Canadian Journal of Chemistry

Published by
THE NATIONAL RESEARCH COUNCIL OF CANADA

Volume 56 Number 1 January 1, 1978

Journal canadien de chimie

Publié par
LE CONSEIL NATIONAL DE RECHERCHES DU CANADA

Volume 56 numéro 1 1 janvier 1978

Can. J. Chem. Downloaded from www.nrcresearchpress.com by 210.87.254.105 on 09/05/12
For personal use only.

Summary of gas phase acidity measurements involving acids AH. Entropy changes in proton transfer reactions involving negative ions. Bond dissociation energies D(A—H) and electron affinities EA(A)

J. B. CUMMING AND P. KEBARLE

Chemistry Department, University of Alberta, Edmonton, Alta., Canada T6G 2G2

Received July 15, 1977

J. B. CUMMING and P. KEBARLE. Can. J. Chem. **56**, 1 (1978).

The complete ladder of ΔG_1^0 determinations obtained from measurements of some 110 gas phase proton transfer equilibria $A_1^- + A_2H = A_1H + A_2^-$ involving some 60 acids AH and connecting to the standard acid HCl is given. Evaluation of the entropy changes leads to values for the deprotonation energies ΔH_D^0 and ΔG_D^0 (at room temperature) corresponding to the gas phase process $AH = A^- + H^+$; $\Delta H_D^0 = D(A—H) - EA(A) + 313.6$ kcal/mol. Comparison of the present data with literature determinations of the bond dissociation energies and electron affinities shows agreement within 2 kcal/mol. Some experimentally determined entropy changes ΔS_1^0 are compared with the theoretically calculated values.

J. B. CUMMING et P. KEBARLE. Can. J. Chem. **56**, 1 (1978).

On rapporte une échelle complète des déterminations de ΔG_1^0 qui a été obtenue à partir des mesures de 110 équilibres de transfert de proton en phase gazeuse $A_1^- + A_2H = A_1H + A_2^-$ impliquant environ 60 acides AH et donnant une relation avec l'acide standard HCl. L'évaluation des changements d'entropie conduit à des valeurs pour les énergies de déprotonation, ΔH_D^0 et ΔG_D^0 (à température ambiante), correspondant au processus en phase gazeuse $AH = A^- + H^+$; $\Delta H_D^0 = D(A—H) - EA(A) + 313.6$ kcal/mol. Une comparaison des données obtenues dans ce travail avec les résultats rapportés dans la littérature pour les énergies de dissociation de liaisons et pour les affinités électroniques présentent une bonne corrélation à l'intérieur de 2 kcal/mol. On a aussi comparé quelques changements d'entropie ΔS_1^0 déterminés expérimentalement avec des valeurs calculées théoriquement.

[Traduit par le journal]

Introduction

Gas phase acidities for a variety of compounds AH determined by measuring the equilibrium constants for the gas phase proton transfer reaction 1 were published in several reports from this laboratory.

[1] $$A_1^- + A_2H = A_1H + A_2^-$$

The classes of compounds were: aliphatic carboxylic acids (1–3), substituted benzoic acids (4, 5), phenols (5), and a variety of carbon and nitrogen acids (6–9). The gas phase equilibria [1] were measured with a pulsed electron beam high ion source pressure mass spectrometer. Measurement of $\Delta G_1^0 = -RT \ln K_1$ permits the establishment of quantitative gas phase acidity orders and continuous acidity ladders. The free energy changes can be related to a standard acid A_0H measuring some equilibria [2] involving the standard acid.

[2] $$A_0^- + AH = A_0H + A^-$$
$$Cl^- + AH = ClH + A^-$$

In the acid determinations from this laboratory the standard acid A_0H selected was HCl. All published acidities were obtained by relating the given compound AH through a continuous ladder of multiple proton transfer equilibria to HCl. In some of the publications (5, 6) partial ladders were published, in others (7–9), only the ladders to a secondary reference compound like pyrolle were given. The secondary reference compound had been previously connected with equilibria to HCl.

We feel that the present publication of the com-

Can. J. Chem. Downloaded from www.nrcresearchpress.com by 210.87.254.105 on 09/05/12
For personal use only.

plete ladder connecting all compounds whose acidity was measured in our laboratory will be useful to other workers in the field and users of the data.

The free energy and enthalpy changes for deprotonation ΔH_D^0 and ΔG_D^0 are defined by eq. 3.

$$[3] \qquad AH_{(g)} = A^-_{(g)} + H^+_{(g)} \qquad \begin{matrix} \Delta G_3^0 = \Delta G_D^0 \\ \Delta H_3^0 = \Delta H_D^0 \end{matrix}$$

ΔH_D is identical to the often used expressions: proton affinity of A^-, $PA(A^-)$ and heterolytic bond dissociation energy $D(A^-—H^+)$.

The relationship [4] permits the determination of $D(A—H) - EA(A)$ from ΔH_2 and the known

$$[4] \quad \Delta H_2^0 = \Delta H_D(AH) - \Delta H_D(A_0H) = D(A—H) - EA(A) - D(A_0—H) + EA(A_0)$$

$D(A_0—H)$ and $EA(A_0)$ of the standard acid. For HCl at 300 K: $D(H—Cl) - EA(Cl) = 20$ kcal/mol (10) and $\Delta H_D = 20 + I_p(H^+) = 333.6$ kcal/mol, where $I_p(H^+) = 313.6$ kcal/mol. In order to obtain ΔH_2^0 from ΔG_2^0 either the temperature dependence of the proton transfer equilibria must be measured and ΔH_2^0 obtained from a van't Hoff plot or ΔS_2^0 must be calculated from theory. Most of the acidity measurements (1–9) were done at a single temperature (600 or 500 K) and values for $D(A—H) - EA(A)$ were obtained via [4] and the assumption that $\Delta G_2^0 = \Delta H_2^0$, i.e. that $\Delta S_2^0 = 0$. The relatively high temperatures of 500–600 K were used for the equilibria determinations since at lower temperatures proton bound dimers AHA^- are formed by reaction 5.

$$[5] \qquad A^- + AH = AHA^-$$

The AHA^- are in equilibrium with A^- and AH and at 500–600 K the equilibria [1] can be measured; however, at low temperatures the concentration of A^- becomes too small to measure accurately, particularly when strongly hydrogen bonding AH (halogen, oxygen, or nitrogen acids) are involved. The temperature dependence of several proton transfer equilibria [1] was examined in earlier work and in general $|\Delta S_1^0|$ was found to be small, i.e. less than 2 cal/deg. At 500 K this leads to a difference between ΔG_1^0 and ΔH_1^0 of 1 kcal/mol and to a similar error in the $D(A—H) - EA(A)$ determinations. Considering the almost complete lack of thermochemical data for the AH systems a 1 kcal/mol error seemed quite acceptable.

The assumption that the entropy change in proton transfer reactions is small has been also made for reaction 6 involving positive ions. The assumption was confirmed by measurement of the temperature dependence of K_6 for several such reactions. Mea-

$$[6] \qquad B_1H^+ + B_2 = B_1 + B_2H^+$$

surements of proton transfer equilibria by the ion cyclotron resonance method (icr) can be made at room temperature because the reactions forming the proton held dimers are third order at low pressures and therefore very slow at icr conditions ($\sim 10^{-6}$ Torr). A comparison of ΔG_6^0(600 K) determined by high pressure mass spectrometry and ΔG_6^0(300 K) determined by icr involving a large number of compounds has shown (11) that the assumption $\Delta S_6^0 \approx 0$ is adequate for many reactions and that for nearly all cases ΔS_6^0 can be quite accurately estimated by considering only the rotational symmetry numbers of reactants and products. Measurement of the temperature dependence of K_6 for substituted benzenes was possible over a wide temperature range and these results (12) provided small ΔS_6^0 changes which could be accurately predicted by consideration of symmetry numbers only.

Recently, through the electron photodetachment measurements of Brauman and co-workers (13–16) a number of electron affinities EA(A) have become available. The availability of such new data makes it clearly desirable to improve the quantitative accuracy of the $D(A—H) - EA(A)$ values obtained from the gas phase acidity measurements.

A reexamination of the assumption that the entropy change ΔS_1^0 for the negative ion proton transfer equilibria is small led to the discovery of an oversight. The equilibrium [2] with the standard acid HCl is exactly a reaction where a significant entropy change can be expected. This comes about from the loss of two rotational degrees of freedom in the change $HCl \rightarrow Cl^-$. This loss is generally not fully compensated by the process $A^- \rightarrow AH$. For example if AH is a carboxylic acid or a phenol only one (internal) rotation will be created for the two rotations disappearing in $HCl \rightarrow Cl^-$. For carbon acids like fluorene there will not even be the appearance of one rotation. Unfortunately no experimental determinations of the temperature dependence of K_2 had been made in the previous work.

Another special problem that arises with acids AH is the appearance of barriers to internal rotation. For example for AH = acetone, the change $CH_3COCH_3 \rightarrow CH_3COCH_2^-$ involves conversion of the near free internal rotation of a methyl group to the very hindered rotation of the CH_2 group, because of partial double bond formation in the enolate anion as shown in structure **1**. The problem created by rotational barriers had been recognized earlier (6) and attempts were made to determine the associated

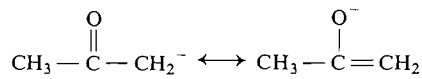

1

Can. J. Chem. Downloaded from www.nrcresearchpress.com by 210.87.254.105 on 09/05/12
For personal use only.

entropy changes by measuring the temperature dependence of selected equilibria [1]. However, the results proved inconclusive (6).

The present work, as already mentioned, combines the previous determinations in one continuous ladder of equilibria. Some new determinations of equilibria [1] were made at key places of the ladder where it appeared necessary to obtain additional multiple cycles. Entropy changes ΔS_2^0 were also evaluated using standard statistical mechanics equations and structural data for AH and A^-. With these ΔS_2^0, ΔH_2^0 and ΔG_D^0 and ΔH_D^0 for AH at 300 K were calculated. Some experimental determinations of entropy changes were also made measuring the temperature dependence of equilibrium constants.

Experimental

The acidity measurements were made by determining the equilibrium constants for the gas phase proton transfer equilibria

[1] $$A_1H + A_2^- = A_1^- + A_2H$$

The method was the same as that used earlier (1–9). A_1H and A_2H at known pressures in the mTorr range were carried in slow flow by ~4 Torr methane carrier gas. The gas also contained some 20 mTorr of NF_3. Short electron pulses through the ion source produced F^- ions by the electron capture reaction $NF_3 + e = F^- + NF_2$. The ions A_1^- and A_2^- resulted from proton transfer from AH to F^-. The reaction mixture was sampled by bleeding a fraction of the gas into a mass spectrometer where the ions were mass analyzed and detected.

Results and Discussion

a. Summary of Equilibrium Measurements and Gas Phase Deprotonation Energies

The free energy changes ΔG_1^0 determined experimentally from $-RT \ln K_1 = \Delta G_1^0$ of reaction 1 are shown in Fig. 1. Almost all of the ΔG_1^0 data shown were published previously (1–9) but only as partial sections of the ladder. Examining the cases where mutiple cycles are available one finds that the ΔG_1^0 values are consistent to ~0.2 kcal/mol. The ΔG_2^0 relating AH to the standard HCl are also shown in Fig. 1. These were obtained by combining the various ΔG_1^0 determinations between AH and HCl. The ΔS_2^0 changes at the experimental temperature were calculated by methods described in the next section. These ΔS_2^0 were used to evaluate the corresponding ΔH_2^0 from $\Delta G_2^0 = \Delta H_2^0 - T\Delta S_2^0$. The ΔH_2^0 at the experimental temperature were corrected to ΔH_2^0 at 300 K by using calculated heat capacity changes $\Delta(C_p)_2$ which require the same data as the ΔS_2^0 evaluations. From $\Delta H_2^0(300)$ and $\Delta S_2^0(300)$, $\Delta G_2^0(300)$ was evaluated. The deprotonation energies $\Delta H_D^0(300)$ and $\Delta G_D^0(300)$ were evaluated from the corresponding $\Delta H_2^0(300)$ and $\Delta G_2^0(300)$ and eqs. 5 and 6 which follow from eq. 4 and the known thermochemical data (10) for HCl.

$$\Delta H_2^0(300) = \Delta H_D^0(AH) - \Delta H_D^0(HCl)$$
$$= \Delta H_D^0(AH) - 333.6 \text{ kcal/mol}$$
$$\Delta G_2^0(300) = \Delta G_D^0(AH) - \Delta G_D^0(HCl)$$
$$= \Delta G_D^0(AH) - 327 \text{ kcal/mol}$$

The ΔH_2^0 at the experimental temperature, and the ΔH_D^0 and ΔG_D^0 at 300 K are given in Fig. 1. Since in the previous publications (1–6), $\Delta S_2^0 = 0$ had been assumed, the D(A—H) − EA(A) data given in these publications actually correspond to the present ΔG_2^0(600 or 500) + D(H—Cl) − EA(Cl), i.e. ΔG_2^0(600 or 500) + 20 kcal/mol.

As shown in the next section, in the average, $\Delta S_2^0 \approx 6$ cal/mol. This leads to a $T\Delta S_2$ term at 600 K of 3.6 kcal/mol. Therefore, the D − EA given in Fig. 1 are, in the average, higher by 3–4 kcal/mol from the D − EA quoted in the earlier work where the assumption $\Delta S_2^0 = 0$ had been made.

Lack of information on energy barriers for internal rotation in the anions A^- introduces some error in the ΔS calculations given in the next section. Therefore it is of interest at this point to compare the present data with data available in the literature. This is done in Table 1. The values compared are D(A—H) − EA(A) from separate determinations of D(A—H) and EA(A) in the literature with D(A—H) − EA(A) = ΔH_D(A—H) − 313.6 kcal/mol from Fig. 1, where 313.6 kcal/mol corresponds to the ionization potential of hydrogen. The EA for compounds other than Cl and HS involve polyatomic species. The literature data for these species are based on electron photodetachment thresholds (Brauman and co-workers (13–16)). Considerable difficulties exist in interpreting the photodetachment threshold curves and extracting electron affinities from them, particularly because of uncertainty whether the photodetaching A^- have vibrational excitation or not. However, the authors (13–16) have made considerable efforts to interpret the threshold curves. Therefore, the electron affinities are probably within a few kcal/mol of the true adiabatic values. The bond dissociation energies D(A—H) for the polyatomic AH are mostly obtained by kinetic methods and are also probably uncertain to within ~2 kcal/mol. Comparing the D − EA literature data with the equilibrium data in Table 1 we find that the agreement is within 1–2 kcal/mol, i.e. certainly within the uncertainty of the literature data and the equilibrium data. The equilibrium data appear to be consistently higher by about 1 kcal/mol. Of special interest is the comparison for H_2S, since the electron

TABLE 1. Comparison between D(A—H) − EA(A) from ion equilibria measurements and thermochemical data[a]

AH	D(A—H)[c]	Ref.	EA(A)[d]	Ref.	D(A—H) − EA(A) Literature	D(A—H) − EA(A) Equilibria
HCl	103	10	83	10	20	20[b]
H_2S	91.1	10	53.5	17	37.6	38.4
Phenol	89.0	17	54.5	14	34.5	36.2
Cyclopentadiene	81.2	18	42.4	13	38.8	41.9
2-Butanone	92.3	19	38.6	15	53.7	54.6
Acetone	98.0	19	40.6	15	57.4	56.2
CH_3CN	92.9	20	34.8	16	58.1	59.3

[a]All values in kcal/mol; D(A—H) − EA(A) (equilibria) is obtained by subtracting I_p(H) = 313.6 kcal/mol from H_D^0 given in Fig. 1.
[b]Primary standard used in equilibria measurements.
[c]Error in literature bond dissociation energy determinations generally ±2 kcal/mol except for HCl which is accurately known.
[d]Error in literature electron affinity generally ±2 kcal/mol except for Cl and HS.

affinity (21) for the diatomic HS is probably accurate to less than 1 kcal/mol. Unfortunately the bond energy appears to be less well known. Thus, Kerr (22) gives limits 90 ± 2 kcal/mol. Taking the upper limit of 92, rather than the 91.1 kcal/mol (10) used in the table, one predicts D − EA of 38.5 which is in complete agreement with the equilibrium result.

Hydrogen sulfide lies roughly halfway up on the energy scale between HCl and the compound with highest ΔH_D^0 (Me_2SO) in Fig. 1. Clearly it would have been desirable to fix the upper part of the scale through measuring equilibria with an AH whose D − EA is accurately known. The suitable compound exists; it is HF for which D(H—F) − EA(F) = 57.4 kcal/mol (23, 24). Experiments were undertaken to measure proton transfer equilibria involving HF. However, the major ion observed was not F^- but SiF_5^-. This ion was evidently formed from F^- and SiF_4, the latter being produced by reaction of the HF with glass present in the apparatus. We hope to report HF equilibria with modified apparatus containing no glass. McIver and co-workers reported recently (25) measurements of proton transfer equilibria performed with an ion cyclotron resonance spectrometer which gave ΔG_D^0(HF) − ΔG_D^0(Me_2SO) = 0.3 kcal/mol at 25°C. Using ΔG_D^0(HF) = ΔH_D(HF) − $T\Delta S_D$ = 57.4 + 313.6 − 5.7 = 365.3 kcal/mol one obtains ΔG_D^0(Me_2SO) = 365 kcal/mol. The ΔG_D^0(Me_2SO) = 367.2 kcal/mol is obtained in the present results (see Fig. 1). The present result is higher by ~2 kcal/mol from the value of McIver and co-workers (25). Considering that the present Me_2SO result is calibrated to HCl which is some 41 kcal/mol and many equilibrium steps away, and that ΔG_D^0 at 300 K involved evaluation of entropy changes, a cumulative error of 2 kcal/mol is not surprising. It seems that the best probable data would be obtained if the ΔH_D^0 and ΔG_D^0 in Fig. 1 for compounds between H_2S and Me_2SO were reduced by ~1 kcal/mol.

b. Evaluation of Entropy Changes and Comparison with Experiment

The evaluation of the entropy changes for reaction 2 can be split up into evaluation of the entropy

[2] $$Cl^- + AH = ClH + A^-$$

change for the two half reactions:

[2*a*] $$Cl^- = ClH$$

[2*b*] $$AH = A^-$$

In both cases, one requires the third law entropies for each species. These are given by the well known expression

[7] $$S^0 = S^0_{trans} + S^0_{rot} + S^0_{vib} + S^0_{el}$$

$\Delta S^0_{trans}(2) \approx 0$ is obtained from the Sackur–Tetrode equation. $S^0_{el} = 0$, since singlet states are involved. Using for S^0_{rot}(HCl) the well known equation for rotational entropy of diatomic molecules and $\Delta S^0_{vib}(2a) = 0$, one obtains ΔS^0(2*a*, 298 K) = 8 cal/deg and ΔS^0(2*a*, 600 K) = 9.4 cal/deg. At 298 K

FIG. 1. Experimental free energy changes in kcal/mol for gas phase proton transfer reactions 1: A_2^- + A_2H = AH + A_2^- shown beside vertical double arrows. Experimental determinations were made at 600 and 500 K. A_1H is the compound shown at the bottom of the double arrow. Acidity increases from top to bottom. ΔG_2^0 and ΔH_2^0 refer to proton transfer reactions involving standard compound HCl (eq. 2) Cl^- + AH = ClH + A^-. ΔH_D^0 and ΔG_D^0 refer to deprotonation of AH: AH = A^- + H^+. These values were obtained from the experimental ΔG_2^0 (500 or 600) and evaluation of the entropy changes. Estimated accuracy of ΔG_1^0 values ±0.2 kcal/mol, ΔH_D^0 and ΔG_D^0 ±2 kcal/mol. Data obtained for substituted phenols and benzoic acids (5) are not included in Fig. 1.

Can. J. Chem. Downloaded from www.nrcresearchpress.com by 210.87.254.105 on 09/05/12
For personal use only.

Can. J. Chem. Downloaded from www.nrcresearchpress.com by 210.87.254.105 on 09/05/12
For personal use only.

300°K		600°K(*500°K)		
ΔH_D^o	ΔG_D^o	ΔH_2^o	ΔG_2^o	Compound
374.6	367.2	41.0	37.3	*Dimethylsulphoxide
373.5	365.6	40.0	35.6	*Acetonitrile
370.0	362.4	36.7	32.5	*Acetone
368.2	361.3	34.9	31.9	*2-Butanone
368.2	361.4	34.9	31.2	*3-Pentanone
367.6	360.5	34.1	31.0	*3-Methyl,2-Butanone
367.0	359.7	33.6	30.1	*Acetaldehyde
366.4	359.4	33.0	29.9	*Propionaldehyde
366.4	358.9	32.8	29.0	*Dimethyl Sulphone
364.5	357.2	30.9	27.6	*Phenyl, Ethyl Sulphone
363.6	356.3	30.0	26.7	*Phenyl, n-Propyl Sulphone
362.7	355.9	29.2	26.1	Diphenyl Methane
362.6	355.4	29.0	25.7 (25.8*)	*Phenyl, isobutyl Sulphone
362.8	355.5	29.4	25.2	Acetophenone
362.7	355.3	29.1	25.6	*Phenyl Methyl Sulphone
361.3	354.9	27.7	25.5	*Phenylcyclopropyl Sulphone
361.2	354.1	27.8	24.7 (22.2*)	*Propiophenone
359.2	351.8	25.8	21.6	Pyrrole
357.6	350.7	24.3	21.1	*Nitromethane
357.3	351.0	24.0	21.0	*Nitroethane
356.6	350.3	23.2	20.9	*2-Nitropropane
355.5	348.7	21.9	18.8	Cyclopentadiene
353.1	345.9	19.6	16.8 (16.4*)	p-Nitrotoluene
352.0	345.6	18.4	16.2	H_2S
351.8	345.4	18.8	16.0	Phenylacetone
352.8	345.8	19.3	15.1	Acetanilide
353.3	345.5	19.7	14.7	Fluorene
351.9	344.9	18.7	14.8	Phenylacetonitrile
351.7	344.9	17.9	14.3	p-Cresol
350.3	343.3	16.9	13.3	Acetonyl Acetate
350.3	343.2	16.9	13.2	Trifluoroacetone
349.8	343.4	16.0	13.2	Phenol
348.3	342.3	15.2	12.4	Diethyl Malonate
348.5	341.5	14.7	11.7	Acetic Acid
348.5	341.1	15.0	11.1	Acetyl Urea
347.3	340.3	13.5	10.5	Propionic Acid
346.8	339.8	13.4	10.2	Diacetamide
346.5	339.5	12.7	9.7	n-Butyric Acid
345.4	338.4	11.6	8.6	γ-Chlorobutyric Acid
345.2	338.2	11.4	8.4	Formic Acid
343.7	336.6	10.6	7.8	Acetyl Acetone
345.4	338.0	11.8	7.6	Succinimide
341.9	334.9	8.1	5.1	β-Chlorobutyric Acid
339.9	333.0	6.9	4.1	Benzoyl Acetone
340.8	333.8	7.0	4.0	β-Chloropropionic Acid
338.8	331.7	5.0	3.1	Benzoic Acid
337.6	331.0	3.9	1.1	Fluoroacetic Acid
337.5	330.9	3.8	1.1	α-Chlorobutyric Acid
338.9	331.1	5.3	0.3	Dimedone
336.4	329.8	2.7	0.0	α-Chloropriopionic Acid
333.6	328.1	0	-	HCl
335.4	328.8	1.7	-1.0	Chloroacetic Acid
334.0	327.4	0.4	-2.2	Bromoacetic Acid
336.0	328.2	2.4	-2.6	Malonitrile
335.1	327.3	1.5	-3.5	Barbituric Acid
330.0	323.5	-3.6	-6.1	Difluoroacetic acid
328.5	322.1	-4.6	-7.4	Trifluoroacetyl acetone
328.4	321.9	-5.2	-7.7	Dichloroacetic acid
322.7	316.3	-10.8	-13.1	Trifluoroacetic acid

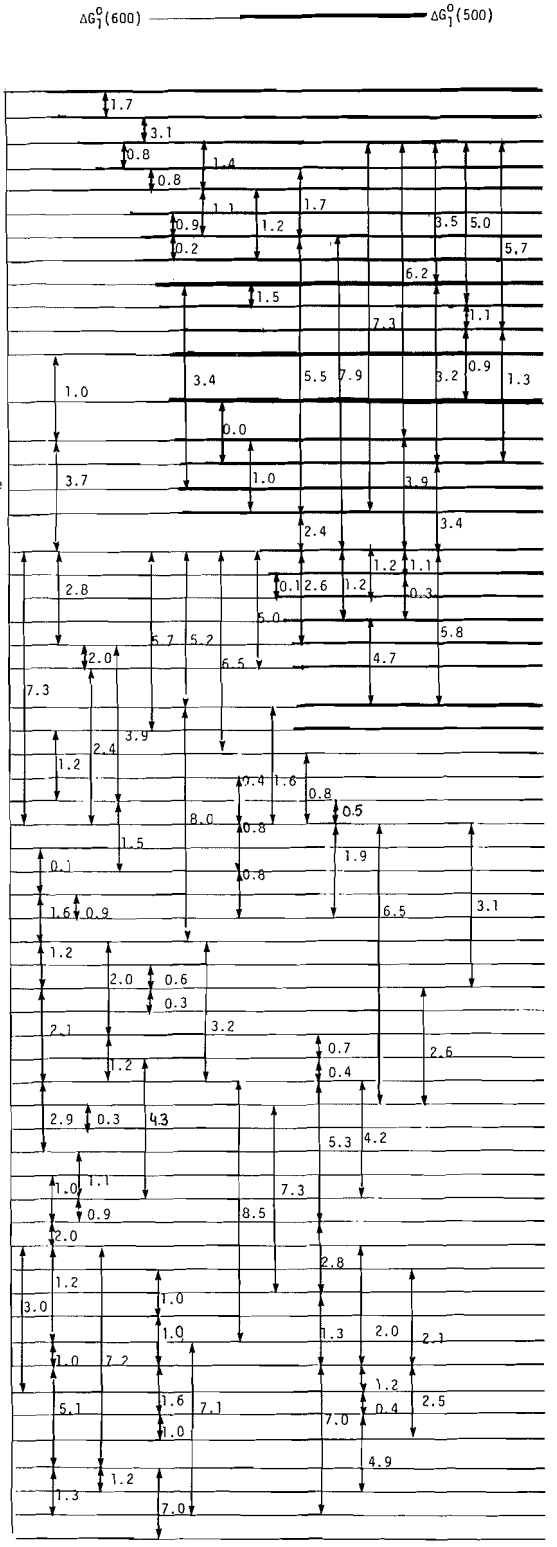

TABLE 2. Barriers V for internal rotation and entropy changes for $AH \rightarrow A^-$

Compound	V(AH) (kcal/mol)	Ref.	$V(A^-)$ (kcal/mol)[d]	σ_{AH}/σ_{A^-}[a]	$\Delta S^o(600)$[b]
Dimethyl sulfoxide	2.94	29	15.3	1	−2.0*
Acetonitrile	—		—	3/2	+0.6*
Acetone	0.78	30	13.0	2/1	−1.1*
2-Butanone	1.0[c]	30	13.3	1	−3.4*
3-Pentanone	1.0[c]	30	13.3	2/1	−2.0*
3-Methyl-2-butanone	2.0[c]	30	14.2	1	−3.3*
Acetaldehyde	1.16	31	13.4	1	−2.4*
Propionaldehyde	1.7[f]		13.9	1	−3.2*
Dimethyl sulfone	4.5	32	20.7	1	−1.8*
Phenyl ethyl sulfone	4.0[e]	—	20.3	1	−2.0*
Phenyl *n*-propyl sulfone	4.0[e]	—	20.3	1	−2.0*
Diphenyl methane	3.0[e] 3.0[e]	—	11.1 11.1	1	−4.2
Phenyl isobutyl sulfone	4.0[e]	—	20.3	1	−2.0*
Phenyl methyl sulfone	4.0[e]	—	20.3	1	−1.6*
Phenyl cyclopropyl sulfone	1[e]	—	17.0	1	−2.8*
Acetophenone	1.2[e]	—	13.4	1	−2.2*
Propiophenone	1.5[e]	—	13.7	1	−3.2*
Pyrrole	—		—	1/2	−2.4
Nitromethane	6.0×10^{-3}	34	12.2	1/2	−3.0*
Nitroethane	0		12.2	1	−3.3*
2-Nitropropane	0		12.2	1/2	−4.9*
Cyclopentadiene	—		—	2/10	−4.2
p-Nitrotoluene	0.014	35	12.2	1/2	−4.7
Hydrogen sulfide	—		—	—	—5.6
Phenyl acetone	2[e]		14.2	1	−4.7
	C—N N—ϕ		N—ϕ		
Acetanilide	11.0[e] 11		19.1 19.1	1	−2.3
Fluorene	—		—	1	−1.0
Phenylacetonitrile	0[e]		8.1	1	−2.9
Cresol	3.4	36	—	1	−3.3
Acetonyl acetate	1.5[e]		13.7	1	−3.3
Trifluoro acetone	1.0[e]		13.2	1	−3.2
Phenol	3.37	36	—	1/2	−4.7
Diethyl malonate	1.5[e] 1.5[e]		9.6 9.6	1	−4.7
Acetic acid	13.4	38		1	−4.4
Acetyl urea	10[e] 10[e]		18.1 18.1	1	−2.8
Propionic acid	13.4	38	—	1	−4.4
Diacetamide	10.0[f]				
n-Butyric acid	13.4	38	—	1	−4.4
α-Chlorobutyric acid	13.4	38	—	1	−4.4
Formic acid	13.4	38	—	1/2	−4.4
Acetyl acetone	1.5[e] 1.5[e]		9.6 9.6	1	−4.7
Succinimide	—		—	1/2	−2.4
β-Chlorobutyric acid	13.4	38	—	1	−4.4
Benzoyl acetone	1.0[e] 1.0[e]		9.1 9.1	1	−4.7
β-Chloropropionic acid	13.4	38	—	1	−4.4
		39			
Benzoic acid	13.4 4.1	39	— 0	1/2	−3.4
	C—O C—C				
Fluoroacetic acid	13.4 1	38, 39	— 2.5	1	−4.7
	C—O C—C				
α-Chlorobutyric acid	13.4 1	38, 39	— 3.0	1	−4.9
Dimedone	—		—	1	−1.0
	C—O C—C				
α-Chloropropionic acid	13.4 1.0	38, 39	— 3.0	1	−4.9
Hydrochloric acid	—		—	—	−9.3
	C—O C—C				
Chloroacetic acid	13.4 1.0	38	— 3.0	1	−4.9
	C—O C—C				
Bromoacetic acid	13.4 15.0	38	4.0	1	−5.1
Malonitrile	—		—	1	−1.0
Barbituric acid	—		—	1	−1.0
	C—O C—C		C—C		

Can. J. Chem. Downloaded from www.nrcresearchpress.com by 210.87.254.105 on 09/05/12
For personal use only.

TABLE 2 (*Concluded*)

Compound	V(AH) (kcal/mol)		Ref.	$V(A^-)$ (kcal/mol)[d]		σ_{AH}/σ_{A^-}[a]	$\Delta S^0(600)$[b]
Difluoroacetic acid	13.4	1.0	38	—	4.0	1	−5.2
Trifluoroacetyl acetone	1.0[e]	1.0[e]	—	9.1	9.1	1	−4.7
	C—O	C—C			C—C		
Dichloroacetic acid	13.4	1.0	38	—	4.0	1	−5.2
	C—O	C—C			C—C		
Trifluoroacetic acid	13.4	1.0	38	—	5.0	1	−5.5

[a]Symmetry numbers for external rotation.
[b]Entropy change (cal/deg) for process AH → A^- at 600 K except numbers with * for which the temperature is 500 K.
[c]Barrier assumed to be equal to that in acetone.
[d]Barrier in A^- estimated as explained in text.
[e]Author's estimate based on barriers given in ref. 33.
[f]Barrier assumed to be equal to that in acetaldehyde.

and 600 K these lead to $T\Delta S$ terms of 2.4 kcal/mol and 5.6 kcal/mol respectively. The $\Delta S_{2a}{}^0$ change makes the major contribution to $\Delta S_2{}^0$. The smaller $\Delta S_{2b}{}^0$ changes are generally negative and amount for the 'average' compound to −3 cal/deg.

The rotational entropy contributions to $\Delta S_{2b}{}^0$ were evaluated by splitting the rotational motion into external rotation and internal rotation. When considering external rotation the changes of the moment of inertia in AH and A^- were taken into account. Significant changes occur only for HCl and H_2S but smaller changes as for example in $CH_3CN \rightarrow CH_2CN^-$ were also considered. Significant rotational entropy changes occur also because of changes in external rotation symmetry numbers. These were evaluated with the standard formula $\Delta S^0{}_{\text{rot sym}} = R \ln (\sigma_{AH}/\sigma_{A^-})$. These corrections are not always unambiguous. Thus for the CH_2CN^- the symmetry number may be 2 or 1 depending on whether the CH_2 group is assumed planar (sp^2) or trigonal (sp^3). In the above case and the enolate systems we have assumed planar carbanions. The symmetry numbers used for the external rotations are shown in Table 2.

Only the internal rotations which would change in the dissociation AH → A^- were considered. The prime examples in this class are the disappearing rotation around the C—O bond on dissociation of hydroxy acids and the already mentioned stiffening of internal rotation in the resonance stabilized ions A^- like the acetonyl ion shown in structure **1**. The calculations of the restricted internal rotation entropies were made by using the table of Pitzer and Gwinn (26, 27). In this table the entropy for internal rotation around a given bond is tabulated as a function of the partition function for free rotation Q_f and the expression V/RT where V is the energy barrier for the internal rotation. Q_f is evaluated (26) by [8],

$$[8] \qquad Q_f = (8\pi^3 I_r kT)^{1/2}/nh$$

where I_r is the reduced moment of inertia for the internal rotation and n is the number of equivalent positions per turn, i.e. the symmetry number for the internal rotation.

The energy barriers V for the internal rotation in the neutrals AH can be estimated to within ~1 kcal/mol. In many cases these barriers are available directly from the literature (28–39). Where no literature data were available estimates by analogy were made. The barriers used in the calculations are summarized in Table 2. No literature data for the internal rotations in A^- are available. Therefore, these had to be estimated. For ions in which charge delocalization occurs equal weighting was given to each possible valence bond structure. Thus the rotation of the CH_2 group in acetonyl$^-$ (see structure **1**) was taken to have a barrier equivalent to that of $\frac{1}{2}\pi$ bond. In the diketones where three resonance structures are possible the barrier for rotation of the CH_3CO group was taken to be that of $\frac{1}{3}\pi$ bond barrier (see structure **2**).

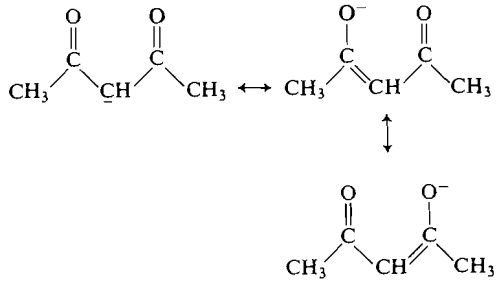

2

The potential barrier V = 26 kcal/mol in ethylene (40) was taken as the π bond barrier. Thus, the assumed barrier in structure **1** was 13 and in **2**, 8.7 kcal/mol. Small adjustments to these barriers were made for cases where the rotating groups were large and could be expected to interfere sterically. The barriers in A^- obtained by such procedures and used in the calculations are shown in Table 2. Evidently errors in V as large as 5 kcal/mol may well be present. These lead to an error of about 1 cal/deg in the entropy.

The tables of Pitzer and Gwinn (26) used for obtaining the values for the hindered rotation $\Delta S^0{}_{\text{rot}}$ are valid for rotation of a symmetric top about a rigid framework. Most of the cases involved in the

Can. J. Chem. Downloaded from www.nrcresearchpress.com by 210.87.254.105 on 09/05/12
For personal use only.

TABLE 3. Comparison of calculated with experimental entropies[a]

A_1	A_2	ΔS_1^0(exp.)	ΔS_1^0(calc.)	ΔH^0(exp.)	ΔH^0(calc.)
Pyrrole	*p*-Nitrotoluene	-2.5 ± 0.4	-2.3	-6.4 ± 0.2	-5.7
Acetone	3-Pentanone	-2.3 ± 0.8	-0.9	-2.7 ± 0.4	-1.1
Acetonitrile	Acetone	-3.5 ± 0.5	-0.5	-4.6 ± 0.2	-3.1
Phenylacetone	Fluorene	$+3.5\pm0.6$	$+3.7$	$+0.9\pm0.3$	$+1.5$

[a] ΔS_1^0 values for reaction $A_1^- + A_2H = A_1H + A_2^-$. Entropies given in (cal/deg), ΔH_1^0 values in kcal/mol. The calculated entropies were taken from Table 2. The experimental data are from Fig. 2.

present systems involve rotating groups that are not symmetric tops and the rest of the molecule is also non-rigid. However, the tables have approximate validity also for such systems when applied as shown in Pitzer (27). In any case the error, because of use of the tables for molecules without symmetric tops, should be smaller than the errors due to the estimates of the potential energy barriers.

Estimates of the small vibrational changes for the reaction $AH \rightarrow A^-$ were obtained by considering only the disappearance of bending vibrations. The frequencies of such vibrations were taken from a table of group frequencies (41). The entropy of the vibration in AH was evaluated from the harmonic oscillator vibrational partition function. The vibrational ΔS changes amounted in the average to a loss of 2 cal/deg at 600 K.

The ΔS_{2b} for the reaction $AH \rightarrow A^-$ obtained by summing all the contributions described above are shown in Table 2.

The experimentally measured entropy changes for proton transfer reactions 1 obtained from van't Hoff plots of the equilibrium constant K_1 are given in Table 3. The corresponding van't Hoff plots are shown in Fig. 2.

Some difficulties in measuring the temperature dependence of K_1 should be mentioned. Because of formation of AHA^- at low temperature by reaction 5 and pyrolysis of AH or A^- at high temperature, the available temperature range is quite restricted. Furthermore in the lower temperature range where appreciable AHA^- is present at equilibrium, dissociation of AHA^- outside the ion source (42) can produce non-equilibrium A^-. This A^- can falsify the temperature dependence of the observed equilibrium constant. As shown by Farneth and Brauman (43), the proton transfer reactions 1 involving delocalized anions A^- are slow even in the exothermic direction. Therefore the establishment of the equilibrium [1] particularly where both A_1^- and A_2^- are delocalized may take milliseconds. Such a long reaction time reduces the accuracy of the measurements since the concentrations of A_1^- and A_2^- are affected by diffusion to the wall and this diffusion has strong temperature dependence (44). Unfortunately all these factors reduce the confidence in the temperature dependence measurements.

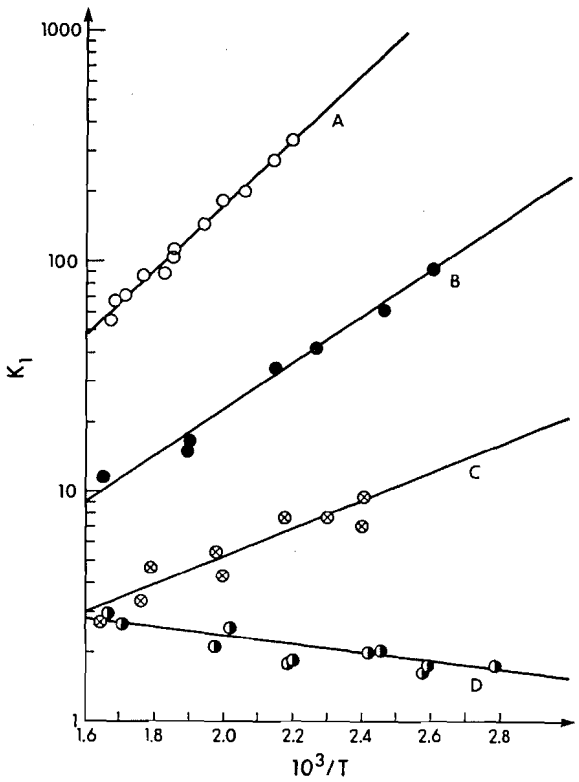

FIG. 2. Van't Hoff plots of experimentally measured temperature dependence of equilibrium constants K_1 for proton transfer reactions $A_1^- + A_2H = A_1H + A_2^-$: (*A*) A_1H pyrrole, A_2H *p*-nitrotoluene, (*B*) A_1H acetonitrile, A_2H acetone, (*C*) A_1H acetone, A_2H diethylketone, (*D*) A_1H $PhCH_2COCH_3$, A_2H fluorene.

Comparing the $\Delta S^0{}_{1(exp)}$ obtained from the van't Hoff plots with the $\Delta S^0{}_{1(calc)}$ obtained from the entropy changes in Table 2 we notice that the agreement is fair. The reaction

$$CH_2CN^- + CH_3COCH_3 = CH_3CN + CH_3COCH_2^-$$

shows the largest deviation between $\Delta S^0{}_{(calc)} = -0.5$ cal/deg and $\Delta S_{(exp)} = -3$ cal/deg. It should be realized that a difference of 2.5 cal/deg is not really large considering some of the difficulties encountered

Can. J. Chem. Downloaded from www.nrcresearchpress.com by 210.87.254.105 on 09/05/12
For personal use only.

Can. J. Chem. Downloaded from www.nrcresearchpress.com by 210.87.254.105 on 09/05/12
For personal use only.

in the measurements and the calculations. As mentioned previously, the C atom in CH_2CN^- is assumed to be sp^2, i.e. planar with a symmetry number $\sigma = 2$ for external rotation. However, if the pyramidal structure (sp^3) is the correct one, this change would lead to $\Delta S^0_{(calc)} \approx -2$ cal/deg, which is much closer to $\Delta S^0_{(exp)} = -3 \pm 0.5$ cal/deg. We believe that neither the calculated nor the experimental ΔS^0 are better than ± 2 cal/deg. For data obtained at 500 and 600 K this leads to an error in the $\Delta H_D{}^0$ of ± 1 kcal/mol. Considering also a sliding error in the acidity ladder, $\Delta H_D{}^0$ given in Fig. 1 should have a confidence of ± 2 kcal/mol. The same conclusion was reached in the preceding section by comparison of the present results with literature data. The relative values $\Delta G_1{}^0$ at the experimental temperature have much smaller errors (± 0.2 kcal/mol) and are better suited for acidity comparisons.

Acknowledgement

The support of this work by grants from the National Research Council of Canada is gratefully acknowledged.

1. R. YAMDAGNI and P. KEBARLE. J. Am. Chem. Soc. **95**, 4050 (1973).
2. K. HIRAOKA, R. YAMDAGNI, and P. KEBARLE. J. Am. Chem. Soc. **95**, 6833 (1973).
3. R. YAMDAGNI and P. KEBARLE. Can. J. Chem. **52**, 861 (1974).
4. R. YAMDAGNI, T. B. MCMAHON, and P. KEBARLE. J. Am. Chem. Soc. **96**, 4035 (1974).
5. T. B. MCMAHON and P. KEBARLE. J. Am. Chem. Soc. **99**, 2222 (1977).
6. T. B. MCMAHON and P. KEBARLE. J. Am. Chem. Soc. **96**, 5940 (1974); **98**, 3399 (1976).
7. J. B. CUMMING and P. KEBARLE. J. Am. Chem. Soc. **99**, (1977).
8. J. B. CUMMING, T. J. MAGNERA, and P. KEBARLE. Can. J. Chem. **55**, 3474 (1977).
9. J. B. CUMMING and P. KEBARLE. J. Am. Chem. Soc. **99**, (1977).
10. Selected Values of Chemical and Thermodynamic Properties. NBS Technical Note 270-3. U.S. Department of Commerce, National Bureau of Standards, Washington, DC. 1968.
11. J. F. WOLF, R. H. STALEY, I. KOPPEL, M. TAAGEPERA, R. T. MCIVER, JR., J. L. BEAUCHAMP, and R. W. TAFT. J. Am. Chem. Soc. **99**. In press.
12. Y. LAU and P. KEBARLE. J. Am. Chem. Soc. **98**, 7452 (1976).
13. J. H. RICHARDSON, L. M. STEPHENSON, and J. I. BRAUMAN. J. Chem. Phys. **59**, 5068 (1973).
14. A. H. ZIMMERMAN and J. I. BRAUMAN. J. Chem. Phys. In press.
15. A. H. ZIMMERMAN, K. J. REED, and J. I. BRAUMAN. J. Am. Chem. Soc. In press.
16. A. H. ZIMMERMAN and J. H. BRAUMAN. J. Am. Chem. Soc. In press.
17. D. H. FINE and J. B. WESTMORE. Chem. Commun. 273 (1969).
18. S. FURNYANA, O. M. GOLDEN, and W. S. BENSON. Int. J. Chem. Kinet. **3**, 237 (1971).
19. R. K. SOLLY, D. M. GOLDEN, and S. W. BENSON. Int. J. Chem. Kinet. **2**, 11 (1970); **2**, 38 (1970).
20. K. D. KING and R. D. GODDARD. Int. J. Chem. Kinet. **7**, 837 (1975).
21. B. STEINER. J. Chem. Phys. **45**, 5057 (1968).
22. J. A. KERR. Chem. Rev. **66**, 465 (1966).
23. S. W. BENSON. J. Chem. Educ. **42**, 502 (1965).
24. K. C. SMYTH and J. I. BRAUMAN. J. Chem. Phys. **56**, 1132 (1972).
25. R. T. MCIVER, J. BARTMESS, and J. S. MILLER. Communication presented at Fifth Structure Energy Conference, Santa Barbara. February 1977.
26. K. S. PITZER and W. D. GWINN. J. Chem. Phys. **10**, 428 (1942).
27. K. S. PITZER. J. Chem. Phys. **14**, 428 (1946).
28. J. C. EVANS. Spectrochim. Acta, **16**, 1382 (1960).
29. H. DREIZLER and G. DENDL. Z. Naturforsch. **20a**, 1431 (1965).
30. R. NELSON and L. PIERCE. J. Mol. Spectrosc. **18**, 344 (1965).
31. R. W. KILB and C. C. LIN. Bull. Am. Phys. Soc. **1**, 198 (1956).
32. A. L. CLEVER and E. F. WESTRUM, JR. J. Phys. Chem. **74**, 1309 (1970).
33. J. P. LOWE. Prog. Phys. Org. Chem. **6**, 1 (1968).
34. E. TANNENBAUM, R. I. MYERS, and W. E. GWINN. J. Chem. Phys. **25**, 42 (1956).
35. C. A. WULFF. J. Chem. Phys. **39**, 1227 (1963).
36. T. PEDERSON, N. W. LARSEN, and L. NYGAARD. J. Mol. Struct. **4**, 59 (1969).
37. W. J. TABOR. J. Chem. Phys. **27**, 974 (1957).
38. D. L. BERNITT, K. D. HARTMAN, and I. C. HISATSUNE. J. Chem. Phys. **42**, 3553 (1965).
39. W. J. HEHRE, L. RADOM, and J. A. POPLE. J. Am. Chem. Soc. **94**, 1496 (1972).
40. S. W. BENSON. Thermochemical kinetics. John Wiley, New York, NY. 1969.
41. G. HERZBERG. Infrared and Raman spectra. van Nostrand, New York, NY. 1945. p. 195.
42. K. HIRAOKA and P. KEBARLE. J. Am. Chem. Soc. **97**, 4175 (1975).
43. W. E. FARNETH and J. I. BRAUMAN. J. Am. Chem. Soc. **98**, 7891 (1976).
44. P. KEBARLE. *In* Interactions between ions and molecules. *Edited by* P. Ausloos. Plenum Press, New York, NY. 1974.

The heterogeneous catalytic reaction between carbon monoxide and nitrous oxide over manganous oxide and cobalto-cobaltic oxide

BORDAN WALTER KRUPAY AND ROBERT ANDERSON ROSS

Department of Chemistry, Lakehead University, Thunder Bay, Ont., Canada P7B 5E1

Received June 27, 1977

BORDAN WALTER KRUPAY and ROBERT ANDERSON ROSS. Can. J. Chem. **56**, 10 (1978).

The catalytic reaction between carbon monoxide and nitrous oxide has been studied on MnO from 493 to 573 K and on Co_3O_4 from 383 to 493 K. The apparent activation energy on MnO was 130 ± 4 kJ mol^{-1}, while for Co_3O_4, a change from 31 ± 4 to 105 ± 4 kJ mol^{-1} was observed at 450 K. The rate-controlling step for the catalytic reaction on MnO was associated with the surface reaction between carbon monoxide and nitrous oxide in a manner similar to that previously reported for NiO, while for Co_3O_4, the rate-determining step was related to the formation of an intermediate surface carbonate. The changes in E_A may be a consequence of the surface reaction proceeding via a concerted redox reaction in the low temperature region and then to a stepwise mechanism at higher temperatures resulting from the presence of structurally and energetically different forms of the intermediate surface carbonate.

BORDAN WALTER KRUPAY et ROBERT ANDERSON ROSS. Can. J. Chem. **56**, 10 (1978).

On a étudié la réaction du monoxyde de carbone et de l'oxyde nitreux catalysée par du MnO entre 493 et 573 K et du Co_3O_4 entre 383 à 493 K. L'énergie d'activation apparente sur MnO est de 130 ± 4 kJ mol^{-1} alors que pour Co_3O_4 on observe un changement de 31 ± 4 à 105 ± 4 kJ mol^{-1} à 450 K. L'étape déterminante de la réaction catalysée par le MnO est associée avec la réaction de surface entre le monoxyde de carbone et l'oxyde nitreux d'une façon semblable à celle rapportée antérieurement pour NiO alors que pour le Co_3O_4, l'étape déterminante est reliée avec la formation d'une carbonate intermédiaire à la surface. Les changements dans les E_A peuvent être une conséquence de la réaction de surface qui procéderait par l'intermédiaire d'une réaction concertée rédox dans la région de basse température; à des températures élevées, la réaction de surface procéderait par étapes grâce à la présence à la surface de formes des carbonates qui diffèrent tant par leur structure que par leur énergie.

[Traduit par le journal]

Introduction

Relationships between the surface chemical properties of manganese oxides and their activities in heterogeneous catalytic reactions have recently been explored in studies of the decomposition of isopropanol (1) and formic acid (2), and also the water–gas shift reaction (3). The rate-controlling step in the mechanism of the latter was related to the reducing action of adsorbed carbon monoxide on a surface oxygen species. These studies have now been extended to include an investigation of the reaction between carbon monoxide and nitrous oxide on manganous oxide catalysts and expanded to include cobalto-cobaltic oxide, Co_3O_4.

The oxidation of carbon monoxide and the decomposition of nitrous oxide have separately received considerable attention as model catalytic reactions (4) and yet few studies have been reported for the interaction of the two gases on solid surfaces. In recent years, however, through technological interest in the development of catalysts suitable for the control of nitrogen oxide emissions, considerable impetus has been given to investigations of reactions between carbon monoxide and nitrogen oxides (5). While most attention has been focussed on the role of the higher oxides of nitrogen, work on the catalytic reaction between carbon monoxide and nitrous oxide has been reported recently for oxides of tin (6), nickel (7), and vanadium (8).

Experimental

Apparatus and Procedure

The all-glass flow system and quartz reactor have been described previously (1–3). High purity helium was used as the carrier gas at atmospheric pressure in the flow system and Beckman GC-5 gas chromatograph. Carbon monoxide, nitrogen, carbon dioxide, and nitrous oxide were analyzed by a thermal conductivity bridge using stainless steel columns, 183 × 0.32 cm od, packed with 61 cm 'Carbosieve B' and the remainder with 'Poropak Q' at a column temperature of 353 K which was sufficient to resolve all components.

The reacting gas mixture consisted of carbon monoxide and nitrous oxide each at a partial pressure of 5.33 kN m^{-2} (40 Torr), except, if stated otherwise, at a total gas flow rate of 350 ml min^{-1} (NTP). All reaction rate measurements were recorded after steady catalyst activity was attained; for example, 3 h at 493 K for Co_3O_4 with a maximum conversion level of ~7% using 1 g samples of the oxide catalysts.

Manganese(II) oxide was prepared by exposing manganese(III) oxide to the same reaction mixture at 573 K for 5 h. At steady catalytic activity the conversion level was 61.3% which was well above the levels usually acceptable for determining kinetic data (9, 10) by this method. The composition of the reaction mixture was then altered to achieve ~17% as a

Can. J. Chem. Downloaded from www.nrcresearchpress.com by 210.87.254.6 on 09/05/12
For personal use only.

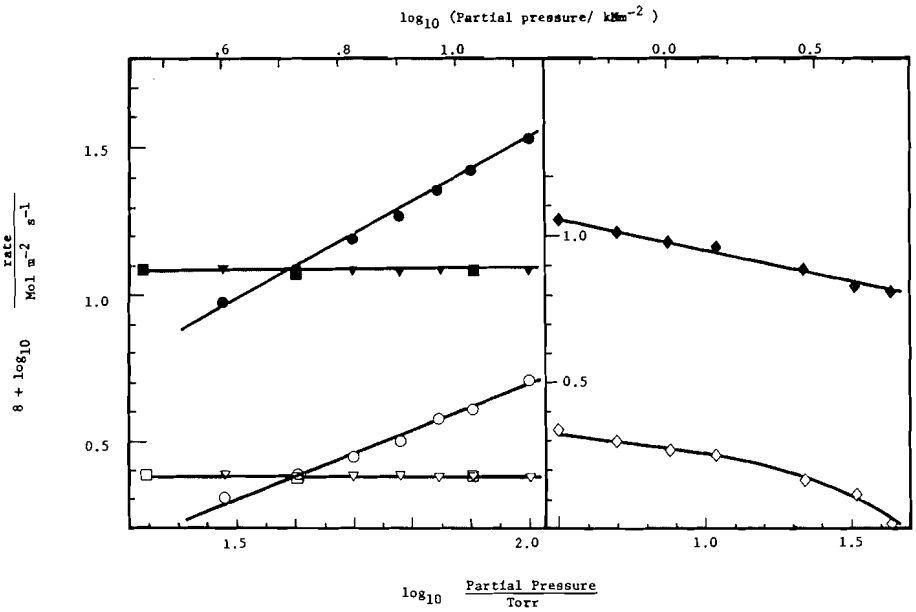

FIG. 1. Reaction rate dependency on variations in the partial pressures of nitrous oxide (●, ○), carbon monoxide (▽), ▼, nitrogen (■, □), and carbon dioxide (◆, ◇) on MnO at 573 and 523 K, respectively.

maximum steady conversion level at 573 K after 5 h by reducing the carbon monoxide partial pressure to 2.67 kN m^{-2} (20 Torr). X-ray powder diffraction photographs taken before and after catalysis were identical for Co_3O_4. For the manganese oxide the structure after catalysis was confirmed to be manganese(II) oxide by X-ray powder diffraction photographs and chemical analysis (3). The brown colour of the samples did indicate, however, that some excess oxygen had been retained (3, 11, 12). In contrast, no perceptible colour change was evident with Co_3O_4 samples after catalysis.

Preliminary experiments with both oxides established that diffusion phenomena did not influence the measurements at the stated conditions (9, 10). 'Blank' runs confirmed that reaction on the quartz wool and reactor walls reached 1% conversion at 853 K. Surface areas were determined by low temperature krypton adsorption (BET; 77K; $\sigma = 21.5$ Å) and values of 9.5 and 4.5 $m^2\ g^{-1}$ were obtained for MnO and Co_3O_4, respectively. The bulk catalyst volumes for the corresponding oxides were 0.82 and 0.94 $cm^3\ g^{-1}$, respectively.

Materials

Cobalto-cobaltic oxide was prepared by heating cobalt carbonate (B.D.H. Ltd.) at 873 K in air for 10 h. Complete decomposition of the carbonate was confirmed by thermogravimetric analysis in air using a Stanton–Redcroft Thermobalance Model HT5A. The preparation of the manganese(III) oxide starting material has been described (1).

Carbon monoxide (C.P.; 99.5% minimum), carbon dioxide (Coleman; 99.99%), nitrogen (super-pure; 99.99%), nitrous oxide (99.9% minimum), and helium (high purity; 99.995%) were used as supplied.

Results

Reaction Rate Order Measurements

Carbon Monoxide

MnO—The dependence of the reaction rate on variations in the carbon monoxide partial pressure from 1.33 to 16.0 kN m^{-2} was examined at 523 and 573 K with nitrous oxide maintained constant at 5.33 kN m^{-2}. At 523 K, the rate order with respect to carbon monoxide partial pressure was zero throughout the range investigated, while at 573 K a sharp change from zero to first order occurred at 8.00 kN m^{-2} (Fig. 1).

Co_3O_4—With nitrous oxide partial pressure fixed at 5.33 kN m^{-2} the reaction rate order with respect to carbon monoxide partial pressure was determined from 1.33 to 18.7 kN m^{-2} at 413 and 453 K. At both temperatures, the reaction rate was independent of the carbon monoxide partial pressure throughout the range (Fig. 2).

Nitrous Oxide

MnO—The effect of variations in nitrous oxide partial pressure on the reaction rate was examined with partial pressures from 2.67 to 10.7 kN m^{-2} at 523 K with the carbon monoxide partial pressure maintained at 2.67 kN m^{-2} (at 573 K the percent conversion rose to 58.8% at 8.00 kN m^{-2} nitrous oxide which limited the range of partial pressure variation). Within these partial pressure ranges, the reaction rate order with respect to nitrous oxide was 1.0 at 523 and 573 K (Fig. 1).

Co_3O_4—With the carbon monoxide partial pressure maintained at 5.33 kN m^{-2}, the nitrous oxide partial pressure was varied from 1.33 to 18.7 kN m^{-2} at 413 and 453 K. Throughout this range and at both temperatures, the reaction rate order with

Can. J. Chem. Downloaded from www.nrcresearchpress.com by 210.87.254.6 on 09/05/12
For personal use only.

Can. J. Chem. Downloaded from www.nrcresearchpress.com by 210.87.254.6 on 09/05/12
For personal use only.

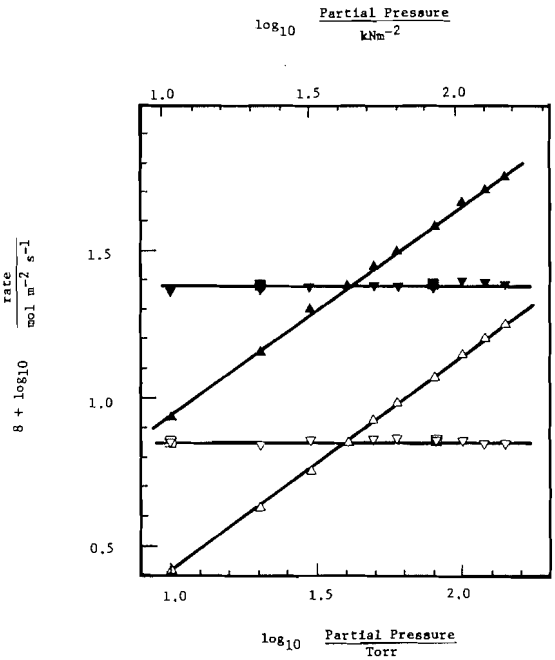

FIG. 2. Reaction rate order for Co_3O_4 at 453 and 413 K for nitrous oxide (▲, △), carbon monoxide (▼, ▽), and nitrogen (■, □).

respect to nitrous oxide partial pressure was 0.7 (Fig. 2).

Nitrogen

MnO—The partial pressures of carbon monoxide and nitrous oxide were fixed at 2.67 and 5.33 kN m^{-2}, respectively, and the partial pressure of nitrogen was varied from 2.67 to 10.7 kN m^{-2}. A zero rate order with respect to nitrogen partial pressure was observed at 523 and 573 K (Fig. 1).

Co_3O_4—The reaction rate order with respect to nitrogen partial pressure in the stated range at 413 and 453 K was zero with the carbon monoxide and nitrous oxide partial pressures each at 5.33 kN m^{-2} (Fig. 2).

Carbon Dioxide

MnO—The composition of the gas mixture with respect to carbon monoxide and nitrous oxide was the same as that in the nitrogen experiments. The effect of variations in carbon dioxide partial pressure on the reaction rate was examined from 0.67 to 5.79 kN m^{-2} at 573 and 523 K (Fig. 1). At both temperatures, a nonlinear relationship was observed in which the inhibitory effect increased with carbon dioxide partial pressure. The reaction rate order with respect to this component at the lowest partial pressures was -0.3 at both temperatures. This value was used in the calculation of rate constants since the levels of carbon dioxide production in the catalytic reaction in the absence of the added component were approached in this partial pressure region.

On the basis of these experiments, the rate of reaction, r (mol m^{-2} s^{-1}), at 523 and 573 K for MnO can be expressed as

$$[1] \qquad r = kP_{N_2O}/P_{CO_2}{}^{0.3}$$

where P_{N_2O} and P_{CO_2} represent the partial pressures of nitrous oxide and carbon dioxide, respectively, and the rate expression applies to the temperature and pressure regions specified.

Co_3O_4—The partial pressures of carbon monoxide and nitrous oxide were maintained at 5.33 kN m^{-2} throughout these experiments. At 453 K, 1.45 kN m^{-2} carbon dioxide was added continuously to the gas stream. The catalytic reaction rate increased from 2.45×10^{-8} mol m^{-2} s^{-1}, in the absence of carbon dioxide, to 83.2×10^{-8} mol m^{-2} s^{-1} measured 3 min after carbon dioxide introduction. After a total of 19 min, the rate decreased to a steady 7.59×10^{-8} mol m^{-2} s^{-1} which was 3.1 times greater than the initial reaction rate observed without the addition of carbon dioxide. Under these circumstances, a rate order dependence upon carbon dioxide partial pressure could not be defined in the usual manner and a rate order of zero was assumed.

Thus, the experimental reaction rate for catalysis on Co_3O_4 becomes

$$[2] \qquad r = kP_{N_2O}{}^{0.7}$$

In separate experiments, Co_3O_4 was exposed to the standard gas mixture at 453 K until activity levels were constant and reproducible with those prior to carbon dioxide admission. Carbon monoxide and nitrous oxide were then turned off and a continuous 5.79 kN m^{-2} of carbon dioxide only was introduced into the helium gas stream. After 2 min no carbon monoxide, nitrous oxide, or carbon dioxide could be detected in the exhaust stream but continuous sampling over a 30 min interval showed a progressive increase in the amount of carbon dioxide present in the gas stream after each sampling. It may be significant that carbon monoxide was not produced during the course of these experiments. The behaviour was markedly different to that observed with MnO (3) where conversion to carbon monoxide was almost completed initially on the introduction of carbon dioxide.

Next, a continuous stream of 5.33 kN m^{-2} nitrous oxide alone was added to the helium carrier and an initial 1.18×10^{-8} mol m^{-2} s^{-1} of nitrogen production was observed which gradually decreased with time. In order to compare the nature of the catalyst surface with that originally obtained at the

Can. J. Chem. Downloaded from www.nrcresearchpress.com by 210.87.254.6 on 09/05/12
For personal use only.

steady level, the standard gas mixture was introduced and the results are shown in Table 1. The catalytic reaction rate prior to these experiments was 2.45×10^{-8} mol m^{-2} s^{-1} and it is apparent from Table 1 that the ratios of the rates of nitrogen and carbon dioxide production were not constant. Thus, the reactions involving carbon monoxide and nitrous oxide would appear to be proceding independently during this stage of catalysis.

The Effect Of Temperature On the Reaction Rate

MnO

After equilibration in the mixture consisting of 5.33 kN m^{-2} nitrous oxide and 2.67 kN m^{-2} carbon monoxide at 573 K for 5 h, the catalytic reaction was examined by cycling from 493 to 573 K at 10 K intervals. Using rate constants calculated by integration of [1], the Arrhenius plot yielded an apparent activation energy of 130 ± 4 kJ mol^{-1} (Fig. 3).

Co_3O_4

When steady catalytic activity was attained at 493 K after 3 h, the reaction rate was determined from 493 to 383 K at 10 K intervals using the standard gas mixture. Rate constants were calculated using [2] and the Arrhenius plot is presented

TABLE 1. Reaction rate results for Co_3O_4 after consecutive exposure to carbon dioxide and nitrous oxide (see text for details)

Time (min)	Reaction rate × 10^8 (mol m^{-2} s^{-1}) Nitrogen (r_1)	Carbon dioxide (r_2)	(r_1/r_2)
3	206	4.42	46.6
13	15.3	1.96	7.8
25	6.57	1.64	4.0

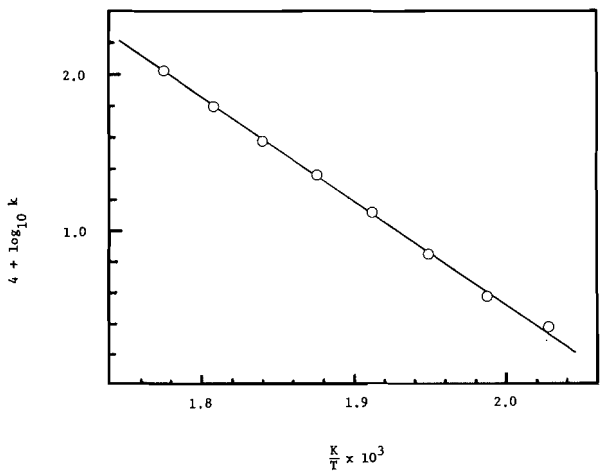

FIG. 3. Arrhenius plot for the reaction of carbon monoxide (2.67 kN m^{-2}) and nitrous oxide (5.33 kN m^{-2}) on MnO.

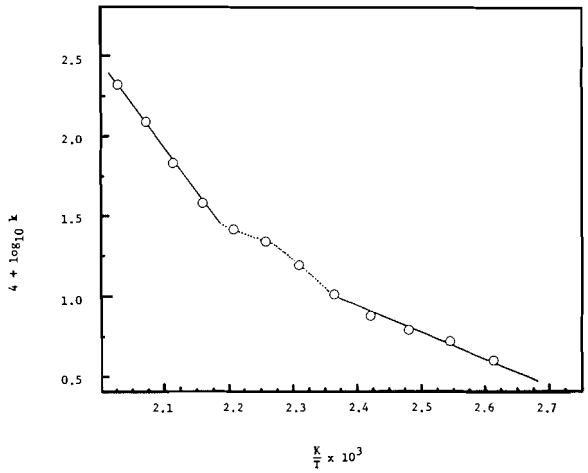

FIG. 4. Arrhenius plot for the reaction of carbon monoxide and nitrous oxide both at 5.33 kN m^{-2} on Co_3O_4.

in Fig. 4. The apparent activation energies were 31 ± 4 kJ mol^{-1} (383 to 433 K) and 105 ± 4 kJ mol^{-1} (453 to 493 K). In the range 433 to 453 K, the rate constants did not lie on the straight lines obtained at the upper and lower temperature regions.

Preliminary experiments had established that diffusion processes did not influence the kinetic data, but considering the low value of apparent activation energy at the lower temperatures, the results of these tests are presented.

Conversion levels were determined at total gas flow rates of 300, 350, and 400 ml min^{-1} (NTP) at both 413 and 383 K. At the former temperature, the corresponding percent conversions were 0.29, 0.30, and 0.32 while at 383 K, the respective values were 0.18 at all total gas flow rates. The slope of the plot, $\log_{10}$ rate versus reciprocal temperature, for the three total gas flow rates gave 20 ± 4, 24 ± 4, and 25 ± 4 kJ mol^{-1}, respectively. The absence of a systematic variation in conversion with total gas flow rate at either temperature, together with the values of the slope, which were within the experimental error, seem to indicate that the measurements represent the intrinsic activity of the oxide catalyst within the accuracy of this method (13).

Discussion

Several plausible reaction schemes for MnO were evaluated using the results of the nitrous oxide and carbon dioxide rate order experiments and the best correlations for both sets of data (Figs. 5 and 6) were obtained with the following kinetic equation:

[3] $$r = k\frac{a\sqrt{P_{N_2O}}}{(1 + a\sqrt{P_{N_2O}} + P_{CO_2})^2}$$

Can. J. Chem. Downloaded from www.nrcresearchpress.com by 210.87.254.6 on 09/05/12
For personal use only.

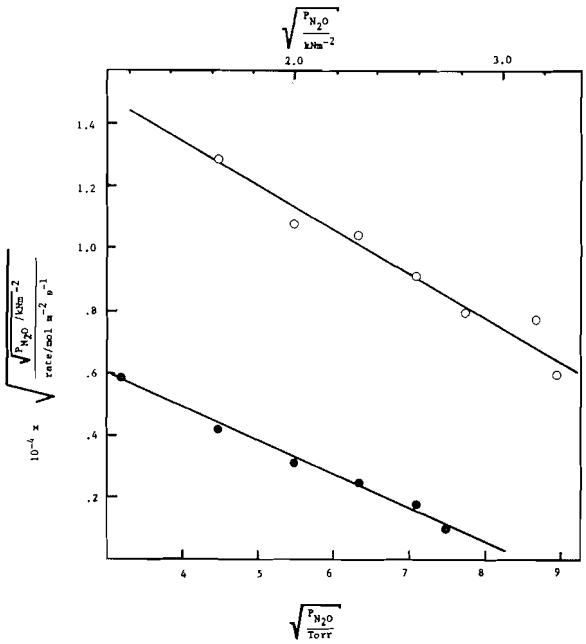

FIG. 5. Reduced plot of the Langmuir–Hinshelwood type expression 3 on MnO. Symbols correspond to Fig. 1.

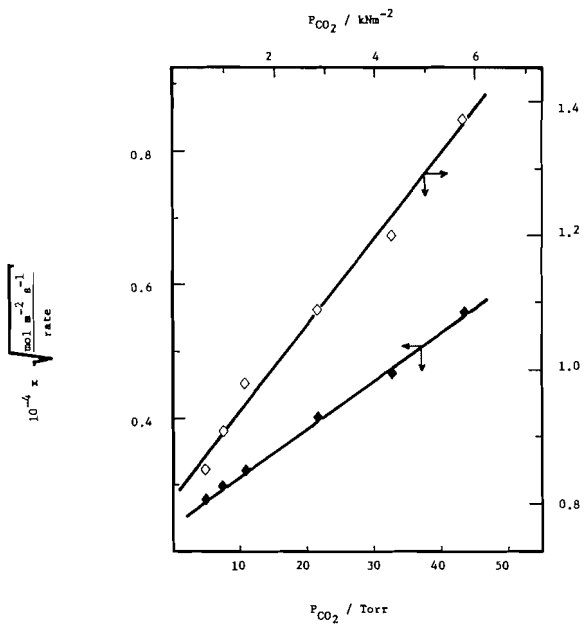

FIG. 6. Reduced plot of the Langmuir–Hinshelwood type expression 3 for carbon monoxide on MnO. Symbols correspond to Fig. 1.

This relationship may be regarded as a Langmuir–Hinshelwood expression. The limitations inherent in adducing correlations between such statistical relationships and the classical Langmuir–Hinshelwood surface reaction model have been documented (14, 15) and thus [3] was regarded as an initial guide to the interpretation of the kinetic results. The following proposal for the surface reaction was consistent with [3] and analogous to the reaction mechanism suggested for NiO (7):

[4] $$CO + S \rightleftharpoons CO(ads.)$$

[5] $$N_2O + S + CO(ads.) \rightarrow N_2 + CO_2(ads.) + S$$

[6] $$CO_2(ads.) \rightarrow CO_2 + S$$

with step 5 rate-controlling; N_2O and CO are absorbed on adjacent adsorption sites, S. Increasing the surface coverage with absorbed CO_2 would inhibit the reaction and catalysis may be regarded as involving a redox cycle similar to that proposed for the water–gas shift reaction on MnO (3). A short-lived, intermediate carbonate may form on the surface (19, 20) but the generation and decomposition of such a species would not be rate-limiting in the present context.

A comparison of the apparent activation energies for reaction on MnO and NiO with those reported (21) for oxygen desorption from the metal oxides (Table 2) shows a close correspondence and suggests that metal–oxygen bond rupture may be involved in the rate-controlling step.

Analysis of the nitrous oxide results for catalysis on Co_3O_4 yielded the expression

[7] $$r = k\frac{aP_{N_2O}\sqrt{P_{N_2O}}}{(1 + a\sqrt{P_{N_2O}} + \ldots)^2}$$

which best accommodated the data (Fig. 7).

A surface mechanism consistent with [7] was formulated:

[8] $$CO + S \rightleftharpoons CO(ads.)$$

[9] $$N_2O + S + CO(ads.) \rightarrow CO_2(ads.) + N_2$$

[10] $$N_2O + CO_2(ads.) \rightarrow CO_3(ads.) + N_2$$

[11] $$CO + CO_3(ads.) \rightarrow 2CO_2 + 2S$$

N_2O adsorption and decomposition would occur on two sites, one of which retains an adsorbed carbon monoxide molecule. Since P_{N_2O} appears in the numerator of [7], step 10 would be rate-controlling while step 11 preserves the stoichiometry of the reaction. No quantitative information concerning

TABLE 2. Activation energies of oxygen desorption (kJ mol^{-1}) (21) and the catalytic reaction between carbon monoxide and nitrous oxide

	State No.	MnO_2	Co_3O_4	NiO	
	0	67	84	105	
	1	126	155	184	
	2	—	213	259	
Observed	—	130±4	105±4	103±4	kJ mol^{-1}

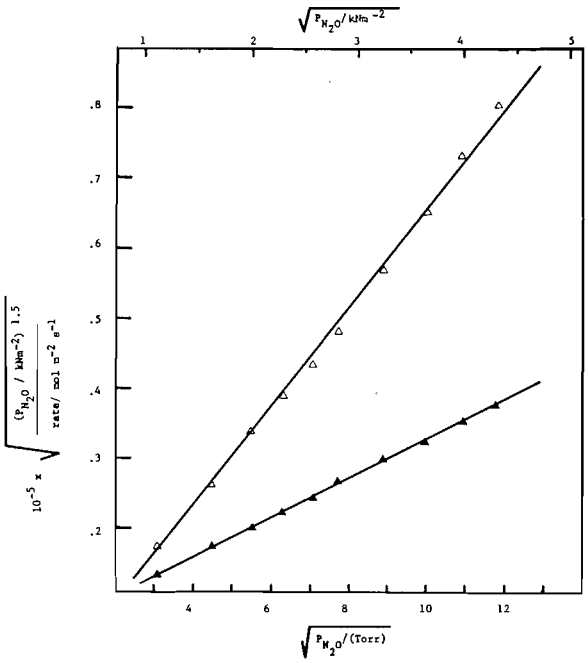

FIG. 7. Reduced plot of the Langmuir–Hinshelwood type expression 7 on Co_3O_4. Symbols correspond to Fig. 2.

the rate dependence on carbon dioxide partial pressure was obtained and hence step 7 must be regarded as an overview.

Certain experimental features can be explained through this mechanism. Thus, absence of carbon monoxide production when the catalyst was exposed only to carbon dioxide can be rationalized since the mechanism is not a simple redox process. Rather, the absorbed carbon dioxide species would appear to occupy a specific catalyst site.

The observed decomposition of nitrous oxide following catalyst exposure to carbon dioxide can be accommodated by step 10 in which a surface carbonate is produced. Similarly, the addition of carbon dioxide to the reacting gas mixture and subsequent increase in the catalytic conversion level may be attributed to the increased presence of reactive carbon dioxide on the surface resulting in a greater proportion of the surface contributing to catalysis.

It has been shown previously (16) that a transition from a concerted redox process (associative), usually observed at lower temperatures, to a sequential process (regenerative) at higher temperatures is accompanied by an increase in the value of the apparent activation energy, E_A. Thus, the low value of E_A observed in the low temperature region can be explained if the surface reaction proceeds on a large number of surface sites via a surface complex involving the catalyst and reactants. The change in surface mechanism to the sequential process would then be accompanied by blockage of the low energy sites. Four distinct adsorbed carbon dioxide species have been observed on a similar preparation of this oxide by temperature programmed desorption (17). The desorption maximum of the third species (γ-form) was noted at 451–456 K, which corresponds to the region in which the E_A changes in this study. The two high-temperature sorption forms of carbon dioxide, γ and δ, have been attributed (17) to the presence of surface and bulk cations of different oxidation states Co^{2+} and Co^{3+} which, respectively, provide energetically different adsorption sites. Thus, the loss of the intermediate γ-carbonate present in the low-temperature region and the formation of the more stable δ form may account for the observed change in E_A. Further, Co^{3+} has been reported (18) to be much less active than Co^{2+} in the decomposition of nitrous oxide and this was related to the different strengths of the metal-to-oxygen bonds. The consequence of the transformation of Co^{2+} to Co^{3+} was a more stable surface oxygen bond and an electronic interaction between these two ions was proposed.

With these considerations, the surface process may be represented by [12].

[12]

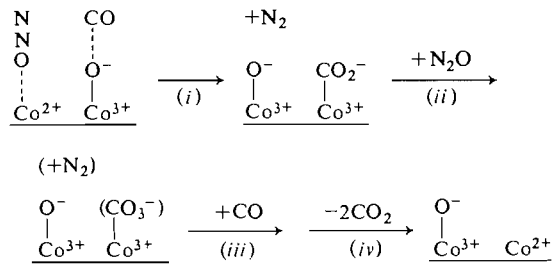

The scheme preserves stationary catalyst composition and suggests that the cobalt oxidation state alternates with each reaction cycle. Stage (*ii*) would be rate-controlling in the formation of the intermediate carbonate, the structure of which has not been specified since it may alter in the two kinetic regions. The subsequent stages (*iii*) and (*iv*) are not clear although reaction with a second carbon monoxide molecule is required while the subsequent desorption of carbon dioxide may proceed in one or two separate stages.

The apparent lack of agreement in Table 2 regarding the closest state for Co_3O_4 may be taken as further evidence supporting the hypothesis of intermediate carbonate formation on this oxide. These E_A values all lie in the region reported for the catalytic oxidation of carbon monoxide (4) while the low value observed for Co_3O_4 corresponds to those found with the oxides of nickel, copper, and manganese near room temperature (4).

Can. J. Chem. Downloaded from www.nrcresearchpress.com by 210.87.254.6 on 09/05/12
For personal use only.

Acknowledgement

We are pleased to acknowledge financial assistance from Imperial Oil Ltd., Toronto.

1. E. F. McCaffrey, D. G. Klissurski, and R. A. Ross. J. Catal. **26**, 380 (1972); Can. J. Chem. **49**, 3778 (1971).
2. B. W. Krupay and R. A. Ross. J. Catal. **39**, 369 (1975).
3. B. W. Krupay and R. A. Ross. Can. J. Chem. **51**, 3520 (1973).
4. O. V. Krylov. Catalysis by nonmetals. Academic Press, New York and London. 1970; A. Clark. The theory of adsorption and catalysis. Academic Press, New York and London. 1970.
5. M. Shelef. Catal. Rev. Sci. Eng. **11**, 1 (1975).
6. M. J. Fuller and M. E. Warwick. J. Catal. **39**, 412 (1975).
7. B. W. Krupay and R. A. Ross. Z. Phys. Chem. N.F. In press.
8. B. W. Krupay and R. A. Ross. J. Catal. In press.
9. C. N. Satterfield. Mass transfer in heterogeneous catalysis. M.I.T. Press, Cambridge, MA. 1970.
10. P. B. Weisz and C. D. Prater. Adv. Catal. **3**, 143 (1951).
11. M. Ellis, T. Moore, and P. W. Selwood. J. Am. Chem. Soc. **72**, 856 (1950).
12. I. Korpenko. J. Am. Ceram. Soc. **51**, 408 (1968).
13. R. P. Chambers and M. Boudart. J. Catal. **6**, 141 (1966).
14. S. W. Weller. Chemical reaction engineering reviews. *Edited by* H. M. Hulburt. American Chemical Society, Washington, DC. 1975. p. 26.
15. M. Boudart. AIChE J. **2**, 62 (1956); **18**, 465 (1972).
16. G. K. Boreskov. Kinet. Catal. **14**, 2 (1973).
17. D. G. Klissurski. J. Catal. **23**, 149 (1974).
18. F. Pepe. Gazz. Chim. Ital. **103**, 1201 (1973).
19. W. E. Garner and F. J. Veal. J. Chem. Soc. 1487 (1935).
20. J. M. Thomas and W. J. Thomas. Introduction to the principles of heterogeneous catalysis. Academic Press, New York and London. 1967. Chapt. 8.
21. B. Halpern and J. E. Germain. J. Catal. **37**, 44 (1975).

Can. J. Chem. Downloaded from www.nrcresearchpress.com by 210.87.254.6 on 09/05/12
For personal use only.

An explanation of reported participation of hydrated electrons as intermediates in electrochemical reduction reactions

JOHN R. DUNCAN[1] AND GRAHAM A. WRIGHT

Chemistry Department, University of Auckland, Auckland, New Zealand

Received October 21, 1976[2]

JOHN R. DUNCAN and GRAHAM A. WRIGHT. Can. J. Chem. **56**, 17 (1978).

Suggestions that $e^-_{(aq)}$ is involved as a reactant in reduction reactions at metal electrodes are examined. It is shown that an experimental test of the participation of $e^-_{(aq)}$ can be devised. The results of this test show that the conventional theory, involving electron transfer directly from the electrode to the species being reduced, provides a better explanation of the reduction process in aqueous solution.

JOHN R. DUNCAN et GRAHAM A. WRIGHT. Can. J. Chem. **56**, 17 (1978).

On examine diverses suggestions à l'effet que $e^-_{(aq)}$ est impliqué comme réactif dans des réactions de réduction à des électrodes métalliques. On montre que l'on peut développer une technique expérimentale pour vérifier la participation des $e^-_{(aq)}$. Les résultats de cette vérification montrent que la théorie conventionnelle impliquant un transfert d'électrons directement de l'électrode vers les espèces qui sont réduites fournit la meilleure explication du processus de réduction en solution aqueuse.

[Traduit par le journal]

There have been many studies carried out on the behaviour of the hydrated electron in electrolytes over the last 15 years, so that its reactions are now well-documented (1–3) and there are quite advanced theories on its structure (4, 5). Formation of solvated electrons under the stimulus of radiation is well-known (5), and it has been known for many years that electrons solvated by ammonia or amines (6, 7) are very stable. However, the suggestion that the hydrated electron may be an important intermediate in electrochemical reduction reactions (8–11) is totally at variance with previously accepted theories of electrode kinetics and electrochemical reduction (12).

The conventional theory of electrochemical reduction, which will be designated as the electrode model in the rest of this paper, requires that the ion or molecule which is to be reduced at the electrode must diffuse from the bulk solution to the electrode surface. During this diffusion, it passes through the diffusion layer and is finally adsorbed into the double layer, i.e. the layer of electrolyte lying immediately adjacent to the electrode surface. The thickness of the diffusion layer, δ, depends on the solution composition and the stirring conditions in the bulk solution, usually being of the order of 10 μm. The double layer is normally only of the order of 1 nm thick, again depending on the solution composition, and has definite structure because of orientation effects exerted by the charge on the electrode. Within the double layer, the substrate species may be adsorbed onto the electrode surface, or there may simply be deformation of its solvation shell. Either of these processes aids the transfer of the electron from the cathode to the substrate. The particular cathode material has been shown to exert a considerable effect on the mechanism and rate of the electrode process, and this is explained for this electrode model in terms of the adsorption effects at the electrode surface (13).

A model of the electrochemical reduction process which involved hydrated electrons as intermediates was first invoked to explain results found in sodium amalgam discharge experiments (8), and has been suggested to apply in hydrogen evolution at an inert metal cathode (9, 10), though this has been disputed since it was first suggested (14). No exact definition of the process involving hydrated electrons has yet been proposed, but analogy with a model proposed for photo-emission from a mercury cathode (15) would require that the electron be ejected from the electrode surface and become thermalised and hydrated, to provide a homogeneous distribution of $e^-_{(aq)}$ throughout a reaction layer which will have a thickness of the same order as that of the double layer invoked in the electrode model. Evidence has been presented to suggest that hydrated electrons may move 2 nm or more from an electrode after photo-emission, before becoming solvated (16). Bulk solution ions which have diffused inwards to this layer must then presumably be reduced by reaction, in a normal ion–ion interaction, with the hydrated electrons in this reaction layer.

The essential difference between the electrode model and the hydrated electron model is thus the

[1]Present address: Building Research Association of New Zealand, Wellington, New Zealand.

[2]Revision received September 12, 1977.

Can. J. Chem. Downloaded from www.nrcresearchpress.com by 210.87.254.5 on 09/05/12
For personal use only.

Can. J. Chem. Downloaded from www.nrcresearchpress.com by 210.87.254.5 on 09/05/12
For personal use only.

involvement of the mobility and reactivity of the hydrated electron in the latter model. The discussion and experiments presented in the rest of this paper were designed to examine the validity of the claims made for $e^-_{(aq)}$ involvement here.

Hughes and Roach (8) measured the total volume, standardized to 273 K and 760 Torr pressure, of gaseous hydrogen evolved per gram of sodium when a known amount of sodium amalgam was reacted to completion with an aqueous solution containing excess hydrogen ions, and compared this volume with that evolved when inorganic metal ions were present as competitors for the hydrated electrons which they believed to be involved as intermediates in the reaction. The results were found to fit a relationship

$$[1] \qquad V_0/V = 1 + A(c_2/c_1)$$

where V_0 = volume of hydrogen evolved in absence of competing ions, V = volume of hydrogen evolved in presence of a concentration c_2 (mol ℓ^{-1}) of competing ions, and c_1 (mol ℓ^{-1}) = hydrogen ion concentration.

These workers proposed reactions 2 to 5 as the mechanism whereby this effect occurred:

$$[2] \qquad Na(Hg) \rightarrow Na^+ + e^-_{(aq)}$$

$$[3] \qquad e^-_{(aq)} + H^+ \rightarrow H$$

$$[4] \qquad H + H \rightarrow H_2$$

$$[5] \qquad S^{z+} + e^-_{(aq)} \rightarrow S^{(z-1)+}$$

The homogeneous rate constants for reactions 3 and 5 are respectively $k_3 = 2.1 \times 10^{10}$ ℓ mol^{-1} s^{-1} (2) and $k_5 = 3 \times 10^{10}$ ℓ mol^{-1} s^{-1} (1), where the competing ion S^{z+} is Cu^{2+}. Hughes and Roach (8) expressed the volumes evolved in terms of the concentrations of the ions present and the homogeneous rate constants of their reactions with the hydrated electron, and assumed that the generation of hydrated electrons would be the rate-determining step. The value of A (in [1]) was then given by the ratio $k_5:k_3$.

There are several reasons for believing that Hughes and Roach have made some incorrect assumptions in deriving this expression. The most important of these is the energetic favorability of sodium oxidation when sodium amalgam is in contact with an aqueous solution; the potential of sodium discharge to form an amalgam is known to be in the region of -1850 mV (nhe) (17), while hydrogen ion discharge occurs at potentials around -1260 mV (nhe) at a dropping mercury electrode (18). It might therefore be expected that supply of electrons at the interface would not be the rate-determining process, and in view of the magnitude of the homogeneous rate constants, the solution reaction might not be expected to be rate determining, either.

Bartlett *et al.* (19) recognized that the model proposed by Hughes and Roach was incompatible with existing theories of electrochemical reduction, and also that the conventional theories would require diffusion of the reacting species to the electrode surface. They therefore proposed that [1] should be rewritten as

$$[6] \qquad \frac{V_0}{V} = 1 + \frac{n_2 D_2}{D_1}\frac{c_2}{c_1}$$

where n_2 = number of electrons transferred to S^{z+} during the reduction, and D_1 and D_2 are respectively the diffusion coefficients of the hydrogen ion and the competing ion in the solution. It was claimed that this equation should represent the relationship between the volume yields and ion concentrations if the electrode model is valid, but this is not true, in that no attention has been paid to electrode kinetic aspects of the reactions in deriving this equation. More accurate relationships will be derived later in this paper.

Bartlett *et al.* (19) found that the values of A in [1] which they found experimentally (in repeating the experiments of Hughes and Roach, and in experiments of their own) did not fit [6] as well as they fitted a different modification of [1], in which $A = k_5'/k_3'$, where $k_n' = 10^{-0.2z}k_n$ (z being the charge on the ion). Barker *et al.* (15) had previously reported that this correction had been found empirically to be required to allow comparison of rate constants determined in pulse radiolysis experiments (at concentrations of the order of 10^{-6} mol ℓ^{-1}) with those found at higher solute concentrations (0.2 to 1 mol ℓ^{-1}). Table 1 contains the results obtained by Hughes and Roach and Bartlett *et al.*, and the theoretical values of n_2D_2/D_1 and $k_5':k_3'$, which have been recalculated where necessary, using the data sources of ref. 19, to remove some errors which appear to have been included in the values computed in ref. 19. The results presented in this table do not lend unequivocal support to any of the relationships discussed so far. The differences in the values observed by the two sets of workers could be attributable to the different amalgam and solution concentrations which were used in the two sets of experiments (Table 2). The experimental method was the same in both cases; a small volume of amalgam was shaken with an excess of solution, so that the concentrations of hydrogen ion and competing ion were maintained essentially constant throughout the experiment.

Though they correctly assumed that diffusion to the reaction site should be an important process,

Can. J. Chem. Downloaded from www.nrcresearchpress.com by 210.87.254.5 on 09/05/12
For personal use only.

TABLE 1. Comparison of predicted results with those found experimentally for values of A in [1]

Competing ion	Hughes and Roach (8)	Ref. 19	$k_5':k_3'^a$	$n_2D_2:D_1^b$
$Co(NH_3)_6^{3+}$	9.3	10.3	1.57	0.10
Cu^{2+}	1.2	1.9	0.81	0.16
Zn^{2+}	1.0	1.5	0.04	0.20
$Fe(CN)_6^{3-}$	0.56	0.5	0.79	0.10
Co^{2+}	0.45	0.7	0.34	0.18*
$Cr_2O_7^{2-}$	—	2.1	5.7	0.72*
Cr^{3+}	—	1.9	1.04	0.24
Mn^{2+}	—	0.02	0.002	0.20*
$CH_2ClCOOH$	—	0.5	0.46	0.14

[a]Values of k_5 taken from refs. 20–24. $k_3 = 2.3 \times 10^{10}$ ℓ mol^{-1} s^{-1} (24). All k values multiplied by $10^{-0.2z}$, as suggested by Barker *et al.* (15).
[b]Values marked by * were calculated from ref. 25. Other D_2 values taken from refs. 26–28. D_1 assumed as average of 7.5×10^{-5} cm^2 s^{-1} (29) and 7.2×10^{-5} cm^2 s^{-1} (30).

TABLE 2. Concentrations (mol ℓ^{-1}) used in sodium amalgam discharge reaction experiments by Hughes and Roach (8) and by Bartlett *et al.* (19)

	Hughes and Roach	Bartlett *et al.*
Sodium amalgam concentration	1–2	~5
Hydrogen ion concentration	0–0.25	~0.5
Competing ion concentration	~0.3	0.1–2.5

Bartlett *et al.* appear to have overlooked a basic difference between the hydrated electron model and the electrode model: while the hydrated electron model predicts a strictly competitive reaction, the electrode model predicts that electrode reactions will proceed at different rates depending on the electrode potential. Thus the formation of a sodium amalgam proceeds at significant rates only at potentials more cathodic than −1850 mV (nhe). The expression which they have derived is therefore not sufficient to describe the electrode model.

When a redox reaction occurs at an electrode, it may be interpreted as the sum of two partial currents of opposite polarity. Electrode kinetic considerations require that these currents are functions of the electrode potential, and the rate of the reaction is limited by the limiting current which the reactants can carry. The limiting cathodic current will flow when the electrode is so negatively charged that the rate-limiting step is diffusion of the reducible species to the cathode, and conversely the limiting anodic current will flow when the electrode potential is so positive that diffusion becomes the rate-limiting step in the charge-transfer process. The limiting current, I_d, may be calculated by [7] for the case of steady-state diffusion through a stationary boundary layer in a stirred solution (31), which is an approximation of the conditions used in the amalgam discharge experiments under discussion.

$$[7] \qquad I_d = nFcDA/\delta$$

n = number of electrons transferred per ion, F = Faraday constant, c = concentration of electro-active species, D = diffusion coefficient, A = area of electrode, and δ = diffuse layer thickness.

Since the relative values of total anodic and total cathodic currents affect the course of the reaction, different reaction paths might be expected for Figs. 1*a* and 1*b*. The potential at which the anodic and cathodic currents are of equal magnitude but opposite sign, so that the total current flowing is zero, is called the mixture potential, E_m, and is the potential at which the system will lie if no external potential is applied. The partial currents flowing at the mixture potential are equivalent to the limiting current for the reaction.

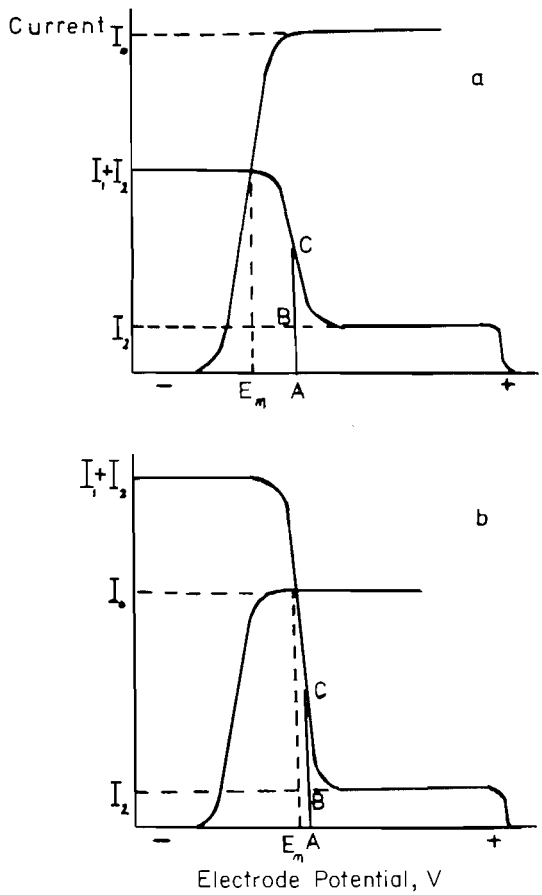

FIG. 1. Schematic mixture potential diagrams for the system Na(Hg)/H^+, scavenger. E_m = mixture potential. (*a*) Total available anodic current exceeds total available cathodic current. (*b*) Total available cathodic current exceeds total available anodic current.

Can. J. Chem. Downloaded from www.nrcresearchpress.com by 210.87.254.5 on 09/05/12
For personal use only.

The concepts outlined above may be applied to predicting the outcome of the amalgam dissolution experiments performed by Hughes and Roach and Bartlett *et al.* Because the aqueous phase reactants were arranged to be in considerable excess over the sodium in the amalgam, there will be virtually no change in scavenging ion or hydrogen ion concentrations during the hydrogen evolution reaction, and thus negligible change in the limiting currents carried by these species.

Consider Fig. 1*a*. The electrode model requires that the limiting current which will flow here will be the total cathodic current, $I_1 + I_2$, where I_1 and I_2 are the limiting currents (derived from [7]) due to hydrogen ion discharge and copper amalgam formation. (The copper amalgam formation reaction may occur as two 1-electron-transfer steps; these will occur at such relatively anodic potentials compared to the hydrogen evolution reaction, however, that the amalgam formation will be assumed to be a single 2-electron transfer for this paper.) I_0 is the current for the anode reaction $Na(Hg) \rightarrow Na^+_{(aq)} + e^-$. Assuming no change in I_1 or I_2, the total currents at the end of the reaction will be anodic current = 0 and cathodic current = $I_1 + I_2$, and V_0/V can be expressed in terms of these partial currents. In absence of a competing ion, the volume of hydrogen evolved is

$$[8] \qquad V_0 = KI_0$$

where K is a proportionality constant. In the presence of a competing ion, the volume V evolved will be the sum of the volumes evolved in the different stages of the reactions; i.e. $V = \sum_i V_i$, where

$$[9] \quad V_1 = \text{volume evolved while } I_0 \text{ decreases to } I_1 + I_2 = K(I_0 - (I_1 + I_2))\frac{I_1}{I_1 + I_2}$$

The last factor in [9] expresses the fraction of the current which is consumed in discharge of hydrogen ions.

$$V_2 = \text{volume evolved while } I_0 \text{ decreases from } I_1 + I_2 \text{ to } I_2 = KI_1 \frac{\text{BC}}{\text{AC}} \text{ on Fig. 1}a$$

where BC/AC is the average fraction of current spent on hydrogen ion discharge, and is approximated by $\frac{1}{2}I_1/(\frac{1}{2}I_1 + I_2)$. Thus

$$V_2 = KI_1^2/(I_1 + 2I_2)$$

$$[10] \quad V_3 = \text{volume evolved while } I_0 \text{ decreases from } I_2 \text{ to } 0 = 0$$

since none of the current which flows is spent on hydrogen ion discharge. During this stage of the process, the mixture potential will have quite positive values. Thus

$$[11] \quad V = V_1 + V_2 + V_3 = \frac{KI_1[I_0(I_1 + 2I_2) - 2I_2(I_1 + I_2)]}{(I_1 + I_2)(I_1 + 2I_2)}$$

and

$$[12] \quad \frac{V_0}{V} = \frac{I_0(I_1 + I_2)(I_1 + 2I_2)}{I_1(I_0(I_1 + 2I_2) - 2I_2(I_1 + I_2))}$$

for the case of Fig. 1*a*.

A similar derivation for the case of Fig. 1*b* gives

$$[13] \qquad \frac{V_0}{V} = \frac{I_0(I_0 + I_2)}{(I_0 - I_2)^2}$$

Plots of V_0/V against c_2/c_1, as predicted by the electrode model, may be drawn by selecting values of amalgam, hydrogen ion, and competing ion concentrations, computing the values of I_0, I_1, and I_2 which correspond to them by using [7], and computing V_0/V by whichever of [12] and [13] is appropriate. Both of these expressions lead to curved plots, so that it should be possible to differentiate between the electrode model (curved plot) and the hydrated electron model (straight-line plot).

Another means of differentiating between the two models is a plot of the ratio of instantaneous rates of gas evolution, v_0/v, against the concentration ratio, c_2/c_1, which is also curved for the electrode model but straight for the hydrated electron model. For Fig. 1*a*, addition of competing ions will not affect the rate of hydrogen evolution until $I_0 = I_1 + I_2$, since until this time the cathodic current is the limiting parameter and hydrogen is being evolved at the maximum rate. When $I_0 = I_1 + I_2$, the case of Fig. 1*b* holds and

$$[14] \qquad v_0 = kI_0$$

$$[15] \qquad v = k(I_0 - I_2)$$

so that

$$[16] \qquad v_0/v = I_0/(I_0 - I_2)$$

Choice of suitable values allows computation of plots such as those shown in Fig. 2.

Using [12] and [13], it is possible to estimate values of concentrations within the ranges used by earlier workers which will allow computation of data which approximates their reported results. An example of this is given in Table 3. While it is not claimed that the values used to compute these data are those used in the actual experiments by Hughes and Roach,

TABLE 3. Comparison of results found by Hughes and Roach (8) with results obtained by calculation from [13]

Concentration ratio $[Cu^{2+}]/[H^+]$ (8)	0.75	1.4	2.4	2.8	3.5
Evolved gas volume ratio V_0/V (8)	1.8	2.7	3.2	4.2	4.8
Amalgam concentration, M	1.4	1.4	1.3	1.1	1.0
H^+ ion concentration, M	0.20	0.20	0.125	0.11	0.09
Cu^{2+} ion concentration, M	0.15	0.28	0.30	0.32	0.31
V_0/V (eq. 13)	1.7	2.7	3.2	4.2	4.7

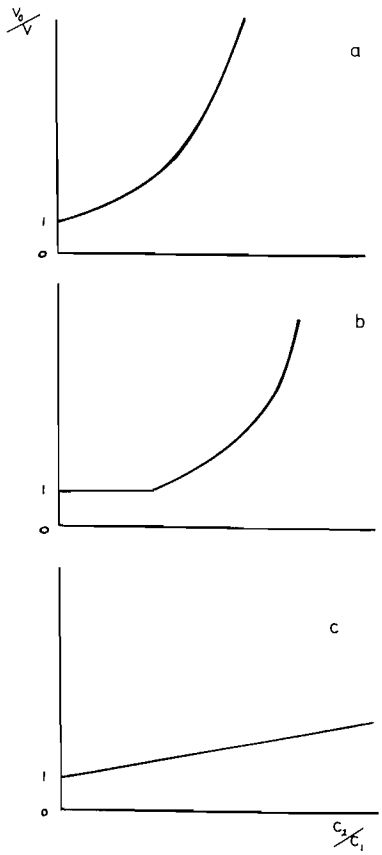

FIG. 2. Schematic representations of plots of v_0/v against c_2/c_1 (see text for definitions). (*a*) Electrode model, $I_0 < I_1$. (*b*) Electrode model, $I_0 > I_1$. (*c*) Hydrated electron model.

Table 3 clearly shows how small changes in reactant concentrations could have significant effects on the V_0/V ratio.

One method of determining more precisely the true mechanism would be to hold all concentrations constant except one, and examine the effect on the reaction rate of changes in this concentration. A cell was designed in which this could be done, and experiments were performed on this theme.

The two-chamber cell (Fig. 3) was built in such a way that sodium amalgam which was manufactured in one chamber by electrolysis of a concentrated sodium hydroxide solution could be transported to the other chamber by the action of a large glass

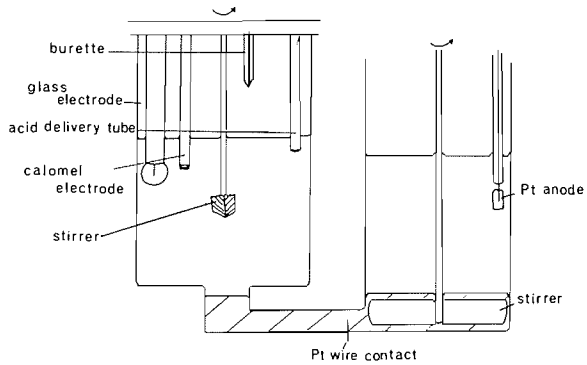

FIG. 3. Cell used to investigate amalgam–solution reaction rates.

paddle, and there reacted with an aqueous solution. The solution in the second chamber was held at a steady pH by a pH-stat (TTTl titrimeter, SBR2 recorder and motor-driven burette (Radiometer, Copenhagen)). This device continuously monitors the solution pH, and adds (in this case) acid automatically from a reservoir to maintain a preset pH value. It was possible to deduce the rate of sodium amalgam reaction at the interface (which had an area of approximately 300 mm^2) from the rate of acid addition needed in absence of competing ions. This enabled balancing of the rates of amalgam formation and reaction, by altering the electrolysis current. This current was supplied by a Duffers Associates Model 600 potentiostat which was operating in a galvanostatic mode, producing currents in the range 0 to 2.5 A.

Experimental

It was decided to investigate thoroughly the effect of added cupric ions on the rate of acid addition needed to maintain constant pH in a solution containing 0.03 M HCl, which was in contact with a 0.1 M sodium amalgam. The amalgam was prepared by passing the appropriate amount of charge through the electrolysis cell, into which had been placed a weighed amount of mercury, before the aqueous solution was introduced to the reaction chamber. During this period, the pH-stat was calibrated using the solution which had been prepared for addition to the reaction chamber. Immediate addition of acid from the reservoir normally occurred when the solution was introduced to the reaction chamber, suggesting that some of the amalgam could have reacted with the atmosphere during its preparation, but a period then followed during which little or no acid addition was necessary. Extrapolation of the slope

Can. J. Chem. Downloaded from www.nrcresearchpress.com by 210.87.254.5 on 09/05/12
For personal use only.

Can. J. Chem. Downloaded from www.nrcresearchpress.com by 210.87.254.5 on 09/05/12
For personal use only.

which was found after this plateau back to zero acid addition usually led to $t \sim 0$.

An adequate steady state was apparently set up for the case $I_0 < I_1$. On three occasions, there was an invariant acid addition rate for more than 45 min, and in these cases calculations of the fluxes from the current in the electrolysis cell and the rate of acid addition gave values which agreed within 8%. For the case $I_0 > I_1$, conditions were never obtained in which the acid addition rate was steady enough for a valid claim to have established a steady state. To reach $I_0 > I_1$, the acid concentration was reduced to 3×10^{-3} M; part of the inaccuracy may have been due to improper deoxygenation of the solution. (An oxygen-saturated solution would have contained approximately 2×10^{-3} M O_2.)

When the rate of acid addition was steady, an aliquot of concentrated $CuCl_2$ solution was added from a burette and the rate allowed to reach a new equilibrium value; this normally took 1 to 2 min to achieve. This process was then repeated until the addition of an aliquot of $CuCl_2$ solution completely inhibited hydrogen evolution, so that no acid addition was required to maintain the pH. On the electrode model, this corresponds to $I_0 < I_2$.

Stirring conditions were kept constant for all experiments, so that values of k in [17] (where $k = AF/\delta$) should remain

$$[17] \qquad I = nkcD$$

constant for all measurements, though k might have different values in the amalgam and solution phases. The value of k in the amalgam, k_0, was determined by assuming a steady state to have been established, in which the current flowing in the electrolysis cell is the limiting current, I_0, flowing at the reaction interface. n, c, and D are known, so that if $I_0 = 0.2$ A (as was used in most experiments), it may be calculated that $k_0 = 2.5 \times 10^8$ C cm mol^{-1}.

The value, k_2, for the solution phase was assumed to be the same for both Cu^{2+} and H^+, though it is known that δ values for these are likely to be different. k_2 was evaluated graphically as 5.1×10^8 C cm mol^{-1}, from the results of spectrophotometric analysis (using a Shimadzu QV50 instrument) for Cu^{2+} of aliquots withdrawn from the reaction chamber at regular time intervals after addition of a known amount of $CuCl_2$.

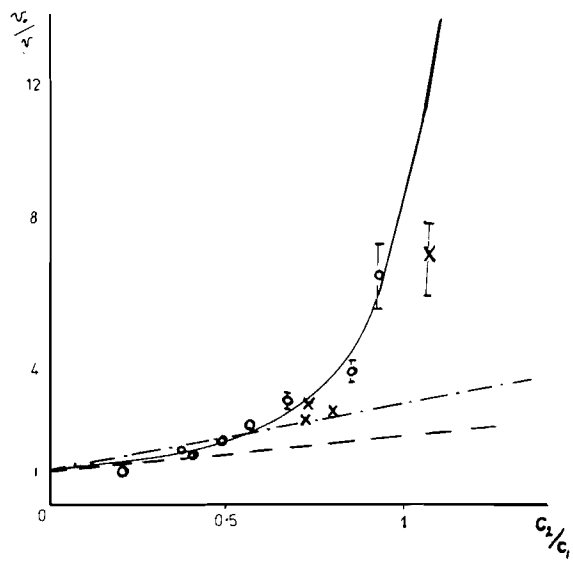

FIG. 4. Comparison of experimental rates of amalgam–solution reaction with theoretical predictions ($I_0 < I_1$). (×, ○) Individual runs. (- ·) After Bartlett *et al.* (19). (--) After Hughes and Roach (8). (—) Electrode model.

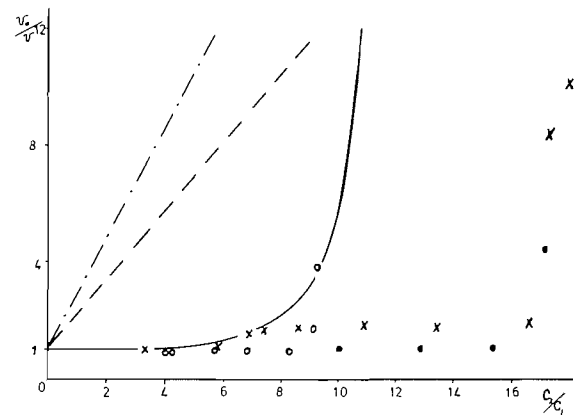

FIG. 5. Comparison of experimental rates of amalgam–solution reaction with theoretical predictions ($I_0 > I_1$). (×, ○) Individual runs. (- ·) After Bartlett *et al.* (19). (--) After Hughes and Roach (8). (—) Electrode model.

It was assumed that c_0 and c_1 were being held constant by the external circuits. The Cu^{2+} ion concentration, c_2, at each point at which the rate v of hydrogen evolution was measured (by calculation from the rate of addition of acid) was calculated using [18]. The ratio v_0/v was plotted against c_2/c_1, and compared with the plots predicted by the hydrated electron and electrode models. The results are shown in Figs. 4 and 5.

$$[18] \qquad C_2(t) = C_2(0) \exp\left[-\frac{D_2 k_2}{FV} t\right]$$

Discussion of Experiments

The results of these experiments suggest that the conventional electrode model provides a better prediction of the behaviour of the Na(Hg)–Cu^{2+}–H^+ system than does the hydrated electron model. There are four possible errors in determining values of v_0/v.

(*1*) Inaccurate measurement from the recorder chart of the rate of addition of acid. Such errors will become more significant as cupric ion concentration rises.

(*2*) Hydrogen evolution by direct reduction of water. It seems unlikely, though, that this will be a major source of hydrogen gas in a solution with pH ~2 to 3.

(*3*) There will be non-uniform transport conditions in the aqueous solution because of the stirring at the interface produced by gas bubble evolution.

(*4*) The surface of the amalgam will become adulterated by the presence of dissolved copper, which may cause variations in the hydrogen evolution.

In spite of these possible errors, the data for the case $I_0 < I_1$ (Fig. 4) fit the prediction of the electrode model fairly well; the best-fit line (correlation

Can. J. Chem. Downloaded from www.nrcresearchpress.com by 210.87.254.5 on 09/05/12
For personal use only.

coefficient = 0.942) corresponds to

$$\frac{v_0}{v} = \frac{0.934 I_0}{I_0 - I_2}$$

compared with the theoretical line given by [16], but does not fit the hydrated electron models proposed by earlier workers (8, 19). A point is reached where $I_2 > I_1$ at $c_2/c_1 = 1.25$, at which the ratio v_0/v is found to be infinite, in accord with the electrode model, while the hydrated electron model predicts $v_0/v = 2.5$ at this concentration ratio. This is compelling evidence for the validity of the electrode model.

The data for the case $I_0 > I_1$ (Fig. 5) are rather scattered, and do not fit any of the models very closely. This scatter is probably due in large part to the absence of a steady state from the system. There is qualitative fit to the electrode model, insofar as the data display a clear plateau region, with a relatively constant value of v_0/v, up to $c_2/c_1 = 15$, with v_0/v then climbing steeply. This qualitative behaviour cannot be reconciled with a hydrated electron model.

Published tables (16) of polarographic constants measured at a dropping mercury electrode suggest that all the depolarizing ions considered by Bartlett *et al.* (19) should reach their limiting currents at potentials more positive than the potential at which sodium amalgam dissolution reaches a limiting current.

This study would therefore appear to refute the claims of Hughes and Roach (8) and Bartlett *et al.* (19) of the occurrence of the hydrated electron as an intermediate in reactions during amalgam dissolution. Conway and Mackinnon (14) have discussed the claim by Pyle and Roberts (10) that $e^-_{(aq)}$ is involved in reactions at platinum electrodes, and deemed this unlikely. There is apparently, therefore, no unequivocal evidence for the existence of hydrated electrons as intermediates in electrochemical reduction mechanisms in the absence of photochemical excitation.

Acknowledgement

We should like to thank the New Zealand University Grants Committee for financial assistance.

1. M. ANBAR and P. NETA. Int. J. Appl. Radiat. **18**, 493 (1967).
2. E. J. HART. Acc. Chem. Res. **2**, 161 (1969).
3. K. EIBEN. Angew. Chem. Int. Ed. Engl. **9**, 619 (1970).
4. K. FUEKI, D. FENG, and L. KEVAN. J. Phys. Chem. **75**, 2297 (1971).
5. J. M. MOSCOWITZ, M. BORING, and J. H. WOOD. J. Chem. Phys. **62**, 2254 (1975).
6. H. A. LAITINEN and C. J. NYMAN. J. Am. Chem. Soc. **70**, 3002 (1948).
7. Colloque Weyl IV. J. Phys. Chem. **79**(26) (1975).
8. G. HUGHES and R. J. ROACH. Chem. Commun. 600 (1965).
9. D. C. WALKER. Can. J. Chem. **44**, 2226 (1966).
10. T. PYLE and C. ROBERTS. J. Electrochem. Soc. **114**, 651 (1967).
11. D. C. WALKER. Can. J. Chem. **45**, 807 (1967).
12. W. R. FAWCETT. J. Chem. Phys. **61**, 3842 (1975).
13. P. DELAHAY. Double layer and electrode kinetics. Interscience, New York, NY. 1965.
14. B. E. CONWAY and D. J. MACKINNON. J. Phys. Chem. **74**, 3663 (1970).
15. G. C. BARKER, A. W. GARDNER, and D. C. SAMMON. J. Electrochem. Soc. **113**, 1182 (1966).
16. Z. A. ROTENBURG and Y. G. GUREVICH. Sov. Electrochem. **9**, 151 (1973).
17. H. DIETRICK, E. YEAGER, and F. HOVORKA. Tech. Rep. No. 3. U.S. Office of Naval Research Project No. WR359-277. 1953.
18. L. MEITES. Polarographic techniques. 2nd ed. Interscience, New York, NY. 1965.
19. H. E. BARTLETT, R. A. BASSON, P. M. CHAMPION, P. CROWTHER, and H. ISAACS. J. S. Afr. Chem. Inst. **23**, 57 (1970).
20. J. H. BAXENDALE, E. M. FIELDEN, C. CAPELLOUS, J. M. FRANCIS, J. V. DAVIES, M. EBERT, C. W. GILBERT, J. P. KEENE, E. J. LAND, A. J. SWALLOW, and J. M. NOSWORTHY. Nature, **201**, 468 (1964).
21. J. K. THOMAS, S. GORDON, and E. J. HART. J. Phys. Chem. **68**, 1524 (1964).
22. M. ANBAR and E. J. HART. J. Phys. Chem. **69**, 973 (1965).
23. E. HAYON and A. O. ALLEN. J. Phys. Chem. **65**, 2181 (1961).
24. S. GORDON, E. J. HART, M. S. MATHESON, J. RABANI, and J. K. THOMAS. J. Am. Chem. Soc. **85**, 1375 (1963).
25. International Critical Tables. Vol. 6. McGraw-Hill, New York, NY. 1929.
26. I. M. KOLTHOFF and J. J. LINGANE. Polarography. Vol. 2. Interscience, New York, NY. 1962.
27. K. ASADA, F. HINE, S. YOSHIZAWA, and S. OKADA. J. Electrochem. Soc. **107**, 242 (1960).
28. A. C. RIDDIFORD. *In* Advances in electrochemistry and electrochemical engineering. Vol. 4. *Edited by* C. Tobias and P. Delahay. Interscience, New York, NY. 1966.
29. W. VIELSTICH and D. JAHN. *In* Advances in polarography. Vol. 1. *Edited by* Longmuir. Pergamon, New York, NY. 1960.
30. R. LANDSBURG, W. FIESSLER, and S. MULLER. Z. Chem. **1**, 169 (1961).
31. G. KORTUM. Treatise on electrochemistry. 2nd Engl. ed. Elsevier, Amsterdam. 1965. p. 451.

Apparent molal heat capacities and volumes of aqueous electrolytes at 25°C: $NaClO_3$, $NaClO_4$, $NaNO_3$, $NaBrO_3$, $NaIO_3$, $KClO_3$, $KBrO_3$, KIO_3, NH_4NO_3, NH_4Cl, and NH_4ClO_4

ALAIN ROUX,[1] GOOLAM M. MUSBALLY,[2] GÉRALD PERRON, AND JACQUES E. DESNOYERS

Département de chimie, Université de Sherbrooke, Sherbrooke (Qué.), Canada J1K 2R1

AND

PREM PAUL SINGH,[3] EARL M. WOOLLEY,[4] AND LOREN G. HEPLER

Department of Chemistry, University of Lethbridge, Lethbridge, Alta., Canada T1K 3M4

Received July 19, 1977

ALAIN ROUX, GOOLAM M. MUSBALLY, GÉRALD PERRON, JACQUES E. DESNOYERS, PREM PAUL SINGH, EARL M. WOOLLEY, and LOREN G. HEPLER. Can. J. Chem. **56**, 24 (1978).

Measurements at 25°C with flow calorimeters and densimeters have led to heat capacities and densities of aqueous solutions of 11 1:1 electrolytes: $NaClO_3$, $NaBrO_3$, $NaIO_3$, $NaNO_3$, $NaClO_4$, NH_4NO_3, $KClO_3$, $KBrO_3$, KIO_3, NH_4Cl, and NH_4ClO_4. The first 6 salts were studied up to near saturation. We have used results of these measurements to obtain apparent molal heat capacities and apparent molal volumes of the various solutes. Extrapolation to infinite dilution on the basis of the Debye–Hückel theory has led to $\phi_C^\ominus$ and $\phi_V^\ominus$ values for each solute. We have compared these standard values with results of earlier investigations.

ALAIN ROUX, GOOLAM M. MUSBALLY, GÉRALD PERRON, JACQUES E. DESNOYERS, PREM PAUL SINGH, EARL M. WOOLLEY et LOREN G. HEPLER. Can. J. Chem. **56**, 24 (1978).

Des mesures de capacités calorifiques et de densités ont été effectuées à 25°C au moyen de microcalorimètres et de densimètres dynamiques sur des solutions aqueuses de 11 électrolytes 1:1: $NaClO_3$, $NaBrO_3$, $NaIO_3$, $NaNO_3$, $NaClO_4$, NH_4NO_3, $KClO_3$, $KBrO_3$, KIO_3, NH_4Cl et NH_4ClO_4. Les 6 premiers sels ont été étudiés presque jusqu'à la saturation. Les capacités calorifiques et volumes molaires apparents ont été calculés et extrapolés à dilution infinie en se basant sur la théorie de Debye–Hückel. Ces valeurs standards $\phi_C^\ominus$ et $\phi_V^\ominus$ ont été comparées aux valeurs antérieurement publiées.

Introduction

As part of our program of determination of thermal and volumetric properties of aqueous solutions, we have made calorimetric measurements leading to apparent molal heat capacities and density measurements leading to apparent molal volumes of 11 1:1 electrolytes at 25°C. Results of these measurements and our thermodynamic calculations are reported in this paper.

Experimental

Heat capacity measurements were made with flow calorimeters that have been described previously (1). A small systematic error in some of the measurements has been identified and corrected as recently described (2, 3).

Densities have been measured with flow densimeters that have been described previously (4).

All results refer to 25.00 ± 0.05°C.

Chemicals used in Sherbrooke were as follows. Fisher Certified samples of $NaClO_3$, $NaBrO_3$, and $NaNO_3$ were dried in a vacuum oven at 100°C. $NaIO_3$ from Mallinckrodt and $NaClO_4$ from Alfa Inorganic Ventron were dried in a vacuum oven at 70°C. NH_4NO_3 (Fisher Certified) was recrystallized from methanol and then dried in vacuum at 80°C.

Chemicals used in Lethbridge were as follows. Reaction of concentrated solution of NH_4NO_3 (Fisher Certified) with concentrated $HClO_4$ (Baker Analytical Reagent) yielded a precipitate of NH_4ClO_4, which was recrystallized several times from 80% ethanol and then twice from water ($pH = 4.5$) before being dried at 105°C. Fisher Certified samples of $KBrO_3$, KIO_3, and NH_4NO_3 were dried at 110°C. $KClO_3$ (BDH Analar) was dried at 96°C and NH_4Cl (BDH Analar) was dried at 110°C.

All solutions used in Sherbrooke were made from known masses of solute and water; most solutions used in Lethbridge were prepared similarly. Some solutions of NH_4ClO_4 were prepared by dilution of stock solutions that had been made by mass, while concentrations of a few solutions of $KBrO_3$ and KIO_3 were determined by titration with $S_2O_3^{2-}$ after reaction with excess I^-.

Results and Discussion

Apparent molal properties of solutions (ϕ_Y) are defined by the expression

$$[1] \qquad \phi_Y = [Y(\text{soln}) - n_1 Y_1^0]/n_2$$

in which the symbols have the following meanings: Y

[1]On leave of absence from Laboratoire de Thermodynamique et de Cinétique, Université de Clermont, Aubière 63170, France.

[2]Present address: Coastguard College, Sidney, N.S., Canada.

[3]On leave from Department of Chemistry, Punjab Agricultural University, Ludhiana, India.

[4]On leave from Department of Chemistry, Brigham Young University, Provo, UT, U.S.A.

Can. J. Chem. Downloaded from www.nrcresearchpress.com by 210.87.254.105 on 09/05/12
For personal use only.

Can. J. Chem. Downloaded from www.nrcresearchpress.com by 210.87.254.105 on 09/05/12
For personal use only.

is the property (heat capacity or volume for our purposes) of a specified quantity of solution, n_1 is the number of moles of solvent in this specified quantity of solution, Y_1^0 is the property (heat capacity or volume) of 1 mol of pure solvent, and n_2 is the number of moles of solute in the specified quantity of solution. Our experimental results (compositions of solutions, heat capacities, densities) have been used to obtain apparent molal heat capacities (ϕ_C) and apparent molal volumes (ϕ_V).[5]

Apparent molal properties of dilute solutions of electrolytes are accurately described by equations of the form of

$$[2] \quad \phi_Y = \phi_Y^\ominus + A_Y(d_1^0 m)^{1/2} + B_Y m + C_Y m^{3/2} + \ldots$$

in which $\phi_Y^\ominus$ is the value of ϕ_Y at infinite dilution, A_Y is the limiting slope derived from the Debye–Hückel theory, d_1^0 is the density of the pure solvent, m is the molality, and B_Y, C_Y, etc. are adjustable parameters. Our principal interest in this work has been in determining $\phi_Y^\ominus$ values which are identical with the corresponding partial molal properties at infinite dilution ($\bar{Y}_2^\ominus$). For our calculations we have used $A_C(d_1^0)^{1/2} = 28.95$ J K^{-1} mol$^{-3/2}$ kg$^{1/2}$ and $A_V(d_1^0)^{1/2} = 1.865$ cm^3 mol$^{-3/2}$ kg$^{1/2}$ as previously reported (2).

One way to treat our experimental results has been to construct graphs of ($\phi_Y - A_Y(d_1^0 m)^{1/2}$) versus m and then obtain values of $\phi_Y^\ominus$ and B_Y from the intercepts, respectively, of the best (judged by eye) straight lines through the points that represent dilute solutions. Another similar approach can be based on a least-squares or other statistical fit of experimental results of [2]. Treatment of all results obtained in Lethbridge has been based on least-squares fits of all results (no points omitted) using [2] up to terms in m from about $m = 0.03$ mol kg^{-1} to about $m = 0.3$ mol kg^{-1}. The derived $\phi_C^\ominus$, B_C, $\phi_V^\ominus$, and B_V are summarized in Table 1.

Results obtained in Sherbrooke are more complicated to analyze since they were made over a much larger concentration range, and the values of $\phi_C^\ominus$ and $\phi_V^\ominus$ depend to some extent on the number of parameters used in [2]. Two approaches have been used for this purpose. First, graphs were made of ($\phi_Y - A_Y(d_1^0 m)^{1/2}$) vs. m. On the basis of these graphs we have made subjective decisions to ignore a few experimental points which appeared definitely out of line and set upper limits on the concentrations where the functions can be considered linear. The data were then treated by linear least squares ([2] with terms to m only) without weight factors. The derived parameters are summarized in Table 2. In the second approach the data up to saturation were treated with [2] using weighted least squares, with as many parameters as needed to reproduce the experimental data. Parameters obtained in this way are given in Table 3 with the standard deviations and the limits of validity. While [2] can reproduce the experimental ϕ_Y inside the expected uncertainties some caution must be used in evaluating partial molal quantities by way of [2] ($\bar{Y} = \phi_Y + m\, d\phi_Y/dm$) at high concentrations since some anomalous curvature is then observed.

The agreement between $\phi_V^\ominus$ in Tables 2 and 3 is, in general, excellent. On the other hand, for $\phi_C^\ominus$ the values in Tables 2 and 3 generally differ by about 1 J K^{-1} mol^{-1} (more for $NaBrO_3$). The linear least-squares treatment emphasizes the low concentration data and should in principle give the most reliable $\phi_C^\ominus$ values. However, because the B_C parameters are quite large, compared with alkali halides (3) for example, it is possible that neglect of higher terms in [2] leads to some error in $\phi_C^\ominus$. These considerations added to previous experience with the calorimeters and densimeters used in this investigation suggest that uncertainties in $\phi_C^\ominus$ values are no more than ± 3 J K^{-1} mol^{-1} and that uncertainties in $\phi_V^\ominus$ values are no more than ± 0.5 cm^3 mol^{-1} for 1:1 electrolytes. Our following comparisons and calculations support these limits on uncertainties.

The $\phi_C^\ominus$ values obtained in Sherbrooke and in Lethbridge for aqueous NH_4NO_3 agree well with each other; we consider our average $\phi_C^\ominus = -2$ J K^{-1} mol^{-1} for NH_4NO_3(aq) to be better than the $\phi_C^\ominus = -6.7$ J K^{-1} mol^{-1} cited in Parker's (5) thorough review of earlier measurements. Our $\phi_V^\ominus = 47.2$ cm^3 mol^{-1} from Sherbrooke and $\phi_V^\ominus = 47.5$ cm^3 mol^{-1} from Lethbridge are in good agreement with $\phi_V^\ominus = 47.24$, 47.4, and 47.56 cm^3 mol^{-1} cited by Millero (6). We recommend $\phi_V^\ominus = 47.4$ cm^3 mol^{-1} as the best value for NH_4NO_3(aq).

The $\phi_C^\ominus = 16.6$ J K^{-1} mol^{-1} obtained in Sherbrooke for $NaClO_4$(aq) agrees well with $\phi_C^\ominus = 15.2$ J K^{-1} mol^{-1} reported earlier (7) from Lethbridge and with $\phi_C^\ominus = 17.6$ J K^{-1} mol^{-1} (based on an estimated C_p^0 for $NaClO_4$(c)) from Mastroianni and Criss (8). We select $\phi_C^\ominus = 17$ J K^{-1} mol^{-1} as the best value for $NaClO_4$(aq). The $\phi_V^\ominus = 43.0$ cm^3 mol^{-1} from Sherbrooke agrees well with $\phi_V^\ominus = 42.8$ cm^3 mol^{-1} from unpublished results obtained in Lethbridge and with several values cited by Millero (6). On the basis of our results and Millero's (6) preferred $\phi_V^\ominus = 42.93$ cm^3 mol^{-1}, we confidently select $\phi_V^\ominus = 42.9$ cm^3 mol^{-1} as the best available value for $NaClO_4$(aq).

'Reasonable' interpretations of the ϕ_C results from

[5] A complete set of the experimental results is available, at a nominal charge, from the Depository of Unpublished Data, CISTI, National Research Council of Canada, Ottawa, Ont., Canada K1A 0S2.

Can. J. Chem. Downloaded from www.nrcresearchpress.com by 210.87.254.105 on 09/05/12
For personal use only.

TABLE 1. Parameters for [2], based on experimental results obtained in Lethbridge

Solute	$\phi_C^\ominus$ ($J\,K^{-1}\,mol^{-1}$)	B_C ($J\,K^{-1}\,mol^{-2}\,kg$)	$\phi_V^\ominus$ ($cm^3\,mol^{-1}$)	B_V ($cm^3\,mol^{-2}\,kg$)
$KClO_3$	−42.5	39.0	46.3	−1.4
$KBrO_3$	−77.3	54.7	44.4	0.40
KIO_3	−58.7	111.8	35.3	1.6
NH_4Cl	−55.6	11.6	36.2	1.6_3
NH_4ClO_4	47.2	33.1	62.2	−1.3
NH_4NO_3	−1.2	26.9	47.5	−1.2

TABLE 2. Parameters for [2], based on low concentration experimental results obtained in Sherbrooke

Solute	$\phi_C^\ominus$ ($J\,K^{-1}\,mol^{-1}$)	B_C ($J\,K^{-1}\,mol^{-2}\,kg$)	$\phi_V^\ominus$ ($cm^3\,mol^{-1}$)	B_V ($cm^3\,mol^{-2}\,kg$)
$NaClO_3$	−16.8	32.3	35.5	0.1
$NaBrO_3$	−50.5	49.0	33.8	0.6
$NaIO_3$	−34.0	130	24.6	3.0
$NaNO_3$	−29	40	28.3	0.3
$NaClO_4$	16.6	37.9	43.0	−0.05
NH_4NO_3	−3.0	13.1	47.2	−0.03

TABLE 3. Parameters of [2] based on all experimental results obtained in Sherbrooke

Electrolyte		$\phi_Y^\ominus$	B_Y	C_Y	D_Y	E_Y	Std. Dev.	Maximum molality
NH_4NO_3	ϕ_V	47.03	−0.378	0.037			0.1	22.4
	ϕ_C	−4.20	26.26	−13.34	2.28	−0.134	1.1	
$NaNO_3$	ϕ_V	28.33	0.246	−0.062				2
	ϕ_C	−30.15	58.5	−23.5			1.6	
$NaClO_3$	ϕ_V	35.54	0.171	−0.038			0.1	7.8
	ϕ_C	−17.73	49.85	−19.85	0.27	0.55	0.7	
$NaBrO_3$	ϕ_V	33.87	0.70	−0.17			0.05	2
	ϕ_C	−53.9	75.5	−25.1			2	
$NaIO_3$	ϕ_V	24.6	3.00				0.2	0.4
	ϕ_C	−34.0	130				5	
$NaClO_4$	ϕ_V	42.97	0.067	−0.04			0.05	16.7
	ϕ_C	17.85	55.93	−33.08	6.76	−0.478	1.4	

Sherbroke for aqueous $NaNO_3$ lead to $\phi_C^\ominus$ values ranging from $-28._3$ to $-30._5$ $J\,K^{-1}\,mol^{-1}$, depending on rejection or acceptance of results for several very dilute solutions and on choice of upper concentration to be included in the analysis. As indicated in Table 2, we have selected $\phi_C^\ominus = -29$ $J\,K^{-1}\,mol^{-1}$ for $NaNO_3$(aq), based on measurements made in Sherbrooke. An earlier investigation (9) in Lethbridge led to $\phi_C^\ominus = -28.9\,J\,K^{-1}\,mol^{-1}$ for $NaNO_3$(aq). Still earlier investigations cited by Parker (5) led to a less certain $\phi_C^\ominus = -40\,J\,K^{-1}\,mol^{-1}$. We therefore adopt $-29\,J\,K^{-1}\,mol^{-1}$ as the best value. The $\phi_V^\ominus = 28.3\,cm^3\,mol^{-1}$ from Sherbrooke and $\phi_V^\ominus = 28.2\,cm^3\,mol^{-1}$ from earlier measurements in Lethbridge (9) are in excellent agreement with each other and in fair agreement with values (27.8, 27.48, and 28.0 $cm^3\,mol^{-1}$) cited by Millero (6). We suggest that $\phi_V^\ominus = 28.2\,cm^3\,mol^{-1}$ is best for $NaNO_3$(aq).

Our measurements in Lethbridge have led to $\phi_C^\ominus = -55.6\,J\,K^{-1}\,mol^{-1}$ for aqueous NH_4Cl. Earlier measurements in Sherbrooke (3) led to $\phi_C^\ominus = -56.6\,J\,K^{-1}\,mol^{-1}$, while Parker (5) has cited a less certain $\phi_C^\ominus = -56.5\,J\,K^{-1}\,mol^{-1}$. We adopt the average of our values ($\phi_C^\ominus = -56\,J\,K^{-1}\,mol^{-1}$) as best for NH_4Cl(aq). Our measurements in Lethbridge have also led to $\phi_V^\ominus = 36.2\,cm^3\,mol^{-1}$ for aqueous NH_4Cl, while earlier measurements in Sherbrooke led (10) to $\phi_V^\ominus = 35.79\,cm^3\,mol^{-1}$. Millero (6) has cited still earlier investigations that led to $\phi_V^\ominus = 35.98$, 36.0, 36.26, and 36.0 $cm^3\,mol^{-1}$. We select $\phi_V^\ominus = 36.0\,cm^3\,mol^{-1}$ as best for NH_4Cl(aq).

We do not know of any prior calorimetric mea-

Can. J. Chem. Downloaded from www.nrcresearchpress.com by 210.87.254.105 on 09/05/12
For personal use only.

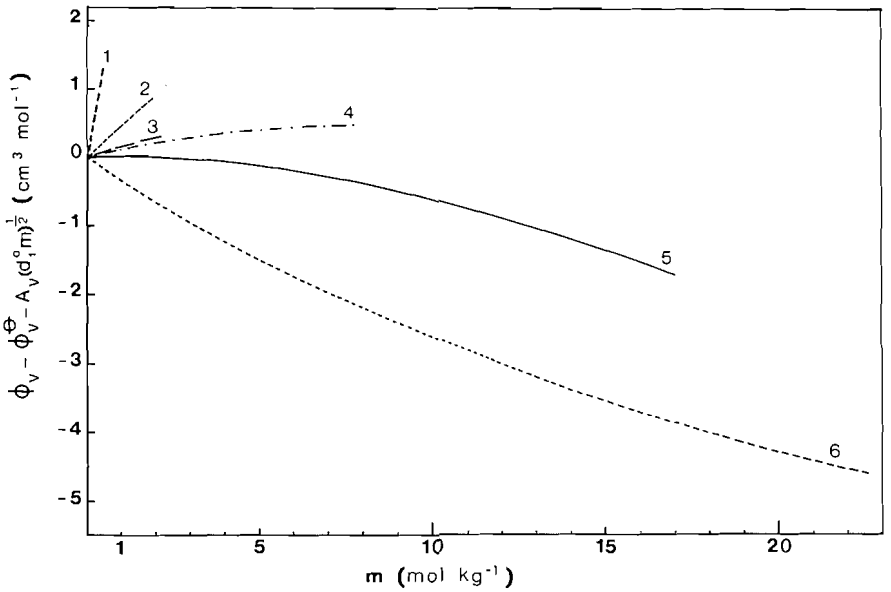

FIG. 1. Apparent molal volumes at 25°C of some 1:1 electrolytes at high concentration: *1*, $NaIO_3$; *2*, $NaBrO_3$; *3*, $NaNO_3$; *4*, $NaClO_3$; *5*, $NaClO_4$; *6*, NH_4NO_3.

TABLE 4. Recommended ionic standard partial molal functions based on $\phi_Y^{\Theta}(H^+) = 0$ at 25°C

Ion	ϕ_V^{Θ} (cm^3 mol^{-1})	ϕ_C^{Θ} (J K^{-1} mol^{-1})
Na^+	−1.2	43
K^+	9.0	13
NH_4^+	17.9	70
Cl^-	18.1	−126
NO_3^-	29.5	−72
ClO_3^-	37.0	−57
BrO_3^-	35.2	−92
IO_3^-	26.0	−74
ClO_4^-	44.2	−25

surements leading to a ϕ_C^{Θ} for $NH_4ClO_4(aq)$ to compare with our $\phi_C^{\Theta} = 47.2$ J K^{-1} mol^{-1} based on measurements made in Lethbridge. There are, however, some simple calculations that will serve to test the relationship of this ϕ_C^{Θ} value to ϕ_C^{Θ} values for some other electrolytes. First, using results reported in this paper, we obtain $[\phi_C^{\Theta}(NH_4ClO_4) - \phi_C^{\Theta}(NaClO_4)] = 47.2 - 17 = 30.2$ J K^{-1} mol^{-1}. We similarly calculate $[\phi_C^{\Theta}(NH_4Cl) - \phi_C^{\Theta}(NaCl)] = -56.1 - (-84.5) = 28.4$ J K^{-1} mol^{-1}, in which $\phi_C^{\Theta}(NH_4Cl)$ is from this paper and $\phi_C^{\Theta}(NaCl)$ is the average of −84.4 and −84.6 J K^{-1} mol^{-1} reported previously from Sherbrooke (3) and Lethbridge (11). The 1.9 J K^{-1} mol^{-1} difference between 30.3 and 28.4 J K^{-1} mol^{-1} is within the limits set by our proposed maximum uncertainty in ϕ_C^{Θ} values. We suggest that our $\phi_V^{\Theta} = 62.2$ cm^3 mol^{-1} may be more accurate than the $\phi_V^{\Theta} = 61.5$ cm^3 mol^{-1} listed in Millero's (6) compilation.

Our ϕ_V^{Θ} values for $NaClO_3$, $NaBrO_3$, $NaIO_3$, $KClO_3$, $KBrO_3$, and KIO_3 are all in satisfactory agreement with results of earlier investigations cited by Millero (6); we suggest that our results are better than those from earlier investigations of these electrolytes. Parker (5) has reviewed earlier investigations of heat capacities and has derived the following: $\phi_C^{\Theta}(NaClO_3) = -36.0$ J K^{-1} mol^{-1}, $\phi_C^{\Theta}(NaBrO_3) = -15.4$ J K^{-1} mol^{-1}, and $\phi_C^{\Theta}(KIO_3) = -102.1$ J K^{-1} mol^{-1}. On the basis of previous assessments of results from our laboratories and those of authors cited by Parker (5) as sources of these values, we suggest that our ϕ_C^{Θ} values listed in Tables 1 and 2 for these solutes are the best ones available.

Using ϕ_C^{Θ} values from Tables 1 and 2, we calculate the following:

$$\phi_C^{\Theta}(KClO_3) - \phi_C^{\Theta}(NaClO_3) = -25.7 \text{ J K}^{-1} \text{ mol}^{-1}$$

$$\phi_C^{\Theta}(KBrO_3) - \phi_C^{\Theta}(NaBrO_3) = -26.8 \text{ J K}^{-1} \text{ mol}^{-1}$$

$$\phi_C^{\Theta}(KIO_3) - \phi_C^{\Theta}(NaIO_3) = -24.7 \text{ J K}^{-1} \text{ mol}^{-1}$$

The almost constancy of these $\Delta\phi_C^{\Theta}$ values is within the limits imposed by our proposed uncertainties in ϕ_C^{Θ} values.

Desnoyers *et al.* (3) have followed the customary procedure of assigning $\phi_C^{\Theta}(H^+) \equiv 0$ and then have developed a table of ionic ϕ_C^{Θ} values based on results of many investigations of heat capacities in Sherbrooke. From their table we calculate $\phi_C^{\Theta}(K^+) - \phi_C^{\Theta}(Na^+) = 13 - 43 = -30$ J K^{-1} mol^{-1}, as compared to the average $\Delta\phi_C^{\Theta} = -26$ J K^{-1} mol^{-1} calculated in the preceding paragraph.

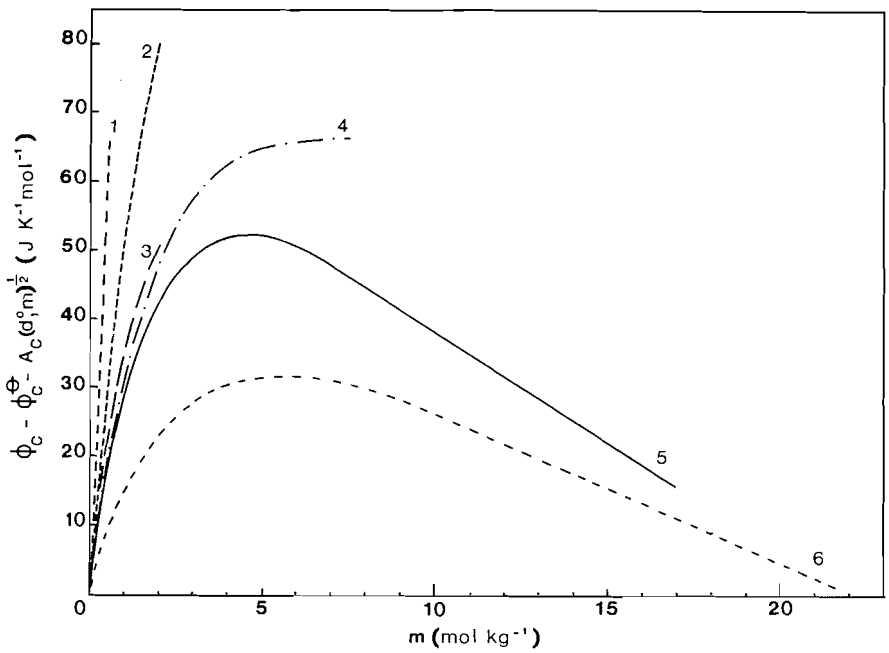

FIG. 2. Apparent molal heat capacities at 25°C of some 1:1 electrolytes at high concentration: *1*, $NaIO_3$; *2*, $NaBrO_3$; *3*, $NaNO_3$; *4*, $NaClO_3$; *5*, $NaClO_4$; *6*, NH_4NO_3.

As previously demonstrated in many investigations, it is useful to assign values for the thermodynamic properties of individual ions in aqueous solution at infinite dilution. To make use of our best ϕ_C^{Θ} and ϕ_V^{Θ} values in this way, we follow the customary procedure of assigning $\phi_C^{\Theta} \equiv 0$ and $\phi_V^{\Theta} \equiv 0$; we also use the ϕ_C^{Θ} values of Desnoyers *et al.* (3) and the ϕ_V^{Θ} values from Millero (6) for $Na^+(aq)$, $K^+(aq)$, and $NH_4^+(aq)$. Results of all of these calculations are summarized in Table 4.

The concentration dependences of ϕ_C and ϕ_V at high concentrations are illustrated in Figs. 1 and 2. For this purpose, $\phi_Y - \phi_Y^{\Theta} - A_Y(d_1^0 m)^{1/2}$ values, based on results obtained in Sherbrooke, are plotted against m.

Acknowledgments

We thank the National Research Council of Canada for support of this research, Brigham Young University for sabbatical leave support to E.M.W., and NATO for a post-doctoral fellowship to A.R.

1. P. PICKER, P.-A. LEDUC, P. R. PHILIP, and J. E. DESNOYERS. J. Chem. Thermodyn. **3**, 631 (1971).
2. G. PERRON, N. DESROSIERS, and J. E. DESNOYERS. Can. J. Chem. **54**, 2163 (1976).
3. J. E. DESNOYERS, C. DE VISSER, G. PERRON, and P. PICKER. J. Solution Chem. **5**, 605 (1976).
4. P. PICKER, E. TREMBLAY, and C. JOLICOEUR. J. Solution Chem. **3**, 377 (1974).
5. V. B. PARKER. Thermal properties of aqueous uni-univalent electrolytes. National Standard Reference Data Series, National Bureau of Standards 2, Washington, DC. 1965.
6. F. J. MILLERO. *In* Water and aqueous solutions; structure, thermodynamics, and transport properties. *Edited by* R. A. Horne. Wiley-Interscience, New York, NY. 1972. Chapt. 13.
7. P. P. SINGH, K. G. MCCURDY, E. M. WOOLLEY, and L. G. HEPLER. J. Solution Chem. **6**, 327 (1977).
8. M. MASTROIANNI and C. M. CRISS. J. Chem. Eng. Data, **17**, 222 (1972).
9. O. ENEA, P. P. SINGH, E. M. WOOLLEY, K. G. MCCURDY, and L. G. HEPLER. J. Chem. Thermodyn. **9**, 731 (1977).
10. P.-A. LEDUC and J. E. DESNOYERS. Can. J. Chem. **51**, 2993 (1973).
11. P. P. SINGH, E. M. WOOLLEY, K. G. MCCURDY, and L. G. HEPLER. Can. J. Chem. **54**, 3315 (1976).

Can. J. Chem. Downloaded from www.nrcresearchpress.com by 210.87.254.105 on 09/05/12
For personal use only.

Comment: On the application of RRKM theory to the unimolecular isomerization of monofluorocyclopropane: a reaction with multiple fall-off characteristics?

MICHAEL C. FLOWERS

Department of Chemistry, The University, Southampton, SO9 5NH, England

Received July 5, 1977

MICHAEL C. FLOWERS. Can. J. Chem. **56**, 29 (1978).

Monofluorocyclopropane isomerizes at 475°C to form *cis*- and *trans*-1-fluoropropene, 2-fluoropropene, and 3-fluoropropene. The relative amounts of these products formed are pressure dependent. It is shown that, using the previously determined Arrhenius parameters for the formation of each product, RRKM theory does account satisfactorily for the pressure dependence of the product yields for *all* the reaction products.

MICHAEL C. FLOWERS. Can. J. Chem. **56**, 29 (1978).

Le monofluorocyclopropane s'isomérise à 475°C pour former des fluoro-1 propène *cis*- et *trans*-, du fluoro-2 propène et du fluoro-3 propène. Les quantités relatives des produits formés dépendent de la pression. On a montré, par l'utilisation des paramètres d'Arrhénius déterminés antérieurement pour la formation de chacun des produits, que la théorie RRKM explique d'une façon satisfaisante la relation qui existe entre la pression et les rendements de *tous* les produits de la réaction.

[Traduit par le journal]

Baghal-Vayjooee, Yau, and Pritchard (BYP) (1) in a recent paper come to the conclusion that conventional RRKM theory cannot account for the fall-off behaviour observed for some of the isomerization products from monofluorocyclopropane. We feel that their interpretation of what constitutes *conventional* RRKM theory is unnecessarily restrictive and that their test of the theory is unreasonable.

Casas *et al.* (2) determined the fall-off characteristics for the formation of the various fluoropropenes (see Fig. 1), measured the Arrhenius parameters of the overall reaction, and observed that 2-fluoropropene and 3-fluoropropene had activation energies ca. 4 kcal mol^{-1} and 1 kcal mol^{-1} respectively higher than for the formation of 1-fluoropropene. The test of the RRKM theory by BYP consisted of applying the theory separately to each product with the additional assumption that the activation energies for all products were the same. It is important to note that even if the experimental activation energies had been the same the fall-off curves would be incorrectly predicted by treating the reactions independently. Presented here are the results of calculations that consider the four reactions as occurring competitively; similar calculations for other reactions have appeared before (3).

Scheme 1 represents the reaction scheme for the isomerization of monofluorocyclopropane. The rate constants, except for k_{-1} which is assumed energy independent, are the specific rate constants for a monofluorocyclopropane molecule of energy ε. The measured unimolecular rate constant for formation

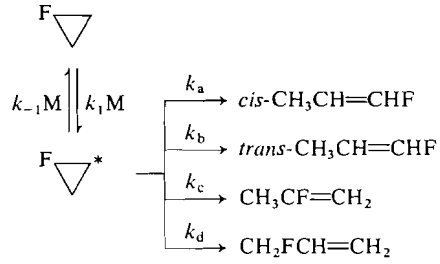

SCHEME 1

of product p is then

$$k_p = \int_{\varepsilon_{0,p}}^{\infty} \frac{k_p \, d(k_1/k_{-1})}{\left(1 + \sum_{p=a,b,c,d} k_p/k_{-1}M\right)}$$

The values of k_a, k_b, k_c, k_d, and $d(k_1/k_{-1})$ are given by the usual RRKM expressions (see refs. 3 or 4 for the actual RRKM equations).

In order to calculate the k_p's transition state (ts) frequencies were assigned so that the experimental and theoretical high pressure rate constants at 475.1°C agreed. The experimental rate constants were calculated from the quoted Arrhenius parameters for the total rate constant (2) and the product distribution also quoted in the paper (unfortunately this is at 453°C). The activation energies used were those estimated by the experimental workers and have not been adjusted in any way. The Appendix to this paper contains details of the various parameters used in the calculation. The vibrational frequencies of fluorocyclopropane are those quoted by BYP.

Can. J. Chem. Downloaded from www.nrcresearchpress.com by 210.87.254.42 on 09/05/12
For personal use only.

Can. J. Chem. Downloaded from www.nrcresearchpress.com by 210.87.254.42 on 09/05/12
For personal use only.

Details of the computational procedure can be found in ref. 3. A step size of 20 cm^{-1} was used in the integration. All collisions were assumed to be strong.

The solid curves in Fig. 1 are the calculated RRKM curves; no shift along the pressure axis has been made. It can be seen that very good agreement between theory and experiment is found for *trans*-1-fluoropropene and 2-fluoropropene. Agreement for *cis*-1-fluoropropene is not quite as good. However, Scheme 1 omits the possible interconversion of *cis*- and *trans*-1-fluoropropene. On the basis of the Arrhenius parameters for the *cis–trans* isomerization of other olefins (4), and group additivity estimates for the heats of formation of fluorocyclopropane and 1-fluoropropene (5, pp. 40–48), the interconversion of the initially formed chemically activated *cis*- and *trans*-1-fluoropropene would be expected to become increasingly important as the pressure is reduced. The results of calculations on a reaction scheme modified to include the above chemical activation effects are included in Fig. 1; the scheme and data used are included in the Appendix. It can be seen that the experimental curve shapes for both *cis*- and *trans*-1-fluoropropene can now be matched but that the position of fall-off is in slight error. Better agreement could no doubt be obtained by changing either the estimated high pressure rate constants or the Arrhenius parameters for these reactions, all of which have significant uncertainties. Experimental data for 3-fluoropropene is badly scattered but agreement between theory and experiment is reasonable, though a higher value for the activation energy of the reaction would perhaps be indicated (the dashed curve in Fig. 1 is calculated for an activation energy of 63.5 kcal mol^{-1}).

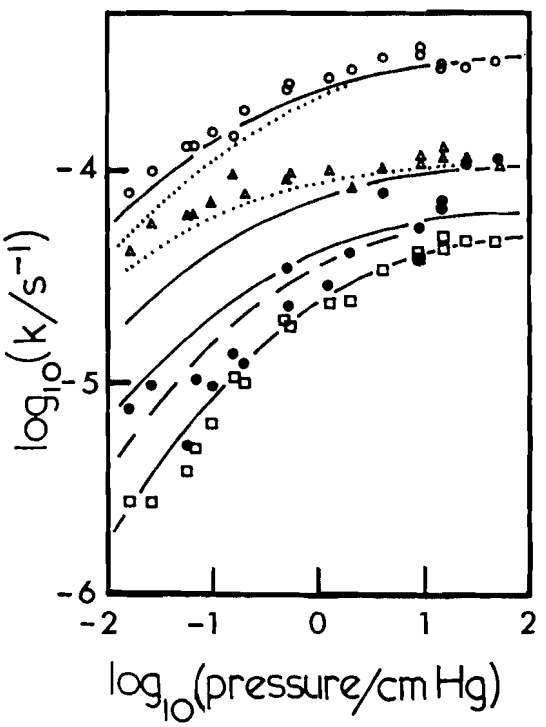

FIG. 1. Experimental rates taken from the work of Casas *et al.* (2) for the formation of *trans*-1-fluoropropene (○), *cis*-1-fluoropropene (△), 2-fluoropropene (□), and 3-fluoropropene (●) from monofluorocyclopropane as a function of pressure at 475.1°C. Solid curves are the calculated RRKM rates based on the experimental data of Casas *et al.* and using the parameters listed in the Appendix of the current paper. The dashed curve is the calculated curve for 3-fluoropropene with an assumed activation energy of 63.5 kcal mol^{-1}. The dotted curves relate to the modified reaction scheme in which interconversion of the initially formed chemically activated *cis*- and *trans*-1-fluoropropene occurs.

It can thus be seen that RRKM theory does fit the data for the isomerization of monofluorocyclopropane and there is no need to invoke alternative theoretical approaches as adopted by BYP, though there may be other valid reasons for so doing. We do, however, support the contention of BYP that the observed fall-off behaviour of the isomerization products from monofluorocyclopropane is consistent with the occurrence of competing reaction pathways having different activation energies; some caution should perhaps be exercised here as doubts as to the reliability of the experimental data have been raised (5, p. 247).

1. M. H. BAGHAL-VAYJOOEE, A. W. YAU, and H. O. PRITCHARD. Can. J. Chem. **55**, 1595 (1977).
2. F. CASAS, J. A. KERR, and A. F. TROTMAN-DICKENSON. J. Chem. Soc. 3655 (1964).
3. M. C. FLOWERS and A. R. GIBBONS. J. Chem. Soc. Perkin Trans. II, 548 (1972); 555 (1972).
4. P. J. ROBINSON and K. A. HOLBROOK. Unimolecular reactions. John Wiley, London. 1972.
5. S. W. BENSON and H. E. O'NEAL. Kinetic data on gas phase unimolecular reactions. NSRDS-NBS 21. U.S. Government Printing Office, Washington, DC. 1970.
6. P. I. ABELL and P. K. ADOLF. J. Chem. Thermodyn. **1**, 333 (1969).

Appendix

Scheme 1

Monofluorocyclopropane: collision diameter 5.2 $\times 10^{-10}$ m; frequencies/cm^{-1} 325, 355, 770, 810, 865, 885, 935, 1025, 1045, 1090, 1165, 1200, 1275, 1305, 1415, 1450, 2980, 3020, 3065, 3095, 3100.

trans-1-Fluoropropene: k(475.1°C) = 3.5×10^{-4} s^{-1}, path degeneracy = 2, $A = 10^{14.36}$ s^{-1}, E_a = 61

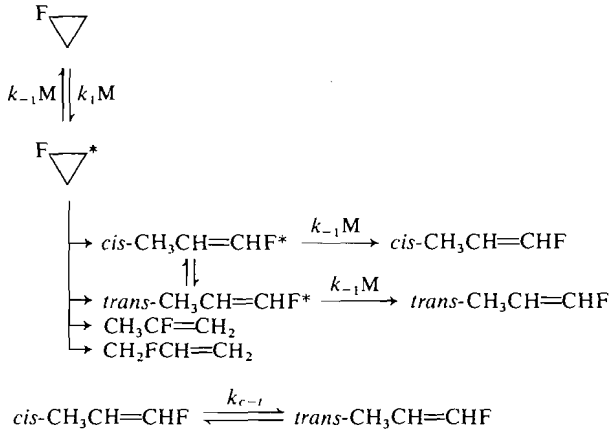

kcal mol^{-1}, ts frequencies/cm^{-1} 200(1), 400(1), 600(1), 800(5), 1000(3), 1200(2), 1400(2), 3000(5).

cis-1-Fluoropropene: k(475.1°C) = 1.1 × 10^{-4} s^{-1}, path degeneracy = 2, A = 10$^{13.84}$ s^{-1}, E_a = 61 kcal mol^{-1}, ts frequencies/cm^{-1} 200(1), 400(1), 800(2), 1000(5), 1200(4), 1400(2), 3000(5).

2-Fluoropropene: k(475.1°C) = 5.3 × 10^{-5} s^{-1}, path degeneracy = 2, A = 10$^{14.70}$ s^{-1}, E_a = 65 kcal mol^{-1}, ts frequencies/cm^{-1} 200(1), 400(2), 600(1), 800(4), 1000(3), 1200(3), 1400(1), 3000(5).

3-Fluoropropene: k(475.1°C) = 6.6 × 10^{-5} s^{-1}, path degeneracy = 4, A = 10$^{13.93}$ s^{-1}, E_a = 62 kcal mol^{-1}, ts frequencies/cm^{-1} 200(1), 800(3), 1000(5), 1200(5), 1400(1), 3000(5).

k_{c-t}(assumed)/s^{-1} = 10$^{13.4}$ exp (−63 kcal mol^{-1}/RT); ΔH^0(*cis* → *trans*) = +750 cal mol^{-1} (6); ΔH^0($\dot{C}H_2\dot{C}H_2CHF$ → *cis*-1-fluoropropene) = −8 kcal mol^{-1} (5, pp. 40–48); path degeneracy (forward and reverse reactions) = 2; frequencies/cm^{-1}: *cis*- and *trans*-1-fluoropropene: 100(1), 200(1), 300(2), 400(2), 700(2), 1000(1), 1150(2), 1450(3), 1650(1), 3000(3), 3100(2); ts *cis*–*trans* isomerization: 100(1), 200(1), 300(1), 400(2), 700(2), 1000(1), 1100(1), 1200(3), 1400(2), 3000(3), 3100(2).

Can. J. Chem. Downloaded from www.nrcresearchpress.com by 210.87.254.42 on 09/05/12
For personal use only.

Differential thermal analysis and infrared studies on the effect of impurities on aragonite–calcite transformation

CHEBROLU RAMA MOHAN RAO AND PRATAP NARAIN MEHROTRA
Department of Chemistry, University of Roorkee, Roorkee – 247 672, India

Received May 24, 1977

CHEBROLU RAMA MOHAN RAO and PRATAP NARAIN MEHROTRA. Can. J. Chem. **56**, 32 (1978).

The transformation of aragonite to calcite (A–C) is an irreversible reconstructive transformation involving a change from 6 to 9 in the primary coordination. Cationic impurities like Na^+, Mg^{2+}, Zn^{2+}, Y^{3+}, La^{3+}, Nd^{3+}, Gd^{3+}, Dy^{3+} have been doped in pure aragonite and their effect on the kinetics and energetics of its transformation to calcite is studied. By employing a DTA technique, the enthalpy and energy of activation for the transformation have been calculated. The ir spectra of aragonite and calcite in pure form and with various impurities have been studied and the effect of impurities on absorption bands discussed.

CHEBROLU RAMA MOHAN RAO et PRATAP NARAIN MEHROTRA. Can. J. Chem. **56**, 32 (1978).

La transformation de l'aragonite en calcite (A–C) est une transformation reconstructive irréversible impliquant un changement de 6 à 9 dans la coordination primaire. On a dopé de l'aragonite pure avec des impuretés cationiques comme Na^+, Mg^{2+}, Zn^{2+}, Y^{3+}, La^{3+}, Nd^{3+}, Gd^{3+}, Dy^{3+} et on a étudié leur effet sur la cinétique et les profils énergétiques de sa transformation en calcite. Faisant appel à la technique de la DTA, on a pu calculer l'enthalpie et l'énergie d'activation de la transformation. On a étudié les spectres infrarouges de l'aragonite et de la calcite sous forme pure et avec diverses impuretés et on discute de l'effet des impuretés sur les bandes d'absorption.

[Traduit par le journal]

Introduction

The aragonite to calcite transformation (A–C) is an irreversible reconstructive transformation involving a change from 6 to 9 in the primary coordination; the transformation is therefore expected to be sluggish and associated with high activation energy (1). Although the thermal transformation of A–C has been examined by several workers, there is limited information in the literature on the effect of impurities on the enthalpy, kinetics, and energetics of the transformation. Such a study is of value because most of the reported preparations of aragonite were in the presence of unknown amounts of different impurities and it has been shown (1) that impurities markedly effect a phase transformation of solids. Furthermore, there is a practical significance for such a study as calcium carbonate finds extensive use in chromatography and its efficiency in such work depends not only on the size of the particles but also on the aragonite–calcite ratio. Again, aragonite and calcite are found in nature and their origin is of particular importance in the interpretation of geological phenomena.

In the present investigation the kinetics and energetics of the A–C transformation with known amounts of different impurity cations have been studied. The values of enthalpy of transformation (ΔH) and energy of activation (E_a), for different impurity doped samples of calcium carbonate, have been evaluated from DTA data. The ir spectra have been used to identify the aragonite and calcite forms of calcium carbonate and also to study the effect of impurities on the absorption bands of each of these two forms.

Experimental

All the samples of aragonite were prepared by hydrolysis of the trichloroacetate salts (2). The procedure yields pure samples and avoids unintentional incorporation of impurities. For the preparation of doped samples known amounts of impurity cations (Na^+, Mg^{2+}, Zn^{2+}, Y^{3+}, La^{3+}, Nd^{3+} Sm^{3+}, Gd^{3+}, Dy^{3+}) were taken in the form of carbonates or oxides along with the sample of pure calcium carbonate before reacting with trichloroacetic acid. The impurity cations were chosen on the basis of their ionic size and their effect on the polymorphic compositions of precipitated calcium carbonate (3). All the chemicals used were of analytical grade.

The DTA curves were obtained by employing a 'Fisher Differential Thermalyzer' Model 260, fitted with an automatic voltage stabilizer, recorder, and an amplifier. The curves were recorded with a constant heating rate of 10°C/min under controlled conditions (packing, particle size, etc.). Calcined α-alumina was used as the reference material. The activation energy was calculated following the method of Borchardt and Daniels (4). ΔH values were computed by comparing the area of the transformation peak for the doped sample with the (orthorhombic–hexagonal) transformation peak of pure potassium sulphate (5, 7) and also with the (orthorhombic(II)–rhombohedral(I)) transformation peak of pure potassium nitrate (6, 7).

The ir spectra of the solid samples were obtained by employing a Beckman IR20 spectrophotometer using Nujol mull as a medium.

Can. J. Chem. Downloaded from www.nrcresearchpress.com by 210.87.254.6 on 09/05/12
For personal use only.

TABLE 1. Values of E_a, ΔH, T_t, and T_i for the A–C transformation of various doped samples of calcium carbonate

No.	Impurity*	E_a (kcal/mol)	ΔH† (cal/mol)	ΔH‡ (cal/mol)	T_t (°C)	T_i (°C)	Ionic radii (nm)
1	None	86	837	849	513	480	$Ca^{2+}=0.099$
2	Na (0.01)	83	770	782	514	484	
3	Na (0.10)	77.5	817	829	518	480	
4	Na (0.50)	55	864	877	523	477	$Na^{+}=0.095$
5	Na (1.00)	83	542	550	518	482	
6	Na (1.5)	64	338	344	514	480	
7	Na (5.0)	49	488	495	524	474	
8	Mg (0.01)	—	1052	1065	518	481	
9	Mg (0.1)	63.7	558	565	512	474	
10	Mg (0.5)	69.5	339	344	510	478	$Mg^{2+}=0.065$
11	Mg (1.0)	72	515	524	513	480	
12	Mg (1.5)	84	575	582	518	483	
13	Zn (0.01)	56.7	511	517	516	481	
14	Zn (0.1)	63.0	464	470	515	482	
15	Zn (0.5)	65	234	237	502	482	$Zn^{2+}=0.074$
16	Zn (1.0)	66.6	520	526	516	482	
17	Zn (1.5)	78.5	584	592	518	483	
18	Y (0.01)	66	700	711	525	481	
19	Y (0.1)	38.2	619	628	523	470	
20	Y (0.5)	105	560	569	522	493	$Y^{3+}=0.094$
21	Y (1.0)	58	549	557	516	486	
22	Y (1.5)	63	636	646	510	488	
23	La (0.5)	168	1166	1183	534	518	$La^{3+}=0.115$
24	Nd (0.5)	144	782	793	532	514	$Nd^{3+}=0.108$
25	Gd (0.5)	120	730	740	513	495	$Gd^{3+}=0.102$
26	Dy (0.5)	89	345	350	512	480	$Dy^{3+}=0.099$

*Impurity concentrations are given in parentheses in at.%.
†ΔH for the transformation peak of pure potassium sulphate is taken as standard.
‡ΔH for the transformation peak of pure potassium nitrate is taken as standard.

Results and Discussion

The ΔH values estimated from the peak areas may have an uncertainty of $\pm 10\%$. The activation energy values obtained by employing the procedure of Borchardt and Daniels may have large uncertainties, but comparison of values in related systems is valid (7).

The temperature at the starting point of the peak (T_i), transformation temperature (T_t), i.e. peak temperature, ΔH, and E_a values for the pure and the various doped samples are listed in Table 1.

It is evident from Table 1 that the incorporation of impurities affects the T_i, T_t, ΔH, and E_a values. The E_a value of 86 kcal/mol for the transformation of pure aragonite to calcite agrees well with a result reported earlier (8). The E_a values for the various doped samples range from 38.2 to 168 kcal/mol in comparison to 60 to 110 kcal/mol for the pure aragonite reported in the literature (8–11). The variation in the value of ΔH is also fairly large ranging from 234 to 1166 cal/mol compared to 837 cal/mol for the pure aragonite when potassium sulphate is taken as standard. A similar variation in the ΔH values was obtained using potassium nitrate as standard. The ΔH values obtained by us are higher than those reported by other workers (8, 12). We have checked these values by taking two standards and obtained almost identical values with both standards. The ΔH for the A–C transformation for a pure sample has also been calculated from heat capacity data (13) which gives the value 500 cal/mol compared to 40–160 cal/mol given by some earlier workers (12). A higher temperature of transformation and a larger particle size are probably responsible for high values of ΔH in our studies.

The increase of sodium ion impurity in aragonite decreases E_a values and increases ΔH values regularly up to 0.5 at.%, but neither E_a nor ΔH values show a regular pattern on further increase in impurity content. The transformation temperature follows the trend of ΔH values. With an increase in Mg^{2+} and Zn^{2+} impurity content from 0.01–1.5 at.%, the E_a values increase regularly, but the ΔH values first decrease up to 0.5 at.% impurity and thereafter they start to increase. The T_i and T_t values follow the trend of the E_a and ΔH values respectively. The same trend is observed in both Mg^{2+} and Zn^{2+} doped

Can. J. Chem. Downloaded from www.nrcresearchpress.com by 210.87.254.6 on 09/05/12
For personal use only.

TABLE 2. The ir absorption bands (in wave number, cm^{-1}) for different impurity doped samples of aragonite and calcite

No.	Impurity (at.%)	Aragonite ν_1	Aragonite ν_2	Aragonite ν_4	Aragonite Overtone of ν_2	Calcite ν_2	Calcite ν_4	Calcite Overtone of ν_2
1	None*	1080	866	706,711	—	879	706	—
2	None†	1080	840	706,711	1780	862	703	1786
3	Na (0.1)	1085	850	700,715	1790	870	700	1790
4	Na (1.5)	1084	845	700,706	1790	855	700	1790
5	Mg (0.1)	1077	835	692,706	1780	865	705	1796
6	Mg (1.5)	1078	845	693,708	1780	862	705	1790
7	Zn (0.1)	1084	850	700,713	1792	865	701	1792
8	Zn (1.5)	1075	844	690,705	1780	865	706	1790
9	Y (0.1)	1075	835, 845	695,708	1790	857	700	1790
10	Y (1.5)	1080	866, 843	700,715	1790	865	706	1798
11	La (0.5)	1076	840, 869	695,706	1784	852	695	1785
12	Nd (0.5)	1076	840, 867	695,704	—	867	703	1795
13	Sm (0.5)	1070	832, 857	684,698	1780	858	700	1795
14	Gd (0.5)	1072	842, 865	690,703	1784	860	700	1793
15	Dy (0.5)	1077	840, 860	690,702	1785	866	710	1803

*Literature values taken from ref. 14.
†Values obtained by the authors.

samples. With the increase in Y^{3+} content the ΔH values decrease up to 1% while the E_a values do not show any regular pattern. The T_i values follow the trend of the ΔH values. In the case of lanthanide impurity doped samples, E_a and ΔH values decrease regularly from lanthanum to dysprosium as the ionic radii decrease (for the same at.% impurity, i.e. 0.5%).

A perusal of the data given in Table 1 for the doped samples in general shows that as the E_a values increase the starting point of the peak also shifts to a higher temperature and with an increase in ΔH values the transformation temperatures increase.

The variation of the T_i, T_i, and E_a of the A–C transformation with impurities is understandable (1, 20) but no reasoning can be put forward for the variation in the ΔH values with impurities. It seems likely that in the case of lanthanide ion impurity doped samples the lower ΔH values may be due to the fact that the A–C transformation occurs over wider temperature ranges causing broad and shallow DTA peaks. Accordingly, the ΔH values are low when the T_t values are low. This statement may become true for other doped samples, provided that the valency, electronic configuration, and the percentage of the impurity cation are similar. The wide variation in the T_t and ΔH values for pure aragonite reported in the literature is mainly due to the fact that most of the samples contained unknown amounts of different impurities. Difference in particle size may be another factor responsible for the wide variation in the ΔH values (6). This has also been observed by us by carrying out the DTA analysis of aragonite samples of different particle size. As the particle size decreases the ΔH of the transformation also decreases considerably. This may be attributed to the variation of surface area and surface energy with particle size.

The present findings reveal that if the valency state of the impurity cations is the same but the ionic radii are different (e.g. Mg^{2+} and Zn^{2+}) the trend in the variation of E_a and ΔH values is more or less similar, although there is a contrast in their behaviour when the absolute values of E_a and ΔH are considered. It is also observed that Na^+ and Y^{3+} impurities in aragonite affect the transformation characteristics in a different manner in spite of their similar ionic sizes. The difference in the behaviour may probably be attributed to their different oxidation states and electronic configuration. There may be some effect from the cation and anion vacancies produced by +1 and +3 ions but these effects are difficult to assess from the present investigation. In the case of lanthanide impurity doped samples, the T_t, T_i, ΔH, E_a values increase with the size of the impurity cation (for the same percentage of the impurity).

We have studied the ir spectra of doped samples of

Can. J. Chem. Downloaded from www.nrcresearchpress.com by 210.87.254.6 on 09/05/12
For personal use only.

aragonite as well as calcite and the data obtained are given in Table 2 along with the data for the pure sample. From site group analysis it can be shown that calcite and aragonite will give ν_2, ν_3, ν_4 and ν_1, ν_2, ν_3, ν_4 bands respectively and that each of the ν_3 and ν_4 bands in aragonite is split into two (14–16). We have made similar observations in our present study. ν_3 is not reported in Table 2 as it is overlapped by Nujol bands. In the case of doped samples, the replacement of calcium ions by different cationic impurities results in an alteration of the site symmetry. It is evident from Table 2 that with the change in site symmetry the vibrational frequencies of the various ir absorption bands of both aragonite and calcite are changed markedly. The extent of change in vibrational frequencies varies with different impurity cations and with their different atomic percentages. Although site group analysis does not predict splitting of the ν_2 band in aragonite, in the case of trivalent impurity doped samples (Y^{3+}, La^{3+}, Nd^{3+}, Sm^{3+}, Gd^{3+}, Dy^{3+}) the ν_2 absorption band of the aragonite splits into two bands. The splitting is attributed to the coupling between neighbouring ions (17) and change in site symmetry (18, 19) which occurs when the valency state of impurity cation is changed from +2 to +3. In the case of pure aragonite and other univalent or bivalent cation doped samples the splitting of the ν_2 band is not observed because the coupling is small due to smaller cationic radii compared to those for trivalent lanthanide impurity cations. That the splitting of the ν_2 band in aragonite is due to coupling between neighbouring ions and change in site symmetry is further supported by the observation that the splitting increases as the size of trivalent cation impurity is increased, and the splitting occurs only when Ca^{2+} ions are replaced by trivalent lanthanide ions which change the site symmetry.

Acknowledgments

The authors are grateful to Dr. I. P. Saraswat, Head of the Chemistry Department, for the research facilities. Thanks are also due to Dr. S. N. Tandon for his interest in this work.

1. C. N. R. Rao and K. J. Rao. *In* Progress in solid state chemistry. Vol. 4. *Edited by* H. Reiss. Pergamon Press, New York, NY. 1967. pp. 131–187.
2. M. S. Rao and S. R. Yoganarasimhan. Am. Mineral. **50**, 1489 (1965).
3. Y. Kitano. Bull. Chem. Soc. Jpn. **35**, 1973 (1962).
4. H. J. Borchardt and F. Daniels. J. Am. Chem. Soc. **79**, 41 (1957).
5. A. J. Majumdar and R. Roy. J. Phys. Chem. **69**, 1684 (1965).
6. M. Natarajan, A. R. Das, and C. N. R. Rao. Trans. Faraday Soc. **65**, 3081 (1969).
7. K. J. Rao and C. N. R. Rao. J. Mater. Sci. **1**, 238 (1966).
8. G. V. Subba Rao, M. Natarajan, and C. N. R. Rao. J. Am. Ceram. Soc. **51**, 179 (1968).
9. H. M. Dufy. Ann. Chim. Paris, **5**, 107 (1960).
10. G. Chaudron, H. Mondange, and M. M. Pruna. *In* Proceedings of the International Symposium on the Reactivity Solids. Gothenburg, 1952. Part I. Gothenburg. 1954. pp. 9–20.
11. B. L. Davis and L. H. Adams. J. Geophys. Res. **70**, 433 (1965).
12. G. J. F. McDonald. Am. Mineral. **41**, 744 (1956).
13. K. Kobayashi. Sci. Rep. Tohoku Univ. **35**, 103 (1951).
14. K. Nakamoto. Infrared spectra of inorganic and coordination compounds. John Wiley, New York, NY. 1963.
15. R. S. Halford. J. Chem. Phys. **14**, 8 (1946).
16. F. A. Cotton. Chemical applications of group theory. Interscience Publishers, Inc., New York, NY. 1964.
17. J. C. Decius. J. Chem. Phys. **22**, 1941 (1954); **23**, 1290 (1955).
18. J. R. Ferraro. J. Mol. Spectrosc. **4**, 99 (1960).
19. C. C. Addison and B. M. Gatehouse. J. Chem. Soc. 613 (1960).
20. J. H. Sharp. Differential thermal analysis. Vol. 2. *Edited by* R. C. Mackenzie. Academic Press, London and New York. 1972. p. 66.

Can. J. Chem. Downloaded from www.nrcresearchpress.com by 210.87.254.6 on 09/05/12
For personal use only.

Limits to barriers to internal rotation in benzal fluoride, chloride, and bromide in solution by the *J* method

TED SCHAEFER, WERNER DANCHURA, AND WALTER NIEMCZURA
Department of Chemistry, University of Manitoba, Winnipeg, Man., Canada R3T 2N2

Received June 27, 1977

TED SCHAEFER, WERNER DANCHURA, and WALTER NIEMCZURA. Can. J. Chem. **56**, 36 (1978).

On the basis of the long-range couplings over six bonds between the protons on the side chain and the ring protons in benzal fluoride, chloride, and bromide and some of their derivatives, a hindered rotor model (*J* method) yields limits to the barriers to internal rotation. These are 0.0 to 1.8, 0.7 to 2.4, and 1.7 to 3.8 kcal/mol for the fluoride, chloride, and bromide, respectively. Refinement of the model suggests barriers of 1.1 ± 0.2, 2.2 ± 0.3, and 3.5 ± 0.6 kcal/mol, respectively. The barrier values in the chloride and bromide are considerably less sensitive to the model parameters than is the barrier in the fluoride. It would be of interest to have gas phase values for these barriers. It is also shown that a σ–π mechanism holds for the six-bond proton–proton coupling constant in benzal fluoride but that the analogous coupling between ^{19}F on the side chain and the *para* ring proton carries a non σ–π contribution of +0.3 Hz.

TED SCHAEFER, WERNER DANCHURA et WALTER NIEMCZURA. Can. J. Chem. **56**, 36 (1978).

Sur la base des couplages à longue distance à travers six liaisons entre les protons de la chaîne latérale et les protons du cycle du fluorure, du chlorure et du bromure de benzal et de quelques-uns de leurs dérivés, un modèle rotor empêché (méthode *J*) fournit les limites pour les barrières à la rotation interne. Celles-ci sont respectivement de 0.0 à 1.8, 0.7 à 2.4 et 1.7 à 3.8 kcal/mol pour le fluorure, le chlorure et le bromure. Un affinement de la méthode suggère des barrières respectives de 1.1 ± 0.2, 2.2 ± 0.3 et 3.5 ± 0.6 kcal/mol. Les valeurs des barrières pour le chlorure et pour le bromure sont beaucoup moins sensibles aux paramètres du modèle que la barrière pour le fluorure. Il serait intéressant d'obtenir des valeurs en phase gazeuse pour ces barrières. On a aussi montré qu'un mécanisme σ–π tient pour la constante de couplage proton–proton à travers six liens dans le fluorure de benzal mais que le couplage analogue entre le ^{19}F de la chaîne latérale et le proton en para du cycle comporte une contribution non σ–π de +0.3 Hz.
[Traduit par le journal]

Introduction

In **1**, the barrier to the internal rotation which interconverts **1***a* and **1***b* rises from about 15 kcal/mol

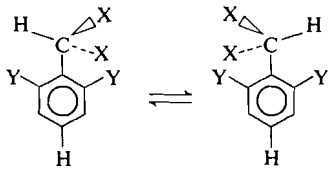

1*a* **1***b*

when X = Y = Cl to 21 kcal/mol when Y = Cl, X = I (1–4). Classical mechanics calculations (3–5) agree with these measurements and strongly indicate a two-fold potential, the high energy form having the C—H bond of the side chain in a plane perpendicular to the benzene plane.

The measurements depend on the well-established broadening of nmr peaks (T_2 effects), caused by dephasing of the magnetization as the nuclear spins hop between sites of different Larmor frequencies. Under even the most favourable experimental conditions, this technique becomes insensitive to rotational barriers below about 5 kcal/mol.

An alternative method (*J* method) for the determination of internal barriers depends on a knowledge of the rotational angle dependence of nuclear spin–spin coupling constants. Coupled with a hindered rotor treatment the method is useful for twofold barriers lying somewhere between about 0.2 and perhaps 3 kcal/mol (6, 7). It has been applied to a variety of benzene derivatives, in particular to phenylethane (8), isopropyl benzene (9), and to phenylcyclopropane (10).

When Y = H in **1**, the line-shape method cannot be applied because the barriers are too small. However, the *J* method may well be useful here and this paper reports on estimates, obtained in this way, of the rotational barriers to internal rotation in benzal fluoride, chloride, and bromide.

Experimental

The preparation of benzal fluoride and of its 3,5-dichloro derivative has been described (11). Benzal chloride and bromide had a commercial origin, while the 3,5-dichlorobenzal chloride was prepared from the toluene by free radical chlorination of the methyl group in a manner described previously (1). 4-Methylbenzal fluoride was prepared from the benzaldehyde derivative in the previous way (11).

Degassed solutions, containing some tetramethylsilane, were carefully calibrated in the frequency sweep mode on an HA100 spectrometer at a probe temperature of 305 K. Manual and sweep oscillator frequencies were read at approximately 5 Hz intervals and the procedure was repeated five times.

Can. J. Chem. Downloaded from www.nrcresearchpress.com by 210.87.254.40 on 09/05/12
For personal use only.

Can. J. Chem. Downloaded from www.nrcresearchpress.com by 210.87.254.40 on 09/05/12
For personal use only.

Deviations from the average peak position were 0.02 Hz or less, comparing well with the rms deviations between observed and calculated peak positions in the analyses described below.

The 10-spin system represented by the spectrum of 4-methylbenzal fluoride was first simplified by decoupling of the methyl protons. The decoupled spectrum was calibrated and analyzed. The fully coupled ^{1}H nmr spectrum was also calibrated. Partial decoupling experiments showed that $^7J_p^{F,CH_3}$ was of the same sign as $^2J^{H,F}$, i.e., positive (11).

Results and Discussion

Spectral Analyses

The computer program LAME (12, 13) led to calculated spectra in satisfactory agreement with the observed spectra. Table 1 gives the spectral data obtained for benzal bromide. In Fig. 1, the observed and calculated spectra of the side-chain proton are displayed to illustrate the resolution and fit. The calculated spectrum assumes a line width at half height of 0.09 Hz.

The analysis of the ^{1}H nmr spectrum of 4-methylbenzal fluoride, methyl protons decoupled, gave the spectral data in Table 2. Use of the program NUMARIT (14) in the noniterative mode allowed the extraction of the couplings to the methyl protons, also given in Table 2. The standard deviations quoted in the table suggest an accuracy of 0.02 Hz or better in the spectral parameters.

Rather than tabulate all spectral parameters for the other compounds, the data of immediate interest, the long-range couplings, are collected in Table 3. All these couplings are thought to be accurate to 0.02 Hz.

The Angular and Substituent Dependence of $^6J_p^{H,CH}$

In toluene, theoretical and experimental data (15–17) agree that $^6J_p^{H,CH} \propto \sin^2\theta$, where θ is the angle by which the C—H bond of the methyl group twists out of the plane of the ring. In other words, ^6J is transmitted by a σ–π mechanism (18, 19). In toluene, ^6J is -1.24 Hz when $\theta = 90°$ (17, 20) and the average or expectation value of $\sin^2\theta$, indicated by angular brackets, is $\langle\sin^2\theta\rangle = 0.5$ because the barrier to internal rotation is only 0.014 kcal/mol (21).

TABLE 1. Proton chemical shifts and spin–spin coupling constants for benzal bromide*

Parameter	Value	Parameter	Value
ν_α†	652.282(7)‡	$^4J_{24}$	1.174(7)
ν_o	744.620(4)	$^4J_{35}$	1.386(6)
ν_m	725.137(4)	$^5J_{25}$	0.554(6)
ν_p	720.303(6)	$^4J_\alpha$	−0.382(6)
$^3J_{23}$§	7.888(7)	$^5J_\alpha$	0.285(7)
$^3J_{34}$	7.474(5)	$^6J_\alpha$	−0.120(10)
$^4J_{26}$	2.143(5)	rms deviation	0.021

*In 10% v/v CS_2.
†In Hz at 100 MHz to low field of internal tetramethylsilane at 305 K.
‡The numbers in brackets give the standard deviations in the last place.
§In Hz.

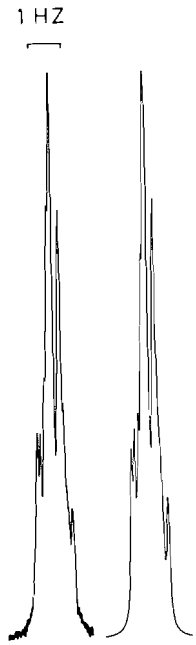

FIG. 1. The observed and calculated proton magnetic resonance spectrum at 100 MHz of the side-chain proton of benzal bromide as a 10 v/v % solution in CS_2. The peak width at half height of the calculated spectrum is set at 0.09 Hz. The peak separation of the small doublet on the left of the observed spectrum is just under 0.1 Hz. The asymmetric structure is a consequence of the relative signs of the couplings to the ring protons.

There exists no evidence that ^6J changes its maximum magnitude when one or two hydrogen atoms are replaced by groups of closely similar electronegativity to that of hydrogen, e.g. CH_3 or SH groups (8, 10, 22). In such molecules, a hindered rotor treatment yields the quantum mechanical expectation value of $\sin^2\theta$ in terms of a twofold hindering potential, the reduced moment of inertia, and the temperature (6, 23). The measured value of $^6J_p^{H,CH}$, divided by -1.24, yields a value of $\langle\sin^2\theta\rangle$, which can be matched to the theoretical values and so yield a barrier.

When X in the CHX_2 fragment is substantially more electronegative than hydrogen, it is conceivable that $^6J(\theta = 90°)$ decreases in magnitude because the X group will polarize the C—H bond, causing smaller σ–π overlap between this σ bond and the adjacent π system of the benzene ring. Theoretical evidence for a reduction in $^6J(\theta = 90°)$ can be adduced. INDO MO FPT calculations of $^6J_p^{H,CH}$ in toluene (18) reproduce the $\sin^2\theta$ dependence and agree exactly with experiment (20). For the CHF_2 group, $^6J(\theta = 90°)$ is calculated as -0.87 Hz (11), the fractional reduction

Can. J. Chem. Downloaded from www.nrcresearchpress.com by 210.87.254.40 on 09/05/12
For personal use only.

TABLE 2. Proton chemical shifts,* $^1H,^1H$ and $^1H,^{19}F$ coupling constants for 4-methylbenzal fluoride, 20 mol% in C_6D_6

Parameter	Value†	Parameter	Value
ν_1	626.828(2)	$^4J_o^{H,CH}$	−0.462(3)
ν_2	716.286(2)	$^5J_m^{H,CH}$	0.247(3)
ν_3	691.883(2)	rms deviation	0.018
ν_4	207.7	Transitions calculated	256
$^2J^{H,F}$	56.622(3)	Peaks observed	92
$^3J^{H,H}$	7.920(4)	Transitions assigned	205
$^4J_{26}^{H,H}$	1.866(4)	$^7J^{H,CH_3}$	0.23±0.02‡
$^4J_{35}^{H,H}$	1.975(4)	$^7J^{F,CH_3}$	1.46±0.02‡
$^5J_{25}^{H,H}$	0.588(3)	$^5J_m^{H,CH_3}$	0.33±0.02‡
$^4J_o^{H,CF}$	−1.169(3)	$^4J_o^{H,CH_3}$	−0.72±0.02‡
$^5J_m^{H,CF}$	0.891(3)		

*In Hz at 100 MHz to low field of internal TMS at 305 K.
†The numbers in brackets give the standard deviation in the last place for the analysis in which the methyl protons were decoupled.
‡These numbers were extracted by a noniterative procedure using the computer program NUMARIT.

TABLE 3. Long-range coupling constants to the sidechain protein in Hz* in toluene derivatives

Compound	$^4J_o^{H,CH}$	$^5J_m^{H,CH}$	$^6J_p^{H,CH}$	Concentration
α,α-diBr	−0.38	0.28_5	−0.12	10% v/v CS_2
α,α-diCl	−0.43	0.26	−0.21	10% v/v CS_2
α,α-diCl-3,5-diCl	−0.45	—	−0.18	10% v/v CCl_4
α,α-diF†	-0.46_5	0.26	-0.24_5	15 mol% C_6D_6
α,α-diF-3,5-diCl†	−0.49	—	−0.28	10 mol% CS_2
α,α-diF-2,6-diCl†	—	0.24	−0.01	15 mol% C_6D_6
α,α-diBr-4-COOEt	−0.38	0.29	—	10 mol% $(CH_3)_2C{=}O$
α,α-diF-4-CH_3	−0.46	0.25	0.23‡	20 mol% C_6D_6

*Standard deviations in these couplings ranged from 0.003 to 0.010 Hz; estimated accuracy is 0.01 to 0.02 Hz.
†Reference 11.
‡$^7J_p^{H,CH_3}$.

in magnitude agreeing very closely with the reduction in magnitude calculated for the β proton hyperfine coupling in the $CF_2H\dot{C}H_2$ radical (24), also transmitted via a σ–π mechanism. The latter calculations are consistent with experimental data (24).

That $^6J(\theta = 0°)$ vanishes is suggested by the nmr spectrum of 2,6-dichlorobenzal bromide, in which $^6J_p^{H,CH}$ is not observable, i.e. < 0.03 Hz, and the C_α—H bond prefers the benzene plane to the extent of 18 kcal/mol (3). Furthermore, this coupling is also unobservable for 2,6-dichlorobenzalfluoride (11) in which the barrier to rotation is known to be not larger than 8 kcal/mol (11).

$^6J_p^{H,CH}$ *and the Barrier to Internal Rotation*

Plots of $\langle\sin^2\theta\rangle$ versus the twofold barrier to rotation at 305 K were prepared in the prescribed way (6) for various reduced moments of inertia, not being very sensitive to the latter. The experimental values of −0.26, -0.19_5, and −0.12 Hz, respectively, for CHF_2, $CHCl_2$, and $CHBr_2$ yield various values of $\langle\sin^2\theta\rangle$, depending on the appropriate value of $^6J(\theta = 90°)$. For example, if $^6J(\theta = 90°)$ were −0.52 Hz for CHF_2, then $\langle\sin^2\theta\rangle$ would be 0.5, corresponding to a zero barrier.

In Fig. 2, the values of the $^6J(\theta = 90°)$ are plotted against the barrier to internal rotation for ^6J ranging from −0.54 to −1.14 Hz and employ reduced moments of inertia of −0.4, 1.02, and 1.27×10^{-38} g cm^2 for CHF_2, $CHCl_2$, and $CHBr_2$, respectively.

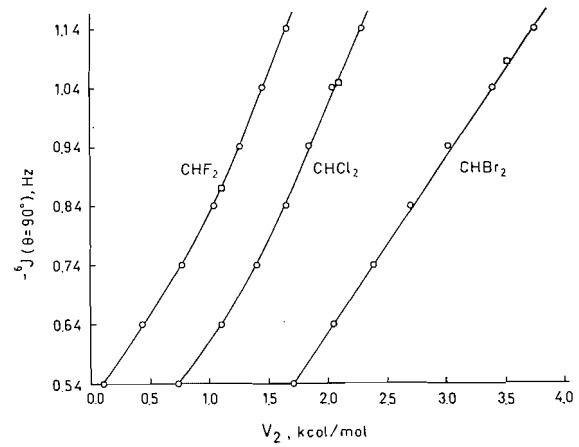

FIG. 2. The value of $^6J_p^{H,CH}$ is plotted versus the twofold barrier to internal rotation as deduced from the hindered rotor model described in the text. The squares indicate preferred values of V_2.

Can. J. Chem. Downloaded from www.nrcresearchpress.com by 210.87.254.40 on 09/05/12
For personal use only.

These plots are obtained for a ground state conformation in which the C—H bond of the side-chain lies in the plane of the benzene ring. If conformations corresponding to **2** and **3** were of lowest energy, a finite barrier would imply that $\langle \sin^2\theta \rangle$ were greater than 0.5, corresponding to a $^6J(\theta = 90°)$ of less than

2 **3**

0.52 Hz in magnitude for each compound, a possibility which we consider absurd.

The assignment of barriers is more problematical. It can be said with confidence (Fig. 2) that the barrier limits are 0.0 to 1.8, 0.7 to 2.4, and 1.7 to 3.8 kcal/mol for CHF_2, $CHCl_2$, and $CHBr_2$, respectively. These limits can be somewhat reduced as follows.

In view of the theoretical value of $^6J(\theta = 90°)$ for CHF_2 of -0.87 Hz, obtained from the same parameterization as that which gives agreement with hyperfine couplings in esr spectra, it can be said with lesser confidence that, for CHF_2, the barrier to internal rotation is 1.1 ± 0.2 kcal/mol, the quoted error arising from the uncertainty in the experimental data only; $\langle \sin^2\theta \rangle = 0.30 \pm 0.02$. If $^6J(\theta = 90°)$ depends linearly on the electronegativity of X, then reasonable estimates are -1.05 Hz for X = Cl and -1.09 Hz for Br (from a plot of $^6J(\theta = 90°)$ versus E_X with endpoints given by X = H and F). It follows that the internal barriers are then 2.2 ± 0.3 and $3.5_5 \pm 0.6$ kcal/mol for Cl and Br; $\langle \sin^2\theta \rangle = 0.19 \pm 0.02$ and 0.11 ± 0.02, respectively.

At 305 K, the shape of the $\langle \sin^2\theta \rangle$ versus barrier curve is such that a change of 0.02 in $\langle \sin^2\theta \rangle$ corresponds to a change of about 0.1 kcal/mol in a barrier of 0.2 kcal/mol, whereas at a barrier of 3.5 kcal/mol such a change in $\langle \sin^2\theta \rangle$ corresponds to a change of 0.7 kcal/mol. In other words, above about 3 kcal/mol the J method becomes rather insensitive for molecules of the present kind, i.e. where $\langle \sin^2\theta \rangle$ varies between 0.0 and 0.5.

The barrier to internal rotation about the sp^2–sp^3 carbon–carbon bond in 3,5-dibromoisopropyl benzene, as derived by present methods, is 2.0 ± 0.2 kcal/mol (9). The van der Waals radius of the methyl group is larger than that of chlorine (25) but for such different substituents the barriers need not be directly proportional to these radii. Hyperconjugation effects should also be considered (26). In fact, even the internal rotational barriers in XH_3—CH_2Y (X = C, Si, Ge; Y = H, CH_3) cannot be interpreted solely in terms of steric repulsions (27).

Ab initio molecular orbital calculations at the STO-3G level (26) yield an internal barrier of 0.18 kcal/mol for benzal fluoride, with **1** as the low-energy conformation. Such a barrier implies that $^6J_p^{H,CH}$ $(\theta = 90°)$ is -0.59 Hz in benzal fluoride. Assuming a linear dependence of $^6J(\theta = 90°)$ on substituent electronegativity ($E_F = 4.0$, $E_{Cl} = 3.0$, $E_{Br} = 2.8$, $E_H = 2.1$), $^6J(\theta = 90°)$ then becomes -0.99 Hz for benzal bromide and -0.93 Hz for benzal chloride. It then follows from Fig. 2 that the internal barrier is 1.8 and 3.2 kcal/mol for the chloride and bromide, respectively.

In other words, the internal barriers in benzal chloride and benzal bromide are considerably less sensitive to the model parameters than is the barrier in benzal fluoride.

The Long-range Coupling to ^{19}F in Benzal Fluoride

The long-range couplings to protons on the side chain in toluene and its derivatives are insensitive to intrinsic substituent effects (28, 29), as are those in the compounds listed in Table 2. For example, in benzal bromide and its *para*-COOEt derivative, $^4J_o^{H,CH}$ and $^5J_m^{H,CH}$ are invariant. $^6J_p^{H,CH}$ in the 3,5-dichloro derivatives is apparently about 0.03 Hz larger in magnitude than in the benzal chloride or fluoride parent. The former have higher reduced moments of inertia and, in principle, should possess somewhat larger magnitudes for ^6J_p, although not to the extent indicated by the data in Table 2. Accordingly, the differences may well arise from experimental error, from unrecognized solvent effects, or from slightly different barriers in the 3,5-disubstituted compounds. In any event, such perturbations are apparently of minor importance in comparison to the uncertainty in $^6J(\theta = 90°)$. That $^6J_p^{H,CH}$ is transmitted by a π electron mechanism in a substituted methyl group has been confirmed for benzyl bromide derivatives (7).

Turning to benzal fluoride, the question arises of the intrinsic substituent dependence of the long-range couplings to ^{19}F and of a pure σ–π mechanism. In benzal fluoride, $^4J_o^{H,CF}$ and $^6J_p^{H,CF}$ are -1.16 and -1.14 Hz, respectively (11). In the 3,5-dichloro derivative, $^4J_o^{H,CF}$ becomes -1.02 Hz and $^6J_o^{H,CF}$ changes to -0.95 Hz, suggesting a substantial intrinsic substituent perturbation by *meta* substituents.

The σ–π dependence was investigated via the spectrum of 4-methylbenzal fluoride. In this compound, $^4J_o^{H,CF}$ is -1.17 Hz and $^5J_m^{H,CF}$ is 0.89 Hz, within experimental error of the data for benzal fluoride (the corresponding values of $^4J_o^{H,CH}$ and $^5J_m^{H,CH}$ also agree to within 0.01 Hz), suggesting a negligible perturbation of these couplings by the methyl substituent. Furthermore, $^7J_p^{H,H}$ is 0.23 ± 0.02 Hz in the methyl derivative, again within ex-

perimental error equal to the magnitude of $^6J_p^{H,CH}$ in benzal fluoride, and confirming the σ–π mechanism, i.e. a $\sin^2\theta$ dependence of $^6J_p^{H,CH}$. Therefore the discussion in the previous sections is unaltered.[1]

On the very reasonable assumption that $^7J_p^{F,CH_3}$ is transmitted solely by a σ–π mechanism, one may argue as follows. $^7J_p^{F,CH_3}$ is 1.46 ± 0.02 Hz in 4-methylbenzal fluoride. Comparison with the value of -1.14 Hz for $^6J_p^{H,CF}$ in benzal fluoride implies $+0.3$ Hz as the component of $^6J_p^{H,CF}$ which is not transmitted by a σ–π mechanism. The θ dependence of this component is unknown. It appears that $^6J_p^{H,CF}$ suffers from two disadvantages from the viewpoint of its use in deriving internal rotational barriers. In contrast to $^6J_p^{H,CH}$, it contains an appreciable non σ–π electron contribution and is sensitive to intrinsic (electronic) perturbations from substituents on the benzene ring. Consequently, although $^6J_p^{H,CF}$ is rather larger in magnitude then $^6J_p^{H,CH}$ and its determination demands less experimental skills, it must be concluded that its use in barrier determinations will be problematical.

For example, the value of $^6J_p^{H,CF}$ ($\theta = 90°$) needed to reproduce the above barrier of 1.1 kcal/mol is -2.43 Hz, i.e. $\langle\sin^2\theta\rangle_F = 0.60 = -1.46/^6J_{90}^{H,CF}$ because for a ground state conformation **1**, $\langle\sin^2\theta\rangle_F$ is decreasing from 0.75 for a very large barrier to 0.50 for a zero barrier. On the dubious assumption that the non σ–π component of $^6J_p^{H,CF}$ is independent of θ and is $+0.3$ Hz, it follows that, at $\theta = 60°$, the observed $^6J_p^{H,CF}$ must be -1.60 Hz, i.e., 0.75 $(-2.43 + 0.3)$ Hz. The observed value in 2,6-dichlorobenzal fluoride is -1.25 Hz, so that the intrinsic substituent effect on $^6J_p^{H,CF}$ would be $+ 0.35$ Hz. This is a reasonable value in view of the substituent perturbation caused by chlorine atoms at the 3,5-positions (see above). Nevertheless, this line of argument illustrates how tenuous would be a barrier derived from $^6J_p^{H,CF}$.

Acknowledgment

We are grateful to the National Research Council of Canada for financial assistance.

[1]Note that, for a σ–π mechanism, $^6J_p^{H,CH_3} = -^7J_p^{CH_3,CH_3}$, as observed in toluene and *p*-xylene and their derivatives (15, 17).

1. B. J. Fuhr, B. W. Goodwin, H. M. Hutton, and T. Schaefer. Can. J. Chem. **48**, 1558 (1970).
2. J. Peeling, T. Schaefer, and C. M. Wong. Can. J. Chem. **48**, 2839 (1970).
3. J. Peeling, L. Ernst, and T. Schaefer. Can. J. Chem. **52**, 849 (1974).
4. J. Peeling, J. B. Rowbotham, L. Ernst, and T. Schaefer. Can. J. Chem. **52**, 2414 (1974).
5. A. Mannschreck and L. Ernst. Chem. Ber. **104**, 228 (1971).
6. T. Schaefer, J. B. Rowbotham, W. J. E. Parr, K. Marat, and A. F. Janzen. Can. J. Chem. **54**, 1322 (1976).
7. T. Schaefer, L. J. Kruczynski, and W. J. E. Parr. Can. J. Chem. **54**, 3210 (1976).
8. T. Schaefer, W. Niemczura, and L. Kruczynski. Chem. Phys. Lett. **38**, 498 (1976).
9. T. Schaefer, W. J. E. Parr, and W. Danchura. J. Magn. Reson. **25**, 167 (1977).
10. W. J. E. Parr and T. Schaefer. J. Am. Chem. Soc. **99**, 1033 (1977).
11. J. B. Rowbotham, A. F. Janzen, J. Peeling, and T. Schaefer. Can. J. Chem. **52**, 481 (1974).
12. S. Castellano and A. A. Bothner-By. J. Chem. Phys. **41**, 3863 (1964).
13. C. W. Haigh and J. M. Williams. J. Mol. Spectrosc. **32**, 398 (1969).
14. A. R. Quirt and J. S. Martin. J. Magn. Reson. **5**, 318 (1971); J. S. Martin, K. M. Worvill, and A. R. Quirt. Abstr. Sixth Int. Symp. Magn. Reson. 176 (1977).
15. C. J. Macdonald and W. F. Reynolds. Can. J. Chem. **48**, 1002 (1970).
16. J. B. Rowbotham and T. Schaefer. Can. J. Chem. **52**, 489 (1974).
17. R. Wasylishen and T. Schaefer. Can. J. Chem. **50**, 1852 (1972).
18. H. M. McConnell. J. Chem. Phys. **30**, 126 (1959).
19. C. Heller and H. M. McConnell. J. Chem. Phys. **32**, 1535 (1960).
20. M. P. Williamson, R. Kostelnik, and S. M. Castellano. J. Chem. Phys. **49**, 2218 (1968).
21. H. Rudolph, H. Dreizler, A. Joeschke, and P. Wendling. Z. Naturforsch. Teil A, **22**, 940 (1967).
22. T. Schaefer and W. J. E. Parr. J. Chem. Soc. Faraday Trans. II, **73**, 1501 (1977).
23. P. B. Ayscough, M. C. Price, and R. E. D. McClung. Mol. Phys. **20**, 41 (1971).
24. K. S. Chen, P. J. Krusic, P. Meakin, and J. K. Kochi. J. Phys. Chem. **78**, 2014 (1974).
25. L. Pauling. The nature of the chemical bond. Cornell University Press. Ithaca, New York, NY. 1960.
26. W. J. Hehre, L. Radom, and J. A. Pople. J. Am. Chem. Soc. **94**, 2496 (1972).
27. J. R. Durig, A. D. Lopata, and P. Groner. J. Chem. Phys. **66**, 1888 (1977).
28. R. Wasylishen and T. Schaefer. Can. J. Chem. **49**, 94 (1971).
29. H. Rottendorf and S. Sternhell. Aust. J. Chem. **17**, 1315 (1964).

Can. J. Chem. Downloaded from www.nrcresearchpress.com by 210.87.254.40 on 09/05/12
For personal use only.

Sur la réduction par $NaBH_4$ de quelques nitriles α,β-insaturés

YVON PÉPIN,[1] HASSAN NAZÉMI[2] ET DANIEL PAYETTE

Département de Chimie, Université du Québec à Montréal, C.P. 8888, Montréal (Qué.), Canada H3C 3P8

Reçu le 18 août 1977

YVON PÉPIN, HASSAN NAZÉMI et DANIEL PAYETTE. Can. J. Chem. **56**, 41 (1978).

L'étude de différentes réactions de réductions par $NaBH_4$ de nitriles α,β-insaturés démontre que celles-ci s'effectuent via une addition 1:4 conduisant aux nitriles saturés. Lorsque le temps de réaction est prolongé, des produits d'hydrolyse ou de substitution du nitrile saturé sont observés. Les vitesses de réduction relatives sont dans l'ordre: phényl-2 butèno-2 nitrile **1** > diphényl-2, 3 propèno-2 nitrile **2** > phényl-3 propèno-2 nitrile **3** > butèno-2 nitrile **4**.

YVON PÉPIN, HASSAN NAZÉMI, and DANIEL PAYETTE. Can. J. Chem. **56**, 41 (1978).

A study of several different reductions of α,β-unsaturated nitriles by $NaBH_4$ shows that these proceed by way of a 1:4 addition to form saturated nitriles. At long reaction times, hydrolysis products or those of substitution of the saturated nitrile are observed. The relative rates of reduction follow the order: 2-phenyl-2-butenenitrile **1** > 2,3-diphenyl-2-propenenitrile **2** > 3-phenyl-2-propenenitrile **3** > 2-butenenitrile **4**.

[Journal translation]

Introduction

L'utilisation du borohydrure de sodium pour la réduction de doubles liaisons conjuguées avec des groupes fonctionnels tels que —COR, —CO_2R, —CN et quelques autres a été largement employée depuis les quelques trente dernières années (1–16). L'étude du mécanisme de ces réactions a aussi fait l'objet de nombreux travaux (17–21). Cependant, aucun mécanisme n'a été proposé pour la réduction de nitriles insaturés quoique plusieurs études sur ce sujet aient été publiées (22–25).

Dans ce travail, nous nous sommes d'abord intéressés à vérifier si le mécanisme de réduction de la double liaison pouvait-être similaire à celui proposé par la réduction des groupes carbonyles α,β-insaturés. Par la suite, nos études ont porté sur la nécessité et l'influence de la position d'un groupe aromatique (phényle) sur la vitesse de réduction. Les molécules modèles utilisées sont le phényl-2 butèno-2 nitrile **1**, le diphényl-2,3 propèno-2 nitrile **2**, le phényl-3 propèno-2 nitrile **3** et le butèno-2 nitrile **4**.

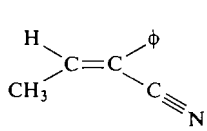

1 (*Z*)

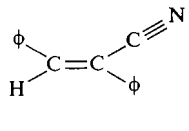

2 (*Z*)

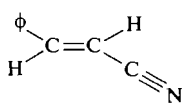

3 (*E*)

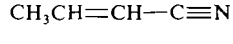

4 (*E* + *Z*)

[1]A qui la correspondance doit-être adressée.

[2]Les résultats rapportés sont tirés en grande partie du mémoire de maîtrise de H. Nazémi (mai 1977).

Résultats

Sur la configuration des produits de départ

Le butèno-2 nitrile **4**, disponible commercialement (Eastman), est un mélange d'isomères *E* et *Z*. Le phényl-3 propèno-2 nitrile **3**, aussi disponible commercialement (Eastman), possède la configuration *E*. Le spectre de rmn ne montre que deux doublets à τ 4.20 et 2.72 ppm, J = 17.3 Hz, qui ne sont compatible qu'avec une configuration *E* (26). Le phényl-2 butèno-2 nitrile **1** possède une configuration *Z* prépondérante (94%). L'attribution de celles-ci est faite par comparaison des protons vinyliques en spectroscopie de rmn avec ceux des phényl-2 crotonates d'alcoyles **5** (15). Le diphényl-2,3 propèno-2 nitrile **2** possède probablement une configuration *Z*. L'attribution de celles-ci est faite par comparaison du spectre uv avec ceux des stilbènes **6** (26) et des diphényl-2,3 acrylates d'alcoyles **7** (27).

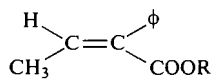

5 (*Z*)

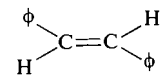

6 (*E*)

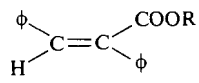

7 (*Z*)

Sur les réductions

La réduction par le borohydrure de sodium des nitriles insaturés **1**, **2** et **3** conduit aux nitriles saturés **8**, **12** et **13** correspondant. Cependant, lorsque la réaction de réduction de **1** est laissée à reflux plusieurs jours, des produits secondaires apparaissent: le phényl-2 butamide **9**, l'acide phényl-2 butanoïque **10** et le phényl-2 propanol **11**.

Can. J. Chem. Downloaded from www.nrcresearchpress.com by 210.87.254.105 on 09/05/12
For personal use only.

Can. J. Chem. Downloaded from www.nrcresearchpress.com by 210.87.254.105 on 09/05/12
For personal use only.

L'apparition du dérivé alcoolique s'est aussi manifestée lors de la réduction prolongée du nitrile **2** pour conduire au diphényl-1,2 éthanol **13**. Le butèno-2 nitrile **4** ne réagit pas dans les conditions présentes de réduction.

La réduction par $NaBD_4$ du dérivé **1** conduit exclusivement au produit monodeutérié en position 3, **8***b*. L'addition de D_2O après une réduction normale avec $NaBH_4$ ne conduit qu'à 25% d'incorporation. Il est nécessaire de faire la réduction directement dans un mélange de tétrahydrofuranne et d'eau deutériée afin d'obtenir au plus 86% d'incorporation conduisant au produit deutérié en position 2, **8***c*.

Les vitesses relatives furent déterminées en réduisant des mélanges équimoléculaires de **1** et **2**, de **1** et **3** et de **2** et **3** par un excès de $NaBH_4$.

ϕ—CR_1CN—CHR_2—CH_3

8*a* $R_1 = R_2 = H$
8*b* $R_1 = H, R_2 = D$
8*c* $R_1 = D, R_2 = H$

ϕ—$CHCONH_2$—CH_2CH_3 **9**

ϕ—$CHOH$—CH_2—CH_3 **11**

ϕ—$CHCOOH$—CH_2—CH_3 **10**

ϕ—$CHOH$—$CH_2\phi$ **13**

ϕ—$CHCN$—$CH_2\phi$ **12**

ϕ—CH_2—CH_2CN **14**

Les analyses des produits de réduction furent principalement faites par la spectrométrie de rmn. Les différents pourcentages relatifs des produits obtenus furent déterminé par intégration du proton méthyne sur les mélanges réactionnels bruts.

Discussion

Sur le mécanisme

La plupart des études rapportées dans la littérature (9, 10, 13–16, 22–25) concernent des systèmes insaturés du type suivant:

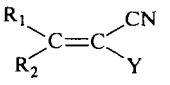

$Y = CN, COOR, CONH_2$
$R_1, R_2 = H, Alkyl, Aryl$

Seuls, à notre connaissance, Knabe *et al.* (11) et Husson *et al.* (12) ont réduit un système insaturé similaire au diphényl-2,3 propèno-2 nitrile **2**.

Considérant l'hypothèse de Kadin (24) sur la création de centre électrophyle et notre propre étude, nous sommes amenés à proposer que le mécanisme de la réduction d'une double liaison conjuguée avec un groupe nitrile est similaire à celui proposé pour la réduction de carbonyles α,β-insaturés (18, 20, 21). Dans la première étape de la réaction, il y aurait une addition 1:4 de l'anion borohydrure pour conduire à un complexe intermédiaire qui s'hydrolyserait par l'action de l'isopropanol ou de l'eau (20, 40) pour conduire au nitrile saturé. Ce mécanisme s'appuie sur les réactions de réductions par $NaBD_4$ où le deutérure s'additionne sur la carbone β de la double liaison, tandis que l'hydrolyse du complexe intermédiaire par l'eau deutérié introduit un atome de deutérium en position α.

La réaction de réduction de **1** étant particulièrement rapide, la formation des produits secondaires **9**, **10** et **11** ne peut que provenir du phényl-2 butanenitrile **8**. Le nitrile **8** fut soumis à l'action de NaOH 5% dans l'isopropanol pour conduire aux trois produits **9**–**11**. La même réaction fut observée lorsque du borohydrure de sodium partiellement hydrolysé (28, 41) remplace l'hydroxyde de sodium. L'amide **9** et l'acide **10** sont donc des produits d'hydrolyse basique du nitrile correspondant.

La substitution du groupe nitrile par un hydroxyle aurait pu se rapprocher de celles rapportées lors de la réduction de cyano stéroides (29–31). Ces auteurs invoquent une oxydation par l'oxygène de l'air en se basant sur les travaux de Stevens et Gasser (32), mais aucun mécanisme n'est proposé.

Lors de notre étude nous avons tenté d'augmenter la quantité d'alcool formé (**8**, **13**) par l'addition durant la réaction de réduction de peroxyde d'hydrogène ou en barbottant de l'air sec, mais sans aucun succès. En se basant sur les réactions du phényl-2 butanenitrile **8** en présence de bases, nous formulons l'hypothèse d'une substitution directe du nitrile par un ion hydroxyle. Il faut noter que la présence d'un phényle en α favorise une telle réaction.

Sur les vitesses de réductions

Les vitesses relatives de réduction sont dans l'ordre: **1** > **2** > **3** > **4**. Ceci implique qu'en plus de l'influence électrophilique (24) du groupe nitrile, la présence et la position d'un groupe phényle a aussi un effet très important sur la vitesse de réduction de la double liaison.

Dans le cas du phényl-1 butèno-2 nitrile **1**, la délocalisation des électrons de la double liaison par le phényle s'additionne à l'effet du nitrile pour créer en β un centre électrophile particulièrement important et la vitesse de réduction est très rapide. Dans le cas du phényl-3 propèno-2 nitrile **3**, les deux effets s'opposent et la vitesse de réduction est relativement lente. Le diphényl-2,3 propèno-2 nitrile **2** cumule les effets positif et négatif des nitriles **1** et **3**, et nous observons une vitesse de réaction intermédiaire entre **1** et **3**. Dans ce dernier cas, il y a peut-être aussi un empêchement stérique à l'approche de l'hydrure qui n'est pas négligeable et qui réduirait la vitesse de la réduction (15, 23). L'absence de réduction de butèno-2 nitrile **4** peut-être comparée à celles rapportées pour d'autres composées aliphatiques similaires (25, 33).

Can. J. Chem. Downloaded from www.nrcresearchpress.com by 210.87.254.105 on 09/05/12
For personal use only.

Il semble contradictoire, cependant, que le dérivé nitrile **3** ayant un phényle en β qui ralentit la réaction, ait une vitesse de réduction quand même beaucoup plus grande que celle de **4** qui ne subit pas cet effet négatif. Autrement dit, le dérivé **4** devrait pouvoir se comparer à **2**, ce qui est loin d'être le cas. La grande réactivité des dérivés **2** et **3** implique donc que la délocalisation des électrons de la double liaison par conjugaison avec des groupes aromatiques semble être une condition nécessaire pour que le centre électrophile puisse se créer (sous l'influence prépondérante du groupe nitrile) et favoriser ainsi l'addition d'un hydrure.

Partie expérimentale

Les points de fusion sont déterminés sur un "Melting Point Apparatus" du type Fisher-Johns de la compagnie Fisher à l'aide d'un thermomètre calibré. Les indices de réfraction sont mesurés sur un réfractomètre Bausch et Lomb du type Abbe de la compagnie Fisher. Les spectres infrarouge sont pris sur un appareil Perkin-Elmer, modèle 457, à double faisceaux, entre deux plaques de NaCl. Les spectres de résonnance magnétique nucléaire sont pris sur un appareil de Perkin-Elmer, modèle R-12. Les déplacement chimiques sont exprimés en valeur τ. Le CCl_4 est utilisé comme solvant et le TMS comme référence interne (s = singlet, d = doublet, t = triplet, q = quartet). Les spectres ultraviolet sont pris dans l'éthanol 95% sur un appareil Perkin-Elmer, modèle 402. Les spectres de masse sont déterminés sur un appareil Hitachi, modèle RMU-6L, à 70 eV.

Les produits suivants sont disponibles commercialement: phényl-3 propèno-2 nitrile **3** (Eastman), butèno-2 nitrile **4** (Eastman), phényl-3 propionitrile **14** (Eastman), diphényl-1,2 éthanol **13** (Eastman), acide phényl-2 butanoïque **10** (Aldrich), phényl-1 propanol-1 **11** (Aldrich).

*Phényl-2 butèno-2 nitrile **1***

Une solution de 2.3 g (0.1 mol) de sodium dans 50 ml d'éthanol absolu est ajoutée goutte à goutte avec forte agitation, dans une solution de 7.5 g (0.17 mol) d'acétaldéhyde et 20 g (0.17 mol) de phényl acétonitrile dans 100 ml d'éthanol. Après une agitation de 10 min la solution est versée dans l'eau et extraite à l'éther de la manière habituelle. L'évaporation des solvants conduit à une huile qui est fractionnée sous vide partiel. On recueille 5 g de **1**, 30% du rendement théorique; péb 150°C/36 Torr (litt. (34) 100–103°C/1 Torr); $\eta^{20°}$ 1.5558 (litt. (34) 1.5555); rmn τ: 2.6 (s, phényl), 3.4 (q, J = 7.4 Hz), méthyne), 7.88 (d, J = 7.4 Hz, méthyle); ir 2210 cm^{-1} (C≡N); uv λ_{max} (ε) 217 (13 000), 222 (11 800), 266 nm (20 200); spectre de masse *m/e* :143 (ion moléculaire, pic majeur).

*Diphényl-2,3 propèno-2 nitrile **2** (35)*

Une solution de 7 g (0.3 mol) de sodium dans 500 ml d'éthanol absolu est ajoutée lentement avec forte agitation, dans une solution de 106 g (1 mol) de benzaldéhyde fraîchement distillé et de 117 g (1 mol) de phényl acétonitrile dans 650 ml d'éthanol. Le mélange réactionnel se solidifie. Celui-ci est refroidit sur la glace et le précipité est filtré, lavé avec 20 ml d'eau et 50 ml d'éthanol 95%. La recristallisation dans 700 ml d'éthanol 95% conduit à 180 g de **2** (88% de rendement), pf 84°C (litt. (35) 88°C); rmn τ: 2–3 (multiplet); ir 2210 cm^{-1} (C≡N); uv λ_{max} (ε) 229 (12 000) et 313.5 nm (22 700); spectre de masse *m/e* 205 (ion moléculaire, pic majeur).

*Diphényl-2,3 propionitrile **12***

A une solution de 0.7 g (0.03 mol) de sodium dans 200 ml d'éthanol absolu sont ajoutés 3.7 g (0.03 mol) de phényl acétonitrile. Le mélange est porté à reflux pendant 3 h et 4 g (0.03 mol) d'α-chlorotoluène sont ajoutés. Le reflux est poursuivi pendant 18 h. Le NaCl formé est filtré et la majeure partie de l'alcool est évaporée. L'huile résiduelle est reprise à l'éther et lavée à l'eau. L'éther est évaporé et le produit est distillé sous vide. Celui-ci se solidifie à la température de la pièce, pf 58°C (litt. (36) 55°C); rmn τ: 2.8 (s, phényles), 6.13 (t, J = 7.4 Hz, méthyne), 7.03 (d, J = 7.4 Hz, méthylène); ir: 2240 cm^{-1} (C≡N); spectre de masse *m/e*: 207 (ion moléculaire).

*Réduction du phényl-2 butèno-2 nitrile **1***

(i) Temps de réaction de 24 h

Un mélange de 3.0 g (0.021 mol) de **1** et 3.0 g (0.079 mol) de $NaBH_4$ dans 200 ml d'isopropanol anhydre est mis à reflux pour 24 h. Le mélange est hydrolysé avec 100 cc d'eau et extrait à l'éther de la manière habituelle. L'évaporation de celui-ci conduit au phényl-2 butanenitrile **8**, rendement quantitatif, péb 128–129°C/22 Torr (litt. (37) 110–112°C/9 Torr); $\eta^{23°}$: 1.5065 (litt. (37) 1.5075); rmn τ: 2.8 (s, phényle), 6.34 (t, J = 7.4 Hz, méthyne), 8.2 (quintet, J = 7.4 Hz, méthylène), 9.04 (q, J = 7.4 Hz, méthyle); ir: 2240 cm^{-1} (C≡N); spectre de masse *m/e*: 145 (ion moléculaire).

(ii) Temps de réaction de 13 jours

Un mélange de 1 g de **1** et 1 g de $NaBH_4$ dans 70 ml d'isopropanol est mis à reflux pendant 13 jours. Après addition d'eau, la solution est extraite à l'éther. La phase organique est séparée, séchée et évaporée pour conduire à une huile, 0.82 g, composés de trois produits: le phényl-2 butanenitrile **8** (44%), le phényle-2 butanamide **9** (14%) et phényl-1 propanol-1 **11** (24%); rmn (mélange brut) τ: 2.8 (s, phényles), 3.86 (s, amide), 6.05 (s, hydroxyle), 6.34 (t, J = 7.4 Hz, méthyne de **8**), 6.70 (t, J = 7.4 Hz, méthyne de **11**), 6.82 (t, J = 7.4 Hz, méthyne de **9**), ≃8.2 (multiplet, méthylène de **8**, **9** et **11**), 9.04 (t, J = 7.4 Hz, méthyle de **8**, **9** et **11**); ir: 3420 (OH), 3340 et 3180 (NH_2), 2240 (C≡N) et 1665 cm^{-1} (C=O).

L'amide **9** peut-être séparé du mélange par extractions répétées au HCl 0.5 *M*. Celui-ci est isolé en neutralisant la phase aqueuse et en extrayant celle-ci par l'éther, pf 84°C (litt. (37) 81–85°C); rmn τ: 2.8 (s, phényle), 4.05 (s, amide), 6.82 (t, J = 7.4 Hz, méthyne), 8.15 (multiplet, méthylène), 9.2 (t, J = 7.4 Hz); ir: 3350 et 3160 (—NH_2) et 1665 cm^{-1} (C=O); spectre de masse *m/e*: 163 (ion moléculaire).

La phase aqueuse de la première extraction est acidifiée avec du HCl 0.5 *M* et extraite à l'éther. L'évaporation de celui-ci conduit à l'acide phényl-2 butanoïque **10**, 0.18 g (18%), pf 46°C (litt. (38) 47.5°C); rmn τ: 2.75 (s, phényle), 6.5 (t, J = 7.4 Hz, méthyne), 8.2 (multiplet, méthylène), 9.06 (t, J = 7.4 Hz, méthyle); ir: 3500–2700 (OH) et 1690 cm^{-1} (C=O); spectre de masse *m/e* 164 (ion moléculaire).

*Réduction de **1** par $NaBD_4$*

Le mode d'opération est identique à celui de la réduction par $NaBH_4$ pendant 24 h. Rendement quantitatif en **8***b*; rmn τ: 2.62 (s, phényle), 6.34 (d, J = 7.4 Hz, méthyne), 8.2 (q, J = 7.4 Hz, méthylène monodeutérié), 9.04 (d, J = 7.4 Hz, méthyle); spectre de masse *m/e*: 146 (ion moléculaire).

Hydrolyse avec D_2O

(i) Dans l'isopropanol

Un mélange de 300 mg de **1** et 300 mg de $NaBH_4$ dans 20 ml d'isopropanol est mis à reflux pendant 3 h. L'hydrolyse est effectuée avec 2 ml de D_2O et l'agitation est continue pendant ½ h. Le mélange réactionnel est extrait de façon habituelle à

Can. J. Chem. Downloaded from www.nrcresearchpress.com by 210.87.254.105 on 09/05/12
For personal use only.

l'éther pour conduire à un mélange de **8** (75%) et de **8***b* (25%); rmn τ: 2.62 (s, phényle), 6.34 (t, J = 7.4 Hz, méthyne (75%)), 8.2 (multiplet, méthylène), 9.02 (t, J = 7.4 Hz, méthyle).

(ii) Dans le THF

Un mélange de 500 mg de **1** et de 450 mg de $NaBH_4$ dans 40 ml de THF anhydre et 6 ml de D_2O est mis à reflux pour 3 h. L'extraction habituelle à l'éther conduit à un mélange de **8** (14%) et de **8***b* (86%); rmn τ: 2.62 (s, phényle), 6.34 (t, J = 7.4 Hz, méthyne (14%)), 8.2 (q, J = 7.4 Hz, méthylène), 9.2 (t, J = 7.4 Hz, méthyle); spectre de masse *m/e*: 146 (ion moléculaire).

*Réaction du phényl-2 butanenitrile **8** avec les bases*

(i) Avec NaOH

Un mélange de 300 mg de **8** dans une solution de 150 mg de NaOH et 60 ml d'isopropanol est gardé à reflux pendant 4 jours. L'extraction à l'éther, selon la méthode décrite pour la réduction de **1** pendant 13 jours, conduit aux produits suivants: phényl-2 butanenitrile **8** (8%), phényl-2 butanamide **9** (54%), acide phényl-2 butanoïque **10** (24%) et phényl-1 propanol-1 **11** (14%). Les proportions de **8**, **9** et **11** sont déterminées par intégration du proton méthyne en rmn: la proportion d'acide **10**, par le rapport des poids des produits d'extraction.

(ii) Avec les produits d'hydrolyse de $NaBH_4$

Les produits d'hydrolyse de $NaBH_4$ sont obtenus par le traitement avec de l'eau, pendant 18 h, de $NaBH_4$ à la température de la pièce. L'eau est évaporée et le résidu solide séché sous vide poussé. Celui-ci devrait contenir un peu de NaOH, de $B(OH)_3$ et du $NaBH_4$ résiduel (41).

Un mélange de 300 mg de **8** et de 300 mg des "produits d'hydrolyse de $NaBH_4$" dans 40 ml d'isopropanol est gardé à reflux pendant 7 jours. L'extraction à l'éther selon la méthode précédente conduit aux produits suivants: phényl-2 butanenitrile **8** (14%), phényl-2 butanamide **9** (23%), acide phényl-2 butanoique **10** (25%) et phényl-1 propanol-1 **11** (38%). Les proportions du mélange sont déterminées comme précédemment.

*Réduction du diphényl-2,3 propèno-2 nitrile **2***

(i) Temps de réaction de 3 h

Un mélange de 500 mg (2.4 mmol) de **2** et de 500 mg (13 mmol) de $NaBH_4$ dans 70 ml d'isopropanol est mis à reflux pendant 3 h. L'hydrolyse avec l'eau et l'extraction habituelle à l'éther conduit au diphényl-2,3 propionitrile **12**, rendement quantitatif, pf 60°C (litt. (36) 57°C). Les spectres sont identiques au produit préparé plus haut.

(ii) Temps de réaction de 18 h

La même réaction qu'en (*i*) est gardée pendant 18 h à reflux. L'extraction habituelle à l'éther conduit au diphényl-2,3 propionitrile **12** (77%) et au diphényl-1,2 éthanol **13** (23%). Spectres des produits bruts: rmn τ: 2.8 (s, phényles), 5.35 (t, J = 6.7 Hz, méthyne de **13** (23%)), 6.13 (t, J = 7.4 Hz, méthyne de **12** (77%)), 7.03 (d, J = 7.4 Hz, méthylène de **12**), 7.1 (d, J = 6.7 Hz, méthylène de **13**); ir: 3480 (OH) et 2240 cm^{-1} (C≡N). L'alcool **13** peut-être isoler par cristallisation de l'éther, pf 68°C (litt. (39) 66–67°C); spectre de masse *m/e*: 198 (ion moléculaire).

*Réduction du phényl-3 propèno-2 nitrile **3***

Un mélange de 500 mg de **3** et de 500 mg de $NaBH_4$ dans 70 ml d'isopropanol est gardé à reflux pendant 48 h. L'extraction habituelle à l'éther conduit à 90% de phényl-3 propionitrile **14** et 10% de produit de départ **3**. Spectres du mélange brut: rmn τ: 2.8 (d, J = 17.4 Hz, proton vinylique de **3** (10%)), 2.86 (s, phényles), 4.3 (d, J = 17.4, proton vinylique de **3** 10%)), 7.20–7.85 (multiplet, méthylènes de **14** (90%)); ir: 2240 cm^{-1} (C≡N); spectre de masse *m/e*: 131 (ion moléculaire). Les spectres sont identiques au produit commercial.

*Réduction du butèno-2 nitrile **4***

La réduction de **4** selon la méthode habituelle pendant 48 h ne conduit qu'au produit de départ **4**.

Vitesses relatives de réduction

Méthode générale

Un mélange de 1 mmol de A et 1 mmol de B et de 8 mmol de $NaBH_4$ dans 40 ml d'isopropanol est mis à reflux pour x min. L'hydrolyse avec l'eau et l'extraction habituelle à l'éther conduit à un mélange brut qui est analysé par rmn.

*(i) Vitesse relative de **1** et **2***—Après un temps de réaction de 15 min, l'on obtient: 100% de phényl-1 butanenitrile **8**, 33–35% de diphényl-2,3 propionitrile **12** et 65–67% de diphényl-3,3 propèno-2 nitrile **2**.

*(ii) Vitesse relative de **1** et **3***—Après un temps de réaction de 30 min, l'on obtient: 100% de phényl-1 butane nitrile **8**, 9% de phényl-3 propionitrile **14** et 91% de phényl-3 propèno-2 nitrile **3**.

*(iii) Vitesse relative de **2** et **3***—Après un temps de réaction de 35 min, l'on obtient: 100% de diphényl-2,3 propionitrile **12**, 9–10% de phényl-3 propionitrile **14** et 90–91% de phényl-3 propèno-2 nitrile **3**.

Remerciements

Un des auteurs (Y.P.) remercie vivement le CNRC pour l'octroi d'une subvention de recherche (A-6180). Des remerciements s'adressent aussi à MM. Pierre Hudon et Réal Lafortune qui ont initié le travail de recherche comme étudiants d'été.

1. R. F. Nystrom et W. G. Brown. J. Am. Chem. Soc. **69**, 2548 (1947).
2. M. S. Brown et H. Rappoport. J. Org. Chem. **28**, 3261 (1963).
3. E. I. Snyder. J. Org. Chem. **32**, 3531 (1967).
4. W. L. Dilling et R. A. Plepys. J. Org. Chem. **35**, 2971 (1970).
5. A. F. Cockerill et D. M. Rackham. J. Chem. Soc. Perkin Trans. II, 2076 (1972).
6. J. C. Richer et A. Rossi. Can. J. Chem. **50**, 438 (1972).
7. J. H. Smith et E. T. Kaiser. J. Org. Chem. **39**, 728 (1974).
8. A. I. Meyers et J. S. Sircar. J. Org. Chem. **32**, 4134 (1967).
9. J. A. Meschino et C. H. Bond. J. Org. Chem. **28**, 3129 (1963).
10. E. Campaigne et W. L. Roelofs. J. Org. Chem. **30**, 396 (1965).
11. J. Knabe, P. Herbort et N. Ruppenthal. Arch. Pharm. **299**, 534 (1966).
12. H. P. Husson, C. Thal et P. Potier. Chem. Commun. 480 (1970).
13. J. S. A. Brunskill. J. Chem. Soc. Perkin Trans. I, 2946 (1972).
14. D. Cabaret et Z. Welvart. C.R. Acad. Sci. Sér. C, **274**, 1200 (1972).
15. J. H. Schauble, G. J. Walter et J. G. Morin. J. Org. Chem. **39**, 755 (1974).
16. T. Kametani, H. Nemoto, H. Ishikawa, K. Shiroyam et K. Fukumoto. J. Am. Chem. Soc. **98**, 3378 (1976).
17. F. A. Hochstein et W. G. Brown. J. Am. Chem. Soc. **70**, 3484 (1948).
18. W. R. Jackson et A. Zurquiyah. J. Chem. Soc. 5280 (1965).
19. K. Yqbal et W. R. Jackson. J. Chem. Soc. 616 (1968).

20. M. R. JOHNSON et B. RICKBORN. J. Org. Chem. **35**, 1041 (1971).
21. J. C. RICHER et Y. PEPIN. Can. J. Chem. **48**, 1226 (1970).
22. R. L. SHIVALKAR et S. V. SUNTHANKAR. J. Am. Chem. Soc. **82**, 718 (1960).
23. J. A. MARSHALL et R. D. CARROLL. J. Org. Chem. **30**, 2748 (1965).
24. S. B. KADIN. J. Org. Chem. **31**, 620 (1966).
25. J. KUTHAN, M. ICHOVA et V. SKALA. J. Chem. Soc. D, 250 (1971).
26. R. M. SILVERSTEIN, G. C. BASSLER et T. C. MORRILL. Spectrometric identification of organic compounds. 3ème éd. John Wiley & Sons, New York, NY. 1974.
27. G. R. NEWKOME et J. M. ROBINSON. J. Org. Chem. **41**, 2536 (1976).
28. H. I. SCHLESINGER, H. C. BROWN, H. R. HOEKSTRA et L. R. RAPP. J. Am. Chem. Soc. **75**, 199 (1953).
29. S. JULIA, H. LINARES et P. SIMON. Bull. Soc. Chim. Fr. 2471 (1963).
30. M. M. JANOT, X. LUSINCHI, L. LABLER et R. GOUTAREL. Bull. Soc. Chim. Fr. 3276 (1966).
31. A. PICOT et X. LUSINCHI. Bull. Soc. Chim. Fr. 1097 (1972).
32. C. L. STEVENS et R. J. GASSER. J. Am. Chem. Soc. **79**, 6057 (1957).
33. F. LIBERATORE, V. CARELLI et M. CARDELLINI. Chem. Ind. (Milan), **51**, 55 (1969).
34. E. C. KNOWLES et J. B. CLOKE. J. Am. Chem. Soc. **54**, 2028 (1932).
35. S. WAWZONEK et E. M. SMOLIN. Org. Synth. III, 716 (1955).
36. F. SALMON-LEGAGNEUR et J. RABADEUX. Bull. Soc. Chim. Fr. 1310 (1967).
37. S. M. MCELVAIN et C. L. STEVENS. J. Am. Chem. Soc. **69**, 2663 (1947).
38. H. SCHEIBLER, E. MARKENKEL et D. BASSANOFF. Ber. **58**, 1198 (1925).
39. M. S. KHARASH et J. H. COOPER. J. Org. Chem. **10**, 46 (1945).
40. D. C. WIGFIELD et F. W. GOWLAND. Tetrahedron Lett. 3373 (1976).
41. F. A. COTTON et G. WILKINSON. Advanced inorganic chemistry. 2ème éd. Interscience Publishers Inc., New York, NY. 1966. p. 203.

Can. J. Chem. Downloaded from www.nrcresearchpress.com by 210.87.254.105 on 09/05/12
For personal use only.

Etudes d'hétérocycles pentagonaux polyhétéroatomiques par résonance magnétique nucléaire du ^{13}C. Thiazoles et thiazolo[2,3-*e*]tétrazoles

ROBERT FAURE,[1] JEAN-PIERRE GALY, EMILE-JEAN VINCENT ET JOSÉ ELGUERO

Laboratoires de Chimie Organique Physique et de Chimie Moléculaire, Rue Henri Poincaré, 13397 Marseille Cedex 4, France

Reçu le 12 juillet

ROBERT FAURE, JEAN-PIERRE GALY, EMILE-JEAN VINCENT et JOSÉ ELGUERO. Can. J. Chem. **56**, 46 (1978).

Les spectres de rmn du carbone-13 de 18 thiazoles diversement substitués (R = CH_3, C_6H_5, Cl, Br, NH_2 et N_3) ont été enregistrés. Les déplacements chimiques $\delta^{13}C$ et les constantes de couplage ^nJ(C,H) sont discutés en fonction de la nature du substituant et de la structure électronique du noyau thiazolique. Les composés substitués en position 2 par un groupement azide présentent la tautomérie azido–tétrazole, ce qui a permis de réaliser une étude comparative des effets de substituant dans les cycles thiazolique et thiazolotétrazolique. Ces études ont été étendues à d'autres hétérocycles: benzothiazole, isothiazole et isoxazole.

ROBERT FAURE, JEAN-PIERRE GALY, EMILE-JEAN VINCENT, and JOSÉ ELGUERO. Can. J. Chem. **56**, 46 (1978).

Carbon-13 nmr spectra of 18 thiazoles with different substituents (R = CH_3, C_6H_5, Cl, Br, NH_2 et N_3) have been recorded. The ^{13}C chemical shifts and the ^nJ(C,H) coupling constants are discussed as a function of the nature of the substituent and the electronic structure of the thiazole ring. The 2-azido substituted thiazoles show azido–tetrazole isomerism, making possible a comparative study of substituent effects in thiazole and thiazolotetrazole rings. These studies have been extended to other heterocycles: benzothiazole, isothiazole, and isoxazole.

Introduction

Différents auteurs (1–4) ont récemment étudié l'influence des substituants sur les déplacements chimiques du ^{13}C et sur les constantes de couplage ^nJ(C,H) du noyau isothiazolique. Par contre, dans le cas de la structure isomère, le thiazole, seulement trois travaux relativement succints ont été réalisés, concernant des alkylthiazoles (5), le benzothiazole (6) et enfin certains thiazoles (en particulier l'amino-2 et le bromo-2) marqués au ^{13}C (42). Dans cette dernière étude les auteurs présentent les valeurs de quelques constantes de couplage ^nJ(C,H).

Dans le but de remédier à ce manque de données structurales et dans le cadre d'une étude sur des systèmes hétérocycliques pentagonaux comportant plus d'un hétéroatome (4–12), nous avons entrepris une analyse des effets de substituant en série thiazolique qui constituera la première partie de ce mémoire.

Certains composés thiazoliques de cette étude possèdent un groupement azide en position 2, et par conséquent présentent la tautomérie azido $\rightleftharpoons$ tétrazole (A $\rightleftharpoons$ T).

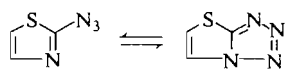

A T

[1]Auteur à qui la correspondance doit être adressée.

Nous avons déjà longuement étudié ce problème en série pentagonale (13–15), et nous connaissons avec certitude la position de l'équilibre pour chacune des structures qui présentent un tel phénomène. Notre intention, et ce sera la deuxième partie de ce travail, est de comparer les effets de substituant observés pour ces structures tétrazoliques avec les résultats obtenus pour le cycle thiazolique.

Dans une troisième partie nous étendrons la comparaison entre cycle simple et bicycle à d'autres systèmes hétéroatomiques: benzothiazole, isothiazole et isoxazole.

Partie expérimentale

Les spectres de ^{13}C ont été enregistrés sur un spectromètre Varian CFT-20. Les composés ont été étudiés à la température de 28 ± 2°C, en solution dans le diméthylsulfoxyde hexadeuterié. Les déplacements chimiques mesurés sur les spectres découplés par bruit par rapport à la raie centrale du solvant, sont ensuite rapportés au signal du TMS par la relation [1] (16), et sont donnés avec une précision supérieure à 0.1 ppm (largeur spectrale de 4000 Hz correspondant à une accumulation sur 8192 points).

$$[1] \quad \delta_{TMS} = \delta_{DMSO\text{-}d_6} + 39.6 \text{ ppm } (\delta \text{ en ppm})$$

Les constantes de couplage sont mesurées sur les spectres non découplés avec une erreur absolue de 0.5 Hz. Pour bénéficier du gain de sensibilité provenant de l'effet nucléaire Overhauser, le système de spins a été irradié durant l'intervalle de temps compris entre deux impulsions successives selon la technique du "gated decoupling." L'analyse des spectres non découplés en haute résolution a été effectuée au premier ordre,

Can. J. Chem. Downloaded from www.nrcresearchpress.com by 210.87.254.105 on 09/05/12
For personal use only.

TABLEAU 1. Déplacements chimiques du ^{13}C.* Dérivés monosubstitués du thiazole

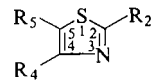

Composé	R_2	R_4	R_5	Déplacements chimiques* C-2	C-4	C-5	Substituants		Référence
1	H	H	H	153.6	143.3	119.6			†
2	CH_3	H	H	165.2	142.3	119.3	CH_3: 18.1		37
3	H	CH_3	H	152.9	153.1	113.7	CH_3: 16.5		†
4	H	H	CH_3	151.8	141.2	133.3	CH_3: 10.9$_5$		‡
5	Br	H	H	136.8	144.0	125.2			†
6	H	H	Br	156.3	144.6	109.1			‡
7	Cl	H	H	150.6	141.4	122.9			38
8	H	Cl	H	154.9	138.8	114.8			38
9	NH_2	H	H	170.3	139.0	107.7			†
10	N_3	H	H	161.8	140.4	117.6			39
11	H	C_6H_5	H	154.2	155.3	114.0	C1′: 134.2 C3′: 128.8	C2′: 126.2 C4′: 128.1	40

*Les déplacements chimiques sont exprimés en ppm du TMS; solvant DMSO-d_6.
†Produits commerciaux.
‡Nous remercions Mme R. M. Zankostian pour le don d'un échantillon de ce produit.

les spectres du proton ayant été eux-mêmes interprétés au premier ordre (13, 17).

Les différents produits étudiés ont été synthétisés selon des méthodes dont les références sont cités dans les tableaux correspondants (tableaux 1, 3, 5, 8 et 9).

Discussion

Cas du thiazole

Effets de substituant sur les déplacements chimiques du thiazole

Dans le tableau 1 sont rassemblées les valeurs des déplacements chimiques du thiazole et de quelques uns de ses dérivés monosubstitués. Les produits **1**, **2** et **3** on déjà fait l'objet d'une étude en rmn du ^{13}C mais n'ont pas été examinés en solution (5); dans l'intention de ne pas apporter d'autres perturbations que celles créées par les substituants, nous avons enregistré de nouveau les spectres de ces composés. Dans le tableau 2 sont présentées les variations de déplacements chimiques engendrées par les différentes substitutions.

Avant d'aborder la discussion en série thiazolique, il est nécessaire de rappeler quelques résultats importants obtenus pour des hétérocycles voisins, le thiophène (18, 19) et l'isothiazole (1–4).

Dans le cas de la molécule de thiophène, les effets α des substituants sont plus prononcés pour les thiophènes substitués en position 2; la seule exception concerne l'atome de brome pour lequel on observe un comportement inverse, l'effet α étant plus important pour le bromo-3 thiophène. En série isothiazolique, et bien que les résultats soient plus fragmentaires, la perturbation directe qui dépend encore de la position du substituant est plus importante en α du soufre (position 5).

D'autre part, en ce qui concerne les thiophènes substitués en 2, et bien qu'on observe quelques différences dans la comparaison des effets de substituant, les positions 3, 4 et 5 peuvent être comparées respectivement aux positions *ortho*, *méta* et *para* des dérivés benzéniques correspondants (20).

TABLEAU 2. Effets de substitution sur les déplacements chimiques des carbones du thiazole

Substituants	Δδ* C-2	C-4	C-5
Méthyl-2	11.6	−1.0	−0.3
Méthyl-4	−0.7	9.8	−5.9
Méthyl-5	−1.8	−2.1	13.7
Bromo-2	−16.8	0.7	5.6
Bromo-5	2.7	1.3	−10.5
Chloro-2	−3.0	−1.9	3.2
Chloro-4	1.3	−4.5	−4.8
Amino-2	16.7	−4.3	−11.9
Azido-2	8.2	−2.9	−2.0
Phényl-4	0.6	12.0	−5.6

*En ppm; les valeurs positives indiquent un déplacement vers les hautes fréquences.

Revenons maintenant à l'étude en série thiazolique. Le groupement méthyle en position 4 provoque sur le carbone en α un déblindage d'environ 10 ppm; cette perturbation est beaucoup plus importante (13.7 ppm) lorsque le substituant alkyle est en position 5, en α de l'atome de soufre. Toutefois pour le méthyl-2 thiazole la perturbation se produit aussi en α du soufre, et cet effet n'est que de 11.6 ppm. Les résultats de la littérature sont comparables, à savoir que, dans le cas du thiophène ou de l'isothiazole, l'effet α d'un groupement méthyle est plus important ($\geq$ 14 ppm) lorsque la perturbation a lieu sur le carbone adjacent à l'atome de soufre.

Can. J. Chem. Downloaded from www.nrcresearchpress.com by 210.87.254.105 on 09/05/12
For personal use only.

Can. J. Chem. Downloaded from www.nrcresearchpress.com by 210.87.254.105 on 09/05/12
For personal use only.

Les carbones en β et γ de la substitution sont relativement sensibles aux effets des méthyles. La perturbation la plus notable est observée pour le carbone-5 du méthyl-4 thiazole (−5.9 ppm), en accord avec les résultats du méthyl-3 thiophène (18, 19) ou du méthyl-4 isothiazole (1–4). Ces effets à longue distance sont plus faibles pour les méthyl-2 et -5 thiazoles, et, dans le cas de **4**, la perturbation est identique en position 4 (β) et en position 2 (γ). Ce comportement est compatible avec la "prédominance" des structures dipolaires suivantes:

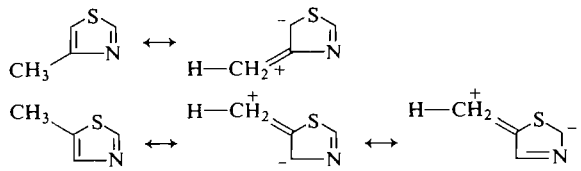

Nous pouvons noter que de telles structures ont déjà été proposées pour expliquer certains effets de substituant en série thiophénique (18, 19) et isothiazolique (1).

Dans le bromo-2 thiazole l'effet de l'halogène sur le déplacement du carbone substitué est plus important (−16.8 ppm) que celui pour le dérivé bromé en 5 (−10.5 ppm). Pour les dérivés chlorés cette perturbation directe est beaucoup plus faible et, si les effets sont pratiquement similaires en position 2 et 4, ils diffèrent nettement des résultats de la littérature concernant le thiophène (4.1 ppm en 2, −1.6 ppm en 3). Comme précédemment, les effets à longue distance des halogènes peuvent être expliqués par l'importance de certaines des structures mesomères; par exemple le blindage en C_5 du chloro-4 thiazole:

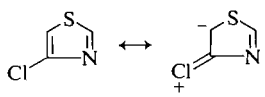

La substitution par un groupement amino perturbe fortement le cycle thiazolique. Si l'effet α de 16.7 ppm est identique à la valeur observée pour le benzothiazole (21), l'effet γ de −11.9 ppm en C_5 est tout à fait comparable à l'effet *para* du groupement amino dans l'aniline (−9.5 ppm) (22). En position 4 l'effet γ est également un effet de blindage, mais sa valeur est moins importante (−4.3 ppm).

En ce qui concerne le groupement azido, l'influence de ce substituant sur les déplacements chimiques du ^{13}C a été très peu étudiée. Les résultats enregistrés pour le cycle thiazolique (tableau 2) sont proches des valeurs observées pour les molécules de phénylazide (23) ou d'azido-3 indazole (24).

Dans le phényl-4 thiazole, le groupement phényle fait un angle de 45° avec le plan contenant le cycle thiazolique (25); cette perte de coplaneité entre les deux cycles peut être mise en évidence par le faible écart enregistré entre les déplacements chimiques des carbones *méta* et *ortho* du noyau benzénique, $\Delta = \delta C_{méta} - \delta C_{ortho}$ (26). La perturbation directe du groupement phényle est très différente de ce que l'on observe en série isothiazolique: 16.5 ppm en 4 et 19.5 ppm en 5 (3). Cette différence dans les effets pourrait traduire l'existence d'une importante interaction entre le groupement phényle et le doublet libre de l'azote. Cette hypothèse est confirmée par les résultats obtenus dans la série du pyrazolo[3,2-*c*]-*s*-triazole (12) pour lequel on observe une perturbation tout à fait comparable en position 5 (l'effet du phényle étant identique à l'effet d'un groupement méthyle).

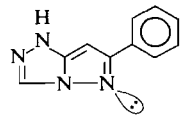

Dans le cas du cycle isothiazolique, ce type de perturbation n'intervient pas pour le phényl-4 isothiazole tandis que, pour la position 5, les interactions du phényle avec les doublets libres du soufre doivent être plus faibles.

Ces résultats permettent de remarquer que les effets de substituant en série thiazolique dépendent de la position de la substitution et que les perturbations en position 2 et 4 sont comparables entre elles.

Additivité des effets de substituant

A partir des effets de substituant du tableau 2, il est possible d'évaluer d'une manière théorique les déplacements chimiques de certains thiazoles disubstitués, par la simple additivité de ces incréments. Dans le tableau 3, nous avons rassemblé les valeurs expérimentales et théoriques (calculées selon le schéma précédent) des déplacements du ^{13}C pour quelques dérivés disubstitués du thiazole. Nous avons récemment montré (27) que les écarts entre théorie et expérience représentaient une perturbation du second ordre qui décrit la disposition relative des différents substituants dans la molécule.

Des résultats du tableau 3 on peut remarquer que les déplacements des dérivés disubstitués en position 2 et 4 étaient dans l'ensemble bien reproduits; par contre, dans le cas des composés 2,5-disubstitués, on observe d'importants écarts entre la théorie et l'expérience. Ces différences pouvant s'expliquer par l'existence d'interactions supplémentaires, certainement de type stérique, qui n'apparaissent pas dans les dérivés monosubstitués.

On peut également noter que, pour l'ensemble des substrats, le déplacement théorique du carbone non substitué est dans l'ensemble en très bon accord avec

TABLEAU 3. Comparaison entre déplacements chimiques théoriques et expérimentaux dans la série des thiazoles disubstitués

	Composé	Atomes	$\delta^{13}C$ Théorique	$\delta^{13}C$ Expérimental	Ecart*	Référence
12	Amino-2 méthyl-4	C_2	169.6	169.4	0.2	
		C_4	148.8	148.0	0.8	†
		C_5	101.8	101.3	0.5	
		CH_3		17.2		
13	Amino-2 méthyl-5	C_2	168.5	167.9	0.6	37
		C_4	136.9	135.4	1.5	
		C_5	121.4	120.3	1.1	
		CH_3		11.8		
14	Amino-2 phényl-4	C_2	169.7	168.8	0.9	
		C_4	151.0	150.2	0.8	†
		C_5	102.1	101.9	0.2	
		C1′		135.1_5		
		C2′		125.8		
		C3′		128.8		
		C4′		127.5		
15	Amino-2 bromo-5	C_2	173.0	169.5	3.5	
		C_4	140.3	139.9	0.4	†
		C_5	97.2	92.1	5.1	
16	Dichloro-2,4	C_2	151.9	151.2	0.7	
		C_4	136.9	135.7	1.2	38
		C_5	118.1	118.2_5	-0.1_5	
17	Azido-2 phényl-4	C_2	162.4	161.4	1.0	
		C_4	152.4	151.5	0.9	
		C_5	112.0	111.3	0.7	
		C1′		133.4		39
		C2′		125.8		
		C3′		128.8		
		C4′		128.3		
18	Azido-2 bromo-5	C_2	164.5	162.2	2.3	
		C_4	141.7	141.6	0.1	15
		C_5	107.1	104.0	3.1	

*Ecart = $\delta^{13}C$ théorique − $\delta^{13}C$ expérimental.
†Produits commerciaux.

la valeur expérimentale, et ce, quelle que soit la position de la substitution.

De plus à partir des effets de substituant du tableau 2, nous pouvons calculer les valeurs des déplacements chimiques des thiazoles **19** et **20**. En effet ces composés présentent un phénomène de tautomérie azido ⇌ tétrazole fortement déplacé vers le tautomère tétrazole, la proportion des formes azides étant inférieure à 3% (15).

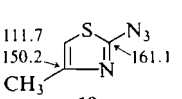

19

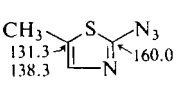

20

En tenant compte des remarques précédentes concernant l'additivité des effets de substituant, on peut s'attendre à ce que les valeurs théoriques des déplacements de **19** et **20** soient surestimées, et que dans le cas de **20** le désaccord entre théorie et expérience soit plus important.

Effets de substituant sur les constantes de couplage du cycle thiazolique

^1J(C,H)—Dans le thiazole la valeur de $^1J(C_5,H)$ est plus élevée que celle de $^1J(C_3,H)$; comme pour l'isothiazole (2,4), le couplage direct est donc plus important pour le carbone en α du soufre que pour celui adjacent à l'atome d'azote.

Ces couplages dépendent de la nature des différentes substitutions comme le montre le tableau 4. En ce qui concerne les dérivés disubstitués, ces effets de substituant présentent un certain caractère d'additivité: par exemple, pour le bromo-5 amino-2 thiazole, la valeur calculée pour $^1J(C_4,H)$ est de 189.3 Hz, soit un écart de 0.7 Hz par rapport à la valeur expérimentale.

Can. J. Chem. Downloaded from www.nrcresearchpress.com by 210.87.254.105 on 09/05/12
For personal use only.

Can. J. Chem. Downloaded from www.nrcresearchpress.com by 210.87.254.105 on 09/05/12
For personal use only.

Les variations de ^1J(C,H) en fonction de la nature du substituant sont comparables à celles que l'on observe en série hétérocyclique (2, 4, 19) ou en série benzénique (28–30).

^2J(C,H)—Considérons le système éthylénique suivant:

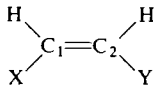

Il est bien connu que les valeurs $^2J(C_2,H_1)$ et $^2J(C_1,H_2)$ dépendent de l'électronégativité des substituants X et Y (31). Si X est plus électronégatif que Y nous aurons alors la relation suivante:

$$^2J(C_2,H_1) > {}^2J(C_1,H_2)$$

Si nous appliquons ce genre d'argument au cas de la liaison C_4—C_5 de la molécule de thiazole, et puisque l'atome d'azote sp^2 N_3 est plus électronégatif que le soufre, l'inégalité suivante devrait être vérifiée:

$$^2J(C_5,H_4) > {}^2J(C_4,H_5)$$

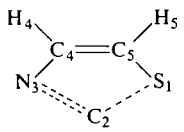

Effectivement on observe (cf. tableau 4) que $^2J(C_5,H_4)$ est le double de $^2J(C_4,H_5)$.

De plus ces couplages géminés ^2J(C,H) sont fonction non seulement des différents substituants en 4 ou 5 (les valeurs diminuent lorsque l'électronégativité du substituant augmente, comme dans le chloro ou nitrobenzène (28, 30, 32)), mais encore de la substitution en 2.

Il convient encore de noter que les valeurs des couplages ^2J(C,H) entre les protons du méthyle et le carbone substitué (~7.0 Hz) sont "habituelles" en série hétérocyclique (4, 5).

^3J(C,H)—A l'inverse des hétérocycles hexagonaux, où ^3J(C,H) est généralement plus grand que ^2J(C,H), dans le thiazole, comme dans l'isothiazole (2, 4), la relation entre ces deux types de couplage est plus complexe et dépend du carbone considéré.

Dans aucun des thiazoles étudiés dans ce mémoire nous n'avons observé de couplages $^3J(C_5,H_2)$. De plus l'inégalité suivante est toujours vérifiée, quel que soit le substrat:

$$^3J(C_2,H_5) < {}^3J(C_4,H_2) \sim {}^3J(C_2,H_4)$$

De ces observations on peut déduire que ces couplages ^3J(C,H) doivent être interprétés en termes de localisation électronique et de conjugaison plutôt qu'en termes d'électronégativité (il est nécessaire de rappeler que la molécule de thiazole est considérée comme peu aromatique et que le doublet libre de l'atome de soufre est peu délocalisé (17)).

Dans les dérivés substitués par un groupement méthyle on observe les couplages suivants:

$$^3J(CH_3,H) \sim 2 \text{ Hz}$$
$$^3J(C,CH_3) \sim 5 \text{ Hz}$$

Pour expliquer la valeur de ces couplages, on peut invoquer la localisation de la liaison C_4—C_5, mais également d'autres facteurs structuraux, tels l'orientation du groupement méthyle ou l'électronégativité des substituants (33, 43).

Vögeli et von Philipsborn (43) ont proposé une relation empirique entre les constantes de couplage vicinales ^3J(C,H) et ^3J(H,H).

$$[2] \qquad {}^3J(CH_3,H) \simeq 0.6\,{}^3J(H,H)$$

En série thiazolique ^3J(H,H) vaut environ 3.5–3.6 Hz (13, 15, 17), tandis qu'en série thiazolotétrazolique ce couplage est légérement plus important: 4.3 Hz (13, 15). En appliquant l'éq. 2, on obtient des couplages vicinaux entre le carbone du méthyle et l'hydrogène qui sont de 2.1 Hz (monocycle) et de 2.5 Hz (bicycle). Expérimentalement (tableaux 4 et 7), on observe des couplages $^3J(CH_3,H)$ plus petits en série thiazolique qu'en série thiazolotétrazolique, c'est à dire un ordre identique à celui que donne [2]; cependant la différence entre les valeurs dans les deux types de structures est de l'ordre de l'erreur expérimentale, ce qui empêche tout autre conclusion.

Par ailleurs, signalons qu'il ne nous a pas été possible d'obtenir les couplages ^nJ(C,H) relatifs au composé **10**, en raison, d'une part de la faible solubilité de ce substrat, et d'autre part du déplacement de l'équilibre azido–tétrazole vers la forme tétrazole (K_e = [A]/[T] = 0.2).

Enfin, notons que les valeurs pour le bromo-2 et l'amino-2 thiazole sont en trés bon accord avec les résultats de la réf. 42.

Série du thiazolo[2,3-e]tétrazole

Les déplacements chimiques du ^{13}C déterminés dans cette série sont rassemblés dans le tableau 5. Nous indiquons dans le tableau 6 les valeurs des perturbations apportées par les différentes substitutions. Le choix des substituants a été conduit de manière à pouvoir réaliser une comparaison de ces effets de substituants avec ceux obtenus en série thiazolique, excepté le composé **26**, puisque le chloro-5 thiazole n'a pas fait l'objet d'une étude de ^{13}C.

Par ailleurs cette structure tétrazolique **26** est en équilibre avec la forme azide **27** dont les paramètres magnétiques sont les suivants:

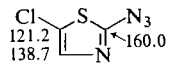

27

Can. J. Chem. Downloaded from www.nrcresearchpress.com by 210.87.254.105 on 09/05/12
For personal use only.

Un calcul CNDO/S[2] (34) des indices de liaison π conduit aux résultats suivants:

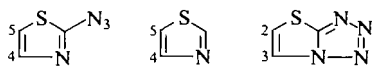

$l_{45} = 0.9055$ $l_{45} = 0.9029$ $l_{23} = 0.9412$

Comme on pouvait d'ailleurs s'y attendre, le calcul indique que la liaison C_{23} du thiazolo[2,3-*e*]tétrazole est plus localisée que la liaison C_{45} du cycle thiazolique. Cependant, la comparaison des effets de substituants (tableau 2 et tableau 6) indique que les perturbations sont tout à fait comparables entre elles.

En réalité, le caractère dienique du thiazole est assez prononcé (17), et notre calcul CNDO/S doit un peu exagérer la différence entre les indices de liaison π, ce qui expliquerait la similitude des effets de substituant.

Dans le tableau 7 sont réunis les constantes de couplage ^nJ(C,H) relatives à quelques unes de ces formes tétrazoliques. Du fait de leur faible solubilité, même dans un solvant polaire comme le diméthylsulfoxyde, nous avons dû nous limiter à l'étude du thiazolo[2,3-*e*]tétrazole et de ses deux dérivés méthylés. De plus, certains couplages n'ont pu être observés, en particulier ceux relatifs au carbone C_{6a} qui se relaxe très lentement.

Les deux résultats les plus frappants que l'on peut tirer de l'analyse de ces couplages sont les suivants. (*i*) D'une part, et contrairement à ce que l'on observe en série thiazolique, le couplage direct du carbone en α du soufre est moins important que celui du carbone adjacent à l'atome d'azote. (*ii*) D'autre part les constantes ^2J(C,H), très différentes dans le thiazole, ont pour cette structure tétrazolique des valeurs très proches: $^2J(C_2,H_3) = 10.6$ Hz tandis que $^2J(C_3,H_2) = 8.3$ Hz.

Une explication simple de ce comportement peut être la suivante: dans les deux structures l'hybridation de l'azote est différente ce qui entraine une variation de l'électronégativité de cet atome, et, par voie de conséquence, une modification des constantes de couplage (35).

Autres systèmes hétérocycliques

Série du benzothiazole

Nous ne discuterons pas dans ce mémoire du problème de l'attribution des déplacements chimiques du benzothiazole **28** et de l'azido-2 benzothiazole **29**, puisque cette étude fait l'objet d'un travail séparé (6, 21). L'analyse du spectre de ^{13}C du tétrazolo[5,1-*b*]benzothiazole **30**, forme tautomère de

[2]Les géométries utilisées dans ce calcul ont déjà été décrites dans un précédent travail (14).

TABLEAU 4. Constantes de couplage $^nJ(^{13}C,^1H)$* en série thiazolique

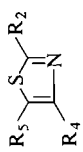

Composé	R_2	R_4	R_5	C-2 H-2	C-2 H-4	C-2 H-5	C-4 H-2	C-4 H-4	C-4 H-5	C-5 H-2	C-5 H-4	C-5 H-5	Autres couplages
1	H	H	H	213.0	15.2	6.0	15.2	187.0	7.1	†	16.2	190.6	
3	H	CH_3	H	211.9	—	6.7	14.5	—	7.2	†	—	188.0	$^2J(C_4,CH_3) = 7.2$; $^3J(C_5,CH_3) = 4.3$
													$^1J(CH_3,CH_3) = 127.9$
4	H	H	CH_3	213.4	15.5	—	13.7	183.6	—	†	14.4	—	$^3J(C_4,CH_3) = 4.9$; $^2J(C_5,CH_3) = 6.9$
													$^1J(CH_3,CH_3) = 129.8$; $^3J(CH_3,H_4) = 1.4$
6	H	H	Br	218.7	15.4	—	13.3	192.8	—	†	12.1	—	
8	H	Cl	H	217.3	—	6.9	18.9	—	3.5	†	—	196.7	
9	NH_2	H	H	—	16.0	7.6	—	183.5	5.8	—	14.6	191.3	
11	H	C_6H_5	H	214.0	—	6.8	13.7	—	4.5	†	—	189.1	
16	Cl	Cl	H	—	—	10.7	—	—	< 1.0	—	—	200.1	
12	NH_2	CH_3	H	—	—	8.1	—	—	6.0	—	—	188.3	$^2J(C_4,CH_3) = 6.0$; $^3J(C_5,CH_3) = 5.3$
													$^1J(CH_3,CH_3) = 127.4$; $^3J(CH_3,H_5) = 2.2$
13	NH_2	H	CH_3	—	16.4	—	—	179.9	—	—	13.5	—	$^3J(C_4,CH_3) = 5.2$; $^2J(C_5,CH_3) = 7.0$
													$^1J(CH_3,CH_3) = 129.0$; $^3J(CH_3,H_4) = 1.8$
15	NH_2	H	Br	—	17.1	—	—	188.6	—	—	10.4	—	
14	NH_2	C_6H_5	H	—	—	8.1	—	—	3.2	—	—	188.2	

*Les couplages sont exprimés en Hz.
†Aucun couplage n'est observé entre le carbone C-5 et le proton H-2.

TABLEAU 5. Déplacements chimiques du ^{13}C.* Série du thiazolo[2,3-*e*]tétrazole

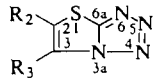

Composé	R_2	R_3	C-2	C-3	C-6a	Substituants		Référence
21	H	H	123.2	118.5_5	159.3_5			39
22	CH_3	H	135.9	115.3	157.7_5	CH_3: 14.1		39
23	H	CH_3	116.8	127.5	158.6	CH_3: 11.9		39
24	H	C_6H_5	117.9	126.7_5	159.5	C-1′: 130.1	C-2′: 126.4	
						C-3′: 129.1	C-4′: 130.1	
25	Br	H	110.7	120.2	157.9			15
26	Cl	H	127.1	118.5	155.9			15

*Les déplacements chimiques sont exprimés en ppm du TMS; solvant DMSO-d_6.

TABLEAU 6. Effets de substitution sur les déplacements chimiques des carbones du thiazolo[2,3-*e*]tétrazole

	Δδ*		
Substituants	C-2	C-3	C-6a
Méthyl-2	12.7	-3.2_5	−1.6
Méthyl-3	−6.4	8.9_5	-0.7_5
Phényl-3	−5.3	8.2	0.1_5
Bromo-2	−12.5	1.6_5	-1.4_5
Chloro-2	3.9	-0.0_5	-3.4_5

*En ppm; les valeurs positives indiquent un déplacement vers les hautes fréquences.

29, a été réalisée par comparaison avec les résultats du triazolo[3,4-*b*]benzothiazole **31** (36).

Nos résultats de rmn protonique (15) indiquent une très forte proportion de forme tétrazole pour l'équilibre **29** ⇌ **30** (K_e = [A]/[T] = 0.08 dans le dimethylsulfoxyde). Par conséquent, pour pouvoir observer les signaux de la forme azide il est nécessaire de déplacer la position de l'équilibre vers ce dernier tautomère, sans pour cela modifier notablement les valeurs des déplacements chimiques. Ces conditions sont réalisées par une élévation de température (14) et les paramètres magnétiques du tableau 8 ont été déterminés à la température de 80°C.

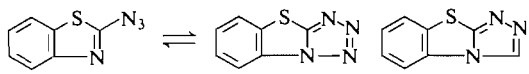

29 **30** **31**

Les perturbations apportées par le groupement azido sur les valeurs des déplacements chimiques du benzothiazole sont les suivantes: δC_2 = 8.0 ppm; δC_{3a} = −3.0 ppm et δC_{7a} = −2.4 ppm. On peut noter que les effets à longue distance (en position γ) sont tout à fait comparables aux résultats obtenus en série thiazolique, tandis que la perturbation directe (effet α) est identique dans cette série benzohétérocyclique.

Par ailleurs, il est possible de réaliser une comparaison des effets engendrés par l'annélation, en série mono et bicyclique; les résultats sont les suivants:

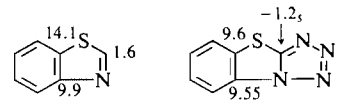

28 **30**

Contrairement aux valeurs obtenues pour une simple substitution (voir précédemment), ce type d'effet dépend du noyau considéré. Cette variation des effets, ainsi qu'une réactivité chimique différente (36) peut s'expliquer par une délocalisation plus importante du système π du noyau benzénique dans les systèmes du type **30** (36), ce qui autorise l'écriture limite suivante pour ces structures:

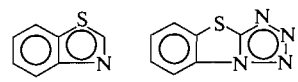

28 **30**

Série de l'isothiazole et de l'isoxazole

L'étude des effets de substituants sur les déplacements du ^{13}C et sur les constantes de couplage ^nJ(C,H) a déjà fait l'objet de plusieurs travaux en série isothiazolique et isoxazolique (1–4); aussi, dans ce chapitre, nous contenterons-nous de déterminer les perturbations apportées par les groupements amino et azido sur ces systèmes aromatiques. L'ensemble des résultats est rassemblé dans les tableaux 9 et 10.

Il convient tout d'abord de noter que, en ce qui concerne l'azido-3 méthyl-5 isoxazole **37**, l'équilibre est totalement déplacé vers la forme azide (15), alors que le méthyl-3 azido-5 isothiazole **34** ne peut présenter une phénomène de tautomérie.

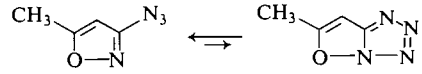

37

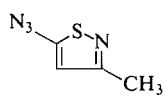

34

Can. J. Chem. Downloaded from www.nrcresearchpress.com by 210.87.254.105 on 09/05/12
For personal use only.

TABLEAU 7. Constantes de couplage ^nJ(C,H) (en Hz) dans la série du thiazolo[2,3-*e*]tétrazole

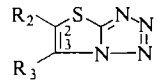

		C_2		C_3		
R_2	R_3	H_2	H_3	H_2	H_3	Autres couplages
H	H	199.8	10.6	8.3	205.6	
CH_3	H	—	9.7	—	203.0	$^3J(C_3,CH_3)$: 6.0; $^2J(C_2,CH_3)$: 7.0 $^1J(CH_3,CH_3)$: 131.5; $^3J(CH_3,H_3)$: 2.0
H	CH_3	197.1	—	8.0	—	$^3J(C_2,CH_3)$: 5.6; $^2J(C_3,CH_3)$: 7.0 $^1J(CH_3,CH_3)$: 132.0; $^3J(CH_3,H_2)$: 2.5

TABLEAU 8. Déplacements chimiques du ^{13}C. Série du benzothiazole*

Composés	δ (en ppm du TMS) C-2	C-3a	C-4	C-5	C-6	C-7	C-7a	Référence
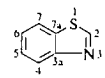 **28**	155.2	153.2	123.1$_5$	125.9	125.2	122.1	133.7	§
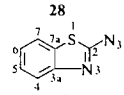 **29**‡	163.2	148.8	121.7†	126.2	124.2	120.7†	131.3	41
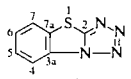 **30**‡	158.1	128.1	114.8	128.1†	127.8†	126.3	132.8	41

*Dans le but de faciliter la mise en page, nous utilisons une nomenclature non correcte pour le noyau tétrazolique.
†Déplacements dont l'attribution peut être inversée.
‡Valeurs mesurées à la température de 80°C (voir texte).
§Produit commercial.

TABLEAU 9. Déplacements chimiques du ^{13}C.* Séries de l'isothiazole et de l'isoxazole

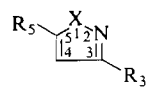

Composé	X	R_3	R_5	C-3	C-4	C-5	Autres déplacements	Référence
32†		CH_3	H	166.1	123.8	148.8	CH_3: 18.5	§
33	S	CH_3	NH_2	166.8 (0.7)	104.0 (−19.8)	174.1 (25.3)	CH_3: 19.2	§
34		CH_3	N_3	167.2 (1.1)	114.2 (−9.6)	164.3 (15.5)	CH_3: 19.2	15
35		H	CH_3	150.7	101.0	168.6	CH_3: 11.3	§
36	O	NH_2	CH_3	164.8 (14.1)	95.0 (−6.0)	168.6 (0.0)	CH_3: 12.2	§
37‡		N_3	CH_3	161.1 (10.4)	96.1 (−4.9)	172.9 (4.3)	CH_3: 12.5$_5$	15

*Les déplacements chimiques sont exprimés en ppm du TMS (solvant DMSO-d_6); les valeurs entre parenthèses représentent les effets de substituant.
†Valeurs tirées de la réf. 1.
‡Le spectre de ^{13}C de ce composé a été enregistré dans l'acétone hexadeuteriée.
§Produits commerciaux.

Le fait le plus marquant que l'on peut relever est l'importance des effets de substitution en position 5 en série isothiazolique. En série isoxazolique, la perturbation a lieu en α de l'azote et les valeurs de ces effets sont très proches des résultats observées en série thiazolique (position 2).

Ce résultat est en bon accord avec les conclusions des chapitres précédents, à savoir qu'en α du soufre

Can. J. Chem. Downloaded from www.nrcresearchpress.com by 210.87.254.105 on 09/05/12
For personal use only.

Can. J. Chem. Downloaded from www.nrcresearchpress.com by 210.87.254.105 on 09/05/12
For personal use only.

TABLEAU 10. Constantes de couplage $^nJ(C,H)$.* Séries de l'isothiazole et de l'isoxazole

Composé	X	R_3	R_5	C-3 H_3	C-3 H_4	C-3 H_5	C-4 H_3	C-4 H_4	C-4 H_5	C-5 H_3	C-5 H_4	C-5 H_5	Autres couplages
32†		CH_3	H	—	7.3	11.0	—	170.7	5.0	—	8.1	185.7	$^2J(C_3,CH_3)$: 6.5; $^3J(C_4,CH_3)$: 3.0 $^1J(CH_3,CH_3)$: 128.0
33	S	CH_3	NH_2	—	6.4	—	—	168.2	—	—	6.0	—	$^2J(C_3,CH_3)$: 6.4; $^3J(C_4,CH_3)$: 2.9 $^1J(CH_3,CH_3)$: 127.4
34		CH_3	N_3	—	6.5	—	—	173.5	—	—	4.3	—	$^2J(C_3,CH_3)$: 6.5; $^3J(C_4,CH_3)$:3.2 $^1J(CH_3,CH_3)$: 128.3
35		H	CH_3	185.6	6.1	—	9.2	182.1	—	4.9	10.4	—	$^2J(C_5,CH_3)$: 6.8; $^3J(C_4,CH_3)$: 3.1 $^1J(CH_3,CH_3)$: 129.8
36	O	NH_2	CH_3	—	4.1	—	—	179.8	—	—	9.6	—	$^2J(C_5,CH_3)$: 6.9; $^3J(C_4,CH_3)$: 3.3 $^1J(CH_3,CH_3)$: 129.4
37‡		N_3	CH_3	—	3.0	—	—	184.6	—	—	8.9	—	$^2J(C_5,CH_3)$: 7.1; $^3J(C_4,CH_3)$: 3.0 $^1J(CH_3,CH_3)$: 130.1

*Les constantes de couplage sont exprimés en Hz (solvant DMSO-d_6).
†Valeurs tirées de la réf. 1.
‡Constantes de couplage mesurées dans l'acétone hexadeuteriée.

(position 5 du thiophène du thiazole et de l'isothiazole), les effets directs et, du moins dans le cas de l'amino-5 et azido-5 méthyl-3 isothiazole, les effets à longue distance sont plus marqués que dans les autres positions.

1. R. E. WASYLISHEN, T. R. CLEM et E. D. BECKER. Can. J. Chem. **53**, 596 (1975).
2. R. E. WASYLISHEN et H. M. HUTTON. Can. J. Chem. **55**, 619 (1977).
3. N. PLAVAC, I. W. J. STILL, M. S. CHAUHAN et D. M. MCKINNON. Can. J. Chem. **53**, 836 (1975).
4. R. FAURE, J. R. LLINAS, E. J. VINCENT et M. RAJZMANN. Can. J. Chem. **53**, 1677 (1975).
5. R. GARNIER, R. FAURE, A. BABADJAMIAN et E. J. VINCENT. Bull. Soc. Chim. Fr. 1040 (1972).
6. J. ELGUERO, R. FAURE, R. LAZARO et E. J. VINCENT. Bull. Soc. Chim. Belg. **86**, 95 (1977).
7. R. FAURE, J. R. LLINAS, E. J. VINCENT et J. L. LARICE. C. R. Acad. Sci. **279**C, 717 (1974).
8. J. ELGUERO, C. MARZIN et J. D. ROBERTS. J. Org. Chem. **39**, 357 (1974).
9. E. GONZALEZ, A. SARLIN et J. ELGUERO. Bull. Soc. Chim. Belg. **85**, 829 (1976).
10. G. ASSEF, J. KISTER, J. METZGER, R. FAURE et E. J. VINCENT. Tetrahedron Lett. 3313 (1976).
11. R. FAURE, E. J. VINCENT, G. ASSEF, J. KISTER et J. METZGER. Org. Magn. Reson. Sous presse.
12. R. FAURE, E. J. VINCENT, R. M. CLARAMUNT et J. ELGUERO. Org. Magn. Reson. **9**, 508 (1977).
13. J. ELGUERO, R. FAURE, J. P. GALY et E. J. VINCENT. Bull. Soc. Chim. Belg. **84**, 1189 (1975).
14. R. FAURE, J. P. GALY, E. J. VINCENT, J. P. FAYET, M. C. VERTUT, P. MAURET et J. ELGUERO. Can. J. Chem. **55**, 1728 (1977).
15. R. FAURE, J. P. GALY, E. J. VINCENT et J. ELGUERO. J. Heterocycl. Chem. Sous presse.
16. G. C. LEVY et G. L. NELSON. ^{13}C NMR for organic chemists. Wiley-Interscience, New York, NY. 1972.
17. E. J. VINCENT. Thèse d'état, Marseille, France. 1966.
18. K. TAKAHASHI, T. SONE et K. FUJIEDA. J. Phys. Chem. **74**, 2765 (1970).
19. S. GRONOWITZ, I. JOHNSON et A. B. HÖRNFELDT. Chim. Scrip. **7**, 76 (1975).
20. S. GRONOWITZ. Advances in heterocyclic chemistry. Vol. 1. Academic Press, New York, NY. 1963.
21. R. FAURE, J. ELGUERO, R. LAZARO et E. J. VINCENT. A paraître.
22. J. B. STOTHERS. ^{13}C NMR spectroscopy. Academic Press. New York, NY. 1972. p. 197.
23. J. ELGUERO. A paraître.
24. A. FRUCHIER, E. ALCALDE et J. ELGUERO. Org. Magn. Reson. **9**, 235 (1977).
25. M. CONTE, T. AVIGNON, J. LAFON et J. METZGER. J. Mol. Struct. **30**, 169 (1976).
26. M. BEGTRUP. Acta Chem. Scand. **28B**, 61 (1974).
27. J. P. MONTI, R. FAURE et E. J. VINCENT. Org. Magn. Reson. **8**, 611 (1977).
28. A. R. TARPLEY, JR et J. H. GOLDSTEIN. J. Phys. Chem. **76**, 515 (1972).
29. M. HANSEN et H. J. JAKOBSEN. J. Magn. Reson. **20**, 520 (1975).
30. L. ERNST, E. LUSTIG et V. WRAY. J. Magn. Reson. **22**, 459 (1976).
31. J. B. STOTHERS. ^{13}C NMR spectroscopy. Academic Press, New York, NY. 1972. Chapt. 10.

32. F. J. WEIGERT et J. D. ROBERTS. J. Am. Chem. Soc. **89**, 2967 (1967).
33. R. E. WASYLISHEN et T. SCHAEFER. Can. J. Chem. **51**, 961 (1973).
34. J. DEL BENE et H. H. JAFFE. J. Chem. Phys. **48**, 1807 (1968).
35. P. LAZLO. Bull. Soc. Chim. Fr. 558 (1966).
36. R. FAURE, J. P. GALY, E. J. VINCENT, J. ELGUERO, J. P. FAYET, M. C. VERTUT et P. MAURET. Bull. Soc. Chim. Fr. 288 (1977).
37. J. MCLEAN et G. D. MUIR. J. Chem. Soc. 383 (1942).
38. A. FRIEDMANN. Thèse d'état, Marseille, France. 1973.
39. L. F. AVRAMENKO, T. A. ZAKHAROVA, V. Y. POCHINOK et Y. S. ROZUM. Khim. Geterosikl. Soedin. **4**, 423 (1968).
40. J. P. AUNE. Thèse d'état, Marseille, France. 1969.
41. G. A. REYNOLDS, J. A. VAN ALLAN et J. F. TINKER. J. Org. Chem. **24**, 1205 (1959).
42. I. N. BOJESEN, J. H. HOG, J. T. NIELSEN, I. B. PETERSEN et K. SCHAUMBURG. Acta Chem. Scand. **25**, 2739 (1971).
43. U. VÖGELI et W. VON PHILIPSBORN. Org. Magn. Reson. **7**, 617 (1975).

Can. J. Chem. Downloaded from www.nrcresearchpress.com by 210.87.254.105 on 09/05/12
For personal use only.

Nuphar thiaspirane sulfoxides. ^{13}C nuclear magnetic resonance determined configuration and utilization in the interconversion of thiaspirane stereochemical types

R. T. LaLonde and C. F. Wong

Department of Chemistry, State University of New York, College of Environmental Science and Forestry, Syracuse, NY 13210, U.S.A.

Received July 15, 1977

R. T. LaLonde and C. F. Wong. Can. J. Chem. **56**, 56 (1978).

The configuration of the sulfoxide oxygen in *syn*- and *anti*-thiobinupharidine sulfoxide was determined by employing the ^{13}C nmr sulfoxidation increments of C-6. Establishment of the ^{13}C nmr line assignments for C-6 included the study of the C-6 and C-6′ deuterated thiobinupharidine and the corresponding sulfoxides. Thermolysis of *syn*-thiobinupharidine sulfoxide in DMSO and subsequent reduction with sodium borodeuteride in methanol yielded thiobinupharidine, labelled with deuterium only at C-6, and thionuphlutine B, labelled with deuterium at both C-6 and C-6′. Treatment of the *anti* sulfoxide in xylene or DMSO resulted in no thiobinupharidine or thionuphlutine B. Similarly, *syn*-neothiobinupharidine sulfoxide gave neothiobinupharidine and a new thiaspirane, thionuphlutine C. These two compounds were not produced from *anti*-neothiobinupharidine sulfoxide heated in xylene.

R. T. LaLonde et C. F. Wong. Can. J. Chem. **56**, 56 (1978).

On a déterminé la configuration de l'oxygène du sulfoxyde dans les sulfoxydes *syn*- et *anti*- de la thiobinupharidine en faisant appel aux incréments de sulfoxydation en C-6 en rmn du ^{13}C. L'attribution des raies en rmn du ^{13}C pour la position C-6 implique l'étude de thiobinupharidines deutérées en C-6 et C-6′ et des sulfoxydes correspondants. La thermolyse du sulfoxyde de la thiobinupharidine *syn* dans le DMSO et la réduction subséquente par le borodeutérure de sodium dans le méthanol fournissent respectivement de la thiobinupharidine marquée par du deutérium uniquement en position C-6 et de la thionuphlutine B marquée avec du deutérium en positions C-6 et C-6′. La réaction du sulfoxyde *anti* dans le xylène ou le DMSO ne conduit à aucune thiobinupharidine ou thionuphlutine B. De la même manière, le sulfoxyde de la néothiobinupharidine *syn* conduit à la néothiobinupharidine et à un nouveau thiaspirane, la thionuphlutine C. Ces deux composés ne se produisent pas lorsque l'on chauffe le sulfoxyde de la néothiobinupharidine *anti* dans le xylène.

[Traduit par le journal]

Three of the four possible stereochemical types of thiaspirane alkaloids isomeric at C-7 and C-7′ have been extracted from *Nuphar*, a genus of fresh-water macrophytes. These are thiobinupharidine (**1**), neothiobinupharidine (**2**), and thionuphlutine B (**3**). The fourth, which we designate thionuphlutine C (**4**), has not been uncovered in nature. The purpose of the work described herein was to demonstrate that **1** could be converted to **3** and **2** to **4** and gain some information regarding the nature of the transformations. These conversions have been achieved by the thermolysis of a mixture of *syn*- (**5**) and *anti*-neothiobinupharidine sulfoxide (**6**)[1] (1) and by the thermolysis of a mixture of *syn*- (**7**) and *anti*-thiobinupharidine sulfoxide (**8**), which has been obtained from the oxidation of thiobinupharidine with hydrogen peroxide in acetic acid.

A knowledge of the sulfoxide configuration was required to establish the dependency of the transformation on configuration. This gave us the opportunity to extend to the thiobinupharidine sulfoxides the ^{13}C nmr method which we had previously employed (1) to ascertain the configuration of sulfoxides **5** and **6**.

The Configuration of syn- *(7) and* anti-*Thiobinupharidine Sulfoxide (8)*

Carbon-6 was used as an indicator carbon for determining the magnitude of the γ-sulfoxidation effect and for probing the configuration of the sulfoxide oxygen in the previously reported case of the neothiobinupharidine sulfoxides (1). The sulfoxidation increment ($\Delta_{C\text{-}6'} = \delta_{C\text{-}6}{}^{S\text{-}O} - \delta_{C\text{-}6}{}^{S}$), the change in chemical shift of C-6 upon sulfoxidation, was a greater negative value when the oxygen atom and the indicator carbon were *syn* than when they were *anti*.

The use of the ^{13}C nmr sulfoxidation increment requires the unequivocal assignment of chemical shifts (δ) for the indicator carbon in thiobinupharidine and its two sulfoxides. The $\delta_{C\text{-}6}{}^{S}$ of thiobinupharidine had been determined previously by model and deuterium labelled compound comparisons (2).

[1]The designations *syn* and *anti* refer to the configuration of the sulfoxide oxygen in relation to the nitrogen atom of the AB quinolizidine ring: X = O, *syn*; Y = O, *anti*.

Can. J. Chem. Downloaded from www.nrcresearchpress.com by 210.87.254.6 on 09/05/12
For personal use only.

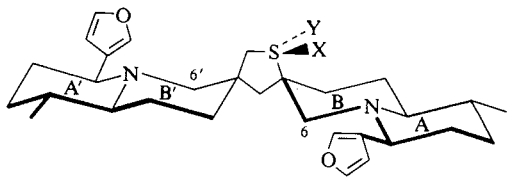

Neothiobinupharidine
2, X = Y = Electron pair
5, X = O; Y = Electron pair
6, X = Electron pair; Y = O

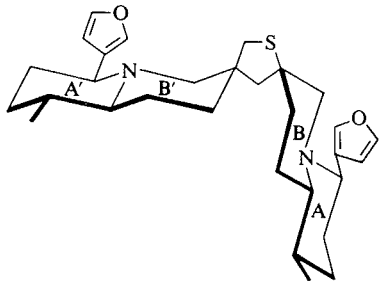

4
Thionuphlutine C

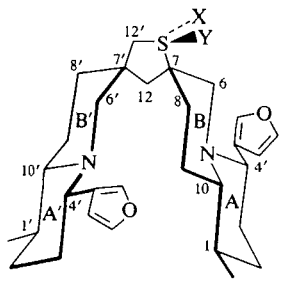

Thiobinupharidine
1, X = Y = Electron pair
7, X = O; Y = Electron pair
8, X = Electron pair; Y = O

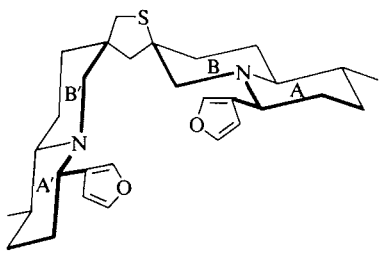

3
Thionuphlutine B

Similarly, the $\delta_{C\text{-}6}{}^{S-O}$ have been determined with the help of the sulfoxides labelled at C-6 and C-6′. Thus the partially ^1H decoupled triplets centered at 63.9 and 59.1 ppm in the spectrum of the unlabelled *anti*-thiobinupharidine sulfoxide (**8**) appeared as slightly shifted triplets in the totally ^1H decoupled spectrum of sulfoxide **8**-6,6′-d_2. The 63.9 ppm signal also appeared as a slightly shifted triplet in the totally ^1H decoupled spectrum of a mixture of *syn*-thiobinupharidine-6′-d_1 sulfoxide (**7**-6′-d_1) and **8**-6′-d_1 while the 59.1 ppm signal appeared as a fully collapsed singlet. Therefore the 59.1 ppm signal was assigned to C-6 and the 63.9 ppm signal was assigned to C-6′.

As for the *syn* sulfoxide (**7**), the partially ^1H decoupled triplets occurring at 64.4 and 56.5 ppm in the spectrum of the unlabelled sample appeared as slightly shifted triplets in the totally ^1H decoupled spectrum of the sulfoxide **7**-6,6′-d_2. The 64.4 ppm signal appeared slightly shifted, overlapping the 63.9 ppm triplet in the totally ^1H decoupled spectrum of the mixture of sulfoxides **7**-6′-d_1 and **8**-6′-d_1. Therefore the 64.4 ppm signal was assigned to C-6′ and the 56.5 ppm signal was assigned to C-6. The ^{13}C shift resulting from the ^2H effect was in all cases -0.5 ppm.

Once the C-6 indicator assignments had been secured, the sulfoxidation increments were determined. The pertinent chemical shift data and sulfoxidation increments for C-6 are summarized in Table 1. Also included in this table are values for C-8, another potential indicator carbon. The values for C-6′ and C-8′ have been added to complete the data for carbons attached to the thiolane ring. However the chemical shift assignments for C-8 and C-8′ rest on an analogy with sulfoxides **5** and **6** (1). The thiobinupharidine sulfoxide having the larger negative $\Delta_{C\text{-}6}$ value was assigned the *syn* configuration. The incremental difference, 2.6 ppm, agrees with the 3–4 ppm difference observed in the study of the neothiobinupharidine sulfoxides and the 2,2,4,4- and 2,2,5,5-tetramethylthiolanes (1).

The Interconversion of Thiaspirane Stereochemical Types

A mixture of *syn*- and *anti*-thiobinupharidine sulfoxides, estimated to consist of 56% *syn* (**7**) and 44% *anti* (**8**) by ^{13}C nmr, was warmed at 135–140°C in DMSO. Thin-layer chromatography indicated the presence of mostly highly polar compounds but a small amount of the less polar bisamines thiobinupharidine (**1**) and thionuphlutine B (**3**) was detected. Reduction of the reaction mixture with sodium borodeuteride in methanol and separation of polar and non-polar components by chromatography yielded a mixture of unconsumed **7** and **8** and **1**-*d* and **3**-*d*. The mixture of unconsumed sulfoxides was estimated by ^{13}C nmr to consist of 43% of the *syn* epimer and 57% of the *anti* epimer. The deuterium labelled bisamines were isolated and identified through tlc, ms, and ^1H nmr comparisons with authentic samples. The region of the ^1H nmr, where C-6-eq, C-6′-eq, or C-4 and C-4′ protons occur, integrated for less than four protons in the case of

Can. J. Chem. Downloaded from www.nrcresearchpress.com by 210.87.254.6 on 09/05/12
For personal use only.

TABLE 1. ^{13}C nmr chemical shifts ($\delta_{C\text{-}i}$) and sulfoxidation increments ($\Delta\delta_{C\text{-}i} = \delta_{C\text{-}i}^{SO} - \delta_{C\text{-}i}^{S}$) for indicator carbon atoms in *syn*- (**7**) and *anti*-thiobinupharidine sulfoxide (**8**)

	C-6		C-6′		C-8*		C-8′†	
Compound	δ	Δδ	δ	Δδ	δ	Δδ	δ	Δδ
Thiobinupharidine, **1**	66.0		63.4		39.6		37.5	
syn-Thiobinupharidine sulfoxide, **7**	56.5	−9.5	64.4	+1.0	32.0	−7.6	40.3, 41.3	+3.8 to +2.8
anti-Thiobinupharidine sulfoxide, **8**	59.1	−6.9	63.9	+0.5	28.6	−11.0	42.1, 38.7	+1.2 to +4.6

*C-8 was identified as the only new resonance appearing within the 27.0–33.0 ppm region when the sulfoxide spectra are compared with that of thiobinupharidine.
†When more than one value is given, one or the other value is the most likely assignment for C-8′ based on comparison with the neothiobinupharidine sulfoxides.

the **1**-*d* and showed slightly less than four protons and a modified splitting pattern in the case of the **3**-*d*.[2]

Mass spectral analysis of the **1**-*d* showed that the latter contained 39.3% d_0 and 59.1% d_1, but virtually all the deuterium was located at C-6. In contrast, the same type of analysis of **3**-*d* demonstrated the presence of 32.0% d_0 and 65.6% d_1 species but the deuterium was distributed between C-6 and C-6′. The ms analysis for location of deuterium was based on earlier work which demonstrated that *m/e* 178 is shifted to *m/e* 179 when deuterium is located at C-6 but *m/e* 178 is retained when the deuterium is located at C-6′ (4). The location of deuterium at only the C-6 and C-6′ positions was supported by observing that each of the peaks in the series *m/e* 136, 107, 94, and 81, a series characteristic of *Nuphar* quinolizidines (5), was retained and indicated no deuterium had found its way into rings A or A′. The retention of *m/e* 447 indicated that no deuterium had been introduced into the thiomethylene center.

On a much smaller scale sulfoxide **7** was heated and subsequently reduced with sodium borohydride as the mixture of epimers had before. No **8** could be detected by tlc before reduction and after reduction **1** and **3**, in addition to unconsumed **7**, were detected by tlc. When the sulfoxide **8** was treated in the same manner, no **7** was detected before reduction and neither **1** nor **3** after.

The epimeric *syn*- (**5**) and *anti*-neothiobinupharidine sulfoxide (**6**) were heated separately in xylene solution. The thermolysis mixtures were then reduced with sodium borohydride. Neothiobinupharidine (**2**) and another non-polar substance, having similar but not the same tlc properties as **1** and **3**, resulted from sulfoxide **5**. The *anti* epimer **6** produced no non-polar substances; none of the thiaspirane bisamines could be detected by the customary tlc analysis.

The two-step thermolysis–reduction sequence was then carried out on a larger quantity of a mixture of **5** and **6**. A solution in DMSO heated to 154–160°C yielded, after sodium borohydride reduction, **2** and thionuphlutine C (**4**), in addition to unconsumed **5** and **6**. The gross structure of **4** was indicated by the molecular formula, determined by high resolution mass spectrometry, and the similarity of the ms fragmentation with those of the other three stereoisomeric thiaspiranes. The infrared spectrum showed Bohlmann bands in the same position and as strong as those of the known thiaspiranes. The ^1H nmr also reflected the presence of the thiaspirane structure in **4**. The resonances attributable to the α- and β-furyl protons, the C-6 and C-6′ equatorial protons, the C-4 and C-4′ protons, and the C-1 and C-1′ methyl groups were observed at their normal positions and with the usual splitting characteristics. The thiomethylene AB quartet, appearing at 2.75 ppm in chloroform, was shifted downfield to 2.90 ppm in benzene. Both the position of the resonance and the direction and magnitude of the benzene induced shift (+9.0 Hz at 60 MHz) were consistent with the same properties for the axial thiomethylene in **2** and similar quinolizidines possessing axial thiomethylene groups but are different from the chemical shift and benzene induced shift of the thiomethylene in **1**, **3**, and similar quinolizidines possessing equatorial thiomethylene groups (6, 7). The spectral indications coupled with tlc properties demonstrate that **4** is isomeric with the other thiaspiranes. The nature of the isomerism was evident from the ^{13}C nmr. Figure 1 gives the correlation of resonances found in the high field half of the spectra. Carbon-12 of **4** and **3** is axial to one quinolizidine ring system and equa-

[2]The modified splitting for the C-6′-eq proton of **3**-*d* is attributed to the presence of some axial deuterium at C-6′. The axial incorporation of deuterium at C-6′ in the reduction of 6,6′-dihydroxythionuphlutine B has been reported (3).

Can. J. Chem. Downloaded from www.nrcresearchpress.com by 210.87.254.6 on 09/05/12
For personal use only.

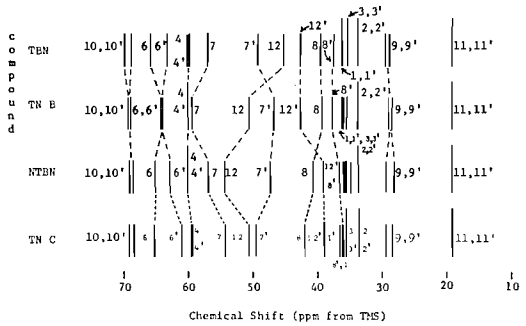

FIG. 1. Chemical shift correlation of thiaspirane bisamines: thiobinupharidine (**1**, TBN); thionuphlutine B (**3**, TN B); neothiobinupharidine (**2**, NTBN); and thionuphlutine C (**4**, TN C).

torial with respect to the other whereas in **1** and **2**, C-12 is respectively axial and equatorial to both quinolizidine systems. Since the chemical shift of C-12 reflects the number of axial and equatorial attachments (2), the appearance of the C-12 resonance of **4** at 50.7 ppm, virtually the same value as the C-12 resonance of **3** (50.6 ppm) and intermediate between the C-12 resonance values of **1** (45.3 ppm) and **2** (54.4 ppm), indicated that C-12 in **4** was axial with respect to one quinolizidine system but equatorial with respect to the other. Since both ^1H and ^{13}C thiomethylene resonances of **2** and **4** were the same and indicated the axial thiomethylene attached to the A′B′ system in both, C-12 in **4** must be axial to the AB quinolizidine system but equatorial to the A′B′ quinolizidine system.

Discussion

Only the *syn* sulfoxides of thiobinupharidine and neothiobinupharidine are thermolyzed to compounds which are reduced by sodium borohydride in methanol to thiaspirane bisamines. Presumably the compounds undergoing reduction are immonium salts or hemiaminals. The dependence of the thermolytic process on sulfoxide stereochemistry is reminiscent of the [2,3] sigmatropic shifts of penicillin sulfoxides wherein hydrogen of the C-2 methyl group *syn* to the sulfoxide migrates to sulfoxide oxygen with simultaneous carbon–sulfur bond rupture and sulfenic acid and carbon–carbon double bond formation (8, 9). Such transformations occur under a wide variety of conditions including those employing acids and anhydrides (10), halogenated solvents (11), and tertiary amines (11, 12). A similar process is envisaged for the thiaspirane sulfoxides as shown in Scheme 1. The thiaspirane structure is reestablished by electrophilic attack of the sulfenic acid sulfur atom on the enamine β carbon. If carbon–sulfur bond formation occurs before rotation or after an even number of 180° rotations of the AB quinolizidine ring about the C-7,C-12 bond, then the original thiaspirane (**1** and **2**) stereochemical type is regenerated. But if carbon–sulfur bond formation occurs after an odd number of 180° rotations then the C-7 stereoisomeric thiaspirane results (**3** and **4**). However, the deuterium location studies carried out in connection with the *syn* sulfoxide **7** investigation indicates a complication. When the immonium ion center in the AB quinolizidine system is *syn* to the nitrogen of the A′B′ quinolizidine system, proton migration from C-6′ to C-6 occurs with resulting transfer of immonium ion location to the A′B′ quinolizidine system.

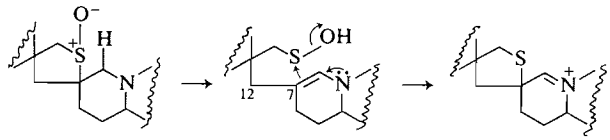

SCHEME 1

The stereoisomerism which we have achieved, albeit in low conversion, indicates a potential for further study: optimization of the isomerization process, identification of other products, and the stereochemical preferences for hydrogen migration from C-6.

Experimental[3]

Spectra were determined as follows: mass spectra (ms) on a Hitachi-Perkin-Elmer RMU6E using a direct inlet, with chamber temperature 200°C and voltage 70 eV, infrared spectra (ir) as indicated on a Perkin-Elmer 137 spectrometer; ^1H nmr at 100 MHz in $CDCl_3$ in 5-mm tubes on an XL-100-15 spectrometer operating in the FT absorption mode (m, s, d, t, and q referring to multiplet, singlet, doublet, triplet, and quartet, respectively); ^{13}C nmr in $CDCl_3$, used also to furnish a secondary reference (77.2 ppm from TMS at δ 0.00 ppm) and the deuterium resonance for field-frequency lock, on an XL-100-15 operating at 25.19 MHz in the FT absorption mode employing 8192 data points. The multiplicity (s, d, t, q) of spectral lines as indicated was determined from the ^1H off-resonance decoupled spectra while the multiplicity of peaks following the designation ^{13}C (^1H) nmr indicates the splitting in the ^1H wide-band noise fully decoupled spectra resulting from the presence of deuterium. In all cases ^{13}C nmr spectral widths were 5000 Hz and acquisition times were 0.8 s. Pulse widths for all spectral determinations ranged from 65–75 μs. Fully ^1H noise decoupled and off-resonance decoupled ^{13}C nmr were determined on 11–102 mg of compound in 0.25–0.30 ml of solvent using 5–97 K transients. High resolution mass spectra (hrms) were performed by the Cornell University Mass Spectrometry Center. Thin-layer chromatography (tlc) was carried out on microscopic size plates uniformly coated with 0.25 mm of SiO_2 or Al_2O_3.

Preparation of syn- *(7) and* anti-*(8) Thiobinupharidine Sulfoxide*

A 199 mg sample of thiobinupharidine (**1**) was treated with

[3]A version of the Experimental Section containing complete ir, ^1H nmr, ^{13}C nmr, and mass spectral data is available, at a nominal charge, from the Depository of Unpublished Data, CISTI, National Research Council of Canada, Ottawa, Ont., Canada K1A 0S2.

Can. J. Chem. Downloaded from www.nrcresearchpress.com by 210.87.254.6 on 09/05/12
For personal use only.

Can. J. Chem. Downloaded from www.nrcresearchpress.com by 210.87.254.6 on 09/05/12
For personal use only.

H_2O_2–HOAc (1) and thereby was obtained 212 mg of a mixture of sulfoxides: tlc (Al_2O_3, five times with C_6H_6) R_f 0.3; (Et_2O–$CHCl_3$, 1:9) R_f 0.8; (Et_2O–hexane, 2:3) R_f 0.6; (Et_2O–C_6H_6) R_f 0.8; (SiO_2, three times with Et_2O–C_6H_6) R_f 0.5. Chromatography of 212 mg on a neutral alumina (4% H_2O) column (13 cm × 1 cm) was effected with 50 ml of C_6H_6 and nine 7-ml portions of CH_2Cl_2 (fractions 2–10). Fractions 2 and 3 combined amounted to 36 mg of pure oily *syn*-thiobinupharidine sulfoxide (7): $[\alpha]_D^{25}$ −7.7° (19.8 mg/ml, 95% EtOH).

A 15 mg sample of the *syn* sulfoxide in 1 ml of MeOH was treated with 2 equiv. of 0.2 *M* aqueous $HClO_4$. The solid residue obtained after evaporating to dryness was recrystallized from MeOH to obtain **7** diperchlorate: mp 228–230°C. *Anal.* calcd. for $C_{30}H_{44}O_{11}N_2SCl_2$: C 50.63, H 6.23, N 3.94, S 4.51; found: C 50.48, H 6.34, N 3.91, S 4.37.

Fractions 4–10 consisted of an oily mixture of *syn* and *anti* epimers which combined amounted to 185 mg. To a 36 mg amount of the mixture was added 6 drops of glacial HOAc and 0.3 ml of $CHCl_3$. The resulting solution was applied to a SiO_2 column which was eluted with portions of $CHCl_3$ and then $CHCl_3$–MeOH. From 5:95 MeOH–$CHCl_3$ was obtained fraction 2, which was dissolved in water. The p*H* was adjusted to 12 with NaOH and the basic solution was extracted with $CHCl_3$. The extract was dried and the solvent was removed by vacuum evaporation to obtain 11 mg of pure *anti*-thionupharidine sulfoxide, **8**: crystalline at 0°C; $[\alpha]_D^{20}$ −70.5 (24 mg/ml, 95% EtOH). *Anal.* calcd. for $C_{30}H_{42}O_3N_2S$: C 70.55, H 8.29, N 5.48, S 6.28; found: C 70.46, H 8.20, N 5.20, S 6.39.

Treatment of later fractions in a manner similar to fraction 2 yielded an additional 13 mg of pure *syn* sulfoxide (**7**).

Thermolysis of a Mixture of syn- *and* anti-*Thiobinupharidine Sulfoxides*

An 88 mg mixture of the sulfoxides was estimated to contain 56% *syn* and 44% *anti* epimers from the relative intensities of the ^{13}C resonance at δ 40.3 ppm (*syn*) and δ 38.7 ppm (*anti*). This mixture in 50 ml of DMSO was degassed repeatedly, put under an atmosphere of N_2, and heated in an oil bath at 135–140°C for 25 h. The DMSO was removed by evacuation at 45°C. The residue in 1 ml of MeOH was treated with three 10-mg portions of $NaBD_4$ periodically over a period of 1 h. Work-up yielded 100 mg of a brown oily residue which was chromatographed on Al_2O_3 (4% H_2O) eluted with C_6H_6 and $CHCl_3$. In this manner were obtained 56 mg of *syn*- and *anti*-thiobinupharidine sulfoxide consisting of 57% *anti* epimer and 43% *syn* epimer estimated from the relative intensities of ^{13}C resonances at δ 40.3 ppm (*syn*) and 38.7 (*anti*), the spectra being determined under precisely the same conditions as the original mixture of isomers.

Also obtained from the benzene fractions were 20 mg which were chromatographed on Al_2O_3 (4% H_2O) using Et_2O–hexane (5:95) in 20 ml, 34 ml, 10 ml, and 50 ml fractions. The second fraction, 3.6 mg, consisted of pure thiobinupharidine-*d*: ^1H nmr (100 MHz, $CDCl_3$) was identical to that of unlabelled thiobinupharidine except that the C-6, C-6′ and C-4, C-4′ proton region (δ 2.70–3.10 ppm) contained 3.4 protons; ms *m/e*: 495 (39.3% d_0, 59.1% d_1, 1.6% d_2), and 179 (100%) (43.6% d_0, 55.9% d_1, and 0.5% d_2). Therefore the deuterium distribution is 39.3% d_0, 59.1% C-6-d_1, and 1.6% C-6′-d_1. Fraction 4, 4.7 mg, consisted of thionuphlutine B-*d*: ^1H nmr (100 MHz, $CDCl_3$) was identical to that of authentic thionuphlutine B (3), except in the C-6_{eq} and C-$6'_{eq}$ region (δ 2.45–2.85 ppm) where differences were observed because of the incorporation of deuterium at both C-6 and C-6′; ms *m/e*: 495 (32.0% d_0, 65.6% d_1, and 2.4% d_2), and 179 (100%) (59.0% d_0, 35.9% d_1, and 5.1% d_2). Therefore the deuterium distribution is 32% d_0, 35.9% C-6 eq-d_1, and 29.7% C-6′ eq-d_1.

Thermolysis of a Mixture of syn- *(5) and* anti- *(6) Neothionupharidine Sulfoxides*

A 70 mg mixture of the title sulfoxides, prepared from neothiobinupharidine (**2**) with H_2O_2–HOAc, was dissolved in 50 ml of DMSO, degassed repeatedly, put under an atmosphere of N_2, and heated in an oil bath at 154–160°C for 20 h. The DMSO was removed by evacuation at 45°C. The dark brown oily residue in 3 ml of MeOH at 25°C was treated with 200 mg of $NaBH_4$ portionwise for 1 h. MeOH was vacuum evaporated and the residue was chromatographed repeatedly on Al_2O_3 (activity 2) with C_6H_6 and then $CHCl_3$. In this manner was obtained pure neothiobinupharidine (10.8 mg) as determined by the identity of its ^1H nmr (100 MHz, $CDCl_3$) with that of an authentic sample. Also obtained was 2 mg of pure thionuphlutine C: $[\alpha]_D^{25}$ −88.4° (6.3 mg/ml, 95% EtOH); tlc (Al_2O_3, three times with Et_2O–hexane, 1:9) R_f 0.73 (neothiobinupharidine, R_f 0.33; thionuphlutine B, R_f 0.61; thiobinupharidine, R_f 0.78); hrms calcd. for $C_{30}H_{42}O_2N_2S$: 494.2967; found: 494.2944.

Preparation of syn- *and* anti-*Thiobinupharidine-6′-*d_1 *Sulfoxides*

Oxidation of 22 mg of thiobinupharidine-6′-d_1 (3), with H_2O_2–HOAc produced 22 mg of a mixture of the labelled sulfoxides: ^{13}C (^1H) nmr δ: 64 ppm (t, C-6′ overlapping in *syn*- and *anti*-thiobinupharidine-6′-d_1, sulfoxides).

Preparation of syn- *and* anti-*Thiobinupharidine-6,6′-*d_2 *Sulfoxides*

Oxidation of 105 mg of thiobinupharidine-6,6′-d_2 (3) with H_2O_2–HOAc produced a 103 mg mixture of the doubly labelled sulfoxides: ^{13}C (^1H) nmr δ: 64 ppm, (t, C-6′ overlapping in *syn*- and *anti*-thiobinupharidine-6,6′-d_2 sulfoxides), 59.1 ppm (t, C-6 in *anti*-thiobinupharidine-6,6′-d_2 sulfoxide), 56.5 ppm (t, C-6 in *syn*-thiobinupharidine-6,6′-d_2 sulfoxide).

Separation of syn- *and* anti-*Thiobinupharidine-6,6′-*d_2 *Sulfoxides*

To a 100 mg mixture of *syn*- and *anti*-thiobinupharidine-6,6′-d_2 sulfoxide was added 5 drops of glacial HOAc and 0.5 ml of $CHCl_3$. The resulting solution was applied to an SiO_2 (10% H_2O) column which was eluted with $CHCl_3$ and then with 2.5% MeOH in $CHCl_3$. An early MeOH–$CHCl_3$ fraction was dissolved in H_2O, the p*H* of the resulting solution was adjusted to 12 with NaOH, and the basic solution was extracted with $CHCl_3$. The extract was dried (Na_2SO_4) and the solvent was removed by vacuum evaporation to obtain 37 mg of pure *anti*-thiobinupharidine-6,6′-d_2 sulfoxide: ^{13}C (^1H) nmr δ: 63.9 ppm (t, C-6′), 59.1 (t, C-6).

A later MeOH–$CHCl_3$ fraction was treated in a similar manner to obtain 50 mg of pure *syn*-thionupharidine-6,6′-d_2 sulfoxide.

Thermolysis of syn-*Neothiobinupharidine Sulfoxide*

A solution of 23 mg of the title compound in 10 ml of xylene was heated at 145–150°C for 72 h. Evaporation of the solvent under vacuum, reduction of the residue with 50 mg of $NaBH_4$ in MeOH for 1 h, evaporation under vacuum to dryness, addition of 10 ml of water, extraction with $CHCl_3$, drying, and evaporation under vacuum resulted in 27 mg of residue: tlc (Al_2O_3, 1:9 Et_2O–hexane) R_f 0.00 (major), 0.42 (neothiobinupharidine), 0.55 (unknown), 0.67 (unknown), 0.73 (thionuphlutine C).

Thermolysis of anti-*Neothiobinupharidine Sulfoxide*

A solution of 11 mg of the title compound in 10 ml of xylene was heated at 145–150°C for 24 h. Reduction and pro-

cessing in the manner applied to the *syn* isomer gave a 9 mg residue: tlc (Al_2O_3, 1:9 Et_2O–hexane) R_f 0.21, 0.35, 0.70 (uv and Dragendorff active), 0.82; tlc of neothiobinupharidine (R_f 0.42), thionuphlutine B (R_f 0.70, Dragendorff active, uv inactive), thionuphlutine C (R_f 0.73), and thiobinupharidine (R_f 0.79) was carried out for comparison.

Thermolysis of syn-*Thiobinupharidine Sulfoxide*

A solution of 10 mg of the *syn* sulfoxide in 1 ml of DMSO was degassed then heated under N_2 at 140°C for 1 h at the end of which time 2 drops were withdrawn and the remainder was heated for an additional 23 h. The solvent was removed from the 1-h sample by vacuum evaporation, the residue was dissolved in 5 drops of $CHCl_3$, and 1 drop of glacial HOAc was added. The 24-h sample was treated in a similar fashion and both samples were examined by tlc (SiO_2, 0.7 ml CH_3OH, 10 ml $CHCl_3$, and 2 drops of HOAc), the 1-h sample showing R_f 0.27 (*syn* sulfoxide), 0.44 but no R_f 0.36 (*anti* sulfoxide) or R_f 0.18, and the 24-h sample showing R_f 0.18, 0.27 (*syn* sulfoxide), 0.44, and 0.50, but no R_f 0.36 (*anti* sulfoxide). The 24-h sample also showed by tlc (Al_2O_3, 10% Et_2O–hexane) R_f 0.0 (*syn* sulfoxide), 0.33, 0.7 (thionuphlutine B), and 0.8 (thiobinupharidine). The 24-h $CHCl_3$–HOAc solution was chromatographed on a 1 cm × 7 cm column of SiO_2 (activity 2) with 2.5% MeOH-$CHCl_3$ in 30 ml (fraction 1, 1.0 mg), 40 ml (fraction 2, 7 mg), and 20 ml (fraction 3, 5 mg) amounts. Fraction 2 (tlc (SiO_2 0.7 ml CH_3OH and 10 ml $CHCl_3$) R_f 0.27, 0.44, and 0.50) in 0.5 ml of MeOH was treated with 20 mg of $NaBH_4$ at 25°C for 1 h. The solvent was removed by vacuum evaporation, the residue was dissolved in 0.5 ml of $CHCl_3$ and the resulting solution was filtered through a 0.5-ml layer of Al_2O_3 which was subsequently washed with 20 ml of $CHCl_3$. The combined filtrate and washing was vacuum-evaporated to afford 2 mg of oil: tlc ($Al_2O_3HF_{254}$, 1:9 Et_2O–hexane) R_f 0.0 (*syn* sulfoxide), 0.7 (thionuphlutine B), and 0.8 (thionuphlutine A).

Acknowledgment

The authors are grateful to the National Institutes of Health, U.S. Public Health Service, for the support of this work.

1. R. T. LALONDE, C. F. WONG, A. I-M. TSAI, J. T. WRÓBEL, J. RUSZKOWSKA, K. KABINSKA, T. I. MARTIN, and D. B. MACLEAN. Can. J. Chem. **54**, 3860 (1976).
2. R. T. LALONDE, T. N. DONVITO, and A. I-M. TSAI. Can. J. Chem. **53**, 1714 (1975).
3. R. T. LALONDE, C. F. WONG, and K. C. DAS. J. Am. Chem. Soc. **95**, 6342 (1973).
4. R. T. LALONDE, C. F. WONG, and K. C. DAS. J. Org. Chem. **39**, 2892 (1974).
5. R. T. LALONDE, C. F. WONG, J. T. WOOLEVER, E. AUER, K. C. DAS, and I-M. TSAI. Org. Mass Spectrum. **9**, 714 (1974).
6. R. T. LALONDE, C. F. WONG, and H. G. HOWELL. J. Org. Chem. **36**, 3703 (1971).
7. R. T. LALONDE, T. N. DONVITO, A. I-M. TSAI, and C. F. WONG. Org. Magn. Reson. **7**, 191 (1975).
8. R. D. G. COOPER and D. O. SPRY. *In* Cephalosarins and penicillins. Chemistry and biology. *Edited by* E. H. Flynn. Academic Press, New York, NY. 1972. p. 216.
9. R. D. G. COOPER. J. Am. Chem. Soc. **92**, 5010 (1970).
10. D. N. MCGREGOR. *In* Progress in the chemistry of organic natural products. Vol. 31. *Edited by* W. Herz, H. G. Rinebach, and G. W. Kirby. Springer Verlag, New York, NY. 1974. p. 28.
11. R. B. MORIN, B. G. JACKSON, R. A. MUELLER, E. R. LAVAGNINO, W. B. SCANLON, and S. L. ANDREWS. J. Am. Chem. Soc. **91**, 1401 (1969).
12. B. DAYAL. Ph.D. thesis. Stevens Institute of Technology, Hoboken, NJ. (1975).

Can. J. Chem. Downloaded from www.nrcresearchpress.com by 210.87.254.6 on 09/05/12
For personal use only.

Total synthesis of indole and dihydroindole alkaloids. XII.[1,2] Selective functionalization of various bisindoles. Efficient syntheses of leurosine and related bisindole alkaloid derivatives

JAMES P. KUTNEY, JOHN BALSEVICH, GORDON H. BOKELMAN, TOSHIHIKO HIBINO, TOSHIO HONDA, ISAMU ITOH, ARNOLD H. RATCLIFFE, AND BRIAN R. WORTH

Department of Chemistry, University of British Columbia, 2075 Wesbrook Place, Vancouver, B.C., Canada V6T 1W5

Received June 30, 1977

JAMES P. KUTNEY, JOHN BALSEVICH, GORDON H. BOKELMAN, TOSHIHIKO HIBINO, TOSHIO HONDA, ISAMU ITOH, ARNOLD H. RATCLIFFE, and BRIAN R. WORTH. Can. J. Chem. **56**, 62 (1978).

Studies involving selective functionalization of the indole unit in a number of bisindole alkaloids and related synthetic derivatives are described. These investigations include such reagents as *tert*-butyl hydroperoxide, which provides an efficient procedure for epoxidation of olefinic linkages, mercuric acetate, osmium tetroxide, and iodine under basic conditions and oxygenation under acidic conditions. Efficient syntheses of leurosine (**8**) and various novel vinblastine derivatives are developed.

JAMES P. KUTNEY, JOHN BALSEVICH, GORDON H. BOKELMAN, TOSHIHIKO HIBINO, TOSHIO HONDA, ISAMU ITOH, ARNOLD H. RATCLIFFE et BRIAN R. WORTH. Can. J. Chem. **56**, 62 (1978).

On décrit des études impliquant la fonctionnalisation sélective d'unités indoliques dans un certain nombre d'alcaloïdes dérivés du bisindole et de dérivés de synthèse qui leur sont reliés. Ces études comprennent des réactifs tels que: l'hydroperoxyde de *tert*-butyle qui permet d'effectuer d'une façon efficace l'époxydation de doubles liaisons, l'acétate mercurique, le tétroxyde d'osmium et l'iode en milieu basique ainsi que l'oxygénation en milieu acide. On a développé des synthèses efficaces de la leurosine (**8**) et de divers dérivés nouveaux de la vinblastine.

[Traduit par le journal]

In a continuing research program directed at the laboratory synthesis of bisindole alkaloids of the vinblastine–vincristine series, we have considered various approaches in the hope of developing efficient procedures for the preparation of these clinically important agents. Our previous investigations (1–3, 5) involved studies in which appropriate indole and dihydroindole units were coupled to provide the desired bisindole systems. In another study we have considered the development of selective reactions which would allow specific functionalization of appropriate bisindole systems already available from previous experiments. The results presented herein illustrate the success of such an approach.

It has already been noted (Part XI, ref. 4) that electrophilic addition to the olefinic linkage of the catharanthine system is complicated by competitive side reactions at the indole or the basic nitrogen site in the molecule. A similar difficulty was observed with the cleavamine system, the indole unit normally present in the bisindole alkaloids. After much frustration with the more common electrophilic reagents generally employed in olefin functionalization, we turned our attention to oxygen and hydroperoxide oxidation of alkenes, a reaction which is not generally utilized by synthetic chemists (6–9).

The intermediate chosen for this study was N_a-carbomethoxy-18β-carbomethoxycleavamine (**1**) since this compound was expected to exhibit properties similar to those of the indole unit present in the bisindole alkaloids. The preparation of this intermediate was accomplished by reacting the readily available 18β-carbomethoxycleavamine (1, 10) with strong base to remove the indolic hydrogen and treating the resultant anion with methyl chloroformate.

Oxidation of **1** with oxygen in a tetrahydrofuran solution containing trifluoroacetic acid provided two main products, which on the basis of their spectral data, were assigned the structures **2** and **3**. The major component (51% yield) was the lactam epoxide **3** while the desired N_a-carbomethoxy-18β-carbomethoxy - 3β,4β - epoxydihydrocleavamine (**2**) was isolated in only 10–15% yield. Of particular importance in allowing the structural assignment for **2** was the characteristic fragmentation pattern in the mass spectrum. The most significant fragmentation occurs in the manner indicated with cleavage at 'a' and 'b' providing the ion **5** (*m/e* 152, 17%; $C_9H_{14}NO$

[1]For part XI see ref. 5.

[2]For preliminary reports on portions of this work, see ref. 19.

Can. J. Chem. Downloaded from www.nrcresearchpress.com by 210.87.254.105 on 09/05/12
For personal use only.

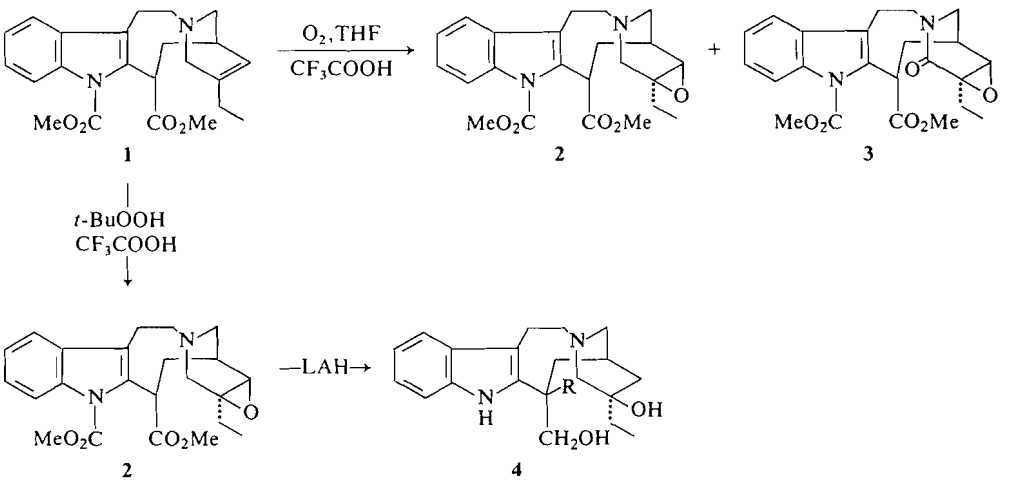

1 2 3 2 4

requires 152.107; found: 152.106) and at 'a' and 'c' to provide ion **6** (*m/e* 224, base peak; $C_{12}H_{18}NO_3$ requires 224.129; found: 224.128).

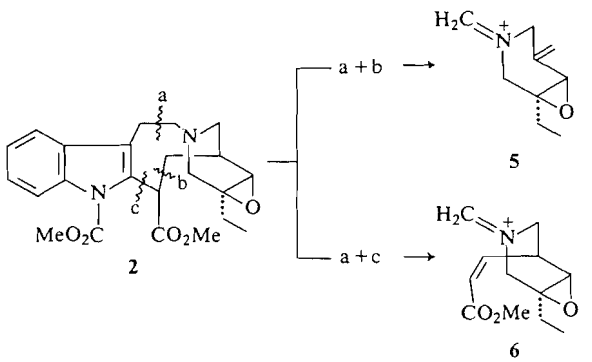

2 5 6

Clearly the data provided thus far did not allow any stereochemical assignment to the epoxide ring as shown in **2** and **3** but further chemical evidence settled this question. Lithium aluminum hydride reduction of **2** in refluxing *N*-methylmorpholine provided the diol **4** (R = H) in 80% yield. The structure of the latter follows directly from the fact that the known triol **4** (R = OH) available from a previous study (11) could be similarly reduced to **4** (R = H). Since the interrelationship of the triol (**4**, R = OH) with isovelbanamine (11) firmly establishes the absolute configuration of the tertiary hydroxy group as shown, it is clear that the epoxide ring in the oxidation products **2** and **3** must be in a β orientation.

Further studies to improve the yield of the desired epoxide intermediate **2** in the oxygenation reaction met with failure but reaction of **1** with the hydroperoxide in aqueous trifluoroacetic acid provided **2** in 67% yield and thereby suggested an attractive application of this reaction to the bisindole series.

The most attractive intermediate from the bisindole series which appeared suitable for studies with the hydroperoxide procedure was 3′,4′-dehydrovinblastine (**7**), a synthetic vinblastine analogue available from our earlier studies (2, 3) and independent investigations conducted elsewhere (12, 13). This compound was treated with *tert*-butyl hydroperoxide and trifluoroacetic acid in tetrahydrofuran as solvent. The product, obtained in 51% yield, was identified as the bisindole alkaloid leurosine **8** by appropriate comparisons with an authentic sample. As already indicated in the previous publication (Part XI, ref. 5) the stereochemistry of the epoxide ring in this alkaloid is as shown in **8**, thereby establishing attack of the hydroperoxide from the α face of the indole unit in **7**. The epoxidation process was selective in that products resulting from reaction at the olefinic linkage in the vindoline unit of **7** were not observed.

An even more efficient route to leurosine (62%) was realized by treatment of the hydrochloride salt of **7** with mercuric acetate and subsequent quenching with sodium borohydride.

In recent isolation studies it has been demonstrated that vicinal diols are present in some bisindole alkaloids as exemplified by vincadioline (14). Thus it appeared appropriate to evaluate selective diol formation with 3′,4′-dehydrovinblastine in the hope that such studies would allow entry into this series of compounds. For this purpose a detailed investigation with osmium tetroxide was initiated and a summary of the results is presented in Fig. 1.

It was found that the nature and relative yields of the products obtained from osmylation of **7** depended markedly on the reaction conditions employed. Initial investigations with **7** and osmium tetroxide revealed a complex reaction product mixture but results with the *N*-oxide derivative **9** were much more encouraging and further studies were performed.

Can. J. Chem. Downloaded from www.nrcresearchpress.com by 210.87.254.105 on 09/05/12
For personal use only.

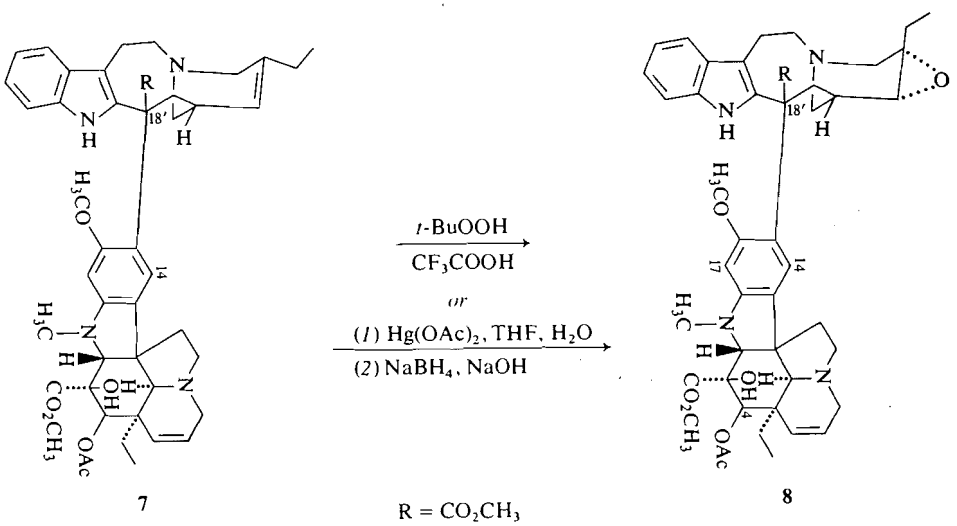

7 R = CO_2CH_3 8

Reaction of **9** with 1 or less than 1 equiv. of osmium tetroxide provided two main products which from spectral and chemical data could be assigned the structures **10** (R_1 = OH) and **11** (R_2 = O).

The major component (53% yield) was 3′,4′-dehydro-19′-oxovinblastine (**11**, R_2 = O) and represented a product in which normal hydroxylation of the olefinic linkage in the indole unit had not occurred but rather oxidation at the basic nitrogen site to provide the lactam. The expected product resulting from hydroxylation of the 3′,4′-double bond in **9** and tentatively assigned the name 3′-hydroxyvinblastine (see later) was isolated only as a minor component (10% yield). In addition, leurosine (3–5% yield) was isolated as a very minor component.

Reaction of **9** with 2 equiv. of osmium tetroxide provided another product (64% yield) which, again on the basis of spectroscopic evidence, was tentatively assigned the name, 3′-hydroxy-19′-oxovinblastine.

More recent studies with several salt derivatives of 3′,4′-dehydrovinblastine provided optimum conditions for obtaining the diol and lactam diol derivatives isolated in the above investigations. Experiments were performed with the hydrochloride and hydrosulfate derivatives, with the latter providing the best results. Thus reaction of the hydrosulfate derivative with 1.2 equiv. of osmium tetroxide afforded a 42% yield of the amine diol, whereas with 2.2 equiv. of this reagent a 63% yield of the lactam diol was obtained. Again leurosine was isolated as a minor component in these reactions.

It is important to emphasize at this point in the discussion that the initial experiments involving *tert*-butyl hydroperoxide, and osmium tetroxide, with 3′,4′-dehydrovinblastine, as reported in preliminary communications (19), were completed prior to our studies (5, 15) which established with certainty the epoxide stereochemistry in leurosine. In those early studies it was assumed that attack of reagents to the 3′,4′-double bond in **7** would occur from the β face of the indole unit. The synthesis of leurosine via the hydroperoxide procedure discussed earlier clearly establishes α attack at the 3′,4′ position in **7**. The isolation of leurosine in the osmylation studies also provides evidence for a similar reaction with osmium tetroxide thereby suggesting stereochemical assignment of the vicinal diol system in **10** and **12** as indicated. On this basis these two compounds are derivatives of leurosidine (**17**, R = CO_2CH_3, R_1 = OH), the C-4′ isomer of vinblastine (16). Conclusive chemical evidence for this stereochemical assignment was obtained in the following manner.

Tosylation of the lactam diol (**12**, R_1 = R_3 = OH, R_2 = O) provided the secondary monotosylate (**12**, R_1 = OH, R_3 = OTos, R_2 = O) and the latter upon reaction with sodium cyanoborohydride afforded leurosine (**8**). This conversion established the α orientation for the tertiary hydroxyl group (R_1) in **12** and, in turn, the same orientation for the secondary function (R_3) since osmylation is well known to be a *cis* hydroxylation process. On this basis the amine diol **10** (R_1 = OH) is given the name, 3′α-hydroxyleurosidine while **12** (R_1 = R_3 = OH, R_2 = O) is 3′α-hydroxy-19′-oxoleurosidine.

The above studies suggested an efficient synthetic entry into a series of novel lactam derivatives in the natural bisindole alkaloid family. The osmylation studies, for example, revealed selective oxidation of the basic nitrogen in the indole unit in the highly functionalized bisindole system and since such intermediates would be important in subsequent investi-

Can. J. Chem. Downloaded from www.nrcresearchpress.com by 210.87.254.105 on 09/05/12
For personal use only.

Can. J. Chem. Downloaded from www.nrcresearchpress.com by 210.87.254.105 on 09/05/12
For personal use only.

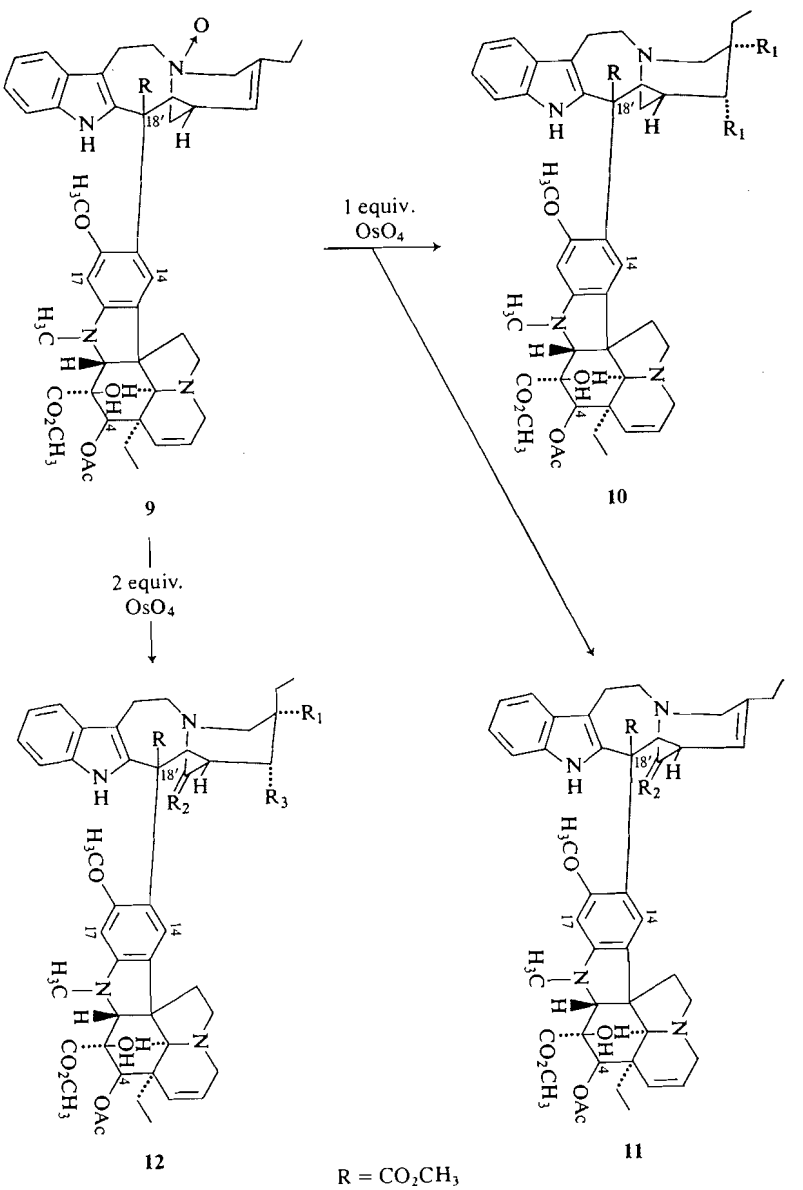

FIG. 1. The reaction of the *N*-oxide intermediate **9** with osmium tetroxide under various conditions.

gations concerned with structure–activity relationships, it was decided to pursue a more thorough investigation in this direction.

We had demonstrated in earlier experiments (4, 17) that conversion of the catharanthine system to the corresponding lactam series could be accomplished by reaction with iodine under basic conditions. The utilization of this reagent with the natural alkaloids vinblastine (**15**, R = CO_2CH_3, R_1 = OH), leurosidine (**17**, R = CO_2CH_3, R_1 = OH), and leurosine (**8**) came under investigation. Figures 2 and 3 provide a summary of the results obtained.

Reaction of vinblastine with iodine and sodium bicarbonate in a tetrahydrofuran solution at room temperature provided 19′-oxovinblastine (**16**, R = CO_2CH_3, R_1 = OH, R_2 = O; 32% yield), whereas a similar oxidation with leurosidine afforded 19′-oxoleurosidine (**18**, R = CO_2CH_3, R_1 = OH, R_2 = O; 62% yield).

The rather unstable alkaloid leurosine can be converted to its lactam derivative **13** (R_1 = O) in 56% yield by means of the iodine oxidation procedure.

The trifluoroacetic acid catalyzed oxygenation

Can. J. Chem. Downloaded from www.nrcresearchpress.com by 210.87.254.105 on 09/05/12
For personal use only.

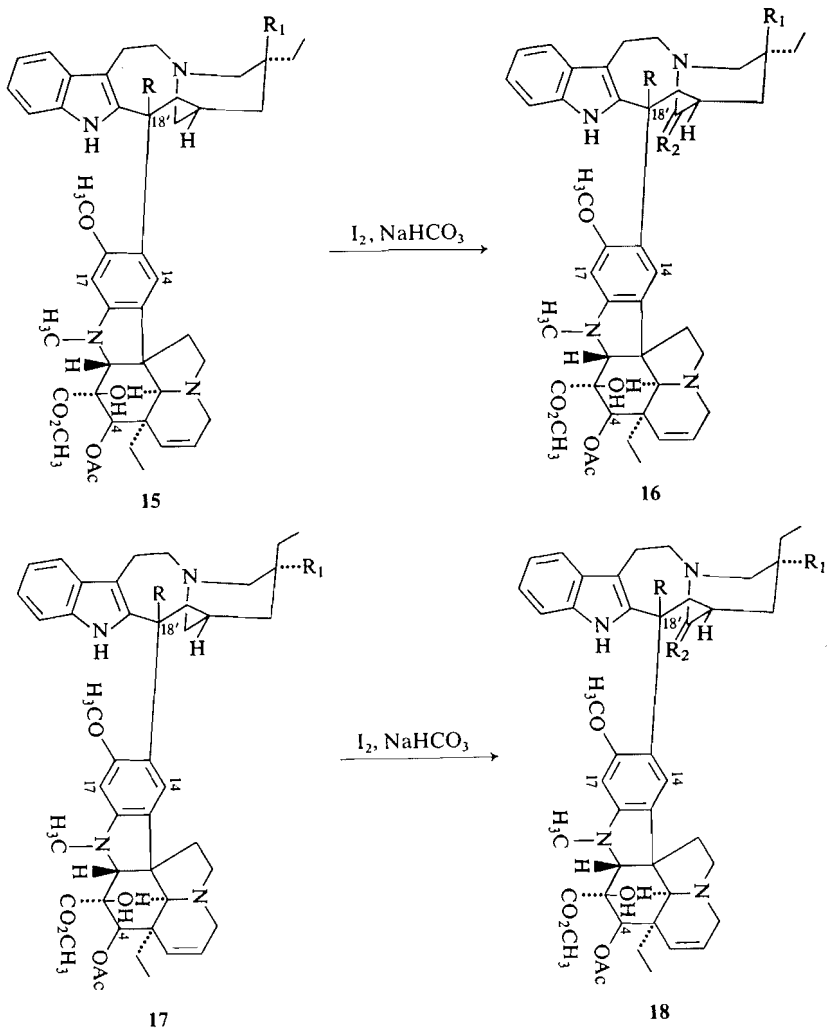

15 16 17 18

FIG. 2. The conversion of vinblastine (**15**, R = CO_2CH_3, R_1 = OH) and leurosidine (**17**, R = CO_2CH_3, R_1 = OH) to lactam derivatives by means of iodine under basic conditions.

procedure discussed earlier was also evaluated for the purpose of providing lactam derivatives in the bisindole area. It was interesting to observe that with this procedure another series of lactams became available. Thus leurosine was converted to 5′-oxoleurosine (**14**, R_1 = O; 15% yield). A more efficient synthesis of this intermediate (34% yield) involved the direct oxygenation of the synthetic derivative, 3′,4′-dehydrovinblastine (**7**).

In summary, the above investigations with various reagents which allow specific functionalization of the indole unit provided reasonably efficient synthetic entries into a whole series of novel bisindole derivatives. The above synthesis of leurosine, by mercuric acetate oxidation, is the most efficient and most easily adaptable for commercial purposes of those reported (5, 15, 18). Further studies in this direction are currently underway.

Experimental

Melting points were determined on a Kofler block and are uncorrected. Ultraviolet (uv) spectra were recorded on a Cary 15 spectrophotometer in ethanol solution. The wavelengths of absorption maxima are reported in nanometres (nm) with log ε values in parentheses. Infrared (ir) spectra were measured on a Perkin Elmer model 710 or 457 spectrophotometer in chloroform solution. The absorption maxima are reported in wavenumbers (cm^{-1}), calibrated with respect to the absorption band of polystyrene at 1601 cm^{-1}. Proton magnetic resonance (^{1}Hmr) spectra were measured in deuterochloroform ($CDCl_3$) solution at ambient temperature on either a Varian HA-100 or XL-100 spectrometer. Chemical shift values are given in the δ (ppm) scale relative to tetramethylsilane (TMS) used as internal standard. The integrated peak areas, signal multi-

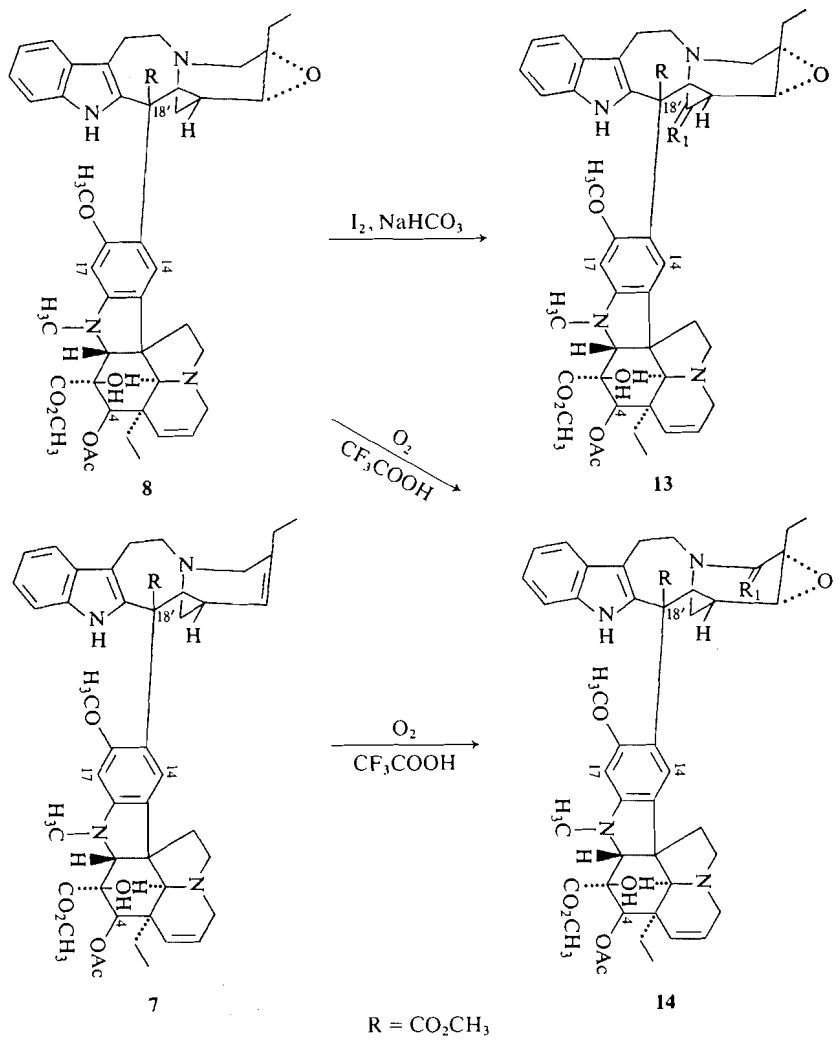

FIG. 3. The conversion of leurosine (**8**) and 3′,4′-dehydrovinblastine (**7**) to lactam derivatives.

plicities and proton assignments are given in parentheses. Low resolution mass spectra (ms) were determined on either an AEI-MS-902 or an Atlas CH-4B spectrometer. High resolution mass spectra were measured on an AEI-MS-902 instrument. Microanalyses were carried out by Mr. P. Borda of the Microanalytical Laboratory, University of British Columbia.

Thin-layer chromatography (tlc) utilized Merck silica gel G (according to Stahl) containing 2% fluorescent indicator. For preparative-layer chromatography (plc), plates (20 × 20 or 20 × 60 cm) of 1 mm thickness were used. Visualization was effected by viewing under ultraviolet light and/or by colour reaction with ceric sulphate spray reagent. Column chromatography utilized Merck silica gel 60 (70–230 mesh) or Merck aluminum oxide 90 (neutral).

As a matter of routine, all reagents and solvents were recrystallized or distilled before use.

N_a-Carbomethoxy-18β-carbomethoxycleavamine (1)

A solution of 18β carbomethoxycleavamine (502 mg, 1.5 mmol) in dry tetrahydrofuran (50 ml) under an atmosphere of nitrogen was treated with a suspension of potassium hydride in mineral oil (300 mg, 22.5% KH, 1.7 mmol). After stirring for 10 min at ambient temperature the resultant mixture was treated with methyl chloroformate (290 mg, 3.1 mmol) and stirred for a further 1 h. Acetic acid (0.5 ml) was added to the mixture and stirring continued for 5 min. The solvent was removed *in vacuo* and the residue chromatographed on alumina (activity III, petroleum ether – benzene) to give N_a-carbomethoxy-18β-carbomethoxycleavamine (**1**) (461 mg, 78%), mp 124–125°C (acetone–ether); uv λ_{max}: 294 (3.66), 283 (3.80), 268 (4.09), 262 (4.11), 228 (4.37); ir ν_{max}: 1725; ^{1}Hmr δ: 8.08 (1H, m, C_{14}-*H*) 7.23 (3H, m, C_{11}-*H*, C_{12}-*H*, C_{13}-*H*), 5.77 (1H, d, J = 6 Hz, C_{18}-*H*), 5.37 (1H, m, C_3-*H*), 3.88 (3H, s, N—CO_2CH_3), 3.53 (3H, s, —CO_2CH_3), 0.98 (3H, t, J = 7 Hz, —CH_2CH_3); ms *m/e* 396 (M^+), 273 (base peak), 136, 124; ^{13}Cmr δ: 12.66 (C-21), 122.25 (C-3), 141.11 (C-4). High resolution molecular weight determination calcd. for $C_{23}H_{28}N_2O_4$: 396.2048; found: 396.2070. *Anal.* calcd. for $C_{23}H_{28}N_2O_4$: C 69.67, H 7.12, N 7.07; found: C 69.86, H 7.10, N 6.87.

Can. J. Chem. Downloaded from www.nrcresearchpress.com by 210.87.254.105 on 09/05/12
For personal use only.

Can. J. Chem. Downloaded from www.nrcresearchpress.com by 210.87.254.105 on 09/05/12
For personal use only.

Autoxidation of N_a*-Carbomethoxy-18β-carbomethoxycleavamine (1)*

A solution of N_a-carbomethoxy-18β-carbomethoxycleavamine (**1**) (400 mg, 1 mmol) in peroxide-free tetrahydrofuran (10 ml) containing aqueous 1% trifluoroacetic acid (1 ml) was stirred at ambient temperature in the presence of air for a period of 8 days. After drying (K_2CO_3) the solvent was removed *in vacuo* to give an amber gum. Chromatography on alumina (activity III) afforded the *epoxide* **2** (40 mg, 10%) and the *epoxy lactam* **3** (230 mg, 54%).

N_a-Carbomethoxy-18β-carbomethoxy-3β,4β-epoxydihydrocleavamine (**2**), mp 131–132°C (ether); uv λ_{max}: 294 (3.66), 283 sh (3.76), 268 (4.08), 262 (4.09), 227 (4.32); ir ν_{max}: 1728; ^{1}Hmr δ: 8.1 (1H, m, C_{14}-*H*), 7.3 (3H, m, C_{11}-*H*, C_{12}-*H*, C_{13}-*H*), 5.84 (1H, d, *J*=6 Hz, C_{18}-*H*), 3.91 (3H, s, N—CO_2CH_3), 3.57 (3H, s, —CO_2CH_3), 1.00 (3H, t, *J* = 7.5 Hz, —CH_2CH_3); ms *m/e* 412 (M^+), 224 (base peak), 152, 138; ^{13}Cmr δ: 8.93 (C-21), 60.6 (C-3), 62.7 (C-4). High resolution molecular weight determination calcd. for $C_{23}H_{28}N_2O_5$: 412.1997; found: 412.2027. *Anal.* calcd. for $C_{23}H_{28}N_2O_5$: C 66.97, H 6.84, N 6.79; found: C 66.81, H 6.87, N 6.71.

N_a-Carbomethoxy-18β-carbomethoxy-5-oxo-3β,4β-epoxydihydrocleavamine (**3**), obtained as a foam from methanol; uv λ_{max}: 293 (3.67), 281 sh (3.78), 265 sh (4.05), 259 (4.06), 227 (4.38); ir ν_{max}: 1732, 1680, 1650; ^{1}Hmr δ: 8.1 (1H, m, C_{14}-H), 7.3 (3H, m, C_{11}-*H*, C_{12}-*H*, C_{13}-*H*), 5.23 (1H, m), 4.00 (3H, bs, N—CO_2CH_3), 3.66 (3H, s, —CO_2CH_3), 1.90 (2H, q, *J* = 7 Hz, —CH_2CH_3), 0.79 (3H, t, *J* = 7 Hz, —CH_2CH_3); ms *m/e* 426 (M^+, base peak), 394, 228. High resolution molecular weight determination calcd. for $C_{23}H_{26}N_2O_6$: 426.1791; found: 426.1795. *Anal.* calcd. for $C_{23}H_{26}N_2O_6 \cdot \frac{1}{2}CH_3OH$:[3] C 63.80, H 6.33, N 6.33; found: C 64.08, H 6.11, N 6.31.

Oxidation of N_a*-Carbomethoxy-18β-carbomethoxycleavamine (1) using* tert*-Butyl Hydroperoxide*

A solution of **1** (1.76 g, 4.4 mmol) in freshly distilled tetrahydrofuran (50 ml) containing aqueous 1% trifluoroacetic acid (10 ml) and *tert*-butyl hydroperoxide (9 ml) was stirred at ambient temperature for 21 h. The mixture was taken up in $NaHCO_3$ solution (40 ml) and extracted with ethyl acetate (2 × 30 ml). The combined organic portion was washed with 5% NaOH solution (1 × 20 ml), water (1 × 20 ml), and brine (1 × 20 ml). After drying (Na_2SO_4) the solvent was removed *in vacuo* to give a viscous oil. Chromatography on alumina (activity III, φH) afforded the epoxide **2** (1.22 g, 67%) identical with that obtained above.

Reduction of N_a*-Carbomethoxy-18β-carbomethoxy-3β,4β-epoxydihydrocleavamine*

A solution of **2** (25 mg, 0.06 mmol) in dry *N*-methylmorpholine (2.5 ml) under an atmosphere of nitrogen was treated with lithium aluminum hydride (75 mg, 2 mmol) in tetrahydrofuran (0.5 ml). The tetrahydrofuran was distilled out of the reaction mixture and the remaining solution was refluxed for 2 h. Excess lithium aluminum hydride was destroyed by careful addition of water (10 ml). The mixture was extracted with ethyl acetate (4 × 5 ml), the combined organic portion was dried (Na_2SO_4), and the solvents were removed *in vacuo*. Chromatography on silica gel (ethyl acetate) afforded the *diol* **4** (R = H) (16 mg, 80%), mp 145–150°C (methanol); uv λ_{max}: 291 (3.81), 283 (3.84), 275 sh (3.79), 228 (4.51); ir ν_{max}: 3600, 1510, 1025; ^{1}Hmr δ: 8.55 (1H, bs, N—*H*), 7.51 (1H, m, C_{14}-*H*), 7.24 (3H, m, C_{11}-*H*, C_{12}-*H*, C_{13}-*H*), 4.24 (1H, quintet, *J* = 5 Hz, C_{18}-*H*), 3.86 (2H, d, *J* = 5 Hz, —CH_2OH), 0.96 (3H, t, *J* = 7 Hz, —CH_2CH_3); ms *m/e* 328 (M^+) 311, 310, 299, 297, 187, 154 (base peak). High resolution molecular weight determination calcd. for $C_{20}H_{28}N_2O_2$: 328.2150; found: 328.2146. *Anal.* calcd. for $C_{20}H_{28}N_2O_2 \cdot \frac{1}{2}CH_3OH$:[3] C 71.48, H 8.78, N 8.13; found: C 71.36, H 8.71, N 8.10.

Reduction of 4β,18-Dihydroxy-18-hydroxymethyldihydrocleavamine (4, R = OH) to 4β-Hydroxy-18β-hydroxymethyldihydrocleavamine

A solution of the triol **4** (R = OH) (37 mg, 0.11 mmol) in *N*-methylmorpholine (3 ml) was treated with lithium aluminum hydride (110 mg, 3 mmol) in tetrahydrofuran (0.75 ml) as described above. Isolation of the product by preparative tlc (silica, ethyl acetate) afforded the diol **4** (R = H) (33 mg, 93%). The physical (tlc, mixture mp) and spectral properties (ir, ^{1}Hmr, ms) showed the product to be identical with the one obtained above.

Synthesis of Leurosine (8) from 3′,4′-Dehydrovinblastine (7) using tert*-Butyl Hydroperoxide*

A solution of 7 (81 mg, 0.1 mmol) in peroxide-free tetrahydrofuran (4 ml) containing aqueous 1% trifluoroacetic acid (0.4 ml) and *tert*-butyl hydroperoxide (0.4 ml) was stirred at ambient temperature for 9 h. The mixture was poured into ice-water (15 ml), made basic with concentrated NH_4OH, and extracted with dichloromethane (3 × 10 ml). The combined organic portion was washed with 3% NaOH solution (1 × 8 ml), dried ($MgSO_4$), and the solvent was removed *in vacuo*. Chromatography on silica gel (ethyl acetate – 10% methanol) afforded leurosine (**8**) (43 mg, 52%) which was identified by comparison with an authentic sample (tlc, ^{1}Hmr, ir, ms, and mixture mp).

Synthesis of Leurosine (8) from 7 using Mercuric Acetate

A solution of the hydrochloride salt of 7 (20 mg) in tetrahydrofuran (1 ml) and water (1 ml) was added at ambient temperature to a suspension of mercuric acetate (16 mg) in tetrahydrofuran (1 ml) and water (1 ml) with stirring. The mixture was stirred for a further 30 min then quenched with 3 *N* NaOH (0.5 ml) and sodium borohydride (excess). After 2 h at ambient temperature the mixture was saturated with sodium chloride and extracted with chloroform. The extract was dried (Na_2SO_4), evaporated, and chromatographed on silica gel to give leurosine (12 mg, 62%) identical with an authentic sample.

The N*-Oxide Derivative (9) of 3′,4′-Dehydrovinblastine*

A solution of 3′,4′-dehydrovinblastine (7) (100 mg, 0.126 mmol) in dichloromethane (5 ml) was cooled to −4°C. *m*-Chloroperbenzoic acid (21.8 mg, 0.126 mmol) was added and the mixture stirred at ca. −4°C for 10 min. Then the solvent was evaporated *in vacuo*. The residue was chromatographed on alumina (grade III, ca. 10 g). Elution with 3:1 ethyl acetate – methanol afforded the *N*-oxide derivative (**9**) (100.7 mg, 99%); mp 194–197°C (methanol); uv λ_{max}: 306 (3.99), 292 (4.24), 283 (4.33), 265 (4.46), 213 (4.98), ir ν_{max}: 3460, 2950, 1735, 1610; ^{1}Hmr δ: 9.76 (1H, bs, O*H*), 8.15 (1H, bs, N*H*), 7.67 (1H, m, $C_{14'}$-*H*), 7.11 (3H, m, $C_{11'}$–$C_{13'}$-*H*'s), 6.43 (1H, s, C_{14}-*H*), 6.10 (1H, s, C_{17}-*H*), 5.83 (1H, m, $C_{7'}$-*H*), 5.39 (1H, m, $C_{3'}$-*H*), 5.39 (1H, s, C_4-*H*), 5.24 (1H, d, *J* = 10 Hz, C_6-*H*), 4.81–3.57 (6H, m, $C_{5'}$, $C_{7'}$, $C_{19'}$-*H*'s), 3.81 (3H, s, OCH_3), 3.77 (3H, s, OCH_3), 3.67 (3H, s, OCH_3), 2.69 (3H, s, NCH_3), 2.07 (3H, s, OCOCH_3), 1.01 (3H, t, *J* = 7 Hz, —CH_2CH_3), 0.61 (3H, t, *J* = 7 Hz, —CH_2CH_3); ms *m/e* 808 (M^+), 792, 610, 136, 135, 122, 121, 120, 107, 106 (base peak). High resolution molecular weight determination calcd. for $C_{46}H_{56}N_4O_9$: 808.4046; found: 808.3995.

[3]For analytical purposes, complete removal of solvent of crystallization was impossible without decomposition of the compounds.

Can. J. Chem. Downloaded from www.nrcresearchpress.com by 210.87.254.105 on 09/05/12
For personal use only.

Osmylation of the N*-Oxide Derivative (**9**) of 3′,4′-Dehydrovinblastine*

(a) With One or Less than One Equivalent of Osmium Tetroxide

A suspension of the *N*-oxide **9** (100 mg, 0.124 mmol) in dry tetrahydrofuran (4 ml) and pyridine (1 ml) was cooled to ca. −5°C under an atmosphere of argon. Osmium tetroxide (31.4 mg, 0.124 mmol) in dry tetrahydrofuran (0.4 ml) was added and the mixture stirred at −5°C for 45 min. Then hydrogen sulfide was bubbled through the mixture for 5 min. The resultant mixture was filtered and the filtrate evaporated *in vacuo*. The oily product was purified by preparative-layer chromatography (silica gel, 19:1 dichloromethane–methanol).

The major product (least polar on tlc) (53 mg, 53%) was identified as 3′,4′-dehydro-19′-oxovinblastine (**11**, R_2 = O), mp 210–212°C (methanol); uv λ_{max}: 293 (4.47), 283 (4.53), 262 (4.63), 213 (5.17); ir ν_{max}: 3460, 2950, 1735, 1655, 1610; ^{1}Hmr δ: 8.10 (1H, bs, N*H*), 7.60 (1H, m, $C_{14'}$-*H*), 7.21 (3H, m, $C_{11'}$–$C_{13'}$-*H*'s), 6.69 (1H, s, C_{14}-*H*), 6.19 (1H, s, C_{17}-*H*), 6.15 (1H, m, $C_{3'}$-*H*), 5.90 (1H, m, $C_{7'}$-*H*), 5.52 (1H, s, C_4-*H*), 5.34 (1H, d, J = 10 Hz, C_6-*H*), 4.92 (1H, m, $C_{2'}$-*H*), 3.84 (6H, bs, 2 × OC*H*$_3$), 3.79 (1H, s, C_2-*H*), 3.62 (3H, s, OC*H*$_3$), 2.75 (3H, s, NC*H*$_3$), 2.13 (3H, s, OCOC*H*$_3$), 1.01 (3H, t, J = 7 Hz, —CH_2CH_3), 0.85 (3H, t, J = 8 Hz, —CH_2CH_3); ms *m/e* 806 (M^+), 748, 670, 136, 135 (base peak), 122, 121, 107, 106. High resolution molecular weight determination calcd. for $C_{46}H_{54}N_4O_9$: 806.3890; found: 806.3873. *Anal.* calcd. for $C_{46}H_{54}N_4O_9 \cdot CH_3OH$: C 67.28, H 6.97, N 6.68; found: C 66.98, H 6.80, N, 6.43.

The second product (more polar on tlc) was leurosine (**8**, R = CO_2CH_3) (3.6 mg, 4%). The identity of this compound was established by tlc mobility, spectral comparison (^{1}Hmr, ms), and mixture melting point determination with an authentic sample.

The third product (most polar on tlc) was 3′α-hydroxyleurosidine (**10**, R_1 = OH; formerly designated '3′-hydroxyvinblastine') (9.4 mg, 9%); uv λ_{max}: 294 (4.37), 285 (4.40), 258 (4.49), 212 (5.00); ir ν_{max}: 3550, 3460, 2960, 1735, 1610; ^{1}Hmr δ: 8.00 (1H, bs, N*H*), 7.50 (1H, m, $C_{14'}$-*H*), 7.15 (3H, m, $C_{11'}$–$C_{13'}$-*H*'s), 6.60 (1H, s, C_{14}-*H*), 6.13 (1H, s, C_{17}-*H*), 5.86 (1H, m, $C_{7'}$-*H*), 5.48 (1H, s, C_4-*H*), 5.30 (1H, d, J = 10 Hz, C_6-*H*), 3.82 (3H, s, OC*H*$_3$), 3.80 (3H, s, OC*H*$_3$), 3.75 (1H, s, C_2-*H*), 3.63 (3H, s, OC*H*$_3$), 2.72 (3H, s, NC*H*$_3$), 2.10 (3H, s, OCOC*H*$_3$), 0.96 (3H, t, J = 7 Hz, —CH_2CH_3), 0.90 (3H, t, J = 8 Hz, —CH_2CH_3); ms *m/e* 826 (M^+), 809, 285 (base peak), 136, 135, 122, 121, 107, 106. High resolution molecular weight determination calcd. for $C_{46}H_{58}N_4O_{10}$: 826.4153; found: 826.4178. The hydrochloride salt had mp > 200°C (dec.). *Anal.* calcd. for $C_{49}H_{59}N_4O_{10}Cl$: C 63.98, H 6.89, N 6.50; found: C 64.18, H 6.85, N 6.17.

(b) With Two Equivalents of Osmium Tetroxide

A suspension of the *N*-oxide **9** (50 mg, 0.062 mmol) in dry tetrahydrofuran (2 ml) and pyridine (0.5 ml) was cooled to 0°C under an atmosphere of argon. Osmium tetroxide (32 mg, 0.126 mmol) in dry tetrahydrofuran (0.4 ml) was added and the mixture stirred at ca. 0°C for 1.5 h. Hydrogen sulfide was then bubbled through the mixture for 5 min. The resultant mixture was filtered and the filtrate evaporated *in vacuo*. The crude product was purified by preparative-layer chromatography (silica gel, 23:2 dichloromethane–methanol).

The major product (33.7 mg, 65%) was 3′α-hydroxy-19′-oxoleurosidine (**12**, R_1 = R_3 = OH, R_2 = O; formerly designated '3′-hydroxy-19′-oxovinblastine'), mp 227–229°C; uv λ_{max}: 293 (4.33), 283 (4.39), 261 (4.45), 213 (5.01); ir ν_{max}: 3600–3500, 3460, 2960, 1735, 1645, 1615; ^{1}Hmr δ: 8.04 (1H, bs, N*H*), 7.54 (1H, m, $C_{14'}$-*H*), 7.18 (3H, m, $C_{11'}$–$C_{13'}$-*H*'s), 6.66 (1H, s, C_{14}-*H*), 6.17 (1H, s, C_{17}-*H*), 5.89 (1H, m, $C_{7'}$-*H*), 5.53 (1H, s, C_4-*H*), 5.33 (1H, d, J = 10 Hz, C_6-*H*), 4.65 (1H, m, $C_{2'}$-*H*), 3.83 (6H, bs, 2 × OC*H*$_3$), 3.81 (1H, s, C_2-*H*), 3.60 (3H, s, OC*H*$_3$), 2.76 (3H, s, NC*H*$_3$), 2.12 (3H, s, OCOC*H*$_3$), 1.04 (3H, t, J = 7 Hz, —CH_2CH_3), 0.85 (3H, t, J = 7 Hz, —CH_2CH_3); ms *m/e* 840 (M^+), 423, 282, 149, 135 (base peak), 122, 121, 107. High resolution molecular weight determination calcd. for $C_{46}H_{56}N_4O_{11}$: 840.3945; found: 840.3904. *Anal.* calcd. for $C_{46}H_{56}N_4O_{11}$: C 65.70, H 6.71, N 6.66; found: C 65.45, H 6.61, N 6.51.

*3′α-Hydroxyleurosidine (**10**, R_1 = OH)*

Osmium tetroxide (36 mg, 0.14 mmol) in dry tetrahydrofuran (0.5 ml) was added to the hydrochloride salt of 3′,4′-dehydrovinblastine 7, (111 mg, 0.135 mmol) in dry tetrahydrofuran (2 ml) at 0°C under an atmosphere of dry nitrogen. After 15 min dry pyridine (0.03 ml, 0.0294 g, 0.372 mmol) was added and stirring continued at 0°C for 2 h. Hydrogen sulphide was bubbled through the solution for 5 min, the mixture diluted with ethyl acetate, washed with dilute ammonia solution, dried (Na_2SO_4) and concentrated *in vacuo*. Chromatography on silica gel gave **10** (R_1 = OH), 25 mg (23%), identical with that obtained earlier.

*3′α-Hydroxy-19′-oxoleurosidine (**12**, R_1 = R_3 = OH, R_2 = O) and 3′α-Hydroxyleurosidine (**10**, R_1 = OH)*

(*a*) Osmylation of the hydrosulfate salt of 7 with osmium tetroxide (2.2 equiv.) in dry tetrahydrofuran at 0°C as described directly above afforded the lactam diol (**12**, R_1 = R_3 = OH, R_2 = O) (63%) and the diol (**10**, R_1 = OH) (12%). These products were identical with the respective authentic samples.

(*b*) Osmylation as in (*a*), using 1.2 equiv. of osmium tetroxide gave the diol (**10**, R_1 = OH) (42%).

*The Tosylate (**12**, R_1 = OH, R_3 = OTos, R_2 = O)*

Toluenesulfonyl chloride (10 mg) was added to a solution of the lactam diol (**12**, R_1 = R_3 = OH, R_2 = O) (18 mg) in dry pyridine (2 ml). The mixture was heated at 40°C for 4 h, allowed to stand at ambient temperature for 16 h, poured into water, and extracted with chloroform. The extracts were combined, dried (Na_2SO_4) and concentrated *in vacuo*. Chromatography on silica gel afforded the monotosylate (6 mg, 63%); mp 218–220°C; uv λ_{max}: 312 (sh, 3.88), 295 (4.18), 286 (4.23), 272 (4.27), and 265 (4.27); ir ν_{max}: 3475, 1730, 1660, 1360; ^{1}Hmr δ: 8.68 (1H, bs, —N*H*), 7.73 (2H, d, J = 8 Hz, Tos protons), 7.60 (1H, m, $C_{14'}$-*H*), 7.41 (2H, d, J = 8 Hz, Tos protons), 7.24 (3H, m, indole aromatic protons), 6.71 (1H, s, C_{14}-*H*), 6.27 (1H, s, C_{17}-*H*), 5.96 (1H, dd, J = 10, 4 Hz, $C_{7'}$-*H*), 5.57 (1H, s, C_4-*H*), 5.36 (1H, d, J = 10 Hz, C_6-*H*), 4.72 (1H, bd, J = 13 Hz, $C_{2'}$-*H*), 4.22 (1H, bs, C*H*—OTos), 3.97 (3H, s, —OC*H*$_3$), 3.86 (3H, s, —OC*H*$_3$), 3.70 (3H, s, —OC*H*$_3$), 2.81 (3H, s, —NC*H*$_3$), 2.53 (3H, s, Ph—C*H*$_3$), 2.17 (3H, s, —OCOC*H*$_3$). *Anal.* calcd. for $C_{53}H_{62}N_4O_{13}S$: C 63.86, H 6.28, N 5.63; found: C 63.81, H 6.40, N 5.25.

Starting material (10 mg) was recovered.

*Leurosine Lactam (**13**, R_1 = O) from the Monotosylate*

Excess sodium cyanoborohydride was added to a solution of **12** (R_1 = OH, R_2 = O, R_3 = OTos) (10 mg) in dry HMPA (2 ml). The mixture was heated at 90°C for 20 h, poured into water and extracted with ethyl acetate. The organic layer was washed with water, dried (Na_2SO_4), and concentrated *in vacuo*. Chromatography on silica gel afforded **13** (R_1 = O) (2.5 mg, 30%), identical with an authentic sample.

*19′-Oxovinblastine (**16**, R = CO_2CH_3, R_1 = OH, R_2 = O)*

Iodine (20 mg) was added to a mixture of vinblastine (**15**, R = CO_2CH_3, R_1 = OH) (18 mg) and sodium bicarbonate

Can. J. Chem. Downloaded from www.nrcresearchpress.com by 210.87.254.105 on 09/05/12
For personal use only.

(20 mg) in aqueous 70% tetrahydrofuran (4 ml). The mixture was stirred at ambient temperature for 10 min, diluted with saturated sodium bicarbonate solution (4 ml), and extracted with dichloromethane. The organic phase was washed with 10% sodium bisulphite solution, dried (Na_2SO_4), and concentrated *in vacuo*. Chromatography on silica gel gave **16** (R = CO_2CH_3, R_1 = OH, R_2 = O) (6 mg, 33%) as a foam from methanol; uv λ_{max}: 311 (sh, 3.74), 294 (3.99), 285 (4.02), 259 (4.14), 213 (4.69); ir ν_{max}: 3475, 1740, 1640; ^{1}Hmr δ: 8.06 (1H, bs, —N—*H*), 7.54 (1H, m, $C_{14'}$-*H*), 7.20 (3H, m, $C_{11',12',13'}$-*H*), 6.68 (1H, s, C_{14}-*H*), 6.18 (1H, s, C_{17}-*H*), 5.91 (1H, dd, *J* = 3.5, 10.5 Hz, C_7-*H*), 5.54 (1H, s, C_4-*H*), 5.34 (1H, d, *J* = 10.5 Hz, C_6-*H*), 4.70 (1H, m, $C_{2'}$-*H*), 3.82 (3H, s, —CO_2CH_3), 3.80 (3H, s, —CO_2CH_3), 3.60 (3H, s, —OCH_3), 2.75 (3H, s, —NCH_3), 2.12 (3H, s, —$OCOCH_3$), 0.87 (6H, bt, *J* = 7.5 Hz, 2 × —CH_2CH_3); ms *m/e* 824 (M^+), 765, 665, 135 (base peak). High resolution molecular weight determination calcd. for $C_{46}H_{56}N_4O_{10}$: 824.3996; found: 824.3971. *Anal.* calcd. for $C_{46}H_{56}N_4O_{10}\cdot CH_3OH$:[3] C 65.89, H 7.01, N 6.54; found: C 65.14, H 7.20, N 6.60.

*19'-Oxoleurosidine (**18**, R = CO_2CH_3, R_1 = OH, R_2 = O)*

Oxidation of leurosidine (**17**, R = CO_2CH_3, R_1 = OH), as described above for the oxidation of vinblastine, gave the lactam (**18**, R = CO_2CH_3, R_1 = OH, R_2 = O) (62%) as a clear glass mp 196–210°C; uv λ_{max}: 309 (sh, 3.74), 294 (4.00), 285 (4.04), 262 (4.11), 214 (4.66); ir ν_{max}: 3477, 1738, 1644; ^{1}Hmr δ: 8.07 (1H, bs, —N*H*), 7.51 (1H, m, $C_{14'}$-*H*), 7.16 (3H, m, $C_{11',12',13'}$-*H*), 6.63 (1H, s, C_{14}-*H*), 6.16 (1H, s, C_{17}-*H*), 5.88 (1H, dd, *J* = 10, 4 Hz, C_7-*H*), 5.50 (1H, s, C_4-*H*), 5.32 (1H, bd, *J* = 10 Hz, C_6-*H*), 4.73 (1H, m, $C_{2'}$-*H*), 3.82 (6H, s, 2 × —CO_2CH_3), 3.60 (3H, s, —OCH_3), 2.74 (3H, s, —NCH_3), 2.11 (3H, s, —$OCOCH_3$), 1.17 (3H, t, *J* = 7.5 Hz, —CH_2CH_3), 0.96 (3H, t, *J* = 7.5 Hz, —CH_2CH_3); ms *m/e* 824 (M^+), 765, 282, 135 (base peak). High resolution molecular weight determination calcd. for $C_{46}H_{56}N_4O_{10}$: 824.3996; found: 824.3953.

*19'-Oxoleurosine (**13**, R = CO_2CH_3, R_1 = O)*

Oxidation of leurosine (**8**, R = CO_2CH_3) as described above gave the lactam (**13**, R = CO_2CH_3, R_1 = O) (56%) as a foam from methanol; uv λ_{max}: 309 (sh, 3.74), 294 (4.00), 284 (4.05), 262 (4.13), 214 (4.66); ir ν_{max}: 3470, 1738, 1644; ^{1}Hmr δ: 8.06 (1H, bs, —N*H*), 7.57 (1H, m, $C_{14'}$-*H*), 7.18 (3H, m, $C_{11',12',13'}$-*H*), 6.65 (1H, s, C_{14}-*H*), 6.19 (1H, s, C_{17}-*H*), 5.90 (1H, dd, *J* = 10.5, 3.5 Hz, C_7-*H*), 5.51 (1H, s, C_4-*H*), 5.33 (1H, bd, *J* = 10.5 Hz, C_6-*H*), 4.76 (1H, m, $C_{2'}$-*H*), 3.85 (3H, s, —CO_2CH_3), 3.83 (3H, s, —CO_2CH_3), 3.63 (3H, s, —OCH_3), 3.04 (1H, d, *J* = 3.5 Hz, $C_{3'}$-*H*), 2.76 (3H, s, —NCH_3), 2.12 (3H, s, —$OCOCH_3$), 1.01 (3H, t, *J* = 7.5 Hz, —CH_2CH_3), 0.84 (3H, t, *J* = 7.5 Hz, —CH_2CH_3); ms *m/e* 822 (M^+), 763, 282, 135 (base peak). High resolution molecular weight determination calcd. for $C_{46}H_{54}N_4O_{10}$: 822.3839; found: 822.3806. *Anal.* calcd. for $C_{46}H_{54}N_4O_{10}\cdot CH_3OH$:[3] C 66.04, H 6.80, N 6.56; found: C 65.26, H 6.91, N 6.76.

*5'-Oxoleurosine (**14**, R_1 = O)*

(*a*) A solution of leurosine (**8**) (30 mg) in tetrahydrofuran (2 ml) containing aqueous 1% trifluoroacetic acid (0.2 ml) was stirred in the presence of air for 11 days. The mixture was diluted with saturated sodium bicarbonate solution (5 ml) and extracted with dichloromethane. The organic layer was dried (Na_2SO_4) and concentrated *in vacuo*. Chromatography on silica gel gave leurosine (4 mg) and the lactam (**14**, R_1 = O) (4 mg, 15%) as a clear glass, mp 185–191°C; uv λ_{max}: 307 (3.91), 290 (4.04), 283 (4.06), 263 (4.15), 215 (4.70); ir ν_{max}: 3425, 1738, 1681, 1652; ^{1}Hmr δ: 8.16 (1H, bs, —N*H*), 6.88 (1H, s, C_{14}-*H*), 5.99 (1H, s, C_{17}-*H*), 5.32 (1H, bd. *J* = 10.5 Hz, C_6-*H*), 3.80 (6H, s, 2 × —OCH_3), 3.70 (3H, s, —OCH_3), 2.68 (3H, s, —NCH_3), 2.10 (3H, s, —$OCOCH_3$), 0.70 (3H, t, *J* = 7.5 Hz, —CH_2CH_3), 0.40 (3H, t, *J* = 7.5 Hz, —CH_2CH_3); ms *m/e* 822 (M^+), 662, 149, 135 (base peak). High resolution molecular weight determination calcd. for $C_{46}H_{54}N_4O_{10}$: 822.3839; found: 822.3915. *Anal.* calcd. for $C_{46}H_{54}N_4O_{10}$: C 67.15, H 6.57, N 6.81; found: C 66.51, H 6.55, N 6.87.

(*b*) Oxidation of (**7**) as described above in (*a*) gave the lactam (**14**, R_1 = O), (34%), identical with that obtained earlier.

Acknowledgments

Financial aid from the National Research Council of Canada and from Contract NO1-CM-23223, National Cancer Institute, National Institutes of Health, Bethesda, Maryland, is gratefully acknowledged. We are grateful to the Lilly Research Laboratories for supplies of catharanthine and vindoline and a sample of leurosine.

1. J. P. KUTNEY, J. BECK, F. BYLSMA, J. COOK, W. J. CRETNEY, K. FUJI, R. IMHOF, and A. M. TREASURYWALA. Helv. Chim. Acta, **58**, 1690 (1975).
2. J. P. KUTNEY, A. H. RATCLIFFE, A. M. TREASURYWALA, and S. WUNDERLY. Heterocycles, **3**, 639 (1975).
3. J. P. KUTNEY, T. HIBINO, E. JAHNGEN, T. OKUTANI, A. H. RATCLIFFE, A. M. TREASURYWALA, and S. WUNDERLY. Helv. Chim. Acta, **59**, 2858 (1976).
4. J. P. KUTNEY, G. H. BOKELMAN, M. ICHIKAWA, E. JAHNGEN, A. V. JOSHUA, P. H. LIAO, and B. R. WORTH. Can. J. Chem. **55**, 3227 (1977).
5. J. P. KUTNEY, G. H. BOKELMAN, A. V. JOSHUA, P. LIAO, and B. R. WORTH. Can. J. Chem. **55**, 3235 (1977).
6. W. F. BRILL. J. Am. Chem. Soc. **85**, 141 (1963).
7. W. F. BRILL and N. INDICTOR. J. Org. Chem. **29**, 710 (1964).
8. N. INDICTOR and W. F. BRILL. J. Org. Chem. **30**, 2074 (1965).
9. M. N. SHENG and J. G. ZAJACEK. Advan. Chem. Ser. **76**, 418 (1968).
10. J. P. KUTNEY, W. J. CRETNEY, J. R. HADFIELD, E. S. HALL, and V. R. NELSON. J. Am. Chem. Soc. **92**, 1704 (1970).
11. J. P. KUTNEY and F. BYLSMA. Helv. Chim. Acta, **58**, 1672 (1975).
12. P. POTIER, N. LANGLOIS. Y. LANGLOIS, and F. GUERITTE. Chem. Commun. 670 (1975).
13. N. LANGLOIS, F. GUERITTE, Y. LANGLOIS, and P. POTIER. J. Am. Chem. Soc. **98**, 7017 (1976).
14. W. E. JONES and G. J. CULLIVAN. U.S. Patent No. 3,887,565; Chem. Abstr. **83**, 97687d (1975).
15. J. P. KUTNEY and B. R. WORTH. Heterocycles, **4**, 1777 (1976).
16. E. WENKERT, E. W. HAGSMAN, B. LAL, G. E. GUTOWSKI, A. S. KATNER, J. C. MILLER, and N. NEUSS. Helv. Chim. Acta, **58**, 1560 (1975).
17. J. P. KUTNEY, G. H. BOKELMAN, M. ICHIKAWA, E. JAHNGEN, A. V. JOSHUA, P. LIAO, and B. R. WORTH. Heterocycles, **4**, 1267 (1976).
18. Y. LANGLOIS, N. LANGLOIS, P. MANGENEY, and P. POTIER. Tetrahedron Lett. 3945 (1976).
19. J. P. KUTNEY, J. BALSEVICH, G. H. BOKELMAN, T. HIBINO, I. ITOH, and A. H. RATCLIFFE. Heterocycles, **4**, 997 (1976); J. P. KUTNEY, J. BALSEVICH, and G. H. BOKELMAN. Heterocycles, **4**, 1377 (1976).

Synthesis of substituted thietanes and thiolanes from α- and β-chloroepoxides and their oxidation to 1,1-dioxides

FRANK S. ABBOTT AND KATSUJI HAYA

Faculty of Pharmaceutical Sciences, University of British Columbia, Vancouver, B.C., Canada V6T 1W5

Received June 16, 1977

FRANK S. ABBOTT and KATSUJI HAYA. Can. J. Chem. **56**, 71 (1978).

Treatment of 3-chloro-1-phenylpropylene oxide-1,2 (**7**) or 1-chloro-4-phenylbutylene oxide-3,4 (**8**) with H_2S saturated ethanolic NaOEt gave 3-hydroxy-2-phenylthietane (**9**) and 3-hydroxy-2-phenylthiolane (**10**) respectively. A similar treatment of 3-chloro-2-phenylpropylene oxide-1,2 (**12**) at low temperatures gave 3-chloro-2-hydroxy-2-phenylpropanethiol (**13**); at reflux temperatures or by refluxing **13** in ethanolic NaOEt, 3-hydroxy-3-phenylthietane (**14**) was formed.

Oxidation of **9**, **10**, and **14** with *m*-chloroperbenzoic acid or H_2O_2–HOAc gave the respective 1,1-dioxides **19**, **20**, and **25**. The alcohols **19** and **20** were dehydrated to their corresponding cyclic olefins through the benzylsulfonate esters. Under the conditions of the Ritter reaction **25** dehydrated to the cyclic olefin. Treatment of **19** with mineral acid gave benzyl methyl ketone, while refluxing **19** in base gave benzyl methyl sulfone. Ethoxylation of 2-phenylthiete 1,1-dioxide (**23**) to the 3-ethoxy derivative **34** was achieved under basic conditions. Attempted chlorination of **9** resulted in desulfurization to 3-chloropropenylbenzene (**5**).

FRANK S. ABBOTT et KATSUJI HAYA. Can. J. Chem. **56**, 71 (1978).

Les réactions du chloro-3 phényl-1 propylèneoxyde-1,2 (**7**) ou du chloro-1 phényl-4 butylène-oxyde-3,4 (**8**) avec du NaOEt éthanolique saturé par H_2S conduisent respectivement à l'hydroxy-3 phényl-2 thiétane (**9**) et à l'hydroxy-3 phényl-2 thiolane (**10**). Un traitement similaire du chloro-3 phényl-2 propylèneoxyde-1,2 (**12**) à basse température conduit au chloro-3 hydroxy-2 phényl-2 propanethiol (**13**); si l'on effectue les réactions au reflux ou si l'on porte **13** au reflux dans du NaOEt éthanolique, il se forme de l'hydroxy-3 phényl-3 thiétane (**14**).

Les oxydations de **9**, **10** et **14** par de l'acide *m*-chloroperbenzoique ou par H_2O_2–HOAc conduisent respectivement aux dioxydes **19**, **20** et **25**. On a déshydraté les alcools **19** et **20** pour obtenir les oléfines cycliques correspondantes par l'intermédiaire de leurs esters benzylsulfonates. Dans des conditions de la réaction de Ritter, **25** se déshydrate pour conduire à une oléfine cyclique. Le traitement de **19** par des acides minéraux conduit à la méthylbenzylcétone alors que le traitement de **19** par de la base au reflux fournit de la méthylbenzylsulfone. On a pu effectuer l'éthoxylation de la phényl-2 thiètedioxyde-1,1 (**23**) conduisant au dérivé éthoxy-3 **34** en travaillant dans des conditions basiques. Des essais de chloruration de **9** ont conduit à sa désulfurisation en chloro-3 propénylbenzène (**5**).

[Traduit par le journal]

Introduction

Several 2-phenyl substituted thietanes were required as intermediary compounds for the synthesis of small ring sulfur compounds of pharmacological interest. Although 2-phenylthietane 1,1-dioxides can be readily prepared, their reduction to 2-phenylthietanes has not been accomplished (1). The exposure of 3-chloropropylene oxide-1,2 (**1**) to a saturated solution of H_2S in $Ba(OH_2)$ gave 3-thietanol (**2**) (2) (Scheme 1), and the application of this procedure to aromatic epoxides seemed to be the most likely route to 2-phenyl substituted thietanes.

Included in this study are a number of experiments which were performed to investigate the chemical properties of substituted thietanes and thiolanes.

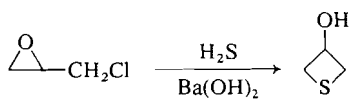

1 **2**

SCHEME 1. Preparation of 3-thietanol

Results and Discussion

The nmr spectrum of commercially available 3-chloropropenylbenzene (**5**) was attributable to that of pure *trans*-**5** (J_{ab} = 16 Hz) (3). As expected the epoxidation of **5** with monoperphthalic acid gave only *trans*-3-chloro-1-phenylpropylene oxide-1,2 (**7**) (Scheme 2); the nmr spectrum showed a coupling constant (J_{ab} = 2 Hz) in agreement with spectra of *trans* substituted epoxides (3). Exposure of **7** to a saturated solution of H_2S in NaOEt gave a highly unstable crystalline material, which decomposed in a few days if left exposed to the atmosphere at room temperature. However, it could be stored at −15°C under nitrogen for at least 1 year without any detectable decomposition. This product proved to be 3-hydroxy-2-phenylthietane (**9**).

Can. J. Chem. Downloaded from www.nrcresearchpress.com by 210.87.254.6 on 09/05/12
For personal use only.

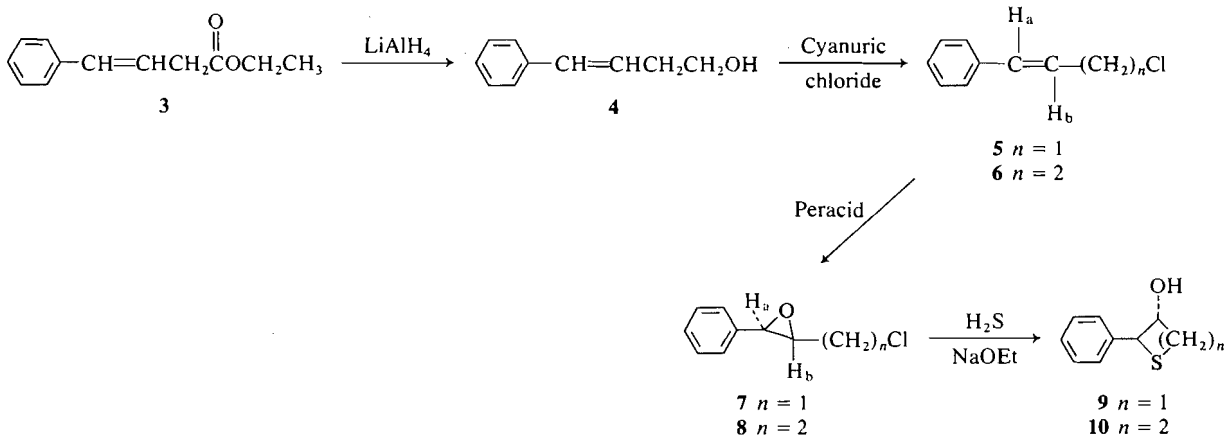

SCHEME 2. Synthetic scheme to 3-hydroxy-2-phenylthietane (**9**) and 3-hydroxy-2-phenylthiolane (**10**)

Reduction of ethyl-*trans*-4-phenyl-3-butenoate (**3**) with $LiAlH_4$ in anhydrous ether gave pure *trans*-4-phenyl-3-buten-1-ol (**4**) (4, 5). Chlorination of **4** with cyanuric chloride (6) at 100°C gave 1-chloro-4-phenyl-3-butene (**6**). The ir spectrum of **6** showed a strong absorption at 975 cm^{-1} and the nmr spectrum showed a vicinal coupling constant, J_{ab} of 16 Hz, both indicative of a *trans* configuration for **6**. Epoxidation of **6** with monoperphthalic acid gave a mixture of *cis*- and *trans*-1-chloro-4-phenylbutylene oxide-3,4 (**8**). A glc analysis of the mixture indicated it to be 70% *trans*-**8** and 30% *cis*-**8**. A pure sample of the *cis*-isomer was obtained by preparative glc and the pure *trans*-isomer was obtained by fractional distillation. The nmr spectrum of *trans*-**8** showed the expected coupling constant (2.5 Hz) for H_aH_b (3). In the nmr spectrum of the *cis*-isomer the peaks due to the ring protons were not sufficiently separated to allow determination of the coupling constants for H_aH_b. From the exposure of *trans*-**8** to a saturated solution of H_2S in ethanolic NaOEt, only 3-hydroxy-2-phenylthiolane (**10**) was isolated.

Treatment of 1,3-dichloro-2-phenylpropan-2-ol (**11**) with base gave 3-chloro-2-phenylpropylene oxide-1,2 (**12**) (Scheme 3). Reaction of **12** with a saturated solution of H_2S in NaOEt gave 3-hydroxy-3-phenylthietane (**14**), a light yellow foul smelling liquid, which has previously been prepared from the reaction of phenylmagnesium bromide with 3-thietanone (7). On the other hand, treatment of the epoxide **12** with a $Ba(OH_2)$ or NaOH solution saturated with H_2S required heating at 80°C to give the thietane **14**. At temperatures of 50°C or less the main product was 3-chloro-2-phenylpropanethiol (**13**). Refluxing the thiol **13** in ethanolic NaOH gave the thietane **14**.

The mechanism for the formation of these heterocyclic sulfur compounds from epoxy halides is described in Scheme 4. Epoxide **7** is used as the example. Nucleophilic attack by sulfhydride ion initially opens the epoxide ring to an intermediate **15** which can then cyclize by nucleophilic displacement of chloride ion. An alternative mechanism whereby sulfhydride ion initially replaces the chloride ion by an S_N2 reaction followed by a ring closure step involving attack on the epoxide seems far less likely. In an analogous system where this latter mechanism has been invoked (8) no compelling evidence was given to substantiate this route. Isolation of the acyclic thiol **13** at the lower reaction temperatures is certainly supportive of the mechanism given in Scheme 4, as were similar results reported for epichlorohydrin reactions with H_2S (9).

Products **9**, **10**, and **14** obtained from the epoxide reactions in the present work appear generally consistent with ring opening reactions of epoxides (9, 10). Under alkaline conditions nucleophilic attack of unsymmetrical epoxides occurs selectively at the less-substituted carbon atom. In the case of **12** the

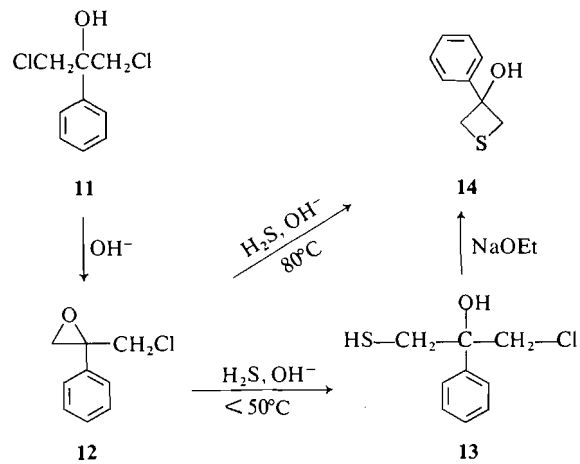

SCHEME 3. Routes to 3-hydroxy-3-phenylthietane

Can. J. Chem. Downloaded from www.nrcresearchpress.com by 210.87.254.6 on 09/05/12
For personal use only.

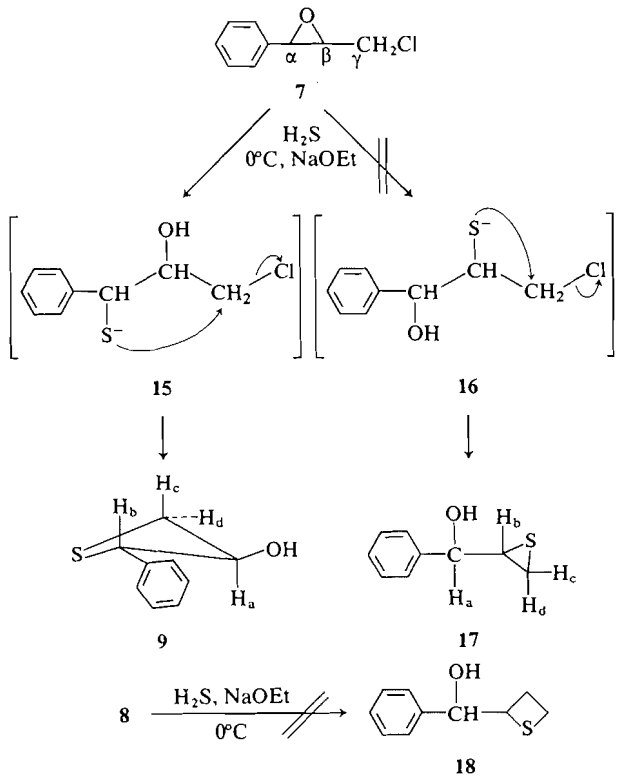

SCHEME 4. Proposed mechanism for the reaction of epoxide with sulfhydride ion

compounds **13** and **14** derived from the ring opening reaction (Scheme 3) are therefore readily predictable. For the epoxides **7** and **8**, however, ring opening at either the α- or β-carbon atom seemed initially to be quite feasible. Hence attack by the sulfur nucleophile at the β-carbon atom of **7** (Scheme 4) to give the intermediate **16**, should also give the thiirane **17**. A similar mechanism for **8** would give the thietane **18**. No evidence was obtained for the presence of either **17** or **18** in the respective reaction mixtures. While the instability of a thiirane could have precluded its isolation, such would not be the case with a thietane such as **18**. This observed predominant, if not exclusive, attack of the sulfur nucleophile at the α-carbon of epoxides **7** and **8** can also be explained in part on the basis of steric effects. But an additional factor is operative with these epoxides, which complements the direction of ring opening favored by the steric considerations. Conjugative effects of the aromatic ring, by stabilizing carbonium ion characteristics at the benzylic carbon atom, would also favor α-attack by an S_N1-type fission (11). For example the isomer ratio of primary and secondary alcohols obtained from the ring opening reaction of styrene oxide by sodium benzene – thiolate in methanol was found to be quite sensitive to *para* substituent effects in the styrene oxide (11).

It follows from the proposed mechanism of the reaction that *trans* substituted epoxides would lead to *trans* substituted thietanes and thiolanes. Because of complexities in the nmr spectra, configurations were not assigned for **9** and **10**. Other evidence supports the *trans* configuration for **9** and **10** (see later).

Infrared, nmr and elemental analysis data of the compound isolated from the reaction of epoxide **7** with sulfhydride ion did not conclusively differentiate between the thietane **9** and the thiirane **17**. The mass spectrum of the product provided evidence in support of **9**. The major fragments at *m/e* 122 ($C_6H_5CHS^{\ddagger}$) the base peak and *m/e* 121 ($C_6H_5CS^+$) are indicative of a thietane (13). If the material isolated had been the thiirane **17**, then strong peaks at *m/e* 105 and 106 due to $(C_6H_5CO)^+$ and $(C_6H_5CHO)^{\ddagger}$ would be expected as these are relatively stable ions and should be readily formed from **17**. Final and conclusive proof of structure **9** was obtained through the conversion of **9** to 2-phenylthiete 1,1-dioxide (**23**) (Scheme 5), which was identical to a sample of **23** prepared by an alternate route (1).

The oxidation of **9** to 3-hydroxy-2-phenylthietane 1,1-dioxide (**19**) with *m*-chloroperbenzoic acid in the present study gave better yields (72% vs. 30–50%) than employing previously published (14, 15) procedures using H_2O_2–HOAc. On the other hand, the oxidation of the thiolane **10** with *m*-chloroperbenzoic acid gave the corresponding 1,1-dioxide **20** in only 27% yield. The oxidation of cyclic sulfides with *m*-chloroperbenzoic acid to the corresponding sulfones, however, appears to be a superior method, particularly from the point of view of safety (16, 17).

The nmr data for **19** and **20** indicated a *trans* configuration between the phenyl and the hydroxyl substituents. In the preferred conformations both groups are equatorial. Assuming Karplus correlations are reliable here (as they are with certain thietane 1,1-dioxides (18, 19)), the coupling constant (6.5 Hz) for H_aH_b in **19** (Scheme 5) indicates a *trans* diaxial interaction. If the protons were in a *cis* relationship, the coupling constants would be expected to be smaller, the dihedral angle being near 90° in the puckered ring. This is supported by the coupling constants observed for the H_a proton with the methylene protons at C-4. The coupling constants were 7.0 and 2.5 Hz which are due to *trans* (diaxial) and *cis* (axial–equatorial) interaction of the protons respectively. The coupling constants of the methylene protons are similar to those found in 3-acetoxy-

Can. J. Chem. Downloaded from www.nrcresearchpress.com by 210.87.254.6 on 09/05/12
For personal use only.

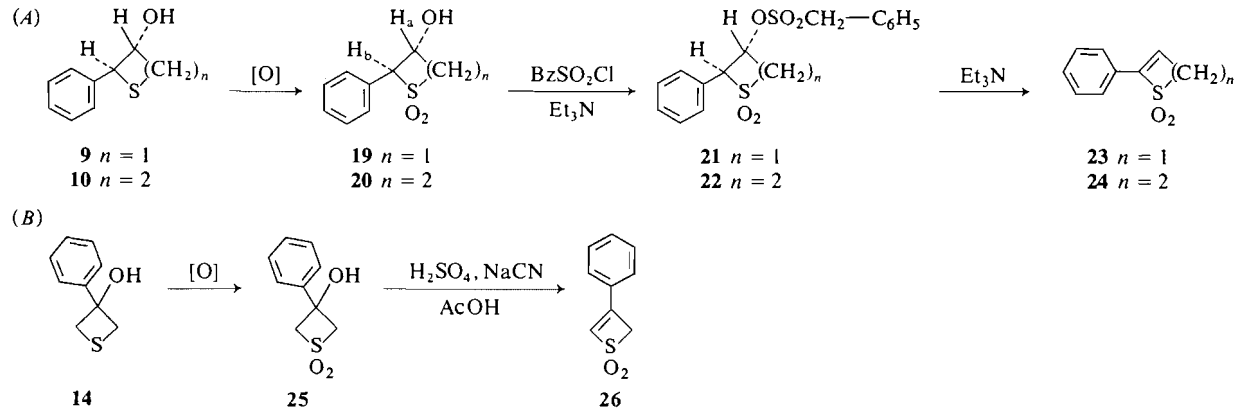

9 $n = 1$ **10** $n = 2$ **19** $n = 1$ **20** $n = 2$ **21** $n = 1$ **22** $n = 2$ **23** $n = 1$ **24** $n = 2$

14 **25** **26**

SCHEME 5. Oxidation of thietane and thiolane; elimination reactions of the 1,1-dioxides

thietane 1,1-dioxide, which was shown to have dihedral angles between the C-3 proton and the methylene protons of 109° and 28° and J values of 3.5 and 8 Hz respectively (20). With **20** the observed coupling constant for H_aH_b (9 Hz) was indicative of an interaction of the protons in a five-membered ring (3). The *trans* relationship of the phenyl and hydroxyl groups in **19** and **20** provides evidence that these substituents were *trans* in **9** and **10**, since the oxidation reaction should not affect the configuration of the compounds. This is the expected relationship from the proposed mechanism for the synthesis of **9** and **10**.

The cyclic sulfones **19** and **20** were dehydrated using triethylamine treatment of the benzylsulfonate esters **21** and **22** (Scheme 5), a method reported for the dehydration of 3-hydroxythietane 1,1-dioxide (21). Under the acidic conditions of the Ritter reaction (see ref. 22 for original references) (Scheme 5) the tertiary alcohol **25** readily dehydrates. Two main components were isolated, 3-phenylthiete 1,1-dioxide (**26**) (23) and a small hexane soluble portion which showed a carbonyl absorption in the ir (1755 cm^{-1} strong), but was not further characterized.

The attempted dehydration of **19** with 85% H_3PO_4 or concentrated H_2SO_4 in glacial acetic acid resulted in the formation of benzyl methyl ketone (**30**) a rather novel reaction in terms of thietane chemistry. This acid catalyzed desulfurization and ring cleavage is postulated to proceed by the mechanism[1] outlined in Scheme 6. Protonation of the sulfone **19** results in the formation of the protonated epoxide **27**, which under the acid conditions rapidly undergoes solvolysis to the glycol **28**. 1-Phenyl-1,2-propanediol under the present conditions has been shown to be converted to benzyl methyl ketone (**30**) (24, 25). Similarly the glycol **28** could give the unstable β-ketosulfinic acid **29** which desulfonates to the ketone **30** (cf. decarboxylation of β-ketocarboxylic acids).

When **19** was heated at reflux in 20% NaOH and then cooled, a 70% yield of benzyl methyl sulfone (**33**) precipitated from the reaction mixture. This type of ring cleavage is well known for thiete 1,1-dioxides (1, 26) and for 3-alkoxythietane 1,1-dioxides (27). The mechanism proposed for the thiete 1,1-dioxides involves a reverse aldol condensation proceeding through an intermediate analogous to **31**, and the ring opened aldehyde **32** (Scheme 7). The isolation of **33** from the base treatment of **19** may be interpreted as supporting this previously proposed mechanism.

Exposure of 2-phenylthiete 1,1-dioxide (**23**) to alcoholic KOH at room temperature results in the addition product, 3-ethoxy-2-phenylthietane 1,1-dioxide (**34**). This is typical of other thiete 1,1-dioxides which have been shown to undergo Michael addition of nucleophiles (26, 28, 29).

When **9** was treated with thionyl chloride in dry $CHCl_3$ (30) the expected 3-chloro-2-phenylthietane (**35**) was not isolated. Distillation of the crude product gave a 48% yield of 3-chloropropenylbenzene (**5**). Thionyl chloride with pyridine or 2,4,6-collidine has been used to chlorinate 3-thietanol 1,1-dioxide (2, 17), but this method resulted in isolation of polymeric material when attempted with **9**. Dehydrohalogenation of 3-chlorothietane 1,1-dioxide to thiete 1,1-dioxide was found to readily occur in base (2). In the attempted chlorination of **9**, it is possible that **35** was formed, but the pyridine or 2,4,6-collidine was sufficiently basic to cause dehydrohalogenation to 2-phenylthiete. Since thietes are known to be unstable compounds and spontaneously polymerize (31, 32) this may explain the

[1]This mechanism developed from the suggestion of a referee and while the initial protonation of the sulfone is less favoured than protonation of the hydroxyl, if the steps are rapid and irreversible, this could be the pathway.

Can. J. Chem. Downloaded from www.nrcresearchpress.com by 210.87.254.6 on 09/05/12
For personal use only.

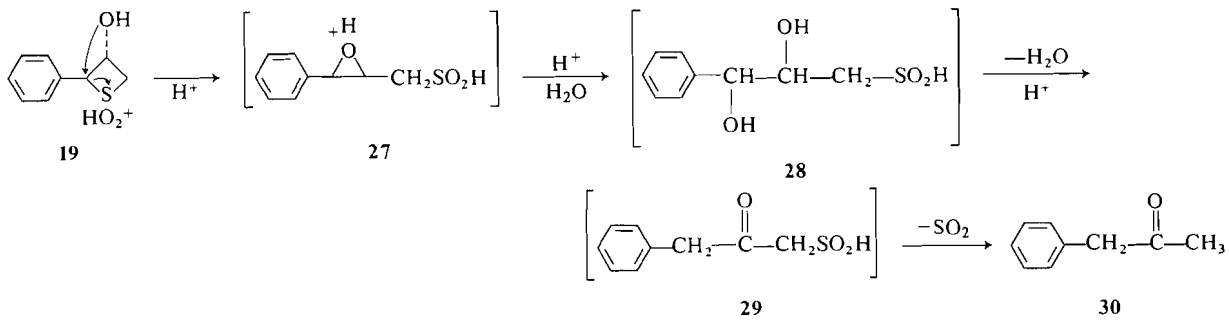

SCHEME 6. Proposed mechanism for the acid catalyzed desulfonation of 3-hydroxy-2-phenylthietane 1,1-dioxide (**19**)

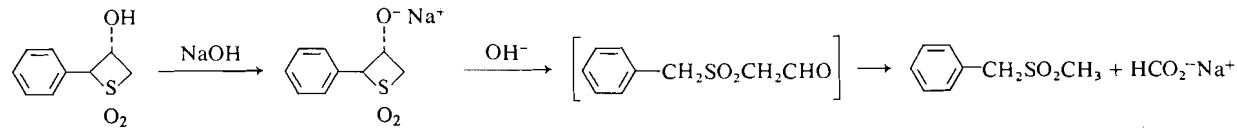

(*A*) 3-Hydroxy-2-phenylthietane 1,1-dioxide (**19**)

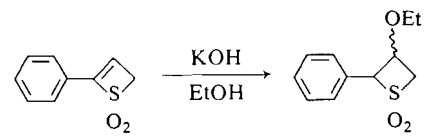

(*B*) 2-Phenylthiete 1,1-dioxide (**23**)

SCHEME 7. Effect of base on thietane 1,1-dioxides

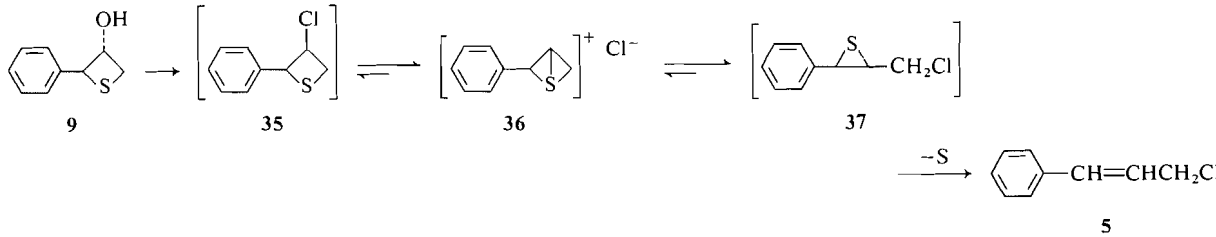

SCHEME 8. Proposed route of desulfurization of 3-hydroxy-2-phenylthietane (**9**)

isolation of polymeric material. Cyanuric chloride has been reported as a convenient chlorinating reagent for alcohols, possessing the advantage that it requires no added base (6). When **9** was treated with cyanuric chloride, again **5** and polymer were obtained. Since the treatment of 3-chlorothietane with triphenylphosphine results in desulfurization and is thought to occur via a sulfonium ion to allyl chloride (33), the desulfurization of **9** may proceed through a similar pathway (Scheme 8). Thus chlorination of **9** results in the rearrangement of **35** through the sulfonium ion **36** to 3-chloromethyl-2-phenylthiirane (**37**). Aromatically substituted thiiranes readily lose elemental sulfur to give the corresponding olefin (12), and thus would explain the isolation of **5**. Several other attempts have been made to displace the —OH in **9** including the use of a crude benzylsulfonate ester and all have proved unsuccessful.

Experimental

Melting points were determined using a Thomas-Hoover capillary melting point apparatus. All melting and boiling points are reported uncorrected. Infrared spectra were recorded on a Beckman IR-10 spectrophotometer, the nmr spectra on a Varian A-60 spectrophotometer, and ms spectra on a Varian MAT-111 GC/MS. The concentrations of the nmr solutions were approximately 10% and trimethylsilane served as the internal standard. Gas–liquid chromatography was carried out using a MicroTek gas chromatograph model MT-200 equipped with a flame ionization detector and a Disc Integrator model 222. Preparative glc was carried out with a Beckman model GC-2 gas chromatograph equipped with a

Can. J. Chem. Downloaded from www.nrcresearchpress.com by 210.87.254.6 on 09/05/12
For personal use only.

Can. J. Chem. Downloaded from www.nrcresearchpress.com by 210.87.254.6 on 09/05/12
For personal use only.

thermoconductivity detector. Microanalyses were performed by Alfred Bernhardt, Microanalytisches Laboratorium, West Germany.

trans-*3-Chloro-1-phenylpropylene Oxide-1,2 (7)*

Freshly distilled 3-chloropropenylbenzene (**5**) (60.84 g, 0.4 mol) (Aldrich) was added to a 500 ml ether solution of monoperphthalic acid (105 g, 0.58 mol) (34).[2] The solution was filtered and washed with 150 ml portions of saturated Na_2CO_3 solution until the washings remained basic. The ether portion was washed with 100 ml of H_2O, dried, and concentrated under vacuum. The resulting yellow oil was vacuum distilled with the aid of Vigreaux stillhead to give 47 g (70% yield) of a colourless liquid: bp 69°C (0.5 Torr) (lit. (35) bp 67°C, 0.3 Torr); ir (neat): 890, 940, 1275 cm^{-1} (epoxide); nmr ($CDCl_3$) δ: 3.22 (dt, 1, J = 2, 5 Hz, CH), 3.64 (d, 2, J = 5 Hz, CH_2Cl), 3.77 (d, 1, J = 2 Hz, ArCH), and 7.30 (m, 5, *Ar*).

3-Hydroxy-2-phenylthietane (9)

Sodium metal (6.13 g, 0.266 g-at.) was added in small fragments to 250 ml of absolute EtOH. When the sodium had completely reacted, the solution was cooled to 0–5°C and saturated with H_2S (Matheson) by bubbling the H_2S through the cooled solution for 1 h. After the 3-chloro-1-phenylpropylene oxide-1,2 (7) (22.27 g, 0.132 mol) was added dropwise over a period of 1 h the H_2S was shut off. A white precipitate began to form almost immediately. The reaction was stirred at 0–5°C for 12 h, filtered, and concentrated under vacuum at room temperature to approximately $\frac{1}{4}$ the original volume, diluted with 200 ml of H_2O, and extracted with 3 × 150 ml of $CHCl_3$. The $CHCl_3$ extracts were pooled, washed with 150 ml of H_2O, dried, and concentrated under vacuum. The yellow oil which remained was solidified by scratching with a glass rod. This solid residue was extracted with successive portions of hot hexane leaving a yellow hexane insoluble gum in the flask. Upon cooling the combined fractions, 13.77 g (62.5% yield) of white needle-like crystals precipitated, mp 52–54°C (56.5–57.5°C upon further recrystallization from hexane); ir (KBr): 1065, 3220, 3310 cm^{-1} (alcohol); nmr ($CDCl_3$) δ: 2.68 (s, 1, OH), 3.17 (dd, 2, J = 1.5, 6 Hz, SCH_2), 4.62 (m, 2, ArCHCH-OH), 7.34 (m, 5, *Ar*); ms *m/e*: 166 (molecular ion), 122 ($(C_6H_5CHS)^+$ base peak), 121 ($(C_6H_5CS)^+$), 91 ($(C_7H_7)^+$), 77 ($(C_6H_5)^+$). *Anal.* calcd. for $C_9H_{10}OS$ (166.3): C 65.02, H 6.06, S 19.29; found: C 64.86, H 5.92, S 19.19.

If the crystals were left at room temperature in contact with the atmosphere, the crystals completely decomposed into a yellow gum within a few days. Storage in a tightly capped container at −15°C under N_2 showed no detectable decomposition after 1 year.

3-Chloro-2-hydroxy-2-phenylpropanethiol (13)

A solution of NaOH (4.8 g, 0.12 mol) in 150 ml of H_2O at 0–5°C was saturated with H_2S. After the dropwise addition of 3-chloro-2-phenylpropylene oxide-1,2 (**12**) (10 g, 0.06 mol) (36), the H_2S was shut off and the reaction mixture was stirred at room temperature for 2 h, then extracted with 3 × 50 ml of ether. The pooled ether extracts were washed with 50 ml of H_2O, dried, and concentrated under vacuum. The residual oil was vacuum distilled and the fraction boiling at 80–85°C (0.05 Torr) was collected. Redistillation through a Vigreaux stillhead gave 8.0 g (65% yield) of a colourless liquid, bp 85°C (0.05 Torr); n_D^{20} 1.5851; ir (neat): 2560 (thiol), 3500 cm^{-1} (alcohol). *Anal.* calcd. for $C_9H_{11}ClOS$ (202.7): C 53.32, H 5.47; found: C 53.57, H 5.53.

3-Hydroxy-3-phenylthietane (14)

(*a*) Using the same procedure as described for (**9**), a solution of sodium (2.76 g, 0.12 g-at.) and H_2S in 200 ml of absolute EtOH was reacted with 3-chloro-2-phenylpropylene oxide-1,2 (**12**) (10 g, 0.06 mol). In this case, the reaction was refluxed for 3 h, cooled, and worked up as previously described for **9**. The residual oil was vacuum distilled to give 7.2 g (36% yield) of a liquid; bp 90–95°C (0.1 Torr). Redistillation gave a yellow liquid, bp 91–93°C (0.1 Torr); n_D^{20} 1.6048 (lit. (7) bp 110–112°C, (0.7 Torr); n_D^{23} 1.6039); ir: 3380 cm^{-1} (alcohol); nmr (CCl_4) δ: 3.52 (s, 4, CH_2SCH_2), 3.75 (s, 1, OH), 7.5 (m, 5, *Ar*). *Anal.* calcd. for $C_9H_{10}OS$ (166.2): C 65.02, H 6.06, S 19.29; found: C 64.86, H 5.96, S 18.96.

(*b*) The reaction was also carried out using aqueous NaOH or $Ba(OH_2)$ as described in the preparation of **13**, except heating at 80°C for 1 h is required. Yields of **14** are 30% or less. (At 50°C or less **13** is the main product.)

(*c*) A solution of sodium (1.5 g, 0.065 g-at.) in 75 ml of absolute EtOH was added dropwise to **13** (8.8 g, 0.043 mol) in 100 ml of absolute EtOH at reflux temperatures. The reaction mixture was refluxed for 4 h, cooled, and worked up as previously described for **9**. The yield of crude thietane **14** was 35%.

4-Phenyl-3-buten-1-ol (4)

Finely powdered $LiAlH_4$ (5.7 g, 0.15 mol) was stirred in 300 ml of Na dried ether for 24 h at room temperature and filtered in an N_2 atmosphere to give a translucent solution. The $LiAlH_4$ was added to a stirred solution of ethyl-4-phenyl-3-butenoate (**3**) (37)[3] (48.3 g, 0.254 mol) in 300 ml of Na dried ether at such a rate to maintain a gentle reflux. The mixture was refluxed for a further 2 h, cooled, and excess $LiAlH_4$ destroyed using 5.7 ml of H_2O, 5.7 ml of 20% NaOH, and 18.1 ml of H_2O. After filtration of the mixture, the ether fraction was separated, dried, and concentrated under vacuum. The residual yellow oil was vacuum distilled with a Vigreaux stillhead to give 28.46 g (77% yield) of a colourless liquid, bp 105–108°C (0.8 Torr) (lit. (4) 137–138°C (12 Torr); ir (neat): 970 (olefin), 1050, 3340 cm^{-1} (alcohol); nmr ($CDCl_3$) δ: 2.05 (s, 1, OH), 2.39 (q, 2, J = 6 Hz, $CHCH_2$), 3.67 (t, 2, J = 6 Hz, CH_2OH), 6.16 (dt, 1, J = 16, 6 Hz, $CHCH_2$), 6.48 (d, 1, J = 16 Hz, ArCH), 7.26 (m, 5, *Ar*).

1-Chloro-4-phenyl-3-butene (6)

Finely powdered cyanuric chloride (20 g, 0.108 mol) (Aldrich) was added in small portions to **4** (28.46 g, 0.192 mol) at 100°C (oil bath temperature). The suspension was heated for another 2 h, cooled, and filtered. The yellow filtrate was vacuum distilled to give 23 g (72% yield) of a clear colourless fraction, bp 98–104°C (0.65 Torr); ir (neat): 975, 3035 cm^{-1} (olefin); nmr ($CDCl_3$) δ: 2.67 (q, 2, J = 7 Hz, $CHCH_2$), 3.62 (t, 2, J = 7 Hz, CH_2Cl), 6.24 (dt, 1, J = 7, 16 Hz, $CHCH_2$), 6.54 (d, 1, J = 16 Hz, ArCH), 7.32 (m, 5, *Ar*).

1-Chloro-4-phenylbutylene Oxide-3,4 (8)

Using the same conditions as in the preparation of **7**, **6** (23 g, 0.138 mol) was reacted with monoperphthalic acid (34.6 g, 0.19 mol). Fractional distillation of the crude oil gave 2 fractions: (*a*) bp 96–105°C (0.8 Torr), (*b*) bp 105–108°C (0.8 Torr). Gas–liquid chromatographic analysis on a Chrom-

[2]The solution was prepared and standardized as described and concentrated to approximately 500 ml prior to use.

[3]Under the conditions of the Wittig reaction the double bond shifts from the 2 to the 3 position.

Can. J. Chem. Downloaded from www.nrcresearchpress.com by 210.87.254.6 on 09/05/12
For personal use only.

port-SE 30 (5%) column, with the oven temperature at 125°C and N_2 flow rate of 45 ml/min showed that (*a*) contained two components of R_t = 4 min (30%) and 6 min (60%), and (*b*) contained 2 components of R_t = 6 min (20%) and 11 min (80%). Preparative glc of (*a*) on a Carbowax column gave the material with the 6 min R_t in 90% purity. Fractional distillation of (*b*) gave pure samples of the materials with R_t = 6 min and 11 min. The R_t = 6 min was taken to be *cis*-**8**, bp 85–87°C (0.45 min); ir (neat): 1040, 1315 cm^{-1} (epoxide); nmr ($CDCl_3$) δ: 1.76 (dt, 2, J = 2, 7 Hz, $CHCH_2$), 2.60 (m, 2, $CHCH$), 3.54 (disturbed t, 2, J = 7 Hz, CH_2Cl), 7.2 (m, 5, *Ar*). The R_t = 11 min was taken to be *trans*-**8**: ir (neat) 895, 950, 1040, 1300 cm^{-1} (epoxide); nmr ($CDCl_3$) δ: 2.12 (m, 2, $CHCH_2$), 3.09 (dt, 1, J = 2.5, 5 Hz, $CHCH_2$), 3.66 (t, 2, J = 5.5 Hz, CH_2Cl), 3.68 (obscured d, 1, J = 2.5 Hz, ArC*H*), 7.26 (m, 5, *Ar*). Fractions (*a*) and (*b*) represented 21.67 g (86% yield) of **8**. In subsequent reactions the crude product upon glc analysis was indicated to be 70% *trans*-**8**.

*3-Hydroxy-2-phenylthiolane (**10**)*

The procedure was the same as outlined for **9**, using 5 g (27.4 mmol) of *trans*-**8**. The residual dark oil was vacuum distilled to give 2.6 g of a colourless liquid, bp 100–114°C (0.1 Torr); ir (neat): 1065, 3400 cm^{-1} (alcohol); nmr ($CDCl_3$) δ: 2.10 (m, 2, $CHCH_2$), 2.36 (s, 1, O*H*), 3.02 (m, 2, SCH_2), 4.32 (m, 2, ArC*H*CH), 7.35 (m, 5, *Ar*).

*3-Hydroxy-2-phenylthietane 1,1-Dioxide (**19**)*

A solution of 3-hydroxy-2-phenylthietane (**9**) (5 g, 0.03 mol) in 50 ml of $CHCl_3$ was added dropwise to a stirred solution of *m*-chloroperbenzoic acid (16.25 g of 80% purity, 0.08 mol) in 150 ml of $CHCl_3$. The resulting pale yellow solution was stirred at room temperature for a further 10 h. The precipitated *m*-chlorobenzoic acid was removed by suction filtration and the filtrate was concentrated under vacuum. The resulting residue was triturated with 3 × 150 ml of H_2O. The H_2O insoluble material was removed by suction filtration. The filtrates were pooled and the H_2O was removed under vacuum to give 5.1 g (85% yield) of a white solid: mp 75–77°C. Recrystallization from ether–petroleum ether (30–60°C) gave 4.39 g (71.5% yield) of white plate-like crystals, mp 76.2–78°C; ir (KBr): 1070, 3500 (alcohol), 1140, 1185, 1285 cm^{-1} (sulfone); nmr ($CDCl_3$), δ: 3.35 (br s, 1, OH), 4.05 (dd, 2, J = 2.5, 7 Hz, SCH_2), 4.70 (m, 1, C*H*OH), 5.30 (d, 1, J = 6.5 Hz, ArC*H*), 7.35 (m, 5, *Ar*); ms *m/e*: 198 (weak molecular ion), 134 ($(C_6H_5CHCHOHCH_2)^+$), 116 ($(C_6H_5CHCHCH)^+$), 105 ($(C_6H_5CO)^+$), 91 ($(C_7H_7)^+$ base peak), 77 ($(C_6H_5)^+$). *Anal.* calcd. for $C_9H_{10}O_3S$ (198.3): C 54.53, H 5.08, S 16.17; found: C 54.62, H 4.96, S 16.29.

*3-Hydroxy-3-phenylthietane 1,1-Dioxide (**25**)*

To a solution of 3-hydroxy-3-phenylthietane (**14**) (12.2 g, 0.07 mol) in 75 ml of 50:50 glacial AcOH–Ac_2O cooled to 0°C was added 30% H_2O_2 (20.67 g) dropwise. The reaction was then stirred at room temperature for 12 h. A small amount of Pd black was added to destroy excess peroxide. The mixture was filtered and the filtrate concentrated. Addition of H_2O to the residual oil caused the precipitation of a buff-coloured solid. The solid was collected by filtration and dried to give 12.5 g (86% yield) of crude product. Recrystallization from EtOH–hexane gave white crystals; mp 105°C; ir (KBr): 1150, 1305 (sulfone) (with splitting at 1160, 1265), 3450 cm^{-1} (alcohol). *Anal.* calcd. for $C_9H_{10}O_3S$ (198.3): C 54.53, H 5.08; found: C 54.38, H 4.99.

*3-Hydroxy-2-phenylthiolane 1,1-Dioxide (**20**)*

The procedure was the same as outlined for **19**. A solution of 3-hydroxy-2-phenylthiolane (**10**) (5 g, 27.8 mmol) in 50 ml of $CHCl_3$ was reacted with *m*-chloroperbenzoic acid (16.25 g of 85% pure, 80 mmol). After filtration of the reaction mixture, it was extracted with saturated Na_2CO_3 solution until the aqueous washings were basic. The organic layer was washed with 25 ml of H_2O, dried, and concentrated under vacuum. The resulting gummy residue was recrystallized from hexane–ether to give 1.61 g (27.3% yield) of white crystals, mp 95–96.5°C; ir (KBr): 1075, 3410 (alcohol), 1130, 1305 cm^{-1} (sulfone); nmr ($CDCl_3$) δ: 1.8–2.9 (m, 2, CH_2CH), 2.38 (s, 1, O*H*) 3.25 (m, 2, SCH_2), 4.00 (d, 1, J = 9 Hz, ArC*H*), 4.58 (dt, 1, J = 6, 9 Hz, C*H*OH), 7.39 (m, 5, *Ar*). *Anal.* calcd. for $C_{10}H_{12}O_3S$ (212.3): C 56.58, H 5.70, S 15.11; found: C 56.65, H 5.70, S 14.95.

*2-Phenylthiete 1,1-Dioxide (**23**)*

Et_3N (240 mg, 2.42 mmol) was added dropwise to a solution of **19** (390 mg, 1.97 mmol) and benzylsulfonyl chloride (410 mg, 2.16 mmol) in 30 ml of freshly distilled THF. The reaction was stirred at room temperature for 45 min, filtered, and concentrated under vacuum. The residue was dissolved in 50 ml of CH_2Cl_2 and washed with 3 × 25 ml of H_2O to remove any residual amount of $Et_3N{\cdot}HCl$. The organic fraction was dried and concentrated under vacuum to give 380 mg (60%) of a light brown scaly residue of **21**, mp 115–122°C dec.; ir (KBr): 1145, 1175, 1320 (sulfone), 1200, 1360 cm^{-1} (sulfonate); ms (no molecular ion) *m/e*: 116 ($(C_6H_5CCHCH_2)^+$), 115 ($(C_6H_5CCCH_2)^+$), 105 ($(C_6H_5CO)^+$), 91 ($(C_7H_7)^+$ base peak).

A solution of Et_3N (1.01 g, 10 mmol) in 3 ml of benzene was added to a solution of **21** (380 mg, 1.18 mmol) in 15 ml of benzene. The reaction was stirred at room temperature for 45 min, filtered, and concentrated under vacuum. The residue was dissolved in 50 ml of ether and washed with 3 × 25 ml of H_2O. The ether layer was dried, and concentrated under vacuum to give a white solid. The solid was recrystallized from EtOH–hexane to give 95 mg (45% yield) of white plate-like crystals, mp 94–95°C (this was identical to a sample of **23** prepared by an alternate method (1)); ir (KBr): 1140, 1180, 1300, 1310 cm^{-1} (sulfone); nmr ($CDCl_3$) δ: 4.52 (d, 2, J = 2 Hz, SCH_2), 7.02 (t, 1, J = 2 Hz, CC*H*), 7.46 (m, 5, *Ar*), ms *m/e*: 180 (weak molecular ion), 116 ($(C_6H_5CCHCH_2)^+$), 115 ($(C_6H_5CCCH_2)^+$ base peak), 105 ($(C_6H_5CO^+$), 89 ($(SO_2CCH)^+$), 77 ($(C_6H_5)^+$).

*2-Phenylthiolene 1,1-Dioxide (**24**)*

The same procedure as outlined for **23** was used starting with 1 g (4.72 mmol) of **20**. This gave 1.25 g (75% yield) of 1,1-dioxy-2-phenyl-3-thiolanyl benzylsulfonate (**22**) as a waxy residue, mp 120–130°C (dec.); ir (KBr): 1130, 1290, 1320 (sulfone), 1183, 1365 cm^{-1} (sulfonate). Treatment of **22** with Et_3N gave a solid residue which was recrystallized from benzene – petroleum ether (30–60°C) to give 0.2 g (46% yield) of **24** as white crystals, mp 113.5–116°C; ir (KBr): 1130, 1200, 1280 cm^{-1} (sulfone); nmr ($CDCl_3$) δ: 2.88 (m, 2, $CHCH_2$), 3.37 (m, 2, SCH_2), 6.70 (t, 1, J = 2.5 Hz, CC*H*), 7.47 (m, 5, *Ar*). *Anal.* calcd. for $C_{10}H_{10}O_2S$ (194.3): C 61.83, H 5.19, S 16.51; found: C 62.00, H 5.08, S 16.48.

Attempted Synthesis of 3-Formamido-3-phenylthietane 1,1-Dioxide (Ritter Reaction)

This reaction was carried out in a fume hood and the apparatus was connected to a 10% NaOH solution trap. NaCN (1.47 g, 0.03 mol) was added in small portions to 15 ml of glacial AcOH at 0°C. A cooled solution of concentrated H_2SO_4 (5.88 g, 0.06 equiv.) in 5 ml of glacial AcOH was then added dropwise, while maintaining the temperature at 20°C. After **25** (5 g, 0.025 mol) was added the reaction was heated at

Can. J. Chem. Downloaded from www.nrcresearchpress.com by 210.87.254.6 on 09/05/12
For personal use only.

50°C for 1 h, then stirred at room temperature overnight. The reaction mixture was poured into 50 ml of ice-cold H_2O and the resulting precipitate was collected and dried. Neutralization of the filtrate with K_2CO_3 resulted in the further precipitation of solid (1 g), which was collected, dried, and recrystallized from xylene and identified as the starting material, **25**. Boiling the initial precipitate in hexane and removal of the insoluble portion by filtration and concentration of the filtrate gave a few milligrams of white solid, mp over 25°C range: ir (KBr): 1755 (carbonyl), 1125, 1315 cm^{-1} (sulfone). Attempts to purify this compound for identification were unsuccessful.

The hexane insoluble portion was decolourized with charcoal in hot EtOH and cooled to give 1 g (22% yield) of 3-phenylthiete 1,1-dioxide **26** as colourless needles, mp 147°C (lit. (23) 145–147°C).

*Treatment of 3-Hydroxy-2-phenylthietane 1,1-Dioxide (**19**) with Acid*

A solution of **19** (1.5 g, 7.6 mmol) in 10 ml of 85% H_3PO_4 (or $AcOH–H_2SO_4$) was refluxed for 25 min and cooled. The dark solution was extracted with $CHCl_3$, and the pooled $CHCl_3$ extracts were dried and concentrated under vacuum. The residual oil was vacuum distilled. No accurate bp was recorded since the product was forced over with a flame (approximately 101°C, 13 Torr). The material isolated (0.5 g, 49.5%) was identified as benzyl methyl ketone (**30**), by virtue of identical ir and nmr spectra given for **30** in Sadtler (38). A crude 2,4-DNPH derivative had a mp of 142–140°C (lit. (39) 153°C, (40) 142–144°C). A methylene chloride extract of the reaction mixture when run on the gc/ms (70°C for 1 min, program at 10°C/min) gave one major peak, the mass spectrum of which showed *m/e* 43 (100), 91 (99), 92 (69), 134 (44), 65 (43), 39 (28). The mass spectrum and retention times were identical to an authentic sample. A very minor gc peak showing *m/e* 105 in the mass spectrum as the base peak indicated some phenylvinyl ketone present. Refluxing a sample of **19** in xylene for 24 h did not result in any detectable reaction.

*Treatment of 3-Hydroxy-2-phenylthietane 1,1-Dioxide (**19**) with Base*

A solution of **19** (0.5 g, 2.53 mmol) in 2% aqueous NaOH was refluxed for 12 h. Upon cooling a white precipitate was collected and recrystallized from EtOH–hexane to give 0.266 g (62% yield) of benzyl methyl sulfone, 124.5–126.5°C (lit. (39) 124–125.5°C); ir identical with that given in Sadtler (38); nmr ($CDCl_3$) δ: 2.76 (s, 3, CH_3), 4.25 (s, 2, CH_2), 7.48 (m, 5, *Ar*).

*3-Ethoxy-2-phenylthietane 1,1-Dioxide (**34**)*

To a solution of **23** (1 g, 5.5 mmol) in 15 ml of EtOH was added a 1 ml portion of a KOH solution (1 g KOH – 5 ml H_2O – 5 ml EtOH) to give a pale yellow solution. The solution was stirred for 1 h then let stand for 1 h, during which time a white precipitate formed. Recrystallization of the precipitate from EtOH–hexane gave fluffy white crystals, mp 107–108°C; ir (KBr): 1105, 1210, 1330 (sulfone), 1080, 1160 cm^{-1} (ethoxy ether); nmr ($CDCl_3$) δ: 1.15 (t, 3, $J = 7$ Hz, CH_3), 3.43 (q, 2, $J = 7$ Hz, OCH_2), 3.95–4.68 (m, 3, $OCHCH_2S$), 5.38 (d, 1, $J = 6$ Hz, $ArCH$), 7.41 (m, 5, *Ar*); ms (no molecular ion) *m/e*: 133 ($(C_6H_5CHCHOCH_2)^+$), 115 ($(C_6H_5CHCCH)^+$), 105 ($(C_6H_5CO)^+$ base peak), 91 ($(C_7H_7)^+$), 90 ($(C_7H_6)^+$). *Anal.* calcd. for $C_{11}H_{14}O_3S$ (226.3): C 58.38, H 6.24, S 14.17; found: C 58.61, H 6.03, S 14.22.

*Attempted Chlorination of 3 Hydroxy-2-phenylthietane (**9**); Isolation of 3-Chloropropenylbenzene (**5**)*

Freshly distilled $SOCl_2$ (3.72 g, 0.0316 mol) in 10 ml of $CHCl_3$ was added dropwise to a solution of **9** (5 g, 0.0316 mol) in 15 ml of $CHCl_3$. After stirring vigorously for 20 h, concentration of the mixture left a thick orange oil. Vacuum distillation of this oil gave 2.2 g of a pale yellow liquid, bp 55–60°C (0.7 Torr). The ir and nmr spectra were superimposable with that of an authentic sample (Aldrich). This represented 48% conversion of **9** to **5**. Similar results were obtained using cyanuric chloride (for procedure see ref. 6).

Acknowledgements

Financial assistance from the Medical Research Council of Canada and the University of British Columbia is acknowledged.

1. J. N. Wells and F. S. Abbott. J. Med. Chem. **9**, 489 (1966).
2. D. C. Dittmer and M. E. Christy. J. Org. Chem. **26**, 1324 (1961).
3. R. H. Bible, Jr. Interpretation of NMR spectra. Plenum Press, New York, NY. 1965.
4. A. R. Rands and A. J. H. Mercer. J. Chem. Soc. C, 2448 (1968).
5. E. Breuer and S. Sarel. Tetrahedron, **24**, 6339 (1968).
6. S. R. Sandler. J. Org. Chem. **35**, 3967 (1970).
7. A. Luttringhaus, S. Kabuss, H. Prinzbach, and F. Langenbucher. Ann. Chem. **653**, 195 (1962).
8. H. Apler and E. C. H. Keung. J. Org. Chem. **37**, 1464 (1972).
9. A. Rosowsky. Heterocyclic compounds with three and four membered rings. *Edited by* A. Weissberger, Interscience, New York, NY. 1964. Part 1. p. 270.
10. D. N. Kirk. Chem. Ind. London, **3**, 109 (1973).
11. A. Behzadi and L. N. Owen. J. Chem. Soc. Perkin Trans. I, **22**, 2733 (1973).
12. M. Sander. Chem. Rev. **66**, 297 (1966).
13. Q. N. Porter and J. Balds. Mass spectrometry of heterocyclic compounds. Wiley, New York, NY. 1971. p. 229.
14. M. Sander. Chem. Rev. **66**, 341 (1966).
15. Y. Etienne, R. Soulas, and H. Lumbroso. Heterocyclic compounds with three and four membered rings. *Edited by* A. Weissberger, Interscience, New York, NY. 1964. Part 2. p. 647.
16. D. C. Dittmer, M. E. Christy, N. Takashina, R. S. Henion, and J. M. Balquist. J. Org. Chem. **36**, 1324 (1971).
17. B. Lamm and K. Gustafsson. Acta Chem. Scand. B, **28**, 701 (1974).
18. W. E. Truce and J. F. Rach. J. Org. Chem. **39**, 1109 (1974) and references cited therein.
19. L. A. Paquette. J. Org. Chem. **29**, 2854 (1964).
20. C. Cistaro, R. Fronza, and R. Mondelli. Tetrahedron Lett. 189 (1973).
21. J. F. King, P. de Mayo, C. L. McIntosh, M. K. Piers, and D. J. H. Smith. Can. J. Chem. **48**, 3704 (1970).
22. J. Ritter and J. Kalish. Org. Synth. **44**, 44 (1964).
23. W. O. Siegl and C. R. Johnson. J. Org. Chem. **35**, 3657 (1970).
24. T. E. Zalasskaya and I. K. Lavrova. Zh. Org. Khim. **5**, 454 (1969); Chem. Abstr. **71**, 2927*x* (1969).
25. I. Hirao. J. Chem. Soc. Jpn. Ind. Chem. Sect. **56**, 265 (1953). Chem. Abstr. **48**, 10534*c* (1954).
26. D. C. Dittmer and M. E. Christy. J. Am. Chem. Soc. **84**, 399 (1962).

27. G. OPITZ, K. RIETH, and G. WALZ. Tetrahedron Lett. 5269 (1969).
28. L. A. PAQUETTE and M. ROSEN. J. Org. Chem. **33**, 3027 (1968).
29. J. E. COATES. Ph.D. Dissertation, University of British Columbia, Vancouver, B.C., Canada. 1972.
30. W. R. KIRNER and W. WINDUS. Org. synth., Coll. Vol. II. John Wiley and Sons, Inc., New York, NY. 1943. p. 136.
31. D. C. DITTMER and F. A. DAVIS. J. Am. Chem. Soc. **87**, 2064 (1965).
32. D. C. DITTMER, K. TAKAHASHI, and F. A. DAVIS. Tetrahedron Lett. 4061 (1967).
33. D. C. DITTMER and S. M. KOTIN. J. Org. Chem. **32**, 2009 (1967).
34. H. BOHME. Org. synth. Coll. Vol. III. John Wiley and Sons, Inc., New York, NY. 1955. p. 619.
35. F. S. ABBOTT. Ph.D. Dissertation, Purdue University, Lafayette, IN. 1966.
36. F. JOHNSON, J. PANELLA, and A. CARLSON. J. Org. Chem. **27**, 2241 (1962).
37. A. MAERCKER. Org. React. **14**, 270 (1965); R. M. GERKIN and B. RICKBORN. J. Am. Chem. Soc. **89**, 5850 (1967).
38. Sadtler-Standard Molecular Spectra. Sadtler Research Laboratories, Inc., Philadelphia, U.S.A. Vol. 2 (1959) and Vol. 3 (1968).
39. A. I. VOGEL. A textbook of practical organic chemistry. 3rd ed. Longmans, Green and Co. Ltd., London. 1956. p. 743.
40. M. GOTTFRIED. Tetrahedron Lett. 1027 (1962).

Can. J. Chem. Downloaded from www.nrcresearchpress.com by 210.87.254.6 on 09/05/12
For personal use only.

The cyclopentadienide anion and tropylium cation analogs of triptycene

DOUGLAS N. BUTLER AND INDRANIL GUPTA
Chemistry Department, York University, Downsview, Ont., Canada M3J 1P3

Received July 18, 1977

DOUGLAS N. BUTLER and INDRANIL GUPTA. Can. J. Chem. **56**, 80 (1978).

The cyclopentadienide analog of triptycene **1** and the tropylium cation analog of triptycene **2** have been synthesized. Some comparative spectroscopic data of these ions relative to triptycene are discussed.

DOUGLAS N. BUTLER et INDRANIL GUPTA. Can. J. Chem. **56**, 80 (1978).

On a synthétisé l'ion cyclopentadiénure, analogue du triptycène **1**, et le cation tropylium, analogue du triptycène **2**. On discute de quelques données spectroscopiques comparées de ces ions par rapport à celles observées pour du triptycène.

[Traduit par le journal]

Can. J. Chem. Downloaded from www.nrcresearchpress.com by 210.87.254.5 on 09/05/12
For personal use only.

The question of intramolecular orbital interaction of the rigid and spatially proximal aromatic rings of triptycene has prompted us to synthesize the triptycene-cyclopentadienide anion analog ('triptycepide') **1***a* and the related tropylium cation analog ('triptopylium') **2**. Shortly after we had succeeded in this goal, the synthesis of **2** was published by Murata and Nakazawa (1), however the simplicity and good yields of our route recommended its description.

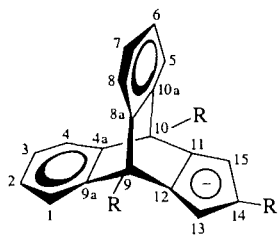

1*a* (R = H)
1*b* (R = D)

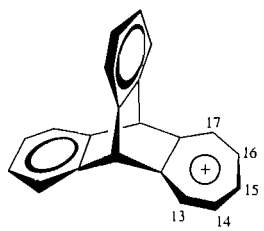

2

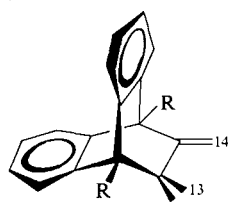

3*a* (R = H)
3*b* (R = D)

The Anion 1

Addition of dichlorocarbene (from phenylbromodichloromethylmercury) to 2,3-dimethylenedibenzobicyclo[2,2,2]octa-5,7-diene **3***a* (2) afforded the adduct **4***a*[1] as the major product together with the bis-adduct **5**. The four sharp singlets in the δ 4–6 ppm region of the proton magnetic resonance spectrum of **4***a* were assigned by a combination of specific deuterium labelling and nuclear Overhauser enhancement (nOe) techniques. Preparation of **4***b* from 9,10-anthracene-d_2 (3) removed the resonances at δ 4.90 and 4.27. The nOe enhancements of the integrated intensities of the four proton singlets are given in Table 1.

Obviously, the proton resonance at δ 4.27 is H_D and is too remote from the other three to exhibit any nOe. The assignment of the δ 5.29 resonance to H_B follows from its large positive enhancement to both H_A (δ 4.90) and H_C (δ 4.58). The other nOe values are typical of a linear three-spin system of this geometry (4).

Following the sequence described by Skattebøl (5), treatment of the adduct **4***a* with excess methyllithium in ether led (after aqueous work-up) directly to 'triptycepene' **6***a* (^{1}Hmr spectrum Fig. 1*a*). Deprotonation of **6***a* using potassium *tert*-butoxide in dimethylsulfoxide (DMSO) instantaneously formed a dark solution of the anion **1***a* (^{1}Hmr spectrum Fig. 1*b*). Addition of water to this basic solution precipitated **6***a* whereas the use of D_2O led to **6***b*. This type of site specificity of anion protonation has also been observed in the anion **7** leading exclusively to **8** (6).

In the present case, repetition of the deprotonation experiment in DMSO-d_6 rapidly removed the vicinal coupling to the vinylic proton at δ 5.32 ppm

TABLE 1. Nuclear Overhauser enhancements (%) of **4***a*

Resonance irradiated (δ)	Resonance observed (δ)			
	5.29	4.90	4.58	4.27
5.29	—	+16	+35	0
4.90	+14	—	−2	0
4.58	+32	−7	—	0
4.27	0	0	0	—

[1]All new compounds have been correctly analyzed and their spectroscopic data are in accordance with the structures shown.

Can. J. Chem. Downloaded from www.nrcresearchpress.com by 210.87.254.5 on 09/05/12
For personal use only.

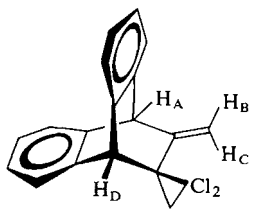

4*a* ($H_{A,B,C,D}$ = H)
4*b* ($H_{A,D}$ = D, $H_{B,C}$ = H)

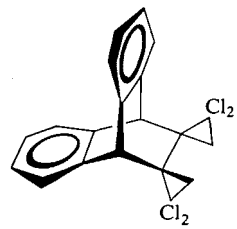

5

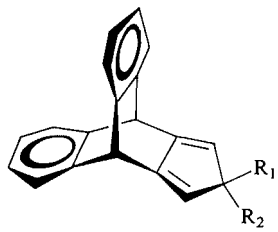

6*a* ($R_{1,2}$ = H)
6*b* (R_1 = H, R_2 = D)
6*c* ($R_{1,2}$ = D)

via D–H solvent exchange at the central site C_{14} in the presence of the strong base (see insert Fig. 1*b*). Quenching at this time with D_2O afforded **6***c*. The remaining vinylic proton ($C_{13,15}$) of **1***b* very slowly exchanged with time being about 80% exchanged after 4 weeks at room temperature under the particular conditions of this experiment.

A simple experiment to test possible [1,5] sigmatropic shifts in **6** was conducted by heating a solution ($CDCl_3$) of **6***c* at 100°C for 8 h. No evidence for diminution of the intensity of the remaining vinylic

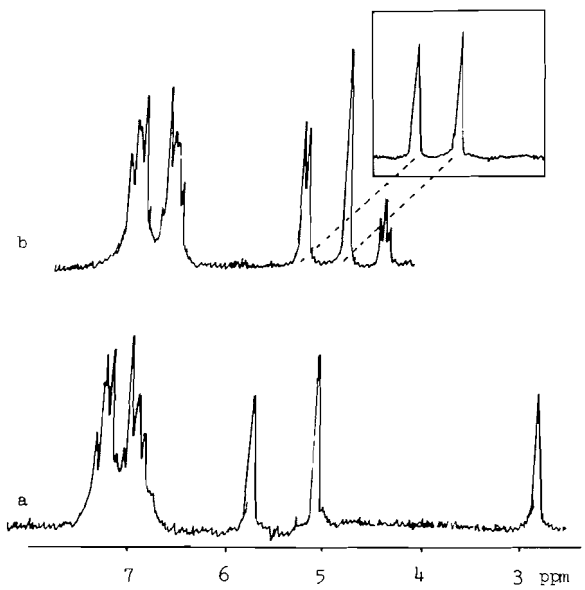

FIG. 1. (*a*) ^{1}Hmr spectrum of **3***a* in DMSO-d_6. (*b*) ^{1}Hmr spectrum of **1***a* in DMSO (inset in DMSO-d_6).

C—H resonance was found. From these results in both the anion **1** and its conjugate acid **6**, incyclic double bond character in the cyclopentadieno two-carbon arm of the dibenzobicyclo[2,2,2]octadiene skeleton appears to be thermodynamically unfavourable. It is worth noting also that the diene **6** shows no tendency to dimerize although Diels–Alder adducts with dimethyl acetylenedicarboxylate and maleic anhydride were readily prepared (compare **8** (6)).

The Cation 2

Our route to the 'triptopylium' cation **2** likewise began with the diene **3** (2). The Diels–Alder adduct **9** with cyclopropene (7) was directly dehydrogenated to the cation **2** using 2,3-dichloro-5,6-dicyanobenzoquinone and converted into the tetrafluoroborate salt (1) with tetrafluoroboric acid. Treatment of the cation **2** (as its perchlorate salt) with sodium hydride suspension in dioxane led to a complex

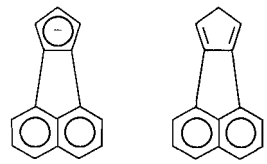

7 **8**

hydrocarbon mixture from which a low yield of the cycloheptatriene **10** could be isolated and shown to be identical to the intermediate described by Nakazawa and Murata (1).

Of relevance to proposed synthetic exercises directed to the 'bi-polar triptycene' **11** ⇄ **12**, the following competitive Diels–Alder reactions also bear upon the relative reactivity of buta-1,3-diene vs. cyclopentadiene toward electron-rich and electron-deficient dienophiles. With the latter, cyclopentadiene is reported to be 1.35×10^3 times more reactive than buta-1,3-diene (8). The two dienes **3** and **6** represent equally substituted examples of the above parent systems; however, the locked *cisoid* form of **3** removes the rotameric uncertainty component of the reported rate difference. In competitive kinetic experiments using dimethyl acetylenedicarboxylate as the dienophile, the cyclopentadiene **6** reacted exclusively (at least as revealed by ^{1}Hmr spectroscopic estimation). Conversely, in competition for the electron-rich dienophile cyclopropene, only **3** could be discerned to have reacted. As mentioned, this impressive differential reactivity provides good augury for a potential synthesis of **11** ⇄ **12** via routes parallel to those described herein.

Comparative Spectroscopic Data

The bridged cyclopentadiene **6** and its conjugate

Can. J. Chem. Downloaded from www.nrcresearchpress.com by 210.87.254.5 on 09/05/12
For personal use only.

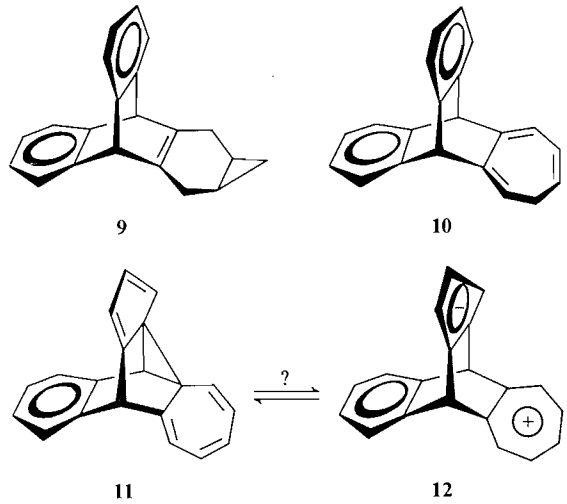

9 10

11 12

anion **1***a* (Li^+ salt) showed no discernable difference in their uv spectra in dry tetrahydrofuran. The uv maximum absorptions of **1** (Table 2) show a small hypsochromic shift relative to those of triptycene **13** (9). These spectra should be compared with that of the cation **2** where a broad charge-transfer band in the 300–450 nm region has been observed (1).

The ^1H and ^{13}C chemical shifts (referenced to TMS) and assignments pertinent to these systems are shown in Fig. 2 together with the $^1J_{^{13}C-H}$ (Hz) coupling constants. Chemical shift corrections between the solvents employed (DMSO for **1***a*, CS_2 for **13** (10), CD_3CN for **2**) have not been applied but they would not be expected to alter the general trends revealed by the data. For the ^1H shifts, a respective shielding for **1***a* and deshielding for **2** relative to triptycene **13** is observed for all the resonances, with the magnitude of these being relatively greater in the cation than in the anion. In both cases, the clear effect of the electric charge is manifest in the chemical shifts of the protons attached to the carbon atoms in the charge bearing rings and these should be compared with the values for the parent six-π aromatic systems (11) (see Fig. 2). The strong shielding of C_{14} in **1***a* is consistent with the protonation results discussed above. For the cation, hydride attack is observed at $C_{14,16}$ for the most deshielded of the perimeter carbon atoms, though this may be simply fortuitous. The published assignments for triptycene (10) suggested those for **1***a* and **2**. These were confirmed by specific ^1H frequency off-resonance decoupling experiments.[2]

For clarity, the ^{13}C shifts and assignments relevant to this discussion are reproduced graphically in Fig. 3 with connections between C atoms having a common structural relationship. The ^{13}C resonances, whilst again generally reflecting the expected direct field effects throughout the systems involved, do show two interesting features. Firstly, the bridgehead resonances ($C_{9,10}$) do not show a monotonic response to the adjacent charged ring relative to **13**. This may be a consequence of the geometric changes associated with the accommodation of the respective five, six, and seven-membered rings in these three systems. Secondly, the four fully substituted carbon atoms ($C_{4a,8a,9a,10a}$) of the uncharged aromatic rings reveal shifts *opposite* to the general trends. We interpret this result as a field-induced π-polarization effect of the type discussed by Reynolds and Hamar (13).

In conclusion it may be noted that the routes to bridged cyclopentadienide anions and tropylium cations described above should be applicable to many of the exocyclic dienes we have previously synthesized (2).

TABLE 2. Ultraviolet spectra

Compound	λ_{max} (log ε)
1*	226 (4.58), 254 (3.72-broad), 267 (3.59), 275 (3.48)
13†	211 (4.80), 264 (3.30-shoulder), 271 (3.55), 279 (3.67)
2‡	240 (4.62), 279 (3.84), 340 (3.51-broad)

*As Li^+ salt in dry THF.
†In ethanol (9).
‡As BF_4^- salt in CH_3CN (1).

Experimental

All melting points are uncorrected. The ir spectra were taken on a Unicam SP1000 spectrophotometer as Nujol mulls or KBr discs. The ^1Hmr spectra were taken on either Varian EM360 or HA100 instruments in the solvents indicated. The cmr spectra were obtained on a Varian CFT20 instrument in the solvents indicated. The uv spectra were run on a Unicam SP800A spectrophotometer. Mass spectra were taken at 70 eV using a Hitachi-Perkin Elmer RMU-6E instrument. Microanalyses were obtained from A. B. Gygli, Toronto.

Dichlorocarbene Adduct ***4***

Phenylbromodichloromethylmercury (14) 4.40 g (0.01 mol) was added to a solution of 11,12-dimethylene-9,10-dihydro-9,10-ethanoanthracene **3***a* (2) 2.30 g (0.01 mol) in dry benzene (10 ml). This mixture was subject to reflux and magnetic stirring for 6 h then cooled; the precipitated phenylmercuric bromide was filtered off with the aid of a pad of Celite and the filtrate passed through a column of alumina (1 × 10 cm Woelm, grade 1) using an additional 150 ml of benzene to wash the column. After solvent evaporation under vacuum the residue was recrystallized from CCl_4 thus providing the adduct **4***a*, 2.57 g (82%), mp 174°C; ^1Hmr ($CDCl_3$) δ_{Me_4Si}: 7.07–7.53 (m, 8H), 5.29 (s, 1H), 4.90 (s, 1H), 4.58 (s, 1H), 4.27 (s, 1H), 1.76 (d, J = 8 Hz, 1H) and 1.36 (d, J = 8 Hz, 1H) ppm; *m/e* M^+ 312, $(M^+ + 2)$ 314, $(M^+ + 4)$ 316 (relative intensities 100:65:11), base peak 178 (anthracene). *Anal.* calcd. for $C_{19}H_{14}Cl_2$: C 72.86, H 4.50; found: C 72.71, H 4.36.

From the mother liquors of the recrystallization of the

[2]For a full discussion on the assignments of α and β carbon atoms in Diels–Alder adducts of anthracene see ref. 12.

Can. J. Chem. Downloaded from www.nrcresearchpress.com by 210.87.254.5 on 09/05/12
For personal use only.

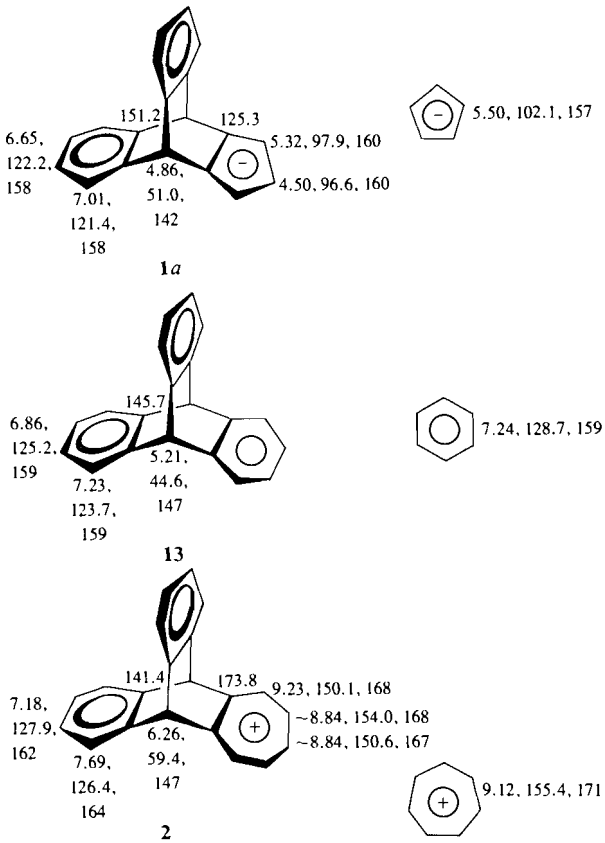

FIG. 2. Chemical shifts in ppm from TMS for ^1H and ^{13}C and coupling constants $^1J_{^{13}C-H}$ (Hz) for **1***a*, **13**, and **2**.

monoadduct **4***a* a small yield of the bis-adduct **5** was obtained, mp 201.5–202°C (ethanol); ^{1}Hmr ($CDCl_3$) δ_{Me_4Si}: 7.10–7.55 (m, 8H), 4.09 (s, 2H), 2.89 (d, J = 8 Hz, 2H) and 1.37 (d, J = 8 Hz, 2H) ppm; *m/e* M^+ 394, $(M^+ + 2)$ 396, $(M^+ + 4)$ 398, $(M^+ + 6)$ 400, and $(M^+ + 8)$ 402 (relative intensities 77:100:47:9:1), base peak 178 (anthracene). *Anal.* calcd. for $C_{20}H_{14}Cl_4$: C 60.64, H 3.56; found: C 60.53, H 3.71.

The synthesis of **3***b* from 9,10-dideuterioanthracene (3) provided the adduct **4***b* via the above method. This material did not show ^{1}Hmr signals at δ 4.90 and 4.27 ppm.

'Triptacepene' 6

To a solution of the adduct **4***a* (1.7 g) in dry ether (75 ml) was added 30 ml of 1.5 *M* methyllithium in ether and the mixture allowed to stand overnight at room temperature before it was cautiously poured over a mixture of ice and water. The organic phase was separated and the aqueous phase extracted with ether (2 × 30 ml). The combined ether phases were then dried ($MgSO_4$) and evaporated under vacuum to afford the crude product which was purified by passage in 3:1 hexane–benzene through a short column of alumina (Woelm, grade 1) and recrystallization from a large volume of ether to give **6***a*, 0.48 g (62%), mp 220°C; ^{1}Hmr ($CDCl_3$) δ_{Me_4Si}: 7.43–7.20 (m, 4H), 7.15–6.97 (m, 4H), 5.87 (t, $J \approx 1$ Hz, 2H), 5.10 (s, 2H), 2.37 (t, $J \approx 1$ Hz, 2H) ppm; ^{13}Cmr (DMSO-d_6) δ_{Me_4Si}: 148.9 (s, $C_{11,12}$), 143.8 (s, $C_{4a,8a,9a,10a}$), 125.9 (d, $C_{2,3,6,7}$), 124.1 (d, $C_{1,4,5,8}$), 118.0 (d, $C_{13,15}$), 47.8 (d, $C_{9,10}$), 43.2 (t, C_{14}) ppm; uv (THF) λ_{max} (log ε_{max}): 226 (4.58), 254 (3.72), 267 (3.59), and 275 (3.48) nm; ir (KBr): 712, 722, 763, 891, 905, 928, 971, 1024, 1150, 1190, 1249, 1354, 1371, 1457, 2951, 3001, 3070 cm^{-1}; *m/e*: M^+ 242 (base peak), 226, 215, 178, 165, 122, 120. *Anal.* calcd. for $C_{19}H_{14}$: C 94.18, H 5.82; found: C 94.30, H 5.58.

Lithium 'Triptacepide' 1a·Li$^+$

The bridged cyclopentadiene **6***a* (42 mg) was dissolved in DMSO (0.4 ml) and excess potassium *tert*-butoxide (≈60 mg) added. This produced a dark brown solution which was directly used to record the ^{1}H and ^{13}C nmr spectra (see text). Addition of water to this solution precipitated **6***a*, whilst D_2O afforded **6***b*. When DMSO-d_6 was used in a similar experiment, the resonance triplet at δ 4.50 disappeared over about 12 min with concurrent collapse of the δ 5.32 doublet to a sharp singlet (see Fig. 1).

At this point, addition of water produced **6***b* whilst D_2O gave **6***c*. After 4 weeks at ambient temperature, the basic DMSO-d_6 solution exhibited a decrease in the δ 5.32 signal to a value about 20% of its original integrated intensity. The uv spectrum was obtained by adding 1 drop of *n*-BuLi (1.2 *M* in hexane) to a solution of **6***a* in dry THF.

Cyclopropene Adduct 9

During 4 h, cyclopropene gas generated by the dropwise

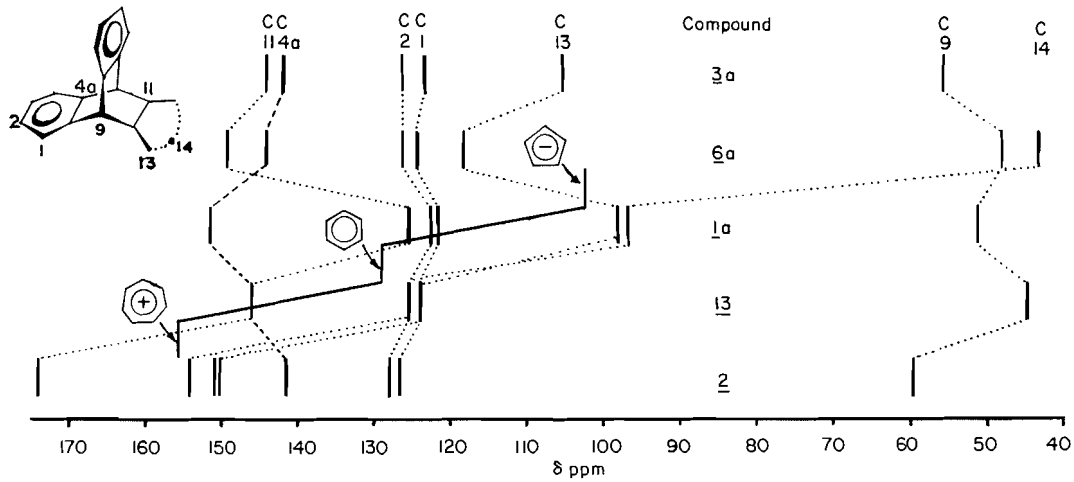

FIG. 3. ^{13}C chemical shifts and assignments for compounds **3***a*, **6***a*, **1***a*, **13**, and **2**.

addition of a solution of allyl chloride (30 g) in mineral oil (150 ml) to a stirred suspension of sodamide (12 g) in mineral oil (50 ml) held at 80°C (7), was passed through a solution of the diene **3***a* (1 g) in CCl_4 (30 ml) until ^{1}Hmr spectroscopy showed the disappearance of the characteristic diene signals. The reaction residue obtained by removal of the solvent was passed in benzene through a short column (1 × 8 cm) of alumina (Woelm, grade 1). Trituration of the evaporated eluate with methanol produced a solid which was recrystallized from ether to afford the adduct **9**, 504 mg (43%), mp 145°C. The mother liquors of this recrystallization were subject to preparative tlc on silica plates developed in hexane–acetone (10:4). A further 287 mg of **9** were obtained (total yield 68%). ^{1}Hmr ($CDCl_3$) δ_{Me_4Si}: 7.37–7.03 (m, 4H), 7.01–6.67 (m, 4H), 4.60 (s, 2H), 2.57 (br. s, 4H), 1.3–0.5 (m, 4H) ppm; ir (KBr): 639, 715, 745, 766, 807, 1018, 1157, 1435, 1457, 2803, 2844, 2865, 2942, 3005 cm^{-1}; *m/e*: M^+ 270. *Anal.* calcd. for $C_{21}H_{18}$: C 93.29, H 6.71; found: C 93.43, H 6.59.

'Triptopylium' Tetrafluoroborate **2**·BF_4^-

To a magnetically stirred solution of the adduct **9** (150 mg) in CH_2Cl_2 (10 ml), DDQ (350 mg) was added and the dark mixture stirred at room temperature for 0.5 h. The CH_2Cl_2 was removed on a rotary evaporator under vacuum and the resulting red complex stirred for 0.5 h with HBF_4 (6 ml, 48%) and CH_3CN (10 ml). The white solid was filtered off and the filtrate concentrated under vacuum and cooled in ice. The yellow green salt was filtered off and recrystallized from CH_3CN and dried over KOH pellets for 14 h under vacuum to afford **2**·BF_4^-, 114 mg (58%) which slowly decomposed at 193–200°C. (See text and ref. 1 for spectroscopic data.)

Bridged Cycloheptatriene **10**

Perchloric acid (1 ml, 60%) was added to a solution of the adduct 9 (200 mg) in glacial acetic acid (8 ml). Then DDQ (400 mg) was added and the mixture stirred overnight. The precipitated solid was filtered off and water (80 ml) added to the filtrate. The crude perchlorate salt of **2** which precipitated was filtered off, dried over KOH pellets in vacuum, then added to a stirred suspension of sodium hydride (200 mg) in dry dioxan (25 ml) and the stirring continued for 3 h under N_2. After this time, the reaction mixture was carefully decomposed with ice-water, extracted with CH_2Cl_2, and the extract washed with water and dried (Na_2SO_4). On evaporation, the residue was passed through a column of alumina (Woelm, grade 1, 1 × 12 cm) in benzene. On evaporation of the eluate and recrystallization of the residue there was obtained the cycloheptatriene **10** (1) 24 mg (12%), mp 202°C. The ^{1}Hmr spectrum was the same as that reported (1); *m/e*: M^+ 268.

Competitive Diels–Alder Reactions of 3a and 6a

The diene **3***a* (23 mg, 0.10 mmol) and the cyclopentadiene **6***a* (24.2 mg, 0.10 mmol) were mixed in an nmr tube with dimethyl acetylenedicarboxylate (DMAD) (11.36 mg, 0.08 mmol) in $CDCl_3$ (0.35 ml) and held at 30°C in a thermostat for 22 h. Inspection of the ^{1}Hmr spectrum revealed no discernable signals for the diene **3***a*–DMAD adduct (15).

The above mixture of **3***a* and **6***a* in $CDCl_3$ was treated with cyclopropene gas (10) until the ^{1}Hmr signals of **3***a* disappeared. Conversely to the DMAD experiment, no signal for the **6***a*-cyclopropene adduct could be detected. In a separate experiment **6***a* in $CDCl_3$ was subjected to a large excess of cyclopropene gas but no evidence for reaction could be found.

Acknowledgments

The authors wish to thank Dr. C. E. Holloway for assistance in obtaining and assigning the ^{13}Cmr spectra and to Dr. W. F. Reynolds for helpful discussions.

1. T. Nakazawa and I. Murata. J. Am. Chem. Soc. **99**, 1996 (1977).
2. D. N. Butler and R. A. Snow. Can. J. Chem. **50**, 795 (1972).
3. J. L. Charlton and R. Agagnier. Can. J. Chem. **51**, 1852 (1973).
4. R. E. Schirmer, J. H. Noggle, J. P. Davis, and P. A. Hart. J. Am. Chem. Soc. **92**, 3266 (1970).
5. L. Skattebøl. Tetrahedron, **23**, 1107 (1967); R. B. Reinarz and G. J. Fonken. Tetrahedron Lett. 4591 (1973).
6. K. Yamamoto, M. Morioka, and I. Murata. Tetrahedron Lett. 3009 (1975).
7. G. L. Closs and K. D. Krantz. J. Org. Chem. **31**, 638 (1966).
8. D. Craig, J. J. Shipman, and R. B. Fowler. J. Am. Chem. Soc. **83**, 2885 (1961).
9. C. F. Wilcox, Jr. J. Chem. Phys. **33**, 1874 (1960).
10. Yu. K. Grishin, N. M. Sergeyev, O. A. Subbotin, and Yu. A. Ustynyuk. Mol. Phys. **25**, 297 (1973); K. G. Kidd, G. Kotowycz, and T. Schaefer. Can. J. Chem. **45**, 2155 (1967).
11. H. Volz and M. Volz-de-Lecea. Ann. Chem. **750**, 136 (1971).
12. D. Axleson. Ph.D. Thesis, York University, Downsview, Ontario. 1976.
13. W. F. Reynolds and G. K. Hamar. J. Am. Chem. Soc. **98**, 7296 (1976).
14. D. Seyferth and J. M. Burlitch. J. Am. Chem. Soc. **84**, 1757 (1962).
15. D. N. Butler and R. A. Snow. Can. J. Chem. **53**, 256 (1975).

Can. J. Chem. Downloaded from www.nrcresearchpress.com by 210.87.254.5 on 09/05/12
For personal use only.

Résonance magnétique nucléaire du carbone-13 de composes oxa- et azabicyclo[3.3.1]- et -[4.2.1]nonaniques

M. Barrelle, M. Apparu et C. Gey

Laboratoire de Chimie Organique, Université Scientifique et Médicale de Grenoble, B.P. 53 Centre de Tri 38041, Grenoble-Cédex, France

Reçu le 6 décembre 1976[1]

M. Barrelle, M. Apparu et C. Gey. Can. J. Chem. **56**, 85 (1978).

Les spectres de rmn du ^{13}C de 25 composés oxa- et azabicyclo[3.3.1]- et -[4.2.1]nonaniques ont été enregistrés. Les résultats obtenus pour les oxa-9 bicyclo[3.3.1]nonanes substitués en position 2 par des groupements hydroxyles ou alkyl- et phénylamino, ainsi que ceux obtenus pour des *N*-alkyl- ou *N*-phényl-aza-9 bicyclo[3.3.1]nonanols-2 apportent des informations supplémentaires, relatives aux structures de ce type déjà étudiées. Suivant le substituant des blindages et des déblindages dûs à des interactions γ et δ stériques sont notés. L'étude relative aux composés oxabicyclo[4.2.1]nonaniques substitués ou non en positions 2 ou 7 (par des groupes hydroxyles) et azabicyclo[4.2.1]nonaniques substitués en position 2 (par les mêmes groupes) apportent d'intéressants renseignements sur l'équilibre conformationnel de ces composés, dû à la flexibilité du cycle à sept chaînons. L'équilibre conformationnel pourrait être déplacé vers la forme bateau du cycle à sept chaînons pour les composés non substitués. Pour les autres composés, des conformations *gauches* sont proposées pour rendre compte des observations expérimentales, les formes chaise et bateau pures étant exclues. Deux cétones sont en outre étudiées.

M. Barrelle, M. Apparu, and C. Gey. Can. J. Chem. **56**, 85 (1978).

Carbon-13 nmr spectra have been recorded for 25 oxa- and azabicyclo[3.3.1]- and -[4.2.1]-nonanes. Results obtained for the 9-oxabicyclo[3.3.1]nonanes, 2-substituted by hydroxyl or alkyl- and phenylamino groups, as well as those obtained for the *N*-alkyl- or *N*-phenyl-9-azabicyclo[3.3.1]nonan-2-ols, provide supplementary information regarding the previously studied structures of these types. Shielding and deshielding due to γ and δ steric interactions were observed depending on the substituent. The study of the oxabicyclo[4.2.1]nonanes, substituted or not substituted in positions 2 and 7 by hydroxyl groups, and of the azabicyclo[4.2.1]-nonanes substituted in position 2 by the same group, yields interesting results on the conformational equilibria in these compounds which is caused by the flexibility of the seven-membered ring. The conformational equilibrium is displaced toward the boat form of the seven-membered ring for the unsubstituted compounds. *Gauche* conformations are proposed for the other compounds in order to account for the experimental observations; the pure chair and boat forms are excluded. Two ketones also have been studied.

[Journal translation]

Introduction

Les effets de substituants sur les déplacements chimiques en rmn du ^{13}C ont été trés étudiés et peuvent apporter d'importants renseignements d'ordre stéréochimique (1–3). En particulier les déplacements chimiques à champ fort de carbones situés en γ de groupes méthyles et éclipsés par ceux-ci sont dus à des interactions stériques (4). L'influence du groupe hydroxyle a été étudiée dans les systèmes bicycliques conformationnellement fixes (série bicyclo[2.2.1]-heptanique ou -[2.2.2]octanique, série de l'adamantane) ou peu flexibles (série bicyclo[3.2.1]octanique) (5–16). Dans des séries de décalols (17) et de stéroïdes (17, 18), l'influence du groupe OH sur les carbones en γ et en δ de ce substituant a aussi été étudiée; des effets γ de -3.3 à -7.3 ppm ont pu ainsi être mis en évidence. Ainsi dans les structures de types cités ci-dessus d'importants résultats conformationnels ont pu être obtenus.

Le passage à l'étude de systèmes conformationnellement flexibles du type bicyclo[3.3.1]nonane est plus récent, les structures ainsi étudiées possédaient en position 9 soit un carbone soit un hétéroatome (N, S, P) et étaient diversement substituées (19–23).

Pour ces composés une conformation prédominante chaise-chaise a été trouvée conformément aux études antérieures ne faisant pas intervenir la rmn du ^{13}C (24), sauf dans le cas ou un substituant en position *endo*-3 subit une interaction répulsive avec une hydrogène du carbone-7 (20, 21): on a alors une conformation chaise-bateau pour la molécule.

Les problèmes conformationnels des systèmes bicyclo[4.2.1]nonaniques n'ont pas à notre connaissance retenu beaucoup l'attention, la flexibilité du cycle à sept chaînons rendant l'étude stéréochimique plus difficile. Signalons toutefois les ré-

[1]Révision reçue le 9 septembre 1977.

Can. J. Chem. Downloaded from www.nrcresearchpress.com by 210.87.254.6 on 09/05/12
For personal use only.

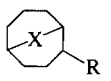

1 X = O; R = H
2 X = O; R = OH *endo*
3 X = O; R = OH *exo*
4 X = O; R = NH_2
5 X = O; R = NMe
6 X = O; R = N*t*Bu
7 X = O; R = NPh
8 X = NMe; R = H
9 X = NMe; R = OH *endo*
10 X = NPh; R = H
11 X = NPh; R = OH *endo*
12 X = NEt; R = OH *endo*

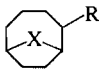

13 X = O; R = H
14 X = O; R = OH *endo*
15 X = O; R = NH_2 *endo*
16 X = O; R = OH *exo*
17 X = O; R = >=O
18 X = NMe; R = H
19 X = NMe; R = OH *endo*
20 X = NMe; R = OH *exo*
21 X = NPh; R = H
22 X = NPh; R = OH *endo*

23 X = O; R = OH *endo*
24 X = O; R = OH *exo*
25 X = O; R = >=O

sultats (obtenus par calculs EFF) de Schleyer et coll. (25), sur le bicyclo[4.2.1]nonane, qui plaident en faveur d'une conformation chaise majoritaire pour le cycle à sept chaînons.

Disposant des produits oxa- et azabicyclo[3.3.1]- et -[4.2.1]nonaniques répertoriés ci-dessus, nous en avons enregistré les spectres de rmn de ^{13}C, analysé les déplacements chimiques et étudié les diverses interactions pouvant conduire à une représentation convenable des conformations, en particulier en série hétérobicyclo[4.2.1]nonanique.

Résultats et discussion

Les déplacements chimiques enregistrés pour ces composés, ainsi que les différences de déplacements chimiques entre les composés substitués et les composés parents (**1**, **8**, **10**, **13**, **18**, **21**) sont consignés dans les tableaux 2 et 4.

Composés bicyclo[3.3.1]nonaniques

*Composés non fonctionnels (**1**, **8**, **10**)*

Dans une récente publication, Lambert et coll. (26) montrent que les déplacements chimiques des carbones d'hétérocycles à six chaînons sont reliés à l'électronégativité de l'hétéroatome: les carbones en α de l'hétéroatome sont déblindés fortement, ceux en β et γ sont blindés par rapport aux carbones du cyclohexane de référence (le blindage du carbone en β étant de plus fonction du substituant porté par l'hétéroatome).

Sur le tableau 1, on s'aperçoit que l'évolution des blindages des carbones α, β, γ des hétérobicyclononanes par rapport au bicyclononane se fait dans le même sens que celle des blindages des hétérocyclohexanes par rapport au cyclohexane.

Le problème du déplacement des carbones 3 et 7 à champ fort n'est pas totalement élucidé.[2] Dans les composés **1**, **8**, **10** auxquels on peut ajouter l'analogue soufré, les déplacements chimiques des carbones 3 et 7 semblent reliés plus directement aux électronégativités des hétéroatomes, la structure rigide du cycle à six chaînons dans ces composés éliminant les perturbations dues à la plus grande flexibilité d'un cycle à six chaînons isolé. Des exemples plus nombreux seraient nécessaires toutefois pour confirmer cette hypothèse.

Composés fonctionnels

Les composés substitués que nous avons étudiés pouvaient à priori présenter des effets similaires à ceux étudiés par Heumann et Kolshorn (19) pour des composés où X = C=O. Répulsion C_3—C_7 conduisant à un plus ou moins grand aplatissement de

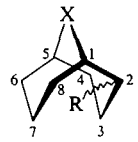

cycle, à laquelle s'ajoute une gêne stérique au niveau de C_4 ou C_8 suivant que R est *exo* ou *endo*, la taille et la nature de R constituant des facteurs supplémentaires à considérer. De même les études de Wiseman et Krabbenhoft (20) ont permis de détailler certains paramètres d'interaction de type γ et δ pour des structures où X = N—R_1.

Indépendamment des comparaisons faites avec les produits de même structure déjà cités ainsi que l'étude des spectres couplés, l'attribution des signaux a pu être menée à bien par les constatations suivantes.

*Composés **2**, **4**, **5**, **6**, **7**, **9**, **11** et **12***

Les déplacements chimiques des carbones C_1, C_2, C_5 sont déterminés sans ambiguïté, les effets de substituants sur le carbone 2 étant cohérents avec ceux déjà décrits dans la littérature à plusieurs reprises (29, 30).

On peut de même attribuer au carbone C_6, quand il n'est pas affecté par des effets de substituants, la

[2]Wiseman et coll. (22*a*) proposent pour différents hétérobicyclo[3.3.1]nonanes un calcul du déplacement chimique des C_3 et C_7 à partir des valeurs du déplacement de C_4 dans les hétérocyclohexanes correspondants. Certaines de ces valeurs sont anciennes et ont été revues récemment dans la réf. 27. A partir de ces nouvelles valeurs, en considérant un effet δ de 4.7 ppm proposé par Wiseman et coll. on trouve un déplacement chimique de 18.9 et 17.4 ppm pour les carbones C_3 et C_7 de **1** et **8** respectivement, ce qui pour **8** est loin de la valeur mesurée (20.4 ppm). Il faut alors considérer que l'effet est différent selon la nature de l'hétéroatome (plus ou moins grand aplatissement des cycles) ou que l'adjonction de 2 méthyles axiaux en α de l'hétéroatome du cycle à six chaînons provoque un blindage du carbone en position γ différent suivant la nature de l'hétéroatome.

Can. J. Chem. Downloaded from www.nrcresearchpress.com by 210.87.254.6 on 09/05/12
For personal use only.

TABLEAU 1. Deplacements chimiques

Composé	X	δ (ppm) Cα	Cβ	Cγ	Référence
	CH_2	27.3	27.3	27.3	2
	S	29.1	27.9	26.6	27
	O	68	26.9	23.8	27
	NMe	57.4	26.7	22.7	27
	NPh	52.4	27.7		28
	CH_2[a]	27.9	31.6	22.5	19
	S	33.2	32.1	21.6	22*a*

[a]Pour X = O, NMe, NPh voir le tableau 3, composés 1, 8 et 10.

TABLEAU 2. Déplacements chimiques en ppm/TMS dans $CDCl_3$ et effets de substituants

Composé	C_1	C_2	C_3	C_4	C_5	C_6	C_7	C_8	N—C
1 Oxa-9 bicyclo[3.3.1]nonane	66.6	29.4	18.9	29.4	66.6	29.4	18.9	29.4	
2 Oxa-9 bicyclo[3.3.1]nonanol-2 *endo*	70.6	68.7	28.7[a]	29.3[a]	66.5	29.3[a]	18.8	22.5	
	(4.0)	(39.3)	(9.8)	(−0.1)	(−0.1)	(−0.1)	(−0.1)	(−6.9)	
3 Oxa-9 bicyclo[3.3.1]nonanol-2 *exo*	73.0	68.8	25.8[a]	24.6[a]	67.0	29.5	17.5	27.1	
	(6.4)	(39.4)	(6.9)	(−4.8)	(0.4)	(0.1)	(−1.4)	(−2.3)	
4 Oxa-9 amino-2 endo bicyclo[3.3.1]-nonane	69.5	53.4	28.4[a]	29.7[a]	66.6	29.5[a]	19.1	23.0	
	(2.9)	(24.0)	(9.5)	(0.3)	(0)	(0.1)	(0.2)	(−6.4)	
5 Oxa-9 méthylamino-2 *endo* bicyclo-[3.3.1]nonane	69.1	58.7	23.2	29.5	66.7	29.5	19.2	27.3	33.4
	(2.5)	(29.3)	(4.3)	(0.1)	(0.1)	(0.1)	(0.3)	(−2.1)	
6 Oxa-9 tertiobutylamino-2 *endo* bicyclo[3.3.1]nonane	71.9	51.3	30.6[a]	29.8[a]	66.1	29.5[a]	19.1	23	Non lu[c]
	(5.3)	(21.9)	(11.7)	(0.4)	(−0.5)	(0.1)	(0.2)	(−6.4)	
7 Oxa-9 phenylamino-2 *endo* bicyclo[3.3.1]nonane	68.0[b]	52.2	27.6	29.8[a]	66.3[b]	29.4[a]	19	23	Non lu[d]
	(1.4)	(22.8)	(8.7)	(0.4)	(−0.3)	(0)	(0.1)	(−6.4)	
8 *N*-Méthyl aza-9 bicyclo[3.3.1]-nonane	52.3	26.4	20.4	26.4	52.3	26.4	20.4	26.4	40.9
9 *N*-Méthyl aza-9 bicyclo[3.3.1]-nonanol-2 *endo*	58.1	69.1	30.1[a]	28.8[a]	51.7	23.5	20.1	16.9	40.8
	(5.8)	(42.7)	(9.7)	(2.4)	(−0.6)	(−2.9)	(−0.3)	(−9.5)	
10 *N*-Phényl aza-9 bicyclo[3.3.1]-nonane	48.4	28.6	20.7	28.6	48.4	28.6	20.7	28.6	150.3[e]
11 *N*-Phényl aza-9 bicyclo[3.3.1]-nonanol-2 *endo*	53.4	69.2	30.1	27.8[a]	47.5	28.4[a]	20.3[b]	20.9[b]	149[f]
	(5.0)	(40.6)	(9.4)	(−0.8)	(−0.9)	(−0.2)	(−0.4)	(−7.7)	
12 *N*-Ethyl aza-9 bicyclo[3.3.1]-nonanol-2 *endo*	55.4	69.6	30.6	28.9	49.5	23.9	20.2	17.2	45.6[g]

[a,b]Valeurs pouvant être interchangées.
[c]$(CH_3)_3$ = 30.2.
[d]C *ortho* 113.2, C *para* 117.5, C *méta* 129.5.
[e]C *ortho* 113.9, C *para* 116.3, C *méta* 129.5.
[f]C *ortho* 114, C *para* 116.9, C *méta* 129.6.
[g]CH_3 = 13.1.

valeur la plus proche de celle d'un carbone identique dans le composé parent, les valeurs attribuées à ce carbone dans **9** et **12** étant justifiées plus loin. Le même raisonnement peut être tenu pour C_7. A ces composés substitués sur le carbone 2 par OH ou N—R en *endo* nous attribuons les déplacements chimiques des carbones restants C_3, C_4 et C_8 en remarquant que C_3 doit être déblindé puisqu'il est en β d'un substituant OH ou N—R, que C_8 doit être blindé à cause de l'effet stérique du substituant (position éclipsée de C_8—H et OH ou N—R). La valeur de déplacement chimique restant est attribuée à C_4 bien que, comme il est noté dans le tableau 2 elle puisse être interchangée parfois avec des valeurs proches attribuées à C_6 ou C_3. Les déplacements des carbones de **12** sont attribués par comparaison avec ceux de **9**. Pour ce dernier composé l'attribution de C_6 a été faite avec certitude par deutériation de ce site en position 6 (cf. partie expérimentale).

Ce blindage du carbone C_6 dans **9**, alors que le

Can. J. Chem. Downloaded from www.nrcresearchpress.com by 210.87.254.6 on 09/05/12
For personal use only.

Can. J. Chem. Downloaded from www.nrcresearchpress.com by 210.87.254.6 on 09/05/12
For personal use only.

reste de la série présente des valeurs cohérentes, est attribué à une effet γ stérique de 2.9 ppm entre le méthyle porté par l'azote et les hydrogènes des carbones C_6 et C_8. On note par ailleurs que l'effet d'un groupement hydroxyle *endo* sur C_8 est de -6.9 et -7.7 ppm environ pour **2** et **11** alors que la valeur pour **9** serait de -9.5 ppm; cette valeur s'explique très bien par l'effet additionnel de l'hydroxyle (-6.6 ppm environ) et du méthyle (-2.9 ppm). Les déblindages observés pour C_4 et C_2 dans **9**, par rapport aux autres composés, montrent inversement que l'effet γ du méthyle vis à vis de ces deux carbones n'a pas lieu et amènent à conclure que l'introduction d'un substituant OH en *endo* produit un aplatissement de cycle qui éloigne les sites susceptibles d'interagir stériquement, ou qu'il y a contribution d'une forme chaise-bateau.

Ce explications données, il ressort que pour les carbones C_1, C_2, C_4, C_5, C_6 et C_7 des composés *endo* on obtient une bonne corrélation des valeurs de déplacement chimique, entre elles, quelques écarts s'expliquent par des effets de substituants sur lesquels nous reviendrons plus loin. Pour les carbones C_3 les valeurs attribuées pour les composés hydroxylés montrent des effets de substituants de 9.4, 9.7 et 9.8 ppm qui correspondent bien aux valeurs de la littérature (17, 19) relatives aux effets d'un hydroxyle en β du carbone considéré. Pour **4** où le substituant est amino un effet similaire de 9.5 ppm, et pour **7** de 8.7 ppm, est trouvé, alors que si l'azote est substitué par un méthyle (**5**) ou un tertiobutyle (**6**) les effets sont différents. La comparaison avec **4** peut permettre d'expliquer ces différences. Dans le cas de **5** le groupement méthyle introduit sur C_3 un effet de blindage γ qui se superpose à l'effet β déblindant, on peut ainsi évaluer l'effet γ à environ -5.2 ppm. Inversement pour **6** le groupement tertiobutyle introduirait sur C_3 un effet δ déblindant d'environ 2.2 ppm (31). A propos de l'étude du composé **9** ci-dessus, nous avons noté l'effet d'un groupement hydroxyle *endo* sur C_8 dans les composés **2** et **11**. Sur ce même carbone C_8 dans les composés aminés **4**, **5**, **6** et **7**, l'effet de blindage γ dû au groupement substituant C_2 est trouvé égal à 6.4 ppm donc du même ordre de grandeur que celui d'un hydroxyle, avec une exception pour **5** (-2.1 ppm) qui s'explique parfaitement si on considère qu'à un effet γ blindant d'environ 6.4 ppm, se superpose un effet δ déblindant dû au méthyle substituant l'azote, cet effet δ serait de 4.3 ppm environ. Pour assurer les bases de cette discussion nous avons étudié un composé supplémentaire obtenu en remplaçant dans **2** le groupement OH par OCH_3; les valeurs de déplacement chimique relatives à ce nouveau composé devenant directement comparables à celles de **2** et **5**. En particulier le groupement méthyle doit jouer le même rôle que dans **5**; nous avons trouvé pour C_3 et C_8 deux valeurs de déplacement de 22.9 et de 26.2 ppm respectivement. Si on considère sur C_3 un effet β d'environ 9.8 ppm, le méthyle introduirait un effet γ blindant de -5.8 ppm environ. Sur C_8 un effet γ blindant de l'hétéroatome d'environ -6.9 ppm se superposerait un effet δ déblindant du méthyle d'environ 3.7 ppm. Ces valeurs sont clairement comparables à celles attribuées au composé **5**. Notons que les autres carbones du composé méthoxylé ont des déplacements comparables à ceux de **2**.

Composé 3

L'attribution des carbones C_3, C_4 et C_8 pour ce composé tient compte des effets de substituant de la manière suivante: on observe en effet qu'une valeur correspond à un déblindage et deux valeurs à des blindages. Comme dans les exemples précédents, C_3 en β du substituant doit être déblindé, raison pour laquelle nous lui attribuons 25.8 ppm soit un blindage de -2.9 ppm par rapport au carbone similaire de **2**, car l'effet d'un groupement OH sur le carbone β est d'environ 6 ppm si l'OH est axial alors qu'il est de 9 ppm environ si l'OH est équatorial. On note encore que la position axiale du groupement OH dans ce cas peut entrainer une déformation de cycle ou la contribution d'un autre conformère puisque le carbone C_7 est blindé de -1.4 ppm contrairement à ce que l'on observe dans tous les autres exemples. Il est logique d'attribuer la valeur de 29.5 ppm à C_6, comme dans les cas précédents. Pour les deux carbones restants C_4 et C_8, l'attribution est faite en considérant que l'un d'eux C_4 subit un blindage par effet γ stérique, alors que l'autre serait blindé par effet *anti*-γ dû à un arrangement *anti* périplanaire du carbone considéré et de l'hétéroatome (32). La valeur la plus faible est attribuée à C_4 comme dans d'autres exemples de la littérature (19) mais aucune preuve ne peut être apportée pour l'instant à cette attribution.

Autres effets observés

Les effets β sur le carbone C_1 en tête de pont sont dans tous les cas les plus faibles que sur C_3 ce qui a déjà été observé par d'autres auteurs (17) ces effets sont plus faibles pour les composés substitués par N—R que pour ceux substitués par OH, sauf dans le cas de **6**, ce qui peut s'expliquer si on envisage un effet stérique δ (environ 2.4 ppm) dû à une interaction entre les hydrogènes des méthyles du groupe tertiobutyle et l'hydrogène en tête de pont (20, 31).

L'effet de la taille du substituant de l'azote sur le déplacement chimique de C_2 est aussi remarquable dans les composés **4**, **5**, **6** et **7**. Le remplacement de NH_2 par $N—CH_3$ déblinde le carbone C_2 de 5.3

TABLEAU 3. Deplacements chimiques

Composé	R	X	δ (ppm) Cα	Cβ	Référence
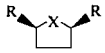	H	CH_2	25.6		2
	H	O	68.6	26.7	27
	H	NMe	56.9	24.6	27
	H	NPh	48.5	28.3	27
	CH_3	O	75.4	33.2	Ce travail

NOTE: Pour les composés **13**, **18** et **21** voir le tableau 4; la réf. 14 donne

ppm. Le remplacement par N—*t*Bu ou N—Ph blinde ce carbone. Il est vraisemblable que dans le cas de **6** et **7** une interaction de type γ-*gauche* a lieu entre l'hydrogène porté par C_2 et les méthyles du groupe tertiobutyle dans le cas de **6**, et un hydrogène *ortho* du groupe phényle dans le cas de **7**. La nécessité pour ces gros groupements de se dégager du système bicyclique impose malgré tout certaines interactions, et l'interaction γ-*gauche* est moindre (en rmn de ^1H le déplacement chimique à champ faible du proton porté par C_2 (3.8 ppm) indique qu'il se situe dans le plan du cycle phényle (33)).

Enfin l'étude du composé **12** a été faite pour voir si le remplacement d'un méthyle par un éthyle avait une grosse influence, ce type de substitution a été reconnu comme déplaçant la résonance des carbones en α de l'éthyle à champ faible et ceux en β à champ fort (dans ce dernier cas, 1.4–4.4 ppm) (14). Les carbones concernés ici sont ceux en tête de pont et sont effectivement blindés de 2.6 ppm pour C_1 et 2.2 ppm pour C_5. On constate par ailleurs que les déplacements chimiques des autres carbones de **9** et **12** sont très proches. Ces blindages, de même que ceux des carbones C_1 et C_5 de **10** par rapport à **8**, et de **11** par rapport à **9**, peuvent encore s'interpréter par un effet de type γ stérique (interactions de CH_3 de l'éthyle et de C—H *ortho* du cycle phényle avec C_1—H).

Composés bicyclo[4.2.1]nonaniques

Composés non fonctionnels

Dans le tableau 3 nous montrons que les déblindages des systèmes bicyclo[3.2.1]octaniques et bicyclo[4.2.1]nonaniques par rapport au composé à cinq chaînons de références présentent des analogies. Par ailleurs les carbones des cycles à six ou sept chaînons situés en tête de pont ou en α des carbones tête de pont sont beaucoup plus déblindés que leurs analogues de la série bicyclo[3.3.1]nonanique. Cette première constatation est insuffisante pour l'attribution des déplacements chimiques mais cette attribution peut se faire sans ambiguïté en comparant les déplacements chimiques de **13**, **18** et **21** avec ceux de l'alcool **24** si on note que dans cet alcool le groupe OH *exo* ne peut donner lieu à aucune interaction stérique. Les quatre couples de déplacement chimique sont ainsi déterminés.

Nous avons publié (34) que l'analyse des déplacements chimiques de **13**, **23** et **24** impliquait la conformation B (bateau pour le cycle à sept chaînons), pour ces composés, ceci sur la base d'analyse des interactions du groupe OH de **23** vis à vis de différents carbones du cycle. Cette conclusion insuffisante doit être modifiée par la possibilité d'un équilibre entre A et B et en particulier si la forme A est présente, un effet γ stérique important doit avoir lieu entre les couples C_3/C_4 et C_7/C_8.

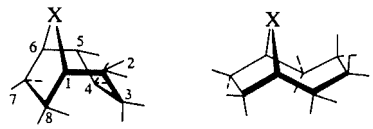

A B

Bien que le diméthyl-2,5 tétrahydrofuranne *cis* ait vraisemblablement une conformation un peu différente de celle de **13** il nous a été suggéré que l'étude de ce composé (réf. 35 et tableau 3) pouvait apporter quelques renseignements par comparaison des déplacements chimiques des carbones C_3/C_4 de ce composé et C_8/C_7 de **13**. Le déplacement chimique trouvé pour ce dernier couple est de 31.6 ppm soit une valeur inférieure de 1.6 ppm par rapport au couple C_3/C_4 du tétrahydrofuranne substitué. Au cas ou ce dernier modèle serait correct pour faire une comparaison valable, on concluerait à un équilibre entre les formes A et B pour **13** sans pouvoir donner les populations respectives des deux conformères. Comme par ailleurs une interconversion rapide entre les conformères C et D impliquerait l'observation de quatre valeurs de déplacements chimiques par rmn, l'étude de ces derniers s'avère insuffisante pour une conclusion en faveur d'une conformation préférentielle.

Pour les composés **18** et **21** on remarque que les couples C_3/C_4 ont à peu prés le même déplacement

Can. J. Chem. Downloaded from www.nrcresearchpress.com by 210.87.254.6 on 09/05/12
For personal use only.

Can. J. Chem. Downloaded from www.nrcresearchpress.com by 210.87.254.6 on 09/05/12
For personal use only.

chimique que dans **13**, ceci impose en particulier pour **18** que le méthyl n'ait pas d'interaction avec C_3/C_4 car ces carbones devraient subir un déblindage par effet δ stérique, dans le cas de la forme bateau; les carbones C_2/C_5 devraient eux subir un blindage par effet γ stérique dans le cas de la forme chaise (comparer le déplacement de C_2 dans **1** et **8** d'une part, **13** et **18** d'autre part). Ceci tend à prouver que le méthyle dans **18** est préférentiellement au-dessus du cycle pyrrolidinique. Donc les déplacements chimiques des couples C_3/C_4 imposent le même équilibre conformationnel pour **13**, **18** et **21**, et subissent ou non la même influence de la part du doublet libre de l'hétéroatome.

Composés fonctionnels

Les composés **23** et **24** ont été analysés dans la réf. 34 et dans ces deux cas la valeur des déplacements chimiques des couples C_3/C_4 proche de celles des composés étudiés ci-dessus semble indiquer que leur comportement conformationnel est similaire à celui des produits précités. Dans le cas de **23** en particulier la présence d'un groupe hydroxyle en *endo* provoque une gêne stérique considérable entre C_3/C_4 et OH, ce qui impose pour le moins un aplatissement important du cycle à sept chaînons, à partir de la position chaise.

*Composés **14**, **15**, **19**, et **22***

Pour ces composés ayant un substituant *endo* en position 2 l'attribution des carbones C_1, C_2 et C_6 est faite sans ambiguïté. On attribue aux carbones C_5 et C_7 les valeurs les plus proches de celles des carbones similaires dans les composés parents, car d'une part, ils sont éloignés du substituant (quatre liaisons) et ne subissent pas d'effet inductif de celui-ci; d'autre part les interactions stériques qu'ils pourraient subir dans certaines conformations envisageables pour la molécule ne conduiraient pas à des valeurs cohérentes pour les déplacements chimiques des autres carbones (nous y reviendrons plus loin à propos de l'étude conformationnelle).

Le carbone C_3 étant situé en β du groupement substituant doit être déblindé, comme nous l'avons vu avec la première série de composés et les écarts de déplacements chimiques observés ont un ordre de grandeur qui justifie l'attribution ainsi faite. Pour les deux carbones restants, C_4 et C_8, l'attribution proposée est basée sur le fait que ces carbones situés en γ du substituant peuvent être blindés. En particulier la valeur attribuée à C_8 correspondrait à un blindage de ce carbone de -8.3 à -9.1 ppm (compatible avec celui du carbone C_5 dans le composé **23** quand l'hydroxyle *endo* est porté par C_7). Sauf si la molécule est en conformation chaise pure (ce qui est improbable, cf. plus loin) le carbone C_8 peut en effet donner lieu à un blindage de la part du substituant en position γ par rapport à lui (éclipse des liaisons C_8—H ... O—H). La valeur restante correspondant à un blindage de -4.9 à -5.1 ppm (pour les substituants OH) est attribuée à C_4.

L'interconversion des valeurs ainsi attribuées à C_8 et à C_4 conduirait à des effets de blindage pour ces deux carbones dans **14**, **19** et **22** beaucoup plus grand pour C_8 et plus petit pour C_4 (**14** par exemple: -12.3 et -1.2 ppm respectivement). De plus ces effets seraient assez différents d'un composé à l'autre alors qu'ils sont dus au même substituant. Il ne semble pas possible de lever cette indétermination pour l'instant.

En ce qui concerne l'étude conformationnelle de ces molécules les formes A et B peuvent être exclues. Dans le cas de A par exemple la valeur de C_7 (plus déblindé que dans le composé parent) exclut une forte interaction entre C_3/C_4 et C_7/C_8. On devrait de même dans ce cas observer un effet δ sur C_5 par exemple dû à l'interaction C_2—H - - - H—C_5. Enfin les blindages de C_4 et C_8 par le substituant *endo*-2 ne sont pas explicables par des effets stériques, ou des dispositions antipériplanaires des atomes concernés (32). On peut exclure la conformation B pure pour des raisons du même type. L'analyse conformationnelle de tous les dérivés bicyclo[4.2.1]nonaniques substitués, à partir des déplacements chimiques est ardue car on ne connait pas les conformations privilégiées des composés non substitués et le déplacement chimique induit par le substituant et celui dû aux changements conformationnels influencent ceux des composés substitués.

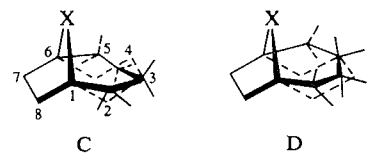

C D

Des conformations *gauches* C et D peuvent être envisagées et se justifient par les valeurs des déplacements chimiques des différents carbones. On peut remarquer que le déplacement du méthyle à bas champ de 1.7 ppm dans **19** pourrait être dû à une interaction de ce dernier et des hydrogènes de C_3 et C_4 suivant que l'équilibre C ⇌ D est en faveur de l'une ou l'autre forme. Le cycle à sept chainons étant flexible il y a peu de chance dans les conditions de température où l'on opère d'avoir une seule conformation, et les valeurs de déplacement ainsi observées sont certainement des valeurs moyennes d'où les difficultés d'attribution et d'interprétation. Il n'en reste pas moins que les formes C et D représentent des modèles où les interactions entre atomes sont moindres et sont certainement celles qui sont statistiquement observées, ce qui n'exclut pas qu'elles

Can. J. Chem. Downloaded from www.nrcresearchpress.com by 210.87.254.6 on 09/05/12
For personal use only.

TABLEAU 4. Déplacements chimiques en ppm/TMS dans $CDCl_3$ et effets de substituants

Composé	C_1	C_2	C_3	C_4	C_5	C_6	C_7	C_8	N—C
13 Oxa-9 bicyclo[4.2.1]nonane	77.7	36.2	24.4	24.4	36.2	77.7	31.6	31.6	
14 Oxa-9 bicyclo[4.2.1]nonanol-2 *endo*	81.5	72.3	33.8	19.3	35.9	76.4	32.6	23.2	
	(3.8)	(36.1)	(9.4)	(−5.1)	(−0.3)	(−1.3)	(1)	(−8.4)	
15 Oxa-9 amino-2 *endo* bicyclo-[4.2.1]nonane	81.0	54.2	34.5	21	36.0	75.9	32.1	23	
	(3.3)	(18.0)	(10.1)	(−3.4)	(−0.2)	(−1.8)	(0.5)	(−8.6)	
16 Oxa-9 bicyclo[4.2.1]nonanol-2 *exo*	84.7	75.2	33.2	18.5	36.4	77.6	31.5	28.6	
	(7.0)	(39.0)	(8.8)	(−5.9)	(0.2)	(−0.1)	(−0.1)	(−3)	
17 Oxa-9 bicyclo[4.2.1]nonanone-2	83.8	218.4	42.0	18.8	35.6	79.8	31.6	26.7	
	(6.1)	(182.2)	(17.6)	(−5.6)	(−0.6)	(2.1)	(0)	(−4.9)	
18 *N*-Méthylaza-9 bicyclo[4.2.1]-nonane	64.7	35.4	24.6	24.6	35.4	64.7	30.2	30.2	42.9
19 *N*-Méthylaza-9 bicyclo[4.2.1]-nonanol-2 *endo*	71.1	72.9	32.8	19.7	35.2	64.1	31.7	21.9	44.6
	(6.4)	(37.5)	(8.2)	(−4.9)	(−0.2)	(−0.6)	(1.5)	(−8.3)	(1.7)
20 *N*-Méthylaza-9 bicyclo[4.2.1]-nonanol-2 *exo*	72.9[a]	73.9[a]	32.5	18.5	35.8	65.3	29.9	26.7	46.6
	(8.2)	(38.5)	(7.9)	(−6.1)	(0.4)	(0.6)	(−0.3)	(−3.5)	(3.7)
21 *N*-Phénylaza-9 bicyclo[4.2.1]-nonane	54.7	32.3	24.1	24.1	32.3	54.7	31.0	31.0	146.0[c]
22 *N*-Phénylaza-9 bicyclo[4.2.1]-nonanol-2 *endo*	59.8	69.3	33.5	19.2	32.3	53.3	32.3	21.9	145.7[d]
	(5.1)	(37)	(9.4)	(−4.9)	(0)	(−1.4)	(1.3)	(−9.1)	(−0.3)
23 Oxa-9 bicyclo[4.2.1]nonanol-7 *endo*	77.4	34.7	24.6[a]	24.1[a]	27.9	79.2	73.2	37.0	
	(−0.3)	(−1.5)	(0.2)	(−0.3)	(−8.3)	(1.5)	(41.6)	(5.4)	
24 Oxa-9 bicyclo[4.2.1]nonanol-7 *exo*	78.2	34.5[b]	24.7[a]	24[a]	33.2[b]	85.1	79.6	39.5	
	(0.5)	(−1.7)	(0.3)	(−0.4)	(−3)	(7.4)	(48.0)	(7.9)	
25 Oxa-9 bicyclo[4.2.1]nonanone-7 D_1-6, D_2-8	76	37.1	24.4	22.3	31.8		219.7		
	(−1.7)	(0.9)	(0)	(−2.1)	(−4.4)		(188.1)		

[a, b]Valeurs pouvant être interchangées.
[c]C *ortho* 111.4, C *para* 114.4, C *méta* 129.4.
[d]C *ortho* 111.2, C *para* 115.1, C *méta* 129.5.

soient les intermédiaires de l'équilibre plus général $A \rightleftharpoons B$

Composés 16 et 20

Les attributions sont faites selon le même principe que dans les molécules précédentes, les atomes C_4 et C_8 étant blindés par effet stérique du substituant pour le premier et par effet *anti*-γ dû à la disposition *anti* périplanaire possible de OH et C_4 pour le second. Dans le composé **20** on note le fort déblindage du méthyle porté par l'azote, 3.7 ppm par rapport à **18** et 2 ppm par rapport à **19**, qui traduit certainement des interactions différentes de celles qui avaient lieu dans les composés précédents. Il n'est pas impossible de penser dans ce dernier cas à un effet sur le méthyle dû à une interaction OH ... H_3C, par exemple.

Composés 17 et 25

Les attributions de déplacements chimiques ont été faites en comparant les effets du groupement C=O de ces deux cétones avec ceux de cétones de structures rigides connues (14–16). La deutériation des carbones 6 et 8 dans **25** permet la mesure des déplacements des seuls carbones du cycle à sept chaînons.

L'examen du tableau 4 permet de voir que le groupement C=O perturbe le déplacement chimique de C_5 (blindage de 4.4 ppm). Des blindages de cette nature ont déjà été relevés pour des cétones cyclohexaniques (31). Le carbone C_4 en position δ par rapport à l'oxygène du groupement carbonyle est blindé de 2.1 ppm, ce qui est cohérent avec ce que l'on observe en série bicyclooctanique où des blindages sont notés pour des carbones situés en position δ par rapport à l'oxygène d'un groupement C=O (13, 15).

Le carbone C_3 ne change pas de déplacement chimique par rapport au composé non substitué, ceci conduit à penser que **25** donne lieu à un équilibre conformationnel identique à celui de **13** par exemple.

Les effets de substituants sur la cétone **17** pré-

sentent deux caractéristiques essentielles. (*i*) Le déblindage du carbone C_1 en β du groupement carbonyle est faible, et du même ordre de grandeur que celui obtenu pour un groupement OH (dans la bicyclo[3.2.1]octanone-2, cet effet est de 15.1 ppm pour C_1); (*ii*) Deux carbones C_4 et C_8 sont blindés respectivement de 5.6 et 4.9 ppm, et ceci peut être dû soit à une double interaction du type =O ... HC, soit à une interaction du type précédent sur C_8 et une interaction γ stérique sur C_4 du doublet de l'oxygène du pont. Il est toutefois difficile de proposer une conformation au vu de ces résultats qui permettent d'éliminer les formes chaise et bateau pour **17**.

Partie expérimentale

Produits

Les produits **1** et **13** ont été préparés selon la réf. 36, **2**, **3**, **14**, **17**, **23** et **24** selon la réf. 37, **25** selon la réf. 38 et **4**, **5**, **6**, **7**, **8**, 9, **10**, **11**, **12**, **15**, **18**, **19**, **21** et **22** selon la réf. 33. Ces derniers produits étant préparés par aminomercuration intramoléculaire d'aziridines ou d'aminoalcools, suivie d'une réduction du mercurique par $NaBH_4$, nous avons ainsi pu deutérer le carbone C_6 du produit 9 en réduisant son mercurique précurseur par $NaBD_4$.

Le produit **20** a été préparé selon la réf. 39.

Appareillage

Les spectres rmn ^{13}C ont été tracés sur un spectromètre à impulsions Brucker-W.P. 60 fonctionnant à 15.08 MHz dans un champ de 14 090 G, avec transformée de Fourier, donnant les déplacements chimiques au $\frac{1}{10}$ de ppm.

Les échantillons utilisés avaient une concentration de l'ordre de 0.5 *M* dans $CDCl_3$ en tubes de 10 mm.

Ils ont été examinés avec irradiation totale par bruit des protons, afin de faire apparaître chaque carbone sous forme de singulet.

Des expériences de découplage "off-resonance" ont été effectuées afin de permettre l'attribution de différents carbones par la multiplicité des raies qu'ils présentaient.

1. J. B. Stothers. Carbon-13 NMR spectroscopy. Academic Press, New York, NY. 1972.
2. G. C. Levy et G. L. Nelson. ^{13}C nuclear magnetic resonance for organic chemists. Wiley Interscience, New York, NY. 1972.
3. N. K. Wilson et J. B. Stothers. Top. Stereochem. **8**, 1 (1974).
4. D. M. Grant et B. V. Cheney. J. Am. Chem. Soc. **89**, 5315 (1967).
5. E. Lippmaa, T. Pehk, J. Paasivirta, N. Belikova et A. Plate. Org. Magn. Reson. **2**, 581 (1970).
6. J. B. Stothers, C. T. Tan et K. C. Teo. Can. J. Chem. **51**, 2893 (1973).
7. J. B. Grutzner, M. Jautelat, J. B. Dence, R. A. Smith et J. D. Roberts. J. Am. Chem. Soc. **92**, 7107 (1970).
8. H. J. Schneider et W. Bremser. Tetrahedron Lett. 5197 (1970).
9. G. E. Maciel et H. C. Dorn. J. Am. Chem. Soc. **93**, 1268 (1971).
10. T. Pehk, E. Lippmaa, V. V. Sevostjanova, M. M. Krayuschkin et A. I. Tarasova. Org. Magn. Reson. **3**, 783 (1971).
11. G. E. Maciel, H. C. Dorn, R. L. Green, W. A. Kleschick, M. R. Peterson et G. H. Wahl. Org. Magn. Reson. **6**, 178 (1974).
12. E. Wenkert, J. S. Binda. C. J. Chang, D. W. Cochran et F. M. Shell. Acc. Chem. Res. **7**, 46 (1974).
13. J. B. Stothers, C. T. Tan et K. C. Teo. Can. J. Chem. **54**, 1211 (1976).
14. E. Lippmaa, T. Pehk, N. A. Belikova, A. A. Bobyleva, A. N. Kalinichenko, M. D. Ordubadi et A. F. Plate. Org. Magn. Reson. **8**, 74 (1976).
15. J. B. Stothers et C. T. Tan. Can. J. Chem. **54**, 917 (1976).
16. J. B. Stothers, J. R. Swenson et C. T. Tan. Can. J. Chem. **53**, 581 (1975).
17. S. H. Grover et J. B. Stothers. Can. J. Chem. **52**, 870 (1974).
18. H. Eggert, C. L. van Antwerp, N. S. Bhacca et C. Djerassi. J. Org. Chem. **41**, 71 (1976).
19. A. Heumann et H. Kolshorn. Tetrahedron, **31**, 1571 (1975).
20. J. R. Wiseman et H. O. Krabbenhoft. J. Org. Chem. **40**, 3222 (1975).
21. J. R. Wiseman et H. O. Krabbenhoft. J. Org. Chem. **41**, 589 (1976).
22. (*a*) J. R. Wiseman, H. O. Krabbenhoft et B. R. Anderson. J. Org. Chem. **41**, 1518 (1976); (*b*) J. A. J. M. Vincent, P. Schipper, A. de Groot et H. M. Buck. Tetrahedron Lett. **24**, 1989 (1975).
23. H. J. Schneider, M. Lonsdorfer et F. F. Weingand. Org. Magn. Reson. **8**, 363 (1976).
24. H. Caldararu et M. Moraru. J. Am. Chem. Soc. **96**, 149 (1974) et références citées.
25. E. M. Engler, J. D. Andose et P. V. R. Schleyer. J. Am. Chem. Soc. **95**, 8005 (1973).
26. J. B. Lambert, D. A. Netzel, Hsiang Nig Sun et K. K. Lilianstrom. J. Am. Chem. Soc. **98**, 3778 (1976).
27. J. A. Hirsch et E. Havinga. J. Org. Chem. **41**, 455 (1976).
28. C. P. Nash et G. E. Maciel. J. Phys. Chem. **68**, 832 (1964).
29. J. D. Roberts, F. J. Weigert, J. I. Kroschwitz et H. J. Reich. J. Am. Chem. Soc. **92**, 1338 (1970).
30. H. Eggert et C. Djerassi. J. Am. Chem. Soc. **95**, 3710 (1973).
31. J. B. Stothers et C. T. Tan. Can. J. Chem. **52**, 308 (1974).
32. E. L. Eliel, W. F. Bailey, L. D. Kopp, R. L. Willer, D. M. Grant, R. Bertrand, K. A. Christensen, D. K. Dalling, M. W. Duch, E. Wenkert, F. M. Schell et D. W. Cochran. J. Am. Chem. Soc. **97**, 322 (1975).
33. M. Barrelle et M. Apparu. Tetrahedron, **33**, 1309 (1977).
34. M. Barrelle, M. Apparu et C. Gey. Tetrahedron Lett. 4725 (1976).
35. V. Speziale, J. Roussel et A. Lattes. J. Heterocycl. Chem. 771 (1974).
36. F. G. Bordwell et M. L. Douglas. J. Am. Chem. Soc. **88**, 993 (1966).
37. M. Barrelle et M. Apparu. Bull. Soc. Chim. 2016 (1972).
38. M. Apparu. Thèse d'Etat. Université Scientifique et Medicale, Grenoble, France. 1977.
39. J. W. Bastable, J. D. Hobson et W. D. Riddell. J. Chem. Soc. Perkin Trans. I, 2205 (1972).

Can. J. Chem. Downloaded from www.nrcresearchpress.com by 210.87.254.6 on 09/05/12
For personal use only.

Stereochemically controlled syntheses of some bicyclo[*n*.3.0]alkane-1-carboxylic acids

E. W. WARNHOFF, W. T. TAI, AND Y. C. TOONG

Department of Chemistry, University of Western Ontario, London, Ont., Canada N6A 5B7

Received August 8, 1977

E. W. WARNHOFF, W. T. TAI, and Y. C. TOONG. Can. J. Chem. **56**, 93 (1978).

Stereospecific methods of synthesis of some *cis*- and *trans*-bicyclo[*n*.3.0]alkane-1-carboxylic acids are described, specifically **5***a*, **5***b*, and **11**. The *cis* ring fusion is insured by use of the Diels–Alder reaction, and the *trans* ring fusion is fixed by the necessity of a *cis* attachment of an intermediate five-membered cyclic lactamol to the existing cyclopentane ring in **9**.

E. W. WARNHOFF, W. T. TAI et Y. C. TOONG. Can. J. Chem. **56**, 93 (1978).

On décrit des méthodes stéréospécifiques de synthèses de quelques acides bicyclo[*n*.3.0]alcanecarboxyliques-1 *cis* et *trans* et en particulier de **5***a*, **5***b* et de **11**. On s'assure de la fusion *cis* du cycle par l'utilisation d'une réaction de Diels–Alder; la fusion *trans* du cycle est déterminée par la nécessité d'avoir un point d'attache *cis* pour un intermédiaire lactamol cyclique à cinq chaînons au noyau cyclopentanique existant dans **9**.

[Traduit par le journal]

As part of a study of certain Favorskii rearrangements (1), authentic samples of several bicyclo-[*n*.3.0]alkane-1-carboxylic acids of unambiguously established geometry were required for comparison with reaction products. An acid corresponding in structure to one of the needed *cis*-acids, bicyclo-[3.3.0]octane-1-carboxylic acid, has already been prepared in three ways (2–4). While the *cis* isomer **5***a* is clearly more stable than the corresponding *trans* epimer, and while each of the three routes probably gave the *cis* isomer, one is left feeling queasy since none of them *guaranteed* a *cis* fusion. One of the routes was the Favorskii rearrangement (2) whose mechanism and stereochemistry were under study (1).[1] The second preparation (3) by the Koch–Haaf carboxylation of the bicyclo[3.3.0]octyl-1-cation unfortunately has associated with it in principle the *cis*/*trans* ambiguities found for the same reaction applied to the bicyclo[4.4.0]decyl-1-cation (5). The third synthesis, the Dieckmann cyclization of the triester of a 1-carboxycyclopentane-1,2-diacetic acid of unknown stereochemistry (4), relies for its assignment of *cis* geometry on the assumption that the *trans*-diacetic ester would not cyclize, which in turn was based on analogy with the closely related, but different, case of cyclopentane-1,2-diacetic ester (6). Further doubt is raised by discrepancies in melting points of the amide derivative (131°C) reported in this last work and of that (107.5 and 108°C) found in the first two syntheses. In view of our need to be certain, this *cis*-acid **5***a* and its higher homolog **5***b* were synthesized by the general procedure outlined in Scheme I which employs the Diels–Alder reaction of a 1-cycloalkenecarboxylic acid with butadiene to insure the *cis* ring fusion. Contraction of the newly formed cyclohexene ring in **2** by oxidative cleavage and subsequent cyclization of the resulting diacid **3**, followed by decarboxylation and Wolff–Kishner reduction yielded the desired *cis*-acids **5**. Since the same bicyclo[3.3.0]octane-1-carboxylic acid was obtained as from the three previously described syntheses (2–4), this acid is now established with certainty to have the *cis* geometry. The melting point of the amide of **5***a* prepared via the Diels–Alder route was 108°C in agreement with refs. 2 and 3.

On the other hand, the synthesis of pure *trans*-bicyclo[5.3.0]decane-1-carboxylic acid was less straightforward. The initial intent was to add cyanide to the conjugated ketone **6**, reduce the carbonyl

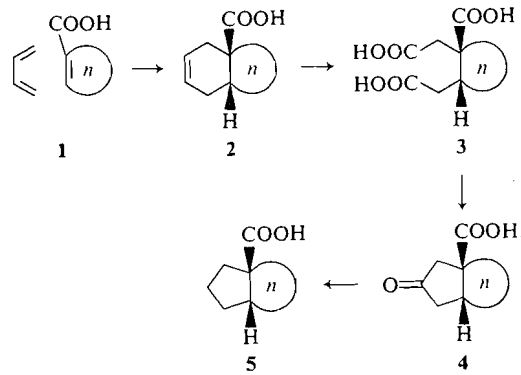

SCHEME I

[1]The correlation of the amide of the bicyclo[3.3.0]octane-1-carboxylic acid with the product of nitration of *cis*-bicyclo-[3.3.0]octane carried out in ref. 2 rests on the assumption that the *cis*-nitro compound is formed.

Can. J. Chem. Downloaded from www.nrcresearchpress.com by 210.87.254.6 on 09/05/12
For personal use only.

Can. J. Chem. Downloaded from www.nrcresearchpress.com by 210.87.254.6 on 09/05/12
For personal use only.

group, and hydrolyze the nitrile. This simple approach seemed worthwhile in view of the ready availability of enone **6**, although it was realized that, even if *anti*-conjugate addition occurred to yield *trans*-keto nitrile **8**, the ring junction was under control of the equilibration permitted by the adjacent carbonyl group (7). In a number of such fused 5/7 ring systems the *cis* and *trans* isomers are of comparable stability (8), but perhaps the *trans* isomer might undergo reduction more rapidly. In the event, conjugate addition of cyanide yielded a mixture of about equal amounts of both *cis*- and *trans*-keto nitriles **7** and **8** (Scheme 2), and unfortunately Wolff–

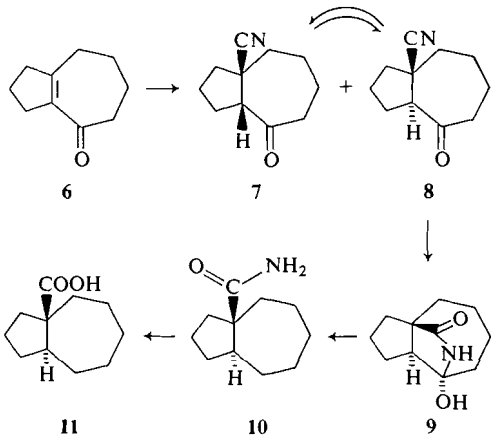

SCHEME 2

Kishner reduction of this mixture produced the *cis*-acid **5***b* plus another acid which was presumed to be the *trans*-acid **11**. Although the acids were separable by glpc of their methyl esters, it was preferable to have a synthesis which would yield unequivocally only the *trans* stereoisomer. Attainment of this goal was aided by a third crystalline product formed in varying amounts in the conjugate addition of cyanide to **6**.

Thus from one conjugate addition reaction, the major product was this crystalline solid containing neither nitrile nor ketone functions. The presence of amide C=O, NH, and OH infrared absorption, in conjunction with Wolff–Kishner reduction of the compound to the *cis*-acid **5***b*, allowed the solid to be identified as a lactamol, R—(C=O)—NH—C—OH. Examination of Dreiding models revealed that only the *trans* ring fusion of keto amide **18** (Scheme 3) would allow a strainless intramolecular addition of the amide NH to the ketone as in **9**; for the *cis*-epimer **12**, lactamol formation would not occur because it would force a strained *trans* fusion of two five-membered rings. This situation is in contrast to that obtaining for similar lactamols **14** and **15** from the octalone **13** (and from its non-methyl derivative)

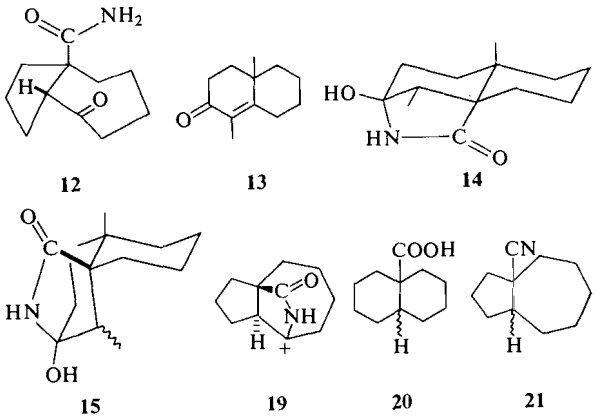

for which both the *cis* and *trans* ring fusions allow strain-free lactamol formation (9).[2] Therefore, since it was known with confidence that the crystalline lactamol **9** possessed the *trans* carbocyclic ring fusion, further efforts to prepare pure *trans* **11** centered around finding conditions to reduce the potential ketone group without allowing epimerization via enolization. The Wolff–Kishner reduction of **9** to **5***b* had occurred with epimerization, and hence the Clemmensen reduction was tried, but it gave a low yield of a mixture of *cis*- and *trans*-acids **5***b* and **11** with *cis* predominating. Finally, resort was had to the just published electrolytic procedure of Throop and Tökés (11) which had been shown to reduce ketones to methylene groups with little or no prior enolization in spite of the strong acid electrolyte. Although the lactamol gave no evidence of any keto tautomer **18** in its infrared spectrum, it was hoped that there would be sufficient **18** for reduction or else that a cationic species such as **19** would be reduced. Gratifyingly, **9** did undergo electroreduction to a single crystalline amide, **10**, mp 156°C, which was converted into the crystalline *trans*-acid **11**, mp 101.5°C, by diazotization. The conceivable possibility that the lactamol **9** or its open keto amide tautomer **18** might have rearranged (12) during reduction in the strong acid medium to a bicyclo-[4,4,0]decane-1-carboxylic acid **20** is excluded by the fact that these known compounds have quite different melting points: *cis*, mp 124°C; *trans*, mp 137°C (5, 10); likewise the melting points of their amides (*cis*, mp 132°C, *trans*, mp 128°C) are different from that of **10**. This synthetic method could presumably be used for other homologous *trans*-bicyclo[*n*.3.0]-1-carboxylic acids.

A remaining point of interest is the differing reactivity exhibited by the cyano group in this series of

[2]The *trans* keto acid corresponding to **18** behaves in the same way as **18** (10).

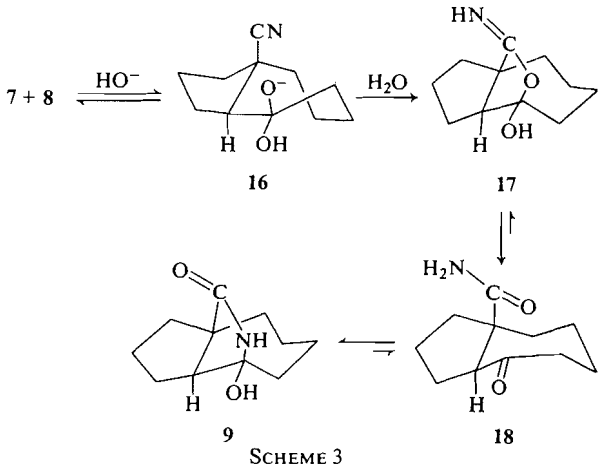

SCHEME 3

compounds. Although hydrolysis occurred under the vigorous high temperature Wolff–Kishner conditions applied to the keto nitrile mixture **7** + **8** and lactamol **9**, in other reactions the inertness of a cyano group at the tertiary junction of a bicyclic system toward the usual hydrolytic reagents was evident. Thus the nitrile **21** from electrolytic reduction of **7** + **8** was not touched by the usually effective hydroxide – hydrogen peroxide reagent, nor was any hydrolysis product formed in hot phosphoric acid. The cyano group of the keto nitrile mixture **7** + **8** was not hydrolyzed by hot phosphoric acid. In view of this demonstrated reluctance to react, the conversion of the keto nitrile mixture **7** + **8** to the lactamol **9** under the relatively mild conditions of refluxing methanolic hydroxide is best interpreted as the result of an intramolecular addition to the nitrile made possible by the nearby ketone function (Scheme 3). The activation energy for the addition **16** → **17** will be less than for an intermolecular reaction of **8** or **21** with hydroxide mainly because in **16** the translational entropy of hydroxide has already been lost in the preceding step. Similar intramolecular effects were noted for the nitriles from **13** (9).

Experimental

General

Melting points were taken on a Reichert Kofler microscope hot stage and are corrected. Infrared spectra were recorded on a Beckman IR-5A or IR-10 spectrophotometer. ^{1}Hmr spectra were determined on a Varian A-60 or T-60 spectrometer. Camag DF-5 silica gel was used for tlc plates developed in various proportions of EtOAc–PE or $CHCl_3$–HOAc (94:6). Mass spectra were obtained by Mr. Doug Hairsine on a MAT 311A instrument. A Glowall Model 400 instrument fitted with a 1.8 × 3.4 mm spiral glass column packed with 5% DEGS on non-acid-washed 60–80 mesh Chromosorb P was used for glpc with argon or helium carrier gas and a hydrogen flame detector. The dc generator for electrolytic reduction was a Harrison Laboratory Model 855B. Organic solutions were washed to neutrality and dried by shaking with saturated NaCl and standing over anhydrous $MgSO_4$. Microanalyses were carried out in the laboratories of A. B. Gygli, Toronto, Ontario, and A. Bernhardt, Mülheim, West Germany. The following abbreviations are used: PE = petroleum ether of bp 60–80°C, pe = petroleum ether of bp 30–60°C, EtOH = ethanol, EtOAc = ethyl acetate, MeOH = methanol, HOAc = acetic acid, s = singlet, t = triplet, and b = broad.

cis-*Bicyclo[4.3.0]non-3-ene-1-carboxylic Acid* **2a**

This acid was prepared by the Diels–Alder reaction between 5 ml of liquefied butadiene and 1.90 g (16.9 mmol) of cyclopentene-1-carboxylic acid **1a** (13), mp 120–121°C, according to the procedure of Kronenthal and Becker (14). A sealed Pyrex tube containing the reactants was heated at 170°C for 26 h. Work-up gave 1.91 g (68%) of crude acid **2a**, mp 65–81°C. Three recrystallizations from HOAc–H_2O raised the mp to 80–81°C (lit. (14) mp 80.5°C).

1-Carboxycyclopentane-cis-*1,2-diacetic Acid* **3a**

To a solution of 3.92 g (23.6 mmol) of unsaturated acid **2a** in 45 ml of water containing 2.0 g of KOH was added with stirring a solution of 9.20 g (58.2 mmol) of $KMnO_4$ in 220 ml of water. The reaction temperature was maintained at 30°C by an ice-water bath. After the $KMnO_4$ had been consumed (30 min), the reaction mixture was acidified (50% H_2SO_4), heated, and filtered while hot. The undissolved MnO_2 was washed with more hot water. The combined aqueous filtrates were concentrated to ~70 ml and chilled. Filtration of the crystallized solid and recrystallization from water yielded 2.76 g (51%) of colorless plates of the *triacid* **3a**, mp 155–160°C. Further recrystallization and drying at 100°C (0.05 Torr) gave an analytical sample, mp 157–160°C (reported (4) for an acid of the same structure but unproven stereochemistry: (150°C). *Anal.* calcd. for $C_{10}H_{14}O_6$ (230.2): C 52.17, H 6.13; found: C 52.74, H 6.20; neutralization equivalent calcd.: 76.7; found: 77.8.

cis-*3-Oxobicyclo[3.3.0]octane-1-carboxylic Acid* **4a**

An intimate mixture of 234 mg (1.01 mmol) of triacid **3a** and 17 mg of BaO under vacuum (150 Torr) in a horizontal tube was slowly heated to 260°C over a period of 2 h and then kept at this temperature until no more product distilled.[3] Redistillation of the product at a lower pressure (0.1 Torr) afforded 55 mg (32%) of oily keto acid **4a**; ir (CCl_4): 3300–2400 (carboxyl OH), 1750 (five-ring C=O), and 1695 cm^{-1} (carboxyl C=O).

The *2,4-dinitrophenylhydrazone* was prepared and partitioned between $CHCl_3$ and aqueous $NaHCO_3$. The ether-washed $NaHCO_3$ solution was acidified (10% H_2SO_4) and extracted with ether. Two recrystallizations from $CHCl_3$–PE gave small golden rosettes, mp 109–111°C. *Mol. Wt.* calcd. for $C_{15}H_{16}N_4O_6$: 348.1070; found (high resolution ms): 348.1066.

cis-*Bicyclo[3.3.0]octane-1-carboxylic Acid* **5a**

(a) Preparation of Semicarbazone

A mixture of 475 mg (2.82 mmol) of crude keto acid **4a**, 500 mg of semicarbazide·HCl, 750 mg of NaOAc, and 4 ml of H_2O were heated with stirring until dissolution. On cooling 530 mg (83%) of semicarbazone crystallized. Three recrystallizations from EtOH–H_2O (decolorizing carbon removed some yellow contaminant) yielded 330 mg of pure derivative, mp 188–190°C dec. *Mol. Wt.* calcd. for $C_{10}H_{15}N_3O_3$: 225.1113; found (high resolution ms): 225.1116.

[3]If the distillation was not conducted slowly, the reaction was incomplete, and the product was mostly the five-ring anhydride carboxylic acid (ir($CHCl_3$): 1850 and 1780 (five-ring anhydride) and 1715 cm^{-1} (carboxyl C=O)).

Can. J. Chem. Downloaded from www.nrcresearchpress.com by 210.87.254.6 on 09/05/12
For personal use only.

Can. J. Chem. Downloaded from www.nrcresearchpress.com by 210.87.254.6 on 09/05/12
For personal use only.

(b) Wolff–Kishner Reduction

A mixture of 165 mg (0.73 mmol) of the semicarbazone of **4***a*, 12 KOH pellets, 1 ml of 85% $H_2NNH_2 \cdot H_2O$, and 3 ml of *tert*-amyl alcohol in a sealed thick-walled glass tube was heated at 165–170°C for 7 h. The reaction was partitioned between water and ether. The aqueous layer was washed once more with ether, acidified (concentrated HCl), and extracted with ether. Evaporation of the water-washed and dried ether solution left 105 mg (95%) of colorless oily **5***a* which crystallized and gave a single tlc spot. A small sample was recrystallized from pe to yield crystals of *cis*-acid **5***a*, mp 43–46°C (reported (2, 4) for an acid of the same structure but unproven stereochemistry: 46–47 and 43–44°C). The rest of the **5***a* was evaporatively distilled at 110°C (40 Torr) to give white crystals; ir (CS_2): 3400–2400 (carboxyl OH) and 1695 cm^{-1} (carboxyl C=O). *Mol. Wt.* calcd. for $C_9H_{14}O_2$: 154.0993; found (high resolution ms): 150.0995. This acid was identical (mp, mixture mp, ir, tlc) with the acid prepared according to ref. 2*b*.

The *amide* of **5***a* was prepared by treatment of 40 mg of **5***a* with $SOCl_2$ at reflux, evaporation of excess $SOCl_2$, addition of benzene, and introduction of NH_3 gas. Recrystallization of the neutral portion of the reaction product from ether–PE gave 10 mg of colorless micaceous flakes, mp 106–108°C (lit. (2*a*) mp 107.5°C); ir (CS_2): 3520, 3440, 3200 (amide NH_2), and 1680 cm^{-1} (amide C=O). *Mol. Wt.* calcd. for $C_9H_{15}NO$: 153.1153; found (high resolution ms): 153.1149.

1-Cycloheptenecarboxylic Acid ***1b***

This acid was prepared in 71% overall yield from cycloheptanone by dehydration and hydrolysis of the cyanohydrin according to Wheeler and Lerner (15). After recrystallization from pe the colorless plates melted at 50.5–51.5°C (lit. (16) mp 49°C); ir (CCl_4): 3200–2500 (carboxyl OH), 1675 (carboxyl C=O), and 1640 cm^{-1} (C=C); ^{1}Hmr ($CDCl_3$) δ: 7.35 (1H, t J = 7 Hz, =CH—(CH_2)) and 11.61 ppm (1H, s, COOH).

cis-*Bicyclo[5.4.0]undec-9-ene-1-carboxylic Acid* ***2b***

The acid **1***b* (3.23 g, 23 mmol) and butadiene (8 ml of liquid) were heated at 170°C for 24 h in two sealed glass tubes. Extraction with aqueous NaOH, washing of the basic solution with benzene and ether, acidification (concentrated HCl), and filtration yielded 2.0 g (44%) of crude acid, mp 73–76°C. Recrystallization from HOAc–H_2O gave colorless plates of the *bicyclic acid* **2***b*, mp 76–77.5°C; ir (CCl_4): 3500–2400 (carboxyl OH) and 1690 cm^{-1} (carboxyl C=O); ^{1}Hmr ($CDCl_3$) δ: 5.60 (2H, bs, CH=CH) and 10.12 ppm (1H, s, COOH). *Anal.* calcd. for $C_{12}H_{18}O_2$ (194.3): C 74.19, H 9.34; found: C 74.39, H 9.43.

1-Carboxycycloheptane-cis-*1,2-diacetic Acid* ***3b***

To a solution of 1.0 g (5.1 mmol) of unsaturated acid **2***b* in 10 ml of 5% aqueous KOH was added in portions with stirring (magnetic bar) 2.40 g of $KMnO_4$. After 0.5 h the reaction mixture was acidified (dilute H_2SO_4), filtered through sintered glass, concentrated to ~30 ml, and chilled to yield 0.40 g (31%) of the *triacid* **3***b*. Three recrystallizations from water gave colorless plates, mp 172–173°C; ir (Nujol): 3500–2250 (carboxyl OH), and 1725–1665 cm^{-1} (broad superimposed carboxyl C=O's). *Anal.* calcd. for $C_{12}H_{18}O_6$ (258.3): C 55.81, H 7.02; found: C 55.65, H 7.04.

cis-*9-Oxobicyclo[5.3.0]decane-1-carboxylic Acid* ***4b***

A thorough mixture of 342 mg (1.32 mmol) of triacid **3***b* and 10 mg of BaO was heated in a horizontal glass tube at 150°C (150 Torr) for 3 h and then at 240°C (60 Torr) until no more product distilled. The 135 mg (52%) of yellow oily *keto acid* **4***b* showed only a trace of impurity on tlc. Evaporative distillation at 133°C (1 Torr) gave a colorless analytical sample: ir (CCl_4): 3500–2400 (carboxyl OH), 1750 (five-ring C=O), and 1700 cm^{-1} (carboxyl C=O). *Anal.* calcd. for $C_{11}H_{16}O_3$ (196.2): C 67.32, H 8.22; found: C 67.29, H 8.18.

The *2,4-dinitrophenylhydrazone* was prepared and isolated by extraction from ether into aqueous $NaHCO_3$. Acidification, extraction into ether, and two recrystallizations from $CHCl_3$ – petroleum ether gave clumps of small golden blades; mp 106–108°C. *Mol. Wt.* calcd. for $C_{17}H_{20}N_4O_6$: 376.1382; found (high resolution ms): 376.1383.

cis-*Bicyclo[5.3.0]decane-1-carboxylic Acid* ***5b***

A mixture of 191 mg (0.98 mmol) of keto acid **4***b*, 1.5 ml of $H_2NNH_2 \cdot H_2O$ (85%), 0.5 g of KOH, and 6 ml of triethylene glycol was refluxed for 1.5 h after which time the excess $H_2NNH_2 \cdot H_2O$ was distilled. The remaining reactants were heated at 200°C for 22 h. The reaction mixture was diluted with water, washed with $CHCl_3$, acidified (concentrated HCl), and extracted with $CHCl_3$ to yield 179 mg (98%) of crude product containing about 5% of **4***b*. Purification by thick-layer chromatography (silica gel developed in PE–EtOAc, 65:35) followed by two recrystallizations from pe gave colorless plates of the *cis-acid* **5***b*, mp 58–60°C; ir (CS_2): 3400–2300 (carboxyl OH) and 1690 cm^{-1} (carboxyl C=O). *Anal.* calcd. for $C_{11}H_{18}O_2$ (182.3): C 72.49, H 9.95; found: C 72.40, H 9.75. *Mol. Wt.* calcd. for $C_{11}H_{18}O_2$: 182.1306; found (high resolution ms): 182.1304.

$\Delta^{1,7}$-*Bicyclo[5.3.0]decen-2-one* ***6***

This conjugated ketone (ir (CCl_4): 1640 cm^{-1} (conjugated C=O)) was prepared in 86% yield by $NaHCO_3$-catalyzed intramolecular condensation of 1,6-cyclodecanedione (17), mp 101–102°C, in turn prepared in 30% yield by ozonolysis of $\Delta^{9,10}$-*octalin* in aqueous HOAc at 0°C (18). Crude $\Delta^{9,10}$-*octalin* (~80% pure) from P_2O_5-catalyzed dehydration of 2-decalol (19) was used.

cis- *and* trans-*1-Cyanobicyclo[5.3.0]decan-6-one* ***7*** + ***8***

A solution of 1.5 g (10 mmol) of conjugated ketone **6**, 1.0 g (20 mmol) of NaCN, and 4 ml of H_2O in 25 ml of MeOH was refluxed for 5 h. The solvent was evaporated and the residue partitioned between $CHCl_3$ and water. Evaporation of the water-washed and dried $CHCl_3$ solution left 1.0 g (57%) of crude product which was mostly a mixture of the *cis*- and *trans*-cyano ketones **7** + **8** (two tlc spots). Purification of a sample by preparative tlc and evaporative distillation at 100°C (0.1 Torr) gave a colorless oil **7** + **8** which still showed two tlc spots; ir (CCl_4): 2225 (C≡N) and 1725 cm^{-1} (seven-ring C=O). *Anal.* calcd. for $C_{11}H_{15}NO$ (177.2): C 74.54, H 8.53, N 7.90; found: C 74.35, H 8.45, N 7.73.

Lactamol ***9*** *of* trans-*Bicyclo[5.3.0]decan-6-one-1-carboxamide*

A solution of 6.0 g (40 mmol) of conjugated ketone **6**, 5.2 g (106 mmol) of KCN, and 16 ml of H_2O in 200 ml of MeOH was refluxed for 5.5 h. The cooled solution was neutralized with HOAc and the solvent was evaporated. The residue was partitioned between $CHCl_3$ and water. Evaporation of the dried $CHCl_3$ solution left 6.0 g (77%) of crude solid **9**. Three recrystallizations from $CHCl_3$–PE gave fine colorless needles of *trans*-lactamol **9**, mp 141–142°C; ir (CCl_4): 3500–3000 (OH, NH) and 1675 cm^{-1} (amide C=O); ^{1}Hmr ($CDCl_3$) δ: 4.47 (1H, s, OH) and 7.10 ppm (1H, bs, NH). *Anal.* calcd. for $C_{11}H_{17}NO_2$ (195.3): C 67.66, H 8.78, N 7.17; found: C 67.12, H 8.90, N 7.46. *Mol. Wt.* calcd. for $C_{11}H_{17}NO_2$: 195.1259; found (high resolution ms): 195.1257.

trans-*Bicyclo[5.3.0]decane-1-carboxamide* ***10***

The reduction (11) was carried out in an H-shaped electrolysis cell with a sintered glass partition between the two 40 ml

Can. J. Chem. Downloaded from www.nrcresearchpress.com by 210.87.254.6 on 09/05/12
For personal use only.

compartments. Each electrode was a 12 cm^2 piece of freshly cleaned lead, the cathode being coated with PbO_2 before use. A stirred (magnetic bar) solution of 746 mg (3.82 mmol) of *trans*-lactamol **9** in 20 ml of 10% aqueous H_2SO_4 and 20 ml of peroxide-free dioxane was electrolyzed at room temperature in the cathode compartment at 18 V and 1.5 A. The anode compartment contained the same electrolyte. After 135 h the cathode solution was extracted with ether to yield 633 mg of crude product. Chromatography on 25 g of silica gel yielded 297 mg of recovered *trans*-lactamol **9** (eluted last) and 190 mg (46% based on recovered **9**) of colorless needles of *trans*-carboxamide **10** which melted at 155–156°C after recrystallization from ether–PE; ir ($CHCl_3$): 3500, 3400, 3100 (NH_2), 1670 (amide C=O), and 1575 cm^{-1} (amide II band); ^{1}Hmr ($CDCl_3$) δ: 5.72 ppm (2H, b lump, $CONH_2$). *Mol. Wt.* calcd. for $C_{11}H_{19}NO$: 181.1466; found (high resolution ms): 181.1462.

trans-*Bicyclo[5.3.0]decane-1-carboxylic Acid* ***11***

The amide **10** (132 mg, 0.73 mmol) was diazotized at room temperature with a solution of 0.7 ml of concentrated H_2SO_4 in 2 ml of 20% aqueous $NaNO_2$; a precipitate appeared immediately. After 3 h the reaction mixture was basified with aqueous KOH, washed with ether, acidified with aqueous HCl, and extracted with ether. Evaporation of the ether left 50 mg (37%) of *trans*-acid **11**, which after slow sublimation at 50–60°C (0.1 Torr) gave colorless crystals, mp 100.5–101.5°C; ir (CCl_4): 3300–2225 (carboxyl OH) and 1690 cm^{-1} (carboxyl C=O); ^{1}Hmr ($CDCl_3$) δ: 1.0–2.8 (17H, CH, CH_2) and 12.10 ppm (1H, s, COOH). *Anal.* calcd. for $C_{11}H_{18}O_2$ (182.3): C 72.49, H 9.95; found: C 72.88, H 9.89. *Mol. Wt.* calcd. for $C_{11}H_{18}O_2$: 182.1306; found (high resolution ms): 182.1302.

Gas–liquid partition chromatography (120°C) of the methyl ester of the reduction product gave a single peak (retention time 4.4 min) with no trace of the methyl ester of the *cis*-acid **5***b* which on co-injection had a retention time of 5.2 min.

The *cis*- and *trans*-acids **5***b* and **11** are also readily distinguished by the pattern of their ir peaks in the 1500–1150 cm^{-1} region (CS_2 or CCl_4 solution); *cis*: 1405 m, 1305 m, 1265 m, and 1210 s cm^{-1}; *trans*: 1450 m, 1410 w, 1265 s, and 1210 m cm^{-1}.

Wolff–Kishner Reduction of Keto Nitriles ***7 + 8***

A solution of 803 mg (4.53 mmol) of **7 + 8**, 3 g of KOH, and 4.5 ml of $H_2NNH_2{\cdot}H_2O$ (85%) in 20 ml of triethylene glycol was heated at 140°C for 1 h and then at 210°C for 5 h while excess $H_2NNH_2{\cdot}H_2O$ was distilled. The cooled reaction mixture was diluted with water, washed with $CHCl_3$, acidified with aqueous HCl, and extracted with $CHCl_3$ to yield 295 mg (35%) of a mixture of the *cis*- and *trans*-acids **5***b* and **11** in a ratio of 88:12 *cis*:*trans* from glpc (120°C) of its methyl ester.

Wolff–Kishner Reduction of trans-*Lactamol* ***9***

A solution of 2.12 g (10.8 mmol) of **9**, 6.0 g of KOH, and 20 ml of $H_2NNH_2{\cdot}H_2O$ (85%) in 30 ml of triethylene glycol were heated at 140°C for 1 h and then at 210°C for 5 h while excess $H_2NNH_2{\cdot}H_2O$ was distilled. The reaction mixture was worked up as described in the preceding experiment to yield 1.07 g of acid which after thick-layer chromatography afforded 940 mg (48%) of *cis*-acid **5***b* (tlc, ir, ^{1}Hmr). Three recrystallizations from PE gave colorless plates of pure **5***b*, mp 58–59°C undepressed on admixture with the authentic specimen from the Diels–Alder route.

Clemmensen Reduction of trans-*Lactamol* ***9***

A mixture of 2.0 g (10 mmol) of **9**, 10 g of amalgamated ($HgCl_2$) mossy zinc, 7.5 ml of water, 10 ml of concentrated HCl, and 10 ml of benzene was refluxed briskly for 48 h during which time a 3 ml portion of concentrated HCl was added every 4 h. The cooled reaction mixture was diluted with ice and extracted with ether to yield only 197 mg of product. Dissolution in aqueous KOH, washing with ether, acidification with aqueous HCl, and extraction with ether gave 97 mg (5%) of acid fraction which glpc (120°C) of the methyl esters revealed to be 75% *cis*-acid **5***b* and 25% *trans*-acid **11**.

1-Cyanobicyclo[5.3.0]decane ***21***

A stirred (magnetic bar) solution of 400 mg (2.26 mmol) of the mixture of keto nitriles **7 + 8** in 20 ml of 10% aqueous H_2SO_4 and 20 ml of peroxide-free dioxane was reduced (11) at room temperature in the cathode compartment of the apparatus described above for electrolytic reduction of **9**. A current of 1.5 A at 18 V was passed for 20 h. Extraction with ether afforded 370 mg (100%) of liquid **21**; ir (CCl_4): 2225 cm^{-1} (C≡N), absence of C=O absorption.

Attempted Hydrolyses of ***21***

(*a*) A solution of 350 mg of **21**, 6 ml of 10% aqueous KOH, 6 ml of 30% H_2O_2, and 6 ml of EtOH was heated at 80°C for 5 h and then refluxed for a further 12 h after addition of 2 ml more of 30% H_2O_2. Acidification of the cooled solution (concentrated HCl) and extraction with $CHCl_3$ yielded 370 mg of an oil whose ir spectrum contained an intense C≡N peak and only weak C=O absorption corresponding to ~10% of amide.

(*b*) The material recovered from (*a*) was dissolved in 10 ml of 85% H_3PO_4 and heated at 180°C for 40 h. The black solution was diluted with ice and extracted with ether to yield 165 mg of dark brown residue which had no C≡N or C=O ir absorption. A retro-Ritter reaction may have occurred.

Attempted Hydrolysis of ***7 + 8***

A solution of 150 mg of the mixture of **7 + 8** in 5 ml of 85% H_3PO_4 was heated at 180°C for 4 h. Dilution with water and extraction with $CHCl_3$ gave 50 mg (33%) of recovered impure **7 + 8**.

Acknowledgment

We would like to thank the National Research Council of Canada for financial support.

1. (*a*) E. W. Warnhoff, C. M. Wong, and W. T. Tai. J. Am. Chem. Soc. **90**, 514 (1968); (*b*) E. W. Warnhoff, C. Bonnice, and Y. C. Toong. Unpublished work.
2. (*a*) A. C. Cope and E. S. Graham. J. Am. Chem. Soc. **73**, 4702 (1951); (*b*) A. C. Cope and M. E. Synerholm. J. Am. Chem. Soc. **72**, 5228 (1950).
3. M. A. McKervey, H. A. Quinn, and J. J. Rooney. J. Chem. Soc. C, 2430 (1971).
4. R. R. Rao and R. Panigrahi. Ind. J. Chem. **14B**, 180 (1976).
5. R. E. Pincock, E. Grigat, and P. D. Bartlett. J. Am. Chem. Soc. **81**, 6332 (1959).
6. R. P. Linstead and E. M. Meade. J. Chem. Soc. 935 (1934).
7. (*a*) W. Nagata, T. Sugasawa, M. Narisada, T. Wakabayashi, and Y. Hayase. J. Am. Chem. Soc. **85**, 2342 (1963); (*b*) W. Nagata, M. Yoshioka, and S. Hirai. Tetrahedron Lett. 461 (1962).
8. (*a*) Y. Mazur and M. Nussim. J. Am. Chem. Soc. **83**, 3911 (1961); (*b*) H. J. E. Loewenthal. J. Chem. Soc. 1367 (1958); (*c*) N. L. Allinger and V. B. Zalkow. J. Am. Chem. Soc. **83**, 1144 (1961); H. L. Goering, A. C. Olson, and H. H. Espy. J. Am. Chem. Soc. **78**, 5371 (1956).

9. (*a*) O. R. RODIG and N. J. JOHNSTON. J. Org. Chem. **34**, 1942 (1969); (*b*) W. NAGATA, S. HIRAI, H. ITAZAKI, and K. TAKEDA. J. Org. Chem. **26**, 2413 (1961); (*c*) W. L. MEYER and N. G. SCHNAUTZ. J. Org. Chem. **27**, 2011 (1962).
10. C. D. GUTSCHE and H. R. ZANDSTRA. J. Org. Chem. **39**, 324 (1974).
11. L. THROOP and L. TÖKÉS. J. Am. Chem. Soc. **89**, 4789 (1967).
12. H. KOCH and W. HAAF. Ann. **618**, 251 (1958).
13. A. H. COOK and R. P. LINSTEAD. J. Chem. Soc. 959 (1934).
14. R. L. KRONENTHAL and E. I. BECKER. J. Am. Chem. Soc. **79**, 1095 (1957).
15. O. H. WHEELER and I. LERNER. J. Am. Chem. Soc. **78**, 63 (1956).
16. E. A. BRAUDE, W. F. FORBES, and E. A. EVANS. J. Chem. Soc. 2202 (1953).
17. A. G. ANDERSON and J. A. NELSON. J. Am. Chem. Soc. **73**, 232 (1951).
18. P. A. PLATTNER and J. HULSTKAMP. Helv. Chim. Acta, **27**, 211 (1944).
19. W. P. CAMPBELL and G. C. HARRIS. J. Am. Chem. Soc. **63**, 2721 (1941).

Can. J. Chem. Downloaded from www.nrcresearchpress.com by 210.87.254.6 on 09/05/12
For personal use only.

Acid-catalyzed reactions of cyclobutanones. III.[1] Formation of substituted 2-tetralones from α-phenylcyclobutanones

VICTOR P. ABEGG,[2] ALAN C. HOPKINSON, AND EDWARD LEE-RUFF
Department of Chemistry, York University, Downsview, Ont., Canada M3J 1P3

Received August 2, 1977

VICTOR P. ABEGG, ALAN C. HOPKINSON, and EDWARD LEE-RUFF. Can. J. Chem. **56**, 99 (1978).

A series of cyclobutanones **1–5** were found to rearrange to β-tetralones **6–10**, respectively, in the presence of phosphorous pentoxide in benzene at room temperature. The structures of the β-tetralones were inferred by conversion of a number of these known naphthalene derivatives. Possible mechanistic pathways are discussed.

VICTOR P. ABEGG, ALAN C. HOPKINSON et EDWARD LEE-RUFF. Can. J. Chem. **56**, 99 (1978).

On a trouvé qu'une série de cyclobutanones **1–5** se réarrangent respectivement en β tétralones **6–10** en présence de pentoxyde de phosphore dans le benzène à la température ambiante. On a déduit les structures des β tétralones du fait que l'on peut en transformer un certain nombre en dérivés naphtaléniques connus. On discute de différents mécanismes possibles.

[Traduit par le journal]

The reactive nature of cyclobutanones with the extensive variation of ring-opening reactions (1–3) has placed these compounds in a class of synthetically important intermediates. With the recent additions of new routes to such systems, cyclobutanone derivatives become accessible synthons to a host of key functional groups required in alkylation reactions (4). During the course of our investigations on the acid-catalyzed rearrangements of cyclobutanones we found that 2-phenylcyclobutanones bearing an activating group in the 3 position are extremely acid labile and undergo facile rearrangements to substituted 2-tetralones.[3] We report here the details of these rearrangements and the supporting evidence for the structural assignments of the rearrangement products.

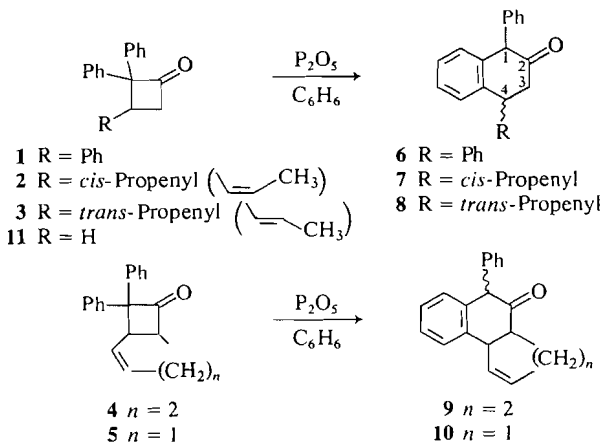

SCHEME 1

Results and Discussion

Cyclobutanones **1–5** and **11** were prepared according to the method of Huisgen and co-workers (5, 6). Treatment of cyclobutanones **1–5** with P_2O_5 in benzene (Scheme 1) gave β-tetralones **6–10**, respectively, with yields exceeding 85%. Reactions were conducted at room temperature and completion times varied from 15 min for **2** and **3** to 24 h for **4**. Carbon 3 of the ring must be bound to an unsaturated carbon or a heteroatom (*vide infra*) for this rearrangement to take place. When 2,2-diphenylcyclobutanone (**11**) is subjected to the same reaction conditions, no apparent reaction takes place after several days.

The existence of inseparable isomeric tetralones (vis-à-vis the 1,4 positions), as indicated by the nmr spectra, made it difficult to obtain physical parameters. Compounds **8**, **9**, and **10** were oils and **6** and **7** had broad melting points. The assignments for the 2-tetralone structure were based on the following evidence. The infrared spectra of all derivatives (**6–10**) exhibited a strong absorption in the region 1713 to 1729 cm^{-1} consistent with a non-conjugated ketone. The nmr spectra of these derivatives were also consistent with the 2-tetralone structure. Worthy of note is the signal at ca. δ 4.80 (singlet) assigned to the diphenylmethyl acyl hydrogen which undergoes rapid exchange with D_2O. Unambiguous proof for the naphthalene backbone was established by their conversion to the substituted naphthalenes via the di-

[1]For part II of this series see ref. 1.

[2]Department of Chemistry, California State Polytechnical University, Pomona, CA.

[3]Earlier examples of such rearrangements involving a 3-substituted heteroatom have been reported by Huisgen and co-workers (9, 10).

Can. J. Chem. Downloaded from www.nrcresearchpress.com by 210.87.254.5 on 09/05/12
For personal use only.

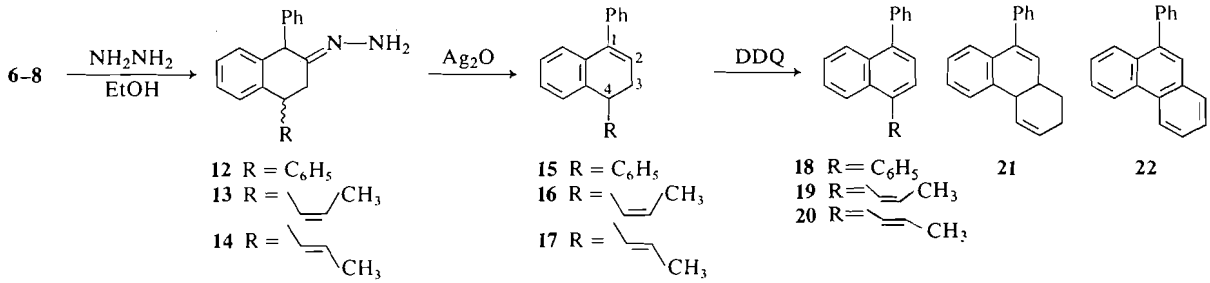

SCHEME 2

hydronaphthalenes. The route to these naphthalenes entailed formation of hydrazones **12–14** (Scheme 2), their oxidation to unstable diazo compounds, and elimination to dihydronaphthalenes. The dihydronaphthalenes were oxidized to the naphthalenes with 2,3-dichloro-5,6-dicyanoquinone (DDQ). In this way the known hydrocarbons **18** and **22** were prepared from **6** and **9**, respectively, and compared with authentic samples (8, 9). Spectral data for all of the dihydronaphthalenes **15–17** and **21** were consistent with the structural assignment and hence pointed to the 4 position for the substituent group R. Evidence for the retention of stereochemistry of the propenyl group in **7** and **8** is based on the following data. Rearrangement products **7** and **8** were shown to have different retention volumes by high pressure liquid chromatography (hplc) (retention volumes of 26.2 and 27.8 ml, respectively). The *trans*-propenyl derivatives **3**, **8**, and **17** all showed strong absorptions at 965–970 cm^{-1} in the ir spectra, attributed to the *trans*-olefinic wagging frequency and which were absent in the *cis*-derivatives.

The mechanism by which the rearrangement of these cyclobutanones to 2-tetralones occurs deserves some comment. Huisgen and co-workers (9, 10) observed that β-naphthols **24** and tetralone **26** were formed (Scheme 3) by thermal and Lewis acid catalyzed rearrangement of cyclobutanones **23** and **25**, respectively.[4] They proposed a zwitterionic intermediate **27** to account for *o*-alkylation of the phenyl group resulting in the observed ring-expanded cyclized products. Alternatively, Lewis acid assisted ring opening of cyclobutanones may involve the intermediacy of diphenylmethyl cation **28** (Scheme 4) which could also undergo *o*-alkylation to one of the phenyl groups. Such a mechanism was postulated to account for the deuterium scrambling between positions 2 and 3 in cyclobutanone **29** (11). Furthermore cyclopropyl carbinyl cations (e.g. **28**) are known resonance contributors to cyclobutyl cations (12).

[4]One of the referees indicated a further example of such rearrangements involving a diphenylketene α-methylstyrene adduct (15).

Our results, however, do not support a mechanism involving a cyclopropyl carbinyl cation **28**. These rearrangements only proceed if the substituent at carbon-3 of cyclobutanone can stabilize a positive

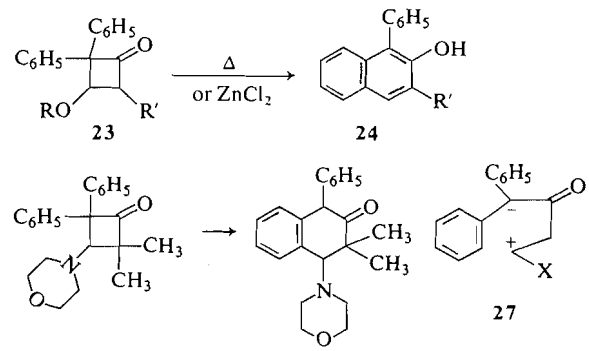

SCHEME 3

charge. No such requirement is necessary for the cyclopropylcarbinyl cation mechanism. Furthermore if intermediate **28** were involved then a mixture of 3- and 4-R-substituted tetralones would be expected. Our data conclusively indicate the substituent R to be located exclusively at carbon-4 of the 2-tetralone

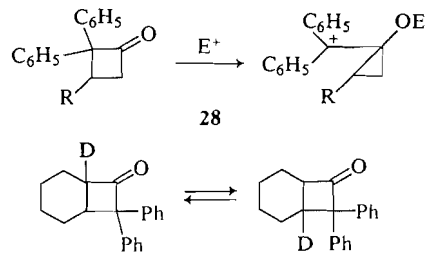

SCHEME 4

system. The retention of stereochemistry of the propenyl group going from **2** and **3** to **7** and **8** respectively can be accounted for by the relatively high energy barrier for rotation for allyl cations. The reported stereomutation of the *cis*, *trans*-allyl cation **30** to the *trans,trans* isomer **31** requires 24 kcal/mol (Scheme 5), the lifetime of **30** being 10 min at 35°C

Can. J. Chem. Downloaded from www.nrcresearchpress.com by 210.87.254.5 on 09/05/12
For personal use only.

TABLE 1. Physical properties of rearrangement products

Starting material	Tetralone	Reaction time	Yield (%)	Melting point (°C) (solvent)[a]	Infrared (cm^{-1}) C=O	Infrared (cm^{-1}) C=C[b]	*m/e* (parent)
1	**6**	1 h	Above 85	105–116 (ethanol)	1727		298[c]
2	**7**	Under 15 min	ca. 85	103–107 (softens above 95)	1717[d] 1729	1663	262[c]
3	**8**	Under 15 min	Above 85	Oil	1723	1661 970	262[c]
4	**9**	24 h	Above 90	104–106 (benzene–hexane at −20°C)	1713		274
5	**10**	Under 12 h	Above 85	Oil	1716		
11			No reaction				

[a]The samples sublime as oils or glasses. On standing these oils and glasses begin to yellow.
[b]It is unclear whether the absorptions at 1663 and 1661 cm^{-1} are due to the isolated unsaturation in the molecules or are shoulders to the carbonyl absorption. These absorptions are not present in the immediate dihydronaphthalene derivatives of the proposed 2-tetralones. The peak at 970 cm^{-1} is clearly due to the *trans*-double bond.
[c]The spectrum is not clean but shows small peaks for higher molecular weight material (oxidation). Such diphenylacylmethyl derivatives are known to undergo air oxidation (7).
[d]Doublet.

(13). It is, therefore, not likely that within the reaction time (15 min) and conditions (25°C) the corresponding allyl cation **32** will equilibrate with its more stable *trans,trans* rotamer.

In summary, we have shown the 2-phenylcyclobutanones with an activating group undergo facile acid-catalyzed rearrangements at room temperature to 2-tetralones.

With the availability of cyclobutanone derivatives, extension of these reactions to other bicyclic derivatives could constitute a novel method in the synthesis of polycyclic systems.

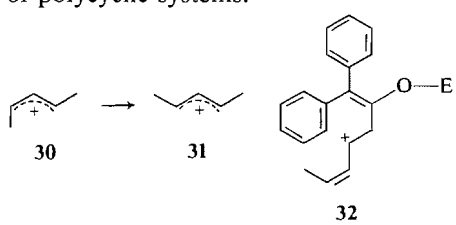

30 **31** **32**

SCHEME 5

Experimental

Melting points were determined on a Fisher-Johns hot-stage melting point apparatus. All melting points and boiling points are uncorrected. Infrared (ir) spectra were determined on a Unicam SP 1000 Spectrophotometer and nuclear magnetic resonance (nmr) spectra were recorded at 60 MHz (Varian EM-360). Chemical shifts are reported in parts per million (δ) relative to Me_4Si (δ 0.0 ppm) as an internal standard. High pressure liquid chromatography was performed on a Waters Model R-400 instrument using a μ Bondapak C_{18} column. Abbreviations used are: s = singlet, d = doublet, t = triplet, m = multiplet, dd = doublet of doublets, td = triplet of doublets, q = quartet, b = broad, w = weak, med = medium, sh = sharp, st = strong.

Diphenylketene was prepared according to the method of Huisgen and Feiler (5).

2,2-Diphenylcyclobutanone (**11**) was prepared according to the method of Huisgen and Feiler (5). The yellow product mixture was treated with diethyl ether to yield a white solid (also insoluble in acetone and benzene) and a yellow solution. The ether insoluble solid became blood red when treated with H_2SO_4. The ethereal solution was extracted with Na_2CO_3. The material contained in the ethereal layer was chromatographed on silicic acid with varying amounts of benzene–hexane to yield 1.70 g of **11** from 5.88 g of diphenylketene (15%).

The Na_2CO_3 extract was acidified and the product shown to be a carboxylic acid mixture by ir and extraction into $NaHCO_3$. Upon treatment with H_2SO_4 and quenching the blood red solution with water, the acids were transformed into ketone products (sh C=O at 1715 cm^{-1}) which could only be extracted into Na_2CO_3 solution and not $NaHCO_3$.

7,7-Diphenylbicyclo[3.2.0]-2-hepten-6-one (**5**), 3-(cis-propenyl)-2,2-diphenylcyclobutanone (**2**), 3-(*trans*-propenyl)-2,2-diphenylcyclobutanone (**3**), and 8,8-diphenylbicyclo[4.2.0]-2-octen-7-one (**4**) were made by the method of Huisgen and Otto (6).

General Method for the P_2O_5-catalyzed Rearrangement of the Cyclobutanones

About 1 g of the cyclobutanone was dissolved in 25–50 ml of benzene and treated with 1–2 g of P_2O_5. Vigorous stirring was continued until tlc indicated completion of rearrangement. The dark red mixture was gravity filtered through paper and the red P_2O_5 cake was washed well with benzene. After concentrating the combined, water-white filtrates by rotary evaporation and chromatographing over silicic acid with benzene as eluent, the product was obtained in high yield. For the sake of a clean and easy chromatography, it is important that the rearrangement be complete, but to avoid decomposition of the product by P_2O_5, the reaction should be allowed to proceed no longer than necessary.

Typical yields after chromatography, reaction times, and physical properties are given in Table 1.

The nmr spectra ($CDCl_3$) of the rearrangement products are as follows:

Compound **6** δ : 2.53–3.30 (m, 2H), 4.23–4.62 (m appears as an unresolved q, 1H), 4.78 (s with a shoulder on the downfield side, 1H), and 6.7–7.6 (m, aromatic, 9H).

Compound **7** δ : 1.71 (td, J_d = 1.5 and J_t = 13.5 Hz, 3H), 2.18–3.03 (m, 2H), 3.98–4.45 (m, 1H), 4.81 (s) and 4.96 (s)

Can. J. Chem. Downloaded from www.nrcresearchpress.com by 210.87.254.5 on 09/05/12
For personal use only.

Can. J. Chem. Downloaded from www.nrcresearchpress.com by 210.87.254.5 on 09/05/12
For personal use only.

(both together represent 1H), 5.21–6.09 (m, vinyl, 2H), and 6.5–7.6 (m, aromatic, 9H).

Compound **8** δ : 1.71 (unresolved d, J = ca. 4 Hz, 3H), 2.25–3.13 (m, 2H), 3.63–4.05 (m, 1H), 4.73 (s with a shoulder on the downfield side, 1H), 5.38–5.67 (m, vinyl, 2H), and 6.8–7.65 (m, aromatic, 9H).

Compound **9** δ : 1.58–2.32 (m, 4H), 2.77–3.07 (m, 1H), 3.68–4.1 (m, 1H), 4.75 (s with spiked shoulder at 4.81, 1H), 5.81 (s, vinyl, 2H), and 6.71–7.45 (m, aromatic, 9H).

Compound **10** δ : 2.41–2.9 (m, 2H), 3.21 (td, J_t = 9 and J_d = 4 Hz, 1H), 4.25–4.63 (s with a spiked shoulder at 4.90, 1H), 5.88 (m, vinyl, 2H, very complex pattern on expansion with very small J values), and 6.8–7.5 (m, aromatic, 9H).

Examination of **7** and **8** by hplc clearly indicated that there had been no isomerization of the double bond during rearrangement; **7** has retention volume of 26.2 ml and **8** of 27.8 ml. A mixture of the two clearly shows two peaks. The individual products show only one peak somewhat broad. This broadening is thought to be due to the isomerism of the 2-tetralones.

General Method for Converting the 2-Tetralones to Dihydronaphthalene Derivatives

About 350 mg of the rearranged product (freshly prepared) was dissolved in 30 ml of ethanol and treated with 1 ml of 97% hydrazine. After stirring for 18 h, the solution was added to diethyl ether and extracted with distilled water until neutral. The dried ethereal layer was reduced to 25 ml and silver oxide (1 g) added. A silver mirror appeared and the mixture was filtered after 24 h. Chromatography on silicic acid using a benzene-hexane mixture (1:3 v/v) afforded the dihydronaphthalene in 23–35% yield. A bright yellow product is also formed, but has not been identified (only two kinds of aliphatic absorptions are noted in the nmr).

On one occasion the heat- and light-sensitive hydrazone **12** was isolated and had ir bands at 3400, 3300, and 3210 (N—H) and 1600 cm^{-1} (broad, involving C=N, C=C conjugated, and C=C aromatic). Its nmr ($CDCl_3$) had absorptions at δ 2.2–3.2 (m, 3.95–4.38 (m), 4.87 (s with a spiked shoulder at 4.93), 4.8 (b, N—H, bordering the 3.95–4.38 m and having the 4.87 s superimposed on it, 4H total), and 6.65–7.4 (m, aromatic, 14H or 15H).

The dihydronaphthalenes formed were all liquids or oils and could not be crystallized. Their ir spectra were similar showing peaks at 3050–2800 (C—H stretch), 1600 (aromatic C=C stretch), 1495–1480 (d), 1440 (methylene band), and 780–690 cm^{-1} (aromatic substitution patterns). In addition **17** displayed a strong absorption at 965 cm^{-1} indicative of the *trans*-unsaturation. Compound **21** shows a strong *m/e* peak at 258 with some minor peaks at higher molecular weight.

The nmr spectra are as follows.

Compound **15** δ : 2.73 (dd, J = 8 and 5 Hz, 2H), 4.17 (t, J = 8 Hz, 1H), 5.99 (t, J = 5 Hz, 1H), and 6.77–7.52 (m, aromatic, 14H).

Compound **16** δ : 1.71 (d, J = 5 Hz, 3H), 2.20–2.60 (m, 2H), 3.60–4.15 (m, 1H), 5.43–5.70 (m, 2H), 5.98 (t, J = 5 Hz, 1H), and 6.95–7.47 (m, aromatic, 9H).

Compound **17** δ : 1.72 (d, J = 5 Hz, 3H), 2.30–2.61 (m, 2H), 3.28–3.72 (m, 1H, appears as an unresolved q), 5.40–5.70 (m, 2H), 5.98 (t, J = 5 Hz, 1H), and 6.90–7.50 (m, aromatic, 9H).

Compound **21** δ : 1.71–2.40 (m, 4H, contains t with J = 5 Hz), 2.70–3.11 (m, 1H), 3.43–3.72 (m, 1H), 5.80 (m, superimposed on d with J = ca. 5 Hz, 3H), and 6.90–7.48 (m, aromatic, 9H).

Other Methods of Preparing the Dihydronaphthalenes

(*i*) Subjecting the hydrazone **12** prepared as indicated above to potassium *tert*-butoxide in DMSO (anhydrous) yielded 18% of **15** after work-up and chromatography.

(*ii*) The freshly prepared, crude hydrazone **13** was treated with activated MnO_2 rather than Ag_2O. After the mixture in anhydrous THF was stirred for 18 h, chromatographic work-up afforded **16** in 27% yield.

(*iii*) The procedure with Ag_2O was repeated using PbO_2 on hydrazone **14**. Dihydronaphthalene **17** was obtained after chromatography in 10% yield.

(*iv*) Treating **6** with hydrazinium sulfate in ethanol, stirring for 18 h, and then refluxing for 3 h yielded 14% of **17** after chromatography.

(*v*) The tosylhydrazone of **6** was prepared, treated with CH_3Li, and heated, affording no hydrocarbon product.

*Oxidation of 1,2-Dihydro-1,4-diphenylnaphthalene (**15**) to 1,4-Diphenylnaphthalene (**18**)*

A 74 mg sample of **14** was refluxed in benzene (50 ml) with an excess (200 mg) of 2,3-dichloro-5,6-dicyanoquinone (DDQ) for 1 h. Chromatographic work-up on silicic acid using benzene–hexane as eluent (1:3 v/v) afforded 70 mg (96%) of **18**. Recrystallization from ethanol afforded material identical to a known sample by ir, nmr, tlc, mixture mp, and mp 136–137°C (lit. (8) mp 134.5–136°C).

*9-Phenylphenanthrene (**22**)*

Oxidation of **21** by DDQ in a manner as above afforded, after chromatography, a near quantitative yield of **22**; ir (KBr): 3060 (b), 2940 (b), 1595 (w), 1490 and 1450 (d, med), 888 (sh, med), 779 (sh), 764 (sh), 753 (sh), 740 (sh, st), 721 (sh, st), and 699 cm^{-1} (sh, st). The nmr was identical to that given in the literature (9). Recrystallization of a sample from ethanol afforded crystals with mp 103–104°C (lit. (14) mp 105–106°C).

*Attempted Oxidation of **16** and **17***

The same procedure was followed as above using an excess of DDQ. No hydrocarbon starting material or product could be found.

*Attempted Addition of Reagents to the Carbonyl of **6***

(*i*) An ethereal solution of **6** (380 mg) was treated with an excess of ethereal CH_3Li (1.56 M, ca. 2 ml). An initial solid dissipated with further addition of CH_3Li and gas evolution accompanied the process. Acidification with dilute HCl, work-up, and chromatography over silicic acid employing 5% diethyl ether in benzene (v/v) afforded 235 mg (ca. 628) of a hydroxyketone (ir: 3615 (w), 3430 (st), and 1713 cm^{-1} (st)). Treatment with P_2O_5 gave an unsaturated ketone (1710 cm^{-1}).

Treatment with methylmagnesium bromide gave the same result.

(*ii*) Reduction of the carbonyl to an alcohol was attempted by adding $NaBH_4$ (30 mg) to 300 mg of **6** in 10 ml of ethanol. Slow evolution of gas resulted. The crude product after acidification with dilute HCl and work-up had an ir similar to the hydroxyketone cited above.

(*iii*) Similar results were obtained on using LAH in THF, but the product was less pure.

Acknowledgements

The authors would like to thank the National Research Council of Canada for financial support and Dr. T. Fyles for assistance with the high pressure liquid chromatography work.

1. E. Lee-Ruff. Can. J. Chem. **50**, 952 (1972).
2. E. Lee-Ruff, N. J. Turro, P. Amice, and J. M. Conia. Can. J. Chem. **47**, 2797 (1969).

3. J. M. CONIA and J. R. SALAUN. Acc. Chem. Res. **5**, 33 (1972).
4. B. M. TROST. Acc. Chem. Res. **7**, 85 (1974).
5. R. HUISGEN and L. A. FEILER. Chem. Ber. **102**, 3391 (1969).
6. R. HUISGEN and P. OTTO. Chem. Ber. **102**, 3475 (1969).
7. G. A. RUSSELL and A. G. BEMIS. J. Am. Chem. Soc. **88**, 5491 (1966).
8. A. ETIENNE, A. SPIRE, and E. TOROMANOFF. Bull. Soc. Chim. Fr. 750 (1952).
9. R. HUISGEN, L. A. FEILER, and P. OTTO. Chem. Ber. **102**, 3405 (1969).
10. L. A. FEILER and R. HUISGEN. Chem. Ber. **102**, 3428 (1969).
11. T. J. KATZ and R. DESSAU. J. Am. Chem. Soc. **85**, 2172 (1963).
12. G. A. OLAH, C. L. JEUELL, D. P. KELLY, and R. D. PORTER. J. Am. Chem. Soc. **94**, 146 (1972).
13. P. v. R. SCHLEYER, T. M. SU, M. SAUNDERS, and J. C. ROSENFELD. J. Am. Chem. Soc. **91**, 5174 (1969).
14. C. F. KOELSCH. J. Am. Chem. Soc. **56**, 480 (1934).
15. R. HUISGEN and P. KOPPITZ. Chem. Ztg. **98**, 461 (1974).

Can. J. Chem. Downloaded from www.nrcresearchpress.com by 210.87.254.5 on 09/05/12
For personal use only.

Crown ether catalysis of decarboxylation: a general survey of reactivity and a detailed analysis of the triphenylacetate anion

D. H. HUNTER, M. HAMITY, V. PATEL, AND R. A. PERRY

Department of Chemistry, University of Western Ontario, London, Ont., Canada N6A 5B7

Received July 29, 1977

D. H. HUNTER, M. HAMITY, V. PATEL, and R. A. PERRY. Can. J. Chem. **56**, 104 (1978).

The effect of 18-crown-6 ether **3** on the decarboxylation rate in THF of sodium salts of carboxylic acids formally derived from hydrocarbons has been investigated and these acids include 9-phenylfluorene-9-carboxylic acid, fluorene-9-carboxylic acid, phenylacetylene carboxylic acid, triphenylacetic acid, and diphenylacetic acid. Addition of equimolar **3** resulted in an increase in decarboxylation rate of 13- to 500-fold and there was a correlation between the decarboxylation rate and the pK_a value of the product hydrocarbon.

The decarboxylation of triphenylacetate was investigated in detail. The effect on reaction rate of cation (Li^+, Na^+, K^+), crown ether concentration, water concentration, and solvent polarity has provided information as to optimum reaction conditions and has helped to clarify the reaction mechanism.

D. H. HUNTER, M. HAMITY, V. PATEL et R. A. PERRY. Can. J. Chem. **56**, 104 (1978).

On a étudié l'effet des couronnes-18 éther-6 (**3**) sur la vitesse de décarboxylation, dans le THF, de sels de sodium d'acides carboxylique dérivés d'une façon formelle d'hydrocarbures; parmi ces acides on retrouve les acides phényl-9 fluorènecarboxylique-9 fluorénecarboxylique-9, phénylacétylènecarboxylique, triphénylacétique et diphénylacétique. Lors de l'addition de quantités équimolaires de **3** les vitesses de décarboxylation sont multipliées par des facteurs allant de 12 à 500 et il existe une corrélation entre la vitesse de décarboxylation et le pK_a de l'hydrocarbure formé.

On a étudié en détail la décarboxylation de l'anion triphénylacétate. Un examen de l'effet, sur la vitesse de réaction, de cations (Li^+, Na^+, K^+), de la concentration de couronne éther, de la concentration d'eau et de la polarité du solvant, a fourni des informations sur les conditions réactionnelles optimum et permet de clarifier le mécanisme de la réaction.

[Traduit par le journal]

Introduction

The decarboxylation of carboxylic acids and their derivatives has received significant attention (1) from biological, synthetic, and mechanistic points of view. From the variety of mechanistic approaches that have been used, reaction pathways involving both the ionized and unionized form of the carboxyl group have been identified. While a range of substrates have been observed to decarboxylate through the ionized or carboxylate form, most detailed studies have payed particular attention to the effect of solvent on the reaction. The effect of micelles (2) and inclusion complexes (3) on decarboxylation rates also have been investigated.

In an important study (4) involving benzisoxazole-3-carboxylates **1**, Kemp and co-workers observed a rate dependence on solvent covering a range of $\sim 10^8$ and demonstrated that hydrogen-bonding of solvent to the carboxylate group is one of the major factors responsible for the observed deactivation by protic solvents. In a less ambitious study (5) of the sodium salt of 3-(fluoren-9-ylidene)-2-phenyl-acrylate **2**, we also observed a strong dependence of decarboxylation rate on solvent which implicated hydrogen bonding. However the role of ion-pairing on the rate of decarboxylation in tetrahydrofuran was also in-

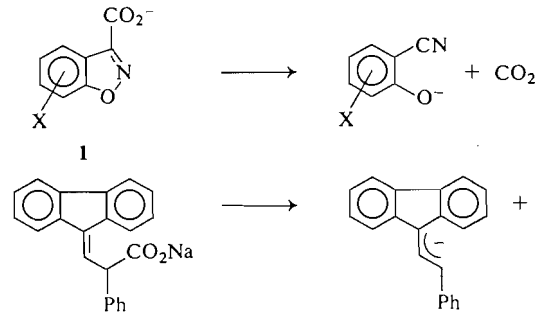

Can. J. Chem. Downloaded from www.nrcresearchpress.com by 210.87.254.5 on 09/05/12
For personal use only.

Can. J. Chem. Downloaded from www.nrcresearchpress.com by 210.87.254.5 on 09/05/12
For personal use only.

vestigated by observing the rate enhancing effect of dibenzo-18-crown-6 ether. An apparent rate enhancement of about 10^3 to 10^5 was sufficient to encourage us to look in more detail at both the source and the generality of this acceleration.

Our study of the effect of crown ethers on decarboxylation in aprotic solvents has involved both a survey of several carboxylate anions and a more thorough study of a selected example, the triphenylacetate anion. The range of carboxylate anions included those formally derived from hydrocarbons as well as several examples of β,γ-unsaturated carboxylic acids. This article will be limited to the results pertaining to the carboxylic anions formally derived from hydrocarbons.

Results and Discussion

For purposes of discussion our study of the effects of crown ethers on decarboxylation of carboxylate anions can be conveniently subdivided. First a general survey of reactivity as a function of structure of the carboxylate will be presented followed by a detailed study of the triphenylacetate anion. In the case of the triphenylacetate anion several variables were systematically changed and these include the nature of the cation, the water concentration, the crown ether concentration, and the solvent polarity. Throughout this study 18-crown-6 ether **3** was used because of its complexing ability with the alkali metal cations, its solubility in a range of solvents and its ready availability.

The Structure of the Carboxylate Anion

A study of a series of carboxylate anions was undertaken to determine: (*i*) the generality of crown ether assistance to decarboxylation; (*ii*) possible correlations between structure and reactivity; and (*iii*) the practical range of usefulness of the crown ether assisted decarboxylations. Initially it seemed likely that the rate of decarboxylation of a carboxylate anion ($R—CO_2^- \rightarrow R^- + CO_2$) might well respond to the stability of the carbanion being produced with changes in the R group having a greater effect on the stability of the carbanion (R^-) than on the carboxylate anion ($R—CO_2^-$).

With this in mind a series of carboxylic acids was selected in which the pK_a values of the derived hydrocarbons (RH) spanned the range 18–32[1] and these are 9-phenylfluorene-9-carboxylic acid **4**, fluorene-9-carboxylic acid **5**, phenylacetylenecarboxylic acid **6**, triphenylacetic acid **7**, and diphenylacetic acid **8**. The pK_a values (DMSO) of the derived hydrocarbons are 17.9 for 9-phenylfluorene, 22.6 for fluorene, 28.8 for phenylacetylene, 30.7 for triphenylmethane, and 32.1 for diphenylmethane. Acids **5** and **8** were available commercially while **4**, **6**, and **7** were prepared via carbonation of the appropriate organolithium. The sodium salts were obtained as solids after lyophilization of a titrated aqueous solution.

To provide a comparison with the previously reported system **2**, the decarboxylation reactions were run in ether solvents (primarily THF) at a temperature at which the decarboxylation both in the presence and absence of 18-crown-6 ether **3** could be followed conveniently. The results of this study are presented in Table 1. In runs 4, 5, 7, and 9 the reactions showed reasonable first-order behaviour over at least two half-lives while often the reactions run in the absence of **3** (runs 3, 6, and 8) were sufficiently slow that the reactions were followed to only about 50% at which point first-order plots were still reasonably linear. For this reason half-lives have been used to facilitate comparisons. Runs 1 and 2 were too fast to follow with ease and runs 10 and 11 were too slow. For purposes of comparison, half-lives were calculated for these runs from a first-order rate expression although we have no firm evidence as to the actual order in substrate. The reactions run in the absence of **3** were two-phase reactions and in dioxane the sodium salt of **6** was only partially soluble even in the presence of equimolar amounts of **3**. In spite of the semiquantitative nature of some of these results and the uncertainty in some cases as to the actual kinetic order, the observed changes are sufficiently large to be of practical significance and to indicate trends.

With the exception of **6** which has limited solubility in dioxane, it is clear that there is a correlation between the rate of decarboxylation and the pK_a of the product, with the most acidic product being formed most rapidly both in the presence and absence of **3**. From the conditions required to decarboxylate **8** it would appear that even compounds with pK_a values near or above 32 can be decarboxylated although in sealed tubes. For all these substrates, the acid forms were quite resistant to decarboxylation and decarboxylation through the salt is the more facile and preferred process. In the presence of equimolar water, the inorganic product is bicarbonate which frequently precipitates so that the entire reaction is run under only mildly basic conditions.

$$R—CO_2M + H_2O \xrightarrow[THF]{3} R—H + MHCO_3\downarrow$$

For all substrates equimolar amounts of the crown ether **3** had an accelerating effect on the rate of decarboxylation which ran from 13 times for **6** (runs

[1]F. G. Bordwell. Private communication.

Can. J. Chem. Downloaded from www.nrcresearchpress.com by 210.87.254.5 on 09/05/12
For personal use only.

TABLE 1. Decarboxylation of sodium carboxylates in the presence and absence of 18-crown-6 ether

		Substrate				
Run	Solvent	Nature	Concentration (*M*)	[CE][a] (*M*)	*T* (°C)	$t_{\frac{1}{2}}$ (min)[b]
1	THF	**4**	0.024		−20	400[c]
2	THF	**4**	0.024	0.027	−20	4[d]
3	THF	**5**	0.026		30	7500
4	THF	**5**	0.024	0.0024	30	90
5	THF	**5**	0.024	0.024	30	15
6	Dioxane	**6**	0.030		100	3600
7	Dioxane	**6**	0.040	0.040	100	280
8	THF	7	0.020		61	3300
9	THF	**7**	0.020	0.020	61	17
10	THF	**8**	0.024		149	35 000[e]
11	THF	**8**	0.028	0.031	149	200[f]

[a]18-Crown-6 ether.
[b]For runs 1, 2, 10, and 11, the $t_{1/2}$ has been calculated assuming first-order kinetics in substrate.
[c]Corresponds to 20.1% reaction at 135 min.
[d]Corresponds to 48% reaction at 4 min.
[e]Corresponds to 20% reaction at 189 h.
[f]Corresponds to 8.4% reaction at 30 min and 38% reaction at 150 min.

6 and 7) to 500 times for **5** (runs 3 and 5). For the substrates that were soluble in the presence of equimolar **3**, the acceleration was in the range of 100–500. Runs 4 and 5 show that changing the crown ether to substrate ratio from 0.1 to 1.0 changes the relative ratio of the half-lives by a factor of 6. Thus while the rate is sensitive to the amount of **3** present, the dependence seems to be less than first order. From a practical point of view, a ratio of 0.1 still produces an acceleration of 83 (runs 3 and 4) which means **3** can be used in reduced amounts. However, a simple extraction procedure has been developed for recovery of **3** (6) which minimizes the disadvantages of using equimolar amounts of **3**.

Interpretation of the accelerating effects of **3** on the various substrates is complicated by the fact that **3** presumably increases the reactivity of *dissolved substrate* but also acts as a phase transfer agent by increasing the solubility of substrate. While the overall reactivity in both the presence and absence of **3** parallels the pK_a value of the product, it is not clear what factors determine the solubilities of substrate in the absence of **3** and thus the net rate of reaction. The fact that the substrates alone have quite limited solubility in THF suggests that the major effect of **3** is as a phase transfer agent.

Decarboxylation of Triphenylacetates

The observation of enhanced decarboxylation rates in a range of substrates upon the addition of a crown ether, **3**, as well as the opportunity to investigate the role of crown ethers in a simple reaction led us to a more detailed study of one of the substrates. Triphenylacetate was chosen because it had appropriate reactivity at readily accessible temperatures. Tetrahydrofuran was used as the solvent for most of the studies because of its ease of handling and because it dissolved the complexed form of most of the salts. A later study of the effect of solvent on reaction rate (*vide infra*) confirmed the accidental sensibility of this initial decision.

Nature of the Cation

Table 2 contains the half-lives for decarboxylation of the lithium, sodium, and potassium salts of triphenylacetate. The reactions were run at reflux in THF both in the absence of **3** and in the presence of equimolar **3**. Again the reactions run in the absence of **3** (runs 12, 8, and 14) and the reaction involving lithium and **3** (run 13) were two-phase reactions. Since the actual kinetic order is in doubt, the times for 50% reaction ($t_{\frac{1}{2}}$) under the stated conditions have been reported for purposes of rough comparison.

Two trends are apparent from the results. First, the presence of **3** produces a rate enhancement of about 100-fold with each of lithium (runs 12 and 13),

TABLE 2. Decarboxylation of lithium, sodium, and potassium triphenylacetates in THF at 61°C

	Substrate			
Run	Concentration (*M*)	Cation	[CE][a] (*M*)	$t_{\frac{1}{2}}$ (min)
12	0.023	Li		30 000[b]
13	0.016	Li	0.016	330
8	0.020	Na		3 300
9	0.020	Na	0.020	17
14	0.020	K		200
15	0.020	K	0.020	≤2[c]

[a]18-Crown-6 ether.
[b]Corresponds to 12% reaction at 96 h.
[c]Corresponds to 90% reaction at 5 min.

Can. J. Chem. Downloaded from www.nrcresearchpress.com by 210.87.254.5 on 09/05/12
For personal use only.

sodium (runs 8 and 9), or potassium (runs 14 and 15) and the magnitude is about the same for all three cations. Second, the reactivity order is K > Na > Li either in the absence of **3** (runs 12, 8, and 14) or in its presence (runs 13, 9, and 15). The magnitude of the change is about the same in either case with the potassium salts (runs 14 and 15) being about 10 times[2] more reactive than sodium (runs 8 and 9) which in turn are about 10 times more reactive than lithium (runs 12 and 13).

From a practical point of view it is clear that the most reactive system involves the complexed potassium salt. From an interpretive point of view the situation is much fuzzier even though the changes are reasonably large. Comparisons involving the two-phase reactions (runs 12, 13, 8, and 14) are clouded by our lack of knowledge of the solubilities of the salts and our ignorance of the actual reactive intermediates. A comparison of the homogeneous reactions involving complexed potassium, sodium, and perhaps lithium (runs 15, 9, and 13) is more justifiable since only the complexed form is appreciably soluble and the solubility behaviour is consistent with a one to one complex between **3** and the cations. As will be discussed later, kinetic results with potassium triphenylacetate **9** suggest that the reactive intermediate is a small equilibrium amount of dissociated triphenylacetate (Scheme 1).

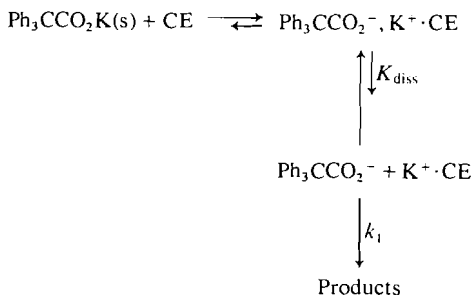

SCHEME 1

The trend with cation above implies that complexed potassium triphenylacetate is more dissociated than sodium than lithium. Analogous observations have been made by esr on alkali metal ketyls with dibenzo-18-crown-6 ether in THF (7). Studies (8) of the effect of dibenzo-18-crown-6 on the relative proportion of solvent separated and contact ion pairs in THF have shown, in contrast, that the preference for solvent separated ion pairs is in the order $Na^+ > Li^+ > K^+$ and in the absence of crown ethers the order is $Li^+ > Na^+ > K^+$ (9). While the reasons for this difference are complex, it has been noted that the equilibria between ion pairs is temperature sensitive. Thus the relative reactivities and perhaps even the order of decarboxylation rates might change with temperature.

Effect of Crown-ether Concentration

Since complexed potassium triphenylacetate was the most reactive of the triphenylacetates and thus is of practical interest, we decided to look in detail at its behaviour. Because of the high rate of reaction at reflux in THF, the temperature was lowered to 30°C for most of the subsequent studies. It was felt that the reaction rate may be sensitive to water in THF, so the concentration of water was monitored by Karl-Fischer titration.

The first parameter to be discussed here is the effect of the concentration of **3**. The results (Table 3) can be conveniently subdivided into those runs involving greater than equimolar **3** (runs 16–23) and those involving less than equimolar **3** (runs 24–30), since equimolar **3** was necessary to effect complete solution of potassium triphenylacetate **9**; a result consistent with formation of a one-to-one complex. In the absence of **3**, potassium triphenylacetate **9** did not have detectable solubility (<0.0001 *M*) in THF at 30°C.

For runs 16–23 which began as homogeneous solutions, the rates of decarboxylation were consistent with a first-order dependence in added triphenylacetate over about 90% reaction and it is these first-order rate constants (k_1^{obs}) that are reported in Table 3. In spite of reasonable kinetic behaviour the solutions did not remain homogeneous throughout the course of the reaction. Filtration (run 17) yielded a white solid (*ca.* 30% yield) whose equivalent weight by titration was consistent with potassium bicarbonate not complexed with **3**.

The results of runs 17, 19, 20, 21, and 22 show the effect of increasing the concentration of **3** with a constant concentration of **9** (0.020 *M*) and of water (0.047–0.053 *M*). While the changes were not large there was a consistent decrease in rate with increase in crown ether concentration beyond equimolar **3**. Because even modest concentrations of **3** can represent fairly substantial weight percentages, it seemed feasible that the rate reducing effect of **3** may be due to changes in solvent polarity. In an attempt to mimic this effect of excess **3** on the solvent polarity, a comparison was made (run 23) using sufficient dioxane to produce a solution of the same weight percentage. There was a rate decrease (3.6×10^{-4} s^{-1}) compared to run 24 (4.6×10^{-4} s^{-1}) but the change was

[2]An extrapolation from rate data at 20, 30, and 40°C yielded a half-life of 1 min at 60°C as well as activation parameters: $\Delta H^{\ddagger} = 21.2$ kcal/mol; $\Delta S^{\ddagger} = -6.5$ eu. The pseudo first-order rate constants ($\times 10^4$, s^{-1}) were 1.18, 3.49, and 11.7, respectively, and were obtained for reaction mixtures 0.020 *M* in substrate, 0.053 *M* in H_2O, and 0.040 *M* in **3**.

Can. J. Chem. Downloaded from www.nrcresearchpress.com by 210.87.254.5 on 09/05/12
For personal use only.

TABLE 3. Effect of 18-crown-6 ether **3** on the decarboxylation of potassium triphenylacetate **9** in THF at 30°C

Run	[9] (M)[a]	[3][b] (M)	[Water] (M)	3/9	k_0^{obs} ($\times 10^7$)	k_1^{obs} (s^{-1}) ($\times 10^4$)
16	0.010	0.010	0.0225	1.0		6.5
17	0.020	0.020	0.047	1.0		4.7
18	0.020 + KBF_4(0.21)	0.047	0.041	1.1[c]		1.5
19	0.020	0.040	0.053	2.0		3.5
20	0.021	0.041	0.053	2.0		3.5
21	0.020	0.080	0.051	4.0		3.3
22	0.020	0.20	0.053	10		2.3
23	0.020	0.020 + 0.53 dioxane[d]	0.054	1.0		3.6
24	0.010		0.028	0	0.075	
25	0.010	0.0011	0.016	0.11	5.8	~10
26	0.010	0.0025	0.016	0.25	10.2	7.0
27	0.010	0.0050	0.015	0.50	15.2	7.5
28	0.010	0.0050	0.054	0.50	10.7	~11
29	0.019	0.0094	0.025	0.50	22.3	4.9
30	0.010	0.0070	0.016	0.70	19.5	9.6

[a]Runs 25–30 were two-phase reactions that started as apparent zero-order reactions and upon complete solution of substrate became apparent first order.
[b]18-Crown-6 ether, 3.
[c]Ratio of 3 to total salts (9 + potassium perfluoroborate).
[d]Contains 0.020 M 3 and enough dioxane (0.53 M) to make a 5 wt.% solution in dioxane.

not as large as that brought about by **3** (2.3×10^{-4} s^{-1} for run 29). Thus the observed effect of excess **3** may well be through the macroscopic properties of the medium since at a microscopic level the expectations seem to be in the opposite direction, e.g. formation of a 2:1 complex should be activating.

A series of experiments was directed at determining the effect of dissolved salt concentration on the reaction rate. One simple comparison is shown in runs 16 and 17 where the ratio of **9** to **3** to water was kept constant but the total dissolved salt concentration was doubled. As can be seen, an increase in salt concentration produced a decrease in rate constant. This is also evidenced in run 18 where added complexed potassium tetrafluoroborate produced a marked decrease in reaction rate. These concentration effects pointed to a reaction passing through a small equilibrium amount of dissociated ions (Scheme 1).

In an attempt to quantify the suggestion that the reaction involves dissociated ions, a series of reactions were run using less than equimolar **3** (runs 24–30). These reactions were characterized by an initial heterogeneous stage which showed zero-order kinetics followed by first-order kinetic behaviour for the remainder of the reaction. The break in the kinetic behaviour coincided with complete dissolution of substrate and appeared to occur when the amount of unreacted **9** equaled the amount of **3** added initially. Qualitatively the zero-order rate constant increases with increasing concentration of dissolved **9**, or added **3** concentration. In runs 25, 26, 27, and 30 the water concentration was held constant and sufficient **9** was added to provide a 0.010 M solution if totally dissolved. The actual dissolved substrate concentration was determined by the amount of **3** added and thus as the complexed substrate concentration was increased from 0.0011 M (run 25) to 0.070 M (run 30) the observed zero-order rate constant (k_0^{obs}) changed from 5.8×10^{-7} to 19.5×10^{-7}. As shown in Fig. 1, the k_0^{obs} showed a half-power dependence on dissolved complexed substrate concentration over the range 0.001–0.01 M.

The mechanism shown in Scheme 1 is consistent with this result provided (*a*) the solution remains saturated with complexed substrate ($Ph_3CCO_2K \cdot CE$) during the heterogeneous stage, (*b*) the dissolved substrate exists primarily as ion pairs, and (*c*) the decarboxylation proceeds through dissociated ions.

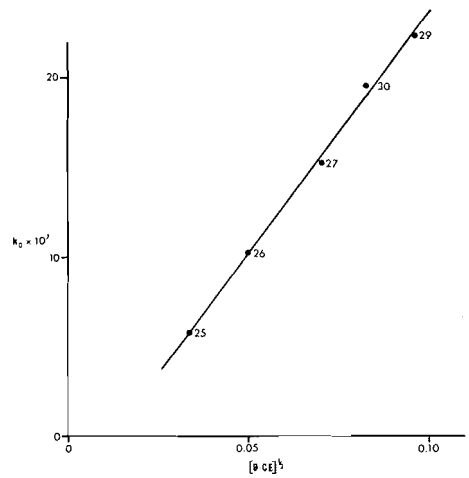

FIG. 1. Plot of zero-order rate constants (runs 25–30 of Table 3) vs. the square root of the dissolved salt concentration $[9 \cdot CE]^{\frac{1}{2}}$.

Can. J. Chem. Downloaded from www.nrcresearchpress.com by 210.87.254.5 on 09/05/12
For personal use only.

Thus the zero-order behaviour during any particular run is a consequence of a constant concentration of both ion-paired and dissociated substrate during the heterogeneous stage. The half-order dependence of the k_0^{obs} on the concentration of dissolved complexed substrate could arise if

$$[K^+\cdot CE] = [Ph_3CCO_2^-] \ll [Ph_3CCO_2K\cdot CE]$$

Since

$$\text{rate} = k_1[Ph_3CCO_2^-]$$

and from the definition of K_{diss} with $[K^+\cdot CE] = [Ph_3CCO_2^-]$

$$[Ph_3CCO_2^-] = (K_{diss}[Ph_3CCO_2K\cdot CE])^{\frac{1}{2}}$$

then

$$\text{rate} = k_1K_{diss}^{\frac{1}{2}}[Ph_3CCO_2K\cdot CE]^{\frac{1}{2}}$$

The apparent first-order behaviour of the homogeneous runs also is consistent with the mechanism in Scheme 1 provided the concentration of $K^+\cdot CE$ remains nearly constant over the course of the reaction. Thus from the definition of K_{diss}

$$\text{rate} = k_1[Ph_3CCO_2^-] = \frac{k_1K_{diss}}{[K^+\cdot CE]}[Ph_3CCO_2K\cdot CE]$$

The assumption that $[K^+\cdot CE]$ may not change a lot during the course of a particular run is supported by the observation that in the presence of equimolar **3** only about 30% of the expected $KHCO_3$ seems to precipitate even at long reaction times. This expression also shows that the rate of the reaction should be decreased by increasing $[K^+\cdot CE]$ either by increasing the substrate concentration (runs 16 and 17) or by adding a different complexed potassium salt (runs 17 and 18).

These results certainly seem consistent with the mechanism of Scheme 1. However, Scheme 1 has not been demonstrated to be the only mechanism consistent with the results. In fact, as will be seen later the mechanism may well be significantly more complex. An indication of this is given in runs 27 and 28 in which just the water concentration was changed producing a rate change. Our concern over the role water might be playing in this reaction, led us to a more thorough study of the effect of water concentration.

Effect of Water Concentration

As is presented in Table 4 and illustrated in Fig. 2, the effect of water on the reaction rates was not simple. The conditions chosen for this study involved homogeneous solutions in THF of **9** (0.020 *M*) and **3** (0.020 *M*) and the ratio of water to complexed substrate was changed from 0.03 to 36. With less than

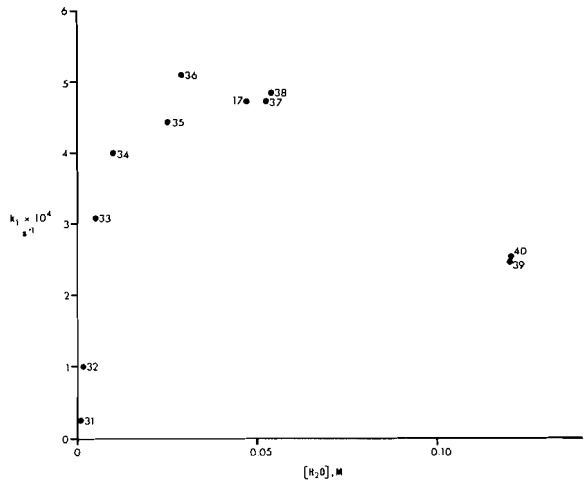

FIG. 2. Plot of first-order rate constants (runs 31–40 of Table 4) vs. the water concentration.

equimolar water [0.020 *M*] the rate increased with increasing water concentration. The rate leveled off when the ratio water/**9** was in the range of 1–3 and then decreased again at higher water concentrations. A second feature of the reactions containing less than 0.010 *M* water was the cessation of reaction when both available water protons had been consumed. Thus run 33 proceeded smoothly until about 40% reaction and run 32 to about 25% reaction. A number of the runs in Table 4 demonstrate the reproducibility of the rate data and confirm the changes with water concentration.

From a practical point of view these results indicate that water is necessary for a successful reaction but with slightly more than equimolar water the rate

TABLE 4. Effect of water on the decarboxylation of potassium triphenylacetate (0.020 *M*) in THF at 30°C with 18-crown-6 ether (0.020 *M*)

Run	[Water][a] (*M*)	$[H_2O]/[9]$	k_1 (s^{-1}) ($\times 10^4$)
31	0.0006[b]	0.03	0.27
32	0.0028[b]	0.14	1.0
33	0.0049	0.24	3.1
34	0.010	0.50	4.0
35	0.025	1.3	4.4
36	0.028	1.4	5.1
17	0.047	2.4	4.7
37	0.052	2.6	4.7
38	0.053	2.6	4.8
39	0.12	6.0	2.5
40	0.12	6.0	2.6
41	0.72	36	0.43
42	0.010[c]	0.50	0.31

[a] ± 0.001 *M*.
[b] Run in the presence of 5A molecular sieves.
[c] The solution was saturated with CO_2 (~0.2 *M*) which also converts the water to carbonic acid.

Can. J. Chem. Downloaded from www.nrcresearchpress.com by 210.87.254.5 on 09/05/12
For personal use only.

is not highly sensitive to water concentration. From the observation that water can both accelerate and decelerate the rate of decarboxylation it is clear that water must be capable of playing a dual role in the reaction scheme. Although there are probably several ways in which excess water could serve to slow the decarboxylation, hydrogen-bonding stabilization of the carboxylate ion is the most obvious and has precedent (4).

More intriguing is the question of how water can act to accelerate the decarboxylation at low water concentrations. One possible role for the water is to assist in the dissociation of the carboxylate ion pair. In this way the water could act to replace the triphenylacetate ion in the coordination shell of the complexed potassium ion. Crystal structures of

$$Ph_3CCO_2K{\cdot}CE + H_2O \rightleftharpoons Ph_3CCO_2^- + H_2O{\cdot}\overset{+}{K}{\cdot}CE$$

crown complexed cations frequently reveal an open face coordinated to the counter anion (10). This suggestion implies that water should be significantly better as a ligand than the solvent, THF, which is present in large excess. Such selectivity has been demonstrated for sodium ions in THF by sodium nmr chemical shift studies (11) and therefore is likely for potassium also. If water is acting to assist in ion pair dissociation, it should be capable of being a fairly general catalyst for crown ether assisted reactions in other solvents.

Another seemingly reasonable way in which water could accelerate decarboxylation is by competitively trapping the intermediate carbanion. This requires extending Scheme 1 to include the protonation step, with loss of CO_2 no longer the rate determining step (Scheme 2). This possibility was tested (run 42) by determining the effect of added CO_2 on the rate of decarboxylation since in Scheme 2 the rate should decrease as the CO_2 concentration increases. Indeed this was the case (run 34 cf. run 42) indicating also that the rate of carbonation of the triphenylmethyl anion must be comparable in magnitude to the rate of its protonation.

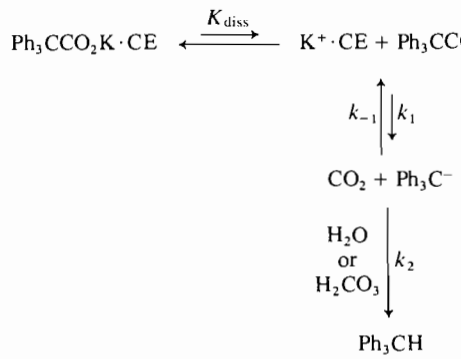

SCHEME 2

While this experiment provides support for Scheme 2 the actual situation is undoubtably more complex. A Karl-Fischer titration of the reaction solution which was originally 0.010 *M* in water showed no free water present (<0.001 *M*) when saturated with CO_2 (~0.2 *M*).[3] Presumably all the water had been converted to carbonic acid in THF. A similar situation appears to occur with ether as solvent (13). Thus in run 42, the reactants competing for the triphenylmethide anion are CO_2 and H_2CO_3 with CO_2 present in about a 10-fold excess. However, during a typical decarboxylation reaction, the water is present in excess and while both H_2O and H_2CO_3 are available for protonation[4] there may be very little CO_2 available for competitive carbonation until after the H_2O has been consumed. While CO_2, when present in excess, can compete with protonation, we think there is still insufficient evidence to confirm this as the way in which water accelerates the rate of decarboxylation.

Effect of Solvent

Since our study has been carried out using THF as solvent, we felt it was important to determine if indeed it was the solvent of choice. Thus the rate of decarboxylation of **9** (0.020 *M*) in the presence of **3** (0.020 or 0.040 *M*) and a 1.5- to 2.5-fold excess of water was measured for seven aprotic solvents of varying polarity (Table 5). While the total range of reactivity was large (~10^4) most of the activating solvents were bunched together within a factor of 10 to each other and THF was among these. From the standpoint of reaction rate, there is little to choose between several of the solvents and a choice of solvent can be made then on other factors such as solubility considerations or ease of removal of solvent.

Since acetonitrile has been chosen for many crown ether catalyzed reactions (14), a comparison was made of the decarboxylation rate in acetonitrile in the presence and absence of **3**. As runs 46 and 47 show, while acetonitrile is among the activating solvents it is at the bottom end of these and at least a factor of 2 slower than THF. Also a comparison of run 47 with run 48 shows a rate enhancement due to the addition of **3** of 60-fold which is somewhat less than that observed in THF (Table 2), although again the reaction in the absence of **3** was a two-phase reac-

[3]Concentration extrapolated from the lower temperature data of Bodor *et al.* (12).

[4]NOTE ADDED IN PROOF: A control study has shown that KOH·**3** in THF will deprotonate triphenylmethane. Thus H_2CO_3 rather than H_2O may be the species that protonates the triphenylmethide anion.

Can. J. Chem. Downloaded from www.nrcresearchpress.com by 210.87.254.5 on 09/05/12
For personal use only.

TABLE 5. Effect of solvent on the decarboxylation of potassium triphenylacetate (0.020 *M*) at 30°C

Run	[CE][a] (*M*)	[Water] (*M*)	Solvent	k_1^{obs} (s^{-1}) ($\times 10^4$)
43	0.020	0.031	Benzene	0.00058[b]
44	0.020	0.036	Dioxane	0.0043[c]
45	0.040	0.056	DME	1.1
19	0.040	0.053	THF	3.5
46	0.040	0.051	Acetonitrile	1.7
47	0.043	0.054	Acetonitrile	1.2
48		0.055	Acetonitrile	0.026[d]
49	0.040	0.048	Pyridine	13
50	0.041	0.050	DMSO	4.8

[a]18-Crown-6 ether.
[b]Calculated from 2.2% reaction at 98 h, 3.0% at 164 h, and 9.0% at 434 h.
[c]Calculated from 3.3% reaction at 19 h and 8.4% reaction at 112 h.
[d]A two-phase reaction which gave a better fit with a zero-order plot ($k_0 = 4.1 \times 10^{-8}$).

tion for which a first-order rate constant is not really valid.

Although the solvents chosen covered a fairly even distribution of polarities, the reaction rates were bunched into two groups with the reaction being about 10^3 slower in either benzene or dioxane than in 1,2-dimethoxyethane, THF, acetonitrile, pyridine, or dimethylsulfoxide. Correlations were sought with many different parameters of solvent polarity or density, but we had no significant success as might be expected. This is illustrated in Fig. 3 where our data have been plotted against values of E_T (15) showing the scatter that typically results.

The lack of correlation between the results of Table 5 and any simple solvent parameter may be attributed to the fact that the decarboxylation does not appear to be a simple one-step reaction. In fact, if Scheme 2 is correct there are at least five rate constants each of which would be altered upon changing solvent and thus any correlation would seem fortuitous. As a result we were rather surprised to discover a reasonable relationship between our data and those of Kemp and Paul (4). They had studied the decarboxylation of 3-carboxy-6-nitrobenzisoxazole **10** in the presence of a large excess of tetramethyl-

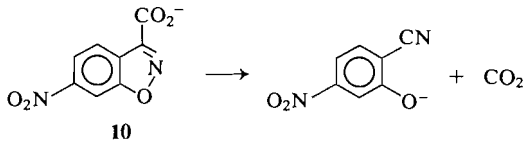

10

guanidine in a wide range of solvents. Five solvents were common between the two studies and Fig. 4 illustrates the common response of both reactions to a change of solvent. While neither reaction correlates with the usual solvent parameters, Kemp and Paul found a correlation of their rate data with the energy of an electronic transition of the reaction

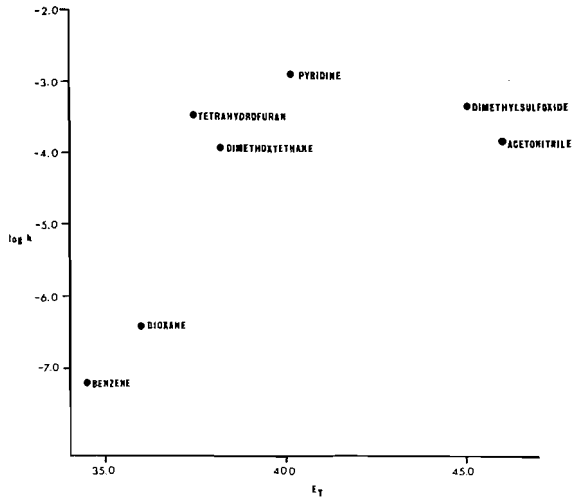

FIG. 3. Plot of log (first-order rate constants) in various solvents vs. the value of E_T (15) for that solvent.

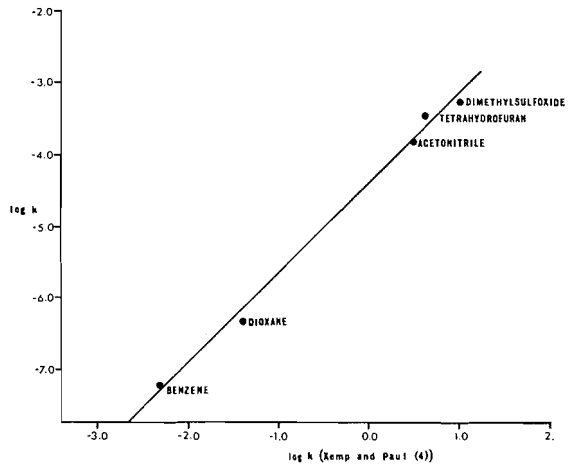

FIG. 4. Plot of the log of the first-order rate constant for decarboxylation of **9** vs. the log of the rate constant for decarboxylation of **10** in various solvents.

product. We made no such study of the triphenylmethyl anion.

While a mechanistic similarity between the two has not been established, from a practical point of view the observed correlation may be of general value. If other decarboxylation reactions proceeding through the salt form can be assumed to behave similarly, then our data and the extensive solvent studies of Kemp and Paul may assist in the choice of reaction conditions.

These studies have demonstrated that catalysis of decarboxylation of sodium carboxylates is a fairly general phenomenon and for those salts which are soluble in THF in the presence of **3**, rate enhancements in the order of 100–500 are observed. Also

Can. J. Chem. Downloaded from www.nrcresearchpress.com by 210.87.254.5 on 09/05/12
For personal use only.

there is a correlation between crown ether assisted decarboxylation rates and the stability of the carbanion produced as a transient intermediate.

An analysis of the behaviour of the triphenylacetate anion has provided results which should be of value to the practitioner and which also give an insight into the mechanism of the catalysis. From a practical point of view, optimum decarboxylation rates should be obtained using the potassium salt in the presence of equimolar **3**.[5] Water is essential to the reaction but should not be in large excess with optimum rates being obtained with a two- to threefold excess of water. While a number of solvents give similar rates, the two best were THF and pyridine.

From a mechanistic point of view, the reaction of **9** in the presence of **3** in THF seems to proceed through dissociated ions which are present in a small equilibrium amount. Water has both an accelerating and decelerating effect on the reaction. The decelerating effect points to hydrogen-bonding of water to the carboxylate while the source of accelerating effect remains ambiguous. The rate depressing effect of added CO_2 indicates that trapping of the intermediate carbanion by CO_2 can be competitive with trapping by protonation.

Experimental

Solvents

The benzene, tetrahydrofuran, and dioxane were freshly distilled from lithium aluminum hydride before use. Spectroscopy quality (Anachemia) acetonitrile, dimethyl sulfoxide, dimethoxyethane, and pyridine were further treated (17) before use. The water content of the solvents and solutions was determined by Karl-Fischer Titration-Photovolt Aquatest.

Substrates

The 18-crown-6 ether was prepared by the usual procedure (18). Fluorene-9-carboxylic acid and diphenylacetic acid were purchased and purified before use. The 9-phenylfluorene-9-carboxylic acid, triphenylacetic acid, and phenylacetylene carboxylic acid were prepared by carbonation of the corresponding organolithium. The preparation of triphenylacetic acid typifies this procedure.

Triphenylmethyllithium was prepared by reacting 12 g (50 mmol) of triphenylmethane in 100 ml of THF at −78°C under an argon atmosphere with 21 ml (50 mmol) of 2.5 *M* *n*-butyllithium in hexane (Ventron). The solution was warmed to room temperature for 15 min and then transferred over about a ½ h period to 75 ml of THF at room temperature that was constantly resaturated with dry carbon dioxide. After most of the THF was removed by rotary evaporator the reaction mixture was extracted using water–ether. After two ether washes, the water layer was acidified and then reextracted with ether. After drying, solvent removal, and recrystallization from toluene, triphenylacetic acid (mp 269°C, lit. (19) mp 270°C) was obtained in 45% yield. Similarly phenylacetylene carboxylic acid (mp 136–137°C, lit. (20) mp 137°C) was obtained in 70% yield and 9-phenylfluorene-9-carboxylic acid (mp 194°C, lit. (21) mp 194°C) was obtained in 78% yield.

The lithium, sodium, and potassium salts of the carboxylic acids were prepared by reaction of the acid with an aqueous solution of the corresponding hydroxide. The titration was stopped short of the equivalence point and the excess acid was removed by filtration. The salts were isolated by lyophilization. The water content was determined by Karl-Fischer titration of THF solutions.

Analytical Procedures

The decarboxylation reactions were run on doubly degassed solutions under an argon atmosphere. Typically 25 ml of solvent were used and sufficient substrate, glc standard, and 18-crown-6 ether to provide concentrations in the range 0.01–0.05 *M*. Aliquots of these solutions were removed for Karl-Fischer water analysis and to determine the progress of the decarboxylation reaction. For the heterogeneous reactions that were run an attempt was made to remove representative samples. Rate constants were obtained by plotting ln (100 − % decarboxylation) vs. time.

The progress of the decarboxylation reactions was measured by glc with added internal standards calibrated for response to the thermal conductivity detector. Typically an aliquot of the reaction mixture was removed and treated by extraction with water–ether to remove the unreacted salt. The ether layer containing the product hydrocarbon, the internal standard and some 18-crown-6 ether was concentrated and an aliquot was injected for glc analysis. Phenanthrene was used as an internal standard for diphenylmethane, triphenylmethane, 9-phenylfluorene, and fluorene while mesitylene was used with phenylacetylene. The glc analysis was performed using a 5 ft × ¼ in. column of 5% SE-30 on Chromsorb W.

[5]For similar accelerating effects of crown ethers in the decarboxylation of alkali metal trichloroacetates see Idemori *et al.* (16). While they observed a decrease in carbene adduct to cyclohexene when using crown ethers, our work on the 18-crown-6 ether catalyzed decomposition of sodium trichloroacetate shows increased yields in chloroform solvent.

Acknowledgment

The authors wish to thank the National Research Council of Canada for their financial support.

1. B. R. Brown. Quart. Rev. **5**, 131 (1951); L. W. Clark. *In* The chemistry of carboxylic acids and esters. *Edited by* S. Patai. J. Wiley and Sons, Toronto, Ont. 1969. Chapt. 12; W. H. Richardson and H. E. O'Neal. *In* Comprehensive chemical kinetics. *Edited by* C. H. Bamford and C. F. H. Tipper. Elsevier, New York, NY. 1972. pp. 447–483; M. L. Bender and L. J. Brubacker. Catalysis and enzyme action. McGraw-Hill, New York, NY. 1973.
2. C. A. Bunton, M. J. Minch, and W. Sepulveda. J. Phys. Chem. **75**, 2707 (1971).
3. T. S. Straub and M. L. Bender. J. Am. Chem. Soc. **94**, 8875 (1972).
4. D. S. Kemp and K. G. Paul. J. Am. Chem. Soc. **97**, 7305 (1975); D. S. Kemp, D. D. Cox, and K. G. Paul. J. Am. Chem. Soc. **97**, 7312 (1975).
5. D. H. Hunter, W. Lee, and S. K. Sim. J. Chem. Soc. Chem. Commun. 1018 (1974).
6. D. H. Hunter and R. A. Perry. Synthesis, 37 (1977).
7. G. F. Pedulli and A. Alberti. J. Chem. Soc. Perkin Trans. II, 137 (1976).
8. B. J. Tabner and T. Walker. J. Chem. Soc. Perkin Trans. II, 1201 (1973).
9. D. Casson and B. J. Tabner. J. Chem. Soc. B, 1560 (1970);

J. W. BURLEY and R. N. YOUNG. J. Chem. Soc. Perkin Trans. II. 835 (1972).
10. M. R. TRUTER. *In* Structure and bonding 16. Springer-Verlag, New York, NY. 1973. pp. 71–111.
11. A. L. VAN GUT. J. Am. Chem. Soc. **94**, 5583 (1972).
12. E. BODOR, G. BOR, M. MALECZKI, G. MESKO, B. MOHAI, and G. SIPOSS. Veszpremi Vegyip. Egy. Kozl. **1**, 89 (1957); Chem. Abstr. **55**, 3176d (1961).
13. G. GATTOW and V. GERWORTH. Angew. Chem. Int. Ed. Engl. **4**, 149 (1965).
14. C. L. LIOTTA and H. P. HARRIS. J. Am. Chem. Soc. **96**, 2250 (1974); C. L. LIOTTA, H. P. HARRIS, M. MCDERMOTT, T. GONZALEZ, and K. SMITH. Tetrahedron Lett. 2417 (1974); C. L. LIOTTA and E. E. GRISDALE. Tetrahedron Lett. 4205 (1975); R. W. ROESKE and P. D. GESELLCHEN. Tetrahedron Lett. 3369 (1976).
15. C. REICHARDT. Angew. Chem. Int. Ed. Engl. **4**, 29 (1965).
16. K. IDEMORI, M. TAKAGI, and T. MATSUDA. Bull. Chem. Soc. Jpn. **50**, 1355 (1977).
17. A. J. GORDON and R. A. FORD. The chemists companion. Wiley-Interscience, New York, NY. 1972.
18. G. W. GOKEL, D. J. CRAM, C. L. LIOTTA, H. P. HARRIS, and F. L. COOK. J. Org. Chem. **39**, 2445 (1974).
19. H. GILMAN and B. J. GAJ. J. Org. Chem. **28**, 1775 (1963).
20. R. C. WEAST (*Editor*). Handbook of chemistry and physics. 53rd ed. The Chemical Rubber Co., Cleveland, OH. 1972.
21. A. L. WILDS, R. L. VON TREBA, and N. F. WOOLSELY. J. Org. Chem. **34**, 2401 (1969).

Can. J. Chem. Downloaded from www.nrcresearchpress.com by 210.87.254.5 on 09/05/12
For personal use only.

Mercury photosensitized decomposition of thietane

DAVID R. DICE AND RONALD P. STEER[1]

Department of Chemistry and Chemical Engineering, University of Saskatchewan, Saskatoon, Sask., Canada S7N 0W0

Received August 2, 1977

DAVID R. DICE and RONALD P. STEER. Can. J. Chem. **56**, 114 (1978).

The mercury photosensitized decomposition of thietane vapour at room temperature has been studied. Quantum yields of the products, ethylene, propylene, cyclopropane, 1,2-dithiocane, and 1,5-hexadiene, have been measured as a function of substrate pressure, percent decomposition, and intensity and the influence of added NO and propylene has been examined. At low pressures quantum yields of thietane decomposition exceed unity. A mechanism involving thiatrimethylene and 4,5-dithiahexamethylene biradicals is proposed.

DAVID R. DICE et RONALD P. STEER. Can. J. Chem. **56**, 114 (1978).

On a étudié la décomposition, photosensibilisée par le mercure, de vapeurs de thiétane à la température ambiante. On a mesuré les rendements quantiques des produits, l'éthylène, le propylène, le cyclopropane, le dithio-1,2 cane et l'hexadiène-1,5, en fonction de la pression du substrat, du pourcentage de décomposition, de l'intensité et de l'influence provoquée par l'addition de NO et de propylène. Aux basses pressions, les rendements quantiques de la décomposition du thiétane sont plus grands que l'unité. On propose un mécanisme impliquant les biradicaux thiatriméthylène et dithia-4,5 hexaméthylène.

[Traduit par le journal]

Introduction

Whereas reports of the direct photodecomposition of cyclic organic sulfides are now relatively numerous (1–8), there have been but two brief previous reports of triplet sensitized photodecomposition of these molecules. Weibe and Heicklen (4) reported that the $Hg6(^3P_1)$ sensitized decomposition of thietane, $\underline{CH_2CH_2CH_2S}$, yielded ethylene, propylene, and cyclopropane with high pressure limiting quantum yields of 0.71, 0.02, and 0.005, respectively, unaffected by the addition of up to 10 Torr of O_2. These authors postulated that ethylene resulted from the molecular fragmentation of a thietane triplet but provided no conclusive evidence against the alternative, two-step decomposition involving a biradical intermediate. In a more recent study (9) of the mercury photosensitized decomposition of *cis*- and *trans*-3-ethyl-2-propylthietane vapour, however, we showed the major product must arise exclusively from the fragmentation of a free biradical intermediate, the lifetime of which is long in comparison with the period of C—C bond rotation.

Several sources suggest that there are a number of interesting aspects of the chemistry of the triplet states of the cyclic sulfides and the biradicals derivable from them which may be amenable to study by sensitization techniques. The lowest triplet state of thiirane, $\underline{CH_2CH_2S}$, has been implicated in the addition of $S(^3P)$ atoms to olefins, and in the thermolysis and photolysis of this compound. This state has been the subject of extensive theoretical and experimental investigation by Strausz and coworkers (1–3, 10–14) and is thought to have a substantial degree of biradical character, to be highly resistant to collisional deactivation, and to be capable of inducing the isomerization of olefins with very large quantum yield via a unique reversible addition reaction in which the sulfide retains its geometric configuration. In the thietane system we have shown (9) that triplet 1,4-biradicals derived from the sensitized photolysis of 2,3-dialkylthietanes are much longer lived than their singlet counterparts despite the fact that the degree of interaction between the two unpaired electrons must be relatively small in these species.

The present study has therefore been undertaken to elucidate the mechanistic details of the mercury photosensitized decomposition of thietane in order to explore further the triplet chemistry of the cyclic sulfides.

Experimental

Most of the apparatus and analytical procedures employed in the present work has been described in detail previously (6, 8). In the mercury photosensitization experiments a Hanovia, Model LO735A-7 low pressure mercury lamp was employed as a light source and either a 254 nm interference filter or short wavelength cut-off filters were used to isolate the 253.7 nm line. The transmitted light intensity was monitored with an RCA 935 phototube coated with sodium salicylate which produced a linear response over the range of intensities employed.

A fresh drop of mercury was placed in a side arm of the cell prior to each run. The temperature of the side arm was maintained at 25.0 ± 0.1°C whereas the cell itself was kept at 28 ± 1°C. After the reactants had been measured into the cell and thoroughly degassed, the contents of the cell were allowed to equilibrate for 1 h prior to photolysis. The cell was cleaned frequently to remove solid deposits.

[1]Author to whom correspondence should be addressed.

Can. J. Chem. Downloaded from www.nrcresearchpress.com by 210.87.254.6 on 09/05/12
For personal use only.

Can. J. Chem. Downloaded from www.nrcresearchpress.com by 210.87.254.6 on 09/05/12
For personal use only.

Lorentz pressure broadening correction factors were measured using the method of Strausz *et al.* (15). For these measurements a Bausch and Lomb high intensity grating monochromator and lens system was used to isolate and collimate the 253.7 nm line; 100% transmittance was set using a freshly cleaned cell containing no mercury vapour. Mercury was then added to the cell side arm and the transmittance of the mercury resonance line measured as a function of addend pressure.

Actinometry was carried out using both the propane ($\phi(H_2) = 0.58$ after pre-irradiation) and N_2O ($\phi(N_2) = 1.00$) systems (16, 17) which yielded identical results. Quantum yields were determined with a precision of $\pm 2\%$ for ethylene; $\pm 5\%$ for propylene, 1,2-dithiocane, and 1,5-hexadiene; and $\pm 25\%$ for cyclopropane which was present in trace amounts only.

Propane (Phillips, Research Grade) was used without further purification. N_2O was purified by passing it through a 5 ft silica gel column at $-95°C$, followed by low temperature vacuum distillation from $-160°C$ to $-196°C$. All other materials were purified as previously described.

Results

The Hg6($^3P_1$) quenching cross section for thietane was measured using the method of Cvetanovic (17) by determining the quantum yield of N_2 from the mercury sensitized photolysis of N_2O-thietane mixtures. The results are shown in Fig. 1. The slope of the $\phi(N_2)^{-1}$ vs. $P(C_3H_6S)/P(N_2O)$ plot is 2.00 ± 0.05, in good agreement with previous results (4), from which a quenching rate constant of $2.86 \times 10^{11}\ M^{-1}\ s^{-1}$ and a cross section of 44.1 Å^2 for thietane may be obtained, assuming that the quenching rate constant for N_2O is $1.43 \times 10^{11}\ M^{-1}\ s^{-1}$ (17).

In addition to the three products, ethylene, propylene, and cyclopropane, previously reported (4), analysis of the $-130°C$ condensable fraction of the reaction mixture revealed the presence of two additional products; 1,2-dithiocane (DTO), previously identified in the direct photolysis of thietane (8), and a product of molecular weight 82, tentatively identified as 1,5-hexadiene (HXD) on the basis of its mass spectrum and gc retention time. CS_2, H_2S, and H_2 were present in trace amounts, and a white solid consisting of a mixture of organosulfide polymer and sulfur was also formed but was not analyzed routinely.

Quantum yields (based on the number of photons absorbed by mercury vapour and corrected for pressure broadening of the mercury absorption line) of all products as a function of thietane pressure are shown in Fig. 2. Previous determinations of the quantum yields of ethylene, propylene, and cyclopropane (4) are in excellent agreement with the present work and are shown for comparison.

Experiments in which product yields from the photolysis of 10 Torr of thietane were measured as a function of exposure time revealed that quantum yields were constant up to about 3% decomposition and declined thereafter. Quantum yield ratios remained constant to much larger percentage decompositions, however, indicating that the decline in quantum yields at long exposure times is likely the result of the deposition of light attenuating solid on the cell windows. Unlike the direct photolysis system (6), no evidence of secondary photolytic reactions was obtained. Nevertheless, in all other experiments reported herein, decomposition was restricted to 3% or less.

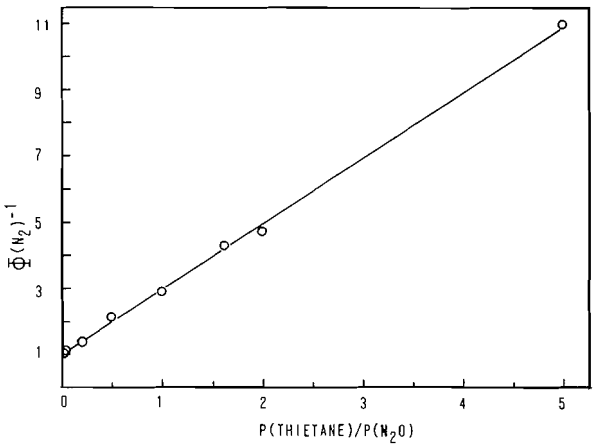

FIG. 1. $\phi(N_2)^{-1}$ vs. $[\square_S]/[N_2O]$ from the Hg6($^3P_1$) sensitization of thietane – nitrous oxide mixtures at a total pressure of 30 Torr.

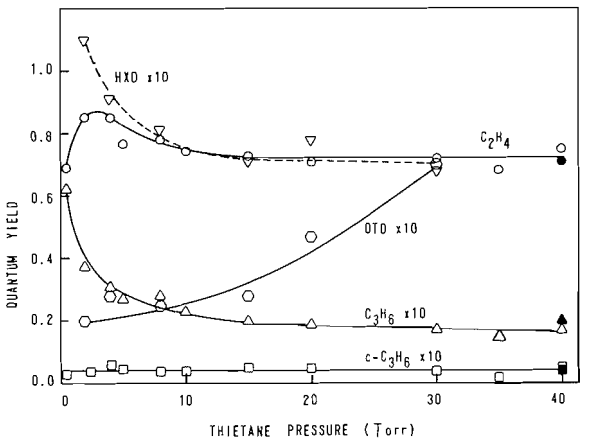

FIG. 2. Quantum yields of products as a function of thietane pressure. $I_a = 3.94 \times 10^{-7}$ einsteins per minute. Solid symbols are data of Weibe and Heicklen (4).

Product quantum yields from the Hg6($^3P_1$) sensitized decomposition of 20 Torr of thietane were found to be independent of absorbed intensity between 1.44×10^{16} and 2.59×10^{17} quanta per second.

In order to determine if free sulfur atoms were produced, 7 Torr of propylene was added to 50

TABLE 1. Effect of NO on the Hg6($^3P_1$) sensitized decomposition of thietane vapour[a]

P(NO) (Torr)	$1/f$[b]	ϕ (C_2H_4)	ϕ (C_3H_6)	ϕ (cyclo-C_3H_6)	ϕ (DTO)	ϕ (HXD)
0	1.00	0.71	0.019	0.005	0.047	0.077
0.5	1.02	0.73	0.019	0.005	0.014	0.066
1.0	1.04	0.72	0.018	0.003	0.009	0.025
2.0	1.07	0.70	0.019	0.006	0.003	0.023

[a] $P(\square_S)$ = 20 Torr. $I_a = 4.30 \times 10^{-7}$ einsteins per minute.

[b] $$f = \frac{P(\square_S)\sigma^2(\square_S)}{P(\square_S)\sigma^2(\square_S) + P(NO)\sigma^2(NO)}.$$

Torr of thietane and subjected to 3% thietane photodecomposition. Under these conditions 90% of the Hg6($^3P_1$) atoms will be quenched by thietane. No propylene episulfide, which results from the addition of S(^3P) to propylene, was detected.

Nitric oxide was added to determine the sensitivity of the product quantum yields to the presence of a free radical scavenger. The results of adding up to 2 Torr of NO to 20 Torr of thietane are given in Table 1. Quantum yields have been corrected for the fraction of Hg6($^3P_1$) quenched by NO. Both DTO and HXD showed significant decreases in quantum yield with increasing NO pressure whereas the C_2 and C_3 hydrocarbon products were unaffected. The latter observation is in agreement with the previous work of Weibe and Heicklen (4) who showed that these products have quantum yields which are unchanged by the addition of up to 10 Torr of O_2.

Discussion

The interaction of Hg6($^3P_1$) with 0.5 Torr of either pure *cis*- or pure *trans*-3-ethyl-2-propylthietane at room temperature has previously been shown (9) to result in the production of both *cis*- and *trans*-3-heptene and isomerized substrate. The ratio of the rates of production of the isomeric 3-heptenes was sensitive to the pressure of argon, added as an inert thermalizing gas, at pressures less than *ca.* 100 Torr, but converged to a common value at high pressures regardless of which thietane isomer was employed. These results indicate that a 1,4-biradical in which free C—C bond rotation takes place must be the precursor of all of the olefin which results from C—C cleavage. There is no evidence that thietane and its 2,3-dialkylderivatives exhibit different pathways leading to C—C cleavage products. Therefore, contrary to the mechanism of Weibe and Heicklen (4), it will be assumed that ethylene is produced exclusively via one or more biradical precursors in the present system.

The following mechanism is in qualitative accord with experiment.

[1] $$Hg6(^1S_0) + h\nu \rightarrow Hg6(^3P_1)$$

[2] $$Hg6(^3P_1) \rightarrow Hg6(^1S_0) + h\nu$$

[3] $$Hg6(^3P_1) + \square_S \rightarrow Hg6(^1S_0) + {}^3\square_S$$

[4] $${}^3\square_S \rightarrow \cdot\!\!\sim\!\!S\cdot$$

[5] $$\cdot\!\!\sim\!\!S\cdot \rightarrow C_2H_4 + CH_2S$$

[6] $$\cdot\!\!\sim\!\!S\cdot \rightarrow \diagup\!\!\diagdown + S(^3P)$$

[7] $$\cdot\!\!\sim\!\!S\cdot \rightarrow \triangle + S(^3P)$$

[8] $$\cdot\!\!\sim\!\!S\cdot \rightarrow HS\cdot + C_3H_5\cdot$$

[9] $$\cdot\!\!\sim\!\!S\cdot \xrightarrow{M} \square_S$$

[10] $$\cdot\!\!\sim\!\!S\cdot \rightarrow \cdot\!\!\sim\!\!S{-}S\!\!\sim\!\!\cdot \xrightarrow{M} DTO$$

[11] $$S(^3P) + \square_S \rightarrow S_2 + \diagup\!\!\diagdown$$

[12] $$S(^3P) + \square_S \rightarrow S_2 + \triangle$$

[13] $$2S(^3P) \xrightarrow[Wall]{M} S_2$$

[14] $$2C_3H_5\cdot \rightarrow C_6H_{10}$$

[15] $$nCH_2S \rightarrow (CH_2S)_n$$

Neither of the minor hydrocarbon products, propylene and cyclopropane, is affected by the free radical scavengers O_2 + NO. However, the propylene yield is clearly pressure sensitive and the total C_3 yield increases substantially with decreasing pressure. We take this as good evidence that propylene is not produced from the isomerization of hot cyclopropane and that neither propylene nor cyclopropane are produced from the trimethylene biradical (18, 19). Both C_3 fragments must result from the loss of sulfur from the substrate either by direct extrusion of a S(^3P) atom or subsequent to attack of the substrate by triplet thietane or a thiatrimethylene biradical.

Attempts to trap S(^3P) atoms yielded inconclusive results. Under the conditions which had to be

Can. J. Chem. Downloaded from www.nrcresearchpress.com by 210.87.254.6 on 09/05/12
For personal use only.

TABLE 2. Quantum yields of products per Hg6($^3P_1$) atom quenched by thietane

$P(\square_S)$ (Torr)	$1/A^a$	Q^b	ϕ' (C_2H_4)	ϕ' (C_3H_6)	ϕ' (cyclo-C_3H_6)	ϕ' (DTO)	ϕ' (HXD)	ΣI^c	ΣII^c
0.50	1.70	1.47	1.01	0.091	0.004	—	—	1.38	1.43
2.0	1.45	1.12	0.95	0.041	0.004	0.022	0.11	1.21	1.24
4.0	1.30	1.06	0.90	0.033	0.006	0.031	0.091	1.13	1.15
5.0	1.11	1.05	0.80	0.028	0.005	—	—	—	—
8.0	1.10	1.03	0.80	0.029	0.004	0.026	0.081	1.00	1.02
10.0	1.06	1.02	0.75	0.023	0.004	—	—	—	—
15.0	1.04	1.02	0.74	0.020	0.005	0.029	0.071	0.92	0.94
20.0	1.02	1.01	0.72	0.019	0.005	0.047	0.078	0.94	0.95
30.0	1.01	1.01	0.73	0.017	0.004	0.071	0.069	0.95	0.96
35.0	1.01	1.01	0.69	0.015	0.002	—	—	—	—
40.0	1.00	1.01	0.76	0.017	0.005	—	—	—	—
47.5	1.00	1.01	0.76	0.016	0.005	—	—	—	—

[a]Lorentz pressure broadening correction factor.
[b]Incomplete quenching correction factor.
[c]See text. Values at 0.50 Torr by extrapolation assuming ϕ'(DTO) = 0.02 and ϕ'(HXD) = 0.15.

employed in the trapping experiments, only a small fraction (likely of the order of 10%) of any S atoms produced would have been scavenged by propylene. Small yields of S(^3P) atoms, such as might accompany the formation of cyclopropane in reaction 7, would have yielded amounts of propylene episulfide too small to detect. Indeed a propylene episulfide yield equal to 10% of the total C_3 yield at high pressure was barely detectable in the presence of large amounts of residual substrate. Since these scavenging experiments could only be carried out at pressures at which the hydrocarbon products had attained their high pressure limiting values, the production of small yields of S(^3P) atoms, particularly at low pressures, cannot be eliminated by the absence of episulfide in these experiments. On the contrary, since sulfur atoms are known to be produced in high yield from triplet thiirane (1–3) the production of S(^3P) in the thietane system might be expected.

The fact that both DTO and HXD have quantum yields which decline with increasing NO pressure indicates that both of these products have scavengeable radical precursors. Because the yield of DTO, unlike all other products, increases with increasing thietane pressure, it must result from the bimolecular reaction of the thiatrimethylene biradical (or alternatively triplet thietane) with substrate. Since there is good evidence (6) that the thiatrimethylene biradical cannot be scavenged by NO, the scavengeable species in the sequence of reactions leading to DTO must be one produced as a result of, or subsequent to, this bimolecular reaction. HXD most likely results from a reaction sequence which, on the basis of its pressure dependence, starts with a unimolecular fragmentation of $\cdot C_3H_6S\cdot$ into HS$\cdot$ and $C_3H_5\cdot$ followed by combination of two $C_3H_5\cdot$ radicals. The $C_3H_5\cdot$ radical is known to be a relatively stable species (20) and is expected to be long lived enough in this system to be scavenged by NO. The fate of HS$\cdot$ is unknown but trace amounts of H_2 and H_2S may result from self-disproportionation and abstraction reactions of this species.

Quantum yields based on the number of photons absorbed by mercury (Fig. 2) must be corrected to account for incomplete quenching at low thietane pressures. Using the value of $k_3 = 2.86 \times 10^{11}\ M^{-1}\ s^{-1}$ and a value of $k_2 = 2.61 \times 10^6\ s^{-1}$ from Holstein's imprisonment formula (21), one may calculate the yields of each product per mercury atom quenched by thietane. These corrected quantum yields are given in Table 2. As presented the mechanism requires that $\phi'(C_2H_4) + \frac{1}{2}\{\phi'(C_3H_6) + \phi'(\text{cyclo-}C_3H_6)\} + 2\phi'(\text{HXD}) + \phi'(\text{DTO}) = \sum\text{I} \leq 1.0$ if $k_{13} \ll k_{11} + k_{12}$ or $\phi'(C_2H_4) + \phi'(C_3H_6) + \phi'(\text{cyclo-}C_3H_6) + 2\phi'(\text{HXD}) + \phi(\text{DTO}) = \sum\text{II} \leq 1.0$ if $k_{13} \gg k_{11} + k_{12}$. The quantum yield of substrate reformation cannot, of course, be measured directly for thietane itself. Nevertheless, the presence of major amounts of isomerized substrate in the mercury photosensitized decomposition of *cis*- and *trans*-2,3-dialkylthietanes (9) requires that such a step be included in the reaction mechanism. Thus either $\sum$I or $\sum$II should equal unity as an upper limit only, based on the mechanism represented by reactions 1 to 15.

The fact that both $\sum$I and $\sum$II substantially exceed unity at low pressures (cf. Table 2) indicates that at least one important additional substrate decomposing reaction must be included in the mechanism. Strausz and co-workers have proposed (13, 14) that the thiirane triplet can undergo a bimolecular reaction with ground state thiirane which results in the decomposition of both reacting molecules.

Can. J. Chem. Downloaded from www.nrcresearchpress.com by 210.87.254.6 on 09/05/12
For personal use only.

[16] 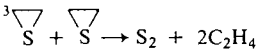

A similar set of reactions in the thietane system would account for the required additional yields of products. However, reaction between thiatrimethylene biradicals and the substrate seems equally plausible and would, additionally, satisfy the requirement that all of the olefin produced by C—C cleavage must have a precursor in which free C—C bond rotation can take place. The following, more detailed reaction sequence is therefore tentatively proposed to replace reaction [10].

[17]

[18] 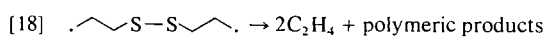

[19] 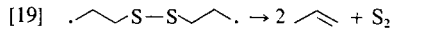

[20] 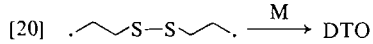

At low pressures where both the thiatrimethylene and 4,5-dithiahexamethylene biradicals are vibrationally hot, the entire reaction sequence would then lead to the required hydrocarbon yield but little DTO. At higher pressures both the rate of ring opening in the thietane triplet and the rate of unimolecular decomposition of the resulting biradicals would be diminished whereas an increased rate of collisionally assisted ring closure of the 4,5-dithiahexamethylene biradical, reaction 20, would lead to increased yields of DTO as required.

Acknowledgement

The authors are grateful to the National Research Council of Canada for financial support.

1. H. E. GUNNING and O. P. STRAUSZ. Adv. Photochem. **4**, 143 (1966).
2. O. P. STRAUSZ, H. E. GUNNING, and E. M. LOWN. *In* Comprehensive chemical kinetics. Vol. 5. *Edited by* C. H. Bamford and C. F. H. Tipper. Elsevier, Amsterdam. 1972. Chapt. 6.
3. P. FOWLES, M. DESORGO, A. J. YARWOOD, O. P. STRAUSZ, and H. E. GUNNING. J. Am. Chem. Soc. **89**, 1352 (1967).
4. H. A. WEIBE and J. HEICKLEN. J. Am. Chem. Soc. **92**, 7031 (1970).
5. S. BRASLAVSKY and J. HEICKLEN. Can. J. Chem. **49**, 1316 (1971).
6. D. R. DICE and R. P. STEER. J. Phys. Chem. **77**, 434 (1973).
7. D. R. DICE AND R. P. STEER. J. Chem. Soc. Chem. Commun. 106 (1973).
8. D. R. DICE and R. P. STEER. Can. J. Chem. **53**, 1744 (1975).
9. D. R. DICE and R. P. STEER. J. Am. Chem. Soc. **96**, 7361 (1974).
10. O. P. STRAUSZ. Adv. Chem. Ser. **110**, 137 (1972).
11. K. S. SIDHU, E. M. LOWN, O. P. STRAUSZ, and H. E. GUNNING. J. Am. Chem. Soc. **88**, 254 (1966).
12. O. P. STRAUSZ, H. E. GUNNING, A. S. DENES, and I. G. CSIZMADIA. J. Am. Chem. Soc. **94**, 8317 (1972).
13. E. M. LOWN, A. JACKSON, P. VITINS, A. JODHAN, and O. P. STRAUSZ. Paper presented to 2nd Joint Conference of the Chemical Institute of Canada and the American Chemical Society, Montreal, 1977.
14. E. M. LOWN, H. S. SANDU, H. E. GUNNING, and O. P. STRAUSZ. J. Am. Chem. Soc. **90**, 7164 (1968).
15. O. P. STRAUSZ, R. J. NORSTROM, D. SALAHUB, R. K. GOSAVI, H. E. GUNNING, and I. G. CSIZMADIA. J. Am. Chem. Soc. **92**, 6395 (1970).
16. R. A. BACK. Can. J. Chem. **37**, 1834 (1959).
17. R. J. CVETANOVIC. Prog. React. Kinet. **2**, 39 (1964).
18. R. G. BERGMAN and W. L. CARTER. J. Am. Chem. Soc. **91**, 7411 (1969).
19. H. E. O'NEAL and S. W. BENSON. J. Phys. Chem. **72**, 1866 (1968).
20. H. E. O'NEAL and S. W. BENSON. *In* Free radicals. Vol. 2. *Edited by* J. K. Kochi. Wiley-Interscience, New York, NY. 1973. Chapt. 17.
21. T. HOLSTEIN. Phys. Rev. **72**, 1212 (1947); **83**, 1159 (1951).

Can. J. Chem. Downloaded from www.nrcresearchpress.com by 210.87.254.6 on 09/05/12
For personal use only.

The chromous chloride promoted addition of *N*-haloamides to olefins. V.[1] The addition of *N*-chloroamides to enol ethers: synthesis of acyloxy and acyl derivatives of α-amino acetals and ketals (aldehydes and ketones) and of 2-amino sugars[2]

HUGUES DRIGUEZ,[3] JEAN-PAUL VERMES, AND JEAN LESSARD

Département de Chimie, Université de Sherbrooke, Sherbrooke (Qué.), Canada J1K 2R1

Received June 3, 1977

HUGUES DRIGUEZ, JEAN-PAUL VERMES, and JEAN LESSARD. Can. J. Chem. **56**, 119 (1978).

The chromous chloride promoted addition of *N*-chlorocarbamates and *N*-chlorocarboxamides to 1-methoxycyclohexene, ethoxyethylene, dihydropyran, and (1-methoxyethylidene)-cyclohexane gave, in 60 to 85% yields, either α-acyloxy- or α-acylamino ketals and acetals, or the corresponding ketones and aldehydes depending on the work-up conditions. The regiospecificity of the addition was higher with the first two enol ethers (≥97%) than with the latter two (≥85%). *N*-Chlorourethane was added to 17-methoxymethylenandrost-4-en-3-one (**19**) and the sole addition product isolated was the 17α-chloro-20-ethoxycarbonylamino derivative **20** in 75% yield. Additions to triacetyl-D-glucal and 3-*O*-acetyl-4,6-*O*-benzylidene-D-glucal followed by solvolysis under Koenigs–Knorr conditions led predominantly to 2-amino-glucopyranosides in 30 to 65% yields, whereas additions to 3-*O*-acetyl-4,6-*O*-benzylidene-D-allal gave 2-amino altropyranosides in 40 to 56% yields.

HUGUES DRIGUEZ, JEAN-PAUL VERMES et JEAN LESSARD. Can. J. Chem. **56**, 119 (1978).

L'addition, catalysée par le chlorure chromeux, de *N*-chloroamides au methoxy-1 cyclohexène, à l'éthoxyéthylène, au dihydropyranne et au (méthoxy-1 éthylidène)cyclohexane donne, suivant le mode opératoire utilisé, soit des α-acyloxy- ou α-acylamino acétals, soit les cétones et aldéhydes correspondants avec des rendements de 60 à 85%. L'addition aux deux premiers éthers d'énol est plus regiospécifique (≥97%) que l'addition aux deux autres (≥85%). Le *N*-chlorouréthane s'additionne au méthoxyméthylène-17 androstène-4 one-3 (**19**) et on isole, comme seul produit d'addition, le dérivé chloro-17α éthoxycarbonylamino-20 (**20**) avec un rendement de 75%. Les additions au triacetyl D-glucal et à l'acétyl-3 benzylidène-4,6 D-glucal, suivies d'une réaction Koenigs–Knorr, donnent comme produits principaux (rendements de 30 à 65%) des glucopyranosides aminés en position 2. Les additions à l'acétyl-3 benzyliden-4,6 D-allal donnent par contre des amino-2 altropyranosides avec des rendements de 40 à 60%.

Introduction

Recently we reported a study of the chromous chloride promoted addition of various *N*-chloro- and *N*-bromoamides to a variety of olefins (1*a*). We also presented a discussion of a working hypothesis concerning the mechanism (1*b*). This paper describes a study of the addition of *N*-chloroamides to enol ethers aimed at evaluating the potential of the method for the synthesis of α-amido acetals and ketals (aldehydes and ketones) and 2-amido sugars (Scheme 1).[4] *N*-Bromoamides cannot be used for that purpose since electrophilic bromination is important under the reaction conditions (see the Experimental for the reaction of *N*-bromocetamide with 1-methoxycyclohexene).

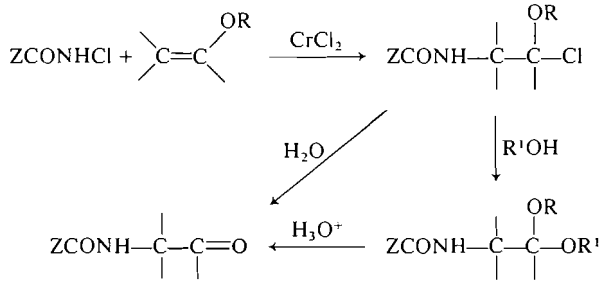

Z = *O*-alkyl, alkyl

SCHEME 1

Results and Discussion

The conditions and results for the additions to various types of enol ethers are reported in Table 1, and those for the additions to glycals are recorded in Table 2. All the compounds had ir and ^{1}Hmr spectra, elemental analyses, and/or mass spectra consistent with their structures. The analysis and interpretation of the spectra are straightforward (see Experimental) and will not be given unless helpful to the discussion.

[1]For parts III and IV, see ref. 1.

[2]Taken in part from the Ph.D. thesis of H. Driguez, Université de Sherbrooke, 1971.

[3]Arts Council of Canada Predoctorate Fellow, 1969–1971. Present address: Centre de Recherches sur les Macromolécules Végétales, C.N.R.S., B.P. 53, 38041, Grenoble, France.

[4]For a preliminary account of part of this work, see ref. 2.

Can. J. Chem. Downloaded from www.nrcresearchpress.com by 210.87.254.5 on 09/05/12
For personal use only.

TABLE 1. The chromous chloride promoted addition of ZCONHCl (**1**) to enol ethers[a]

Entry	Enol ether	Z	Work-up[b]	Addition products: Acetal or ketal	Yield[c] (%)	Aldehyde or ketone	Yield[c] (%)	Others	Yield[c] (%)
1	1-Methoxycyclohexene (**2**) (Scheme 2)	CH_3CH_2O[d]	H_2SO_4			**4***a*	85(90)[e]		
2		$ClCH_2CH_2O$	H_2O	**3***b*	6	**4***b*	80(81)[e]		
3			CH_3ONa	**3***b*	74				
4		CCl_3CH_2O	H_2SO_4			**4***c*	86		
5			CH_3ONa	**3***c*	75	**4***c*	7		
6		$C_6H_5CH_2O$	CH_3ONa	**3***d*	60	**4***d*	3		
7		CH_3	H_2SO_4			**4***e*	82		
8	Ethoxyethylene (**5**) (Scheme 3)	$ClCH_2CH_2O$	CH_3ONa	**6***b*(R=CH_3)	74				
9		$C_6H_5CH_2O$	CH_3ONa	**6***d*(R=CH_3)	81				
10		$ClCH_2$	C_2H_5ONa	**6***f*(R=C_2H_5)	78				
11	Dihydropyran (**8**) (Scheme 4)	CH_3CH_2O	CH_3OH	**10***a trans*	77	**12***a*	5	**13***a*	~5[f]
				11*a cis*	4			**14***a*	~7[f]
12		$C_6H_5CH_2O$	CH_3OH/Ag^+	**10***d trans*	72	**12***d*	9	[g]	
				11*d cis*	4				
13		CH_3O	CH_3OH	**10***g trans*	66[h]				
14	(1-Methoxyethylidene)cyclohexane (**15**)[i] (Scheme 6)	CH_3CH_2O	H_2SO_4			**16**	59(62)[e]	17	10
15	Steroid **19**[i] (Scheme 7)	CH_3CH_2O	CH_3ONa					20	75
16	2-Trimethylsiloxy-2-norbornene (**22**)[i] (Scheme 8)	$C_6H_5CH_2O$	CH_3OH			23	19		

[a]Unless specified otherwise, the reactions were carried out under the usual conditions, that is at a cooling bath temperature of −78°C, in a mixture of chloroform–methanol as solvent, using a 2:1 molar ratio of enol ether to *N*-chloroamide, and the yields are based on the *N*-chloroamide.
[b]H_2SO_4: the reaction mixture was allowed to warm up to room temperature, dilute sulfuric acid was added, and the mixture was stirred for 4 h; H_2O: addition of water to the reaction mixture followed by stirring for 4 h at room temperature; CH_3ONa: addition of sodium methoxide to the reaction mixture at −78°C; C_2H_5ONa: the reaction was carried out in chloroform–ethanol and was followed by the addition of sodium ethoxide at −78°C; CH_3OH: the reaction was carried out in methanol only at −78°C and was followed by stirring at room temperature for 1 h; CH_3OH/Ag^+: the reaction, carried out under the usual conditions, was immediately followed by rapid extraction in the presence of ice, then the crude product, containing the α-chloro ether **9**, was treated under Koenigs–Knorr conditions (dry methanol, Ag_2CO_3, Drierite).
[c]Unless specified otherwise the yields refer to products isolated by chromatography and homogeneous according to tlc.
[d]Taken from ref. 1*a*.
[e]By vpc.
[f]The adducts **13***a* (most probably a mixture of *cis* and *trans* isomers) and **14***a* were obtained as a mixture and the proportion was calculated from elemental analysis (see the Experimental).
[g]No attempt was made to isolate the adducts **13***d* and **14***d*.
[h]Yield after chromatographic separation and short path distillation. No attempt was made to isolate the *cis* acetal **11***g*, the hemiacetal **12***g*, and the adducts **13***g* and **14***g*.
[i]A 1:2 molar ratio of enol ether to *N*-chloroamide was used and the yields are based on the enol ether.

TABLE 2. Addition of ZCONHCl (**1**) to glycals followed by solvolysis[a]

	Z	2-Amidopyranosides[b]: Product	Yield[c] (%)	Product	Yield[c] (%)	Recovered glycal (%)
Triacetyl-D-glucal (**24**) (Scheme 9)	CH_3CH_2O	**28***a*(R=CH_3)	42(61)[d]			18
		(R=CH_3CO)	41			18
		(R=$C_6H_5CH_2$)	53			17
	$ClCH_2CH_2O$	**28***b*(R=CH_3)	55(62)[d]	**29***b*(R=CH_3)	7	5
	$C_6H_5CH_2O$	**28***d*(R=CH_3)	46			18
		(R=CH_3CO)	32			10
		(R=$C_6H_5CH_2$)	22			11
	CH_3	**28***e*(R=CH_3)	31			39
	$ClCH_2$	**28***f*(R=CH_3)	48			7
Acetylbenzylidene-D-glucal (**31**) (Scheme 11)	CH_3CH_2O	**32**	12	**29***a*(R=CH_3)[e]	9	7
		28*a*(R=CH_3)[e]	30			
Acetylbenzylidene-D-allal (**34**) (Scheme 12)	CH_3CH_2O	**35***a*	40			13
		36*a*[e]	16			
	CCl_3CH_2O	**36***c*[e]	65			
	CH_3	**37**(oxazoline)[e]	18			18

[a]The additions were carried out with an excess of *N*-chloroamide **1** (2 mol per mol of glycal) under the usual conditions ($CHCl_3$–CH_3OH, −78°C). The reaction mixture was then poured into an ice-cold saturated sodium bicarbonate solution then rapidly extracted in the cold. The crude products, containing 2-amidopyranosyl chlorides according to the ^{1}Hmr spectra, were solvolyzed under Koenigs–Knorr conditions.
[b]The following 2-amidopyranosides have been reported in the literature: **28***a*(R = CH_3CO), ref. 7; **28***d*(R = CH_3), ref. 8; **28***d*(R = CH_3CO), ref. 7; **28***d*(R = $C_6H_5CH_2$), ref. 8; **28***e*(R = CH_3), ref. 9; **28***f*(R = CH_3), ref. 10.
[c]The yields refer to compounds obtained by recrystallization of chromatographic fractions and are based on the glycal.
[d]The yield between brackets include the additional amount obtained by deacetylation of the mother liquors, recrystallization, then reacetylation of the crystals.
[e]See text.

Can. J. Chem. Downloaded from www.nrcresearchpress.com by 210.87.254.5 on 09/05/12
For personal use only.

Can. J. Chem. Downloaded from www.nrcresearchpress.com by 210.87.254.5 on 09/05/12
For personal use only.

Additions to the Enol Ethers of Table 1

In the additions to *1-methoxycyclohexene* (**2**) (Scheme 2), it was possible to obtain either the ketal **3** or the ketone **4** depending on the work-up procedure. The sodium methoxide work-up allowed the isolation of ketal **3**[5] in good yields (entries 3, 5, and 6) but small amounts of ketone **4** were also formed by hydrolysis of the intermediate α-chloro ether due to the water (6.3 mol per mol of Cr(II)) present in the chromous chloride solution (1*a*). When using the dilute sulfuric acid work-up, hydrolysis of ketal **3** was complete after 4 h to give the ketone **4** in very good yields (entries 1, 4, and 7). If water only was added, the hydrolysis was not complete after 4 h (entry 2). These additions appear to be highly regiospecific, the material balance (ketal **3** and/or ketone **4** plus amide) accounting for more than 96% of starting *N*-chloroamide. α-Chlorocyclohexanone, which could be derived from addition of the amido radical at C-1 and/or electrophilic chlorination followed by hydrolysis, was present in very small amounts (< 1%) in the crude products according to vpc analysis.

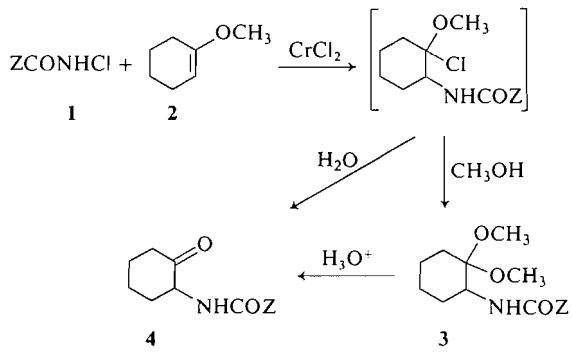

SCHEME 2

In the additions to *ethoxyethylene* (**5**) (Scheme 3), we used the alkoxide work-up and the acetal **6** was isolated in good yields. The addition of *N*-chlorochloroacetamide (**1***f*) was carried out in chloroform–ethanol in order to avoid the formation of a mixed acetal. We did not isolate any aldehyde **7** from the chromatographic fractions although it was probably formed to a small extent by reaction of the intermediate α-chloro ether with the water present in the reaction medium. The acetal **6** and the parent amide accounted for 90% or more of the starting *N*-chloroamide. No 1-amido-2-chloro-1-ethoxyethane or 1-amido-1-ethoxyethane resulting from addition of the amido radical at C-1 was isolated or detected. Such adducts have been isolated from radical additions to disubstituted enol ethers derived from aldehydes (18) (see the addition of *N*-chlorourethane (NCU) to **19** below). Thus the additions to **5** appear to be highly regiospecific also.

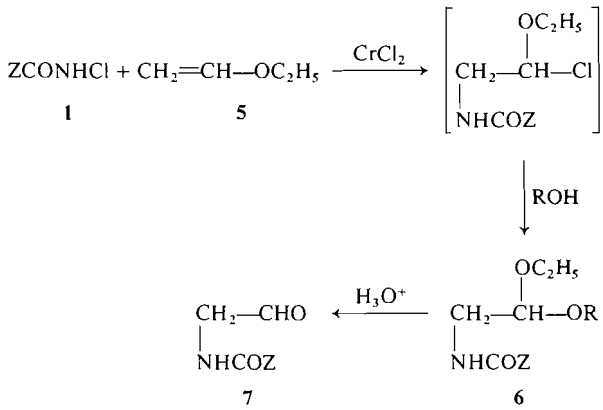

SCHEME 3

The acetals **6***b* and **6***d* were hydrolyzed to the corresponding aldehydes **7***b* and **7***d* (Scheme 3) with 70% aqueous acetic acid at 70°C in 65 and 80% yield, respectively (based on the conversion to their 2,4-DNP derivatives).

The additions to *dihydropyran* (**8**) (Scheme 4) led to the *trans* α-amido acetal **10** as the major product probably as a result of participation of the carbamate group in the methanolysis of the intermediate α-chloro ether **9**[6] (Scheme 5). The *cis* acetal **11** could result from direct attack of methanol on the cation B and/or from partial isomerization of the *trans* acetal **10** since the reaction medium is acidic. Equilibration of either the *trans* isomer **10***a* or the *cis* isomer **11***a* with hydrogen chloride in methanol led to a 1:1.8 mixture of **10***a* and **11***a*. The more stable isomer was assigned the *cis* configuration **11** with the carbamate group equatorial and the methoxy group axial, a consequence of the anomeric effect (3): $J_{2,3}$ = 3.0 Hz for **11***a*, 3.5 Hz for **11***d*, in $CDCl_3$. The *trans* isomer **10** exists predominantly in the *trans* diaxial conformation ($J_{2,3}$ = 2.6 Hz for **10***a* and **10***g*, 2.0 Hz for **10***d*, in $CDCl_3$) again as a result of the anomeric effect (3); the proportion of diaxial conformer decreases as the polarity of the solvent increases in agreement with the greater polarity of the diequatorial conformer and with the fact that the anomeric effect varies inversely with the dielectric constant of the solvent (4): $J_{2,3}$ for **10***a* = 2.0 Hz in CS_2, 2.6 Hz in $CDCl_3$, 3.9 Hz in CD_3OD. The ^{1}Hmr spectrum of the *trans* adducts **10***a* and **10***g* was studied at low temperature. At 173 K, only the

[5]The pure ketals **3***b*, **3***c*, and **3***d* were hydrolysed to the corresponding ketones **4***b*, **4***c*, and **4***d* in 98, 92, and 89% yield, respectively.

[6]The *cis* isomer is probably predominant as in the additions to cyclohexene and norbornene (1*a*) and to triacetylglucal (**24**) (see below).

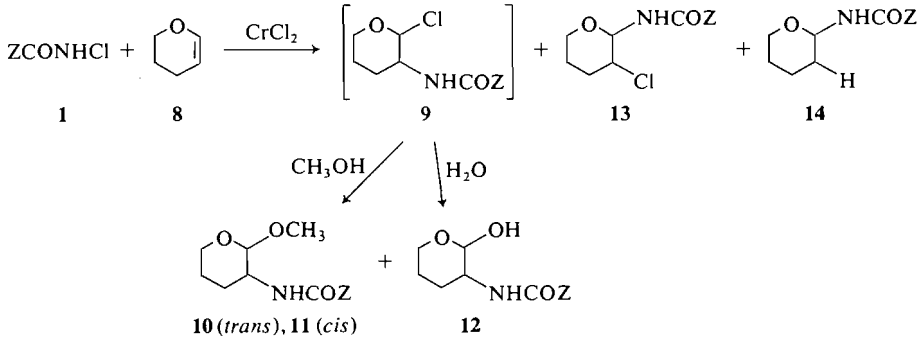

1 8 9 13 14

10 (*trans*), 11 (*cis*) 12

SCHEME 4

diaxial conformer could be observed even in CD_3OD: the proton at C-3 appeared as a singlet, the width at half height being less than 2 Hz ($J_{2,3}$ < 2 Hz).[7]

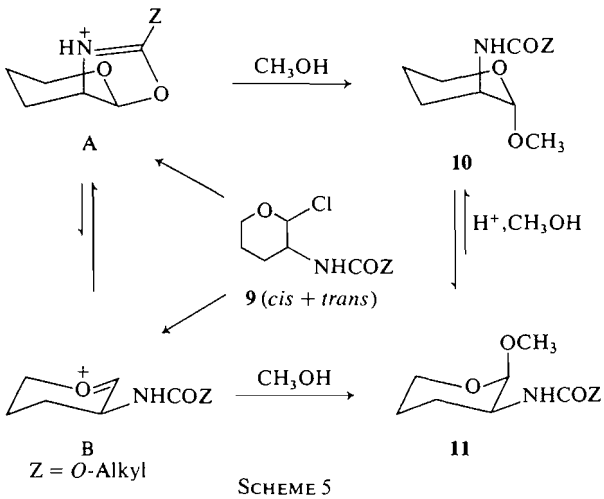

SCHEME 5

The hemiacetal **12** results most probably from reaction of the α-chloro ether **9** with the water present in the reaction medium. Isolation of the adducts **13***a* and **14***a* resulting from addition of the amido radical at C-2 indicates that the additions to dihydropyran (**8**) are less regiospecific than the additions to 1-methoxycyclohexene (**2**) and ethoxyethylene (**5**).[8]

[7]We thank Professor R. R. Fraser, Ottawa University, for recording these spectra.

[8]One of the referees suggested that the adducts **13***a* and **14***a* might be formed by electrophilic addition. However, we believe it is not very probable for the following reasons. On one hand, treatment of ethyl vinyl ether and methoxymethylenecyclohexane with *N*-chlorourethane (**1***a*) in methanol or in methanol containing chromic chloride for 5 h at room temperature led exclusively to the corresponding α-chloro acetal (>95%); there was no detectable reaction after 5 h at −78°C (18). On the other hand the formation of **14***a* by electrophilic addition would imply the reduction of **13***a* and we have shown that 1,2-adducts of *N*-chloroamides (and even *N*-bromoamides) to olefins are not reduced by chromous chloride under such mild conditions as those used for the additions (**1***a*).

The addition of NCU (**1***a*) to *(1-methoxyethylidene)cyclohexane* (**15**) (Scheme 6), a fully substituted enol ether, is noteworthy since no addition was observed upon photochemical initiation (19). Besides **16** and **17**, the other compounds present in the crude product were acetylcyclohexane and urethane according to vpc analysis. The α-chloro ketone **17** could result either from addition of the ethoxycarbonylamino radical to the carbon bearing the methoxy group or from electrophilic chlorination.

In the addition of NCU (**1***a*) to *17-methoxymethylene-androst-4-en-3-one* (**19**) (Scheme 7), the sole addition product isolated in a 75% yield was the 17α-chloro-20-ethoxycarbonylamino-20-methoxy derivative **20** (mixture of diastereoisomers) resulting from the addition of the ethoxycarbonylamino radical on the less hindered carbon of the double bond. No addition occurred on the unreactive Δ^4-3-keto system as expected (1*a*). Hydrolysis of the adduct **20** (70% aqueous acetic acid at 70°C) gave the α-chloro aldehyde **21** in an 82% yield (Scheme 7). The α configuration was tentatively assigned to the chlorine on the basis that the chlorine-atom transfer on the intermediate adduct radical should be easier from the α side. The preparation of enol ether **19** (mixture of geometrical isomers) from 3β-acetoxyan-

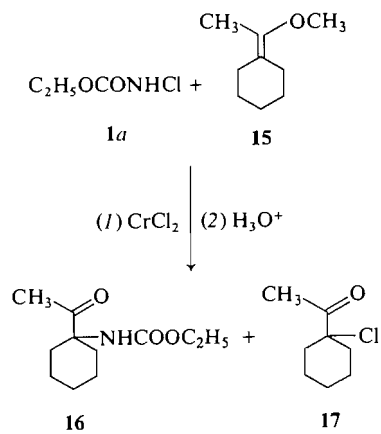

1*a* 15

16 17

SCHEME 6

ERRATA, The yield of 16 is 59% (62% by VPC)
(17 is 10% (by VPC))

Can. J. Chem. Downloaded from www.nrcresearchpress.com by 210.87.254.5 on 09/05/12
For personal use only.

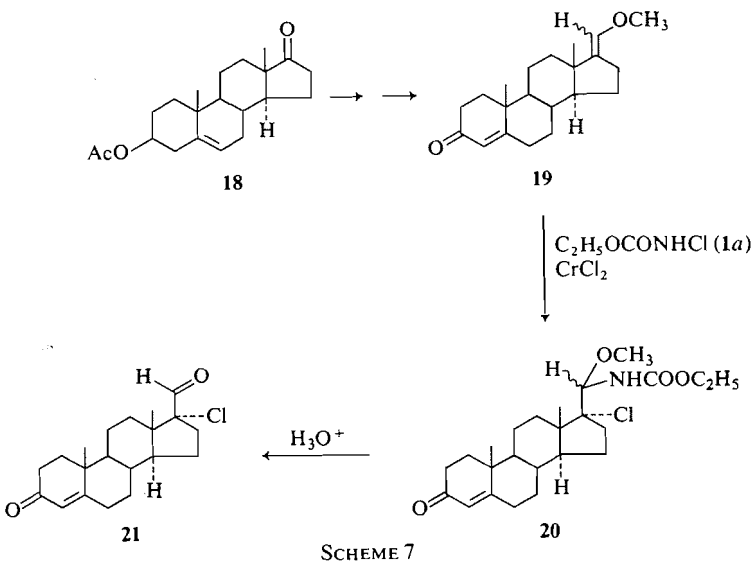

SCHEME 7

drost-5-en-3-one (**18**) is described in the Experimental.

The addition of *N*-chlorobenzylcarbamate (**1***d*) to *2-trimethylsiloxy-2-norbornene* (**22**) (Scheme 8) gave a low yield (19%) of the expected α-benzyloxycarbonylaminonorbornanone (**23**),[9] the other product isolated besides benzylcarbamate being norbornanone (80%). It would be surprising if the silyl enol ether **22** would be much less reactive than norbornene which gave high yields of addition with *N*-chlorocarbamates (1*a*), and we attribute the low yield of **23** to the fact that hydrolysis of **22** under the reaction conditions was faster than the addition reaction. Edwards *et al.* (5) added calcium carbonate to the chromous chloride solution in order to remove the acid but did not observe any improvement of the yield of addition. However, water was always present and they used a longer reaction time.

The orientation of radical additions to olefins depends on the interplay of steric effects, polar effects (e.g. preferential attack of an electrophilic radical on the carbon having the highest electron density), and bond-strength terms according to Tedder and Walton (6).[10] The orientation of the addition to the steroid enol ether **19** must be governed mainly by steric effects; the polar effect would be expected to favor the addition of an amido radical at C-17 whether the radical is free or complexed with a metal ion (1*b*). In the additions to 1-methoxycyclohexene (**2**), ethoxyethylene (**5**), and the silyl enol ether **22**, both steric and electronic effects (e.g. the polar effect) should favor the addition of the amido radical on the less substituted carbon atom, hence the high regioselectivity observed. The lower regioselectivity of the addition to dihydropyran (**8**) probably reflects the fact that, both ends of the double bond being monosubstituted, the steric effects at C-2 and C-3, although not identical (C—O bonds are shorter than C—C bonds), should not be appreciably different; the orientation of the addition is probably controlled by electronic effects to a large extent. In the case of (1-methoxyethylidene)cyclohexane (**15**), the preferential addition at the ring carbon is most probably determined by electronic effects.

Additions to Glycals

The yields given in Table 2 represent minimum yields of addition since the ^{1}Hmr spectra of the mother liquors from recrystallization of the chromatographic fractions (footnote *a*) showed that they still contained appreciable amounts of 2-amino derivatives, and since the Koenigs–Knorr reactions were not quantitative. In all the isolated products, the amido group at position 2 and the oxygenated

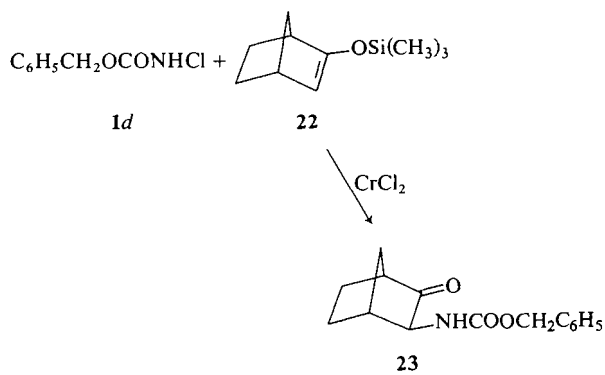

SCHEME 8

[9]We thank Dr. O. E. Edwards, National Research Council of Canada, for providing us with samples of **22** and **23**.

[10]It seems difficult to dissociate the bond-strength terms from other effects since both steric and electronic effects should have a bearing on the strength of the new bond formed in the initial addition step.

Can. J. Chem. Downloaded from www.nrcresearchpress.com by 210.87.254.5 on 09/05/12
For personal use only.

Can. J. Chem. Downloaded from www.nrcresearchpress.com by 210.87.254.5 on 09/05/12
For personal use only.

function at position 1 are *trans* most probably as a result of the participation of the amido group during solvolysis of the pyranosyl chlorides (e.g. Scheme 5).

The main products from the additions to *triacetyl-*D*-glucal* (**24**) (Scheme 9) are the β-D-gluco derivatives **28**. Some α-D-manno derivatives **29** were also formed, but in smaller amount, as suggested by the ^{1}Hmr spectrum of chromatographic fractions and/or mother liquors from recrystallizations. Methyl 2-chloroethoxycarbonylamino-α-D-mannopyranoside **29***b* (R = CH_3) was the sole manno derivative isolated in a pure state and characterized; the doublet of H-1 at 4.80 ppm, J = 1.6 Hz, in the ^{1}Hmr spectrum shows clearly the equatorial orientation of H-1 and H-2.

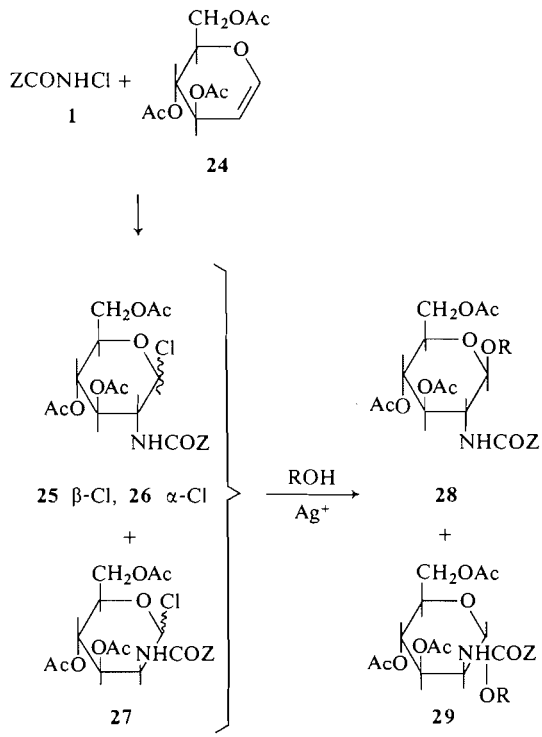

SCHEME 9

The two anomeric chlorides **25***a* and **26***a* were prepared from the β-acetate **28***a* (R = $COCH_3$) in 62 and 87% yield, respectively, as shown in Scheme 10. Anomerization of the β-chloride **25***a* with titanium tetrachloride in chloroform at room temperature took 3 days and was quantitative (Scheme 10).

Methanolysis of the β-chloride **26***a* under Koenigs–Knorr conditions afforded the pure methyl β-D-glucopyranoside **28***a* (R = CH_3)[11] in 87% yield; from the α-chloride **25***a*, the yield of **28***a* (R = CH_3) was 98%. However, when the methanolysis under the same conditions was carried out on a 2:2:1 mixture of β-chloride **25***a*, α-chloride **26***a*, and triacetyl-D-glucal (**24**), the yield of pure methyl β-D-glucopyranoside **28***a* (R = CH_3) was 65% only after chromatographic separation. Anomerization of **28***a* (R = CH_3) with titanium tetrachloride in chloroform at room temperature was complete after 3 days according to the ^{1}Hmr spectrum. Chromatographic separation yielded 70% of pure methyl α-D-glucopyranoside **30**.

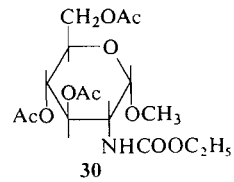

30

We compared the ^{1}Hmr spectrum of the crude reaction product from the addition of NCU (**1***a*) (before the Koenigs–Knorr reaction) with that of a 2:2:1 mixture by weight of β-chloride **25***a*, α-chloride **26***a*, and triacetyl-D-glucal (**24**). In both spectra, the doublet of H-1 of the α-chloride **26***a* at 6.28 ppm (J = 3.7 Hz) and the signal of H-1 of **24** at 6.56 ppm (d of d, J = 6 and 1 Hz) were easily seen whereas the signal of H-1 of the β-chloride **25***a* was masked by other peaks. By integrating the signals at 6.28 and 6.56 ppm and taking the quantity of triacetylglucal (**24**) recovered after the Koenigs–Knorr reaction as the amount present in the crude reaction mixture, the yield of α-chloride **26***a* was estimated to be approximately 59%. Since 18% of **24** was recovered, the maximum yield of β-chloride **25***a* would be 23%. Thus the 1,2-addition of NCU to triacetylglucal (**24**) appears to be predominantly *cis* as with other cyclic olefins (e.g. cyclohexene, norbornene) (1*a*).

The addition of NCU (**1***a*) to *3-O-acetyl-4,6-O-benzylidene-*D*-glucal* (**31**) followed by methanolysis is described in Scheme 11. Chromatographic separation gave a mixture of urethane and pyranosides from which 12% of methyl benzylidene-β-glucopyranoside **32** could be isolated after sublimation of urethane and recrystallization. Hydrolysis of the mother liquors and of chromatographic fractions followed by acetylation and chromatographic separation led to the isolation of methyl β-glucopyranoside **28***a* (R = CH_3) in 30% yield (total yield of gluco derivative, 42%) and methyl α-mannopyranoside **29***a* (R = CH_3) in 9% yield. The gluco-to-manno ratio appears to be slightly lower (~4.4) than in the additions to triacetylglucal (**24**), e.g. **28***b*:**29***b* ≃ 7.8.

In the additions to *3-O-acetyl-4,6-O-benzylidene-*D*-allal* (**34**) (Scheme 12), the sole products isolated were methyl 2-amido altrosides (**35** and/or **36**) re-

[11]We thank professor S. Hanessian, Université de Montréal, for providing us with a sample of methyl 2-methoxycarbonylamino-β-D-glucopyranoside **28** (Z = OCH_3, R = CH_3) for comparison purposes.

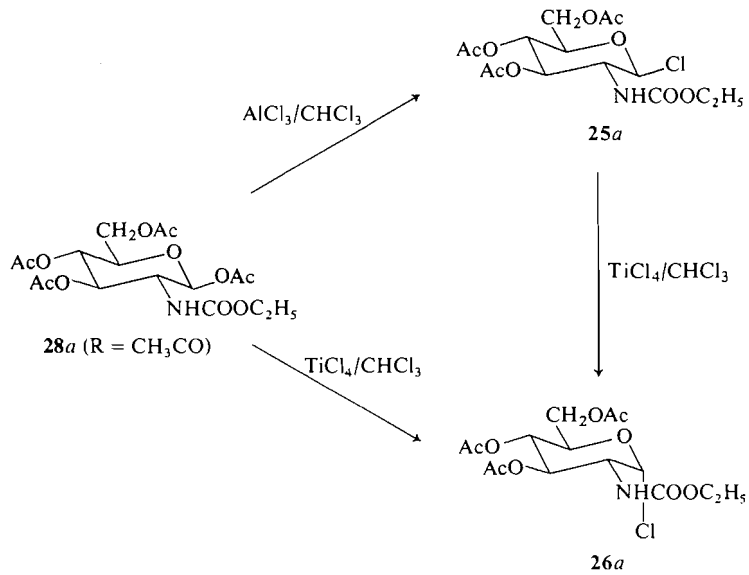

SCHEME 10

sulting from addition of the amido radical on the β face of **34**. Partial deacetylation and partial acetal cleavage occurred upon chromatographic separation. In the case of the addition of NCU (**1***a*), some 40% of methyl benzylidenaltropyranoside **35***a* was nevertheless isolated from the chromatographic fractions; 16% of methyl triacetylaltroside **36***a* (total yield of 2-amido altrosides, 56%) could be obtained by hydrolysis then acetylation of the more polar fractions. In the case of *N*-chlorotrichloroethylcarbamate (**1***c*), part of the chromatographic fractions were hydrolyzed then acetylated to yield 65% of methyl triacetylaltroside **36**. Another part was treated with zinc in glacial acetic acid then acetylated to yield 63% of methyl benzylidenaltropyranoside **35***e* (11) which proved identical to an authentic sample.[12] Finally, from the addition of *N*-chloroacetamide (**1***e*), the sole addition product that could be obtained pure was the oxazoline **37** (18% yield). Its mass spectrum showed the characteristic fragments of oxazolines (12) (see the Experimental). It was converted to the known **36***e* (11) by treatment with *p*-toluenesulfonic acid in methanol and acetylation.

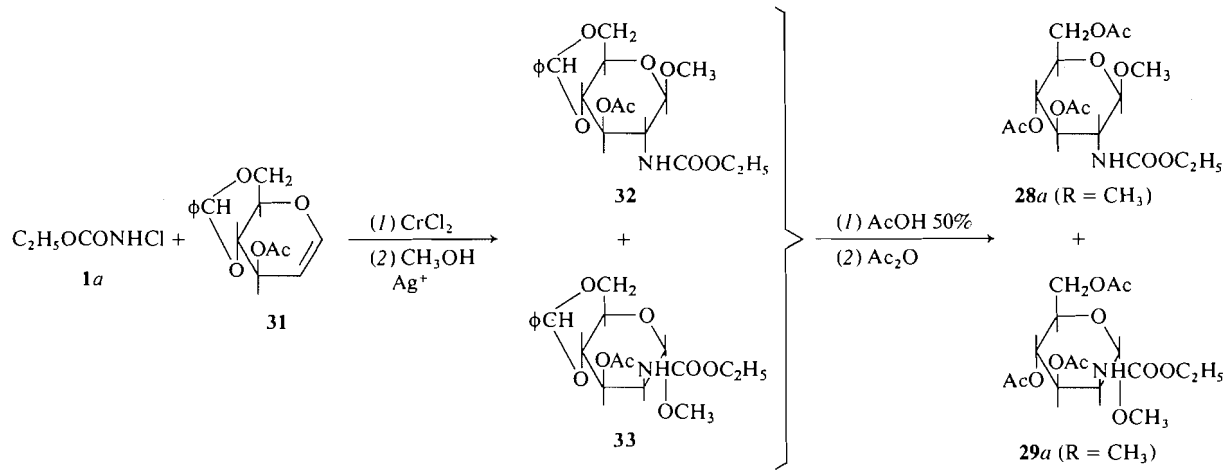

SCHEME 11

Thus the addition of *N*-chloroamides, in particular of *N*-chlorocarbamates, to the glucals **24** and **31** and to the allal **36**, followed by solvolysis under Koenigs–Knorr conditions, led to 2-amido derivatives in yields that can be of preparative value. Higher yields

[12]We thank professor R. U. Lemieux, University of Alberta, for providing us with a generous sample of **35***e*.

Can. J. Chem. Downloaded from www.nrcresearchpress.com by 210.87.254.5 on 09/05/12
For personal use only.

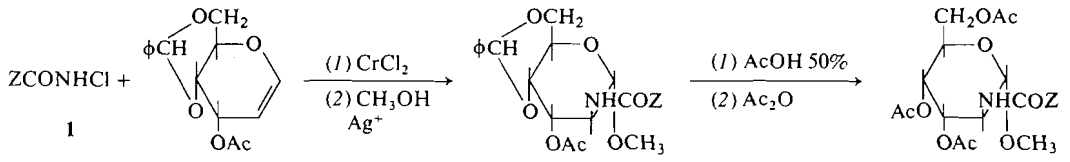

SCHEME 12

could probably be obtained by using a larger excess of *N*-chloroamide (the excess *N*-chloroamide is simply reduced to the amide which can be recovered) and by using improved Koenigs–Knorr conditions.[13] The influence of the configuration of the acetoxy group at C-3 on the direction of attack of the double bond by an amido radical is noteworthy. When the acetoxy group is α as in allal **34** the attack occurs preferentially from the β face leading to 2-amido altrosides; no 2-amido allosides were isolated. When the acetoxy group is β as in the glucals **24** and **31**, the attack occurs preferentially from the α face leading to 2-amido gluco derivatives; 2-amido manno derivatives were formed and isolated but in much smaller amounts. The steric hindrance to the attack of the π electrons at C-2, in a direction perpendicular to the plane of the double bond and on the same side as the 3-acetate, could be greater in the allal **34** than in the glucals **24** and **31**, assuming a quasi-axial orientation of the 3-acetate in **34** and a quasi-equatorial orientation of the 3-acetate in **24** and **31**. The preferential addition of an amido radical on the α face of **24** and **31** is in contrast with the preferentrial addition of the thioacetyl radical (13*a*)

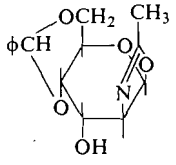

37

and the chlorine atom (13*b*) on the β face of triacetylglucal **24**: β attack:α attack = 2.2–3.3 (13). One possible explanation could be the larger size of an amido radical with respect to that of a thioacetyl radical or a chlorine atom.[14] One could argue. that the amido radical is complexed with a metal ion (1*b*) and thus effectively much larger. However, in the photochemical addition of *N*-chlorochloroacetamide (**1***f*) to triacetyl-D-glucal (**24**) in methylene chloride, the addition of the free amido radical occurs preferentially from the α face also. Indeed the sole product isolated after methanolysis was the 2-amidoglucopyranoside **28***f* (R = CH_3) (19).

Conclusion

The results presented in this paper show that α-alkoxycarbonylamino and α-acylamino acetals, ketals, aldehydes, and ketones can be obtained in high yields by the chromous chloride promoted addition of *N*-chloroamides to enol ethers. The method was even successful with a fully substituted enol ether. However, it cannot be applied to a β,β-disubstituted enol ether since the addition of the amido radical occurs preferentially on the less hindered α position ($CHOCH_3$ end).[15] It was not successful either with a trimethylsilyl enol ether because, under the reaction conditions, hydrolysis of the enol ether was faster than the addition reaction. With glycals, 2-alkoxycarbonylamino and 2-acylamino sugars were obtained in good yields. The use of *N*-chloro-2,2,2-trichloroethylcarbamate (**1***c*) and of *N*-chlorobenzylcarbamate (**1***d*) illustrates the potential of these additions for the synthesis of *N*-protected α-amino acetals and ketals or of the corresponding *N*-protected α-amino carbonyl derivatives. For instance 2-trichloroethoxycarbonylaminocyclohexanone (**4***c*) was converted into 2-acetylaminocyclohexanone (**4***e*) (15) in a 90% yield by zinc reduction followed by acetylation; also the α-benzyloxycarbonylamino ketal **3***d* was converted into the acetylamino ketal **3***c* in an 87% yield by hydrogenolysis and acetylation. It is noteworthy that in all the additions to the various enol ethers, we did not isolate any β-amido ether (e.g. ZCONH—C—CH—OCH_3) resulting from chromium(II) reduction of the intermediate adduct radical (e.g. ZCONH—C—Ċ—OCH_3) followed by protonolysis (1,H-addition) even with *N*-chloroacetamide (**1***e*) which was shown to lead predominantly to 1,H-addition with 1-octene, cyclohexene, and norbornene (1*a*).

[13]R. U. Lemieux, private communication.

[14]From the conformational energies of monosubstituted cyclohexanes (14), an NH_2 group appears to be larger than a SH group which, however, would be larger than a chlorine.

[15]A detailed study of the orientation of radical additions to β,β-disubstituted enol ethers will be presented in a forthcoming paper (see ref. 18).

Can. J. Chem. Downloaded from www.nrcresearchpress.com by 210.87.254.5 on 09/05/12
For personal use only.

Can. J. Chem. Downloaded from www.nrcresearchpress.com by 210.87.254.5 on 09/05/12
For personal use only.

Experimental[16]

The pertinent general information and a description of the apparatus used for the chromous chloride promoted additions have been given in part III (*1a*). The solvents from extractions were evaporated on a rotating evaporator. Unless specified otherwise, the chromatographic separations were carried out on silica gel. The *N*-chloroamides were prepared by the sodium hypochlorite method (16).

Typical Procedure for the Chromous Chloride Promoted Addition of N-*Chloroamides to Enol Ethers*

Addition of N-*Chloro-2,2,2-trichloroethylcarbamate (1c) to 1-Methoxycyclohexene (2)*

The *N*-chlorocarbamate **1***c* (1.33 g, 98% active chlorine, 5.74 mmol) was dissolved in chloroform (4 ml) and absolute methanol (1.2 ml) and the solution was cooled to ca −78°C. A solution of 1-methoxycyclohexene (**2**) (1.5 ml, ~12 mmol) in chloroform (2 ml), pre-cooled to −78°C, was added. The 1 *M* chromous chloride solution was then added dropwise until the starch–iodide paper test was negative: 5 ml (5 mmol) added over 60 min.

Acid work-up—The cooling bath was removed and air was allowed in the reaction vessel. Dilute sulfuric acid was added (1 ml of a 1 *N* solution) and the mixture was stirred at room temperature for 4 h. It was poured into water (50 ml) then extracted with methylene chloride (3 × 100 ml). The organic phases were washed with water (2 × 25 ml) then combined and dried. The solvent was evaporated and the crude product (1.51 g) separated by preparative-layer chromatography (plc) (ether–hexane 1:4) to afford two fractions. The less polar fraction consisted of *2-(N-trichloroethoxycarbonyl)aminocyclohexanone* (**4***c*), mp 75–78°C (1.302 g, 86%). One recrystallization from hexane afforded the analytical sample, mp 80–80.5°C; ν_{max} (CCl_4): 3405 (NH), 1745 (C=O), 1720 (C=O), 1500 (NH), 1310 1205, 1110, and 1050 cm^{-1}; ν_{max} (CS_2): 785 and 765 cm^{-1} (C—Cl); (CCl_4) δ: 4.22 (t of d with J = 12 and 6 Hz; d of d with J = 11.5 and 6 Hz after exchange with D_2O; H-2), 4.63 (s, OCH_2CCl_3), 5.92 ppm (m, NH). *Anal.* calcd. for $C_9H_{12}Cl_3NO_3$: C 37.44, H 4.19, Cl 36.89, N 4.85; found: C 37.43, H 4.17, Cl 37.10, N 5.02. The other fraction consisted 2,2,2-trichloroethylcarbamate, mp 60–62°C (0.185 g), identical (ir, ^{1}Hmr) to an authentic sample.

Sodium methoxide work-up—The reaction was carried out as above on similar quantities. A sodium methoxide solution (0.59 g of Na in 15 ml of absolute methanol) was added to the reaction mixture at −78°C which was then allowed to warm up to room temperature. It was poured into water (50 ml) then extracted with methylene chloride (3 × 100 ml). The organic phases were washed with water (2 × 25 ml) then dried and the solvent evaporated. The crude product was separated by plc (ether–hexane 1:4) to afford three fractions. The less polar fraction consisted of *2-(N-trichloroethoxycarbonyl)aminocyclohexanone dimethyl acetal* (**3***c*) (1.44 g, 75%), an oil which was purified by microdistillation at 80–82°C/0.01 Torr; ν_{max} (CCl_4): 3440 (NH), 1742 (C=O), 1512 (NH), 1215, 1120, 1105, 1070, and 1055 cm^{-1}; ($CDCl_3$) δ: 3.18 (s, OCH_3), 3.23 (s, OCH_3), 3.87 (m, $\Delta\nu_{1/2}$ = 20 Hz, H-2), 4.73 (OCH_2CCl_3), and 5.47 ppm (br d, J = 8 Hz, NH). *Anal.* calcd. for $C_{11}H_{18}Cl_3NO_4$: Cl 31.78; found: Cl 31.61. The second fraction consisted of *2-(N-trichloroethoxycarbonyl)aminocyclohexanone* (**4***c*), mp 76–78°C (0.116 g, 7%), identical (ir, ^{1}Hmr) to the sample obtained above. The third fraction consisted of 2,2,2-trichloroethylcarbamate, mp 59–61°C (0.192 g).

The addition of *N*-bromoacetamide to **2** carried out as above using the acid work-up gave *α-bromocyclohexanone* (20% by vpc) and *2-acetylaminocyclohexanone* (**4***e*), mp 88–91°C (14% by plc), identical (ir, ^{1}Hmr) to the sample obtained from the addition of *N*-chloroacetamide (**1***e*).

The other additions to 1-methoxycyclohexene (**2**), the additions to ethoxyethylene (**5**) and dihydropyran (**8**), the addition of NCU (**1***a*) to (1-methoxyethylidene)cyclohexane (**15**) and 2-trimethylsiloxy-2-norbornene (**22**), the hydrolysis of ketals **3***b*, **3***c*, **3***d*, and **3***e*, and the hydrolysis of acetals **6***b* and **6***d* are described in the supplementary material.[16]

Removal of the Trichloroethoxycarbonyl Group of Ketone 4c

The ketone **4***c* (577 mg, 2 mmol) was treated with freshly activated zinc dust (600 mg added in 200 mg portions) in glacial acetic acid (6 ml) at room temperature for 1 h. The reaction mixture was made alkaline (pH = 13) with ice-cold 4 *N* NaOH then extracted with ether (5 × 100 ml) in the presence of ice. The ether layer was dried and the solvent evaporated. The resulting liquid was acetylated in the usual way (Ac_2O, 1 ml; pyridine, 2 ml) to give *2-acetylaminocyclohexanone* (**4***e*) (15), mp 90–92°C (363 mg, 90%), identical (ir and ^{1}Hmr) to the sample obtained from *N*-chloroacetamide (**1***e*) and 1-methoxycyclohexene (**2**).

Hydrogenolysis of 2-Benzyloxycarbonylaminocyclohexanone Dimethyl Acetal (3d)

The acetal **3***d* (205 mg, 0.7 mmol) in methanol (60 ml) was hydrogenated over 10% palladium-on-charcoal at atmospheric pressure for 24 h. The catalyst was filtered and the solvent evaporated to yield *2-aminocyclohexanone dimethyl acetal* as a liquid (107 mg, 96%); ν_{max} (CCl_4): 3400 and 3330 (NH_2), 1110 and 1060 cm^{-1} (C—O—C); (CCl_4) δ: 1.53 ppm (m, 10H) and 3.13 ppm (s, OCH_3). It was acetylated to give *2-acetylaminocyclohexanone dimethyl acetal* (**3***e*), mp 110–112°C (123 mg, 87%). Recrystallization from methylene chloride – ether afforded the analytical sample, mp 117–118°C; ν_{max} ($CHCl_3$): 3410 (NH), 1670 (C=O), 1510 (NH), 1110 and 1065 cm^{-1} (C—O—C); ($CDCl_3$) δ: 1.98 (s, $COCH_3$), 3.22 and 3.28 (two s, OCH_3), 4.15 (m, $\Delta\nu_{1/2}$ = 18 Hz, H-2) and 5.82 ppm (m, NH); *m/e*: 201 (M^+). *Anal.* calcd. for $C_{10}H_{19}NO_3$: C 59.68, H 9.52, N 6.96; found: C 59.26, H 9.48, N 6.68.

Equilibration of 10a and 11a

The *trans* adduct **10***a* (748 mg, 3.7 mmol) was dissolved in methanolic HCl (40 ml of a 0.6 *N* solution, 24 mmol) and kept at room temperature for 6 days. Sodium bicarbonate (2.5 g, 25 mmol) was added. The solution was filtered, evaporated to dryness, and an aliquot (516 mg) of the crude product (736 mg) was separated by plc (ether–hexane 1:1) to yield the *cis* adduct **11***a*, mp 62–63°C (298 mg) and the *trans* isomer **10***a* (164 mg), identical (ir, ^{1}Hmr, tlc) to authentic samples (**11***a*:**10***a* = 1.8). The *cis* adduct **11***a* (140 mg, 0.7 mmol) was treated as above with methanolic HCl (5.5 ml) for 20 h. Work-up and separation gave the *cis* isomer **11***a*, mp 62–63°C (83 mg) and the *trans* isomer **10***a* (46 mg) (**11***a*:**10***a* = 1.8).

Preparation of 17-Methoxymethylenandrost-4-en-3-one (19)

A Wittig reaction on 3β-acetoxyandrost-5-en-17-one (**18**) (8.25 g, 125 mmol) was carried out according to Corey's modification (17) with methoxymethylenetriphenylphosphonium chloride (42.8 g, 125 mmol), sodium hydride (5.23 g, 125

[16]Reactions and products not included in the Experimental are fully described in the Supplementary Material placed in the Depository of Unpublished Data. Photocopies of this material are available, at a nominal charge, from the Depository of Unpublished Data, CISTI, National Research Council of Canada, Ottawa, Ont., Canada K1A 0S2.

Can. J. Chem. Downloaded from www.nrcresearchpress.com by 210.87.254.5 on 09/05/12
For personal use only.

mmol), and DMSO (150 ml). The mixture was kept at 40°C for 18 h then poured into cold water and extracted with ether. The crystals (ϕ_3PO) obtained after evaporation of the solvent were filtered, washed with ether, and the solvent evaporated. The residue was separated on basic alumina activity III (ether–pentane 1:2) to yield *17-methoxymethylenandrost-4-en-3β-ol*, mp 135–140°C (5.30 g, 67%); ν_{max} ($CHCl_3$): 3550 (OH) and 1670 cm^{-1} (C=C); ($CDCl_3$) δ: 0.88 (s, 18-CH_3), 1.03 (s, 19-CH_3), 3.45 and 3.55 (two s, OCH_3 of geometric isomers), 5.34 (m, H-4), and 5.72 ppm (t, J = 2 Hz, H-20). An Oppenauer oxidation was carried out on the above alcohol (1.67 g, 5 mmol) with potassium tertiobutylate (0.58 g, 5 mmol) and benzophenone (1.82 g, 10 mmol) in refluxing benzene (80 ml) for 18 h. The mixture was poured into cold water and extracted with ether. Separation of the crude product (3.27 g) on basic alumina activity III (ether–pentane 1:2) gave *17-methoxymethylenandrost-4-en-3-one* (**19**), mp 156–159°C (1.16 g, 72%); ν_{max} ($CHCl_3$): 1665 cm^{-1} (C=O and C=C); ($CDCl_3$) δ: 0.87 (s, 18-CH_3), 1.19 (s, 19-CH_3), 3.43 and 3.50 (two s, OCH_3 of geometric isomers), and 5.58 ppm (H-4 and H-20); *m/e* 316 (M^+).

Addition of NCU (1a) to 17-Methoxymethylenandrost-4-en-3-one (19)

The reaction was carried out with 2 mmol of NCU, 1 mmol of **19**, $CHCl_3$ (5 ml), CH_3OH (1 ml), and $CrCl_2$ (14 mmol) for 2 h. The crude product (470 mg) was separated by plc on Florisil (ether–methanol 99:1) to yield the *adduct* **20** as a mixture of diastereoisomers, mp 108–138°C (330 mg, 75%); λ_{max} (EtOH): 240 nm (ε 16 000); ν_{max} ($CHCl_3$): 3440 and 3340 (NH), 1730 (carbamate), 1680 and 1620 (C=C—C=O), 1490 (NH), 1225, 1100, 1070 cm^{-1}; ($CDCl_3$) δ: 0.95 (br s, 18-CH_3), 1.20 (two very closed s, 19-CH_3), 1.26 (t, J = 7 Hz, OCH_2CH_3), 3.32 (s, OCH_3) 4.15 (q, J = 7 Hz, OCH_2CH_3), 5.04 and 5.10 (two d, J = 10 Hz, H-20), 5.45 (br d, J = 10 Hz, NH), 5.65 ppm (s, H-4); *m/e*: 437, 439 (3:1, M^+). *Anal.* calcd. for $C_{24}H_{36}ClNO_4$: Cl 8.11; found: Cl 8.28.

Hydrolysis of the Steroid Adduct 20

The adduct **20** (175 mg, 0.4 mmol) was heated at 70°C for 2 h in 70% aqueous acetic acid (5 ml). Evaporation to dryness after adding benzene and plc (ether–pentane 5:1) yielded the *aldehyde* **21**, mp 158–160°C (109 mg, 81%). It was recrystallized from ether–pentane, mp 162–163°C; λ_{max} (EtOH): 240 nm (ε 18 100); ν_{max} (CCl_4): 2720 and 2830 (C—H of aldehyde), 1730 (C=O of aldehyde), 1670 and 1620 cm^{-1} (C=C—C=O); ($CDCl_3$) δ: 0.80 (s, 18-CH_3) 1.18 (s, 19-CH_3) 5.67 (s, H-4), and 9.44 ppm (s, H-20); *m/e*: 334, 336 (3:1, M^+) *Anal.* calcd. for $C_{20}H_{27}ClO_2$: C 71.73, H 8.13, Cl 10.59; found: C 71.17, H 8.29, Cl 10.34.

Typical Procedure for the Chromous Chloride Promoted Addition of N-*Chloroamides to Glycals*

Addition of NCU (1a) to Triacetyl-D-glucal (24) Followed by Solvolysis

A solution of **24** (5.445 g, 20 mmol) in chloroform (20 ml) and absolute methanol (4 ml) was cooled to ca. −78°C. A solution of NCU (4.74 g, 96% active chlorine, 40 mmol) in chloroform (20 ml) and absolute methanol (4 ml), pre-cooled to −78°C, was then added. The 1 *M* methanolic chromous chloride solution (80 ml, 80 mmol) was added dropwise over 8 h. The reaction mixture was poured into an ice-cold saturated $NaHCO_3$ solution (100 ml) then extracted rapidly with ether (4 × 200 ml) in the presence of ice. The organic layers were washed with ice-cold water (2 × 50 ml) then dried. The solvent was evaporated, the temperature of the water bath being maintained at 30–35°C, to yield 9.76 g of crude product; ($CDCl_3$) δ: 1.25 (t, J = 7 Hz, OCH_2CH_3), 205 and 2.09 (two s, $OCOCH_3$), 3.9–4.6 (m), 4.89 (d of d, J = 6 and 3 Hz, H-2 of **24**), 5.1–5.5 (m), 5.62 (d, J = 9 Hz, NH), 6.28 (d, J = 3.7 Hz, H-1 of α-chloride **26***a*), and 6.56 ppm (d of d, J = 6 and 1 Hz, H-1 of **24**); the relative integration of the absorptions at 2.05–2.09, 6.28, and 6.56 ppm gave 42:2.6:1. The relative integration of the same peaks in a standard 2:2:1 mixture by weight of triacetylglucal **24**, α-chloride **26***a*, and β-chloride **25***a* gave 31:1.1:1 (the absorption of H-1 of the β-chloride **25***a* was masked by other signals). Thus the molar ratio of α-chloride **26***a* to **24** in the crude product was about 3.3. Since 3.6 mmol (18%) of **24** was recovered, the minimum amount of α-chloride **26***a* would be 11.9 mmol (59%).

Methanolysis—An aliquot (570 mg) of the above crude product was dissolved in absolute methanol (20 ml) and cooled in an ice bath. A solution of silver nitrate (285 mg) and pyridine (0.15 ml) in methanol (20 ml) was then added. A precipitate was formed immediately. The mixture was stirred at room temperature overnight then filtered and the solvent evaporated. The residue was taken in chloroform and filtered again. The filtrate was evaporated to dryness after adding benzene. Separation by plc (ether–hexane 2:1) gave two main fractions. The less polar fraction consisted of unreacted **24**, mp 44–50°C (56 mg, 18%) identical (ir, ^{1}Hmr) to an authentic sample. The other fraction (360 mg) was crystalline, mp 90–95°C. It was recrystallized from ether–chloroform to give *methyl-2-deoxy-2-ethoxycarbonylamino-3,4,6-tri-O-acetyl-β-D-glucopyranoside* (**28***a*, R = CH_3), mp 133–135°C (193 mg, 42%). Two additional recrystallizations afforded the analytical sample, mp 136.5–137°C; $[\alpha]_D^{25}$ +6.0° (*c* 2.0, $CHCl_3$); ν_{max} ($CHCl_3$): 3440 and 3420 (NH), 1740 (C=O), 1515 (NH), 1240 and 1040 cm^{-1} (C—O—C); ($CDCl_3$) δ: 1.25 (t, J = 7 Hz, OCH_2CH_3), 2.02 and 2.10 (two s, $OCOCH_3$) 3.52 (s, OCH_3), 4.15 (q, J = 7 Hz, OCH_2CH_3), 4.62 (d, J = 8 Hz, H-1), 5.22 ppm (d, J = 9 Hz, NH). *Anal.* calcd. for $C_{16}H_{25}NO_{10}$: C 49.10, H 6.43, N 3.57; found: C 49.22, H 6.24, N 3.54. The mother liquors from the first recrystallization (168 mg) were deacetylated by sodium methoxide (~1 mg) in methanol (10 ml) at room temperature for 20 h. The solvent was evaporated and the residue (99 mg) recrystallized in methanol–ether. Acetylation of the crystals in the usual way, Ac_2O (2 ml) and pyridine (4 ml), gave 84 mg of β-pyranoside **28***a* (R = CH_3), mp 137°C (total yield 277 mg, 61%).

Acetolysis—A mixture of silver acetate (2 g) and glacial acetic acid (40 ml) was heated to reflux then cooled to room temperature. This solution was added to a solution of a second aliquot (5.76 g) of the crude product in glacial acetic acid (20 ml) and acetic anhydride (20 ml). After stirring for 3 h, the reaction mixture was filtered then evaporated to dryness. The residue was washed with water (2 × 10 ml), dried, and the solvent evaporated. Separation by column chromatography (ether–hexane 3:1) gave some unreacted **24**, mp 40–50°C (0.560 g, 18%), and a crystalline fraction, mp 120–129°C (3.41 g). Recrystallization from chloroform and ether gave *2-deoxy-2-ethoxycarbonylamino-1,3,4,6-tetra-O-acetyl-β-D-glucopyranose* (**28***a*, R = $COCH_3$), mp 139–142°C (1.99 g, 41%). Another recrystallization gave a sample melting at 144.5°C; $[\alpha]_D^{25}$ +18° (*c* 2.0, $CHCl_3$) (lit. (7) mp 144–145°C, $[\alpha]_D^{25}$ +16.1° (*c* 0.6, $CHCl_3$)); ν_{max} $CCHCl_3$): 3420 (NH), 1750 (br, C=O), 1515 (NH), 1235 (br), 1085, and 1050 cm^{-1} (C—O—C); ($CDCl_3$) δ: 1.25 (t, J = 7 Hz, OCH_2CH_3), 2.02, 2.08, and 2.12 (three s, $OCOCH_3$), 5.50 (d, J = 9 Hz, NH), and 5.78 ppm (d, J = 8.5 Hz, H-1). The ^{1}Hmr of the mother liquors from the first crystallization showed a doublet at 6.10 ppm (J = 1 Hz), which could be attributed to the mannopyranose **29***a* (R = $COCH_3$), in addition to the doublet at 5.78 ppm (J = 8.5 Hz) due to the glucopyranose **28***a* (R = $COCH_3$).

Can. J. Chem. Downloaded from www.nrcresearchpress.com by 210.87.254.5 on 09/05/12
For personal use only.

Solvolysis in benzyl alcohol—A third aliquot (527 mg) of the crude product was stirred at room temperature for 24 h in benzyl alcohol (5 ml) in the presence of silver carbonate (100 mg) and Drierite (100 mg). After filtration of the solids and evaporation to dryness, the residue was separated by plc (ether–hexane 1:1) to give some unreacted **24**, mp 142–155°C (53 mg, 17%), and a crystalline fraction, mp 142–155°C (318 mg). Recrystallization from chloroform–ether gave *benzyl 2-deoxy-2-ethoxycarbonylamino-3,4,6-tri-O-acetyl*-β-D-*glucopyranoside* (**28***a*, R = $CH_2C_6H_5$), mp 153–155°C (270 mg, 53%). One additional recrystallization gave the analytical sample, mp 157–158°C; $[\alpha]_D^{25}$ −28° (*c* 1.6, $CHCl_3$); ν_{max} ($CHCl_3$): 3430–3410 (NH), 1750 (br, C=O), 1240, 1220, and 1050 cm^{-1} (C—O—C); ($CDCl_3$) δ: 1.20 (t, *J* = 7 Hz, OCH_2CH_3), 2.00 and 2.08 (two s, $OCOCH_3$), 3.5–5.3 (complex, 12H), and 7.32 ppm (s, aromatic H). *Anal.* calcd. for $C_{22}H_{29}NO_{10}$: C 56.53, H 6.25, N 3.00; found: C 56.57, H 6.45, N 3.42.

The other additions to triacetyl-D-glucal (**24**), the addition of NCU (**1***a*) to 3-*O*-acetyl-4,6-*O*-benzylidene-D-glucal (**31**), and the additions to 3-*O*-acetyl-4,6-*O*-benzylidene-D-allal (**34**) are described in the supplementary material.[16]

Synthesis of β-*Chloride* **25***a*

The β-glucopyranose **28***a* (R = $COCH_3$) (1.0 g, 2.4 mmol) was dissolved in chloroform (25 ml) freshly distilled over P_2O_5. Aluminum chloride (0.180 g, 1.35 mmol) was added and the mixture stirred at room temperature for 45 min. After the addition of dry benzene (25 ml) and silicic acid (0.25 g), the mixture was filtered and the filtrate poured into ice-cold water (7 ml). The organic phase was separated, dried, and the solvent evaporated, all these operations being carried out quickly and in a cold bath. Crystallization in ether gave *2-deoxy-2-ethoxycarbonylamino-3,4,6-tri-O-acetyl*-β-D-*glucopyranosyl chloride* **25***a*, mp 115–116°C (0.576 g, 61%). One recrystallization in ether afforded the analytical sample, mp 115–116°C; $[\alpha]_D^{25}$ +17.5° (*c* 2.0, $CHCl_3$); ν_{max} ($CHCl_3$): 3410 (NH), 1745 (C=O), 1515 (NH), 1235 and 1040 cm^{-1} (C—O—C); ($CDCl_3$) δ: 1.25 (t, *J* = 7 Hz, OCH_2CH_3), 2.10 and 2.15 (two s, $OCOCH_3$), 4.18 (q, *J* = 7 Hz, OCH_2CH_3) 5.55 ppm (d, *J* = 8 Hz, H-1), the NH is masked by other signals. *Anal.* calcd. for $C_{15}H_{22}ClNO_9$: C 45.52, H 5.60, Cl 8.96, N 3.54; found: C 45.47, H 5.54, Cl 8.25, N 3.56. The mother liquors from the first crystallization contained essentially the α-*chloride* **26***a* (174 mg, 18%) according to the ^{1}Hmr spectrum (see below).

Synthesis of α-*Chloride* **26***a*

From β-*Glucopyranose* **28***a* (*R* = $COCH_3$)

The glucopyranose **28***a* (R = $COCH_3$) (119 mg, 0.29 mmol) and titanium tetrachloride (0.5 ml) in chloroform (2 ml) were heated to reflux for 3 h. The mixture was poured into cold water (10 ml) then extracted with chloroform (3 × 50 ml). The organic phases were washed with cold water, dried, and the solvent evaporated (cold bath) to yield pure *2-deoxy-2-ethoxycarbonylamino-3,4,6-tri-O-acetyl*-α-D-*glucopyranosyl chloride* (**26***a*) (97 mg, 85%) as an amorphous solid which crystallized after many months in the refrigerator, mp 47–52°C; $[\alpha]_D^2$ +11° (*c* 1.62, $CHCl_3$); ν_{max} ($CHCl_3$): 3410 (NH), 1740 (C=O), 1510 (NH), 1240 and 1040 cm^{-1} (C—O—C); ($CDCl_3$) δ: 1.22 (t, *J* = 7 Hz, OCH_2CH_3), 2.05 and 2.10 (two s, $OCOCH_3$), 4.15 (q, *J* = 7 Hz, OCH_2CH_3), and 6.22 ppm (d, *J* = 3.5 Hz, H-1). *Anal.* calcd. for $C_{15}H_{22}ClNO_9$: C 45.52, H 5.60, Cl 8.96; found: C 45.41, H 5.43, Cl 8.89.

By Anomerization of the β-*Chloride* **25***a*

The anomerization of **25***a* (110 mg, 0.28 mmol) by titanium tetrachloride (0.6 ml) in chloroform (30 ml) was complete after 3 days at room temperature according to the ^{1}Hmr spectrum. The reaction mixture was poured into ice-cold saturated $NaHCO_3$ solution and the product was extracted with chloroform (3 × 50 ml). The organic phases were washed with cold water (2 × 10 ml), dried, and the solvent evaporated (cold bath) to yield quantitatively (109 mg) the pure α-chloride **26***a*, identical (ir, ^{1}Hmr) to the sample obtained above.

Methanolysis of Chlorides **25***a and* **26***a*

β-*Chloride* **25***a*

The chloride **25***a* (40 mg, 0.1 mmol) was treated by silver nitrate (70 mg) in methanol (10 ml) containing pyridine (4 drops) as described above to give *methyl* β-*glucopyranoside* **28***a* (R = CH_3), mp 132–134°C (39 mg, 98%), identical (ir, ^{1}Hmr) to an authentic sample.

α-*Chloride* **26***a*

The chloride **26***a* (93 mg, 0.23 mmol) was solvolyzed in methanol (12 ml) in the presence of Ag_2CO_3 (200 mg) and Drierite (200 mg) under the usual conditions to give *methyl* β-*glucopyranoside* **28***a* (R = CH_3), mp 131–134°C (78 mg, 86%).

Mixture of Triacetylglucal (**24**), **25***a, and* **26***a*

A mixture of **24** (17.5 mg), β-chloride **25***a* (35 mg), and α-chloride **26***a* (35 mg) was solvolyzed in the conditions used for the methanolysis of **25***a* (see above). The crude product was separated by plc (ether–hexane 2:1) to give triacetylglucal (**24**) (17 mg) and a crystalline fraction, mp 121–129°C (66 mg). It was recrystallized from ether–chloroform to yield pure *methyl* β-*glucopyranoside* **28***a* (R = CH_3), mp 136–136.5°C (45 mg, 64%).

Anomerization of Methyl β-*Glucopyranoside* **28***a* (*R* = CH_3)

Titanium tetrachloride (1 ml) in dry chloroform (10 ml) was added to a solution of **28***a* (R = CH_3) (136 mg, 0.34 mmol) in chloroform (20 ml). The reaction was followed by ^{1}Hmr spectroscopy and was complete after 3 days at room temperature. The reaction mixture was poured into an ice-cold saturated $NaHCO_3$ solution (20 ml) and extracted with chloroform (4 × 30 ml). The organic phases were washed with water (2 × 20 ml), dried, and the solvent evaporated. The crude product (151 mg) was filtered over silica gel to afford pure *methyl 2-deoxy-2-ethoxycarbonylamino-3,4,6-tri-O-acetyl*-α-D-*glucopyranoside* (**30**), amorphous (97 mg, 70%); $[\alpha]_D^{25}$ +99° (*c* 1.5, $CHCl_3$); ν_{max} ($CHCl_3$): 3420 (NH), 1740 and 1720 (sh) (C=O), 1510 (NH), 1235 and 1040 cm^{-1} (C—O—C); ($CDCl_3$) δ: 1.22 (t, *J* = 7 Hz, OCH_2CH_3), 2.06 and 2.13 (two s, $OCOCH_3$), 3.50 (s, OCH_3), 4.19 (q, *J* = 7 Hz, OCH_2CH_3), 4.85 ppm (d, *J* = 3.8 Hz, H-1). *Anal.* calcd, for $C_{16}H_{25}NO_{10}$: C 49.10, H 6.43, N 3.57; found: C 49.26, H 6.53, N 3.64.

Acknowledgements

We are grateful to the Ministère de l'Education du Québec and the National Research Council of Canada for financial assistance.

1. (*a*) H. DRIGUEZ, J. M. PATON, and J. LESSARD. Can. J. Chem. **55**, 700 (1977); (*b*) H. DRIGUEZ and J. LESSARD. Can. J. Chem. **55**, 720 (1977).
2. J. LESSARD, H. DRIGUEZ, and J. P. VERMES. Tetrahedron Lett. 4887 (1970).
3. R. U. LEMIEUX and N. J. CHÜ. Abstr. Pap. Am. Chem. Soc. **133**, 31N (1958); N. J. CHÜ. Ph.D. thesis, University of Ottawa, Ottawa, Ont. 1959.
4. G. O. PIERSON and O. A. RUNQUIST. J. Org. Chem. **33**, 2572 (1968); E. L. ELIEL and C. A. GIZA. J. Org. Chem. **33**, 3754 (1968).

5. O. E. EDWARDS, J. W. ELDER, M. LESAGE, and R. W. RETALLACK. Can. J. Chem. **53**, 1019 (1975).
6. J. M. TEDDER and J. C. WALTON. Acc. Chem. Res. **9**, 183 (1976).
7. W. H. BROMUND and R. M. HERBST. J. Org. Chem. **10**, 267 (1945).
8. P. H. GROSS and H. X. ZIMMERMAN, JR. Ann. Chem. **674**, 211 (1964).
9. G. WULFF and G. RÖHLE. Angew. Chem. Int. Ed. Engl. **13**, 157 (1974); S. HANESSIAN and J. BANOUB. Carbohydr. Res. **53**, C13 (1977).
10. T. OSAWA. Chem. Pharm. Bull. Tokyo, **8**, 597 (1960).
11. W. H. MYERS and G. J. ROBERTSON. J. Am. Chem. Soc. **65**, 8 (1943).
12. N. S. WULFSON, V. N. BOCHKAREV, G. M. ZOIOTAREVA, T. R. RAJACOPOLAN, A. J. KHORLIN, J. M. PRIVALOVA, and M. L. SHULMAN. Carbohydr. Res. **10**, 351 (1969).
13. (*a*) K. IGARASHI and T. HONMA. J. Org. Chem. **35**, 606 (1970); (*b*) K. IGARASHI and T. HONMA. J. Org. Chem. **35**, 617 (1970).
14. E. L. ELIEL, N. L. ALLINGER, S. J. ANGYAL, and G. A. MORRISON. Conformational analysis. John Wiley and Sons, Inc., New York, NY. 1965. pp. 438 and 439.
15. R. K. HILL, J. A. JOULE, and L. L. LOEFFLER. J. Am. Chem. Soc. **84**, 4951 (1962).
16. C. BACHAND, H. DRIGUEZ, J. M. PATON, D. TOUCHARD, and J. LESSARD. J. Org. Chem. **39**, 3136 (1974).
17. R. GREENWALD, M. CHAYKOVSKY, and E. J. COREY. J. Org. Chem. **28**, 1128 (1963).
18. G. CARON. Ph.D. thesis, Université de Sherbrooke, Sherbrooke, Qué. 1976.
19. D. TOUCHARD. Ph.D. thesis, Université de Sherbrooke, Sherbrooke, Qué. 1974.

Can. J. Chem. Downloaded from www.nrcresearchpress.com by 210.87.254.5 on 09/05/12
For personal use only.

Experimental and theoretical studies of proton removal from propene

GERVASE I. MACKAY, MIN H. LIEN, ALAN C. HOPKINSON, AND DIETHARD K. BOHME[1]

Department of Chemistry, York University, Downsview, Ont., Canada M3J 1P3

Received June 21, 1977

GERVASE I. MACKAY, MIN H. LIEN, ALAN C. HOPKINSON, and DIETHARD K. BOHME. Can. J. Chem. **56**, 131 (1978).

The kinetics and energetics of proton removal from propene, which contains several sites of different acidities, were investigated both theoretically and experimentally. Rate and equilibrium constants were measured for the proton-transfer reaction $OH^- + C_3H_6 \rightleftharpoons C_3H_5^- + H_2O$ at 296 ± 2 K using the flowing afterglow technique. The rate constants were determined to be $k_{forward} = (1.1 \pm 0.3) \times 10^{-9}$ cm^3 molecule^{-1} s^{-1} and $k_{reverse} = (5.4 \pm 1.9) \times 10^{-10}$ cm^3 molecule^{-1} s^{-1}. The ratio of rate constants, $k_f/k_r = 2.1 \pm 0.7$, was found to be in agreement with the equilibrium constant, $K = 2.2 \pm 0.8$, determined from equilibrium concentrations. *Ab initio* molecular orbital calculations predicted the removal of a methyl proton from propene to yield the allyl anion to be energetically favoured. This prediction was supported by measurements of deuteron removal from CD_3CHCH_2. The measured value of K corresponds to a standard free energy change, ΔG^0_{298}, of -0.44 ± 0.14 kcal mol^{-1} which provided values for the standard enthalpy change $\Delta H^0_{298} = +0.5 \pm 0.4$ kcal mol^{-1}, the proton affinity, $PA_{298}(C_3H_5^-) = 391 \pm 1$ kcal mol^{-1}, the heat of formation, $\Delta H^0_{f,298}(C_3H_5^-) = 29.0 \pm 0.8$ kcal mol^{-1}, and the electron affinity $EA(CH_2CHCH_2) = 12.4 \pm 1.9$ kcal mol^{-1}. The experimentally established value for the proton affinity of the allyl anion was in reasonable accord with the value of 422.3 kcal mol^{-1} determined by calculation. The electron affinity of the allyl radical derived in this study is supported by previous calculations and several limiting values obtained experimentally.

GERVASE I. MACKAY, MIN H. LIEN, ALAN C. HOPKINSON et DIETHARD K. BOHME. Can. J. Chem. **56**, 131 (1978).

On a examiné, tant du point de vue théorique qu'expérimental, la cinétique et les énergies impliquées lors de l'enlèvement d'un proton du propène qui contient plusieurs sites différents par leur acidité. On a mesuré les vitesses et les constantes d'équilibre de la réaction de transfert de proton: $OH^- + C_3H_6 \rightleftharpoons C_3H_5^- + H_2O$ à 296 ± 2 K en faisant appel à la technique d'écoulement post-luminescent. On a déterminé les constantes de vitesse k_f (réaction) = $(1.1 \pm 0.3) \times 10^{-9}$ cm^3 molécule^{-1} s^{-1} et k_r (réaction inverse) = $(5.4 \pm 1.9) \times 10^{-10}$ cm^3 molécule^{-1} s^{-1}. Le rapport des constantes de vitesse $k_f/k_r = 2.1 \pm 0.7$ est en bon accord avec la constante d'équilibre de $K = 2.2 \pm 0.8$ déterminée à partir de concentrations à l'équilibre. Des calculs d'orbitales moléculaires *ab initio* ont prédit que l'enlèvement d'un proton du méthyle du propène conduisant à l'anion allyle serait favorisé d'un point de vue énergétique. Cette prédiction est appuyée par des mesures d'enlèvements de deutérons à partir du CD_3CHCH_2. La valeur mesurée de K correspond à un changement d'énergie libre standard ΔG^0_{298} de -0.44 ± 0.14 kcal mol^{-1} qui fournit des valeurs de changement d'enthalpie standard $\Delta H^0_{298} = +0.5 \pm 0.4$ kcal mol^{-1}, d'affinité de proton $PA_{298}(C_3H_5^-) = 391 \pm 1$ kcal mol^{-1}, de chaleur de formation $\Delta H^0_{f,298}(C_3H_5^-) = 29.0 \pm 0.8$ kcal mol^{-1}, et d'affinité électronique $EA(CH_2CHCH_2) = 12.4 \pm 1.9$ kcal mol^{-1}. L'accord entre la valeur établie expérimentalement pour l'affinité du proton de l'anion allylique avec la valeur de 422.3 kcal mol^{-1} déterminée à partir de calculs est raisonnable. L'affinité pour un électron du radical allyle obtenue dans cette étude est en accord avec des calculs antérieurs et plusieurs valeurs limitantes obtenues expérimentalement.

[Traduit par le journal]

Introduction

Gas-phase measurements of rate and equilibrium constants for proton-transfer reactions of the type

[1] $$X^- + YH \rightleftarrows Y^- + XH$$

constitute an important means of determining intrinsic thermochemical properties for Brønsted acids and their conjugate bases (1–5). In particular, such measurements have provided proton affinities and heats of formation of anions and electron affinities of their corresponding radicals of sufficient accuracy to be of both academic and practical value. When the proton donor, YH, has only one acidic site the structure of the anion, Y^-, is likely to be unique so that the corresponding measurements and thermodynamic assignments should be unambiguous. For proton donors with more than one acidic site, YH_n ($n > 1$), several tautomeric forms of the conjugate base, YH^-_{n-1}, having different energies, may become both thermodynamically and kinetically acces-

[1]Alfred P. Sloan Research Fellow, 1974–1976.

Can. J. Chem. Downloaded from www.nrcresearchpress.com by 210.87.254.42 on 09/05/12
For personal use only.

Can. J. Chem. Downloaded from www.nrcresearchpress.com by 210.87.254.42 on 09/05/12
For personal use only.

sible although the higher energy forms will be discriminated against as the reaction exothermicity decreases.

This study is directed towards the determination of the proton affinity, PA, and heat of formation, ΔH^0_f, of the allyl anion, and the electron affinity, EA, of the allyl radical. The allyl anion was derived from propene by proton removal according to the reaction:

[2] $$OH^- + CH_3CHCH_2 \rightarrow \ddot{C}H_2\ddot{C}H\ddot{C}H_2 + H_2O$$

In its optimum conformation propene has been shown (6, 7) to have one hydrogen of the methyl group in the plane of the carbon nuclei as shown in structure **1**. The rationale for this eclipsed structure

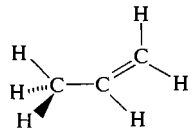

1

being preferred is that this configuration maximizes the distance between the out-of-plane hydrogen atoms and the double bond, thereby decreasing the destabilizing 4π-electron interaction. In this conformation the propene molecule has five chemically different protons and deprotonation could therefore conceivably produce five different anions. Reaction 2, which was chosen deliberately for its low exothermicity (2), should be selective in establishing the allyl anion which is expected to be the lowest energy tautomer. This was confirmed by *ab initio* molecular orbital calculations. An attempt was also made to establish experimentally additional confidence in the assignment of the allylic structure to the carbanion by measurements of the reaction of OH^- with propene-3,3,3-d_3 designed to identify the most acidic site on propene.

Experimental

The experiments were carried out in a flowing plasma-mass spectrometer (flowing afterglow) system for which the details of construction and the method of operation and data analysis have been described elsewhere (8). Hydrogen and helium were both used as the carrier gas. The OH^- ions were produced either via proton transfer from H_2O to NH_2^- or to H^- according to the rapid reactions (9)

[3] $$NH_2^- + H_2O \rightarrow OH^- + NH_3$$

[4] $$H^- + H_2O \rightarrow OH^- + H_2$$

or by electron impact on water vapour added upstream from the ionizer (10). NH_2^- and H^- were generated by dissociative ionization of NH_3 introduced upstream of the electron gun. When helium was used as the carrier gas small amounts of H_2 were added to remove the O^- (also produced by electron impact of H_2O) according to the associative detachment reaction (11):

[5] $$O^- + H_2 \rightarrow H_2O + e$$

In these experiments the filament of the electron gun was biased negatively in the range from 35 to 70 V with respect to the grid envelope held at ground potential. The emission current was typically 1 mA. The water vapour, which also served as the neutral back reactant, was introduced through a capillary tube in the usual manner either in its pure form at pressures below its vapour pressure, or diluted with helium (1 part H_2O to 9 parts He). The mixtures were prepared by allowing the H_2O vapour to equilibrate in the gas inlet system to the ambient temperature (at a pressure <0.8 of the vapour pressure) and subsequently adding helium. Measurement of the H_2O flow required a separate determination of the viscosity of both the pure and diluted vapour (4). The propene was added sufficiently downstream of the ion production region to ensure that all the reactions producing OH^- had gone to completion and that the OH^- ions experienced enough collisions with the carrier gas to become thermalized at the ambient temperature (296 ± 2 K). The ions present in the flowing plasma were sampled through a small orifice in the tip of a nose cone situated at the end of the reaction region and mass analyzed with a quadrupole mass filter. The variation in the reactant and product ion signals as a function of neutral reagent addition provided the raw data from which the rate and equilibrium constants were determined (8).

A number of tests were carried out to establish confidence in the attainment of true equilibrium. The forward and reverse rate constants and the ratio of the ion concentrations were determined at different relaxation and reaction times, various flows of neutral back reactant, in both helium and hydrogen at several pressures, at various electron and ion densities, and under different sampling conditions.

The gases used were helium (Linde, Prepurified Grade, 99.995% He), hydrogen (Linde, Very Dry Grade, 99.95% H_2), ammonia (Matheson, anhydrous, >99.99% NH_3 (liquid phase)), propene (Matheson, C.P. Grade 99.0% C_3H_6 (liquid phase)), and propene-3,3,3-d_3 (Merck, Sharp & Dohme, >98% D). The water vapour was derived from either boiled tap water or boiled distilled water.

Results

Experimental

Figure 1 shows the data obtained upon the addition of C_3H_6 into a He–H_2O plasma in which OH^- is initially a dominant negative ion. The negative ions with m/e = 17, 35, 37, 41, and 46, the major ions present in the range m/e = 1–60 for the range of C_3H_6 flows used, were monitored as a function of C_3H_6 addition. These ions were identified as OH^-, Cl^- (m/e = 35 and 37), $C_3H_5^-$, and NO_2^- respectively. Cl^- and NO_2^-, which are unreactive impurity ions generally present in the negative ion spectrum, were monitored to confirm constant sampling throughout an experiment. The behaviour shown is representative of the observations made in 12 separate experiments performed under the following conditions: effective reaction length, L = 61 cm (in 7 experiments) and 85 cm (in 5 experiments), average flow velocity, $\bar{v} = 7.7$ to 8.1×10^3 cm s^{-1}, total pressure, $P = 0.390$ to 0.76 Torr, and flow of $H_2O = 7.9 \times 10^{16}$ to 3.47×10^{18} molecules s^{-1}.

Can. J. Chem. Downloaded from www.nrcresearchpress.com by 210.87.254.42 on 09/05/12
For personal use only.

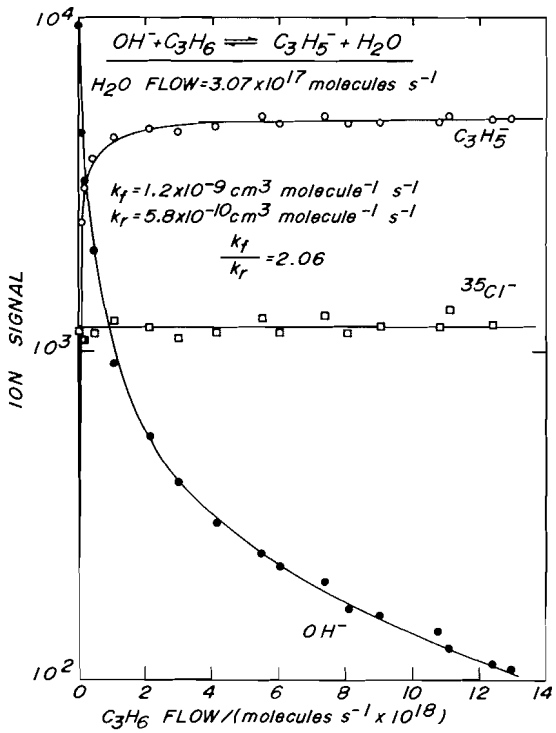

FIG. 1. The variation of the major negative ion signals recorded upon the addition of C_3H_6 into a flowing H_2O–He plasma in which OH^- is initially a dominant negative ion. The solid line through the OH^- decay is a computer fit. T = 296 K, P = 0.54 Torr, $\bar{v}$ = 8.1 × 10^3 cm s^{-1}, and L = 61 cm.

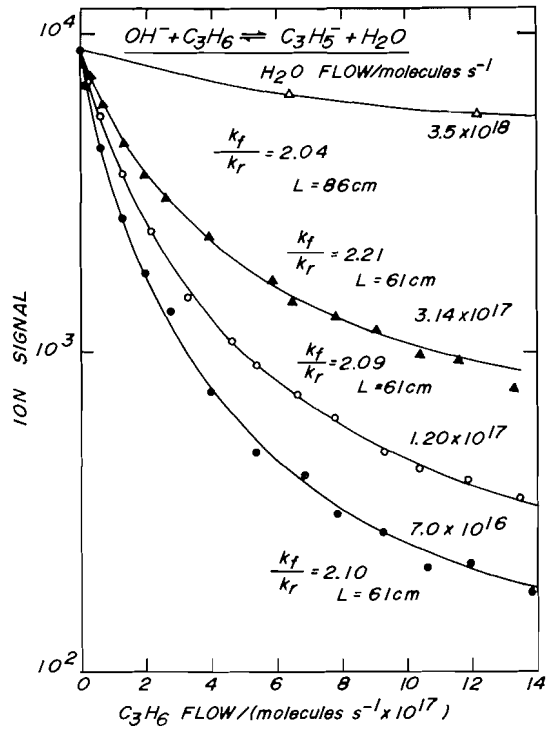

FIG. 2. The variation of the OH^- signals as a function of C_3H_6 addition at various additions of H_2O. P = 0.54 Torr, T = 296 K, and $\bar{v}$ = 7.7–8.1 × 10^3 cm s^{-1}. The points are experimental and the solid lines are computer fits.

Addition of C_3H_6 gave rise to the rapid decline of the OH^- signal and the concomitant increase in the $C_3H_5^-$ signal. There was no evidence for the occurrence of competing reactions so that the entire variation in the OH^- and $C_3H_5^-$ signals with C_3H_6 addition could be ascribed to the transfer of a proton. The curvature in the logarithmic decay of the OH^- signal can be attributed to the occurrence of the reverse proton transfer from H_2O to $C_3H_5^-$. The solid curve drawn through the data points for the OH^- decay represents the best computer fit obtained using analysis B of ref. 8.

In eight investigations the amount of back-reaction was sufficient to introduce curvature in the OH^- decay without attaining equilibrium at low C_3H_6 flows. This allowed the determination of unique values for k_f = (1.1 ± 0.1) × 10^{-9} cm^3 molecule^{-1} s^{-1}, for k_r = (5.4 ± 1.0) × 10^{-10} cm^3 molecule^{-1} s^{-1} and for $(k_f/k_r)_{ne}$ = 2.1 ± 0.3. In three other investigations the reaction was already so close to equilibrium at low C_3H_6 flows that the application of the fitting procedure could only yield a unique value for the ratio of rate constants, $(k_f/k_r)_e$ = 2.1 ± 0.1. Figure 2 shows a family of OH^- decays which encompass the range of back-reactant H_2O flows as well as the two values of the reaction length employed in this study.

In all 12 experiments equilibrium was established at high flows of C_3H_6 and fits to the linear portions of the ratio plots (analysis C in ref. 8) allowed the determination of the equilibrium constant, K, from the equilibrium concentrations. The ratio of the ion signals, $I(C_3H_5^-)/I(OH^-)$, when corrected for mass discrimination, is a measure of the ratio of the ion concentrations $[C_3H_5^-]/[OH^-]$. The method employed for the determination of the mass discrimination factor, m, has been reported previously (8). Figure 3 indicates the approach to and attainment of equilibrium at several flows of back-reactant H_2O. At the highest flow of H_2O equilibrium is established at the lowest measurable addition of C_3H_6. The 12 measurements led to a mean value for K of 2.2 ± 0.1.

The sampling conditions were altered in several of the 12 experiments either by varying the potential of the nose cone with respect to the flow tube (NP) at a fixed potential difference between the nose cone and the axis of the quadrupole mass filter (AP) or by adjusting AP at a fixed value for NP. Both k_f/k_r and K were observed to be independent of these variations within the experimental uncertainty.

Our analysis of the approach to and attainment

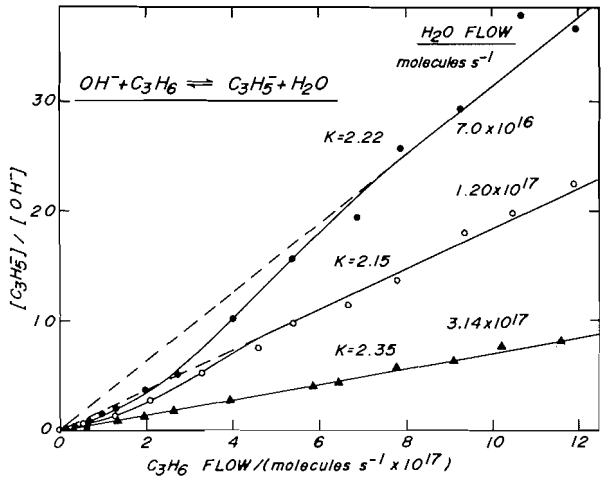

FIG. 3. The variation of $[C_3H_5^-]/[OH^-]$ as a function of C_3H_6 flow at various additions of H_2O. The slopes of the straight lines through the experimental points are proportional to the equilibrium constant K. $L = 61$ cm, $P = 0.54$ Torr, $T = 296$ K, and $\bar{v} = 8.1 \times 10^3$ cm s^{-1}. $m = 2.11$, 2.98, and 2.35 respectively from high to low H_2O flow.

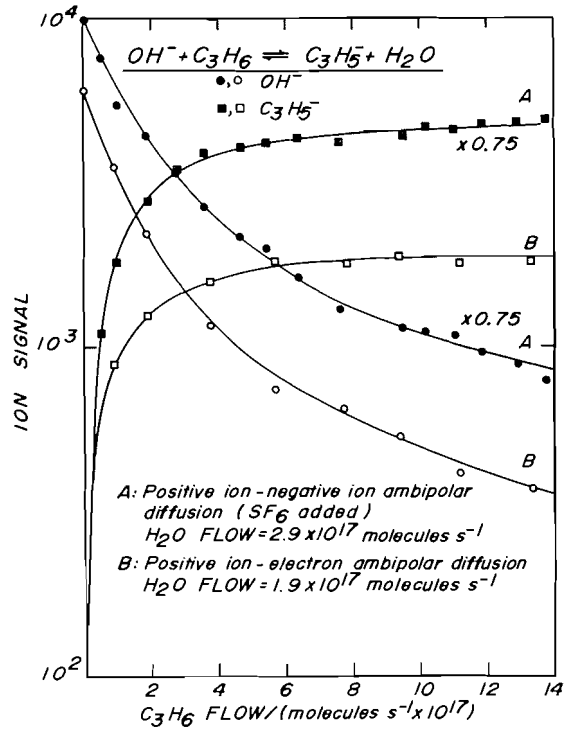

FIG. 4. The effect of SF_6 addition on the variation of the OH^- and $C_3H_5^-$ signals with C_3H_6 addition. The experimental operating conditions were otherwise quite similar. The curves drawn through the OH^- decays represent best computer fits to the experimental points: curve A, $k_f/k_r = 2.3$; curve B, $k_f/k_r = 2.1$. $P = 0.53$ Torr, $\bar{v} = 8.1 \times 10^3$ cm s^{-1}, $T = 296$ K, and $L = 61$ cm.

of equilibrium in the flowing afterglow assumes equal diffusive losses for the reactant and product ions (8). Under normal operating conditions the loss of negative ions due to diffusion in the flowing plasma is controlled by positive ion–electron ambipolar diffusion. In these experiments H_3O^+ ($m/e = 19$) was the dominant positive ion present in the H_2O–He(H_2) plasma. As C_3H_6 was added to the reaction region the H_3O^+ was observed to react rapidly via proton transfer to give $C_3H_7^+$ ($m/e = 43$) as the dominant positive ion with $k = (1.5 \pm 0.3) \times 10^{-9}$ cm^3 $molecule^{-1}$ s^{-1}. For positive ions with $m/e > 20$ the ion–electron ambipolar diffusion coefficients in hydrogen and helium are very similar (12). Therefore, the assumption of equal losses for OH^- and $C_3H_5^-$ by diffusion should not represent a serious error. It is possible to test the validity of this assumption experimentally by adding trace amounts of SF_6 into the reaction region (13). The addition of SF_6 changes the diffusion mode from positive ion – electron to positive ion – negative ion which is less rapid and less discriminating.

Figures 4 and 5 explore the effect of diffusion on the equilibrium constant measurements. Figure 4 shows the expected enhancement of the ion signals as SF_6 is added. However, the shape of the OH^- decay and hence the value of k_f/k_r derived from a fit to this decay remains essentially unchanged as would be expected if OH^- and $C_3H_5^-$ have similar diffusion coefficients. The equilibrium constants derived from the ion–signal ratio at equilibrium in the absence and presence of SF_6 again agree within experimental error when a correction is made for mass discrimination (Fig. 5).

Table 1 summarizes the experimental results and includes an assessment of the accuracy in each case. The sources of error have been described previously (8, 13). In these experiments the largest uncertainty in the determination of k_f/k_r and K was introduced by the uncertainty in the measurement of the flow of water vapour.

Figure 6 shows the observed variation in the major negative ion signals detected upon the addition of propene-3,3,3-d_3 into a He–H_2O plasma in which OH^- was initially a dominant negative ion. The introduction of CD_3CHCH_2 into the reaction region gave rise to a decrease in the OH^- signal and a concomitant increase in the ion signals at $m/e = 18$ (OD^-), $m/e = 41$ ($C_3H_5^-$), $m/e = 42$ ($C_3DH_4^-$), $m/e = 43$ ($C_3D_2H_3^-$), and $m/e = 44$ ($C_3D_3H_2^-$). There was no evidence for subsequent rapid reaction of any of the carbanions with CD_3CHCH_2.

Theoretical

The possible anions derived from the abstraction

Can. J. Chem. Downloaded from www.nrcresearchpress.com by 210.87.254.42 on 09/05/12
For personal use only.

Can. J. Chem. Downloaded from www.nrcresearchpress.com by 210.87.254.42 on 09/05/12
For personal use only.

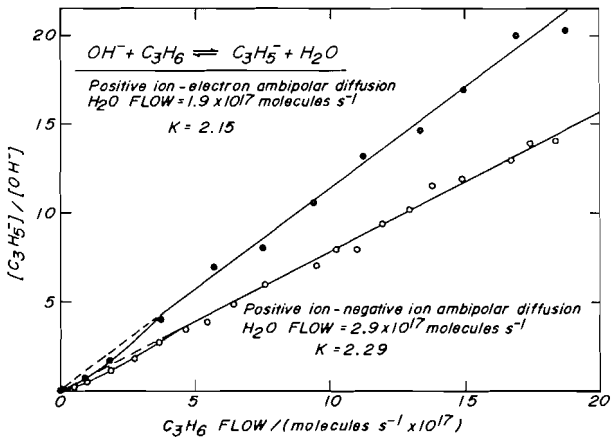

FIG. 5. The effect of SF_6 addition on the variation of ion ratio $[C_3H_5^-]/[OH^-]$ as a function of C_3H_6 addition. $L = 61$ cm, $P = 0.54$ Torr, $\bar{v} = 8.1 \times 10^3$ cm s^{-1}, $T = 296$ K, and $m = 2.98$ (without SF_6) and 1.84 (with SF_6 added).

TABLE 1. Experimental results for the reaction $OH^- + C_3H_6 \rightleftharpoons C_3H_5^- + H_2O$ at 296 ± 2 K

	Number of measurements	Results and precision	Accuracy (%)
k_f	8	$(1.1 \pm 0.1) \times 10^{-9a}$	±30
k_r	8	$(5.4 \pm 1.0) \times 10^{-10a}$	±35
$(k_f/k_r)_{nc}$	8	2.1 ± 0.3	±30
$(k_f/k_r)_c$	3	2.1 ± 0.1	±30
K	12	2.2 ± 0.1	±35

[a]Units of cm^3 $molecule^{-1}$ s^{-1}.

of the five chemically different protons of propene were examined using *ab initio* molecular orbital calculations. The removal of any proton from the methyl group was found to produce the same *planar* allyl anion. This reduces the number of possible anions to four (structures **2** to **5**). The cyclopropyl anion, another possible tautomer, was not examined in this study. It cannot be established directly by proton removal from propene and, furthermore, earlier calculations have established it to be very unstable (14).

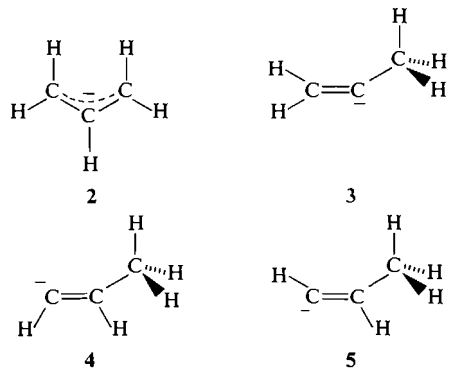

2 **3** **4** **5**

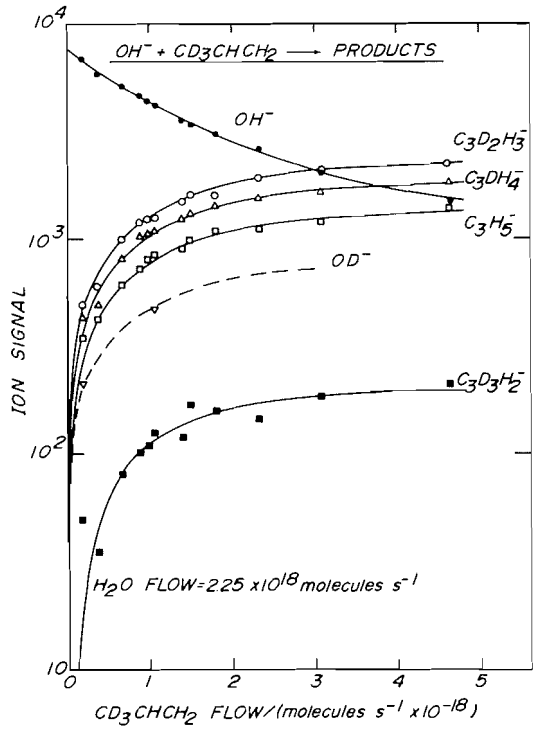

FIG. 6. Observed variation of major negative ion signals recorded upon the addition of propene-3,3,3-d_3 into a flow H_2O–He plasma in which OH^- is initially a dominant negative ion. The product ion signals have not been corrected for mass discrimination. $T = 296$ K, $P = 0.357$ Torr, $v = 7.8 \times 10^3$ cm s^{-1}, and $L = 59$ cm.

The geometry of propene has been optimized with the minimal STO-3G basis set (15) and there is good agreement between the experimental (16) and computed (6) geometries. This same basis set was employed to optimize the geometries of the four anions. Larger basis set (6-31G) calculations (17) using these optimum geometries were then performed to obtain more reliable energies for these anions.

Removal of a proton from the methyl group produces the planar allyl anion (**2**) in which both terminal methylene groups are equivalent. In this structure (Fig. 7) the carbon–carbon bond lengths (1.370 Å) are intermediate between single and double bond lengths and are close to previously calculated values of 1.38 Å (14) and 1.388 Å (18). The internal angle between the carbon atoms (132.9°) is almost 8° larger than in propene, a fact which is attributable to the negative charge formally located on the terminal carbon atoms. Again there is good agreement with the literature values of 133.1° (18) and 134° (19).

Preliminary studies on the other three anions showed the methyl group to prefer the same conformation as in propene. In the subsequent geometry

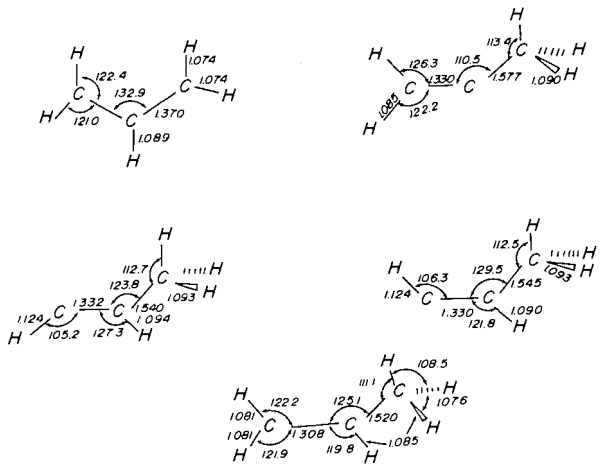

FIG. 7. Optimum geometries of propene and the tautomeric forms of $C_3H_5^-$ as computed with the STO-3G basis set. Bond lengths are given in angstroms and angles in degrees.

optimizations it was assumed that the bond lengths and angles for all three hydrogens in a methyl group were the same. This approximation reduced the number of geometric parameters and thereby reduced the computational cost of the optimizations. An estimate of the magnitude of the error introduced by this approximation is available from the same type of optimization on propene. The overall geometry computed for propene using this approximation is almost identical to that produced in the *complete* optimization and the total energy is inferior by only 0.5 kcal/mol (at STO-3G level) and by less than 0.13 kcal/mol with the more extensive 6-31G basis set.

Geometry optimizations on anions **3**, **4**, and **5** produced bond lengths similar to, but slightly longer than, the corresponding bonds in propene, showing the valence bond structures to be satisfactory descriptions of the molecular structure. The angle between the three carbon atoms appears to be particularly sensitive to the site of deprotonation. Removal of the proton from the central carbon atom produces a decrease in this angle by almost 15°, possibly caused by the newly generated σ-lone pair repelling the two bonds. Deprotonation of the methylene group produces less dramatic changes and these can also be attributed to lone pair – bond pair repulsions. Comparison of the relative energies of the carbanions as computed by both the STO-3G and 6-31G basis sets shows the allyl anion (**2**) to be the most stable by a substantial margin (Table 2 and Fig. 8).

Table 2 also includes proton removal energies taken as the difference in the computed energies of C_3H_6 and $C_3H_5^-$ for the reaction

$$[6] \qquad C_3H_6 \rightarrow C_3H_5^- + H^+$$

Since these proton removal energies may also be regarded as acidities, the order of acidities as computed by both the STO-3G and 6-31G basis sets is $CH_3 \gg CH > CH_2$. This order, deduced from the equilibrium energies, differs from that predicted by the computed net-atomic charges from a Mulliken overlap population on propene (using the 6-31G basis set), showing use of a ground state property is unsatisfactory to predict equilibrium stabilities.

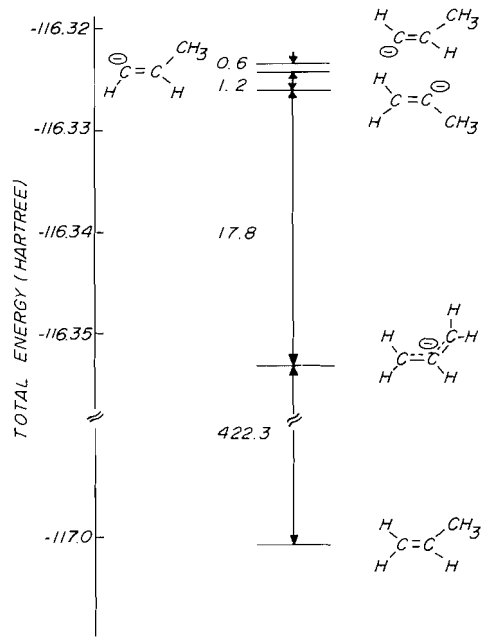

FIG. 8. Relative energies of propene and the tautomeric forms of $C_3H_5^-$ as computed with the 6-31G basis set. Energy differences are in kcal mol^{-1}.

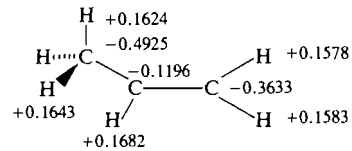

Discussion

Flowing afterglow studies of the reaction of OH^- with propene have been performed previously by Bohme *et al.* (2) who reported a value for $k_f = 2.7 \times 10^{-10}$ cm^3 $molecule^{-1}$ s^{-1} and by Bierbaum *et al.* (20) who determined a value for $k_f = 2.5 \times 10^{-10}$ cm^3 $molecule^{-1}$ s^{-1}. The observations reported here, which provided a value for $k_f = 1.1 \times 10^{-9}$ cm^3 $molecule^{-1}$ s^{-1}, suggest that these earlier numbers should be regarded as lower limits to the true value of k_f. Our experience indicates that only small amounts of H_2O are needed to achieve equilibrium for this reaction under typical flowing afterglow operating conditions even at low propene additions. Indeed we have observed that impurity amounts of

Can. J. Chem. Downloaded from www.nrcresearchpress.com by 210.87.254.42 on 09/05/12
For personal use only.

TABLE 2. Computed total energies and proton removal energies

Species	Total energy (hartree) STO-3G	Total energy (hartree) 6-31G	Proton removal energy[a] (kcal mol^{-1}) STO-3G	Proton removal energy[a] (kcal mol^{-1}) 6-31G
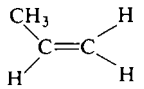	−115.66030[b]	−117.02768[b]		
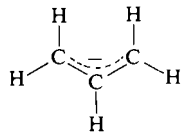	−114.83832	−116.35495	516.0	422.3
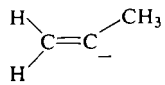	−114.82613	−116.32655	523.6	440.1
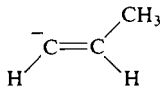	−114.82164	−116.32468	526.4	441.3
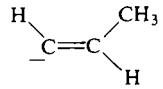	−114.82225	−116.32368	526.1	441.9

[a]Not corrected for zero-point energy or thermal energy.
[b]Reference 6.

H_2O can result in sufficient back-reaction to modify the OH^- decay to such an extent that the application of the standard rate constant analysis can only provide a lower limit to the true value of the forward rate constant (8).

The results given in Table 1 indicate that satisfactory agreement is found in this study between the following quantities: (*1*) the ratio of rate constants, $(k_f/k_r)_{ne}$, determined from the fit to the OH^- ion decays obtained under nonequilibrium conditions; (*2*) the ratio of rate constants, $(k_f/k_r)_e$, determined from the fit to the OH^- ion decays under equilibrium conditions; and (*3*) the equilibrium constant, K, determined from equilibrium concentrations. It should be emphasized here that $(k_f/k_r)_{ne}$ and $(k_f/k_r)_e$ do not require the correction for mass discrimination necessary in the determination of K from the equilibrium concentrations. These results, together with the observed independence of the measured ratio of rate constants and the equilibrium constant on the range of reaction times, neutral concentrations, electron and ion densities (diffusion mode), and the potentials in the sampling region, provide confidence that these measured values represent a true equilibrium constant.

The values of k_f/k_r and K provide a best estimate (21) of the true value (a weighted mean) of the equilibrium constant at 296 ± 2 K of 2.1 with a standard error of ±0.5. The thermodynamic information which can be derived from a knowledge of this equilibrium constant is summarized in Table 3. The value of $K = 2.1 \pm 0.5$ corresponds to a standard free energy change, ΔG^0_{298}, of -0.44 ± 0.14 kcal mol^{-1}. A standard entropy change, ΔS^0_{298}, of 3 ± 1 eu may be calculated from the reported values of the standard entropies of H_2O, C_3H_6, and OH^- (22, 23) and an estimated value for S^0_{298} ($C_3H_5^-$) of 63 ± 1 cal deg^{-1} mol^{-1}. This leads to a standard enthalpy change, ΔH^0_{298}, of $+0.5 \pm 0.4$ kcal mol^{-1}.

The standard enthalpy change determined in this study corresponds to a difference in proton affinity $PA(C_3H_5^-) - PA(OH^-) = +0.5 \pm 0.4$ kcal mol^{-1}. Adoption of the values for $\Delta H^0_{f,298}$ (H_2O, OH, H^+) given in the JANAF tables (22) and $EA_0(OH) = 42.09 \pm 0.043$ kcal mol^{-1} (24) leads to a value for $PA_{298}(OH^-) = 390.9 \pm 0.09$ kcal mol^{-1} and thus a value for $PA_{298}(C_3H_5^-) = 391.4 \pm 0.5$ kcal

TABLE 3. Thermodynamic parameters for the reaction $OH^- + C_3H_6 \rightleftharpoons C_3H_5^- + H_2O$ at 296 ± 2 K. The standard error is given along with the best estimate of the true value

$K = 2.1 \pm 0.5$
$\Delta G^0 = -0.44 \pm 0.14$ kcal mol^{-1}
$\Delta S^0 = +3 \pm 1$ cal deg^{-1} mol^{-1} (estimated)
$\Delta H^0 = +0.5 \pm 0.4$ kcal mol^{-1}

Can. J. Chem. Downloaded from www.nrcresearchpress.com by 210.87.254.42 on 09/05/12
For personal use only.

Can. J. Chem. Downloaded from www.nrcresearchpress.com by 210.87.254.42 on 09/05/12
For personal use only.

mol^{-1}. However, the equilibrium measurements per se do not unequivocably establish the tautomeric form of $C_3H_5^-$. Although it is reasonable to expect that the equilibrium involves the allyl anion which our calculations have shown to be the most stable form, the possibility remains that the reaction of OH^- with propene produces a higher energy tautomer which does not isomerize in the helium or hydrogen bath to the allylic form prior to reverse reaction with H_2O. In this case the proton affinity determined from these measurements would refer to the higher energy form and not to the allyl anion. However, this possibility can be readily discounted by a comparison of the ~18 kcal mol^{-1} difference between the allyl anion and the next lowest energy tautomer established by our calculations and the difference allowed by experimental observations. A proton affinity of 391 kcal mol^{-1} for the high energy tautomer would require a proton affinity for the allyl anion of only 373 kcal mol^{-1}. Such a low value would make the allyl anion thermodynamically accessible to the reaction

[7] $$CH_3O^- + C_3H_6 \rightleftharpoons C_3H_5^- + CH_3OH$$

since $PA_{298}(CH_3O^-) = 381 \pm 2$ kcal mol^{-1} (25). However, equilibrium measurements made in this laboratory indicate a value for $K_7 < 10^{-5}$ which requires the proton affinity for the allyl anion to be >388 kcal mol^{-1} and, when combined with the value for $PA_{298}(C_3H_5^-) = 391$ kcal mol^{-1}, would allow a proton affinity difference of at most 3 kcal mol^{-1} between the allyl ion and the next lowest energy tautomer. This result is clearly not supported by the theoretical expectations. On this basis we conclude that the carbanion produced by the reaction of OH^- with propene is indeed the allyl anion.

Our assignment of the allylic structure to the observed $C_3H_5^-$ is also supported, albeit indirectly, by the deuterated propene experiments whose results were considerably more complex than we had naively anticipated. Although the expected $C_3D_2H_3^-$ was the dominant product ion, significant concentrations of other carbanions with various extents of deuteration, viz. $C_3DH_4^-$, $C_3H_5^-$, and $C_3D_3H_2^-$, as well as some OD^- were observed. The $C_3H_5^-$, which cannot arise from the reaction of OH^- with CD_3CHCH_2, is presumed to result from secondary hydrogen–deuterium exchange reactions of the various deuterated carbanions with water vapour (the parent gas of OH^-) present in the reaction region according to

[8] $$C_3D_2H_3^- + H_2O \rightarrow C_2DH_4^- + HOD$$
$$\rightarrow C_3H_5^- + D_2O$$

[9] $$C_3DH_4^- + H_2O \rightarrow C_3H_5^- + HOD$$

The exchange is believed to proceed in the reaction

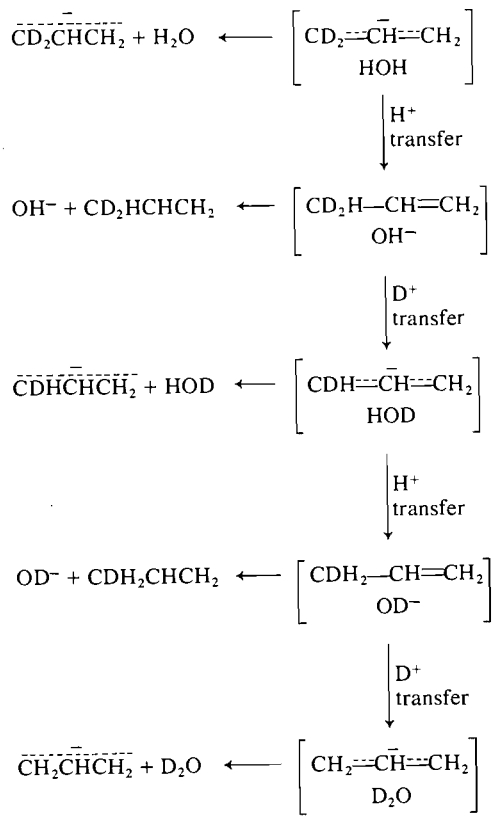

SCHEME 1

intermediate via sequential proton–deuteron transfer made possible by the symmetry of the allylic structure (Scheme 1). This sequence, which is meant only to be illustrative of the general nature of the mechanism, does not include all modes of proton–deuteron transfer. An analogous mechanism should also be involved for the forward reaction (Scheme 2). This reaction sequence (again abridged) allows the formation of $C_3D_3H_2^-$ in addition to the other anions observed.[2]

The thermochemical values for the allyl anion and radical derived from the equilibrium constant measurement for reaction 2 are summarized in Table 4. A value for $\Delta H^0_{f,298}$ (allyl anion) of 29.0 ± 0.8 kcal mol^{-1} is obtained when the values for $\Delta H^0_{f,298}(OH^-) = -34.3 \pm 0.4$ (22, 24), $\Delta H^0_{f,298}(H_2O) = 57.7979$ kcal mol^{-1} (22), $\Delta H^0_{f,298}(C_3H_6) = 4.88 \pm 0.1$ kcal mol^{-1} (23), and the present value of ΔH^0_{298} for reaction 2 are combined according to

[10] $$\Delta H^0_f(\bar{C}H_2\bar{C}H\bar{C}H_2) = \Delta H^0_f(C_3H_6) - \Delta H^0_f(H_2O) + \Delta H^0_f(OH^-) + \Delta H^0$$

[2]J. H. Stewart, R. H. Shapiro, C. H. DePuy, and V. M. Bierbaum have independently proposed a similar mechanism of sequential proton–deuteron transfer in connection with their flowing afterglow studies of reactions of carbanions with D_2O (C. H. DePuy, private communication).

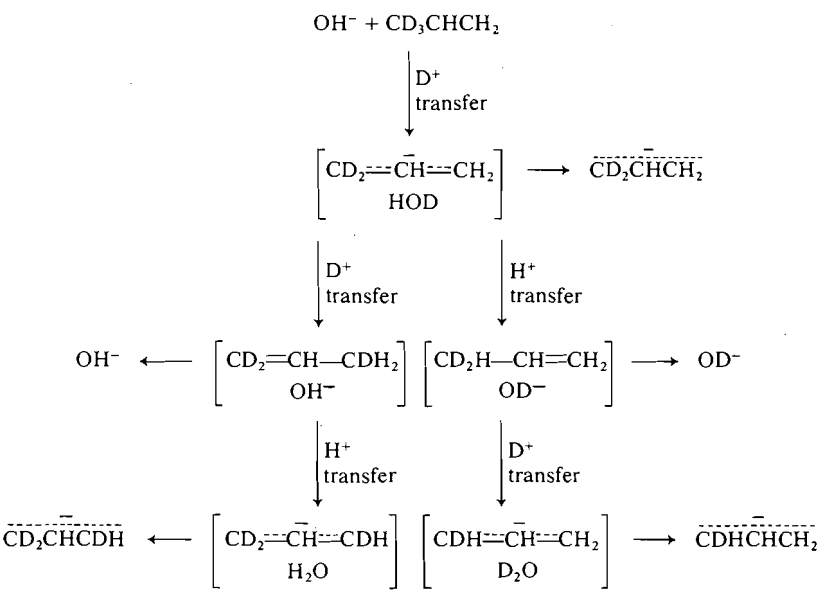

SCHEME 2

TABLE 4. Thermochemical values determined in this study

$PA_{298}(\bar{C}H_2\bar{C}H\bar{C}H_2)$	$= 391.4 \pm 0.5$ kcal mol^{-1}
$\Delta H^0_{f,298}(\bar{C}H_2\bar{C}H\bar{C}H_2)$	$= 29.0 \pm 0.8$ kcal mol^{-1}
$EA_{298}(CH_2CHCH_2)$	$= 12.4 \pm 1.9$ kcal mol^{-1}

Combination of this result for the heat of formation of the allyl anion with a value of 41.4 ± 1 kcal mol^{-1} for the heat of formation of the allyl radical (26) according to

$$EA(CH_2CHCH_2) = \Delta H^0_f(CH_2CHCH_2) - \Delta H^0_f(\bar{C}H_2\bar{C}H\bar{C}H_2)$$

leads to a value for $EA_{298}(CH_2CHCH_2) = 12.4 \pm 1.9$ kcal mol^{-1}.

Our experimental value for PA_{298}(allyl anion) $= 391.4 \pm 0.5$ kcal mol^{-1} is somewhat ($\sim 8\%$) lower than the absolute value (not corrected for zero-point energy or thermal energy) of 422.3 kcal mol^{-1} derived from our molecular orbital calculations with the 6-31G basis set. Such a difference between theory and experiment is not unexpected (4) and could be reduced with the use of a more extensive basis set. Other theoretical studies have provided a variety of values for the electron affinity of the allyl radical. An early molecular orbital calculation by Hush and Pople (27) provided a value for $EA(CH_2CHCH_2) = 5.5$ kcal mol^{-1}. Subsequent calculations by Ehrenson (28) and Hoyland and Goodman (29) led to values of -3.2 and 12 kcal mol^{-1}, respectively. Reliable experimental values were not available for comparison at that time. More recently, flowing afterglow measurements have provided an upper limit for $EA_{298}(CH_2CHCH_2) \leq 12.6 \pm 0.8$ kcal mol^{-1} (corrected for entropy changes), based on the observation of the electron transfer reaction

[11] $\bar{C}H_2\bar{C}H\bar{C}H_2 + O_2 \rightarrow O_2^- + CH_2CHCH_2$

with $k_{11} = 2.8 \times 10^{-10}$ cm^3 molecule^{-1} s^{-1} (28). The electron affinity of O_2 at 298 K is 11.6 kcal mol^{-1} (30) and we have allowed for a possible endoergicity of 0.5 kcal mol^{-1} given by $-RT \ln k_{11}/k_L$, where k_L is the Langevin collision rate constant (31). A lower limit for $EA_{298}(CH_2CHCH_2)$ of 12.1 ± 1.8 kcal mol^{-1} (corrected for entropy changes) can be derived (2) from the observation of reaction 2. These limiting values and the value calculated most recently by Hoyland and Goodman (29) are in accord with the value of 12.4 ± 1.9 kcal mol^{-1} determined in the present study. Very recently Zimmerman and Brauman (32) have reported electron photodetachment measurements for $\bar{C}H_2\bar{C}H\bar{C}H_2$ produced by reaction 2. A theoretical fit to the relative cross-sections near threshold provided a value for the electron affinity at 0 K of 12.7 ± 1.2 kcal mol^{-1} where the error limits reflect the lack of data at threshold.

Acknowledgements

The financial support of the National Research Council of Canada and the Sloan Foundation are gratefully acknowledged.

1. J. I. BRAUMAN and L. K. BLAIR. J. Am. Chem. Soc. **92**, 5987 (1970).
2. D. K. BOHME, E. LEE-RUFF, and L. B. YOUNG. J. Am. Chem. Soc. **94**, 5132 (1972).
3. R. T. MCIVER, JR. and J. SCOTT MILLER. J. Am. Chem. Soc. **96**, 4323 (1974).

Can. J. Chem. Downloaded from www.nrcresearchpress.com by 210.87.254.42 on 09/05/12
For personal use only.

4. G. I. MACKAY, R. S. HEMSWORTH, and D. K. BOHME. Can. J. Chem. **54**, 1624 (1976).
5. T. B. MCMAHON and P. KEBARLE. J. Am. Chem. Soc. **98**, 3399 (1976).
6. L. RADOM, W. A. LATHAN, W. J. HEHRE, and J. A. POPLE. J. Am. Chem. Soc. **93**, 5339 (1971).
7. W. J. HEHRE and L. SALEM. Chem. Commun. 754 (1973).
8. D. K. BOHME, R. S. HEMSWORTH, H. W. RUNDLE, and H. I. SCHIFF. J. Chem. Phys. **58**, 3504 (1973).
9. D. BETOWSKI, J. D. PAYZANT, G. I. MACKAY, and D. K. BOHME. Chem. Phys. Lett. **31**, 321 (1975).
10. D. K. BOHME, G. I. MACKAY, H. I. SCHIFF, and R. S. HEMSWORTH. J. Chem. Phys. **61**, 2175 (1974).
11. F. C. FEHSENFELD, E. E. FERGUSON, and A. L. SCHMELTEKOPF. J. Chem. Phys. **45**, 1844 (1966).
12. E. W. MCDANIEL and E. A. MASON. The mobility and diffusion of ions in gases. Wiley, New York, NY. 1973.
13. J. D. PAYZANT, H. I. SCHIFF, and D. K. BOHME. J. Chem. Phys. **63**, 149 (1975).
14. D. T. CLARK and D. R. ARMSTRONG. Theoret. Chim. Acta, **14**, 870 (1969).
15. W. J. HEHRE, R. F. STEWART, and J. A. POPLE. J. Chem. Phys. **51**, 2657 (1969).
16. D. R. LIDE and D. CHRISTENSEN. J. Chem. Phys. **35**, 1374 (1961).
17. W. J. HEHRE, R. DITCHFIELD, and J. A. POPLE. J. Chem. Phys. **56**, 2257 (1972).
18. A. Y. MEYER and M. CHRIVOTZKY. J. Mol. Struct. **12**, 157 (1972).
19. S. D. PEYERIMHOFF and R. J. BUENKER. J. Chem. Phys. **51**, 2528 (1968).
20. V. M. BIERBAUM, C. H. DEPUY, R. H. SHAPIRO, and J. H. STEWART. J. Am. Chem. Soc. **98**, 4229 (1976).
21. N. C. BARFORD. Experimental measurements: precision error and truth Addison-Wesley, London. 1967.
22. JANAF Thermochemical Tables. Vol. 37. 2nd ed. Natl. Stand. Ref. Data Ser., Natl. Bur. Stand. (1971); JANAF Thermochemical Tables, 1974 Supplement, J. Phys. Chem. Ref. Data, **3** (1974).
23. S. W. BENSON, F. R. CRUICKSHANK, D. M. GOLDEN, G. R. HAUGIN, H. E. O'NEAL, A. S. RODGERS, R. SHAW, and R. WALSH. Chem. Rev. **69**, 279 (1969).
24. H. HOTOP, T. A. PATTERSON, and W. C. LINEBERGER. J. Chem. Phys. **60**, 1806 (1974).
25. G. I. MACKAY and D. K. BOHME. Can. J. Chem. To be submitted.
26. D. M. GOLDEN and S. W. BENSON. Chem. Rev. **69**, 125 (1969).
27. N. S. HUSH and J. A. POPLE. Trans. Faraday Soc. **51**, 600 (1955).
28. S. EHRENSON. J. Phys. Chem. **66**, 706 (1962).
29. J. R. HOYLAND and L. GOODMAN. J. Chem. Phys. **36**, 21 (1962).
30. R. J. CELOTTA, R. A. BENNETT, J. L. HALL, M. W. SIEGEL, and J. LEVINE. Phys. Rev. A, **6**, 631 (1972).
31. G. GIOUMOUSIS and D. P. STEVENSON. J. Chem. Phys. **39**, 1413 (1963).
32. A. H. ZIMMERMAN and J. I. BRAUMAN. J. Am. Chem. Soc. **99**, 3568 (1977).

Can. J. Chem. Downloaded from www.nrcresearchpress.com by 210.87.254.42 on 09/05/12
For personal use only.

Hydrogen bonding in organic synthesis. Part 9. The sulphenylation of fluoride-activated β-dicarbonyls

JAMES H. CLARK AND JACK M. MILLER

Department of Chemistry, Brock University, St. Catharines, Ont., Canada L2S 3A1

Received August 4, 1977

JAMES H. CLARK and JACK M. MILLER. Can. J. Chem. **56**, 141 (1978).

Various α-arylthio-β-dicarbonyls have been prepared by the room temperature reaction of β-dicarbonyltetraethylammonium fluoride monosolvates with aryl disulphides. The disulphides are formed by the *in situ* fluoride-assisted air oxidation of aryl thiols.

JAMES H. CLARK et JACK M. MILLER. Can. J. Chem. **56**, 141 (1978).

On a préparé divers composés α-arylthio β-dicarbonylés en faisant réagir, à température ambiante, le complex monosolvaté du fluorure de tétraéthylammonium et de la forme énolique d'un dérivé β-dicarbonylé avec des disulfures d'aryles. On forme les disulfures par l'oxydation *in situ* d'aryles thiols effectuée par l'air assisté par des fluorures.

[Traduit par le journal]

A variety of synthetic methods for the preparation of α-thio-β-dicarbonyls have been developed since these compounds are considered as valuable synthetic intermediates. For example, α-arylthiodialkyl malonates have been used as intermediates in the synthesis of a number of heterocycles (1) including coumarins and α-pyrones (2). Furthermore, α-thio-β-diketones have been shown to represent interesting examples of strong intramolecular hydrogen bonding (3). Previous methods of preparation have usually involved the use of sulphenyl halides (4–6) or of α-halodicarbonyls (3) although an alternative method involving sulphenamides has been proposed (7).

We now wish to report a new simple procedure for the preparation of α-thio-β-dicarbonyls which involves the reaction of β-dicarbonyltetraethylammonium fluoride monosolvates with aryl disulphides, the latter being formed *in situ* by the fluoride-assisted air oxidation of arylthiols. To the best of our knowledge, this is the first reported one-pot synthesis of α-arylthio-β-dicarbonyls starting from the β-dicarbonyl and arylthiol.

Experimental

^{1}H nmr spectra were recorded in $CDCl_3$ with a Varian A60 (60 MHz) spectrometer ($SiMe_4$ standard). Mass spectra were obtained on an AE1 MS-30 double-beam mass spectrometer.

Tetraethylammonium fluoride was prepared by neutralisation of 20% aqueous tetraethylammonium hydroxide with 51% aqueous hydrofluoric acid. Pentane-2,4-dione was distilled before use. Other reagents were generally commercial grade samples used without further purification.

Reactions

Two techniques are available for the preparation of β-dicarbonyltetraethylammonium fluoride monosolvates. For β-diketones, an aqueous solution of the fluoride was evaporated in the presence of the β-dicarbonyl, whereas for dialkyl malonates and ethyl acetoacetate, the aqueous fluoride was first reduced to a solid hydrate by evaporation, followed by treatment, at room temperature, with a dimethylformamide solution of the β-dicarbonyl. Details of these methods are given elsewhere (8, 9). An equimolar amount of the arylthiol was added to the dimethylformamide solution of the monosolvate and the whole stirred at room temperature over 5 Å molecular sieves in an open vessel. Reactions were monitored by ^{1}H nmr spectroscopy and/or by tlc and were usually stopped when complete unless stated otherwise in Table 1. Most reactions were complete within 16–20 h. The technique of separation used in each case was virtually the same, with only minor modifications. Diethyl ether was added and any precipitated fluoride was removed by filtration. The ethereal extracts were then shaken with equal volumes of water (3×) to remove the DMF and any remaining fluoride. The ethereal solution was dried ($MgSO_4$) and evaporated. Most products were solids and once crystallised by cooling were recrystallised usually from EtOH. Liquid products were purified by column chromatography (silica gel).

All products are known compounds and gave melting points or boiling points consistent with those reported in the literature (see Table 1) and ^{1}H nmr and mass spectra consistent with their structure and, where reported data is available, consistent with those reported in the literature (3).

Details of a representative preparation are given below.

Preparation of 2-Benzenethio-1,3-diphenylpropane-1,3-dione

An aqueous solution of tetraethylammonium fluoride containing 0.02 mol of the fluoride was briefly concentrated (ca. 5 min) by evaporation at ca. 80°C (water bath) under a mild vacuum (aspirator). 1,3-Diphenylpropane-1,3-dione (0.02 mol) in dimethylformamide (ca. 25 ml) was added and the whole evaporated (same conditions) with shaking for 10–15 min or until no further ebullition occurred. Benzene thiol (0.02 mol) in dimethylformamide (ca. 25 ml) was added dropwise to the cooled solution of the solvate giving a red coloration. The resulting solution was then stirred at room temperature (25°C) over 5 Å molecular sieves for 16 h at which point sampling and ^{1}H nmr analysis showed no starting material remaining. The reaction mixture was extracted in diethyl ether, washed with water (3×), dried ($MgSO_4$), and evaporated. The partially solid residue was extracted in hot EtOH–ligroin (60–100°C) and cooled giving a solid which on recrystallization from hexane gave crystals of 2-benzenethio-1,3-diphenylpropane-1,3-dione (0.0168 mol, 84%); mp 86°C

Can. J. Chem. Downloaded from www.nrcresearchpress.com by 210.87.254.105 on 09/05/12
For personal use only.

Can. J. Chem. Downloaded from www.nrcresearchpress.com by 210.87.254.105 on 09/05/12
For personal use only.

TABLE 1. Sulphenylation of β-dicarbonyls in the presence of tetraethylammonium fluoride

β-Dicarbonyl	Thiol	Product	Yield (%)	Melting point (°C)		Boiling point (°C) (Torr)	
				Exptl.	Literature	Exptl.	Literature
Pentane-2,4-dione	PhSH	MeCOCH(SPh)COMe (enol)	81[a]			157–158 (30)	142–143 (12)[d]
1,3-Diphenylpropane-1,3-dione	PhSH	PhCOCH(SPh)COPh	84[a]	86	83–84[d]		
1-Phenylbutane-1,3-dione	PhSH	PhCOCH(SPh)COMe (enol)	78[a]	67	63[d]		
Diethyl malonate	PhSH	EtOCOCH(SPh)CO_2Et	78[a]			187–190 (28)	148 (1.7)[e]
Ethyl acetoacetate	PhSH	MeCOCH(SPh)CO_2Et	86[a]			169–170 (23)	165 (19)[d]
Pentane-2,4-dione	*p*-MeC_6H_4SH	MeCOCH(S—C_6H_4—Me)COMe (enol)	85[a]	48	53[f]		
Pentane-2,4-dione	*p*-$NO_2C_6H_4SH$	MeCOCH(S—C_6H_4—NO_2)COMe (enol)	41[b]			128	130–131[g]
Pentane-2,4-dione	2-Mercaptopyridine	MeCOCH(S—py)COMe (enol)	68[c]	35–36			

[a]Recovered yields after 16–20 h (100% reaction).
[b]Recovered yield after 60 h (ca. 50% reaction).
[c]Recovered yield after 30 h (100% reaction).
[d]Reference 3.
[e]Reference 7.
[f]Reference 16.
[g]Reference 17.

(lit. (3) mp 83–84°C); δ 6.08 (1H, s, CH), ca. 7.3 (11H, m, aromatic CH), and ca. 7.9 (4H, m, aromatic CH); *m/e* 332.

Results and Discussion

β-Dicarbonyl compounds are capable of behaving as H-bond electron acceptors in the presence of fluoride ions (8, 9). Although the situation is less clear with malonates, β-diketones are totally enolised in the presence of tetraethyl- or tetrabutylammonium fluorides and stable, crystalline monosolvates containing very strong enol hydroxy–fluoride H-bonds have been isolated (8, 9). The synthetic utility of these H-bond activated β-dicarbonyls as sources of highly reactive β-dicarbonyl nucleophiles has already been demonstrated in their reaction with alkyl iodides (8, 9).

Despite the very strong H-bonding that exists in dimethylformamide solutions of tetraethylammonium fluoride and β-dicarbonyls, the equilibrium [1]

[1]

at room temperature will be such that significant amounts of free fluoride ions are present in solution. A comparable system is the very strongly H-bonded tetrabutylammonium fluoride – acetic acid monosolvate in chloroform which has been shown to contain about 7% free fluoride at room temperature and a solvate molarity of 1.0 (10). The free fluoride in the β-dicarbonyl system provides the opportunity for secondary H-bonding between fluoride and the much weaker H-bond electron acceptor thiol molecule (11), which will provide the driving force for air oxidation of the thiol to disulphide [2].

[2] $2R^2—SH\cdots\bar{F} \xrightarrow{[O]} R^2—SS—R^2 + HOH\cdots\bar{F}$

Although water is consequently introduced into the reaction system at this stage, its presence does not affect the outcome of the reaction.

Thus, on stirring a solution of the β-dicarbonyl-fluoride monosolvate (8, 9) in dimethylformamide (tetrahydrofuran may also be used with some loss in reactivity) with an equimolar amount of an arylthiol at room temperature, the α-arylthio-β-dicarbonyl is formed via the aryl disulphide giving the overall reaction 3.

[3] $RCOCH_2COR' + R^2SH + [O] \xrightarrow{\bar{F}} RCOCH(SR^2)COR' + H_2O$

Recently, a general method for the sulphenylation of ketones using disulphides in the presence of a strong base, such as lithium diisopropylamide, was

Can. J. Chem. Downloaded from www.nrcresearchpress.com by 210.87.254.105 on 09/05/12
For personal use only.

reported (12). Presumably, this method could be used for the sulphenylation of β-dicarbonyls although no examples were given in the article. The essential advantage of our method for the preparation of α-arylthio-β-dicarbonyls over such an alternative lies in the choice of 'base.' Strong bases such as lithium amides are destroyed by air and hence sulphenylations using such bases cannot involve the *in situ* air oxidation of a thiol to a disulphide. Thus, reactions must start with a disulphide so that one half of the disulphide is 'wasted' and a quantitative amount of thiol or disulphide would be generated on quenching the reaction mixture, perhaps leading to potential separation problems.

With regard to the previously reported methods for preparing the title compounds, that is, those involving sulphenyl halides or α-halodicarbonyls, it is clear that direct reaction of the more readily available thiol and β-dicarbonyl is the more desirable. Furthermore, tetraalkylammonium fluorides are considerably easier to prepare and use than many more conventional strong organic bases and in the reactions described here and indeed in many other reactions (13–15) they operate essentially as a catalyst and may be removed and recovered in water and subsequently re-used.

The reactions that have been attempted are summarised in Table 1. It is interesting to note that on increasing the acidity of the thiol, the time required for sulphenylation increases. The reason for this is not readily apparent as one might expect that the more acidic the thiol, the weaker the S—S bond in the corresponding disulphide. It may be that the products of the reactions involving the more acidic thiols are better H-bond electron acceptors than the original β-dicarbonyls assuming that the sulphenyl group behaves as an electron withdrawing substituent through $p\pi$–$d\pi$ conjugation at the sulphur atom directly attached to the α-position of the β-dicarbonyl. The products would act to partly block the fluoride to a degree dependent on the overall electron withdrawing powers of the sulphenyl group.

Attempts to introduce a second sulphenyl group into these molecules were unsuccessful. This is not unexpected when one considers that most β-dicarbonyls are totally enolised in the presence of fluoride (8, 9) and β-dicarbonyls containing one α-substituent (particularly where that substituent is electron withdrawing) will have their one remaining acidic hydrogen firmly locked in a very strong H-bond to fluoride.

1. A. LEFEUVRE. Mem. Mus. Natl. Hist. Nat. Paris, Ser. D, **3**, 1 (1966); Chem. Abstr. **69**, 35898a (1968).
2. A. LEFEUVRE and C. MENTZER. Bull. Soc. Chim. Fr. 623 (1964).
3. Z. YOSHIDA, H. OGASHI, and T. TOKUMITSU. Tetrahedron, **26**, 2987 (1970).
4. H. BRINTZINGER and H. ELLWANGER. Chem. Ber. **87**, 300 (1954).
5. H. BÖHME, F. FREIMUTH, and E. MUNDLOS. Chem. Ber. **87**, 1661 (1954).
6. J. A. BARLTROP and K. J. MORGAN. J. Chem. Soc. 4486 (1960).
7. T. MUKAIYAMA, S. KOBAYASHI, and T. KUMAMATO. Tetrahedron Lett. **59**, 5115 (1970).
8. J. H. CLARK and J. M. MILLER. J. Chem. Soc. Chem. Commun. 64 (1977).
9. J. H. CLARK and J. M. MILLER. J. Chem. Soc. Perkin Trans. I, 1743 (1977).
10. J. H. CLARK and J. EMSLEY. J. Chem. Soc. Dalton, 2154 (1973).
11. J. H. CLARK and J. M. MILLER. J. Am. Chem. Soc. **99**, 498 (1977).
12. B. M. TROST, T. N. SALZMANN, and K. HIROI. J. Am. Chem. Soc. **98**, 4887 (1976).
13. J. H. CLARK and J. M. MILLER. J. Chem. Soc. Perkin Trans. I, 2063 (1977).
14. I. KUWAJIMA, T. MUROFUSHI, and E. NAKAMURA. Synthesis, 602 (1976).
15. S. HOZ, M. ALBECK, and Z. RAPPOPORT. Synthesis, 162 (1975).
16. S. SMILES. J. Chem. Soc. 1723 (1926).
17. P. F. HU. Sci. Rep. Natl. Tsing Hua Univ. Ser. A5, 260 (1948); Chem. Abstr. **43**, 6634h (1949).

Can. J. Chem. Downloaded from www.nrcresearchpress.com by 210.87.254.105 on 09/05/12
For personal use only.

Syntheses related to the octodiose in apramycin. Part II

HAROLD C. JARRELL AND WALTER A. SZAREK
Department of Chemistry, Queen's University, Kingston, Ont., Canada K7L 3N6

Received November 10, 1977

HAROLD C. JARRELL and WALTER A. SZAREK. Can. J. Chem. **56**, 144 (1978).

Derivatives of two octodioses have been synthesized from methyl α-D-glucopyranoside and have been shown to possess a *trans*-decalin structure. The new octodiose derivatives may be useful in the synthesis of aminooctodioses which occur in apramycin and oxyapramycin.

HAROLD C. JARRELL et WALTER A. SZAREK. Can. J. Chem. **56**, 144 (1978).

On a effectué la synthèse de dérivés de deux octodioses à partir de l'α-D-glucopyrannoside de méthyle et on a démontré qu'ils possèdent une structure *trans*-décalinique. Les nouveaux dérivés de l'octodiose peuvent être utiles dans la synthèse d'aminooctodioses qui se retrouvent dans l'apramycine et l'oxyapramycine.

[Traduit par le journal]

Recently, apramycin (**1**) (1) and oxyapramycin (**2**) (2) have been shown to be components of an aminocyclitol antibiotic complex, namely, nebramycin (3). Structural studies (2, 4) have shown that the unusual aminooctodioses **3** and **4** are components of compounds **1** and **2**, respectively. It may be seen from structures **1** and **2** that the interesting features are the presence of a nonreducing disaccharide linkage, an octodiose having a *trans*-decalin structure, and 2-deoxystreptamine. In addition to its unique structural features, apramycin is of interest because it has been found to be a potent antibiotic relative to neamine (for a summary of biological data see ref. 5) and has not been reported to be inactivated by any of the known aminoglycoside-inactivating enzymes (5, 6). Interestingly, replacement of the terminal 4-amino-4-deoxy-D-glucose moiety in apramycin with a methyl group yields a cyclitol derivative which has a similar antimicrobial spectrum (5). In view of the latter result, pseudodisaccharides containing the unique aminooctodioses **3** and **4** or their analogs may prove to be of value. Part of the initial work done in this laboratory has been to investigate the preparation of octodioses which are related to structures **3**

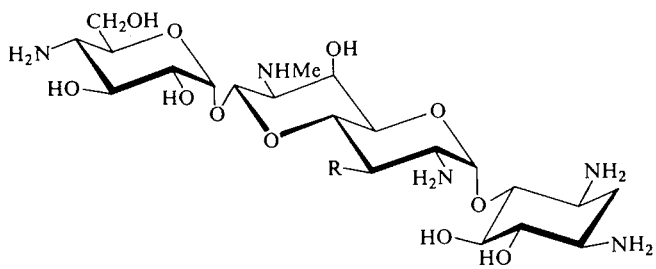

1 R = H
2 R = OH

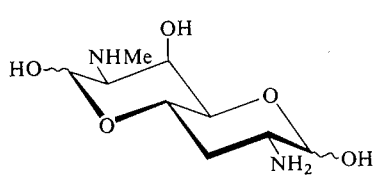

3

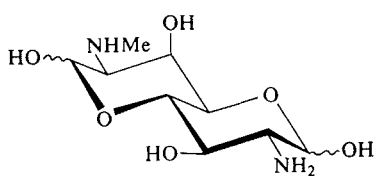

4

Can. J. Chem. Downloaded from www.nrcresearchpress.com by 210.87.254.105 on 09/05/12
For personal use only.

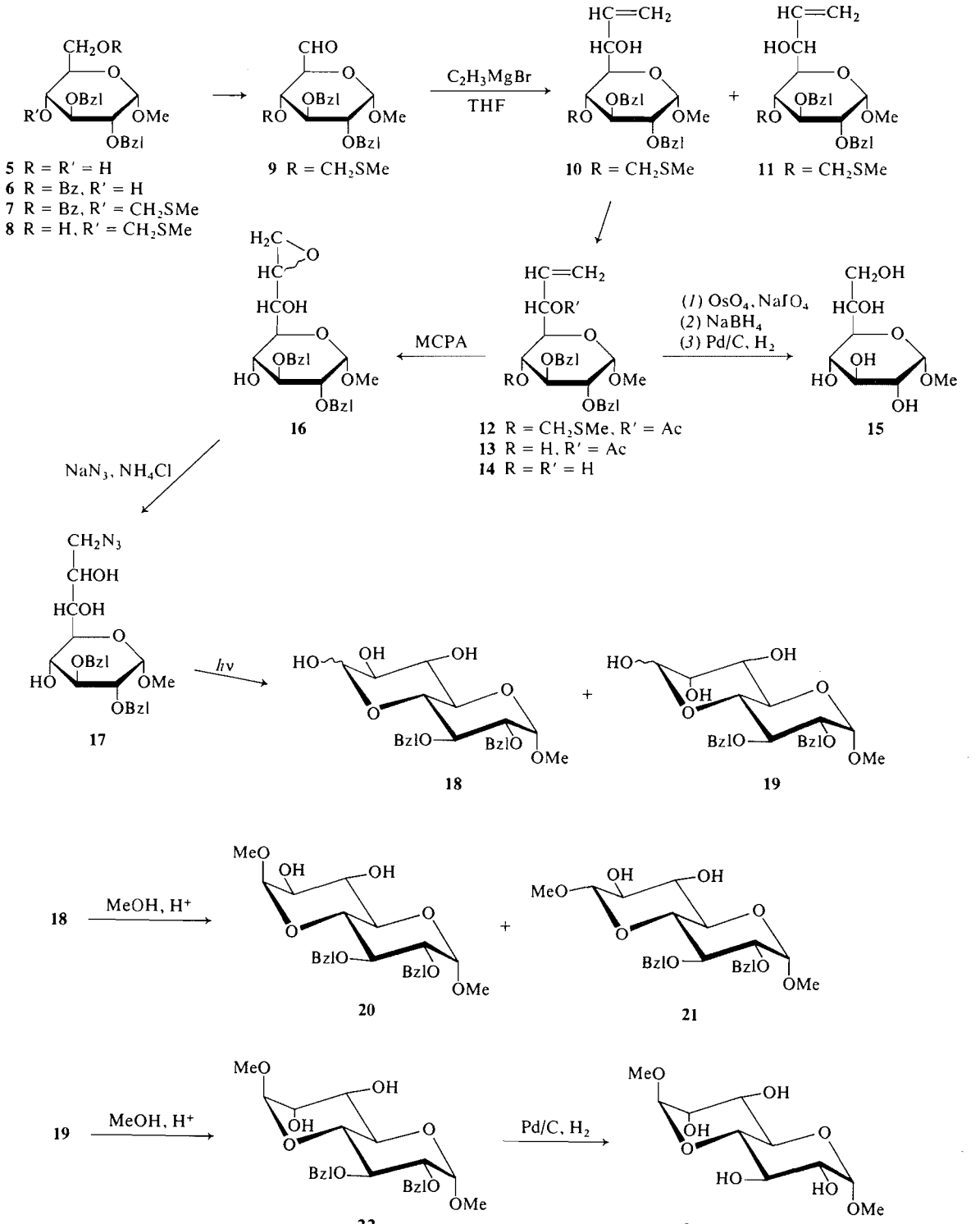

SCHEME 1. **6**, mp 75–77°C, $[\alpha]_D$ +22°; **8**, mp 88.5–89.5°C, $[\alpha]_D$ +153°; **10**, syrup, $[\alpha]_D$ +109.7°; **11**, mp 93–94°C, $[\alpha]_D$ +115.5°; **12**, syrup, $[\alpha]_D$ +82.3°; **13**, syrup, $[\alpha]_D$ +2.9°; **14**, mp 109–110°C, $[\alpha]_D$ −1.6°; **17**, mp 122–128°C, $[\alpha]_D$ +9.9°; **16**, mp 118.5–120°C, $[\alpha]_D$ +9.0°; **18**, syrup, $[\alpha]_D$ +14.8°; **19**, mp 88–89°C, $[\alpha]_D$ +20.6°; **20** + **21**, mp 120–122°C, $[\alpha]_D$ +15.2°; **22**, mp 148.5–150°C, $[\alpha]_D$ −12°; **23**, mp 192–196°C, $[\alpha]_D$ +56° (H_2O).

Can. J. Chem. Downloaded from www.nrcresearchpress.com by 210.87.254.105 on 09/05/12
For personal use only.

and **4**, and which might be of use in their synthesis. In an earlier report (7) the synthesis of two octodioses and an unsuccessful attempt to convert one of them into a *trans*-decalin structure were presented. In this Communication we report what we believe to be the first synthetic examples of octodioses which have a *trans*-decalin structure.

The synthetic approach which was used is outlined in Scheme 1.[1] Readily available compound **5** (8) was selectively benzoylated to give crystalline **6** in 77% yield. Compound **6** was converted, by a known procedure (9), into **7** which was debenzoylated to give crystalline **8** in 66% yield (from **6**). A Grignard reaction with aldehyde **9**[2] (prepared by the oxidation (10) of **8**) afforded a mixture of epimeric products **10** (67.4%) and **11** (12.2%) which were readily separable with **10** being the preponderant isomer. Acetylation of **10** gave **12** in 91% yield; removal of the methylthiomethyl group (9) from **12** gave **13** in 84% yield. Conversion of **13** into **15** was effected in three steps; the product had mp 163–165°C and $[\alpha]_D$ +137.8° (H_2O). The enantiomer of **15** has been reported (11) to have mp 167.5–169°C and $[\alpha]_D$ −142° (H_2O). These data establish that the configuration at C-6 in **15**, **10**, and **11** is that which is shown.

Deacetylation of **13** afforded crystalline **14** (80%) which on treatment with *m*-chloroperbenzoic acid gave compound **16** in 76% yield. Opening the anhydro ring in **16** with azide (12) afforded a mixture of epimeric azides **17** (79%) which could not be resolved. Photolysis of **17** by a standard procedure (13) gave a mixture of **18** and **19** in a yield of 33%. Methanolysis of **18** afforded a mixture of glycosides **20** and **21** (48.5%), whereas **19** afforded **22** (68%) as the only isolated product. The structures assigned to compounds **20**, **21**, and **22** were established by ^1H and ^{13}C nmr spectroscopy. Compound **22** was debenzylated to give crystalline **23** in 84% yield.

The present approach has been demonstrated to provide a viable access to structures which are analogs of those found in **3** and **4**. It is evident that the present scheme is flexible in that, by a suitable choice of starting monosaccharide, other octodioses may be prepared and, by a judicious choice of protecting groups, linkages at C-1 and C-8 may be introduced in which the aglycons may be different as is the case in **1** and **2**.

[1]All compounds gave correct elemental analyses and had pmr and ^{13}C nmr spectra which were in accord with their structures. Optical rotations were measured at 25°C in chloroform, unless otherwise stated. Melting points are uncorrected.

[2]Aldehyde **9** was characterized by treatment with *N,N'*-diphenyl-1,2-diaminoethane to give the corresponding imidazolidine derivative.

Acknowledgements

The authors are grateful to the National Research Council of Canada for its generous financial support of this work in the form of a scholarship (to H.C.J.) and a grant (to W.A.S.). They also wish to acknowledge the encouragement and interest of the late Professor J. K. N. Jones.

1. S. O'Connor and L. K. T. Lam. Abstr. Pap. Am. Chem. Soc. Meeting, **165**, MEDI6 (1973).
2. D. E. Dorman, J. W. Paschal, and K. E. Merkel. J. Am. Chem. Soc. **98**, 6885 (1976).
3. W. M. Stark, M. M. Hoehn, and N. G. Knox. Antimicrob. Agents Chemother. 314 (1968).
4. S. O'Connor, L. K. T. Lam, N. D. Jones, and M. O. Chaney. J.Org. Chem. **41**, 2087 (1976).
5. K. E. Price and J. C. Godfrey. Adv. Appl. Microbiol. **18**, 191 (1974).
6. H. Umezawa. Adv. Carbohydr. Chem. Biochem. **30**, 183 (1974).
7. H. C. Jarrell and W. A. Szarek. Carbohydr. Res. In press.
8. D. J. Bell and J. Lorber. J. Chem. Soc. 453 (1940).
9. P. M. Pojer and S. J. Angyal. Tetrahedron Lett. 3067 (1976).
10. J. G. Moffatt. *In* Oxidation. Vol. 2. *Edited by* R. L. Augustine and D. J. Trecker. Marcel Dekker, Inc., New York, NY. 1971.
11. B. Pettersson and O. Theander. Acta Chem. Scand. B, **29** (1974).
12. R. D. Guthrie and D. Murphy. J. Chem. Soc. 5288 (1963).
13. D. Horton, A. E. Luetzow, and J. C. Wease. Carbohydr. Res. **8**, 366 (1968).

Canadian Journal of Chemistry
Published by
THE NATIONAL RESEARCH COUNCIL OF CANADA

Journal canadien de chimie
Publié par
LE CONSEIL NATIONAL DE RECHERCHES DU CANADA

Volume 56 Number 2 January 15, 1978 Volume 56 numéro 2 15 janvier 1978

Can. J. Chem. Downloaded from www.nrcresearchpress.com by 210.87.254.40 on 09/05/12
For personal use only.

The radiation chemistry of nitrogen: primary neutral dissociative excitation yield and the isotopic exchange mechanism[1]

A. W. BOYD AND O. A. MILLER
Physical Chemistry Branch, Atomic Energy of Canada Limited, Chalk River Nuclear Laboratories, Chalk River, Ont., Canada K0J 1J0
AND
C. WILLIS
Division of Chemistry, National Research Council of Canada, Ottawa, Ont., Canada K1A 0R6

Received August 11, 1977

A. W. BOYD, O. A. MILLER, and C. WILLIS. Can. J. Chem. **56**, 147 (1978).

Measurements of the yield of NO_2 in N_2–NO mixtures give a neutral dissociative excitation yield of $G(N_2 \rightsquigarrow 2N) = 2.8 \pm 0.2$ in good agreement with those derived from excitation cross-section measurements and from product yield measurement in the radiolysis of N_2–O_2 mixtures.

The dependence of exchange yields in the radiolysis of $^{28}N_2$–$^{30}N_2$ mixtures on pressure, O_2 concentration, and dose-rate has been measured. The results are consistent with a significant contribution to these yields from the isotopic exchange reaction of N^+ with N_2. They also indicate that dose-rates of the order of $> 10^{22}$ eV g^{-1} s^{-1} are required for the N_2^+ ions to contribute to the exchange yield.

A. W. BOYD, O. A. MILLER et C. WILLIS. Can. J. Chem. **56**, 147 (1978).

En mesurant les rendements en NO_2 dans des mélanges de N_2–NO, on peut évaluer que le rendement d'excitation dissociative neutre $G(N_2 \rightsquigarrow 2N)$ est de 2.8 ± 0.2; cette valeur est en bon accord avec des valeurs obtenues à partir de mesures de sections efficaces d'excitation et de mesures de rendements de produits lors de la radiolyse de mélanges de N_2–O_2.

On a pu évaluer la relation qui existe entre les rendement d'échange lors de la radiolyse de mélanges de $^{28}N_2$–$^{30}N_2$ et la pression, la concentration en O_2 et l'intensité de radiation. Les résultats sont en accord avec une interprétation impliquant une contribution importante à ces rendements provenant de la réaction d'échange isotopique de N^+ avec N_2. Ils indiquent aussi qu'il est nécessaire d'utiliser des intensités de l'ordre de $> 10^{22}$ eV g^{-1} s^{-1} pour que les ions N_2^+ contribuent au rendement d'échange.

[Traduit par le journal]

Introduction

Two major uncertainties remain in the radiation chemistry of nitrogen (1). Firstly, the yield of neutral dissociative excitation is based on two rather indirect measurements: a value of $G(N_2 \rightarrow 2N) = 2.5 \pm 0.5$ has been derived (1) from the total dissociative excitation cross section measured by heterogeneous absorption of N-atoms (2); a value of $G(N_2 \rightarrow 2N) = 2.9 \pm 0.2$ has been deduced from product yields in the radiolysis of N_2–O_2 mixtures (3). Secondly, the observed exchange yields in the radiolysis of $^{28}N_2$–$^{30}N_2$ mixtures (4–7) are apparently mechanistically inconsistent with the yields of ions and excited states (1). In the absence of isotope effects, in the irradiation of an equimolal mixture of $^{28}N_2$ and $^{30}N_2$ half of the molecules formed by N-atoms will be $^{29}N_2$ and thus the exchange yield is defined as $G(\text{exch.}) = 2G(^{29}N_2)$. Experimental measurements give $G(\text{exch.})$ in the range 7.3 to 9.5 (4–7) for pressures in the range 13 to 53 kPa, doses in the range 6×10^{20} to 1.5×10^{22} eV g^{-1} and for dose-rates from 10^{15} to 10^{17} eV g^{-1} s^{-1}. The most reliable value appears to be $G(\text{exch.}) = 7.5 \pm 0.5$ (5, 7). The primary ionization yields in the radiolysis of nitrogen can be derived by combining cross-section measurements with the W-value to give $G(N_2 \rightarrow N_2^+ + e) = 2.2$;

[1]Issued as AECL 6004 and as NRCC 16312.

Can. J. Chem. Downloaded from www.nrcresearchpress.com by 210.87.254.40 on 09/05/12
For personal use only.

$G(N_2 \rightarrow N^+ + N + e) = 0.7$ (1). The primary neutral dissociation yield as discussed above can be taken to be $G(N_2 \rightsquigarrow 2N) = 2.7 \pm 0.3$. At the dose-rates used in these studies (4–7) it is very unlikely that N_2^+ will contribute to the total N-atom yield. Once it has undergone the rapid clustering reaction to form N_4^+ (8), its lifetime with respect to charge neutralization is so long that it will undergo charge exchange with impurities in the system. The N^+ primary ion will cluster to give N_3^+ (8) and either on charge transfer or charge neutralization, this should give just one N-atom. On the basis of these arguments the total N-atom yield should be:

$$G(N)_{total} = 2G(N_2 \rightsquigarrow N^+ + N + e) + 2G(N_2 \rightsquigarrow 2N)$$
$$= 2 \times 0.7 + 2 \times 2.7 \pm 0.3 = 6.8 \pm 0.6$$

Thus G(exch.) should be in the range 3.1 to 3.7. Clearly this prediction is at variance with the experimental yields.

Since the experimental exchange yields were reported and our review written the rate constant for isotopic exchange of N^+ with N_2 has been published (9).

[1] $$^{15}N^+ + {}^{28}N_2 \rightarrow {}^{14}N^+ + {}^{29}N_2$$
or
$$^{14}N^+ + {}^{30}N_2 \rightarrow {}^{15}N^+ + {}^{29}N_2$$
$$k_1 = 3.3 \times 10^{-10} \text{ cm}^3 \text{ molecule}^{-1} \text{ s}^{-1}$$

Including reaction 1 in the exchange mechanism leads to a chain reaction. This possibility had previously been ruled out because of the observed lack of dose-rate dependence on the exchange yields. However, the chain length will be determined not only by reaction 1, the propagation step, but also by reaction 2 which will presumably be the termination step.

[2] $$N^+ + 2N_2 \rightarrow N_3^+ + N_2$$
$$k_2 = 5 \times 10^{-29} \text{ cm}^6 \text{ molecule}^{-2} \text{ s}^{-1} \text{ (8)}$$

Simple kinetic considerations lead to expression [3]

[3] $$G(\text{exch.})_{N^+ \text{ chain}} = 2G(N_2 \rightsquigarrow N^+ + N + e) \cdot k_1/k_2[N_2]$$

for the contribution of this process to the exchange yield. Since this expression is derived from terms which are all first order in the concentration of primary species the contribution to the exchange yield should be independent of dose-rate. There are some qualitative uncertainties in the above treatment, for example the three body limit of reaction 2 is not known, but, as will be discussed, it does provide at least a partial explanation for the observed high exchange yield.

We have measured the yield of the neutral dissociation process by a more direct method and we have investigated the contribution of reaction 1 to the radiolytic exchange by varying the pressure and by the use of additives.

Experimental

Dosimetry

A single dosimeter system, N_2O containing 1 mol% SF_6, was used for the Gammacell, Van de Graaff, and linear accelerator irradiations so that all the data would be as self-consistent as possible. The initial yield from this mixture, $G(N_2) = 8.0$ (10–12), is independent of dose-rate over the range 10^{16}–10^{28} eV g^{-1} s^{-1}. The absorbed dose in the $^{28}N_2$–$^{30}N_2$ sample irradiations with the linear accelerator and the Van de Graaff was obtained by monitoring with a secondary electron counter which was then normalized against the N_2O–SF_6 dosimeter system. To reduce any error due to this monitoring the N_2O–SF_6 dosimeters were given doses in the range 5×10^{20} to 2×10^{21} eV g^{-1}. As the yields of N_2 from N_2O–SF_6 at these high doses have not been previously reported they were determined by irradiations of this dosimeter in the Gammacell. The results are given in Table 1.

Irradiations

Gammacell-220 (CRNL)

Samples were irradiated in Pyrex cells either 1 cm or 4 cm in diameter (volumes ~10 and ~100 cm^3 respectively). The absorbed dose-rate was 2.5×10^{16} eV g^{-1} s^{-1}.

Van de Graaff (CRNL)

In the present experiments we used pulses 1 μs long of 2.25 MeV electrons at a frequency of 20 Hz. Samples were contained in Pyrex cells 0.8 cm diameter, 10 cm long fitted with 0.05 cm thick windows. The absorbed dose per pulse was 2×10^{17} eV g^{-1} giving a dose-rate of 2×10^{23} eV g^{-1} s^{-1}.

Linear Accelerator (NRCC)

With this source we used pulses 40 ns long of 35 MeV electrons at a frequency of 720 Hz. Sample cells were similar to those used with the Van de Graaff. The absorbed dose per pulse was 2.5×10^{17} eV g^{-1} giving a dose-rate of 6×10^{24} eV

TABLE 1. Dose dependence of nitrogen yields from Gammacell irradiations of N_2O-1% SF_6 mixtures

Time (h)	Dose[a] (eV g^{-1}/10^{20})	Amount of N_2 per g of N_2O (molecules/10^{18})	$G(N_2)$
1	0.918	7.22	8.0
2	1.82	14.30	8.0
3	2.73	21.93	8.0
4	3.64	29.07	8.0
5	4.56	37.8	8.0
6	5.46	43.33	8.0
7	6.38	48.32	7.58
8	7.29	54.57	7.49
10.67	9.71	62.41	7.05
16	14.58	92.90	6.38
20	18.22	109.8	6.03
22.5	20.5	125.5	6.13
30	27.33	168.5	6.17
40	36.4	215.8	5.92
61.5	56.0	326.3	5.83
87	79.3	431.5	5.44
106	96.6	524.3	5.42

[a]Calculated from first 6 values using $G(N_2) = 8.0$ (10, 12) as the rates of N_2 production of these are the same.

Can. J. Chem. Downloaded from www.nrcresearchpress.com by 210.87.254.40 on 09/05/12
For personal use only.

g^{-1} s^{-1}. Because of the high rate of energy deposition the temperature of the samples rose some 200–300°C during irradiation. Previous work (13) has shown that exchange yields in nitrogen are independent of temperature in the range 300–1300 K so that this temperature excursion should not be significant.

Febetrons (CRNL)

Both a Febetron 705 and a Febetron 706 were used. The samples were irradiated in quartz cells 4 cm diameter × 7 cm long for the 705 and 2.5 cm diameter × 2 cm long for the 706 with both cells having 0.05 cm windows. The absorbed doses per pulse in these cells from N_2O dosimetry $G(N_2) = 12.4$ (10, 14, 15) were 1×10^{20} eV g^{-1} ($\sim 2 \times 10^{27}$ eV g^{-1} s^{-1}) and 7.2×10^{19} eV g^{-1} ($\sim 2 \times 10^{28}$ eV g^{-1} s^{-1}) for the 705 and 706 respectively.

Materials and Analyses

The $^{28}N_2$–$^{30}N_2$ mixture was prepared using nitrogen supplied by Monsanto with a specified ^{15}N content of > 99% and a purity > 99.99%. This was mixed with Matheson research grade nitrogen. Analysis of this mixture gave $^{28}N_2$ 48.5%, $^{29}N_2$ 1.2%, $^{30}N_2$ 50.3%. Because there was some uncertainty regarding the oxygen content of samples in some experiments the substrate was exposed to a sodium mirror before irradiation. These experiments gave results which were indistinguishable from those where no exposure to a sodium mirror was made.

The O_2, SF_6, NO, and N_2O were all obtained from Matheson. The SF_6 and N_2O were freed of permanent gases. The NO was freed from NO_2 and N_2O_3 by distillation at 195 K and from N_2O by passing through 3A molecular sieve.

Isotopic analysis was done with a CEC-2-610 mass spectrometer.

The NO_2 formed in the N_2–NO mixtures was determined measuring its optical density after all NO had been removed by low temperature distillation to prevent formation of N_2O_3. A Cary 17 spectrophotometer was used and the extinction coefficients were taken from ref. 16. Corrections were made for the equilibrium $2NO_2 \rightleftharpoons N_2O_4$.

Results

Yield of N-atoms in Radiolysis of Nitrogen

The primary yield of N-atoms was determined by irradiating mixtures of nitrogen with added NO in the Gammacell. All samples contained 0.5 mol% SF_6 which was added to eliminate the possibility of charge neutralization yielding any N-atoms. The measured yields of NO_2 given in Table 2 are independent of dose and of the concentration of NO in the range 2–4%.

Exchange Yields

The calculation of the exchange yields was done as described previously (4–6).

Gammacell Irradiations

Preliminary experiments with 1-cm diameter cells gave results with a good deal of scatter at pressures below 13 kPa both with and without the addition of O_2. This was attributed to the importance of wall effects and impurities at these low pressures and we attempted to lessen the effects by using larger diameter cells in subsequent experiments. The exchange yields for both sets of irradiations are given in Table 3. In agreement with previous work (4, 5) the yields are decreased by the addition of O_2. Only one previous measurement at pressures below 13 kPa has been reported: at 4.4 kPa G(exch.) = 11 (5) which is 15% higher than the value found by the same authors at 13 to 50 kPa.

TABLE 2. Yields of NO_2 in the Gammacell radiolysis of N_2–NO–SF_6 mixtures absorbed dose-rate 2.5×10^{16} eV g^{-1} s^{-1}

Pressure[a] (kPa)			
N_2	NO	Dose (10^{20} eV)	$G(NO_2)$
93	1.9	1.87	6.04
93	3.8	1.87	5.68
93	1.9	3.75	6.84
93	1.9	3.75	6.61
93	3.8	3.75	6.31
93	3.8	11.2	6.37
Average $G(NO_2) = 6.31 \pm 0.4$			

[a]Each sample contained 0.5 kPa SF_6.

TABLE 3. Exchange yields from the Gammacell irradiation[a,b] of $^{28}N_2$–$^{30}N_2$ mixtures

	Sample composition		
Cell	N_2 (kPa)	O_2 (kPa)	G(exch.)[c]
1-cm diameter	0.6	0	7.9
	1.2	0	9.5
	1.3	0	9.1
	2.5	0	11.4
	2.7	0	9.3
	4.0	0	9.5
	5.3	0	11.1
	6.7	0	9.1
	8.0	0	8.9
	25	0	7.6 ± 0.5[d]
	25	0.025	4.6
	25	0.25	4.7
	25	0.5	4.4
	25	1.25	2.2
	2.5	1.25	0.6
4-cm diameter	0.67	0	16.8
	1.33	0	15.2
	5.3	0	13.6
	6.7	0	12.2
	8.0	0	11.6
	9.3	0	11.5
	10.7	0	11.4
	13.3	0	11.1
	19.3	0	10.3
	25.3	0	9.7
	30.9	0	9.2
	37.5	0	9.4

[a]Absorbed dose-rate 2.5×10^{16} eV g^{-1} s^{-1}.
[b]All samples irradiated to a total absorbed dose of $5–9 \times 10^{21}$ eV g^{-1}.
[c]Calculated based upon the energy absorbed by the entire gas sample.
[d]Average of 3 experiments.

Can. J. Chem. Downloaded from www.nrcresearchpress.com by 210.87.254.40 on 09/05/12
For personal use only.

Van de Graaff and Linear Accelerator

The results of these irradiations are given in Table 4. The scatter in the results at low pressures is again attributed to wall effects and impurities.

Febetrons

The yields in the Febetron irradiations which were expected to be the same as those with the Van de Graaff and linear accelerator are given in Table 5. Possible explanations for the anomalously high values observed are given at the end of the discussion.

Discussion

To provide a basis for the discussion of the results the rate constants for reactions that can take place in the mixtures we have irradiated are listed in Table 6. The lifetimes of ions and atoms under various conditions derived from these rate constants are given in Table 7.

Yields of NO_2 in the N_2–NO–SF_6 Mixtures

At low doses all N-atoms produced in these mixtures should undergo reaction with NO,

[28] $$N + NO \rightarrow N_2 + O$$

and, the O-atoms produced should react to give NO_2 by reaction 29.

[29] $$O + NO + N_2 \rightarrow NO_2 + N_2$$

At larger doses, the concentration of NO_2 may be high enough to give back reactions and make the interpretation of the yields difficult; however, the lack of dependence of our values on dose (Table 2) shows that sufficiently low doses were maintained. The data given in the table also show that amounts of O_2 in the samples did not contribute significantly to the NO_2 levels measured at low doses.

The situation as regards reaction of ionic species is not quite so clear. There should be no contribution to the NO_2 yield from N_2^+ ions. In these mixtures, N_2^+ will cluster to form N_4^+ (8) and by analogy with other reactions of N_4^+, this can be expected to undergo charge transfer with NO, reaction 18′.

[18′] $$N_4^+ + NO \rightarrow NO^+ + 2N_2$$

Dissociative neutralization of NO^+ is suppressed by the addition of SF_6.[2]

The N^+ ions will first form N_3^+, reaction 2, which can then react with NO,

[16] $$N_3^+ + NO \rightarrow N_2O^+ + N_2$$

[17] $$N_3^+ + NO \rightarrow NO^+ + N_2 + N$$

$$k_{16} + k_{17} = 1.4 \times 10^{-10}\ \text{cm}^3\ \text{molecule}^{-1}\ \text{s}^{-1}$$

As pointed out in ref. 23, $k_{16} + k_{17}$ is much smaller than the limiting Langevin simple charge transfer rates which suggests that a reaction intermediate is formed thereby favouring the more exothermic channel, reaction 16. Thus, to a fair degree of approximation, the dominant contribution to the NO_2 yield from the primary process ($N_2 \rightsquigarrow N^+ + N + e$) will be from the N-atoms formed directly. On the basis of the above arguments, the yield of NO_2 should be

$$G(NO_2) = 2G(N_2 \rightsquigarrow 2N) + G(N_2 \rightsquigarrow N^+ + N + e)$$

Taking the present value of $G(NO_2) = 6.3 \pm 0.4$ gives

$$G(N_2 \rightsquigarrow 2N) = (6.3 \pm 0.4 - 0.7)/2 = 2.8 \pm 0.2$$

This falls between the value derived from excitation cross-sections of 2.5 (1) and that deduced from product yields in N_2–O_2 radiolysis of 2.9 (3).

Exchange Yields

Gammacell Experiments

The yields obtained using 1-cm diameter cells at pressures of 13 kPa or greater give $G(\text{exch.}) = 7.5 \pm 0.5$ which is in good agreement with those of Dawes and Back (5) and Wood and Mascall (6). The results at lower pressures show an increase but with considerable scatter. The yields with the 4-cm diameter cells show a fairly consistent increase with decreasing pressure and this supports our suggestion that the variation in the small cell yields is due to wall effects and impurities.

We suggest in the Introduction that there are three main contributions to the exchange yield: that from the primary dissociative excitation giving N-atoms, that from the neutralization (or charge transfer) from

TABLE 4. Exchange yields in the Van de Graaff and linear accelerator irradiations of $^{28}N_2$–$^{30}N_2$ mixtures. Absorbed dose 3 to 12 × 10^{21} eV g^{-1}

Sample		G(exch.)	
$^{28}N_2$ (kPa)	O_2 (kPa)	Van de Graaff[a] irradiations	Linear accelerator[b] irradiations
8–100	—	10.3±0.6[c]	11.7±1[d]
6.7	—	7.8	
5.3	—	8.4	
4	—	9.3	
2.7	—	9.5	
1.3	—	13.8	
25	0.5	3±0.5	4±0.5

[a]Absorbed dose-rate 2 × 10^{23} eV g^{-1} s^{-1}.
[b]Absorbed dose-rate 6 × 10^{24} eV g^{-1} s^{-1}.
[c]Average of 14 samples with and without exposure to Na mirror.
[d]Average of 5 samples.

[2]A. W. Boyd and O. A. Miller. Unpublished results.

Can. J. Chem. Downloaded from www.nrcresearchpress.com by 210.87.254.40 on 09/05/12
For personal use only.

TABLE 5. Exchange yields from the Febetron irradiations of $^{28}N_2$–$^{30}N_2$ mixtures

Sample composition ~80 kPa $^{28}N_2$–$^{30}N_2$	Dose-rate (eV g^{-1} s^{-1})	Dose (eV g^{-1})	G(exch.)
Pure	$\sim 2\times10^{27}$	0.45×10^{22}	20 ± 1
Pure	$\sim 2\times10^{27}$	0.89×10^{22}	
Pure	$\sim 2\times10^{27}$	1.38×10^{22}	
+3.3 kPa SF_6	$\sim 2\times10^{27}$	0.83×10^{22}	10 ± 1
+3.3 kPa SF_6	$\sim 2\times10^{27}$	0.95×10^{22}	
Pure	$\sim 2\times10^{28}$	0.18×10^{22}	11 ± 0.6
Pure	$\sim 2\times10^{28}$	0.36×10^{22}	
+0.8 kPa SF_6	$\sim 2\times10^{28}$	0.72×10^{22}	15
+4 kPa SF_6	$\sim 2\times10^{28}$	0.72×10^{22}	16.6
+8 kPa SF_6	$\sim 2\times10^{28}$	0.72×10^{22}	16.6

TABLE 6. Reactions in irradiated N_2 and its mixtures with O_2, NO, and SF_6

Reaction	Rate constant (cm^3 $molecules^{-1}$ s^{-1})	Ref.
[1] $^{14}N^+ + {}^{30}N_2 \rightarrow {}^{15}N^+ + {}^{29}N_2$	$3.3\pm0.8\times10^{-10}$[a]	9
[2] $N^+ + 2N_2 \rightarrow N_3^+ + N_2$	5×10^{-29}[b]	8
[4] $N^+ + N_2 \rightarrow N_3^+$	1.3×10^{-12}[c]	8
[5] $N_2^+ + 2N_2 \rightarrow N_4^+ + N_2$	8×10^{-29}[b]	8
[6] $N_2^+ + N_2 \rightarrow N_4^+$	5×10^{-10}[d]	
[7] $N^+ + O_2 \rightarrow O_2^+ + N$	7×10^{-10}	17
[8] $N^+ + O_2 \rightarrow NO^+ + O$		
[9] $N^+ + SF_6 \rightarrow SF_5^+ + NF$	1.4×10^{-9}	18
[10] $N_2^+ + O_2 \rightarrow O_2^+ + N_2$	1×10^{-10}	19
[11] $N_4^+ + O_2 \rightarrow O_2^+ + 2N_2$	4×10^{-10}	20
[12] $N_2^+ + O_2 \rightarrow NO^+ + NO$	$<2\times10^{-13}$	19
[13] $N_2^+ + e \rightarrow 2N$	1×10^{-7}	21
[14] $N_2^+ + O_2^- \rightarrow 2N + O_2$	2×10^{-6}	21
[15] $N^+ + NO \rightarrow NO^+ + N$	8×10^{-10}	22
[16] $N_3^+ + NO \rightarrow N_2O^+ + N_2$	$k_{15}+k_{16} = 1.4\times10^{-10}$	23
[17] $N_3^+ + NO \rightarrow NO^+ + N_2 + N$		
[18] $N_2^+ + NO \rightarrow NO^+ + N_2$	5×10^{-10}	24
[19] $O_2^+ + NO \rightarrow NO^+ + O_2$	7.2×10^{-10}	22
[20] $e + 2O_2 \rightarrow O_2^- + O_2$	2×10^{-30}[b]	25
[21] $e + 2NO \rightarrow NO^- + NO$	1.3×10^{-31}[b]	26
[22] $e + SF_6 \rightarrow SF_6^-$	2.2×10^{-7}	27
[23] $NO^- + NO_2 \rightarrow NO_2^- + NO$	7.4×10^{-10}	28
[24] $O_2^- + NO_2 \rightarrow NO_2^- + NO$	1.5×10^{-9}	29
[25] $NO_2^- + NO_2 \rightarrow NO_3^- + NO$	4×10^{-12}	30
[26] $N + N + N_2 \rightarrow 2N_2$	5×10^{-33}[b]	31
[27] $N + O_2 \rightarrow NO + O$	1×10^{-16}	32
[28] $N + NO \rightarrow N_2 + O$	2.2×10^{-11}	33
[29] $O + NO + M \rightarrow NO_2 + M$	7×10^{-32}[b]	34
[30] $O + NO_2 \rightarrow NO + O_2$	9×10^{-12}	35
[31] $O + NO_2 + M \rightarrow NO_3 + M$	8×10^{-32}[b]	36
[32] $N + NO_2 \rightarrow N_2O + O$	7.7×10^{-12}	37
[33] $N + NO_2 \rightarrow 2NO$	5.9×10^{-12}	37
[34] $N + NO_2 \rightarrow N_2 + 2O$	2.3×10^{-12}	37
[35] $N + NO_2 \rightarrow N_2 + O_2$	1.8×10^{-12}	37

[a]This is the more recent value of ref. 9*b*.
[b]Three body rate constants (cm^6 $molecules^{-2}$ s^{-1}).
[c]The data in (8) are also consistent with this 2-body rate constant over the pressure range used.
[d]Assumed value above 25 kPa.

the primary N^+ ion, and that arising from the N^+-chain sequence.

From our N_2–NO measurements and the previous measurements of $G(N_2 \rightsquigarrow 2N)$ the contribution of the first of these to the exchange yield is

$$G(\text{exch.})_{\text{N atoms}} = (6.3 \pm 0.4)/2$$

The value of $G(N^+) = 0.7$ gives

$$G(\text{exch.})_{N^+} = 0.7/2$$

The contribution of the N^+ chain is then the difference between the observed G(exch.) and the above two values

Can. J. Chem. Downloaded from www.nrcresearchpress.com by 210.87.254.40 on 09/05/12
For personal use only.

TABLE 7. Ion and atom lifetimes in irradiated nitrogen at 100 kPa

Species	Reaction	Conditions	Lifetime (s)
N_2^+	$N_2^+ + 2N_2 \rightarrow N_4^+ + N_2$		8×10^{-11}
N_2^+	$N_2^+ + e \rightarrow N + N$	2×10^{27} to 2×10^{28} eV g^{-1} s^{-1}	5 to 15×10^{-9}
N_4^+	$N_4^+ + O_2 \rightarrow 2N_2 + O_2^+$	10 ppm O_2	10^{-5}
N_4^+	$N_4^+ + e \rightarrow 2N + N_2$	2.5×10^{16} eV g^{-1} s^{-1}	10^{-3}[a]
		2×10^{23} eV g^{-1} s^{-1}	5×10^{-7}[a]
		6×10^{24} eV g^{-1} s^{-1}	10^{-7}[a]
N	$N + N + N_2 \rightarrow 2N_2$	2.5×10^{16} eV g^{-1} s^{-1} for $G(N) = 7$	2
N	$N + O_2 \rightarrow NO + O$	10 ppm O_2	40

[a]Assuming $k_{(N_4^+ + e)} = 1 \times 10^{-6}$ cm^3 molecule^{-1} s^{-1}.

$$G(\text{exch.})_{N^+ \text{ chain}} = G(\text{exch.})_{obs} - [G(\text{exch.})_{N^+} + G(\text{exch.})_{N \text{ atoms}}]$$

Therefore,

$$G(\text{exch.})_{N^+ \text{ chain}} = G(\text{exch.})_{obs} - 3.5 \pm 0.4$$

To test the applicability of expression 3 the contribution from N^+ chain processes for both the 1-cm and 4-cm diameter cell experiments are plotted in Fig. 1 as a function of the reciprocal pressure. As we have previously stated we attribute the difference between the two sets of data as being due to impurities and we further attribute the obvious curvature in the 4-cm cell data at low pressures to increasing effects of impurities and walls.

The non-zero intercept of the plot is presumably due to the clustering reaction 2 becoming effectively 2-body. The limiting contribution of $G(\text{exch.})_{N^+ \text{ chain}} = 4.0$ gives a total $G(\text{exch.}) = 7.5$ which is in very good agreement with that of other workers already discussed. The value of the intercept suggests a high pressure limiting rate for reaction 2 of

$$k_2 \text{ (high pressure limit)} = \frac{2G(N^+)}{G(\text{exch.})_{N^+ \text{ chain}}} \times k_1$$

$$= \frac{2 \times 0.7}{4.0} \times 3.3 \times 10^{-10}$$

$$= 1.2 \times 10^{-10} \text{ cm}^3 \text{ molecule}^{-1} \text{ s}^{-1}$$

The pressures used for the measurement of the rate constant for the addition of N^+ to N_2 at 300 K (ref. 8) were 0.08 to 0.16 kPa. These gave values of k_2 in the range 4 to 6×10^{-29} cm^6 molecule^{-2} s^{-1}. The value of k_2 calculated from extrapolation of the straight line drawn in Fig. 1 to this pressure range and substituting in expression 3 is $k_2 = 4.4 \times 10^{-29}$ cm^6 molecule^{-1} s^{-1}.

We conclude that the high and low pressure extrapolations provide reasonable support for assuming that the high exchange yields arise from reaction 1.

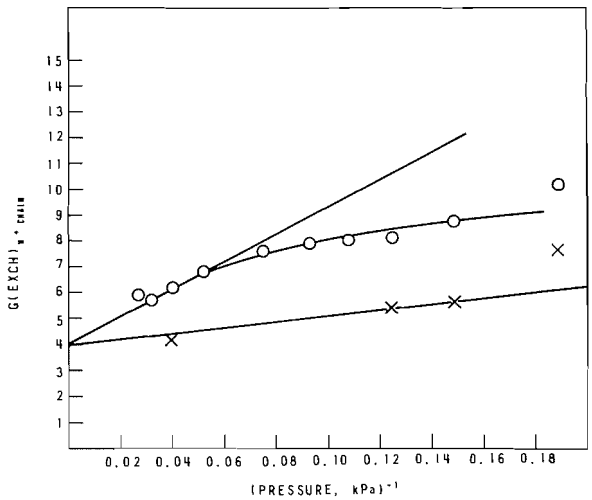

FIG. 1. Pressure dependence of the exchange yield attributed to the N^+ chain reaction. ○, 4-cm cells; ×, 1-cm cells.

O_2 Dependence

It might be hoped that the exchange yields as a function of O_2 concentration would give the contribution of reaction 1 to these yields as the rate constants for $N^+ + O_2$, reactions 7 and 8 are very much larger than that for $N + O_2$, reaction 2. However as a result of the high doses used the concentrations of NO and NO_2 became significant. The reactions of these with N^+, N_3^+, N_4^+, and N make the interpretation of the results very difficult.

It appears that all that can be said is that the effect of O_2 is not inconsistent with the proposed mechanism.

Van de Graaff and Linear Accelerator Exchange Yields

The limiting exchange yield at Gammacell dose-rates where no contribution from N_2^+ ions is expected is $G(\text{exch.})_{\text{Gammacell}} = 7.5 \pm 0.5$. The limiting value obtained in Van de Graaff irradiations is $G(\text{exch.})_{\text{VdG}} = 10.3 \pm 0.6$. The difference between these values, $\Delta G(\text{exch.}) = 2.8 \pm 0.8$ agrees within

Can. J. Chem. Downloaded from www.nrcresearchpress.com by 210.87.254.40 on 09/05/12
For personal use only.

the wide experimental error with the primary yield of N_2^+ ions of $G(N_2 \rightarrow N_2^+ + e) = 2.2$ (1). The results from the linear accelerator experiments show more scatter but are consistent with this.

The reduction in the exchange yields at lower pressures shown in Table 4 is presumably due to the sensitivity of the N_4^+ contribution to G(exch.) to very small impurity levels.

Febetron Results

From the above discussion of the yields from the irradiations with the other accelerators and the Gammacell the expected exchange yield from the Febetron irradiations of pure $^{28}N_2$–$^{30}N_2$ mixtures is G(exch.) = 10.5 ± 0.5. The addition of SF_6 should reduce this considerably as it will lead to the suppression of dissociative neutralization and will react with N^+ (reaction 18). Although the yield in pure $^{28}N_2$–$^{30}N_2$ with the Febetron 706, G(exch.) = 11 ± 0.6 is consistent with this reasoning, none of the other yields are. The yield in the pure isotopic mixture with the Febetron 705 is twice as large as expected and with 4% added SF_6 it should be less than 8 instead of the observed value of G(exch.) = 10 ± 1. Even more inconsistent is the exchange yield in the Febetron 706 irradiations which increases by about 50% on the addition of 1 to 10% SF_6.

The increase in the values in the Febetron 705 irradiations could possibly have an explanation similar to that proposed to account for the anomalously high yields in N_2O, NH_3, and the hydrogen halides with the 705 (38). In these irradiations the yields increased with decreasing pressure below ~80 kPa. We suggested that the electrons in the very intense beam were accelerated across the beam and at low pressures could attain sufficient energy to cause dissociation. It is not clear that such a mechanism occurred in the $^{28}N_2$–$^{30}N_2$ irradiations but it seems reasonable to suggest that the relative rates of reactions 1 and 2 could be changed under such extreme conditions. This does not account for the results with Febetron 706. However we have observed that in Febetron 705 irradiations of N_2O at pressures below 6 kPa the addition of SF_6 increases the amount of nitrogen produced.[3] The mechanism of this is not understood but it may involve an ionic chain reaction. A similar effect might be operating on the addition of SF_6 at the higher dose-rate of the Febetron 706.

It is obviously not possible to establish precise mechanisms for the Febetron yields. We believe though, that the anomalies are due to the sensitivity of the N^+–N_2 exchange reaction to the high intensities of the Febetron pulses. Unfortunately these results do not provide any reliable yields in irradiated nitrogen.

[3]A. W. Boyd and C. Willis. Unpublished data.

Conclusions

The yields of neutral dissociative excitation in the radiolysis of N_2 derived from cross-section measurements (1), O_3 yields in N_2–O_2 mixtures (3), and NO_2 yields in N_2–NO mixtures (this work) are in good agreement and give $G(N_2 \rightsquigarrow 2N) = 2.7 \pm 0.2$.

The high exchange yield in the radiolysis of $^{28}N_2$–$^{30}N_2$ mixtures which was previously thought to be contrary to primary yield data can be explained by the exchange reaction between N^+ ions and N_2 molecules. The pressure dependence of this yield suggests that the three body limit of the addition of N^+ to N_2 is above 30 kPa.

The increase in the exchange yield between dose-rates of 10^{16} eV g^{-1} s^{-1} and 10^{23} eV g^{-1} s^{-1} is consistent with the yield of N_2^+ ions and the lifetimes of the ions with respect to possible O_2 impurities and neutralization.

Acknowledgements

We are most grateful to W. A. Seddon and F. C. Sopchyshyn for carrying out the Van de Graaff irradiations and to H. A. Gillis for the linear accelelator irradations.

1. C. Willis and A. W. Boyd. Int. J. Radiat. Phys. Chem. **8**, 71 (1976).
2. H. F. Winters. J. Chem. Phys. **44**, 1472 (1966).
3. C. Willis, A. W. Boyd, and M. J. Young. Can. J. Chem. **48**, 1515 (1970).
4. M. Anbar and P. Perlstein. J. Phys. Chem. **68**, 1234 (1964).
5. D. H. Dawes and R. A. Back. J. Phys. Chem. **69**, 2385 (1965).
6. C. J. Wood and R. A. Mascall. J. Chem. Soc. Faraday Trans. I, **71**, 1678 (1975).
7. J. A. Mahoney. Ph.D. Thesis. Princeton University, NJ. 1968.
8. A. Good, D. A. Durden, and P. Kebarle. J. Chem. Phys. **52**, 212 (1970).
9. (*a*) F. C. Fehsenfeld, D. L. Albritton, Y. A. Bush, P. G. Fournier, T. R. Govers, and J. Fournier. J. Chem. Phys. **61**, 2150 (1974); (*b*) V. G. Anicich, W. T. Huntress, Jr., and J. H. Futrell. Chem. Phys. Lett. **47**, 488 (1977).
10. C. Willis, A. W. Boyd, and D. A. Armstrong. Can. J. Chem. **47**, 3783 (1969).
11. S. Takao, S. Shida, Y. Hatano, and H. Yamagashi. Bull. Chem. Soc. Jpn. **41**, 2221 (1968).
12. C. Willis, A. W. Boyd, and P. E. Bindner. Can. J. Chem. **50**, 1557 (1972).
13. R. K. Lyon. Can. J. Chem. **50**, 1437 (1972).
14. C. Willis, O. A. Miller, A. E. Rothwell, and A. W. Boyd. Adv. Chem. Ser. **81**, 539 (1968).
15. C. Willis, A. W. Boyd, and O. A. Miller. Radiat. Res. **46**, 428 (1971).
16. T. C. Hall, Jr. and F. E. Blacet. J. Chem. Phys. **20**, 1745 (1952).

17. A. L. FARRAGHER. Trans. Faraday Soc. **66**, 1411 (1970).
18. F. C. FEHSENFELD. J. Chem. Phys. **54**, 438 (1971).
19. E. W. MCDANIEL, V. CERMAK, A. DALGARNO, E. E. FERGUSON, and L. FRIEDMAN. *In* Ion molecule reactions. Wiley, New York, NY. 1970.
20. D. B. DUNKIN, F. C. FEHSENFELD, A. L. SCHMELTEKOPF, and E. E. FERGUSON. J. Chem. Phys. **54**, 3817 (1971).
21. E. E. FERGUSON. Adv. Electron. Electron Phys. **24**, 1 (1968).
22. P. D. GOLDAN, A. L. SCHMELTEKOPF, F. C. FEHSENFELD, H. I. SCHIFF, and E. E. FERGUSON. J. Chem. Phys. **44**, 4095 (1966).
23. W. LINDINGER. J. Chem. Phys. **64**, 3720 (1976).
24. P. WARNECK. J. Geophys. Res. **72**, 1651 (1967).
25. J. L. PACK and A. V. PHELPS. J. Chem. Phys. **44**, 1870 (1966).
26. C. S. WELLER and M. A. BIONDI. Phys. Rev. **172**, 198 (1968).
27. F. C. FEHSENFELD. J. Chem. Phys. **53**, 2000 (1970).
28. M. MCFARLAND, D. B. DUNKIN, F. C. FEHSENFELD, A. L. SCHMELTEKOPF, and E. E. FERGUSON. J. Chem. Phys. **56**, 2358 (1972).
29. J. A. RUTHERFORD and B. R. TURNER. J. Geophys. Res. **72**, 3795 (1967).
30. F. C. FEHSENFELD, E. E. FERGUSON, and D. K. BOHME. Planet. Space Sci. **17**, 1759 (1969).
31. M. A. A. CLYNE and D. H. STEDMAN. J. Phys. Chem. **71**, 3071 (1967).
32. A. S. VLASTERAS and C. A. WINKLER. Can. J. Chem. **45**, 2837 (1967).
33. L. F. PHILLIPS and H. I. SCHIFF. J. Chem. Phys. **36**, 1509 (1962).
34. K. H. BECKER, W. GROTH, and D. THRAN. Chem. Phys. Lett. **15**, 215 (1972).
35. A. A. WESTENBERG and N. DEHAAS. J. Chem. Phys. **50**, 707 (1969).
36. A. B. HARKER and H. S. JOHNSTON. J. Phys. Chem. **77**, 1153 (1973).
37. L. F. PHILLIPS and H. I. SCHIFF. J. Chem. Phys. **42**, 3171 (1965).
38. A. W. BOYD, D. A. ARMSTRONG, C. WILLIS, and O. A. MILLER. Radiat. Res. **40**, 255 (1969).

Can. J. Chem. Downloaded from www.nrcresearchpress.com by 210.87.254.40 on 09/05/12
For personal use only.

An aid to the interpretation of electrochemical data measured with spherical and cylindrical electrodes: corrections to the Cottrell equation

NAROTTAM P. BANSAL[1] AND JAMES A. PLAMBECK

Department of Chemistry, University of Alberta, Edmonton, Alta., Canada T6G 2G2

Received June 17, 1977

NAROTTAM P. BANSAL and JAMES A. PLAMBECK. Can. J. Chem. **56**, 155 (1978).

An analysis of the theoretical correction factors for diffusion toward spherical and cylindrical electrodes has been made. The Cottrell equation is a limiting case for spherical and cylindrical diffusion and is accurate only when both $D^{1/2}/r_0$ and t are small.

NAROTTAM P. BANSAL et JAMES A. PLAMBECK. Can. J. Chem. **56**, 155 (1978).

On a effectué une analyse des facteurs théoriques de corrections pour la diffusion vers des électrodes sphériques et cylindriques. L'équation de Cottrell est un cas limite pour les diffusions sphériques et cylindriques et n'est exacte que lorsque $D^{1/2}/r_0$ et t sont petits en même temps.
[Traduit par le journal]

Introduction

The effect of electrode sphericity and cylindricity upon chronopotentiometric results has been reported (1, 2) as modifications of the Sand equation. For a chronopotentiometric process controlled by semi-infinite linear diffusion at a planar electrode, the time dependence of the current is described by the Cottrell (3) equation. The Cottrell equation predicts that, under conditions of semi-infinite linear diffusion, the current decays as $t^{-1/2}$ and the quantity $It^{1/2}$ should be constant at all times after application of the potential step. For linear diffusion, the area from which the electroactive substance can diffuse is independent of the thickness of the diffusion layer, while for spherical and cylindrical diffusion the area from which material can diffuse constantly increases with time as the diffusion layer extends further into the solution; thus $It^{1/2}$ continues increasing with time.

For diffusion towards a spherical electrode such as the hanging mercury drop electrode (hmde) a ratio of the spherical diffusion current I_{sph} (4) to the linear Cottrell diffusion current I_{lin} yields

$$[1] \qquad I_{sph}/I_{lin} = 1 + \pi^{1/2}t^{1/2}D^{1/2}/r_0$$

The second term on the right-hand side, henceforth called R, is the relative difference between spherical and linear diffusion and is a function of time t, diffusion coefficient D, and electrode radius r_0.

For cylindrical diffusion, as to a wire electrode, the ratio of the cylindrical diffusion current I_{cyn} (4) to the Cottrell diffusion current yields

$$[2] \qquad I_{cyn}/I_{lin} = 1 + \pi^{1/2}t^{1/2}\frac{D^{1/2}}{r_0'} \times [\tfrac{1}{2} - \tfrac{1}{4}(\phi/\pi)^{1/2} + \tfrac{1}{8}\phi + \ldots]$$

where r_0' and A are the radius and area of the cylindrical electrode, ϕ represents the dimensionless quantity $Dt/r_0'^2$, and the other terms have the same significance as in [1]. Excluding unity, the right-hand side, henceforth called R', is the relative difference between linear and cylindrical diffusion and is a function of t, D, and r_0'.

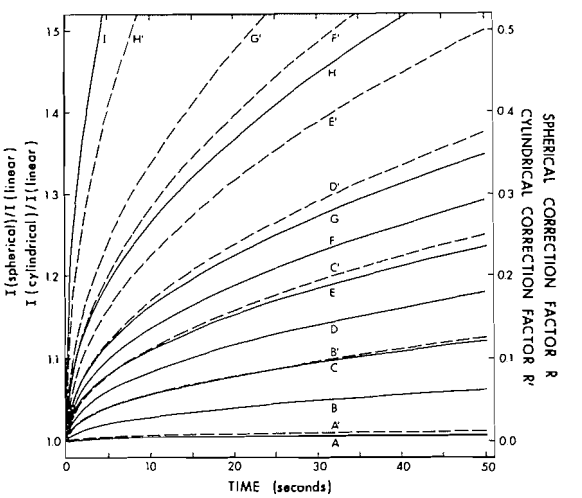

FIG. 1. Ratios of spherical and cylindrical to linear currents and the correction factors R and R' for spherical and cylindrical electrodes as a function of electrolysis time for various selected values of $D^{1/2}/r_0$ ($s^{-1/2}$): A,A', 0.001; B,B', 0.01; C,C', 0.020; D,D', 0.030; E,E', 0.040; F,F', 0.050; G,G', 0.060; H,H', 0.10; I, 0.30; solid line, cylindrical; dashed line, spherical diffusion.

[1]On leave of absence from Department of Chemistry, Ramjas College, University of Delhi, Delhi-110 007 (India).

Can. J. Chem. Downloaded from www.nrcresearchpress.com by 210.87.254.5 on 09/05/12
For personal use only.

Results and Discussion

The values of the correction factors R and R' were calculated using the AMDAHL 470/V6 computer system and have been deposited in the Depository of Unpublished Data.[2] Plots of the ratio I_{sph}/I_{lin} and I_{cyn}/I_{lin} as a function of the electrolysis time t for a few selected values of $D^{1/2}/r_0$ are depicted in Fig. 1. The value of R is approximately, but not exactly, twice that of R' for the same values of the experimental parameters; this is because the first term in the square brackets of [2] is the most significant.

By a judicious choice of the experimental conditions, the effect of sphericity or cylindricity can be made negligible. For example, to make the correction R or R' less than 0.01 (1%), r_0 and r_0' must be greater than 0.53 and 0.26 cm for $D = 10^{-5}$ cm^2/s and electrolysis times of 1 s. Since $D \leq 10^{-5}$ cm^2/s for most species in media of analytical interest, chronoamperometric measurements made with spherical or cylindrical electrodes of practical and usual size will differ significantly from those calculated using the simple Cottrell equation.

[2]Copies of material on deposit may be obtained, at a nominal charge, from the Depository of Unpublished Data, CISTI, National Research Council of Canada, Ottawa, Ont., Canada K1A 0S2.

Acknowledgement

This work was supported by the National Research Council of Canada through an operating grant (to J.A.P.).

1. B. J. Welch, H. C. Gaur, A. K. Adya, and R. K. Jain. Indian J. Chem. **14A**, 150 (1976).
2. D. H. Evans and J. E. Price. J. Electroanal. Chem. **5**, 77 (1963).
3. F. G. Cottrell. Z. Phys. Chem. **42**, 385 (1902).
4. P. Delahay. New instrumental methods in electrochemistry. Interscience, New York, NY. 1954. pp. 61 and 69.

Can. J. Chem. Downloaded from www.nrcresearchpress.com by 210.87.254.5 on 09/05/12
For personal use only.

Metal complexes as antioxidants. V. Inhibition of hydrocarbon autoxidation by cupric complexes of dialkyldithiophosphoric and dialkyldithiocarbamic acids[1]

J. H. B. CHENIER, J. A. HOWARD,[2] AND J. C. TAIT[3]

Division of Chemistry, National Research Council of Canada, Ottawa, Ont., Canada K1A 0R9

Received May 2, 1977

J. H. B. CHENIER, J. A. HOWARD, and J. C. TAIT. Can. J. Chem. **56**, 157 (1978).

Liquid-phase reactions of alkylperoxy radicals with cupric complexes of dialkyldithiophosphoric and dialkyldithiocarbamic acids have been examined. These complexes have been shown to be extremely efficient peroxy radical scavenging antioxidants for hydrocarbon autoxidation. Initial rates of oxygen absorption by typical hydrocarbons were extremely slow implying inhibition rate constants $>10^6\ M^{-1}\ s^{-1}$. The initial rate of disappearance of the dithiocarbamate was equal to the rate of chain initiation (R_i) whereas the rate of disappearance of the dithiophosphate was twice as fast as R_i. In both cases the rate of complex disappearance slowed down as the complex was consumed. Autoxidation of styrene commenced as soon as the complex disappeared while cumene did not absorb oxygen for a considerable length of time after complex destruction. Cumylperoxy radicals were converted to α-cumyl alcohol, α-methylstyrene, and acetophenone by reaction with these complexes and the copper ions were eventually precipitated as copper sulphate. In the case of the dithiocarbamate three intermediate cupric complexes were detected by epr spectroscopy.

J. H. B. CHENIER, J. A. HOWARD et J. C. TAIT. Can. J. Chem. **56**, 157 (1978).

On a étudié les réactions en phase liquide des radicaux alkylpéroxy avec des complexes cuivriques d'acides dialkyldithiophosphorique et dialkyldithiocarbamique. On a montré que ces complexes sont des antioxydants extrêmement efficaces pour piéger les radicaux péroxy responsables de l'autoxydation des hydrocarbures. Les vitesses initiales d'absorption d'oxygène par des hydrocarbures typiques sont entrêmement lentes; ce qui implique des constantes de vitesse d'inhibition supérieures à $10^6\ M^{-1}\ s^{-1}$. Le taux initial de disparition du dithiocarbamate est égal à la vitesse d'initiation de la chaîne (R_i) alors que le taux de disparition du dithiophosphate est deux fois plus grand que R_i. Dans chacun des cas, la vitesse de disparition du complexe est ralentie à mesure que le complexe est consumé. L'autoxydation du styrène commence aussitôt que le complexe est disparu alors que l'absorption d'oxygène par le cumène ne commence que longtemps après la destruction du complexe. Les radicaux cumylpéroxy sont transformés en alcool α-cumylique, en α-méthylstyrène et en acétophénone par réaction avec ces complexes et les ions cuivriques précipitent éventuellement sous forme de sulfate de cuivre. Dans le cas du dithiocarbamate, on a pu détecter trois complexes intermédiaires par spectroscopie rpe.

[Traduit par le journal]

Introduction

Zinc and nickel complexes of dialkyldithiophosphoric acids, $[(RO)_2PS_2]_2M$, and dialkyldithiocarbamic acids, $[R_2NCS_2]_2M$, where M is Zn or Ni and R is CH_3, C_2H_5, i-C_3H_7, etc., are reasonably efficient alkylperoxy radical (R'OO·) scavenging antioxidants (1–3). Inhibition rate constants (k_{inh}) fall in the range 10^3–$10^4\ M^{-1}\ s^{-1}$ with the nature of the transition metal and ligand having no obvious influence on antioxidant activity. The principal peroxy radical derived product is the alcohol, R'OH, while the transition metal ion is eventually precipitated as the sulphate.

The related cupric complexes also inhibit autoxidation (4–7) and in this paper we report the results of an investigation of the inhibition kinetics for these complexes and a product study of their reaction with alkylperoxy radicals.

Experimental

The preparation of the cupric complexes, purification of the oxidizable substrates and solvents, procedures used to measure rates of autoxidation, induction periods, cupric complex concentrations, and volatile reaction product analyses have been described in previous papers in this series (1, 2, 8). Bis(dimethyldithiocarbamoyl) disulphide was prepared by oxidation of sodium dimethyldithiocarbamate (Aldrich) with ammonium persulphate. The crude product was recrystallized from methanol–benzene, mp 157–161°C. *tert*-Butylperoxy and α-cumylperoxy radicals were prepared by photolysis of 2,2,4,4-tetramethyl-3-pentanone (Chemical Samples Co.) and thermolysis of azocumene (50°C), respectively, in air saturated solvent.

Liquid chromatography was conducted on a Spectra-Physics (3500) chromatograph employing a 2.1 × 20 cm column packed with 5 μ Spherisorb and a uv detector (SP 8200). The eluting solvent was hexane–chloroform (5:1) at a flow rate of 1 $cm^3\ min^{-1}$.

[1]NRCC No. 16303.

[2]To whom correspondence should be addressed.

[3]NRCC Research Associate.

Can. J. Chem. Downloaded from www.nrcresearchpress.com by 210.87.254.6 on 09/05/12
For personal use only.

Can. J. Chem. Downloaded from www.nrcresearchpress.com by 210.87.254.6 on 09/05/12
For personal use only.

Results and Discussion

(i) Inhibition of Hydrocarbon Autoxidation Kinetics

We have previously suggested (1, 2) that *initial* rates of oxygen absorption by hydrocarbons (tetralin, styrene, cumene, etc.) containing a free-radical initiator (α,α′-azobisisobutyronitrile) and zinc and nickel complexes of dialkyldithiocarbamic and dialkyldithiophosphoric acids (A) at 30–50°C are approximately described by the rate expression

$$[1] \qquad \left(\frac{-\mathrm{d}[O_2]}{\mathrm{d}t}\right) = \frac{k_p[RH]R_i}{nk_{inh}[A]_0} + R_i$$

where R_i is the rate of chain initiation, k_p is the propagation rate constant, k_{inh} is the termination rate constant, n is the number of peroxy radicals scavenged by each molecule of A, and the subscript zero refers to initial rates and concentrations.

This expression is consistent with a mechanism in which there is a competition for the chain propagating peroxy radicals between the hydrocarbon [2] and the complex [3]

$$[2] \qquad ROO^{\cdot} + RH \xrightarrow{k_p} ROOH + R^{\cdot}$$

$$[3] \qquad ROO^{\cdot} + A \xrightarrow{k_{inh}} X$$

$$[4] \qquad ROO^{\cdot} + X \xrightarrow{\text{fast}} \text{Non-radical products}$$

Cupric dialkyldithiophosphates and dialkyldithiocarbamates inhibit hydrocarbon autoxidation (4–7) and if the reaction mechanism is the same as that for the zinc and nickel complexes, inhibited rates of oxygen absorption should obey [1].

Recently we have suggested (8) that the reaction of peroxy radicals with these cupric complexes is best described by reactions 5–9, where A_1, A_2, A_3, and

$$[5] \qquad ROO^{\cdot} + A \xrightarrow{k_{inh}} RO^{\cdot} + A_1$$

$$[6] \qquad ROO^{\cdot} + A_1 \longrightarrow RO^{\cdot} + A_2$$

$$[7] \qquad ROO^{\cdot} + A_2 \longrightarrow RO^{\cdot} + A_3$$

$$[8] \qquad ROO^{\cdot} + A_3 \longrightarrow RO^{\cdot} + A_4$$

$$[9] \qquad ROO^{\cdot} + A_4 \longrightarrow \text{Non-radical products}$$

A_4 are oxidized forms of A. Under steady state conditions consideration of reactions 5 to 9 rather than 3 and 4 gives the rate expression [1] with $n = 1$.

Preliminary experiments on the 2,2,3,3-tetraphenylbutane (TPB) initiated autoxidation of tetralin and cumene at 30°C indicated that $Cu[(RO)_2PS_2]_2$ and $Cu[R_2NCS_2]_2$ were extremely efficient peroxy radical scavenging antioxidants. Thus rates of oxidation were very close to the rate of chain initiation at complex concentrations as low as 10^{-4} M.

Detectable differences between $(-\mathrm{d}[O_2]/\mathrm{d}t)$ and R_i were observed in styrene at 30°C. The kinetic data obtained in this substrate are given in Table 1 and presented as a plot of $(-\mathrm{d}[O_2]/\mathrm{d}t)/2[TPB]$ against [RH]/[A] in Fig. 1. The intercept of this plot on the ordinate axis should be equal to k_d, the first-order rate constant for the formation of radicals from TPB, while the slope is equal to $k_d k_p/k_{inh}$ (9). The value of the intercept for $Cu[Et_2NCS_2]_2$ and $Cu[(i\text{-}PrO)_2PS_2]_2$ is $\sim 3 \times 10^{-6}$ M^{-1} s^{-1} while $k_d = 2 \times 10^{-6}$ M^{-1} s^{-1} (10). This difference between the intercept and k_d is probably associated with the difficulties in accurately measuring initial rates rather than a mechanistic complexity. The value of $k_d k_p/k_{inh}$ from Fig. 1 is $< 10^{-11}$ s^{-1} for both complexes and since $k_p = 41$ M^{-1} s^{-1} (11) $k_{inh} > 8 \times 10^6$ M^{-1} s^{-1}.

Kinetic data for the cupric complex inhibited autoxidation of the α,α′-azobisisobutyronitrile initiated autoxidation of 9,10-dihydroanthracene at 50°C are summarized in Table 2. Equation 1 would appear to be obeyed by this system with $k_{inh} \sim 10^6$ M^{-1} s^{-1} for the dithiophosphate and $\sim 2 \times 10^6$ M^{-1} s^{-1} for the dithiocarbamate.

It is clear from these results that cupric dialkyldithiophosphates and dithiocarbamates are very efficient peroxy radical scavenging antioxidants and are significantly more efficient than the analogous zinc and nickel complexes. The rate constants for reaction with $ROO^{\cdot}$ must be greater than 10^6 M^{-1} s^{-1}. Unfortunately it is not possible to accurately determine rate constants of this magnitude by conventional kinetic studies of inhibited hydrocarbon autoxidation.

Induction Periods

The decrease in complex concentration and concentration of oxygen absorbed, as a function of time, for TPB (0.0085 M) initiated autoxidation of styrene containing $Cu[Et_2NCS_2]_2$ (1.24×10^{-4} M) are shown in Fig. 2. The rate of complex disappearance was almost linearly dependent on its concentration unlike most radical scavenging antioxidants which disappear by a zero order process at a constant rate of chain initiation. This result suggests that termination reactions other than reaction of the chain propagating peroxy radical with the complex become rate determining as the complex is consumed. The initial rate of disappearance of $Cu[Et_2NCS_2]_2$ was nearly equal to R_i indicating an *initial* stoichiometric factor of one.

The disappearance of $Cu[Et_2NCS_2]_2$ was accompanied by the appearance of the cupric transient I which we have previously observed in the reaction

Can. J. Chem. Downloaded from www.nrcresearchpress.com by 210.87.254.6 on 09/05/12
For personal use only.

TABLE 1. Kinetic data for the $Cu[(i\text{-}PrO)_2PS_2]_2$ and $Cu[Et_2NCS_2]_2$ inhibited tetraphenylbutane[a] initiated autoxidation of styrene (7.83 M) at 30°C

Ligand	$10^4[A]_0$ (M)	$10^7(-d[O_2]/dt)_{obs}$ ($M\ s^{-1}$)	10^7R_i ($M\ s^{-1}$)	$10^7(-d[O_2]/dt)_0$ ($M\ s^{-1}$)
$(i\text{-}PrO)_2PS_2$	1.25	0.51	0.37	0.14
	2.5	0.83	0.37	0.46
	5	0.64	0.37	0.27
	10	0.76	0.37	0.39
	50	0.6	0.37	0.23
	50	1.2	0.74	0.46
Et_2NCS_2	1.25	0.55	0.33	0.22
	100	0.52	0.33	0.16
$i\text{-}Pr_2NCS_2$	1.25	0.58	0.37	0.21
	5.0	0.7	0.37	0.33

[a]$[TPB]_0 = 0.008 - 0.02\ M$.

TABLE 2. Kinetic data for the $Cu[(i\text{-}PrO)_2PS_2]_2$ and $Cu[Et_2NCS_2]_2$ inhibited autoxidation of 9,10-dihydroanthracene (0.5 M)[a] at 50°C

Ligand	$10^4[A]_0$ (M)	$10^7(-d[O_2]/dt)_0$ ($M\ s^{-1}$)	Chain length	$\frac{10^{-5}k_p[RH]R_i}{[A]_0(-d[O_2]/dt)_0}$ [b] ($M^{-1}\ s^{-1}$)	$10^{-3}\tau_{O_2}$ (s)	$\frac{\tau_{O_2}R_i}{[A]_0}$
$(i\text{-}PrO)_2PS_2$	1.0	3.0	5	8	1.27	0.7
	1.5	2.1	3.5	8	—	—
	2	0.77	1.3	17	3.3	0.9
	4	0.42	0.7	15	—	—
Et_2NCS_2	0.5	—	—	—	1.4	1.6
	1.0	1.1	1.8	23	3.9	2.2
	2.0	0.7	~1	18	10.8	3.2
	4.0	~0	0	—	24	3.6

[a]Solvent: *o*-dichlorobenzene.
[b]$R_i = 2 \times 0.7 \times 2.37 \times 10^{-6} \times [AIBN]$; k_p, the homopropagation rate constant for 9,10-dihydroanthracene, at 50°C can be calculated to be 843 $M^{-1}\ s^{-1}$ from $\log(A_p/M^{-1}\ s^{-1}) = 8.5$ (12) and $k_p = 330\ M^{-1}\ s^{-1}$ at 30°C (11).

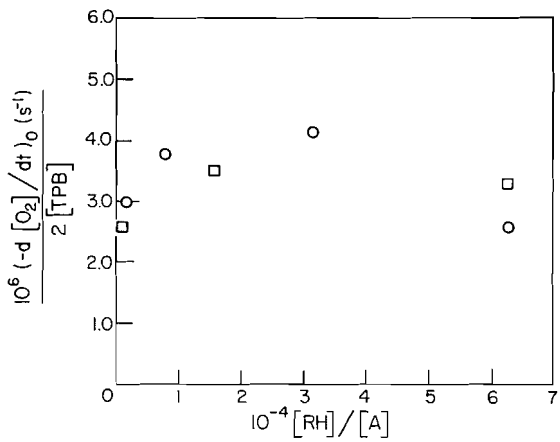

FIG. 1. Rates of oxygen absorption by styrene and TPB at 30°C inhibited by $Cu[(RO)_2PS_2]_2$ (○) and $Cu[R_2NCS_2]_2$ (□).

of this complex with *tert*-butyl hydroperoxide (8) and was also observed by Zverev *et al.* (5) during the $Cu[Et_2NCS_2]_2$ inhibited autoxidation of ethylbenzene. This transient reached a maximum concentration equal to 32% of the initial concentration of $Cu[Et_2NCS_2]_2$ when 90% of the complex had disappeared. The concentration of I then declined and two other cupric transients (II and III) were evident. I, II, and III disappeared when rapid absorption of oxygen commenced at a rate equal to the uninhibited rate.

$(-d[Cu[Et_2NCS_2]_2]/dt)_0$ was also equal to R_i in cumene but did not slow down as rapidly as in styrene. The complex was, therefore, consumed in a shorter period of time (Fig. 3). The cupric transient I was formed in this substrate, again reaching a maximum concentration when the $Cu[Et_2NCS_2]_2$ had almost disappeared. Unlike the inhibited autoxidation of styrene, oxygen absorption by cumene did not commence for a considerable length of time after both the $Cu[Et_2NCS_2]_2$ and I had disappeared. A further difference between cumene and styrene was that oxygen absorption by the former substrate, after the induction period, decreased very rapidly after the absorption of a small amount of O_2 (typically 10^{-2} M). $-d[O_2]/dt$ was then equal to R_i for a considerable length of time.

In chlorobenzene containing TPB, $-d[Cu(Et_2NCS_2)_2]/dt$ was zero order with respect to the complex concentration and I accumulated and was

TABLE 3. Induction periods and initial rates of complex disappearance for $Cu[Et_2NCS_2]_2$ inhibited autoxidation[a]

Substrate	$10^{-4}\tau_{O_2}$ (s)	$\frac{\tau_{O_2}R_i}{[A]}$	$10^8(-d[A]/dt)_0$ ($M\ s^{-1}$)	$\frac{R_i}{(-d[A]/dt)_0}$
Styrene	1.87	5.0	3.4	1.0
Tetralin	2.9	7.6	3.1	1.1
Cumene	2.6	6.9	4.4	0.74
Chlorobenzene	—	—	3.3	1.0
Styrene[b]	0.66	2.0	—	—

[a]$[A]_0 = 1.25 \times 10^{-4}\ M$; $[TPB]_0 = 0.0085\ M$, $R_i = 3.3 \times 10^{-8}\ M\ s^{-1}$.
[b]Data for the BMeOP ($1.1 \times 10^{-4}\ M$) inhibited autoxidation.

destroyed in the same way as was observed in the oxidizable substrates.

The $Cu[Et_2NCS_2]_2$ inhibited autoxidation of 9,10-dihydroanthracene at 50°C behaved just like the inhibited autoxidation of cumene at 30°C (Fig. 4). There was a very slow rate of oxygen uptake while the complex was destroyed. The rate then increased slightly and was autoretarding until the uninhibited rate was reached. During the period from complete complex destruction and rapid oxygen uptake, the concentration of cupric species was below the concentration detectable by the esr spectrometer. While the $Cu[Et_2NCS_2]_2$ was being destroyed, the transient species I was formed but its maximum concentration was much lower than the concentration detected at 30°C.

Values of the stoichiometric factor, n, for peroxy radical scavenging antioxidants, such as hindered phenols (AH), can be calculated from

$$\tau_{O_2} = n[AH]/R_i \qquad [10]$$

where τ_{O_2} is the induction period. The values of τ_{O_2} and n for $Cu[Et_2NCS_2]_2$ in styrene, tetralin, and cumene are given in Table 3 and, for comparison, the value for 2,6-di-*tert*-butyl-4-methoxyphenol.

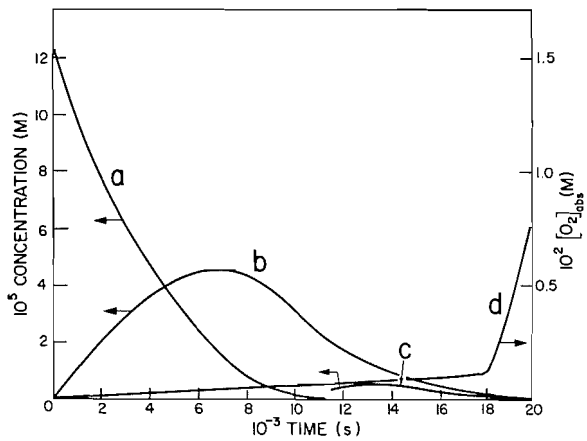

FIG. 2. Concentration–time profiles for $Cu[Et_2NCS_2]_2$ ($1.25 \times 10^{-4}\ M$) inhibited autoxidation of styrene ($7.83\ M$) at 30°C. (*a*) $Cu[Et_2NCS_2]_2$, (*b*) I, (*c*) II and III, (*d*) O_2.

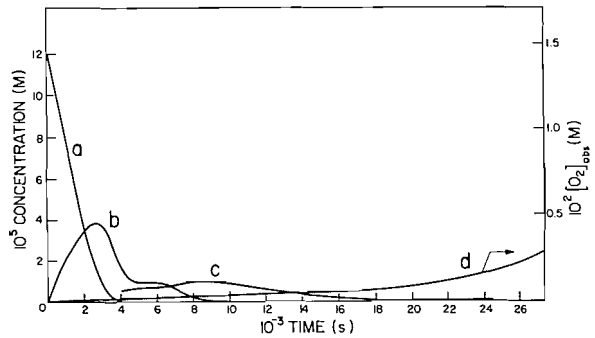

FIG. 3. Concentration–time profiles for $Cu[Et_2NCS_2]_2$ ($1.25 \times 10^{-4}\ M$) inhibited autoxidation of cumene ($7.17\ M$) at 30°C. (*a*) $Cu[Et_2NCS_2]_2$, (*b*) I, (*c*) II and III, (*d*) O_2.

Alternatively, n can be calculated from the initial rate of scavenger disappearance since

$$n = R_i/(-d[A]/dt)_0 \qquad [11]$$

The initial rates of disappearance of $Cu[Et_2NCS_2]_2$ are given in Table 3 along with the n values calculated from [11].

It is clear from the data in Table 3 that each molecule of complex reacts with *one* peroxy radical whereas the *overall* stoichiometry of ~5 must be the result of peroxy radical scavenging by complex derived products.

The induction periods obtained in the aralkanes were slightly longer than in styrene. This may be because of heterolytic decomposition of the small amount of aralkyl hydroperoxide to a phenol during the induction period.

Induction periods and initial rates of complex disappearance for cupric dialkyldithiophosphate inhibited hydrocarbon autoxidation are given in Table 4. Initial rates of complex disappearance were approximately twice as fast as R_i implying a stoichiometric factor of 0.5. This rate was nearly proportional to the complex concentration in styrene while in the other substrates an almost zero-order dependence was observed. A careful examination of the concentration–time profile for the complex revealed that after an initial first- or zero-order decay the

Can. J. Chem. Downloaded from www.nrcresearchpress.com by 210.87.254.6 on 09/05/12
For personal use only.

Can. J. Chem. Downloaded from www.nrcresearchpress.com by 210.87.254.6 on 09/05/12
For personal use only.

TABLE 4. Induction periods and initial rates of complex disappearance for $Cu[i\text{-}PrO)_2PS_2]_2$ inhibited autoxidation[a]

Substrate	$10^{-4}\tau_{O_2}$ (s)	$\frac{\tau_{O_2}R_i}{[A]}$	$10^8(-d[A]/dt)_0$ ($M\ s^{-1}$)	$\frac{R_i}{(-d[A]/dt)_0}$
Styrene	1.37	3.5	5.2	0.6
Tetralin	1.8	5.5	7.0	0.5
Cumene	1.75	5.2	9.0	0.4
Chlorobenzene	—	—	9.0	0.4

[a]$[A]_0 = 1.2 \times 10^{-4}\ M$; $[TPB]_0 = 0.0085\ M$.

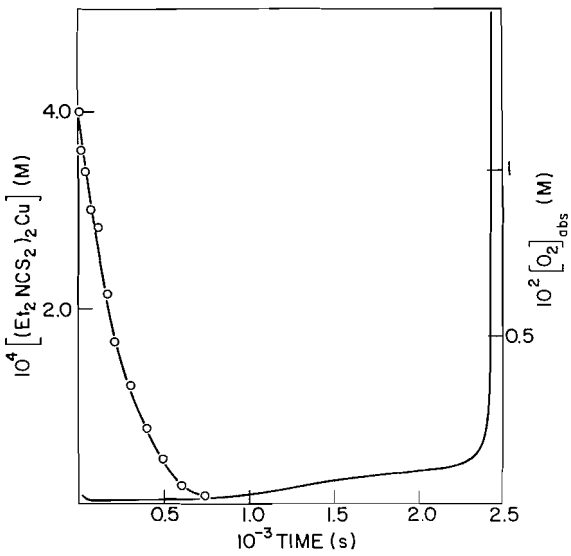

FIG. 4. Concentration–time profiles for $Cu[Et_2NCS_2]_2$ ($1.25 \times 10^{-4}\ M$) inhibited autoxidation of 9,10-dihydroanthracene (0.5 M) in *o*-dichlorobenzene at 50°C.

rate of complex disappearance slowed down until 5% of the complex remained, whereupon the rate increased to complete complex destruction. This overall behavior is very similar to the concentration–time profiles obtained for the destruction of $Cu[(RO)_2PS_2]_2$ by alkyl hydroperoxides (8).

Oxygen absorption by styrene at the uninhibited rate commenced immediately the complex had disappeared while much longer induction periods were observed with the other substrates. Oxygen absorption by cumene was extremely autoretarding after the induction period and the rate fell to R_i after the absorption of as little as $7.5 \times 10^{-3}\ M\ O_2$.

Although the overall behavior of hydrocarbon autoxidation inhibited by dithiophosphates and dithiocarbamates during and after the induction period were similar transient cupric complexes analogous to I, II, and III were not detected with the thiophosphate.

(ii) Pro-oxidant Effect

Addition of $Cu[(i\text{-}PrO)_2PS_2]_2$ (0.016 M) to styrene (1.74 M) in chlorobenzene at 30°C containing $(CH_3)_3COOH$ (0.01 M) gave an initial rate of oxygen absorption of $1.2 \times 10^{-6}\ M\ s^{-1}$. We have previously shown (8) that the rate of radical production from a mixture of $Cu[(i\text{-}PrO)_2PS_2]_2$ and $(CH_3)_3COOH$ is given by the rate expression $d[R^\cdot]/dt = 2.4\ [A][ROOH]$. Substitution of this rate into the inhibition rate expression [1] gives

$$(-d[O_2]/dt)_0 = 2.4k_p[RH][ROOH]/k_{inh}$$

and since $k_p = 41\ M^{-1}\ s^{-1}$, $k_{inh} = 1.4 \times 10^6\ M^{-1}\ s^{-1}$ which is in good agreement with rate constants obtained using conventional initiators. This agreement must be somewhat fortuitous because chain lengths were very much less than 1.0 and alkoxy as well as peroxy radicals could be propagating the chain.

Mixtures of $Cu[Et_2NCS_2]_2$ and $(CH_3)_3COOH$ also gave measurable inhibited rates of oxidation of styrene. The kinetics for the generation of radicals by this binary system are, however, not simple (8) and we have not attempted to calculate k_{inh} from the pro-oxidant effect produced by this complex.

(iii) Low Temperature Electron Spin Resonance Studies

Rates of disappearance of *tert*-butylperoxy radicals in the presence of excess complex could not be followed by the esr method (1, 2) because the copper complex $M_I = -\frac{1}{2}$ transition occurs at the same field position as the signal from $(CH_3)_3COO^\cdot$. Direct evidence for a rapid reaction between $(CH_3)_3COO^\cdot$ and $Cu[R_2NCS_2]_2$ and $Cu[(RO)_2PS_2]_2$ was, however, obtained by this method. Thus $(CH_3)_3COO^\cdot$ ($2.5 \times 10^{-5}\ M$) was rapidly destroyed upon addition of the complex ($5 \times 10^{-5}\ M$) in the dark at −90°C. At this temperature approximately two peroxy radicals were destroyed by each molecule of complex. There was no evidence for the production of transient cupric complexes probably because they were destroyed by reaction with peroxy radicals.

(iv) Products

Peroxy Radical Derived Products

α-Methylstyrene and α-cumyl alcohol were the principal volatile products from reaction of cumylperoxy radicals with $Cu[i\text{-}Pr_2NCS_2]_2$ in chloro-

Can. J. Chem. Downloaded from www.nrcresearchpress.com by 210.87.254.6 on 09/05/12
For personal use only.

TABLE 5. Volatile products from reaction of cumylperoxy radicals with cupric complexes in chlorobenzene at 50°C

$[Azocumene]_0$ (M)	Complex	Concn. (M)	$[O_2]_{abs}$ (M)	Acetophenone[a]	α-Methylstyrene[a]	α-Cumyl alcohol[a]
0.026	—	—	0.04	0.5	—	0.27
0.025	$Cu[(i\text{-}PrO)_2PS_2]_2$	0.025	0.056	0.11	0.65	0.04
0.025	$Cu[i\text{-}Pr_2NCS_2]_2$	0.025	0.067	0.01	0.62	0.27

[a]Yields relative to the total concentration of cumylperoxy radicals produced.

benzene at 50°C. Acetophenone was also formed in low yield (Table 5). α-Methylstyrene was almost certainly produced by dehydration of α-cumyl alcohol by a Lewis acid formed in the system while acetophenone was formed by β-scission of cumyloxy radicals. The overall ratio of α-cumyl alcohol to acetophenone was, therefore, 89:1 which can be compared with a ratio of 0.54 produced in the absence of the complex.

The same three products were formed from reaction of cumylperoxy radicals with $Cu[(i\text{-}PrO)_2PS_2]_2$. The relative yields were, however, quite different. In this case the α-cumyl alcohol was more efficiently dehydrated while the ratio of α-methylstyrene + α-cumyl alcohol to acetophenone was 6.3:1.

Complex Derived Products

$Cu[Et_2NCS_2]_2$ (10^{-4} M) was rapidly destroyed when it was photolysed in air-saturated toluene–chlorobenzene (5:1) containing di-*tert*-butyl ketone. Photolysis of this ketone in the presence of oxygen is an efficient method of generating *tert*-butylperoxy radicals and it was by reaction with these radicals that the complex was destroyed.

$$[12]\quad (CH_3)_3CC(=O)(CH_3)_3 \xrightarrow{h\nu,\ O_2} 2(CH_3)_3COO^{\cdot} + CO$$

$$[13]\quad (CH_3)_3COO^{\cdot} + Cu[Et_2NCS_2]_2 \longrightarrow \text{Reaction products}$$

At least three transient cupric complexes, I, II, and III were formed by this reaction before the copper ions were finally quantitatively precipitated as copper sulphate. These transients were readily distinguished from each other and $Cu[Et_2NCS_2]_2$ by their g-factors which increased in the order $Cu[Et_2NCS_2]_2 < I < II < III$ (Table 6). The concentration–time profiles for the disappearance of $Cu[Et_2NCS_2]_2$ and the appearance and disappearance of I, II, and III at −40°C are shown in Fig. 5. This temperature was chosen for these experiments because line broadening was at a minimum.

The rate of disappearance of $Cu[Et_2NCS_2]_2$ was approximately 5–6 times slower than $+d[(CH_3)_3COO^{\cdot}]/dt$ while $+d[I]/dt$ was approximately equal to $-d[Cu[Et_2NCS_2]_2]/dt$. The complex I reached a maximum concentration of 4.6×10^{-5} M when

TABLE 6. Isotropic esr parameters[a] for cupric diethyldithiocarbamate and the cupric complex transients I, II, and III formed by reaction with *tert*-butylperoxy radicals

Complex	g-factor	a_{Cu} (G)
$Cu[Et_2NCS_2]_2$	2.0458	78.3
I	2.0643	76.8
II	2.0857	77.4
III	2.0891	71.0

[a]Measured in toluene–chloroform (1.5:1) at −30°C.

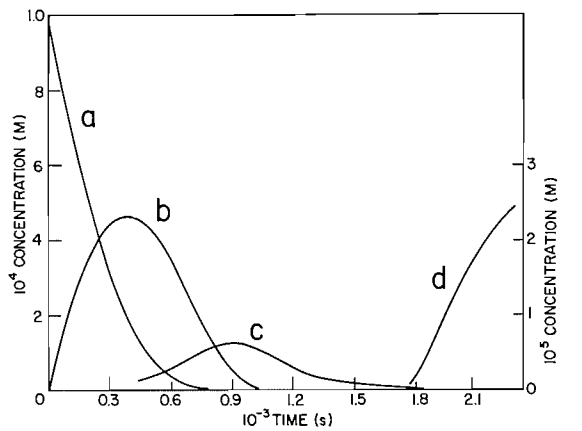

FIG. 5. Concentration–time profiles for the products of photolysis of di-*tert*-butyl ketone (0.5 M) in air-saturated toluene–chlorobenzene (5:1) containing $Cu[Et_2NCS_2]_2$ ($10^{-4}M$) at −40°C. (*a*) $Cu[Et_2NCS_2]_2$, (*b*) I, (*c*) II and III, (*d*) $(CH_3)_3COO^{\cdot}$.

8×10^{-5} M of $Cu[Et_2NCS_2]_2$ had disappeared. The concentration of I then began to fall and it was completely destroyed just after the disappearance of $Cu[Et_2NCS_2]_2$. The maximum concentrations of II and III seemed to occur soon after I had disappeared and *tert*-butylperoxy radicals did not reach a detectable concentration until these complexes had disappeared.

If the light was shuttered when I had reached its maximum concentration the concentration of this complex increased slowly by a further 20% while the concentration of $Cu[Et_2NCS_2]_2$ decreased slowly to a lower stationary concentration. Since the generation of $(CH_3)_3COO^{\cdot}$ would have stopped immediately photolysis was ceased this observation is best explained by a reaction between $(CH_3)_3COO^{\cdot}$

Can. J. Chem. Downloaded from www.nrcresearchpress.com by 210.87.254.6 on 09/05/12
For personal use only.

and $Cu[Et_2NCS_2]_2$ which gives an intermediate that decomposes to I and a species that leads to the production of peroxy radicals and the further destruction of $Cu[Et_2NCS_2]_2$.

We could find no direct evidence for the production of bis(dimethyldithiocarbamoyl) disulphide during the reaction of $Cu[Me_2NCS_2]_2$ with *tert*-butylperoxy radicals. This does not prove that the disulphide was not formed as it is not stable in the presence of photochemically generated *tert*-butylperoxy radicals.

Conclusions

This work confirms the findings of other workers (4–7) that cupric dialkyldithiocarbamates and dialkyldithiophosphates are extremely efficient peroxy radical scavenging antioxidants. Our kinetic results indicate that they are at least several orders of magnitude more efficient than the related zinc and nickel complexes. Further advantages of these complexes are the long *overall* induction periods that they produce before substrate oxidation commences which must result from the production of efficient radical scavengers during inhibited autoxidation.

The principal advantage of cupric complexes as models for this class of antioxidant is their paramagnetism. Their concentration can, therefore, be easily followed by the epr method, a technique that is considerably more informative than the uv spectroscopic method that we used for the nickel complexes (2). This is certainly true for the dithiocarbamates for which we detected three transient cupric complexes in the conversion to copper sulphate.

From a mechanistic viewpoint we believe that our results for the dithiocarbamate are best explained on the basis of the production of an intermediate **1** by reaction of a peroxy radical at the metal centre. This intermediate could rearrange to give the cupric complex I and an alkoxy radical

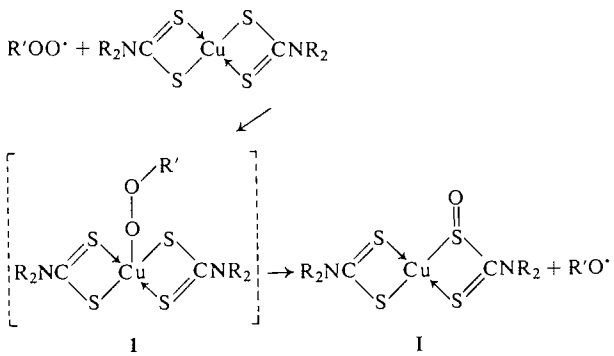

1 I

The cupric complexes I, II, and III detected by epr are almost certainly the products A_1, A_2, and A_3 of reactions [5], [6], and [7]. We have spectroscopic evidence that the structure of A_1 or I takes the form shown above.[4] This structure is analogous to the one suggested by Chien and Boss (13) for the initial complex-derived product from reaction of alkyl hydroperoxide with nickel dialkyldithiocarbamates. These workers, however, speculated that this intermediate was produced by non-radical reduction of the hydroperoxide to alcohol. We previously concluded (8) that the cupric transients I, II, and III observed during the destruction of $Cu[R_2NCS_2]_2$ by alkyl hydroperoxides were produced by reaction of alkylperoxy radicals with the complex. The results of the present work confirm this conclusion and show that the reaction is extremely facile.

1. J. A. Howard, Y. Ohkatsu, J. H. B. Chenier, and K. U. Ingold. Can. J. Chem. **51**, 1543 (1973) and references cited therein.
2. J. A. Howard and J. H. B. Chenier. Can. J. Chem. **54**, 382 (1976).
3. R. P. R. Ranaweera and G. Scott. Eur. Polym. J. **12**, 825 (1976).
4. V. G. Vinogradova and Z. K. Maizus. Kinet. Kat. **13**, 298 (1972).
5. A. N. Zverev, V. G. Vinogradova, Z. K. Maizus, and E. G. Rukhadze. Izv. Akad. Nauk SSSR Ser. Khim. 2224 (1975).
6. V. G. Vinogradova, A. N. Zverev, and Z. K. Maizus. Kinet. Katal. **15**, 323 (1974).
7. V. G. Vinogradova and A. N. Zverev. Izv. Akad. Nauk SSSR Ser. Khim. 2217 (1975).
8. J. H. B. Chenier, J. A. Howard, and J. C. Tait. Can. J. Chem. **55**, 1644 (1977).
9. L. R. Mahoney. J. Am. Chem. Soc. **88**, 3035 (1966).
10. E. Müller and G. Roscheinsen. Ber. **90**, 543 (1957).
11. J. A. Howard. Adv. Free-Radical Chem. **4**, 49 (1972).
12. D. G. Hendry, T. Mill, L. Piszkiewicz, J. A. Howard, and H. K. Eigenmann. J. Phys. Chem. Ref. Data, **3**, 937 (1974).
13. J. C. W. Chien and C. R. Boss. J. Polym. Sci. Part A-1, **10**, 1579 (1972).

[4]J. A. Howard and J. C. Tait. Part VI. This issue.

Metal complexes as antioxidants. VI. An electron spin resonance study of the transient cupric complexes formed in the reaction of cupric dialkyldithiocarbamates with alkylperoxy radicals and alkyl hydroperoxides[1]

JAMES ANTHONY HOWARD[2] AND JOHN CHARLES TAIT[3]

Division of Chemistry, National Research Council of Canada, Ottawa, Ont., Canada K1A 0R9

Received June 14, 1977

JAMES ANTHONY HOWARD and JOHN CHARLES TAIT. Can. J. Chem. **56**, 164 (1978).

The epr spectra of three intermediate copper(II) complexes formed by oxidation of bis[*N*,*N*-dialkyl(dithiocarbamato-*S*,*S*′)] copper(II) by alkyl hydroperoxides and alkylperoxy radicals are reported. Isotropic and anisotropic spectra of the complexes formed from alkylperoxy radicals enriched with ^{17}O are consistent with the following structures: $[Cu(S_2CNR_2)(OS_2CNR_2)]$ (I), $[Cu(OS_2CNR_2)_2]$ (II), and $[Cu(OS_2CNR_2)(O_2S_2CNR_2)]$ (III). The isotropic ^{17}O hyperfine interaction of I is 19.2 G while the anisotropic spectrum of II indicates that the two oxygen nuclei are equivalent. The anisotropic ^{17}O hyperfine splitting constants are consistent with a structure for these complexes in which the S—O bond(s) is directed out of the plane of the complex and not coordinated to the copper.

JAMES ANTHONY HOWARD et JOHN CHARLES TAIT. Can. J. Chem. **56**, 164 (1978).

On rapporte les spectres rpe de trois complexes de cuivre formés comme intermédiaires lors de l'oxydation du bis[*N*,*N*-dialkyl(dithiocarbamato-*S*,*S*′)] cuivre(II) par les hydroperoxydes d'alkyle et des radicaux alkylperoxy. Les spectres isotropes et anisotropes des complexes formés à partir de radicaux alkylperoxy enrichis avec du ^{17}O sont en accord avec les structures suivantes: $[Cu(S_2CNR_2)(OS_2CNR_2)]$ (I), $[Cu(OS_2CNR_2)_2]$ (II) et $[Cu(OS_2CNR_2)(O_2S_2CNR_2)]$ (III). L'interaction hyperfine isotrope de ^{17}O de I est 19.2 G alors que le spectre anisotrope de II indique que les deux noyaux d'oxygène sont équivalents. Les constantes de couplage hyperfines anisotropes de ^{17}O sont en accord avec une structure pour ces complexes dans lesquels le(s) lien(s) S—O est dirigé hors du plan du complexe et n'est pas coordonné avec le cuivre.

[Traduit par le journal]

In 1972 Vinogradova and Maizus (1) detected a transient paramagnetic copper species during the bis-hexamethylenimine-dithiocarbamato copper(II) inhibited, α,α′-azobisisobutyronitrile initiated, autoxidation of ethylbenzene at 75°C. They concluded that this species was produced by reaction of the dithiocarbamate with 1-phenylethylperoxy radicals ($RO_2^{\cdot}$) according to [1], where R = $C_6H_5CH(CH_3)$, L =

[1] $$RO_2^{\cdot} + CuL_2 \rightarrow Cu(L_{ox})_2$$

$R_2'NCS_2$ and L_{ox} is an oxidized form of the ligand. These workers also discovered that this transient was formed by reaction of the dithiocarbamate with 1-phenylethyl hydroperoxide.

More recently, Zverev *et al.* (2) demonstrated that a transient cupric complex was formed during the bisdiethyldithiocarbamato copper inhibited autoxidation of ethylbenzene and attributed it to 1-phenylethylperoxo diethyldithiocarbamato copper, **1**, formed by substitution of a diethyldithiocarbamato radical from copper by a 1-phenylethylperoxy radical [2].

[2] $$Cu[Et_2NCS_2]_2 + RO_2^{\cdot} \rightarrow \{Cu[Et_2NCS_2]_2 \ldots RO_2\} \rightarrow \{Cu[Et_2NCS_2]_2^{+} \ldots RO_2^{-}\} \rightarrow ROOCuS_2CNEt_2 + Et_2NCS_2^{\cdot}$$

1

Furthermore these workers suggested that **1** was destroyed by reaction with a second peroxy radical to give bis(1-phenylethylperoxo) copper coordinated to a diethyldithiocarbamato radical, **2**, which subsequently dimerized to give an insoluble species **3**.

[3] 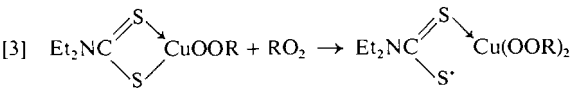

2

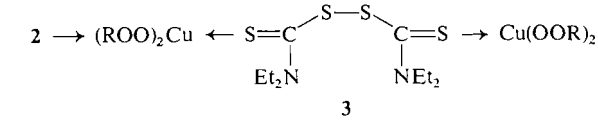

3

The electron spin resonance spectrum attributed to **1** was characterized by an isotropic *g*-factor (2.066) that was larger than the *g*-factor for the dithiocarbamate (2.047) while the isotropic copper hyperfine splitting constants for the two complexes were very similar.

[1]NRCC No. 16237.

[2]Author to whom all correspondence should be addressed.

[3]NRCC Research Associate 1975–1977.

Can. J. Chem. Downloaded from www.nrcresearchpress.com by 210.87.254.6 on 09/05/12
For personal use only.

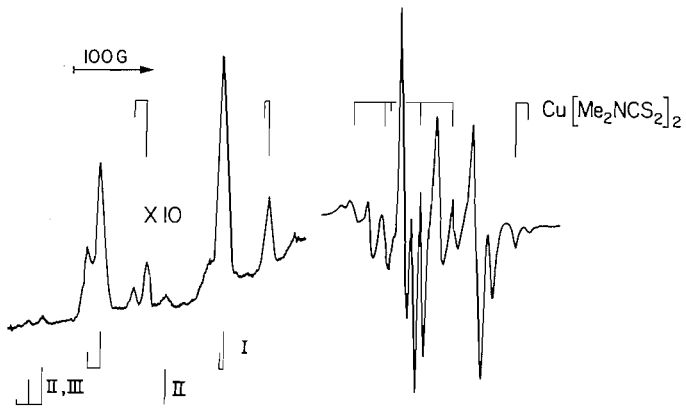

FIG. 1. The epr spectrum at 135 K of products from reaction of $Cu[Me_2NCS_2]_2$ (0.02 *M*) and *t*-BuOOH 0.2 *M* in toluene at 263 K.

In the course of our kinetic and product studies of the reaction of cupric dialkyldithiocarbamates with alkyl hydroperoxides (3) we also found that a cupric complex I was formed as the original $Cu[R_2NCS_2]_2$ was destroyed. This copper species was not stable in the presence of excess hydroperoxide and as it was destroyed at least two other transient cupric species, II and III, were detected before the copper ions were quantitatively precipitated as copper sulphate. Thus at least three cupric complexes are involved as intermediates in the overall conversion of cupric dialkyldithiocarbamates to copper sulphate rather than one as originally reported (1, 2). We have also detected these three complexes during cupric dialkyldithiocarbamate inhibited hydrocarbon autoxidation and during the continuous generation of *tert*-butylperoxy radicals in the presence of the dithiocarbamate (4).

Our previous experimental observations would appear to confirm Vinogradova and Maizus' conclusion that the transient cupric species I formed in oxidizing systems is produced by reaction of the dithiocarbamate with alkylperoxy radicals. The observation of at least two other cupric transients does, however, cast considerable doubt on the conclusion that I is an alkylperoxo dialkyldithiocarbamato copper complex. Our observations are, perhaps, more consistent with a mechanism that involves successive oxidation of the ligand sulphur atoms.

In experiments designed to eliminate the other transient radicals involved in autoxidation as possible sources of I, II, and III, we found that anaerobic, thermal generation of *tert*-butoxy and *tert*-butyl radicals from di-*tert*-butyl hyponitrite and azoisobutane in $Cu[R_2NCS_2]_2$ solutions resulted only in the destruction of the complex. Only when oxygen was admitted to these systems were the transient Cu(II) species observed, confirming that they are due to ligand oxidation by peroxy radicals.

We have previously reported (4) that during photolysis of an oxygenated toluene solution of di-*tert*-butyl ketone (DTBK) (0.4 *M*) and $Cu[Et_2NCS_2]_2$ (0.0001 *M*) a transient cupric species I was produced from the beginning of the reaction at a rate equal to the rate of disappearance of the dithiocarbamate. This species reached a maximum concentration equal to about 50% of the $Cu[Et_2NCS_2]_2$ when about 90% of the latter had been destroyed. The concentration of I then slowly decreased and it finally disappeared just after the complete disappearance of $Cu[Et_2NCS_2]_2$. The two other transient cupric species II and III were observed to build up and decay in a similar manner to I when all of the $Cu[Et_2NCS_2]_2$ and most of I had decayed.

Experiments on the dithiocarbamate initiated decomposition of *tert*-butyl hydroperoxide and cumene hydroperoxide at 253 K revealed a behaviour identical to the photolysis results.

In order to characterize the new species formed, a $Cu[Me_2NCS_2]_2$-hydroperoxide solution in toluene at 263 K was rapidly cooled to 135 K at successive stages of the reaction to observe the changes in the frozen solution spectrum. From Fig. 1 it is evident that $g_{\parallel}$ and $g_{\perp}$ for the newly formed species are significantly larger than the original complex. The analysis of the $g_{\perp}$ region is hindered by the strong overlap of lines from the various species; however, main features can be distinguished when different stages of the reaction are compared. As can be seen from Fig. 1, at least three new copper(II) species have been formed, each exhibiting successively higher $g_{\parallel}$ values (and consequently higher g_{iso}). The changes in $A_{\parallel}$ and $A_{\perp}$ are much less significant.

Can. J. Chem. Downloaded from www.nrcresearchpress.com by 210.87.254.6 on 09/05/12
For personal use only.

Can. J. Chem. Downloaded from www.nrcresearchpress.com by 210.87.254.6 on 09/05/12
For personal use only.

The epr spectrum of the Cu(II) transients was the same for both hydroperoxides and it was assumed that the species formed were identical. In reaction with the hydroperoxides, the final stages of reaction were difficult to observe due to the formation of solid $CuSO_4$ which obscured the spectral region of interest. To circumvent this, aerated solutions of DTBK and $Cu[Me_2NCS_2]_2$ in toluene were photolysed for short intervals at 3650 Å (where photolytic decomposition of the complex was shown to be insignificant), and the samples were centrifuged and then degassed by flushing the solution with a stream of argon. The species formed in this reaction were found to have identical epr parameters with those formed in the hydroperoxide reaction and there was no reason to suspect that they were due to different species.

In order to establish the nature of the new species, the DTBK experiments were repeated, except that pure oxygen enriched to 50% with ^{17}O was used to saturate the solution. When an appreciable concentration of the species I was achieved, the solution was degassed to eliminate line broadening by oxygen. In Fig. 2 superhyperfine structure due to the interaction of one ^{17}O nucleus ($I = \frac{5}{2}$) was observed on the high field side of the isotropic ($-\frac{3}{2}$) line of the $Cu[Et_2NCS_2]_2$ (^{17}O hyperfine on the lower field lines was obscured by their inherently broad linewidth). The spectrum was consistent with species I containing *one* ^{17}O nucleus (a_{iso} (^{17}O) = 19.2 G). Spectra run under high gain revealed no evidence for a second equivalent oxygen or an oxygen with a hyperfine ≥ 1.5 G which would be the smallest observable splitting.

Hyperfine structure was also observed in the spectrum of the frozen solution in both the $g_{\parallel}$ and $g_{\perp}$ regions (Fig. 3) and was again consistent with only one observable ^{17}O nucleus. Upon continued photolysis in the presence of ^{17}O enriched oxygen, species II could be observed before the complete decay of $Cu[Et_2NCS_2]_2$. Again it was apparent that this species contained one ^{17}O nucleus with $a_{iso} = 19.2$ G. There was also evidence for a second, equivalent ^{17}O at half the intensity of species II with one ^{17}O consistent with an ^{17}O enrichment of 50%. This would suggest that a second sulfur in the dithiocarbamate complex was oxidized before subsequent oxidation occurred. The epr parameters for the cupric dialkyldithiocarbamates and the transient species formed are collected in Tables 1 and 2. The anisotropic hyperfine and g-tensor parameters were calculated from a second-order solution to the Hamiltonian (5) by varying the g and A tensor components until agreement was reached with the observed line positions. The spectra were then simulated using a polycrystalline lineshape simulation program (6).

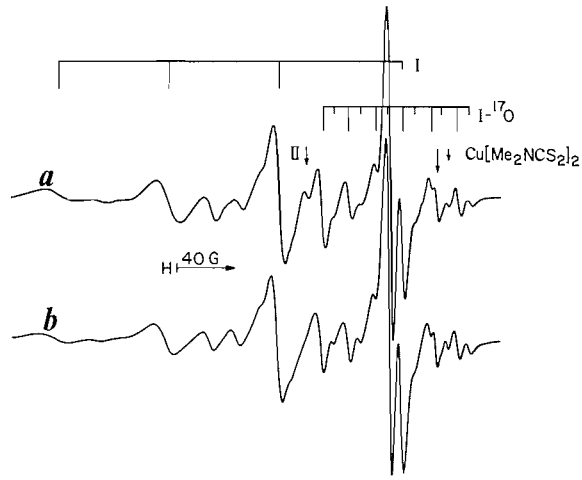

FIG. 2. (*a*) The epr spectrum at 243 K of reaction products from the photolysis of a 60% toluene – 40% $CHCl_3$ solution of $Cu[Me_2NCS_2]_2$ and DTBK which had been saturated with O_2 containing 50% $^{17}O_2$. (*b*) Computer simulation using epr parameters in Tables 1 and 2 and allowing for the M_I dependence of linewidth of Cu. The species included $Cu[Me_2NCS_2]_2$, I and I + ^{17}O and both isotopes of Cu.

In all cases contributions from nuclear Zeeman and quadrupole terms were neglected as have slight deviations from axiality because the overlap of species in the $\perp$ region precluded accurate parameter determination. A typical simulation is shown in Fig. 4.

In an attempt to synthesize the transient cupric species, H_2O_2 (0.01 mol) was reacted with an aqueous solution of $Na[Me_2NCS_2]$ (0.02 mol) at $-5°C$ and the resulting salt reacted with an aqueous solution of $CuSO_4$ (7). This would supposedly have given the mixed salt $Cu[Me_2NCS_2][Me_2NCS_2O]$. This product, however, could not be isolated in a pure form, despite repeated recrystallizations. The epr spectrum of the product in toluene showed that several salts of oxidized forms of $Cu[Me_2NCS_2]_2$ as well as ~10% of the unoxidized complex were present. The epr spectrum of a solution of these salts in 60% toluene – 40% chloroform at 135 K was identical to that obtained from species I, II, and III in the photolysis of DTBK and $Cu[Me_2NCS_2]_2$.

The recrystallized reaction products were extracted with toluene to give a toluene soluble fraction (A) whose composition by epr intensities was ~10% $Cu[Me_2NCS_2]_2$, 80% I, and 10% II + III. The toluene insoluble fraction was extracted with chloroform to give after removal of the solvent a fraction (B) which contained <2% of the dithio-

TABLE 1. The epr parameters for polycrystalline Cu(II) species[a]

	g_{iso}	a	$g_{\|}$	$g_{\perp}$	$A_{\|}$	$A_{\perp}$
$Cu[Me_2NCS_2]_2$	2.0448	79.4	2.0881	2.0215	163.5	45.
I*a*	2.0641	77.6	2.1288	2.0345	165.5	43.
II*a*	2.0908	72.9	2.1827	2.0385	169.	32.
III*d*	2.1012	~72.9	—	—	—	—
$Cu[Et_2NCS_2]_2$	2.0458	78.3	2.0890	2.0195	166.	45.
I*b*	2.0643	76.8	2.1301	2.0356	167.	45.
II*b*	2.0857	77.4	2.1816	2.0517	171.	45.
III*b*	2.0891	71.0	—	—	—	—

[a] ^{63}Cu hyperfine splitting constants in gauss, isotropic parameters measured in toluene–chloroform (3:2) at 243 K and anisotropic parameters measured in toluene–chloroform (3:2) at 141 K.

TABLE 2. ^{17}O hyperfine splittings (G) for some cupric complexes

Complex	A_x	A_y	$A_z(\|\|)$	a_{iso}	Ref.
I[a]	−20	−20	−17.5	−19.2	This work
$CuOx_2$[b]	−10.6	−26.8	−10.6	−16	9
$Cupic_2$[c]	−10.1	−20.2	−8.3	−12.7	9
$Cu(acac)_2$	−10	−24	−10	−14.6	10
$Cu(hfac)_2$[d]	—	—	−10–11	—	11
$Cu^{2+}(H_2O)_6$	−22.1	−11.9	−9.7		12
	−9.2	−16	−8.7		

[a] Species I from $Cu[i\text{-}Pr_2NCS_2]_2$.
[b] Copper(II)-8-hydroxy quinolate in phthalimide.
[c] Copper(II)picolinate in zinc picolinate.
[d] Adduct with tetrahydrothiophene (parameter estimated from Fig. 3 of ref. 11).

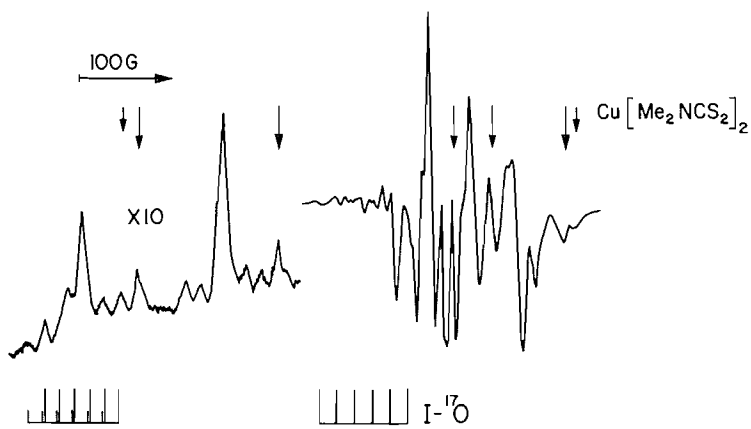

FIG. 3. The epr spectrum at 135 K of a frozen solution of the sample shown in Fig. 2. Stick diagram shows ^{17}O hyperfine lines for species I in the parallel and perpendicular region.

carbamate. Fraction B was then passed down an alumina column and a fraction whose composition by epr was >95% II was collected.

The results of elemental analyses on these fractions are presented in Table 3. Fraction A is consistent with a mixture whose composition is 10% $Cu[Me_2NCS_2]_2$ and 80% $Cu[Me_2NCS_2][Me_2NCS_2O]$ + 10% $Cu[Me_2NCS_2O]_2$. The analysis of fraction B is consistent with the molecular formula $Cu[Me_2NCS_2O]_2$. Mass spectra were run on these samples; however, the only parent peaks observable were at m/e = 303, 305, 307 corresponding to the isotopes of $Cu[Me_2NCS_2]_2^+$ and at m/e = 120, 88 corresponding to the $Me_2NCS_2^+$ and $Me_2N{=}C{=}S^+$ fragments (8). It is evident that thermal deoxygenation of the compounds must occur during vaporization in the mass spectrometer since the epr spectrum and elemental analysis on fraction B showed <1% $Cu[Me_2NCS_2]_2$.

The ^{17}O hyperfine coupling constants for a number of oxygen chelated Cu(II) complexes have been reported (9–12) and are presented in Table 2 along

Can. J. Chem. Downloaded from www.nrcresearchpress.com by 210.87.254.6 on 09/05/12
For personal use only.

Can. J. Chem. Downloaded from www.nrcresearchpress.com by 210.87.254.6 on 09/05/12
For personal use only.

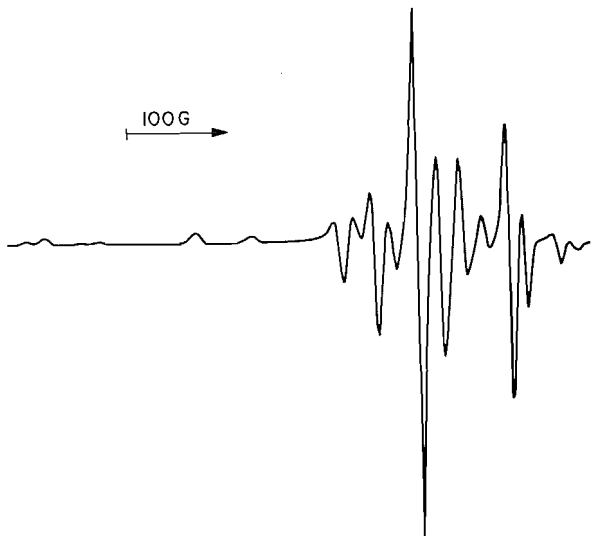

FIG. 4. Computer simulation of the epr spectrum at 135 K using parameters in Table 1 for species I*a* and $Cu[Me_2NCS_2]_2$.

TABLE 3. Elemental analyses of Cu(II) complexes

Complex	C (%)	H (%)	N (%)
$Cu[Me_2NCS_2]_2$	23.95(23.72)	4.06(3.95)	9.30(9.22)
Fraction A[a]	22.57(22.53)	3.94(3.75)	8.73(8.76)
Fraction B[b]	21.59(21.46)	3.61(3.57)	8.35(8.34)

[a]Composition ~80% I, 10% $Cu[Me_2NCS_2]_2$, 10% II and III by epr.
[b]Composition ~95% II, 5% I + III. Theoretical analyses in parentheses.

with those evaluated in this work. All of these previously studied chelates exhibit similar ^{17}O hyperfine tensors in which the dipolar tensor is close to being axial with the largest component directed along the Cu—O bond and associated with the $g_\perp$ features. This is not unexpected, as the unpaired electron occupies the Cu $d_{x^2-y^2}$ orbital in these square planar complexes which allows direct interaction with the ligand *s* and p_σ orbitals. That the transient species observed is also due to the unpaired electron occupying the $d_{x^2-y^2}$ or d_{xy} orbital on Cu, is confirmed by the *g*-tensor which is very similar to other Cu(II) species with square planar coordination. If the highest occupied orbital were d_{z^2}, $g_\perp$ values in the range 2.15–2.25 and $g_\parallel \simeq 2.03$ would be expected (13).

For the transient species, the ^{17}O hyperfine tensor is nearly isotropic and the largest component of the dipolar tensor is associated with $g_\parallel$, suggesting that the bonding orbital is directed parallel to the *z* axis of the Cu complex, and not basally coordinated as in the cases in Table 2. If the oxygen were apically coordinated to Cu, a considerably weaker hyperfine coupling from that observed for the basally coordinated oxygen would be expected since the p_z ligand orbital would be orthogonal to the $d_{x^2-y^2}$ orbital (12). From the ^{17}O hyperfine tensor then, it is suggested that the oxygen is bonded to the sulfur ligand and takes a position in which the S—O bond is directed out of the plane of the complex.

It is supposed that the major source of the ^{17}O hyperfine splitting is due to electron delocalization via sulfur to the oxygen atom by a mechanism similar to that in dialkyldithiophosphato copper complexes, where a large isotropic ^{31}P hyperfine coupling is observed (14). The oxygen is expected to be weakly π bonded to sulfur by donation from the filled *p*-orbitals to the unfilled *d*-orbitals on sulfur, and will not be very effective in delocalizing the unpaired electron. Thus the main mechanism for delocalization must be through direct *s–s* and *s–p* overlap between oxygen and sulfur. Spin polarization of the *s* electrons on O by the unpaired electron in the in-plane $d_{x^2-y^2}$ orbital on Cu could also be a contributing factor.

The more highly oxidized species II and III are almost certainly due to successive oxidation of the sulfur ligands. Due to the larger uncertainties in the epr parameters, it is difficult to propose a structure for these species. It is evident, however, that the *g*-values continue increasing while a_{iso} decreases substantially for species III. The increase in *g*-value is indicative of a lowering in covalency of the Cu—S bond and the decrease in a_{iso} is also consistent with an increase in delocalization of the electron onto the ligands. It is possible that the oxygen eventually becomes the coordinating ligand, which would form a more ionic bond, further increasing the *g*-value. Unfortunately this cannot be confirmed from these experiments due to the loss of spectral resolution as the species are successively oxidized.

Reaction Mechanism

The results presented here are not consistent with the mechanism suggested by Zverev *et al.* (2) for the reaction of alkylperoxy radicals with cupric dialkyldithiocarbamates and summarized by [2] and [3]. It is evident that the initial paramagnetic product cannot be alkylperoxo dialkyldithiocarbamato copper ($ROO{\cdot}Cu{\cdot}S_2CNR_2$) as predicted by an S_H2 or electron transfer mechanism.

We believe that our results are more consistent with the reaction mechanism given by [4]–[6] with

[4] 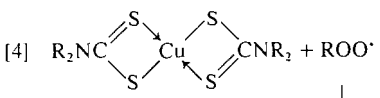

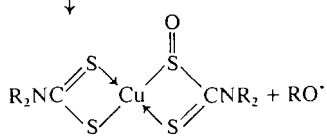

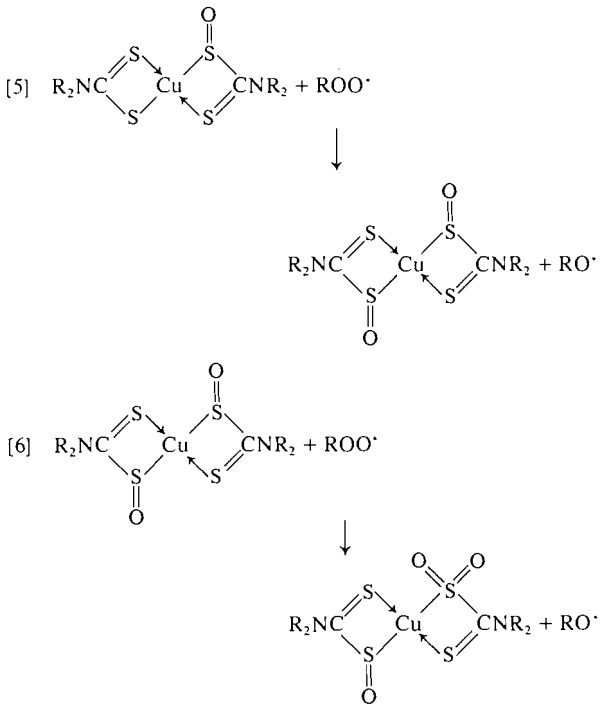

further oxidation of the cupric complexes until the copper is eventually precipitated as copper sulphate. This mechanism is similar to the one proposed by Chien and Boss (15) for the reaction of nickel dialkyldithiocarbamates with alkyl hydroperoxides. These workers did, however, propose that the hydroperoxide was the oxidizing species whereas we believe alkylperoxy radicals are the oxidizing species.

Experimental

Cupric dialkyldithiocarbamates were prepared by the procedure described previously (3). ^{17}O enriched oxygen was obtained from Yeda Inc., Israel. The spectra were recorded on a Varian E-4 spectrometer equipped with a variable temperature accessory. The microwave frequency was measured with a Syntron-Donner Model 6016 frequency counter, which also monitored the frequency of a proton magnetometer used to measure the magnetic field.

1. V. G. Vinogradova and Z. K. Maizus. Kinet. Katal. **13**, 298 (1972).
2. A. N. Zverev, V. G. Vinogradova, and Z. K. Maizus. Izv. Akad. Nauk. SSSR Ser. Khim. 2224 (1975).
3. J. H. B. Chenier, J. A. Howard, and J. C. Tait. Can. J. Chem. **55**, 1644 (1977).
4. J. H. B. Chenier, J. A. Howard, and J. C. Tait. Can. J. Chem. This issue.
5. R. E. D. McClung. Can. R. Phys. **46**, 2271 (1968).
6. R. Lefebvre and J. Maruani. J. Chem. Phys. **42**, 1480 (1965).
7. L. A. Brooks and R. T. O'Shaugnessy. U.S. Patent No. 3,322,802 (1967).
8. F. I. Onuska and M. E. Comba. J. Assoc. Off. Anal. Chem. **59**, 622 (1976).
9. A. R. Lorenz and Hs. H. Günthard. Chem. Phys. **14**, 327 (1976).
10. D. Getz and B. L. Silver. Inorg. Chem. **15**, 1240 (1976).
11. D. R. McMillin, R. S. Drago, and J. A. Nusz. J. Am. Chem. Soc. **98**, 3120 (1976).
12. D. Getz and B. L. Silver. J. Chem. Phys. **61**, 630 (1974).
13. B. J. Hathaway and D. E. Billing. Coord. Chem. Rev. **5**, 143 (1970).
14. J. R. Wasson. Inorg. Chem. **10**, 1531 (1971).
15. J. C. W. Chien and C. R. Boss. J. Polym. Sci. Part A-1, **10**, 1579 (1972).

Can. J. Chem. Downloaded from www.nrcresearchpress.com by 210.87.254.6 on 09/05/12
For personal use only.

Absolute rate constants for hydrocarbon autoxidation. 24. Rate constants and Arrhenius parameters for reaction of *tert*-butylperoxy radicals with 3-methylpentane[1]

J. A. HOWARD, J. H. B. CHENIER, AND D. A. HOLDEN[2]

Division of Chemistry, National Research Council of Canada, Ottawa, Ont., Canada K1A 0R9

Received February 18, 1977[3]

J. A. HOWARD, J. H. B. CHENIER, and D. A. HOLDEN. Can. J. Chem. **56**, 170 (1978).

Autoxidation of 3-methylpentane in the presence of *tert*-butyl hydroperoxide gives, after reduction with triphenylphosphine, 3-methyl-3-pentanol and 3-methyl-2-pentanol as the major reaction products. The overall rate constant for reaction of $(CH_3)_3COO^\cdot$ with this substrate at 30°C is 0.008 ± 0.001 M^{-1} s^{-1} which consists of k/tertiary C—H = 0.007 ± 0.001 M^{-1} s^{-1} and k/secondary C—H = 0.0002 ± 0.0001 M^{-1} s^{-1}. The products from cooxidation of cumene and 3-methylpentane in the presence of *tert*-butyl hydroperoxide are formed in yields which are consistent with these rate constants relative to a value of 0.16 M^{-1} s^{-1} for cumene. The Arrhenius equations for reaction of $(CH_3)_3COO^\cdot$ with the *t*-C—H and *s*-C—H of 3-methylpentane relative to the Arrhenius equation for reaction of $(CH_3)_3COO^\cdot$ with cumene (log $(k_{10}/M^{-1}\ s^{-1}) = (8.7 \pm 0.3) - (13.2 \pm 0.4)/\theta$) are

$$\log (k_4(t)/M^{-1}\ s^{-1}) = (9.5 \pm 0.5) - (16.3 \pm 0.7)/\theta$$

$$\log (k_4(s) \text{ per H}/M^{-1}\ s^{-1}) = (8.9 \pm 0.7) - (17.5 \pm 0.8)/\theta$$

respectively, where $\theta = 2.303RT$ kcal mol^{-1}.

J. A. HOWARD, J. H. B. CHENIER et D. A. HOLDEN. Can. J. Chem. **56**, 170 (1978).

L'autoxydation du méthyl-3 pentane en présence d'hydroperoxyde de *tert*-butyle conduit, après réduction avec la triphénylphosphine, aux méthyl-3 pentanol-3 et méthyl-3 pentanol-2 comme produits principaux de la réaction. La constante de vitesse globale pour la réaction de $(CH_3)_3COO^\cdot$ avec ce substrat à 30°C est de 0.008 ± 0.001 M^{-1} s^{-1}; cette valeur est formée de k/C—H tertiaire = 0.007 ± 0.001 M^{-1} s^{-1} et k/C—H secondaire = 0.0002 ± 0.0001 M^{-1} s^{-1}. Les rendements des produits de la cooxydation du cumène et du méthyl-3 pentane en présence d'hydroperoxyde de *tert*-butyle sont en accord avec ces constantes de vitesse elles-même relatives à une valeur de 0.16 M^{-1} s^{-1} pour le cumène. Les équations d'Arrhénius pour la réaction de $(CH_3)_3COO^\cdot$ avec le C—H tertiaire et le C—H secondaire du méthyl-3 pentane par rapport à l'équation d'Arrhénius pour la réaction de $(CH_3)_3COO^\cdot$ avec le cumène (log $(k_{10}/M^{-1}\ s^{-1}) = (8.7 \pm 0.3) - (13.2 \pm 0.4)/\theta$) sont respectivement

$$\log (k_4(t)/(M^{-1}\ s^{-1}) = (9.5 \pm 0.5) - (16.3 \pm 0.7)/\theta$$

$$\log (k_4(s) \text{ par H}/M^{-1}\ s^{-1}) = (8.9 \pm 0.7) - (17.5 \pm 0.8)/\theta$$

où $\theta = 2.303RT$ kcal mol^{-1}.

[Traduit par le journal]

Introduction

Absolute rate constants for reaction of alkylperoxy radicals with a wide variety of aralkanes, aralkenes, and C—H bonds adjacent to a functional group have been determined by the rotating sector technique and the hydroperoxide method (1–8). In contrast there have been few measurements of absolute rate constants for alkanes although rate constants for reaction of *tert*-butylperoxy with the secondary aliphatic C—H bonds in cyclohexane, hexadecane, and tridecane have been reported (4, 8). These rate constants are, however, of low accuracy because of the very short kinetic chain lengths involved in the autoxidations (4). Alkanes with tertiary C—H bonds are much more susceptible to autoxidation than alkanes such as cyclohexane. We have, therefore, employed the hydroperoxide method to measure the reactivity of 3-methylpentane to the *tert*-butylperoxy radical at 30°C. This substrate undergoes reaction at the tertiary and secondary C—H's and relative product yields enable the overall rate constant to be separated into contributions from reaction at each position. These rate constants have been confirmed by product yields from co-oxidation of cumene and 3-methylpentane in the presence of *tert*-butyl hydroperoxide. In addition these co-oxidations have been performed over a temperature range and we are able to report Arrhenius parameters for reaction of *t*-$BuO_2^\cdot$ with the *t*-C—H and *s*-C—H bonds in 3-

[1]NRCC No. 16302.
[2]NRCC summer student 1976.
[3]Revision received August 26, 1977.

Can. J. Chem. Downloaded from www.nrcresearchpress.com by 210.87.254.6 on 09/05/12
For personal use only.

Can. J. Chem. Downloaded from www.nrcresearchpress.com by 210.87.254.6 on 09/05/12
For personal use only.

methylpentane relative to the Arrhenius parameters for cumene.

Experimental

Materials

3-Methylpentane and cumene (Phillips Research Grade) were used after distillation from triphenylphosphine and percolation through basic alumina. *tert*-Butyl hydroperoxide (Lucidol) was purified by fractional distillation and α,α′-azo-bis-isobutyronitrile, AIBN, (Aldrich) by recrystallization from ethyl alcohol below 40°C, mp = 102°C. 3-Methyl-3-pentanol, 3-methyl-2-pentanol, and α-cumyl alcohol were commercial samples which were used without further purification.

Kinetic Procedure

Rates of oxygen absorption were determined by means of the automatic recording gas apparatus previously described (9). Rates of chain initiation were measured for *all* kinetic experiments by the induction period method (10) using 2,6-di-*tert*-butyl-4-methylphenol as the radical scavenger. Because of the substantial vapour pressure of 3-methylpentane induction periods of >20 h were needed to ensure that both sides of the pressure transducer were at the same pressure before oxygen absorption commenced.

Co-oxidation

3-Methylpentane and cumene were co-oxidized in the presence of AIBN and *tert*-butyl hydroperoxide from 30 to 80°C. These runs were performed in glass-lined stainless steel high pressure vessels at ca. 5 atm of O_2.

Reaction Products

The major products from autoxidation of 3-methylpentane and co-oxidation of 3-methylpentane and cumene in the presence of *tert*-butyl hydroperoxide were identified (after reduction with a slight excess of triphenylphosphine) and relative yields were estimated by standard gas chromatography procedures.

Steady-state alkylperoxy radical concentrations were measured relative to a standard solution of 2,2,6,6-tetramethylpiperid-4-one 1-oxyl (10^{-4} *M*) by electron spin resonance spectroscopy (6).

Results

Oxidation of 3-Methylpentane

Oxygen was absorbed very slowly by 3-methylpentane (RH) at 30°C containing α,α′-azo-bis-isobutyronitrile (0.05 *M*) and the kinetic chain length was about 1. Upon addition of *tert*-butyl hydroperoxide (1.0 *M*) there was a significant increase in the overall rate and kinetic chain lengths of 7–30 were obtained. We have previously demonstrated (4, 6) that autoxidation of most hydrocarbons in the presence of this concentration of *tert*-butyl hydroperoxide can be described by the elementary reactions [1]–[6], where X· represents

Initiation

$$[1] \qquad R'N_2R' \xrightarrow{O_2} R'O_2\cdot + N_2$$

Chain transfer

$$[2] \qquad X\cdot + (CH_3)_3COOH \rightarrow XH + (CH_3)_3COO\cdot$$

$$[3] \qquad 2(CH_3)_3COO\cdot \xrightarrow{2k_3} 2(CH_3)_3CO\cdot + O_2$$

Propagation

$$[4] \qquad (CH_3)_3COO\cdot + RH \xrightarrow{k_4} (CH_3)_3COOH + R\cdot$$

$$[5] \qquad R\cdot + O_2 \xrightarrow{k_5} ROO\cdot$$

Termination

$$[6] \qquad 2(CH_3)_3COO\cdot \xrightarrow{2k_6} (CH_3)_3COOC(CH_3)_3 + O_2$$

radical species other than $(CH_3)_3COO\cdot$ and $R'N_2R'$ represents AIBN. Thus *tert*-butylperoxy radicals are the only radicals involved in rate controlling propagation and termination reactions.

The observed rate of oxygen absorption is given by

$$[7] \quad \left\{\frac{-d[O_2]}{dt}\right\}_{obs} = k_5[R\cdot][O_2] + 2ek_1[R'N_2R'] - k_1[R'N_2R'] - k_3[(CH_3)_3COO\cdot]^2 - k_6[(CH_3)_3COO\cdot]^2$$

where $k_1[R'N_2R']$ is the rate of nitrogen evolution from AIBN. Under steady state conditions [7] becomes

$$[8] \quad \left\{\frac{-d[O_2]}{dt}\right\}_{obs} = \frac{k_4[RH]R_i^{1/2}}{(2k_6)^{1/2}} + 2ek_1[R'N_2R'] - k_1[R'N_2R'] - \left\{\frac{k_3 + k_6}{k_6}\right\}\frac{R_i}{2}$$

where R_i is the rate of chain initiation which may be greater than $2ek_1[R'N_2R']$ because of initiation by homolysis of *t*-BuOOH.

We have previously shown that $(k_3 + k_6)/2k_6 = 2.6$ and $e = 0.5$ at 30°C (4). The rate of absorption of oxygen by RH is, therefore, given by

$$[9] \quad \left\{\frac{-d[O_2]}{dt}\right\}_{corr} = \left\{\frac{-d[O_2]}{dt}\right\}_{obs} + 2.6R_i = \frac{k_4[RH]R_i^{1/2}}{(2k_6)^{1/2}}$$

where k_4 is the rate controlling propagation rate constant and is the overall rate constant for reaction of $(CH_3)_3COO\cdot$ with RH and $2k_6$ is the rate controlling termination rate constant.

The kinetic data presented in Table 1 indicate that the overall rate was independent of the hydroperoxide concentration after allowance was made for its effect on the rate of chain initiation, in accordance with eq. 9.

The steady state alkylperoxy radical concentration in the AIBN initiated autoxidations was too weak to be measured with any degree of accuracy. More intense signals were obtained using 2,2′,3,3′-

TABLE 1. Kinetic data for autoxidation of 3-methylpentane in the presence of *tert*-butyl hydroperoxide at 30°C[a]

[RH] (M)	[ROOH] (M)	$10^7 R_i$ ($M\ s^{-1}$)	$10^7(-d[O_2]/dt)_{obs}$ ($M\ s^{-1}$)	$10^7(-d[O_2]/dt)_{corr}$[b] ($M\ s^{-1}$)	$\frac{10^4(-d[O_2]/dt)_{corr}}{[RH]\ R_i^{1/2}}$ ($M^{-1/2}\ s^{-1/2}$)
7.75	—	0.068	~0.06	~0.06	—
3.1	1.1	0.07	0.44	0.62	2.4
7.4	0.66	0.054	1.06	1.2	2.2
7.06	1.1	0.022	0.74	0.79	2.4
6.9	1.3	0.098	1.41	1.67	2.4
6.27	2.2	0.11	1.2	1.5	2.3
6.27	2.2	0.22	1.75	2.32	2.5
6.27	2.2	0.7	2.16	4.0	2.4

[a]All runs were performed in the presence of α,α'-azobisisobutyronitrile (0.05 M) and 2,6-di-*tert*-butyl-4-methylphenol (0.8–4 × 10^{-4} M).
[b]Obtained from eq. 9.

tetraphenylbutane and rate constants calculated from

$$R_i = 2k_6[ROO^\cdot]_{ss}^2$$

were close to the 'best' value of $(1.2 \pm 0.3) \times 10^3$ $M^{-1}\ s^{-1}$ calculated from $\log (2k_6/M^{-1}\ s^{-1}) = (9.2 \pm 0.2) - (8.5 \pm 0.2)$ kcal $mol^{-1}/2.303RT$ (4).

The average value of $k_4/(2k_6)^{1/2} = (2.4 \pm 0.1) \times 10^{-4}$ $M^{-1/2}\ s^{-1/2}$ in conjunction with the 'best' value of $2k_6$ gives $k_4 = 0.008 \pm 0.001$ $M^{-1}\ s^{-1}$ for the *overall* reactivity of 3-methylpentane.

Autoxidation of 3-methylpentane at 30°C gave, after reduction with triphenylphosphine, two major products, 3-methyl-3-pentanol and 3-methyl-2-pentanol, indicating that both the secondary and tertiary C—H bonds had been attacked by *tert*-butylperoxy radicals.

$$(CH_3)_3COO^\cdot + CH_3CH_2\underset{\displaystyle CH_3}{\underset{|}{C}}HCH_2CH_3 \xrightarrow{k_4(t)} CH_3CH_2\underset{\displaystyle CH_3}{\underset{|}{\overset{\displaystyle \cdot}{C}}}CH_2CH_3 + (CH_3)_3COOH$$

$$(CH_3)_3COO^\cdot + CH_3CH_2\underset{\displaystyle CH_3}{\underset{|}{C}}HCH_2CH_3 \xrightarrow{k_4(s)} CH_3CH_2\underset{\displaystyle CH_3}{\underset{|}{C}}\overset{\displaystyle \cdot}{C}HCH_3 + (CH_3)_3COOH$$

The average relative yield of 3-methyl-3-pentanol to 3-methyl-2-pentanol from 8 runs was 8.2 ± 0.8 which indicates that the tertiary C—H bond is ca. eight times more reactive than the secondary C—H bonds. The absolute value of $k_4(t)$ is, therefore, 0.007 ± 0.001 $M^{-1}\ s^{-1}$ and $k_4(s)$ per active hydrogen is 0.0002 ± 0.0001 $M^{-1}\ s^{-1}$.

Co-oxidation of Cumene and 3-Methylpentane

The rate controlling propagation reactions for the co-oxidation of 3-methylpentane and cumene in the presence of >0.5 M *tert*-butyl hydroperoxide are [4] and [10].

$$[10]\quad (CH_3)_3COO^\cdot + C_6H_5C(CH_3)_2H \xrightarrow{k_{10}} (CH_3)_3COOH + C_6H_5\dot{C}(CH_3)_2$$

The ratio of α-cumyl alcohol to 3-methyl-3-pentanol is therefore given by

$$\frac{[C_6H_5C(CH_3)_2OH]}{[t\text{-ROH}]} = \frac{k_{10}[C_6H_5C(CH_3)_2H]}{k_4(t)[RH]}$$

and the ratio of α-cumyl alcohol to 3-methyl-2-pentanol by

$$\frac{[C_6H_5C(CH_3)_2OH]}{[s\text{-ROH}]} = \frac{k_{10}[C_6H_5C(CH_3)_2H]}{k_4(s)[RH]}$$

Typical yields of these three alcohols produced after co-oxidations of cumene and 3-methylpentane and reduction with $(C_6H_5)_3P$ from 30 to 80°C were measured and are summarized in Table 2.

At 30°C $k_{10}/k_4(t) = 24 \pm 2$ and $k_{10}/k_4(s) = 190 \pm 22$. Since $k_{10} = 0.16 \pm 0.01$ $M^{-1}\ s^{-1}$, $k_4(t) = 0.007 \pm 0.001$ $M^{-1}\ s^{-1}$, and $k_4(s)$ per active H = 0.0002 ± 0.0001 $M^{-1}\ s^{-1}$, rate constants that are in excellent agreement with the values obtained from rate measurements on the oxidation of 3-methylpentane in the presence of *t*-BuOOH.

Accurate values of k_4 cannot be obtained above 30°C by the hydroperoxide method because of the high vapour pressure of 3-methylpentane. Accurate values of k_{10} can, however, be obtained from 30–60°C by this technique (Table 3). The Arrhenius plot of these data was linear (Fig. 1) and a least squares analysis yielded the Arrhenius expression

Can. J. Chem. Downloaded from www.nrcresearchpress.com by 210.87.254.6 on 09/05/12
For personal use only.

Can. J. Chem. Downloaded from www.nrcresearchpress.com by 210.87.254.6 on 09/05/12
For personal use only.

TABLE 2. Relative yields of α-cumyl alcohol, 3-methyl-3-pentanol (*t*-ROH), and 3-methyl-2-pentanol (*s*-ROH) produced by co-oxidation of cumene and 3-methylpentane in the presence of *tert*-butyl hydroperoxide at different temperatures[a]

T (°C)	$\frac{[C_6H_5C(CH_3)_2H]}{[C_6H_{14}]}$	$\frac{[C_6H_5C(CH_3)_2OH]}{t\text{-ROH}}$	$\frac{[C_6H_5C(CH_3)_2OH]}{s\text{-ROH}}$
30	0.023	0.62	5.2
30	0.048	1.14	8.1
40	0.023	0.52	4.4
40	0.048	1.2	9.8
50	0.023	0.49	3.3
50	0.048	1.02	6.6
60	0.023	0.42	2.5
60	0.048	0.93	5.3
70	0.023	0.327	1.9
70	0.048	0.69	4.6
80	0.048	0.56	3.4
80	0.048	0.55	4.9

[a]Oxidations were taken to 1–10% conversion and then reduced with $(C_6H_5)_3P$.

TABLE 3. Rate constants for reaction of *tert*-butylperoxy radicals with cumene at different temperatures[a]

T (°C)	k_{10} (M^{-1} s^{-1})
30	0.16
35	0.24
40	0.34
45	0.47
50	0.67
55	0.98
60	1.10

[a]Averages of at least two runs at each temperature at different cumene and *tert*-butyl hydroperoxide concentrations. Above 40°C *tert*-butyl benzene was used as diluent.

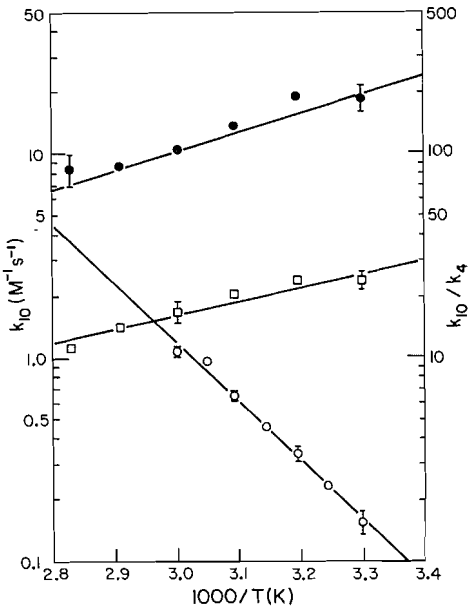

FIG. 1. Arrhenius plots of log $(k_{10}/M^{-1}$ s$^{-1})$ ⊙, log $(k_{10}/k_4(t))$ □, and log $(k_{10}/k_4(s))$ ● against $1000/T$ (K).

$$\log (k_{10}/M^{-1}\ s^{-1}) = (8.7 \pm 0.3) - (13.2 \pm 0.4)/\theta$$

where $\theta = 2.303RT$ kcal mol^{-1}.

These Arrhenius parameters are very similar to those reported by Howard *et al.* (11) for reaction of cumylperoxy with cumene (2×10^8 M^{-1} s^{-1} and 12.4 kcal mol^{-1}) and are quite different to those recently reported (12) for the rate controlling propagation reaction for the liquid-phase autoxidation of cumene with lead oxide (2×10^5 M^{-1} s^{-1} and 7.2 kcal mol^{-1}). The difference between these two sets of data is well beyond the limits of error and raises doubt about the validity of kinetic data obtained from the heterogeneous autoxidation.

The yields of 3-methyl-3-pentanol and 3-methyl-2-pentanol relative to α-cumyl alcohol from co-oxidations over a temperature range were measured and plots of log $(k_{10}/k_4(t))$ and log $(k_{10}/k_4(s))$ against the reciprocal of the absolute temperature (Fig. 1) gave

$$\log (A_{10}/A_4(t)) = -0.82 \pm 0.18$$
$$E_4(t) - E_{10} = 3.1 \pm 0.3 \text{ kcal mol}^{-1}$$
$$\log (A_{10}/A_4(s)) = -0.80 \pm 0.4$$
$$E_4(s) - E_{10} = 4.3 \pm 0.4 \text{ kcal mol}^{-1}$$

The Arrhenius equations for 3-methylpentane relative to cumene are, therefore,

$$\log (k_4(t)/M^{-1}\ s^{-1}) = (9.5 \pm 0.5) - (16.3 \pm 0.7)/\theta$$

$$\log (k_4(s) \text{ per C—H}/M^{-1}\ s^{-1}) = (8.9 \pm 0.7) - (17.5 \pm 0.8)/\theta$$

Discussion

Neat 3-methylpentane does not absorb oxygen at a significant rate at 30°C whereas chain lengths of 7–30 are obtained in the presence of *tert*-butyl hydroperoxide. Product studies on the latter system

Can. J. Chem. Downloaded from www.nrcresearchpress.com by 210.87.254.6 on 09/05/12
For personal use only.

suggest that significant concentrations of the secondary hydroperoxide, 3-methyl-2-pentyl hydroperoxide are formed, indicating a significant contribution from secondary alkylperoxy radicals to the overall concentration of *substrate* derived peroxy radicals. Thus chain termination for neat 3-methylpentane must involve 3-methyl-2-pentylperoxy (*s*-ROO•) as well as 3-methyl-3-pentylperoxy (*t*-ROO•) radicals.

[11] $t\text{-ROO}^\bullet + t\text{-ROO}^\bullet \rightleftharpoons t\text{-ROOOOR-}t \begin{cases} \rightarrow 2t\text{-RO}^\bullet + O_2 \\ \rightarrow t\text{-ROOR-}t + O_2 \end{cases}$

[12] $t\text{-ROO}^\bullet + s\text{-ROO}^\bullet \xrightarrow{2k_{12}}$

[13] $s\text{-ROO}^\bullet + s\text{-ROO}^\bullet \xrightarrow{2k_{13}}$ Non-radical products

The *overall* termination rate constant for the neat liquid will consist of contributions from $2k_{11}$, $2k_{12}$, and $2k_{13}$ and also contributions from the rate constants associated with the alkylperoxy radicals produced by β-scission of the 3-methyl-3-pentoxy radicals formed in reaction [11]. This overall rate constant will be significantly larger than the value expected for 3-methyl-3-pentylperoxy radicals and must be the principal reason for the resistance to autoxidation exhibited by 3-methylpentane. This substrate, therefore, behaves like other hydrocarbons with more than one type of reactive C—H bond, such as *p*-cymene which is more resistant to autoxidation than cumene because *p*-isopropylbenzylperoxy radicals are involved in termination (13, 14).

The average value of $k_4(t) = 0.007 \pm 0.001$ M^{-1} s^{-1} at 30°C for 3-methylpentane, determined by the hydroperoxide method and co-oxidation, is slightly larger than the estimated value of $k_4(t) = 0.003$–0.005 M^{-1} s^{-1} for isobutane (3, 4, 15). There is, however, no reason to believe that there will be any difference in reactivity between these two hydrocarbons. The experimental values of log $(A_4(t)/M^{-1}$ $s^{-1})$ and $E_4(t)$ are 9.5 and 16.3 kcal mol^{-1} relative to values of 8.7 and 13.2 kcal mol^{-1} for cumene. This preexponential factor is in good agreement with the estimated value of 9.4 for reaction of $t\text{-RO}_2^\bullet$ with a tertiary aliphatic C—H bond (3) while the activation energy is slightly larger than the value calculated from the overall activation energy for autoxidation of isobutane $(E_4 - \frac{1}{2}E_6) = 11.3$ kcal mol^{-1} quoted by Allara and co-workers (16) and our value of $E_6 = 8.5$ kcal mol^{-1} (4).

Extrapolation of our Arrhenius equation to 753 K gives $k_4(t) = 5.8 \times 10^4$ M^{-1} s^{-1} which compares favorably with the rate constant of 8.5×10^4 M^{-1} s^{-1} estimated by Baldwin for $HO_2^\bullet + i\text{-}C_4H_{10}$ in the gas phase (17), considering that $HO_2^\bullet$ may be slightly more reactive than $(CH_3)_3COO^\bullet$ at this temperature (18).

The value of $k_4(s)$ per active hydrogen $= 0.0002 \pm 0.0001$ M^{-1} s^{-1} at 30°C for 3-methylpentane is of similar magnitude to the values of $k_4(s) = 0.00026$ M^{-1} s^{-1} for cyclohexane, 0.00031 M^{-1} s^{-1} for tridecane, and 0.00034 M^{-1} s^{-1} for hexadecane, rate constants that were obtained by the hydroperoxide method on the individual hydrocarbons (4).

The activation energy for reaction of $s\text{-BuO}_2^\bullet$ with *n*-butane can be calculated to be 16.6 ± 3 kcal mol^{-1} from $E_p - E_t/2 = 15.3 \pm 3$ kcal mol^{-1} (19) and $E_t = 2.7$ kcal mol^{-1} (20). We have previously shown (4) that $s\text{-RO}_2^\bullet$ is about 5 times more reactive than $t\text{-RO}_2^\bullet$ in hydrogen abstraction from the same hydrocarbon at 30°C, which corresponds to a difference in activation energy of ~1 kcal mol^{-1}. We can, therefore, estimate that the activation energy for abstraction of a secondary hydrogen from *n*-butane by $t\text{-BuO}_2^\bullet$ is 17.6 ± 3 kcal mol^{-1}, very similar to our value for 3-methylpentane.

Bennett *et al.* (21) have recently determined the overall propagation rate constant for autoxidation of 2,6,10,14-tetramethylpentane at 413 K as 38 M^{-1} s^{-1}. Using the Arrhenius equations reported in this work for reaction of $t\text{-BuO}_2^\bullet$ with tertiary and secondary aliphatic C—H bonds we can calculate an overall reactivity of 2,6,10,14-tetramethylpentane to $t\text{-BuO}_2^\bullet = 4 \times 7.5 + 18 \times 0.44 = 38$ M^{-1} s^{-1} at 413 K, a value in excellent agreement with the directly measured value (21).

In conclusion the kinetic parameters reported in this work can be compared with kinetic parameters for Br•, a free radical that has the same endothermicities as ROO• in its reaction with aliphatic C—H bonds. Thus the selectivity of $t\text{-BuO}_2^\bullet$ to aliphatic *s*-C—H and *t*-C—H is ~1:35 at 30°C while the selectivity of Br• to these two bonds at 40°C is ~1:40 (15). Furthermore, $E^s - E^t$ for Br• is 2.5 kcal mol^{-1} (22) while this difference is 1.2 ± 1.5 kcal mol^{-1} for $t\text{-BuO}_2^\bullet$.

1. J. A. HOWARD. Adv. Free-Radical Chem. **4**, 49 (1972).
2. J. A. HOWARD. Free radicals. Vol. II. *Edited by* J. K. Kochi. Wiley, New York, NY. 1973. Chapt. 1.
3. D. G. HENDRY, T. MILL, L. PISZKIEWICZ, J. A. HOWARD, and H. K. EIGENMANN. J. Phys. Chem. Ref. Data, **3**, 937 (1974).
4. S. KORCEK, J. H. B. CHENIER, J. A. HOWARD, and K. U. INGOLD. Can. J. Chem. **50**, 2285 (1972).
5. J. A. HOWARD and J. H. B. CHENIER. J. Am. Chem. Soc. **95**, 3054 (1973).
6. J. A. HOWARD and J. H. B. CHENIER. Int. J. Chem. Kinet. **6**, 527 (1974).
7. J. H. B. CHENIER, J.P-A. Tremblay, and J. A. HOWARD. J. Am. Chem. Soc. **97**, 1618 (1975).

8. D. G. HENDRY, C. W. GOULD, D. SCHUETZLE, M. G. SYZ, and F. R. MAYO. J. Org. Chem. **41**, 1 (1976).
9. J. A. HOWARD and K. U. INGOLD. Can. J. Chem. **47**, 3809 (1969).
10. C. E. BOOZER, G. S. HAMMOND, C. E. HAMILTON, and J. N. SEN. J. Am. Chem. Soc. **77**, 3233 (1955).
11. J. A. HOWARD, W. J. SCHWALM, and K. U. INGOLD. Adv. Chem. Ser. **75**, 6 (1968).
12. S. FUKUZUMI and Y. ONO. J. Chem. Soc. Perkin Trans. II, 784 (1977).
13. G. A. RUSSELL. J. Am. Chem. Soc. **78**, 1047 (1956).
14. J. A. HOWARD and J. C. ROBB. Trans. Faraday Soc. **59**, 1590 (1963).
15. K. U. INGOLD. Free radicals. Vol. I. *Edited by* J. K. Kochi. Wiley, New York, NY. 1973. Chapt. 2.
16. D. L. ALLARA, T. MILL, D. G. HENDRY, and F. R. MAYO. Adv. Chem. Ser. **76**, 40 (1968).
17. R. R. BALDWIN, D. H. LANGFORD, M. J. MATCHAN, R. W. WALKER, and D. A. YORK. 13th Int. Combustion Symp. The Combustion Institute, Pittsburgh, PA. 1971. p. 251.
18. D. G. HENDRY and D. SCHUETZLE. J. Org. Chem. **41**, 3179 (1976).
19. T. MILL, F. MAYO, H. RICHARDSON, K. IRWIN, and D. L. ALLARA. J. Am. Chem. Soc. **94**, 6802 (1972).
20. J. A. HOWARD and J. E. BENNETT. Can. J. Chem. **50**, 2374 (1972).
21. J. E. BENNETT, J. A. EYRE, and R. SUMMERS. J. Chem. Soc. Perkin Trans. II, 797 (1974).
22. M. L. POUTSMA. Free radicals. Vol. II. *Edited by* J. K. Kochi. Wiley, New York, NY. 1973. Chapt. 15.

Can. J. Chem. Downloaded from www.nrcresearchpress.com by 210.87.254.6 on 09/05/12
For personal use only.

Electron paramagnetic resonance spectra of the *tert*-butylperoxy and *tert*-butoxy adducts to phenyl *tert*-butyl nitrone and 2-methyl-2-nitrosopropane. Oxygen-17 hyperfine coupling constants[1]

JAMES ANTHONY HOWARD AND JOHN CHARLES TAIT[2]

Division of Chemistry, National Research Council of Canada, Ottawa, Ont., Canada K1A 0R9

Received July 13, 1977

JAMES ANTHONY HOWARD and JOHN CHARLES TAIT. Can. J. Chem. **56**, 176 (1978).

tert-Butylperoxy radicals enriched with oxygen-17 react with phenyl *tert*-butyl nitrone to give α-*tert*-butylperoxybenzyl *tert*-butyl nitroxide with a_N = 13.42 G, a_H = 0.95 G, a_O^β = 2.9 G, g = 2.0064. The O-hfsc decreases with an increase in temperature while the H-hfsc increases with an increase in temperature. This radical is not stable above about 273 K and is replaced by α-*tert*-butoxybenzyl *tert*-butyl nitroxide, a_N = 13.62 G, a_H = 1.72 G, a_O^β = 5.05 G, g = 2.0064.

Alkylperoxy radicals are also trapped by 2-methyl-2-nitrosopropane to give alkylperoxy *tert*-butyl nitroxide a_N = 28.7 G, a_O^{ROO} = 4.6 G, g = 2.0056 while the epr parameters for alkoxy *tert*-butyl nitroxide are a_N = 27.25 G, a_O^{RO} = 1.03 G, g = 2.0057.

JAMES ANTHONY HOWARD et JOHN CHARLES TAIT. Can. J. Chem. **56**, 176 (1978).

Les radicaux *tert*-butylperoxy enrichis en oxygène-17 réagissent avec la phényle *tert*-butyle nitrone pour conduire au nitroxyde de l'α-*tert*-butylperoxybenzyle et de *tert*-butyle avec a_N = 13.42 G, a_H = 0.95 G, a_O^β = 2.9 G, g = 2.0064. Le O-hfsc diminue avec une augmentation de la température alors que le H-hfsc augmente avec une augmentation de température. Ce radical n'est pas stable au dessus d'environ 273 K et est remplacé par le nitroxyde de l'α-*tert*-butoxybenzyle et de *tert*-butyle, a_N = 13.62 G, a_H = 1.72 G, a_O^β = 5.05 G, g = 2.0064.

On peut aussi piégé les radicaux alkylperoxy par le méthyl-2 nitroso-2 propane pour conduire aux nitroxydes d'alkylperoxy et de *tert*-butyle a_N = 28.7 G, a_O^{ROO} = 4.6 G, g = 2.0056 alors que les paramètres rpe pour le nitroxyde d'alkoxy et de *tert*-butyle sont a_N = 27.25 G, a_O^{RO} = 1.03 G, g = 2.0057.

[Traduit par le journal]

Can. J. Chem. Downloaded from www.nrcresearchpress.com by 210.87.254.5 on 09/05/12
For personal use only.

Introduction

Merritt and Johnson (1) have recently reported the preparation and epr spectra of alkylperoxy radical (ROO·) adducts to phenyl *tert*-butyl nitrone (PBN).

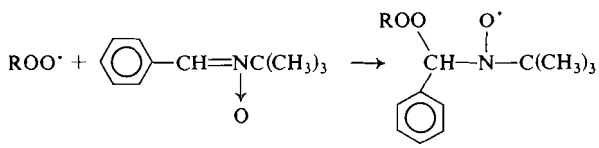

These radicals were prepared by reaction of $Pb(OAc)_4$ at −80°C with the alkyl hydroperoxide (ROOH) in the presence of PBN. The reported epr parameters for the nitroxide with R = *t*-Bu were a_N = 13.39 G, a_H = 1.19 G, and g = 2.0062. The only other authentic peroxy radical adduct to PBN is the hydroperoxy adduct with R = H (a_N = 14.8 G, a_H^β = 2.75 G, and g = 2.0057) which was prepared by photolysis of 30% H_2O_2 containing the nitrone (2).

We have studied the *direct* reaction of the *tert*-butylperoxy radical with phenyl *tert*-butyl nitrone, 2-methyl-2-nitrosopropane, and some other spin traps by the epr method. Two oxy radical adducts were observed with each trap using peroxy radicals enriched with ^{17}O. One of these was the alkoxy adduct while the second has been identified as the alkylperoxy adduct. Unambiguous identification of alkylperoxy radical adducts to phenyl *tert*-butyl nitrone and 2-methyl-2-nitrosopropane means that these traps can be used as probes for the intermediacy of alkylperoxy radicals in free-radical reactions.

Experimental

tert-Butylperoxy radicals were prepared directly in the cavity of the spectrometer by photolysis of di-*tert*-butyl ketone in oxygen-saturated solvent (toluene, fluorotrichloromethane, and carbon tetrachloride). ^{17}O enriched oxygen was purchased from Yeda Inc., Israel. The spin traps were gifts from Dr. E. Janzen (Guelph) and Dr. K. U. Ingold (NRCC, Ottawa).

The epr spectra were observed using a Varian E-4 spectrometer equipped with a variable temperature accessory. The microwave frequency was measured with a Syntron-Donner Model 6016 frequency counter, which also monitored the frequency of a proton magnetometer used to measure the magnetic field.

Results

tert-BuO_2· + *PBN*

The *tert*-butylperoxy radical is extremely persistent at −80°C and photolysis of di-*tert*-butyl ketone in oxygen-saturated toluene gave ca. 10^{-5} *M* of radical

[1]NRCC No. 16238.

[2]NRCC Research Associate 1975–1977.

Can. J. Chem. Downloaded from www.nrcresearchpress.com by 210.87.254.5 on 09/05/12
For personal use only.

which to all intents and purposes was completely stable. The radical did, however, disappear slowly upon the addition of PBN (10^{-2} *M*) to give two nitroxides **1** (a_N = 12.85 G, g = 2.0063) and **2** (a_N = 7.79 G; g = 2.0071). Neither of these radicals exhibited proton hyperfine splitting at this temperature.

The spectrum did not change as the temperature of the solution was slowly increased until −20°C when **1** resolved into a triplet of doublets (a_N = 13.42 G; a_H = 0.95 G; g = 2.0064). This nitroxide was not stable above 0°C and was replaced by the *tert*-butoxy adduct to PBN, **3** (a_N = 13.62 G; a_H = 1.72 G, g = 2.0064) (3).

The epr parameters for **1** are very similar to the parameters assigned to the *tert*-butylperoxy adduct to PBN by Merritt and Johnson (1). Confirmation that **1** was indeed α-*tert*-butylperoxybenzyl *tert*-butyl nitroxide was obtained by preparing ^{17}O enriched *tert*-butylperoxy and allowing it to react with PBN. The nitroxide **1** exhibited hyperfine splitting from one oxygen nucleus ($I = \frac{5}{2}$), a_O^{β} = 2.9 G at −60°C. There was no observable hyperfine splitting from the second oxygen.

The *tert*-butoxy adduct to PBN also exhibited hyperfine splitting from one oxygen nucleus, a_O^{β} = 5.05 G at 25°C.

It should be noted that the hydrogen and oxygen hyperfine splitting constants (hfsc) of the *tert*-butylperoxy and *tert*-butoxy adducts to PBN were dependent on the temperature. The oxygen-17 hfsc decreased with an increase in temperature while the proton hfsc increased with an increase in temperature. These temperature dependent hfsc's suggest that the nitroxides prefer a conformation with the oxyl group partially eclipsed by the *p* orbital containing the unpaired electron at low temperatures. Rotation about the N—C bond would increase as the temperature was increased with an associated decrease in a_O and increase in a_H.

The H-hfsc for **1** is comparatively small and the value at −20°C reflects an average C—H dihedral angle, θ_H = 74°. The value of θ_O is, therefore, most probably 14°.

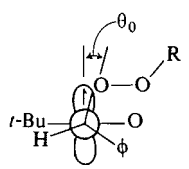

The H-hfsc for **3** is larger than it is for **1** and θ_H = 70°. The dihedral angle between the orbital containing the unpaired electron and the alkoxy group is, therefore, 10°. It would, therefore, appear that the most stable conformation for **3** has the alkoxy group eclipsed to a greater extent than the peroxy group in **1**.

tert-BuO$_2^{\cdot}$ + *tert-BuNO*

tert-Butylperoxy radicals reacted slowly with 2-methyl-2-nitrosopropane in toluene at −90°C to give di-*tert*-butyl nitroxide (a_N = 15.7 G, g = 2.0063) and *tert*-butoxy *tert*-butyl nitroxide (a_N = 27.25 G, g = 2.0057). At −20°C the concentration of these radicals increased substantially and the spectrum from benzyl *tert*-butyl nitroxide (4) developed (a_N = 14.75 G, a_H = 7.35 G; g = 2.0063). This latter radical almost certainly arose by addition of benzyl, formed by H-atom abstraction from the solvent, to the trap. There was no evidence for a spectrum that could be attributed to *tert*-butylperoxy *tert*-butyl nitroxide. If the *tert*-butylperoxy radical was prepared from ^{17}O enriched oxygen the spectrum from *tert*-butoxy *tert*-butyl nitroxide contained a hyperfine splitting from one oxygen-17 nucleus, a_O^{RO} = 1.03 G, at −40°C.

In a somewhat different experiment di-*tert*-butyl peroxide was photolyzed at −170°C in propane containing ^{17}O enriched oxygen. At this temperature some of the 2-propylperoxy radicals must combine with *tert*-butoxy radicals to give 2-propyl-*tert*-butyl trioxide (5) according to reactions 1, 2, and 3.

[1] $$(CH_3)_3COOC(CH_3)_3 \rightarrow 2(CH_3)_3CO^{\cdot}$$

[2] $$(CH_3)_3CO^{\cdot} + CH_3CH_2CH_3 \xrightarrow{O_2} (CH_3)_3COH + (CH_3)_2CHOO^{\cdot}$$

[3] $$(CH_3)_2CHOO^{\cdot} + (CH_3)_3CO^{\cdot} \rightarrow (CH_3)_2CHOOOC(CH_3)_3$$

The temperature of the solution was then increased and solid 2-methyl-2-nitrosopropane was added at −90°C. At this temperature epr spectra from di-*tert*-butyl nitroxide and the *tert*-butylperoxy radical were evident. Toluene was then added and the solution was saturated with argon. At −40°C the propane evaporated and no radicals could be detected. Upon warming to −10°C, di-*tert*-butyl nitroxide, an alkoxy *tert*-butyl nitroxide, benzyl-*tert*-butyl nitroxide, and a fourth radical, **4**, with a_N = 28.7 G, a_O = 4.6 G, g = 2.0056 were detected. This latter radical was either *tert*-butylperoxy *tert*-butyl nitroxide or isopropylperoxy *tert*-butyl nitroxide or a mixture of these radicals. It would, therefore, appear that the O-hfsc for alkylperoxy *tert*-butyl nitroxide is larger than a_O^{RO} for alkoxy *tert*-butyl nitroxide. This difference in O-hfsc's must reflect a difference in the extent of transfer of spin from the nitrogen nucleus to the oxygen orbitals arising from spin polarization. This difference is not unexpected as the ROO adduct has an electron

withdrawing group attached to the α-oxygen while the RO adduct has an electron donating group attached to this oxygen.

Other Spin Traps

tert-Butylperoxy radicals react rapidly at −90°C with a variety of other spin traps (nitrosobenzene, 2,4,6-tri-*tert*-butyl nitrosobenzene, and 5,5-dimethyl-1-pyrrolene-1-oxide). The epr spectra of the *tert*-$BuO_2^{\bullet}$ adducts were, however, either too complex or too unstable for these traps to be of much use as diagnostic probes for the intermediacy of alkylperoxy radicals in free-radical reactions.

1. M. V. MERRITT and R. A. JOHNSON. J. Am. Chem. Soc. **99**, 3713 (1977).
2. J. R. HARBOUR, V. CHOW, and J. R. BOLTON. Can. J. Chem. **52**, 3549 (1974).
3. (*a*) E. G. JANZEN and C. A. EVANS. J. Am. Chem. Soc. **95**, 8205 (1973); (*b*) B. B. ADELEKE, S-K. WONG, and J. K. S. WAN. Can. J. Chem. **52**, 2901 (1974).
4. G. CHAPELET-LETOURNEUX, H. LEMAIRE, R. LENK, M. A. MARECHAL, and A. RASSAT. Bull. Soc. Chim. Fr. 3963 (1968).
5. J. A. HOWARD. Can. J. Chem. **50**, 1981 (1972).

Can. J. Chem. Downloaded from www.nrcresearchpress.com by 210.87.254.5 on 09/05/12
For personal use only.

Studies of the rhenium–oxygen bond. II.[1] The crystal and molecular structure of μ-oxobis(*cis*-dichloro-*cis*-di(pyridine)-*trans*-oxorhenium(V)), $ORe(C_5H_5N)_2Cl_2ORe(C_5H_5N)_2Cl_2O$

COLIN JAMES LYNE LOCK[2] AND GRAHAM TURNER

Institute for Materials Research, McMaster University, Hamilton, Ont., Canada L8S 4M1

Received June 28, 1977

COLIN JAMES LYNE LOCK and GRAHAM TURNER. Can. J. Chem. **56**, 179 (1978).

The crystal structure of μ-oxobis(*cis*-dichloro-*cis*-di(pyridine)-*trans*-oxorhenium(V)), $ORe(C_5H_5N)_2Cl_2{\cdot}O{\cdot}Re(C_5H_5N)_2Cl_2O$ has been studied by single crystal X-ray methods. The crystals were orthorhombic with lattice parameters $a = 15.367(2)$, $b = 10.283(2)$, $c = 16.685(2)$ Å. The space group was $Pna2_1$ and there were four formula weights per unit cell. A total of 3339 reflections, of which 2990 were observed, were examined, and the structure refined by full matrix least squares (treating the pyridine rings as groups) to an R_2 value of 0.0449. The dimer had a roughly rectilinear O—Re—O—Re—O backbone with pairs of chlorine atoms and pyridine molecules arranged *cis* in each half of the dimer. The two halves of the dimer were arranged such that the pairs of *cis* atoms in one half were rotated about the Re(1)–Re(2) axis almost 113° when compared to the corresponding pair in the other half. Important bond lengths (Re—O(terminal), 1.715(16), 1.764(16); Re—O(bridging), 1.943(16), 1.903(16); Re—Cl, 2.356(5)–2.390(5); Re—N, 2.116(16)–2.180(16)) were close to previously observed values. The molecule was markedly disturbed from the idealized structure and this was caused by intramolecular non-bonded interactions.

COLIN JAMES LYNE LOCK et GRAHAM TURNER. Can. J. Chem. **56**, 179 (1978).

On a étudié la structure cristalline du μ-oxobis(*cis*-dichloro-*cis*-di(pyridine)-*trans* oxorhénium(V)), $ORe(C_5H_5N)_2Cl_2{\cdot}O{\cdot}Re(C_5H_5N)_2Cl_2O$, par la diffraction de rayons-X de monocristaux. Les cristaux sont orthorhombiques avec des paramètres de mailles $a = 15.367(2)$, $b = 10.283(2)$, $c = 16.685(2)$ Å. Le groupe d'espace est $Pna2_1$ et il y a quatre unités par maille. On a examiné un total de 3339 réflexions desquelles on a observé 2990; la structure a été affinée par la méthode des moindres carrés (matrice complète) (en traitant les cycles pyridiniques comme groupe) jusqu'à une valeur de R_2 de 0.0449. Le dimère possède un squelette O—Re—O—Re—O qui est approximativement rectiligne avec des paires d'atomes de chlore et de molécules de pyridine arrangées *cis* dans chaque moitié du dimère. L'arrangement des deux portions du dimère est tel que, par rapport à l'axe Re(1)–Re(2), les paires d'atomes *cis* dans une moitié sont tournés d'environ 113° lorsqu'on les compare avec la paire correspondante dans l'autre moitié. Les longueurs des liaisons importantes (Re—O(terminal), 1.715(16), 1.764(16); Re—O (le pont), 1.943(16), 1.903(16); Re—Cl, 2.356(5)–2.390(5); Re—N, 2.116(16)–2.180(16)) se rapprochent des valeurs observées antérieurement. La molécule existe sous une forme qui diffère considérablement de la structure idéalisée et ce phénomène provient d'interactions intramoléculaires non-liées.

[Traduit par le journal]

Introduction

We have been attempting to derive a relationship between Re—O bond lengths and the Re—O stretching frequencies and derived force constants. Although over 40 structures have been determined that contain Re—O bonds, relatively few compounds have both been examined in detail by vibrational spectroscopy, and have had the structures determined to an accuracy that allows a detailed mathematical relationship to be derived. We have been attempting to determine structures of compounds that might be suitable for spectroscopic examination and to redetermine other structures accurately where good spectroscopic data are available. One series of compounds that appeared to be worth investigating contained pyridine as a counter ligand. One of the compounds in this series is $Re_2O_3(C_5H_5N)_4Cl_4$. We have determined the structure of this compound by single crystal X-ray diffraction. Despite very careful work, the structure determination is not of sufficient accuracy to fulfil the original purpose of the work. Nevertheless, the structure is of interest since it is different from the structure assumed previously (2, 3). We report the structure of $Re_2O_3(C_5H_5N)_4Cl_4$ here.

[1]We regard the first paper in this series as the paper shown as ref. 1.

[2]To whom correspondence should be addressed.

Can. J. Chem. Downloaded from www.nrcresearchpress.com by 210.87.254.5 on 09/05/12
For personal use only.

Can. J. Chem. Downloaded from www.nrcresearchpress.com by 210.87.254.5 on 09/05/12
For personal use only.

Experimental

Preparation of μ-Oxo-bis(cis-dichloro-cis-di(pyridine)-trans-oxorhenium(V))

$Re_2O_3Cl_4(C_5H_5N)_4$

The compound was prepared by reacting $ReOCl_3((C_6H_5)_3P)_2$ (yellow–green isomer) with pyridine in benzene according to Method B of Johnson *et al.* (2). *Anal.* calcd. for $C_{20}H_{20}Cl_4N_4O_3Re_2$: C 27.3, H 2.3, N 6.4, Cl 16.1; found: C 27.4, H 2.4, N 6.4, Cl 15.3. Crystals suitable for X-ray studies were obtained by crystallization from acetone at 5°C.

Crystallography

The title compound crystallizes as green orthorhombic prisms. An irregularly shaped small crystal, roughly 0.10 × 0.07 × 0.16 mm, showing sharp extinctions every 90° when viewed by polarized light, was mounted along the longest dimension. Preliminary precession photographs indicated orthorhombic symmetry; photographs of the hkn (n = 0–2) and mkl (m = 0–2) layers showed systematic absences of the type $0kl$, $k + l = 2n + 1$ and $h0l$, $h = 2n + 1$, which indicated the possible space groups as $Pna2_1$ (#33) or $Pnam$ (an unconventional setting of $Pnma$) (#62).

The space group $Pna2_1$ was chosen; choice of this space group will be justified later.

The density of a few single crystals was obtained by flotation in a carefully degassed aqueous solution of zinc bromide. The crystal was transferred to a Syntex $P\bar{1}$ automatic diffractometer and accurate unit cell parameters were obtained by least squares refinement of 15 accurately centered reflections in the range $20° < 2\theta < 25°$. Crystal data were:

$C_{20}H_{20}Cl_4N_4O_3Re_2$ fw = 879
Orthorhombic, a = 15.367(2), b = 10.283(2), c = 16.685(2) Å, V = 2636.5(5) Å^3, $Pna2_1$, (#33), ρ_o = 2.20(1) g cm^{-3}, Z = 4, ρ_c = 2.21(1) cm^{-3} (22°, MoKα, λ = 0.71069 Å, μ = 101.2 cm^{-1}).

Intensity data were collected using MoKα radiation made monochromatic by reflection from the 002 face of an oriented mosaic single crystal of graphite. Data were collected using a coupled θ(crystal)–2θ(counter) scan up to $2\theta = 35°$. The scan rate was chosen by the program supplied with the instrument and varied from 8 to 24 deg min^{-1}. Above 35° most reflections were not significantly above background. The intensity of a standard reflection was monitored after every 49 reflections; the intensity of this standard showed only random fluctuation with a standard deviation of 2.4%. A total of 2705 reflections were collected in one quadrant (h, k, $\pm l$). After the removal of 328 reflections that were not above background, the remaining reflections were averaged, yielding 1347 symmetry independent reflections, of which 1025 were considered observed and 322 were considered unobserved (see ref. 4 for a detailed discussion of data processing). Data were corrected for Lorentz and polarization effects, but not for absorption. The coarse features of the structure were obtained from this data set.

A second data set was obtained from a larger crystal, which was hand cut from a very large plate. The crystal used was a parallelpiped with one corner removed and was bounded by the faces {100}, {010}, {001}, and {1$\bar{1}$0}. The sets of faces were 0.182, 0.090, 0.060, and 0.104 mm, respectively, from the centre of the crystal. The only difference in instrumental conditions was that the scan rate was varied from 4 to 24 deg min^{-1}. A total of 4349 reflections were collected in the hemisphere $\pm h$, $\pm k$, l to $2\theta = 55°$, the standard reflection, 2, 0, 4, being measured after every 49 reflections. The standard reflection showed only statistically random variation: the standard deviation was 1.43%. The 495 reflections that were not significantly above background were rejected. The remaining reflections were corrected for absorption on the basis of the dimensions given above,[3] and corrected for Lorentz and polarization effects as described previously. Symmetry equivalent reflections were averaged, leaving 2328 unique reflections of which 2015 were considered observed.

The final refinement obtained from this second data set was still unsatisfactory. The space group chosen was acentric, and because of the large anomalous dispersion correction of the rhenium atoms, Friedel's law should not apply. The independent data for the space group $Pna2_1$ are ($hkl = h\bar{k}l = \bar{h}kl = \bar{h}\bar{k}l$) ≠ ($hkl = \bar{h}kl = h\bar{k}l = \bar{h}\bar{k}l$). No data had been obtained for the hemisphere with negative l, where the Friedel's law inequivalencies would show up. A third data set was therefore collected.

This data set consisted of a complete sphere ($\pm h$, $\pm k$, $\pm l$) of low angle ($2\theta \leq 30°$) reflections. These data were collected on a Syntex $P2_1$ diffractometer with scan rates varying from 1.8 to 24 deg min^{-1}, depending on the intensity of the reflection. Three standard reflections from different areas of reciprocal space (5 −1 2, 7 −1 −2, and −2 0 −4) were measured after every 97 reflections. These standard reflections showed only statistically random variations with an overall standard deviation of 1.8%. A total of 3339 reflections were collected, of which 349 were rejected as being not significantly above background. The remaining 2990 reflections were corrected for absorption, Lorentz, and polarization effects. The crystal used for collecting these data was a regular parallelpiped, bounded by {100}, {010}, and {001}, these faces being 0.081, 0.013, and 0.032 mm, respectively, from the centre of the crystal. The crystal was mounted about b^*, and deliberately misset by 3° from this axis. The symmetry equivalent reflections were then averaged, leaving 1067 unique reflections, all of which were considered observed. These data were used in the final stages of refinement as outlined below. Of the 478 pairs of reflections of type hkl and $hk\bar{l}$ that were collected, 412 pairs did not differ by more than 3σ, 50 pairs differed by between 3σ and 5σ, and 16 pairs differed by more than 5σ.

Solution of the Structure

The Patterson diagram was solved, with some difficulty, to give two independent rhenium atoms at 0.29, 0.52, 0.5 and 0.20, 0.48, 0.29. This solution ruled out the centrosymmetric space group $Pnam$, with an eight-fold general position. In the chosen space group, $Pna2_1$, the coordinate z was defined by fixing the z coordinate of one rhenium atom. The two rhenium atom positions could not be transformed into one other by any of the symmetry operations of the space group $Pnam$. The space group choice was confirmed by the successful solution of structure.[4] There was, however, pseudosymmetry

[3]All calculations were carried out on a CDC6400 computer. The programs DATCO3, ABSORB, DATRDN, ORTEP were taken from the X-RAY 71 package. The full matrix least squares program CUDLS and group least squares program GROUPLS were written locally by J. S. Stephens. The Fourier program SYMFOU was written by J. S. Rutherford and the least squares plans program PALS by P. G. Ashmore.

[4]To eliminate completely the possibility of the space group $Pnam$, refinement was tried in this space group using each of the rhenium positions. R factors were 0.50. Attempts to add chlorine atoms led to no improvement in the R factor and caused the temperature factors to rise to completely unacceptable values.

Can. J. Chem. Downloaded from www.nrcresearchpress.com by 210.87.254.5 on 09/05/12
For personal use only.

between the two rhenium atom positions ($x_1 + x_2 \approx \frac{1}{2}$, $y_1 + y_2 \approx 1$). These values of y, close to, but not exactly, $\frac{1}{2}$, lead to broad peaks in the Patterson diagram. An initial structure factor calculation, phased on the two rhenium atoms, with fixed isotropic temperature factors and varying only the scale factor, gave $R_1 = 0.22$.[5] Variation of rhenium positional parameters and isotropic temperature factors (eight parameters, one rhenium atom z coordinate being fixed) gave $R_1 = 0.18$. An electron density difference synthesis revealed the positions of four chlorine, three oxygen, four nitrogen, and seven carbon atoms. Refinement of positional and isotropic temperature factors for all atoms gave $R_1 = 0.105$ (80 parameters). Subsequent refinement cycles and difference syntheses did not reveal the positions of four of the remaining carbon atoms of one pyridine ring. The final R factor was $R_1 = 0.079$, with the rhenium and chlorine atoms having anisotropic temperature factors, for a total of 125 variable parameters. The esd's in bond lengths were quite large (e.g. Re—O(terminal), 1.74(6) Å), in view of the relatively low R factor. A decision was made at this point to recollect data using a well shaped larger crystal, and then to apply an absorption correction.

The data from the second crystal and the final atom parameters from the first crystal were used as the basis for the least squares refinement. One cycle of refinement, varying only the scale factor, gave $R_1 = 0.0722$. A difference synthesis revealed the remaining four carbon atoms (C12, C13, C14, and C15). In all further cycles of refinement the chlorine and rhenium atoms were given anisotropic temperature factors. Refinement converged to $R_1 = 0.0563$ for 163 variable parameters. The pyridine rings did not show the expected geometry. Carbon–carbon bond lengths varied from 1.25 to 1.6 Å, and individual pyridine ring atoms showed large random shifts in each cycle without improving the refinement. The pyridine rings were treated as rigid groups, using the known geometry (5) by a method similar to that of Scheringer (6) and LaPlaca and Ibers (7). The program GROUPLS was used, which allows the variation of six group positional parameters and individual isotropic temperature factors for each atom in the group. Atom positions from the CUDLS refinement were used to generate the exact atomic positions of a rigid pyridine ring of standard geometry. The refinement converged to $R_1 = 0.0541$ (114 variable parameters). At this stage, the errors in the various Re—O bond lengths had dropped to 0.025 Å, which was still considered large. All refinements using this second set of data gave atomic positions that resulted in certain 'chemically' equivalent bond lengths in the different halves of the dimer being significantly different. Although there are no symmetry requirements relating equivalent parts of the two halves of the dimer, it seems reasonable to suppose that atoms that have superficially similar environments should have similar bond lengths. It was felt that many of the difficulties in refinement and in the structural parameters would be resolved if the Friedel independent data (in this case hkl and $hk\bar{l}$) were used in refinement. Accordingly, the third set of data was collected and used in refinement. These data were included in a third refinement of the structure. This third refinement used the following reflection data: 1067 reflections with $2\theta \leq 30°$, collected from the third crystal, which were averaged with the equivalent reflections from the second crystal; 1754 reflections with $30° < 2\theta < 55°$ from the second crystal; a total of 2821 reflections were used in this final refinement.

After correction for secondary extinction by the method of Larsen (8) a weighting scheme was applied such that $\omega/||F_o| - |F_c||^2$ was locally independent of F_o and sin θ/λ.[6] Refinement converged to $R_1 = 0.0453$ and $R_2 = 0.0449$. In the final cycle of refinement, no parameter shifted by more than 1/12 of its error; the average shift was 0.01σ. A final difference synthesis revealed no peak greater than 0.93 e/Å^3 (at 0.29, 0.51, 0.50, close to Re(1)) and no valley less than -0.52 e/Å^3 (at 0.28, 0.49, 0.49, also close to Re(1)). In all calculations the atomic scattering factors for the neutral atoms were taken from the *International Tables for X-ray Crystallography* (9) and anomalous dispersion corrections (10) were used for rhenium and chlorine. The final atom parameters are given in Table 1 and the moduli for F_o and F_c are given in Table 2.[7]

Discussion

The molecule is pictured in Fig. 1 and selected interatomic distances and angles are given in Table 3. The molecule has a pseudo-two-fold axis through O(2). The pairs of pyridine rings in each half of the dimer are *cis*, in contrast to the suggested structure (3), in which, on the basis of vibrational spectra, the pyridine groups were considered to be *trans*. There are no symmetry requirements relating equivalent parts of the two halves of the dimer, but chemically equivalent bond lengths do not, in general, differ significantly. There are, however, marked differences in certain pairs of angles which might be expected to be equivalent. We suggest these effects may be caused by the exigencies of intramolecular packing.

The Re—N bond lengths (2.116(16)–2.180(16) Å) do not differ significantly and are similar to distances observed previously for similar compounds (range 2.11(2)–2.17(5) Å) (11, 12). The Re—Cl distances are not equivalent: the minimum and maximum values (2.356(5), 2.390(5) Å) differ by $4.80(\sigma_1^2 + \sigma_2^2)^{1/2}$. Nevertheless, neither of these values differs significantly from the intermediate values and all distances lie well within the range observed for Re—Cl bond lengths (2.182(7)–2.563(4) Å) (13, 14) and are close to the range, 2.37–2.38 Å, considered by Ibers and co-workers to be 'normal' (14, 15).

The Re—O(terminal) bonds (1.715(16), 1.764(16) Å) do not differ significantly, nor do the Re—O (bridge) bonds (1.903(16), 1.943(16) Å). Again, both sets of bonds agree reasonably well with values found with similar compounds containing the O—Re—O—Re—O framework (Re—O(terminal), range, 1.67(5)–1.723(7) Å; Re—O(bridge), range 1.903(5)–1.917(5)) (16–18).

[5] $R_1 = \dfrac{\Sigma||F_o| - |F_c||}{\Sigma|F_o|}$; $R_2 = \left\{\dfrac{\Sigma\,\omega(|F_o| - |F_c|)^2}{\Sigma\,\omega F_o^2}\right\}^{1/2}$

[6] ω was chosen such that

$$\omega = 1/(47.1 - 0.594|F_o| + 0.00255|F_o|^2).$$

[7] Table 2 is available, at a nominal charge, from the Depository of Unpublished Data, CISTI, National Research Council of Canada, Ottawa, Ont., Canada K1A 0S2.

Can. J. Chem. Downloaded from www.nrcresearchpress.com by 210.87.254.5 on 09/05/12
For personal use only.

TABLE 1

(*a*) Atom parameters for $ReO(C_5H_5N)_2Cl_2 \cdot O \cdot ReO(C_5H_5N)_2Cl_2$ ($\times 10^3$)*

Atom	*x*	*y*	*z*	*U* (Å²)
Re(1)	296.10(5)	521.58(7)	499.64(5)	See (*b*)
Re(2)	201.01(5)	467.92(7)	289.31(5)	See (*b*)
Cl(1)	436.4(3)	560.2(6)	447.9(4)	See (*b*)
Cl(2)	330.5(3)	297.4(5)	515.5(3)	See (*b*)
Cl(3)	60.8(3)	518.5(5)	342.8(4)	See (*b*)
Cl(4)	180.0(3)	245.0(5)	320.8(3)	See (*b*)
O(1)	321(1)	572(1)	598(1)	53(4)
O(2)	244(1)	493(1)	398(1)	22(2)
O(3)	164(1)	467(1)	192(1)	52(4)
N(1)	265(1)	722(1)	485(1)	36(4)
N(2)	166(1)	479(2)	544(1)	43(4)
N(3)	330(1)	422(2)	255(1)	44(4)
N(4)	228(1)	672(2)	273(1)	42(4)
C(11)	322(1)	812(2)	501(1)	41(4)
C(12)	303(1)	950(2)	496(1)	39(4)
C(13)	221(1)	984(2)	466(1)	53(4)
C(14)	160(1)	887(2)	443(1)	37(4)
C(15)	185(1)	757(2)	456(1)	39(4)
C(21)	127(1)	372(2)	514(1)	42(4)
C(22)	42(1)	329(2)	541(1)	44(5)
C(23)	0(1)	407(2)	597(1)	50(5)
C(24)	43(2)	521(2)	625(2)	60(7)
C(25)	123(1)	551(2)	598(1)	30(4)
C(31)	380(1)	347(2)	298(1)	47(5)
C(32)	466(1)	307(2)	277(1)	45(5)
C(33)	495(1)	356(2)	202(1)	56(6)
C(34)	447(2)	430(2)	155(2)	60(6)
C(35)	358(2)	464(2)	181(2)	58(7)
C(41)	308(1)	721(2)	295(1)	36(4)
C(42)	331(1)	849(2)	289(1)	48(5)
C(43)	265(1)	938(2)	260(1)	50(5)
C(44)	185(1)	882(2)	240(1)	55(6)
C(45)	164(1)	753(2)	245(1)	40(5)

(*b*) Anisotropic temperature factors U_{ij}($\times 10^3$)†

	U(11)	*U*(22)	*U*(33)	*U*(12)	*U*(13)	*U*(23)
Re(1)	22.4(4)	31.9(5)	27.7(6)	−1.5(3)	−5.3(4)	2.1(4)
Re(2)	26.7(5)	37.8(6)	30.7(6)	3.5(3)	−7.8(4)	−3.1(4)
Cl(1)	17(2)	74(4)	57(4)	−6(2)	0(2)	1(3)
Cl(2)	59(3)	36(3)	41(3)	9(2)	−7(2)	4(2)
Cl(3)	33(2)	48(3)	57(3)	2(2)	−4(2)	−6(3)
Cl(4)	47(3)	39(3)	41(3)	−8(2)	−3(2)	−9(2)

*Estimated standard deviations from the least squares program are given in parentheses in terms of the least significant figure.

†The temperature factor parameters U_{ij} were obtained from $\beta_{ij} = 2\pi^2 b_i b_j U_{ij}$ where β_{ij}'s appear as a temperature effect through $\exp[-(\beta_{11}h^2 + \ldots + \beta_{12}hk + \ldots)]$ in the structure factor expression and b_i are the reciprocal lattice vectors.

Examination of the least squares planes data (Table 4) and angular parameters (Table 3) shows some fairly marked distortions in the structure. In both planes 6 and 7 the ligand atoms lie in a plane, but for plane 7 the rhenium atom is displaced 0.10 Å from this plane. Figure 1*A* shows this displacement clearly; Re(2) is displaced away from O(2) and towards O(3). Of the other two ligand atom planes containing Re(2) and roughly at right angles to plane 7, plane 9 shows only a small distortion but the distortion in plane 8 is more marked. Any distortion is towards tetrahedral geometry. Thus, in plane 9, O(3) and O(2) are out of the plane in the opposite direction to Cl(4) and N(4). The two corresponding planes on Re(1) (10 and 11) showed a greater distortion, again towards a tetrahedral geometry. It should be noted that in planes 8, 10, and 11, if one considers the rhenium atom not to be displaced, then most of the distortion appears to arise from the position of the oxygen atoms.

In considering further details of the structure it is of interest to consider the other O—Re—O—Re—O

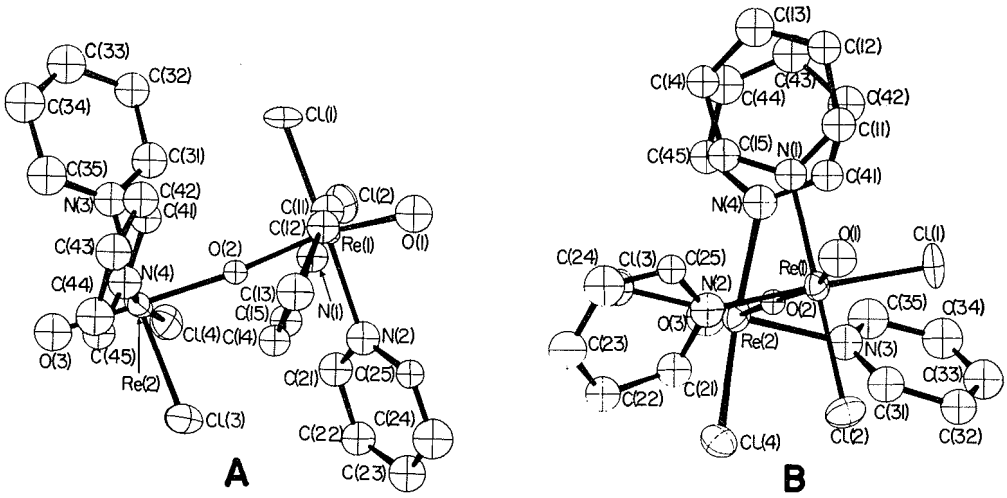

FIG. 1. The molecular structure of $ORe(C_5H_5)_2Cl_2 \cdot O \cdot Re(C_5H_5N)_2Cl_2O$ viewed from different directions. The numbering of the atoms is the same as in Table 1.

structures, namely those of $Re_2O_3(S_2CN(C_5H_5)_2)_4$ (17), $Re_2O_3Cl_4(NH_2 \cdot CH_2 \cdot CH_2 \cdot NH_2)_2$ (16), and $K_4Re_2O_3(CN)_8$ (18). Both $Re_2O_3Cl_4(NH_2 \cdot CH_2 \cdot CH_2 \cdot NH_2)_2$ and $K_4Re_2O_3(CN)_8$ have a centre of symmetry at the bridging oxygen atom and thus Re—O—Re is constrained to be rectilinear and the 'equatorial' ligands in one half of the dimer are eclipsed with respect to the other half. Fletcher and Skapski (17) have noted that for $Re_2O_3(S_2CN(C_2H_5)_2)_4$, where there is no centre of symmetry, the two halves of the dimer are rotated about the Re—O—Re bond by about 40° from the eclipsed position, but they have suggested no reason for this. In our compound no centre of symmetry is present and a similar twist is observed, although it is larger (113°). We suggest that in our molecule this twist is caused by the intramolecular packing requirements of the pyridine rings.

In considering the asymmetry of our molecule we were faced with questions such as "Why is there so much asymmetry in a formally very symmetric molecule?", "Why is this particular shape adopted; why not a system similar to $Re_2O_3Cl_4(en)_2$, where although the nitrogen atom positions in each half of this dimer are *cis*, the two halves are related by an inversion centre?", or "Since the monomer precursor has been postulated to have the pyridine rings *trans*, and the monomer ethanolysis product has been shown to have the pyridine rings *trans* (19), why is the structure not that postulated by Johnson *et al.* (2) and Cotton *et al.* (3)?"

Pyridine rings are very restrictive in their packing requirements (11), the α-protons interacting with other groups attached to the metal, and it appeared that interactions of the pyridine rings might provide the answer to all the above questions. We therefore made a series of very simple calculations, based on idealized structures and normal values for bond lengths and van der Waals radii.[8] Arguments on stability were based on differences between calculated non-bonded distances and sums of van der Waals radii. The calculations were applied first to the idea form of the structure observed, and in light of their success, to the other structures shown in Fig. 2.

To move the α-hydrogen atom away from a *cis* chlorine atom to the van der Waals contact distance it was necessary to rotate the pyridine ring about the Re—N bond by 61° from the position where all atoms are coplanar. Similarly, when the chlorine atom was replaced by an oxygen atom, the rotation of the pyridine ring was 66° (terminal) or 63° (bridging). Clearly, rotation of 60° could not be achieved, since in rotating away from a chlorine atom the ring rotated towards an oxygen atom. We could not calculate the final rotational angle, but since the ideal angle is close to 60° in each case, it seemed reasonable that the angle would be close to

[8]The following assumptions were made in all calculations: Re—Cl, 2.377 Å, Re—O (terminal), 1.73 Å; Re—O (bridging), 1.92 Å; Re—N, 2.15 Å; N—C, 1.34 Å; C—H, 1.08 Å; Re—N—C, 121.6°; N—C—H, 115.9°, the pyridine ring and the Re—N bond were coplanar, all *cis* angles at rhenium were 90°, van der Waals radii, Cl, 1.81 Å; O, 1.40 Å; H, 1.29 Å, pyridine ring half thickness, 1.7 Å. In the isomer calculations it was assumed the pyridine rings were rotated 45°, about the Re—N bond, from the position where the pyridine ring was coplanar with the rhenium–chlorine bond, unless another angle is specifically mentioned. In describing the direction of rotation, in every case it was assumed that the pyridine ring was viewed from the rhenium atom to which it was bonded.

Can. J. Chem. Downloaded from www.nrcresearchpress.com by 210.87.254.5 on 09/05/12
For personal use only.

Can. J. Chem. Downloaded from www.nrcresearchpress.com by 210.87.254.5 on 09/05/12
For personal use only.

TABLE 3. Selected interatomic distances and angles for $ORe(C_5H_5N)_2Cl_2 \cdot O \cdot Re(C_5H_5N)_2Cl_2O$

Atoms	Distance (Å)	Atoms	Distance (Å)
Re(1)—O(1)	1.764(16)	Re(2)—O(3)	1.715(16)
Re(1)—O(2)	1.903(16)	Re(2)—O(2)	1.943(16)
Re(1)—Cl(1)	2.356(5)	Re(2)—Cl(3)	2.390(5)
Re(1)—Cl(2)	2.380(5)	Re(2)—Cl(4)	2.374(5)
Re(1)—N(1)	2.135(14)	Re(2)—N(3)	2.116(16)
Re(1)—N(2)	2.180(16)	Re(2)—N(4)	2.156(16)
Atoms	**Angle (deg)**	**Atoms**	**Angle (deg)**
O(1)—Re(1)—O(2)	165.5(7)	O(3)—Re(2)—O(2)	172.8(7)
O(1)—Re(1)—Cl(1)	95.4(5)	O(3)—Re(2)—Cl(3)	93.3(6)
O(1)—Re(1)—Cl(2)	97.8(5)	O(3)—Re(2)—Cl(4)	99.1(5)
O(1)—Re(1)—N(1)	82.4(7)	O(3)—Re(2)—N(3)	92.8(7)
O(1)—Re(1)—N(2)	86.7(7)	O(3)—Re(2)—N(4)	87.3(6)
Cl(1)—Re(1)—Cl(2)	90.0(2)	Cl(3)—Re(2)—Cl(4)	90.3(2)
Cl(1)—Re(1)—N(1)	90.0(4)	Cl(3)—Re(2)—N(3)	173.9(5)
Cl(1)—Re(1)—N(2)	177.6(5)	Cl(3)—Re(2)—N(4)	90.4(4)
Cl(1)—Re(1)—O(2)	94.9(5)	Cl(3)—Re(2)—O(2)	85.9(5)
Cl(2)—Re(1)—N(1)	179.8(5)	Cl(4)—Re(2)—N(3)	88.3(5)
Cl(2)—Re(1)—N(2)	88.5(5)	Cl(4)—Re(2)—N(4)	173.5(4)
Cl(2)—Re(1)—O(2)	92.4(5)	Cl(4)—Re(2)—O(2)	88.1(5)
N(1)—Re(1)—N(2)	91.6(6)	N(3)—Re(2)—N(4)	90.3(6)
N(1)—Re(1)—O(2)	87.5(6)	N(3)—Re(2)—O(2)	88.1(6)
N(2)—Re(1)—O(2)	83.3(6)	N(4)—Re(2)—O(2)	85.6(6)
Re(1)—N(1)—C(11)	121(2)	Re(2)—N(3)—C(31)	122(2)
Re(1)—N(1)—C(15)	119(2)	Re(2)—N(3)—C(35)	118(2)
Re(1)—N(2)—C(21)	116(2)	Re(2)—N(4)—C(41)	120(2)
Re(1)—N(2)—C(25)	124(2)	Re(2)—N(4)—C(45)	120(2)
Re(1)—O(2)—Re(2)	174.5(9)		

Non-bonded distances

Atoms	Distance (Å)	Atoms	Distance (Å)
Cl(1)–O(1)	3.07(2)	Cl(1)–O(2)	3.15(2)
Cl(2)–O(1)	3.15(2)	Cl(2)–O(2)	3.11(2)
Cl(3)–O(3)	3.02(2)	Cl(3)–O(2)	2.97(2)
Cl(4)–O(3)	3.14(2)	Cl(4)–O(2)	3.02(2)
Cl(1)–N(1)	3.18(2)	Cl(1)–Cl(2)	3.350(7)
Cl(2)–N(2)	3.18(2)	Cl(3)–Cl(4)	3.378(7)
Cl(3)–N(4)	3.23(2)	N(1)–N(2)	3.10(2)
Cl(4)–N(3)	3.13(2)	N(3)–N(4)	3.08(2)
O(1)–N(1)	2.58(2)	O(2)–N(1)	2.80(2)
O(1)–N(2)	2.72(2)	O(2)–N(2)	2.72(2)
O(3)–N(4)	2.69(2)	O(2)–N(3)	2.83(2)
O(3)–N(3)	2.79(2)	O(2)–N(4)	2.79(2)
Cl(3)–C(21)	3.38(2)	Cl(1)–C(31)	3.44(2)
Cl(2)–Cl(4)	4.02(1)	C(14)–C(42)	3.71(2)
N(1)–C(41)	3.24(2)	C(14)–C(43)	3.51(2)
N(1)–N(4)	3.62(2)	C(14)–C(44)	3.42(2)
N(1)–C(42)	3.67(2)	C(14)–C(45)	3.60(2)
C(11)–Cl(42)	3.56(2)	C(15)–N(4)	3.24(2)
C(12)–C(42)	3.63(2)	C(15)–C(41)	3.31(2)
C(13)–C(42)	3.68(2)	C(15)–C(42)	3.71(2)
C(13)–C(43)	3.54(2)	C(15)–C(45)	3.55(2)

45° from either chlorine or oxygen atoms. Angles of rotation of roughly 45° are well established (20–23) and where no rotation is observed unusually long M—N distances are observed (24). In Table 4 it can be seen that the pyridine rings are rotated 37–51° from the position where they are coplanar with the rhenium and chlorine atoms.

Considering now the whole molecule, (*f*) in Fig. 2, when the first and fourth pyridine rings are rotated in the same sense by 45° their interplanar

TABLE 4. Planes and interplanar angles in $ORe(C_5H_5N)_2Cl_2 \cdot O \cdot ReCl_2(C_5H_5N)_2O$

Plane	Atoms	Distance from the plane (Å)
1	Re(1)O(2)Re(2)	
2	N(1)C(11)C(12)C(13)C(14)C(15)	N(1) + 0.02; C(11) − 0.03; C(12) + 0.02; C(13) + 0.01; C(14) − 0.02; C(15) + 0.01
3	N(2)C(21)C(22)C(23)C(24)C(25)	N(2) − 0.01; C(21) + 0.02; C(22) − 0.01; C(23)0; C(24) + 0.01; C(25)0
4	N(3)C(31)C(32)C(33)C(34)C(35)	N(3) + 0.01; C(31)0; C(32) − 0.01; C(33) + 0.01; C(34)0; C(35) − 0.01
5	N(4)C(41)C(42)C(43)C(44)C(45)	N(4)0; C(41) + 0.01; C(42) − 0.01; C(43)0; C(44) + 0.01; C(45) − 0.01
6	N(1)N(2)Cl(1)Cl(2)Re(1)	N(1) + 0.01; N(2) − 0.02; Cl(1) − 0.02; Cl(2) + 0.01; Re(1) + 0.02
7	N(3)N(4)Cl(3)Cl(4)Re(2)	N(3) + 0.02; N(4) + 0.03; Cl(3) + 0.02; Cl(4) + 0.03; Re(2) − 0.10
8	N(3)Cl(3)O(3)O(2)Re(2)	N(3) − 0.06; Cl(3) − 0.05; O(3) + 0.08; O(2) + 0.07; Re(2) − 0.04
9	N(4)Cl(4)O(3)O(2)Re(2)	N(4) + 0.02; Cl(4) + 0.02; O(3) − 0.02; O(2) − 0.02; Re(2)0.0
10	N(1)Cl(2)O(1)O(2)Re(1)	N(1) + 0.08; Cl(2) + 0.05; O(1) − 0.10; O(2) − 0.10; Re(1) + 0.07
11	N(2)Cl(1)O(1)O(2)Re(1)	N(2) − 0.10; Cl(1) − 0.08; O(1) + 0.11; O(2) + 0.10; Re(1) − 0.05

Planes	Dihedral angle (deg)	Planes	Dihedral angle (deg)
1–8	29	2–6	41
1–11	10	2–10	48
8–11	25	3–6	44
1–6	87	3–11	44
1–7	89	4–7	51
6–7	5	4–8	37
1–9	62	5–7	40
1–10	84	5–9	51
9–10	22	2–5	8
2–11	88	3–10	90
4–9	90	5–8	87

contact distance is 2.7 Å, much less than the van der Waals contact distance of 3.4 Å. The rings can be moved away from each other if one half of the dimer is twisted about the Re(1)—Re(2) vector. Calculations for an ideal model suggest this angle should be 26° compared with the observed angle of 23°. The twist can be seen in Fig. 1*B* and is illustrated more clearly in Fig. 3. Figure 1 *A* and *B* also shows that the effect of this twist is that, while it increases the interpyridine ring distance, it also brings the rings to a position where each lies more nearly over the other, which will increase the attractive London interaction between the polarizable π-clouds.

Further consideration of the twists of the second and third pyridine rings shows that the second ring comes in contact with Cl(3) (Cl(3)—C(21), 3.38(2) Å) and the third ring with Cl(1) (Cl(1)—C(31), 3.44(2) Å). The result is a very tightly packed molecule, and in particular, O(2), which should be the attack point for any reaction, such as hydrolysis or ethanolysis, which gives a monomer, is particularly well protected. Indeed, the only contact distance between the two halves of the dimer that is greater than the van der Waals contact distance is Cl(3)—Cl(4) at 4.02(1) Å. This may explain why ethanolysis of this molecule is such a slow reaction (19).

The twist of the second and third pyridine rings causes two further short interactions, namely between the hydrogen atom on C(31) and Cl(2) and the hydrogen atom on C(21) and Cl(4). These interactions can be relieved in two ways, either by angular distortions or by increasing the lengths of the Re—N or Re—Cl bonds.

The twist about the Re(1)—Re(2) axis required to move py1 and py4 apart shortens both the C(31)—Cl(2) and C(21)—Cl(4) distances. Other relevant angles show significant differences, however. Ignoring errors at this point, Re(2)—N(3)—C(31), 122(2)°, is the second largest Re—N—C angle, whereas Re(1)—N(2)—C(21), 116(2)°, is the smallest. O(2)—Re(2)—N(3), 88.1(6), is the largest O(2)—Re—N angle, while O(2)—Re(1)—N(2), 83.3(6) is the

Can. J. Chem. Downloaded from www.nrcresearchpress.com by 210.87.254.5 on 09/05/12
For personal use only.

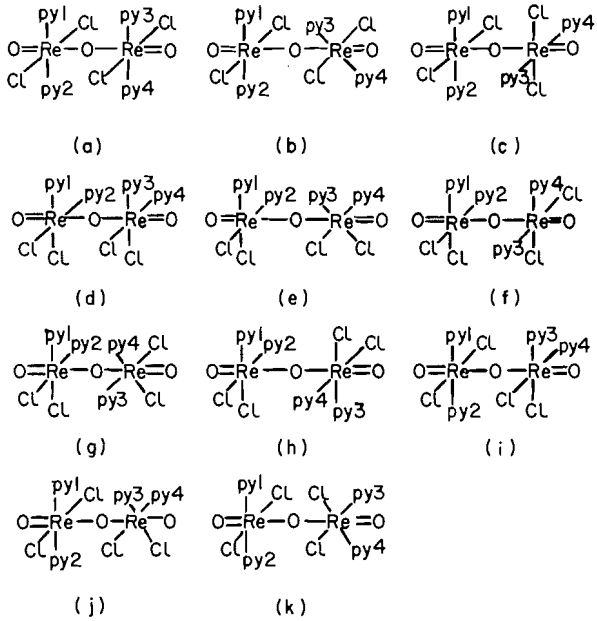

FIG. 2. Possible structures for conformations of $ORe(C_5H_5N)_2Cl_2{\cdot}O{\cdot}Re(C_5H_5N)_2Cl_2O$.

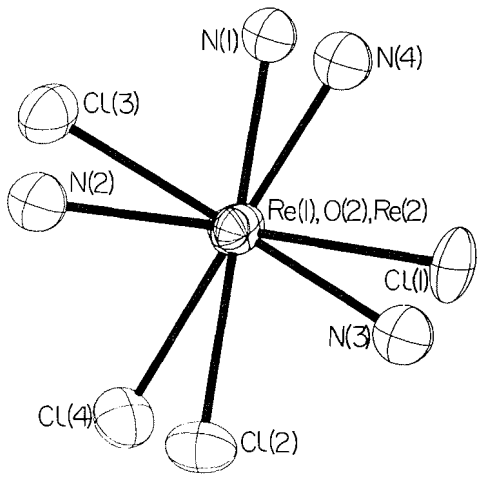

FIG. 3. The nearest neighbour 'equatorial' atoms of the rhenium atoms viewed as a projection down Re(1)—Re(2), and showing the rotation between the two halves of the dimer in $ORe(C_5H_5N)_2Cl_2{\cdot}O{\cdot}Re(C_5H_5N)_2Cl_2O$.

smallest of the four angles. Further, while O(2)—Re(1)—Cl(2), 92.4(5), is the second largest O(2)—Re—Cl angle and O(2)—Re(2)—Cl(4), 88.1(5) is the third largest angle they are significantly different as are all the pairs given above. Thus, angular relief may minimize the C(31)—Cl(2) interaction, but it is unlikely to do so for C(21)—Cl(4). Further calculation of the H—Cl distance, using H positions calculated from the ideal pyridine geometry (5), show that both H(C(21))—Cl(4) and H(C(31))—Cl(2) distances are ~2.7 Å. Thus, we suggest that for C(31)—Cl(2), the steric interaction is minimized by angular distortion but although Re(1)—N(2) has the longest mean Re distance, errors preclude the conclusion that the C(21)—Cl(4) interaction is relieved by bond lengthening.

Because the calculations we had undertaken on our molecule gave answers that were close to the observed parameters, (i.e., answering the first question) we have applied the calculations to other possible structures. The structures considered are shown in Fig. 2.

In (*c*), if the pyridine rings on one end of the dimer are rotated in the clockwise sense, then those on the other end must be rotated anticlockwise to minimize ring interaction. In this position there is interaction between an α-hydrogen on a ring and its eclipsed chlorine atom on the other end of the dimer. The distance is 2.80 Å. No reduction of this distance can be achieved by simple twists without increasing other repulsive interactions. The distance is very close to that observed for the two α-hydrogen–chlorine interactions in our molecule, although there are four such interactions in (*c*). The structure may be possible. A similar argument applies to (*h*).

For case (*a*), py1 and py3 must rotate in the same sense, as must py2 and py4. Further, a twist of about 25° must be introduced about the Re—O—Re bond between the two halves of the dimer to keep py1 and py3 (or py2 and py4) far enough apart. This twist is only possible if both py1 and py2 (and py3 and py4) are rotated in the same sense. In this position, however, the shortest distance between the α-hydrogen on a pyridine ring on one half of the dimer and a chlorine atom on the other half of the dimer is 2.53 Å, about 0.57 Å shorter than the van der Waals radii sum. Since there are four such contacts, and any angular distortion to increase one separation will only shorten another, it seems unlikely such an isomer can exist.

Similar calculations for (*b*) indicate an α-hydrogen chlorine interaction, with a distance of 2.56 Å. There are four such interactions, and again they cannot be relieved through angular distortion without increasing other interactions. Similar arguments apply to (*g*) and (*k*). Thus, we think these isomers are unlikely.

Any system with all rings eclipsed or with a ring on one end of the dimer lying between two rings on the other end (*d*, *e*, *j*) can be ruled out because of ring–ring interactions.

The final structure to consider is (*i*). As the structure is drawn, if py1 is rotated clockwise, so must py3 and py4 and this causes py2 to rotate anticlockwise. The molecule must rotate about Re—Re by

Can. J. Chem. Downloaded from www.nrcresearchpress.com by 210.87.254.5 on 09/05/12
For personal use only.

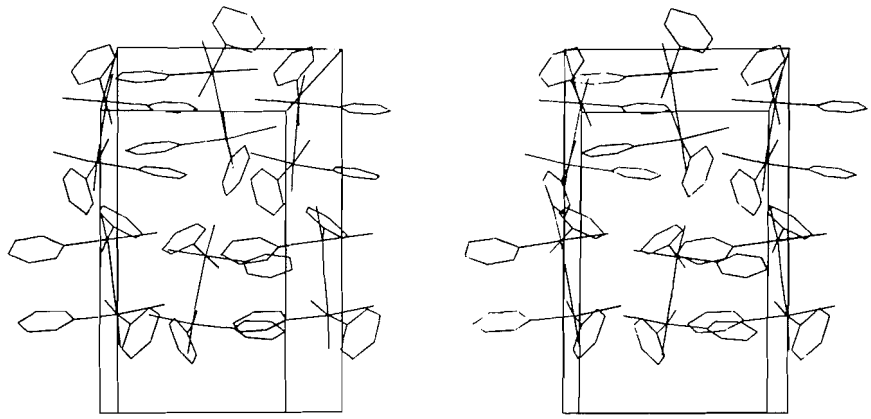

FIG. 4. Stereogram (stereoscopic pair of perspective projections) showing the packing of $ORe(C_5H_5N)_2Cl_2 \cdot O \cdot Re(C_5H_5N)_2Cl_2O$ within the unit cell. Six molecules are shown. The cell is viewed down the ***a*** axis and the ***b*** axis is parallel to the top of the page and the ***c*** axis is parallel to the side of the page.

23° to relieve the py1, py3 interaction and this twist causes py4 to interact with py2. Indeed, if py1, py2, and py3 are rotated to position and then the 23° twist is applied, py4 cannot rotate at all before coming into contact with py2. Thus, (*i*) is not possible.

In doing the calculations we ignored minor distortion that might stabilize a structure, but on the basis of calculations we can divide the structures into groups. They are: not possible, *d*, *e*, *i*, *j*; possible, unlikely, *a*, *b*, *g*, *k*; possible (four repulsions), *c*, *h*; possible (two repulsions), *f*; which is the conformation whose structure is reported in this paper. Thus, all the anomalies in the chemistry, and the answers to the questions posed earlier can be explained in terms of the intramolecular packing requirements of the pyridine rings.

The packing of the molecules in the unit cell is shown in Fig. 4. In the ***b*** direction the atoms Cl(2) and Cl(4) on one molecule are in contact with the hydrogen atoms on the first and fourth pyridine rings in the next translationally equivalent molecule. The small angle between the Re(1)—Re(2) axis and the *ac* plane means that Cl(4) actually fits in between the hydrogen atoms attached to C(13) and C(43).

In both the ***a*** and ***c*** directions the packing pattern is more complicated but the most important feature appears to be contact between chlorine or oxygen atoms and the pyridine rings. There is no parallel contact between pyridine rings, such as we have already noted in each individual molecule, or as we have observed before between molecules containing phenyl rings (25). In the ***c*** direction the chlorine and oxygen atoms on one molecule contact pyridine rings on a neighbour related by the 2_1 operation. In the ***a*** direction the packing can be described in two ways. The molecules are arranged such that the pair of parallel pyridine rings (1 and 4) point roughly along the ***b*** direction. The packing can then be considered about the glide planes at $y = 1/4$ and 3/4. In one case the pairs of molecules related by the *n* glide lie with the pairs of pyridine rings pointing towards the glide planes; in the other case it is Cl(2) and Cl(4) on each molecule which points at the planes. Nevertheless, in both cases the prime contact in the ***a*** direction is between chlorine atoms and pyridine rings, although there are pyridine–pyridine contacts close to the $y = 1/2$ plane. Thus there are no anomalous packing features in the structure and since all distances mentioned above are greater than or equal to the van der Waals contact distances, we conclude that intermolecular packing factors are not of major importance in determining the intramolecular structure.

Acknowledgment

We thank the National Research Council of Canada for financial support of this work.

1. C. J. L. LOCK and G. TURNER. Acta Crystallogr. Sect. B, **31**, 1764 (1975).
2. N. P. JOHNSON, F. I. M. TAHA, and G. WILKINSON. J. Chem. Soc. 2614 (1964).
3. F. A. COTTON, W. R. ROBINSON, and R. A. WALTON. Inorg. Chem. **6**, 223 (1967).
4. R. P. HUGHES, N. KRISHNAMACHARI, C. J. L. LOCK, J. POWELL, and G. TURNER. Inorg. Chem. **16**, 314 (1977).
5. B. BAK, L. HANEEN-HYGAARD, and J. RASTRUP-ANDERSEN. J. Mol. Spectrosc. **2**, 361 (1958).
6. C. SCHERINGER. Acta Crystallogr. **16**, 546 (1963).
7. S. J. LAPLACA and J. A. IBERS. Acta Crystallogr. **18**, 511 (1965).
8. A. C. LARSEN. Acta Crystallogr. **23**, 664 (1967).
9. D. T. CROMER and J. T. WABER. International tables for X-ray crystallography. Vol. IV. *Edited by* J. A. Ibers and W. C. Hamilton. Kynoch Press, Birmingham, England. 1974. Table 2.2A.

Can. J. Chem. Downloaded from www.nrcresearchpress.com by 210.87.254.5 on 09/05/12
For personal use only.

10. D. T. CROMER. International tables for X-ray crystallography. Vol. IV. *Edited by* J. A. Ibers and W. C. Hamilton. Kynoch Press, Birmingham, England. 1974. Table 2.3.1.
11. C. CALVO, N. KRISHNAMACHARI, and C. J. L. LOCK. J. Cryst. Mol. Struct. **1**, 161 (1971).
12. G. BETZNER. M.Sc. Thesis. McMaster University, Hamilton, Ontario. 1967.
13. C. CALVO, P. W. FRAIS, and C. J. L. LOCK. Can. J. Chem. **50**, 3607 (1972).
14. P. W. R. CORFIELD, R. J. DOEDENS, and J. A. IBERS. Inorg. Chem. **6**, 197 (1967).
15. R. J. DOEDENS and J. A. IBERS. Inorg. Chem. **6**, 204 (1967).
16. T. GLOWIAK, T. LIS, and B. JEZOWSKA-TRZEBIATOWSKA. Bull. Acad. Pol. Sci., Ser. Sci. Chim. **20**, 199 (1972).
17. S. R. FLETCHER and A. C. SKAPSKI. J. Chem. Soc., Dalton Trans. 1073 (1972).
18. R. SHANDLES, E. O. SCHLEMPER, and R. K. MURMANN. Inorg. Chem. **10**, 2785 (1971).
19. C. J. L. LOCK and G. TURNER. Can. J. Chem. **55**, 333 (1977).
20. F. MADAULE-AUBRY and G. M. BROWN. Acta Crystallogr. Sect. B, **24**, 745 (1968).
21. A. C. ANTSYSHKINA and M. A. PORAI-KOSHITS. Sov. Phys. Crystallogr. **3**, 684 (1958); **3**, 694 (1958).
22. M. A. PORAI-KOSHITS. Trudy Inst. Kristallogr., Akad. Nauk SSSR, **10**, 269 (1954).
23. D. J. HAMM, J. BORDNER, and A. F. SCHREINER. Inorg. Chim. Acta, **7**, 637 (1973).
24. R. J. DOEDENS and L. F. DAHL. J. Am. Chem. Soc. **88**, 4847 (1966).
25. C. J. L. LOCK and C. WAN. Can. J. Chem. **53**, 1548 (1975).

Can. J. Chem. Downloaded from www.nrcresearchpress.com by 210.87.254.5 on 09/05/12
For personal use only.

General method for the synthesis of [*n*.3.3]propellanes, $n \geq 3$

ROBERT W. WEBER AND JAMES M. COOK

Department of Chemistry, University of Wisconsin-Milwaukee, Milwaukee, WI 53201, U.S.A.

Received July 4, 1977

ROBERT W. WEBER and JAMES M. COOK. Can. J. Chem. **56**, 189 (1978).

Reaction of alicyclic-1,2-diones (**2***a–d*) with dimethyl 3-ketoglutarate **1** at room temperature in aqueous buffer (p*H* = 5.6) provided good yields of the tetramethylpropellanedione tetracarboxylates (**3***a–d*), respectively. Hydrolysis and decarboxylation of the β-ketoester functions, followed by Wolff–Kishner reduction of the corresponding propellanediones (**4***a–d*) has resulted in synthesis of [10.3.3]-, [6.3.3]-, [4.3.3]-, and [3.3.3]propellanes (**5***a–d*). The ^{13}C nmr of propellanes **5***a–c* are also reported.

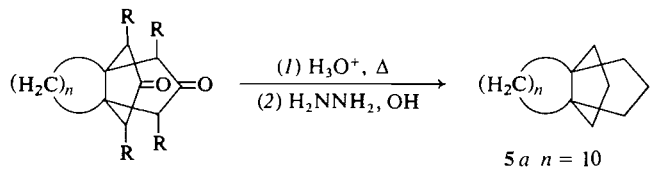

3 *a* $n = 10$ R = CO_2CH_3
b $n = 6$ R = CO_2CH_3
c $n = 4$ R = CO_2CH_3
d $n = 3$ R = CO_2CH_3

5*a* $n = 10$
b $n = 6$
c $n = 4$
d $n = 3$

ROBERT W. WEBER et JAMES M. COOK. Can. J. Chem. **56**, 189 (1978).

Les réactions de diones-1,2 alicycliques (**2***a–d*) avec le céto-3 glutarate de diméthyle (**1**) à température ambiante, dans un tampon aqueux (p*H* = 5.6) fournissent respectivement les tétraméthylpropellanedione tétracarboxylates **3***a–d* avec de bons rendements. L'hydrolyse et la carboxylation des fonctions β-cétoesters, suivie par une réduction de Wolff–Kishner des propellanediones correspondantes (**4***a–d*) conclut la synthèse des [10.3.3]-, [6.3.3]-, [4.3.3]- et [3.3.3]propellanes (**5***a–d*). On rapporte aussi les spectres rmn ^{13}C des propellanes **5***a–c*.

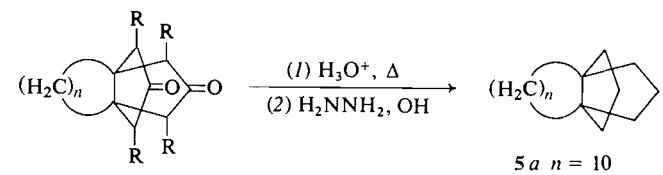

3 *a* $n = 10$ R = CO_2CH_3
b $n = 6$ R = CO_2CH_3
c $n = 4$ R = CO_2CH_3
d $n = 3$ R = CO_2CH_3

5*a* $n = 10$
b $n = 6$
c $n = 4$
d $n = 3$

[Traduit par le journal]

In 1965 the first reports of the preparation of compounds termed propellanes (1) appeared, and since that time these Y-shaped molecules have received much attention. Investigation of members of the series comprised of small rings has been stimulated by interest in the hybridization (2) and reactivity (3) of the bridgehead–bridgehead, central bond. Ultimately, this has resulted in the construction of a derivative of [2.2.2]propellane (4). In addition, interactions between blades of the individual propellane derivatives have been observed both chemically (5) and spectroscopically (5–7).

The reaction of α-dicarbonyl compounds with dimethyl 3-ketoglutarate **1**, studied recently in some detail, has resulted in preparation of several interesting cyclopentanoid compounds (8*a–d*). Most important for the present work is the reaction of 1,2-cyclododecanedione **2***a* with **1** to yield tetramethyl-[10.3.3]propellane-14,17-dione 13,15,16,18-tetracarboxylate **3***a* which was eventually converted into [10.3.3]propellane **5***a* (8*b*) (Scheme 1). This result, coupled with earlier work in the area (8*a*), has provided a facile, general method for the synthesis of [*n*.3.3]propellanes, $n \geq 3$.

Can. J. Chem. Downloaded from www.nrcresearchpress.com by 210.87.254.105 on 09/05/12
For personal use only.

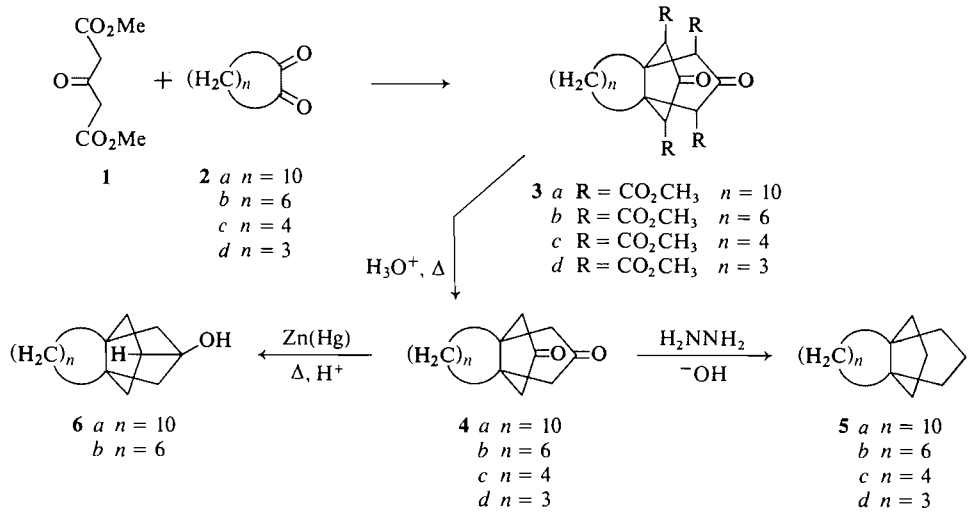

SCHEME 1

The appropriate cycloalkane-1,2-diones were dissolved in aqueous acidic buffer[1] and **1** was added to the mixture. After the mixture was stirred for several days, the tetramethylpropellanedione tetraesters precipitated from the solution. Using this method, the cyclic 1,2-diones **2***a–d* were converted into the corresponding β-ketoesters **3***a–d*, respectively, in yields ranging from 70–95%. Acid hydrolysis of the ester functions and decarboxylation, followed by Wolff–Kishner reduction of the appropriate propellanediones **4***a–d*, provided [10.3.3]-, [6.3.3]-, [4.3.3]-, and [3.3.3]propellanes **5***a–d*, respectively. Because of the various equilibria involved in formation of the tetraesters (8*c*) the proposed preparation of the [3.3.2]propellane system, via dimethylsquarate was unsuccessful. Presumably the strain involved in forming the [3.3.2] system was too great, hence the above procedure is limited to alicyclic-1,2-diones composed of five carbon atoms or more. Conversion of the β-ketoesters **3***a–d* into the propellanediones **4***a–d* was carried out in yields greater than 80%. The poorest reaction in the three-step sequence was the Wolff–Kishner reduction but this transformation was effected consistently at a level of 50% for propellanediones **4***a–d* (60% yield based on recovered starting material).

Clemmensen reduction of the propellanediones **4***a* and **4***b*, under reflux, provided the tetracyclic alcohols **6***a* and **6***b* but not the parent hydrocarbons (8*c*) **5***a* and **5***b*. However, if the Clemmensen reduction of **4***a–d* was carried out at room temperature for 3 weeks a 2–5% yield of the corresponding propellanes **5***a–d* could be obtained.

Although the prospect of rearrangement of the propellanediones under the conditions of reduction is somewhat limited, the ^{13}C nmr of the [10.3.3]-, [6.3.3]-, and [4.3.3]propellanes were recorded to determine if this had occurred. The propellanes described here belong to the C_{2v} point group; consequently, the number of lines in the ^{13}C nmr spectrum should correspond to half the number of equivalent carbon atoms present in the parent hydrocarbon. On examination of the carbon spectra this was found to be the case. In addition, the quaternary carbons could be easily identified at 51.21 ppm, 53.32 ppm, and 54.79 ppm in the [4.3.3]-, [6.3.3]-, and [10.3.3]propellanes, respectively, while the other signals appeared at chemical shifts quite consistent with the structures of the hydrocarbons (see Table 1). The signals in the proton nmr spectra of the propellanes **5***a–d* likewise correlate well with the chemical shifts of adsorptions from methylene groups contained in cyclopentane, cyclohexane, cyclooctane, and cyclododecane rings (9).

This route provides facile entry into a variety of [*n*.3.3]propellanes and could be extended to substituted [*n*.3.3]propellane derivatives. The limitations on extension of the method require that the starting dione **2** contain functionality stable both to acid hydrolysis and to base catalyzed reduction. Entry into these systems should provide templates for study of the steric interactions between blades of a homologous series of propellane derivatives.

Experimental

Microanalyses were performed on an F & M Scientific Corp. carbon, hydrogen, nitrogen analyzer model 185; some

[1]The actual citrate–phosphate buffer employed in this work had a p*H* of 5.6; however, addition of methanol to the reaction to solubilize the α-dicarbonyl compounds resulted in a p*H* of 6.0 to 6.8 depending on the amount of methanol necessary for dissolution of the diones.

Can. J. Chem. Downloaded from www.nrcresearchpress.com by 210.87.254.105 on 09/05/12
For personal use only.

TABLE 1. ^{13}C nmr chemical shifts[a]

Compound	Carbon atom	Chemical shift[b]	Signal intensity[c]	Proton coupled signal
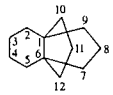	3+4[d]	21.42	59	t[e]
	2+5[d]	21.62	60	t
	8+11	31.98	49	t
	7+9, 10+12	37.54	100	t
5*c*	1+6	51.21	19	s[f]
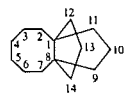	3+6[d]	24.41	54	t
	2+7[d]	24.24	49	t
	4+5[d]	27.04	54	t
	10+13	36.61	52	t
	9+11, 12+14	43.35	100	t
5*b*	1+8	53.32	19	s
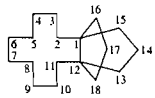	3+10[d]	23.73	58	t
	2+11[d]	24.03	61	t
	4+9[d]	24.05	61	t
	5+8[d]	26.26	54	t
	6+7[d]	27.92	54	t
	14+17	37.11	55	t
	13+15, 16+18	40.43	100	t
5*a*	1+12	54.79	17	s

[a]Measured in $CDCl_3$.
[b]$(CH_3)_4Si$ internal standard.
[c]Percent relative to intensity.
[d]The assignment of the shift to the methylene signals in the larger rings is tentative and is reported here solely to ensure a value for each set of carbon atoms.
[e]Triplet.
[f]Singlet.

analyses were carried out at the National Institutes of Health, Bethesda, MD. Melting points were taken on a Thomas-Hoover apparatus and are uncorrected. Nuclear magnetic resonance spectra were recorded on Varian T-60 and CFT-20 spectrometers. Infrared spectra were recorded on a Beckman Acculab-1 instrument while mass spectra were taken on an Hitachi RMU-6 mass spectrometer.

The citrate–phosphate buffer was prepared by dissolving $Na_2HPO_4 \cdot 7H_2O$ (11.67 g) and citric acid (3.68 g) in water (900.00 ml). Cyclohexane-1,2-dione was purchased from Aldrich Chemical Co.

Cyclododecane-1,2-dione **2***a* (10), cyclooctane-1,2-dione **2***b* (11), and cyclopentane-1,2-dione **2***d* were prepared by published methods. In a previous paper in this series we described the preparation of [10.3.3]propellane **5***a*, tetramethyl[6.3.3]propellane-10,13-dione 9,11,12,14-tetracarboxylate **3***b*, and [6.3.3]-propellane-10,13-dione **4***b* (8*b*).

[6.3.3]Propellane 5b

The propellanedione **4***b* (2 g, 9.1 mmol), hydrazine (11 ml of 95%), and KOH (9 g) were added to diethyleneglycol (40 ml). The resulting mixture was refluxed at 135°C for 2.5 h, at which time the water was distilled from the solution until the pot temperature reached 220°C. The water which distilled from the reaction was extracted with ether (4 × 25 ml) and the combined extracts were dried (Na_2SO_4). The pot residue, which remained, was acidified (aqueous HCl) and then extracted with benzene (5 × 25 ml). The benzene extracts were combined and dried over Na_2SO_4. Evaporation of solvent from either the benzene extract or the ether extract provided a clear oil which contained **5***b*. The oils were combined and chromatographed on alumina (Skelly-B) to yield **5***b* (0.85 g, 50% yield), bp 275–277°C at 760 Torr; ir (neat): 2940 and 2860 cm^{-1}; nmr ($CDCl_3$) δ: 1.50–1.60 (two overlapping singlets); ms *m/e*: 192 (M^+, 81.3), 164 (100), 149 (97.3), 135 (100), 122 (98), and 108 (60). *Anal.* calcd. for $C_{14}H_{24}$: C 87.42, H 12.58; found: C 87.30, H 12.30.

Tetramethyl[4.3.3]propellane-8,11-dione 7,9,10,12-Tetracarboxylate 3c

Cyclohexane-1,2-dione **2***c* (10 g, 0.09 mol) was dissolved in citrate–phosphate buffer (500 ml, p*H* = 5.6) and **1** (31 g, 0.18 mol) was added. After the solution was stirred at room temperature for 2 h, a white precipitate began to form. The mixture was stirred for an additional 2 weeks and then the solid was filtered from the reaction to provide **3***c* (25 g, 70% yield), mp 171–175°C (from methanol); ir (KBr): 2940 (C—H), 1730 (C=O), and 1650 cm^{-1} (enol form of β-ketoester); nmr ($CDCl_3$) δ: 1.45 (4H, m), 1.91 (4H, m), 3.66 (15H, several overlapping singlets of unequal intensity), and 9.90 (1H, s); ms *m/e*: 424 (M^+). *Anal.* calcd. for $C_{20}H_{24}O_{10}$: C 56.60, H 5.70; found: C 56.33, H 5.74.

When **2***c* and **1** were stirred for 2 weeks at p*H* = 8.4 and the solution was then acidified, an 81% yield of crystalline **3***c* was obtained.

[4.3.3]Propellane-8,11-dione 4c

The tetraester **3***c* (5 g, 0.012 mol) was added to hydrochloric acid (100 ml, 6 *N*) and the resulting mixture refluxed for 10 h. A portion of the acid was removed under reduced pressure. The residue was basified with aqueous sodium bicarbonate and then extracted with chloroform (5 × 25 ml). The combined organic extracts were dried over Na_2SO_4. Removal of solvent under reduced pressure furnished an oil which crystallized from methanol to provide **4***c* (1.6 g) in 71% yield, mp 173–174°C; nmr and ir spectra were identical to the spectra obtained on an authentic sample of **4***c* (8*a*).

[4.3.3]Propellane 5c

The propellanedione **4***c* (2 g, 0.01 mol) was added to a mixture of hydrazine (11 ml of 95%), potassium hydroxide (9 g), and diethyleneglycol (40 ml). The slurry was refluxed at 136°C for 2.5 h after which the water was distilled from the reaction until the pot temperature reached 220°C. During the distillation **5***c* crystallized on the condenser. The product was re-

Can. J. Chem. Downloaded from www.nrcresearchpress.com by 210.87.254.105 on 09/05/12
For personal use only.

moved from the condenser and the distillate by washing with ether. The combined extracts were dried (Na_2SO_4) and the ether removed under reduced pressure to provide a white solid **5***c* (0.7 g, 41% yield), mp 100–101°C (from methanol). When the residue from the distillation was acidified and extracted with ether, additional amounts of **5***c* (0.2 g) were obtained: total yield 50%. The combined solids were chromatographed on alumina (Skelly-B) and further purified by vacuum sublimination; nmr ($CDCl_3$) δ: 1.40 (8H, s) and 1.58 (12H, s); ir (KBr): 2920 and 2860 (C—H); ms *m/e* 164 (40, M^+), 136 (60), 121 (100), 107 (13). *Anal.* calcd. for $C_{12}H_{20}$: C 87.73, H 12.27; found: C 87.48, H 12.00.

[3.3.3]Propellane **5***d*

The [3.3.3]propellanedione **4***d* was prepared from **1** and **2***d* by a sequence of reactions exactly analogous to those reported for preparation of the [4.3.3]propellanedione **4***c* (see above), mp 185–187°C (lit. (8*a*) 183°C). The dione **4***d* was then reduced to [3.3.3]propellane **5***d* by the same method employed to prepare the [4.3.3]propellane. The yield of **5***d* was 49%, mp 130°C (lit. 133°C); ir (KBr): 2940 and 2860 cm^{-1}; nmr ($CDCl_3$) δ: 1.50 (this compound **5***d* was prepared independently by Professor Roger Alder, private communication, who kindly provided us with the experimental details of his procedure).

*Conversion of the [*n*.3.3]Propellanediones to [*n*.3.3]Propellanes by Clemmensen Reduction*

Mercuric chloride (0.2 g) was dissolved in a mixture of water (2 ml) and concentrated hydrochloric acid (0.4 ml). To the resulting solution zinc dust (2 g) was added slowly, with stirring. After 5 min the stirring was discontinued and the aqueous solution was decanted from the small lumps of zinc amalgam which had formed. The propellanedione was then added to the amalgam, followed by addition of a solution of concentrated HCl (4 ml), glacial acetic acid (2 ml), and water (1 ml). Many of the propellanediones were not soluble under the above reaction conditions; therefore, acetic acid was added to the reaction 3 days later. Because acetic acid would decompose the amalgam, small portions of amalgam (1 g) had to be added to the mixture five times over the course of a 3 week period. The reaction mixture was stirred at room temperature for 3 weeks.

The amalgam was filtered from the mixture and the mother liquor then made basic with sodium hydroxide (50 ml, 6 *N*). Extraction of the basic solution with ether followed by removal of the ether under reduced pressure provided an oil which was chromatographed on Al_2O_3 to provide small amounts (2–5%) of the propellanes **5***a–d*.

1. G. Snatzke and G. Zanati. Liebigs Ann. **684**, 62 (1965); F. Nerdel, K. Janowsky, and D. Frank. Tetrahedron Lett. 2979 (1965); S. Welner and D. Ginsburg. Isr. J. Chem. **4**, 39 (1966).
2. J. V. Silverton, G. W. A. Milne, P. Eaton, K. Nyi, and G. H. Temme III. J. Am. Chem. Soc. **96**, 7429 (1974); W. D. Stohrer and R. Hoffmann. J. Am. Chem. Soc. **94**, 779 (1972).
3. K. B. Wiberg and G. J. Burgmaier. J. Am. Chem. Soc. **94**, 7396 (1972); M. D. Newton and J. M. Schulman. J. Am. Chem. Soc. **94**, 4392 (1972); J. J. Dannenberg and T. M. Prociv. J. Chem. Soc. Chem. Commun. 291 (1973); K. B. Wiberg, J. B. Hiatt, and G. J. Burgmaier. Tetrahedron Lett. 5855 (1968); P. E. Eaton and N. Kyi. J. Am. Chem. Soc. **93**, 2786 (1971).
4. P. E. Eaton and G. H. Temme III. J. Am. Chem. Soc. **95**, 7508 (1973).
5. D. Ginsburg. Propellanes—structure and reactions. Verlag Chemie, Weinheim. 1975.
6. J. J. Bloomfield and R. E. Moser. J. Am. Chem. Soc. **90**, 5625 (1968); S. C. Neely, R. Fink, D. Van der Helm, and J. J. Bloomfield. J. Am. Chem. Soc. **93**, 4903 (1971); J. M. Fritsch and J. J. Bloomfield. Spectroscopy Lett. **1**, 277 (1968); R. Gleiter, E. Heilbronner, L. A. Paquette, G. L. Thompson, and R. E. Wingard, Jr. Tetrahedron, **29**, 565 (1973).
7. J. F. Arnett and S. P. McGlynn. Presented at the 172nd National Meeting of the American Chemical Society, San Francisco, CA. 1976. Abstr. No. 198.
8. (*a*) U. Weiss and J. M. Edwards. Tetrahedron Lett. 4885 (1968); (*b*) S. Yang and J. M. Cook. J. Org. Chem. **41**, 1903 (1976); (*c*) S. Yang-Lan, M. Mueller-Johnson, J. Oehldrich, D. Wichman, J. M. Cook, and U. Weiss. J. Org. Chem. **41**, 4053 (1976); (*d*) J. Oehldrich, J. M. Cook, and U. Weiss. Tetrahedron Lett. 4549 (1976).
9. C. J. Pouchert and J. R. Campbell. The Aldrich Library of nmr spectra. Vol. I. Aldrich Chemical Co., Inc., Milwaukee, WI. 1974. pp. 31–32.
10. K. B. Sharpless, R. F. Laver, O. Repic, A. Y. Teranishi, and D. R. Williams. J. Am. Chem. Soc. **93**, 3303 (1971).
11. N. L. Allinger. Organic synthesis. Coll. Vol. IV. Wiley, New York, NY. 1963. p. 840; A. T. Blomquist and A. Goldstein. Organic synthesis. Coll. Vol. IV. Wiley, New York, NY. 1963. p. 838.

Can. J. Chem. Downloaded from www.nrcresearchpress.com by 210.87.254.105 on 09/05/12
For personal use only.

Rate and equilibrium constant measurements for gas-phase proton-transfer reactions involving H_2O, H_2S, HCN, and H_2CO

KENICHIRO TANAKA,[1] GERVASE I. MACKAY, AND DIETHARD K. BOHME[2]

Department of Chemistry and Centre for Research in Experimental Space Science, York University, Downsview, Ont., Canada M3J 1P3

Received July 15, 1977

KENICHIRO TANAKA, GERVASE I. MACKAY, and DIETHARD K. BOHME. Can. J. Chem. **56**, 193 (1978).

The flowing afterglow technique has been employed in the measurement of rate and equilibrium constants at 296 ± 2 K for unsolvated proton transfer reactions of the type $XH^+ + Y \leftrightarrows YH^+ + X$ and several solvated proton transfer reactions of the type $XH^+\cdot X + Y \leftrightarrows YH^+\cdot X + Y$ where X and Y may be H_2O, H_2S, HCN, or H_2CO. Where possible, direct comparisons are made with similar measurements performed with other techniques. The equilibrium constant measurements provide a measure of the relative proton affinities of H_2O, H_2S, HCN, and H_2CO and absolute values for $PA(H_2O) = 166.4 \pm 2.4$ kcal mol^{-1}, $PA(H_2S) = 170.2 \pm 1.8$ kcal mol^{-1}, and $PA(HCN) = 171.0 \pm 1.7$ kcal mol^{-1} when reference is made to $PA(H_2CO) = 170.9 \pm 1.2$ kcal mol^{-1} which can be derived from available thermochemical information. The rate constant measurements reinforce the generalization that unsolvated proton transfer involving simple molecules proceeds with high efficiency and provide information about the influence of solvation on this efficiency.

KENICHIRO TANAKA, GERVASE I. MACKAY et DIETHARD K. BOHME. Can. J. Chem. **56**, 193 (1978).

On a utilisé la technique d'écoulement post-luminescent dans le but de mesurer les constantes de vitesse et d'équilibre à 296 ± 2 K des réactions de transfert de protons non-solvatés du type $XH^+ + Y \leftrightarrows YH^+ + X$ et pour plusieurs réactions de transfert de protons solvatés du type $XH^+\cdot X + Y \leftrightarrows YH^+\cdot X + Y$ où X et Y peuvent être H_2O, H_2S, HCN ou H_2CO. Lorsque la possibilité existait, on a fait des comparaisons directes avec des mesures semblables effectuées par d'autres techniques. Les mesures de constante d'équilibre nous ont fourni une mesure des affinités relatives des protons pour H_2O, H_2S, HCN et H_2CO et des valeurs absolues pour $PA(H_2O) = 166.4 \pm 2.4$ kcal mol^{-1}, $PA(H_2S) = 170.2 \pm 1.8$ kcal mol^{-1} et $PA(HCN) = 171.0 \pm 1.7$ kcal mol^{-1} lorsque l'on se réfère à une valeur de $PA(H_2CO) = 170.9 \pm 1.2$ kcal mol^{-1} qui peut être obtenue à partir de données thermochimiques. Les mesures de constantes de vitesse renforcent la généralisation à l'effet que le transfert d'un proton non-solvaté impliquant des molécules simples se produit avec une grande efficacité et fournissent une information concernant l'influence de la solvatation sur cette efficacité.

[Traduit par le journal]

Introduction

Over the past few years a variety of gas-phase experimental techniques have been applied to the determination of the relative proton affinities of molecules through measurements which attempt to establish values for equilibrium constants of proton-transfer reactions of the type

$$[1] \qquad XH^+ + Y \rightleftarrows YH^+ + X$$

proceeding in partially ionized gas mixtures at both low and high total pressures (1). Such measurements have led to reports of relative proton affinity 'ladders' incorporating a large number and variety of inorganic and organic molecules. Absolute scales are assigned to such ladders usually with the aid of thermodynamic information gained from (nonequilibrium) photon or electron impact studies.

The purpose of this study is twofold. It is directed in part towards a determination of the absolute proton affinities of HCN, H_2S, and H_2O. Equilibrium constant measurements are attempted for reactions of type [1] which allow the construction of a relative proton affinity ladder which links these molecules to H_2CO. Absolute values for proton affinities are derived to within ±2 kcal mol^{-1} by referring to the proton affinity of H_2CO which can be established from the photoionization appearance potential measurements of H_2COH^+ from CH_3OH reported by Refaey and Chupka (2). Such an accuracy is acceptable for most chemical applications. The proton affinity of H_2O is, of course, of special importance and interest. Unfortunately, its value has experienced a considerable variation with time. Only very recently, equilibrium constant measurements made

[1]Present address: Institute for Molecular Science, Myodaiji, Okazaki, Aichi, Japan.

[2]Alfred P. Sloan Research Fellow, 1974–1976.

Can. J. Chem. Downloaded from www.nrcresearchpress.com by 210.87.254.40 on 09/05/12
For personal use only.

Can. J. Chem. Downloaded from www.nrcresearchpress.com by 210.87.254.40 on 09/05/12
For personal use only.

with a high-pressure pulsed electron-beam ion source mass spectrometer (3) and with low-pressure pulsed ion cyclotron resonance (4) have suggested values for $PA_{298}(H_2O) = 169 \pm 2$ and 170 ± 2 kcal mol^{-1}, respectively, which are somewhat higher than the value of 165 ± 3 kcal mol^{-1} previously preferred by Long and Munson (5).

Secondly, the equilibrium constant measurements chosen in this study allow direct comparisons to be made with similar measurements performed with other techniques which employ a variety of modes of ion production, containment, and detection and encompass a wide range of operating conditions such as total pressure, ion and neutral concentrations, temperature, reaction time, and ambient electric fields. Such comparisons, which have not been as frequent as one might have expected, are instructive in establishing the applicability and reliability of the various techniques which have been employed for such measurements (6–8).

Experimental

The experiments were performed with a flowing afterglow system in the manner described previously (9). The reactant ions $XH^+ = H_3O^+$, H_3S^+, H_2CN^+, and H_2COH^+ were established in a flowing hydrogen plasma by fast proton-transfer reactions of the type

$$[2] \qquad H_3^+ + X \rightarrow XH^+ + H_2$$

which proceed upon the addition of the appropriate gas X downstream of the ionizer. H_3^+ was established by the fast reaction

$$[3] \qquad H_2^+ + H_2 \rightarrow H_3^+ + H$$

Sufficient X was added to ensure that reaction 2 reached completion prior to the reaction region. H_3O^+ was also generated in a helium–water vapour plasma by the reaction

$$[4] \qquad H_2O^+ + H_2O \rightarrow H_3O^+ + OH$$

The neutral reactants were added sufficiently downstream of the ion production region to ensure thermalization of the XH^+ ions by collisions with the carrier gas molecules to the ambient temperature of 296 ± 2 K prior to reaction. The total pressure in the reaction region was in the range $P = 0.27$ to 0.65 Torr, the effective reaction length had values in the range $L = 59$–85 cm, and the average flow velocity had values in the range $\bar{v} = 7.3$–8.2×10^3 cm s^{-1}. At the end of the reaction region the plasma was sampled with a quadrupole mass spectrometer through a small orifice mounted at the tip of a sampling nose cone. The observed variations in the reactant and product ion signals as a function of reactant gas addition at a fixed addition of the back-reactant gas provided the raw data from which the rate and equilibrium constants were derived.

The gases used were helium (Linde, Prepurified Grade, 99.995% He), hydrogen (Linde, Very Dry Grade, 99.95% H_2), and H_2S (Matheson, C.P. Grade, 99.5% H_2S). The water vapour was derived from either boiled tap water or boiled distilled water. The HCN was prepared by the action of sulfuric acid on an aqueous solution of KCN (10), dried by passing over anhydrous $CaCl_2$, and further purified by distillation *in vacuo*. Monomeric formaldehyde was prepared from paraformaldehyde (Fisher Scientific, Purified Grade) by an adaptation of the method developed by Spence and Wild (11). Paraformaldehyde was distilled at low pressures at ~370 K. The formaldehyde was then dried by passing it through a cold trap at 195 K and frozen out at liquid nitrogen temperatures. A gaseous mixture of ~5% formaldehyde in helium was used in these studies. The partial pressure of the formaldehyde was maintained at between 5 and 7 Torr to avoid polymerization. The monomer could be stored at these pressures for several days with negligible polymerization.

All experiments were carried out at a room temperature of 296 ± 2 K.

Results

The results of the measurements of rate and equilibrium constants for the proton-transfer reactions investigated in this study are summarized in Tables 1 and 2. An account of the data analysis and sources of error has been given previously (9, 14). Complications which may arise as a result of diffusion, competing reaction channels, and clustering reactions of the reactant and product ions have also been dealt with in detail elsewhere (14, 15).

Reaction 5

$$[5] \qquad H_3O^+ + H_2S \rightleftharpoons H_3S^+ + H_2O$$

The reaction of H_3O^+ with H_2S was observed to proceed rapidly by proton transfer to produce H_3S^+. Equilibrium was achieved in both H_2 (eight experiments) and He (five experiments) carrier gases over a range of $P = 0.290$–0.65 Torr and flow of H_2O from 2.13 to 4.96×10^{18} molecules s^{-1}. There was no evidence for the occurrence of competing reaction channels and no serious complications were introduced into the data analysis under these conditions by the clustering reactions of H_3O^+ with H_2O and H_3S^+ with H_2S. Figure 1 illustrates the determination of k_5, k_{-5} and k_5/k_{-5} from a fit to the H_3O^+ decay, whereas Fig. 2 indicates the determination of K_5 from the variation of the product to reactant ion signal ratio (corrected for mass discrimination) with H_2S addition. The cluster ions $H_3O^+ \cdot H_2O$ and $H_3O^+ \cdot 2H_2O$ did not react rapidly with H_2S, $k \lesssim 10^{-12}$ cm^3 $molecule^{-1}$ s^{-1}. Their initial decay shown in Fig. 1 is due to the depletion in the reaction region of the precursor ions, H_3O^+ and $H_3O^+ \cdot H_2O$, respectively.

Trace amounts of SF_6 were added in one H_2 and one He experiment to test the validity of the assumption of equal diffusion losses for H_3O^+ and H_3S^+. The values derived for k_5/k_{-5} (from the fit to the H_3O^+ decay) and K_5 (from the ratio plot) were observed to be insensitive to the change in the mode of diffusion from ion–electron to ion–ion brought about by the added SF_6.

Can. J. Chem. Downloaded from www.nrcresearchpress.com by 210.87.254.40 on 09/05/12
For personal use only.

Reaction 6

[6] $H_3O^+ + HCN \rightleftharpoons H_2CN^+ + H_2O$

H_3O^+ was observed to react rapidly with HCN to produce H_2CN^+ in four experiments in which H_2 was used as the carrier gas. Equilibrium was achieved in all four experiments over a range of $P = 0.342$–0.405 Torr and a range of H_2O flow from 3.61 to 4.59×10^{18} molecules s^{-1}. Again there was no evidence for the occurrence of competing reaction channels and no serious complications were introduced into the data analysis by the occurrence of clustering reactions. $H_3O^+ \cdot H_2O$ appeared to react with HCN, $k = 1 \times 10^{-10}$ cm^3 $molecule^{-1}$ s^{-1}. A concomitant increase in the $m/e = 46$ signal suggested the occurrence of what might, in this context, be more appropriately regarded as a solvated proton-transfer reaction:

[7] $H_3O^+ \cdot H_2O + HCN \rightarrow H_2CN^+ \cdot H_2O + H_2O$

rather than a solvent 'switching' reaction:

[8] $H_3O^+ \cdot H_2O + HCN \rightarrow H_3O^+ \cdot HCN + H_2O$

The analysis of the behaviour of the $H_3O^+ \cdot 2H_2O$ signal was complicated by its overlap at $m/e = 55$ with $H_2CN^+ \cdot HCN$.

Reaction 9

[9] $H_3S^+ + HCN \rightleftharpoons H_2CN^+ + H_2S$

The equilibrium for this reaction was approached from both directions in H_2 carrier gas. Seven experiments were carried out in the forward direction over a range of $P = 0.362$–0.51 Torr and flow of H_2S from 0.247 to 3.24×10^{18} molecules s^{-1}. Proton transfer was the only observed reaction channel. Equilibrium was achieved in six experiments. The product H_2CN^+ was observed to react further at large additions of HCN to produce the cluster ion $H_2CN^+ \cdot HCN$. Our standard analysis (9) allowed a good fit to the H_3S^+ decay and the H_2CN^+/H_3S^+ ion signal ratio plot at additions of HCN below $\sim 1 \times 10^{18}$ molecule s^{-1}. At higher additions the rate of the reaction of H_2CN^+ with HCN appeared to approach that for the back reaction of H_2CN^+ with H_2S to an extent sufficient to drive the reaction slightly out of equilibrium (case 5 in ref. 14).

The perturbation introduced by the further reaction of the product ion with the added reactant gas apparent in the attainment of equilibrium in the forward direction was observed to be less severe in the reverse direction presumably as a result of the lower rate of association of H_3S^+ with H_2S. Five experiments were carried out in the reverse direction in H_2 carrier gas at pressures $P = 0.363$–0.61 Torr

TABLE 1. Summary of the measured values of k_f/k_r and K at 296 ± 2 K together with estimates of their accuracies

Reaction	k_f/k_r[a]				K[b]			
	N[c]	Forward	N	Reverse	N	Forward	N	Reverse
$H_3O^+ + H_2S \rightleftharpoons H_3S^+ + H_2O$	13	$(5.5 \pm 1.7) \times 10^2$			13	$(6.2 \pm 2.2) \times 10^2$		
$H_3O^+ + HCN \rightleftharpoons H_2CN^+ + H_2O$	4	$(4.1 \pm 1.2) \times 10^3$			4	$(3.8 \pm 1.3) \times 10^3$		
$H_3S^+ + HCN \rightleftharpoons H_2CN^+ + H_2S$	7	5.6 ± 1.4	5	4.8 ± 1.0	6	5.7 ± 1.4	5	4.8 ± 1.0
$H_3S^+ + H_2CO \rightleftharpoons H_2COH^+ + H_2S$	4	≤ 13	4	≥ 9.3	4	11.3 ± 4.5	4	9.2 ± 3.7
$H_2CN^+ + H_2CO \rightleftharpoons H_2COH^+ + HCN$	1	< 4	3	1.9 ± 0.7	2	1.6 ± 0.6	3	1.4 ± 0.5
$H_2CN^+ \cdot HCN + H_2CO \rightleftharpoons H_2COH^+ \cdot HCN + HCN$	1	8.9 ± 2.2			1	8.8 ± 2.2	3	8.6 ± 3.0
$H_2COH^+ \cdot H_2CO + HCN \rightleftharpoons H_2CN^+ \cdot H_2CO + H_2CO$					3	1.6 ± 0.6		

[a]Determined from a fit to the decay of the reactant ion (analysis B ref. 9) with a precision $\lesssim 20\%$.
[b]Determined from the slope of the ratio plot and corrected for mass discrimination (analysis C ref. 9) with a precision $\lesssim 20\%$.
[c]N represents the number of measurements.

Can. J. Chem. Downloaded from www.nrcresearchpress.com by 210.87.254.40 on 09/05/12
For personal use only.

TABLE 2. Summary of the experimental measurements of rate constants (10^{-9} cm^3 molecule^{-1} s^{-1}) and equilibrium constants at 296 ± 2 K

Reaction	$k_{forward}$[a]	N[b]	K[c]	N
$H_3O^+ + H_2S \rightleftharpoons H_3S^+ + H_2O$	1.9±0.1	13	(5.8±1.3)×10^2	26
$H_3O^+ + HCN \rightleftharpoons H_2CN^+ + H_2O$	3.5±0.3	11[d]	(4.0±0.9)×10^3	8
$H_3S^+ + HCN \rightleftharpoons H_2CN^+ + H_2S$	1.5±0.1	7	5.1±0.6	23
$H_3S^+ + H_2CO \rightleftharpoons H_2COH^+ + H_2S$	2.2±0.1	3	10.0±2.9	8
$H_2CN^+ + H_2CO \rightleftharpoons H_2COH^+ + HCN$	>1.6		1.6±0.3	8
$H_2CN^+\cdot HCN + H_2CO \rightleftharpoons H_2COH^+\cdot HCN + HCN$	0.60	1	8.8±1.8	5
$H_2COH^+\cdot H_2CO + HCN \rightleftharpoons H_2CN^+\cdot H_2CO + H_2CO$	≳0.1		1.6±0.6	3
$H_3O^+\cdot H_2O + H_2S \rightarrow H_3S^+\cdot H_2O + H_2O$	≲0.001			
$H_3O^+\cdot 2H_2O + H_2S \rightarrow H_3S^+\cdot 2H_2O + H_2O$	≲0.001			
$H_3O^+\cdot H_2O + HCN \rightarrow H_2CN^+\cdot H_2O + H_2O$	0.10	2		
$H_2CN^+\cdot HCN + H_2S \rightarrow H_3S^+\cdot HCN + HCN$	≲0.001			

[a]Values for $k_{forward}$ were determined using either analysis A or B (9). The limits given along with the mean value represent the precision. The accuracy is estimated to be ±20% for the reactions of H_3O^+, ±25% for the reactions of H_3S^+, and ±30% for the reactions of $H_2CN^+\cdot HCN$ and $H_3O^+\cdot H_2O$.

[b]N represents the number of measurements.

[c]The value of K represents the weighted mean together with the standard error of measurements of k_f/k_r and K in one or both directions of the reaction (12).

[d]Includes seven previous determinations (13).

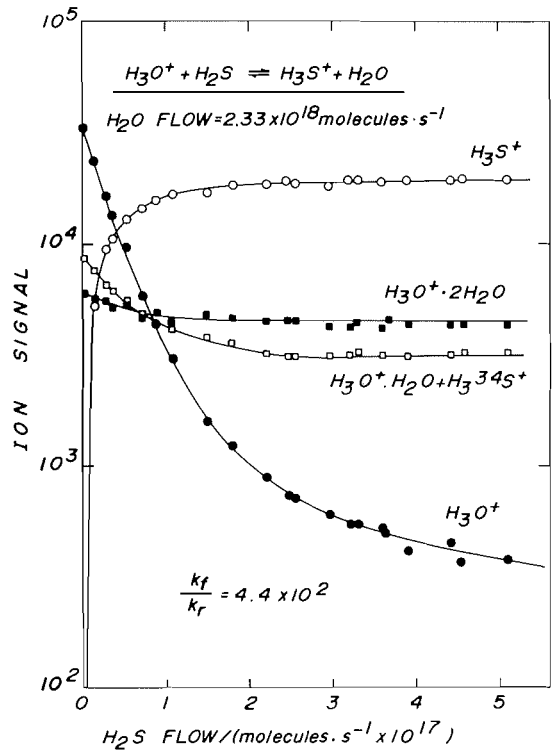

FIG. 1. The observed variation of H_3O^+, $H_3O^+\cdot H_2O$, and $H_3O^+\cdot 2H_2O$ upon the addition of H_2S into a H_2O–H_2 plasma in which H_3O^+ is initially a dominant ion. The solid line drawn through the H_3O^+ decay is a fit which provides the values $k_f = 1.9 \times 10^{-9}$ cm^3 molecule^{-1} s^{-1}, $k_r = 4.4 \times 10^{-12}$ cm^3 molecule^{-1} s^{-1}, and $k_f/k_r = 4.4 \times 10^2$ for the proton transfer to H_2S; $T = 296$ K, $P = 0.432$ Torr, $\bar{v} = 7.7 \times 10^3$ cm s^{-1}, and $L = 85$ cm.

and HCN flows in the range from 0.92 to 3.05 × 10^{17} molecules s^{-1}. The equilibrium constant derived from fits to the observed H_2CN^+ decays and the H_3S^+/H_2CN^+ ion signal ratio plots corrected

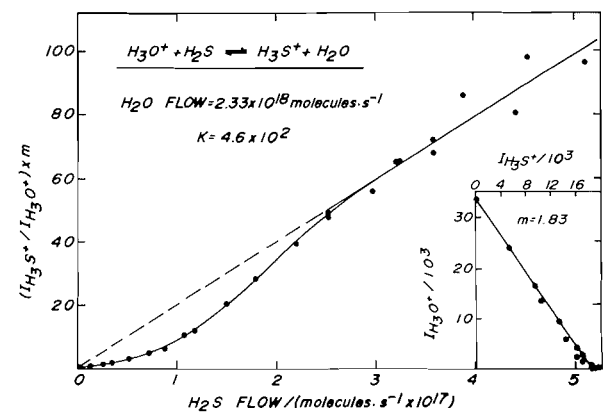

FIG. 2. The observed variation of the product to reactant ion signal ratio (corrected for mass discrimination) with the flow of neutral reactant, H_2S, at constant flow of neutral back reactant, H_2O. The initial curvature reflects the approach to equilibrium. The insert illustrates the determination of the mass discrimination factor, m; $T = 296$ K, $P = 0.432$ Torr, $\bar{v} = 7.7 \times 10^3$ cm s^{-1}, and $L = 85$ cm.

for mass discrimination was in good agreement with that determined from the study of the forward direction. The $H_2CN^+\cdot HCN$ present in the reaction region was observed not to react rapidly with the added H_2S, $k \gtrsim 10^{-12}$ cm^3 molecule^{-1} s^{-1}.

Reaction 10

[10] $H_3S^+ + H_2CO \rightleftharpoons H_2COH^+ + H_2S$

This reaction was also investigated in both directions in H_2 carrier gas. Four experiments were carried out in the forward direction over a range of P = 0.268–0.336 Torr and flow of H_2S from 2.04 to 9.6 × 10^{17} molecules s^{-1}. The results for one of these experiments is shown in Fig. 3 which indicates the production of H_2COH^+ from H_3S^+ as H_2CO is added into the flowing plasma. H_2COH^+ appears to

Can. J. Chem. Downloaded from www.nrcresearchpress.com by 210.87.254.40 on 09/05/12
For personal use only.

react further with H_2CO to form the cluster ion $H_2COH^+ \cdot H_2CO$ presumably via a three-body association reaction. The production of CH_3S^+, which was observed to be enhanced at the higher flows of H_2S, can be attributed to reaction 11 which is exothermic by several kcal mol^{-1}. Both reaction 11 and the association reaction of H_2COH^+ with H_2CO act as sinks for H_2COH^+ which compete with the reverse proton transfer [−10] and can prevent the establishment of true equilibrium. The incorporation of reasonable rates for these reactions into an extended analysis (case 2 and case 5 in ref. 14) indicated that the decay of H_3S^+ shows decreased curvature under these conditions so that the apparent value of k_{10}/k_{-10} determined from a fit to the H_3S^+ decay should be regarded as an upper limit to the true value. However the apparent value of the equilibrium constant determined from the ratio plot should still be nearly equal to the true value under these same conditions.

[11] $$H_2COH^+ + H_2S \rightarrow CH_3S^+ + H_2O$$

Four experiments were carried out in which H_2S was added into a flowing H_2 plasma in which H_2COH^+ was initially the dominant ion. Values of P were in the range 0.296–0.339 Torr and the flow of H_2CO had values in the range 0.71–1.95 × 10^{17} molecules s^{-1}. The proton-transfer reaction −10 was again observed to proceed in competion with reaction 11. Neither H_3S^+ nor CH_3S^+ appeared to react further with H_2S, $k \gtrsim 10^{-12}$ cm^3 $molecule^{-1}$ s^{-1}. The H_3S^+/CH_3S^+ ion signal ratio at saturation which was observed to be independent of H_2CO addition led to a value for $k_{-10}/k_{11} \cong 5$. In this case the extended analysis (case 4 in ref. 14) indicated that the apparent value of k_{-10}/k_{10} determined from a fit to the H_2COH^+ decay should be regarded as an upper limit to the true value and hence a lower limit to the true value of k_{10}/k_{-10}. However, the ratio plot should again provide a good measure of the true equilibrium constant.

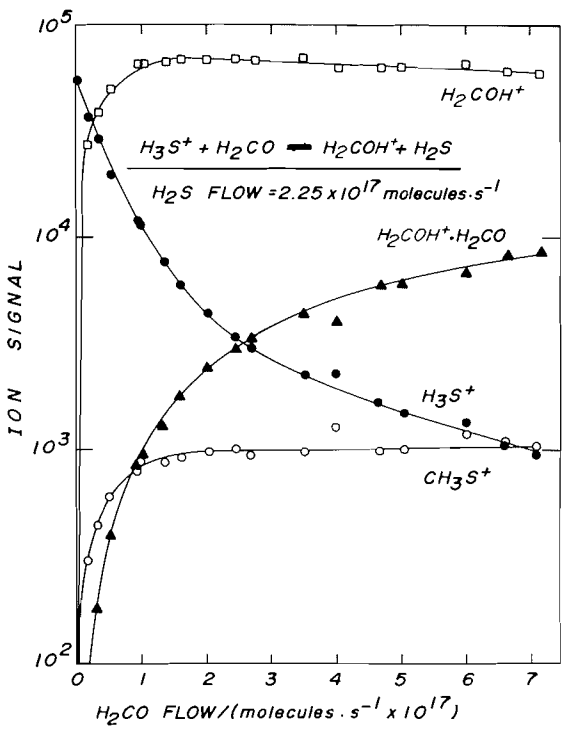

FIG. 3. The observed variation of ion signals with the flow of H_2CO at constant flow of H_2S. The solid line drawn through the H_3S^+ decay is a fit which provides values for $k_f = 2.1 \times 10^{-9}$ cm^3 $molecule^{-1}$ s^{-1} and $k_f/k_r \leq 15$; $T = 297$ K, $P = 0.308$ Torr, $\bar{v} = 7.5 \times 10^3$ cm s^{-1}, and $L = 59$ cm.

Reaction 12

[12] $$H_2CN^+ + H_2CO \rightleftharpoons H_2COH^+ + HCN$$

The interconversion of ions observed upon the addition of H_2CO into a flowing HCN–H_2 plasma in which H_2CN^+ is initially a dominant ion is illustrated in Fig. 4. H_2CN^+ appeared to react with H_2CO by proton transfer only to produce H_2COH^+ which reacted further with H_2CO to form the

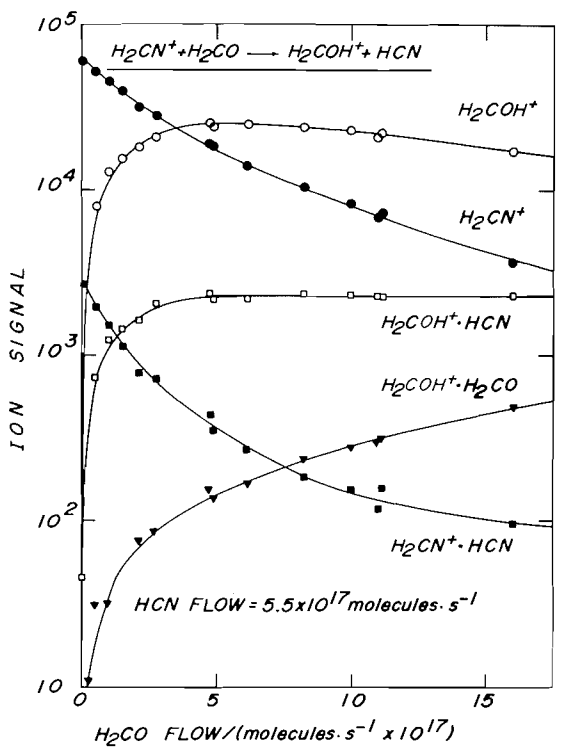

FIG. 4. The observed variation of ion signals with the flow of H_2CO at constant flow of HCN. The solid line drawn through the H_2CN^+ decay is a fit which provides values for $k_f \geq 1.6 \times 10^{-9}$ cm^3 $molecule^{-1}$ s^{-1} and $k_f/k_r < 4$; $T = 297$ K, $P = 0.371$ Torr, $\bar{v} = 8.1 \times 10^3$ cm s^{-1}, and $L = 85$ cm.

Can. J. Chem. Downloaded from www.nrcresearchpress.com by 210.87.254.40 on 09/05/12
For personal use only.

$H_2COH^+ \cdot H_2CO$ cluster ion. The rate of this latter reaction was sufficient to allow the determination of only a reliable upper limit to k_{12}/k_{-12} (case 5 in ref. 14) from a fit to the H_2CN^+ decay while the corresponding ratio plot still allowed a reasonable measure of K_{12}.

It is also apparent from Fig. 4 that $H_2CN^+ \cdot HCN$ reacts with H_2CO in a manner which may be represented by the solvated proton-transfer reaction

[13] $H_2CN^+ \cdot HCN + H_2CO \rightarrow H_2COH^+ \cdot HCN + HCN$

The decay of the $H_2CN^+ \cdot HCN$ signal and the $H_2COH^+ \cdot HCN/H_2CN^+ \cdot HCN$ ratio plot provided values for $k_{13} = (6 \pm 2) \times 10^{-10}$ cm^3 molecules^{-1} s^{-1} and $K_{13} = 8.9 \pm 2.2$.

The study of reaction 12 in its reverse direction allowed a more reliable determination of its equilibrium constant largely as a result of the somewhat slower rate of clustering of H_2CN^+ with HCN in the H_2 carrier gas. The values of k_{-12}/k_{12}, determined from a fit to the H_2COH^+ decay, and K_{-12}, determined from the H_2CN^+/H_2COH^+ ratio plot, were found to be in agreement within experimental error in three experiments in which P had values from 0.363 to 0.370 Torr and the flow of H_2CO had values in the range 4.72–8.1 $\times 10^{16}$ molecules s^{-1}. The $H_2COH^+ \cdot H_2CO$ cluster ion present in the flowing H_2CO–H_2 plasma was observed to react with HCN ($k \gtrsim 1 \times 10^{-10}$ cm^3 molecule^{-1} s^{-1}) in a manner which can be represented by the solvated proton-transfer reaction

[14] $H_2COH^+ \cdot H_2CO + HCN \rightarrow H_2CN^+ \cdot H_2CO + H_2CO$

The $H_2CN^+ \cdot H_2CO/H_2COH^+ \cdot H_2CO$ ratio plots indicated that equilibrium was established for this reaction at all flows of HCN and provided a value for $K_{14} = 1.6 \pm 0.6$. A ratio plot analysis of the further reaction of $H_2CN^+ \cdot H_2CO$ with HCN provided three additional determinations of $K_{13} = 8.6 \pm 3.0$ with the equilibrium state now being approached from the reverse direction.

Discussion

Equilibrium Constant Measurements

Confidence in the assertion that the equilibrium constants measured in this study represent true equilibrium is provided by the following observations, each of which is required for equilibria of elementary reactions such as those investigated in this study (7, 9, 15):

(*i*) The agreement between the ratios of rate constants determined from fits to the primary ion decays (which are independent of mass discrimination in the sampling system) and the equilibrium constants determined from the measured equilibrium ion concentrations (corrected for mass discrimination).

(*ii*) The constancy of the measured ratios of rate constants and equilibrium constants over the range in reaction time, neutral concentrations and total pressure adopted in these experiments. In the case of reaction 5, constancy was also observed over the range of electron and ion densities achieved by the addition of SF_6.

(*iii*) The independence of the measured ratios of rate constants and equilibrium constants on the direction of approach to equilibrium (in the case of reactions 9, 10, and 12).

(*iv*) The internal consistency between single-step and multi-step measurements. The equilibrium constant of $(5.8 \pm 1.3) \times 10^2$ determined from a direct study of the H_3O^+/H_3S^+ system agrees within experimental error with the value of $(7.8 \pm 2.7) \times 10^2$ determined indirectly from a study of the H_3O^+/H_2CN^+ and H_3S^+/H_2CN^+ systems. Also the value of 5.1 ± 0.6 for the equilibrium constant of the H_3S^+/H_2CN^+ system compares favourably with the value of 6.3 ± 3.0 which can be derived from the equilibrium constants determined for the H_3S^+/H_2COH^+ and H_2CN^+/H_2COH^+ systems.

A number of reported equilibrium constant measurements performed with a variety of experimental techniques are available for comparison, particularly in the case of reaction 5. These are summarized in Table 3. The deuterium analogue of reaction 5:

[15] $D_3O^+ + D_2S \rightleftarrows D_3S^+ + D_2O$

was investigated by Chong *et al.* (16) in electron impact ion source mass spectrometer experiments involving intensity measurements of D_3O^+ and D_3S^+ in mixtures of D_2O and D_2S in various known proportions at total pressures in the range 0.339–0.680 Torr. Chong *et al.* (16) reported a value for the equilibrium constant of 14.4 ± 1.9 at an ion source temperature of 340 ± 5 K. Hopkins and Bone (17) approached the equilibrium state for [5] in the reverse direction in a photoionization source in mixtures of pure H_2O and H_2S at total pressures ≤ 1.22 Torr and temperatures of 296, 355, and 426 K at which somewhat lower values of 6.7, 2.8, and 1.6, respectively, were obtained for the apparent equilibrium constant. Yamdagni and Kebarle (3) have recently investigated this equilibrium at higher temperatures in the range 570 to 660 K at total pressures in the range 0.5–4 Torr in a pulsed electron-beam ion source. High purity methane was used as the carrier gas in these latter experiments. Moet-Ner and Field (18) have also examined this equilibrium in a pulsed electron-beam ion source in a four-component mixture of 3% H_2O + 1% H_2S + 1% CS_2 in CH_4. In

Can. J. Chem. Downloaded from www.nrcresearchpress.com by 210.87.254.40 on 09/05/12
For personal use only.

TABLE 3. Measured equilibrium constants

Reaction	K	T/K	Method[a]
$D_3O^+ + D_2S \rightleftharpoons D_3S^+ + D_2O$	14.4 ± 1.9	340 ± 5	IS
$H_3O^+ + H_2S \rightleftharpoons H_3S^+ + H_2O$	6.7	296	IS–PI
	2.8	355	
	1.6	426	
	~ 10 to ~ 20	570 to 660	HPIS(YK)
	~ 30 to ~ 100	480 to 580	HPIS(MF)
	$(4.4 \pm 0.5) \times 10^{2}$[b]	303	ICR
	$(5.8 \pm 1.3) \times 10^{2}$	296 ± 2	FA
$H_3O^+ + HCN \rightleftharpoons H_2CN^+ + H_2O$	$(4.0 \pm 0.9) \times 10^{3}$	296 ± 2	FA
$H_3S^+ + HCN \rightleftarrows H_2CN^+ + H_2S$	2.8 ± 0.3	303	ICR
	5.1 ± 0.6	296 ± 2	FA
$H_3S^+ + H_2CO \rightleftarrows H_2COH^+ + H_2S$	6.2 ± 0.8	303	ICR
	10.0 ± 2.9	296 ± 2	FA
$H_2CN^+ + H_2CO \rightleftarrows H_2COH^+ + HCN$	2.3 ± 0.3	303	ICR
	1.6 ± 0.3	296 ± 2	FA

[a]IS, electron beam ion source mass spectrometer (16); IS-PI, photoionization source mass spectrometer (17); HPIS, pulsed electron beam high-pressure ion source mass spectrometer (3, 18); ICR, pulsed ion cyclotron resonance (4); FA, flowing afterglow, this work.
[b]Determined indirectly via proton transfer to CF_3CH_2OH but borne out by one direct measurement (see text).

these experiments the temperature was varied between 480 and 580 K at total pressures in the range 0.7–2.5 Torr. Recent pulsed ion cyclotron resonance measurements (4) of the equilibrium state at 303 K for the reactions

[16] $H_3O^+ + CF_3CH_2OH \rightleftarrows CF_3CH_2OH_2^+ + H_2O$

[17] $CF_3CH_2OH_2^+ + H_2S \rightleftarrows H_3S^+ + CF_3CH_2OH$

also provide a value for $K_5 = K_{16}K_{17} = (4.4 \pm 0.5) \times 10^2$ which was borne out by one direct measurement of K_5. These measurements were taken at a total pressure of $\sim 10^{-6}$ Torr in the absence of a carrier gas. The flowing afterglow measurements reported here were carried out at 296 ± 2 K in the presence of a large excess of either H_2 or He at total pressures in the range 0.290–0.65 Torr. The results of all six groups of investigators are compared in the Van't Hoff plot shown in Fig. 5. Reasonable agreement is apparent only between the extrapolated high-pressure ion source results of Yamdagni and Kebarle (3), the ion cyclotron resonance measurement at 303 K and the flowing afterglow result reported here. The higher values and temperature dependence of the equilibrium constant implied by the measurements of Moet-Ner and Field (18) lead to a difference of almost an order of magnitude at room temperature. The values of the equilibrium constants reported by Chong *et al.* (16) and Hopkins and Bone (17) are both lower by more than one order of magnitude from the corresponding extrapolated values. In the case of reactions 9, 10, and 12 further comparisons can be made between the results obtained with the ion cyclotron resonance and flowing afterglow techniques. It is apparent from the values given in Table 3 that the equilibrium constants determined with these two techniques for these three reactions disagree within the quoted experimental uncertainties, albeit never by more than a factor of 2.

There are several possible origins for the discrepancies between the various types of measurements. Differences may arise from uncertainties associated with the detection and measurement of ion signals and the measurement of neutral concentrations and temperature. The extent to which such uncertainties contribute to the observed differences could not be ascertained since an adequate assessment of the overall accuracy of the measurements was not always reported. Discrepancies may also arise from differences in conditions prevailing in the actual reaction regions of the various techniques, especially as regards the presence of ambient electric fields, the magnitudes of the temperatures as well as the partial and total pressures and the presence of a carrier gas. The influence of an ambient electric field on equilibrium constant measurements has recently been carefully investigated by Meisels *et al.* (8) particularly in conjunction with such measurements as they are carried out by high-pressure ion source mass spectrometry of the type employed by Chong *et al.* (16). In their systematic study of the equilibrium

[18] $CO_2H^+ + CH_4 \rightleftarrows CH_5^+ + CO_2$

these authors have observed a strong variation of the value of the equilibrium constant with field strength: for this exothermic reaction the equilibrium constant was observed to decrease substantially as the strength of the ambient field increased, viz. as the average ion energies were shifted upward and the ion velocity distributions lost Maxwell–Boltzmann character. On

Can. J. Chem. Downloaded from www.nrcresearchpress.com by 210.87.254.40 on 09/05/12
For personal use only.

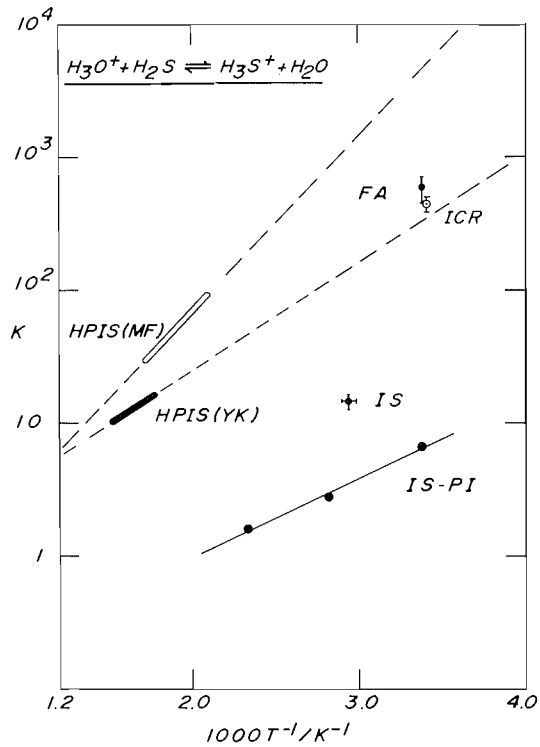

FIG. 5. Van't Hoff plot showing a comparison of the apparent equilibrium constants measured for the reaction $H_3O^+ + H_2S \rightleftarrows H_3S^+ + H_2O$ with a variety of experimental techniques: IS, electron beam ion source mass spectrometer (16); IS–PI, photo-ionization source mass spectrometer (17); HPIS, pulsed electron beam high-pressure ion source mass spectrometer (3, 18); ICR, pulsed ion cyclotron resonance (4); and FA, flowing afterglow, this work.

the basis of these observations, Meisels *et al.* (8) drew attention to the systematic error that can generally be introduced into equilibrium constant measurements with techniques which employ external fields unless the field strength approaches zero. A second complication is readily apparent from the observations reported by Hopkins and Bone (17) in their study of reaction 5 in its reverse direction. At the temperatures, partial pressures of H_2O and total pressures employed in their experiments, complications were introduced by the clustering of H_3O^+ to higher hydrates, an extraneous sink for H_3O^+ which must be properly taken into account in a complete data analysis. Apparently the rate of clustering of H_3O^+ in these experiments was sufficiently high to prevent the establishment of equilibrium between H_3O^+ and H_3S^+ at all convenient operating conditions. Not being able to determine equilibrium constants directly from a measured H_3O^+ ion signal ratio, these authors were led instead to analyze their data kinetically in terms of a steady state assumption. While the partial pressures of H_2O employed by Chong *et al.* (16) were similar to those used in the photoionization source experiments of Hopkins and Bone (17), those used in the flowing afterglow experiments, the ion cyclotron resonance experiments and the ion source experiments of Yamdagni and Kebarle (3) were many orders of magnitude lower. In the latter two sets of experiments the tendency of H_3O^+ to cluster was reduced still further by the lower total pressures and higher prevailing temperatures, respectively. We have recently considered in detail the constraints introduced into equilibrium constant determinations under flowing afterglow conditions by the occurrence of clustering reactions, indeed of competing reactions generally (14, 15). It was evident from these considerations that a judicious choice of partial pressures of the neutral reagents and the direction of approach to equilibrium is often required to ensure a successful determination of an equilibrium constant. A similar analysis has since been reported by ion cyclotron resonance practitioners (19) who have come to similar conclusions. Finally, only in the high-pressure ion source measurements and the flowing afterglow measurements reported here was it common practice to add a carrier gas in large excess. A carrier gas is normally required to allow both the reactants and products to establish thermal equilibrium with their common surroundings prior to reaction. The uncertainties introduced by the failure to use a carrier gas will be determined in part by the extent to which the product ions are initially formed in disequilibrium and can therefore be expected to be reaction specific. The extent to which the low values of equilibrium constant for [5] obtained in the experiments by Chong *et al.* (16) and Hopkins and Bone (17) which were carried out in pure H_2O/H_2S (D_2O/D_2S) mixtures and the differences between the ion cyclotron resonance and flowing afterglow results for reactions 5, 9, 10, and 12 can be accounted for in this way is uncertain.

Thermochemistry

The changes in standard free energy derived from the equilibrium constant measurements for the five unsolvated proton-transfer reactions and the two solvated proton-transfer reactions investigated in this study are summarized in Table 4. Changes in standard entropy were estimated from changes in molecular rotational symmetry numbers; viz, it was assumed that $\Delta S^0 \approx \Delta S^0_{rot}$ (3, 4). Such a treatment has recently been found to be valid to within ± 1.5 cal mol^{-1} deg^{-1} for a large number and variety of proton-transfer reactions (4). In the determination of the rotational symmetry numbers of the ions, account has been taken of what is known from calculations about their geometry (20, 21). The use of

TABLE 4. Changes in the standard free energy (kcal mol^{-1}), standard entropy (cal mol^{-1} deg^{-1}), and standard enthalpy (kcal mol^{-1}) at 298 K

Reaction	$-\Delta G^0_{298}$[a]	ΔS^0_{298}[b]	$-\Delta H^0_{298}$[c]
$H_3O^+ + H_2S \rightleftharpoons H_3S^+ + H_2O$	3.8±0.2	0 ±1.5	3.8±0.6
$H_3O^+ + HCN \rightleftharpoons H_2CN^+ + H_2O$	4.9±0.1	0.8±1.5	4.7±0.5
$H_3S^+ + HCN \rightleftharpoons H_2CN^+ + H_2S$	1.0±0.1	0.8±1.5	0.7±0.5
$H_3S^+ + H_2CO \rightleftharpoons H_2COH^+ + H_2S$	1.4±0.2	2.2±1.5	0.7±0.6
$H_2CN^+ + H_2CO \rightleftharpoons H_2COH^+ + HCN$	0.3±0.1	1.4±1.5	−0.1±0.5
$H_2CN^+ \cdot HCN + H_2CO \rightleftharpoons H_2COH^+ \cdot HCN + HCN$	1.3±0.2		
$H_2COH^+ \cdot H_2CO + HCN \rightleftharpoons H_2CN^+ \cdot H_2CO + H_2CO$	0.3±0.3		

[a]Calculated from the measured equilibrium constants.
[b]Entropy change due to change in rotational symmetry number (3, 4).
[c]Determined with the relationship $\Delta H^0 = \Delta G^0 + T\Delta S^0$.

entropies of isoelectronic species (given in parentheses) for the ions H_3O^+ (NH_3), H_3S^+ (PH_3), and H_2CN^+ (C_2H_2) provides values for ΔS^0_{298} of 0 ± 0.5, −1.1 ± 1.0, and −1.2 ± 1.0 cal mol^{-1} deg^{-1} for reactions 5, 6, and 9, respectively, when the entropies are taken from the JANAF tables (22). The agreement with the results obtained from the calculations using symmetry numbers is good in the case of reaction 5 but poor for the latter two reactions since the isoelectronic arguments fail to take into account the difference in the rotational symmetry numbers of H_2CN^+ ($H—C\equiv\overset{+}{N}—H$) and C_2H_2. Previous direct experimental determinations of standard entropy changes are available only for reaction 5 and the reaction

[19] $$H_3O^+ + H_2CO \rightleftarrows H_2COH^+ + H_2O$$

Yamdagni and Kebarle (3) obtained a value of −1.0 ± 0.4 cal mol^{-1} deg^{-1} for ΔS^0 of reaction 5 but these authors were quick to point out that this value is not supported by what is known about the geometrics of H_3O^+ and H_3S^+. Allowing for possible inaccuracies in their experimental determination of ΔS^0, they preferred the value of 0 cal mol^{-1} deg^{-1} arrived at from the isoelectronic and symmetry considerations just mentioned. The value of −5.5 ± 0.2 cal mol^{-1} deg^{-1} derived by Hopkins and Bone (17) from their Van't Hoff plot is clearly unreasonable, while the value of −2.2 ± 1.0 cal mol^{-1} deg^{-1} reported by Moet-Ner and Field (18) appears to be too high. Reaction 19 has been investigated in a variable-temperature flowing afterglow by Fehsenfeld and co-workers (23) who obtained a standard entropy change at a mean temperature of 470 K of 2.2 ± 3.0 cal mol^{-1} deg^{-1} for this reaction which agrees remarkedly well with the sum of the standard entropy changes derived for reactions 5 and 10 from the rotational symmetry arguments.

The value of −3.8 ± 0.6 kcal mol^{-1} for ΔH^0_{298} determined here for reaction 5 may be compared with those which have derived from the Van't Hoff plots shown in Fig. 5: −3.7 ± 0.3 kcal mol^{-1} (3), −2.9 ± kcal mol^{-1} (17), and −5.0 ± 0.4 kcal mol^{-1} (18). Good agreement is apparent only with the results of Yamdagni and Kebarle (3). A comparison may also be made with the value for ΔH^0_{298} which can be derived indirectly from the standard enthalpy changes determined previously by pulsed high-pressure ion source mass spectrometer measurements of the temperature dependence of the equilibrium constants for the reactions [20]–[22]:

[20] $$H_3O^+ + H_2O \rightleftarrows H_3O^+ \cdot H_2O$$

[21] $$H_3O^+ \cdot H_2O + H_2S \rightleftarrows H_3S^+ \cdot H_2O + H_2O$$

[22] $$H_3S^+ \cdot H_2O \rightleftarrows H_3S^+ + H_2O$$

[5] $$H_3O^+ + H_2S \rightleftarrows H_3S^+ + H_2O$$

Cunningham *et al.* (24) report a value of −31.6 ± 1 kcal mol^{-1} for ΔH^0 of reaction 20. The very recent measurements of Moet-Ner and Field (25) yielded $\Delta H^0 = -33.0 \pm 1.5$ kcal mol^{-1} for this reaction. These two values combine to yield a weighted mean of −32.1 kcal mol^{-1} with a standard error of ±0.8 kcal mol^{-1} (12). Hiraoka and Kebarle (26) report a value of +6.7 ± 1 kcal mol^{-1} for ΔH^0 of reaction 21 while Moet-Ner and Field (25) obtained a value of +17 ± 1.5 kcal mol^{-1} for ΔH^0 of reaction 22. When these values are adopted, the analysis of the thermodynamic cycle represented by the above four reactions provides a value of −8.4 ± 3.3 kcal mol^{-1} for ΔH^0_{298} of reaction 5 which is considerably higher than the values obtained from the direct measurements of the equilibrium constant for [5]. We are unable to assign the exact origin of this large discrepancy. It appears likely, however, that it reflects a serious shortcoming, presumably of the type discussed in the previous section, in one or more of the equilibrium constant measurements for reactions 20–22. The variable-temperature flowing afterglow measurements for [19] provided a value for $\Delta H^0_{470} = -5.2 \pm 0.8$ kcal mol^{-1} (23) which agrees, within experimental error, with the value for

Can. J. Chem. Downloaded from www.nrcresearchpress.com by 210.87.254.40 on 09/05/12
For personal use only.

TABLE 5. Summary of proton affinities and heats of formation (kcal mol^{-1}) at 298 K derived from the flowing afterglow equilibrium constant measurements

X	ΔH^0	ΔH^0 (XH$^+$ to CH$_2$O)	PA(X)	ΔH_f^0(XH$^+$)[a]
HCN	0.1	+0.1	171.0±1.7	228.5±3.7
H_2CO	0.7	0	170.9±1.2[b]	170.3±1.1[b]
H_2S	4.7	−0.7	170.2±1.8	192.1±2.0
H_2O	3.8	−4.5	166.4±2.4	143.0±2.4

[a]$\Delta H_f^0(XH^+) = \Delta H_f^0(X) + \Delta H_f^0(H^+) - PA(X)$. Values for $\Delta H_f^0(X)$ and $\Delta H_f^0(H^+)$ were taken from the JANAF tables (22).
[b]Reference value, see text.

$\Delta H^0_{298} = -4.5 \pm 1.1$ kcal mol^{-1} derived from the standard enthalpy changes determined in this study for reactions 5 and 10.

When combined with those of the corresponding unsolvated proton-transfer reactions, the standard free energy changes derived from the equilibrium constant measurements for the solvated proton transfer reactions provide information about the standard free energies of dissociation of the solvated ions. In the case of 'heterogeneous' solvated ions, XH^+Y in which the proton is shared between two different molecules, we can distinguish between two paths of dissociation and therefore two free energies of dissociation which are related according to the following thermochemical cycle:

[23]
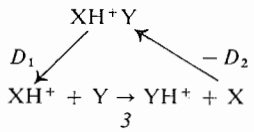

The standard free energies of dissociation D_1 and D_2 differ by an amount given by the standard free energy change associated with the proton-transfer step *3*. This notion is expressed explicitly by the manner in which we have chosen to write the molecular formula of the solvated ions, viz. we have artificially distinguished between $XH^+\cdot Y$ and $YH^+\cdot X$. This convention facilitates the comparison of unsolvated and solvated proton transfer and is not meant to imply a difference in structure or energy. It is readily apparent from a comparison of reaction 1 and the generalized solvated proton-transfer reaction

[24] $$XH^+\cdot X + Y \rightleftarrows YH^+\cdot X + X$$

that the standard free energy change associated with a solvated proton-transfer reaction will differ from that associated with its unsolvated counterpart by the difference in the standard free energies of dissociation of the two solvated ions, viz. $D(XH^+ - X) - D(YH^+ - X)$. Thus a comparison of the values for ΔG^0 determined for reactions 12 and 13 provides a value for the difference in standard free energies of dissociation, $D(H_2COH^+ - HCN) - D(H_2CN^+ - HCN)$, of $+1.0 \pm 0.3$ kcal mol^{-1} whereas such a comparison for reactions 12 and 14 provides a value for $D(H_2CN^+ - H_2CO) - D(H_2COH^+ - H_2CO)$ of $+0.6 \pm 0.4$ kcal mol^{-1}. A value of $+0.3 \pm 0.1$ kcal mol^{-1} is obtained for $D(H_2CN^+ - H_2CO) - D(H_2COH^+ - HCN)$ when ΔG^0 determined for reaction 12 is incorporated into the thermochemical cycle [23]. This result simply reflects the slightly higher basicity (expressed as a free energy) of H_2CO. Finally a thermochemical analysis of the cycle comprising reactions 12–14 provides a value for $D(H_2COH^+ - H_2CO) - D(H_2CN^+ - HCN) = +0.7 \pm 0.5$ kcal mol^{-1}.

Proton Affinities

The standard enthalpy changes determined in this investigation for the reactions of type [1] are presented in Table 5 in the form of a proton affinity 'ladder' together with the corresponding proton affinities and heats of formation of the protonated species. The proton affinity ladder is referenced to the proton affinity of H_2CO which was derived from the photoionization appearance potential of 11.67 ± 0.03 eV for H_2COH^+ from CH_3OH as measured by Refaey and Chupka (2). Adoption of the values for $\Delta H^0_{f,0}(H)$ and $\Delta H^0_{f,0}(CH_3OH)$ tabulated in the recent compilation by Rosenstock *et al.* (27) leads to a value for $\Delta H^0_{f,0}(H_2COH^+) = 172.1 \pm 0.7$ kcal mol^{-1} and for $\Delta H^0_{f,298}(H_2COH^+) = 170.3 \pm 1.1$ kcal mol^{-1} when a correction is made for temperature by comparison with similar molecules (2); (we have assigned an uncertainty of ±20% to this correction). A value for $PA_{298}(CH_2O) = 170.9 \pm 1.2$ kcal mol^{-1} can then be derived using $\Delta H^0_{f,298}(CH_2O) = -25.95 \pm 0.11$ kcal mol^{-1} as determined by Fletcher and Pilcher (28) and the $\Delta H^0_{f,298}(H^+)$ in the JANAF tables (22).

Our values for $PA_{298}(HCN)$ and $PA_{298}(H_2S)$ agree within experimental error with the value 170 ± 3 kcal mol^{-1} derived for the proton affinity of these two molecules by Haney and Franklin (29). The value of $PA(H_2S)$ was determined by these latter authors

Can. J. Chem. Downloaded from www.nrcresearchpress.com by 210.87.254.40 on 09/05/12
For personal use only.

TABLE 6. Summary of rate constants (10^{-9} cm^3 molecule^{-1} s^{-1}) at 296 ± 2 K

Reaction	k_{expt1}	$k_{capture}$	$k_{expt1}/k_{capture}$
$H_3O^+ + H_2S \rightarrow H_3S^+ + H_2O$	1.9±0.4	1.65	1.1 ±0.2
$H_3O^+ + HCN \rightarrow H_2CN^+ + H_2O$	3.5±0.7	3.20	1.1 ±0.2
$H_3S^+ + HCN \rightarrow H_2CN^+ + H_2S$	1.5±0.4	2.74	0.56±0.14
$H_3S^+ + H_2CO \rightarrow H_2COH^+ + H_2S$	2.2±0.6	2.23	1.0 ±0.3
$H_2CN^+ + H_2CO \rightarrow H_2COH^+ + HCN$	≥1.6	2.35	≥0.69

[a]The mean value together with the estimated accuracy of the measurements.
[b]Calculated using the cos 0 model of the Average-Dipole-Orientation theory (32). C = 0.144, 0.252, and 0.234 for the reactions with H_2S, HCN, and H_2CO respectively; $\alpha(HCN)$ = 2.59 Å^3 (33), $\alpha(H_2S)$ = 3.64 Å^3 (34), $\alpha(H_2CO)$ = 2.81 Å^3 (35); $\mu_D(HCN)$ = 2.98 D, $\mu_D(H_2S)$ = 0.97 D, $\mu_D(H_2CO)$ = 2.33 D (36).

from appearance potential measurements for electron impact fragmentation of ethanethiol and dimethylsulfide while PA(HCN) was tied to PA(H_2S) through the observation of proton transfer between these two molecules. Our value for $PA_{298}(H_2O)$ agrees within experimental error with the 'best' value of 165 ± 3 kcal mol^{-1} adopted by Long and Munson (5) in their consideration of the proton affinities of oxygenated compounds but is somewhat lower than the values of 168.9 ± 2 kcal mol^{-1} derived recently by Yamdagni and Kebarle (3) and 170.3 ± 2 kcal mol^{-1} preferred by Wolf *et al.* (4).

One problem generally encountered in equilibrium studies directed towards the determination of an accurate absolute value of the proton affinity of a specific molecule has been to incorporate that molecule into a proton affinity ladder in close proximity to a reference molecule whose absolute proton affinity has been accurately established with other methods. The uncertainty in the proton affinity of the desired molecule is then determined both by the uncertainty in the absolute standard and the uncertainty which accumulates according to the number of equilibrium steps between that molecule and the reference molecule. In the case of single temperature measurements this uncertainty will include that associated with the estimation of ΔS^0. As regards the determination of $PA_{298}(H_2O)$, we are fortunate in this study to have available as a reference a relatively accurate value for $PA_{298}(CH_2O)$ with CH_2O being only two equilibrium steps removed from H_2O. In the equilibrium studies of Yamdagni and Kebarle (3) isobutene was chosen as the reference molecule. It was only three equilibrium steps removed from NH_3, the molecule whose proton affinity was desired, but at least ten equilibrium steps removed from H_2O. For each step between isobutene and H_2O, including the H_2S/H_2O equilibrium for which a value for ΔH^0 had actually been derived from a Van't Hoff plot, ΔG^0_{600} was assumed to be equal to ΔH^0_{298}. These considerations, including the uncertainty in PA_{298} (isobutene) which we estimate to be ≲4 kcal mol^{-1} (largely due to the uncertainty in ΔH_f(*tert*-butyl radical) (30)), are probably sufficient to account for the apparent discrepancy between the values for $PA(H_2O)$ determined by these authors and in the present study. The origin of the value for $PA(H_2O)$ of 170.3 ± 2 kcal mol^{-1} was not discussed in the paper by Wolf *et al.* (4). It is due to appear in a separate publication by these authors.

Rate Constant Measurements

The unsolvated proton-transfer reactions investigated in this study were all observed to proceed rapidly ($k \gtrsim 1 \times 10^{-9}$ cm^3 molecule^{-1} s^{-1}) in the forward (exoergic) direction, in accord with expectations based on our growing experience for such reactions (31). The measured rate constants for the individual reactions are summarized in Table 6. They appear not to have been determined previously by other workers although Chong *et al.* (16) have reported a rate constant in the range 0.8–1.9 × 10^{-9} cm^3 molecule^{-1} s^{-1} for reaction 15, the deuterium analogue of reaction 5. Table 6 also includes a comparison of the measured reaction rate constants with collision rate constants calculated using the Average-Dipole-Orientation theory (32). The consonance between these two sets of values is again not surprising (31).

The much larger range in values observed for the rate constants of the solvated proton-transfer reactions (see Table 2) is most readily understood in terms of overall reaction energetics. For several of these reactions the difference in the standard free energies of dissociation of the two solvated ions appears to be sufficient to cause a change in the sign of the standard free energy change associated with the unsolvated counterpart. This is not surprising in view of the low exoergicity, $\Delta G^0_{298} \lesssim 5$ kcal mol^{-1}, generally exhibited by the corresponding unsolvated reactions. In the case of reactions 12–14 our equilibrium constant measurements indicate that the solvation of H_2CN^+ by one HCN molecule actually increases the exoergicity for proton transfer by 1.0 kcal mol^{-1} while solvation by one H_2CO molecule decreases the exoergicity from −0.3 to +0.3 kcal mol^{-1}. These observations are borne out by the corresponding rate constant measurements which

Can. J. Chem. Downloaded from www.nrcresearchpress.com by 210.87.254.40 on 09/05/12
For personal use only.

Can. J. Chem. Downloaded from www.nrcresearchpress.com by 210.87.254.40 on 09/05/12
For personal use only.

indicate that $H_2CN^+ \cdot HCN$ still undergoes proton transfer with H_2CO with a relatively large rate constant, albeit slightly lower than that for its unsolvated counterpart, and that $H_2COH^+ \cdot H_2CO$ reacts rapidly with HCN to produce $H_2CN^+ \cdot H_2CO$. The rate constant for proton transfer between H_3O^+ and HCN is decreased significantly upon the solvation of H_3O^+ with one H_2O molecule. The low value for k_7 of 1×10^{-10} cm^3 molecule^{-1} s^{-1} suggests that this solvated reaction may in fact be slightly endoergic with $D(H_3O^+ - H_2O) - D(H_2CN^+ - H_2O) \approx 6$ kcal mol^{-1}. There is much less doubt about the overall energetics of the reaction of unsolvated and solvated H_3O^+ with H_2S. The recent measurements of Hiraoka and Kebarle (26) indicate standard free energy changes at 300 K for the reactions

[25] $$H_3O^+ \cdot H_2O + H_2S \rightleftarrows H_3S^+ \cdot H_2O + H_2O$$

[26] $$H_3O^+ \cdot 2H_2O + H_2S \rightleftarrows H_3S^+ \cdot 2H_2O + H_2O$$

of $+7.1 \pm 0.5$ and $+6.3 \pm 0.6$ kcal mol^{-1}, respectively, which correspond to a decrease of ~ 10 kcal mol^{-1} in ΔG^0 upon hydration of H_3O^+. Our observations indicate a concomitant decrease in the value of k by more than 10^3 from 1.9×10^{-9} to $\lesssim 1 \times 10^{-12}$ cm^3 molecule^{-1} s^{-1}. Finally the drop in the value of k from 3×10^{-10} to $\lesssim 1 \times 10^{-12}$ cm^3 molecule s^{-1} observed for the endoergic proton transfer from H_2CN^+ to H_2S suggests an even larger endoergicity for the $H_2CN^+ \cdot HCN$ reaction with $D(H_2CN^+ - HCN) > D(H_3S^+ - HCN)$.

Acknowledgements

We thank Dr. Fehsenfeld for a preprint of ref. 23 and Professor R. W. Taft for a preprint of ref. 4 and for providing us with the values of the equilibrium constants measured with the pulsed ion cyclotron resonance technique. We are grateful to the National Research Council of Canada and the Sloan Foundation for financial support.

1. P. Ausloos (*Editor*). Interactions between ions and molecules. Plenum Press, New York, NY. 1975.
2. K. M. A. Refaey and W. A. Chupka. J. Chem. Phys. **48**, 5205 (1968).
3. R. Yamdagni and P. Kebarle. J. Am. Chem. Soc. **98**, 1320 (1976).
4. J. F. Wolf, R. H. Staley, I. Koppel, M. Taagepera, R. T. McIver, J. L. Beauchamp, and R. W. Taft. J. Am. Chem. Soc. In press.
5. J. Long and B. Munson. J. Am. Chem. Soc. **95**, 2427 (1973).
6. R. H. Staley and J. L. Beauchamp. J. Chem. Phys. **62**, 1998 (1975).
7. D. Betowski, G. Mackay, J. Payzant, and D. Bohme. Can. J. Chem. **53**, 2365 (1975).
8. G. G. Meisels, R. K. Mitchum, and J. P. Freeman. J. Phys. Chem. **80**, 2845 (1976).
9. D. K. Bohme, R. S. Hemsworth, H. W. Rundle, and H. I. Schiff. J. Chem. Phys. **58**, 3504 (1973).
10. G. Brauer (*Editor*). Handbook of preparative inorganic chemistry. Academic Press, New York, NY. 1965.
11. R. Spence and W. Wild. J. Chem. Soc. 338 (1935).
12. N. C. Barford. Experimental measurements: precision, error and truth. Addison-Wesley, London. 1967.
13. G. I. Mackay, L. D. Betowski, J. D. Payzant, H. I. Schiff, and D. K. Bohme. J. Phys. Chem. **80**, 2919 (1976).
14. G. I. Mackay, R. S. Hemsworth, and D. K. Bohme. Can. J. Chem. **54**, 1624 (1976).
15. D. K. Bohme and G. I. Mackay. 24th Am. Conf. Mass Spectrom. Allied Topics, San Diego, California, May, 1976.
16. S. L. Chong, R. A. Myers, and J. L. Franklin. J. Chem. Phys. **56**, 2427 (1972).
17. J. M. Hopkins and L. I. Bone. J. Chem. Phys. **58**, 1473 (1973).
18. M. Meot-Ner and F. H. Field. J. Chem. Phys. **66**, 4527 (1977).
19. W. R. Davidson, M. T. Bowers, T. Su, and D. H. Aue. Intern. J. Mass Spectrom. Ion Phys. **24**, 83 (1977).
20. A. C. Hopkinson. Prog. Theor. Org. Chem. **2**, 194, (1977).
21. A. C. Hopkinson, N. K. Holbrook, K. Yates, and I. G. Csizmadia. J. Chem. Phys. **49**, 3596 (1968).
22. JANAF Thermochemical Tables. 2nd ed. Natl. Stand. Ref. Data Serv. Natl. Bur. Stand. **37** (1971).
23. F. C. Fehsenfeld, I. Dotan, D. L. Albritton, C. J. Howard, and E. E. Ferguson. J. Geophys. Res. In press.
24. A. J. Cunningham, J. D. Payzant, and P. Kebarle. J. Am. Chem. Soc. **94**, 7627 (1972).
25. M. Meot-Ner and F. H. Field. J. Am. Chem. Soc. **99**, 998 (1977).
26. K. Hiraoka and P. Kebarle. Can. J. Chem. **55**, 24 (1977).
27. H. M. Rosenstock, K. Draxl, B. W. Steiner, and J. T. Herron. J. Phys. Chem. Ref. Data, **6** (1977).
28. R. A. Fletcher and G. Pilcher. Trans. Faraday Soc. **65**, 113 (1968).
29. M. A. Haney and J. L. Franklin. J. Chem. Phys. **50**, 2028 (1968).
30. W. Tsang. J. Phys. Chem. **76**, 143 (1972).
31. D. K. Bohme. *In* Interactions between ions and molecules. *Edited by* P. Ausloos. Plenum Press, New York, NY. 1975.
32. L. Bass, T. Su, W. J. Chesnavich, and M. T. Bowers. Chem. Phys. Lett. **34**, 119 (1975).
33. J. O. Hirschfelder, G. F. Curtiss, and R. B. Bird. Molecular theory of gases and liquids. John Wiley and Sons, New York, NY. 1954.
34. E. R. Lippincott and J. M. Stutman. J. Phys. **31**, 1619 (1959).
35. E. W. Rothe and R. B. Bernstein. J. Chem. Phys. **31**, 1619 (1959).
36. R. D. Nelson, D. R. Lide, and A. A. Marjott. Natl. Stand. Ref. Data Ser. Natl. Bur. Stand. **10** (1966).

Reactivity of cyclopropylalkenes with *p*-chlorobenzenesulfenyl chloride[1]

TIMOTHY R. CERKSUS, VALERIA M. CSIZMADIA, GEORGE H. SCHMID, AND THOMAS T. TIDWELL

Department of Chemistry, University of Toronto, Toronto, Ont., Canada M5S 1A1

Received August 10, 1977

TIMOTHY R. CERKSUS, VALERIA M. CSIZMADIA, GEORGE H. SCHMID, and THOMAS T. TIDWELL. Can. J. Chem. **56**, 205 (1978).

The reactivity of a series of cyclopropylalkenes, as well as norbornene and cyclohexene, with *p*-chlorobenzenesulfenyl chloride in CH_2Cl_2 at 25°C have been measured. Rates of reaction of several of the substrates were also measured in acetic acid and 1,1,2,2,-tetrachloroethane so that factors for converting rates from one solvent to another could be obtained. The rates of the sulfenyl halide additions varied over a total range of 193 from the least reactive alkene, ethylene, to the most reactive, 1,1-dicyclopropylethylene. This relatively small variation is in accord with all of these reactions involving bridged rate-determining transition states. The corresponding range in reactivity for acid-catalyzed hydration, a reaction involving protonation on carbon to give an open carbonium ion, is 10^{16}. These two reactions are proposed as bases for structure–reactivity comparisons to determine whether other reactions involve bridged or open transition states.

TIMOTHY R. CERKSUS, VALERIA M. CSIZMADIA, GEORGE H. SCHMID et THOMAS T. TIDWELL. Can. J. Chem. **56**, 205 (1978).

On a mesuré la réactivité d'une série de cyclopropylalcènes de même que celle du norbornène et du cyclohexène vis-à-vis le chlorure de *p*-chlorosulfényle dans le CH_2Cl_2 à 25°C. On a aussi mesuré les vitesses de réaction de plusieurs substrats dans de l'acide acétique et du tétrachloro-1,1,2,2 éthane de façon à obtenir les facteurs permettant d'évaluer les vitesses dans un solvant à l'aide des vitesses dans un autre solvant. Les vitesses d'addition de l'halogénure de sulfényle varient de 1 à 193 lorsque l'on passe de l'alcène le moins réactif, l'éthylène, vers le plus réactif le dicyclopropyl-1,1 éthylène. Cette variation relativement faible est en accord avec un mécanisme suggérant que toutes ces réactions impliquent des ions pontés comme états de transition déterminant la vitesse. L'écart correspondant de réactivité pour l'hydration acido-catalysée, une réaction impliquant la protonation d'un carbone conduisant à un carbocation ouvert, est de 10^{16}. On suggère que ces deux réactions peuvent servir de base pour des comparaisons de structure et de réactivité afin de déterminer si d'autres réactions impliquent des états de transition pontés ou ouverts.

[Traduit par le journal]

The intermediates in electrophilic additions to olefins, and the transition states leading to them, may be divided into two distinctive types. On the one hand there are those reactions that proceed through bridged transition states and intermediates [1] and on the other hand there are those that involve rate determining attack at carbon to form open carbonium ions (the $A_{SE}2$ mechanism) as shown in eq. 2 (1, 2). The best example of the first class of reaction

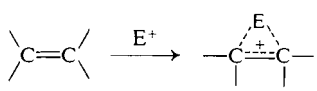

[1]

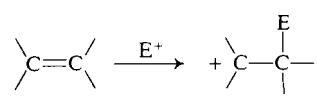

[2]

is addition of sulfenyl halides (3) to olefins [3]. Protonation of alkenes in acid-catalyzed hydrations is a reaction which clearly fits in the second category (4).

[1]Reactions of sulfenyl chlorides and their derivatives, Part 18. For Part 17, see ref. 12*b*.

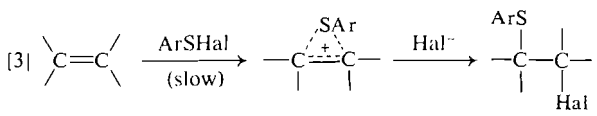

[3]

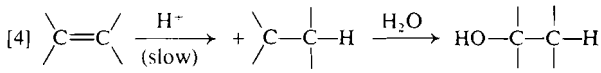

[4]

The mechanism of sulfenyl halide additions are securely based on rate–structure correlations, product stereochemistry, and direct observation of the bridged intermediates (3). In turn the mechanism of the hydration reaction is supported by the correlation of rates with structure, solvent isotope effects, acidity dependence, and other kinetic criteria (4). Interestingly, these reactions had been the object of only sporadic quantitative investigations and their mechanisms have been clearly defined only rather recently, as reviewed in refs. 1–4.

It is somewhat anomalous that two much more ambiguous electrophilic reactions of alkenes, namely bromination and oxymercuration, have been the object of earlier and generally more intensive mech-

Can. J. Chem. Downloaded from www.nrcresearchpress.com by 210.87.254.105 on 09/05/12
For personal use only.

Can. J. Chem. Downloaded from www.nrcresearchpress.com by 210.87.254.105 on 09/05/12
For personal use only.

anistic study. Bromonium ion formation as in eq. 1 was proposed in 1937 (5) and mercurinium ions were suggested as intermediates in 1939 (6). Both bromination (7) and oxymercuration (8) of olefins have been the subject of intensive examination since that time.

Despite the immense amount of careful work which has been devoted to these reactions there is still some ambiguity as to the respective contribution of bridged and open ions in such additions. We believe that a useful approach to solving this problem is to compare the effect of systematic variations of alkene structure on the different types of reaction. By comparing the structure–reactivity profiles of the reactions in question with sulfenyl halide additions, which are known to involve bridging, and hydrations, which are known to involve open ions, it should be possible to gain an insight into the details of the borderline cases.

A substituent which has proved particularly informative is cyclopropyl (4, 9). This substituent is capable of strong electron donation by resonance to an adjacent empty *p* orbital, assuming that the proper bisected (Fig. 1) geometry can be attained. For example cyclopropyl is 1000 times more effective than phenyl at accelerating the solvolysis of *p*-nitrobenzoate esters RMe_2COPNB (10). On the other hand this group is inductively electron withdrawing if resonance donation is precluded by geometrical constraints (11). Bridging should also prevent the cation stabilizing effect of this substituent from being effective by preempting the adjacent *p* orbitals, so the substituent effect of cyclopropyl should provide a critical test of transition state structure.

We have completed and published (4) a survey of the effects of representative substituents on alkene hydrations. This paper deals with the assessment of the effect of the cyclopropyl substituent on arylsulfenyl halide additions. Also a limited study of the effect of solvent variation on rates of sulfenyl halide addition has been carried out. Rate measurements on some cycloalkenes were also included for comparison. The use of the rates of sulfenyl halide addition in the elucidation of the mechanism of oxymercuration (12*a*) and bromination (12*b*) has been reported elsewhere. It was also of interest to briefly compare the effect of cyclopropyl on the product determining steps in sulfenyl halide additions relative to other electron-donating substituents (13, 14).

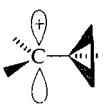

FIG. 1. Favourable bisected geometry.

Results

Kinetics of the sulfenyl halide additions were measured by stopped-flow ultraviolet spectroscopy as described previously (14). The observed rate constants are given in Table 1.

The rates of addition agree well with published results where comparisons can be made. Thus our average value for the ratio k(cyclohexene)/k(1-hexene) of 6.6 agrees with a reported value of 9.5 (15) and our average value of 11.0 for k(norbornene)/k(cyclohexene) agrees with that reported of 12.9 (16).

The products were examined by ^1H nmr spectroscopy by mixing the reactants in an nmr tube at $-20°C$ and immediately observing the spectra, which were then rescanned at intervals until the product composition ceased to change. In this way an estimate could be made of both the kinetic products formed initially and the thermodynamic product which was favored on extended reaction time. The assignments of the signals are given in Table 2 and the basis of these assignments is given in the Appendix.

Discussion

The products of the reactions were not a major concern but were given some attention to insure there was no untoward behavior which might complicate the analysis of the kinetic results. These observations of the products are consistent with the reactions proceeding by usual addition of the sulfenyl halide to the double bond, with isomerization and ring cleavage (17) occurring subsequently in some cases. Details are given in the Appendix.

The rates of addition of *p*-chlorobenzenesulfenyl chloride show a vivid contrast to the rates of acid-catalyzed hydration. The total range in relative rates for the former reaction is 193, whereas for the latter it is 1.3×10^{16}. This vast difference in the sensitivity of the rates to changes in substitution confirms the fundamental difference in the reaction mechanisms, namely that sulfenyl halide addition proceeds through a bridged rate-determining transition state, whereas acid-catalyzed hydration involves an open ion. This effect is especially noticeable when comparing the isomeric dicyclopropylethylenes. The 1,1,-isomer is 10^6 more reactive than the 1,2-isomers in hydration but only five-fold faster in sulfenyl halide addition. This result emphasizes the value of the cyclopropyl group as a transition state probe.

The observed solvent effects show that the greater reactivity in hydration does not arise from a more polar solvent. Indeed the *p*-chlorobenzenesulfenyl halide additions are slower in more polar solvents. Average relative rate factors for the solvents acetic

Can. J. Chem. Downloaded from www.nrcresearchpress.com by 210.87.254.105 on 09/05/12
For personal use only.

TABLE 1. Rates of addition of *p*-chlorobenzenesulfenyl chloride to alkenes at 25°C

Alkene	Solvent	$k_2(M^{-1}\ s^{-1})$	$k_{rel}(CH_2Cl_2)$	$k_{rel}(H_3O^+)^a$
c-PrCH=CH_2(**1**)	CH_2Cl_2	130	3.5	5.9×10^4
	HOAc	68.3		
	$C_2H_2Cl_4$	410		
c-Pr_2C=CH_2(**2**)	CH_2Cl_2	3050	83	2.5×10^9
c-PrCMe=CH_2(**3**)	CH_2Cl_2	1430	39	4.6×10^7
c-PrCH=CH-*c*-Pr(*E*)(**4**)	CH_2Cl_2	417	11	1.7×10^3
c-PrCH=CH-*c*-Pr(*Z*)(**5**)	CH_2Cl_2	782	21	4.4×10^3
c-PrCH=CHMe(*E*)(**6**)	CH_2Cl_2	620	17	6.3×10^3
c-PrCH=CHMe(*Z*)(**7**)	CH_2Cl_2	853	23	1.4×10^4
1-Hexene	CH_2Cl_2	36.8	1.0	1.0
	HOAc	17.8[b]		
	$C_2H_2Cl_4$	130		
Cyclohexene	CH_2Cl_2	260	7.1	10
	$C_2H_2Cl_4$	786		
Norbornene	CH_2Cl_2	2710	74	7.9×10^3
	HOAc	1030		
	$C_2H_2Cl_4$	9010		
CH_2=CH_2	HOAc	7.68[c]	(0.43)[g]	3.4×10^{-7}
	$C_2H_2Cl_4$	65[d]		
MeCH=CH_2	HOAc	13.7[c]	(0.76)[g]	0.55
	$C_2H_2Cl_4$	205[d]		
EtCH=CH_2	HOAc	18.0[c]	(1.0)[g]	
	$C_2H_2Cl_4$	248[d]		
PhCH=CH_2	HOAc	15.9[e]	(0.89)[g]	56
	$C_2H_2Cl_4$	62.0[f]		

[a]Reference 4.
[b]This value supersedes that reported earlier (9).
[c]Reference 21.
[d]Reference 3*a*.
[e]Reference 9.
[f]Reference 14.
[g]Comparison in HOAc.

TABLE 2. Proton nmr parameters of 4-chlorobenzenesulfenyl chloride adducts in CCl_4

		Group assignments[a]			Chemical shifts		
Alkene	Product	1	2	3	1	2	3
c-PrCH=CH_2(**1**)	**8**	C*H*Cl	CH_2S		3.38(s)	3.34(s)	
c-PrCH=CHMe(*Z*)(**7**)	**9**	*c*-PrC*H*Cl	C*H*S	Me	3.44(dd)[b]	3.60(m)[c]	1.42(d)[d]
	10	*c*-PrC*H*S	C*H*Cl	Me	2.75(dd)[e]	4.22(m)[f]	1.60(d)[d]
c-PrCH=CHMe(*E*)(**6**)	**11**	*c*-PrC*H*Cl	C*H*S	Me	3.36(dd)[b]	3.52(m)[c]	1.44(d)[d]
	12	*c*-PrC*H*S	C*H*Cl	Me	2.61(dd)[b]	4.21(m)[c]	1.62(d)[d]
c-PrCH=CH-*c*-Pr(*Z*)(**5**)	**13**	C*H*Cl	C*H*S		3.28(dd)[b]	2.74(dd)[b]	
c-PrCH=CH-*c*-Pr(*E*)(**4**)	**14**	C*H*Cl	C*H*S		3.53(dd)[b]	2.80(dd)[b]	
c-PrCMe=CH_2(**3**)	**15**	CH_2S	Me		3.37(s) or	1.52(s)	
	16	CH_2Cl	Me		3.50(s)	1.50(s)	
c-Pr_2C=CH_2(**2**)	**17**	CH_2X			3.52(s)		

[a]The cyclopropyl protons appeared as a multiplet between δ 0.6–1.5, and the aryl protons appeared as a multiplet at 7.2. In 9–14 the methine proton of the cyclopropyls were coupled to the vicinal C*H*X proton by 9 Hz.
[b]J = 9 and 3 Hz.
[c]J = 7 and 3 Hz.
[d]J = 7 Hz.
[e]J = 9 and 5 Hz.
[f]J = 7 and 5 Hz.

acid, CH_2Cl_2, and $CHCl_2CHCl_2$ are 1.0, 2.3, and 7.8, respectively. This fact suggests a decrease in polarity of the reactants in attaining the transition state for addition. By contrast the addition of 2,4-dinitrobenzenesulfenyl chloride to cyclohexene is 10^3 times faster in acetic acid than in carbon tetrachloride (18). Evidently this sulfenyl halide has much less polar character in the S—Cl bond in the reactant so there is an increase in polarity in the transition state which is aided by a more ionic medium.

Can. J. Chem. Downloaded from www.nrcresearchpress.com by 210.87.254.105 on 09/05/12
For personal use only.

This assessment depends upon the assignment of relative solvent polarity as HOAc > CH_2Cl_2 > $C_2H_2Cl_4$ > CCl_4. The dielectric constants of the first three of these solvents are almost identical (6.2, 8.9, and 8.2, respectively) but the E_T and Z solvent parameters indicate acetic acid is much more polar than methylene chloride (19). Apparently these solvent parameters have not been reported for $C_2H_2Cl_4$.

The determination of the rates of *p*-chlorobenzenesulfenyl chloride addition in acetic acid make comparisons possible with published rates for 2,4-dinitrobenzenesulfenyl chloride addition. The former halide is more reactive toward 1-hexene (3*b*, 15), cyclohexene (15, 16), norbornene (16), and styrene (20) by factors of 15×10^3, 8.1×10^3, 6.9×10^3, and 22×10^3, respectively (the rates for the dinitro compound were measured at 30°C for cyclohexene and norbornene and the rate of the *p*-Cl compound with cyclohexene was calculated using the rates in the other solvents). The low reactivity of the dinitrobenzenesulfenyl chloride may be interpreted in terms of the electron deficiency on sulfur in the transition state being destabilized by the nitro groups.

In summary this study provides a structure–reactivity correlation for a reaction known to involve bridged transition states. This provides a standard by which to judge the transition state geometries of other reactions, which we have done for oxymercuration (12*a*) and bromination (12*b*). Our preliminary study of solvent effects on sulfenyl halide additions has been suggestive of the relative charge distributions in the reactants and products in this reaction, but a thorough study of this topic is clearly warranted.

Experimental

Cyclopropylalkenes were obtained as reported previously (4) and the other alkenes were commercial material. Acetic acid was purified by refluxing with acetic anhydride for 10 days followed by slow distillation. Methylene chloride was shaken three times with concentrated sulfuric acid, twice with water, and twice with sodium bicarbonate solution and was then dried successively over $CaCl_2$ and K_2CO_3. Freshly distilled material was used in kinetic runs. Commercial tetrachloroethane (*Caution*, toxic vapour) was purified by the same procedure as methylene chloride.

Kinetic measurements were carried out using a Durrum D110 Stopped Flow Spectrophotometer as previously described (3*a*). Product studies were carried out by adding 1.5 mmol *p*-chlorobenzenesulfenyl chloride to 1.4 mmol alkene in 0.5 mL $CDCl_3$ in an nmr tube cooled to −20°C with Dry Ice. The reactions were exothermic, particularly for the more reactive alkenes. After mixing the solutions were frozen, and then melted, placed in the probe of the Varian T-60 operating at normal room temperature and recorded immediately. Spectra were remeasured after standing at room temperature at various intervals until the spectra no longer appeared to change.

In the kinetic runs alkene concentrations typically in the range 0.005–0.015 *M* were used and the arylsulfenyl chloride concentrations were less by a factor of 10. The calculated second-order rate constants were independent of the initial concentrations of reagents within this range.

Acknowledgements

Acknowledgement is made to the Bickell Foundation, the National Research Council of Canada, and to the Donors of the Petroleum Research Fund, administered by the American Chemical Society for support of this research.

1. G. H. SCHMID and D. G. GARRATT. *In* Chemistry of double bonded functional groups. Supplement A, Part 2. *Edited by* S. Patai. Wiley Interscience, New York, NY. 1977. p. 725.
2. T. H. LOWRY and K. S. RICHARDSON. Mechanism and theory in organic chemistry. Harper and Row, New York, NY. 1976. Chapt. 7.
3. (*a*) G. H. SCHMID, C. L. DEAN, and D. G. GARRATT. Can. J. Chem. **54**, 1253 (1976); (*b*) G. M. BEVERLY and D. R. HOGG. J. Chem. Soc. B, 175 (1971); (*c*) G. MEHTA and P. N. PANDEY. Tetrahedron Lett. 3567 (1975); (*d*) W. A. SMIT, M. Z. KRIMER, and E. A. VOROB'EVA. Tetrahedron Lett. 2451 (1975); (*e*) G. CAPOZZI, O. DELUCCHI, V. LUCCHINI, and G. MODENA. Tetrahedron Lett. 2603 (1975); (*f*) K. IZAWA, T. OKUYAMA, and T. FUENO. Bull. Chem. Soc. Jpn. **47**, 1480 (1974); (*g*) N. S. ZEFIROV, N. K. SADOVAJA, A. M. MAGGERRAMOV, I. V. BODRIKOV, and V. R. KASRTASHOV. Tetrahedron, **31**, 2948 (1975).
4. (*a*) K. OYAMA and T. T. TIDWELL. J. Am. Chem. Soc. **98**, 947 (1976); (*b*) W. K. CHWANG, P. KNITTEL, K. M. KOSHY, and T. T. TIDWELL. J. Am. Chem. Soc. **99**, 3395 (1977); (*c*) S. Y. ATTIA, J. P. BERRY, K. M. KOSHY, Y.-K. LEUNG, E. P. LYZNICKI, JR., V. J. NOWLAN, K. OYAMA, and T. T. TIDWELL. J. Am. Chem. Soc. **99**, 3401 (1977); (*d*) P. KNITTEL and T. T. TIDWELL. J. Am. Chem. Soc. **99**, 3408 (1977); (*e*) W. K. CHWANG, V. J. NOWLAN, and T. T. TIDWELL. J. Am. Chem. Soc. **99**, 7233 (1977).
5. I. ROBERTS and G. E. KIMBALL. J. Am. Chem. Soc. **59**, 947 (1937); H. WEISS. J. Am. Chem. Soc. **99**, 1670 (1977).
6. H. J. LUCAS, F. R. HEPNER, and S. WINSTEIN. J. Am. Chem. Soc. **61**, 3102 (1939).
7. (*a*) D. GROSJEAN, G. MOUVIER, and J.-E. DUBOIS. J. Org. Chem. **41**, 3869, 3872 (1976); (*b*) K. YATES, G. H. SCHMID, T. W. REGULSKI, D. G. GARRATT, H.-W. LEUNG, and R. MCDONALD. J. Am. Chem. Soc. **95**, 160 (1973); (*c*) P. B. D. DE LA MARE. Electrophilic halogenation reaction pathways involving attack by electrophilic halogens on unsaturated compounds. Cambridge University Press, Cambridge. 1976.
8. (*a*) D. S. MATTESON. Organometallic reaction mechanisms of the nontransition elements. Academic Press, New York, NY. 1974. pp. 202–218; (*b*) D. SEYFERTH. J. Organomet. Chem. **98**, 133 (1975).
9. D. G. GARRATT, A. MODRO, K. OYAMA, G. H. SCHMID, T. T. TIDWELL, and K. YATES. J. Am. Chem. Soc. **96**, 5295 (1974).
10. H. C. BROWN and E. N. PETERS. J. Am. Chem. Soc. **95**, 2400 (1973).
11. (*a*) H. C. BROWN and J. D. CLEVELAND. J. Org. Chem. **41**, 1792 (1976); (*b*) Y. E. RHODES and V. G. DIFATE. J. Am. Chem. Soc. **94**, 7582 (1972); (*c*) B. R. REE and J. C. MARTIN. J. Am. Chem. Soc. **92**, 1660 (1970); (*d*) V. BUSS, R. GLEITER, and P. VON R. SCHLEYER. J. Am. Chem. Soc. **93**, 3927 (1971).
12. (*a*) I. C. AMBIDGE, S. K. DWIGHT, C. M. RYNARD, and T. T. TIDWELL. Can. J. Chem. **55**, 3086 (1977); (*b*) G. H. SCHMID and T. T. TIDWELL. J. Org. Chem. In press.

Can. J. Chem. Downloaded from www.nrcresearchpress.com by 210.87.254.105 on 09/05/12
For personal use only.

13. (*a*) V. M. CSIZMADIA. Ph.D. Thesis, University of Toronto, Toronto, Ont. 1971; (*b*) D. G. GARRATT. Ph.D. Thesis, University of Toronto, Toronto, Ont. 1975; (*c*) G. M. UNDERWOOD, C. T. WATTS, and C. A. KINGSBURY. J. Org. Chem. **38**, 1553 (1973); (*d*) C. L. DEAN, D. G. GARRATT, T. T. TIDWELL, and G. H. SCHMID. J. Am. Chem. Soc. **96**, 4958 (1974); (*e*) G. H. SCHMID and V. J. NOWLAN. J. Org. Chem. **37**, 3086 (1972); Can. J. Chem. **54**, 695 (1976).
14. G. H. SCHMID and D. G. GARRATT. Can. J. Chem. **52**, 1807 (1974).
15. W. M. BALUZOW, G. JUST, and W. PRITZKOW. J. Prakt. Chem. **316**, 1051 (1974).
16. H. KWART and L. J. MILLER. J. Am. Chem. Soc. **83**, 4552 (1961).
17. (*a*) S. SAREL, J. YOVELL, and M. SAREL-IMBER. Angew. Chem. Int. Ed. Engl. **7**, 577 (1968); (*b*) E. DUNKELBAUM. Tetrahedron, **30**, 3991 (1974).
18. D. R. HOGG and N. KHARASCH. J. Am. Chem. Soc. **78**, 2728 (1956).
19. C. REICHARDT. Angew. Chem. Int. Ed. Engl. **4**, 29 (1965).
20. W. L. ORR and N. KHARASCH. J. Am. Chem. Soc. **78**, 1201 (1956).
21. G. H. SCHMID, A. MODRO, and K. YATES. J. Org. Chem. **42**, 871 (1977).

Appendix

The structures of the products from **4**–**7** were assigned according to Scheme 1 on the basis of their proton nmr spectra, which agreed well with the large body of these reported in the literature (3*a*). In particular the resonances of the protons on chlorine-bearing carbon and sulfur-bearing carbon were in the region of δ 2.5–4.0. In accordance with the normally observed behaviour (3*a*), the higher field resonance was assigned to the latter protons when these were well separated (in **10**, **12**, **13**, and **14**). Products **10** and **12** from *Z*- and *E*-1-cyclopropyl-

[5] *c*-PrCH=CHMe → *c*-PrCHClCHMeSAr → *c*-PrCHSArCHMeCl
7 (*Z*) **9** (*threo*) **10** (*threo*)

[6] *c*-PrCH=CHMe → *c*-PrCHClCHMeSAr → *c*-PrCHSArCHMeCl
6 (*E*) **11** (*erythro*) **12** (*erythro*)

[7] *c*-PrCH=CH-*c*-Pr → *c*-PrCHClCHSAr-*c*-Pr
5(*Z*) **13** (*threo*)

[8] *c*-PrCH=CH-*c*-Pr → *c*-PrCHClCHSAr-*c*-Pr
4 (*E*) **14** (*erythro*)

SCHEME 1

propene, respectively, were not the initially formed products but were derived from rearrangement of the original adducts **9** and **11**. Accordingly, **9** and **11** were assigned as having the positions of the Cl and S reversed from **10** and **12**.

The additions to **4**–**7** were assigned as being *anti* on the basis that the initial additions were stereospecific, and the fact that this is the normal mode of addition. Normally the *threo* and *erythro* isomers which result from addition of sulfenyl halides to 1,2-disubstituted ethylenes may be differentiated on the basis of the larger vicinal coupling constant between

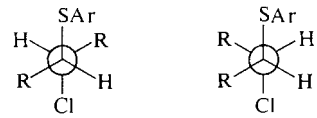

erythro *threo*

the protons shown in the *erythro* isomer than in the *threo* (*cf*, J = 6.0 and 3.0 (R = Me (13*a*)), J = 6.8 and 3.2 (R = Et (13*b*)), J = 10.5 and 5.6 (R = *i*-Pr (13*c*)), and J = 3.2 and 0.5 Hz (R = *t*-Bu (13*d*), respectively). However, in the case of adducts **9**–**14** the differences in these coupling constants were too small to serve as reliable bases for determination. The only examples of sulfenyl halide additions that do not give *anti* addition are cases in which one of the substituents is a powerful electron donor, such as *p*-anisyl. In such cases both *syn* and *anti* addition is observed, and these results have been interpreted in terms of a bridged rate-determining transition state but with an open ion intervening before the product-determining transition state (13*e*). We have found cyclopropyl to be a stronger electron donor than *p*-anisyl (ref. 4*b*, as measured by the σ^+ parameter for the entire group) but the stereospecific formation of a single initial product from these reactions indicates that only bridged ions are formed from **4**–**7**. The assigned stereochemistries of the kinetically controlled products are thus as shown in eqs. 5–8.

The nmr spectrum of the product from cyclopropylethylene (**1**) was unusual in that the protons on the carbons bearing Cl and S appeared as two closely spaced singlets without the normal vicinal coupling or the coupling to the methine proton of the cyclopropyl group. The structure may confidently be assigned the structure *c*-PrCHClCH$_2$SAr (**8**) as the protons on the carbon bearing sulfur are consistently shifted to higher field by an adjacent cyclopropyl in **10**, **12**, **13**, and **14**. This regiochemistry is also consistent with the result observed with styrene, which gives 83% Markovnikoff adduct in the kinetic product and 100% at equilibrium (14).

The reaction of 2-cyclopropylpropene (**3**) showed the initial formation of two adducts in the approximate ratio of 5:1. The observed chemical shifts were consistent with the formation of *c*-PrMeCClCH$_2$SAr and *c*-PrMeCSArCH$_2$Cl but because of the similarity of the spectra the isomers could not be positively identified. For comparison 2-phenylpropene gives an 87% preference for Markovnikoff addition in the kinetic product (14). The initial adducts from **3** underwent further reaction, presumably rearrange-

ment by cyclopropane homoallylic ring opening (4*a*, 17), which has been documented in the addition of arylsulfenyl halide to α-cyclopropylstyrene (eq. 9) (17*b*).

$$[9]\quad c\text{-PrCPh}{=}CH_2 \xrightarrow{\text{ArSCl}} c\text{-PrCPh}{=}CHSAr + ClCH_2CH_2CH{=}CPhCH_2SAr$$

1,1-Dicyclopropylethylene (**2**) underwent rapid initial conversion to an adduct with a singlet resonance at δ 3.52 which rapidly disappeared with the emergence of a complex spectrum. The chemical shift of the signal noted of the initial adduct is consistent with the formation of either $c\text{-Pr}_2CClCH_2SAr$ or $c\text{-Pr}_2CSArCH_2Cl$, and the further changes in the spectrum suggest a mixture of products are then formed with ring opening of one of the cyclopropane rings with formation of a double bond.

Can. J. Chem. Downloaded from www.nrcresearchpress.com by 210.87.254.105 on 09/05/12
For personal use only.

The synthesis of D,L-*cis*-*N*-oxalamido-3-*N*-phenylacetamido-4-methoxymethyl-2-azetidinone

GEORGE JUST AND TENG-JIAM LIAK

Department of Chemistry, McGill University, Montreal, P.Q., Canada H3A 2K6

Received August 15, 1977

GEORGE JUST and TENG-JIAM LIAK. Can. J. Chem. **56**, 211 (1978).

The title compound γ_{max} 1810 cm^{-1}, has been synthesized in 18% yield, starting from L-serine.

GEORGE JUST et TENG-JIAM LIAK. Can. J. Chem. **56**, 211 (1978).

En commencant avec la L-serine, le composé **17**, γ_{max} 1810 cm^{-1}, a été synthétisé avec un rendement de 18%.

A high β-lactam absorption frequency is a necessary prerequisite for high antimicrobial activity of β-lactam antibiotics (penicillin: γ_{max} 1790 cm^{-1}; cephalosporin: γ_{max} 1785 cm^{-1}) but does not necessarily lead to antibiotic activity. The only exception to that rule is provided by the monocyclic nocardicin, where other factors such as an in vivo oxidation may play an important role.

We therefore set out to synthesize β-lactams, in which the ring strain of penicillin and cephalosporin, which seem to be responsible for the high frequency of the β-lactam absorption, are replaced by electronic activation. Lowe and Yeung (1) had synthesized β-lactam analogs A, based on the same principle. The diester of A absorbs at 1790 cm^{-1}.

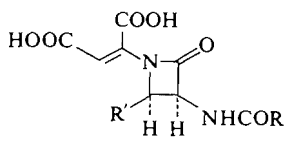

A R′ = H, CH_3

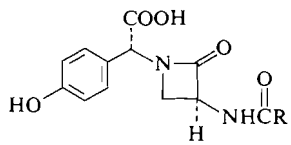

Nocardicin

No absorption frequency was reported for the free acid. Compound A showed no significant antibacterial activity but it could not be ruled out that this lack of activity may be due to reduced electron-withdrawing capacity of the acrylate moiety in A due to anion formation.

Our synthetic goal was **17**, in which the electronic activation is provided by a carbonyl group attached to the β-lactam nitrogen. The side chain at C-4 should not influence unduly the biological activity since it has been shown that the sulphur atom of cephalosporin may be replaced by oxygen or carbon (2–4). The nature of the side-chain derives from its mode of synthesis, in which the essential *cis*-substitution at C-3 and C-4 had to be maintained. The substituent at C-3 is a conventional group known to confer antibiotic activity to β-lactam antibiotics (5).

We chose as our starting material readily available L-serine methyl ester hydrochloride (**6**). It was converted in nearly quantitative yield to its *tert*-butyldimethylsilyl derivative **7**. Using the procedure recently described by Doyle *et al.* (6), **7** was transformed to its stable Schiff base **1**, which upon reaction with azidoacetyl chloride and triethylamine in methylene chloride at −10°C gave β-lactam **2**, mp 74.5–75.5°C in 50% yield based on **7** (Scheme 1).

The nmr spectrum and tlc behaviour of the crude reaction product and of the mother liquors of crystallization indicated that there was one isomer only, in addition to some impurities which made recrystallization of the mother liquors difficult.

β-Lactam **2** appeared to be one compound, since it and all substances derived from it travelled as one spot on tlc, using different systems, and since its ^{1}Hmr spectrum and that of all compounds derived from it never indicated the presence of more than one isomer. The coupling constant of the two hydrogens attached to the β-lactam ring indicated in all cases in which they did not seriously overlap with other signals that the fusion was *cis* (J = 5.5 Hz (7, 8)). The geometry at C-1 will be discussed later, as well as the fact that all β-lactams formed were racemic. However, it should be pointed out that this 'diastereomeric purity' is quite remarkable, since it has been found in our and other laboratories (6, 9–11) that similar additions give rise to both possible diastereomers in approximate equal yields. We have no explanation for this phenomenon. β-Lactam **2** was reduced with triethylamine – hydrogen sulphide in methylene chloride (6) to give amine **8**, mp 94–95°C, which could be transformed without purification to the corresponding phenylacetamide **9**, mp

Can. J. Chem. Downloaded from www.nrcresearchpress.com by 210.87.254.5 on 09/05/12
For personal use only.

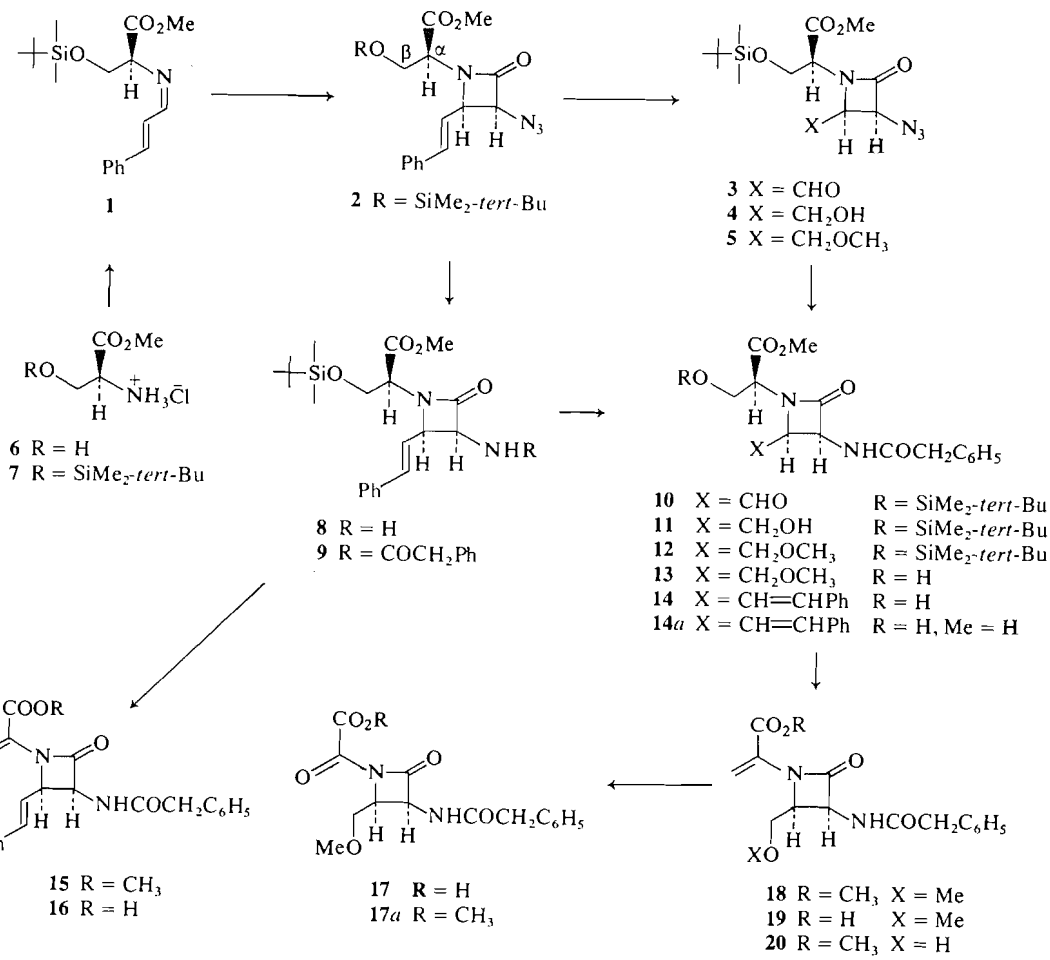

SCHEME 1

72–73°C, in high yield. An attempt to remove the silyl protecting group in **9** by means of tetraethylammonium fluoride in dry tetrahydrofuran (THF) gave an easily separable 1:4 mixture of alcohol **14**, mp 154–155°C, and acrylic ester **15**, mp 161–162°C. Alcohol **14** could be obtained as the sole product when the reaction was repeated, adding 2 equiv. of acetic acid. It was converted quantitatively to acrylate **15**, mp 161–162°C, γ_{max} 1780 cm^{-1}, by treatment with mesyl chloride and triethylamine at −78°C.

In order to ascertain whether the acrylic ester could be hydrolysed in the presence of the strained β-lactam function, **15** was treated with 3 equiv. of sodium hydroxide in H_2O–MeOH or H_2O–THF. In either case, a mixture of acrylic acid **16** and the corresponding β-hydroxy acid **14***a*, was obtained, implying that the rate of hydrolysis of the ester and the rate of Michael addition of hydroxide ion to the ester are approximately equal. Since it is known (12) that rates of hydrolysis of esters in 85% aqueous dimethyl sulfoxide are two orders of magnitude larger, the hydrolysis was repeated using the latter solvent system, and 1 or 3 equiv. of sodium hydroxide. Pure acrylic acid **16**, mp 147–148°C, was obtained in quantitative yield in each case. Having elaborated methods to introduce the acrylic acid function, we next turned our attention to the removal of the side chain. Ozonolysis of **9** in methanol at −78°C, followed by reaction with sodium borohydride at −40°C, gave exclusively the unstable hydroxyacrylate **20** (ir and nmr, only) which seemed to cyclize over a period of a few hours to give **23**, the structure of which was not rigorously established (Scheme 2). When the ozonolysis was carried out in methylene chloride and the ozonide reduced with dimethyl sulphide (13), the resulting aldehyde **10**, mp 176–177°C, could be cleanly converted to the desired alcohol **11** by means of lithium aluminum tri-*tert*-butoxy hydride in dry THF at 0°C. Attempts to convert **11** to its methyl ether **12** by means of methyl iodide – silver oxide (14) failed and dia-

Can. J. Chem. Downloaded from www.nrcresearchpress.com by 210.87.254.5 on 09/05/12
For personal use only.

Can. J. Chem. Downloaded from www.nrcresearchpress.com by 210.87.254.5 on 09/05/12
For personal use only.

zomethane–borontrifluoride etherate (15) led either to recovered starting material (0.1 mol equiv. of $BF_3{\cdot}Et_2O$) or to complete degradation (1 mol equiv. of $BF_3{\cdot}Et_2O$). This is not surprising in view of the results of Doyle *et al.* on an attempted BF_3-catalysed cyclization of a similar alcohol with an acetal.

Since it was essential to block the alcohol function in order to avoid at a later stage cyclizations of type **20** → **23**, and since it had been shown that methylation of a similar alcohol function could be carried out in the presence of an azide function,[1] the styrene **2** was ozonized in methylene chloride at −78°C. Treatment with dimethyl sulphide gave aldehyde **3** and the epoxide or the ozonide[2] of **2** in a ratio of 1:3. Ozonolysis of **2** in methanol followed by treatment with dimethyl sulphide, gave aldehyde **3** as its methanol adduct. Slow distillation of its benzene solution gave pure aldehyde **3**, mp 72–73°C in quantitative yield. Reduction with lithium aluminum tri-*tert*-butoxy hydride gave **4**, mp 67–69°C, which was converted to its methyl ether **5**, mp 71–72°C, by means of diazomethane – boron trifluoride etherate.

Reduction of the azide function, followed by acylation, gave **12**, mp 76–77°C. Treatment of **12** with $\overset{+}{N}Et_4F^-$ in THF containing 2 equiv. of acetic acid gave **13**, mp 93–94°C, which was converted quantitatively to acylate **18**, mp 133–134°C, by means of MsCl–NEt_3 at −78°C. Hydrolysis with a slight excess of sodium hydroxide in DMSO–H_2O (85:15) gave acrylic acid **19**, mp 195–196°C (dec.). Ozonolysis of acrylic acid **19** in methanol, followed by dimethyl sulphide reduction, gave a product which did not contain a β-lactam absorption in its infrared spectrum. When the reaction was repeated in methylene chloride containing a few drops of DMSO in order to solubilize the acid, the oxalic acid derivative **17**, mp 102–103°C, was obtained. The overall yield for the sequence **6** → **7** → **1** → **2** → **3** → **4** → **5** → **13** → **19** → **17** was approximately 18%.

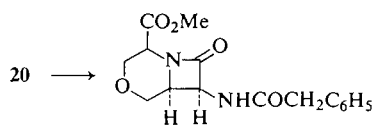

23

SCHEME 2

Ozonolysis of **18** gave **17***a*, which was identical to **17***a*, obtained by methylation of **17** with diazomethane. β-Lactam **17** possessed the remarkable ir absorption at 1810 cm^{-1} for its β-lactam carbonyl, which was in accordance with what we expected. Its ^{1}Hmr in DMSO-d_6 and D_2O, showed a three-proton singlet for methoxy ether at 3.07 ppm, a two-proton multiplet at 3.20–3.40 ppm (CH_2OCH), a two-proton singlet at 3.50 ($CH_2C_6H_5$), a one-proton multiplet for β-lactam C_4 proton, a doublet (J = 7 Hz) for β-lactam C_3 proton, and a sharp singlet for aromatic proton at 7.26 ppm.

Although ozonolysis of acrylic acid **19** in methanol had destroyed the β-lactam function, presumably by opening of the ring by methanol, acid **17** and its ester **17***a* were reasonably stable in DMSO-D_2O (5:1), as ascertained by ^{1}Hmr, which indicated that the half-life of **17** at room temperature was 2 days, whereas $T/2$ for **17***a* was 4 days.

To establish the relative stereochemistry of the carbomethoxy group with respect to the β-lactam hydrogens, the silyl group of aldehyde **3** was hydrolysed (Scheme 3). The resulting aldehyde alcohol

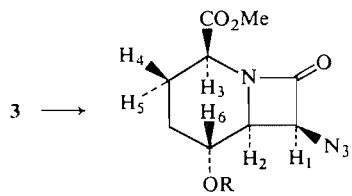

21 R = H
21*a* R = Ac

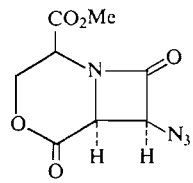

22

SCHEME 3

was isolated as the corresponding lactol **21**. Attempts to convert **21** to lactone **22** using Jones, Fetizon or Moffatt reagents failed. In the latter case, a good yield of crystalline acetate **21***a* was obtained.

Proton magnetic resonance analysis of **21***a*, assuming a chair conformation of the six-membered ring, indicated that the acetate and carbomethoxy group had an equatorial conformation, and was fully consistent with the structure proposed. Thus $J_{1,2}$ was 5.0 Hz, and $J_{2,6}$ 8.0 Hz; H_4 and H_5 appeared as an AB quartet (J = 12.2 Hz), in which the low-field equatorial proton H_5 was further split ($J_{3,5}$ = 2.2 Hz), whereas the high-field hydrogen showed an appropriate axial–equatorial coupling constant $J_{3,4}$ = 5.5 Hz. A boat conformation for the six-

[1]R. Zamboni, personal communication.

[2]We wish to thank the referee for this suggestion. The ^{1}Hmr data (δ 5.51, 5.91 ppm) are more consistent with the latter possibility.

membered ring with opposite relative stereochemistry for the carbomethoxy group would be equally consistent with the ^{1}Hmr data but is quite unlikely since it would result in two severe flagpole interactions, namely H_3–H_6 and H_2–H_5.

It has been suggested by Doyle *et al.* that the mechanism of azidoacetyl chloride addition to cinnamyl Schiff base of type **1** involves the formation of an acylimmonium ion **24**. Our present work supports this view since it could be demonstrated that Schiff base **1** does not racemize during its formation, or upon addition of triethylamine at −10°C, but that the further addition of azidoacetyl chloride results in complete racemization as evidence by complete lack of optical rotation of several intermediates. It seems that acyl immonium ions labilize α-hydrogens more than the corresponding Schiff bases.

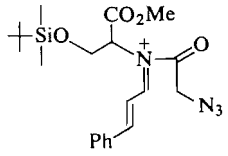

24

Biological tests indicated that **17** was inactive against gram-negative and gram-positive organisms at a level of 128 μg/ml.

Experimental

L-*Serine Methyl Ester* tert-*Butyldimethylsilyl Ether (7)*

To L-serine methyl ester hydrochloride **6** (1.00 g, 6.34 mmol) in dry *N,N*-dimethylformamide (5 ml) was added imidazole (1.53 g, 22.47 mmol) and *tert*-butyldimethylchlorosilane (1.05 g, 6.97 mmol). The solution was stirred at room temperature overnight, then partitioned between ether (100 ml) and water (30 ml). The organic layer was further washed with water (3 × 25 ml), dried (Na_2SO_4), and evaporated. The crude silyl ether was chromatographed on silica gel. Elution with ethyl ether afforded a quantitative yield of amine **7**; ^{1}Hmr (CCl_4) δ: 0.05 (s, 6H, Si(CH_3)$_2$), 0.85 (s, 9H, Si—*tert*-Bu), 1.44 (s, 2H, exchangeable with D_2O, NH_2), 3.27 (t, 1H, J = 4.0 Hz), 3.53 (s, 3H, COOCH_3), 3.63, 3.66, ppm (each d, 2H, J = 4.0 Hz); ir (film) γ_{max}: 3400–3200 (NH_2), 1745 (C=O), 1250 cm^{-1}; ms (60°C) *m/e*: 218 ($M^+ - CH_3$), 204, 176 (M^+ − *tert*-Bu), 175 ($M^+ - COOCH_3$), 144, 116.

*Methyl α-Amino-(*N*-cinnamylidine)-β-tert-butyldimethylsilyloxypropionate (1)*

To amino ester **7** (1.20 g, 0.515 mmol) in 60 ml dry methylene chloride was added cinnamaldehyde (0.68 g, 0.515 mmol). The solution was heated, and methylene chloride distilled off slowly with the constant addition of more dry methylene chloride. After 1 h the solution was cooled and magnesium sulfate added. The suspension was stirred for 1 h, filtered, and evaporated to give a quantitative yield of Schiff base **1**; ^{1}Hmr ($CDCl_3$) δ: 0.05 (s, 6H, Si(CH_3)$_2$), 0.85 (s, 9H, Si—*tert*-Bu), 3.60 (s, 3H, COOCH_3), 3.78–4.10 (m, 3H), 6.78 (d, 2H, J = 4.0 Hz, C_6H_5CH=CH), 7.18 (m, 5H, C_6H_5), 7.78 ppm (t, 1H, J = 4.0 Hz, CH=N); ir (film) γ_{max}: 1735 (C=O), 1670 (C=N), 1630 cm^{-1} (C=C).

cis-N-*(α-Carbomethoxy-β-tert-butyldimethylsilyloxyethyl)-3-azido-4-styryl-2-azetidinone (2)*

To a solution of Schiff base **1** (1.73 g, 5 mmol) and triethylamine (505 mg, 5 mmol) in 100 ml dry methylene chloride at −10°C (ice–methanol bath) was added azidoacetyl chloride (595 mg, 5 mmol) in 10 ml methylene chloride dropwise over a period of 1 h. After the addition was complete, the solution was stirred an additional 15 min and washed with water (50 ml × 3). The organic layer was dried over sodium sulfate, filtered, and evaporated. The crude product (brown oil) was treated with active charcoal (neutral) in 100 ml of anhydrous ether, filtered through Celite, and evaporated to give a yellow solid. Recrystallization from ether–hexane afforded 1.08 g (50%) of β-lactam **2** as colourless crystals, mp 74.5–75.5°C; ^{1}Hmr ($CDCl_3$) δ: 0.05 (s, 6H, Si(CH_3)$_2$), 0.85 (s, 9H, Si—*tert*-Bu), 3.64 (s, 3H, COOCH_3), 3.90 (d, 2H, J = 5 Hz, SiOCH_2), 4.38 (t, 1H, J = 5 Hz, CHCOOCH$_3$), 4.46–4.88 (m, 2H, CH—CH—N$_3$), 6.18 (ddt, 1H, J_1 = 16 Hz, J_2 = 6 Hz, J_3 = 1.5 Hz, C_6H_5—CH=CH), 6.60 (d, 1H, J = 16 Hz, C_6H_5—CH=CH), 7.20 ppm (s, 5H, C_6H_5); ir (KBr) γ_{max}: 2100 (N$_3$), 1780 (β-lactam C=O), 1755 and 1740 cm^{-1} (COOCH$_3$); ms (180°C) *m/e*: 415 ($M^+ - CH_3$), 402 ($M^+ - N_2$), 345 ($M^+ - N_2$—*tert*-butyl), 290 (M^+ − COCHN$_3$—*tert*-butyl). *Anal.* calcd. for $C_{21}H_{30}N_4O_4Si_1$: C 58.60, H 6.97, N 13.02; found: C 58.81, H 7.09, N 13.16.

cis-N-*(α-Carbomethoxy-β-tert-butyldimethylsilyloxyethyl)-3-amino-4-styryl-2-azetidinone (8)*

To a solution of azido-β-lactam **2** (860 mg, 2 mmol) and triethylamine (212 mg, 2.1 mmol) in methylene chloride (30 ml) at 0°C was bubbled in hydrogen sulfide gas for 5 min and the solution allowed to stand for 1 h (evolution of nitrogen was observed). Nitrogen gas was passed in for 15 min and the solvent evaporated under reduced pressure. An additional 50 ml of methylene chloride was added and the solution again evaporated. This procedure was repeated twice more. The crude oil was then redissolved in 40 ml of methylene chloride, washed with water (20 ml × 3), dried (Na_2SO_4), and evaporated. Trituration with hexane gave a pale yellow solid. Recrystallization from ether–hexane afforded 647 mg (80%) of amine **5** as colourless crystals, mp 94–95°C; ^{1}Hmr ($CDCl_3$) δ: 0.05 (s, 6H, Si(CH_3)$_2$), 0.85 (s, 9H, Si—*tert*-Bu), 1.68 (bs, 2H exchangeable with D_2O, NH_2), 3.67 (s, 3H, COOCH_3), 3.9 (d, 2H, SiOCH_2), 4.26–4.76 (m, 3H), 6.10 (dd, 1H, J_1 = 16 Hz, J_2 = 7 Hz, C_6H_5CH=CH), 6.60 (d, 1H, J = 16 Hz, C_6H_6 CH=CH), 7.20 ppm (m, 5H, C_6H_5); ir (film) γ_{max}: 3360 and 3280 (NH_2), 2900, 2820, 1745 (β-lactam C=O and COOCH$_3$), 1240 cm^{-1}.

cis-N-*(α-Carbomethoxy-β-tert-butyldimethylsilyloxyethyl)-3-*N*-phenylacetamido-4-styryl-2-azetidinone (9)*

To a solution of amine **8** (808 mg, 2 mmol) and pyridine (158 mg, 2 mmol) in 30 ml dry methylene chloride was added dropwise phenylacetyl chloride (308 mg, 2 mmol) in 5 ml methylene chloride. After the addition was completed, the solution was stirred an additional 5 min and washed with water (20 ml × 2). The organic layer was dried (Na_2SO_4), filtered, and evaporated. The crude oil was chromatographed on silica gel. Elution with ether afforded amide **9** in quantitative yield, mp 72–73°C; ^{1}Hmr ($CDCl_3$) δ: 0.01, 0.05 (each s, Si(CH_3)$_2$), 0.85 (s, 9H, Si—*tert*-Bu), 3.51 (s, 2H, $C_6H_5CH_2$), 3.76 (s, 3H, COOCH$_3$), 4.0 (dd, 2H, SiOCH_2, J_1 = 4.5 Hz, J_2 = 2 Hz), 4.50 (t, 1H, J = 4.5 Hz), 4.80 (dd, 1H, C_6H_5CH=$CHCH$, J_1 = 8 Hz, J_2 = 5 Hz), 5.46 (dd, 1H, $C_6H_5CH_2CONHCH$, J_1 = 8.5 Hz, J_2 = 5 Hz), 6.0 (dd, 1H, C_6H_5CH=CH, J_1 = 8 Hz, J_2 = 16 Hz), 6.50 (d, 1H, NH, J = 8.5 Hz), 6.61 (d, 1H, C_6H_5CH=CH, J = 16 Hz), 7.02 (s,

Can. J. Chem. Downloaded from www.nrcresearchpress.com by 210.87.254.5 on 09/05/12
For personal use only.

Can. J. Chem. Downloaded from www.nrcresearchpress.com by 210.87.254.5 on 09/05/12
For personal use only.

5H, C_6H_5), 7.24 ppm (s, 5H, C_6H_5); ir ($CHCl_3$) γ_{max}: 3380 (NH), 1750 (β-lactam C=O), 1735 ($COOCH_3$), 1670 cm^{-1} (amide C=O); ms (150°C) *m/e*: 522 (M^+), 465 (M^+ – *tert*-Bu). *Anal.* calcd. for $C_{29}H_{38}N_2O_5Si_1$: C 66.66, H 7.27, N 5.36; found: C 66.87, H 7.09, N 5.03.

cis-N-*(α-Carbomethoxy-β-hydroxyethyl)-3*-N-*phenylacetamido-4-styryl-2-azetidinone (**14**)*

To the silyl protected β-lactam **9** (400 mg, 0.76 mmol) and glacial acetic acid (182 mg, 3.04 mmol) in dry tetrahydrofuran (10 ml) was added tetraethylammonium fluoride (223 mg, 1.50 mmol). After stirring at room temperature for 3 h the solvent was removed under reduced pressure. The residue was dissolved in ethyl acetate (30 ml), washed with saturated sodium bicarbonate solution and water, dried, and evaporated. Recrystallization from methylene chloride – ether afforded 264 mg (85%) of alcohol **14**, mp 154–155°C; ^{1}Hmr ($CDCl_3$) δ: 3.36 (s, 2H, $C_6H_5CH_2$), 3.63 (s, 3H, $COOCH_3$), 3.63–4.06 (bm, 3H, one exchangeable with D_2O, CH_2OH), 4.18–4.46 (m, 1H, $CHCOOCH_3$), 4.61 (dd, 1H, J_1 = 5 Hz, J_2 = 8 Hz, C_6H_5CH=$CHCH$), 5.28 (dd, 1H, J_1 = 5 Hz, J_2 = 8.5 Hz, $C_6H_5CH_2CONHCH$), 5.97 (dd, 1H, J_1 = 16 Hz, J_2 = 8 Hz, C_6H_5CH=CH), 6.52 (d, J_1 = 16 Hz, C_6H_5CH=CH), 6.92 (s, 5H, C_6H_5), 7.06 (d, 1H, J=8.5 Hz, NH), 7.18 ppm (s, 5H, C_6H_5); ir (KBr) γ_{max}: 3490 and 3425 (OH), 3270 (NH), 1770 (β-lactam C=O), 1740 and 1720 ($COOCH_3$), 3050, 2920, 1650 cm^{-1} (amide C=O); ms (150°C) *m/e*: 407 (M^+ – 1), 390 (M^+ – H_2O), 273 ((M^+ – 1) – $C_6H_5CH_2CONH$), 233 (M^+ – $C_6H_5CH_2CONHCHCO$). *Anal.* calcd. for $C_{23}H_{24}N_2O_5$: C 67.65, H 5.88, N 6.86; found: C 67.95, H 5.76, N 6.76.

cis-N-*(α-Methylacrylyl)-3*-N-*phenylacetamido-4-styryl-2-azetidinone (**15**)*

To a solution of alcohol **14** (204 mg, 0.5 mmol) and triethylamine (101 mg, 1 mmol) in 25 ml dry methylene chloride at −78°C was added dropwise methanesulfonyl chloride (112 mg, 0.5 mmol) in 3 ml methylene chloride. After the addition was completed the mixture was washed with p*H* 4.4 buffer (0.2 *M*, KH_2PO_4 solution) and water, dried (Na_2SO_4), and evaporated. Recrystallization from methylene chloride – hexane afforded a quantitative yield of olefin **15**, mp 161–162°C; ^{1}Hmr ($CDCl_3$) δ: 3.40 (s, 2H, $C_6H_5CH_2$), 3.63 (s, 3H, $COOCH_3$), 5.0 (dd, 1H, J_1 = 5 Hz, J_2 = 8 Hz, C_6H_5CH=CH—CH), 5.40 (dd, 1H, J_1 = 5 Hz, J_2 = 8.5 Hz, $C_6H_5CH_2CONHCH$), 5.83 (dd, 1H, J_1 = 16 Hz, J_2 = 8 Hz, C_6H_5CH=CH), 5.77, 5.90 (each s, 2H, C=CH_2), 6.40 (d, 1H, J = 16 Hz, C_6H_5CH=CH), 6.41 (d, 1H, J = 8.5 Hz, NH), 6.90 (s, 5H, C_6H_5), 7.10 ppm (s, 5H, C_6H_5); ir (KBr) γ_{max}: 3260 (NH), 3020, 2930, 1760 (β-lactam C=O), 1725 ($COOCH_3$), 1650 cm^{-1} (amide C=O). *Anal.* calcd. for $C_{23}H_{22}N_2O_4$: C 70.77, H 5.64, N 7.18; found: C 70.75, H 5.71, N 7.41.

cis-N-*(α-Acrylyl)-3*-N-*phenylacetamido-4-styryl-2-azetidinone (**16**)*

To β-lactam ester **15** (55 mg, 0.14 mmol) at room temperature was added 1.6 ml sodium hydroxide (0.1 *N*) in aqueous dimethyl sulfoxide (H_2O–DMSO 15:85). The suspension was stirred until all the ester dissolved, giving a clear solution to which p*H* 4.4 phosphate buffer (15 ml) was added. The mixture was extracted with ethyl acetate (10 ml × 4), washed with a small amount of water, dried (Na_2SO_4), and evaporated. Recrystallization from chloroform afforded 41 mg (80%) acid **16**, mp 147–148°C (dec.); ^{1}Hmr (acetone-d_6) δ: 3.50 (s, 2H, $C_6H_5CH_2$), 3.89–4.55 (m, 2H, two β-lactam protons), 5.77, 5.94 (each s, 2H, CH_2=C), 6.20 (dd, 1H, J_1 = 16 Hz, J_2 = 8 Hz, C_6H_5CH=CH), 6.62 (d, 1H, J = 16 Hz, C_6H_5-CH=CH), 7.04 (m, 5H, C_6H_5), 7.23 (s, 5H, C_6H_5), 7.60–8.05 ppm (b, 1H, NH); ir (KBr) γ_{max}: 3350 (NH), 3040, 3070, 2800–2500 (COOH), 1745 (β-lactam C=O), 1725 (C=O), 1655 cm^{-1} (amide C=O).

cis-N-*(α-Methylacrylyl)-3*-N-*phenylacetamido-4-hydroxymethyl-2-azetidinone (**20**)*

A solution of β-lactam **9** (300 mg, 0.57 mmol) in dry methanol (30 ml) was ozonized at −78°C (Dry Ice – acetone bath) until the solution turned blue. The excess ozone was removed by passing in dry nitrogen for 10 min. Sodium borohydride (23 mg, 0.6 mmol) was added and the solution was allowed to warm up slowly to room temperature. The solvent was removed under reduced pressure. The residue after addition of p*H* 4.4 phosphate buffer was extracted with chloroform (10 ml × 4), washed with water, and dried over sodium sulfate. Evaporation of the solvent afforded a mixture of unstable olefinic alcohol **20** and benzyl alcohol; ^{1}Hmr ($CDCl_3$) δ: 3.60 (s, 2H, $C_6H_5CH_2$), 3.79 (s, 3H, $COOCH_3$), 3.92–4.26 (b, 3H, CH_2—OH), 4.42 (m, 1H, $CHCH_2OH$), 5.41 (dd, 1H, J_1 = 5 Hz, J_2 = 8.5 Hz, $C_6H_5CH_2CONHCH$), 5.89, 6.09 (each s, 2H, CH_2=CH), 7.16 ppm (bs, 6H, C_6H_5 and NH); ir (CH_2Cl_2) γ_{max}: 3600–3200 (OH), 3420 (NH), 2920, 2840, 1780 (β-lactam C=O), 1770 ($COOCH_3$), 1695 (amide C=O), 1620 cm^{-1} (C=C).

cis-N-*(α-Carbomethoxy-β-tert-butyldimethylsilyloxyethyl)-3*-N-*phenylacetamido-4-formyl-2-azetidinone (**10**)*

A solution of β-lactam **9** (400 mg, 0.76 mmol) in dry methylene chloride (50 ml) was ozonized at −78°C (Dry Ice – acetone bath) until the solution turned blue. The excess ozone was removed by passing in dry nitrogen. Dimethyl sulfide (0.5 ml) was added and the solution was allowed to warm up slowly to room temperature. The solution was washed with water (20 ml × 3), dried (Na_2SO_4), and evaporated. The semisolid residue was heated under high vacuum for 20 h at 50°C to remove benzaldehyde. Recrystallization from methylene chloride – ether afforded 294 mg (86%) aldehyde **10**, mp 176–177°C; ^{1}Hmr ($CDCl_3$) δ: 0.01 (s, 6H, $Si(CH_3)_2$), 0.80 (s, 9H, Si—*tert*-Bu), 3.44 (s, 2H, $C_6H_5CH_2$), 3.63 (s, 3H, $COOCH_3$), 4.12 (dd, 2H, J_1 = 3 Hz, J_2 = 7 Hz, $SiOCH_2$), 4.50–5.0 (m, 3H, 2 β-lactam protons and $CHCOOCH_3$), 6.36 (bd, 1H, J = 6 Hz, NH), 7.10 (s, 5H, C_6H_5), 9.66 ppm (d, 1H, J = 1.5 Hz, CHO); ir (KBr) γ_{max}: 3250 (NH), 3080, 2960, 2860, 1775 (β-lactam C=O), 1740 ($COOCH_3$), 1720 (CHO), 1645 cm^{-1} (amide C=O).

cis-N-*(α-Carbomethoxy-β-tert-butyldimethylsilyloxyethyl)-3*-N-*phenylacetamido-4-hydroxymethyl-2-azetidinone (**11**)*

To aldehyde **10** (448 mg, 1 mmol) in dry tetrahydrofuran (30 ml) at 0°C under nitrogen was added lithium aluminum tri-(*tert*-butoxy) hydride (431 mg, 1.5 mmol). The mixture was stirred at 0°C for 3 h. Dilute hydrochloric acid (2%) was added slowly (in ice bath) to the mixture until p*H* 5, followed by 1 g of Celite. The suspension was stirred for 20 min, filtered through Celite, and the Celite washed twice with tetrahydrofuran (10 ml × 2). The combined solution was evaporated under reduced pressure. To the residue was added 30 ml of water. The solution was extracted with ethylacetate (20 ml × 3), washed with water, dried (Na_2SO_4), and evaporated. The crude product was chromatographed on silica gel (activity II–III). Elution with chloroform afforded a colorless solid. Recrystallization from ether–hexane afforded 365 mg (81%) alcohol **11**, mp 81–82°C; ^{1}Hmr ($CDCl_3$) δ: 0.1 (s, 6H, $Si(CH_3)_2$), 0.86 (s, 9H, Si—*tert*-Bu), 3.40–3.60 (b, 1H, D_2O exchangeable, OH), 3.53 (s, 2H, $C_6H_5CH_2$), 3.66 (s, 3H, $COOCH_3$), 3.73–4.26 (m, 5H), 4.46 (m, 1H, CH—CH_2OH),

Can. J. Chem. Downloaded from www.nrcresearchpress.com by 210.87.254.5 on 09/05/12
For personal use only.

5.50 (dd, 1H, J_1 = 10 Hz, J_2 = 5 Hz, $C_6H_5CH_2CONHCH$), 6.73 (bd, 1H, J = 10, NH), 7.16 ppm (s, 5H, C_6H_5); ir (KBr) γ_{max}: 3200 (OH), 3060, 3040, 2960, 2925, 2860, 1780 (β-lactam C=O), 1745 ($COOCH_3$), 1660 cm^{-1} (amide C=O). *Anal. calcd.* for $C_{22}H_{34}N_2O_6Si_1$: C 58.67, H 7.56, N 6.22; found: C 58.61, H 7.82, N 6.51.

cis-N-*(α-Carbomethoxy*-β-tert-*butyldimethylsilyloxyethyl)-3-azido-4-formyl-2-azetidinone (**3**)*

A solution of azido-β-lactam **2** (1.505 g, 3.50 mmol) in dry methanol (150 ml) was ozonized at −30°C for 90 min. The excess ozone was removed by passing in dry nitrogen. Dimethyl sulfide (1.5 ml) was added and the solution was allowed to warm up slowly to room temperature. Methanol was removed under reduced pressure and the residue was dissolved in 60 ml of benzene, washed with water (20 ml × 3), and dried over sodium sulfate. The benzene solution was azeotroped for 1 h followed by evaporation. The oily residue was heated under high vacuum for 20 h at 50°C to remove benzaldehyde. The aldehyde **3** was obtained in quantitative yield, mp 72–73°C; ^{1}Hmr ($CDCl_3$) δ: 0.01 (s, 6H, $Si(CH_3)_2$), 0.81 (s, 9H, Si—*tert*-Bu), 3.63 (s, 3H, $COOCH_3$), 3.82–4.35 (m, 2H, CH_2—OSi), 4.52 (m, 2H), 4.95 (d, 1H, J = 5.7 Hz, CHN_3), 9.32 ppm (d, 1H, J = 3 Hz, CHO); ir (KBr) γ_{max}: 2960, 2940, 2895, 2860, 2140, and 2110 (N_3), 1790 (β-lactam C=O), 1750 ($COOCH_3$), 1745 cm^{-1} (CHO).

cis-N-*(α-Carbomethoxy*-β-tert-*butyldimethylsilyloxyethyl)-3-azido-4-hydroxymethyl-2-azetidinone (**4**)*

To aldehyde **3** (1.246 g, 3.5 mmol) in tetrahydrofuran (80 ml) at 0°C was added lithium aluminium tri(*tert*-butoxy) hydride (1.78 g, 7 mmol). After stirring under nitrogen for 3 h (0°C), the mixture was acidified with dilute hydrochloric acid (2%) to pH 5, and 1 g of Celite was added. The suspension was stirred for 10 min, filtered, and evaporated. To the residue was added 60 ml ethyl acetate, washed with brine (20 ml × 3), dried (Na_2SO_4), and evaporated. The crude alcohol was chromatographed on silica gel. Elution with chloroform afforded 1.00 g (80%) of alcohol **4**, mp 67–69°C; ^{1}Hmr ($CDCl_3$) δ: 0.1 (s, 6H, $Si(CH_3)_2$), 0.89 (s, 9H, Si—*tert*-Bu), 2.84 (t, 1H, D_2O exchangeable, J = 7 Hz, OH), 3.66 (s, 3H, $COOCH_3$), 3.69–4.03 (m, 4H), 4.03–4.29 (m, 1H, CH—CH—N_3), 4.52 (t, 1H, J = 5 Hz, $CHCOOCH_3$), 4.65 ppm (d, 1H, J = 5 Hz, CHN_3); ^{1}Hmr ($CDCl_3$ + D_2O) δ: 0.1 (s, 6H, $Si(CH_3)_2$), 0.89 (s, 9H, Si—*tert*-Bu), 3.66 (s, 3H, $COOCH_3$), 3.79 (d, 2H, J = 4 Hz, CH_2—OD), 3.93, 3.94 (each d, J = 5 Hz, CH_2—OSi), 4.03–4.29 (m, 1H, CH—CH—N_3), 4.52 (t, 1H, J = 5 Hz, $CHCOOCH_3$), 4.65 ppm (d, 1H, J = 5 Hz, CHN_3); ir (KBr) γ_{max}: 3460 (OH), 2960, 2940, 2900, 2860, 2140 (N_3), 1770 (β-lactam C=O), 1750 cm^{-1} ($COOCH_3$). *Anal.* calcd. for $C_{14}H_{26}N_4O_5Si_1$: C 46.93, H 7.26, N 15.64; found: C 46.81, H 7.50, N 15.68.

cis-N-*(α-Carbomethoxy*-β-tert-*butylmethylsilyloxyethyl)-3-azido-4-methoxymethyl-2-azetidinone (**5**)*

To azido alcohol **4** (358 mg, 1 mmol) and boron trifluoride etherate (0.1 mmol) in dry methylene chloride (40 ml) at 0°C was added diazomethane (10 mmol) in absolute ether in portions over a period of 30 min. After stirring for another hour the solution was washed with saturated sodium bicarbonate solution (15 ml × 2) and water (15 ml × 2), dried (Na_2SO_4), and evaporated. The crude product was chromatographed on silica gel. Elution with chloroform – methylene chloride afforded 316 mg (85%) methyl ether **5**, mp 71–72°C; ^{1}Hmr (CCl_4) δ: 0.06 (s, 6H, $Si(CH_3)_2$), 0.92 (s, 9H, Si—*tert*-Bu), 3.27 (s, 3H, OCH_3), 3.50 (d, 2H, J = 5.5 Hz, CH_2OCH_3), 3.63 (s, 3H, $COOCH_3$), 3.76–4.39 (m, 4H), 4.57 ppm (d, 1H, J = 5 Hz); ir (KBr) γ_{max}: 2940, 2900, 2860, 2120 (N_3), 1780 (β-lactam C=O), 1755 and 1745 cm^{-1} ($COOCH_3$).

cis-N-*(α-Carbomethoxy*-β-tert-*butylmethylsilyloxyethyl)-3-amino-4-methoxymethyl-2-azetidinone (**8a**)*

To a solution of azido-β-lactam **5** (372 mg, 1 mmol) and triethylamine (106 mg, 1.05 mmol) in methylene chloride (20 ml) at 0°C was bubbled in hydrogen sulfide gas for 3 min and the solution allowed to stand for 1 h (evolution of nitrogen was observed). Nitrogen gas was passed in for 15 min and the solvent evaporated under reduced pressure. An additional 30 ml methylene chloride was added and the solution again evaporated. This procedure was repeated twice more. The residue was redissolved in 30 ml of methylene chloride, washed with water (15 ml × 3), dried (Na_2SO_4), and evaporated. The crude product was chromatographed on silica gel. Elution with chloroform – ethyl acetate afforded 284 mg (82%) amine **8*a***; ^{1}Hmr ($CDCl_3$) δ: 0.06 (s, 6H, $Si(CH_3)_2$), 0.86 (s, 9H, Si—*tert*-Bu), 1.91 (bs, 2H, NH_2), 3.27 (s, 3H, OCH_3), 3.36–3.70 (m, 2H, CH_2OCH_3), 3.66 (s, 3H, $COOCH_3$), 3.76–4.06 (m, 3H), 4.15 (d, 1H, J = 5 Hz, $CHNH_2$), 4.42 ppm (t, 1H, J = 4 Hz, $CHCOOCH_3$); ir (film) γ_{max}: 3380 and 3320 (NH_2), 2940, 2895, 2860, 1760 (β-lactam C=O), 1745 cm^{-1} ($COOCH_3$).

cis-N-*(α-Carbomethoxy*-β-tert-*butyldimethylsilyloxyethyl)-3-N-phenylacetamido-4-methoxymethyl-2-azetidinone (**12**)*

To a solution of amine **8*a*** (360 mg, 1 mmol) and pyridine (79 mg, 1 mmol) in dry methylene chloride (20 ml) was added dropwise phenylacetyl chloride (154 mg, 1 mmol) in 3 ml methylene chloride. After the addition was complete, the solution was stirred an additional 5 min and washed with water (15 ml × 2). The organic layer was dried (Na_2SO_4), filtered, and evaporated. The crude oil was chromatographed on silica gel. Elution with ether–chloroform afforded the amide **12** in quantitative yield, mp 76–77°C; ^{1}Hmr ($CDCl_3$) δ: 0.01 (s, 6H, $Si(CH_3)_2$), 0.82 (s, 9H, Si—*tert*-Bu), 2.84 (s, 3H, OCH_3), 2.85–3.23 (m, 2H, CH_2OCH_3), 3.50 (s, 2H, $CH_2C_6H_5$), 3.60 (s, 3H, $COOCH_3$), 3.62–4.15 (m, 3H), 4.40 (t, 1H, J = 4 Hz, $CHCOOCH_3$), 5.41 (dd, 1H, J_1 = 5.5 Hz, J_2 = 10 Hz, CHNH), 6.37 (bd, 1H, J = 10 Hz, NH), 7.08 ppm (s, 5H, C_6H_5); ir (KBr) γ_{max}: 3250 (NH), 2940, 2920, 2880, 2840, 1768 (β-lactam C=O), 1740 ($COOCH_3$) 1645 cm^{-1} (amide C=O).

cis-N-*(α-Carbomethoxy*-β-*hydroxyethyl)-3*-N-*phenylacetamido-4-methoxymethyl-2-azetidinone (**13**)*

To the silyl protected β-lactam **12** (464 mg, 1 mmol) and glacial acetic acid (240 mg, 4 mmol) in dry tetrahydrofuran (10 ml) was added tetracthylammonium fluoride (294 mg, 2 mmol). After stirring at room temperature for 3 h the solvent was removed under reduced pressure. The residue was dissolved in ethyl acetate (30 ml), washed with saturated sodium bicarbonate solution and water, dried, and evaporated. Recrystallization from ether–hexane afforded 294 mg (84%) of alcohol **13**, mp 93–94°C; ^{1}Hmr ($CDCl_3$) δ: 2.97 (s, 3H, CH_2OCH_3), 3.03–3.43 (m, 2H, CH_2OCH_3), 3.50 (s, 2H, $CH_2C_6H_5$), 3.66 (s, 3H, $COOCH_3$), 3.67–3.99 (m, 3H, (CH_2OH), 4.13 (m, 1H, $CHCH_2OCH_3$), 4.42 (m, 1H, $CHCOOCH_3$), 5.51 (dd, 1H, J_1 = 5 Hz, J_2 = 9 Hz, CHNH), 6.50 (bd, 1H, J = 9 Hz, NH), 7.10 ppm (s, 5H, C_6H_5); ^{1}Hmr ($CDCl_3$ + D_2O) δ: 2.97 (s, 3H, CH_2OCH_3), 3.03–3.43 (m, 2H, CH_2OCH_3), 3.50 (s, 2H, $CH_2C_6H_5$), 3.66 (s, 3H, $COOCH_3$), 3.73 (d, 2H, J = 5 Hz, CH_2OD), 4.13 (m, 1H, $CHCH_2OCH_3$), 4.42 (t, 1H, J = 5 Hz, CH—$COOCH_3$), 5.51 (dd, 1H, J_1 = 5 Hz, J_2 = 9 Hz, CHNH), 6.93 (bd, 1H, J = 9 Hz, NH), 7.10 ppm (s, 5H, C_6H_5); ir (KBr) γ_{max}: 3400 (OH), 3300 (NH), 3040, 3010, 2940, 2910, 2885, 1750 (β-lactam C=O), 1730 ($COOCH_3$), 1660 cm^{-1} (amide C=O).

cis-N-*(α-Methylacrylyl)-3*-N-*phenylacetamido-4-methoxymethyl-2-azetidinone (**18**)*

To a solution of alcohol **13** (350 mg, 1 mmol) and triethyl-

Can. J. Chem. Downloaded from www.nrcresearchpress.com by 210.87.254.5 on 09/05/12
For personal use only.

amine (202 mg, 2 mmol) in 30 ml dry methylene chloride at −78°C was added dropwise methane sulfonyl chloride (224 mg, 1 mmol) in 5 ml methylene chloride. After the addition was completed the mixture was washed with p*H* 4.4 buffer (0.2 *M* KH_2PO_4 solution) and water, dried (Na_2SO_4), and evaporated. Recrystallization from methylene chloride–ether afforded a quantitative yield of olefin **18**, mp 133–134°C; ^{1}Hmr ($CDCl_3$) δ: 2.90 (s, 3H, CH_2OCH_3), 2.97–3.46 (m, 2H, CH_2OCH_3), 3.53 (s, 2H, $CH_2C_6H_5$), 3.70 (s, 3H, $COOCH_3$), 4.42 (m, 1H, $CHCH_2OCH_3$), 5.48 (dd, 1H, J_1 = 6 Hz, J_2 = 10 Hz, CHNH), 5.81, 6.07 (each s, 2H, CH_2=C), 6.37 (bd, 1H, J = 10 Hz, NH), 7.13 ppm (s, 5H, C_6H_5); ir (KBr) γ_{max}: 3295 (NH), 3010, 2930, 2910, 1755 (β-lactam C=O), 1725 ($COOCH_3$), 1658 (amide C=O), 1612 cm^{-1} (C=C). *Anal.* calcd. for $C_{17}H_{20}N_2O_5$: C 61.45, H 6.02, N 8.43; found: C 61.49, H 6.29, N 8.69.

cis-N-*(α-Acrylyl)-3*-N-*phenylacetamido-4-methoxymethyl-2-azetidinone (19)*

To β-lactam ester **18** (166 mg, 0.5 mmol) at room temperature was added 5.72 ml sodium hydroxide (0.1 *N*) in aqueous dimethyl sulfoxide (H_2O–DMSO 15:85). The suspension was stirred until all the ester dissolved, giving a clear solution to which p*H* 4.4 phosphate buffer (15 ml) was added. The mixture was extracted with ethyl acetate (15 ml × 4), washed with a small amount of water, dried (Na_2SO_4), and evaporated. The solid residue was washed with ether and filtered to afford 129 mg (81%) acid **19**, mp 195–196°C (dec.); ^{1}Hmr ($CDCl_3$ + DMSO-d_6) δ: 3.04 (s, 3H, OCH_3), 3.35 (d, 2H, J = 4.2 Hz, CH_2OCH_3), 3.43 (s, 2H, $CH_2COCH_2C_6H_5$), 4.36 (bm, COOH, H_2O, and $CHCH_2OCH_3$), 5.12 (dd, 1H, J_1 = 5 Hz, J_2 = 9 Hz, CHNH), 5.59, 5.74 (each s, 2H, CH_2=C), 7.03 (s, 5H, C_6H_5), 8.12 ppm (d, 1H, J = 9 Hz, NH); ir (KBr) γ_{max}: 3250 (NH), 2800–2600 (b, COOH), 1758 (β-lactam C=O), 1695 (acid, C=O), 1658 (amide, C=O), 1596 cm^{-1} (C=C).

cis-N-*Methyloxalamido-3*-N-*phenylacetamido-4-methoxymethyl-2-azetidinone (17a)*

A solution of β-lactam **18** (50 mg, 0.15 mmol) in dry methylene chloride (25 ml) was ozonized at −78°C until the solution turned blue. The excess ozone was removed by passing in dry nitrogen. Dimethyl sulfide (0.2 ml) was added and the solution was allowed to warm up slowly to room temperature. The solution was washed with water (10 ml × 3), dried (Na_2SO_4), and evaporated to afford a quantitative yield of oxalate derivative **17***a*, mp 112–113°C; ^{1}Hmr ($CDCl_3$) δ: 2.97 (s, 3H, CH_2OCH_3), 3.10–3.36 (m, 2H, CH_2OCH_3), 3.56 (s, 2H, $CH_2C_6H_5$), 3.83 (s, 3H, $COOCH_3$), 4.26 (m, 1H, $CHCH_2OCH_3$), 5.64 (dd, 1H, J_1 = 7 Hz, J_2 = 10 Hz, CHNH), 6.44 (bd, 1H, J = 10 Hz, NH), 7.16 ppm (s, 5H, C_6H_5); ir (CH_2Cl_2) γ_{max}: 3370 (NH), 1810 (β-lactam C=O), 1775 ($COOCH_3$), 1700 (C=O), 1680 (amide C=O), 1508, 1372 cm^{-1}.

cis-N-*Oxalamido-3*-N-*phenylacetamido-4-methoxymethyl-2-azetidinone (17)*

The acid **19** (80 mg, 0.25 mmol) was ozonized at −78°C in a mixture of methylene chloride (20 ml) and dimethyl sulfoxide (0.25 ml) until the solution became blue. The excess ozone was removed by passing in dry nitrogen. Dimethyl sulfide (0.25 ml) was added and the solution was allowed to warm up slowly to room temperature. After removal of solvent under high vacuum, the β-lactam **17**, mp 102–103°C, was obtained in quantitative yield; ^{1}Hmr (D_2O + DMSO-d_6) δ: 3.07 (s, 3H, OCH_3), 3.20–3.40 (m, 2H, CH_2OCH_3), 3.50 (s, 2H, $CH_2C_6H_5$), 4.32 (m, 1H, $CHCH_2OCH_3$), 5.38 (d, 1H, J = 7 Hz, CHND), 7.26 ppm (s, 5H, C_6H_5); ir (CH_2Cl_2) γ_{max}: 3230 (NH), 2900, 2720–2440 (COOH), 1810 (β-lactam C=O), 1750–1660 (b, C=O, COOH, NHCO), 1530 cm^{-1}.

1-α-Hydroxy-4-β-carbomethoxy-7-β-azido-O-2-isocepham (21) (3)

To aldehyde **3** (150 mg, 0.42 mmol) and glacial acetic acid (101 mg, 1.68 mmol) in dry tetrahydrofuran (10 ml) was added tetraethylammonium fluoride (124 mg, 0.84 mmol). After stirring at room temperature for 2.5 h the solvent was removed under reduced pressure. The residue was dissolved in ethyl acetate (25 ml), washed with brine (10 ml × 3), dried (K_2CO_3), and evaporated to afford 73 mg (~70%) lactol **21**; pmr ($CDCl_3$ + D_2O) δ: 3.76 (s, 3H, $COOCH_3$), 3.77–4.45 (m, 5H), 4.83 (d, 1H, J = 8 Hz, O—CH—OH), 4.93 ppm (d, 1H, J = 5 Hz, CHN_3); ir (CH_2Cl_2) γ_{max}: 3600 and 3400 (OH), 2140 (N_3), 1786 (β-lactam C=O), 1760 cm^{-1} ($COOCH_3$).

1-α-Acetoxy-4-β-carbomethoxy-7-β-azido-O-2-isocepham (21a)

A solution of lactol **21** (50 mg, 0.21 mmol) in dimethyl sulfoxide (1.5 ml) and acetic anhydride (1 ml) was stirred at room temperature overnight. To the mixture chloroform (30 ml) was added and washed with water (10 ml × 2), dried (Na_2SO_4), and evaporated. The crude product was chromatographed on silica gel. Elution with chloroform afforded 45 mg (75%) of acetate **21***a*; ^{1}Hmr ($CDCl_3$) δ: 2.09 (s, 3H, $COCH_3$), 3.75 (s, 3H, $COOCH_3$), 3.81 (dd, 1H, J_1 = 5 Hz, J_2 = 8 Hz, $CHCH—N_3$), 3.95 (dd, 1H, J_1 = 5.5 Hz, J_2 = 12.2 Hz, OCH_4), 4.21 (dd, 1H, J_1 = 2.2 Hz, J_2 = 12.2 Hz, OCH_5), 4.39 (dd, 1H, J_1 = 2.2 Hz, J_2 = 5.5 Hz, $CHCOOCH_3$), 4.91 (d, 1H, J = 5.0 Hz, CHN_3), 5.75 (d, 1H, J = 8 Hz, $CHOCOCH_3$); ir (film) γ_{max}: 2995, 2160 (N_3), 1790–1740 cm^{-1} (β-lactam C=O, $COOCH_3$, $OCOCH_3$).

Acknowledgement

We wish to thank the National Research Council of Canada for generous financial support.

1. G. Lowe and H. W. Yeung. J. Chem. Soc. Perkin Trans. 1, 2907 (1973).
2. L. D. Cama and B. G. Christensen. J. Am. Chem. Soc. **96**, 7582 (1974).
3. R. N. Guthikonda, L. D. Cama, and B. G. Christensen. J. Am. Chem. Soc. **96**, 7584 (1974).
4. S. Wolfe, J. B. Ducep, K. C. Tin, and S. N. Lee. Can. J. Chem. **52**, 3996 (1974).
5. E. H. Flynn. Cephalosporins and penicillins. Academic Press, New York and London. 1972.
6. T. W. Doyle, B. Belleau, B. Luh, C. F. Ferrari, and M. P. Cunningham. Can. J. Chem. **55**, 468 (1977).
7. H. B. Kagan, J. J. Basselier, and J. L. Luche. Tetrahedron Lett. 941 (1964).
8. P. J. Decazes, J. L. Luche, and H. B. Kagan. Tetrahedron Lett. 3661 (1970).
9. T. W. Doyle, B. Belleau, B. Luh, T. T. Conway, M. Menard, J. L. Douglas, D. T. Chu, G. Lim, L. E. Morris, P. Riverst, and M. Casey. Can. J. Chem. **55**, 484 (1977).
10. T. W. Doyle, B. Luh, and A. Martel. Can. J. Chem. **55**, 2700 (1977).
11. T. W. Doyle, A. Martel, and B. Luh. Can. J. Chem. **55**, 2708 (1977).
12. D. D. Roberts. J. Org. Chem. **29**, 2039 (1964).
13. J. J. Pappas, W. P. Keaveney, E. Gancher, and M. Berger. Tetrahedron Lett. 4273 (1966).
14. R. Kuhn, J. Trischmann, and I. Löw. Angew. Chem. **67**, 32 (1955).
15. M. Neehman, M. C. Caserio, J. D. Roberts, and W. S. Johnson. Tetrahedron, **6**, 36 (1966).

Preparation of substituted 2,3-diphenylindoles and 2,3-diphenylindolenyl-3-hydroperoxides via reduction of α-(*o*-nitrophenyl)deoxybenzoins

M. JAWDOSIUK, I. KMIOTEK-SKARŻYŃSKA, AND W. WILCZYŃSKI

Institute of Organic Chemistry and Technology, Polytechnical University, 00-662 Warsaw, Poland

Received June 1, 1977

M. JAWDOSIUK, I. KMIOTEK-SKARŻYŃSKA, and W. WILCZYŃSKI. Can. J. Chem. **56**, 218 (1978).

Substituted *o*-nitrohalobenzenes react in aprotic solvents in the presence of powdered potassium hydroxide with deoxybenzoin to form corresponding nitroarylated deoxybenzoins. The latter on reduction form substituted 2,3-diphenylindoles which under certain conditions undergo oxidation with atmospheric oxygen to form 2,3-diphenylindolenyl-3-hydroperoxides.

M. JAWDOSIUK, I. KMIOTEK-SKARŻYŃSKA et W. WILCZYŃSKI. Can. J. Chem. **56**, 218 (1978).

Dans des solvants aprotiques et en présence d'hydroxyde de potassium en poudre, les *o*-nitrohalobenzènes substitués réagissent avec la déoxybenzoine pour conduire aux déoxybenzoines nitroarylés correspondantes. Ces dernières, par réduction, donnent naissance aux diphényl-2,3 indoles substitués. Ces indoles subissent dans certaines conditions des oxydations par l'oxygène atmosphérique pour conduire à des diphényl-2,3 indolénylehydroperoxydes-3.

[Traduit par le journal]

Can. J. Chem. Downloaded from www.nrcresearchpress.com by 210.87.254.6 on 09/05/12
For personal use only.

For nearly a century, the Fischer synthesis of indoles involving intramolecular cyclization of suitable phenylhydrazones has been employed as one of the most useful methods for the synthesis of these compounds (1). The original method has undergone substantial modification and improvement. For example, Dave (2) has recently described a one-step procedure for the synthesis of 2,3-dialkylindoles from appropriate ketones and phenylhydrazine hydrochlorides. The versatility of indoles in organic synthesis, as well as their biological activity gives the stimulus for the further search for new, convenient methods for the preparation of indole derivatives (3, 4).

It has been known from the literature, that one of the possible routes leading to indole formation is the reductive ring closure of suitable aromatic nitro compounds (1, 4). Unfortunately there are not many potential precursors for such cyclizations. Our past work on nitroarylation of carbanions (5) and subsequent cyclization of the products to heterocyclic compounds (6) suggested a new route to indoles via nitroarylation of ketone enolates.

The goal of the present paper is to show a new, simple route leading to substituted 2,3-diphenylindoles which have been the subject of some recent studies on their synthetic (7) and practical (8) applications. In the course of this work we also succeeded in the preparation of 2,3-diphenylindolenyl-3-hydroperoxides. Earlier attempts to obtain these hydroperoxides have failed (9).

Our method consists of aromatic nucleophilic substitution of a halogen atom in substituted *o*-halonitrobenzenes by deoxybenzoin enolate anion (10) and subsequent reduction of the products resulting in the closure of the five-membered ring as shown in Scheme 1. Deoxybenzoin anion produced in dipolar aprotic solvents by the action of powdered potassium hydroxide displaces chlorine in substituted *o*-halonitrobenzenes to afford the corresponding aromatic nucleophilic substitution products. The latter when reduced with iron in acetic acid or hydrogenated on a Pd–C catalyst give indoles in yields exceeding 80%. The results and analytical data are presented in Table 1. *o*-Nitrobenzylphenylketone (2-nitrodeoxybenzoin) also undergoes cyclization under the same conditions to produce 2-phenylindole in 91% yield. This method can be recommended as an alternative source of the title indoles which have been prepared previously from phenylhydrazones of deoxybenzoin (11) or by condensation of primary aromatic amines with benzoin (12).

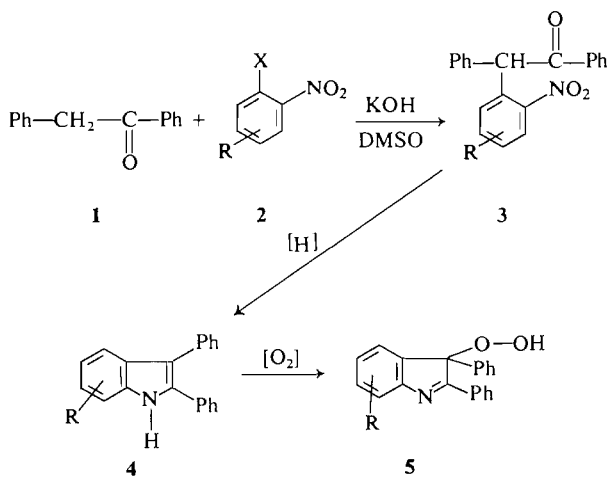

SCHEME 1

Can. J. Chem. Downloaded from www.nrcresearchpress.com by 210.87.254.6 on 09/05/12
For personal use only.

TABLE 1. Summary of analytical data for substituted 2,3-diphenylindoles **4**

Compound R	Formula (mol. wt.)	Yield[a] (%)	Melting point (°C) This work	Melting point (°C) Literature (ref.)
H	$C_{20}H_{15}N$ 269.35	92	123–126	122–123 (14) 124–125 (15)
5-Cl	$C_{20}H_{14}ClN$ 303.80	85	134–136	135 (16)
6-Cl	$C_{20}H_{14}ClN$ 303.80	81	116–118[b]	
6-CH_3	$C_{21}H_{17}N$ 283.38	83	110–112	114–116 (7)

[a]Yields obtained when compounds **3** were reduced with iron in acetic acid. Yields obtained by hydrogenation were of comparable range if some precautions against auto-oxidation were taken.
[b]*Anal.* calcd. for $C_{20}H_{14}ClN$: C 79.07, H 4.65, N 4.61; found: C 79.03, H 4.55, N 4.52.

In the course of this work we observed that reduction of nitro compounds **3** with iron in acetic acid always gave good and reproducible yields of **4**, and the resulting compounds were resistant to auto-oxidation. Although catalytic hydrogenation of **3** seemed to be the simplest way of reduction, and indeed reactions proceeded easily and rapidly, we encountered some unexpected difficulties. When a reduced sample was processed immediately the yields of **4** exceeded 90%; however when it was exposed to air for several hours the characteristic blue fluorescence of the solution disappeared, and after partial evaporation of solvent a corresponding hydroperoxide **5** crystallized in high yield. Undoubtedly auto-oxidation of **4** was catalyzed by traces of the catalyst present in the solution even after filtration of the mixture through a paper filter. The catalytic oxidation of 2,3-disubstituted indoles was reported in the literature a long time ago; however, the resulting hydroperoxyindolenines were unstable and formed 2,3-disubstituted-3-hydroxy-indolenines (13). Interestingly samples of indoles, obtained by reduction with iron, which were dissolved in benzene and agitated with a stream of air for 24 h did not form any detectable amount of hydroperoxide even at elevated temperatures. Addition of a small quantity of the catalyst used for hydrogenation did not change the result. So far we have not been able to convert such indoles into their hydroperoxides. On the other hand the reaction mixtures maintained overnight in open flasks, after hydrogenation was completed, produced **5** exclusively. To our knowledge these hydroperoxides are new compounds. The analytical data are presented in Table 2. Hydroperoxides **5** undergo typical transformations for hydroperoxides of this structure. For instance, methanolic solutions of **5** (R = H, 6-CH_3) when refluxed with some quantity of 2 *N* aqueous sodium hydroxide formed corresponding 2-benzamidobenzophenones (Scheme 2).

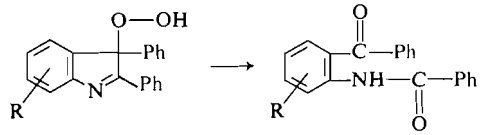

SCHEME 2

Experimental

Reaction of Deoxybenzoin with Substituted o-*Nitrobenzenes*

General Procedure (10)

In a three-necked flask equipped with an efficient mechanical stirrer, thermometer, and dropping funnel 19.6 g (0.1 mol) of deoxybenzoin, 12 g of powdered KOH, and 60 ml of DMSO were stirred for 5–10 min. Then 0.1 mol of nitrocompound dissolved in 30 ml of DMSO was added dropwise to the stirred mixture. The reaction was carried out for 1–1.5 h at 45–50°C and then the mixture was poured into water. The product was filtered off or extracted with benzene and then recrystallized from methanol. Recrystallized products were obtained in a 50–60% yield.

Substituted 2,3-Diphenylindoles 4

Reduction with Iron-dust

A portion (3 g) of nitrocompound **3** was dissolved in 30 ml of warm acetic acid. To this solution 6 g of powdered iron was added and the mixture was refluxed for 3 h. The solution was poured into 100 ml of water and the precipitated product was filtered off, dried, and finally powdered in a mortar. The resulting material was refluxed with benzene and the filtered

TABLE 2. Summary of analytical data for substituted 2,3-diphenylindolenyl-3-hydroperoxides **5**

Compound R	Formula	Yield (%)	Melting point[a] (°C)	Analyzes C Found	C Calcd.	H Found	H Calcd.	N Found	N Calcd.
H[b]	$C_{20}H_{15}NO_2$	85	238–240	79.33	79.72	5.07	5.02	4.61	4.65
5-Cl	$C_{20}H_{14}ClNO_2$	50	232–234	71.34	71.54	4.18	4.20	4.12	4.17
6-Cl	$C_{20}H_{14}ClNO_2$	60	258–260	71.04	71.54	4.15	4.20	4.11	4.17
6-CH_3[c]	$C_{21}H_{17}NO_2$	60	235–236	79.84	79.98	5.62	5.43	4.30	4.44

[a]All compounds melted with decomposition.
[b]Mass spectrum 70 eV, *m/e* (relative intensity, %): 301 (M^+, 29), 285 (53), 284 (35), 270 (19), 256 (59), 224 (15), 196 (34), 119 (100), 105 (44), 77 (40).
[c]Mass spectrum 70 eV, *m/e* (relative intensity, %): 315 (M^+, 25), 299 (52), 283 (37), 270 (37), 210 (31), 196 (10), 195 (16), 181 (17), 165 (25), 133 (100), 105 (47), 77 (63).

solution was concentrated and precipitated with petroleum ether. Yields and analytical data for **4** are given in Table 1.

Catalytic Hydrogenation

Compound **3** (2 mmol) was hydrogenated in 30 ml of methanol or dioxane in the presence of 0.1 g of a 5% Pd–C (Degussa Typ E1ON) or $Pd–Al_2O_3$ catalyst (Degussa Typ E207R). After the reaction mixture had consumed 6 mmol of hydrogen, the catalyst was immediately filtered off, the solvent was evaporated to dryness, and the residual oil was recrystallized from methanol or ligroin as quickly as possible to avoid excessive exposure to air. Following this procedure indoles **4** were obtained in 50–80% yields depending on the duration of the processing of the reaction mixture. The residual filtrates after subsequent evaporation yielded hydroperoxides **5** in a 15–45% yield.

Substituted 2,3-Diphenylindolenyl-3-hydroperoxides 5

A portion (2 mmol) of **3** was hydrogenated as described above. The reaction mixture was left for 2 days and then the catalyst was filtered off and the filtrate was partially evaporated to give a 50–85% yield of **5**. To accelerate the formation of **5** a slow stream of oxygen was passed through the solution at 50°C. After a period of 4–5 h glc did not show the presence of **4** and the only isolable product was **5**. Analytical data are presented in Table 2.

Decomposition of 5 to 6

Hydroperoxide **5** (1 g) was dissolved in 40 ml of boiling methanol. To this solution 5 ml of 2 *N* aqueous NaOH was added and the mixture was refluxed for 2 h. The mixture was diluted with water and the product was extracted with benzene; the extract was dried over $MgSO_4$, evaporated, and recrystallized from ethanol. Compound **5**, R = H, gave a 85% yield of 2-benzamidobenzophenone, mp 84–86°C (7); compound **5**, R = 6-CH_3, gave a 70% yield of 2-benzamido-4-methyl-benzophenone.

Acknowledgement

The authors wish to thank the National Science Foundation, U.S.A., for the financial support of this work, Grant-INT-76-14966.

1. R. J. SUNDBERG. The chemistry of indoles. Academic Press, New York, NY. 1970; R. K. BROWN. *In* Indoles. Part I. *Edited by* W. J. Houlihan. Wiley-Interscience, New York, NY. 1972. p. 246.
2. V. DAVE. Org. Prep. Proc. Int. **8**, 41 (1976).
3. P. G. GASSMAN, T. J. VAN BERGEN, D. P. GILBERT, and B. W. CUE. J. Am. Chem. Soc. **96**, 5495 (1974).
4. R. L. AUGUSTINE, A. J. GUSTAVSEN, J. F. WANAT, I. C. PATTISON, K. S. HOUGHTON, and G. KOLETAR. J. Org. Chem. **38**, 3004 (1973); A. D. BATCHO and W. LEIMGRUBER. Ger. Patent No. 2,057,840; Chem. Abstr. **75**, 63605v (1971).
5. M. MĄKOSZA. Tetrahedron Lett. 673 (1969); M. MĄKOSZA, J. M. JAGUSZTYN-GROCHOWSKA, and M. JAWDOSIUK. Rocz. Chem. **45**, 851 (1971); M. MĄKOSZA, M. JAGUSZTYN-GROCHOWSKA, M. LUDWIKOW, and M. JAWDOSIUK. Tetrahedron, **30**, 3723 (1974).
6. M. JAWDOSIUK and M. MĄKOSZA. Rocz. Chem. **50**, 857 (1976); M. JAWDOSIUK, J. CZYŻEWSKI, and M. MĄKOSZA. J. Chem. Soc. D, 794 (1973); M. MĄKOSZA, I. KMIOTEK-SKARZYŃSKA, and M. JAWDOSIUK. Synthesis, 56 (1977).
7. C. A. MUDRY and A. R. FRESCA. Tetrahedron, **30**, 2983 (1974).
8. J. J. KRUTAK. U.S. Patent No. 3,905,999; Chem. Abstr. **83**, 193080w (1975); W. H. DEKKER, H. A. SELLING, and J. C. OVEREEM. J. Agric. Food Chem. **23**, 785 (1975); Chem. Abstr. **83**, 109650b (1975).
9. R. J. S. BEER, T. DONAVANIK, and A. ROBERTSON. J. Chem. Soc. 4139 (1954).
10. M. JAWDOSIUK, W. WILCZYŃSKI, and W. ĆWIKIEWICZ. Rocz. Chem. **51**, 595 (1977).
11. D. W. OCKENDEN and K. SCHOFIELD. J. Chem. Soc. 612 (1953).
12. E. RITCHIE. J. Proc. R. Soc. N.S.W. **80**, 33 (1946); Chem. Abstr. **41**, 3094c (1947).
13. B. WITKOP and J. B. PATRICK. J. Am. Chem. Soc. **73**, 2188 (1951); J. W. KERSHAW and W. TAYLOR. J. Chem. Soc. 4320 (1964).
14. E. FISCHER. Ann. **236**, 116, 136 (1886).
15. U. SIMON, O. SÜS, and L. HORNER. Ann. **697**, 17, 39 (1966).
16. M. MĄKOSZA, J. M. JAGUSZTYN-GROCHOWSKA, and M. JAWDOSIUK. Rocz. Chem. **50**, 1841 (1976).

Can. J. Chem. Downloaded from www.nrcresearchpress.com by 210.87.254.6 on 09/05/12
For personal use only.

Pyrrole chemistry. XVIII. The thio-Claisen rearrangement

KANG-ER TEO, GRAHAM H. BARNETT, HUGH J. ANDERSON, AND CHARLES E. LOADER
Department of Chemistry, Memorial University of Newfoundland, St. John's, Newfoundland, Canada A1B 3X7

Received August 30, 1977

KANG-ER TEO, GRAHAM H. BARNETT, HUGH J. ANDERSON, and CHARLES E. LOADER. Can. J. Chem. **56**, 221 (1978).

The thio-Claisen rearrangement has been carried out on 2-allylthiopyrrole, 1-methyl-2-allylthiopyrrole, and 2,5-diallylthiopyrrole. The products were trapped by acetylation of the β-allyl-α-thiols. Raney nickel desulfurization of these products gave the corresponding β-propylpyrroles but attempts to functionalize the β-allyl group failed. 1-Methyl-3-propylpyrrole and 3,4-dipropylpyrrole were also synthesized by other routes for comparison.

KANG-ER TEO, GRAHAM H. BARNETT, HUGH J. ANDERSON et CHARLES E. LOADER. Can. J. Chem. **56**, 221 (1978).

On a effectué un réarrangement de thio-Claisen sur l'allylthio-2 pyrrole, le méthyl-1 allylthio-2 pyrrole et le diallylthio-2,5 pyrrole. On a piégé les produits par acétylation des β-allyl α-thiols. La désulfurisation, par le nickel de Raney, de ces produits conduit aux β-propylpyrroles correspondants mais des essais pour fonctionnaliser le groupe β-allyle n'ont donné aucun résultat. Pour fins de comparaison on a aussi synthétisé les méthyl-1 propyl-3 pyrrole et dipropyl-3,4 pyrrole par d'autres méthodes.

[Traduit par le journal]

The thio-Claisen rearrangement apparently has not been investigated in the pyrrole series, possibly because of the expected instability of the allyl pyrrolethiol reaction products (1). In view of the recent success of the thio-Claisen rearrangement of indoles (2, 3), it seemed worthwhile to examine the potential of this rearrangement with 2-allylthio pyrroles as it offered an approach to 2,3-disubstituted pyrroles. If the reaction was fruitful, Raney nickel desulfurization of the product would lead to a β-substituted pyrrole. It was also of interest to see whether or not a double thio-Claisen rearrangement would take place.

Thiocyanation (4, 5) of pyrrole and 1-methylpyrrole in methanol with copper(II) thiocyanate furnished 2-thiocyanopyrrole (**1***a*) and 1-methyl-2-thiocyanopyrrole (**1***b*), respectively, in fair yield

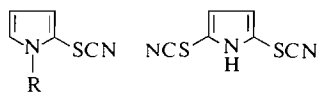

1 **2**

(*a*) R = H
(*b*) R = CH_3

(48–68%), whereas pyrrole with thiocyanogen in methanol gave a low yield of 2,5-dithiocyanopyrrole (**2**) as the only isolated product. Treatment of a methanolic solution of the thiocyanopyrroles, **1***a*, **1***b*, or **2**, and allyl bromide at 0°C with an excess of aqueous methanolic potassium hydroxide furnished, essentially quantitatively according to nmr spectra, the corresponding allylthiopyrroles **3***a*, **3***b*, and **4**. However purification by column chromatography followed by repeated short path, reduced pressure distillations resulted in considerable loss of material. The allylthiopyrroles were light yellow liquids which

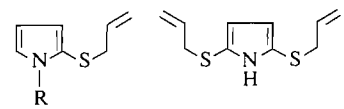

3 **4**

had the expected spectroscopic properties including the correct molecular ion peaks in their mass spectra.

The mass spectra of all these allylthiopyrroles have a fragmentation peak corresponding to the loss of a vinyl group ($M - 27$) and an allyl group ($M - 41$). The loss of a thiol unit ($M - 33$) from **3***a* and **3***b* may arise from a thermal thio-Claisen rearrangement to the thiol followed by a loss of the SH group. The corresponding peak for **4** is at $M - 67$, presumably from the loss of two SH groups and a hydrogen atom.

The microanalyses of all of the allylthiopyrroles, **3***a*, **3***b*, and **4** were unsatisfactory; each being low in carbon. The corresponding sulfones, **5***a*, **5***b*, and **6**, proved more stable and gave the expected ir, uv, nmr, and mass spectra. Correct microanalyses were obtained for **5***a* and **6** but **5***b* was repeatedly low in carbon.

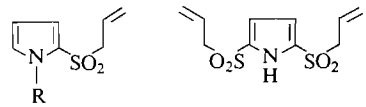

5 **6**

Can. J. Chem. Downloaded from www.nrcresearchpress.com by 210.87.254.40 on 09/05/12
For personal use only.

Can. J. Chem. Downloaded from www.nrcresearchpress.com by 210.87.254.40 on 09/05/12
For personal use only.

Several attempts to rearrange 2-allylthiopyrrole (**3***a*) in triethylene glycol or in quinoline under nitrogen at 100 or 170°C for several hours led to deep red gums which showed no pyrrolic proton absorption in the nmr spectrum. At shorter reaction times, most of the starting material **3***a* was recovered unchanged with a small amount of the red gum. As *N*-alkylpyrroles are often more stable, attention was turned to 1-methyl-2-allylthiopyrrole (**3***b*) and it was decided to attempt to trap the expected thiol by acetylation. The rearrangement of 1-methyl-2-allylthiopyrrole with quinoline and acetic anhydride was successful, and the acetylated product **7***b* was isolated. These conditions were then found to be satisfactory for 2-allylthiopyrrole (**3***a*).

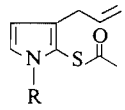

7

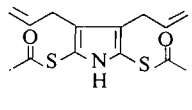

8

Both **3***a* and **3***b* were shown to rearrange efficiently and the *S*-acylated products **7***a* and **7***b* were isolated in good yield under two sets of conditions: (*i*) in quinoline at 170°C under nitrogen for 15 min; (*ii*) in *N*,*N*-dimethylaniline at 90–100°C under nitrogen for 15 h.

The nmr spectrum of the rearrangement product **7***a* showed two triplets in the aromatic region which collapsed to two doublets upon the treatment with deuterium oxide. The coupling constant, ($J_{4,5} \approx 2.8$ Hz) supported a 2,3-disubstituted pyrrole (6). The rearrangement product **7***b* also showed the expected nmr spectrum. The ir spectra of **7***a* and **7***b* showed carbonyl absorption consistent with an acetylated thiol (7) and not with an acetyl group directly attached to the pyrrole ring (8). When 2,5-diallylthiopyrrole (**4**) was heated in the presence of acetic anhydride and quinoline at 170°C for 15 min a double thio-Claisen rearrangement occurred to afford **8** in excellent yield. Products **7***a* and **8** were fairly stable whereas **7***b* darkened considerably on standing but all three gave good microanalytical results. Mass, ir, and nmr spectra of these compounds were consistent with the structures assigned.

Several attempts were made to modify the double bond of the rearrangement products **7***a* and **7***b* so that, after the removal of the sulfur side chain, a β-functionalized pyrrole might be obtained. Attempted hydration of **7***a* with mercury(II) acetate in water–tetrahydrofuran followed by sodium borohydride – sodium hydroxide reduction (9) gave only recovered starting material. Attempted oxidative rearrangement of **7***a* with thallium(III) nitrate in methanol (10) gave a brown liquid showing no pyrrolic proton in its nmr spectrum. Lemieux – von Rudloff oxidation (11) on **7***a* resulted in loss of the starting material. With *m*-chloroperoxybenzoic acid in methylene chloride at 25°C for 25 h (12), **7***a* did not react, while after refluxing for several hours about 30% of the starting material was recovered and no desired epoxide was obtained. An attempt to ozonize **7***b* also resulted in the loss of starting material. Thus the double bond resisted mild conditions but the pyrrole ring did not survive stronger conditions.

Attempts to remove the sulfur side chain from **7***b* using zinc dust – aqueous acetic acid reflux gave only starting material. Stirring and refluxing **7***a* with Raney nickel in acetone gave a moderate yield of 3-propylpyrrole (**9***a*), together with a very small amount of 2-acetyl-3-propylpyrrole (**10**). A comparable yield of 1-methyl-3-propylpyrrole (**9***b*) was obtained under similar conditions from **7***b* accompanied by a trace of a compound whose spectral properties corresponded to 1-methyl-3-propyl-2-acetylthiopyrrole (**11**). Compound **8** gave the expected Raney nickel product, 3,4-dipropylpyrrole (**12**), and some 2-acetyl-3,4-dipropylpyrrole (**13**).

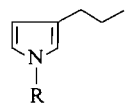

9

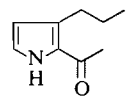

10

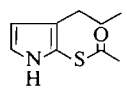

11

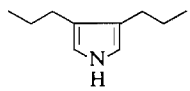

12

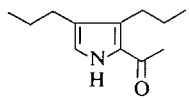

13

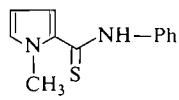

14

The new β-propyl pyrroles **9***b* and **12** were then synthesized by other methods to confirm structures and to compare ease of preparation. Friedel–Crafts propanoylation of 1-methyl-2-pyrrolethiolcarboxylate prepared via the thiocarbanilide (**14**) gave the desired 4-propanoyl derivative as well as a small amount of the dipyrrolyl ketone (**15**). When milder conditions were used for propanoylation another dipyrrolyl ketone by-product (**16**) was obtained together with significant amounts of unreacted starting material.

The Wolff–Kishner reduction of compound **14** also caused hydrolysis of the thiol ester but not decarboxylation (13), giving 1-methyl-3-propyl-2-pyrrolecarboxylic acid (**17**). It was found that the addition of copper chromite and more potassium hydroxide to the Wolff–Kishner reaction mixture then

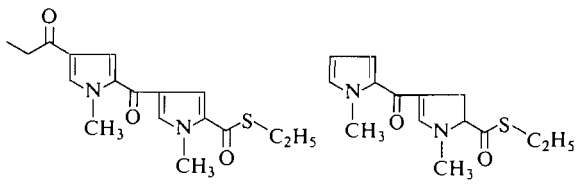

15 16

led to decarboxylation and formation of the desired product (**9***b*) in good yield.

The reaction of ethylmagnesium bromide with 2-hexenal gave 4-octen-3-ol which could be oxidized with 2,3-dichloro-5,6-dicyano-1,4-benzoquinone (DDQ) to 4-octen-3-one (**18**). Condensation of **18** with *p*-toluenesulfonylmethyl isocyanide (14) then gave 3-propanoyl-4-propylpyrrole (**19**) which was reduced with lithium aluminum hydride to 3,4-

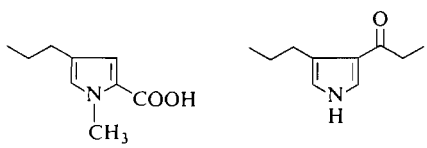

17 19

dipropylpyrrole (**12**). Thus, thio-Claisen rearrangement of readily prepared allylthiopyrroles followed by Raney nickel desulfurization is a way to synthesize β-propylpyrroles but functionalization of the β-allyl group has not been accomplished. Other synthetic approaches to these β-propylated pyrroles proved quite competitive, much less offensive from an odor standpoint, and produced more stable intermediates.

Experimental

Melting points were determined on a Thomas–Hoover apparatus and are not corrected. The proton magnetic resonance spectra were obtained with a Varian EM360 spectrometer at 60 MHz in $CDCl_3$, unless otherwise stated, and are recorded on the δ scale. Analyses were determined by Atlantic Microlab, Inc., Atlanta, GA, U.S.A., Memorial University Water Analysis Facility, and Alfred Bernhardt, West Germany. Other instruments were as described in ref. 13. Ultraviolet spectra were recorded in 95% ethanol and infrared spectra in carbon tetrachloride unless otherwise specified.

2-Thiocyanopyrrole and 2,5-Dithiocyanopyrrole

The copper(II) thiocyanate method of Matteson and Snyder (4) gave 48% of 2-thiocyanopyrrole. Spectral data corresponded to those of ref. 5.

From the thiocyanogen method (4) for 2-thiocyanopyrrole about 17% of 2,5-dithiocyanopyrrole was obtained. Spectral data corresponded to those of ref. 15.

1-Methyl-2-thiocyanopyrrole

The method of Matteson and Snyder afforded 68% of 1-methyl-2-thiocyanopyrrole, bp 40–45°C/0.2 Torr (lit. (16) bp 108–110°C/13 Torr); ir ν: 2155 cm^{-1}(C≡N); nmr δ: 7.10 (1H, m), 6.57 (1H, m), 6.10 (1H, m), 3.68 (3H, s).

2-Allylthiopyrrole

The method of Matteson and Snyder (4) for 2-methylthiopyrrole was adapted using allyl bromide to give 82% of 2-allylthiopyrrole (**3***a*), bp 40–44°C/0.2 Torr, as a yellow oil which darkened rapidly; ir showed a free N—H at ν 3450 cm^{-1}; nmr δ: 8.23 (1H, br, D_2O exchanged); 6.70 (1H, m), 6.30 (1H, m), 6.12 (1H, m), 5.75 (1H, m), 4.87 (2H, d), 3.20 (2H, d); ms showed M^+ 139. *Anal.* calcd. for C_7H_9NS: C 60.39, H 6.52, N 10.06; found: C 59.46, H 6.45, N 9.76.

1-Methyl-2-allylthiopyrrole

1-Methyl-2-thiocyanopyrrole was converted by the above procedure to 90% of 1-methyl-2-allylthiopyrrole (**3***b*), a colorless liquid, bp 60°C/0.3 Torr, pure by tlc and nmr; uv λ_{max}: 222 (ε 6100), 248 nm (ε 6700); nmr δ: 6.68 (1H, m), 6.28 (1H, m), 6.03 (1H, m), 5.70 (1H, m), 4.87 (2H, m), 3.63 (3H, s), 3.19 (2H, d). Analyses repeatedly low in carbon.

2,5-Diallylthiopyrrole

2,5-Dithiocyanopyrrole was converted by the above procedure to 85% of 2,5-diallylthiopyrrole (**4**), pale yellow liquid, bp 80°C/0.3 Torr, pure by tlc and nmr; uv λ_{max}: 220 (ε 8500) 264 nm (ε 11 100); ir ν: 3445 cm^{-1}; nmr δ: 8.3 (1H, broad s), 6.25 (2H, d), 5.75 (2H, m), 4.85 (4H, m), 3.22 (4H, d). Analyses repeatedly low in carbon.

2-Allylsulfonylpyrrole

2-Allylthiopyrrole (1.39 g, 10.0 mmol) was dissolved in acetic acid (8 ml) and cooled in an ice bath with stirring. Hydrogen peroxide (30% aq, 9 ml, 100 mmol) was added in portions. The solution became black and heat was evolved. After stirring at room temperature for 50 h the colour of the solution had changed to orange. The mixture was diluted with water and then extracted three times with methylene chloride. The combined organic extracts were washed (5% aqueous $NaHCO_3$, H_2O, saturated brine), dried ($MgSO_4$), and then the solvent was removed. The thick yellow-brown oil residue was chromatographed on silica gel. The eluate containing the product gave an oil which was distilled bulb-to-bulb (0.35 Torr, oven temperature 100°C) to give (350 mg, 20%) of 2-allylsulfonylpyrrole (**5***a*), a colorless oil; ir ν: 3430, 3350 (NH, free and H-bonded), 1318, 1131 cm^{-1} (sulfone); uv λ_{max}: 237 nm (ε 10 100); nmr δ: 9.7 (1H, broad s), 6.92 (1H, m), 6.74 (1H, m), 6.16 (1H, m), 5.30 (3H, m), 3.80 (2H, d), $J_{3,4} = 3.8$, $J_{4,5} = 2.8$, $J_{3,5} = 1.4$ Hz. *Anal.* calcd. for $C_7H_9NO_2S$: C 49.11, H 5.30, N 8.18; found: C 49.16, H 5.34, N 8.03.

1-Methyl-2-allylsulfonylpyrrole

The procedure above was applied to 1-methyl-2-allylthiopyrrole. After failure to obtain an analytically pure specimen it was rechromatographed on thick-layer plates of silica gel giving 15% of 1-methyl-2-allylsulfonylpyrrole (**5***b*) a colorless semi-solid; ir ν: 1320, 1140 cm^{-1} (sulfone); nmr δ: 7.10 (1H, q), 6.60 (1H, q), 6.39 (1H, q), 5.3 (3H, m), 3.78 (2H, d), 3.69 (3H, s). *Anal.* calcd. for $C_8H_{11}NO_2S$: C 51.87, H 5.99; found: C 50.66, H 5.97. This analysis could not be improved.

2,5-Bis(allylsulfonyl)pyrrole

The oxidation procedure above was applied to 2,5-diallylthiopyrrole. After repeated crystallization from methylene chloride – hexane, a 35% yield of 2,5-bis(allylsulfonyl)pyrrole (**6**) was obtained as a white solid mp 115–117°C; uv λ_{max}: 237 nm (ε 17 400); ir (Nujol) ν: 1314, 1142 cm^{-1} (sulfone); nmr δ: 10.5 (1H, broad s), 6.84 (2H, d), 5.4 (6H, m), 3.95 (4H, d). *Anal.* calcd. for $C_{10}H_{13}NO_4S_2$: C 43.62, H 4.76, N 5.09, S 23.29; found: C 43.60, H 4.78, N 5.06, S 23.21.

Rearrangement of 2-Allylthiopyrrole

(*a*) A mixture of 2-allylthiopyrrole (1.39 g, 10.0 mmol) and

Can. J. Chem. Downloaded from www.nrcresearchpress.com by 210.87.254.40 on 09/05/12
For personal use only.

Can. J. Chem. Downloaded from www.nrcresearchpress.com by 210.87.254.40 on 09/05/12
For personal use only.

acetic anhydride (6 ml) was added all at once with stirring to quinoline (6 ml) which had been heated to 170°C under nitrogen. These conditions were maintained for 15 min then the reaction mixture was cooled and diluted with ethyl ether. This solution was successively washed three times with 2 *M* HCl, water, 5% aqueous $NaHCO_3$, saturated brine, and dried ($MgSO_4$). Removal of the solvent gave a brown oil which was chromatographed on silica gel. The fractions containing solid were combined and recrystallized from hexane to give (1.28 g, 71%) colorless 3-allyl-2-acetylthiopyrrole (*7a*), mp 42.5–43.5°C; uv λ_{max}: 226 (ε 10 500), 241 nm (ε 10 900); ir ν: 3468, 1735, 1702 cm^{-1}; nmr δ: 8.3 (1H, broad s, D_2O exchanged), 6.83 (1H, t) 6.15 (1H, t), 5.11 (1H, m), 4.87 (1H, m), 3.21 (2H, d), 2.26 (3H, s), $J_{4,5}$ = 2.8 Hz. *Anal.* calcd. for $C_9H_{11}NOS$: C 59.64, H 6.12, N 7.73; found: C 59.46, H 6.15, N 7.81.

(*b*) A solution of 2-allylthiopyrrole (280 mg, 2 mmol) in *N*,*N*-dimethylaniline (1.5 ml) and acetic anhydride (1.5 ml) was stirred at 90–100°C under nitrogen for 15 h. It was worked up as above to give 335 mg (92%) of crude crystalline product after solvent removal.

Rearrangement of 1-Methyl-2-allylthiopyrrole

Following procedure (*a*) above, 1-methyl-2-allylthiopyrrole (1.47 g, 9.6 mmol) was rearranged and worked up to give (1.77 g, 95%) 1-methyl-3-allyl-2-acetylthiopyrrole (*7b*), a pale yellow oil which was almost pure by tlc and nmr. The analytical sample was prepared by two bulb-to-bulb distillations: uv λ_{max}: 227 (ε 10 600), 245 nm (ε 11 700); ir ν: 1720 cm^{-1}; nmr δ 6.75 (1H, d), 6.03 (1H, d), 5.02 (1H, m), 4.80 (1H, m), 3.47 (3H, s), 3.18 (2H, d), 2.23 (3H, s), $J_{4,5}$ = 2.8 Hz. *Anal.* calcd. for $C_{10}H_{13}NOS$: C 61.51, H 6.71, N 7.17; found: C 61.61, H 6.75, N 7.04.

Rearrangement of 2-5-Diallylthiopyrrole

Following procedure (*a*) above, 2,5-diallylthiopyrrole (1.75 g, 8 mmol) was rearranged and worked-up to give (2.01g, 85%) 3,4-diallyl-2,5-diacetylthiopyrrole (**8**) as a pale brown oil. Rechromatographed to give single tlc spot: uv λ_{max}: 256 nm (ε 15 300); ir ν: 1702 cm^{-1}; nmr δ: 8.7 (1H, broad s) 5.7 (2H, m), 5.00 (2H, m), 4.73 (2H, m), 3.18 (4H, d), 2.28 (6H, s). *Anal.* calcd. for $C_{14}H_{17}NO_2S_2$: C 56.92, H 5.80, N 4.74; found: C 56.88, H 5.73, N 4.87.

Desulfurization of 3-Allyl-2-acetylthiopyrrole

3-Allyl-2-acetylthiopyrrole (980 mg, 5.42 mmol) was dissolved in a small amount of acetone and W-5 Raney nickel (10 g), which had been washed three times with acetone, was added. The volume was made up to 100 ml with acetone and the mixture stirred and refluxed for 1 h. The Raney Ni was removed by filtration through a pad of Celite and the solvent removed to give a yellow oil. Thick-layer chromatography on silica gel gave (350 mg, 58%) of liquid with spectral properties corresponding to those reported for 3-propylpyrrole (**9***a*) (17) and a colorless solid, (12 mg after sublimation) 2-acetyl-3-propylpyrrole (**10**) mp 63–64°C; uv λ_{max}: 291 nm (ε 12 700); ir ν: 3433, 3275, 1641 cm^{-1}; nmr δ: 9.7 (1H, broad s), 6.83 (1H, m), 6.04 (1H, m), 2.72 (2H, m), 2.41 (3H, s), 1.7 (2H, m), 0.95 (3H, t). Mass calcd. for $C_9H_{13}NO$: M^+ 151.0997; found: 151.0999.

Desulfurization of 1-Methyl-3-allyl-2-acetylthiopyrrole

Repetition of the above procedure with 1-methyl-3-allyl-2-acetylthiopyrrole (400 mg, 2.05 mmol) gave (130 mg, 53%) of 1-methyl-3-propylpyrrole (**9***b*) as a pale yellow oil from thick-layer chromatography; nmr δ: 6.36 (1H, m), 6.24 (1H, m), 5.85 (1H, m), 3.52 (3H, s), 2.38 (2H, t), 1.5 (2H, m), 0.91 (3H, t). *Anal.* calcd. for $C_8H_{13}N$: C 77.99, H 10.64; found: C 77.73, H 10.77.

After repeated thick-layer chromatography about 10 mg of a pale yellow oil was obtained whose spectra suggested 1-methyl-3-propyl-2-acetylthiopyrrole (**11**): ir ν: 1708 cm^{-1}; ms M^+ 197; nmr δ: 6.76 (1H, d), 6.07 (1H, d), 3.49 (3H, s), 2.7 (2H, m), 2.28 (3H, s), 1.7 (2H, m), 0.9 (3H, m), $J_{4,5}$ = 2.9 Hz.

Desulfurization of 3,4-Diallyl-2,5-diacetylthiopyrrole

Repetition of the above procedure using 3,4-diallyl-2,5-diacetylthiopyrrole (540 mg, 1.8 mmol) gave (180 mg, 66%) of pale yellow liquid obtained from thick-layer chromatography on silica gel, 3,4-dipropylpyrrole (**12**), bp 69.5–70.5°C/1 Torr; nmr δ: 7.6 (1H, broad s), 6.37 (2H, d), 2.37 (4H, m), 1.5 (4H, m), 0.93 (6H, t), $J_{2,5}$ = 2.5 Hz. *Anal.* calcd. for $C_{10}H_{17}N$: C 79.41, H 11.33; found: C 79.30, H 11.35.

In addition, 60 mg of colorless solid was isolated, 2-acetyl-3,4-dipropylpyrrole (**13**), mp 71–73°C; uv λ_{max}: 297 nm (ε 19 600); ir ν: 3430, 3240, 1635 cm^{-1}; nmr δ: 9.3 (1H, broad s), 6.69 (1H, d), 2.40 (3H, s), 2.8–0.7 (14H, complex m). *Anal.* calcd. for $C_{12}H_{19}NO$: C 74.57, H 9.91; found: C 74.37, H 9.95.

Alternate Synthesis of 1-Methyl-3-propylpyrrole

(a) 1-Methyl-2-pyrrolethiocarbanilide

To a stirred suspension of aluminum chloride (67 g, 0.50 mol) in dichloromethane (200 ml) maintained at 0°C under N_2 was added 1-methylpyrrole (40.5 g, 0.50 mol) in dichloromethane (150 ml). A solution of phenyl isothiocyanate (67.5 g, 0.50 mol) in dichloromethane (200 ml) was added dropwise over about 45 min and allowed to stir at room temperature a further 2 h under N_2. The mixture was poured onto ice and the two-phase system stirred vigorously 15 min. The organic layer was separated, washed (H_2O), and dried ($MgSO_4$). After removal of solvent, a yellow crystalline mass was obtained which was triturated with ether and filtered, giving yellow needles. More product was recovered from the filtrate after evaporation. The product (64.7 g, 60%) 1-methyl-2-pyrrolethiocarbanilide (**14**) was recrystallized from chloroform–petroleum and sublimed, mp 100–100.5°C; nmr δ: 8.8 (1H, broad s), 7.3 (5H, m), 6.71 (1H, t), 6.46 (1H, q), 6.01 (1H, q), 3.89 (3H, s). *Anal.* calcd. for $C_{12}H_{12}N_2S$: C 66.65, H 5.59, N 12.96; found: C 66.78, H 5.60, N 13.02.

(b) Ethyl 1-Methyl-2-pyrrolethiolcarboxylate

A mixture of 1-methyl-2-pyrrolethiocarbanilide (59 g, 0.27 mol), 6 *M* aqueous NaOH (175 ml), and bromoethane (43.6 g, 0.40 mol) was heated on a steam bath with vigorous stirring for 2.5 h. The solution was cooled and extracted with ether. The ether layer was washed thoroughly with water, then 3 *M* aqueous H_2SO_4 (180 ml) was added and the two-phase system heated under N_2 on a steam bath, allowing the ether to escape. After 1 h, the mixture was cooled and the dark supernatant oil was extracted into ether. The aqueous phase was carefully neutralized (solid Na_2CO_3) and extracted thoroughly with ether. The combined ether extracts were washed (aqueous $NaHCO_3$, water) and dried ($MgSO_4$). Removal of solvent and distillation gave the crude product (31.0 g, 66%) as a yellow oil. Redistillation gave pure ethyl 1-methyl-2-pyrrolethiolcarboxylate, bp 96–96.5°C/25 Torr; ir ν: 1635 cm^{-1}; nmr δ: 6.93 (1H, q), 6.65 (1H, t), 5.97 (1H, q), 3.82 (3H, s), 2.93 (2H, q), 1.26 (3H, t). *Anal.* calcd. for $C_8H_{11}NOS$: C 56.77, H 6.55; found: C 56.77, H 6.49.

(c) Ethyl 1-Methyl-4-propanoyl-2-pyrrolethiolcarboxylate

Following the acetylation procedure of ref. 18, ethyl 1-methyl-2-pyrrolethiolcarboxylate (4.65 g, 27 mmol) was acylated with propanoyl chloride (2.78 g, 30 mmol) to give a yellow oil after evaporation of the dried solution. The product was chromatographed on neutral alumina (40 g) eluting with dichloromethane–petroleum to give a pale yellow oil which crystallized. Recrystallization from ether–petroleum gave (4.50 g, 73%) ethyl 1-methyl-4-propanoyl-2-pyrrolethiolcarboxylate, mp 60–61.5°C; ir (Nujol) ν: 1645 cm^{-1}; nmr δ: 7.3 (2H, m), 3.88 (3H, s), 2.99 (2H, q), 2.75 (2H, q), 1.31 (3H, t),

Can. J. Chem. Downloaded from www.nrcresearchpress.com by 210.87.254.40 on 09/05/12
For personal use only.

1.16 (3H, t). *Anal.* calcd. for $C_{11}H_{15}NO_2S$: C 58.64, H 6.71; found: C 58.62, H 6.74.

Continued elution of the column gave (0.27 g) ethyl 4-(1′-methyl-4′-propanoyl-2′-pyrrolecarbonyl)-1-methyl-2-pyrrolethiolcarboxylate (**15**), mp 151–152.5°C (dichloromethane–petroleum); ir (Nujol) ν: 1610, 1635, 1670 cm^{-1}; nmr δ: 7.41 (3H, m), 7.22 (1H, m), 3.94 (6H, s), 2.99 (2H, q), 2.76 (2H, q), 1.30 (3H, t), 1.17 (3H, t). *Anal.* calcd. for $C_{17}H_{20}N_2O_3S$: C 61.42, H 6.06, N 8.43; found: C 61.41, H 6.05, N 8.44.

Under conditions where the propanoylation was incomplete and starting material was recovered, ethyl 4-(1′-methyl-2′-pyrrolecarbonyl)-1-methyl-2-pyrrolethiolcarboxylate (**16**) was also obtained, mp 79.5–81.5°C (dichloromethane–petroleum); ir (Nujol) ν: 1600, 1645 cm^{-1}; nmr δ: 7.36 (1H, d), 7.25 (1H, d), 6.74 (2H, m), 6.02 (1H, m), 3.88 (6H, s), 2.95 (2H, q), 1.28 (3H, t), $J_{3,5} = 2.0$ Hz). *Anal.* calcd. for $C_{14}H_{16}N_2O_2S$: C 60.85, H 5.84, N 10.14; found: C 60.89, H 5.84, N 10.14.

(d) 1-Methyl-3-propylpyrrole

A solution of ethyl 1-methyl-4-propanoyl-2-pyrrolethiolcarboxylate (1.125 g, 5.0 mmol), potassium hydroxide pellets (1.00 g, 18.0 mmol), and hydrazine hydrate 85% aqueous (1.00 g, 17.0 mmol) in triethylene glycol (10 ml) was heated at ca. 125°C under N_2 for 1.5 h. Water was allowed to distil off through a short-path condenser. Then copper chromite powder (0.30 g) and potassium hydroxide pellets (3.0 g) were added and the mixture heated at 210–220°C for 2 h. The mixture was cooled and the p*H* reduced to 6–7 with 6 *M* aqueous HCl, then reheated to distil water and the product as a supernatant oil which could be removed by pipetting. Yield of crude 1-methyl-3-propylpyrrole (**9b**) was 0.442 g (72%). This material was identical to that obtained from the desulfurization synthesis above.

When the combined Wolff–Kishner, hydrolysis and decarboxylation procedure described in ref. 13 was followed, no product distilled. Acidification of that reaction mixture gave (0.51 g, 71%) 1-methyl-4-propyl-2-pyrrolecarboxylic acid (**17**), mp 69.5–70.5°C (sublimation); ir (Nujol) ν: 1665 cm^{-1}; nmr δ: 6.86 (1H, d), 6.56 (1H, d), 3.82 (3H, s), 2.37 (2H, t), 1.5 (2H, m), 0.91 (3H, t), $J_{3,5} = 1.6$ Hz. *Anal.* calcd. for $C_9H_{13}NO_2$: C 64.65, H 7.84, N 8.38; found: C 64.69, H 7.85, N 8.39.

Alternate Synthesis of 3,4-Dipropylpyrrole

(a) 4-Octen-3-ol

Ethylmagnesium bromide (0.30 mol in ether) was prepared and treated with *trans*-2-hexenal (9.8 g, 0.10 mol) in ether and worked up to give (11.2 g, 88%) 4-octen-3-ol, bp 89–92°C/27 Torr; ir ν: 3300 cm^{-1} (broad); nmr δ: 5.4 (2H, m), 3.89 (1H, q), 2.13 (1H, s, exchanges), 1.97 (2H, q), 1.4 (4H, m), 0.87 (6H, t). *Anal.* calcd. for $C_8H_{16}O$: C 74.94, H 12.58; found: C 75.07, H 12.66.

(b) 4-Octen-3-one

A solution of 4-octen-3-ol (4.10 g, 32 mmol) and 2,3-dichloro-5,6-dicyano-1,4-benzoquinone (8.0 g, 35 mmol) in anhydrous benzene (80 ml) was stirred in a stoppered flask for 8 h at room temperature (19). After removal of most of the solvent and filtration, the solution was chromatographed on neutral alumina (dichloromethane) and distilled to give (3.07 g, 76%) 4-octen-3-one (**18**), bp 95.5–96.5°C/40 Torr; ir ν: 1660, 1620 cm^{-1}; nmr (CCl_4) δ: 6.63 (1H, m), 5.90 (1H, d), 2.43 (2H, q), 2.09 (2H, t), 1.5 (2H, m), 0.9 (6H, m). *Anal.* calcd. for $C_8H_{14}O$: C 76.14, H 11.18; found: C 76.14, H 11.21.

(c) 4-Propyl-3-propanoylpyrrole

Following the method of van Leusen *et al.* (14) but working under nitrogen, using degassed solvents and extending the addition over 2.5 h, 4-octen-3-one (4.43 g, 35 mmol), *p*-toluenesulfonylmethyl isocyanide (7.8 g, 40 mmol), and sodium hydride (2.0 g of 58% mineral oil dispersion, 50 mmol) gave a pale yellow oil and solid mixture. Ether was added and the solid collected by filtration and washed with more cold ether. More solid product was obtained by chromatography of the filtrate on neutral alumina. Yield of 4-propyl-3-propanoylpyrrole (**19**) was 2.34 g (40%), mp 113.5–114.5°C (sublimation); ir ($CHCl_3$) ν: 3220, 1635 cm^{-1}; nmr δ: 9.3 (1H, broad s), 7.32 (1H, q), 6.53 (1H, m), 2.7 (4H, m), 1.7 (2H, m), 1.15 (3H, t), 0.93 (3H, t). *Anal.* calcd. for $C_{10}H_{15}NO$: C 72.68, H 9.14; found: C 72.71, H 9.18.

(d) 3,4-Dipropylpyrrole

Following the procedure of Hinman and Theodoropulos (20), 4-propyl-3-propanoylpyrrole (1.65 g, 10 mmol) was reduced with $LiAlH_4$, (0.070 g, 20 mmol) in tetrahydrofuran (100 ml) and worked-up to give (0.776 g, 51%) a colorless oil, 3,4-dipropylpyrrole (**12**), identical to the product from the desulfurization synthesis.

Acknowledgements

The authors gratefully acknowledge the continued financial support of the National Research Council of Canada and the Memorial University of Newfoundland. They also thank D. Embree of NRCC, Halifax, for the high resolution mass spectrum.

1. R. L. N. Harris. Aust. J. Chem. **25**, 985 (1972).
2. B. W. Bycroft and W. London. Chem. Commun. 168 (1970).
3. H. Plieninger, H.-P. Kraemer, and H. Sirowej. Chem. Ber. **107**, 3915 (1974).
4. D. S. Matteson and H. R. Snyder. J. Org. Chem. **22**, 1500 (1957).
5. S. Gronowitz, A. B. Hörnfeldt, B. Gestblom, and R. A. Hoffman. Arkiv Kemi, **18**, 151 (1961).
6. A. Gossauer. Die Chemie der Pyrrole. Springer Verlag, Berlin, Heidelberg, New York, NY. 1974. p. 84.
7. K. Nakanishi. Infrared absorption spectroscopy. Holden-Day, San Francisco, CA. 1962. p. 47.
8. H. Rapoport and C. D. Willson. J. Am. Chem. Soc. **84**, 630 (1962).
9. H. C. Brown and P. Geoghegan. J. Am. Chem. Soc. **89**, 1522 (1967).
10. A. McKillop, J. D. Hunt, F. Kienzle, E. C. Bigham, and E. C. Taylor. J. Am. Chem. Soc. **95**, 3635 (1973).
11. R. U. Lemieux and E. von Rudloff. Can. J. Chem. **33**, 1701 (1955).
12. B. J. Burreson, C. Christophersen, and P. J. Scheuer. Tetrahedron, **31**, 2015 (1975).
13. J. K. Groves, H. J. Anderson, and H. Nagy. Can. J. Chem. **50**, 2427 (1971).
14. A. M. van Leusen, H. Siderius, B. E. Hoogenboom, and D. van Leusen. Tetrahedron Lett. 5337 (1972).
15. E. Söderback, S. Gronowitz, and A. B. Hörnfeldt. Acta Chem. Scand. **15**, 227 (1961).
16. N. V. Philips' Gloeilampenfabrieken. Neth. Patent. Appl. 6, 617, 755; Chem. Abstr. **68**, 68877 (1968).
17. (*a*) P. S. Skell and G. P. Bean. J. Am. Chem. Soc. **84**, 4655 (1962); (*b*) N. S. Bhacca, L. F. Johnson, and J. N. Schoolery (*Compilers*). NMR Spectra Catalog. Varian Associates, Palo Alto, CA. 1962. No. 177.
18. C. E. Loader and H. J. Anderson. Tetrahedron, **25**, 3879 (1969).
19. D. Burn, V. Petrow, and G. O. Weston. Tetrahedron Lett. No. 9, **14** (1960).
20. R. L. Hinman and S. Theodoropulos. J. Org. Chem. **28**, 3052 (1963).

Synthesis of 3-carboxylated 2,5-dihydrothiophenes[1]

JOHN M. MCINTOSH AND ROBERT A. SIELER

Department of Chemistry, University of Windsor, Windsor, Ont., Canada N9B 3P4

Received July 21, 1977

JOHN M. MCINTOSH and ROBERT A. SIELER. Can. J. Chem. **56**, 226 (1978).

Vinylphosphonates **11**, readily prepared from diethyl carbomethoxymethyl phosphonate (**10**) react with α-mercaptocarbonyl compounds to afford substituted 3-carbomethoxy-2,5-dihydrothiophenes in excellent yields. The scope of this synthesis is indicated and the use of the products in the synthesis of substituted 2-carboxy-1,3-butadienes is illustrated.

JOHN M. MCINTOSH et ROBERT A. SIELER. Can. J. Chem. **56**, 226 (1978).

Les vinylphosphonates **11** qui peuvent être préparés facilement à partir du phosphonate de carbométhoxyméthyle et de diéthyle (**10**), réagissent avec des composés α-mercaptocarbonyle pour conduire aux carbométhoxy-3 dihydro-2,5 thiophènes substitués et ceci avec d'excellents rendements. On indique la généralité de cette synthèse et on illustre aussi l'utilisation des produits dans la synthèse de carboxy-2 butadiènes-1,3 substitués.

[Traduit par le journal]

In recent years, we have been engaged in delineating the reactions of mercaptocarbonyl compounds with various types of Michael acceptors. Much of that work has centered on the use of vinylphosphonium salts (**1**) and we have shown that substituted 2,5-dihydrothiophenes (1) and dihydrothiopyrans (2) are readily prepared using these reagents. These products are useful synthons for a variety of organic structures, in particular, as sources of specifically alkylated conjugated dienes (3). While the synthesis is highly successful for alkylated materials, compounds having functional groups directly attached to the ring offer more obstacles. For instance, methoxy- or carboalkoxy-substituted dienes would require the preparation of dihydrothiophenes of general structure **2**. These in turn would necessitate the use of either **3** as the vinyl salt or **4** as the mercaptocarbonyl compound. Esters (**4***a*) do not gen-

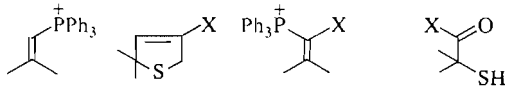

1 **2***a* X = OR **2***b* X = COOR **3***a* X = OR **3***b* X = COOR **4***a* X = OR **4***b* X = COOR

erally give olefins on treatment with a phosphorane (4) although some exceptions are known (5), and α-keto-β-mercaptoesters (**4***b*) are both difficult to prepare and offer ambiguity in the site of attack by a phosphorane. A single example of **3***a* is known (6) and it does not behave satisfactorily in the annulation reaction (1*c*). Finally, compounds of type **3***b* are not readily available and the phosphorane formed by attack of thiolate ion would be of a type (**5***a*) well known to react with aldehydes but very poorly with ketones (7).

[1]Dihydrothiophenes, Part VII. For Part VI, see ref. 1*c*.

It is known that phosphonate anions (**5***b*) are more nucleophilic than **5***a* (4) and thus the use of vinylphosphonates (**6**) was suggested. Furthermore, a considerable number of compounds of type **6** bearing a variety of functionality are known (see for example ref. 8) and they have been shown to undergo addition reactions with nucleophiles (9). However, there is

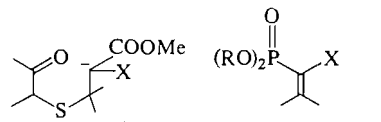

5*a* X = $Ph_3\overset{+}{P}$ **5***b* X = P(O)(OR)$_2$ **6***a* X = OR **6***b* X = COOR

ample evidence in the literature (10) to indicate that a Wittig-type reaction of phosphonate anions only proceeds well when electron-withdrawing substituents are adjacent to phosphorus. Thus, we centered our attention on the preparation and use of compounds of type **6***b*.

The importance of these functionalized dihydrothiophenes lies in their ready conversion to functionalized dienes. While terminally carboxylated conjugated dienes can be prepared using Knoevenagel-type conditions (11) compounds of type **7** cannot and their obvious utility in the Diels–Alder reaction makes them of considerable synthetic interest. The parent compound **7***a*(12) rapidly polymerizes and the possibility of storing **7** in the form of sulfone **8**, which can be easily converted to **7** as required, was a distinctly attractive possibility. In addition, **2***b* has excellent dienophilic character as was shown by Stork and Stotter (13) and desulfurization of the Diels–Alder adducts can lead to easy assembly of complex organic structures.

Can. J. Chem. Downloaded from www.nrcresearchpress.com by 210.87.254.6 on 09/05/12
For personal use only.

TABLE 1. Vinylphosphonates[a] 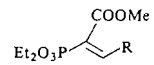

R		Method[b]	bp (Torr)	Yield (%)	Infrared (cm^{-1})[c]	Nuclear magnetic resonance[d]
H	(**11***a*)	*A*	92–94°C(0.08)	76		7.23(dd, 1, J = 26,2 Hz), 6.70(dd, 1, J = 4,2 Hz), 4.25(quin., 4, J = 7 Hz), 3.88(s, 3), 1.37(t, 6, J = 7 Hz)
n-C_3H_7	(**11***b*)	*B*	96–102°C(0.05)	87	3000, 1730, 1260, 1030	5.6(m, 1), 4.18(quin., 4, J = 7.5 Hz), 3.82 and 3.78(2 s, total = 3), 2.90–1.80(m, 2), 1.32(t, 6, J = 7.5 Hz), 1.6–0.9(m, 5).
Ph	(**11***c*)	*B*	160–165°C(1)	55		7.40(s, 5), 4.20(quin., 4, J = 7 Hz), 3.80(s, 3), 1.35(t, 6, J = 7 Hz)
cyclo-C_6H_{11}		*B*	120–122°C(0.02)	74	3010, 2940, 1730, 1260, 1035	6.95(dd, 1, J = 22.5, 9 Hz), 4.50–3.96(m, 4), 3.80(s, 3), 3.0–1.3(m, 11), 1.30(t, 6, J = 7.5 Hz)

[a]All new products gave acceptable elemental analyses.
[b]See experimental section.
[c]Four most intense peaks.
[d]See Experimental section for coding and solvent.

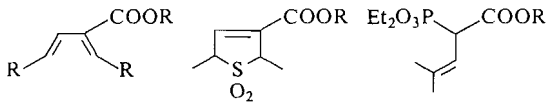

7 8 9

7*a* R = H

Results and Discussion

Synthesis of Phosphonates

Although the literature on the preparation of vinylphosphonates is enormous, reports of the preparation of **6***b* are not common. We chose not to pursue the isomerization of the allylic isomer **9**, the approach which proved so successful in the preparation of **1** (1), since **9** is a significant synthetic challenge in itself.

Several reports suggest that, under proper conditions, interaction of phosphonate **10** with aldehydes leads, not to a Wittig olefination reaction, but rather to an aldol type condensation. This would allow the formation of a series of vinylphosphonates (10) from a common precursor [1]. Using a method based on

[1] $(EtO)_2P(O)CH_2COOMe$ + RCHO

10

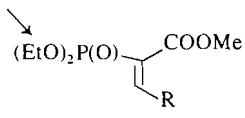

11

the work of Patai and Schwartz (14) we have prepared three vinylphosphonates (**11***b* → **11***d*). In addition, the unsubstituted phosphonate **11***a* was prepared by condensation of formaldehyde with **10** in methanolic solution (15). The yield and simplicity of these reactions obviate the need for the more exotic and costly sequence recently published (16).[2] It should be noted that we have been unsuccessful in condensing ketones with **10**. In these cases the selenium-mediated (16) route may be advantageous. The phosphonates prepared and their spectral data are summarized in Table 1. In all cases, the methyl ester was used to simplify the nmr spectra.

The stereochemistry of the phosphonates has not been investigated in detail, but is undoubtedly a mixture of *E* and *Z* isomers (17).[3]

Synthesis of 2,5-Dihydrothiophenes

The reaction used to prepare the dihydrothiophenes **13–23** is shown in [2]. The proposed mech-

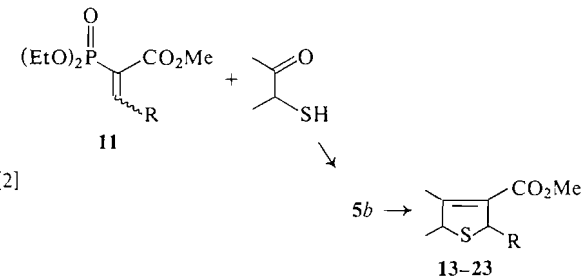

11

[2]

13–23

anism is entirely analogous to that proposed for the vinylphosphonium salt reactions (1). Since the acidity of phosphonates is substantially lower than the corresponding phosphonium salts, we initially employed sodium hydride as the basic reagent. Subsequently, it was found that triethyl amine was sufficiently basic to catalyze the condensations of α-mercaptoaldehydes.

[2]We thank Prof. Heathcock for informing us of his experimental procedure before publication.

[3]^{31}P spectra indicate such a mixture.

Can. J. Chem. Downloaded from www.nrcresearchpress.com by 210.87.254.6 on 09/05/12
For personal use only.

TABLE 2. Dihydrothiophenes prepared[a]

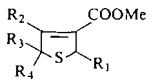

Carbonyl	Phosphonate	Product[a] No.	R_1	R_2	R_3	R_4	Yield (%)[d]
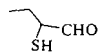 (12*a*)	**11***a*	**13**	H	H	H	Et	71
(12*b*)	**11***a*	**14**[b]	H	H	—$(CH_2)_5$—		94
12*a*	**11***b*	**15**	Pr	H	H	Et	67
12*b*	**11***b*	**16**	Pr	H	—$(CH_2)_5$—		90
(12*c*)	**11***b*	**17**	Pr	Me	Me	Me	81
(12*d*)	**11***b*	**18**	Pr	Et	H	Me	54
12*a*	**11***c*	**19**	Ph	H	H	Et	74
12*b*	**11***c*	**20**[c]	Ph	H	—$(CH_2)_5$—		90
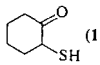 (12*e*)	**11***c*	**21**	Ph	—$(CH_2)_4$—		H	82
12*a*	**11***d*	**22**	*cyclo*-C_6H_{11}	H	H	Et	86
12*b*	**11***d*	**23**	*cyclo*-C_6H_{11}	H	—$(CH_2)_5$—		89

[a]All products gave acceptable elemental analyses.
[b]Melting point 49–50°C.
[c]Melting point 53–55°C (from hexane).
[d]Determined by glc.

TABLE 3. Spectral data for products

Compound	n_D^{25}	Infrared (cm^{-1})[a,b]	Nuclear magnetic resonance[c]
13	1.5080	2970, 1715, 1440, 1265	6.85(dd, 1, J = 3.7,2 Hz), 4.35(m, 1), 3.92(dd, 2, J = 3.7,2 Hz), 3.80(s, 3), 2.0–1.25(m, 2), 1.01(t, 3, J = 7 Hz).
14	[d]	2940, 1720, 1440, 1250	6.60(t, 1, J = 2 Hz), 3.85(d, 2, J = 2 Hz), 3.72(s, 3), 1.95–1.0(m, 10).
15	1.4942	2970, 1715, 1440, 1260	6.72(dd, 1, J = 1.3,3 Hz), 4.5–4.0(m, 2), 3.75(s, 3), 2.3–1.2(m, 6), 1.2–0.8(m, 6).
16	1.5141	2940, 1715, 1440, 1205	6.75(d, 1, J = 1.5 Hz), 4.5–4.25(m, 1), 3.80(s, 3), 2.2–1.15(m, 14), 1.00(t, 3, J = 6 Hz).
17	1.4936	2970, 1715, 1295, 1165	4.4(m, 1), 3.80(s, 3), 2.06(d, 3, J = 1.5 Hz), 1.8–1.2(m, 4), 1.55(s, 3), 1.50(s, 3), 1.10–0.8(m, 3).
18	1.4944	2970, 1715, 1440, 1290, 1080	4.6–4.0(m, 2), 3.80(s, 3), 3.1–2.1(m, 4), 1.8–0.75(m, 11).
19	1.5436	3040, 1720, 1260, 1100	7.20(s, 5), 6.9(dd, 1, J = 5.8,1.5 Hz), 5.46(dd, 1, J = 5.8,1.5 Hz), 4.70–4.05(m, 1), 3.57(s, 3), 2.62–2.00(m, 2), 1.05(t, 3, J = 6.5 Hz).
20	[d]	2930, 1720, 1285, 1265	7.28(s, 5), 6.85(d, 1, J = 2 Hz), 5.45(d, 1, J = 2 Hz), 3.52(s, 3), 2.2–1.15(m, 10).
21	1.5825	2950, 1715, 1285, 1265	7.26(s, 5), 5.56(m, 1), 4.63–4.00(m, 1), 3.56(s, 3), 2.5–1.3(m, 8).
22	1.5168	2940, 1715, 1265, 1100	6.75(bt, 1, J = 1.5 Hz), 4.60–3.90(m, 2), 3.75(s, 3), 2.4–0.8(m, 16).
23	1.5346	2930, 1715, 1450, 1255	6.62(d, 1, J = 1.5 Hz), 4.48(dd, 1, J = 3,1.5 Hz), 3.75(s, 3), 2.4–0.8(m, 21).

[a]Four most intense peaks.
[b]All compounds show medium strength absorption at 1650 cm^{-1}.
[c]See Experimental for coding.
[d]Solids.

Can. J. Chem. Downloaded from www.nrcresearchpress.com by 210.87.254.6 on 09/05/12
For personal use only.

TABLE 4. Diene products

Dihydrothiophene	Diene[a,b]	Infrared (cm^{-1})[c]	Nuclear magnetic resonance[d]
15	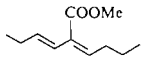 (28)	2980, 1715 1440, 1245	6.60(t, 1, J = 7.5 Hz), 6.2–5.7(m, 2), 3.80 and 3.75(2 s, total = 3), 2.52–1.97(m, 4), 1.80–1.25(m, 2), 1.20–0.75(m, 6).
16	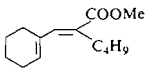 (39*a*)	3050, 1720, 1245, 1210	7.00(s, 1), 5.85(m, 1), 3.70(s, 3), 2.60–1.90(m, 6), 1.81–1.10(m, 8), 0.87(t, 3, J = 6 Hz).
17	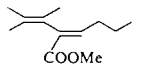 (30)	2970, 1710, 1270, 915	5.85(t, 1, J = 7.5 Hz), 3.75(s, 3), 2.48(quin, 2, J = 7.5 Hz), 1.74(s, 6), 1.68(s, 3), 1.6–1.15(m, 2), 0.9(t, 3, J = 6.7 Hz).

[a]All products gave acceptable elemental analyses.
[b]No stereochemistry implied.
[c]Four most intense peaks.
[d]See Experimental for coding and solvent.

The reactions run and products obtained are shown in Table 2, and the physical and spectral characteristics are summarized in Table 3. As can be seen, excellent yields of the cyclized products are obtained in almost every instance.

In two cases (**19** and **21**), the corresponding thiophenes (**19***a* and **21***a*) were also formed as byproducts. These structures were confirmed by comparison with authentic samples. Thiophene formation was minimized by rigorous exclusion of air from the reaction mixture.

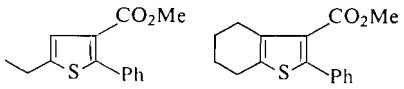

19*a* **21***a*

In only one case did the reaction take an unexpected course. The condensation of **11***c* with **12***c* led to a low yield of a mixture of two products, tentatively identified as **24** and **25** on the basis of their spectral characteristics [3]. The transesterification of the carboxylic ester was not observed in any other case. Finally, when the reaction of ketone **12***d* with

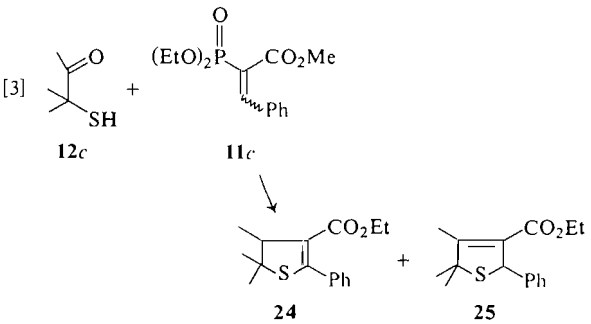

12*c* **11***c* **24** **25**

phosphonate **11***c* was attempted, no dihydrothiophene of any type was isolated. The only product which was isolated in very low yield, appeared to be the simple addition product $EtCOCH(CH_3)SCH(Ph)CH(COOMe)PO_3Et_2$ (**26**).

At this time, the stereochemical composition of the products is unknown. However, the product **19** derived from **11***c* and **12***a* shows a clear doublet of doublets for the benzylic proton (δ 5.46). If, as seems likely, these signals are due to stereoisomers, the isomeric ratio appears to be approximately 60:40, but the identity of the major isomer is not clear. Further work on the stereochemistry of compounds **13–23** is in progress.

Diene Formation

The peracid oxidation of dihydrothiophenes leads to sulfolenes (1). However, in some cases thiophenes have been formed when the ring bears strongly electronegative substituents (18). In order to test our diene synthesis, it was necessary to verify the proposed oxidation–pyrolysis sequence of reactions [4]. This has been done in three cases (Table 4). In

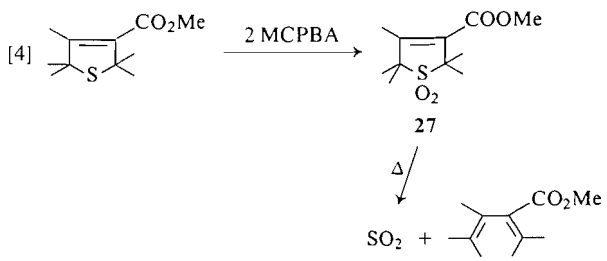

every instance, peracid oxidation gave the sulfone **27** with no trace (nmr) of thiophene. Injection of **26** into a gas chromatograph effected elimination of sulfur dioxide and the dienes were isolated by collection. Since these reactions have been performed on a small scale, it is difficult to obtain accurate yields. However, nmr analysis of crude **27** indicated no significant impurities and no other volatile products were eluted from the gas chromatograph. Thus it appears that the yields of dienes are excellent. In the case of **16**, rearrangement of the initially formed **29** to **29***a* occurred [5]. This isomerization may be avoided by

Can. J. Chem. Downloaded from www.nrcresearchpress.com by 210.87.254.6 on 09/05/12
For personal use only.

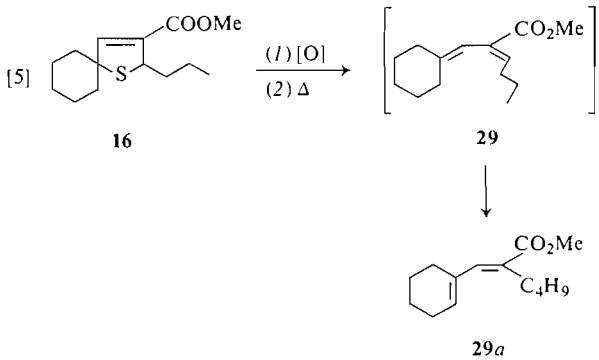

16 29 29*a*

conducting the pyrolysis at a lower temperature in the presence of a dienophile (cf. ref. 1*a*).

In conclusion, it appears that the synthesis of dihydrothiophenes from vinyl phosphonates is a viable synthetic route to compounds of type **2***b* and that these can be converted to dienes. We are currently engaged in applying the method to the synthesis of more complex organic materials.

Experimental

Infrared spectra were recorded on a Beckman IR-12 in chloroform solution; nmr spectra were obtained on either a JEOL C60HL or Varian EM 360 spectrometer in deuteriochloroform solution and are reported in parts per million downfield from Me_4Si as internal standard. The tabulation of nmr data follows the order: chemical shift (δ); multiplicity; number of protons; and coupling constant. Mass spectra were obtained on a Varian MAT CH-5DF instrument. Gas–liquid chromatographic analyses were carried out on an F and M Model 720 instrument using either a 20% SE 30 on Chromosorb W or a 10% Dexsil on Chromosorb W column. Compositions of mixtures were determined using a disc integrator. Unless otherwise noted the drying agent used was anhydrous sodium sulfate, solvents were removed at reduced pressure and preparative tlc was performed on 2 mm thick plates coated with silica gel GF-270. Microanalyses were performed by A. B. Gygli, Microanalysis Laboratory, Toronto.

Preparation of Phosphonates ***11***

Method A

Phosphonate **11***a* was prepared by a variation of the literature procedure (15). Paraformaldehyde (6 g, 0.06 mol) was dissolved in methanol (300 ml) containing 10 drops of piperidine, by refluxing the solution for 0.5 h. Phosphonate **10** (19) (20 g, 0.095 mol) was added all at once and the solution was heated at reflux for 19 h. Evaporation of the methanol afforded an oil which showed no vinyl proton absorption in the nmr spectrum. This oil was dissolved in toluene, a catalytic amount of toluenesulfonic acid was added, and the mixture was refluxed under a Dean–Stark water separator for 8 h. The solvent was removed and the residue distilled to give **11***a*, 16 g (76%), bp 93–99 (1 Torr) (lit (15) 100–101 (1 Torr)).

Method B

Phosphonates **11***b–d* were prepared as follows (14). The aldehyde (0.1 mol) and phosphonate **10** (0.1 mol) were dissolved in benzene (150 ml) containing a mixture of acetic acid (1.5 ml) and piperidine (0.3 g). The mixture was heated at reflux under a Dean–Stark water separator for 22 h. In the case of volatile aldehydes, the use of a five-fold excess was beneficial. The solvent was removed and the residue distilled to give the products shown in Table 1.

General Procedures for Dihydrothiophene Preparation

(A) For Mercaptoaldehydes ***12a*** *(20),* ***12b*** *(16)*

A solution of 0.01 mol of phosphonate **11** and 0.01 mol of triethyl amine in 75 ml dry pyridine was put under a nitrogen atmosphere. To this was added a solution of the appropriate mercaptoaldehyde in 25 ml of pyridine, dropwise with stirring at room temperature. The mixture was stirred at ambient temperature for 1.5 h after the final addition and then at reflux for 18–20 h. The cooled solution was diluted with 200 ml of water and extracted with 4 × 50 ml of ether and 4 × 50 ml of pentane. The combined extracts were washed with 10% hydrochloric acid and water, dried and evaporated under nitrogen to afford a brown oil which was purified by tlc using 1:1 pentane–ether as eluant. Analytical samples were collected from glc. The yields shown in Table 2 were derived by multiplying the crude weight of product by the purity as determined by glc analysis.

(B) For Mercaptoketones ***12c*** *(21),* ***12d*** *(3), and* ***12e*** *(22)*

To a slurry of 0.012 mol of sodium hydride in 50 ml of dry pyridine was added a solution of 0.01 mol of ketone in 50 ml of the same solvent, dropwise with stirring under a nitrogen atmosphere. After hydrogen evolution had ceased, phosphonate **11** was added slowly at room temperature and stirring was continued for 1.5 h. After refluxing for 18–20 h, the solution was worked up as in the previous method.

Formation of isomers ***24*** *and* ***25***

When the reaction between **11***c* and **12***c* was carried out using the sodium hydride procedure, an oil was obtained which contained two components. These were separated by glc and shown to be ethyl 2-phenyl-4,5,5-trimethyl-2,5-dihydrothiophene-3-carboxylate (**25**); nmr: 7.32 (s, 5), 5.55 (q, 1, J = 1.8 Hz), 4.05(d, q, 2, J = 7, 2 Hz), 2.20(d, 3, J = 1.8 Hz), 1.62(s, 3), 1.58(s, 3), 0.97(t, 3, J = 7 Hz); and ethyl 2-phenyl-4,5,5-trimethyl-4,5-dihydrothiophene-3-carboxylate (**24**); mp 49–51°C; nmr: 7.27(s, 5), 3.98(q, 2, J = 7 Hz), 3.09(q, 1, J = 6.7 Hz) 1.57(s, 3), 1.40(s, 3), 1.25(d, 3, J = 6.7 Hz), 1.00(t, 3, J = 7 Hz); *m/e* 276 (M^+, 100%); ir: 2990, 1690, 1330, 1265 cm^{-1}.

Peracid Oxidation of Dihydrothiophenes ***15–17***

The oxidation was carried out according to a published procedure (3). Injection of the crude sulfones into the glc effected elimination of sulfur dioxide and the dienes were collected directly. The spectral data for the products are given in Table 4.

Thiophene ***21a***

This was prepared according to the procedure of Bohlmann and Bresinsky (23). To a solution of 2.6 g (0.02 mol) of **12***e* in 50 ml DMSO was added 30 mg of potassium *tert*-butoxide and 3.2 g (0.02 mol) of methyl phenylpropiolate. The flask was purged with nitrogen and heated at 85–90°C for 90 min with stirring. The cooled solution was poured into 200 ml of 10% sulfuric acid and extracted with 4 × 100 ml of ether. The extracts were washed with water, dried and evaporated to give an oil which solidified on standing and which was recrystallized from ether – petroleum ether to give **21***a*; mp 62–64°C; nmr: 7.47(s, 5), 3.65(s, 3), 2.78(m, 4), 1.82(m, 4); ir: 1710, 1280, 1150 cm^{-1}; *m/e* 272 (M^+, 100%). *Anal.* calcd. for $C_{16}H_{16}O_2S$: C 70.56, H 5.92; found: C 70.41, H 5.81.

Thiophene ***19a***

Using the same procedure and molar amounts, the condensation of **12***a* and methyl phenylpropiolate gave an orange

Can. J. Chem. Downloaded from www.nrcresearchpress.com by 210.87.254.6 on 09/05/12
For personal use only.

oil which was distilled to give thiophene **19***a*, bp 140–150°C (0.23 Torr); nmr: 7.32(m, 5), 7.12(bs, 1), 3.68(s, 3), 2.82(q, 2, J = 7.5 Hz), 1.32(t, 3, J = 7.5 Hz); ir: 1710, 1280, 1160 cm^{-1}; *m/e* 246 (M^+, 90%). *Anal.* calcd. for $C_{14}H_{14}O_2S$: C 68.28, H 5.73; found: C 67.98, H 5.49.

Acknowledgement

This work was made possible by financial support from the National Research Council of Canada and the University of Windsor.

1. (*a*) J. M. McINTOSH, H. B. GOODBRAND, and G. M. MASSE. J. Org. Chem. **39**, 202 (1974); (*b*) J. M. McINTOSH and R. S. STEEVENSZ. Can. J. Chem. **52**, 1934 (1974); (*c*) J. M. McINTOSH and R. S. STEEVENSZ. Can. J. Chem. **55**, 2442 (1977).
2. J. M. McINTOSH and H. KHALIL. Can. J. Chem. **54**, 1923 (1976).
3. J. M. McINTOSH and G. M. MASSE. J. Org. Chem. **40**, 1294 (1975).
4. A. MAERKER. Organic reactions. Vol. 14. Wiley, New York, NY. 1965. p. 270.
5. V. SUBRAMANYAM, E. H. SILVER, and A. H. SOLWAY. J. Org. Chem. **41**, 1272 (1976).
6. J. M. McINTOSH and H. B. GOODBRAND. Synthesis, 862 (1974).
7. G. WITTIG and H. REIFF. Angew. Chem. Int. Ed. Engl. **7**, 7 (1968).
8. A. N. PUDOVIK and T. K. GAZUZON. J. Gen. Chem. USSR, **38**, 139 (1968); A. N. PUDOVIK and G. E. YASTREBOVA. J. Gen. Chem. USSR, **43**, 1647 (1973), and references therein.
9. S. D. DARLING and N. SUBRAMANIAN. J. Org. Chem. **40**, 2851 (1975); S. D. DARLING and V. B. MURALIDHARAN. American Chemical Society 172nd National Meeting, San Francisco, August 1976. Abstracts. No. 13.
10. G. BUCHI and M. PAWLAK. J. Org. Chem. **40**, 100 (1975).
11. G. JONES. Organic reactions. Vol. 15. Wiley, New York, NY. 1967. p. 204.
12. T. TSUANETSUGU, T. FUENO, and J. FURUKAWA. Makromol. Chem. **112**, 220 (1968).
13. G. STORK and P. L. STOTTER. J. Am. Chem. Soc. **91**, 7780 (1969).
14. S. PATAI and A. SCHWARTZ. J. Org. Chem. **25**, 1232 (1960).
15. A. N. PUDOVIK, G. E. YASTREBOVA, and V. I. NIKITINA. J. Gen. Chem. USSR, **37**, 2660 (1967).
16. W. A. KLESCHICK and C. H. HEATHCOCK. American Chemical Society 173rd National Meeting, New Orleans, March 1977. Abstracts. No. 95.
17. D. C. WYSOCKI. PhD. Thesis, University of Pittsburgh, Pittsburgh, PA. 1967; Diss. Abstr. B. **28**, 1437 (1967).
18. T. TAKAYA, S. KOSAKA, Y. OTSUJI, and E. IMOTO. Bull. Chem. Soc. Jpn. **41**, 2086 (1968).
19. H. O. HOUSE, V. K. JONES, and G. A. FRANK. J. Org. Chem. **29**, 3327 (1964).
20. A. KIRRMANN, J. CANTACUZENE, and L. VIO. Rev. Chim. Acad. Rep. Populaire Roumaine, **7**, 1011 (1962).
21. F. ASINGER, M. THIEL, and G. ESSER. Justus Liebig's Ann. Chem. **610**, 33 (1953).
22. G. GIESELER and F. STACHE. Chem. Ber. **94**, 337 (1961).
23. F. BOHLMANN and E. BRESINSKY. Chem. Ber. **97**, 2109 (1964).

Can. J. Chem. Downloaded from www.nrcresearchpress.com by 210.87.254.6 on 09/05/12
For personal use only.

Resonance Raman labels: spectroscopic studies on *cis*- and *trans*-4-benzylidene-2-phenyl-Δ^2-oxazolin-5-one and an isotopically substituted analog[1]

K. KUMAR, D. J. PHELPS, AND P. R. CAREY

Division of Biological Sciences, National Research Council of Canada, Ottawa, Ont., Canada K1A 0R6

Received June 22, 1977

K. KUMAR, D. J. PHELPS, and P. R. CAREY. Can. J. Chem. **56**, 232 (1978).

The absorption and preresonance Raman spectra of *cis*- and *trans*-4-benzylidene-2-phenyl-Δ^2-oxazolin-5-one are reported. Although steric considerations suggest that the π electron pathway in the *cis* isomer is considerably distorted compared to the *trans* isomer, the Raman and absorption spectra of the two isomers are strikingly similar. Preresonance Raman excitation profiles for the *cis* and *trans* isomers indicate that the main features in the Raman spectra owe their intensity to coupling to the 360 nm absorption band present in both isomers. It is proposed that both the electronic dipole transition responsible for this absorption and the vibrational modes giving rise to the intense Raman bands are localized in the —C=C—N=C—Ph part of the molecule. Thus the main Raman and absorption bands are insensitive to isomerization in the benzylidene portion. Support for a localized electronic transition, polarized along the —C=C—N=C—Ph long axis, comes from Raman depolarization ratio (ρ) measurements which show that all intense Raman features in both *cis* and *trans* isomers have $\rho \sim 0.33$. Further support comes from ir and resonance Raman spectra of *trans*-4-(4-dimethylamino-3-nitrobenzylidene)-2-phenyloxazolin-5-one substituted either with ^{13}C in the 4 position, or with ^{15}N, in the oxazolinone ring. These spectra indicate that the main Raman feature seen in all 4-benzylidene-2-phenyloxazolinones at 1561 cm^{-1} is a symmetric stretching mode associated with the —C=C—N=C— chain and that this feature has some C=N stretching character. The substitution experiments also show that the weak 1654cm^{-1} Raman band has a high degree of C=C stretching character and may represent an essentially antisymmetric mode from the C=C—N=C moiety. The preresonance Raman excitation profiles show that the intensity enhancement follows an F_B^2 type dependence. The utility of the Raman spectrum as a probe for the chromophore responsible for the electronic transition in a highly conjugated system is discussed.

K. KUMAR, D. J. PHELPS et P. R. CAREY. Can. J. Chem. **56**, 232 (1978).

On rapporte les spectres d'absorption et de pré-résonance Raman des benzylidène-4 phényl-2 Δ^2-oxazolinones-5 *cis* et *trans*. Quoique des considérations stériques suggèrent que les voies des électrons π dans l'isomère *cis* devraient être considérablement déformées par rapport à l'isomère *trans*, les spectres Raman et d'absorption des deux isomères sont très semblables. Les profils d'excitation Raman en pré-résonance pour les isomères *cis* et *trans* indiquent que les principales caractéristiques du spectre Raman doivent leur intensité à un couplage avec la bande d'absorption à 360 nm présente dans chacun des isomères. On suggère que la transition dipolaire électronique responsable pour cette absorption ainsi que les modes de vibrations donnant lieu aux bandes Raman intenses sont localisés dans la portion —C=C—N=C—Ph de la molécule. Ainsi les bandes principales des spectres Raman et d'absorption seraient insensibles à l'isomérie dans la portion benzylidène. On trouve des données permettant d'appuyer le concept d'une transition électronique localisée, polarisée le long de l'axe —C=C—N=C—Ph, à partir de mesures de rapports de dépolarisation Raman (ρ) qui montrent que toutes les caractéristiques Raman intenses dans les isomères *cis* et *trans* ont un ρ d'environ 0.33. On obtient un soutien supplémentaire en se basant sur les spectres ir et de résonance Raman de la (diméthylamino-4 nitro-3 benzylidène)-4 phényl-2 oxazolinone-5 *trans* substituée soit par du ^{13}C en position 4 ou du ^{15}N dans le cycle oxazolinone. Ces spectres indiquent que la principale caractéristique Raman qui peut être observée dans tous les benzylidène-4 phényl-2 oxazolinones à 1561 cm^{-1} est une vibration de valence symétrique associée avec la chaîne —C=C—N=C— et que cette caractéristique possède un peu du caractère de vibration de valence du C=N. Des expériences de substitution montrent aussi que la bande Raman faible à 1654 cm^{-1} possède un haut degré de caractère de vibration de valence C=C et peut représenter un mode essentiellement antisymétrique de la portion C=C—N=C. Les profils d'excitation Raman en pré-résonance indiquent que l'augmentation d'intensité varie suivant une relation du type F_B^2. On discute de l'utilisation des spectres Raman comme sonde pour déterminer le chromophore responsable d'une transition électronique dans un système hautement conjugué.

[Traduit par le journal]

---

[1]NRCC No. 16305.

Can. J. Chem. Downloaded from www.nrcresearchpress.com by 210.87.254.42 on 09/05/12
For personal use only.

Can. J. Chem. Downloaded from www.nrcresearchpress.com by 210.87.254.42 on 09/05/12
For personal use only.

Introduction

Resonance Raman labels enable detailed vibrational spectra to be obtained from a ligand at a key site in a complex biological system (1). For example, by using chromophoric substrates resonance Raman spectroscopy has provided unique information on enzyme–substrate interactions during enzymolysis (2–4). Laser excitation within an absorption band of the substrate gives an intense resonance Raman spectrum of the substrate and in mixture of enzyme, substrate, and solvent it is possible to obtain and monitor the vibrational spectrum of the substrate throughout the course of the reaction. Interpretation of these spectra in terms of enzyme mechanism requires an understanding of the interrelation between structure, absorption, and resonance Raman spectra for chromophoric substrates and the present work represents a step towards this goal.

Oxazolinones[2] were chosen since some molecules in this class are chromophoric substrates for proteolytic enzymes (5, 6) and thus offer an additional source of systems to study by the resonance Raman technique. Furthermore it has been suggested that oxazoline type intermediates may occur in some enzyme catalyzed reactions (3, 7). In the most general and important sense, however, the ideas and principles enunciated for oxazolinones are directly transferable to other chromophoric substrate systems. For oxazolinones it has been possible to explore the relationships between group conjugation in a π electron system and the appearance of features in the Raman spectrum and between the electronic dipole transition and Raman depolarization ratios. In this paper these relationships are investigated for the *cis* and *trans* isomers of 4-benzylidene-2-phenyl-Δ^2-oxazolin-5-one (Fig. 1). Isotopic substitution using ^{15}N and ^{13}C in a *trans* analog of this compound provides important supportive evidence. Raman intensity excitation profiles are used to test theoretical predictions and to identify the chromophore responsible for Raman intensity enhancement.

Experimental

Raman and absorption spectral measurements were performed as detailed in previous publications (3, 4). Infrared spectra were recorded on a Perkin Elmer 521 spectrometer. Neither photodecomposition nor photoisomerization was observed in the laser beam. Raman spectra recorded using stationary cells were identical to those taken using the rotating cell technique (8). In the latter the sample molecules are only exposed to the laser beam for tens of microseconds.

Syntheses

Syntheses of *trans*-4-benzylidene-2-phenyl-Δ^2-oxazolin-5-one and isotopically labelled *trans*-4-(4-dimethylamino-3-nitrobenzylidene)-2-phenyloxazolin-5-one were carried out by literature methods (9, 10). They were characterized by mp, nmr, ir, and Raman spectroscopy.

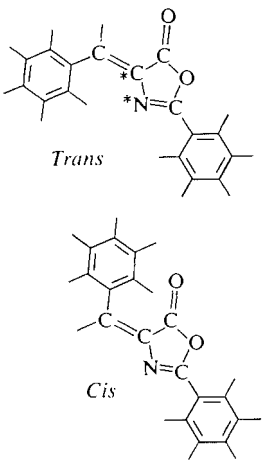

FIG. 1. *trans*- and *cis*-4-Benzylidene-2-phenyl-Δ^2-oxazoline-5-one (adapted from ref. 17).

cis-*4-Benzylidene-2-phenyloxazoline-5-one (11)*

The *trans* isomer (1.0 g, mp 165–167°C) was suspended in 48% aqueous hydrobromic acid (20 ml) and cooled in an ice bath. The stirring suspension was treated with hydrogen bromide gas for ½ h, maintaining the temperature between 0 and 5°C, and the reaction flask was stoppered and stored in the cold overnight. The reaction mixture was then poured on ice (100 g) and, after the ice had melted, collected by suction and dried to yield 0.97 g (97%) of a pale yellow solid, mp 144–147°C (lit. (11) mp 148.5); mixture mp with authentic *trans* isomer 124–126°C. *Anal.* calcd. for $C_{16}H_{11}NO_2$: C 77.09, H 4.53, N 5.62; found for *cis* isomer: C 76.40, H 4.29, N 5.53; found for *trans* isomer (starting material): C 76.10, H 4.21, N 5.53.

Results and Discussion

Absorption Spectra and the Use of Depolarization Ratios as a Test for a Localized Electronic Transition

The absorption spectra of many oxazolinones have been studied by a number of workers (12–15). The spectra of the *cis* and *trans* isomers of 4-benzylidene-2-phenyl-Δ^2-oxazolin-5-one (Fig. 1) were first reported by Buckles *et al.* (16) and more recently by Brocklehurst and Williamson (5). The absorption spectra reported herein (Fig. 2) are in excellent agreement with those of Brocklehurst and Williamson. The spectra of the *cis* and *trans* isomers are strikingly similar, with the isomers possessing identical λ_{max}'s in the near uv and very similar extinction coefficients. However the fine structure is less well resolved in the long wavelength band of the *cis* isomer and the intensity distribution differs in the components of the high energy band centered at 240 nm (Fig. 2).

The salient features of the stereochemistry of *cis*- and *trans*-oxazolinones can be derived from the recently published crystallographic study on 4-(2,4-

[2]Throughout this paper oxazolinones refers to analogs of 4-benzylidene-2-phenyl-Δ^2-oxazolin-5-one.

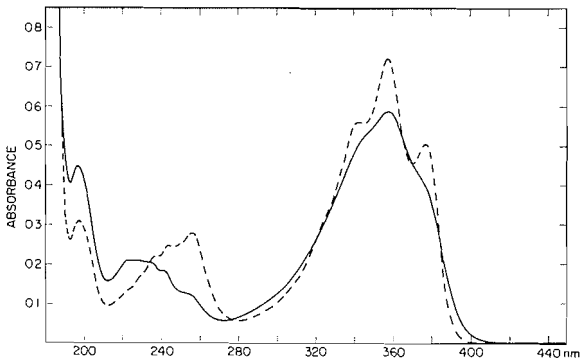

FIG. 2. Absorption spectra of *trans* (---) and *cis* (—) isomers of 4-benzylidene-2-phenyl-Δ^2-oxazolin-5-one. Both compounds 2.0×10^{-5} *M* in CH_3CN; 1-cm path length.

dinitrobenzylidene)-2-phenyloxazolin-5-one (17). The nitro substituted molecule crystallized in the *trans* form and is approximately planar. From the X-ray data it is immediately apparent that the *trans* form experiences little steric hindrance. However, in the *cis* isomer considerable repulsion would occur between the carbonyl oxygen and the ortho hydrogen on the benzylidene ring. For the *cis* isomer in solution this will result in twisting about the Ph—C bond in Ph—C(H)=C with a concomitant loss in conjugation through that bond. As it appears, on the basis of the present study, that substitution on the benzylidene ring only causes minor perturbations to the benzylidene-2-phenyloxazolinone structure it will be assumed that these conclusions may be transferred to the unsubstituted molecule (Fig. 1) viz. the *trans* isomer is essentially planar while the *cis* is non-planar with twisting probably occurring about the Ph—C bond in Ph—C(H)=C.

Two compounds, stilbene and 1,4-diphenyl-1,3-butadiene, are classic examples on the behaviour of long wavelength absorption bands upon *cis–trans* isomerization. *trans*-Stilbene is sterically unhindered while the *cis* isomer undergoes considerable distortion. Compared to the *trans* isomer, *cis*-stilbene shows a blue shift in λ_{max} and a reduction in molar extinction coefficient for this band (18). Similar behaviour is observed in the absorption spectra of *trans-trans*, *trans-cis*-, and *cis-cis*-1,4-diphenyl-1,3-butadiene (19, 20) and the important generalization established by these and other examples is that a decrease in conjugation causes a blue shift in λ_{max} with a concomitant decrease in the extinction coefficient of that band. Thus the problem in interpreting the absorption spectra of *cis*- and *trans*-oxazolinone is that although the X-ray data establish that for the *cis* isomer distortion from planarity of the benzylidene ring almost certainly takes place, no change in λ_{max} is observed, and very little, if any, change is observed in the integrated absorption intensity centered at 360 nm.

The apparent contradiction between the X-ray data suggesting strong steric hindrance in the *cis* isomer and the lack of evidence for this in the absorption spectra is resolved by assuming that the benzylidene ring makes only a minimal contribution to the electronic transition centered at 360 nm. Furthermore it will be seen that although the benzylidene ring may be necessary as a reservoir of π electrons it makes only a minor contribution to the Raman and preresonance Raman spectra. It is thus relegated to the role of an end group such as a keto moiety at the end of a polyene chain which has only very weak intensity in preresonance and resonance Raman spectra. This analogy is strengthened by the fact that subtle changes at the end of polyene chains have no effect in the position of λ_{max} or in the resonance Raman spectrum but can have a marked effect on the appearance of vibronic structure in the absorption spectra (21). In the *cis*-oxazolinone the benzylidene may cause a loss of resolution of vibronic structure by perturbing solvent interactions around the C=O or possibly by existing in more than one conformation about the Ph—C(H)=C single bond.

The position of λ_{max} for the oxazolinones is red shifted compared to e.g. 1,4-diphenyl-1,3-butadiene and this may be due to the presence of the N atom and a mechanism such as π–π^* n–π^* mixing. It is likely that the C=O acts as only an ineffectual end group in terms of its properties in absorption and Raman spectra and thus does not appreciably affect the position of λ_{max}.

The 'end group concept' of the benzylidene ring, in which this ring does not participate in the electronic transition, received support from isotopic substitution (below), from the substituted compounds discussed in the following paper and from measurements of the depolarization ratios of unsubstituted *cis* and *trans* isomers. As has been discussed by Behringer (22) measurements of depolarization ratios, ρ, can provide some evidence about the linearity of an electronic transition.

Starting with a delocalized π electron system in which the electronic transition is essentially linear the depolarization ratios equal $\frac{1}{3}$. Any isomerization in the system which perturbs this linearity makes $\rho \neq \frac{1}{3}$. Thus by monitoring ρ values for two isomers, e.g. *cis*- and *trans*-oxazolinones, participation of the group undergoing isomerization, in this case the benzylidene group, in the transition can be probed.

Although the qualitative origin of resonance Raman intensity will be discussed under Excitation Profiles, the relationship between Raman depolarization ratios and the polarization of an electronic

Can. J. Chem. Downloaded from www.nrcresearchpress.com by 210.87.254.42 on 09/05/12
For personal use only.

Can. J. Chem. Downloaded from www.nrcresearchpress.com by 210.87.254.42 on 09/05/12
For personal use only.

transition can be derived from the following considerations (22). Raman scattering intensity is proportional to the square of the polarizability tensor α_{ik}' ($i, k, = x, y, z$). Using the approximations of Behringer (22) the elements of α_{ik}' are related to the transition moments of the electronic dipole moment operator μ by

$$\alpha_{ik}' = \mu_{eg,i}(0)\mu_{ge,k}(0)\left(\frac{\partial f}{\partial Q}\right)_0$$

where e and g are quantum numbers for pure electronic excited and ground states, respectively, $\mu(0)$ is the value of the electronic moment at zero point amplitude and $\partial f/\partial Q$ is the frequency factor depending on ν_0, ν_{eg} and ν, the frequencies of the exciting radiation, the first coupled electronic transition, and the Raman mode, respectively.

When the electronic transition moment $\mu_{eg}(0)$ has a definite direction, e.g. x, all α_{ik}' except α_{xx} vanish. Then in the case of plane polarized light and a symmetric scattering tensor $\rho = \frac{1}{3}$ (23). This should hold true for all nondegenerate fundamental vibrations in molecules with a single Raman active absorption band which is electronically allowed and which results from a transition lying in a definite molecular direction. Although this derivation supposes Raman intensity enhancement occurs by coupling with a single excited electronic state, and some evidence is found from excitation profiles (*vide infra*) that two excited states are involved, we shall continue to use it as a working hypothesis.

cis- and *trans*-Stilbene (Fig. 3) illustrate how a change in polarization of the electronic dipole affects the Raman depolarization ratios. For *trans*-stilbene the intense bands have $\rho \sim 0.33$ (Table 1) suggesting a well-defined linear electronic transition; however for *cis*-stilbene $\rho \neq 0.33$ strongly suggesting that the electronic transition does not lie in a definite molecular axis.

For the *cis*- and *trans*-oxazolinones the measured depolarization ratios for the three intense bands in 1500–1600 cm^{-1} region are given in Table 2. Taking into account the intrinsic experimental errors in measuring intensities these values are considered to be indistinguishable from 0.33. This strongly suggests that the electronic transition responsible for Raman intensity enhancement has a fixed linear direction for both *cis* and *trans* isomers and that it is not perturbed by isomerization. This is consistent with the benzylidene ring not participating in the 360 nm electronic transition.

Excitation Profiles

The variation of Raman intensities with excitation wavelength, the excitation profile, is capable of

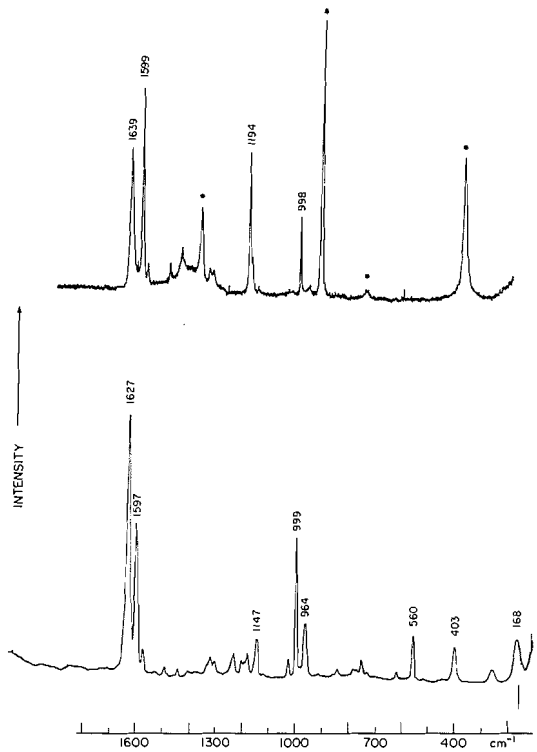

FIG. 3. Preresonance Raman spectra of *cis*- (bottom) and *trans*- (top) stilbene: *cis* neat liquid, *trans* 2.8×10^{-2} *M* in CH_3CN; 441.6 nm; 50 mW; spectral slit 3 cm^{-1}; * indicates CH_3CN.

TABLE 1. Depolarization ratios* for *cis*- and *trans*-stilbene

	ρ	
Band (cm^{-1})	*Cis*	*Trans*
998	0.08	0.15
1194		0.25
1598	0.51	0.29
1639		0.29
1627	0.24	

*Using 441.6 nm excitation; the spectra are shown in Fig. 3.

TABLE 2. Depolarization ratios* for *cis*- and *trans*-4-benzylidene-2-phenyl-Δ^2-oxazolin-5-one

	ρ	
Band (cm^{-1})	*Cis*	*Trans*
1561	0.32	0.29
1589	0.26	0.30
1601	0.36	0.33

*Using 514.5 nm excitation. Very similar results were obtained using 647.1 nm excitation.

TABLE 3. Theoretical and experimental Raman intensity enhancements* for the 1561, 1588, and 1601 cm^{-1} bands

ν_0(kK) (λ_0(nm))	Theory		Experiment $I_{\lambda_0}/I_{\lambda 488.0}$					
			Cis			*Trans*		
	$F_A^2(\lambda_0)/F_A^2(488.0)$	$F_B^2(\lambda_0)/F_B^2(488.0)$	1561	1588	1601	1561	1588	1601
19.435 (514.5)	0.48	0.56	0.63	0.60	0.69	0.66	0.65	0.70
19.932 (501.7)	0.66	0.76	0.78	0.78	0.78	0.79	0.79	0.82
20.140 (496.5)	0.77	0.84	0.85	0.85	0.87	0.90	0.91	0.91
20.492 (488.0)	1	1	1	1	1	1	1	1
20.987 (476.5)	1.44	1.29	1.16	1.16	1.15	1.17	1.19	1.14
21.155 (472.7)	1.64	1.41	1.20	1.20	1.17	1.30	1.34	1.29
21.469 (465.8)	2.20	1.67	1.54	1.54	1.47	1.55	1.69	1.48
21.837 (457.9)	3.08	1.94	1.73	1.71	1.62	1.81	1.74	1.69

*The value at 488.0 is arbitrarily taken as 1. The calculated values in columns two and three do not vary by more than 1% for 1561, 1588, and 1601 cm^{-1}.

providing information on vibronic structure which lies unresolved in an absorption spectrum (21, 24, 25). However in the present case, in which excitation frequencies do not closely approach absorption bands, the major utility of excitation profiles is to indicate the identity of an absorption band responsible for the intensity enhancement of Raman bands and to provide a comparison of experimental Raman intensity enhancements with those predicted by theory.

Qualitatively, the origin of the resonance Raman effect has been understood for some time (for recent reviews see ref. 26). There are essentially two scattering mechanisms, called by Albrecht A and B terms, which depend on coupling to one and more than one excited electronic state, respectively. The A term is based on a shift of equilibrium nuclear position along the normal mode upon exciting into its first excited state (in the present case in the near uv). The B term deals with the vibronic coupling of the first excited electronic state with a whole family of states in the deep ultraviolet having similar polarizations. The frequency dependence of the A and B terms are given by the factors F_A and F_B, respectively (27):

$$F_A = \frac{\nu^2(\nu_e^2 + \nu_0^2)}{(\nu_e^2 - \nu_0^2)^2}$$

$$F_B = \frac{\nu^2(\nu_e\nu_s + \nu_0^2)}{(\nu_e^2 - \nu_0^2)(\nu_s^2 - \nu_0^2)}$$

The functions F_A and F_B carry the full ν_0 dependence and in the case of a single mechanism Raman intensity is proportional to F_A^2 or F_B^2. ν_0 is the frequency of the exciting radiation and ν the frequency of the scattered photons. ν_e is the frequency of the major active electronic state and it is assumed that active virtual states, s, lie at sufficiently high energies to permit the use of an average ν_s. The frequency for ν_s is normally taken as the frequency of an electronic transition in the far uv having the same polarization as the major active electronic state. The F_A and F_B terms have been derived using the assumption that only one of the components α_{xx}, α_{yy}, or α_{zz} is active. For *cis*- and *trans*-oxazolinones this condition is satisfied since the depolarization ratios have a value ~0.33 under all conditions (see above and Table 2). The frequency factors F_A and F_B can be easily calculated from the absorption spectrum and the theoretical relative intensity of Raman lines subsequently determined, provided that the Raman intensity is uniquely derived from either F_A or F_B terms.

The experimental Raman intensities were obtained by measuring the intensities at different exciting frequencies relative to a CH_3CN line at 924 cm^{-1} as internal standard. Use of dilute solutions obviated the need for a correction for self absorption. However a ν^4 correction was made where the experimental intensity is defined as

$$S = \frac{I}{I_a}\left(\frac{\nu_a}{\nu}\right)^4$$

where ν and I denote the frequency and intensity of the sample's line, ν_a and I_a denote the frequency and intensity of the acetonitrile peak at 924 cm^{-1}. The measured intensities were also corrected for spectral sensitivity and Table 3 shows the calculated and

Can. J. Chem. Downloaded from www.nrcresearchpress.com by 210.87.254.42 on 09/05/12
For personal use only.

Can. J. Chem. Downloaded from www.nrcresearchpress.com by 210.87.254.42 on 09/05/12
For personal use only.

measured Raman intensities of the *cis*- and *trans*-oxazolinones in the preresonance region. F_A^2 and F_B^2 were calculated using $\nu_c = 27.77$ kK and $\nu_s = 41.66$ kK. Due to availability of laser lines measurements could not be made below 457.9 nm. Upon going from normal to preresonance conditions there were no drastic changes in the intensities of the Raman bands around 1600 cm^{-1} and the overall pattern of the spectra remained the same. This and the agreement between experiment and theory in the preresonance region suggests that all the intense modes are coupled to the strong electronic transition ~360 nm. Both *cis* and *trans* isomers show good agreement between experimental and the theoretical F_B^2 terms for intensity enhancement. Although some studies on dependence of Raman intensity upon frequency have reported better agreement with F_A type terms it now appears (23, 25, 27) that in compounds based on a substituted benzenoid nucleus that F_B^2 mechanism is predominant. This could be due, in part, to the fact that these compounds *viz.* nitroanilines, substituted azobenzenes, cinnamic acid derivatives, and oxazolinones have a nitrogen atom in the π electron pathway. Thus the opportunity for π–π^* n–π^* mixing exists and this could result in both an F_B^2 two state type dependence in the Raman intensity enhancement and red shifted intense absorption bands. Similar effects have been characterized in nitrogen heterocycles by Ito and coworkers (28).

Preresonance Raman Spectra and Isotopic Substitution

The preresonance Raman spectra of *cis*- and *trans*-oxazolinone are shown in Fig. 4 and are dominated by three bands at 1561, 1588, and 1601 cm^{-1}. These bands also dominate the normal Raman spectrum (647.1 nm excitation). They are at the same frequency for both *cis* and *trans* isomers and show a similar intensity distribution in both (Fig. 4). This, at first a surprising finding, is related to the localized nature of the electronic transition and the relationship between the electronic transition and Raman intensity which were both discussed above. It was shown that the three intense bands in the 1550 cm^{-1} region gain intensity by coupling to the electronic transition at 360 nm. Since this transition and the 1550 cm^{-1} modes are localized in the —C=C—N=C—Ph portion this part of the Raman spectrum is insensitive to *cis-trans* isomerization of the benzylidene ring.

The most intense Raman band at 1561 cm^{-1} has a major contribution from the —C=C—N=C— chain (*vide infra*). However its occurrence at 1561 cm^{-1} is difficult to explain on the basis of (*a*) delocalized π electrons in a diphenylpolyene-like system, or (*b*) the effect of the oxazolinone ring, or (*c*) the effect of the C=O group.

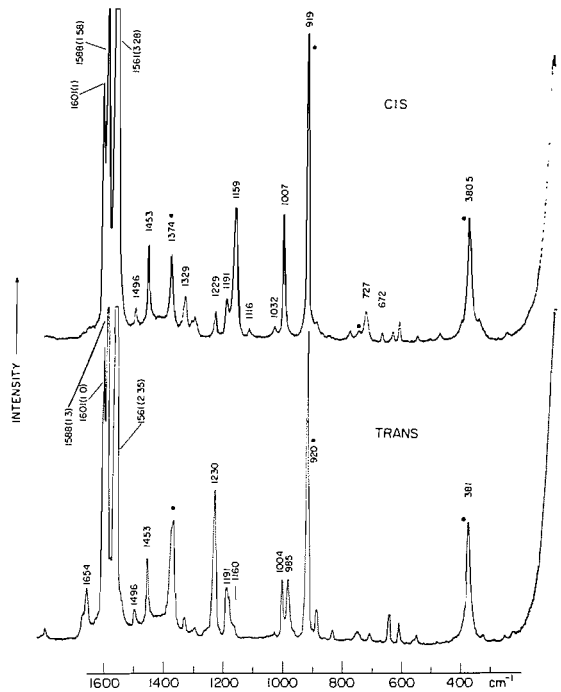

FIG. 4. Preresonance Raman spectra of *trans*- and *cis*-4-benzylidene-2-phenyl-Δ^2-oxazolin-5-one: approx. 10^{-2} M in CH_3CN (indicated by *); 514.5 nm; ~100 mW, 5 cm^{-1} spectral slit.

The major features in the Raman spectra of linear polyenes are bands in the region 1500–1650 cm^{-1} and 1100–1250 cm^{-1} (29). The strong peak near 1600 cm^{-1} is due to a coupled —C=C motion of the chain. In the case of diphenylpolyenes there are two very strong bands in the 1580–1600 cm^{-1} and they have been assigned to polyene —C=C— stretch and benzene ring normal modes (30). However the low frequency of the 1561 cm^{-1} band in *cis*- and *trans*-oxazolinones cannot be ascribed to the effects of conjugation in the Ph—C=C—N=C—Ph system since it is not until four double bonds are interposed between the rings that the chain mode approaches 1570 cm^{-1} (30).

The effect of ring size on —C=C— frequencies has been discussed by Bellamy (31). On the basis of simple theory and given the bond angles shown in Fig. 1, $\nu_{C=N}$ of the oxazolinone ring is expected to be greater than 1610 cm^{-1}. This is borne out experimentally by measurements on 2-phenyl-Δ^2-oxazolin-5-one, where $\nu_{C=N}$ occurs at ~1660 cm^{-1}.[3]

The possibility of the 1561 cm^{-1} band being mainly $\nu_{C=C}$ which is lowered by conjugation with C=O can be ruled out by isotopic substitution (below) and by analogy with the vibrational spectra

[3]K. Kumar, D. J. Phelps, and P. R. Carey. Unpublished work.

Can. J. Chem. Downloaded from www.nrcresearchpress.com by 210.87.254.42 on 09/05/12
For personal use only.

of cinnamic acid derivatives in which $\nu_{C=C}$ normally occurs between 1620 and 1640 cm^{-1} (4).

Crucial evidence on the nature of the 1561 cm^{-1} band comes from the combined Raman and ir data on isotopically labelled 4-(4-dimethylamino-3-nitrobenzylidene)-2-phenyl-Δ^2-oxazolin-5-ones. The ^{15}N and ^{13}C substituted compounds were separately labelled at the positions denoted * in Fig. 1. The Raman spectra are shown in Fig. 5, and are very similar, in the 1500–1600 cm^{-1} region, to those of the *trans* and *cis* isomers of unsubstituted oxazolinone (Fig. 4). Figures 6 and 7 compare the ir spectra of the labelled and unlabelled compounds and the shifts in features which can be identified in both the ir and Raman spectra between 1550 and 1650 cm^{-1} are given in Table 4. Care was taken to reduce error to less than ± 1 cm for intense bands in this region. These results are consistent with the following interpretation which applies for all the substituted oxazolinones having as a basic skeleton the structure shown in Fig. 1. The —C=C—N=C— grouping

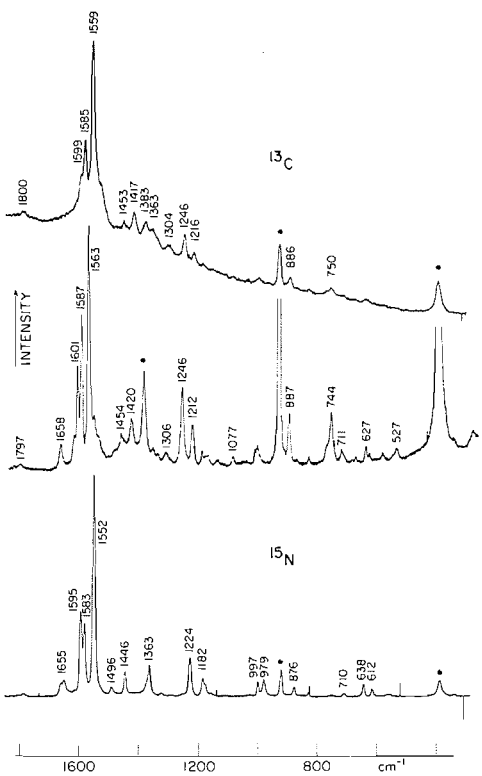

FIG. 5. Resonance Raman spectra of isotopically substituted *trans*-4-(4-dimethylamino-3-nitrobenzylidene)-2-phenyl-Δ^2-oxazolin-5-one: Top ^{13}C in 4 position of oxazolinone ring (see Fig. 1); bottom, ^{15}N in oxazolinone ring; middle, unsubstituted; 441.6 nm; 50 mW; spectral slit ~9 cm^{-1}; approx 10^{-4} *M* in CH_3CN (indicated by *).

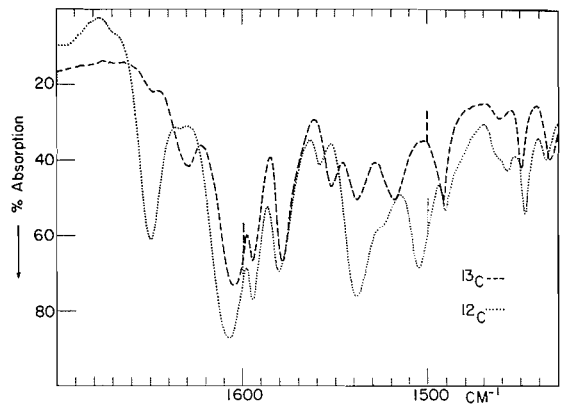

FIG. 6. Infrared spectra ^{12}C and ^{13}C substituted *trans*-4-(4-dimethylamino-3-nitrobenzylidene)-2-phenyl-Δ^2-oxazolin-5-one. Substitution is in the 4 position of oxazolinone ring. KBr pellet.

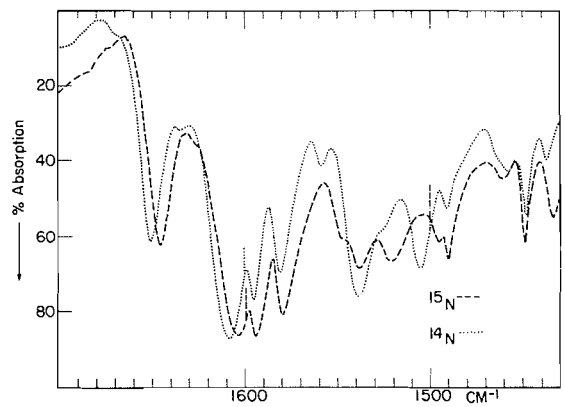

FIG. 7. Infrared spectra of ^{14}N and ^{15}N substituted *trans*-4-(4-dimethylamino-3-nitrobenzylidene)-2-phenyl-Δ^2-oxazoline-5-one. Substitution is in the oxazolinone ring. KBr pellet.

gives rise to two vibrations, one an essentially symmetric mode (intense Raman, weak ir) near 1560 cm^{-1} and the other an essentially asymmetric mode (very weak Raman and medium ir) near 1650 cm^{-1}. The 1560 cm^{-1} band has a degree of C=N character and the 1650 cm^{-1} feature a high degree of C=C character. The latter designation receives support from the Raman of the unsubstituted *cis*- and *trans*-oxazolinones (Fig. 4) in which, for the sterically crowded *cis* isomer, the weak 1650 cm^{-1} band is not observed. This could possibly be due to the reduced polarizability of the C=C following reduction of conjugation with the benzylidene ring.

Figure 5 and Table 4 show that the Raman spectrum is far more sensitive to ^{15}N compared to ^{13}C substitution. The shift from 1246 → 1224 cm^{-1} upon ^{15}N substitution indicates that this band may have C—N single bond stretching character. The bands

TABLE 4. ^{13}C and ^{15}N shifts of features which may be common to the ir and resonance Raman spectra of 4-(4-dimethylamino-3-nitrobenzylidene)-2-phenyl-Δ^2-oxazolin-5-one

Resonance Raman (cm^{-1})*		Infrared (cm^{-1})†	
^{15}N	^{13}C	^{15}N	^{13}C
1563 → 1552	1563 → 1559	1559 → 1546(sh)	1558 → 1552
1587 → 1583			
1601 → 1595		1608 → 1603	1608 → 1604
1658 → 1655	1658 → ~1630(sh)	1650 → 1646	1650 → 1630

*CH_3CN solutions, 441.6 nm excitation.
†KBr pellets.

at 1587 and 1601 cm^{-1} are probably benzene ring modes, from the N=C—Ph, which on the basis of the ^{15}N shifts are coupled to the 1561 cm^{-1} mode. Indeed the many shifts in the weaker features seen upon ^{15}N substitution indicate that the majority of weaker bands in the Raman spectra emanate from the —N=C—Ph portion of the molecule.

The important conclusion from the present work is that extensive π electron conjugation is a necessary but not sufficient condition for the appearance of relatively intense preresonance or even normal Raman features. Raman bands of high or medium intensity appear only from that part of the molecule associated with the electronic transition. Isotopic substitution and in some cases depolarization ratio may be used to locate the position of the electronic dipole transition in the conjugated system. The use of the Raman spectrum to locate the electronic transition appears to be a novel application of the Raman technique.

1. P. R. CAREY, H. SCHNEIDER, and H. J. BERNSTEIN. Biochem. Biophys. Res. Commun. **47**, 588 (1972).
2. P. R. CAREY and H. SCHNEIDER. Biochem. Biophys. Res. Commun. **57**, 831 (1974).
3. P. R. CAREY, R. G. CARRIERE, K. R. LYNN, and H. SCHNEIDER. Biochemistry, **15**, 2387 (1976).
4. P. R. CAREY and H. SCHNEIDER. J. Mol. Biol. **102**, 679 (1976).
5. K. BROCKLEHURST and K. WILLIAMSON. Tetrahedron, **30**, 351 (1974).
6. J. DE JERSEY and B. ZERNER. Biochemistry, **8**, 1975 (1969).
7. E. C. LUCAS and A. WILLIAMS. Biochemistry, **8**, 5125 (1969).
8. W. KIEFER and H. H. BERNSTEIN. Appl. Spectrosc. **25**, 501 (1971).
9. R. K. GRIFFITH and H. J. HARWOOD. J. Org. Chem. **29**, 2658 (1964).
10. P. R. CAREY, R. G. CARRIERE, D. J. PHELPS, and H. SCHNEIDER. Biochemistry. In press.
11. Y. S. RAO and R. FILLER. Synthesis, 749 (1975).
12. T. ASAHINA. Bull. Chem. Soc. Jpn. **4**, 202 (1929); Bull. Chem. Soc. Jpn. **5**, 354 (1930).
13. D. A. BASSI, V. DEULOFEU, and F. A. F. ORTEGA. J. Am. Chem. Soc. **75**, 171 (1953).
14. E. L. BENNETT and E. HOERGER. J. Am. Chem. Soc. **74**, 5975 (1952).
15. F. W. SCHUELER and S. C. WANG. J. Am. Chem. Soc. **72**, 2220 (1950).
16. R. E. BUCKLES, R. FILLER, and L. HILFMAN. J. Org. Chem. **17**, 233 (1952).
17. A. W. HANSON. Acta Crystallogr. B, **33**, 594 (1977).
18. J. DALE. Acta Chem. Scand. **11**, 971 (1957).
19. J. H. PINCKARD, B. WILLE, and L. ZECHMEISTER. J. Am. Chem. Soc. **70**, 1938 (1948).
20. G. WETTERMARK and R. SCHOR. Theor. Chim. Acta (Berlin), **9**, 57 (1967).
21. V. R. SALARES, R. MENDELSOHN, P. R. CAREY, and H. J. BERNSTEIN. J. Phys. Chem. **80**, 1137 (1976) and references therein.
22. J. BEHRINGER. *In* Raman spectroscopy. *Edited by* H. A. Szymanski. Plenum Press, New York, NY. 1967. p. 203.
23. K. KUMAR and P. R. CAREY. J. Chem. Phys. **63**, 3697 (1975).
24. B. P. GABER, V. MISKOWSKI, and T. G. SPIRO. J. Am. Chem. Soc. **96**, 6868 (1974).
25. K. KUMAR and P. R. CAREY. Can. J. Chem. **55**, 1444 (1977).
26. P. P. SHORYGIN. Sov. Phys.-Usp. **16**, 99 (1973); J. BEHRINGER. *In* Molecular spectroscopy. Vol. 2. *Edited by* R. F. Barrow, D. A. Long, and D. J. Millen. Specialist Periodical Reports, The Chemical Society, London. 1974; J. TANG and A. C. ALBRECHT. *In* Raman spectroscopy. Vol. 2. *Edited by* H. Szymanski. Plenum Press, New York, NY. 1970.
27. A. C. ALBRECHT and M. C. HUTLEY. J. Chem. Phys. **55**, 4438 (1971).
28. K. KAMOGAWA and M. ITO. J. Mol. Spectrosc. **60**, 277 (1976) and references therein.
29. L. RIMAI, M. E. HEYDE, and D. GILL. J. Am. Chem. Soc. **95**, 4493 (1973).
30. E. D. SCHMID and B. BROSA. J. Chem. Phys. **58**, 3871 (1973).
31. L. J. BELLAMY. Advances in infrared group frequencies. Methuen, London. 1969. p. 22.

Can. J. Chem. Downloaded from www.nrcresearchpress.com by 210.87.254.42 on 09/05/12
For personal use only.

Preresonance Raman spectra and excitation profiles of some chemically and isotopically substituted *trans*-4-benzylideneoxazolin-5-ones[1]

D. J. PHELPS, R. G. CARRIERE, K. KUMAR, AND P. R. CAREY

Division of Biological Sciences, National Research Council of Canada, Ottawa, Ont., Canada K1A 0R6

Received June 22, 1977

D. J. PHELPS, R. G. CARRIERE, K. KUMAR, and P. R. CAREY. Can. J. Chem. **56**, 240 (1978).

Resonance and preresonance Raman spectra of nine substituted *trans*-4-benzylidene-Δ^2-oxazolin-5-ones are reported. The seven analogs with phenyl in the 2 position of the oxazolinone ring have either an electron donating or attracting group on one of the phenyl rings. Although shifts in λ_{max} of up to 100 nm are observed the Raman spectra are very similar to that of the unsubstituted *trans* isomer. However, in the substituted compounds modes from the benzylidene portion may become weakly intensity enhanced. Replacing the 2-phenyl group by 2-methyl in the oxazolinone ring results in quite gross changes in the Raman spectrum. Substitution by ^{15}N in the ring of a 2-methyloxazolinone reveals that a change in the vibrational coupling scheme occurs. Excitation profiles for the 2-phenyl and the 2-methyl analogs of 4-(*p*-nitrobenzylidene)-oxazolinone indicate that in each compound all intensity enhanced modes are coupled to the intense low energy absorption band near 350 nm and the intensity enhancement fits the F_B^2 terms of Albrecht and Hutley. However, differences in the relative intensity of the benzylidene nitro feature in the 2-methyl and 2-phenyl analogs, taken with the excitation profiles, suggest that in the 2-methyl compound the electronic transition responsible for Raman intensity enhancement is no longer primarily located in the C=C—N=C—Ph moiety.

D. J. PHELPS, R. G. CARRIERE, K. KUMAR et P. R. CAREY. Can. J. Chem. **56**, 240 (1978).

On rapporte les spectres Raman de résonance et de pré-résonance de neuf benzylidène-4 Δ^2-oxazolinones-5 *trans* substituées. Les sept analogues avec un phényle en position 2 du cycle oxazolinone possèdent soit un groupe électrodonneur ou électroaffinitaire sur l'un des cycles phényle. Quoique l'on peut observer des déplacements allant jusqu'à 100 nm dans le λ_{max}, les spectres Raman sont très semblables à ceux de l'isomère *trans* non-substitué. Toutefois, dans les composés substitués, les modes de la portion benzylidène peuvent avoir des intensités qui ont subi une faible augmentation. En remplaçant le groupe phényle en position 2 du cycle oxazolinone par un méthyle, il se produit des changements très importants dans le spectre Raman. L'introduction d'un ^{15}N dans le cycle d'une méthyl-2 oxazolinone révèle qu'il se produit un changement dans le schéma de couplage vibrationnel. Les profils d'excitation pour les analogues phényl-2 et méthyl-2 de la (*p*-nitrobenzylidène)-4 oxazolinone indiquent que, dans chacun de ces composés, tous les modes où l'intensité est augmentée sont couplés avec la bande d'absorption intense de basse énergie près de 350 nm et que l'augmentation d'intensité est une fonction des termes F_B^2 d'Albrecht et Hulley. Toutefois, les différences dans l'intensité relative des caractéristiques du benzylidènenitro des analogues méthyl-2 et phényl-2 de concert avec les profils d'excitation suggèrent que, dans le composé méthyl-2, la transition électronique responsable pour l'augmentation de l'intensité du spectre Raman n'est plus liée principalement avec la portion C=C—N=C—Ph.

[Traduit par le journal]

Introduction

In the preceding and accompanying paper (1) the unsubstituted *cis* and *trans* isomers of 4-benzylidene-2-phenyl-Δ^2-oxazolin-5-one were discussed. To explain the unexpected similarity between the absorption and preresonance Raman spectra of the two isomers it was proposed that the electronic dipole transition responsible for the intense low energy absorption band and the vibrational modes responsible for the intense Raman lines are localized in the —C=C—N=C—Ph part of the molecule. Support for this concept came from depolarization ratio measurements and isotopic substitution. The present paper explores the consequences of adding an electron donating or accepting group to the benzylidene phenyl ring (Fig. 1) and in separate experiments replacing the 2-phenyl on the oxazolinone ring by a methyl group. Although large shifts in λ_{max} are

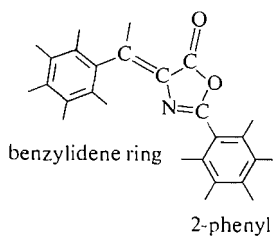

FIG. 1. *trans*-4-Benzylidene-2-phenyl-Δ^2-oxazolin-5-one.

[1]NRCC No. 16306.

Can. J. Chem. Downloaded from www.nrcresearchpress.com by 210.87.254.5 on 09/05/12
For personal use only.

Can. J. Chem. Downloaded from www.nrcresearchpress.com by 210.87.254.5 on 09/05/12
For personal use only.

sometimes observed, substituents in the benzylidene ring have little effect on the Raman spectra indicating only minor perturbations in the factors responsible for Raman intensity. However, replacement of the 2-phenyl by a methyl group results in far more radical changes in both the vibrational and vibronic coupling schemes.

Experimental

Raman, ir, and absorption spectroscopic measurements were made using procedures outlined in previous publications (2, 3). As in the preceding and accompanying paper (1) no evidence was found for photodecomposition or photoisomerization. Synthesis of the oxazolinones was carried out by literature methods (4). All oxazolinones were determined pure by tlc and were characterized by nmr, ir, and Raman spectroscopy. Their melting points are as follows: 4-(4-nitro)benzylidene-2-phenyl- mp 235–239°C (lit. (5) mp 240–242°C); 4-(2-nitro)benzylidene-2-phenyl- mp 163–164°C (lit. (6) mp 160–164°C); 4-(3-nitro)benzylidene-2-phenyl- mp 174–176°C (lit. (7) mp 175–176°C); 4-(4-dimethylamino)benzylidene-2-phenyl- mp 210–212°C (lit. (8) mp 220); 4-(4-dimethylamino-3-nitro)benzylidene-2-phenyl- mp 180–181°C (lit. (9) 181°C); 4-benzylidene-2-(4-nitro)phenyl- mp 236–237°C (lit. (10) 206°C); 4-benzylidene-2-methyl- mp 149–151°C (lit. (11) mp 152–154°C; 4-(4-nitro)benzylidene-2-methyl mp 172°C (dec) (lit. (12) mp 186–187°C). 4-(2,4-Dinitro)benzylidene-2-phenyloxazolin-5-one was generously donated by Dr. H. Schneider.

It has been concluded that stable oxazolinones have the *trans* configuration from nmr (13–15), X-ray (16, 17), and other considerations (18, 19).

Results and Discussion

o-, m-, *and* p-*Nitro Substitutions in the Benzylidene Ring*

The absorption and preresonance Raman spectra of these analogs are shown in Figs. 2 and 3, respectively. The absorption spectra of *m*- and *p*-NO_2 show clear structure in the main bands while *o*-NO_2 does not. The loss of structure may reflect steric interactions between the *o*-nitro and ethylenic hydrogen atoms (1, 17). The preresonance Raman spectra (Fig. 3) are very similar, and, for the *cis* and *trans* unsubstituted compounds, are dominated by the three bands in the 1560–1610 cm^{-1} region. This similarity is strong evidence that the vibronic interactions responsible for the Raman intensity enhancement are essentially unperturbed. However, the presence of the —NO_2 chromophore in the benzylidene ring does result in a Raman feature of weak-to-medium intensity from this part of the molecule, e.g. the 1349 cm^{-1} band in the *p*-NO_2 compound (Fig. 3, bottom).

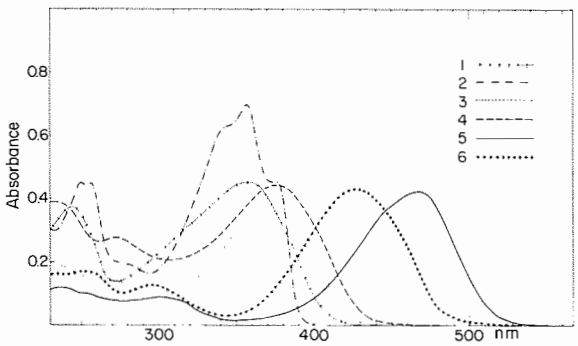

FIG. 2. Absorption spectra of 4-benzylidene-2-phenyl-Δ^2-oxazolin-5-one substituted in the benzylidene ring: (*1*) *o*-nitro 2×10^{-5} *M*, (*2*) *m*-nitro- 1.99×10^{-5} *M*, (*3*) *p*-nitro- $\sim 2 \times 10^{-5}$ *M*, (*4*) 2,4-dinitro- 2×10^{-5} *M*, (*5*) *p*-dimethylamino- 0.82×10^{-5} *M*, (*6*) 4-dimethylamino-3-nitro- 1.05×10^{-5} *M*; solvent CH_3CN, 1-cm path length.

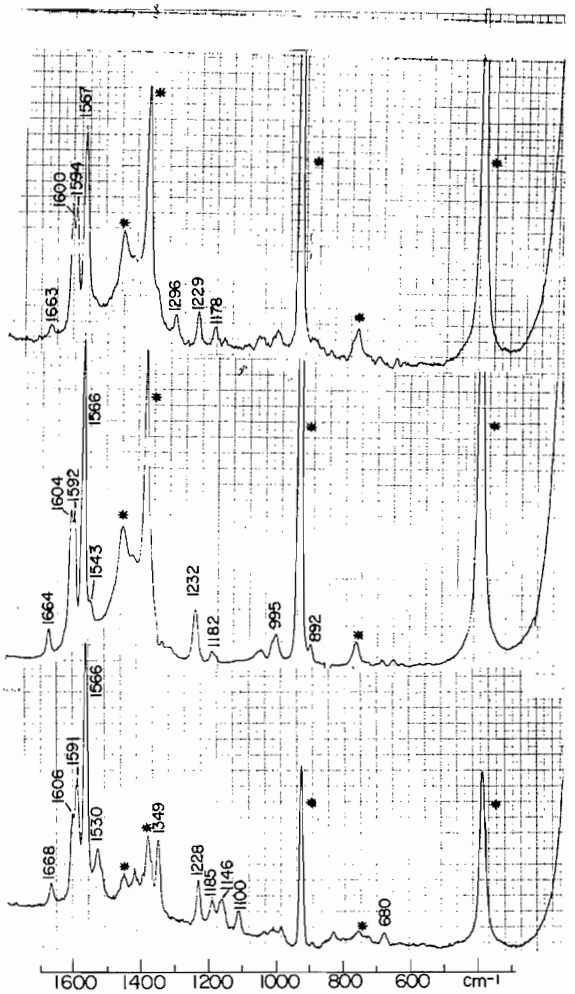

FIG. 3. Preresonance Raman spectra of 4-(*o*-nitrobenzylidene)- (top), 4-(*m*-nitrobenzylidene)- (center), and 4-(*p*-nitrobenzylidene)-2-phenyl-Δ^2-oxazolin-5-one (bottom): $\sim 2 \times 10^{-3}$ *M* in CH_3CN (indicated by *); 457.9 nm; 100 mW; 9-cm^{-1} spectral slit.

Other Nitro Substitutions

Nitro groups in the 2,4 positions of the benzylidene ring give rise to an absorption spectrum (Fig. 2)

Can. J. Chem. Downloaded from www.nrcresearchpress.com by 210.87.254.5 on 09/05/12
For personal use only.

with a λ_{max} similar to that of the compound substituted in the 4 position alone. However, structure is not resolved in the absorption spectrum and this may be again due to steric interactions of the *o*-nitro group. The preresonance Raman spectrum is shown in Fig. 4 and its strong resemblance to the *o*-, *m*-, and *p*-monosubstituted and unsubstituted compounds again testifies to the minor role played by the benzylidene ring in the mechanism of Raman intensity enhancement. The absorption spectrum of the analog substituted *para* in the 2-phenyl ring is shown in Fig. 6. Its preresonance Raman spectrum (Fig. 5) still bears strong resemblance to that of the unsubstituted molecules. However, slight differences, e.g. in the position of the 1580 cm^{-1} band, are detectable and these differences are greater than those found within the series characterized by NO_2 substitutions in the benzylidene ring.

p-*Dimethylamino Substitution in the Benzylidene Ring*

In keeping with the strong electron donating power of the dimethylamino group, this substitution results in a large red shift in λ_{max} (Fig. 2). The resonance Raman spectrum (Fig. 4) is still dominated by features in the 1540–1610 cm^{-1} region but there is evidence of a shoulder at 1545 cm^{-1} not appearing in the compounds discussed above. However, it is apparent that the electron rearrangement caused by the dimethylamino group has had only a minor effect

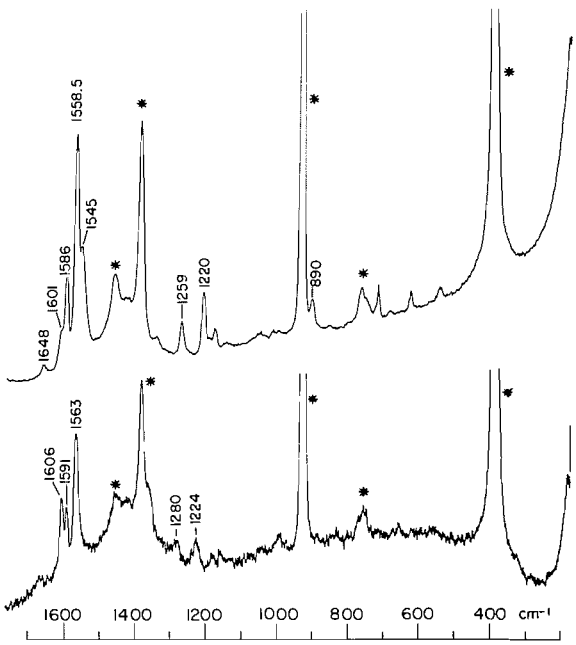

FIG. 4. Raman spectra of 4-(4-dimethylaminobenzylidene)- (top) and 4-(2,4-dinitrobenzylidene)-2-phenyl-Δ^4-oxazolin-5-one (bottom); $\sim 2 \times 10^{-3}$ *M* in CH_3CN (indicated by *); 647.1 nm; 300 mW, 8-cm^{-1} spectral slit.

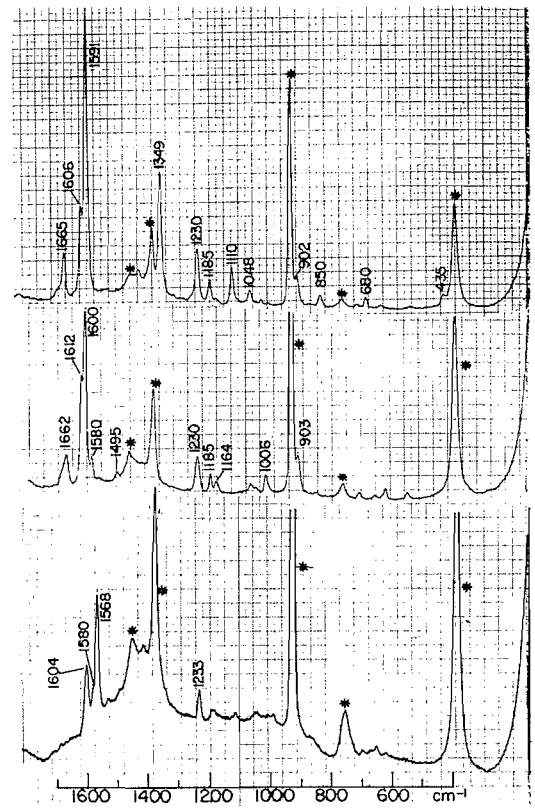

FIG. 5. Preresonance Raman spectra of 4-(*p*-nitrobenzylidene)-2-methyloxazolin-5-one (top), 4-benzylidene-2-methyloxazolin-5-one (center), and 4-benzylidene-2-(*p*-nitrophenyl)-oxazolin-5-one (bottom); 1–2 $\times 10^{-3}$ *M* in CH_3CN (indicated by *); 457.9 nm; 100 mW, 8 cm^{-1} spectral slit.

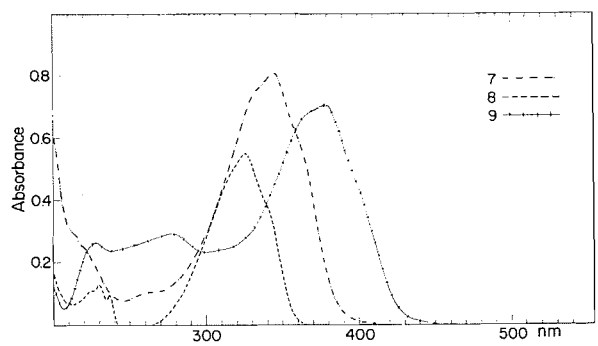

FIG. 6. Absorption spectra of (*7*) 4-(*p*-nitrobenzylidene)-2-methyloxazolin-5-one 2.85×10^{-5} *M*, (*8*) 4-benzylidene-2-methyloxazolin-5-one 2×10^{-5} *M*, (*9*) 4-benzylidene-2-(*p*-nitrophenyl)oxazolin-5-one 2.4×10^{-5} *M*; solvent CH_3CN; 1-cm path length.

on the vibrational coupling scheme in the oxazolinone skeleton and on the position of the electronic dipole responsible for Raman intensity enhancement. It is interesting to compare this case with the changes observed during some enzyme–substrate reactions. In certain of the latter (9), large red shifts in substrate

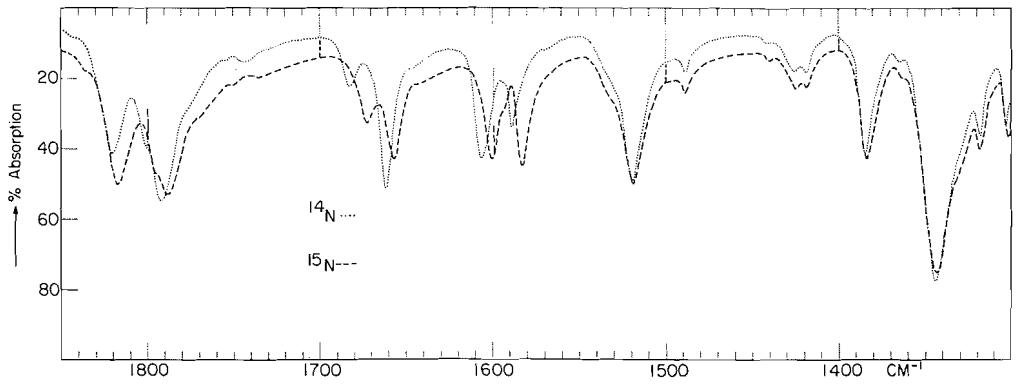

FIG. 7. Infra red spectra of ^{14}N and ^{15}N (substituted in the oxazolinone ring) 4-(*p*-nitrobenzylidene)-2-methyloxazolin-5-one; KBr pellet.

absorbance upon forming an enzyme–substrate complex are accompanied by a total change in the appearance of the resonance Raman spectrum. Good model systems, which mimic these absorption and Raman properties, have been found for the effects of the enzyme.[2] These enzyme–substrate and model systems thus contrast strongly with the present case in which a large red shift is accompanied by a minimal perturbation of the resonance Raman spectrum.

4-(4-Dimethylamino-3-nitrobenzylidene)-2-phenyl-Δ^2-oxazolin-5-one

Again this compound illustrates that substitution in the benzylidene ring does little to affect the overall appearance of the Raman spectra. Resonance Raman and ir data are reported for ^{13}C and ^{15}N substituted analogs of this compound in the preceding paper and the absorption spectrum is shown in Fig. 2. The isotopically substituted analogs established that the intense Raman band at 1563 cm^{-1} had a degree of C=N stretching character but only a small degree of C=C stretching character while for the weak Raman band at 1658 cm^{-1} this situation is reversed. The 1563 cm^{-1} band was assigned to an essentially symmetric mode from the —C=C—N=C portion of the molecule while the band at 1658 cm^{-1} represents an essentially antisymmetric vibration of this moiety.

Replacing the 2-Phenyl on the Oxazolinone Ring by Methyl

In contrast to the above examples replacement of the 2-phenyl ring by methyl causes a substantial change in the appearance of the Raman spectra. This change is not predictable on the basis of the absorption spectra (Fig. 6). The characteristic three Raman bands in the 2-phenyl compounds of medium and high intensity between 1560 and 1610 cm^{-1} are replaced, in the 2-methyl analogs, by two bands whose center of gravity shifts 25–30 cm^{-1} to higher wave numbers. Furthermore the NO_2 feature near 1350 cm^{-1} has a much higher relative intensity in the 2-methyl substituted 4-(*p*-nitrobenzylidene)oxazolinone compared to the 2-phenyl analog. There appear to be two sources for these changes, firstly a change in vibrational coupling and secondly a partial relocation of the electronic transition responsible for Raman intensity enhancement. The change in vibrational coupling in the 2-methyl compared to the 2-phenyl analog is revealed by ^{15}N substitution in the oxazolinone ring of 4-(*p*-nitrobenzylidene)-2-methyloxazolin-5-one. The intense Raman peak at 1591 cm^{-1} shows a ^{15}N shift of about 5 cm^{-1} as do less intense peaks at 1607 and 1662 cm^{-1} (Table 1). Figure 7 compares the ir spectra of the ^{14}N and ^{15}N compounds. All four intense ir features between 1580 and 1700 cm^{-1} move significantly upon ^{15}N substitution; the 1682 cm^{-1} (Fig. 7) band is a very weak shoulder in the Raman (Fig. 5). Thus the present situation contrasts strongly with the 2-phenyl substituted compounds where the most intense Raman band at 1563 cm^{-1} showed the greatest ^{15}N shift (14 cm^{-1}, see preceding

TABLE 1. Raman spectra of ^{15}N substituted 4-(*p*-nitrobenzylidene)-2-methyl-Δ^2-oxazolin-5-one*

	Band positions (cm^{-1})	
	^{14}N	^{15}N
Solid	1588	1581
CH_3CN solution	1665	1661
	1607	1600(sh)
	1591	1586
	1230, 1185, 1110	No detectable shift

*Using 441.6 nm excitation. Differences are thought to be accurate to ± 1 cm^{-1}.

[2]P. R. Carey, R. G. Carriere, D. J. Phelps, and H. Schneider. Unpublished results.

Can. J. Chem. Downloaded from www.nrcresearchpress.com by 210.87.254.5 on 09/05/12
For personal use only.

Can. J. Chem. Downloaded from www.nrcresearchpress.com by 210.87.254.5 on 09/05/12
For personal use only.

paper, ref. 1). It is apparent that in the 2-methyl substituted compounds the modes in the double bond region are mixed and no single band can be assigned a high degree of C=N stretching character.

The relationship between Raman intensity and the electronic dipole transition is discussed under Excitation Profiles in the preceding paper. Evidence that in the 2-methyl compounds the electronic transition is no longer primarily in the C=C—N=C—Ph moiety comes from considering both the relative intensities of the Raman bands and their excitation profiles. The experimental excitation profiles of 4-(4-nitro-benzylidene)oxazolin-5-one substituted with 2-methyl or 2-phenyl (Fig. 8) demonstrate that in both compounds the NO_2 feature at 1349 cm^{-1} and the intense bands in the double bond region have the same degree of enhancement upon going from 514.5 nm to 457.9 nm. The depolarization ratios for the intense features in both 4-(*p*-nitrobenzylidene)-2-methyl-Δ^2-oxazolin-5-one (Table 2) and the 2-phenyl analog are all ~0.33 showing that only one element of the scattering tensor is dominant and permitting the calculation of theoretical excitation profiles. Good agreement is observed between experimental intensity enhancement and theoretical F_B^2 terms (1, 20) using the transition at ~350 nm for the theoretical calculation (Fig. 8). Moreover the relative intensities in each spectrum remain essentially the same using 647.1 nm excitation. Thus for both the 2-phenyl and 2-methyl analogs in the preresonance region the nitro and double bond features are coupled to the intense electronic transition at ~350 nm. However, comparing the 2-methyl and 2-phenyl spectra, the relative intensities of the nitro band and the double bond features are very different. The integrated intensity of the 1349 cm^{-1} band compared to the total integrated intensity of the bands between 1550 and 1650 cm^{-1} is 1:2.7 for the 2-methyl molecule and 1:6.2 for the 2-phenyl molecule. The intensity ratio for the 2-methyl is quite close to that for *p*-nitro cinnamic acid, which is 1:2.1 (Fig. 9). Recent theoretical studies (21) have emphasized the importance of relative Raman intensities as a source of molecular information and these, together with the data presented here, lead us to propose that in the 2-methyl substituted compounds the electronic dipole transition responsible for intensity enhancement is no longer primarily located in the C=C—N=C—Ph moiety. In the 2-methyl compounds the benzylidene ring becomes important in the Raman intensity enhancement mechanism. In this sense the chromophore can be said to have switched in part from C=C—N=C—Ph to the benzylidene portion.

TABLE 2. Depolarization ratios for 4(*p*-nitrobenzylidene)-2-methyl-Δ^2-oxazolin-5-one*

Band position (cm^{-1})	ρ
1662	0.31
1606(sh)	0.30
1591	0.33
1350	0.31
1228	0.28
1185	0.29
1110	0.31

*Using 514.5 nm excitation.

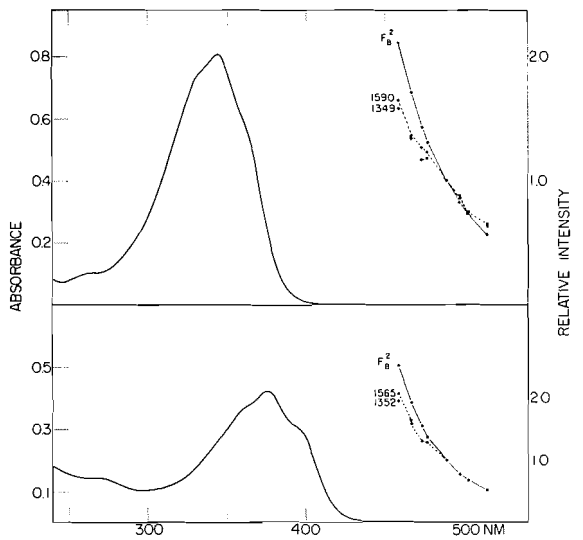

FIG. 8. Theoretical (F_B^2) and experimental excitation profiles for 4-(*p*-nitrobenzylidene)-2-methyloxazolin-5-one (top) and the 2-phenyl analog (bottom); CH_3CN 1376 and 920 cm^{-1} features used as internal standards for experimental data. For 2-phenyl calculations ν_e = 375 nm, ν_s = 280 nm, F_B^2 shown for 1570 cm^{-1} Raman line; for 2-methyl ν_e = 345 nm, ν_s = 260 nm, F_B^2 shown for 1590 cm^{-1} Raman line.

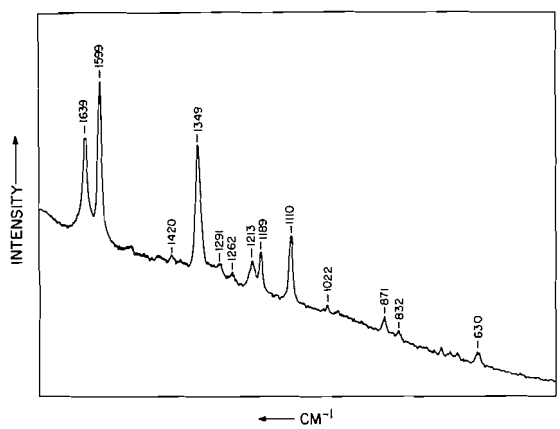

FIG. 9. Preresonance Raman spectrum of *p*-nitrocinnamic acid: KBr pellet; rotating cell; 457.9 nm; 100 mW; 9-cm^{-1} spectral slit.

Two conclusions stem from the present work. Firstly, although strongly electron attracting or donating groups attached to the benzylidene ring may cause large shifts in λ_{max}, the position and relative intensities of the Raman peaks are only minimally perturbed. Secondly it is shown that replacement of the 2-phenyl group by methyl on the oxazolinone ring results in rearrangement of the vibrational coupling scheme and in a partial relocation of the electronic transition responsible for Raman intensity enhancement with the benzylidene moiety assuming increasing importance.

Acknowledgement

We are grateful to Dr. R. N. Jones for use of his Perkin Elmer 521 IR spectrometer.

1. K. KUMAR, D. J. PHELPS, and P. R. CAREY. Can. J. Chem. This issue.
2. K. KUMAR and P. R. CAREY. Can. J. Chem. **55**, 1444 (1977).
3. K. KUMAR and P. R. CAREY. J. Chem. Phys. **63**, 3697 (1975).
4. R. K. GRIFFITH and H. J. HARWOOD. J. Org. Chem. **29**, 2658 (1964).
5. A. PEDRAZZOLI. Helv. Chim. Acta, **40**, 80 (1957).
6. S. I. LUR'E, E. S. CHAMAN, and G. A. RAVDEL. Zhur. Obsch. Khim. **23**, 1392 (1953); Chem. Abstr. **47**, 12246a (1953).
7. V. G. DUBENKO. Dopov. Akad. Nauk Ukr. RSR. Ser. B, **30**, 547 (1968); Chem. Abstr. **69**, 106596p (1968).
8. L. HEILERMAN, C. C. PORTER, H. J. LOWE, and H. F. KOSTER. J. Am. Chem. Soc. **68**, 1890 (1946).
9. P. R. CAREY, R. G. CARRIERE, K. R. LYNN, and H. SCHNEIDER. Biochemistry, **15**, 2387 (1976).
10. M. M. BOTVINIK and S. M. AVAEVA. Uchenye Zapiski, Moskov. Gosudarst. Univ. L'm M.V. Lomonosova No. 132 Org. Khim. No. 7, 288 (1950); Chem. Abstr. **49**, 3944d (1955).
11. G. CARRARA and G. WEITNAUER. Gazz. Chim. Ital. **79**, 856 (1949).
12. D. O. HOLLAND, P. A. JENKINS, and J. H. C. NAYLER. J. Chem. Soc. 273 (1953).
13. A. P. MORGENSTERN, C. SCHUTIJ, and W. T. NAUTA. Chem. Commun. 321 (1969).
14. P. O. LARSEN and E. WIECZORKOWSKA. Acta Chem. Scand. B, **28**, 92 (1974).
15. R. GLASER and M. TWAIK. Tetrahedron Lett. 1219 (1976).
16. K. BROCKLEHURST, R. P. BYWATER, R. A. PALMER, and R. PATRICK. Chem. Commun. 632 (1971).
17. A. W. HANSON. Acta Crystallogr. B, **33**, 594 (1977).
18. K. BROCKLEHURST and K. WILLIAMSON. Tetrahedron, **30**, 351 (1974).
19. Y. S. RAO and R. FILLER. Synthesis, 749 (1975).
20. A. C. ALBRECT and M. C. HUTLEY. J. Chem. Phys. **55**, 4438 (1971).
21. A. WARSHEL. J. Chem. Phys. In press. Quoted in A. Warshel. Ann. Rev. Biophys. Bioeng. **6**, 273 (1977).

Can. J. Chem. Downloaded from www.nrcresearchpress.com by 210.87.254.5 on 09/05/12
For personal use only.

Terpenoids. Part 44. Oxidative rearrangement of 17-nor-13β-kauran-16-one with thallium(III) nitrate

EIICHI FUJITA AND MASAHITO OCHIAI

Institute for Chemical Research, Kyoto University, Uji, Kyoto-Fu 611, Japan

Received July 6, 1977

EIICHI FUJITA and MASAHITO OCHIAI. Can. J. Chem. **56**, 246 (1978).

17-Nor-13β-kauran-16-one (**1**) on treatment with thallium(III) nitrate in acetic acid gives an oxidatively rearranged product, 9,10-*friedo*-17-norkaur-5(10)-en-12-one (**2**). On heating in the presence of acid, compound **2** undergoes rearrangement to give an αβ-unsaturated ketone, 17-norkaur-9(11)-en-12-one (**8**). The structure and stereochemistry of the compound **8** were established by the total synthesis of its racemate.

EIICHI FUJITA et MASAHITO OCHIAI. Can. J. Chem. **56**, 246 (1978).

Traitée par le nitrate de thallium(III) dans l'acide acétique, la nor-17 kauran-13β one-16 (**1**) donne un produit transformé oxydiquement, la *friedo*-9,10 nor-17 kaurèn-5(10) one-12 (**2**). Par chauffage en présence d'acide, le composé **2** subit la transformation, en donnant une cétone non-saturée, la nor-17 kaurèn-9(11) one-12 (**8**). La structure et la stéréochimie ont été établies par la synthèse totale de son composé racémique.

Can. J. Chem. Downloaded from www.nrcresearchpress.com by 210.87.254.40 on 09/05/12
For personal use only.

It is well known that oxidation (1) and/or oxidative rearrangements (2) occur in the reaction of carbonyl compounds with thallium(III) salts. The oxidative rearrangements are of two types, *A* and *B*, as shown in Scheme 1.

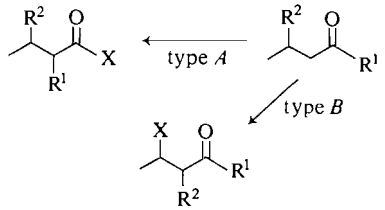

SCHEME 1

Recently we reported (3) the type *B* rearrangement in the reaction of *ent*-17-norkauran-16-one with thallium(III) nitrate (TTN), for which the type *A* reaction seemed unfavorable because it would have to form a highly strained product. It appeared interesting to check the same reaction with other carbonyl compounds, for which both types of rearrangements seem disadvantageous for some reason. Thus we chose 17-nor-13β-kauran-16-one (**1**) (4): its type *A* rearrangement should be difficult for the same reason as in the case of *ent*-norkauranone; its type *B* rearrangement should also be difficult because of the severe strain in two of the rings of the expected product resulting from the migration of the 8,9-bond to the 15-carbon atom.

Compound **1** on treatment with TTN in acetic acid at room temperature for 4 days, gave a product in 81% yield. Its molecular formula was shown to be $C_{19}H_{28}O$ and the presence of a cyclohexanone system was suggested by its infrared spectrum. A tetrasubstituted double bond (or a fifth ring) was suggested by the number of sites of unsaturation and its nmr spectrum. Its cd spectrum showed a large positive maximum (5). These data as well as consideration of the following facts led to the tentative assignment of structure **2** to this product.

In 1974, Murray *et al.* (6) published the transformation of **3** into **4** in which carbons 11 and 12 of **3** become carbons 15 and 16 in the product **4** and carbons 15 and 16 of **3** become carbons 11 and 12 of the product. A mechanism for the transformation was proposed (6).

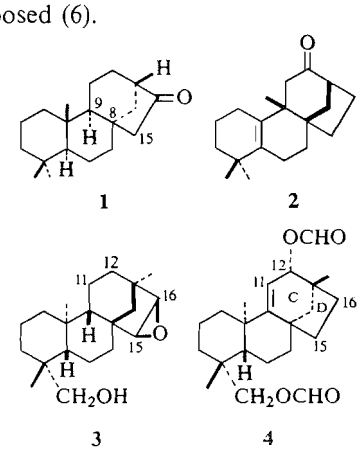

Consideration of the same type of mechanism for our rearrangement is reasonable. Thus, as shown in Scheme 2, the initial electrophilic attack of TTN from the less-hindered α side of the enol form of compound **1** yields a π complex, which immediately forms the 15α-Tl substituted compound **5**. The

Can. J. Chem. Downloaded from www.nrcresearchpress.com by 210.87.254.40 on 09/05/12
For personal use only.

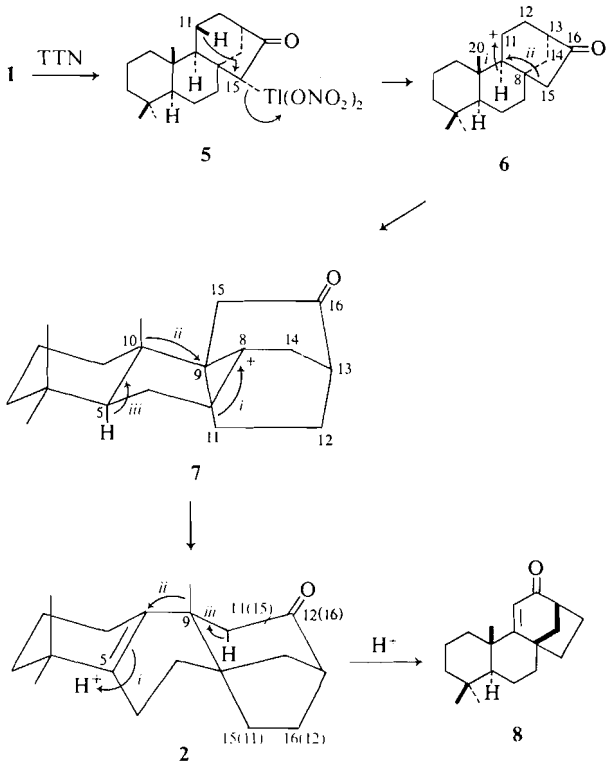

SCHEME 2

successive heterolysis of the C-15—Tl bond cannot be followed by rearrangement of the 8,9 bond into the 15-carbon atom (*vide supra*) but instead is followed by a 1,4-hydride shift of the 11β-H, which is suitably located, to give a cation **6**. Subsequent 1,2-hydride shift from 9α to 11α followed by a 1,2-alkyl shift from 8 (15) to 9 forms a cation **7**. An alternative 1,2-hydride shift of 12α-H to 11α and subsequent 1,2-alkyl shift of the 13,16-bond to 12 forming a bicyclo[2.2.2.]octane system must be unfavorable because of large nonbonded interaction between the 15-methylene and the 20-methyl group. The final deprotonation of the 5α-H after the two successive 1,2-shifts from cation **7** as shown yields the product **2**.

Compound **2** on treatment with a little nitric acid in acetic acid at 100°C gave a rearranged product in 92% yield. It was shown to have the same molecular formula ($C_{19}H_{28}O$) as the starting material. The presence of an αβ-unsaturated ketone in the molecule was suggested by the spectroscopic data (uv (EtOH) λ_{max}: 244 nm; ir ($CHCl_3$) ν_{max}: 1655 and 1593 cm^{-1}; nmr δ: 5.72 (1H, d, J = 1.5 Hz)). The initial protonation at C-5 from the α side, the 1,2-shift of the methyl group on C-9, and subsequent deprotonation of 11α-H would convert the compound **2** into a product having structure **8**. The assignment of this structure to the rearranged product was confirmed by a total synthesis of its racemate.

rac-17-Norkaur-9(11)-en-16β-ol (**9**) which had been synthesized[1] from 5-methoxy-2-tetralone was subjected to successive Jones' oxidation, Wolff–Kishner reduction, and oxidation with chromium trioxide in acetic acid to give *rac*-17-norkaur-9(11)-en-12-one (**8**) via the ketone **10** and the unsaturated hydrocarbon **11**. Compound **8** formed in this manner was identical with the optical active form described above. Compound **11** was auto-oxidized to ketone **8** on standing for a few months.

Thus the product from the reaction of 17-nor-13β-kauran-16-one (**1**) with TTN in acetic acid is now established to be 9,10-*friedo*-17-norkaur-5(10)-en-12-one (**2**).

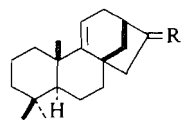

9 R = α-H, β-OH
10 R = O
11 R = H_2

Experimental

Melting points were determined on a micro hot-stage apparatus. The ir spectra were recorded on a Hitachi EPI-S2 spectrometer and the nmr spectra on a Varian T-60 spectrometer for solutions in deuteriochloroform (tetramethylsilane as internal standard). Mass spectra were determined with a JEOL JMS-OISG double-focusing spectrometer. The uv spectrum was recorded on a Hitachi model EPS-3 spectrophotometer. The circular dichroism was measured with a JASCO J-20 spectropolarimeter. Optical rotations were measured with a JASCO DIP-180 automatic polarimeter. Extracts were dried over anhydrous Na_2SO_4. Mallinckrodt silicic acid and Kieselgel 0.05–0.2 mm (Merck) were used for column chromatography.

*9,10-*friedo*-17-Norkaur-5(10)-en-12-one (2)*

TTN (139 mg) was added to a solution of the ketone **1** (56 mg) in acetic acid (3 ml). The mixture was stirred vigorously for 4 days at room temperature, precipitating white thallium(I) nitrate gradually. The inorganic salt was filtered off and a small amount of water was added to the filtrate. Extraction with *n*-hexane, washing with sodium carbonate and water, and then evaporation left a crystalline residue, which was purified by chromatography to give the rearranged ketone, *9,10-*friedo*-17-norkaur-5(10)-en-12-one* (**2**), (45 mg, 81% yield) as needles, mp 110–113°C (recrystallized from acetonitrile); $[\alpha]_D^{25}$ −60° (*c* 0.22, MeOH); cd (*c* 0.017, MeOH) : $[\theta]_{320}$ 0, $[\theta]_{284}$ −29 000, $[\theta]_{233}$ 0, $[\theta]_{212}$ +14 000, $[\theta]_{199}$ 0; ir ($CHCl_3$) ν_{max} : 1705, 910 cm^{-1}; nmr δ : 0.75, 0.86, 1.01 (each 3H, s); ms *m/e* : 272 (M^+), 257 ($M^+ - CH_3$). *Anal.* calcd. for $C_{19}H_{28}O$: C 83.77, H 10.36; found: C 83.60, H 10.35.

17-Norkaur-9(11)-en-12-one (8)

To a solution of the ketone **2** (13 mg) in acetic acid (2 ml) was added nitric acid (*d*, 1.42) (0.3 ml) and the mixture was heated at 100°C for 2 h. Water was added and the mixture was extracted with ether. After washing with sodium carbonate and water and drying, evaporation left a crystalline mass,

[1]The detailed manuscript has been accepted by Chem. Pharm. Bull. (Jpn).

which was chromatographed to give *17-norkaur-9(11)-en-12-one* (**8**) (11 mg, 92% yield). The analytical sample was prepared by crystallization from acetonitrile as colorless prisms, mp 111°C; $[\alpha]_D^{25}$ −96° (*c* 0.28, MeOH); cd (*c* 0.014, MeOH): $[\theta]_{372}$ 0, $[\theta]_{319}$ −21 000, $[\theta]_{276}$ 0, $[\theta]_{245}$ +47 000, $[\theta]_{226}$ 0, $[\theta]_{217}$ −15 000; ir ($CHCl_3$) ν_{max}: 1655, 1593, 885 cm^{-1}: nmr δ: 0.88, 0.97, 1.17 (each 3H, s), 5.72 (1H, d, J = 1.5 Hz, 11-H); uv (EtOH) λ_{max}: 244 (ε 15 800), 319 (ε 120) nm; ms *m/e*: 272 (M^+), 257 ($M^+ - CH_3$). *Anal.* calcd. for $C_{19}H_{28}O$: C 83.77, H 10.36; found: C 83.69, H 10.54.

rac-*17-Norkaur-9(11)-en-16-one* (***10***)

To an ice-cooled solution of *rac*-17-norkaur-9(11)-en-16β-ol (**9**) (50 mg) in acetone (7 ml), Jones' reagent was added dropwise until yellow color persisted. Excess of the reagent was decomposed with isopropyl alcohol, and the solution was concentrated *in vacuo*. Extraction with ethyl acetate after addition of a little water and the usual work-up gave a crude crystalline product, which was chromatographed to yield *rac-17-norkaur-9(11)-en-16-one* (**10**) (40 mg, 81% yield). The analytical sample was prepared by crystallization from aqueous methanol as needles, mp 89-89.5°C; ir ($CHCl_3$) ν_{max}: 1735 cm^{-1}; nmr δ: 0.82, 0.92, 1.08 (each 3H, s), 5.20 (1H, m, 11-H); ms *m/e*: 272 (M^+). *Anal.* calcd. for $C_{19}H_{28}O$: C 83.77, H 10.36; found: C 83.87, H 10.13.

rac-*17-Norkaur-9(11)-ene* (***11***)

To a solution of the ketone **10** (108 mg) in triethylene glycol (4 ml) hydrazine was added (heated at reflux over sodium hydroxide and distilled) (1 g) and the mixture was heated at 160°C for 4 h under a nitrogen atmosphere. After the addition of hydrazine (0.5 g), a solution of sodium (200 mg) in triethyl ene glycol (4 ml) was added, then the temperature was raised to 220°C by distilling off the low boiling material and the solution was heated at this temperature for 1 h. After cooling, water was added and the solution extracted with *n*-hexane. Usual work-up of the extract gave an oily substance, which was purified by chromatography to yield rac-*17-norkaur-9(11)-ene* (**11**) (102 mg, 100% yield) as an oil; nmr δ: 0.83, 0.90, 1.05, (each 3H, s), 5.12 (1H, m, 11-H).

rac-*17-Norkaur-9(11)-en-12-one* (***8***)

To a solution of *rac*-17-norkaur-9(11)-ene (**11**) (52 mg) in acetic acid (2 ml) was added chromium trioxide (50 mg) at room temperature and the solution was stirred for 2 h. Excess reagent was decomposed with isopropyl alcohol and the solution was concentrated *in vacuo*. After addition of a little water, extraction with *n*-hexane and the usual work-up gave a crystalline mass, which was chromatographed to yield rac-*17-norkaur-9(11)-en-12-one* (**8**) (35 mg, 64% yield). Recrystallization from acetonitrile gave colorless plates, mp 78–79°C; its ir (in $CHCl_3$), nmr, and mass spectra were identical with those of (−)-17-norkaur-9(11)-en-12-one (**8**).

Acknowledgements

We are indebted very much to Prof. R. C. Cambie, University of Auckland, for the gift of 13β-kaur-16-ene. We thank Dr. S. Takahashi, Mrs. J. Tanaka, and Miss T. Hirasawa for the cd and mass spectra and elemental analyses.

1. H. J. Kabbe. Ann. **656**, 204 (1962); S. Uemura, T. Nakano, and K. Ichikawa. J. Chem. Soc. Jpn. **88**, 111 (1967).
2. K. B. Wiberg and W. Koch. Tetrahedron Lett. 1779 (1966); A. McKillop, B. P. Swann, and E. C. Taylor. J. Am. Chem. Soc. **93**, 4919 (1971); A. McKillop, J. D. Hunt, and E. C. Taylor. J. Org. Chem. **37**, 3381 (1972); G. Ortar and A. Romeo. J. Chem. Soc. Perkin Trans. I, 111 (1976); E. C. Taylor, C. S. Ching, A. McKillop, and J. F. White. J. Am. Chem. Soc. **98**, 6750 (1976).
3. E. Fujita and M. Ochiai. J. Chem. Soc. Perkin Trans. I, 1182 (1977).
4. R. A. Appleton, P. A. Gunn, and R. McCrindle. J. Chem. Soc. C, 1148 (1970).
5. W. Klyne. Tetrahedron, **13**, 29 (1961).
6. R. D. H. Murray, R. W. Mills, A. J. McAlees, and R. McCrindle. Tetrahedron, **30**, 3399 (1974).

Can. J. Chem. Downloaded from www.nrcresearchpress.com by 210.87.254.40 on 09/05/12
For personal use only.

Studies related to antitumor antibiotics. Part XIII. Reactivity of 2- and 3-indolylcarbinyl compounds as models for mitosane action

J. WILLIAM LOWN AND GORDON L. WEIR[1]

Department of Chemistry, University of Alberta, Edmonton, Alta., Canada T6G 2G2

Received May 16, 1977

J. WILLIAM LOWN and GORDON L. WEIR. Can. J. Chem. **56**, 249 (1978).

The base-catalyzed methanolyses of 1-methylgramine methiodide **2**, 1-methylisogramine methiodide **3**, and 1-methylindol-2-ylmethyl *N-tert*-butylcarbamate **4** were studied in the temperature range 50–90°C in order to gain information about the relative reactivity of 2- and 3-indolylcarbinyl systems, analogous to the proposed reactive sites of the mitosane antitumor antibiotics when enzymatically reduced. The leaving groups were also analogous to those found in the mitosanes. The methanolysis of **2** proceeds with strict first-order kinetics in accord with indole nitrogen lone pair assistance of the displacement. The comparable reactions of **3** and **4** proceed with second-order kinetics in accord with a direct S_N2 process and the carbamate moiety is the better leaving group by a factor of 10. Gramine methiodide **5** undergoes a very rapid elimination of the elements of $(CH_3)_3\overset{+}{N}HI^-$ followed by addition of a nucleophile such as methanol at a rate which is too rapid to follow kinetically even at −78°C. In accord with the model for the mode of action of the mitosanes, 2.2 m*M* **5** alkylates and cross-links DNA to the extent of 71% at p*H* 7 and 37°C. The extent of cross-linking is proportional to the (G + C) content of DNA's as was found for the mitosanes and occurs at a position other than N-7 on guanine. The results suggest that in the reaction of the mitosane antibiotics with DNA the inherent greater reactivity of the 10-carbamate moiety towards nucleophilic displacement is more than offset by the rate enhancement of the 1 position due to relief of aziridine ring strain.

J. WILLIAM LOWN et GORDON L. WEIR. Can. J. Chem. **56**, 249 (1978).

On a étudié la méthanolyse, catalysée par les bases, de l'iodométhylate de méthyl-1 gramine (**2**), de l'iodométhylate de méthyl-1 isogramine (**3**) et du *N-tert*-butylcarbamate de méthyl-1 indolylméthyle-2 (**4**) à des températures allant de 50–90°C; on a réalisé ces études afin d'obtenir des informations concernant les réactivités relatives des systèmes indolylcarbinyles-2 et -3 qui, lorsqu'ils sont réduits d'une façon enzymatique, sont des sites réactifs proposés pour les antibiotiques antitumoraux mitosanes. Les nucléofuges sont aussi analogues à ceux trouvés dans les mitosanes. La méthanolyse de **2** se produit d'après une cinétique de premier ordre strict tel que prévu si l'on fait l'hypothèse que la paire d'électrons libres de l'azote de l'indole fournit une aide lors du déplacement. Les réactions comparables de **3** et **4** se produisent suivant des cinétiques du deuxième ordre tel que l'on peut le supposer pour une réaction S_N2; par opposition au groupe iodométhylate le groupe carbamate est un meilleur nucléofuge par un facteur de 10. L'iodométhylate de gramine **5** subit une élimination très rapide de $(CH_3)_3\overset{+}{N}HI^-$ qui est suivie par une addition de nucléophiles, comme le méthanol, à une vitesse qui est trop rapide pour être mesurée même à −78°C. Tel qu'on peut le supposer en se basant sur le modèle pour le mode d'action des mitosanes, le composé **5**, à des concentrations de 2.2 m*M*, provoque une alkylation et une réticulation avec l'DNA jusqu'à un taux de 71% à un p*H* 7 et une température de 37°C. Comme on l'a montré avec les mitosanes, le taux de réticulation est proportionnel au contenu (G + C) des DNA et cette réticulation ne se produit par à la position N-7 de la guanine. Les résultats suggèrent que, dans la réaction des antibiotiques misotanes avec la DNA, le groupe carbamate en 10 est beaucoup plus réactif vis-à-vis une substitution nucléophile mais cette réactivité inhérente est plus que contrebalancée par une augmentation de vitesse en position 1 qui provient de l'élimination de la contrainte stérique dans le cycle aziridine.

[Traduit par le journal]

Introduction

The mitosane antitumor antibiotics **1**, isolated from *Streptomyces caespitosus* (1) have a unique four-ring structure (2, 3) and contain three carcinostatic groups: quinone, urethane, and aziridine (4). Although quite toxic, the mitosanes exhibit broad spectrum activity against a variety of neoplasms and mitomycin C and porfiromycin are currently used clinically in Japan for the treatment of breast, stomach, lung, and colon cancer (5).

Considerable evidence indicates the nucleic acids of the cell are the principal targets for mitosane action (6). The action is twofold: (*i*) after NADPH mediated reduction the 'activated' mitosanes become bifunctional alkylating agents which can covalently link the complementary strands of DNA and (*ii*) the extensive degradation of DNA which we have shown proceeds by the autoxidation of acti-

[1]NRCC Studentship holder 1970–1973.

Can. J. Chem. Downloaded from www.nrcresearchpress.com by 210.87.254.5 on 09/05/12
For personal use only.

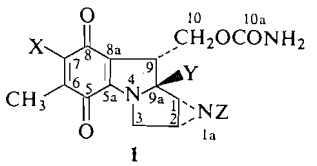

1

	X	Y	Z
Mitomycin A	OCH_3	OCH_3	H
N-Methylmitomycin A	OCH_3	OCH_3	CH_3
Mitomycin C	NH_2	OCH_3	H
Porfiromycin	NH_2	OCH_3	CH_3
7-Hydroxyporfiromycin	OH	OCH_3	CH_3

vated mitosanes to produce superoxide and hydroxyl radicals (7).

A plausible mechanism for the cross-linking process put forward by Iyer and Szybalski (6), suggests aromatization of ring A in the enzymatic reduction generates two potential alkylating sites at the 2 and 3 position of the *indole* moiety which are presumed to react with DNA bases, principally guanine (Scheme 1). Szybalski and Iyer showed that the rate

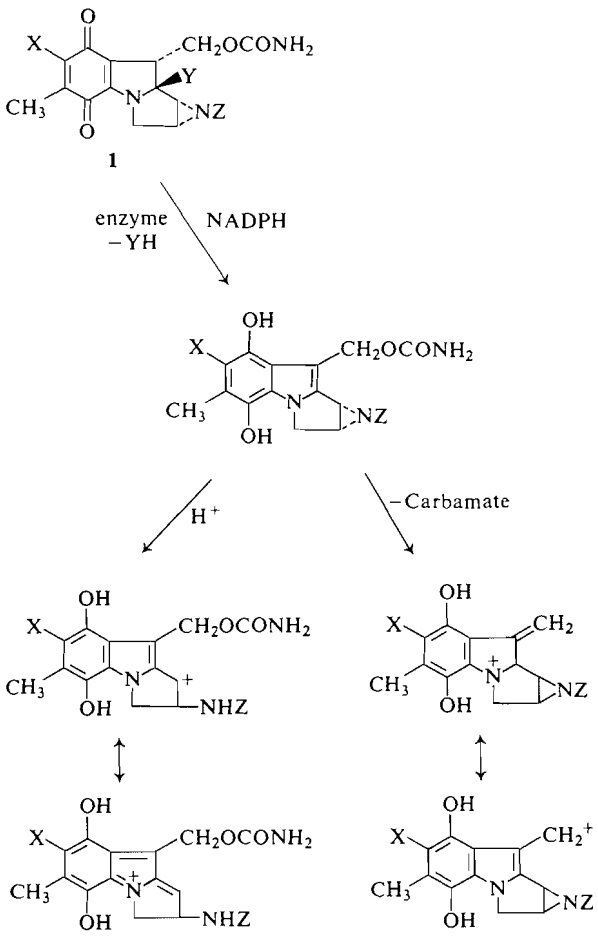

SCHEME 1

of cell death correlated well with the degree of DNA cross-linking (7). While synthetic analogues of the mitosanes bearing the carcinostatic moieties of the parent antibiotics cross-link DNA efficiently in vitro (8) there have been virtually no chemical studies on the relative reactivities of substituted 2- and 3-indolylcarbinyl systems which are structurally analogous to the activated mitosanes.

To this end a number of 2- and 3-indolyl compounds have been synthesized and their relative reactivities in nucleophilic displacements examined as well as the comparative reactivity of the trialkylammonium and carbamate leaving groups.

Synthesis of 2- and 3-Indolylcarbinyl Compounds

To gain an insight into the step-wise nature of the cross-linking process the 2- and 3-indolylcarbinyl reaction sites were studied separately on model compounds **2** and **3** with the same leaving group (comparable with that at position 1 of the activated mitosanes). In addition, one of the reacting sites was studied with different leaving groups (**3** and **4**) analogous to those at positions 1 and 10 of the reduced mitosanes, respectively. It was not possible

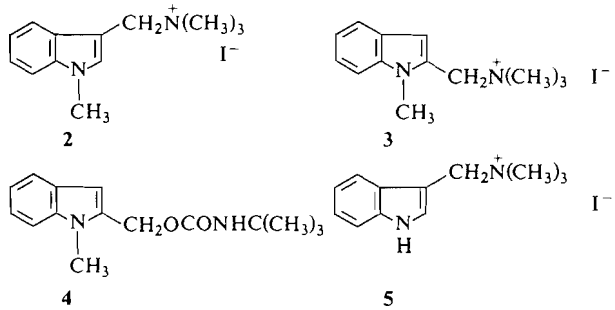

to synthesize compound **6** isomeric with **4** although this failure in itself is consistent with the other findings for this series of compounds. Gramine

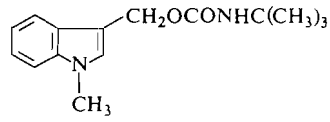

6

methiodide **5** was also investigated in conjunction with the study of its *N*-methyl derivative **2** and proved to have quite different properties with DNA.

Compounds **2** and **3** were prepared by known procedures involving the Fischer indole synthesis, followed by a Mannich reaction and quaternization (9–13). The literature preparation of gramine methiodide **5** was found to give substantial amounts of **7** as evidenced by the nmr spectrum (singlets at 2.85 and 7.30 δ in $CDCl_3$) (14). An improved method was devised involving the addition of a nearly

Can. J. Chem. Downloaded from www.nrcresearchpress.com by 210.87.254.5 on 09/05/12
For personal use only.

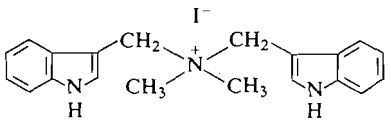

7

saturated ethereal solution of gramine to neat methyl iodide which provided **5** free from contamination by **7**.

Compound **4** was synthesized as outlined in Scheme 2.

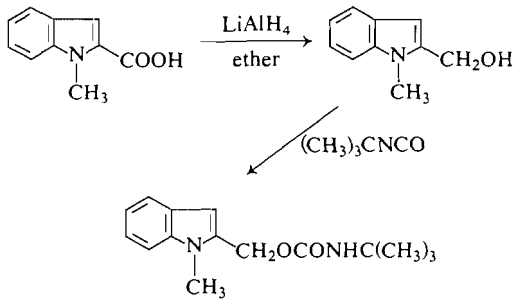

SCHEME 2

Kinetic Study of Nucleophilic Displacements of 2- and 3-Indolylcarbinyl Derivatives

Since the reduced mitosanes cross-link DNA by attack on the two exposed electrophilic centers (corresponding to the 2- and 3-indolylcarbinyl positions) by nucleophiles principally on guanine, we examined the base-catalyzed solvolysis of model compounds, **2–5** (Scheme 3).

By performing the reaction with the gramine derivatives in a sealed nmr tube, using deuterated methanol, it was possible to follow kinetically the disappearance of the singlet in the nmr spectrum due to $-\overset{+}{N}(CH_3)_3$ (3.09 δ from hexamethyldisilane, HMDS for **2** and 3.13 δ for **3**) together with the appearance of the singlet at 2.18 δ from HMDS due to $N(CH_3)_3$.

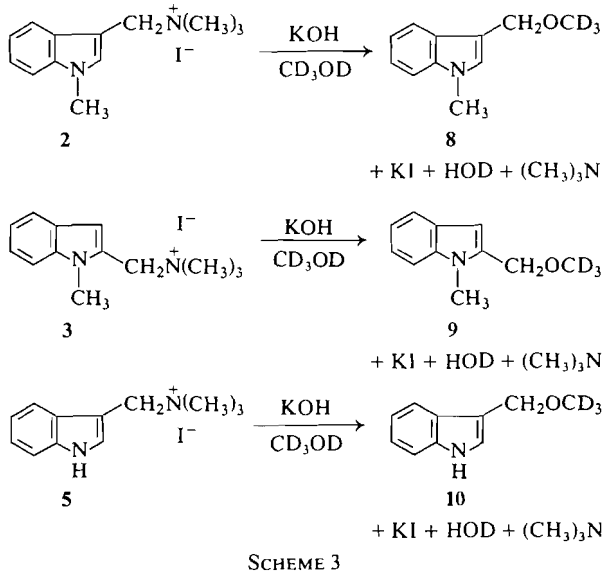

SCHEME 3

The corresponding reaction of the carbamate **4** gave the same indole product **9** (Scheme 4). However the nmr absorption of the *tert*-butyl group in the product had virtually the same chemical shift as that of the *tert*-butyl group in **4** and so this signal could not be followed in a kinetic study. However, the methylene protons absorbed at 5.12 δ from HMDS in the carbamate **4** and at 4.68 δ from HMDS in the ether **9**, thus facilitating the kinetic study.

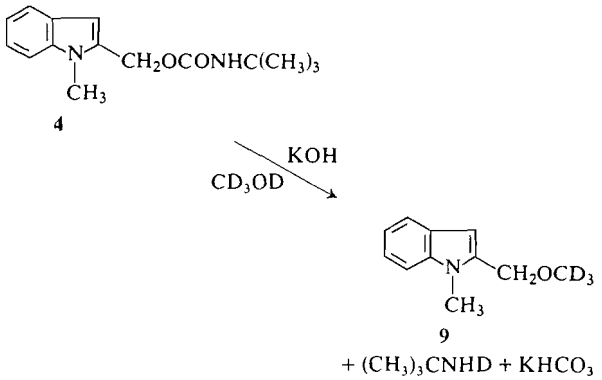

SCHEME 4

Results

The product of the solvolysis reaction of **2** was established by carrying the reaction to completion in methanol with potassium hydroxide. Recovery of the protium analogue of **8** was quantitative. A reaction performed with sodium hydroxide as base and water as solvent gave an orange oil the mass spectrum and nmr spectrum of which are consistent with structure **11**. The formation of **11** is in accord with the known chemistry of hydroxymethylindoles (such as the presumed intermediate) in the presence of base (15). Reaction of **2** with sodium methoxide in *tert*-butyl alcohol gave a low yield of the *tert*-butyl ether **12**. The rate of the reaction of **2** to **8** was studied at five temperatures 50, 60, 70, 80, and 90°C. In all cases a plot of the integrated first-order rate expression against time gave a straight line. Two additional kinetic runs were carried out at 80°C in which the base concentration was in turn approximately doubled and halved. The reaction rates were virtually unchanged (see Table 1) in accord with a unimolecular process.

In the product run of **3**, compound **9** was recovered in 94% yield (based on the unreacted **3**). The rate of

Can. J. Chem. Downloaded from www.nrcresearchpress.com by 210.87.254.5 on 09/05/12
For personal use only.

Can. J. Chem. Downloaded from www.nrcresearchpress.com by 210.87.254.5 on 09/05/12
For personal use only.

TABLE 1. Summary of first-order rate constants for the base-catalyzed solvolysis of 1-methylgramine methiodide **2** in methanol

[KOH]M	[**2**]M	[KOH]:[**2**]	Temperature (°C)	$k_1(s^{-1})$
0.0977	0.0978	0.990	50.0	$(6.04\pm0.09)\times10^{-6}$
0.1411	0.1016	1.389	60.0	$(2.14\pm0.01)\times10^{-5}$
0.1105	0.1153	0.958	70.0	$(5.24\pm0.01)\times10^{-5}$
0.1075	0.1078	0.997	80.0	$(1.67\pm0.04)\times10^{-4}$
0.1184	0.1083	1.093	90.0	$(4.20\pm0.06)\times10^{-4}$
0.2228	0.1069	2.084	80.0	$(2.03\pm0.02)\times10^{-4}$
0.0452	0.1060	0.426	80.0	$(1.78\pm0.10)\times10^{-4}$

NOTE: activation parameters: E_a, 24.6 ± 0.6 kcal/mol; $\Delta H^{\ddagger}$, 23.8 ± 0.6 kcal/mol; $\Delta S^{\ddagger}$, −8.5 ± 1.8 eu.

TABLE 2. Summary of second-order rate constants for the base-catalyzed solvolysis of 1-methylisogramine methiodide **3** and 1-methylindol-2-ylmethyl *N-tert*-butylcarbamate **4** in methanol

Compound	[KOH]M	[Reactant]M	[KOH]:[Reactant]	Temperature (°C)	$k_2(\ell\ mol^{-1}\ s^{-1})^a$
3	0.0695	0.0477	1.457	70.0	$(6.02\pm0.07)\times10^{-6}$
3	0.0846	0.0474	1.785	80.0	$(2.52\pm0.03)\times10^{-5}$
3	0.0362	0.0460	0.787	90.0	$(1.58\pm0.02)\times10^{-4}$
3	0.0877	0.0477	1.838	90.0	$(1.07\pm0.02)\times10^{-4}$
3	0.2317	0.438	5.29	90.0	$(6.08\pm0.03)\times10^{-5}$
4	0.1341	0.0768	1.746	50.0	$(3.83\pm0.06)\times10^{-6}$
4	0.1267	0.0769	1.648	70.0	$(7.80\pm0.18)\times10^{-5}$
4	0.1051	0.0660	1.592	80.0	$(2.59\pm0.08)\times10^{-4}$

NOTE: activation parameters: **3**: E_a, 35.6 ± 0.7 kcal/mol; $\Delta H^{\ddagger}$, 34.9 ± 0.7 kcal/mol; $\Delta S^{\ddagger}$, +18.9 ± 2.0 eu; **4**: E_a, 32.0 ± 1.1 kcal/mol; $\Delta H^{\ddagger}$, 31.1 ± 0.1 kcal/mol; $\Delta S^{\ddagger}$, +13.0 ± 2.8 eu.

[a]Individual runs showed strict linear adherence to least-square analysis of second-order kinetics. The results of adding rather high concentrations of KOH appear to be due to medium effects on the rate of reaction.

this reaction was determined at 70, 80, and 90°C and was found to follow second-order kinetics over 80% of the reaction as demonstrated by straight line computer least-squares analysis with 12 points for an individual run. An additional run at 90°C with 0.428 of the original amount of base proceeded at a rate consistent with this reaction order (Table 2).

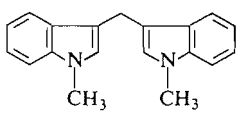

11

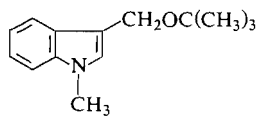

12

The product run of **4** afforded the ether **9** also obtained from **3**. This confirms that nucleophilic attack occurs at the 2-indolylcarbinyl position and not at the carbamate carbonyl which would be expected to yield the 2-indolylcarbinol. A kinetic study of this reaction at the temperatures 50, 70, and 80°C revealed as in the solvolysis of **3** strict second-order kinetics (Table 2). Using the rate constants to plot ln (k_1) vs. ($1/T$) and ln (k_1/T) vs. ($1/T$) the activation parameters E_a, $\Delta H^{\ddagger}$, and $\Delta S^{\ddagger}$ were calculated (16).

Preparative scale base catalyzed methanolysis of **5** gave the deuterium analog of the known methyl ether **10** quantitatively. Since the reaction of gramine methiodide **5** with even very low concentrations of base and in methanol was found to be extremely rapid even at −78°C, it was not possible to follow this reaction kinetically.

Reaction of 3-Indolylcarbinyl Derivatives with Natural DNA's

If the interpretation of the mode of antitumor action of the mitosanes proposed by Iyer and Szybalski (6) is correct one would anticipate that a suitably substituted indolylcarbinyl derivative would alkylate and/or produce interstrand links in DNA. Treatment of PM2-ccc-DNA[2] (85% ccc) with **5** at a concentration of 7.0 mM resulted in a progressive fall in the ethidium fluorescence before heat denaturation characteristic of removal of potential ethidium intercalation sites as a result of alkylation of the bases (7). The corresponding fluorescence readings taken after heat denaturation and cooling showed an initial rapid fall interpreted as thermally induced removal of alkylated bases followed by rapid alkaline hydrolysis of the exposed ribosephosphate backbone in the pH 11.8 assay medium (17). Subsequently the fluorescence readings rose suggestive of interstrand cross-links which provide nucleation sites for renaturation of the PM2-oc-DNA (7, 8).

The cross-linking of DNA by **5** was confirmed by reaction with linear λ-DNA at 37°C. At pH 7 and 37°C, 2.2 mM **5** produced 71% cross-linking of

[2]Abbreviations: clc, covalently linked complementary; ccc, covalently closed circular; oc, open circular.

Can. J. Chem. Downloaded from www.nrcresearchpress.com by 210.87.254.5 on 09/05/12
For personal use only.

λ-DNA after 300 min, and at p*H* 8.7 and 37°C 2.9 m*M* **5** produced 79% cross-linking after 170 min.

The dependence of the extent of cross-linking by **5** on the (G + C) content was determined by using the following DNA's: *Clostridium perfringens* (30% G + C), calf thymus (40%), and *Escherichia coli* (50%). Allowance was made for differences in their average molecular weights which were determined by sedimentation velocity. Assuming a Poisson's distribution of the links and further, that one link is sufficient to permit spontaneous renaturation of the molecule (18) the average number of cross links per nucleotide m ($m = \ln(1/P_0)$ where P_0 is the proportion of unlinked molecules) was estimated to be ($\times 10^5$) 1.77, 3.46, and 20.6 for the three DNA's at a concentration of **5** of 3.4×10^{-3} *M* (see fig. 1). When the clc assay was performed at p*H* 7.0 as well as at the normal assay conditions of p*H* 11.8 it was found that the fluorescence readings taken before heat denaturation values were constant for 1 h at both p*H* values. None of the compounds **2**, **3**, or **4** cross-links DNA.

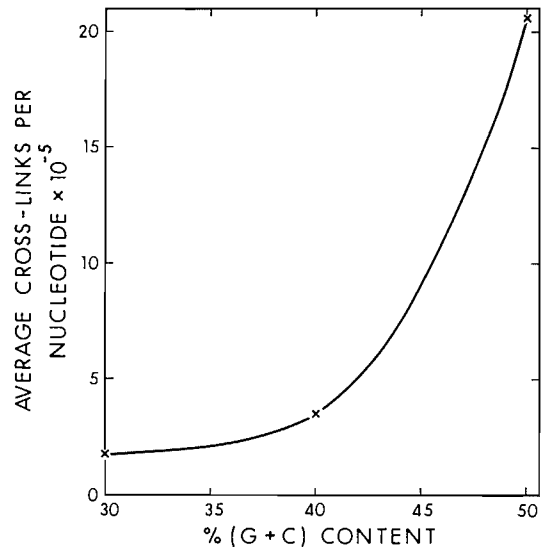

FIG. 1. Dependence of efficiency of covalent cross-linking of DNA's by gramine methiodide **5** on the (G + C) content of the DNA. Reactions were performed at 37°C and contained DNA at 1.25 A_{260}, 0.05 *M* phosphate buffer p*H* 8.7, and gramine methiodide **5** at 3.4×10^{-3} *M*.

Discussion

The kinetics of the solvolysis of 1-methylgramine methiodide **2** are consistent with a rate-determining unimolecular elimination of trimethylamine followed by a faster attack by the nucleophile (Scheme 5). This elimination can be assisted and the resulting intermediate stabilized by the lone pair of the indole nitrogen.

The role of the base in this reaction appears to be more than just that of a proton sponge. One possible explanation is that the active nucleophile is the methoxide ion formed in a prior equilibrium with the low available concentration of hydroxide ion. The pK_a values of water and methanol in aqueous solution at 25°C are, respectively, 15.74 and 15.5 (19), which would give a substantial proportion of available methoxide ion by equilibration.

The negative entropy value is unusual for unimolecular reactions which involve a molecular fragmentation with a concomitant increase in disorder. However this may be due in the present case to the restricted rotation at the indole 3 position as the hybridization of the reaction center changes from sp^3 (in **2**) to sp^2 (in **2**A).

The nucleophilic displacement of the same leaving group for 1-methylisogramine **3** is not only slower but also exhibits second-order behavior. This result suggests that the type of electron pair assistance analogous to that for the 1-methylgramine **2** does not

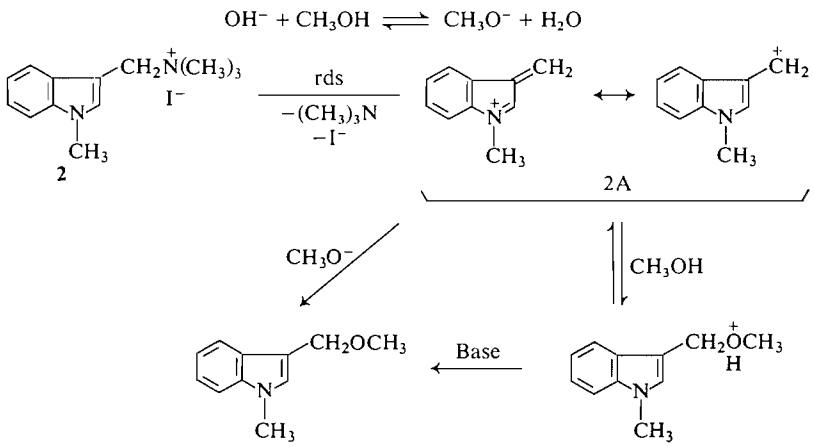

SCHEME 5

Can. J. Chem. Downloaded from www.nrcresearchpress.com by 210.87.254.5 on 09/05/12
For personal use only.

make a significant contribution to the reaction process despite suggestions to the contrary by Iyer and Szybalski (6) and by Sartorelli and co-workers (20).

Since the carbenium ion process is not favored in this way, compound **3** behaves as a normal primary system and undergoes an S_N2 type of displacement. The positive value observed for $\Delta S^{\ddagger}$ may be rationalized in terms of the partial neutralization of unlike charges taking place in the transition state. This in turn would bring about less ordering of the solvent shell surrounding the substrate ions.

The studies with the corresponding carbamate **4** show that this compound reacts more rapidly than the trimethylammonium salt **3** (about 10-fold at 80°C) and suggest that the carbamate moiety is a better leaving group for this series of reactions.

This greater reactivity of the carbamate compounds would also explain why it is not possible to synthesize the isomeric carbamate **6**, in which the more reactive leaving group is located on the more reactive 3 position of the indole.

All attempts to prepare such a carbamate, even under the mildest conditions, resulted in mixtures which showed extensive decomposition.

Gramine methiodide **5** undergoes a very rapid elimination of the elements of $(CH_3)_3\overset{+}{N}H\ I^-$ followed by an addition of a nucleophile such as solvent methanol (Scheme 6). The process is too fast to

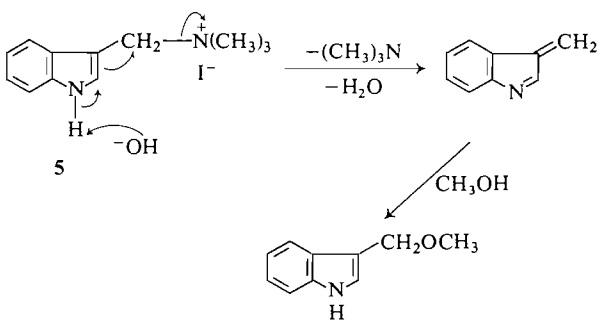

SCHEME 6

follow kinetically even at very low base concentrations due to the acceleration of the S_N1 displacement provided by the indole anion. Nevertheless such a mechanism could account for the method by which this compound alkylates DNA and why the alkylation and cross-linking of the latter by **5** is promoted by higher p*H* values. The rates of nucleophilic displacement of **2–4** are evidently too slow to allow alkylation of DNA.

Despite the fact that **5** contains only one obvious alkylating center it cross-links DNA quite efficiently and the cross-linking shows a similar dependence on (G + C) content as for the comparable reaction with mitomycin C (16, 17). The dependence of the extent of cross-linking on $(G + C)^2$ content suggests the necessity of locating two adjacent G residues on the complementary DNA strands to complete the cross-link. The constancy of the fluorescence readings at p*H* 11.8 suggests alkylation of DNA by **5** takes place at a position other than N-7 on guanine (21). Interstrand cross-linking of DNA by monofunctional alkylating agents (e.g. methyl methanesulfonate) has been observed but only after heating at 50°C at p*H* 8 for 4 h (22). In that case since the extent of cross-linking is proportional to depurination, the mechanism appears to involve exposure of an aldehyde function at C-1 of the deoxyribose at the depurination site which subsequently reacts with a chemical group in the opposite DNA strand creating a cross-link.

However, since neither mitomycin C nor synthetic analogues which cross-link DNA cause any depurination (7, 8) it follows that a second reactive site in **5** is responsible for completion of the cross-link. The N-1 position of the indole is implicated because of the lack of reactivity towards DNA of the 1-methyl derivative. Murakami has postulated involvement of the N-4 position (tertiary in this case) of the activated mitomycins acting as polyfunctional agents in bonding to DNA bases (23).

The ability of **5** to cross-link DNA provides evidence for the participation in the cross-linking process of the site corresponding to the methylurethane group in the mitosanes. The present studies support the conclusion that the C-10 carbenium ion in the activated mitosanes, once formed, is more stable than the C-1 cationic center. Yet evidence has accumulated to show that the 1 position is in fact the first to react (6, 7). This suggests that a rate enhancement for the 1 position due to relief of the aziridine ring strain is more than sufficient to offset the inherent comparative stabilities of these two cationic centres.

Experimental

Melting points were determined on a Fisher-Johns apparatus and are uncorrected. Infrared spectra were recorded on a Perkin-Elmer grating infrared spectrophotometer Model 421 and generally only the principal peaks are reported. Absorption spectra were measured in either distilled water or spectrograde solvents and were run on either a Beckman DB spectrophotometer, a Gilford 250 spectrophotometer, or a Unicam SP1700 uv spectrophotometer. Proton magnetic resonance spectra were recorded on Varian A-60 and HA-100 analytical instruments and were generally measured on 10–15% (w/v) solutions of the compound in the appropriate deuterated solvent. The reference compound was tetramethylsilane (TMS), except for the nmr kinetic runs, where hexamethyldisilane (HMDS) was used as the reference because of its lower volatility. Line positions are reported in ppm from the reference. Mass spectra were determined with Associated

Can. J. Chem. Downloaded from www.nrcresearchpress.com by 210.87.254.5 on 09/05/12
For personal use only.

Electrical Industries MS2, MS9, MS12, or MS50 (DS50) mass spectrometers. In general the ionization energy was 70 eV.

Materials

Ethidium bromide, and calf thymus DNA were purchased from Sigma Chemical Co. The λ and PM2-ccc-DNA's were prepared as before (25). *Escherichia coli* and *C. perfringens* DNA's were obtained from Dr. A. R. Morgan.

Anhydrous methanol for the product runs was prepared from commercially available methanol by treatment with magnesium methoxide and distilled as described by Fieser (ref. 25, p. 289).

2,6-Lutidine was prepared as follows: Eastman practical grade 2,6-lutidine was dried over potassium hydroxide for 24 h then refluxed and distilled from barium oxide as described by Fieser for the preparation of anhydrous pyridine (ref. 25, p. 291). The center cut (138–140°C) was treated with boron trifluoride etherate as described by Brown *et al.* (26).

1-Methylgramine

This compound was prepared from 1-methylindole (9) as an amber oil in 63% yield by a method similar to that reported by Snyder and Eliel (10); nmr ($CDCl_3$) δ_{TMS}: 2.27 (s, 6H, $N(CH_3)_2$, 3.61 (s, 2H, CH_2), 3.69 (s, 3H, indole NCH_3), 6.97 (s, 1H, indole 2-H), 7.05–7.91 (m, 4H, aryl protons).

1-Methylgramine Methiodide **2**

This compound was prepared according to Snyder and Eliel (10) by the alkylation of 1-methylgramine with methyl iodide. The crude material was formed in 98% yield as a pink solid which was recrystallized from methanol–ether to give small white leaflets, mp 177–178°C (dec.) (lit. (10) inst. decomposition point 195°C); (DMSO-*d*) δ_{TMS}: 3.12 (s, 9H, $^+N(CH_3)_3$), 3.88 (s, 3H, indole NCH_3), 4.79 (s, 2H, CH_2), 7.74 (s, 1H, indole 2-H), 7.09–8.09 (m, 4H, aryl protons). *Anal.* calcd. for $C_{13}H_{19}N_2I$: C 47.29, H 5.80, N 8.48, I 38.43; found: C 47.31, H 5.88, N 8.37, I 38.29.

*Indole-1-methyl-2-(*N,N-*dimethyl)carboxamide*

Patterned after the method of Schindler (11) 9.2 g of 1-methylindole-2-carboxylic acid was suspended in 135 ml of benzene (freshly distilled from sodium) under a nitrogen atmosphere. Thionyl chloride (13.5 ml) distilled from quinoline was added dropwise with magnetic stirring over a period of 45 min. The mixture was then heated to 45–50°C for 1 h, during which time the acid dissolved and the solution became dark green. The solvent and excess thionyl chloride were then removed on a high-vacuum distillation apparatus, 70 ml of dry benzene was added to the residue, and this solution was added dropwise to 150 ml of benzene which had been saturated with dimethylamine gas. After the addition was completed, more dimethylamine gas was bubbled into the brown solution to ensure an excess of the amine.

After standing overnight in a refrigerator, the mixture was treated with water to dissolve the dimethylamine hydrochloride. The organic layer was removed and dried (Na_2SO_4). Removal of the solvent gave a quantitative yield of a brown oil which solidified on standing to a material with mp 83–84°C (lit. (12) mp 95°C); ir ν_{max}(film): 1620 (C=O), 1455 (C—N) cm^{-1}.

1-Methylisogramine

Following the general method of Schindler (11) 6 g of lithium aluminum hydride was mixed with 110 ml of tetrahydrofuran and cooled to below 10°C. Over a period of 2 h at ambient temperature a solution of 11.0 g of indole-1-methyl-2-(*N,N*-dimethyl)carboxamide in 90 ml of tetrahydrofuran was added dropwise with stirring. The mixture was then stirred overnight, cooled in ice water, and carefully treated with water to decompose the unreacted lithium aluminum hydride. The mixture was filtered and the solvent removed from the filtrate to give a residue which was treated with 25 ml of 2 *M* sodium hydroxide solution and extracted with ether. The ether extract was dried (Na_2SO_4) and evaporated to give 9.1 g (89% yield) of product as a brown liquid; nmr ($CDCl_3$) δ_{TMS}: 2.21 (s, 6H, $N(CH_3)_2$), 3.48 (s, 2H, CH_2), 3.72 (s, 3H, indole NCH_3), 6.36 (s, 1H, indole 3-H), 6.93–7.70 (m, 4H, aryl protons).

1-Methylisogramine Methiodide **3**

Following the procedure of Schindler (11) 9.0 g of 1-methylisogramine was alkylated with methyl iodide to give 14.0 g (89% yield) of a brownish solid. A portion of this was recrystallized from methanol–ether to give a cream-colored solid, mp 207°C (lit. (11) mp 217–219°C); nmr (DMSO-d_6) δ_{TMS}: 3.16 (s, 9H, $^+N(CH_3)_3$), 3.88 (s, 3H, indole NCH_3), 4.92 (s, 2H, CH_2), 6.90 (s, 1H, indole 3-H), 7.00–7.87 (m, 4H, aryl protons). *Anal.* calcd. for $C_{13}H_{19}N_2I$: C 47.29, H 5.80, N 8.48, I 38.43; found: C 47.04, H 5.82, N 8.51, I 38.80.

2-Hydroxymethyl-1-methylindole

A solution of 5 g of 1-methylindole-2-carboxylic acid in 100 ml of tetrahydrofuran was treated cautiously with 3.5 g of lithium aluminum hydride, then refluxed for 1 h. The mixture was then cooled and treated with ethyl acetate and then water to decompose the excess of lithium aluminum hydride. The resulting mixture was filtered and the filtrate dried (Na_2SO_4). Upon evaporation of the solvent this solution yielded 4.0 g (87% yield) of a light yellow solid, mp 92–93°C (lit. (13) mp 108–110°C). The nmr spectrum indicated a purity sufficient for subsequent steps; nmr ($CDCl_3$) δ_{TMS}: 1.95 (br, 1H, OH), 3.67 (s, 3H, CH_3), 4.67 (s, 2H, CH_2), 6.37 (s, 1H, indole 3-H), 6.96–7.68 (m, 4H, aryl protons).

1-Methylindol-2-ylmethyl N-tert-*Butylcarbamate* **4**

A mixture of 1.50 g of 2-hydroxymethyl-1-methylindole and 2.3 ml of *tert*-butyl isocyanate was warmed on a steam bath until all the solid material had dissolved. The solution was then cooled overnight in a refrigerator, the resulting precipitate collected, washed with petroleum ether (bp 60–100°C), and evaporated to give 1.51 g of a dark brown material. Extraction of this substance with ether left a brown earthy residue and gave a solution from which 0.78 g (32% yield) of a cream-colored material precipitated upon concentration. This substance was recrystallized from either acetone–water or ether–*n*-pentane to give crystals, mp 103°C; ir ($CHCl_3$) ν_{max}: 3440, 2970, 1720 (carbamate C=O), 1495, 1460, 1390, 1360, 1335, 1315, 1255, 1135, 1065 cm^{-1}; nmr ($CDCl_3$) δ_{TMS}: 1.33 (s, 9H, $C(CH_3)_3$), 3.74 (s, 3H, NCH_3), 4.47–4.95 (br, 1H, NH), 5.23 (s, 2H, CH_2), 6.57 (s, 1H, indole 3-H), 6.93–7.70 (m, 4H, aryl protons). *Anal.* calcd. for $C_{15}H_{20}N_2O_2$: C 69.20, H 7.74, N 10.76; found: C 59.32, H 7.89, N 10.88. *Mol. Wt.* calcd. for $C_{15}H_{20}N_2O_2$: 260.1524; found (mass spectrum): 260.1519.

Gramine Methiodide **5**

The method of Geissman and Armen (14) was found to give a sticky material containing impurities of dimethyldi-(3-indolylmethyl)ammonium iodide **7**, as evidenced by the nmr spectrum (singlets at 2.85 and 7.30 δ_{TMS} in $CDCl_3$).

An improved method involved first dissolving 2.75 g of gramine in 300 ml of ether and adding this nearly saturated solution dropwise with stirring to 100 g of methyl iodide. As the addition proceeded a white-to-pale-yellow solid precipitated from the reaction mixture in quantitative yield. The product was recrystallized from methanol–ether as white crystals, mp 168–170°C (lit. (14) mp 168–169°C); nmr (DMSO-d_6) δ_{TMS}: 3.12 (s, 9H, $^+N(CH_3)_3$), 4.80 (s, 2H, CH_2), 7.76 (d, J =

Can. J. Chem. Downloaded from www.nrcresearchpress.com by 210.87.254.5 on 09/05/12
For personal use only.

2.5 Hz, 1H, indole 2-H), 7.05–8.03 (m, 4H, aryl protons), 11.57 (br, 1H, NH). *Anal.* calcd. for $C_{12}H_{17}N_2I$: C 45.58, H 5.42, N 8.86, I 40.14; found: C 45.63, H 5.67, N 8.65, I 40.14.

Treatment of 1-Methylgramine Methiodide **2** *with Sodium Hydroxide in Methanol*

A solution of 1.495 g (4.53 mmol) of 1-methylgramine methiodide **2** and 0.181 g (4.53 mmol) of sodium hydroxide in 100 ml of anhydrous methanol was placed in a stoppered volumetric flask and suspended for 209 h in an oil bath thermostated at 70.0°C. The solvent was then removed *in vacuo* and the organic portion of the residue extracted with ether. Recovery was 0.790 g (4.51 mmol, 99.6%) of 3-methoxymethyl-1-methylindole (protium analogue of **8**) as a brown oil which became hard and vitreous on prolonged standing; ir ($CHCl_3$) ν_{max}: 2900, 1635, 1590, 1450, 1350, 1305, 1130, 990 cm^{-1}; nmr ($CDCl_3$) δ_{TMS}: 3.36 (s, 3H, OCH_3), 3.67 (s, 3H, NCH_3), 4.63 (s, 2H, CH_2), 6.99 (s, 1H, indole 2-H), 7.07–7.82 (m, 4H, aryl protons). *Mol. Wt.* calcd. for $C_{11}H_{13}NO$: 175.0997; found (mass spectrum): 175.0993.

Treatment of 1-Methylgramine Methiodide **2** *with Sodium Hydroxide in Water*

A solution of 0.159 g (0.483 mmol) of 1-methylgramine methiodide **2** and 0.021 g (0.531 mmol) of sodium hydroxide in 10 ml of distilled water was stoppered in a 25-ml pear-shaped flask and suspended for 48 h in an oil bath at 70.0°C. The ether extract of the residue after evaporation gave 60 mg of an orange oil. The mass spectrum (m = 274) and the aryl:CH_2 and aryl:CH_3 ratios of the nmr integrations indicated that this product was di-(1-methylindoyl)methane **11**.

Treatment of 1-Methylgramine Methiodide **2** *with 2,6-Lutidine in Methanol*

A solution of 0.115 g (0.347 mmol) of 1-methylgramine methiodide **2** and 0.044 g (0.409 mmol) of 2,6-lutidine in 5 ml of anhydrous methanol was sealed in a test tube and placed into a 70.0°C oil bath for 259 h. The work-up as described above gave only 1 mg of the ether (protium analogue of **8**) (mass spectrum, m = 175) plus 50 mg of solid materials which could not be identified.

Treatment of 1-Methylgramine Methiodide **2** *with Sodium Methoxide in* tert-*Butyl Alcohol*

1-Methylgramine methiodide **2** (0.136 g (0.412 mmol)) and 0.024 g (0.437 mmol) of sodium methoxide were suspended in 10 ml of *tert*-butyl alcohol and placed in a 70.0°C oil bath for 187 h. From the work-up was isolated 20 mg of a yellowish oil which from the nmr spectrum and mass spectrum (m = 217) was identified as 3-*tert*-butoxymethyl-1-methylindole **12**; nmr ($CDCl_3$) δ_{TMS}: 1.35 (s, 9H, $C(CH_3)_3$), (s, 3H, NCH_3), 3.72 (s, 3H, NCH_3), 4.65 (s, 2H, CH_2), 6.97–7.36 (br m, 5H, aryl plus indole 2-H protons).

Treatment of 1-Methylisogramine Methiodide **3** *with Sodium Hydroxide in Methanol*

A solution of 1.257 g (3.81 mmol) of 1-methylisogramine methiodide **3** and 0.152 g (3.81 mmol) of sodium hydroxide in 100 ml of anhydrous methanol was placed in a 70.0°C oil bath for 425 h. The solution was then evaporated to dryness and extracted with ether to give 0.19 g (31% yield) of 2-methoxymethyl-1-methylindole as a yellow solid, mp 44–47°C; 69% of unreacted **3** was also obtained from the ether-insoluble residue; ir ($CHCl_3$) ν_{max}: 2930, 1660, 1605, 1460, 1395, 1335, 1310, 1135, 1075, 905 cm^{-1}; ($CDCl_3$) δ_{TMS}: 3.31 (s, 3H, OCH_3), 3.73 (s, 3H, NCH_3), 4.57 (s, 2H, CH_2), 6.46 (s, 1H, indole 3-H), 6.87–7.73 (m, 4H, aryl protons). *Mol. Wt.* calcd. for $C_{11}H_{13}NO$: 175.0997; found (mass spectrum): 175.0994.

Treatment of 1-Methylindol-2-ylmethyl N-tert-*Butylcarbamate* **4** *with Potassium Hydroxide in Methanol-*d_4

1-Methylindol-2-ylmethyl *N-tert*-butylcarbamate **4** (20.00 mg, 0.0768 mmol) and 8.18 mg of 86.5% potassium hydroxide (0.126 mmol) were sealed in an nmr tube with 1.0 ml of methanol-d_4 containing 1 drop of HMDS. The nmr spectrum was recorded and the tube was then placed in a 90.0°C oil bath for 164 h. After this the nmr spectrum was again recorded and found to be that of *tert*-butylamine plus 2-(trideuteromethoxy)-methyl-1-methylindole **9**; nmr (CD_3OD) δ_{HMDS} before heating: 1.25 (s, 9H, $C(CH_3)_3$), 3.66 (s, 3H, NCH_3), 4.90 (s, exchangeable protons), 5.12 (s, 2H, CH_2), 6.41 (s, 1H, indole 3-H), 6.82–7.52 (m, 4H, aryl protons); after heating: 1.24 (s, 9H, $C(CH_3)_3$, 3.72 (s, 3H, NCH_3), 4.90 (s, exchangeable protons), 4.68 (s, 2H, CH_2), 6.32 (s, 1H, indole 3-H), 6.82–7.50 (m, 4H, aryl protons).

Treatment of Gramine Methiodide **5** *with Sodium Hydroxide in Methanol*

A solution of 1.405 g (4.44 mmol) of gramine methiodide **5** and 0.178 g (4.45 mmol) of sodium hydroxide in 100 ml of anhydrous methanol was placed in a pressure bottle in an oil bath at 70.0°C for 99 h. The solvent was then removed and the residue extracted with ether to give 0.700 g (4.34 mmol, 98% yield) of 3-methoxymethylindole (protium analogue of **10**) as a solid, mp 94–95°C after recrystallization from benzene–*n*-pentane (lit. (27) mp 99–100°C). Thin-layer chromatography on silica gel with either benzene of benzene–*n*-pentane 10:90 as the developing solvent showed a single component. The mass spectrum showed a parent ion at m/e = 161; ir ($CHCl_3$) ν_{max}: 3475, 3000, 2930, 1455, 1415, 1335, 1085 cm^{-1}; nmr ($CDCl_3$) δ_{TMS}: 3.40 (s, 3H, OCH_3), 4.67 (s, 2H, CH_2), 6.99 (d, J = 2.5 Hz, 1H, indole 2-H), 7.08–7.89 (m, 4H, aryl protons), 8.21 (br, 1H, NH).

Kinetic Studies

For each kinetic run, the salt or carbamate ester was weighed into a clean nmr tube. The calculated amount of 86.5% potassium hydroxide was dissolved in about 0.5 ml of CD_3OD in a 1-ml volumetric flask. The flask was then filled to the mark with CD_3OD and 2 drops of HMDS as an internal standard. The contents of the volumetric flask were transferred to the nmr tube which was then sealed.

The slower reactions were conducted in a constant temperature bath with the tube being quenched in ice water prior to the spectrum recordings; for the faster reactions, the reaction was conducted directly in the heated probe of the nmr instrument. The technique consisted of monitoring the integrals of the *N*-trimethyl signals for the salts, and the methylene signal for the carbamate ester. The percentage reaction at timed intervals was established by calculating the ratio of the *N*-trimethyl (or methylene) integral due to the reaction product, to the total *N*-trimethyl (or methylene) integral.

Except for the faster runs, integrations of the spectra were usually run in duplicate or triplicate, and the results averaged to reduce random fluctuations.

Interstrand Cross-linking of λ-DNA by Gramine Methiodide **5** *Fluorescence Assay for Detecting Covalently Linked Complementary Sequences in DNA and Synthetic Polynucleotides and the p*H *Dependence*

All measurements were performed on a G. K. Turner and Associates model 430 spectrofluorometer equipped with a cooling fan to minimize fluctuations in the xenon lamp source. Wavelength calibration was performed as described in the manual for the instrument. One-centimetre square cuvettes

Can. J. Chem. Downloaded from www.nrcresearchpress.com by 210.87.254.5 on 09/05/12
For personal use only.

were used. The excitation wavelength was 525 nm and the emission wavelength 600 nm. The 100×-scale of medium sensitivity was generally used and water was circulated between the cell compartment and a thermally regulated bath at 22°C. The alkylation experiments with gramine methiodide **5** were conducted on a 200 μl scale at 37°C. The reaction mixture contained PM2-ccc-DNA (86% ccc) at 1.0 A_{260}, 0.05 *M* potassium phosphate buffer p*H* 7.0, and **5** at 7.0 m*M*. A control was run containing no compound **5**. Samples of 20 μl were withdrawn at intervals over a period of 130 min.

The cross-linking of DNA by **5** was performed with λ-DNA at 1.2 A_{260}, 0.05 *M* potassium phosphate p*H* 7.0 or 8.7, and **5** at 2.2×10^{-4} *M*. For both p*H* values a control experiment was run with no **5**. In each case samples (15 μl) were withdrawn at intervals and analyzed for the extent of cross-linking by addition to 2 ml of the standard p*H* 11.8 assay solution. This contained 20 m*M* potassium phosphate p*H* 11.8, 0.4 m*M* EDTA, and 0.5 μg/ml ethidium bromide. The fluorescence was measured using a blank without added sample. For the heat denaturation, the solutions were heated for 3 min at 96°C on a tempblok and cooled to 23°C. Under these conditions only clc DNA shows return of fluorescence since the covalent links provide a nucleation site for renaturation (7, 28). The ratio of the fluorescence intensity after the heat denaturation to the fluorescence before the heat denaturation gave the extent of covalent cross-linking of the DNA.

Procedure for Determining Covalent Cross-linking of DNA's of Different (G + C) Content by Gramine Methiodide **5**

The DNA's used in this study were *C. perfringens* (mol. wt. 11.4×10^6, (G + C) content 30%), calf thymus (mol. wt. 9.1×10^6, (G + C) content 40%), and *E. coli* (mol. wt. 7.7×10^5, (G + C) content 50%). The molecular weights were determined by sedimentation velocity studies. Reactions were performed at 37°C and contained DNA at 1.25 A_{260}, 0.05 *M* potassium phosphate buffer p*H* 8.7, and **5** at 3.4 m*M*. Aliquots were removed at intervals and analyzed for the extent of covalent cross-linking by the ethidium assay as described above.

Acknowledgements

This research was supported by grants to J.W.L. from the National Cancer Institute of Canada, the National Research Council of Canada, and by the Department of Chemistry, University of Alberta.

1. T. Hata, Y. Sano, R. Sugawara, A. Matsumae, K. Kanamori, T. Shima, and T. Hoshi. J. Antibiot. Ser. A, **9**, 141 (1956).
2. J. S. Webb, D. B. Cosulich, J. H. Mowat, J. B. Patrick, R. W. Broschard, W. E. Meyer, R. P. Williams, C. F. Wolf, W. Fulmor, C. Pidacks, and J. E. Lancaster. J. Am. Chem. Soc. **84**, 3185 (1962); **84**, 3187 (1962).
3. A. Tulinsky. J. Am. Chem. Soc. **84**, 3188 (1962).
4. E. J. Kirsch. *In* Mitomycins. *In* Antibiotics II. *Edited by* D. Gottlieb and P. D. Shaw. Springer-Verlag Publishers, New York, NY. 1967. p. 66.
5. G. E. Moore, I. D. J. Bross, R. Ausman, S. Nadler, R. Jones, N. Slack, and A. A. Rimm. Cancer Chemother. Rep. **52**, 675 (1968).
6. W. Szybalski and V. N. Iyer. *In* The mitomycins and porfiromycins. *In* Antibiotics I. *Edited by* D. Gottlieb and P. D. Shaw. Springer-Verlag Publishers, New York, NY. 1967. p. 211.
7. J. W. Lown, A. Begleiter, D. Johnson, and A. R. Morgan. Can. J. Biochem. **54**, 110 (1976).
8. M. H. Akhtar, A. Begleiter, D. Johnson, J. W. Lown, L. McLaughlin, and S. K. Sim. Can. J. Chem. **53**, 2891 (1975).
9. E. Fischer and O. Hess. Chem. Ber. **17**, 559 (1884).
10. H. R. Snyder and E. L. Eliel. J. Am. Chem. Soc. **70**, 1703 (1948).
11. W. Schindler. Helv. Chim. Acta, **40**, 2156 (1957).
12. J. A. Eenkhoorn, S. O. de Silva, and V. Snieckus. Can. J. Chem. **51**, 792 (1973).
13. K. Eiter and O. Svierak. Monatsh. Chem. **83**, 1453 (1952).
14. T. A. Geissman and A. Armen. J. Am. Chem. Soc. **74**, 3916 (1952).
15. E. Leete. J. Am. Chem. Soc. **81**, 6023 (1959).
16. (*a*) S. Glasstone and D. Lewis. Elements of physical chemistry. 2nd ed. D. Van Nostrand Co. Inc., Princeton, NJ. 1960. p. 627; (*b*) K. B. Wiberg. Physical organic chemistry. Wiley and Sons, Inc., New York, NY. 1964. p. 377.
17. J. W. Lown, K. C. Majumdar, A. I. Meyers, and A. Hecht. Bioorg. Chem. In press.
18. V. N. Iyer and W. Szybalski. Proc. Natl. Acad. Sci. **50**, 355 (1963).
19. C. H. Rochester. *In* The chemistry of the hydroxyl group. *Edited by* S. Patai. Interscience Publishers, London. 1971. Part 1, p. 369.
20. A. J. Lin, L. A. Cosby, and A. C. Sartorelli. Cancer Chemother. Rep. Part 2, **4**, 23 (1974).
21. H. Hsiung, J. W. Lown, and D. Johnson. Can. J. Biochem. **54**, 1047 (1976).
22. J. Burnotte and W. G. Verly. Biochim. Biophys. Acta, **262**, 449 (1972).
23. H. Murakami. J. Theoret. Biol. **10**, 236 (1966).
24. A. R. Morgan and D. E. Pulleyblank. Biochem. Biophys. Res. Commun. **61**, 396 (1974).
25. L. F. Fieser. Experiments in organic chemistry. 3rd ed. D. Heath and Co., Boston, MA. 1957.
26. H. C. Brown, S. Johnson, and H. Podall. J. Am. Chem. Soc. **76**, 5556 (1954).
27. J. Madinaveitia. J. Chem. Soc. 1927 (1937).
28. A. R. Morgan and V. Paetkau. Can. J. Biochem. **50**, 210 (1972).

Nitration of 4-*tert*-butyl-*o*-xylene in acetic anhydride. Formation and rearomatization of adducts

ALFRED FISCHER AND KHAY CHUAN TEO

Department of Chemistry, University of Victoria, Victoria, B.C., Canada V8W 2Y2

Received August 18, 1977

ALFRED FISCHER and KHAY CHUAN TEO. Can. J. Chem. **56**, 258 (1978).

Nitration of 4-*tert*-butyl-1,2-dimethylbenzene in acetic anhydride gives *trans*-1-*tert*-butyl-3,4-dimethyl-4-nitro-1,4-dihydrophenyl acetate (**6**), *trans*-1-*tert*-butyl-3,4-dimethyl-4-nitro-1,4-dihydrophenol, 2-*tert*-butyl-4,5-dimethylphenyl acetate, 5-*tert*-butyl-2-methylbenzaldehyde, 4-*tert*-butyl-1,2-dimethyl-5-nitrobenzene, and 4-*tert*-butyl-1,2-dimethyl-6-nitrobenzene. 2-*tert*-Butyl-4,5-dimethylphenyl acetate and 3,4-dimethylphenyl acetate are the major products of solvolysis of **6** in moist acetic acid. Both of these compounds are likely formed via the cation generated by ionization of the nitro group. Under more acidic conditions 5-*tert*-butyl-2-methylbenzaldehyde and 4-*tert*-butyl-1,2-dimethyl-6-nitrobenzene, formed via the cation generated by acid-catalysed loss of acetate, become dominant, the balance between these products being controlled by the basicity of the solvent. More basic solvents deprotonate the cation to a triene, a key step in the formation of the aldehyde, at a competitive rate with the nitro group migration.

ALFRED FISCHER et KHAY CHUAN TEO. Can. J. Chem. **56**, 258 (1978).

La nitration du *tert*-butyl-4 diméthyl-1,2 benzène dans l'anhydride acétique conduit à l'acétate du *tert*-butyl-1 diméthyl-3,4 nitro-4 dihydro-1,4 phényle *trans* (**6**), au *tert*-butyl-1 diméthyl-3,4 nitro-4 dihydro-1,4 phénol *trans*, à l'acétate du *tert*-butyl-2 diméthyl-4,5 phényle, au *tert*-butyl-5 méthyl-2 benzaldéhyde, au *tert*-butyl-4 diméthyl-1,2 nitro-5 benzène et au *tert*-butyl-4 diméthyl-1,2 nitro-6 benzène. Les acétates du *tert*-butyl-2 diméthyl-4,5 phényle et diméthyl-3,4 phényle sont les produits principaux de la solvolyse de **6** dans l'acide acétique humide. Chacun de ces composés se forme vraisemblablement par l'intermédiaire du cation produit par l'ionisation du groupe nitro. Utilisant des conditions plus acides, la perte acido-catalysée du groupement acétate conduit à la formation d'un cation qui fournit du *tert*-butyl-5 méthyl-2 benzaldéhyde et du *tert*-butyl-4 diméthyl-1,2 nitro-6 benzène comme produits prédominants; les quantités relatives de ces produits sont contrôlées par la basicité du solvant. Dans les solvants les plus basiques la vitesse de déprotonation du cation conduisant à un triène, une étape clé dans la formation de l'aldéhyde, devient compétitive avec la migration du groupe nitro.

[Traduit par le journal]

Can. J. Chem. Downloaded from www.nrcresearchpress.com by 210.87.254.40 on 09/05/12
For personal use only.

Nitration of appropriately substituted arenes in acetic anhydride is accompanied by the formation of nitronium acetate (acetyl nitrate) adducts initiated by the attack of nitronium ion at a substituted (*ipso* (1)) position (2–4). Only in the case of *p*-*tert*-butyltoluene has a 1,2 adduct, **1***a*, been obtained, in addition to the normal 1,4 adduct (2).[1] Formation of the 1,2 adduct has attributed to the steric effect of the *tert*-butyl substituent. The present study of 4-*tert*-butyl-1,2-dimethylbenzene (4-*tert*-butyl-*o*-xylene) was undertaken in order to determine if a general preference for 1,2 adduct formation existed in *tert*-butylbenzene derivatives. Related studies are those on 1,2,4-trimethylbenzene (pseudocumene (5)) and, less directly, other substituted *o*-xylenes such as 3,4-dimethylacetophenone (6). In all of these compounds, as in the parent *o*-xylene itself, the position *ipso* to one methyl group is activated by the second, *ortho* methyl and as a result *ipso* nitration and adduct formation is a dominant reaction (7, 8).

[1]These descriptions retain the enumeration of the parent hydrocarbon for the adducts. Thus the 1(nitronium), 4(acetate) adduct is 4-acetoxy-1-nitro-1,4-dihydro-*p*-*tert*-butyltoluene (more appropriately named 1-*tert*-butyl-4-methyl-4-nitro-1,4-dihydrophenyl acetate), whereas the 1,2 adduct is 2-acetoxy-1-nitro-1,2-dihydro-*p*-*tert*-butyltoluene (5-*tert*-butyl-2-methyl-2-nitro-1,2-dihydrophenyl acetate).

Results and Discussion

Nitration and Formation of Adducts

Nitration of 4-*tert*-butyl-*o*-xylene (**2**) in acetic anhydride gave a product mixture containing ca. 68% of diene adducts. Since 13% of **2** was recovered it is evident that *ipso* attack and addition in this system occurs to the extent of at least 78% of all attack by the nitrating electrophile. Low-temperature chromatography of the product gave the unreacted **2**, the 5- and 6-nitro derivatives **3***a* and **4***a*, respectively, 5-*tert*-butyl-2-methylbenzaldehyde (**5**), 2-*tert*-butyl-4,5-dimethylphenyl acetate (**3***b*), one diastereoisomer of 1-*tert*-butyl-3,4-dimethyl-4-nitro-1,4-dihydrophenyl

Can. J. Chem. Downloaded from www.nrcresearchpress.com by 210.87.254.40 on 09/05/12
For personal use only.

acetate (**6**),[2] and the corresponding diastereoisomer of 1-*tert*-butyl-3,4-dimethyl-4-nitro-1,4-dihydrophenol (**7**).[3] The correspondence of the stereochemistry was established by reduction of the acetate **6** to the alcohol **7** with aluminum hydride. The sample of **7** so obtained had identical ir and nmr to that isolated from the nitration mixture. That the adducts isolated are 1,4 rather than 1,2 is clearly indicated by their uv absorption: only end-absorption to 225 nm was observed with ε being 150 for the acetate and 120 m^2mol^{-1} for the alcohol. These values are consistent with the 2,5 diene pattern of structures **6** and **7** but inconsistent with the 2,4 (conjugated) diene structures **1***b* or **1***c*. The 1,2 adduct **1***a* has an appropriate absorption peak for a conjugated cyclohexadiene: 255 nm, ε 580 m^2mol^{-1} (2). At the same wavelength the acetate **6** and alcohol **7** both have ε 20 m^2mol^{-1}. Additional evidence is provided by the nmr spectra. The *tert*-butyl absorption of **1***a* is at 1.07 whereas that of its 1,4 isomers is at 0.93 and 0.96 ppm (2), the 0.1 ppm difference being a consequence of the attachment of the *tert*-butyl to a vinylic carbon in **1***a* and to a saturated carbon in the 1,4 isomers. For acetate **6** and alcohol **7** the absorption is at 0.99 and 0.97 ppm, respectively.[4] The shift reagent *tris*(1,1,1,2,2,3,3-heptafluoro-7,7-[$^2H_6$]dimethyl-4,6-[$^2H_3$]octanedionato)europium(III) {Eu([$^2H_9$]fod)$_3$} moves the *tert*-butyl peak relatively rapidly downfield (relative gradient 0.40), as is appropriate if the *tert*-butyl and acetate or hydroxyl are attached to the same carbon (Table 1). In **1***a* with the acetate and *tert*-butyl isolated and thus with the europium comparatively distant from the *tert*-butyl, the peak moves very slowly (relative gradient 0.04 (2)), whereas in the 1,4 isomer of **1***a* it again moves rapidly (relative gradient 0.40). Additional arguments can be adduced to rule out structures **1***b* and **1***c* and also to reject other isomeric 1,2 and 1,4 adduct structures (cf. 9).

TABLE 1. Relative gradients of proton chemical shifts for diene adducts resulting from the addition of Eu([$^2H_9$]fod)$_3$

6		7	
Assignment	Relative gradient[a]	Assignment	Relative gradient[b]
1-C(CH$_3$)$_3$	0.40	1-C(CH$_3$)$_3$	0.137
2-H	0.87	2-H	0.221
3-CH$_3$	0.31	3-CH$_3$	0.043
4-CH$_3$	0.50	4-CH$_3$	0.032
5-H	0.51	5-H	0.082
6-H	0.96	6-H	0.215

[a]Gradient 1-OCOCH$_3$ = 1.00; absolute gradient 1-OCOCH$_3$ = 1.7 ppm mol of substrate per mol of shift reagent.
[b]Gradient 1-OH = 1.00; absolute gradient 1-OH = 31 ppm mol of substrate per mol of shift reagent.

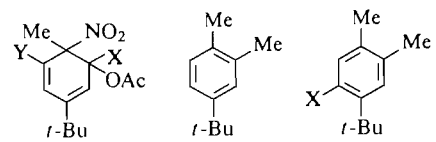

1 **2** **3**

a X = H, Y = H
b X = H, Y = Me
c X = Me, Y = H

a X = NO_2
b X = OAc
c X = OH
d X = Cl

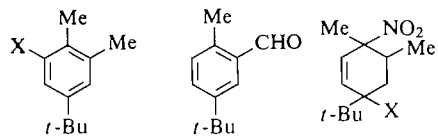

4 **5**

a X = NO_2
b X = OAc
c X = OH
d X = Cl

6 X = OAc
7 X = OH

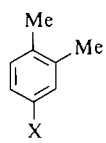

8

a X = NO_2
b X = OAc
c X = OH

Calculations based on the known susceptibility of the 1(*ipso*), 3, and 4 positions of *o*-xylene to attack by nitronium ion (8), and on partial rate factors for nitration of *tert*-butylbenzene in acetic anhydride (10) predict that in 4-*tert*-butyl-*o*-xylene attack at the 1 position should occur to the extent of more than 90%. Attack at the other ring positions is predicted to occur to at most a few percent in each case. It is, therefore, not surprising that no 2,5 adduct, or 4,1 adduct,[5] or 3-nitroarene was detected. The 3 position is activated by two *ortho* alkyl groups but is very hindered. The 4 position, being *ipso* to the bulky *tert*-

[2]4-Acetoxy-1-nitro-1,4-dihydro-4-*tert*-butyl-*o*-xylene.
[3]4-Hydroxy-1-nitro-1,4-dihydro-4-*tert*-butyl-*o*-xylene.

[4]In the mother liquors from recrystallization of **6** there was an absorption 0.1 ppm further downfield, indicative of the presence of the expected 1,2 adduct. Chromatography of the residues from the mother liquors gave fractions in which the 1,2 adduct was a major component. This adduct decomposed in the course of determining the ^{13}C nmr spectrum of combined fractions.

[5]The nitro-de-*tert*-butylation product, 4-nitro-*o*-xylene (**8***a*), is the expected product from nitration at the 4 position, rather than the 4,1 adduct (cf. (11)). However, no **8***a* was obtained. The absence of attack *ipso* to the *tert*-butyl group parallels the behaviour of *p*-*tert*-butyltoluene (2).

Can. J. Chem. Downloaded from www.nrcresearchpress.com by 210.87.254.40 on 09/05/12
For personal use only.

butyl group, is also very hindered. 5-*tert*-Butyl-2-methylbenzaldehyde (**5**), a side-chain substitution product, and the aryl acetate **3***b* are rearomatization products of adduct **6**. Their formation is discussed further below but here it might be noted that if account is taken of the fact that these are formed from **6** then the extent of *ipso* attack is more complete than it first appears. The hydroxynitrodiene **7** is probably not formed directly but is, rather, a solvolysis product from the acetoxynitrodiene **6** or, perhaps, a nitritonitrodiene (12). Support for this suggestion is provided by the observation that when aqueous acetic acid was added to a nitration mixture after the nitration had been carried out at −40°C, and the resulting solution stirred at 0°C before work-up, the acetoxynitrodiene **6** was not obtained but good yields of aryl acetate **3***b* and hydroxynitrodiene **7** were formed. The formation of hydroxynitrodienes has been noted in the nitration of durene (12) *p*-cymene (13) and *p*-xylene (14). When the *p*-xylene nitration mixture is worked up under completely anhydrous conditions, no hydroxynitrodiene is obtained.[6]

Although in each case only one of the pair of diastereoisomers of **6** and **7** was isolated it is likely that the other diastereomer of each pair was also formed. From the nmr spectra of some of the column fractions it was evident that small amounts of other dienes, with absorptions in positions appropriate for the diastereoisomers, were present. Both diastereoisomers of the 1,4 nitronium acetate adduct of *p*-*tert*-butyltoluene were formed but one was obtained in much smaller amount than the other (2). It is likely that the acetate and alcohol diastereomers isolated have the nitro and acetoxy or hydroxy groups *trans*. For **6** the gradient of the chemical shift of the 4-Me group on the addition of Eu([$^2H_9$]fod)$_3$ is larger than that for the 3-Me group and is similar to that for the 5-H. This implies that the protons in each of these groups are of comparable distances from the europium, complexed at the acetate. This would seem possible in the *trans* isomer (with 4-Me *cis* to acetate and europium) but unlikely in the *cis* isomer with 4-Me on the other side of the ring to the europium.

Rearomatization Reactions

Adduct **6** is a tertiary acetate. Under conditions of low acidity tertiary acetate adducts undergo loss of nitrous acid accompanied by 1,2 shift of the acetate group to a neighbouring position, to form an aryl acetate (7*b*, 14). Myhre and co-workers (15*a*) have presented convincing evidence that the elimination of nitrous acid from the secondary acetate, 3,4,5-trimethyl-4-nitrocyclohexa-2,5-dienyl acetate (the adduct of 1,2,3-trimethylbenzene), to form the unrearranged aryl acetate, is a two-step (E1 type) process, involving initial loss of the nitro group as nitrite anion to form a cyclohexadienyl cation, which loses the proton in a subsequent step to form the aryl acetate. A similar mechanism involving initial formation of the acetoxycyclohexadienyl cation **9** (a *tert*-acetate) by ionization of the nitro group, followed by shift of the acetate group to form the secondary acetate, cation **10**, which is rapidly deprotonated, is likely to apply to tertiary acetate adducts (15*b*) and is depicted in the upper part of Scheme 1 (a one-step, concerted, process was proposed earlier for the elimination to aryl acetate (14)). At higher acidities the *ipso*-nitrocyclohexadienyl cation **11** is formed by protonation of the acetate group and loss of acetic acid. If the solvent is of low nucleophilicity the lifetime of the cation is sufficiently long for shift of the nitro group to occur to form the (secondary) nitrocyclohexadienyl cation **12** which is rapidly deprotonated to the nitroarene (Scheme 1, middle). If the solvent is more nucleophilic, capture of cation **11** occurs, before rearrangement, to form a new adduct and/or the cation is deprotonated at that methyl group originally *ipso* to the acetate group in the adduct, to form a triene **13**, which is the precursor to benzylic derivatives (12, 14) (Scheme 1, lower). In the earlier paper it was proposed that the conversion of the triene to benzylic derivative(s) is an S_N1' or S_N2' process, the group Z being introduced as a nucleophile. Now that the nitro group has been shown to ionize readily from an adduct (15) the unimolecular pathway, involving formation of the benzyl cation **14**, seems the more probable. Thus the products obtained on rearomatization of tertiary acetate adducts (as typified by the *p*-xylene adduct) depend, in the first instance, upon competition between the ionization of nitro to form the cyclohexadienyl cation **9**, leading to 2,5-dialkylphenyl acetate, and the loss of acetate to form cation **11**, leading to 1,4-dialkyl-2-nitrobenzene and 4-alkylbenzyl compounds. Apparently nitro is a better anionic leaving group than acetate (the 2,5-dimethylphenyl acetate obtained from the *p*-xylene adduct had only exchanged with [$^2H_4$] acetic acid solvent to a small extent (14)). Thus neutral, strongly ionizing, conditions favour ionization of the nitro group and the formation of the aryl acetate product, whereas strongly acidic conditions enhance the *catalysed* loss of acetate as acetic acid, allowing this pathway to supersede the noncatalysed loss of the nitro group, and thus these conditions favour the formation of nitroarene and benzyl products. The balance between nitroarene and benzyl compound(s) is determined by the basicity of the solvent, which controls the outcome of the secondary competition between **11** → **12** and **11** → **13**. The

[6]Unpublished work with R. J. Thompson.

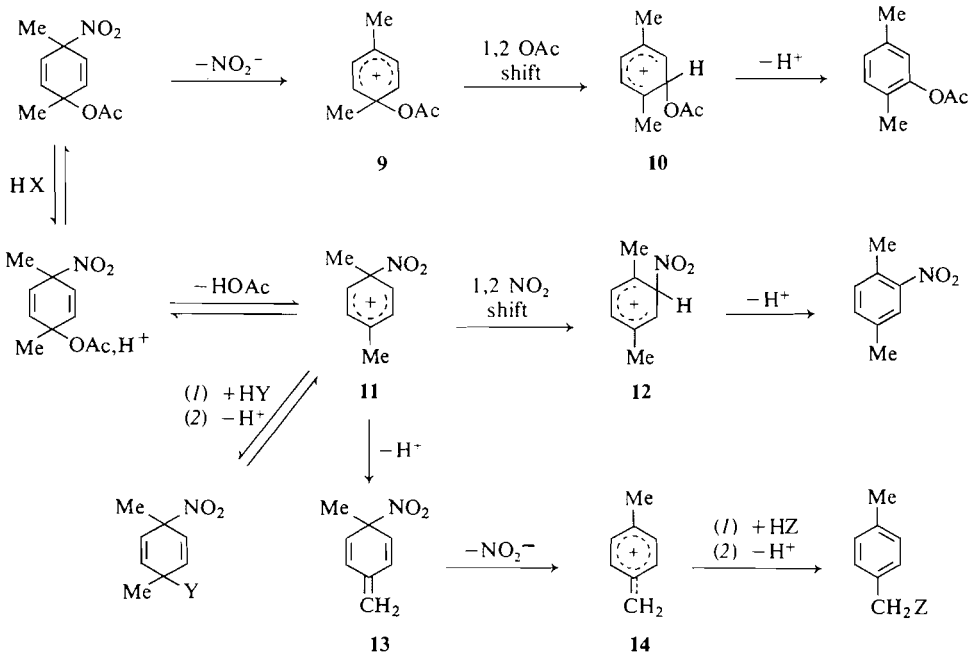

SCHEME 1

exchange of acetate for another nucleophile and thus the interconversion of dienes, which also involves cation **11** as an intermediate, should be most favoured by a nucleophilic solvent made sufficiently acid such that the formation of **11** just supersedes formation of **9**. At higher levels of acidity, or on prolonged reaction times, reversion of the exchanged diene to **11** gives further opportunity for the competing irreversible rearomatization to nitroarene and benzyl compounds to occur.

In the case of the 1,4-nitroacetoxy adduct of *p-tert*-butyltoluene the above scenario is modified (2). Under weakly acidic ionizing conditions the predominant rearomatization product is *p*-tolyl acetate, formed by elimination of the nitro and *tert*-butyl groups. The likely mechanism of this reaction is shown in Scheme 2, a parallel of that proposed by Myhre for the formation of aryl acetate from secondary acetate adducts. Only the *tert*-butyl cation is sufficiently stable to be eliminated in this way, in contrast to other alkyl groups. The cleavage of the *tert*-butyl cation in **15** is faster than the 1,2 acetate shift, which would convert **15** into **16** and ultimately 2-*tert*-butyl-5-methylphenyl acetate, since none of this expected product was formed under any of the conditions investigated. 5-*tert*-Butyl-2-methylphenyl acetate was obtained under all (acidic) conditions investigated and was the major product when acetic acid made more acidic by the addition of 1% trifluoroacetic acid was used. The 1,2 adduct **1***a* has been suggested to be an intermediate in this reaction (2). Support for this suggestion is provided by the observation that, when the reaction is carried out at a higher concentration of trifluoroacetic acid but at lower temperature, the 1,2 adduct is obtained with little rearomatization.[7] Thus the sequence involving acid-catalysed loss of acetate from the 4 position, (formation of **17**) its recombination at the 2 position (formation of **1***a*), followed by ionization of the

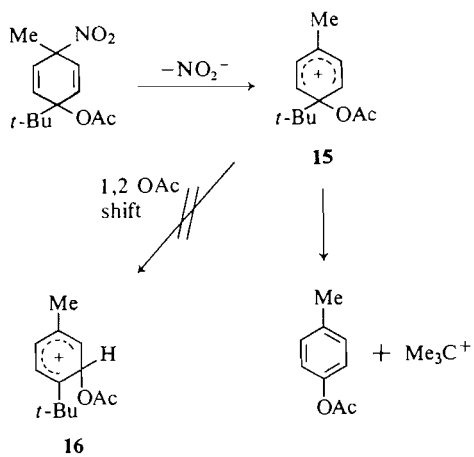

SCHEME 2

nitro group in **1***a* to form cation **18** (Y = OAc), which is deprotonated, is predicated (Scheme 3). Formation of 4-*tert*-butyl-2-nitrotoluene also occur-

[7]Unpublished work with L. M. Iyer.

Can. J. Chem. Downloaded from www.nrcresearchpress.com by 210.87.254.40 on 09/05/12
For personal use only.

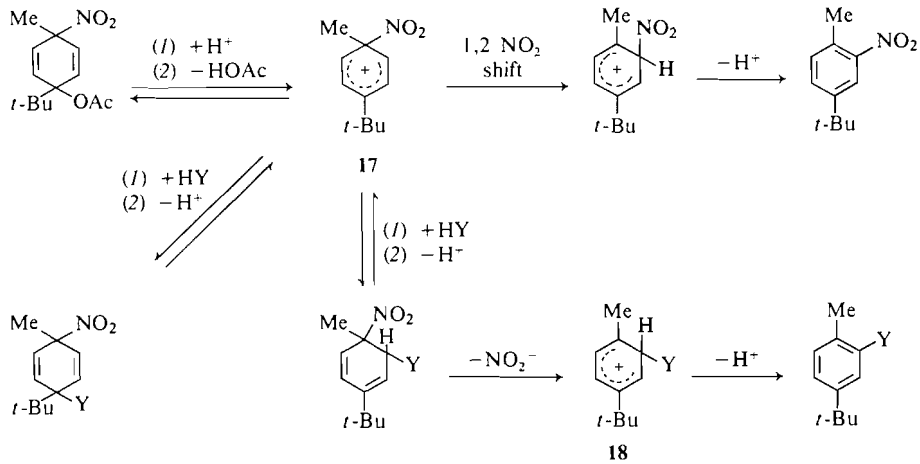

SCHEME 3

red and it was the dominant product under strongly acidic conditions, as expected. Thus, as in the case of the *p*-xylene adduct, the rearomatization products are determined by a primary competition between ionization of nitro and acid-catalysed loss of acetate, but these products are *p*-tolyl acetate, on the one hand, and the nitroarene plus 5-*tert*-butyl-2-methylphenyl acetate on the other. The secondary competition which determines the ratio of the last two products is controlled by the acidity and nucleophilicity of the solvent; strongly acidic conditions and weakly nucleophilic solvents favouring the formation of the nitroarene. No benzyl derivatives are formed since the quaternary centre prevents the formation of the triene analog of **13** from cation **17**.

The reactions of adduct **6** can be interpreted in terms of the pathways shown in Schemes 1–3. Under the most favourable conditions investigated for ionization of the nitro group and formation of cation **19**, reaction in aqueous acetic acid, 87% of the product (70% **3***b*, 17% **8***b*) can be accounted for as being derived via this intermediate (Scheme 4) and a further 3% were the corresponding phenols presumably formed via the analog of **19** containing OH in place of OAc. This cation is the product of ionization of nitro from **7**, itself obtained from **6** by prior exchange with solvent water via **21**. Unlike the case of *p*-*tert*-butyltoluene the 1,2 shift of the acetate is not superseded by the cleavage of the *tert*-butyl group, indeed the acetate shift is predominant. This is understandable in terms of the greater stability of **20** than **16** and of corresponding relationship between the transition states leading to these ions. Compared with **16** cation **20** has an electron-donating methyl substituent located at one of the three centres of positive charge.[8] It is interesting that although the rearomatization reactions of cation **19** dominate those of **21** the latter ion is formed more rapidly. Both the **3***b* and the **8***b* formed contained [$^2H_3$]acetate and it follows that formation of **21** and its recombination with [$^2H_4$]acetic acid must have preceded the formation of **19** and from it the labelled **3***b* and **8***b*. The other reactions of **21** (Scheme 5) must be slower than these reactions of **19**. In these weakly acidic ionizing conditions not more than a few percent of the products were derived by rearomatization of **21**.

When the reaction was repeated in less ionizing conditions, acetic acid made anhydrous by addition

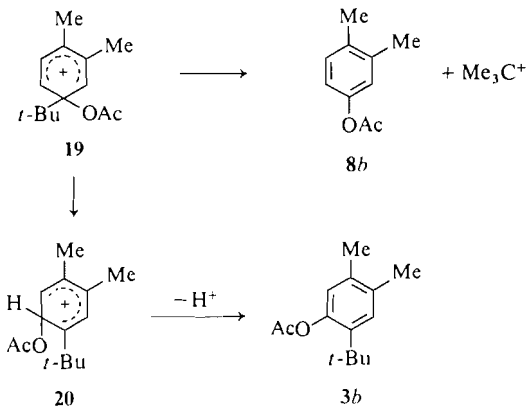

SCHEME 4

[8]Acetate **3***b* obtained in the nitration of **2** is clearly formed from adduct **6**, since, as noted above, when aqueous acetic acid was added to the reaction mixture before work-up (conditions known to favour formation of aryl acetate (14)) the yield of **3***b* was enhanced at the expense of **6**. (As discussed earlier **7** was also formed during work-up).

Can. J. Chem. Downloaded from www.nrcresearchpress.com by 210.87.254.40 on 09/05/12
For personal use only.

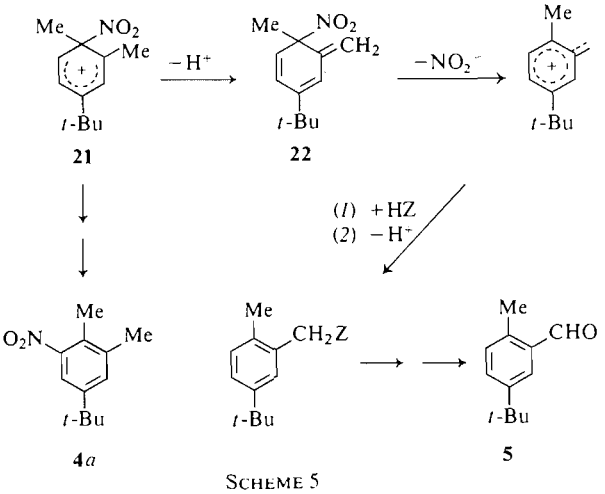

SCHEME 5

of acetic anhydride, the products formed via **19** were reduced (46% **3***b*, 5% **8***c*) and the products formed via **21** were enhanced (10% **4***a*, 6% **5**). The nitroarene **4***a* would be expected to be formed by the normal 1,2 nitro shift and deprotonation. The sequence shown in Scheme 5 (Z = ONO_2 (16) or ONO (17)) is the likely pathway to the aldehyde **5**. Normally the methyl group substituted in forming benzyl derivatives is that *para* to the position of *ipso* attach by the nitronium ion. In the absence of this possibility in **21** the unusual deprotonation at the 2-methyl group occurs to form **22** and eventually **5**. The benzaldehyde **5** was also obtained from the nitration of **2** (see above), presumably through the same sequence of intermediates. As in aqueous acetic acid, exchange of acetate in **6** for acetate from the solvent was noted.

When rearomatization was carried out in acetic acid containing acetic anhydride and made successively more acidic by the addition of sulfuric acid the yield of products from **19** steadily decreased and those from **21** increased, reaching 78% in 50% sulfuric acid. Furthermore, in the competition between benzaldehyde, **5** and nitroarene **4***a* the aldehyde was favoured when the sulfuric acid constituted only a small portion of the solvent and thus the acetic acid was effective in deprotonating **21** to **22**. In the very acidic solutions in which the solvent would be much less available for deprotonation the nitroarene **4***a* became the dominant product. All of this is in accord with the foregoing discussion. The absence of other than a trivial amount of acetate **4***b* in the rearomatization of **6** (contrast the *p-tert*-butyltoluene adduct) correlates with the greater difficulty of forming the 1,2 adduct **1***b* or **1***c* as compared with **1***a* of the *p-tert*-butyltoluene case. Furthermore, the 1,2 adduct, once formed, may be relatively less reactive than in the *p-tert*-butyltoluene case. The additional methyl group in **21** is suitably located for maximum stabilization of the cation, in contrast to the situation in the cations generated by ionization of nitro from **1***b* or **1***c*. This difference should be reflected in the relative stabilities and ease of formation of the transition states leading to these ions. In the more dilute sulfuric acid solutions the initial formation of adducts isomeric with **6** could be followed. These reactions provide further evidence of the rapid formation of cation **21**.

When rearomatization reactions were carried out using trifluoroacetic acid or boron trifluoride etherate as reagents, nitroarene **4***a* was formed effectively instantly and in over 90% yield at −70°C. Under these strongly acidic conditions **21** is formed very rapidly. The solvent species are too weakly basic to be effective in the deprotonation of **21** to triene **22** thus formation of benzylic derivatives cannot compete with the 1,2 nitro shift leading to **4***a*.

Reaction of diene **6** in ether with hydrogen chloride gave a mixture which appeared to contain a chloronitro diene, i.e. exchange of chloride for acetate had occurred. However, after work-up and chromatography only a mixture of the chloroarenes **3***d* and **4***d* was obtained. Formation of **4***d* could conceivably involve an intermediate 1,2 nitrochloro adduct which subsequently eliminates nitrous acid. Formation of **3***d* could involve formation of a 1,4 nitrochloro adduct which undergoes 1,2 shift of the chloride and elimination of nitrous acid.

Reaction of the diene acetate **6** with sodium methoxide in methanol gave the phenol **3***c* as the major product and lesser amounts of 3,4-dimethylphenol (**8***c*) the phenol **4***c*, the aryl acetate **3***b*, a nitroarene and small amounts of unidentified products. The main reaction is rearomatization of the adduct to aryl acetate **3***b* accompanied by cleavage of the acetate group. The formation of **8***c* parallels the formation of *p*-cresol from the 1,4 nitroacetoxy adduct of *p-tert*-butyltoluene on reaction with sodium methoxide (2).

Thermolysis of the acetate adduct **6** gave the parent hydrocarbon **2** as the major product. Thermolysis of the nitrohydroxy adduct **7** gave similar amounts of parent hydrocarbon **2** and 3,4-dimethylphenol (**8***c*) as well as other products.

Experimental

Infrared spectra were obtained on a Perkin-Elmer 337 spectrophotometer. ^1H nuclear magnetic resonance spectra at 90 MHz were determined using a Perkin-Elmer R32 spectrometer. ^{13}C nuclear magnetic resonance spectra were measured on solutions in deuteriochloroform with tetramethylsilane reference, using a Nicolet TT-14 spectrometer, operating in the

Can. J. Chem. Downloaded from www.nrcresearchpress.com by 210.87.254.40 on 09/05/12
For personal use only.

TABLE 2. ^{13}C Chemical shifts (δ_C, ppm) of 4-*tert*-butyl-*o*-xylene (**2**) and its derivatives[a]

Compound	*C*-1	*C*-2	*C*-3	*C*-4	*C*-5	*C*-6	1-CH_3	2-CH_3	$C(CH_3)_3$	$C(CH_3)_3$
2	133.3	135.8	126.6	148.6	122.7	129.4	19.1	20.0	31.5	34.2
3*a*	135.4	139.6	129.5	149.3	138.5	124.8	18.7	19.7	31.0	35.1
3*b*[b]	135.0	133.6	128.3	137.9	146.9	125.0	19.0	19.4	30.4	34.0
3*c*	134.8	127.6	128.2	133.3	152.2	118.1	18.9	18.9	29.8	34.1
3*d*[c]	138.2	134.8	129.4	149.6	125.7	130.7	19.1	19.6	31.2	34.3
4*a*	127.5	138.9	131.0	151.5	118.5	149.6	14.7	20.6	31.0	34.5
4*d*[c]	131.3	137.8	125.4	149.6	123.9	134.4	15.8	21.1	31.2	34.3

[a]Enumeration of all compounds in this table follows that of **2**; **3***a–d* are 5-substituted derivatives of **2**; **4***a–d* are 6-substituted derivatives of **2**.
[b]21.5 ($OCOCH_3$), 169.6 ($OCOCH_3$).
[c]From a 3:1 mixture of **3***d* and **4***d*.

Fourier transform (FT) mode at 15.1 MHz, under optimized conditions of complete noise decoupling. Mass spectra were obtained on an Hitachi Perkin-Elmer RMU-7 spectrometer and, for glc mass studies, on a Finnigan 3300 system. Microanalyses were by Dr. D. McGillivray. Gas–liquid chromatography analyses were performed on a Varian Aerograph 2400 gas chromatograph using stationary phases SE 30 (3%) and DEGS (10%) on acid-washed Chromosorb W. Nitric acid, ether and pentane were purified as previously described (6). Alumina was deactivated with 3% of 10% acetic acid. *o*-Xylene (Eastman), *tert*-butyl alcohol (Mallinckrodt), and [$^2H_4$]acetic acid (99.5%, Aldrich) were commercial products.

4-tert-*Butyl-1,2-dimethylbenzene (2)*

A mixture of *tert*-butylalcohol (2.0 mol) and *o*-xylene (0.50 mol) was added dropwise with stirring, over 0.5 h, to a mixture of *o*-xylene (2.0 mol) and pulverized anhydrous aluminium chloride (1.0 mol) at −8°C (18). The reaction mixture was heated to ca. 65°C and maintained at that temperature for 1.5 h. The dark red solution was cooled to 0°C and decomposed with 6 *M* HCl (400 cm^3) and extracted with pentane (4 × 100 cm^3). The pentane extracts were combined and washed with brine (300 cm^3), saturated sodium bicarbonate (200 cm^3), and brine (3 × 150 cm^2) and dried over anhydrous magnesium sulfate. Rotatory evaporation under reduced pressure afforded 357 g of crude product which contained 78% of 4-*tert*-butyl-1,2-dimethylbenzene (**2**) by glc, an 86% yield. Pure (> 99.9%) **2** was obtained by distillation at 45°C/65 Pa using a spinning band column and had ir (CCl_4): 1500, 1450, 1275, 1145, 1020, 994, 815 cm^{-1}; ^1H nmr ($CDCl_3$) δ: 1.26 (s, 9H, $C(CH_3)_3$), 2.18 (s, 3H, 1-CH_3), 2.21 (s, 3H, 2-CH_3), 6.93–7.14 ppm (m, 3H, ArH_3); ^{13}C nmr listed in Table 2; mass spectrum (70 eV) *m/e* (relative intensity): 162.150 (42, M_r ($^{12}C_{12}{}^1H_{18}$) 162.141), 148 (21), 147 (100, $M-CH_3$), 119 (25), 107 (17).

Nitration of 4-tert-*Butyl-1,2-dimethylbenzene (2) in Acetic Anhydride*

A solution of freshly distilled nitric acid (12.6 g, 0.20 mol) in acetic anhydride (35 cm^3) was added to **2** (16.2 g, 0.10 mol) in acetic anhydride (40 cm^3) at −65°C over a period of 5 min. The reaction mixture was stirred for 20 min at −60°C and then allowed to warm to ca. −40°C and maintained at that temperature for 30 min. The mixture was cooled to −78°C and cold dry ether (200 cm^3) was stirred in slowly. Ammonia was condensed into the solution (ca. 1 drop/5 s) with constant stirring. The temperature during neutralization was held below −50°C. Aqueous ammonia (150 cm^3) was added to the mixture to dissolve the ammonium salts and acetamide, and the aqueous phase was extracted with ether (2 × 100 cm^3). The combined ethereal solution was washed with 10% brine (4 × 100 cm^3) and dried over anhydrous magnesium sulfate. Removal of the ether solvent under reduced pressure (below 20°C) yielded an oily yellow crystalline solid. The ^1H nmr spectrum indicated that the crude product contained ca. 68% of diene(s).

Chromatography of the crude product on 3% deactivated alumina at −45°C and elution first with pentane and then with ether–pentane gave unreacted **2** (2.1 g, 13 mmol) in the first 5% ether fraction. The second 5% ether fraction (2.1 g) was rechromatographed and the various constituents were isolated or enriched in different sub-fractions as follows. Mixtures of 4-*tert*-butyl-1,2-dimethyl-5-nitro- and -6-nitrobenzene (**3***a* and **4***a*) in the ratio of ca. 75:25 (1.76 g, 8.5 mmol) and 50:50 (0.65 g, 3.1 mmol) were obtained from the pentane and 0.4% ether fractions, respectively. 4-*tert*-Butyl-1,2-dimethyl-5-nitrobenzene (**3***a*) from the pentane fraction had ir (liquid film): 1520, 1360 (NO_2), 1282, 875, 809 cm^{-1}; ^1H nmr ($CDCl_3$) δ: 1.35 (s, 9H, $C(CH_3)_3$), 2.18 (s, 3H, 1-CH_3), 2.24 (s, 3H, 2-CH_3), 7.04 (s, 1H, 3-*H*), 7.25 ppm (s, 1H, 6-*H*); mass spectrum (70 eV) *m/e* (relative intensity): 207.136 (7, M_r ($^{12}C_{12}{}^1H_{17}{}^{14}N^{16}O_2$) 207.126), 192 (14, $M-CH_3$), 162 (20), 161 (100). The 0.8% ether fraction, after rechromatography for a second time yielded 5-*tert*-butyl-2-methylbenzaldehyde (5, 0.11 g, 0.6 mmol) as a yellow oil, ir (liquid film): 1680 (CHO), 1215, 1195, 1140, 825 cm^{-1}; ^1H nmr ($CDCl_3$) δ: 1.34 (s, 9H, $C(CH_3)_3$), 2.62 (s, 3H, 2-CH_3), 7.17 (d, 1H, J = 7.8 Hz, 3-*H*), 7.49 (d-d, 1H, J = 2.3 and 7.8 Hz, 4-*H*), 7.81 ppm (d, 1H, J = 2.3 Hz, 6-*H*); mass spectrum (70 eV) *m/e* (relative intensity): 176.124 (51, M_r ($^{12}C_{12}{}^1H_{16}{}^{16}O$) 176.120), 162 (19), 161 (100, $M-CH_3$), 133 (22), 105 (24).

In the first 10% ether fraction a mixture of 2-*tert*-butyl-4,5-dimethylphenyl acetate **3***b* and one diastereoisomer of 1-*tert*-butyl-3,4-dimethyl-4-nitro-1,4-dihydrophenyl acetate (**6**) with a little nitroarene was obtained (1.85 g). The second 10% and the 15% ether fractions gave essentially pure diene acetate **6** 11.0 g, 41.2 mmol). Recrystallization (×3) from a mixture of pentane – methylene chloride gave pure **6** (6.2 g) as white prismatic crystals, mp 73.0–73.5°C; uv (CH_3OH): 225 nm (ε 150 m^2 mol^{-1});[9] ir (CCl_4): 1740 and 1250 ($OCOCH_3$), 1540 and 1365 cm^{-1} (NO_2); ^1H nmr ($CDCl_3$) δ: 0.99 (s, 9H, $C(CH_3)_3$), 1.78 (s, 3H, 4-CH_3), 1.85 (d, 3H, 3-CH_3), 1.95 (s, 3H, $OCOCH_3$), 5.79 (m, 1H, 2-*H*), 5.99 (d, 1H, 6-*H*), 6.00 ppm (s, 1H, 5-*H*), $J_{2,3\text{-}CH_3}$ = 1.5, $J_{2,6}$ = 1.3 Hz; addition of Eu([$^2H_9$]fod)$_3$ moved the 6-H to lower field than the 5-H and revealed the 10 Hz coupling between the 5-H (d) and 6-H (d of d); ^{13}C nmr ($CDCl_3$) δ_C: (TMS) 18.4 (3-CH_3), 21.7 ($OCOCH_3$), 22.3 (4-CH_3), 25.2 ($C(CH_3)_3$), 39.1 ($C(CH_3)_3$), 80.5 (*C*-1), 88.7 (*C*-4), 127.7 (*C*-6), 129.7 (*C*-2 or *C*-5), 130.1 (*C*-5 or *C*-2), 133.9 (*C*-3), 169.4 ppm ($OCOCH_3$). *Anal.* calcd. for $C_{14}H_{21}NO_4$: C 62.90, H 7.92, N 5.24; found: C 63.29, H 7.81, N, 5.15.

[9]The limit of measurement under the conditions used was 225 nm, where only end absorption was observed.

Can. J. Chem. Downloaded from www.nrcresearchpress.com by 210.87.254.40 on 09/05/12
For personal use only.

Can. J. Chem. Downloaded from www.nrcresearchpress.com by 210.87.254.40 on 09/05/12
For personal use only.

Rotatory evaporation of the combined mother liquors from recrystallization of **6**, under reduced pressure, at 15°C, yielded a dark brown oil (2.1 g). ^{1}H and ^{13}C nmr spectra of the oil established[10] that a significant component was the 1,2-diene acetate **1***b*, which was relatively unstable since it decomposed with evolution of nitrogen dioxide when the decoupled and off-resonance ^{13}C nmr spectra were taken over a period of 1 and 1.5 h, respectively, at a probe temperature of +37°C.

The 50–80% ether fractions gave one diastereoisomer of 3,4-dimethyl-1-*tert*-butyl-4-nitro-1,4-dihydrophenol (**7**, 2.97 g, 13.2 mmol). After recrystallization (×3) from pentane-methylene chloride pure **7** (1.0 g) was obtained as white prismatic crystals, mp 81–82°C; uv (CH_3OH): 225 nm (ε 120 m^2 mol^{-1}); ir: (CCl_4) 3620 (OH), 1530, 1320 (NO_2), 1217, 1127, 1053, 990, 970, 963, 650 cm^{-1}; nmr ($CDCl_3$) δ : 0.97 (s, 9H, C-(CH_3)$_3$), 1.72 (s, 1H, 1-O*H*), 1.76 (s, 3H, 4-CH_3), 1.87 (d, 3H, 3-CH_3), 5.92 (d, 1H, 5-*H*), 5.98 (m, 1H, 2-*H*), 6.17 (d-d, 1H, 6-*H*), $J_{2,3\text{-}CH_3}$ = 1.2, $J_{2,6}$ = 2.1, $J_{5,6}$ = 10.2 Hz; addition of Eu([$^2H_9$]fod)$_3$ moved the 2-H downfield from its overlapping position with 5-H and clearly revealed the 10 Hz coupling in the 5-H; ^{13}C nmr ($CDCl_3$) δ_C (TMS): 18.8 (3-CH_3), 24.9 (4-CH_3), 25.4 (C(CH_3)$_3$), 38.4 (*C*(CH_3)$_3$), 72.7 (*C*-1), 87.1 (*C*-4), 128.4 (*C*-5), 132.2 (*C*-3), 132.5 (*C*-6), 134.6 ppm (*C*-2). *Anal.* calcd. for $C_{12}H_{19}NO_2$: C 63.98, H 8.50, N 6.22; found: C 63.89, H 8.57, N 6.08.

Nitration of **2** *in Trifluoroacetic Acid: 4-*tert*-Butyl-1,2-dimethyl-6-nitrobenzene (**4***a*)*

A solution of nitric acid (5.0 g, 80 mmol) in a mixture of trifluoroacetic anhydride (4 cm^3) and trifluoroacetic acid (36 cm^3) was added to a solution of **2** (8.1 g, 50 mmol) at −78°C. The mixture was allowed to warm to 5°C and maintained at that temperature for 10 min. The solution was then cooled and worked up to give a product consisting of 50% nitroarene and 50% **2** (by nmr). Chromatography on alumina and elution with pentane gave 4-*tert*-butyl-1,2-dimethyl-6-nitrobenzene (**4***a*), ir (film): 1525, 1360 (NO_2), 880; ^{1}H nmr ($CDCl_3$) δ: 1.31 (s, 9H, C(CH_3)$_3$), 2.31 (s, 3H, 2-CH_3), 2.35 (s, 3H, 1-CH_3), 7.38 (d, 1H, J = 1.9 Hz, 3-*H*), 7.59 ppm (d, 1H, J = 1.9 Hz, 5-*H*); mass spectrum (70 eV) *m/e* (relative intensity): 207.137 (67, M_r ($^{12}C_{12}{}^1H_{17}{}^{14}N^{16}O_2$) 207.126), 193 (35), 192 (100, $M-CH_3$), 190 (70, $M-OH$), 14 (37, $M-CH_3NO_2$), 131 (30, $M-C_2H_6NO_2$), 91 (29).

Nitration of **2** *in Acetic Anhydride with Hydrolytic Work-up: 2-*tert*-Butyl-4,5-dimethylphenol (**3***c*) and 5-*tert*-Butyl-2,3-dimethylphenol (**4***c*)*

The hydrocarbon **2** (8.1 g, 50 mmol) was nitrated by preparing a solution of it with nitric acid (4.7 g, 75 mmol) in acetic anhydride (15 cm^3) at −60°C and then allowing the temperature of the mixture to rise to −40°C. Aqueous (10%) acetic acid (20 cm^3) was added, the temperature allowed to rise to 0°C and stirring continued at that temperature for 10 min. After work-up ^{1}H nmr indicated that the composition of the product was hydrocarbon **2** (20%), acetate **3***b* (30%), diene **7** (20%), nitroarene **4***a* (5%), and unidentified compounds (25%). Chromatography on alumina and elution with pentane and ether–pentane mixtures gave in the 20% ether fraction 2-*tert*-butyl-4,5-dimethylphenyl acetate (**3***b*), ir (CCl_4): 1750 and 1215 (C=O), 1440, 1370, 1355, 875, 860 cm^{-1}; ^{1}H nmr ($CDCl_3$) δ: 1.31 (s, 9H, C(CH_3)$_3$), 2.16 (s, 3H, CH_3), 2.18 (s, 3H, CH_3), 2.24 (s, 3H, OCOCH_3), 6.72 (s, 1H, 6-*H*), 7.08 ppm (s, 1H, 3-*H*); mass spectrum (70 eV) *m/e* (relative intensity): 220.146 (28, M_r ($^{12}C_{14}{}^1H_{20}{}^{16}O_2$) 220.146), 178 (77), 164 (29), 163 (100, $M-C_4H_9$), 135 (18). The 50–70% ether fractions gave 2-*tert*-butyl-4,5-dimethylphenol (**3***c*), ir (CCl_4): 3620 (s), 3530 (m), ~3250–3450 (broad) (OH); 1185 (s, C—O), 880 (m), 840 (m) cm^{-1}; ^{1}H nmr ($CDCl_3$) δ: 1.37 (s, 9H, C(CH_3)$_3$), 2.12 (s, 3H, CH_3), 2.14 (s, 3H, CH_3), 4.65 (broad, 1H, O*H*), 6.41 (s, 1H, 6-*H*), 6.98 ppm (s, 1H, 3-*H*); mass spectrum (70 eV) *m/e* (relative intensity): 178 (32, M), 163 (100, $M-CH_3$), 135 (28, $M-C_3H_7$). The 85–100% ether fractions gave 5-*tert*-butyl-2,3-dimethylphenol (**4***c*), ir (CCl_4): 3625, 3600–3200 (broad) (OH), 1610, 1570, 1440, 1390, 1340, 1280, 1180 (C—O), 1075, 1045, 939, 880, 840 cm^{-1}; ^{1}H nmr ($CDCl_3$) δ: 1.25 (s, 9H, C(CH_3)$_3$), 2.10 (s, 3H, 2-CH_3), 2.22 (s, 3H, 3-CH_3), ~4.6 (s, 1H, O*H*), 6.63 (b, 1H, J ~ 1.5 Hz, 6-*H*), 6.77 ppm (b, 1H, J ~ 1.5 Hz, 4-*H*); mass spectrum (70 eV) *m/e* (relative intensity): 178 (36, M), 164 (16), 163 (100, $M-CH_3$), 135 (23, $M-C_3H_7$), 123 (12).

Aluminium Hydride Reduction of Diene **6**

Diene **6** (140 mg, 0.53 mmol) in dry tetrahydrofuran (THF) was added to a solution of excess AlH_3 (2.75 mmol in 15 cm^3 THF) and stirred at 0°C for 10 min. The nmr and ir spectra of the oily solid obtained on work-up showed that the product was the hydroxy diene **7** (ir (CCl_4): 3620 (OH), 1530, 1320 (NO_2); nmr ($CDCl_3$) δ: 0.97, 1.76, 1.87, 5.92, 5.98, 6.17 ppm).

Reaction of Diene **6** *with Moist* [$^2H_4$]*Acetic Acid*

A solution of the diene **6** (50 mg, 0.19 mmol) in a mixture of H_2O (10 mm)[3] and CD_3COOD (500 mm^3) was prepared at 0°C and the reaction was observed by nmr at 35°C. No obvious reaction took place over a period of 40 min. A vigorous reaction took place with the evolution of brown fumes of nitrogen dioxide, when the temperature was raised to 100°C. After work-up, nmr and glc – mass spectrometry established the major product to be the deuterated acetate **3***b* (70%, M^+ 223), with lesser amounts of the deuterated acetate **8***b* (17%, M^+ 167), the phenol **8***c* (2%, M^+ 122), an isomer of **3***b* (2%, M^+ 223), a nitroarene (2%, M^+ 207), an isomer of **8***b* (6%, M^+ 167) and a phenol, probably **3***c* (1%, M^+ 178).

Reaction of Diene **6** *with Sulfuric Acid in Acetic Anhydride – [$^2H_4$]Acetic Acid*

A solution of diene **6** (107 mg, 0.4 mmol) in $CDCl_3$ (150 mm^3) was treated in successive experiments with a solution of 0, 0.05, 0.5, 5, and 50% H_2SO_4 (by weight) in 10% Ac_2O–CD_3CO_2D (250 mm^3). The reactions were followed by nmr as the temperature was raised from 0°C to ambient (23°C). After work-up, the product distributions, shown in Table 3, were determined by nmr and glc – mass spectrometry.

Rearomatization was slow ($t_{\frac{1}{2}}$ ~ 56 h) in the case of the reaction carried out in the absence of sulfuric acid. The diene acetate group was exchanged with the deuterated solvent and this was essentially complete (90%) after 47 h. Under sulfuric acid catalysis the diene acetate also exchanged the acetate group with the solvent prior to rearomatization and the rapid formation of isomeric adducts could be observed when the sulfuric acid concentration was 0.05% and 0.5%.

[10]The ^{1}H nmr spectra exhibited a *tert*-butyl peak at 1.12 ppm and vinylic-allylic absorptions at 5.9 ppm as well as the peaks characteristic of **6**. The *tert*-butyl peak in **6** is at 0.99 ppm and the lower-field *tert*-butyl peak is characteristic of a *tert*-butyl group attached to a double bond (2). The ^{13}C spectra exhibited peaks, in addition to those of **6**, at 29.8 (CH_3 of *tert*-butyl), 35.0 (4°-*C* of *tert*-butyl), 65.2 and 65.1 (3°-*C* of ring), and 87.8 and 89.6 ppm (4°-*C* of ring). The peaks for the tertiary and quaternary carbons were assigned with the aid of undecoupled spectra. The *tert*-butyl absorptions are closely similar to those of the 1,2 adduct of 4-*tert*-butyltoluene (2) and significantly shifted from the absorptions of the 1,4 adduct. The 3°-*C* absorption can only be attributed to a 1,2 adduct. The doubling of the ring carbon peaks indicates that a *pair* of diastereoisomeric 1,2 adducts was formed.

Can. J. Chem. Downloaded from www.nrcresearchpress.com by 210.87.254.40 on 09/05/12
For personal use only.

TABLE 3. Yields[a] of products of rearomatization of diene **6** with sulfuric acid and 10% acetic anhydride in [$^2H_4$]acetic acid

% H_2SO_4	**3***b*	**4***a*	**5**	**8***c*	Others
0	46	10	6	5	12,[b] 8,[c] 13[c]
0.05	43	17	21	3	17[b]
0.5	37	29	22	3	6,[b] 3[c]
5.0	26	57	15	3	
50		66	12	5	17[d]

[a]From glc – mass spectral data, peaks appeared in the order with observed M^+: **8***c* (122), **5** (176), **3***b* (223, [$^2H_3$]acetate), nitroarene (207), **4***a* (207).
[b]Nitroarene, probably benzylic derivative or **3***a*.
[c]Unidentified compound.
[d]A nitroarene (M^+ 207), probably **3***a* or benzylic derivative.

*Reaction of Diene **6** with Trifluoroacetic Acid*

Diene **6** (107 mg, 0.40 mmol) in $CDCl_3$ (200 mm^3) was cooled to −60°C and mixed with CF_3COOH (200 mm^3). The nmr spectrum showed that the reaction was complete on mixing. After work-up,[11] nmr and glc – mass spectral analyses established the major product as **4***a* (92%). Two minor products (4% each) appeared to be isomeric nitroarenes (M^+ 207), one of them the benzylic derivative (^{1}H nmr ($CDCl_3$) δ: 5.25 ppm).

*Reaction of Diene **6** with Boron Trifluoride*

Diene **6** (107 mg, 0.40 mmol) was dissolved in $CDCl_3$ (200 mm^3), cooled to −70°C and $BF_3 \cdot Et_2O$ (200 mm^3) was added. Observation by nmr indicated that the reaction was complete at −70°C. After work-up and examination by ^{1}H nmr and glc – mass spectrometry, the products were identified as **4***a*, (97%) and an isomeric nitroarene (3%, M^+ 207).

*Reaction of Diene **6** with Hydrogen Chloride*

A solution of diene **6** (500 mg, 1.87 mmol) in dry ether (25 cm^3) was cooled to −5°C and hydrogen chloride was bubbled through the solution for ca. 20 min. The ^{1}H nmr spectrum after work-up indicated that chloronitrodiene adducts had been formed. Chromatography on alumina yielded a pale greenish liquid. Nuclear magnetic resonance and glc – mass spectrometry showed the products after chromatography to be 4-*tert*-butyl-5-chloro-1,2-dimethylbenzene (**3***d*), (76%) and 4-*tert*-butyl-6-chloro-1,2-dimethylbenzene (**4***d*), (24%). The chloronitrodiene adducts had decomposed.

*Reaction of Diene **6** with Sodium Methoxide in Methanol*

A solution of diene **6** (100 mg, 0.38 mmol) in $CDCl_3$ (200 mm^3) was treated with a solution of CH_3ONa (0.75 mmol) in CH_3OH (250 mm^3) at 0°C. After 10 min the solution turned bright orange and sodium acetate precipitated. The product was acidified and worked up, and the composition was established by nmr and glc – mass spectrometry: **8***c* (15%, M^+ 122), two unidentified compounds (2% each), **4***c* (13%, M^+ 178), **3***c* (56%, M^+ 178), **3***b* (8%, M^+ 220), nitroarene (4%, M^+ 207).

[11]Small-scale reactions were worked up by adding the solution to methylene chloride (5 cm^3) followed by neutralization with gaseous ammonia, aspiration of the excess ammonia, drying over magnesium sulfate, filtration, and removal of the solvent under reduced pressure.

*Thermolysis of Diene **6***

A solution of **6** in pentane was injected into the inlet of a gas chromatograph at 260°C. Thermolysis proceeded smoothly giving rise to five well-resolved peaks. These peaks were identified by comparison of their retention times with those of authentic samples, and by glc – mass spectrometry. The products were in the order of retention time: parent hydrocarbon **2** (68%, M^+ 162), **8***b* (8%, M^+ 164), a nitroarene (1%, M^+ 207), **3***b* (16%, M^+ 220), **4***a* (7%, M^+ 207).

*Thermolysis of Diene **7***

An ethereal solution of **7** was injected into the inlet of a gas chromatograph at 260°C. Thermolysis proceeded smoothly giving rise to seven well-resolved peaks. Five peaks were identified by comparison of their retention times with those of authentic samples and by glc – mass spectrometry. The compounds were in order of retention time: parent hydrocarbon **2** (32%, M^+ 162), **8***c* (30%, M^+ 122), two unidentified compounds (3%, 5%), **4***c* (19%, M^+ 178), **3***c* (5%, M^+ 178), a nitroarene (6%, M^+ 207).

1. C. L. PERRIN and G. A. SKINNER. J. Am. Chem. Soc. **93**, 3389 (1971).
2. A. FISCHER and R. RÖDERER. Can. J. Chem. **54**, 3978 (1976).
3. M. W. GALLEY and R. C. HAHN. J. Am. Chem. Soc. **96**, 4337 (1974).
4. P. C. MYHRE. J. Am. Chem. Soc. **94**, 7921 (1972).
5. A. FISCHER and J. N. RAMSAY. J. Am. Chem. Soc. **96**, 1614 (1974); J. N. RAMSAY. Ph.D. Thesis, University of Victoria, Victoria, B.C. 1973.
6. A. FISCHER, C. C. GREIG, and R. RÖDERER. Can. J. Chem. **53**, 1570 (1975).
7. (*a*) D. J. BLACKSTOCK, A. FISCHER, K. E. RICHARDS, J. VAUGHAN, and G. J. WRIGHT. Chem. Commun. 641 (1970); (*b*) D. J. BLACKSTOCK, J. R. CRETNEY, A. FISCHER, M. P. HARTSHORN, K. E. RICHARDS, J. VAUGHAN, and G. J. WRIGHT. Tetrahedron Lett. 2793 (1970).
8. A. FISCHER and G. J. WRIGHT. Aust. J. Chem. **27**, 217 (1974).
9. A. FISCHER and C. C. GREIG. Can. J. Chem. **52**, 1231 (1974); A. FISCHER and D. R. A. LEONARD. Can. J. Chem. **50**, 3367 (1972); A. FISCHER, C. C. GREIG, A. L. WILKINSON, and D. R. A. LEONARD. Can. J. Chem. **50**, 2211 (1972).
10. J. R. KNOWLES, R. O. C. NORMAN, and G. K. RADDA. J. Chem. Soc. 4485 (1960).
11. G. A. OLAH and S. J. KUHN. J. Am. Chem. Soc. **86**, 1067 (1964).
12. A. FISCHER and D. A. R. LEONARD. Can. J. Chem. **54**, 1795 (1976).
13. A. FISCHER and R. RÖDERER. Can. J. Chem. **54**, 423 (1976).
14. A. FISCHER and J. N. RAMSAY. Can. J. Chem. **52**, 3960 (1974).
15. (*a*) T. BANWELL, C. S. MORSE, P. C. MYHRE, and A. VOLLMAR. J. Am. Chem. Soc. **99**, 3042 (1977); (*b*) P. C. MYHRE. Personal communication.
16. H. SUZUKI and K. NAKAMURA. Synthesis, 606 (1972); S. D. ROSS, F. R. COBURN, and M. FINKLESTEIN. J. Org. Chem. **33**, 585 (1968).
17. R. G. GILLIS. J. Org. Chem. **21**, 805 (1956).
18. M. J. SCHLATTER. J. Am. Chem. Soc. **76**, 4952 (1954).

Can. J. Chem. Downloaded from www.nrcresearchpress.com by 210.87.254.5 on 09/05/12
For personal use only.

Canadian Journal of Chemistry

Published by
THE NATIONAL RESEARCH COUNCIL OF CANADA

Journal canadien de chimie

Publié par
LE CONSEIL NATIONAL DE RECHERCHES DU CANADA

Volume 56 Number 3 February 1, 1978

Volume 56 numéro 3 1 février 1978

Crystal and molecular structure of bis(perchlorato)(γ-*C*-*meso*-5,5,7,12,14,14-hexamethyl-1,4,8,11-tetraazacyclotetradecane)copper (II)

EI-ICHIRO OCHIAI, STEVEN J. RETTIG, AND JAMES TROTTER

Department of Chemistry, University of British Columbia, 2075 Wesbrook Mall, Vancouver, B.C., Canada V6T 1W5

Received August 22, 1977

EI-ICHIRO OCHIAI, STEVEN J. RETTIG, and JAMES TROTTER. Can. J. Chem. **56**, 267 (1978).

Crystals of bis(perchlorato) (γ-*C*-*meso*-5,5,7,12,14,14-hexamethyl-1,4,8,11-tetraazacyclotetradecane)copper(II) are monoclinic, $a = 14.061(1)$, $b = 8.908(1)$, $c = 19.710(1)$ Å, $\beta = 90.912(5)°$, $Z = 4$, space group $P2_1/c$. The structure was solved by Patterson and Fourier syntheses and was refined by full-matrix least-squares procedures to a final R of 0.054 and R_w of 0.069 for 2945 reflections with $I \geq 3\sigma(I)$. The copper(II) ion has tetragonally distorted octahedral coordination geometry. The four nitrogen atoms of the macrocyclic ligand occupy the equatorial sites and two perchlorate oxygen atoms are in the axial positions. Bond lengths (corrected for libration) are: Cu—N, 2.024(4)–2.051(4), Cu—O, 2.657(5) and 2.697(5), Cl—O, 1.420(4)–1.473(6), N—C, 1.463(6)–1.508(6), and C—C, 1.498(8)–1.542(8) Å.

EI-ICHIRO OCHIAI, STEVEN J. RETTIG et JAMES TROTTER. Can. J. Chem. **56**, 267 (1978).

Les cristaux du bis(perchlorato) (γ-*C*-*méso*-hexaméthyl-5,5,7,12,14,14 tétraaza-1,4,8,11 tétradécane)cuivre(II) sont monocliniques: $a = 14.061(1)$, $b = 8.908(1)$, $c = 19.710(1)$ Å, $\beta = 90.912(5)°$, $Z = 4$, groupe d'espace $P2_1/c$. On a résolu la structure par des synthèses de Patterson et Fourier et on l'a affinée par la méthode des moindres carrés (matrice complète) jusqu'à une valeur finale de R de 0.054 et R_w de 0.069 pour 2945 réflexions avec $I \geq 3\sigma(I)$. L'ion cuivrique-(II) possède un géométrie de coordination octaédrique déformée d'une façon tétraédrique. Les quatre atomes d'azote du ligand macrocyclique occupent des sites équatoriaux et les deux atomes d'oxygène du perchlorate sont en positions axiales. Les longueurs de liaison (corrigées pour les librations) sont: Cu—N, 2.024(4)–2.051(4), Cu—O, 2.657(5) et 2.697(5), Cl—O, 1.420(4)–1.473(6), N—C, 1.463(6)–1.508(6) et C—C, 1.498(8)–1.542(8) Å.

[Traduit par le journal]

Introduction

The metal complexes of synthetic macrocyclic ligands have attracted considerable attention in recent years (1–4). Nickel(II) and cobalt(II) derivatives dominated earlier studies, partly because of their interesting stereochemistries (1, 5).

Cobalt(II or III) (6) and iron(II or III) (7) derivatives of synthetic macrocycles obviously serve as model compounds for such important biologically active molecules as cobalamin (vitamin B_{12}), and iron porphyrins in hemoglobin and peroxidase.

The macrocyclic ligand in the present study, *meso*-5,5,7,12,14,14-hexamethyl-1,4,8,11-tetraazacyclotetradecane(1,4-CTH), is derived from 5,7,7,12,12,14-hexamethyl-1,4,8,11-tetraazacyclotetradeca-1(14),4-diene (1,4-CT) (2, 8). The ligand was allowed to react with copper(II) perchlorate, forming the present complex, $[Cu(1,4\text{-}CTH)](ClO_4)_2$.

Earlier studies of related macrocycle copper(II) complexes include work on $[Cu(1,4\text{-}CT)]^{2+}$ and $[Cu(1,7\text{-}CT)]^{2+}$ (9) where 1,7-CT refers to 5,5,7,12,12,14-hexamethyl-1,4,8,11-tetraazacyclotetradeca-1(14),7-diene. The crystal structures of $[Ni(1,7\text{-}CT)](ClO_4)_2$ (10) and $[Ni(1,4\text{-}CT)](ClO_4)_2$ (11) were determined as early as 1966. The skeletal structure of both 1,4-CTH and 1,7-CTH is represented by cyclam (1,4,8,11-tetraazacyclotetradecane). A number of transition metal complexes incorporating saturated macrocyclic tetraaza ligands have been characterized by X-ray crystallography: $[Ni(cyclam)]Cl_2$ (12),

Can. J. Chem. Downloaded from www.nrcresearchpress.com by 210.87.254.5 on 09/05/12
For personal use only.

TABLE 1. Final positional parameters (fractional × 10^4, Cu and Cl × 10^5, H × 10^3) with estimated standard deviations in parentheses

Atom	x	y	z
Cu	24931(4)	50304(7)	62009(3)
Cl(1)	5265(10)	24440(15)	58040(7)
Cl(2)	44714(11)	75562(18)	66806(7)
O(1)	957(3)	3258(6)	6353(2)
O(2)	−303(3)	1722(6)	5995(2)
O(3)	392(4)	3434(7)	5265(3)
O(4)	1226(4)	1382(6)	5619(3)
O(5)	4177(3)	6383(6)	6226(3)
O(6)	3737(4)	8667(6)	6648(4)
O(7)	4479(4)	6991(8)	7340(2)
O(8)	5341(3)	8174(7)	6501(3)
N(1)	3119(3)	3044(5)	6002(2)
N(2)	2758(3)	4550(5)	7192(2)
N(3)	1866(3)	7028(5)	6402(2)
N(4)	2223(3)	5534(5)	5204(2)
C(1)	3638(4)	2597(6)	6626(3)
C(2)	3019(4)	2956(6)	7226(3)
C(3)	2030(4)	5013(6)	7684(2)
C(4)	1878(4)	6692(6)	7641(3)
C(5)	1316(3)	7335(5)	7034(2)
C(6)	1382(5)	7517(7)	5762(3)
C(7)	2022(5)	7143(6)	5188(3)
C(8)	2817(3)	4951(6)	4632(2)
C(9)	3045(5)	3299(7)	4763(3)
C(10)	3672(4)	2896(6)	5371(3)
C(11)	2298(8)	4576(11)	8407(3)
C(12)	1254(7)	9044(7)	7139(4)
C(13)	331(4)	6662(10)	6981(4)
C(14)	2238(7)	5041(11)	3969(3)
C(15)	3715(5)	5869(9)	4564(4)
C(16)	4091(8)	1337(10)	5285(5)
H(N1)	264(3)	243(5)	601(2)
H(N2)	313(3)	498(5)	725(2)
H(N3)	222(3)	752(5)	642(2)
H(N4)	176(3)	524(5)	516(2)
H(1a)	431(3)	319(4)	669(2)
H(1b)	372(3)	149(5)	664(2)
H(2a)	235(4)	233(5)	716(2)
H(2b)	332(3)	270(5)	767(2)
H(3)	133(4)	434(6)	760(2)
H(4a)	147(3)	699(4)	800(2)
H(4b)	247(4)	715(6)	767(3)
H(6a)	66(3)	693(4)	576(2)
H(6b)	129(5)	858(8)	577(3)
H(7a)	273(5)	762(8)	524(3)
H(7b)	177(4)	746(6)	476(3)
H(9a)	342(3)	311(4)	446(2)
H(9b)	246(5)	272(8)	477(3)
H(10)	428(3)	365(6)	546(2)
H(11a)	286(3)	534(5)	850(2)
H(11b)	170(6)	465(9)	861(4)
H(11c)	247(6)	351(10)	846(4)
H(12a)	93(4)	913(6)	761(3)
H(12b)	189(5)	937(8)	720(3)
H(12c)	80(6)	954(9)	680(4)
H(13a)	−6(5)	669(7)	743(3)
H(13b)	−13(5)	720(7)	663(3)
H(13c)	36(5)	548(8)	677(3)
H(14a)	169(6)	450(9)	405(4)
H(14b)	195(4)	620(8)	386(3)
H(14c)	257(6)	464(10)	364(4)

TABLE 1 (*Concluded*)

Atom	x	y	z
H(15a)	420(4)	545(6)	421(3)
H(15b)	357(5)	688(9)	433(4)
H(15c)	399(4)	603(6)	500(3)
H(16a)	351(4)	76(6)	532(3)
H(16b)	443(6)	142(9)	488(4)
H(16c)	454(5)	84(9)	563(4)

$[Cu(cyclam)](ClO_4)_2$ (13), $[Co(cyclam)](ClO_4)_2$ (14), $[Mn(1,7\text{-CTH})Cl_2]Cl\cdot 3H_2O$ (15), two isomers of $[Ni(1,7\text{-CTH})](ClO_4)_2$ (16), $[Ni(1,7\text{-CTH})]ZnCl_4\cdot H_2O$ (16), $[Ni(N,N,N,N\text{-tetramethylcyclam})]_2(N_3)_3I$ (17), $[Co(cyclam)Cl_2]Cl$ (18), $[Co(cyclam)(H_2NCH_2\text{-}CH_2NH_2)]Cl_3\cdot 3H_2O$ (19), $[Cu(1,7\text{-CTH})]_2Cl(ClO_4)_3$ (20), and $[Ni(1,7\text{-CTH})(C_5H_8O_2)]ClO_4$ (21).

Experimental

Preparation of Bis(perchlorato) (γ-C-meso-5,5,7,12,14,14-hexamethyl-1,4,8,11-tetraazacyclotetradecane)copper(II)

The complex was prepared by a method similar to the one described by Curtis (22). (5,7,7,12,12,14-Hexamethyl-1,4,8,11-tetraazacyclotetradeca-1(14),4-diene)nickel(II) perchlorate was prepared from acetone and tris(ethylenediamine)nickel(II) perchlorate (2), and was then hydrogenated with platinum oxide catalyst (22). The ligand was isolated by adding sodium cyanide to the nickel complex. The stoichiometric amounts of copper(II) perchlorate and the perchlorate salt of the ligand were mixed, and the solution was slowly evaporated to give needle crystals. *Anal.* calcd. for $Cu(C_{16}H_{36}N_4)(ClO_4)_2$: C 35.14, H 6.63, N 10.24; found: C 35.00, H 6.67, N 10.15.

X-Ray Crystallographic Analysis of Bis(perchlorato) (γ-C-meso-5,5,7,12,14,14-hexamethyl-1,4,8,11-tetraazacyclotetradecane)copper(II)

The crystal chosen for study was mounted with *b* parallel to the goniostat axis and had dimensions of ca. 0.3 × 0.4 × 0.25 mm. Unit-cell and space group data were obtained from film and diffractometer measurements. The unit-cell parameters were refined by least squares on 2 sin θ/λ values for 30 reflections measured on a diffractometer with Cu K_α radiation (λ = 1.5418 Å). Crystal data (at 22°C) are:

$C_{16}H_{36}Cl_2CuN_4O_8$ fw = 546.9

Monoclinic, a = 14.061(1), b = 8.908(1), c = 19.710(1) Å, β = 90.912(5)°, V = 2468.5(5) Å^3, Z = 4, ρ_c = 1.472 g cm^{-3}, $F(000)$ = 1148, μ(Cu K_α) = 37.2 cm^{-1}. Absent reflections: $0k0$, $k \neq 2n$ and $h0l$, $1 \neq 2n$ define uniquely the space group $P2_1/c$ (C_{2h}^5, No. 14).

Intensities were measured with nickel-filtered Cu K_α radiation on a Datex-automated General Electric XRD-6 diffractometer. A θ–2θ scan at 2° min^{-1} over a range of (1.80 + 0.86 tan θ) degrees in 2θ was employed; 10 s background counts were measured at each end of the scan. Data were measured to 2θ = 145°. The intensities of the check reflections, measured every 40 reflections throughout the data collection, decreased slowly and uniformly to values which were 0.84 times the initial values. Lorentz and polarization corrections and batch check reflection scaling were applied, and the structure amplitudes were derived. No absorption correction was made due to irregularity of the crystal surface. Of the 4890 independent reflections measured, 2957 (60%) had intensities greater than 3σ(I) above background where $\sigma^2(I) = S + B +$

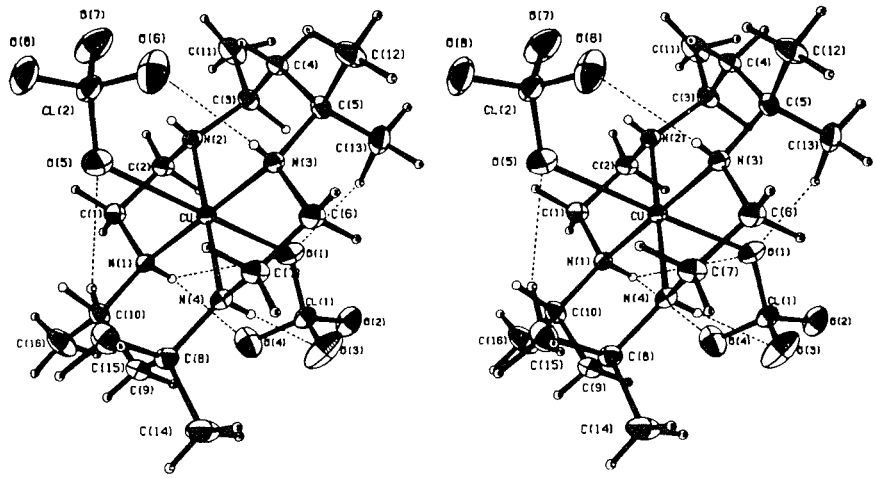

FIG. 1. A stereo view of the bis(perchlorato)(γ-*C*-*meso*-5,5,7,12,14,14-hexamethyl-1,4,8,11-tetraazacyclotetradecane)-copper(II) molecule, 50% ellipsoids are shown for the nonhydrogen atoms. Hydrogen atoms have been assigned artificially small thermal parameters for the sake of clarity.

TABLE 3. Bond lengths (Å) with estimated standard deviations in parentheses
(*a*) Nonhydrogen atoms

	Distance			Distance	
Bond	Uncorrected	Corrected	Bond	Uncorrected	Corrected
Cu—O(1)	2.697(5)		N(2)—C(3)	1.480(6)	1.483
Cu—O(5)	2.657(5)		N(3)—C(5)	1.500(6)	1.502
Cu—N(1)	2.018(4)	2.024	N(3)—C(6)	1.490(6)	1.492
Cu—N(2)	2.028(4)	2.035	N(4)—C(7)	1.462(6)	1.463
Cu—N(3)	2.028(4)	2.034	N(4)—C(8)	1.506(6)	1.508
Cu—N(4)	2.045(4)	2.051	C(1)—C(2)	1.513(7)	1.517
Cl(1)—O(1)	1.429(4)	1.470	C(3)—C(4)	1.514(7)	1.518
Cl(1)—O(2)	1.390(4)	1.420	C(3)—C(11)	1.520(8)	1.522
Cl(1)—O(3)	1.391(5)	1.431	C(4)—C(5)	1.534(7)	1.537
Cl(1)—O(4)	1.417(5)	1.459	C(5)—C(12)	1.540(8)	1.542
Cl(2)—O(5)	1.434(5)	1.475	C(5)—C(13)	1.511(8)	1.514
Cl(2)—O(6)	1.430(6)	1.473	C(6)—C(7)	1.494(8)	1.498
Cl(2)—O(7)	1.393(5)	1.436	C(8)—C(9)	1.528(8)	1.532
Cl(2)—O(8)	1.392(4)	1.422	C(8)—C(14)	1.530(8)	1.533
N(1)—C(1)	1.476(6)	1.479	C(8)—C(15)	1.512(8)	1.515
N(1)—C(10)	1.482(6)	1.485	C(9)—C(10)	1.519(7)	1.523
N(2)—C(2)	1.467(6)	1.471	C(10)—C(16)	1.519(9)	1.522

$(0.06S)^2$ with S = scan count and B = time averaged background count.

The initial stages of the structure determination and refinement were carried out using the 1299 observed reflections with $2\theta \leq 90°$. The positions of the copper and chlorine atoms were determined from the three-dimensional Patterson function. Two cycles of full-matrix least-squares refinement of the Cu and Cl atoms with isotropic thermal parameters gave R = 0.451. An electron density difference map gave positions for the oxygen, nitrogen, and 10 of the 16 carbon atoms. These atoms were refined for two cycles giving R = 0.216 and a difference map revealed the positions of the remaining carbon atoms. The 31 nonhydrogen atoms were refined for one cycle with isotropic thermal parameters, and then for two cycles with anisotropic thermal parameters, resulting in an R value of 0.076. The hydrogen atom positions were taken from a difference map calculated at this point. The entire structure (hydrogen atoms having isotropic thermal parameters and using the complete data set) was refined for three cycles giving a final R of 0.054 and R_w of 0.069 for 2945 reflections with $I \geq 3\sigma(I)$ (12 observed and 2 unobserved reflections which had $|F_o| - |F_c| > 3\sigma(F)$ were treated as unobserved in the final stages of refinement; instrumental error was suspected for these reflections but it seemed unwise to bias the data by remeasuring them; none of the disagreements were exceptionally bad). For all 4890 reflections R = 0.094 and R_w = 0.088.

A correction for secondary extinction was approximated by basing the least-squares refinement on the minimization of $\Sigma w[|F_o| - |F_c|/(1 + gI)|]^2$ where g is the extinction parameter and I the uncorrected intensity. The final value of g was 3.7 $\times 10^{-8}$. The scattering factors of ref. 23 were used for the nonhydrogen atoms and those of ref. 24 for the hydrogen atoms. Anomalous scattering factors from ref. 25 were used for the nonhydrogen atoms. The weighting scheme, $w = 1/\sigma^2(F)$

Can. J. Chem. Downloaded from www.nrcresearchpress.com by 210.87.254.5 on 09/05/12
For personal use only.

Can. J. Chem. Downloaded from www.nrcresearchpress.com by 210.87.254.5 on 09/05/12
For personal use only.

TABLE 4. Bond angles (deg) with estimated standard deviations in parentheses
(*a*) Nonhydrogen atoms

Bonds	Angle(deg)	Bonds	Angle(deg)
O(1)—Cu—O(5)	168.2(2)	Cu—N(2)—C(2)	106.9(3)
O(1)—Cu—N(1)	82.0(2)	Cu—N(2)—C(3)	117.0(3)
O(1)—Cu—N(2)	84.5(2)	C(2)—N(2)—C(3)	114.5(4)
O(1)—Cu—N(3)	98.1(2)	Cu—N(3)—C(5)	123.6(3)
O(1)—Cu—N(4)	95.7(2)	Cu—N(3)—C(6)	106.5(3)
O(5)—Cu—N(1)	90.6(2)	C(5)—N(3)—C(6)	114.5(4)
O(5)—Cu—N(2)	85.9(2)	Cu—N(4)—C(7)	105.6(3)
O(5)—Cu—N(3)	89.3(2)	Cu—N(4)—C(8)	123.2(3)
O(5)—Cu—N(4)	94.0(2)	C(7)—N(4)—C(8)	115.5(4)
N(1)—Cu—N(2)	85.9(2)	N(1)—C(1)—C(2)	108.1(4)
N(1)—Cu—N(3)	179.9(2)	N(2)—C(2)—C(1)	108.4(4)
N(1)—Cu—N(4)	94.6(2)	N(2)—C(3)—C(4)	109.7(4)
N(2)—Cu—N(3)	94.0(2)	N(2)—C(3)—C(11)	112.3(5)
N(2)—Cu—N(4)	179.5(2)	C(4)—C(3)—C(11)	109.8(5)
N(3)—Cu—N(4)	85.5(2)	C(3)—C(4)—C(5)	118.9(4)
O(1)—Cl(1)—O(2)	111.3(3)	N(3)—C(5)—C(4)	108.3(4)
O(1)—Cl(1)—O(3)	108.1(4)	N(3)—C(5)—C(12)	108.9(5)
O(1)—Cl(1)—O(4)	104.7(3)	N(3)—C(5)—C(13)	110.8(5)
O(2)—Cl(1)—O(3)	113.7(3)	C(4)—C(5)—C(12)	107.0(5)
O(2)—Cl(1)—O(4)	110.4(3)	C(4)—C(5)—C(13)	111.4(5)
O(3)—Cl(1)—O(4)	108.2(4)	C(12)—C(5)—C(13)	110.3(6)
O(5)—Cl(2)—O(6)	106.4(3)	N(3)—C(6)—C(7)	107.7(4)
O(5)—Cl(2)—O(7)	108.8(4)	N(4)—C(7)—C(6)	108.7(4)
O(5)—Cl(2)—O(8)	111.1(3)	N(4)—C(8)—C(9)	108.8(4)
O(6)—Cl(2)—O(7)	106.7(4)	N(4)—C(8)—C(14)	109.1(5)
O(6)—Cl(2)—O(8)	110.5(3)	N(4)—C(8)—C(15)	110.7(5)
O(7)—Cl(2)—O(8)	113.1(3)	C(9)—C(8)—C(14)	107.6(5)
Cu—O(1)—Cl(1)	122.9(3)	C(9)—C(8)—C(15)	111.2(5)
Cu—O(5)—Cl(2)	126.2(3)	C(14)—C(8)—C(15)	109.2(6)
Cu—N(1)—C(1)	106.6(3)	C(8)—C(9)—C(10)	118.6(5)
Cu—N(1)—C(10)	118.5(3)	N(1)—C(10)—C(9)	109.6(4)
C(1)—N(1)—C(10)	114.6(4)	N(1)—C(10)—C(16)	112.6(5)
C(9)—C(10)—C(16)	110.5(6)		

where $\sigma^2(F)$ is derived from the previously defined $\sigma^2(I)$ gave uniform average values of $w(|F_o| - |F_c|)^2$ over ranges of $|F_o|$ and was employed in the final stages of refinement.

On the final cycle of refinement the mean parameter shift was 0.38σ and the largest shift (3.2σ) was associated with a hydrogen atom. The mean error in an observation of unit weight was 1.503. The final positional and thermal parameters appear in Tables 1 and 2, respectively; measured and calculated structure factors have been placed in the Depository of Unpublished Data.[1]

The ellipsoids of thermal motion for the nonhydrogen atoms are shown in Fig. 1. The thermal motion has been analysed in terms of the rigid-body modes of translation (T), libration (**L**), and screw (**S**) motion (26) using the computer program MGTLS. The rms standard error in the temperature factors σU_{ij} (derived from the least-squares analysis) is 0.0035 Å^2. Analyses of the two perchlorate and [Cu, N(1)–N(4), C(1)–C(10)] groups (rms ΔU_{ij} = 0.0026, 0.0016, and 0.0039 Å^2, respectively) gave physically reasonable rigid-body thermal parameters.

The appropriate bond distances have been corrected for

[1]The structure factor table and Tables 2 (thermal parameters), 3*b*, and 4*b* (bond lengths and angles involving hydrogen), 7 (mean plane), and 6*a* (nonbonded distances) are available, at a nominal charge, from the Depository of Unpublished Data, CISTI, National Research Council of Canada, Ottawa, Canada K1A 0S2.

TABLE 5. Intra-annular torsion angles (deg)

Bond	Angle observed	Bond	Angle observed
	Five-membered chelate rings		
Cu—N(1)	15.6(3)	Cu—N(3)	−13.0(3)
N(1)—C(1)	−41.2(4)	N(3)—C(6)	40.1(4)
C(1)—C(2)	55.0(4)	C(6)—C(7)	−57.2(5)
C(2)—N(2)	−49.6(4)	C(7)—N(4)	43.7(4)
N(2)—Cu	13.5(3)	N(4)—Cu	−16.7(3)
	Six-membered chelate rings		
Cu—N(2)	−36.8(3)	Cu—N(4)	27.4(3)
N(2)—C(3)	58.4(4)	N(4)—C(8)	−42.3(4)
C(3)—C(4)	−74.7(4)	C(8)—C(9)	65.7(5)
C(4)—C(5)	64.4(5)	C(9)—C(10)	−74.9(5)
C(5)—N(3)	−44.1(4)	C(10)—N(1)	55.9(4)
N(3)—Cu	31.3(3)	N(1)—Cu	−33.2(3)
	Cyclam ring		
N(1)—C(1)	−174.5(4)	N(3)—C(6)	−179.6(4)
C(1)—C(2)	55.0(4)	C(6)—C(7)	−57.2(5)
C(2)—N(2)	−170.8(4)	C(7)—N(4)	−176.6(4)
N(2)—C(3)	−175.5(4)	N(4)—C(8)	−174.3(4)
C(3)—C(4)	−74.7(4)	C(8)—C(9)	65.7(5)
C(4)—C(5)	64.4(5)	C(9)—C(10)	−74.9(5)
C(5)—N(3)	−176.8(4)	C(10)—N(1)	−176.7(4)

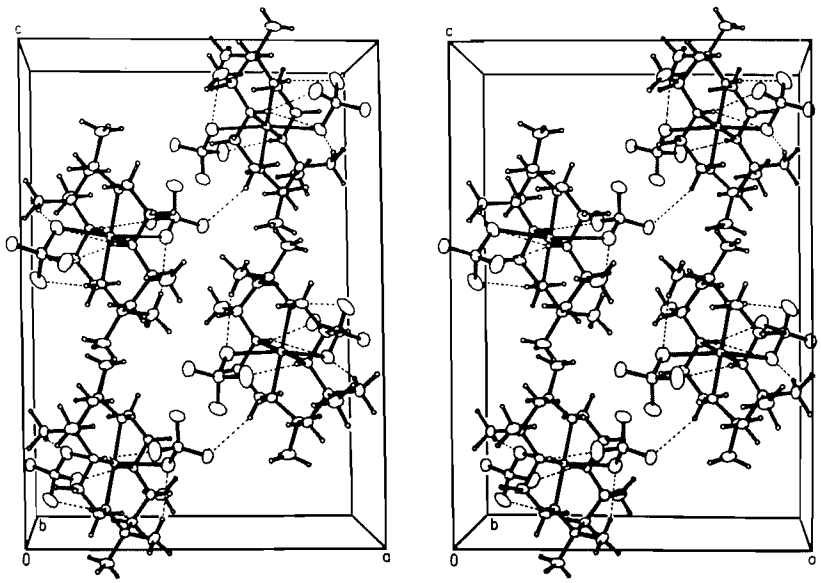

FIG. 2. The crystal structure of bis(perchlorato)(γ-*C*-*meso*-5,5,7,12,14,14-hexamethyl-1,4,8,11-tetraazacyclotetradecane)-copper(II) viewed along *b*.

libration (27, 28), using shape parameters q^2 of 0.08 for all atoms involved. Bonds involving the methyl groups were corrected for independent motion based on the ΔU_{ij} (29, 30). Corrected bond lengths appear in Table 3[1] along with the uncorrected values. Corrected bond angles are not significantly different from the uncorrected value listed in Table 4.[1]

Results and Discussion

A general view of the complex, with the crystallographic numbering scheme, is shown in Fig. 1 and the packing arrangement is shown in Fig. 2. Intraannular torsion angles are given in Table 5 and the geometry of the O···H contacts in Table 6*b*. Deviations of atoms from the CuN_4 mean plane (Table 7) and selected nonbonded distances (Table 6*a*) have been deposited.[1]

The crystal structure consists of discrete molecules of Cu(1,4-CTH)$(ClO_4)_2$ linked by a network of weak C—H···O interactions (there are five intermolecular O···H distances between 2.5 and 2.6 Å, see Table 6*b*).

The copper(II) ion has a typical tetragonally distorted octahedral coordination geometry. The four nitrogen atoms of the macrocyclic ligand occupy the equatorial sites at distances ranging from 2.024(4) to 2.051(4) Å. The axial positions are occupied by perchlorate oxygen atoms at distances of 2.657(5) and 2.697(5) Å. The equatorial CuN_4 group is planar within experimental error ($\chi^2 = 0.76$). Bond angles at the copper atom within the equatorial group differ significantly, those in the five-membered chelate rings being 85.9(2) and 85.5(2)° and those in the six-membered rings being 94.6(2) and 94.0(2)°. The angle between the axial oxygen atoms is 168.2(2)° and angles between equatorial and axial substituents range from 82.0(2) to 98.1(2)°. These values are in good agreement with those found in other complexes which have saturated tetraaza ligands occupying equatorial coordination sites (12–17).

The Cu—O bonds are longer than the value of 2.57(4) Å in the centrosymmetric complex Cu(cyclam)$(ClO_4)_2$ (13), probably as a result of steric interactions with the six methyl groups. The geometry of the weakly coordinated perchlorate groups is similar to that found for a number of octahedral copper(II) complexes (summarized in ref. 13) and the related complex bis(perchlorato)(1,4,8,11-tetrathiacyclotetradecane)copper(II) (31). In addition to weak Cu—O bonds, the perchlorate groups are also linked to the rest of the molecule by a number of weak intramolecular N (and C) —H···O interactions (summarized in Table 6*b*). The Cu—N distances are as expected for this type of complex (13, and summaries in ref. 32).

The complex has approximate C_2 symmetry with the twofold axis passing through the midpoints of the C(1)—C(2) and C(6)—C(7) bonds and the copper atom. The ligand has the energetically favorable γ conformation (18) with both amine hydrogen atoms of one six-membered chelate ring on one side of the molecular plane and both amine hydrogen atoms of the second six-membered ring on the opposite side of the plane. The saturated macrocyclic tetraaza ligands sometimes adopt folded conformations and occupy *cis* coordination sites about an octahedral metal (18, 19, 21, 22) or occupy two equatorial and two axial positions about a trigonal bipyramidal metal (20). The α conformation of the ligand (with adjacent

Can. J. Chem. Downloaded from www.nrcresearchpress.com by 210.87.254.5 on 09/05/12
For personal use only.

TABLE 6*b*. Geometry of O···H contacts < 2.6 Å. Distances in Å and angles in deg*

D—H···A	H···A	D···A	∠DHA	∠XAH
N(1)—H(N1)···O(1)	2.58(5)	3.135(6)	123(4)	92(1)
N(1)—H(N1)···O(4)	2.31(5)	3.128(6)	156(4)	104(1)
N(3)—H(N4)···O(6)	2.40(4)	3.041(7)	163(5)	111(1)
N(4)—H(N4)···O(3)	2.52(4)	3.186(6)	159(4)	112(1)
C(1)—H(1b)···O(6)[5]	2.51(5)	3.504(8)	174(3)	134(1)
C(2)—H(2b)···O(8)[6]	2.51(5)	3.386(8)	147(4)	115(1)
C(4)—H(4a)···O(2)[7]	2.60(4)	3.510(8)	158(3)	134.9(9)
C(6)—H(6a)···O(3)[1]	2.50(4)	3.299(8)	126(2)	127.1(9)
C(6)—H(6b)···O(4)[8]	2.52(7)	3.461(8)	170(5)	131(1)
C(13)—H(13c)···O(1)	2.30(7)	3.40(1)	160(5)	123(2)
C(15)—H(15c)···O(5)	2.44(6)	3.36(1)	162(5)	138(1)

*Superscripts refer to atoms at positions: [1] $-x, 1-y, 1-z$; [2] $1-x, 1/2+y, 3/2-z$; [3] $1-x, 1-y, 1-z$; [4] $x, 3/2-y, 1/2+z$; [5] $x, y-1, z$; [6] $1-x, y-1/2, 3/2-z$; [7] $-x, 1/2+y, 3/2-z$; [8] $x, 1+y, z$.

amine hydrogen atoms alternately above and below the molecular plane) is particularly prone to folding. Structural examples of all three possible ligand conformations exhibiting planar coordination are given for $[Ni(1,7\text{-CTH})]^{2+}$ (16).

The torsion angles around the 14-membered ring (Table 5) (which are ideally ± 60 or 180° for planar coordination) indicate relatively low ring strain, intermediate between that observed for cyclam and 1,7-CTH complexes (see Table III in ref. 31 for example). The five-membered chelate rings have slightly distorted *gauche* conformations and the six-membered chelate rings have distorted chair conformations (torsion angles are given in Table 5).

Bond lengths and angles in the macrocyclic ligand itself are in good agreement with those in related metal complexes (12–22) and those in $(H_2cyclam)(ClO_4)_2$ (33).

Acknowledgments

We thank the National Research Council of Canada for financial support and the University of British Columbia Computing Centre for assistance. The synthetic work on the title compound was initiated while one of the authors (E.I.O.) was at Ohio State University. He wishes to thank Dr. D. H. Busch for providing him with the opportunity.

1. D. H. BUSCH. Helv. Chim. Acta, Special Issue, 174 (1967).
2. N. F. CURTIS. Coordin. Chem. Rev. **3**, 3 (1968).
3. L. F. LINDOY and D. H. BUSCH. Prep. Inorg. React. **6**, 1 (1971).
4. J. J. CHRISTENSEN, D. J. EATOUGH, and R. M. IZATT. Chem. Rev. **74**, 351 (1974).
5. E. I. OCHIAI and D. H. BUSCH. Inorg. Chem. **8**, 1474 (1969).
6. E. I. OCHIAI, K. M. LONG, C. R. SPERATI, and D. H. BUSCH. J. Am. Chem. Soc. **91**, 3201 (1969).
7. J. P. COLLMAN, R. R. GAGNE, R. H. REED, W. T. ROBINSON, and G. A. RODLEY. Proc. Nat. Acad. Sci. U.S.A. **71**, 1326 (1974); J. E. BALDWIN and J. HUFF. J. Am. Chem. Soc. **95**, 5757 (1973).
8. N. F. CURTIS. J. Chem. Soc. 4409 (1960).
9. N. SADASIVAN and J. F. ENDICOTT. J. Am. Chem. Soc. **88**, 5468 (1966); J. I. LOVE and H. K. J. POWELL. Inorg. Nucl. Chem. Lett. **3**, 113 (1967).
10. M. F. BAILEY and I. E. MAXWELL. J. Chem. Soc. Chem. Commun. 908 (1966).
11. R. R. RYAN, B. T. KILBOURN, and J. D. DUNITZ. J. Chem. Soc. Chem. Commun. 910 (1966).
12. B. BOSNICH, R. MASON, P. PAULING, G. B. ROBERTSON, and M. L. TOBE. J. Chem. Soc. Chem. Commun. 97 (1965).
13. P. A. TASKER and L. SKLAR. J. Cryst. Mol. Struct. **5**, 329 (1975).
14. J. F. ENDICOTT, J. LILLIE, J. M. KOSZAJ, B. S. RAMASWAMY, W. G. SCHMONSEES, M. G. SIMIC, M. D. GLICK, and D. P. RILLEMA. J. Am. Chem. Soc. **99**, 429 (1977).
15. E. BRACKETT and C. PFLUGER. Am. Cryst. Assoc. Summer Meeting, Pennsylvania State University, University Park, PA, 1974. Abstr. p. 228.
16. N. F. CURTIS, D. A. SWANN, and T. N. WATERS. J. Chem. Soc. Dalton Trans. 1963 (1973).
17. F. WAGNER, M. T. MOCELLA, M. J. D'ANIELLO, JR., A. H. J. WANG, and E. K. BAREFIELD. J. Am. Chem. Soc. **96**, 2625 (1974).
18. P. O. WHIMP, M. F. BAILEY, and N. F. CURTIS. J. Chem. Soc. (A), 1956 (1970).
19. T. F. LAI and C. K. POON. Inorg. Chem. **15**, 1562 (1976).
20. R. A. BAUER, W. R. ROBINSON, and D. W. MARGERUM. J. Chem. Soc. Chem. Commun. 289 (1973).
21. N. F. CURTIS, D. A. SWANN, and T. N. WATERS. J. Chem. Soc. Dalton Trans. 1408 (1973).
22. N. F. CURTIS. J. Chem. Soc. 2644 (1964).
23. D. T. CROMER and J. B. MANN. Acta Cryst. A**24**, 321 (1968).
24. R. F. STEWART, E. R. DAVIDSON, and W. T. SIMPSON. J. Chem. Phys. **42**, 3175 (1965).
25. D. T. CROMER and D. LIBERMAN. J. Chem. Phys. **53**, 1891 (1970).
26. V. SCHOMAKER and K. N. TRUEBLOOD. Acta Cryst. B**24**, 63 (1969).
27. D. W. J. CRUICKSHANK. Acta Cryst. **9**, 747 and 754 (1956).
28. D. W. J. CRUICKSHANK. Acta Cryst. **14**, 896 (1961).
29. W. R. BUSING and H. A. LEVY. Acta Cryst. **17**, 142 (1964).
30. C. K. JOHNSON. *In* Crystallographic computing. Munksgaard, Copenhagen. 1970. pp. 207–226.
31. M. D. GLICK, D. P. GAVEL, L. L. DAIDDARIO, and D. B. RORABACHER. Inorg. Chem. **15**, 1190 (1976).
32. M. H. MEYER, P. SINGH, W. E. HATFIELD, and D. J. HODGSON. Acta Crystallogr. Sect. B, **28**, 1607 (1972); P. J. J. BONNET and Y. JEANNIN. Acta Crystallogr. Sect. B, **26**, 318 (1970).
33. C. NAVE and M. R. TRUTER. J. Chem. Soc. Dalton Trans. 2351 (1974).

Can. J. Chem. Downloaded from www.nrcresearchpress.com by 210.87.254.5 on 09/05/12
For personal use only.

Comparison of orbital symmetry allowed and forbidden ring opening of aziridines

A. C. OEHLSCHLAGER, A. S. YIM, AND M. H. AKHTAR
Department of Chemistry, Simon Fraser University, Burnaby, B.C., Canada V5A 1S6

Received May 17, 1977

A. C. OEHLSCHLAGER, A. S. YIM, and M. H. AKHTAR. Can. J. Chem. **56**, 273 (1978).

The rates of reactions of *N*-aryl-*cis*-2,3-diphenyl aziridines (**4***a–d*) with dimethyl acetylenedicarboxylate (DMAD) are dependent only on aziridine concentration suggesting slow conversion of aziridines to azomethine ylides which subsequently react in 1,3-dipolar cycloadditions to yield Δ^3-pyrrolines. The Hammett reaction constant (-0.80) determined for the *N*-substituents in the slow ring opening further suggests direct generation of azomethine ylides from these aziridines. The stereochemistry of the cycloaddition products derived from *cis*-1,2,3-triphenylaziridine with DMAD, maleic anhydride, dimethyl maleate, and dimethyl fumarate is consistent with the conrotatory generation of the ylides followed by their stereospecific *cis-cis* cycloaddition to the dipolarophiles.

Similarly, cycloaddition of 7-aryl-6a,7a-dihydroacenaphtha-[1,2]-aziridines (**5***a–f*) with DMAD yields bicyclic Δ^3-pyrrolines and the rate is dependent only on aziridine concentration. This suggests the reaction proceeds via a slow disrotatory cleavage of the aziridine rings producing azomethine ylides which undergo subsequent addition to DMAD. The Hammett reaction constant for the ring opening step is $+0.74$ suggesting that the transition state for the ring cleavage is electron deficient in the aziridinyl ring but the cycloaddition reactions of **5***a* with isomeric dipolarophiles as well as several dienes and cycloheptatriene reveal only stereospecific 1,2-cycloadditions expected of an azomethine ylide intermediate.

A. C. OEHLSCHLAGER, A. S. YIM et M. H. AKHTAR. Can. J. Chem. **56**, 273 (1978).

Les vitesses de réaction des *N*-aryl diphényl-2,3 aziridines *cis* (**4***a–d*) avec l'acétylènedicarboxylate de diméthyle (DMAD) dépendent uniquement de la concentration des aziridines; ces résultats suggèrent qu'il s'effectue une conversion lente des aziridines en ylures d'azométhine qui réagissent subséquemment par des cycloadditions dipolaires 1,3 pour fournir des Δ^3-pyrrolines. La constante de Hammett de la réaction (-0.80), déterminée pour des substituants sur l'azote dans l'ouverture lente du cycle, suggère de plus, qu'il peut se produire une formation directe d'ylures d'azométhine à partir de ces aziridines. La stéréochimie des produits de cycloaddition, obtenus par réactions de la triphényl-1,2,3 aziridine *cis* avec la DMAD, l'anhydride maléique, le maléate de méthyle et le fumarate de méthyle, est en accord avec une formation conrotatoire des ylures suivie par une cycloaddition *cis-cis* stéréospécifique avec le dipolarophile.

De la même manière, les cycloadditions d'aryl-7 dihydro-6a,7a acénaphta [1,2]aziridines (**5***a–f*) avec de la DMAD conduisent à des Δ^3-pyrrolines bicycliques et les vitesses de réaction dépendent uniquement de la concentration des aziridines. Ces résultats suggèrent que la réaction se produit par l'intermédiaire d'une coupure lente disrotatoire des cycles aziridines pour conduire à des ylures d'azométhine qui réagissent d'une façon subséquente avec la DMAD. La constante de Hammett pour la réaction de l'étape d'ouverture du cycle est de $+0.74$. Cette valeur suggère que l'état de transition pour l'ouverture du cycle est déficient en électron au niveau du cycle aziridinyle; toutefois les réactions de cycloaddition de **5***a* avec des dipolarophiles isomères, de même qu'avec plusieurs diènes et le cycloheptatriène, conduisent uniquement aux cycloadditions-1,2 stéréospécifiques attendues pour des ylures d'azométhine intermédiaires.

[Traduit par le journal]

Introduction

The value and validity of the orbital symmetry rules of Woodward and Hoffmann (1) and others for predicting the stereoselectivity of concerted pericyclic reactions are well established. Most interpretations of pericyclic reactions are in terms of correlations of bonding states or orbitals between reactants and products and do not provide predictions of how electron density changes at the reacting atoms during the course of reaction will influence the progress of reaction.[1]

As the organic chemist endeavors to achieve forbidden reactions of high stereospecificity he will undoubtedly turn not only to alteration of the steric environment but to the electronic environment of the reacting atoms to achieve his desired goals.

Since it is becoming increasingly apparent (3, 4) that the magnitude of the differences in activation energies between analogous allowed and forbidden reactions is not so large as to prevent forbidden concerted processes it is now indeed possible to consider methods for achieving forbidden reactions with low activation energies.

It occurred to us that for the conversion of three-membered heterocycles to their open-chain analogs,

[1]For investigation into the effect of substituents on the course of pericyclic reactions see ref. 2.

Can. J. Chem. Downloaded from www.nrcresearchpress.com by 210.87.254.105 on 09/05/12
For personal use only.

Can. J. Chem. Downloaded from www.nrcresearchpress.com by 210.87.254.105 on 09/05/12
For personal use only.

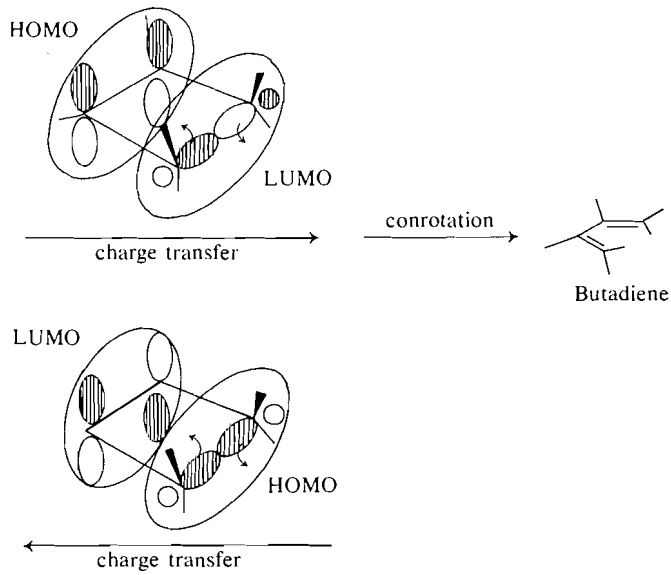

FIG. 1. Modes of the HOMO–LUMO interaction in the ring opening of cyclobutene.

the analysis of Fukui (5*a*) contained intriguing implications with regard to how to approach the design of three-membered heterocycles capable of undergoing forbidden processes. In Fukui's (5*a*) analysis of pericyclic transformations, reaction is considered to be initiated by mutual charge transfer from the highest occupied molecular orbital (HOMO) of one bond undergoing reaction and the lowest unoccupied molecular orbital (LUMO) of another bond participating in the reaction (5). According to Fukui the stereochemical course of such reactions is strongly biased in a direction which achieves maximum overlapping of the HOMO and LUMO of the participating bonds. For most electrocyclic reactions the several possible choices of HOMO–LUMO interaction lead to the prediction of the same stereochemical outcome. Thus, thermal conrotatory cyclobutene to butadiene conversion is predicted regardless of the dominant HOMO–LUMO interaction (Fig. 1).

In the case of electrocyclic opening of three-membered rings the implications of this analysis are that the stereochemical sense of ring opening will be influenced by the dominant HOMO–LUMO interaction and perhaps vice versa (Fig. 2).

Thus, if interaction *a* is predominant the ring

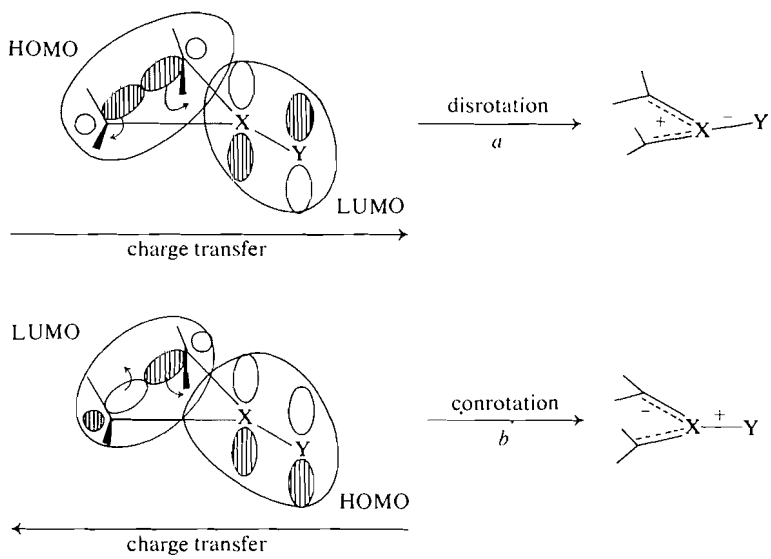

FIG. 2. Modes of HOMO–LUMO interaction in ring opening of a three-membered ring.

Can. J. Chem. Downloaded from www.nrcresearchpress.com by 210.87.254.105 on 09/05/12
For personal use only.

opening would be expected to occur in a disrotatory sense. If *b* is predominant conrotation is to be expected. The favored interaction is expected to be determined by the electronegativities of X and Y since the relative electronegativities of these ring substituents will determine the amplitude of the participating HOMO or LUMO at X. In general, the greater the amplitude of a given MO at X the greater the predominance of the interaction involving the participation of that MO. In cyclopropanones (X = C, Y = O) interaction *a* will be favorable because the relative electronegativities of carbon and oxygen give the carbonyl LUMO a large amplitude at the carbonyl carbon (5). A disrotatory ring opening of cyclopropanone is thus expected (6). Although the stereochemical sense of cyclopropanone opening remains to be determined, the ring-opened forms of substituted cyclopropanones have been trapped in 1,4-cycloaddition to 1,3-dienes and thus appear to possess the dipolar character indicated in Fig. 2*a* (6). The solvolysis of cyclopropyl halides (7) (X = C, Y = halogen) and *N*-chloroaziridines (8) (X = N, Y = Cl) proceed via ionization of the halogen with simultaneous disrotatory C_2—C_3 bond cleavage in which interaction *a* must predominate.

The cycloaddition reactions of substituted aziridines (9) and epoxides (10) (**1**; X = N—R, O) have been interpreted as involving preferred conrotatory ring opening via C_2—C_3 bond scission generating ylides (**2**; X = N—R, O) which in the presence of dipolarophiles undergo *cis-cis*-cycloaddition giving high yields of heterocycles **3** (Scheme 1). Indeed the direct conversion of these heterocycles to ylides must involve charge flow as indicated in Fig. 2*b* (10).

From Scheme 1 one can easily develop the point of view that thermal disrotatory cleavage of aziridines would involve predominantly interaction *a*. If this is a valid opinion then to aid a disrotatory aziridine ring opening one might further reason that electron withdrawing groups attached to nitrogen would be beneficial. To investigate these expectations we have ascertained the effect of *N*-aryl substitution on the rates of conrotatory opening of triaryl aziridines **4***a–d* and on the rates of disrotatory opening of the tetracyclic arylaziridines **5***a–f*. Since we obtained evidence for the predominance of interaction *b* in the reactions involving conrotation and interaction *a* in the reactions involving disrotation we have trapped the ring-opened species from both processes to determine their cycloadditive properties.

Although it was certain that thermal conrotatory cleavage of the arylaziridines **4***a–d* studied would lead to an azomethine ylide that would react stereospecifically with added dipolarophiles we were uncertain as to the expected behavior of the species

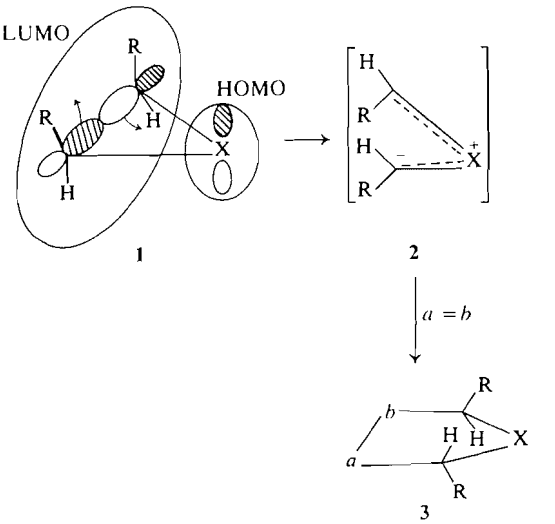

SCHEME 1

generated from thermal disrotatory cleavage of the tetracyclic aziridines (**5***a–f*) studied.

Since disrotatory aziridine cleavage occurred with predominance of interaction *a* (Fig. 2) attendant cycloaddition reactions might be expected to occur involving 4π dipolarophiles via a $\sigma 2s + \pi 4s$ process (1). Hence, we considered it of prime importance in these trapping experiments to determine the stereochemistry of the cycloadditions and examine any tendency of the ring-opened species from the tetracyclic aziridines studied to undergo addition to 4π systems.

Results

The reactions of **4***a–d* with dimethyl acetylenedicarboxylate (DMAD) in benzene gave 1:1 cycloadducts (**6**) in nearly quantitative yield. Kinetic investigation of the reaction was carried out by nmr

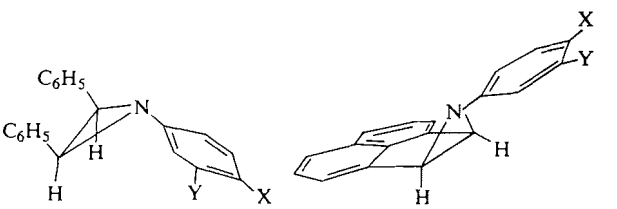

4
a X = Y = H
b X = CH_3, Y = H
c X = Cl, Y = H
d X = Y = Cl

5
a X = Y = H
b X = CH_3, Y = H
c X = OCH_3, Y = H
d X = Br, Y = H
e X = NO_2, Y = H
f X = Y = Cl

integration of the carbomethoxy resonances due to DMAD and adducts vs. toluene as an internal standard. It was found that when both reactants were present in comparable concentrations, the reaction rate was dependent only on the concentra-

Can. J. Chem. Downloaded from www.nrcresearchpress.com by 210.87.254.105 on 09/05/12
For personal use only.

tion of the aziridine. This observation parallels that made (9) for the reaction of closely related carboalkoxy substituted aziridines with dipolarophiles and implies a slow conversion of aziridine to an azomethine ylide that subsequently reacts rapidly with DMAD. Such a sequence may be treated kinetically by application of the steady-state approximation to the azomethine ylide.

This formulation leads to the rate expression

$$\text{Aziridine} \underset{k_{-1}}{\overset{k_1}{\rightleftharpoons}} \text{[Azomethine ylide]}$$

$$\text{[Azomethine ylide]} + \text{DMAD} \xrightarrow{k_2} \text{Cycloadduct}$$

$$[1] \qquad \frac{d[P]}{dt} = \frac{k_1 k_2 [Az][DMAD]}{k_{-1} + k_2[DMAD]}$$

where [P] = [Cycloadduct] and [Az] = [Aziridine].

From eq. 1 it is apparent that if product k_2 [DMAD] is sufficiently large, compared to k_{-1}, the latter may be neglected in the denominator and eq. 1 reduces to eq. 2.

$$[2] \qquad \text{rate} = k_1[Az]$$

This will obtain if k_2 is large compared to k_1 or if high concentrations of DMAD are present. Inspection of Table 1 reveals that the overall rate of aziridine reaction is relatively insensitive to changes in concentration of DMAD at moderate concentration levels, indicating the steady state approximation is valid, i.e. k_2[DMAD] $\gg k_{-1}$. By this analysis k_1 is rate limiting and represents the conversion of aziridine to azomethine ylide. The increase in the observed changes in the rate of reaction with *N*-aryl substitution (treated in a Hammett plot in Fig. 3) are thus ascribed to their effect on the ring-opening reaction.

That this ring opening proceeds in a conrotatory fashion producing ylide **7**, which subsequently adds in a *cis-cis* fashion to the reacting dipolarophile is supported by several observations. Huisgen and co-workers (9*g*) have put forward convincing arguments to indicate the C_2 and C_5 phenyl groups in **6***a* are *trans*. This stereochemistry is expected from *cis* addition of a ylide having the geometry of **7** to DMAD. The geometry of **7** is that expected from conrotatory opening of an *N*-aryl-*cis*-2,3-diphenylaziridine, **4**. That the *N*-aryl aziridines made by the method of Taylor (11, used in this study) indeed possess *cis*-2,3 substitution was indicated by independent synthesis of *cis*-1,2,3-triphenylaziridine (**4***a*) from *cis*-2,3-diphenylaziridine (12) and benzyne (13).

One could consider the possibility that the *cis*-2,3-diphenylaziridines **4***a–d* were converted to their *trans* isomers in rapid equilibrium reactions. Such a pre-equilibrium followed by rate determining addition of the *trans* aziridines to the olefins used would alter somewhat the structural similarity of the systems under study. Two considerations indicate such a *cis-trans* pre-equilibrium does not occur in the present cases. First, a search by nmr (detection limit ~5%) and by tlc of the reaction mixture of **4***b* and DMAD failed to reveal resonances or chromatographic bands attributable to *trans* **4***b*. Secondly, addition of *trans* isomers of **4***a–d* to olefins would be expected to yield adducts in which the phenyl substituents are *cis*.

To confirm that the cycloadditions of the ylides produced from *N*-aryl-2,3-diphenyl aziridines were *cis* with respect to the dipolarophile we repeated the previously reported (14) cycloaddition of **4***a* to maleic anhydride, dimethyl maleate, and dimethyl fumarate (Scheme 2). Reaction of **4***a* with maleic anhydride gave the previously reported (14) adduct **8** in which the two phenyl groups are *trans*. Reaction

TABLE 1. First-order rate constants for the reaction of aziridines **4***a–d* and dimethyl acetylene dicarboxylate in benzene at 110.1 ± 0.1°C

Aziridine	$[Aziridine]_0$ (mol/ℓ)	$[DMAD]_0$ (mol/ℓ)	$k_1(\pm 0.2) \times 10^4$ (s^{-1})
4*a*	0.211	0.543	2.35
	0.213	0.742	2.59
	0.204	1.043	2.28
4*b*	0.206	0.547	3.17
	0.208	0.753	3.29
	0.198	0.973	3.38
	0.101	0.074	3.01
4*c*	0.205	0.529	1.73
	0.216	0.738	1.64
	0.204	0.941	1.87
4*d*	0.213	0.498	0.91
	0.221	0.741	1.05
	0.141	0.542	0.98

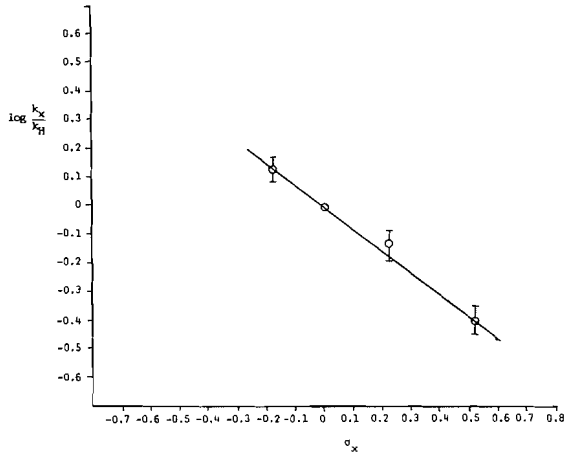

FIG. 3. Correlation of $\log k_x/k_H$ and σ_x for the decomposition of monocyclic aziridines (**4***a–d*).

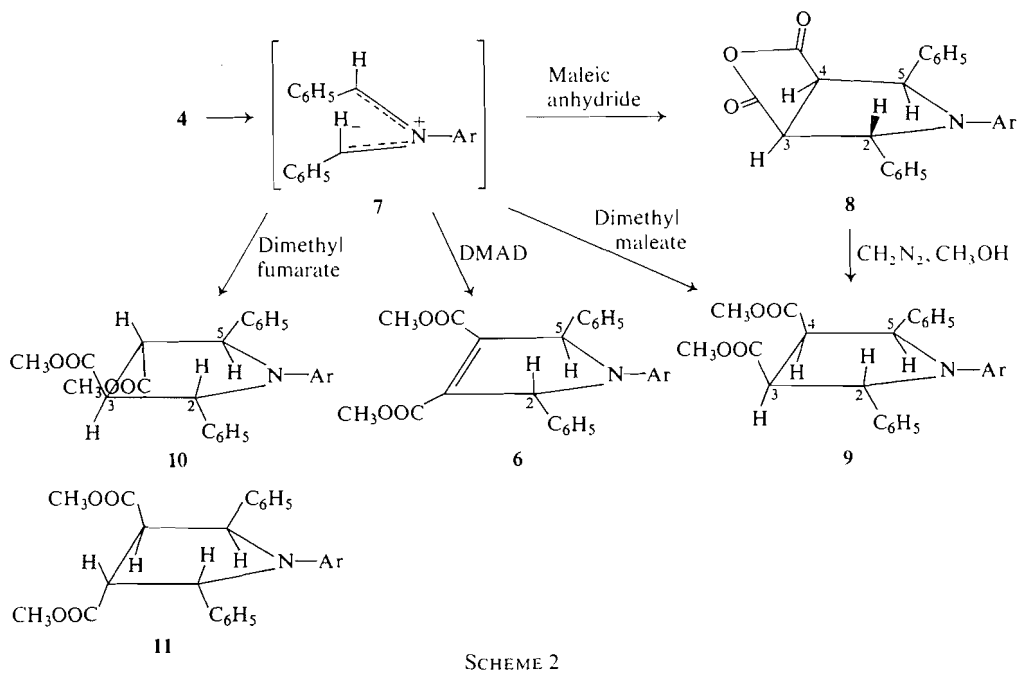

SCHEME 2

of **4***a* with dimethyl maleate gave **9** which was also formed upon reaction of **8** with ethereal methanolic diazomethane. Our mild conversion of **8** to **9** by ethereal diazomethane was chosen to avoid C_3,C_4 isomerization. The maintenance of *cis*-3,4-stereochemistry, although not obvious from the vicinal couplings (9*h*) observed in the nmr spectrum of **9** ($J_{2,3} = 7.5$ Hz, $J_{3,4} = 7.5$ Hz, and $J_{4,5} = 7.0$ Hz), is apparent from the appearance of H_3 and H_4 at different positions (δ 3.39, 3.89). This would be expected only if there had been no isomerization to the thermodynamically more stable **10** or **11** since both have a twofold symmetry axis. Heine has previously assigned the stereochemistry of **11** to the adduct produced upon reaction of **4***a* with diethyl maleate (although see Huisgen and co-workers (9*f*, *g*) for assignment of structure **9**). Structure **10** is easily assigned to the major adduct obtained from **4***a* and dimethyl fumarate since the twofold symmetry axis produces equivalent chemical shifts for the C_2 and C_5 as well as the C_3 and C_4 hydrogens. The *trans* stereochemistry of all groups in **10** is indicated by small vicinal couplings (9*h*) (2.5 Hz). Huisgen and coworkers (9*h*, *g*) have reported that **11** is also formed in minor amounts in the **4***a* dimethyl fumarate reaction. In all of these cycloadditions the stereochemistry of the dipolarophile is maintained and there is a *trans* relationship between the two phenyl groups at C_2 and C_5 indicating *cis* reaction of an azomethine ylide produced upon conrotatory opening of *cis*-1,2,3-triphenyl aziridine.

Aziridines **5***a–f* were obtained by reaction of a 1.5–2.0 molar excess of the appropriately substituted aryl azide with acenaphthylene for 4–15 days at 60–70°C. After this time the aziridines precipitated in 60–80% yield. Thus, the reaction of phenyl azide with acenaphthylene gave an addition product, $C_{18}H_{13}N$, the nmr spectrum of which possessed a 2 hydrogen singlet at δ 4.33 and an 11 hydrogen multiplet in the δ 6.67–7.63 region. Only the imine (**12**) and aziridine (**5***a*) structure are compatible with this spectral pattern (15). The absence of a strong infrared absorption in the 1600–1700 cm^{-1} region (C=N stretching (16)) as well as the failure of the azide–acenaphthylene adducts to undergo hydrolytic cleavage to aniline and a ketone indicated the adduct was not an imine and thus was aziridine **5***a*.

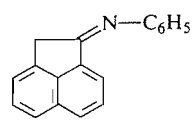

12

Aziridines **5***a–f* condense readily with DMAD to form 1:1 cycloadducts in high yield. These reactions displayed first-order kinetics with respect to aziridine and were zero order with respect to DMAD. The changes in the rates of reaction (Table 2) of these tetracyclic aziridines with alteration of the *N*-aryl (Fig. 4) indicate the effect of this substitution on the necessarily disrotatory ring-opening reaction.

To compare the activation parameters for the ring

Can. J. Chem. Downloaded from www.nrcresearchpress.com by 210.87.254.105 on 09/05/12
For personal use only.

Can. J. Chem. Downloaded from www.nrcresearchpress.com by 210.87.254.105 on 09/05/12
For personal use only.

TABLE 2. First-order rate constants for the reaction of the aziridines **5***a–f* with DMAD in benzene at 119.5°C

Aziridine	$[Aziridine]_0$ (mol/ℓ)	$[DMAD]_0$ (mol/ℓ)	$k_1(\pm 0.3) \times 10^5$ (s^{-1})
5*a*	0.187	0.137	4.85
	0.183	1.002	5.02
	0.113	0.087	5.43
5*b*	0.184	0.129	4.09
	0.163	1.014	4.50
	0.110	0.068	4.07
5*c*	0.185	0.141	3.45
	0.187	0.285	3.67
	0.201	1.008	3.81
5*d*	0.182	0.151	7.54
	0.147	0.603	6.93
	0.118	1.741	7.18
5*e*	0.035	0.055	16.64
	0.038	0.116	17.28
	0.029	0.504	16.97
5*f*	0.181	0.147	10.95
	0.204	0.704	10.43
	0.192	1.253	10.74
	0.143	0.456	10.14

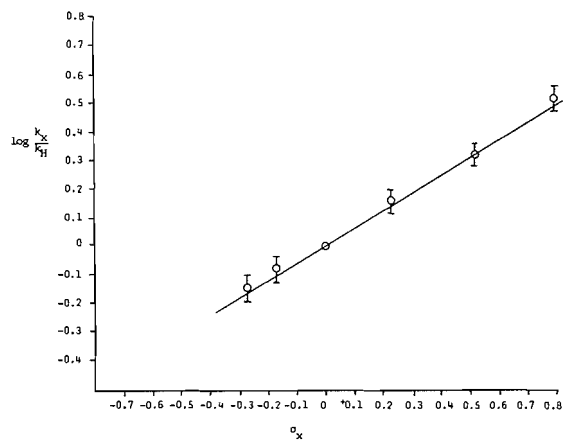

FIG. 4. Correlation of $\log k_x/k_H$ and σ_x for the decomposition of tetracyclic aziridines (**5***a–f*).

opening of monocyclic aziridines with their tetracyclic analogs we investigated the rate of reaction of monocyclic aziridine **4***a* and its tetracyclic analog (**5***a*) with DMAD each at six temperatures over the range of 90–130°C. Analysis of the rates as a function of temperature by standard methods (15) yielded activation parameters of $\Delta H^{\ddagger} = 21.6 \pm 0.4$ kcal and $\Delta S^{\ddagger} = -0.4 \pm 1$ eu for the ring opening of **4***a*. The calculated activation parameters for the ring opening of **5***a* were $\Delta H^{\ddagger} = 25.1 \pm 0.4$ kcal and $\Delta S^{\ddagger} = -0.1 \pm 1$ eu.

The structures of the cycloadducts produced from reaction of **5***a–f* with DMAD were deduced from inspection of their infrared and nmr spectra. Thus, the infrared spectrum of the adduct obtained (93%) upon reaction of **5***a* with DMAD showed an absorption at 1720 cm^{-1} attributable to a conjugated ester. An absorption at 1645 cm^{-1} is attributed to a tetrasubstituted double bond conjugated with a carbonyl. Two structures **14** and **15** are consistent with the elemental analysis and infrared spectrum. The former was eliminated by inspection of the nmr spectrum of the adduct which exhibited a 6 hydrogen resonance at δ 3.73, a 2 hydrogen singlet at δ 5.78, and an 11 hydrogen multiplet in the δ 6.45–7.71 region. Reaction of aziridine, **5***a*, with maleic anhydride gave **16** and **17** which upon treatment with methanolic ethereal diazomethane gave **18** and **19**, respectively (Scheme 3). The latter two compounds were the only adducts produced upon reaction of **5***a* with dimethyl maleate. The *endo-cis*-3,4-stereochemistry of **18** was indicated by its production upon catalytic reduction of **15**. Inspection of molecular models of **16–20** revealed that in the *endo* adducts (**16** and **18**) the *exo*-C_3,C_4 hydrogens lie near the periphery of the naphthyl system (deshielding area) and the dihedral angle of these hydrogens with their bridgehead neighbors (H_2 and H_5) is approximately 30° for which couplings of 6–7 Hz are expected. The *exo*-C_3,C_4 hydrogens in *cis-endo* adducts should thus be at lower field and coupled strongly with the bridgehead hydrogens compared to those at C_3 and C_4 in *cis-exo* adducts since the hydrogens at C_3 and C_4 in *exo* adducts are below the plane of the naphthyl ring (shielding area) and have dihedral angles of nearly 90° with the neighboring bridgehead hydrogens.

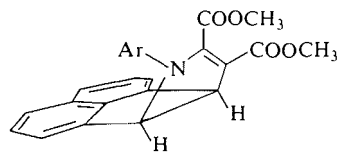

14

In accord with these expectations the nmr spectrum of **18** revealed both ester methyls were identical and resonated at higher field (δ 3.29) than those of **19** (δ 3.73). The nmr spectrum of **18** also revealed the signals due to the C_3 and C_4 pyrrolidine hydrogens in an A_2X_2 pattern ($J_{2,3} = J_{4,5} = 6.7$ Hz) at lower field (δ 3.86) than their counterparts in **19** (δ 3.47) which appeared as a singlet. Similar differences were observed in the nmr spectra of **16** and **17** and have been used by Cava and co-workers (18) to deduce the structures of similar adducts of 2-thiaphenalene.

The reaction of dimethyl fumarate with **5***a* gave a single adduct (**20**) which possessed two different ester functions. The infrared spectrum of **20** possessed absorption at 1730 and 1748 cm^{-1} while its nmr spectrum contained signals due to two different ester groups at δ 3.46 (*endo*) and 3.75 (*exo*). A one

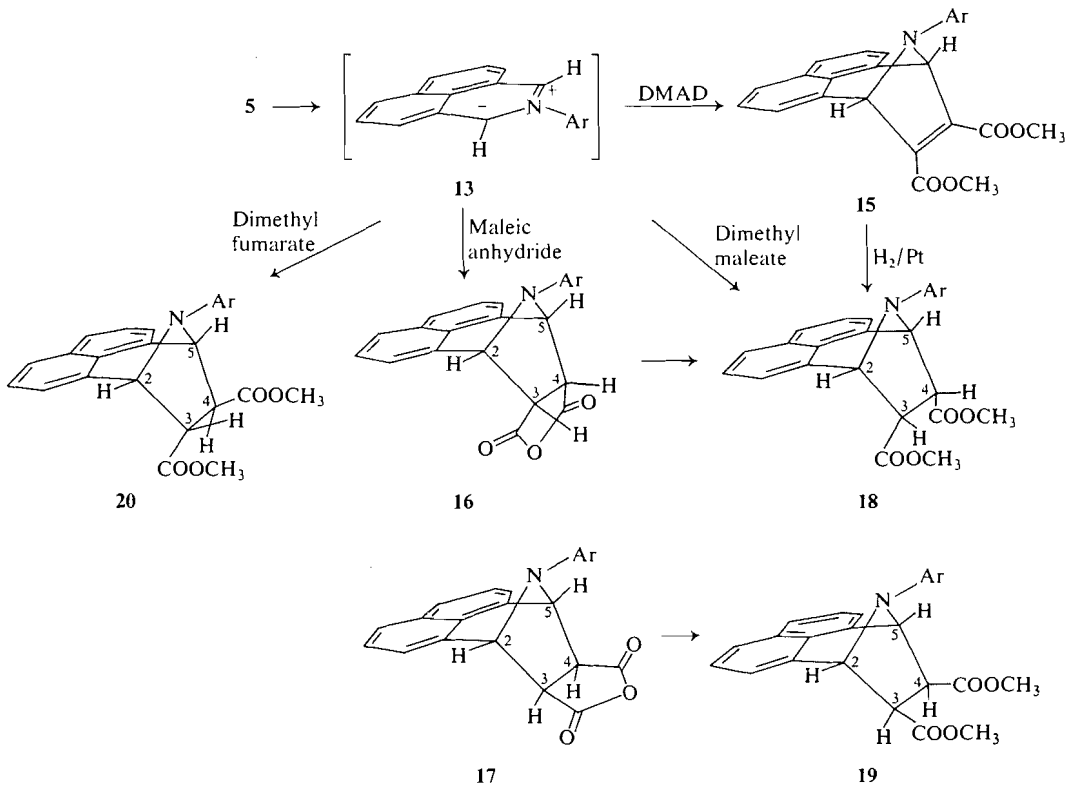

SCHEME 3

TABLE 3. *Exo*:*endo* ratio for thermal and photolytic cycloaddition of **5***a–e* to dimethyl maleate

	Thermal		Photolytic		
Aziridine	*Exo*:*endo*	Total *cis* yield (%)	*Exo*:*endo*	Total *cis* yield (%)	*Trans* yield (%)
5*a*	31:69	89	34:66	84	5
5*b*	30:70	79	36:64	91	4
5*c*	34:66	78	40:60	89	4
5*d*	24:76	85	29:71	81	~5
5*e*	14:86	93	13:87	75	~5

hydrogen doublet at δ 3.66 ($J_{3,4}$ = 5.7 Hz) was assigned to an *endo* hydrogen at C_4. A one hydrogen doublet of doublets at δ 4.28 ($J_{3,4}$ = 5.7 Hz; $J_{4,5}$ = 7.0 Hz) was assigned to an *exo*-C_3 hydrogen. The hydrogen at C_5 was observed as a singlet (δ 5.55) while the C_2 hydrogen was a doublet (δ 5.49, J = 7.0 Hz).

Since the structures of aziridines **5***a–e* made them suitable for studying the effect of nitrogen substitution on *exo*:*endo* addition ratio in the absence of steric effects this aspect of the cycloaddition of these aziridines to dimethyl maleate under both thermal and photochemical conditions was undertaken. Reaction of **5***a–e* with dimethyl maleate under both thermal and photochemical conditions gave mixtures of adducts. The relative amounts of *exo* and *endo* addition (Table 3) of these were assigned by comparison of the chemical shifts of the methoxyl groups in each set of adducts according to the arguments presented above.

To investigate the possible σ2*s* behavior of the ring-opened species generated from the tetracyclic aziridines under study (to give adducts of the general structure **21**) we attempted the cycloaddition of these aziridines to numerous dienes and trienes. In the majority of cases only aziridine dimers were detected but with three polyenes we obtained cycloaddition products.

Reaction of **5***a* with dimethyl *trans-trans*-1,3-butadiene-1,4-dicarboxylate gave a low melting 1:1

Can. J. Chem. Downloaded from www.nrcresearchpress.com by 210.87.254.105 on 09/05/12
For personal use only.

Can. J. Chem. Downloaded from www.nrcresearchpress.com by 210.87.254.105 on 09/05/12
For personal use only.

adduct **22**, (63%) and a high melting *bis* adduct, **23** (31%) derivable from the monoadduct by further reaction with **5***a* (Scheme 4). That 1,2- and not 1,4-

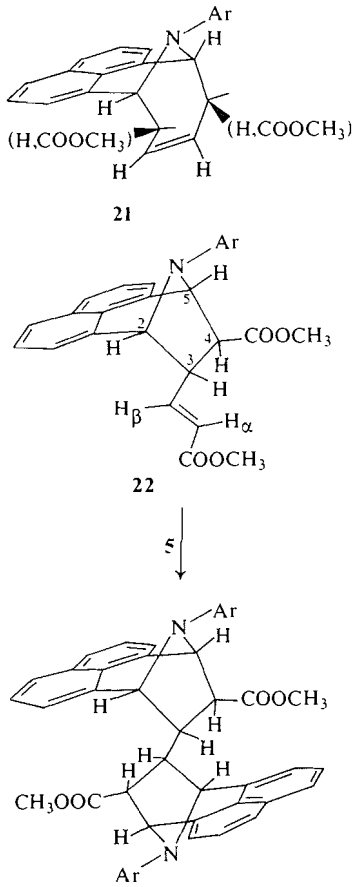

SCHEME 4

addition had occurred to give the 1:1 adduct was deduced from the presence of both an unconjugated (1733 cm^{-1}) and an α,β-unsaturated ester (1710 cm^{-1}) as well as a *trans*-disubstituted alkene (970 cm^{-1}) function. The stereochemistry of adduct **22** was deduced from its nmr spectrum which possessed a singlet (δ 5.52) attributable to the C_5 hydrogen indicating an *endo*-C_4 hydrogen, a doublet ($J_{3,4}$ = 6.2 Hz) at δ 2.93 assignable to the latter, and a doublet at δ 5.20 ($J_{2,3}$ = 6.0 Hz) assignable to the C_2 hydrogen suggesting an *exo*-C_3 hydrogen. The latter appeared at δ 3.98 as a multiplet which collapsed to a triplet upon irradiation of the β-vinyl hydrogen. Further evidence for the *exo* stereochemistry of the ester function in **22** may be obtained from the observation that the chemical shifts of the C_5 hydrogens in **21** and **20** are nearly identical whereas the positions of C_2—H,C_3—H, and C_4—H resonance in the 1:1 adduct show a positive shift in comparison to their counterparts in **20**. This is attributable to the shielding effect of the *endo*-α,β-unsaturated ester. If this group had been in an *exo* position an appreciable positive shift of the C_5 hydrogen in **22** as compared to **20** would have been anticipated.

The reaction of *trans-trans*-2,4-hexadiene with **5***d* gave a single 1:1 adduct (**24**) in 58% yield. In addition aziridine dimer **25***d* was obtained in 22% yield. That **24** was derived via 1,2-addition was deduced from the presence of resonance due to two *trans*-vinyl hydrogens (δ_α 4.96 and δ_β 5.50, $J_{\alpha\beta}$ = 15.0 Hz) and a vinyl methyl (δ 1.47, J_α = 6.5 Hz, J_β = 1.0 Hz) in its nmr spectrum. Upon catalytic reduction of **24** to **26** the vinyl methyl resonance is replaced by a triplet at δ 0.78 (J = 6.5 Hz), whereas the doublet (δ 1.31) assigned to the methyl at C_4 remained unaffected.

The stereochemistry of the adduct was deduced by examination of the signals assigned to the bridgehead hydrogens. Thus, a singlet (δ 4.57) due to the C_5-H indicated an *endo*-hydrogen at C_4 whereas a doublet ($J_{2,3}$ = 6.0 Hz) at δ 4.96 assigned to the C_2-H indicated an *exo*-C_3-H. The *trans* relationship of the C_3 and C_4 hydrogens is also indicated by the quintet structure of the signal (δ 2.89) attributable to the C_4-H requiring $J_{3,4}$ to be 6.5 Hz.

The reaction of 1,3-cyclohexadiene with **5***f* gave a 1:1 adduct in 72% yield along with small amounts of aziridine dimers (**25** and **27**). The nmr spectrum of the 1:1 adduct revealed two multiplets due to four methylene hydrogens (δ 1.21–1.81) and to two methine hydrogens (δ 2.90–3.45). The two bridge-

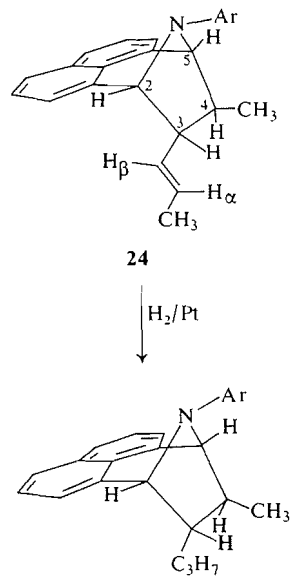

Can. J. Chem. Downloaded from www.nrcresearchpress.com by 210.87.254.105 on 09/05/12
For personal use only.

head hydrogens (C_2,C_5) were exhibited as a doublet (J = 6.2 Hz) at δ 5.07 whereas the two vinyl hydrogens were exhibited as a multiplet centered at δ 5.48. Although it could not be discerned from the above whether 1,2- or 1,4-addition had occurred, the former was confirmed by reduction of the 1:1 adduct **28** to the adduct (**29**) obtained (7%) when cyclohexene was reacted with **5***f*. The *endo* configuration of the cyclohexene ring in the latter was evident from the coupling (J = 6.2 Hz) between the bridgehead hydrogens (C_2,C_5); one doublet at δ 5.03, and their vicinal neighbors (C_3,C_4).

The less reactive aziridine, **5***a*, gave only a 34% yield of 1:1 adduct with 1,3-cyclohexadiene along with appreciable amounts of aziridine dimers.

Reaction of tetracyclic aziridines with tropone and cycloheptatriene were also investigated. Only the latter reaction led to identifiable products. The reaction of **5***d* with cycloheptatriene gave a 37% yield of a 1:1 adduct and major amounts of aziridine dimers. The structure of the 1:1 adduct was deduced to be as in **30** by reduction to the 1:1 adduct **31** obtained from **5***d* and cycloheptene. That the alternate product of π4*s* + π2*s* cycloaddition, **32**, was not the correct formulation for the cycloheptatriene–**5***d* adduct was also deduced by observation of coupling ($J_{4,6}$ = 2.5 Hz, $J_{4,7}$ = 12 Hz) between a methine hydrogen (H-4) and the methylene hydrogens (H-6 and H-7) of the cycloheptyl ring. That the adduct was asymmetric with respect to a plane bisecting the fused aromatic rings was also evident from the distinctly different chemical shifts observed for the two bridgehead hydrogens (δ$_2$ 4.98 and δ$_5$ 5.08). The *endo* stereochemistry of the cycloheptyl rings in both **30** and **31** was deduced from the coupling of the bridgehead hydrogens with their methine neighbors (J = 6 Hz) in both compounds.

Several of the reactions of tetracyclic aziridines, **5**, with alkenes not possessing conjugated carbonyls resulted in low yields of cycloaddition products and competing formation of aziridine dimers. Heating aziridine **5***a* in benzene at 140°C for 14 h resulted in complete consumption of the aziridine and the formation of two separable dimers **25***a* and **27***a*. The mass spectrum of each showed a parent ion peak at *m*/*e* 486 and a base peak at *m*/*e* 243. Assignment of structures to **25***a* and **27***a* was made by comparison

28

H_2/Pt

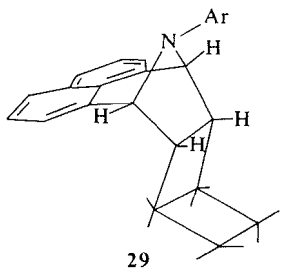

29

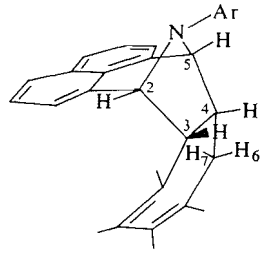

30

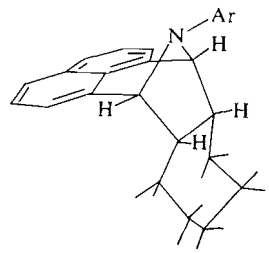

31

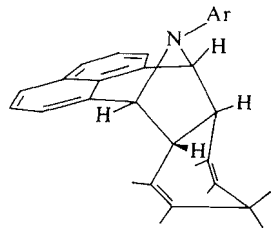

32

of the relative chemical shifts of the bridgehead hydrogens (δ 5.09 and 5.79, respectively) and the naphthyl hydrogens (δ 7.33–7.83 and 6.63–7.03, respectively) with those of the analogous hydrogens in the acenaphthylene photodimers (19–21). Thus, the nmr spectrum of α-heptacyclene, **33**, revealed the benzylic hydrogens at δ 4.07 vs. 4.78 for these hydrogens in β-heptacyclene, **34**. Furthermore the naphthyl hydrogens of **33** appear in the region δ 7.76–7.83 whereas in **34** these hydrogens occur in the δ 6.58–7.28 region. The differences between the chemical shifts of the aromatic hydrogens in **25***a* and **27***a* as well as between **33** and **34** are readily attributable to the shielding effects of the naphthyl rings in the *cis* isomers. In the *trans* isomers (**25***a* and **33**) the methine hydrogens are shielded by these rings.

Discussion

We examined cycloaddition reactions of monocyclic (**4***a–d*) and tetracyclic aziridines (**5***a–f*) with numerous 2π, 4π, and 6π systems. In all cases only

Can. J. Chem. Downloaded from www.nrcresearchpress.com by 210.87.254.105 on 09/05/12
For personal use only.

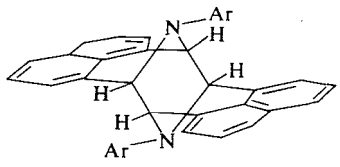

25

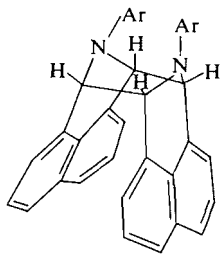

27

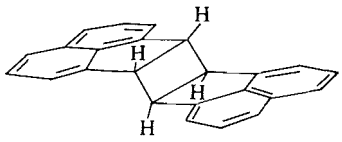

33

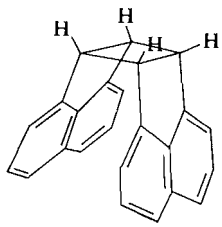

34

stereospecific *cis*-1,2-addition to the reacting dipolarophiles was observed. These results indicate the respective azomethine ylides **7** and **13** are the reactive intermediates in these reactions and support the suggestion (17) that the lack of stereospecificity previously noted in similar aziridine cycloadditions resulted from alkene isomerization prior to reaction.

Evidence that azomethine ylides are the product forming intermediates in the thermal cycloaddition of tetracyclic aziridines (**5**) to dipolarophiles such as dimethyl maleate also comes from a comparison of the ratios of *exo* to *endo* adducts that are formed during the thermal and photochemical cycloaddition of these reactants. It is established (9) that photochemical C—C bond cleavage of substituted aziridines such as **5** proceeds by disrotatory ring opening to produce azomethine ylides that are the product forming intermediates in subsequent cycloaddition reactions. If azomethine ylides are the product forming intermediates in the thermal cycloaddition of the tetracyclic aziridines (**5**) used in the present study then the ratio of *exo* to *endo* adduct formation with olefins such as dimethyl maleate should be similar for both photochemical and thermal cycloaddition of a given aziridine.

Examination of the *exo*:*endo* ratios of adducts from **5***a–e* and dimethyl maleate (Table 3) reveals no significant difference in this reaction parameter when a given aziridine is consumed under photochemical or thermal conditions.

An additional argument that can be brought to bear on the question of the involvement of azomethine ylides in the cycloaddition of the tetracyclic aziridines (**5**) to dipolarophiles makes use of the variation of *exo*:*endo* ratio observed in Table 3 with the nature of the *N*-aziridinyl substituent. It can be predicted on the basis of secondary orbital interactions (1, 22) that attraction between LUMO of a 4π electron system such as an azomethine ylide and the HOMO of a reacting olefinic dipolarophile leads to a bonding interaction favoring *cis-endo* addition. As the electronegativity of the *N*-substituent in such ylides increases so does the coefficient of the N–*p* orbital in the LUMO of the ylide making this bonding interaction stronger. The relative amount of *endo* adduct for such a ylide would therefore be expected to increase if steric factors remained unchanged. The data reported in Table 3 indeed reveals that as the *N*-substituent of the reacting aziridines becomes more electronegative the relative amount of *endo* addition increases.

The above argument, based on secondary orbital interactions between the N–*p* orbital in the ylide LUMO and π_{CO} orbitals in the dipolarophile HOMO, predicts the trend of *exo*:*endo* ratios observed but

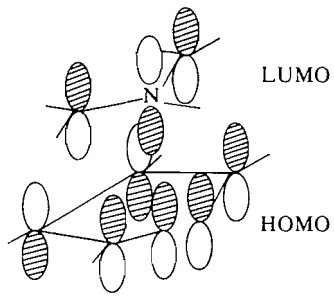

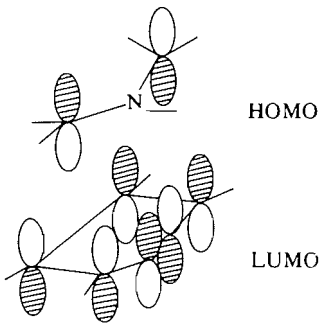

does not predict the *endo* adduct as the major product. It can be argued that since azomethine ylides are HOMO controlled 1,3-dipoles which react best with electron deficient alkenes the addition of ylides **5***a–f* to dimethylmaleate should involve a predominant ylide HOMO-dipolarophile LUMO interaction. If this is the case there should be no interaction between the N–*p* orbital of the ylide and the π_{CO} of the dipolarophile since there is a node at the N atom in the HOMO of the former.

Secondary orbital interaction leading to *endo*

Can. J. Chem. Downloaded from www.nrcresearchpress.com by 210.87.254.105 on 09/05/12
For personal use only.

adduct is possible between the π_{CO} in the LUMO of dimethylmaleate and the π-naphthalene HOMO. This interaction could be stronger than π_{CO} dipolarophile LUMO–π_{Ar}–dipole HOMO interaction which would lead to *exo* adduct formation. The changes in *exo*:*endo* ratios may, in this argument, be attributed to differences in magnitudes of the secondary orbital interactions between π_{CO} and π_{Ar}. As electron-withdrawing substituents decrease interactions between the π_{Ar} HOMO and the π_{CO} dipolarophile LUMO a decrease in the *exo*:*endo* adduct ratio should be observed.[2]

The present observations complement the reports that the carbonyl ylides produced upon both thermal conrotatory (10) and thermal disrotatory (21) cleavages of tetracyclic epoxides undergo stereospecific cycloaddition to 2π-dipolarophiles.

Thus, available evidence indicates that regardless of the rotatory motion involved in the thermal conversion of aziridines and epoxides to their respective ylides the latter are generated in a form for which stereospecific 1,2-cycloaddition is the usual mode of reaction.

It is noteworthy that we saw no evidence for nonstereospecific addition of either the monocyclic or tetracyclic aziridines to dimethyl maleate or dimethyl fumarate expected (23) if a diradical species were involved in these cycloadditive processes. This is an especially important observation in the case of addition of the tetracyclic aziridines to these dipolarophiles since, according to the arguments of Dewar and Kirschner (**4***c*), diradical behavior of species generated during thermally forbidden disrotatory opening of aziridines would be most likely in those cases (such as **5**) where symmetry is enforced by severe geometrical constraint on the transition state leading to the ring-opened species.

In agreement with recent calculations by Dewar and co-workers (4), indicating there is often a fairly small difference in the activation energies for analogous allowed and forbidden reactions, we found the enthalpy of activation for the disrotatory ring opening of the tetracyclic aziridine, **5***a*, to be only 3.5 kcal greater than that for the conrotatory opening of its monocyclic analog, **4***a*.

The observation (Fig. 3) that increasing electron donating power of *N*-aryl substituents of the monocyclic aziridines (**4***a–d*) increased their rate of conrotatory opening was expected. This indicates that the interaction in Fig. 2*b* predominates during this ring opening and that the azomethine ylide (**7**) is the product of the process.

The observation that electron withdrawal from nitrogen (Fig. 4) increases the rate of disrotatory opening of the tetracyclic aziridines (**5***a–f*) indicates the interaction described in Fig. 2*a* predominates during this ring-opening process. This means that during the approach to the transition state for this process electron density decreases in the aziridinyl portion of the molecule. Since all evidence points to azomethine ylide **13** as the reactive intermediate involved in the cycloaddition reactions of the tetracyclic aziridines, the electron density in the aziridinyl region of these compounds must increase to full 4π electron status after the transition state for disrotatory opening is achieved.

The kinetic behavior of the *N*-substituted tetracyclic aziridines studied can be viewed in two ways. First, one could conclude that Fukui's analysis (Fig. 2) has validity in terms of net charge flow during electrocyclic reactions of three-membered rings and that we have observed a manifestation of predominant HOMO–LUMO interactions in both possible directions. Secondly, in a broader context one might view the flow of electron density from the aziridine nitrogen to its aryl appendage during disrotatory opening as an attempt to achieve minimum electron density in the reacting portion of the molecule during this forbidden process. On further thought one might expect this behavior to be generally observed since, by this decrease, electronic interactions attending thermally forbidden reactions are minimized in those orbitals where the greatest destabilizing interactions occur.

Experimental

Melting points were determined on a Fisher–Johns apparatus and are uncorrected. Elemental analyses were performed either by Alfred Berhardt Microanalysisches Laboratorium, Mulheim, Germany, or in this laboratory. The infrared spectra were determined with a Unicam SP200 or a Beckman IR-12 instrument. Ultraviolet spectra were recorded on either a Unicam SP800 or Cary 14 spectrometer. The nmr spectra were recorded at 60 MHz on a Varian A56/60 instrument using tetramethylsilane as an internal standard. Mass spectra were obtained on a Hitachi Perkin-Elmer RMU-6E spectrometer using an ionization voltage of 70 eV and an inlet temperature of 175–200°C.

Preparation of N-*Aryl*-cis-*2,3-diphenyl Aziridines (4a–d)*

These aziridines (Table 4) were prepared in good yields

TABLE 4. Physical properties of aziridines **4***a–d*

Aziridine	Melting point (°C)	Nuclear magnetic resonance (δ $CDCl_3$)
4*a*	98–99.5 (lit. (11) 99°C)	3.43(s, 2H), 6.95–7.36(m, 15H)
4*b*	113–114.5	2.25(s, 3H), 3.51(s, 2H), 6.93–7.26(m, 14H)
4*c*	92–93.5	3.50(s, 2H), 6.80–7.22(m, 14H)
4*d*	114–155	3.73(s, 2H), 6.74–7.26(m, 13H)

[2]We would like to thank a referee for suggesting this argument.

Can. J. Chem. Downloaded from www.nrcresearchpress.com by 210.87.254.105 on 09/05/12
For personal use only.

TABLE 5. Yields, melting points, and analyses of *N*-aryl-6*b*,7*a*-dihydroacenaphtha[1,2-*b*]aziridines (**5***a–f*)

Aziridines	Yield (%)	Melting point (°C)	Analysis			
			Calculated		Found	
			C	H	C	H
5*a*	75	171–172.5	88.85	5.37	88.67	5.42
5*b*	69	167–168.5	88.68	5.88	88.54	5.73
5*c*	57	145–146.5	83.49	5.55	83.35	5.64
5*d*	81	188–190	67.08	3.75	66.97	3.91
5*e*	83	225–227	74.98	4.16	75.21	4.13
5*f*	80	139.5–141	69.21	3.55	69.08	3.43

using the procedures described (11) for the preparation of **4***a* except that the yields in the reduction of the hydroxy imine intermediates were appreciably improved by slowly leaching the hydroxy imines into ethereal solutions of LAH (Soxhlet).

Stereospecific Synthesis of **4***a*

To a solution of 3.5 g of *cis*-2,3-diphenylaziridine (12) in 80 ml of THF was added 2.55 g of benzenediazonium-2-carboxylate (13). The suspension was stirred at 50°C until the solid dissolved, then concentrated, and approximately $\frac{1}{3}$ of the concentrate chromatographed on 40 g of silica gel. Elution with 4:1 benzene – petroleum ether gave initial fractions (2 × 50 ml) containing *cis*- and *trans*-stilbenes (50 mg). Subsequent fractions gave a mixture of stilbenes and *N*-phenyl-*cis*-2,3-diphenylaziridine, **4***a* (60 mg), mp 98–100°C. Mixture mp with **4***a* prepared above 98–100°C.

*Preparation of 7-Aryl-6a,7a-dihydroacenaphtha-[1,2-*b*]-aziridines 5a–f*

Solutions of acenaphthylene (~3 g) and a 1.5–2.0 molar equivalent of the appropriately substituted aryl azide in 15 ml of benzene were heated at 60–70°C for 4 (Ar = *p*-NO_2—C_6H_4) to 15 (Ar = *p*-$CH_3OC_6H_4$) days during which time a granular product deposited. Removal of the solvent and recrystallization from ether – petroleum ether gave aziridines **5***a–f* in yields recorded in Table 5.

In the absence of excess azide the dimerization and polymerization of acenaphthylene become undesirable side reactions. Reaction temperatures above 100°C caused dimerization of aziridines.

Kinetic and Product Analysis of Reaction of **4***a–d and* **5***a–f with DMAD*

Materials

The aziridines **4***a–d* and **5***a–f* were purified by at least three recrystallizations from appropriate solvents followed by drying at 70–75°C (0.1 Torr). The dimethyl acetylene dicarboxylate was prepared by a published procedure (24), was distilled twice, bp 130–131°C (10 Torr), and stored at 0°C until used. Spectroscopic grade benzene was distilled over LAH prior to use.

The requisite amounts of aziridine, toluene (internal standard), and dimethyl acetylenedicarboxylate were weighed into 10 ml volumetric flasks and made up to volume with solvent. The nmr tubes were filled with samples of the reaction mixture using a hypodermic syringe and sealed under N_2 atmosphere. The tubes were withdrawn at appropriate intervals, and the reaction was quenched by cooling to −70°C. The tubes were allowed to warm to room temperature, and the nmr spectra were recorded.

The concentration of aziridines, products, and esters were calculated by comparison of the spectra of the respective peak area with that of the peak area of known concentrations of toluene (internal standard). The rates of adduct formation were determined by comparison of the adduct methoxyl resonance intensities with that of the toluene methyl internal standard. In the case of **4***b*, the area of methyl signals was used in calculating the concentration of the product. The nmr spectra were recorded using sweep width of 250 Hz and sweep time of 250 s.

The yields of products from the kinetic runs were obtained by placing the tubes in an oil bath at 140°C after recording the spectra, for varying lengths of time to ensure complete reaction. The reaction mixtures were then transferred to a flask. The solvent was removed at 50–55°C and the residue was diluted with methanol (10 ml) to precipitate the product which was filtered, washed, dried, and weighed.

The yields of adducts and their physical properties are collected in Tables 6 and 7.

Reaction of **4***a with Maleic Anhydride*

Refluxing a toluene (25 ml) solution of **4***a* (275 mg) and maleic anhydride (100 mg) for 6 h gave, after evaporation of the solvent, **8** as a pale yellow solid which after washing with methanol yielded 342 mg (93%), mp 212–214°C. Recrystallization from benzene – petroleum ether (1:10) gave mp 215–216°C (lit. (14) mp 214–215.5°C). Reaction of **8** with an excess of ethereal diazomethane containing methanol gave **9** in 90% yield, mp 180–181.5°C. Mixture mp with **9** prepared from **4***a* and dimethyl maleate was 180–181°C.

Reaction of **4***a with Dimethyl Maleate*

A solution of **4***a* (273 mg) and dimethyl maleate (145 mg) was refluxed in toluene (25 ml) for 14 h. Removal of the solvent *in vacuo* gave a light yellow oil which solidified on standing to give **9** which further precipitated by treating the reaction mixture with methanol, 385 mg (92%), mp 178–181°C. An analytical sample was obtained by recrystallization from methanol, mp 180–181.5°C. *Anal.* calcd. for $C_{26}H_{25}NO_4$: C 75.16, H 6.06; found: C 75.04, H 6.24. *Mol. wt.* calcd. for $C_{26}H_{25}NO_4$: 415; found: 415.

Reaction of **4***a with Dimethyl Fumarate*

A toluene solution (25 ml) of **4***a* (276 mg) and dimethyl fumarate (147 mg) was refluxed for 15 h. After removal of solvent, a pale yellow oil was obtained. Trituration of the oil with methanol gave **10**, 392 mg (94%), mp 218–221°C. Recrystallization from hot methanol gave an analytical sample, mp 221–222°C. *Anal.* calcd. for $C_{26}H_{25}NO_4$: C 75.16, H 6.06; found: C 75.25, H 6.20. *Mol. wt.* calcd. for $C_{26}H_{25}NO_4$: 415; found: 415.

Can. J. Chem. Downloaded from www.nrcresearchpress.com by 210.87.254.105 on 09/05/12
For personal use only.

TABLE 6. Properties of adducts of **4***a–d* and DMAD

Adduct	Yield (%)	Melting point (°C)	Nuclear magnetic resonance (δ $CDCl_3$)	Infrared (KBr, cm^{-1}) (C=O)	Mass spectra M^+	$\frac{(M+1)^+}{M^+}$	$\frac{(M+2)^+}{M^+}$
6*a* (Ar = C_6H_5	92	164–166	3.59(s, 6H) 6.25(s, 2H) 6.30–7.50(m, 15H)	1710	Calcd.: 413 Found: 413	0.289 0.283	0.0489 0.0493
6*b* (Ar = *p*-$CH_3C_6H_4$)	91	214–215	2.09(s, 3H) 3.57(s, 6H) 6.18(s, 2H) 6.37–7.43(m, 14H)	1720	Calcd.: 427 Found: 427	0.333 0.330	0.052 0.059
6*c* (Ar = *p*-ClC_6H_4)	89	197–199	6.63(s, 6H) 6.25(s, 2H) 6.28–7.37(m, 14H)	1720	Calcd.: 447 Found: 447	0.289 0.295	0.368 0.338
6*d* (Ar = *m,p*-$Cl_2C_6H_3$)	90	178–180	3.60(s, 6H) 6.18(s, 2H) 6.24–7.41(m, 13H)	1717	Calcd.: 481 Found: 481	0.289 0.297	0.695 0.641

TABLE 7. Properties of adducts of **5***a–f* and DMAD

Adduct	Yield (%)	Melting point (°C)	Nuclear magnetic resonance (δ, $CDCl_3$)	Infrared (KBr, cm^{-1}) (C=O)	Mass spectra (or analysis) M^+	$\frac{M^++1}{M^+}$	$\frac{M^++2}{M^+}$
15*a*	93	211–212.5	3.73(s, 6H) 5.78(s, 2H) 6.61–7.71(11H)	1720	Calcd.: $C_{24}H_9NO_4$: C 74.79, H 4.96 Found: C 74.96, H 4.68		
15*b* (Ar = *p*-CH_3—C_6H_4)	87	295–297	2.13(s, 3H) 3.74(s, 6H) 5.72(s, 2H) 6.59–7.56(m, 10H)	1707	Calcd.: 399 Found: 399	0.278 0.291	0.0458 0.0491
15*c* (Ar = *p*-CH_3O—C_6H_4)	81	225–227	3.16(s, 3H) 3.73(s, 6H) 5.68(s, 2H) 6.71–7.64(m, 10H)	1717	Calcd.: 415 Found: 415	0.278 0.292	0.0478 0.0492
15*d* (Ar = *p*-Br—C_6H_4)	89	286–288	3.75(s, 6H) 5.70(s, 2H) 6.52–7.71(m, 10H)	1710	Calcd.: 463 Found: 463	0.267 0.262	1.017 1.000
15*e* (Ar = *p*-NO_2—C_6H_4)	93	255–257	3.76(s, 6H) 5.84(s, 2H) 6.51–7.91(m, 10H)	1702	Calcd.: 430 Found: 430	0.267 0.281	0.0468 0.049
15*f* (Ar = *m,p*-Cl_2—C_6H_3)	91	243–245	3.74(s, 6H) 5.75(s, 2H) 6.65–7.82(m, 9H)	1700	Calcd.: 453 Found: 453	0.281 0.279	0.688 0.691

Reaction of 5a with Maleic Anhydride

A solution of **5***a* (500 mg) and maleic anhydride (200 mg) in benzene (15 ml) was heated in a sealed tube at 140°C for 8 h. Removal of the solvent gave a semisolid which was washed with ether to yield **17** as a solid. The solid was filtered, washed with ether, and dried to give 400 mg (60%); mp 255–257°C. Recrystallization from hot toluene afforded a pure sample of **17**, mp 256–257.5°C. *Mol. wt.* calcd. for $C_{22}H_{15}NO_3$: 341 (M^+); found: 341 (M^+).

Evaporation of the filtrate gave a beige oil, **16**, which resisted crystallization. Its ir spectrum (thin film) showed absorption due to an anhydride moiety at 1853 and 1776 cm^{-1}, and the nmr ($CDCl_3$) had two sets of doublets centered at δ 4.19 (2H), and another two sets of doublets centered at δ 5.42 (2H).

Conversion of 16 to 18

The oil from above in 10 ml of methanol was treated with an excess of ethereal diazomethane. Evaporation of the solvent at 50°C left a semicrystalline material which was treated with methanol to give **18**, 210 mg (28%); mp 202–204°C. The nmr and ir spectra of **18** prepared in this manner were identical to those of **18** prepared upon reaction of dimethyl maleate with **5***a*. The mixture melting point of **18** from the two sources was undepressed.

Conversion of 17 to 19

A suspension of anhydride adduct **17** (200 mg) in ether–methanol solution (20 ml) was treated with an excess of ethereal diazomethane solution at −70°C and was allowed to warm to room temperature. The usual work-up procedure

Can. J. Chem. Downloaded from www.nrcresearchpress.com by 210.87.254.105 on 09/05/12
For personal use only.

afforded needles, 200 mg (90%), mp 188–190°C. The nmr and ir spectra of this dimethyl ester were identical to those of the diester **19** obtained from reaction of dimethyl maleate with **5***a*.

Reaction of 5a with Dimethyl Maleate

A benzene solution (10 ml) of **5***a* (750 mg) and dimethyl maleate (450 mg) was heated in a sealed tube at 140°C for 14 h. Removal of the solvent left a red oil which was taken up in 75–80 ml of boiling ethanol. Standing at room temperature for 6–8 h gave a thick layer of **18**, 340 mg, mp 201–203°C. The filtrate was concentrated to half its volume. On standing this concentrate gave another 150 mg of **18** (41%). An analytical sample was obtained by recrystallization from hot methanol: mp 202–203°C. *Anal.* calcd. for $C_{24}H_{21}NO_4$: C 74.40, H 5.46; found: C 74.31, H 5.42. *Mol. wt.* calcd. for $C_{24}H_{21}NO_4$: 387; found: 387.

Further concentration of the mother liquor gave 137 mg of a mixture of **18** and **19**, mp 180–195°C. The filtrate was concentrated and treated with petroleum ether which on standing overnight yielded **19**, 390 mg (32%), mp 188–190.5°C. Evaporation of the solvent to dryness gave a mixture of **18** and **19**, 70 mg, mp 187–190°C. An analytical sample of **19** was prepared by recrystallization from benzene – petroleum ether (1:10), mp 189–190.5°C. *Anal.* calcd. for $C_{24}H_{21}NO_4$: C 74.40, H 5.46; found: C 74.68, H 5.28. *Mol. wt.* calcd. for $C_{24}H_{21}NO_4$: 387; found: 387.

Hydrogenation of 15

A solution of **15** (245 mg) in toluene (10 ml) and methanol (50 ml) containing 50 mg of 5% Pt-on-charcoal was stirred under H_2 at 50 psi for 24 h. The removal of the solvent gave **18**, 232 mg (94%), mp 201–203°C. The nmr and the ir spectra of **18** prepared in this manner were identical to those of **18** prepared by reaction of dimethyl maleate with **5***a*. The mixture melting point of **18** from these two sources was undepressed.

Reaction of 5a with Dimethyl Fumarate

A benzene solution (10 ml) of **5***a* (500 mg) and dimethyl fumarate (291 mg) was heated at 140°C for 14 h in a sealed tube. Removal of the solvent under reduced pressure gave a red liquid which crystallized from methanol – petroleum ether (1:10) to afford **20**, 683 mg (89%), mp 144–146.5°C. An analytically pure sample was obtained by further crystallization from methanol – petroleum ether, mp 145–146.5°C. *Anal.* calcd. for $C_{24}H_{21}NO_4$: C 74.40, H 5.46; found: C 74.24, H 5.55. *Mol. wt.* calcd. for $C_{24}H_{21}NO_4$: 387; found: 387.

Thermal Reaction of 5a–e with Dimethyl Maleate

Benzene-d_6 solutions 0.2 *M* each in **5** and dimethyl maleate were degassed, sealed in nmr tubes, and heated at 110°C for 1–3 days. After consumption of the aziridine the reaction mixture was analyzed directly by nmr. The relative amounts of adducts (**18** and **19** respectively) reported in Table 3 are based on integration of the ester resonances of the adducts.

After evaporation of the solvent the *exo* adducts crystallized easily from boiling ethanol while the *endo* adducts crystallized from cold ethanol in total overall yields of 80–90%.

Prolonged (10 days) heating of benzene-d_6 solutions of pure **18** or **19** or the reaction mixture at 110°C indicated (nmr) no interconversion of **18** and **19** occurred under the reaction conditions.

Photolytic Reaction of 5a–e with Dimethyl Maleate

Benzene-d_6 solutions 0.2 *M* in each aziridine **5** and dimethyl maleate were degassed and sealed in nmr tubes. The tubes were suspended approximately 1 in. from a Pyrex jacketed 200 W Hanovia mercury lamp for 1–3 days. After completion of reaction the ratios of **18** to **19** were determined by integration of the nmr spectra of the ester groups of the adducts. Under the photochemical conditions using benzene-d_6 solutions of **18** and **19** were stable as was the fumarate adduct. The fumarate adduct was detected (by nmr) in the photolysate of all photolyses. Dimethyl maleate was observed to photoequilibrate with dimethyl fumarate under the conditions used for the addition of **5** to the former.

Reaction of 5a with Dimethyl trans,-trans-*1,3-Butadiene-1,4-dicarboxylate*

A benzene solution (15 ml) of **5***a* (500 mg) and dimethyl muconate (340 mg) was heated in a sealed tube at 140°C for 14 h. The reaction mixture on cooling at room temperature gave white needles of unreacted diester, 70 mg (19%), mp 155–157°C (lit. (25) mp 156–157°C).

Evaporation of the filtrate afforded an oil which was crystallized from hot methanol. The crystalline product was filtered, washed with cold methanol, and dried to yield **23**, 210 mg (31%), mp 296–299°C, Further crystallization from benzene – petroleum ether (1:10) gave **23**, mp 298–300°C. *Anal.* calcd. for $C_{44}H_{36}N_2O_4$: C 80.48, H 5.48; found: C 80.57, H 5.65. *Mol. wt.* calcd. for $C_{44}H_{36}N_2O_4$: 656; found: 656.

The mother liquor was evaporated and treated with hot petroleum ether to give **22**, 520 mg (63%), mp 146–149°C. An analytical sample was obtained by recrystallization from benzene – petroleum ether (1:10): mp 148–149.5°C. *Anal.* calcd. for $C_{26}H_{23}NO_4$: C 75.53, H 5.61; found: C 75.48, H 5.52. *Mol. wt.* calcd. for $C_{26}H_{23}NO_4$: 413; found: 413.

Conversion of 22 to 23

Heating a benzene (10 ml) solution of **22** (100 mg) and **5***a* (68 mg) in a sealed tube at 140°C for 14 h gave a red oil. Dilution of the oil with ether deposited a small amount of dimer **25** which was removed by filtration. The filtrate was concentrated to dryness and treated with hot methanol to yield **23**, 120 mg (75%), mp 297–300°C.

*Reaction of 2,4-*trans-trans-*Hexadiene with 5d*

A benzene solution of **5***d* (650 mg) and 2,4-*trans-trans*-hexadiene (400 mg) was allowed to react at 140°C for 16 h in a sealed tube. Removal of the solvent afforded a red liquid which on dilution with ether gave dimer **25** which was filtered, washed with ether, and dried to yield 142 mg (22%), mp > 300°C. Mass calcd. for $C_{36}H_{24}Br_2N_2$: 642 (M^+); found: 642 (M^+).

The ethereal mother liquor was evaporated and treated with hot methanol – petroleum ether (1:10) to give on cooling **24**, 469 mg (58%), mp 197–199.5°C. Recrystallization from benzene – petroleum ether (1:10) gave mp 198–199.5°C. *Anal.* calcd. for $C_{24}H_{22}BrN$: C 71.29, H 5.48; found: C 71.13, H 5.59. *Mol. wt.* calcd. for $C_{24}H_{22}BrN$: 403; found: 403.

Catalytic Hydrogenation of 24

To a suspension of 50 mg of 5% Pt-on-charcoal in methanol (50 ml) was added **24** (110 mg). Reaction under hydrogen at 50 psig for 8 h followed by filtration and evaporation of the solvent yielded **26** as an oil which solidified on standing, 107 mg (97%), mp 134–137°C. A pure sample was obtained by crystallization from methanol – petroleum ether (1:10) mixture mp 136–137.5°C. *Mol. wt.* calcd. for $C_{24}H_{24}BrN$: 405 (M^+); found: 405 (M^+).

Reaction of 5f with 1,3-Cyclohexadiene

A benzene solution (10 ml) of **5***f* (315 mg) and 1,3-cyclohexadiene (400 mg) was heated in a sealed tube at 140°C for 16 h. On cooling a small amount of solid deposited which was removed by filtration. Evaporation of the solvent and treatment with ether deposited the dimer, **25**, which was washed

Can. J. Chem. Downloaded from www.nrcresearchpress.com by 210.87.254.105 on 09/05/12
For personal use only.

with ether, and dried to yield 40 mg (13%), mp > 300°C. Removal of the solvent to dryness gave a semisolid compound which on dilution with benzene – petroleum ether (1:10) deposited 280 mg (72%) of **28**, mp 193–196°C. A pure sample was obtained by crystallization from hot benzene – petroleum (1:10) ether, mp 197–198.5°C. *Anal.* calcd. for $C_{24}H_{19}Cl_2N$: C 73.45, H 4.88; found: C 73.33, H 4.78. *Mol. wt.* calcd. for $C_{24}H_{19}Cl_2N$: 391; found: 391.

Reaction of 5f with Cyclohexene

A benzene solution (10 ml) of **5***f* (700 mg) and cyclohexene (1.5 g) was heated in a sealed tube at 140°C for 14 h. On cooling dimer **25** deposited (20 mg). Evaporation of the solvent and treatment with ether gave additional dimer which was washed with ether and dried to yield 460 mg, 38%, mp > 300°C. Removal of the solvent to dryness gave a semisolid which upon dilution with petroleum ether deposited **29**, which was filtered and dried to yield 12 mg, 7%, mp 180–182°C.

Hydrogenation of 28

A solution of **28** (70 mg) in distilled methanol (25–30 ml) containing 20 mg of 5% Pt-on-charcoal was placed under 45 psig of hydrogen. Hydrogen uptake was completed in 3 h. After reaction for an additional 2 h the catalyst was removed and the solvent evaporated to yield **29**, 68 mg (96%), mp 180–182°C. A pure sample was prepared by recrystallization from warm petroleum ether, mp 181–182.5°C. A mixture of this hydrogenated product, mp 181–182.5°C, with **29** from reaction of **5***f* with cyclohexene, mp 180–182°C, gave mp 180–182°C.

Reaction of 1,3-Cyclohexadiene with 5a

A benzene solution (10 ml) of **5***a* (500 mg) and 1,3-cyclohexadiene (200 mg) was heated at 140°C for 14 h in a sealed tube. On cooling the reaction mixture dimer **25** deposited and was removed by filtration, washed twice with benzene, and dried to yield 120 mg (24%), mp 318–322°C (dec.).

The filtrate was evaporated to dryness and on treatment with methanol gave dimer **27**, which was washed with methanol, and dried to yield 97 mg (20%), mp 278–282°C (dec.).

The methanolic solution was evaporated to dryness to give an oil which was then dissolved in warm benzene – petroleum ether (1:10). On cooling the **28** (Ar = C_6H_5) which deposited was filtered, washed with benzene – petroleum ether (1:20), and dried to yield 207 mg (32%), mp 172–176°C. An analytical sample was obtained by recrystallization from hot benzene – petroleum ether (1:10); mp 175–176.5°C. *Anal.* calcd. for $C_{24}H_{21}N$: C 89.13, H 6.54; found: C 88.97, H 6.63. *Mol. wt.* calcd. for $C_{24}H_{21}N$: 323; found: 323.

Reaction of 5d with Cycloheptatriene

A benzene solution (10 ml) of **5***d* (0.5 g) and cycloheptatriene (1.5 g) was heated in a sealed tube at 110°C for 3 days. Upon cooling dimer **25** precipitated and was removed. The solvent was evaporated and methanol added to precipitate dimer **27**. The filtrate from this filtration was evaporated to dryness and the residue crystallized from benzene – petroleum ether (1:10) to give **30**, 234 mg (37.6%), mp 182–184°C. *Mol. wt.* calcd. for $C_{25}H_{20}BrN$: 413, 415 (M^+); found: 413, 415 (M^+).

Hydrogenation of 30

A solution of **30** (200 mg) in methanol (50 ml) was reduced using PtO_2 (100 mg) and 60 psig H_2 pressure for 21 h. Removal of the catalyst and evaporation of the solvent *in vacuo* afforded a yellow oil which crystallized from ether – petroleum ether (1:3) to give **31**, mp 280–282°C. The **31** produced in this manner gave no melting point depression upon mixture with **31** derived from cycloheptene and **5***d* as described below.

Reaction of 5d with Cycloheptene

A solution of **5***d* (250 mg) and cycloheptene (250 mg) in 10 ml benzene were heated at 110°C in a sealed tube for 4 days. After cooling dimer **25** precipitated and was removed. Addition of methanol precipitated dimer **27**. The filtrate from this filtration was evaporated to dryness to give **31** which precipitated from benzene – petroleum ether (1:10 64 mg 20%), mp 281–282°C. *Mol. wt.* calcd. for $C_{25}H_{22}BrN$: 415, 417 (M^+); found: 415, 417 (M^+).

Thermal Dimerization of 5a

A benzene solution (10 ml) of **5***a* (250 mg) was heated at 140°C in a sealed tube for 14 h. On cooling the reaction mixture **25** precipitated, was filtered, washed with benzene, and dried to yield 117 mg (47%), mp 318–321°C (dec.). A pure sample was obtained by crystallization from boiling toluene: mp 322–324°C (dec.). *Anal.* calcd. for $C_{36}H_{26}N_2$: C 88.85, H 5.38; found: C 88.61, H 5.47. *Mol. wt.* calcd. for $C_{36}H_{26}N_2$: 486; found: 486.

Evaporation of the solvent gave **27**, 102 mg (41%), mp 278–281°C (dec.). Recrystallization from benzene – petroleum ether (1:10) gave mp 280–282°C (dec.). *Anal.* calcd. for $C_{36}H_{26}N_2$: C 88.85, H 5.38; found: C 88.57, H 5.52. *Mol. wt.* calcd. for $C_{36}H_{26}N_2$: 486; found: 486.

Acknowledgements

We wish to thank the National Research Council of Canada for generous support of this work.

1. R. B. WOODWARD and R. HOFFMANN. The conservation of orbital symmetry. Academic Press, New York, NY. 1970.
2. N. D. EPIOTIS. J. Am. Chem. Soc. **95**, 1191 (1973); **95**, 1200 (1973); **95**, 1206 (1973); **95**, 1214 (1973); **95**, 5624 (1973), and other papers from this group.
3. (*a*) J. E. BALDWIN, A. H. ANDRIST, and R. K. PINSCHMIDT, JR. Acc. Chem. Res. **5**, 402 (1972); (*b*) J. A. BERSON. Acc. Chem. Res. **5**, 406 (1972).
4. (*a*) M. J. S. DEWAR, S. KIRSCHNER, and H. W. KOLLMAR. J. Am. Chem. Soc. **96**, 5240 (1974); (*b*) M. J. S. DEWAR, S. KIRSCHNER, H. W. KOLLMAR, and L. E. WADE. J. Am. Chem. Soc. **96**, 5242 (1974); (*c*) M. J. S. DEWAR and S. KIRSCHNER. J. Am. Chem. Soc. **96**, 5244 (1974).
5. (*a*) K. FUKUI. Acc. Chem. Res. **4**, 57 (1971); (*b*) R. G. PEARSON. Acc. Chem. Res. **4**, 152 (1971).
6. N. J. TURRO. Acc. Chem. Res. **2**, 25 (1969).
7. U. SCHÖLLKOPF. Angew. Chem. Int. Ed. Engl. **7**, 588 (1968).
8. P. G. GASSMAN, D. K. DYGOS, and J. E. TRENT. J. Am. Chem. Soc. **92**, 2084 (1970).
9. (*a*) R. HUISGEN, W. SCHEER, and H. HUBER. J. Am. Chem. Soc. **89**, 1753 (1967); (*b*) R. HUISGEN and H. MÄDER. J. Am. Chem. Soc. **93**, 1777 (1971); (*c*) H. HERMANN, R. HUISGEN, and H. MÄDER. J. Am. Chem. Soc. **93**, 1779 (1971); (*d*) R. HUISGEN, W. SCHEER, and H. MÄDER. Angew. Chem. Int. Ed. Engl. **8**, 602 (1969); (*e*) R. HUISGEN, W. SCHEER, H. MÄDER, and E. BRUNN. Angew. Chem. Int. Ed. Engl. **8**, 604 (1969); (*f*) J. H. HALL and R. HUISGEN. Chem. Commun. 1187 (1971); (*g*) J. H. HALL, R. HUISGEN, C. H. ROSS, and W. SCHEER. Chem. Commun. 1188 (1971); (*h*) P. B. WOLLER and N. H. CROMWELL. J. Org. Chem. **35**, 888 (1970).
10. H. HAMBERGER and R. HUISGEN. Chem. Commun. 1190 (1971); A. DAHMEN, H. HAMBERGER, R. HUISGEN, and V. MARKOWSKI. Chem. Commun. 1192 (1971).
11. T. W. J. TAYLOR, J. S. OWEN, and D. WHITTAKER. J. Chem. Soc. 206 (1938).

12. A. HASSNER and F. W. FOWLER. J. Am. Chem. Soc. **90**, 2869 (1968).
13. F. M. LOGULLO, A. H. SEITZ, and L. FRIEDMAN. Org. Synth. **48**, 12 (1968).
14. H. W. HEINE, R. E. PEAVY, and A. J. DURBETAKI. J. Org. Chem. **31**, 3924 (1966).
15. R. S. MCDANIEL and A. C. OEHLSCHLAGER. Tetrahedron, **25**, 1381 (1969).
16. L. J. BELLAMY. The infrared spectra of complex molecules. Methuen and Company Ltd., London, England. 1958.
17. J. W. LOWN and K. MATSUMOTO. J. Org. Chem. **36**, 1405 (1971).
18. M. P. CAVA, N. M. POLLACK, and D. A. RAPELLA. J. Am. Chem. Soc. **89**, 3640 (1967); R. H. SCHLESSINGER and I. S. PONTICELLO. J. Am. Chem. Soc. **89**, 3641 (1967); M. P. CAVA and N. M. POLLACK. J. Am. Chem. Soc. **89**, 3639 (1967).
19. J. D. DUNITZ and L. WEISSMAN. Acta Crystallogr. **2**, 62 (1949).
20. D. CURTIN, H. GRUEN, and B. SHOULDERS. Chem. Ind. (London), 1205 (1958); D. J. CRAM, C. K. DALTON, and G. R. KNOX. J. Am. Chem. Soc. **85**, 1088 (1963); H. SCHECHTER, W. L. LINK, and G. TIERS. J. Am. Chem. Soc. 1601 (1963).
21. D. R. ARNOLD and L. A. KARNISCHKY. J. Am. Chem. Soc. **92**, 1404 (1970).
22. K. N. HOUK. Acc. Chem. Res. **8**, 361 (1975).
23. R. HUISGEN. J. Org. Chem. **41**, 403 (1976).
24. E. H. HUNTRESS, T. E. LISSLIE, and J. BORNSTEIN. Org. Synth. **4**, 329 (1963).
25. J. A. ELVIDGE, R. P. LINSTEAD, B. A. ORKIN, P. SIMS, H. BAER, and D. B. PATTISON. J. Chem. Soc. 2228 (1950).

Can. J. Chem. Downloaded from www.nrcresearchpress.com by 210.87.254.105 on 09/05/12
For personal use only.

Photoreactions of iminophosphoranes

A. S. YIM, M. H. AKHTAR, A. M. UNRAU, AND A. C. OEHLSCHLAGER
Department of Chemistry, Simon Fraser University, Burnaby, B.C., Canada V5A 1S6

Received August 23, 1977

A. S. YIM, M. H. AKHTAR, A. M. UNRAU, and A. C. OEHLSCHLAGER. Can. J. Chem. **56,** 289 (1978).

The irradiation of *N*-aryltriphenyliminophosphoranes in inert solvents leads to efficient production of triphenylphosphine and the diaryl azo compounds derived from the *N*-aryl ylide substituent. The irradiation of *N*-alkyltriphenyliminophosphoranes leads to rearrangements of the *N*-alkyl substituent analogous to those observed during the irradiation of the corresponding azides. Triphenyliminophosphoranes which possess *N*-substituents capable of strong delocalization of the nitrogen lone pair (e.g. benzene sulfonyl, benzoyl) are photostable. Since all attempts to trap nitrene intermediates suspected to be formed during the photoreactions of the photolabile iminophosphoranes were unsuccessful, the reactions are considered to proceed via excited ylide intermediates.

A. S. YIM, M. H. AKHTAR, A. M. UNRAU et A. C. OEHLSCHLAGER. Can. J. Chem. **56,** 289 (1978).

L'irradiation de *N*-aryltriphényliminophosphoranes dans des solvants inertes conduit à une formation efficace de triphénylphosphine et de composés diarylazo provenant du substituant *N*-aryl de l'ylure. L'irradiation de *N*-alkyltriphényliminophosphoranes conduit à des réarrangements de substituants *N*-alkyles semblables à ceux observés durant l'irradiation des azotures correspondants. Les triphényliminophosphoranes portant, au niveau de l'azote, des substituants pouvant favorisés une délocalisation importante de la paire d'electrons libres sur l'azote (e.g. benzènesulfonyle ou benzoyle) sont photostables. On avait cru que des intermédiaires nitrènes pouvaient se former au cours des photoréductions des iminophosphoranes photolabiles; toutes les tentatives effectuées en vue de piéger ces intermédiaires se sont avérées vaines. On considère donc que les réactions se produisent par l'intermédiaire d'ylures excités.
[Traduit par le journal]

Introduction

Many ylides are susceptible to photolytic fragmentation of the ylide bond. In theory, homolytic dis-

$$R_nX{=}YR_m \xrightarrow{h\nu} R_nX{:}\quad {:}YR_m$$

sociation of the heteromultiple bonds of phosphorus–carbon, phosphorus–nitrogen, and analogous sulfur ylides can lead to stable phosphorus and sulfur derivatives and carbene or nitrene species. Most of the evidence for the intervention of carbene and nitrene intermediates in the photoreactions of P=C (1), S=C (2), and S=N (3) ylides comes from comparisons of the products formed in such reactions with those formed when these reactive intermediates are generated by alternate routes.

The relatively few investigations of photoreactions of phosphorus–nitrogen ylides have revealed that a variety of reactions are possible.

Zimmer and Jayawant (4) studied the irradiation of *N*-tert-butyltriphenyliminophosphorane in cyclohexene. They observed the formation of triphenylphosphine, its oxide, *tert*-butylamine, di-*tert*-butylamine, *tert*-butylcyclohexenylamine, 3,3′-bicyclohexenyl, benzene, nitrogen, and hydrogen, which were considered to be derived from competing P—N and C—N bond cleavage as shown in Scheme 1.

Irradiation of cycloiminophosphoranes in hydrocarbon solvents results in low yields of the organo substituted derivatives as the only characterizable products (5).

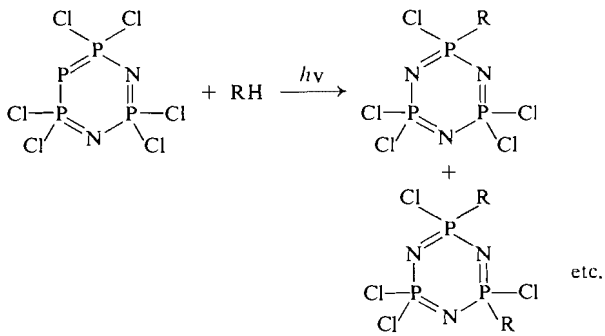

Our main objective in the present study was to investigate the course of the photoreactions of triphenyliminophosphoranes. Since the uv irradiation of these ylides yields triphenylphosphine and characterizable products derived from the nitrogen containing fragment, we sought to ascertain if the latter were derived from nitrenes formed via photodis-

Can. J. Chem. Downloaded from www.nrcresearchpress.com by 210.87.254.40 on 09/05/12
For personal use only.

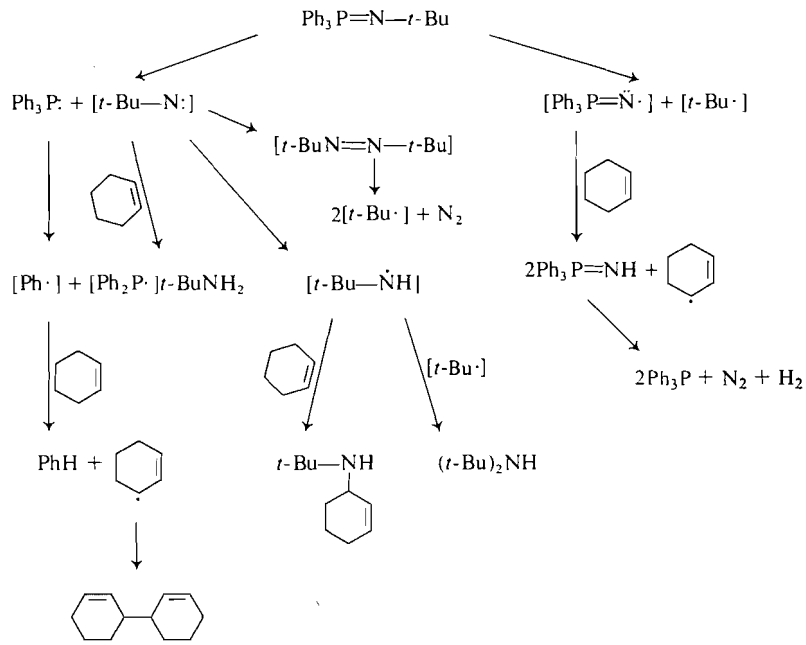

SCHEME I

sociation of the iminophosphoranes. The fates of the ylide-derived nitrogen species were therefore compared with those of nitrene intermediates suspected to be involved in the photoreaction of related azides.

$$Ar_3P{=}N{-}R \xrightarrow{h\nu} Ar_3P{:} + [:\ddot{N}{-}R] \longrightarrow \text{Products}$$

$$R{-}N_3 \xrightarrow{h\nu} N_2 + [:\ddot{N}{-}R] \longrightarrow \text{Products}$$

Experimental

General Description of Equipment and Services

Infrared spectra were recorded with Unicam SP200 or Beckman IR-12 spectrophotometer. The nmr spectra were taken on a Varian A 56-60 spectrometer with tetramethylsilane as an internal standard. Ultraviolet spectra were recorded on either Unicam SP/800 or Cary 14 spectrophotometers.

Mass spectra were obtained on a Perkin-Elmer Hitachi RMU-6E spectrometer using an ionization voltage of 70 eV and an inlet temperature of 175–200°C.

Preparation of Azides

Azides were prepared according to established (16) procedures and purified by passing through a Woelm Alumina (Activity I) column (wt. ratio 10:1) in petroleum ether. Further purification was carried out by recrystallization as ylide.

Preparation of Ylides

Triphenylphosphine (0.1 mol) in benzene (100 ml) was added dropwise at room temperature to 0.11 mol of azides in 100 ml benzene under anhydrous conditions. Evolution of nitrogen occurred instantaneously. The mixtures were stirred overnight, the solvent removed, and the ylides crystallized from benzene – petroleum ether in 60–90% yields (see Table 1).

General Conditions of Irradiation

All solvents were distilled over lithium aluminum hydride or dried over molecular sieve 5A. The reaction mixtures (8–10 m*M*) were made up under dry nitrogen atmosphere. After transfer to the photocell, the photolysates were purged for an hour with helium dried through three trains of anhydrous calcium chloride. A condenser was fitted on the purge gas outlet with an anhydrous calcium chloride drying tube. The source of irradiation was a 200 W Hanovia mercury lamp with the appropriate filter cooling jacket.

Analyses were carried out by gas–liquid partition chromatography on Varian Aerograph Autoprep and Series 1200 gas chromatography units. The column used was 6 ft × $\frac{1}{8}$ in. (6 ft × $\frac{1}{4}$ in. for preparative gas chromatography), 20% SE-30 silicone oil stationary phase on 100–200 mesh HMDS washed Chromosorb W support. Each analysis was temperature programmed from 60–300°C at a rate of 4°C per minute.

Yields were determined by inclusion of an octadecane internal standard (IS) in the reaction solution and applying the usual equations:

$$\text{Specific response} = \frac{\text{Wt. X}}{\text{Response X}} \div \frac{\text{Wt. IS}}{\text{Response IS}}$$

$$\text{Wt. X} = \text{Specific response} \times \frac{\text{Response X}}{\text{Response IS}} \times \text{Wt. IS}$$

Irradiation of Ylides 1–4

A 30 m*M* solution of the ylide in 110 ml of benzene (with octadecane as internal standard) was irradiated for 8 h through a Pyrex filter cooling jacket. The reaction mixture was concentrated to ~10 ml and subjected to glpc analysis. The ratio of ylide to octadecane remained unchanged from the initial concentrations and no triphenylphosphine was detected. Evaporation of the solvent and recrystallization from benzene/petroleum ether gave 90% recovery of the ylide.

Irradiation of Ylides 5, 8–11, 18

A 25–30 m*M* solution (clear to pale yellow) of each ylide in benzene (110 ml) with octadecane internal standard was irradiated for 1 h through a Pyrex filter cooling jacket. The

Can. J. Chem. Downloaded from www.nrcresearchpress.com by 210.87.254.40 on 09/05/12
For personal use only.

Can. J. Chem. Downloaded from www.nrcresearchpress.com by 210.87.254.40 on 09/05/12
For personal use only.

TABLE 1. Properties of triphenyliminophosphoranes

Azide	Imino-phosphorane	Melting point (°C) Exptl.	Melting point (°C) Lit. (17)	Molecular weight Calcd.	Molecular weight Found
Benzenesulfonyl azide	**1**	155–157	157–158		
Benzoyl azide	**2**	195–197	196–197		
Methylazidoformate	**3**	135–137	136–137		
cis-1,2-Diphenyl vinylazide (ref. 18)	**4**	157–159 dec.		$C_{32}H_{26}NP$: 455 M^+	455 M^+
Phenyl azide	**5**	133–134	131–132		
p-Bromophenyl azide	**8**	133–135		$C_{24}H_{14}NPBr$: 432 M^+	432 M^+
p-Anisyl azide	**9**	117–118	118		
p-Nitrophenyl azide	**10**	161–162	160–162		
o-Tolylazide	**11**	129–130	129–130		
o-Butylphenyl azide	**13**	134–135		$C_{24}H_{19}NP$: 409 M^+	409 M^+
o-Azidobiphenyl	**14**	140–141		$C_{30}H_{24}NP$: 429 M^+	429 M^+
p-Tolyl azide	**18**	135–136	135–136		
Cyclohexyl azide	**19**	71–73		$C_{24}H_{26}NP$: 359 M^+	359 M^+
Benzyl azide	**23**	112–113		$C_{25}H_{22}NP$: 367 M^+	367 M^+
Trityl azide (ref. 19)	**26**	228–229	228–229		

photolysate (brick red to brown) was concentrated to ~10 ml and subjected to glpc analysis. The identity of azoaryl, aryl amine, triphenylphosphine, and triphenylphosphine oxide was determined by mixed injection with authentic samples. The yields given in Table 2 were determined as described above. The photoreactions listed in Table 3 were carried out in a similar manner except that the initial ylide concentrations were 10 m*M*.

Quantum Yield Determination for **5**

The method of Hatchard and Parker (20) was followed. The light source was found to emit 1.05×10^{15} photons per second. Ylide consumption as well as triphenylphosphine and azobenzene formation for the first 10 min, when absorption interference from azobenzene was negligible, were determined by glpc with authentic samples using octadecane as internal standard.

Irradiation of Ylide **13**

A 25 m*M* solution (110 ml) of ylide **13** in benzene was irradiated through a Pyrex filter for 3 h. The photolysate was concentrated to 10 ml and analyzed by glpc. Comparison of the retention characteristics of the photolysate components with 2-ethyl-2,3-dihydroindole and 2-methyltetrahydroquinoline generated by photocyclisation of *o*-butylphenyl azide (9) revealed these components were not formed (<0.1%) during irradiation of ylide **13**. Two components were detected (85%) in addition to triphenylphosphine (90%) and 2-butylaniline (5%) and were isolated from the photolysate by preparative glpc. Mass calcd. for $C_{20}H_{26}N_2$: 295 (M^+); found: 294 (M^+).

They were found to interconvert upon separate irradiation and possessed uv_{max} at 320 and 285 nm. By analogy with *trans* (λ_{max} 319 nm) and *cis* (λ_{max} 280 nm) azobenzene (21) these two compounds are considered to be the *trans*- and *cis*-*o*,*o*′-dibutylazobenzenes.

Irradiation of Ylide **14**

Solutions (110 ml) of ylide **14** (27 m*M*) in the solvents given in Table 4 containing octadecane standard were each irradiated for 9 h through a Pyrex filter. The photolysate was concentrated to 10 ml and analyzed by glpc. Biphenyl, *o*-aminobiphenyl, carbazole, triphenylphosphine, and azobiphenyl were identified by mixed injection with authentic samples. Yields given in Table 4 were calculated in the usual manner.

Irradiation of 2-Aminobiphenyl with Triphenylphosphine

A 110 ml benzene solution of 2-aminobiphenyl (0.856 g) and triphenylphosphine (1.336 g) with octadecane as internal standard was irradiated for 6 h with air as purge gas. *o*-Aminobiphenyl remained unreacted but triphenylphosphine was partially converted to triphenylphosphine oxide (46.8%).

Irradiation of **3** *in Presence of Phenyl Azide*

A 110 ml benzene solution of ylide **3** (1.0 g) and phenyl azide (0.8 g) containing octadecane standard was irradiated for 6 h through Pyrex filter. Analysis of the concentrated photolysate by glpc indicated no asymmetric azobenzene or triphenylphosphine was formed. Azobenzene (40%) and aniline (<1%) were formed. Ylide **3** remained unreacted.

Irradiation of p-*Tolyl Azide and Ylide* **5** *Mixture*

A 110 ml benzene solution of *p*-tolyl azide (0.37 g) and ylide **5** (1.0 g) containing octadecane standard was irradiated for 3 h through a Pyrex filter. The photolysate was concentrated to 10 ml and analyzed by glpc (see Discussion).

Irradiation of **18** *and Phenyl Azide Mixture*

A benzene solution (110 ml) of phenyl azide (0.40 g) and ylide **18** (1.05 g) was irradiated for 3 h through a Pyrex filter. The photolysate was concentrated to 10 ml and analyzed by glpc (see Discussion).

Irradiation of **5** *and* **18**

A 110 ml benzene solution of ylide **5** (0.7 g) and ylide **18** (0.6 g) was irradiated for 3 h through a Pyrex filter. The photolysate was concentrated to 10 ml and analyzed by glpc (see Discussion).

Irradiation of Methyl Azidoformate and **5**

A 110 ml benzene solution of methyl azidoformate (0.3 g) and ylide **5** (1.0 g) was irradiated for 3 h through a Pyrex filter. The photolysate was concentrated to 10 ml and analyzed by glpc. Ylide **3** and azobenzene were the only products formed.

Irradiation of Ylide **19**

An ether solution (110 ml) of ylide **19** (1 g) containing octadecane standard was irradiated for 12 h through a Pyrex filter. The photolysate was concentrated to 10 ml and analyzed by glpc. Products listed in Table 6 were identified by mixed injection with the authentic samples. The major products, **20** and

Can. J. Chem. Downloaded from www.nrcresearchpress.com by 210.87.254.40 on 09/05/12
For personal use only.

triphenylphosphine were isolated by preparative glpc. Mass calcd. for $C_{12}H_{21}N$: 179 (M^+); found: 179 (M^+).

Irradiation of Ylide **23**

A 110 ml ether solution of ylide **23** (1 g) containing octadecane standard was irradiated for 12 h through a Pyrex filter. The photolysate was concentrated to 10 ml and analyzed by glpc. Triphenylphosphine and imine, **24**, were isolated by preparative glpc. For **24** mass calcd. for $C_{14}H_{13}N$: 195 (M^+); found: 195 (M^+). Acid hydrolysis of **24** afforded benzaldehyde and benzylamine.

Irradiation of Ylide **26**

A benzene solution (110 ml) of ylide **26** (0.5 g) containing octadecane standard was irradiated for 6 h through a Pyrex filter. The photolysate was concentrated to 10 ml and analyzed by glpc. Triphenylphosphine and *N*-phenylbenzophenone imine, **27**, were the only products formed. For **27** mass calcd. for $C_{19}H_{15}N$: 257 (M^+); found: 257 (M^+). The imine (**27**) was identical to the condensation product of aniline and benzophenone.

Results and Discussion

The triphenyliminophosphoranes used in this study were prepared by reacting triphenylphosphine with the corresponding azide (6). The iminophosphorane products were characterized (Table 1, Experimental) and stored under dry nitrogen until use. Irradiations were generally carried out using a medium pressure Hg lamp in a Pyrex vessel (>300 nm). Because of the hydrolytic instability of most iminophosphoranes, irradiations were conducted in freshly distilled, dry solvents under dry nitrogen or helium. Under these irradiation conditions, *N*-benzenesulfonyl- (**1**), *N*-benzoyl- (**2**), *N*-carbomethoxy- (**3**), and *N-cis*-1,2-diphenylvinyl-triphenyliminophosphoranes (**4**) are stable. These ylides were recovered in nearly quantitative yield after 8 h of irradiation.

$Ph_3P{=}N{-}R$
1 R = $SO_2C_6H_5$
2 R = COC_6H_5
3 R = CO_2CH_3
4 R = (*cis*)CPh=CHPh

The photochemical stability of **1–4** parallels the stability of such ylides toward hydrolysis and reaction with polar bonds (6). Ylides **1–4** possess the common feature of nitrogen substituents that allow extensive resonance delocalization of the nitrogen lone pair. This delocalization leads to an alteration of the uv absorption spectra of these ylides compared to photolabile triphenyliminophosphoranes. The uv spectra of all triphenyliminophosphoranes studied possess an intense ($\varepsilon \approx 1.35 \times 10^4$) broad absorption in the 220–280 nm region due to the aromatic phosphorous substituents. In addition there is a weak ($\varepsilon \approx 10^2$) absorption shoulder centered at 315 nm in photolabile triaryliminophosphoranes. This latter absorption is in the borosilicate transparent region of the uv and undoubtedly is receiving irradiation in the present experiments. We attribute this absorption to the $n \rightarrow \pi^*$ transition of the ylide nitrogen lone pair. In the photostable ylides (**1–4**) the 315 nm absorption is not noticeable.

Irradiation of *N*-phenyltriphenyliminophosphorane (**5**) in benzene led to nearly quantitative yields of triphenylphosphine (**6**) and azobenzene (**7**). These products were identified by chromatographic isolation and comparison with authentic samples. The quantum yield for this irradiation based on azobenzene formation was 0.7. In several runs of this and other ylide photoreactions the formation of both triphenylphosphine oxide and amine (aniline in this case) was noted. The yield of these products was reduced when moisture was rigorously excluded from the photolysis solution. We therefore attribute their formation to ylide hydrolysis.

Substitution of the *N*-aryl ring with electron withdrawing (*p*-Br (**8**), *p*-NO_2 (**10**)) or electron donating (*p*-OCH_3 (**9**), *o*-tolyl (**11**), and *p*-tolyl (**18**)) groups did not noticeably alter the course of the photoreaction (Table 2).

Comparison of the course of photolysis of phenyl azide with the photolysis of ylide, **5**, in benzene revealed that only a small amount of azobenzene was formed from the azide photolysis (7). Most of the azide was converted to aniline.

Several attractive mechanisms come to the fore in considering the photoconversion of iminophosphoranes to azo compounds. These can be envisioned as involving reaction via an excited ylide (reaction sequence *a,c* or *a,d*) or a nitrene (*b,e*; *b,c*; or *a,d*). Since reaction between highly reactive species, i.e. excited ylide and nitrene generated in low concentration, is less probable than reaction of these same species with available solvent or ylide, pathways such as *a,d* and *b,e* can be eliminated from consideration. One is therefore led to consider the reaction as proceeding via excited ylide combination with ylide (*a,c*) or nitrene combination with ylide (*b,c*). To

TABLE 2. Effect of *N*-phenyl substitution on the photolysis of *N*-aryltriphenyliminophosphoranes (10 m*M*) in benzene for 3 h

N-Aryl group	% reaction	Azoaryl (%)	Aromatic amine (%)	Ph_3P (%)
Phenyl (**5**)	100	100		100
p-Bromophenyl (**8**)	81	75	1	80
p-NO_2-Phenyl (**10**)	100	10	0.5	70*
o-Tolyl (**11**)	85	75	5	8
p-Tolyl (**18**)	80	79	0.5	75
p-Anisyl (**9**)	85	81	1	81

*Ph_3PO: photolysis of *p*-NO_2-phenyl ylide yields many additional, very complicated products probably due to deoxygenation by Ph_3P formed during photolysis.

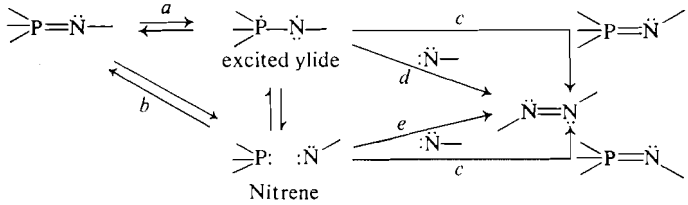

differentiate between these two routes, a search for independent evidence for the intervention of aryl nitrenes in these reactions was conducted.

It was considered likely that the failure of aryl azides to produce the high yields of azo compounds which are ordinarily obtained from ylide photoreactions could be due to the lesser nucleophilicity of azides compared to that of ylides. This difference would lead to a lower rate of reaction of any nitrene intermediates with their parent azides allowing alternate reactions such as hydrogen abstraction to proceed.

To increase the likelihood that any nitrene generated during ylide photolysis would be trapped by reaction with substrates other than ylide, we investigated the photolysis of **5** in the presence of various solvents (Table 3). We varied the reactivity of the solvent to include nucleophilic olefins (cyclohexene, styrene, dihydropyran), solvents capable of undergoing facile hydrogen abstraction reactions (cumene), and nucleophilic solvents capable of reaction with any nitrene generated (acetonitrile, diethylamine). In only one case were products detected which were attributable to reaction other than azo compound formation or ylide hydrolysis. This was the formation of aniline (but no triphenylphosphine oxide) from irradiation of **5** in cyclohexene. Although this was presumably due to allylic hydrogen abstraction of the photogenerated intermediate with cyclohexene, no products such as 3,3′-dicyclohexenyl were detected.

The irradiation of **5** in diethylamine was designed to trap any nitrene formed as an azepine. This and related nucleophiles have been reported to trap phenylnitrene generated from a variety of sources (8) with the concomitant formation of azepines (**12**).

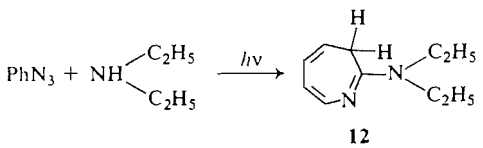

12

We repeated (7, 8) the irradiation of phenyl azide in diethylamine and indeed isolated azepine **12**. When irradiation of the corresponding ylide **5** was conducted under the same reaction conditions, no azepine was detected by glpc or tlc.

Failing to obtain any evidence for intermolecular reaction of suspected nitrene intermediates in the foregoing ylide irradiations, attention was directed to the detection of intramolecular reactions. We irradiated the triphenyliminophosphoranes **13** and **14**, respectively, from *o*-butylphenyl azide and its *o*-phenyl analog. Irradiation of ylide **13** in benzene gave only triphenylphosphine, 2-butylaniline, and azoaryls. No insertion into the *ortho* aliphatic side chain of the ylide was observed. This contrasts with the reported production of moderate yields of C—H insertion products when *o*-butylnitrobenzene is reduced with triethylphosphite (9) or when the corresponding azide is irradiated in inert solvent (10).

Irradiation of the azide from which ylide **14** was derived has been studied in some detail. The important azide reaction characteristics for the present study were considered to be the reported efficient formation of carbazole (**15**) when the reaction was carried out under singlet sensitization (11) and the variation of product distribution with solvent (11). Both facets of the reaction were used in arguments that were later confirmed by flash irradiation (12) to invoke a nitrene intermediate. Irradiation of ylide **14** in a variety of solvents gave nearly quantitative yields of azobiphenyl, small amounts of *o*-aminobiphenyl, triphenylphosphine, and its oxide but no carbazole. Singlet sensitization of the reaction did not yield any detectable amount of carbazole and the nature of the solvent had no appreciable effect on product distribution (Table 4).

When dry air was used as a purge gas during the irradiation of ylide **14** in benzene, carbazole was formed in good yield (Table 5). Since it is known (13) that 2-aminobiphenyl undergoes oxidative cyclization to carbazole under similar conditions 2-aminobiphenyl was irradiated in the presence of triphenylphosphine with oxygen as the purge gas. The amine was recovered unreacted and no carbazole was detected.

The most attractive remaining route for the formation of carbazole from ylide in the presence of oxygen is via triphenylphosphine deoxygenation of *o*-nitrosobiphenyl (**16**) formed by oxygenation of ylide **14** (Scheme 2). Indeed *o*-nitrosobiphenyl was detected in the photolysate when the irradiation of **14** was conducted using oxygen as a purge gas, condi-

Can. J. Chem. Downloaded from www.nrcresearchpress.com by 210.87.254.40 on 09/05/12
For personal use only.

Can. J. Chem. Downloaded from www.nrcresearchpress.com by 210.87.254.40 on 09/05/12
For personal use only.

TABLE 3. Irradiation of *N*-phenyltriphenyliminophosphorane (**5**) in different solvents

Solvent	Reaction time	Products (yield)
Benzene	1 h	Ph_3 (100%) + PhN=NPh (100%)
Cyclohexene	3 h	Ph_3P (78%) + Aniline (17%) + PhN=NPh (55%)
Styrene in cyclohexene	5 h	Ph_3P (79%) + Ph_3P=O (8%) + Aniline (7%) + PhN=NPh (73%)
Dihydropyran	3 h	Ph_3P (64%) + Ph_3P=O (13%) + Aniline (12%) + PhN=NPh (34%)
1,1,2,2-Tetramethylethylene	4 h	Ph_3P (93%) + PhN=NPh (70%)
Acetonitrile	6 h	Ph_3P (80%) + PhN=NPh (75%)
1% Cumene in cyclohexene	4 h	Ph_3P (87%) + PhN=NPh (83%) + Dicumyl (1%)
Diethylamine	12 h	Ph_3P (80%) + PhN=NPh (78%) + No azepine (**12**, ref. 8)

TABLE 4. Solvent effect on product distribution of the irradiation of ylide **14** (% yield)

Compounds	Benzene	Anthracene in benzene	Dioxane	Ether	Piperylene in ether
Biphenyl	<0.1	<0.1	4 ±0.5	<0.1	<0.1
o-Aminobiphenyl	2.0±0.5	1.0±0.5	<0.1	2.0±0.5	1.0±0.5
Carbazole	<0.1	<0.1	<0.1	<0.1	<0.1
Ph_3P	69 ±5	71 ±5	78 ±5	80 ±5	85 ±5
Ph_3PO	7.3±0.5	5.0±0.5	1.2±0.5	10.0±0.5	5.0±0.5
Azobiphenyl	93 ±5	90 ±5	100 ±5	90 ±5	95 ±5

tions which might be expected to result in the consumption of triphenylphosphine prior to its reaction with *o*-nitrosobiphenyl.

It should be pointed out that azobiphenyl can be formed from ylide **14** by thermal or photoreaction with *o*-nitrosobiphenyl.

To determine whether aryl nitrenes could be trapped by ylides under our conditions, phenylnitrene was generated photochemically and thermally from phenyl azide in the presence of a photochemically stable ylide (**3**). The ylide remained unreacted under both sets of conditions and no triphenylphosphine, its oxide or carbomethoxyazoaryl (**17**) was formed.

When *p*-tolylnitrene from *p*-tolyl azide was generated thermally in the presence of ylide **5**, the ylide remained unreacted. However, when *p*-tolyl azide and **5** were irradiated in benzene, the expected azoaryls were formed. The same three azoaryls were formed when *N*-*p*-tolyltriphenyliminophosphorane (**18**) and phenyl azide were irradiated and when ylides **5** and **18** were irradiated together. When methyl azidoformate and ylide **5** were irradiated together, azobenzene and photostable ylide (**3**) were formed.

We conducted several irradiations to determine the course of reaction of *N*-alkyltriphenyliminophosphoranes (Table 6). As seen from these data, the irradiation of these ylides induces both P—N and C—N cleavage depending on the substitution. The most prominent reaction observed was migration

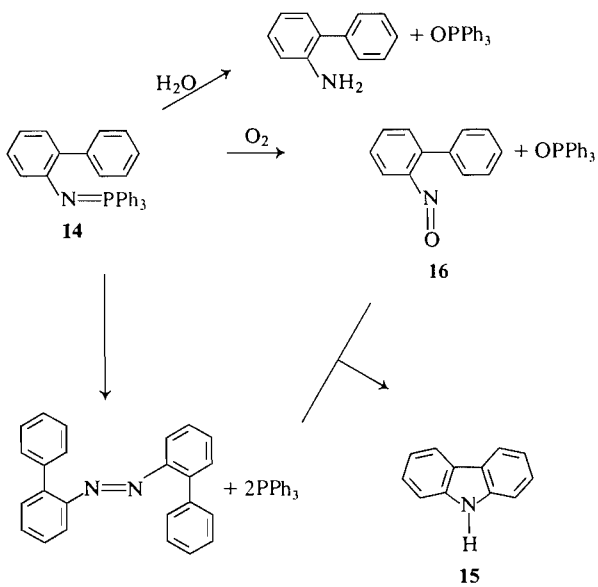

SCHEME 2

Can. J. Chem. Downloaded from www.nrcresearchpress.com by 210.87.254.40 on 09/05/12
For personal use only.

TABLE 5. Effect of purge gas on product distribution on irradiation of **14** in benzene (% yield)

Compounds	Helium	Air	Oxygen
o-Aminobiphenyl	2.0±0.5	3.7±0.5	7.3±0.5
Biphenyl	<0.1	<0.1	<0.1
o-Nitrosobiphenyl (**16**)	<0.1	Trace	5.0±0.5
Carbazole (**15**)	<0.1	26.4±0.5	19.2±0.5
Ph_3P	69 ±5	8.3±0.5	<0.1
Ph_3PO	7.3±0.5	76 ±5	91 ±5
Azobiphenyl	93 ±5	41 ±5	20 ±5

TABLE 6. Product distribution from irradiation of *N*-alkyliminophosphoranes

Ylids	Solvents	Time	Products (yield)
$Ph_3P{=}N$–⬡ **19**	Ether	6 h	Ph_3P (70%) + Ph_3PO (12%) + ⬡–NH_2 (5%) **21** + ⬡=N–⬡ (60%) **20**
$Ph_3P{=}NCH_2Ph$ **23**	Benzene	12 h	Ph_3P (80%) + Ph_3PO (10%) + $PhCH_2N{=}CHPh$ (48%) + $PhCH_2NH_2$ (3%)
$Ph_3P{=}NCPh_3$ **26**	Benzene	6 h	Ph_3P (80%) + $Ph_2C{=}NPh$ (65%)

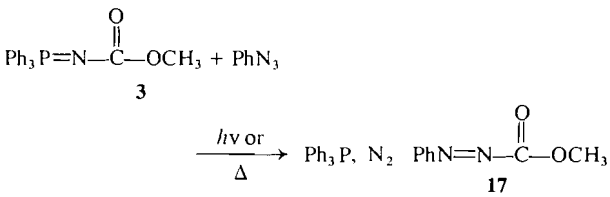

or loss of a substituent bound to the carbon bearing nitrogen.

Irradiation of *N*-cyclohexyltriphenyliminophosphorane (**19**) gave triphenylphosphine, its oxide, *N*-cyclohexylcyclohexanone imine (**20**), and cyclohexylamine (**21**) (Scheme 3). Subtracting the amount of cyclohexylamine formed from presumed hydrolysis of the ylide (equimolar to triphenylphosphine oxide formed) revealed that the ratio of cyclohexanone imine (**22**) to amine (**21**) formed from the photoreaction is in good agreement with that formed during photolysis of cyclohexyl azide (14). The interpretation that this photoreaction involves a nitrene can't be made with certainty since imine **20** could also be derived from reaction of cyclohexanone with ylide **19**.

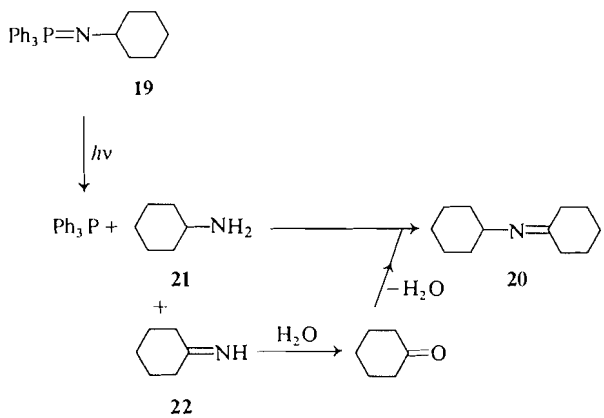

SCHEME 3

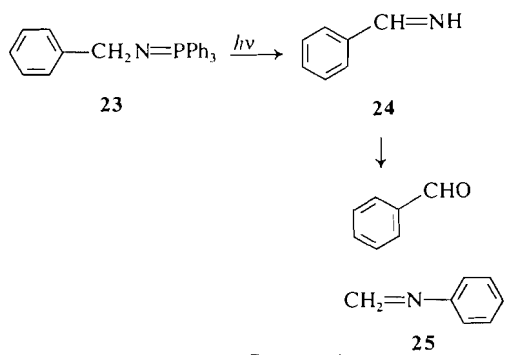

SCHEME 4

Irradiation of *N*-benzyltriphenyliminophosphorane (**23**) gave essentially the same type of product distribution as ylide **19** (Scheme 4). Although both phenyl and hydrogen migration occur to the same extent during the photolysis of benzyl azide (14), only products (**24**) of hydrogen migration are isolated from the irradiation of ylide **23**. The trimer of imine **25** which should have been derived from phenyl migration was synthesized independently from

aniline and formaldehyde but not detected in the photolysate of ylide **23**. Irradiation of *N*-tritylimino-phosphorane, **26**, gave imine **27**, the product of trityl azide photodecomposition (15).

$$\underset{\mathbf{26}}{Ph_3CN{=}PPh_3} \xrightarrow{h\nu} \underset{\mathbf{27}}{Ph_2C{=}N{-}Ph} + Ph_3P$$

The reactions observed upon irradiation of the triaryliminophosphoranes studied are easily attributable to excited ylide intermediates. In all instances where ylide structure would allow detection of characteristic nitrene reactions, such were not observed. From a synthetic point of view the photoreactions of triaryliminophosphoranes represent an extremely efficient route to diaryl azo compounds.

Acknowledgements

We wish to thank the National Research Council of Canada, the Defence Research Board, and the Simon Fraser University Research Fund for support of this project. The authors also wish to acknowledge the assistance of Carol Emory in the preparation of several of the ylides studied.

1. H. Tschesche. Chem. Ber. **98**, 3318 (1965); A. Ritter and B. Kim. Tetrahedron Lett. 3449 (1968).
2. E. J. Corey and M. Chaykovsky. J. Am. Chem. Soc. **86**, 1640 (1964); B. M. Trost. J. Am. Chem. Soc. **88**, 1587 (1966); **89**, 138 (1967).
3. D. J. Anderson, T. L. Gilchrist, D. C. Horwell, and C. W. Rees. Chem. Commun. 146 (1969).
4. H. Zimmer and M. Jayawant. Tetrahedron Lett. 6061 (1966).
5. B. R. Disshon and Y. Hirshberg. J. Polym. Sci. **4**, 75 (1949).
6. A. W. Johnson. Ylid chemistry. Academic Press, New York and London. 1966.
7. W. E. Doering and R. A. Odum. Tetrahedron, **22**, 81 (1966).
8. (*a*) R. Huisgen and M. Appl. Chem. Ber. **91**, 1 (1958); (*b*) B. A. DeGraff, D. W. Gillespie, and R. J. Sundberg. J. Am. Chem. Soc. **96**, 7491 (1974).
9. R. J. Sundberg. J. Am. Chem. Soc. **88**, 3781 (1966).
10. G. Smolinsky and B. Feuer. J. Org. Chem. **31**, 3883 (1966).
11. J. S. Swenton. J. Am. Chem. Soc. **92**, 3103 (1970).
12. P. A. Lehman and R. S. Berry. J. Am. Chem. Soc. **95**, 8614 (1973).
13. H. Suhr, V. Schoch, and G. Rosskamp. Chem. Ber. **104**, 674 (1971).
14. R. M. Moriarty and R. C. Reardon. Tetrahedron, **26**, 1379 (1970).
15. F. D. Lewis and W. H. Saunders. J. Am. Chem. Soc. **89**, 645 (1967).
16. N. Rabjohn (*Editor*). Organ. Syn. **4**, 75 (1963).
17. H. J. Bestmann and R. Zimmerman. *In* Organic phosphorus compounds. Vol. 3. *Edited by* G. M. Kosolapoff and L. Maier. John Wiley and Sons. 1972. Chapt. 5A.
18. F. W. Fowler, A. Hassner, and L. A. Levy. J. Am. Chem. Soc. **89**, 2077 (1967).
19. W. H. Saunders, Jr. and J. A. Ware. J. Am. Chem. Soc. **80**, 3328 (1958).
20. C. G. Hatchard and C. A. Parker. Proc. R. Soc. A, **235**, 518 (1956).
21. P. P. Birnbaum, J. H. Lingford, and D. W. G. Style. Trans. Faraday Soc. **49**, 735 (1953).

Can. J. Chem. Downloaded from www.nrcresearchpress.com by 210.87.254.40 on 09/05/12
For personal use only.

Some stereochemical aspects of two-bond $^{13}C-^{1}H$ spin–spin coupling. Sign determination in natural abundance ^{13}C nuclear magnetic resonance spectra[1]

NATSUKO CYR, GORDON K. HAMER, AND ARTHUR S. PERLIN

Department of Chemistry, McGill University, Montreal, P.Q., Canada H3A 2A7

Received July 19, 1977

NATSUKO CYR, GORDON K. HAMER, and ARTHUR S. PERLIN. Can. J. Chem. **56**, 297 (1978).

The magnitudes and signs of two-bond $^{13}C-^{1}H$ coupling constants (^{2}J) in the array $O-^{13}C_A-C_B-^{1}H$, appear to be determined by the relative orientations of the $O-^{13}C_A$ and $C_B-^{1}H$ bonds, as shown with a variety of carbohydrate derivatives. The data have been observed from natural abundance ^{1}H-coupled ^{13}C nmr spectra, and signs of ^{2}J have been determined by the 'selective population transfer' technique. When C_B bears one oxygen atom, the observed ^{2}J values range from -6 to 0 Hz, whereas a range of 0 to $+8$ Hz is found when C_B bears two oxygen atoms. By contrast, for arrays in which C_B bears one oxygen atom and C_A two, the ^{2}J values vary from -6 to $+6$ Hz. In general, the results confirm earlier indications that the larger the torsional angle between the $O-^{13}C_A$ and $C_B-^{1}H$ bonds, the more positive is the value of ^{2}J. These findings are supported by calculations for model compounds, i.e., propane-1,1,2-triol and butane-2,3-diol.

NATSUKO CYR, GORDON K. HAMER et ARTHUR S. PERLIN. Can. J. Chem. **56**, 297 (1978).

Les amplitudes et les signes des constantes de couplage $^{13}C-^{1}H$ à travers deux liaisons (^{2}J) dans des arrangements $O-^{13}C_A-C_B-^{1}H$ semblent être déterminées par les orientations relatives des liaisons $O-^{13}C_A$ et $C_B-^{1}H$; ces conclusions dérivent d'observations faites à l'aide d'un certain nombre de dérivés de carbohydrate. On a obtenu des données à partir de spectres rmn ^{13}C en abondance naturelle et couplés avec le proton; on a déterminé les signes de ^{2}J par la technique de transfert sélectif de population. Lorsque C_B porte un atome d'oxygène, les valeurs ^{2}J observées varient de -6 à 0 Hz alors que l'on trouve des valeurs allant de 0 à $+8$ Hz lorsque C_B porte deux atomes d'oxygène. Par opposition, les arrangements dans lesquels C_B et C_A portent respectivement un et deux atomes d'oxygène, les valeurs de ^{2}J varient de -6 à $+6$ Hz. En général les résultats confirment des indications antérieures à l'effet que des angles de torsion plus grands entre les liens $O-^{13}C_A$ et $C_B-^{1}H$, provoquent des valeurs plus positives de ^{2}J. On trouve des données expérimentales appuyant des conclusions obtenues à l'aide de calcul sur des composés modèles comme le propanetriol-1,1,2 et de butanediol-2,3.

[Traduit par le journal]

Introduction

Coupling between a carbon-13 nucleus and a proton across two bonds ($^{2}J_{C-H}$) varies with the orientation of substituents appended to the carbon atom (1–5). For experimental reasons, studies of ^{2}J values in the sugar series have dealt mainly with ^{1}H spectra of ^{13}C-enriched compounds (2–5), and have been restricted largely to terminally-labelled positions (i.e. coupling between C-1 and H-2, or C-6 and H-5). Due to recent developments in FT nmr spectroscopy, natural abundance ^{13}C spectra offer a far more convenient and versatile source of $^{13}C-^{1}H$ coupling information (6–8). The current data have been obtained in this manner, making possible a much fuller description than heretofore available of the stereochemical dependence of ^{2}J in carbohydrate molecules.

Results and Discussion

Influence of Substituent Orientation

A wide variety of structural and geometrical arrangements of ^{13}C and ^{1}H nuclei separated by two bonds is found among carbohydrate molecules. In the vicinity of the anomeric centre, stereochemical differences give rise to a large range of values for coupling between C-1 and H-2: as shown recently by ^{1}H spectroscopy of ^{13}C-1 labelled β-D-glucopyranose, α-D-glucopyranose, and 1,2:5,6-di-*O*-isopropylidene-α-D-glucofuranose, respectively, $^{2}J_{C\text{-}1,H\text{-}2}$ is -5.7 Hz, 0 Hz, and $+5.5$ Hz (5). During the current study, these results were confirmed with non-enriched samples of the same compounds by ^{13}C nmr spectroscopy, in combination with the 'selective population transfer' (spt) technique for sign determination (9–12) (see below). That is, the respective $^{2}J_{C\text{-}1,H\text{-}2}$ values were found to be -5.7, 0, and $+5.5$ Hz.[2]

In accounting empirically for such differences, it has been suggested (4, 5) that the magnitude of ^{2}J is

[1]Presented in part at the 59th Canadian Chemical Conference, Chemical Institute of Canada, London, Ont., June 6–9, 1976.

[2]It should be noted that these values and others presented below (Table 1) are *observed spacings*. Undoubtedly, some are not true ^{2}J values, owing to second order effects, as discussed earlier (8). The estimated error in the measurement of these spacings is ± 0.2 Hz, due to the limits of the computer digital resolution.

Can. J. Chem. Downloaded from www.nrcresearchpress.com by 210.87.254.105 on 09/05/12
For personal use only.

Can. J. Chem. Downloaded from www.nrcresearchpress.com by 210.87.254.105 on 09/05/12
For personal use only.

affected by the orientation of the O—^{13}C—O bonds with respect to the C-2—^{1}H-2 bond. For example, in β-glucose the ^{13}C-1—O-1 and C-2—^{1}H-2 bonds are *gauche* (**1**) whereas the corresponding bonds are *antiperiplanar* (**2**) in the α-anomer. It appears, therefore, that when the dihedral angle between these bonds is large, a *positive* contribution is made to ^{2}J.

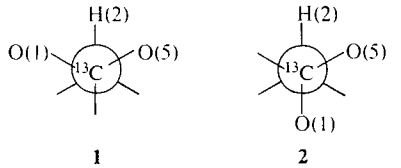

1 **2**

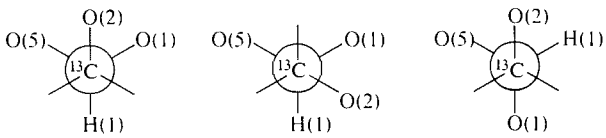

3 **4*a*** **4*b***

Other arrays of ^{13}C and ^{1}H nuclei described below were previously not amenable to the ^{13}C-enrichment and ^{1}Hmr approach because of experimental limitations, as already noted. One such system involves coupling between ^{13}C-2 and the anomeric proton (^{1}H-1), which is the converse of the pathway in **1** and **2**, in that the carbon bears only a single oxygen whereas the proton is flanked by two oxygens. Two basically different spatial arrays of this kind have been examined in (*a*) β-D-mannopyranose, methyl β-D-mannopyranoside, and 1,2:5,6-di-*O*-isopropylidene-α-D-glucofuranose, which exhibit spacings ($^{2}J_{\text{C-2,H-1}}$) of 8, 7, and 5.6 Hz, respectively, and (*b*) in α- and β-D-glucopyranose, α- and β-D-galactopyranose, and α-D-mannopyranose, for each of which $^{2}J < 1$ Hz. That is, a large spacing is observed when the ^{13}C-2—O-2 bond is *anti* (or approaches such an orientation) with respect to the C-1—^{1}H-1 bond (**3**, $\phi \sim 120$–$180°$), whereas there is no appreciable two-bond coupling when they are *gauche* (e.g., **4*a*** or **4*b***).[3] As illustrated below for the di-*O*-isopropylidene derivative, representative of **3**, a sign determination by the spt technique showed that $^{2}J_{\text{C-2,H-1}}$ is +5.6 Hz; analogously, the ^{2}J values for the β-*manno* compounds are taken to be +8 and +7 Hz. Therefore, these findings are consistent with the earlier comments (4, 5) to the effect that a ^{13}C—O bond makes a *positive* contribution to ^{2}J when angle ϕ is large, as in **3**.

A type of array that is most common in carbohydrate molecules is one in which each of the vicinal carbons bears only a single oxygen and hydrogen: i.e., two-bond coupling involving secondary carbons of aldo- and ketopyranoses. Data for some 90 examples in this general category have been accumulated during the course of studies in this laboratory, and representative values are given in Table 1. In a number of instances, regioselectively deuterated analogs have been used to check the origin of ^{1}H coupling with the ^{13}C nucleus of interest. As shown in Table 1, the data fall into two categories: invariably, the observed spacing is close to 5 Hz when a *gauche* arrangement of the ^{13}C—O—C—^{1}H bonds (**5*a*–5*c***) pertains, whereas when these bonds are *anti* (**6**) there is no detectable interaction between the nuclei ($^{2}J < 1$ Hz).

As a representative of **5**, methyl β-D-glucopyranoside was selected in order to determine the sign of coupling between ^{13}C-2 and ^{1}H-3 by the spt technique. It was found in this instance that ^{2}J is *negative*, and therefore it appears reasonable to

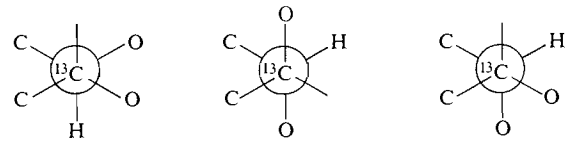

5*a* (O_e,O_e) **5*b*** (O_a,O_a) **5*c*** (O_a,O_e)

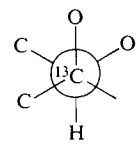

6

assume that the other examples of **5** studied, each of which exhibits a two-bond coupling of ~5 Hz, also represent negative values of ^{2}J. Hence, in comparing the geometries illustrated in **5** and **6**, an *anti* orientation of the ^{13}C—O bond relative to the C—^{1}H bond is again found to be associated with a *positive* contribution to the absolute value of ^{2}J.

For purposes of comparison with these findings, MO calculations have been carried out for model systems. The theoretical angular dependence of $^{2}J_{\text{C–H}}$ in structures such as **1** and **2**, or **3** and **4**, was assessed through calculations with propane-1,1,2-triol, and with butane-2,3-diol for structures of type **5** and **6**. Each of the plots obtained for these calculated values of $^{2}J_{\text{C–H}}$ vs. dihedral angle takes the general shape illustrated in Fig. 1, which is similar to results calculated earlier for simpler alcohols. Most of the coupling constants obtained either by the CNDO/2 (13) or INDO finite perturbation (14) method, were of negative sign and were smaller than

[3]Differences in the relative orientations of the *vic*-O atoms, as in **4*a*** as compared with **4*b***, appear to have no appreciable influence on the magnitude of ^{2}J.

TABLE 1. Representative values of two-bond coupling (^2J) involving secondary ^{13}C and ^1H nuclei in carbohydrates and derivatives*

	^2J (Hz)						
	C-2,H-3	C-3,H-2	C-3,H-4	C-4,H-3	C-4,H-5	C-5,H-4	C-6,H-5
	Examples of projection 5a						
α-D-Glucopyranose	5.0		5.0				
α-D-Glucopyranose pentaacetate	5.9						
β-D-Glucopyranose	4.8						
β-D-Glucopyranose pentaacetate	6.0						
α-D-Mannopyranose				4.8			
α-D-Mannopyranose pentaacetate			4.7				
β-D-Galactopyranose	4.0	4.0					
	Examples of projection 5b						
Methyl 2,3-di-*O*-acetyl-4,6-*O*-benzylidene-α-D-altropyranoside	4.5						
Methyl β-D-gulopyranoside			3.6				
1,6-Anhydro-β-D-galactopyranose		4.5				4.0	
1,6-Anhydro-β-D-galactopyranose triacetate						4.2	
2,7-Anhydro-β-D-glucoheptulopyranose				4.4	4.4		
	Examples of projection 5c						
α-D-Mannopyranose		4.0					
α-D-Mannopyranose pentaacetate		4.7					
β-D-Galactopyranose			4.0				
Methyl β-D-galactopyranoside			4.7				
1,6-Anhydro-β-D-allopyranose		5.0	5.0				
1,6-Anhydro-β-D-allopyranose triacetate		5.0	5.0				
	Examples of projection 6						
Methyl α-D-mannopyranoside	0						
Methyl β-D-mannopyranoside	0						
1,6-Anhydro-β-D-gulopyranose	0						
1,6-Anhydro-β-D-gulopyranose triacetate	0						
2,7-Anhydro-β-D-mannoheptulopyranose				0			0

*Data for the anhydrosugars were obtained in collaboration with R. G. S. Ritchie.

observed values. Nevertheless, the trend represented by Fig. 1, in which an increase of ϕ from 60 → 180° is accompanied by an increasingly positive value of ^2J, is in accord with the experimental results of this study.

These calculated results show consistency also with another feature of the observed data. That is, the ^{13}C–^1H coupling pathway represented by structures **3**, **4***a*, and **4***b*, in which the proton is bonded to a carbon bearing two oxygens is characterized by ^2J values more positive than those of the other arrays of nuclei. Experimentally, the effect is similar to that found (15) in comparing $^2J_{C\text{-}2,H\text{-}1}$ in the series: ethane (−4.8 Hz), chloroethane (2.6 Hz), and 1,1-dichloroethane (~1 Hz) (although the signs of the latter two values are not known), which implies that an electronegative element makes a positive contribution to ^2J. Hence, this effect is reproduced qualitatively in Fig. 1 by the more positive values of coupling between C-2 and H-1 than between C-1 and H-2 in 1,1,2-propanetriol.

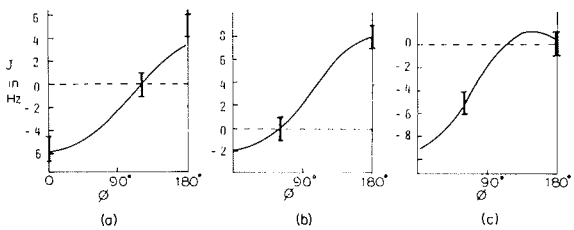

FIG. 1. Dependence of $^2J_{C-H}$ on the magnitude of the torsional angle (ϕ). The curves represent values of ^2J calculated by the CNDO/2 method for the following model compounds. (*a*) $(OH)_2{}^{13}CH—C^1H(OH)CH_3$, for types **1** and **2**; (*b*) $(OH)_2C^1H—{}^{13}CH(OH)CH_3$, for types **3** and **4**; (*c*) $CH_3—(OH)^{13}CH—C^1H(OH)CH_3$, for types **5** and **6**. The vertical bars are examples of ^2J values observed for carbohydrate molecules containing arrays of nuclei analogous to those in the model compounds. The calculated values are proportional to these ^2J values, although on an arbitrary scale.

Determination of the Sign of $^2J_{C-H}$

The sign of $^2J_{C-H}$ was determined by the pulsed double resonance selective population transfer (spt) technique (10–12). In the spt experiment, a selective pulse applied to a given ^1H transition alters the equilibrium distribution of spins in the upper and lower energy levels. The effect on the ^{13}C spectrum

Can. J. Chem. Downloaded from www.nrcresearchpress.com by 210.87.254.105 on 09/05/12
For personal use only.

Can. J. Chem. Downloaded from www.nrcresearchpress.com by 210.87.254.105 on 09/05/12
For personal use only.

is monitored by a conventional $\pi/2$ pulse applied immediately after the ^1H irradiation. There are three practical requirements for the experiment (12): (*a*) the power of the ^1H pulse ($\gamma H_2/2\pi$) must be low enough that adjacent transitions are not perturbed (i.e. $\gamma H_2/2\pi < {}^3J_{HH}$); (*b*) the pulse time (t) must be adjusted to give a significant population redistribution (e.g., complete population inversion requires that $t = \pi/\gamma H_2$); (*c*) the pulse must not be so long that secondary population changes occur (i.e. $t \ll T_1$ where T_1 is the shortest spin-lattice relaxation time for all connected transitions). For monosaccharides, where $T_1(^{13}C) \sim 0.5$–1 s (16–18) and ${}^3J_{HH} \sim 3$–8 Hz, these requirements dictate that $t \sim 0.2$ s and $\gamma H_2/2\pi \sim 1$–4 Hz.

In analyzing the spt experiments the ^{13}CH–CH spin system was treated as an AMX case; i.e., $^{13}C(X)H(A)$—CH(M) (Fig. 2); J_{AM} was obtained from the ^1H nmr spectrum (${}^3J_{HH}$), whereas J_{AX} and J_{MX} were obtained from the ^1H-coupled ^{13}C spectrum (${}^1J_{CH}$ and ${}^2J_{CH}$, respectively). The exact resonance frequency of H_A (ν_A) was determined graphically (19) from a series of single-frequency off-resonance decoupled ^{13}C spectra (decoupler power, $\gamma H_2/2\pi = 350$ Hz). Selective population transfer experiments were then carried out at each of the four A transition frequencies ($\nu_A \pm \frac{1}{2}(J_{AX} \pm J_{AM})$), using a ^1H power level $\gamma H_2/2\pi \sim 2$–3 Hz and a pulse time of 0.2 s (these parameters being adjusted to give the maximum response). Generally 1000–1500 transients were accumulated (sample concentration ~ 2 *M*). Selective population transfer difference spectra (20, 21) were recorded by subtracting the normal ^1H-coupled ^{13}C spectrum (obtained under otherwise identical conditions) from the spt response. Typical experimental results are shown in Figs. 3 and 4.

The Sign of ${}^2J_{C\text{-}1,H\text{-}2}$ *in* β-D-*Glucose (Solvent, D_2O)*

Here ${}^1J_{C\text{-}1,H\text{-}1} = 161$ Hz, ${}^3J_{H\text{-}1,H\text{-}2} = 8.1$ Hz and $|{}^2J_{C\text{-}1,H\text{-}2}| = 5.7$ Hz. Selective irradiation of A1 ($\nu_A - \frac{1}{2}J_{AX} - \frac{1}{2}J_{AM}$) at a power level $\gamma H_2/2\pi = 3$ Hz caused partial inversion of transition X2 and

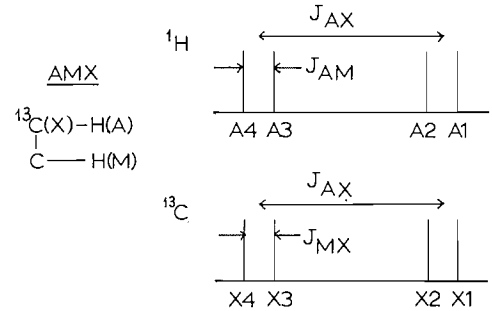

FIG. 2. Stick diagram of the $^1H(A)$ and $^{13}C(X)$ nmr spectra of the $^{13}C(X)H(A)$—CH(M) spin system.

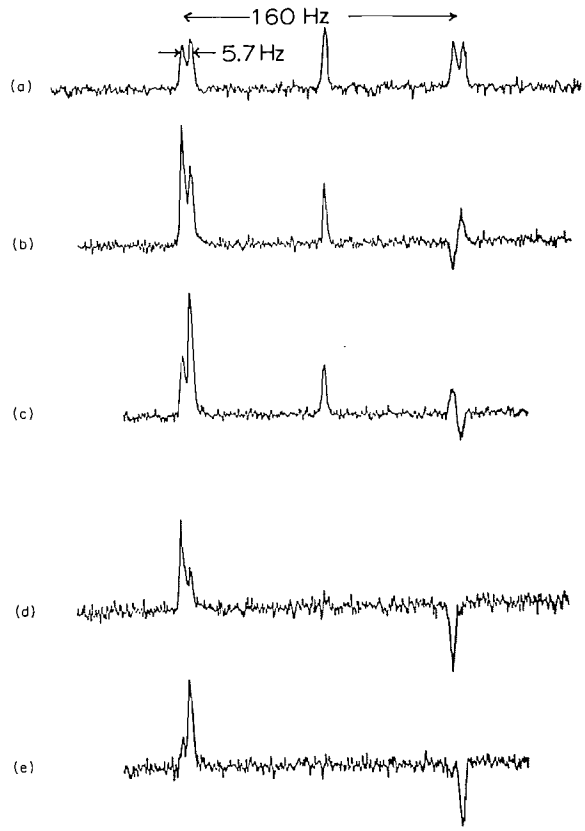

FIG. 3. ^{13}C nmr spectra of the C-1 carbon of β-D-glucopyranose: (*a*) normal ^1H-coupled spectrum; (*b*) spt spectrum obtained by pulsed irradiation at the frequency of transition A1, and (*c*) of transition A2; (*d*) and (*e*) spt-difference spectrum of (*b*) *minus* (*a*), and (*c*) *minus* (*a*), respectively.

enhancement of X4 (Fig. 3*b*). Irradiation of A2 ($\nu_A - \frac{1}{2}J_{AX} + \frac{1}{2}J_{AM}$) caused inversion of X1 and enhancement of X3 (Fig. 3*c*). These results indicate that ${}^2J_{C\text{-}1,H\text{-}2}$ and ${}^3J_{H\text{-}1,H\text{-}2}$ are of opposite sign; i.e. ${}^2J_{C\text{-}1,H\text{-}2} < 0$. Consistent results were obtained for irradiation of lines A3 and A4. The spt-difference spectra (Figs. 3*d* and 3*e*) show that the ^1H irradiation was not completely selective; in Fig. 3*d* for example, X3 is also perturbed. However, since all four A transitions have been examined, there is no ambiguity in this experiment as to the correct sign of ${}^2J$.

The Sign of ${}^2J_{C2,H1}$ *in 1,2:5,6-di-*O*-Isopropylidene-*α*-*D*-Glucofuranose-3-*d*(Solvent, $CDCl_3$)*

The 3-*d* analog of the diketal was used to simplify the ^{13}C–^1H and ^1H–^1H coupling patterns. Here ${}^1J_{C\text{-}2,H\text{-}2} = 160$ Hz, ${}^3J_{H\text{-}1,H\text{-}2} = 3.6$ Hz and $|{}^2J_{C\text{-}2,H\text{-}1}| = 5.6$ Hz. Selective irradiation of A1 ($\gamma H_2/2\pi = 2$ Hz, $t = 0.2$ s) nulled transition X1 and enhanced X3 (Fig. 4*b*). Irradiation of A2 nulled X2 and enhanced X4 (Fig. 4*c*). Thus ${}^2J_{C\text{-}2,H\text{-}1} > 0$. Again, consistent results were obtained for irradiation of A3 and A4.

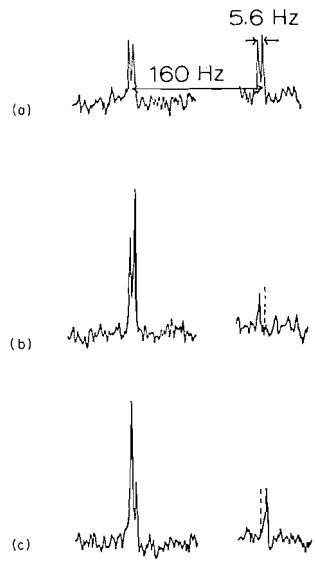

FIG. 4. ^{13}C nmr spectra of the C-2 carbon of 1,2:5,6-di-*O*-isopropylidene-α-D-glucofuranose-3-*d*: (*a*) normal ^{1}H-coupled spectrum; (*b*) spt spectrum obtained by pulsed irradiation at the frequency of transition A1, and (*c*) of transition A2.

In this set of experiments inversion of lines was not clearly evident. This is a consequence of the reduced power level of the ^{1}H irradiation (required for selectivity) and, possibly, secondary population changes during the pulse.

Experimental

Natural abundance ^{13}C nmr spectra were recorded on a Bruker WH-90 FT spectrometer equipped with a B-SV WH model decoupler. However, the 500 ohm 1-turn decoupler output power control was replaced with a 10-turn potentiometer so that the low ^{1}H power levels required in the spt experiments could be set more precisely. A Heathkit model 1B-1103 rf frequency counter was used to monitor the decoupler frequency. Pulse timing was controlled by the Bruker gated multipulser.

Acknowledgements

Generous support by the Faculty of Graduate Studies, McGill University, the National Research Council of Canada, and the Pulp and Paper Research Institute of Canada is gratefully acknowledged. The authors also express their thanks to Dr. R. G. S. Ritchie for valuable assistance.

1. R. M. LYNDEN-BELL. Mol. Phys. **6**, 537 (1963).
2. A. S. PERLIN and B. CASU. Tetrahedron Lett. 2921 (1969).
3. A. S. PERLIN. *In* Carbon-13 in organic chemistry. Isotopes in organic chemistry. Vol. 3. *Edited by* E. Buncell and C. C. Lee. Elsevier, Oxford, 1977. p. 171.
4. J. A. SCHWARCZ and A. S. PERLIN. Can. J. Chem. **50**, 3667 (1972).
5. J. A. SCHWARCZ, N. CYR, and A. S. PERLIN. Can. J. Chem. **53**, 1872 (1975).
6. D. E. DORMAN. Ann. N.Y. Acad. Sci. **222**, 915 (1973).
7. A. S. PERLIN, N. CYR, R. G. S. RITCHIE, and A. PARFONDRY. Carbohydr. Res. **37**, C 1 (1974).
8. N. CYR, R. G. S. RITCHIE, T. M. SPOTSWOOD, and A. S. PERLIN. Can. J. Spectrosc. **19**, 190 (1974).
9. R. FREEMAN. Mol. Phys. **4**, 385 (1961).
10. K. G. R. PACHLER and P. L. WESSELS. J. Magn. Reson. **12**, 337 (1973).
11. A. A. CHALMERS, K. G. R. PACHLER, and P. L. WESSELS. Org. Magn. Reson. **6**, 445 (1974).
12. S. SORENSEN, R. S. HANSEN, and H. J. JAKOBSEN. J. Magn. Reson. **14**, 243 (1974).
13. J. A. POPLE and G. A. SEGAL. J. Chem. Phys. **43**, S 136 (1965).
14. J. A. POPLE, J. W. MCIVER, and N. S. OSTLUND. J. Chem. Phys. **49**, 2960 (1968); **49**, 2965 (1968).
15. G. MIYAZIMA, Y. UTSUMI, and K. TAKAHASHI. J. Phys. Chem. **73**, 1370 (1969).
16. A. ALLERHAND, D. DODDRELL, and R. KOMOROSKI. J. Chem. Phys. **55**, 189 (1971).
17. C. F. BREWER, D. MARCUS, A. P. GROLLMAN, and H. STERNLICHT. Ann. N.Y. Acad. Sci. **222**, 978 (1973).
18. K. BOCK and L. D. HALL. Carbohydr. Res. **40**, C 3 (1975).
19. B. BIRDSALL, N. J. M. BIRDSALL, and J. FEENEY. J. Chem. Soc. Chem. Commun. 316 (1972).
20. A. A. CHALMERS, K. G. R. PACHLER, and P. L. WESSELS. J. Magn. Reson. **15**, 415 (1974).
21. J. FEENEY and P. PARTINGTON. J. Chem. Soc. Chem. Commun. 611 (1973).

Can. J. Chem. Downloaded from www.nrcresearchpress.com by 210.87.254.105 on 09/05/12
For personal use only.

Photolysis of 1,2-dipropyl-3,5-diethyl-1,2-dihydropyridine. A model for some elastin cross-links

MIREILLE GUAY AND FRANÇOIS LAMY

Département de Biochimie, Faculté de Médecine, Université de Sherbrooke, Sherbrooke, Qué., Canada J1H 5N4

Received December 21, 1976[1]

MIREILLE GUAY and FRANÇOIS LAMY. Can. J. Chem. **56**, 302 (1978).

Photolysis of 1,2-dipropyl-3,5-diethyl-1,2-dihydropyridine **4**, at $\lambda > 300$ nm, results in the opening of the ring to give an iminodiene **5**, which upon reduction leads to an aminodiene **6**. The imine **5** releases propylamine at acid p*H*. The dihydropyridine **4** is a model for analogous dihydro compounds which cross-link polypeptide chains in elastin. Thus photolysis would seem to be a specific method for breaking this type of cross-link in the insoluble fibrous protein.

MIREILLE GUAY et FRANÇOIS LAMY. Can. J. Chem. **56**, 302 (1978).

Le noyau du dipropyl-1,2-diéthyl-3,5-dihydro-1,2 pyridine **4**, s'ouvre par photolyse à $\lambda > 300$ nm pour donner un iminodiène **5** qui après réduction conduit à l'aminodiène **6**. L'imine **5** s'hydrolyse à p*H* acide pour produire de la propylamine. La dihydropyridine **4** sert de modèle pour des composés dihydro analogues des liaisons croisées entre les chaînes polypeptidiques de l'élastine. Ainsi la photolyse semblerait être une méthode spécifique pour briser ces liaisons croisées dans la protéine fibreuse insoluble.

Introduction

Elastin, a fibrous protein from connective tissue, is an elastomer composed of polypeptide chains cross-linked by special amino acids: desmosine and isodesmosine **1**, **2**. These consist of tetrasubstituted pyridinium rings.[2] We have studied the photolysis of these compounds at 254 nm (1) and found that in analogy to the work of Kaplan *et al.* (9) the pyridinium salt most probably rearranged to an azabicyclo-[3.1.0]hexenyl carbonium ion which was trapped by water. The resulting product could then open at low p*H* to yield an imine which hydrolysed to give free lysine and an analogue of glutaconaldehyde **3**. Other

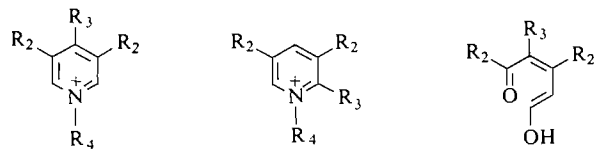

1 **2** **3**

$R_n = (CH_2)_n-CH(CO_2H)(NH_2)$

compounds in addition to these aromatic compounds, can cross-link the polypeptide chains in elastin. For example, Paz *et al.* (2) have shown by mass spectrometry that tetrasubstituted dihydro- and tetrahydropyridines were present. Since the general aim of our work is to develop techniques for the selective attack of the elastin cross-links in order to obtain soluble subunits, we thought it appropriate to study the action of uv light upon dihydropyridine compounds. In this paper, we present a study of the photolysis of 1,2-dipropyl-3,5-diethyl-1,2-dihydropyridine, **4**, a model of dihydroisodesmosine.

Compound **4** was synthesized from *N*-butylidenepropylamine (3) by the method of Patrick (4). It was a liquid which was readily oxidized to the corresponding aromatic compound. The final product was obtained by distillation under nitrogen. The structure was confirmed by observing an uv absorption band at 330 nm and nmr signals at 5.43 ppm for the olefinic protons and 3.51 ppm for the methine proton. A specific rotation of +1.68 indicated that the product was a racemic mixture.

Irradiation of **4** was carried out at $\lambda > 300$ nm. To determine the kinetics of the reaction a solution (4.1×10^{-4} M/ℓ) in anhydrous ethanol was irradiated under nitrogen at 15°C, for various lengths of time. The logarithm of the absorbance at 330 nm decreased linearly with time, giving a first-order rate constant $k = 1.46 \times 10^{-3}$ s^{-1}. The quantum yield of the reaction ($\Phi = 0.213$) was determined by a method described by Parker and Hatchard (5), in which a solution of ferrous oxalate was photolysed under exactly the same conditions as those used for **4**. The photochemical susceptibility was calculated to be 571.

For preparative purposes 80 mg of **4** in anhydrous ethanol was photolysed under nitrogen at 15°C for 4 h (Scheme 1). The nmr spectrum exhibited two singlets at 7.76 and 6.04 ppm, and a triplet at 5.26 ppm ($J = 7$ Hz). This suggested that the product of photolysis was **5**, an iminodiene. Attempts to purify

[1]Revision received August 31, 1977.

[2]Trivial names: desmosine, 4-(4-amino-4-carboxybutyl)-1-(5-amino-5-carboxypentyl)-3,5-bis(3-amino-3-carboxypropyl)-pyridinium; isodesmosine, 2-(4-amino-4-carboxybutyl)-1-(5-amino-5-carboxypentyl)-3,5-bis(3-amino-3-carboxypropyl)-pyridinium).

Can. J. Chem. Downloaded from www.nrcresearchpress.com by 210.87.254.105 on 09/05/12
For personal use only.

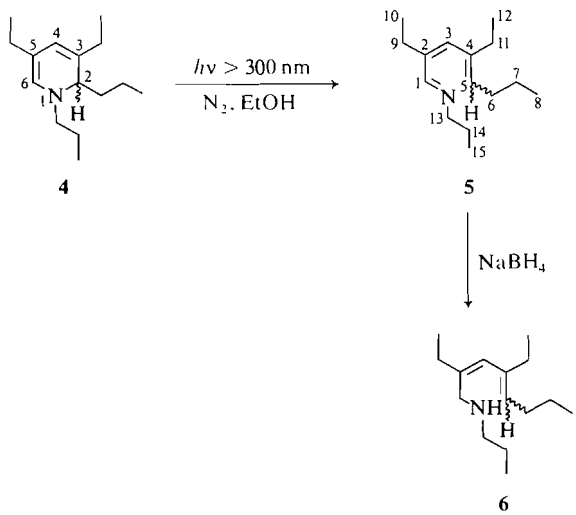

SCHEME 1

5 by chromatography on silica gel, even at 4°C, led to the decomposition of the product. Consequently we were unable to determine if the two isomers **5***a* and **5***b* were present or if only one was favored. In any case **5** was reduced with sodium borohydride to give **6** which was purified by silica gel chromatography. In the nmr spectrum the signal at 7.76 ppm disappeared indicating that the imino group was reduced. It showed signals at 5.65 and 5.20 ppm characteristic of olefinic protons. The structure **6** was confirmed by other spectral data such as the infrared band at 3500–3200 cm^{-1} characteristic of N—H and the observation of a molecular ion with an $m/e = 223$ by mass spectroscopy. A ^{13}C nmr spectrum was recorded and indicated the presence of only one isomer. The elucidation of the structure of this isomer is not simple, even with the help of ^{13}C nmr spectroscopy since in acyclic compounds, several conformations may exist. Four planar conformations are possible for the diene moiety in compound **6**: *cisoid* and *transoid* **6***a* and *cisoid* and *transoid* **6***b*. For the *transoid* conformation of **6***b* an Overhauser effect should be observed between the protons in positions 3 and 5 since these protons have an internuclear distance of 2.4 Å (6). For the *cisoid* conformation of **6***b* this effect would occur between the protons in positions 1 and 5 as these protons are in close proximity. For the two rotamers of **6***a* no effect should be observed at either olefinic proton by irradiation of the protons 1 and 3. The nOe experiments (i.e. irradiation of protons at C(3) and then C(1) were carried out and no area increases were observed, showing that the **6***a* isomer was present.[3] The only uncertainty which remains concerns the *transoid* or *cisoid* nature of the conformation. However this is of little consequence for the mechanism of the photolytic opening itself.

Baldwin and Krueger (7) and Courtot (8) studied the mechanism of the photolytic opening of cyclohexadienes. They have shown that the mechanism is conrotatory, and that the substituents on the saturated carbons rotate in a direction which depends upon the helicity of the diene; therefore two antipodes will give the same open product and two conformers will give two different isomers.

For the original dihydropyridine compound, we can draw the two conformations **4***a*′ and **4***b*′ for one isomer and the two conformations, **4***a* and **4***b*, for the other (Scheme 2). In each case we assume that the unpaired electrons on the nitrogen atom are in a pseudo-axial position. From the examination of models, one can assume that the conformations **4***a* and **4***a*′ of the enantiomeric pair are more stable than **4***b* and **4***b*′ since the propyl group in position 2 is pseudo-axial. Taking into account the general mechanism of cyclohexadiene ring opening (7, 8) we conclude that isomers **4***a* and **4***a*′ will give exclusively **5***a* while **4***b* and **4***b*′ will give **5***b*. Since reduction of the iminodiene gave only **6***a* it is clear that the most stable form of the dihydropyridine is also its most reactive form.

The yield of **6** was only 52%, although **5** was obtained practically quantitatively from **4**. This was because **6** is very volatile and unstable, and was partially lost during experimental manipulations.

The open-chain compound **5** can be easily hydrolysed at acid p*H*, releasing propylamine as detected by chromatography in an amino acid analyzer.

In conclusion, we have shown that dihydropyridine compounds can be photolysed, like the corresponding aromatic compounds, albeit at a different wavelength and according to a different mechanism. In both cases at acid p*H*, an amine is released by the hydrolysis of the imino group which results from the photolytic reactions. The differences observed between the photolysis of the two classes of compound should be useful in the study of the cross-link distribution in elastin itself.

Experimental

The uv spectra were taken on a model 118-C Cary spectrophotometer. The ir spectra were recorded on a Perkin-Elmer spectrophotometer, model 457. Proton nmr spectra (δ value) were taken on a Varian T-60 spectrometer in CCl_4 with TMS as internal standard. The ^{13}C nmr spectra were recorded on a Bruker HX-90 spectrometer with a Nicolet 1083 computer operating in the Fourier transform mode. The solvent was CCl_4 containing 15% deuterated benzene. Chemical shifts were recorded relative to TMS. Mass spectra were recorded in an AEI MS 30 double beam spectrometer. The nOe experi-

[3]To illustrate the sensitivity of the method we detected an average increase of 26% in the intensity of the signals due to olefinic protons, when protons in position 6 were irradiated.

Can. J. Chem. Downloaded from www.nrcresearchpress.com by 210.87.254.105 on 09/05/12
For personal use only.

Can. J. Chem. Downloaded from www.nrcresearchpress.com by 210.87.254.105 on 09/05/12
For personal use only.

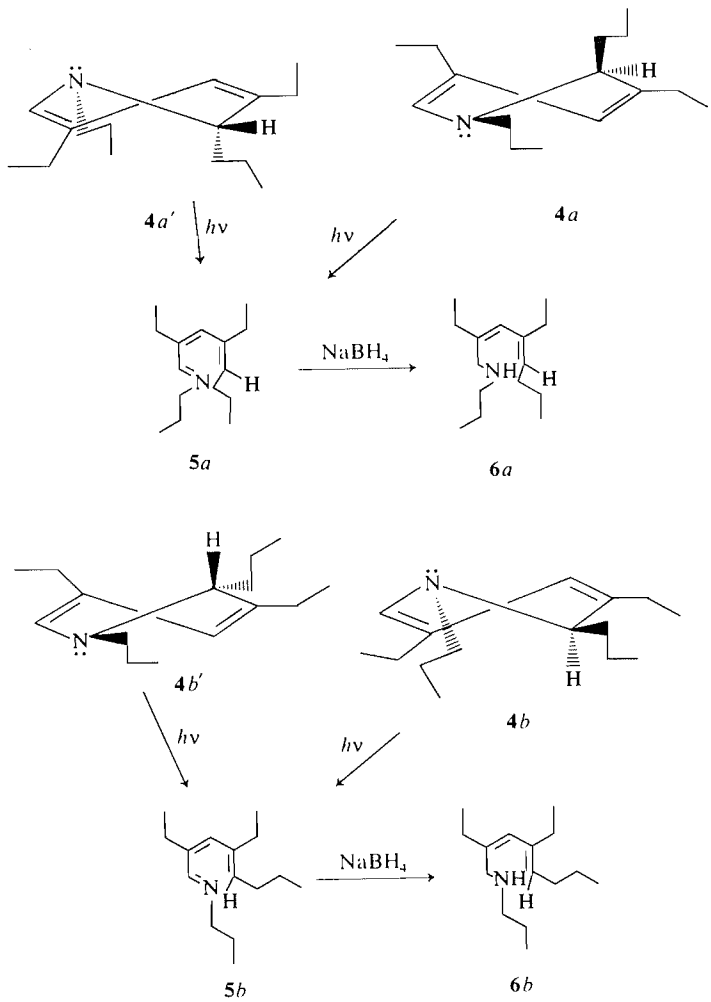

SCHEME 2

ments were recorded on a Bruker WP-60 operating in the Fourier transform mode. Silica gel (100 mesh) for column chromatography was obtained from Malinckrodt chemical works.

System of Photolysis

One Pyrex test tube (diameter = 17 mm) was placed inside a larger one (diameter = 35 mm). The volume between the two contained the solution to be irradiated. A low pressure mercury lamp (model PCQ, Ultraviolet Product Inc., San Gabriel, CA) was placed inside the smaller test tube. The system was closed with a three-holed rubber stopper which permitted the bubbling of nitrogen and the removal of samples. The inside test tube (between the lamp and the solution) served to filter the light at $\lambda > 300$ nm. The effectiveness of this filter was confirmed by irradiating a solution of 3,5-diethyl-1,2-dipropylpyridinium. At a concentration of 1.86×10^{-4} *M* (*A* = 0.980 at 278 nm) the absorbance remained constant for 35 min while a similar solution irradiated with the same lamp for the same length of time, but without the Pyrex filter, decreased in absorbance by 40%.

1,2-Dipropyl-3,5-diethyl-1,2-dihydropyridine 4

Compound **4** was synthesized according to the method of Patrick (4). The nmr spectrum of the crude product showed that it was a mixture of 2-ethyl-2-hexenal, *N*-(2-ethyl-2-hexenylidene)propylamine, 1,2-dipropyl-3,5-diethyl-1,2-dihydropyridine, and an unknown product. Distillation to isolate compound **4** was carried out under nitrogen. The sample, a yellow oil, was at once transferred under nitrogen into bottles with serum stoppers and kept in a freezer. Yield 62%; uv (EtOH) λ_{max}: 330 nm (ε 2510); nmr (CCl_4) δ: 2.88 (2H, t, J = 6.5 Hz, —CH_2—N), 3.51 (1H, bs, C(2)-H), 5.43 (2H, bs, C(4)-H and C(6)-H); ms *m/e* 221 (M^+), 220 ($M^+ - H$), 206 ($M^+ - CH_3$), 192 ($M^+ - C_2H_5$), 178 ($M^+ - C_3H_7$); $[\alpha]_{578}^{25}$ +1.68 (*c* 1.01, EtOH).

N-(2,4-diethyl-2,4-octadienylidene)propylamine 5

The dihydropyridine (84 mg, 0.38 mmol in 140 ml anhydrous ethanol) was irradiated for 4 h at 15°C, under constant nitrogen bubbling. The alcohol was vacuum evaporated at room temperature. The unstable product obtained proved to be *N*-(2,4-diethyl-2,4-octadienylidene)propylamine **5**, ir (liquid film) ν_{max}: 1665 (C=N), 1635 and 1615 cm^{-1} (C=C); nmr (CCl_4) δ: 3.33 (2H, bt, J = 7 Hz, —C(13)H_2—N=), 5.26 (1H, bt, J = 7 Hz, =C(5)H—CH_2), 6.04 (1H, bs, =C(3)H—C), 7.76 (1H, s, —C(1)H=N—); uv (EtOH) λ_{max}: 226 nm (ε 7150).

1-Propylamino-2,4-diethyl-2,4-octadiene **6**

The photolytic product **5** (254 mg, 1.15 mmol) was dissolved in 10 ml of cold methanol. Sodium borohydride (50 mg, 1.3 mmol) was added. The reaction proceeded at 0°C, for 2 h under agitation. The methanol was then evaporated under vacuum at room temperature and the residue was dissolved in 25 ml H_2O. The solution was extracted four times with 15 ml of ether. The combined extracts were dried on sodium sulfate, filtered, and vacuum evaporated at room temperature. The residue (266 mg) was chromatographed on silica gel at 4°C. The reduced compound **6**, 1-propylamino-2,4-diethyl-2,4-octadiene was recognized by thin-layer chromatography. It was a volatile, pale yellow liquid; 113 mg was recovered which represented a yield of 52% taking in account the presence of 15% of impurities in the starting material **4**; ir (liquid film) ν_{max}: 3500–3200 (N—H) and 1650 cm^{-1} (C=C); nmr (CCl_4) δ: 3.14 (2H, s, C(1)H_2N), 5.20 (1H, split t, $J = 7$ Hz, $J = 1.3$ Hz —C(5)H—CH_2), 5.65 (1H, bs, =C(3)H); uv (EtOH) λ_{max}: 220 nm (ε 6150); ms *m/e*: 223 (M^+), 208 ($M^+ - CH_3$), 194 ($M^+ - C_2H_5$), 180 ($M^+ - C_3H_7$); ^{13}C nmr (CCl_4) δ: 10.5, 11.8, 11.8, 12.6 (C(8)H, C(10)H, C(12)H, C(15)H), 21.5, 21.9, 26.4, 30.1, 30.2, (C(6)H, C(7)H, C(9)H, C(11)H, C(14)H), 48.3, 50.5 (C(1)H, C(13)H) 125.2, 126.7 (C(3)H, C(5)H), 139.5, 163.2 (C(2)H, C(4)H). No picrate derivative could be obtained and the compound itself was not stable enough to give good elemental analysis.

Propylamine

The compound was identified on the short column of an amino acid analyzer (Beckman 120-C, at 55.5°C). Resin UR-35 (Beckman) was used and the eluting buffer consisted of 0.4 *N* sodium citrate p*H* 5.35. Under these conditions propylamine was eluted approximately 37 min after ammonia.

Acknowledgements

We wish to express our sincere appreciation to Dr. J. K. Saunders, Department of Chemistry, University of Sherbrooke, without whom the nOe experiment would not have been performed and much less conceived. We thank also Mr. R. Langlois, who recorded the mass spectra with competence, and J. R. Martin and D. Viens for their technical assistance in the nOe experiments. This work was supported by the Medical Research Council, Grant MT-4003.

1. R. BAURAIN, J. F. LAROCHELLE, and F. LAMY. Eur. J. Biochem. **67**, 155 (1976).
2. M. A. PAZ, B. PEREYRA, P. M. GALLOP, and S. SEIFTER. J. Mechanochem. Cell. Motil. **2**, 231 (1974).
3. K. N. CAMPBELL, A. H. SOMMERS, and B. K. CAMPBELL. J. Am. Chem. Soc. **66**, 82 (1944).
4. T. M. PATRICK, JR. J. Am. Chem. Soc. **74**, 2984 (1952).
5. C. A. PARKER and C. G. HATCHARD. Proc. R. Soc. London, A, **235**, 518 (1956).
6. J. NOGLE and A. SCHERMER. *In* The nuclear Overhauser effect: chemical applications. Academic Press, New York, NY. 1971.
7. J. E. BALDWIN and S. M. KRUEGER. J. Am. Chem. Soc. **91**, 6444 (1969).
8. P. COURTOT. *In* Elements de photochimie avancée. Hermann Editions, Paris. 1972. p. 190.
9. L. KAPLAN, J. W. PAVLIK, and K. E. WILZBACH. J. Am. Chem. Soc. **94**, 3283 (1972).

Can. J. Chem. Downloaded from www.nrcresearchpress.com by 210.87.254.105 on 09/05/12
For personal use only.

A simple synthesis of aucantene

HSING-JANG LIU AND ERIC N. C. BROWNE
Department of Chemistry, University of Alberta, Edmonton, Alta., Canada T6G 2G2

Received August 15, 1977

HSING-JANG LIU and ERIC N. C. BROWNE. Can. J. Chem. **56**, 306 (1978).

Aucantene (**1**) has been synthesized from propynal in three stages involving the conjugate addition of lithium di-(*E*)-propenylcuprate to α,β-unsaturated aldehyde **2** as a key step.

HSING-JANG LIU et ERIC N. C. BROWNE. Can. J. Chem. **56**, 306 (1978).

On a synthétisé l'aucatène (**1**) à partir du propynal; cette transformation implique trois étapes dont une addition conjuguée du di-(*E*)-propénylcuprate de lithium à l'aldéhyde α,β non-saturé **2** comme étape clé.

[Traduit par le journal]

Since several methods were developed in the early 1970's for the conjugate addition of lithium divinylcuprates to α,β-unsaturated ketones (1–3), this approach has been widely used for the preparation of γ,δ-enones (4). A logical extension to the synthesis of γ,δ-unsaturated aldehydes, however, is little known. We wish to describe a three-step synthesis, in racemic form, of aucantene (**1**) (5), a constituent of the anisogamous brown alga *Cutleria multifida*. In addition to providing an efficient alternative route to the naturally occurring hydrocarbon (6), the synthesis also demonstrates the feasibility of constructing γ,δ-unsaturated aldehydes by 1,4-addition using lithium divinylcuprates.

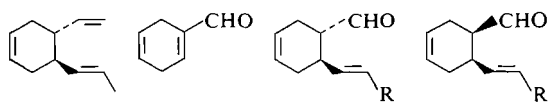

1 **2** **3** R = CH_3, **5** R = H **4** R = CH_3, **6** R = H

Aldehyde **2**[1] was prepared in 58% yield from propynal (8) by Diels–Alder reaction with 1,3-butadiene at room temperature using boron trifluoride etherate as a catalyst. This compound was subsequently treated with lithium di-(*E*)-propenylcuprate (9) in ether at −78°C for 1 h. Under these conditions,[2,3] the addition reaction proceeded smoothly with retention of the stereochemical integrity of the reagent, to give, in 77% yield, a mixture of two epimers **3**[4] and **4** in a ratio of ca. 3:2 as determined by gas chromatographic analysis. Preparative liquid chromatography of the mixture resulted in the separation of pure **3** and another mixture containing mainly **4** (~80%) in a total recovery of 74%. When the latter mixture was subjected to base treatment (10% aqueous potassium carbonate in methanol), an equilibrium was established after 4 h. Gas chromatographic analysis showed that the resulting mixture was composed of two parts of **3** and one part of **4**. In addition to confirming the epimeric nature of these two compounds, this finding strongly supported the stereochemical assignments since the *trans* isomer **3** is expected to be more stable and thus should be formed preferentially under thermodynamically controlled conditions. Moreover, the epimerization of **4** → **3** proved that the former compound is equally useful for the present synthesis.

Wittig reaction of **3** with methylenetriphenylphosphorane prepared from methyltriphenylphosphonium bromide and *n*-butyllithium in ether gave rise to a 74% yield of aucantene (**1**) whose ir and nmr spectra were found to be in agreement with those reported (5, 6).

Experimental

General

Mass spectra were recorded on AEI MS-50 and MS-12 spectrometers. Infrared spectra were obtained by using Perkin Elmer model 457 and 257 spectrophotometers. Nuclear magnetic resonance spectra were recorded on an HR-100 spectrometer using tetramethylsilane as internal standard. Elemental analyses were performed by the microanalytical laboratory of this department. Gas chromatographic (gc) analyses were performed using an Hewlett-Packard model 5750 instrument with an 8 ft × 1/8 in. stainless steel column of Carbowax 20 M on 80–100 mesh Chromosorb W.

1-Formyl-1,4-cyclohexadiene (2)

Propynal was prepared from propargyl alcohol according to the described procedure (8).

[1]A previous preparation involves the thermal Diels–Alder reaction of propynal and 1,3-butadiene (7).

[2]It is interesting to note that, whereas 1,4-additions of lithium divinylcuprates to conjugated enones are facilitated by a complexing agent, e.g., tetrakis(iodo(tri-*n*-butylphosphinecopper(I)) (1) or diisopropylsulfide (3), such an additional reagent is unnecessary in the present case.

[3]The addition of lithium divinylcuprate to **2** carried out in a similar manner resulted in the formation of a mixture of **5** and **6** in 72% yield and in a ratio of 1:2. The two aldehydes have been previously prepared by Marner and Jaenicke (6) using a different route and applied to their synthesis of **1** and its epimer.

[4]A mixture of **3** and a skeletal isomer has previously been synthesized in poor yield by a different approach (6).

Can. J. Chem. Downloaded from www.nrcresearchpress.com by 210.87.254.6 on 09/05/12
For personal use only.

Can. J. Chem. Downloaded from www.nrcresearchpress.com by 210.87.254.6 on 09/05/12
For personal use only.

To a solution of propynal (20 g, 0.37 mol) in ether (500 ml) under a nitrogen atmosphere, was added dropwise over a period of 20 min a solution of boron trifluoride etherate (26.26 g, 0.185 mol) in ether (100 ml). The resulting solution was stirred at room temperature for 15 min and a solution of benzene (500 ml) saturated with 1,3-butadiene was introduced dropwise over 40 min. After stirring for 20 h, the reaction mixture was cooled to 0°C and saturated aqueous sodium bicarbonate (200 ml) was slowly added. The organic layer was separated and the aqueous solution extracted three times with ether. The organic solutions were washed with water, combined, dried ($MgSO_4$), filtered, and concentrated to give 31.742 g of reddish oil. A portion (1.015 g) of the crude product was purified by column chromatography on silica gel. Elution with a solution of 5% ether in *n*-pentane gave 0.739 g (58% yield) of **2** as a colorless liquid. The remaining crude product was distilled at 78–79°C/16 Torr to give 20.361 g of **2**. The following properties were observed for **2**: ir (KBr, film): 3030 (C=CH and HC=CH), 2805, 2705 (CHO), 1685 (C=O), 1633 (C=C), and 760 (HC=CH); nmr (CCl_4) δ: 2.75, 3.01 (both m, 2H each, $-CH_2-$), 5.70 (m, 2H, $-CH=CH-$), 6.71 (m, 1H, $-C=CH-$), and 9.41 (s, 1H, —CHO); ms M^+ 108.0572 (calcd. for C_7H_8O: 108.0576). *Anal.* calcd. for C_7H_8O: C 77.75, H 7.46; found: C 77.75, H 7.57.

trans- *(3) and* cis-*4-((E)-1-Propenyl)-5-formylcyclohexene (4) and Epimerization*

To a suspension of cuprous iodide (4.73 g, 24.8 mmol) in ether (30 ml) under nitrogen at −78°C, was added a 1.075 *N* solution of (*E*)-1-propenyllithium (9) in ether (46.2 ml, 49.6 mmol) in a dropwise manner over a period of 40 min. The temperature was allowed to rise to −35°C over 1 h, and tetrahydrofuran (40 ml) was added over a 20 min period. After stirring at −35°C for 15 min, the mixture was cooled to −78°C. A solution of **2** (1.7 g, 18.3 mmol) in ether (30 ml) was then added dropwise over 30 min. The resulting mixture, after stirring for 30 min, was poured into 200 ml of ice-cold saturated aqueous ammonium chloride and filtered. The residue was washed thoroughly with ether. The organic layer of the filtrate was separated and the aqueous solution extracted four times with ether. The organic solutions were washed with 10% aqueous ammonium chloride (adjusted to ~p*H* 7 with concentrated ammonium hydroxide), water, and saturated aqueous sodium chloride, dried ($MgSO_4$), filtered, and concentrated. Column chromatography of the crude product thus obtained on silica gel using a solution of 4% ether in Skelly B gave 1.818 g (77% yield) of a mixture of **3** and **4** in a ratio of ca. 3:2 by gc analysis. A portion (1.186 g) of this material was subjected to preparative liquid chromatography (Waters Associates Prep LC/System 500; silica gel cartridge). Elution with a solution of 100% ether in petroleum ether gave 0.417 g of pure **3**: ir (KBr, film): 3010 (HC=CH), 2820, 2700 (CHO), 1722 (C=O), 1655 (C=C), 970 (*trans* HC=CH), and 720 (*cis* HC=CH); nmr (CCl_4) δ: 1.66 (dd, 3H, $J = 5$, $J' = 2.5$ Hz, $-CH_3$), 1.80–3.00 (complex, 6H, $-CH_2CHCHCH_2-$), 5.15–5.55 (complex, 2H, $-CH=CHCH_3$), 5.62 (br s, 2H, —CH=CH—), and 9.54 (d, 1H, $J = 2$ Hz, —CHO); ms M^+ 150.1041 (calcd. for $C_{10}H_{14}O$: 150.1044). *Anal.* calcd. for $C_{10}H_{14}O$: C 79.96, H 9.39; found: C 79.58, H 9.40.

Further elution with the same solvent system gave a mixture of **3** and **4** in a ratio of ca. 1:4 (gc and nmr). The nmr spectrum (CCl_4) showed a set of signals corresponding to **3** and another, set for **4** consisting of signals at δ 1.64 (d, 3H, $J = 4$ Hz, $-CH_3$), 1.80–3.20 (complex, 6H, $-CH_2CHCHCH_2-$), 5.20–5.60 (complex, 2H, $-CH=CHCH_3$), 5.62 (m, 2H, —CH=CH—), and 9.59 (s, 1H, —CHO). The ir spectrum was found to be similar to that of **3**.

The above mixture (85 mg) was dissolved in methanol (2 ml) and a 100% aqueous potassium carbonate solution (2 ml) was added. The mixture was stirred at room temperature under a nitrogen atmosphere and the reaction was monitored by gc. Within 4 h, an equilibrium (**3**:**4** ≃ 2:1) was established. The mixture was poured into water and extracted with methylene chloride. Work-up of the extracts in the usual manner followed by column chromatography of the crude product on silica gel using a solution of 5% ether in *n*-pentane as eluent gave 74 mg (87% recovery) of a mixture of **3** and **4** in a ratio of ~2:1 (gc).

Aucantene (1)

To a suspension of methyltriphenylphosphonium bromide (625 mg, 1.75 mmol) in ether (10 ml), was added a 1.72 *N* solution of *n*-butyllithium in hexane (1.02 ml, 1.75 mmol). The mixture was stirred at room temperature under a nitrogen atmosphere for 1 h and a solution of **3** (210 mg, 1.40 mmol) in ether (10 ml) was added dropwise over a 15 min period. Afterstirring for 3.5 h, the reaction mixture was poured into ice-cold water. The organic layer was separated and the aqueous layer extracted three times with ether (total 50 ml). The organic solutions were washed with saturated aqueous sodium chloride, dried ($MgSO_4$) and filtered. The volume of the filtrate was reduced under aspirator pressure without heating to ~2 ml. This solution was filtered to remove a small amount of triphenylphosphine oxide which was washed with *n*-pentane (~1 ml). The filtrate was concentrated using the same procedure described above. Column chromatography of the crude product on neutral alumina (activity I, ~1 g) using *n*-pentane as an eluent gave 153 mg (74% yield) of **1**. The ir and nmr spectra were shown to be in agreement with those reported (5, 6) and the mass spectrum displayed M^+ at 148.

Acknowledgements

We are grateful to the National Research Council of Canada and the University of Alberta for financial support.

1. J. Hooz and R. B. Layton. Can. J. Chem. **48**, 1626 (1970).
2. F. Näf and P. Degen. Helv. Chim. Acta, **54**, 1939 (1971).
3. E. J. Corey and R. L. Carney. J. Am. Chem. Soc. **93**, 7318 (1971).
4. G. Posner. *In* Organic reactions. Vol. 19. J. Wiley and Sons, Inc., New York, NY. 1972. Chapt. 1.
5. L. Jaenicke, D. G. Müller, and R. E. Moore. J. Am. Chem. Soc. **96**, 3324 (1974).
6. F.-J. Marner and L. Jaenicke. Chem. Ber. **108**, 2202 (1975).
7. A. A. Petrov. Zh. Obshch. Khim. **24**, 2136 (1954); Chem. Abstr. **50**, 233b (1956).
8. J. C. Sauer. Org. Synth. **36**, 66 (1956).
9. G. Linstrumelle, J. K. Krieger, and G. M. Whitesides. Org. Synth. **55**, 103 (1976).

Thermolysis of Δ^3-1,3,4-oxadiazolin-2-ones and 2-phenylimino-Δ^3-1,3,4-oxadiazolines derived from α,β-epoxyketones. An alternative method for the conversion of α,β-epoxyketones to alkynones and alkynals[1]

GERALD A. MACALPINE AND JOHN WARKENTIN

Department of Chemistry, McMaster University, Hamilton, Ont., Canada L8S 4M1

Received September 23, 1977

GERALD A. MACALPINE and JOHN WARKENTIN. Can. J. Chem. **56**, 308 (1978).

Thermolyses in polar solvents, of Δ^3-1,3,4-oxadiazolin-2-ones or 2-phenylimino-Δ^3-1,3,4-oxadiazolines derived from α,β-epoxyketones, yields acetylenic carbonyl compounds. Good yields of acetylenic aldehydes and ketones are obtained for those cases in which the epoxide is ring fused. Extension to acyclic cases failed primarily due to predominance of a parallel decomposition pathway. The method complements the procedures developed by Eschenmoser and co-workers for the conversion of α,β-epoxyketones into acetylenic carbonyl compounds.

GERALD A. MACALPINE et JOHN WARKENTIN. Can. J. Chem. **56**, 308 (1978).

La thermolyse, dans des solvants polaires, de Δ^3-oxadiazoline-1,3,4 ones-2 ou de phénylimino-2 Δ^3-oxadiazolines-1,3,4 obtenues à partir d'α,β-époxycétones, conduit à des composés carbonylés acétyléniques. On obtient de bons rendements d'aldéhydes et de cétones acétyléniques dans tous les cas ou l'époxyde est juxtaposé à un cycle. Il n'a pas été possible d'étendre ces conclusions à des cas acycliques; dans ces cas une voie parallèle de décomposition devient prédominante. La méthode sert de complément aux propositions de Eschenmoser et de ses collaborateurs pour la conversion d'α,β-époxycétones en composés carbonylés acétyléniques.

[Traduit par le journal]

Introduction

The transformation of α,β-epoxyketones into acetylenic carbonyl compounds is a useful synthetic procedure. New syntheses of exaltone and muscone (1, 2), which are macrocyclic ketones of importance in the fragrance industry, a stereoselective synthesis of *exo*-brevicomin (3), which is the principal sex attractant of the western pine beetle *Dendrocotnus brevicomis*, an 8-methylprostanoid synthon (4), as well as the synthesis of several acetylenic seco-steroids (5, 6) have all involved this fragmentation process. Several methods are known which bring about this transformation. *p*-Toluenesulfonylhydrazine was first used by Eschenmoser and Ohloff (1, 2, 7) and independently by Tanabe and co-workers (5, 6). Later Corey and Sachdev (4) introduced 2,4-dinitrobenzenesulfonylhydrazine as a milder reagent. The transformation may be viewed as outlined in Scheme 1.

Although the *p*-toluenesulfonylhydrazine method works well for β-substituted cyclic α,β-epoxyketones, β-unsubstituted and acyclic α,β-epoxyketones do not give good yields of the fragmentation products. To overcome some of these shortcomings, Eschenmoser and co-workers (8–10) developed an alternative method based on the thermolysis of hydrazones of α,β-epoxyketones derived from *N*-aminoaziridines (8, 9, 10). This process probably proceeds through the intermediacy of a diazoalkane as outlined in Scheme 2. This method has been successfully employed for a wide range of α,β-epoxyketones and works well for cyclic as well as acyclic cases.

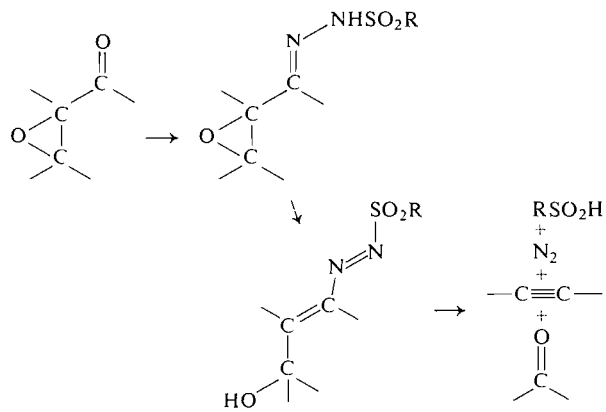

SCHEME 1

A number of related fragmentations have also been reported. Treatments of oximes of α,β-epoxyketones with hydroxylamine-*O*-sulfonic acid yields the corresponding acetylenic carbonyl compounds in a number of steroidal cases (11). As well, certain suitably functionalized diazirines undergo fragmentation to acetylenic carbonyl compounds under acidic conditions (12). It is probable that these two reactions also proceed through a diazoalkane intermediate.

Lead tetraacetate (LTA) oxidation of ketone

[1]Presented in part at the Canadian Chemical Conference of the Chemical Institute of Canada, London, Ontario, June 1976.

Can. J. Chem. Downloaded from www.nrcresearchpress.com by 210.87.254.105 on 09/05/12
For personal use only.

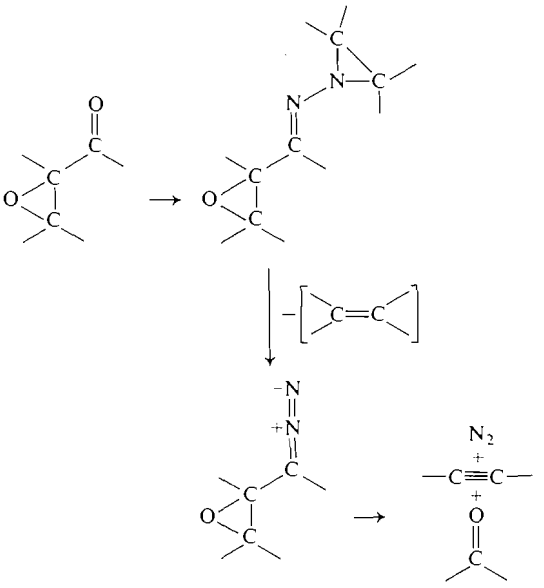

SCHEME 2

semicarbazones gives 5,5-disubstituted-2-imino-Δ^3-1,3,4-oxadiazolines (13–15). These interesting compounds can be hydrolyzed to the corresponding oxadiazolinones which are easily purified by crystallization or sublimation. Compounds of this type undergo thermolysis (16), by two competing paths, to give diazoalkane and heterocumulene or ketone and the appropriate cofragments (Scheme 3). Which pathway predominates may be controlled by choice of the solvent. In polar solvents, the formation of diazoalkane is favoured, whereas in nonpolar solvents ketone formation is the main process.

Since ketone semicarbazones are easily prepared and LTA oxidation to oxadiazolines proceeds in good yield, it seemed of value to investigate the thermolysis of oxadiazolines derived from the semicarbazones of α,β-epoxyketones as an alternative method to bring about the transformation of α,β-epoxyketones to acetylenic carbonyl compounds. The advantages of such an alternative were expected to be: (*i*) a simpler product isolation because of gaseous by-products (i.e., CO_2 and N_2 for oxadiazolinones); (*ii*) mild reaction conditions; and, (*iii*) generality for all types of α,β-epoxyketones. It should be noted that the use of α,β-epoxyaldehydes is not feasible because aldehyde semicarbazones are

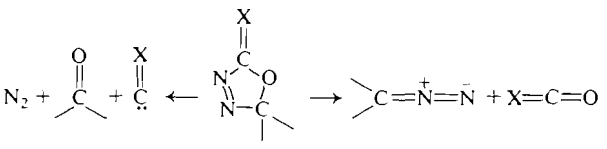

X = O, NR

SCHEME 3

cyclized to 2-amino-1,3,4-oxadiazoles on LTA oxidation (17–20).

Results and Discussion

We initially chose to investigate the decomposition of oxadiazolinones derived from α,β-epoxyketones instead of the corresponding imino oxadiazolines. The reasons for this were twofold: the thermolyses could be carried out at lower temperatures and the co-products for the desired process would be gases, nitrogen and carbon dioxide, whereas for the imino oxadiazolines the co-products would be nitrogen and an isocyanate. We felt that the presence of an isocyanate could complicate product isolation.

It was necessary to demonstrate that α,β-epoxyketones are suitable substrates for oxadiazolinone formation (see Table 1). This required that the semicarbazones be formed in good yield and that subsequent LTA oxidation and hydrolysis should not affect the epoxide ring. To this end we first looked at isophorone oxide (**1**) (20). The semicarbazone was easily prepared and underwent LTA oxidation followed by aqueous acid hydrolysis to give crystalline, solid oxadiazolinone (**13**) in 75% yield, mp 97–100°C. Compound **13**[2] was obtained as a mixture of diastereoisomers as evidenced by its ^{1}Hmr and ^{13}Cmr spectra. Thermolysis of **13** in refluxing acetonitrile gave a mixture of 4,4-dimethyl-6-heptyn-2-one (**20**) and isophorone oxide (**1**) in the approximate ratio 3:1 (glc and ^{1}Hmr). The two products formed are the result of competitive decomposition via the two pathways. The product composition from reaction in ethylene glycol at 150°C was essentially the same. The two products were separated by chromatography on neutral alumina; 4,4-dimethyl-6-heptyn-2-one (**20**) was obtained in 44% yield.

The semicarbazones of some epoxyketones could not be prepared by reaction with semicarbazide under a number of conditions. It seems probable that in these cases the initially formed semicarbazone is unstable and undergoes further reaction with opening of the epoxide ring (Scheme 4). This is ana-

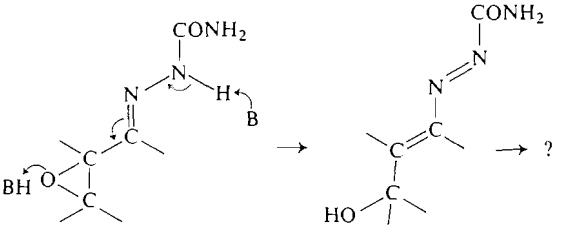

SCHEME 4

[2]The name of this compound is 4,4,6-trimethylspiro[7-oxabicyclo[4.1.0]-heptane-2,2′-[Δ^3-1,3,4]oxadiazolin]-5′-one. We are indebted to Dr. Kurt Loening, Nomenclature Director, Chemical Abstracts Service, Columbus, Ohio for his assistance in this matter.

Can. J. Chem. Downloaded from www.nrcresearchpress.com by 210.87.254.105 on 09/05/12
For personal use only.

TABLE 1. α,β-Epoxyketone derivatives and thermolysis products

α,β-Epoxyketone	Semicarbazone	Oxadiazoline	Acetylenic carbonyl	Isolated yield (%)
1	6 R = H; 7 R = C_6H_5	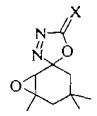 13 X = O; 14 X = NC_6H_5	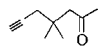 20	44[a], 71[b]
2	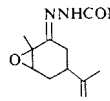 8	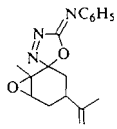 15	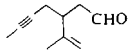 21	53[b]
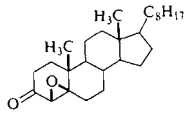 3	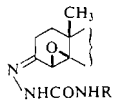 9 R = H; 10 R = C_6H_5	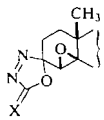 16 X = NH; 17 X = NC_6H_5	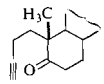 22	38[c], 64[b]
4	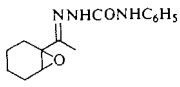 11	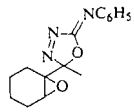 18	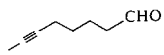 23	36[b]
5	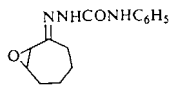 12	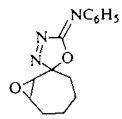 19	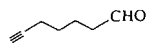 24	74[b]
			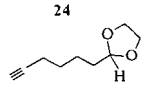 25	47[d]

[a]Thermolysis of oxadiazolinone.
[b]Thermolysis of phenylimino oxadiazoline; product isolated as 2,4-DNP.
[c]Thermolysis of imino oxadiazoline.
[d]See text.

logous to the known dehydrohalogenation of α-haloketones by 2,4-dinitrophenylhydrazine (22).

Even when semicarbazone formation proceeds readily an additional problem arises when an attempt is made to hydrolyze the intermediate imino oxadiazoline. Compound **16**, obtained by LTA oxidation of β-4,5-epoxycholestan-3-one semicarbazone (**9**) (23), hydrolyzed in a mixture of dilute aqueous hydrochloric acid and dichloromethane to yield substantial quantities of cholest-4-en-3-one. The enone is most likely formed by the process outlined in Scheme 5.[3] To overcome this problem, the crude oxidation product (**16**) was thermolyzed in nitrobenzene at 110°C to give a 38% yield of oily, acetylenic ketone (**22**) after purification by chromatography on neutral alumina. Thus the use of oxadiazolinones is limited not only at the semicarbazone-forming step but also at the hydrolysis stage.

We next turned our attention to preparing and studying the thermolysis of substituted imino oxadiazolines derived from α,β-epoxyketones. Since 4-phenylsemicarbazide is stable and easily prepared (24) we chose to use it as the substituted semicarbazide. It reacted with equivalent quantities of α,β-epoxyketones in dichloromethane at ambient temperature to give nearly quantitative yields of 4-phenylsemicarbazones of all the α,β-epoxyketones studied (Table 1). LTA oxidation of the 4-phenylsemicarbazones proceeded readily to give phenyl-

[3]Oxadiazolin-2-ones derived from α,β-epoxyketones are very susceptible to attack by nucleophiles. For example, compound **13** gave a near quantitative yield of 3-hydroxy-3,5,5-trimethylcyclohexanone on reaction with an aqueous methanolic solution of sodium cyanide.

Can. J. Chem. Downloaded from www.nrcresearchpress.com by 210.87.254.105 on 09/05/12
For personal use only.

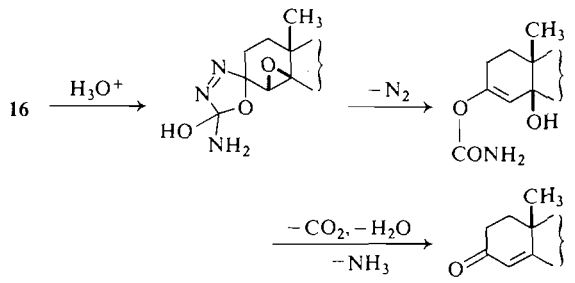

SCHEME 5

imino oxadiazolines as crystalline, yellow solids in good yield. These compounds are more stable than the corresponding oxadiazolinones and thus, if necessary, can be chromatographically purified. Usually the oxidation produced a mixture of diastereoisomers. In the steroidal case, the diastereoisomers (**17**) could be chromatographically separated but no difference in their thermolytic behaviour was observed.

Thermolyses were generally carried out in ethylene glycol. Ethylene glycol served not only as a suitable polar solvent, but also to scavenge the phenyl isocyanate produced as a co-product. Temperatures of the order of 140°C were necessary to initiate decomposition; refluxing methanol or acetonitrile did not result in appreciable decomposition. In general, acetylenic carbonyl compounds were formed in good yield in a clean reaction. Only small amounts of α,β-epoxyketones, derived from the alternative decomposition pathway, were detected. In contrast to decomposition of oxadiazolinone **13**, where a 3:1 ratio of acetylenic ketone to α,β-epoxyketone was observed, only a trace amount of **1** was formed on thermolysis of **14**. It should be noted that acetylenic aldehydes were formed in good yield. The carbonyl compounds were usually isolated as their 2,4-dinitrophenylhydrazones. In one case compound **19** was thermolyzed in the presence of a catalytic amount of *p*-toluenesulfonic acid and the aldehyde was isolated as the acetal (**25**). This may be an important feature for cases in which the newly formed carbonyl is highly reactive.

Attempts to extend the method to acyclic cases failed. Thermolysis of compound **27** in ethylene glycol or in a number of other polar solvents gave complex product mixtures. No synthetically useful yield of the desired aldehyde was obtained. The main product in the thermolysis was the α,β-epoxyketone **26**. Thermolysis of neat **27** resulted in formation of a low yield of aldehyde **28** plus a substantial quantity of α,β-epoxyketone **26**.

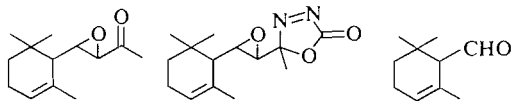

26 **27** **28**

In summary, oxidation and thermolysis of phenylsemicarbazones derived from cyclic α,β-epoxyketones is a useful alternative to bring about their conversion to acetylenic carbonyl compounds. Use of oxadiazolinones is less general as problems arise in making the required semicarbazones and in the isolation of unstable oxidation products. Furthermore, it appears that phenylimino oxadiazolines are more selective, in the desired sense, in the choice of decomposition pathway.

Experimental

General

Melting points were determined on a Thomas Hoover capillary melting point apparatus and are uncorrected. Microanalyses were performed by Schwarzkopf Microanalytical Laboratory. Infrared (ir) spectra ($CHCl_3$ solutions unless otherwise indicated) were taken on either a Beckman-IR5 or a Perkin-Elmer model 283 spectrophotometer. ^{1}Hmr spectra were measured on either a Varian T-60 or EM-390 spectrometer in deuteriochloroform with tetramethylsilane as internal reference unless otherwise noted. Mass spectra (ms) were recorded on a CEC-21-110B spectrometer. Gas chromatographic (glc) analyses were performed using an Aerograph A90-P3 with a column of 15% Carbowax 20M on 60-80 Mesh Chromosorb P. Thin-layer chromatography (tlc) was carried out on Merck plates (0.25 mm thick) pre-coated with silica gel 60F-254 or aluminum oxide F-254 (type E). Preparative-layer chromatography (plc) was done on plates (20 × 20 cm; 2 mm thick) prepared from silica gel GF-254 or aluminum oxide GF-254 (type 60/E). Chlorocarbon extracts were dried over anhydrous sodium sulfate and diethyl ether extracts over anhydrous magnesium sulfate. Light petroleum refers to the fraction boiling between 30–60°C; hexane refers to 'Baker analyzed' reagent, boiling point range 68.5–69.3°C.

Materials

4-Phenylsemicarbazide was prepared by the method of Wheeler, mp 120–122°C (lit. (24) mp 120–123°C). 2,4-Dinitrophenylhydrazine reagent refers to a solution of 2,4-dinitrophenylhydrazine (1 g) in methanol (30 ml) and concentrated H_2SO_4 (2 ml).

General Procedure for Epoxidation of α,β-Unsaturated Ketones

The temperature of a solution of α,β-unsaturated ketone (~1 *M*) in anhydrous methanol containing 30% aqueous H_2O_2 (1.2 equiv.) was adjusted to between 0–15°C by means of an ice-water bath. Sodium hydroxide (6 *N*) was added dropwise to the rapidly stirred solution and the reaction was monitored by tlc. In some cases the temperature was allowed to rise to 20°C. When all the starting material had been consumed the reaction mixture was diluted with H_2O and extracted with ether. The organic extracts were combined and washed several times with a cold, saturated solution of $FeSO_4$, then H_2O, and finally brine. Drying and removal of the solvent at reduced pressure gave crude α,β-epoxyketone. Usually the α,β-epoxyketone was used without further purification.

4,4,6-Trimethyl-7-oxabicyclo[4.1.0]heptan-2-one (Isophorone Oxide) 1

This compound was prepared from isophorone by the method of House and Wasson (21) in 70% yield, bp 80–84°C/10 Torr (lit. (21) bp 70–73°C/5 Torr).

Can. J. Chem. Downloaded from www.nrcresearchpress.com by 210.87.254.105 on 09/05/12
For personal use only.

Can. J. Chem. Downloaded from www.nrcresearchpress.com by 210.87.254.105 on 09/05/12
For personal use only.

1,6-Epoxy-p-*menth-8-en-2-one* **2**

This compound was prepared by the general procedure from (−)-carvone (1 h at 0–4°C) in 50% yield, bp 73–76°C/1 Torr (lit. (25) bp 160°/7 Torr) as a mixture of diastereoisomers; ^{1}Hmr δ: 1.40 (s, 3H, CH_3), 1.72 (s(b), 3H, C=C—CH_3), 1.80–2.93 (m, 5H, CH and CH_2), 3.43 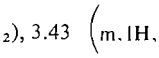 , 4.77 (m, 2H, C=CH_2); ir: 1706 (s, C=O), 1644 (w, C=CH_2).

β-*4,5-Epoxycholestan-3-one* **3**

This compound was prepared from 4-cholesten-3-one by the method of Plattner, mp 117–117.5°C (lit. (23) mp 116°C).

1-Acetyl-7-oxabicyclo[4.1.0]heptane **4**

This compound was prepared by the general method (20 h at 20°C) in 70% crude yield; ^{1}Hmr δ: 1.20–2.43 (m, 8H, CH_2), 2.05 (s, 3H, $COCH_3$), 3.33 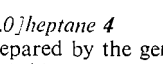 .

8-Oxabicyclo[5.1.0]octan-2-one **5**

This compound was prepared by the general method (3 h at 0°C) in 94% crude yield; ^{1}Hmr δ: 1.50–2.50 (m, 8H, CH_2), 2.53–2.87 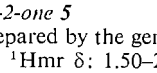 , 3.33–3.50 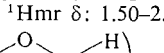 .

3,4-Epoxy-4-(2′,6′,6′-trimethyl-2′-cyclohexenyl)-butan-2-one **26**

This compound was prepared from α-ionone in 60% yield by the method of Eschenmoser and co-workers (10), mp 34.5–35.5°C (lit. (10) mp 36–38°C).

General Procedure for the Preparation of Semicarbazones and 4-Phenylsemicarbazones

For semicarbazone formation the α,β-epoxyketone was added to an aqueous solution of semicarbazide hydrochloride (1.2 *M*) containing 1 equiv. of sodium acetate trihydrate at 20°C. Sufficient 95% ethanol was added to bring about a homogeneous solution. The semicarbazone usually began to precipitate immediately, it was then filtered and dried under vacuum over P_2O_5. For 4-phenylsemicarbazone formation, a CH_2Cl_2 solution (~1 *M*) of the α,β-epoxyketone containing 1.1 equiv. of 4-phenylsemicarbazide was stirred over anhydrous Na_2SO_4 at 20°C for 4–20 h. The reaction was followed by tlc and was usually complete after 4 h. The Na_2SO_4 was removed by filtration and the solvent removed at reduced pressure. One crystallization furnished pure 4-phenylsemicarbazone.

Preparation of Semicarbazone 6 from 4,4,6-Trimethyl-7-oxabicyclo[4.1.0]heptan-2-one **(1)**

This compound was prepared by the general procedure in 84% yield, mp 213°C (lit. (26) mp 216°C (dec.)) from 95% ethanol.

Preparation of 4-Phenylsemicarbazone 7 from 4,4,6-Trimethyl-7-oxabicyclo[4.1.0]heptan-2-one **(1)**

This compound was prepared by the general procedure in 84% yield, mp 204–205°C (dec.) from ethyl acetate; ^{1}Hmr δ: 0.93 (s, 3H, CH_3), 1.03 (s, 3H, CH_3), 1.43 (s, 3H, CH_3), 1.51–2.53 (m, 4H, CH_2), 3.42 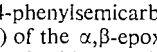 , 6.97–7.67 (m, 5H, C_6H_5), 8.37 (s, 1H, $CONHC_6H_5$), 9.97 (s, 1H, C=NNHCO); ir: 3390 (m, NH), 1690 (s, C=N and C=O); ms: M^+ 287.

Preparation of 4-Phenylsemicarbazone 8 from 1,6-Epoxy-p-*menth-8-en-2-one* **(2)**

This compound was prepared by the general procedure, in nearly quantitative yield, as a mixture of diastereoisomers. As this mixture was difficult to crystallize, it was used without purification, ^{1}Hmr δ: 1.58 and 1.68 (s, 6H, 2 CH_3), 1.81–2.91 (m, 5H, CH_2 and CH), 3.41 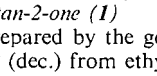 , 4.80 (s(b), 2H, C=CH_2), 6.91–7.61 (m, 5H, C_6H_5), 8.37 (s, 1H, $CONHC_6H_5$), 9.78 (s, 1H, C=NNHCO); ir (KBr): 3370 (m, NH), 1685 (s, C=N and C=O).

Preparation of Semicarbazone 9 from β-*4,5-Epoxycholestan-3-one* **(3)**

This compound was prepared in 60% yield, mp 189–192°C (dec.) from ether–hexane by the general procedure, ^{1}Hmr δ: 3.33 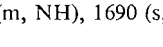 , 6.87–7.63 (m, 5H, C_6H_5), 8.3 (s(b), 1H, $CONHC_6H_5$), 9.4 (s(b), 1H, C=NNHCO); ir: 3390 (m, NH), 1700 (s, C=N and C=O).

Preparation of 4-Phenylsemicarbazone **11** *from 1-Acetyl-7-oxabicyclo[4.1.0]heptane* **(4)**

This compound was prepared in 57% yield by the general procedure, mp 153–155°C from ethyl acetate – hexane, ^{1}Hmr δ: 1.47 (m, 4H, CH_2), 1.78 (s, 3H, $COCH_3$), 1.83–2.62 (m, 4H, CH_2), 3.23 , 7.00–7.67 (m, 4H, C_6H_5), 8.20 (s(b), 1H, $CONHC_6H_5$), 8.8 (s(b), 1H, C=NNHCO); ir: 3390 (m, NH), 1695 (s, C=N and C=O).

Preparation of 4-Phenylsemicarbazone **12** *from 8-Oxabicyclo-[5.1.0]octan-2-one* **(5)**

The 4-phenylsemicarbazone was prepared by the general method in 84% yield, mp 180–181°C (dec.) from ethyl acetate, ^{1}Hmr δ: 1.14–3.00 (m, 8H, CH_2), 3.24–3.58 , 3.70 and 3.99 (both d, $J \sim 5$ Hz, total of 1H, *syn*- and *anti*-4-phenylsemicarbazones), 6.93–7.63 (m, 5H, C_6H_5), 8.30 (s(b), 1H, $CONHC_6H_5$), 9.77 and 10.13 (both s(b), 1H, C=NNHCO, *syn*- and *anti*-4-phenylsemicarbazones); ir: 3390 (m, NH), 1695 (s, C=N and C=O).

The Preparation of 4-Phenylsemicarbazone of 3,4-Epoxy-4-(2′,6′,6′-trimethyl-2′-cyclohexenyl)butan-2-one **(26)**

The 4-phenylsemicarbazone was prepared by the general method in 78% yield, mp 180–181°C from chloroform-hexane, ^{1}Hmr δ: 0.97 (s, 3H, CH_3), 1.24 (s, 3H, CH_3), 1.31–1.70 (m, 3H, CH_2 and CH), 1.59 (s, 3H, CH_3), 2.04 (m, 2H, allylic CH), 2.83 , 3.49 , 5.53 (m, 1H, C=CH), 6.99–7.63 (m, 5H, C_6H_5), 8.25 (s(b), 1H, $CONHC_6H_5$), 9.12 (s(b), 1H, C=NNHCO); ir: 3390 (m, NH), 1695 (s, C=N and C=O).

Lead Tetraacetate Oxidation of Semicarbazones and 4-Phenylsemicarbazones

A specific procedure is given below for the oxidation of

Can. J. Chem. Downloaded from www.nrcresearchpress.com by 210.87.254.105 on 09/05/12
For personal use only.

semicarbazone **6** and 4-phenylsemicarbazone 7 derived from isophorone oxide (**1**). For all other cases, a similar procedure was followed.

LTA Oxidation of Semicarbazone 6

Lead tetraacetate (5.40 g, 0.012 mol) was added to a stirred suspension of the semicarbazone (2.11 g, 0.01 mol) in dry CH_2Cl_2 (100 ml) at −10°C. There was an immediate formation of a yellow, homogeneous solution which formed a precipitate over the next 0.5 h. After 4 h at −10°C ice-cold H_2O (50 ml) was added to the now colourless reaction mixture, followed by 2.4 *N* HCl (30 ml). The reaction mixture was stirred at 0°C for 0.5 h to ensure complete hydrolysis of the intermediate imino oxadiazoline. The reaction mixture was then filtered through Celite, the organic phase separated, and the aqueous phase extracted with CH_2Cl_2 (3 × 20 ml). The organic extracts were combined, washed with H_2O (20 ml), dried, and the solvent removed at reduced pressure to give crude oxadiazolinone **13** (1.87 g) in 87% yield. Crystallization from ether–hexane gave 1.52 g (75%) of pure **13**, mp 97–100°C as a mixture of diastereoisomers; ^{1}Hmr (DMSO-d_6) δ: 0.98, 1.18, 1.35 and 1.37 (all s, total 9H, $3CH_3$), 1.63 (s(b), 2H, CH_2), 1.83 (s(b), 2H, CH_2), 3.05 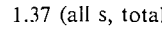 ; ir (KBr): 1825 (s, C=O); *Anal.* calcd. for $C_{10}H_{14}N_2O_3$: C 57.13, N 6.71, N 13.33; found: C 57.31, H 6.77, N 13.05.

LTA Oxidation of 4-Phenylsemicarbazone 7

A solution of LTA (3.55 g, 0.008 mol) in dry CH_2Cl_2 (25 ml) was added dropwise over 0.3 h to a stirred solution of 4-phenylsemicarbazone **7** (2.16 g, 0.0075 mol) in dry CH_2Cl_2 (50 ml) at 0°C. After all the LTA solution had been added, the reaction mixture was stirred at 0°C for 3 h, diluted with cold H_2O (15 ml), and stirred an additional 0.25 h. The reaction mixture was filtered through Celite and the organic phase separated. The aqueous phase was extracted with CH_2Cl_2 (3 × 20 ml). The extracts were combined, washed with H_2O, and dried. Removal of the solvent at reduced pressure gave crude **14** (2.17 g). Crystallization from CH_2Cl_2 – light petroleum gave **14** as a mixture of diastereoisomers (1.19 g) mp 112–126°C (dec.) in 50% yield; tlc (SiO_2, 3:7 ether–hexane) R_F 0.64 and 0.55; ^{1}Hmr δ: 1.08, 1.10, 1.31, 1.42 and 1.48 (all s, total of 9H, 3 CH_3), 1.64–2.01 (m, 4H, CH_2), 2.63 (minor diastereoisomer) and 2.67 (major diastereoisomer) 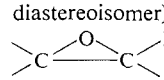 , 7.11–7.63 (m, 5H, C_6H_5); ir: 1700 (s, C=N); *Anal.* calcd. for $C_{16}H_{19}N_3O_2$: C 67.35, H 6.71, N 14.73; found: C 67.37, H 6.80, N 14.71.

LTA Oxidation of 4-Phenylsemicarbazone 8

Compound **8** (1.50 g, 0.005 ml) was oxidized at −15°C and the crude product purified by chromatography on neutral alumina (grade III) using 10% ether – light petroleum as eluant to give a 53% yield (0.79 g) of **15** as a mixture of diastereoisomers. An analytical sample was prepared by three crystallizations from ether–hexane, mp 114–115.5°C; tlc (SiO_2, 1:1 ether–hexane R_F 0.8; ^{1}Hmr δ: 1.07 (s(b), 3H, CH_3), 1.33–2.83 (m, total of 8H, CH, CH_2 and CH_3, latter s(b) at 1.73), 3.38 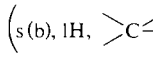 , 4.80 (m, 2H, C=CH_2), 7.13–7.77 (m, 5H, C_6H_5); ir: 1695 (s, C=N); *Anal.* calcd. for $C_{17}H_{19}N_3O_2$: C 68.66, H 6.44, N 14.13; found: C 68.47, H 6.44, N 13.99.

LTA Oxidation of Semicarbazone 9

Semicarbazone **9** (0.192 g, 0.004 mol) was oxidized at 0°C and the crude imino oxadiazoline **16** (0.19 g) isolated as an oil. Since this compound was unstable it was used directly for fragmentation without further purification.

LTA Oxidation of 4-Phenylsemicarbazone 10

4-Phenylsemicarbazone **10** (0.33 g, 6.8 mmol) was oxidized at 0°C for 4 h and then at 20°C for 16 h to give crude **17** as a mixture of diastereoisomers (0.28 g) in 83% yield. The two diastereoisomers were separated by chromatography on neutral alumina (grade III) using 10% ether – light petroleum as eluant. An analytical sample of the major diastereoisomer was obtained by crystallization from ether–hexane, mp 177–179°C; tlc (SiO_2, 3:7 ether–hexane) R_F 0.93; ^{1}Hmr δ: 2.67 , 7.13–7.70 (m, 5H, C_6H_5); ir: 1700 (s, C=N); *Anal.* calcd. for $C_{34}H_{49}N_3O_2$: C 76.79, H 9.29, N 7.90; found: C 76.88, H 9.13, N 7.98. A pure sample of the minor diastereoisomer was obtained by crystallization from ether–hexane, mp 128–129°C; tlc (SiO_2, 3:7 ether–hexane) R_F 0.83; ^{1}Hmr δ: 2.65 , 7.23–7.62 (m, 5H, C_6H_5); ir: 1700 (s, C=N).

LTA Oxidation of 4-Phenylsemicarbazone 11

Compound **11** was oxidized at 0°C for 3 h and then at 20°C for 1 h. The crude product was purified by chromatography on neutral alumina (grade III) using 10% ether – light petroleum as eluant. Compound **18** was obtained in 77% yield (0.455 g) as a mixture of diastereoisomers, mp 75–80°C. An analytical sample was prepared by two crystallizations from ether–hexane, mp 82–83°C; tlc (SiO_2, 1:1 ether–hexane) R_F 0.77; ^{1}Hmr δ: 1.12–1.59 (m, 4H, CH_2), 1.72 (s, 3H, CH_3), 1.79–2.23 (m, 4H, CH_2), 3.30 and 3.40 diastereoisomers), 7.16–7.60 (m, 5H, C_6H_5); ir: 1700 (s, C=N); *Anal.* calcd. for $C_{15}H_{17}N_3O_2$: C 66.40, H 6.32, N 15.49; found: C 66.73, H 6.37, N 15.32.

LTA Oxidation of 4-Phenylsemicarbazone 12

Compound **12** (0.52 g, 0.002 mol) was oxidized at 0°C for 3 h. Crystallization from ether–hexane gave **19** as a mixture of diastereoisomers in 60% yield, mp 96–97°C (dec.). An analytical sample was prepared by two crystallizations from ether–hexane, mp 132.5–135°C (dec.); tlc (SiO_2, 3:7 ether–hexane) R_F 0.68; ^{1}Hmr δ: 1.10–2.57 (m, 8H, CH_2), 2.71 , 3.31 , 7.13–7.70 (m, 5H, C_6H_5); ir: 1700 (s, C=N); *Anal.* calcd. for $C_{14}H_{15}N_3O_2$: C 65.35, H 5.88, N 16.33; found: C 65.50, H 5.97, N 16.30.

4,4-Dimethyl-6-heptyn-2-one 20

(*A*) A solution of oxadiazolinone **13** (1.05 g, 0.005 mol) was refluxed in dry acetonitrile (50 ml) under a nitrogen atmosphere for 7 h. The solvent was removed by careful distillation; glc and ^{1}Hmr analysis indicated that the ratio of alkynone **20** to α,β-epoxyketone **1** was approximately 3:1. Chromatography of the residue on neutral alumina (50 g, grade III) using 20% ether – light petroleum gave 0.30 g (44%) of 4,4-dimethyl-6-heptyn-2-one (**20**): tlc (Al_2O_3, 3:7 ether–hexane) R_F 0.9; ^{1}Hmr δ: 1.05 (s, 6H, *gem*-dimethyl), 2.04 (t, J = 2.5 Hz, 1H, C=CH), 2.12 (s, 3H, $COCH_3$), 2.24 (d, J = 2.5 Hz, 2H, CH_2), 2.47

Can. J. Chem. Downloaded from www.nrcresearchpress.com by 210.87.254.105 on 09/05/12
For personal use only.

(s, 2H, CH_2); ir: 3330 (m, C≡CH), 2120 (w, C≡C), 1721 (s, C=O). There was also obtained 0.14 g of a mixture of compounds **20** and **1**, as well as 0.07 g of pure α,β-epoxyketone **1**.

(*B*) Phenylimino oxadiazoline **14** (0.143 g, 0.50 mmol) was added to ethylene glycol (5 ml) at 150–160°C (oil bath temperature). Gas evolution began at once and after 0.5 h the reaction mixture had turned from yellow to colourless. The reaction mixture was cooled to 20°C, poured into H_2O, and extracted with ether. The extracts were combined, washed with brine, water, and dried. The solvent was removed by careful distillation to give crude alkynone **20**. The residue was dissolved in CH_3OH (2 ml) and treated with 2,4-DNP reagent (3 ml). After standing at ambient temperature for 16 h 0.103 g (71%) of the 2,4-DNP of compound **20** was obtained, mp 102–103°C from 95% ethanol: ^{1}Hmr δ: 1.23 (s, 6H, *gem*-dimethyl), 2.09 (t, J = 2.5 Hz, 1H, C≡CH), 2.16 (s, 3, CH_3), 2.23 (d, J = 2.5 Hz, 2H, CH_2), 2.50 (s, 2H, CH_2), 7.98 (d, J = 10 Hz, 1H, ArH), 8.34 (dd, J = 10 and 2 Hz, 1H, ArH), 9.17 (d, J = 2 Hz, 1H, ArH), 11.09 (s(b), 1H, NH); *Anal.* calcd. for $C_{15}H_{18}N_4O_4$: C 56.59, H 5.70, N 17.60; found: C 56.38, H 5.69, N 17.31.

3-Isopropenyl-5-heptynal ***21***

Phenylimino oxadiazoline **15** (0.297 g, 1.0 mmol) was added to ethylene glycol (10 ml) at 150°C under a nitrogen atmosphere. After 0.75 h the reaction mixture was cooled to 20°C and diluted with H_2O (10 ml). The product was extracted with ether and the combined ethereal extracts washed with brine, H_2O, and dried. Careful removal of the solvent by distillation gave crude alkynal **21**. This material was treated with 2,4-DNP reagent (15 ml) and after 16 h the 2,4-DNP (0.273 g, 83%) was isolated by chloroform extraction and chromatography on neutral alumina (grade III) using 20% ether – light petroleum as eluant, mp 91–93°C from methanol. An analytical sample was prepared by crystallization from 95% ethanol, mp 93–94°C: ^{1}Hmr δ: 1.70–1.87 (complex, 6H, $2CH_3$), 1.98–2.97 (m, 5H, CH and CH_2), 4.86 (m, 2H, C=CH_2), 7.53 (t, J = 5 Hz, 1H, CH=N), 7.94 (d, J = 10 Hz, 1H, ArH), 8.31 (dd, J = 10 and 2 Hz, 1H, ArH), 9.1 (d, J = 2 Hz, 1H, ArH), 11.05 (s(b), 1H, NH); *ir* (KBr): *1625* (s, C=N); *Anal.* calcd. for $C_{16}H_{18}N_4O_4$: C 58.17, H 5.49, N 16.96; found: C 58.37, H 5.67, N 16.96. The alkynal **21** could be isolated by plc on SiO_2 using 1:1 ether – light petroleum as eluant: ^{1}Hmr δ: 1.70–1.83 (complex, 6, $2CH_3$), 2.19–2.82 (m, 5H, CH and CH_2), 4.83 (m, 2H, C=CH_2), 9.79 (t, J = 1.5 Hz, 1H, CHO); ir: 2730 (w, aldehydic CH), 1725 (s, C=O).

4,5-Seco-3-cholestyn-5-one ***22***

(*A*) Crude imino oxadiazoline **16** (1.12 g) prepared by LTA oxidation of semicarbazone **9** (1.16 g) was heated in nitrobenzene (50 ml) at 110°C for 5 h. The solvent was removed at reduced pressure and the residue chromatographed on neutral alumina (grade III) using 20% ether – light petroleum as eluant to give compound **22** (4) (0.30 g) as a colourless oil in 38% overall yield: tlc (Al_2O_3, 1:7 ether–hexane) R_F 0.50; ^{1}Hmr δ: 0.75, 0.85, 0.91 and 1.1 (complex, CH_3's); ir: 3310 (m, C≡CH), 2110 (w, C≡C), 1700 (s, C=O); *Mol. Wt.* calcd. for $C_{27}H_{44}O$: 384.3392; found (high resolution ms): 384.3402. There was also obtained from the column 0.19 g of a mixture of compounds **3** and **22**.

(*B*) Phenylimino oxadiazoline **17**, mp 177–179°C (major diastereoisomer), (0.037 g, 0.07 mmol) was dissolved in dry HMPA (5 ml) and heated at 150°C under a nitrogen atmosphere for 1 h. The reaction mixture was cooled to 20°C, diluted with H_2O (30 ml) and extracted with ether. After drying the solvent was removed at reduced pressure and the residue chromatographed (plc) on neutral alumina (5:1 ether–hexane as eluant; developed three times). 4,5-seco-3-cholestyn-5-one (**22**) was obtained in 63% yield (0.017 g) and β-4,5-epoxycholestan-3-one (**3**) in 12.5% yield (0.0035 g). Similar results were obtained using the minor diastereoisomer.

6-Octynal ***23***

Phenylimino oxadiazoline **18** (0.136 g, 0.50 mmol) was added to ethylene glycol (5 ml) at 140°C under a nitrogen atmosphere. The reaction mixture was stirred at this temperature for 0.5 h, cooled to ambient temperature, poured into H_2O (20 ml), and extracted with ether (4 × 20 ml). After washing the combined ether extracts with brine (20 ml) and H_2O (20 ml), and drying, the solvent was removed by careful distillation and the residue treated with 2,4-DNP reagent (5 ml). After 5 h at 20°C the 2,4-DNP was isolated by extraction with CH_2Cl_2 and plc on neutral alumina using 1:4 ether – light petroleum. The 2,4-DNP of 6-octynal (**23**) was obtained in 36% yield (0.054 g), mp 118–121°C from methanol; ^{1}Hmr δ: 1.41–1.98 (complex, 7, CH_2 and CH_3, latter at 1.79, t, J = 2 Hz), 2.00–2.62 (m, 4, CH_2), 7.6 (t, J = 5 Hz, 1H, CH=N), 7.97 (d, J = 10 Hz, 1H, ArH), 8.33 (dd, J = 10 and 2 Hz, 1H, ArH), 9.14 (d, J = 2 Hz, 1H, ArH), 11.1 (s(b), 1H, NH); ir: 1620 (s, C=N); *Anal.* calcd. for $C_{14}H_{16}N_4O_4$: C 55.25, H 5.30, N 18.41; found: C 55.45, H 5.58, N 18.28.

7-Heptynal ***24***

Phenylimino oxadiazoline **19** (0.0129 g, 0.5 mmol) was added to ethylene glycol (5 ml) at 140°C. The reaction mixture was heated for 5 h under a nitrogen atmosphere, cooled to 20°C, diluted with H_2O, and extracted with ether (4 × 20 ml). The combined ethereal extracts were washed with brine, H_2O, and dried. The residue was treated with 2,4-DNP reagent (9 ml) at ambient temperature for 24 h. The 2,4-DNP was isolated by extraction with CH_2Cl_2 and plc on silica gel using 1:1 ether–hexane as eluant. The 2,4-DNP of 7-heptynal (**24**) was obtained in 74% yield (0.107 g), mp 103–103.5°C from methanol; ^{1}Hmr δ: 1.40–1.93 (m, 4H, CH_2), 1.99 (t, J = 2 Hz, 1H, C≡CH), 2.1–2.67 (m, 4H, CH_2), 7.6 (t, J = 5 Hz, 1H, CH=N), 7.97 (d, J = 10 Hz, 1H, ArH), 8.34 (dd, J = 10 and 2 Hz, 1H, ArH), 9.16 (d, J = 2 Hz, 1H, ArH), 11.5 (s(b), 1H, NH); ir: 3310 (m, C≡CH), 2115 (w, C≡C), 1620 (s, C=N); *Anal.* calcd. for $C_{13}H_{14}N_4O_4$: C 53.79, H 4.86, N 19.30; found: C 53.58, H 4.92, N 19.03.

8,8-Ethylenedioxy-1-heptyne ***25***

Phenylimino oxadiazoline **19** (0.025 g, 0.10 mmol) was heated in ethylene glycol (5 ml) containing *p*-toluenesulfonic acid monohydrate (12 mg) at 150°C for 0.25 h. The reaction mixture was cooled to 20°C, poured into saturated aqueous sodium bicarbonate solution, and extracted with ether. After drying the solvent was removed by careful distillation and the residue subjected to plc on silica gel using 1:1 ether–hexane as eluant, to give **25** (7.3 mg, 47%); ^{1}Hmr δ: 1.42–1.83 (m, 6H, CH_2), 1.89 (t, J = 2 Hz, 1H, C≡CH), 2.07–2.33 (m, 2H, CH_2), 3.81–4.06 (m, 4H, CH_2), 4.89 (m, 1H, O—CH—O); ir: 33.0 (m, C≡CH), 2115 (w, C≡C).

Thermolysis of Phenylimino Oxadiazoline ***27***

Phenylimino oxadiazoline **27** (0.33 g, 0.97 mmol) was heated under vacuum at 170°C for 0.75 h. The residue was chromatographed by plc on silica gel using 1:2 ether–hexane as eluant to give α,β-epoxyketone **26** (34 mg) and aldehyde **25** (10) (15 mg); ^{1}Hmr δ: 0.90 and 1.00 (s, 6H, *gem*-dimethyl), 1.20–2.43 (m, 8H, CH_2 and CH_3, latter at 1.61d, J = 1.5 Hz), 5.72 (m, 1H, C=CH), 9.52 (d, J = 6 Hz, 1H, CHO); ir: 2720 (w aldehydic CH), 1715 (s, C=O).

Acknowledgement

This work was supported by the National Research Council of Canada.

1. A. Eschenmoser, D. Felix, and G. Ohloff. Helv. Chim. Acta, **50**, 708 (1967).
2. D. Felix, J. Schreiber, K. Piers, U. Horn, and A. Eschenmoser. Helv. Chim. Acta, **54**, 2896 (1971).
3. P. J. Kocienski and R. W. Ostrow. J. Org. Chem. **41**, 398 (1976).
4. E. J. Corey and H. S. Sachdev. J. Org. Chem. **40**, 579 (1975).
5. M. Tanabe, D. F. Crowe, R. L. Dehn, and G. Detre. Tetrahedron Lett. 3739 (1967).
6. M. Tanabe, D. F. Crowe, and R. L. Dehn. Tetrahedron Lett. 3943 (1967).
7. J. Schreiber, D. Felix, A. Eschenmoser, M. Winter, F. Gautschi, K. H. Schulte-Elte, E. Sundt, G. Ohloff, J. Kalvoda, H. Kaufmann, P. Wieland, and G. Annev. Helv. Chim. Acta, **50**, 2101 (1967).
8. R. K. Müller, D. Felix, J. Schreiber, and A. Eschenmoser. Helv. Chim. Acta, **53**, 1479 (1970).
9. D. Felix, J. Schreiber, K. Piers, U. Horn, and A. Eschenmoser. Helv. Chim. Acta, **51**, 1461 (1968).
10. D. Felix, R. K. Müller, U. Horn, R. Joos, J. Schreiber, and A. Eschenmoser. Helv. Chim. Acta, **55**, 1276 (1972).
11. P. Wieland, H. Kaufmann, and A. Eschenmoser. Helv. Chim. Acta, **50**, 2108 (1967).
12. P. Borrevang, J. Hjort, R. T. Rapala, and R. Edie. Tetrahedron Lett. 4905 (1968).
13. A. M. Cameron, P. R. West, and J. Warkentin. J. Org. Chem. **34**, 3230 (1969).
14. S. L. Lee, G. B. Gubelt, A. M. Cameron, and J. Warkentin. Chem. Commun. 1074 (1970).
15. P. Knittel, S. L. Lee, and J. Warkentin. Can. J. Chem. **50**, 3248 (1972).
16. S. L. Lee, A. M. Cameron, and J. Warkentin. Can. J. Chem. **50**, 2326 (1972).
17. G. Valenti and F. Maggio. Ann. Chim. (Rome), **42**, 18 (1952).
18. F. Maggio, G. Werber, and G. Lombardo. Ann. Chim. (Rome), **42**, 18 (1952).
19. M. S. Gibson. Tetrahedron, **18**, 1377 (1962).
20. H. Gehlen and K. Möckel. Ann. Chem. **651**, 133 (1962).
21. H. O. House and R. L. Wasson. *In* Organic syntheses. Vol. IV. *Edited by* Norman Rabjohn. John Wiley and Sons Inc., New York, NY. 1963. p. 552.
22. V. R. Mattox and E. C. Kendall. J. Am. Chem. Soc. **72**, 2290 (1950).
23. Pl. A. Plattner, H. Heussen, and A. B. Kulkarni. Helv. Chim. Acta, **31**, 1822 (1948).
24. A. S. Wheeler. *In* Organic syntheses. Vol. I. *Edited by* A. H. Blatt. John Wiley and Sons Inc., New York, NY. 1932. p. 450.
25. V. K. Homoad, E. Siscovic, and A. S. Rao. Indian J. Chem. **5**, 234 (1967).
26. W. Treibs. Ber. **66**, 1483 (1933).

Can. J. Chem. Downloaded from www.nrcresearchpress.com by 210.87.254.105 on 09/05/12
For personal use only.

Evidence for five-coordination in titanium(IV) complexes. A nuclear magnetic resonance investigation

ARPAD SOMOGYVARI AND NICK SERPONE

Department of Chemistry, Sir George Williams Campus, Concordia University, Montreal, P.Q., Canada H3G 1M8

Received August 11, 1977

ARPAD SOMOGYVARI and NICK SERPONE. Can. J. Chem. **56**, 316 (1978).

Diketonato complexes of titanium(IV), $(X_3Ti(dik))_2$ (X = Cl, Br; dik = anions of dipivaloylmethane and benzoylacetone), of apparent five-coordinate stoichiometry have been prepared and investigated in nitrobenzene solutions using the variable temperature nuclear magnetic resonance technique. The nmr spectra reveal the existence of two equilibrium species; a five-coordinate $X_3Ti(dik)$ and a six-coordinate $X_2Ti(dik)_2$ complex. The data are interpreted in terms of a symmetric dissociation of the six-coordinate titanium(IV) dimer, $(X_3Ti(dik))_2$, into two five-coordinate monomers which then undergo a disproportionation reaction to the four-coordinate titanium tetrahalide and the six-coordinate $X_2Ti(dik)_2$ species.

ARPAD SOMOGYVARI et NICK SERPONE. Can. J. Chem. **56**, 316 (1978).

On a préparé des complexes dicétonato du titane (IV), $(X_3Ti(dik))_2$ (X = Cl, Br; dik = les anions du dipivaloylméthane et de la benzoylacétone), qui possèdent apparemment une stoechiométrie pentacoordonnée; on les a aussi étudié en solution dans le nitrobenzène en faisant appel à la technique de la résonance magnétique nucléaire à température variable. Les spectres rmn indiquent la présence de deux espèces en équilibre; un complexe pentacoordonné $X_3Ti(dik)$ et un complexe hexacoordonnée $X_2Ti(dik)_2$. On interprète les données en termes d'une dissociation symétrique du dimère hexacoordonné du titane (IV), $(X_3Ti(dik))_2$, en deux monomères pentacoordonnés qui subissent alors une réaction de disproportionation conduisant à un tétrahalogénure de titane tétracoordonné et à des espèces hexacoordonnées $X_2Ti(dik)_2$.

[Traduit par le journal]

Introduction

The characterization of titanium(IV) complexes possessing six-coordinate (1, 2) geometry has been the object of much activity. In contrast, the corresponding five-coordination in these species has received less attention in the light of current interest in less common coordination geometries (3–7).

Apparent five-coordination for titanium(IV) has been postulated by Yamamoto and Kambara (8) and by Mehrotra and co-workers (9–11) for various alkoxy $(OR)_3Ti(dik)$ and $Cl_3Ti(acac)$ complexes (dik = a 1,3-diketonate anion; acac = anion of acetylacetone) on the basis of elemental analyses, infrared spectra, and chemical reactions. Later, after a systematic characterization (molecular weights and molar conductivities in nitrobenzene and benzene) of several diketonate $X_3Ti(dik)$ complexes, Thompson,[1] and Thompson, Somers, and Workman (12) concluded that these species of stoichiometry $X_3Ti(dik)$ are monomeric and nonelectrolytes. Holloway and Sentek (13), on the other hand, have suggested that this apparent five-coordination in titanium(IV) may actually be an equilibrium mixture of the more familiar four- and six-coordinate complexes, weakly associated in solution according to

[1] $$(dik)_2TiX_2 + TiX_4 \rightleftharpoons (dik)_2TiX_2TiX_4$$

reaction 1 in which the two titanium atoms are bridged by the two X ligands.

To establish the stereochemistry of these apparent five-coordinate species, we (14, 15) recently undertook a study of the crystal and molecular structure of one such $X_3Ti(dik)$ species. In particular, when X is Cl and dik is acac, the solid state structure of di-μ-chlorotetrachlorobis(acetylacetonato)dititanium(IV) consists of a cyclic dimer with the two titanium(IV) atoms linked by two chlorine bridges, and the observed space group ($P2_1/n$) requires this dimer to be centrosymmetric and not as suggested in reaction 1. It appears therefore that a structural disproportionation must take place upon dissolution of the dimer to be consistent with the monomeric and non-ionic nature of these species in solution. In agreement with this expectation, nmr and infrared spectral evidence suggests that $Cl_3Ti(bzac)$ is five-coordinate in nitrobenzene solutions and is involved in the equilibrium (16)

[2] $$2\ Cl_3Ti(bzac) \rightleftharpoons TiCl_4 + Cl_2Ti(bzac)_2$$

In a more recent study on the stereochemical nature of $(OR)_3TiL$, where L is a uninegative bidentate ligand with an ethane backbone (e.g., Me_2NCH_2-CH_2NMe), Alyea and Merrell (17) report that some

[1] D. W. Thompson, personal communication of unpublished results.

Can. J. Chem. Downloaded from www.nrcresearchpress.com by 210.87.254.105 on 09/05/12
For personal use only.

TABLE 1. Chemical shift data in the identification of the two species in solutions[a]

Solution	δ (ppm) of CH_3 groups	
	Five-coordinate	Six-coordinate
(*i*) $Cl_3Ti(dpm)$	1.38	1.28
$Cl_2Ti(dpm)_2$	—	1.25
$Cl_3Ti(dpm) + Cl_2Ti(dpm)_2$	1.38	1.29
$Cl_3Ti(dpm) + TiCl_4$	1.38	—
(*ii*) $Br_3Ti(dpm)$	1.40	1.29
$Br_2Ti(dpm)_2$	—	1.29
$Br_3Ti(dpm) + Br_2Ti(dpm)_2$	1.40	1.28
$Br_3Ti(dpm) + TiBr_4$	1.40	—
(*iii*) $Cl_3Ti(bzac)$	2.53(2.52)[b]	2.39(2.36)[b]
$Cl_2Ti(bzac)_2$	—	2.37(2.36)[b]
$Cl_3Ti(bzac) + Cl_2Ti(bzac)_2$	2.53(2.52)[b]	2.40(2.36)[b]
$Cl_3Ti(bzac) + TiCl_4$	2.60(2.52)[b]	—
$Cl_2Ti(bzac)_2 + TiCl_4$	(2.56)[b]	—
(*iv*) $Br_3Ti(bzac)$	2.48	2.38(2.30)[c]

[a]Solvent is nitrobenzene–TMS; ca. 37°C.
[b]Reference 16.
[c]In dichloromethane, ref. 18.

of these species truly represent pentacoordinate titanium(IV) complexes in solutions and, further, have questioned the validity of equilibria 1 and 2 above.

In an attempt to verify this five-coordination in titanium(IV) complexes, we have investigated the nature of the species $X_3Ti(dik)$, where X is Cl or Br and dik is bzac or dpm, in nitrobenzene solutions using the variable temperature nuclear magnetic resonance technique.

Experimental

Titanium tetrachloride (Fisher Certified Reagent), titanium tetrabromide (Alfa), and Aldrich benzoylacetone were used without further purification. Dipivaloylmethane was prepared[2] by reacting pinacolone (Aldrich) with phenyl pivalate in the presence of $NaNH_2$ in ether. The dimeric species $(X_3Ti(dik))_2$ (X = Cl, Br; dik = bzac, dpm) were synthesized from procedures reported earlier (15). Their purity was checked by nmr and infrared spectra, and by melting point determinations.[1] The corresponding six-coordinate $X_2Ti(dik)_2$ complexes were prepared by standard methods (18). Nitrobenzene (Fisher Reagent) was purified by a modified procedure of that of Taylor and Krauss (19), and stored over molecular sieves (Linde, 4A). A nmr spectrum of this solvent revealed no impurities even under very high amplification.

Syntheses, handling of compounds, and subsequent physical measurements were carried out under anhydrous conditions in an inert nitrogen atmosphere.

Infrared spectra were taken on a Perkin-Elmer 457 grating spectrophotometer as Nujol mulls between KBr windows.

Variable temperature nuclear magnetic resonance spectra were recorded in the temperature range 28–100°C with a high resolution Varian A60-A nmr spectrometer operating at 60 MHz, and equipped with a V-6040 variable temperature controller. All spectra were taken from samples in vacuum-sealed tubes. The sweep width of the spectrometer was calibrated against a standard sample of $CHCl_3$–TMS in carbon tetrachloride. Temperatures were estimated with the Van Geet (20) equations. Reported chemical shifts are believed accurate to ±0.01 ppm.

[2]We thank Prof. R. C. Fay for providing us with the recipe.

Results and Discussion

Nuclear magnetic resonance spectra for the four titanium(IV) species, $X_3Ti(dik)$, in nitrobenzene solution are depicted in Fig. 1. While conductivity and molecular weight data[1] (16) are consistent with non-ionic and monomeric five-coordinate $X_3Ti(dik)$ (X = Cl, Br; dik = bzac, dpm) complexes, the proton resonance spectra indicate two methyl proton resonances of unequal intensity. Consideration of the parentage of these resonances suggests that the species in solution are neither the dimer $(X_3Ti(dik))_2$, nor the monomer alone possessing a trigonal bipyramidal or a square pyramidal stereochemistry. The observation of two such proton signals of different intensity implies the presence of two distinct ketoenolate species. To identify these two species, an experiment was carried out in which solutions were made up containing (*i*) only the 'dimer,' (*ii*) only the corresponding six-coordinate $X_2Ti(dik)_2$, (*iii*) a mixture of the 'dimer' and $X_2Ti(dik)_2$, and (*iv*) the 'dimer' and the parent titanium tetrahalide. The results have been summarized in Table 1.

When X is Cl and dik is dpm, the methyl proton spectrum of solution *i* reveals a signal at 1.38 and one at 1.28 ppm. The latter resonance corresponds closely to the chemical shift of the time-averaged methyl signal of $Cl_2Ti(dpm)_2$. Also, the sample with the mixture 'dimer' and $Cl_2Ti(dpm)_2$ shows only two methyl group resonances with chemical shifts 1.38 and 1.29 ppm, albeit with a different intensity ratio from that of solution *i*. Moreover, the sample containing the 'dimer' and an excess of $TiCl_4$ reveals only *one* methyl proton signal at 1.38 ppm.

Can. J. Chem. Downloaded from www.nrcresearchpress.com by 210.87.254.105 on 09/05/12
For personal use only.

Can. J. Chem. Downloaded from www.nrcresearchpress.com by 210.87.254.105 on 09/05/12
For personal use only.

Analogously, in the case of $Br_3Ti(dpm)$ resonances are observed at 1.40 and 1.29 ppm; the time-averaged methyl signal for $Br_2Ti(dpm)_2$ occurs at 1.29 ppm. Addition of the six-coordinate complex to solution *i* shows signals also at 1.40 and 1.28 ppm, whereas addition of an excess of $TiBr_4$ to solution *i* quenches the upfield resonance. When X is Cl and dik is bzac, our data (Table 1) are in agreement with those reported by Thompson *et al.* (16). Interestingly, the nmr spectrum (16) of $Cl_2Ti(bzac)_2$ in nitrobenzene containing an excess of $TiCl_4$ shows only a single resonance whose chemical shift (2.56 ppm) corresponds closely to that of the downfield signal (2.53 ppm) observed for the sample containing the 'dimer' alone. Lastly, in the case of $Br_3Ti(bzac)$, the methyl nmr spectrum reveals signals at 2.48 and 2.38 ppm.

On the basis of the above data (see Table 1), the upfield resonance line in the spectrum of solution *i* is attributed to the methyl groups of the six-coordinate $X_2Ti(dik)_2$ complex, while the downfield signal is assigned to the methyl groups of the five-coordinate $X_3Ti(dik)$ species. We interpret[3] the experimental evidence in terms of the following scheme in

$$[3]\quad (X_3Ti(dik))_2 \xrightarrow{PhNO_2} 2\,X_3Ti(dik) \rightleftharpoons X_2Ti(dik)_2 + TiX_4$$

which dissolution of the dimer leads to a symmetric cleavage of the TiX_2Ti bridge bonds in the dimeric structure (15) to yield the five-coordinate complex. The latter subsequently disproportionates, probably via a rapid intermolecular ligand exchange process, to give the six-coordinate $X_2Ti(dik)_2$ and four-coordinate TiX_4 species in equilibrium with $X_3Ti(dik)$. The small resonance line (noted x) in Fig. 1 is observed for the dpm complexes only, and can be attributed neither to a solvent impurity nor to the free ligand as the methyl resonance of dipivaloylmethane occurs upfield (1.20 ppm) from the highest field signal. If this resonance were attributable to the dimer, it would indicate that the dimer is not involved in the equilibrium reaction.

Chemical evidence also lends credence to the above scheme [3]. First, the five-coordinate species can be prepared either by reacting TiX_4 with Hdik in a 1:1 molar ratio or by reacting the six-coordinate $X_2Ti(dik)_2$ complexes with TiX_4 also in a 1:1 molar ratio (12, 15). Second, a solution of $X_3Ti(dik)$ reacts with a variety of other ligands[4] (e.g., 1,3-diketones, pyridines, phosphines, etc.) to give six-coordinate species. Third, Frazer and Rimmer (21) have also reported evidence for equilibrium 4

$$[4]\quad Cl_2Sn(C_6H_9NO)_2 + SnCl_4 \rightleftharpoons 2\,Cl_3Sn(C_6H_9NO)$$

where C_6H_9NO is the quinolate anion.

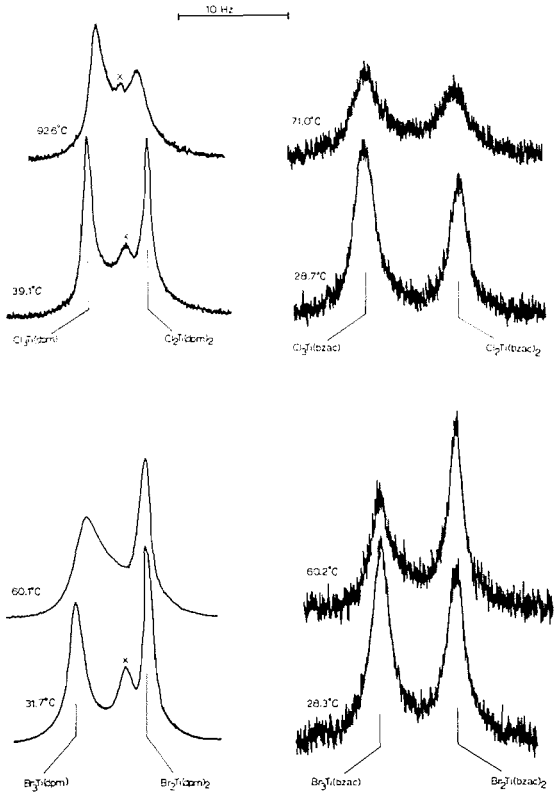

FIG. 1. The 50 Hz methyl proton resonance spectra for the $X_3Ti(dik)$ species investigated. For the significance of the small resonance denoted x in the dpm spectra, see text.

Acknowledgement

Partial support of this work from the National Research Council of Canada is gratefully appreciated.

1. R. J. H. CLARK. The chemistry of titanium and vanadium. Elsevier, New York, NY. 1968.
2. N. SERPONE and D. G. BICKLEY. Progr. Inorg. Chem. **17**, 391 (1972).

[3]A referee has suggested that the equilibrium in reaction 3 could equally be represented as a fluxional dimer breaking symmetrically to give the six- and four-coordinate species, and that the dimer merely represents an unstable intermediate state. We wish to point out, however, that to get the $X_2Ti(dik)_2$ and TiX_4 species, the dimer would have to undergo intramolecular ligand exchange *prior* to the asymmetric breakup to produce as some intermediate state a dimeric species of the type shown in equilibrium 1 (see text). Unfortunately, the solubility of the $(X_3Ti(dik))_2$ dimer precludes studies designed to distinguish between the two types of cleavage.

[4]Unpublished results from this laboratory (D. G. Bickley).

3. D. F. LEWIS and R. C. FAY. J. Am. Chem. Soc. **96**, 3843 (1974).
4. A. FELTA. Z. Chem. **7**, 158 (1967).
5. N. W. ALCOCK, M. PIERCE-BUTLER, and G. R. WILLEY. J. Chem. Soc. Dalton Trans. 707 (1976); J. Chem. Soc. Chem. Commun. 627 (1974).
6. H. HOPPE and W. HAASE. Acta Crystallogr. B**24**, 281 (1968).
7. K. WATENPAUGH and C. N. CAUGHLAN. Inorg. Chem. **5**, 1782 (1966).
8. A. K. YAMAMOTO and S. KAMBARA. J. Am. Chem. Soc. **79**, 4344 (1957).
9. D. M. PURI and R. C. MEHROTRA. J. Less-Common Met. **3**, 247 (1961); J. Less-Common Met. **3**, 253 (1961).
10. D. M. PURI and R. C. MEHROTRA. J. Less-Common Met. **5**, 2 (1963).
11. D. M. PURI, K. C. PANDE, and R. C. MEHROTRA. J. Less-Common Met. **4**, 481 (1962); J. Less-Common Met. **4**, 393 (1962).
12. D. W. THOMPSON, W. A. SOMERS, and M. O. WORKMAN. Inorg. Chem. **9**, 1252 (1970).
13. C. E. HOLLOWAY and A. E. SENTEK. Can. J. Chem. **49**, 519 (1971).
14. N. SERPONE, P. H. BIRD, D. G. BICKLEY, and D. W. THOMPSON. J. Chem. Soc. Chem. Commun. 217 (1972).
15. N. SERPONE, P. H. BIRD, A. SOMOGYVARI, and D. G. BICKLEY. Inorg. Chem. **16**, 2381 (1977).
16. D. W. THOMPSON, R. W. ROSSER, and P. B. BARRETT. Inorg. Nucl. Chem. Lett. **7**, 931 (1971).
17. E. C. ALYEA and P. H. MERRELL. Inorg. Nucl. Chem. Lett. **9**, 69 (1973).
18. N. SERPONE and R. C. FAY. Inorg. Chem. **6**, 1835 (1967).
19. E. G. TAYLOR and C. A. KRAUSS. J. Am. Chem. Soc. **69**, 1731 (1947).
20. A. L. VAN GEET. Anal. Chem. **40**, 2227 (1968); **42**, 679 (1970).
21. M. J. FRAZER and B. RIMMER. J. Chem. Soc. A, 69 (1968).

Can. J. Chem. Downloaded from www.nrcresearchpress.com by 210.87.254.105 on 09/05/12
For personal use only.

Synthesis of cyclohexapyrrolizidines: *C*-methylation of vinylogous amides

RONALD B. KELLY AND SANDRA J. ALWARD

Department of Chemistry, University of New Brunswick, P.O. Box 5050, Saint John, N.B., Canada E2L 4L5

Received September 8, 1977

RONALD B. KELLY and SANDRA J. ALWARD. Can. J. Chem. **56**, 320 (1978).

A synthesis of the cyclohexapyrrolizidines **32** and **33** is described; the structure of the latter was determined by X-ray crystallography. It is anticipated that this synthesis will serve as a model for the construction of a similar pyrrolizidine system during a projected synthesis of thelepogine **2**.

A convenient method for the *C*-methylation of cyclic vinylogous amides is also described. This procedure, which is similar to published procedures, affords high yields of methylated product and is regiospecific.

RONALD B. KELLY et SANDRA J. ALWARD. Can. J. Chem. **56**, 320 (1978).

On décrit une synthèse des cyclohexapyrrolizidines **32** et **33**; on a déterminé la structure du dernier composé par crystallographie de rayon-X. On croit que cette synthèse pourra servir de modèle dans la préparation d'un système pyrrolizidine semblable au cours d'une synthèse en voie d'élaboration de la thélépogine **2**.

On décrit aussi une méthode convenable de *C*-méthylation d'amides vinylogues cycliques. Cette méthode, qui est semblable à celles qui ont déjà été publiées, fournit de bons rendements de produit méthylé et elle est régiospécifique.

[Traduit par le journal]

The cyclohexapyrrolizidine derivative **1** represents a moiety of the novel structure assigned to the diterpenoidal alkaloid thelepogine **2** (1). For this reason we are interested in devising methods for the synthesis of such cyclohexapyrrolizidine systems. Another structural moiety of thelepogine, the

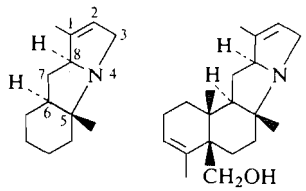

1 **2**

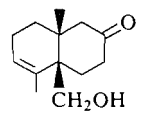

3

stereospecific synthesis of which has recently been described by us (2), is the octalone **3**. Obviously, the successful fusion of the appropriate pyrollizidine moiety onto **3** would constitute a total synthesis of thelepogine. With this in mind we undertook some model studies, substituting cyclohexanone for **3**, which were aimed at the delineation of methods for the conversion of **3** into thelepogine. We now wish to describe some aspects of this work.

Our initial approach involved the utilization of our experience with the condensation of cyclic ketones with cyclic β-amino esters (3). Such condensations afford vinylogous amides as the result of internal enamine acylations (3). Applied to the present work, this approach is illustrated in Scheme 1.

The vinylogous amide **4**, possessing the required tricyclic system, was prepared from cyclohexanone and ethyl prolinate by a procedure similar to those already described (4). We then attempted to introduce the angular methyl group by the sequence shown in Scheme 1 and thereby obtain **6**. This involved converting **4** to the iminium salt **5** by treatment with triethyloxonium fluoroborate (Meerwein's reagent (5)). The appearance of bands at 1620 and 1525 cm^{-1} attests to the successful formation of the iminium salt. The salt **5**, however, failed to undergo alkylation with either methyl lithium or methyl magnesium iodide, as demonstrated by the absence in the nmr spectrum of any signal for a methyl group. The properties of the crude intractable product are in accord with structure **7** which

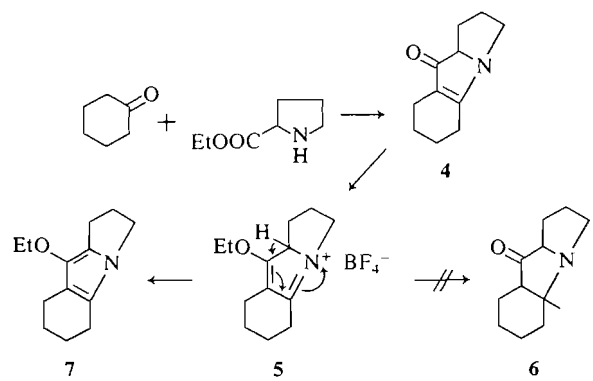

7 **5** **6**

SCHEME 1

Can. J. Chem. Downloaded from www.nrcresearchpress.com by 210.87.254.42 on 09/05/12
For personal use only.

Can. J. Chem. Downloaded from www.nrcresearchpress.com by 210.87.254.42 on 09/05/12
For personal use only.

possesses a substituted pyrrole nucleus and would likely be impervious to methylation by the procedure employed. The ir spectrum of the crude product showed bands at 1655 and 1590 cm^{-1} attributable to pyrrole double bonds. The formation of **7** from **5** can be explained in terms of abstraction of the methine proton next to the nitrogen atom by the reagents (methyl lithium or methyl magnesium iodide) followed by bond rearrangement as indicated in **5**. Thus, the inherent basicity of the methylating agents precluded the methylation of **4** to give **6**.

The failure of **4** to undergo methylation by the sequence just described (Scheme 1) is in direct contrast to the behavior of its analog **8** (*3b*, see Experimental) when subjected to the same sequence (Scheme 2). Treatment of **8** with the Meerwein reagent and subsequent treatment of the resulting iminium salt **9** with methyl lithium afforded the enol ether **10** in 81% yield. A three-proton singlet in the nmr spectrum of **10** revealed the presence of the angular methyl group. Treatment of **10** with ethanolic hydrochloric acid and purification of the product through the picrate afforded **11** (ν_{max} 1700 cm^{-1}; nmr δ 0.75 (s, 3H, angular CH_3) in 74% yield. The methylation of **8** in good yield, as described above, and reports (6) of similar alkylations demonstrates the usefulness of this approach for the *C*-alkylation of vinylogous amides.

Despite the failure to methylate **4**, it was hoped that this enamino ketone would yet prove to be a useful intermediate and that it might be transformed, by a different approach, into **1** or stereoisomers thereof. To this end, it was envisaged that **4** could be reduced to the amine **15** which might then be oxidized to the iminium salt **16**. Methylation of the latter would afford **17** which might be oxidized to provide functionality for the introduction of the vinylic methyl group (Scheme 3).

The amine **15** was obtained without difficulty by the following sequence (Scheme 3). The enamino ketone **4** was reduced with sodium in liquid ammonia to the amino ketone **12** (ν_{max} 1740 cm^{-1})

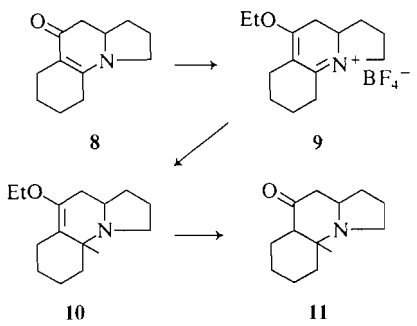

SCHEME 2

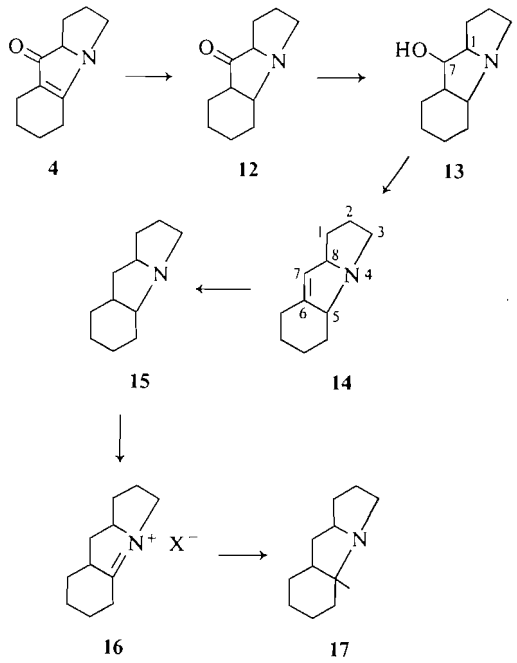

SCHEME 3

which was reduced quantitatively to the crystalline amino alcohol **13** (ν_{max} 3050 cm^{-1} (hydrogen bonded OH); nmr δ 3.58 (m, 1H, proton at C-7)). Dehydration of **13** gave the olefin **14** (ν_{max} 1660 cm^{-1}; nmr δ 5.18 (s, 1H, vinylic proton)). The assignment of the double bond in **14** to the 6–7 position rather than the 7–8 position is based on the absence of bands attributable to a conjugated enamine in the ir spectrum.

Hydrogenation of **14** over a platinum catalyst in ethanol containing hydrochloric acid afforded, quantitatively, the hydrochloride of **15** from which the free amine was obtained. The ir and nmr spectra of **15** provided evidence for the absence of an olefinic bond. Unfortunately, we were unable to satisfactorily oxidize **15** to the iminium salt **16** and were therefore obliged to abandon this approach.

Eventually, application of the sequence outlined in Scheme 4 resulted in a synthesis of **32** and **33**, stereoisomers of **1**. The fact that these two isomers, rather than **1** and its C_8 epimer, were the end products of the model studies is the consequence of the arbitrary choice of the intermediate *cis*-isomer **22** rather than the *trans*-isomer **21**. This choice was made under circumstances whereby we were unable to distinguish between the two intermediates. It was only after completion of the model synthesis that X-ray crystallographic studies[1] on the picrolonate of one of the end products revealed that it had

[1]P. White and E. Stanley. To be published.

Can. J. Chem. Downloaded from www.nrcresearchpress.com by 210.87.254.42 on 09/05/12
For personal use only.

stereostructure **33** and that we had therefore chosen the *cis*-isomer **22**. The structures assigned to **21**, **22** and all succeeding compounds in Scheme 4 are based on structure **33**.

It was felt that, with the completion of the synthesis of **32** and **33**, the model studies had served their purpose in that the sequence outlined in Scheme 4 could as well be applied to the intermediate **21**. In the latter case the expected end products would be **1** and its C_8 epimer.

The sequence outlined in Scheme 4 was carried out as follows. The hexahydroindole **18**, prepared from cyclohexanone by a published procedure (7), was converted into the iminium salt **19** by treatment with benzyl bromide. Treatment of **19** with methyl magnesium iodide afforded the angularly methylated perhydroindole **20**, subsequently found to be a mixture of *cis*- and *trans*-isomers. A three-proton singlet in the nmr spectrum at δ 1.07 attested to the presence of the angular methyl group in **20**.

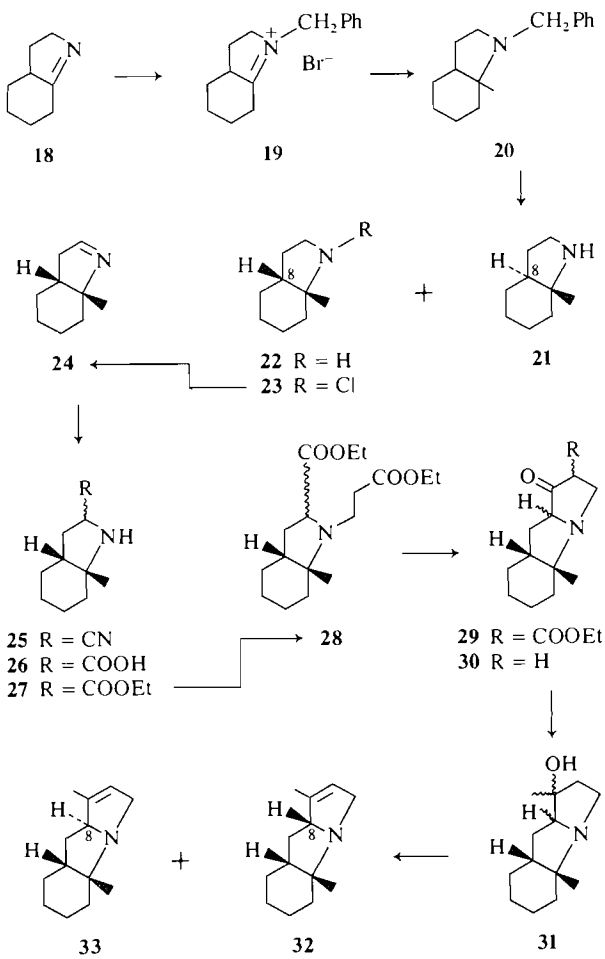

SCHEME 4

Removal of the benzyl group from **20** by hydrogenolysis afforded a mixture of two isomeric amines, **21** and **22**. The presence of two three-proton singlets at δ 1.00 and 1.12 in the nmr spectrum of the hydrogenolysis product revealed the presence of the two amines and showed that **20** was also a mixture of two isomers. Fractional crystallization of the hydrochlorides derived from the hydrogenolysis product left an essentially pure hydrochloride (40%) in the mother liquors which was later shown to be the hydrochloride of **22** (*vide supra*).

The *cis*-amine **22** was transformed, via the chloroamine **23** into the imine **24**. Cyanation of **24** afforded the epimeric amino nitriles **25**. The presence of epimers in the cyanation product was revealed by the appearance of two cyano bands at 2250 and 2200 cm^{-1} in the ir spectrum and two methyl singlets at δ 1.13 and 1.20 in the nmr spectrum.

Hydrolysis of **25** to the corresponding acid **26** followed by esterification afforded the amino ester **27**, also as a mixture of epimers (two methyl singlets at δ 1.12 and 1.18). Condensation of the epimeric mixture **27** with ethyl acrylate afforded a mixture of epimeric diesters, **28**. Cyclization of **28** afforded the keto ester **29**, which after saponification and decarboxylation of the acid gave the epimeric amino ketones **30**. Treatment of **30** with methyl lithium gave a mixture of isomeric alcohols **31** the nmr spectrum of which displayed three methyl singlets at δ 1.17, 1.27 and 1.30.

Finally, dehydration of the mixture of alcohols **31** followed by chromatography of the product on alumina afforded two amines one of which was shown, by X-ray crystallography (*vide supra*), to possess stereostructure **33**. The other amine could therefore be assigned stereostructure **32**.

Experimental

Instrumentation, Methods, and Materials

Melting points were determined on a Fisher-Johns apparatus and are uncorrected. The ir spectra were recorded on a Perkin-Elmer model 237B spectrophotometer and uv spectra were determined with a Perkin-Elmer Coleman model 124 instrument. The nmr spectra were recorded with a Varian T-60 instrument; chemical shifts were expressed in ppm (δ values) downfield from the signal for tetramethylsilane which is used as an internal standard.

Petroleum ether refers to the fraction with boiling point range 30–60°C.

Brine refers to a saturated solution of sodium chloride.

Enamino Ketone **4** *(cf. ref. 4)*

A solution of 2.0 g of ethyl prolinate, 1.6 g of cyclohexanone and a few crystals of *p*-toluenesulfonic acid in 18 ml of dry benzene was refluxed, under nitrogen, for 68 h. Water produced was absorbed by molecular sieve (Linde, type 4A) in a small Soxhlet apparatus. The appearance and gradual increase in intensity of a peak at 334 nm in the uv spectrum was observed. Evaporation of the solvent and distillation of the

Can. J. Chem. Downloaded from www.nrcresearchpress.com by 210.87.254.42 on 09/05/12
For personal use only.

residue *in vacuo* afforded 1.73 g (70%) of **4** as an oil, bp 136–138°C (0.9 Torr), (lit. (*4a*) bp 150°C (2.5 Torr)); λ_{max} (EtOH): 334 nm (ε 9000); ν_{max} (film): 1670 and 1595 cm^{-1} (vinylogous amide); nmr (CCl_4) δ: 3.07 (m, 2H, N—CH_2), 3.60 (m, 1H, N—CH); *m/e* calcd. for $C_{11}H_{15}NO$: 177; found: 177.

Attempted Formation of Amino Ketone 6

A solution of 177 mg of **4** (4) in 2 ml of methylene chloride was added, under nitrogen, to a solution of 190 mg of Meerwein's reagent (5) in 7 ml of methylene chloride at room temperature. The mixture was stirred for 1 h and left to stand overnight. The solvent was evaporated *in vacuo* to give the iminium salt **5**, ν_{max} (film) 1620 and 1525 cm^{-1} (conjugated iminium salt).

A solution of the iminium salt in 5 ml of ether was cooled in an ice bath and treated with 2 ml of an ether solution of 2.2 *M* methyl lithium. The mixture was stirred at room temperature for 5 h and then the excess methyl lithium was destroyed with 15 ml of saturated aqueous ammonium chloride. Work-up in the usual manner with ether, 1 *M* ammonium hydroxide and brine gave 183 mg of intractable oil with spectral properties indicative of **7**, ν_{max} (film): 1655 and 1590 cm^{-1} (pyrrole double bonds); nmr (CCl_4) δ: 1.22 (t, J = 6.5 Hz, 3H, OCH_2—CH_3) and 3.63 (q, J = 6.5 Hz, OCH_2—CH_3).

The same results were obtained when the preceding reaction was repeated employing methylmagnesium iodide as the alkylating agent.

Enamino Ketone 8

A solution of 2.35 g of ethyl 2-pyrrolidineacetate, 0.63 ml of trifluoroacetic acid, 2.2 g of cyclohexanone, and 47 ml of dry toluene was refluxed under a nitrogen atmosphere for 28 h. Water formed during the reaction was absorbed by Linde, type 4A, molecular sieve in a Soxhlet apparatus. The solution was worked up in the usual manner with benzene, saturated sodium bicarbonate solution, and water. The benzene extracts were dried over anhydrous potassium carbonate and evaporated *in vacuo* to give 3.06 g of oil. Crystallization from ether – petroleum ether yielded 1.83 g (64%) of **8**, mp 48–49°C; λ_{max} EtOH: 343 nm (ε 14 800); ν_{max} ($CHCl_3$): 1603 and 1540 cm^{-1} (vinylogous amide); nmr ($CDCl_3$) δ: 3.45 (m, 3H, N—CH_2 and N—CH). *Anal.* calcd. for $C_{12}H_{17}NO$: C 75.30, H 8.95, N 7.32; found: C 75.48, H 8.56, N 7.15.

Enol Ether 10 and Amino Ketone 11

The enamino ketone **8** (573 mg) was converted, via the iminium salt **9**, to the enol ether **10** by the same procedure as was attempted in the case of the enamino ketone **4** (*vide supra*). Utilization of methyl lithium as the alkylating agent gave 570 mg of **10** (81%) as an oil, ν_{max} (film): 1670 cm^{-1} (olefin); nmr (CCl_4) δ: 0.93 (s, 3H, angular methyl), 1.13 (t, J = 6.0 Hz, 3H, OCH_2—CH_3) and 3.55 (q, J = 6.0 Hz, 2H, OCH_2—CH_3).

A solution of 1.1 g of **10**, 66 ml of ethanol and 45 ml of 1 *M* aqueous hydrochloric acid was refluxed for 4 h. The ethanol was evaporated *in vacuo* and the aqueous solution worked up in the usual manner with methylene chloride, 1 *M* ammonium hydroxide and brine to give 650 mg (74%) of **11** as an oil, ν_{max} film): 1700 cm^{-1} (ketone); nmr (CCl_4) δ: 0.75 (s, 3H, angular methyl).

The amino ketone **11** was analysed as its picrate, mp 225°C. *Anal.* calcd. for $C_{19}H_{24}N_4O_8$: C 52.29, H 5.54, N 12.84; found: C 52.16, H 5.42, N 12.74.

Amino Ketone 12

A solution of 2.01 g of **4** (4) in 50 ml of dry tetrahydrofuran was added dropwise to 0.8 g of lithium in 280 ml of liquid ammonia. After stirring on a Dry Ice – acetone bath for 2 h, excess reagent was destroyed by the addition of solid ammonium chloride and the ammonia was allowed to evaporate at room temperature. To the residue was added 500 ml of ice water and the resulting aqueous solution was acidified with 1 *N* hydrochloric acid, washed with ether, rendered alkaline with 1 *M* sodium carbonate and extracted with methylene chloride. The methylene chloride extracts were evaporated and the resulting residue was converted in the usual manner to a crystalline picrate derivative. The amino ketone **12** (1.07 g) was obtained from the picrate as an oil, ν_{max} (film): 1740 cm^{-1}, and was analysed as the picrate, mp 202°C. *Anal.* calcd. for $C_{17}H_{20}N_4O_8$: C 50.00, H 4.94, N 13.72; found: C 50.32, H 4.95, N 13.72.

Amino Alcohol 13

A mixture of 610 mg of **12**, 750 mg of lithium aluminum hydride, and 120 ml of ether was refluxed under a nitrogen atmosphere overnight. The excess lithium aluminum hydride was destroyed with aqueous sodium sulfate solution and the resulting mixture was stirred for 1 h. Then anhydrous sodium sulfate was added and the mixture was stirred for another 30 min. The residue was removed by filtration and washed with methylene chloride. The filtrate was evaporated *in vacuo* to give 616 mg (100%) of the amino alcohol **13**, mp 114–117°C; ν_{max} (Nujol): 3050 cm^{-1} (OH); nmr (DMSO) δ: 3.58 (m, 1H, *CH*—OH) and 4.30 (broad singlet, 1H, hydroxyl). *Anal.* calcd. for $C_{11}H_{19}NO$: C 72.88, H 10.56, N 7.73; found: C 72.42, H 10.49, N 7.78.

Enamine 14

The alcohol (**13**, 2.21 g) was dissolved in 65 ml pyridine and cooled in an ice bath. Then 5.2 ml of phosphorous oxychloride was added and the mixture was kept in the dark at room temperature for 20 h. The solution was then added to 200 ml of ice water and stirred for 15 min. After basifying with 1 *M* sodium carbonate, the resulting aqueous solution was worked up in the usual manner with methylene chloride and 1 *M* sodium carbonate to give 1.356 g (68%) of **14** as an oil, ν_{max} (film): 1660 cm^{-1} (olefin); nmr ($CDCl_3$) δ: 5.18 (m, 1H, vinylic proton).

The enamine **14** was analysed as its picrate, mp 165–167°C. *Anal.* calcd. for $C_{17}H_{20}N_4O_7$: C 52.03, H 5.15, N 14.28; found: C 52.20, H 5.36, N 14.52.

Amine 15

A mixture of 106 mg of **14** and 80 mg of platinum oxide, in 10 ml of ethanol with a few drops of hydrochloric acid, was hydrogenated at 4 atm pressure for 3 h. The mixture was filtered to remove the catalyst and the catalyst was washed with methanol. Evaporation of the filtrate *in vacuo* gave 140 mg (100%) of the hydrochloride of **15**, mp 195–200°C. *Anal.* calcd. for $C_{11}H_{20}NCl$: C 65.47, H 10.01, N 6.96, Cl 17.57; found: C 65.31, H 9.93, N 6.88, Cl 17.66.

Extraction of an alkaline sodium carbonate solution of the hydrochloride with methylene chloride gave 98 mg of the amine **15** as a liquid.

Benzyl Amine 20

A solution of 1.23 g of imine **18** (7), 6.13 g of benzyl bromide, and 20 ml of ethanol was refluxed under a nitrogen atmosphere for 90 min. The solvent was evaporated *in vacuo* and the residue washed with dry ether. The residue (**19**) was then treated dropwise with 100 ml of a 1 *M* ether solution of methyl magnesium iodide and the resulting mixture was refluxed for 40 h.

The reaction mixture was then cooled and a saturated solution of ammonium chloride was added. The aqueous phase was diluted with 300 ml of brine, basified with ammonium hydroxide and then worked up in the usual manner

Can. J. Chem. Downloaded from www.nrcresearchpress.com by 210.87.254.42 on 09/05/12
For personal use only.

with ether and brine to give 2.114 g of oil. The oil was purified by column chromatography using grade II neutral alumina with hexane as solvent. This gave 1.513 g (66%) of **20** as an oil, ν_{max} (film): 3000 to 3100, 1600 to 2000, and 700 to 800 cm^{-1} (multiple aromatic bands); nmr ($CDCl_3$) δ: 1.07 (s, 3H, angular methyl), 3.37 and 3.58 (doublets, J = 12 Hz, 1H each N—CH_2—Ph) and 7.20 (m, 5H, aromatic protons).

The benzyl amine **20** was analysed as its hydrobromide, mp 179–180°C. *Anal.* calcd. for $C_{16}H_{24}NBr$: C 61.94, H 7.80, N 4.52; found: C 61.88, H 7.98, N 4.33.

Amine 21

A mixture of 2.17 g of **20**, 800 mg of 10% palladium-on-charcoal and 40 ml of acetic acid was hydrogenated at 4 atm pressure for 3 days. The mixture was filtered to remove the catalyst and the catalyst was washed with methanol. The combined filtrates were treated with 1.5 ml of concentrated hydrochloric acid and the solvent was evaporated *in vacuo*. Acid–base work-up of the residue with ether gave 1.185 g (90%) of the free amine as a mixture of *cis*- and *trans*-isomers **21** and **22**. The nmr indicated an approximate ratio of 3:2 of *cis*:*trans* on the basis of the angular methyl signal which occurs at δ 1.12 in the case of the *cis*-isomer **22** and at δ 1.00 in the case of the *trans*-isomer **21**.

Fractional crystallization of the mixture of hydrochlorides from methylene chloride and ether and subsequent freeing of the amine resulted in the isolation from the mother liquors of the *cis*-amine **22** (40%) as an oil; ν_{max} (film): 3250 cm^{-1} (NH); nmr ($CDCl_3$) δ: 1.12 (s, 3H, angular methyl), 2.40 (s, 1H, NH) and 3.00 (t, J = 6.0 Hz, 2H, N—CH_2).

The amine **22** was analysed as its picrate, mp 216–219°C. *Anal.* calcd. for $C_{15}H_{20}N_4O_7$: C 48.91, H 5.47, N 15.21; found: C 48.89, H 5.53, N 15.17.

Amino Nitrile 25

An ice-cold solution of 112 ml of 0.67 *N* aqueous sodium hypochlorite was treated dropwise with 5.2 g of the *cis*-amine **22** in 7.5 ml of 5 *M* acetic acid. The resulting mixture was immediately extracted with ether and the ether was dried and evaporated *in vacuo* to give the chloroamine **23**.

The chloroamine **23** was added to a hot solution of 2.5 g of potassium hydroxide in 25 ml of 95% ethanol. The mixture was refluxed for 20 min and then stirred at room temperature for 1 h. Water (12 ml) and 4 g of potassium cyanide were added and the reaction mixture was treated dropwise with 82 ml of 1 *N* hydrochloric acid, while cooling in an ice bath. The solution was stirred overnight at room temperature, made alkaline with 2 *N* sodium hydroxide and extracted with methylene chloride. Evaporation of the methylene chloride extracts gave 6 g of oil which was purified by column chromatography on grade III basic alumina with petroleum ether – ether as solvent. This yielded 1.938 g (32%) of the amino nitrile **25** as a mixture of epimers, ν_{max} (film): 3360 (NH), 2250 and 2200 cm^{-1} (CN); nmr ($CDCl_3$) δ: 1.13 and 1.20 (two singlets, 3H, angular methyls of two isomers), 4.03 (t, J = 6.5 Hz, 1H, methine next to nitrogen).

Amino Ester 27

The amino nitrile **25** (1.85 g) was refluxed in 30 ml of 6 *N* hydrochloric acid for 6 h. The solvent was evaporated *in vacuo* to give 3 g of the hydrochloride of the amino acid **26** which was dissolved in 150 ml of ethanol. The alcoholic solution was saturated with hydrogen chloride gas with cooling on an ice bath. The reaction solution was left for 3 h at room temperature and the solvent was evaporated *in vacuo* to give 2.92 g of the hydrochloride of **27**. The amine was freed from its hydrochloride to give 2.4 g (100%) of the amino ester **27**, ν_{max} (film): 3350 (NH) and 1730 cm^{-1} (ester); nmr ($CDCl_3$) δ: 1.12 and 1.18 (two singlets, 3H, angular methyls of two isomers), 1.27 (t, J = 7.0 Hz, 3H, OCH_2—CH_3), 3.83 and 4.16 (q, J = 7.0 Hz, 2H, OCH_2—CH_3).

The amino ester **27** was analysed as its picrate, mp 139–145°C. *Anal.* calcd. for $C_{18}H_{24}N_4O_9$: C 49.09, H 5.49, N 12.72; found: C 49.17, H 5.73, N 12.80.

Amino Ketone 30

A solution of 2.0 g of **27** and 4 ml of ethyl acrylate was heated in a sealed tube at 135°C for 20 h. Acid–base work-up of the product with ether gave 2.22 g (75%) of the amino diester **28** as an oil, ν_{max} (film): 1730 cm^{-1} (ester); nmr ($CDCl_3$) ca. δ: 1.27 (two triplets, J = 7.0 Hz, 3H each, OCH_2—CH_3) and 4.07 and 4.13 (two quartets, J = 7.0 Hz, 2H each, OCH_2—CH_3).

A solution of 700 mg of 57% sodium hydride (oil dispersion) in 35 ml of toluene, under a nitrogen atmosphere, was treated dropwise with 2.1 g of **28** in 35 ml of toluene. The solution was heated at 60°C for 5 h. Then the reaction mixture was extracted with 70 ml of 1 *N* hydrochloric acid and two 35-ml portions of water. The combined aqueous phases were then refluxed for 3 h with 98 ml of a concentrated aqueous solution of hydrochloric acid. Evaporation of the solvent *in vacuo* and trituration of the residue with chloroform gave 1.185 g (76%) of the hydrochloride of the amino ketone **30**.

Extraction of an aqueous alkaline solution of the hydrochloride with ether and evaporation of the extract gave the amino ketone **30**, ν_{max} (film): 1740 cm^{-1} (ketone); nmr ($CDCl_3$) δ: 1.12 (s, 3H, angular methyl), 3.15 (m, 2H, N—CH_2), and 3.63 (m, 1H, N—CH).

The amino ketone **30** was analysed as its picrolonate, mp 156–157°C. *Anal.* calcd. for $C_{22}H_{27}N_5O_6$: C 57.76, H 5.95, N 15.31; found: C 57.37, H 6.03, N 15.36.

Amines 32 and 33

An ice-cold solution of 10 ml of 1.5 *M* methyl lithium (ether solution) in 10 ml of tetrahydrofuran, under a nitrogen atmosphere, was treated dropwise with 400 mg of the hydrochloride of **30** in 20 ml of tetrahydrofuran. The reaction mixture was stirred at room temperature for 22 h. The excess methyl lithium was destroyed with 16 ml of 1 *N* hydrochloric acid and the solvent was evaporated *in vacuo*. The residue was basified with 10 *N* sodium hydroxide and the solution was extracted continuously with methylene chloride for 3 h. The extract was evaporated *in vacuo* to give 358 mg (98%) of amino alcohol **31** as an oil, ν_{max} (film): 3400 cm^{-1} (OH); nmr ($CDCl_3$) δ: 1.17, 1.27 and 1.30 (three singlets, 3H, angular methyls of isomers), 1.73 (s, 1H, hydroxyl proton), 2.80 (m, 2H, N—CH_2) and 3.40 (m, 1H, N—CH).

An ice-cold solution of 500 mg of alcohol **31** in chloroform (5 ml) was treated with phosphorous pentachloride (1.5 g). The reaction mixture was refluxed for 1 h. Acid–base work-up with 1 *N* hydrochloric acid, 10 *N* sodium hydroxide, and methylene chloride gave 381 mg of an oil. Purification of the product by column chromatography on grade II basic alumina (employing petroleum ether, benzene, and ether as solvents) yielded the amino olefins **32** and **33**.

The faster moving isomer **32** (48 mg) was isolated as an oil, ν_{max}: 1650 cm^{-1} (olefin); nmr ($CDCl_3$) δ: 1.18 (s, 3H, angular methyl), 1.70 (d, J = 2 Hz, 3H, vinylic methyl) and 4.88 (m, 1H, vinylic proton); *m/e* calcd. for $C_{13}H_{21}N$: 191; found: 191.

The slower moving isomer **33** (73 mg) was also isolated as an oil; ν_{max} (film): 1640 cm^{-1} (olefin); nmr ($CDCl_3$) δ: 1.12 (s, 3H, angular methyl), 1.68 (d, J = 2.0 Hz, 3H vinylic methyl), 3.57 (m, 2H, N—CH_2), 4.13 (m, 1H, N—CH) and 5.22 (m, 1H, vinylic proton).

The amine **33** was analysed as its picrolonate, mp 222–

225°C. *Anal.* calcd. for $C_{23}H_{29}N_5O_5$: C 60.64, H 6.42, N 15.38; found: C 60.47, H 6.56, N 15.40.

Acknowledgements

Financial assistance from the National Research Council of Canada in the form of a grant to R.B.K. and a Postgraduate Scholarship to S.J.A. is gratefully acknowledged. The authors also thank Drs. P. White and E. Stanley, University of New Brunswick, for X-ray crystallographic studies and Dr. H-K. Hung for the preparation of compounds **8** and **11**.

1. J. FRIDRICHSON and A. M. MATHIESON. Tetrahedron Lett. **26**, 18 (1960): W. D. CROW. Aust. J. Chem. **15**, 159 (1962).
2. R. B. KELLY, S. J. ALWARD, and J. ZAMECNIK. Can. J. Chem. **53**, 2441 (1975).
3. (*a*) R. B. KELLY, B. A. BECKETT, I. MUMTAZ, E. STANLEY, and P. S. WHITE. Can. J. Chem. **54**, 1512 (1976); (*b*) M. I. MUMTAZ, M.Sc. Thesis, University of New Brunswick, Saint John, N.B. (1974).
4. (*a*) K. HIROI, K. ACHIWA, and S. YAMADA. Chem. Pharm. Bull. **20**, 246 (1972); (*b*) P. W. HICKMOTT and K. N. WOODWARD. J. Chem. Soc. Perkin Trans. I, 904 (1976).
5. H. MEERWEIN. Org. Synth. **46**, 113 (1966).
6. M. E. KUEHNE. Synthesis, 510 (1970) and references cited.
7. B. BELLEAU. Can. J. Chem. **35**, 651 (1957).

Can. J. Chem. Downloaded from www.nrcresearchpress.com by 210.87.254.42 on 09/05/12
For personal use only.

Synthetic routes to nucleoside analogs of *N*-substituted 1,3-thiazolidines

MASAHARU IWAKAWA, B. MARIO PINTO, AND WALTER A. SZAREK[1]

Department of Chemistry, Queen's University, Kingston, Ont., Canada K7L 3N6

Received July 4, 1977

MASAHARU IWAKAWA, B. MARIO PINTO, and WALTER A. SZAREK. Can. J. Chem. **56**, 326 (1978).

Nucleoside analogs, namely 6-benzamido-9-(3-benzoyl-4(*R*)-methoxycarbonyl-2,2-dimethylthiazolidin-5(*S*)-yl)-9*H*-purine (**7**) and 6-chloro-9-[(3-benzoyl-2,2-dimethylthiazolidin-4(*R*)-yl)-methyl]-9*H*-purine (**8**), were obtained from 3-benzoyl-5(*S*)-benzoyloxy-4(*R*)-methoxycarbonyl-2,2-dimethylthiazolidine (**23**) and 3-benzoyl-4(*R*)-hydroxymethyl-2,2-dimethylthiazolidine (**24**), respectively, the former, by treatment with 6-benzamidochloromercuripurine and titanium tetrachloride in 1,2-dichloroethane and the latter, by treatment with 6-chloropurine, triphenylphosphine, and diethyl azodicarboxylate in tetrahydrofuran. Compound **23** was obtained from 3-benzoyl-4(*R*)-methoxycarbonyl-2,2-dimethylthiazolidine (**13**) by treatment with benzoyl peroxide in refluxing benzene whereas compound **24** was obtained from **13** by borohydride reduction. The stereochemistry of the isomeric sulfoxides **18***a* and **18***b*, obtained from **13** by treatment with *m*-chloroperbenzoic acid, was assigned by means of ^{1}Hmr spectroscopy. Reaction of the sulfoxides **18***a* and **18***b* under the Pummerer-reaction conditions afforded the rearranged product, 4-benzoyl-3(*R*)-methoxycarbonyl-5-methyl-3,4-dihydro-2*H*-1,4-thiazine (**20**). The chiral shift reagent, tris-[3-(trifluoromethylhydroxymethylene)-*d*-camphorato]europium(III), was used to confirm the enantiomeric purity of the key intermediates and the product nucleosides. The carbon-13 nmr spectra of the key compounds are reported.

MASAHARU IWAKAWA, B. MARIO PINTO et WALTER A. SZAREK. Can. J. Chem. **56**, 326 (1978).

On a pu obtenir des analogues de nucléosides, soit la benzamido-6[benzoyl-3 méthoxycarbonyl-4(*R*) diméthyl-2,2 thiazolidinyl-5(*S*)]-9 9*H* purine (**7**) et la chloro-6[(benzoyl-3 diméthyl-2,2 thiazolidinyl-4(*R*))méthyl]-9 9*H* purine (**8**), en faisant réagir d'une part la benzoyl-3 benzoyloxy-5(*S*) méthoxycarbonyl-4(*R*) diméthyl-2,2 thiazolidine (**23**) avec la benzamido-6 dichloro mercuripurine et le tétrachlorure de titane dans le dichloro-1,2 éthane et d'autre part la benzoyl-3 hydroxyméthyl-4(*R*) diméthyl-2,2 thiazolidine (**24**) avec la chloro-6 purine, la triphénylphosphine et l'azodicarboxylate de diéthyle dans le tétrahydrofuranne. On a obtenu le composé **23** à partir de la benzoyl-3 méthoxycarbonyl-4(*R*) diméthyl-2,2 thiazolidine (**13**) par réaction du peroxyde de benzoyle dans le benzène au reflux alors que l'on a obtenu le composé **24** à partir de **13** par réduction avec du borohydrure. On a attribué la stéréochimie des sulfoxydes isomères **18***a* et **18***b*, obtenus à partir de **13** par réaction avec l'acide *m*-chloroperbenzoique, en se basant sur des données de spectroscopie rmn ^{1}H. La réaction des sulfoxydes **18***a* et **18***b* dans des conditions de la réaction de Pummerer fournit un produit de réarrangement, le benzoyl-4 méthoxycarbonyl-3(*R*) méthyl-5 dihydro-3,4 2*H* thiazine-1,4 (**20**). On a utilisé le tris[(trifluorométhylhydroxyméthylène-3) *d*-camphorato] europium(III) pour confirmer la pureté d'énantiomère des intermédiaires clés et des nucléosides obtenus comme produits. On rapporte les spectres rmn ^{13}C des composés clés.

[Traduit par le journal]

Introduction

An active area of research in this laboratory has been the synthesis of novel nucleoside analogs in which the carbohydrate moiety has been replaced with a variety of heterocyclic systems. Thus far, we have reported the synthesis (1, 2) and conformational analysis (3) of nucleoside-base derivatives of six-membered heterocycles, namely 1,4-oxathiane (**1** and **2**), 1,4-dithiane (**3**), 1,4-dioxane (**4**), 1-oxa-4-azacyclohexane (**5**), and 1-thia-4-azacyclohexane (**6**); some of these compounds have exhibited anticancer activity.[2] We now wish to report the synthesis of nucleoside analogs containing a five-membered heterocyclic ring, namely 6-benzamido-9-(3-benzoyl-4(*R*)-methoxycarbonyl-2,2-dimethylthiazolidin-5-(*S*)-yl)-9*H*-purine (**7**) and 6-chloro-9-[(3-benzoyl-2,2-dimethylthiazolidin-4(*R*)-yl)-methyl]-9*H*-purine (**8**) from the amino-acid precursor, L-cysteine. It is noteworthy that thiazolidine derivatives having diazo ketone and chloro ketone functions have been investigated as potential antitumor agents (5). Carbon-13 magnetic resonance (Cmr) and proton magnetic resonance (^{1}Hmr) spectroscopic data of all intermediates and product nucleosides are also reported in this paper; these data have been employed for proof of structure and assignment of stereochemistry. We also report the use of the chiral shift reagent, tris-[3-(trifluoromethylhydroxymethylene)-

[1]Author to whom inquiries should be addressed.

[2]W. A. Szarek, D. M. Vyas, B. M. Pinto, and A. Bloch. Unpublished results.

Can. J. Chem. Downloaded from www.nrcresearchpress.com by 210.87.254.105 on 09/05/12
For personal use only.

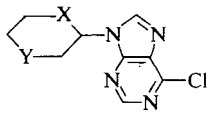

1 X = O, Y = S
2 X = S, Y = O
3 X = Y = S
4 X = Y = O
5 X = O, Y = N—Bz
6 X = S, Y = N—Bz

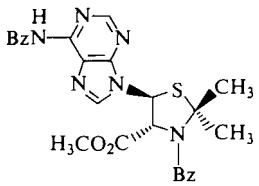

7

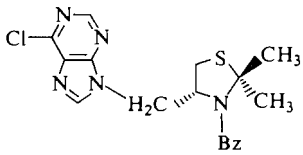

8

d-camphorato]europium(III), in the confirmation of enantiomeric purity of the key intermediates and the product nucleoside analogs.

Results and Discussion

Commercially available L-cysteine hydrochloride monohydrate (**9**) was readily converted into 2,2-dimethyl-4(*R*)-carboxythiazolidine hydrochloride (**10**) (see Scheme 1) by condensation with acetone (6). Interestingly, the benzoylation of compound **10** yielded results that were dependent on the amount of pyridine used in the reaction. Thus, treatment of **10** with benzoyl chloride in 200 equiv. of pyridine and subsequent methylation of the product **11** with diazomethane (7) afforded 3-benzoyl-4(*R*)-methoxycarbonyl-2,2-dimethylthiazolidine (**13**), whereas treatment of **10** with benzoyl chloride in chloroform containing 2 equiv. of pyridine and subsequent methylation of the product **12** with diazomethane afforded a racemic mixture (**14**) of the 4(*R*) and 4(*S*) isomers. It would appear that racemization at C-4 of **10** is a consequence of an equilibrium reaction involving deprotonation and protonation at C-4, possibly by means of an elimination–addition mechanism. The results also seem to suggest that the reaction involving abstraction of H-4 in the zwitterion formed from **10** and the benzoylation reaction are competitive, parallel reactions, although the former process, namely, the abstraction of the hydrogen α to the carboxylate anion, seems unlikely. Nevertheless, the observation that the benzoylation of **10** in an excess of pyridine proceeds with predominant retention of configuration at C-4 suggests that, in this case, the rate of the benzoylation reaction is greatly enhanced relative to the rate of the reaction involving loss of H-4. To gain some understanding of the dependence of the stereochemical outcome of this reaction on the type of system involved, 4(*R*)-carboxythiazolidine hydrochloride (**15**), prepared from L-cysteine hydrochloride monohydrate (**9**) by treatment with formaldehyde (8), was subjected to each of the benzoylation conditions (see Scheme 2). Thus, treatment of **15** with benzoyl chloride in pyridine and subsequent methylation of the product afforded optically active 3-benzoyl-4(*R*)-(methoxycarbonyl)thiazolidine (**16**). Similarly, the optically active compound **16** was obtained upon treatment of **15** with benzoyl chloride in aqueous sodium bicarbonate solution. However,

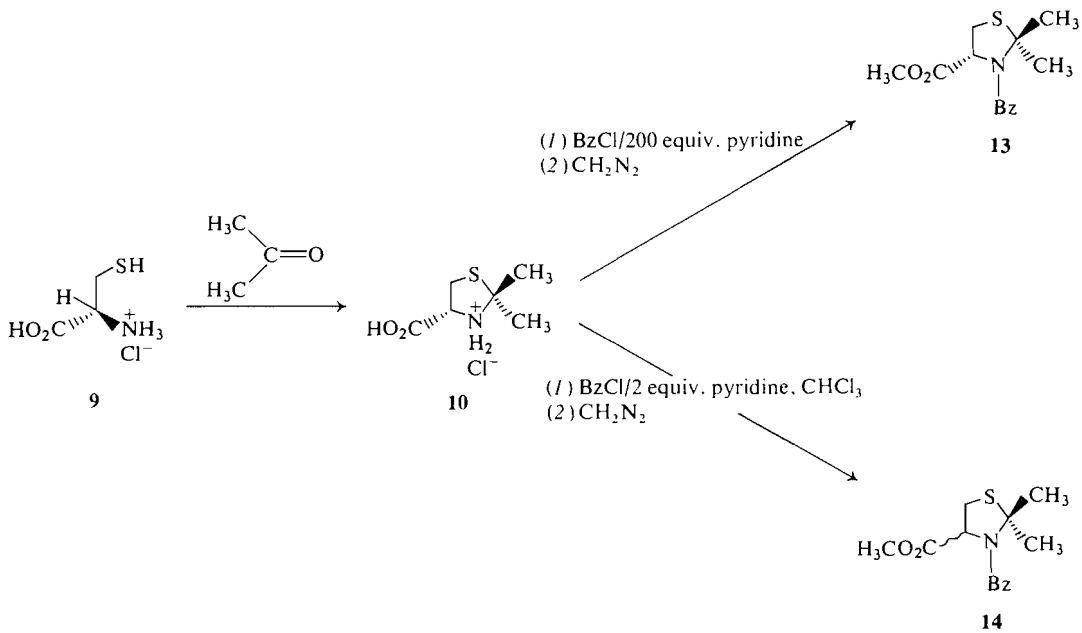

9 **10** **13** **14**

SCHEME 1

Can. J. Chem. Downloaded from www.nrcresearchpress.com by 210.87.254.105 on 09/05/12
For personal use only.

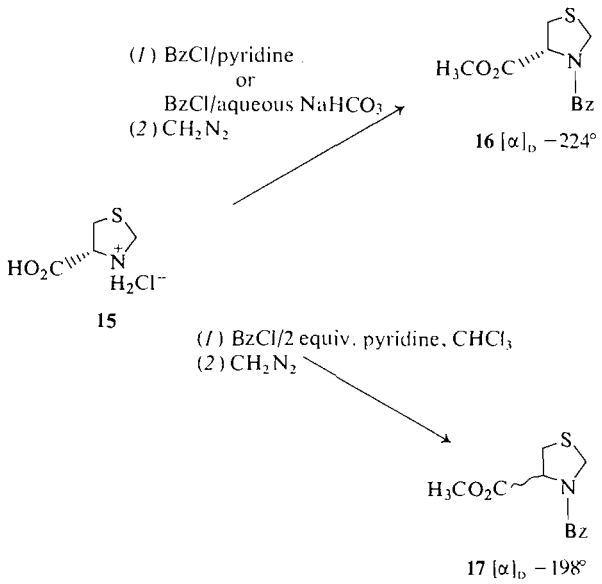

SCHEME 2

when the benzoylation reaction was carried out in chloroform containing 2 equiv. of pyridine, the product **17** obtained after methylation showed a slight loss of optical activity. The lack of total racemization of **15** in this reaction is in contrast to the earlier observation that compound **10** racemizes under the same conditions, a result which is probably indicative of the relative stabilities of the thiazolidine and 2,2-dimethylthiazolidine ring systems. The fact that the thiazolidine system is more stable to ring opening than the 2,2-dimethylthiazolidine system is also evidenced by the decomposition of 2,2-dimethyl-4(*R*)-carboxythiazolidine hydrochloride (**10**) in water to give the constituent amino acid in contrast to the stability of 4(*R*)-carboxythiazolidine hydrochloride (**15**) in water. The enantiomeric purity of 3-benzoyl-4(*R*)-methoxycarbonyl-2,2-dimethylthiazolidine (**13**) was confirmed by use (9) of the chiral shift reagent, tris-[3-(trifluoromethylhydroxymethylene)-*d*-camphorato]europium(III). Thus, the nmr spectrum of **13** in chloroform containing 0.2 equiv. of the chiral shift reagent exhibited two singlets for the C-2 methyl resonances, whereas the nmr spectrum of the racemate **14** in chloroform with 0.2 equiv. of the chiral shift reagent exhibited a differential shift of 0.07 ppm between the C-2 methyl resonances in the two enantiomers; interestingly, a separation of only one of the diastereotopic methyl group signals was observed in the spectrum of **14** upon addition of the shift reagent.

Parallel syntheses of the product nucleosides utilizing the optically active compound **13** and the racemic compound **14** as starting materials were performed. The enantiomeric purity of the key intermediates and the product nucleosides was confirmed by their nmr spectra in deuterochloroform containing the chiral shift reagent; in each case, the optimum amount of shift reagent used and the signals that provided differentiation of the enantiomers in the racemic compounds are indicated in the Experimental.

Oxidation of 3-benzoyl-4(*R*)-methoxycarbonyl-2,2-dimethylthiazolidine (**13**) with *m*-chloroperbenzoic acid afforded a mixture of the isomeric sulfoxides **18***a* and **18***b* in a ratio of 1.5:1, as indicated by its nmr spectrum. Crystallization from methanol–hexane afforded the pure isomer **18***a* as a white crystalline solid; this permitted the unambiguous assignment of signals to the two isomers **18***a* and **18***b* in the ^{1}Hmr and Cmr spectra of the isomeric mixture of sulfoxides. The chemical shifts and coupling constants obtained from the LAOCN-4A analysis (10) of the two ABX systems, corresponding to the methine and methylene proton signals in **18***a* and **18***b*, in the 220-MHz spectrum recorded at 293 K are given in Table 1. The assignment of sulfoxide stereochemistry in **18***a* and **18***b* was made on the basis of the signs and magnitudes of the sulfoxidation chemical-shift increments ($\Delta\delta H\text{-}i = \delta H\text{-}i^{S\to O} - \delta H\text{-}i^{S}$) of the methine and methylene proton signals in the ^{1}H nmr spectra of the two isomers. Examination of the spectra of **13** and **18***a* shows that the H-4 signal in the spectrum of isomer **18***a* is shifted downfield by 0.6 ppm relative to the corresponding signal in the spectrum of the sulfide **13**. This deshielding has been ascribed to electric field effects and/or the acetylene-like anisotropy of the S=O bond, and is consistent with a *syn*-axial relationship of H-4 to the sulfinyl group (11, 12). In contrast, the spectrum of sulfoxide **18***b* shows that the H-4 signal is shifted downfield by only 0.2 ppm relative to the corresponding signal in the sulfide **13**. The isomer **18***a* is therefore, assigned the *R* stereochemistry and the isomer **18***b* is assigned the *S* stereochemistry at sulfur. An analogous assignment has been made by Jonsson and Holmquist (13) in the case of the isomeric sulfoxides of thiolane-3,4-dicarboxylic acid.

The nmr spectral data recorded in Table 1 also

TABLE 1. Calculated chemical shifts[a] and coupling constants (Hz) for nmr signals of methine and methylene protons in **18**

	Signal			Coupling constant		
Isomer	H-4	*pro-R* H-5	*pro-S* H-5′	$J_{4,5}$	$J_{4,5'}$	$J_{5,5'}$
18*a*	5.41	3.38	3.09	6.9	10.3	−13.6
18*b*	4.99	3.22	3.51	7.7	0.2	−14.6

[a]In ppm from tetramethylsilane at 220 MHz and 293 K.

Can. J. Chem. Downloaded from www.nrcresearchpress.com by 210.87.254.105 on 09/05/12
For personal use only.

Can. J. Chem. Downloaded from www.nrcresearchpress.com by 210.87.254.105 on 09/05/12
For personal use only.

allow one to comment on the conformational preferences of the thiazolidine ring in the isomeric sulfoxides. Previous studies (14) of the conformations of five-membered rings containing hetero atoms have indicated that the ring may exist in a variety of interconverting pseudorotational forms, although the presence of potential energy barriers in certain systems owing to the nature, number, positions, and steric requirements of the substituents sometimes restricts such pseudorotation and gives rise to preferred conformations of the five-membered ring having definite energy minima (15–17). The diastereotopic methylene proton signals appear in the spectrum of **18***b* at 3.22 and 3.51 ppm; the higher field signal appears as a doublet of doublets with a vicinal coupling constant ($J_{4,5}$) of 7.7 Hz, whereas the lower field signal appears as a broadened doublet with a vicinal coupling constant ($J_{4,5'}$) of about 0 Hz. Examination of Dreiding models suggests a preponderance of conformation B having dihedral angles of 20° and 90°, and the sulfinyl group in a pseudoaxial orientation, as illustrated in Fig. 1. Baldwin *et al.* (18) have suggested the preponderance of the same conformation for a series of similar thiazolidine derivatives. The signal at 3.22 ppm is therefore assigned to the hydrogen at C-5 having a *cis* relationship to H-4, namely, the *pro-R* methylene hydrogen, and that at 3.51 ppm to the *pro-S* methylene hydrogen in isomer **18***b*. In the spectrum of **18***a*, the H-5′ and H-5 signals appear as distinct AB quartets at 3.09 and 3.38 ppm with vicinal coupling constants of 10.3 and 6.9 Hz, respectively. Examination of Dreiding models suggests a preponderance of conformation A (see Fig. 1) having dihedral angles of about 170° and 30°, and the sulfinyl group in a pseudoaxial orientation. Parthasarathy *et al.* (17) have assigned similar twist conformations to the thiazolidine ring, having the S and C(5) atoms displaced in opposite directions with respect to the plane of C(2), N(3), and C(4), in the stable conformers of *N*-acetyl-2-(*p*-tolyl)-thiazolidine 4-carboxylic acid by X-ray and nmr studies; the H(4)—C(4)—C(5)—*pro-R*H(5) torsion angles in the preferred conformers were found to be −31° and −35°, respectively. The signal having the larger vicinal coupling constant may be assigned to the methylene proton having an *anti* relationship to the hydrogen at C-4. Wilson and Bazzone (16) have assigned the larger vicinal coupling constant in the spectrum of 2-*tert*-butyl-1,3-thiazolidine to coupling between protons in a *trans*-diaxial orientation.

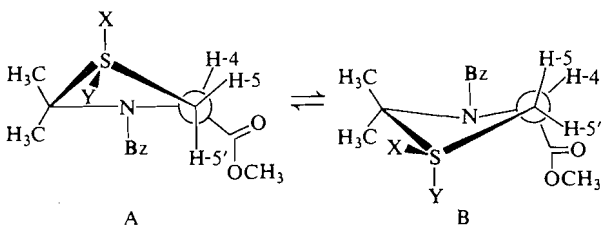

18*a* X = O, Y = Electron pair
18*b* X = Electron pair, Y = O

FIG. 1. Conformational equilibrium in 3-benzoyl-4(*R*)-(methoxycarbonyl)-2,2-dimethylthiazolidine 1(*R*)-oxide (**18***a*) and 3-benzoyl-4(*R*)-(methoxycarbonyl)-2,2-dimethylthiazolidine 1(*S*)-oxide (**18***b*).

The resonance at 3.09 ppm is therefore assigned to the *pro-S* methylene hydrogen and that at 3.38 ppm to the *pro-R* hydrogen in isomer **18***a*. It is interesting to note that the signal of the *pro-R* methylene hydrogen in the spectrum of **18***a* is shifted downfield by 0.29 ppm relative to the signal of the *pro-S* methylene hydrogen, whereas the *pro-S* methylene hydrogen signal in the spectrum of **18***b* is shifted downfield by 0.29 ppm relative to the signal of the *pro-R* methylene hydrogen. Since the magnitude of the chemical shift difference between the methylene hydrogen signals is the same in both isomers (**18***a* and **18***b*), it is indicative of a similar orientation of the lone pair of electrons of the sulfinyl group relative to the α-methylene hydrogens (19) in both isomeric sulfoxides and is consistent with the assignment of the sulfinyl group to the pseudoaxial orientation in both isomers. Further evidence for the similarity in orientation of the lone pair with respect to the methylene hydrogens in **18***a* and **18***b* may be obtained by consideration of the geminal coupling constants in the two isomers. Previous studies (19, 20) have indicated a significant difference in geminal coupling constants for the α-methylene protons when the lone pair was axial or equatorial. In our case, however, the geminal coupling constants in the two isomers differ by only 1.0 Hz. The result is also in accord with the proposed acetylene-like anisotropy of the S=O bond since, in both isomers, the α proton *syn* to the sulfinyl group is deshielded with respect to its diastereotopic counterpart *anti* to the sulfinyl group. This observation is not in agreement with results obtained in some sulfoxides in which the α-proton *syn* to the sulfinyl group was found to be shielded with respect to the α proton *anti* to the sulfinyl group (11, 20), thereby suggesting a carbonyl-like anisotropy of the S=O bond.

Treatment of a mixture of the isomeric sulfoxides **18** with 5 equiv. of acetic anhydride in refluxing benzene containing a trace of *p*-toluenesulfonic acid monohydrate afforded 4-benzoyl-3(*R*)-methoxycarbonyl-5-methyl-3,4-dihydro-2*H*-1,4-thiazine (**20**) and not the Pummerer-reaction product (**19**) (see Scheme 3). A possible mechanism for the conversion of **18** to **20** involves the rearrangement of the sulfoxide **18**

Can. J. Chem. Downloaded from www.nrcresearchpress.com by 210.87.254.105 on 09/05/12
For personal use only.

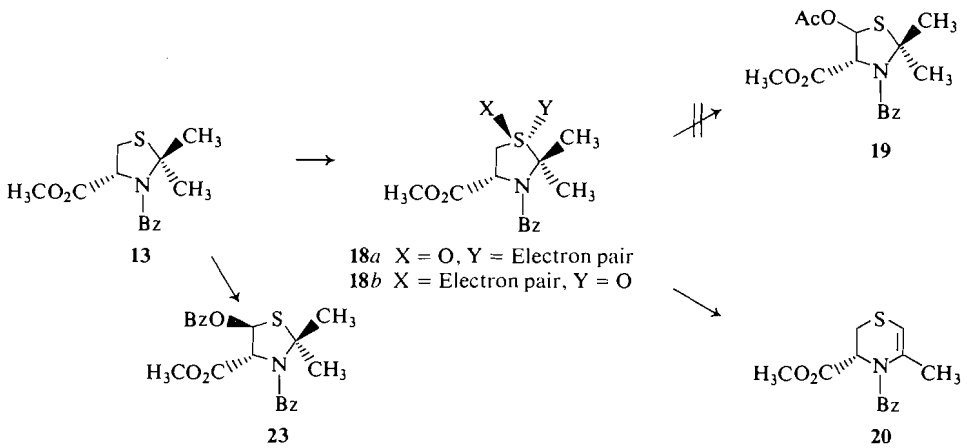

SCHEME 3

to the sulfenic acid intermediate **21** which, after ring closure, gives the nitrogen-stabilized carbonium ion **22** which, in turn, gives **20** upon deprotonation, as illustrated in Scheme 4. Some evidence for such a mechanism has been obtained by Chen (21) for the ring expansion reaction of 1,3-dithiolane 1-oxides to the dihydro-1,4-dithiins. Analogous rearrangements of the halosulfonium salts of some 1,3-oxathiolane derivatives to give the corresponding 1,4-oxathienes have also been reported (22).

Functionalization at C-5 of 3-benzoyl-4(*R*)-methoxycarbonyl-2,2-dimethylthiazolidine (**13**) was achieved by treatment with dibenzoyl peroxide in refluxing benzene, as described by Baldwin *et al.* (18). This resulted in the stereospecific conversion of **13** into 3-benzoyl-5(*S*)-benzoyloxy-4(*R*)-methoxycarbonyl-2,2-dimethylthiazolidine (**23**), as illustrated in Scheme 3; the stereospecificity of the reaction is presumably due to shielding of one face of the molecule by the methoxycarbonyl group. Compound **23** was converted stereospecifically into the nucleoside analog, namely, 6-benzamido-9-(3-benzoyl-4(*R*)-

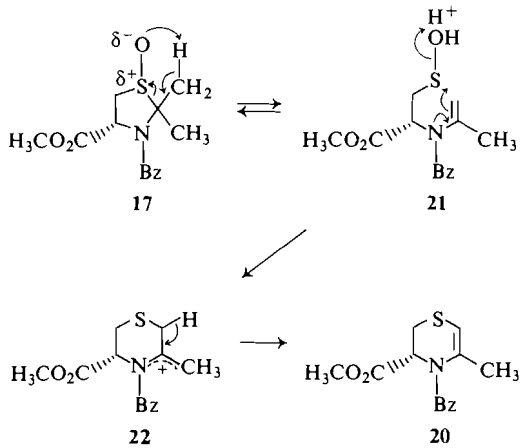

SCHEME 4

methoxycarbonyl-2,2-dimethylthiazolidin-5(*S*)-yl)-9*H*-purine (**7**), in 40% yield by treatment with 6-benzamidochloromercuripurine and titanium tetrachloride in 1,2-dichloroethane (23) (Scheme 5); the

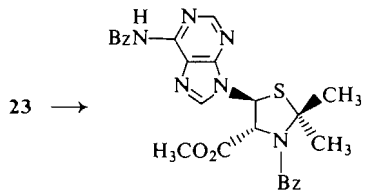

SCHEME 5

observed stereospecificity results from double inversion at C-5 of **23** via the intermediate chloride. The enantiomeric purity of compound **7** was confirmed by use of the chiral shift reagent. Thus, for example, the ^{1}H nmr spectrum at 220 MHz of optically active **7** in chloroform-*d* containing 0.2 equiv. of the shift reagent exhibited slightly broadened singlets for the C-2 methyl proton signals, whereas the corresponding signals in the spectrum of the optically inactive nucleoside analog in chloroform-*d* with 0.2 equiv. of shift reagent exhibited differential shifts of 0.11 and 0.15 ppm between the C-2 methyl group signals in the two enantiomers, as illustrated in Fig. 2. The maximal uv absorptions for **7** at 232 and 281 nm in neutral solution and at 285 nm in acidic solution are in agreement (24) with a 9-substituted 6-benzamidopurine.

In addition, the synthesis of an analog of a 1′-homonucleoside, namely, 6-chloro-9-[(3-benzoyl-2,2-dimethylthiazolidin-4(*R*)-yl)methyl]-9*H*-purine (**8**), was readily achieved in 62% yield by treatment (2) of 3-benzoyl-4(*R*)-hydroxymethyl-2,2-dimethylthiazolidine (**24**), obtained from **13** (see Scheme 6) by borohydride reduction, with 6-chloropurine, triphenylphosphine, and diethyl azodicarboxylate in tetra-

Can. J. Chem. Downloaded from www.nrcresearchpress.com by 210.87.254.105 on 09/05/12
For personal use only.

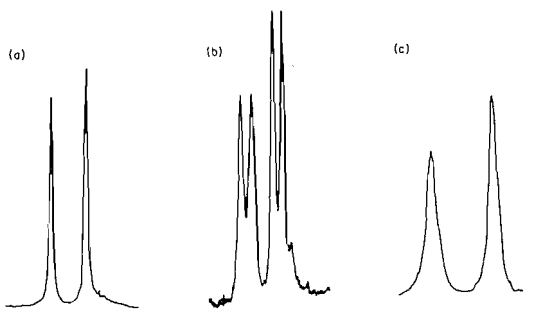

FIG. 2. C-2 methyl signals in the ^{1}H nmr spectrum ($CDCl_3$) at 220 MHz of the nucleoside analog **7**: (*a*) mixture of enantiomers; (*b*) mixture of enantiomers with 0.8 equiv. chiral shift reagent; (*c*) (4*R*,5*S*)-isomer with 0.8 equiv. chiral shift reagent.

hydrofuran at room temperature. The maximal uv absorption for **8** at 265 nm in neutral, acid, or basic solution is in agreement (25) with a 9-substituted 6-chloropurine. The enantiomeric purity of compound **8** was confirmed by use of the chiral shift reagent. Thus, for example, the C-2 methyl group signals in the spectrum of **8** in chloroform-*d* with 0.2 equiv. of the shift reagent appeared as singlets, whereas differential shifts of 0.10 and 0.14 ppm between the C-2 methyl signals in the two enantiomers were observed in the spectrum of the corresponding racemic compound in chloroform-*d* with 0.2 equiv. of the shift reagent.

The carbon-13 nmr data of the 1,3-thiazolidine derivatives that were prepared in this study are presented in Tables 2 and 3. The chemical shift assignments in all the compounds were facilitated by consideration of the substituent effects on the ^{13}C chemical shifts in the spectra of related heterocyclic compounds containing sulfur and nitrogen (2), and were confirmed by means of gated decoupling experiments.

The assignment of signals to the diastereotopic methyl groups in the spectra of the isomeric sulfoxides **18***a* and **18***b* was made on the basis of knowledge of the chemical shift dependence of the C-2 methyl group signals on the orientation of the sulfinyl group in related sulfoxides. For example, it has been demonstrated (26) in the case of the sulfoxides of tetramethylthiolanes, that the C-2 methyl group *cis* to the sulfoxide oxygen is shielded to a greater extent than is the C-2 methyl group *trans* to the sulfoxide oxygen relative to the corresponding methyl groups in the parent sulfide. This has also been found to be the case in certain penicillin sulfoxides (27, 4). Thus, the methyl signal appearing at 20.6 ppm in the spectrum of **18***a* may be assigned to the methyl group *cis* to the sulfoxide oxygen, namely, the *pro-S* methyl group and that at 23.0 ppm to the *pro-R* methyl group. Similarly, the signal appearing at 19.3 ppm in the spectrum of **18***b* may be assigned to the *pro-R* methyl group and that at 22.7 ppm to the *pro-S* methyl group.

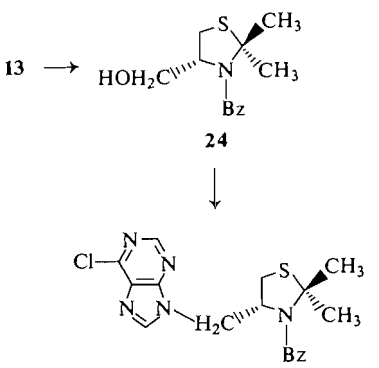

SCHEME 6

Experimental

Melting points were determined with a Fisher-Johns melting point apparatus and are uncorrected. The ir spectra were recorded on a Perkin-Elmer 180 spectrophotometer. Ultraviolet (uv) spectra were recorded on a Beckman ACTA MIV spectrophotometer. Proton magnetic resonance (^{1}Hmr) spectra at 60 MHz were recorded on a Varian EM-360 or Bruker HX-60 spectrometer in chloroform-*d* with tetramethylsilane as the internal standard. The ^{1}Hmr spectra at 220 MHz were measured on a Varian HR-220 spectrometer at the Canadian 220 MHz NMR Centre. The Cmr spectra were recorded in chloroform-*d* solution on a Bruker HX-60 spectrometer equipped with an FT60M Fourier transform accessory at 15.09 MHz; chemical shifts are given in ppm downfield from TMS. A chiral shift reagent, (tris-[3-trifluoromethylhydroxymethylene)-*d*-camphorato]europium(III), was purchased from Aldrich Chemical Co. Optical rotations were determined on a Perkin-Elmer 141 polarimeter. Thin-layer chromatography was performed with silica gel G (E. Merck) as adsorbent in the following solvent systems (v/v): (*A*) benzene – ethyl acetate, 9:1; (*B*) 4:1; (*C*) 1:1; (*D*) 1:4; (*E*) ethyl acetate. The developed plates were air-dried, and exposed to uv light and/or sprayed with a solution of cerium sulfate (1%) and molybdic acid (1.5%) in 10% aqueous sulfuric acid, and heated at ~150°C. Column chromatography was performed on Brinkmann silica gel 60 (E. Merck). Solvents were evaporated under reduced pressure and below 40°C.

*3-Benzoyl-2,2-dimethyl-4(*R*)-carboxythiazolidine (**11**)*

To a solution of 2,2-dimethyl-4(*R*)-carboxythiazolidine hydrochloride (**10**) (4.0 g, 20 mmol), prepared from L-cysteine hydrochloride monohydrate (**9**) by the method of Sheehan *et al.* (6), in pyridine (400 ml, 4.95 mol) at 0°C was added benzoyl chloride (2.87 g, 20 mmol) dropwise. The mixture was stirred at room temperature for 8 h and then pyridine was evaporated. The residue was dissolved in dichloromethane (150 ml) and the solution was washed with water. The organic layer was dried over anhydrous sodium sulfate and the solvent evaporated to afford a half crystalline mass. Compound **11** was obtained from chloroform–hexane as needles (4.0 g, 74%), mp 180–182°C (dec.), $[\alpha]_D^{24}$ −154° (*c* 0.83, chloroform), −266° (*c* 1.2, pyridine); ^{1}Hmr 60 MHz δ: 1.98 (6-H, bs, Me), 3.08 (1-H, d of d's, $|J_{5,5'}| = 10$ Hz, $J_{4,5} = 4$ Hz, H-5), 3.38 (1-H,

TABLE 2. Carbon-13 chemical-shift data[a] of 1,3-thiazolidine derivatives

Compound	Carbon 2	4	5	CH_3	OCH_3	CO	Ph	CH_2OH
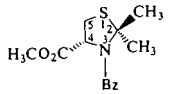 **13**	73.2	67.7	31.3	28.2 29.6	52.7	170.8	125.8, 128.5 129.4, 138.5	—
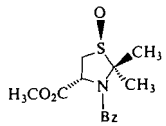 **18*a***	84.1	63.8	48.5	20.6[b] 23.0[c]	52.9	171.2	127.3, 128.5 130.6, 136.7	—
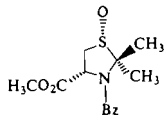 **18*b***	83.2	63.4	49.0	19.3[c] 22.7[b]	52.9	169.9	125.6, 128.7 129.8, 137.5	—
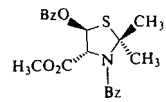 **23**	74.2	73.1	78.7	28.5 32.5	53.2	165.0 167.9	125.7, 128.8 129.2, 129.6, 133.8, 138.2	—
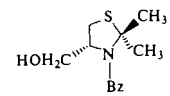 **24**	72.1	66.3	29.8	29.8	—	169.8	125.8, 128.5, 129.3, 138.6	62.3

[a]In ppm downfield from internal tetramethylsilane (TMS) in chloroform-*d*.
[b]The signal is assigned to the *pro-S* methyl group at C-2.
[c]The signal is assigned to the *pro-R* methyl group at C-2.

TABLE 3. Carbon-13 chemical-shift data[a] for nucleoside analogs

Compound	Carbon 2′	4′	5′	CH_3	OCH_3	CH_2	NCO*Ph*	Purine
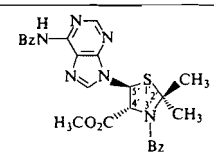 **7**	74.5	72.2	60.5	29.5 31.6	53.5	—	125.9, 128.7 128.2, 130.1 132.9	142.3, 152.7
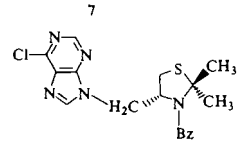 **8**	72.7	64.2	31.4	29.8 30.2	—	47.5	125.8, 128.1, 128.5, 128.9, 129.8, 131.8 132.4	144.9, 151.9

[a]In ppm downfield from internal tetramethylsilane (TMS) in chloroform-*d*.

d of d's, $J_{4,5'} = 6$ Hz, H-5′), 5.35 (1-H, m, H-4), 7.38 (5-H, s, Ph).

3-Benzoyl-2,2-dimethyl-4-carboxythiazolidine (12)

To an ice-water cooled suspension of 2,2-dimethyl-4(*R*)-carboxythiazolidine hydrochloride (**10**) (0.404 g, 2.0 mmol) in chloroform (10 ml) was added pyridine (0.361 g, 4.6 mmol) in chloroform (8 ml) over a period of 5 min with stirring, and then benzoyl chloride (0.22 g, 1.6 mmol) in chloroform (7 ml) over a period of 20 min. The mixture was stirred at room temperature for 16 h and then diluted with chloroform (100 ml). The chloroform solution was washed successively with 2 *N* hydrochloric acid (2 × 70 ml) and aqueous sodium chloride solution (2 × 50 ml), and dried over anhydrous sodium

Can. J. Chem. Downloaded from www.nrcresearchpress.com by 210.87.254.105 on 09/05/12
For personal use only.

Can. J. Chem. Downloaded from www.nrcresearchpress.com by 210.87.254.105 on 09/05/12
For personal use only.

sulfate. The solvent was evaporated to afford crystals, which were recrystallized from chloroform–hexane to give **12** as fine prisms (404 mg, 71%), mp 180–180.5°C, $[\alpha]_D^{30}$ −0.8° (*c* 2.4, chloroform).

*3-Benzoyl-4(*R*)-methoxycarbonyl-2,2-dimethylthiazolidine (**13**)*

To a solution of 3-benzoyl-2,2-dimethyl-4(*R*)-carboxythiazolidine (**11**) (1.06 g, 4 mmol) in methanol (20 ml) at 0°C was added a slight excess of diazomethane in ether. The mixture was stirred for 12 h and then the solvent evaporated to afford a white crystalline product. Compound **13** was obtained from ether–hexane as white prisms (0.93 g, 83%), mp 105–106.5°C, $[\alpha]_D^{23}$ −180° (*c* 0.92, chloroform), R_F 0.40 (solvent *A*). A racemic mixture of 3-benzoyl-4-methoxycarbonyl-2,2-dimethylthiazolidine (**14**) was obtained in the same manner from the corresponding carboxylic acid **12**; ir (KBr): 1745 (O=C), 1640 (N–C=O) cm^{-1}; ^{1}Hmr δ: 1.95 (3-H, s, Me), 2.01 (3-H, s, Me), 3.22 (2-H, m, 2 H-5's), 3.64 (3-H, s, OMe), 4.79 (1-H, m, H-4), 7.34 (5-H, s, Ph); optically active **13** (with 0.2 equiv. chiral shift reagent); δ: 2.74 (3-H, s's, Me), 3.07 (3-H, s, Me); optically inactive **14** (with 0.2 equiv. chiral shift reagent); δ: 2.59 (3-H, bs, Me), 2.79, 2.86 (3-H, s, Me). *Anal.* calcd. for $C_{14}H_{17}NO_3S$: C 60.19, H 6.13, N 5.01, S 11.48; found: C 60.17, H 6.13, N 4.93, S 11.54.

*4(*R*)-Carboxythiazolidine Hydrochloride (**15**)*

4(*R*)-Carboxythiazolidine (1.34 g, 10 mmol), obtained from L-cysteine hydrochloride monohydrate (**9**) by the method of Ratner and Clarke (8) was dissolved into 2*N* hydrochloric acid (5 ml) and then water was immediately evaporated to give the hydrochloride **15** as white crystals (1.72 g, 100%).

*3-Benzoyl-4(*R*)-(methoxycarbonyl)thiazolidine (**16**)*

To a solution of 4(*R*)-carboxythiazolidine hydrochloride (**15**) (500 mg, 3 mmol) in pyridine (50 ml, 620 mmol) at 0°C was added benzoyl chloride (424 mg, 3 mmol) and the mixture was stirred for 8 h at room temperature. Pyridine was evaporated and the residue was dissolved in dichloromethane (100 ml). The organic layer was washed with aqueous sodium chloride (3 × 50 ml) and dried (anhydrous sodium sulfate); evaporation of the solvent gave a syrup which was treated with an ethereal solution of diazomethane to give a thick oil whose tlc indicated the presence of three components having R_F values of 0.41, 0.2, and 0.06 (solvent *B*). The component having an R_F value of 0.41 was isolated by column chromatography on silica gel and then distilled under vacuum to give compound **16** (7) as a clear oil; bp 130–140°C/0.07 Torr $[\alpha]_D^{23}$ −224° (*c* 1.6, chloroform); ir: 1750 (O=C), 1650 (N–C=O) cm^{-1}; ^{1}Hmr (60 MHz) δ: 3.3 (2-H, d, J = 6 Hz, 2 H-5's), 3.78 (3-H, s, OMe), 4.62 (2-H, bs, 2 H-2's), 5.22 (1-H, b, H-4), 7.45 (5-H, s, Ph).

*3-Benzoyl-4-(methoxycarbonyl)thiazolidine (**17**)*

To a vigorously stirred suspension of 4(*R*)-carboxythiazolidine hydrochloride (**15**) (500 mg, 3 mmol) in chloroform (15 ml) at 0°C was added pyridine (512 mg, 6.6 mmol) in chloroform (8 ml) and then benzoyl chloride (422 mg, 3 mmol) in chloroform (7 ml). The mixture was stirred for 16 h at room temperature and then diluted with chloroform (100 ml). The chloroform solution was washed successively with 2 *N* hydrochloric acid (2 × 50 ml) and aqueous sodium chloride solution (2 × 50 ml), and dried over anhydrous sodium sulfate. Evaporation of the solvent afforded a syrup which was treated with ethereal diazomethane solution to give a thick oil. Thin-layer chromatography of the oil indicated the presence of three components having R_F values of 0.42, 0.19, and 0.06 (solvent *B*). The component having an R_F value of 0.42 was isolated by column chromatography on silica gel; subsequent distillation afforded **17** as a clear oil; bp 120–140°C/0.06 Torr $[\alpha]_D^{23}$ −198° (*c* 1.1, chloroform).

*3-Benzoyl-4(*R*)-(methoxycarbonyl)-2,2-dimethylthiazolidine 1-Oxide (**18**)*

To a solution of the methyl ester **13** (614 mg, 2.2 mmol) in dichloromethane (20 ml) at 0°C was added *m*-chloroperbenzoic acid (444 mg, 2.2 mmol) in dichloromethane (25 ml). The mixture was stirred at room temperature for 3 h and then diluted with dichloromethane (30 ml). The solution was washed successively with aqueous sodium bicarbonate solution (2 × 25 ml), aqueous sodium chloride solution (25 ml), and dried over magnesium sulfate. Evaporation of the solvent afforded an isomeric mixture of **18***a* and **18***b* as a solid (648 mg, 99%) in a ratio of 1.5:1, as determined by ^{1}Hmr spectroscopy. The isomer **18***a* was obtained from methanol–hexane as white crystals (112 mg); mp 169–170°C, $[\alpha]_D^{22}$ −283° (*c* 0.2, 5% ethanol in chloroform); R_F 0.14 (solvent *C*); ir (KBr): 1770 (O–C=O), 1640 (N–C=O), 1050 (S=O) cm^{-1}; ^{1}Hmr (220 MHz) of **18***a*; δ: 1.72 (3-H, s, Me), 1.84 (3-H, bs, Me), 3.09 (1-H, d of d's, $|J_{5,5'}|$ = 13.6 Hz, $J_{5',4}$ = 10.5 Hz, *pro-S* H-5'), 3.38 (1-H, d of d's, $J_{5,4}$ = 7.2 Hz, *pro-R* H-5), 3.49 (3-H, s, OMe), 5.41 (1-H, m, H-4), 7.46 (5-H, d, Ph); ^{1}Hmr (220 MHz) of **18***b*; δ: 1.50 (3-H, s, Me), 1.97 (3-H, s, Me), 3.22 (1-H, d of d's, $|J_{5,5'}|$ = 14.6 Hz, $J_{5,4}$ = 8.0 Hz, *pro-R* H-5), 3.51 (1-H, bd, *pro-S* H-5'), 3.48 (3-H, s, OMe), 4.99 (1-H, bd, H-4), 7.37 (5-H, d, Ph); **18***a* (60 MHz); δ: 3.47 (3-H, s, OMe); optically active **18***a* (with 0.3 equiv. chiral shift reagent); δ: 3.67 (3-H, s, OMe); optically inactive **18***a* (with 0.3 equiv. chiral shift reagent); δ: 3.63, 3.71 (3-H, s's, OMe). *Anal.* calcd. for $C_{14}H_{17}NO_4S$: C 56.93, H 5.80, N 4.74, S 10.86; found: C 56.89, H 5.86, N 4.79, S 10.79.

*4-Benzoyl-3(*R*)-methoxycarbonyl-5-methyl-3,4-dihydro-2H-1,4-thiazine (**20**)*

A solution of sulfoxides **18***a* and **18***b* (294 mg, 1 mmol) in benzene (25 ml) containing acetic anhydride (0.5 ml, 5.3 mmol) and *p*-toluenesulfonic acid (~10 mg) was stirred at room temperature for 3.5 h and a further 2.5 h at reflux temperature. Aqueous sodium bicarbonate solution (20 ml) was added to the reaction mixture and then the mixture was stirred for 10 h at room temperature. The benzene layer was separated and washed with water (15 ml), and dried (magnesium sulfate). Evaporation of the solvent afforded a syrup. Chromatography on silica gel (10% ethyl acetate in benzene) gave compound **20** as a pale yellow solid (157 mg, 60%), mp 93–94°C, $[\alpha]_D^{23}$ −391° (*c* 0.8, chloroform), R_F 0.38 (solvent *A*); ir (KBr): 1750 (O–C=O), 1650 (N–C=O) cm^{-1}; ^{1}Hmr (60 MHz) δ: 1.65 (3-H, s, Me), 3.40 (2-H, m, H-2, H-2'), 3.78 (3-H, s, OMe), 5.47 (1-H, bs, H-6), 5.89 (1-H, m, H-3), 7.44 (5-H, m, Ph); optically active **20** (with 0.2 equiv. chiral shift reagent) δ: 2.41 (3-H, s, Me); optically inactive **20** (with 0.2 equiv. chiral shift reagent) δ: 2.16, 2.24 (3-H, s's, Me). *Anal.* calcd. for $C_{14}H_{15}NO_3S$: C 60.63, H 5.45, N 5.05, S 11.56; found: C 60.79, H 5.44, N 5.22, S 11.56.

Can. J. Chem. Downloaded from www.nrcresearchpress.com by 210.87.254.105 on 09/05/12
For personal use only.

*3-Benzoyl-5(*S*)-benzoyloxy-4(*R*)-methoxycarbonyl-2,2-dimethylthiazolidine (**23**)*

A solution of 3-benzoyl-4(*R*)-methoxycarbonyl-2,2-dimethylthiazolidine (**13**) (2.62 g, 9.4 mmol) and dibenzoyl peroxide (4.54 g, 18.8 mmol) in benzene (250 ml) was refluxed for 20 h under nitrogen. The solution was washed with aqueous sodium bicarbonate solution and dried over magnesium sulfate. Evaporation of the solvent afforded a syrup. Thin-layer chromatography indicated the presence of a major component having R_F value of 0.45 (solvent system *A*). Chromatography on silica gel (3% ethyl acetate in benzene) and recrystallization gave compound **23** (0.76 g, 20%), mp 142°C, $[\alpha]_D^{25}$ +195° (*c* 0.4, chloroform); ir (KBr): 1740, 1720 (O—C(=O)—), 1640 (—N—C(=O)—) cm^{-1}; ^{1}Hmr (60 MHz) δ: 2.05, 2.15 (two 3-H s's, 2 Me's), 3.74 (3-H, s, OMe), 5.16 (1-H, s, H-4), 6.63 (1-H, s, H-5), 7.38 (5-H, s, NCOPh), 7.50, 8.05 (5-H, m's, OCOPh); optically active **23** (with 0.3 equiv. chiral shift reagent) δ: 2.60, 2.88 (two 3-H, s's, 2 Me's); optically inactive **23** (with 0.3 equiv. chiral shift reagent) δ: 2.88 (3-H, s, Me), 2.98, 3.08 (3-H, s's, Me). *Anal.* calcd. for $C_{21}H_{21}NO_5S$: C 63.14, H 5.30, N 3.51, S 8.03; found: C 63.25, H 5.39, N 3.67, S 7.89.

*6-Benzamido-9-(3-benzoyl-4(*R*)-methoxycarbonyl-2,2-dimethylthiazolidin-5(*S*)-yl)-9*H*-purine (**7**)*

A mixture of the benzoate **23** (212 mg, 0.53 mmol), 6-benzamidochloromercuripurine (306 mg, 0.65 mmol), and Celite (200 mg) in dry 1,2-dichloroethane (30 ml) was heated to reflux, and about 7 ml of the solvent was distilled to remove moisture, and then titanium tetrachloride (0.075 ml, 0.68 mmol) in 1,2-dichloroethane (2 ml) was added dropwise. The mixture was refluxed for 7 h and then cooled to room temperature. Saturated aqueous sodium bicarbonate solution (10 ml) was added with vigorous stirring and the mixture was filtered through a layer of Celite, which was thoroughly washed with chloroform. The organic layer was separated and washed successively with water (30 ml), 30% aqueous potassium iodide (2 × 25 ml) and dried over anhydrous sodium sulfate. The solvent was evaporated to leave a brown syrup which contained a major component having an R_F value of 0.64 (solvent *E*) on tlc. Preparative tlc (ethyl acetate) on silica gel afforded compound **7** as a white foam (105 mg, 38%), $[\alpha]_D^{24}$ +53.8° (*c* 1.2, chloroform); ir (KBr): 3250 (NH), 1740 (—O—C(=O)—), 1690, 1590, and 1570 (aromatic, purine ring), 1650 (—N—C(=O)—) cm^{-1}; uv λ_{max} (ethanol): 281 (ε 21 300) (purine ring), 262 (ε 13 000) sh (purine ring), 232 nm (ε 16 230); λ_{max} (ethanol containing a trace amount of hydrochloric acid): 285 nm (ε 21 300); ^{1}Hmr (60 MHz) δ: 2.02, 2.11 (two 3-H s's, Me), 3.83 (3-H, s, OMe), 5.86 (1-H, s, H-4′), 6.41 (1-H, s, H-5′), 6.66–7.66, 7.8–8.15 (10-H, m's, Ph), 8.62, 8.66 (two 1-H, s's, H-4, H-8), 9.3 (1-H, bs, NH); (220 MHz) δ: 2.04, 2.15 (two 3-H, s's, Me); optically active **7** (220 MHz with 0.8 equiv. chiral shift reagent): 2.14, 2.29 (two 3-H, s's, Me); optically inactive **7** (220 MHz with 0.8 equiv. chiral shift reagent) δ: 2.12, 2.15 (3-H, s's, Me), 2.27, 2.31 (3-H, s's, Me). *Anal.* calcd. for $C_{26}H_{24}N_6O_4S$: C 60.45, H 4.68, N 16.27, S 6.21; found: C 60.30, H 4.88, N 16.09, S 6.14.

*3-Benzoyl-4(*R*)-hydroxymethyl-2,2-dimethylthiazolidine (**24**)*

To a suspension of sodium borohydride (5.0 g, 132 mmol) in methanol at ~25°C was added the methyl ester **13** (1.83 g, 6.6 mmol) in methanol (15 ml) over the period of 30 min with stirring and then the mixture was further stirred for 3 h. Thin-layer chromatography (solvent *B*) indicated the presence of a new component having an R_F value of 0.23 together with the unreacted starting material **13** (R_F 0.60). The mixture was cooled and water (30 ml) was added. Methanol was evaporated under reduced pressure and then the residue was extracted with dichloromethane (2 × 50 ml). The organic layer was washed with water, dried over anhydrous sodium sulfate, and the solvent evaporated to afford a syrup which was chromatographed on silica gel with solvent *B* as eluant to give the component having an R_F value of 0.23. Compound **24** was obtained from ether–hexane as prisms (1.31 g, 80%), mp 114.5–116.5°C, $[\alpha]_D^{24}$ −104° (*c* 2.3, ethanol); ir: 3320 (OH), 1600 (—N—C(=O)—) cm^{-1}; ^{1}Hmr (60 MHz) δ: 1.86 (6-H, s, Me), 2.68–3.9 (5-H, m's, 2 H-5's, CH_2OH, OH), 4.0–4.5 (1-H, m, H-4), 7.32 (5-H, s, Ph); optically active **24** (with 0.4 equiv. chiral shift reagent) δ: 3.05, 3.13 (3-H, s's, Me); optically inactive **24** (with 0.4 equiv. chiral shift reagent) δ: 3.31, 3.41 (3-H, s's, Me), 3.68 (3-H, s, Me). *Anal.* calcd. for $C_{13}H_{17}NO_2S$: C 62.12, H 6.82, N 5.57, S 12.76; found: C 62.25, H 6.98, N 5.62, S 12.59.

*6-Chloro-9-[(3-benzoyl-2,2-dimethylthiazolidin-4(*R*)-yl)-methyl]-9*H*-purine (**8**)*

To a mixture of 6-chloropurine (74 mg, 0.48 mmol), triphenylphosphine (125 mg, 0.48 mmol), and diethyl azodicarboxylate (103 mg, 0.59 mmol) in dry tetrahydrofuran (3 ml) was added 3-benzoyl-4(*R*)-hydroxymethyl-2,2-dimethylthiazolidine (**24**) (120 mg, 0.48 mmol) in dry tetrahydrofuran (2 ml) with stirring. The stirring was continued for 16 h. The reaction mixture was concentrated, and the residue was chromatographed on silica gel, with solvent *D* as eluant, to give a component having an R_F value of 0.45 in solvent *D*. Compound **8** was obtained by preparative tlc of the component (solvent *D*), and recrystallized (ethanol–hexane) to give prisms (115 mg, 62%), mp 156.5–159°C, $[\alpha]_D^{25}$ +4.9° (*c* 1.2, chloroform); ir (KBr): 1585, 1552 and 1492 (purine ring), 1615 (C=O) cm^{-1}; uv λ_{max} (ethanol): 265 nm (ε 6191) (purine ring); λ_{max} (ethanol containing a trace of hydrochloric acid): 264.8 nm (ε 6137) (purine ring); λ_{max} (ethanol containing a trace of sodium hydroxide): 265 nm (ε 6280) (purine ring); ^{1}Hmr (60 MHz) δ: 1.93, 2.05 (two 3-H, s's, Me), 2.64–4.6 (4-H, m, 2 H-5's, CH_2—N), 4.65–5.15 (1-H, m, H-4′), 6.85–7.35 (5-H, m's, Ph), 7.52, 8.46 (two 1-H, s's, purine); optically active **8** (with 0.2 equiv. chiral shift reagent) δ: 1.95, 2.1 (two 3-H, s's, Me); optically inactive **8** (with 0.2 equiv. chiral shift reagent) δ: 2.38, 2.52 (3-H, s's, Me), 2.52, 2.62 (3-H, s's, Me). *Anal.* calcd. for $C_{18}H_{18}N_5OSCl$: C 55.74, H 4.68, N 18.06, S 8.27; found: C 55.52, H 4.85, N 17.87, S 8.37.

Acknowledgements

The authors are grateful to the National Research Council of Canada for financial support of this work. They also thank the Canadian 220 MHz NMR Centre for providing facilities for the recording of spectra, Dr. D. M. Vyas for helpful discussions on many aspects of the project, and Dr. B. Achmatowicz for some preliminary work.

1. W. A. SZAREK, D. M. VYAS, and B. ACHMATOWICZ. J. Heterocycl. Chem. **12**, 123 (1975).
2. B. M. PINTO, D. M. VYAS, and W. A. SZAREK. Can. J. Chem. **55**, 937 (1977).
3. W. A. SZAREK, D. M. VYAS, A.-M. SEPULCHRE, S. D. GERO, and G. LUKACS. Can. J. Chem. **52**, 2041 (1974); W. A. SZAREK, D. M. VYAS, and B. ACHMATOWICZ. Tetrahedron Lett. 1553 (1975).
4. P. HODGE and C. H. HARRISON. J. Chem. Soc. Perkin Trans. I, 1772 (1976).
5. B. PAUL and W. KORYTNYK. J. Med. Chem. **19**, 1002 (1976).
6. J. C. SHEEHAN and D.-D. H. YANG. J. Am. Chem. Soc. **80**, 1158 (1958).
7. A. W. A. JEFFREY. M.Sc. Thesis, Queen's University, Kingston, Ontario, Canada. 1975.
8. S. RATNER and H. I. CLARKE. J. Am. Chem. Soc. **59**, 200 (1937).
9. C. KUTAL. *In* Nuclear magnetic resonance shift reagents. *Edited by* R. E. Sievers. Academic Press, New York, NY. 1973.
10. J. A. MUSSO. Nuclear magnetic resonance spectra analysis by least squares with magnetic equivalence factoring, self-assignment, and plots. Program 232, Quantum Chemistry Program Exchange, Indiana University, Bloomington, IN. 1973.
11. D. N. HARPP and J. G. GLEASON. J. Org. Chem. **36**, 1314 (1971).
12. E. JONSSON. Ark. Kemi. **26**, 357 (1967).
13. E. JONSSON and S. HOLMQUIST. Ark. Kemi. **29**, 301 (1968).
14. C. ROMERS, C. ALTONA, H. R. BUYS, and E. HAVINGA. *In* Topics in stereochemistry. Vol. 4. *Edited by* E. L. Eliel and N. L. Allinger. Wiley Interscience, New York. NY. 1969.
15. S. TOPPET, P. CLAES, and J. HOOGMARTENS. Org. Magn. Reson. **6**, 48 (1974).
16. G. E. WILSON, JR. and T. J. BAZZONE. J. Am. Chem. Soc. **96**, 1465 (1974).
17. R. PARTHASARATHY, B. PAUL, and W. KORYTNYK. J. Am. Chem. Soc. **98**, 6634 (1976).
18. J. E. BALDWIN, A. AU, M. CHRISTIE, S. B. HABER, and D. HESSON. J. Am. Chem. Soc. **97**, 5957 (1975).
19. J. B. LAMBERT and R. G. KESKE. J. Org. Chem. **31**, 3429 (1966).
20. R. R. FRASER, T. DURST, M. R. MCCLORY, R. VIAU, and Y. Y. WIGFIELD. Int. J. Sulfur Chem. A, **1**, 133 (1971).
21. C. H. CHEN. Tetrahedron Lett. 25 (1976).
22. G. E. WILSON, JR. J. Am. Chem. Soc. **87**, 3785 (1965); G. E. WILSON, JR. and M.-G. HUANG. J. Org. Chem. **41**, 966 (1976).
23. R. G. S. RITCHIE and W. A. SZAREK. Chem. Commun. 686 (1973).
24. M. MIYAKI and B. SHIMIZU. Chem. Pharm. Bull. **18**, 732 (1970).
25. E. E. LEUTZINGER, W. A. BOWLES, R. K. ROBINS, and L. B. TOWNSEND. J. Am. Chem. Soc. **90**, 127 (1968); L. B. TOWNSEND, R. K. ROBINS, R. N. LOEPPKY, and N. J. LEONARD. J. Am. Chem. Soc. **86**, 5320 (1964).
26. R. T. LALONDE, C. F. WONG, A. I-M. TSAI, J. T. WROBEL, J. RUSZKOWSKA, K. KABZINSKA, T. I. MARTIN, and D. B. MACLEAN. Can. J. Chem. **54**, 3860 (1976).
27. R. A. ARCHER, R. D. G. COOPER, P. V. DEMARCO, and L. F. JOHNSON. Chem. Commun. 1291 (1970).

Can. J. Chem. Downloaded from www.nrcresearchpress.com by 210.87.254.105 on 09/05/12
For personal use only.

The electrochemical formation of mercuric oxide in alkaline solution

REMIGIO GERMANO BARRADAS, STEPHEN FLETCHER, AND JOHN DOUGLAS PORTER

Department of Chemistry, Carleton University, Ottawa, Ont., Canada K1S 5B6

Received May 9, 1977

REMIGIO GERMANO BARRADAS, STEPHEN FLETCHER, and JOHN DOUGLAS PORTER. Can. J. Chem. **56**, 336 (1978).

The electrochemical formation of mercuric oxide on mercury in alkaline solutions is described. The reaction was investigated because of its importance as a reference electrode system, and also because it provides a model test of recent theoretical developments. Various derived data are compared to computer simulations of the growth mechanism.

REMIGIO GERMANO BARRADAS, STEPHEN FLETCHER et JOHN DOUGLAS PORTER. Can. J. Chem. **56**, 336 (1978).

On décrit la formation électrochimique d'oxyde mercurique sur du mercure en solutions alcalines. On a étudié la réaction à cause de son importance comme système d'électrode de référence et aussi parce qu'elle fournit un bon modèle pour vérifier de récents développements théoriques. On peut comparer diverses données déduites avec des simulations par ordinateur du mécanisme de croissance.

[Traduit par le journal]

Can. J. Chem. Downloaded from www.nrcresearchpress.com by 210.87.254.6 on 09/05/12
For personal use only.

Introduction

The anodic behaviour of mercury in hydroxide ion solutions was studied by Armstrong *et al.* (1), who demonstrated that a layer of mercuric oxide in the (010) orientation was formed. The first stage in the growth of the layer was shown to be the formation of a monolayer by the nucleation and subsequent growth of two-dimensional centres at the electrode surface. This was followed by the generation of a three-dimensional layer, the growth of which caused the electrode to passivate. In particular, models of the growth processes were described at constant overpotential. Verification of the models was then achieved by the potential step technique. The slow step in both two- and three-dimensional growth was concluded to be at the edge of the expanding crystal lattices, whilst it was assumed that sufficient nuclei were present in both cases for the Avrami (2) theorem to be applicable.

Recently we extended these models by computer simulation to include the linear potential sweep technique (lps) and the staircase voltammogram technique (sv). The simulations were based on the assumption that the surface coverage functions $S(t)$ responded instantaneously to small changes of potential, ΔE, so that a steady-state rate of nucleation was observed at any given potential. Under these circumstances (3–5) the current corresponding to a given mechanism was evaluated as a function of both potential and time. Furthermore, it was possible to investigate the influence of uncompensated ohmic overpotential on the experimental data. This is clearly desirable, because the large current densities observed in passivation studies are invariably distorted by ohmic effects.

The purpose of the present paper, therefore, is to report the results of a comparison between certain results of the computer simulations and experimental data obtained using the model Hg/HgO system.

Experimental

All computer programs were written in either FORTRAN IV or BASIC, and the computations were performed on a Xerox SIGMA-9 computer. The electrodes, considered to be sections of a sphere, were generated *in situ* by the extrusion of mercury via a micrometer-controlled syringe through the tip of a wide-bore glass capillary (0.05 cm). The all-Pyrex cell (illustrated in Fig. 1) was undivided, a cylindrical platinum gauze concentric with the working electrode serving as the counter electrode. An adjustable luggin reference probe was also incorporated in the cell design, in order to minimize the ohmic contribution to the applied potential. Deoxygenation was performed by bubbling purified nitrogen through the apparatus between measurements. Potentials were measured ± 0.05 mV, and are quoted vs. the mercury/mercuric oxide reference electrode in the same solution (5 *M* KOH). The strong KOH solution was chosen in order to minimize the solution component of the total ohmic potential drop. Experimental data were recorded photographically from Tektronix type 549 and 503 oscilloscopes and subsequently analyzed by enlargement.

Results

(a) The Potential Step Technique

In this section the results obtained from the potential step technique will be reported. Only data relating to three-dimensional growth will be described because of the poor definition of two-dimensional growth in this instance (see, for example, Fig. 11). As shown previously (3) the computer simulation predicts that the current maximum in the experimental transients (i_m (in mA)) obeys an equation of the form

Can. J. Chem. Downloaded from www.nrcresearchpress.com by 210.87.254.6 on 09/05/12
For personal use only.

[1] $$\log (i_m) = a_1(E - i_mR) + b_1$$

where a_1 and b_1 are experimentally determined constants, E is the applied potential (mV), R is the resistance (Ω, Ω cm^{-2}), and the product i_mR is the ohmic overpotential at the current maximum. Simple differentiation gives

[2] $$\frac{\partial E}{\partial \log (i_m)} = \frac{1}{a_1} + 2.303 i_m R$$

so that the experimentally determined plot of $\partial E/\partial \log(i_m)$ as a function of i_m should be linear, the intercept giving $1/a_1$ whilst the gradient gives R. Unfortunately, the potential step technique necessitates the acquisition of data one point at a time, so that the gradient $\partial E/\partial \log(i_m)$ may not be easily obtained as a continuous function in i_m. In order to resolve this problem a combination of spline function approximations with least squares best-fit procedures (6) was utilized in order to fit an accurate continuous function to the $\log(i_m)$ vs. E data. The gradient of this function at each i_m value could then be obtained exactly. A typical result is shown in Fig. 2. It is clear that [2] is closely obeyed for low i_m. Insertion of resistors of variable value (1 Ω, 2 Ω, etc.) into the electrical circuit between the potentiostat and the working electrode also confirmed the validity of [2], since identical intercepts at $i_m = 0$ were obtained in each case.

Once R values have been obtained in this way, it is possible to substitute back into [1] and hence compensate for ohmic distortions in log (i_m) vs. E plots by shifting the potential scales by an amount i_mR. This results in an extraordinary improvement in the resolution of log (i_m) vs. E data as demonstrated in Fig. 3. For the first time the presence of a discontinuity becomes apparent, bounded by two approximately linear sections. In the past such a discontinuity has not been observed because of the dominance of ohmic effects; the effect of only 1 Ω, say, would be to shift the discontinuity by $\sim$100 mV. Further evidence of discontinuous behaviour may be observed by applying a similar compensation procedure to log (t_m) vs. E data where t_m is the time

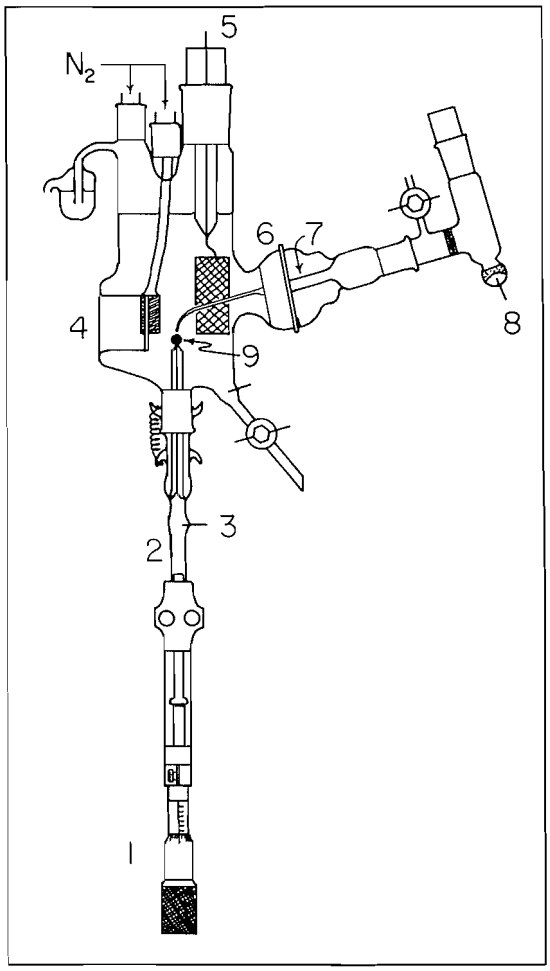

FIG. 1. Cell design for minimization of ohmic effects. (1) Micrometer attachment, (2) glass syringe, (3) working electrode contact, (4) optical flat, (5) platinum gauze counter electrode (shown displaced for clarity), (6) adjustable ball joint, (7) luggin capillary, (8) Hg/HgO reference electrode, (9) mercury drop working electrode.

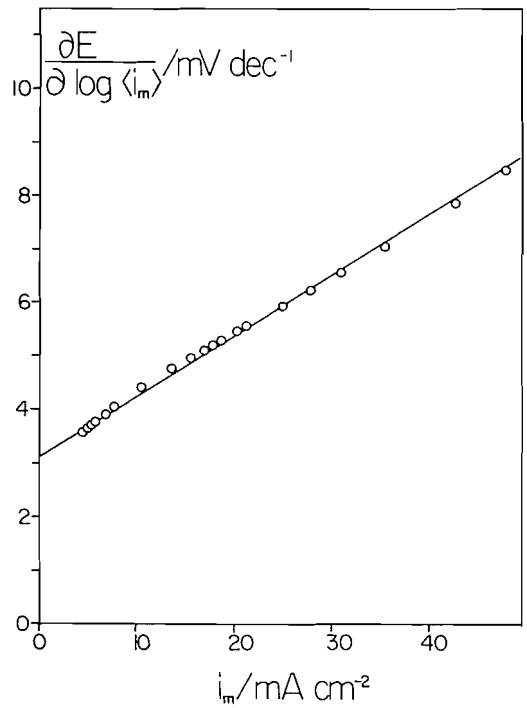

FIG. 2. $\partial E/\partial \log \langle i_m \rangle$ vs. i_m. Gradient function obtained by spline function approximation.

Can. J. Chem. Downloaded from www.nrcresearchpress.com by 210.87.254.6 on 09/05/12
For personal use only.

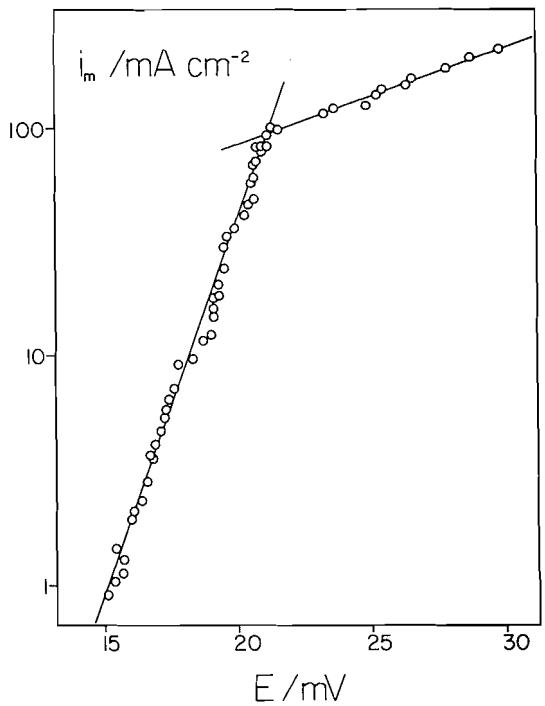

FIG. 3. Log (i_m) vs. E, after correction for ohmic overpotential. 5 M KOH, A = 0.073 cm^2.

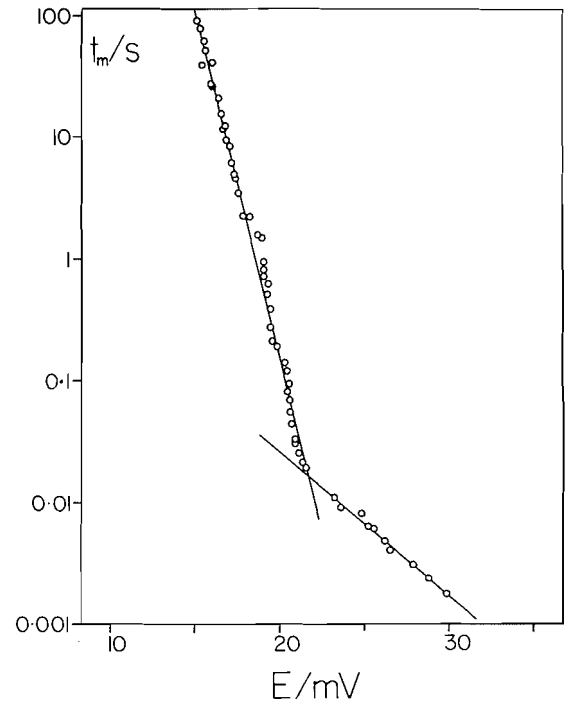

FIG. 4. Log (t_m) vs. E, after correction for ohmic overpotential. 5 M KOH, A = 0.073 cm^2.

taken to achieve i_m (s), although in this case the procedure has been shown to become increasingly inaccurate as E increases (3). Even so, the improvement in the data is substantial and allows the observation of a similar discontinuity to the log (i_m) case (Fig. 4).

Figure 5 shows the variation of log ($i_m t_m$) as a function of E, without including ohmic compensation. Because $i_m t_m \propto Q$ (the charge required to form the 3-D layer (in mC cm^{-2})) this is essentially a plot of log (Q) vs. E. A linear dependence is observed at low overpotentials. Such a variation is a diagnostic criterion of 3-D growth; obviously 2-D (monolayer) growth involves smaller, constant, charge consumption during formation of a layer.

(b) The Linear Potential Sweep Technique

The response of the Hg/KOH (aq) interface to lps is illustrated in a sequence of photographs in Fig. 6. The smaller peak corresponds to monolayer formation whilst the larger peak results from the formation of the three-dimensional multilayer. Concurrent with the observed monolayer formation is the dissolution of Hg(II) species into the bulk of solution. This dissolution reaction is observed in the potential region in which a faradaic pseudo-capacitance was reported by Armstrong *et al.* (1), which was attri-

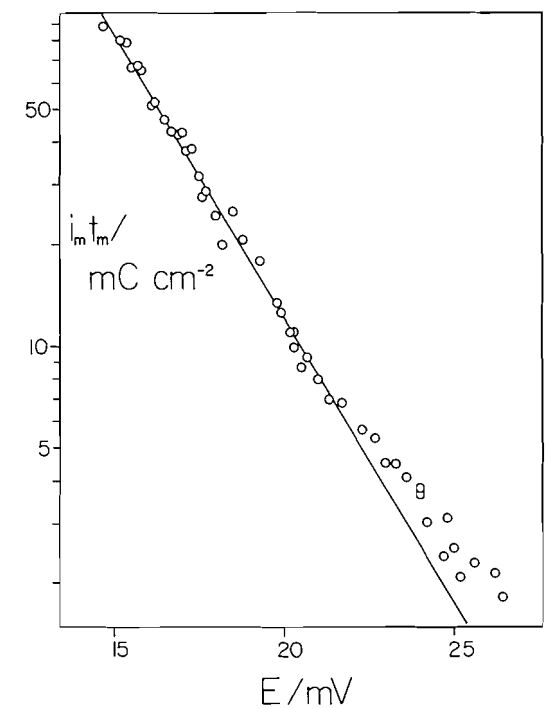

FIG. 5. Log ($i_m t_m$) vs. E, without ohmic correction. 5 M KOH, A = 0.073 cm^2.

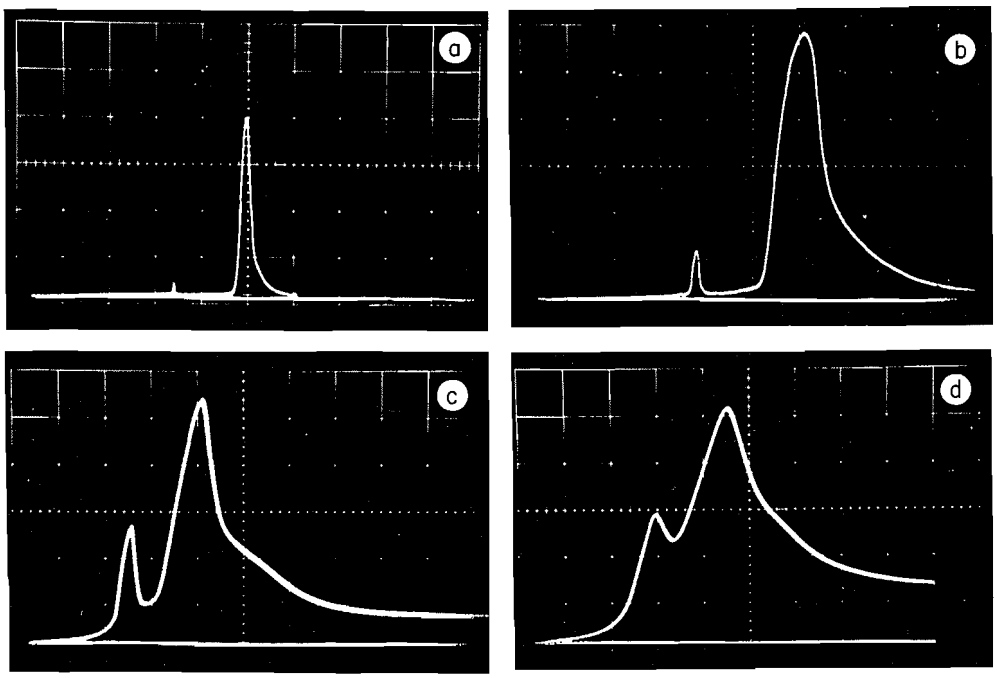

FIG. 6. (*a*) Successive linear potential scans, $\nu = 10$ mV s^{-1}. Horizontal scale: 1 s cm^{-1}; vertical scale: 1 mA cm^{-1}. 5 *M* KOH, $A = 0.073$ cm^2. Scan begins -20 mV. (*b*) Successive linear potential scans, $\nu = 500$ mV s^{-1}. Horizontal scale: 20 ms cm^{-1}; vertical scale: 2.5 mA cm^{-1}. 5 *M* KOH, $A = 0.073$ cm^2. Scan begins -20 mV. (*c*) Successive linear potential scans, $\nu = 10$ V s^{-1}. Horizontal scale: 2 ms cm^{-1}; vertical scale: 5 mA cm^{-1}. 5 *M* KOH, $A = 0.073$ cm^2. Scan begins -20 mV. (*d*) Successive linear potential scans, $\nu = 50$ V s^{-1}. Horizontal scale: 0.5 ms cm^{-1}; vertical scale: 10 mA cm^{-1}. 5 *M* KOH, $A = 0.073$ cm^2. Scan begins -20 mV.

buted to

$$[3] \qquad 2OH^- + Hg \overset{-2e}{\rightleftharpoons} Hg(OH)_2$$

However the contribution to the overall current from this reaction is small. An interesting observation here, clear from Fig. 6, is that the presence of the monolayer does not appear to inhibit the dissolution reaction at all, in agreement with the observations of Armstrong *et al.* (1). A further interesting feature of the voltammograms of Fig. 6 is that the current maximum in voltammograms (i_p (mA)) corresponding to the two-dimensional nucleation and growth process 'catches up' with the current maximum due to the three-dimensional nucleation and growth process as the potential scan rate is increased. At the low scan rates this is in accordance with predictions made on the basis of the computer-simulated data, which may be summarized:

$$[4] \qquad \frac{\partial \log (i_p)}{\partial \log (\nu)} = \text{constant} \; (= 1)$$

where ν is the scan rate (mV s^{-1}), for monolayer formation (4), and

$$[5] \qquad \frac{\partial \log (i_p)}{\partial \log (\nu)} = \text{constant} \; (< 1)$$

for thick layer formation. These predictions are tested experimentally in Figs. 7 and 8 for low values of ν. The expected linearity is observed, although the monolayer case is found to have a gradient slightly less than unity, possibly because of the presence of background currents due to the dissolution process. At high scan rates (and hence high current densities) the influence of ohmic overpotential becomes important, as is also clear in Fig. 6. Although the overall effect is complex (3), the effect of R on i_p and E_p (the peak current and the peak potential at current maximum (mV) respectively) may be determined both in the case of the experiment and the computer simulation. The results are shown in Figs. 9 and 10 for thick layer formation. Identical trends are observed in theory and practice. The diminution of i_p with increasing R is close to exponential, whilst E_p varies almost linearly with R at high R values.

Discussion

(a) Monolayer Growth

A typical current–time transient corresponding to the progressive nucleation and subsequent growth of a monolayer of the (010) plane of mercuric oxide is shown in Fig. 11. The experimental curve is highly distorted because of the presence of uncompensated

Can. J. Chem. Downloaded from www.nrcresearchpress.com by 210.87.254.6 on 09/05/12
For personal use only.

Can. J. Chem. Downloaded from www.nrcresearchpress.com by 210.87.254.6 on 09/05/12
For personal use only.

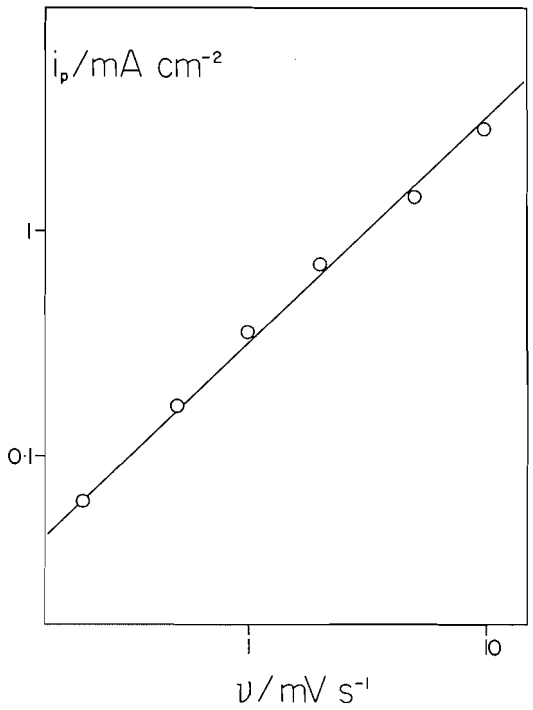

FIG. 7. Linear potential scan, monolayer region. Log (i_p) vs. log (v). 5 *M* KOH, $A = 0.073$ cm^2. Gradient $\simeq 1$.

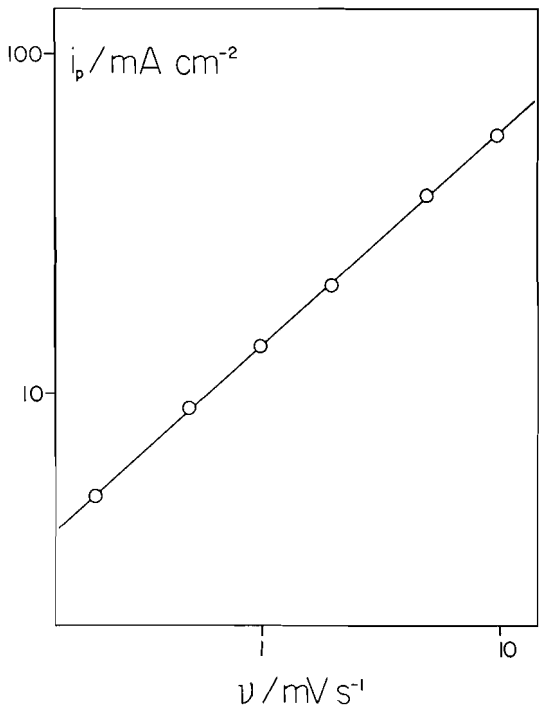

FIG. 8. Linear potential scan, multilayer region. Log (i_p) vs. log (v). 5 *M* KOH, $A = 0.073$ cm^2. Gradient = 0.62.

ohmic overpotential. However, in the absence of any ohmic contribution the current response (i) is given by

$$[6] \quad i = \frac{nFl\pi k^2 A t^2 M}{\rho} \exp\left[\frac{-\pi M^2 k^2 A t^3}{3\rho^2}\right]$$

where l is the height of a monolayer (cm), k is the rate constant for lattice growth (mol cm^{-2} s^{-1}), A is the steady-state nucleation rate constant (nuclei cm^{-2} s^{-1}), M is the gram-molecular weight, and ρ is the density of the layer (g cm^{-3}). Comparison of Fig. 11 with Fig. 6 indicates that when it is desired to minimize ohmic effects on observable parameters, monolayer growth may be more clearly investigated by linear sweep methods than by potential pulse techniques. The theoretical voltammogram has recently been described, and the interested reader is referred to the original paper for details (3). A further advantage of lps techniques is that complications, such as those which frequently arise from dissolution reactions in the potential step method, may be minimized by appropriate adjustment of the scan rate. Furthermore, at very high scan rates the qualitative features of a given system may also be easily identified. This is illustrated in Fig. 6 for the present case of HgO formation.

(b) Multilayer Growth

A model for the growth of the thick layer of HgO on mercury has been described by Armstrong *et al.* (1). Individual nuclei are approximated as right circular cones expanding on the electrode surface. In the absence of ohmic effects the current response of the system at constant step potential is

$$[7] \quad i = nFk_2[1 - \exp(-\pi M^2 k_1^2 A t^3/3\rho^2)] \times \exp(-\pi M^2 k_1^2 A t^3/3\rho^2)$$

where k_1 is the rate constant describing crystal growth parallel to the electrode surface (mol cm^{-2} s^{-1}), k_2 is the rate constant describing crystal growth orthogonal to the electrode surface, and A is the nucleation rate constant. Expressions for i_m and t_m, the current and time at the transient maximum, can be obtained from this equation. Thus

$$[8] \quad i_m = nFk_2/4$$

$$[9] \quad t_m = [3\rho^2 \ln(2)/\pi M^2 k_1^2 A]^{1/3} = \left[\frac{\ln(2)}{\beta}\right]^{1/3}$$

where β is a constant. Combination of [8] and [9] yields

$$[10] \quad i_m t_m = 0.221 nFk_2(3\rho^2/\pi M^2 k_1^2 A)^{1/3}$$

The expression for the charge consumed in the

Can. J. Chem. Downloaded from www.nrcresearchpress.com by 210.87.254.6 on 09/05/12
For personal use only.

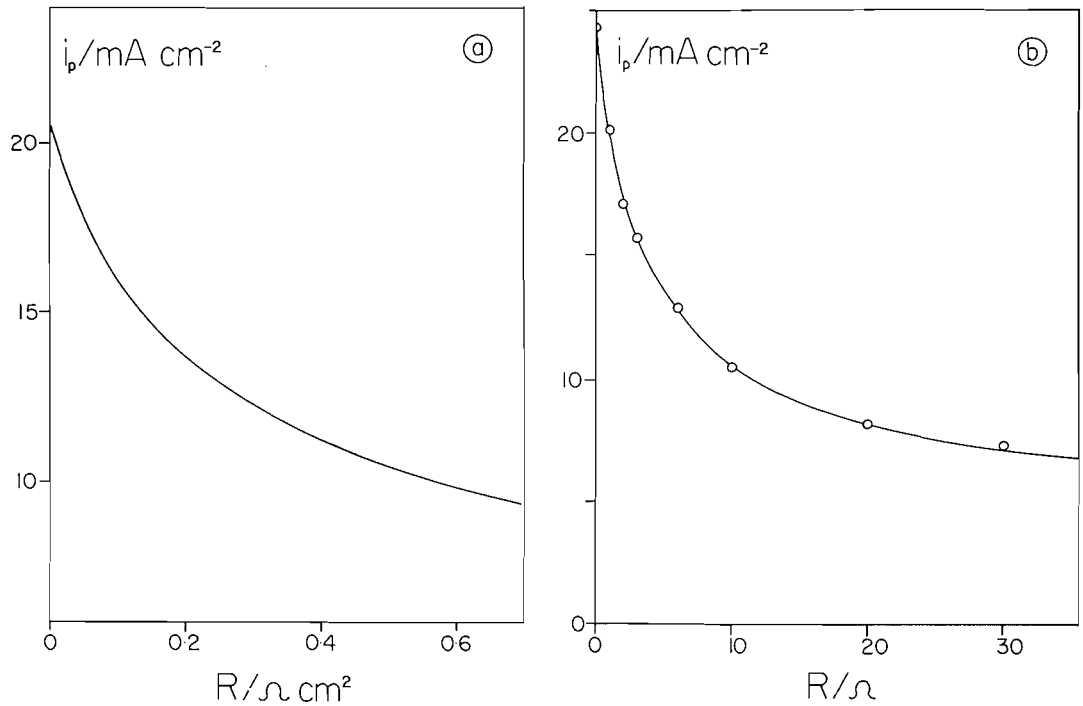

FIG. 9. (*a*) Computer simulation, multilayer case. Effect of R (Ω cm^{-2}) on i_p in linear potential scans. $\nu = 100$ mV s^{-1}, $\Delta E = 0.01$ mV, $\partial E/\partial \log (i_m) = 8$ mV, $\partial E/\partial \log (t_m) = -7$ mV. (*b*) Experimental result, multilayer case. Effect of R (Ω, added) on i_p in linear potential scans. $\nu = 5$ mV s^{-1}, 5 M KOH, $A = 0.073$ cm^2.

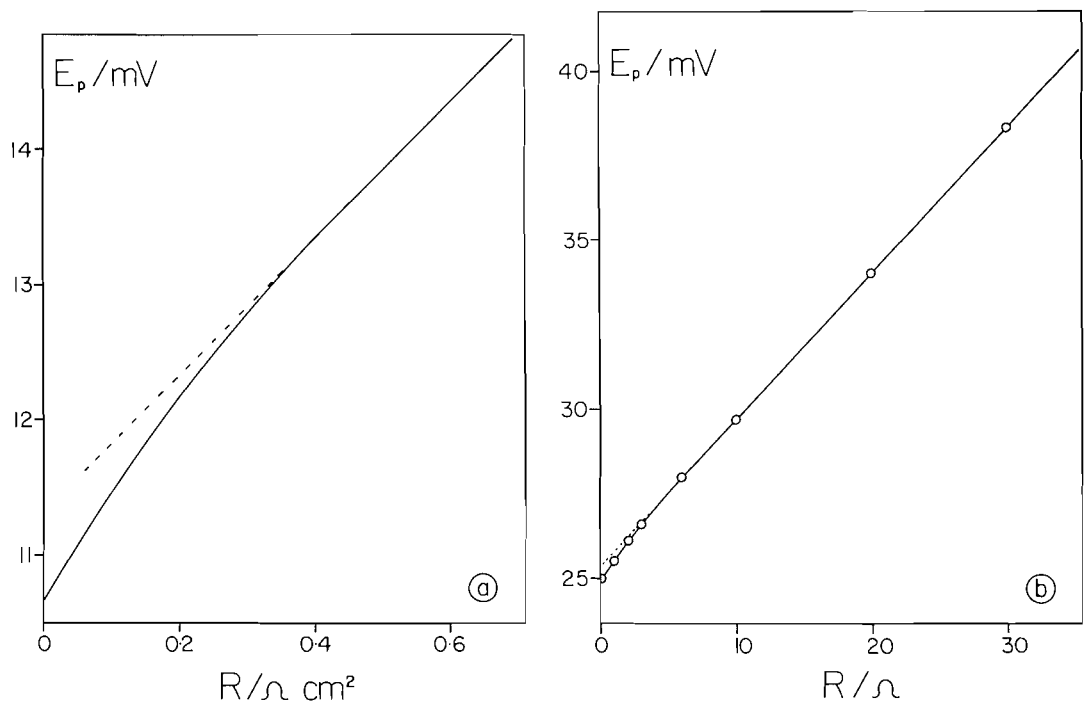

FIG. 10. (*a*) Computer simulation, multilayer case. Effect of R (Ω cm^{-2}) on E_p in linear potential scans. $\nu = 100$ mV s^{-1}, $\Delta E = 0.01$ mV, $\partial E/\partial \log (i_m) = 8$ mV, $\partial E/\partial \log (t_m) = -7$ mV. (*b*) Experimental result, multilayer case. Effect of R (Ω, added) on E_p in linear potential scans. $\nu = 5$ mV s^{-1}, 5 M KOH, $A = 0.073$ cm^2.

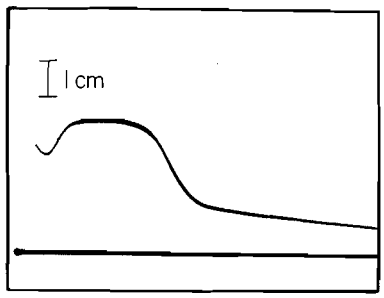

FIG. 11. Potentiostatic pulse from −100 mV to +22.6 mV. Horizontal scale: 0.5 ms cm^{-1}; vertical scale: 1.5 mA cm^{-1}. $A = 0.073$ cm^2. Formation of monolayer.

creation of the thick layer is

$$[11] \qquad Q = \int_0^\infty i\,dt$$

Substitution of [7] in [11] gives the result that

$$[12] \qquad Q = \tfrac{1}{3}nFk_2\Gamma(\tfrac{1}{3})[\beta^{-1/3} - (2\beta)^{-1/3}] = 0.184nFk_2(3\rho^2/\pi M^2 k_1{}^2 A)^{1/3}$$

where Γ is the gamma function. Combination of [10] and [12] shows that

$$[13] \qquad i_m t_m = 1.20Q$$

Equations 10 and 12 contain typographical errors in the original paper (1). The potential dependences of $k_1{}^2A$, k_2, and Q may now be evaluated from the ohmically corrected data shown in Figs. 3 and 4. The results at low overpotentials are

$$[14] \quad \partial \log (k_2)/\partial E = (3.1 \pm 0.2 \text{ mV decade}^{-1})^{-1}$$

$$[15] \quad \partial \log (k_1{}^2A)/\partial E = (0.7 \pm 0.1 \text{ mV decade}^{-1})^{-1}$$

$$[16] \quad \partial \log Q/\partial E = (-5.7 \pm 0.4 \text{ mV decade}^{-1})^{-1}$$

As described earlier, it is apparent that discontinuities appear in the corrected experimental data at high overpotentials. Comparison with the computer-simulated data indicates that only $\partial \log (k_2)/\partial E$ may be evaluated with complete accuracy in such overpotential regions, via eq. 8. The result is that, at high overpotentials,

$$[17] \quad \partial \log (k_2)/\partial E = ((30 \pm 5) \text{ mV decade}^{-1})^{-1}$$

Unfortunately, no model in the literature is able to explain the observed discontinuities, although k_2 is expected to behave according to

$$[18] \quad k_2 = k'\left[\exp\frac{\alpha nF}{RT}\eta - \exp\frac{(1-\alpha)nF}{RT}\eta\right]$$

where k' is a constant and η is the overpotential (mV), in regions of high overpotential (7). For a reversible two-electron transfer reaction this equation predicts a 30 mV decade^{-1} Tafel slope in close agreement with that obtained. Further discussion of this point may be found elsewhere (3, 5).

Using the assumption that the rate constants for lattice growth (k_1,k_2) exhibit an exponential dependence on overpotential (1), the computer simulation is able to predict the response of both the monolayer (4) and the thick layer (8) to linear scans of potential. Typical experimental data are shown in Fig. 6, and the theory is tested in Figs. 7 and 8. The expected dependences are observed in accordance with [4] and [5], but some residual doubt remains concerning the accuracy of the derived gradients. This is more true of the monolayer than the thick layer, because of its proximity to the dissolution reaction. The observed value of $\partial \log(i_p)/\partial \log(v)$ for the thick layer is 0.62. This should be compared with the value 0.50 which would be observed for a diffusion-controlled reaction.

Finally, the computer-simulated dependence of i_p and E_p on R for the thick layer is compared to experiment in Figs. 9 and 10. The experimental trends are in very close agreement with prediction, although exact numerical correlation is naturally precluded because of the arbitrary values of the growth parameters employed in the simulation.

Conclusion

The formation of mercuric oxide on mercury has been examined in aqueous alkaline solution. The system was investigated because of its importance as a reference electrode system, and also because it provides a model with which to test recent theoretical predictions. An improvement in the accuracy of experimentally determined parameters is reported, principally due to the application of developments in ohmic compensation procedures (3). The results are compared to computer simulations of the growth mechanisms, and good agreement has been found.

Acknowledgement

This work has been financially supported by a grant from the National Research Council of Canada.

1. R. D. ARMSTRONG, J. FLEISHMANN, and H. R. THIRSK. J. Electroanal. Chem. **11**, 208 (1966).
2. M. AVRAMI. J. Chem. Phys. **9**, 177 (1941).
3. R. G. BARRADAS, F. C. BENSON, S. FLETCHER, and J. D. PORTER. J. Electroanal. Chem. **85**, 57 (1977).
4. R. G. BARRADAS, F. C. BENSON, and S. FLETCHER. Electrochim. Acta, **22**, 1197 (1977).
5. R. G. BARRADAS, F. C. BENSON, S. FLETCHER, and J. D. PORTER. J. Electroanal. Chem. **85**, 67 (1977).
6. C. DEBOOR. *In* Spline functions and approximation theory. *Edited by* A. Meir and A. Sharma. Birkhäuser Verlag, Basel. 1973.
7. E. B. BUDEVSKI. Prog. Surf. Membr. Sci. **11**, 71 (1976).
8. R. G. BARRADAS, F. C. BENSON, and S. FLETCHER. J. Electroanal. Chem. **80**, 305 (1977).

Can. J. Chem. Downloaded from www.nrcresearchpress.com by 210.87.254.6 on 09/05/12
For personal use only.

Complex fluoroanions in solution. VII. Replacement of fluoride by trifluoroacetate[1]

S. BROWNSTEIN

Division of Chemistry, National Research Council of Canada, Ottawa, Ont., Canada K1A 0R9

Received August 2, 1977

S. BROWNSTEIN. Can. J. Chem. **56**, 343 (1978).

Binary fluorides of groups III, IV, V, VI, and VII of the periodic table form complex fluoroanions with the trifluoroacetate ion. There is frequently disproportionation to yield species containing more than one trifluoroacetate group. Fluorine and trifluoroacetate exchange reactions are usually slow on the nmr time scale at −70°C.

S. BROWNSTEIN. Can. J. Chem. **56**, 343 (1978).

Les fluorures binaires des groupes III, IV, V, VI et VII de la table périodique forment des fluoroanions complexes par réaction avec l'ion trifluoroacétate. Il se produit fréquemment une dismutation conduisant à des espèces contenant plus qu'un groupe trifluoroacétate. Les réactions d'échange du fluor et du trifluoroacétate sont généralement lentes par comparaison avec l'échelle de temps de la rmn à −70°C.

[Traduit par le journal]

Introduction

Trifluoroacetates have been extensively studied and in some ways are similar to fluorides (1). Only three fully substituted anionic species, $B(TFA)_4^-$, $Ge(TFA)_6^{2-}$, and $Te(TFA)_6^{2-}$, where TFA is trifluoroacetate, have been reported (1). The only mixed species containing both fluoride and TFA radicals found thus far are $HSbF_5TFA$ and perhaps $(SbF_5)_2TFA^-$ (2). Fluoroanions frequently form fluorine bridged complex fluoroanions with binary fluorides (3). It is of interest to see if mixed fluoride, TFA species can be prepared and if they are capable of complex anion formation.

Experimental

Fluorine resonance spectra were obtained at 94.1 MHz on either a 'Varian Associates' HA-100D or XL-100A spectrometer. In the latter case Fourier transform spectra were obtained with a 'Nicolet Instruments' TT100A accessory. Chemical shifts are reported in ppm with respect to $CFCl_3$ as zero and with shifts to high field considered negative. Samples were prepared with great care to exclude moisture using standard vacuum line and dry box techniques. Vapor pressure studies were done in a manner previously described except for pressure measurement by a 'Baratron' diaphragm manometer rather than a constant volume mercury manometer (4).

Tetramethylammonium trifluoroacetate (TMATFA) and tetrabutylammonium trifluoroacetate (TBATFA) were prepared by reaction of sodium trifluoroacetate with the corresponding ammonium chloride in methanol as solvent. After filtration of the sodium chloride the solvent was evaporated and the product recrystallized from a suitable solvent (acetone in the case of TMATFA and methylene chloride – ether for TBATFA).

Aluminum trifluoride, purchased from Ozark-Mahoning, was used as received. Tin tetrafluoride, titanium tetrafluoride, and zirconium tetrafluoride were purified by vacuum sublimination shortly before use. These four solids were manipulated at all times in a vacuum dry box.

Silicon tetrafluoride, purchased from Matheson, germanium tetrafluoride, sulfur tetrafluoride, and tellurium hexafluoride, purchased from Ozark-Mahoning, and phosphorus trifluoride, purchased from PCR Research Chemicals, were used directly from the cylinder. Iodine pentafluoride, purchased from Allied Chemical, was purified by trap to trap distillation. Boron trifluoride, phosphorus, arsenic, vanadium, niobium, and tantalum pentafluorides and molybdenum and tungsten hexafluorides were handled as described in earlier articles in this series (3).

Results and Discussion

It is found that complexing of binary fluorides with the trifluoroacetate ion is very widespread. The complexes will be described according to the position of the binary fluoride in the periodic table.

Group III

Boron Trifluoride

Reaction proceeds according to eqs. 1 and 2 from the results of fluorine resonance spectroscopy. The nuclear resonance parameters are listed in Table 1.

$$[1] \qquad BF_3 + CF_3COO^- \rightarrow BF_3CF_3COO^-$$

$$[2] \qquad 2BF_3CF_3COO^- \rightleftharpoons BF_4^- + BF_2(CF_3COO)_2^-$$

Further disproportionation to $BF(CF_3COO)_3^-$ or $B(CF_3COO)_2^-$ cannot be excluded, although a large percentage of $BF(CF_3COO)_4^-$ would have been observed in the fluorine resonance spectrum. Assignment of the line for BF_4^- was made by comparison with an authentic sample, and the remainder from relative intensities. The spectrum is shown in Fig. 1. With an excess of BF_3 there is an averaging of all the signals from fluorine bonded to boron, even at −100°C. From vapor pressure measurements of BF_3 over a methylene chloride solution of TBATFA it is found that 1.59 equivalents of BF_3 is complexed at −40°C and 1.64 equivalents at −53°C. Com-

[1]NRCC No. 16379.

Can. J. Chem. Downloaded from www.nrcresearchpress.com by 210.87.254.40 on 09/05/12
For personal use only.

Can. J. Chem. Downloaded from www.nrcresearchpress.com by 210.87.254.40 on 09/05/12
For personal use only.

TABLE 1. Fluorine chemical shifts and coupling constants in complex species

Species	δF_1	J_{M-F_1} (Hz)	δF_2	J_{M-F_2} (Hz)	$J_{F_1-F_2}$ (Hz)	δF_3	δF_4	δF_5
$^{11}BF_4^-$	−139.80	1						
$^{10}BF_4^-$	−139.75	—						
$^{11}BF_3TFA^-$	−141.00	4.5						
$^{10}BF_3TFA^-$	−140.98	—						
$BF_2(TFA)_2^-$	−142.3	9						
PF_5TFA^-	− 78.0	740	−63.2	770	60			
AsF_5TFA^-	−66.3		−54.4		125			
$V_2F_9(TFA)_2^-$	492		421		90	−14	254	236
NbF_5TFA^-			128					
TaF_5TFA^-	73.7		56.6		27.5			
$TaF_4(TFA)_2^-$	70.3		86.9		26.5			
cis $SF_4(TFA)_2^-$	72.6		32.5		60			
$MoF_7(TFA)^{2-}$	142.8	69	−129.1		54			
$MoF_5(TFA)_3^{2-}$	134.8		−60.3		54			
$WF_7(TFA)^{2-}$	65.6	72	−145.0	48	57.3			
$WF_5(TFA)_3^{2-}$	57.3	73	−67.1	60	51			
WF_8^{2-}	63.8	68						
IF_5TFA^-	53.6		4.1		68			

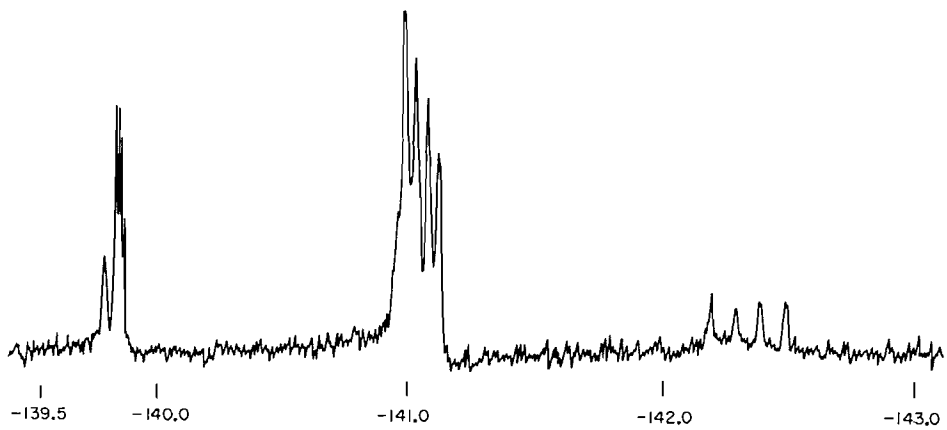

FIG. 1. The fluorine bonded to boron region of the reaction products of BF_3 and $(CH_3)_4NTFA$.

plexes containing more than one BF_3 per anion are required to explain this result.

Aluminum Trifluoride

No complex formation is observed.

Group IV

Silicon Tetrafluoride

A complex is formed in sulfur dioxide solution at −70°C with a fluorine chemical shift of −130.6 (sharp line).

Germanium Tetrafluoride

Complexes are formed which give many well resolved fluorine resonance lines from −87 to −100 ppm.

Tin Tetrafluoride

The situation is the same as for germanium tetrafluoride except for the chemical shifts from −110 to −130 ppm and a different pattern of lines.

Titanium Tetrafluoride

More than 80 well resolved resonance lines are observed for fluorine bonded to titanium, probably from a variety of complexes. Bridging fluorine signals are found from −10 to −20 ppm and directly bonded fluorine signals appear from 150 to 240 ppm. These are in the regions previously reported for binary complex fluoroanions of titanium, but do not correspond with any of the previously reported species (5).

Zirconium Tetrafluoride

No complex formation is observed.

Group V

Phosphorus Trifluoride

No complex formation is observed.

Phosphorus Pentafluoride

With an excess of TFA^- a complex of structure **1**

Can. J. Chem. Downloaded from www.nrcresearchpress.com by 210.87.254.40 on 09/05/12
For personal use only.

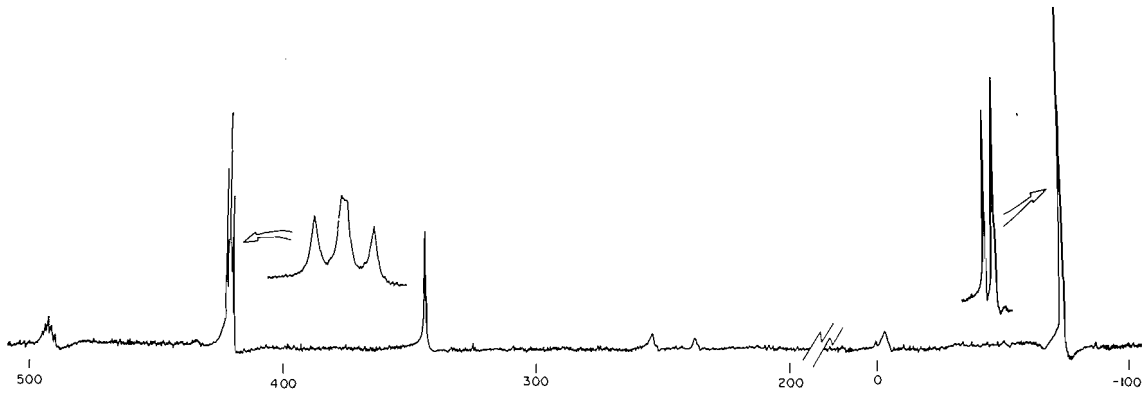

FIG. 2. The fluorine resonance spectrum of an equimolar solution of TBATFA and VF_5 in SO_2ClF at $-100°C$.

is formed. Its fluorine resonance parameters are listed in Table 1. With an excess of PF_5 only a single broad line is observed for fluorine bonded to phosphorus because of rapid averaging. There is no evidence, from vapor pressure measurements, for complexing of PF_5 beyond a 1:1 ratio.

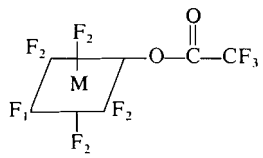

1

Arsenic Pentafluoride

With an excess of TFA^- and at $-120°C$ fluorine exchange is sufficiently slowed that a complex of structure I may be identified by its fluorine resonance spectrum. The parameters are listed in Table 1.

Vanadium Pentafluoride

The spectrum from equivalent amounts of VF_5 and TBATFA, shown in Fig. 2, may be explained as

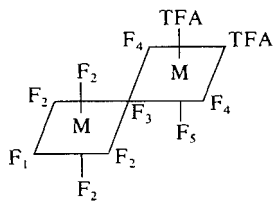

2

arising from structure **2**. The quintet is attributed to F_1. In similar complex fluoroanions the terminal fluorine is found at about 500 ppm (3). The doublet of doublets is assigned to F_2, spin coupled to F_1 and F_3. Fluorines in this environment have been observed near 430 ppm. The bridging fluorine, F_3, is allocated to the broad line at -14 ppm, in agreement with the value 13 in polymeric vanadium pentafluoride. The lines at 254 and 236 ppm are assigned to F_4 and F_5 respectively. These are halfway between 345 and 130 ppm, the chemical shifts of VF_6^- and $VF_4(OH)_2^-$. A possible mode of formation is given by eqs. 3 and 4.

[3] $$2VF_5TFA^- \rightarrow cis\ VF_4(TFA)_2^- + VF_6^-$$

[4] $$cis\ VF_4(TFA)_2^- + VF_5 \rightarrow V_2F_9(TFA)_2^-$$

These reactions are consistent with the formation of a *cis* 1:2 complex by TaF_5 and further complexing with the binary fluoride as found with BF_3. It would be difficult to fit the observed spectrum to a species with a bridging trifluoroacetate group. The fluorine resonance parameters are listed in Table 1.

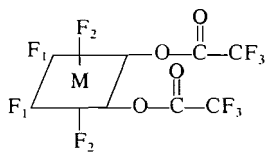

3

Niobium Pentafluoride

Solutions of NbF_5 and TBATFA give a single rather broad line for fluorine bonded to niobium at 128 ppm. It was not possible to lower the temperature sufficiently to slow the fluorine exchange. The chemical shift value indicates that complex formation has occurred.

Tantalum Pentafluoride

A 1:1 complex of structure **1** and a 1:2 complex of structure **3** are both formed. The fluorine resonance parameters are listed in Table 1.

Group VI

Sulfur Tetrafluoride

A 1:2 complex of structure **3** is formed. An additional line in the fluorine resonance spectrum at 16.8 may be from the *trans* 1:2 complex. The com-

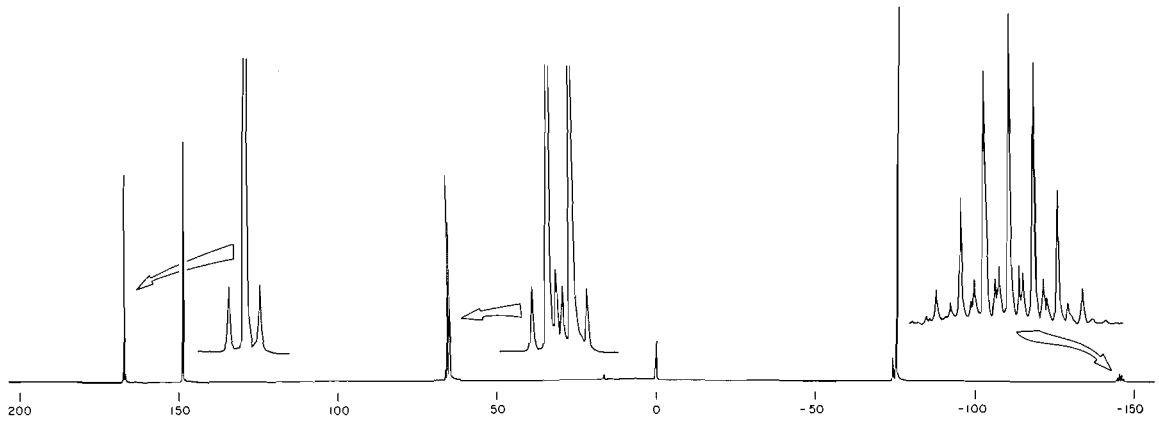

FIG. 3. The fluorine resonance spectrum of an equimolar solution of TMATFA and WF_6 in SO_2 at $-70°C$.

TABLE 2. Relative intensities of fluorine resonance signals in TFA–WF_6 samples[a]

	Species 1		Species 2		Species 3		Species 4		Species 5	
Time	Shift	Intensity	Shift	Intensity	Shift	Intensity	Shift	Intensity	Shift	Intensity
					1:1 Sample					
Initial	166.70	547	148.50	1068	65.50	373				
1 h	166.70	323	148.51	820	65.53	377				
4 h	166.72	245	145.64	684	65.65	556				
					2:1 Sample					
Initial	166.67	44	148.51	532			172	—	—	
1 h	—	—	148.62	217			140	57.92	134	
4 h	—	—	148.78	171			138	58.11	202	

[a]Relative to $CFCl_3$ as 100.

plexes are completely dissociated at room temperature.

Tellurium Hexafluoride

In SO_2 solution at $-70°C$ there is a broad weak peak at -53.8 in the fluorine resonance spectrum which may be due to partial complex formation. In CH_2Cl_2 as solvent there is no complex formation even at $-100°C$.

Molybdenum Hexafluoride

Two complexes have been identified with structures **4** and **5**. The fluorine resonance parameters are listed in Table 1. Justification for these assignments will be given for the corresponding complexes with tungsten hexafluoride.

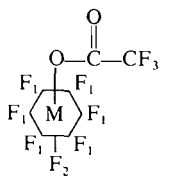

4

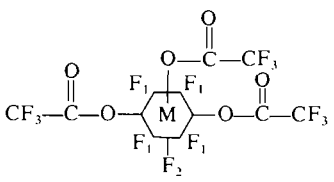

5

Tungsten Hexafluoride

Several complexes are formed with the trifluoroacetate ion. The fluorine resonance spectrum of an equilibrated sulfur dioxide solution of equimolar quantities of TMATFA and WF_6 at $-70°C$ is shown in Fig. 3. It is difficult to find a reasonable structure, other than **4** which has six and one magnetically equivalent fluorines. The proposed hexagonal bipyramid structure is also consistent with that proposed for $WF_6[(CH_3)_2S]_2$ (6). There is rapid exchange on the nmr time scale at room temperature for the fluorines in the different chemical environments. It is found that after some time at room temperature and subsequent cooling to $-70°C$ the fluorine resonance spectra of TMATFA + WF_6 samples are changed. This behaviour is presented in Table 2. Species 1 (WF_6) and Species 2 decrease in concentration with time while Species 3 (WF_7TFA^{2-}) increases. These results may be explained by the reactions shown in eqs. 5 and 6.

$$[5] \qquad WF_6 + TFA^- \rightarrow WF_6TFA^-$$

$$[6] \qquad 2WF_6TFA^- \rightarrow WF_7TFA^{2-} + WF_5TFA$$

The line at 148.5 (Species 2) must then be attributed to a rapidly averaging mixture of WF_6TFA^- and WF_5TFA since these are the only species not accounted for. The chemical shift and absence of satellites from fluorine–tungsten spin coupling for

Can. J. Chem. Downloaded from www.nrcresearchpress.com by 210.87.254.40 on 09/05/12
For personal use only.

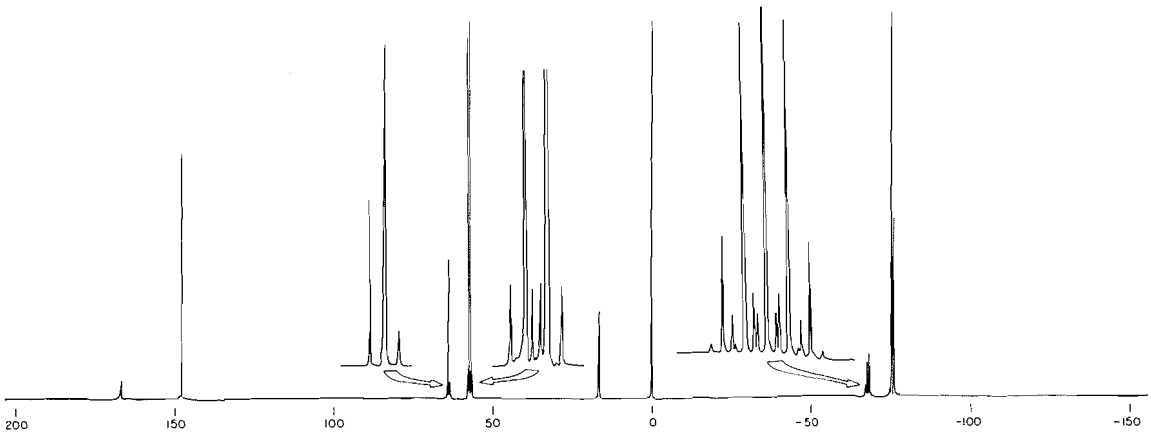

FIG. 4. The fluorine resonance spectrum at −70°C of an SO_2 solution of WF_6 and two equivalents of TMATFA.

this signal are consistent with the results obtained with other Lewis bases (6), and with rapid averaging. A solution of the same composition but with $CHFCl_2$ as solvent has the same fluorine resonance spectrum with the addition of a weak doublet at 56.4 (J = 51 Hz).

With two equivalents of TFA for each WF_6 in $CHFCl_2$ as solvent an additional line is found at 60.8 with satellites from W–F spin coupling. A solution of the same composition in sulfur dioxide, when well equilibrated, has the fluorine resonance spectrum shown in Fig. 4. The doublet and quintuplet are assigned to $WF_5(TFA)_3^{2-}$ with the geometry of Structure **5**, and may be formed according to eq. 7 or 8.

[7] $3WF_6TFA^- + 3TFA^- \rightarrow WF_8^{2-} + 2WF_5(TFA)_3^{2-}$

[8] $3WF_7TFA^{2-} \rightarrow 2WF_8^{2-} + WF_5(TFA)_3^{2-}$

Support for this scheme comes from the time dependence of the fluorine resonance spectrum of a 2:1 sample as listed in Table 2. Free WF_6 rapidly disappears and the 1:1 complex slowly disappears as reactions 6 and 7 occur. Further study is needed to fully elucidate the details of this system. The fluorine resonance parameters are listed in Table 1.

Group VII

Iodine Pentafluoride

A 1:1 complex of structure **1** is formed at low temperature and has the fluorine resonance parameters given in Table 1.

Conclusions

The trifluoroacetate ion complexes readily with binary fluorides to yield mixed fluoroanions. In some cases these undergo disproportionation to yield anions containing more than the original number of trifluoroacetate groups. With boron, vanadium, titanium, and tin there is strong evidence for complex fluoroanion formation via fluorine bridging.

1. C. D. GARNER and B. HUGHES. Adv. Inorg. Chem. Radiochem. **17**, 1 (1975).
2. M. G. HARRISS and J. B. MILNE. Can. J. Chem. **49**, 2937 (1971).
3. S. BROWNSTEIN and G. LATREMOUILLE. Can. J. Chem. **52**, 2236 (1974).
4. S. BROWNSTEIN and J. PAASIVIRTA. Can. J. Chem. **43**, 1645 (1965).
5. P. A. W. DEAN. Can. J. Chem. **51**, 4024 (1973).
6. S. BROWNSTEIN, B. H. CHRISTIAN, G. LATREMOUILLE, and A. STEIGEL. Can. J. Chem. **54**, 2343 (1976).

Can. J. Chem. Downloaded from www.nrcresearchpress.com by 210.87.254.40 on 09/05/12
For personal use only.

Vapour pressures of aqueous solutions of (Ag, Tl, Cd)NO_3 at 98.5°C. I. Brunauer–Emmett–Teller isotherms

JAMES MALCOLM SANGSTER[1]

Département de Génie Chimique, Ecole Polytechnique, Campus de l'Université de Montréal, Case postale 6079, Succursale A, Montréal (Qué.), Canada H3C 3A7

AND

MARIE-CHRISTINE ABRAHAM AND MAURICE ABRAHAM

Département de Chimie, Université de Montréal, Case postale 6210, Succursale A, Montréal (Qué.), Canada H3C 3V1

Received June 22, 1977

JAMES MALCOLM SANGSTER, MARIE-CHRISTINE ABRAHAM, and MAURICE ABRAHAM. Can. J. Chem. **56**, 348 (1978).

Vapour pressures of aqueous solutions of the mixed melt $AgNO_3$ + $TlNO_3$ + $Cd(NO_3)_2$ have been measured at 98.5°C by the static technique. The Ag/Tl mole ratio was fixed at 1.06, and the mole fractions Cd/(Ag + Tl + Cd) of Cd in the melt were 0, 0.05, 0.075, 0.10, and 0.125. Adapted BET isotherms and their constants were obtained for each of the five melt mixtures. It has been shown, in the present study, from the BET equation itself, and verified experimentally, that certain systems can give rise to a 'crossover point', that is, a reversal of sign of the deviation from Raoult's law. The BET constants of the systems conform to simple additivity rules. The water concentration range over which the BET equation is valid is unexpectedly wide.

JAMES MALCOLM SANGSTER, MARIE-CHRISTINE ABRAHAM et MAURICE ABRAHAM. Can. J. Chem. **56**, 348 (1978).

Par mesure des pressions de vapeur, à l'aide de la méthode statique, on a déterminé les constantes BET de dissolution de l'eau dans cinq mélanges fondus $AgNO_3$ + $TlNO_3$ + $Cd(NO_3)_2$ à 98.5°C, pour un rapport molaire Ag/Tl = 1.06 et des rapports molaires Cd/Ag + Tl + Cd = 0, 0.05, 0.075, 0.1 et 0.125. On a montré, dans cette étude, par application de la théorie BET adaptée, et vérifié expérimentalement, que certains systèmes peuvent présenter un point dit "de compensation", situé hors du domaine d'idéalité de Raoult, où l'activité de l'eau est égale à sa fraction molaire. Les constantes de la théorie BET adaptée suivent des règles d'additivité que l'on a discutées. Ces systèmes sont remarquables pour le grand intervalle de concentration en eau où la théorie BET adaptée s'applique d'une manière satisfaisante.

Introduction

In an earlier article (1), we reported the results of vapour pressure measurements of the system (Ag, Tl)NO_3 + H_2O at 98.5°C, at the mole ratio Ag/Tl = 1.14. When this ratio is near 1, the system is liquid at temperatures near 100°C at all water concentrations (2). This system showed positive deviations from Raoult's law throughout the water concentration range studied. This behaviour is quite rare among aqueous electrolyte solutions, and it was postulated that this observation is connected with the fact that Ag^+ and Tl^+ are both relatively weakly hydrated ions.

To test this idea, it was decided to add another cation which was more strongly hydrated than Ag^+ or Tl^+, and which would form melts with the same water solubility as previous ones. Cadmium answered these requirements, and we report here vapour pressure measurements of the system (Ag, Tl, Cd)NO_3 + H_2O at 98.5°C, varying separately the Cd content of the melt, and the water concentration as before. This first article presents the vapour pressure data and discusses the Raoult's law behaviour and BET isotherms of five Cd concentrations in the melt. The second article will discuss the results in terms of Henry's law and the excess free energy.

[1]Author to whom correspondence should be addressed.

Experimental

Vapour pressures were measured by the static technique, the details of which were given previously (1). The same sample manipulation was used, except that $Cd(NO_3)_2 \cdot 4H_2O$ (Fisher, 99.9%) was added to the melt to give the desired cadmium content, and the water was driven off by heating *in vacuo* at about 200°C. The Ag/Tl ratio was fixed at 1.06, corresponding to the composition of an $AgNO_3/TlNO_3$ eutectic (3); this ratio is very close to the one used previously (1). All measurements were done at 98.50 ± 0.05°C.

The data were treated in the same manner as before, the fugacity f being calculated from the pressure p by means of the second virial coefficient of water vapour at 98.5°C, and the water activity a_w from the ratio f/f_0, f_0 being the fugacity of pure water at the same temperature. The mole fraction activity

Can. J. Chem. Downloaded from www.nrcresearchpress.com by 210.87.254.105 on 09/05/12
For personal use only.

Can. J. Chem. Downloaded from www.nrcresearchpress.com by 210.87.254.105 on 09/05/12
For personal use only.

coefficient of water, γ_w, was the ratio a_w/x_w, where x_w is the mole fraction of water in the solution.

Results and Discussion

To facilitate the presentation and discussion of the results, we have adopted the designation S_X to indicate the cadmium content of the melt[2] in a solution. The subscript X indicates the mole percentage of $Cd(NO_3)_2$ in the melt, and Table 1 gives this information explicitly for the five Cd contents used in this work. For example, S_5 indicates a solution $AgNO_3 + TlNO_3 + Cd(NO_3)_2 + H_2O$, obtained by adding water to the melt whose composition is, in mole fractions: $AgNO_3$, 0.489; $TlNO_3$, 0.461: $Cd(NO_3)_2$, 0.050.

Experimental values of p, f, a_w, and γ_w for the systems S_0, S_5, $S_{7.5}$, S_{10}, and $S_{12.5}$ are given elsewhere.[3]

Raoult's Law

Plots of a_w vs. x_w are given in Fig. 1 for the systems S_0, $S_{7.5}$, and $S_{12.5}$. (To avoid undue clutter in the figure, the curves for S_5 and S_{10} are not included; they lie, however, in the appropriate positions intermediate among the three shown.) As was found previously (1), the cadmium-free system shows positive deviations throughout. As Cd is added successively, the curves are pushed downward in a regular manner, i.e., for any x_w, a_w decreases step by step as the Cd content of the melt is increased. This tends to confirm our expectation that positive and negative deviations from Raoult's law are connected with the presence of weakly and strongly hydrated cations respectively.

The curve is at the same time distorted into an S shape upon addition of Cd. As a consequence, each of the curves for intermediate Cd concentrations (S_5, $S_{7.5}$, and S_{10}) crosses the ideal Raoult's law line at one point (and one point only). The crossover point is displaced toward the pure water end as the Cd concentration increases and the curve, originally concave to the abscissa (system S_0), gradually becomes more convex. The change from concave to convex does not proceed via a general flattening (as one might naively have expected), but via the S shape.

BET Isotherms

This rather complicated behaviour can perhaps be better understood in the light of the conformity of these systems to the BET isotherm equation. This

TABLE 1. Explanation of the nomenclature used for designating the composition of the melt

	Composition (mole fraction)		
Designation	$AgNO_3$	$TlNO_3$	$Cd(NO_3)_2$
S_0	0.515	0.485	0
S_5	0.489	0.461	0.050
$S_{7.5}$	0.476	0.449	0.075
S_{10}	0.464	0.436	0.100
$S_{12.5}$	0.451	0.424	0.125

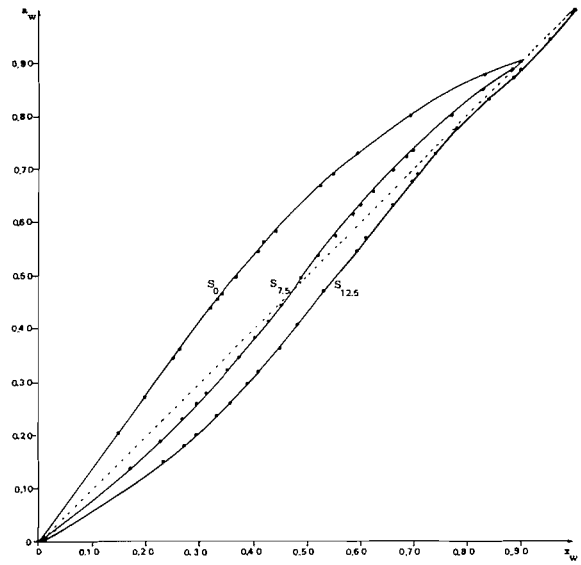

FIG. 1. Raoult's law curves for the system (Ag, Tl, Cd)NO_3 + H_2O at 98.5°C, for three Cd concentrations in the melt. Dashed line represents ideal behaviour.

equation was adapted by Stokes and Robinson (4) to very concentrated electrolyte solutions, and can be written as

$$[1] \quad a_w(1 - x_w)/x_w(1 - a_w) = 1/cr + (c - 1)a_w/cr$$

in which r and c are the BET constants. The number of water molecules adsorbed per complete monolayer on a solute molecule is r, and c is given approximately by $c = \exp[-(E - E_L)/RT]$, $(E - E_L)$ being the difference between the energy of adsorption of water in the monolayer and the energy of liquefaction of bulk water.

Figure 2 shows that all five systems studied here conform to the BET equation over the same wide range of water concentration, as previously observed (1). It follows from this result that the Raoult's law curve may have *only one* crossover point, as suggested by Fig. 1. At the crossover point, $a_w = x_w$; making this substitution in eq. 1, we solve for x_w and

[2]The word 'melt' in this article signifies the anhydrous electrolyte mixture.

[3]A complete set of the actual experimental data is available, at a nominal charge, from the Depository of Unpublished Data, CISTI, National Research Council of Canada, Ottawa, Ont., Canada K1A 0S2.

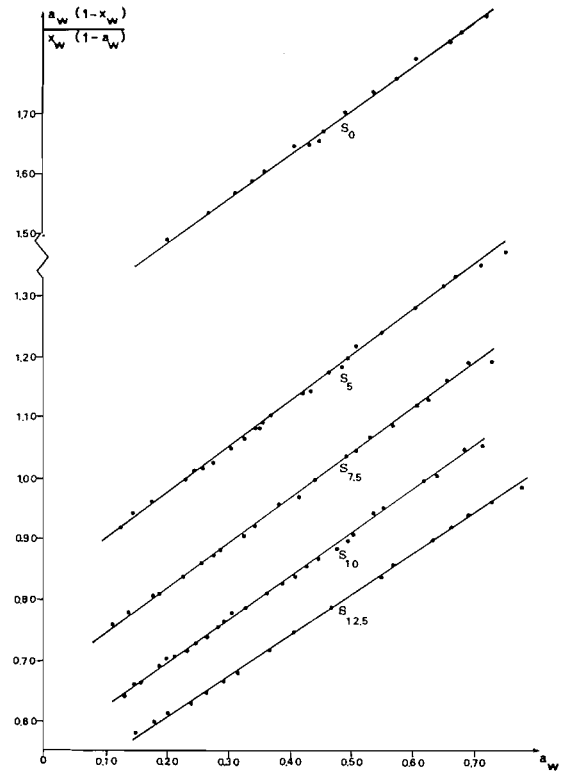

FIG. 2. The BET isotherms for the system (Ag, Tl, Cd)NO_3 + H_2O at 98.5°C, for five Cd concentrations in the melt.

obtain

$$[2] \qquad x_w = (cr - 1)/(c - 1)$$

Equation 2 shows that the crossover point is uniquely determined by the BET constants. Since $0 \leq x_w \leq 1$, eq. 2 also implies that

$$[3] \qquad 0 \leq (cr - 1)/(c - 1) \leq 1$$

for any system exhibiting a crossover point. This ratio is given in Table 2 for the five systems studied. It is seen that eq. 3 is a necessary, *though not sufficient*, condition for the appearance of a crossover point in these systems.

Additivity Rules

Table 2 shows that r and $-(E - E_L)$ increase regularly with Cd concentration. This suggests the possibility of finding linear dependences upon Cd mole fraction (say). For r, we take r_0 as the number of moles of water in the complete monolayer of 1 mol of solute in system S_0 (we shall suppose that cations only are hydrated). The corresponding number of moles of water for 1 mol of Cd^{2+} in S_5, $S_{7.5}$, S_{10}, and $S_{12.5}$ is r_1. We would expect r to be a weighted sum of r_0 and r_1, such as

TABLE 2. The constants of the BET equation (eq. 1) for the system (Ag, Tl, Cd)NO_3 + H_2O at 98.5°C, and the upper a_w limit of validity of this equation

	r	c	$-(E - E_L)$ (kcal/mol)	$\frac{cr - 1}{c - 1}$	a_w limit
S_0	0.486	1.54	0.317	−0.47	0.75
S_5	0.639	1.90	0.474	0.24	0.70
$S_{7.5}$	0.715	2.10	0.548	0.55	0.70
S_{10}	0.801	2.27	0.605	0.64	0.70
$S_{12.5}$	0.883	2.39	0.642	0.80	0.80

$$[4] \qquad r = X_{(Ag+Tl)}r_0 + X_{Cd}r_1$$

where the X's are cationic mole fractions in the melt (for example, if n represents number of moles, $X_{Cd} = n_{Cd}/(n_{Ag} + n_{Tl} + n_{Cd})$). If the substitution $X_{(Ag+Tl)} = 1 - X_{Cd}$ is made in eq. 4, then upon rearrangement we have

$$[5] \qquad r = r_0 + (r_1 - r_0)X_{Cd}$$

It has been assumed here that r_1 and r_0 are independent of X_{Cd}.

A plot of r vs. X_{Cd} is given in Fig. 3*a*. The slope and intercept of the straight line, found from least squares analysis, are 3.19 and 0.48 respectively, from which are found the values $r_0 = 0.48$ and $r_1 = 3.67$. The value for r_0 is close to that found in the previous work ($r_0 = 0.5$) and the value for r_1 is the same as that determined from isopiestic measurements for $Ca(NO_3)_2$ at this temperature (5). It is probably not fortuitous that r_1 is also close to the number of waters of hydration in the hydrate $Cd(NO_3)_2 \cdot 4H_2O$.

The validity of an additivity rule for r (eq. 4 or 5) suggests the possibility of a similar rule for the quantity rE, where E is the energy of adsorption per mole of water, defined after eq. 1. The equation for rE, precisely analogous to eq. 5, is

$$[6] \qquad rE = r_0E_0 + (r_1E_1 - r_0E_0)X_{Cd}$$

where E_0 and E_1 are individual energies of adsorption defined in the same manner as r_0 and r_1 above. In order to test eq. 6, we have to transform it into one containing energy *differences* $(E - E_L)$, etc. This is accomplished by multiplying eq. 5 by E_L,

$$[7] \qquad rE_L = r_0E_L + (r_1E_L - r_0E_L)X_{Cd}$$

and subtracting eq. 6 from eq. 7 to give

$$[8] \qquad -r(E - E_L) = -r_0(E_0 - E_L) - [r_1(E_1 - E_L) - r_0(E_0 - E_L)]X_{Cd}$$

In Fig. 3*b* the quantity $-r(E - E_L)$ is plotted against X_{Cd}, and the straight line obtained has slope 3.34 and intercept 0.15. Using these values and the previously determined value $r_1 = 3.67$, we arrive at the energy

Can. J. Chem. Downloaded from www.nrcresearchpress.com by 210.87.254.105 on 09/05/12
For personal use only.

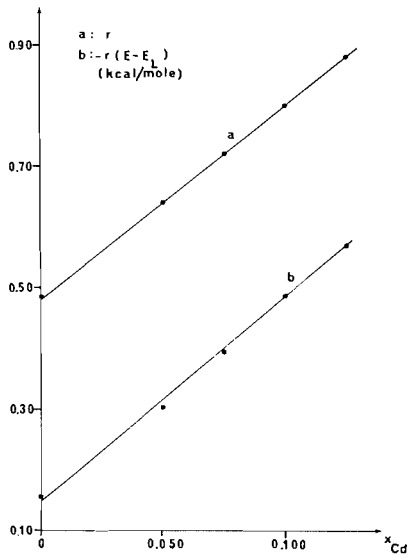

FIG. 3. (*a*) The BET constant r as a function of the cadmium content of the melt. (*b*) The product, $-r(E - E_L)$, of two BET parameters as a function of cadmium content of the melt.

of adsorption term for $Cd(NO_3)_2$, $-(E_1 - E_L) = 0.95$ kcal/mol. This value can be compared with those for other nitrates at 100°C (5), as shown in the series: $Ca(NO_3)_2$, 1.5; $LiNO_3$, 1.2; (Ca, Cs)NO_3, 1.0; $Cd(NO_3)_2$, 0.95 (this work); (Li, K)NO_3, 0.7.

Range of BET Linearity

The upper a_w limit to which the BET equation remains valid is given in Table 2; this limit is ≥ 0.7 in these systems. This is as high, or higher, than the upper limits previously observed (6) for systems containing at least 50 mol% of strongly hydrated cation in the melt (e.g. Li, Ca). This is surprising, since considering the assumptions of the BET theory, one would expect the equation to become invalid when the monolayers become complete. In the case of the weakly hydrated Ag^+ and Tl^+, one might have expected this limit to be noticeably less than $a_w = 0.7$.

Acknowledgement

We thank le Ministère de l'Education de la Province de Québec for financial aid.

1. M.-C. TRUDELLE, M. ABRAHAM, and J. SANGSTER. Can. J. Chem. **55**, 1713 (1977).
2. M. ABRAHAM and J. J. HECHLER. Electrochim. Acta, **17**, 1849 (1972).
3. M. LEDUC. Mémoire de Maîtrise. Université de Montréal, Montréal (Qué.), Canada. 1970.
4. R. H. STOKES and R. A. ROBINSON. J. Am. Chem. Soc. **70**, 1870 (1948).
5. H. BRAUNSTEIN and J. BRAUNSTEIN. J. Chem. Thermodyn. **3**, 419 (1971).
6. J. BRAUNSTEIN. *In* Ionic interactions: from dilute solutions to fused salts. Vol. 1. *Edited by* S. Petrucci. Academic Press, New York, NY. 1971. p. 197.

Can. J. Chem. Downloaded from www.nrcresearchpress.com by 210.87.254.105 on 09/05/12
For personal use only.

The dielectric relaxation of some diols in *p*-dioxane solution

J. CROSSLEY

Department of Chemistry, Lakehead University, Thunder Bay, Ont., Canada P7B 5E1

Received August 2, 1977

J. CROSSLEY. Can. J. Chem. **56**, 352 (1978).

Dielectric constant and loss data at up to nine microwave frequencies have been obtained for 1-butanol, 1,4-butanediol, 1,7-heptanediol, 1,8-octanediol, 1,10-decanediol, and 1,12-dodecanediol at 25°C, and for 1,6-hexanediol at 15, 25, 40, and 55°C, in *p*-dioxane. In each case the dielectric dispersion is adequately described by a Cole–Cole distribution. The relaxation times for the diols are almost independent of the length of the alkyl group. An intramolecular relaxation process appears to be primarily responsible for the dielectric absorption.

J. CROSSLEY. Can. J. Chem. **56**, 352 (1978).

On a obtenu des données relatives aux constantes diélectriques, à diverses (jusqu'à neuf) fréquences de microonde, pour le butanol-1, le butanediol-1,4, l'heptanediol-1,7, l'octanediol-1,8, le décanediol-1,10 et le dodécanediol-1,12 à 25°C et pour l'hexanediol-1,6 à 15, 25, 40 et 55°C dans le *p*-dioxanne. Dans chaque cas, la dispersion diélectrique est décrite d'une façon adéquate par une distribution Cole–Cole. Les temps de relaxation pour les diols sont pratiquement indépendants de la longueur de la chaîne carbonée. Il semble que l'absorption diélectrique est principalement due à un processus de relaxation intramoléculaire.

[Traduit par le journal]

Introduction

Dielectric measurements have provided valuable information on the nature of association in liquid alcohols. Monohydric *n*-alcohols show a single Debye-type principal dielectric dispersion (1). In contrast, the principal dispersion region for many polyhydroxyl alcohols is better described by the Cole–Davidson (2) empirical relation (3, 4). It is generally considered that relaxation in all alcohols occurs via cooperative motions of molecules and involves the formation and rupture of hydrogen bonds. Intramolecular hydrogen bonding in polyhydroxyl alcohols leads to a less regular liquid structure, and evidently hinders the cooperative relaxation. The effect is determined by the proximity of the OH groups in the same molecule (3, 5).

Dielectric constant, dipole moment, and dielectric relaxation measurements on monohydric alcohols diluted with non-polar hydrocarbon solvents have been particularly useful in examining the nature of the hydrogen bonding (6). Because of their sparse solubility in most non-polar solvents, no such work has been reported for polyhydroxyl alcohols. Diols, however, are sufficiently soluble in *p*-dioxane to allow accurate dielectric constant and loss measurements, and it seemed that an examination of such solutions would be of interest. This paper reports the work on *p*-dioxane solutions of a series of diols with hydroxyl groups at the chain ends. The results are compared with earlier data for monohydric alcohols in non-polar solvents.

Experimental

The apparatus and procedure used to determine the dielectric constant (ε') and loss (ε'') at up to nine microwave frequencies between 1 and 35 GHz have been described previously (7, 8). Low frequency dielectric constants (ε_0) were measured at 2 MHz using a WTW Dipdmeter. Dioxane itself has a small dielectric dispersion. The solvent was measured at each frequency and the solution ε' and ε'' values were corrected accordingly. All the chemicals were dried and distilled or recrystallized prior to use.

Results

The Cole–Cole (9) plots for all the solutions gave smooth depressed centre arcs (Fig. 1). The experi-

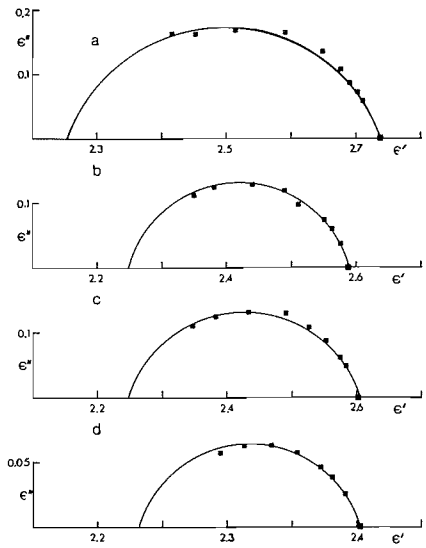

FIG. 1. Cole–Cole plots for (*a*) 1,4-butanediol, (*b*) 1,6-hexanediol ($f_2 = 0.0408$), (*c*) 1,8-octanediol, and (*d*) 1,10-decanediol in *p*-dioxane at 25°C. The frequencies in GHz are: 35, 24, 16.2, 9.3, 5.4, 3.5, 2.4, and 1.5 (except for 1,10-decanediol); with an additional 2 GHz point on plot (*a*).

Can. J. Chem. Downloaded from www.nrcresearchpress.com by 210.87.254.40 on 09/05/12
For personal use only.

TABLE 1. Relaxation times, distribution parameters, dielectric constants, and dipole moments for alcohols at mol fraction f_2 in *p*-dioxane solution

Solute	f_2	T (°C)	τ_0 (ps)	α	ε_0	ε_∞	μ (D)
1-Butanol	0.0534	25	5.9	0.17	2.474	2.234	1.79
1,4-Butanediol	0.0503	25	10.0	0.20	2.738	2.244	2.61
1,6-Hexanediol	0.0335	15	12.5	0.15	2.563	2.265	2.47
	0.0335	25	9.8	0.14	2.518	2.242	2.43
	0.0335	40	7.6	0.13	2.482	2.234	2.37
	0.0335	55	5.6	0.12	2.440	2.202	2.39
	0.0220	25	8.5	0.16	2.408	2.226	2.43
	0.0408	25	10.3	0.14	2.581	2.250	2.41
	0.0555	25	11.3	0.16	2.739	2.257	2.47
1,7-Heptanediol	0.0385	25	10.6	0.15	2.571	2.249	2.40
1,8-Octanediol	0.0415	25	11.1	0.19	2.600	2.234	2.53
1,10-Decanediol	<0.02	25	9.4	0.16	2.402	2.234	—
1,12-Dodecanediol	<0.02	25	10.1	0.16	2.305	2.227	—

mental ε_0, ε', and ε'' data were fitted to the Cole–Cole equation as described previously (10) to obtain the high frequency dielectric constant (ε_∞), mean relaxation time (τ_0), and distribution parameter (α) values listed in Table 1. The apparent dipole moments (μ) given in Table 1 were calculated from:

$$\mu = \left[\frac{9kT(\varepsilon_0 - \varepsilon_\infty)(2\varepsilon_0 + \varepsilon_\infty)}{4\pi N\varepsilon_0(\varepsilon_\infty + 2)^2}\right]^{1/2}$$

where N is the number of alcohol molecules per ml of solution and k is the Boltzmann constant.

Discussion

The ε' and ε'' values reported here for diols in *p*-dioxane solution are well represented by a Cole–Cole distribution. A similar result is observed for 1-butanol (Table 1), methanol, and decanol in *p*-dioxane (11). This is in contrast to the Cole–Davidson skewed arc behaviour (2) shown by many pure liquid diols (3, 4). Johari and Smyth (11) reported τ_0 values of 3, 5, and 9 ps for methanol, 1-butanol, and 1-decanol, respectively, at about 0.05 mol fraction in *p*-dioxane solution at 25°C. Their result for 1-butanol, which showed a Cole–Cole α of 0.17, is in good agreement with that reported here (Table 1). The remarkable feature of the results presented in Table 1 is that the τ_0 values for the C_4 to C_{12} diols at 25°C are very similar. The relaxation times for corresponding 1-alkenes and 1-bromoalkanes, which are by no means rigid molecules, are considerably longer than those found here for diols (12).

A 1,6-hexanediol solution was measured at four temperatures (Table 1). The Cole–Cole α values show the usual small decrease with increased temperature. The plot of $\ln \tau T$ against $1/T$ is linear and yields an activation energy of 3.1 kcal/mol. This value is almost identical with those calculated from Johari and Smyth's (11) data for 1-butanol in *p*-dioxane/*n*-heptane mixtures.

The close similarity in the τ_0 values for diols of quite different size strongly suggests that an intramolecular relaxation process is the dominant factor in the dielectric absorption. Hydroxyl group rotation for alcohols and phenols gives rise to relaxation times of about 3 ps (11, 13, 14). The longer values obtained here may be partially explained in terms of OH rotation which is restricted by solute–solvent interactions. In fact, such interactions have a significant effect upon the OH group relaxation time in phenols (15). If hydroxyl group rotation were solely responsible for the dielectric absorption of the dioxane solutions, then one would expect τ_0 for 1-butanol and 1,4-butanediol to be similar, which is not the case. It is quite possible that this observation and the increase in τ_0 from methanol to 1-butanol to 1-decanol is due to a small contribution from some molecular species. The results for 1,6-hexanediol reveal that τ_0 has detectable concentration dependence. The limited solubility of the higher molecular weight diols meant that they were studied at lower concentrations than some of the other diols. A comparison of the τ_0 values in Table 1 for (*i*) 1,4-butanediol and 1,6-hexanediol ($f_2 = 0.0555$), (*ii*) 1,6-hexanediol ($f_2 = 0.0408$), 1,7-heptanediol, and 1,8-octanediol, and (*iii*) 1,6-hexanediol ($f_2 = 0.022$), 1,10-decanediol, and 1,12-dodecanediol does reveal a quite small, but consistent, lengthening of τ_0 with increased molecular size. These observations support a dielectric absorption dominated by an intramolecular process with a small contribution from 'molecular' reorientation. Attempts have been made to analyze the ε' and ε'' data for these solutions in terms of two discrete relaxation times. Meaningful analyses were not obtained. This is perhaps not altogether surprising since 'molecular' reorientation referred to above could involve diol

Can. J. Chem. Downloaded from www.nrcresearchpress.com by 210.87.254.40 on 09/05/12
For personal use only.

monomers and diol–dioxane complexes. In view of this, the distribution of relaxation times is only to be expected.

Acknowledgement

The author wishes to thank the National Research Council of Canada for an operating grant which supported this work.

1. S. K. GARG and C. P. SMYTH. J. Phys. Chem. **69**, 1294 (1965).
2. D. W. DAVIDSON and R. H. COLE. J. Chem. Phys. **19**, 1484 (1951).
3. D. W. DAVIDSON. Can. J. Chem. **39**, 2139 (1961).
4. E. IKADA. J. Phys. Chem. **75**, 1240 (1971).
5. M. W. SAGAL. J. Chem. Phys. **36**, 2437 (1962).
6. J. CROSSLEY. Adv. Mol. Relaxation Processes, **2**, 69 (1970).
7. W. F. HASSELL, M. D. MAGEE, S. W. TUCKER, and S. WALKER. Tetrahedron, **20**, 2137 (1964).
8. S. E. KEEFE and E. H. GRANT. Rev. Sci. Instrum. **39**, 1800 (1965).
9. K. S. COLE and R. H. COLE. J. Chem. Phys. **9**, 341 (1941).
10. J. CROSSLEY, S. P. TAY, and S. WALKER. Adv. Mol. Relaxation Processes, **6**, 69 (1974).
11. G. P. JOHARI and C. P. SMYTH. J. Am. Chem. Soc. **91**, 6215 (1969).
12. J. CROSSLEY. Adv. Mol. Relaxation Processes, **6**, 39 (1974).
13. M. D. DAVIES and R. J. MEAKINS. J. Chem. Phys. **26**, 1584 (1957).
14. F. K. FONG and C. P. SMYTH. J. Am. Chem. Soc. **85**, 1565 (1963).
15. M. D. MAGEE and S. WALKER. J. Phys. Chem. **74**, 2378 (1970).

Can. J. Chem. Downloaded from www.nrcresearchpress.com by 210.87.254.40 on 09/05/12
For personal use only.

Electrolytes in mixed solvents: indium trichloride in water–dimethylsulfoxide mixtures

ALAN N. CAMPBELL

Department of Chemistry, University of Manitoba, Winnipeg, Man., Canada R3T 2N2

Received July 8, 1977

ALAN N. CAMPBELL. Can. J. Chem. **56**, 355 (1978).

This paper is concerned with the investigation of the conductances (some 160 determinations) of potassium chloride and of indium trichloride in water–dimethylsulfoxide mixtures. The behaviour of potassium chloride in these mixtures is practically identical with its behaviour in water, up to 50 wt% DMSO. Thus Walden's rule is followed very closely, implying that the only effect on the speeds of the ions is that of viscosity. The behaviour of indium trichloride is very different. The conductance increases rapidly with dilution, in the dilute region, and it is time dependent. It is practically certain that the ionization of indium trichloride takes place in steps and that, in dilute solution, progressive hydrolysis occurs. By extrapolating the measurements as a straight line, below concentrations of 0.01 *N*, an approximation to the limiting value of Λ is obtained.

ALAN N. CAMPBELL. Can. J. Chem. **56**, 355 (1978).

Dans cet article, on rapporte les résultats d'une étude sur la conductivité (environ 160 déterminations) du chlorure de potassium et du trichlorure d'indium dans des mélanges d'eau et de diméthylsulfoxyde. Le comportement du chlorure de potassium dans des mélanges contenant jusqu'à 50% en poids de DMSO est pratiquement identique avec son comportement dans l'eau. La règle de Walden est donc suivie très fidèlement et ceci implique que les seuls effets agissant sur les vitesses des ions sont ceux de la viscosité. Le comportement du trichlorure d'indium est très différent. Dans la région diluée, la conductivité augmente rapidement avec la dilution et dépend du temps. Il est pratiquement certain que l'ionisation du trichlorure d'indium se produit par étapes et qu'en solution diluée, une hydrolyse progressive se produit. En extrapolant les mesures sous forme de ligne droite à des concentrations plus basses que 0.01 *N*, on peut obtenir une approximation de la valeur limite de Λ.

[Traduit par le journal]

Can. J. Chem. Downloaded from www.nrcresearchpress.com by 210.87.254.6 on 09/05/12
For personal use only.

Introduction

Because of the hydrolysis of indium trichloride in dilute aqueous solutions, it is impossible to determine the limiting conductance of indium trichloride and, therefore, that of the indium ion, $\frac{1}{3}In^{3+}$, by the usual method of conductance. The matter is further complicated by the probability, indeed almost the certainty, that the ionization of the indium trichloride molecule occurs in stages. It has recently been shown by Jarv *et al.* (1) that the ionization of the $InCl_3$ molecule gives rise to the species: $(InCl(H_2O)_5)^{2+}$, $(InCl_2(H_2O)_4)^{+}$, $(InCl_3(H_2O)_3)$, and $(InCl_4(H_2O)_2)^{-}$, as well as, no doubt, $(In(H_2O)_6)^{3+}$. The method used by Jarv *et al.* (1) was that of Raman spectroscopy. Conductance measurements give no evidence of the existence of the negatively charged complex ion. The conductance decreases with increasing concentration of indium trichloride to a very low value for the saturated solution. If an appreciable amount of the negative ion were present, the conductance would pass through a minimum but it decreases continuously. This is not to say that the negative ion does not exist in solution but that the amount of it cannot be large in comparison with those of the other ions.

Alternatively, the limiting conductance of the $\frac{1}{3}In^{3+}$ ion can be obtained from transport number determinations but a very high degree of accuracy in the determination of transport number is necessary to obtain even moderate accuracy in the ionic conductance. The author has attempted this on two occasions (2, 3) and hopes that his last figure, if not definitive, is at least an improvement on his previous one.

On the face of it, it would seem that if measurements of conductance were made in a solvent other than water, in which hydrolysis could not occur, at least part of the problem would be solved. If Λ^0 were obtained in a given solvent, the value of $\Lambda^0\eta$ for the non-aqueous solvent should yield Λ^0 for water. Admittedly, Walden's rule ($\Lambda^0\eta$ = constant) has little theoretical justification but it does apply in many instances. At least, this seemed a justification for further experimental work.

As solvent, dimethylsulfoxide was chosen, since it has a reasonably high dielectric constant (ε = 46.7, as against 78.3 for water) and it can be obtained cheaply in a pure condition. A great practical advantage is the ease of purification, as compared with, for example, formamide. Passage through a

Can. J. Chem. Downloaded from www.nrcresearchpress.com by 210.87.254.6 on 09/05/12
For personal use only.

molecular sieve is sufficient to remove any trace of water. In the present work, passage through a molecular sieve did not lower the already very low specific conductance, and the product was used as it came from the supplier.

An obvious objection to dimethylsulfoxide is the (relatively) low dielectric constant, which would imply that complex ions would occur even more abundantly than in water. By lowering the concentration to the practical limit of 0.0005 N, however, it was hoped that a straight line plot of Λ vs. $\sqrt{C}$ would yield Λ^0. At least, this is what was done by Gordon and his school (4) working in methanol; their limiting concentration was 0.0001 N. Since the dielectric constant of methanol is so low (32.63) one is inclined to wonder if the extrapolation is justified.

In addition to a series of measurements in pure dimethylsulfoxide, complete series of measurements were made in solvents containing 10, 20, etc., up to 90 wt% water. The densities, viscosities, and dielectric constants of each of these solvents were determined. It was hoped that the plots of $\Lambda\eta$ vs. $\sqrt{C}$ would yield a value for $\Lambda^0\eta$ in pure dimethylsulfoxide and hence, by application of Walden's rule, the value of Λ^0 for pure water. To some extent, this expectation has been justified.

Because of the complicated form of the ionization of indium trichloride, an identical set of measurements was made with potassium chloride as solute, potassium chloride being the ideal normal electrolyte. These extensive measurements have yielded a family of curves which is very instructive as to the nature of the ionization of the two solutes.

Starting with an electrolyte concentration of 0.1 N, the solutions were diluted by weighing down to 0.001 N and lower. The values of $\Lambda\eta$ were then plotted against $\sqrt{C}$.

The heats of mixing of water and dimethylsulfoxide were determined over the complete concentration range, as well as the heats of solution of indium trichloride in water–dimethylsulfoxide mixtures, but the latter measurements could not be pushed to high concentrations of DMSO, because of the decreasing solubility of indium trichloride.

Experimental

Materials

The potassium chloride was reagent grade, analysed. It was dried in a platinum dish over a Meker burner, avoiding fusion. Fisher certified dimethylsulfoxide was used as supplied. Specific conductance = 7.2×10^{-7} mho. All the methods of determination have been described previously (2, 3, 6). The anhydrous indium trichloride was a Ventron Alfa Product.

Results

The data for density, dielectric constant, and viscosity of dimethylsulfoxide–water mixtures are to be found in 'Physical Chemistry of Organic Solvent Systems' (5).

The conductance measurements, amounting to some 160 in all, were made both for potassium chloride and for indium trichloride. In each case, the strongest or starting solution (about 0.1 N) was analysed gravimetrically as chloride and subsequent dilutions were made by weighing. The densities were taken as those of the pure solvent as were the viscosities, a procedure which may have introduced a slight error into the measurements on the strongest (0.1 N) solution. These numerous numerical results are to be found in the Depository of Unpublished Data in Tables 1 and 2.[1] The results are expressed graphically (for certain strengths only, to avoid confusion in the diagram) as the product $\Lambda\eta$ vs. $\sqrt{N}$ in Figs. 1 and 2.

The heats of mixing of dimethylsulfoxide and water are given in Table 3.[1] The results are expressed graphically in Fig. 3. There is a pronounced maximum at about 45 mol% dimethylsulfoxide. The heats of solution of indium trichloride in water and water–dimethylsulfoxide mixtures are given in Table 4.

Discussion

The extensive measurements of conductance are to be found in the Depository material but an inspection of Figs. 1 and 2 reveals the main features. The straight line plot of $\Lambda\eta$ vs. $\sqrt{N}$ of potassium chloride is hardly influenced by the presence of dimethylsulfoxide and Walden's rule is very closely followed, as shown by Table 5.

Walden's rule applies exactly at a weight concentration of 10.5% giving a Λ_0 value of 121.1 for KCl in 10.5 wt% DMSO. The rule continues to apply approximately up to 51.83 wt% DMSO (ratio $(\Lambda\eta)_0(\text{water})/(\Lambda\eta)_0(\text{solvent}) = 1.054$). Within the limits of this approximation Λ_0 for KCl has been reduced from 149.8 mho cm^{-1} to 44.79, principally as a result of increased viscosity of the medium. Further increase of DMSO content results in rather serious deviation from the Walden rule.

The state of affairs is very different for $InCl_3$, as Fig. 2 shows. At concentrations less than 0.01 N, the conductance rises rapidly with dilution and at concentrations less than 0.001 N becomes time dependent. The explanation of this is twofold. The time dependence is due to increasing hydrolysis with time, as the products of hydrolysis separate from solution. In addition, however, the step-wise ionization of $InCl_3$ must be taken into account. The ionization in

[1]Copies of Tables 1–3 are available, at a nominal charge, from the Depository of Unpublished Data, CISTI, National Research Council of Canada, Ottawa, Ont., Canada K1A 0S2.

Can. J. Chem. Downloaded from www.nrcresearchpress.com by 210.87.254.6 on 09/05/12
For personal use only.

TABLE 4. Heat of solution of indium trichloride in water and in water–dimethylsulfoxide mixtures

Composition of solvent	Molarity of $InCl_3$	ΔH/mol of $InCl_3$† (kcal)
100% H_2O	0.1171	−20.01*
9.861 mol% DMSO	0.03863	−19.30
9.861 mol% DMSO	0.08037	−18.90

*Previous result (6) = 16.77 kcal (m = 0.5).
†Qualitatively, it appears that ΔH of solution is decreasing with increasing DMSO content of the solvent.

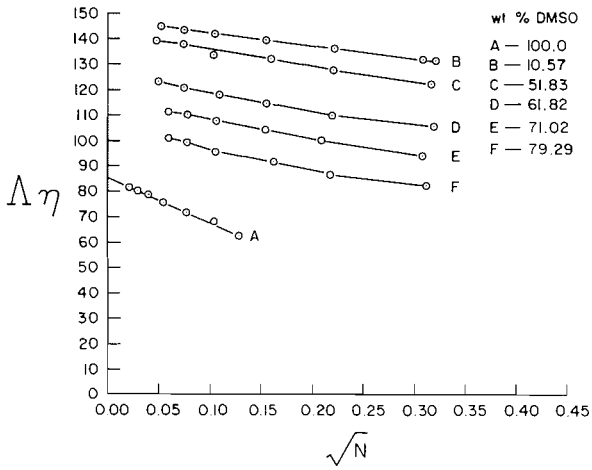

FIG. 1. Conductance × viscosity (Λη) of KCl in DMSO–water mixture.

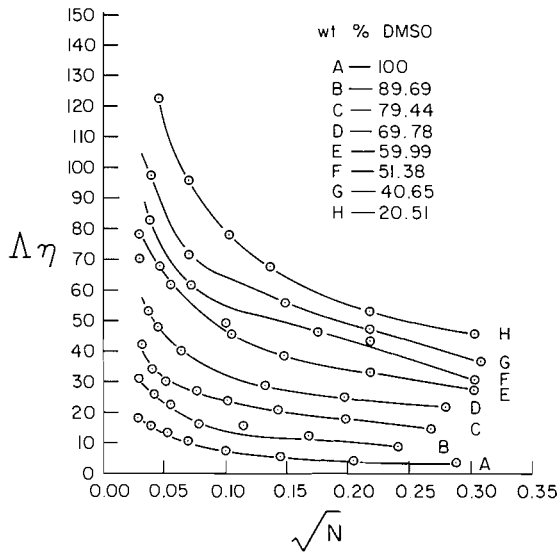

FIG. 2. Conductance × viscosity (Λη) of $InCl_3$ in DMSO–water mixtures.

steps was assumed by the author to account for the very low conductance of indium trichloride in saturated (aqueous) solution. This assumption has been confirmed by Jarv *et al.* (1) (see Introduction).

Since the conductance reading of $InCl_3$ begins to be

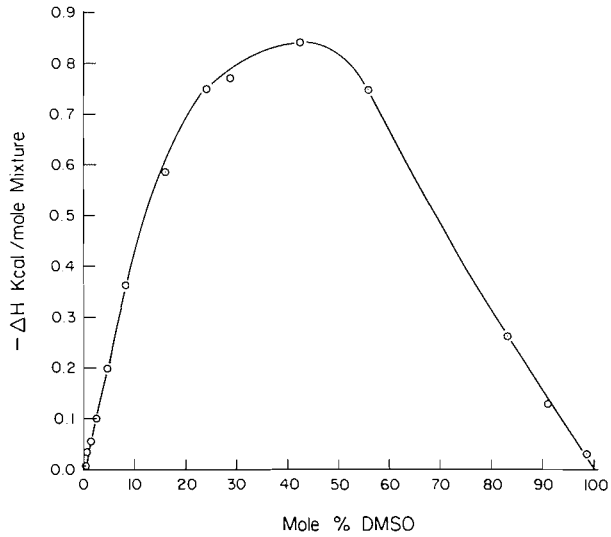

FIG. 3. Heat of mixing of DMSO and water.

TABLE 5. Limiting values of Λη (extrapolated to zero concentration) and Λ for potassium chloride

Concentration of DMSO (mol%)	$(\Lambda\eta)_0$	Λ_0	Ratio of $(\Lambda\eta)_0$(water) to $(\Lambda\eta)_0$(solvent)
100.00	86.1	39.98	149.8/86.1 = 1.739
10.57	149.8	121.1	1.000
21.63	146.8	93.92	1.021
31.66	146.4	74.62	1.024
41.22	145.5	58.86	1.030
51.83	142.2	44.79	1.054
61.82	127.8	33.73	1.173
71.02	116.6	29.24	1.285
79.29	106.9	28.89	1.402

TABLE 6. Straight line extrapolation of Λη for indium trichloride

Concentration in wt% DMSO	$(\Lambda\eta)^0$ KCl	$(\Lambda\eta)^0$ $InCl_3$	Ratio $(\Lambda\eta)^0(KCl)/(\Lambda\eta)^0(InCl_3)$
100	80.9	11.8	6.856
80	104.0	31.8	3.270
70	114.8	39.1	2.936
60	127.8	50.7	2.520
50	142.2	66.4	2.142
40	146.6	77.4	1.894
30	147.4	92.6	1.592
20	149.86	137.0	1.094
0.0	149.86	125.9	1.190

time dependent with increasing water content, $(\Lambda\eta)$'s have been calculated by extending the experimental results down to a concentration of 0.01 N only and extrapolating as a straight line from that point. The results are given in Table 6.

The data in Table 6 would suggest that $(\Lambda\eta)_0$ and

therefore Λ_0 ($\eta = 1.000$) for $InCl_3$ lie between 137 and 125.9. The figure of the author's last determination of Λ_0 (3) is 132.9.

Table 4 gives the heats of solution of indium trichloride in water and a water–dioxane mixture. It would seem that the enthalpy of solution decreases with increasing DMSO content. This is to be expected. The molar volume, viscosity, and heat of mixing all indicate that the DMSO molecule is strongly hydrated. If the solution of indium trichloride can only take place in 'free' water, some dissociation of the DMSO–water complex, with absorption of energy, will have to occur before solution of $InCl_3$ is possible.

1. T. JARV, J. T. BULMER, and D. E. IRISH. J. Phys. Chem. **81**, 649 (1977).
2. A. N. CAMPBELL. Can. J. Chem. **51**, 3006 (1973).
3. A. N. CAMPBELL. Can. J. Chem. **54**, 3732 (1976).
4. J. P. BUTLER, H. I. SCHIFF, and A. R. GORDON. J. Chem. Phys. **19**, 752 (1951); R. E. JERVIS, D. R. MUIR, J. P. BUTLER, and A. R. GORDON. J. Am. Chem. Soc. **75**, 2855 (1953).
5. A. K. COVINGTON and T. DICKINSON (*Editors*). Physical chemistry of organic solvent systems. Plenum Press, London and New York. 1973. p. 19; R. G. LE BEL and D. A. GORING. J. Chem. Eng. Data, **7**, 600 (1962).
6. A. N. CAMPBELL, E. M. KARTZMARK, and O. N. BHATNAGER. Can. J. Chem. **52**, 1954 (1974).

Can. J. Chem. Downloaded from www.nrcresearchpress.com by 210.87.254.6 on 09/05/12
For personal use only.

Raman and nuclear quadrupole resonance studies of the phase transition in pentachlorophenol

H. F. SHURVELL, J. KORPPI-TOMMOLA, AND R. J. C. BROWN
Department of Chemistry, Queen's University, Kingston, Ont., Canada K7L 3N6

Received April 20, 1977

H. F. SHURVELL, J. KORPPI-TOMMOLA, and R. J. C. BROWN. Can. J. Chem. **56**, 359 (1978).

Raman and nqr spectra of pentachlorophenol (PCP) have been recorded at temperatures above and below the transition at 62 ± 2°C. The complete loss of structure in the Raman external mode region and the disappearance of the ^{35}Cl nuclear quadrupole resonances above the transition temperature indicate a disordered structure for the high temperature phase. Supercooling is observed in nqr and Raman spectra when the sample is cooled through the transition temperature. No evidence for any new crystal phase is observed on cooling the sample to liquid nitrogen temperature. Eleven of the 12 external modes predicted from the reported crystal structure of PCP have been observed in the Raman spectrum at 77 K.

H. F. SHURVELL, J. KORPPI-TOMMOLA et R. J. C. BROWN. Can. J. Chem. **56**, 359 (1978).

On a enregistré les spectres Raman et rqn du pentachlorophénol (PCP) à des températures supérieures et inférieures à celle de la transition (62 ± 2°C). La perte complète de structure dans la région de mode externe du spectre Raman et la disparition des résonances quadrupolaires nucléaires du ^{35}Cl au-dessus de la température de transition indiquent la présence d'une structure désordonnée dans la phase existant à température élevée. On observe de la surfusion dans les spectres rqn et Raman lorsque l'on refroidit l'échantillon à une température inférieure à celle de la transition. On n'observe aucune indication relative à la présence d'une nouvelle phase cristalline lorsque l'on refroidit l'échantillon jusqu'à la température de l'azote liquide. Dans le spectre Raman du PCP mesuré à 77 K, on a observé 11 des 12 modes externes qui avaient été prédits à partir de la structure cristalline déterminée antérieurement.

[Traduit par le journal]

Introduction

Pentachlorophenol (PCP) is an important industrial chemical widely used as a plant pesticide. It is of interest from the point of view of hydrogen bonding, since it does not appear to self-associate in solution and forms H-bonded complexes with various other molecules.

In the crystalline state, PCP is known to undergo a phase transition near 62°C (1). The transition has been studied by Rohleder and co-workers using near-infrared spectroscopy (2) and microcalorimetry (3). A nuclear quadrupole resonance and X-ray study of the crystal structure was carried out at room temperature (4) following an earlier nqr study at 77 K (5).

An infrared spectrum of PCP is found in the Aldrich Library of Infrared Spectra (6) and in ref. 2. However, we are not aware of any published Raman spectrum of this compound in the chemical literature. We are therefore including a Raman survey spectrum in this paper.

As the title suggests, our main interest lies in the nature of the phase transition in solid PCP. To study this, we have recorded Raman spectra of the external (lattice) mode region and the ^{35}Cl nuclear quadrupole resonance of PCP at various temperatures above and below the reported (2, 3) transition temperature.

Experimental

Reagent grade pentachlorophenol was obtained from J. T. Baker Chemical Co. Samples for Raman spectroscopy were recrystallized from CCl_4 solution and sublimed under vacuum. Pellets were prepared by means of the apparatus usually used to make KBr pellets for ir studies. The sample pellet was mounted on a copper block in our low temperature Raman cell (7). The spectra were excited by the 514.5 nm line of an Ar^+ laser operating at a power of 200 mW. Even at this relatively low power it was noticed that some sublimation and recrystallization of the sample occurred during several hours of illumination. This resulted in a considerable improvement in signal to noise ratio in the spectrum.

Raman spectra were recorded using a Jarrell-Ash 25-100 monochromator, a cooled RCA C31034-02 photomultiplier, and photon counting electronics. The spectra were calibrated using emission lines from a neon lamp (8). Spectra were recorded at liquid nitrogen temperature and at various temperatures between room temperature and 100°C. The latter temperatures were obtained by means of a controlled 'Firerod' heater (Watlow Electric Co.), immersed in ethylene glycol in the refrigerant container of the low temperature cell. Temperatures were monitored with a Fe/constantan thermocouple and are believed to be accurate to within ±2°C.

For the nqr spectra, the pentachlorophenol was used without further purification. Samples were sealed in glass tubes under vacuum and placed in a gas-flow cryostat, which maintained

Can. J. Chem. Downloaded from www.nrcresearchpress.com by 210.87.254.105 on 09/05/12
For personal use only.

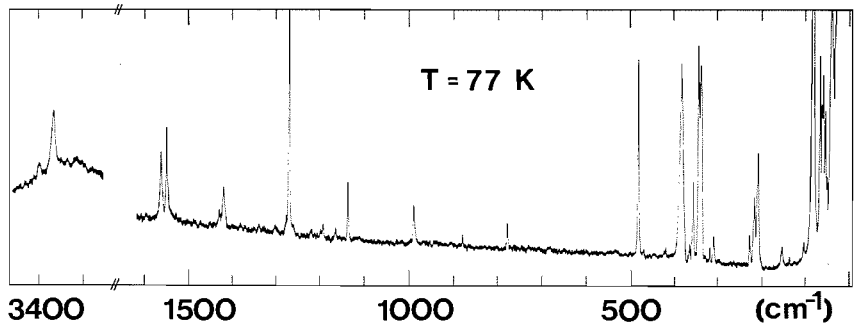

FIG. 1. A Raman survey spectrum of PCP at 77 K.

the temperature constant to ±0.2°C. The temperature was measured with a Cu/constantan thermocouple taped to the outside of the sample tube. The nuclear quadrupole resonances were recorded using a conventional super-regenerative spectrometer.

Results

A Raman survey spectrum of PCP is shown in Fig. 1 and the observed wave numbers and relative intensities are listed in Table 1. Figure 2 shows the external mode region at liquid nitrogen and room temperatures and Table 2 lists the observed Raman wave numbers. Figure 3 shows the results of typical temperature cycling through the transition temperature.

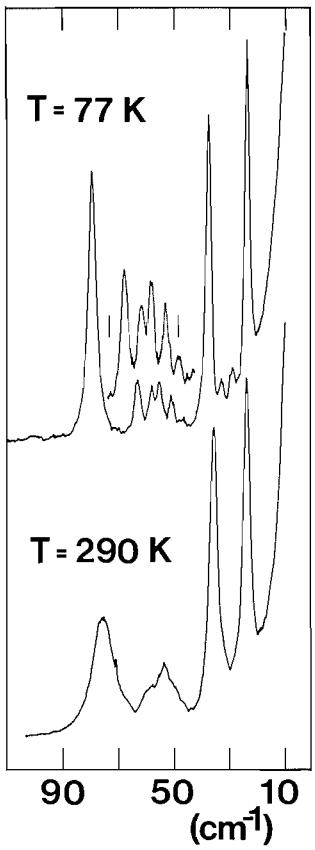

FIG. 2. The external mode region of the Raman spectrum of PCP at 77 and 290 K.

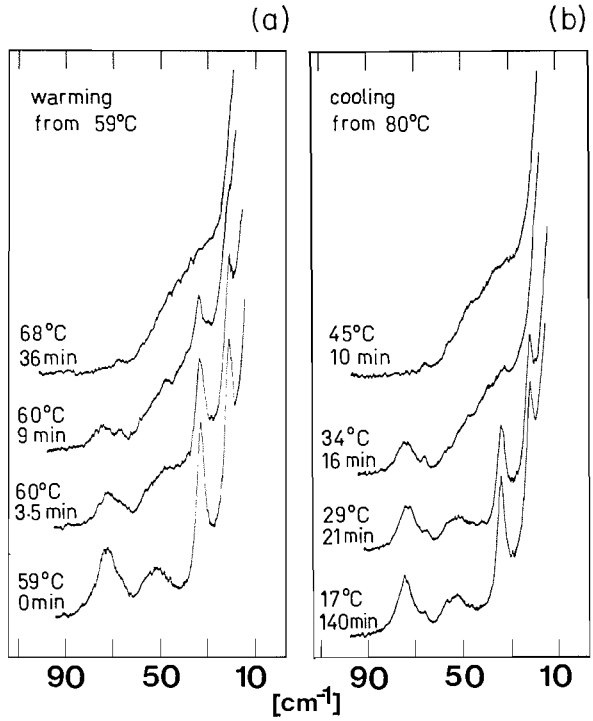

FIG. 3. A temperature cycling study of the external mode Raman spectrum of PCP.

TABLE 1. Observed Raman wave numbers (cm^{-1}) for the internal modes of PCP

3398 vw	1303 vw	986 w	341 s
3365 w	1278 sh	877 vw	336 s
1562 w	1272 vs	776 w	317 vw
1552 m	1261 sh	479 s	309 w
1431 vw	1221 vw	417 vw	226 w
1420 w	1194 vw	381 s	216 w
1383 vw	1164 vw	363 vw	208 m
1338 vw	1136 m	353 w	152 vw
			137 vw

Can. J. Chem. Downloaded from www.nrcresearchpress.com by 210.87.254.105 on 09/05/12
For personal use only.

Can. J. Chem. Downloaded from www.nrcresearchpress.com by 210.87.254.105 on 09/05/12
For personal use only.

TABLE 2. External modes (wave numbers in cm^{-1}) observed in the Raman spectra of PCP

$T = 290$ K	$T = 77$ K
103 vw	103 vw
76.0 m	82.4 s
60 w	66.4 w
56 sh	61.2 w
54 w	58.4 w
49 sh	54.2 w
—	50.0 vw
35.6 s	40.3 s
32 sh	35.6 vw
28 sh	31.4 vw
23.8 s	26.0 s

TABLE 3. Observed nuclear quadrupole resonance frequencies

Resonance (following Sakurai (4))	Frequency (25°C) (kHz)	$(\partial\nu/\partial T)_P$ (kHz K^{-1})
ν_3	38 029	−3.36
ν_4	37 762	−2.76
ν_2	37 716	−2.46
ν_1	36 985	−2.38
ν_5	36 668	−2.62

Five nqr frequencies were observed at 25°C. These are listed in Table 3, together with their temperature coefficients. The resonance frequencies are linear functions of temperature above room temperature up to 64.2°C. No resonance was detected at temperatures above 64.2°C in the frequency range 36.02–39.20 MHz. The intensities of the resonances appeared to be independent of temperature below 64.2°C.

Discussion

Crystal Structure and External Modes

The crystal structure of PCP at room temperature is reported to be monoclinic with eight molecules per unit cell (4). The space group is $C2/c$ (C_{2h}^6) and the eight molecules are located on general sites (Wykoff position *f*). Using the method of Adams (9, 10), we find that the 24 external vibrations of the unit cell comprise

$$6A_g + 6B_g + 6A_u + 6B_u \text{ modes}$$

of which $1A_u + 2B_u$ are acoustic modes. Thus, the low frequency Raman spectrum should contain 12 lines and the far ir spectrum 9 absorption bands due to external modes. The observed ir and Raman wave numbers may not be coincident due to the centrosymmetric unit cell.

The low temperature Raman spectrum of the lattice mode region (Fig. 2) shows 10 clearly resolved lines and a very weak band is observed at 103 cm^{-1} (Fig. 1). Thus, we appear to have observed 11 of the 12 predicted Raman active external modes.

Although there is a marked improvement in the Raman spectrum on cooling to 77 K from room temperature, there is no indication of any new crystalline phase at low temperatures. The sharpening of lines, with resulting improvement in resolution, together with some frequency shifts as the temperature is lowered are observations normally expected in the external mode spectrum of a crystal.

Temperature Cycling Studies

As the sample is warmed from room temperature to about 59°C, there is no noticeable change in the Raman spectrum (Fig. 3*a*). However, if the temperature is maintained at 60°C for several minutes, the external modes decrease in intensity and broaden, until no structure remains, apart from a broad feature centred near 40 cm^{-1}. The Rayleigh line also broadens considerably. No significant changes were observed in the internal mode spectrum during the transition.

On cooling the sample from 80°C to below 60°C, the lattice modes reappear in the spectrum. However, there is a considerable relaxation time involved. Under our experimental conditions, it was not possible to obtain reproducible times for the reappearance of the spectrum but this aspect of the phase transition has been studied previously by microcalorimetry (3). A typical supercooling effect is shown in Fig. 3*b* (upper trace) where it is seen that the high temperature spectrum is still present at 45°C. After cooling to room temperature over a period of 20–30 min, the spectrum of the low temperature phase is obtained.

The nqr spectrum shows a similar result. The resonance frequencies (Table 3) decrease as the temperature is increased from room temperature up to a temperature of 64.2°C. At this point, the signal disappears and no resonance at all is detected above this temperature. On recooling to below 64.2°C, the signals reappear, but again, a supercooling effect is observed.

Conclusions

The disappearance of both the external modes and the ^{35}Cl nuclear quadrupole resonances above the transition temperature suggests rapid reorientation of the molecules in the high temperature phase. It has been suggested previously (2, 3) that the low temperature phase can be considered to be an intermolecular (OH...O) hydrogen bonded solid polymer, whereas the high temperature form consists of

monomeric PCP units, with intramolecular (OH...Cl) hydrogen bonds. This change from hydrogen bonded polymer to monomeric molecules can be seen in the infrared spectrum (2). The ir spectrum of the high temperature phase is very similar to that of a dilute solution of PCP in carbon tetrachloride. The interpretation of the infrared studies is consistent with the present spectroscopic observations, since an intramolecular hydrogen bonded structure would be able to reorient rapidly in the plane of the benzene ring.

There is no reason to suppose that a disordered structure is obtained on rapid cooling through the transition temperature. The structure of the high temperature phase is temporarily retained below the equilibrium temperature. This is ordinary supercooling, which is common and characteristic of first order phase changes.

Acknowledgments

The authors are grateful to the National Research Council of Canada for financial support. J.K-T. thanks the Canada Council for a fellowship offered under a programme of cultural exchange between Canada and Finland.

1. J. MEINNEL, Y. BALCOU, and P. GREGOIRE. Proc. Colloq. AMPERE, **12**, 429 (1963); Chem. Abstr. **62**, 9895 (1965).
2. J. W. ROHLEDER and B. JAKUBOWSKI. Acta Phys. Pol. **31**, 1047 (1967).
3. B. JAKUBOWSKI, M. LAZNIEWSKI, and J. W. ROHLEDER. Rocz. Chem. **43**, 1987 (1969).
4. T. SAKURAI. Acta Crystallogr. **15**, 1164 (1962).
5. P. J. BRAY and D. ESTEVA. J. Chem. Phys. **22**, 570 (1954).
6. C. POUCHERT. The Aldrich library of infrared spectra. 2nd. ed. The Aldrich Chemical Company, Milwaukee. 1975. Spectrum 590D.
7. S. J. DAUNT, H. F. SHURVELL, and L. PAZDERNIK. J. Raman Spectrosc. **4**, 205 (1975).
8. J. LOADER. Basic laser Raman spectroscopy. Heyden, London. 1969.
9. D. M. ADAMS. Coord. Chem. Rev. **10**, 183 (1973).
10. D. M. ADAMS and D. C. NEWTON. Tables for factor group and point group analysis. Beckman-R11C Ltd., London. 1970.

Can. J. Chem. Downloaded from www.nrcresearchpress.com by 210.87.254.105 on 09/05/12
For personal use only.

Hydrothermal reaction kinetics. The decomposition of nickel(II) hydroxide

THOMAS W. SWADDLE[1] AND TONY C. T. WONG

Department of Chemistry, The University of Calgary, Calgary, Alta., Canada T2N 1N4

Received August 2, 1977

THOMAS W. SWADDLE and Tony C. T. WONG. Can. J. Chem. **56**, 363 (1978).

The fractional extent α of decomposition of ripened $Ni(OH)_2$ into green NiO in alkaline hydrothermal conditions under nitrogen is given by the rate law $\alpha^{1/3} = k_c[OH^-]t$, where $k_c = 2.4 \times 10^{-5}$ kg mol^{-1} s^{-1} at 561 K. The Arrhenius activation energy is 220 $\pm$ 25 kJ mol^{-1}. The reaction is accelerated moderately by O_2 (giving black $NiO_{1+\delta}$) and strongly by added NiO. A reaction mechanism involving dissolution of $Ni(OH)_2$ as $Ni(OH)_3^-$(aq) and rate-determining, surface-controlled reprecipitation of this as NiO is proposed.

THOMAS W. SWADDLE et TONY C. T. WONG. Can. J. Chem. **56**, 363 (1978).

A 561 K, on peut exprimer la fraction, α, de la décomposition de $Ni(OH)_2$ vieilli en NiO *vert dans des conditions hydrothermiques alcalines sous atmosphère d'azote par la loi de* vitesse $\alpha^{1/3} = k_c[OH^-]t$ ou $k_c = 2.4 \times 10^{-5}$ kg mol^{-1} s^{-1}. L'énergie d'activation d'Arrhénius est de 220 $\pm$ 25 kJ mol^{-1}. Il y a une légère accélération de la réaction par la présence de O_2 (conduisant à du $NiO_{1+\delta}$ noir) et une forte accélération par l'addition de NiO. On propose un mécanisme de réaction impliquant la dissolution de $Ni(OH)_2$ sous forme de $Ni(OH)_3^-$(aq) et une reprécipitation sous forme NiO, contrôlée par la surface, déterminant la vitesse.

[Traduit par le journal]

Introduction

The study of the kinetics and thermodynamics of the conversion of nickel(II) hydroxide into nickel(II) oxide under hydrothermal conditions is of tech-

$$[1] \qquad Ni(OH)_2(c) \rightarrow NiO(c) + H_2O(l)$$

nological interest in connection with the corrosion of nickel alloy components (such as heat exchangers in water-cooled nuclear power plants) by neutral or alkaline water at elevated temperatures (1–3). It may also be expected to provide an experimentally convenient model for the mechanisms of hydrothermal reactions of transition metal hydroxides and oxides in general.

There is, however, no general agreement regarding the thermodynamics of reaction 1. Data published by the U.S. National Bureau of Standards (NBS) (4), and calculations based on these (5), indicate that reaction 1 should proceed spontaneously at or near the saturated vapor pressure throughout the entire liquid range of water, whereas experimentally it has, with one exception (6), been found not to occur below about 545 K (7–15), although decomposition of $Ni(OH)_2$ can be observed at 470 K or less in the 'dry' state (14, 16–23).

This apparent discrepancy arises partly because nickel(II) hydroxide can exist in more than one form. When freshly precipitated at or near room temperature, it takes the form of poorly crystalline particles (21) of size on the order of 3–8 nm (24, 25) and composition best represented by $Ni(OH)_2 \cdot xH_2O$ where $x = 0.5$–0.7 (12) which grow on standing in water ('aging' or 'Ostwald ripening') into hexagonal plates with the brucite structure following loss of intercalary water, ultimately reaching some 40 nm in diameter and 7 nm in thickness (25–27). The poorly crystalline (turbostratic) initial material, often designated α-$Ni(OH)_2$, is characterized by a reflection in the powder X-ray diffraction pattern corresponding to a spacing of 0.81–0.85 nm (11, 14, 25, 28), and an idealized crystal structure based on an expanded brucite-type lattice corresponding to the formula $3Ni(OH)_2 \cdot 2H_2O$ has been proposed (11), but detailed consideration of this poorly reproducible material has provoked controversy (13, 20, 29). The fully 'aged' or β-$Ni(OH)_2$ form, however, is relatively well-crystallized and reproducible; a similar material of composition $Ni(OH)_2 \cdot xH_2O$ (where $x = 0.17 \pm 0.10$, decreasing to 0.07 on warming) can be obtained by precipitating $Ni(OH)_2$ in *boiling* water (16), while hydrothermal ripening (7, 10–14, 30) gives essentially stoichiometric β-$Ni(OH)_2$ in platelets with crystallite dimensions around 30 nm thick and 50 nm across (30). Hydrothermal ripening is generally favored by high temperatures (up to 543 K in plain water) (11) and high hydroxide ion concentrations (up to 40% KOH at 513 K) (12), although other standard hydrothermal 'mineralizers' such as KCl or NH_4I seem to be ineffective (10).

It is clearly β-$Ni(OH)_2$ which is relevant to the present hydrothermal study. The solubility product of 6.5×10^{-18} reported by Gayer and Garrett (31) evidently refers to the β form, since these authors prepared $Ni(OH)_2$ by precipitation from hot solutions.

[1]Author to whom correspondence should be sent.

Can. J. Chem. Downloaded from www.nrcresearchpress.com by 210.87.254.105 on 09/05/12
For personal use only.

Can. J. Chem. Downloaded from www.nrcresearchpress.com by 210.87.254.105 on 09/05/12
For personal use only.

Combining this result with thermodynamic data for NiO and H_2O (4), we obtain $\Delta G_f^0 = -458.1$ kJ mol^{-1} for β-Ni(OH)$_2$(c), which is 10.9 kJ mol^{-1} more negative than the NBS value (4) (which evidently refers to the ill-defined α-Ni(OH)$_2$(c)) but which agrees well with the value adopted by Naumov *et al.* (32). This leads to $\Delta G^0 = +9.25$ kJ mol^{-1} for reaction 1 at 298 K, i.e., NiO(c) is actually *unstable* with respect to β-Ni(OH)$_2$(c) in liquid water at 298 K, as pointed out by Baes and Mesmer (33), although it is stable relative to α-Ni(OH)$_2$(c). Knowledge of the temperature dependence of ΔG_f^0 of β-Ni(OH)$_2$(c) is needed to determine the minimum temperature at which reaction 1 becomes thermodynamically favored in water at its saturated vapor pressure; such data seem to be lacking, although Mukaibo *et al.* (3) have estimated this temperature to be about 440 K, whereas others (7, 9, 10) have published purported phase relationships which suggest transition temperatures of about 560 K.

A major factor contributing to the confusion over the occurrence of reaction 1 is its slowness, even at temperatures on the order of 500 K. A primary objective of this study was to demonstrate that failure to observe reaction 1 at elevated temperatures (7–15) may result from a combination of the form of the rate law and a high activation energy, rather than from unfavorable thermodynamic factors.

Experimental Section

Nickel(II) hydroxide was prepared using only polyethylene or polytetrafluoroethylene laboratory ware. Contact between the solutions and glassware led to the appearance of one well-defined and one diffuse extraneous reflection, corresponding to spacings at 0.725 and 0.95 nm respectively, in the powder X-ray diffraction pattern of the final product, indicating the hydrothermal formation of nickel antigorite ($Ni_3Si_2O_5(OH)_4$) and a trace of nickel montmorillonite ($Ni_3Si_4O_{10}(OH)_2$) (34). Typically, 1 mol nickel(II) nitrate or chloride in 400 cm^3 water was added dropwise with stirring to 4 mol NaOH in 600 cm^3 water at room temperature. The mixture was stirred overnight and filtered under suction, and the solid was washed with 1000 cm^3 NaOH (1.0 *m*; *m* = mol kg^{-1}) followed by several dm^3 water until the filtrate was neutral. Then, the wet solid was either dried under reduced pressure at 110°C for 1–3 h and the resulting cake ground to a fine powder for future use, or else dispersed in 1.0 *m* NaOH (about 0.1 mol Ni(OH)$_2$ to 25 cm^3), sealed under nitrogen in PTFE-lined autoclaves of 35 cm^3 capacity (35), and heated at 200°C for 24 h. The resulting 'ripened' solid β-Ni(OH)$_2$ was filtered, washed with water until the filtrate was neutral, and dried under reduced pressure at 110°C.

The ripened solid was seen under the transmission electron microscope to consist of hexagonal lamellae, 70–160 nm in diameter. Powder X-ray diffraction patterns detected no crystalline compounds other than β-Ni(OH)$_2$, and indicated the lamellae to be about 20–40 nm thick according to the Scherrer formula (36) (which, however, was at the limit of its applicability). The BET(N_2) surface area of the ripened material was determined using a Micromeritics Model 2200 High-Speed Surface Area Analyzer to be ~16 m^2 g^{-1}, as compared with over 200 m^2 g^{-1} for the dry, unripened Ni(OH)$_2$.

Kinetics of the Hydrothermal Reaction

Weighed amounts of β-Ni(OH)$_2$ were placed in capped 35 cm^3 PTFE liners with (usually) 20 cm^3 NaOH solution, and sealed into titanium/0.2% palladium alloy autoclaves (35) leaving ~25 cm^3 gas space. These operations were carried out in a nitrogen-filled glovebox, when oxygen was to be excluded; measurements using a Rexnord oxygen meter showed the O_2 content of solutions handled in this way to be less than 0.1 μg/g (cf. 8 μg/g for water in equilibrium with air at 294 K and 90 kPa). The sealed vessels were thermostatted (±0.2 K) in a preheated forced-convection oven as described previously (37), and quenched in cold water after chosen intervals t_f. The solid reaction products were filtered, washed with water, and dried under reduced pressure at 110°C for 1 h. Thermogravimetric analysis of 5–10 mg portions over the range 300–800 K with a Perkin-Elmer TGS-1 thermobalance gave the relative amounts of Ni(OH)$_2$ and NiO. These analyses were confirmed semi-quantitatively by powder X-ray diffraction measurements, which also showed that NiO and β-Ni(OH)$_2$ were the only detectable solid phases present.

Kinetics of Decomposition of Ni(OH)$_2$ in Dry Environments

Isothermal thermogravimetric analyses were carried out with the Ni(OH)$_2$ in a shallow layer in an open dish in atmospheres of helium or, as desired, oxygen. Sample temperature measurements were calibrated against the magnetic transition temperatures of alumel, nickel, perkalloy, and iron.

Results

Despite the availability of much data in the literature (14, 16–23), the isothermal decomposition kinetics of dry Ni(OH)$_2$ in helium were investigated again in the present study for purposes of direct comparison with the hydrothermal measurements on similarly prepared material, since the mode of preparation of Ni(OH)$_2$ is known to affect the decomposition rate (10, 14, 18, 19). The rate in helium decreased progressively, and could be represented by the equation

$$[2] \qquad 1 - (1 - \alpha)^{1/n} = k_n t/nN_0^{1/n}$$

where α is the mole fraction of NiO formed by time t, N_0 is the molar amount of Ni(OH)$_2$ originally present, k_n is a rate coefficient, and the index n is 2 for a 'contracting area' and 3 for a 'contracting volume' process (18). Hazell and Irving (19) interpreted their rate data for the decomposition of dry Ni(OH)$_2$ on the basis of the contracting area formula, arguing that the brucite-type layer structure would favor inward progress of decomposition along the planes of the lamellae from the edges. Marcellini and Teichner (18), however, found empirically that n was close to 3 for samples in an open dish, and this is supported by the correlation coefficients r listed in Table 1. The distinction is, however, a fine one, especially since the effective zero of the reaction time scale had to be treated as a parameter to be calculated (in practice, the calculated zero time followed

TABLE 1. Isothermal decomposition of nickel(II) hydroxide[a] in dry gaseous environments

T (K)	Gas[b]	Flow rate ($cm^3\ s^{-1}$)	Correlation coefficient r		$10^5 k_3$[c] ($mol^{1/3}\ s^{-1}$)
			$n = 3$	$n = 2$	
508	He	25	0.9998	0.9986	3.9
513	He	25	0.9992	0.9971	5.0
	He	25	0.9908	0.9882	14.0[d]
	He	0	0.9971	0.9952	3.5
	O_2	30	0.9991	0.9978	4.8
	O_2	0	0.9997	0.9995	2.5
518	He	25	0.9981	0.9945	7.2
523	He	25	0.9992	0.9969	9.3

[a]Hydrothermally ripened (specific surface ~16 $m^2\ g^{-1}$) except as indicated; initial quantity N_0 = 0.08–0.10 mmol.
[b]Pressure 90 kPa.
[c]Standard error ±2%.
[d]Unripened $Ni(OH)_2$ (specific surface ≥ 200 $m^2\ g^{-1}$).

the beginning of the formal reaction time scale t_f by as little as 35–70 s). The reaction was not followed beyond $\alpha \sim 0.8$ because of the retention of some water by the NiO product (18, 19, 22); indeed Erkelens and Egginck-DuBurck (22) took $\alpha = 0.8$ to represent complete reaction, which gave $n \sim 1$.

The rate coefficients k_3 listed in Table 1 are obviously influenced not only by the particle size but also by the nature and flow rate of the gas, as suggested by the results of Marcellini and Teichner (18), and furthermore the omission of the factor $N_0^{1/n}$ by other authors makes direct comparison of our k_n values with their data difficult. Our isothermal measurements give an Arrhenius activation energy E_a of 132 ± 8 kJ mol^{-1} in helium (flowing or still) for the decomposition of dry, hydrothermally ripened $Ni(OH)_2$, and this value was confirmed by thermal volatilization measurements *in vacuo*; unripened $Ni(OH)_2$ gave E_a = 114 kJ mol^{-1} in isothermal thermogravimetry. These values are similar to, or slightly higher than, those reported by other authors (14, 18, 19, 22).

For the hydrothermal decomposition reaction, Table 2 shows that the fractional extent of decomposition of β-$Ni(OH)_2$ per given time is independent of the quantities both of the aqueous phase and of $Ni(OH)_2$, so that the mole fraction α of NiO product is again a useful quantity for expressing reaction rate. It is seen that α is reproducible to ±0.02.

Table 3 presents values of α, determined in four independent series of hydrothermal experiments, which are to be correlated with the effective reaction time t, where t is the time t_f spent by the vessels in the furnace less the warm-up time (shown previously (37) to be about 0.8 h for reaction temperatures near 570 K). In contrast with the dry decomposition reaction, the hydrothermal reaction is seen to be very slow initially but to accelerate progressively, and one is faced with the problem of choosing an appropriate mathematical function to represent the data. Such a

TABLE 2. Decomposition of $Ni(OH)_2$ in aqueous NaOH under nitrogen

Initial mass $Ni(OH)_2$ (g)	Volume 0.474 *m* NaOH (cm^3 at 294 K)	$Ni(OH)_2$ remaining after 10 h at 573 K (%)
0.80	30	39
0.80	20	43
0.80	10	41
0.40	20	42

TABLE 3. Decomposition of $Ni(OH)_2$ in aqueous NaOH at 561.2 K under nitrogen[a]

Experiment No.	Time t_f in furnace (h)	α	$10^5 k_{obsd}$[b] (s^{-1})
1	3.9	0.02	2.4
	4.9	0.03	2.1
	6.0	0.11	2.6
	6.9	0.16	2.5
	8.0	0.26	2.5
	9.0	0.42	2.5
	10.0	0.54	2.5
2	9.2	0.40	2.4
	10.1	0.51	2.4
	11.3	0.76	2.4
	12.1	0.84	2.3
3	9.9	0.64	2.6
	11.0	0.75	2.5
	12.0	0.94	2.4
4	9.0	0.39	2.5
	9.5	0.53	2.6

[a]$Ni(OH)_2$ (0.8 g) initially in 20 cm^3 aqueous NaOH (0.474 mol kg^{-1}).
[b]Calculated from $k_{obsd} = \alpha^y/t$ with $y = 1/3$, and $t = t_f - 0.8$ h (to correct for warm-up time).

dependence of α upon t is typical of topotactic dry decomposition reactions of certain other ionic solids, and can be represented by the Erofeyev equation (38)

$$[3] \qquad -\ln(1 - \alpha) = (k_E t)^{n_E}$$

or similar generalized equations (39); the data of Table 3 fit eq. 3 satisfactorily, with n_E = 3.76 ± 0.15,

Can. J. Chem. Downloaded from www.nrcresearchpress.com by 210.87.254.105 on 09/05/12
For personal use only.

Can. J. Chem. Downloaded from www.nrcresearchpress.com by 210.87.254.105 on 09/05/12
For personal use only.

$k_E = (2.9 \pm 0.3) \times 10^{-5}$ s^{-1}, and correlation coefficient $r = 0.9894$, using all 16 data points.

Equations such as [3] were originally developed for solid state reactions on the basis of assumed rate control by propagation of reaction product growth from nuclei within crystals of the starting material, and, even though more detailed theoretical considerations (40) indicate that the empirical usefulness of eq. 3 beyond the stage where α is small is somewhat fortuitous, the choice of eq. 3 implies the assignment of a solid-state, internal nucleation mechanism to reaction 1. There are, however, several reasons for rejecting this assignment in favor of a dissolution mechanism.

Firstly, the rate law for the decomposition of $Ni(OH)_2$ in the dry state (eq. 2) bears no resemblance to eq. 3, and suggests surface rather than internal nucleation. It could, however, be argued that the surface nucleation process involves reversible dehydration and that this is suppressed in liquid water; indeed, the hydrothermal reaction is much slower than dry decomposition, the rate of which is sensitive to the gaseous environment.

Secondly, the rate of hydrothermal decomposition of $Ni(OH)_2$ is essentially proportional to $[OH^-]$ at high pH (see below). This suggests a dissolution mechanism, but could still be accommodated by an intracrystalline nucleation mechanism of the type proposed by Ball and Taylor (41) for the decomposition of dry brucite ($Mg(OH)_2$, isomorphous with β-$Ni(OH)_2$), which depends on chain transfers of protons from internal nuclei to surfaces and which could be facilitated by surface adsorption of OH^-.

Thirdly, transmission electron microscopy showed that, even after only 4% reaction in 0.474 m NaOH under N_2 at 573 K, the newly formed cubes of NiO were typically of 1 μm edge, whereas the diameters of the hexagonal $Ni(OH)_2$ crystals had increased only slightly and were on the order of 100–200 nm (BET measurements confirmed that the $Ni(OH)_2$ had undergone some further hydrothermal ripening at this high temperature, reducing the surface area by a factor of about 3, but it was established that neither NiO nor $Ni(OH)_2$ could have reached dimensions on the order of 1 μm by hydrothermal ripening under these conditions). Towards the end of the reaction, the well-crystallized NiO cubes had reached sizes of 3–6 μm side, i.e., their masses had increased in proportion to the extent of reaction α. These observations rule out all topotactic mechanisms, and indicate growth of NiO by crystallization from solution on to a fixed number of nuclei in the sample.

[4a] $Ni(OH)_2(c) + xOH^-(aq) \rightleftharpoons Ni(OH)_{2+x}{}^{x-}(aq)$

[4b] $Ni(OH)_{2+x}{}^{x-}(aq) \rightarrow NiO(c) + xOH^-(aq) + H_2O$

The importance and relatively rapid establishment of the equilibrium 4a at 540–575 K is demonstrated by the effectiveness of alkali in promoting hydrothermal growth of β-$Ni(OH)_2$ even at 470 K, although the absence of massive dissolution of $Ni(OH)_2$ indicates that the equilibrium 4a still lies far to the left. Thus, step 4b must be rate controlling, involving deposition of fresh NiO on pre-existing NiO crystals or nuclei, and the rate of the overall reaction 4 will be proportional to the xth power of the hydroxide ion activity a_{OH} and to the available surface area of NiO.

If this mechanism is correct, added NiO should accelerate the reaction greatly; this was found to be true (see below), and so we can write, for a single NiO crystal and hydroxide activity a_{OH},

$$[5] \qquad dm/dt = k(\text{area of NiO})a_{OH}{}^x = ka_{OH}{}^x\sigma m^{2/3}V^{2/3}$$

where k is the rate coefficient, m is the mass (in mol) of NiO in the given NiO crystal, V is the molar volume of NiO, and σ is a shape factor (6, for a perfect cube). The total mass M of NiO in a $Ni(OH)_2$ sample containing N growth centers (i.e., NiO crystals) is Nm, and, if p is the number of such centers per mol of original $Ni(OH)_2$, then

$$[6] \qquad N = pM_0$$

where M_0 is *either* the molar amount of $Ni(OH)_2$ originally present in the decomposing sample *or* the molar amount of NiO seeds deliberately added at the start of the reaction (in the latter case, all NiO growth would occur on the seeds, to the exclusion of latent nuclei in the $Ni(OH)_2$). Then,

$$[7] \qquad m = M/pM_0$$

$$[8] \qquad \frac{1}{pM_0}\left(\frac{dM}{dt}\right) = ka_{OH}{}^x\sigma(V/pM_0)^{2/3}M^{2/3}$$

Integration then gives

$$[9] \qquad (M_2{}^{1/3} - M_1{}^{1/3})/M_0{}^{1/3} = (\tfrac{1}{3}k\sigma p^{1/3}V^{2/3})a_{OH}{}^x t$$

$$[10] \qquad = k'a_{OH}{}^x t$$

$$[11] \qquad = k_{obsd}t \quad \text{at a given } [OH^-]$$

where M_2 = NiO in mol present at time t, and M_1 = NiO present at $t = 0$. When $M_1 = 0$, M_2 ranges from 0 at $t = 0$ to M_0 at the end of the reaction, so

$$[12] \qquad (M_2/M_0)^{1/3} = \alpha^{1/3} = k_{obsd}t$$

The validity of eq. 12 was tested by carrying out a linear regression analysis of ln t on ln α, using the data of Table 3 (which are unedited experimental

TABLE 4. Rate coefficients[a] for the decomposition of $Ni(OH)_2$ to NiO in aqueous NaOH

T (K)	Atmosphere[b]	[NaOH] (mol kg^{-1})	$10^5 k_{obsd}$[c] (s^{-1})	No. of data	Range of α	$10^5 k_c$ (kg mol^{-1} s^{-1})
542.2	N_2	1.026	0.64±0.09	11	0.13–1.00	0.62
552.5	N_2	1.027	0.97±0.05	11	0.13–0.93	0.95
561.2	N_2	1.026	2.5±0.1	16	0.02–0.94	2.4
561.2	Air	1.026	4.5±0.5	4	0.10–0.97	4.4
561.2	O_2	1.026	6.0±0.9	8	0.06–0.92	5.9
572.5	N_2	1.027	6.6±0.8	7	0.08–0.94	6.4
570.7	N_2	0.474	2.5±0.3	11	0.24–0.86	5.3
572.2	N_2	0.098	0.47±0.07	5	0.22–0.93	4.8

[a] $k_{obsd} = \alpha^{1/3}/t$; $k_c = k_{obsd}/[NaOH]$.
[b] Originally 90 kPa at 294 K.
[c] Uncertainties are standard deviations.

results); the correlation coefficient r was 0.9915 for all 16 data points, giving a slope (index of α) of 0.32 ± 0.01 and $k_{obsd} = (2.49 \pm 0.05) \times 10^{-5}$ s^{-1}. Similarly, the constancy of the calculated values of k_{obsd} in Table 3 (mean $k_{obsd} = (2.45 \pm 0.12) \times 10^{-5}$ s^{-1}) is remarkably good (fortuitously so, for $\alpha <$ 0.10), and vindicates the use of eq. 12. Table 3 refers only to hydrothermally ripened $Ni(OH)_2$ as the starting material; experiments using unripened $Ni(OH)_2$ gave somewhat faster but poorly reproducible rates.

Activity coefficients for aqueous hydroxide ion are not available for the conditions of this study, but, by analogy with values for 298 K, it may be assumed that they remain tolerably constant from 0.1 to 1.0 mol kg^{-1} NaOH. Thus, the data of Table 4 show that x in eqs. 4, 5, and 8–10 may be taken to be unity, and we can write

$$[13] \qquad \alpha^{1/3} = k_c[OH]t$$

This confirms that the main nickel(II) species present in strongly alkaline water is indeed $Ni(OH)_3^-(aq)$ (or, more generally, $[HNiO_2 \cdot yH_2O]^-$), as has been assumed by Gayer and Garrett (31). Attempts to follow reaction 1 at pH values near neutral led to poorly reproducible, very slow reaction rates.

The activation energy E_a from Table 4 is 220 ± 25 kJ mol^{-1}, i.e., roughly twice that of the dry decomposition reaction. Table 4 also shows that the presence of O_2 causes a marked acceleration of the hydrothermal decomposition, the product being black $NiO_{1+\delta}$ rather than the leaf green, stoichiometric (42–44) NiO that was obtained in the reactions under nitrogen. Green NiO prepared hydrothermally was not visibly affected by subsequent exposure to air, whereas green NiO prepared by decomposition of dry $Ni(OH)_2$ *in vacuo* turned black immediately on contact with air; this difference may be attributed to the much larger specific surface of the small, porous (30) NiO particles formed by the vacuum decomposition relative to the small ($\leq$0.2 m^2 g^{-1}, BET) specific surface of the hydrothermal NiO.

In principle, eq. 11 permits the calculation of the time-dependence of reaction 1 catalyzed by added NiO (hydrothermally prepared, to ensure the appropriate value of σ). In practice, the separate hydrothermal preparations of NiO tend to yield agglomerates of crystals which must be completely broken up and dispersed in the fresh reaction medium without crushing the individual crystals, and this is difficult to achieve. Nevertheless, the experimental fractional extents of reaction ($M_2 - M_1$) listed in Table 5 approach the calculated values sufficiently closely to indicate that eqs. 9–11 and the underlying theory describe the hydrothermal decomposition of $Ni(OH)_2$ accurately.

The large catalytic effect of NiO illustrated by Table 5 was considerably reduced when undispersed NiO agglomerates were used, as expected for a surface-controlled reaction.

Discussion

In practical terms, k_{obsd} represents the reciprocal of the time required for reaction 1 to reach 100% completion. More significantly, eq. 13 and the k_c values of Table 4 permit extrapolations to be made

TABLE 5. Decomposition of $Ni(OH)_2$ in aqueous NaOH in the presence of added NiO[a]

Time t_f (h)	M_2[b] (mmol)	$M_2 - M_1$[b] (%)	($M_2 - M_1$), calculated (%)	
			NiO catalysis[c]	No catalysis[d]
0	4.28	0	0	0
2.0	4.87	17	19	0.007
3.75	5.50	35	52	0.1
5.0	5.92	48	78	0.3
9.0	7.17	84	Complete	2.4

[a] NaOH (1.026 *m*), 553.2 K, under N_2; added NiO prepared hydrothermally under these same conditions.
[b] M_2 = total NiO present at time t; M_1 = NiO present initially = 4.28 mmol; $M_0 = (M_2)_{max}$ = NiO present at end of reaction = 7.73 mmol.
[c] Calculated from $(M_2/M_0)^{1/3} = (M_1/M_0)^{1/3} = k_{obsd}t$.
[d] Calculated from $(M_2 - M_1)/(M_0 - M_1) = \alpha = (kt)^3$.

Can. J. Chem. Downloaded from www.nrcresearchpress.com by 210.87.254.105 on 09/05/12
For personal use only.

Can. J. Chem. Downloaded from www.nrcresearchpress.com by 210.87.254.105 on 09/05/12
For personal use only.

to calculate the times needed for an experimentally significant extent of reaction to occur in the absence of pre-existing NiO; thus, the first 1% reaction requires about 80 days at 523 K, or over 2 years at 473 K, in 1.0 *m* NaOH, and proportionately longer times at lower $[OH^-]$.

This initial slowness of reaction 1 raises doubts concerning the thermodynamic validity of the experimental pressure–temperature phase relations reported for the $Ni(OH)_2$–NiO–H_2O system (7, 9, 10). The calculations of Mukaibo *et al.* (3), on the other hand, seem realistic; a thermodynamic threshold of about 440 K is predicted for reaction 1 at the saturated vapor pressure of water, which accommodates the considerable thermodynamic stability of β-$Ni(OH)_2$ at 298 K noted in the Introduction and also its apparent catalytic conversion to NiO in some ferrite syntheses at 473 K (6). This explains why all attempts to demonstrate the hydration of NiO to $Ni(OH)_2$ have failed (1, 7, 9, 10); the reaction is probably thermodynamically possible only below about 440 K, and even at this temperature 1% conversion would require over 200 years in 1.0 *m* NaOH (since $k_c \sim 3 \times 10^{-11}$ kg mol^{-1} s^{-1}, and the forward and back reactions would have the same rates).

The slightly faster and rather poorly reproducible rates observed for reaction 1 when unripened $Ni(OH)_2$ was used in place of the hydrothermally prepared hydroxide are unlikely to originate in the relatively rapid pre-equilibrium

$$[14] \quad Ni(OH)_2(c) + OH^-(aq) \rightleftharpoons Ni(OH)_3^-(aq)$$

but may reflect a greater (and variable) number of growth centers p per mol of unripened $Ni(OH)_2$, which would facilitate the rate determining step

$$[15] \quad Ni(OH)_3^-(aq) \rightarrow NiO(c) + OH^-(aq) + H_2O(l)$$

Similarly, the accelerating effect of O_2 may originate in the creation of Ni^{3+} defects in NiO, so assisting the formation of growth spirals; certainly, $NiO_{1+\delta}$ is the product when O_2 is present. Alternatively, the normal mechanism of reactions 14 and 15 may be supplemented by a sequence of the type

$$[16] \quad \beta\text{-}Ni(OH)_2 \overset{O_2}{\rightleftharpoons} \beta\text{-}NiO_{2\delta}(OH)_{2-2\delta} \quad (0 < 2\delta < 1)$$

$$[17] \quad \beta\text{-}NiO_{2\delta}(OH)_{2-2\delta} \rightarrow \gamma\text{-}NiO_{2\delta}(OH)_{2-2\delta}$$

$$[18] \quad \gamma\text{-}NiO_{2\delta}(OH)_{2-2\delta} \rightarrow NiO_{1+\delta} + (1-\delta)H_2O$$

Under hydrothermal conditions, reaction 17 evidently proceeds at about 513 K, and reaction 18 near 563 K (10, 12, 45). Reaction 16 may be expected to occur to a small extent on the surface of a β-$Ni(OH)_2$ crystal, as the electrochemical analogue of this reaction proceeds smoothly with 2δ ranging from 0 to 1 without changing the main structural features of the crystal (reaction 18 similarly involves minimal structural changes) (12, 46).

To conclude, the alkaline hydrothermal decomposition of $Ni(OH)_2$ in the absence of oxygen consists of a rate-determining, autocatalytic precipitation reaction following relatively rapid dissolution of the metastable β-$Ni(OH)_2$ as $Ni(OH)_3^-$(aq). This is in accordance with the general observation (47) that dissolution and ripening reactions (reaction 14) occur by relatively rapid diffusion-controlled processes, whereas precipitation of new phases (reaction 15) occurs by slower, interfacial processes. For this reason, the dissolved nickel(II) species of eqs. 4, 14, and 15 is more appropriately written as $Ni(OH)_3^-$ than as $NiO(OH)^-$, etc., implying readier reprecipitation as $Ni(OH)_2$ than as NiO. The practical significance of this reaction mechanism and the large E_a ($\sim$220 kJ mol^{-1}) associated with it is that $Ni(OH)_2$ can exist metastably in water at temperatures on the order of 570 K for remarkably long periods, especially if the pH is not high and there is little O_2 or solid NiO in the system. It follows that β-$Ni(OH)_2$ will often be an important product of the hydrothermal corrosion of nickel alloys, and that its thermodynamic properties should be used in place of those of NiO in calculations relating to the courses of chemical reactions in high-temperature aqueous systems. The same is probably true of cobalt(II) hydroxide, the pink β-form of which is isostructural with β-$Ni(OH)_2$ and forms hydrothermally from the blue α-$Co(OH)_2$ (6).

Finally, this study serves to emphasize the importance of reaction mechanism, as well as thermodynamics, in determining the outcome of hydrothermal reactions.

Acknowledgments

We thank Miss Margaret Sisley for some preliminary experiments, Dr. P. Bayliss for X-ray diffraction measurements, Alberta Sulphur Research, Ltd., for assistance with thermogravimetry, Drs. D. W. Shoesmith, T. E. Rummery, and A. G. Wikjord for discussions, and Atomic Energy of Canada, Ltd., for financial support.

1. N. S. McIntyre, T. E. Rummery, M. G. Cook, and D. Owen. J. Electrochem. Soc. **123**, 1164 (1976).
2. R. Gasparini and E. Ioanilli. Proc. Am. Power Conf. **33**, 776 (1971).
3. T. Mukaibo, S. Masukawa, M. Maeda, and M. Hoshido. Denki Kagaku, **34**, 388 (1966).
4. D. D. Wagman, W. H. Evans, V. B. Parker, I. Halow, S. M. Bailey, and R. H. Schumm. Selected values of chemical thermodynamic properties. NBS Technical Notes 270-3 (1968) and 270-4 (1969), U.S. Department of Commerce, Washington, DC.

Can. J. Chem. Downloaded from www.nrcresearchpress.com by 210.87.254.105 on 09/05/12
For personal use only.

5. R. E. VON MASSOW, G. R. SULLIVAN, and G. N. WAUGH. Solubility of nickel and cobalt ferrite in water up to 300°C. Report No. AECL-4582, Atomic Energy of Canada, Ltd., Ottawa, Ont., Canada. 1975.
6. A. R. GAINSFORD, M. J. SISLEY, T. W. SWADDLE, and P. BAYLISS. Can. J. Chem. **53**, 12 (1975).
7. L. A. ROMO. J. Phys. Chem. **60**, 1021 (1956).
8. C. KLINGSBERG and R. ROY. Am. Mineral. **44**, 819 (1959).
9. C. W. F. T. PISTORIUS. Z. Phys. Chem. Frankfurt am Main, **34**, 287 (1962).
10. M. A. AIA. J. Electrochem. Soc. **113**, 1045 (1966).
11. H. BODE, K. DEHMELT, and J. WITTE. Electrochim. Acta, **11**, 1079 (1966).
12. R. S. MCEWEN. J. Phys. Chem. **75**, 1782 (1971).
13. S. LE BIHAN and M. FIGLARZ. Electrochim. Acta, **18**, 123 (1973).
14. S. LE BIHAN and M. FIGLARZ. Thermochim. Acta, **6**, 319 (1973).
15. V. CHERTOV and R. S. TYUTYUNNIK. Kolloidn. Zh. **37**, 323 (1975).
16. A. MERLIN and S. TEICHNER. C. R. Acad. Sci. **236**, 1892 (1953).
17. S. J. TEICHNER, R. P. MARCELLINI, and P. RUÉ. Adv. Catal. **9**, 458 (1957).
18. R. P. MARCELLINI and S. J. TEICHNER. J. Chim. Phys. **58**, 625 (1961).
19. I. F. HAZELL and R. J. IRVING. J. Chem. Soc. A, 669 (1966).
20. W. DENNSTEDT and W. LÖSER. Electrochim. Acta, **16**, 429 (1971).
21. M. SAKASHITA and N. SATO. Bull. Chem. Soc. Jpn. **46**, 1983 (1973).
22. J. ERKELENS and S. H. EGGINCK-DUBURCK. Rec. Trav. Chim. Pays-Bas, **92**, 658 (1973).
23. M. TOPIC, F. J. MICALE, C. L. CRONAN, H. LEIDHEISER, JR., and A. C. ZETTLEMOYER. Adsorption at interfaces. A.C.S. Symposium Series No. 8, 225 (1975).
24. A. OBERLIN. Bull. Soc. Fr. Mineral. **77**, 833 (1954).
25. S. LE BIHAN, J. GUENOT, and M. FIGLARZ. C. R. Acad. Sci. Ser. C, **270**, 2131 (1970).
26. D. LOUËR, D. WEIGEL, and J. I. LANGFORD. J. Appl. Crystallogr. **5**, 353 (1972).
27. V. P. KOTOV. Zavod. Lab. **10**, 503 (1941).
28. S. LE BIHAN and M. FIGLARZ. J. Cryst. Growth, **13/14**, 458 (1972).
29. W. DENNSTEDT. Electrochim. Acta, **19**, 535 (1974).
30. F. FIEVET and M. FIGLARZ. J. Catal. **39**, 350 (1975).
31. K. H. GAYER and A. B. GARRETT. J. Am. Chem. Soc. **71**, 2973 (1949).
32. G. B. NAUMOV, B. N. RYZHENKO, and J. L. KHODAKOVSKI. Handbook of thermodynamic data. Atomizdat, Moscow, Russia. 1971.
33. C. F. BAES, JR. and R. E. MESMER. The hydrolysis of cations. J. Wiley and Sons, New York, NY. 1976. pp. 245–246.
34. J. J. B. VAN EIJK VAN VOORTHUIJSEN and P. FRANZEN. Rec. Trav. Chim. Pays-Bas, **70**, 793 (1951).
35. T. W. SWADDLE, J. H. LIPTON, G. GUASTALLA, and P. BAYLISS. Can. J. Chem. **49**, 2433 (1971).
36. E. SUONINEN, T. JUNTUNEN, H. JUSTEN, and M. PESSA. Acta Chem. Scand. **27**, 2013 (1973).
37. M. HENDERSON, V. I. MIASEK, and T. W. SWADDLE. Can. J. Chem. **49**, 317 (1971).
38. B. V. EROFEYEV. C. R. Dokl. Acad. Sci. URSS, **52**, 511 (1946).
39. J. H. TAMPLIN. Aust. J. Chem. **29**, 27 (1976).
40. A. R. ALLNATT and P. W. M. JACOBS. Can. J. Chem. **46**, 111 (1968).
41. M. C. BALL and H. F. W. TAYLOR. Mineral. Mag. **32**, 754 (1961).
42. S. P. MITOFF. J. Chem. Phys. **35**, 882 (1961).
43. R. NEWMAN and R. M. CHRENKO. Phys. Rev. **114**, 1507 (1959).
44. F. J. MORIN. Phys. Rev. **93**, 1199 (1954).
45. R. W. CAIRNS and E. OTT. J. Am. Chem. Soc. **55**, 527 (1933); **55**, 534 (1933).
46. H. BODE, K. DEHMELT, and J. WITTE. Z. Anorg. Allg. Chem. **366**, 1 (1969).
47. A. G. WALTON. The formation of precipitates. Interscience, New York, NY. 1967. Chapt. 2.

State equation parameters of three homologous series: tetraalkyltin compounds, tetraalkoxysilanes, trialkylamines

ROBERT PHILIPPE

Université de Lyon, Laboratoire de Chimie Analytique I, 43, Boulevard du 11 Novembre 1918, 69621-Villeurbanne, France

AND

GENEVIÈVE DELMAS AND MICHÈLE COUCHON

Université du Québec à Montréal, Département de Chimie, C.P. 8888, Montréal (Qué.), Canada H3C 3P8

Received June 30, 1977

ROBERT PHILIPPE, GENEVIÈVE DELMAS, and MICHÈLE COUCHON. Can. J. Chem. **56**, 370 (1978).

Expansion coefficients and thermal pressure coefficients γ have been measured at 25°C for members of the following series of compounds: (*1*) SnR_4 (R = CH_3, C_2H_5, C_3H_7, C_4H_9, $C_{12}H_{25}$). (*2*) $Si(OR)_4$ (R = being the same except for C_6H_{13} and C_8H_{17} instead of $C_{12}H_{25}$). (*3*) NR_3, R from C_2H_5 to $C_{12}H_{25}$ except C_9H_{19} and $C_{11}H_{23}$; two NR_3' where R′ is a branched (br) alkyl radical isopentyl and isooctyl and $N(CH_3)_2(C_{12}H_{25})$. (*4*) *n*-C_7H_{16}, 3-3-diethylpentane (3,3-DEP), dimethylsulfoxide (DMSO), 2,2,4,4,6,8,8-heptamethylnonane (br-C_{16}). The variation of γ between 25 and 80°C is obtained for the following compounds: br-C_{16}, $N(isopent)_3$ and $N(Dec)_3$. The comparison of the cohesive energies for the different members of a series or from one series to another is made with P^* rather than with γ. $P^* = \gamma\tilde{v}^2T$. For the three series the limiting values, when *n* increases, of the pressure reduction parameter P^* and of the expansion coefficients are very similar. The P^* do not have regular values for the NR_3, SnR_4, and $Si(OR)_4$ series for low values of the molecular weights. One explanation of these irregularities is the different shape of the molecules. The surface to volume ratios of the different molecules are calculated with a spherical model or a cylindrical model. Values of cohesive energies per unit surface P^*/s are compared. P^*/s for the linear and branched alkanes are on the same curve while the P^* were not. However, no similar smoothing is accomplished for the lower members of the other series. The high values of P^*/s for the sterically hindered $SnEt_4$, $SnPr_4$, and 3,3-DEP seem to indicate that measurements of γ and P^* can be a method to evaluate steric hindrance in the different members of a series. Report is made of calorimetric results on the same sterically hindered compounds in solution. Higher P^*'s may also come from increased polarity in the lower members of a series.

ROBERT PHILIPPE, GENEVIÈVE DELMAS et MICHÈLE COUCHON. Can. J. Chem. **56**, 370 (1978).

Les coefficients d'expansion et les coefficients thermiques de pression γ ont été mesurés à 25°C pour les séries des composés suivants: (*1*) SnR_4 (R = CH_3, C_2H_5, C_3H_7, C_4H_9, $C_{12}H_{25}$). (*2*) $Si(OR)_4$ (R est le même sauf pour C_6H_{13} et C_8H_{17} au lieu de $C_{12}H_{25}$). (*3*) NR_3, R varie de C_2H_5 à $C_{12}H_{25}$ excepté C_9H_{19} et $C_{11}H_{23}$, deux NR_3' où R′ est un radical alkyle ramifié, isopentyl et isooctyl ainsi que $N(CH_3)_2(C_{12}H_{25})$. (*4*) *n*-C_7H_{16}, diethyl-3,3 pentane (3,3-DEP), diméthylsulfoxyde (DMSO), heptaméthyl-2,2,4,4,6,8,8 nonane (br-C_{16}). La variation de γ entre 25 et 80°C est obtenue pour les composés suivants br-C_{16}, $N(isopent)_3$ et $N(Dec)_3$. La comparaison des énergies de cohésion d'une série à l'autre ou pour les différents composés d'une même série se fait sur P^* plutôt que sur γ, $P^* = \gamma\tilde{v}^2T$. Pour les trois séries, les valeurs limites, quand *n* augmente, du paramètre de pression réduite P^* et des coefficients d'expansion sont très similaires. Les paramètres P^* pour les *n*-alcanes donnent une courbe régulière quand *n* augmente tandis que les valeurs obtenues pour les composés à bas poids moléculaire des séries NR_3, SnR_4 et $Si(OR)_4$ ne donnent rien de semblable. Ces irrégularités peuvent s'expliquer par la différence de forme de ces molécules. Les rapports surface–volume des différentes molécules sont calculés à partir d'un modèle sphérique ou d'un modèle cylindrique. On compare alors les énergies de cohésion par unité de surface P^*/s. P^*/s pour les alcanes linéaires et les alcanes ramifiés apparaissent sur une même courbe alors que les P^* sont dispersés. Cependant aucun lissage similaire n'est obtenu pour les premiers composés des autres séries. Les valeurs élevées des P^*/s pour les composés stériquement encombrés tels $SnEt_4$, $SnPr_4$ et 3,3-DEP semblent indiquer que les mesures de γ et P^* peuvent être une méthode d'évaluation de l'encombrement stérique pour les différents composés d'une série. On rapproche alors ces résultats de ceux de calorimétrie obtenus sur les mêmes composés stériquement encombrés, en solution. Un P^* plus élevé peut aussi provenir de l'augmentation de polarité des premiers composés d'une série.

Introduction

Modern theories of solutions of non-polar molecules (Prigogine (1), Patterson and Delmas (2), Flory *et al.* (3)) have shown the importance of two main contributions to the excess thermodynamic properties. The first one depends on the difference

Can. J. Chem. Downloaded from www.nrcresearchpress.com by 210.87.254.5 on 09/05/12
For personal use only.

Can. J. Chem. Downloaded from www.nrcresearchpress.com by 210.87.254.5 on 09/05/12
For personal use only.

in chemical nature of the two components. This chemical term gives a positive contribution to the heats of mixing and to the excess volume and a negative one to the excess entropy. The second contribution, which has been recognized more recently, depends on the difference of state of expansion (or free volume) of the two components mixed. It gives a negative contribution to H^E, TS^E, and V^E. Solution properties of mixtures (4–6) consisting of molecules of different shape, such as a globular molecule and a linear one, have shown that a third contribution depending on the shape of the molecule should be added. In the case of the heats, this third contribution can be a positive term related to the destruction of orientational order (4–6) and a negative one due to the 'condensation' or steric hindrance effect (7, 8).

The prediction of these different contributions depends on the knowledge of the expansion coefficient $\alpha = 1/V(\partial V/\partial T)_P$ and the thermal pressure coefficient $\gamma = (\partial P/\partial T)_V$.

The thermal pressure coefficient of a liquid is sensitive to the shape of its molecules. For instance, γ (5) is higher (0.888 J cm^{-3} K^{-1}) for the linear *n*-octane than for the branched isomer 2,2,4-trimethylpentane (0.798 J cm^{-3} K^{-1}). It has seemed interesting to us to measure the variation of γ for molecules in a series such as the SnR_4 and $Si(OR)_4$, where R is an alkyl radical. The characteristic of these series is that the shape of the molecule changes gradually from globular to linear when the chain length increases. Heat of mixing (9, 10) measurements on members of these series do not vary regularly with the chain length. This has been explained by the existence of different degrees of steric hindrance among members of the same series. For this reason, we would like to call these series the 'differently sterically hindered' series (dsh) to distinguish them from a normal series such as the *n*-alkanes.

On the other hand, the knowledge of the thermal pressure coefficient of the pure components is needed to calculate the pressure reduction parameter P^*. The comparison of V^E(calc.) and V^E(exp.) is possible only if the P^* are known, since an important contribution to V^E(calc.) comes from the difference in P^* of the components (2, 7). It should be noted that for the calculation of H^E the difference in expansion coefficients or of free volume is more important than that of P^*.

Moreover, it is hoped that the measurement of this macroscopic property on the pure compounds in the series would possibly give information on the 'condensation effect' (7–10) which has been seen in solutions: heats of mixing of the SnR_4 series with $Sn(Laur)_4$ (10) show an unexpected negative contribution with $SnEt_4$. Other heats[1] give similar results. The origin of this effect, which cannot be explained by free volume contributions, may be related to steric hindrance but it is not clearly understood.

Measurements of the thermal pressure coefficients have been made on some *n*-alkanes (12, 13) and branched (br) alkanes (14), cycloalkanes (15), aromatic and polar compounds (16), and polymers (17). Apparently, no measurements have been done on the SnR_4, $Si(OR)_4$, and NR_3 series. α and γ measurements at 25°C of the following 29 compounds are presented here: (*a*) SnR_4, R = CH_3, C_2H_5, C_3H_7, C_4H_9, $C_{12}H_{25}$. (*b*) $Si(OR)_4$ for the same alkyl radicals except that R = $C_{12}H_{25}$, which was not available, has been replaced by R = C_6H_{13} and R = C_8H_{17}. (*c*) NR_3, R from C_2H_5 to $C_{12}H_{25}$ except C_9H_{19} and $C_{11}H_{23}$, two NR_3' where R′ is a branched alkyl radical (isopentyl and isooctyl) and $N(CH_3)_2C_{12}H_{25}$. (*d*) *n*-C_7H_{16}, 3,3-diethylpentane (3,3-DEP), dimethylsulfoxide (DMSO), 2,2,4,4,6,8,8-heptamethylnonane (br-C_{16}). The variation of between 25 and 80°C is obtained for the following compounds: br-C_{16}, $N(isopent)_3$ and $N(Dec)_3$. In the text, the dodecyl derivatives will be called Lauryl, $N(Laur)_3$ for instance.

Experimental

Solvents

The sources of solvents are indicated in Table 1 and have been used without further purification. Their density and refractive index have been measured as a test of their purity and are given in the same table.

Thermal Expansion Coefficients

Values of thermal expansion coefficients have been measured with an Anton Paar digital precision density meter (distributed by the Fisher Co.). The temperature was read on the same quartz thermometer used for the thermal pressure coefficients and the densities were measured over a 10 deg interval (20–30°C).

Thermal Pressure Coefficients

The basic experimental procedure is that of Westwater *et al.* (18) and the method has been used by several other workers (13–17). The equipment used was built by Bardin (14) and consists of a constant volume pressure vessel, Pyrex glass cell, thermometer, pressure gauge, and a constant temperature bath. The schematic diagram of this is presented in Fig. 1.

The constant volume pressure vessel built by the American Instrument Co. was made of stainless steel with a 1.5 ℓ capacity and could withstand a pressure greater than 200 bars at 350°C.

Procedure

The liquid sample, about 8 cm^3, is placed in the Pyrex glass cell and degassed by repeated freezing with liquid nitrogen and

[1]R. Philippe, G. Delmas, and Phuong Nguyen Hong, unpublished results on the following systems: SnR_4 + *n*-C_{16}, NR_3 + $N(R')_3$, and NR_3 + alkanes.

TABLE 1. Refractive index and densities of compounds at 25°C

	Origin	n_D (this work)	d (this work)
$SnMe_4$	C.P.L.	1.4388	1.2865
$SnEt_4$	K and K	1.4675	1.1873
$SnPr_4$	C.P.L.	1.4722	1.1013
$Sn(But)_4$	Aldrich	1.4713	1.0492
$Sn(Laur)_4$	C.P.L.	1.4708	0.9170
$Si(OMe)_4$	K and K	1.3656	1.0231
$Si(OEt)_4$	K and K	1.3805	0.9301
$Si(OPr)_4$	Cygni	1.3981	0.9065
$Si(OBut)_4$	Cygni	1.4112	0.8976
$Si(OHex)_4$	I.C.N.	1.4273	0.8808
$Si(OOct)_4$	C.P.L.	1.4339	0.8806
$Si(OLaur)_4$	ROC/RIC		0.8719
NEt_3	Eastman	1.3980	0.7234
NPr_3	Aldrich	1.4141	0.7524
$N(But)_3$	Eastman	1.4268	0.7746
$N(Pent)_3$	Eastman	1.4351	0.7870
$N(Hex)_3$	C.P.L.	1.4404	0.7964
$N(Hept)_3$	Eastman	1.4470	0.8023
$N(Oct)_3$	Aldrich	1.4478	0.8105
$N(Dec)_3$	Eastman	1.4527	0.8151
$N(Laur)_3$	Merck	1.4568	0.8211
$N(Isopent)_3$	Eastman	1.4304	0.7790
$N(Isooct)_3$	C.P.L.	1.4495	0.8147
$(CH_3)_2N(Laur)$	K and K	1.4370	0.7846
n-Heptane	Fisher	1.3846	0.6541
br-C_{16}	Chem-Samples	1.4380	0.7819
3,3-DEP	Chem-Samples		0.7500
DMSO	Anachemia	1.47726	1.0958

melting under vacuum. The capillary is then filled with a known weight of degassed mercury and the mercury level adjusted at the extremity of the tungsten wire for the desired temperature. As the mercury rises up the capillary of the cell, it makes contact with the sharpened tungsten wire (ec) and shuts off an electric circuit.

The temperature of the bomb is measured by a Hewlett-Packard quartz thermometer (model 2801 A) with a temperature-sensing probe (S/N 980-2 type 2880 C model). The probe,

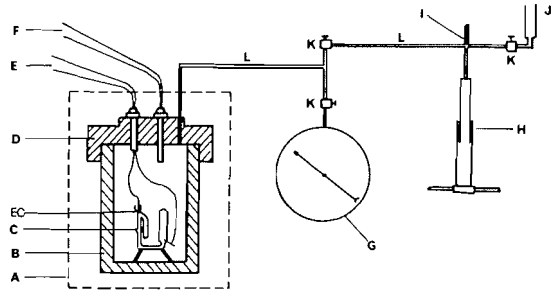

FIG. 1. Schematic diagram of the equipment used in the determination of thermal pressure coefficients: A thermoregulated water bath, B pressure vessel, C glass cell, D pressure vessel cap, E leads for the constant volume checking circuit, F temperature probe leads, G high pressure gauge, H pressure generator, I safety head assembly, J reservoir for the pressure fluid, K valves, L high pressure tubing, ec contact between the mercury and the tungsten wire.

screwed into the top of the bomb, gives the pressure-transmitting fluid (200 Dow Corning) temperature with a resolution of 10^{-4}°C and a precision of ± 0.02°C. The large mass of the bomb minimizes temperature fluctuations of the thermoregulated bath.

The pressure is applied with a manual pump (High Pressure Equipment Co., capacity 20 cm^3) and is measured with a precalibrated Bourdon-type gauge (Seegers Instrument Co. SS 2792 A 600). This gauge operates between 0 and 40 bars and gives a visual display of the pressure measured with a resolution of 0.02 bar.

Calculation

As pointed out previously (17), the application of small temperature increments increases the reproducibility of the results. The total temperature interval for one γ measurement is not larger than 2°C and the data can be fitted adequately by a straight line.

A least squares fitting procedure is employed on four to six (p, T) points to obtain the slope of the line, γ_{obs}, and the temperature at zero pressure. The γ_{obs} data are then corrected using eq. 1 (13):

$$[1] \qquad \gamma = \gamma_{obs} \frac{\alpha_l V_l}{\alpha_l V_l + (\alpha_{Hg} - \gamma_{obs}\beta_{Hg})V_{Hg} - (\alpha_g - \gamma_{obs}\beta_g)V_g}$$

where α is the thermal expansion coefficient, β the isothermal compressibility, and V the volume. The indices g, Hg, and l refer to the glass, mercury, and liquid samples respectively. Data needed in eq. 1 have been found in the literature or measured.

Comparison with Literature Data

Data are given in the text table below. As these data have been obtained on two different compounds (non-polar and polar) the agreement is quite satisfactory.

Theory

Equation of State Parameters

The simple Van der Waals relation between energy and volume, $\tilde{U} = -1/\tilde{v}$, gives equally good predictions as the more complex expressions (2). It has been used with the Flory model to obtain the volume, pressure, and temperature reduction parameters V^*, P^*, and T^*. The experimental densities,

Compounds	$T - 273.15$ (K)	γ (J cm^{-3} K^{-1}) This work	Literature	(Ref.)
n-Heptane	25.67	0.808 ± 0.002	0.8090 ± 0.0003	(13)
DMSO	25.22	1.703 ± 0.003	1.730 ± 0.008	(16)

Can. J. Chem. Downloaded from www.nrcresearchpress.com by 210.87.254.5 on 09/05/12
For personal use only.

Can. J. Chem. Downloaded from www.nrcresearchpress.com by 210.87.254.5 on 09/05/12
For personal use only.

TABLE 2. Parameters for the pure compounds

		Experimental				Calculated						
											$s = S/V$ (Å)$^{-1}$	
Compounds	$T - 273.15$ (K)	γ (J cm^{-3} K^{-1})	σ_γ (J cm^{-3} K^{-1})	$10^3\alpha_{25°C}$ (K^{-1})	$\gamma_{25°C}$ (J cm^{-3} K^{-1})	$\tilde{v}_{25°C}$	P^* (J cm^{-3})	V^* (cm^3 mol^{-1})	T^* (K)	c	Sphere	Cylinder
$SnMe_4$	24.28	0.811	0.003	1.280[a]	0.809	1.3024	409.1	106.73	4606	1.15	0.96	0.88
$SnEt_4$	20.48	0.997	0.005	1.000[a]	0.977	1.2477	453.5	158.59	5231	1.68	0.75	0.86
$SnPr_4$	22.34	1.088	0.003	0.890[a]	1.071	1.2247	478.9	215.79	5589	2.22	0.68	0.84
$Sn(But)_4$	21.00	1.022	0.003	0.818[a]	1.006	1.2092	438.6	273.63	5876	2.56	0.61	0.83
$Sn(Laur)_4$	26.00	1.092	0.009	0.767[a]	1.107	1.1978	473.3	724.68	6113	7.76		0.82
$Si(OMe)_4$	25.81	1.051	0.010	1.118[a]	1.055	1.2713	508.11	117.03	4601	1.59	0.841	0.93
$Si(OEt)_4$	25.46	0.936	0.007	1.168[a]	0.938	1.2810	458.73	174.84	4817	2.01	0.732	0.89
$Si(OPr)_4$	25.04	0.964	0.073	1.026[a]	0.965	1.2529	451.43	232.83	5157	2.46	0.667	0.86
$Si(OBut)_4$	26.09	0.946	0.003	0.975[a]	0.951	1.2425	437.48	287.39	5303	2.86	0.624	0.85
$Si(OHex)_4$	25.16	0.994	0.003	0.889[a]	0.995	1.2244	444.50	398.48	5591	3.82		0.84
$Si(OOct)_4$	25.25	1.033	0.004	0.829[a]	1.035	1.2115	452.68	510.79	5828	4.78		0.83
$Si(OLaur)_4$				0.757[a]		1.1956	455.78	737.28	6163	6.57		
NEt_3	20.02	0.927	0.002	1.290[b]	0.906	1.3042	459.2	107.31	4590	1.29	0.85	0.94
NPr_3	25.14	0.864	0.002	1.064[b]	0.865	1.2606	409.6	151.06	5059	1.49	0.77	0.90
$N(But)_3$	20.86	0.981	0.005	0.97[b]	0.963	1.2414	442.3	192.76	5322	1.93	0.71	0.88
$N(Pent)_3$	24.66	0.978	0.002	0.92[a]	0.977	1.2310	441.2	234.76	5484	2.08		0.86
$N(Hex)_3$	24.88	0.993	0.003	0.879[a]	0.993	1.2223	442.1	276.87	5631	2.62		0.854
$N(Hept)_3$	25.15	1.013	0.001	0.854[a]	1.014	1.2169	447.5	319.16	5728	3.00		0.848
$N(Oct)_3$	25.75	1.024	0.005	0.832[a]	1.029	1.2121	450.5	359.93	5819	3.36		0.84
$N(Dec)_3$	24.82	1.072	0.006	0.808[a]	1.072	1.2069	465.3	445.10	5922	4.21		0.835
—	42.27	0.982	0.006				458.9					
—	54.28	0.926	0.002				454.3					
—	71.34	0.856	0.002				449.0					
—	86.62	0.777	0.006				431.6					
$N(Laur)_3$	24.98	1.104	0.004	0.787[a]	1.104	1.2022	475.5	528.7	6020	5.03		0.83
$N(Isopent)_3$	24.77	0.918	0.004	0.956[a]	0.917	1.2385	419.2	235.7	5362	2.21	0.66	0.86
—	32.48	0.885	0.003				418.3					
—	45.40	0.798	0.007				398.5					
—	67.24	0.654	0.003				356.9					
$N(Isooct)_3$	24.69	1.006	0.001	0.89[c]	1.001	1.2245	449.5	354.50	5588	3.43		0.84
$(CH_3)_2N(Laur)$	24.92	1.016	0.001	0.91	1.015	1.2290	457.1	221.3	5517	2.20		0.92
n-Heptane	25.67	0.808	0.002	1.388[a]	0.811	1.3222	422.7	115.85	4434	1.33		1.01
br-C_{16}	20.02	0.925	0.003	0.853[d]								
—	24.86	0.912	0.005	0.857[d]	0.912	1.2177	396.6	237.84	5712	1.99	0.77	0.766
—	39.25	0.810	0.005	0.871[d]								
—	55.43	0.744	0.005	0.888[d]								
—	76.31	0.682	0.002	0.912[d]								
3,3-DEP	24.19	0.925	0.004	0.957[d]	0.921	1.2388	421.4	138.05	5361	1.30	0.79	0.906
DMSO	25.22	1.703	0.003	0.88	1.705	1.2226	759.8	58.31	5626	0.95		

[a]This work.
[b]Reference 22.
[c]Estimated.
[d]Reference 14.

Can. J. Chem. Downloaded from www.nrcresearchpress.com by 210.87.254.5 on 09/05/12
For personal use only.

expansion coefficients, thermal pressure coefficients given in Tables 1 and 2 are used with eq. 2 (3, 19). The reduced volume and the reduction parameters are respectively:

$$\tilde{v}^{1/3} = ((4/3)\alpha T + 1)/(\alpha T + 1)$$
$$V^* = V/\tilde{v} \text{ with } V = M/d$$
$$T^* = T/\tilde{T} = T\tilde{v}/(1 - \tilde{v}^{-1/3}) \quad [2]$$
$$P^* = \gamma\tilde{v}^2 T$$

The number of external degrees of freedom for the whole molecule is given by c in eq. 3

$$c = P^*V^*/RT^* \quad [3]$$

Results and Discussion

Table 2 gives the experimental values of γ for the different compounds. The first three columns show the temperature of the measurement, the γ value, and the standard deviation. Columns 4 to 6 indicate the expansion coefficient α, the γ value computed at 25°C exactly, and the reduced volume $\tilde{v}$. Columns 7 to 10 give pressure, volume, and temperature reduction parameters P^*, V^*, T^*, and c. The last two columns are calculated surface to volume ratios for the different molecules using the spherical and cylindrical models. The temperature variation of γ, $(d\gamma/dT)_{P=0} = (2\alpha T + 1)\gamma/T$ has been used to obtain $\gamma_{25°C}$. Although this relation does not predict well the temperature variation of γ, its use on a small temperature interval does not change the results significantly.

Comparison of P* *for Members of a Series and for the Different Series*

Comparison of the cohesive energy of the compounds will be made on P^* rather than on γ, since γ also reflects the state of expansion which varies considerably along the series. P^* is calculated from eq. 2 and the experimental values of α and γ. As can be seen from Fig. 2 the characteristic features of these results are the following: (*a*) The P^*'s tend towards a limiting value when the molecular weight increases.

The limiting values do not vary by more than about 5% and the order appears to be $Si(OR)_4 < SnR_4 < NR_3 < n\text{-}C_n$. The branched alkanes and the branched amines have distinctively lower P^*'s but the limiting value cannot be extrapolated. (*b*) The P^* values for the lower members of the DSH series do not vary smoothly with molecular weight as is the case for the normal or the three branched alkanes shown on Fig. 2. The high values found for NEt_3, $Si(OMe)_4$, and $Si(OEt)_4$ can be explained by the more polar character of these molecules compared to the longer members of the series. The higher values of P^* for $SnEt_4$, $SnPr_4$, and possibly $NBut_3$,

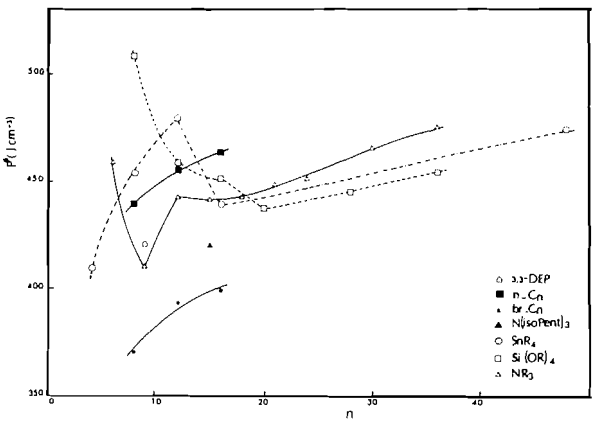

FIG. 2. Pressure reduction parameter P^* plotted against n the total number of carbon atoms for SnR_4 (○), $Si(OR)_4$ (□), n-C_n (■), br-C_n (●), $N(isopent)_3$ (▲), 3,3-DEP (△). The points for $N(isooct)_3$ and $(CH_3)_2N(laur)$ which are very close to $N(oct)_3$ and n-C_{14} have not been put on the graph. The abcissa n for the $Si(OR)_4$ has been calculated as if the oxygen atoms were carbon atoms. br-C_n stands for three highly branched alkanes 2,2,4-trimethylpentane (br-C_8), 2,2,4,6,6,-pentamethylheptane (br-C_{12}), and br-C_{16} used in previous work for comparison with n-alkanes.

$Si(OEt)_4$, and $Si(OPr)_4$ must be related to the steric hindrance of these molecules. A similar feature exists for 3,3-diethylpentane (3,3-DEP) whose P^* (420 J/mol) is higher than that of a hydrocarbon in C_9 of the same shape, 2,2-dimethylpentane (390 J/mol). $SnEt_4$ and 3,3-DEP with four ethyl groups attached to a tetravalent central atom have similar shapes.

The irregularities of P^* in the series are assumed not to be due to the inadequacy of the theory to obtain P^* from the experimental quantity γ. This assumption is reasonable for two reasons: the same theory gives a smooth P^* variation for the n-alkanes and the experimental γ values in the series do not vary smoothly.

External Degrees of Freedom

The number of external degrees of freedom c can be calculated from d, α, and γ and from eqs. 2 and 3. It would be interesting to see if the steric hindrance of $SnEt_4$ and $SnPr_4$ changes the number of external degrees of freedom in a series The column before the last in Table 2 gives c for the different series. A plot of c versus n, the total number of carbon atoms for the three series, not shown here, gives a single curve for the series with some scatter of the points for the low molecular weight compounds. In this plot, as in Fig. 2, the oxygen atoms of the $Si(OR)_4$ compounds have been counted as a carbon atom. The points corresponding to $SnEt_4$ and $SnPr_4$ have higher values of the external degrees of freedom due to their high P^*. The external degrees of freedom can be

Can. J. Chem. Downloaded from www.nrcresearchpress.com by 210.87.254.5 on 09/05/12
For personal use only.

expressed by segment for chain-like molecules. The Prigogine definition of a segment has been used to calculate c/r as shown in Fig. 3: the number of segments, r, of a linear molecule with n carbon atoms is $(n + 1)/2$. In the present case, the central atom has not been counted and the oxygen atom of the $Si(OR)_4$ compounds has been considered equivalent to a carbon atom. Figure 3 shows that the external degrees of freedom have comparable values in the four series for $n \geq 14$. The higher values for the shorter members of the series can be due to higher cohesive energies which increases c, having no relation with external degrees of freedom. On the other hand, one would expect that the globular shape of the shorter compounds would cause the c/r values to increase towards 1. It does not seem possible to separate the different contributions (shape and polarity) to this increase. In any case, the sterically hindered compounds show c/r higher on the plot: this means that steric hindrance changes P^* more than it does V^* and T^*. Available data on isomers of different steric hindrance indicate that the sterically hindered compounds have lower V and higher T^* since the molecule has a higher density and lower expansion coefficient and also a lower core volume V^*.

Surface to Volume Ratio s *for a Molecule and Values of* P*/s

As interactions of molecules take place between molecular surfaces, the comparison of energies by unit surface P^*/s is more meaningful than that of energies by unit volume P^*. s depends on the shape of the molecule and can be calculated from S and V the molecular surface and molecular volume. s can be obtained from a spherical or cylindrical model.

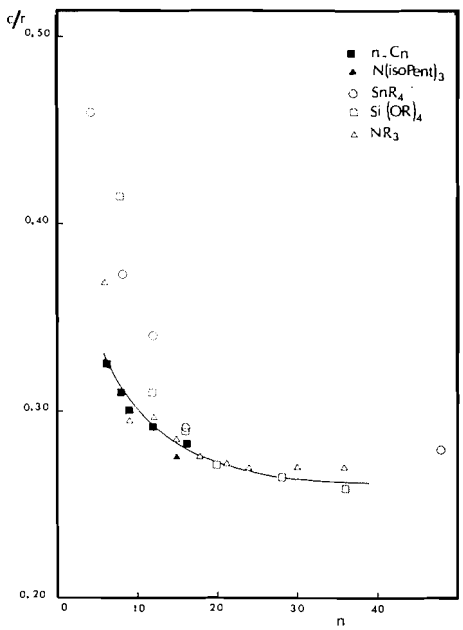

FIG. 3. External degrees of freedom by segment c/r plotted against the total number of carbons for SnR_4 (○), $Si(OR)_4$ (□), NR_3 (△), n-C_n (■), $N(isopent)_3$ (▲). $c = P^*V^*/RT^*$ and $r = (n + 1)/2$ even for the lower members of the series.

Sphere

A globular molecule can be approximated to a sphere which gives a value of $s = 4.083(V^*)^{-1/3}$ (V^* expressed in cm^3).

Cylinders

Linear alkanes can be represented by a right cylinder having a diameter of 4.98 Å (23*b*) and very branched alkanes by a 6.98 Å diameter cylinder (23*a*).

Group of Cylinders

The SnR_4, $Si(OR)_4$, NR_2 molecules are represented as an assembly of three or four cylinders attached to the central atom, the cylinder having the same diameter as a free alkane chain. The surface of the central atom which could be available for contact with other molecules has been neglected, its core volume obtained by extrapolating to zero carbon atom the V^* of the other members of the series. For the N, Si, Sn atoms, the core volumes are found to be 26, 40, 49 cm^3 respectively. The surface of the base of the cylinder attached to the central atom has been neglected in the counting of the surface available for contacts with other molecules. Accordingly s is given by

$$s = (n/V^*)(0.473D^2 - V^*_{ca}(4/nD))$$

n is the number of branches, D the cylinder diameter in Å, and V^* and V^*_{ca} the core volume of the molecule and of the central atom respectively in cm^3. The P^*/s values are plotted on Fig. 4 versus the carbon atom number. The P^*/s values of the linear and branched alkanes are now quite comparable. This is also true for $N(isopent)_3$ and $N(isooct)_3$. For $N(isopent)_3$, a 6 Å diameter cylinder has been used, a value between that of a linear and a branched alkane. The spherical model would give a small s and an unreasonable value of P^*/s. This must mean that even with a branched alkyl chain, there is a surface available for extramolecular contacts in between the three chains of the NR_3 molecule when R contains more than three carbon atoms.

SnR_4 Series

Contrary to the case of the branched and linear alkanes, the relative values per unit surface, P^*/s, with s(cylinder) are not significantly different from those of P^*. The values for $SnEt_4$ and $SnPr_4$ are still higher than expected from a regular curve and would

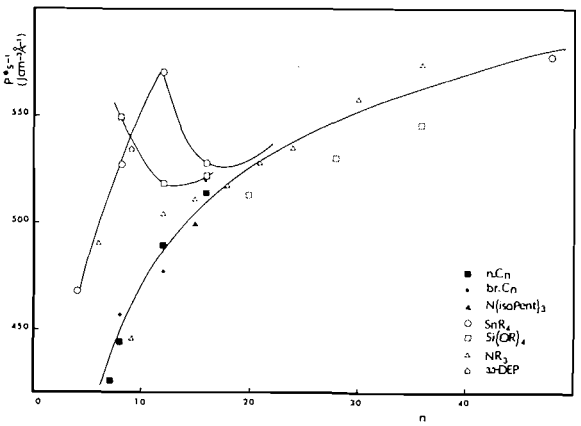

FIG. 4. P^*s^{-1} plotted against the total number of carbon atoms for SnR_4 (○), $Si(OR)_4$ (□), NR_3 (△), n-C_n (■), br-C_n (●), N(isopent)$_3$ (▲), 3,3-DEP (□). The surface to volume ratio s Å^{-1}, characteristic of the molecular shape, is obtained from molecular models of the molecules.

be much larger if the spherical model were used for the shorter members of the series.

NR_3 Series

The P^*/s values with s(cylinder) give a smooth curve for the derivatives longer than that of propyl. The low value for NPr_3 appears relatively normal if compared to the alkane with the same carbon atom number. It is possible that the higher value for NEt_3 comes from increased polarity. However, the spherical model would bring the P^*/s values to 534 J/mol for both NEt_3 and NPr_3 while the s intermediate between the two models would give $P^*/s = 495$ for NEt_3.

Heats of mixing of the NR_3 series with the branched and normal alkanes[1] indicate that the heats with NPr_3 and $NBut_3$ are nearer to each other than NPr_3 from NEt_3. This could be in agreement with the rather similar P^*/s for the NPr_3 and $NBut_3$ and with a somewhat higher value for NEt_3. Detailed analysis of the heats of mixing of the $NR_3 + NR_3'$ systems[1] currently being done could give more information on the relative cohesive energies of the different members of the NR_3 series.

$Si(OR)_4$ Series

The P^*/s are somewhat lower than those of the NR_3 or SnR_4 compounds but are likely to reach the same limiting value for large n. $Si(OPr)_4$ has a higher P^*/s and this may be due to steric hindrance. It is not possible to decide the proportion of increased polarity and that of steric hindrance in the higher $Si(OEt)_4$ value.

Temperature Dependence of the Thermal Pressure Coefficient

Measurements of γ versus T were made in order to investigate the effect of the shape of the molecule on the change of the cohesive energy of the molecule with temperature, a change which could not be due only to molecular expansion. The relation $P^* = \gamma\tilde{v}^2T$ takes account of the volume variation with temperature but at the same time introduces a non-experimental quantity $\tilde{v}$ obtained from the expansion coefficient and the model. In the variation of P^* with temperature, we would like to ascertain whether it is possible to separate the part due to an imperfection of the theory and the part which depends on the change of orientational order with temperature. Measurements were made on N(isopentyl)$_3$, N(Dec)$_3$, and br-C_{16} and compared to literature data (13) on linear alkanes like n-C_{16}. N(Dec)$_3$ and n-C_{16} have in the pure state correlation of molecular orientations which disappear rapidly when the temperature increases while the more globular molecules like N(isopent)$_3$ and br-C_{16} have much less order or 'structure'. It could be expected that P^* would diminish faster for ordered compounds. The P^* values (J cm^{-3}) at different temperatures are given in Table 2 but they can be represented between 25 and 80°C by the following equations with T in K: N(isopent)$_3$ $P^* = 972 - 1.8T$, N(Dec)$_3$ $P^* = 583 - 0.40T$, br-C_{16} $P^* = 380$ between 40 and 80°C (399 at 25°C).

Patterson (11) has shown that the reducing parameter of the compressibilities P^* does not vary over a wide range of temperature and chain length from butane to polymethylene when it is obtained from the corresponding state principle rather than from an equation of state. However, if values of P^* for different T and n are plotted against αT (or $\alpha\tilde{T}$) a single curve is obtained. This could be a way of separating the different contributions in the temperature variations of P^*. On Fig. 5, P^*/s is plotted against αT for the different members of the series and for some alkanes from published data: the P^*/s values situated on the main curve should be due to the imperfect equation of state; the P^*/s values outside the curve may have a physical significance. One can see it is possible to make the P^*/s points corresponding to the NR_3 compounds and the octane at different temperatures fit on the same curve. It seems, however, that there is not a unique dependence of P^*/s on αT. More globular molecules like N(isopent)$_3$ and octane show a more rapid decrease than the linear compounds such as N(Dec)$_3$ and n-C_{16}. The sterically hindered br-C_{16} shows no decrease of P^*/s between 40 and 80°C. These results seem to indicate that for relatively low molecular weight compounds there is a rapid decrease of P^*/s with αT. For larger molecules P^*/s decreases more slowly but there seems to be a difference between ordered liquids such as n-C_{16} and N(Dec)$_3$ and

Can. J. Chem. Downloaded from www.nrcresearchpress.com by 210.87.254.5 on 09/05/12
For personal use only.

Can. J. Chem. Downloaded from www.nrcresearchpress.com by 210.87.254.5 on 09/05/12
For personal use only.

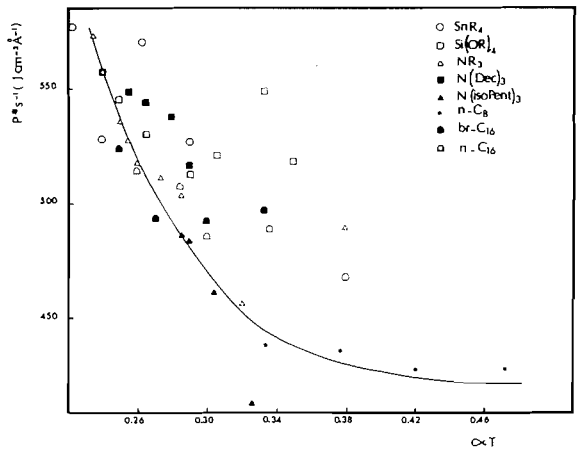

FIG. 5. P^*s^{-1} plotted against the equation of state parameter αT. Most of the points correspond to α and γ measurements at 25°C. For n-C_8 (ref. 13 (●)), n-C_{16} (ref. 13 (⏢)), N(isopent)$_3$ (this work (▲)), br-C_{16} (this work (⬟)), N(Dec)$_3$ (this work (■)), the different points correspond to α and γ measurements at different temperatures. SnR_4 (○), $Si(OR)_4$ (□), NR_3 (△).

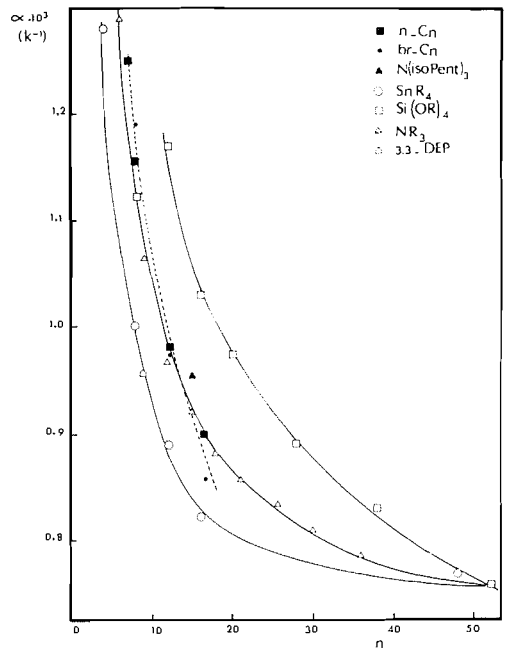

FIG. 6. Expansion coefficients α measured at 25°C plotted against n the total number of carbon atoms for the different series: SnR_4 (○), $Si(OR)_4$ (□), NR_3 (△), n-C_n (■), br-C_n (●), N(isopent)$_3$ (▲), 3,3-DEP (⏢).

not ordered liquids as br-C_{16}. P^*/s for ordered liquids apparently diminishes faster than for globular ones. However, measurements on more systems would be necessary to ascertain that it is a general feature. The four points well outside the curve belong to more polar molecules or to sterically hindered molecules. Table 2 gives results of γ and P^*/s obtained on other compounds for comparison purposes; P^*/s for N(isooct)$_3$ is very similar to that of N(Oct)$_3$ since a methyl at the end of a relatively long chain does not alter too much its molecular shape.

Figure 6 shows the experimental values of α for the different series against the atom carbon number. At short or intermediate chain lengths the order of increasing α is $SnR_4 < NR_3 < n\text{-}C_n < Si(OR)_4$ but the expansion coefficients tend to the same limit when the chain length increases. The branched alkanes usually have higher values of α than the linear alkanes except for the sterically hindered br-C_{16}. It is impossible to see any irregularity in the expansion coefficient curve for the sterically hindered $SnEt_3$ and $SnPr_3$ because of the very rapid decrease of α with n from one member to the next one. Comparison of the temperature dependence of α for the different members could give some complementary information. However, these measurements have not been done since it is known that the theory predicts a too large temperature dependence for the n-alkanes (13).

Thermal Pressure Coefficients and Steric Hindrance

Steric hindrance within the molecule has a marked effect on the macroscopic properties of the liquid especially on the equation of state quantities such as the molar volume, thermal expansion coefficient, and thermal pressure coefficient. This can be seen for isomers of the same alkane which have different degrees of steric hindrance (9, 24).

These different degrees of steric hindrance are more difficult to deduce from density comparison between members of a series since the effect of molecular weight on density overcomes that of steric hindrance. It is therefore particularly valuable to find, by this work, that the thermal pressure coefficient indicates the presence of steric hindrance in cases where densities and expansion coefficients cannot give the information.

Steric Hindrance and Solution Properties

Heats of mixing of non-polar, alkane-like compounds have been measured for a few years (4, 9). It has been possible to separate them in an almost quantitative way, into different contributions such as the h^E_{dis} (disorder) present when long-chains are disordered by the second component and the negative free volume contribution h^E_{fv} due to the difference in expansion coefficients of the components. However, unexpected results have been found in the heats of mixing of linear alkanes, for instance with some globular alkanes (9, 10, 24). An exothermic contribution has to be added to explain the small endothermic heats or exothermic heats. The importance

of this term seems to be related to the steric hindrance of the branched alkane. A strong effect called 'the condensation effect' or the steric hindrance contribution is found with 3,3-diethylpentane and $SnEt_4$ (9, 10, 24). For instance the heat of mixing of the 2,2,4,4-tetramethylpentane with n-C_{16} is 235 J/mol at $x = 0.5$ while it is 18.3 for the sterically hindered isomer 3,3-diethylpentane. It is worthwhile noting that the steric hindrance of a compound can be seen on the thermal pressure coefficient, thus confirming the heats of mixing results.

Acknowledgements

We would like to thank the France Quebec scientific collaboration for financial assistance to two of us (R.P., M.C.). We are grateful to Professor Donald Patterson and M. Pierre de Saint-Romain for advice and discussion in the thermal pressure coefficient measurements and also to Phuong Nguyen Hong who has measured the expansion coefficients.

1. I. PRIGOGINE (*with the collaboration of* A. BELLEMANS and V. MATHOT). The molecular theory of solutions. North-Holland, Amsterdam. 1957.
2. D. PATTERSON and G. DELMAS. Discuss. Faraday Soc. **49**, 1 (1970).
3. P. J. FLORY, R. A. ORWOLL, and A. VRIJ. J. Am. Chem. Soc. **86**, 3507 (1964); **86**, 3515 (1964).
4. S. TURRELL and G. DELMAS. J. Chem. Soc. Faraday Trans. 1, **70**, 572 (1974).
5. V. T. LAM, P. PICKER, D. PATTERSON, and P. TANCRÈDE. J. Chem. Soc. Faraday Trans. II, **70**, 1465 (1974).
6. G. DELMAS and NG. T. THANH. J. Chem. Soc. Faraday Trans. I, **71**, 1172 (1975).
7. G. DELMAS, P. DE SAINT-ROMAIN, and P. PURVES. Trans. Faraday Soc. **71**, 1181 (1975).
8. P. TANCRÈDE, P. BOTHOREL, and D. PATTERSON. J. Chem. Soc. Faraday Trans. II, **73**, 29 (1977).
9. P. TANCRÈDE, P. BOTHOREL, P. DE SAINT-ROMAIN, and D. PATTERSON. J. Chem. Soc. Faraday Trans. II, **73**, 15 (1977).
10. G. DELMAS and NG. T. THANH. J. Phys. Chem. **81**, 1730 (1977).
11. D. PATTERSON and J. M. BARDIN. Trans. Faraday Soc. **66**, 321 (1970).
12. (*a*) G. ALLEN, G. GEE, and G. J. WILSON. Polymer, **1**, 456 (1960); (*b*) G. ALLEN, G. GEE, D. MANGARAJ, D. SIMS, and G. J. WILSON. Polymer, **1**, 467 (1960).
13. R. A. ORWOLL and P. J. FLORY. J. Am. Chem. Soc. **89**, 6814 (1967).
14. J. M. BARDIN. Ph.D. thesis, McGill University, Montreal, P.Q. 1972.
15. (*a*) E. D. BAGLEY, T. P. NELSON, J. W. BARLOW, and S. A. CHEN. Ind. Eng. Chem. Fundam. **9**, 93 (1970); (*b*) E. D. BAGLEY, T. P. NELSON, S. A. CHEN, and J. BARLOW. Ind. Eng. Chem. Fundam. **10**, 27 (1971).
16. C. F. LAU, G. N. MALCOM, and D. V. FENBY. Aust. J. Chem. **22**, 855 (1969).
17. U. BIANCHI, G. AGABIO, and A. TURTTURRO. J. Phys. Chem. **69**, 4392 (1965).
18. W. WESTWATER, N. W. FRANTZ, and J. H. HILDEBRAND. Phys. Rev. **31**, 135 (1928).
19. D. PATTERSON, S. N. BHATTACHARYYA, and P. PICKER. Trans. Faraday Soc. **64**, 648 (1968).
20. (*a*) V. MATHOT. Bull. Soc. Chim. Belg. **59**, 111 (1950); (*b*) I. PRIGOGINE and V. MATHOT. J. Chem. Phys. **18**, 765 (1950).
21. J. NAGY, S. FRENCZI-GRESZ, and R. FARKAS. Acta Chim. Acad. Hung. Tomus. **52**, 319 (1967).
22. J. TIMMERMANS. Physico-chemical constants of pure organic compounds. Vol. 2. Elsevier, Amsterdam. 1965.
23. (*a*) B. E. EICHINGER and P. J. FLORY. Trans. Faraday Soc. **64**, 2053 (1968); (*b*) **64**, 2066 (1968).
24. D. PATTERSON. Pure Appl. Chem. **47**, 305 (1976).

Can. J. Chem. Downloaded from www.nrcresearchpress.com by 210.87.254.5 on 09/05/12
For personal use only.

A simpler method to evaluate the isotopic shifts in fundamental stretching frequencies of polyatomic molecules

JAN BRON AND R. WALLACE

Department of Chemistry, University of Manitoba, Winnipeg, Man., Canada R3T 2N2

Received May 12, 1977

JAN BRON and R. WALLACE. Can. J. Chem. **56**, 379 (1978).

As an alternative to the more exact, but much more complex theory, a simpler method to estimate the isotope shifts in fundamental (stretching) frequencies of molecules is proposed. By means of examples, it is shown that good agreement between calculated and observed frequencies can be obtained.

JAN BRON et R. WALLACE. Can. J. Chem. **56**, 379 (1978).

On propose une nouvelle méthode plus simple pour remplacer la théorie beaucoup plus complexe et plus exacte qui existe déjà pour trouver un estimé des déplacements isotopiques dans les fréquences fondamentales (vibration) des molécules. Aux moyens d'exemples, on montre qu'il existe un bon accord entre les valeurs calculées et les fréquences observées.

[Traduit par le journal]

Can. J. Chem. Downloaded from www.nrcresearchpress.com by 210.87.254.42 on 09/05/12
For personal use only.

Introduction

In view of current interest in vibrational pumping as a means to achieve isotopic separation and the very substantial complexity of calculating isotopic shifts in the spectra of polyatomic molecules by conventional normal mode theory (1), a simpler model capable of predicting isotopic shifts would seem appropriate. In this connection it has been shown recently (2) that many of the features of polyatomic vibrational spectra (fundamental, anharmonic overtones, etc.) can be predicted on the basis of a simple internal coordinate anharmonic model. The present work is essentially an adaptation of that model, designed to obtain isotopic shifts in the vibrational spectra of polyatomic molecules.

All of the molecules currently considered (H_2O/D_2O; CH_4/CD_4; $^{235}UF_6/^{238}UF_6$) are of the type AX_n, in which the mass of X is much less than that of A. To a good degree of approximation, this permits the separation of bending from stretching vibrations. For convenience we shall restrict consideration to the isotopic shifts in the stretching vibrations only. Relatively simple expressions will be obtained for the various fundamental frequencies. Since the effect of particle masses is explicitly contained in these expressions, it is a simple matter to obtain isotopic shift information. The results for the molecules mentioned above compare favourably with experimental data and have been obtained with relatively little labour.

The Schrödinger Equation

The vibrational Hamiltonian operator to be used has the form

$$[1]\quad \hat{H} = \sum_i \hat{H}_i^{(0)} - \hbar^2 \sum_{i<j}\sum G_{ij}(\partial^2/\partial S_i \partial S_j) + \sum_{i<j}\sum R_{ij}S_iS_j$$

in which

$$[2]\quad \hat{H}_i^{(0)} = -\tfrac{1}{2}\hbar^2 G_{ii}(\partial^2/\partial S_i^2) + V_i$$

The quantities G_{ij} are Wilson's **G** matrix elements (3), R_{ij} is a force constant, and S_i is an *internal stretching coordinate*. The potential energy term in [2] is defined by means of the Morse function (1)

$$[3]\quad V_i = D_i[\exp(-2a_iS_i) - 2\exp(-a_iS_i)]$$

where D_i and a_i are the Morse parameters. Compared to the expression used previously (1), [1] contains the additional interaction terms $R_{ij}S_iS_j$, which are necessary to obtain the correct isotopic shift for the fundamental frequencies. It may be observed that D_i, a_i, and R_{ij} are isotope independent and are, therefore, the same for molecules differing only in isotopic substitution.

The vibrational energy levels of a molecule can be determined by means of [1] and the variation method. A suitable linear variation function has the form

$$[4]\quad \phi = \sum_i \gamma_i \psi_i$$

In [4], the coefficients γ_i are parameters to be determined by minimizing the variational integral (4). The functions ψ_i are in turn defined as

$$[5]\quad \psi_i = N_i \sum_j c_{ij} f_j$$

in which f_i has been defined as (1)

$$[6]\quad f_i = \prod_{i=1}^{n} |\alpha_i(S_i)\rangle$$

There are n bonds in the molecule. As before, $|\alpha_i(S_i)\rangle$ are the eigenfunctions in the equation

$$[7]\quad \hat{H}_i^{(0)}|\alpha_i(S_i)\rangle = -A_i^{-2}(K_i - v_i - \tfrac{1}{2})^2|\alpha_i(S_i)\rangle$$

The constants A_i and K_i are equal to

Can. J. Chem. Downloaded from www.nrcresearchpress.com by 210.87.254.42 on 09/05/12
For personal use only.

$$[8] \qquad A_i = (2\mu_i)^{1/2}(a_i\hbar)^{-1}$$
$$K_i = A_i D_i^{1/2}$$

while v_i is a quantum number, refering to the ith Morse oscillator, and μ_i is the reduced mass of the two atoms defining the ith bond. Finding the eigenvalues of the secular determinant requires the evaluation of the integrals (4)

$$[9] \qquad H_{ij} = \langle\psi_i|\hat{H}|\psi_j\rangle = H_{ji}$$

and

$$[10] \qquad S_{ij} = \langle\psi_i|\psi_j\rangle = S_{ji}(= \delta_{ij})$$

The integral S_{ij} is for our purposes equal to the Kronecker δ_{ij}. The matrix element H_{ij} can also be written as

$$[11] \quad H_{ij} = \langle\psi_i|\hat{H}|\psi_j\rangle$$
$$= N_iN_j\langle\textstyle\sum_i c_{ik}f_k|\sum_r H_r^{(0)} - \hbar^2\sum_{r<s}\sum G_{rs}(\partial^2/\partial S_r\partial S_s) + \sum_{r<s}\sum R_{rs}S_rS_s|\sum_j c_{jl}f_l\rangle$$
$$= N_iN_j\Big[\textstyle\sum_k\sum_l c_{ik}c_{jl}\sum_r\langle f_k|H_r^{(0)}|f_l\rangle - \hbar^2\sum_k\sum_l c_{ik}c_{jl}\sum_{r<s}\sum G_{rs}\langle f_k|\partial^2/\partial S_r\partial S_s|f_l\rangle + \sum_k\sum_l c_{ik}c_{jl}\sum_{r<s}\sum R_{rs}\langle f_k|S_rS_s|f_l\rangle\Big]$$

Although [11] suggests that many matrix elements are to be evaluated in order to obtain H_{ij}, in actual fact many matrix elements are zero or, using *harmonic* oscillator selection rules, so small that they can be ignored. At this point it is best to use examples to illustrate how numerical values for H_{ij} can be obtained. It should be noted that no tedious transformation of internal to dimensionless normal coordinates is required (5).

H_2O and D_2O

To determine the fundamental frequencies of X_2O (X = H, D), the ground and first excited states should be evaluated (Bohr frequency rule: $\Delta E = h\nu$). For H_2O and D_2O the variation functions may be defined as

$$[12] \qquad \phi = \gamma_1\psi_1 + \gamma_2\psi_2$$

To diagonalize the secular determinant, ψ_1 and ψ_2 will be symmetrized states (3)

$$[13] \qquad \psi_1 = 2^{-1/2}(f_1 + f_2)$$
$$\psi_2 = 2^{-1/2}(f_1 - f_2)$$

The functions f_1 and f_2 are

$$[14] \quad f_1 = |\alpha_1(S_1, v_1)\rangle|\alpha_2(S_2, v_2)\rangle = |v_1, v_2\rangle$$
$$f_2 = |\alpha_1(S_1, v_2)\rangle|\alpha_2(S_2, v_1)\rangle = |v_2, v_1\rangle$$

The quantum numbers v_1 and v_2 are, in this case, restricted to zero or unity. Let us start by determining the energy of the first (two) excited states.

For X_2O the functions ψ_1 and ψ_2 are

$$[15] \qquad \psi_1 = 2^{-1/2}(|10\rangle + |01\rangle)$$
$$\psi_2 = 2^{-1/2}(|10\rangle - |01\rangle)$$

These functions will diagonalize the secular determinant and, hence, values for H_{11} and H_{22} only need to be found. Because $a_1 = a_2$ and $D_1 = D_2$, the subscripts of a, D, K, and A will be dropped. Therefore:

$$[16] \quad H_{11} = \langle\psi_1|\hat{H}|\psi_1\rangle$$
$$= \tfrac{1}{2}\langle f_1 + f_2|\hat{H}|f_1 + f_2\rangle$$
$$= \langle f_1|\hat{H}|f_1\rangle + \langle f_1|\hat{H}|f_2\rangle$$
$$= \langle 10|\hat{H}|10\rangle + \langle 10|\hat{H}|01\rangle$$
$$= \langle 10|\hat{H}_1{}^{(0)} + \hat{H}_2{}^{(0)}|10\rangle - \hbar^2G_{12}\langle 10|\partial^2/\partial S_1\partial S_2|10\rangle + R_{12}\langle 10|S_1S_2|10\rangle + \langle 10|\hat{H}_1{}^{(0)} + \hat{H}_2{}^{(0)}|01\rangle - \hbar^2G_{12}\langle 10|\partial^2/\partial S_1\partial S_2|01\rangle + R_{12}\langle 10|S_1S_2|01\rangle$$

Equation 16 can now be reduced to[1]

$$[17] \quad H_{11} = \langle 1|\hat{H}^{(0)}|1\rangle + \langle 0|\hat{H}^{(0)}|0\rangle + \hbar^2G_{12}\left\langle 1\left|\frac{d}{dS}\right|0\right\rangle^2 + R_{12}\langle 1|S|0\rangle^2$$

The relationship [17] follows from [16], if redundant subscripts are dropped, small matrix elements ignored, and use is made of the fact that d/dS is an anti-Hermitian operator. The matrix element $\langle 1|S|0\rangle$ is difficult to evaluate when Morse oscillator eigenfunctions are used. Therefore, $\langle 1|S|0\rangle$ will be determined by harmonic oscillator functions. This is reasonable, since anharmonicity at the bottom of the well, defined by the Morse potential, is not so important yet. After evaluating matrix elements, [17] becomes

[1]In this case G_{ij} is equal to the product of the cosine of the bond angle and inverse of the mass of oxygen atom (3). Note also that R_{12} refers to the interaction force constant of the *internal* coordinates S_1 and S_2.

Can. J. Chem. Downloaded from www.nrcresearchpress.com by 210.87.254.42 on 09/05/12
For personal use only.

$$[18]\quad H_{11}(\mathrm{cm}^{-1}) = -[(K-\tfrac{3}{2})^2 + (K-\tfrac{1}{2})^2](hcA^2)^{-1} + hG_{12}a^2(2K-1)(16\pi^2c)^{-1} + R_{12}(16\pi^2c^2\mu F)^{-1/2}$$

In [18] the force constant F is equal to $(2a^2D)$; an equality obtained from [3]. Similarly, the expression for H_{22} is

$$[19]\quad H_{22}(\mathrm{cm}^{-1}) = -[(K-\tfrac{3}{2})^2 + (K-\tfrac{1}{2})^2](hcA^2)^{-1} - hG_{12}a^2(2K-1) \times (16\pi^2c)^{-1} - R_{12}(16\pi^2c^2\mu F)^{-1/2}$$

The ground state energy is simply

$$[20]\quad E_0(\mathrm{cm}^{-1}) = \langle 00|\hat{H}|00\rangle \simeq -2(K-\tfrac{1}{2})^2(hcA^2)^{-1}$$

The fundamental (stretching) frequencies, ν_1 and ν_3, are then

$$[21]\quad \nu_1(\mathrm{cm}^{-1}) = H_{11} - E_0 = C_1 + G_{12}C_2 + R_{12}C_3$$
$$\nu_3(\mathrm{cm}^{-1}) = H_{22} - E_0 = C_1 - G_{12}C_2 + R_{12}C_3$$

where

$$[22]\quad C_1 = 2(K-1)(hcA^2)^{-1}\ \mathrm{cm}^{-1}$$
$$C_2 = hF(2K-1)(32\pi^2cD)^{-1}\ \mathrm{g\ cm}^{-1}$$
$$C_3 = (16\pi^2c^2\mu F)^{-1/2}\ \mathrm{dyn}^{-1}$$

In [22], a^2 has been replaced by $(F/2D)$. A close examination of [21] and [22] reveals that ν_1 and ν_3 are determined by three parameters (F, D, and R_{12}), which are independent of isotopic substitution in the molecule X_2O. Two other examples will be discussed below.

CH_4, CD_4 and $^{235}UF_6$, $^{238}UF_6$

The symmetrized functions, ψ_i, for CX_4 are (3)

$$[23]\quad \psi_1(A_1) = \tfrac{1}{2}(f_1 + f_2 + f_3 + f_4)$$
$$\psi_2(F_2) = \tfrac{1}{2}(f_1 + f_2 - f_3 - f_4)$$

and two other functions, where f_1 is equal to $|1000\rangle$ etc. By means of [1], [4], [23], and the above example X_2O, the two stretching frequencies $\nu_1(A_1)$ and $\nu_3(F_2)$ become

$$[24]\quad \nu_1(A_1) = C_1 + 3C_2G_{12} + 3R_{12}C_3$$
$$\nu_3(F_2) = C_1 - C_2G_{12} - R_{12}C_3$$

The constants C_i have been defined by [22]. It follows from the symmetry of CX_4 that all quantities G_{ij} and R_{ij} $(i \neq j)$ are the same and, therefore, have been equated to G_{12} and R_{12}. Although CX_4 has two more bonds than X_2O, the fundamentals in [24] are also functions of three parameters only.

The molecules $^xUF_6$ have octahedral structures (six U—F bonds). The symmetrized functions are (6)

$$\psi_1(A_{1g}) = 6^{-1/2}(f_1 + f_2 + f_3 + f_4 + f_5 + f_6)$$
$$[25]\quad \psi_2(E_g) = \tfrac{1}{2}(f_1 + f_4 - f_3 - f_6) \quad [\text{one other}]$$
$$\psi_3(F_{1u}) = 2^{-1/2}(f_1 - f_4) \quad [\text{two others}]$$

The bonds 1 and 4, 2 and 5, and 3 and 6 form angles of 180°, while all other bond angles are 90°. The only non-zero matrix elements are G_{14}, G_{26}, and G_{36}; all three **G** matrix elements are equal to the negative value of the reciprocal mass of the central uranium atom in $^xUF_6$ (3). Symmetry reduces the number of force constants to two types only: R_{14} and R_{12}. The constant R_{14} accounts for interaction between bonds forming an angle of 180°, while R_{12} is the interaction force constant of bonds making a 90° angle. It is known from experiment (7) that R_{14} is much smaller than R_{12}.

By means of [25] and other equations given above, it follows that for $^xUF_6$ the three frequencies are:

$$[26]\quad \nu_1(A_{1g}) = C_1 + C_2G_{14} + (4R_{12} + R_{14})C_3$$
$$\nu_2(E_g) = C_1 + C_2G_{14} + (R_{14} - 2R_{12})C_3$$
$$\nu_3(F_{1u}) = C_1 - C_2G_{14} - R_{14}C_3$$

In this case there are four parameters that determine ν_1, ν_2, and ν_3: F, D, R_{12}, and R_{14}.

Numerical Results and Discussion

As pointed out above, the fundamentals of H_2O and D_2O depend upon three unknown parameters: F, D, and R_{12}. In general, a value for these parameters may be obtained by analogy to other, closely related molecules (8). Another method is to assume a reasonable value for F and find D and R_{12} by means of [21] from the two observed fundamentals of H_2O: two equations with two unknowns are obtained when F is fixed. Stated differently: it is possible to choose such values for F, D, and R_{12} that will give exact agreement with the observed frequencies (9) of H_2O and then, by means of [21] and [22], ν_1 and ν_3 for D_2O can be calculated. The numerical results for D_2O obtained by the method of fitting are displayed in Table 1. It can be seen that the agreement with the observed values of ν_i is quite satisfactory, even though no interaction of any kind with the bending mode has been assumed. The calculated values for ν_1 and ν_3 given in Table 1 are based on $F = 8.454$ mdyn Å^{-1} (10), determined from harmonic frequencies, $D = 8.18 \times 10^{-12}$ erg and $R_{12} = -0.092$ mdyn Å^{-1}.

TABLE 1. A comparison of observed and calculated frequencies (cm^{-1})

	ν_1		ν_2		ν_3	
Compound	Obs.	Calc.	Obs.	Calc.	Obs.	Calc.
D_2O	2672 (9)	2680	—	—	2788	2789
CD_4	2085 (10)	2082	—	—	2258	2259
$^{235}UF_6$	667[a]	667.05	534[a]	533.98	626.65 (7)	626.56

[a]See text.

The calculated fundamentals for CD_4 are also shown in Table 1. The listed values of ν_1 and ν_3 for CD_4 are based on $F = 5.2$ mdyn Å^{-1}, $D = 10.81 \times 10^{-12}$ erg, and $R_{12} = 0.043$ mdyn Å^{-1}. Again, the magnitudes of the parameters F, D, and R_{12} have been chosen in such a way as to obtain complete agreement between the observed (11) and calculated frequencies for CH_4. As can be seen in Table 1, the agreement between the observed and calculated frequencies for CD_4 is improved with respect to D_2O. This better fit is a result of optimization of F. The dependence of the calculated results on F is shown in Fig. 1. It can be seen that the relationship is (almost) linear. The calculated values of the fundamentals in Fig. 1 have been obtained as follows. For a given F, D and R_{12} can be formed by means of [24] and the observed fundamentals for CH_4. The parameters evaluated in such a way were then used to calculate ν_1 and ν_3 for CD_4. Figure 1 also shows that unreasonably large values of F, which is approximately the stretching force constant of the C—X bond, result in large deviations from the observed frequencies.

Finally, Table 1 shows results for UF_6. The calculated isotopic shift in ν_1 and ν_2 cannot be compared with experiment, since spectroscopic techniques do not allow such small shifts to be measured. The observed shift in ν_3 is 0.65 ± 0.09 cm^{-1}, hence the calculated shift of 0.56 cm^{-1} agrees within experimental error. The calculated values are based on $F = 3.85$ mdyn Å^{-1}, $D = 5.085 \times 10^{-12}$ erg, $R_{14} = -0.02$ mdyn Å^{-1}, and $R_{12} = 0.3$ mdyn Å^{-1}. As above, the quantities D, R_{12}, and R_{14} have been calculated by means of [26], the observed values (7) for ν_1, ν_2, and ν_3 and $F = 3.85$ mdyn Å^{-1}.

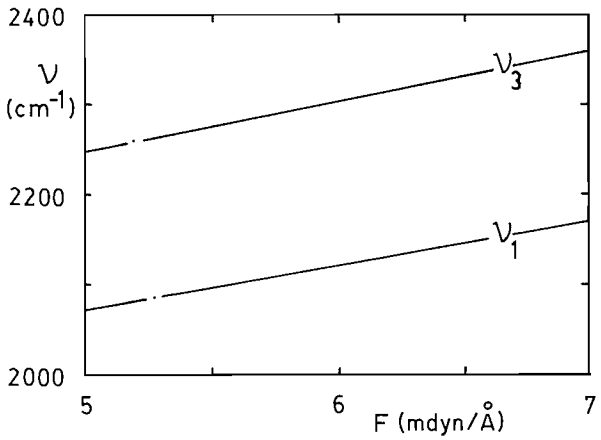

FIG. 1. A plot of the fundamental frequencies, ν_1 and ν_3, of CD_4 versus the force constant F. The dots represent the observed frequencies.

The main features of the method presented in this paper to evaluate the isotopic shifts may be summarized as follows:

(*1*) The method is a simpler alternative to the more exact but much more complicated normal mode theory (1).

(*2*) The tedious and computer time consuming transformation of isotope dependent force constants in dimensionless normal coordinates to isotope independent force constants internal coordinates (5) has been eliminated; this transformation is the main reason why 'large' molecules such as UF_6 cannot be considered in normal mode theory.

(*3*) The algebraic complexity of the (quantum mechanical) problem is greatly reduced.

(*4*) The number of parameters is much smaller: in order to deal with anharmonicity the normal mode theory requires a knowledge of numerous cubic and quartic force constants (5, 9).

(*5*) Equation 1 and a slight modification of the above techniques may be used to determine the isotopic shifts in overtone and combination bonds.

1. H. H. NIELSEN. Rev. Mod. Phys. **23**, 90 (1951).
2. R. WALLACE. Chem. Phys. **11**, 189 (1975).
3. E. B. WILSON, J. C. DECIUS, and P. C. CROSS. Molecular vibrations. McGraw-Hill Book Company, Toronto, Ont., Canada. 1955.
4. I. N. LEVINE. Quantum chemistry. Allyn and Bacon, Boston, MA, U.S.A. 1970.
5. A. R. HOY, I. M. MILLS, and G. STREY. Mol. Phys. **24**, 1265 (1972).
6. C. W. F. T. PISTORIUS. J. Chem. Phys. **29**, 1328 (1958).
7. R. S. MCDOWELL, L. B. ASPREY, and R. T. PAINE. J. Chem. Phys. **61**, 3571 (1974).
8. J. BRON and R. WALLACE. Can. J. Chem. **55**, 2292 (1977).
9. D. FOSS SMITH, JR. and J. OVEREND. Spectrochim. Acta, Part A, **28**, 471 (1972).
10. K. KUCHITSU and Y. MORINO. Bull. Chem. Soc. Jpn. **38**, 814 (1965).
11. G. HERZBERG. Molecular spectra and molecular structure. II. Infrared and Raman spectra of polyatomic molecules. Van Nostrand Reinhold Company, New York, NY, U.S.A. 1945.

Can. J. Chem. Downloaded from www.nrcresearchpress.com by 210.87.254.42 on 09/05/12
For personal use only.

Solidaline. A modified protoberberine alkaloid from *Corydalis solida*

RICHARD H. F. MANSKE AND RUSSELL RODRIGO

Department of Chemistry, Guelph-Waterloo Centre for Graduate Work in Chemistry, The University of Waterloo, Waterloo, Ont., Canada N2L 3G1

HERBERT L. HOLLAND,[1] DONALD W. HUGHES, AND DAVID B. MACLEAN

Department of Chemistry, McMaster University, Hamilton, Ont., Canada L8S 4M1

AND

JOHN K. SAUNDERS

Département de Chimie, Université de Sherbrooke, Sherbrooke (Que.), Canada J1K 2R1

Received August 16, 1977

RICHARD H. F. MANSKE, RUSSELL RODRIGO, HERBERT L. HOLLAND, DONALD W. HUGHES, DAVID B. MACLEAN, and JOHN K. SAUNDERS. Can. J. Chem. **56**, 383 (1978).

Re-investigation of the alkaloids of *Corydalis solida* yielded two further bases, ochotensine and solidaline. Spectral analysis has shown the latter to be representative of a new class of protoberberine-related isoquinoline alkaloids.

RICHARD H. F. MANSKE, RUSSELL RODRIGO, HERBERT L. HOLLAND, DONALD W. HUGHES, DAVID B. MACLEAN et JOHN K. SAUNDERS. Can. J. Chem. **56**, 383 (1978).

Une nouvelle étude des alcaloïdes du *Corydalis solida* a permis d'isoler deux nouvelles bases, l'ochotensine et la solidaline. Sur la base d'une analyse spectrale, on a pu montrer que ce dernier composé correspond à une nouvelle classe d'alcaloïdes de l'isoquinoléine qui se rapproche de la protoberbérine.

[Traduit par le journal]

Reinvestigation of the alkaloids of *Corydalis solida* (L.) Swartz (1) has yielded two further bases. One is identical with ochotensine from *C. ochotensis* (2), and the second is a hitherto unreported alkaloid, to which we have assigned the name solidaline.

Spectral analysis of solidaline, $C_{23}H_{27}NO_6$ (see Experimental) did not permit unequivocal assignment to any known group of isoquinoline alkaloids. The mass spectrum, however, indicated a protoberberine alkaloid: fragment ions at *m/e* 206 ($C_{12}H_{14}O_3$) and 207 ($C_{11}H_{13}NO_3$) which together comprise the entire molecule, may readily arise from the molecular ion at *m/e* 413 by a fragmentation characteristic of this class of alkaloid (3). Spectral data showed the presence of non-phenolic hydroxyl, one tertiary *C*-methyl, four methoxy groups, and two tetrasubstituted aromatic rings. The ^{1}Hmr data, although suggestive of a protoberberine skeleton (4), were not uniquely interpretable, but a combination of ^{1}Hmr and ^{13}Cmr spectral data enabled us to assign tentatively structure **2** to solidaline (Fig. 1).

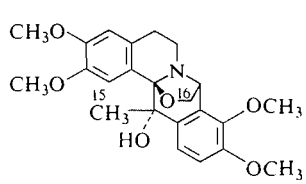

FIG. 1. Proposed structure of solidaline **2**.

[1]Present address: Department of Chemistry, Brock University, St. Catharines, Ont., Canada L2S 3A1.

Comparison of the ^{13}Cmr spectrum of **2** with that of corydaline (**1***a*) (also in *C. solida*) (5), mesocorydaline (**1***b*) (5), ophiocarpine (**1***c*), and hydrastinine

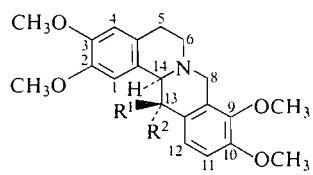

Corydaline **1***a*: $R^1 = CH_3$, $R^2 = H$
Mesocorydaline **1***b*: $R^1 = H$, $R^2 = CH_3$

(**3**) strengthened the proposal of structure **2** for solidaline. The Cmr assignments for **2** are given in Table 1, those with an asterisk being tentative. The

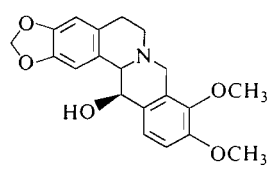

1*c* Ophiocarpine

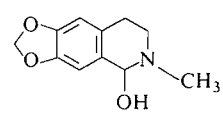

3 Hydrastinine

chemical shift of C-15 of **2** is similar to that in **1***b*: the deshielding effect of the OH at the α carbon is compensated for by the shielding effect of the oxygen at C-14. The resonance for C-8 of **2** should be deshielded from that of **1***b*, as observed, and the resonance at 78.3 ppm, assigned to C-14, is shielded from the corresponding carbon, C-1, of **3**. Quaternary carbons are often shielded relative to methine carbons (of steroids) in similar environments due to

Can. J. Chem. Downloaded from www.nrcresearchpress.com by 210.87.254.5 on 09/05/12
For personal use only.

TABLE 1. ^{13}Cmr chemical shifts of **1***a–c*, **2**, and **3**

Carbon	Compound				
	1*a*	**1***b*	**1***c*	**2**	**3**
1	109.0	112.1	105.6	113.0*	108.8
2	147.3	146.7	146.1	146.1*	146.4
3	147.8	148.0	146.5	147.9*	147.5
4	111.3	111.1	108.4	110.9*	109.1
4a	128.5	127.7	128.5	130.0	132.4
5	29.4	28.1	29.3	30.7	29.6
6	51.5	47.0	50.8	46.3	45.5
8	54.5	51.1	53.8	60.9	
8a	128.6	126.5	127.2	126.9	
9	150.2	150.2	151.6	150.7*	
10	145.1	145.4	144.5	149.6*	
11	111.7	111.1	111.1	111.7*	
12	124.1	123.2	123.4	123.6	
12a	135.1	133.0	129.4	134.2	
13	38.4	34.6	69.8	69.0	
14	63.1	64.2	64.6	78.3	85.7
14a	128.6	130.7	130.9	130.0	129.1
15	18.4	22.4	—	22.2	
16	—	—	—	68.7	
OCH_2O	—	—	100.7	—	101.8
2,3-OMe	55.8, 55.9	55.9	—	55.9, 56.0	
9-OMe	60.1	60.4	60.0	60.9	
10-OMe	56.2	56.4	55.7	55.9*	
N—Me	—	—	—	43.1	

*Tentative assignments.

different gauche interactions (6). This may also account for the slight shielding of C-13 of **2** relative to **1***c*.

The Cmr spectrum also showed resonances corresponding to CH_2 carbons at 30.7 and 46.3 ppm which were assigned to C-5 and C-6 of a *cis*-quinolizidine structure by comparison with the spectrum of the *cis*-quinolizidine **1***b* (5). The observation of the C-15 resonance of **2** at 22.2, corresponding with the value for C-15 of **1***b* rather than that of **1***a* (see Table 1), strengthens the assignment of the *cis*-quinolizidine stereochemistry to **2**. The aliphatic carbon resonances, other than those corresponding to C-5, C-6, and OCH_3 groups, appeared at 22.2 (CH_3), 68.7 (CH_2), 60.9 (CH), and 78.3 ppm (C). The ABX system observed in the ^{1}Hmr spectrum (*vide infra*) must therefore correspond to a CH_2—CH moiety.

The location of the C-methyl of **2** pseudoequatorial at C-13 was confirmed by the observation of a 21% nuclear Overhauser enhancement (^{1}H spectrum, 100 MHz, CD_2Cl_2 solution) of one half of the AB quartet (δ 7.25), upon irradiation at δ 1.73 (C-methyl). This irradiation also caused a 24% enhancement of signal intensity at δ 7.15. These data suggest a substitution pattern identical with that of corydaline, namely methoxyl groups at C-2, -3, -9, and -10, and a methyl at C-13. The observed nOe is between the methyl group and hydrogens at C-1 and

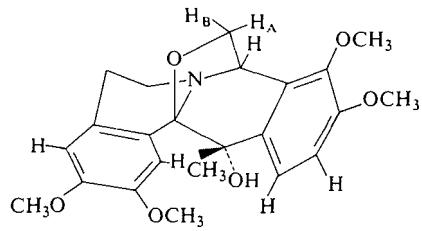

FIG. 2. Relative stereochemistry of solidaline.

C-12. The data also suggest the relative stereochemistry at C-13 and C-14 shown in Fig. 2, in which the β methyl at C-13 is located close to the hydrogens at both C-1 and C-12. Inspection of models reveals that significant nOe's such as those described above would not be anticipated if the methyl were located α at C-13.

The ^{1}Hmr spectrum also showed signals at δ 3.61 (1H, d, J = 7 Hz), 4.03 (1H, q, J = 4, 7 Hz) and 4.70 (1H, d, J = 4 Hz). Irradiation at δ 3.61 caused collapse of the signal at δ 4.03 to a doublet (J = 4 Hz), while irradiation at δ 4.70 also caused collapse at δ 4.03 to a doublet (J = 7 Hz). These data may be interpreted in the light of the structure shown in Fig. 2. The C-8 hydrogen, assigned resonance at δ 4.70, is coupled only to the C-16 hydrogen at δ 4.03 (J_{vic} = 4 Hz). The downfield shift of C-8 H relative to the analogous hydrogen of other *cis*-quinolizidine protoberberine alkaloids (eg. *meso*-corydaline, **1***b*, C-8 H at δ 3.97 (4)) is attributed to additional deshielding by the nitrogen lone pair and the aromatic ring D. A similar effect is observed in the synthetic homoprotoberberine alkaloids (7). Inspection of models reveals that the dihedral angle between C-8 H and C-16 H_A is close to 90°; coupling will therefore be close to zero, indicating resonance of the latter at δ 3.61 and its coupling only to C-16 H_B at δ 4.03 (J_{gem} = 7 Hz). The assignment of C-16 H_A at δ 3.61 and C-16 H_B at δ 4.03 is also consistent with shielding of the former hydrogen by the aromatic ring D, above which it is rigidly held. The observed value of J_{gem} is similar to that noted in analogous tetrahydrooxazole systems (8), militating against a structure for solidaline in which the ether bridge to C-14 and the hydroxyl at C-13 are transposed. This alternate structure would also be inconsistent with the magnitude of the vicinal coupling between the C-8 and C-16 hydrogens.

Structure **2** accounts for all the major fragment ions of the mass spectrum (Scheme 1). The fragmentation parallels the pattern observed for the protoberberine alkaloids (3). The failure of the ion at *m/e* 207 to lose hydrogen, giving a fully aromatic system (as is observed with the protoberberine alkaloids) may be attributed to the presence of oxygen at

Can. J. Chem. Downloaded from www.nrcresearchpress.com by 210.87.254.5 on 09/05/12
For personal use only.

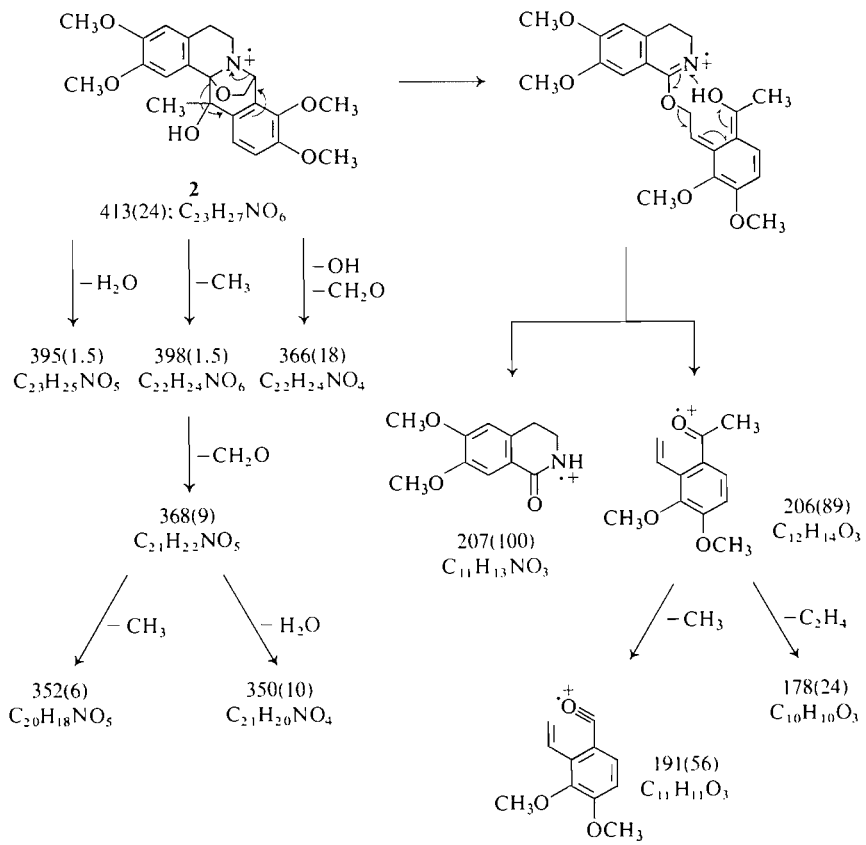

SCHEME 1. Mass spectrum of solidaline

C-14; *m/e* 207 is essentially an amidic ion, as indicated in Scheme 1.

This structure is also compatible with the irreversible change observed in the uv spectrum of solidaline on heating with acid. Addition of acid at room temperature caused a reversible change in the spectrum (see Experimental) but on heating a further irreversible change occurred. This phenomenon is interpreted as resulting from a reversible immonium ion – carbinolamine ether equilibrium (Scheme 2), followed by a dehydration under more vigorous acidic conditions to give the berberine like structure **4**: the uv and ir spectra of **4** (see Experimental) indicate a structure similar to that of tetradehydrocorydaline **5** (λ_{max} (log ε): 268 (4.43), 336 (4.35), 420 (3.81); ν_{max} (cm^{-1}): 1600, 1500, 1460, 1370, 1340, 1280, 1170, 1150, 1110, 1025).

We have considered the possibility that solidaline

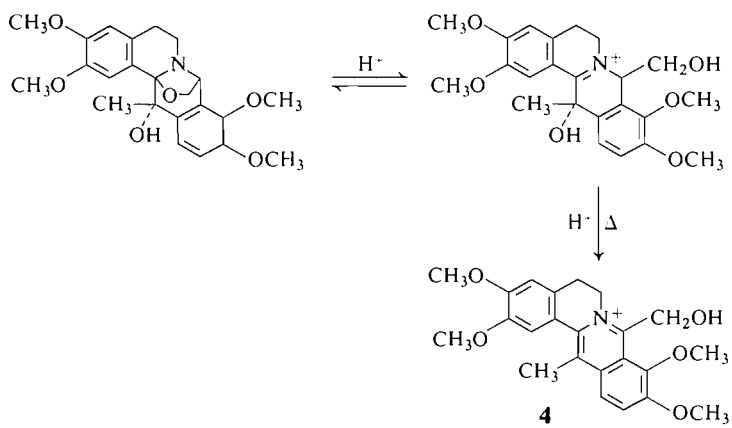

SCHEME 2. Treatment of solidaline with acid

Can. J. Chem. Downloaded from www.nrcresearchpress.com by 210.87.254.5 on 09/05/12
For personal use only.

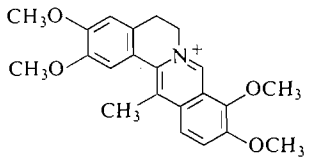

5

may be an artefact of isolation, produced by the addition of formaldehyde to ring C of tetradehydrocorydaline **5**. However, we feel that this hypothesis may be discounted on two grounds; firstly, we have been unable to effect reaction of formaldehyde with **5** under a variety of conditions, and secondly, such reaction, if it were to occur, would be expected to produce a bridged species in which the nucleophilic C-8 is bonded to oxygen, and not carbon as observed in solidaline. Further evidence for the natural origin of solidaline is provided by the existence of analogous benzophenanthridine alkaloids containing a C-8 hydroxymethyl group (9).

The biosynthetic origin of the C-8 substituted protoberberines such as solidaline and the related benzophenanthridines (9) is not clear. The presence of solidaline in a plant whose major alkaloid is corydaline (**1***a*) suggests that it may be derived *in vivo* from the latter by the addition of a one carbon unit (e.g. from methionine) (10), but the possibility that solidaline is formed from an *N*-ethyl or *N*-acetyl precursor, prior to closure of the berberine bridge, cannot be exluded.

Experimental

Materials and Methods

Melting points are uncorrected. Infrared spectra were obtained with a Perkin-Elmer 337 spectrophotometer, and ultra violet spectra in methanol solution with a Bausch and Lomb Spectronic 600 spectrophotometer. ^1H nuclear magnetic resonance spectra were obtained at 100 MHz on a Varian HA 100, and at 220 MHz on the Varian HR 220 instrument of the Ontario Research Foundation, Sheridan Park, Ontario. ^{13}C magnetic resonance spectra (broad band and off-resonance) were obtained in both $CDCl_3$ and CD_2Cl_2–CCl_4 solution at 22.628 MHz on a Bruker HX 90 instrument at the University of Sherbrooke, Sherbrooke, Quebec. Mass spectra were recorded on a CEC 21-110B spectrometer. High resolution mass measurements were performed by the reported method (11).

Isolation of the Alkaloids

In a typical extraction, *Corydalis solida* (L) Swartz (2.5 kg) was extracted by the reported procedure (1). Ochotensine (8 mg), isolated from fractions BCE and EEC, was identified by mp and spectral comparisons with an authentic sample (2). The mother liquors from fraction BC from which corydaline and stylopine had been removed were treated with oxalic acid and extracted exhaustively with ether. The bases were regenerated with potassium hydroxide and extracted with a large volume of ether. Solidaline crystallized from the dried (Na_2SO_4) ether solution, mp 197°C. Recrystallization from chloroform–methanol yielded 9 mg, mp 198°C; ir (KBr): 3400, 1285 cm^{-1}; ($CHCl_3$): 3550, 1270 cm^{-1}; uv λ_{max} (log ε): 364(3.33), 316(3.42), 281(3.51), 233(4.03); after addition of HCl λ_{max} (log ε): 367(3.90), 318(3.92), 248(4.02). This change was reversed by the addition of aqueous ammonia. The ms *m/e* (%), composition:[2] 413(24), $C_{23}H_{27}NO_6$; 398 (1.5), $C_{22}H_{24}NO_6$; 395(1.5), $C_{23}H_{25}NO_5$; 368(9), $C_{21}H_{22}NO_5$; 367(14), $C_{22}H_{25}NO_4$; 366(18), $C_{22}H_{24}NO_4$; 365(12.5), $C_{22}H_{23}NO_4$; 352(6), $C_{20}H_{18}NO_5$; 350(10), $C_{21}H_{20}NO_4$; 207(100), $C_{11}H_{13}NO_3$; 206(89), $C_{12}H_{14}O_3$; 205(25), $C_{12}H_{13}O_3$; 192(14), $C_{11}H_{12}O_3$; 191(56), $C_{11}H_{11}O_3$; 179(8), $C_{10}H_{11}O_3$, 178(24), $C_{10}H_{10}O_3$. ^1Hmr (220 MHz, CD_2Cl_2) δ: 1.73 (3H, s C—CH_3), 2.50–3.23 (4H, m, C-5 and C-6 H's), 3.61 (1H, d, J = 7 Hz, C-16 H), 3.83 (6H, s, 2 × OCH_3), 3.84 (6H, s, 2 × OCH_3), 4.03 (1H, q, J = 4, 7 Hz, C-16 H), 4.70 (1H, d, J = 4 Hz, C-8 H), 6.64 (1H, s, C-4 H), 6.86, 7.25 (2H, ABq, J = 8.5 Hz, C-11 and C-12 H's), 7.15 (1H, s, C-1 H). At 100 MHz ($CDCl_3$) a signal at δ 2.55 (1H, br s, disappears on adding D_2O) has been assigned to OH. *Anal.* calcd. for $C_{23}H_{27}NO_6$: C 66.81, H 6.58, N 3.38, 4(OCH_3) 30.02; found: C 66.55, H 6.25, N 3.77, OCH_3 30.14.

Treatment of Solidaline with Acid

A solution of solidaline (28 mg) in methanol (10 ml) and concentrated HCl (2 ml) was refluxed for 3 h. The solution was then cooled and evaporated to give a residue which was dissolved in aqueous ammonia and extracted several times with chloroform. The extract was washed with water, dried, and evaporated; ir ($CHCl_3$) ν_{max}: 1600, 1495, 1460, 1370, 1340, 1280, 1160, 1100, 1020 cm^{-1}; uv λ_{max} (log ε): 266(4.63), 344(4.41), 405(4.22). Addition of aqueous ammonia caused no appreciable change in the uv spectrum.

Acknowledgement

We thank the National Research Council of Canada for financial support.

1. R. H. F. MANSKE. Can. J. Chem. **34**, 1 (1956).
2. R. H. F. MANSKE. Can. J. Res. **18B**, 75 (1940).
3. C-Y. CHEN and D. B. MACLEAN. Can. J. Chem. **46**, 2501 (1968).
4. C. K. YU, D. B. MACLEAN, R. G. A. RODRIGO, and R. H. F. MANSKE. Can. J. Chem. **48**, 3673 (1970).
5. D. W. HUGHES, H. L. HOLLAND, and D. B. MACLEAN. Can. J. Chem. **54**, 2252 (1976).
6. J. W. APSIMON, H. BEIERBECK, and J. K. SAUNDERS. Can. J. Chem. **53**, 338 (1975).
7. M. SHAMMA and M. J. HILLMAN. Tetrahedron, **27**, 1363 (1971).
8. P. CERUTTI and H. SCHMID. Helv. Chim. Acta, **45**, 1992 (1962).
9. H. ISHII, K. HOSOYA, and N. TAKAO. Tetrahedron Lett. 2429 (1971).
10. H. L. HOLLAND, M. CASTILLO, D. B. MACLEAN, and I. D. SPENSER. Can. J. Chem. **52**, 2818 (1974).
11. C. K. YU and D. B. MACLEAN. Can. J. Chem. **49**, 3025 (1971).

[2]Observed masses agreed with the calculated values for the compositions given within ±0.005 amu.

Can. J. Chem. Downloaded from www.nrcresearchpress.com by 210.87.254.5 on 09/05/12
For personal use only.

Deactivation of HF($v = 1, 2$) by fluoroethylenes

S. J. ARNOLD AND G. H. KIMBELL

Defence Research Establishment Valcartier, P.O. Box 880, Courcelette, P.Q., Canada G0A 1R0

Received August 4, 1977

S. J. ARNOLD and G. H. KIMBELL. Can. J. Chem. **56**, 387 (1978).

A discharge flow tube technique has been used to measure the deactivation of HF($v = 1, 2$). Effective vibrational deactivation rate constants for HF($v = 1, 2$) relaxed by C_2H_4, C_2H_3F, 1,1-$C_2H_2F_2$, *cis*-1,2-$C_2H_2F_2$, *trans*-1,2-C_2H_2F, C_2HF_3, and C_2F_4 have been determined. For HF($v = 1$) the values of the rate constants range from 4.9×10^4 s^{-1} $Torr^{-1}$ for C_2H_4 to 3.5×10^3 s^{-1} $Torr^{-1}$ for C_2F_4 and for HF($v = 2$) from 1.3×10^5 s^{-1} $Torr^{-1}$ to 8.8×10^3 s^{-1} $Torr^{-1}$. The cross sections for the deactivation of HF($v = 1$) and HF($v = 2$) by C_2H_4 and the fluoroethylenes are observed to scale linearly with the number of hydrogen atoms.

S. J. ARNOLD et G. H. KIMBELL. Can. J. Chem. **56**, 387 (1978).

On a utilisé la "technique du tube d'écoulement de décharge" pour mesurer la désactivation de HF($v = 1, 2$). On a pu évaluer les constantes de vitesse pour la désactivation vibrationnelle effective de HF($v = 1, 2$) relaxé par C_2H_4, C_2H_3F, $C_2H_2F_2$-1,1, $C_2H_2F_2$-1,2 *cis*, C_2H_2F-1,2 *trans*, C_2HF_3 et C_2F_4. Pour HF($v = 1$), les valeurs des constantes de vitesse varient de 4.9×10^4 s^{-1} $Torr^{-1}$ pour le C_2H_4 à 3.5×10^3 s^{-1} $Torr^{-1}$ pour C_2F_4 alors que pour HF($v = 2$) les valeurs s'étalent entre 1.3×10^5 s^{-1} $Torr^{-1}$ à 8.8×10^3 s^{-1} $Torr^{-1}$. On a observé que les sections efficaces pour la désactivation de HF($v = 1$) et HF($v = 2$) par du C_2H_4 et des fluoroéthylènes varient d'une façon linéaire avec le nombre d'atomes d'hydrogène.

[Traduit par le journal]

Introduction

With the increasing interest in and development of HF and DF lasers, numerous studies have been undertaken to supply the requisite information on both vibrational–vibrational and vibrational–translational deactivation of vibrationally excited HF and DF. The three principal experimental methods used were: laser-excited fluorescence (1, 2), discharge flow tube technique (3, 4), and the 'steady state' chemiluminescence technique (5). For the deactivation of HF by CO_2, one of the few reactions studied by all three techniques, the agreement among the results obtained by all three techniques appears to be very good.

Very little attention has been given to the deactivation of HF by either fluorinated or unsaturated hydrocarbons. Anlauf *et al.* (3) measured the rate of deactivation of HF($v = 1, 2$) by C_2H_4 to be 5×10^4 $Torr^{-1}$ s^{-1} and 2.2×10^5 $Torr^{-1}$ s^{-1} respectively. Bott and Cohen (1) obtained values of $(4.2 \pm 0.6) \times 10^2$, $(1.6 \pm 0.5) \times 10^2$, and $(6.3 \pm 1.0) \times 10^2$ $Torr^{-1}$ s^{-1} respectively for the deactivation of HF($v = 1$) by CF_4, C_2H_6, and C_4H_8. Recent studies by Jones and Matinopoulous (6) of the infrared chemiluminescence produced by the reaction of H atoms with fluoroethylenes has prompted an interest in the rates of deactivation of HF($v = 1, 2$) by fluoroethylenes. Consequently, the present study using the discharge flow tube technique was undertaken to determine the rates of deactivation of HF($v = 1, 2$) by C_2H_4 and all the fluoroethylenes.

Experimental

The experimental apparatus consisted of a medium pressure (~ 1.7 Torr) flow tube having a diameter of 3.4 cm (Fig. 1). The F atoms were generated by passing SF_6 diluted with argon through a 2450 MHz microwave discharge in a 13 mm side arm. The discharge and the flow tube were both coated with phosphoric acid to inhibit atom recombination. The fuel, CH_4, and the deactivant along with additional argon were injected into the F atom argon stream by means of a moveable probe. This probe consisted of a glass tube with a Teflon tip having four spokes with 16 holes of 0.25 mm diameter per spoke. The holes were oriented perpendicular to the flow axis. The probe position could be varied from the observation position to a point 15 cm upstream. Characterization of the flow was accomplished by measuring pressure with a quartz spiral gauge (Texas Instruments) and the flow rates of the reactant gases with Fisher Porter flowmeters.

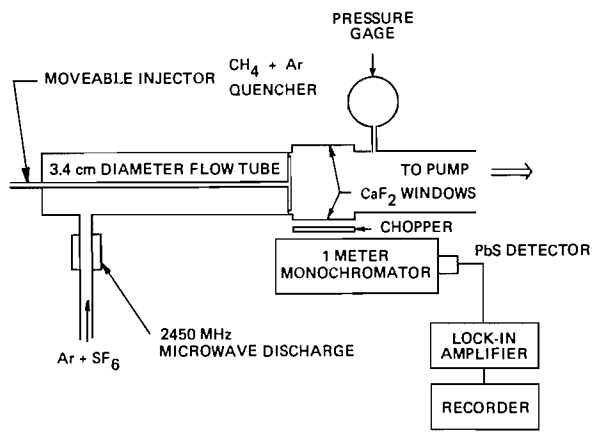

FIG. 1. Experimental apparatus.

Can. J. Chem. Downloaded from www.nrcresearchpress.com by 210.87.254.105 on 09/05/12
For personal use only.

Can. J. Chem. Downloaded from www.nrcresearchpress.com by 210.87.254.105 on 09/05/12
For personal use only.

The detection system consisted of CaF_2 windows mounted flush with the walls of the flow tube, a McPherson 1 m monochromator equipped with a Dry ice – acetone cooled PbS detector chopped at 200 Hz by a Bulova L8HH optical chopper and a Hewlett-Packard lock-in amplifier. The 2 mm slit of the chopper acted as an iris limiting the field of view. This gave a spatial resolution of 4.4 mm along the flow axis.

Typical experimental conditions were: molar flow rates (μmol s^{-1}) Ar 884, SF_6 0.45, CH_4 5.24; pressure 1.65 Torr; average linear velocity 1.85×10^3 cm s^{-1}; temperature (298 ± 2) K.

Results and Discussion

Vibrationally excited HF is produced by the fast reaction

$$[1] \qquad CH_4 + F \rightarrow HF(v \leq 3) + CH_3$$

which has a rate constant $k = 5.48 \times 10^{-10} \exp(-575/T)$ cm^3 $molecules^{-1}$ s^{-1} (7). The emission spectrum of the HF fundamental vibrational rotational band is well resolved permitting the use of the $R_1(2)$ and $R_2(4)$ lines as a monitor of the HF($v = 1$) and HF($v = 2$) concentration.

HF($v = n$) is deactivated by the quenching reaction

$$[2] \qquad HF(v = n) + Q \rightarrow HF(v = n - 1) + Q$$

where Q is the added quencher, as well as undergoing collisional deactivation with reactants and products, radiative decay, and wall deactivation. The method of analysis employed is similar to that used by Kwok and Wilkins (8). The flow is treated as fully developed, viscous, laminar, axially symmetric pipe flow having a parabolic radial dependence. Axial diffusion and coupling between HF(v) levels is assumed to be negligible. Mixing of the reactants at the injector is assumed to be instantaneous. The value of the number density averaged along the tube diameter, $\bar{N}_v$, as a function of the radial coordinate z is approximately

$$[3] \qquad \bar{N}_v(z) = \bar{N}_v(z = 0) \exp(-z/\tau_v U')$$

where $\tau_v^{-1}(z)$ is the overall decay rate. The velocity U' compensates for the distortion of the density $\bar{N}_v$ caused by the paraboloidal velocity profile. $U' = \phi\bar{U}$ where $\bar{U}$ is the average velocity calculated from the continuity equation. The correction factor ϕ can be calculated for specified diffusion coefficients and given wall loss conditions using the method outlined by Poirier and Carr (9). Figure 2 shows a typical plot of observed number density, $\bar{N}_v$, against distance along the z axis. The decay slopes obtained from these plots

$$[4] \qquad \text{Slope} = S_v = \frac{d(\ln \bar{N}_v)}{dz} = (\tau_v U')^{-1}$$

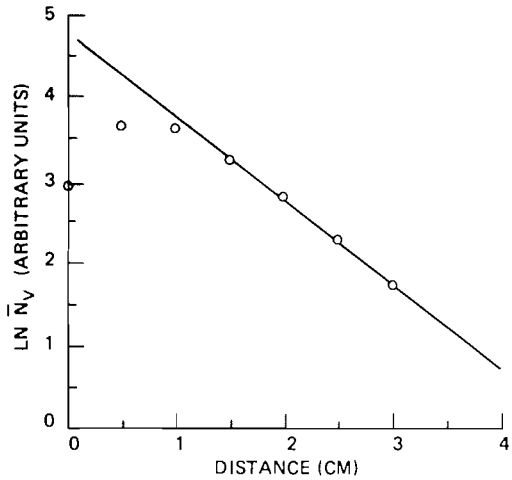

FIG. 2. Plot of observed number density, $\bar{N}_v$, against distance along the z axis.

are then plotted against quencher concentration Q to give the quenching rate constant

$$[5] \qquad dS_v/dQ = k_q/U'$$

Figure 3 shows a representative plot of S_v vs. Q for the deactivation of HF($v = 2$) by C_2HF_3.

The flow system was very steady during the measurements with changes in gas pressure and discharge parameters being less than 5%. The flows were steady to within 5% with the uncertainty in their absolute values calculated to be less than 20% of value. Detector sensitivity was sufficient to permit the decay of HF($v = 1$) to be monitored over a distance of 10 cm and HF($v = 2$) over a distance of 5 cm. The signal for $\bar{N}_1$ at the 1 cm position varied by less than 2% over 10 min and at the 10 cm posi-

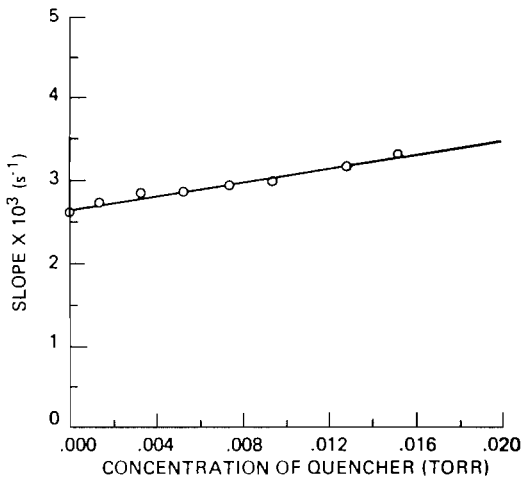

FIG. 3. Plot of S_v vs. Q for the deactivation of HF($v = 2$) by C_2HF_3.

Can. J. Chem. Downloaded from www.nrcresearchpress.com by 210.87.254.105 on 09/05/12
For personal use only.

TABLE 1. Comparison of rate constants for the deactivation of HF($v = 1$) by CH_4, C_2H_6, and CO_2

Quencher	k_q (Torr^{-1} s^{-1})	Temperature (K)	Method	Reference
CH_4	3.5×10^4	298	Discharge flow tube	Present work
	2.1×10^4	298	Discharge flow tube	Kwok and Cohen (4)
	6.4×10^4	298	Discharge flow tube	Anlauf *et al.* (3)
	$(5.3 \pm 0.8) \times 10^4$	295	Laser fluorescence	Hancock and Green (2)
C_2H_6	9.3×10^4	298	Discharge flow tube	Present work
	$(1.1 \pm 0.16) \times 10^5$	295	Laser fluorescence	Hancock and Green (2)
	5.6×10^4	298	Discharge flow tube	Anlauf *et al.* (3)
CO_2	4.0×10^4	298	Discharge flow tube	Present work
	4.1×10^4	298	Discharge flow tube	Kwok and Cohen (4)
	$(3.6 \pm 0.2) \times 10^4$	295	Laser fluorescence	Bott and Cohen (10)
	4.0×10^4	298	Steady-state chemiluminescence	Airey and Smith (5)
	$(5.9 \pm 0.2) \times 10^4$	294	Laser fluorescence	Hancock and Green (11)
	$(4.25 \pm 0.6) \times 10^4$	299	Laser fluorescence	Lucht and Cool (12)
	$(3.9 \pm 0.4) \times 10^4$	295	Laser fluorescence	Bott (13)

tion by less than 5%. As can be seen from Fig. 2 the scatter about the least-squares line drawn through the straight portion of the curve is small permitting an accurate determination of the slope. Similarly plots of S_v vs. Q exhibit only small fluctuations from the expected linearity (Fig. 3).

In order to test the experimental method and the assumptions made in the analysis, the rate of deactivation of HF($v = 1$) by CH_4, C_2H_6, and CO_2 was determined. The values of the rate constants obtained in the present study together with literature values are given in Table 1. Good agreement with the literature values is obtained in the case of CO_2 and good agreement with the preferred value in the case of C_2H_6. For CH_4 the present value lies intermediate between the two preferred values.

The rate of deactivation of HF($v = 2$) by CH_4 and CO_2 was also determined. For CH_4 a value of 7.5×10^4 Torr^{-1} s^{-1} was obtained, which is in reasonable agreement with the Kwok and Cohen (4) value of 6.9×10^4 Torr^{-1} s^{-1}. For CO_2, the value of 1.3×10^5 Torr^{-1} s^{-1} is somewhat lower than the values of 1.6×10^5 Torr^{-1} s^{-1} (4), 1.6×10^5 Torr^{-1} s^{-1} (5), and $(2.0 \pm 0.2) \times 10^5$ Torr^{-1} s^{-1} (13) obtained by other workers.

The rate constants for the deactivation of HF($v = 1$) and HF($v = 2$) by C_2H_4 and all the fluoroethylenes are given in Table 2. Several determinations of each rate constant were made, six being the normal number with three being the minimum. The maximum deviation between values was 15% with the average deviation being considerably less. The values of the rate constants are considered to have uncertainties of less than a factor of 2 although the agreement between the values obtained for the deactivation of HF($v = 1$) by CH_4, C_2H_6, and CO_2 and the literature values indicates that the uncertainty is probably considerably less. The values of 4.9×10^4 and 2.2×10^5 obtained for the deactivation of HF($v = 1$) and HF($v = 2$) by C_2H_4 are thus in good accord with the approximate values of 5×10^4 and 2.2×10^5 given by Anlauf *et al.* (3).

TABLE 2. Rate constants for the deactivation of HF($v = 1$, 2) by fluoroethylenes

Quencher	k_q (Torr^{-1} s^{-1}) HF($v = 1$)	HF($v = 2$)
C_2H_4	4.9×10^4	1.3×10^5
C_2H_3F	3.4×10^4	8.7×10^4
1,1-$C_2H_2F_2$	2.7×10^4	6.5×10^4
cis-1,2-$C_2H_2F_2$	3.1×10^4	5.9×10^4
trans-1,2-$C_2H_2F_2$	2.9×10^4	6.6×10^4
C_2HF_3	1.9×10^4	4.2×10^4
C_2F_4	3.5×10^3	8.8×10^3

The cross section for the deactivation of HF($v = 1$) and HF($v = 2$) by fluoroethylenes ($C_2H_{2x-m}F_m$) appears to scale linearly with the number of hydrogen atoms ($2x - m$) which is equal to the number of CH stretching frequencies (Figs. 4 and 5). Since the CH stretching frequencies for the fluoroethylenes fall within the range 3060 ± 75 cm^{-1}, the energy defect, ΔE, for each member of the series of reactions

$$[6] \quad HF(v = n) + C_2H_{2x-m}F_m \rightarrow HF(v = n - 1) + C_2H_{2x-m}F_m + \Delta E$$

is essentially the same and the increased efficiency can be attributed to an increase in the number of CH stretching modes available. Hancock and Green (2) observed a similar dependence of collision cross section on the number of hydrogen atoms for the deactivation of HF($v = 1$) by alkanes.

Can. J. Chem. Downloaded from www.nrcresearchpress.com by 210.87.254.105 on 09/05/12
For personal use only.

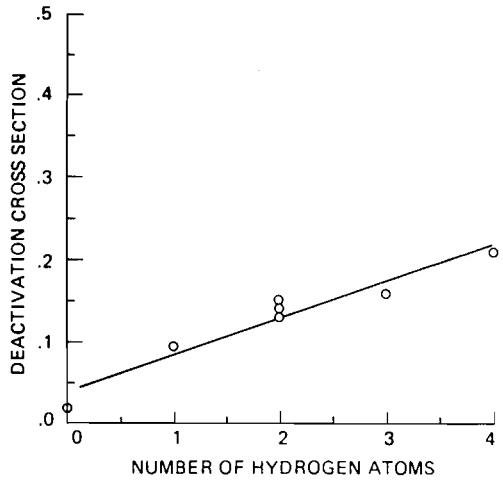

FIG. 4. Plot of deactivation cross section (σ (Å^2)) for HF(v = 1) against number of hydrogen atoms in fluoroethylene.

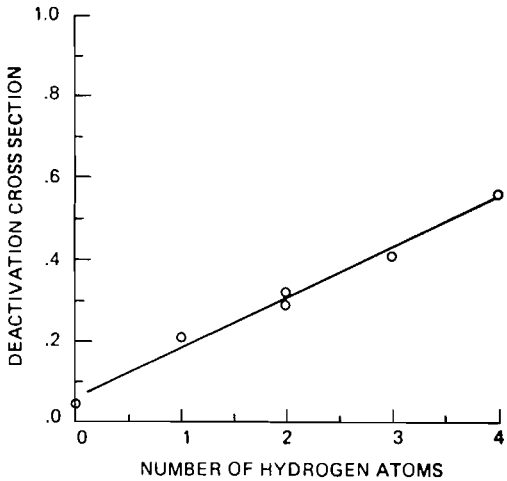

FIG. 5. Plot of deactivation cross section (σ (Å^2)) for HF(v = 2) against number of hydrogen atoms in fluoroethylene.

Conclusions

A discharge flow tube method has been used to determine the rate of deactivation of HF(v = 1) and HF(v = 2) by CO_2, CH_4, C_2H_6, C_2H_4, and all the fluoroethylenes. The values of the rate constants obtained for the deactivation of HF(v = 1) by CO_2, CH_4, and C_2H_6 are in good agreement with the literature values indicating that the discharge flow tube method with the assumptions made in the analysis is capable of yielding satisfactory results. For the deactivation of HF(v = 1) the value of the rate constants ranged from 4.9×10^4 Torr^{-1} s^{-1} for C_2H_4 to 3.5×10^3 Torr^{-1} s^{-1} for C_2F_4 and for HF(v = 2) from 1.3×10^5 Torr^{-1} s^{-1} for C_2H_4 to 8.8×10^3 Torr^{-1} s^{-1} for C_2F_4. The cross sections for the deactivation of HF(v = 1) and HF(v = 2) by C_2H_4 and the fluoroethylenes is observed to scale linearly with the number of hydrogen atoms.

Acknowledgements

The authors wish to thank Mr. A. Blanchard for his assistance in the solution of the continuity equation. The interest of Prof. W. Jones and Dr. G. Matinopoulous in this work is also acknowledged.

1. J. F. BOTT and N. COHEN. J. Chem. Phys. **61**, 681 (1974).
2. J. K. HANCOCK and W. G. GREEN. J. Chem. Phys. **58**, 6350 (1973).
3. K. G. ANLAUF, P. H. DAWSON, and J. A. HERMAN. J. Chem. Phys. **58**, 5354 (1973).
4. M. A. KWOK and N. COHEN. J. Chem. Phys. **61**, 5221 (1974).
5. J. R. AIREY and I. W. M. SMITH. J. Chem. Phys. **57**, 1669 (1972).
6. W. E. JONES and G. MATINOPOULOUS. Submitted to J. Chem. Soc. Faraday Trans.
7. H. G. WAGNER, J. WARNATZ, and C. ZETZSCH. An. Acos. Quim. Argent. **59**, 169 (1971).
8. M. A. KWOK and R. L. WILKINS. J. Chem. Phys. **63**, 2453 (1975).
9. R. V. POIRIER and R. W. CARR, Jr. J. Phys. Chem. **75**, 1593 (1971).
10. J. F. BOTT and N. COHEN. J. Chem. Phys. **58**, 4539 (1973).
11. J. K. HANCOCK and W. H. GREEN. J. Chem. Phys. **57**, 4515 (1972).
12. R. A. LUCHT and T. A. COOL. J. Chem. Phys. **63**, 3962 (1975).
13. J. F. BOTT. J. Chem. Phys. **65**, 4239 (1976).

Appendix

The data were analysed in the manner described by Kwok and Wilkins (8) and Poirier and Carr (9). Consequently, only a brief resume of the method will be given here. The flow reactor is axially symmetrical with flow in the axial direction only. The reactions are assumed to occur isothermally in laminar flow. Thus, the differential equation describing the system is

$$[A.1] \quad -v_z\left(\frac{\partial C_i}{\partial_z}\right) + D_i\left(\frac{\partial^2 C_i}{\partial r^2} + \frac{1}{r}\frac{\partial C_i}{\partial r} + \frac{\partial^2 C_i}{\partial_z{}^2}\right) - R_i = 0$$

$$i = 1, 2, \ldots, n$$

where v_z = axial velocity, z = axial coordinate measured from the reactor inlet, r = radial coordinate measured from the tube axis, C_i = concentration, D_i = molecular diffusivity, R_i = reaction rate of the ith component. When the velocity profile is described by Poiseuille's equation, axial diffusion is negligible in comparison to radial diffusion and when there is no volume change on reaction, [A.1] for an irreversible first order reaction is

[A.2] $$-v_0\left(1-\left(\frac{r}{R}\right)^2\right)\frac{\partial C}{\partial_z} + D\left(\frac{\partial^2 C}{\partial r^2}+\frac{1}{r}\frac{\partial C}{\partial r}\right) - kC = 0$$

where v_0 = center line velocity and R = tube radius. In dimensionless form [A.2] is

[A.3] $$-(1-u^2)\frac{\partial C}{\partial \lambda}+\alpha\left(\frac{\partial^2 C}{\partial U^2}+\frac{1}{U}\frac{\partial C}{\partial U}\right) - C = 0$$

with $C = 1$ at $\lambda = 0$, $\partial C/\partial\lambda = 0$ at $U = 0$, and $-\alpha\partial C/\partial U = \beta C$ at $U = 1$; where $U = r/R$, $C = C/C_0$, $\lambda = k_z/v_0$, $\alpha = D/kR^2$, and $\beta = k_w/kR$. For a homogeneous first order reaction with a concurrent first order wall reaction, the parameter β in the boundary condition $-\alpha\partial C/\partial U = \beta C$ has positive values. The continuity equation (eq. A.3) was solved using a finite difference technique. Concentrations were averaged along a principal diameter of the reactor

[A.4] $$\bar{C}_1 = \int_0^1 C\,du$$

and plots of $-\log \bar{C}_1/C_0$ vs. λ were obtained as a function of α and β as is done in ref. 9. The slope, $(-\log \bar{C}_1/C_0)/\lambda$ for the experimentally determined values of α and β, is ϕ, the correction to the average flow velocity required to compensate for the distortion of the number density, $\bar{N}_v$, caused by the parabolic velocity profile.

Can. J. Chem. Downloaded from www.nrcresearchpress.com by 210.87.254.105 on 09/05/12
For personal use only.

Mesure de la constante de vitesse de réaction des atomes d'hydrogène sur l'éthane et le propane en réacteurs tubulaire et parfaitement agité ouverts

JACQUES LEDE ET JACQUES VILLERMAUX

Laboratoire des Sciences du Génie Chimique, C.N.R.S. – E.N.S.I.C, 1, rue Grandville, 54042 Nancy Cedex, France

Reçu le 16 novembre 1976[1]

JACQUES LEDE et JACQUES VILLERMAUX. Can. J. Chem. **56**, 392 (1978).

On étudie la constante de vitesse de la réaction des atomes d'hydrogène produits par décharge électrique, sur l'éthane et le propane dans deux types de réacteurs ouverts: tubulaire et parfaitement autoagité par jets gazeux. Les mesures sont faites grâce à l'utilisation d'une nouvelle méthode très sensible de dosage des atomes. Les résultats obtenus au voisinage de la température ambiante sont parfaitement compatibles avec ceux d'autres auteurs résultant d'études effectuées sous des températures nettement plus élevées. Il est possible de proposer les estimations suivantes:

$$H + C_2H_6 \xrightarrow{k_5} H_2 + C_2H_5: \quad k_5 = 10^{13.7\pm0.6} \exp -((9100 \pm 600)/RT)\ (cm^3\ mol^{-1}\ s^{-1})$$

$$H + C_3H_8 \xrightarrow{k_{13}} H_2 + C_3H_7: \quad k_{13} = 10^{13.8\pm0.3} \exp -((7800 \pm 100)/RT)\ (cm^3\ mol^{-1}\ s^{-1})$$

JACQUES LEDE and JACQUES VILLERMAUX. Can. J. Chem. **56**, 392 (1978).

The rate constant for the reaction of hydrogen atoms, generated by electrical discharge, with ethane and propane has been studied in tubular and perfectly stirred open reactors. Measurements are made with a new and very sensitive method of analysis of the hydrogen atom concentration. The results obtained near room temperature are in good agreement with those of other authors operating at much higher temperatures. The following estimates may be made:

$$H + C_2H_6 \xrightarrow{k_5} H_2 + C_2H_5: \quad k_5 = 10^{13.7\pm0.6} \exp -((9100 \pm 600)/RT)\ (cm^3\ mol^{-1}\ s^{-1})$$

$$H + C_3H_8 \xrightarrow{k_{13}} H_2 + C_3H_7: \quad k_{13} = 10^{13.8\pm0.3} \exp -((7800 \pm 100)/RT)\ (cm^3\ mol^{-1}\ s^{-1})$$

Introduction

Un certain nombre d'articles de revues rassemblant les principales réactions des atomes d'hydrogène apparaissent régulièrement dans la littérature (1–3). Parmi elles, les réactions sur les alcanes ont suscité d'assez nombreux travaux.

Il est généralement admis que le processus initial correspond à l'arrachement d'un atome H avec formation d'une molécule H_2 et d'un radical alkyle R (processus métathétique):

$$H + RH \rightarrow H_2 + R$$

Les expériences sont menées dans des systèmes très variés (limite d'explosion du mélange H_2–O_2; flammes; radiolyse; photolyse; décharge; etc). Très souvent, les méthodes sont assez indirectes, la constante de ce processus étant déduite d'autres constantes supposées parfaitement connues. Dans la majorité des cas, la température de travail est nettement supérieure à 400 K et, dans les systèmes en écoulement, la pression totale inférieure à 10 Torr.

Les effets de paroi (recombinaison d'une fraction des atomes H sur les parois de l'enceinte) peuvent avoir une grande importance sur la cinétique apparente. Pour s'y soustraire, les auteurs effectuent soit des traitements de parois destinés à en minimiser les effets (4, 5) (mais ces processus étant activés peuvent prendre une importance insoupçonnée à haute température); soit des corrections (6); soit des mesures quantitatives préalables (7, 8).

Dans une étude récente, Lede et coll. (9, 10) ont préconisé l'utilisation de deux types de réacteurs ouverts en vue de l'étude de réactions homogènes: le réacteur tubulaire en régime d'écoulement laminaire et le réacteur parfaitement autoagité par jets gazeux turbulents. Ils ont notamment proposé plusieurs méthodes de dépouillement d'expériences permettant de calculer des constantes de vitesse homogènes après avoir déterminé sur le plan expérimental la constante de vitesse de la réaction parasite aux parois, le coefficient de diffusion moléculaire du réactif et l'importance de l'hydrodynamique de l'écoulement gazeux.

Ces méthodes sont applicables à des réactions modérément rapides et se justifient donc parfaitement pour l'étude de réactions de métathèse dans des conditions où celles-ci sont peu étudiées: au voisinage de la température ambiante et sous une pression totale pouvant atteindre l'atmosphère. Un autre

[1]Revision reçue le 26 août 1977.

Can. J. Chem. Downloaded from www.nrcresearchpress.com by 210.87.254.6 on 09/05/12
For personal use only.

Can. J. Chem. Downloaded from www.nrcresearchpress.com by 210.87.254.6 on 09/05/12
For personal use only.

intérêt d'une telle étude est de faire appel à une technique nouvelle de mesure de la concentration en atome H (11) applicable à des concentrations très faibles.

Dispositif expérimental

Il est le même quel que soit le réacteur utilisé. Ayant déjà décrit ce dispositif à plusieurs reprises (12, 13), nous n'en rappellerons que les points essentiels.

Généralités

Un courant d'hydrogène de qualité "U" de l'"Air Liquide" ($[H_2] > 99.995\%$) traverse une vanne à aiguille puis une zone dans laquelle il est partiellement dissocié par décharge électrique Corona. A cette zone, délimitée en sortie par une pastille en PTFE percée d'un trou de 0.01 cm^2, succède le réacteur où la réaction est étudiée en obervant la concentration résiduelle des atomes d'hydrogène. Les gaz traversent ensuite une seconde vanne à aiguille et une pompe pour vide primaire. Le domaine de pressions étudié va de quelques Torr à la pression atmosphérique et les débits volumiques de 50 à 1000 $cm^3\ s^{-1}$ (mesurés sous la pression de travail).

Une canalisation secondaire munie d'une troisième vanne à aiguille permet d'introduire dans le réacteur un débit secondaire connu (rotamètres) d'alcane de qualité "N 35" (pureté $>99.95\%$). Celui-ci est auparavant débarrassé de toute trace d'oxygène et d'éthylène par passage sur un lit d'amiante palladiée et platinée en présence d'une très faible concentration d'hydrogène.

Réacteurs tubulaires

Il s'agit de tubes cylindriques en Pyrex dont les parois peuvent être modifiées facilement grâce à différents chemisages internes. Trois types de réacteurs tubulaires à parois différentes ont été utilisés: un réacteur à parois en PTFE (diamètre 1.2 cm); un réacteur à parois en Pyrex (diamètre 1.45 cm); un réacteur à parois en platine (diamètre 1.16 cm).

Des mesures ont été faites à différentes températures. Le réacteur est à cet effet entouré d'un tube coaxial dans lequel circule de l'eau thermostatée, l'ensemble étant calorifugé par un manchon de laine de verre. Avant la zone de mesure, la surface interne du réacteur est tapissée sur une longueur de 80 cm par un tube en PTFE ce qui permet (compte tenu du faible pouvoir catalytique de ce matériau) de transporter les atomes avec un minimum de recombinaison tout en permettant la mise en régime thermique du gaz.

Le courant d'alcane (éthane ou propane) est introduit par un simple tube débouchant à l'entrée du réacteur. Le parfait mélangeage avec le courant principal est assuré par de nombreuses chicanes en PTFE. Les mesures ne sont effectuées qu'après une abscisse l telle que le régime d'écoulement laminaire stable soit réétabli. Des expériences de visualisation de l'écoulement ont permis de proposer la relation (13):

$$l = 2R(0.035Re + 1)$$

dans laquelle R est le rayon du réacteur et Re le critère de Reynolds correspondant à l'expérience.

Réacteur agité

Sa conception technique est entièrement décrite dans la réf. 10. Rappelons simplement que le flux d'hydrogène pénètre dans le réacteur (sphère en "Pyrex" ayant un volume utile de 26 cm^3) par l'intermédiaire d'un injecteur ayant la forme d'un croissillon portant quatre tuyères situées à mi-rayon. Celles-ci ont un diamètre tel que les jets d'hydrogène soient turbulents et assurent grâce à de nombreux recyclages internes un vigoureux brassage du milieu gazeux. Les conditions de parfaite autoagitation ont été énoncées par David et coll. (14, 15). L'injecteur est en PTFE afin de minimiser la quantité d'atomes susceptibles de se recombiner entre la sortie de la décharge électrique et le débouché des tuyères.

L'arrivée d'alcane se fait par un simple tube débouchant dans le réacteur, le mélangeage étant, dans ce cas, parfaitement assuré par la turbulence que règne dans le milieu. Les expériences sont faites dans une gamme de temps de passage où les déterminations préalables de distributions de temps de séjour (13) ont prouvé la parfaite agitation du réacteur.

Les mesures ont été faites à la température ambiante.

Mesure de la concentration en atomes d'hydrogène

Il s'agit d'une méthode nouvelle décrite en détail dans la réf. 11. Son principe de fonctionnement repose sur le fait que l'oxyde de mercure HgO est sélectivement réduit par les atomes d'hydrogène pour former du mercure, libéré en phase gazeuse lorsque l'on opère avec de faibles concentrations atomiques. En réacteur ouvert, la vapeur de mercure est entraînée en continu et son dosage est effectué en sortie par la mesure spectrophotométrique de l'absorption d'un faisceau de rayonnement 253.7 nm.

La comparaison de cette méthode avec d'autres utilisant des sondes de natures très différentes (16) a permis d'en souligner la fiabilité et la linéarité. Les risques encourus par un éventuel dépôt de mercure sur les parois peuvent être exclus, aucune variation du coefficient de recombinaison hétérogène des atomes sur celles-ci n'ayant été observée en utilisant d'autres types de sondes (17). Si cette technique est essentiellement relative, des évaluations absolues de concentrations peuvent être faites grâce notamment à des expériences d'étalonnage réalisées en introduisant des concentrations connues de vapeur de mercure (11). La limite inférieure de concentration atomique détectable peut être ainsi estimée proche de 5×10^{-13} at-g cm^{-3}.

D'un point de vue pratique, la sonde proprement dite est constituée par une fine grille en verre "Pyrex" interceptant le courant gazeux et sur laquelle est déposé l'oxyde. La position de la surface sensible peut être réglée à volonté depuis l'extérieur du montage grâce à un système d'aimant.

Les études cinétiques en réacteur tubulaire sont menées en positionnant la sonde à différentes abscisses. L'information expérimentale est donc le profil axial de concentration. Les études cinétiques en réacteur agité sont menées grâce au jeu de deux sondes parfaitement identiques positionnées à l'entrée et à la sortie du réacteur. L'information expérimentale est donc cette fois le rapport des concentrations d'entrée et de sortie.

Méthodes de dépouillement des expériences

Ces méthodes ont déjà fait l'objet de descriptions détaillées, rappelons cependant ici les points nécessaires à la compréhension de cet article. Que ce soit avec le réacteur tubulaire ou le réacteur agité, les deux méthodes ont en commun le fait que les expériences sont menées en deux étapes correspondant aux cas où la réaction homogène existe ou non (arrivée d'alcane mise en service ou bien coupée).

Expériences en réacteur tubulaire

Les conditions sont telles que réactions homogène et hétérogène et processus diffusionnels soient com-

Can. J. Chem. Downloaded from www.nrcresearchpress.com by 210.87.254.6 on 09/05/12
For personal use only.

pétitifs. La pression de travail est suffisamment forte pour que l'hypothèse d'un écoulement piston ne puisse être formulée. Les dépouillements tiennent donc compte du profil radial parabolique des vitesses dans le réacteur.

(*1*) On se propose dans la première étape, de mesurer les deux constantes caractérisant les phénomènes chimiques (rendement de recombinaison hétérogène γ) et diffusionnel (coefficient de diffusion D) dans les conditions de l'expérience. En accord avec ce qui est généralement rapporté dans la littérature (12) l'expérience montre que la réaction de recombinaison des atomes aux parois est un phénomène d'ordre un (mécanisme de Rideal): allure parfaitement exponentielle des profils axiaux de concentration et indépendance de ceux-ci avec la concentration atomique initiale (13, 18).

Les atomes parviennent à la paroi par un processus de diffusion en phase gazeuse. Villermaux (19) a montré dans ces conditions que le phénomène global reste d'ordre un avec une constante de temps caractéristique τ qui peut s'écrire sous la forme:

$$[1] \qquad \tau = \frac{2R}{\gamma \bar{C}} + \frac{R^2}{3.66D}$$

R est le rayon du réacteur; $\bar{C}$ est la vitesse moyenne d'agitation thermique des atomes; γ est le rendement de recombinaison sur les parois; D est le coefficient de diffusion moléculaire; 3.66 est un coefficient numérique traduisant la nature de l'écoulement gazeux (laminaire avec profil parabolique).

L'expression 1 montre que les variations de τ en fonction de la pression sont linéaires, ce qui offre une méthode expérimentale originale d'accès à γ et D.

Cette étude a été menée systématiquement entre 50 et 760 Torr et de 277 à 333 K dans trois réacteurs ayant des parois de nature catalytique différentes (12). Elle a permis de calculer l'énergie d'activation de la recombinaison sur Pyrex ainsi que les paramètres d'interaction moléculaire du couple H,H_2. Les résultats se sont avérés être en très bon accord avec ceux d'autres auteurs ayant opéré dans des conditions très différentes.

(*2*) Dans la seconde étape, un débit connu et constant d'alcane est introduit, toutes autres conditions étant restées inchangées. Si l'on désigne par k la constante de vitesse d'ordre ou de pseudo ordre un de cette réaction homogène, on peut montrer (9) que si $k \ll 30D/R^2$, le profil axial de concentration reste en première approximation exponentiel malgré les forts couplages entre phénomènes chimiques, diffusionnels et hydrodynamiques:

$$[2] \qquad C_m \sim \exp(-\lambda z/R)$$

C_m est la concentration moyenne en atomes dans une section droite du réacteur; λ est une fonction de γ, D et k.

Les paramètres γ et D ont été obtenus dans l'étape précédente; λ est calculé par la méthode des moindres carrés sur les droites expérimentales $\log C_m$ en fonction de z; une procédure d'optimisation menée sur ordinateur (9) permet de calculer la meilleure valeur de k.

Expériences en réacteur agité

Ici encore les conditions sont telles que réactions homogène et hétérogène sont compétitives. La pression de travail est suffisamment forte pour que l'agitation soit assurée par la turbulence du milieu et non pas par diffusion moléculaire.

(*1*) Dans la première étape, on mesure le rapport des concentrations d'entrée et de sortie $(C_0/C_S)'$ qui peut s'écrire (10):

$$[3] \qquad \left(\frac{C_0}{C_S}\right)' = 1 + \frac{(\gamma\bar{C}/4)k_g}{(\gamma\bar{C}/4) + k_g}\frac{S}{Q}$$

S est la surface active intérieure; Q est le débit volumique total du gaz; k_g est la conductance de transfert du réactif à travers la couche limite qui isole la paroi du milieu gazeux turbulent.

Notons que l'expression 3 permet la mesure expérimentale du rendement de recombinaison sur le matériau constituant la surface intérieure du réacteur agité, compte tenu d'une hypothèse sur les valeurs de k_g. Les résultats obtenus sur le verre Pyrex recoupent très favorablement ceux d'autres déterminations (10).

(*2*) Dans la second étape, un débit constant et connu d'alcane est introduit, toutes autres conditions étant restées inchangées. On mesure cette fois un rapport des concentrations d'entrée et de sortie C_0/C_S tel que:

$$[4] \qquad \frac{C_0}{C_S} = 1 + \frac{(\gamma\bar{C}/4)k_g}{(\gamma\bar{C}/4) + k_g}\frac{S}{Q} + k\frac{V}{Q}$$

V désignant le volume du réacteur, l'association de [3] et [4] permet de calculer simplement k:

$$\frac{C_0}{C_S} - \left(\frac{C_0}{C_S}\right)' = k\frac{V}{Q}$$

Une telle procédure ne nécessite pas de faire le moindre calcul ou hypothèse sur la part quantitative de la réaction aux parois et des phénomènes de transfert, les paramètres γ et k_g disparaissant dans la différence.

Résultats et discussion

Les mesures ont été faites avec l'éthane et le propane dans les conditions suivantes:

Can. J. Chem. Downloaded from www.nrcresearchpress.com by 210.87.254.6 on 09/05/12
For personal use only.

$[H] \ll [C_2H_6, C_3H_8]$: condition de réaction de pseudo premier ordre.

$[C_2H_6, C_3H_8] \ll [H_2]$: condition nécessaire pour que la présence de l'alcane ne modifie pas sensiblement les propriétés de transport du milieu par rapport aux expériences faites sans alcane.

Les concentrations initiales en atomes d'hydrogène ont été ajustées en agissant sur la tension appliquée entre les deux électrodes de la décharge électrique de telle manière que les concentrations atomiques régnant dans la zone de mesure soient compatibles avec les limites de sensibilité de la sonde à oxyde mercurique (5×10^{-11} à 5×10^{-13} at-g cm^{-3}). Le fait que tous les phénomènes observés soient du premier ordre a rendu inutile la mesure précise des concentrations initiales absolues correspondant à chaque expérience.

Réaction avec l'éthane

On se propose de mesurer la constante de vitesse k_5 de la réaction:

$$[5] \qquad H + C_2H_6 \xrightarrow{k_5} H_2 + C_2H_5$$

La cinétique est suivie en observant la baisse de concentration des atomes H et il convient de tenir compte de réactions secondaires et en premier lieu de leur réaction de combinaison avec les radicaux C_2H_5 formés par [5]:

$$[6] \qquad H + C_2H_5 \xrightarrow{k_6} C_2H_6^*$$

Ce processus donne naissance à une molécule d'éthane dont l'excès d'énergie est suffisant pour rompre la liaison C—C:

$$[7] \qquad C_2H_6^* \xrightarrow{k_7} 2CH_3$$

Les radicaux méthyle ainsi formés réagissent à leur tour sur les atomes H pour former du méthane, seul produit effectivement détecté (7, 21):

$$[8] \qquad 2(CH_3 + H \xrightarrow{(M)\,k_8} CH_4)$$

On peut noter que les processus de cette séquence constituent les étapes essentielles consécutives à l'addition d'atomes H sur l'éthylène (22–26).

L'intégration numérique complète des équations de vitesse représentant les processus [5] à [8] a été menée sur ordinateur en prenant $k_5 = 1.29 \times 10^7$ cm^3 mol^{-1} s^{-1}; $k_6 = 3 \times 10^{13}$ cm^3 mol^{-1} s^{-1}; $k_7 = 3 \times 10^8$ s^{-1}; $k_8 = 3 \times 10^{13}$ cm^3 mol^{-1} s^{-1} et avec les conditions moyennes suivantes: concentration en atomes d'hydrogène à l'instant initial: 10^{-11} at-g cm^{-3}; pression totale: 300 Torr; titre en éthane: 4%; température: 300 K.

Sauf pour les tout premiers temps de réaction, la loi d'atteinte de l'état stationnaire pour les espèces intermédiaires peut être représentée avec une bonne approximation par une relation du type:

$$R_t = R_\infty(1 - e^{-300t})$$

R_t: concentration en espèce intermédiaire à un instant t; R_∞: concentration stationnaire.

En se fixant une borne $(R_\infty - R_t)/R_\infty < 0.1$, on trouve que ces conditions sont atteintes après 8×10^{-3} s, limite au delà de laquelle les expériences devront être effectuées. Dans ces conditions, le schéma cinétique proposé conduit à l'équation stoechiométrique:

$$[9] \qquad 4H + C_2H_6 = H_2 + 2CH_4$$

La constante apparente de pseudo premier ordre k_{app} mesurée dans nos conditions vaut alors

$$[10] \qquad k_{app} = 4k_5[C_2H_6]$$

Il ne faut pas exclure, à priori, la possibilité d'intervention de la réaction 11 inverse de [5]:

$$[11] \qquad H_2 + C_2H_5 \xrightarrow{k_{11}} H + C_2H_6$$

étant donné la valeur élevée du rapport $[H_2]/[H]$ prévalant dans nos expériences. En prenant les valeurs suivantes à 300 K: $[H_2] = 1.6 \times 10^{-5}$ mol cm^{-3} (300 Torr); $[C_2H_5] = 3 \times 10^{-13}$ mol cm^{-3} (valeur stationnaire donnée par l'intégration numérique); $[H] = 10^{-11}$ mol cm^{-3}; $[C_2H_6] = 6.4 \times 10^{-7}$ mol cm^{-3} (4% d'éthane); $k_5 = 1.29 \times 10^7$ cm^3 mol^{-1} s^{-1}; $k_{11} = 3.7 \times 10^2$ cm^3 mol^{-1} s^{-1} (20); le rapport des vitesses des processus [5] et [11] vaut:

$$\frac{k_5[H][C_2H_6]}{k_{11}[H_2][C_2H_5]} = 4.6 \times 10^4$$

Le processus [11] peut donc être parfaitement négligé.

Le tableau 1[2] donne pour quelques expériences typiques: la température, la nature de la paroi du réacteur, les valeurs de D et de $2R/\gamma\bar{C}$ obtenues dans la première étape sans éthane, les conditions de pression et de titre en éthane, la valeur de λ (argument de l'exponentielle de décroissance de concentration en atomes H mesuré expérimentalement le long de l'axe du réacteur en présence d'éthane) et la valeur de k_5 obtenue par optimisation. Figurent également dans le tableau, les moyennes des valeurs

[2]On peut obtenir la série complète des tableaux 1 et 2 à un prix nominal, en s'adressant au Depôt de données non publiées, ICIST, Conseil national de recherches du Canada, Ottawa (Ont.), Canada K1A 0S2.

Can. J. Chem. Downloaded from www.nrcresearchpress.com by 210.87.254.6 on 09/05/12
For personal use only.

TABLEAU 1. Valeurs de k_5 obtenues en réacteur tubulaire

T (K)	Parois	P (Torr)	Domaine axial des mesures (cm) origine: point d'addition de C_2H_6	Débit total mesuré sous 760 Torr, 295 K ($cm^3\ s^{-1}$)	D ($cm^2\ s^{-1}$)	$(2R/\gamma\bar{C}) \times 10^3$ (s)	Titre en C_2H_6 (%)	λ	$k_5 \times 10^{-7}$ ($cm^3\ mol^{-1}\ s^{-1}$)
281	PTFE	403	7–20	153.26	3.49	60	5.15	0.104	0.80
	Pyrex	264	8–16	110.50	5.89	8.1	0.87	0.141	0.84
					Moyenne de 4 mesures différentes				0.75
					Valeurs extrêmes				0.80–0.51
283	PTFE	227	7–27	129.66	6.70	130	5.09	0.052	0.98
	Pyrex	317	7–14	121.21	5.13	10.3	0.74	0.135	1.11
					Moyenne de 7 mesures différentes				1.01
					Valeurs extrêmes				0.75–1.35
286	PTFE	336	7–18	130.08	4.29	49	5.11	0.108	0.98 Une seule mesure
295	PTFE	202	11–23	85.11	7.97	60	2.76	0.060	1.29
	Pyrex	380	6–14	150.38	4.29	4	1.36	0.154	1.53
	Platine	279	7–15	147.06	5.79	0.1	2.58	0.120	1.45
					Moyenne de 56 mesures différentes				1.46
					Valeurs extrêmes				0.87–2.29
305	PTFE	250	7–25	155.34	6.75	70	3.18	0.074	2.70
					Moyenne de 4 mesures différentes				2.80
					Valeurs extrêmes				2.65–2.93
316	PTFE	90	6–15	36.50	18.83	43.4	7.26	0.129	3.35
	Pyrex	160	6–17	156.25	11.40	6.3	2.58	0.115	3.68
	Platine	398	7–12	145.45	4.65	0.46	1.79	0.168	3.35
					Moyenne de 14 mesures différentes				3.45
					Valeurs extrêmes				2.25–4.73
322	PTFE	219	9–17	144.14	8.45	28	2.50	0.093	5.22
	Platine	345	10–23	347.83	5.50	0.10	0.58	0.057	6.91
					Moyenne de 6 mesures différentes				5.38
					Valeurs extrêmes				3.43–7.16
336	Pyrex	182	8–19	148.15	11.23	4	0.63	0.130	8.80
					Moyenne de 5 mesures différentes				8.50
					Valeurs extrêmes				6.44–9.57
347	Pyrex	189	7–16	159.05	10.84	2.8	0.57	0.122	10.22
					Moyenne de 3 mesures différentes				9.98
					Valeurs extrêmes				8.43–11.30

Can. J. Chem. Downloaded from www.nrcresearchpress.com by 210.87.254.6 on 09/05/12
For personal use only.

de k_5 obtenues à même température mais dans d'autres conditions de pression, de débit et de titre en éthane. La non dépendance des valeurs de k_5 avec le type de paroi est une preuve de la validité de la méthode de dépouillement utilisée (9), compte tenu des valeurs du rendement de recombinaison des atomes très différents dans chaque cas.

Dans un diagramme d'Arrhénius, la fig. 1 reproduit les valeurs de k_5 comparées aux résultats d'autres auteurs. Très peu de mesures ont été réalisées au voisinage de la température ambiante. Celles effectuées par Yang (27) nécessitaient une hypothèse sur la constante de vitesse de la réaction entre H et C_3H_6. Seuls les travaux de Berlie et Le Roy (7) (mesure des concentrations par sonde calorimétrique) et de Azatyan et coll. (4, 5) (technique rpe) ont été effectués en mesurant la variation de la concentration des atomes H. Ces auteurs ont opéré également en réacteur tubulaire mais sous des pressions telles (<4 Torr) que le régime piston pouvait être très valablement supposé (coefficient de diffusion élevé).

Si l'énergie d'activation proposée par Berlie et coll. (6.8 kcal mol^{-1}) apparaît trop faible compte tenu des valeurs généralement admises pour ce genre de réaction, l'accord entre les valeurs de Azatyan et coll. et celles du présent travail obtenues dans des conditions d'écoulement laminaire avec profil parabolique des vitesses est très satisfaisant compte tenu également des méthodes de dosage très différentes.

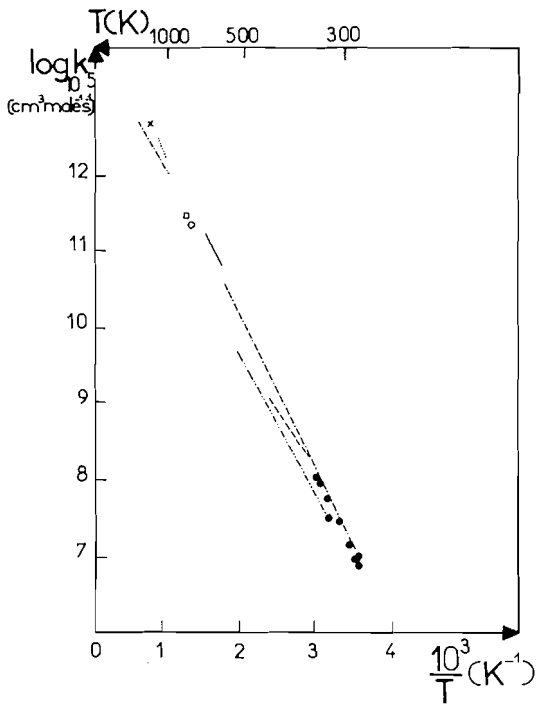

FIG. 1. Comparaison de la moyenne des valeurs de la constante de vitesse k_5 de la réaction $H + C_2H_6 \rightarrow H_2 + C_2H_5$ obtenues dans le présent travail ((●) réacteur tubulaire) avec celles publiées par d'autres auteurs: (---) réf. 5; (--) réf. 7; (-·-) réf. 22; (-·-·-) réf. 26; (□) réf. 27; (···) réf. 28; (—) réf. 29; (○) réf. 30; (×) réf. 31.

Cet accord indique en outre que le processus:

[12] $$C_2H_6^* + M \rightarrow C_2H_6 + M$$

concurrent de [7] et susceptible d'interrompre la séquence réactionnelle de consommation des H reste négligeable même sous les pressions assez fortes régnant dans nos conditions.

L'étude de la compétition entre les réactions 7 et 12 a été souvent abordée par les auteurs étudiant les réactions consécutives à l'acte d'addition des atomes H sur l'éthylène. Après stabilisation du radical éthyle formé par le processus $H + C_2H_4 \rightarrow C_2H_5^*$ les atomes restant peuvent en effet donner lieu aux réactions 6, 7, 8 et 12. Barker et coll. (24) citant les travaux de Rabinovitch et Setser (29) indiquent que le processus [12] est négligeable sous des pressions inférieures à 10 Torr de C_2H_4 pur, la production de radicaux CH_3 étant largement majoritaire. Michael et coll. (26) précisent que ce processus devient compétitif sous une pression voisine de une atmosphère en supposant une efficacité de collision égale à 1. Des conclusions comparables ont été également apportées par Kurylo et coll. (30). D'autres auteurs (2, 23) enfin envisagent directement le processus

$$H + C_2H_5 \rightarrow 2CH_3$$

Tous ces travaux indiquent que, dans nos conditions, le processus [12] peut être négligé devant [7] même en supposant que seuls les chocs sur d'autres molécules C_2H_6 sont à prendre en compte (pression partielle en alcane toujours inférieure à 10 Torr).

Il y a tout lieu de penser cependant que sous des pressions partielles d'éthane modérément plus élevées, [12] pourrait devenir compétitif, ce qui aurait pour conséquence d'arrêter la séquence réactionnelle après cette étape. Dans ce cas, la stoechiométrie de la réaction vis-à-vis des atomes H passerait de la valeur 4 à la valeur 2. Notre système expérimental capable de fonctionner sous des pressions élevées ne peut cependant se prêter directement à cette vérification. Les importantes concentrations d'éthane nécessaires auraient pour effet d'augmenter fortement la valeur de la constante apparente de pseudo premier ordre et le profil axial de concentration atomique deviendrait trop abrupt pour pouvoir être mesuré avec précision. Les mesures devraient également être faites à proximité de la zone de mélange où le régime d'écoulement laminaire stable n'est pas encore établi.

Il apparaît enfin tout à fait raisonnable de ne pas tenir compte d'un éventuel processus de désactivation des molécules $C_2H_6^*$ à la paroi. En effet, en

Can. J. Chem. Downloaded from www.nrcresearchpress.com by 210.87.254.6 on 09/05/12
For personal use only.

supposant les limitations diffusionnelles négligeables, la constante de temps $2R/\gamma\bar{C}$ de ce phénomène hétérogène vaut 3.3×10^{-5} s dans le cas extrême où $\gamma = 1$. Cette valeur est 10^3 fois supérieure à celle de la constante de temps du processus [7] proposée par Growcock et coll. (28).

La fig. 1 indique également que nos valeurs recoupent très bien celles obtenues dans le domaine des hautes températures (31–36) et en particulier celles publiées par Baldwin et coll. (32, 35).

Clark et Dove (37) ont proposé la relation:

$$k_5 = 10^{-3.27} T^{3.5} \exp\left(-\frac{5200}{RT}\right) (\text{cm}^3\ \text{mol}^{-1}\ \text{s}^{-1})$$

susceptible de rendre compte d'un éventuel écart au comportement "Arrhénius" de k_5 entre 300 et 1800 K. Cette relation rend bien compte des résultats des réfs 7, 31, 32, 35. Par contre, ceux de Azatyan et coll. (4, 5) ainsi que ceux du présent travail tendent à montrer que cette relation est trop sévère au voisinage de la température ambiante. La précision de l'ensemble de tous les résultats reproduits sur la fig. 1 semble interdire de pouvoir déceler expérimentalement un tel écart.

En prenant l'ensemble de toutes ces valeurs on obtient entre 281 et 1485 K l'estimation suivante:

$$k_5 = 10^{13.7 \pm 0.6} \exp -\left(\frac{9100 \pm 600}{RT}\right) \quad (\text{cm}^3\ \text{mol}^{-1}\ \text{s}^{-1})$$

Les marges d'erreur figurant dans cette relation sont relativement faibles compte tenu du large domaine de températures représenté et des méthodes expérimentales fort différentes utilisées par les divers auteurs.

Réaction avec le propane

On se propose de mesurer la constante de vitesse k_{13} de la réaction:

$$[13] \qquad H + C_3H_8 \xrightarrow{k_{13}} H_2 + C_3H_7$$

Ici encore la cinétique est étudiée en observant la vitesse de consommation des atomes d'hydrogène.

Ceux-ci donnent lieu à une séquence de processus radicalaires débutant par une combinaison d'un H et d'un radical C_3H_7 pour former une molécule de propane porteuse d'un excès d'énergie vibrationnelle:

$$[14] \qquad H + C_3H_7 \rightarrow C_3H_8^*$$

Cet excès d'énergie est suffisant pour rompre une liaison C—C avec formation de deux radicaux CH_3 et C_2H_5:

$$[15] \qquad C_3H_8^* \rightarrow CH_3 + C_2H_5$$

dont la combinaison avec d'autres atomes H conduit à une suite de réactions identiques à celles prévalant dans le cas de l'éthane: processus [6], [7] et [8].

Ce mécanisme consiste donc en un craquage de proche en proche de la chaine tricarbonée avec formation de méthane, seul produit important de la réaction qui ait été observé (8, 16).

L'intégration numérique complète des équations de vitesse représentant cette séquence réactionnelle n'a pas été menée compte tenu des temps de calculs nécessaires. Nous supposerons que l'ordre de grandeur des résultats obtenus avec l'éthane sont transposables au cas du propane.

Les conditions de l'état quasi stationnaire étant atteintes au bout d'un certain temps t en réacteur tubulaire, on peut se demander s'il en est de même dans un réacteur parfaitement agité fonctionnant sur un temps de passage $t_S = t$. La concentration en espèces intermédiaires R_a en réacteur agité est donnée par l'expression:

$$R_a = \int_0^\infty R_t \frac{1}{t_S} e^{-t/t_S}\, dt = R_\infty \frac{300 t_S}{1 + 300 t_S}$$

En se fixant une borne $(R_\infty - R_a)/R_\infty < 0.1$, on constate qu'il convient d'opérer avec des valeurs $t_S > 3 \times 10^{-2}$ s. On est donc en droit de baser nos calculs sur la relation stoechiométrique suivante:

$$[16] \qquad 6H + C_3H_8 = H_2 + 3CH_4$$

à condition d'opérer avec le réacteur tubulaire sur des temps de réaction supérieurs à 8×10^{-3} s et avec le réacteur agité sur des temps de passage supérieurs à 3×10^{-2} s.

La constante apparente de pseudo premier ordre k'_{app} mesurée dans nos conditions vaut alors:

$$k'_{app} = 6k_{13}[C_3H_8]$$

Le tableau 2^2 donne les résultats de quelques expériences typiques réalisées dans divers types de réacteurs et accompagnées des conditions expérimentales correspondantes. On retrouve à nouveau la non dépendance des valeurs de k_{13} avec le type de paroi de même qu'un accord très satisfaisant entre les mesures effectuées en réacteur tubulaire et agité. La fig. 2 permet de comparer ces résultats avec ceux publiés par d'autres auteurs.

La littérature est moins riche en valeurs de k_{13} que dans le cas de l'éthane, aucune mesure n'ayant semble-t-il été faite auparavant à température ambiante. Les valeurs proposées dans le présent travail sont compatibles avec celles issues des mesures assez indirectes de Yang (38) et en accord excellent avec celles, extrapolées, de Kazmi et coll. (8) obtenues dans des conditions semblables à celles de la réf. 7.

Cet accord indique en outre que les processus:

Can. J. Chem. Downloaded from www.nrcresearchpress.com by 210.87.254.6 on 09/05/12
For personal use only.

TABLEAU 2. Valeurs de k_{13}

(*a*) Réacteur tubulaire

T (K)	Parois	P (Torr)	Domaine axial des mesures (cm) origine: point d'addition de C_3H_8	Débit total mesuré sous 760 Torr, 295 K ($cm^3\ s^{-1}$)	D ($cm^2\ s^{-1}$)	$(2R/\gamma\bar{C}) \times 10^3$ (s)	Titre en C_3H_8 (%)	λ	$k_{13} \times 10^{-8}$ ($cm^3\ mol^{-1}\ s^{-1}$)
295	PTFE	237	9–17	196.56	6.88	34	0.99	0.126	1.53
	Pyrex	68	6–10	76.92	19.22	4.8	10.92	0.471	1.53
					Moyenne de 18 mesures différentes				1.53
					Valeurs extrêmes				0.89–2.02

(*b*) Réacteur agité

T (K)	Parois	P (Torr)	Débit total mesuré sous 760 Torr 295 K ($cm^3\ s^{-1}$)	Titre en C_3H_8 (%)	C_0/C_S	$(C_0/C_S)'$	$k_{13} \times 10^{-8}$ ($cm^3\ mol^{-1}\ s^{-1}$)
295	Pyrex	100	50.38	2.26	10.49	4.10	1.32
	Pyrex	271	184.33	0.60	8.53	4.08	1.75
	Pyrex	630	219.78	0.41	25.41	11.16	1.79
			Moyenne de 11 mesures différentes				1.46
			Valeurs extrêmes				0.92–1.95

Can. J. Chem. Downloaded from www.nrcresearchpress.com by 210.87.254.6 on 09/05/12
For personal use only.

[17] $C_3H_8^* + M \rightarrow C_3H_8 + M$

[18] $C_3H_8^* + \text{paroi} \rightarrow C_3H_8 + \text{paroi}$

susceptibles ici encore d'interrompre la séquence réactionnelle de consommation des atomes d'hydrogène restent négligeables dans nos conditions.

Il convient de signaler que s'il en était ainsi, le coefficient stoechiométrique passerait de la valeur 6 à la valeur 2 et le facteur 3 ainsi introduit rendrait nos valeurs de k_{13} nettement incompatibles avec celles des autres auteurs (fig. 2) et en particulier Kazmi et coll. (8). D'un point de vue plus quantitatif on peut montrer que dans le cas du réacteur tubulaire, dans l'hypothèse où tous les chocs hétérogènes sont efficaces ($\gamma = 1$) et sans limitation diffusionnelle, la constante de temps du processus [18] vaut 2.7×10^{-5} s. Celle-ci est supérieure d'au moins une puissance de 10 à celle caractérisant le processus de décomposition [15] voisine, elle, de 2×10^{-6} s (43). Nos résultats indiquent par contre que l'efficacité de désactivation homogène par choc d'une molécule $C_3H_8^*$ serait inférieure à 2×10^{-2} (fréquence de collision sous 10 Torr voisine de 10^{-8} s) ce qui peut paraître assez faible.

Comme dans le cas de l'éthane, le domaine des basses températures se raccorde assez bien à celui des hautes températures où les travaux ont été plus nombreux (39–42), sans qu'il soit possible de pouvoir observer une éventuelle courbure dans la représentation d'Arrhénius de la constante k_{13}.

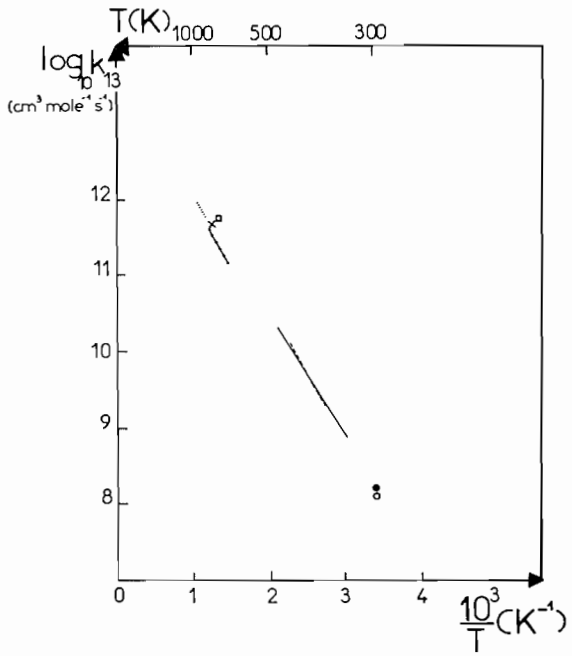

FIG. 2. Comparaison de la moyenne des valeurs de la constante de vitesse k_{13} de la réaction $H + C_3H_8 \rightarrow H_2 + C_3H_7$ obtenues dans le présent travail ((●) réacteur tubulaire; (○) réacteur agité) avec celles publiées par d'autres auteurs: (--) réf. 8; (—) ref. 38; (·–·–·) réf. 39; (×) réf. 40; (···) réf. 41; (□) réf. 42.

L'ensemble de ces valeurs permet de proposer entre 295 et 953 K l'estimation suivante:

$$k_{13} = 10^{13.8 \pm 0.3} \exp\left(-\frac{7800 \pm 100}{RT}\right) \times (\text{cm}^3\ \text{mol}^{-1}\ \text{s}^{-1})$$

Ici encore les marges d'erreur sont faibles compte tenu de la diversité des conditions opératoires prévalant dans les mesures effectuées par les divers auteurs.

Conclusion

Les travaux exposés dans cet article ont permis de montrer les points suivants:

Le réacteur tubulaire et le réacteur parfaitement agité peuvent être très valablement utilisés pour des études de cinétiques d'espèces très réactives même sous des pressions avoisinant l'atmosphère.

Les méthodes de dépouillement proposées permettent de mesurer des constantes de vitesse de réactions en phase gazeuse dans des conditions où ces processus homogènes sont concurrencés par des phénomènes hétérogènes, diffusionnels et hydrodynamiques.

L'utilisation de techniques de conception très simples et peu onéreuses a permis de déterminer les constantes de vitesse de réaction des atomes d'hydrogène sur l'éthane et le propane indépendamment du type de paroi utilisé. Les valeurs obtenues par d'autres auteurs sous des températures nettement plus élevées peuvent être extrapolées jusqu'au voisinage de la température ambiante par l'utilisation d'une simple loi d'Arrhénius.

1. B. A. THRUSH. Prog. React. Kinet. **3**, 63 (1965).
2. H. G. WAGNER et J. WOLFRUM. Angew. Chem. **15**, 561 (1971).
3. W. E. JONES, S. D. MACKNIGHT et L. TENG. Chem. Rev. **73**, 407 (1973).
4. V. V. AZATYAN, J. B. FILIPPOV, A. B. NALBANDYAN et L. B. ROMANOVITCH. Arm. Khim. Zh. **22**, 193 (1969).
5. V. V. AZATYAN et J. B. FILIPPOV. Dokl. Akad. Nauk SSSR, **184**, 625 (1969).
6. R. R. BALDWIN et R. F. SIMMONS. Trans. Faraday Soc. **53**, 964 (1957).
7. M. R. BERLIE et D. J. LE ROY. Discuss. Faraday Soc. **14**, 50 (1953).
8. H. A. KAZMI, R. J. DIEFENDORF et D. J. LE ROY. Can. J. Chem. **41**, 690 (1963).
9. J. LEDE et J. VILLERMAUX. J. Chim. Phys. **74**, 459 (1977).
10. J. LEDE et J. VILLERMAUX. J. Chim. Phys. **74**, 468 (1977).
11. J. LEDE et J. VILLERMAUX. Anal. Chim. Acta, **87**, 291 (1976).
12. J. LEDE et J. VILLERMAUX. J. Chim. Phys. **71**, 85 (1974).
13. J. LEDE. Thèse. Institut National Polytechnique de Lorraine, Nancy. 1975.

14. R. DAVID et D. MATRAS. Can. J. Chem. Eng. **53**, 297 (1975).
15. R. DAVID. Thèse. Institut National Polytechnique de Lorraine, Nancy. 1976.
16. J. VILLERMAUX, J. LEDE et D. CHERY. J. Chim. Phys. **65**, 1673 (1968).
17. J. LEDE et J. VILLERMAUX. Chem. Phys. Lett. **43**, 283 (1976).
18. J. LEDE et J. VILLERMAUX. J. Chim. Phys. **67**, 847 (1970).
19. J. VILLERMAUX. Int. J. Heat Mass Transfer, **14**, 1963 (1971).
20. L. E. REID et D. J. LE ROY. Can. J. Chem. **46**, 3275 (1968).
21. W. R. TROST et E. W. R. STEACIE. J. Chem. Phys. **16**, 361 (1948).
22. A. A. WESTENBERG et N. DE HAAS. J. Chem. Phys. **50**, 707 (1969).
23. M. P. HALSTEAD, D. A. LEATHARD, R. M. MARSHALL et J. H. PURNELL. Proc. R. Soc. London, Ser. A, **316**, 575 (1970).
24. J. R. BARKER, D. G. KEIL, J. V. MICHAEL et D. T. OSBORNE. J. Chem. Phys. **52**, 2079 (1970).
25. L. TENG et W. E. JONES. J. Chem. Soc. Faraday Trans. **68**, 1267 (1972).
26. J. V. MICHAEL, D. T. OSBORNE et G. N. SUESS. J. Chem. Phys. **58**, 2800 (1973).
27. K. YANG. J. Phys. Chem. **67**, 562 (1963).
28. F. B. GROWCOCK, W. L. HASE et J. W. SIMONS. Int. J. Chem. Kinet. **5**, 77 (1973).
29. B. S. RABINOVITCH et D. W. SETSER. Adv. Photochem. **3**, 1 (1964).
30. M. J. KURYLO, N. C. PETERSON et W. BRAUN. J. Chem. Phys. **53**, 2776 (1970).
31. C. P. FENIMORE et G. W. JONES. Symp. Int. Combust. Proc. 9th, 597 (1963).
32. R. R. BALDWIN et A. MELVIN. J. Chem. Soc. 1785 (1964).
33. G. B. SKINNER et G. H. RINGROSE. J. Chem. Phys. **43**, 4129 (1965).
34. N. I. PARSAMYAM, E. A. ARAKELYAN, V. V. AZATYAN et A. B. NALBANDYAN. Izv. Akad. Nauk SSSR, 496 (1968).
35. R. R. BALDWIN, D. E. HOPKINS et R. W. WALKER. Trans. Faraday Soc. **66**, 189 (1970).
36. T. C. CLARK, T. P. J. IZOD et G. B. KISTIAKOWSKY. J. Chem. Phys. **54**, 1295 (1971).
37. T. C. CLARK et J. E. DOVE. Can. J. Chem. **51**, 2147 (1973).
38. K. YANG. J. Am. Chem. Soc. **84**, 3795 (1962).
39. N. I. GORBAN et A. B. NALBANDYAN. Zh. Fiz. Khim. **36**, 1757 (1962).
40. R. R. BALDWIN. Trans. Faraday Soc. **60**, 527 (1964).
41. N. I. PARSAMYAM et A. B. NALBANDYAN. Izv. Akad. Nauk SSSR. Ser. Khim. 750 (1968).
42. R. R. BAKER, R. R. BALDWIN et R. W. WALKER. Trans. Faraday Soc. **66**, 2812 (1970).
43. M. J. LEXTON, R. M. MARSHALL et J. H. PURNELL. Proc. R. Soc. London, Ser. A, **324**, 433 (1971).

Can. J. Chem. Downloaded from www.nrcresearchpress.com by 210.87.254.6 on 09/05/12
For personal use only.

Hydrothermal preparation of magnetite from iron chelates

MEINDERT BOOY AND THOMAS WILSON SWADDLE

Department of Chemistry, The University of Calgary, Calgary, Alta., Canada T2N 1N4

Received August 24, 1977

MEINDERT BOOY and THOMAS WILSON SWADDLE. Can. J. Chem. **56**, 402 (1978).

The hydrothermal decomposition of iron(II) or iron(III) aminopolycarboxylate complexes can produce well-crystallized, stoichiometric Fe_3O_4. Best results were obtained when 0.1 *m* nitrilotriacetatoiron(III) was decomposed under N_2 in 0.2–0.4 *m* NaOH at 497 K for 70 h or more.

MEINDERT BOOY et THOMAS WILSON SWADDLE. Can. J. Chem. **56**, 402 (1978).

La décomposition hydrothermique de complexes aminopolycarboxylates de fer(II) ou de fer(III) peut conduire à du Fe_3O_4 bien cristallisé et stoechiométrique. On obtient les meilleurs résultats quand on décompose une solution de 0.1 *m* de nitrilotriacétatofer(III) sous une atmosphère d'azote en présence de NaOH 0.2–0.4 *m* à 497 K pour 70 h ou plus.

[Traduit par le journal]

Can. J. Chem. Downloaded from www.nrcresearchpress.com by 210.87.254.6 on 09/05/12
For personal use only.

The preparation of stoichiometric magnetite (Fe_3O_4) as reproducible, roughly monodisperse samples consisting of well-formed discrete crystals of size on the order of 1 μm to 1 mm is often desired, e.g., for dissolution studies in connection with corrosion phenomena but presents several difficulties. Preparative methods involving solid reactants, e.g., the oxidation of elemental iron by steam containing hydrogen (1), tend to give a sintered product, are usually slow, and leave room for doubt concerning the homogeneity and purity of the product. The latter problems persist in heterogeneous hydrothermal syntheses of Fe_3O_4 from metallic iron and hematite (α-Fe_2O_3) (2, 3) or from solid iron(II) hydroxide by the Schikorr reaction (4, 5).

$$[1] \qquad 3Fe(OH)_2 = Fe_3O_4 + 2H_2O + H_2$$

although hydrothermal methods can produce well-crystallized magnetite (2, 6, 7).

The hydrothermal syntheses of magnetite reported to date (2–7) require rather severe conditions and depend upon the maintenance of the correct redox potential, which can be difficult when done through the hydrogen pressure (6). We now report a hydrothermal synthesis in which magnetite is directly deposited at relatively low temperature and pressure from homogeneous alkaline solutions of decomposing iron chelates which maintain an appropriate reducing environment automatically (8).

Experimental

Analytical grade reagents were used throughout. Nitrilotriacetatoiron(III) monohydrate ($FeNTA \cdot H_2O$) was prepared as a yellow solid by boiling 20 g ammonium iron(III) sulfate 12-hydrate and 8 g nitrilotriacetic acid in 400 cm^3 water for 1 h; the precipitate was washed with water and dried in air overnight.

The hydrothermal reactions were carried out in capped PTFE liners in small autoclaves of type 316 stainless steel (free volume ~17 cm^3). For $FeNTA \cdot H_2O$, the solid was weighed into the liner and 10 cm^3 of the desired aqueous solution was added; in the other cases, the required amounts of iron(II) or iron(III) chloride or sulfate were mixed in solution with the chelating agent and sodium hydroxide. These operations and the closure of the autoclaves were in general carried out under nitrogen in a glove box. The autoclaves were heated in a forced convection oven (± 1 K) for the desired time then quenched in cold water and the precipitated solid was filtered, washed with water, and dried in a vacuum oven at ~380 K for 1 h.

Results

The hydrothermal decomposition of iron(II) or iron(III) chelates in the absence of oxygen under appropriate conditions of alkalinity, concentration, and temperature yielded well-formed octahedra of magnetite of size up to 0.1 mm. The effectiveness of various aminopolycarboxylate ligands in this respect, as gauged by the size and regularity of the magnetite crystals, was nitrilotriacetate > methyliminodiacetate > iminodiacetate ≫ ethylenedinitrilotetraacetate. Better results were obtained when the iron was present initially as *either* iron(II) *or* iron(III) than when as a mixture of these. When the iron was initially present as iron(III) reduction of part of this to iron(II) occurred as the organic ligand decomposed. The optimal initial molar ratio of iron(II) or iron(III) to chelating agent was 1:1, at a concentration of up to 0.2 *m*. A reaction temperature of at least 490 K for $Fe^{III}NTA^0$ (or 530 K for $Fe^{II}NTA^-$) was required and the longer the reaction time the larger were the crystals (reaction times of over 70 h were not tried), although the addition of unmounted seed crystals seemed not to facilitate the growth of large crystals significantly.

For $Fe^{III}NTA^0$, the size of the Fe_3O_4 crystals produced by hydrothermal decomposition was not significantly affected by the presence of NaCl (up to 4.0 *m*) or NH_4Cl (up to 0.5 *m*), or by the degree of filling of the vessel, but the presence of a platinum

Can. J. Chem. Downloaded from www.nrcresearchpress.com by 210.87.254.6 on 09/05/12
For personal use only.

surface or of very high [NaOH] ($\gtrsim 1.3$ *m*) resulted in the formation of maghemite (γ-Fe_2O_3), presumably by facilitating direct decomposition of $Fe^{III}NTA^0$ without reduction of the iron ion. Insufficient NaOH (≤ 0.1 *m*, with [Fe^{III}NTA] = 0.1 *m*), however, led to the precipitation of the iron(II) compound $Fe_3(NTA)_2 \cdot H_2O$, at 497 K. The presence of O_2 produced hematite in various amounts together with Fe_3O_4.

The optimal conditions for magnetite preparation were found to be [Fe^{III}NTA] = 0.10 *m*, $0.20 \leq$ [NaOH] ≤ 0.40 *m*, under nitrogen at 497 K for 70 h or more; these give shining, well-formed, jet-black octahedra, 10–100 μm in diameter. These crystals can easily be freed from the surface of the liner, in 70% yield. The unit cell parameters, derived using a Debye-Scherrer X-ray diffraction camera and an internal silicon standard (9), were 839.71 ± 0.06 and 839.65 ± 0.04 pm for two independently-prepared samples of magnetite. These are not significantly different from the value of 839.67 pm derived from the 10 highest-angle reflections in the accepted X-ray diffraction data for stoichiometric magnetite (JCPDS file number 19-629), and correspond to a bulk composition of $Fe_{3.00\pm0.01}O_4$ at the 99.5% confidence level, or $Fe_{3.000\pm0.007}O_4$ at 95%, based on an assumed linear relationship between unit cell dimensions and composition for magnetite–maghemite solid solutions. Determination of the oxygen content of the same samples by thermogravimetry in a stream of hydrogen, though relatively imprecise, confirmed the validity of these analyses ($Fe_{3.01\pm0.05}O_4$) and the absence of significant amounts of substances other than magnetite. Analysis of samples with different degrees of crystallinity by flame emission spectrophotometry showed that the sodium ion content was less than 0.02%.

Discussion

The observation (5) that solid iron(II) hydroxide and 'green rusts' decompose to magnetite under hydrothermal conditions *at the solid–water interface* strongly suggests that the Schikorr reaction [1] proceeds by decomposition of *dissolved* $Fe(OH)_2$. It is therefore likely that the hydrothermal syntheses of magnetite described in this article proceed by a modified Schikorr reaction in which the supply of iron(II) hydroxide is strictly limited by the slow decomposition of the iron chelate in homogeneous solution, thereby leading to controlled and regular growth of magnetite crystals without the intermediate formation of solid iron(II) hydroxide or green rusts.

The decomposition of the organic ligand creates and helps maintain a mildly reducing environment (8), so that oxidation of the product to maghemite or a magnetite–maghemite solid solution is prevented. The relatively low specific surfaces of the magnetite crystals also help suppress oxidation; our attempts to produce stoichiometric Fe_3O_4 powders by hydrothermal ripening of aqueous suspensions of $Fe(OH)_2 + 2Fe(OH)_3$ at about 470 K (cf. hydrothermal ferrite syntheses (10, 11)) invariably produced black or chocolate-brown ferromagnetic powders intermediate in composition between Fe_3O_4 and γ-Fe_2O_3 when reasonable precautions were taken to exclude air, and pure γ-Fe_2O_3 when air was freely admitted. The BET surface areas of these latter powders were typically 100 $m^2\ g^{-1}$, as against 0.1 $m^2\ g^{-1}$ or less for magnetite made by alkaline hydrothermal decomposition of Fe^{III}NTA.

Acknowledgements

We thank Atomic Energy of Canada Ltd., for financial support and Drs. P. Taylor and H. L. Yeager for analytical measurements.

1. F. H. Sweeton and C. F. Baes, Jr. J. Chem. Thermodyn. **2**, 479 (1970).
2. A. Matthews. Am. Mineral. **61**, 927 (1976).
3. J. J. Bartel, E. F. Westrum, Jr., and J. L. Haas, Jr. J. Chem. Thermodyn. **8**, 575 (1976).
4. J. E. Castle and R. G. Thompson. J. Appl. Chem. **17**, 177 (1967).
5. T. W. Swaddle, J. H. Lipton, G. Guastalla, and P. Bayliss. Can. J. Chem. **49**, 2433 (1971).
6. E. D. Kolb, A. J. Caporaso, and R. A. Laudise. J. Crystal Growth, **19**, 242 (1973).
7. R. A. Laudise and J. W. Nielsen. Solid State Phys. **12**, 149 (1961).
8. M. Booy and T. W. Swaddle. Can. J. Chem. **55**, 1762 (1977); **55**, 1770 (1977).
9. W. Parrish. Acta Cryst. **13**, 838 (1960).
10. W. J. Schuele and V. D. Deetscreek. J. Appl. Phys. **32**, 235S (1961).
11. A. R. Gainsford, M. J. Sisley, T. W. Swaddle, and P. Bayliss. Can. J. Chem. **53**, 12 (1975).

Aminocyclitols. 2,5-Dideoxystreptamine and derivatives

GERRY KAVADIAS,[1] STEPHAN VELKOF, and BERNARD BELLEAU

Bristol Laboratories of Canada, 100 Industrial Boulevard, Candiac, P.Q., Canada J5R 1J1

Received July 12, 1977

GERRY KAVADIAS, STEPHAN VELKOF, and BERNARD BELLEAU. Can. J. Chem. **56**, 404 (1978).

2,5-Dideoxystreptamine (**11**) was synthesized via the cyclic hydrazine intermediate **10**, itself obtained by reaction of the *cis*-1,4-diepoxycyclohexane (**7**) with hydrazine. Compound **11** was converted into *d,l*-*N*-ethoxycarbonyl-2,5-dideoxystreptamine (**12**) and the latter resolved into its optical isomers (1*N*-ethoxycarbonyl- and 3*N*-ethoxycarbonyl-2,5-dideoxystreptamines **16** and **14**). 1,6-*N,O*-carbonyl-3*N*-ethoxycarbonyl-2,5-dideoxystreptamine (**1**) and 3,4-*N,O*-carbonyl-1*N*-ethoxycarbonyl-2,5-dideoxystreptamine (**2**) were synthesized from **14** and **16** respectively. A practical process for the preparation of *cis*-1,4-diepoxycyclohexane is described.

GERRY KAVADIAS, STEPHAN VELKOF et BERNARD BELLEAU. Can. J. Chem. **56**, 404 (1978).

On a synthétisé la didéoxy-2,5 streptamine (**11**) par l'intermédiaire de l'hydrazine cyclique **10** qui a elle même été obtenue par réaction du diépoxy-1,4 cyclohexane *cis* (**7**) avec de l'hydrazine. On a pu transformer le composé **11** en *d,l*-*N*-éthoxycarbonyle didéoxy-2,5 streptamine (**12**) et on a résolu ce dernier en isomères optiques (éthoxycarbonyl-1*N* et éthoxycarbonyl-3*N* didéoxy-2,5 streptamine **16** et **14**). Utilisant respectivement les composés **14** et **16** comme produits de départ, on a synthétisé le *N,O*-carbonyl-1,6 éthoxycarbonyl-3*N* didéoxy-2,5 streptamine (**1**) et le *N,O*-carbonyl-3,4 éthoxycarbonyl-1*N* didéoxy-2,5 streptamine (**2**). On décrit un procédé pratique pour la préparation du diépoxy-1,4 cyclohexane *cis*.

[Traduit par le journal]

In a research project directed at the synthesis of 5-deoxyaminoglycoside antibiotics (e.g. the 5-deoxykanamycins, gentamycins, and nebramycins) a properly protected, 2,5-dideoxystreptamine was required as the aglycon component. It became apparent that the protected 2,5-dideoxystreptamine should meet the following structural requirements: (*a*) all the functional groups except for one hydroxyl group should be protected. If both hydroxyls were free, the glycosidation reaction would yield a mixture of pseudodisaccharides (two diastereoisomers) and a symmetrical pseudotrisaccharide; and (*b*) the protected, 2,5-dideoxystreptamine should be resolved into its optical antipodes. If the *d,l* mixture were to be used, two diastereoisomeric pseudodisaccharides would be formed.

The carbamates **1** and **2** meet the above requirements since their functional groups are all protected except for their respective 4- and 6-OH, groups.[2] It is therefore possible to introduce one aminosugar either at the 4- or 6-position of the 2,5-dideoxystreptamine molecule. The position of attachment of the aminosugar is expected to be of importance for antibiotic activity, since in the aminoglycosides possessing a 2-deoxystreptamine entity, the positional isomers greatly differ in antibiotic activity. For example, 4-*O*-(6-amino-6-deoxy-α-D-glucopyranosyl)-2-deoxystreptamine is biologically active whereas the 6-*O*-isomer is not (1). After glycosidation of the free OH in **1** or **2** the remaining OH can be deprotected and functionalized by another aminosugar.

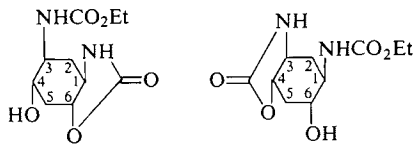

1 **2**

The present paper describes the synthesis of **1** and **2** and provides evidence for their assigned structures.

The key intermediate in the present synthesis was *cis*-1,4-diepoxycyclohexane (**7**) and an easy access to this valuable intermediate will be described first. Craig *et al.* (2) have described the synthesis of **7** via the bromohydrin **4** by epoxidation followed by alkaline hydrolysis (Scheme 1). These authors have reported that bisepoxidation of 1,4-cyclohexadiene (**3**) with perbenzoic acid or monoperphthalic acid produced exclusively the *trans*-bisepoxide **8** whereas bisepoxidation with *m*-chloroperbenzoic or peracetic acids produced 2:1 mixtures of *trans*- and *cis*-bisepoxides, respectively. They further reported that the *cis*-bisepoxide **7** could not be separated from the mixture owing to its tendency to form a 1:1 crystalline complex with the *trans*-isomer. Initially, we adopted the above process for the synthesis of **7** and several modifications and improvements were introduced. Reaction of 1,4-cyclohexadiene with *N*-

[1]Author to whom correspondence concerning this paper may be addressed.

[2]The numbering of the position of the substituted 2,5-dideoxystreptamines follows the proposal of Hickens and Rinehart (12) and this numbering has been rationalized by Lemieux *et al.* (13).

Can. J. Chem. Downloaded from www.nrcresearchpress.com by 210.87.254.5 on 09/05/12
For personal use only.

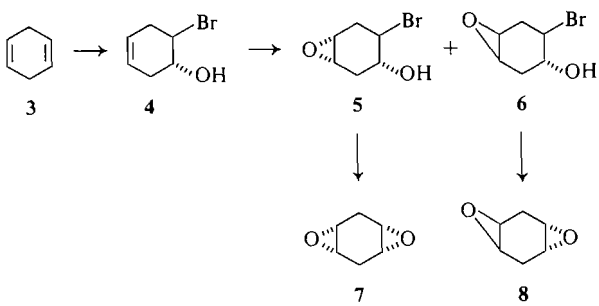

SCHEME 1

bromosuccinimide (NBS) in water produced the bromohydrin **4** in yields ranging from 65 to 88% depending on the source of NBS. However, reproducible yields of 85–88% were obtained when recrystallized NBS was used (3). Epoxidation of compound **4** with *m*-chloroperbenzoic acid produced a mixture of the epoxybromohydrins **5** and **6** in high yield (90%) and the isomer ratio was the same when monoperphthalic acid (2) was used. The ratio of **5** to **6** was slightly dependent on the reaction temperature. Thus, at 0 and 25°C the ratios of **5** to **6** were 85:15 and 75:25, respectively. The *cis*-bromohydrin **5** was separated from the mixture as previously described and several recrystallizations were necessary for the pure product to be obtained. Treatment of **5** with base produced the bisepoxide **7**.

Bisepoxidation of 1,4-cyclohexadiene with *m*-chloroperbenzoic acid turned out to be the most convenient method for the synthesis of the *cis*-bisepoxide **7**. It led to a mixture of the bisepoxides **7** and **8** (90%) where, contrary to the previous report (2), the *cis*-bisepoxide **7** was the predominant isomer (70%). The ratio of **7** to **8** varied slightly with the reaction temperature. At 0 and 25°C the ratio was 70:30 and 63:37 respectively. Separation of the *cis*-bisepoxide **7** from the mixture was easily effected by liquid–liquid extraction. Isomers **7** and **8** exhibited markedly different solubilities in water and in organic solvents. As would be expected on the basis of their dipole moments (2) (compound **7**, 3.3 D; **8**, 0.0 D), the *trans*-isomer **8** had a substantially higher partition coefficient than the *cis*-isomer **7** in ether–water and petroleum ether – water systems. Extraction of an aqueous solution of **7** and **8** with ether or continuous extraction with petroleum ether selectively removed the *trans*-bisepoxide **8** leaving the *cis*-isomer in the aqueous phase. The latter was then extracted with an organic solvent.

A most promising potential route for the synthesis of 2,5-dideoxystreptamine (**11**) involves the reaction of *cis*-bisepoxide **7** with hydrazine to form **10** followed by hydrogenolysis. (Scheme 2). It was anticipated that one epoxide ring in **7** would initially open diaxially to give **9** through attack by a hydrazine molecule and that subsequently the second epoxide ring of the latter would suffer intramolecular attack by the hydrazino group at position 3 rather than 4 as would be required by the rule of diaxial opening. Indeed, reaction of **7** with hydrazine in ethanol produced the 1,3-hydrazino compound **10** in 84.5% yield. Hydrogenation of **10** in aqueous acetic acid in the presence of a palladium catalyst (11) afforded the acetate salt of **11** in 78% yield. The free base **11** was obtained simply by treatment with an anion exchange resin. The structure of **11** was confirmed by nmr spectroscopy. The nmr spectrum of the hydrochloride salt of **11** showed a two-proton double triplet at δ 3.78 with spacings of 4.5 and 11.0 Hz which were assigned to the magnetically equivalent H-4 and H-6. It also showed a two-proton double triplet at δ 3.25 with spacings of 4.5 and 11.0 Hz which were assigned to H-1 and H-3. Thus, all the substituents in **11** are equatorially oriented as expected. After completion of our work, two reports appeared in the literature describing the synthesis

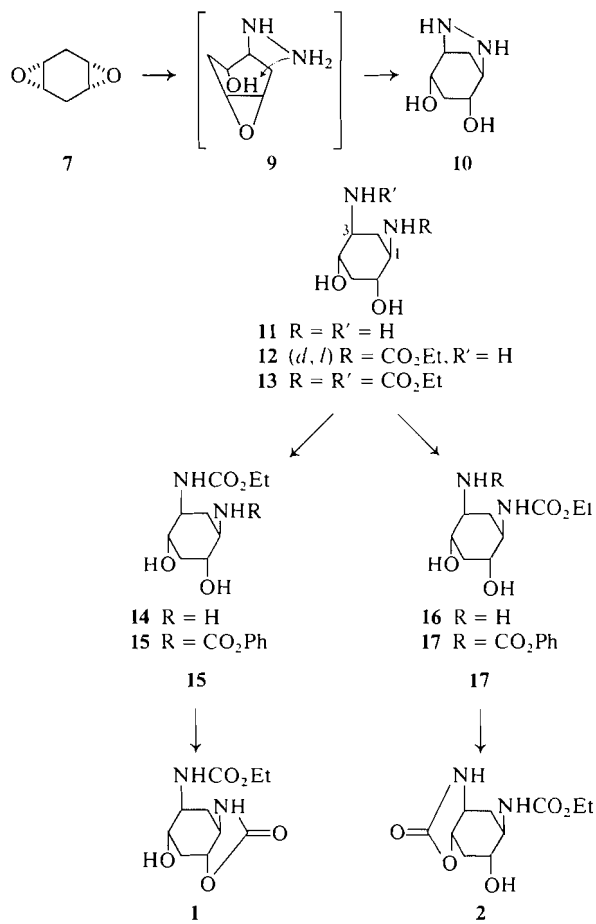

SCHEME 2

Can. J. Chem. Downloaded from www.nrcresearchpress.com by 210.87.254.5 on 09/05/12
For personal use only.

Can. J. Chem. Downloaded from www.nrcresearchpress.com by 210.87.254.5 on 09/05/12
For personal use only.

of **11** by similar methods (4, 5). However, the preparation of key dissymmetric intermediates was not reported. This gap was filled as follows: reaction of 2,5-dideoxystreptamine (**11**) with 1 mol of ethylchloroformate in aqueous methanol, in the absence of base, produced a mixture of the monocarbethoxy compound **12** (53%) and the biscarbethoxy derivative **13** (23%) from which **12** was easily separated. Obviously, the liberated hydrogen chloride in the mono acylation reaction effectively protects the second amino group against acylation. In the presence of a base the reaction yielded mainly the biscarbethoxy compound **13** as expected.

The monocarbethoxy compound **12** was resolved into the optical isomers **14** and **16** via the 2-nitrotartranilate salts. Treatment of a solution of **12** with $\frac{1}{2}$ mol of (−)-2-nitrotartranilic acid (6) gave a tartranilate salt ($[\alpha]_D$ −43.4) from which the free base **14** ($[\alpha]_D$ +37.3) was generated by treatment with an anion exchange resin. Treatment of the mother liquors with (+)-2-nitrotartranilic acid (6) yielded a salt ($[\alpha]_D$ +43.3) from which the free base **16** ($[\alpha]_D$ −37.6) was generated as above.

The configurations of 3-*N*-ethoxycarbonyl- and 1-*N*-ethoxycarbonyl-2,5-dideoxystreptamines (**14** and **16**) were established by determination of their respective $\Delta[M]$ values in tetramine copper(II) sulfate solutions (TACu) (7). The dextrorotary isomer had a $\Delta[M]$TACu of +600, thus indicating a positive projected angle between the adjacent amino and hydroxyl groups (7, 8). On that basis absolute configuration **14** is assigned to this isomer. The other isomer had a $\Delta[M]$TACu of −550 and is thus assigned configuration **16**. The magnitudes of the $\Delta[M]$TACu values for **14** and **16** are lower than would be expected (7) (~900) and this might be due to partial conversion of **14** and **16** to the corresponding optically inactive 1,3-cyclic ureas in the tetramine copper sulfate solutions.

The conversion of **14** and **16** to the corresponding cyclic carbamates **1** and **2** respectively, was carried out by the general procedure of Umezawa *et al.* (9) as applied to the conversion of 1,2-*trans*-di-equatorial amino alcohols to cyclic carbamates. Thus, reaction of **14** with phenylchloroformate in aqueous acetone in the presence of sodium bicarbonate afforded crystalline **15** in 91% yield. Treatment of the latter with triethylamine in aqueous acetone gave carbamate **1** in high yield (92%). When, however, a solution of **15** in aqueous acetone was treated with a strong anion-exchange resin (9) the yield of **1** was appreciably lower (~60%) because of partial hydrolysis of **1** to **14** under these conditions.

Application of the same sequence of reactions to **16** led to carbamate **2** in high yield.

The structures of **1** and **2** were verified by elemental analysis and spectroscopic determinations. Furthermore, when **1** and **2** were treated with a catalytic amount of sodium ethoxide in ethanol the cyclic carbamate functions suffered opening (9) to give the optically inactive 1,3-*N*,*N*′-diethoxycarbonyl-2,5-dideoxystreptamine (**13**).

Experimental

The melting points were determined on a Mel-Temp melting point apparatus and are uncorrected. Optical rotations were measured with a Perkin-Elmer Model 141 polarimeter. Nuclear magnetic resonance spectra were taken with a Varian A-60A spectrometer. Tetramethylsilane (for solution other than deuterium oxide) and sodium 4,4-dimethyl-4-silapentane-1-sulfonate (for the solutions of deuterium oxide) were used as internal standards. Thin-layer chromatography (tlc) was carried out on microscope slides coated with silica gel, and the spots were visualized with perchloric acid.

Preparation of Starting Materials

trans-*4-Hydroxy-5-bromocyclohexene (4)*

This compound was prepared by reaction of 1,4-cyclohexadiene with an equimolar amount of *N*-bromosuccinimide (NBS) by the procedure described by Craig *et al* (2). Compound **4** was obtained in reproducibly high yields of 85–88% when recrystallized (3) NBS was used. The yields varied from 65–88% when unpurified NBS from various suppliers was used; bp 109–110°C/15 Torr. (lit. (2) bp 109–110°C/15 Torr).

cis-*4,5-Epoxy*-trans-*2-bromocyclohexanol (5)*

To a stirred suspension of 49.0 g (240 mmol) *m*-chloroperbenzoic acid (Aldrich, technical grade, 85% pure) in methylene chloride (200 ml) previously cooled to 0°C, was added dropwise with stirring a solution of 41.0 g of **4** in methylene chloride (100 ml) at a rate to maintain the solution temperature at 0–2°C. After the addition (15 min), stirring in the cold was continued for 4 h and the mixture stored at 0°C overnight. The reaction mixture was filtered and the solids were washed with methylene chloride (2 × 60 ml). The combined filtrates and washings were washed with 20% aqueous sodium sulfite (100 ml) and then with 8% aqueous sodium bicarbonate (2 × 100 ml). The washings were combined and back-extracted with methylene chloride (2 × 100 ml); these extracts were combined with the first methylene chloride extract and after drying (Na_2SO_4) the solvent was removed under reduced pressure to give 41.0 g (92.5%) of a mixture of the epoxybromohydrins **5** and **6** as an oil. The proportions of the two isomers in the mixture were determined as follows. A sample was treated with aqueous sodium hydroxide and converted to a mixture of the bisepoxides **7** and **8**. The latter mixture was analyzed by nmr and found to contain 85% of the *cis*-bisepoxide **7** and 15% of the *trans*-isomer **8**, thus establishing that the bromohydrin mixture contained 85% of the *cis*-isomer **5** and 15% of the *trans*-isomer **6**.

The crude product was dissolved in ether (60 ml), diluted with hexane (40 ml) and allowed to crystallize first at room temperature and then at 0°C to give 26 g of **5**, mp 51–54°C. Recrystallization from the same solvent system gave 19.0 g, mp 53–58°C. Two additional recrystallizations raised the mp to 58–60°C (lit. (2) mp 55–56°C).

In another experiment where the epoxidation was carried out at 25°C, the ratio of **5** to **6**, determined as above, was 75:25.

cis-*4,8-Dioxatricyclo*[*5.1.0.0*^{3,5}]*octane (7)* (cis-*1,4-diepoxycyclohexane, by Epoxidation of 1,4-Cyclohexadiene with* m-*Chloroperbenzoic Acid*

To a stirred suspension of 335 g of *m*-chloroperbenzoic acid

Can. J. Chem. Downloaded from www.nrcresearchpress.com by 210.87.254.5 on 09/05/12
For personal use only.

(Aldrich, 85% pure) in methylene chloride (1.6 ℓ), previously cooled to 0°C, was added dropwise a solution of 64.2 g (800 mmol) of 1,4-cyclohexadiene (Aldrich, 97% purity) in methylene chloride (170 ml) at a rate to maintain the solution temperature at 0–2°C. After completion of the addition (1 h), stirring at 0°C was continued for 8 h and the mixture kept at room temperature overnight (16 h). The mixture was filtered and the cake was washed with methylene chloride (2 × 150 ml). The combined filtrates and washings were rigorously stirred with 20% aqueous sodium sulfite solution (100 ml), at room temperature for 1 h, to decompose the excess peracid. The organic phase was separated and the aqueous phase was extracted with methylene chloride until tlc (silica, ether) indicated complete recovery (8 × 50 ml). All the methylene chloride extracts were combined and stirred with powdered calcium hydroxide (10) (100 g) to remove *m*-chlorobenzoic acid. The mixture was filtered and the solids washed with methylene chloride. After combining the filtrates and washings, the solvent was removed *in vacuo* at 40°C to give 85.0 g (95%) of a liquid that slowly crystallized. Thin-layer chromatography (silica, ether) showed two components with respective R_F values of 0.10 (*cis*-isomer **7**) and 0.50 (*trans*-isomer **8**). The nmr spectrum indicated that the ratio of **7** to **8** was 70:30. When the epoxidation was carried out at 25°C, the ratio was 63:37.

Separation of the Two Epoxides

Method A—The crude product (85.0 g) was dissolved in warm water (100 ml) and the solution filtered to remove some insoluble matter (2.5 g). This material seemed to be calcium *m*-chloroperbenzoate (only aromatic protons in the nmr spectrum; it gave a slow iodine test, it exploded when heated, it left a residue after burning and was insoluble in ethanol). The aqueous solution was placed in a separatory funnel and extracted with an equal volume of ether (100 ml). The ether phase was transferred to a second funnel containing water (100 ml) and after shaking, the ether-phase was removed. This process was repeated 10 times (10 × 100 ml). The combined ether extracts were dried and evaporated to dryness (at 40°C) to give 22.5 g of solids which contained about 80% *trans*-bisepoxide **8** and 20% *cis*-bisepoxide **7** as ascertained by nmr. Two recrystallizations from ethanol (20 ml) gave 14.5 g (17% based on 1,4-cyclohexadiene) of **8**, mp 108–109°C (lit. (2) mp 106.5–107.5°C); nmr ($CDCl_3$), δ 2.26 (b s, 4H, $2CH_2$) 2.96 (b s, 4H, 4 epoxide hydrogens). The mother liquors yielded 8.0 g of a syrup after evaporation of the solvent. This syrup was recycled. The aqueous phases from the two funnels were combined (200 ml), sodium chloride was added, followed by extraction with 70 ml portions of methylene chloride until tlc of the aqueous phase showed complete removal of **7** (10 extractions). The methylene chloride extracts were combined, dried and evaporated to dryness at 40°C to give 52.5 g solid material shown by nmr to contain 92% *cis*-bisepoxide **7** and 8% of the *trans*-isomer **8**. This mixture could be used without further purification in the next step. When pure **7** was required, the crude product was dissolved in boiling petroleum ether (bp 90–120°C) (750 ml), ether (50 ml) was added and the product allowed to crystallize first at room temperature and then at 0°C to give 38.5 g of **7**, mp 59–60°C (lit. (2) mp 60–61°C); nmr ($CDCl_3$) δ 2.50 (b q, 4H, J= 17 Hz, 2—CH_2—) and 3.09 (b s, 4H, 4 epoxide hydrogens). The mother liquors were evaporated to dryness (40°C) and the residue dissolved in 250 ml of boiling petroleum ether, the solution diluted with 50 ml ether and the product allowed to crystallize as above to give an additional 6.5 g of **7**, mp 59–60°C. The two crops were combined to give a total of 45.0 g (52% based on **3**). The mother liquors were kept for recycling. This method was quite effective for the separation of as much as 350 g of a mixture of **7** and **8**.

Method B—The crude mixture of solid epoxidation product (43.0 g) was dissolved in water (200 ml) and the solution filtered to remove insoluble matter (see above). The p*H* of the aqueous solution was adjusted to 7.0 with sodium bicarbonate and extracted continuously with petroleum ether (bp 39–47°C). The progress of the extraction was followed by tlc (silica, ether) of the aqueous and the organic phases and was continued until all or most of the *trans*-isomer **8** was removed. After 16 h the petroleum ether solution was evaporated to dryness to give 15.5 g solid material shown by nmr to be a mixture of *trans*- and *cis*-epoxides in a ratio of 60:40. Fresh petroleum ether was added and extraction continued for an additional 4 h. The extract was dried and evaporated to leave 1.3 g of a residue shown by nmr to consist of a mixture of *trans*- and *cis*-epoxide in a ratio of 22:78. The solid material from the first extract (15.5 g) was recrystallized twice from ethanol (2 ml/g) to give 8.0 g of **8**, mp 108–109°C. The mother liquor was kept for recycling. The aqueous phase was extracted continuously with ether for 48 h (or repeatedly with methylene chloride as in method A above). The extracts, after drying and evaporation yielded 22.0 g of solid material shown by nmr to consist of 95–98% *cis*-bisepoxide **7** and 2–5% *trans*-isomer. This material was used as such in the next reaction with hydrazine. When pure **7** was required, it was recrystallized as described above in method A. In another run, 350 g of a mixture of **7** and **8** was effectively fractionated by the above process.

*6,7-Diazabicyclo[3.2.1]octane-(2S,4R)-2,4-diol (**10**)*

A solution of 17.2 g (153.5 mmol) of the *cis*-epoxide **7** and 6.6 g (206 mmol) anhydrous hydrazine in dry EtOH (100 ml) was refluxed under nitrogen. After 1 h, a crystalline precipitate appeared. The progress of the reaction was followed by tlc (silica, 5% EtOH in ether). After 12 h, the spot corresponding to **7** (R_F 0.40) had disappeared and a new spot with R_F 0 (**10**) had appeared. After boiling for 17 h, the reaction mixture was cooled in ice. The crystalline product was collected, washed with ether (25 ml), and dried to give 17.5 g of **10** (79.5%) mp 180–190°C (dec.). The mother liquors were evaporated to dryness. Ethanol (35 ml) was added to the residue and the solution left in the refrigerator overnight. The crystalline precipitate, collected by filtration, consisted of 1.0 g of **10**; mp 180–190°C (dec.). The combined yield amounted to 18.5 g (84.5%). The analytical sample was obtained by recrystallization from ethanol, mp 185–190°C (dec.). *Anal.* calcd. for $C_{16}H_{12}N_2O_2$: C 49.97, H 8.38, N 19.42; found: C 50.16, H 8.54, N 19.17.

The yield of **10** was not affected when hydrazine hydrate was used. Crystalline **10** was also obtained when crude **7** (containing 5–8% of *trans*-isomer **8**) was used.

*2,5-Dideoxystreptamine (**11**)*

A solution of 17.7 g (122.5 mmol) of compound **10** in a mixture of glacial acetic acid – water (1:1, 100 ml) and 2.0 g of 10% Pd/C was shaken under hydrogen in a Parr apparatus at 60°C and an initial pressure of 50 psi. When uptake had ceased (7 h), the mixture was cooled to room temperature and filtered. The catalyst was washed with acetic acid and the washings and filtrate combined. The solution was colorless in the beginning but it turned brown on evaporation and exposure to the atmosphere. The acetic acid was removed by evaporation and the solid residue was stirred with 100 ml of boiling ethanol. After cooling to room temperature, the mixture was filtered and the solid washed with ice-cold ethanol and dried to give 20.0 g of the acetate salt of **11**, mp 205–207°C (dec.), (darkens at 185°C). Evaporation of the mother liquor, left a residue which was treated with 30 ml ethanol as above to give an additional 3.0 g of the acetate salt of **11**. The combined crops weighed 27.0 g (78%). The mother liquor, after evaporation gave 5.5 g of a dark brown sticky residue. *Anal.*

Can. J. Chem. Downloaded from www.nrcresearchpress.com by 210.87.254.5 on 09/05/12
For personal use only.

calcd. for $C_{10}H_{22}N_2O_6 \cdot H_2O$: C 42.24, H 8.51, N 9.85; found: C 43.14, H 8.64, N 10.00.

The acetate salt (27.0 g) was dissolved in water (75 ml) and the solution passed through a column containing 220 g of Rexyn 201 (Fisher Scientific Co., strongly basic resin, OH form) and the column washed with water (600 ml). The effluent was evaporated to dryness to give in quantitative yield the amine **11**, mp 173–180°C (darkens at 165°C). A sample of 2.7 g was recrystallized from water (2.0 ml) – ethanol (25 ml) to give 1.95 g, mp 182-183°C (monohydrate) and resolidifies to melt at 198–199°C. *Anal.* calcd. for $C_6H_{14}N_2O_2 \cdot H_2O$: C 43.88, H 9.82, N 17.06; found: C 43.91, H 9.95, N 17.13.

The hydrochloride salt of **11** had mp >350°C; nmr (D_2O), δ: 3.78 (d of t, 2, H-4 and H-6, J = 11 and 4.5 Hz) 3.25 (d of t, 2, H-1 and H-3, J = 11 and 4.5 Hz).

d,l-N-*Ethoxycarbonyl-2,5-dideoxystreptamine* (*12*)

A solution of 54.0 g (329 mmol) of 2,5-dideoxystreptamine (**11**) in 270 ml water was diluted with 180 ml of methanol and cooled in an ice-bath while stirring. Ethylchloroformate (37.4 g or 345 mmol) was added dropwise and at a rate to maintain the solution temperature at 4–6°C. After completion of the addition (45 min), stirring was continued for 1 h at 4–6°C and then at room temperature for an additional h. The solvent was removed by evaporation at 55–60°C and the traces of water removed by coevaporation with ethanol (3 × 100 ml). The partly solid residue consisted of a mixture of the hydrochloride of **12**, the *bis*-hydrochloride of **11** and the *bis*-carbamate **13**. A sample was basified and examined by tlc (silica, 10% MeOH – ethyl acetate): two spots with R_F 0.34 (**13**) and 0 (**11** and **12**) were observed.

The crude product was treated while stirring with boiling dry ethanol for 5–10 min, the mixture cooled to room temperature, the insoluble *bis*-hydrochloride of **11** removed by filtration and the solid washed with hot ethanol (2 × 50 ml) to give a mass weighing 14.0 g. The combined filtrate and washings were evaporated to dryness, the sticky residue dissolved in water and the solution extracted continuously with ethyl acetate until all the biscarbethoxy compound **13** was removed (48 h). The ethyl acetate extract was evaporated to dryness to give 21.7 g (22.8%) of crystalline **13**, mp 204–205°C. *Anal.* calcd. for $C_{12}H_{22}N_2O_6$: C 49.64, H 7.64, N 9.65; found: C 49.58, H 7.70, N 9.61.

The aqueous phase containing mainly the hydrochloride of **12** and some salt of **11** was decolorized with charcoal, evaporated to dryness and the traces of water removed by coevaporation with ethanol (3 × 100 ml). The sticky residue was dissolved in boiling ethanol (200 ml) and after cooling to room temperature the solution was diluted with ether (100 ml) while cooling in ice. The precipitated bishydrochloride of **11** was removed by filtration (2.5 g) and the filtrate evaporated to dryness to give 43.1 g (52%) of the hydrochloride of **12** as a brittle foam.

Regeneration of ***12*** *from the Hydrochloride Salt*

Some Rexyn 201 resin (220 g) was packed into a column and washed with 6% NaOH (1.5 ℓ) to generate the hydroxide form. It was then washed with distilled water until the effluent was neutral. The size of the column bed was 37.5 cm × 3.5 cm id. A solution of 35.0 g (137.5 mmol) of the hydrochloride of **12** in 50 ml water was poured onto the column and the column subsequently washed with distilled water at a rate of 1.5 ℓ/h. A fast elution was important since prolonged contact with the resin resulted in conversion of **12** to 1,3-cyclic urea. The first 175 ml of the effluent was neutral and discarded. The following 400 ml had a pH > 7.0 and was evaporated to dryness (at 40–45°C) to give 28.8 g (96%) of crystalline **12**. Thin-layer chromatography (silica, 10% water in ethanol, iodine as developer) showed one spot with R_F 0.29 and a faint spot with R_F 0. This material was thus pure enough for purposes of resolution into its optical isomers, A sample of 1.0 g was recrystallized from ethanol (2 ml) – ether (4 ml) and gave 0.7 g of an analytical sample, mp 132–134°C. *Anal.* calcd. for $C_9H_{18}N_2O_4$: C 49.51, H 8.31, N 12.83; found: C 49.34, H 8.35, N 12.80.

*l-*N*-Ethoxycarbonyl-2,5-dideoxystreptamine* (***16***) *and 3-*N*-Ethoxycarbonyl-2,5-dideoxystreptamine* (***14***) *by Resolution of* d,l-N-*Ethoxycarbonyl-2,5-dideoxystreptamine* (***12***)

A warm solution of 20.0 g (91.5 mmol) of **12** in 95% ethanol–water (100 ml) was added to a warm solution of 12.38 g (45.8 mmol) (−)-2-nitrotartranilic acid (6) in the same solvent (100 ml) and crystallization allowed to take place at room temperature. In some experiments the crystalline precipitate was mixed with a jelly-like solid. In such cases, the mixture was heated to selectively dissolve the jelly and the solution allowed to stand at room temperature overnight. The crystalline salt was collected, washed with absolute ethanol (40 ml) and dried to give 19.2 g (86%) of the nitrotartranilate salt of **14** mp 195–199°C (dec.) $[\alpha]_D^{25}$ −45.4 (*c* 1.0, H_2O). The rotation indicated an optical purity of 94%. A sample was dissolved in a boiling water – ethanol mixture (1 : 1), (3 ml/g), the solution diluted with absolute ethanol (13.4 ml/g) and the product allowed to crystallize at room temperature. Two more recrystallizations from the same solvent system afforded the analytical sample mp 207–209°C, $[\alpha]_D^{25}$ −43.4 (*c* 1.0, H_2O). *Anal.* calcd. for $C_{19}H_{28}N_4O_{11}$: C 46.71, H 5.77, N 11.50; found: C 46.50, H 5.84, N 11.52.

The mother liquors containing the other optical isomer mainly as the free base were evaporated to dryness at 40°C and the residue dissolved in 35 ml of water. Rexyn 201 resin (OH form, 15 ml) was added, the mixture shaken for 2–3 min and filtered. The resin was washed with water (2 × 10 ml) and the combined filtrate and washings evaporated to dryness at 40°C to give 10.2 g of a solid residue. This was dissolved in 95% EtOH–H_2O (90 ml) and the solution added to a warm solution of 10.8 g (40 mmol) (+)-2-nitrotartranilic acid (6) in the same solvent (90 ml). The product was allowed to crystallize at room temperature overnight and was then collected, washed with dry EtOH (40 ml) and dried to give 17.4 g of the nitrotartranilate salt of **16**, mp 207–208°C (dec.) $[\alpha]_D^{25}$ + 43.36(*c* 1.0, H_2O). Two recrystallizations from 90% EtOH–water did not alter the mp or the rotation. *Anal.* calcd. for $C_{19}H_{28}N_4O_{11}$: C 46.71, H 5.77, N 11.50; found: C 47.06, H 5.84, N 11.51.

Free Bases ***14*** *and* ***16*** *from their 2-Nitrotartranilate salts Compound* ***16***

A column of 3.4 cm id was packed with Rexyn 201 resin (200 g) and the resin washed with 6% sodium hydroxide (1.5 ℓ) followed by distilled water until the effluent was neutral. A solution of 44.0 g (90 mmol) of the dextrorotary salt of **16** ($[\alpha]_D^{25}$ +43.3) in 70 ml of water (initially warmed to facilitate dissolution) was poured onto the column followed by washing with water at a rate of 3 ℓ/h. A fast elution of the product is very important at this stage because at slow elution rates, the effluent was colored yellow owing to decomposition of the 2-nitrotartranilic acid by the resin. Also, prolonged contact with the resin resulted in formation of the 1,3-cyclic urea. The first 200 ml of effluent was neutral and was discarded. The next 600 ml (pH > 7.0) of effluent containing the desired material was quickly evaporated to dryness at 40–45°C (receiver cooled in an ice-ethanol mixture). Evaporation at higher temperatures and prolonged heating favored urea formation. To the syrupy residue was added ethanol which

Can. J. Chem. Downloaded from www.nrcresearchpress.com by 210.87.254.5 on 09/05/12
For personal use only.

after evaporation, gave 18.2 g (93%) of crystalline **16**. A sample was recrystallized from ethanol–ether (1:10); mp 154–156°C, $[\alpha]_D^{25}$ −37.6 (*c* 1.0, H_2O). $\Delta[M]$TACu −550.

*Compound **14***

A solution of 33.0 g (67.5 mmol) of the levorotary salt ($[\alpha]_D^{25}$ −43.7) in 70 ml of water was processed as described above to yield 14.6 (99%) of compound **14**; mp 154–156°C (ethanol–ether), $[\alpha]_D^{25}$ +37.3 (*c* 1.0, H_2O); $\Delta[M]$TACu +600.

1-N-*Ethoxycarbonyl-3*-N-*phenoxycarbonyl-2,5-dideoxystreptamine (**17**)*

To a solution of 8.44 g (38.6 mmol) of **16** and 3.70 g (44 mmol) of sodium bicarbonate in water (40 ml) was added 40 ml acetone and the mixture cooled in an ice-bath while stirring. Phenylchloroformate (6.73 g or 43 mmol) was added dropwise (over 10 min), the mixture stirred in the cold for 1 h and then diluted with water (80 ml). The precipitate was collected, washed with water (2 × 30 ml) and dried in a vacuum desiccator to give 10.6 g of **17**. From the filtrate, after concentration *in vacuo* to ¼ of the volume and addition of water (50 ml), an additional 0.9 g of **17** was obtained to give a total of 11.5 g (88.5%); mp 136–141°C; $[\alpha]_D^{25}$ +6.0 (*c* 1.0, EtOH).

*3*N-*Ethoxycarbonyl-1*N-*phenoxycarbonyl-2,5-dideoxystreptamine (**15**)*

Reaction of **14** (13.55 g, 62 mmol) with phenylchloroformate by the procedure described above gave 19.18 g (91.5%) of **15**; mp 135–140°C; $[\alpha]_D^{25}$ −6.7 (*c* 1.0, ethanol).

3,4-N,O-*Carbonyl-1*-N-*ethoxycarbonyl-2,5-dideoxystreptamine (**2**)*

A suspension of 11.2 g (33.2 mmol) of **17** in 90% acetone–water (90 ml) containing 2.4 ml triethylamine was stirred at room temperature until dissolution (45 min). After stirring for 5 h, 20 ml of Dowex 50W-X4 resin (H^+ form) previously washed with water and acetone was added and the mixture stirred for 3 min (to remove the triethylamine). The resin was removed by filtration and the filtrate evaporated to dryness (40–45°C). The crystalline residue was stirred for 10 min with acetone (15 ml), the mixture diluted with ether (50 ml), the solid collected, washed with ether and dried under vacuum at 65°C overnight to give 7.5 g (92.5%) of **2**; mp 203–205°C, $[\alpha]_D^{25}$ −58.5 (*c* 1.0, H_2O). *Anal.* calcd. for $C_{10}H_{16}N_2O_5$: C 49.17, H 6.60, N 11.47; found: C 48.84, H 6.48, N 11.64.

1,6-N,O-*Carbonyl-3*-N-*ethoxycarbonyl-2,5-dideoxystreptamine (**1**)*

Compound **15**, (18.85 g or 55.7 mmol) was treated with triethylamine (4.0 ml) as described above to give 12.6 g (92.5%) of **1**; mp 203–205°C; $[\alpha]_D^{25}$ +57.5 (*c* 1.0, H_2O). *Anal.* calcd. for $C_{12}H_{16}N_2O_5$: C 49.17, H 6.60, N 11.47; found: C 49.13, H 6.71, N 11.47.

1. Y. Nishimura, T. Tsuchiya, and S. Umezawa. Bull. Chem. Soc. Jpn. **44**, 2521 (1971).
2. T. W. Craig, G. P. Harvey, and G. A. Berchtold. J. Org. Chem. **32**, 3743 (1967).
3. H. J. Dauben, Jr. and L. L. McCoy. J. Am. Chem. Soc. **81**, 4863 (1959).
4. R. T. Testa, G. H. Wagman, P. J. L. Daniels, and M. J. Weinstein. J. Antib. **27**, 917 (1974).
5. T. Suami, S. Ogawa, H. Uchino, and Y. Funaki. J. Org. Chem. **40**, 456 (1975).
6. T. A. Montzka, T. L. Pindell, and J. D. Mattiskella. J. Org. Chem. **33**, 3993 (1968).
7. S. Umezawa, T. Tsuchiya, and K. Tatsuta. Bull. Chem. Soc. Jpn. **39**, 1235 (1966).
8. R. E. Reeves. Advances in carbohydrate chemistry. Vol. 6. Academic Press, New York, NY. 1951. p. 107.
9. S. Umezawa, Y. Tagaki, and T. Tsuchiya. Bull. Chem. Soc. Jpn. **44**, 1411 (1971).
10. H. B. Henbest and B. Nicholls. J. Chem. Soc. 4608 (1957).
11. G. D. Daves, Jr., R. K. Robins, and C. C. Cheng. J. Am. Chem. Soc. **84**, 1724 (1962).
12. M. Hickens and K. L. Rinehart, Jr., J. Am. Chem. Soc. **85**, 1547 (1963).
13. R. U. Lemieux, T. L. Nagabhushan, K. J. Clemetson, and L. C. N. Tucker. Can. J. Chem. **51**, 53 (1973).

The α-alkoxycarbonylation of saturated carbonyl compounds. The synthesis of 17α-hydroxymethyl 20-keto steroids[1,2]

D. MUKHERJEE[3] AND CH. R. ENGEL

Department of Chemistry, Laval University, Quebec, P.Q., Canada G1K 7P4

Received July 26, 1977

D. MUKHERJEE and CH. R. ENGEL. Can. J. Chem. **56**, 410 (1978).

It is shown that enolate ions, in particular lithium enolates obtained from enol acetates of saturated ketones by reaction with methyllithium, may not only be alkylated and carboxylated, but also alkoxycarbonylated (in position α to the original saturated keto group). By this method, saturated 20-keto steroids were transformed into 17α-methoxycarbonyl 20-ketones. Thus, from pregnenolone, 17-methoxycarbonylpregnenolone was prepared and was then converted to 17-hydroxymethylprogesterone and to some of its esters. This method for preparing 17-hydroxymethylated hormone analogues of the progesterone-corticoid group is simpler and more efficient than the pathway implying a free-radical functionalization of a 17α-methyl group.

D. MUKHERJEE et CH. R. ENGEL. Can. J. Chem. **56**, 410 (1978).

Des ions énolate, en particulier des énolates de lithium, obtenus par réaction d'acétates d'énols de cétones saturées avec du méthyllithium, peuvent non seulement être alkylés et carboxylés mais aussi alkoxycarbonylés, en position α par rapport à la fonction carbonyle saturée originale. Par cette méthode des 20-céto stéroïdes ont été transformés en 20-cétones 17α-méthoxycarbonylées. Nous avons préparé, à l'aide de cette réaction, à partir de la pregnénolone, la 17-méthoxycarbonylpregnénolone qui fut convertie en 17-hydroxyméthylprogestérone et en certains de ses esters. Cette méthode de préparation d'analogues d'hormones 17-hydroxyméthylés du groupe progestéro-corticoïde est plus simple et plus efficace que celle impliquant une fonctionnalisation radicalaire d'un groupe 17α-méthyle.

Recently (1) we reported the first synthesis of 17-hydroxymethyl- and 17-acetoxymethylprogesterone (**9** and **9***a*). The novel 17α-substituent had been arrived at (1, 5) by functionalization of the 17α-methyl group of a 17α-methyl 12α-hydroxy etio ester (**4**), by a photolytic Barton transfer reaction (cf. refs. 6, 7) on its 12-nitrite (**4***a*), the 17-methyl etio ester having been prepared from a 17-bromo 20-ketone (**1***c*) with the help of a Favorsky rearrangement (5*b*, 8) (sequence **1***b* → **1***c* → **4** → **4***a* → **7** → **8** → **9** in Scheme 1). While the yields in the various steps of this synthesis had been, with the exception of the moderate result of the Barton reaction, very satisfactory, the overall pathway was lengthy and not entirely rewarding since a 21-methyl 20-ketone had to be transformed into a 17-methyl etianate, the 20-ester function of which had to be reconverted at a later stage to a 21-methyl 20-keto side chain. Furthermore, the 12-hydroxy group, necessary for the transfer reaction, had to be removed after having served its purpose and, finally, the starting material, 3α,12α-diacetoxy-5β-pregnan-20-one (**1***b*), is not readily available anymore.

Under the circumstances an alternate pathway to 17-hydroxymethyl derivatives of steroid hormones of the progesterone-corticoid group seemed desirable. An attractive approach towards the direct introduction of a 17α-substituent into 20-keto steroids appeared to consist of their α-alkoxycarbonylation, since this should open the way not only to 17-alkoxycarbonyl and 17-carboxy derivatives but also to 17-hydroxymethylated products.

For the realization of this objective, the use of enolate ions seemed promising. Deghenghi and colleagues (9) and, independently, Weiss and coworkers (10) have shown that enolate ions generated by metal hydride reduction from 16-unsaturated 20-ketones, according to a general method described by Stork *et al.* (11), or from 17-hydroxy, 17-acetoxy, or 17-bromo 20-ketones (10), could be alkylated in position 17α. Stork *et al.* (11) also showed that lithium enolates generated from α,β-unsaturated ketones could be carboxylated with solid carbon dioxide. On the other hand, it is known (12) that enolate ions may be formed readily from saturated ketones by treatment of the corresponding enol acetates with alkyllithium or Grignard reagents, in aprotic, polar solvents. Since 16,17-saturated 20-keto steroids are in general readily available, sometimes

[1]Paper XLIV in our series on Steroids and Related Products. For paper XLIII, see ref. 1.

[2]The main results of this paper were contained in a communication to the 9th International (IUPAC) Symposium on the Chemistry of Natural Products, Ottawa, Ontario, June 24–28, 1974 (see ref. 2); other results of this paper were part of an invited symposium paper presented to the 4th International Congress on Hormonal Steroids, Mexico, September 2–7, 1974 (see refs. 3, 4).

[3]Abbreviated from part of the doctoral thesis of D. Mukherjee, School of Graduate Studies, Laval University, Quebec, 1976.

Can. J. Chem. Downloaded from www.nrcresearchpress.com by 210.87.254.6 on 09/05/12
For personal use only.

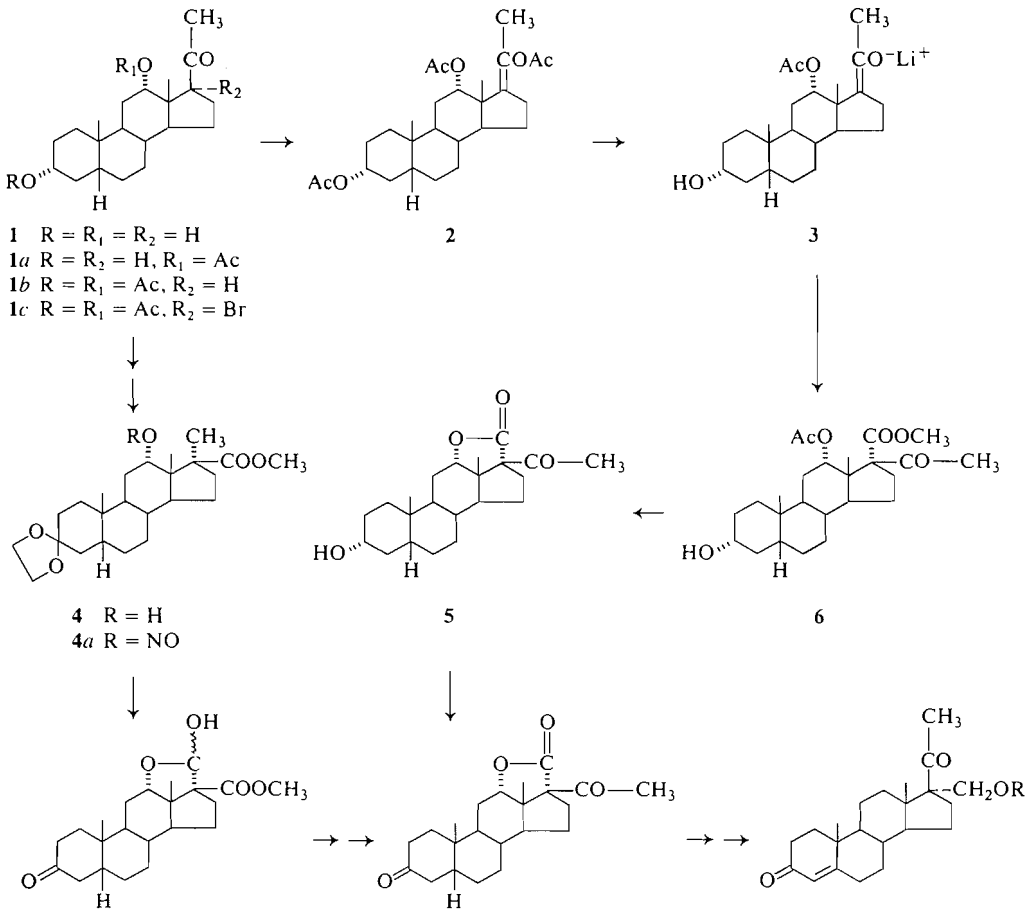

SCHEME 1

more readily than the corresponding 16-unsaturated derivatives, and since they are easily converted to 17-en-20-ol acetates (13, 14), we decided to attempt the transformation of unconjugated 20-keto steroids into lithium 17,20-enolates and to explore the alkoxycarbonylation of such enolate ions; finally, in the case of success, to investigate the conversion of the resulting 17-alkoxycarbonyl 20-ketones to 17α-hydroxymethylated 20-keto steroids (cf. Schemes 1 and 2).

In a preliminary experiment (Scheme 1), we wished not only to establish the feasibility of a 17α-alkoxycarbonylation of an unconjugated 20-keto steroid but also its stereochemical course, by choosing a substrate which would lead to a product already obtained, sterically unequivocally, with the help of the Barton transfer reaction (see above). We therefore transformed 3α,12α-diacetoxy-5β-pregnan-20-one (**1***b*) with acetic anhydride and *p*-toluenesulfonic acid into the *cis*/*trans* mixture of its 17,20-enol acetates (**2**) (15), which we subjected to the action of methyllithium in dimethoxyethane at 5°C. The resulting mixture of lithium enolates (**3**) was treated in its original solution with dimethyl carbonate. The product contained, apart from partly hydrolyzed starting material (**1***a*), the crude 3-hydroxy 17α-methoxycarbonyl 20-ketone **6**. Without purification, the material was saponified with methanolic potassium hydroxide at reflux temperature; ether extraction of the alkaline solution afforded the hydrolyzed starting material **1**. Acidification of the remaining aqueous product led to the hydroxy lactone **5** which was immediately oxidized with Jones' reagent (16) to the 3-oxo 12α-hydroxy 17α-acetyl 17β-etianic acid lactone (20 → 12) (**8**) which we had previously prepared (1) by functionalization of a 17α-methyl group. Thus, the feasibility of α-alkoxycarbonylations of lithium enolates, formed from 16,17-saturated 20-ketones, was demonstrated and the stereochemistry of this reaction, which proceeded, as expected, from the less hindered side, was established. In this preliminary experiment we

Can. J. Chem. Downloaded from www.nrcresearchpress.com by 210.87.254.6 on 09/05/12
For personal use only.

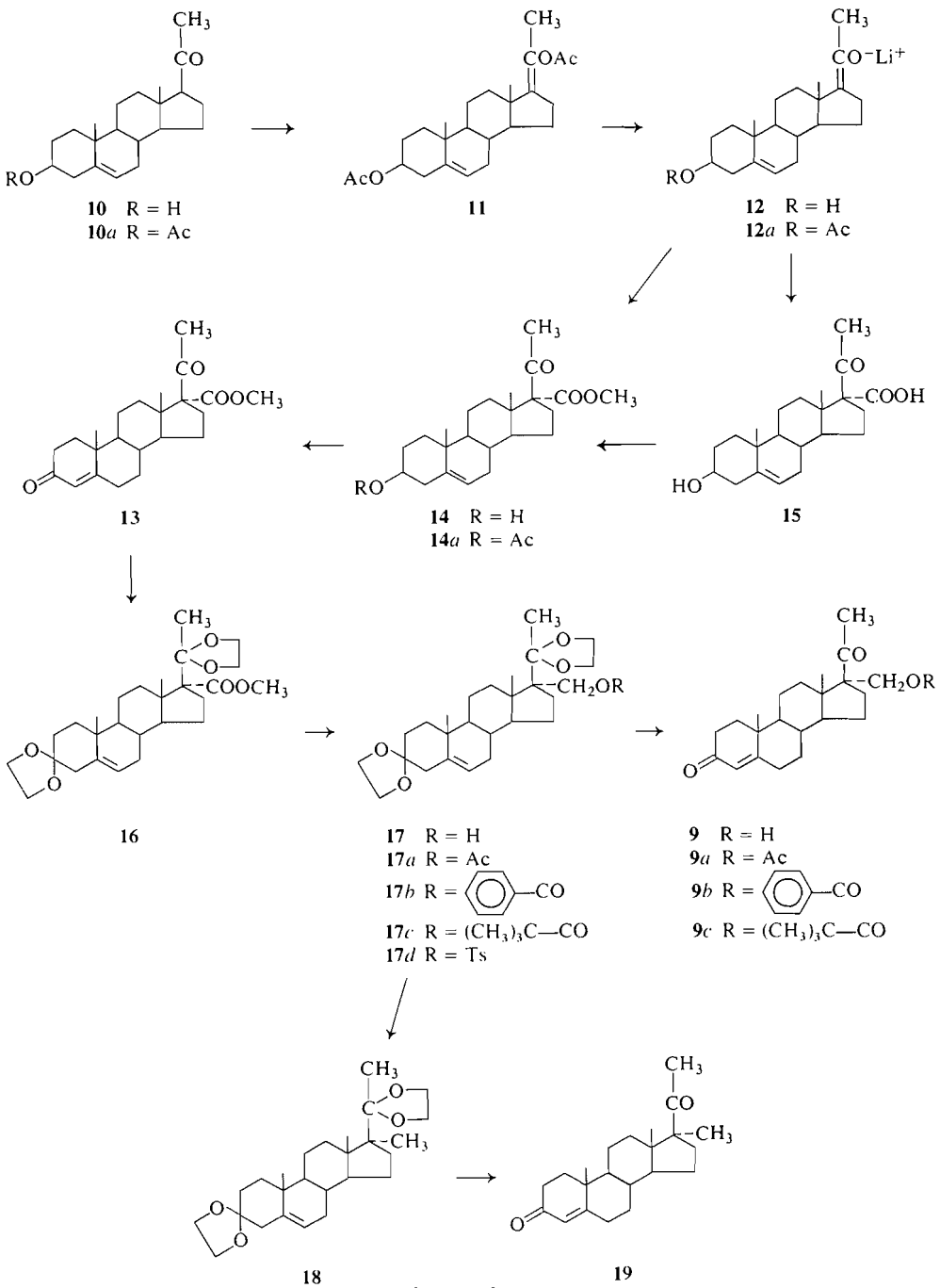

SCHEME 2

did not attempt to isolate the intermediates and to optimize the yields.

We now applied this method of α-alkoxycarbonylation of a saturated ketone to the synthesis of 17-hydroxymethylprogesterone (**9**) and some of its esters (Scheme 2). The very readily available pregnenolone **10** was transformed with acetic anhydride and *p*-toluenesulfonic acid into the *cis*/*trans* mixture of its enol acetates (**11**) (13, 14, 17) which was treated, as described above, in dimethoxyethane with methyllithium. The resulting mixture of lithium enolates (**12** and **12***a*) was subjected, as described above, to the action of dimethyl carbonate. By crystallization, 17-methoxycarbonyl pregnenolone acetate (**14***a*) was isolated. From the mother liquors, the 3-hydrolyzed product (**14**) was obtained. Ace-

Can. J. Chem. Downloaded from www.nrcresearchpress.com by 210.87.254.6 on 09/05/12
For personal use only.

Can. J. Chem. Downloaded from www.nrcresearchpress.com by 210.87.254.6 on 09/05/12
For personal use only.

tylation of the mother liquors gave the acetylated starting material, pregnenolone acetate (**10***a*). Considering this recovery of starting material, the yield of the acetoxy methyl ester **14***a* amounted to 53%, that of the hydroxy methyl ester **14** to 4.5%. The acetate of ester **14***a* could be selectively hydrolyzed with potassium bicarbonate in aqueous methanol in approximately 95% yield to the hydroxy methyl ester **14**. When the crude mixture obtained upon methoxycarbonylation of the lithium enolates was directly treated with potassium bicarbonate in aqueous methanol, the yield of the 3-hydroxy 17-methoxycarbonyl pregnenolone **14**, from pregnenolone (**1**), was raised to 60% (taking into account the recovery of starting material).

Alternatively, the 3-hydroxy 17-methoxycarbonyl 20-ketone **14** was obtained by carboxylation of the mixture of the lithium enolates **12** and **12***a*, by treatment with solid carbon dioxide, under the conditions described by Stork *et al.* (11*b*). From the ether extract of the resulting product the starting material **10** was isolated. Acidification of the remaining aqueous solution led to the 17-carboxy derivative **15** which was methylated with diazomethane. The resulting 3-hydroxy ester **14** was thus obtained in a yield of 63% from pregnenolone (**10**), considering the recovery of starting material.

The transformation of 17-methoxycarbonylpregnenolone (**14**) into 17-hydroxymethylprogesterone (**9**) was now performed by well-established methods. Jones' oxidation (16), followed by treatment with hydrochloric acid (see also ref. 18), gave in 85% yield the pure 4-unsaturated 3,20-diketo ester **13**, also obtained in 80% yield by Oppenauer oxidation with cyclohexanone and aluminum *tert*-butoxide. The keto functions were protected (in 88% yield) by ketalization with ethylene glycol and *p*-toluenesulfonic acid and the 17-methoxycarbonyl diketal **16** was reduced in 90% yield with lithium aluminum hydride to the 17-hydroxymethyl diketal **17**, which was transformed, again in 90% yield, with acetone and *p*-toluenesulfonic acid, into 17-hydroxymethylprogesterone (**9**). Alternatively, the 17-hydroxymethyl diketal **17** was acetylated to its acetate **17***a* whose ketal groups were removed, as just described, in 99% yield. The hydrolysis with potassium carbonate of the resulting 17-acetoxymethylprogesterone (**9***a*) to 17-hydroxymethylprogesterone (**9**) has already been described (1). This product (**9**), as well as its acetate **9***a*, proved in every respect identical with the products previously synthesized from 3α,12α-diacetoxy-5β-pregnane 20-one (**1***b*) (1).

We have already reported (1) that 17-hydroxymethylprogesterone (**9**) and its acetate **9***a* showed, unexpectedly, no appreciable progestational activity in the Clauberg–McPhail test (19). It seemed possible that the primary acetate group of 17-acetoxymethylprogesterone (**9***a*) would be hydrolyzed in vivo and that the free 17-hydroxymethylprogesterone (**9**) lacked noteworthy progestational activity because of the conformation of the 17β-methyl ketone side chain which, as a result of hydrogen bonding between the 20-carbonyl group and the 17^1-hydroxyl group, should differ from that of the biologically active progesterones (cf. ref. 20). We therefore prepared less readily hydrolyzable esters of 17-hydroxymethylprogesterone (**9**), namely the benzoate (**9***b*) and the pivalate (**9***c*). For that purpose the 17-hydroxymethyl diketal **17** was transformed, on one hand with benzoyl chloride and pyridine into the benzoate **17***b* and, on the other hand, with trimethylacetyl chloride in pyridine to the pivalate **17***c*. The benzoate **9***b* and pivalate **9***c* of 17-hydroxymethylprogesterone (**9**) were obtained in high yields by exchange reactions with acetone and *p*-toluenesulfonic acid. Both the benzoate **9***b* and the pivalate **9***c* now proved, even at high dose levels, progestationally practically inactive in the Clauberg–McPhail test. Since the hydrolysis of these ester groups, especially of the trimethylacetate group, under physiological conditions, seems unlikely, one has to rule out that the progestational inactivity of 17-hydroxymethylprogesterone and its esters is due to hydrogen bonding in the unesterified product (**9**), and thus to the particular side chain conformation of this hormone analogue. Under the circumstances, we wished to prove once more and by a direct method the 17β-configuration of the methyl ketone side chain of 17-hydroxymethylprogesterone (**9**) and its esters. We therefore prepared (in 85% yield) the tosylate **17***d*, and reduced it with lithium aluminum hydride to the 17α-methyl diketal **18** which we transformed with acetone and *p*-toluenesulfonic acid into the well-known and progestationally very active 17α-methylprogesterone (**19**) (17). This sequence of reactions confirmed the configuration in position 17 of 17-hydroxymethylprogesterone (**9**) and its esters. These products thus represent the first progesterone analogues with bulky 17α-substituents which exhibit no appreciable progestational activity.

From a chemical point of view, the experiments reported demonstrate that saturated ketones may not only be carboxylated, but also, and readily, alkoxycarbonylated by reaction, with dialkyl carbonates, of their lithium enolates, prepared from their enol acetates. One thus disposes of another, simple, route to a variety of α-substituted ketones.

Experimental

The melting points were taken in evacuated capillaries and the temperatures were corrected. For elution chromatography, neutral aluminum oxide Woelm, activity III, and Davison's

Can. J. Chem. Downloaded from www.nrcresearchpress.com by 210.87.254.6 on 09/05/12
For personal use only.

silica gel no. 923 were employed, unless otherwise stated. Dry-column chromatography was performed with Woelm dry-column chromatography silica gel, activity III; thin-layer chromatography with Merck-Darmstadt silica gel. The ir spectra were recorded on Beckman IR-4 and IR-12 spectrophotometers, and the uv spectra on a Beckman DK-1A instrument. The nmr spectra were taken at 60 and 90 MHz on Varian A-60 and Brucker HFX-90 spectrometers, tetramethylsilane serving as internal standard and deuteriochloroform as solvent. The microanalyses were performed by the late Dr. F. Pascher, Bonn, Germany, and by Ayerst Laboratories, Montreal (under the direction of Dr. G. Schilling).[4]

(Z)- and (E)-3α,12α,20-Triacetoxy-5β-pregn-17-enes (2)

To a solution of 30 g of 3α,12α-diacetoxy-5β-pregnan-20-one (**1***b*), mp 139–141°C, in 1.5 ℓ of absolute acetic anhydride, 8.43 g of *p*-toluenesulfonic acid was added. The solution was heated and the solvent was then slowly distilled during 8 h. The volume was further reduced to approximately 100 ml by distillation *in vacuo*. The reaction mixture was cooled and extracted with ether. The ethereal solution was washed with water, a saturated sodium bicarbonate solution, again with water, and was dried over sodium sulfate. Removal of the solvent gave 36.5 g of a dark-brown semicrystalline product which was chromatographed on 1 kg of aluminum oxide. Petroleum ether – benzene (9:1 and 4:1) eluted 26.9 g (82%) of a crystalline mixture of the enol acetates **2**, mp 160–166°C. Recrystallization from ether–hexane raised the mp to 172–174°C. A sample was recrystallized twice from ether–hexane for analysis; mp 172–174°C; $[\alpha]_D^{26}$ +160.7° (*c* 1.000, $CHCl_3$); ν_{max} (KBr):1735 and 1250 cm^{-1} (acetates); δ (90 MHz): 0.95 (s, 3H, 19-CH_3), 0.98 (s, 3H, 18-CH_3), 1.8 (s, 3H, 21-CH_3), 2.06 (s, 6H, 3,12-$OCOCH_3$), 2.10 (s, 3H, 20-$OCOCH_3$). *Anal.* calcd. for $C_{27}H_{40}O_6$: C 70.40, H 8.75; found: C 70.59, H 8.61.

3-Oxo-12α-hydroxy-17β-acetyl-5β,17α-etianic Acid Lactone (20 → 12) (8)

The solvent was removed from 20 ml of a 1.5 *M* ethereal methyllithium solution and the residue was taken up in 30 ml of absolute dimethoxyethane. A few crystals of triphenylmethane were added and the mixture was cooled to 5°C. To this solution was added, dropwise and with stirring, a solution of 2 g of the above-described mixture of the enol acetates **2**, mp 160–166°C, in 50 ml of absolute dimethoxyethane, until the red colour was almost completely discharged, 40 ml of the enol acetate solution having been consumed. To this product, 5 ml of dimethyl carbonate in 20 ml of absolute dimethoxyethane was added and, after 5 min, the reaction mixture was carefully acidified, in the cold, with 2 *N* hydrochloric acid, to the Congo-blue reaction. Subsequently, the mixture was poured into ice water, the precipitate was extracted with ether, and the ethereal solution was washed with water and was dried over sodium sulfate. Evaporation of the solvent provided 1.65 g of a yellow foam, representing a mixture containing partially hydrolyzed starting material, *3α-hydroxy-12α-acetoxy-5β-pregnan-20-one* (**1***a*), and crude *methyl 3α-hydroxy-12α-acetoxy-17β-acetyl-5β,17α-etianate* (**6**); ν_{max} (KBr): 3440–3420 (OH), 1750–1740 (esters), 1705 (ketone), 1270 and 1250 cm^{-1} (methyl ester and acetate). The product was treated without purification with 75 ml of a 6.8% methanolic potassium hydroxide solution, for 4 h at reflux temperature. After cooling, the solution was poured onto ice, the precipitate was extracted with ether, the ethereal solution was washed with water, and was dried over sodium sulfate. Evaporation of the solvent provided 923 mg of the 'neutral fraction'. The aqueous alkaline solution remaining after the extraction, together with the first washings of the 'neutral fraction', were acidified with 2 *N* sulfuric acid to the Congo-blue reaction. The mixture was extracted with ether and the ethereal layer was washed with water and was dried over sodium sulfate. Evaporation of the solvent gave 230 mg of the 'acid fraction',[5] a yellow foam, representing crude *3α,12α-dihydroxy-17β-acetyl-5β,17α-etianic acid lactone (20 → 12)* (**5**); ν_{max} (KBr): 3400 (OH), 1775 (lactone), 1705 cm^{-1} (ketone).

The 'neutral fraction' was acetylated with 2 ml of acetic anhydride in 4 ml of pyridine at reflux temperature, for 1.5 h. The usual work-up gave 1.2 g of an amorphous product which was chromatographed on 36 g of aluminum oxide. Petroleum ether – benzene (4:1 and 1:1) eluted 723 mg of *3α,12α-diacetoxy-5β-pregnan-20-one* (**1***b*), mp 126–128°C. The identity of the product was established by the determination of a mixture melting point and by the comparison of its infrared spectrum with that of an authentic sample.

The 'acid fraction' was dissolved in 10 ml of absolute acetone and was treated at 0°C with 0.4 ml of Jones' reagent (16). The product was stirred for 5 min. The usual work-up gave 228 mg of a partly crystalline product which was chromatographed on 8 g of aluminum oxide. Elutions with petroleum ether – benzene (4:1) gave 130 mg of *3-oxo-12α-hydroxy-17β-acetyl-5β,17α-etianic acid lactone (20 → 12)* (**8**), mp 176–180°C. The identity of the product was established by the determination of a mixture melting point and by the comparison of its infrared and nmr spectra with those of an authentic sample (1).

3β-Acetoxy-17-methoxycarbonyl-5-pregnen-20-one (14a) and 3β-Hydroxy-17-methoxycarbonyl-5-pregnen-20-one (14)

According to the procedure of Fieser and Huang-Minlon (14), 50 g of pregnenolone (**10**), mp 182–187°C, was transformed with 2.5 ℓ of acetic anhydride and 13.9 g of *p*-toluenesulfonic acid into 62.3 g of a crude mixture of the (*Z*)- and (*E*)-*3β,20-diacetoxy-5,17-pregnadienes* (**11**), presenting itself as a dark-brown semi-crystalline product. Filtration through 1.5 kg of aluminum oxide (eluent: petroleum ether – benzene (1:1)) gave 49.8 g of a purified, crystalline, product, mp 137–143°C; ν_{max} (KBr):1750 (enol acetates), 1730 (3-acetate), 1250 and 1230 cm^{-1} (acetates); δ (90 MHz): 0.82 and 1.00 (s's, 18- and 19-CH_3), 1.85 (s, 3H, 21-CH_3), 2.00 (s, 3H, 3-acetate), 2.15 (s, 3H, 20-acetates), 5.40 (m, 1H, 6-H).

From 27 ml of a 1.5 *M* ethereal methyllithium solution, the solvent was removed *in vacuo* under slight nitrogen pressure. The residue was dissolved in 40 ml of absolute dimethoxyethane at 5°C, the solution was treated with 10 mg of triphenylmethane and there was added, dropwise and with stirring, a solution of 4 g of the above-described mixture of the enol acetates **11**, mp 137–143°C, in 100 ml of absolute dimethoxyethane. When 90 ml of the enol acetate solution had been used, the red colour almost disappeared. The addition was interrupted and the reaction mixture was treated with a solution of 0.9 ml of dimethyl carbonate in 3 ml of dimethoxyethane. After 5 min the product was poured into cold 2 *N* hydrochloric acid, the precipitate was extracted with ether, and the ethereal solution was washed with water and was dried over sodium sulfate. Removal of the solvent gave 3.53 g of a foam which crystallized upon addition of a few drops of ether. Recrystallization from dichloromethane–methanol

[4]We pay tribute to Dr. Pascher and express our sincere appreciation to the management and staff of the analytical laboratories.

[5]The name 'acid fraction' merely indicates its origin, not its acidity.

Can. J. Chem. Downloaded from www.nrcresearchpress.com by 210.87.254.6 on 09/05/12
For personal use only.

afforded 1.05 g (30% yield) of *3β-acetoxy-17-methoxycarbonyl-5-pregnen-20-one* (**14***a*), mp 178–181°C. A sample was recrystallized twice from dichloromethane–methanol for analysis; colourless, fine plates, mp 182–184°C; $[\alpha]_D^{23}$ +45° (*c* 1.000, $CHCl_3$); ν_{max} (KBr): 1745 (acetate), 1735 (methyl ester), 1705 (ketone), 1250 cm^{-1} (acetate); δ (90 MHz): 0.70 and 0.98 (s's, 6H, 18- and 19-CH_3), 2.12 (s, 3-acetate), 2.18 (s, $COCH_3$), 3.70 (s, $OCOCH_3$), 4.42 (m, 3α-H), 5.40 (t, 6-H). *Anal.* calcd. for $C_{25}H_{36}O_5$: C 72.08, H 8.71; found: C 71.98, H 8.87.

The mother liquors of the crystallization were taken to dryness and chromatographed on 60 g of aluminum oxide. Elutions with benzene gave 93 mg (2.5%) of *3α-hydroxy-17-methoxycarbonyl-5-pregnen-20-one* (**14**), mp 221–223°C. A sample was recrystallized twice from methanol for analysis; colourless needles, mp 221–223°C; $[\alpha]_D^{23}$ +63° (*c* 1.000, $CHCl_3$); ν_{max} (KBr):3500 (OH), 1735 (methyl ester), 1700 cm^{-1} (ketone); δ (90 MHz):0.71 and 0.98 (s's, 6H, 18- and 19-CH_3), 2.18 (s, 3H, $COCH_3$), 3.70 (s, 3H, $OCOCH_3$), 5.40 (t, 6-H). *Anal.* calcd. for $C_{23}H_{34}O_4$: C 73.76, H 9.15; found: C 73.75, H 9.23.

The other eluates were acetylated in 6 ml of pyridine with 3 ml of acetic anhydride at reflux temperature for 45 min. The usual work-up gave 2.78 g of a product which, upon crystallization from ether–hexane, afforded 1.43 g (44%) of acetylated starting material, *pregnenolone acetate* (**10***a*), mp 149–151°C, identified by the determination of a mixture melting point and by comparison of its infrared spectrum with that of an authentic sample. Considering the recovery of starting material, the yield of 3β-acetoxy-17-methoxycarbonyl-5-pregnen-20-one (**14***a*) amounted to 53%, that of 3β-hydroxy-17-methoxycarbonyl-5-pregnen-20-one (**14**) to 4.5%.

Partial Hydrolysis of 3β-Acetoxy-17-methoxycarbonyl-5-pregnen-20-one (14a)

To a solution of 800 mg of the acetoxy keto ester **14***a*, mp 178–181°C, in 200 ml of methanol, a solution of 230 mg of potassium bicarbonate in 10 ml of water and 25 ml of methanol was added. The mixture was stirred at room temperature and the course of the reaction was followed by tlc analysis. After 5 days, no starting material was left and the solution was poured into ice water. The precipitate was extracted with ether, the ethereal solution was washed with water, and was dried over sodium sulfate. Evaporation of the solvent provided 697 mg (94% yield) of *3β-hydroxy-17-methoxycarbonyl-5-pregnen-20-one* (**14**), mp 218–221°C. Recrystallization from methanol afforded 610 mg of the same product, melting at 221–223°C. The material was found identical, by the determination of a mixture melting point and by the comparison of the infrared and nmr spectra, with that described in the previous section.

3β-Hydroxy-17-methoxycarbonyl-5-pregnen-20-one (14) from the Enol Acetates 11 without Isolation of 3β-Acetoxy-17-methoxycarbonyl-5-pregnen-20-one (14a)

Ether was removed *in vacuo* from 140 ml of a 0.7 *M* methyllithium solution. The residue was dissolved in 200 ml of absolute dimethoxyethane and a solution of 10 g of the mixture of enol acetates **11**, mp 137–143°C, in 250 ml of absolute dimethoxyethane was added dropwise, with vigorous stirring, at 0°C, 2,2′-bipyridyl serving as indicator. The red colour was almost discharged when 200 ml of the solution (corresponding to 8 g of the enol acetates) had been consumed. The addition was stopped, and the mixture was treated with 1.5 ml of dimethyl carbonate in 10 ml of dimethoxyethane. After 5 min of stirring at 0°C, 200 ml of a 20% ammonium chloride solution was added. The product was extracted with ether, the ethereal solution was washed with water and was dried over sodium sulfate. Removal of the solvents gave 6.49 g of a brown foam (ν_{max} (KBr): 3540 (sharp) and 3400 (br) (OH), 1735 (esters), 1708 (ketone), 1250 (esters); δ (60 MHz): 0.7 and 0.82 (18-CH_3), 1.05 (s, 19-CH_3), 2.18 and 2.20 (s's, $COCH_3$), 3.73 (s, $COOCH_3$), 5.40 (m, 5-H)). This product was dissolved without purification in 250 ml of methanol and a solution of 1 g of potassium bicarbonate in 40 ml of water and 100 ml of methanol was added. The mixture was left at room temperature for 22 h and then poured into cold water. The product was extracted with ether, the ethereal layer was washed with water, and was dried over sodium sulfate. Removal of the solvents gave 6.28 g of a semisolid product which was chromatographed on 150 g of aluminum oxide, activity IV. Petroleum ether – benzene mixtures (1:1 and 1:4) eluted 2.25 g (30%) of *17-methoxycarbonylpregnenolone* (**14**), mp 216–220°C; benzene–ether (1:1) and pure ether eluted 3.2 g of *pregnenolone* (**10**) (50.5% yield). The identities of the products were established in the usual fashion. Considering the recovery of pregnenolone (**10**), the yield of 17-methoxycarbonylpregnenolone (**14**) amounted to 60%.

3β-Hydroxy-17α-methoxycarbonyl-5-pregnen-20-one (14) from the Lithium Enolates 12 and 12a by Carboxylation and Subsequent Methylation

A mixture of the lithium enolates **12** and **12***a*, prepared as described above from 1 g of the isomeric mixture of the enol acetates **11**, mp 137–143°C, in 50 ml of ether, and from 6 ml of an ethereal 1.5 *M* methyllithium solution, was treated in the original solution in the presence of 2,2′-bipyridyl which served as indicator, with an excess of solid carbon dioxide (solid carbon dioxide remaining in the mixture). The product was poured into ice water and the organic material was extracted with ether. The ethereal solution was washed with water and dried. Evaporation of the solvent gave 227 mg of a product which was dissolved in 1 ml of pyridine and treated at reflux temperature for 90 min with 0.5 ml of acetic anhydride. The usual work-up provided 300 mg of a solid which was recrystallized from ether–hexane to give 230 mg of *pregnenolone acetate* (**10***a*), mp 149–151°C. The identity of the product was established by the determination of a mixture melting point and by the comparison of its infrared spectrum with that of an authentic sample.

The aqueous solution remaining after the ether extraction was acidified with 2 *N* sulfuric acid to the Congo-blue reaction and the thus precipitated *3β-hydroxy-17-carboxy-5-pregnen-20-one* (**15**) was extracted with ether. The ethereal solution was dried and was then treated with 50 ml of a 2% ethereal diazomethane solution. The excess diazomethane was destroyed with a few drops of acetic acid and the solvents were removed to give 515 mg (51.5% yield) of *3β-hydroxy-17-methoxycarbonyl-5-pregnen-20-one* (**14**), mp 212–217°C. Considering the recovery of acetylated starting material (**10***a*), the yield of the unpurified hydroxy keto ester **14** amounted to 63%. One recrystallization from dichloromethane–methanol gave 437 mg of pure product, mp 221–223°C, identified by the determination of a mixture melting point and by the comparison of its ir and nmr spectra with those of an authentic sample (see above).

17-Methoxycarbonyl-4-pregnene-3,20-dione (13)

(a) By Jones' Oxidation

To a solution of 1 g of the hydroxy keto ester **14**, mp 221–223°C, in 50 ml of absolute acetone, there was added, at 0°C, dropwise and with stirring, 1 ml of Jones' reagent (16), in the course of 15 min. The mixture was left at 0°C for another 10 min and then poured into ice water. The organic product was extracted with ether, the ethereal solution was washed with water, and was dried over sodium sulfate.

Can. J. Chem. Downloaded from www.nrcresearchpress.com by 210.87.254.6 on 09/05/12
For personal use only.

Removal of the solvent gave 985 mg of a crystalline product which was dissolved in 30 ml of methanol and 0.5 ml of water containing a drop of concentrated hydrochloric acid. The solution was warmed to 50°C for 5 min, cooled, and diluted with 300 ml of cold water. The mixture was extracted with ether, the ethereal solution was washed with water, and was dried over sodium sulfate. Evaporation of the solvent gave 975 mg (98% yield) of crystalline 17-methoxycarbonyl-4-pregnene-3,20-dione (**13**), mp 178–184°C. Recrystallization from ether–hexane gave 845 mg (85% yield) of pure product, mp 190–192°C. A sample was recrystallized twice from ether–hexane for analysis; colourless prisms, mp 190–192°C; $[\alpha]_D^{23}$ +192° (*c* 1.000, $CHCl_3$); λ_{max} (EtOH): 240 nm (log ε 4.2); ν_{max} (KBr): 1735 (ester), 1705 (20-ketone), 1673 and 1618 cm^{-1} (Δ^4-3-keto doublet); δ (60MHz): 0.71 (s, 3H, 18-CH_3), 0.98 (s, 3H, 19-CH_3), 2.10 (s, methyl ketone), 3.70 (s, $COOCH_3$), 5.70 (4-H). *Anal.* calcd. for $C_{23}H_{32}O_4$: C 74.16, H 8.66; found: C 74.04, H 8.50.

(b) By Oppenauer Oxidation

A solution of 300 mg of 3β-hydroxy-17-methoxycarbonyl-5-pregnen-20-one (**14**), mp 221–223°C, in 30 ml of absolute benzene was refluxed for 18 h with 267 mg of aluminum *tert*-butoxide and 1 ml of freshly redistilled cyclohexanone. The mixture was cooled and poured into ice water. The precipitate was extracted with ether, the organic solution was washed with water, and was dried over sodium sulfate. Evaporation of the solvent left 287 mg (96% yield) of crystalline diketo ester **13**. Recrystallization from ether–hexane provided 238 mg (80% yield) of pure product, mp 188–190°C. The identity of the material with the product described under (*a*) was established by the usual methods.

3,20-Bis(ethylenedioxy)-17-methoxycarbonyl-5-pregnene (16)

From a solution of 1.86 g of the diketo ester **13**, mp 188–190°C, and of 75 mg of *p*-toluenesulfonic acid in 200 ml of freshly distilled ethylene glycol, the solvent was slowly distilled at 78–80°C at 0.5 Torr, during 6 h. The residue was cooled and poured into an ice-cold saturated sodium bicarbonate solution. The product was extracted with dichloromethane, the organic layer was washed with water and was dried over sodium sulfate. Removal of the solvent gave 2.35 g of a solid which, upon crystallization from ether, gave 2.02 g (88% yield) of diketal **16**, mp 185–187°C. A sample was recrystallized twice from ether–dichloromethane for analysis; colourless needles, mp 187–189°C; $[\alpha]_D^{23}$ +23° (*c* 1.000, $CHCl_3$); ν_{max} (KBr): 1730 and 1255 (ester), 1090 and 1080 cm^{-1} (ketals); δ (90 MHz): 0.98 and 1.1 (s's, 18- and 19-CH_3), 1.60 (s, 3H, 21-CH_3), 3.7 (s, 3H, $COOCH_3$), 3.9 (s, 8H, ketals); mass calcd. for $C_{27}H_{40}O_6$: 460; found: 460. *Anal.* calcd. for $C_{27}H_{40}O_6$: C 70.40, H 8.75; found: C 70.06, H 8.65.

3,20-Bis(ethylenedioxy)-17-hydroxymethyl-5-pregnene (17)

A solution of 1 g of the diketal ester **16**, mp 185–187°C, in 200 ml of absolute tetrahydrofuran was added dropwise and with vigorous stirring to a suspension of 1.75 g of lithium aluminum hydride in 100 ml of absolute tetrahydrofuran. The mixture was refluxed for 15 h with continuous stirring. The excess reagent was destroyed with ice, the organic solution was filtered and was dried over sodium sulfate. Removal of the solvent gave 930 mg of a solid which, upon recrystallization from ether, gave 880 mg (93% yield) of the 17-hydroxymethyl diketal **17**, mp 172–175°C. A sample was recrystallized twice from ether for analysis; colourless needles, mp 175–177°C; $[\alpha]_D^{23}$ +15° (*c* 1.000, $CHCl_3$); ν_{max} (KBr): 3360 (br) and 3520 (hydroxyl), 1105 and 1080 cm^{-1} (ketals); δ (90 MHz): 0.92 and 1.02 (s's, 18- and 19-CH_3), 1.40 (s, 3H, 21-CH_3), 3.85 (2H, dd, ν = 21 Hz, *J* = 8 Hz, 17-CH_2OH), 3.90 (s, 8H, ketals), 5.33 (m, 1H, 6-H); mass calcd. for $C_{26}H_{40}O_5$: 432; found: 432. *Anal.* calcd. for $C_{26}H_{40}O_5$: C 72.19, H 9.32; found: C 72.51, H 9.25.

17¹-Acetate 17a

A solution of 500 mg of the hydroxy diketal **17**, mp 172–175°C, in 2.5 ml of pyridine was treated at room temperature for 18 h with 0.3 ml of acetic anhydride. After addition of a few drops of methanol, the solvents were removed under reduced pressure and the product was dried by repeated evaporation of its benzene solutions. Thus, 543 mg (99.8% yield) of crystalline acetate **17***a*, mp 146–150°C, was obtained. Recrystallization from ether–hexane gave 491 mg (86% yield) of pure 3,20-bis(ethylenedioxy)-17-acetoxymethyl-5-pregnene (**17***a*), mp 150–152°C. A sample was recrystallized twice from ether–hexane for analysis; colourless needles, mp 152–154°C; $[\alpha]_D^{23}$ +31° (*c* 1.000, $CHCl_3$); ν_{max} (KBr): 1735 and 1250 (acetate), 1100 and 1080 cm^{-1} (ketals); δ (90 MHz): 0.96 and 1.05 (s's, 18- and 19-CH_3), 1.42 (s, 3H, 21-CH_3), 3.90 (s, 8H, ketals), 4.26 (dd, ν = 18 Hz, *J* = 12 Hz, 2H, 17-CH_2OAc), 5.33 (m, 1H, 6-H). *Anal.* calcd. for $C_{28}H_{42}O_6$: C 70.85, H 8.92; found: C 70.74, H 8.85.

17¹-Benzoate (17b)

A solution of 100 mg of the hydroxymethyl diketal **17**, mp 172–175°C, in 0.25 ml of absolute pyridine was left with 0.1 ml of benzoyl chloride at room temperature for 18 h. Subsequently, the mixture was diluted with ether, the ethereal solution was washed with a cold 2 *N* sodium carbonate solution and with water, and was dried over sodium sulfate. The solvents were evaporated and the product was dried for 24 h in high vacuum. Thus, 120 mg of crude, solid, 3,20-bis-(ethylenedioxy)-17-benzoyloxymethyl-5-pregnene (**17***b*) was obtained; ν_{max} (KBr): 1720 and 1270 (benzoate), 1100 cm^{-1} (ketals). The product was converted without purification to 17-benzoyloxymethylprogesterone (**9***b*) (see below).

17¹-Pivalate (17c)

A solution of 100 mg of the hydroxymethyl diketal **17**, mp 172–175°C, in 0.25 ml of absolute pyridine was left for 18 h at room temperature with 0.1 ml of trimethylacetyl chloride. The mixture was taken to dryness *in vacuo* and the solid residue was dried in high vacuum for 24 h. This gave 118 mg of crude, solid, 3,20-bis(ethylenedioxy)-17-trimethylacetoxymethyl-5-pregnene (**17***c*); ν_{max} (KBr): 1725 and 1270 (ester), 1100 (ketals). This product was transformed without purification into 17-hydroxymethylprogesterone pivalate (**9***c*) (see below).

17¹-Tosylate (17d)

A solution of 200 mg of the hydroxy diketal **17**, mp 173–176°C, and of 300 mg of *p*-toluenesulfonyl chloride, mp 67–69°C, in 5 ml of absolute pyridine was flushed with nitrogen and the flask was sealed. The mixture was heated for 3 days at 50°C. The product was then poured into 100 ml of an ice-cold saturated sodium bicarbonate solution, the precipitate was extracted with ether, the ethereal layer was washed with a cold saturated sodium bicarbonate solution and with water, and was dried over sodium sulfate. Removal of the solvent *in vacuo* gave 230 mg (85%) of crystalline 3,20-bis(ethylenedioxy)-17-tosyloxymethyl-5-pregnene (**17***d*), mp 130–138°C. One recrystallization from ether gave 189 mg (70% yield) of purified product, mp 149–151°C; λ_{max} (EtOH): 227 nm (log ε 4.1). This product was not further purified but used directly in the formation of 17-methylprogesterone (**19**) (see below).

17-Hydroxymethylprogesterone (9)

A solution of 100 mg of 3,20-bis(ethylenedioxy)-17-hydroxymethyl-5-pregnene (**17**), mp 173–176°C, and of 50 mg of *p*-toluenesulfonic acid in 50 ml of absolute acetone was allowed to stand for 10 h at room temperature. Ice and a potassium

Can. J. Chem. Downloaded from www.nrcresearchpress.com by 210.87.254.6 on 09/05/12
For personal use only.

bicarbonate solution were added and the precipitate was extracted with ether. The ethereal solution was washed with water and was dried over sodium sulfate. Removal of the solvent gave 82 mg (86% yield) of crystalline 17-hydroxymethylprogesterone (**9**), mp 216–220°C. Recrystallization from dichloromethane–ether gave 74 mg (80% yield) of pure product, mp 220–222°C, identified by the determination of a mixture melting point and by the comparison of the infrared, ultraviolet, and nmr spectra with those of an authentic sample (1).

*17-Acetoxymethylprogesterone (**9a**)*

*(a) From the Acetoxy Diketal **17a***

A solution of 300 mg of 3,20-bis(ethylenedioxy)-17-acetoxymethyl-5-pregnene (**17a**), mp 150–152°C, and of 35 mg of *p*-toluenesulfonic acid in 140 ml of absolute acetone was left at room temperature for 7 h. The mixture was worked up as described above for 17-hydroxymethylprogesterone (**9**). Thus, 244 mg (99% yield) of crude acetate **9a** was obtained. Recrystallization from ether gave 195 mg (80% yield) of pure 17-acetoxymethylprogesterone (**9a**), mp 169–171°C, identified by the determination of a mixture melting point and by the comparison of the infrared, ultraviolet, and nmr spectra with those of an authentic sample (1).

*(b) From 17-Hydroxymethylprogesterone (**9**)*

A solution of 200 mg of 17-hydroxymethylprogesterone (**9**), mp 216–220°C, in 1 ml of pyridine was treated at room temperature for 12 h with 0.5 ml of acetic anhydride. The excess acetic anhydride was destroyed with methanol and the mixture was taken to dryness *in vacuo*, and was further dried in high vacuum for 24 h. The crystalline residue (220 mg, 98% yield) melted at 160–167°C. Recrystallization from ether–hexane gave 178 mg (85% yield) of pure 17-acetoxymethylprogesterone (**9a**), mp 169–171°C, the identity of which was established in the usual fashion by comparison with an authentic sample (1).

*17-Benzoyloxymethylprogesterone (**9b**)*

A solution of the crude 3,20-bis(ethylenedioxy)-17-benzoyloxymethyl-5-pregnene (**17b**) (120 mg) described above and of 20 mg of *p*-toluenesulfonic acid in 25 ml of absolute acetone was left at room temperature for 12 h and was then poured into cold water. The mixture was extracted with ether, the ethereal solution was washed with a cold sodium bicarbonate solution and with water, and was dried with sodium sulfate. Removal of the solvent left 82 mg (81% yield) of crystalline benzoate **9b**, mp 172–180°C. Recrystallization from ether–hexane gave 57 mg (56%) of purified product, mp 183–185°C. For analysis a sample was recrystallized twice from ether–hexane; white needles, mp 184–186°C; $[\alpha]_D^{30}$ +42° (*c* 1.000, $CHCl_3$); λ_{max} (EtOH): 238 nm (log ε 4.15); ν_{max} (KBr): 1720 (benzoate), 1700 (20-ketone), 1675 and 1620 (Δ^4-3-keto doublet), 1610 and 1530 (aromatic), 1270 cm^{-1} (benzoate); δ (60 MHz): 0.8 (s, 3H, 18-CH_3), 1.16 (s, 3H, 19-CH_3), 2.18 (s, 3H, CO-CH_3), 4.26 (dd, ν = 21 Hz, *J* = 12 Hz, 17-CH_2—O—CO—), 5.80 (s, 1H, 4-H), 7.3 (m, 5H, aromatic protons). *Anal.* calcd. for $C_{29}H_{36}O_4$: C 77.64, H 8.09; found: C 77.68, H 8.21.

*17-Trimethylacetoxymethylprogesterone (**9c**)*

A solution of the crude 3,20-bis(ethylenedioxy)-17-trimethylacetoxymethyl-5-pregnene (**17c**) (118 mg) described above and of 20 mg of *p*-toluenesulfonic acid in 25 ml of absolute acetone was left at room temperature for 12 h and was then poured into cold water. The mixture was extracted with ether, the ethereal solution was washed with a cold saturated sodium bicarbonate solution and with water, and was dried over sodium sulfate. Removal of the solvent gave 89 mg (90% yield) of crystalline pivalate **9c**, mp 160–168°C. Three recrystallizations from ether–hexane gave 59 mg (61% yield) of pure pivalate **9c**, mp 169–171°C. For analysis a sample was recrystallized twice from ether–hexane; colourless prisms, mp 175–177°C; $[\alpha]_D^{30}$ +85° (*c* 1.000, $CHCl_3$); λ_{max} (EtOH): 237 nm (log ε 4.1); ν_{max} (KBr): 1725 (ester), 1708 (20-ketone), 1675 and 1620 (Δ^4-3-keto doublet), 1270 cm^{-1} (ester); δ (90 MHz): 0.72 (s, 3H, 18-CH_3), 1.10 (s, 9H, $(CH_3)_3C$—COO), 1.18 (s, 3H, 19-CH_3), 2.16 (s, 3H, CO—CH_3), 4.26 (dd, ν = 18 Hz, *J* = 12 Hz, 2H, CH_2—O—CO—), 5.80 (s, 1H, 4-H); mass calcd. for $C_{27}H_{40}O_4$: 428; found: 428. *Anal.* calcd. for $C_{27}H_{40}O_4$: C 75.66, H 9.41; found: C 75.80, H 9.43.

*17-Methylprogesterone (**19**)*

A solution of 180 mg of the tosyloxymethyl diketal **17d**, mp 149–151°C, (see above) in 20 ml of absolute tetrahydrofuran was added dropwise and with vigorous stirring to a suspension of 200 mg of lithium aluminum hydride in 25 ml of absolute tetrahydrofuran. Subsequently, the mixture was refluxed for 18 h with continuous stirring and was then cooled. The excess reagent was destroyed by addition of ice. The organic solution was filtered and dried over sodium sulfate. Removal of the solvent gave 129 mg of crude *3,20-bis(ethylenedioxy)-17-methyl-5-pregnene* (**18**), transparent to ultraviolet light in the region of 227 nm; ν_{max} (KBr): 1100 and 1080 cm^{-1} (ketals); δ (90 MHz): 0.85 and 1.12 (s's, 18- and 19-CH_3), 1.23 (s, 17-CH_3), 1.43 (s, 21-CH_3), 3.9 (s, ketals), 5.35 (m, 6-H).

Without purification, 120 mg of this crude diketal (**18**) and 60 mg of *p*-toluenesulfonic acid were dissolved in 60 ml of absolute acetone and the mixture was allowed to stand for 12 h at room temperature. Subsequently, the product was diluted with ether, the ethereal solution was washed with a sodium carbonate solution and with water, and was dried over sodium sulfate. Removal of the solvent gave 90 mg (91% from tosylate **17d**) of crude, crystalline, *17α-methylprogesterone* (**19**), mp 116–122°C. Recrystallization from ether–hexane gave 64 mg (65% from tosylate **17d**) of 17α-methylprogesterone (**19**), mp 122–125°C. A second recrystallization from methanol raised the melting point to 129–130°C. The identity of the product was established by the comparison of its infrared spectrum with that of an authentic sample and by the determination of a mixture melting point.

Acknowledgements

Sincere thanks are extended to Dr. T. Iwadare for fruitful discussions, and to Mrs. J. Capitaine and Mr. J. Zee for excellent collaboration. We gratefully acknowledge the devoted technical assistance of Mrs. G. Pelletier and Miss D. Thibault. Part of this study was performed pursuant to contract NIH-NICHD No. 72-2714 with the National Institutes of Health, U.S. Department of Health, Education, and Welfare, to whom we are also indebted for the majority of the biological assays, summarily mentioned in this paper. We express our gratitude for this support and cooperation, especially to Dr. M. Karten of the NICHD, Bethesda, MD. We also assure Dr. E. G. Shipley and her coworkers of our appreciation for some tests carried out at Endocrine Laboratories, Madison WI. We acknowledge with sincerest thanks the financial assistance of the National Research Council of Canada, of the Ministère de l'Education du Québec, and of Ayerst Laboratories, Montreal.

1. CH. R. ENGEL and D. MUKHERJEE. Steroids, **29**, 827 (1977).
2. CH. R. ENGEL, G. DIONNE, and D. MUKHERJEE. 29th International Symposium on the Chemistry of Natural Products, Ottawa, Canada, June 24–29, 1974. Abstract 43A.
3. CH. R. ENGEL, D. MUKHERJEE, M. N. ROY CHOWDHURY, G. RAMANI, and V. S. SALVI. 4th International Symposium on Hormonal Steroids, Mexico, September 2–7, 1974. Symposium Abstract S-17(2).
4. CH. R. ENGEL, D. MUKHERJEE, M. N. ROY CHOWDHURY, G. RAMANI, and V. S. SALVI. J. Steroid Biochem. **6**, 585 (1975).
5. (*a*) CH. R. ENGEL and G. J. BEAUDOIN. Tetrahedron Lett. 1887 (1968); (*b*) CH. R. ENGEL, D. MUKHERJEE, and G. J. BEAUDOIN. Steroids, **21**, 857 (1973).
6. (*a*) D. H. R. BARTON, J. M. BEATON, L. E. GELLER, and M. M. PECHET. J. Am. Chem. Soc. **82**, 2640 (1960); **83**, 4076 (1961); (*b*) D. H. R. BARTON and J. M. BEATON. J. Am. Chem. Soc. **82**, 2641 (1960); **83**, 4083 (1961).
7. (*a*) A. L. NUSSBAUM and C. H. ROBINSON. Tetrahedron, **17**, 35 (1962); (*b*) K. HEUSLER and J. KALVODA. Angew. Chem. Int. Ed. **3**, 525 (1964).
8. CH. R. ENGEL, K. F. JENNINGS, and G. JUST. J. Am. Chem. Soc. **78**, 6153 (1956).
9. (*a*) R. DEGHENGHI and R. GAUDRY. J. Am. Chem. Soc. **83**, 4668 (1961); Tetrahedron Lett. 498 (1962); (*b*) R. DEGHENGHI, C. REVESZ, and R. GAUDRY. J. Med. Chem. **6**, 301 (1963); (*c*) R. DEGHENGHI. U.S. Patent No. 3,219,672 (Nov. 23, 1965).
10. (*a*) M. J. WEISS, R. E. SCHAUB, J. F. POLETTO, J. R. ALLEN, JR., and C. J. COSCIA. Chem. Ind. 118 (1963); (*b*) M. J. WEISS, R. E. SCHAUB, J. R. ALLEN, JR., J. F. POLETTO, C. PIDACKS, R. D. CONROW, and C. J. COSCIA. Tetrahedron, **20**, 357 (1964).
11. (*a*) G. STORK, P. ROSEN, and N. GOLDMAN. J. Am. Chem. Soc. **83**, 2965 (1961); (*b*) G. STORK, P. ROSEN, N. GOLDMAN, R. V. COOMBY, and J. TSUJI. J. Am. Chem. Soc. **87**, 275 (1965).
12. H. HOUSE. Rec. Chem. Prog. **28**, 99 (1967).
13. (*a*) C. W. MARSHALL, T. H. KRITCHEVSKY, S. LIEBERMAN, and T. F. GALLAGHER. J. Am. Chem. Soc. **70**, 1937 (1948); (*b*) T. H. KRITCHEVSKY and T. F. GALLAGHER. J. Biol. Chem. **79**, 507 (1949).
14. L. F. FIESER and HUANG-MINLON. J. Am. Chem. Soc. **71**, 1840 (1949).
15. J. ZEE. M.Sc. Thesis, Université Laval, 1973. pp. 36, 37, 67, 68.
16. (*a*) K. BOWDEN, J. M. HEILBRON, E. R. H. JONES, and B. C. L. WEEDON. J. Chem. Soc. 39 (1946); (*b*) A. BOWERS, H. G. HALSALL, E. R. H. JONES, and A. J. LEMIN. J. Chem. Soc. 2548 (1953).
17. H. HEUSSER, CH. R. ENGEL, P. TH. HERZIG, and PL. A. PLATTNER. Helv. Chim. Acta, **33**, 2229 (1950).
18. CH. R. ENGEL and H. JAHNKE. Can. J. Biochem. Physiol. **35**, 1047 (1957).
19. M. K. MCPHAIL. J. Physiol. **83**, 145 (1935).
20. S. RAKHIT and CH. R. ENGEL. Can. J. Chem. **40**, 2163 (1962).

Can. J. Chem. Downloaded from www.nrcresearchpress.com by 210.87.254.6 on 09/05/12
For personal use only.

Cyanoethylations and Michael additions. VIII.[1] The use of preformed enolate ions in Michael additions. Part I[2,3]

GERVAIS DIONNE[4] AND CH. R. ENGEL

Department of Chemistry, Laval University, Quebec, P.Q., Canada G1K 7P4

Received August 4, 1977

GERVAIS DIONNE and CH. R. ENGEL. Can. J. Chem. **56**, 419 (1978).

Some Michael additions involving preformed enolate ions as nucleophiles were studied. High regioselectivity was observed in the additions of the lithium enolate of 2-methylcyclohexanone to ethyl acrylate and to methyl β-chloroacrylates, the latter reactions being by far superior to those involving classical Michael additions. The addition to *cis*- and *trans*-β-chloroacrylates proceeded with appreciable stereoselectivity. Michael addition of a preformed enolate ion, derived from a ketone, to a *cis*-β-chloroacrylate constitutes an efficient pathway to 6-substituted α-pyrones, as exemplified by the synthesis of 5,6,7,8-tetrahydrocoumarin from cyclohexanone.

GERVAIS DIONNE et CH. R. ENGEL. Can. J. Chem. **56**, 419 (1978).

On rapporte des additions de Michael impliquant comme nucléophiles des ions énolate préformés. Une régiosélectivité marquée s'observe lors d'additions de l'énolate de lithium de la méthyl-2 cyclohexanone à l'acrylate d'éthyle et aux β-chloroacrylates de méthyle, les dernières réactions s'avérant bien supérieures à des réactions de Michael classiques. Les additions aux *cis*- et *trans*-β-chloroacrylates procèdent en plus avec une stéréosélectivité appréciable. L'addition de Michael d'un *cis*-β-chloroacrylate et d'un ion énolate préformé, dérivé d'une cétone, représente un procédé efficace pour le formation d'α-pyrones 6-substituées, comme le montre la synthèse de la tétrahydro-5,6,7,8 coumarine à partir de la cyclohexanone.

Our success in employing preformed enolate ions for α-alkoxycarbonylations of ketones, useful for the synthesis of 17-substituted 20-keto steroids (4), as well as our interest in α-pyrone syntheses, prompted us to investigate the potential of lithium enolates for Michael additions of relevance to the preparation of α-pyrones. We were particularly interested in syntheses involving acrylates and β-chloroacrylates as electrophiles.

In a preliminary exploration, we studied the replacement of the not highly regioselective Michael addition of 2-methylcyclohexanone (**1**) to an alkyl acrylate under classical conditions (catalysis with *tert*-butoxide) (5) by a reaction involving a preformed enolate ion as Michael donor (Scheme 1). The reaction of ethyl acrylate with the lithium enolate **3**, prepared via the enol acetate **2**, gave a mixture from which we isolated only products arising from addition in position 2, the 'normal' Michael addition product **4** (isolated in approximately 28% yield) and products arising from a double Michael addition, followed by cyclizations: the hydroxy dicarbethoxy derivative **5** (obtained in the pure state in 25% yield), formed by an aldol cyclization of the di-addition product, and the diketo bicyclo[3.3.1]nonane **6** (isolated in 17% yield), formed by a Dieckmann condensation of the di-addition adduct.

The structures of the products are apparent from their analytical and spectroscopic data. In the mass spectrum of the mono-addition product **4** appear, apart from the molecular peak (*m/e* 212), a peak at *m/e* 167 (*M* − OEt), and one at *m/e* 112 (resulting from a McLafferty rearrangement). The product was further characterized by its 2,4-dinitrophenylhydrazone **4***a*. The relatively low infrared frequency of one of the ester groups of the aldol condensation product **5** (1715 cm^{-1} in CCl_4) seems to indicate that its carbonyl group is chelated (6). We also note the particularly high frequency of the carbonyl absorptions of the keto groups of the Dieckmann cyclization product **6** (1750 and 1730 cm^{-1} in KBr) which is not surprising since β-diketones which are not enolizable in a classical fashion are known to show high infrared absorption frequencies (7). For analytical and spectral details we refer to the Experimental.

The main result of the experiment is the confirmation that the use of preformed enolate ions as nucleophiles has, over classical Michael donors, the advantage of a significantly higher regioselectivity.[5]

[1]For paper VII, see ref. 1.

[2]This communication represents paper IV in our series on α-pyrones. For paper III, see ref. 2.

[3]The results of this paper were part of communications to the 9th International (IUPAC) Symposium on the Chemistry of Natural Products, Ottawa, Ont., June 24–28, 1974 (see ref. 3).

[4]Abbreviated from part of the doctoral thesis of G. Dionne, presented to the School of Graduate Studies, Laval University, Quebec, P.Q., 1975.

[5]Indeed, although in the case of the performance of the reaction under classical Michael conditions (5) the mono-addition product contained 7–12% of the adduct arising from addition in position 6, no 6-addition product could be detected in our reaction mixture.

Can. J. Chem. Downloaded from www.nrcresearchpress.com by 210.87.254.5 on 09/05/12
For personal use only.

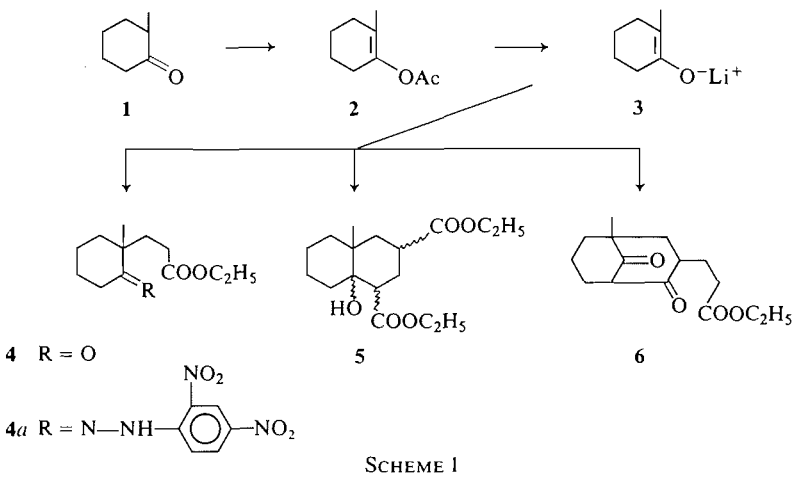

SCHEME 1

The fact that a greater proportion of di-addition products was formed in the reaction under investigation, in comparison with the classical Michael addition (5), was only of secondary interest and not surprising. In 1972, Kretchmer *et al.* (8) reported that in the reaction of methyl vinyl ketone with the iodomagnesium enolate of 3-methylcyclohexanone a di-addition product was formed, and Stork and coworkers (9) have shown that polyadditions of Michael electrophiles to preformed lithium enolates may be avoided when the electrophile carries a trialkylsilyl substituent in position α to the carbonyl function, and that such a substituent may readily be removed after the Michael addition (see also ref. 10).[6]

In view of our interest in the synthesis of α-pyrones, we now turned our attention to the attachment of a 2-butenoic acid or ester moiety in position α to a carbonyl group. For that purpose the addition of a preformed enolate ion, derived from a carbonyl compound, to a propiolic ester could have been taken into consideration; however, in this case again, the addition of a second molecule of the Michael electrophile to the anion formed by the first addition had to be contended with. It seemed logical that the second addition would be suppressed if the propiolic ester were to be replaced by a β-halo acrylic ester since, by elimination of the halogen anion from the anionic mono-addition product, the negative charge responsible for the second addition would be removed (Scheme 2).

In a first experiment (Scheme 3), we thus allowed the lithium enolate **3** of 2-methylcyclohexanone (**1**) to react with methyl *trans*-β-chloroacrylate. We obtained in over 40% crude yield (the completely pure product was isolated in 25% yield) the *trans*-cyclohexylacrylate **7**, arising from addition in position 2.

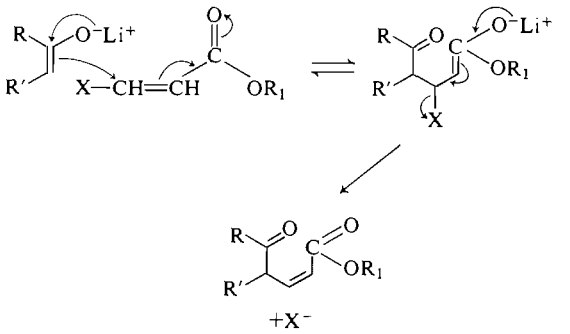

SCHEME 2

No product formed by addition in position 6 could be detected.

Addition of methyl *cis*-β-chloroacrylate to the lithium enolate **3** gave a mixture of three products arising from a Michael addition in position 2. Indeed, we isolated by dry-column chromatography in 18% yield the *trans* acrylic ester **7**, in 29% yield the *cis* isomer **8**, and in 20% yield diketone **9**, which represents the Dieckmann condensation product of the *cis* keto ester **8**. The structure of these products follow from their analytical and spectral characteristics (see Experimental). The *trans* configuration of adduct **7** and the *cis* configuration of its isomer **8** are evident from the coupling constants of the olefinic protons (16 Hz for compound **7**, 12 Hz for compound **8**). The ultraviolet spectrum of the bicyclic diketone **9**, which shows a maximum (in ethanol) at 225 nm, agrees well with that of an α,β-unsaturated β-monosubstituted ketone, and one notes in the infrared (film) a doublet at 1680 and 1615

[6]Under the circumstances, we made no attempt to minimize the formation of products arising from polyadditions by changing the experimental conditions. However, in applying Michael additions involving preformed enolate ions to the synthesis of α-pyrones, we chose Michael electrophiles, the constitution of which excludes the formation of polyaddition products (see the following paragraph and also the subsequent paper of this series (11)).

Can. J. Chem. Downloaded from www.nrcresearchpress.com by 210.87.254.5 on 09/05/12
For personal use only.

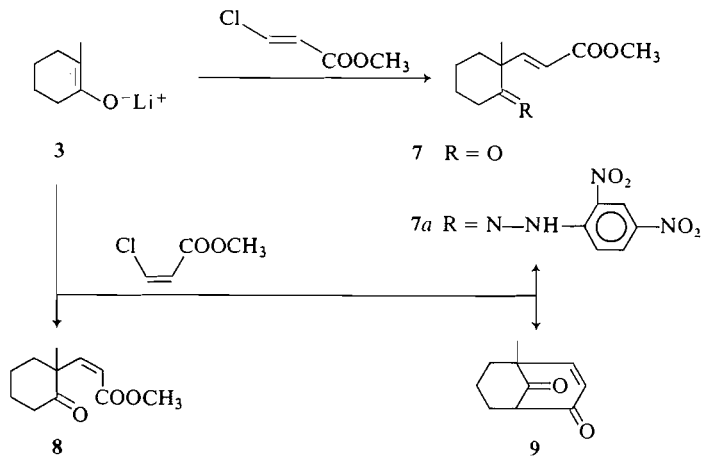

SCHEME 3

cm^{-1}, typical of an α,β-unsaturated ketone, and the absorption of the non-enolizable saturated ketone at 1735 cm^{-1}. The coupling constant of the olefinic protons (10 Hz) is again indicative of a *cis* configuration.

These results must be compared with those reported by House *et al.* (5) for corresponding Michael additions under classical conditions. In the case of the reaction of 2-methylcyclohexanone (**1**) with methyl *trans*-β-chloroacrylate they obtained in only 5–15% yield a mixture of 2- and 6-addition products (the latter predominating) and thus observed no regioselectivity. In the case of the reaction with methyl *cis*-β-chloroacrylate, they obtained no Michael addition product at all but, rather, observed the formation of an adduct arising from an aldol addition to ketone **1** of methyl propiolate, generated by dehydrochlorination of the chloroacrylate. Our experiments thus demonstrate that the use of preformed enolate ions in this kind of reaction may have considerable advantages.[7]

We may remark also on the stereochemistry of the reaction. The addition of *trans*-β-chloroacrylate had given exclusively the *trans*-acrylate **7**, whereas the addition of the *cis*-β-chloroacrylate had led in a proportion of 73% to the *cis*-acrylate **8** and its cyclization product **9**. A similar stereoselectivity has already been observed, and explained, by Jones *et al.* (13) in the reaction of ethyl β-chlorocrotonates with thiophenoxide and ethyl mercaptide (cf. also ref. 14).

We now applied the above-described reaction to an α-pyrone synthesis, by subjecting (Scheme 4) the lithium enolate **12** of unsubstituted cyclohexanone (**10**), prepared via the enol acetate **11**, to the action of methyl *cis*-β-chloroacrylate. Spectral analysis of the crude reaction product revealed that it contained some 32% of the desired α-pyrone, 5,6,7,8-tetrahydrocoumarin (**14**), accompanied by the non-cyclized product **13**. When the crude reaction mixture was treated at reflux temperature with hydrochloric acid in methanol, the pure tetrahydrocoumarin **14** could be obtained by distillation, 30% yield from enol acetate **11**. We have not attempted to optimize the yields but even so this simple sequence of reactions represents one of the most efficient syntheses of 5,6,7,8-tetrahydrocoumarin (**14**) and should be considered a truly useful approach to the preparation of 6-substituted α-pyrones.

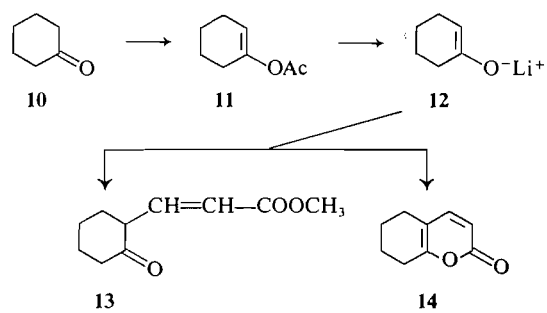

SCHEME 4

Experimental

Melting points were taken in evacuated capillaries and temperatures were corrected. For dry-column chromatography, silica gel Woelm, activity III, was used. The ir spectra were recorded on Beckman IR-12 and Perkin-Elmer 457 instruments, the ultraviolet spectra on Beckman DK-1A and Zeiss DMR-21 spectrometers, the nmr spectra at 60 MHz on a Varian A-60 instrument, tetramethylsilane being used as internal reference, and, if not otherwise stated, deuteriochloroform as solvent. The mass spectra were recorded on a

[7]However, it must be pointed out that the use of preformed enolate ions in Michael additions does not *always* represent a synthetic advantage over 'classical' Michael reactions. In this respect we may refer to the recent article by House and Lusch (12). In the perspective of practical synthetic utility, the situation is thus not without analogy to the one with which one is confronted when deciding whether to use classical Michael electrophiles or Mannich salts.

Can. J. Chem. Downloaded from www.nrcresearchpress.com by 210.87.254.5 on 09/05/12
For personal use only.

Can. J. Chem. Downloaded from www.nrcresearchpress.com by 210.87.254.5 on 09/05/12
For personal use only.

Varian M-66 spectrometer. The microanalyses were performed by the late Dr. and Mrs. F. Pascher, Bonn, Germany, by Dr. C. Daesslé, Montreal, and by Ayerst Laboratories (under the direction of Dr. G. Schilling), Montreal.[8]

Lithium 2-Methylcyclohexenolate (3)

With exclusion of moisture and under nitrogen, 47 ml of an ethereal 1.82 *M* methyllithium solution was introduced through a diaphragm with the help of a syringe into a three-neck flask containing 10 mg of 2,2-bipyridyl, and the ether was removed *in vacuo*. The residue was dissolved in 150 ml of anhydrous 1,2-dimethoxyethane, the solution was cooled to 0°C, and there was added, dropwise and with vigorous stirring, a solution in 10 ml of dimethoxyethane, of 6.1 g of enol acetate **2**, bp 81–82°C 18 Torr, prepared according to the method of Gall and House (15) from 2-methylcyclohexanone (**1**). The persistence of an orange coloration indicated the presence of an excess of methyllithium. This product, containing lithium 2-methyl cyclohexenolate (**3**), was used directly in the following reaction.

Reaction of Lithium Enolate 3 with Ethyl Acrylate

To the above-described solution of the lithium enolate **3** in dimethoxyethane, there was added, rapidly, at 0°C, 4.7 ml of ethyl acrylate. The solution was stirred for 3 min at 0°C and was then poured into 500 ml of cold 2 *N* sulfuric acid. The product was extracted with ether, the ethereal layer was washed with water and was dried over sodium sulfate. Evaporation of the solvent gave 8.32 g of a yellowish oil. A portion of 3.11 g of that product was subjected to dry-column chromatography on 450 g of silica gel, petroleum ether – ether (4:1) serving as eluent. Thus, 892 mg (28%) of crude *ethyl 3-(1′-methyl-2′-oxocyclohexyl)propanoate* (**4**) was obtained; bp 92–95°C 1 Torr (lit. (16) bp 150°C 15 Torr); ν_{max} (film): 1735 (ester), 1710 (ketone), 1190 cm^{-1} (ester); δ: 1.01 (s, 1′-CH_3), 1.2 (t, J = 7 Hz, $COOCH_2CH_3$), 4.01 (q, J = 7 Hz, $COOCH_2CH_3$); ms *m/e* 212 (M^+), 167 (M − OEt), 112.

2,4-Dinitrophenylhydrazone 4a

The 2,4-dinitrophenylhydrazone **4***a* was prepared in the usual fashion (17): mp 88–90°C; λ_{max} (EtOH): 365 nm (log ε 4.3); ν_{max} (KBr): 3220 (NH), 3120 (aromatic C—H), 1730 (ester), 1630 and 1600 (aromatic), 1520 and 1340 (nitro functions), 1280 (ester), 830 cm^{-1} (aromatic); δ: 1.22 (t, J = 7 Hz, $COOCH_2CH_3$), 1.25 (s, 1′-CH_3), 4.13 (q, J = 7 Hz, $COOCH_2CH_3$), 7.95 (d, J = 9 Hz), 8.25 (m) and 9.16 (d, J = 2.5 Hz), (aromatic protons), 10.8 (s, N*H*). *Anal.* calcd. for $C_{18}H_{24}N_4O_6$: C 55.09, H 6.17, N 14.28; found: C 54.90, H 5.88, N 14.44.

From the above-mentioned dry-column chromatogram, there was further obtained 1.146 g (25% yield) of *2ξ,5ξ-bis(ethoxycarbonyl)-8aξ-methyldecal-4a-ol* (**5**). A sample was purified for analysis by vacuum distillation; bp 102°C 0.02 Torr; n^{25} 1.4842; ν_{max} ($CHCl_3$): 3520 (OH), 1735, 1715, and 1185 cm^{-1} (esters); δ: 1.01 (s, 3H, 8a-CH_3), 1.21 and 1.25 (t, 6H, J = 7 Hz, $COOCH_2CH_3$), 3.1 (1H, exchanged with D_2O, OH), 4.03 and 4.15 (q, 4H, J = 7 Hz, $COOCH_2CH_3$); ms *m/e* 312 (M^+), 294 (M − H_2O), 112 (base peak). *Anal.* calcd. for $C_{17}H_{28}O_5$: C 65.36, H 9.03; found: C 65.81, H 8.97.

Finally, from the above-described chromatogram, 680 mg (17.3%) of *ethyl 3-(1′-methyl-4′,9′-dioxo-3′-bicyclo[3.3.1]-nonanyl)propanoate* (**6**), mp 85–88°C, was obtained. For analysis, a sample was recrystallized three times from ether–hexane; prisms, mp 91–91.5°C; ν_{max} (KBr): 1750 and 1730 (ketones), 1220 cm^{-1} (ester); δ: 1.22 (s, 3H, 1′-CH_3), 1.27 (t, 3H, J = 7 Hz, $COOCH_2CH_3$), 2.03 (m, 1H, 3′-H), 2.94 (dd, 1H, J = 9.5 Hz and 3.5 Hz, 5′-H), 4.6 (q, 2H, J = 7 Hz, $COOCH_2CH_3$); ms *m/e* 266 (M^+), 221 (M − OEt), 220. *Anal.* calcd. for $C_{15}H_{22}O_4$: C 67.64, H 8.33; found: C 67.50, H 8.47.

Reaction of Methyl trans-β-*Chloroacrylate with Lithium 2-Methylcyclohexenolate (3)*

As described above, 2.3 g of methyl *trans*-β-chloroacrylate, obtained by diazomethane methylation of *trans*-β-chloroacrylic acid, synthesized according to the method of Kurtz *et al.* (18) from propiolic acid via *cis*-β-chloroacrylic acid, was treated at 0°C for 3 min in 80 ml of dimethoxyethane with a solution of the lithium enolate **3**, prepared from 2.7 g of the enol acetate **2** and 20.8 ml of a 1.82 *M* ethereal methyllithium solution in 70 ml of dimethoxyethane. The usual work-up gave 3.29 g of a crude product, a 2.8 g portion of which was subjected to dry-column chromatography on 200 g of silica gel, petroleum ether – ether (1:3.5) serving as eluent. Thus, 613 mg (25% yield) of pure *methyl trans-3-(1′-methyl-2′-oxocyclohexyl)acrylate* (**7**) was obtained; bp 75–76°C 0.02 Torr; λ_{max} (EtOH): 212 nm (log ε 3.9); ν_{max} (film): 1720 (carbonyls), 1645 (double bond), 1180 cm^{-1} (ester); δ (CCl_4): 1.16 (s, 3H, 1′-CH_3), 3.64 (s, 3H, $COOCH_3$), 5.65 (d, 1H, J = 16 Hz, H_α), 7.0 (d, 1H, J = 16 Hz, H_β); ms *m/e* 196 (M^+), 165 (M − OCH_3), 137 (M − $COOCH_3$), 93.

2,4-Dinitrophenylhydrazone 7a

The dinitrophenylhydrazone **7***a* of the keto ester **7** was prepared in the usual fashion (17): mp 121–123°C; λ_{max} (EtOH): 355 nm (log ε 4.3); ν_{max} (KBr): 3300 (NH), 3120 and 3090 (aromatic and olefinic C—H), 1720 (ester), 1625 and 1600 (aromatic), 1520 and 1340 (nitro groups), 1290 (ester), 835 cm^{-1} (aromatic); δ: 1.45 (s, 1′-CH_3), 3.75 (s, $COOCH_3$), 5.76 (d, J = 16 Hz, H_α), 7.15 (d, J = 16 Hz, H_β), 7.88 (d, J = 10 Hz), 8.3 (dd, J = 10 and 2.5 Hz) and 9.15 (d, J = 2.5 Hz) (aromatic protons), 11.28 (s, large, NH). *Anal.* calcd. for $C_{17}H_{20}N_4O_6$: C 54.25, H 5.36, N 14.89; found: C 54.35, H 5.11, N 14.92.

Reaction of Methyl cis-β-*Chloroacrylate with Lithium 2-Methylcyclohexenolate (3)*

As described above, 4.6 g of methyl *cis*-β-chloroacrylate, prepared by methylation of *cis*-β-chloroacrylic acid, synthesized according to the method of Kurtz *et al.* (18), was treated at 0°C for 3 min in 160 ml of dimethoxyethane with a solution of the lithium enolate **3** of 2-methylcyclohexanone (**1**), prepared from 5.5 g of enol acetate **2** and 50 ml of an ethereal 1.5 *M* methyllithium solution in 150 ml of dimethoxyethane. The usual work-up gave 6.74 g of a yellowish oil, 3.45 g of which was purified by dry-column chromatography on 300 g of silica gel, petroleum ether – ether (1:1) serving as eluent. Thus, 636 mg (18% yield) of *methyl* trans-*3-(1′-methyl-2′-oxocyclohexyl)acrylate* (**7**), bp 76–78.5°C 0.03 Torr, was obtained. The identity of the product with the one described above was established by the comparison of the ir, uv, nmr, and mass spectra.

From the chromatogram, there was also obtained 1.044 g (29%) of *methyl* cis-*3-(1′-methyl-2′-oxocyclohexyl)acrylate* (**8**), bp 80–82°C 0.03 Torr; n^{25} 1.5035; λ_{max} (EtOH): 210 nm (log ε 3.8); ν_{max} (film): 1720 (carbonyls), 1645 (double bond), 1205 cm^{-1} (ester); δ (CCl_4): 1.22 (s, 3H, 1′-CH_3), 3.56 (s, 3H, $COOCH_3$), 5.72 (d, 1H, J = 12 Hz, H_α), 6.18 (d, 1H, J = 12 Hz, H_β); ms *m/e* 196 (M^+) (base peak), 168 (M − CO), 165 (M − OCH_3), 137 (M − $COOCH_3$). *Anal.* calcd. for $C_{11}H_{16}O_3$: C 67.32, H 8.22; found: C 67.50, H 8.29.

Treatment, under usual conditions, of the *cis* keto ester **8** with 2,4-dinitrophenylhydrazine in methanol at room temperature did not lead to the formation of a dinitrophenylhydrazone derivative. However, when the reaction was carried out for 3 h at 100°C, there was obtained, upon cooling, a crystalline precipitate, representing the 2,4-dinitrophenyl-

[8]We pay tribute to the late Dr. and Mrs. Pascher and express our appreciation to the management and the staff of the analytical laboratories mentioned.

Can. J. Chem. Downloaded from www.nrcresearchpress.com by 210.87.254.5 on 09/05/12
For personal use only.

hydrazone **7***a* of the *trans* keto ester **7**. The identity of the material with the above-described product was established by the determination of a mixture melting point and by the comparison of the infrared, ultraviolet, and nmr spectra.

Finally, from the above-described chromatogram, there was obtained 605 mg (20% yield) of *1-methylbicyclo[3.3.1]non-2-ene-4,9-dione* (**9**), bp 125°C 0.02 Torr; n^{25} 1.5135; λ_{max} (EtOH): 225 nm (log ε 3.8); ν_{max} (film): 1735 (saturated ketone), 1680 and 1615 cm^{-1} (α,β-unsaturated keto doublet); δ (CCl_4): 1.22 (s, 3H, 1-CH_3), 3.15 (m, 1H, 5-H), 6.30 (d, 1H, J = 10 Hz, 2-H), 6.77 (d, 1H, J = 10 Hz, 3-H); ms *m/e* 164 (M^+) (base peak), 121, 108. *Anal.* calcd. for $C_{10}H_{12}O_2$: C 73.14, H 7.34; found: C 72.81, H 7.21.

*1-Acetoxycyclohexene (**11**)*

For 14 h, 105 ml of cyclohexanone (**10**) and of 200 ml of isopropenyl acetate were refluxed with 1 g of *p*-toluenesulfonic acid. After cooling, approximately 100 ml of isopropenyl acetate was removed *in vacuo* and 1 g of sodium carbonate was added. The product was subjected to fractional distillation. Thus, 123.5 g (86%) of enol acetate **11** was obtained. For analysis, a sample was redistilled under vacuum; bp 83°C 25 Torr (lit. (19) bp 84–85°C 25 Torr); n^{25} 1.4595 (lit. (19) n_D^{25} 1.4555); ν_{max} (film): 1755 (enol acetate), 1690 cm^{-1} (double bond); δ:1.96 (s, acetate), 5.22 (m, olefinic proton). *Anal.* calcd. for $C_8H_{12}O_2$: C 68.54, H 8.63; found: C 68.49, H 8.64.

*5,6,7,8-Tetrahydrocoumarin (**14**)*

As described above, 2.8 g of methyl *cis*-β-chloroacrylate was treated for 10 min at −15°C in dimethoxyethane with a solution of the lithium enolate **12** of cyclohexanone (**10**), prepared from 3 g of enol acetate **11** and 25 ml of an ethereal 1.9 *M* methyllithium solution in 80 ml of dimethoxyethane. The usual work-up gave 3.64 g of a yellowish oil containing some methyl *cis*-β-chloroacrylate which was removed by heating the product for 15 h under vacuum to 50°C. The resulting oil (2.762 g) represented a mixture of tetrahydrocoumarin (**14**) and of non-cyclized addition products (cf. **13**); λ_{max} (EtOH): 308 nm (log ε 3.4); ν_{max} (film): 1740 (large, carbonyls), 1635 and 1570 cm^{-1} (diene); δ (CCl_4): 3.6 (s, $COOCH_3$), 5.6–7.1 (m, olefinic protons). To a solution of this mixture in 500 ml of methanol, 50 ml of concentrated hydrochloric acid was added and the product was refluxed for 41 h. After cooling, most of the methanol was evaporated *in vacuo*. The product was poured into 500 ml of water and the mixture was extracted with ether. The organic solution was washed with a saturated sodium bicarbonate solution and with water, and was dried over sodium sulfate. Evaporation of the solvent gave 2.22 g of an oil, λ_{max} (EtOH) 308 nm (log ε 3.5), which was purified by fractional vacuum distillation, followed by crystallization from ether – petroleum ether. Thus 958 mg (30% yield from enol acetate **11**) of *5,6,7,8-tetrahydrocoumarin* (**14**) was obtained; mp 55–60°C. Recrystallization from ether – petroleum ether raised the melting point to 57–61°C (lit. (20) mp 64.5–65°C); λ_{max} (EtOH): 222 nm (log ε 3.5), 308 nm (log ε 3.8) (lit. (20) 222 nm (log ε 3.46), 309 nm (log ε 3.85)); ν_{max} (film) 3100 (double bonds), 1720 (lactone), 1650 and 1570 (diene); δ (CCl_4): 1.5–1.98 (m, 4H, 6- and 7-CH_2), 2.2–2.6 (m, 4H, 5- and 8-CH_2), 6.14 (d, 1H, J = 9 Hz, 3-H), 7.1 (d, 1H, J = 9 Hz, 4-H); ms *m/e* 150 (M^+), 122, 94, 66.

*Maleic Anhydride Derivative of Tetrahydrocoumarin **14***

This derivative was prepared according to Dreiding and Tomasewski (20). From 250 mg of the above-described tetrahydrocoumarin **14**, 177 mg of the addition product, mp 301.5–302°C, was obtained. Recrystallization from xylene gave prisms, mp 305–305.5°C (lit. (20) mp 310–311°C); ν_{max} (KBr): 3080 (double bond), 1860 and 1780 (anhydride), 1630 cm^{-1} (double bond). *Anal.* calcd. for $C_{16}H_{14}O_6$: C 63.57, H 4.67; found: C 63.65, H 4.63.

Acknowledgements

Sincere thanks are extended to Mrs. J. Capitaine for much appreciated assistance in some of the experiments. We acknowledge gratefully the technical cooperation of Mrs. G. Pelletier and Miss D. Thibault. High appreciation is expressed to the National Research Council of Canada, the Ministère de l'Education du Gouvernement du Québec, and to Ayerst Laboratories, Montreal, Quebec, for financial assistance. One of us (G.D.) extends sincere thanks to the National Research Council of Canada for the award of a scholarship.

1. J. Lessard, L. Ruest, and Ch. R. Engel. Can. J. Chem. **50**, 1433 (1972).
2. A. Bélanger, P. Brassard, G. Dionne, and Ch. R. Engel. Steroids, **24**, 377 (1974).
3. (*a*) Ch. R. Engel, G. Dionne, and D. Mukherjee. 9th IUPAC Symposium on the Chemistry of Natural Products, Ottawa, June 24–29, 1974, Abstract 43A; (*b*) P. Brassard, Ch. R. Engel, G. Dionne, and A. Bélanger. 9th IUPAC Symposium on the Chemistry of Natural Products, Ottawa, June 24–29, 1974, Abstract 44A.
4. D. Mukherjee and Ch. R. Engel. Can. J. Chem. This issue.
5. H. O. House, W. L. Roelafs, and B. M. Trost. J. Org. Chem. **31**, 646 (1966).
6. C. N. R. Rao. Chemical applications of infrared spectroscopy. Academic Press, New York, NY. 1963. Chapt. III, p. 209.
7. S. M. Anachenko, I. V. Berezin, and I. V. Torgov. Otdel. Khim. Nauk. 1644 (1960).
8. R. A. Kretchmer, E. D. Mihelich, and J. J. Waldron. J. Org. Chem. **37**, 4483 (1972).
9. (*a*) G. Stork and B. Ganem. J. Am. Chem. Soc. **95**, 6152 (1973); (*b*) G. Stork and M. E. Jung. J. Am. Chem. Soc. **96**, 3682 (1974); (*c*) G. Stork and J. Singh. J. Am. Chem. Soc. **96**, 6181 (1974).
10. R. K. Boeckmann, Jr. J. Am. Chem. Soc. **96**, 6179 (1974).
11. Ch. R. Engel and G. Dionne. Can. J. Chem. This issue.
12. H. O. House and M. J. Lusch. J. Org. Chem. **42**, 183 (1977).
13. D. E. Jones, R. O. Morris, C. A. Vernon, and R. F. M. White. J. Chem. Soc. 2349 (1960).
14. E. L. Eliel. Stereochemistry of carbon compounds. McGraw-Hill Inc., New York, NY. 1962. pp. 368–369.
15. M. Gall and H. O. House. Org. Synth. **52**, 39 (1972).
16. L. Ruzicka, D. R. Koolhas, and A. H. Wind. Helv. Chim. Acta, **14**, 1151 (1931).
17. R. L. Shriner, R. C. Fuson, and D. Y. Curtin. The systematic identification of organic compounds. John Wiley and Sons, Inc., New York, NY. 1967. p. 253.
18. A. N. Kurtz, W. E. Billups, R. B. Greenlee, H. F. Hamil, and W. T. Pace. J. Org. Chem. **30**, 3141 (1965).
19. N. J. Leonard and F. H. Owens. J. Am. Chem. Soc. **80**, 6039 (1958).
20. A. S. Dreiding and A. J. Tomasewski. J. Am. Chem. Soc. **76**, 6388 (1954).

α-Pyrones. V.[1,2] The synthesis of bufadienolides. Part IV[3,4]

CH. R. ENGEL AND GERVAIS DIONNE[5]

Department of Chemistry, Laval University, Quebec, P.Q., Canada G1K 7P4

Received September 1, 1977

(Dedicated to Professor EDGAR LEDERER on the occasion of his seventieth birthday)

CH. R. ENGEL and GERVAIS DIONNE. Can. J. Chem. **56**, 424 (1978).

Additions of preformed enolate ions, derived from esters, to α-methylene carbonyl compounds, the methylene group of which carries in the terminal position a leaving group, were studied. The reaction of steroidal 20-chloromethylene 21-aldehydes with preformed diethyl sodiomalonate results in a Michael addition which allowed an efficient synthesis of a 23-alkoxycarbonyl bufadienolide. In contrast, the reactions of the same chloromethylene aldehydes and of an analogous 20-methoxymethylene 21-aldehyde with ethyl lithioacetate give rise to 1,2-additions. The reaction of lithioacetate with the methoxymethylene aldehyde was used for the most efficient bufadienolide synthesis yet realized. Treatment with lithioacetate of 20-acetoxymethylene and 20-hydroxymethylene 21-aldehydes gave no addition products. The reactions of preformed sodiomalonate and lithioacetate with α-chloromethylene and α-methoxymethylene cyclohexanones proceeded analogously to those of the steroidal aldehydes.

CH. R. ENGEL et GERVAIS DIONNE. Can. J. Chem. **56**, 424 (1978).

L'étude concerne des additions d'ions énolate, préformés à partir d'esters, à des composés carbonylés α-méthyléniques dont le groupe méthylène porte en position terminale un substituant nucléofuge. La réaction de 21-aldéhydes stéroïdiques 20-chlorométhyléniques avec le sodiomalonate de diéthyle préformé résulte en une addition de Michael qui fut utilisée pour une synthèse efficace d'un bufadiénolide 23-alkoxycarbonylé. Par contre, les réactions des mêmes aldéhydes chlorométhyléniques, ainsi que d'un 21-aldéhyde 20-méthoxyméthylénique analogue, avec le lithioacétate d'éthyle donnèrent lieu à des additions aldoliques. La réaction du lithioacétate avec l'aldéhyde méthoxyméthylénique permit la réalisation d'une synthèse d'un bufadiénolide qui dépasse en efficacité toutes les synthèses connues de ce type de cardiotoniques. Le traitement avec un lithioacétate des 21-aldéhydes 20-hydroxyméthylénique et 20-acétoxyméthylénique ne conduit pas à des produits d'addition. Les réactions du sodiomalonate de diéthyle et du lithioacétate d'éthyle préformés avec les α-chlorométhylène et α-méthoxyméthylène cyclohexanones procèdent de la même façon que les réactions avec les aldéhydes stéroïdiques correspondants.

Some years ago we published (6) a bufadienolide synthesis which consisted of the Michael addition of diethyl malonate to a 20-methylene 21-aldehyde and the transformation of the resulting aldehydo diester into an enol lactone which was then dehydrogenated to the α-pyrone (Scheme 1). Since the yields of the last step were not very satisfactory, we attempted to 'prefigure' the non-enolic double bond in the Michael nucleophile by using bromomalonate as Michael

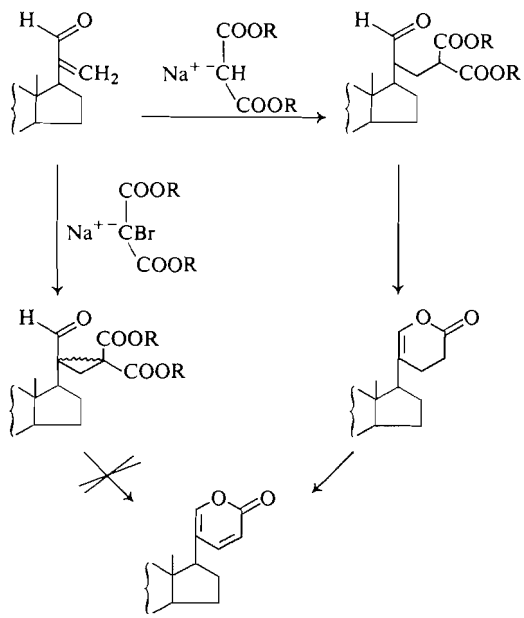

SCHEME 1

[1]For Part IV, see ref. 1.

[2]This publication also represents paper IX in our series on Cyanoethylations and Michael additions (for paper VIII, see ref. 1); paper XLV in our series on Steroids and Related Products (for paper XLIV, see ref. 2), and paper VI in our series on Cardiotonic Steroids (for paper V, see ref. 3).

[3]For Part III, see ref. 3.

[4]Reported in part to the 9th International (IUPAC) Symposium on the Chemistry of Natural Products, Ottawa, Ontario, June 24-28, 1974 (4), and to the 25th International (IUPAC) Congress of Chemistry, Jerusalem, Israel, July 6–11, 1975 (5).

[5]Abbreviated from part of the doctoral thesis of G. Dionne, presented to the School of Graduate Studies, Laval University, Quebec, P.Q., December 1975.

Can. J. Chem. Downloaded from www.nrcresearchpress.com by 210.87.254.6 on 09/05/12
For personal use only.

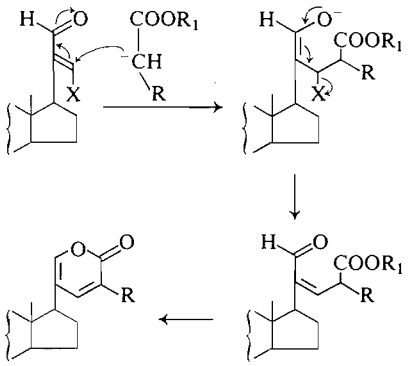

SCHEME 2

donor (7). This indeed led to the expected cyclopropane derivative but the conversion of that product to an α-pyrone proved unsuccessful (Scheme 1).

It now seemed conceivable to retain the basic strategy of our approach, by incorporating an appropriate leaving group, not in the Michael nucleophile, but in the Michael electrophile, as depicted in Scheme 2 (for related reactions, see ref. 8). We therefore prepared derivatives of the 20-methylene 21-aldehyde which had served for our first bufadienolide synthesis, in which the methylene group carries a leaving group (structures **2**-**2***d*, **3**, and **5** of Scheme 3).

The dimethyl acetal **1***a* of aldehyde **1**, previously prepared in our laboratory (6), was subjected, according to the method employed by the Roussel group in the first bufadienolide synthesis (9), to a Vilsmeier-Haack reaction (10, see also ref. 11). This led to a mixture of the geometrically isomeric methoxymethylene aldehydes **2***d* and **3**, the *Z*-isomer **2***d* being obtained in 64% yield, the *E*-isomer **3** in 15% yield. The ultraviolet maxima (in ethanol), 253 nm for the *Z*-isomer and 275 nm for the *E*-isomer, agree well with those reported by Sondheimer *et al.* (12) for similar products. The configurational assignment is substantiated by the consideration that it is known that α-hydroxymethylene ketones and aldehydes exist as '*cis*'-isomers (13, 14) and that the methylation and acetylation of the 3-hydroxy (*Z*)-hydroxymethylene aldehyde **2**, whose configuration was confirmed by its infrared spectrum (see below), led indeed to the 3-acetoxy 20-methoxymethylene aldehyde **2***d*.[6]

The 3-hydroxy-(*Z*)-20-hydroxymethylene 21-aldehyde **2** was obtained in 85% yield by vinylogous saponification (cf. refs. 9, 12) of the (*Z*)-methoxymethylene aldehyde **2***d*. Again, the ultraviolet spectrum of this derivative corresponds to that of an analogous product reported by Sondheimer *et al.* (12). In the infrared spectrum we note an intramolecular hydrogen bond, confirming the *Z*-configuration (cf. refs. 13, 14). Treatment of the 3-hydroxy-(*Z*)-hydroxymethylene aldehyde **2** with acetic anhydride in pyridine gave in almost quantitative yield the diacetate **2***b* which is, however, unstable in solution.

According to the procedure employed by Skoldinov and co-workers (15) for the preparation of β-chloroacroleins from β-methoxyacroleins, both the (*Z*)-methoxymethylene aldehyde **2***d* and its *E*-isomer **3** were transformed, in 85% and 68% yield, respectively, by reaction with thionyl chloride in dichloromethane and by subsequent treatment of the resulting dichloro derivative with ice, into a mixture of geometrically isomeric 20-chloromethylene 21-aldehydes (**5**) which could not be separated. The presence of both isomers was revealed by the nmr spectrum which shows two signals for each, the olefinic (7.0 and 7.16 δ) and the aldehydic protons (9.60 and 10.04 δ).

In a first series of experiments, we explored the applicability of the general pathway outlined in Scheme 2 to the synthesis of bufadienolides, by investigating the addition of diethyl malonate to the (*Z*)-hydroxymethylene aldehyde **2** and to the (*Z*)-methoxymethylene aldehyde **2***d*. In contradistinction to the situation in the case of a number of hydroxymethylene and methoxymethylene ketones (8*a*,*b*, 16), no 1,4-additions could be observed under a variety of conditions; using, as basic catalysts, sodium ethoxide, potassium hydroxide, or Triton B, and as solvents ethanol, *tert*-butanol, or dioxane, no reaction took place. A negative result was also encountered when a reaction was attempted with preformed diethyl sodiomalonate in hexamethylphosphoric triamide.[7] On the other hand, when piperidine in boiling ethanol was used as a base, aldehyde **2***d* gave in 80% yield the 21-nor 23-ethoxycarbonyl cholenic ester **4***a*. Under similar conditions, the hydroxymethylene aldehyde **2** gave in 45% yield the corresponding 3-hydroxy derivative **4**, readily acetylated to acetate **4***a*. The structure of ester **4***a* follows from the results of its elemental analysis and from its spectra (see Experimental). The nmr spectrum reveals a single olefinic proton, appearing as a triplet, which confirms the presence of an adjacent methylene group, and the ultraviolet spectrum (λ_{max} (EtOH) 217 nm (log ε 4)) corresponds well to that of an α,β-unsaturated α,β-disubstituted ester (17). In the mass spectrum, apart from the molecular ion, appear peaks arising from the

[6]The comparison of the spectral data of the non-acetylated methoxymethylene aldehyde **2***c* and of the acetylated product **2***d* confirms that no isomerization occurred during acetylation.

[7]These negative experiments are not recorded in the Experimental.

Can. J. Chem. Downloaded from www.nrcresearchpress.com by 210.87.254.6 on 09/05/12
For personal use only.

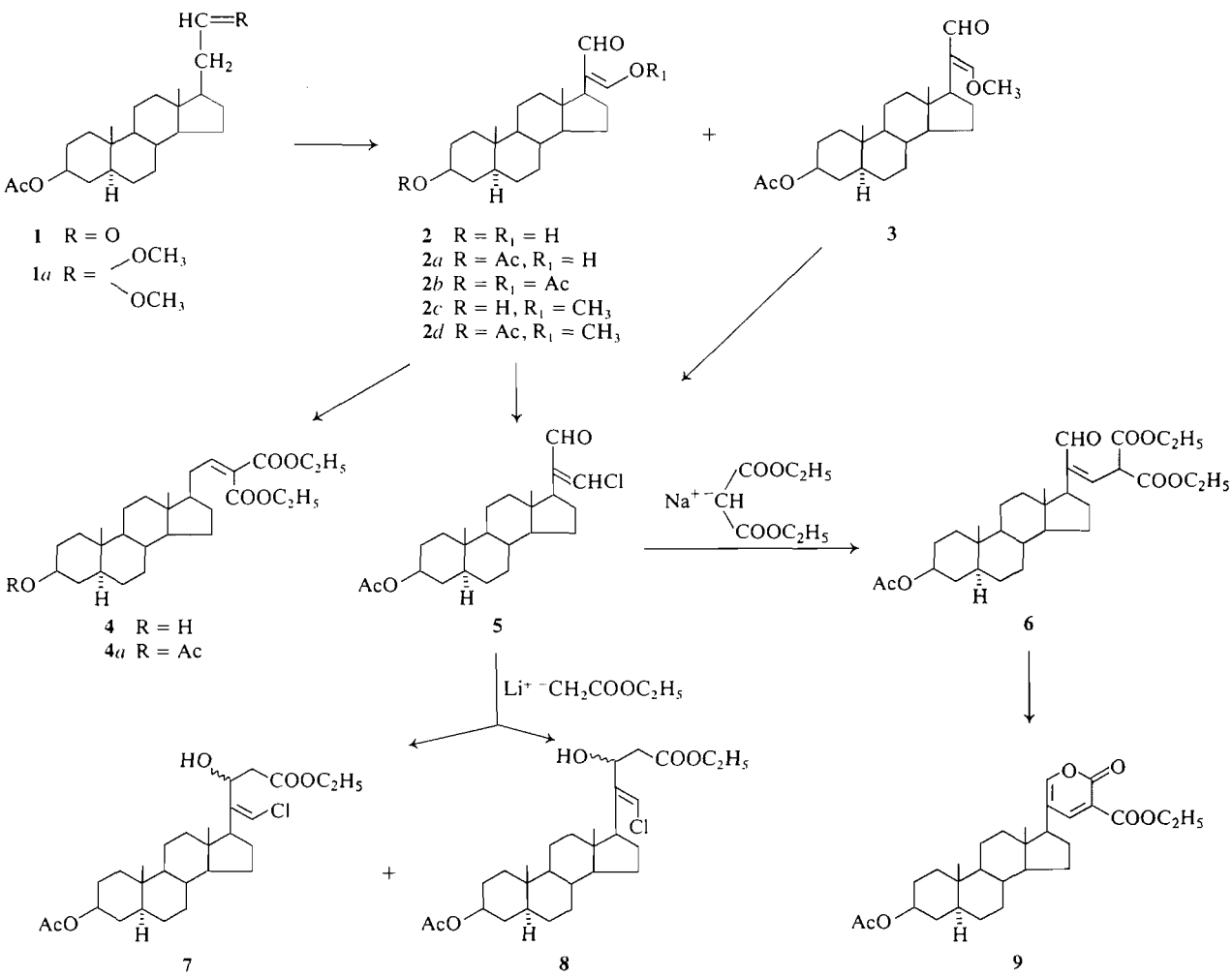

SCHEME 3

rupture of the side chain in position 17. The analytical and spectral results of the 3-hydroxy derivative **4** again agree with the suggested structure. The formation of the esters **4** and **4***a* may be explained by an aldol condensation of the Knoevenagel type, followed by deformylation which, in the case of the reaction of the methoxymethylene derivative, is preceded by the hydrolysis of the enol ether.

The desired Michael addition (Schemes 2 and 3) could be realized when the 20-chloromethylene 21-aldehydes **5** were used as electrophiles. Under classical Michael conditions, no reaction occurred with diethyl malonate but the addition succeeded well with preformed sodiomalonate in hexamethylphosphoric triamide (HMPT). The infrared spectrum of the resulting product (**6**) revealed the presence of the α,β-unsaturated aldehyde and that of the ester groups. The structure was confirmed by the nmr spectrum and by the ultraviolet characteristics, typical of an α,β-disubstituted α,β-unsaturated aldehyde. The aldehydo diester **6** could not be isolated in the pure state since it cyclizes spontaneously to the α-pyrone **9**, a 23-alkyloxycarbonyl bufadienolide. The cyclization is accelerated when the crude reaction mixture containing the aldehydo ester **6** is heated, when it is treated with acid, or when it is passed through a silica gel column. The bufadienolide **9** was obtained directly, in 38% yield from the chloromethylene aldehydes **5**, by simply subjecting the reaction product to dry-column chromatography on silica gel. The 3-alkoxycarbonyl α-pyrone structure is shown by the ultraviolet absorption (in ethanol) at 322 nm and the constitution of the product is confirmed by elemental analysis and by its infrared and nmr spectra. We note, for instance, that the absorptions of the 21- and 22-protons correspond to those of the corresponding protons of the 5-unsubstituted 3-ethoxycarbonyl-α-pyrone (ref. 7, see also ref. 18).

While the above described synthesis represents an efficient pathway to 23-alkoxycarbonyl bufadieno-

Can. J. Chem. Downloaded from www.nrcresearchpress.com by 210.87.254.6 on 09/05/12
For personal use only.

Can. J. Chem. Downloaded from www.nrcresearchpress.com by 210.87.254.6 on 09/05/12
For personal use only.

lides and their derivatives, it would not be useful for the synthesis of 23-unsubstituted products since it is known (8*d*, 19) that decarboxylations of 3-carboxy α-pyrones are difficult to realize. The addition of a preformed enolate ion, derived from an alkyl acetate, to a 20-methylene 21-aldehyde with a suitable leaving group in position 22 would constitute an elegant and direct route to 23-unsubstituted bufadienolides, if the course of the reaction were analogous to that of the addition of preformed sodiomalonate to the 20-chloromethylene 21-aldehydes **5**. However, the sodium enolate of an alkyl acetate should not lend itself well to such a reaction because of its instability and of its facile self-condensation (20). On the other hand, alkyl lithioacetates can be readily prepared (21), but it is known (22) that in reactions of organolithium compounds with α,β-unsaturated carbonyl products, 1,2-additions are favoured over 1,4-additions;[8] thus, the reaction of lithioacetates with chloromethylene aldehydes of type **5** did not appear very promising for bufadienolide syntheses. However, it seemed reasonable to assume that in the case of the addition of a lithioacetate to α-methylene 21-aldehydes, possessing as β-substituent a group such as an alkoxy function, the reaction product should lend itself to a ready transformation, by hydrolysis and dehydration, into an unsaturated δ-oxo ester, easily convertible to an α-pyrone (see below).

Considering that Dreiding and Nickel (16*b*) had observed an appreciable proportion of a 1,4-addition upon reaction of an organolithium compound with an α-alkoxymethylene cyclohexanone, we still investigated the addition of ethyl lithioacetate to the 20-chloromethylene 21-aldehydes **5**. Indeed, it could be assumed that the improbability of hydrolysis, in the medium, of the chlorine substituent should allow us to differentiate readily a 1,2-addition product from a 1,4-addition product. No 1,4-addition product could be isolated. Instead, the reaction gave rise, in very high yield, to the geometrically isomeric 1,2-addition products **7** and **8**, the *Z*-isomer **7** being isolated in 50% yield, the *E*-isomer **8** in 41% yield. The infrared spectra of the products are indicative of hydrogen bonding between the hydroxy group and the ester carbonyl function, as evidenced by a weak carbonyl absorption and by the position of the hydroxyl maximum (at 3520 cm^{-1} in CCl_4 and 3480 cm^{-1} in KBr). The configurations could be deduced from the chemical shifts of the olefinic protons which appear at 5.94 and 6.48 δ. The values calculated according to the rules of Pascual *et al.* (23) would correspond to 5.88 δ for the *Z*-isomer and to 5.96 δ for the *E*-isomer. On the basis of the important difference of the chemical shift of the relevant proton of one of the isomers with respect to either calculated value, we assign to this product the *E*-configuration, since this difference may be attributed to deshielding, due to the diamagnetic anisotropy of the carbonyl group of the ester, and since this effect should only be felt significantly by the olefinic proton of the *E*-isomer.

It is known (24) that certain salts, particularly copper salts, favour a 1,4-addition over a 1,2-addition in reactions of organometallic compounds with α,β-unsaturated carbonyl derivatives. However, even in the presence of cuprous chloride, the addition of ethyl lithioacetate to the aldehydes **5** proceeded as described above.

As expected, addition of ethyl lithioacetate to the 20-methoxymethylene 21-aldehyde **2***d* took an analogous course and allowed us to realize a most fruitful bufadienolide synthesis (Scheme 4). Treatment of the reaction product with hydrochloric acid led in 78% yield to a mixture of the (*Z*)- and (*E*)-aldehydo cholenic esters **12** and **13**. Nuclear magnetic resonance spectroscopy revealed that the major constituent was the *Z*-isomer **12**. The mixture could not be separated into its components; when it was recrystallized from dichloromethane–hexane, the *E*-isomer **13** was converted quantitatively to the *Z*-isomer **12**.[9] The structures of the products follow from analytical and spectral data. Treatment of the aldehydo cholenic ester **12** with hydrochloric acid in boiling ethanol, followed by reacetylation, gave in 60% yield the bufadienolide **11**, previously prepared in our laboratory (6). The over-all yield of the bufadienolide **11** from the methoxymethylene aldehyde **2***d* amounted to 47% and this pathway to bufadienolides thus seems to represent the most efficient method for the synthesis of that class of compounds, its yield exceeding even that realized (3) by the use of Bélanger and Brassard's α-pyrone synthesis (25).[10]

The fact that the aldehydo esters **12** and **13** were not formed by a 1,4-addition of the Michael type, could be proved by omitting treatment with acid in the work-up. This allowed the isolation, in good yield, of the aldol-type addition product **10** which was converted in quantitative yield, by reaction with hydrochloric acid at room temperature, to the

[8]This does, however, not mean that 1,4-additions are excluded (see below).

[9]The geometry around the double bond of the two isomers **12** and **13** was deduced by comparing the chemical shifts of the C(22)-protons with the values calculated according to the rules of Pascual *et al.* (23).

[10]For other direct pathways to bufadienolides, see refs. 6, 9, and 26. Pettit and co-workers also developed an interesting method for the transformation of cardenolides into bufadienolides (27).

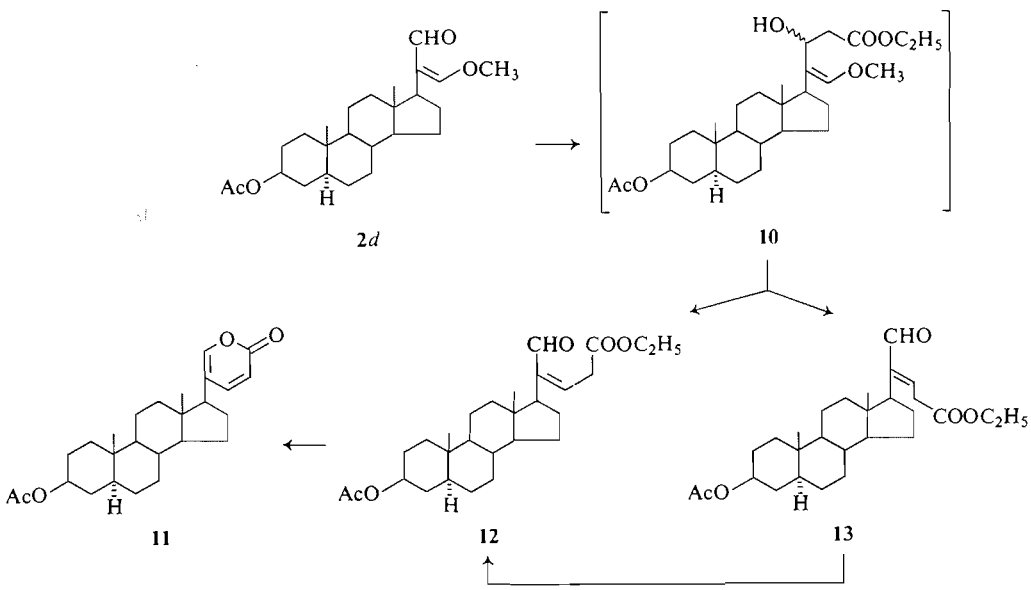

SCHEME 4

mixture of the aldehydo cholenic esters **12** and **13**.[11] Our new bufadienolide synthesis is thus, mechanistically, analogous to the α-pyrone synthesis of Plattner *et al.* (28), involving a Reformatzky reaction on an α-benzoyloxymethylene ketone and not to the α-pyrone synthesis realized by Dreiding and Tomasewski (16*c*), by treatment of the corresponding hydroxymethylene ketone with the Reformatzky reagent.

It seemed of interest to establish whether or not ethyl lithioacetate could be added also to the hydroxymethylene aldehyde **2**. This would correspond to substituting a lithioacetate for the Reformatzky reagent employed in the first successful but, in the perspective of yields, not too attractive pathway to bufadienolides (9, see also ref. 12). However, when the hydroxymethylene aldehyde **2** was treated with ethyl lithioacetate, the starting material was recovered quantitatively. Apparently, the reaction resulted only in the formation of the lithium enolate of the 'dialdehyde' **2**. When the 3-acetoxy 20-acetoxymethylene 21-aldehyde **2***b* was treated with ethyl lithioacetate, it was merely transformed into the 3-acetoxy 20-hydroxymethylene 21-aldehyde **2***a*. These results contrast with those observed in the case of analogous reactions involving Reformatzky reagents (9, 16*c*, 28).

The courses of the reactions of preformed sodiomalonates and lithioacetates with α-chloromethylene and α-methoxymethylene carbonyl compounds, established for steroidal 21-aldehydes, were confirmed with analogously constituted cyclic ketones. We used 2-chloromethylenecyclohexanone (**15**) and 2-methoxymethylenecyclohexanone (**20**) as substrates (Scheme 5). Upon addition (in HMPT) of preformed diethyl sodiomalonate to the chloromethylene ketone **15**, we obtained directly the ethoxycarbonyl tetrahydrocoumarin **18**. As in the case of the reaction with the analogous steroidal α-chloromethylene aldehydes **5**, a Michael-type 1,4-addition must have occurred (cf. intermediate **16**, which could not be isolated), since a 1,2-aldol-type addition would have afforded the chloromethylene diester **14**, the transformation of which into an α-pyrone (under the reaction conditions, in any case, highly improbable)[12] would have led to the ethoxycarbonyl α-pyrone **17**. The nmr spectrum of the tetrahydrocoumarin obtained (**18**), clearly differentiates it from its isomer **17**; the only proton (in position 4) of its α-pyrone system appears at 7.97 δ, which corresponds well to the chemical shift of the corresponding proton of 3-ethoxycarbonyl-2-pyrone (7), whereas the only proton of the α-pyrone system of a product of structure **17** should appear around 8.35 δ (7).

On the other hand, treatment of the methoxy-

[11]The difference in the course of the additions of sodiomalonates and lithioacetates to α,β-unsaturated aldehydes was corroborated by a preliminary experiment (not reported in the Experimental) which establishes that the reaction of ethyl lithioacetate with the unsubstituted 20-methylene 21-aldehyde leads to an aldol-type addition product, whereas, as shown previously (ref. 6, see also the introduction to this paper), the reaction of this aldehyde with sodiomalonate results in a Michael-type addition.

[12]Not only on theoretical grounds; indeed, treatment with hydrochloric acid of the steroidal β-hydroxy-γ-chloromethylene esters **7** and **8** (see above) did not lead to an α-pyrone.

Can. J. Chem. Downloaded from www.nrcresearchpress.com by 210.87.254.6 on 09/05/12
For personal use only.

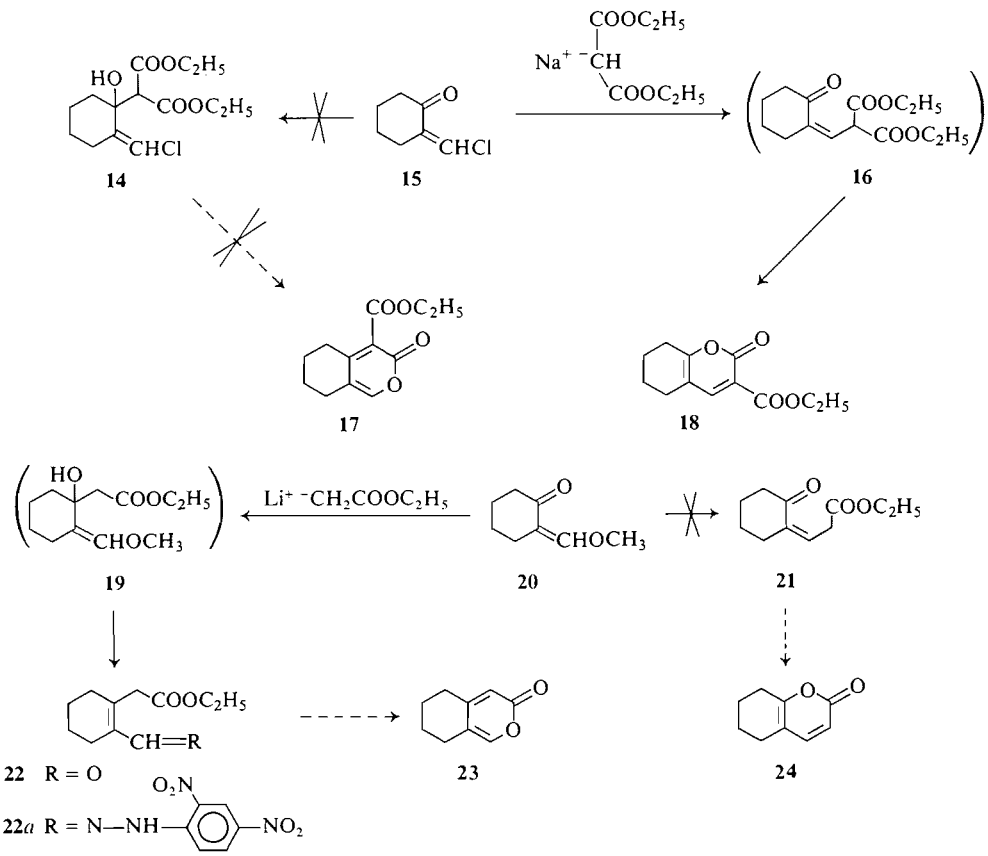

SCHEME 5

methylene cyclohexanone **20** with ethyl lithioacetate resulted exclusively, as in the case of the corresponding steroidal 20-methoxymethylene 21-aldehyde **2***d*, in a 1,2-addition; the intermediate β-hydroxy-γ-methoxymethylene ester **19** was not isolated, but the unsaturated aldehydo ester **22** was obtained in approximately 65% yield.[13] A conjugate (Michael-type) addition would have afforded the keto ester **21**.[14] The structure of the aldehydo ester **22** was substantiated by its spectral data and by the characteristics of its dinitrophenylhydrazone derivative **22***a*.

In summary, whereas the reactions of the α-methoxymethylene and α-chloromethylene carbonyl compounds with ethyl lithioacetate resulted in 1,2-additions, leading in the case of the methoxymethylene derivatives to β,γ-unsaturated γ-formyl esters which can be transformed into 5-substituted (in the case of ketonic starting materials, into 4,5-disubstituted) α-pyrones, the reactions of the α-chloromethylene carbonyl compounds with preformed diethyl sodiomalonate gave rise to 1,4-additions which lead, through cyclization, to 5-substituted (in the case of ketonic starting materials, to 5,6-disubstituted) 3-ethoxycarbonyl α-pyrones.

Experimental

Melting points were taken in evacuated capillaries and the temperatures were corrected. For elution chromatography, neutral aluminum oxide Woelm and Davison's silica gel 923 were employed. Dry-column chromatography was performed with Woelm dry-column chromatography silica gel, activity III; for thin-layer chromatography, Merck silica gel GF-254 and Baker silica gel 7G were used. The ir spectra were recorded on Beckman IR-12 and Perkin-Elmer 457 instruments, uv spectra on Beckman DK-1A and Zeiss DMR-21 spectrometers. The nmr spectra were obtained at 60 and 90 MHz on Varian A-60 and Bruker HX-90 instruments, tetramethylsilane serving as internal standard and, if not otherwise stated, deuteriochloroform as solvent. Mass spectra were recorded, if not otherwise indicated, on a Varian A-66 instrument. For the drying of organic extracts, sodium sulfate was used. The microanalyses were performed by the late Dr. and Mrs. F. Pascher, Bonn, Germany, and by the microanalytical section of Ayerst Laboratories, Montreal (under the direction of Dr. G. Schilling), as well as by Dr. C. Daesslé, Montreal.[15]

[13]Cyclization of the aldehydo ester **22** would lead to the α-pyrone **23**.

[14]The cyclization of that ester would lead to the α-pyrone **24**.

[15]We pay tribute to the late Dr. and Mrs. Pascher and express our appreciation to the staff and management of the analytical laboratories.

Can. J. Chem. Downloaded from www.nrcresearchpress.com by 210.87.254.6 on 09/05/12
For personal use only.

Can. J. Chem. Downloaded from www.nrcresearchpress.com by 210.87.254.6 on 09/05/12
For personal use only.

3β-Acetoxy-21,21-dimethoxy-5α-pregnane (1a)

A solution of 12.36 g of 3β-acetoxy-5α-pregnan-21-al (**1**) (6) and of 360 mg of *p*-toluenesulfonic acid in 380 ml of anhydrous methanol was refluxed for 1 h. The solution was concentrated to 200 ml at atmospheric pressure and then to 75 ml under vacuum. The product was precipitated in 1 ℓ of ice water and the mixture was extracted with ether. The ethereal layer was washed with an iced sodium bicarbonate solution and with water, and was dried. Evaporation of the solvents left 14.01 g of a viscous oil, the infrared spectrum of which revealed partial hydrolysis of the 3-acetate group (ν_{max} (film) 3420 cm^{-1}). The product was treated in 80 ml of pyridine with 40 ml of acetic anhydride for 18 h at room temperature. The majority of the pyridine and of the acetic anhydride was removed by vacuum distillation and the product was precipitated in 500 ml of ice water. The mixture was extracted with ether, the ethereal layer was washed with iced dilute hydrochloric acid, cold sodium bicarbonate solution, and water, and was dried. Evaporation of the solvent left 14.31 g (98% yield) of crystalline acetal **1a**, mp 76–79°C. For analysis a sample was recrystallized three times from methanol – water; mp 81.5–82°C; $[\alpha]_D^{25}$ + 7.9° (*c* 1.042, $CHCl_3$); ν_{max} (KBr): 1720 (acetate), 1258 and 1248 (C—O), 1120 cm^{-1} (acetal); δ (60 MHz): 0.56 (s, 3H, 18-CH_3), 0.83 (s, 3H, 19-CH_3), 2.01 (s, 3H, acetate), 3.30 and 3.33 (s, 6H, acetal), 4.46 (m, 1H, 3α-H). *Anal.* calcd. for $C_{25}H_{42}O_4$: C 73.85, H 10.41; found: C 74.04, H 10.34.

(Z)-3β-Acetoxy-20-methoxymethylene-5α-pregnan-21-al (2d) and (E)-3β-Acetoxy-20-methoxymethylene-5α-pregnan-21-al (3)

To 13 ml of anhydrous dimethylformamide, 6 ml of freshly redistilled phosphorous oxychloride was added dropwise at 0°C. Subsequently, the mixture was heated for 0.5 h to 50°C and then cooled to 0°C. To this product a solution of 7.52 g of acetal **1a**, mp 76–79°C, in 60 ml of DMF was added. The mixture was heated for 3 h to 50°C then cooled and poured into an iced sodium carbonate solution. The precipitate was extracted with ether and the organic layer was washed with water and dried. The solvent was removed and the residue, still containing some dimethylformamide, was dissolved in ether, the ethereal solution was washed repeatedly with water and was dried. Evaporation left 7.22 g of a yellowish foam which was subjected to dry-column chromatography on 400 g of silica gel, petroleum ether – ether (1:2) serving as eluent. Thus, 4.7 g (64% yield) of (Z)-*3β-acetoxy-20-methoxymethylene-5α-pregnan-21-al* (**2d**), mp 148–150°C, was isolated. For analysis, a sample was recrystallized 3 times from methanol–water; colorless powder, mp 152–153.5°C; $[\alpha]_D^{22}$ −15.7° (*c* 0.900, $CHCl_3$); λ_{max} (EtOH): 253 nm (log ε 4.2); ν_{max} (KBr): 2780 (aldehyde), 1735 (acetate), 1675 and 1640 (doublet of α,β-unsaturated aldehyde), 1250 cm^{-1} (acetate); δ (90 MHz): 0.63 (s, 3H, 18-CH_3), 0.81 (s, 3H, 19-CH_3), 2.0 (s, 3H, acetate), 3.88 (s, 3H, OCH_3), 4.17 (m, 1H, 3α-H), 6.85 (s, 1H, olefinic proton), 9.18 (s, 1H, aldehyde); ms *m/e* 402.5 (M^+), 371, 213, 111. *Anal.* calcd. for $C_{25}H_{38}O_4$: C 74.59, H 9.52; found: C 74.72, H 9.57.

From the above described chromatogram, there was also obtained 1.08 g (15% yield) of (E)-*3β-acetoxy-20-methoxymethylene-5α-pregnan-21-al* (**3**), mp 178–181°C. For analysis a sample was recrystallized 3 times from chloroform–methanol; colorless prisms, mp 182–184.5°C; $[\alpha]_D^{22}$ −23.1° (*c* 1.110, $CHCl_3$); λ_{max} (EtOH): 275 nm (log ε 3.95); ν_{max} (KBr): 3100 (double bond), 1735 (acetate), 1665 and 1635 (doublet of α,β-unsaturated aldehyde), 1260 cm^{-1} (acetate); δ (90 MHz): 0.60 (s, 3H, 18-CH_3), 0.79 (s, 3H, 19-CH_3), 1.97 (s, 3H, acetate), 3.79 (s, 3H, OCH_3), 4.66 (m, 1H, 3α-H), 6.85 (s, 1H, olefinic proton), 10.13 (s, 1H, aldehyde); ms *m/e* 402.5 (M^+), 370.5, 316, 217. *Anal.* calcd. for $C_{25}H_{38}O_4$: C 74.59, H 9.52; found: C 74.53, H 9.63.

(Z)-3β-Hydroxy-20-hydroxymethylene-5α-pregnan-21-al (2)

A portion of 1 ml of an aqueous ethanolic NaOH solution, prepared from 1.5 g of NaOH, 1.5 ml of water, and 7 ml of ethanol, was added to a solution of 500 mg of the *3β*-acetoxy aldehyde **2d** in 8 ml of ethanol. The mixture was heated for 18 h under nitrogen to 30°C, was subsequently diluted with 25 ml of water and was acidified to the Congo-blue reaction with 2 *N* hydrochloric acid. The product was poured into 100 ml of ice water and the precipitate was extracted with a (3:1) ether–dichloromethane mixture. The organic phase was washed with water and was dried. Evaporation of the solvent gave 362 mg (85% yield) of (*Z*)-3β-hydroxy-20-hydroxymethylene-5α-pregnan-21-al (**2**), mp 192–196°C. A sample was recrystallized 3 times from ethanol–water for analysis; colorless powder, mp 198–198.5°C; $[\alpha]_D^{22}$ −22.5° (*c* 0.930, CH_3OH); λ_{max} (EtOH): 253 nm (log ε 4.1); ν_{max} (KBr): 3500–2300 (hydroxyls), 2720 (aldehyde), 1635 (chelated β-dicarbonyl structure (29)), 1600 (double bond), 1260 and 1250 (C—O), 1040 and 1030 cm^{-1} (hydroxyls); δ (90 MHz, CD_3OD): 0.62 (s, 3H, 18-CH_3), 0.82 (s, 3H, 19-CH_3), 2.64 (m, 1H, 17α-H), 8.33 (s, 2H, protons of the mesomeric aldehydes); ms *m/e* 346.5 (M^+), 328.5, 217. *Anal.* calcd. for $C_{22}H_{34}O_3$: C 76.26, H 9.89; found: C 76.09, H 9.90.

Methylation and Acetylation

A solution of 233 mg of (*Z*)-3β-hydroxy-20-hydroxymethylene-5α-pregnan-21-al (**2**) in 10 ml of tetrahydrofuran was treated for 18 h with 10 ml of a 1.2% ethereal diazomethane solution. The usual work-up gave 240 mg (quantitative yield) of (Z)-*3β-hydroxy-20-methoxymethylene-5α-pregnan-21-al* (**2c**), as a foam; λ_{max} (EtOH): 253 nm (log ε 4.2); ν_{max} (KBr): 3440 (hydroxyl), 2750 (aldehyde), 1675 and 1630 cm^{-1} (doublet of α,β-unsaturated aldehyde); δ (90 MHz): 0.57 (s, 3H, 18-CH_3), 0.79 (s, 3H, 19-CH_3), 3.88 (s, 3H, OCH_3), 6.88 (s, 1H, olefinic proton), 9.31 (s, 1H, aldehyde). This product was dissolved in 10 ml of pyridine and treated with 5 ml of acetic anhydride for 15 h at room temperature. The mixture was poured into 150 ml of ice water and the product was extracted with ether. The usual work-up afforded 259 mg (96% yield) of (Z)-*3β-acetoxy-20-methoxymethylene-5α-pregnan-21-al* (**2d**), mp 140–146°C. Recrystallization from methanol–water gave 202 mg of pure product, mp 147.5–150°C; its identity with the product obtained by the Vilsmeier–Haack reaction (see above) was established in the usual fashion.

Diacetylation

A solution of 1.0 g of the dihydroxy aldehyde **2** in 14 ml of pyridine was treated for 20 h at room temperature with 7 ml of acetic anhydride. The mixture was precipitated into 300 ml of ice water. The usual work-up gave 1.216 g (98% yield) of a foamy product, representing (Z)-*3β-acetoxy-20-acetoxymethylene-5α-pregnan-21-al* (**2b**), mp 54–58°C; λ_{max} (EtOH): 245 nm (log ε 4); ν_{max} (KBr): 2710 (aldehyde), 1780 (enol acetate), 1730 (acetate), 1690 and 1650 cm^{-1} (doublet of α,β-unsaturated aldehyde); δ (60 MHz): 0.61 (s, 3H, 18-CH_3), 0.85 (s, 3H, 19-CH_3), 1.95 (s, 3H, 3-acetate), 2.26 (s, 3H, enol acetate), 4.6 (m, 1H, 3α-H), 7.98 (s, 1H, olefinic proton), 9.42 (s, 1H, aldehyde); ms[16] *m/e* 430 (M^+), 388, 370, 310, 215. Since the product is unstable, particularly in solution, it was impossible to purify it sufficiently to obtain satisfactory results of an elemental analysis.

[16]We express sincere thanks to Dr. G. Schilling of Ayerst Laboratories, Montreal, for kindly having performed this mass spectral analysis for us.

Can. J. Chem. Downloaded from www.nrcresearchpress.com by 210.87.254.6 on 09/05/12
For personal use only.

(Z)- *and* (E)-*3β-Acetoxy-20-chloromethylene-5α-pregnan-21-als* (*5*)

(*a*) To a solution of 3.28 g of (*Z*)-3β-acetoxy-20-methoxymethylene-5α-pregnan-21-al (**2***d*) in 80 ml of dichloromethane, 1.08 ml of thionyl chloride was added dropwise and with stirring at 0°C. The mixture was heated for 3 h to 56°C, and then was cooled and taken to dryness *in vacuo*. There were added 50 ml of dichloromethane and 100 ml of ice water and the mixture was shaken vigorously for 45 min; its ether extract was washed with water and was dried. Evaporation gave 3.37 g of a yellow solid which was filtered through 60 g of aluminum oxide, activity III. Elutions with benzene gave 2.67 g (81%) of a mixture of the *Z* and *E* aldehydes **5**, mp 195–199°C. For analysis a sample was recrystallized 3 times from ether – petroleum ether; colorless prisms, mp 203–204°C; $[\alpha]_D^{25}$ −73.6° (*c* 1.010, $CHCl_3$); λ_{max} (EtOH): 247 nm (log ε 4.1); ν_{max} (KBr): 3080 and 3060 (double bond), 2740 (aldehyde), 1725 (acetate), 1690 and 1590 (α,β-unsaturated aldehyde), 1250 cm^{-1} (acetate); δ (60 MHz): 0.63 (s, 3H, 18-CH_3), 0.80 (s, 3H, 19-CH_3), 1.98 (s, 3H, acetate), 7.0 and 7.16 (s, 1H, olefinic proton), 9.60 and 10.04 (s, 1H, aldehyde); ms *m/e* 409 (M^+ + 2), 407 (M^+), 346, 331, 226. *Anal.* calcd. for $C_{24}H_{35}O_3Cl$: C 70.82, H 8.67, Cl 8.71; found: C 71.05, H 8.61, Cl 8.75.

(*b*) An analogous reaction was carried out with 200 mg of (*E*)-3β-acetoxy-20-methoxymethylene-5α-pregnan-21-al (**3**) and 0.6 ml of thionyl chloride. This led to 198 mg of the crude mixture of the chloromethylene aldehydes **5**. Filtration through 10 g of aluminum oxide, activity III, gave 140 mg of the pure mixture, mp 196–198°C. The identity of the product with that described under (*a*) was established by the determination of a mixture melting point and by the comparison of the uv, ir, and nmr spectra.

Ethyl 3β-Hydroxy-23-ethoxycarbonyl-21-nor-5α-chol-22-en-24-oate (*4*) *and Ethyl 3β-Acetoxy-23-ethoxycarbonyl-21-nor-5β-chol-22-en-24-oate* (*4a*)

(*a*) A solution of 1.0 g of aldehyde **2***d*, mp 148–150°C, of 0.46 ml of diethyl malonate and of 0.29 ml of piperidine in 24 ml of absolute ethanol was refluxed under nitrogen for 3 h. The product was cooled and precipitated into 250 ml of ice water. The mixture was extracted with ether, the ethereal layer was washed with an iced dilute hydrochloric acid solution, a cold sodium bicarbonate solution and water, and was dried. Evaporation of the solvent gave 1.12 g of an oil which was subjected to dry-column chromatography on 250 g of silica gel, petroleum ether – ether (1:2) being used as eluent. Thus, 885 mg of *ethyl 3β-acetoxy-23-ethoxycarbonyl-21-nor-5α-chol-22-en-24-oate* (**4***a*) was obtained; the product crystallized from petroleum ether, mp 98–100°C. A quantity of 118 mg of starting material (**2***d*) was recovered; considering this recovery, the yield of ester **4***a* corresponded to 80%. For analysis, a sample of ester **4***a* was recrystallized 3 times from petroleum ether; colorless needles, mp 102–103°C; $[\alpha]_D^{23}$ +20.9° (*c* 1.080, $CHCl_3$); λ_{max} ($CHCl_3$): 217 nm (log ε 3.5); ν_{max} (KBr): 1720 (esters), 1650 (double bond), 1250 cm^{-1} (esters); δ (90 MHz): 0.61 (s, 3H, 18-CH_3), 0.94 (s, 3H, 19-CH_3), 1.28 (t, *J* = 7 Hz, 3H) and 1.33 (t, *J* = 7 Hz, 3H), $COOCH_2CH_3$), 2.0 (s, 3H, acetate), 4.23 (q, *J* = 7 Hz, 2H), and 4.30 (q, *J* = 7 Hz, 2H) ($COOCH_2CH_3$), 7.0 (t, *J* = 8 Hz, 1H, 22-H); ms *m/e* 502.5 (M^+), 457, 317, 185.5. *Anal.* calcd. for $C_{30}H_{46}O_6$: C 71.68, H 9.22; found: C 71.52, H 9.00.

(*b*) A quantity of 266 mg of the dihydroxy aldehyde **2**, mp 192–196°C, was treated with 0.18 ml of diethyl malonate and 0.11 ml of piperidine in 18 ml of absolute ethanol, as described under (*a*) for the acetate **2***d*. The usual work-up gave 264 mg of a yellowish oil which was subjected to dry-column chromatography on 50 g of silica gel, ether being used as eluent. Thus, 80 mg of starting material (**2**) was recovered and 111 mg of *ethyl 3β-hydroxy-23-ethoxycarbonyl-21-nor-5α-chol-22-en-24-oate* (**4**), mp 125–130°C, was obtained (yield, considering the recovery of starting material, 45%); λ_{max} (EtOH): 215 nm (log ε 3.8); ν_{max} (KBr): 3380 (hydroxyl), 1730 (esters), 1650 (double bond), 1250 cm^{-1} (esters): δ (90 MHz): 0.58 (s, 18-CH_3), 0.80 (s, 19-CH_3), 1.25 (m, 6H, $COOCH_2CH_3$), 2.38 (s, 1H, exchanged with D_2O, OH), 3.57 (m, 1H, 3α-H), 4.22 (m, 4H, $COOCH_2CH_3$), 7.0 (t, *J* = 8 Hz, 1H, 22-H).

A quantity of 95 mg of this product (**4**) was acetylated in the usual fashion at room temperature with 1 ml of acetic anhydride in 2 ml of pyridine. Thus, 103 mg (quantitative yield) of *ethyl 3β-acetoxy-23-ethoxycarbonyl-21-nor-5α-chol-22-en-24-oate* (**4***a*), mp 97–100°C, was obtained. The identity of the product with the one described under (*a*) was established by the determination of a mixture melting point and by the comparison of the uv, ir, and nmr spectra.

3β-Acetoxy-23-ethoxycarbonyl-5α,14α-bufa-20,22-dienolide (*9*)

A solution of sodium ethoxide, prepared from 30 mg of sodium and 5 ml of absolute ethanol, was taken to dryness. The residue was dissolved in 10 ml of anhydrous hexamethylphosphoric triamide (HMPT) and 0.25 ml of freshly redistilled diethyl malonate was added. After 0.5 h, a solution of 500 mg of the *cis–trans* mixture of the chloromethylene aldehydes **5** in 20 ml of HMPT was added with stirring. The mixture was further stirred for 2.5 h at room temperature and was subsequently kept for 18 h at 0°C. After acidification with a few drops of glacial acetic acid, the product was poured into 400 ml of ice water. The mixture was extracted with ether, the ethereal layer was washed with a saturated sodium bicarbonate solution and water, and was dried. Evaporation of the solvent gave 658 mg of an oil, containing *ethyl 3β-acetoxy-23-ethoxycarbonyl-21-oxo-5α-chol-20-en-24-oate* (**6**); λ_{max} (EtOH): 238 nm (log ε 3.75); ν_{max} (film): 2710 (aldehyde), 1730 (esters), 1700 (aldehyde), 1640 (double bond), 1250 cm^{-1} (esters); δ (90 MHz): 0.60 (s, 3H, 18-CH_3), 0.85 (s, 3H, 19-CH_3), 1.3 (t, *J* = 7 Hz, 6H, $COOCH_2CH_3$), 1.93 (s, 3H, acetate), 4.21 (q, *J* = 7 Hz, 4H, $COOCH_2CH_3$), 6.4 (d, *J* = 10 Hz, 1H, 22-H), 10.06 (s, 1H, aldehyde). This product could not be purified since it cyclized as a consequence of the corresponding operations. It was subjected to dry-column chromatography, first on 150 g of silica gel, activity III, using petroleum ether – ether (1:2) as eluent, and again on 150 g of the same absorbent, using petroleum ether – ether (2:1) as eluent. There was recovered 90 mg of the starting material, the mixture of the isomeric aldehydes **5**, and there was further obtained 185 mg (38% yield, considering the recovery of starting material) of *3β-acetoxy-23-ethoxycarbonyl-5α,14α-bufa-20,22-dienolide* (**9**). This product did not crystallize but was found homogeneous by thin-layer analysis; $[\alpha]_D^{23}$ +42.2° (*c* 0.920, $CHCl_3$); λ_{max} (EtOH): 322 nm (log ε 3.7); ν_{max} (KBr): 1760 (lactone), 1730 (ester), 1640 and 1550 (conjugated diene), 1240 cm^{-1} (ester); δ (90 MHz): 0.53 (s, 3H, 18-CH_3), 0.82 (s, 3H, 19-CH_3), 1.28 (t, *J* = 7 Hz, 3H, $COOCH_2CH_3$), 2.0 (s, 3H, acetate), 4.37 (q, *J* = 7 Hz, 2H, $COOCH_2CH_3$), 4.68 (m, 1H, 3α-H), 7.45 (d, *J* = 2.5 Hz, 1H, 22-H), 8.12 (d, *J* = 2.5 Hz, 1H, 21-H); ms[16] *m/e* 484.5 (M^+), 345, 302, 287, 248, 216. *Anal.* calcd. for $C_{29}H_{40}O_6$: C 71.87, H 8.32; found: C 71.47, H 8.48.

Ethyl (Z)-*21-Chloro-3β-acetoxy-22ξ-hydroxy-5α-chol-20(21)-enoate* (*7*) *and Ethyl* (E)-*21-Chloro-3β-acetoxy-22ξ-hydroxy-5α-chol-20(21)-enoate* (*8*)

To a solution of 0.27 ml of hexamethyldisilazane in 1 ml of absolute ether and 3 ml of anhydrous *n*-pentane, there was added, with exclusion of moisture and in a nitrogen atmosphere, with a syringe, through a septum, 0.825 ml of a 1.52 *M* *n*-butyllithium solution in *n*-pentane. The mixture was

Can. J. Chem. Downloaded from www.nrcresearchpress.com by 210.87.254.6 on 09/05/12
For personal use only.

refluxed for 0.5 h and was subsequently cooled. The solvent was evaporated *in vacuo* and the residue was dissolved in 3 ml of absolute tetrahydrofuran. This solution was cooled to −78°C and, with vigorous stirring, 0.1 ml of anhydrous ethyl acetate was added slowly. The mixture was stirred at −78°C for 15 min and, through a septum, a solution of 407 mg of the *cis–trans* mixture of the chloromethylene aldehydes **5** in 5 ml of THF was added. The product was stirred for 10 min at −78°C, treated with 8 ml of 2 *N* hydrochloric acid, and then allowed to reach room temperature. The mixture was precipitated into water and the product was extracted with ether. The ethereal layer was washed with a saturated sodium bicarbonate solution and water, and was dried. Evaporation of the solvent gave 526 mg of a mixture of the isomeric cholenates 7 and **8**. Recrystallization from ether–hexane gave 200 mg (41% yield) of *ethyl* (E)-*21-chloro-3β-acetoxy-22ξ-hydroxy-5α-chol-20(21)-enoate* (**8**), mp 141–144°C. For analysis, a sample was recrystallized 3 times from ether–hexane; colorless powder, mp 161–162°C; $[\alpha]_D^{25}$ −21.6° (*c* 1.250, $CHCl_3$); ν_{max} (KBr): 3410 (hydroxyl), 3100 (double bond), 1730 (acetate), 1710 (ethyl ester), 1625 (double bond), 1280 cm^{-1} (esters); δ (90 MHz): 0.72 (s, 3H, 18-CH_3), 0.93 (s, 3H, 19-CH_3), 1.26 (t, J = 7 Hz, 3H, $COOCH_2CH_3$), 2.4 (d, J = 9 Hz, 2H, $CH_2COOC_2H_5$), 4.16 (q, J = 7 Hz, 2H, $COOCH_2CH_3$), 4.66 (m, 2H, 3α-H and 21-H), 6.48 (s, 1H, olefinic proton). *Anal.* calcd. for $C_{28}H_{43}O_5Cl$: C 67.92, H 8.75, Cl 7.16; found: C 67.54, H 8.70, Cl 7.05.

Recrystallization of the mother liquors from ether–hexane gave 249 mg (50% yield) of *ethyl* (Z)-*21-chloro-3β-acetoxy-22ξ-hydroxy-5α-chol-20(21)-enoate* (7), mp 101–108°C. For analysis a sample was recrystallized 3 times from ether–hexane; colorless powder, mp 107–110°C; $[\alpha]_D^{25}$ +14.5° (*c* 1.035, $CHCl_3$); ν_{max} (KBr): 3480 (hydroxyl), 3100 (double bond), 1730 (acetate), 1710 (ethyl ester), 1625 (double bond), 1270 cm^{-1} (esters); ν_{max} (CCl_4): 3520 cm^{-1}; δ (90 MHz): 0.67 (s, 3H, 18-CH_3), 0.81 (s, 3H, 19-CH_3), 1.28 (t, J = 7 Hz, 3H, $COOCH_2CH_3$), 2.6 (d, J = 9 Hz, 2H, $CH_2COOC_2H_5$), 4.16 (q, J = 7 Hz, 2H, $COOCH_2CH_3$), 4.66 (m, 1H, 3α-H), 5.16 (m, 1H, 21-H), 5.94 (s, 1H, olefinic proton). *Anal.* calcd. for $C_{28}H_{43}O_5Cl$: C 67.92, H 8.75, Cl 7.16; found: C 67.80, H 8.68, Cl 6.90.

The reaction was repeated, employing the same procedure, in the presence of 5 mg of cuprous chloride, which led to an identical result.

Ethyl (Z)-*3β-Acetoxy-21-oxo-5α-chol-20(22)-enoate* (**12**) *from* (Z)-*3β-Acetoxy-20-methoxymethylene-5α-pregnan-21-al* (**2***d*) *without Isolation of the Hydroxy Cholenoate* **10**

Using the procedure described in the previous experiment leading to the chloro cholenoates **7** and **8**, 1.206 g of the methoxymethylene aldehyde **2***d*, mp 148–150°C, was treated in THF at −78°C for 10 min with a solution of ethyl lithioacetate obtained from 0.3 ml of ethyl acetate and a solution of lithium hexamethyldisilazine, the latter having been prepared from 2.58 ml of 1.52 *M* *n*-butyllithium and 0.81 ml of hexamethyldisilazane. The usual work-up gave 1.463 g of a product which was subjected to dry-column chromatography on 80 g of silica gel, petroleum ether – ether (1:1) serving as eluent. Thus, 1.047 g (78% yield) of a *cis–trans* mixture of the *ethyl 3β-acetoxy-21-oxo-5α-chol-20(22)-enoates* **12** and **13**, mp 149–154°C, was obtained; λ_{max} (EtOH): 233 (log ε 3.95), 300 nm (log ε 3.25); ν_{max} (KBr): 2740 (aldehyde), 1745 (shoulder) and 1730 (esters), 1683 and 1630 (α,β-unsaturated aldehyde), 1250 cm^{-1} (esters); ν_{max} (film) 2720 (broad, aldehyde), 1742, 1730 (esters), 1697 and 1636 (α,β-unsaturated aldehyde), 1250 cm^{-1} (esters); δ (90 MHz): 0.6 (s, 3H, 18-CH_3), 0.8 (s, 3H, 19-CH_3), 1.25 and 1.27 (t, J = 7 Hz, 3H, $COOCH_2CH_3$), 2.0 (s, 3H, acetate), 3.42 (d, J = 7 Hz, 2H, 23-H_2), 4.16 and 4.18 (q, J = 7 Hz, 2H, $COOCH_2CH_3$), 6.52 and 6.77 (t, J = 7 Hz, 1H, olefinic proton), 9.46 and 9.96 (s, 1H, aldehyde). Recrystallization from dichloromethane–hexane raised the melting point to 157–160°C. The nmr spectra of the recrystallized product and of its mother liquors indicated the presence of only the *Z-isomer* **12**. For analysis, a sample was recrystallized 3 times from dichloromethane–hexane; colorless prisms, mp 163.5–165°C; $[\alpha]_D^{25}$ −56.7° (*c* 1.180, $CHCl_3$); λ_{max} (EtOH): 233 nm (log ε 4.05), 300 nm (log ε 3.4); ν_{max} (KBr): 2740 (aldehyde), 1745 and 1730 (esters), 1685 and 1630 (α,β-unsaturated aldehyde), 1250 cm^{-1} (esters); δ (90 MHz): 0.61 (s, 3H, 18-CH_3), 0.81 (s, 3H, 19-CH_3), 1.27 (t, J = 7 Hz, 3H, $COOCH_2CH_3$), 2.0 (s, 3H, acetate), 3.43 (d, J = 7 Hz, 2H, $CH_2COOC_2H_5$), 4.18 (q, J = 7 Hz, 2H, $COOCH_2CH_3$), 6.77 (t, J = 7 Hz, 1H, olefinic proton), 9.48 (s, 1H, aldehyde). *Anal.* calcd. for $C_{28}H_{42}O_5$: C 73.32, H 9.23; found: C 73.58, H 9.21.

Ethyl (Z)-*3β-Acetoxy-21-methoxy-22ξ-hydroxy-5α-chol-20(21)-enoate* (**10**)

As described above, 602 mg of aldehyde **2***d* was treated in THF at −78°C for 10 min with a solution of ethyl lithioacetate, obtained from 0.15 ml of ethyl acetate and a solution of lithium hexamethyldisilazine, prepared from 1.3 ml of a 1.52 *M* *n*-butyllithium solution and 0.40 ml of hexamethyldisilazane. However, in contradistinction to the experiment described in the previous section, in the work-up the product was not hydrolyzed with hydrochloric acid but with water. Thus, 646 mg of a material was obtained which was subjected to dry-column chromatography on 42 g of silica gel, petroleum ether – ether (1:1) being used as eluent. This gave 306 mg (42% yield) of the hydroxy cholenoate **10**, mp 139–143°C. For analysis, a sample was recrystallized 3 times from ether–hexane; colorless powder, mp 143.5–145°C; $[\alpha]_D^{25}$ −18.8° (*c* 1.120, $CHCl_3$); ν_{max} (KBr): 3450 (hydroxyl), 1730 (acetate), 1715 (ethyl ester), 1655 (double bond), 1250 cm^{-1} (esters); δ (90 MHz): 0.64 (s, 3H, 18-CH_3), 0.81 (s, 3H, 19-CH_3), 1.25 (t, J = 7 Hz, 3H, $COOCH_2CH_3$), 2.53 (d, J = 6 Hz, 2H, $CH_2COOC_2H_5$), 3.51 (s, 3H, CH_3O), 4.15 (q, J = 7 Hz, 2H, $COOCH_2CH_3$), 4.3–4.9 (m, 2H, 3α-H and 21-H), 6.24 (s, 1H, olefinic proton). *Anal.* calcd. for $C_{29}H_{46}O_6$: C 70.98, H 9.45; found: C 71.03, H 9.39.

Ethyl (Z)-*3β-Acetoxy-21-oxo-5α-chol-20(22)-enoate* (**12**) *from the Hydroxy Cholenoate* **10**

For 10 min, at room temperature, 102 mg of ethyl (*Z*)-3β-acetoxy-21-methoxy-22ξ-hydroxy-5α-chol-20(21)-enoate (**10**), mp 139–143°C, was treated in 10 ml of tetrahydrofuran with 6 ml of 2 *N* hydrochloric acid. The usual work-up gave 96 mg (quantitative yield) of the *cis–trans* mixture of the aldehydo cholenoates **12** and **13**. One recrystallization from dichloromethane–hexane gave the *Z*-isomer **12**, mp 155–159°C, identified by the determination of a mixture melting point and by the comparison of its ir, uv, and nmr spectra with those of the product described above.

3β-Acetoxy-5α,14α-bufa-20,22-dienolide (**11**)

A solution of 347 mg of ethyl (*Z*)-3β-acetoxy-21-oxo-5α-chol-20(22)-enoate (**12**), mp 157–160°C, in 65 ml of ethanol was refluxed with 6.5 ml of concentrated hydrochloric acid, under nitrogen, for 18 h. The mixture was cooled and was then precipitated into 650 ml of ice water. After 1 h, the product was filtered, the solid material was washed with water and was dissolved in dichloromethane. The solution was dried, the solvent was evaporated, and the residue (292 mg) was dissolved in 25 ml of pyridine and treated for 16 h at room temperature with 12.5 ml of acetic anhydride. The product was precipitated into 300 ml of ice water and the mixture was extracted with ether. The ethereal solution was washed with iced dilute

Can. J. Chem. Downloaded from www.nrcresearchpress.com by 210.87.254.6 on 09/05/12
For personal use only.

hydrochloric acid, a cold sodium bicarbonate solution, and water, and was dried. Evaporation of the solvent gave 317 mg of a solid which was subjected to dry-column chromatography on 20 g of silica gel, petroleum ether – ether (2:3) serving as eluent. Thus, 138 mg of the bufadienolide **11**, mp 175–180°C, and 92 mg of the starting material, the aldehydo ester **12**, were obtained (yield, considering the recovery of starting material, 60%). Recrystallization of the bufadienolide **11** from ether–hexane raised the melting point to 180–183°C; λ_{max} (EtOH): 298–300 nm (log ε 3.7); ν_{max} (KBr): 3100 (double bond), 1755 (lactone), 1735 (acetate), 1645 and 1545 (conjugated diene), 1240 cm^{-1} (acetate); δ (90 MHz): 0.51 (s, 3H, 18-CH_3), 0.81 (s, 3H, 19-CH_3), 2.0 (s, 3H, acetate), 4.72 (m, 1H, 3α-H), 6.25 (d, J = 10 Hz, 1H, 22-H), 7.22–7.33 (m, 2H, 21-H and 23-H). The identity of the product was confirmed by the determination of a mixture melting point and by the comparison of its spectra with those of an authentic sample (6).

Treatment of (Z)-*3β-Acetoxy-20-acetoxymethylene-5α-pregnan-21-al (2b) with Ethyl Lithioacetate*

Using the above described method, 430 mg of (*Z*)-3β-acetoxy-20-acetoxymethylene-5α-pregnan-21-al (**2***b*) was treated in THF at −78°C for 10 min with a solution of ethyl lithioacetate, prepared from 0.1 ml of ethyl acetate and a solution of lithium hexamethyldisilazine, obtained from 0.825 ml of a 1.52 *M n*-butyllithium solution and 0.27 ml of hexamethyldisilazane. The usual work-up gave 444 mg of a crude product, mp 240–245°C, consisting essentially of *3β-acetoxy-20-hydroxymethylene-5α-pregnan-21-al* (**2***a*). One recrystallization from dichloromethane–hexane gave 175 mg of the pure product, mp 243–247°C; λ_{max} (EtOH): 253 nm (log ε 4.1); ν_{max} (KBr): 3500–2400 (hydroxyl), 2700 (aldehyde), 1730 (acetate), 1640 and 1585 (strong, α,β-unsaturated aldehyde), 1240 (ester), 1025 cm^{-1} (hydroxyl); δ (60 MHz): 0.53 (s, 3H, 18-CH_3), 0.83 (s, 3H, 19-CH_3), 2.03 (s, 3H, acetate), 8.4 (s, 2H, mesomeric aldehyde groups)

Reacetylation

A quantity of 25 mg of the acetoxy hydroxymethylene aldehyde **2***a* was acetylated with 3 ml of acetic anhydride in 6 ml of pyridine in the usual fashion. This led to 26 mg (quantitative yield) of *3β-acetoxy-20-acetoxymethylene-5α-pregnan-21-al* (**2***b*), obtained as a foam. The identity of the product was established by the comparison of its uv, ir, and nmr spectra with those of authentic diacetate **2***b* (see above).

Treatment of (Z)-*3β-Hydroxy-20-hydroxymethylene-5α-pregnan-21-al (2) with Ethyl Lithioacetate*

Using the above described method, 345 mg of the hydroxymethylene aldehyde **2** was treated in THF at −78°C for 1 h with an excess of ethyl lithioacetate (5.5 equiv.), obtained from 0.55 ml of ethyl acetate and a solution of lithium hexamethyldisilazine, prepared from 4.53 ml of a 1.52 *M n*-butyllithium solution and 1.48 ml of hexamethyldisilazane. The usual work-up gave 337 mg (quantitative yield) of a yellowish solid which was identified, by thin-layer, ultraviolet, infrared, and nmr analyses, as starting material **2**.

3-Ethoxycarbonyl-5,6,7,8-tetrahydrocoumarin (18)

A solution of sodium ethoxide, prepared from 10 ml of absolute EtOH and 90 mg of Na, was taken to dryness. The product was dissolved in 30 ml of anhydrous HMPT and 0.67 ml of freshly redistilled diethyl malonate was added. After 0.5 h, a solution of 557 mg of 2-chloromethylenecyclohexanone (**15**) (30) in 3 ml of HMPT was added with stirring. The mixture was further stirred for 1.5 h at room temperature and was then left for 18 h at 0°C. After acidification with a few drops of glacial acetic acid, the product was poured into 300 ml of ice water. The product's ether extract was washed with a saturated sodium bicarbonate solution and with water, and was dried. Evaporation of the solvent gave 1.012 g of a dark-brown oil, the ir and nmr spectra of which indicated the presence, to a considerable extent, of the starting materials, the uv spectrum of which, however, showed a maximum at 243 nm. The product was left for 2 days at room temperature. The black material was dissolved in ether, the ethereal solution was washed with water and was dried. Evaporation gave 780 mg of a brown oil, showing an α-pyronic structure (λ_{max} (EtOH) 332 nm (log ε 3.95); ν_{max} (film): 1645 and 1570 cm^{-1} (conjugated diene); δ (90 MHz): 7.88 (s, α-pyronic proton)). This product was subjected to dry-column chromatography on 50 g of silica gel, petroleum ether – ether (1:1) serving as eluent. Thus, 192 mg of the tetrahydrocoumarin **18**, mp 86–89°C, and 117 mg of the starting material **15** were obtained. For analysis, a sample of the tetrahydrocoumarin **18** was recrystallized twice from ether – petroleum ether; colorless prisms, mp 90.5–90°C; λ_{max} (EtOH): 335 nm (log ε 4); ν_{max} (KBr): 3040 (double bond), 1755 (large, lactone and ester), 1640 and 1570 (conjugated diene), 1235 cm^{-1} (ester); δ (90 MHz): 1.34 (t, J = 7 Hz, 3H, $COOCH_2CH_3$), 1.7–1.9 (m, 4H, 6-H_2 and 7-H_2), 2.4–2.6 (m, 4H, 5-H_2 and 8-H_2), 4.33 (q, J = 7 Hz, 2H, $COOCH_2CH_3$), 7.97 (s, 1H, 4-H). *Anal.* calcd. for $C_{12}H_{14}O_4$: C 64.85, H 6.35; found: C 64.96, H 6.33.

1-Formyl-2-carbethoxymethyl-1-cyclohexene (Ethyl (2′-Formylcyclohexenyl) Acetate) (22)

Using the above described procedure, 3.0 g of 2-methoxymethylenecyclohexanone (**20**) (31) prepared from 2-hydroxymethylenecyclohexanone according to the method employed by Gusakova *et al.* (32) for the synthesis of 2-ethoxymethylenecyclohexanone, was treated at −78°C in THF for 10 min with a solution of ethyl lithioacetate, prepared from 2.0 ml of ethyl acetate and a solution of lithium hexamethyldisilazine, obtained from 16.5 ml of 1.52 *M n*-butyllithium and 5.4 ml of hexamethyldisilazane. The usual work-up gave 3.65 g of a product which was subjected to dry-column chromatography on 300 g of silica gel, petroleum ether – ether (3:1) being used as eluent. Thus, 2.74 g (64% yield) of the aldehydo ester **22**, bp 94–97°C/1.0 Torr, was obtained; λ_{max} (EtOH): 247 nm (log ε 4.1); ν_{max} (film): 2740 (aldehyde), 1730 (ester), 1670 and 1640 (α,β-unsaturated aldehyde), 1230 cm^{-1} (ester); δ (90 MHz): 1.25 (t, J = 7 Hz, 3H, $COOCH_2CH_3$), 1.55–1.8 (m, 4H, 4-H_2 and 5-H_2), 2.2–2.5 (m, 4H, 3-H_2 and 6-H_2), 3.58 (s, 2H, $CH_2COOC_2H_5$), 4.2 (q, J = 7 Hz, 2H, $COOCH_2CH_3$), 10.2 (s, 1H, aldehyde).

2,4-Dinitrophenylhydrazone 22a

The 2,4-dinitrophenylhydrazone **22***a* was prepared in the usual fashion (33): mp 199.5–200°C (lit. (16*c*) 196–197°C); λ_{max} (EtOH): 261 (log ε 4.2), 292 (log ε 3.95), 380 nm (log ε 4.45) (lit. (16*c*) 257.5 (log ε 4.22), 291 (log ε 3.99), 381 nm (log ε 4.48)); ν_{max} (KBr): 3260 (NH), 3100 (aromatic C—H), 1705 (ester), 1615 and 1595 (aromatic), 1515 and 1330 (nitro groups), 1280 (ester), 835 cm^{-1} (aromatic); δ (90 MHz): 1.27 (t, J = 7 Hz, 3H, $COOCH_2CH_3$), 1.60–1.85 (m, 4H, 4-H_2 and 5-H_2), 2.22–2.60 (m, 4H, 3-H_2 and 6-H_2), 3.3 (s, 2H, $CH_2COOC_2H_5$), 4.17 (q, J = 7 Hz, 2H, $COOCH_2CH_3$), 8.22 (s, 1H, CH=N), 7.92 (d, J = 9 Hz, 1H), 8.20–8.35 (m, 1H), 9.1 (d, J = 2.5 Hz, 1H) (aromatic protons), 11.7 (s, large, 1H, NH). *Anal.* calcd. for $C_{17}H_{20}N_4O_6$: C 54.25, H 5.36, N 14.89; found: C 54.48, H 5.20, N 14.82.

Acknowledgements

Sincere thanks are extended to Mrs. J. Capitaine for her excellent cooperation in this study. We express our appreciation to Mrs. G. Pelletier and

Miss D. Thibault for devoted technical assistance. We are very grateful to the National Research Council of Canada, to the Ministère de l'Education du Gouvernement du Québec, and to Ayerst Laboratories, Montreal, for financial support, to Ayerst Laboratories also for very kind cooperation. One of us (G.D.) wishes to acknowledge scholarships from the National Research Council of Canada and the Ministère de l'Education du Québec.

1. G. DIONNE and CH. R. ENGEL. Can. J. Chem. This issue.
2. D. MUKHERJEE and CH. R. ENGEL. Can. J. Chem. This issue.
3. A. BÉLANGER, P. BRASSARD, G. DIONNE, and CH. R. ENGEL. Steroids, **24**, 377 (1974).
4. P. BRASSARD, CH. R. ENGEL, G. DIONNE, and A. BÉLANGER. Abstract 44A, 9th International (IUPAC) Symposium on the Chemistry of Natural Products, Ottawa, Ontario, June 24–28, 1974.
5. CH. R. ENGEL, D. MUKHERJEE, and G. DIONNE. Abstracts of Papers, 5th International (IUPAC) Congress of Chemistry, Jerusalem, July 6–11, 1975, p. 101.
6. CH. R. ENGEL, R. BOUCHARD, A. F. DE KRASSNY, L. RUEST, and J. LESSARD. Steroids, **14**, 637 (1969).
7. CH. R. ENGEL, A. F. DE KRASSNY, A. BÉLANGER, and G. DIONNE. Can. J. Chem. **51**, 3263 (1973).
8. (*a*) J. WALKER. J. Chem. Soc. 120 (1939); (*b*) P. R. HILLS and F. J. MCQUILLIN. J. Chem. Soc. 4060 (1953); (*c*) N. K. KOCHETKOV and L. I. KUDRYASHOV. Zhur. Obsch. Khim. **27**, 248 (1957); (*d*) M. J. D. VAN DAM. Recl. Trav. Chim. Pays-Bas, Belg. **83**, 31 (1964); (*e*) F. SCOTTI and E. J. FRAZZA. J. Org. Chem. **29**, 1800 (1964).
9. D. BERTIN, L. NÉDÉLEC, and J. MATHIEU. C. R. Acad. Sci. **253**, 1219 (1961).
10. A. VILSMEIER and A. HAACK. Ber. **60**, 119 (1927).
11. M. R. DE MEHEAS. Bull. Soc. Chim. Fr. 1989 (1962).
12. F. SONDHEIMER, W. MCCRAE, and W. G. SALMOND. J. Am. Chem. Soc. **91**, 1228 (1969).
13. L. BARDOU, J. ELGUERO, and R. JACQUIER. Bull. Soc. Chim. Fr. 289 (1967).
14. E. W. GARBISCH, JR. J. Am. Chem. Soc. **87**, 505 (1965).
15. V. T. KLIMKO, T. V. PROTOPOVA, and A. P. S. SKOLDINOV. Zhur. Obsch. Khim. **34**, 109 (1964).
16. (*a*) C. M. HILL, R. A. WALKER, and M. E. HILL. J. Am. Chem. Soc. **73**, 1663 (1951); (*b*) A. S. DREIDING and S. N. NICKEL. J. Am. Chem. Soc. **76**, 3965 (1954); (*c*) A. S. DREIDING and A. J. TOMASEWSKY. J. Am. Chem. Soc. **76**, 6388 (1954).
17. R. B. WOODWARD. J. Am. Chem. Soc. **63**, 1123 (1941); **64**, 72 (1942); **64**, 76 (1942).
18. H. PLIENINGER and HE DUCK MAH. Chem. Ber. **105**, 2766 (1972).
19. D. MOLHO and M. GIRAUD. Bull. Soc. Chim. Fr. 2603 (1968).
20. C. R. HAUSER and B. ABRAMOVITCH. J. Am. Chem. Soc. **62**, 1763 (1940).
21. M. W. RATHKE. J. Am. Chem. Soc. **92**, 3222 (1970).
22. I. N. ROZHKOV and S. M. MAKIN. J. Gen. Chem. (USSR), **34**, 57 (1964).
23. C. PASCUAL, J. MEIER, and W. SIMON. Helv. Chim. Acta, **49**, 164 (1966).
24. (*a*) M. S. KHARASCH and P. O. TAWNEY. J. Am. Chem. Soc. **63**, 2308 (1941); (*b*) H. O. HOUSE, W. L. RESPESS, and G. M. WHITESIDE. J. Org. Chem. **31**, 3128 (1966).
25. A. BÉLANGER and P. BRASSARD. J. Chem. Soc. Chem. Commun. 863 (1972); Can. J. Chem. **53**, 195 (1975); **53**, 201 (1975).
26. (*a*) G. R. PETTIT, D. C. FESSLER, K. D. PAULL, P. HOFER, and J. C. KNIGHT. J. Org. Chem. **35**, 1398 (1970); (*b*) G. R. PETTIT and J. R. DIAS. J. Org. Chem. **36**, 3207 (1971); (*c*) K. RADSCHEIDT, U. STACHE, W. HAEDE, W. FRITSCH, and H. RUSCHIG. Tetrahedron Lett. 3029 (1969); (*d*) W. HAEDE, W. FRITSCH, K. RADSCHEIDT, U. STACHE, and H. RUSCHIG. Justus Liebigs Ann. Chem. **741**, 92 (1970); (*e*) U. STACHE, K. RADSCHEIDT, W. FRITSCH, W. HAEDE, H. KOHL, and H. RUSCHIG. Justus Liebigs Ann. Chem. **750**, 149 (1971).
27. R. PETTIT, L. E. HOUGHTON, J. C. KNIGHT, and F. BRUSCHWEILER. J. Org. Chem. **35**, 2895 (1970).
28. PL. A. PLATTNER, P. TREADWELL, and C. SCHOLZ. Helv. Chim. Acta, **28**, 771 (1945).
29. C. N. R. RAO. Chemical applications of infrared spectroscopy. Academic Press, New York, NY. 1963. p. 210.
30. J. WOLINSKY, D. CHAN, and R. NOVAK. Chem. Ind. 720 (1965).
31. (*a*) E. E. ROYALS and K. N. BRANNOCK. J. Am. Chem. Soc. **75**, 2050 (1953); (*b*) L. BARDOU, J. ELGUERO, and R. JACQUIER. Bull. Soc. Chim. Fr. 297 (1967).
32. G. S. GUSAKOVA, E. A. PANFEROV, and E. P. POLUBNEVA. J. Gen. Chem. (USSR), **29**, 2732 (1959).
33. R. L. SHRINER, R. C. FUSON, and D. Y. CURTIN. The systematic identification of organic compounds. John Wiley and Sons Inc. New York, NY. 1967. p. 253.

Can. J. Chem. Downloaded from www.nrcresearchpress.com by 210.87.254.6 on 09/05/12
For personal use only.

Can. J. Chem. Downloaded from www.nrcresearchpress.com by 210.87.254.42 on 09/05/12
For personal use only.

Canadian Journal of Chemistry

Published by
THE NATIONAL RESEARCH COUNCIL OF CANADA

Journal canadien de chimie

Publié par
LE CONSEIL NATIONAL DE RECHERCHES DU CANADA

Volume 56 Number 4 February 15, 1978

Volume 56 numéro 4 15 février 1978

Hydrolysis of Co(II) at elevated temperatures[1]

GAÉTAN GIASSON[2] AND PARAM H. TEWARI[3]

Research Chemistry Branch, Atomic Energy of Canada Limited, Whiteshell Nuclear Research Establishment, Pinawa, Man., Canada R0E 1L0

Received May 25, 1977

GAÉTAN GIASSON and PARAM H. TEWARI. Can. J. Chem. **56**, 435 (1978).

Hydrolysis of Co(II) has been studied up to 200°C using a concentration cell with liquid junction of the type $Pt(H_2)|H^+(a_1)||H^+(a_2)|(H_2)Pt$. The effect of varying the initial solution p*H* and cobalt concentration has been studied at different ionic strengths. The hydrothermal hydrolysis for cobalt solutions between p*H* 3.9 and 9.6 is consistent with the equilibrium $Co^{2+} + H_2O \rightarrow CoOH^+ + H^+$. Higher hydrolytic species are not important. Hydrolysis increases with temperature and produces a buffering action at 200°C. Thermodynamic quantities for the hydrolysed species are reported.

GAÉTAN GIASSON et PARAM H. TEWARI. Can. J. Chem. **56**, 435 (1978).

On a étudié l'hydrolyse de Co(II) à des températures allant jusqu'à 200°C; pour y parvenir, on a fait appel à une cellule de concentration avec une jonction liquide du type $Pt(H_2)|H^+(a_1)||H^+(a_2)|(H_2)Pt$. On a étudié l'effet produit par la variation du p*H* et de la concentration du cobalt à diverses forces ioniques. L'hydrolyse hydrothermique de solutions de cobalt à des p*H* allant de 3.9 à 9.6 est en accord avec l'équilibre $Co^{2+} + H_2O \rightarrow CoOH^+ + H^+$. Les espèces hydratées plus élevées ne sont pas importantes. L'hydrolyse augmente avec la température et provoque une action de tampon à 200°C. On rapporte les paramètres thermodynamiques des espèces hydrolysées.

[Traduit par le journal]

Introduction

The hydrolysis of Co(II) ion has been studied by several workers (1–5) but these studies are limited to temperatures up to 50°C. The reported hydrolysis constants, even at 25°C, vary by a factor of more than 10^4. Therefore there is a need for more reliable values for the constants.

We have shown that hydrolysis enhances the adsorption of Co(II) on oxide surfaces (6, 7) in aqueous suspensions. Since oxides containing Co(II) become a contributing factor in the transport of ^{60}Co radioactivity in the coolant circuits of nuclear reactors, hydrolysis of Co(II) has been studied to understand its adsorption on oxides. To obtain better values for the hydrolysis constants, especially at higher temperatures, we have also studied the hydrolysis of Co(II) up to 200°C, using electrometric acidity measurements. In this work, hydrolysis studies between 25 and 200°C are reported as a function of p*H* of the initial solution, Co(II) concentration, and the ionic strength of the medium.

Experimental

The concentration cell with liquid junction of the type $Pt(H_2)|H^+(a_1)||H^+(a_2)|(H_2)Pt$ used to measure the acidity up to 200°C is shown in Fig. 1. The cell consists of two Teflon compartments housed in a high pressure autoclave. The two compartments contain solutions connected through a liquid junction (plug) of porous Teflon which was soaked in a saturated potassium chloride solution. The leakage rate through the plug was 2 μl/h but this was insufficient to introduce any significant error in the acidity of the solutions. The two compartments achieved a balanced H_2 pressure through a 1 mm hole located at the top of the inner Teflon wall.

Two platinum-encased thermocouples served as temperature sensors as well as reversible hydrogen electrodes for the cell. The electrodes were electrically isolated from the cell body by

[1]AECL No. 6027.

[2]Present address: Aluminum Company of Canada Limited, Arvida, Quebec, Canada.

[3]To whom correspondence should be addressed.

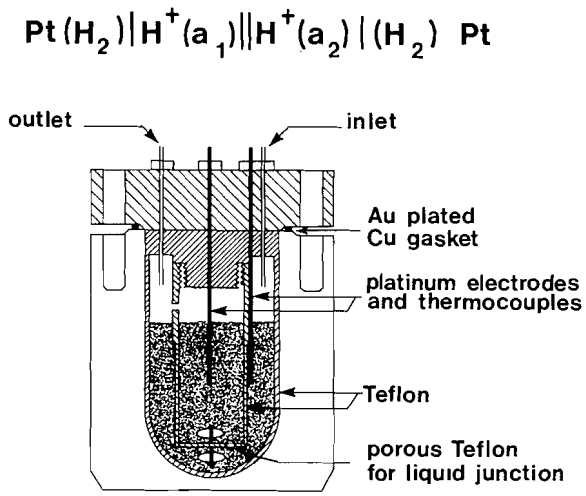

FIG. 1. High temperature concentration cell with liquid junction.

Teflon washers. The lower parts of the electrodes were platinized before each new set of measurements.

The entire autoclave assembly was put in a flush-fitting heating jacket and its heating was regulated by a thermocouple. The temperature of the two compartments was monitored continuously on a chart recorder and readings of cell emf were taken only after the temperature readings on the recorder were constant for an hour. The temperature was controlled between 25°C and 200°C to ±0.2°C. The potential difference of the cell was measured on a high-impedance digital millivoltmeter. Equilibrium emf values, as shown by their constancy on the recording chart paper, were used for calculations. The instrument could detect 0.1 mV changes in voltage between the two hydrogen electrodes. The solutions in the two compartments were stirred by Teflon-coated magnetic stirrers. All solutions were bubbled with H_2 before putting them into the cell and then were pressurized and purged repeatedly with H_2 to remove all traces of air or oxygen. Finally the cell was pressurized with 0.7 kPa of H_2 and sealed. At 25°C the equilibrium potential was attained in about 3 to 4 h after sealing the cell. The cell was then heated to the desired temperatures and at each equilibrium temperature the potential difference was noted.

Materials

Analytical grade $CoCl_2$, KCl, and HCl were used. KCl was further recrystallized. Deionized double-distilled water of conductivity $< 5.0 \times 10^{-6}$ Ω^{-1} m^{-1} was used. The reference (outer) compartment contained an HCl/KCl mixture with $H^+ = 1.0 \times 10^{-2}$ mol/kg and the inner compartment contained Co(II)/KCl solution mixtures at different initial acidities. Cobalt concentration was varied between 10^{-3} and 10^{-1} mol/kg and KCl concentration was varied between 0 and 1.0 mol/kg. Solutions of cobalt were prepared by weighing $CoCl_2 \cdot 6H_2O$ and their concentrations were checked by atomic absorption spectroscopy. The concentration of Cl^- and the ionic strength of the medium were maintained at the same value in both compartments by addition of KCl. The pH of the reference solution was periodically checked against a standard solution at 25°C and was found to remain constant to within 0.005 pH.

Acidity Measurements at Higher Temperatures

The potential difference E between the two hydrogen electrodes of the concentration cell $Pt(H_2)|H^+(a_1)||H^+(a_2)|(H_2)Pt$ is given by eq. 1,

$$[1] \qquad E = \frac{2.303RT}{F} \log \frac{a_2}{a_1} + E_J$$

$$= \frac{2.303RT}{F} \log \frac{\gamma_2 m_2}{\gamma_1 m_1} + E_J$$

$$= \frac{2.303RT}{F} (pH_1 - pH_2) + E_J$$

where a_1 and a_2 refer to the activities, γ_1 and γ_2 the activity coefficients, and m_1 and m_2 the molalities of H^+ in the inner and outer compartments respectively. E_J is the liquid junction potential. E_J was estimated by the method described by Macdonald and others (8) using diffusion coefficient, molality, and equivalent conductance data for ionic species in the solution. The liquid junction potential thus calculated for solutions of different ionic strengths seldom exceeded 0.1 mV, an insignificant fraction of the total measured potential difference (100–200 mV). Also, since the ionic strength of the two compartments was kept the same, the term $\log \gamma_2/\gamma_1$ can be eliminated without introducing significant error (8). Therefore, from the values of the potential difference E, and the pH_1 and m_1 of the reference compartment, pH_2 and m_2 for the cobalt containing solutions were calculated at different temperatures using [1].

Some hysteresis was observed with cobalt concentrations $> 10^{-1}$ mol/kg. This was probably due to hydrolytic precipitation on the electrodes; however, no detectable precipitation was observed. The electrodes were scraped to analyse for any precipitated material on them by X-ray diffraction but apart from platinum lines the patterns were very weak and no cobalt was detected. Also no metallic cobalt was detected under the reducing H_2 atmosphere at 200°C.

To test the reliability of the high temperature cell, K_w, the ionisation constant of water as a function of temperature was studied with acidic and alkaline (H^+ and OH^-) solutions in the outer and inner compartments respectively. The results were in close agreement (within 6%) with those reported in the literature (8, 9) which indicated that the cell was working satisfactorily.

Results and Discussion

Values for pH decreased with increasing temperature (Fig. 2). For solutions with higher initial pH, the drop in p$H(T)$ with temperature was steep; however, for solutions with lower pH, the decrease was small. Steeper p$H(T)$ changes showed a larger degree of hydrolysis for solutions of higher initial pH in contrast to solutions of lower pH. However, for all cobalt solutions with initial pH ranging from 3.9 to 9.6, the p$H(T)$ converged at higher temperatures and the final p$H(T)$ at 200°C for all the solutions was 3.78 ± 0.05. Thus the acidity at 200°C was insensitive to the pH at 25°C. This buffering action of the hydrolysis equilibria for cobalt is apparent from Fig. 3, where a p$H(T)$ vs. p$H(25)$ graph shows that p$H(T)$ was dependent on p$H(25)$ at lower temperatures but became almost independent at 200°C. Only at the highest pH (>5.5) does p$H(T)$ increase significantly from 3.75 at 200°C.

Can. J. Chem. Downloaded from www.nrcresearchpress.com by 210.87.254.42 on 09/05/12
For personal use only.

Can. J. Chem. Downloaded from www.nrcresearchpress.com by 210.87.254.42 on 09/05/12
For personal use only.

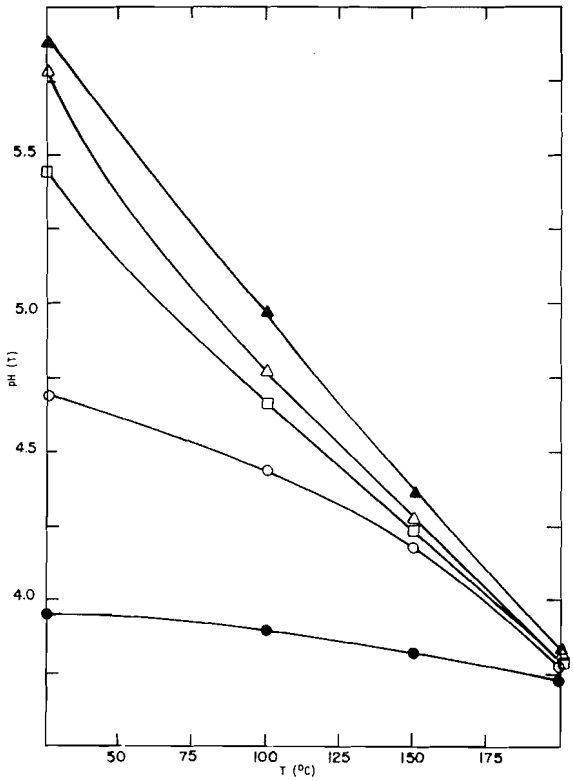

FIG. 2. p$H(T)$ versus temperature for different initial solution p$H(25)$, Co(II) 0.010 mol/kg and KCl 1.02 mol/kg: ●, pH 3.94; ○, pH 4.70; □, pH 7.92; △, pH 9.10; ▲, pH 9.62.

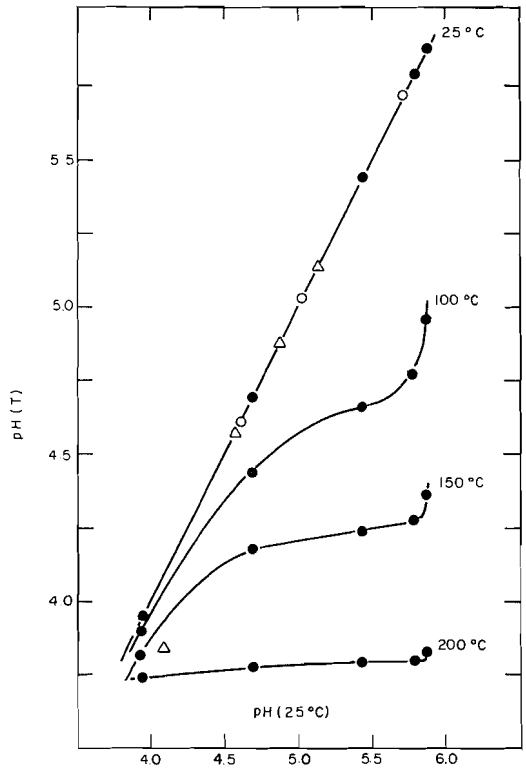

FIG. 3. p$H(T)$ versus p$H(25)$ at different temperatures: Co(II) = ●, 0.010, ○, 0.05, △, 0.102 mol/kg; Cl^- = 1.02 mol/kg.

High Temperature Hydrolysis

The temperature dependence of hydrolysis may be understood by defining a term $Z(T)$ as equal to the average number of OH^- ions bound per metal ion in the system. $Z(T)$ can be evaluated from experimental data of the hydrogen ion concentration in the solution before and after hydrolysis at each temperature (8–10) by [2], where h is the acidity after hydrolysis, H is the acidity before hydrolysis, $Q_{w(T)}$ is the equilibrium quotient for self-dissociation of water at temperature T, $Q_{w(25)}$ is the equilibrium quotient for self-dissociation of water at 25°C, and M_{Co} is total cobalt concentration.

$$[2] \quad Z(T) = \left[\left(h - \frac{Q_{w(T)}}{h}\right) - \left(H - \frac{Q_{w(25)}}{H}\right)\right] \Big/ M_{Co}$$

$Z(T)$ increases rapidly with temperature above 100°C (Fig. 4). The increase in $Z(T)$ is greater for solutions of higher pH at the same temperatures, indicating higher hydrolysis which is also evident from Fig. 2 where the largest drops in p$H(T)$ values, with temperature, are seen for solutions of higher pH.

In a plot of $Z(T)$ versus p$H(T)$ (T = 25°C) for different initial concentrations of Co(II) (Fig. 5), all the points fall on the same curve, i.e., $Z(T)$ is independent of cobalt concentration. This shows that the complexes present in appreciable amounts are homonuclear (1, 11, 13) and are probably represented by the hydrolysis equilibrium

$$[3] \quad Co^{2+} + H_2O \rightleftarrows CoOH^+ + H^+$$

Similarly at 200°C (Fig. 6), the points for the three concentrations of cobalt, with two exceptions, fall on one curve, showing that even at 200°C only homonuclear species are present. The two points which do not fit well on the curve are for solutions at the initial pH of 3.94 where hydrolysis is least and, therefore, the error in $Z(T)$ is high for these least hydrolysed samples.

Values of $Z(T)$ versus p$H(T)$ (Figs. 4, 7) at three Cl^- concentrations (from 0.02–1.02 mol/kg) at different temperatures fall on the same curve. Also a plot of $Z(T)$ against $Z(25)$ for different chloride ion concentrations is insensitive to chloride concentration. These results indicate that there is no formation of CoOHCl or mixed hydroxochloro complexes, and that OH^- is a stronger ligand than Cl^- for Co.

Hydrolysis Equilibria

The formation of different cobalt complexes in the

Can. J. Chem. Downloaded from www.nrcresearchpress.com by 210.87.254.42 on 09/05/12
For personal use only.

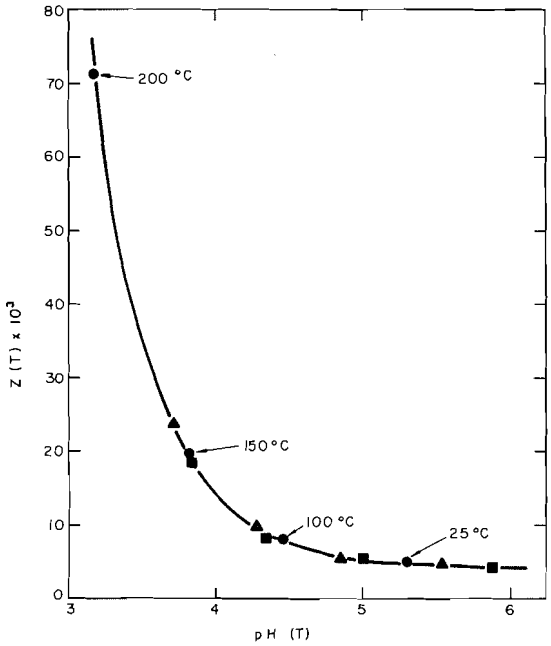

FIG. 4. Variation of $Z(T)$ with $pH(T)$ for different chloride concentrations; starting $pH(25)$ in the range 9.62–9.65: Co(II) = 0.01 mol/kg; Cl^- = ●, 0.02, ▲, 0.10, ■, 1.02 mol/kg.

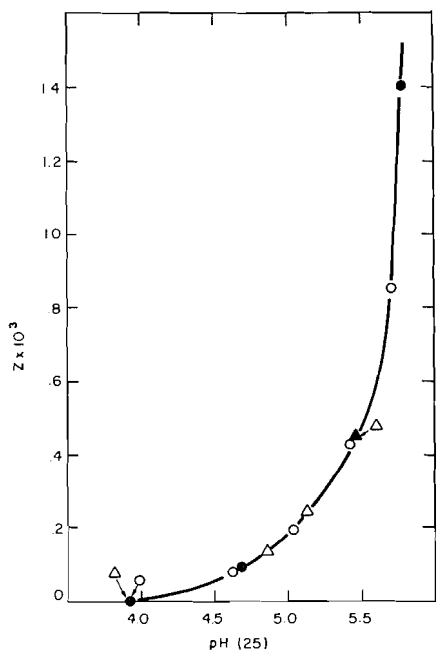

FIG. 5. Variation of $Z(T)$ with $pH(T)$ at T = 25°C: Co(II) = ●, 0.010, ○, 0.051, △, 0.102 mol/kg; Cl^- = 1.02 mol/kg.

KCl solution can be represented by

$$[4]\quad x\mathrm{Co}^{2+} + y\mathrm{H_2O} + z\mathrm{Cl}^- \overset{K_n}{\rightleftharpoons} \mathrm{Co}_x(\mathrm{OH})_y\mathrm{Cl}_z^{(2x-y-z)+} + y\mathrm{H}^+$$

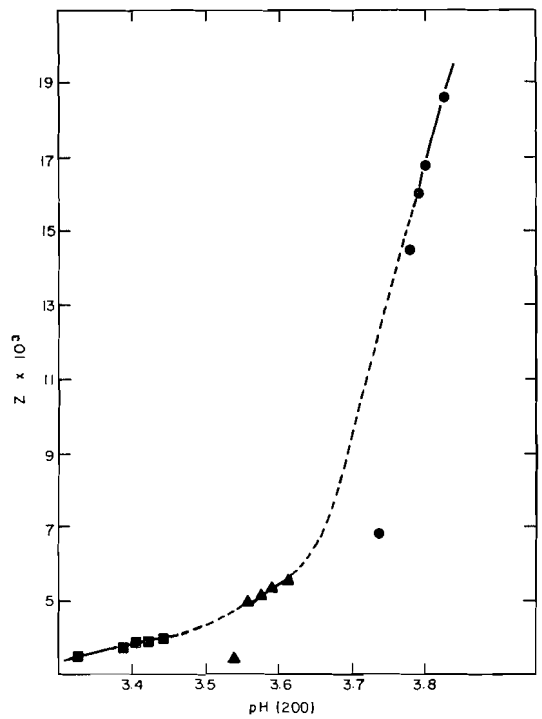

FIG. 6. Variation of $Z(T)$ with $pH(T)$ at T = 200°C: Co(II) = ●, 0.010, ▲, 0.051, ■, 0.102 mol/kg; Cl^- = 1.02 mol/kg.

where $x = 1, \ldots, n$, $y = 0, \ldots, n$, and $z = 0, \ldots, n$. K_n is the nth hydrolysis constant of [3].

$Z(T)$ is related to M_{Co} (total cobalt), x, y, z, and K_n at the temperature of interest through [5] and [6].

$$[5]\quad M_{Co} = [\mathrm{Co}^{2+}]_{free} + \sum_z \sum_y \sum_x xK_n \frac{[\mathrm{Co}^{2+}]^x[\mathrm{Cl}^-]^z}{[\mathrm{H}^+]^y}$$

$$[6]\quad [\mathrm{OH}^-]_{bound} = \sum_z \sum_y \sum_x yK_n \frac{[\mathrm{Co}^{2+}]^x[\mathrm{Cl}^-]^z}{[\mathrm{H}^+]^y}$$

Values of K_n were derived using a modified version of the computer program SCOGS, adopted for potentiometric measurements (12), which calculates K_n by minimizing the difference between $Z(T)$ calculated ([5] and [6]), and $Z(T)$ measured ([2]).

Since the fit of the experimental data (Table 1) is better when only $CoOH^+$ is considered, the results seem to be consistent with the presence of only $CoOH^+$, with little contribution from $Co(OH)_2$, under the conditions of the experiment (between pH 3 and 9.6 and for Co(II) solutions between 10^{-3} and 10^{-1} mol/kg).

At 25°C, our calculated value of pK_1 is similar to that reported by Bolzan and Arvia (1) but lower than that of Shanker and DeSouza (4) and Collados *et al.* (5). However, in these cases 1–5 mol/kg $Ba(ClO_4)_2$ and $NaClO_4$ were used to control the ionic strength,

TABLE 1. Calculated pK's

Species considered	Temperature (°C) 25	100	150	200
Only $CoOH^+$	$pK_1 = 9.82 \pm 0.02$	7.62 ± 0.03	6.59 ± 0.02	6.02 ± 0.04
$\mu = 1.0$	$\sigma = 1 \times 10^{-4}$	$\sigma = 3 \times 10^{-4}$	$\sigma = 7 \times 10^{-4}$	$\sigma = 3 \times 10^{-3}$
$CoOH^+$ and $Co(OH)_2$	$pK_1 = 9.84 \pm 0.09$	7.60 ± 0.10	6.63 ± 0.08	6.08 ± 0.12
	$pK_2 = 16.12 \pm 0.15$	12.89 ± 0.19	11.53 ± 0.18	9.64 ± 0.16
	$\sigma = 2 \times 10^{-4}$	$\sigma = 4 \times 10^{-4}$	$\sigma = 6 \times 10^{-4}$	$\sigma = 4.8 \times 10^{-3}$
pK_1 at zero ionic strength	10.02 ± 0.02	7.79 ± 0.02	6.86 ± 0.03	6.10 ± 0.06
pK_1 from literature	9.8 (1)			
	10.82 (4)			
	10.20 (5)			

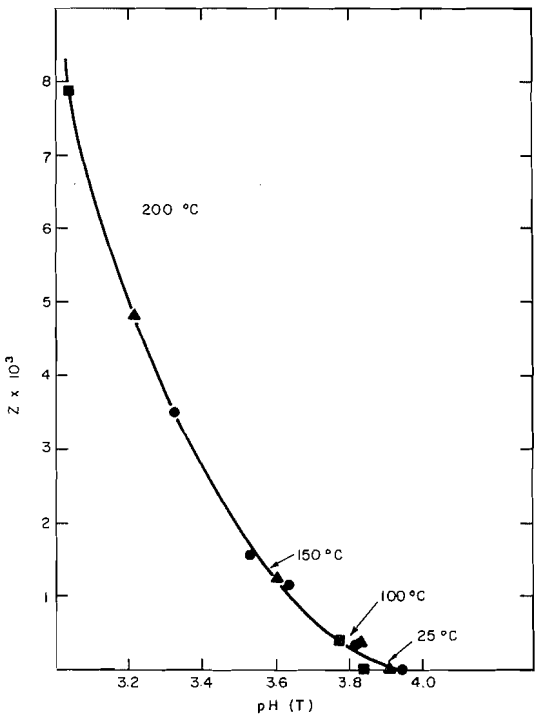

FIG. 7. Variation of $Z(T)$ with p$H(T)$ for different chloride concentrations; starting p$H(25)$ = 3.84 to 3.94: Cl^- = ●, 0.205, ▲, 0.512, ■, 1.02 mol/kg; Co(II) = 0.102 mol/kg.

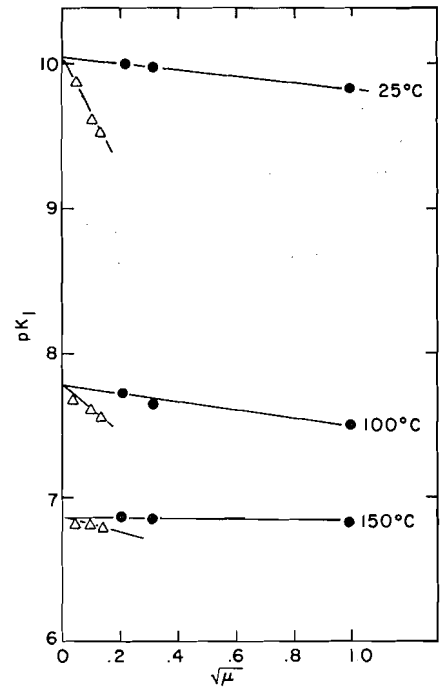

FIG. 8. Variation of pK_1 with $\sqrt{\mu}$ (ionic strength = μ) at different temperatures for Co(II) = ●, 1.0×10^{-2}, △, 1.0×10^{-3} mol/kg.

as compared to 1.0 mol/kg KCl used in this study. The difference may be due either to the anions or to some oxidation of Co(II) to Co(III) in the previous studies. There are no reported data for pK_1 at higher temperatures to which our data may be compared.

Higher hydrolytic polymers like $Co_2(OH)^{3+}$ and $Co_4(OH)_4{}^{4+}$ at relatively higher concentrations of Co(II) ($\approx$1.0 mol kg^{-1}) have been reported but their formulae are not uniquely established (13). In the concentration range of Co(II) used in our experiments, higher hydrolytic polymeric species do not appear to be present in significant quantities. When the results are analysed assuming the presence of both $CoOH^+$ and $Co(OH)_2$, pK_1 values do not differ significantly from those where only $Co(OH)^+$ is considered, and the pK_2 value, at 25°C, is lower than that reported in the literature (13) ($pK_2 \approx 18$). There are no data to compare at higher temperatures.

Calculation of Thermodynamic Functions

The hydrolysis constants have also been evaluated at different ionic strengths of the medium, and pK_1 versus $\sqrt{\mu}$, the square root of ionic strength, is plotted for different temperatures in Fig. 8. The

Can. J. Chem. Downloaded from www.nrcresearchpress.com by 210.87.254.42 on 09/05/12
For personal use only.

curves are extrapolated to zero ionic strength. At all temperatures and for two concentrations of cobalt, the extrapolated values at zero ionic strength are within the experimental errors, which reinforces the validity of the data obtained for pK_1.

Between 25 and 200°C, the free energy change ΔG^0 for the hydrolysis reaction $Co^{2+} + H_2O \rightarrow CoOH^+ + H^+$ does not change significantly. At 25°C the ΔG value is 57 ± 3 kJ/mol and at 200°C, 55 ± 3 kJ/mol. The enthalpy change ΔH, calculated from a linear plot of pK_1 versus $1/T$, at zero ionic strength is 60 ± 3 kJ/mol and ΔS^0 is 20 ± 8 J/(mol K) at 25°C. This value for ΔS^0 compares with values of 4 J/(mol K) and 13 ± 13 J/(mol K) for hydrolysis of Fe(II) (14) and Ni(II) (15) respectively. Our value is more reasonable than that of Bolzan and Arvia (1) (73 J/mol) which was calculated from results for temperatures up to only 40°C and without extrapolating to zero ionic strength.

In summary, hydrolysis of Co(II) increases with temperature and produces a buffering action at 200°C. For Co(II) solutions between 10^{-3} and 10^{-1} mol/kg with initial pH between 3.9 and 9.6, $CoOH^+$ is the dominant species with no detectable contributions from higher hydrolytic species.

Acknowledgements

The authors thank Dr. P. Tremaine for helpful discussions of thermodynamic quantities and one of us (G.G.) gratefully acknowledges the award of a National Research Council of Canada Postdoctoral Fellowship.

1. J. A. Bolzan and A. J. Arvia. Electrochim. Acta, **7**, 589 (1962).
2. K. H. Gayer and L. Wootner. J. Am. Chem. Soc. **74**, 1436 (1952).
3. S. Chaberek, R. C. Courtney, and A. E. Martell. J. Am. Chem. Soc. **74**, 5057 (1952).
4. J. Shankar and B. S. DeSouza. Aust. J. Chem. **16**, 1119 (1963).
5. M. P. Collados, F. Brito, and R. D. Cadavieco. An. Fis. Quim. **63B**, 843 (1967).
6. P. H. Tewari, A. B. Campbell, and Woon Lee. Can. J. Chem. **50**, 1642 (1972).
7. P. H. Tewari, R. H. Tuxworth, and Woon Lee. Proceedings of Symposium on oxide–electrolyte interfaces. J. Electrochem. Soc. 1973.
8. (*a*) D. D. Macdonald, P. Butler, and D. Owen. J. Phys. Chem. **77**, 2424 (1973); (*b*) R. E. Mesmer, C. F. Baes, and F. H. Sweeton. J. Phys. Chem. **74**, 1937 (1970).
9. C. F. Baes. Inorg. Chem. **4**, 588 (1965).
10. D. D. Macdonald, P. Butler, and D. Owen. Can. J. Chem. **51**, 2590 (1973).
11. L. G. Sillen. Q. Rev. **13**, 147 (1959).
12. I. G. Sayce. Talanta, **15**, 1397 (1968).
13. C. F. Baes, Jr. and R. E. Mesmer. The hydrolysis of cations. John Wiley and Sons, N.Y., NY. 1976.
14. P. Tremaine, R. Von Massow, and G. Sherman. Thermochim. Acta, **19**, 287 (1977).
15. D. D. Perrin. J. Chem. Soc. 3644 (1964).

Can. J. Chem. Downloaded from www.nrcresearchpress.com by 210.87.254.42 on 09/05/12
For personal use only.

Reactions of K_2PtCl_4 with pyridine derivatives in dimethylformamide and synthesis of potassium trichloro(pyridine)platinum(II)

PI-CHANG KONG AND F. D. ROCHON

Département de chimie, Université du Québec à Montréal, C.P. 8888, Montréal (Qué.), Canada H3C 3P8

Received May 24, 1977

PI-CHANG KONG and F. D. ROCHON. Can. J. Chem. **56**, 441 (1978).

The reactions of K_2PtCl_4 with pyridine derivatives L (L = py = pyridine, pic = picoline, and lut = lutidine) were studied in dimethylformamide (DMF).

$$K_2PtCl_4 \xrightarrow[L]{-KCl} K[Pt(L)Cl_3] \xrightarrow[L]{-KCl} \textit{cis}\text{-}[Pt(L)_2Cl_2] \xrightarrow{L} \textit{trans}\text{-}[Pt(L)_2Cl_2]$$

1 **2** **3**

The complexes (**1**) were isolated and the yield decreased with the order, 2,4-lut = 2-pic > 2,6-lut > 4-pic = py, which can be correlated to the steric hindrance of the *ortho* methyl groups. The compounds (**2**) can be converted to the compounds (**3**), the free ligand acting as catalyst and (**3**) is the final product of the above reactions. The compounds (**3**) can also be obtained from a DMF solution of $[Pt(L)_4]Cl_2$ (L = py) at room temperature. A comparison of the above reactions in water and in DMF was also made.

PI-CHANG KONG et F. D. ROCHON. Can. J. Chem. **56**, 441 (1978).

Les réactions entre K_2PtCl_4 et des dérivés de la pyridine L (L = py = pyridine, pic = picoline et lut = lutidine) ont été étudiées en milieu diméthylformamide (DMF).

$$K_2PtCl_4 \xrightarrow[L]{-KCl} K[Pt(L)Cl_3] \xrightarrow[L]{-KCl} \textit{cis}\text{-}[Pt(L)_2Cl_2] \xrightarrow{L} \textit{trans}\text{-}[Pt(L)_2Cl_2]$$

1 **2** **3**

Les complexes (**1**) ont été isolés et les rendements diminuent dans l'ordre, lut-2,4 = pic-2 > lut-2,6 > pic-4 = py. L'ordre peut être relié à l'encombrement stérique des groupements méthyles en position *ortho*. Les complexes *cis* (**2**) peuvent être convertis en (**3**), le ligand agissant comme catalyseur. (**3**) est le produit final des réactions mentionnées ci-haut. $[Pt(L)_4]Cl_2$ (L = py) en solution DMF à la température ambiante se décompose pour donner également (**3**). Une comparaison entre les réactions dans l'eau et dans le DMF a été faite.

Introduction

The recent chemotherapic results of platinum compounds are very promising, and compounds with high antitumour activity, low toxicity, and better solubility in the solvents used for dissolving drugs are being sought by investigators (1). So far, most compounds tested are of the type *cis*-$[Pt(am)_2Cl_2]$ and *cis*-$[Pt(py)_2Cl_2]$ (2, 3) (am = amine, py = pyridine) with two identical neutral ligands, since they can easily be prepared from the direct reaction between K_2PtCl_4 and the base in water. If compounds with two different neutral ligands such as *cis*-$[Pt(am)(am')Cl_2]$, *cis*-$[Pt(py)(py')Cl_2]$ and *cis*-$[Pt(py)(am)Cl_2]$ (am ≠ am' and py ≠ py') could be systematically synthesized, the screening range of platinum complexes could be largely extended and antitumour activity, toxicity, and solubility could be significantly modified.

In order to prepare such complexes, one has to use $K[Pt(am)Cl_3]$ or $K[Pt(py)Cl_3]$ as a starting material and react it with another kind of amine or pyridine. However, these two compounds are not easily prepared. Although $K[Pt(NH_3)Cl_3]$ (4) and $K[Pt(py)Cl_3]$ (5) have been known for a long time, the methods used are not suitable for other amine or pyridine derivatives. Recently, Kukushkin *et al.* (6, 7) prepared some alkylamine complexes from $[Pt(DMSO)(am)Cl_2]$ (DMSO = dimethylsulphoxide) through a long process of oxidation, replacement, and reduction.

$$[Pt(DMSO)(am)Cl_2] \xrightarrow{Cl_2} [Pt(DMSO)(am)Cl_4] \xrightarrow[KCl]{HCl} K[Pt(am)Cl_5] \xrightarrow{N_2H_4} K[Pt(am)Cl_3]$$

These complexes were precipitated as $[Pt(NH_3)_4][Pt(am)Cl_3]_2$ because of the difficulty of isolating the potassium salt.

Can. J. Chem. Downloaded from www.nrcresearchpress.com by 210.87.254.105 on 09/05/12
For personal use only.

Can. J. Chem. Downloaded from www.nrcresearchpress.com by 210.87.254.105 on 09/05/12
For personal use only.

In a recent communication (8) we reported a method for preparing mononucleoside platinum complexes by the direct reaction of K_2PtCl_4 and the nucleoside in dimethylformamide (DMF). This method is also applicable to pyridine analogues. Here we report the isolation and properties of the complexes $K[Pt(L)Cl_3]$ (L = py = pyridine, pic = picoline, and lut = lutidine). The reaction between K_2PtCl_4 and the bases in DMF is also discussed.

Experimental

Microanalyses were done by Chemalytics Inc., Tempe, Arizona, U.S.A. Melting points were measured on a Fischer-Johns apparatus and are uncorrected. Nuclear magnetic resonance spectra were measured on a Perkin-Elmer R-12 spectrometer. Infrared spectra were measured on a Perkin-Elmer 621 grating spectrophotometer.

The platinum salt, K_2PtCl_4, was obtained from Johnson Matthey & Co. Limited. Pyridine, picoline, and lutidine were purchased from Aldrich and Eastman and used without further purification. Dimethylformamide, A.C.S. reagent, was purchased from Anachemia and distilled with BaO, under reduced pressure (9). $[Pt(NH_3)_4]Cl_2$ (10) and $[Pt(py)_4]Cl_2$ (11) were prepared according to the already published methods. All the complexes were dried at 65°C, under vacuum in the presence of P_2O_5.

1. (a) K[Pt(py)Cl$_3$] and (b) [Pt(NH$_3$)$_4$][Pt(py)Cl$_3$]$_2$

K_2PtCl_4 (1.245 g) and pyridine (0.277 g) were mixed in 100 ml of dimethylformamide and heated at 75°C for 3 h. The DMF was then evaporated to dryness under reduced pressure at 40°C and the residue dissolved in a minimum volume of 0.5 *M* HCl solution. The insoluble material (mainly $[Pt(py)_2Cl_2]$) was separated by filtration. (*a*) To the HCl filtrate, KCl was added till saturation and $K[Pt(py)Cl_3]$ precipitated. The precipitate was filtered and dried. It was then dissolved in acetone and filtered to remove KCl and K_2PtCl_4. The acetone filtrate was evaporated to dryness. The solid compound, $K[Pt(py)Cl_3]$, was washed with chloroform and collected by filtration. Yield 35%. (*b*) To the HCl filtrate, an excess of $[Pt(NH_3)_4]Cl_2$ was added. The precipitate consisting of $[Pt(NH_3)_4][Pt(py)Cl_3]_2$ and $[Pt(NH_3)_4][PtCl_4]$ was filtered, dried, and dissolved in DMF. $[Pt(NH_3)_4][PtCl_4]$, being insoluble in DMF, was filtered off. The DMF filtrate of $[Pt(NH_3)_4][Pt(py)Cl_3]_2$ was evaporated to dryness, and the yellow product was washed with chloroform and collected by filtration. Yield 30%.

2. (a) K[Pt(4-pic)Cl$_3$] and (b) [Pt(NH$_3$)$_4$][Pt(4-pic)Cl$_3$]$_2$

K_2PtCl_4 (1.245 g) and 4-picoline (0.326 g) were mixed in 100 ml of DMF and heated at 75°C for 3 h. The DMF was then evaporated to dryness under reduced pressure at 40°C and the residue was washed with ether and dried. It was then dissolved in a minimum volume of 0.5 *M* HCl solution and the insoluble material (mainly $[Pt(4\text{-pic})_2Cl_2]$) was separated out by filtration. (*a*) To the HCl filtrate, KCl was added till saturation and $K[Pt(4\text{-pic})Cl_3]$ was precipitated. The precipitate was filtered, washed with a saturated aqueous solution of KCl, and dried. $K[Pt(4\text{-pic})Cl_3]$ was dissolved in a minimum amount of DMF and separated from KCl by filtration. $K[Pt(4\text{-pic})Cl_3]$ was precipitated by adding the DMF filtrate to 100 ml of a mixture of acetone (20 ml) and ether (80 ml). The compound was filtered and washed with chloroform. Yield: 40%. (*b*) Same as in section 1(*b*). Yield: 35%.

3. (a) K[Pt(2, 6-lut)Cl$_3$] and (b) [Pt(NH$_3$)$_4$][Pt(2, 6-lut)Cl$_3$]$_2$

K_2PtCl_4 (0.83 g) and 2,6-lutidine (0.214 g) were mixed in 75 ml of DMF and heated at 65°C overnight. The DMF was then evaporated to dryness and the solid residue washed with ether. It was then dissolved in a minimum volume of 0.5 *M* HCl solution and the insoluble black material removed by filtration. (*a*) Same as in section 2(*a*). Yield: 60%. (*b*) Same as in section 1(*b*). Yield: 50%.

4. K[Pt(2-pic)Cl$_3$] and K[Pt(2,4-lut)Cl$_3$]

K_2PtCl_4 (1.245 g) and 2-picoline (0.290 g) (or 0.340 g of 2,4-lutidine) were mixed in 75 ml of DMF at 80°C for 3 h. The DMF was then evaporated to dryness and the crude product was washed with ether and dried. $K[Pt(2\text{-pic})Cl_3]$ (or $K[Pt(2,4\text{-lut})Cl_3]$) was dissolved in acetone and separated from KCl and K_2PtCl_4 by filtration. The acetone filtrate was evaporated to dryness, and the yellow product was washed with chloroform and collected by filtration. Yield: 83% (2,4-lut, yield: 90%).

Results and Discussion

All the complexes are yellow and decompose on heating. Their analytical data and decomposing points are listed in Table 1. They are all insoluble in chloroform and the complexes of py, 2-pic, and 2,4-lut are soluble in acetone. $[Pt(NH_3)_4][Pt(L)Cl_3]_2$ can be formed as a precipitate when $K[Pt(L)Cl_3]$ (L = py, 4-pic, and 2,6-lut) reacts with $[Pt(NH_3)_4]Cl_2$ in acidic solution.

The complexes are stable in hydrochloric acid solution and can be gradually dissolved in potassium hydroxide solution. The KOH solutions are light yellow. When an excess HCl is added to a fresh KOH solution of a complex, the solution becomes darker yellow and the complex can be recovered by evaporating the solution.

In a few hours, all the complexes $K[Pt(L)Cl_3]$, except when L = 2,6-lut, form *cis*-$[Pt(L)_2Cl_2]$ with L in aqueous solution. The aqueous solution of $K[Pt(2,6\text{-lut})Cl_3]$ and 2,6-lut only becomes turbid, even on standing for two days, and no *cis*-$[Pt(2,6\text{-lut})_2Cl_2]$ can be isolated. The typical method to prepare *cis*-$[Pt(L)_2Cl_2]$ is to isolate the precipitate from the aqueous solution of K_2PtCl_4 and L. Again, *cis*-$[Pt(2,6\text{-lut})_2Cl_2]$ cannot be prepared by this method, since the solution of K_2PtCl_4 and 2,6-lut becomes black in 3 h and no yellow precipitate appears.

From a perchloric acid solution of $K[Pt(L)Cl_3]$, $KClO_4$ crystallizes out, and $[Pt(L)Cl_2]_2$, a dimer, can be isolated by evaporating the solution. When $K[Pt(L)Cl_3]$ is treated with $AgNO_3$ in DMF, $[Pt(L)(DMF)Cl_2]$ can be isolated.

When DMF was evaporated to dryness in the isolation of $K[Pt(py)Cl_3]$ and $K[Pt(4\text{-pic})Cl_3]$, a product soluble in chloroform was found. Upon the

TABLE 1. Element analysis and decomposing point of pyridine complexes*

Compound	Analysis (%) C	H	N	Cl	Decomposing points (°C)
$K[Pt(py)Cl_3]$	14.29	1.19	3.33	25.50	230
	14.53	1.21	3.44	24.90	
$K[Pt(4\text{-pic})Cl_3]$	16.59	1.61	3.22	24.52	230
	17.14	1.26	3.55	23.63	
$K[Pt(2\text{-pic})Cl_3]$	16.59	1.61	3.22	24.52	170
	17.12	1.60	3.30	23.80	
$K[Pt(2,4\text{-lut})Cl_3]$	18.79	2.01	3.12	23.75	220
	19.04	1.92	3.44	23.48	
$K[Pt(2,6\text{-lut})Cl_3]$	18.79	2.01	3.13	23.71	230
	19.00	2.01	2.97	23.47	
$[Pt(NH_3)_4][Pt(py)Cl_3]_2$	11.70	2.15	8.20	20.76	200
	12.28	2.20	8.20	20.58	
$[Pt(NH_3)_4][Pt(2,6\text{-lut})Cl_3]_2$	15.55	2.79	7.77	19.68	190
	15.84	2.88	8.69	19.51	

*Calculated value in first row.

evaporation of the chloroform, it became an oily paste which was difficult to crystallize. Its infrared spectrum showed that it contained py and DMF. However, it is not pure $[Pt(py)(DMF)Cl_2]$ which was isolated in our laboratory. It also was soluble in hydrochloric solution and can be converted at least partially to $K[Pt(py)Cl_3]$ in the presence of excess KCl.

From the Experimental section, we know that the yield in the synthesis of $K[Pt(L)Cl_3]$ is in the order:

$$2,4\text{-lut} \sim 2\text{-pic} > 2,6\text{-lut} > 4\text{-pic} \sim \text{py}$$

This order can be correlated to the steric hindrance of the *ortho*-methyl groups. During the preparation of *cis*-$[Pt(pic)_2Cl_2]$, Ivanova (12) found that 2-picoline had more difficulty entering the coordinating sphere of platinum than 3-picoline. In this work, both $K[Pt(L)Cl_3]$ and $[Pt(L)_2Cl_2]$ were isolated and the ligand difficulty in entering the platinum coordinating sphere can be determined by studying the following reactions.

$$[PtCl_4]^{2-} \xrightarrow[-Cl]{L} [Pt(L)Cl_3]^- \xrightarrow[-Cl]{L} \textit{cis}\text{-}[Pt(L)_2Cl_2]$$

Both $K[Pt(2,4\text{-lut})Cl_3]$ and $K[Pt(2\text{-pic})Cl_3]$ were produced in high yields (83–90%) and gave few by-products of $[Pt(L)_2Cl_2]$. This indicated that the second ligand, and not the first one, has difficulty in entering the coordinating sphere of the metal. However, pyridine and 4-picoline have no *ortho*-methyl groups and there is little difficulty in both steps of the above reactions. Formation of $[Pt(L)_2Cl_2]$ is at the expense of $K[Pt(L)Cl_3]$ and that is why the yield of $K[Pt(py)Cl_3]$ and $K[Pt(4\text{-pic})Cl_3]$ is low. Pearson and Muir (13) have found that the rates of the above reactions for $[PtBr_4]^{2-}$ and pyridine are comparable.

As for 2,6-lutidine, the methyl groups slow down even the first step of the above reaction and the formation of $[Pt(2,6\text{-lut})_2Cl_2]$ is almost impossible. $K[Pt(2,6\text{-lut})Cl_3]$, in DMF, decomposes slowly in the presence of 2,6-lut. This probably explains why the yield of $K[Pt(2,6\text{-lut})Cl_3]$ cannot be increased by increasing the reaction time. The steric hindrance from 2,6-lutidine can be further demonstrated by the observation mentioned in a preceding paragraph, i.e. 2,4-lut can form *cis*-$Pt(2,4\text{-lut})_2Cl_2]$ in aqueous solution with K_2PtCl_4 while 2,6-lut cannot.

Some characteristic bands of the infrared spectra of the $K[Pt(L)Cl_3]$ complexes are shown in Table 2. Quite similar to the complexes of $[Pt(L)_2Cl_2]$ (14), most bands of the pyridine ligands in $K[Pt(L)Cl_3]$ shift to a higher frequency region upon coordination. There should be three stretching modes for Pt—Cl bonds, two (sym ν(Pt—Cl) and asy ν(Pt—Cl)) for the bonds *cis* to L and one for the bond *trans* to L. The former two are generally close together in the infrared spectra and less affected by L (15). If L has a higher *trans*-effect the *trans* ν(Pt—Cl) shifts to a lower frequency and is well separated from *cis* ν(Pt—Cl), such as in the case of L = ethylene, phosphine, and carbonyl (15). With a ligand having a low *trans*-effect like pyridine the ν(Pt—Cl) is not expected to be well separated. However, some complexes show a little splitting in the ν(Pt—Cl) stretching, but we believe that it is due to crystal effect rather than to the *trans*-effect.

The chemical shifts in nuclear magnetic resonance of the protons and the coupling constants of the protons with ^{195}Pt are listed in Table 3. The upfield

Can. J. Chem. Downloaded from www.nrcresearchpress.com by 210.87.254.105 on 09/05/12
For personal use only.

TABLE 2. Some strong characteristic absorptions for platinum(II)–pyridine complexes

	$K[Pt(py)Cl_3]$	$K[Pt(2\text{-pic})Cl_3]$	$K[Pt(4\text{-pic})Cl_3]$	$K[Pt(2,4\text{-lut})Cl_3]$	$K[Pt(2,6\text{-lut})Cl_3]$
	1608s	1611s	1622vs	1628vs	1610s
	1568m	1570s	1500vs	1555m	1570m
	1145vs	1157vs	1204s	1185m	1164vs
	1067s	1035m	964m	1032s	1015s
	768vs	775vs	815vs	822vs	794vs
	695vs	723s			
	445m	489m	500vs	455s	
ν(Pt—Cl)	330vs	332vs	348vs	335sh	328vs
		324vs	322s	328vs	
				310s	

TABLE 3. ^1H nmr spectra of pyridine derivatives and their complexes*

Compound	H_o	H_m	H_p	J_{Pt-H_o}	$(CH_3)_o$	$(CH_3)_p$	$J_{Pt-(CH_3)_o}$
2,4-Lutidine	7.78	6.52			2.46	2.30	
$K[Pt(2,4\text{-lut})Cl_3]$	8.22	6.63		40	3.14	2.38	13
2-Picoline	7.98	6.72	7.18		2.50		
$K[Pt(2\text{-pic})Cl_3]$	8.38	6.86	7.18	40	3.24		13
2,6-Lutidine		6.48	7.06		2.45		
$K[Pt(2,6\text{-lut})Cl_3]$		6.78	7.16		3.40		17
4-Picoline	7.88	6.68				2.30	
$K[Pt(4\text{-pic})Cl_3]$†	8.28	6.68		40		2.40	
Pyridine	8.08	6.86	7.28				
$K[Pt(py)Cl_3]$	8.38	6.92	7.48	40			

*Spectra of the aromatic protons were taken in 0.4 *M* solution of dimethylacetamide (DMA) by using CH_2Cl_2 at 5.28 ppm as standard and those of the methyl protons were taken in 0.2 *M* solution of D_2O by using sodium 2,2-dimethyl-2-silapentane-5-sulfonate as standard. Chemical shift in δ (ppm) and coupling constant in Hz.
†Because of low solubility, the spectra were taken in 0.1 *M* DMA solution and 0.05 *M* D_2O solution respectively.

spectra were recorded in D_2O, while the downfield spectra were measured in dimethylacetamide. Couplings of both the *ortho* protons and the methyl groups can be observed; the former being larger than the latter.

The by-products, $[Pt(py)_2Cl_2]$ and $[Pt(4\text{-pic})_2Cl_2]$ largely formed in the preparation of $K[Pt(py)Cl_3]$ and $K[Pt(4\text{-pic})Cl_3]$, were found to be a mixture of the *cis* and *trans* isomers. The two isomers can be separated by their different solubility in organic solvents. They can be identified by their infrared spectra in the solid state in the region of 750–780 cm^{-1} and 320–350 cm^{-1}. In these regions the *cis*-isomer has a doublet while the *trans*-isomer has a singlet (14). The *cis*-isomer is a typical product of the reaction

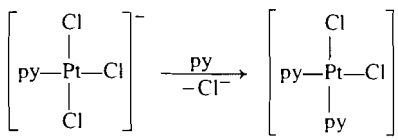

because Cl has a greater *trans*-directing influence than py. The *trans* chlorine atoms destabilize each other and the *cis*-isomer is favored.

The following tests demonstrate the formation of the *trans*-isomer with catalysis of the free pyridine (16).

(*a*) The *cis*-isomer or the *trans*-isomer in DMF overnight at 80°C was found unchanged. Therefore, no isomerization reaction occurs between the *cis*- and the *trans*-isomer in the preparative conditions.

(*b*) The *trans*-isomer in DMF with pyridine at 80°C overnight was found unchanged. Tetra(pyridine)platinum chloride, $[Pt(py)_4]Cl_2$, converted in DMF, even at room temperature, to the *trans*-isomer $[Pt(py)_2Cl_2]$. Therefore, *trans*-$[Pt(py)_2Cl_2]$ is the final product of the reaction between K_2PtCl_4 and pyridine in DMF.

(*c*) *cis*-$[Pt(py)_2Cl_2]$ in DMF with pyridine at 80°C was converted to the *trans*-isomer. The addition of pyridine to the DMF solution of the *cis*-isomer produced no change in conductivity. Therefore, no ionic species are formed in the reaction between the *cis*-isomer and pyridine.

It is interesting to compare the reactions of K_2PtCl_4 and pyridine in water to the reactions in DMF (Scheme 1). (*a*) In water, *cis*-$[Pt(py)_2Cl_2]$ is first formed, which reacts further with pyridine to reach a final product, $[Pt(py)_4]Cl_2$; in DMF, the first formed *cis*-$[Pt(py)_2Cl_2]$ is converted to the *trans*-isomer by the catalysis of free pyridine. (*b*) In water, *trans*-$[Pt(py)_2Cl_2]$ is obtained by prolonged reflux of $[Pt(py)_4]Cl_2$ in concentrated HCl solution; in DMF, $[Pt(py)_4]Cl_2$ is spontaneously converted

Can. J. Chem. Downloaded from www.nrcresearchpress.com by 210.87.254.105 on 09/05/12
For personal use only.

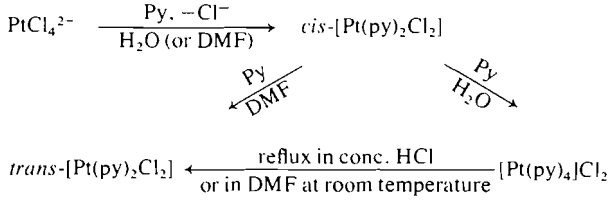

SCHEME 1

to *trans*-$[Pt(py)_2Cl_2]$ at room temperature. A method to prepare *trans*-compounds may therefore be developed by the reaction of K_2PtCl_4 and pyridine in DMF or by dissolving $[Pt(py)_4]Cl_2$ in DMF. This method would be useful to prepare *trans*-compounds of pyridine derivatives with substituent groups sensitive to acids.

Acknowledgments

Grateful acknowledgments are made to the National Research Council of Canada and to the Cancer Research Society Inc. for financial support and to Johnson Matthey & Co. Limited for the loan of potassium chloroplatinite.

1. J. L. MARX. Science, **192**, 774 (1976).
2. M. J. CLEARE. Coord. Chem. Rev. **12**, 349 (1974).
3. P. D. BRADDOCK, T. A. CONNORS, M. JONES, A. R. KHOKKAR, D. H. MELZACK, and M. K. TOBE. Chem. Biol. Interaction, **11**, 145 (1975).
4. A. COSSA. Gazzetta, **20**, 725 (1890).
5. A. WEMER and F. FASSBENDER. Z. Anorg. Chem. **15**, 123 (1897).
6. YU. N. KUKUSHKIN, E. D. AGEEVA, and V. N. SPEVAK. Russ. J. Inorg. Chem. **19**, 614 (1974).
7. YU. N. KUKUSHKIN, E. D. AGEEVA, V. N. SPEVAK, and YU. V. FADEEV. Russ. J. Inorg. Chem. **19**, 1024 (1974).
8. P. C. KONG and F. D. ROCHON. J. Chem. Soc. Chem. Commun. 599 (1975).
9. B. B. WAYLAND, R. J. FITZGERALD, and R. D. DRAGO. J. Am. Chem. Soc. **88**, 4600 (1966).
10. R. N. KELLER. Inorg. Synth. Vol. II, 250 (1946).
11. A. B. KAUFFMAN. Inorg. Synth. Vol. VII, 249 (1963).
12. M. I. IVANOVA. Zh. Neorg. Khim. **2**, 1317 (1957).
13. R. G. PEARSON and M. M. MUIR. J. Am. Chem. Soc. **88**, 2163 (1966).
14. M. PFEFFER, P. BRAUNSTEIN, and J. DEHAND. Spectrochim. Acta, **30**, (*a*) 331; (*b*) 341 (1974).
15. R. J. GOODFELLOW, P. K. GOGGIN, and D. A. DUDDELL. J. Chem. Soc. A, 504 (1968).
16. F. A. COTTON and G. WILKINSON. Advanced inorganic chemistry. 3rd ed. Interscience Publishers, New York. 1972. Chapt. 21, p. 667.

Can. J. Chem. Downloaded from www.nrcresearchpress.com by 210.87.254.105 on 09/05/12
For personal use only.

The enthalpy of formation of potassium chromate(V), K_3CrO_4(c)

LAWRENCE H. JOHNSON AND LOREN G. HEPLER

Department of Chemistry, University of Lethbridge, Lethbridge, Alta., Canada T1K 3M4

AND

CARLOS E. BAMBERGER AND DONALD M. RICHARDSON[1]

Chemistry Division, Oak Ridge National Laboratory, P.O. Box X, Oak Ridge, TN 37830, U.S.A.

Received September 30, 1977

LAWRENCE H. JOHNSON, LOREN G. HEPLER, CARLOS E. BAMBERGER, and DONALD M. RICHARDSON. Can. J. Chem. **56**, 446 (1978).

Calorimetric measurements on potassium chromate(V), K_3CrO_4(c), and related substances have provided enthalpies that lead to $\Delta H_f^0 = -370 \pm 2$ kcal mol^{-1} for K_3CrO_4(c) at 298 K.

LAWRENCE H. JOHNSON, LOREN G. HEPLER, CARLOS E. BAMBERGER et DONALD M. RICHARDSON. Can. J. Chem. **56**, 446 (1978).

Des mesures calorimétriques effectuées sur du chromate(V) de potassium, K_3CrO_4(c), et sur d'autres composés apparents ont permis d'obtenir des enthalpies conduisant à une valeur de $\Delta H_f^0 = -370 \pm 2$ kcal mol^{-1} pour le K_3CrO_4(c) à 298 K.

[Traduit par le journal]

Introduction

There is considerable contemporary interest in production of hydrogen from water by way of thermochemical processes. For example, such processes can be utilized in obtaining maximum useful energy from nuclear reactors (1). There is also potential value in using thermochemical cycles that result in decomposition of water to yield hydrogen in fields where hydrogen may be needed as a chemical reactant, such as in bitumen processing and coal gasification. Proper design and evaluation of possible thermochemical processes must be based on thermodynamic properties of the various chemicals involved in the cycle. We have therefore undertaken the investigations reported here that lead to the enthalpy of formation of K_3CrO_4, which is a promising component of one thermochemical cycle (2) for production of hydrogen from water.

We also note that results of this investigation can contribute to our understanding of the stability of chromium in the 'unusual' 5+ oxidation state.

Experimental

Potassium chromate(V), K_3CrO_4(c), may be prepared by means of any of the following reactions:

[1*a*] $Cr_2O_3 + 6\,KOH \rightleftharpoons 2\,K_3CrO_4 + H_2O + 2\,H_2$ (ref. 3*a*)

[1*b*] $4\,K_2CrO_4 + 4\,KOH \rightleftharpoons 4\,K_3CrO_4 + 2\,H_2O + O_2$ (ref. 3*b*)

[1*c*] $Cr_2O_3 + 4\,K_2CrO_4 + 10\,KOH \rightleftharpoons 6\,K_3CrO_4 + 5\,H_2O$ (ref. 3*a*)

[1]Deceased.

The choice of reaction for synthesis of K_3CrO_4 in Oak Ridge was reaction 1*a* because it readily provided for means of monitoring the course of reaction and yield of desired product. Unlike [1*c*], reaction 1*a* permits unambiguous analysis of product by means of conventional chemical methods. Reaction 1*b* presents the undesirable feature of requiring a large excess (beyond that required by stoichiometry) of KOH.

The experimental procedure in Oak Ridge consisted of heating the reagents, mole ratio of $KOH/Cr_2O_3 \cong 6.2$, to ~850°C in a tall covered cylindrical crucible of gold or platinum, under a flow of ~100 ml min^{-1} of argon until there was no more evolution of hydrogen. A tall crucible was used instead of a boat because the mixture foamed considerably during early stages of the reaction and would have spilled out of a container with low sides. The noble metal crucible was placed inside a quartz tube, which in turn was placed in a larger quartz tube that was provided with the required gas lines. This tube-within-tube arrangement was made necessary by the volatilization of KOH and subsequent reaction of this KOH with quartz that led to cracking of a single tube on cooling and thence exposure of the product to air; our double-tube arrangement made use of the inner tube as a 'getter' for KOH so that the outer tube remained intact on cooling. The exiting gases, a mixture of argon, hydrogen, and water vapor, were passed through a Drierite column and then through a thermal conductivity cell (Gow-Mac Gas Analyzer) that was calibrated for hydrogen in argon. Auxiliary equipment included thermocouples, flow meters, a wet test meter for measuring integrated gas volume, and chart read-outs for temperature and volume percent of hydrogen in exit gas.

The material resulting from the above procedure was ground in a dry box and loaded into a covered noble metal boat for further heating at ~850°C. After preliminary analysis of this material, an appropriate amount of KOH was added and the mixture subjected to final heating for 24 h at ~1000°C. Material from this third heating was sealed in evacuated glass containers to await subsequent analyses and calorimetric measurements.

Analytical characterization of the material prepared as described above was carried out in Oak Ridge as follows. Total chromium content was determined by refluxing a weighed sample in concentrated perchloric acid, followed by dilution, reduction of Cr(VI) to Cr(III) with Fe^{2+}, and back-titration

Can. J. Chem. Downloaded from www.nrcresearchpress.com by 210.87.254.5 on 09/05/12
For personal use only.

Can. J. Chem. Downloaded from www.nrcresearchpress.com by 210.87.254.5 on 09/05/12
For personal use only.

with previously standardized $KMnO_4$ solution; this procedure led to 24.9 ± 0.2% Cr. Oxidizing power was determined by adding a weighed sample to a dilute acidic solution containing excess I^-, followed by titration with a previously standardized solution of $Na_2S_2O_3$; this procedure led to 8.81 ± 0.12 milliequivalents of oxidant per gram of solid material. Flame spectrophotometric measurements led to $46._7$ ± 1.4% potassium.

The analytical data above are consistent with the following overall composition of the solid material: 85.8 ± 0.4 mass% K_3CrO_4, 9.4 ± 1.0 mass% K_2CrO_4, and 4.8 ± 0.6 mass% Cr_2O_3. The proposed presence of K_2CrO_4 is attributed to the high temperature reaction (3*a*).

$$K_3CrO_4 \rightleftharpoons K_2CrO_4 + K$$

X-Ray diffraction patterns obtained in Oak Ridge showed the presence of two polymorphs, a minor phase similar to the high temperature form of K_3CrO_4 described by Olazcuaga *et al.* (4) and a major phase with diffraction pattern very similar to that of K_3MnO_4 as described by Herbstein *et al.* (5).

All calorimetric measurements were made in Lethbridge with an LKB 8700 Precision Calorimetry System. The standard LKB 100 ml glass reaction calorimeter was used with 1 ml glass ampoules. All of our calorimetric results refer to 25.0 ± 0.1°C and are reported in terms of the defined thermochemical calorie (1 cal = 4.184 J).

A suitable sequence of calorimetric reactions involving K_3CrO_4(c) and other compounds of chromium must be one in which all reactions are reasonably rapid under practical calorimetric conditions and in which products of various reactions can be 'identified' in the sense described below. Both of these requirements present substantial difficulties because of the well known slowness of many reactions involving Cr(III) and because many aqueous species of Cr(III) are poorly characterized. We have therefore carried out a number of preliminary investigations of reactions of K_3CrO_4(c) with water and various aqueous solutions at 25°C, along with related investigations of other compounds of chromium that can be used as thermochemical references.

We have established that the reaction of K_3CrO_4(c) with aqueous acid at 25°C leads to solutions with two-thirds of the chromium in the 6+ oxidation state and one-third in the 3+ oxidation state, after allowance has been made for presence of Cr_2O_3 and K_2CrO_4 in the sample; these results are consistent with the anticipated chemical behavior of Cr(V) and with the analyses done in Oak Ridge. Unfortunately, the Cr(III) resulting from such reactions with acidic solutions was present as complicated mixtures of various complex species. Because we were unable to produce these same mixtures by starting with other chromium-containing compounds that could be used as thermochemical references, we turned to consideration of reaction sequences involving alkaline solutions.

Investigations of the reactions of K_3CrO_4(c) and various other compounds of chromium with several alkaline solutions led us to adopt 1.75 *M* KOH as the solvent for all of our calorimetric measurements. For convenience we describe Cr(III) in this solvent as 'chromite' with formula CrO_2^-; all that is really necessary is that the 'chromite' formed from K_3CrO_4(c) be the same as that formed from chromic nitrate, which we have verified by ultraviolet spectroscopic investigation of various solutions as described by Schug and King (6).

Calorimetric ampoules were loaded with K_3CrO_4(c) and sealed in a dry box with a nitrogen atmosphere.

Calorimetric samples of chromic nitrate were prepared by recrystallizing Fisher certified $Cr(NO_3)_3 \cdot 9H_2O$ from dilute nitric acid. Two different samples of recrystallized material were air dried and then stored six weeks over silica gel; these samples were gently ground and lumps were broken nearly every day during this storage period to make the samples as nearly homogeneous as possible. Weighed samples were dissolved in aqueous KOH, oxidized by H_2O_2 with the excess decomposed by boiling, followed by acidification, reduction with a known amount of Fe^{2+} and titration of the remaining Fe^{2+} with standard $Cr_2O_7^{2-}$ solution. Results of these analyses were consistent with the compositions $Cr(NO_3)_3 \cdot yH_2O$ with $y = 5.55_0$ and 7.35_0. Samples of both of these substances were dissolved in water to form solutions whose p*H* was then measured to confirm that there was no significant trapped or adsorbed nitric acid in or on the crystals. Calorimetric ampoules were loaded and sealed at the same time samples were taken for analysis and calorimetric runs were made as soon as possible afterwards to minimize the possibility of change in hydration number.

Other chemicals used in calorimetric measurements were reagent grade materials that were handled in well established ways.

Results and Calculations

All calorimetric measurements on K_3CrO_4(c) have been made on samples of material having the composition described earlier in this paper. The calorimetric measurements have led directly to enthalpies of reaction listed as Δh in Table 1. On the basis of analytical results given earlier, we have assumed that each sample contained 4.8% Cr_2O_3(c) and have further assumed that this Cr_2O_3(c) is inert to our solvent system on the time scale of our measurements. Our recovery of Cr_2O_3(c) from the calorimeter after completion of calorimetric runs was consistent with this combination of assumptions. We have also assumed that our samples contained 9.4% K_2CrO_4(c) as indicated by the analyses described earlier; our enthalpies of solution of K_2CrO_4(c) given later in this paper have been used in making an appropriate correction for presence of this substance. Finally, we have assumed that our material contained 85.8% K_3CrO_4(c) as indicated by the analyses. On the basis of all this, we have obtained the ΔH_2 values also listed in Table 1 that refer to the reaction represented by

$$[2] \quad 3\,K_3CrO_4(c) + 2\,H_2O(s) \rightleftharpoons CrO_2^-(s) + 2\,CrO_4^{2-}(s) + 9\,K^+(s) + 4\,OH^-(s)$$

in which we have used (s) to indicate that the pre-

TABLE 1. Enthalpies of reaction of K_3CrO_4(c) with 1.75 *M* KOH as in eq. 2

Mass of sample (g)	Δh (cal)	ΔH_2* (kcal mol^{-1})
0.4117_5	-48.1_6	−96.8
0.3789_7	-45.2_5	−98.8
0.3905_5	-46.4_9	−98.5
0.2854_2	-34.0_6	−98.7

*Average $\Delta H_2 = -98._2$ kcal (mol of CrO_2^-)$^{-1}$.

Can. J. Chem. Downloaded from www.nrcresearchpress.com by 210.87.254.5 on 09/05/12
For personal use only.

ceding species are in solution in our 1.75 *M* KOH solvent system. We have verified by analyses of the calorimetric solutions that amounts of chromium in the 3+ ('chromite') and 6+ oxidation states were consistent with this reaction and the assumed composition of the calorimetric samples.

We have also made calorimetric measurements leading to enthalpies of reactions represented by the following equations:

[3] $K_2CrO_4(c) \rightleftharpoons 2K^+(s) + CrO_4^{2-}(s)$

[4] $Cr(NO_3)_3 \cdot yH_2O(c) + 4OH^-(s) \rightleftharpoons CrO_2^-(s) + 3NO_3^-(s) + (y + 2)H_2O(s)$

[5] $H_2O(liq) \rightleftharpoons H_2O(s)$

[6] $KNO_3(c) \rightleftharpoons K^+(s) + NO_3^-(s)$

[7] $HCl \cdot zH_2O(liq) + OH^-(s) \rightleftharpoons (z + 1)H_2O(s) + Cl^-(s)$

[8] $KCl(c) \rightleftharpoons K^+(s) + Cl^-(s)$

Results of all these measurements are summarized in Table 2 where the listed ΔH_n values are averages from three calorimetric runs of each reaction.

Appropriate combination of the seven reaction equations above and the corresponding enthalpies leads to the following:

[9] $3K_3CrO_4(c) + 3KNO_3(c) + 8HCl \cdot zH_2O(liq) \rightleftharpoons 2K_2CrO_4(c) + Cr(NO_3)_3 \cdot yH_2O(c) + (8z - y + 4)H_2O(liq) + 8KCl(c)$

[10] $\Delta H_9 = \Delta H_2 - 2\Delta H_3 - \Delta H_4 - (8z - y + 4)\Delta H_5 + 3\Delta H_6 + 8\Delta H_7 - 8\Delta H_8$

Values of ΔH_9 for the various combinations of y and z are listed in Table 3.

To derive the desired ΔH_f^0 of $K_3CrO_4(c)$ from the various values of ΔH_9 in Table 3 we need to know several enthalpies of formation as follows.

For $H_2O(liq)$ we have $\Delta H_f^0 = -68.315$ kcal mol^{-1} from NBS Tech. Note 270-3 (7). We also obtain $\Delta H_f^0 = -459.05$ kcal mol^{-1} and $\Delta H_f^0 = -592.99$ kcal mol^{-1} for $HCl \cdot zH_2O(liq)$ when $z = 6.16_7$ and $z = 8.12_0$ from this same source (7). Because the excellent NBS Tech. Note 270 series has not yet reached KCl(c) and $KNO_3(c)$, we calculate the ΔH_f^0 values for these compounds in the following way. The NBS Tech. Note 270-3 (7) does list ΔH_f^0 values for $K^+(aq)$, $Cl^-(aq)$, and $NO_3^-(aq)$; we combine these values with the standard enthalpies of solution of KCl(c) and $KNO_3(c)$ listed by Parker (8) to obtain $\Delta H_f^0 = -104.39$ kcal mol^{-1} for KCl(c) and $\Delta H_f^0 = -118.22$ kcal mol^{-1} for $KNO_3(c)$. We also use $\Delta H_f^0 = -335.4$ kcal mol^{-1} for $K_2CrO_4(c)$ from the recent review by Dellien, Hall, and Hepler (9).

We have carried out our own new calorimetric measurements leading to the desired ΔH_f^0 of $Cr(NO_3)_3 \cdot yH_2O(c)$. An equation representing the calorimetric reaction is

[11] $Cr(NO_3)_3 \cdot yH_2O(c) \rightleftharpoons Cr^{3+}(aq) + 3NO_3^-(aq) + yH_2O(liq)$

Measurements of the enthalpy of solution of the crystalline material (0.2 g in 100 ml of 10^{-2} *M* nitric acid) have led to $\Delta H_{11} = -4.50$ kcal mol^{-1} for $y = 5.55_0$ and to $\Delta H_{11} = -4.65$ kcal mol^{-1} for $y = 7.35_0$. We have estimated the enthalpy of dilution to zero concentration by analogy to other salts of similar charge type, weighting the value from NBS Tech. Note 270-7 (10) for $La(NO_3)_3(aq)$ most heavily, to obtain $\Delta H_{11}^0 = -4.9$ kcal mol^{-1} for $y = 5.55_0$ and $\Delta H_{11}^0 = -5.1$ kcal mol^{-1} for $y = 7.35_0$. Combination of ΔH_{11}^0 values with ΔH_f^0 values for $NO_3^-(aq)$ and $H_2O(liq)$ cited above and $\Delta H_f^0 = -60$ kcal mol^{-1} for $Cr^{3+}(aq)$ from the recent calorimetric investigation of Dellien and Hepler (11) leads to $\Delta H_f^0 = -583$ kcal mol^{-1} for $Cr(NO_3)_3 \cdot yH_2O(c)$ with $y = 5.55_0$ and to $\Delta H_f^0 = -706$ kcal mol^{-1} for $y = 7.35_0$.

Finally, combination of the y, z, and ΔH_9 values from Table 3 with various ΔH_f^0 values cited above leads to the ΔH_f^0 values for $K_3CrO_4(c)$ that are also listed in Table 3. We choose $\Delta H_f^0 = -370 + 2$ kcal mol^{-1} for $K_3CrO_4(c)$ in which ± 2 kcal mol^{-1} represents our estimate of the maximum likely uncertainty based on considerations of uncertainties in com-

TABLE 2. Summary of ΔH_n values for reactions represented by eqs. 3 to 8

Reaction n	ΔH_n (kcal mol^{-1})
3	3.51
4 ($y = 5.55_0$)	−28.1
4 ($y = 7.35_0$)	−29.3
5	−0.0043
6	7.01
7 ($z = 6.16_7$)	-16.1_3
7 ($z = 8.12_0$)	-15.8_9
8	3.78

TABLE 3. ΔH_f^0 values for $K_3CrO_4(c)$ at 298 K

y	z	ΔH_9^0 (kcal mol^{-1})	ΔH_f^0 (K_3CrO_4) (kcal mol^{-1})
5.55_0	6.16_7	−215.2	$-370._4$
5.55_0	8.12_0	−213.2	$-369._7$
7.35_0	6.16_7	−214.0	$-370._8$
7.35_0	8.12_0	−212.0	$-370._1$

position, homogeneity, and polymorphism of the calorimetric samples, uncertainties in our various measured enthalpies, and uncertainties in various auxiliary data used in our calculations.

Acknowledgment

This research has been sponsored by the Division of Basic Energy Sciences of the U.S. Energy Research and Development Administration under contract with Union Carbide Corporation and by the National Research Council of Canada.

1. C. E. BAMBERGER and D. M. RICHARDSON. Cryogenics, 197, April (1976).
2. C. E. BAMBERGER and D. M. RICHARDSON. U.S. Patent 3,927,192, Dec. 16 (1975).
3. (*a*) R. SCHOLDER, F. SCHWOCHOW, and H. SCHWARZ. Z. Anorg. Allg. Chem. **363**, 10 (1968); (*b*) N. BAILEY and M. C. R. SYMONS. J. Chem. Soc. 203 (1957).
4. R. OLAZCUAGA, J.-M. REAU, G. LEFLEM, and P. HAGENMULLER. Z. Anorg. Allg. Chem. **412**, 271 (1975).
5. F. H. HERBSTEIN, G. RON, and A. WEISSMAN. J. Chem. Soc. A, 1821 (1971).
6. K. SCHUG and E. L. KING. J. Am. Chem. Soc. **80**, 1089 (1958).
7. D. D. WAGMAN, W. H. EVANS, V. B. PARKER, I. HALOW, S. M. BAILEY, and R. H. SCHUMM. National Bureau of Standards Technical Note 270-3. U.S. Government Printing Office, Washington, DC. 1968.
8. V. B. PARKER. Thermal properties of aqueous uni-univalent electrolytes. National Standard Reference Data Series, U.S. National Bureau of Standards NSRDS-NBS 2, U.S. Government Printing Office, Washington, DC. 1965.
9. I. DELLIEN, F. M. HALL, and L. G. HEPLER. Chem. Rev. **76**, 283 (1976).
10. R. H. SCHUMM, D. D. WAGMAN, S. BAILEY, W. H. EVANS, and V. B. PARKER. National Bureau of Standards Technical Note 270-7. U.S. Government Printing Office, Washington, DC. 1973.
11. I. DELLIEN and L. G. HEPLER. Can. J. Chem. **54**, 1383 (1976).

Can. J. Chem. Downloaded from www.nrcresearchpress.com by 210.87.254.5 on 09/05/12
For personal use only.

The crystal structure of *cis*-chlorobis(triethylphosphine)-1,8-naphthyridineplatinum(II) tetrafluoroborate, $[PtCl(PEt_3)_2(naph)]BF_4$, a complex containing a monodentate 1,8-naphthyridine ligand

GORDON W. BUSHNELL, KEITH R. DIXON, AND MASOOD A. KHAN

Department of Chemistry, University of Victoria, Victoria, B.C., Canada V8W 2Y2

Received July 28, 1977

GORDON W. BUSHNELL, KEITH R. DIXON, and MASOOD A. KHAN. Can. J. Chem. **56**, 450 (1978).

The crystal structure of *cis*-chlorobis(triethylphosphine)-1,8-naphthyridineplatinum(II) tetrafluoroborate has been determined by single crystal X-ray diffraction and refined to an *R*-value of 0.063. The cell dimensions are $a = 1.4246$, $b = 1.2676$, $c = 1.6530$ nm, $\beta = 115.66°$. The space group is $P2_1/c$ with 4 molecules per unit cell, and the measured density is 1.665 g cm^{-3}. The structure is essentially a 4-coordinate square planar platinum(II) complex containing monodentate 1,8-naphthyridine. Interatomic distances to platinum are: Pt—Cl, 236.6(4); Pt—P(1), 225.4(4); Pt—P(2), 225.2(4); Pt—N(1), 208.3(11); and Pt—N(2), 304.5(14) pm. The structure is discussed in relation to variable temperature nmr studies of solutions, which indicate fluxional behaviour of the heterocyclic ligand.

GORDON W. BUSHNELL, KEITH R. DIXON et MASOOD A. KHAN. Can. J. Chem. **56**, 450 (1978).

On a déterminé la structure cristalline du tétrafluoroborate du chlorobis(triéthylphosphine) naphtyridine-1,8 platine(II) *cis* par diffraction de rayon-X d'un monocristal et on a affiné la structure jusqu'à une valeur finale *R* de 0.063. Les dimensions de la maille sont: $a = 1.4246$, $b = 1.2676$, $c = 1.6530$ nm, $\beta = 115.66°$. Le groupe d'espace est $P2_1/c$ avec quatre molécules par maille et la densité mesurée est de 1.665 g cm^{-3}. La structure consiste essentiellement d'un complexe de platine(II) tétracoordonné plan carré contenant la naphtyridine-1,8 sous forme de monodentate. Les distances interatomiques vers le platine sont: Pt—Cl, 236.6(4); Pt—P(1), 225.4(4); Pt—P(2), 225.2(4); Pt—N(1), 208.3(11); et Pt—N(2), 304.5(14) pm. On discute de la structure par rapport à des études de rmn à température variable en solution qui indiquent un comportement fluxionel du ligand hétérocyclique.

[Traduit par le journal]

Can. J. Chem. Downloaded from www.nrcresearchpress.com by 210.87.254.5 on 09/05/12
For personal use only.

Introduction

A crystal structure determination on the apparently five co-ordinate complex, *cis*-$[PtCl(PEt_3)_2phen][BF_4]$, has shown that the actual geometry is close to four co-ordinate square planar and the complex contains the first example of a monodentate 1,10-phenanthroline ligand (1).[1] This highly unusual result raised interesting questions regarding the solution behaviour of the complex since nmr studies had shown chemical equivalence of the two heterocyclic rings (2). The most likely interpretation of this result is a solution structure similar to that in the solid state but with fluxional motion of the heterocyclic ligand. Thus the platinum is bound first at one nitrogen and then at the other, with rapid interchange between the two possibilities. A more detailed nmr study (3) strongly favours this interpretation even though the lowest accessible temperatures did not yield a slow exchange limiting spectrum. Moreover, the closely related complex, *cis*-$[PtCl(PEt_3)_2(naph)][BF_4]$, naph = 1,8-naphthyridine, showed chemical inequivalence of the heterocyclic rings at low temperatures. As the temperature was raised the spectrum changed until above −30°C the two rings were equivalent. These observations suggested a fluxional process similar to that postulated for the phenanthroline complex and it was of interest to determine whether the two complexes have similar co-ordination geometry in the crystalline state.

Several previous authors have been interested in 1,8-naphthyridine complexes on the grounds that the small 'bite' of this ligand is expected to stabilize unusually high co-ordination numbers (4–8). In practice, the co-ordination geometry of the naphthyridine varies widely. For example, in $[Fe(naph)_4][ClO_4]_2$, one ligand is fairly symmetric (Fe—N = 228.4, 233.5 pm), one markedly asymmetric (Fe—N = 218.4, 275.6 pm), and the others intermediate (4). Thus, it was also of interest to determine how naphthyridine co-ordinates in a situation where even phenanthroline is essentially monodentate. Since the

[1] In this type of complex it is, of course, impossible to discount weak interactions between the platinum and the second nitrogen. However, the very asymmetric nature of the geometry is unique (Pt—N(1) = 214(2), Pt—N(2) = 284(2) pm).

Can. J. Chem. Downloaded from www.nrcresearchpress.com by 210.87.254.5 on 09/05/12
For personal use only.

completion of our work a crystal structure determination of *trans*-[$CuCl_2$(2,7-dimethyl-1,8-naphthyridine)$_2$] showing very asymmetric naphthyridine co-ordination (Cu—N = 198.2, 280.1 pm) has been reported (8). Our complex, with Pt—N(1) = 208, and Pt—N(2) = 305 pm, seems to be even more asymmetric than this, and is essentially monodentate.

Experimental

The preparation and characterization of the complex is described elsewhere (3). Crystals were grown by a vapour diffusion method (ref. 9, p. 65) using acetone as solvent 1 and ether as solvent 2. The crystal used for intensity measurements was approximately a rectangular block with dimensions 0.14, 0.5, 0.2 mm in the x, y, and z directions respectively.

Weissenberg and precession photographs were taken with CuK_α radiation. The space group $P2_1/c$ was thus established unequivocally. A crystal was mounted on the b-axis and centred on a Picker 4-circle diffractometer. The $\theta/2\theta$ peaks were measured for 25 reflections using both $MoK_{\alpha 1}$ (λ = 70.926 pm) and $MoK_{\alpha 2}$ (λ = 71.354 pm) at 22°C. The dimensions of the unit cell were refined using the method of least squares. The results and other crystal data are given in Table 1. The density was measured by flotation in a carbon tetrachloride/bromoform solution. Intensity measurements were done manually at room temperature using MoK_α radiation and a Zr filter. Reflections were scanned in the $\theta/2\theta$ mode for 1 min at a rate of 2° min^{-1} in 2θ. The instrument was operated in the bisecting position with $\omega = 0$. The background measurements were for 30 s at each end of the scan. The orientation of the crystal was checked twice daily using a set of three reflections. One of these reflections was measured for every batch of 30 reflections and used as an intensity standard. No crystal decomposition was noted. All reflections up to 2θ = 40° were measured. A total of 2110 reflections were given observed status using the criterion that the net count must be greater than the standard deviation of the background count. The intensities were corrected for the Lorentz and polarization effects. An absorption correction was applied as a function of the angle ϕ on the diffractometer. The absorption correction function was determined experimentally using reflections at χ = 90°.

Structure Determination

The structure was solved by the heavy atom method. A set of programs supplied by Penfold (10) was used for all calculations. The atomic scattering factors of Cromer and Waber (11) were used for Pt, P, and Cl. Atomic scattering factors for F, N, C, and B were taken from the International Tables (12). All atoms were assumed to be uncharged and a correction was applied for the anomalous dispersion of Pt (13). In the full-matrix least-squares refinement the function $\Sigma w(|F_o| - |F_c|)^2$ was minimized. Weights were derived from the counting statistics and an experimentally determined instrument instability constant of 0.04 using the formula given by Stout and Jensen, Appendix H (9). The unobserved reflections were included in the structure factor calculations but excluded from the least-squares sums. The final agreement factors were R = 0.054, R_w = 0.058 (unobserved reflections excluded) and R = 0.063, R_w = 0.062 (all reflections). Shifts in the final cycle of refinement were less than 3% of the standard deviations. A final difference map gave no indication of any misplaced atoms, and the maximum electron density difference was 7.2×10^{-7} e pm^{-3}. Estimated standard deviations for the results are derived from the full inverted matrix. The structure factor table is in the Depository for Unpublished Data.[2]

TABLE 1. Crystal data for $[PtCl(naph)(PEt_3)_2]BF_4$

System	Monoclinic
Space group	$P2_1/c$ (No. 14)
Molecular formula	$C_{20}H_{36}BClF_4N_2P_2Pt$
Molecular weight	683.81
Cell dimensions	a = 1.4246(1) nm
	b = 1.2676(3) nm
	c = 1.6530(1) nm
	β = 115.66(1) deg
Cell volume	2.6907(8) nm^3
Density (calculated)	1.658 g cm^{-3}
Density (observed)	1.665 g cm^{-3}
No. of molecules per unit cell	4
Absorption coefficient (MoK_α)	57.5 cm^{-1}

Results and Discussion

The molecular structure with labels is shown in Fig. 1 and the crystal packing in Fig. 2. The atomic parameters are given in Table 2 and bond lengths and angles in Tables 3 and 4.

Within the triethylphosphine ligand the mean angles, C—P—C = 104.3° and P—C—C = 112°, and the mean bond length, P—C = 183 pm, are normal for this ligand, as is the mean Pt—P—C angle of 114.1°. Similarly the fluoroborate anion does not require comment. Table 5 gives the least-squares planes for the naphthyridine ligand and also for the platinum co-ordination. The χ^2 values indicate that the naphthyridine ligand is deviating slightly from planarity but this is also the case in most of the naphthyridine complexes studied previously (8) and

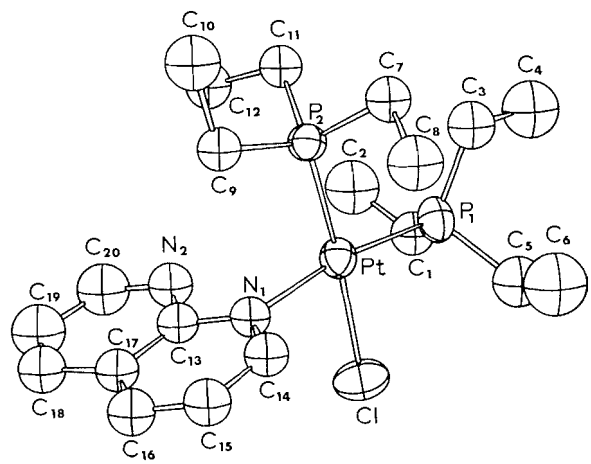

FIG. 1. The molecular structure of *cis*-chlorobis(triethylphosphine)naphthyridineplatinum(II) tetrafluoroborate.

[2]Copies may be obtained at a nominal charge, upon request, from the Depository of Unpublished Data, CISTI, National Research Council of Canada, Ottawa, Ont., Canada K1A 0S2.

Can. J. Chem. Downloaded from www.nrcresearchpress.com by 210.87.254.5 on 09/05/12
For personal use only.

TABLE 2

(*a*) Positional parameters for the heavy F(1)—F(4) and B atoms in *cis*-chloro-(naph)bis(triethylphosphine)platinum(II) tetrafluoroborate

Atom	*X*	*Y*	*Z*
Pt	0.21704(4)	0.25020(5)	0.14402(4)
Cl	0.1093(3)	0.2788(4)	−0.0102(3)
P(1)	0.1424(3)	0.3947(3)	0.1705(3)
P(2)	0.3298(3)	0.2107(3)	0.2859(3)
F(1)	0.3745(16)	−0.3391(14)	0.3438(13)
F(2)	0.3194(16)	−0.2232(16)	0.4188(15)
F(3)	0.3319(15)	−0.1698(13)	0.3005(11)
F(4)	0.4672(11)	−0.2136(13)	0.4186(12)
B	0.3675(23)	−0.2407(27)	0.3647(20)

(*b*) Anisotropic temperature parameters for the heavy F(1)—F(4) and B atoms[a]

Atom	U_{11}	U_{22}	U_{33}	U_{12}	U_{13}	U_{23}
Pt	43.5(4)	43.7(4)	47.7(5)	−2.8(4)	17.6(2)	−1.2(2)
Cl	61(3)	99(4)	53(2)	8(2)	16(2)	10(2)
P(1)	46(2)	42(2)	68(3)	2(2)	14(2)	−4(2)
P(2)	48(2)	47(2)	41(2)	4(2)	20(2)	2(2)
F(1)	232(20)	122(13)	221(19)	−20(14)	64(16)	−30(6)
F(2)	223(18)	229(21)	289(23)	14(16)	200(18)	48(9)
F(3)	220(18)	155(14)	153(14)	34(14)	74(14)	60(12)
F(4)	112(11)	175(15)	187(15)	24(10)	28(5)	−52(12)
B	103(19)	87(22)	118(17)	−19(19)	53(18)	14(20)

[a] $T = \exp -2\pi^2(U_{11}h^2a^{*2} + U_{22}k^2b^{*2} + U_{33}l^2c^{*2} + 2U_{12}hka^*b^* + 2U_{13}hla^*c^* + 2U_{23}klb^*c^*)$. Tabulated values should be multiplied by 10 to obtain mean square amplitudes in pm².

(*c*) Positional and isotropic temperature parameters of N(1)—N(2), C(1)—C(20) atoms in *cis*-chloro-(naph)bis(triethylphosphine)platinum(II) tetrafluoroborate[a]

Atom	*X*	*Y*	*Z*	$U \times 10^{-1}$ (pm)²
N(1)	0.2740(9)	0.1260(9)	0.0957(7)	47(3)
N(2)	0.1535(10)	0.0191(11)	0.1113(9)	64(4)
C(1)	0.0026(13)	0.3742(14)	0.1335(12)	72(5)
C(2)	−0.0203(18)	0.2895(18)	0.1876(15)	107(7)
C(3)	0.1883(14)	0.4488(15)	0.2819(12)	80(5)
C(4)	0.1209(18)	0.5455(19)	0.2912(16)	116(8)
C(5)	0.1409(16)	0.5053(16)	0.0972(13)	86(6)
C(6)	0.2552(19)	0.5390(20)	0.1131(16)	126(8)
C(7)	0.4250(12)	0.3148(13)	0.3395(10)	58(4)
C(8)	0.4837(14)	0.3386(15)	0.2801(12)	80(6)
C(9)	0.4065(11)	0.0934(12)	0.2912(10)	54(4)
C(10)	0.4882(15)	0.0650(15)	0.3907(13)	84(6)
C(11)	0.2736(12)	0.1816(13)	0.3650(10)	59(5)
C(12)	0.2079(13)	0.0819(14)	0.3400(12)	71(5)
C(13)	0.2295(12)	0.0294(12)	0.0833(10)	54(4)
C(14)	0.3501(12)	0.1430(12)	0.0711(10)	55(4)
C(15)	0.3873(13)	0.0659(13)	0.0334(11)	64(5)
C(16)	0.3421(12)	−0.0309(13)	0.0169(10)	62(4)
C(17)	0.2603(12)	−0.0521(12)	0.0426(10)	57(4)
C(18)	0.2148(13)	−0.1545(14)	0.0373(11)	70(4)
C(19)	0.1392(16)	−0.1643(16)	0.0637(13)	91(6)
C(20)	0.1072(15)	−0.0760(16)	0.1009(13)	85(6)

[a] Estimated standard deviations in parentheses.

Can. J. Chem. Downloaded from www.nrcresearchpress.com by 210.87.254.5 on 09/05/12
For personal use only.

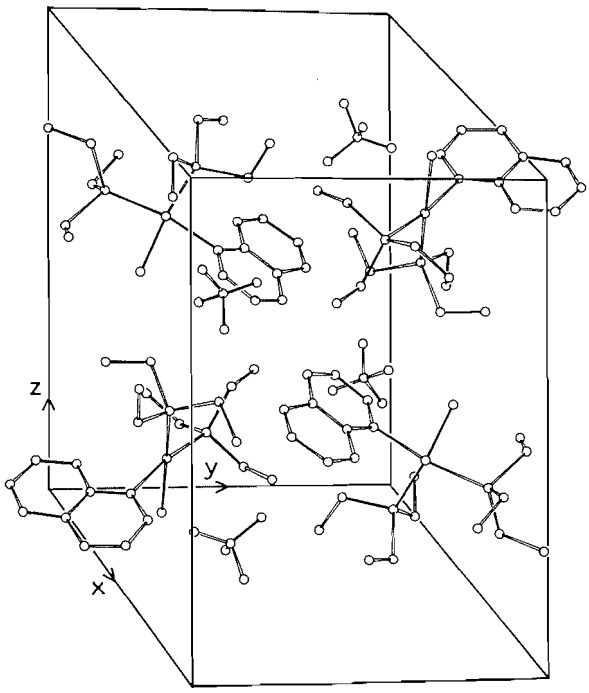

FIG. 2. The crystal packing diagram of *cis*-chlorobis(triethylphosphine)naphthyridineplatinum(II) tetrafluoroborate.

even in crystalline 1,8-naphthyridine (14).[3] The bond lengths and angles within the co-ordinated naphthyridine are similar to those in free naphthyridine and we note that the N(1)—C(13)—N(2) angle (115°) is essentially identical to the 115.3° found in the free ligand (14). A narrowing of this angle by 3.7° in $[Fe(naph)_4][ClO_4]_2$ has been attributed to decreased repulsion of the nitrogen lone pairs when they become shared pairs in the complex (14). The absence of this narrowing when the naphthyridine is essentially monodentate may therefore have some significance.

The naphthyridine ligand is almost perpendicular to the square co-ordination plane around platinum (Table 5). The platinum co-ordination is significantly non-planar with N(1) deviating furthest from the least-squares plane.

The shortest interionic contacts are of the type F---HC, the minimum F—C length being 312(2) pm. Six such contacts are less than 350 pm in length.

The bond angles around platinum are very similar to those in the analogous phenanthroline complex, the angle P—Pt—P being approximately 99° in both cases and Cl—Pt—N(1) being 83 and 81° respectively. The lengths to platinum are compared to those found in the phenanthroline complex in Table 6. The bond lengths in the square plane are identical but the Pt—N(2) distances are not the same, since the ligand structures differ.

It follows quite naturally from these structures that naphthyridine with the shorter N(1)—N(2) bite gives a longer Pt—N(2) distance. This is illustrated in Fig. 3 using hexagons, 120° angles, and the correct

[3] $\chi^2 = \Sigma_i |P_i^2/\sigma^2(P_i)|$, where P_i = perpendicular distance of atom i from the plane.

TABLE 3. Bond distances in *cis*-chloro(naph)bis(triethylphosphine)platinum(II) tetrafluoroborate[a]

(*a*) The platinum atom co-ordination

Bond	Length (pm)	Bond	Length (pm)
Pt—N(1)	208(1)	Pt—N(2)	305(1)
Pt—P(1)	225.4(4)	Pt—P(2)	225.2(4)
Pt—Cl	236.6(4)		

(*b*) The naphthyridine ligand

Bond	Length (pm)	Bond	Length (pm)
N(1)—C(13)	135(2)	N(2)—C(13)	136(2)
N(1)—C(14)	133(2)	N(2)—C(20)	135(2)
C(14)—C(15)	138(2)	C(20)—C(19)	144(3)
C(15)—C(16)	136(2)	C(19)—C(18)	133(3)
C(16)—C(17)	143(2)	C(18)—C(17)	144(2)
C(13)—C(17)	140(2)		

(*c*) The triethylphosphine ligands

Bond	Length (pm)	Bond	Length (pm)
P(1)—C(1)	183(2)	P(2)—C(7)	182(2)
P(1)—C(3)	180(2)	P(2)—C(9)	183(2)
P(1)—C(5)	185(2)	P(2)—C(11)	184(2)
C(1)—C(2)	152(3)	C(7)—C(8)	157(3)
C(3)—C(4)	160(3)	C(9)—C(10)	159(3)
C(5)—C(6)	159(3)	C(11)—C(12)	152(3)

(*d*) The tetrafluoroborate ion

Bond	Length (pm)	Bond	Length (pm)
B—F(1)	130(3)	B—F(2)	137(3)
B—F(3)	132(2)	B—F(4)	135(3)

[a]Estimated standard deviations in parentheses.

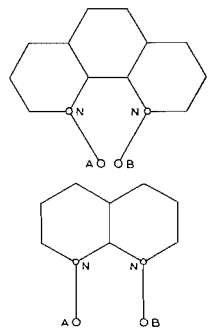

FIG. 3. Alternative metal positions A and B for fluxional monodentate *o*-phenanthroline and naphthyridine.

Can. J. Chem. Downloaded from www.nrcresearchpress.com by 210.87.254.5 on 09/05/12
For personal use only.

TABLE 4. Bond angles in *cis*-chloro(naph)bis(triethylphosphine)platinum(II) tetrafluoroborate[a]

(*a*) The platinum atom co-ordination

Bonds	Angle (deg)	Bonds	Angle (deg)
Cl—Pt—P(2)	173.6(1)	P(1)—Pt—N(1)	169.7(3)
Cl—Pt—P(1)	86.8(2)	Cl—Pt—N(1)	83.2(3)
P(1)—Pt—P(2)	99.3(1)	P(2)—Pt—N(1)	90.6(3)

(*b*) The naphthyridine ligand

Bonds	Angle (deg)	Bonds	Angle (deg)
C(13)—N(1)—C(14)	119(2)	C(13)—N(2)—C(20)	118(2)
N(1)—C(13)—C(17)	121(2)	N(2)—C(13)—C(17)	124(2)
N(1)—C(14)—C(15)	123(2)	N(2)—C(20)—C(19)	121(2)
C(14)—C(15)—C(16)	119(2)	C(20)—C(19)—C(18)	121(2)
C(15)—C(16)—C(17)	119(2)	C(19)—C(18)—C(17)	118(2)
C(16)—C(17)—C(13)	118(2)	C(18)—C(17)—C(13)	118(2)
N(1)—C(13)—N(2)	115(2)	C(18)—C(17)—C(16)	124(2)
C(13)—N(1)—Pt	121(1)	C(14)—N(1)—Pt	120(1)

(*c*) The triethylphosphine ligands

Bonds	Angle (deg)	Bonds	Angle (deg)
C(1)—P(1)—C(3)	104.8(8)	C(7)—P(2)—C(9)	105.2(7)
C(1)—P(1)—C(5)	100.8(9)	C(7)—P(2)—C(11)	105.2(7)
C(3)—P(1)—C(5)	106.1(9)	C(9)—P(2)—C(11)	103.8(7)
Pt—P(1)—C(1)	110.9(6)	Pt—P(2)—C(7)	113.0(5)
Pt—P(1)—C(3)	121.0(6)	Pt—P(2)—C(9)	111.9(5)
Pt—P(1)—C(5)	111.2(7)	Pt—P(2)—C(11)	116.8(5)
P(1)—C(1)—C(2)	113(2)	P(2)—C(7)—C(8)	109(2)
P(1)—C(3)—C(4)	115(2)	P(2)—C(9)—C(10)	113(2)
P(1)—C(5)—C(6)	112(2)	P(2)—C(11)—C(12)	112(2)

(*d*) The tetrafluoroborate ion

Bonds	Angle (deg)	Bonds	Angle (deg)
F(1)—B—F(2)	116(3)	F(2)—B—F(3)	106(3)
F(1)—B—F(3)	119(3)	F(2)—B—F(4)	102(3)
F(1)—B—F(4)	105(3)	F(3)—B—F(4)	107(3)

[a]Estimated standard deviation in parentheses.

Pt—N(1) lengths. Figure 3 also shows that to change its point of attachment from N(1) to N(2) the metal atom would have to move relative to the ligand through a shorter distance for phenanthroline than for naphthyridine. To explain the fluxional and kinetic behaviour of these complexes in solution we need to estimate the order of activation energies. In Figure 3, positions A or B represent low energy co-ordinates for the platinum atom as observed in the crystalline state. The transition point of the reaction is expected to lie close to the midpoint of A, B. In the phenanthroline compound A and B are close together and it is hence unlikely that the activation energy for reaction will be high. The transition state has a five membered ring. For the naphthyridine compound, it is likely that the activation energy will be higher because A and B are further apart. Considerable distortion of the nitrogen sp^2 σ bonds from their preferred direction would be necessary in the transition state which has a four membered ring. The coalescence temperature observed by nmr spectroscopy was $-30°C$ for the naphthyridine compound, whereas the fluxional motion in the phenanthroline complex was not arrested at $-85°C$, the lowest temperature obtainable before viscosity broadening of the spectrum and crystallization of the complex spoiled the experiment.

The X-ray diffraction results for the crystalline materials thus provide insight into the processes occurring in solutions as observed by nmr, and the two techniques are in mutual accord. These results also emphasize that when the concept of ligand span

TABLE 5. Least-squares planes ($k_1x + k_2y + k_3z = k_4$) of *cis*-chloro(naph)bis(triethylphosphine)platinum(II) tetrafluoroborate[a]

Plane[b]	k_1	k_2	k_3	k_4	χ^2
1	0.812	0.579	−0.075	335	136
2	−0.321	0.271	−0.907	−189	24.0

Plane	Atom	Significant distance of atom from least-squares plane
1	Pt	−0.16(6)
	Cl	3.1(5)
	P(1)	1.3(5)
	P(2)	2.9(5)
	N(1)	8(1)
	N(2)	−220(2)
2	C(16)	3.1(15)
	C(17)	4.4(15)
	C(18)	−4.1(17)
	Pt	14.28(6)

[a]*x*, *y*, *z* are co-ordinates in pm along an orthogonal axis system, defined as *x* along *a*, *y* in the (*a*,*b*) plane, and *z* along *c**.
[b]Plane *1* is defined by Pt, Cl, P(1), P(2), and N(1); plane *2* is defined by N(1), N(2), C(13)—C(20). The angle between planes *1* and *2* is 92.0°.

TABLE 6. Comparison of bond lengths (pm) between complexes

Bond	Length (pm) naph	Length (pm) phen	Δ
Pt—N(1)	208(1)	214(2)	6(3)
Pt—N(2)	305(1)	284(2)	21(3)
Pt—P(1)	225.4(4)	223.9(7)	1.5(8)
Pt—P(2)	225.2(4)	224.1(6)	1.1(7)
Pt—Cl	236.6(4)	236.1(6)	0.5(7)

(or 'bite') is used in coordination chemistry, it is important to consider the convergence or divergence of the co-ordinate bond directions.

Acknowledgement

We thank the University of Victoria and the National Research Council of Canada for research grants.

1. G. W. BUSHNELL, K. R. DIXON, and M. A. KHAN. Can. J. Chem. **52**, 1367 (1974).
2. K. R. DIXON and A. D. RATTRAY. Can. J. Chem. **51**, 618 (1973).
3. K. R. DIXON. Inorg. Chem. **16**, 2618 (1977).
4. P. SINGH, A. CLEARFIELD, and I. BERNAL. J. Co-ord. Chem. **1**, 29 (1971).
5. J. M. EPSTEIN, J. C. DEWAN, D. L. KEPERT, and A. H. WHITE. J. Chem. Soc. Dalton, 1949 (1974).
6. J. C. DEWAN, D. L. KEPERT, and A. H. WHITE. J. Chem. Soc. Dalton, 490 (1975).
7. A. CLEARFIELD, R. GOPAL, and R. W. OLSEN. Inorg. Chem. **16**, 911 (1977).
8. C. MEALLI and L. SACCONI. Acta Crystallogr. **B33**, 710 (1977).
9. G. H. STOUT and L. H. JENSEN. X-Ray structure determination. MacMillan, New York. 1968.
10. B. R. PENFOLD. University of Canterbury Crystallographic Programs, Christchurch, New Zealand.
11. D. T. CROMER and J. T. WABER. Acta Crystallogr. **18**, 104 (1965).
12. J. A. IBERS. International Tables for X-ray Crystallography. I. U. Cr. by the Kynoch Press, Birmingham. Vol. III, Table 3.3.1A, 201 (1962).
13. D. T. CROMER. Acta Crystallogr. **18**, 17 (1965).
14. A. CLEARFIELD, M. J. SIMS, and P. SINGH. Acta Crystallogr. **B28**, 350 (1972).

Can. J. Chem. Downloaded from www.nrcresearchpress.com by 210.87.254.5 on 09/05/12
For personal use only.

Vinyl ether hydrolysis. XI. The effect of α-phenyl substitution[1]

Y. CHIANG, W. K. CHWANG, A. J. KRESGE,[2]
L. H. ROBINSON, D. S. SAGATYS, and C. I. YOUNG

Department of Chemistry, University of Toronto, Scarborough College, West Hill, Ont., Canada M1C 1A4 and Department of Chemistry, Illinois Institute of Technology, Chicago, Illinois 60616 U.S.A.

Received August 29, 1977

Y. CHIANG, W. K. CHWANG, A. J. KRESGE, L. H. ROBINSON, D. S. SAGATYS, and C. I. YOUNG. Can. J. Chem. **56**, 456 (1978).

The unexpected inability of an α-phenyl group to accelerate the rate of vinyl ether hydrolysis more strongly than an α-methyl substituent, $k(CH_2{=}CPhOEt)/k(CH_2{=}CMeOEt) = 0.2$ for catalysis by H_3O^+ at 25°C, is examined and is found to be the result of two effects: (*i*) preferential initial state stabilization by phenyl and (*ii*) weak resonance interaction with the developing alkoxy carbonium ion in the transition state induced by the reactant-like character of the latter. A curved Brønsted relation for the hydrolysis of 3-methoxyindene catalyzed by carboxylic acids and monohydrogen phosphonate anions gives the Marcus theory parameters $\Delta G_0^{\ddagger} = 3 \pm 1$ kcal/mol and $w^r = 12 \pm 1$ kcal/mol.

Y. CHIANG, W. K. CHWANG, A. J. KRESGE, L. H. ROBINSON, D. S. SAGATYS et C. I. YOUNG. Can. J. Chem. **56**, 456 (1978).

Les vitesses d'hydrolyse, catalysée par H_3O^+ et à 25°C, d'éthers vinyliques substitués en α par des groupes phényle ou méthyle ne sont pas très différentes; $k(CH_2{=}CPhOEt)/k(CH_2{=}CMeOEt) = 0.2$; on a trouvé que ce résultat inattendu est dû à deux effets: (*i*) une stabilisation préférentielle de l'état initial par le phényle et (*ii*) une interaction faible de résonance avec le carbocation alcoxy qui se développe dans l'état de transition et qui est induit par le caractère ressemblant au réactif de l'état de transition. La courbe représentant la relation de Brønsted pour l'hydrolyse du méthoxy-3 indène catalysée par les acides carboxyliques et les anions monophosphate conduit à des paramètres pour la théorie de Marcus de $\Delta G_0^{\ddagger} = 3 \pm 1$ kcal/mol et $w^r = 12 \pm 1$ kcal/mol.

[Traduit par le journal]

Carbonium ions are generally stabilized to a greater extent by α-phenyl substituents than by α-methyl groups. The triphenylmethyl cation, **1**, for example, is formed from triphenylmethanol in

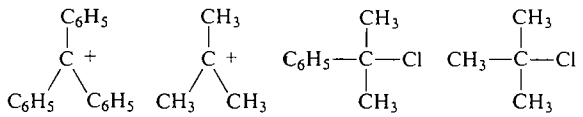

1 **2** **3** **4**

50% aqueous H_2SO_4 but 'superacids' such as FSO_3H–SbF_5 or HF–SbF_5 are needed to generate the *tert*-butyl cation, **2**, from *tert*-butyl alcohol (1) and cumyl chloride, **3**, undergoes solvolysis in ethanol solution 5000 times more rapidly than *tert*-butyl chloride, **4** (2).

We were somewhat surprised, therefore, when we discovered (3) that an α-phenyl group was actually *less* effective than an α-methyl group in promoting vinyl ether hydrolysis. This is a reaction which takes place via rate-determining formation of an alkoxy carbonium ion (eq. 1) (4) and yet the ratio of specific rates for R = C_6H_5 to R = CH_3 in **5** is 0.2. In this

[1] $CH_2{=}C(R)OC_2H_5 \xrightarrow[\text{slow}]{H^+}$ **5**

$CH_3\overset{+}{C}(R)OC_2H_5 \xrightarrow[\text{fast}]{H_2O} CH_3C(=O)R + HOC_2H_5$

paper we report our further study of this unexpected phenomenon.

Results and Discussion

Sigma–Rho Relationships

Phenyl groups stabilize adjacent carbonium ion centers by a conjugative or resonance mechanism; when resonance is inhibited, a destabilizing inductive effect takes over.[3] The fact that an α-phenyl group does facilitate reaction in the present case (although not as much as α-methyl): the rate ratio for R = C_6H_5 to R = H in **1** is 70 (3), indicates that some conjugative stabilization is available. To assess the magnitude of this resonance effect, we examined the influence of substituents in the *para* position of the phenyl group on the rate of methyl α-phenylvinyl ether hydrolysis catalyzed by the hydronium ion.

[1]For part X, see ref. 13*d*.

[2]Author to whom correspondence should be addressed at the University of Toronto.

[3]For a recent example of such inhibition of resonance, see ref. 5.

Can. J. Chem. Downloaded from www.nrcresearchpress.com by 210.87.254.6 on 09/05/12
For personal use only.

Can. J. Chem. Downloaded from www.nrcresearchpress.com by 210.87.254.6 on 09/05/12
For personal use only.

TABLE 1. Summary of rate constants for the hydrolysis of some vinyl ethers in aqueous solution at 25°C under catalysis by H^+

Substrate	k_{H^+} (M^{-1} s^{-1})
Ethyl α-*p*-nitrophenylvinyl ether	2.01[a]
Ethyl α-*p*-bromophenylvinyl ether	36.1[b]
Ethyl α-phenylvinyl ether	118[a]
Ethyl α-*p*-methylphenylvinyl ether	277[b]
Ethyl α-*p*-methoxyphenylvinyl ether	645[b]
3-Methoxyindene	57.9[b]
Methyl α-phenylvinyl ether	53.3[a]

[a]Reference 3.
[b]This work.

The results are detailed in Table S1[4] and are summarized in Table 1. They show a response to substitution, especially to introduction of methyl and methoxyl groups, which is rather less than expected for a strong resonance interaction, and the specific rates in fact correlate better with σ than with σ^+. Treatment of the data by the Yukawa–Tsuno method (6) gives 0.14 ± 0.07 for the resonance parameter *r*, which rates the conjugative effect on a scale from zero for no resonance to unity for a resonance interaction equivalent to the rather strong conjugative effect in the cumyl cation **6**. The value

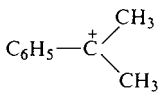

6

of ρ is also low: ρ = −2.23 ± 0.14. Thus, these experiments reveal a rather weak resonance interaction.

3-Methoxyindene

Resonance effects of phenyl groups have a strong conformational requirement, and reduced conjugation may often be traced back to steric effects which prevent the system from adopting its optimum configuration. In the present case there would seem to be no obvious interference of this kind: the α-phenylvinyl group is not a crowded one, and the benzene ring should easily be able to assume the necessary arrangement coplanar with the carbon–carbon double bond.

It is, however, a simple matter to test this idea experimentally; for example, by examining a substance in which coplanarity is forced upon the system through the presence of a small ring, as in 3-methoxyindene, **7**. We therefore measured the rate of hydrolysis of this substance. The data, detailed in Table S2[4] and summarized in Table 1, show the rate

[4]Tables S1, S2, and S3 of rate data are available, at a nominal charge, from the Depository of Unpublished Data, CISTI, National Research Council of Canada, Ottawa, Ont., Canada K1A 0S2.

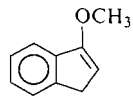

7

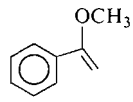

8

of this reaction to be virtually identical with that of its acyclic analog: for 3-methoxyindene k_{H^+} = 58 M^{-1}s^{-1} while for methyl α-phenylvinyl ether, **8**, k_{H^+} = 53 M^{-1}s^{-1}. Steric inhibition of resonance may therefore be ruled out as the cause of the weak resonance effect.

Initial State Stabilization

An additional factor which must be taken into account in the present comparison of phenyl and methyl group effects is the interaction between these groups and the carbon–carbon double bonds in the vinyl ether substrates of the initial states of these reactions. It is well known that phenyl groups stabilize double bonds; a recent study (7) puts this effect, in free energy terms, at $\delta_R G$ = 4.9 kcal/mol. Methyl groups also lower the energy of carbon–carbon double bonds but by a smaller amount: $\delta_R G$ = 3.2 kcal/mol. The difference between these two values, 1.7 kcal/mol, is the amount by which the initial state for methyl α-phenylvinyl ether hydrolysis is stabilized relative to that for ethyl α-methylvinyl ether hydrolysis. This energy difference is equivalent to a rate factor of 20 at 25°C, which is more than enough to offset the rate ratio of 0.2 actually found for these two compounds.

This analysis suggests, therefore, that an α-phenyl group is in fact better at stabilizing positive charge in an alkoxy carbonium ion than is a methyl group in the same position but this superiority is not reflected in rates of vinyl ether hydrolysis because of overwhelming initial state effects. This conclusion is supported by the fact that benzaldehyde diethyl acetal, **9**, undergoes acid-catalyzed hydrolysis 30

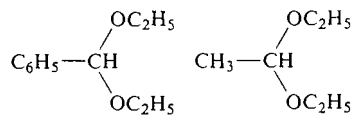

9 **10**

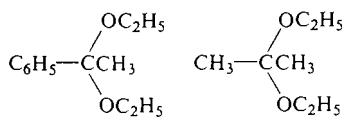

11 **12**

times faster than does acetaldehyde acetal, **10** (8). These reactions occur by rate-determining formation of alkoxy carbonium ions, eq. 2,[5] similar to those generated in vinyl ether hydrolysis but the substrates

[5]For a recent review of the evidence, see ref. 9.

Can. J. Chem. Downloaded from www.nrcresearchpress.com by 210.87.254.6 on 09/05/12
For personal use only.

[2] $$RCH(OC_2H_5)_2 \xrightarrow{H^+} RCHOC_2H_5^+ + C_2H_5OH$$

here do not contain carbon–carbon double bonds and the initial state effects found in vinyl ether hydrolysis are therefore absent. Phenyl substitution in the ketals **11** and **12**, on the other hand, is less effective at promoting hydrolysis than is methyl substitution: the rate ratio **11**:**12** is 0.3 (10). But this system is much more crowded than the acetal series **9** and **10**, and complicating steric effects may well be present (10, 11).

It is interesting also that 'inverted' phenyl to methyl rate ratios have been found in a number of other reactions involving rate-determining proton addition to carbon–carbon double bonds. In fact, of the six systems for which data are available (Table 2), only one gives a phenyl to methyl rate ratio greater than unity.

Brønsted Relation

Weak phenyl group resonance effects such as those observed here seem to be characteristic of fairly stable carbonium ions. They have been observed before in reactions which give alkoxy carbonium ions and have been attributed to a substituent saturation effect or diminished demand for additional stabilization in already quite stable species (12). Some insight into how this saturation effect operates is provided by a Brønsted relation for one of the present vinyl ether hydrolysis reactions.

This Brønsted relation was constructed using 3-methoxyindene as the substrate. Catalytic coefficients were determined for carboxylic acids and for monohydrogen phosphonate anions by measuring rates of hydrolysis in buffer solutions of these acids. The data, summarized in Table S3,[4] when treated by methods we have described before (13), give the rate constants listed in Table 3.

Here, as before in the hydrolysis of other vinyl ethers (13*c* and *d*), the monohydrogen phosphonate anions prove to be better catalysts than neutral carboxylic acids of the same acid strength; this difference may be understood as the result of electrostatic interactions in the transition states of these reactions (13*b* and *c*). The two kinds of catalysts give separate Brønsted relations (Fig. 1) of different slope, $\alpha = 0.64 \pm 0.05$ for RCO_2H and $\alpha = 0.78 \pm 0.02$ for RPO_3H^-. These may be regarded as linear segments of more extensive curved correlations, and, as before (13*c* and *d*) a single curved Brønsted relation (Fig. 2) may be obtained by a simple vertical displacement of the phosphonate anion points.

TABLE 2. Comparison of phenyl and methyl substituent effects in double bond protonation reactions

System	$k(C_6H_5)/k(CH_3)$ (Ref. No.)
$CH_2{=}CHR$	6.6 (20, 21)
$CH_2{=}C(R)CH_3$	0.26 (20, 22)
$CH_2{=}C(R)cPr$	0.065 (20)
$CH_2{=}C(R)OCOCH_3$	0.63 (23)
$CH_2{=}C(R)PO_2(OEt)_2$	0.65 (24, 25)
$CH_2{=}C(R)OC_2H_5$	0.20 (3)

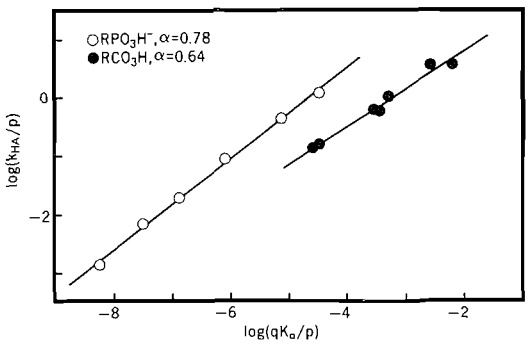

FIG. 1. Separate linear Brønsted relations for the hydrolysis of 3-methoxyindene catalyzed by carboxylic acids and by monohydrogen phosphonate anions.

This curved Brønsted relation shows that α diminishes with increasing catalyst acid strength. For an acid as strong as H_3O^+, the catalyst which was used in the rate comparisons and σ–ρ correlations discussed above, the value $\alpha = 0.39$ may be extrapolated. Insofar as Brønsted exponents may be used as a measure of the degree of proton transfer (14), this implies that the proton is only some 40% transferred, and the carbonium ion only 40% developed, in the transition states of these reactions. Resonance stabilization of this incipient carbonium ion can therefore be no more than 40% of that in a fully developed carbonium ion, and it could be less if resonance effects in carbonium ion-forming reactions lag behind proton transfer just as they seem to do in carbanion formation (14, 15). The weak resonance effects observed in these vinyl ether hydrolyses thus appear to be natural consequences of the early transition states these reactions possess.

Curved Brønsted relations such as that of Fig. 2, when analyzed using Marcus rate theory, give certain parameters by which proton transfer reactions may be characterized (15*b*, 16). This treatment in the present case provides the intrinsic barrier $\Delta G_0^{\ddagger} = 3.4 \pm 0.9$ kcal/mol and the work term $w^r = 12.2 \pm 1.2$ kcal/mol. Thus, in the hydrolysis of 3-methoxyindene, just as in most other vinyl ether hydrolysis reactions (3, 13*c*), rather more energy is required to bring the catalyst and the substrate together and form them into a reaction

Can. J. Chem. Downloaded from www.nrcresearchpress.com by 210.87.254.6 on 09/05/12
For personal use only.

TABLE 3. Summary of catalytic coefficients for the hydrolysis of 3-methoxyindene in aqueous solution at 25°C

Catalyst	pK_a (Ref. No.)	k_{HA} ($M^{-1}s^{-1}$)
$CNCH_2CO_2H$	2.47 (26)	3.85
$ClCH_2CO_2H$	2.87 (27)	3.87
$CH_3OCH_2CO_2H$	3.57 (28)	1.02
HCO_2H	3.75 (29)	0.577
$HOCH_2CO_2H$	3.83 (30)	0.618
CH_3CO_2H	4.76 (31)	0.162
$CH_3CH_2CO_2H$	4.88 (32)	0.150
$CCl_3PO_3H^-$	4.93 (33)	1.24
$CHCl_2PO_3H^-$	5.60 (33)	0.464
$CH_2ClPO_3H^-$	6.59 (33)	0.0889
$HOCH_2PO_3H^-$	7.36 (33)	0.0200
$CH_3PO_3H^-$	8.00 (33)	0.00690
$(CH_3)_3CPO_3H^-$	8.71	0.00138

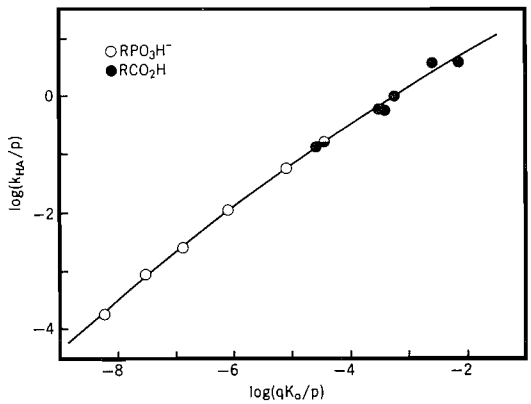

FIG. 2. Curved Brønsted relation for the hydrolysis of 3-methoxyindene by carboxylic acids and monohydrogen phosphonate anions.

complex (w^r) than is needed to surmount the kinetic barrier to proton transfer within this complex ($\Delta G_0^{\neq}$).

Experimental

Materials

Vinyl ethers were prepared from the corresponding ketones via the dimethyl or diethyl ketals. The latter were made by treating the ketones with trimethyl or triethyl orthoformate in alcohol (methanol or ethanol) solution in the presence of a catalytic amount of *p*-toluenesulfonic acid; the ketals were isolated and characterized, and alcohol was then eliminated, by heating under reflux with *p*-toluenesulfonic acid catalyst, to produce the vinyl ethers. The identity of all ketals and vinyl ethers was confirmed by their nmr and ir spectra, and satisfactory carbon and hydrogen analyses were obtained for all new substances.

Phosphoric acids were samples prepared previously for pK_a determinations (17); all other substances were best available commercial grades. Solutions were prepared using deionized water purified further by distillation from alkaline permanganate.

Kinetics

Rates were measured spectroscopically by monitoring the increase in product ketone absorption in the region 240–270 nm. Runs with half-lives greater than 2–3 min were performed using a Cary 118 spectrometer, and faster reactions were measured with a Durrum-Gibson stopped-flow spectrometer; both instruments were thermostatted at 25.0 ± 0.1°C. Rate constants were evaluated graphically, either as plots of ln $(A - A_\infty)$ vs. time (using infinite-time readings made after 10–12 half-lives) or by the Guggenheim (18) or Swinbourne (19) methods.

Acknowledgements

We are grateful to the National Research Council of Canada, the National Science Foundation of the United States, and the donors of the Petroleum Research Fund administered by the American Chemical Society for their generous support of this research.

1. G. A. OLAH and C. U. PITTMAN, JR. Adv. Phys. Org. Chem. **4**, 304 (1966).
2. H. C. BROWN and M. H. REI. J. Am. Chem. Soc. **86**, 5008 (1966).
3. A. J. KRESGE, D. S. SAGATYS, and H. L. CHEN. J. Am. Chem. Soc. **90**, 4174 (1968); in Press.
4. P. SALOMAA, A. KANKAANPERA, and M. LAJUNEN. Acta. Chem. Scand. **20**, 1790 (1966); A. J. KRESGE and Y. CHIANG. J. Chem. Soc. B, 53 (1967); 57 (1967).
5. Y. CHIANG, A. J. KRESGE, P. SALOMAA, and C. I. YOUNG. J. Am. Chem. Soc. **96**, 4494 (1974).
6. Y. YUKAWA and Y. TSUNO. Bull. Chem. Soc. Jpn. **32**, 965, 971 (1959).
7. J. HINE and N. W. FLACKSHAM. J. Am. Chem. Soc. **95**, 1179 (1973); J. HINE. Structural effects on equilibria in organic chemistry. John Wiley and Sons, New York, NY. 1975. p. 270.
8. M. M. KREEVOY, and R. W. TAFT. J. Am. Chem. Soc. **77**, 5590 (1955).
9. E. H. CORDES and H. G. BULL. Chem. Rev. **74**, 581 (1974).
10. T. H. FIFE and L. HAGOPIAN. J. Org. Chem. **31**, 1772 (1966).
11. V. P. VITULLO, R. M. POLLACK, W. C. FAITH, and M. L. KEISER. J. Am. Chem. Soc. **96**, 6682 (1974).
12. G. M. LOUDON and C. BERKE. J. Am. Chem. Soc. **96**, 4508 (1974).
13. (*a*) A. J. KRESGE, H. L. CHEN, Y. CHIANG, E. MURRILL, M. A. PAYNE, and D. S. SAGATYS. J. Am. Chem. Soc. **93**, 413 (1971); A. J. KRESGE and H. J. CHEN. J. Am. Chem. Soc. **94**, 2818 (1972); (*b*) A. J. KRESGE and Y. CHIANG. J. Am. Chem. Soc. **95**, 803 (1973); (*c*) W. K. CHWANG, R. ELIASON, and A. J. KRESGE. J. Am. Chem. Soc. **99**, 805 (1977); (*d*) A. J. KRESGE and W. K. CHWANG. J. Am. Chem. Soc. Submitted.
14. A. J. KRESGE. *In* Proton transfer reactions. *Edited by* E. F. Caldin and V. Gold. Chapman and Hall, London. 1975. Chapt. 7.
15. (*a*) A. J. KRESGE, D. A. DRAKE, and Y. CHIANG. Can. J. Chem. **52**, 1889 (1974); A. J. KRESGE. Can. J. Chem. **52**, 1897 (1974); M. H. DAVIES. J. Chem. Soc. Perkin II, 1018 (1974); (*b*) A. J. KRESGE. Chem. Soc. Rev. **2**, 475 (1973).
16. R. A. MARCUS. J. Phys. Chem. **72**, 891 (1968).
17. A. J. KRESGE and Y. C. TANG. J. Org. Chem. **42**, 757 (1977).
18. F. A. GUGGENHEIM. Philos. Mag. **2**, 538 (1926).
19. E. S. SWINBOURNE. J. Chem. Soc. 2371 (1960).
20. K. OYAMA and T. T. TIDWELL, J. Am. Chem. Soc. **98**, 947 (1976).
21. B. T. BALIGA and E. WHALLEY. Can. J. Chem. **42**, 1019 (1964).

22. F. G. CIAPETTA and M. L. KILPATRICK. J. Am. Chem. Soc. **70**, 639 (1948).
23. D. S. NOYCE and R. M. POLLACK. J. Am. Chem. Soc. **91**, 119, (1969); **91**, 7158 (1969).
24. S. Y. ATTIA, J. P. BERRY, K. M. KOSHY, Y. K. LEUNG, E. P. LYZNICKI, V. J. NOWLAN, K. OYAMA, and T. T. TIDWELL. J. Am. Chem. Soc. **99**, 3401 (1977).
25. C. A. BUNTON and L. ROBINSON. J. Am. Chem. Soc. **91**, 6072 (1969).
26. F. S. FEATES and D. J. G. IVES. J. Chem. Soc. 2798 (1956); D. J. G. IVES and P. D. MARSDEN. J. Chem. Soc. 649 (1965).
27. D. J. G. IVES and J. H. PRYOR. J. Chem. Soc. 2104 (1955).
28. E. J. KING. J. Am. Chem. Soc. **82**, 3575 (1960).
29. H. S. HARNED and N. D. EMBREE. J. Am. Chem. Soc. **56**, 1042 (1934).
30. L. F. NIMS. J. Am. Chem. Soc. **58**, 987 (1936).
31. H. S. HARNED and R. W. EHLERS. J. Am. Chem. Soc. **55**, 652 (1933).
32. D. H. EVERETT, D. A. LANDSMAN, and B. R. W. PINSENT. Proc. R. Soc. Ser. A, **215**, 403 (1952).
33. A. J. KRESGE, and Y. C. TANG. J. Org. Chem. **42**, 757 (1977).

Can. J. Chem. Downloaded from www.nrcresearchpress.com by 210.87.254.6 on 09/05/12
For personal use only.

Vinyl ether hydrolysis. XII. Use of *cis–trans* isomerism to probe the reaction mechanism[1]

Y. CHIANG, A. J. KRESGE,[2] AND C. I. YOUNG

Department of Chemistry, University of Toronto Scarborough College, West Hill, Ontario M1C 1A4 and Department of Chemistry, Illinois Institute of Technology, Chicago, Illinois 60616, U.S.A.

Received August 29, 1977

Y. CHIANG, A. J. KRESGE, and C. I. YOUNG. Can. J. Chem. **56**, 461 (1978).

Rates of hydrolysis of *cis*- and *trans*-β-phenylvinyl methyl ethers, *cis*- and *trans*-β-(*p*-nitrophenyl)vinyl methyl ethers, and *cis*- and *trans*-β-cyanovinyl ethyl ethers were measured in concentrated (10–55 wt%) aqueous perchloric acids. The results show that these *cis* and *trans* isomers do not interconvert under the hydrolysis reaction conditions, and that formation of the alkoxy carbonium ion intermediate in these reactions is therefore not reversible.

Y. CHIANG, A. J. KRESGE et C. I. YOUNG. Can. J. Chem. **56**, 461 (1978).

On a mesuré les vitesses d'hydrolyse des β-phénylvinylméthyl éthers *cis* et *trans*, des β-(*p*-nitrophényl)vinylméthyl éthers *cis* et *trans* et des β-cyanovinyléthyl éthers *cis* et *trans* dans des solutions aqueuses concentrées (10–55% en poids) d'acide perchlorique. Des résultats indiquent qu'il n'y a pas d'interconversion entre isomères *cis* et *trans* dans les conditions de réaction d'hydrolyse et que la formation du carbocation alcoxy intermédiaire dans ces réactions n'est donc pas réversible.

[Traduit par le journal]

The acid-catalyzed hydrolysis of simple vinyl ethers occurs through rate-determining proton transfer from the catalyst to the substrate (eq. 1), followed by rapid hydration of the ensuing alkoxy carbonium ion (eq. 2) and subsequent fast breakdown of the hemiacetal intermediate (eq. 3). There is

$$[1]\qquad CH_2{=}CHOR + HA \rightarrow CH_3\overset{+}{C}HOR + A^-$$

$$[2]\qquad CH_3\overset{+}{C}HOR + H_2O \rightarrow CH_3\overset{OH}{\overset{|}{C}}HOR + H^+$$

$$[3]\qquad CH_3\overset{OH}{\overset{|}{C}}HOR \rightarrow CH_3\overset{O}{\overset{\|}{C}}H + HOR$$

reason to believe, however, that the hydration reaction (eq. 2) is not very much faster than the reverse of the proton transfer step (eq. 1) (1) and a change in mechanism from rate-determining protonation to rate-determining hydration has in fact been observed in the case of the difunctional cyclic vinyl ether, 2-methoxy-2,3,4,5,6,7-hexahydrooxonin, **1** (2).

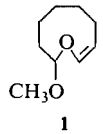

1

Our interest in vinyl ether hydrolysis has prompted us to explore the borderline between these two mechanistic variations and we have already reported (1) that we were unable to obtain any evidence for a change in mechanism with substrates containing carbon–carbon double-bond stabilizing groups; such substituents would be expected to lower the free energy of activation for the deprotonation step while leaving that for hydration largely unaffected, and that might cause protonation to become reversible and make hydration rate-determining. The criteria of reaction mechanism we used in these studies consisted of isotope effects, isotopic labelling, and the form of acid-catalysis. We now report the results of applying yet another mechanistic test, *cis–trans* isomerism.

This diagnostic tool depends for its operation upon the fact that reversal of the protonation step provides a route for inversion of configuration about the vinyl ether double bond (eq. 4). This mechanistic criterion has been applied before to the hydrolysis of vinyl ethers (3), but not to substrates containing double-bond stabilizing groups.

Experimental

Materials

cis-β-Phenylvinyl methyl ether was prepared as before (1*a*) by the addition of methanol to phenylacetylene in the presence of sodium methoxide, which occurs in a stereospecific *trans* manner (4). The *trans* isomer was obtained by treating phenylacetaldehyde dimethyl acetal with an excess of *n*-butyl lithium at room temperature for 48 h; it was purified by liquid chromatography on a silica gel column using *n*-hexane to elute impurities and benzene to remove pure product. The nmr spectra of both isomers were consistent with their structures; in particular the *cis* isomer gave vinyl proton signals at

[1]For part XI see accompanying paper in this issue.

[2]Author to whom correspondence should be addressed at the University of Toronto.

Can. J. Chem. Downloaded from www.nrcresearchpress.com by 210.87.254.5 on 09/05/12
For personal use only.

[4]

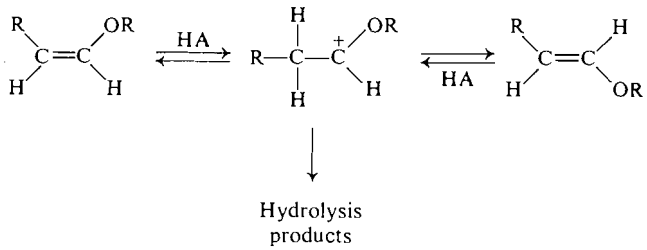

δ = 5.1 (d) and 5.8 (d) ppm with a coupling constant of J_{HH} = 7 Hz, whereas the *trans* isomer showed signals at δ = 5.7 (d) and 6.9 (d) ppm with J_{HH} = 13 Hz.

trans-β-(*p*-Nitrophenyl)vinyl methyl ether was prepared by treating β-fluoro-*p*-nitrostyrene (kindly supplied by Dr. F. Naso) with sodium methoxide (5). Irradiation of this substance with a sun lamp gave an equilibrium mixture consisting of two parts *cis*- and one part *trans*-β(*p*-nitrophenyl)vinyl methyl ether from which the pure *cis* isomer was obtained by liquid chromatography on silica gel; elution with cyclohexane containing 1% ethyl ether released the *cis* isomer first and provided good separation from the *trans*. The *cis* isomer gave vinyl proton nmr signals at δ = 6.7 (d) and 7.9 (d) ppm with J_{HH} = 8 Hz, and the *trans* isomer showed signals at δ = 5.8 (d) and 7.2 ppm with J_{HH} = 13 Hz.

A mixture of *cis*- and *trans*-β-cyanovinyl ethyl ether was prepared by decarboxylation of 2-cyano-3-ethoxyacrylic acid (Aldrich) at reduced pressure (0.5 mm) (6); this mixture was separated into pure *cis* and *trans* isomers by gas chromatography using a 20% carbowax on Chromosorb-P column. The *cis* isomer gave vinyl proton nmr signals at δ = 4.1 (d) and 4.4 (d) ppm, J_{HH} = 7 Hz, and the *trans* isomer showed signals at δ = 4.1 (d) and 4.9 (d) ppm with J_{HH} = 13 Hz.

Kinetics

Rates were measured spectroscopically by monitoring the decrease in strong vinyl ether absorption at 225 nm for *cis*- and *trans*-β-cyanovinyl ethyl ether, 260 nm for *cis*- and *trans*-β-phenylvinyl methyl ether, and 350 nm for β-(*p*-nitrophenyl)-vinyl methyl ether. Measurements were made using a Cary Model 11 spectrometer with cell compartment thermostatted at 25.0 ± 0.05°C.

Results

Each of the six vinyl ethers investigated proved to be too unreactive to hydrolyze at convenient rates in dilute aqueous acid solutions, and measurements were therefore made using concentrated perchloric acid in the range 10–55 wt%. All of the data so obtained obeyed the first-order rate law exactly. Rate constants were evaluated graphically as slopes of plots of ln $(A - A_\infty)$ vs. time, with infinite-time readings (A_∞) taken after 10–12 half-lives. The results are summarized in Tables 1–3.

It may be seen that for all three *cis–trans* vinyl ether pairs, the *cis* isomer hydrolyzed substantially more rapidly than the *trans*; *cis*:*trans* rate ratios ranged from 4.2 for β-phenylvinyl methyl ether to 5.5 for β-cyanovinyl ethyl ether. Increased hydrolytic reactivity of *cis* over *trans* vinyl ethers of this order of magnitude has been observed before (3, 7, 8) and has been attributed to preferential stabilization of the *cisoid* conformation in the transition state (*7a*) (by analogy with the eclipsed conformation of propionaldehyde (9)) and also to initial-state steric congestion in the *cis* isomer (3).

In all cases, rates of reaction increased rapidly with increasing acid concentration, and for all substrates plots of log k_{obs} vs. the H_0 acidity function were linear with slopes near unity: $d(\log k_{obs})/d(-H_0) = 0.95 \pm 0.01$ for *cis*- and 0.96 ± 0.01 for *trans*-β-cyanovinyl ethyl ether, 1.11 ± 0.01 for *cis*- and 1.13 ± 0.01 for *trans*-β-phenylvinyl methyl ether, and 1.15 ± 0.02 for *cis*- and 1.10 ± 0.01 for *trans*-β-(*p*-nitrophenyl)vinyl methyl ether. In this respect these reactions resemble the hydration of simple olefins whose rates also correlate well with the H_0 function (10).

TABLE 1. Rates of hydrolysis of *cis*- and *trans*-β-phenylvinyl methyl ethers in aqueous perchloric acid at 25°C

wt% $HClO_4$	$-H_0$	$10^3 k_{obs}$ (s^{-1}) *cis*	$10^3 k_{obs}$ (s^{-1}) *trans*
8.72	0.18	5.38, 5.39	—
10.26	0.30	7.60, 7.60, 7.62	—
13.58	0.53	13.7, 13.7, 13.7	3.20, 3.29
16.01	0.68	21.2, 21.3, 20.5	4.63, 4.70, 4.70
19.05	0.89	31.7, 32.0, 32.0	7.62, 7.62, 7.62
21.95	1.04	50.6, 49.7, 50.2	11.7, 11.9, 11.8
27.33	1.38	—	30.2, 29.9, 29.6
30.16	1.57	—	45.5, 46.5, 46.5

TABLE 2. Rates of hydrolysis of *cis*- and *trans*-β-(*p*-nitrophenyl)vinyl methyl ethers in aqueous perchloric acid at 25°C

wt% $HClO_4$	$-H_0$	$10^3 k_{obs}$ (s^{-1}) *cis*	$10^3 k_{obs}$ (s^{-1}) *trans*
16.01	0.68	2.93, 2.95	—
19.05	0.89	4.82, 4.82, 4.72	—
21.95	1.04	7.90, 7.86, 7.90	—
27.33	1.38	19.5, 18.7, 18.7	3.61, 3.62
30.16	1.57	30.2, 30.2, 28.9	5.59, 5.61, 5.59
33.33	1.79	—	10.1, 10.1, 10.5
36.35	2.01	—	18.9, 18.4, 18.3
40.40	2.35	—	42.0, 40.5, 40.7

Can. J. Chem. Downloaded from www.nrcresearchpress.com by 210.87.254.5 on 09/05/12
For personal use only.

Can. J. Chem. Downloaded from www.nrcresearchpress.com by 210.87.254.5 on 09/05/12
For personal use only.

TABLE 3. Rates of hydrolysis of *cis*- and *trans*-β-cyanovinyl ethyl ethers in aqueous perchloric acid at 25°C

wt% $HClO_4$	$-H_0$	$10^3 k_{obs}$ (s^{-1}) *cis*	$10^3 k_{obs}$ (s^{-1}) *trans*
43.28	2.62	3.44, 3.45	—
44.18	2.72	4.42, 4.44	—
45.79	2.90	6.58, 6.25	—
46.88	3.02	8.15, 8.20	1.49, 1.49
49.87	3.42	20.1, 19.9, 19.8	3.77, 3.77
50.44	3.50	—	4.70, 4.72
52.38	3.79	—	8.30, 8.20
53.42	3.96	—	12.4, 12.1
55.41	4.30	—	26.2, 25.7, 26.0

Discussion

In each of the three cases examined here, *cis* and *trans* isomeric vinyl ethers underwent acid-catalyzed hydrolysis at substantially different rates. This indicates that no mechanism for rapid isomer interconversion exists under the hydrolysis reaction conditions, for, if such a mechanism were operative, the two isomers would give a single hydrolysis rate constant characteristic of the equilibrium *cis–trans* mixture. This, in turn, shows that deprotonation of the alkoxy carbonium ion intermediates formed in these hydrolysis reactions (eq. 1) cannot be rapid relative to their rates of hydration (eq. 2).

Slow interconversion of *cis–trans* isomers under hydrolysis reaction conditions, on the other hand, would allow the two isomers to hydrolyze at different rates, at least initially. In this circumstance, however, conversion of one isomer into the other during the hydrolysis reaction would upset the smooth first-order disappearance of vinyl ether normally observed in vinyl ether hydrolysis. Some calculations we have done simulating such a system show that substantial deviations from first-order kinetic behavior occur even when the alkoxy carbonium ion intermediate partitions equally between deprotonation and hydration reaction paths. Such systems, moreover, though they show different reaction rates for the two isomers initially, settle down to identical rates of reaction after one to two half-lives. The fact that accurate first-order kinetic behavior was observed in all of the reactions investigated here, and that no tendency toward convergence to similar rate constant for members of the *cis–trans* pair could be detected, implies that no kinetically significant isomerization is occurring under the hydrolysis reaction conditions.

This conclusion is supported by additional direct examination of the reaction mixture during hydrolysis of one of the kinetic substrates, *cis*-β-phenylvinyl methyl ether. It had been found earlier, by direct equilibration studies, that this substance is less stable than its *trans* isomer (3). We corroborated that result here: using samples of both *cis*- and *trans*-vinyl ether plus catalytic amounts of mercuric acetate and following the isomerization by nmr, we found a *cis*:*trans* equilibrium ratio of 0.31 ± 0.02. We allowed this less stable isomer to hydrolyze in solution, in a 20% H_2O – 80% D_2O solvent containing 1.5 *M* perchloric acid (ca. 15 wt%), while taking samples, extracting them with an organic solvent (carbon tetrachloride) and examining the extracts by nmr. Although, as the reaction progressed, we could see *cis*-β-phenylvinyl methyl ether disappear and the product of hydrolysis, phenylacetaldehyde, appear, we could detect no *trans*-β-phenylvinyl methyl ether whatsoever; we could also not discern any of the characteristic alteration in the vinyl-hydrogen portion of the nmr spectrum which would have occurred had deuterium been incorporated into the substrate.

This total lack of evidence for reversal of the proton transfer step in these vinyl ether hydrolysis reactions is consistent with our previous experience. We were unable before to detect proton transfer reversal in the hydrolysis of β-phenyl-α-methyl vinyl ether (1*a*) and α-cyclopropylvinyl methyl ether (1*b*), despite the fact that these substrates contain phenyl and cyclopropyl groups in positions from which they can interact to stabilize the carbon–carbon double bond. We can now add cyano and *p*-nitrophenyl to the list of double-bond stabilizing groups which do not render the proton transfer step reversible. It is of particular interest that the *p*-nitrophenyl substituent does not function in this way, for the nitro group is a powerful electron acceptor. It should therefore interact strongly with the ether oxygen atom, which is a good electron donor, and set up a particularly favorable conjugated system involving the carbon–carbon double bond. In the closely analogous *N*,*N*-dimethylaniline system, for example, introduction of a nitro group into the *para* position raises the barrier to rotation about the C–N bond, which is a measure of the resonance interaction, from 5 to 8 kcal/mol (11).

It is likely that the inability of these groups to promote proton transfer reversal is related to the strong retarding effect they have upon the rate of the hydrolysis reaction. Extrapolation of the log k_{obs} vs. H_0 relationships described above gives dilute-solution hydrogen ion catalytic coefficients which range from 2.7×10^{-3} M^{-1} s^{-1} (for *cis*-β-phenylvinyl methyl ether) to 2.1×10^{-6} M^{-1} s^{-1} (for *trans*-β-cyanovinyl ethyl ether); these are lower than any values previously reported for vinyl ether hydrolysis. The slowness of these reactions implies

that they have late, product-like transition states with not much carbon-carbon double bond character; double-bond stabilizing substituents are therefore likely to have little effect on the mechanism of the reaction.

Acknowledgements

We are grateful to the National Research Council of Canada, the National Science Foundation of the United States, and the donors of the Petroleum Research Fund administered by the American Chemical Society for their generous support of this research.

1. (*a*) A. J. KRESGE and H. J. CHEN. J. Am. Chem. Soc. **94**, 2818 (1972); (*b*) A. J. KRESGE and W. K. CHWANG. J. Am. Chem. Soc. In press.
2. J. D. COOPER, V. P. VITULLO, and D. L. WHALEN. J. Am. Chem. Soc. **93**, 6294 (1971).
3. T. OKUYAMA, T. FUENO, H. NAKATSUJI, and J. FURUKAWA. J. Am. Chem. Soc. **89**, 5826 (1967).
4. J. E. BALDWIN and L. E. WALKER. J. Org. Chem. **31**, 3985 (1966).
5. G. MARCHESE, F. NASO, and G. MODENA. J. Chem. Soc. B, 290 (1969).
6. M. A. DOLLIVER, T. L. GRESHAM, G. B. KISTIAKOWSKY, E. A. SMITH, and W. E. VAUGHN. J. Am. Chem. Soc. **60**, 441 (1938); S. RUHEMAN and W. WRAGG. J. Chem. Soc. 1185 (1901).
7. (*a*) P. SALOMAA and P. NISSI. Acta Chem. Scand. **21**, 1366 (1967); (*b*) A. KANKAANPERA, P. SALOMAA, P. JUHALA, R. AALTONEN, and M. MATTSEN. J. Am. Chem. Soc. **95**, 3618 (1973).
8. A. J. KRESGE, D. S. SAGATYS, and H. L. CHEN. J. Am. Chem. Soc. **99**, 7228 (1977).
9. R. J. ABRAHAM and J. A. POPLE, Mol. Phys. **3**, 609 (1960); S. S. BUTCHER and E. B. WILSON, JR. J. Chem. Phys. **45**, 1984 (1966).
10. R. W. TAFT, JR. J. Am. Chem. Soc. **74**, 5372 (1952); R. W. TAFT, JR., E. L. PURLEE, P. RIESZ, and C. A. DEFAZIO. J. Am. Chem. Soc. **77**, 1584 (1955).
11. R. K. MACKENZIE and D. D. MACNICOL. J. Chem. Soc. Chem. Commun. 1299 (1970).

Can. J. Chem. Downloaded from www.nrcresearchpress.com by 210.87.254.5 on 09/05/12
For personal use only.

Studies of silyl and germyl Group VI species. Part II. Bis(methylgermyl) and bis(dimethylgermyl) chalcogenides and related species

JOHN E. DRAKE,[1] BORIS M. GLAVINČEVSKI, AND H. ERNEST HENDERSON
Department of Chemistry, University of Windsor, Windsor, Ont., Canada N9B 3P4

AND

RAYMOND T. HEMMINGS
Department of Chemistry, University of the West Indies, Mona, St. Andrew, Jamaica, W. I.

Received May 24, 1977

JOHN E. DRAKE, BORIS M. GLAVINČEVSKI, H. ERNEST HENDERSON, and RAYMOND T. HEMMINGS. Can. J. Chem. **56**, 465 (1978).

Comparative reactions of some halogenogermanes with lithium(I), lead(II), and organosilicon Group VI species have been investigated, leading to the efficient syntheses of the chalcogermanes of the formula $(Me_nH_{3-n}Ge)_2E$, where E = O, S, Se, Te; $n = 0 \rightarrow 3$. The spectroscopic properties of the new bis(methylgermyl) and bis(dimethylgermyl) chalcogenides are discussed. Germanethiols and germaneselenols, viz. $Me_nH_{3-n}GeEH$ (E = S, Se; $n = 0, 3$) are isolated as intermediates in the reaction of digermoxanes with H_2E and from equilibrium mixtures of $(Me_nH_{3-n}Ge)_2E$ with excess H_2E. Evidence is presented for the condensation of the chalcogermanes to species of the type $Me_nH_{2-n}Ge(EGeH_{3-n}Me_n)_2$ ($n = 1, 2$) and for the elimination of metallic selenium or tellurium giving digermanes of the type $(Me_nH_{3-n}Ge)_2$ ($n = 1, 2$).

JOHN E. DRAKE, BORIS M. GLAVINČEVSKI, H. ERNEST HENDERSON et RAYMOND T. HEMMINGS. Can. J. Chem. **56**, 465 (1978).

On a étudié les réactions comparatives de quelques halogermanes avec du lithium(I), du plomb(II) et des espèces du groupe VI d'organosilicium; ces réactions conduisent à des synthèses efficaces de chalcogermanes de formule $(Me_nH_{3-n}Ge)_2E$ où E = O, S, Se, Te; $n = 0 \rightarrow 3$. On discute des propriétés spectroscopiques des nouveaux bis(méthylgermyl) et bis-(diméthylgermyl)-chalcogénures. On a isolé des germanethioles et germanesélénoles, $Me_nH_{3-n}GeEH$ (E = S, Se; $n = 0, 3$), comme intermédiaires dans la réaction de digermoxanne avec H_2E et à partir de mélanges à l'équilibre de $(Me_nH_{3-n}Ge)_2E$ avec un excès de H_2E. On présente des données concernant la condensation de chalcogermanes produisant les composés du type $Me_nH_{2-n}Ge(EGeH_{3-n}Me_n)_2$ ($n = 1, 2$) et l'élimination de sélénium ou de tellure métallique conduisant à des digermanes du type $(Me_nH_{3-n}Ge)_2$ ($n = 1, 2$).

[Traduit par le journal]

Introduction

In a recent report (1) we demonstrated, via small scale preparations, the susceptibility of the Ge—N linkage in bis(methylgermanium) carbodiimides to Group VI protic species, giving bis(methylgermanium) chalcogenides. Attempts to increase the scale of production generally met with unsatisfactory results because of a variety of side reactions. Therefore, we examined a number of alternative methods of forming the germanium–chalcogen linkage and report herein the preparation of the germyl species, viz. $(Me_nH_{3-n}Ge)_2E$ (E = O, S, Se, Te; $n = 0 \rightarrow 3$), from the metathesis reactions of various halogenogermanes with lithium(I), lead(II), and organosilicon chalcogenides. The new bis(methylgermyl) and bis(dimethylgermyl) chalcogenides are identified by their ^1H nmr, infrared, Raman, and mass spectral parameters and by their cleavage reactions with known quantities of gaseous hydrogen halides. Self-condensation reactions of the methyl(hydrido)chalcogermanes and subsequent elimination of the chalcogen moiety provide further chracterization. Co-condensation with Group VI hydrides results in the formation of the monomeric chalcogermane intermediates, germanethiols and germaneselenols, which are identified by ^1H nmr and mass spectral techniques.

[1]To whom correspondence should be addressed.

Experimental

Manipulations and spectroscopic measurements were as previously described (1). Halogenogermanes were either commercially obtained or prepared by literature methods (2–8). Lithium selenide and telluride were prepared from the elements: typically, powdered selenium (0.403 g, 5.10 mmol) and clean lithium wire (0.069 g, 10 mmol) were allowed to react in dry ammonia (ca. 10–15 ml) at −78°C in a reactor (ca. 70 ml) attached to the vacuum system via a Teflon-in-glass stopcock. The reaction was accelerated by occasional removal of the −78°C bath with shaking and cautious warming while monitoring the NH_3 pressure. After typically 12 h the NH_3 was pumped off. The light grey salt was heated at 150–170°C for 6 h *in vacuo* and stored under nitrogen. Hydrolysis gave typically 98% of the Se content required for Li_2Se as H_2Se, whilst ca. 80% resulted for the release of H_2Te from Li_2Te. Bis(tri-

Can. J. Chem. Downloaded from www.nrcresearchpress.com by 210.87.254.105 on 09/05/12
For personal use only.

Can. J. Chem. Downloaded from www.nrcresearchpress.com by 210.87.254.105 on 09/05/12
For personal use only.

TABLE 1. Exchange reactions of iodogermanes with Li_2E[a]

$$2Me_nH_{3-n}GeI + Li_2E \rightarrow (Me_nH_{3-n}Ge)_2E + 2LiI$$
(I) (II)

	E = S			E = Se			E = Te		
$Me_nH_{3-n}Ge$	I (mmol)	II (mmol)	Yield (%)	I (mmol)	II (mmol)	Yield (%)	I (mmol)	II (mmol)	Yield (%)
H_3Ge	2.76	0.92	67	4.16	1.61	77	8.45	3.52	83
MeH_2Ge	4.32	1.80	83	3.56	1.43	80	7.14	3.17	89
Me_2HGe	1.71	0.70	82	8.80	3.90	89	9.88	4.20	85
Me_3Ge	3.16	1.43	91	12.25	5.23	85	5.78	2.49	86

[a]When E = O, incomplete conversion of the iodogermanes afforded mixtures of $(Me_nH_{3-n}Ge)_2O$ and $Me_nH_{3-n}GeI$ (n = 0, 1, 2).

methylsilyl)selenide and -telluride were prepared from Me_3SiCl and Li_2E (E = Se, Te) in Et_2O at 25°C. The purity of the volatile materials was confirmed by ^1H nmr and vibrational spectroscopic analysis. Hydrogen sulfide and hydrogen selenide were obtained via the hydrolysis of the respective aluminum chalcogenides (9, 10). The remainder of the materials was of commercial origin.

Reactions of Halogenogermanes with Lithium Salts

(i) With Lithium Sulfide, Selenide, and Telluride

In a typical reaction, the ampule which contained Li_2Se (ca. 0.46 g, 5.0 mmol) and which was attached to the vacuum line, was thoroughly evacuated. Then, Me_2O (ca. 10–15 ml) and Me_2HGeI (8.80 mmol) were condensed in with the ampule held at −196°C. The ampule was isolated and warmed to −78°C with occasional shaking. After ca. 96 h the ampule was opened and the volatile materials fractionated at −78 and −196°C. The latter trap retained Me_2O and traces of Me_2GeH_2 and Me_2Se which were identified spectroscopically (4, 11). The material at −78°C was further fractionated through traps at −45 and −78°C. The −45°C trap contained pure bis(dimethylgermyl) selenide, $((Me_2HGe)_2Se$, 3.90 mmol, 89%; ms peak m/e 279–294 $(C_4H_nGe_2Se)^+$). No Me_2HGeI was recovered. The analogous reactions with trimethylbromo- or trimethyliodogermane were allowed to occur at 25°C either in Me_2O or Et_2O. Details of the preparations are collected in Table 1.

(ii) With Lithium Oxide

Typically, Me_2HGeI (0.80 g, 3.47 mmol) and Li_2O (0.060 g, 2.00 mmol) were allowed to react as in (*i*). Upon fractionation of the volatile materials a mixture of $(Me_2HGe)_2O$ and Me_2HGeI (ca. 0.39 g) and small amounts of immiscible droplets of water were retained at −78°C, as identified spectroscopically (see Results and Discussion). Attempts to separate the $(Me_2HGe)_2O$ from Me_2HGeI by trap to trap fractional distillation were unsuccessful. Longer reaction times and appreciable excesses of Li_2O had little effect on the product mixture. By contrast, trimethylbromogermane, Me_3GeBr (0.58 g, 2.94 mmol) and Li_2O (0.18 g, ca. 6 mmol) in Et_2O at 25°C with continuous stirring for ca. 80 h gave $(Me_3Ge)_2O$ (0.357 g, 1.42 mmol, 98%). The purity of $(Me_3Ge)_2O$ was confirmed by the absence of the stretching vibration, ν(Ge—Br), in the Raman spectrum.

Reactions of $Me_nH_{3-n}GeX$ with Lead(II) Salts

(i) $Me_nH_{3-n}GeBr$ with PbO

Typically, MeH_2GeBr (1.56 mmol) was condensed onto PbO (ca. 14 g) contained in a reaction flask (ca. 40 ml; equipped with a Teflon-in-glass stopcock) held at −196°C. The −196°C bath was removed and the contents of the reaction flask were shaken and allowed to react at 25°C for ca. 20 min. Fractionational condensation at −78°C gave bis(methylgermyl)oxide, $(MeH_2Ge)_2O$ (0.76 mmol, 97.4%). By similar procedures Me_2HGeBr (2.98 mmol), Me_3GeBr (3.67 mmol), and H_3GeBr (0.92 mmol) reacted with PbO (12–15 g) to give $(Me_2HGe)_2O$ (1.47 mmol, 98.7%), $(Me_3Ge)_2O$ (1.83 mmol, 99.7%), and $(H_3Ge)_2O$ (0.35 mmol, 76.1%), respectively. However, when gaseous MeH_2GeBr (1.41 mmol) was allowed to pass back and forth six times at room temperature over a mixture of PbO (ca. 40 g) and a small amount of powdered glass held in a column on glass wool the recovery of MeH_2GeBr (1.39 mmol) was almost quantitative.

(ii) $Me_nH_{3-n}GeI$ with PbO

Typically, Me_2HGeI (1.46 mmol) was condensed onto excess of PbO in an analogous manner to (*i*). After ca. 15 min at 25°C, fractionation of the volatile materials through traps at −78 and −196°C gave $(Me_2HGe)_2O$ (0.45 mmol, 61.6%) in the former and Me_2GeH_2 (0.20 mmol) in the latter. Similarly, H_3GeI (0.86 mmol), MeH_2GeI (1.22 mmol), and Me_3GeI (3.67 mmol) were converted by PbO to the corresponding oxides, viz. $(H_3Ge)_2O$ (0.15 mmol, 34.9%), $(MeH_2Ge)_2O$ (0.28 mmol, 45.9%), and $(Me_3Ge)_2O$ (1.82 mmol, 99.2%).

In the alternative preparation, when $Me_nH_{3-n}GeI$ (n = 0, 1, 2) was streamed as a gas over a previously evacuated column of PbO as in (*i*) very little formation of germoxanes (5–15%) was achieved as estimated by the relative intensity of the stretching vibrations ν(Ge—O) and ν(Ge—I) in the Raman spectra.

(iii) MeH_2GeBr and Me_3GeBr with PbS

A mixture of MeH_2GeBr (1.89 mmol) and excess of PbS was allowed to react at 25°C for ca. 25 min as in (*i*). Fractionation of the volatile material gave unchanged MeH_2GeBr (1.80 mmol). No reaction occurred even when the mixture of Me_3GeBr (2.96 mmol) and excess of PbS was heated at 85°C for ca. 2 h.

(iv) MeH_2GeI and Me_3GeI with PbS

In a typical reaction, MeH_2GeI (1.03 mmol) was allowed to react with excess of PbS at 25°C for ca. 30 min. Fractionation of the volatile materials through traps held at −78 and −196°C gave a mixture of $(MeH_2Ge)_2S$ and MeH_2GeI in the former, and small amounts of $MeGeH_3$ in the latter. The conversion of MeH_2GeI into $(MeH_2Ge)_2S$ was 39% as estimated by their respective peak ratios in the ^1H nmr spectrum. Me_3GeI (2.40 mmol) at 80°C for 2 h gave $(Me_3Ge)_2S$ (0.90 mmol, 75.0%).

Reactions of Fluorogermanes with Organosilicon Chalcogenides

In a typical reaction, $(Me_3Si)_2S$ (0.24 mmol) and excess H_3GeF (0.61 mmol) were distilled into an ampule and allowed to react at room temperature for 5–10 min. The volatile materials were then fractionated at −45 and −196°C. The

Can. J. Chem. Downloaded from www.nrcresearchpress.com by 210.87.254.105 on 09/05/12
For personal use only.

TABLE 2. Exchange reactions of $(Me_3Si)_2E$ species with fluorogermanes
$(Me_3Si)_2E$ + excess $Me_nH_{3-n}GeF \rightarrow (Me_nH_{3-n}Ge)_2E + Me_3SiF$
(I) (II)
E = S, Se, Te; $n = 0 \rightarrow 3$

	E = S			E = Se			E = Te		
$Me_nH_{3-n}Ge$	I (mmol)	II (mmol)	Yield (%)	I (mmol)	II (mmol)	Yield (%)	I (mmol)	II (mmol)	Yield (%)
MeH_2Ge	0.43	0.43	100	1.02	1.00	98	1.32	1.30	98
Me_2HGe	0.23	0.22	96	0.79	0.78	99	1.22	1.22	100
Me_3Ge	0.14	0.14	100	0.85	0.85	100	0.85	0.85	100
H_3Ge	0.24	0.23	96	0.23	0.23	100	0.95	0.94	99

former trap held $(H_3Ge)_2S$ (0.23 mmol, 96%) while the latter retained Me_3SiF (11) and unreacted H_3GeF (12), identified spectroscopically. Similar experiments using excess $MeGeH_2F$ and Me_2GeHF gave $(MeGeH_2)_2S$ (100%) and $(Me_2HGe)_2S$ (95%). The analogous reaction of $(Me_3Si)_2S$ (3.28 mmol) with excess Me_3GeF (8.15 mmol) for 45 min at room temperature gave a mixture of $(Me_3Ge)_2S$, $(Me_3Si)_2S$, and the mixed sulfide $Me_3SiSGeMe_3$ at −23°C, and Me_3SiF and MeGeF at −196°C. All species were identified by their ^1H nmr parameters (12–14). Similar product distribution was obtained with longer reaction times. However, when $(Me_3Si)_2S$ (0.14 mmol) and Me_3GeF (0.41 mmol) were allowed to react in a sealed tube at high temperature (≥80°C) and left overnight, then $(Me_3Ge)_2S$ (0.14 mmol) was formed quantitatively. Details of all preparations are collected in Table 2.

Reactions of Chalcogermanes with Hydrogen Sulfide and Selenide

In a typical reaction, $(Me_3Ge)_2O$ (1.25 mmol) and H_2S (1.28 mmol) were introduced into an ampule (ca. 7.5 ml) and isolated for 5 min at 25°C. Fractional condensation at −78°C afforded $(Me_3Ge)_2S$ (1.24 mmol, 99.2%; ms peak *m/e* 262–274 $(C_6H_{18}Ge_2S)^+$) and traces of H_2S at −196°C. Immiscible droplets of water were removed by passage of the mixture over a small amount of P_2O_5. The formation of the thiol, Me_3GeSH, resulted when excess H_2S was used as was confirmed by its ^1H nmr parameters (δ(Me) 0.56, δ(SH) −0.32 ppm, $|J_{^{13}CH}|$ 129.0 Hz). The thiol was sufficiently stable at low temperatures to permit the recording of its mass spectrum, peak *m/e* 147–155 $(CH_4GeS)^+$. Thus, with the vessel held at −78°C, H_2S was pumped away and the thiol was passed into the mass spectrometer. The identical reaction of $(H_3Ge)_2O$ with H_2S gave high yields of $(H_3Ge)_2S$, ms peak *m/e* 172–190 $(H_nGe_2S)^+$. With excess H_2S, formation of H_3GeSH resulted as was confirmed by its ^1H nmr (18) and mass spectral parameters (δ(GeH) 4.33, δ(SH) −0.23 ppm and ms peak *m/e* 102–112 $(H_nGeS)^+$. The analogous reactions with H_2Se gave the corresponding germyl selenides, $(Me_3Ge)_2Se$ (ms peak *m/e* 306–322 $(C_6H_{18}Ge_2Se)^+$) and $(H_3Ge)_2Se$ (ms peak *m/e* 216–238 $(H_nGe_2Se)^+$), and germaneselenols Me_3GeSeH (ms peak *m/e* 191–204 $(C_3H_{10}GeSe)^+$, δ(Me) 0.66, δ(SeH) −2.38 ppm, $|J_{^{13}CH}|$ 128.7, $|J_{^{77}SeH}|$ 42.55 Hz) and H_3GeSeH (ms peak *m/e* 146–162 $(H_nGeSe)^+$δ (GeH)4.26, δ(SeH) −2.23 ppm $|J_{^{77}SeH}|$ 41.1 Hz). The chalcogenols were also formed as mixtures with the sulfides and selenides with excess H_2S and H_2Se respectively and their ^1H nmr and mass spectra were recorded as above. Alternatively, the germyl selenides and selenols were formed from the sulfides with H_2Se.

Cleavage Reactions of Chalcogermanes with Hydrogen Halides

Analysis of the $Me_nH_{3-n}Ge$— moiety in the chalcogenide species, viz. $(Me_nH_{3-n}Ge)_2E$, was accomplished by protolytic cleavage of the Ge—E bond with an excess of gaseous hydrogen bromide. Typically, $(MeH_2Ge)_2S$ (1.25 mmol) and HBr (3.12 mmol) were condensed *in vacuo* into a small ampule (ca. 25 ml equipped with a Teflon-in-glass stopcock) held at −196°C. The contents were subsequently allowed to warm to room temperature for ca. 20 min. Fractionation of the products at −95 and −196°C gave MeH_2GeBr (2.46 mmol, 98%; identified by ^1H nmr (2) and vibrational (3) spectroscopy) condensing in the former and a mixture of H_2S and unreacted HBr (identified by their infrared parameters (15)) in the latter. Similar reactions with other chalcogenides provided indirect evidence for the stoichiometric and monomeric nature of $(Me_nH_{3-n}Ge)_2E$.

Results and Discussion

Heavy metal salts (16–20), as well as lithium salts (21, 22) have been widely used in the conversion of halogenosilanes and germanes into the corresponding chalcogenides. We find that iodogermanes react with lithium sulfide, selenide and telluride in ether to give high yields (Table 1) of the chalcogenides [1]. The

[1] $2Me_nH_{3-n}GeI + Li_2E \rightarrow (Me_nH_{3-n}Ge)_2E + 2LiI$
(E = S, Se, Te; $n = 0 \rightarrow 3$)

corresponding reaction of mono- and dimethyliodogermane with lithium oxide does not go to completion at −78°C, but trimethyliodo- and trimethylbromogermane afford high yields of hexamethyldigermoxane at ambient temperature. It is interesting to note that we have observed rapid exchange (on the nmr time scale) in the systems $(Me_nH_{3-n}Ge)_2O$–$Me_nH_{3-n}GeX$ (X = Br, I). Thus, the ^1H nmr spectrum shows a single, well resolved resonance intermediate to the resonance positions of the pure compounds (a 1:1 mixture of $(Me_2HGe)_2O$ (δ (Me) 0.40, δ (GeH) 5.40 ppm) and Me_2HGeI (δ (Me) 1.08, δ (GeH) 4.12 ppm) gives a well resolved doublet-septet ^1H nmr spectrum: δ (Me) 0.78, δ (GeH) 5.17 ppm). This observation places some doubt on the reported conversions of H_3GeI to $(H_3Ge)_2O$ with HgO and of $(H_3Ge)_2O$ to H_3GeI with HgI_2 (18). We also examined the use of lead(II) oxide in these syntheses. In ambient temperature reactions without the use of solvent, lead(II) oxide provides facile

Can. J. Chem. Downloaded from www.nrcresearchpress.com by 210.87.254.105 on 09/05/12
For personal use only.

conversion of $Me_nH_{3-n}GeBr$ into $(Me_nH_{3-n}Ge)_2O$ in high yield. The corresponding reaction using $Me_nH_{3-n}GeI$ gives lower yields (ca. 35–60%) of $(Me_nH_{3-n}Ge)_2O$ and appreciable amounts of the decomposition by-product, methylgermane. By contrast, when iodo- and bromogermanes are passed as gases over PbO there is essentially no reaction. Bromogermanes do not react with PbS but there is partial conversion of iodogermanes into the corresponding sulfides. Nevertheless, the lower reactivity of iodogermanes towards PbS relative to Li_2S is also shown in the reactions with PbSe contrasted with Li_2Se.

However, it is essential that Li_2Se be prepared properly because, when Me_2HGeI is reacted with excess Li_2Se, where the samples still contain quantities of NH_3, Li_2NH, and $LiNH_2$ or when excess of selenium is used, a considerable reduction in the yield of bis(dimethylgermyl) selenide results with increased yields of the condensed selenide, $Me_2Ge(SeGeHMe_2)_2$ [2]. During the fractionation of these mixtures, a deposit of metallic selenium is observed with the evolution of a more volatile component, 1,1′,2,2′-tetramethyldigermane, $(Me_2HGe)_2$ (23) [3]. The latter reacts readily with hydrogen chloride or bromide without a catalyst according to reaction 4.

[2] $2(Me_2HGe)_2Se \rightarrow Me_2Ge(SeGeHMe_2)_2 + Me_2GeH_2$

[3] $Me_2Ge(SeGeHMe)_2 \rightarrow (Me_2HGe)_2 + (Me_2GeSe)_n + Se \qquad (n = 2, 3)$

[4] $2(Me_2GeH)_2 + 3HX \rightarrow Me_2HGeGeXMe_2 + (Me_2GeX)_2 + 3H_2 \qquad (X = Cl, Br)$

Pure samples of the chalcogermanes, in general, showed little evidence for condensation or elimination. However, increased condensation is observed in the telluro species, as is evident from the slow condensation of $(MeH_2Ge)_2Te$ at room temperature over an extended period of time. Moderate heating of

[5] $2(MeH_2Ge)_2Te \rightarrow MeHGe(TeGeH_2Me)_2 + MeGeH_3$

[6] $2MeGeH(TeGeH_2Me)_2 \rightarrow MeGe(TeGeH_2Me)_3 + MeGeH_2$

the condensed species in this instance leads to the elimination of tellurium and the formation of $(MeH_2Ge)_2$ (23). Similarly, condensation and elimination of tellurium are observed when tellurogermanes are sealed over extended periods (ca. 1 month) in cyclohexane solution.

The exchange reactions involving bis(trimethylsilyl) chalcogenides, viz. $(Me_3Si)_2E$ (E = S, Se, Te) and fluorogermanes, which occur in the absence of solvent, follow the general rule that the harder moiety (24*b*) prefers to be attached to silicon, so that the reactions to give Ge—S, Ge—Se and Ge—Te bonds are essentially quantitative. Attempts to prepare

[7] $(Me_3Si)_2E + 2Me_nH_{3-n}GeF \rightarrow (Me_nH_{3-n}Ge)_2E + 2Me_3SiF$

chalcogermanes by this method using the more readily available chlorides were unsuccessful because mixtures containing mixed species of the type $Me_3SiEGeMe_3$ were obtained.

The chalcogermanes are all colourless liquids with obnoxious odours. When the hydridic species are pure, they show little tendency to decompose when stored at ambient temperature. They are characterized by ^1H nmr, ir, Raman, and mass spectra and by reactions with anhydrous hydrogen halides, as well as hydrogen chalcogenides. The former cleaves the Ge—E bond quantitatively [8] to give well known compounds. Previous reports (24, 25) have shown

[8] $(Me_nH_{3-n}Ge)_2E + 2HBr \rightarrow 2Me_nH_{3-n}GeBr + H_2E$

that hydrogen sulfide and selenide react with either germylphosphine or -arsine to give $(H_3Ge)_2S$ and $(H_3Ge)_2Se$ via H_3GeSH and H_3GeSeH. These intermediates thio- and selenogermanes are also observed when digermoxane is treated with an excess of the hydrogen chalcogenide [9].

[9] $(H_3Ge)_2O + H_2E\,(\text{excess}) \rightarrow (H_3Ge)_2E + H_2O$, with H_3GeEH as intermediate

TABLE 3. The ^1H nmr parameters[a] of $(Me_nH_{3-n}Ge)_2E$ (E = O, S, Se, Te; $n = 0 \rightarrow 3$) species

Compound	δ(Me)	δ(GeH)	$\lvert J_{HH}^{vic}\rvert$	$\lvert J_{CH}\rvert$
$(H_3Ge)_2O$[b]	—	5.28	—	—
$(MeH_2Ge)_2O$[c]	0.59	5.28	2.91	129.1
$(Me_2HGe)_2O$[c,d]	0.40	5.40	2.43	128.2
$(Me_3Ge)_2O$[e]	0.29	—	—	125.9
$(H_3Ge)_2S$[f]	—	4.62	—	—
$(MeH_2Ge)_2S$	0.66	4.87	3.30	129.4
$(Me_2HGe)_2S$	0.54	4.93	2.91	129.0
$(Me_3Ge)_2S$[e]	0.51	—	—	127.5
$(H_3Ge)_2Se$[g]	—	4.23	—	—
$(MeH_2Ge)_2Se$	0.77	4.55	3.38	129.6
$(Me_2HGe)_2Se$	0.69	4.73	2.96	129.4
$(Me_3Ge)_2Se$[e]	0.58	—	—	128.4
$(H_3Ge)_2Te$[g]	—	3.59	—	—
$(MeH_2Ge)_2Te$[h]	0.93	4.12	3.53	132.6
$(Me_2HGe)_2Te$[h]	0.80	4.65	3.37	131.7
$(Me_3Ge)_2Te$[i]	0.71	—	—	129.1

[a]The spectra were recorded at ambient temperature in CCl_4 solution (ca. 5% v/v). Chemical shifts (δ ± 0.02 ppm) are in ppm to lowfield of Me_4Si as internal standard. Deviations for coupling constants are J(HH) ± 0.05 Hz, $J(^{13}CH)$ ± 0.2 Hz.
[b]See ref. 22.
[c]Compare with the values $(MeH_2Ge)_2O$ (δ(Me) 0.49, δ(GeH) 5.12 ppm) and $(Me_2HGe_2)_2O$ (δ(Me) 0.42, δ(GeH) 5.34 ppm) in ref. 28.
[d]Compare with δ(Me) 0.13, δ(GeH) 5.45 ppm (Et_2O solvent) in ref. 35.
[e]Compare with δ(Me) of $(Me_3Ge)_2E$ (CCl_4 solution) of 0.31 (O), 0.53 (S), 0.66 (Se) ppm in ref. 14.
[f]See ref. 25.
[g]See ref. 22, J(SeGeH) 12.1 Hz, J(TeGeH) 19.4 Hz.
[h]Recorded in C_6H_{12} (5% v/v).
[i]0.74 ppm (C_6H_6 solution) in ref. 36.

Can. J. Chem. Downloaded from www.nrcresearchpress.com by 210.87.254.105 on 09/05/12
For personal use only.

TABLE 4. The ir and Raman spectra (cm^{-1}) of the bis(methylgermanium)chalcogenides[a]

Tentative assignment		$(MeH_2Ge)_2O$		$(MeH_2Ge)_2S$		$(MeH_2Ge)_2Se$		$(MeH_2Ge)_2Te$	
		ir (gas)	Raman (liq)	ir (gas)	Raman (liq)	ir (gas)	Raman (liq)	ir (liq)	Raman (liq)
$\nu(CH_3)$	(a)	2997m	2990m,dp	2999m (2970)m	2988m,dp	2998m (2967)w	2987m,dp	2991m	2984m,dp
	(s)	2923w	2920s,p	2923m	2919s,p	2923w	2916s,p	2916m	2915ms,p
$\nu(GeH_2)$	(a)	2077sh	2071vs,p	2082vs		2078vs		2061vs	
	(s)	2057vs	2058m,p	2070vs	2060vs,p	2066vs	2057vs,p		2048vs,p
$\delta(CH_3)$	(a)	1418vw	1420w,dp	1420w	1416w,dp	1413w	1414w,dp	1409m	1407w,dp
	(s)	1259m	1248m,p	1262m	1243m,p	1263w	1240m,p	1238m	1238m,p
$\delta(GeH_2)$	(sc)	876s[b] 872vs[c]	875m,dp	873sh	871m,dp	873s	868m,dp	865s	865m,dp
$\rho(CH_3)$	(a)	840s	845wsh	852s		853s	848sh,p	832vs	837w
	(s)	800vs		831vs	823w	823vs	820w,dp	808vs	815w
$\delta(GeH_2)$	(wag)	725s	728w,dp	709s	708m,dp	698s	695m,dp	674s	677m,dp
	(tw)		661m,dp		632sh,dp		625sh,dp		ca. 619sh,dp
$\nu(GeC)$		610ms	610vs,p	605s	603vs,p	604s	602vs,p	595s	597s,p
$\rho(GeH_2)$		454vw	453m,p	445ms	461m,p	450w,br	451m,p	430m	429w,p
$\nu(Ge—E)$	(a)	901sh[b] (883)[c]	900sh,dp	409s	402m,dp			235ms	
	(s)	486m	501m,p	378vw	371vs,p		279vs,p		226vs,p
$\delta(C—Ge—E)$			236w		163ms,p		158ms,p		147s,p
$\delta(Ge—E—Ge)$			182m,p		101ms,p		84ms,p		77ms,p

[a]Spectra recorded at room temperature; m = medium, s = strong, w = weak, v = very, sh = shoulder, br = broad, ms = moderately strong, p = polarized, dp = depolarized.
[b]Gas.
[c]In CCl_4 solution.

Can. J. Chem. Downloaded from www.nrcresearchpress.com by 210.87.254.105 on 09/05/12
For personal use only.

TABLE 5. The ir and Raman spectra (cm^{-1}) of the bis(dimethylgermanium)chalcogenides[a]

Tentative assignment		$(Me_2HGe)_2O$		$(Me_2HGe)_2S$		$(Me_2HGe)_2Se$		$(Me_2HGe)_2Te$	
		ir (gas)	Raman (liq)	ir (gas)	Raman (liq)	ir (liq)	Raman (liq)	ir (liq)	Raman (liq)
$\nu(CH_3)$	(a)	2997s	2987m,dp	2987m	2988m,dp	2983s	2979m,dp	2982s	2978m,dp
	(s)	2926m	2918vs,p	2915m	2917vs,p	2914s	2915vs,p	2912s	2910s,p
$\nu(GeH)$		2040vs	2034vs,p	2042vs	2044s,p	2039vs	2044s,p	2036vs	2038s,p
$\delta(CH_3)$	(a)	1422m	1418m,dp	1410m	1412w,dp	1410m	1415w,dp	1408m	1414w,dp
	(s)	1255s	1247m,p	1248m	1244m,p	1238s	1246m,p	1236s	1241m,p
$\rho(CH_3)$	(a)	849s	847m,p	847s	852m,p	846vs	898w	839vs	843m,p
	(s)	805vs	800w	824vs	826w	820vs	820sh	819vs	820sh
	(a,s)	762m	758w	763m	752w	758m	751w	756m	752w
$\delta(GeH)$	(a)	702s	698m,dp	678s	683m,dp	668s	666m,dp	650s	650m,dp
	(s)	664w	634m,dp	662w	630m,dp	634w	630m,dp		625m,dp
$\nu(GeC)$	(a)	613s	609m,dp	607s	609m,dp	607vs	603m,dp	603s	601m,dp
	(s)	591s	593vs,p	587s	590vs,p	583s	587vs,p	579s	581s,p
$\nu(Ge—E)$	(a)	882s	883w,sh	410s	409m,dp	280s		234s	
	(s)	480m	485m,p		379vs,p		273vs,p		232vs,p
$\delta(C—GeC)$			250sh		198s,p		189m,p		188m,p
$\delta(C—Ge—E)$	(s)		214sh						
	(a)		193sh		162s,p		158s,p		152s,p
$\delta(Ge—E—Ge)$			169m,p		95m,p		76m,p		63m,p

[a]See footnote to Table 4.

Can. J. Chem. Downloaded from www.nrcresearchpress.com by 210.87.254.105 on 09/05/12
For personal use only.

This method is quite useful for the preparation of $(Me_nH_{3-n}Ge)_2E$ when stoichiometric quantities of H_2E and $(Me_nH_{3-n}Ge)_2O$ are used (26).

Characterization of the Chalcogermanes

The ^1H nmr spectra of the chalcogermanes provide the initial characterization of the species and confirmed their purity (>99% based on the absence of any other proton containing species). The chalcogermanes, $(Me_nH_{3-n}Ge)_2E$ give first-order spectra (Table 3) consistent with free rotation about the Ge—E bonds. The chemical shifts of the germyl and methyl protons show similar changes with substituent electronegativity as do the halogenogermanes $Me_nH_{3-n}GeX$. Thus, for any series, as E = O → S → Se → Te the GeH resonance moves to high field consistent with a decrease in inductive deshielding. The accompanying downfield shift in the Me resonance may be related to anisotropic factors (14). Satellites arising from interaction with ^{77}Se and ^{125}Te are observed, indicating there is no rapid exchange of germyl groups under these conditions.

The hydridic chalcogenols, H_3GeEH (E = S, Se) give long range, first-order coupling between the three hydrogen atoms attached to germanium and the lone hydrogen attached to the chalcogen atom. The resultant doublet-quartet pattern (intensity 3:1) has been observed previously (24*a*, 25, 27). H–H coupling is not observed in the case of Me_3GeEH nor is the longer range H–H coupling observed in Me_3GeE-GeH_3 (E = S, Se, Te), where the spectra show two singlet peaks (intensity 3:1) attributable to δ(Me) and δ(GeH).[2] The condensed chalcogermanes give simple first order spectra, similar to the parent analogues. Overlap of the resonances with those of the parent compounds allows only tentative assignments to δ(Me) and δ(GeH) as follows: $Me_2'Ge(SeGeHMe_2)_2$; δ(Me) 0.31, δ(GeH) 3.73, δ(Me') 0.37 ppm; $Me'H'Ge(TeGeH_2Me)_2$: δ(Me) ca. 0.93, δ(GeH) ca. 4.12, δ(Me') 1.53, δ(GeH') 5.75 ppm; $Me'Ge(TeGeH_2Me)_3$: δ(Me) ca. 0.93, δ(GeH) ca. 4.12, δ(Me') 2.13 ppm.

The vibrational spectra of $(Me_3Ge)_2E$ and $(H_3Ge)_2E$ where E = O, S, Se, Te have appeared elsewhere (18, 22, 29–32) so we will only concern ourselves with the intermediate species (Tables 4 and 5). Assignments of the vibrational modes in $(MeH_2Ge)_2E$ and $(Me_2HGe)_2E$ are based on the aforementioned chalcogermanes and related monohalogeno- and pseudohalogenogermanes (3, 4, 33).

General features in the spectra of the chalcogermanes, which are characteristic of the Ge—E—Ge linkage, appear as follows: Ge—E stretching (2 bands) at ca. 882 (ir) and 501–480m,p (Raman) [O]; ca. 410s (ir) and ca. 371vs,p (Raman) [S]; 280s (ir) and ca. 276vs,p (Raman) [Se]; 235m (ir) and ca. 229vs,p (Raman) [Te]. The Ge—E—Ge deformation mode is clearly observed in the Raman spectra of the chalcogermanes and the resulting trend of O > S > Se > Te is a direct consequence of the weight of the chalcogen atom. Thus for $(MeH_2Ge)_2E$ we observe a shift in the Ge—E—Ge deformation as follows: 182m,p [O]; 101ms,p [S]; 84ms,p [Se]; 77ms,p [Te] which is similar to that of the $(Me_2HGe)_2E$ series, viz. 169m,p [O]; 95m,p [S]; 76m,p [Se]; 63m,p [Te]. The methyl stretching and deformation modes are clearly observed in the expected 3000–2920 cm^{-1} and 1420–1240 cm^{-1} regions as are the Ge—H stretching modes at 2080–2030 cm^{-1}. The remainder of the assignments for the $Me_nH_{3-n}Ge$— moieties (i.e. ρCH_3, δGeH_2, ρGeH_2, δGeH) are comparable to the related monohalogeno and pseudohalogenogermanes (3, 4, 33).

The mass spectroscopic data for the chalcogermanes are complicated due to the presence of polyisotopic atoms and to the stripping of hydrogen from the hydridic species, viz. $(Me_nH_{3-n}Ge)_2E$, n = 0–2. Summation of the hydrogen loss for each fragment, however, greatly reduces the complexity of the problem, resulting in 'generalized' assignments. The mass spectra of the intermediate chalcogenides, viz. $(Me_nH_{3-n}Ge)_2E$, n = 1, 2 have been analyzed and are displayed in Tables 6 and 7. The molecular ion is present in all cases although in larger abundances for the monomethyl chalcogermanes. Fragmentation along the CGeEGeC skeleton affords large abundances of ions resulting from the loss of Me, $Me_nH_{3-n}Ge$ and $Me_nH_{3-n}GeE$. The most abundant ion in the dimethyl species is due to Me_3GeH_n (n = 0, 1) suggesting a migration of a methyl group from one germanium atom to the

TABLE 6. Ion clusters in the mass spectra of the bis(methylgermyl)chalcogenides[a]

Ion fragment	Relative abundance (%) E = O	E = S	E = Se	E = Te
$(Me_2H_nGe_2E)^+$	23.1	8.9	14.4	19.2
$(MeH_nGe_2E)^+$	33.3	11.8	14.5	15.8
$(Me_2H_nGe_2)^+$		17.0	14.2	4.0
$(H_nGe_2E)^+$	11.4		10.9	11.2
$(MeH_nGeE)^+$	13.4	12.4	12.6	25.0
$(Me_2H_nGe)^+$		17.5	—	—
$(H_nGeE)^+$	15.6		7.3	7.3
$(MeH_nGe)^+$		24.5	20.0	13.6
$(MeH_nGe_2)^+$	[b]	1.1	—	—
$(H_nGe_2)^+$	0.7	0.7	0.5	0.9
$(H_nGe)^+$	2.5	6.1	5.6	3.0

[a]The value of n is summed from 0 → 2 for Ge and 0 → 4 for Ge_2.
[b]$(MeH_nGe_2)^+$ may give some contribution to the $(H_nGe_2O)^+$ fragment but it is expected to be very small in abundance.

[2]J. E. Drake, B. M. Glavinčevski, and R. T. Hemmings. Unpublished results.

TABLE 7. Ion clusters in the mass spectra of the bis(dimethylgermyl)chalcogenides[a]

Ion fragment	Relative abundance (%) E = O	E = S	E = Se	E = Te
$(Me_4H_nGe_2E)^+$	8.8	5.3	8.2	9.0
$(Me_3H_nGe_2E)^+$	23.5	11.5	8.5	4.0
$(Me_4H_nGe_2)^+$		10.3	14.6	[b]
$(Me_2H_nGe_2E)^+$	8.8		1.8	3.7
$(MeH_nGe_2E)^+$	4.0	3.9	0.7	6.2
$(H_nGe_2E)^+$	4.7	2.8	4.9	5.3
$(Me_2H_nGeE)^+$	26.3	5.2	4.0	14.0
$(Me_3H_nGe)^+$		20.4	21.0	15.3
$(MeH_nGeE)^+$	11.4	3.6	3.0	12.8[b]
$(Me_2H_nGe)^+$		19.8	17.1	15.6
$(H_nGeE)^+$	11.0		1.5	1.9
$(MeH_nGe)^+$		13.7	12.4	9.6
$(H_nGe)^+$	1.5	3.5	2.3	2.6

[a]The value of n is summed from $0 \rightarrow 1$ for Ge and $0 \rightarrow$ for Ge_2.
[b]Contribution summed with $(MeH_nGeE)^+$.

other. A similar rearrangement is not observed in the methylseleno and -telluro derivatives but could occur in the oxides and sulfides where the overlapping of fragments makes such an assignment speculative. The $(C_2H_nGe_2)^+$ and $(C_4H_nGe_2)^+$ fragments observed in the spectra of $(MeH_2Ge)_2Se$ and $(Me_2HGe)_2E$, where E = Se, Te, result from the effective elimination of the central chalcogen atom. For the other species in Tables 6 and 7, the *m/e* values of these fragments overlap those of other probable molecular ions. The elimination of the central atom now appears to be a common feature in the cleavage of silyl and germyl Group V and VI species (*1*, 34).

Acknowledgements

We wish to thank the National Research Council of Canada for financial support and Allan J. F. Clark for helpful discussions.

1. J. E. DRAKE, R. T. HEMMINGS, and H. E. HENDERSON. J. Chem. Soc. Dalton, 366 (1976).
2. J. E. DRAKE, R. T. HEMMINGS, and C. RIDDLE. J. Chem. Soc. (A), 3359 (1970).
3. G. K. BARKER, J. E. DRAKE, R. T. HEMMINGS, and B. RAPP. J. Chem. Soc. (A), 3291 (1971); Spectrochim. Acta, **28A**, 1113 (1972).
4. G. K. BARKER, J. E. DRAKE, and R. T. HEMMINGS. Can. J. Chem. **52**, 2622 (1974).
5. H. J. EMELÉUS and L. E. SMYTHE. J. Chem. Soc. 609 (1958).
6. E. A. V. EBSWORTH, M. ONYSZCHUK, and N. SHEPPARD. J. Chem. Soc. 1453 (1958).
7. H. J. EMELÉUS, A. G. MADDOCK, and C. REID. J. Chem. Soc. 1353 (1941).
8. J. W. ANDERSON, G. K. BARKER, J. E. DRAKE, and R. T. HEMMINGS. Synth. Inorg. Metalorg. Chem. **3**, 125 (1973).
9. G. R. WAITKINS and R. SHUTT. Inorg. Synth. **2**, 183 (1946).
10. A. TIAN and S. AUBANEL. Compt. Rend. Trav. Faculte Sci. Marseille, **1**, 97 (1942).
11. T. R. ALLKINS and P. J. HENDRA. Spectrochim. Acta, **22**, 2075 (1966).
12. E. A. V. EBSWORTH and S. G. FRANKISS. Trans. Faraday Soc. **63**, 1574 (1967).
13. H. SCHMIDBAUR. J. Am. Chem. Soc. **85**, 2336 (1963).
14. H. SCHMIDBAUR and I. RUIDISCH. Inorg. Chem. **3**, 599 (1964).
15. R. H. PIERSON, A. N. FLETCHER, and E. S. C. GANTZ. Anal. Chem. **28**, 1218 (1956).
16. K. BURSCHKIES. Chem. Ber. **69**, 1143 (1936); C. W. N. CRUMPER, A. MELNIKOFF, and A. I. VOGEL. J. Chem. Soc. (A), 242 (1966); J. SATGÉ and M. LESBRE. Bull. Soc. Chim. Fr. 2578 (1965).
17. T. N. SRIVASTAVA, J. E. GRIFFITHS, and M. ONYSZCHUK. Can. J. Chem. **40**, 739 (1962).
18. S. SUJISHI. XVIIth Int. Congr. Pure Appl. Chem. Munich, 1959 Abstr. p. 53; T. D. GOLDFARB and S. SUJISHI. J. Am. Chem. Soc. **86**, 1679 (1964).
19. H. J. EMELÉUS, A. G. MACDIARMID, and A. G. MADDOCK. J. Inorg. Nucl. Chem. **1**, 194 (1955); H. J. EMELÉUS, M. ONYSZCHUK, and W. KUCHEN. Z. Anorg. Chem. **283**, 74 (1956); H. J. EMELÉUS and L. E. SMYTHE. J. Chem. Soc. 609 (1958); L. G. L. WARD and A. G. MACDIARMID. J. Inorg. Nucl. Chem. **21**, 287 (1961).
20. R. S. STOBART and P. C. ANGUS. J. Chem. Soc. Dalton Trans. **22**, 2342 (1975).
21. H. BÜRGER and U. GOETZE. Inorg. Nucl. Chem. Lett. **3**, 549 (1967).
22. S. CRADOCK, E. A. V. EBSWORTH, and D. W. H. RANKIN. J. Chem. Soc. (A), 1628 (1969).
23. R. D. GEORGE and K. M. MACKAY. J. Chem. Soc. (A), 2122 (1969).
24. (*a*) J. E. DRAKE and C. RIDDLE. J. Chem. Soc. (A), 1573 (1969); (*b*) R. G. PEARSON. J. Am. Chem. Soc. **85**, 3533 (1963).
25. J. E. DRAKE and C. RIDDLE. J. Chem. Soc. (A), 2710 (1968).
26. J. E. DRAKE, B. M. GLAVINČEVSKI, and H. E. HENDERSON. Inorg. Nucl. Chem. Lett. Pt. I, **13**, 565 (1977).
27. C. GLIDEWELL, D. W. H. RANKIN, and G. M. SHELDRICK. Trans. Faraday Soc. **65**, 1409 (1969).
28. V. F. MIRONOV, L. N. KALININA, E. M. BERLINER, and T. K. GAR. Zh. Obshch. Khim. **40**, 2597 (1970).
29. A. MARCHAND, M-T. FOREL, M. LEBEDEFF, and T. VALADE. J. Organomet. Chem. **26**: 69 (1971).
30. J. RUIDISCH and M. SCHMIDT. J. Organomet. Chem. **1**, 160 (1963).
31. H. SCHUMANN, R. MOHTACHEMI, H.-J. KROTH, and U. FRANK. Chem. Ber. **106**, 1555 (1973); **106**, 2049 (1973).
32. S. CRADOCK. J. Chem. Soc. (A), 1426 (1968).
33. J. E. DRAKE and R. T. HEMMINGS. Can. J. Chem. **51**, 302 (1973).
34. S. CRADOCK, E. A. V. EBSWORTH, G. DAVIDSON, and L. A. WOODWARD. J. Chem. Soc. (A), 1229 (1967); C. GLIDEWELL, and D. W. H. RANKIN. J. Chem. Soc. (A), 753 (1969).
35. A. R. DAHL, C. A. HEIL, and A. D. NORMAN. Inorg. Chem. **10**, 2562 (1975).
36. H. SCHUMANN, R. MOHTOCHEMI, H. J. KROTH, and U. FRANK. Chem. Ber. **106**, 2049 (1973).

Can. J. Chem. Downloaded from www.nrcresearchpress.com by 210.87.254.105 on 09/05/12
For personal use only.

Flow nuclear magnetic resonance study of the addition, dehydration, and cyclization steps for reaction between hydrazine and ethyl acetoacetate[1]

MICHAEL COCIVERA, KYU W. WOO,[2] AND PETER LIVANT[3]

Guelph-Waterloo Centre for Graduate Work in Chemistry, University of Guelph, Guelph, Ont., Canada N1G 2W1

Received August 18, 1977

MICHAEL COCIVERA, KYU W. WOO, and PETER LIVANT. Can. J. Chem. **56**, 473 (1978).

The proton nuclear magnetic resonance spectra of a reaction mixture of hydrazine and ethyl acetoacetate (EAA) in aqueous solution under flowing and stopped-flow conditions provides kinetic information concerning the rapid addition step to form the carbinolamine (CA) intermediate and the slower dehydration and cyclization steps to form the *anti* hydrazone and 3-methylpyrazol-5-one, respectively. The addition step was studied while flowing at rates faster than the dehydration and cyclization rates so that no product signal was observed. Under these conditions, a broad signal resulting from the coalescence of the CH_3 proton resonances of EAA and CA is observed. Analysis of the line shape of this broad signal yields the addition rate constant, which has a value that appears to be p*H* dependent and is of the order of $10^3\ M^{-1}\ s^{-1}$. Stopped-flow spectra provide the time dependence for the reactant and product signals. Analysis of these time dependences provides information concerning the mechanism of product formation. In contrast with hydroxylamine, CA appears to undergo dehydration and cyclization at comparable rates in the p*H* range, 8.8–9.2 when hydrazine is the nucleophile. In addition, the *anti* hydrazone cyclizes at an appreciable rate. These intramolecular cyclization rates are compared with the intermolecular values.

MICHAEL COCIVERA, KYU W. WOO et PETER LIVANT. Can. J. Chem. **56**, 473 (1978).

Les spectres de résonance magnétique nucléaire du proton du mélange réactionnel de l'hydrazine et de l'acétoacétate d'éthyle (AAE) en solution aqueuse dans des conditions de flux et de flux stoppé fournissent de l'information cinétique concernant l'étape d'addition rapide pour former l'intermédiaire carbinolamine (CA) et les étapes plus lentes de déshydratation et de cyclisation formant respectivement l'hydrazone *anti* et la méthyl-3 pyrazolone-5. On a étudié l'étape d'addition alors que les vitesses d'écoulement étaient plus grandes que les vitesses de déshydratation et de cyclisation de façon à ce que l'on n'observe aucun signal de produit. Dans ces conditions, on observe un signal large provenant de la coalescence des résonances des protons CH_3 de l'AAE et du CA. L'analyse des formes des raies de ce signal large fournit la constante de vitesse de l'addition qui a une valeur qui semble dépendre du p*H* et qui est de l'ordre de $10^3\ M^{-1}\ s^{-1}$. Le spectre à flux stoppé fournit une relation en fonction du temps pour les signaux des réactifs et des produits. Une analyse de ces fonctions fournit de l'information concernant le mécanisme de la formation du produit. Par opposition avec l'hydroxylamine, il semble que, si l'hydrazine agit comme nucléophile, la CA subit des réactions de déshydratation et de cyclisation avec des vitesses qui sont comparables à des p*H* allant de 8.8–9.2. De plus l'hydrazone *anti* se cyclise à une vitesse élevée. On compare ces vitesses de cyclisation intramoléculaire avec les valeurs intermoléculaires.

[Traduit par le journal]

Introduction

By means of nuclear magnetic resonance spectroscopy of flowing liquids, it was possible to measure directly the rates for the addition, dehydration, and cyclization steps for the reaction between hydroxylamine and ethyl acetoacetate (EAA) (1). At p*H* 6.5 and above, the addition step to form the carbinolamine intermediate CA is much faster than the dehydration of this intermediate, permitting its detection and the measurement of the rate of addition by means of nmr line shape analysis. It was also found that cyclization of CA was not competitive with dehydration to form the *syn* and *anti* oximes. The *syn* isomer subsequently cyclizes to form 3-methylisoxazol-5-one at an appreciable rate whereas the conversion of the *anti* isomer is substantially slower. In the present paper, we report the results of a study of the reaction between hydrazine (HYD) and EAA. Hydrazine offers an interesting comparison with hydroxylamine since the intramolecular addition to the acyl carbonyl, which follows the formation of CA, involves nitrogen rather than oxygen. Unlike the hydroxylamine case, the cyclization of the CA intermediate formed from HYD appears to be competitive with the dehydration step, and no *syn* hydrazone is detected. Furthermore,

[1]This study was supported in part by The National Research Council of Canada.

[2]Present address: Department of Chemistry, EWHA Women's University, Seoul, Korea.

[3]Present address: Department of Chemistry, Auburn University, Auburn, Alabama, U.S.A.

Can. J. Chem. Downloaded from www.nrcresearchpress.com by 210.87.254.40 on 09/05/12
For personal use only.

Can. J. Chem. Downloaded from www.nrcresearchpress.com by 210.87.254.40 on 09/05/12
For personal use only.

the *anti* isomer converts to the cyclic product, 3-methylpyrazol-5-one (MPY) at an appreciable rate. Since the *anti* isomer must first convert to the *syn* form before cyclizing and since no *syn* isomer is detected, the rate of cyclization of the *anti* isomer is equal to the rate of conversion of *anti* into *syn* isomer. In addition, the intramolecular addition of nitrogen to the acyl carbonyl proceeds faster than the intermolecular process.

Experimental

All chemicals except acetoacetamide were obtained from suppliers. Ethyl acetoacetate and hydrazine were distilled before use. The buffers were used without additional purification. Acetoacetamide was prepared from diketene according to the procedure used to prepare *p*-fluoroacetoacetanilide (2). This procedure was modified slightly in that the temperature was maintained between -35 and -30°C and a slight excess of diketene was used. The yield of amide was 91%, and after recrystallizing from acetone – petroleum ether, the melting point was 54–55°C. The kinetic method involved measurement of the proton nmr spectra at 100 MHz and 30.0 ± 0.3°C under static and flowing conditions using a Varian HA-100-15 equipped with a flow system as described earlier (3). The rate constant k_n for the addition step was obtained by analysis of the line shape of signals in spectra obtained while the liquid was flowing. The rate of decomposition of the tetrahedral intermediate to form products and growth of products was obtained from the time dependence of the spectra measured after the flow had been stopped. For these cases, the reaction mixture was made by mixing equal volumes of an aqueous ethyl acetoacetate and an aqueous hydrazine solution at an ionic strength of 1.0 (KCl).

The equilibrium constant K_n for the addition step was determined from the uv absorbance decrease measured with a Cary 118 when equal volumes of hydrazine and ethyl acetoacetate were mixed under the same conditions as the nmr kinetic measurements. A flow system was used for this measurement. The p*H* of the solutions was measured using a Radiometer PHM 63 digital p*H* meter with an accuracy of ± 0.02 unit. The p*H* of the reaction mixture was measured as a function of time at 5-s intervals immediately after mixing. This interval was expanded to several minutes as the reaction progressed.

Results

Sample spectra obtained under static and flowing conditions at 30°C are illustrated in Fig. 1. The spectrum labeled EAA illustrates only the proton resonance of the carbonyl CH_3 of EAA (for reference) obtained under static conditions without spinning for an aqueous solution containing 0.2 *M* EAA and 0.2 *M* diazabicyclooctane DABCO at p*H* 9.0. The complete spectrum of EAA under similar conditions has been reported earlier (1). The spectrum labeled FLOW was obtained by mixing the EAA solution with an equal volume of an aqueous solution of 0.8 *M* HYD at a flow rate of 20 ml/min. The STOP spectrum was obtained just after the flow had been stopped and the spectrum at the end of the reaction is labeled FINAL. The assignment of the

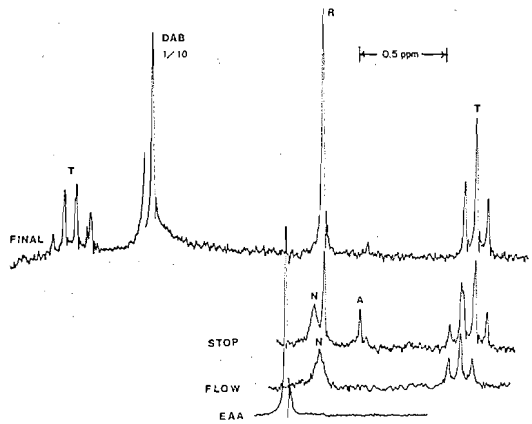

FIG. 1. Proton nmr spectra of aqueous solutions at p*H* 9.0 obtained at 100 MHz and 30°C under static and flowing conditions without spinning. Only the portion of the spectral range upfield from the water signal, which is used as the lock signal, is illustrated. The EAA spectrum is the keto CH_3 resonance of 0.20 *M* EAA. The flow spectrum was obtained after mixing the EAA solution with 0.8 *M* HYD (total). The stop spectrum was obtained immediately after stopping the flow. The final spectrum was recorded after the anti hydrazone had disappeared. For the assignment of the resonances, see the text.

signals is analogous to that given previously for the reaction of hydroxylamine with EAA (1). Thus, the triplet and quartet labeled T are due to ethanol (CH_3 and CH_2 protons, respectively); and the signals labeled R and A are due to the CH_3 protons of 3-methylpyrazol-5-one (MPY) and *anti* hydrazone of EAA, respectively. The triplets due to the ethoxy CH_3 protons of EAA and the isomeric hydrazones have identical chemical shifts (at the same position as the triplet illustrated in the flow spectrum). The signal due to DABCO (labeled DAB) was recorded at 1/10 the gain used for the rest of the spectrum. As in the case of the reaction of EAA with hydroxylamine (1), the broad signal labeled N is a coalescence of two CH_3 proton resonances, one due to EAA and the other due to the carbinolamine CA formed by the addition of HYD to the keto carbonyl carbon of EAA. Thus, in the flow spectrum obtained after mixing, the EAA signal is not observed in its original position and, instead, has moved upfield and merged with the CA signal because the equilibrium, EAA + HYD $\rightleftharpoons$ CA, is rapid on the nmr time scale (4). Consequently, although the forward and reverse rates for this equilibrium are too fast relative to the flow rates employed, they may be obtained by analysis of the line shape of N, which is related to the average lifetime τ for exchange between the CH_3 protons of EAA and those of CA (4).

The value for τ is calculated using the equation for fast exchange between two sites (4), $\Delta = p_1 p_2 \delta^2 \tau$. In the present case, the CH_3 protons are exchanging as

Can. J. Chem. Downloaded from www.nrcresearchpress.com by 210.87.254.40 on 09/05/12
For personal use only.

a group between the EAA and the CA environments. Consequently, p_1 and p_2 represent the proton fractions of the carbonyl CH_3 protons of EAA and CA, respectively, and δ is the chemical shift between the signals due to these two types of protons. For pH values of 9.0 or greater the proton fractions are calculated from the initial concentrations of EAA and HYD using K_n, the equilibrium constant for the equilibrium, EAA + HYD $\rightleftharpoons$ CA, which was determined to have a value of 0.50 M^{-1} based on the decrease in uv absorbance measured when an EAA solution was mixed with a HYD solution in a flow system. Below pH 9.0, the protonation of HYD and CA has been taken into account in the calculation of the proton fractions. This was done by considering the following equilibria to calculate the equilibrium concentrations of all the species indicated:

$$NH_2NH_3^+ \underset{H^+}{\overset{-H^+}{\rightleftharpoons}} NH_2NH_2 + EAA \overset{K_n}{\rightleftharpoons} CA \underset{-H^+}{\overset{H^+}{\rightleftharpoons}} CAH^+$$

For this purpose, 8.20 was used as the pK_a for hydrazine at 1.0 ionic strength (5). Although the pK_a for CAH^+ could not be measured, it is estimated to be 7.3, (the pK_a value of the more basic of the two possible types of protonated species), based on the values for hydrazine and 1,2-dimethylhydrazine (6) and correcting for substituent effects as discussed below. By suitable combination of all of the equilibrium constant expressions, equilibrium concentrations may be specified at any pH for given total concentrations of HYD and EAA. In practice, these calculations were programmed conveniently on an HP-65 calculator.

At pH 8.5, the extent of protonation is small so that the proton fraction for the intermediate is almost the same as that at higher pH for solutions containing the same initial concentrations of reactants. However, below this pH, protonation becomes more important, and the proton fraction of the intermediate decreases. The extent of this decrease depends on the interpretation of the details of the exchange, i.e. does the exchange with EAA involve either CA alone or CA plus CAH^+? For the former, the proton fraction of the intermediate is obtained from the concentration of CA; for the latter, it is obtained from the sum of the concentrations of CA and CAH^+. We conclude that the exchange involves the latter because the equilibrium between CA and CAH^+ is probably much faster than the one between EAA and the intermediate (CA and/or CAH^+). This conclusion is based on the following considerations. Acid–base proton transfer reactions have second-order rate constants of about 5×10^8 s^{-1} M^{-1} (7). In addition to CA and CAH^+, the solution contains the acid and base forms of the buffer and HYD, all of which can undergo proton transfer reactions with CA and CAH^+. Consequently since the concentration for acid and for base is at least 0.1 M, the lifetime for conversion of CA to CAH^+ is estimated to be about 2×10^{-8} s, which is about 4 orders of magnitude smaller than the lifetime for exchange between EAA and the intermediate (see below). Thus, the CH_3 signals due to CA and CAH^+ are coalesced and the exchange between EAA and the intermediate reduces to a two-site process in which the proton fraction for the intermediate p_I is obtained from the sum of the concentrations of CA and CAH^+. The rest of the calculation to obtain τ is the same as that used for the higher pH solutions, except that the chemical shift δ is slightly lower than the value at higher pH (90 Hz vs. 96 Hz). The value for the chemical shift of the intermediate is obtained by determining the position of the coalescence signal as a function of HYD concentration when the EAA concentration is held constant, as has been described previously (3*a*).

For each run, the value for Δ (in rad s^{-1}) is obtained from the line width of the coalescence signal by subtracting out the weighted average of the line widths in the absence of exchange for the signals due to each of the two CH_3 groups that are involved in the exchange. This line width for the CH_3 group of EAA is obtained in the absence of HYD. For the CH_3 group of CA, this line width could not be measured directly because the exchange rate could not be slowed sufficiently. Consequently, it was assumed to be the same as that for the CH_3 signal of the structurally similar carbinolamine derived from acetaldehyde (8). To account for any changes due to field homogeneity or flow rate from one run to the next, the line widths were related to the one for the CH_3 signal of methanol, which was present in all kinetic runs.

The forward k_n and reverse k_{-n} rate constants for the equilibrium are obtained from the equilibrium constant K_n and the exchange rate $1/\tau$, which is related to τ_E, the average lifetime for the CH_3 protons at the EAA site by the expression, $1/\tau_E = p_I/\tau$. Thus, since $1/\tau_E = k_n[NH_2NH_2]$ in which $[NH_2NH_2]$ is the equilibrium concentration of HYD free base, k_n may be calculated, and values are listed in Table 1 for various conditions of pH and concentration. Values for k_{-n} are not listed in the table because they are not obtained independently, i.e. k_{-n} is calculated using k_n and K_n.

Each value of k_n listed in Table 1 is an average of at least three measurements with a precision of $\pm 20\%$. For each pH, k_n appears to be independent of buffer concentration since the values do not vary

Can. J. Chem. Downloaded from www.nrcresearchpress.com by 210.87.254.40 on 09/05/12
For personal use only.

TABLE 1. Rate constants for the formation and decomposition of the tetrahedral intermediate and the formation of MPY from *anti*-hydrazone in the presence of various concentrations of buffer and hydrazine at 30°C in aqueous solutions containing 0.1 *M* EAA after mixing[a]

p*H*		[Buffer][b] (*M*)	[NH_2NH_2][c] (*M*)	$k_n \times 10^{-3}$ ($M^{-1}s^{-1}$)	$k_I \times 10^2$ (s^{-1})	$k_{ac} \times 10^3$ (s^{-1})
7.5	Phos[d]	0.2	0.2		58	
			0.5		45	
8.0	Imid[e]	0.5	0.2		16	
			0.5		17	
8.5	DABCO[f]	0.2	0.2	2.7	5.1	
			0.3		6.6	
			0.4	3.3	8.4	
			0.5	2.9		
			0.6	3.7		
8.8	DABCO	0.2	0.2	1.9	5.2	3.9
		0.3		1.2	7.4	5.2
		0.4		1.2	8.8	
		0.5		1.7	8.7	
		0.2	0.3	1.7	5.7	4.8
			0.4	1.5	5.4	
	Boric[g]	0.2	0.2	1.3	4.6	3.0
		0.3		1.3	5.7	
		0.4		1.3	6.9	
		0.5		1.4	6.9	
9.0	DABCO	0.1	0.2	1.1	6.1	
		0.2		1.3	3.8	3.6
		0.3		1.3	7.1	4.1
		0.4		1.4	7.1	3.8
		0.5		1.3		
		0.2	0.1	1.5	5.9	
			0.3	1.2	4.7	
			0.4	1.2	4.2	
			0.5	1.3		
9.2	DABCO	0.2	0.2	1.2		3.9
			0.3	1.4	4.4	4.4
			0.4	1.2	4.3	6.0
	Boric	0.2	0.2	1.0	5.8	3.6
		0.3		0.8	4.2	4.0
		0.4		1.0		
		0.5		0.9	6.2	

[a]See text for details of the calculation of rate constants using either the time dependence of the signal intensities or line width measurements.
[b]Approximate total concentration after mixing, includes all degrees of protonation. The exact values deviated by no more than ± 10% from those indicated in the table.
[c]Approximate total initial concentration after mixing, includes all degrees of protonation. The exact values, which were used in all calculations, deviated by no more than ± 10% from those indicated in the table.
[d]Sodium phosphate buffer.
[e]Imidazole buffer.
[f]Diazabicyclooctane buffer.
[g]Boric acid buffer.

systematically and the differences are within experimental error. A similar result was found previously for the addition of hydroxylamine to EAA (1). On the other hand unlike the hydroxylamine case, k_n appears to be p*H* dependent, increasing approximately linearly as the hydronium ion concentration increases. For the hydroxylamine reaction, the absence of buffer and hydronium ion catalysis was considered to be evidence in favor of a rate limiting addition step to form the zwitterion $CA^{\pm}$ which rapidly converts to CA. For the HYD reaction, the results do not give a clear indication of the mechanistic details since the buffers do not catalyze the exchange process but the exchange rate increases with hydronium ion concentration. Unfortunately the p*H* range over which the p*H* effect is tested is small because the EAA CH_3 signal in the absence of HYD broadens for p*H* values larger than 9.2. Furthermore below p*H* 8.5, the contribution to the line width made by the EAA–CA exchange process is insufficient for accurate measurement because the small value for K_n coupled with protonation of HYD makes the proton fraction of the intermediate very small. In fact the results at p*H* 8.5 are somewhat marginal since Δ is not the dominant contribution to the line width. For example for 0.8 *M* HYD, the

Can. J. Chem. Downloaded from www.nrcresearchpress.com by 210.87.254.40 on 09/05/12
For personal use only.

largest concentration, Δ is 5.3 rad s^{-1} while the total line width is 12.0 rad s^{-1}. Consequently, the hydronium ion dependence must be considered somewhat tentative.[4] A test of the p*H* dependence for HYD addition is planned for another ketone for which K_n is appreciably larger.

The evaluation of rate constants for the formation of products from the time dependence of the coalescence signal depends upon the mechanism proposed. For the reaction of EAA with hydroxylamine, the mechanism appears to involve dehydration of the carbinolamine to form the *syn* and *anti* oximes with subsequent cyclization of the *syn* isomer (1). Cyclization via the *anti* isomer is substantially slower, and after the *syn* isomer has completely disappeared the cyclic compound and the *anti* oxime are present in about equal amounts. However in the present case with hydrazine as the nucleophile, no *syn* isomer is observed, and the *anti* isomer decays at an appreciable rate, indicating two possibilities: (*a*) dehydration of CA is faster than cyclization, and in the sequence CA → *syn* → MPY, the formation of *syn* is rate limiting; (*b*) same as *a* except CA → MPY is an additional path. To decide between these two possibilities, it is necessary to know the relative rates of formation of the *syn* and *anti* isomers. Since the cyclization step(s) cannot be slowed sufficiently to allow direct measurement of these rates, the following approach has been employed. The relative rates of formation of *syn* and *anti* hydrazones of acetoacetamide AAM were measured and assumed to be identical to those for EAA. If mechanism *a* obtains, this ratio should be identical to the ratio of MPY to *anti* isomer since all the *syn* isomer converts to MPY. For this purpose, the initial ratio of MPY to *anti*, which is obtained by extrapolation back to zero time, was used since the *anti* isomer also converts to MPY. For measurements between p*H* 8.8 and 9.2, this ratio is 1.1 ± 0.2. On the other hand, the ratio is 0.55 ± 0.03 for the hydrazones of AAM. Since the difference between these two ratios is well outside of experimental error and since mechanism *a* cannot account for this difference, it seems likely that mechanism *b* obtains, i.e. the cyclization of the carbinolamine of EAA is competitive with the dehydration step. Estimation of the rate constant for this cyclization step will be discussed below.

One question which must be considered concerns the validity of equating the ratio of rates obtained for EAA to that obtained for AAM. Fortunately, this approach can be tested with the oximes of EAA and AMM since the rate of conversion of *anti* oxime to cyclic compound is very slow in both cases, and cyclization via CA does not appear to occur for EAA (1). The ratio of rates of formation of *syn* vs. *anti* oxime was found to be identical for EAA and AAM, namely, 0.91 (1) and 0.92, respectively, at p*H* 7.0 in the presence of 0.3 *M* imidazole.

Since it appears that the carbinolamine intermediate cyclizes and dehydrates at comparable rates, the mechanism illustrated in Scheme 1 is proposed[5,6]. According to Scheme 1, the cyclic compound is formed only via intermediate CA whereas the *syn* and *anti* hydrazones are formed via intermediates CA and CAH_2^+. Cyclization via intermediate CAH_2^+ is expected to be slower than the other route since the nitrogen that is to add has no nonbonded electron pairs. On the other hand, a more complex reaction involving cyclization of CAH_2^+ after intramolecular proton transfer to the acyl carbonyl oxygen cannot be precluded. However, inclusion of this possibility makes only a minor alteration in the form of the rate expression as discussed below. Dehydration and cyclization via intermediate CAH_1^+ is assumed to occur more slowly than via the other two intermediates because the protonation is expected to make both nitrogens less electron donating. However, including this possibility does not alter the general form of the rate expression. The rate expression, which was derived to describe the rate of change of the total concentration of EAA according to this scheme, is

$$[1]\quad \frac{-d[EAA]_\Upsilon}{dt} = \frac{(k_d + k_d^+[H^+]/K_{a1} + k_c)K_n[N][EAA]_\Upsilon}{1 + K_n[N](L[H^+] + 1)}$$

in which the subscript d denotes dehydration to both *syn* and *anti* hydrazones, subscript Υ denotes total concentration, the superscript + denotes reaction via CAH_2^+, [N] is the equilibrium concentration of HYD free base, and $L = 1/K_{a1} + 1/K_{a2}$ in which the subscripts 1 and 2 denote CAH_1^+ and CAH_2^+,

[4]As pointed out by one of the referees, the p*H* dependence observed for k_n would require a very large third-order rate constant. In view of the possible error associated the results at p*H* 8.5, the reliability of this rate constant may be questionable.

[5]Although the reaction is written as stopping at MPY, MPY may, in fact, tautomerize to give the heterocyclic enamine. Since the ring CH proton resonance is not observed, we cannot determine whether most of the MPY converts to the enamine or only part of it does and the ring CH proton resonance is not observed because it is too broad due to rapid equilibration between the two tautomers.

[6]An intramolecular proton switch resulting in direct conversion of $CA^\pm$ to CA may also occur (see ref. 9) although we estimate that the intermolecular protonation may be somewhat faster in the present study since appreciable quantities of general acids are present.

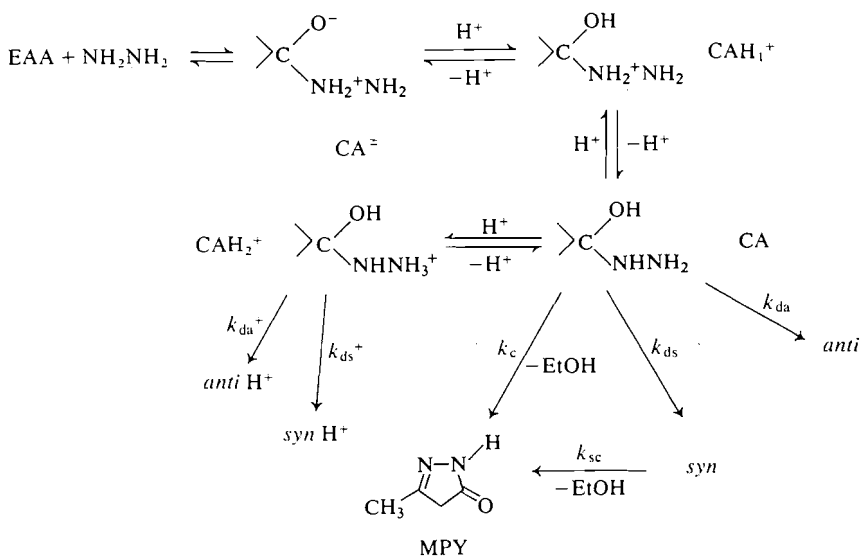

SCHEME 1

respectively. The values for pK_{a1} and pK_{a2} are estimated to be 7.3 and 5.1, respectively, in the following manner.[7] For CAH_1^+ and CAH_2^+, 1,2-dimethylhydrazine (6) and hydrazine, respectively, are used as models and adjusted for substituent effects using σ^* values (10) and a ρ^* value of about -3 (11). For CAH_1^+, $\Delta pK = -2.45$ based on σ^* values of 0.555 for the HO—C group (10) and 0.26 estimated for the EtOOC—C—C group using the value for COOMe (10) and allowing that $\sigma_X = 2.8\sigma_{XCH_2}$ (12). For CAH_2^+, the σ^* values were estimated from those given above and assuming that the relation $\sigma_X = 2.8\sigma_{XCH_2}$ holds when the CH_2 group is replaced by the isoelectronic NH group, and ΔpK is estimated to be -0.88. In practice the sum of the rate constants, $k_d + k_d^+[H^+]/K_{a1} + k_c$, is calculated by a linear least-squares fit of the logarithm of the intensity of the coalescence signal vs. $K_n[N]t/[1 + K_n[N](L[H^+] + 1)]$ in which t is the time in seconds and [N] is determined at each t using the appropriate equilibrium constants and the total concentrations of HYD and EAA, which have been adjusted for product formation. The accuracy of this method of calculation was tested by using it to calculate the rate constant from data for the time dependence of $[EAA]_T$ that had been simulated by an incremental method using eq. 1 and specified rate constants. For this purpose, the incremental method was programmed for a HP 25 calculator to give $[EAA]_T$ and [N] for various time intervals, and it was found that time increments of 2 s or less give an accurate measure of dt. For all simulations, time increments of 0.5 s were used. It was found that the least-squares procedure gives a calculated rate constant that is always larger than the specified 'real' value and that this deviation depends upon the extent to which the concentration of one reactant exceeds that of the other. Thus, when the initial concentration of EAA is held constant at 0.1 M, the percentage error in the accuracy of the rate constant is 24.9, 10.3, and 6.0% for initial HYD concentrations of 0.1, 0.2, 0.4 M, respectively. In principle, the values calculated by the least-squares method could be corrected for this systematic error. However, the precision of the data does not warrant this correction, and the uncorrected first-order rate constants are reported as k_1 in Table 1. In addition, with the exception of one value, all the results reported in this table are derived from solutions for which the concentration of HYD is at least a factor of two larger than that for EAA so that the systematic error due to the method of calculation is 10% or less.

The values listed in Table 1 are for the sum of the rate constants, $k_d + k_d^+[H^+]/K_{a1} + k_c$. As mentioned above, product formation via CAH_1^+ and cyclization via CAH_2^+ have been neglected. Including these possibilities merely adds more terms to this sum but does not change the other parts of the rate expression and, therefore, does not alter the values in the table. The data in Table 1 do not give a clear indication concerning catalysis by the buffers. On the other hand, the rate constant k_1 increases as the initial pH is lowered from 8.5 to 7.5. Unfortunately, below pH 8.8 there is an appreciable decrease in pH during the reaction and any quantitative treatment of the pH dependence of k_1 is precluded. For

[7]We are grateful to one of the referees for pointing out this method.

Can. J. Chem. Downloaded from www.nrcresearchpress.com by 210.87.254.40 on 09/05/12
For personal use only.

Can. J. Chem. Downloaded from www.nrcresearchpress.com by 210.87.254.40 on 09/05/12
For personal use only.

example, at an initial pH of 8.8, the pH decreases to a final value of 8.7, but for initial values of 8.5 and 7.5, it decreases to 8.0 and 7.0, respectively. As a result, below pH 8.8, the reported k_1 values must be considered averages over the pH change.

On the other hand, a dissection into a term for cyclization and one for dehydration is possible since the *syn* to *anti* hydrazone ratio measured for acetoacetamide appears to be identical to that for EAA, as discussed above. At pH 9.0, this ratio is 0.55 for the amide. If cyclization were occurring only via the *syn* hydrazone of EAA, the initial cyclic to *anti* ratio should also be 0.55. However, the initial cyclic to *anti* ratio is 1.1 in the pH range, 8.8–9.2, indicating that MPY is also formed from the carbinolamine intermediate. Using these two ratio (i.e. from AAM and EAA) and the expression $k_1 = k_c + k_{ds} + k_{da}$, for the EAA reaction, we find that $k_{da} = 0.48\ k_1$, $k_{ds} = 0.26\ k_1$, and $k_c = 0.26\ k_1$ in which k_c, k_{da}, and k_{ds} are the rate constants for conversion of carbinolamine to MPY and *anti* and *syn* hydrazone, respectively, with no restriction concerning protonation of the intermediate.

As discussed above, the signal due to the anti hydrazone decays at an appreciable rate with a concomitant growth in the MPY signal, indicating that the anti hydrazone converts to MPY. It is possible to calculate the rate constant k_{ac} for this conversion using a nonlinear least-squares fit of the concentration ratio $[MPY]/[EAA]_{r_0}$ vs. t according to the expression,

$$\frac{[MPY]}{[EAA]_{r_0}} = 1 - \exp(-k_1 t/X) + B(\exp(-k_{ac}t) - \exp(-k_1 t/X))$$

in which $B = k_{da}/(k_{ac}X - k_1)$, $X = (K_n[N] + 1)/K_n[N]$, t is the time, and k_{da}, which is the first-order rate constant for the formation of *anti* hydrazone from the various possible protonated forms of the intermediate, is obtained as just described. This expression was derived for the mechanism in the scheme for the case in which the pH is 8.8 or larger. For the fit, X and t are independent variables; [N] is obtained as a function of time as discussed above. The values listed in Table 1 for k_{ac} obtained in this manner have standard errors of about $\pm 10\%$ based on the fit of the data. Since the *syn* hydrazone is not detected, cyclization via this isomer is presumably faster than the *anti* to *syn* interconversion. Consequently, k_{ac} represents the first-order rate constant for *anti* to *syn* interconversion, and a comparison with k_c is not meaningful.

A measure of the effectiveness of the intramolecular cyclization steps relative to that for the analogous intermolecular nucleophilic reactions can be inferred. Since the carbinolamine is too reactive for the intermolecular study, the *O*-methyloxime of EAA was chosen as a model compound rather than EAA itself to prevent any complications resulting from nucleophilic addition to the keto carbonyl. Furthermore, since the carboethoxy group is separated from the oxime group by a CH_2 group, the rate difference caused by electronic differences between CA and the oxime of EAA is expected to be substantially less than an order of magnitude for the intermolecular process. 1,1-Dimethylhydrazine was chosen to be the intermolecular nucleophile because its primary nitrogen is expected to have a nucleophilicity similar to that for the primary nitrogen of the carbinolamine. Since these reactions were studied at pH 9.2, the ester hydrolysis rate of the *O*-methyloxime of EAA at this pH in the absence of the hydrazine was also measured as a control experiment. The rate of ester hydrolysis at this pH was found to be the same in the presence and in the absence of the hydrazine. Allowing for the fact that a 20% difference in the rate between the two solutions could have been detected, we estimate that the upper limit for the rate constant for ester hydrolysis catalyzed by 1,1-dimethylhydrazine is $4 \times 10^{-6} M^{-1}\,s^{-1}$. Since the average first-order rate constant for cyclization via the carbinolamine at pH 9.2 is about $2 \times 10^{-2}\ s^{-1}$, the lower limit for the effective molarity[8] of the nucleophile in the intramolecular process is about 10^4 M.

Since the cyclization of the *syn* hydrazone is apparently faster than the *anti* to *syn* interconversion, k_{ac} must be considered to be a lower limit to k_{sc}. Consequently comparison of the intermolecular hydrazone catalysis of the rate of ester hydrolysis with the cyclization of the *anti* hydrazone of EAA can provide only a lower limit to the effective molarity. The intermolecular catalysis of the ester hydrolysis by hydrazone was measured using a solution containing the *O*-methyloxime of EAA and the hydrazone of acetone. The oxime is expected to provide electronic effects similar to the hydrazone of EAA, and the primary nitrogen of hydrazone of acetone is expected to have a nucleophilicity similar to that for the primary nitrogen of the hydrazone of EAA. As a control, the rate of ester hydrolysis of this solution at pH 9.2 was compared to the rate for a solution that was exactly the same except that the hydrazone was absent. The rates were identical in both cases, and an upper limit for the rate constant for intermolecular hydrazone catalysis is estimated (in the same manner as described above) to be

[8]For a definition of effective molarity see ref. 13.

$4 \times 10^{-6} M^{-1} s^{-1}$. Consequently, the lower limit for the effective molarity of the primary nitrogen of the *syn* hydrazone of EAA is 10^3 *M*, based on an average value for k_{ac} at p*H* 9.2 (Table 1).

1. M. COCIVERA, A. EFFIO, H. CHEN, and S. VAISH. J. Am. Chem. Soc. **98**, 7362 (1976).
2. B. WILSON. J. Org. Chem. **28**, 314 (1963).
3. (*a*) M. COCIVERA and A. EFFIO. J. Am. Chem. Soc. **98**, 7371 (1976); (*b*) C. FYFE, M. COCIVERA, S. DAMJI, T. HOSTETTER, D. SPROAT, and J. O'BRIEN. J. Magn. Res. **23**, 377 (1976).
4. J. POPLE, W. SCHNEIDER, and H. BERNSTEIN. High resolution nuclear magnetic resonance. McGraw-Hill, New York, NY. 1959. p. 222.
5. A. FERSHT. J. Am. Chem. Soc. **93**, 3504 (1971).
6. R. HINMAN. J. Org. Chem. **23**, 1587 (1958).
7. E. GRUNWALD and M. COCIVERA. Discuss. Faraday Soc. 105 (1965).
8. M. COCIVERA, C. FYFE, A. EFFIO, S. VAISH, and H. CHEN. J. Am. Chem. Soc. **98**, 1573 (1976).
9. S. ROSENBERG, S. SILVER, J. SAYER, and W. JENCKS. J. Am. Chem. Soc. **96**, 7986 (1974).
10. J. CLARK and D. D. PERRIN. Q. Rev. **18**, 295 (1964).
11. F. E. CONDON. J. Am. Chem. Soc. **87**, 4491 (1965).
12. (*a*) R. W. TAFT. *In* Steric effects in organic chemistry. *Edited by* M. S. Newman. J. Wiley and Sons, New York, NY. 1956. p. 556; (*b*) C. RITCHIE and W. SAGER. *In* Progress in physical organic chemistry. Vol. II. *Edited by* S. Cohen, A. Streitwieser, Jr., and R. W. Taft. Interscience Publishers, New York, NY. 1964.
13. T. FIFE, J. HUTCHINS, and M. WANG. J. Am. Chem. Soc. **97**, 5878 (1975).

Can. J. Chem. Downloaded from www.nrcresearchpress.com by 210.87.254.40 on 09/05/12
For personal use only.

Cyclopropanediols. VII. Comportement chimique des cyclopropanediols et reactions de bis(trimethylsiloxy)-1,2 cyclopropanes

RAYMOND LE GOALLER ET JEAN-LOUIS PIERRE

Laboratoire de Chimie Organique, Université Scientifique et Médicale de Grenoble, B.P. 53, 38041 Grenoble Cedex, France

Reçu le 5 mai 1977

RAYMOND LE GOALLER et JEAN-LOUIS PIERRE. Can. J. Chem. **56**, 481 (1978).

Le texte décrit le comportement chimique des bis(triméthylsiloxy)-1,2-cyclopropanes. Les réactions de solvolyses acides et basiques, ainsi que les réactions du chlore et du brome se font avec ouverture du cycle conduisant à des α cétols, des énones et des β dicétones. Cétols et énones proviennent d'une ouverture type cyclopropanol, tandis que les β dicétones résultent de l'oxydation de siloxycyclopropanols ou de cyclopropanediols intermédiaires.

RAYMOND LE GOALLER and JEAN-LOUIS PIERRE. Can. J. Chem. **56**, 481 (1978).

The chemical behaviour of 1,2-bis(trimethylsiloxy)cyclopropanes is described. Acid and base solvolyses as well as reactions with chlorine and bromine occur with opening of the ring leading to α-ketols, enones and β-diketones. Ketols and enones arise from a cyclopropanol type ring opening while the β-diketones result from the oxidation of the intermediate siloxycyclopropanols or cyclopropanediols.

[Journal translation]

Introduction

Nous avons récemment décrit deux méthodes générales d'obtention de dérivés de cyclopropanediols (1). Nous nous proposons d'examiner ici leur comportement chimique. Les quelques cyclopropanediols libres obtenus à ce jour (2–6) sont représentés dans le schéma 1. Leur instabilité à l'air permettant difficilement l'étude de leur réactivité chimique, la littérature présente peu de données sur ce point.

Armand et Boulares (5) signalent simplement leur oxydabilité. Chen et Ainsworth (6) indiquent en outre la réaction de **3** avec le méthylate de sodium et son instabilité en milieu acide. Seuls, Curphey et coll. (3) et Reusch et coll. (4, 7, 8) ont effectué des études plus poussées sur leurs cyclopropanediols, mais ceux-ci sont exceptionnellement et anormalement stables en milieu acide (ils restent inchangés sous l'action de HCl méthanolique 2 *M*) et ne semblent donc pas représentatifs de cette classe de composés. Cette stabilité est d'ailleurs restée inexpliquée, une espèce homoaromatique ayant été suggérée, mais non confirmée. La réaction de **2** avec HCl 9 *M* fournit lentement l'α cétol **5**; par action de différents oxydants on obtient une dicétone **6**; l'action de la potasse le transforme en β cétol **7** et le chlorure d'acétyle en diacétate.

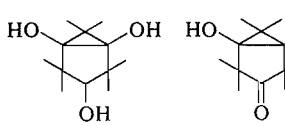

1(4) **2**(3,4) **3**(6) **4**(5)

4*a* $R_1 = R_2 = Ph, R_3 = R_4 = Me$
4*b* $R_1 = R_2 = Ph, R_3 = H, R_4 = Me$
4*c* $R_1 = Ph, R_2 = R_3 = R_4 = Me$
4*d* $R_1 = Ph, R_2 = R_3 = Me, R_4 = Ch_2Ph$

SCHÉMA 1. Les cyclopropanediols libres actuellement connus.

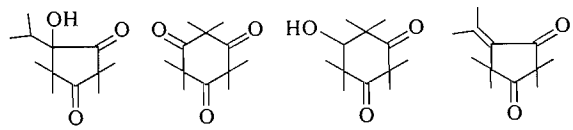

5 **6** **7** **8**

SCHÉMA 2

Les quelques réactions réalisées par Curphey et coll. (3) sur le diacétoxycyclopropane dérivé de **2** ne peuvent pas non plus être considérées comme caractéristiques du fait du squelette trop particulier. L'action de HCl méthanolique conduit au diol **2** et a des traces d'énone **8** et celle de HCl 9 *M* à l'α cétol **5** avec des traces de la même énone.

D'autre part, on sait que la réduction de Clemmensen des β dicétones conduit généralement à des α cétols et des cétones provenant de cyclopropanediols intermédiaires (9). Dans certains cas on a également obtenu des β cétols (schéma 3)

L'objet de ce travail est donc de cerner de plus près les propriétés des cyclopropanediols et éventuellement d'en dégager leur utilité en tant qu'intermédiaires de réactions, en étudiant le comportement chimique des bis(triméthylsiloxy)-1,2 cyclopropanes considérés comme des cyclopropanediols potentiels.

Resultats

Synthèse de diacétoxy-1,2 cyclopropanes

L'action du bromure d'acétyle dans l'éther sur les

Can. J. Chem. Downloaded from www.nrcresearchpress.com by 210.87.254.40 on 09/05/12
For personal use only.

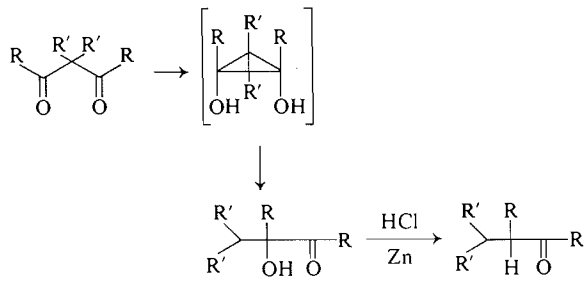

SCHÉMA 3

bis(triméthylsiloxy)-1,2 cyclopropanes **9***a*–**17***a* conduit quantitativement aux diacétates correspondants **9***b* à **17***b* (schéma 4). La réaction est beaucoup plus rapide qu'avec le chlorure d'acétyle. Sans solvant et en présence d'un excès de bromure d'acétyle on obtient également des produits d'ouverture. C'est ainsi que le mélange des deux isomères de **9***a* conduit à l'acétoxy-3 méthyl-3 butanone-2 à côté des deux isomères de **9***b*. Dans tous les cas, hormis **14** les isomères cis et trans ont été séparés.

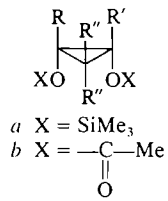

a X = $SiMe_3$
b X = —C(=O)—Me

9 R = R′ = Me, R″ = H
10 R = R′ = Et, R″ = H
11 R = R′ = Pr, R″ = H
12 R = R′ = isoPr, R″ = H
13 R = Me, R′ = Et, R″ = H
14 R = R′ = —$(CH_2)_4$—, R″ = H
15 R = R′ = Me, R″ = Me
16 R = R′ = Ph, R″ = Me
17 R = Me, R′ = H, R″ = Me

SCHÉMA 4. Disiloxy et diacetoxy 1,2-cyclopropanes.

Solvolyses

Réactions induites par les acides

Les acétates de cyclopropanediols restent inchangés dans du méthanol pur, mais nous avons pu réaliser la méthanolyse de **9***b* au reflux en ajoutant un peu d'acide *p*-toluènesulfonique (TsOH). Les résultats au bout de 4 h de réaction, indiqués dans le schéma 5, montrent qu'ils diffèrent beaucoup de

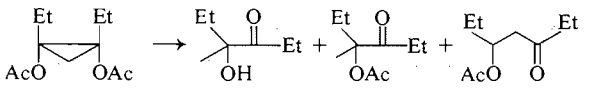

10*b* **21** 47% **21***b* 50% **24***b* 3%

SCHÉMA 5

ceux de Curphey et coll. (3) et que nous avons une ouverture du cycle. Toutes ces réactions, comme les suivantes sont menées sous atmosphère d'azote.

En ce qui concerne les bis(triméthylsiloxy)-1,2 cyclopropanes, nous avons réalisé la méthanolyse dans les mêmes conditions que précédemment après avoir constaté qu'ils ne réagissent pas en milieu parfaitement neutre. Le composé de départ disparait entièrement au bout de 10 min de reflux. D'autre part, leur hydrolyse a été menée de trois façons différentes: (*i*) En milieu neutre: H_2O en quantité nécessaire et solvant[1]. Les bis(triméthylsiloxy) cyclopropanes ne sont pas affectés. La réaction a lieu dès que l'on ajoute un peu d'acide *p*-toluènesulfonique. Les résultats pratiquement analogues à ceux obtenus par méthanolyse ne dépendent pas de façon appréciable du solvant et sont résumés dans le schéma 6. (*ii*) La réaction de HCl gazeux et sec dans l'éther a été réalisée sur **9***a*, **10***a* et **17***a*. Dans chaque cas la réaction est immédiate et conduit exclusivement aux α cétols (indiqués entre crochets dans le schéma 4 pour **17***a*), sauf pour **9***a* qui donne un peu d'énone (moins de 10%). Nous n'avons pas observé de produits chlorés. (*iii*) La réaction de **9***a*, **10***a* et **17***a*, avec une solution chlorydrique N est également instantanée et conduit aux α cétols (≃80%) et aux énones (≃20%) pour **9***a* et **10***a* et à l'α cétol exclusivement pour **17***a*. Les résultats semblent donc indiquer que plus les conditions sont acides, plus on obtient d'α cétol.

D'autre part au cours de la méthanolyse de **9***a*, suivie en cpv, nous avons pu observer la formation, à côté de **19** et **20** d'un composé qui disparaît au cours de la réaction au profit de l'acétylacétone. Ce produit a été séparé par cpv préparative et identifié à partir de ses données spectroscopiques ir et rmn comme étant le monotriméthylsiloxycyclopropanol **9***c* (schéma 7). En présence d'air, même en solution dans l'éther, ce composé se transforme rapidement en acétyl acétone également obtenue seule, en présence de méthanol–eau–TsOH, c'est-à-dire dans les conditions d'ouverture des bis(triméthyl siloxy) cyclopropanes.

Réactions induites par les bases

Nous avons examiné la comportement de **9***a*, **10***a* et **17***a* dans la soude méthanolique 0.2 *M* au reflux.[2] Le produit de départ est entièrement consommé au bout de 6 heures et on obtient un mélange d'α cétols, d'énones et de composés dicarbonylés. Les résultats sont indiqués dans le schéma 8. Nous avons vérifié que les résultats ne dépendent pas de la stéréochimie des produits de départ. Cependant les proportions de produits obtenus varient sensiblement d'une expérience à une autre et les proportions indiquées au schéma 8 représentent des moyennes de plusieurs expériences. D'autre part, une expérience sur **10***a*, conduite avec de la potasse au lieu de la soude, nous

[1]MeOH, C_6H_6, diglyme et DMSO conduisent aux mêmes résultats, de même que MeOH sec. Dans tous les cas, les deux stéréoisomères donnent les mêmes résultats.

[2]Les réactions de **9***a* et **10***a* avec le méthyl lithium ont également été envisagées et aboutissent pratiquement aux mêmes résultats.

Can. J. Chem. Downloaded from www.nrcresearchpress.com by 210.87.254.40 on 09/05/12
For personal use only.

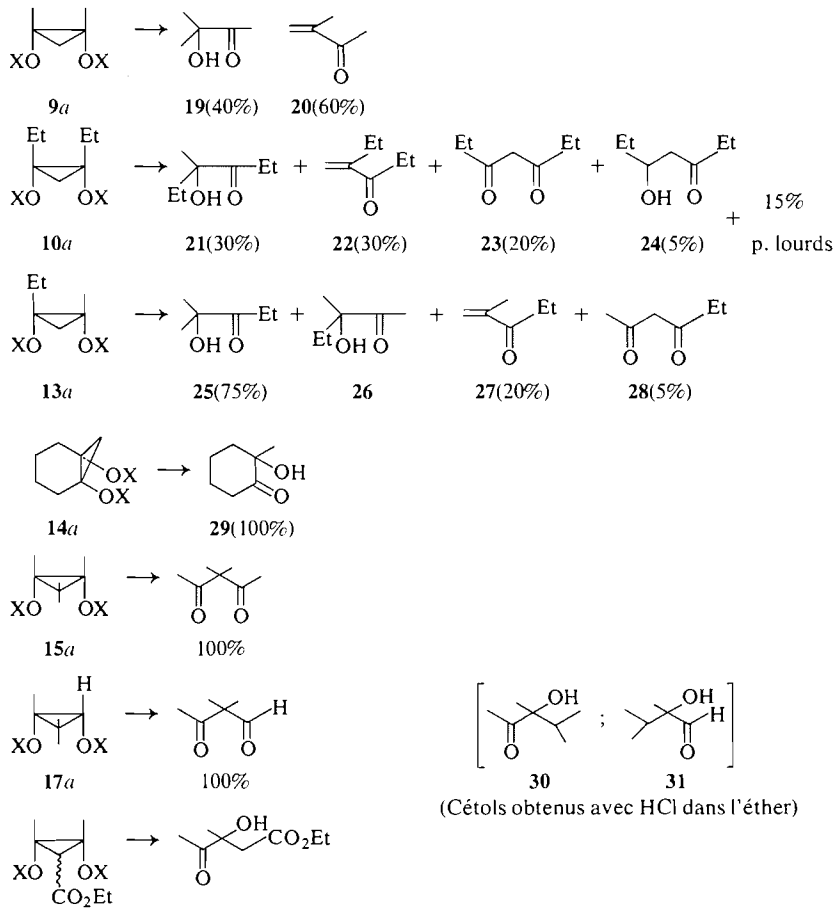

SCHÉMA 6. Resultats obtenus avec le melange H_2O–solvant en presence d'acide paratoluene sulfonique (X = —$SiMe_3$).

a permis d'isoler **10***c* qui se décompose également rapidement en β dicétone. Nous n'avons pu obtenir **10***c* en utilisant de la soude, mais la réaction semble si sensible aux conditions que nous ne pouvons en tirer de conclusion. Cette fois encore, si on remet **10***c* dans les conditions réactionnelles, on n'obtient que de la β dicétone.

Halogénations

Nous avons envisagé les réactions de **10***a*, **14***a* et **17***a* avec du chlore et du brome dans l'éther. Les réactions sont rapides et on obtient les composés halogénés du schéma 9. Ces composés séparés par chromatographie sur colonne de silice, noircissent et se décomposent rapidement, ce qui nous empêche de donner des rendements.[3] Les réactions menées avec NaOCl se sont avérées négatives.

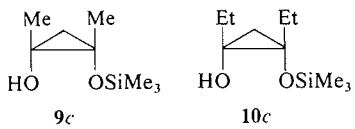

SCHÉMA 7

Discussion et conclusion

La réaction de formation des α cétols par action des acides sur les cyclopropanediols libres de Curphey et coll. (3) et de Reusch et coll. (4) est tout à fait analogue à l'ouverture acide des cyclopropanols et on accepte généralement la même conclusion pour les cyclopropanediols intermédiaires de la réduction de Clemmensen des β dicétones. En réalisant l'hydrolyse des bis(triméthylsiloxy)-1,2 cyclopropanes, nous pensions pouvoir obtenir les cyclopropanediols correspondants. En fait nous n'avons jamais pu observer ces composés même en milieu trés peu acide et nos résultats impliquent que les composés ob-

[3]Les composés chlorés sont nettement plus stables, mais il est certain que les rendements en produits isolés sont nettement plus faibles que les rendements en produits formés, la décomposition étant toujours importante.

Can. J. Chem. Downloaded from www.nrcresearchpress.com by 210.87.254.40 on 09/05/12
For personal use only.

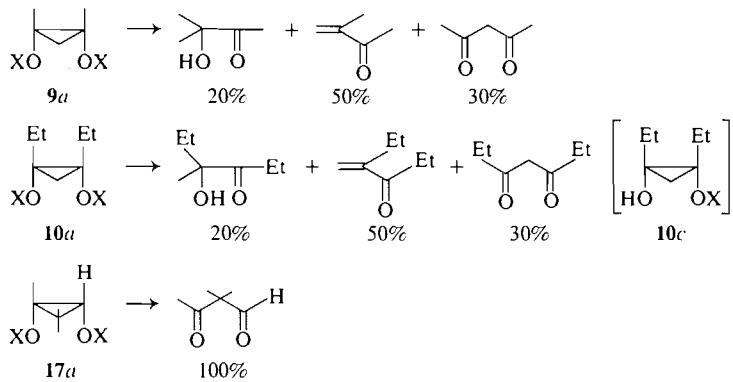

SCHÉMA 8. Résultats obtenus par hydrolyse basique (X = $SiMe_3$).

tenus proviennent, partiellement ou totalement, des dérivés bissiloxylés et non des diols libres intermédiaires.

Le fait que les monosiloxycyclopropanols **9***c* et **10***c* se transforment uniquement en β dicétone, aussi bien en présence d'air qu'en milieu MeOH–H_2O–TsOH, montre que les α cétols sont obtenus à partir de **9***a* et **10***a*.[4]

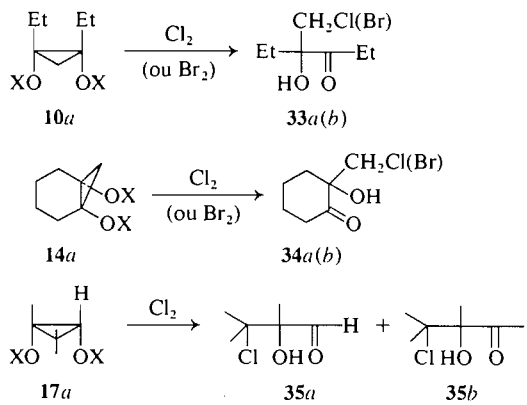

SCHÉMA 9

Il faut également noter qu'en présence d'air les bis(trimethylsiloxy) cyclopropanes présentent un comportement différent de **9***c* et sont lentement transformés (en un ou deux mois) en un mélange contenant les mêmes produits que ceux obtenus par solvolyse acide. Nous avons établi le fait que les énones ne proviennent pas des α cétols dans les conditions réactionnelles envisagées,[5] ce qui suggère que, comme les α cétols, elles sont obtenues directement à partir des dérivés bissiloxylés. Nous pensons donc que dans le cas des diéthers cyclopropaniques, les α cétols sont obtenus par un processus analogue à l'ouverture acide des cyclopropanols (2) et la formation des énones par un processus analogue à l'ouverture des tosylates de cyclopropyle, ce qui indique que la protonation peut concerner aussi bien le site cyclopropyle que le site oxygéné (schéma 10).

Les β cétols obtenus dans certains cas (ainsi d'ailleurs que dans la réduction des β dicétones) proviendraient de l'autre orientation possible de l'ouverture 'type cyclopropanol,' mais nous n'avons trouvé aucune corrélation avec la structure.

A notre avis, les β dicétones (ou le β cétoaldéhyde provenant de **17***a*) sont obtenues soit via l'intermédiaire siloxycyclopropanol soit via l'intermédiaire diol libre non isolé. Cette oxydation des cyclopropane-diols en β dicétones a été étudiée par Curphey et coll. (3*b*) et Priddy et Reusch (8) et semble analogue à l'oxydation des cyclopropanols.

En milieu basique, les résultats sont très analogues à ceux obtenus en milieu acide, avec moins de cétols et plus d'énones et de β dicétones. Ici encore le comportement de **10***c* fait penser que les α cétols et les énones sont obtenus à partir des dérivés bissiloxylés par coupure initiale d'une liaison O—Si, selon

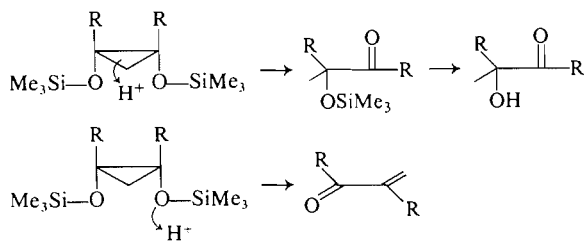

SCHÉMA 10

schéma 11, et non des diols libres. Nous avons vérifié que dans les conditions réactionnelles les cétols ne se transforment pas en énones.

La formation des composés dicarbonylés (seul produit de réaction pour **17***a*) peut être expliqué par oxydation de l'intermédiaire cyclopropanediol, non isolé. On voit cependant que quand le diol obtenu

[4]Conclusion en contradiction avec l'interprétation de Curphey et coll. (3) qui admet, dans le cas d'un diacétate, que les diols libres sont les précurseurs des α cétols.

[5]Observation en contradiction avec l'interprètation de Priddy et Reusch (7).

Can. J. Chem. Downloaded from www.nrcresearchpress.com by 210.87.254.40 on 09/05/12
For personal use only.

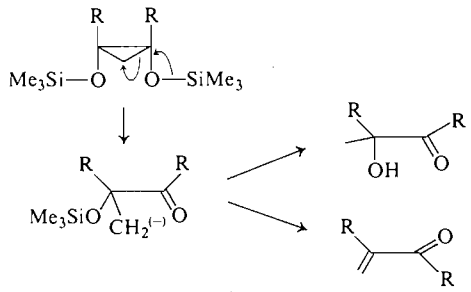

SCHÉMA 11

est moins oxydable, (i.e. non substitué en position 3) on obtient plus de cétol et d'énone et donc que dans ce cas le réarrangement serait plus rapide que l'oxydation.

En ce qui concerne les halogénations, les résultats peuvent être interprétés comme une ouverture électrophile, analogue à celle induite par les acides (schéma 12).

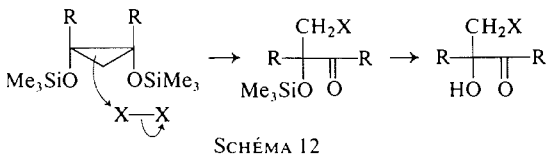

SCHÉMA 12

En conclusion, la réactivité chimique des cyclopropanediols ressemble incontestablement à celle des cyclopropanols et semble totalement différente de celles des α diols aliphatiques: les α cétols et halohydrines qui pourraient être obtenus par transposition pinacolique ne sont jamais observés et les énones sont obtenues par une toute autre voie. Dans certains cas les bis(triméthylsiloxy)-1,2 cyclopropanes peuvent constituer d'utiles synthons pour la synthèse de β dicétones dans des conditions très douces, ainsi que d'α cétols, et ils remplacent avantageusement les cyclopropanediols eux mêmes, trop instables. Nous explorons actuellement l'utilisation de ces dérivés en synthèse.

Partie experimentale

Les spectres ir ont été réalisés sur Perkin-Elmer 221 et les spectres rmn sur Perkin-Elmer R 10 ou sur Varian A60 (60 MHz). Tous les déplacements chimiques sont donnés en $\delta \times 10^6$ par rapport au TMS utilisé comme référence interne (s: singulet, d: doublet, t: triplet, q: quadruplet, h: heptuplet, m: multiplet). Les analyses en chromatographie en phase gazeuse ont été réalisées sur Aérograph 1420 et les séparations sur Aérograph autoprep A 700 équipés de colonnes Apiezon ou Carbowax.

Substrats

Les bissiloxy 1,2-cyclopropanes ont été préparés au laboratoire (1) et purifiés par cpv préparative. Le chlore a été préparé par réaction de HCl concentré sur $KMNO_4$, puis séché sur H_2SO_4. L'azote a été séché sur P_2O_5, puis KOH avant de traverser une solution d'hydroquinone dans l'éther. Les autres réactifs sont des produits commerciaux utilisés tels quels.

Préparation des acétates de cyclopropanediol

Les diacétates **9***b*–**17***b* sont obtenus quantitativement en faisant réagir 1 g de bis(triméthylsiloxy) cyclopropane sur 0.6 g de bromure d'acétyle dans 5 ml d'éther anhydre au reflux. Au bout de 30 min, le produit initial ayant totalement disparu, l'éther est évaporé et les diacétates séparés par cpv (Carbowax). Ont été ainsi obtenus:

9*b cis*: ir: 1750 et 3010 cm^{-1}; rmn (CCl_4) δ: 1.45 (s, 6H), 1.92 (s, 6H), 51 et 60 Hz A–B, J = 8.5 Hz. **9***b trans*: id sauf A_2 à 0.82 (2 H). *Anal.* calc.: C 58.06, H 9.67; trouvé: C 58.15, H 9.48.

10*b* isomères non séparés: ir: 1745 et 3030 cm^{-1}; rmn (CCl_4) δ: 1.00 (t, 6H), 1.7 (q, 4H), 1.95 (s, 6H), 0.75 (2H). *Anal.* calc.: C 58.06, H 9.67; trouvé: C 58.15, H 9.48.

11*b*: ir: 3040, 1750 cm^{-1}; rmn (CCl_4) δ: 1.94 (s, 6H), 1.2–1.8 (m, 8H), 0.8–1.15 (8H). *Anal.* calc.: C 64.46, H 9.09; trouvé: C 63.98, H 9.09.

12*b cis*: ir: 3040 et 1745 cm^{-1}; rmn (CCl_4) δ: 1.98 (s, 6H), 1.4 (h, 2H), 1.1 (d, 12H), 0.8–1.2 (m, 2H). Dans le benzène le AB analysable indique δ A 32 Hz, δ B 54 Hz, J = 6 Hz.

12*b trans*: id sauf A_2 à 0.8 (2H). *Anal.* calc.: C 64.46, H 9.09; trouvé: C 64.18, H 9.21.

14*b*: ir: 1655 cm^{-1}; rmn (CCl_4) δ: 1.95 (s, 6H), 1.8–2.2 et 1.1–1.8 (2 massifs, 18H), 1.00 (s, 2H); dans le benzène on lit δ A 36.2 Hz, δ B 53.4 Hz et J_{AB} = 8 Hz.

15*b cis*: ir: 1750 cm^{-1}; rmn (CCl_4) δ: 0.9 (s, 3H), 0.97 (s, 3H), 1.39 (s, 6H), 1.95 (s, 6H). **15***b trans*: 1.09 (s, 6H), 1.39 (s, 6H), 1.95 (s, 6H). *Anal.* calc.: C 61.68, H 8.41, O 29.91; trouvé: C 61.67, H 8.85, O 30.33.

16*b*: rmn (CCl_4) δ: 7.3 (massif, 5H), 2.1 (s, 3H), 1.1 (s, 3H), 1.3 (s, 3H). *Anal.* calc.: C 74.58, H 6.5; trouvé: C 74.48, H 6.32.

17*b*: rmn (CCl_4) δ: 0.90 (s, 3H), 0.95 (s, 3H), 1.25 (s, 3H), 2.45 et 2.84 (2s, 1H). *Anal.* calc.: C 60.00, H 8.00; trouvé: C 60.15, H 8.43.

Hydrolyse de 10

On porte au reflux pendant 4 h 1 g du produit dans 10 ml de méthanol additionné de quelques mg de TsOH, puis les produits obtenus sont séparés par cpv. On obtient: 50% d'acétoxy 3, méthyl-3 hexanone-4 (ir: 1735 et 1690 cm^{-1}, rmn δ: 0.85 (t, 3H), 2.4 (q des CH_2—C(=O)—, 2H)) 47% de **21** et 3% d'acétoxy-5 heptanone-3 identique au produit obtenu par estérification de **24**.

Hydrolyses des bissiloxy 1,2-cyclopropanes en milieu acide

Nous avons utilisé quatres méthodes que nous décrivons ici à titre d'exemple pour **9***a*.

(*a*) On porte au reflux 1 g de **9***a* dans 10 ml de méthanol en présence de 5 mg d'acide paratoluènesulfonique, sous atmosphère d'azote. La réaction est suivie en cpv et en chromatographie sur plaque jusqu'àdisparition totale de **9***a*. On observe à côté de **19** et **20** la formation de **9***c* qui disparait rapidement ($t_{\frac{1}{2}}$ = 12–13 min). Ce produit, séparé sur colonne Apiézon recueilli dans du CCl_4 et maintenu sous atmosphère inerte montre en ir des bandes à 3450–3500, 1250 et 840 cm^{-1}, et en rmn δ: 0.05 (s, 9H), 0.3–0.5 (doublet d'intensité 1, représentant la partie A des protons cyclopropaniques, la partie B étant masquée par le $SiMe_3$), 0.98 et 1.03 (2s, 6H), plus le proton hydroxylique variant avec la dilution. Ce produit isolé se transforme uniquement en **20**, et on obtient en fin de réaction 40% de **19** et 60% de **20** (étalon interne: diphényl éther).

(*b*) A 1 g de **9***a* (0.004 mol) on ajoute 72 µl de H_2O (0.004 mol) et 10 ml de solvant (méthanol, ou bien benzène plus méthanol jusqu'à ce qu'on obtienne une solution homogène,

Can. J. Chem. Downloaded from www.nrcresearchpress.com by 210.87.254.40 on 09/05/12
For personal use only.

Can. J. Chem. Downloaded from www.nrcresearchpress.com by 210.87.254.40 on 09/05/12
For personal use only.

ou bien DMSO). Le mélange est ensuite chauffé au reflux pour les deux premiers cas, à 80°C pour le troisième. La réaction est suivie en cpv et en chromatographie couches minces. Les études rmn réalisées en cours de réaction, après évaporation du solvant sous vide et remplacement par $CDCl_3$ ne nous ont pas permis de conclure à la présence de diol. Les composées **19** et **20** sont ensuite séparés en cpv et comparés à des échantillons authentiques.

(*c*) On fait arriver un courant de HCl sec dans une solution éthérée de **9***a*. La réaction est instantanée et **19** et **20** sont identifiés par cpv dans le rapport 9:1.

(*d*) On ajoute 1 ou 2 gouttes d'acide chlorhydrique N à une solution méthanolique de 1 g de **9***a*. La réaction est instantanée et conduit à **19** et **20** dans le rapport 8:2.

Les produits obtenus ont été identifiés sans ambiguité par comparaison avec des échantillons authentiques sauf **9***c* et **10***c* et par les analyses spectrales rapportées ci-dessous:

19: ir: 3450, 1625 cm^{-1}; rmn ($CDCl_3$) δ: 2.03(3H), 1.4(6H).

20: ir: 3090, 1685, 1640 cm^{-1}; rmn (CCl_4) δ: 1.87(3H, s), 2.3(3H, s), 5.75 et 5.81 (1H et 1H s et s).

21: ir: 3480 et 1705 cm^{-1}; rmn ($CDCl_3$) δ: 1(6H, 2t), 2(2H, q), 2.5(2H, q), 2.3(3H, s).

22: ir: 3105, 1690, 1640 cm^{-1}; rmn (CCl_4)δ: 1 et 1.05: (2 t, imbriqués, 3H et 3H), 2.27 (q, 2H), 2.67 (q, 2H), 5.9 et 5.61 (1H et 1H).

23: ir: 1710–1720, 1600 cm^{-1}; rmn (CCl_4) δ: 1.15 (t, 6H), 2.3 (q, 4H), et s à 5.4 et 3.5 (1H).

24: ir: 3540 et 1610 cm^{-1}; rmn ($CDCl_3$) δ: 1.05 (t, 6H), multiplets à 1.4(2H), 2.4(2H), 3.9(1H).

25: ir: 3430 et 1685 cm^{-1}; rmn ($CDCl_3$) δ: 1.1 (t, 3H) -s-(6), 2.9 (q, 2H).

26: rmn ($CDCl_3$) δ: 0.95 (t, 3H), 1.3 (s, 3H), 2.3 (q, 2H) 2.6 (s, 3H).

27: ir: 1675, 1630, 3125 cm^{-1}; rmn (CCl_4) δ: 1.1 (t, 3H), 2.7 (q, 2H), 1.88 (s, 3H), 5.8 et 6 (s, 1H et 1H).

29: ir: 3470 et 1730 cm^{-1}; rmn ($CDCl_3$) δ: 1.4 (s), 1.75–2.5 (6H et 2H).

30: ir: 3450 et 1605 cm^{-1}; rmn ($CDCl_3$) δ: 2.12 (s, 3H), 3.91 (d 1H), 1.4 (m 1H), 0.7, 1.1 (2d, 3H et 3H).

31: rmn δ: 1.3 (d, 6H), 1.42 (s, 3H), 2.4 (h, 1H), 9.7 (s, 1H).

Hydrolyse en milieu basique

(*a*) On porte au reflux 10 ml d'une solution de soude méthanolique 0.2 *M* (ou soude 0.2 *M* dans le glyme à 80°C) contenant 1 g de produit cyclopropanique. Le produit disparait au bout de 6–10 h. La réaction est suivie par cpv et en chromatographie sur plaques de silice. Des analyses rmn en cours de réaction ne nous ont pas permis de conclure à la présence de cyclopropanediols.

Dans le cas de **10***a* on observe l'apparition d'un composé qui disparait au cours de la réaction en se transformant en dicétone. Ce produit séparé en cpv Apiézon présente en ir une bande OH à 3450 cm^{-1} des protons cyclopropaniques à 3080 cm^{-1} et les bandes caractéristiques du groupement $SiMe_3$ à 1250 et 830 cm^{-1}.

(*b*) *L'action du MeLi*—L'action du MeLi obtenu à partir de MeI en solution éthérée est très lente: on porte au reflux 1 g de produit cyclopropanique dans la quantité nécessaire de MeLi. La réaction dure 10–15 h. On obtient les mêmes produits que précédemment.

Action du chlore—On fait barbotter du chlore sec, dans une solution éthérée de produit. Après évaporation de l'éther les produits obtenus sont analysés en chromatographie sur plaque de silice.

Action du brome—On ajoute du brome sur le produit en solution dans l'éther. Il est rapidement consommé (20–30 min) et il y a noircissement rapide. Les produits sont séparés par chromatographie colonne.

33*a*: rmn ($CDCl_3$) δ: 1.1 et 1.2 (2t imbriqués, 6H), 1.65 (massif, 2H), 2.5 (q, 2H), 3.65 (AB, 2H (CH_2Cl) inéquivalents).

34*b*: ir: 3450 et 1720 cm^{-1}; rmn δ: 2 massif cyclohexane à 1.4 et 2.3 (6H), et 2.4 et 2.7 (2H), protons AB à 3.66 J = 8 Hz δA 212 Hz et δB 230 Hz.

35*a*: rmn δ: 9.7 (s, 1H), 1.6 (s, 3H), 1.25 et 1.3 (s, 3H et 3H).

35*b*: rmn δ: 2.2 (s, 3H), 4.1 (s, 1H), 1.1 et 1.2 (s, 3H) et 3H).

1. R. Le Goaller et J. L. Pierre. Can. J. Chem. **55**, 757 (1977).
2. D. H. Gibson et C. H. Depuy. Chem. Rev. **74**, 605 (1974).
3. (*a*) T. J. Curphey et R. L. McCartney. Tetrahedron Lett. 5295 (1969); (*b*) T. J. Curphey, C. W. Amelotti, T. P. Layloff, R. L. McCartney et S. M. Williams. J. Am. Chem. Soc. **91**, 2817 (1969).
4. W. Reusch et D. B. Priddy. J. Am. Chem. Soc. **91**, 3677 (1969).
5. J. Armand et L. Boulares, Can. J. Chem. **54**, 1197 (1976).
6. F. Chen et C. Ainsworth. J. Am. Chem. Soc. **94**, 4037 (1972).
7. D. B. Priddy et W. Reusch. Tetrahedron Lett. 5291 (1969).
8. D. B. Priddy et W. Reusch. Tetrahedron Lett. 2637 (1970).
9. T. J. Curphey et R. L. McCartney. J. Org. Chem. **34**, 1964 (1969) et références citées.

Oligoribonucleotide synthesis. XI.[1] Improved preparation of 2′-*O*-tetrahydropyranyl derivatives of guanosine and adenosine necessary for insertion in phosphotriester synthesis

RENE J. GREGOIRE AND THOMAS NEILSON

Department of Biochemistry, McMaster University, Hamilton, Ont., Canada L8S 4J9

Received July 18, 1977

RENE J. GREGOIRE and THOMAS NEILSON. Can. J. Chem. **56**, 487 (1978).

Treatment of N^2-benzoyl-2′,3′,5′-*O*-triacetylguanosine and 2′,3′,5′-*O*-triacetyladenosine with buffered hydrazine gave equilibrium mixtures of N^2-benzoyl-2′(3′),5′-diacetylguanosine and 2′(3′),5′-diacetyladenosine, greatly enriched in the desired 3′-acetates. Fractional crystallization effected recovery of pure 3′,5′-diacetates in 60% yields. From these were prepared the 2′-*O*-tetrahydropyranyl derivatives required for guanosine and adenosine insertion in phosphotriester oligonucleotide synthesis.

RENE J. GREGOIRE et THOMAS NEILSON. Can. J. Chem. **56**, 487 (1978).

La réaction de la N^2-benzoyl tri-*O*-acétyl-2′,3′,5′ guanosine et de la tri-*O*-acétyl-2′,3′,5′ adénosine avec de l'hydrazine tamponnée conduisent à des mélanges à l'équilibre de N^2-benzoyl diacétyl-2′(3′),5′ guanosine et diacétyl-2′(3′),5′ adénosine, dans lesquelles les acétates-3′ désirés ont été grandement enrichis. La cristallisation fractionnée permet de récupérer des diacétates-3′,5′ purs avec des rendements de 60%. Utilisant ces derniers, on a pu préparer les dérivés *O*-tétrahydropyranyl-2′ requis pour l'insertion de la guanosine et de l'adénosine dans la synthèse d'oligonucléotides de phosphotriestères.

[Traduit par le journal]

Introduction

All successful polymer syntheses are dependent on (*i*) convenient supply of monomers and (*ii*) efficient coupling. Recent improvements in phosphotriester oligoribonucleotide synthesis in these areas include (*i*) new nucleoside protecting groups such as alkylsilyl ethers (2) and levulinic esters (3), and (*ii*) more efficient internucleotide coupling with various mesitylene sulfonamides (3, 4).

Several oligoribonucleotides of biological significance (1, 5, 6) have been prepared by the general synthesis developed in this laboratory. This communication describes an improved, convenient synthetic route to two purine ribofuranoside monomers widely used in oligoribonucleotide synthesis.

Guanosine is presently inserted as N^2-benzoyl-2′-*O*-tetrahydropyranylguanosine (**3**), obtained by a synthesis (7) containing (*a*) two acidic steps leading to loss via depurination and (*b*) a wasteful fractional crystallization from an approximately 1:1 isomeric mixture of 3′(2′)-*O*-acetates.

A recent report of supposed regioselective hydrazinolysis (8) of 2′-*O*-acyl groups in fully acylated purine ribofuranosides was of interest, since such a scheme would eliminate the acid-catalyzed 2′,3′-orthoacetate ring opening. Difficulty was experienced in ^{1}Hmr monitoring of the hydrazine-catalyzed debenzoylation of N^2,2′,3′,5′-*O*-tetrabenzoylguanosine (**1**: $R_1 = R_2 =$ Ph). Also, crystallization of N^2,3′,5′-*O*-tribenzoylguanosine (**2**: $R_1 = R_2 =$ Ph) was unsuccessful. Deacetylation of N^2-benzoyl-2′,3′,5′-*O*-triacetylguanosine (**1**: $R_1 = R_2 = CH_3$) on the other hand, was convenient to monitor by ^{1}Hmr, and the 3′-acetyl product (**2**: $R_1 = R_2 = CH_3$) crystallized well.

N^2-Benzoyl-2′,3′,5′-*O*-triacetylguanosine (**1**: $R_1 = R_2 = CH_3$) was prepared from N^2-benzoylguanosine (**1**: $R_1 = R_2 =$ Ph). Also, crystallization of N^2,3′,5′-*O*-tribenzoylguanosine (**2**: $R_1 = R_2 =$ Ph) was unsuccessful. Deacetylation of N^2-benzoyl-2′,3′,5′-*O*-triacetylguanosine (**1**: $R_1 = R_2 = CH_3$) on the other hand, was convenient to monitor by ^{1}Hmr, and the 3′-acetyl product (**2**: $R_1 = R_2 = CH_3$) crystallized well.

N^2-Benzoyl-2′,3′,5′-*O*-triacetylguanosine (**1**: $R_1 = R_2 = CH_3$) was prepared from N^2-benzoylguano-

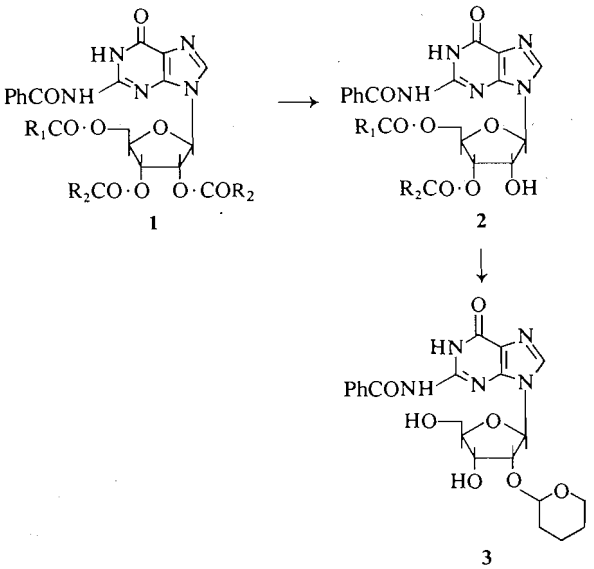

SCHEME 1

[1]For Part X see ref. 1.

Can. J. Chem. Downloaded from www.nrcresearchpress.com by 210.87.254.6 on 09/05/12
For personal use only.

sine (9) and treated with buffered hydrazine solution (8). Work-up gave N^2-benzoyl-3′,5′-*O*-diacetylguanosine (**2**: $R_1 = R_2 = CH_3$) as the major product, in 61% yield, from an equilibrium mixture of 2′- and 3′-acetates enriched (ca. 5:1) in the latter. Compound **2** was successfully converted to **3** (Scheme 1).

Scheme 2 summarizes the overall yields of **3** from the present and previous methods. Elimination of depurination and crystallization of **2** from an enriched isomeric mixture allows the overall yield of **3** to rise from 33 to 50%.

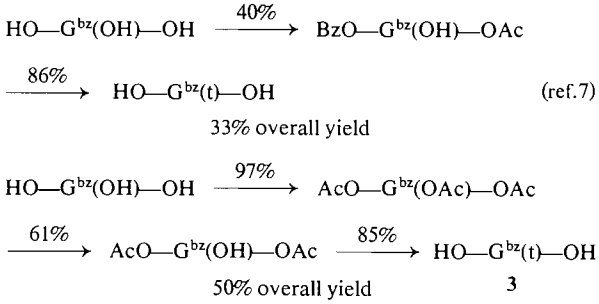

SCHEME 2

The improved synthesis of **3** prompted us to consider a parallel synthesis for the adenosine analogue (**6**) (Scheme 3). Similar hydrazinolysis (8) on 2′,3′,5′-*O*-triacetyladenosine (**4**) (10) gave a similarly enriched (ca. 5:1) mixture of isomers, from which 3′,5′-*O*-diacetyladenosine (**5**) was recovered in 59% yield. This offers some improvement in yield over the previously published method (11), as shown in Scheme 4. Conversion of **5** to **6** remained as before (12).

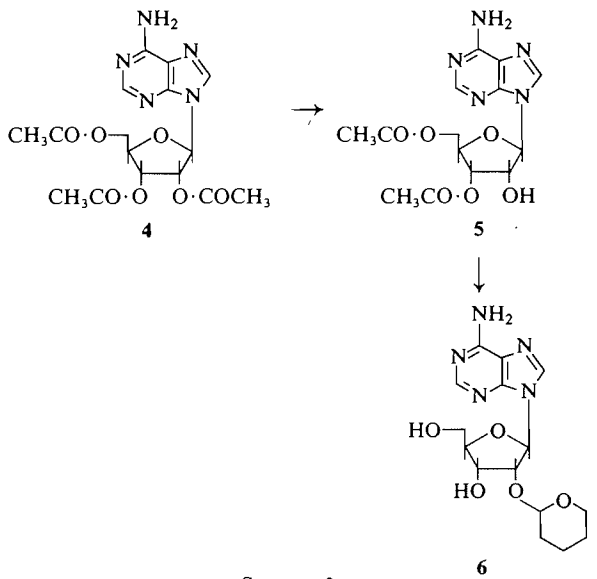

SCHEME 3

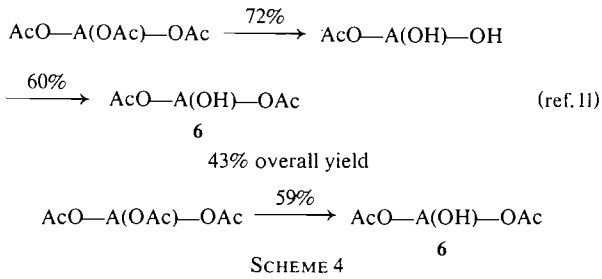

SCHEME 4

Although hydrazinolysis is deemed to be regioselective (8), base-catalyzed acetyl migration is also in operation. The resulting equilibrium mixture of 2′(3′)-acetates favours the 3′-acetate isomer by ca. 5:1, which improves fractional crystallization of the desired isomer.

Composition of acetate samples was readily determined from ^{1}Hmr spectra. Table 1 compares the ^{1}Hmr data of the 2′- and 3′-acetates. Chemical shifts (ppm) of the anomeric proton are typically less for the 3′-acetate, whereas the $J_{1',2'}$ coupling constants (Hz) of the 3′-acetates are larger (13).

Experimental

Proton magnetic resonance spectra were recorded on a Varian T60 spectrometer in DMSO-d_6/D_2O/CD_3COOD (0.5 g/0.05 ml/0.05 ml) solutions. Silica gel (Baker Analyzed Reagent) was used for column chromatography, and Analtech prescored silica gel plates for tlc. The plates were developed in 10% methanol in methylene chloride mixtures, then sprayed with 1% (w/v) $H_4Ce(SO_4)_4$ in 10% (v/v) aqueous sulfuric acid and heated to 300–400°F for detection.

*N²-Benzoyl-2′,3′,5′-O-triacetylguanosine (**1**: $R_1 = R_2 = CH_3$)*

Cold acetic anhydride (146 ml, 1.55 mol) was added, portionwise, over 30 min, to an ice-cold stirring solution of N^2-benzoylguanosine (9) (18.29 g, 47.2 mmol) in dry pyridine (500 ml). The mixture was cooled for 60 min, then warmed to room temperature. Acetylation (R_F 0.07 → 0.30 → 0.55 → 0.70) was complete after 2½ h. The reaction was cooled briefly and quenched with excess methanol. After 30 min, the mixture was reduced to ca. 450 ml, and extracted from water (200 ml) into methylene chloride (3 × 150 ml). Combined organic extracts were washed with water (150 ml), then saturated sodium bicarbonate solution (3 × 150 ml) and water (150 ml). This was followed by evaporation *in vacuo* to a reddish-brown foaming oil for chromatography on silica gel (150 g) in methylene chloride. The product (**1**: $R_1 = R_2 = CH_3$), a yellowish white foam (23.43 g, 97%) was eluted with 3–4% methanol in methylene chloride. A pilot reaction had previously yielded 1.57 g (95%) of foam from 1.2 g of starting material.

The ^{1}Hmr spectrum of the material showed signals (δ TMS) at 8.26 (1H, sharp s, 8 proton of G), 8.10–7.60 (5H, m, C_6H_5CO protons), 6.20 (1H, d, $J \simeq 6.0$ Hz, 1′ anomeric sugar proton), 2.08 (3H, sharp s, CH_3CO protons), and 2.00 ppm (6H, sharp s, 2 CH_3CO protons).

*N²-Benzoyl-3′,5′-O-diacetylguanosine (**2**: $R_1 = R_2 = CH_3$)*

Hydrazine hydrate (2.44 ml, 50.4 mmol) was added to a solution of the N^2-benzoyl-2′,3′,5′-*O*-triacetylguanosine (**1**: $R_1 = R_2 = CH_3$) (23.43 g, 45.8 mmol) prepared above, in a 4:1 pyridine – acetic acid mixture. After overnight stirring at

Can. J. Chem. Downloaded from www.nrcresearchpress.com by 210.87.254.6 on 09/05/12
For personal use only.

TABLE 1. The ^{1}Hmr data of 2′- and 3′-acetate isomers

Ribonucleoside* derivatives	H-1′ chemical shift (ppm)	$J_{1',2'}$ (Hz)	Acetyl protons (ppm)	Reference
AcO—G^{bz}(OH)—OAc	5.98	7.0	2.12 2.05	
AcO—G^{bz}(OAc)—OH	6.18	5.0	2.12 2.05	
BzO—G^{bz}(OH)—OAc	6.00	6.0	2.20	7
BzO—G^{bz}(OAc)—OH	6.20	4.5	2.15	7
AcO—A(OH)—OAc	6.00	6.0	2.12 2.02	13
AcO—A(OAc)—OH	6.20	4.0	2.09 1.98	13

*Single line shorthand is used to condense structural formula

AcO—G^{bz}(OH)—OAc

↑ 5′ ↑ 2 ↑ 2′ ↑ 3′

where G is guanosine and A is adenosine.

room temperature, tlc indicated a trace of starting material, diacetylated products (R_F 0.50, ca. 90%), and monoacetylated by-products (R_F 0.30, ca. 10%). The reaction was quenched with acetone. After 30 min, the yellowish brown mixture was partially evaporated and extracted from water (150 ml) into methylene chloride (4 × 150 ml). The combined organic extracts were washed with water (2 × 100 ml), then saturated sodium bicarbonate solution (4 × 100 ml), and water (2 × 100 ml). Combined organic extracts were evaporated *in vacuo* to a green foam for chromatography on silica gel (150 g) in methylene chloride. The diacetate mixture was eluted with 5–6% methanol in methylene chloride. The ^{1}Hmr analysis of the crude diacetate mixture showed a mixture of 2′-and 3′-acetates as indicated by the additional anomeric doublet ($J \simeq 5.0$ Hz) at 6.18 ppm. Integration of the anomeric doublets showed an approximate 1:5 mixture of 2′(3′)-acetates. Crystallization of the yellow foam (14.92 g) from warm methanol yielded as a single crop, N^2-benzoyl-3′,5′-*O*-diacetylguanosine (**2**: $R_1 = R_2 = CH_3$) (13.1 g, 61%) as a fluffy white solid (mp 131–133°C). Thin-layer chromatography indicated only trace quantities remaining in the mother liquor. A pilot reaction had previously yielded 1.92 g (60%) of the desired isomer from 3.5 g of starting material.

The ^{1}Hmr spectrum of the material (**2**: $R_1 = R_2 = CH_3$) showed signals (δ TMS) at 8.30 (1H, sharp s, 8 proton of G), 8.16–7.60 (5H, m, C_6H_5CO protons), 5.98 (1H d, $J \simeq 7.0$ Hz, 1′ anomeric sugar proton), 3.67 (2H, sharp s, H_2O protons), 2.12 (3H, sharp s, CH_3CO protons) and 2.05 ppm (3H, sharp s, CH_3CO protons). *Anal.* calcd. for $C_{21}H_{21}N_5O_8 \cdot H_2O$ (mol. wt. 489.444): C 51.53, H 4.74, N 14.31; found: C 51.39, H 4.91, N 14.32.

N^2-*Benzoyl-2′-O-tetrahydropyranylguanosine (3)*

A solution of *p*-toluenesulfonic acid monohydrate (142 mg, 0.75 mmol) in dry *p*-dioxan (15 ml) containing molecular sieves (500 mg) was cooled on ice, to solidification. 2,3-Dihydro-4*H*-pyran (5 ml, 59.6 mmol) was then added dropwise, with stirring, causing partial melting of the frozen solution. N^2-Benzoyl-3′,5′-*O*-diacetylguanosine (**2**: $R_1 = R_2 = CH_3$) (1.4 g, 2.98 mmol) suspended in dry *p*-dioxan (10 ml) was added portionwise, with stirring. After 45 min, the reaction was allowed to warm to room temperature. Reaction (R_F 0.50 → 0.70) was ca. 60% complete after 6 h, and finished by standing at room temperature overnight. After brief chilling, and neutralization with concentrated ammonia, ammonium tosylate was filtered off and washed with methylene chloride. Filtrate and washings were evaporated *in vacuo* to a yellow-green oil, which was dissolved in absolute ethanol (15 ml) and pyridine (10 ml). To this rapidly stirred solution was added a mixture of aqueous 2 *N* sodium hydroxide (7.5 ml) and ethanol (7.5 ml). Reaction (R_F 0.68 → 0.45 and 0.35) was quenched after 5 min by neutralization with Dowex 50W-X8 resin (pyridinium form). After filtration, and washing with ethanol, the filtrate and washings were evaporated *in vacuo* to a yellow-green foam for chromatography on silica gel (25 g). The two diastereoisomers of **3** (R_F 0.35 and 0.45) eluted as a mixture (755 mg) with 3–4% methanol in methylene chloride. Pure low R_F **3** (490 mg) eluted with 4–6% methanol. Combined yield of the two isomers corresponds to 85%, compared to 86% (7) starting from 3′-*O*-acetyl-N^2,5′-*O*-dibenzoylguanosine (**2**: R_1 = Ph, $R_2 = CH_3$). The ^{1}Hmr spectrum of the low R_F product was identical to that obtained previously from **2**: R_1 = Ph, $R_2 = CH_3$ (7).

2′,3′,5′-O-*triacetyladenosine (4)*

Adenosine was acetylated with a five-fold excess of acetic anhydride in dry pyridine. 2′,3′,5′-*O*-Triacetyladenosine (**4**) was recovered in 90% yield as white crystals, mp 172–173°C (lit. (10) mp 174°C) from toluene.

3′,5′-O-*diacetyladenosine (5)*

Hydrazine hydrate (1.36 ml, 28 mmol) was added to a solution of 2′,3′,5′-*O*-triacetyladenosine (**4**) (10 g, 25.5 mmol) in a 4:1 pyridine – acetic acid mixture (8). After overnight reaction, tlc indicated unreacted material (R_F 0.65, ca. 10%), diacetylated products (R_F 0.45, ca. 85%) and monoacetylated by-products (R_F 0.25, ca. 5%). Reaction was quenched with acetone (10 ml, 134 mmol). After 30 min, the mixture was partially evaporated *in vacuo* and continuously extracted into methylene chloride (2 × 300 ml). Combined extracts were evaporated *in vacuo* to a foaming oil for chromatography on silica gel (150 g) in methylene chloride. Unreacted triacetate eluted with 3% methanol in methylene chloride. The diacetate mixture eluted with 4–6% methanol.

The ^{1}Hmr spectrum of the crude diacetate mixture showed a mixture of 2′- and 3′-acetates, as indicated by the additional anomeric doublet ($J \simeq 4.0$ Hz) at 6.20 ppm and additional acetyl singlets at 2.08 and 1.98 ppm. Integration of the anomeric protons indicated an approximate 1:5 mixture of 2′(3′)-acetates.

The ^{1}Hmr spectrum of the material (**5**) showed signals

Can. J. Chem. Downloaded from www.nrcresearchpress.com by 210.87.254.6 on 09/05/12
For personal use only.

(δ TMS) at 8.38 (1H, sharp s, 8 proton of A), 8.25 (1H, sharp s, 2 proton of A), 6.00 (1H, d, $J \simeq 6.0$ Hz, 1′ anomeric sugar proton), and 2.12 and 2.02 ppm (3H, 3H, sharp s, two CH_3CO protons). Crystallization of the yellow foam (6.60 g) from warm ethanol yielded 3′,5′-*O*-diacetyladenosine (**5**) (5.27 g, 59%) as white crystals, mp 146–148°C. This compared favourably with a yield of 43% previously obtained by 2′,3′-orthoacetate ring opening (11).

Acknowledgements

Financial assistance from the J. P. Bickell Foundation and the National Research Council of Canada is gratefully acknowledged.

1. E. S. Werstiuk and T. Neilson. Can. J. Chem. **54**, 2689 (1976).
2. K. K. Ogilvie, S. L. Beaucage, D. W. Entwistle, E. A. Thompson, M. A. Quilliam, and J. B. Westmore. J. Carbohydr. Nucleosides, Nucleotides, **3**, 197 (1976).
3. J. H. van Boom and P. M. J. Burgers. Tetrahedron Lett. 4875 (1976).
4. J. Stawinski, T. Hozumi, and S. A. Narang. Can. J. Chem. **54**, 670 (1976).
5. T. E. England and T. Neilson. Can. J. Chem. **54**, 1714 (1976).
6. M. C. Ganoza. Can. J. Chem. **55**, 267 (1977).
7. Thomas Neilson, E. V. Wastrodowski, and E. S. Werstiuk. Can. J. Chem. **51**, 1068 (1973).
8. Y. Ishido, N. Nakazaki, and N. Sakairi. J. Chem. Soc. Chem. Commun. 832 (1976).
9. C. Chládek and J. Smrt. Coll. Czech Chem. Commun. **29**, 214 (1964).
10. H. Bredereck and A. Martini. Chem. Ber. **80**, 401 (1949).
11. H. P. M. Fromageot, B. E. Griffin, C. B. Reese, and J. E. Sulston. Tetrahedron, **23**, 2315 (1967).
12. B. E. Griffin, M. Jarman, and C. B. Reese. Tetrahedron, **24**, 639 (1968).
13. H. P. M. Fromageot, B. E. Griffin, C. B. Reese, J. E. Sulston, and D. R. Trentham. Tetrahedron, **22**, 705 (1966).

Can. J. Chem. Downloaded from www.nrcresearchpress.com by 210.87.254.6 on 09/05/12
For personal use only.

Sesquiterpene lactones from *Centaurea linifolia* Vahl[1]

A. G. González, J. Bermejo, J. M. Amaro, G. M. Massanet, A. Galindo, and I. Cabrera

Department of Organic Chemistry and Biochemistry, University of La Laguna, Instituto de Productos Naturales Organicos del CSIC, Tenerife, Spain

Received July 19, 1977

A. G. González, J. Bermejo, J. M. Amaro, G. M. Massanet, A. Galindo, and I. Cabrera. Can. J. Chem. **56**, 491 (1978).

Three new sesquiterpene lactones, linichlorins A, B, and C were isolated from the aerial parts of *Centaurea linifolia* Vahl and their structures were determined by physical and chemical methods. The sesquiterpene lactones chlorohyssopifolins A, B, C, D, E, aguerin B, and vahlenin were also isolated from the same plant.

A. G. González, J. Bermejo, J. M. Amaro, G. M. Massanet, A. Galindo et I. Cabrera. Can. J. Chem. **56**, 491 (1978).

Trois nouvelles lactones sesquiterpéniques ont été isolées a partir de *Centaurea linifolia* Vahl; ses structures ont été determinées par des méthodes physiques et chimiques. On a isolé aussi les lactones sesquiterpéniques, chlorohyssopifolins A, B, C, D, E, aguerin B et vahlenin.

Can. J. Chem. Downloaded from www.nrcresearchpress.com by 84.22.46.98 on 09/08/12
For personal use only.

As part of our studies of the chemical constituents of the genus *Centaurea* (Compositae) we examined *Centaurea linifolia* Vahl, endemic to the Iberian peninsula. The plant was gathered in July at Los Monegros (Zaragoza) and extracted as usual (see Experimental). By column chromatography 10 sesquiterpene lactones were separated and 7 were identified, by comparison with authentic samples, as centaurepensin (chlorohyssopifolin A) (**1***b*), acroptilin (chlorohyssopifolin C) (**2***b*), chlorohyssopifolins B (**1***a*), D (**1***c*), and E (**1***d*), vahlenin (**4***e*), and aguerin B (**3***e*), isolated from other species of *Centaureae* (1–6). The other three lactones were chlorinated guaianolides found for the first time and were named linichlorin A (**1***e*), B (**3***b*), and C (**5***b*).

Linichlorin A (**1***e*): $C_{19}H_{23}O_6Cl$, mol. wt. (ms) 382, mp 153–155°C, $[\alpha]_D$ +89°. The ir spectrum showed bands at 3450 (OH), 1740 (α,β′-unsaturated γ-lactone), 1710 (ester), and 1640 cm^{-1} (double bonds). Its nmr (Table 1) and mass spectra clearly show that it is a methacrylic acid ester (doublets at δ 6.20 and 5.65 (J = 2 Hz), singlet of a vinyl methyl at δ 2.0, and prominent peaks at m/e 296 ($M^+ - C_4H_6O_2$) and 69 (C_4H_5O)). A pair of doublets at δ 4.35 and 3.95 (J = 11 Hz) is attributable to a —C—(OH)—CH_2Cl group at C-4, a pair of lowfield doublets at δ 6.20 and 5.60 (J = 3 Hz) confirms the presence of an exocyclic methylene in **1***e* while two signals at δ 5.10 and 4.80 represent a methylene at C-10.

From these data, linichlorin A was assigned the formula **1***e*. $NaBH_4$ reduction led to the corresponding 11,13-dihydroderivative (**6***e*), with a new doublet at δ 1.25 (J = 9 Hz) typical of a secondary methyl. This compound proved to be the same as 8α-metacryloyl-11,13α-dihydrochlorohyssopifolin B, obtained in this laboratory (7) by treating centaurepensin with a zinc–copper couple.

Linichlorin B (**3***b*): $C_{19}H_{23}O_6Cl$, mol. wt. (ms) 382, mp 144–146°C, $[\alpha]_D$ +95° has an ir spectrum similar to that of linichlorin A. Its nmr shows signals in the vinyl region which correspond to three methylenes, at C-4, C-10, and C-11 (Table 1). A β-chloro-α-hydroxyisobutyric group is indicated by nmr (pair of doublets at δ 3.90 and 3.65 (J = 11 Hz), singlet at 1.50 (—C—(OH)*Me*—CH_2Cl)) and by ms (m/e 244 ($M^+ - C_4H_7O_3Cl$)). These data suggest the formula **3***b* for linichlorin B. By $NaBH_4$ treatment of **3***b*, the 11,13α-dihydroderivative (**7***b*) was obtained (8α,β-chloro-α-hydroxyisobutyrate of 11,13α-dihydrocynaropicrin) plus its saponification product **7***a* (11,13α-dihydrodeacylcynaropicrin). Both of these had been obtained in this laboratory from centaurepensin, the structure and stereochemistry of which, in its turn, had previously been established by González *et al.* (7) by dehalogenation and saponification, thus giving the deacyldihydrocynaropicrin derivative of cynaropicrin for which the assymetrical centres C-1 [α-H], C-5 (α-H), C-6 (β-H), and C-7 (α-H) have been rigorously established. By reductive elimination of the spiroepoxide at C-4 with $MgBr_2$–(H_g)Mg (8), **3***b* can be obtained from acroptilin (**2***b*), further confirming the structure of this lactone as **3***b*.

Linichlorin C (**5***b*): mp 160–162°C, $[\alpha]_D$ +83°, $C_{21}H_{27}O_9Cl$ from its elemental analysis and ms (fragment at m/e 427 ($M^+ - CH_2OH$)), shows bands of hydroxyl groups, of an α,β′-unsaturated γ-lactone, esters and double bonds in its ir. Its nmr and ms reveal an acetyl group (singlet at 2.20 and peak at m/e 43 (C_2H_3O)) and a β-chloro-α-hydroxy-

[1]Part 35 of the series "Chemical constituents of the *Compositae*." For Part 34 see ref. 6.

Can. J. Chem. Downloaded from www.nrcresearchpress.com by 84.22.46.98 on 09/08/12
For personal use only.

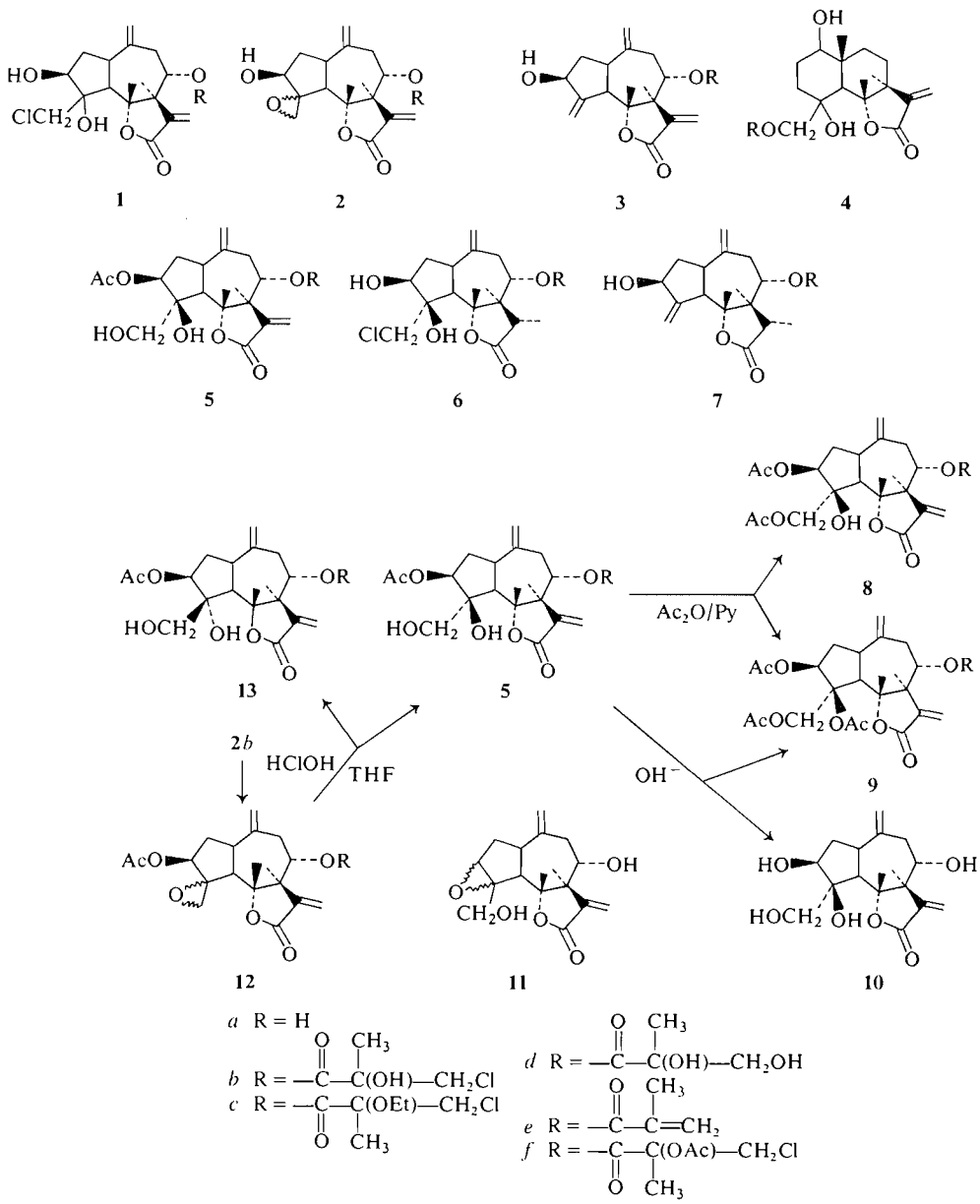

isobutyric grouping. A prominent peak in its ms spectrum at *m/e* 31 (CH_2OH) suggests the existence of a primary hydroxyl group in the molecule. By mild acetylation **8***b* was formed with a paramagnetic shift of 0.5 ppm from the CH_2OH signals recorded in the nmr of **5***b*. Protracted treatment produced **9***f*. Alkaline hydrolysis of **5***b* gave **10** as major product and **11** in lower yield. Compound **11** proved to be identical (nmr and mp) to the compound obtained by Rybalko *et al.* (9) upon saponifying acroptilin. Compound **8***b* showed no reaction on treatment with Jones' reagent, leading to the assumption that the acetate group in **5***b* esterified the hydroxyl at C-3. This was confirmed when **5***b* was obtained from acroptilin. In fact the acetylation at 0°C of **2***b* yielded a mixture of **12***b* and **12***f* and treatment of **12***b* with $HClO_4$ at room temperature (10) caused the opening of the oxiran ring to give a mixture of diols (**5***b*) epimeric at C-4 and identical to **5***b* and **13***b*. A comparison of the nmr spectra of both diols showed a downfield chemical shift of the H-6 in **5***b* relative to **13***b* ($\Delta\delta = +0.30$ ppm probably due to the 1–3

TABLE 1. Proton chemical shifts of linichlorins and related compounds*

Compound	H-3	H-6(q)	H-8(c)	H-13(d)	H-14	H-15(d)	3'H-2†	2'Me†	OAc
1*e*	4.15	4.75	5.05	6.20 (3)	5.10	4.35 (11)	6.20 (2)	2.0 s	
				5.60 (3)	4.80	3.95 (11)	5.65 (2)		
3*b*	4.55	4.30	5.25	6.25 (3)	5.20	5.45 (6)	3.90 (11)	1.50 s	
				5.60	5.10		3.65 (11)		
5*b*	4.90	4.85	5.20	6.20 (3)	5.15	3.90 (11)	3.90 (11)	1.55 s	2.20 s
				5.60 (3)	5.02	3.65 (11)	3.65 (11)		
6*e*	4.15	4.65	5.05	1.25 (7)	5.10	4.25 (11)	6.15 (2)	1.95 d	
					4.90	3.85 (11)	5.60 (2)		
7*a*		4.50		1.32 (7)	5.05	5.25			
					4.95				
7*b*	4.55	4.20	5.20	1.25 (7)	5.15	5.43	3.86 (11)	1.50 s	
					5.10	5.35	3.59 (11)		
8*b*	4.45		5.25	6.25 (3)	5.20	4.65 (11)	3.90 (11)	1.55 s	2.10 s
				5.60 (3)	5.10	4.30 (11)	3.65 (11)		
9*b*	4.45		5.40	6.25 (3)	5.13	4.95 (11)	4.05 (11)	1.70 s	2.10 c
				5.78 (3)	5.03	4.70 (11)	3.75 (11)		
10	4.05	4.55	4.10	6.15 c	5.10	4.05 (11)			
					4.95	3.80 (11)			
11	3.60	4.20	3.80	6.30 c	5.05	3.95 s			
12*b*	4.90	4.40	5.25	6.20 (3)	5.20	3.25 (6)	3.85 (11)	1.50 s	2.0 s
				5.55 (3)	5.10	3.05 (6)	3.55 (11)		
13*b*	5.05	4.55	5.20	6.25 (3)	5.20	4.35 (11)	3.85 (11)	1.55 s	2.10 s
				5.65 (3)	5.10	4.15 (11)	3.65 (11)		

*All values are in δ relative to internal TMS; s, singlet; d, doublet; q, quartet; c, complex; *J* values (Hz) in parentheses.
†Acyl group C(1')—C(2')Me—C(3').

diaxial interaction between the β H-6 and the C-4 OH. This suggests a β orientation for the C-4 OH in **5***b*.

Experimental

Melting points were taken on a Kofler block and are uncorrected. Optical activities were measured in $CHCl_3$, ir spectra in $CHCl_3$ on a Perkin–Elmer spectrophotometer, and nmr spectra in $CDCl_3$ with TMS as internal standard on a 90 MHz Perkin–Elmer instrument.

Extraction and Separation

The dried plant (12 kg) collected at Los Monegros (Zaragoza) in July was chopped and exhaustively extracted with EtOH in a Soxhlet. The extract was filtered, concentrated to 500 ml and, after adding $Pb(OAc)_2$ (15 g) in hot H_2O (500 ml), was left for 24 h. It was then filtered, concentrated until free of EtOH and the residue (630 g) was extracted with $CHCl_3$ and chromatographed on a column of silica gel. Elution with benzene – ethyl acetate yielded, in order of increasing polarity, linichlorin A, aguerin B, chlorohyssopifolins A, D, and C, linichlorin B, chlorohyssopifolins B and E, vahlenin, and linichlorin C.

Linichlorin A (**1***e*) was purified by preparative tlc with petrol – ethyl acetate (7:3) (six elutions) and crystallized from chloroform – isopropyl ether: mp 153–155°C, $[\alpha]_D$ +89° (*c* 0.58); ir (KBr) ν_{max}: 3450, 1740, 1710, 1630, and 740 cm^{-1}; ms *m/e*: 382 (M^+), 296, 278, 260, 69. *Anal.* calcd. for $C_{19}H_{23}O_6Cl$: C 59.60, H 6.01, Cl 9.28; found: C 59.81, H 6.24, Cl 9.32.

Linichlorin B (**3***b*): mp 144–146°C (EtOAc–petrol), $[\alpha]_D$ +95° (*c* 0.45); ir ν_{max}: 3560, 3540, 1760, 1740, and 1640 cm^{-1}; ms *m/e*: 382 (M^+), 296, 278, 260, 69. *Anal.* calcd. for $C_{19}H_{23}O_6Cl$: C 59.60, H 6.01, Cl 9.28; found: C 59.59, H 6.13, Cl 8.98.

Linichlorin C (**5***b*): mp 160–162°C (EtOAc–petrol), $[\alpha]_D$ +83° (*c* 0.36); ir (KBr) ν_{max}: 3550, 3360, 1760, 1720, and 1660 cm^{-1}; ms *m/e*: 427 ($M^+ - 31$), 391, 368, 320, 302, 260, 242, 93, 57, 43. *Anal.* calcd. for $C_{21}H_{27}O_9Cl$: C 55.02, H 5.89, Cl 7.75; found: C 54.79, H 6.11, Cl 7.77.

*$NaBH_4$ Reduction of **1***e*

Sodium borohydride (600 mg) was added to compound (**1***e*) (300 mg) dissolved in methanol (50 ml) and the solution was stirred for 10 min at 0°C. The solution was evaporated and the residue acidified with 5% hydrochloric acid and extracted with ethyl acetate. The resulting solid was chromatographed on silica gel, yielding the product (**6***e*): mp 164–167°C, $[\alpha]_D$ +33.4° (*c* 0.25); ir ν_{max}: 3540, 1760, and 1640 cm^{-1}; ms *m/e*: 298 ($M^+ - 86$), 280, 262, 91, and 69.

*$NaBH_4$ Reduction of **3***b*

A solution of compound (**3***b*) (500 mg) in methanol (30 ml) was treated with sodium borohydride (100 mg). Under the same conditions as above, a mixture of two products was obtained which was separated by preparative tlc with petrol – ethyl acetate (4:6). Derivative **7***b*, oil: $[\alpha]_D$ +88° (*c* 0.24); ir ν_{max}: 3460, 1770, 1730, and 1640 cm^{-1}; ms *m/e*: 384 (M^+), 264, 246, 93. Derivative **7***a*: mp 134–136°C (EtOAc–petrol), $[\alpha]_D$ +70° (*c* 0.27 in MeOH); ir (KBr) ν_{max}: 3330, 1730, and 1635 cm^{-1}; ms *m/e*: 264 (M^+), 246, 218, and 200.

*Treatment of **2***b* with $MgBr_2$–Mg(Hg)*

A solution of **2***b* (500 mg) in THF (20 ml) was added to magnesium amalgam (Hg 3.53 g, Mg 0.072 g) under argon atmosphere. A solution of $MgBr_2$ (180 mg) in THF was then introduced and the mixture was continually stirred for 1 night under argon atmosphere. It was filtered, the solvent being eliminated, poured into water, and extracted with ethyl acetate. By chromatography on silica gel (petrol – ethyl

Can. J. Chem. Downloaded from www.nrcresearchpress.com by 84.22.46.98 on 09/08/12
For personal use only.

acetate 6:4), two products were separated, one proving to be linichlorin B (**3***b*).

*Diacetate (**8***b*)

A solution of **5***b* (300 mg) in pyridine (0.2 ml) and Ac_2O (1 ml) was left standing for 2 h at room temperature. By silica gel chromatography (petrol–EtOAc 7:3) monoacetyllinichlorin C (**8***b*) was obtained, oil: $[\alpha]_D$ +82° (*c* 0.43); ir ν_{max} 3530, 1770, 1740, and 1640 cm^{-1}; ms *m/e*: 464 ($M^+ - 36$), 427, 462, 302, 242, 93, and 43.

*Tetraacetate (**9***f*)

Treatment of **5***b* (150 mg) with Ac_2O (3 ml) in pyridine (0.2 ml) at room temperature during 48 h yielded a liquid tetraacetate (**9***f*) which was purified by silica gel chromatography (benzene – ethyl acetate 1:1), $[\alpha]_D$ +56° (*c* 0.36); ir ν_{max}: 1770, 1740, and 1640 cm^{-1}; ms *m/e* 524 ($M^+ - 60$), 481, 421, 404, 284, 241, 224, 93, 43.

*Alkaline Hydrolysis of **5***b*

A solution of compound (**5***b*) (500 mg) in methanol (10 ml) was treated with aqueous 5% potassium carbonate (50 ml) during 48 h at room temperature. The soln was acidified with 5% hydrochloric acid until p*H* 6, saturated with NaCl and continuously extracted with EtOAc. The crude product (350 mg) was eluted on a column of silica gel (benzene–EtOAc 1:4). Crystallization from EtOAc–petrol gave a solid (**11**): mp 164–166°C, $[\alpha]_D$ +61° (*c* 0.2); ir (KBr) ν_{max}: 3460, 1760, and 1640 cm^{-1}; ms *m/e* 278 (M^+), 260, 247, 231. The other product was an amorphous solid (**10**): $[\alpha]_D$ +32° (*c* 0.64 in MeOH); ir (film) ν_{max}: 3500–3300, 1740, and 1640 cm^{-1}; ms *m/e* 296 (M^+), 278, 265, 248, 229. *Anal.* calcd. for $C_{15}H_{20}O_6$: C 60.80, H 6.80; found: C 60.88, H 6.82.

Treatment of Diacetate with Jones' Reagent

Diacetate **8***b* (250 mg) was dissolved in acetone (20 ml) and Jones' reagent (8 ml) was added in drops. The solution was stirred for 1 h at 0°C and then brought to room temperature and kept overnight. Excess reagent was destroyed with MeOH and the solution was filtered and evaporated at reduced pressure. The residue was extracted with EtOAc, dried on Na_2SO_4, and concentrated, recovering the starting material.

*Acetylation of **2***b*

Treatment of **2***b* (500 mg) with Ac_2O–Py at 0°C produced a mixture of acetates (480 mg) separated by silica gel chromatography (petrol–EtOAc 6:4). Monoacetate (**12***b*): mp 173–176°C (CH_3Cl – isopropyl ether), $[\alpha]_D$ +79° (*c* 0.48); ir ν_{max}: 3540, 1765, 1740, and 1650 cm^{-1}; ms *m/e* 440 (M^+), 380, 370, 302, 93, 43. Diacetate (**12***f*): mp 111–112°C, $[\alpha]_D$ +72° (*c* 1.75); ir ν_{max}: 1765, 1735, and 1640 cm^{-1}; ms *m/e* 302 ($M^+ - 180$), 259, 242, 91, 43.

*Treatment of **12***b* *with $HClO_4$*

One millilitre of 3 *N* $HClO_4$ was added to a solution of **12***b* (300 mg) in THF (15 ml) and the mixture was left at room temperature. The reaction was followed by tlc until the starting material was virtually eliminated (1 h). The products were extracted with $CHCl_3$, dried, distilled, and the residue was separated by preparative tlc with $CHCl_3$–Me_2CO (8:2) (three elutions). Diol **5***b*: mp 160°C, $[\alpha]_D$ +83° (identical with natural linichlorin C (mixture mp, ir, nmr, and chromatography results)). Diol **13***b*: $[\alpha]_D$ +41° (*c* 0.53); ir ν_{max}: 3520, 1760–1710, and 1640 cm^{-1}; ms *m/e* 427 ($M^+ - 31$), 368, 321, 302, 260, 242, 229, and 93.

1. J. Harley-Mason, A. T. Hewson, O. Kennard, and R. C. Pettersen. Chem. Commun. 460 (1972).
2. A. G. González, J. Bermejo, J. L. Bretón, and J. Triana. Tetrahedron Lett. 2017 (1972).
3. A. G. González, J. Bermejo, I. Cabrera, and G. M. Massanet. Anal. Quim. **70**, 74 (1974).
4. A. G. González, J. Bermejo, J. L. Bretón, G. M. Massanet, and J. Triana. Phytochemistry, **13**, 1193 (1974).
5. R. I. Evstratova, V. I. Scheichenko, and K. S. Rybalko. Khim. Prir. Soedin. **9**, 161 (1973).
6. A. G. González, J. Bermejo, I. Cabrera, A. Galindo, G. M. Massanet, and H. Mansilla. Phytochemistry, **16**, 1836 (1977).
7. A. G. González, J. Bermejo, J. L. Bretón, G. M. Massanet, B. Domínguez, and J. M. Amaro. J. Chem. Soc. Perkin Trans. 1, 1663 (1976).
8. F. Bertini, P. Grasselli, G. Zubiani, and G. Cainelli. Chem. Commun. 144 (1970).
9. R. I. Evstratova, K. S. Rybalko, and V. I. Scheichenko. Khim. Prir. Soedin. **8**, 451 (1972).
10. E. Ali, P. P. Ghosh-Dastidar, S. C. Pakrashi, J. L. Durham, and A. M. Duffield. Tetrahedron, **28**, 2285 (1972).

Can. J. Chem. Downloaded from www.nrcresearchpress.com by 84.22.46.98 on 09/08/12
For personal use only.

Photoelectron spectra of substituted benzamides

E. J. McAlduff and B. M. Lynch

Department of Chemistry, St. Francis Xavier University, Antigonish, N.S., Canada B0H 1C0

AND

K. N. Houk[1]

Department of Chemistry, Louisiana State University, Baton Rouge, LA 70803, U.S.A.

Received June 16, 1977

E. J. McAlduff, B. M. Lynch, and K. N. Houk. Can. J. Chem. **56**, 495 (1978).

The photoelectron spectra of the following substituted benzamides have been determined: *p*-CH_3O, *p*-CH_3, *p*-Cl, H, *p*-F, *p*-CN, *p*-NO_2, *m*-CH_3O, *m*-CH_3, *m*-Cl, and *m*-NO_2. The first six ionization potentials have been assigned with reference to the phenyl and amide moieties. As an aid to the assignment CNDO/S calculations have been performed on the methoxy, methyl, and nitro benzamides. Linear relationships have been shown to exist between the first phenyl IP of disubstituted and monosubstituted benzenes. The slopes of these relationships have been shown to be related to the electron releasing ability of the substituent.

By comparison of the pes data with nmr chemical shifts, the first phenyl IP has been shown to be related to the electron density at the position of substitution of the amide group. Likewise, the amide IP centered on the nitrogen has been shown to be related to the electron density on nitrogen.

E. J. McAlduff, B. M. Lynch et K. N. Houk. Can. J. Chem. **56**, 495 (1978).

On a déterminé les spectres photoélectroniques des benzamides substituées suivantes: *p*-CH_3O, *p*-CH_3, *p*-Cl, H, *p*-F, *p*-CN, *p*-NO_2, *m*-CH_3O, *m*-CH_3, *m*-Cl et *m*-NO_2. On a attribué les six premiers potentiels d'ionisation en se référant aux portions phényle et amide. Afin d'aider à l'attribution, on a effectué des calculs CNDO/S sur les benzamides substituées par des groupements méthoxy, méthyle et nitro. On a montré qu'il existe des relations linéaires entre le potentiel d'ionisation du premier phényle de benzènes disubstitués et monosubstitués. On a démontré que les pentes de ces relations sont reliées à l'habilité du substituant à donner des électrons.

En effectuant une comparaison de données de spectres photoélectroniques avec des déplacements chimiques en rmn, on a montré que le potentiel d'ionisation du premier phényle est relié à la densité électronique au niveau de la position de substitution de groupe amide. De la même manière le potentiel d'ionisation de l'amide centré au niveau de l'azote est relié à la densité au niveau de l'azote.

[Traduit par le journal]

Introduction

Electronic effects of substituents upon reactivity have been empirically quantified in Hammett relationships and other extra thermodynamic treatments (1). Various experimental and theoretical criteria have been used to divide gross substituent effects into polar, steric, and resonance effects but experimental reactivity probes, with the exception of ion cyclotron resonance studies (2), are always subject to uncertainties involving solvent effects or uncontrollable variables. Until recently theoretical treatments (3) were too inexact to yield reliable results.

Photoelectron spectroscopy can be used to measure directly the influence of a substituent upon the elementary ionization event, and upon the relative energies of the ground state and various radical cation states of the molecule. By the investigation of substituent effects upon ionization potentials of substituted benzenes, we hoped to determine how the presence of a substituent on the benzene ring influences the ability of a second substituent to stabilize or destabilize the radical cation states formed by ionization.

Finally, through Koopmans' theorem (4), we can utilize the information obtained from photoelectron spectroscopy to map the electron densities in filled molecular orbitals of substituted benzenes.

By determining the photoelectron spectra of a series of *para* and *meta* substituted benzamides we hoped to study a range of substituents from strong donors to strong acceptors and their effect on the phenyl IP values of benzamides. In addition, the amido substituent is particularly significant in that its influence is secondary to the other substituents. It is also useful to determine the photoelectron spectra of benzamides since three of the IP values can be associated with the amide moiety and thus the in-

[1]Alfred P. Sloan Foundation Fellow 1975–1977; Camille and Henry Dreyfus Teacher–Scholar Grant Recipient 1972–1977.

Can. J. Chem. Downloaded from www.nrcresearchpress.com by 210.87.254.42 on 09/05/12
For personal use only.

Can. J. Chem. Downloaded from www.nrcresearchpress.com by 210.87.254.42 on 09/05/12
For personal use only.

fluence of substituents on the ring on the energy of an orbital not effectively connected with the ring can be determined.

A number of investigators (5–9) have studied the photoelectron spectra of mono- and disubstituted benzenes. In monosubstituted benzenes the substituent interacts with the phenyl moiety to remove the degeneracy of the e_{1g} π orbitals of benzene. At the point of substitution one of the benzene orbitals (b_1 in C_{2v} symmetry) has its maximum electron density whereas the other orbital (a_2 in C_{2v} symmetry) has a node. As can be seen from Fig. 1, electron releasing substituents interact conjugatively with the phenyl orbital, e_{1g} (S) via a high lying occupied lone pair orbital to produce a new π ionization substantially shifted to lower IP. The other phenyl orbital e_{1g} (A) (termed Ph_A in this discussion) is found essentially unchanged from its position in benzene. Electron withdrawing groups shift both bands to higher IP values. The location of the first ionization potential in substituted benzenes which will be termed Ph_S in this discussion has been correlated with the σ constants of the substituent (9).

In disubstituted benzenes Turner and co-workers (5, 6) have pointed out that the separation between the two highest π levels is nearly equal to the sum of the separations in the corresponding monosubstituted benzenes. Rao (9) has pointed out that this approximation fails in the case of substituents interacting strongly with the phenyl π system. Rao has correlated all three π ionization potentials of substituted benzenes with the Hammett σ constants (10) of the substituent. Lindberg *et al.* (11) have correlated esca shifts of *meta* and *para* carbon in disubstituted benzenes with Hammett σ constants and have established the fact that esca shifts can be treated as linear free energy relationships.

The photoelectron spectra of formamide and acetamide have been determined (5) and the spectra of similar alkyl carbonyl compounds extensively described (12).

In this investigation we have studied the effect on the photoelectron spectrum of combining the phenyl and amide moieties in benzamide and the perturbation on its energy levels by a variety of substituents in the *meta* and *para* positions.

Results and Discussion

The photoelectron spectra of *m*-benzamides and benzamide are shown in Fig. 2. Figure 3 contains the photoelectron spectra of the *p*-benzamides. The IP values for the various band maxima and their

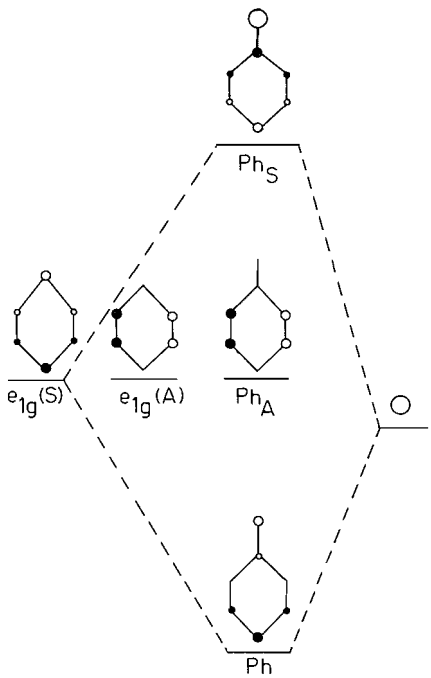

FIG. 1. Orbital energy diagram showing Ph_S, Ph_A, and Ph orbitals of donor substituted benzene.

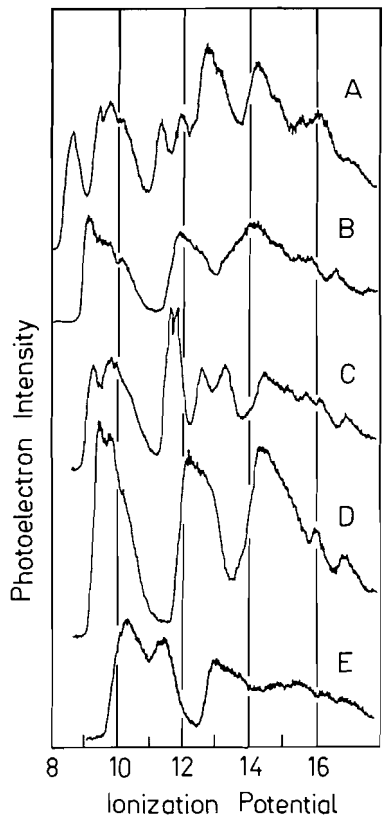

FIG. 2. Photoelectron spectra of benzamide and *meta* benzamides: (*A*) *m*-OCH_3; (*B*) *m*-CH_3; (*C*) *m*-Cl; (*D*) benzamide; (*E*) *m*-NO_2.

Can. J. Chem. Downloaded from www.nrcresearchpress.com by 210.87.254.42 on 09/05/12
For personal use only.

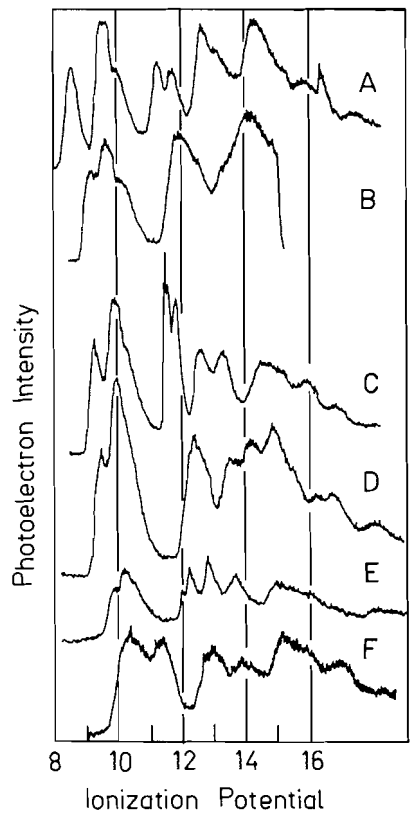

FIG. 3. Photoelectron spectra of *para* benzamides: (*A*) p-OCH_3; (*B*) p-CH_3; (*C*) p-Cl; (*D*) p-F; (*E*) p-CN; (*F*) p-NO_2.

assignments are listed in Table 1. Using the energy level designation which is applied to the constituent moieties, three of these levels are related to the phenyl group and are designated Ph_S, Ph_A, and Ph. The other three are derived from the amide group and are termed n_0, π_0, and $\pi_{C=O}$.

In considering the photoelectron spectrum of benzamide (Fig. 2*D*) it can be seen that the first band at 9.45 eV has shoulders at 9.78 and 10.20 eV. In addition the band with maximum at 12.16 eV has a shoulder at 14.16 eV. When a strong donor group such as OCH_3 or CH_3 is introduced into the *para* position of benzamide the first band is separated from its shoulder components (Fig. 3*A* and *B*) with its maximum appearing at 8.62 and 9.14 eV in p-OCH_3 benzamide and p-CH_3 benzamide, respectively. The peak which appeared at 9.78 eV in benzamide is destabilized to a smaller extent and appears at 9.57 and 9.62 in p-OCH_3 benzamide and p-CH_3 benzamide. Thus the first band at 9.45 eV is assigned to the Ph_S orbital which is characterized by high electron density at the position of substitution and *para* to it. The shoulder at 9.78 eV in benzamide is assigned to Ph_A. This orbital is generally less influenced by donor substituents and is characterized by high electron density in the *ortho* and *meta* positions and a node at the position of substitution and *para* to it. The substituent effect of $CONH_2$ on benzene is analogous to that of other electron withdrawing groups in that it has affected the Ph_A orbital to a larger extent than Ph_S. Ph_S has been stabilized by 0.21 eV and Ph_A by 0.54 relative to benzene. In benzonitrile (7) Ph_S is stabilized by 0.48 and Ph_A by 0.90 and in nitrobenzene (15) Ph_S is stabilized by 0.75 eV and Ph_A by 1.08. The amide group being less strongly electron withdrawing than the cyano or nitro results in less stabilization of the phenyl orbitals but the trend of $Ph_A > Ph_S$ is maintained.

In the amide moiety, the n_0 orbital corresponds to the oxygen lone pair on the carbonyl group. The analogous lone pair in formaldehyde at 10.88 is lowered to 10.20 in acetaldehyde by methyl substitution (12). Phenyl substitution in benzaldehyde lowers it further to 9.69 eV (14). Thus the phenyl substituent effect is 1.75 times as great as methyl. The n_0 IP in formamide at 10.32 eV is lowered to 9.96 eV in acetamide. If the phenyl substituent effect on the oxygen lone pair observed in benzaldehyde is duplicated in the case of benzamide the oxygen lone pair IP might be expected to occur in the region of 9.7 eV. This result together with the fact that the Ph_A band is considerably larger in area than Ph_S in the *para* substituted benzamides leads to the assignment in which n_0 is assumed to be accidentally degenerate with Ph_A of benzamide at 9.78 eV. In the *meta* benzamide this accidental degeneracy is removed.

The orbital designated π_N is largely located on the N atom and is an antibonding combination of the carbonyl π and the nitrogen p orbital. In formamide this IP occurs at 10.52 eV (5) and in acetamide it is found at 10.32 eV. If the phenyl substituent effect on π_N is assumed to be of the same order of magnitude as was observed for n_0 (i.e. 1.75 times the CH_3 substituent effect) the π_N IP might be expected to be found in the region of 10.17 eV. For this reason the

TABLE 1. Ionization potentials (eV) and assignments

R	Ph_S	Ph_A	n_0	π_N	Ph	$\pi_{C=O}$
p-CH_3O	8.62	9.57	9.57	10.02	11.72	14.24
p-CH_3	9.14	9.62	9.62	10.08	11.87	14.06
H	9.45	9.78	9.78	10.20	12.16	14.16
p-Cl	9.35	9.94	9.94	10.29	12.60	14.47
p-F	9.50	10.00	10.00	10.28	12.73	14.80
p-CN	9.99	10.29	10.29	10.60		14.93
p-NO_2	10.33	10.33	10.33	10.69	12.84	15.12
m-CH_3O	8.60	9.45	9.77	10.13	11.81	14.08
m-CH_3	9.11	9.48	9.72	10.08	11.88	13.98
m-Cl	9.34	10.06	9.82	10.31	12.59	14.47
m-NO_2	10.28	10.55	10.05	10.55	12.95	14.66

Can. J. Chem. Downloaded from www.nrcresearchpress.com by 210.87.254.42 on 09/05/12
For personal use only.

shoulder at 10.20 eV in the benzamide spectrum is assigned to the π_N orbital.

The band at 12.16 eV in benzamide is assigned to the phenyl orbital which has been stabilized from 11.67 eV in benzene. This stabilization is comparable to that observed for the Ph_A orbital. The shoulder in this band at 14.16 eV is assigned to $\pi_{C=O}$ which has been destabilized from 14.5 eV in formamide. This is comparable to the destabilization observed in the π_N orbital from formamide to benzamide. The $\pi_{C=O}$ orbital is the bonding combination of $\pi_{C=O}$ and the nitrogen lone pair. There is more uncertainty associated with the latter two ionization potentials than with the others because they are located in broad bands which probably include overlapping σ components and orbitals from the substituents.

Substituent Effect on Phenyl Orbitals

Electron releasing groups such as OCH_3 and CH_3 increase the Ph_S level of benzamide by 0.83 and 0.31 eV, respectively, whereas electron withdrawing groups such as CN and NO_2 lower the Ph_S level of benzamide by 0.54 and 0.88 eV, respectively. As expected the magnitude of the destabilization or stabilization is an indication of the electron releasing or withdrawing ability of the substituent. Figure 4 shows a plot of the Ph_S IP of *para*-substituted benzamides vs. the Ph_S IP of the corresponding substituted benzenes. As can be seen, a linear relationship is observed with a slope of 1.04. The significance of this slope will be considered when Ph_S IP values of

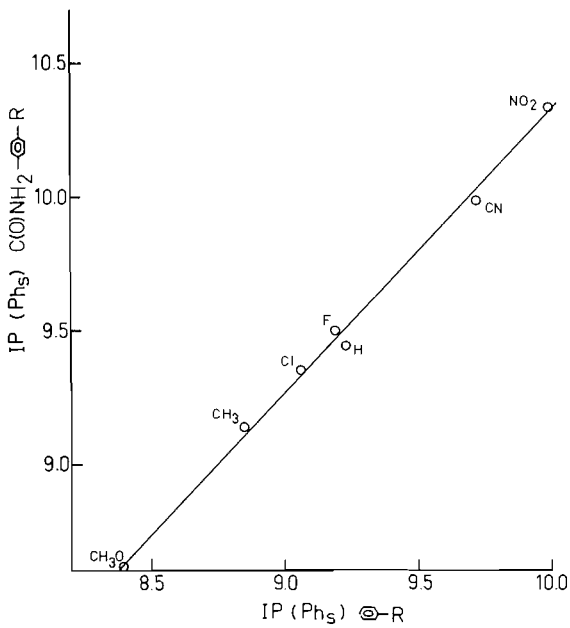

FIG. 4. Ph_S IP of *para* benzamides vs. Ph_S IP of substituted benzenes.

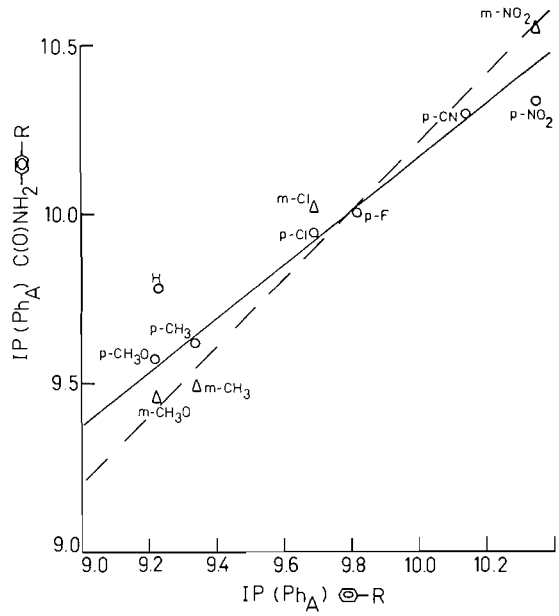

FIG. 5. Ph_A IP values of *para* ○ and *meta* △ benzamides vs. Ph_A IP of substituted benzenes.

other disubstituted benzenes are discussed. The Ph_S IP's of the *meta* substituted benzamides are identical to the *para* substituted benzamides within experimental error. In contrast to this the Ph_A orbitals are found to be separated by at least 0.1 eV in *para* and *meta* benzamides. Discussion of this distinction will be considered after the Ph_A data are presented.

Figure 5 shows a plot of Ph_A IP values for substituted benzamides vs. those for the corresponding substituted benzenes. As in the case of Ph_S orbital linear relationships between substituted benzamide and substituted benzene IP's are found. Unlike the Ph_S orbital, there is a significant difference between the Ph_A IP's for *meta* and *para* substituted compounds. The shapes of the Ph_S and Ph_A orbitals obtained from CNDO/S calculations on *m*-OCH_3 benzamide are shown in Schemes 1 and 2.

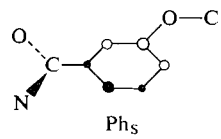

Ph_S

SCHEME 1

The strong donor or strong acceptor substituents used in this study exert the major 'orbital orienting' effect, that is, determine the effective C_{2v} symmetry of the disubstituted molecules. In Schemes 1 and 2 the size of the circles at each position is approximately proportional to the coefficient of the wave function at that position. As can be seen in Scheme 2, as one shifts the amido substituent from the *para* to

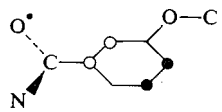

Ph_A

SCHEME 2

the *meta* position one goes from essentially a node to a position of high electron density. The actual coefficients from the calculation are 0.043 and −0.467 for the Ph_A orbital for the carbons *para* and *meta* to the methoxy group. From Scheme 1 it is obvious that the change is not so dramatic for Ph_S as the amido group is moved from *para* to *meta* to the OCH_3 group. The calculated coefficients for the Ph_S orbital at the *para* and *meta* positions are 0.511 and 0.215, respectively. Since the square of the coefficient is assumed to be proportional to the extent of interaction then if the large change in the *para* and *meta* coefficients for Ph_A is only producing a change in the energy level of 0.1–0.2 eV, it would be impossible to observe any change in Ph_S energy level as one changed the amido substituent from *para* to *meta* where the relative change in coefficient size is much smaller.

The phenyl orbital IP values are listed in Table 1 and the general trend of increasing orbital energy with increasing electron donating ability of the substituent is also observed. Because the IP of the phenyl orbital increases for electron withdrawing groups it moves up into the region of the σ bands. In *p*-CN benzamide it becomes impossible to assign the Ph orbital.

Substituent Effect on Amide Orbitals

The substituent effect on the n_0 orbital is shown in Fig. 6 where its IP is plotted against the σ value of the substituent. Separate linear relationships are found for both *para* and *meta* substituted benzamides. Thus, the inductive effect of the substituent is being transmitted to the carbonyl oxygen from either the *meta* or *para* position. The influence of substituent on n_0 IP is obviously less than that on an orbital such as Ph_S which is directly associated with the phenyl group. Thus, the n_0 orbital changes by 0.76 through the series from *p*-CH_3O benzamide to *p*-NO_2 benzamide whereas Ph_S changes by 1.71 eV over the same series of compounds.

The dependence of π_N on substituent is also shown in Fig. 6. The π_N IP is also linearly related to the σ value of the substituent with *para* and *meta* substituents showing parallel trends. The change in π_N IP from *p*-CH_3O benzamide to *p*-NO_2 benzamide is 0.67 eV which is comparable to that observed for the n_0 orbital. As observed for all orbitals discussed thus far, the introduction of donor groups results in higher energy levels (decrease in IP's) and acceptor

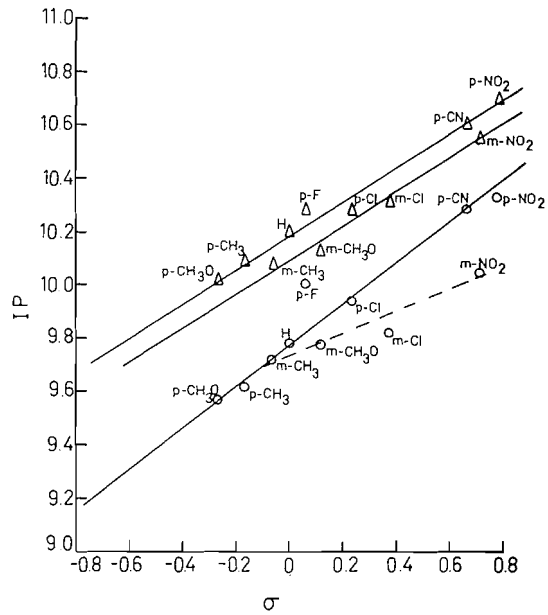

FIG. 6. n_0 IP of benzamides ○ and π_N IP of benzamides △ vs. σ of substituents.

group introduction lowers the energy levels (increases IP's). There is a general trend of decreasing $\pi_{C=O}$ IP with electron donating ability of the substituent. However, both *p*-CH_3O and *m*-CH_3O seem to be exceptions to this trend in that the $\pi_{C=O}$ IP for them is higher than the corresponding IP in *p*-CH_3 and *m*-CH_3 benzamide. Thus, there is less of a correlation between IP and substituent than there was for some of the lower IP's.

Other Levels

Ionizations from other orbitals which can be identified in the photoelectron spectra in Figs. 2 and 3 are principally due to lone pairs on the various substituents. In *p*-CH_3O benzamide and *m*-CH_3O benzamide the IP's at 11.27 and 11.21 eV, respectively, are assigned to ionization from the nonbonding oxygen of the methoxy group. The analogous IP is at 11.06 eV in anisole (7). In *p*-Cl benzamide the peaks at 11.52 and 11.83 eV are assigned to the nonbonding chlorine orbitals. In *m*-Cl benzamide these two levels occur at 11.62 and 11.79 eV. The analogous levels in chlorobenzene are located at 11.42 and 11.76 eV (6). The chlorine lone pair orbital which is perpendicular to the plane of the phenyl ring would be expected to interact more strongly with the phenyl π electrons. As a consequence it should be lowered and its IP should be slightly higher than that of the orbital which is in the plane of the phenyl ring. The orbital with the higher IP should have lost some of its nonbonding character and should be broader than the one at lower IP. As

Can. J. Chem. Downloaded from www.nrcresearchpress.com by 210.87.254.42 on 09/05/12
For personal use only.

TABLE 2. CNDO/S calculated ionization potentials for benzamides

	Ph_S		Ph_A		n_0		π_N	
	$IP_{(calcd)}$	Ratio	$IP_{(calcd)}$	Ratio	$IP_{(calcd)}$	Ratio	$IP_{(calcd)}$	Ratio
p-CH_3O	9.13	0.944	10.07	0.950	10.20	0.938	11.36	0.882
m-CH_3O	9.25	0.930	9.87	0.957	10.24	0.954	11.46	0.884
p-CH_3	9.51	0.961	10.05	0.957	10.20	0.943	11.43	0.882
m-CH_3	9.64	0.945	9.90	0.958	10.22	0.951	11.47	0.879
H	9.83	0.961	10.09	0.970	10.26	0.953	11.50	0.887
p-NO_2	10.50	0.984	10.68	0.967	10.44	0.989	10.78	0.992
m-NO_2	10.46	0.983	10.65	0.965	10.37	0.969	10.81	0.976

can be seen from the spectra of the chlorobenzamides this is the case. In *p*-CN benzamide there are three levels whose IP's are 12.20, 12.82, and 13.54 eV. Two of these levels are probably the C≡N π orbitals whose IP's are 11.84 and 12.11 eV in benzonitrile (7). If the first two are assigned to the C≡N π orbitals then the third at 13.54 eV seems unusually high for a phenyl orbital as compared to other phenyl orbitals in the series. Alternatively 13.54 eV seems unreasonable for C≡N π, when compared to benzonitrile. Thus, a definite assignment of these three levels cannot be made. In *p*-NO_2 benzamide and *m*-NO_2 benzamide the IP's at 11.34 and 11.33 eV are assigned to nonbonding oxygen orbitals of the nitro group. These are located at 11.15 and 11.30 eV in nitrobenzene (15). No splitting of the nitro group orbitals into two levels is observed here as in the nitrobenzene case.

Calculations

As an aid in assignment of the photoelectron spectra of the benzamides CNDO/S calculations (16) have been performed on several of the compounds under investigation. Table 2 shows the results of these calculations for the first four ionization potentials. These values were obtained by the use of Koopmans' theorem (4) in which the negative of the calculated molecular orbital energy is equated to the ionization potential. The halogen substituted benzamides are not included since the program is not equipped to handle halogen orbitals. Standard geometries were used throughout the calculation. Ionization potentials beyond the first four are not included for two reasons: (*i*) the program begins to overestimate the orbital energies of σ levels and places them in this range and (*ii*) the Ph and $\pi_{C=O}$ levels are mixed with other levels so that they become difficult to distinguish.

The ratio of IP_{exp}/IP_{calcd} is also included in Table 2 for comparison purposes. The calculated IP is always larger than the experimental. It is also worth noting that with the exception of the nitrobenzamides the ratio of the experimental to calculated IP's is virtually constant for each type of orbital: 0.95 for Ph_S, 0.96 for Ph_A, 0.95 for n_0, and 0.88 for π_N. This relative constant deviation between calculated and experimental IP's can be used as an aid in assignment. If an IP is assigned incorrectly for one compound in the series the ratio will show a large deviation from the remainder of the series.

In the benzamides for which calculations were performed, the trends in calculated IP's parallel those of the experimental values. Thus, the Ph_S IP undergoes the greatest change from the parent benzamide to *p*-CH_3O benzamide. Ph_A IP's are more affected by substituents in the *meta* position than in the *para* position. The calculated and experimental π_N IP change by a comparable amount from *p*-CH_3O benzamide to benzamide. One notable exception to these trends in the n_0 orbital whose calculated IP is virtually unchanged from *p*-CH_3O benzamide to benzamide whereas the experimental IP changes by 0.21 eV over this series of compounds. Another significant difference between calculated and experimental IP's appears when one compares the Ph_S IP's of the *para* and *meta* substituted compounds. Experimentally, these IP's are identical whereas calculationally they differ by ~0.1 eV with the *meta* compound having the higher IP. In summary, the use of semiempirical molecular orbital calculations aids qualitatively in assignment of the photoelectron spectra of the benzamides in this investigation.

Ionization Potential Relationships in Disubstituted Benzenes

As discussed previously the photoelectron spectra of series of dimethylanilines (8), nitrobenzenes (8), acetophenones (8), and nitrosobenzenes (17) have been determined. In each case linear correlations between phenyl π IP and σ for the substituent have been obtained. In view of the fact that we have obtained a linear relationship between the Ph_S IP of substituted benzamides (Fig. 4) and the Ph_S IP of the corresponding substituted benzenes, we have attempted a similar correlation for the above series of disubstituted benzenes. The results are shown in Fig. 7.

Can. J. Chem. Downloaded from www.nrcresearchpress.com by 210.87.254.42 on 09/05/12
For personal use only.

Can. J. Chem. Downloaded from www.nrcresearchpress.com by 210.87.254.42 on 09/05/12
For personal use only.

The Ph_S IP's for substituted benzenes have been compiled from various sources and these values together with the sources are listed in Table 3. As can be seen from Fig. 7, a linear relationship is found for each series of compounds. The slope of this linear relationship is approximately unity for all series of compounds except the *N,N*-dimethylanilines. In the latter case the slope is 0.40.

An analogous plot is shown in Fig. 8 for substituted anilines, chlorobenzenes, and benzonitriles. The Ph_S IP's of substituted anilines and benzonitriles are not available directly but Rao (9) has tabulated the changes in first IP of substituted benzenes brought about by substituting amino and cyano groups in the *para* position. Thus, we have added these group contributions to the Ph_S IP's of monosubstituted benzenes in Table 3 to obtain the data for anilines and benzonitriles in Fig. 8. The substituted chlorobenzene data is listed in Table 3. All three series of compounds in Fig. 8 show linear relationships with slopes of 1.06 for benzonitriles,

TABLE 3. Values of Ph_S ionization potentials and their sources for disubstituted benzenes

R	R′	Ph_S IP	Reference
H	H	9.24	13
H	$N(CH_3)_2$	7.45	8
H	NH_2	8.05	7
H	OH	8.73	7
H	CN	9.72	7
H	NO_2	9.99	15
H	$CONH_2$	9.45	This work
H	NO	9.84	17
H	F	9.19	5
H	Br	9.05	5
H	Cl	9.06	5
H	CHO	9.80	6
H	$COCH_3$	9.55	7
H	CH_3	8.85	7
CH_3	$N(CH_3)_2$	7.25	8
CH_3	NH_2	7.62	7
CH_3	CH_3	8.71	6
CH_3	OH	8.38	7
CH_3	NO_2	9.53	8
CH_3	$CONH_2$	9.14	This work
CH_3	NO	9.53	17
H	OCH_3	8.39	7
OCH_3	$N(CH_3)_2$	7.22	8
OCH_3	$COCH_3$	8.6	8
OCH_3	$CONH_2$	8.62	This work
OCH_3	NO_2	8.98	8
OCH_3	NO	8.94	17
OCH_3	CH_3	8.18	7
OCH_3	OCH_3	7.90	6
OCH_3	Br	8.49	6
OCH_3	CHO	8.87	6
CH_3	Br	8.71	6
CH_3	Cl	8.90	6
Cl	$CONH_2$	9.35	This work

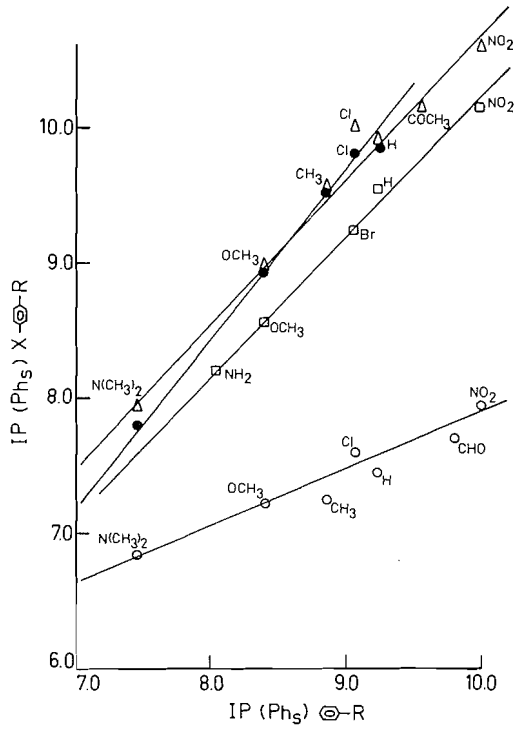

FIG. 7. Ph_S IP of disubstituted benzenes vs. Ph_S IP of monosubstituted benzenes: dimethylanilines (ref. 8) ○, acetophenones (ref. 8) □, nitrobenzenes (ref. 8) △, nitrosobenzenes (ref. 17) ●; (substituted benzene IP values from Table 3).

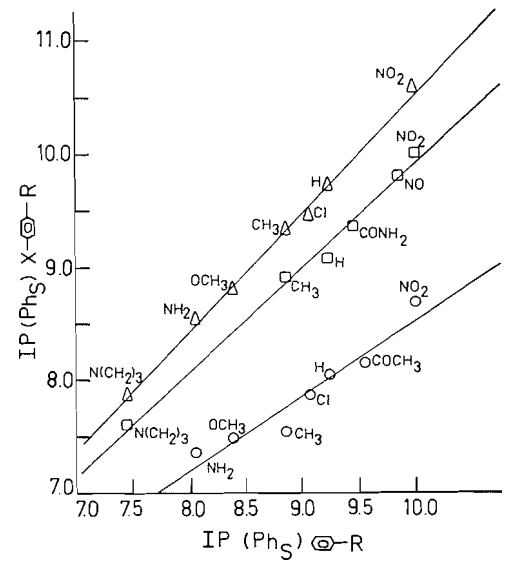

FIG. 8. Ph_S IP of disubstituted benzenes vs. Ph_S IP of monosubstituted benzenes: anilines (ref. 9) ○, chlorobenzenes (Table 3) □, benzonitriles (ref. 9), △; (substituted benzene IP values from Table 3).

Can. J. Chem. Downloaded from www.nrcresearchpress.com by 210.87.254.42 on 09/05/12
For personal use only.

0.92 for chlorobenzenes, and 0.67 for anilines. As previously observed in Fig. 7, it is only a strong electron releasing group ($—NH_2$) which shows a slope much less than unity.

To investigate further the generality of this relationship between phenyl IP's of disubstituted and monosubstituted benzenes it was decided to examine the phenyl IP's of substituted toluenes and anisoles. The results are shown in Fig. 9 for toluenes and Fig. 10 for anisoles. Since several sources of IP's are used, the values of the IP's used in Figs. 9 and 10 and their sources are listed in Table 3. A linear relationship with a slope of 0.95 exists between the Ph_s IP of substituted toluenes and the Ph_s IP of substituted benzenes. Figure 10 demonstrates similar behavior for the *para* substituted anisoles with the slope being 0.69. Thus, it seems that electron releasing groups such as CH_3, OCH_3, NH_2, and $N(CH_3)_2$ have a distinct influence on the Ph_s IP of benzene. Electron withdrawing groups do not display this effect and show slopes of $COCH_3$ 1.01, $CONH_2$ 1.06, CN 1.06, NO_2 1.12, and NO 1.20. It is of interest to note that the slopes exhibited by the electron releasing groups are in the order of their electron releasing abilities with the furthest deviation from unity being the most electron releasing viz. 0.9 for CH_3, 0.7 for OCH_3, 0.67 for NH_2, and 0.40 for $N(CH_3)_2$.

Donor substituents are known to interact with the e_{1g} orbital of benzene through high lying occupied lone pair orbitals producing the phenyl $S(b_1)$ and phenyl $A(a_2)$ levels of substituted benzenes. The fact that a second electron releasing substituent produces

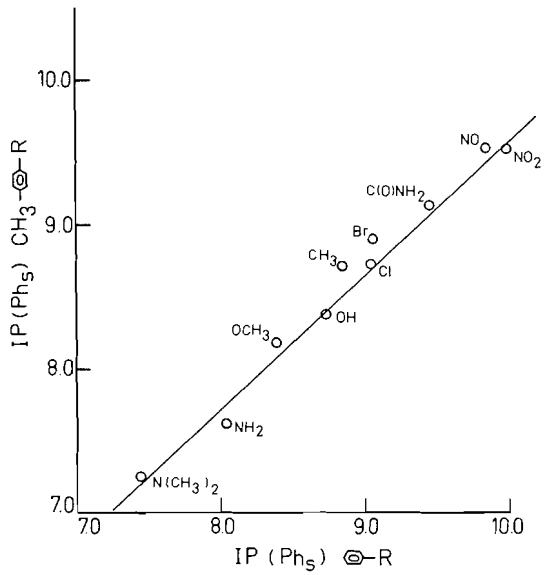

FIG. 9. Ph_s IP for substituted toluenes vs. Ph_s IP for substituted benzenes; IP values from Table 3.

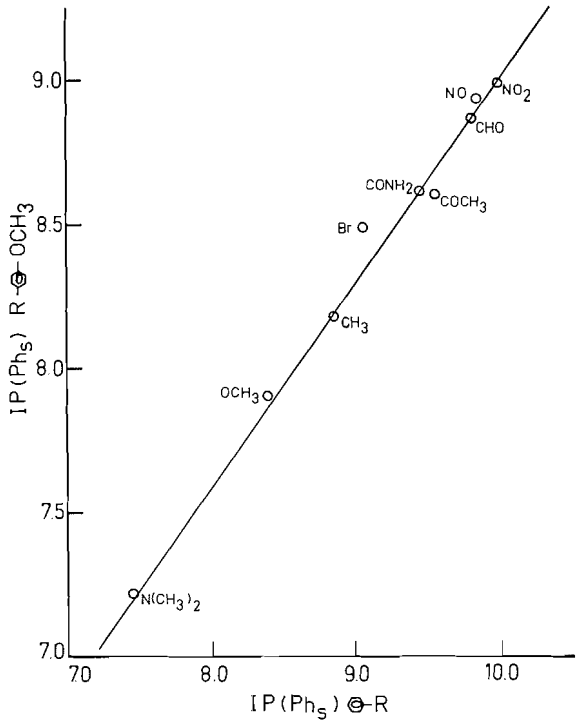

FIG. 10. Ph_s IP for substituted anisoles vs. Ph_s IP for substituted benzenes; IP values from Table 3.

less of an effect on Ph_s than the first can be attributed partly to the fact that there is a larger separation, hence decreased interaction, between Ph_s of the monosubstituted benzene and the lone pair of the substituent than between the benzene e_{1g} orbital and the lone pair of the substituent. The nitrogen lone pair in dimethylamine occurs at 8.9 eV (18). The interaction between this orbital and one of the e_{1g} orbitals of benzene at 9.24 eV produces a destabilization of 1.78 eV in *N,N*-dimethylaniline (Table 3). When a second dimethylamino group is introduced, the interaction is a much weaker one between the lone pair orbital at ~8.9 and the Ph_s at 7.45 eV and produces a destabilization of 0.61 to 6.84 eV (8). In addition the HOMO of substituted benzene has less benzene character i.e. all the coefficients are smaller than in the benzene HOMO.

The energy consideration above would suggest that acceptors should lower Ph–donor orbitals more than they lower Ph—H, since the acceptor LUMO is involved and will be closer in energy to the Ph–donor HOMO. The combination of inductive withdrawal plus the low lying vacant π orbital in acceptors is responsible for producing a larger effect than anticipated when an acceptor is added to a donor substituted benzene. The smaller slope observed for donor substituents can then be considered to result from both decreased interaction by a second donor and

Can. J. Chem. Downloaded from www.nrcresearchpress.com by 210.87.254.42 on 09/05/12
For personal use only.

enhanced interaction when the second substituent is an acceptor group.

An additional feature of the plots of Ph_S IP values of disubstituted benzenes vs. those of monosubstituted benzenes is that the graphs can aid in assignment of photoelectron spectra of some of these compounds. Two conflicting assignments have been reported for the photoelectron spectrum of nitrobenzene. Kobayashi and Nagakura (7) and Egdell and co-workers (8) have proposed an inversion of the b_1 and a_2 levels in nitrobenzene. Rabalais (15) has concluded that the normal ordering of substituted benzene levels is followed and b_1 is the HOMO with a_2 at a lower energy. If one uses the inverted assignment the b_1 or Ph_S point does not fall on the curve for nitrobenzenes (Fig. 7). A prediction of inversion of energy levels for nitrosobenzenes (17) has also been made, whereas Rabalais and Colton (14) have predicted the normal ordering in their assignment. Again an attempt to use the second highest IP in nitrosobenzene to represent Ph_S results in a point which does not correlate with the remainder of the nitrosobenzene curve (Fig. 7). In an independent study[2] the normal ordering (b_1 or Ph_S above a_2 or Ph_A) in nitrobenzene has been confirmed from the photoelectron spectra of *p*-NO_2 styrene and *m*-NO_2 styrene.

Photoelectron Spectra Correlations with Nuclear Magnetic Resonance Data

Figure 11 shows a plot of the IP's assigned to Ph_S in the *para* benzamides vs. chemical shifts of C-4 carbon (19). In this designation the C-4 carbon represents the carbon at which the amide group is substituted. As can be seen a linear relationship is observed between IP and chemical shift which is to be expected since the extent of chemical shift is proportional to the electron density and the Ph_S orbital is expected to be one in which there is high electron density at the position of substitution of the amide. This high electron density results both from actual charge donation and polarization of the benzamide HOMO by substituents. As pointed out by Santiago *et al.* (20), the higher in energy the HOMO, the more it has mixed with the donor orbital and the more polarization towards the *para* carbon occurs. Acceptor substitution does the opposite with polarization towards the substituent taking place. This polarization will influence the chemical shift of the *para* carbon in the direction observed with larger values of the chemical shift associated with acceptor substituents. Figure 12 shows a correlation of the π_N IP's of *para* benzamides with ^{15}N chemical shifts as determined by Randall and co-workers (21). In their studies an acceptor group produced a low field shift (i.e. to higher frequency) and a donor group produced a high field shift. The ^{15}N shifts correlate well with the IP of the orbital with high electron density on the atom to which the shift is referred and the substituents which act to remove electron density from that atom provide both a large chemical shift and high IP.

[2]E. J. McAlduff, C. Gallo, R. W. Strozier, and K. N. Houk. To be published.

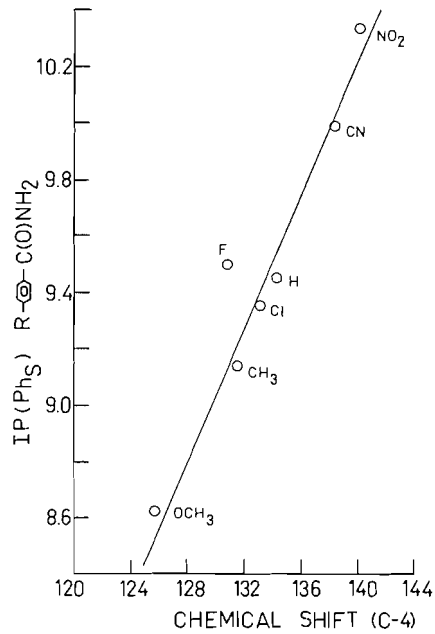

FIG. 11. Ph_S IP *para* benzamides vs. chemical shift (carbon-4) (ref. 20).

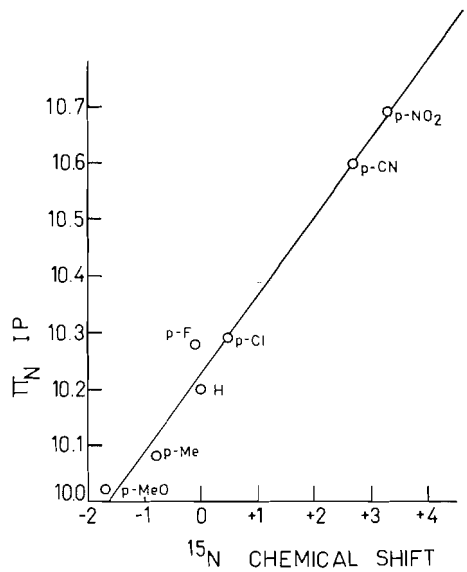

FIG. 12. π_N IP *para* benzamides vs. ^{15}N chemical shift (ref. 22).

Experimental

Photoelectron spectra were recorded on a Perkin-Elmer Ltd., PS-18 Photoelectron Spectrometer with heated probe. A mixture of xenon and argon was used as internal calibrants and the recorded peak positions represent an average of five determinations. Resolution as measured on the argon peak at 15.76 eV was 25–30 meV. The substituted benzamides were prepared by ammonolysis of the commercially available benzoyl chlorides using a standard procedure (22).

Acknowledgements

Financial support of the National Research Council of Canada and St. Francis Xavier University Council for Research is acknowledged by E.J.M. and B.M.L. K.N.H. acknowledges support from the National Science Foundation and the National Institutes of Health (GM-21311). The authors are also indebted to Ruth Gandour for assistance with the calculations.

1. O. EXNER. *In* Advances in linear free energy relationships. *Edited by* N. B. Chapman and J. Shorter. Plenum Press, New York, NY. 1972. Chapt. 1.
2. Y. K. LAU and P. KEBARLE. J. Am. Chem. Soc. **98**, 7452 (1976).
3. W. J. HEHRE, L. LANDOM, and J. A. POPLE. J. Am. Chem. Soc. **94**, 1496 (1972); J. M. MCKELVEY, S. ALEXANDRATOS, A. STREITWEISER, JR., J. L. M. ABBOUD, and W. J. HEHRE. J. Am. Chem. Soc. **98**, 244 (1976).
4. T. KOOPMANS. Physica, **1**, 104 (1934).
5. D. W. TURNER, C. BAKER, A. D. BAKER, and C. R. BRUNDLE. Molecular photoelectron spectroscopy. Wiley-Interscience, New York, NY. 1970.
6. A. D. BAKER, D. P. MAY, and D. W. TURNER. J. Chem. Soc. B, 22, (1968).
7. T. KOBAYASHI and S. NAGAKURA. Bull. Chem. Soc. Jpn. **47**, 2563 (1974).
8. R. EGDELL, J. C. GREEN, and C. N. R. RAO. Chem. Phys. Lett. **33**, 600 (1975).
9. C. N. R. RAO. Tetrahedron, **32**, 1561 (1976).
10. H. H. JAFFE. Chem. Rev. **53**, 191 (1953).
11. B. LINDBERG, S. SVENSSON, P. Å. MALMQUIST, E. BASILIER, U. GELIUS, and K. SIEGBAHN. Chem. Phys. Lett. **40**, 175 (1976).
12. J. L. MEEKS, H. J. A. MARIA, P. BRINT, and S. P. MCGLYNN. Chem. Rev. **75**, 603 (1975).
13. L. ÅSBRINK, E. LINDHOLM, and O. EDQVIST. Chem. Phys. Lett. **5**, 609 (1970).
14. J. W. RABALAIS and R. J. COLTON. J. Electron Spectrosc. Relat. Phenom. **1**, 83 (1972).
15. J. W. RABALAIS. J. Chem. Phys. **57**, 960 (1972).
16. J. DEL BENE, H. H. JAFFE, R. L. ELLIS, and G. KUEHNLENZ. CNDO/S program. University of Cincinnati, Cincinnati, OH. QCPE Program No. 174.
17. R. EGDELL, J. C. GREEN, C. N. R. RAO, B. G. GOWENLOCK, and J. PFAB. J. Chem. Soc. Faraday Trans. II, **72**, 988 (1976).
18. A. B. CORNFORD, D. C. FROST, F. G. HERRING, and C. A. MCDOWELL. Can. J. Chem. **49**, 1135 (1971).
19. B. M. LYNCH. Can. J. Chem. **55**, 541 (1977).
20. C. SANTIAGO, K. N. HOUK, R. A. SNOW, and L. A. PAQUETTE. J. Am. Chem. Soc. **98**, 7443 (1976).
21. P. S. PREGOSIN, E. W. RANDALL, and A. I. WHITE. J. Chem. Soc. Perkin Trans. II, 513 (1972).
22. A. I. VOGEL. A textbook of practical organic chemistry. Longman, London. 1950. p. 755.

Can. J. Chem. Downloaded from www.nrcresearchpress.com by 210.87.254.42 on 09/05/12
For personal use only.

Preparation of cyclobutenones and cyclopent-2-enones via epoxy sulfone cyclizations

BERNARD CORBEL,[1] JOHN M. DECESARE, AND TONY DURST

Department of Chemistry, University of Ottawa, Ottawa, Ont., Canada K1N 6N5

Received July 29, 1977

BERNARD CORBEL, JOHN M. DECESARE, and TONY DURST. Can. J. Chem. **56**, 505 (1978).

Epoxysulfones of the type $PhSO_2(CH_2)_nCH\overset{O}{\frown}CH_2$ (n = 1, 2) react with about 2 equiv. of CH_3MgI in THF to give 3-phenylsulfonylcyclobutanols and 3-phenylsulfonylcyclopentanols in good to excellent yields. 3-Alkyl-3-phenylsulfonylcyclobutanols and -cyclopentanols can be obtained either from the appropriately substituted epoxides or by alkylation of the dianion of the parent 3-phenylsulfonylcycloalkanols. Oxidation of these alcohols with Jones' reagent followed by treatment of the crude ketones with triethylamine leads to 3-substituted cyclobutenones and cyclopent-2-enones.

BERNARD CORBEL, JOHN M. DECESARE et TONY DURST. Can. J. Chem. **56**, 505 (1978).

Les époxysulfones du type $PhSO_2(CH_2)_nCH\overset{O}{\frown}CH_2$ (n = 1,2) réagissent avec environ 2 équiv. de CH_3MgI dans le THF pour conduire aux phénylsulfonyl-3 cyclobutanols et aux phénylsulfonyl-3 cyclopentanols avec des rendements allant de bon à excellent. On peut obtenir des alkyl-3 phénylsulfonyl-3 cyclobutanols et cyclopentanols soit à partir des époxydes substitués d'une façon appropriée soit par alkylation du dianion des phénylsulfonyl-3 cycloalkanols correspondants. L'oxydation de ces alcools par le réactif de Jones, suivi par un traitement des cétones brutes par la triéthylamine, conduit aux cyclobutenones et aux cyclopentène-2 ones substitués en position 3.

[Traduit par le journal]

We have shown in a recent communication (1) that γ-epoxysulfones **1** can be effectively cyclized to 3-phenylsulfonylcyclobutanols **2**. We would now like to report the conversion of the homologous δ-epoxysulfones **3** to cyclopentanols **4**, and the conversion of **2** and **4** in good overall yield to cyclobutenones and cyclopent-2-enones, respectively. This route adds significantly to the synthetic methodology available

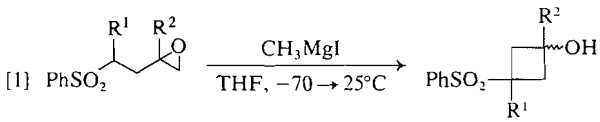

1 **2**

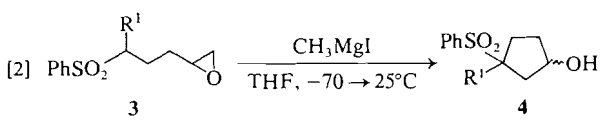

3 **4**

for the preparation of cyclobutenones, especially those having substituents only in the 3 position (2).

The starting materials **1** and **3** required for the cyclization reactions were readily prepared by several simple routes outlined in eqs. 3–5. For details, see the Experimental.

The cyclizations of the epoxysulfones were carried out in dry THF, initially at −70°C and then at room temperature over a 24 h period, using about 2 equiv. of Grignard reagent. The yields of chromatographically pure cyclized material were usually in the good to excellent range (Table 1). The structures of these compounds were confirmed by their nmr, ir, and analytical data (see Table 1). The mechanism of the cyclization reactions, which involves initial opening of the epoxide to a haloalkoxide, subsequent formation of an α-sulfonyl Grignard reagent

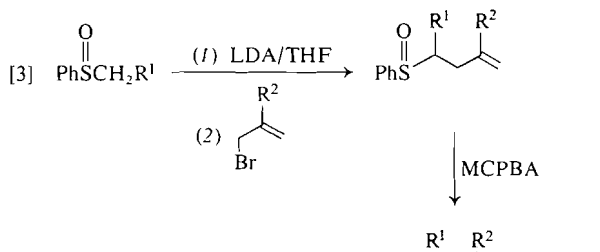

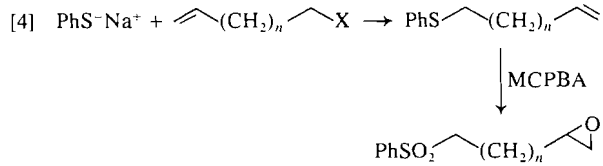

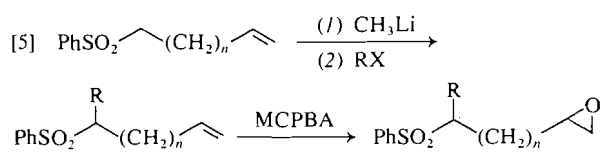

[1]NRCC–France exchange visitor 1975–1976.

TABLE 1. Physical characteristics of cyclobutanols and cyclopentanols from the cyclization of epoxy sulfones

Epoxy sulfone	Method of preparation (eq.)	Product	% yield	Ethyl acetate: hexane[a]	Nuclear magnetic resonance data (δ)	Analysis			
						Calculated		Found	
						C	H	C	H
$PhSO_2CH_2CH_2CH(O)CH_2$	4	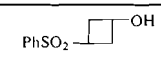	96	1:1	2.3–2.8 (m, 4H) 3.95 (d, 1H, OH) 3.36 (approx. quintet 1H) 4.25 (quintet, $J \sim 7.5$ Hz, 1H) 7.4–8.0 (m, 5H)	56.60	4.66	56.93	4.48
			72[b]						
$PhSO_2(CH_2)_2CH(O)CH_2$ CH_3	3	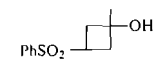	51	1:2	1.40 (s, 3H) 1.2–1.8 (m, 4H) 3.44 (quintet, $J = 8$Hz, 1H) 3.35 (s, 1H, OH) 7.4–8.0 (m, 5H)				
$PhSO_2CHCH_2CH(O)CH_2$ Ph	3	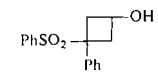	98	1:2	2.9–3.3 (m, 4H) 4.18 (quintet, $J \sim 6.5$ Hz, 1H) 6.8–7.7 (m, 10H)	66.64	5.92	66.58	5.64
		(mp 132°C)							
$PhSO_2CHCH_2CH(O)CH_2$ CH_2Ph	5	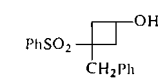	89	1:4	2.3–2.8 (m, 4H) 2.88 (s, 2H) 2.9–3.2 (m, 1H) 7.0–8.0 (m, 10H)[c]	67.52	6.00	67.59	6.06
$PhSO_2CHCH_2CH(O)CH_2$ $(CH_2)_3CH_3$	5	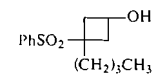	92	1:3	0.8–1.8 (m, 9H) 2.4–3.0 (m, 4H) 4.22 (quintet $J \sim 6.5$ Hz, 1H) 7.4–7.9 (m, 5H)[c]	62.66	7.51	62.48	7.58
		(mp 178°C)							
$PhSO_2CHCH_2CH(O)CH_2$ $(CH_2)_nCH_3$	5	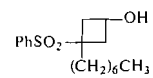	95	1:3	0.9–1.8 (m, 15H) 2.3–2.6 (m, 2H) 2.7–3.0 (m, 2H) 4.22 (quintet $J = 7$Hz, 1H) 7.4–7.9 (m, 5H)	65.77	8.44	65.77	8.53
$PhSO_2(CH_2)_3CH(O)CH_2$	4	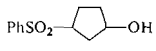	75	1:4	1.7–2.4 (m, 6H) 2.9–3.1 (1H, OH) 3.5–3.9 (m, 1H) 4.2–4.6 (m, 1H) 7.4–7.8 (m, 5H)	58.41	6.19	58.17	6.16

[a]The ratio of ethyl acetate:hexanes used as the eluent for chromatography (silica gel as support).
[b]CH_3CH_2MgBr used as the base.

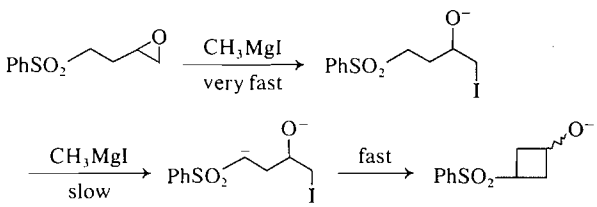

SCHEME 1. Mechanism of cycloalkanol formation from epoxy sulfones.

and finally cyclization has been discussed (1) (Scheme 1).

The preparation of both the β-phenylsulfonylcyclobutanols and -cyclopentanols could also be carried out under 'one-pot' conditions according to Scheme 2. Thus reaction of phenyl methyl sulfone **5** (R = H) with 1 equiv. of CH_3Li in THF containing 5% of hexamethylphosphoramide (HMPTA) at −70°C followed by sequential addition of epibromohydrin and CH_3MgI and warming to room temperature overnight gave **2** ($R^1 = R^2 = H$) in 46% isolated yield; the cyclobutanol **2**, R^1 = Ph, R^2 = H, was similarly prepared from benzyl phenyl sulfone (**6**, R = Ph) in 60% yield. Replacement of epibromohydrin by 4-bromo-1,2-epoxybutane in the above sequence lead to the formation of 3-phenylsulfonylcyclopentanol and 3-phenyl-3-phenylsulfonylcyclopentanol in 35 and 75% yield, respectively.

The parent ring compounds **7** and **8** could readily be alkylated, halogenated or sulfenylated at the 3 position via the dianion **9** and **10** (Scheme 3). The yields of product derived from these reactions are remarkably high considering the fact that a quaternary system is being generated (Table 2). Interestingly, in the cyclization of the epoxysulfones only one isomer was detected by nmr examination of the product, whereas two isomers were obtained in nearly equal amounts from the alkylation procedure. The stereochemical assignments of the isomers has not as yet been made and thus no explanation can be offered for the high stereoselectivity in the epoxysulfone cyclization.

Oxidation of the cyclobutanols or cyclopentanols with Jones' reagent led in excellent yield to the corresponding ketones (Scheme 4, Table 3). The

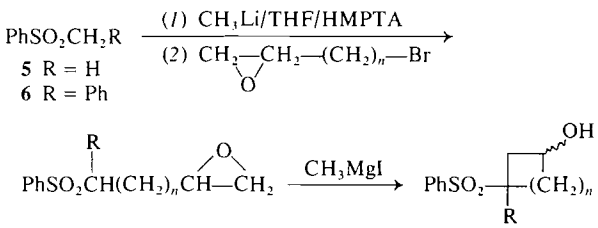

SCHEME 2. 'One-pot' formation of 3-phenylsulfonylcycloalkanols.

β-sulfonylcyclobutanones **11** were generally isolated and purified. Subsequent treatment with triethylamine in CH_2Cl_2 at room temperature furnished the cyclobutenones. Because of the ease of elimination of the phenylsulfonyl group from the cyclopentanones **12**, these compounds were directly converted to cyclopentenones without attempts at their purification. The facile β-elimination of a phenylsulfonyl moiety to yield αβ-unsaturated ketones is well known (3).

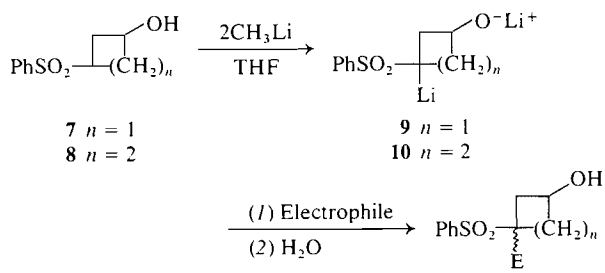

SCHEME 3

The 3-phenylsulfonyl substituted cyclobutanones were identified by their analytical data, nmr spectra (see Experimental) and the characteristic carbonyl frequency, 1780–1800 cm^{-1}, in the infrared. The cyclobutenones showed the carbonyl frequency at about 1760 cm^{-1}. In their nmr spectra these substances each had two slightly broadened singlets at about δ 3.2 (2H) and 5.8–6.0 (1H) assignable to the remaining methylene and olefinic hydrogen in the

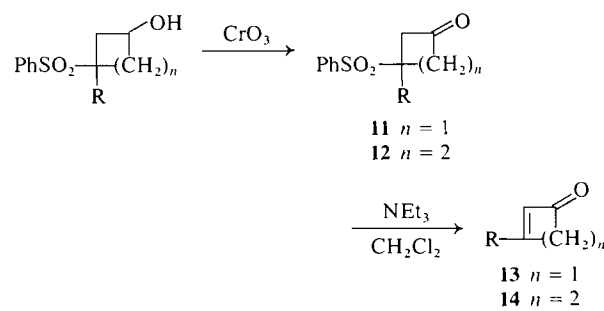

SCHEME 4

ring. For **13** (R = Ph) these absorptions occurred at δ 3.54 and 6.40 (4). 3-Benzylcyclobutenone (**13**, R = CH_2Ph) readily isomerized in the presence of triethylamine to benzylidenecyclobutanone (nmr δ: 3.9–4.0 (m, 4H), 6.6 (m, 1H) and 7.3 (s, 5H)). In the presence of D_2O/NEt_3 all non-aromatic ring hydrogens underwent H–D exchange. The various 3-alkylcyclopentenones each showed a one proton multiplet in the δ 5.9–6.0 region (5).

TABLE 2. Physical characteristics of the products of the reaction outlined in Scheme 3

R—X	*n*	Product	% yield	Nuclear magnetic resonance data (δ)	Analysis					
					Calculated			Found		
					C	H	I	C	H	I
C_4H_9—Br	1	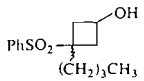	68	See Table 1	See Table 1					
C_4H_9—Br	2	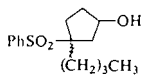	80	0.8—2.8 (m, 15H) 3.4–3.7(1H, OH) 4.2–4.6 (m, 1H) 7.4–8.0 (m, 5H)	63.53	7.80		63.93	7.97	
C_7H_{15}—Br	2	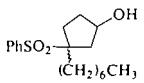	88	0.8–2.8 (m, 21H) 3.4—3.6 (1H, OH) 4.2–4.6 (m, 1H) 7.4–7.9 (m, 5H)	Correct analysis was obtained for the DNP of the corresponding cyclopent-2-enone					
$PhCH_2$—Br	2	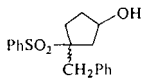	76	0.8–2.8 (m, 6H) 3.3–3.4 (1H, OH) 3.7–4.0 and 4.1–4.4 (2m, total 1H) 7.0–8.2 (m, 10H)	68.35	6.33		68.17	6.28	
$(CH_3)_2CH$—Br	1	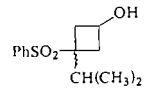	71	0.90 (d, J = 7 Hz, 6H) 1.8–3.4 (m, 6H) 4.1–4.6 (m, 1H) 7.4–8.0 (m, 5H)	61.42	7.09		61.74	7.82	
I—I	1	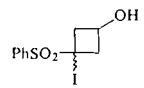 (mp 102–107°C)	32	2.6–3.4 (m, 5H) 4.4–4.8 (m, 1H) 7.4–8.0 (m, 5H)	35.51	3.26	37.56	35.32	3.32	37.66
CH_3S-SCH_3		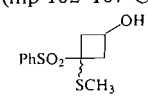	62	2.20 (S, 3H) 2.3–3.9 (m, 5H) 4.2–4.9 (m, 6H) 7.4–7.8 (m, 5H)						

TABLE 3. Product yields for the reaction outlined in Scheme 4

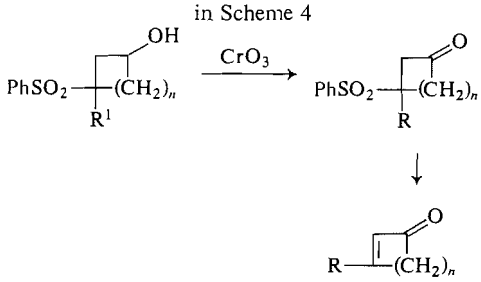

n	R	%
1	Ph	80(100)
1	n-C_7H_{15}	83
1	iso-C_3H_7	82
1	CH_2Ph	94
2	Ph	75
2	n-C_7H_{15}	75
2	H	85
2	CH_2Ph	87
2	C_4H_9	85
1	C_4H_9	80

Experimental

General Comments

All nmr spectra were recorded on a Varian T-60 or HA-100 Spectrometers using $CDCl_3$ – 1% TMS as solvent; the chemical shifts are reported in ppm downfield from TMS. Infrared spectra were obtained as thin films or $CHCl_3$ solution on a Beckman IR-20 instrument. Melting points are not corrected. Usual work-up refers to washing the reaction mixture with water, drying the organic extracts with $MgSO_4$, and evaporating the organic solvent on a rotary evaporator. The intermediates epoxysulfones and their precursors were not subjected to elemental analysis. Their structures follow unambiguously from their method of synthesis and are supported by the nmr spectra.

Preparation of Epoxysulfones

General Procedures

Via eq. 3—The anion of an alkyl phenyl sulfoxide was generated by reaction with 1.1 equiv. of lithium diisopropylamide (LDA) in THF at either −70 or 0°C. One equivalent of an alkyl halide was then introduced and the reaction mixture was then allowed to warm to room temperature. Usual workup gave the crude sulfoxide olefin which was generally purified by silica gel chromatography. The purified product was then oxidized with slightly more than 2 equiv. of *m*-chloroperbenzoic acid (MCPBA) in refluxing CH_2Cl_2 (overnight). The reaction mixture was then washed with 10% NaOH and then water. The crude product was purified by chromatography on silica gel or recrystallization.

Via eq. 4—Potassium phenyl mercaptide was generated in CH_3OH and reacted with slightly less than 1 equiv. of alkyl halide usually by refluxing the methanol solution for up to 18 h. The sulfide was isolated by diluting the reaction mixture with water and extracting several times with CH_2Cl_2. The organic phase was then processed in the usual manner. The crude sulfide, which was generally sufficiently pure for further use was oxidized in one of two ways. The use of 2 equiv. of MCPBA in CH_2Cl_2 at room temperature furnished only olefin sulfones whereas epoxysulfones could be obtained directly by reacting the sulfide olefin for 18 h with >3 equiv. of MCPBA in refluxing CH_2Cl_2. In each instance the reaction was processed as described above.

Via eq. 5—The phenylsulfonylalkenes $PhSO_2CH_2(CH_2)_n$ $CH{=}CH_2$ obtained via eq. 4 above were dissolved in dry THF at 0°C, treated with 1.1 equiv. of CH_3Li and the resultant anion was then alkylated. After a 15–30 min reaction time the reaction mixture was diluted with water and extracted with CH_2Cl_2. The crude organic products isolated in the usual way were purified by column chromatography.

4-Phenylsulfonyl-1,2-epoxybutane

This compound was prepared in 85% overall yield starting with 5.4 g of 4-bromobut-1-ene according to eq. 4. The nmr spectrum of the epoxysulfone showed peaks at δ 1.7–3.5 (m, 7H) and 7.4–7.8 (m, 5H).

2-Methyl-4-phenylsulfonyl-1,2-epoxybutane

Alkylation of the anion derived from 2.45 g (17.5 mmol) of phenyl methyl sulfoxide and 20 mmol of LDA with 2.5 g methallyl bromide gave after purification by silica gel chromatography 2.23 g (66%) of 2-methyl-4-phenylsulfinyl-but-1-ene; nmr δ: 1.84 (s, 3H), 2.1–3.1 (m, 4H), 3.7–3.9 (m, 2H) 7.4–7.8 (m, 5H).

Oxidation of this material with 2.2 equiv. of MCPBA gave 2.33 g (84%) of the desired epoxysulfone whose nmr spectrum showed peaks at δ 1.32 (s, 3H) 1.7–2.2 (m, 2H), 2.60 (s, 2H), 3.1–3.3 (m, 2H), and 7.5–8.0 (m, 2H).

4-Phenyl-4-phenylsulfonyl-1,2-epoxybutane

This compound was prepared according to eq. 3. Thus 4.15 g (19.2 mmol) of benzyl phenyl sulfoxide in 70 ml of THF at −20°C was converted to its lithio salt by reaction with 21.5 mmol of CH_3Li. The yellow anion solution was then quenched with 40 mmol of allyl bromide. The yield of 4-phenyl-4-phenylsulfinyl-but-1-ene was 86%.

The sulfide-olefin was refluxed overnight in CH_2Cl_2 with 2.5 equiv. of MCPBA. The yield of epoxysulfone, mp 98°C (CH_2Cl_2–hexane) was 90%; nmr δ: 2.2–3.2 (m, 6H), 4.2–4.4 (m, 1H), 7.0–7.6 (m, 10H).

5-Phenyl-4-phenylsulfonyl-1,2-epoxypentane

Via eq. 5: 4-phenylsulfonylbut-1-ene (7.5 mg, 3.64 mmol) was dissolved in 25 ml THF and 1 ml hexamethylphosphorus triamide (HMPTA) at −70°C and then converted to its α-sulfone anion with CH_3Li. The resultant anion was reacted with 1.5 equiv. of $PhCH_2Br$ and the reaction mixture allowed to warm to room temperature workup, followed by column chromatography on silica gel gave 780 mg (77%) of a clear oil whose nmr spectrum showed peaks at δ: 2.3–2.6 (m, 5H), 4.9–5.9 (m, 3H), 7.0–8.0 (m, 10H).

The above alkene was oxidized with MCPBA in refluxing CH_2Cl_2. The yield of epoxide, mp 67°C, was 95%; nmr δ: 1.5–2.3 (m, 3H), 2.4–3.0 (m, 3H), 3.1–3.6 (m, 2H), 7.1–7.4 (m, 5H), 7.5–8.0 (m, 5H).

4-Phenylsulfonyl-1,2-epoxyundecane

Via eq. 5: alkylation of the lithio salt from 1.12 g of $PhSO_2CH_2CH_2CH{=}CH_2$ with 1-bromoheptane in THF–HMPTA (25:1) at −70°C followed by warming to room temperature gave 1.18 g (76%) of 4-phenylsulfonylundec-1-ene; nmr δ: 0.8–2.0 (m, 15H), 2.1–2.7 (m, 2H), 2.8–3.1 (m, 1H), 4.9–6.0 (m, 3H), 7.5–8.0 (m, 5H). This latter upon oxidation with MCPBA in the usual manner furnished, after column chromatography (4:1 hexane – ethyl acetate), a 92% yield (1.15 g) of epoxysulfone; nmr δ: 0.8–2.2 (m, 17H), 2.4–2.6 (m, 1H), 2.7–2.9 (m, 1H), 3.0–3.4 (m, 2H), 7.5–8.0 (m, 5H).

4-Phenylsulfonyl-1,2-epoxyoctane

Via eq. 5: 4-phenylsulfonyl-but-1-ene (2.09 g) dissolved in 35 ml THF and 2 ml of HMPTA at −70°C was converted to its anion with CH_3Li and then reacted with excess 1-bromobutane. The crude product was chromatographed to yield

1.86 g (77%) of alkene sulfone; nmr δ: 0.8–2.0 (m, H), 2.1–2.7 (m, 2H), 2.8–3.2 (m, 1H), 4.9–6.0 (m, 3H), 7.5–8.0 (m, 5H).

Epoxidation of the above intermediate with MCPBA gave 92% of the desired epoxysulfone after purification on silica gel column (4:1 ethyl acetate – hexane); nmr δ: 0.8–2.2 (m, 17H), 2.4–2.6 (m, 1H), 2.7–2.9 (m, 1H), 3.0–3.3 (m, 2H), 7.5–8.0 (m, 5H).

5-Phenylsulfonyl-1,2-epoxypentane

4-Penten-1-ol (9.9 g) was dissolved in 150 ml CH_2Cl_2 containing 14 g of triethylamine. To this mixture, cooled to 0°C was added dropwise 11.4 g of CH_3SO_2Cl dissolved in 50 ml of CH_2Cl_2. The reaction mixture was washed successively with water and 5% HCl solution and the organic extract was dried and evaporated. The crude yield of mesylate was 18.0 g (96%); nmr δ: 1.5–2.3 (m, 4H), 2.92 (s, 3H), 4.0–4.3 (2H), and 4.7–6.0 (m, 3H).

The crude mesylate was added to a methanol solution containing PhS^-K^+ and stirred overnight. The reaction mixture was then diluted with H_2O and extracted with 5 × 100 ml of CH_2Cl_2. The combined organic extracts were washed with 4 × 100 ml of 5% NaOH, dried, and evaporated yielding 17.8 g (97%) of 4-phenylthiopent-1-ene; nmr δ: 1.4–2.4 (m, 4H), 2.79 (t, J = 7 Hz, 2H), 4.7–6.0 (m, 3H), 7.0–7.4 (m, 5H).

Oxidation of 16.3 g (92 mmol) of the above sulfide-alkene with 70 g (330 mmol) of MCPBA in refluxing CH_2Cl_2, overnight, followed by washing with 5% NaOH solution and further usual work-up gave 18.0 g (90%) of the desired epoxy-sulfone, mp 120–121°C; nmr δ: 1.2–2.2 (m, 4H), 2.4–3.4 (m, 5H), and 7.3–8.1 (m, 5H).

Reaction of Epoxysulfones with CH_3MgI Preparation of Cyclobutanols and Cyclopentanols. General Procedure

Epoxysulfone (2 mmol) was dissolved in about 25 ml of THF at −70°C. The solution was then treated with 4–5 mmol of CH_3Mg (~2.5 M) in ether. A white solid precipitated immediately. The reaction mixture was allowed to warm to room temperature and stirred for about 4–18 h depending on convenience. The crude product obtained in the usual manner was purified by silica gel chromatography (see Table 1).

Alkylation of 3-Phenylsulfonylcyclopentanol. General Procedure

A solution of 3-phenylsulfonylcyclopentanol was dissolved in THF at −70°C and converted to the dianion upon treatment with 2.1 equiv. of CH_3Li. The dianion formation was allowed to proceed for 5 min and 1 equiv. of the alkyl halide was introduced. The acetone – Dry Ice bath was then removed and the reaction stirred until the disappearance of starting material (tlc). Work-up, as described for the formation of 3-phenylsulfonylcyclopentanol gave the crude products which were purified by chromatography using 1:2 ethyl acetate – hexane as eluent (see Table 2).

'One-pot' Preparation of Cyclobutyl- and Cyclopentanols

3-Phenyl-3-phenylsulfonylcyclopentanol

Benzyl phenyl sulfone 786 mg (3.3 mmol) was dissolved in 25 ml of THF containing 1 ml of HMPTA. The solution was cooled to −70°C and reacted with 3.6 mmol of CH_3Li followed by 543 mg (3.6 mmol) of 4-bromo-1,2-epoxybutane. The reaction mixture was warmed to room temperature and kept until the starting material had disappeared. The reaction mixture was then cooled to −70°C and treated with 2.1 equiv. of CH_3MgI, warmed to room temperature and stirred for 48 h. Work-up was accomplished by pouring the reaction mixture into saturated NH_4Cl solution, extracting with ether and then CH_2Cl_2, drying the organic extracts, and evaporating the solvents. The crude product was purified by chromatography using 1:2 ethyl acetate – hexane as eluent. The yield of viscous oil was 750 mg (75%); ir: 3500 (broad), 1300(s), 1130(s) cm^{-1}; nmr δ: 2.0–3.4 (m, 6H), 3.4–3.8 (1H, OH), 4.2–4.6 (m, 1H), 7.0–7.6 (m, 10H). *Anal.* calcd. for $C_{17}H_{18}O_3S$: C 67.55, H 5.96; found: C 67.33, H 6.10.

Also prepared by this route were 3-phenylsulfonylcyclopentanol (35%); 3-phenylsulfonylcyclobutanol (46%), and 3-phenyl-3-phenylsulfonylcyclobutanol (60%).

Oxidation of Cyclobutanols to Cyclobutanones

(a) 3-Phenylsulfonylcyclobutanone

3-Phenylsulfonlycyclobutanol (270 mg, 1.29 mmol) was dissolved in 6 ml of acetone and reacted with 2 ml of Jones' reagent (6) for 3 h at room temperature. The reaction mixture was diluted with CH_2Cl_2 and then washed successively with 10% $NaHSO_3$ and 10% $NaHCO_3$. Chromatography of the crude reaction product yielded 148 mg (56%) of 3-phenylsulfonylcyclobutanol as colorless crystals, mp 99–100°C; ir: 1790 cm^{-1}; nmr δ: 3.1–4.1 (m, 5H), 7.5–8.0 (m, 5H.) *Anal.* calcd. for $C_{10}H_{10}O_3S$: C 57.13, H 4.79; found: C 57.11, H 4.92.

(b) 3-Phenyl-3-phenylsulfonylcyclobutanone

The precursor cyclobutanol 560 mg (1.94 mmol) was dissolved in 5 ml of acetone and treated with 2 ml of Jones' reagent. After a 30 min reaction time the reaction was worked up as above. Recrystallization of the crude product gave 450 mg (80%) of cyclobutanone, mp 144°C from 95% ethanol; nmr δ: 3.4–3.7 (m, 2H), 4.1–4.4 (m, 2H), 6.9–7.8 (m, 10H).

(c) 3-Benzyl-3-phenylsulfonylcyclobutanone

The precursor alcohol (140 mg, 0.48 mmol) was oxidized as above in 5 ml of acetone with 1.5 ml of Jones' reagent for 1 h. Recrystallization gave 134 mg (94%) of 3-benzyl-3-phenylsulfonylcyclobutanone, mp 134°C (CH_2Cl_2–hexane); ir: 1800(s), 1310(s), and 1150(s) cm^{-1}; nmr δ: 219–3.3 (m, 2H), 3.26 (s, 2H), 3.6–3.9 (m, 2H), 6.9–8.1 (m, 10H).

(d) 3-Butyl-3-phenylsulfonylcyclobutanone

This compound was prepared in 92% yield after column chromatography on silica gel (1:5 ethyl acetate – hexane); colorless viscous oil; ir: 1800(s), 1305(s), 1150(s) cm^{-1}; nmr δ: 0.8–2.0 (m, 9H), 2.8–3.2 (m, 2H), 3.6–4.0 (m, 2H), 7.5–8.0 (m, 5H). The crude sample was contaminated with some of the enone.

(e) 3-Heptyl-3-phenylsulfonylcyclobutanone

Oxidation of 205 mg (0.68 mmol) of the precursor alcohol as above gave 196 mg of a viscous oil whose nmr indicated a mixture of cyclobutanone and cyclobutenone. The two compounds were separated by column chromatography. Yield of 3-heptyl-3-phenylsulfonylcyclobutanone, 152 mg (74%), ir 1800(s), 1305(s), 1150(s); nmr δ: 0.7–2.0 (15H), 2.8–3.2 (m, 2H), 3.7–4.0 (m, 2H), 7.5–8.0 (m, 5H); 3-heptylcyclobutenone (22 mg, 20%) was obtained in an earlier fraction.

Cyclobutenones

(a) 3-Phenylcyclobutenone

3-Phenyl-3-phenylsulfonylcyclobutanol (1 mmol) was dissolved in CH_2Cl_2 and stirred with 10% Na_2CO_3 solution containing a small amount of benzyltriethylammonium chloride. After 20 min of reaction time, work-up yielded 140 mg (>98%) of 3-phenylcyclobutenone; nmr δ: 3.54 (s, 2H), 6.40 (s, 1H), 6.2–6.8 (m, 1H); ir: 1770 cm^{-1} (4).

(b) 3-Benzylcyclobutenone

3-Benzyl-3-phenylsulfonylcyclobutanone (80 mg) was dissolved in 3 ml of CH_2Cl_2 and reacted with 0.5 ml of triethylamine for 30 min. After the usual work-up the reaction mixture was separated into two components by column chromatography using 1:5 ethyl acetate – hexane as eluent. The faster moving fraction (23%) was identified as 3-benzylidene cyclobutanone on the basis of its ir and nmr spectra; ir: 1760(s),

1585(s) cm^{-1}; nmr δ: 6.5 (m, 1H), 3.90 (m, 4H), and 7.2–7.6 (aromatic H). 3-Benzylcyclobutanone had a strong ir peak at 1802 cm^{-1} and nmr bands at δ 3.18 (2H), 3.90 (2H), 5.92 (1H), and 7.2–7.6 (5H). The combined yield was about 90%.

In a second experiment an 82% yield of a 1:1 mixture of conjugated and unconjugated enones was obtained. The compounds decomposed on standing and were not analyzed.

(c) 3-Butylcyclobutenone

3-Butyl-3-phenylsulfonylcyclobutanol 250 mg (0.93 mmol) was oxidized with 1.2 ml of Jones' reagent in 5 ml of acetone for 1 h. The crude product obtained from the typical oxidation reaction work-up was dissolved in 6 ml of CH_2Cl_2 and reacted with 0.15 ml of triethylamine for 30 min at room temperature. Usual work-up followed by filtration through silica gel using CH_2Cl_2 as eluent afforded 92 mg (80%) of 3-butylcyclobutenone; ir: 1770(s) and 1590(m) cm^{-1}; nmr δ: 0.91 (m, 3H), 1.2–1.9 (m, 4H), 2.62 (t, 2H), 3.10 (s, 2H), 5.88 (s, 1H).

(d) 3-Heptylcyclobutenone

This compound was obtained in 83% yield from 200 mg of 3-heptyl-3-phenylsulfonylcyclobutanol using the same procedure as for the 3-butyl derivative; nmr δ: 0.85 (m, 3H), 1.1–2.0 (m, 10H), 2.57 (t, 2H), 3.15 (s, 2H), and 5.87 (s, 1H).

(e) 3-Isopropylcyclobutenone

This compound was obtained in 80% yield from 261 mg of 3-isopropyl-3-phenylsulfonylcyclobutanol using the same procedure as the other 3-alkyl derivatives; nmr δ: 1.16 (d, J = 7 Hz, 6H), 2.4–3.0 (m, 1H), 3.1 (s, 1H), 5.8 (broad s, 1H).

Conversion of 3-Phenylsulfonylcyclopentanols into Cyclopent-2-enones. General Procedure

About 500 mg of the 3-phenylsulfonylcyclopentanol was dissolved in 5 ml of reagent grade acetone at room temperature and reacted with 1.1 equiv. of Jones' reagent (6); dropwise addition was carried out over 10 min. The progress of the reaction was followed by tlc and most oxidations were complete within 30 min. Excess oxidizing agent was destroyed by addition of 10% Na_2SO_3 solution. The reaction mixture was then poured into saturated NH_4Cl solution and extracted with 2 × 50 ml of CH_2Cl_2. The organic layer was dried over $MgSO_4$ and concentrated to a few milliliter on a rotary evaporator. To this crude product was added about 1 ml of triethylamine. The reaction was followed by tlc. When complete, the product was isolated by washing with 2 × 25 ml of 5% HCl solution, drying, and evaporating the organic solvent. The cyclopentenones were purified by column chromatography using 1:4 ethyl acetate – hexane as eluent: (*a*) 3-phenylcyclopent-2-enone: colorless oil, yield 75%; ir: 1690(s), 1610(m) cm^{-1}; nmr δ: 2.5–2.7 (m, 2H), 2.9–3.2 (m, 2H), 6.52 (narrow spaced triplet, 1H), 7.2–7.7 (5H); (*b*) 3-benzylcyclopent-2-enone: colorless oil, 87%; nmr δ: 2.3–2.7 (m, 4H), 2.74 (s, 2H), 5.88 (broad s, 1H), 7.1–7.5 (m, 5H); (*c*) 3-butylcyclopent-2-enone: colorless oil 86%; nmr δ: 0.98 (t, J = 7 Hz, 3H), 1.2–1.8 (m, 4H), 2.3–2.8 (m, 6H), 5.86–5.98 (m, 1H); (*d*) 3-heptylcyclopent-2-enone: colorless oil, 75%; nmr δ: 0.7–2.8 (m, 13H), 2.3–2.7 (m, 6H), 5.85–5.95 (m, 1H). *Anal.* calcd. for the DNP derivative: C 60.00, H 6.66, N 15.55; found: C 59.89, H 6.76, N 15.44.

Acknowledgements

Financial assistance by the National Research Council of Canada and Hoffmann-LaRoche Co. (Nutley, New Jersey) is gratefully acknowledged.

1. B. CORBEL and T. DURST. J. Org. Chem. **41**, 3648 (1976).
2. H. H. WASSERMAN, J. U. PIPER, and E. V. DEHMLOW. J. Org. Chem. **38**, 1451 (1973); R. HUISGEN and H. MAYR. Tetrahedron Lett. 2965, 2969 (1975); T. R. KELLY and R. W. MCNUTT. Tetrahedron Lett. 285 (1975).
3. K. KONDO and D. TUNEMOTO. Tetrahedron Lett. 1007 (1975); K. UNEYAMA and S. TORII. Tetrahedron Lett. 443 (1976).
4. S. L. MANATT, M. VOGEL, D. KNUTSON, and J. D. ROBERTS. J. Am. Chem. Soc. **86**, 2645 (1964).
5. The Aldrich Library of NMR spectra. Vol. II. p. 139.
6. H. E. BAUMGARTEN (*Editor*). Organic synthesis. Vol. 5. John Wiley and Sons, Inc., New York, NY. 1973. p. 310.

Photochemical extrusion of sulfur dioxide from sultines

TONY DURST, JOHN C. HUANG, AND NARENDRA K. SHARMA
Department of Chemistry, University of Ottawa, Ottawa, Ont., Canada K1N 6N5
AND
DAVID J. H. SMITH
Department of Chemistry, University of Leicester, Leicester, England LE1 7RH

Received July 29, 1977

TONY DURST, JOHN C. HUANG, NARENDRA K. SHARMA, and DAVID J. H. SMITH. Can. J. Chem. **56**, 512 (1978).

γ-Sultines having an aryl substituent α to the oxygen atom have been shown to undergo photochemically induced loss of SO_2 via radical intermediates. In the case of the monocyclic derivatives, arylcyclopropanes are formed in excellent yield. 3-Phenylbenz-2,1-thiole-2-oxides yield fluorene derivatives as the major photolysis product.

TONY DURST, JOHN C. HUANG, NARENDRA K. SHARMA et DAVID J. H. SMITH. Can. J. Chem. **56**, 512 (1978).

On a montré que les γ sultines possèdant un substituant aryle en α de l'atome d'oxygène subissent des pertes de SO_2 induites photochimiquement; ces réactions se produisent par des intermédiaires radicalaires. Dans le cas de dérivés monocycliques, il y a formation d'arylcyclopropanes avec d'excellents rendements. Les phényl-3 benzthiazol-2,1 oxydes-2 conduisent à des dérivés fluorènes comme produits majeurs de la photolyse.

[Traduit par le journal]

Can. J. Chem. Downloaded from www.nrcresearchpress.com by 210.87.254.40 on 09/05/12
For personal use only.

Several years ago we reported the thermal extrusion of SO_2 from β-sultines **1** to yield alkenes. In addition, several examples of the formation of phenylcyclopropanes from the photolysis of 5-phenyl-1,2-oxathiolan 2-oxides (γ-sultines) **2**, were also described (1).

We have since investigated several aspects of the photochemical reaction. Structurally, only those sultines which have an aryl group α to the ring oxygen atom undergo SO_2 elimination and cyclopropane formation; no photochemistry was observed for sultines such as **4** or **5** which do not have this feature. Since the sultine **4** has no uv absorption near 253 nm ($\lambda_{max} \sim 225$, $\varepsilon < 500$), the 5-aryl group appears to be required for energy absorption and not simply to stabilize a radical at that carbon. From the two

[1] 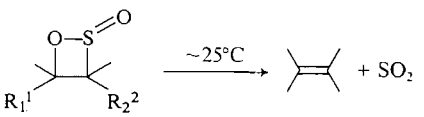

[2] 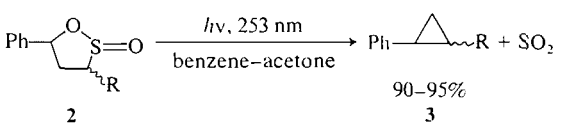

2 3

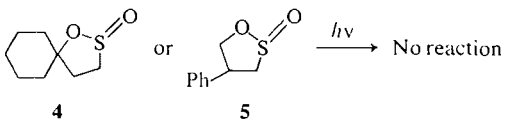

4 5

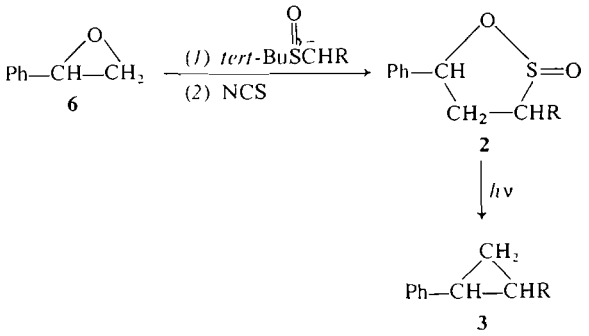

R	% sultine	% cyclopropane
H	82	95
CH_3	84	98

examples which we have studied, the γ-sultine route represents a viable three-step process for converting epoxides to cyclopropanes. The overall yields in the sequence approach 80%.

The photochemical behavior of γ-sultines is similar to that of the structurally related γ-lactones. The latter compounds have been studied quite thoroughly by Givens and Oettle (2) who have shown that a variety of aryl substituted γ-lactones of the type **7** yield arylcyclopropanes. The yields were generally under 50% and are thus considerably lower than those obtained from the sultines.

The reverse of eq. 2, i.e., the preparation of γ-sultines by photolysis of mixtures of arylcyclopropanes and sulfur dioxide in the presence of visible light has recently been accomplished. Such reactions which

Can. J. Chem. Downloaded from www.nrcresearchpress.com by 210.87.254.40 on 09/05/12
For personal use only.

[3] 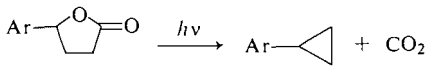

involve initial excitation of SO_2 occasionally also give thietan *S,S*-dioxides **8** in addition to γ-sultines (3).

[4] 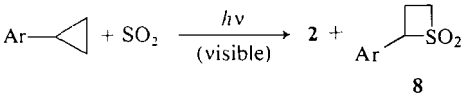

8

The mechanism of the sultine photolysis has not been studied in detail. The available evidence is completely consistent with initial generation of the diradical **9**, which loses SO_2 and couples to give cyclopropanes.[1] In agreement with this, is the observation that 2-phenylthietane *S,S*-dioxide, **10**, also yields phenylcyclopropane (>95%) on photolysis in methanol with **9** being a reasonable intermediate.[2] Furthermore, irradiation of the δ-sultine **11** rapidly afforded the unsaturated sulfinic acid **12** which was isolated and identified as the methyl sulfone **13**. The formation of **12** via the diradical **14** is easily visualized.

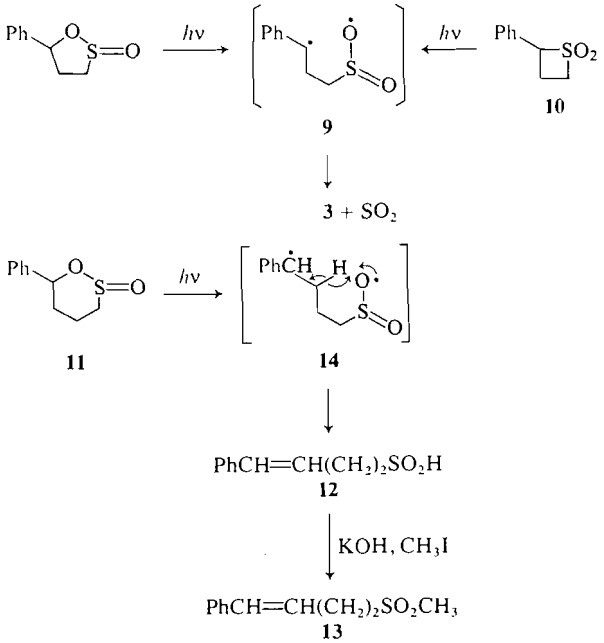

The photolysis of the benz-fused sultines **15** was then studied as a potential route to benzocyclopropenes. Depending on the substitution pattern desired, these compounds were synthesized by one of the two following routes. The parent, dimethyl, and diphenyl derivatives were most easily prepared by controlled oxidation of the mercaptoalcohols **16** using SO_2Cl_2 in acetic acid (4). These intermediates in turn were readily available by reduction of *o*-mercaptobenzoic acid with $LiAlH_4$ in the case of **15***a*, and reaction of methyl *o*-mercaptobenzoate with excess methyl- or phenylmagnesium bromide for **15***b* and **15***c*, respectively. All the mercaptoalcohols were highly susceptible to air-oxidation and were best processed further without undue delay. The diastereomeric monosubstituted sultines, **17***a* and *b*, were obtained via a more arduous route based on our earlier sultine synthesis (5). Thus, *o*-mercaptobenzoic acid was alkylated with α-phenethyl bromide, esterified, and reduced with lithium aluminum

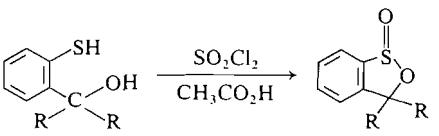

16
a R = H
b R = CH_3
c R = Ph

15
a R = H
b R = CH_3
c R = Ph

hydride. The resultant alcohol was oxidized with CrO_3–pyridine to give the aldehyde **18**. This aldehyde was then treated with PhMgBr and the product oxidized and cyclized with SO_2Cl_2. The diastereomeric alcohols were easily separated by column chromatography. Their spectroscopic properties are described in the Experimental. Individual stereochemical assignments have not been made conclusively. The less polar isomer, **17***a*, mp 122–123°C, shows the benzylic hydrogen at δ 6.57 whereas in the more polar one **17***b*, this proton resonates at δ 7.06. On the basis of the generally observed *trans*-annular deshielding by a *syn*-S=O bond (6) we assign the S=O and C—H *cis* relationship to the latter isomer. The chromatographic behavior of the isomers, in which the isomer having the S=O and C—H groups *cis* would be expected to be more polar because of the greater steric accessibility of the S=O group than when the S=O and phenyl groups are *cis*, supports the assignments (7).

Upon photolysis of the compounds **15***b* and **17**, two types of products were isolated, neither of which requires the intermediacy of benzocyclopropenes, but suggest that possibly under appropriate experimental conditions, e.g. lower temperatures, benzocyclopropenes might be obtainable (8). Thus, irradiation of either of the diastereomeric monophenyl sultines **17** in CH_3OH resulted first in epimerization, a result consistent with a diradical intermediate which can collapse back to starting materials with loss of stereochemistry at both sulfur and carbon. Prolonged irradiation of **17** led to a mixture from which

[1]The photochemical decarboxylation likewise has been shown to involve radical intermediates (2).

[2]D. J. H. Smith and J. Finlay. Private communication.

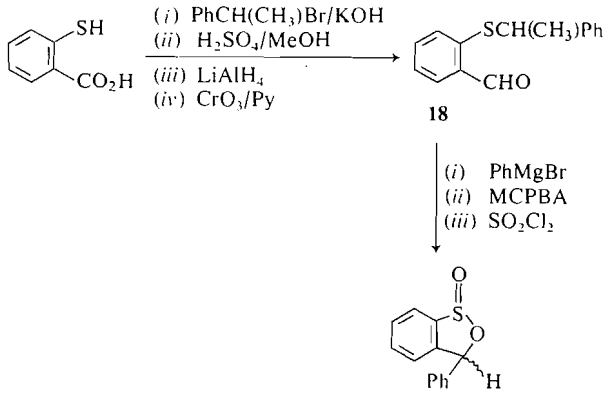

fluorene (**19**) and diphenylmethyl methyl ether (**20**) were isolated in 27 and 32% yields, respectively. The rationalization of fluorene formation via the diradicals **21** and **22** is shown below. The benzocyclopropene **23**, if formed, would not have been expected to be stable under the reaction conditions and be converted to fluorene (9). The isolation of **20** suggests the intermediacy of diphenylcarbene; examples of the trapping of this carbene by methanol to form **20** are well documented (10).

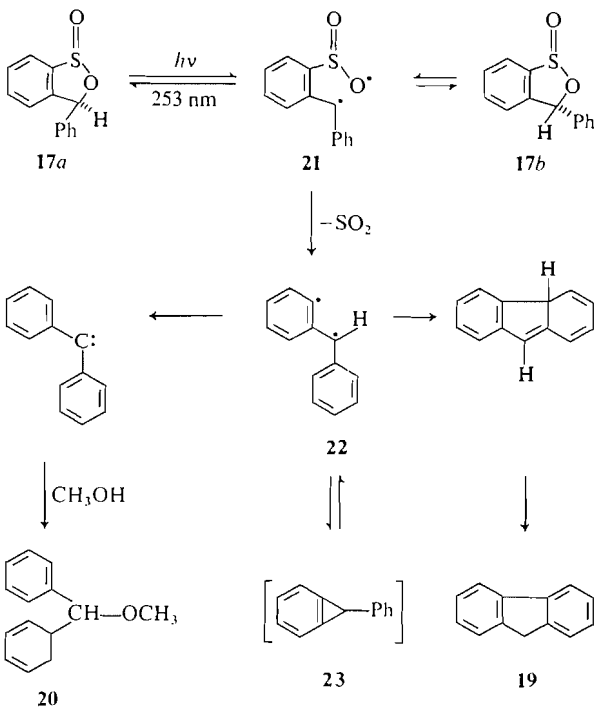

The diphenyl sultine **15***c* gave 9-phenylfluorene as the only isolable product in 42% yield. Its genesis must be similar to that of fluorene from **17**. In contrast to these reactions, the parent benz-fused sultine **15***a* and the dimethyl derivative **15***b* were quite unreactive and gave, after prolonged irradiation (>48 h), unidentifiable decomposition products.

The six- and eight-membered ring sultines **24** and **25**,[3] when photolyzed in CH_3OH gave, respectively, the sulfone **26** and 9,10-dihydrophenanthrene (**27**). The photolysis of **24** to **26** required about 1 h at 25°C; this interconversion can also be accomplished thermally at 80°C (11).

Experimental

All proton nmr spectra were recorded on either Varian T-60 or HA-100 spectrometers using $CDCl_3$ – 1% TMS as solvent; shifts are reported in ppm (7) downfield from TMS. Infrared spectra were obtained on a Beckman IR-20 either neat, or as $CHCl_3$ solutions. Melting points are not corrected.

Usual work-up of reactions refers to partitioning of the reaction mixture between CH_2Cl_2 and water, drying the organic phase over $MgSO_4$, and evaporating the solvent using a rotary evaporator.

The structures of most intermediates were assigned on the basis of spectroscopic data. Key compounds were also sent for elemental analysis and/or exact mass spectral measurements. Sultines **2** (R = H and R = CH_3), **4**, **5**, **11**, and **15***a* have been described (5).

o-Mercaptobenzyl Alcohol (16a)

This compound was prepared in 80% yield by reduction of *o*-mercaptobenzoic acid with $LiAlH_4$ in THF. The crude reaction product was a slightly orange oil; nmr δ: 3.26 (broad s, OH and SH), 4.60 (s, 2H), 7.0–7.4 (m, 4H); ir 3360 and 2530 cm^{-1}.

2-(o-Mercaptophenyl)propan-2-ol (16b)

A stirred solution of 4.89 g of methyl *o*-mercaptobenzoate (prepared by H_2SO_4-catalyzed esterification of the corresponding acid) was dissolved in 200 ml of dry ether at 0°C under N_2 and reacted with 50.5 ml of 1.7 *M* CH_3Li. The reaction was stirred for 5 min, then washed with 200 ml of 10% HCl. The separated aqueous layer was saturated with NaCl and re-extracted with ether. The combined organic extracts were dried and evaporated to yield 4.22 g (86%) of the desired product as a yellowish oil; nmr δ: 1.74 (s, 6H), 2.74 (1H, OH), 4.12 (1H, SH), and 6.9–7.5 (m, 4H). The substance was considered sufficiently pure for the next transformation.

(o-Mercaptophenyl)diphenylmethanol (16c)

Phenylmagnesium bromide (~80 mmol) was prepared in 100 ml of ether. To this solution was added 4.6 g (27.2 mmol) of methyl *o*-mercaptobenzoate. The solution was stirred for about 30 min at room temperature. The usual Grignard work-up gave 8.2 g (95%) of crude thiol alcohol; ir: 3480, 2540 cm^{-1}, no C=O. The crude product was sufficiently pure for the next step.

3H-2,1-Benzoxathiole 1-Oxide (15a)

To a solution of 5.71 g. of mercaptobenzyl alcohol in 100 ml of a 9:1 mixture of CH_2Cl_2 and acetic acid at 0°C was added dropwise 4.4 ml of SO_2Cl_2 in 20 ml of methylene chloride. The mixture was stirred for 1 h and washed with 200 ml of 10% Na_2CO_3. The organic extracts were dried and the solvent evaporated. The crude brown oil was chromatographed on

[3]The authors would like to thank Mr. K. Steliou and Prof. D. N. Harpp (McGill University) for a sample of this compound.

Can. J. Chem. Downloaded from www.nrcresearchpress.com by 210.87.254.40 on 09/05/12
For personal use only.

Can. J. Chem. Downloaded from www.nrcresearchpress.com by 210.87.254.40 on 09/05/12
For personal use only.

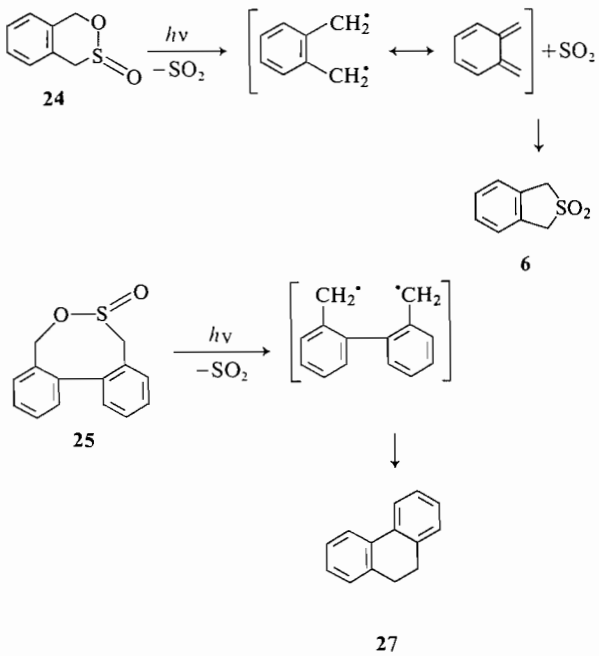

24 6 25 27

300 g of silica gel. The sultine was eluted with 1:5 ethyl acetate – hexane; yield, 2.60 g, 40%. The ir and nmr spectra were identical to those of the compound previously prepared by a different route (5).

*3,3-Dimethyl-2,1-benzoxathiole 1-Oxide (**15c**)*

To a mixture of 0.511 g. of *o*-mercaptophenylpropan-2-ol and 2 ml of acetic acid in 25 ml of CH_2Cl_2 at 0°C was added dropwise 0.25 ml of SO_2Cl_2 in 5 ml of CH_2Cl_2. The reaction was subsequently stirred for 1 h and then worked up as in the case of **15***b*. The crude product was chromatographed on 30 g of silica (hexane). The yield of sultine **15***c*, colorless oil, bp 125°C/4.5 Torr, was 0.274 g (50%); nmr δ: 1.67 (s, 3H), 1.83 (s, 3H), 7.05–7.75 (m, 4H); ir: 1130 and 1105 cm^{-1} (S=O); ms calcd. for $C_9H_{10}O_2S$: 182; found 182; other peaks (relative intensities) were: 182(78), 167(32), 148(88), 134(52), 118(100), 103(68), 91(52), 77(78).

*3,3-Diphenyl-2,1-benzoxathiole 1-Oxide (**15b**)*

A solution of 0.56 ml (6.9 mmol) of sulfuryl chloride dissolved in 10 ml of CH_2Cl_2 was added dropwise with stirring to 2.03 g (6.9 mmol) of (*o*-mercaptophenyl)diphenyl methanol in 70 ml of CH_2Cl_2 and 10 ml of acetic acid at 0°C. The reaction mixture was stirred for 1 h after completion of the addition, then washed with 10% Na_2CO_3 until the p*H* of the aqueous layer was 8. The crude organic product was chromatographed on 150 g of silica gel using hexane – ethyl acetate as eluent. The sultine **15***b* was obtained as colorless crystals, 0.651 g (30%), mp 125–126°C; nmr δ: 7.1–7.8 (m); ir: 1110 and 1120 cm^{-1} (S=O); ms calcd. for $C_{19}H_{14}O_2S$: 306; found 306; other peaks (relative intensity), 258(4), 242(100), 197(44), 165(76), 118.5(40), 105(47), 77(62).

*2-(1-Phenylethylthio)benzaldehyde (**18**)*

2-(1-Phenylethylthio)benzyl alcohol (5) (14.0 g) was dissolved in dry pyridine (87 ml) and reacted with 35 g of CrO_3 using the procedure of Ratcliffe and Rodehurst (13). The yield of the aldehyde **18** was 10.0 g (72%), pale yellow oil; nmr δ: 1.67 (J = 7.5 Hz, 3H), 4.33 (q, J = 7 Hz, H), 7.2–7.4 (m, 5H), 7.4–7.6 (m, 3H), 7.7–8.1 (m, 1H), 10.4 (s, 1H); ir: 1685 cm^{-1}.

2-[(1-Phenylethylsulphinyl)phenyl]methanol

The above aldehyde (3.5 g) dissolved in 10ml of dry ether was added to a solution of PhMgBr prepared from 4.3 g of bromobenzene, 1.8 g Mg in 50 ml of dry ether. The reaction mixture was stirred for an additional hour after completion of the addition then poured into 50 ml of H_2O. Separation, drying and evaporation of the organic extracts gave 3.3 g (72%) of alcohol; ir: 3440 cm^{-1}; nmr δ: 1.57 (d, J = 7 Hz, 3H), 2.3 (s, 1H), 4.00 (q, J = 7 Hz, 1H), 6.10 and 6.13 (2s, 1H), 7.0–7.5 (m, 14H). To this alcohol, dissolved in 100 ml of ethyl acetate at −30°C was added dropwise with vigorous stirring 2.09 g of MCPBA in 30 ml of ethyl acetate. The reaction mixture was kept at −30°C for 2 h, washed with 100 ml of 10% $Na_2S_2O_3$, and 2 × 100 ml of 10% NaOH solution. The crude oily product was chromatographed on 250 g of silica gel. Elution with CH_2Cl_2 gave 2.0 g (57%) of one isomer mp 124–125°C, from methylene chloride – hexane; nmr δ: 1.30 (d, J = 7.5 Hz, 3H), 4.1 (q, J = 7.5 Hz, 1H), 5.63 (1H, OH), 7.0–7.6 (m, 14H), 7.7–8.0 (m, 1H). *Anal.* calcd. for $C_{21}H_{20}O_2S$: C 75.00, H 5.95, S 9.52; found: C 74.91, H 6.07, S 9.68.

*3-Phenyl-2,1-benzoxathiole 1-Oxide (**17a and b**)*

To a solution of 2.0 g of 2-[(1-phenylethylsulfinyl)phenyl]-methanol in 70 ml of CH_2Cl_2 at 0°C was added dropwise 0.80 g of SO_2Cl_2 in 15 ml of CH_2Cl_2. The reaction mixture was kept at 0°C for 1 h and then the solvent was removed on the rotary evaporator. Chromatography on 150 g of silica gel provided, on elution with 4:1 hexane – ethyl acetate, both isomers. Isomer **17***a*: 41% yield mp 122–123°C (CH_2Cl_2–hexane); ir: 1125 cm^{-1}; nmr δ: 6.57 (s, 1H), 7.1–7.8 (m, 9H). *Anal.* calcd. for $C_{13}H_{10}O_2S$: C 67.92, H 4.35, S 13.91; found: C 67.59, H 4.44, S 13.70. Isomer **17***b*: 32% yield; mp 102°C from CH_2Cl_2–hexane; ir: 1125 cm^{-1}; nmr δ: 7.06 (s, 1H) 7.1–7.8 (m, 9H). *Anal.* found: C 67.99, H 4.48, S 13.83.

Photolysis Reactions

These were carried out using a Rayonet-type photochemical apparatus, unless otherwise stated. The photolyses were carried out under N_2 until tlc indicated the disappearance of starting material.

5-Phenyl-1,2-oxathiolane 2-Oxide

Sultine (1.40 g) was dissolved in 40 ml of benzene and 10 ml of acetone and photolyzed using a 450 W Hannovia lamp (immersion apparatus) for 14 h. The yield of phenylcyclopropane, identified by a comparison of the nmr with the published spectrum, was 850 mg (93%).

3-Methyl-5-phenyl-1,2-oxathiolane 2-Oxide

Sultine (250 mg) was photolyzed as above for 4 h. Vapour phase chromatographic analysis indicated a 98% yield of 2-methyl-1-phenylcyclopropane. The nmr of the product obtained after evaporation, 180 mg (~98%) showed absorption from δ 0.5–2.1 (m, 7H) and 6.8–7.3 (m, 5H).

Sultines **4** and **5** were photolyzed under identical conditions to **2***a* and *b* for 36 h. No indication of cyclopropane formation was observed and the starting materials were largely recovered.

Photolysis of 6-Phenyl-1,2-oxathian 2-Oxide

Sultine (0.25 g) was photolyzed in 40 ml of benzene and 10 ml of acetone using a 450 W Hannovia lamp under the above conditions for 3 h. Thin-layer chromatography indicated the disappearance of starting material and the formation of a single very polar product identified as **12** by nmr δ: 2.5–3.0 (m, 4H), 5.3–5.6 (m, 2H), 7.2 (m, 5H), and 9.8 (broads, 1H, OH).

The sulfinic acid was characterized as the sulfone **13** by stirring with methanolic KOH and CH_3I overnight. The reaction mixture was worked-up in the usual manner and the product chromatographed on silica gel using benzene as eluent.

The yield of the sulfone **13** was 180 mg (82%), mp 112°C; nmr δ 2.90 and 3.0 (two s, 3H), 3.0–3.4 (m, 4H), 5.3–6.6 (m, 2H) 7.2 (5H); ir 1120 and 1300 cm^{-1}. *Anal.* calcd. for $C_{11}H_{14}O_2S$: C 50.81, H 5.82, S 13.23; found: C 50.65, H 5.89, S 13.51.

*Photolysis of Sultine **15b***

Sultine (363 mg) was dissolved in 120 ml of anhydrous methanol and photolyzed at 253 nm in a Rayonet apparatus for 14 h. Nitrogen was passed through the reaction mixture during the photolysis. At the end of the photolysis period, the reaction mixture was foggy yellow. The solvent was removed on a rotary evaporator and the product chromatographed on 80 g of silica gel. Elution with 1:1 hexane – ethyl acetate gave two fractions. The less polar material was identified as 9-phenylfluorene, mp 182°C, 42% yield, by comparison with an authentic sample prepared by reduction of 9-hydroxyphenylfluorene with zinc in acetic acid (13). The more polar fraction (61 mg) of yellowish oil was not identified; nmr δ: 7.06–7.83 (m).

Photolysis of 3-Phenyl-2,1-benzoxathiole 1-Oxide in Methanol

Sultine (107 mg, mixture of isomers) was irradiated for 19 h in 120 ml of anhydrous methanol under N_2 as above. The reaction mixture changed from colorless to foggy yellow. The solvent was evaporated and the dark brown paste was chromatographed. The less polar product, 20 mg (27%), had nmr peaks at δ 3.90 (s, 2H) and 7.1–7.9 (m, 8H) and was identified as fluorene by comparison of its spectrum with that of a standard sample (14). Further elution furnished 29 mg (32%) of a colorless oil; nmr δ: 3.3 (s, 3H), 5.2 (s, 1H) and 6.9–7.5 (m, 10H); ir: 1090 cm^{-1}, which was identified as diphenylmethyl ether.

In a second experiment, the photolysis of a single isomer was interrupted after approximately 5 h. Nuclear magnetic resonance investigation of the crude reaction product indicated the presence of approximately equal amounts of both isomers, together with some fluorene and diphenyl methyl ether.

*Photolysis of **24***

A solution of 260 mg of **24** in 30 ml benzene and 10 ml of acetone was photolyzed in the immersion apparatus for 1 h. The solvent was removed and the product identified as the five-membered ring sulfone **26** (11). The yield was essentially quantitative.

*Photolysis of Sultine **25***

A solution of 302 mg of sultine in 120 ml of CH_3OH was photolyzed as above under a stream of N_2 for 18 h. During the photolysis the solution changed from colorless to yellow and the walls of the reaction vessel became coated with polymer. The solvent was evaporated and the brown paste obtained was chromatographed. Elution with hexane gave 161 mg of a 1:1 mixture of 9,10-dihydrophenanthrene and phenanthrene (nmr analysis). In another experiment, the solution was initially purged with N_2, then photolyzed for 17 h. The product obtained was a mixture of 9,10-dihydrophenanthrene and phenanthrene in about a 10:1 ratio.

Acknowledgements

Financial assistance by the National Research Council of Canada and the NATO organization, Grant 1122, is gratefully acknowledged.

1. N. K. Sharma, F. Jung, and T. Durst. Tetrahedron Lett. 2863 (1973).
2. R. S. Givens and W. F. Oettle. J. Org. Chem. **37**, 4325 (1972).
3. D. E. Applequist and L. F. McKenzie. J. Org. Chem. **42**, 1251 (1977).
4. E. N. Givens and L. A. Hamilton. J. Org. Chem. **32**, 2857 (1967).
5. N. K. Sharma, F. de Reinach-Hirtzbach, and T. Durst. Can. J. Chem. **54**, 3012 (1976).
6. E. Jonsson and S. Holmquist. Ark. Kemi. **29**, 301 (1969); C. R. Johnson and W. O. Siegl. J. Am. Chem. Soc. **91**, 2796 (1969).
7. W. O. Siegl and C. R. Johnson. J. Org. Chem. **35**, 3657 (1970).
8. B. Halton. Chem. Rev. **73**, 113 (1973).
9. G. Baum, R. Bernard, and H. Shechter. J. Am. Chem. Soc. **89**, 5307 (1967); H. A. Staab and J. Ipaktschi. Chem. Ber. **101**, 1457 (1968).
10. G. W. Griffin and A. Manmade. J. Org. Chem. **37**, 2589 (1972).
11. F. Jung, M. Molin, R. Van den Elzen, and T. Durst. J. Am. Chem. Soc. **96**, 935 (1974).
12. R. Ratcliffe and R. Rodehurst. J. Org. Chem. **35**, 4000 (1970).
13. A. F. Cockerill and J. E. Lamper. J. Chem. Soc. (B), 503 (1971).
14. The Aldrich Library of NMR Spectra. Vol. IV. p. 31.

Can. J. Chem. Downloaded from www.nrcresearchpress.com by 210.87.254.40 on 09/05/12
For personal use only.

Synthesis of dehydrocycloroyleanone

ROBERT H. BURNELL and MICHEL RINGUET
Département de Chimie, Université Laval, Québec (Qué.), Canada G1K 7P4

Received July 18, 1977

ROBERT H. BURNELL and MICHEL RINGUET. Can. J. Chem. **56**, 517 (1978).

A degradation product (**14**) obtained during the elucidation of the structure of lycoxanthol has been synthesized from podocarpic acid. Several model series of experiments are also described, leading to quinones and furan derivatives.

ROBERT H. BURNELL et MICHEL RINGUET. Can. J. Chem. **56**, 517 (1978).

On a synthétisé, à partir de l'acide podocarpique, un produit de dégradation (**14**) obtenu au cours de l'élucidation de la structure du lycoxanthole. On décrit aussi plusieurs séries d'expériences modèles permettant d'obtenir des dérivés de quinones et de furannes.
[Traduit par le journal]

Can. J. Chem. Downloaded from www.nrcresearchpress.com by 210.87.254.105 on 09/05/12
For personal use only.

During work on the non-alkaloidal constituents of *Lycopodium lucidulum*, we isolated a diterpenoid hydroquinone (lycoxanthol) which was shown (1) to be **1**. One of the degradation products arising from

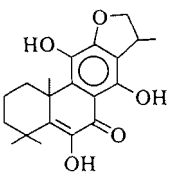

1

the hydrogenolysis of lycoxanthol was assigned the structure **14** (dehydrocycloroyleanone) and the synthesis of this compound, which contains the intact carbon skeleton of lycoxanthol seemed a desirable corroboration of the structures proposed.

Since the final synthesis would be effected from podocarpic acid (**9***a*) and the reduction of the carboxylic acid function to a methyl group is laborious (2), we used the suitably substituted dimethylanisole **2***a* for model studies. Our intention was to oxidize the latter to the known quinone **3***a*, hydrolyze the methoxyl to give the hydroxyquinone **3***b* and then effect a free-radical (Fieser type) annelation (3) to construct the dihydrofuran ring. The hydrolysis step did not afford satisfactory results although hydrolysis had evidently occurred, so it was decided to try the same sequence using a protecting group removable under neutral conditions. Peracid oxidation (4) of the *O*-benzylxylenol **2***b* lead to the *O*-benzylquinone **3***c* but rather than remove the protecting group at this stage, the quinone was subjected to reductive acetylation to give the *O*-benzyldiacetoxyxylenol **4***a*. While this product was readily hydrolyzed to **4***b*, the latter was even more readily oxidized in air to give back the quinone **3***c*. By using conditions whereby simultaneous hydrolysis and methylation are possible the diacetoxy derivative was converted to the dimethoxy compound **4***c* but the reaction was far from complete. Hydrogenolysis of the *O*-benzyl residue in **4***a* afforded the phenol **4***d* which was hydrolyzed to **4***e*, too unstable to isolate but quantitatively oxidized to hydroxyquinone **3***b*. The dimethoxy phenol **4***f* was obtained by similar hydrogenolysis of **4***c*.

Hoping that manipulation of the products might prove easier on the larger molecule, we performed most of these operations on the podocarpane

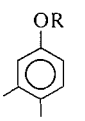

2*a* R = Me
b R = CH_2Ph
c R = COMe

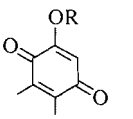

3*a* R = Me
b R = H
c R = CH_2Ph

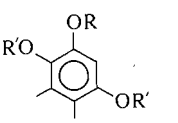

4*a* R′ = Ac, R = CH_2Ph
b R′ = H, R = CH_2Ph
c R′ = Me, R = CH_2Ph
d R′ = Ac, R = H
e R′ = R = H
f R′ = Me, R = H

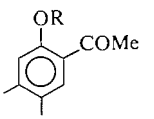

5*a* R = H
b R = CH_2COOEt
c R = CH_2COOH

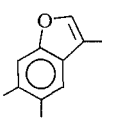

6

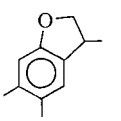

7

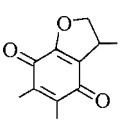

8

Can. J. Chem. Downloaded from www.nrcresearchpress.com by 210.87.254.105 on 09/05/12
For personal use only.

skeleton. We originally followed published methods (2) to reduce the carboxyl moiety of podocarpic acid **9** to the methyl group (as in **9***d*). Recently however we have found that the photochemical reduction of esters described by Deshayes *et al.* (5) for certain acetates, formates, and benzoates:

$$[1]\quad R^1COOR^2 \xrightarrow[HMPT\text{–}H_2O]{h\nu} R^2H(\text{major}) + R^1OH(\text{minor})$$

can be applied to convert the methoxy-*O*-acetyl compound **9***c* to the podocarpane derivative **9***d*. While this reaction is only moderately successful (42%), the only other product is the primary alcohol **9***b* (46%) which can be acetylated and recycled. The methoxypodocarpane **9***d* was then oxidized with peracid and the methoxyquinone **10***a* obtained in 18% yield after chromatography over deactivated alumina. Hydrolysis of the methoxyl proved as unmanageable in this case as in the simpler model **3***a*. Oxidation of the benzyloxypodocarpane **9***f* gave the quinone **10***b*.

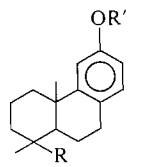

9*a* R = COOH, R′ = H
b R = CH_2OH, R′ = Me
c R = CH_2OAc, R′ = Me
d R = Me, R′ = Me
e R = Me, R′ = H
f R = Me, R′ = CH_2Ph
g R = Me, R′ = COMe

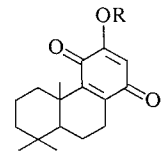

10*a* R = Me
b R = CH_2Ph

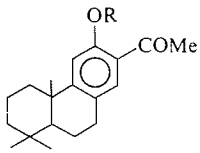

11*a* R = Me
b R = H
c R = CH_2COOEt
d R = CH_2COOH

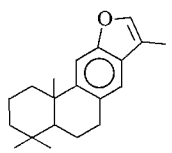

12

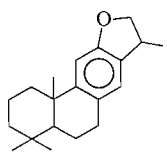

13

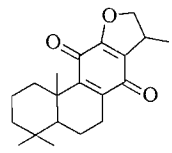

14

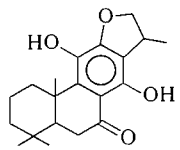

15

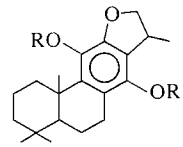

16

In a parallel series of experiments on the model xylenol establishment of the dihydrofuran ring was found to be much simpler. The *O*-acetylxylenol **2***c* was subjected to a Fries rearrangement and gave almost exclusively the properly oriented acetylxylenol **5***a*. Ethyl bromoacetate in the presence of sodium carbonate afforded the ester **5***b* which was hydrolyzed to the acid **5***c*. The latter, on heating in acetic anhydride containing sodium acetate, cyclized and decarboxylated affording the benzofuran **6** which readily absorbed hydrogen in ethanol containing palladium-on-charcoal to give the dihydrofuran **7**. Exploratory peracid oxidation of the small quantity of product available at this stage was shown to be successful both by the required colour change during the reaction and the spectra of the isolated product **8**. The nmr spectrum of this material (and that of **7**) bore a striking resemblance to that of lycoxanthol in the δ 3–4 region.

Applying this sequence in the podocarpane series necessitated certain experimental modifications. Fries rearrangement of the *O*-acetylpodocarpane **9***c* could not be effected so the acetyl residue was introduced by Friedel–Crafts acylation of the methoxypodocarpane **9***d* and the methoxyl group (in **11***a*) was then hydrolyzed by the aluminium chloride technique (6). *O*-Alkylation of the phenol **11***b* with bromoacetate and hydrolysis of the product **11***c* afforded the acid **11***d*. Cyclization and decarboxylation gave the furan **12**. Unlike the model furan **6**, this podocarpane derivative was only sluggishly hydrogenated even in the presence of perchloric acid. The dihydrofuran product **13** contains a newly established asymmetric centre but no evidence suggested the presence of two epimers. Peracid oxidation of the benzodihydrofuran **13** followed by careful chromatography afforded a yellow glass which showed very similar spectral properties and identical tlc behaviour to dehydrocycloroyleanone **14**. Repeated thick-layer chromatography finally removed traces of a minor product affording a synthetic product identical with the dehydrocycloroyleanone **14** obtained previously from lycoxanthol (**1**).

Monache[1] has informed us that this quinone **14** is also a transformation product arising from the naturally occurring ketone **15** and both our synthetic and natural quinones (**14**) are identical with the sample obtained from this source. Despite repeated experimentation we have been unable to proceed further towards synthesis of Monache's ketone **15** or lycoxanthol **1** due to the reluctance of hydroquinone derivatives such as **16** (R = H, Me, or Ac) to Ring B

[1]F. D. Monache. Instituto di Chimica, University Cattolica del Sacro Cuore, Rome. Personal communication, June 1975.

Can. J. Chem. Downloaded from www.nrcresearchpress.com by 210.87.254.105 on 09/05/12
For personal use only.

oxidation. Other workers have described similar difficulties (7).

Experimental

The normal conditions and instruments for the spectra quoted are: optical rotations, chloroform solutions ($c = 1.0$); uv ethanol solutions (ε in parentheses), Beckman DK-1A; ir Perkin Elmer 457 and Beckman IR 12; nmr deuteriochloroform solutions with internal TMS standard, coupling constants in Hz, Varian A60 and Bruker HX 90; mass spectra, Varian M66. Elemental analyses by Chemalytics, Arizona.

4-Benzyloxy-o-xylene **2b**

To 3,4-dimethylphenol (6.11 g) in dioxane (40 ml) under nitrogen was added potassium hydroxide (2.81 g) in water (3 ml). The mixture was heated to 100°C and benzyl chloride (7.03 g) was added drop by drop then the heating was continued for 36 h. After cooling, pouring into water (90 ml), ether extraction and washing with 2 *N* sodium hydroxide, the benzyl ether was obtained as a colourless oil (6.4 g, 60%) which crystallized slowly on standing, mp 39–40°C: λ_{max}: 278 (1800) and 283 nm (1700); δ: 2.18 and 2.22 (s's, aromatic methyls), 5.00 (s, —O—CH_2—), 6.87 (m, 3H, aromatic protons), 7.45 (bs, 5H). *Anal.* calcd. for $C_{15}H_{16}O$: C 84.87, H 7.60; found: C 84.68, H 7.85.

*5-Benzyloxy-2,3-dimethyl-*p*-benzoquinone* **3c**

Sulfuric acid (10 ml) was added to acetic anhydride (920 ml) at 0°C followed by the dropwise addition of hydrogen peroxide (400 ml of 30%) at 5°C. The benzyloxy-*o*-xylene **2b** (30 g) was added in acetic anhydride (60 ml) and the reaction mixture stirred in darkness for 20 h. The product which precipitated when the mixture was poured into cold water was filtered and recrystallized from methanol (3.2 g, 9.5%) mp 134–135°C; λ_{max}: 270 (21 500) and 370 nm (450); ν_{KBr}: 3050, 1680, 1650, and 1610 cm^{-1}; δ: 2.00 (s, C-methyls), 5.00 (s, —O—CH_2—), 5.95 (s, vinyl proton), 7.35 (s, phenyl). *Anal.* calcd. for $C_{15}H_{14}O_3$: C 74.36, H 5.83; found: C 74.52, H 5.83.

4-Benzyloxy-3,6-diacetoxy-o-xylene **4a**

The *p*-quinone **3c** (1.5 g) was dissolved in acetic anhydride (7.5 ml). Powdered zinc (1.5 g) and sodium acetate (0.3 g) were added and the mixture heated until the yellow colour disappeared and then for 1 min longer. Acetic acid (6 ml) was added and after boiling for several minutes the solution was decanted. The residue was washed with hot acetic acid and the combined supernatant was diluted with water to a faint turbidity when cooling in ice gave the hydroquinone derivative **4a** (1.5 g, 75%) mp 118–120°C (from ethanol): λ_{max} 276 nm (1800); ν_{KBr} 2950, 1770, 1635, 1600, 1230, and 1200 cm^{-1}; δ: 2.00 and 2.10 (s's, aromatic methyl), 2.35 and 2.37 (s, CH_3CO), 4.98 (s, —O—CH_2—), 6.55 (s, aromatic proton), 7.35 (s, phenyl). *Anal.* calcd. for $C_{19}H_{20}O_5$: C 69.50, H 6.14; found: C 69.76, H 6.12.

2,5-Diacetoxy-3,4-dimethylphenol **4d**

The benzyloxy derivative **4a** (500 mg) was dissolved in a 9:1 mixture of ethanol–toluene (100 ml) and added to 10% palladium-on-charcoal (200 mg) in ethanol (10 ml). Hydrogenation was continued at 3 atm for 30 min. Filtration and evaporation afforded the phenol **4d** (290 mg, 80%) after crystallization from ether–hexane, mp 115–117°C: λ_{max} 278 nm (2100); ν_{KBr} 3400, 3050, 2930, 1745, 1630, 1230, and 1190 cm^{-1}; δ: 1.98 and 2.04 (s's, aromatic methyls), 2.27 (s, 6H, CH_3CO), 5.9 (bs, D_2O, phenolic OH), 6.75 (s, aromatic proton). *Anal.* calcd. for $C_{12}H_{14}O_5$: C 60.50, H 5.92; found: C 60.54, H 5.89.

Hydrolysis and Oxidation of **4d**

The acetylated hydroquinone **4d** (500 mg) was dissolved in methanol (25 ml). One drop of concentrated hydrochloric acid was added and the mixture was heated on the steam bath for 30 min. The solution was evaporated *in vacuo* at 40°C leaving an oil which crystallized on standing. Without purification the unstable product **4e** was taken up in water (50 ml) and oxidized with ferric chloride (9.7 g) in water (10.7 ml) containing concentrated hydrochloric acid (10.7 ml). After 30 min the hydroxyquinone **3b** (160 mg, 50%), was isolated in the usual manner (ether), mp 115–116°C (lit. (8) mp 115–116°C).

4-Benzyloxy-3,6-dimethoxy-o-xylene **4c**

The diacetoxy compound **4a** (0.328 g) was dissolved in methanol (3 ml) under nitrogen and dimethyl sulfate (0.5 g) was then added. The flask contents were cooled to, and maintained at, 5°C while a solution of sodium hydroxide (0.5 g) in water (0.5 g) was added. The mixture was stirred for 2 h, diluted with water (3.5 ml) and stirring continued for 1 h. Concentrated ammonia (0.02 ml) was then added and the mixture extracted with benzene. The crude product was chromatographed over silica gel and the benzene eluate contained the dimethoxy derivative **4c** (0.13 g, 48%), white needles, mp 54–55°C: λ_{max} 283 nm (2500); δ ($CDCl_3$): 2.08 and 2.21 (s's, aromatic methyls), 3.72 and 3.78 (s's, O-methyls), 5.11 and 7.39 (bs, 2H, 5H, O—CH_2—Ph), 6.42 (bs, lone aromatic proton). *Anal.* calcd. for $C_{17}H_{20}O_3$: C 74.97, H 7.40; found: C 74.93, H 7.20.

2,5-Dimethoxy-3,4-dimethylphenol **4f**

Hydrogenolysis of the benzyl residue in **4c**, as described for **4d**, afforded the phenol **4f** (76%), mp 70–71°C: λ_{max} 284 nm (2480); δ ($CDCl_3$): 2.02 and 2.15 (s's, aromatic methyl), 3.67 and 3.71 (s's, O-methyls), 5.67 (bs, D_2O, OH), 6.38 (s, aromatic proton). *Anal.* calcd. for $C_{10}H_{14}O_3$: C 65.91, H 7.74; found: C 65.96, H 7.95.

2-Hydroxy-4,5-dimethylacetophenone **5a**

Aluminium chloride (4 g) was added in small portions to the 4-acetoxy-*o*-xylene **2c** (25 g) and the mixture heated at 160°C for 2 h. Good yields depend on the exclusion of moisture. After cooling, the hard mass was broken up and added to ice (100 g). Dilute hydrochloric acid (200 ml, 13%) was added and finally the precipitated acetophenone **5a** was filtered and recrystallized from hexane (17.1 g, 68%), mp 69–72°C: λ_{max} 263 (13 000) and 333 nm (4000); ν_{KBr} 3050, 1655, 1630 cm^{-1}; δ: 6.82 and 7.63 (s's, aromatic methyls); 11.62 (s, chelated OH). *Anal.* calcd. for $C_{10}H_{12}O_2$: C 73.14, H 7.34; found: C 73.17, H 7.14.

The Ester **5b**

Under nitrogen, the hydroxyacetophenone **5a** (3.4 g) was dissolved in acetone (100 ml), anhydrous potassium carbonate (2.4 g) was added and the mixture heated to gentle reflux. Ethyl bromoacetate (4.5 g) was added dropwise and after 2 h a further portion (1.5 g) of bromoacetate was added and refluxing was continued until a ferric chloride test was negative (ca. 2 h). After cooling, the solid was filtered off, the volume reduced and the solution filtered again before evaporating. The white residue was recrystallized from ethanol–water (5.2 g, 90%), mp 89–90°C: λ_{max} 255 (11 800) and 310 nm (4800); ν_{KBr} 1760, 1660, 1605, and 1270 cm^{-1}; δ: 1.28 (t, $J = 7.0$ Hz), 4.26 (q, $J = 7.0$ Hz), and 4.68 (s, CH_3CH_2OOC—CH_2—O—), 2.16 and 2.33 (s's, aromatic methyls), 2.66 (s, CH_3CO), 6.65 and 7.58 (s's, aromatic protons). *Anal.* calcd. for $C_{14}H_{18}O_4$: C 67.18, H 7.25; found: C 67.30, H 7.37.

The Acid **5c**

The acetophenone **5b** (5 g) was heated on a steam bath with

Can. J. Chem. Downloaded from www.nrcresearchpress.com by 210.87.254.105 on 09/05/12
For personal use only.

aqueous sodium hydroxide (100 ml, 4%) for 1 h, then cooled and neutralized with dilute hydrochloric acid. The acid **5***c* was filtered, washed with cold water, and recrystallized from ethanol (4.25 g, 95%) mp 185–187°C: λ_{max} 255 (9800) and 312 nm (4400); ν_{KBr} 3200, 1720, and 1660 cm^{-1}; δ: 2.39 and 2.47 (s's, aromatic methyls), 2.95 (s, CH_3CO), 5.04 (s, —O—CH_2—), 7.00 and 7.85 (s's, aromatic protons). *Anal.* calcd. for $C_{12}H_{14}O_4$: C 64.85, H 6.35; found: C 64.55, H 6.28.

3,5,6-Trimethylbenzofuran ***6***

The acid product **5***c* (4.4 g), sodium acetate (17.6 g), and acetic anhydride (60 g) were refluxed for 1.5 h and then cooled and poured onto ice (400 g). The ether extract was evaporated to a small volume then poured into ice water causing the low melting product to crystallize. The benzofuran **6** was sublimed (2.9 g, 90%), mp 40–42°C: λ_{max} 248 (10 300), 278 (3000), 284 (3000), and 290 nm (3600); δ: 2.07 and 2.25 (s's, aromatic methyls), 2.12 (d, J = 1.0 Hz, furan methyl), 7.19 and 7.28 (bs, s, aromatic protons), 7.22 (d, J = 1.0 Hz, furan proton). *Anal.* calcd. for $C_{11}H_{12}O$: C 82.46, H 7.55; found: C 82.42, H 7.55.

3,5,6-Trimethyl-2,3-dihydrobenzofuran ***7***

The benzofuran **6** (5.35 g) in acetic acid (50 ml) was added to prehydrogenated palladium charcoal (500 mg) in acetic acid (10 ml). After the uptake of 1 mol of hydrogen (ca. 1 h), the catalyst was removed and the solution evaporated. The residue was taken up in water, extracted with ether which was washed with sodium bicarbonate solution. The dihydrofuran was finally distilled, (5.0 g, 92%) bp 45–46°C/0.3 Torr; λ_{max} 287 nm (3800); δ: 1.25 (d, J = 7.0 Hz), 3.43 (m), 3.98 (dd, J = 7.0 and 8.5 Hz), and 4.60 (dd, J = 8.5 and 8.5 Hz, CH_3—CH—CH_2—O—), 2.16 (s, 6H, aromatic methyl), 6.57 and 6.87 (s's, aromatic protons). *Anal.* calcd. for $C_{11}H_{14}O$: C 81.44, H 8.70; found: C 81.58, H 8.81.

The Quinone ***8***

The peracid solution was prepared as described for **3***c* using acetic anhydride (9.2 ml), sulfuric acid (0.1 ml), and hydrogen peroxide (4 ml of 30%). To this solution, the dihydrobenzofuran **7** (2.5 g) was added in acetic anhydride (0.8 ml). After 3 h in darkness, the reaction mixture was poured into cold water (25 ml) and was extracted with methylene chloride. After washing with sodium bicarbonate (5%), the residue obtained by evaporation was lyophilized to give an orange oil from which the quinone **8** (90 mg) was obtained by repeated preparative tlc; mp 101–104°C: λ_{max} 285 (19 000) and 420 nm (400); ν(CCl_4): 2950, 1680, 1655 and 1645 cm^{-1}; δ: 1.29 (d, J = 8.0 Hz), 3.57 (m), 4.26 (dd, J = 8.0 and 9.0 Hz), and 4.74 (dd, J = 9.0 and 9.0 Hz, CH_3—CH—CH_2—O—), 1.98 (s, 6H, quinone methyls); *m/e* 192 (M^+, 100), 177 (80), 160 (40), 149 (50), 145 (25), 95 (20), and 53 (30).

12-Methoxypodocarpa-8,11,13-trien-16-ol ***9b***

The primary alcohol was prepared from methyl podocarpane methyl ether following essentially the procedure of Zeiss *et al.* (9) ($LiAlH_4$ in ether), yield 90%, mp 89–91°C (lit. (9) mp 91°C).

The *acetate* **9***c* was prepared by reacting **9***b* (1 g) with acetic anhydride (2 ml) and pyridine (1 ml) at 25°C for 40 h; yield 0.95 g (82%), mp 72–74°C (from hexane), $[\alpha]_D^{25}$ +65.99°: λ_{max} 280 (2700) nm; ν_{KBr} 1730 and 1240 cm^{-1}; δ($CDCl_3$): 1.02 and 1.19 (s's, *C*-methyls), 2.04 (s, CH_3CO), 2.81 (m, benzylic CH_2), 3.63 (s, *O*-methyl), 4.14 (ABq, J = 11 Hz, —CH_2—O—), 6.77 (m, aromatic protons, 3H). *Anal.* calcd. for $C_{20}H_{28}O_3$: C 75.91, H 8.92; found: C 75.98, H 8.78.

12-Methoxypodocarpa-8,11,13-triene ***9d***

By Irradiation of the Acetate ***9c***

The acetate **9***c* (0.5 g) was dissolved in HMPT (95 ml) and water (5 ml) and the solution irradiated with a low pressure mercury lamp (254 nm) in a quartz vessel for 3 h. After evaporation, the residue was taken up in ether and washed well. The oily product was separated by chromatography over silica gel affording the primary alcohol **9***b* (0.19 g, 46%) which followed the reduced product **9***d* (0.17 g, 42%), mp 30–31°C (lit. (9) mp 30.5–31.5°C), $[\alpha]_D^{25}$ +71.8°: δ: 1.03, 1.27, and 3.86 (s, methyls). *Anal.* calcd. for $C_{18}H_{26}O$: C 83.66, H 10.14; found: C 83.87, H 10.40.

12-Hydroxypodocarpa-8,11,13-triene ***9e***

Under nitrogen, the methoxy derivative **9***d* (6.0 g) was dissolved in dry methylene chloride (180 ml) which was then cooled to −70°C. Drop by drop, a solution of boron tribromide (6.0 g) in methylene chloride (20 ml) was added and the temperature allowed to rise to ambiant during 16 h of stirring. Water (100 ml) was added and the organic layer yielded the phenol **9***e* (5.0 g, 88%) in the usual manner, mp 139–141°C (lit. (10) 140–141°C).

The *O-benzyl ether* ***9f*** was prepared in 65% yield using the procedure described for **2***b*. Colorless oil, n_D^{20} 1.5745, $[\alpha]_D^{25}$ +67.2°: λ_{max} 278 (3000) and 283 nm (2600); ν_{film} 3050, 2960, 1620, 1590, 1510, 1460, 1390, 1260, 1200, 1080 and 1040 cm^{-1}; δ: 0.95 (s, 6H, *gem*-dimethyl), 5.05 and 7.42 (s, bs, —O—CH_2—Ph), 6.95 (m, other aromatic protons); *Anal.* calcd. for $C_{28}H_{30}O$: C 86.18, H 9.04; found: C 86.01, H 9.08.

The *O-acetyl derivative* ***9g*** was prepared from the phenol **9***e* (9.7 g) by heating at 70°C with anhydrous sodium acetate (0.7 g) in acetic anhydride (125 ml) for 2 days. The acetate **9***g* (10.2 g, 90%) was recrystallized from methanol, mp 75–77°C (lit. (4) 75–76°C).

12-Methoxypodocarpa-8,12-dien-11,14-dione ***10a***

A peracid solution was prepared as described for **3***c* (acetic anhydride 40 ml, sulfuric acid 0.5 ml and 30% hydrogen peroxide 20 ml). The methoxypodocarpatriene **9***d* (2.4 g) in acetic anhydride (5 ml) was added and the mixture stirred in darkness for 20 h and then poured into cold water (125 ml). Methylene chloride extraction, washing with sodium bicarbonate solution, and evaporation gave a yellow oil which was chromatographed over alumina (deactivated by adding 5% by weight of 10% aqueous acetic acid). Petroleum ether elutes starting material (0.7 g) but the petroleum ether – benzene (1:4) eluate was the yellow methoxyquinone **10***a* (320 mg), mp 168°C (lit. (4) 171°C), $[\alpha]_D^{25}$ +89.6°: λ_{max}: 272 (20 700) and 370 nm (645); ν_{KBr}: 1670, 1645, and 1595 cm^{-1}; δ: 0.95, 1.31, and 3.83 (s's, methyls), 2.64 (m, —CH_2—C=C), 5.86 (s, vinyl proton). *Anal.* calcd. for $C_{18}H_{24}O_3$: C 75.0, H 8.4; found: C 75.2, H 8.6.

Further elution of the column (benzene–ether 1:1) gave 8β-hydroxypodocarpa-9(11),13-dien-12-one (0.5 g).

12-Benzyloxypodocarpa-8,12-dien-11,14-dione ***10b***

The benzyl ether **9***f* (1.4 g) was oxidized as described above but the orange crude product was chromatographed over silica gel affording the crystalline benzyloxyquinone **10***b* (160 mg, 10%) in the hexane–benzene (7:3) eluate, mp 232–233°C, $[\alpha]_D^{25}$ +85.3°; λ_{max}: 272 (17 000) and 360 nm (500); ν_{KBr}: 1675, 1655, and 1605 cm^{-1}; δ: 0.93 (s, 6H, *gem*-dimethyl), 1.32 (s, angular methyl), 5.00 and 7.40 (bs, s, —O—CH_2Ph), and 5.88 (s, vinyl proton). *Anal.* calcd. for $C_{24}H_{28}O_3$: C 79.09, H 7.74; found: C 79.10, H 7.84.

13-Acetyl-12-methoxypodocarpa-8,11,13-triene ***11a***

To a stirred cooled solution of the methoxy compound **9***d* (2.0 g) and acetyl chloride (1.17 ml) in nitrobenzene (25 ml) was added aluminum chloride (2.05 g) in small portions over a 30 min period (12). The mixture was stirred for 20 h and then hydrolyzed with cold 10% hydrochloric acid (200 ml). The

Can. J. Chem. Downloaded from www.nrcresearchpress.com by 210.87.254.105 on 09/05/12
For personal use only.

nitrobenzene was removed by steam distillation and the residue extracted with ether to give the acetyl compound **11***a* (1.7 g, 75%) after crystallization from hexane, mp 76–77°C, $[\alpha]_D^{25}$ +69.9°: λ_{max} 258 (10 700) and 318 nm (4200); ν(CCl_4). 2840 and 1670 cm^{-1}; δ (CCl_4): 6.75 (s, H) and 7.33 (s, C(14)-H) *Anal.* calcd. for $C_{20}H_{28}O_2$: C 79.95, H 9.39; found: C 79.72, H 9.44.

13-Acetyl-12-hydroxypodocarpa-8,11,13-triene ***11b***

This preparation is adapted from the method of Cambie *et al.* (6). Under nitrogen, the methoxy compound **11***a* (0.75 g) in methylene chloride (15 ml) was refluxed for 15 h with aluminum chloride (1.0 g). The cooled reaction mixture was poured into cold dilute hydrochloric acid. The organic layer was extracted with 0.5% sodium hydroxide and the phenolic product **11***b* isolated in the usual manner, mp 129–130°C (from hexane), $[\alpha]_D^{25}$ +83.4° (0.6 g, 85%): λ_{max} 263 (14 500) and 340 nm (4200); ν(CCl_4) 2950, 2860, 1655 and 1585 cm^{-1}; δ: 0.93, 0.94 and 1.17 (s's, methyls), 2.54 (s, CH_3CO), 6.83 and 7.35 (s's, C(11)-H, C(14)-H, aromatic protons), 11.82 (s, chelated OH). *Anal.* calcd. for $C_{19}H_{26}O_2$: C 79.68, H 9.15; found: C 79.60, H 9.38.

13-Acetyl-12-(carbethoxymethoxy)podocarpa-8,11,13-triene ***11c***

To phenol **11***b* (1.75 g) and anhydrous potassium carbonate (5.4 g) in dry acetone (50 ml) was added ethyl bromoacetate (1.8 g). The mixture was refluxed 12 h and after cooling and filtering, evaporation afforded a yellow oil (2.0 g, 88%) which resisted crystallization after chromatography over silica gel, n_D^{20} 1.5436, $[\alpha]_D^{25}$ +54.9°: λ_{max} 255 (10 000) and 312 nm (3450); ν_{film} 1755, 1670 and 1610 cm^{-1}; δ: 0.90, 0.92 and 1.15 (s's, methyls), 1.28 (t, J = 7.5 Hz), 4.27 (q, J = 7.5 Hz), 4.65 (s, $CH_3CH_2OOC—CH_2—O$), 2.63 (s, CH_3CO), 6.73 and 7.45 (s's, C(11)-H, C(14)-H, aromatic protons). *Anal.* calcd. for $C_{23}H_{32}O_4$: C 74.16, H 8.66; found: C 74.26, H 8.60.

13-Acetyl-12-(carboxymethoxy)podocarpa-8,11,13-triene ***11d***

The ester **11***c* (1.9 g) in ethanol (20 ml) was hydrolyzed by refluxing for 1 h with 10% sodium hydroxide (12.5 ml). The cooled mixture was poured into ice water, acidified (5% hydrochloric acid) and the precipitated acid was filtered off (gummy) and then taken up in ether. Silica gel chromatography afforded the acid **11***d* (1.7 g, 97%) as a yellow glass which has never crystallized: λ_{max} 255 (11 800) and 315 nm (4300); ν_{film} 3400, 2500, 1730, 1675 and 1615 cm^{-1}; δ(CCl_4): 0.90 (s, 6H, *gem*-dimethyl), 1.13 (s, angular methyl), 2.57 (s, CH_3CO), 4.64 and 11.65 (s, bs, $O—CH_2—COOH$), 6.75 and 7.38 (s's, aromatic protons). *Anal.* calcd. for $C_{21}H_{28}O_4$: C 73.22, H 8.19; found: C 73.15, H 8.21.

3,7,7,10aβ-Tetramethyl-5,6,6a,7,8,9,10,10a-octahydrophenanthrofuran(2,3,b) ***12***

To the acid **11***d* (1.7 g) in acetic anhydride (35 ml) was added anhydrous sodium acetate (7.0 g) and the mixture was refluxed for 3 h. After cooling and pouring into ice water (200 ml), the gummy precipitate was taken up in ether and washed with dilute sodium bicarbonate. Evaporation gave a yellow oil (**12**) which was purified by short path distillation, bp 140°C/0.15 Torr, n_D^{20} 1.5671 (1.2 g, 86%), $[\alpha]_D^{25}$ +66.0°; λ_{max} 253 (13 500), 286 (5500) and 295 nm (5100); δ: 0.95 (s, 6H, *gem*-dimethyl), 1.19 (s, angular methyl) 2.16 (d, J = 1.0 Hz, furan methyl), 3.00 (m, benzylic CH_2) 7.10 and 7.31 (s's, C(11)-H, C(14)-H) aromatic protons, and 7.24 (d, J = 1.0 Hz, furan). *Anal.* calcd. for $C_{20}H_{26}O$: C 85.05, H 9.28; found: C 84.76, H 9.40.

3,7,7,10aβ-Tetramethyl-2,3,5,6,6a,7,8,9,10,10a-decahydrophenanthrofuran(2,3,b) ***13***

The furan **12** (0.5 g) was hydrogenated at 3 atm. for 12 h in acetic acid (200 ml) containing a small drop of perchloric acid. The residue obtained by evaporating the filtered solution was taken up in hexane and washed with dilute sodium bicarbonate. The usual workup afforded the dihydrofuran **13** as a colorless oil (0.48 g, 95%), n_D^{20} 1.5877, $[\alpha]_D^{26}$ +72.1°: λ_{max} 292 nm (5100); δ: 0.91 (s, *gem*-dimethyl), 0.93 (s), 1.15 (s, angular methyl), 1.28 (d, J = 7.0 Hz), 3.35 (m), 3.95 (dd, J = 8.5 and 8.5 Hz), and 4.58 (dd, J = 8.5 and 8.5 Hz, $CH_3—CH—CH_2—O—$), 6.61 and 6.72 (s's, C(11)-H and (C14)-H, aromatic protons). *Anal.* calcd. for $C_{20}H_{28}O$: C 84.45, H 9.92; found: C 84.48, H 9.94.

Dehydrocycloroyleanone ***14***

To a peracid solution, prepared as described for **3***a* using acetic anhydride (80 ml), sulfuric acid (0.5 ml) and 30% hydrogen peroxide (35 ml), was added the dihydrofuran **13** (4.4 g) in acetic anhydride (20 ml). After stirring in darkness for 2.5 h the mixture was poured into ice water (250 ml) and extracted with chloroform. After rigorous washing with 1% sodium hydroxide, the crude product was chromatographed over Florisil and the yellow band eluted with benzene was rechromatographed over alumina deactivated with 10% acetic acid (5% by weight). The yellow fraction (303 mg) still showed a slight impurity (weak acetate peaks in the infrared) which could only be removed by repeated preparative tlc. The quinone **14** was finally sublimed, mp 142–143°C: identical in all respects with the dehydrocycloroyleanone obtained by hydrogenolysis of lycoxanthol (1): λ_{max} 285 (21 000) and 380 nm (400); δ($CDCl_3$): 0.89 (s, 3H), 0.92 (s, 3H), 1.25 (s, 3H), 1.30 (d, J = 8.0 Hz, 3H), and dihydrofuran protons centred at 3.49, 4.18, and 4.71 (J = J = 8.5 Hz); *m/e* 314.1880 (M^+, $C_{20}H_{26}O_3$ requires 314.1882).

Acknowledgements

We acknowledge aid in the form of operating grants from the National Research Council of Canada and from the Commission de la Recherche Scientifique, Gouvernement du Québec, and as graduate bursaries (M.R.) from the National Research Council of Canada and the Quebec Government.

1. R. H. Burnell, L. Mo, and M. Moinas. Phytochemistry, **11**, 2815 (1972).
2. (*a*) W. P. Campbell and D. Todd. J. Am. Chem. Soc. **64**, 928 (1942); (*b*) K. Mori and M. Matsui. Tetrahedron, **26**, 3467 (1970).
3. (*a*) L. F. Fieser and M. T. Teffler. J. Am. Chem. Soc. **70**, 3179 (1948); (*b*) A. C. Baillie and R. H. Thomson. J. Chem. Soc. C, 48 (1968).
4. G. F. Burkinshaw and B. R. Davis. Tetrahedron, **23**, 4147 (1967).
5. M. Deshayes, J. P. Pete, C. Portella, and D. Scholler. J. Chem. Soc. Chem. Commun. 439 (1975).
6. R. C. Cambie, K. P. Mathai, and A. W. Missen. Aust. J. Chem. **25**, 1253 (1972).
7. T. Matsumoto, Y. Tachibana, M. Hayashi, and K. Fukui. J. Sci. Hiroshima Univ. Ser. A, **39**, 111 (1975).
8. L. F. Fieser and M. I. Ardao. J. Am. Chem. Soc. **78**, 779 (1956).
9. H. H. Zeiss, C. E. Slimowicz, and V. Z. Pasternak. J. Am. Chem. Soc. **70**, 1981 (1948).
10. R. Hodges and R. A. Raphael. J. Chem. Soc. 52 (1960).

Ribo-2′-deoxyribo hybrid dinucleoside monophosphates. Proton magnetic resonance studies of 3′,5′- and 2′,5′-uridylyl-2′-deoxythymidine

JAMES PEELING[1] AND FRANK E. HRUSKA
Department of Chemistry, University of Manitoba, Winnipeg, Man., Canada R3T 2N2
AND
PETER C. LOEWEN
Department of Microbiology, University of Manitoba, Winnipeg, Man., Canada R3T 2N2

Received July 14, 1977

JAMES PEELING, FRANK E. HRUSKA, and PETER C. LOEWEN. Can. J. Chem. **56**, 522 (1978).

This ^{1}Hmr study initiates our examination of the conformations of dinucleoside monophosphates possessing ribo 2′- or 3′-nucleotidyl units linked to 5′-nucleotidyl units possessing the 2′-deoxyribo sugar. The syntheses of uridylyl-3′,5′-2′-deoxythymidine (3′,5′-UpdT) and its 2′,5′-isomer, 2′,5′-UpdT, were carried out with standard techniques. The ^{1}Hmr data were obtained at frequencies up to 270 MHz and used to derive the dominant conformation of the dimers in aqueous solution. Comparison with data for the component mononucleotides reveals that dimerization does not lead to drastic changes in the molecular conformation. Literature data for dimers possessing only the ribo sugar (3′,5′-UpU) and the 2′-deoxyribo sugar (3′,5′-d(TpT)) are also presented. The results indicate that, at least for our dipyrimidine dimers, the molecular conformation of a particular fragment is not critically dependent on the nature (ribo or 2′-deoxyribo) of the other nucleotide unit.

JAMES PEELING, FRANK E. HRUSKA, et PETER C. LOEWEN. Can. J. Chem. **56**, 522 (1978).

Cette étude par rmn ^{1}H marque le début de nos travaux sur les conformations de monophosphates de nucléosides possédant des unités ribo 2′- ou 3′-nucléotidyles qui sont liées à des unités 5′-nucléotidyles possédant un sucre 2′-déoxyribo. On a effectué des synthèses d'uridylyl-3′,5′ 2′-déoxythymidine (3′,5′-UpdT) et de son isomère 2′,5′-UpdT, en faisant appel à des techniques standards. On a obtenu des données de rmn ^{1}H à des fréquences allant jusqu'à 270 MHz et on les a utilisées pour déterminer la conformation prédominante des dimères en solution aqueuse. Une comparaison de ces données avec celles obtenues pour les composants mononucléotides indique que la dimérisation ne conduit pas à des changements importants dans la conformation moléculaire. On présente aussi des données provenant de la littérature au sujet de dimères ne possédant que le sucre ribo (3′,5′-UpU) et le sucre 2′-déoxyribo (3′,5′-d(TpT)). Les résultats indiquent, au moins pour nos dimères dipyrimidines, que la conformation moléculaire d'un fragment particulier ne dépend pas d'une façon critique de la nature (ribo ou 2′-déoxyribo) de l'autre unité nucléotide.

[Traduit par le journal]

Introduction

Conformational studies of oligonucleotides in solution have been directed mainly at molecules containing solely either the ribose or 2′-deoxyribose sugar (1–6) though structures with covalently linked ribo- and 2′-deoxyribonucleotides are known (7). Maurizot *et al.* (8) examined the temperature dependence of the circular dichroic spectra of the four possible hybrid dinucleoside-3′,5′-monophosphates of adenine, i.e., ApA, dApA, ApdA, and d(ApA),[2] with a view to elucidating the conformational role of a 2′-hydroxyl group, and suggested that the observed spectral differences were most likely due to an intramolecular hydrogen bond to the adjacent 3′-phosphate. Kondo *et al.* (9) carried out uv, cd, and proton nmr of these same molecules, and concluded that the mode and extent of intramolecular base stacking was influenced by the 2′-hydroxyl group but they suggested that its effect is exerted through steric hindrance.

In the earlier nmr studies of the hybrid dimers (9), spectral parameters obtainable from the bands of the base, the H_1' and H_2' protons were considered, and thus, though comments about base stacking and sugar pucker could be made, no information about the conformational situation about the $C_{4'}$—$C_{5'}$ and $C_{5'}$—$O_{5'}$ bonds was obtained. Here we present proton nmr data for the hybrid dimer, uridylyl-3′,5′-2′-deoxythymidine (3′,5′-UpdT) (Fig. 1) as well as for its isomer possessing the 2′,5′-phosphodiester linkage (2′,5′-UpdT). Dimers containing only the pyrimidine bases (U, T) were chosen for our initial studies; since base stacking is

[1]Post-doctoral fellow; present address: University of Petroleum and Minerals, Dhahran, Saudi Arabia.

[2]A 'd' outside the parenthesis indicates that both fragments are 2′-deoxyderivatives, d(ApA) for example. A 'd' immediately before a base symbol (A, T, etc.) indicates that that unit has the 2′-deoxy sugar. A ribose nucleoside fragment will not be prefixed.

Can. J. Chem. Downloaded from www.nrcresearchpress.com by 210.87.254.105 on 09/05/12
For personal use only.

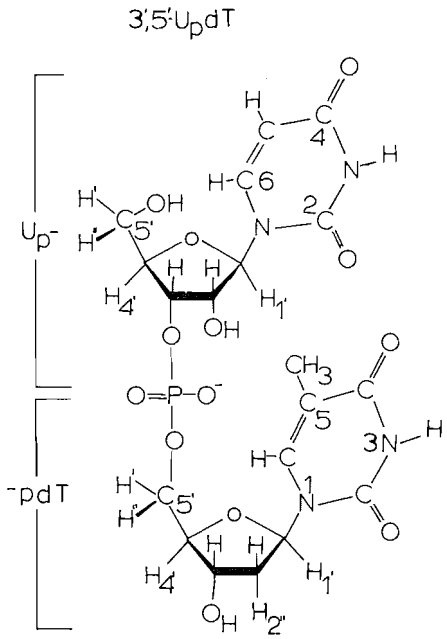

FIG. 1. Structural formula of uridylyl-(3',5')-2'-deoxythymidine or 3',5'-UpdT. Up- and -pdT refer to the 3'- and 5'-linked fragments, respectively.

expected to be less important here than in purine-containing dimers, the interpretation of the data is simplified but forms the basis for extension of the work to the more complex situation of stacked dimers.

Experimental

3',5'-UpdT and 2',5'-UpdT were prepared following the procedure of Lapidot and Khorana (10). Details of the preparation and purification are available upon request.

Proton spectra were obtained on a variety of spectrometers (Bruker WH-90DS, Manitoba; Bruker WH-270, Madison; Varian HA-100, Manitoba; Varian HR-220, Canadian 220 MHz Centre) operating in the CW or FT modes. Sodium-3-trimethylsilylpropionate, 2,2,3,3-d_4 (TSP) was used as an internal ^{1}Hmr reference. Solutions (0.05 *M* or less) were freeze-dried three times and dissolved in 100% D_2O. For the dimers the p*D* of the solution was adjusted to neutrality with NaOD and DCl; for the monomers the solution p*D* was adjusted to about 5.0. In all instances, then, the phosphate is monoanionic. Calibration of the spectra was carried out by standard methods. Spectral analysis was carried out using LAME (11) and computer simulated spectra were generated as a final test of the data. A sample spectrum of 3,5-UpdT is shown in Fig. 2.

The chemical shift (δ) and coupling constant (*J*) data for the *ribose* and *2'-deoxyribose* fragments of the hybrid dimers are listed in Tables 1 and 2, respectively. For purposes of comparison data for the mononucleotide, 5'dTMP, and the homodimers, 3',5'-UpU and 3',5'-d(TpT), are included in the appropriate table; the source of these data is indicated in the footnotes to the tables.

Results and Discussion

Spectral Assignment and Chemical Shifts

The assignment of the spectral bands of the Up- and -pdT fragments was accomplished by comparison with published spectra of mono- and oligonucleotides (1, 3, 12, 13). Following the work of Ritchie and Perlin (14) on selectively deuterated adenosine and that of Remin and Shugar (15) and Davies and Rabczenko (16), the low-field portion of the $H_{5'}$,$H_{5''}$ bands was assigned to $H_{5'}$ for all ribose and 2'-deoxyribose fragments (Fig. 3).

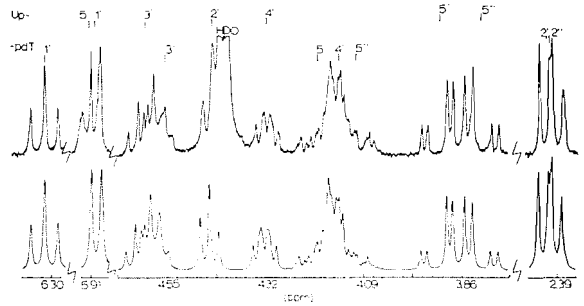

FIG. 2. (*a*) Single scan, continuous wave, 220 MHz spectrum of the ribose protons 3',5'-UpdT (p*D* = 6.8, 65°C, ~0.05 *M* in D_2O). Sweep width 250 Hz. (*b*) Computer simulated spectrum.

In the -pdT unit of 3',5'-UpdT there exists a substantial shift between the 5'- and 5''-hydrogens (0.13 ppm at 20°C; Table 2). In contrast $H_{5'}$ and $H_{5''}$ in -pdT of 2',5'-UpdT are nearly isochronous. Furthermore, the $\delta_{5'}$ and $\delta_{5''}$ values of -pdT (2',5'-isomer) are similar to those of the monomer 5'dTMP. This is not the case in either 3',5'-UpdT or 3',5'-d(TpT) where large deshielding effects (up to 0.19 ppm, relative to 5'dTMP) are evident in the $\delta_{5'}$ and $\delta_{5''}$ values of the -pdT units. Thus, incorporation of 5'-dTMP into a dimer induces magnetic nonequivalence in the $H_{5'}$,$H_{5''}$ pair if the second fragment is 3'-linked, the magnitude of the induced effect being dependent on the nature (ribo or 2'-deoxyribo) of the 3'-linked fragment. Ezra *et al.* (4) have seen an analogous situation for the ribose homodimers 2',5'-CpC and 3',5'-CpC. In the -pC fragment of the former the $H_{5'}$,$H_{5''}$ hydrogens are isochronous whereas in that of the latter they are separated by 0.22 ppm.

It is interesting to note that, whereas the $\delta_{5''}$ values for the -pdT units of 3',5'-UpdT and 3',5'-d(TpT) differ by only 0.03 ppm, the $\delta_{5'}$ values differ by a larger amount, 0.09 ppm. Thus, the $H_{5'}$ hydrogen on the -pdT fragment appears to be more sensitive to the nature (hydrogen or hydroxyl) of the *exo* substituent on the $C_{2'}$ carbon of the 3'-linked nucleotidyl fragment. This supports our assignment of the $H_{5'}$,$H_{5''}$ hydrogens in the -pdT fragment of both dimers and provides as well some conformational information. (See below).

The $H_{2'}$ and $H_{2''}$ of the -pdT units of 3',5'-UpdT,

Can. J. Chem. Downloaded from www.nrcresearchpress.com by 210.87.254.105 on 09/05/12
For personal use only.

Can. J. Chem. Downloaded from www.nrcresearchpress.com by 210.87.254.105 on 09/05/12
For personal use only.

TABLE 1. Proton chemical shifts (δ) and coupling constants (J)[a] of 2′UMP, 3′UMP, 3′,5′-UpU, and the ribose protons of 2′,5′-UpdT and 3′,5′-UpdT in D_2O

		Up-				Up-	
			3′,5′-UpdT			2′,5′-UpdT	
Parameter	3′UMP	3′,5′-UpU[b] 20°C	20°C	65°C	2′UMP (23°C)	20°C	65°C
$\delta_{1'}$	5.96	5.89	5.85	5.90	6.02	6.06	6.03
$\delta_{2'}$	4.46	4.46	4.46	4.45	4.75	4.73	4.76
$\delta_{3'}$	4.57	4.55	4.55	4.60	4.37	4.39	4.37
$\delta_{4'}$	4.31	4.34	4.33	4.32	4.15	4.14	4.14
$\delta_{5'}$	3.93	3.94	3.94	3.91	3.87	3.87	3.87
$\delta_{5''}$	3.85	3.85	3.84	3.83	3.81	3.80	3.80
δ_6	7.91	7.93	7.95	7.86	7.84	7.81	7.77
δ_5	5.92	5.87	5.86	5.91	5.91	5.74	5.81
$J_{1'2'}$	4.9	4.2	4.3	4.6	5.7	4.5	5.5
$J_{2'3'}$	5.2	5.2	5.1	4.8	5.4	4.6	5.8
$J_{3'4'}$	5.2	5.3	5.6	4.9	4.4	4.1	4.9
$J_{4'5'}$	2.9	2.4	2.7	2.9	3.0	3.1	2.7
$J_{4'5''}$	4.2	4.0	3.3	4.0	4.7	3.8	4.7
$J_{5'5''}$	−12.8	−13.1	−13.1	−13.0	−12.7	−13.7	−12.7
J_{56}	8.2	8.1	8.2	8.1	8.1	7.7	8.1
$J_{P2'}$	—	—	—	—	8.4	9.4	8.9
$J_{P3'}$	8.2	8.2	8.3	7.8	—	—	—
Σ[c]	7.1	6.4	6.0	6.9	7.7	6.9	7.4

[a]Chemical shifts reported in ppm from TSP. Coupling constants in Hz. Estimated error: J, ±0.2 Hz; δ, ±0.01 ppm.
[b]Data from ref. 3; pD = 7.4, 0.05 M.
[c]$\Sigma = J_{4'5'} + J_{4'5''}$.

3′,5′-d (TpT) and 5′dTMP are nearly isochronous. Furthermore, $\delta_{2'}$ and $\delta_{2''}$ fall in the narrow range from 2.37 to 2.41 ppm from TSP. This constancy of the $\delta_{2'}$ values on the one hand and of $\delta_{2''}$ on the other, for these three molecules, is perhaps predictable from space-filling models of the dimers in either the extended (unstacked) conformation or in the right-handed stacked arrangement. In both conformations the $C_{2'}$ hydrogens on -pdT are distant from the 3′-linked unit.

In contrast with 5′dTMP and the 3′,5′-dimers, a substantial chemical shift (0.06 ppm) exists between the $H_{2'}$ and $H_{2''}$ protons of the -pdT fragment of 2′,5′-UpdT, a consequence of the differential shielding effect induced by the formation of the 2′,5′-phosphodiester bond. Thus, relative to 3′,5′-UpdT, $H_{2'}$ and $H_{2''}$ of the 2′,5′-isomer are shifted upfield by 0.10 and 0.04 ppm, respectively. (Our assignment of the $H_{2'}$ and $H_{2''}$ hydrogens is based on the observation that $J_{2'3'}$ is generally larger than $J_{2''3'}$ (1, 12, 13).) This shielding effect is not simply explained. It could be due to changes in the sugar-base torsion angle (χ) (4, 17) of the -pdT unit which determines the disposition of $H_{2'}$ and $H_{2''}$ relative to the magnetically anisotropic 2-keto oxygen of the base. (In this regard it is relevant to point out that $H_{1'}$ is also shifted (upfield) in -pdT of 2′,5′-UpdT relative to the 3′,5′-isomer.) The need for change in χ could in turn be traced to the stacking properties of the 2′,5′- and 3′,5′-isomers, but further comment here would require extensive cd measurements.

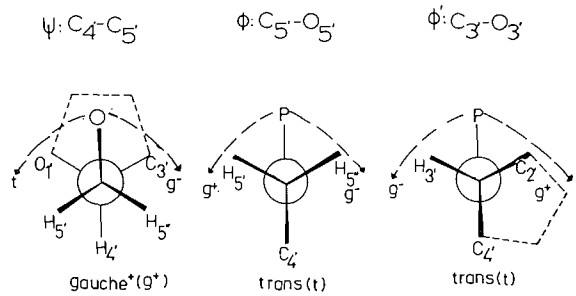

FIG. 3. Newman projections of the dominant conformations viewed along the $C_{4'}$—$C_{5'}$, $C_{5'}$—$O_{5'}$, and $C_{3'}$—$O_{3'}$ bonds. Definitions according to ref. 18.

The Sugar-base Torsion Angle (χ)

A variety of methods have been employed for evaluating χ. One method is based on the characteristic shielding changes observed for the $H_{2'}$ and $H_{3'}$ protons when, in the *syn* conformation, the 2-keto oxygen is located over the sugar ring (19, 20). Following the reasoning outlined (19), we propose on the basis of the chemical shifts (Table 2) that the *syn* ⇆ *anti* balance is not drastically altered by incorporation of the monomers into the dimer molecules. The general consensus is that in solution pyrimidine nucleosides prefer the *anti* conformation but the *syn* can be significantly populated (2).

TABLE 2. Proton chemical shifts and coupling constants[a] for 5′dTMP, 3′5′-d(TpT), and the 2′-deoxyribose fragment of 2′,5′-UpdT and 3′,5′-UpdT

		-pdT				
		3′,5′-d(TpT)[b]	3′,5′-UpdT		2′,5′-UpdT	
Parameter	5′dTMP[b] 30°C	18°C	20°C	65°C	20°C	65°C
$\delta_{1'}$	6.34	6.34	6.33	6.31	6.28	6.27
$\delta_{2'}$	2.37[c]	2.38[c]	2.39[c]	2.40[c]	2.30	2.31
$\delta_{2''}$	2.38[c]	2.39[c]	2.40[c]	2.41[c]	2.36	2.38
$\delta_{3'}$	4.58	4.60	4.59	4.57	~4.54[d]	~4.52[d]
$\delta_{4'}$	4.17	4.13	4.16	4.16	~4.08[e]	~4.07[e]
$\delta_{5'}$	4.06[c]	4.16	4.25	4.20	~4.08[e]	~4.07[e]
$\delta_{5''}$	4.05[c]	4.09	4.12	4.12	~4.08[e]	~4.07[e]
δ_6	7.77	7.71	7.75	7.68	7.71	7.66
$\delta_5(CH_3)$	1.93	1.91	1.91	1.92	1.92	1.93
$J_{1'2'}$	[7.0[f]	[6.9	[6.2	[6.9	6.8	6.9
$J_{1'2''}$	[7.0	[6.9	[6.2	[6.9	6.8	6.7
$J_{2'2''}$[g]	−13.8	−14.1	−14.2	−14.2	−13.2	−14.5
$J_{2'3'}$	[4.8	[5.8	[5.4	[5.2	6.4	7.6
$J_{2''3'}$	[4.8	[5.8	[5.4	[5.2	5.7	4.5
$J_{3'4'}$	2.9	4.0	3.2	3.9	—[i]	—
$J_{4'5'}$	3.8	2.5	2.4	2.8	—	—
$J_{4'5''}$	3.8	4.0	4.0	4.2	—	—
$J_{5'5''}$[g]	−12.1	−12.1	−11.2	−11.5	—	—
$J_{CH_3,6}$	1.1	1.3	1.0	1.2	1.0	1.0
$J_{P4'}$	1.6	1.6	1.7	1.8	—	—
$J_{P5'}$	[5.0	[4.0	4.0	5.0	—	—
$J_{P5''}$	[5.0	[4.0	3.8	5.7	—	—
Σ[h]	7.6	6.5	6.4	7.0	—	—
Σ'	10.0	8.0	7.8	10.7	—	—

[a]Chemical shifts in ppm from TSP. Coupling constants in Hz. Estimated error: J, ±0.2 Hz; δ, ±0.01 ppm.
[b]Data from ref. 14; 5′dTMP: 0.1 M, pD 5.8; 3′,5′-d(TpT), 0.1 M, pD = 7.0.
[c]The 0.01 ppm is arbitrary if $\delta_{2'} \simeq \delta_{2''}$ or $\delta_{5'} \simeq \delta_{5''}$.
[d]Taken from centre of broad $H_{3'}$ band; featureless since $\delta_{4'} \simeq \delta_{5'} \simeq \delta_{5''}$.
[e]Taken from centre of doublet $H_{4'}$, $H_{5'}$, $H_{5''}$ band.
[f]Only sum of connected couplings is significant.
[g]Arbitrary if $\delta_{2'} \simeq \delta_{2''}$ or $\delta_{5'} \simeq \delta_{5''}$.
[h]$\Sigma = J_{4'5'} + J_{4'5''}$; $\Sigma' = J_{P5'} + J_{P5''}$.
[i]Not measurable.

Sugar Pucker

The conformation of a ribose or 2′-deoxyribose ring, described in terms of the pseudorotational parameters (P), the amplitude of pucker (τ_m), and the populations of the 2′*endo* (S) and 3′*endo* (N) puckers in the N ⇆ S blend (21), can be evaluated from the magnitudes of the vicinal couplings ($J_{1'2'}$ etc.) (22, 23). In Table 3 are presented the % 3′*endo* values for the entries in Table 1, calculated according to Davies and Danyluk (22).

A striking feature of the $J_{1'2'}$, $J_{2'3'}$, and $J_{3'4'}$ data (Table 1) is their similarity in the monomer, 3′UMP, and the 3′-linked uridylyl fragments of 3′,5′-UpU and 3′,5′-UpdT. Clearly, the sugar pucker of the 3′-linked uridine fragment is not critically dependent on whether its 5′-linked pyrimidine nucleotidyl partner is a ribose or 2′-deoxyribose derivative. The data in Table 3 show a slight bias for the 3′*endo* conformation which is little affected by temperature change.

With few exceptions, 2′-deoxyribose derivatives display a preference for the 2′*endo* pucker, both in the crystal and solution states (18, 24). The -pdT fragment of 3′,5′-UpdT is not, in this respect, exceptional. Calculations (Table 3) show contributions of 32 and 39% from the 3′*endo* pucker at 20 and 65°C, respectively, results which are similar to those of the -pdT unit of 3′,5′-d(TpT) and to that of the monomer, 5′dTMP. Thus the pucker of a -pdT unit is not critically dependent on the nature (ribo or 2′-deoxyribo) of its 3′-linked pyrimidine nucleotidyl partner. (At 20°C the magnitude of the sum $J_{1'2'} + J_{1'2''}$ is 12.4 and 13.8 Hz for the -pdT units of 3′,5′-UpdT and 3′,5′-d(TpT), respectively. Thus, some dependence on the nature of the 3′-linked unit is indicated; however, it is difficult to assess since only the sum, and not the individual couplings, could be obtained owing to the chemical shift equivalence of $H_{2'}$ and $H_{2''}$.)

The data for the 2′-phosphorylated uridine fragments provide some contrast. For 2′UMP there is a shift, relative to 3′UMP, in the 3′*endo* bias (Table 3).

Can. J. Chem. Downloaded from www.nrcresearchpress.com by 210.87.254.105 on 09/05/12
For personal use only.

Can. J. Chem. Downloaded from www.nrcresearchpress.com by 210.87.254.105 on 09/05/12
For personal use only.

TABLE 3. Calculated rotamer populations

	T(°C)	% 3′*endo*	% $g^+(\psi)$	% $t(\phi)$
2′- or 3′-Linked uridylyl				
3′UMP[a]	18	52	59	—
3′-Up- (3′,5′-UpU)[b]	20	56	66	—
3′-Up- (3′,5′-UpdT)	20	57	70	—
3′-Up- (3′,5′-UpdT)	65	51	61	—
2′UMP	23	44	53	—
2′Up- (2′,5′-UpdT)	20	48	61	—
2′Up- (2′,5′-UpdT)	65	47	56	—
5′-Linked-2′-deoxythymidylyl				
5′dTMP[c]	30	29	54	71
-pdT[c] (3′,5′-d(TpT))	18	40	65	81
-pdT (3′,5′-UpdT)	20	32	66	82
-pdT (3′,5′-UpdT)	65	39	60	68
-pdT (2′,5′-UpdT)	20	—	—	—
-pdT (2′,5′-UpdT)	65	—	—	—

[a]Reference 23.
[b]Reference 4.
[c]Reference 14.

Furthermore, dimerization of 2′UMP to yield the Up- unit of 2′,5′-UpdT results at 20°C in a decrease in $J_{1'2'}$, $J_{2'3'}$, and $J_{3'4'}$. This decrease in $J_{2'3'}$ is indicative of an increase in the amplitude of pucker (21) and is not observed upon dimerization of 3′UMP. Dimerization also leads to a slight increase in the 3′*endo* contribution (Table 3). Elevation of the temperature to 65°C leads to an increase of 1.2 Hz in the magnitude of $J_{2'3'}$, indicating a decrease in the τ_m value of 65°C. This pronounced decrease in τ_m with increasing temperature is not observed for the Up- unit of 3′,5′-UpdT (Table 3) or of 3′,5′-UpU (3). Ezra *et al.* (4) have found that 2′,5-dimerization of 2′CMP to yield 2′,5′-CpC leads to an increase in $J_{2'3'}$ (decrease in τ_m) at 20°C, results which contrast with our results for 2′,5′-UpdT. It seems therefore, that a systematic study of the influence of the base, sugar, temperature, etc., is warranted for the 2′,5′-isomers.

Conformation about the $C_{4'}$—$C_{5'}$ (ψ) and $C_{5'}$—$O_{5'}$ (ϕ) Bonds

Contributions from $g^+(\psi)$ and $t(\phi)$ conformers (Fig. 3), calculated[3] by the usual methods, are listed in Table 3. The following comments can be made about the $C_{4'}$—$C_{5'}$ conformation of the uridine units. (*a*) The data define a range from 53 to 70%, indicating a bias for $g^+(\psi)$ over $t(\psi)$ and $g^-(\psi)$ in all instances. (*b*) 3′-Elongation of 3′UMP with either a U fragment or a dT fragment enhances % $g^+(\psi)$ (7–11%). Thus, the ψ conformer distribution is not strongly dependent on the nature (ribo or 2′-deoxyribo) of the 5′-nucleotidyl unit. (*c*) Relative to 3′UMP the bias for $g^+(\psi)$ is reduced in 2′UMP. This reduction is probably a reflection of the shift in the 3′*endo* ⇆ 2′*endo* balance (Table 3) which is known (24) to influence the ψ conformer distribution. Elongation of 2′UMP with a dT unit (2′,5′-UpdT) leads to a slight increase in % $g^+(\psi)$. It is interesting that our 2′,5′- and 3′,5′-dimerization effects are in line with observations on 2′,5′- and 3′,5′-CpC (4); in both isomers dimerization leads to an increase in % $g^+(\psi)$.

Ezra *et al.* (4) have noted a significant magnetic nonequivalence for $H_{5'}$ and $H_{5''}$ of -pC of 3′,5′-CpC and that this pair of hydrogens are, along with $H_{4'}$ of -pC, essentially isochronous in the 2′,5′-isomer. In like fashion, we observe magnetic nonequivalence for $H_{5'}$ and $H_{5''}$ of -pdT of 3′,5′-UpdT but a collapse of $H_{5'}$, $H_{5''}$, and $H_{4'}$ in the 2′,5′isomer. Thus, in this respect, a parallel behavior exists for the 5′-nucleotidyl units of the CpC and UpdT isomers. An unfortunate consequence of this spectral collapse is that the couplings required for discussion of the ϕ,ψ conformational features of the 2′,5′-isomers cannot be obtained.

However, we may make the following comments about the $C_{4'}$—$C_{5'}$ (ψ) and $C_{5'}$—$O_{5'}$ (ϕ) conformer distributions for the -pdT unit of 3′,5′-UpdT. (*a*) The $g^+(\psi)$ conformer is dominant in 5′dTMP (Table 3). (*b*) The magnitude of % $g^+(\psi)$ is enhanced to about 65% when (at 20°C) 5′dTMP is incorporated into 3′,5′-UpdT and 3′,5′-d(TpT). With dimerization of 5′dTMP there occurs also an increase in % t (ϕ) regardless of the nature (Up- or dTp-) of the 3′-unit. It is, then, clear that neither the ϕ nor the ψ conformer distribution of -pdT is dependent on the nature of the sugar moiety of the 3′-unit. This, of course, need not be the case for purine derivatives nor for that matter in pyrimidine dimers in the fully stacked conformation. (*c*) Increasing temperature leads to decreases in % $g^+(\psi)$ and % $t(\phi)$. This is also the case for -pdT of 3′,5′-d(TpT) (4) and -pU of 3′,5′-UpU (3). It seems, however, that Σ' is somewhat more sensitive to temperature in 3′,5′-UpdT than in the other dimers, increasing by 3.7 Hz in the 20–65°C interval. In the 18–65°C range Σ' increases by about only 1 Hz for -pdT of 3′,5′-d(TpT) (14) and by 0.9 Hz for -pU of 3′,5′-UpU in the 20–85°C interval (3). Thus, the ϕ orientation is not entirely insensitive to the nature of the 3′-linked sugar.

The long-range $^4J_{P4'}$ couplings provide information about the $C_{4'}$—$C_{5'}$ and $C_{5'}$—$O_{5'}$ conformer distribution (26, 27) although, owing to their small size, they may be less reliable than Σ and Σ' as conformational probes. However, the magnitudes of the observed $^4J_{P4'}$ couplings for the 5′-nucleotidyl fragments (1.6–1.8 Hz, Table 2) are in line with our observations based on Σ and Σ', namely, that $g^+(\psi)$ and $t(\phi)$ are the dominant conformations.

[3]% $g^+(\psi) = (13 - \Sigma)/10$ where $\Sigma = J_{4'5'} + J_{4'5''}$ and % $t(\phi) = (25 - \Sigma')/21$ where $\Sigma' = J_{P5'} + J_{P5''}$ (12, 25).

Can. J. Chem. Downloaded from www.nrcresearchpress.com by 210.87.254.105 on 09/05/12
For personal use only.

Conformation about $C_{3'}$—$O_{3'}$ and $C_{2'}$—$O_{2'}$

Information about the conformations about these bonds in 3′- and 2′-nucleotidyl units may be obtained from $^3J_{P3'}$ and $^3J_{P2'}$. On the basis of steric considerations and a wealth of X-ray data (18), the $g^+(\phi')$ conformation (Fig. 3) may be excluded from consideration. However, the $H_{3'}$ ($H_{2'}$) and P atoms are *gauche* in the two remaining possibilities, $g^-(\phi')$ and $t(\phi')$, and thus no unambiguous distinction between the two can be made on the basis of ^1H–^{31}P couplings alone. They provide, however, the following important information about our 3′(2′)-uridylyl units if we assume the applicability of eq. 1 (25).

$$[1] \qquad {}^3J_{PH}\,(\text{Hz}) = 18.1\cos^2\theta - 4.8\cos\theta$$

where θ is the dihedral angle in the relevant H—C—O—P fragment. Note that $\theta = 60°$ corresponds to the classical $g^-(\phi')$ and $t(\phi')$ staggered conformers whereas $\theta = 0$ corresponds to the conformation in which $H_{2'}$ (of the 2′-nucleotidyl units) and $H_{3'}$ (of the 3′-nucleotidyl units) eclipse the phosphorus atom, i.e. $\phi' = -120°$.

The $^3J_{P3'}$ and $^3J_{P2'}$ values (Table 1) are significantly larger than expected for the classical $g^-(\phi')$ and $t(\phi')$ conformers (ca. 2 Hz) and since the $g^+(\phi')$ conformation is excluded (expected $^3J_{P3',2'} = 23$ Hz), a substantial bias towards the $\phi' = -120°$ situation is indicated. In this conformer which separates the g^- and t ranges, the phosphorus and $H_{2'}$($H_{3'}$) atoms are eclipsed ($\theta = 0°$) and a large (13.3 Hz) ^1H–^{31}P coupling is expected. Using eq. 4 we obtain $\theta \simeq 35°$ for 2′- and 3′-UMP and the Up- units of 3′,5′UpU and 3′,5′UpdT from the low temperature data, corresponding to ϕ' angles of -85 and $-155°$ in the g^- and t conformer range, respectively. Increasing temperature leads to a small decrease in $^3J_{P3'}$ and an increase (ca. 1°) in θ for the 3′-units of the dimers. For Up- of 2′,5′-UpdT $\theta \simeq 30°$, corresponding to $\phi' = -90$ and $-150°$. It appears then that in the 2′,5′-dimer the $C_{2'}$—$O_{2'}$ bond is somewhat more constrained towards the eclipsed ($\phi' = -120°$) situation than is the $C_{3'}$—$O_{3'}$ bond in the 3′,5′-isomer. (A similar trend has been noted (4) for the Cp- units of 2′,5′-CpC ($^3J_{P2'} = 9.1$ Hz) and 3′,5′CpC ($^3J_{P3'} = 8.3$ Hz).) Thus 3′,5′-dimerization appears to have little influence on $^3J_{P3'}$, regardless of the nature (ribo or 2′-deoxyribo) of the 5′-nucleotidyl unit. 2′,5′-Dimerization appears to bias the angle about the $C_{2'}$—$O_{2'}$ bond towards the $\phi' = -120°$ situation but again the nature of the 5′-linked sugar is unimportant.

The bias towards the $\phi' = -120°$ eclipsed conformer is consistent with X-ray data. Thus, in Sundaralingam's review (18), we note that for 3′-nucleotides (five entries) the ϕ' values lie in the range from -91 to $-165°$, with one entry, 3′AMP, having a ϕ' value of $-123°$, just 3° from the $H_{3'}$–P eclipsed situation.

In general, the $^3J_{P3'}$ values for the Up- units are considerably larger than those measured for dTp- units (6.8 Hz for dTp- of 3′,5′-d(TpT) (4) and 6.1–6.4 Hz for the dTp- units of 3′,5′-d(TpTp) (16) and 3′,5′-d(TpTpA) (1)). Thus, the bias towards the eclipsed conformer is less pronounced in the 2′-deoxyribo units ($\theta \simeq 44°$; $\phi' = -76, -164°$). This greater bias for $\phi' = -120°$ in the ribo units is most likely due to steric interactions involving the 2′-hydroxyl group. Support for this contention is provided by the observation (28) that 2′-*O*-methylation of the Ap- unit of ApA results in an increase of 1.4 Hz in $^3J_{P3'}$.

The similarity in the $^3J_{P3'}$ values suggests that the ϕ' conformer distribution is similar for the Up- units of 3′,5′-UpdT, and 3′,5′-UpU and for 3′UMP itself. This suggestion is supported by the chemical shift data. In the $g^-(\phi')$ conformer $H_{4'}$ is near to the charged nonester oxygens of the phosphate while $H_{2''}$ is distant; in $t(\phi')$, the converse is true. Thus, changes in the $g^-(\phi') \rightleftarrows t(\phi')$ blend should be manifest in $\delta_{2''}$ and $\delta_{4'}$. However, in Table 1 we note a remarkable constancy for these species in, on the one hand, $\delta_{2''}$, and, on the other hand, $\delta_{4'}$, which is inconsistent with major differences in the conformer weighting.

Conformation about the $O_{3'}$—P and $O_{5'}$—P Bonds

Our measured coupling constants cannot provide information on the orientations about the internucleoside O—P bonds. Recently, however, variations in the $H_{5'}$ shift of the 5′-unit of 3′,5′-ribodimers have been related (3) to the proximity of $H_{5'}$ to the 2′-hydroxyl of the 3′-unit. When the $O_{3'}$—P and $O_{5'}$—P bond are g^-, as in the right handed (g^-g^-) stacked conformation, van der Waals contact between these atoms is possible and appears to lead to a specific deshielding of $H_{5'}$ (3). These effects are best discussed in terms of the dimerization shifts, Δ, defined as the shift of a proton in the dimer relative to its shift in the corresponding mononucleotide, with positive values indicating increased shielding at the dimer level. For the -pdT fragments we obtain from the low temperature data in Table 2: $\Delta_{5'}$ ($\Delta_{5''}$ in brackets) in ppm: -0.10 (-0.04), -0.19 (-0.07), -0.02 (-0.03) for 3′,5′-d(TpT), 3′,5′-UpdT, and 2′,5′-UpdT, respectively. For 3′,5′-UpdT a significant deshielding effect upon dimerization is noted for the $H_{5'}$, that for $H_{5''}$ being greatly attenuated. Following the reasoning outlined (3), we conclude that $H_{5'}$ is located in the vicinity of the 2′-OH of the Up- unit for a significant fraction of the time and

Can. J. Chem. Downloaded from www.nrcresearchpress.com by 210.87.254.105 on 09/05/12
For personal use only.

therefore, that the g^-g^- conformer makes a significant (but quantitatively undeterminable here) contribution to the time-averaged conformation of 3′,5′-UpdT. It is important to point out, however, that a large (ca -0.10 ppm) $\Delta_{5'}$ value is observed for -pdT of 3′,5′-d(TpT), but the effect is certainly smaller than that noted for the mixed dimer. Clearly factors other than the proximity of the 2′-OH of the 3′-unit can contribute to the $\Delta_{5'}$ values and thus the interpretation of these Δ values in quantitative terms will be difficult. Interestingly, the $\Delta_{5'}$ and $\Delta_{5''}$ values are small (less than -0.03 ppm) for the 2′,5′-isomer. In the g^-g^- conformer of a 2′,5′-dimer $H_{5'}$ does not approach any position of the furanose moiety of the 3′-unit and thus the appearance of this conformer may not be reflected in the $\Delta_{5'}$. However, with molecular models one may construct a compact, g^-g^- stacked arrangement of a 2′,5′-dimer in which $H_{5'}$ is placed in juxtaposition with the magnetically anisotropic 2-keto oxygen of the pyrimidine base on the 3′-unit. The minimal value of $\Delta_{5'}$ for 2′,5′-UpdT cannot, therefore, be unambiguously interpreted; it could be a reflection of the virtual exclusion of the g^-g^- arrangement or it may be a consequence of an insensitivity of $\Delta_{5'}$ to the orientation of the O—P bonds.

Comparison of some other chemical shift data (Table 1) provides some evidence for base-base interaction in the 2′,5′-dimer. Thus, in particular, the large (0.17 ppm) upfield shift (relative to 3′UMP) experienced by the 5-hydrogen of the uracil base is only reasonably explained if some stacking of the U and T bases occurs. For the 3′,5′-isomer an upfield shift (0.06 ppm) for the H_5 hydrogen of the uracil is observed, in line with the evidence given above for some contribution from the g^-g^- conformer. That the H_5 dimerization shift is larger for the 2′,5′-UpdT isomer could be a consequence of more extensive base stacking as well as to alternations in the spatial arrangement of the bases in the stack.

Conclusions

The ^{1}Hmr data of mixed dimers 3′,5′-UpdT and 2′,5′-UpdT are compared with data for the component mononucleotides, 3′UMP, 2′UMP, and 5′dTMP, and for the dimers 3′,5′-UpU and 3′,5′-d(TpT), and discussed in terms of their molecular conformations in aqueous solution. For the greater part the conformations (sugar pucker and the $C_{4'}$—$C_{5'}$, $C_{5'}$—$O_{5'}$, and $C_{3'}$—$O_{3'}$ conformer distributions) of the 3′- and 5′-linked dimer units are similar to those of the corresponding mononucleotides. Furthermore, the sugar phosphate conformation of a particular nucleotidyl unit (3′- or 5′-linked) does not appear to be critically dependent upon the nature (ribo or 2′-deoxyribo) of the other unit. This conclusion is, of course, restricted to our dipyrimidine dimers which exist to a large extent in an extended rather than stacked orientation.

Acknowledgements

This research was supported by operating grants from the National Research Council of Canada and Rh Institute of Manitoba. We thank the NRCC, the University of Manitoba, and its Faculty of Graduate Studies for capital grants for purchase of a Bruker WH-90 spectrometer. We thank Dr. A. A. Grey of the Canadian 220 MHz centre and Dr. W. A. Gibbons of the University of Wisconsin (Madison) for obtaining 220 MHz and 270 MHz spectra, respectively. We are grateful to Dr. Donald Wood for his generous aid in the spectral analysis, and to Mr. A. George and W. Niemczura for obtaining spectra for 2′UMP.

1. C. Altona, J. H. Van Boom, and C. A. G. Haasnoot. Eur. J. Biochem. **71**, 557 (1976).
2. C. Chachaty, T. Yokono, T.-D. Son, and W. Guschlbauer. Biophys. Chem. **6**, 151 (1977).
3. C.-H. Lee, F. S. Ezra, N. S. Kondo, R. H. Sarma, and S. S. Danyluk. Biochemistry, **15**, 3627 (1976).
4. F. S. Ezra, N. S. Kondo, C. F. Ainsworth, and S. S. Danyluk. Nucl. Acid Res. **3**, 2549 (1976).
5. N. S. Kondo and S. S. Danyluk. Biochemistry, **15**, 756 (1976).
6. F. S. Ezra, C. H. Lee, N. S. Kondo, S. S. Danyluk, and R. H. Sarma. Biochemistry, **16**, 1977 (1977).
7. A. L. Lehninger. Biochemistry. 2nd ed. Worth Publishers, New York, NY. 1975. p. 909.
8. J. C. Maurizot, J. Brahms, and F. Eckstein. Nature, **222**, 559 (1969).
9. N. S. Kondo, K. N. Fang, P. S. Miller, and P. O. P. Ts'O. Biochemistry, **11**, 1991 (1972).
10. Y. Lapidot and H. G. Khorana. J. Am. Chem. Soc. **85**, 3852 (1963).
11. C. W. Haigh and J. M. Williams. J. Mol. Spectrosc. **32**, 398 (1969).
12. D. J. Wood, F. E. Hruska, and K. K. Ogilvie. Can. J. Chem. **52**, 3353 (1974).
13. D. J. Wood, K. K. Ogilvie and F. E. Hruska. Can. J. Chem. **53**, 2781 (1975).
14. R. G. S. Ritchie and A. S. Perlin. Carbohydr. Res. **55**, 121 (1977).
15. M. Remin and D. Shugar. Biochem. Biophys. Res. Commun. **48**, 636 (1972).
16. D. B. Davies and A. Rabczenko. J. Chem. Soc. Perkin Trans. II, 1703 (1975).
17. J. Prestegard and S. I. Chan. J. Am. Chem. Soc. **91**, 2843 (1969).
18. M. Sundaralingam. *In* Proceedings international symposium on the conformation of biological molecules and polymers, symposia on quantum chemistry and biochemistry. Vol. 5. *Edited by* B. Pullman and E. D. Bergmann. Academic Press, Jerusalem. 1973. p. 417.
19. H. Dugas, B. J. Blackburn, R. K. Robins, R. Des-

LAURIERS, and I. C. P. SMITH. J. Am. Chem. Soc. **93**, 3468 (1971).
20. J. CADET, R. DUCLOMB, and C. TAIEB. Tetrahedron Lett. 3455 (1975).
21. C. ALTONA and M. SUNDARALINGAM. J. Am. Chem. Soc. **95**, 2333 (1973).
22. D. B. DAVIES and S. S. DANYLUK. Biochemistry, **14**, 543 (1975).
23. T. SCHLEICH, B. J. BLACKBURN, R. D. LAPPER, and I. C. P. SMITH. Biochemistry, **11**, 137 (1972).
24. F. E. HRUSKA. *In* Proceedings international symposium on the conformation of biological molecules and polymers, symposia on quantum chemistry and biochemistry. Vol. 5. *Edited by* B. Pullman and E. D. Bergmann. Academic Press, Jerusalem. 1973. p. 345.
25. C. H. LEE and R. H. SARMA. Biochemistry, **15**, 697 (1976).
26. R. H. SARMA, R. J. MYNOTT, D. J. WOOD, and F. E. HRUSKA. J. Am. Chem. Soc. **95**, 6457 (1973).
27. P. J. COZZONE and O. JARDETZKY. Biochemistry, **15**, 4860 (1976).
28. H. SINGH, M. H. HERBUT, C. H. LEE, and R. H. SARMA. Biopolymers, **15**, 2167 (1976).

Can. J. Chem. Downloaded from www.nrcresearchpress.com by 210.87.254.105 on 09/05/12
For personal use only.

The microwave spectrum and structure of cyclopropyl carbinol. II. Four deuterated forms

W. V. F. BROOKS AND C. K. SASTRI

Department of Chemistry, University of New Brunswick, Fredericton, N.B., Canada E3B 5A3

Received August 31, 1977

W. V. F. BROOKS and C. K. SASTRI. Can. J. Chem. **56**, 530 (1978).

The microwave spectra of four deuterated species of cyclopropyl carbinol have been studied. The rotational constants *A*, *B*, and *C* (in MHz) are: $C_3H_5CH_aD_bOH$, 11 742.86, 3205.17, 2830.41; $C_3H_5CD_aH_bOH$, 11 853.44, 3188.10, 2878.28; $C_3H_5CH_aD_bOD$, 11 321.30, 3145.87, 2762.23; $C_3H_5CD_aH_bOD$, 11 433.85, 3129.30, 2809.81. The measured dipole moments of $C_3H_5CH_aD_bOH$ and $C_3H_5CH_aD_bOD$ are, respectively, 1.91 and 1.873 D. This confirms the essential details of the conformation proposed in an earlier paper.

W. V. F. BROOKS et C. K. SASTRI. Can. J. Chem. **56**, 530 (1978).

On a étudié les spectres de microonde de quatre espèces deutérées de cyclopropylcarbinol. Les constantes de rotation *A*, *B* et *C* (en MHz) sont: $C_3H_5CH_aD_bOH$, 11 742.86, 3205.17, 2830.41; $C_3H_5CD_aH_bOH$, 11 853.44, 3188.10, 2878.28; $C_3H_5CH_aD_bOD$, 11 321.30, 3145.87, 2762.23; $C_3H_5CD_aH_bOD$, 11 433.85, 3129.30, 2809.81. Les moments dipolaires mesurés pour $C_3H_5CH_aD_bOH$ et $C_3H_5CH_aD_bOD$ sont respectivement 1.91 et 1.873 D. Ces résultats confirment les détails essentiels de la conformation proposée dans une publication antérieure.

[Traduit par le journal]

Introduction

An earlier paper (1) hereafter referred to as I, reported the microwave spectra and dipole moments of cyclopropyl carbinol ($CH_2—CH_2—CH—CH_2OH$) and a deuterated (—OD) form, and proposed a conformation of the molecule which is diagrammed in Fig. 1. Note that the diagram shows only one of two forms; the mirror image conformation is identical in its spectroscopic properties. Note also that the two hydrogens labelled *a* and *b* are not equivalent. The microwave spectra of species deuterated at these *a* and *b* positions may be used to test the validity of the proposed conformation, and to determine some of the structural constants (interatomic distances and angles) more precisely.

Experimental

The deuterium labelled molecules were prepared by oxidizing cyclopropyl carbinol (Aldrich Chemical Company) to the aldehyde (2), reducing the aldehyde to the sodium salt with $NaBD_4$, and adding H_2O to the reaction mixture. The doubly deuterated (C_3H_5CHDOD) forms were made by allowing the singly deuterated substance to exchange with excess D_2O in the cell of the microwave spectrometer. The purity and composition of the intermediate aldehyde and singly deuterated product were checked with infrared, mass, and nmr spectra.

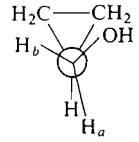

FIG. 1. Newman projection of gaseous cyclopropyl carbinol.

Microwave spectra and Stark coefficients were measured as described in I.

Spectra

All samples contained at least two separate species (D in the *a* and D in *b* positions). The predicted spectra, calculated from the structure of I, made the assignment easy. Enough isolated lines were available to clarify assignment problems and a few Stark coefficients were measured (measured and calculated coefficients are given in Table 2).

Four species were identified, two singly deuterated (on the carbinol C atom) and two doubly deuterated. More than 20 lines for each species[1] (mostly *a*-type R and *c*-type Q with *J* values from 0 to 8) were assigned, measured, and used in a least-squares determination of the rotational constants (listed in Table 1). Only lines for which observed and calculated values differed by less than 0.5 MHz were used in the final least-squares computations. No attempt was made to identify vibrationally excited states or other conformational species.

Structure and Discussion

The dipole moment results (Table 3) are in excellent agreement with the previous measurements except for the large value of μ_c for $C_3H_5CH_aD_bOH$ (this component is very poorly determined by the data available). The rotation of the principal axes due to deuterium substitutions are small enough that

[1]The assigned and measured line measurements are available from the Depository of Unpublished Data, CISTI, National Research Council of Canada, Ottawa, Ont., Canada K1A 0S2.

Can. J. Chem. Downloaded from www.nrcresearchpress.com by 210.87.254.6 on 09/05/12
For personal use only.

TABLE 1. Rotational constants (observed and calculated)[a] of six species of cyclopropyl carbinol

Parameter	Value					
	$C_3H_5CH_2OH$[b]	$C_3H_5CH_2OD$[b]	$C_3H_5CH_aD_bOH$	$C_3H_5CD_aH_bOH$	$C_3H_5CH_aD_bOD$	$C_3H_5CD_aH_bOD$
A obs.	12 484.99(8)	12 063.95(10)	11 742.86(10)	11 853.44(11)	11 321.30(10)	11 433.85(6)
A calc.	12 460.87	12 050.76	11 723.23	11 855.64	11 329.51	11 471.76
B obs.	3 236.46(1)	3 177.23(2)	3 205.17(2)	3 188.10(3)	3 145.87(2)	3 129.30(2)
B calc.	3 230.78	3 163.76	3 204.01	3 186.24	3 140.40	3 122.24
C obs.	2 894.38(1)	2 826.18(2)	2 830.41(2)	2 878.28(3)	2 762.23(2)	2 809.81(2)
C calc.	2 904.75	2 829.49	2 841.85	2 890.38	2 769.84	2 815.84

[a]Observed values are from least-squares fitting to microwave frequencies; calculated values are from best geometry. All in MHz.
[b]From paper I, but values slightly altered due to reprocessing of data.

TABLE 2. Stark effect and dipole moments, $\Delta\nu/E^2$ in MHz m^2/V^2

Transition	*M*	$\Delta\nu/E^2$	
		Observed	Calculated
$C_3H_5CH_aD_bOH$			
2_{12}–1_{11}	1	5.4	5.4
2_{02}–1_{01}	0	−0.19	−0.189
3_{13}–2_{12}	1	0.179	0.184
	2	0.771	0.769
4_{23}–3_{22}	0	−0.050	−0.050
$C_3H_5CH_aD_bOD$			
2_{12}–1_{11}	1	5.26	5.25
2_{02}–1_{01}	0	−0.20	−0.20
3_{13}–2_{12}	1	0.181	0.181
	2	0.756	0.756
4_{23}–3_{22}	0	0.019	0.019

the components can be compared directly without considering rotation.

The rotational constants of all four species are sufficiently close to the predicted values that the proposed conformation of the molecule may be regarded as confirmed. The 12 new pieces of data were combined with the earlier 6 to determine the structure more precisely. The most interesting structural questions concern the amounts of rotation of the CH_2OH and OH groups about the C_{ring}—$C_{carbinol}$ and $C_{carbinol}$—O bonds respectively, the C—O—H angle and the distortion of the ring due to the unsymmetrical interaction between the ring and the carbinol group.

Using the same fitting procedure as described in I, we first tried adjusting the dihedral angles H—C_{ring}—$C_{carbinol}$—O, C_{ring}—$C_{carbinol}$—O—H, and the C—O—H angle as these were the items of greatest interest in the proposed structure. The new best least-squares values changed H—C—C—O from $\pm$124.2 to $\pm$123.7°, C—C—O—H from $\mp$32.3° to $\mp$32.9° and C—O—H from 116.7° to 117.8°. These changes seem insignificant. We also tried several adjustments of coordinates that either move the carbinol carbon into a less symmetrical position with respect to the ring or make the ring less symmetrical. No adjustments of these gave any significant improvement of the fit between calculation and observation. We conclude, therefore, that the carbinol carbon must lie very close (within 0.1 nm) of the plane that is perpendicular to and bisects the ring.

Penn and Boggs (3) consider another type of ring distortion due to substitution on the ring; the ring bond opposite to the point of substitution is shortened or lengthened. This effect is fairly easily measured when the substituent group and the ring have a common plane of symmetry. The lack of symmetry in this molecule makes the problem more difficult; we have not been able to extract any information about such a distortion from our data. Thus the remaining differences between observed and calculated rotational constants (Table 1) must be due to a combination of experimental and model errors (the rigid rotor model plus all the assumed distances and angles). A more precise determination of the ring shape will require isotopic substitution on

TABLE 3. Dipole components and total moments of four species of cyclopropyl carbinol in debye units

Parameter	Value			
	$C_3H_5CH_2OH$[a]	$C_3H_5CH_2OD$[a]	$C_3H_5CH_aD_bOH$	$C_3H_5CH_aD_bOD$
μ_a	1.81(1)	1.78(2)	1.816(5)	1.810(1)
μ_b	0.36(7)	0.32(1)	0.30(6)	0.364(1)
μ_c	0.31(4)	0.30(2)	0.51(12)	0.317(3)
μ_{total}	1.87(2)	1.84(2)	1.91(3)	1.873(1)

[a]From paper I.

Can. J. Chem. Downloaded from www.nrcresearchpress.com by 210.87.254.6 on 09/05/12
For personal use only.

the ring itself and perhaps corrections for vibration and centrifugal distortion.

Acknowledgements

We are grateful for financial support from the National Research Council of Canada, and for much experimental help from Dr. S. C. Dass.

1. A. BHAUMIK, W. V. F. BROOKS, S. C. DASS, and K. V. L. N. SASTRY. Can. J. Chem. **48**, 2949 (1970).
2. L. B. YOUNG and W. S. TRAHANOVSKY. J. Org. Chem. **32**, 2349 (1967).
3. R. E. PENN and J. E. BOGGS. J. Chem. Soc. Chem. Commun. 666 (1972).

Can. J. Chem. Downloaded from www.nrcresearchpress.com by 210.87.254.6 on 09/05/12
For personal use only.

Ion–molecule reactions in the binary mixture of acetaldehyde and trioxane. II. Mechanism for the reaction of acetaldehyde molecular ion with trioxane

MINORU KUMAKURA, KAZUO ARAKAWA, AND TOSHIO SUGIURA[1]

Takasaki Radiation Chemistry Research Establishment, Japan Atomic Energy Research Institute, Takasaki, Gunma, Japan

Received April 21, 1977

MINORU KUMAKURA, KAZUO ARAKAWA, and TOSHIO SUGIURA. Can. J. Chem. **56**, 533 (1978).

The ionic reaction of CH_3CHO^+ with trioxane in acetaldehyde–trioxane mixtures has been studied using a time-of-flight mass spectrometer. The product ions, $C_3H_5O_2^+$, $C_3H_6O_2^+$, and $C_3H_7O_2^+$, were formed by condensation–elimination reactions, which involve the elimination of a formaldehyde molecule. The dissociation of the intermediate-complex, $CH_3CHO(CH_2O)_3^{+*}$, leads to the formation of the product ions. The structure of the complex is linear with localized positive charge. Rearrangement of hydrogen atoms occurs in the complex but not extensive scrambling. From the distribution of the isotopic product ions in acetaldehyde-d_4–trioxane mixtures it was proposed that the origins of the product ions are the acetaldehyde molecule (reactant ion) and fragments from trioxane. The rate constants for the product ions formed in acetaldehyde (or acetaldehyde-d_4)–trioxane mixtures were obtained.

MINORU KUMAKURA, KAZUO ARAKAWA et TOSHIO SUGIURA. Can. J. Chem. **56**, 533 (1978).

Faisant appel à un spectromètre de masse à temps de vol, on a étudié la réaction ionique de CH_3CHO^+ avec le trioxanne dans des mélanges d'acétaldéhyde–trioxanne. Les ions qui se forment comme produits, $C_3H_5O_2^+$, $C_3H_6O_2^+$ et $C_3H_7O_2^+$, proviennent de réactions de condensation–élimination qui impliquent l'élimination d'une molécule de formaldéhyde. La dissociation du complexe intermédiaire, $CH_3CHO(CH_2O)_3^{+*}$, conduit à la formation des ions. La structure du complexe est linéaire avec une charge positive localisée. Dans le complexe, il se produit des transpositions des atomes d'hydrogène, mais il ne se produit pas d'une manière importante de répartition au hasard. En se basant sur la distribution isotopique dans les ions qui se forment comme produits dans des mélanges d'acétaldéhyde-d_4–trioxanne, on propose que les produits ioniques ont comme origine la molécule d'acétaldéhyde (ion réactif) et des fragments provenant du trioxanne. On a évalué les constantes de vitesse pour les formations des ions obtenus comme produits dans des mélanges d'acétaldéhyde (ou acétaldéhyde-d_4)–trioxanne.

[Traduit par le journal]

Introduction

In an earlier work the reaction of ethylene oxide molecular ion with trioxane in ethylene oxide–trioxane mixtures was studied as a part of our program for examination of the thermal ion–molecule reactions occurring in binary mixtures of oxygen-containing molecules (1). From the distribution of isotopic product ions in the mixture it was concluded that the intermediate-complex formed has a cyclic structure and delocalized positive charge (1). The ion–molecule reactions in ethylene oxide and acetaldehyde have been studied in order to obtain information concerning the behavior of structural isomers in oxygenated fragment ions such as CHO^+ and $C_2H_4O^+$ (2, 3); it was found that the reactions are intimately related to the structure and properties of the neutral molecules. It was felt that a study of the ion-molecule reactions in acetaldehyde–trioxane mixtures is important to obtain information to elucidate any structure effect of the reactant ion in the reactions involving structural isomers of oxygen-containing cyclic molecules. The ion–molecule reactions in acetaldehyde have been studied by several workers (4–8); however, reactions in binary mixtures of acetaldehyde and large-ring cyclic ether molecules, such as trioxane, have not been studied containing cyclic molecules. The ion–molecule thus far. The behavior of protonated molecular ions resulting from proton and hydrogen atom transfer reactions in acetaldehyde–trioxane mixtures has been studied at low pressures (9). Since the condensation–elimination reactions involving the acetaldehyde molecular ion in acetaldehyde have been studied at elevated pressures (3), the present work is concerned with exploring the structural consequences of the condensation–elimination reaction of the acetaldehyde molecular ion with trioxane on the ion chemistry of acetaldehyde–trioxane mixtures at elevated pressures.

Experimental

The instrument used was a Bendix Model 12-101 time-of-flight mass spectrometer which has been modified to study

[1]Present address: Japan Atomic Energy Research Institute, Shinbashi, Minato-ku, Tokyo, Japan.

Can. J. Chem. Downloaded from www.nrcresearchpress.com by 210.87.254.6 on 09/05/12
For personal use only.

Can. J. Chem. Downloaded from www.nrcresearchpress.com by 210.87.254.6 on 09/05/12
For personal use only.

ion–molecule reactions as described in a previous paper (2). A Hewlett-Packard 214A pulse generator and a pulse generator (Sanwa Denshi Production Co. Ltd.) were used as the source of the ionizing and ion withdrawal pulses. The retarding potential differential technique (rpd) was adopted for appearance potential and ionization efficiency curve measurement and a detailed description of this technique was reported earlier (10). The measurement of the ionization efficiency curves of two ions was performed simultaneously by a two-channel ion detection method. The ion current of two different ions was recorded with a three-pen recorder. A gas-sample inlet system consisting of a dual leak and a dual reservoir was used. The samples were introduced individually into the ionization chamber through two separate leaks from separate reservoirs. The partial pressure of the two samples was measured with an MKS Baratron 90-X RP-2 capacitance manometer and the pressure was calibrated by the known rate constant (1.11×10^{-9} cm^3 molecule^{-1} s^{-1}) for the formation of CH_5^+ in methane. Acetaldehyde and acetaldehyde-d_4 were obtained from Merck Sharp and Dohme of Canada and trioxane from Celanese Chemical Co. Ltd. These samples were used after vacuum distillation.

Results and Discussion

Delay Time and Pressure Dependence

The delay time dependence of major fragment and product ions in a 1:1 mixture of acetaldehyde and trioxane at 2.65×10^{13} molecules cm^{-3} is shown in Figs. 1 and 2. $C_3H_5O_3^+$ (*m/e* 89), $C_2H_5O_2^+$ (*m/e* 61), CH_3O^+ (*m/e* 31), and CHO^+ (*m/e* 29) are fragment ions from trioxane, while CH_3CHO^+ (*m/e* 44), CH_3CO^+ (*m/e* 43), and CHO^+ (*m/e* 29) are those from acetaldehyde. The molecular ion from trioxane

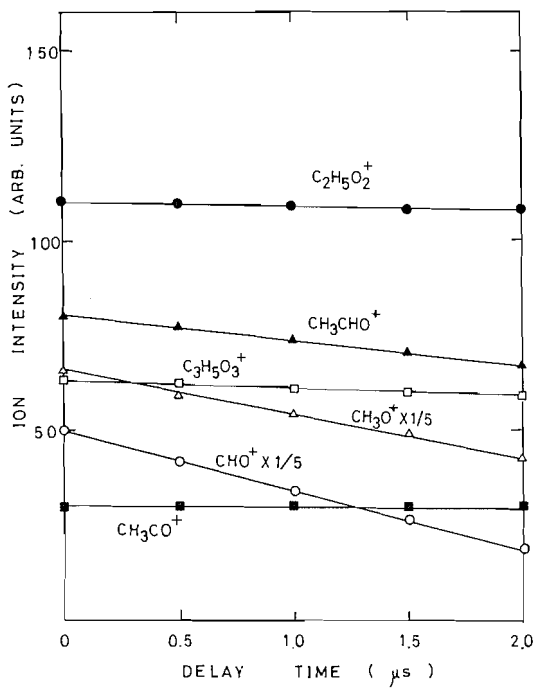

FIG. 1. Delay time dependence of major fragment ions in acetaldehyde–trioxane mixtures.

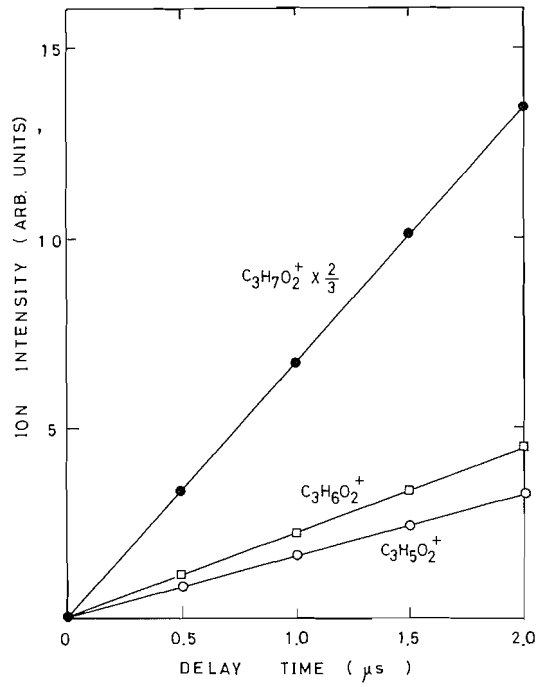

FIG. 2. Delay time dependence of product ions in acetaldehyde–trioxane mixtures.

was less abundant and its ion intensity was comparable with the ion intensity of the ^{13}C isotope of $C_3H_5O_3^+$. The remarkable decrease of the ion intensities of CHO^+ and CH_3O^+ with increasing delay time was due to the participation of these ions in proton transfer reactions (9). Since the behavior of the product ions (homo-reaction product ions) formed in each individual system has been described previously (3), these ions are not shown in Fig. 2. New product ions of $C_3H_5O_2^+$ (*m/e* 73), $C_3H_6O_2^+$ (*m/e* 74), and $C_3H_7O_2^+$ (*m/e* 75) were observed in acetaldehyde–trioxane mixtures at elevated pressures and long delay times. In order to clarify the formation mechanism and the structures of the product ions, the ion–molecule reactions in acetaldehyde-d_4–trioxane mixtures were studied under the same conditions as for acetaldehyde–trioxane mixtures. The delay time dependence of the product ions is shown in Fig. 3, and the isotopic product ions ($C_3H_2D_3O_2^+$ (*m/e* 76), $C_3HD_4O_2^+$ (*m/e* 77), $C_3H_2D_4O_2^+$ (*m/e* 78), and $C_3H_3D_4O_2^+$ (*m/e* 79)) correspond to the ions ($C_3H_5O_2^+$, $C_3H_6O_2^+$, and $C_3H_7O_2^+$) formed in acetaldehyde–trioxane mixtures.

The ion intensity variation of the product ions with pressure in each gas was examined in order to clarify the contribution of both compounds (acetaldehyde and trioxane). The dependence of the product ions ($C_3H_5O_2^+$, $C_3H_6O_2^+$, and $C_3H_7O_2^+$)

Can. J. Chem. Downloaded from www.nrcresearchpress.com by 210.87.254.6 on 09/05/12
For personal use only.

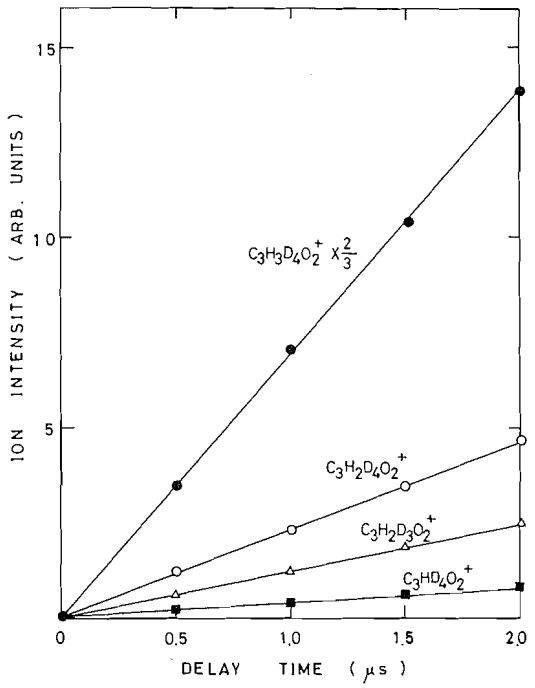

FIG. 3. Delay time dependence of product ions in acetaldehyde-d_4–trioxane mixtures.

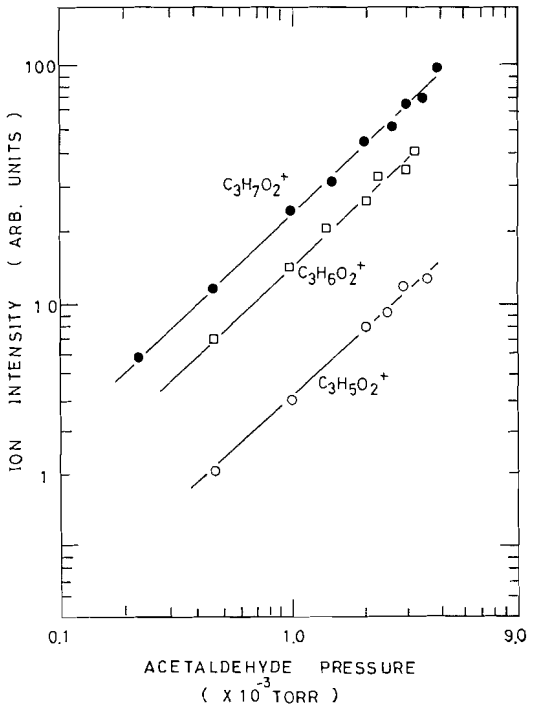

FIG. 4. Pressure dependence of product ions on acetaldehyde at 2.0 μs.

on acetaldehyde pressure, shown in Fig. 4, was obtained by variation of the acetaldehyde pressure using the dual leak at constant trioxane pressure and at a delay time of 2.0 μs. Similarly, the pressure dependence of the product ions in trioxane at constant acetaldehyde pressure is shown in Fig. 5. In Figs. 4 and 5, the product ions are first order in acetaldehyde and trioxane, indicating that these ions result from a cross reaction (reaction between ions of one compound and the molecules of the other) in acetaldehyde–trioxane mixtures.

Ionization Efficiency Curve

The appearance potentials and ionization efficiency curves of the fragment and product ions were measured to determine the precursors (reactants) of the product ions. The fragment ion whose appearance potential lies closest to that of the product ion generally is taken to be the precursor. If more than one fragment ion is responsible for the formation of a given product ion, a change in the slope of the ionization efficiency curve will often denote the onset of the reaction involving a different precursor. The ionization efficiency curves of major fragment and product ions ($C_3H_5O_2^+$, $C_3H_6O_2^+$, and $C_3H_7O_2^+$) in acetaldehyde–trioxane mixtures are shown in Fig. 6. All the ionization efficiency curves of the product ions coincide in onsets as well as shape. This indicates that the product ions have a common precursor. The onsets of the ionization efficiency curves

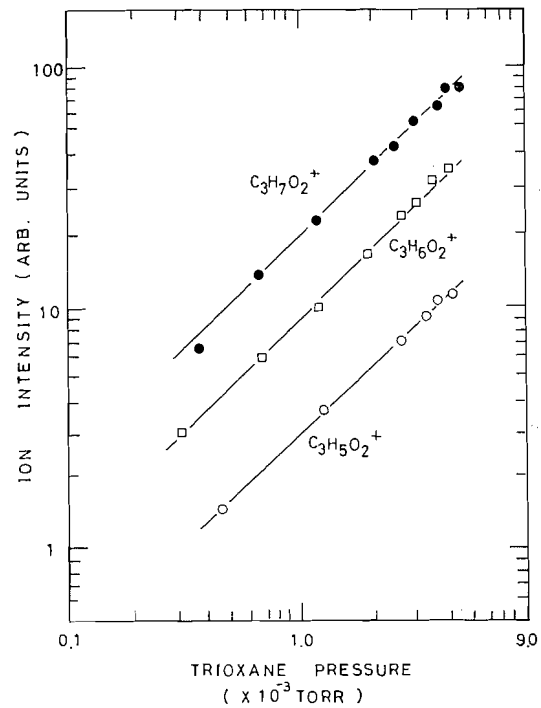

FIG. 5. Pressure dependence of product ions on trioxane at 2.0 μs.

Can. J. Chem. Downloaded from www.nrcresearchpress.com by 210.87.254.6 on 09/05/12
For personal use only.

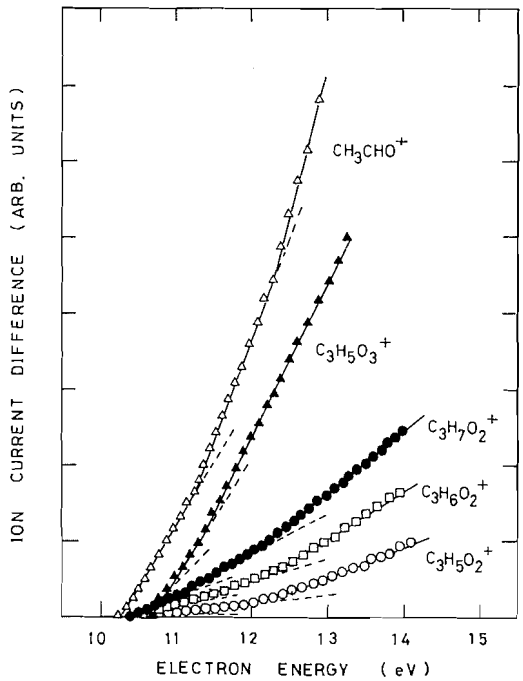

FIG. 6. Ionization efficiency curves of major fragment and product ions in acetaldehyde–trioxane mixtures.

of the product ions agree with the ionization potential (10.32 ± 0.05 eV) of acetaldehyde. The break points in the ionization efficiency curves of the product agree with those of acetaldehyde molecular ion. The onsets and break points in the ionization efficiency curves of the product ions did not agree with that of $C_3H_5O_3^+$ from trioxane. The appearance potentials of the fragment ions, CH_3CO^+, CHO^+, and CH_3^+, from acetaldehyde were 11.42 ± 0.05, 12.12 ± 0.05, and 14.32 ± 0.05 eV (3), while the appearance potentials of $C_2H_5O_2^+$, CH_3O^+, and CHO^+ from trioxane were 10.79 ± 0.05, 11.49 ± 0.05, and 13.59 ± 0.05 eV, respectively (10). Thus, the appearance potentials of these fragment ions were considerably higher than those of the product ions, and the break points in the ionization efficiency curves of the product ions did not agree with those in the curves of these fragments. CHO^+ and CH_3O^+ did not participate in the formation of the product ions in acetaldehyde–trioxane mixtures. The CHO^+ was generated from acetaldehyde as an intense fragment ion; however, $C_3H_5O_2^+$ was not formed in the ionic reactions in acetaldehyde. The CHO^+ and CH_3O^+ are proton donor ions which participate in proton transfer reactions (9). From the results of the ionization efficiency curve measurement it is concluded that the acetaldehyde molecular ion is the precursor of the product ions.

Reaction Mechanism and Ion Structures

The product ions result from the condensation–elimination reaction of CH_3CHO^+ with trioxane. From the distribution of the isotopic product ions in acetaldehyde-d_4–trioxane mixtures it is proposed that the product ions are formed by means of the dissociation of an unstable intermediate-complex resulting from the reaction of CH_3CHO^+ with trioxane (Scheme 1). The rate constants for the

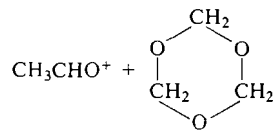

$$\rightarrow CH_3CHO{-}CHO^+ + C_2H_5O_2 \quad m/e\ 73 \quad (1)$$

$$\rightarrow CH_3CHO{-}CH_2O^+ + C_2H_4O_2 \quad m/e\ 74 \quad (2)$$

$$\rightarrow CH_3CHO{-}CH_2OH^+ + C_2H_3O_2 \quad m/e\ 75 \quad (3)$$

SCHEME 1

product ions in acetaldehyde (or acetaldehyde-d_4)–trioxane mixtures are given in Table 1. The sum of the rate constants for $CD_3CO{-}CH_2O^+$ and $CD_3CDO{-}CHO^+$ formed in acetaldehyde-d_4–trioxane mixtures is nearly equal to that for $CH_3CHO{-}CHO^+$ formed in those of acetaldehyde–trioxane. In addition, the rate constants for $CD_3CDO{-}CH_2O^+$ and $CD_3CDO{-}CH_2OH^+$ in acetaldehyde-d_4–trioxane mixtures are comparable with those for $CH_3CHO{-}CH_2O^+$ and $CH_3CHO{-}CH_2OH^+$ in those of acetaldehyde–trioxane. From the distribution of the isotopic product ions in both systems, the empirical formulae for the product ions shown in Table 1 are reasonable. The origins of the product ions are the acetaldehyde molecule (reactant ion) and fragments from trioxane. This suggests that the formation of the product ions involves an abstraction reaction by CH_3CHO^+ in the complex. From the formula of the product ions, it is probable that the complex resulting from the reaction of CH_3CHO^+ with trioxane has the linear structure shown in Fig. 7. As can be seen in Fig. 3, the ion intensity of $CD_3CDO{-}CH_2OH^+$ increased with increasing delay time and the rate constant for its formation was the largest of those for that of any of the product ions observed. The formation of $CD_3CDO{-}CH_2OH^+$ involves the rearrangement of a hydrogen atom in the complex. The rate constant for $CD_3CDO{-}CHO^+$ resulting from CHO^+ transfer in the complex is relatively small. From the empirical formulae of the product ions we estimate that extensive scrambling does not occur in the complex.

TABLE 1. Rate constants of the reactions in acetaldehyde (or acetaldehyde-d_4)–trioxane mixtures

Reactant ion			Product ion					$k \times 10^{10}$ (cm^3 molecule^{-1} s^{-1})
CH_3CHO^+	+	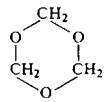	$CH_3CHO—CHO^+$ *m/e* 73	+	$2CH_2O$	+	H	0.51
			$CH_3CHO—CH_2O^+$ *m/e* 74	+	$2CH_2O$			0.75
			$CH_3CHO—CH_2OH^+$ *m/e* 75	+	CH_2O	+	CHO	4.30
CD_3CDO^+	+	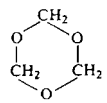	$CD_3CO—CH_2O^+$ *m/e* 76	+	$2CH_2O$	+	D	0.37
			$CD_3CDO—CHO^+$ *m/e* 77	+	$2CH_2O$	+	H	0.10
			$CD_3CDO—CH_2O^+$ *m/e* 78	+	$2CH_2O$			0.71
			$CD_3CDO—CH_2OH^+$ *m/e* 79	+	CH_2O	+	CHO	4.10

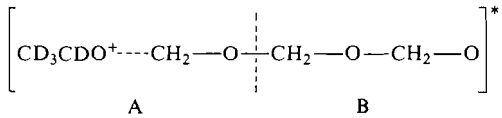

FIG. 7. Possible structure of the intermediate-complex.

It is well known that ring opening of trioxane occurs by means of positive species and radiation (11). It is presumed that the ring of the trioxane molecule is subsequently opened after the reaction of acetaldehyde molecular ion with trioxane. The constituent atoms of the product ions consist only of those in the A-site in the complex (Fig. 7) and the ion having the atoms of the B-site is not observed. This indicates that the positive charge is mainly localized on the site of the acetaldehyde molecule in the complex. The complex would be dissociated to the product ions due to the cleavage of the C—O bond in the trioxane molecule site, in which the neutral products involving a formaldehyde molecule are eliminated. If the complex has a cyclic structure, some product ions containing fragments from both origins (acetaldehyde and trioxane) would be formed as observed in the condensation–elimination reaction in ethylene oxide–trioxane mixtures (1). It would be impossible that a formaldehyde molecule is abstracted from trioxane by a stripping mechanism. The structure of the complex elucidated in acetaldehyde–trioxane mixtures is different from that in ethylene oxide–trioxane mixtures (1). Thus is is found that the nature of the condensation–elimination reaction involving a cyclic ether is related to the structure of the reactant ion.

Acknowledgment

We wish to express our sincere thanks to Dr. I. Kuriyama for helpful advice during the course of this work.

1. M. KUMAKURA, K. ARAKAWA, and T. SUGIURA. Bull. Chem. Soc. Jpn. **51**, 54 (1978).
2. M. KUMAKURA, A. ITO, and T. SUGIURA. Mass Spectrosc. **22**, 61 (1971).
3. M. KUMAKURA, K. ARAKAWA, and T. SUGIURA. Int. J. Mass Spectrom. Ion Phys. In press.
4. A. S. BLAIR and A. G. HARRISON. Can. J. Chem. **51**, 703 (1973).
5. J. L. BEAUCHAMP and R. C. DUNBAR. J. Am. Chem. Soc. **92**, 1477 (1970).
6. M. S. B. MUNSON. J. Am. Chem. Soc. **87**, 5313 (1965).
7. H. PRICHARD and A. G. HARRISON. J. Chem. Phys. **48**, 5623 (1968).
8. V. K. POTAPOVE. Dokl. Akad. Nauk SSSR, **183**, 386 (1968).
9. M. KUMAKURA, K. ARAKAWA, and T. SUGIURA. Bull. Chem. Soc. Jpn. **51**, 49 (1978).
10. M. KUMAKURA, T. SUGIURA, and S. OKAMURA. Mass Spectrosc. **16**, 16 (1968).
11. M. SAKAMOTO, I. ISHIGAKI, M. KUMAKURA, H. YAMASHINA, T. IWAI, A. ITO, and K. HAYASHI. J. Macromol. Chem. **1**, 639 (1966).

Can. J. Chem. Downloaded from www.nrcresearchpress.com by 210.87.254.6 on 09/05/12
For personal use only.

X-ray photoelectron spectra of C_6F_5X compounds (X = CH_3, CF_3, CN, CHO, OH, OCH_3, NH_2, NO_2)

BARRY C. TRUDELL AND S. JAMES W. PRICE[1]

Department of Chemistry, University of Windsor, Windsor, Ont., Canada N9B 3P4

Received August 4, 1977

BARRY C. TRUDELL and S. JAMES W. PRICE. Can. J. Chem. **56**, 538 (1978).

The gas phase photoelectron spectra, XPS, were observed for the series C_6F_5X (X = CH_3, CF_3, OCH_3, OH, CHO, NO_2, NH_2, CN). Binding energies were determined from the spectra by using computer curve fitting. Charge calculations were carried out using CNDO/2 and ACHARGE techniques. The CNDO/2 analysis led to the following correlation for the C 1*s* binding energies and the atomic charges, q_i

$$E_i, (\text{C } 1s) = 290.01 + 23.74q_i + \sum_{i \neq j} q_i/R_{ij}$$

Correlations were also obtained for O 1*s* and N 1*s*:

$$E_i, (\text{O } 1s) = 538.12 + 9.59q_i + \sum_{i \neq j} q_i/R_{ij}$$

$$E_i, (\text{N } 1s) = 405.99 + 24.26q_i + \sum_{i \neq j} q_i/R_{ij}$$

These equations are based on only four and three points respectively. However, the N 1*s* values cover a wide range (E_i, 402 to 419 eV; q_i, −0.2 to 0.5) and show a better correlation than those for oxygen.

BARRY C. TRUDELL et S. JAMES W. PRICE. Can. J. Chem. **56**, 538 (1978).

On a déterminé les spectres photoélectroniques en phase gazeuse, XPS, pour la série C_6F_5X (X = CH_3, CF_3, OCH_3, OH, CHO, NO_2, NH_2, CN). On a déterminé les énergies de liaison à partir des spectres en faisant appel a une correspondance de courbe effectuée par ordinateur. On a calculé les charges à l'aide des techniques CNDO/2 et ACHARGE. L'analyse CNDO/2 a conduit à la corrélation suivante pour les énergies de liaison des atomes de C 1*s* et les charges atomiques q_i

$$E_i, (\text{C } 1s) = 290.01 + 23.74q_i + \sum_{i \neq j} q_i/R_{ij}$$

On a aussi obtenu les corrélations pour O 1*s* et N 1*s*:

$$E_i, (\text{O } 1s) = 538.12 + 9.59q_i + \sum_{i \neq j} q_i/R_{ij}$$

$$E_i, (\text{N } 1s) = 405.99 + 24.26q_i + \sum_{i \neq j} q_i/R_{ij}$$

Toutefois ces équations ne sont basées respectivement que sur quatre et trois données. Toutefois les valeurs de N 1*s* couvrent un spectre plus grand (E_i 402 à 419 eV, q_i −0.2 à 0.5) et présentent une meilleure corrélation que celles obtenues pour l'oxygène.

[Traduit par le journal]

Introduction

We have shown in a recent paper (1) that charge distributions in molecules of the type C_6F_5X (X = F, Cl, Br, I, H) can be calculated from XPS data and compared with CNDO/2 calculations successfully. This paper presents a similar study of C_6F_5X compounds where X = OH, CHO, NO_2, CN, OCH_3, NH_2, CF_3, CH_3.

Experimental

All of the C_6F_5X compounds were obtained from the Imperial Smelting Corporation with the exception of C_6F_5OH which was obtained from Bristol Organics Ltd. The chemicals were distilled twice, with only middle fractions taken for use. Boiling points agreed with literature values (2).

Spectra were measured (1) using a McPherson Esca 36 spectrometer[2] employing MgK_α radiation (1253.6 eV). Spectra for each level were run a minimum of three times and were reproducible to within ±0.1 eV.

Results and Discussion

The binding energies of the various levels in each of the compounds are reported in Table 1. The areas calculated were used in some cases to decide how many, but not which, carbons were to be assigned to a particular binding energy (e.g. $C_6F_5OCH_3$ 6:1).

[1]To whom correspondence should be addressed.

[2]Located at the University of Western Ontario, London, Ontario.

Can. J. Chem. Downloaded from www.nrcresearchpress.com by 210.87.254.6 on 09/05/12
For personal use only.

Can. J. Chem. Downloaded from www.nrcresearchpress.com by 210.87.254.6 on 09/05/12
For personal use only.

TABLE 1. Binding energies in compounds of the type C_6F_5X

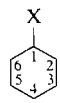

Compound	Level	BE[a]	Area[b]	Assignments
$C_6F_5CH_3$	C 1*s*	293.6	255(13)	C_2—C_6
		291.6	90(13)	C_1, C_x
	F 1*s*	693.7	582(16)	
$C_6F_5CF_3$	C 1*s*	299.3	134(18)	C_x
		294.4	534(21)	C_2—C_5
		292.5	129(17)	C_1
	F 1*s*	694.2	876(22)	
C_6F_5OH	C 1*s*	293.8	399(13)	C_1—C_6, C_x
	O 1*s*	540.3	324(19)	
	F 1*s*	693.9	744(19)	
C_6F_5CHO	C 1*s*	294.1	349(12)	C_2—C_5, C_x
		292.0	50(6)	C_1
	F 1*s*	694.2	345(14)	
	O 1*s*	538.4	77(10)	
$C_6F_5OCH_3$	C 1s	293.6	292(21)	C_1—C_6
		292.6	44(10)	C_x
	F 1*s*	693.8	517(17)	
	O 1*s*	539.5	104(7)	
$C_6F_5NO_2$	C 1*s*	294.4	293(17)	C_2—C_5
		293.2	88(15)	C_6
	F 1*s*	694.4	308(13)	
	O 1*s*	539.6	233(12)	
	N 1*s*	412.7	136(10)	
C_6F_5CN	C 1*s*	294.4	262(16)	C_2—C
		293.0	141(14)	C_x, C_1
	F 1*s*	694.5	355(14)	
	N 1*s*	405.9	96(11)	
$C_6F_5NH_2$	C 1*s*	293.5	331(16)	C_2—C_6
		292.5	69(13)	C_1
	F 1*s*	693.6	801(70)	
	N 1*s*	406.2	219(11)	

[a]All binding energy values relative to argon $2p_{3/2} = 248.62$ eV.
[b]Relative values. Values in parentheses are uncertainties calculated by computer curve fitting.

The binding energies of the carbon atoms varied over a wide range (290.0–299.3) depending on the particular environment. The pattern for the chemical shifts of the carbon atom joined to the substituting group was found to be OH > OCH_3 > NO_2 > CN > CF_3 = NH_2 > CHO > CH_3. The position of CH_3 in this series is consistent with the idea that the first seven groups are all −I groups while CH_3 is +I. Each of these groups also has the capability of a resonance effect (either +R or −R) on the ring system. The pattern of chemical shifts for the carbon atoms on the C_5F_5 portion of the ring was found to be CN = NO_2 = CF_3 > CHO > OH > CH_3 > OCH_3 > NH_2. The first four groups are all −R groups while the last four are +R groups which is consistent with the overall ordering. (The method by which carbon atoms were assigned to particular binding energy values will be discussed later in the paper.) There were no separate peaks seen for the fluorine atoms in any of the molecules, although the fluorine in the aliphatic side chain in $C_6F_5CF_3$ did lead to peak broadening.

In all cases where comparison was possible, the binding energies of all atoms of the C_6F_5X series are higher than in the corresponding C_6H_5X (3) series in accordance with the idea that the fluorine atoms are largely −I moderated by a small +R effect.

CNDO/2 Calculations and Chemical Shifts

The use of the electrostatic potential model to correlate binding energies of atoms in molecules with their respective CNDO/2 charges is well documented (3–8). The technique involves an equation of the type,

$$[1] \qquad E_i - \sum_{i \neq j} q_j/R_{ij} = E_0 + k_A q_i$$

A plot of the term on the left vs. q_i, the CNDO/2 charges, should allow calculation of k_A and E_0 which are parameters necessary for ACHARGE analysis of the molecules.

The CNDO/2 charge calculations for the series of molecules in this present paper were carried out using QCPE No. 290.[3] The program was discussed in a previous paper (1) and no alterations were made. The CNDO/2 charges are reported in Table 2. In three cases (X = OH, CHO, OCH_3) the optimized geometry (minimum energy) predicts an unsymmetric configuration. The values listed in Table 2 for these three molecules are for this minimum energy structure.

If one substitutes these CNDO/2 values for q_i in [1] along with the necessary R_{ij} values which were derived from the optimized geometry calculated by QCPE No. 290, the plot shown in Fig. 1 is obtained. This plot is for the carbon atoms only. As can be seen the correlation for these values is excellent. A least-squares calculation returns the values 289.93 eV and 23.80 eV/e for E_0 and k_c respectively. If points from previous calculations of similar molecules are included, the following equation is obtained.

$$[2] \quad E_i(\text{C } 1s) = 290.01 + 23.74q_i + \sum_{j \neq i} q_j/R_{ij}$$

In the case where the assignment of a particular binding energy to a particular carbon atom in the molecule was not clear, e.g. $C_6F_5OCH_3$, Fig. 1 was used as an aid to work out the problem. In $C_6F_5OCH_3$ there is one carbon atom with a binding energy higher than all the rest. It is impossible to determine whether it is the C_1 carbon or the CH_3

[3]Developed by Dr. D. Rinaldi, Université de Nancy. Available through Quantum Chemistry Program Exchange, University of Indiana.

TABLE 2. CNDO/2 charges, ACHARGE charges, and molecular potentials of compounds of the type

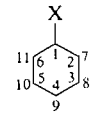

Compound	Parameter	Value						
		C_1	C_2	C_3	C_4	X		
$C_6F_5CH_3$						C		H
	CNDO/2	−0.013	0.179	0.143	0.162	0.013		0.016
	ACHARGE	−0.058	0.178	0.148	0.149	0.037		−0.019
	M.P.[a]	2.60	−1.42	0.21	0.06	0.96		—
$C_6F_5CF_3$						C		F
	CNDO/2	−0.148	0.234	0.133	0.186	0.654		−0.213
	ACHARGE	−0.129	0.198	0.166	0.155	0.682		−0.205
	M.P.	5.84	−0.77	0.95	0.22	−7.15		—
C_6F_5OH[b]						O		H
	CNDO/2	0.155	0.137	0.161	0.146	−0.204		0.165
	ACHARGE	0.130	0.132	0.145	0.146	−0.225		0.196
	M.P.	0.75	0.49	0.16	0.38	—		—
C_6F_5CHO[c,e]						C	O	H
	CNDO/2	−0.074	0.213	0.131	0.188	0.242	−0.215	−0.019
	ACHARGE	−0.084	0.181	0.152	0.155	0.293	−0.268	−0.012
	M.P.	4.10	−0.49	0.91	0.12	−2.39	—	—
$C_6F_5OCH_3$[d,e]						C	O	H
	CNDO/2	0.116	0.141	0.157	0.149	0.152	−0.169	−0.007
	ACHARGE	0.117	0.134	0.144	0.145	0.157	−0.148	−0.004
	M.P.	0.73	0.36	0.14	0.25	−1.41	—	—
$C_6F_5NO_2$						N		O
	CNDO/2	−0.045	0.224	0.136	0.196	0.561		−0.312
	ACHARGE	−0.060	0.188	0.162	0.163	0.511		−0.255
	M.P.	4.87	0.01	1.35	0.54	—		—
C_6F_5CN						C		N
	CNDO/2	−0.023	0.206	0.139	0.177	0.107		−0.131
	ACHARGE	−0.027	0.180	0.157	0.159	0.240		−0.279
	M.P.	3.24	−0.69	0.82	−1.18	−0.90		—
$C_6F_5NH_2$						N		H
	CNDO/2	0.106	0.129	0.166	0.130	−0.215		0.127
	ACHARGE	0.039	0.153	0.144	0.146	−0.122		0.096
	M.P.	0.61	0.24	−0.21	0.27	—		—

[a]M.P. ≡ molecular potential.
[b]$k_0 = 9.2$.
[c]$k_0 = 11.5$.
[d]$f_0 = 10.5$.
[e]Minimum energy states unsymmetric. Charge on C_3 and C_5 nearly equal but in C_6F_5CHO and C_6H_5OH the charge on C_6 exceeds that on C_2 by 0.008 and 0.015 respectively. F_7–F_{11} charges all −0.148 to −0.184 with in general F_7 and F_{11} more negative than F_8–F_{10} by 0.01 to 0.02 charge units.

carbon by inspection. However, if the two sets of assignments are made it is found that in one case both of the points fall well off the line, while the second choice leads to excellent correlation indicating correct assignments have probably been made. This procedure was also adopted for C_6F_5CHO.

Although the molecular potential terms are not dominant in all cases, in every case it certainly adds or subtracts a significant amount to or from the chemical shift. Only in molecules where there is no significant charge distribution, e.g. C_6H_6, could the molecular potential term be successfully left out.

In order to be able to carry out the ACHARGE analysis for this series of molecules, it is necessary to have values for E_0 and k_A for carbon, fluorine, nitrogen, and oxygen (suitable values for fluorine were used in a previous paper (1) and the values for carbon have already been discussed). In order to obtain the values for nitrogen and oxygen, plots similar to that of Fig. 1 for carbon were made for nitrogen and oxygen. These are shown in Figs. 2 and 3.

The nitrogen plot contains only three points (NO_2, NH_2, CN) but gives a reasonable correlation over a wide range of binding energies (402–419 eV) and atomic charges ($-0.2 \rightarrow 0.5$). The corresponding parameters were found to be 406.0 eV for E_0 and 24.26 eV/e for k_N.

The oxygen plot although having four points

Can. J. Chem. Downloaded from www.nrcresearchpress.com by 210.87.254.6 on 09/05/12
For personal use only.

Can. J. Chem. Downloaded from www.nrcresearchpress.com by 210.87.254.6 on 09/05/12
For personal use only.

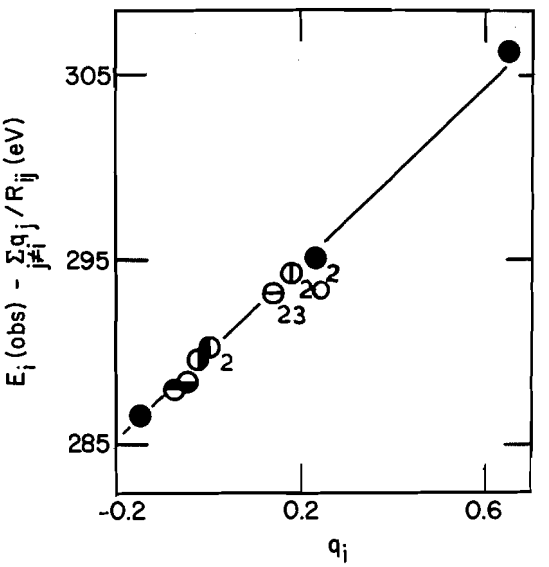

FIG. 1. Binding energies of C 1*s* electrons in C_6F_5X (X = CF_3, CH_3, NH_2, OH, OCH_3, CN, NO_2, CHO) corrected for interatomic potentials vs. the charge on the respective carbon atom. All *q* values are from CNDO/2 calculations. ● $C_6F_5CF_3$, ◐ $C_6F_5CH_3$, ◑ C_6F_5CN, ◒ $C_6F_5NO_2$, ◓ C_6F_5CHO. Subscripts indicate number of C 1*s* values averaged to obtain the given point. For the two multicompound points contributions are as follows (X, number of C 1*s* values from C_6F_5X): ⊕ CF_3, 1; CH_3, 2; NO_2, 5; CN, 6; CHO, 6. ⊖ CF_3, 2; CH_3, 3; NH_2, 6; OH, 6; OCH_3, 6.

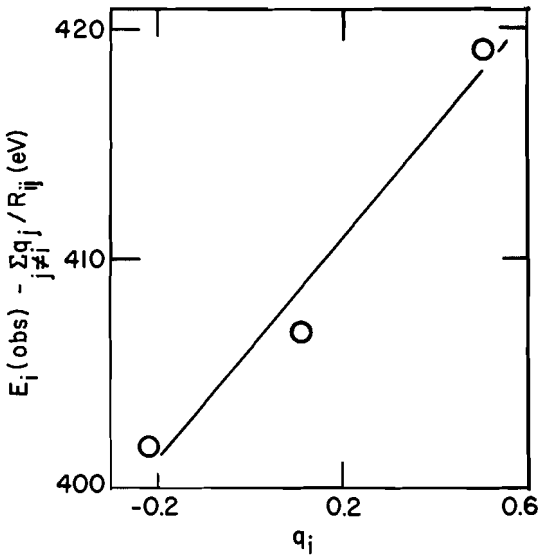

FIG. 2. Binding energies of N 1*s* electrons in C_6F_5X (X = NH_2, CN, NO_2) corrected for interatomic potentials vs. the charge on the respective nitrogen atom. All *q* values are from CNDO/2 calculations. Points from left to right are for $C_6F_5NH_2$, C_6F_5CN, and $C_6F_5NO_2$ respectively.

(NO_2, CHO, OH, OCH_3) gave a poorer correlation. This was probably due to the narrow range of binding energies (538.5–540.3 eV) and charges ($-0.31 \rightarrow -0.17$). The necessary values were calculated as 538.1 eV for E_0 and 9.59 eV/e for k_0. The value for k_0 of oxygen was lower than expected although other experiment slopes have varied from roughly 8 (9, 10) to 26 (11) eV/e. Accordingly, it was thought that the value of 9.59 eV/e was probably acceptable for ACHARGE calculation on these molecules.

ACHARGE Analysis

Using chemical shift data and a knowledge of molecular geometry, atomic charges can be calculated by ACHARGE Analysis (3–7).

In the preceding section E_0 and k_A values for carbon, nitrogen, and oxygen were established. Values for fluorine have been documented (1, 7). Thus, if we assume only that all hydrogens in the molecules have an equal charge (e.g. the hydrogen in $C_6F_5CH_3$) and that the molecule is neutral, the calculation can be carried out.

The charge densities calculated by the ACHARGE technique are shown in Table 2.

In most cases the correlation between these 'experimentally' determined charge densities and the CNDO/2 result is excellent. In the case of

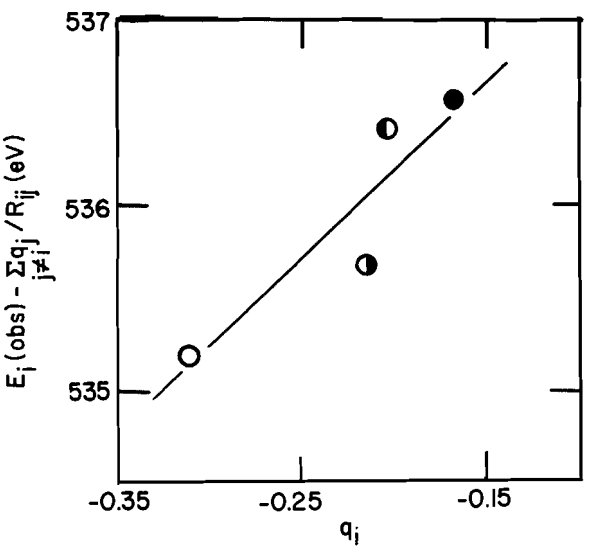

FIG. 3. Binding energies for O 1*s* electrons is C_6F_5X (X = NO_2, CHO, OH, OCH_3) corrected for interatomic potentials vs. the charge on the respective oxygen atom. ○ $C_6F_5NO_2$, ◑ C_6F_5CHO, ◐ C_6F_5OH, ● $C_6F_5OCH_3$.

$C_6F_5OCH_3$, C_6F_5CHO, and C_6F_5OH, because of the lower precision in the value for k_0 slightly different values ranging from 9.2 to 11.5 eV/e were used to give the best fit. It was found that the charges on the oxygen atom and its immediate neighbours were extremely sensitive to the values of k_0 used. The fact that E_0 for oxygen may also be in error is considered but the effect on the charge densities was less pronounced.

Acknowledgements

The authors would like to thank Mr. R. Lazier for his assistance in running the spectra, Mr. R. M. Baillageon for his co-operation in setting up the programmes used in this paper, and Dr. C. S. Lin for many fruitful discussions. This work was supported by a grant from the National Research Council of Canada.

1. B. C. TRUDELL and S. J. W. PRICE. Can. J. Chem. **55**, 1279 (1977).
2. Highly Fluorinated Aromatic and Alicyclic Compounds. Imperial Smelting Co., St. Andrews Rd., Avonmouth, Bristol BS11 9HP, England.
3. T. OHTA, T. FUJIKAWA, and H. KURODA. Bull. Chem. Soc. Jpn. **48**, 2017 (1975).
4. D. T. CLARK, D. KILCAST, D. B. ADAMS, and W. K. R. MUSGRAVE. J. Electron Spectrosc. **1**, 227 (1972/73).
5. D. T. CLARK, D. KILCAST, D. B. ADAMS, and W. K. R. MUSGRAVE. J. Electron Spectrosc. **6**, 117 (1975).
6. T. D. THOMAS. J. Chem. Phys. **52**, 1373 (1970).
7. D. W. DAVIS, D. A. SHIRLEY, and T. D. THOMAS. J. Am. Chem. Soc. **94**, 6565 (1972).
8. V. GELIUS. Phys. Scr. **9**, 147 (1974).
9. K. SIEGBAHN *et al.* ESCA applied to free molecules. North Holland Publishing Co., Amsterdam, The Netherlands. 1969.
10. D. A. SHIRLEY (*Editor*). Electron spectroscopy. North Holland Publishing Co., Amsterdam, The Netherlands. 1972. Chapt. V.
11. W. J. STEC, W. E. MORGAN, J. R. VAN WAZER, and V. G. PROCTOR. J. Inorg. Nucl. Chem. **34**, 1100 (1972).

Can. J. Chem. Downloaded from www.nrcresearchpress.com by 210.87.254.6 on 09/05/12
For personal use only.

The effect of *p*, *d*, and *f* Gaussian polarization functions on the computed one-electron properties of AH_n oxygen and sulfur hydrides

RAYMOND POIRIER AND ROY KARI

Department of Chemistry, Laurentian University, Sudbury, Ont., Canada P3E 2C6

Received August 12, 1977

RAYMOND POIRIER and ROY KARI. Can. J. Chem. **56**, 543 (1978).

A series of LCAO-MO-SCF calculations, using various basis sets of Gaussian-type functions, has been made in order to study the effects of *p*, *d*, and *f* polarization functions on calculated one-electron properties for a 10-electron isoelectronic series of oxygen hydrides and for an 18-electron series of sulfur hydrides. Conclusions from these results suggest that several one-electron properties have a predictable, although not monotonic convergence pattern. Except for calculated field gradients, *f* GPF's have only a small effect on the calculated values.

RAYMOND POIRIER et ROY KARI. Can. J. Chem. **56**, 543 (1978).

On a effectué une série de calculs LCAO-MO-SCF, faisant appel à divers ensembles de base de type Gaussien, de façon à étudier les effets des fonctions de polarisation *p*, *d* et *f* sur les propriétés uniélectroniques calculées pour une série isoélectronique de 10 électrons d'hydrures d'oxygène, et pour une série de 18 électrons d'hydrures de soufre. Les conclusions que l'on peut tirer de ces résultats suggèrent que plusieurs propriétés uniélectroniques possèdent un type de convergence qui peut être prèdit mais qui n'est pas monotone. A l'exception des gradients de champs calculés, *f* l'effet des valeurs GPF sur les valeurs calculées est minime.

[Traduit par le journal]

Introduction

Physical properties may be divided into two general classes: those that involve energy, specifically energy differences such as ionization potentials and proton affinities, and those that represent molecular properties other than energy. In this paper, attention will be focussed on certain properties of the latter class, namely properties such as dipole and quadrupole moments, which may be computed as expectation values of one-electron operators (one-electron properties).

The sources of error in *ab initio* calculations may be divided into four distinct categories: (*1*) Born–Oppenheimer and relativistic effects, (*2*) variation with internuclear distance, (*3*) correlation effects, and (*4*) finite expansion basis set effects. The purpose of this article is to examine the fourth category in detail for it is well known (1) that a deficiency in the SCF basis will not be corrected by subsequent beyond Hartree–Fock calculations.

The importance of *d* Gaussian polarization functions (GPF's) in molecules containing first and second row atoms and *p* GPF's on molecules containing hydrogen in the determination of molecular properties have been the subject of many investigations (2, 3). However, these investigations have been confined usually and only to those properties involving energy, which generally converges monotonically and relatively quickly with the addition of GPF's. On the other hand, molecular one-electron properties converge more slowly and furthermore do not usually converge to their limiting values in a monotonic manner. This makes it difficult if not often impossible to predict limiting values for one-electron properties. Also, although one property may be adequately represented by a given basis set, this does not imply that any other property will be equally well represented.

Recognizing the relative intractability of computed one-electron properties, the present study included an analysis of the importance of *f* GPF's in determining one-electron properties for oxygen and sulfur hydrides. The inclusion of a *f* GPF also allows a comparison to be made with a parallel study (3) undertaken to determine the energetic effects of GPF's.

Calculations

In order to investigate the basis set dependence of each operator, two series of calculations were performed on three isoelectronic oxygen hydrides OH^-, OH_2, and OH_3^+ and on three isoelectronic sulfur hydrides SH^-, SH_2, and SH_3^+. The first series included as *s* only basis set on the hydrogens and a *sp*, then *spd*, and finally an *spdf* basis set on either oxygen or sulfur. The second series repeated the oxygen or sulfur basis set but this time each hydrogen was represented by an *sp* basis set. The basis sets will be hereafter abbreviated by the symbols (*sp*/*s*), (*spd*/*s*), etc., where the letters before the solidus indicate the basis set used to represent the heavy atom while the letters after the solidus indicate the basis set used to represent each hydrogen atom.

The actual basis sets used incorporated 10^s, 5^p, 1^d, and 1^f GTO's contracted to 4^s, 2^p, 1^d, and 1^f GTO's

Can. J. Chem. Downloaded from www.nrcresearchpress.com by 210.87.254.105 on 09/05/12
For personal use only.

Can. J. Chem. Downloaded from www.nrcresearchpress.com by 210.87.254.105 on 09/05/12
For personal use only.

on oxygen, 12^s, 9^p, 2^d, and 1^f GTO's contracted to 6^s, 4^p, 2^d, and 1^f GTO's on sulfur, and finally 4^s and 1^p GTO's contracted to 2^s and 1^p GTO's on hydrogen. Due to the nature of Gaussian functions, the six *d*-type functions will combine to form linear combinations which correspond to the traditionally accepted five 3*d*-AO and one 3*s*-AO. Similarly, the 10 *f*-type Gaussians will produce seven 4*f*-AO and three 4*p*-AO. No attempt was made to separate the Gaussians into the more traditional forms. The oxygen α exponent (0.706328) and the sulfur *d* exponents (0.25 and 1.3225) were chosen so as to describe electron densities for both ionic and neutral species. The *f* exponent was arbitrarily set equal to unity. As a result of these compromises, none of the GPF exponents are optimum for any one species. However, because the dependence of expectation values on the choice of exponent values is small (3, 4) relative to their dependence on the actual inclusion of one or more polarization functions, it is not expected that the present choice of exponents will cause any qualitative discrepancies in the relative results and conclusions presented here. The reader is referred to previous publications (3–6) for more specific details about the basis sets and the nuclear geometries for all of the species investigated. It should be noted that the nuclear geometries used here were not necessarily identical to experimental geometries. Hence, the values of the properties calculated here are not directly comparable to experimentally determined values in so far as these values vary with small changes in the internuclear distances or valence angles.

All of the one-electron properties calculations were performed via the POLYATOM (version 2) system of programs (QCPE # I99). The one-electron properties package was locally modified to compute properties over *f* Gaussian-type orbitals.

Balanced Basis Sets

Mulliken (7) introduced the terms physical and formal balance to describe the nature of basis sets. A physically balanced set is one which gives reasonable calculated values for well defined experimental quantities. A formally balanced set exists when reasonable charges are calculated for atoms. Both of these definitions are somewhat arbitrary in that one must define what is meant by reasonable. For discussion purposes, it will be assumed that the (*spdf*/*sp*) basis set Mulliken populations display formally balanced charge distributions.

The absolute effect of GPF's on Mulliken population is illustrated in Fig. 1 for oxygen and sulfur hydrides. For convenience, these have been shown relative to the (*sp*/*sp*) basis set. The relative effect of adding GPF's in the order *d*, *p*, and *f* is given in Table 1. Assuming that the (*spdf*/*sp*) basis set is formally balanced, the addition of *d* or *f* GPF's on the heavy atom will exaggerate the charge on the heavy atom. Figure 1 reveals a simple rule. Electron density will flow to the nuclear centre where the GPF is added. Therefore, in order to obtain a formally balanced basis set when adding *d* and *f* GPF's to the heavy atom, a *p* GPF must be included in the hydrogen basis set. In Fig. 1 and Table 1, *p* and *f* GPF show a significantly larger effect for the oxygen hydrides than for the sulfur hydrides while the reverse is true for addition of a *d* GPF.

Mulliken population is an excellent example of predictable convergence where the addition of GPF's on a given centre increases the population at that centre and addition at a second centre will lower the population at the first centre.

Although physical balance requires that the basis set produce reasonable results for well defined experimental quantities, Fig. 3 shows that the dipole moments, for example, do not exhibit a simple or predictable convergence. As a result, one basis set may accidentally give a reasonable result for one quantity but may also give an unreasonable description of another property. For this reason, a discussion of physical balances would seem inappropriate unless consideration is simultaneously given to many different physical properties. One method of incorporating all of the calculated properties is to discuss the basis set in terms of their relative effects on negative, neutral, and positive species.

On addition of *d*, *f*, and *p* GPF's to an (*sp*/*s*) basis set, the minimum change in the dipole moment was noted for the anion and the maximum change was noted for the cation. Table 2 indicates similar maximum and minimum changes for all of the other one-electron properties. If it is assumed that the (*spdf*/*sp*) basis set is the most physically balanced basis set, then any other basis set which is equally balanced should exhibit a similar minimum and maximum effect for each property. For example, if the (*spd*/*s*) basis set were as balanced as the (*spdf*/*sp*) basis set, then we would expect the addition of a *d* GPF to least affect the dipole moment of the anion and to most affect the dipole moment of the cation. A summary of the mismatches which were observed for the (*spd*/*s*), (*sp*/*sp*), (*spd*/*sp*), and (*spdf*/*s*) basis sets is listed in Table 3. From this table, it may be concluded that the (*sp*/*sp*) basis sets for both the oxygen and sulfur hydrides and the (*spd*/*s*) basis set for oxygen hydride are furthest from physical balance and the (*spd*/*sp*) and (*spdf*/*s*) are closest to physical balance.

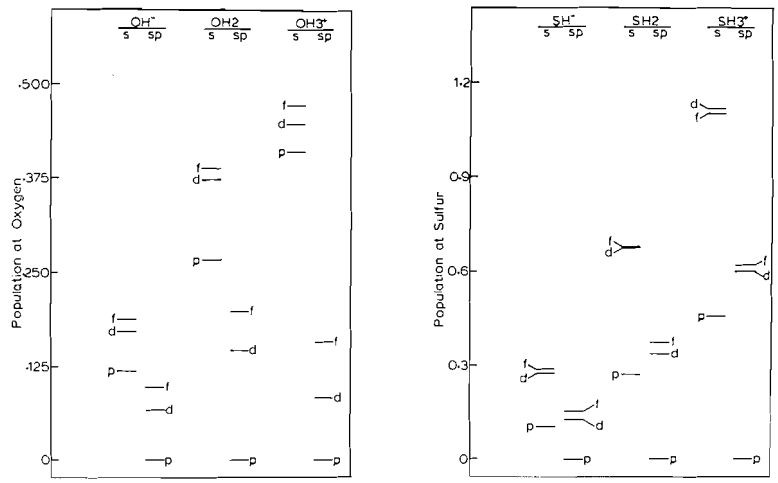

FIG. 1. The gross Mulliken electron population at the oxygen and sulfur nuclei for oxygen and sulfur hydrides.

TABLE 1. Percentage[a] effects of *d*, *p*, and *f* GPF's on the calculated Mulliken population of oxygen or sulfur atom

Species	Basis set[b]	Percentage effect
OH^-	*d*	0.57
	p	−198
	f	58
OH_2	*d*	1.22
	p	−212
	f	48
OH_3^+	*d*	0.70
	p	−598
	f	122
SH^-	*d*	1.01
	p	−85
	f	16
SH_2	*d*	2.48
	p	−83
	f	9
SH_3^+	*d*	4.16
	p	−78
	f	3

[a]For a definition of percentage effect see text.
[b]Symbols *d*, *p*, and *f* refer to (*spd*/*s*), (*spd*/*sp*), and (*spdf*/*sp*) basis sets respectively.

Relative Effects of Polarization Functions

In order to measure the relative effects of GPF's, an order of addition of GPF's was assumed. Thus, the basis sets were built up in the order; (*sp*/*s*), (*spd*/*s*), (*spd*/*sp*), and (*spdf*/*sp*). As the addition of a *d* GPF to a (*sp*/*s*) basis set will change the calculated expectation value of any operator, the value of this change (Ad) may be defined as

$$\mathrm{Ad} = \langle spd/s \rangle - \langle sp/s \rangle$$

where $\langle sp/s \rangle$ and $\langle spd/s \rangle$ refer to the expectation values of an operator as calculated with (*sp*/*s*) and (*spd*/*s*) basis sets respectively. As well, the value of a similar change on addition of *p* (Ap) or *f* (Af) GPF's may be defined as

$$\mathrm{Ap} = \langle spd/sp \rangle - \langle spd/s \rangle$$

$$\mathrm{Af} = \langle spdf/sp \rangle - \langle spd/sp \rangle$$

For convenience, the percentage effect of adding a *d* GPF was defined relative to the change calculated with the (*sp*/*s*) basis set while the percentage effects of additional *p* and *f* GPF's was defined relative to the change occurring on addition of a *d* GPF. That is,

$$\text{Percentage effect of a } d \text{ GPF} = \frac{\mathrm{Ad}}{\langle sp/s \rangle} \times 100\%$$

$$\text{Percentage effect of a } p \text{ GPF} = \frac{\mathrm{Ap}}{\mathrm{Ad}} \times 100\%$$

$$\text{Percentage effect of a } f \text{ GPF} = \frac{\mathrm{Af}}{\mathrm{Ad}} \times 100\%$$

TABLE 2. Species for which the minimum (min) and maximum (max) effects were observed on addition of *p*, *d*, and *f* polarization function to an (*sp*/*s*) basis set. The species are identified by the symbols A for anion, C for cation, and N for neutral

	Oxygen hydrides		Sulfur hydrides	
Property	Min	Max	Min	Max
Dipole moment	A	C	A	C
Second moment	A	C	A	C
Third moment	A	C	N	C
Potential at O or S	N	C	A	C
Potential at (H)	A/C	N	A	C
Field gradient at O or S	C	N	A	C
Field gradient at (H)	A	N	N	C
Electric field at O or S	N	C	A	N
Electric field at (H)	C	A	N	A
Population	A	C	A	C
Total negative	6	1	7	2
neutral	2	3	3	1
positive	2	6	0	7

Can. J. Chem. Downloaded from www.nrcresearchpress.com by 210.87.254.105 on 09/05/12
For personal use only.

Can. J. Chem. Downloaded from www.nrcresearchpress.com by 210.87.254.105 on 09/05/12
For personal use only.

TABLE 3. Number of mismatches of other basis sets relative to the *spdf/sp* basis set for the oxygen and sulfur hydrides[a]

Basis set	Property	Species substituted	Effect (min or max)	No. mismatches/ correlation
		Oxygen	Hydrides	
spd/s	Electric field at (H)	N	Min	
	Second moment	N	Max	4/0.80
	Field gradient	A	Max	
	Population	N	Max	
sp/sp	Potential at (O)	A	Min	
	Electric field at (O)	A	Min	3/0.85
	Second moment	N	Max	
spd/sp	Field gradient at (O)	A	Max	1/0.95
spdf/s	Population	N	Max	1/0.95
		Sulfur	Hydrides	
spd/s	Field gradient at (H)	A	Min	
	Field gradient at (S)	N	Max	2/0.90
sp/sp	Third moment	A	Min	
	Third moment	C	Max	
	Field gradient at (S)	N	Max	
	Field gradient at (H)	A	Max	6/0.70
	Electric field at (S)	C	Max	
	Electric field at (H)	C	Max	
spd/sp	Field gradient at (S)	N	Max	1/0.95
spdf/s	—	—	—	0/1.00

[a]Symbols A for anion, C for cation, and N for neutral.

TABLE 4. Percentage[a] effects of *d*, *p*, and *f* Gaussian polarization functions on the calculated energy $\langle E \rangle$, dipole $\langle r \rangle$, second $\langle r^2 \rangle$, and third $\langle r^3 \rangle$ moment expectation values of oxygen and sulfur hydrides

Property	Basis set[b]	Species OH^-	SH^-	OH_2	SH_2	OH_3^+	SH_3^+
$\langle E \rangle$	*d*	0.02	0.00	0.04	0.01	0.02	0.02
	p	36	34	39	42	116	18
	f	27	30	5	6	14	1
$\langle r \rangle$	*d*	9.44	5.74	13.36	13.96	28.91	15.72
	p	16	1	14	0	9	1
	f	−13	−9	−1	−1	0	1
$\langle r^2 \rangle$	*d*	−0.05	−0.72	−0.71	−2.03	−0.46	−3.69
	p	533	1	75	5	174	6
	f	−1852	−86	−9	−7	51	2
$\langle r^3 \rangle$	*d*	1.53	−9.05	4.02	0.01	63.69	6.00
	p	159	−11	117	−4755	32	12
	f	−313	18	−27	−4184	7	2

[a]For a definition of percentage effect see text.
[b]Symbols *d*, *p*, and *f* refer to (*spd/s*), (*spd/sp*), and (*spdf/sp*) basis sets respectively.

A summary of the percentage effects of *p*, *d*, and *f* GPF's is listed in Tables 4 and 5 for a variety of operators. A few of the calculated expectation values are also illustrated in Figs. 2 and 3. In these figures, all values are shown relative to the expectation value as calculated with the (*sp/s*) basis set which is indicated by the *p* line under the s column for each species. Actual computed one-electron property values for the (*spdf/sp*) basis set are listed in Tables 6 and 7. Persons interested in obtaining additional computed values for the various other basis sets may do so by writing to one of the authors (RK).

Energy

The absolute and relative effects of GPF's on the energy have been fully discussed in a previous publication (3) but are summarized for convenience in Table 4. Here, it may be noted that the percentage effect on the energy of added *d* GPF's is relatively small, for example 0.04% for OH_2 and 0.01% for SH_2. Similarly, a *p* and a *f* GPF both have very small additional effects and the GPF's cause a monotonic convergence of the energy to the Hartree–Fock limit. The general preference for the addition of polarization functions is in the order $d > p > f$.

TABLE 5. Percentage[a] effects of *d*, *p*, and *f* Gaussian polarization functions on the calculated potentials $\langle 1/r \rangle$, electric fields $\langle 1/r^2 \rangle$, and field gradients $\langle 1/r^3 \rangle$ of sulfur and oxygen hydrides

Property	Basis set[b]	Species					
		OH^-	SH^-	OH_2	SH_2	OH_3^+	SH_3^+
		Values at the oxygen or sulfur nucleus					
$\langle 1/r \rangle$	*d*	0.04	0.01	0.02	0.02	−0.04	0.04
	p	−21	33	−97	15	121	14
	f	−118	92	57	−3	62	10
$\langle 1/r^2 \rangle$	*d*	91.70	40.71	90.02	46.24	129.77	43.16
	p	12	6	10	6	7	7
	f	6	0	5	0	5	0
$\langle 1/r^3 \rangle$	*d*	−7.98	−5.96	−5.42	−31.49	−4.28	17.35
	p	16	24	17	11	−53	13
	f	−11	160	170	−25	118	64
		Values at the hydrogen nucleus					
$\langle 1/r \rangle$	*d*	0.25	0.30	0.33	0.46	0.15	0.64
	p	85	44	68	37	162	30
	f	−18	−16	1	−2	8	2
$\langle 1/r^2 \rangle$	*d*	2.79	2.68	1.30	2.09	−2.79	2.14
	p	49	100	119	134	−73	134
	f	9	0	13	0	−12	0
$\langle 1/r^3 \rangle$	*d*	1.73	1.44	−7.91	−2.52	2.09	−9.55
	p	−27	25	−6	−33	−23	−46
	f	51	24	−21	−30	48	−9

[a]For a definition of percentage effect see text.
[b]Symbols *d*, *p*, and *f* refer to (*spd*|*s*), (*spd*|*sp*), and (*spdf*|*sp*) basis sets respectively.

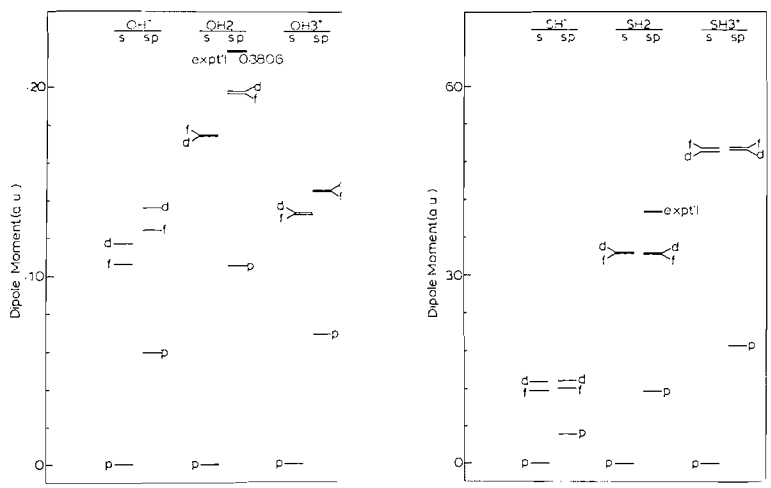

FIG. 2. The calculated dipole moments of oxygen and sulfur hydrides.

Dipole Moment

The absolute effect of GPF's on the calculated dipole moment is illustrated in Fig. 2 for the oxygen and sulfur hydrides respectively. The percentage effect of adding GPF's in order *d*, *p*, and *f* is given in Table 4. Whereas *d* GPF's had little effect on the energy this is not the case for the dipole moment. For example, the dipole moment changes by 13.36% for OH_2 and by 13.96% for SH_2. For the oxygen hydrides there is a small effect when a *p* GPF is added but a *f* GPF has relatively no effect. For the sulfur hydrides neither *p* nor *f* GPF's have significant effects on the calculated dipole moments. Figure 2 shows that for OH_2, addition of a *f* GPF to the (*spd*|*sp*) basis set will not cause any further convergence towards the experimental dipole moment (8). Similarly for SH_2, the addition of a *p* or *f* GPF will not cause any further convergence towards the experimental dipole moment (9). The poor agreement between the calculated and experimental dipole

Can. J. Chem. Downloaded from www.nrcresearchpress.com by 210.87.254.105 on 09/05/12
For personal use only.

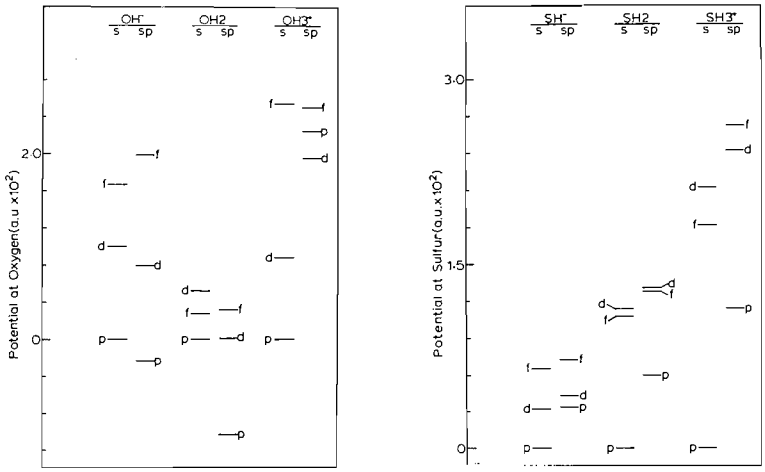

FIG. 3. The potential at the oxygen and sulfur nuclei as calculated with different basis sets.

TABLE 6. Nuclear components (au) of the one-electron properties for the oxygen and sulfur hydrides

Property	Components	CH^-	OH_2	OH_3^+	SH^-	SH_2	SH_3^+
Dipole moment	Z	1.8000	−2.4125	−1.2265	2.5000	−3.2167	−4.5047
Second moment	XX	0.0	0.0	4.6093	0.0	0.0	5.2580
	YY	0.0	3.5698	4.6093	0.0	6.3464	5.2580
	ZZ	2.0361	2.4434	0.3885	5.9562	4.7268	5.9163
Third moment	ZZZ	4.7187	−2.4471	−0.1198	14.1439	−6.9270	−7.7157
	XXX	0.0	0.0	−4.0399	0.0	0.0	−4.9221
	XXZ	0.0	0.0	−1.5849	0.0	−7.0720	−7.2147
	XYY	0.0	0.0	4.0399	0.0	0.0	4.9221
	YYZ	0.0	−3.8281	−1.5849	0.0	−9.6083	−7.2147
	RZ	4.7187	−6.2752	−3.2805	14.1439	−16.5352	−22.1452
Quadrupole moment	XX	−1.4681	−3.0066	2.1104	−2.9781	−5.5366	−0.3292
	YY	−1.4681	2.3482	2.1104	−2.9781	3.9830	−0.3292
	ZZ	2.9351	0.6584	−4.2208	5.9562	1.5536	0.0583
Octopole moment	ZZZ	4.7187	3.2951	4.6349	14.1439	7.4854	13.9285
	XXX	0.0	0.0	−10.0998	0.0	0.0	−12.3053
	XXZ	−2.3594	3.1376	−2.3174	−7.0720	8.2676	−6.9642
	YYX	0.0	0.0	10.0998	0.0	0.0	12.3053
	YYZ	−2.3594	−6.4327	−2.3174	−7.0720	−15.7530	−6.9642
Potential at O		0.5556	1.1111	1.6667	0.4000	0.8333	1.2500
Potential at H		4.4444	4.8157	5.1032	6.4000	6.9474	7.2834
Field gradient at A	XX	0.1715	0.3429	−0.2174	0.0640	0.1447	0.0189
	YY	0.0640	0.0944	0.0189	0.1715	−0.2238	−0.2174
	ZZ	−0.3429	−0.1191	0.4348	−0.1280	−0.0502	−0.0378
Field gradient at H	XX	1.3717	1.4242	−2.6205	1.0240	1.1795	1.1721
	YY	1.3717	−1.0002	1.3896	1.0240	−0.7997	−1.0290
	ZZ	−2.7435	−0.4240	1.2309	−2.0480	−0.3798	−0.1431
	YZ	0.0	2.0469	−0.9103	0.0	1.7271	1.6947
Electric field at A	Z	−0.3086	0.4137	0.2103	−1.600	0.2327	0.3259
	X	0.0	1.9727	−2.5925	0.0	2.1405	2.2317
Electric field at H	Z	2.4691	−1.6547	−0.5608	2.5600	−1.8615	−1.7379

moment in the case of OH_2 may be due to any one or all of the following reasons: poor (*sp*/*s*) basis sets, incorrect geometry, or electron correlation effects.

Second Moment

The relative effect of adding GPF in the order *d*, *p*, and *f* is given in Table 4. The effect of adding *d* GPF's is much smaller than for the dipole moment but again larger than for energy, for example 0.71% of OH_2 and 2.03% for SH_2. The effect of *d* GPF have a larger percentage effect for all hydrides, although somewhat exaggerated in an absolute sense by the small affect of a *d* GPF. Table 4 reveals for both OH_2 and SH_2 a convergence of the second moment except for the addition of *f* GPF to the (*spd*/*sp*) basis set, which causes a divergence. In

Can. J. Chem. Downloaded from www.nrcresearchpress.com by 210.87.254.105 on 09/05/12
For personal use only.

TABLE 7. Electronic components (au) of the one-electron properties of oxygen and sulfur hydrides as calculated with an (*spdf*/*sp*) basis set

Property	Component[a]	OH^-	H_2O	H_3O^+	SH^-	SH_2	SH_3^+
Dipole moment	*Z*	−1.3592	1.5007	0.6076	−2.3896	2.7478	3.6641
Second moment	*XX*	−6.2509	−5.4251	−6.3803	−13.5994	−12.2745	−13.1825
	YY	—	−6.9546	—	—	−15.3255	—
	ZZ	−7.8932	−6.5769	−4.9638	−17.4060	−14.8342	−14.1031
	⟨⟩	−20.3950	−18.9566	−17.7245	−44.6048	−42.4342	−40.4682
Third moment	*ZZZ*	−4.1660	1.4823	−0.1122	−16.2525	7.1062	7.2355
	XXX/*XXZ*	−0.0885	0.0223	1.6024	−0.3420	0.3376	3.7531
	XXZ/*YYZ*	—	2.2699	0.5874	—	8.6421	5.9983
	RZ	−4.3430	3.7745	1.0626	−16.9366	16.0859	19.2320
Quadrupole moment	*XX*	—	1.3407	—	—	2.8053	—
	YY	—	−0.9536	—	—	−1.7712	—
	ZZ	−1.6423	−0.3871	1.4165	−3.8065	−1.0341	−0.9206
	⟨⟩	−20.3950	−18.9566	−17.7245	−44.6048	−42.4342	−40.4682
Octopole moment	*ZZZ*	−3.9004	−1.9561	−1.8743	−15.2264	−6.3634	−10.7593
	XXX/*XXZ*	—	−1.8315	3.9988	—	−7.1990	9.3814
	XXZ/*YYZ*	—	3.7875	0.9372	—	13.5624	5.3796
Potential at A		−23.3535	−23.4506	−23.5508	−59.9899	−60.0474	−60.0858
Potential at H		−5.8679	−5.8214	−5.6894	−7.7454	−7.9696	−7.9789
Field gradient at A	*XX*	—	1.6221	—	—	2.5049	—
	YY	—	−1.3178	—	—	−2.2287	—
	ZZ	−1.7013	−0.3070	1.6140	−2.8931	−0.2924	1.6101
Asymmetry at A		0.0048	0.5663	0.0048	0.0159	0.7413	−0.0049
Field gradient at H	*XX*	—	−1.1198	2.1861	—	−0.9718	0.8764
	YY	—	0.7844	−1.1881	—	0.6656	−1.0089
	ZZ	2.1368	0.3354	−0.9940	1.7299	0.3061	0.1326
	XZ/*YZ*	—	−1.6668	−0.7464	—	−1.4707	−1.4497
Asymmetry at H		−0.0050	0.1325	0.1465	−0.0005	0.1477	0.0305
Electric field at A	*Z*	0.2284	−0.3110	−0.1472	0.1497	−0.2201	−0.3234
Electric field at H	*Z*	−2.4596	1.6612	0.5554	−2.5464	1.8260	1.7134
	X/*YZ*	—	−1.9490	−2.5631	—	−2.1029	−2.2648
Mulliken population	A	9.1729	8.6770	8.4526	16.9920	16.3878	16.0729
	H	0.8271	0.6615	0.5158	1.0080	0.8061	0.6424

[a]Components before the solidus refer to AH_3^+ species while components after the solidus refer to AH_2 species.

general the relative importance again appears to be in the order $d > p > f$.

Third Moment

From Table 4, the percent effect of adding *d* GPF's is generally greater for the third moment than it is for the second moment.

Overall, dipole, and third moments are the most affected while the second moment is least affected by the addition of GPF.

Potential, Electric Field, and Field Gradient at the Heavy Atom

The absolute effects of GPF on the potential as calculated at the heavy atom are illustrated in Fig. 3. The relative effects of adding GPF in the order *d*, *p*, and *f* are given in Table 5 for all of the above properties. The potential is almost invariant to the addition of GPF's. The reason for this invariance is that the potential operator ($\langle 1/r \rangle$) is part of the Hamiltonian and the wavefunction is initially designed to represent this property optimally. Figure 3 also illustrates the oscillatory convergence of the potential. There are no obvious rules for the order of addition, which varies from species to species.

Very large effects are observed for the calculated electric field on addition of a *d* GPF with 90.02% change for H_2O and 46.24% change for SH_2. The total force on the nuclei, like energy, decreases monotonically to the H–F limit of zero. As seen from Table 4, *p* and *f* GPF's have a significant additional effect on the net force on the nuclei for the oxygen hydrides but no significant effect on the sulfur hydrides. For oxygen hydrides the preferable order of addition is $d > p > f$ and for sulfur hydrides addition of a *d* GPF appears sufficient.

For field gradients, *d* GPF also have a large effect. For example, the effect is 5.42% for OH_2 and 31.49% for SH_2. As with electric field, *p* GPF have a minimal effect on field gradient, but this effect is somewhat larger than was the case for electric field. In addition it may be noted that *f* GPF have a substantial and unpredictable effect on the calculated field gradient. For example, the field gradient of OH_2 at the oxygen is increased by 17% on addition of a *p* GPF to an (*spd*/*s*) basis set but increased by 170% on

Can. J. Chem. Downloaded from www.nrcresearchpress.com by 210.87.254.105 on 09/05/12
For personal use only.

Can. J. Chem. Downloaded from www.nrcresearchpress.com by 210.87.254.105 on 09/05/12
For personal use only.

addition of an *f* GPF. For SH_2 the effect of a *p* GPF is plus 11% whereas the subsequent effect of a *f* GPF is −25%.

In summary, Table 4 shows that the general trend for the effect of *d* GPF is electric field ($\langle 1/r^2 \rangle$) greater than field gradient ($\langle 1/r^3 \rangle$) much greater than potential ($\langle 1/r \rangle$). This may be contrasted with the general trend dipole moment ($\langle r \rangle$) approximately equal to third moment ($\langle r^3 \rangle$) much greater than second moment ($\langle r^2 \rangle$) noted before.

Potential, Electric Field, and Field Gradients at the H Atom

It is generally expected that the addition of a GPF to a particular nuclear centre will affect a property calculated at another nuclear centre. As shown in Table 5, the relative effect of *d*, *p*, and *f* GPF's on the properties calculated at the sulfur or oxygen atoms is consistent with this expectation. However, the properties calculated at the hydrogen atom are generally more affected by the addition of a *d* GPF to sulfur or oxygen than by the addition of a *p* GPF to hydrogen. Only four exceptions may be noted: the potential for OH_3^+ and the electric field for OH_2, SH_2, and SH_3^+.

The general trend for the effect of a *d* GPF is electric field approximately equal to field gradient much greater than potential. As well, the potential at the hydrogen atom is more affected by the *d* GPF than was the potential at the sulfur or oxygen atom. This indicates that the *s* basis set for hydrogen atom is not as adequate as the *sp* basis set for the heavy atom and also agrees with previous studies on optimal basis sets (4, 10). The *f* GPF is of little importance for the calculation of potential or electric field at the hydrogen. Although, *f* GPF's contribute from one-third to one-half as much as *p* GPF's, *f* GPF's are of less importance here than they were in the calculation of field gradients at the heavy atom nucleus.

Conclusions

Energy

While the energy decreases monotonically as it must for the addition of GPF's to a given centre, GPF's should be added in the order *d*, *p*, and *f* for maximum effectiveness.

Convergence of One-electron Properties

Both Mulliken population and net force (electric field) have a predictable convergence behaviour. In a Mulliken population analysis, the charge flows to the centre where the GPF is added. The convergence pattern for the net force on the nuclei is monotonic and similar to the pattern observed for total energy.

Although the multipole moments (dipole, second, and third moments) do not converge in a monotonic manner, if the basis sets are considered in the order (*sp*/*s*), (*spd*/*s*), (*spd*/*sp*), and (*spdf*/*sp*) there is an observable pattern. For all neutral and anionic species the value of the moment either increases or decreases when proceeding through the series (*sp*/*s*), (*spd*/*s*), (*spd*/*sp*). The value then reverses slightly on addition of a *f* GPF to the (*spd*/*sp*) basis set. For cationic species, a similar pattern can be observed for the (*sp*/*s*) to (*spd*/*sp*) series but on addition of a *f* GPF the value continues to either increase or decrease as before. That is, the *f* GPF reinforces the effect of *d* and *p* GPF's for cationic species. These patterns indicate that GPF's have a tendency to increase the magnitude of the electronic component of the dipole moment which in turn indicates increased charge separation. Increased charge separation cannot be obtained from a Mulliken population analysis with certainty except when changing an (*sp*/*s*) basis set to an (*spd*/*sp*) basis set.

The other one-electron properties have an unpredictable convergence behaviour. For example, although the field gradients of OH^-, OH_2, and OH_3 are all increased on addition of a *d* GPF, the subsequent addition of a *p* GPF causes an increase for OH^- and OH_2 but a decrease for OH_3^+. The final addition of an *f* GPF causes an increase for OH_2 and OH_3^+ but a decrease for OH^-. In addition the sulfur hydrides display a pattern different from the above.

Effectiveness

In almost every case there is a substantially greater effect when adding a *d* GPF rather than a *p* GPF. This suggests that an (*spd*/*s*) basis set is both more effective and more efficient than an (*sp*/*sp*) basis set.

Addition of a *d* GPF to an (*sp*/*s*) basis set has a larger absolute effect on the sulfur hydrides than on the oxygen hydrides. However, these effects are similar in percentage terms.

Except for the calculated field gradients, *f* GPF's have a small effect on the calculated properties of neutral and positively charged species.

The effect on the calculated properties of anions is substantially greater. Previous studies (11, 12) on anionic species have shown that additional diffuse *s* and *p* basis functions have a marked effect on the energy of anionic species but only a minimal effect on the neutral or positively charged species. Hence, it has been concluded that diffuse *s* and *p* basis functions are required to adequately represent anions. Here, the additional effect of an *f* GPF on the anion properties is likely due to the lack of such diffuse functions rather than the intrinsic need for an *f* GPF. For neutral and positively charged molecules, there appears to be little obvious advantage to

including *f* GPF in the basis set. The addition of an *f* GPF to an (*spd*|*sp*) basis set of OH^- increases the number of integrals to be evaluated from 26 796 integrals for the (*spd*|*sp*) basis set to 123 256 integrals for the (*spdf*|*sp*) basis set. Taking into account that *f* integral computation is approximately twice as slow as *d* integral computation and considering that the addition of one *f* GPF increases the integral computation time for OH^- by 720%, there is little economic justification for using *f* GPF's.

In terms of balance, reliability, and effectiveness, the best basis set to use for either oxygen or sulfur hydrides is an (*spd*|*sp*) basis set. For sulphur hydrides, the (*spd*|*s*) basis set will give relatively good results except for Mulliken population. The (*sp*|*sp*) basis should never be used.

Acknowledgements

This work was financially supported by the National Research Council of Canada. One of us (R.P.) wishes to thank the National Research Council of Canada for a graduate scholarship.

1. S. GREEN. Adv. Chem. Phys. **25**, 179 (1974).
2. (*a*) D. NEUMANN and J. W. MOSKOWITZ. J. Chem. Phys. **49**, 2056 (1968); (*b*) B. ROOS and P. SIEGBAHN. Theor. Chim. Acta, **17**, 199 (1970); (*c*) S. ROTHENBERG, R. H. YOUNG, and H. D. SCHAEFFER. J. Am. Chem. Soc. **92**, 3243 (1970); (*d*) P. C. HARIHARAN and J. A. POPLE. Theor. Chim. Acta, **28**, 213 (1973); Mol. Phys. **27**, 209 (1974).
3. R. KARI and I. G. CSIZMADIA. Int. J. Quantum Chem. **11**, 441 (1977).
4. J. D. GODDARD, I. G. CSIZMADIA, P. G. MEZEY, and R. E. KARI. J. Chem. Phys. **66**, 3545 (1977).
5. R. KARI and I. G. CSIZMADIA. Can. J. Chem. **53**, 3747 (1975).
6. R. KARI and I. G. CSIZMADIA. J. Am. Chem. Soc. **99**, 4539 (1977).
7. R. S. MULLIKEN. J. Chem. Phys. **36**, 3428 (1962).
8. D. EISENBERG and W. KAUZMANN. The structure and properties of water. Oxford University Press, London. 1969.
9. A. L. MCLELLAN. Tables of experimental dipole moments. Freeman and Co., London. 1963.
10. P. G. MEZEY, R. E. KARI, and I. G. CSIZMADIA. J. Chem. Phys. **66**, 964 (1977).
11. B. WEBSTER. J. Phys. Chem. **79**, 2809 (1975).
12. J. PACANSKY, U. WAHLGREN, and P. S. BAGUS. J. Chem. Phys. **62**, 2740 (1975).

Can. J. Chem. Downloaded from www.nrcresearchpress.com by 210.87.254.105 on 09/05/12
For personal use only.

Thermodynamics of the salting effect; free energies, enthalpies, entropies, heat capacities, and volumes of the ternary systems electrolyte–alcohol–water at 25°C

GÉRALD PERRON, DANIEL JOLY, AND JACQUES E. DESNOYERS[1]

Department of Chemistry, Université de Sherbrooke, Sherbrooke (Qué.), Canada J1K 2R1

AND

LÉVON AVÉDIKIAN AND JEAN-PIERRE MOREL

Laboratoire des Interactions Soluté–Solvant, Université de Clermont, 63170 Aubière, France

Received August 15, 1977

GÉRALD PERRON, DANIEL JOLY, JACQUES E. DESNOYERS, LÉVON AVÉDIKIAN, and JEAN-PIERRE MOREL. Can. J. Chem. **56**, 552 (1978).

The thermodynamic pair interaction parameters of the ternary systems electrolyte (alkali halides and tetraalkylammonium bromides) – nonelectrolyte (*n*-alcohols and *tert*-butylalcohol) – water were measured at 25°C through enthalpies of solution, of mixing and of dilution, densities and heat capacities per unit volume. Some freezing point and electromotive force data were also combined with previously published data to obtain free energies. From these pair parameters the complete thermodynamics of the salting in and salting out of alcohols can be derived and were used to test various theoretical approaches. Most results are consistent with the cosphere overlap structural model, and the various trends can also be correlated through the scaled-particle theory.

GÉRALD PERRON, DANIEL JOLY, JACQUES E. DESNOYERS, LÉVON AVÉDIKIAN et JEAN-PIERRE MOREL. Can. J. Chem. **56**, 552 (1978).

Des mesures, effectuées à 25°C, d'enthalpie de dissolution, de mélange et de dilution, de densité et de capacité calorifique permettent le calcul des paramètres thermodynamiques d'interaction par paire dans les systèmes ternaires: électrolyte (halogénures alcalins, bromure de tétraalkylammonium) – non-électrolyte (alcools normaux et alcool *tert*-butylique) – eau. Certaines mesures d'abaissement du point de fusion et de force électromotrice conduisent, en utilisant des résultats déjà publiés, aux valeurs des enthalpies libres. Des paramètres d'interaction par paire, on peut déduire la thermodynamique complète du relargage des alcools et vérifier diverses théories. Les résultats proposés sont en accord avec ceux prévus par le modèle structural de recouvrement des cosphères d'hydratation. L'allure des variations des différentes grandeurs peut aussi être prédite par la théorie des particules calibrées (scaled particle).

Introduction

Electrolytes are known to modify the properties of nonelectrolytes in water. An example of this is the familiar salting effect. The several reviews (1–3) written in the last 25 years illustrate the large quantity of data that has been cumulated on this topic. Still, our understanding of these phenomena is far from satisfactory, and recently a number of vastly different theoretical approaches have been proposed with the claim that they can account at least semi-quantitatively for the experimental data (4).

The main difficulty with our understanding of the interactions between electrolytes and nonelectrolytes is that most investigations have been limited to free energies. Other thermodynamic properties can readily be obtained provided the nonelectrolytes are sufficiently soluble for direct measurements. This excludes most gases and alkanes, but alcohols are usually considered good substitutes in view of the similarity of the OH group with water.

Any property which measures the activities of the electrolyte, of the nonelectrolyte, or of water can be used in principle to determine the non-ideal free energies. For example, freezing point (4, 5) electromotive forces (6, 7), vapor pressures (8, 9), and distribution (10) measurements have all been used successfully to study ternary aqueous systems.

The purpose of the present study is to report enthalpies, heat capacities, and volumes of alcohols with alkali halides and tetraalkylammonium bromides in water. Some free energy data were also measured and combined with previously published data. The complete thermodynamics of the interactions between typical nonelectrolytes and electrolytes could then be derived.

Theoretical Relations

The usual way of expressing thermodynamic properties of ternary systems is in terms of transfer functions. For any function F the transfer of a nonelectrolyte N from pure water W to an electrolyte E solution can be expressed as $\Delta F_N(W \rightarrow W + E)$. If the component N is in the standard state (hypothetical ideal 1 mol kg^{-1} or infinite dilution), we

[1]To whom all correspondence to be addressed.

Can. J. Chem. Downloaded from www.nrcresearchpress.com by 210.87.254.42 on 09/05/12
For personal use only.

Can. J. Chem. Downloaded from www.nrcresearchpress.com by 210.87.254.42 on 09/05/12
For personal use only.

refer to standard transfer functions. In the particular case of free energies the standard function is related to the salting constant k_S by

$$[1] \qquad \Delta G_N^0(W \rightarrow W + E) = RTk_S m_E$$

provided the molality m_E of the electrolyte is relatively low (4). The factor 2.303 is usually added on the right-hand side of eq. 1.

To generalize to all thermodynamic functions it is advantageous to use a virial expansion in m (11–15) which related the non-ideal contribution of any total thermodynamic function to a series of pair (f_{NE}, f_{NN}, f_{EE}), triplet (f_{NNN}, f_{NNE}, ...), and higher order interaction parameters. For a transfer function it can readily be shown that

$$[2] \quad \Delta F_N(W \rightarrow W + E) = 2\nu f_{NE} m_E + 3\nu^2 f_{NEE} m_E^2 + 3\nu f_{NNE} m_E m_N + \ldots$$

where m_E and m_N are the molalities defined per kg of pure water and ν is the number of ions into which E dissociates. In many instances ν is included in the interaction parameters. For simplicity in deriving the equations E is not separated into its ionic components. A similar equation can be written for the converse transfer function,

$$[3] \quad \Delta F_E(W \rightarrow W + N) = 2\nu f_{NE} m_N + 3\nu f_{NNE} m_N^2 + 3\nu^2 f_{NEE} m_N m_E + \ldots$$

For standard functions the higher terms in m_N or m_E on the right-hand side of eqs. 2 and 3 vanish, and the limiting slopes of the standard transfer function, $2\nu f_{NE}$, must be identical for the two converse functions. This has been verified experimentally (16). For free energies it immediately follows from eqs. 1 and 2 that

$$[4] \qquad RTk_S = 2\nu g_{NE}$$

The pair and triplet interaction parameters are all readily measurable experimentally for any thermodynamic function. Most of the free energy data were obtained from the freezing point depression θ for the ternary and binary systems (4, 5) using the expression

$$[5] \quad \frac{RT\{\theta(m_N, m_E) - \theta(m_N) - \theta(m_E)\}}{1.858 m_N m_E} = 2\nu g_{NE} + \text{terms in } m_N \text{ and } m_E$$

or from the emf of a cell using a specific ion glass cathode and a silver – silver halide anode as described by Pointud *et al.* (7). In this latter technique the emf is measured for the electrolyte in water and also after the addition of N. Then it follows that the standard emf variation ΔU^0 is given by

$$[6] \quad -\mathcal{F}\Delta U^0/m_N = \Delta G_E^0(W \rightarrow W + N)/m_N = 2\nu g_{NE} + 3\nu g_{NNE} m_N + \ldots$$

where $\mathcal{F}$ is the Faraday.

For enthalpies, the parameters are derived either from enthalpies of solution or enthalpies of mixing and of dilution (15). In the first instance standard enthalpies of transfer are calculated from the standard enthalpies of solution of the solute in the binary mixture and in pure water;

$$[7] \quad \Delta H_N^0(W \rightarrow W + E)/m_E = 2\nu h_{NE} + 3\nu^2 h_{NEE} m_E + \ldots$$

and

$$[8] \quad \Delta H_E^0(W \rightarrow W + N)/m_N = 2\nu h_{NE} + 3\nu h_{NNE} m_N + \ldots$$

With the second technique, solutions in pure W, initially at molalities m_N and m_E, are mixed and the final molalities are $d_N m_N$ and $d_E m_E$, where d_N and d_E are the dilution ratios (d_N is equal to the weight of W in the initial solution of N divided by the weight of W in the final solution). From the enthalpy of mixing ΔH_M, expressed in J per kg of W in the final mixture, and the corresponding integral enthalpies of dilution of both components it follows that

$$[9] \quad \left\{\Delta H_M\begin{pmatrix} m_N \rightarrow d_N m_N \\ m_E \rightarrow d_E m_E \end{pmatrix} - d_N m_N \Delta H_N(m_N \rightarrow d_N m_N) - d_E m_E \Delta H_E(m_E \rightarrow d_E m_E)\right\} \Big/ d_N d_E m_N m_E = 2\nu h_{NE} + 3\nu h_{NNE} m_N + 3\nu^2 h_{NEE} m_E + \ldots$$

For volumes and constant pressure heat capacities the parameters are given by the apparent molal quantities at low m_N in the ternary and binary systems (17, 18);

$$[10] \quad \{\phi_{V_N}(m_E, m_N) - \phi_{V_N}(m_N)\}/m_E = 2\nu v_{NE} + 3\nu^2 v_{NEE} m_E + \ldots$$

and

$$[11] \quad \{\phi_{C_N}(m_E, m_N) - \phi_{C_N}(m_N)\}/m_E = 2\nu c_{NE} + 3\nu^2 c_{NEE} m_E + \ldots$$

Similar equations can be written for the apparent molal quanities of E in solution of W + N.

The pair interaction parameters are related to each other in the usual way. Assuming c_{NE} to be independent of temperature, the enthalpic pair parameter at temperature T is given by

$$[12] \qquad h_{NE}^T = h_{NE}^{T_0} + c_{NE}(T - T_0)$$

Can. J. Chem. Downloaded from www.nrcresearchpress.com by 210.87.254.42 on 09/05/12
For personal use only.

where T_0 is a reference temperature, usually 298.15 K. From the Gibbs–Helmholtz equation it also follows that the free energy parameter $g_{NE}{}^T$ at any temperature is given by

$$[13] \quad g_{NE}{}^T = (T/T_0)g_{NE}{}^{T_0} + \frac{T_0 - T}{T_0} h_{NE}{}^{T_0} - \left\{T_0 - T + T \ln \frac{T}{T_0}\right\} c_{NE}{}^{T_0}$$

Depending on the units of $c_{NE}{}^{T_0}$ the last term of eq. 13 is sometimes divided by T_0. Similarly the value of $g_{NE}{}^P$ at any pressure is given by

$$[14] \quad g_{NE}{}^P = g_{NE}{}^{P_0} + v_{NE}(P - P_0)$$

For a large range of pressures, compressibility parameters would also have to be considered. From a knowledge of $g_{NE}{}^T$ and $g_{NE}{}^P$ and eq. 4, the salting constant can be calculated over a large range of temperature or pressure (5). From the parameters g_{NE} and h_{NE} it is also straightforward to obtain the entropies,

$$[15] \quad s_{NE} = (h_{NE} - g_{NE})/T$$

Experimental

The procedure for the measurement of free energies has been described elsewhere (4, 7). The freezing point technique is in general quite reliable for differential measurements (4) but can lead to larger uncertainties with *n*-pentyl alcohol. This alcohol has a strong tendency to unmix especially in the presence of NaCl and it was hard to reproduce the freezing temperatures. In addition triplet interactions become important at relatively low concentrations with the long-chain alcohols, and again this may lead to larger uncertainties in the determination of g_{NE}.

Enthalpies have been measured with an LKB precision calorimeter and a flow microcalorimeter as described elsewhere (15). In the heat of mixing technique corrections have to be made for enthalpies of dilution of both binary systems. In general this presented no difficulty and the parameter h_{NE} was determined with reasonable precision. For alcohols the heats of dilution were remeasured but for the electrolytes literature values were used (22, 23). With a few alkali halides the heat of dilution had not been measured previously in our laboratory and it was more difficult to estimate the uncertainty on these literature data. The largest uncertainty arises with the large alcohols and R_4NBr since here the corrections for the enthalpies of dilution become quite important. Still, as it will be shown in the next section, the agreement with the enthalpy of solution method is in general quite satisfactory.

The volumes and heat capacities (19–21) presented no special problem. In all cases the densities and heat capacities per unit volume were repeated for the corresponding binary systems to minimize sources of errors. In all cases where data on the binary systems were available in the literature the agreement of the new data was within the experimental error.

The origin and purification of chemicals and general procedure for the preparation of solutions have all been given elsewhere (4, 5, 7, 24, 25).

Results

In this study on ternary aqueous sytems the chosen nonelectrolytes were alcohols and the electrolytes were alkali halides and tetraalkylammonium bromides. For *tert*-butylalcohol (TBA) the effect of additivity of the pair parameters and the effect of ionic size were investigated. With NaCl the effect of nonelectrolyte size was examined. The following solutes were therefore used: alkali chlorides (MCl), KI, KBr, sodium halides (NaX), the five first symmetrical tetraalkylammonium bromides (R_4NBr), the first five normal alcohols (ROH) and TBA.

The free energies obtained from freezing point data (4, 5), electromotive force (6, 7), and distribution studies at 20°C (10) are compared in Table 1. The parameters g_{NE} at the freezing point were corrected to 298.15 K with eq. 13. Some discrepancy was observed between the different sets of data, especially with RbCl and CsCl. These measurements were repeated by both techniques[2] (freezing point and emf) and the differences essentially disappeared. The only disagreement remaining which is probably larger than the experimental uncertainty is with NaCl and NaBr. Although they were repeated g_{NE} still differ by 40 J mol^{-2} kg. However, the trends in g_{NE} with ionic size are hardly affected by this difference.

The enthalpies of mixing[2] were determined for variable m_N and m_E in the range 0.1 to 1 mol kg^{-1}. For most systems the enthalpies of transfer of both N and E were measured for the same concentration range of the variable component. Some examples of the function $\Delta H^* = 2v h_{NE} + 3v h_{NNE} m_N + 3v^2 h_{NNE} m_E + \ldots$ are shown in Fig. 1 for the enthalpies of mixing and enthalpies of solution. The agreement is quite good considering that with the enthalpies of solution one of the components is at a much lower concentration than in the mixing experiments. Both sets of data were analysed separately. The enthalpies of transfer were assumed to be standard values (final concentration is of the order of 0.01 mol kg^{-1}) and the pair parameters were obtained through a least-squares treatment using eq. 7 or eq. 8. For the mixing data the function ΔH^* was treated by least-squares using a function of the type $Z = a + bx + cy$. The parameters h_{NE}, given in Table 1 for both sets of data, are in excellent agreement. On the other hand the agreement is less satisfactory for the triplet interaction parameters derived from both approaches and in some cases even the signs are different. These

[2]Complete set of the actual experimental data is available, at a nominal charge, from the Depository of Unpublished Data, CISTI, National Research Council of Canada, Ottawa, Ont., Canada K1A 0S2.

Can. J. Chem. Downloaded from www.nrcresearchpress.com by 210.87.254.42 on 09/05/12
For personal use only.

TABLE 1. Pairs interactions parameters for ternary systems at 25°C

		g_{NE} (J mol^{-2} kg)		h_{NE} (J mol^{-2} kg)		Ts_{NE}	c_{NE}	v_{NE}
E	N	F.P.	EMF	ΔH_M	ΔH_{IS}	(J mol^{-2} kg)	(J K^{-1} mol^{-2} kg)	(cm^3 mol^{-2} kg)
LiCl	TBA	223	214	302[f]	312	79	-8.7_5	-0.17_5
NaCl		310	275	483[f]	490	173	−10.5	−0.10
KCl		279	284	468[e]	450	189	−9.5	−0.11
RbCl		258	267	477[e]	433[c]	194	−11.0	-0.02_5
CsCl		249	254	493[e]	485[c]	247	−11.3	-0.03_5
NaF		384		502[f]		118	-7.7_5	−0.12
NaBr		266	226	501[e]		235	−11.2	−0.05
NaI		161	169	711[f]		550	−14.0	0.02_5
KBr		235	234	555[e]	500	320	−10.5	-0.05_5
KI			180		633			
Me_4NBr		−94			480	574	−13.2	−0.50
Et_4NBr		−147		805[d]		1088	−13.5	-1.1_5
Pr_4NBr		−170		1420[d]		1590	−1.5	-1.7_5
Bu_4NBr		−227			2340	2567	6.0	−2.0
Pen_4NBr		−281		3280[d]		3561	17.5	−2.3
NaCl	MeOH	99	94[a]	175	150	76	−3.5	-0.12_5
	EtOH	173	168	326	290	153	−6.0	−0.05
	PrOH	211	236	368	370	157	−7.0	0
	n-BuOH	254	266[b]	404	356[b]	150 (90[b])	−7.5	−0.05
	n-PenOH	265	292[b]	450	428[b]	185 (136[b])		

[a]Wilcox and Schrier (6).
[b]Aveyard and Heselden (10) corrected to 25°C.
[c]Values at 5% in TBA.
[d]Values for $m_E \approx 0.05$ *m*.
[e]Enthalpies of dilution from Parker (23).
[f]Enthalpies of dilution from Fortier *et al.* (22).

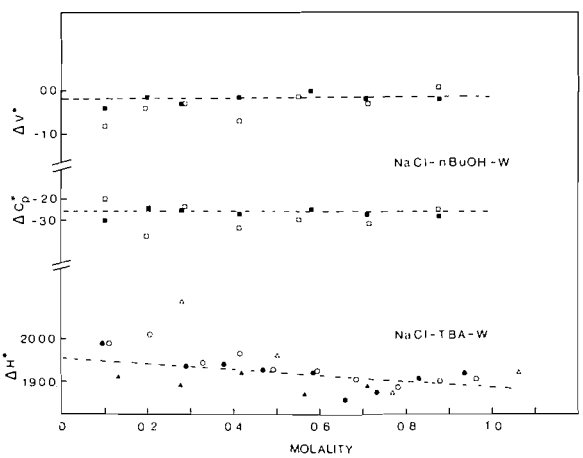

FIG. 1. Dependence of the functions $\Delta F^* = 2vf_{NE} + 3vf_{NNE}m_N + 3vf_{NEE}m_E + \ldots$ on m_N and m_E at 25°C: □, *n*-BuOH in NaCl (variable component); ■, NaCl in *n*-BuOH; ○, mixing of NaCl with TBA, NaCl variable; ●, mixing of NaCl with TBA, TBA variable; △, enthalpies of solution of TBA in NaCl; ▲, enthalpies of solution of NaCl in TBA.

parameters are in general small and are associated with a large uncertainty. All we can say at this stage is that h_{NNE} is zero or negative with all the systems investigated while h_{NEE} are also small but sometimes positive and sometimes negative.

The volumes and heat capacities were measured for a fixed m_N (0.25 mol kg^{-1}) and a variable m_E between 0.1 to 1 mol kg^{-1}. It has been verified that under these conditions the triplet terms $3vv_{NNE}m_N$ and $3vc_{NNE}m_N$ contribute little to the overall data. Examples of the functions $\Delta V^* = 2vv_{NE} + 3v^2v_{NEE}m_E + \ldots$ and $\Delta C^* = 2vc_{NE} + 3v^2c_{NEE}m_E + \ldots$ are shown in Fig. 1. The original data for densities and heat capacities per unit volume are also available elsewhere.[2] The pair interaction parameters obtained from a least-squares fit are given in Table 1. The entropic pair parameters derived from g_{NE} and h_{NE} using eq. 15 are also given in Table 1.

The pair parameters should, by definition, be additive for various ionic pairs. The additivity test was verified for g_{NE} at the freezing temperature elsewhere (4). The values from emf measurements also show very good additivity although the differences between various pairs are slightly different for both sets of data. The parameters h_{NE}, v_{NE}, and c_{NE} show little ionic size dependence and the differences between pairs are therefore rather small. Still the additivity test, combined with a comparison of parameters obtained by various techniques, serves as an indication of the accuracy of the parameters: g_{NE}, ±20 J mol^{-2} kg; h_{NE}, ±20 J mol^{-2} kg; v_{NE}, ±0.05 cm^3 mol^{-2} kg; c_{NE}, ±1 J K^{-1} mol^{-2} kg.

Can. J. Chem. Downloaded from www.nrcresearchpress.com by 210.87.254.42 on 09/05/12
For personal use only.

Discussion

It was shown that the salting out (4) and salting in (5) of alcohols by alkali halides and tetraalkylammonium bromides follow the same general pattern as typical nonelectrolytes such as benzene or alkanes. It is therefore reasonable to expect that the trends observed with all the thermodynamic parameters will be similar to those of nonpolar nonelectrolytes.

The pair parameters for the NaCl–ROH–W system are plotted against the standard partial molal volumes of the alcohols $\bar{V}^0_{ROH}$ (26) in Fig. 2. Inside the experimental uncertainty all the parameters are linear function of $\bar{V}^0_{ROH}$ of normal alcohols and pass through the origin. This is the kind of behavior we would expect from the McDevit and Long theory (1). Electrostatic type theories (3) and the scaled-particle theory (6, 27–29) also predict a strong dependence on the size of the nonelectrolyte but the functions do not necessarily pass through the origin. The data for TBA or *n*-PenOH are slightly out of line. It could be that a better linear function exists with the $\bar{V}^0$ of MeOH, EtOH, *i*-PrOH, TBA, etc. but the uncertainty on the data is too large to prove this.

The pair parameters for the system MCl–TBA–W, NaX–TBA–W, and R_4NBr–TBA–W are given as a function of the cationic and anionic size in Fig. 3; g_{NE}, h_{NE}, and Ts_{NE} are not shown for NaX for clarity of presentation. The data points for the variable anions are very similar to the cationic size dependence. While g_{NE} shows a significant ionic size dependence, becoming negative with the R_4NBr, the other parameters shown relatively little size dependence with the alkali halides. On the other hand, h_{NE}, c_{NE}, and v_{NE} show a very large dependence on the cationic size of R_4NBr. These trends are remarkably similar to the transfer functions of electrolytes from water to urea–water (U + W) mixtures and to D_2O (D) (30–36). These transfer functions are also rather insensitive to the ionic size with alkali halides (except with Li^+ and I^- which are usually out of line) and very dependent on the size of the R_4NBr. The simplest way of seeing the similarities and differences between these functions is to compare the pair parameters for TBA and U with the transfer functions $\Delta F^0_E(W \rightarrow D)$ for the three electrolytes NaCl, Me_4NBr, and Bu_4NBr; pair interaction parameters were derived from the transfer functions $\Delta F^0_E\{W \rightarrow W + U)$.

It is interesting to compare these three systems since TBA is usually considered a typical hydrophobic structure maker, U a structure breaker, and D_2O more structured than H_2O, at least at low temperatures.

The first observation we can make from the data in Table 2 is that for all alkali halides the sign of the

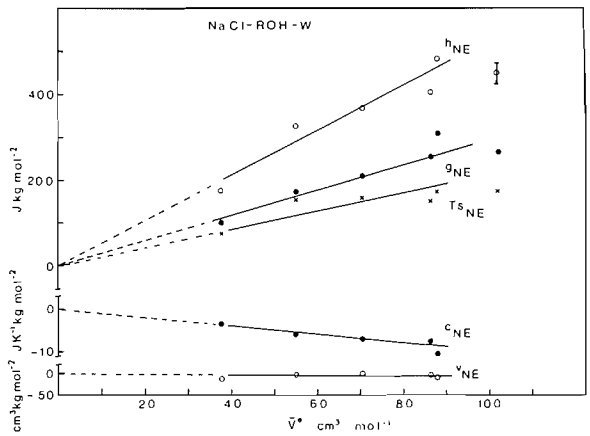

FIG. 2. Dependence of pair functions of NaCl on the standard partial molal volumes of the alcohols.

pair parameters f_{NE} for TBA are always opposite f_{NE}(U) and of the same sign as $\Delta F^0_E(W \rightarrow D)$. This is also true for Me_4NBr for all the properties except for the parameter g_{NE}(TBA) which is slightly negative. The situation is more complex with Bu_4NBr (and the other large R^4NBr). The parameters v_{NE}(TBA) and c_{NE}(TBA) are again opposite those for U and the same as $\Delta V^0_E(W \rightarrow D)$ and $\Delta C^0_E(W \rightarrow D)$. Such relations do not exist with free energies, enthalpies, and entropies; h_{NE}(TBA) and s_{NE}(TBA) now have the same sign as U and opposite sign to the transfer functions to D_2O, and g_{NE}(TBA), g_{NE}(U), and $\Delta G^0_E(W \rightarrow D)$ are all negative.

Although h_{NE} and s_{NE} for the systems TBA–Bu_4NBr and U–Bu_4NBr have the same sign, they are not reflecting similar interactions. It was shown (36) that $\Delta H^0_{Bu_4NBr}(W \rightarrow W + U)$ decreases rapidly with temperature and probably changes sign above 50°C. The opposite was observed with $\Delta H^0_{Bu_4NBr}(W \rightarrow D)$ and $\Delta S^0_{Bu_4NBr}(W \rightarrow D)$. On the other hand, the temperature dependence of h_{NE} can readily be calculated from eq. 12 and, as seen from Fig. 4, it increases significantly with temperature with the more hydrophobic R_4NBr. If the temperature dependences of c_{NE} were known, h_{NE} would most probably show some curvature as a function of temperature.

It is relatively easy to find a model or theory that can account for the sign, magnitude, and trends if only one property and one chemical system is examined. It is much more difficult to find such a model or theory if we try to account for all the thermodynamic properties with typical hydrophobic and hydrophilic, ionic and non-ionic solutes.

The parameters f_{NE} represent the contribution to the thermodynamic function F when the two solutes N and E approach each other from infinity to some critical distance. Contributions will arise from inter-

Can. J. Chem. Downloaded from www.nrcresearchpress.com by 210.87.254.42 on 09/05/12
For personal use only.

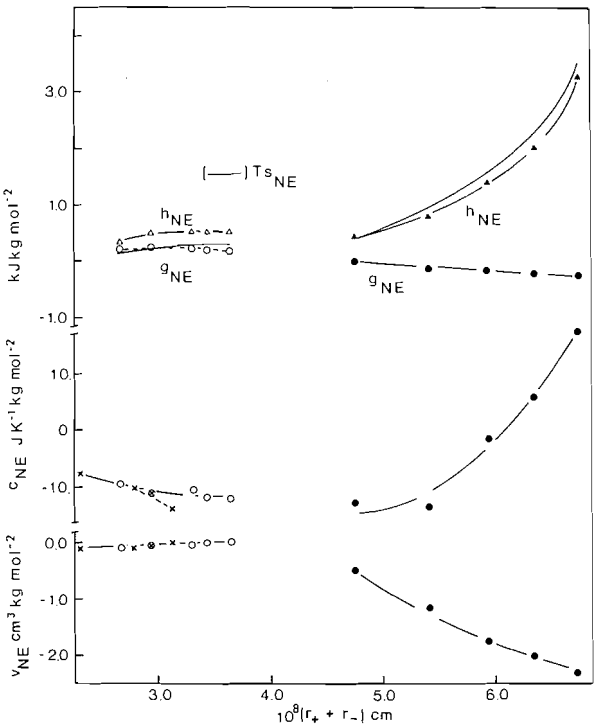

FIG. 3. Dependence of pair functions of TBA on the sum of ionic radii: △ and ○, MBr; ×, NaX; ▲ and ●, R_4NBr; data not shown for the NaX with g_{NE}, h_{NE}, and Ts_{NE} (see text).

actions such as charge-dipole, polarization, and dispersion forces and also from modification of the solute–solvent interactions.

Most electrostatic theories of the salting effect can explain reasonably well the dependence of g_{NE} or k_S on the charge and size of the ions and on the size and polarity of the nonelectrolytes (1–3). However, they fail to account for the salting in by R_4NBr (5) of solutes which lower the relative permittivity of the solvent and which are salted out by inorganic salts. They also generally fail to account for the trends, magnitude, and sometimes even the sign of the other functions, h_{NE}, s_{NE}, v_{NE}, and c_{NE}. The probable explanation for this failture is that while electrostatic interactions may be the leading contribution to g_{NE}, these interactions do not vary significantly with temperature and pressure. On the other hand, structural hydration interactions (related to the modification of the overall solute–solvent interactions) do not have a large contribution to g_{NE} or k_S but, being quite temperature dependent, rapidly becomes the leading effect with the other functions.

The concept of structural interactions, introduced by Frank and Robinson (37) in 1940, has been used successfully by many authors to explain the anomalous concentration dependence of thermodynamic functions of electrolytes in water (24, 38). The same

TABLE 2. Comparison of pair interaction parameters and transfer functions from H_2O to D_2O at 25°C

Compound	g_{NE}(TBA)	g_{NE}(U)	$\Delta G_E(W \rightarrow D)$	h_{NE}(TBA)	h_{NE}(U)	$\Delta H_E(W \rightarrow D)$	Ts_{NE}(TBA)	Ts_{NE}(U)	$T\Delta S_E(W \rightarrow D)$
NaCl	310	−123[a]	(+)[a]	483	−632[a]	(+)[a]	173	−504[a]	(+)[a]
Me_4NBr	−94	−310[b]	(+)[a]	475	−820[c]	(+)[a]	479	−513[c]	(+)[a]
Bu_4NBr	−186	−347[b]	(−)[a]	2340	975[c]	(−)[a]	2567	1324[c]	(−)[a]

Compound	v_{NE}(TBA)	v_{NE}(U)	$\Delta V_E(W \rightarrow D)$	c_{NE}(TBA)	c_{NE}(U)	$\Delta c_E(W \rightarrow D)$
NaCl	−0.10	0.34[e]	−0.87[f]	−10.5	8.6[e]	−40[f]
Me_4NBr	−0.50	0.17[g]	−0.44[g]	−13.2	4.5[g]	−22.7[g]
Bu_4NBr	−2.0	0.18[g]	−0.90[g]	6.0	−25.3[g]	29.3[g]

[a]Schrier *et al.* (30).
[b]Wen and Chen (31).
[c]Cassel and Wen (32).
[d]Friedman and Krishnan (33).
[e]Desrosiers *et al.* (34).
[f]Fortier *et al.* (35).
[g]Perron *et al.* (36).

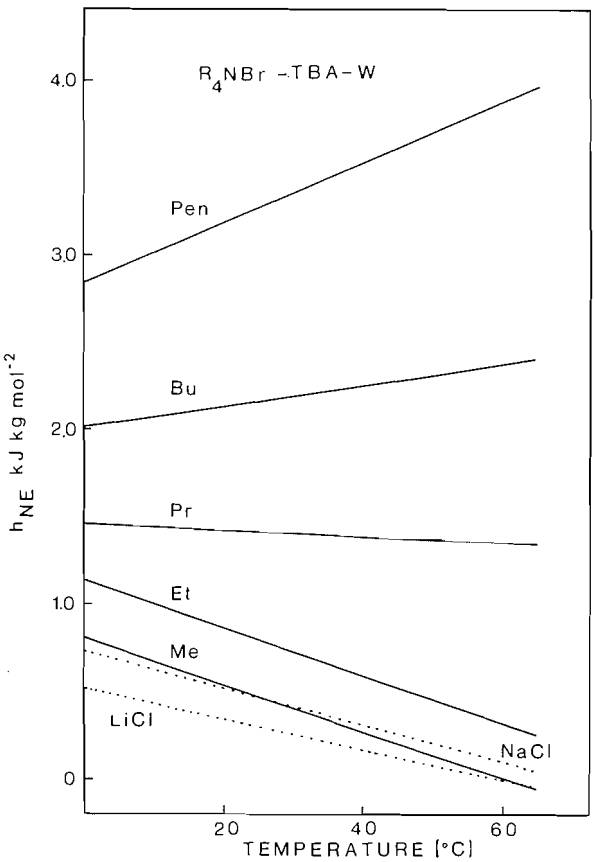

FIG. 4. Dependence of h_{NE} for the systems R_4NBr–TBA–W on temperatures.

idea was used to interpret salting in by R_4NBr (39), the transfer functions of electrolytes to TBA–W mixtures (17) and to U–W mixtures (30). For example h_{NE} for the two hydrophobic solutes Bu_4N^+ and TBA will have the same sign as the pair parameters h_{NN} and h_{EE} (obtained from enthalpies of dilution) since they are all reflecting hydrophobic–hydrophobic interactions. This explains why h_{NE} has a sign different from $\Delta H^0_E(W \rightarrow D)$ since this latter function is reflecting differences in solute–solvent interactions. A general discussion of these structural interactions is given elsewhere (18). The signs of all the pair parameters can be explained with this approach. In most cases, the overlap of the cospheres are destructive in that the net effect is the reduction of the hydration contribution of both solutes. Pair functions related to second derivatives of the free energy (heat capacities, expansibilities, and compressibilities) are more complicated in that they cannot be accounted for with a simple destructive overlap approach; new interactions must be called upon.

Friedman and co-workers (38, 40) have treated structural interactions quantitatively by introducing a contribution (Gurney term) to the potential of average force, from which the solute pair correlation function is obtained, using the hypernetted chain equation. Franks and co-workers (41, 42) have extended this approach to mixtures of alcohols and their results are not inconsistent with the existence of some cooperative effects. Unfortunately there is at present no way of predicting the Gurney terms which must be derived from the experimental data. While this is a small term with excess free energies of electrolyte solutions, it becomes the leading term with excess heat capacities of R_4NBr (43) and with ternary systems (40). Therefore, although the statistical thermodynamic theories in terms of a potential of average force between the solute molecules is the logical approach to account for the pair interaction parameters, these theories are not very useful at present since we cannot predict from basic principles the Gurney terms.

The most successful theories for the prediction of the pair interaction parameters are, probably at present, those based on a thermodynamic approach. McDevit and Long (1) have related the salting out effect to the energy necessary to create a cavity in a medium characterized by ion–solvent interactions. This theory has been refined recently by Cross (44), and it can account for the salting out of various nonelectrolytes up to very concentrated KOH solutions. However, this theory fails to account for salting in by R_4NBr (5), and it is also difficult to extend it to thermodynamic functions other than free energies.

The scaled-particle theory (SPT), as applied to aqueous systems by Pierotti (45), was shown to account for the salting out and salting in of gases (27, 28), and of alcohols (6, 10) and for the temperature dependence of the salting effect (5, 29). Using reasonable values for the size parameters, Philip and Jolicoeur (46) have shown that this theory explains most of the transfer functions of R_4N^+ from H_2O to D_2O and Desrosiers and Desnoyers (47) applied it to the transfer functions of Bu_4N^+ from water to TBA–W and U–W mixtures. In all cases the agreement with experiment is amazingly good. In this approach the thermodynamic functions are calculated in three steps: formation of a cavity in the solution, transfer of the solute in the cavity, and interaction of the solute with the molecules in the solvent. For g_{NE} and h_{NE} the interaction terms are important but for the other functions the cavity term rapidly becomes the leading one.

The SPT is probably the only theory which can predict nearly quantitatively the pair interaction parameters and many transfer functions over a large concentration range of cosolvent for polar and nonpolar nonelectrolytes, for simple and hydrophobic

Can. J. Chem. Downloaded from www.nrcresearchpress.com by 210.87.254.42 on 09/05/12
For personal use only.

Can. J. Chem. Downloaded from www.nrcresearchpress.com by 210.87.254.42 on 09/05/12
For personal use only.

electrolytes, and for all thermodynamic functions. Still this theory is not ideal and can be criticized on many aspects. It is very sensitive to the choice of the molecular diameters of the various components and the interaction energy parameters required are not always easy to evaluate. However, the main drawback of this theory is that the experimental mixed-solvent density is introduced to account for the attractive forces in the system, and, as a result, much of the information on solute–solvent and solute–solute interactions is lost in the process. The SPT is therefore more of a correlation device between thermodynamic properties of ternary and binary solutions (g_{NE} is related to the apparent molal volume ϕ_V of the electrolyte solution, h_{NE} to the apparent molal expansibility ϕ_E, and c_{NE} to $d\phi_E/dT$), and sometimes the binary data ($d\phi_E/dT$) might be more difficult to measure than the ternary data (c_{NE}).

The thermodynamic theory based on surface tension (10) is also successful but f_{NE} are not correlated to factors that are readily accessible and such an approach again does not give us much insight on the interactions on the molecular level.

Acknowledgements

The authors are grateful to the National Research Council of Canada, to the Quebec Ministry of Education, and to the Centre National de la Recherche Scientifique (France) for financial assistance and for the award of a travel fellowship to one of us (G.P.).

1. F. A. Long and W. F. McDevit. Chem. Rev. **51**, 119 (1952).
2. V. F. Sergeeva. Russ. Chem. Rev. **34**, 309 (1965).
3. B. E. Conway and D. M. Novak. Chemistry and physics of aqueous gas solutions. *Edited by* W. A. Adams. The Electrochemical Society, Princeton, NJ. 1975. p. 115.
4. J. E. Desnoyers, M. Billon, S. Léger, G. Perron, and J.-P. Morel. J. Solution Chem. **5**, 681 (1976).
5. J. E. Desnoyers, G. Perron, S. Léger, B. Y. Okamoto, T. N. Lilley, and R. H. Wood. J. Solution Chem. In press.
6. F. L. Wilcox and E. E. Schrier. J. Phys. Chem. **75**, 3757 (1971).
7. Y. Pointud, J. Juillard, J.-P. Morel, and L. Avédikian. Electrochim. Acta, **19**, 229 (1974).
8. H. Uedaira. Bull. Chem. Soc. Jpn. **45**, 3068 (1972).
9. C. Treiner. J. Chim. Phys. **70**, 1183 (1973).
10. R. Aveyard and R. Heselden. J. Chem. Soc. Faraday Trans. I, **70**, 1953 (1974); **71**, 312 (1975).
11. J. J. Kozak, W. S. Knight, and W. Kauzmann. J. Chem. Phys. **48**, 675 (1968).
12. H. L. Friedman and C. V. Krishnan. J. Solution Chem. **2**, 2460 (1973).
13. R. B. Cassel and R. H. Wood. J. Phys. Chem. **78**, 2465 (1974).
14. F. Franks, M. Pedley, and D. S. Reid. J. Chem. Soc. Faraday Trans. I, **72**, 359 (1976).
15. J. E. Desnoyers, G. Perron, L. Avédikian, and J.-P. Morel. J. Solution Chem. **5**, 631 (1976).
16. J. E. Desnoyers, G. Perron, J.-P. Morel, and L. Avédikian. Chemistry and physics of aqueous gas solutions. *Edited by* W. A. Adams. The Electrochemical Society, Princeton, NJ. 1975. p. 172.
17. L. Avédikian, G. Perron, and J. E. Desnoyers. J. Solution Chem. **4**, 331 (1975).
18. C. de Visser, G. Perron, and J. E. Desnoyers. J. Am. Chem. Soc. **99**, 5894 (1977).
19. P. Picker, E. Tremblay, and C. Jolicoeur. J. Solution Chem. **3**, 377 (1974).
20. P. Picker, P.-A. Leduc, P. R. Philip, and J. E. Desnoyers. J. Chem. Thermodyn. **3**, 631 (1971).
21. J. E. Desnoyers, C. de Visser, G. Perron, and P. Picker. J. Solution Chem. **5**, 605 (1976).
22. J.-L. Fortier, P.-A. Leduc, and J.-E. Desnoyers. J. Solution Chem. **3**, 323 (1974).
23. V.-B. Parker. Thermal properties of aqueous univalent electrolytes. NSRDS-NBS2 (1965).
24. J. E. Desnoyers, M. Arel, G. Perron, and C. Jolicoeur. J. Phys. Chem. **73**, 3346 (1969).
25. B. E. Conway, R. E. Verrall, and J. E. Desnoyers. Trans. Faraday Soc. **62**, 2738 (1966).
26. C. Jolicoeur and G. Lacroix. Can. J. Chem. **54**, 624 (1976).
27. A. Feillolay and M. Lucas. J. Phys. Chem. **76**, 3068 (1972).
28. S. K. Shoor and K. E. Gubbins. J. Phys. Chem. **73**, 498 (1969).
29. W. L. Masterton and T. P. Lee. Chemistry and physics of aqueous gas solutions. *Edited by* W. A. Adams. The Electrochemical Society, Princeton, NJ. 1975. p. 199.
30. M. Y. Schrier, P. J. Turner, and E. E. Schrier. J.Phys. Chem. **79**, 1391 (1975).
31. W.-Y. Wen and C. M. Chen. J. Phys. Chem. **73**, 2895 (1969).
32. R. B. Cassel and W.-Y. Wen. J. Phys. Chem. **76**, 1369 (1972).
33. H. L. Friedman and C. V. Krishnan. Water, a comprehensive treatise. Vol. 3. *Edited by* F. Franks. Plenum Press, New York. 1973. p. 1.
34. N. Desrosiers, G. Perron, J. G. Mathieson, B. E. Conway, and J. E. Desnoyers. J. Solution Chem. **3**, 789 (1974).
35. J.-L. Fortier, P. R. Philip, and J. E. Desnoyers. J. Solution Chem. **3**, 523 (1974).
36. G. Perron, N. Desrosiers, and J. E. Desnoyers. Can. J. Chem. **54**, 2163 (1976).
37. H. S. Frank and R. L. Robinson. J. Chem. Phys. **8**, 933 (1940).
38. H. L. Friedman. Modern aspects of electrochemistry. Vol. 6. *Edited by* J. O'M. Bockris and B. E. Conway. 1971. p. 1.
39. J. E. Desnoyers, G. E. Pelletier, and C. Jolicoeur. Can. J. Chem. **43**, 3232 (1965).
40. C. V. Krishnan and H. L. Friedman. J. Solution Chem. **3**, 727 (1974).
41. A. H. Clark, F. Franks, M. D. Medley, and D. S. Reid. J. Chem. Soc. Faraday Trans. I, **73**, 290 (1977).
42. F. Franks, M. Medley, and D. S. Reid. J. Chem. Soc. Faraday Trans. I, **72**, 359 (1976).
43. W. H. Streng and W.-Y. Wen. J. Solution Chem. **3**, 865 (1974).
44. R. F. Cross. J. Phys. Chem. **79**, 1822 (1975).
45. R. A. Pierotti. J. Phys. Chem. **67**, 1840 (1963).
46. P. R. Philip and C. Jolicoeur. J. Solution Chem. **4**, 105 (1975).
47. N. Desrosiers and J. E. Desnoyers. Can. J. Chem. **54**, 3800 (1976).

Crystal structure of methyl,2-mercaptopyrimidinatomercury(II)

CHUNG CHIEH

Guelph-Waterloo Centre for Graduate Work in Chemistry, Department of Chemistry, University of Waterloo, Waterloo, Ont., Canada N2L 3G1

Received August 19, 1977

CHUNG CHIEH. Can. J. Chem. **56**, 560 (1978).

Methyl,2-mercaptopyrimidinatomercury(II) was synthesized from methylmercuric hydroxide and 2-mercaptopyrimidine in aqueous solution. The crystal is orthorhombic with $a = 4.063(2)$, $b = 9.901(4)$, $c = 18.808(15)$ Å, $D_m = 2.88(1)$, $Z = 4$, $D_c = 2.867$ g cm^{-3}, space group $P2_12_12_1$. The structure was solved by the heavy atom method using 605 diffractometer measured reflections. The final R factor was 0.069. The key bond lengths and angles are: Hg—S, 2.39(2) Å, Hg—CH_3, 2.13(6) Å, ∠SHgC, 174°. The CH_3HgS— group bends out of the plane of the pyrimidine ring and the Hg atom interacts rather strongly with one of the ring nitrogens with an Hg—N distance of 2.83 Å. However, the Hg...N interaction is very labile in solution, since the two hydrogen atoms in the *meta* positions are equivalent from the ^{1}H nmr spectra in both $CDCl_3$ and DMSO solutions. The solution of the compound is not optically active.

CHUNG CHIEH. Can. J. Chem. **56**, 560 (1978).

On a effectué la synthèse du mercapto-2 pyrimidinatomercure(II) de méthyle à partir de l'hydroxyde de méthylmercure(II) et de la mercapto-2 pyrimidine en solution aqueuse. Les cristaux sont orthorhombiques avec $a = 4.063(2)$, $b = 9.901(4)$, $c = 18.808(15)$ Å, $D_m = 2.88(1)$, $Z = 4$, $D_c = 2.867$ g cm^{-3}, groupe d'espace $P2_12_12_1$. On a résolu la structure par la méthode des atomes lourds utilisant 605 réflexions mesurées par un diffractomètre. Le facteur final R est de 0.069. Les longueurs de liaisons et les angles les plus importants sont: Hg—S, 2.39(2) Å, Hg—CH_3, 2.13(6) Å, ∠SHgC, 174°. Le groupe CH_3HgS se trouve à l'extérieur du plan du cycle pyrimidine et l'atome Hg interagit d'une façon assez forte avec un des azotes du cycle avec une distance Hg—N de 2.83 Å. Toutefois, l'interaction Hg...N est très labile en solution puisque les deux atomes hydrogène en position *meta* sont équivalents dans les spectres rmn ^{1}H soit en solution dans le $CDCl_3$ soit dans le DMSO. La solution du composé n'est pas optiquement active.

[Traduit par le journal]

Introduction

Numerous sulfur-substituted pyrimidines and purines have found applications as clinically useful drugs. Many sulfur derivatives of nucleic acid have shown anticarcinogenic properties (1). Because 6-mercaptopurine had been used in the treatment of acute lymphocytic and chronic mylelocytic leukemias, interest in other sulfur derivatives of purines and pyrimidines remains high (2). Recently, anticarcinogenic activities were found for palladium and bismuth complexes with 6-mercaptopurine; but the platinum complex was not active (3). We have been interested in the interaction of sulfur-containing drugs with mercurials (4) and have studied the reaction between methylmercuric hydroxide and 2-mercaptopyrimidine. The mercaptopyrimidines are interesting intermediates in many reactions (5). Methylmercury does not form stable coordination complexes with nitrogen bases such as pyridine (6). It is predictable that methylmercury will bind to the deprotonated thio-group of 2-mercaptopyrimidine, but it was not known how the nitrogen atoms on the ring will interact with the mercury.

Experimental

Methylmercuric hydroxide from Ventron, 2-mercaptopyrimidine from Aldrich Chemical and solvents of standard reagent grade were used.

When two aqueous solutions containing (not completely dissolved) 0.3 g 2-mercaptopyrimidine and 0.62 g methylmercuric hydroxide were mixed, a fine white precipitate was obtained leaving a clear colorless filtrate. The fine prismatic crystals were soluble in ethanol, chloroform, acetone, and benzene. Recrystallization by slow evaporation of an ethanol solution gave crystals of suitable size for X-ray diffraction studies. Crystals of the same form were also obtained by slow evaporation of the filtrate.

Photographic methods were used to estimate the unit cell constants. These were refined based on the 2θ (Zr-filtered Mo Kα) values of 22 reflections measured on a G.E. XRD-6 diffractometer.

Crystal Data

$C_5H_6HgN_2S$ fw = 326.7

Orthorhombic space group $P2_12_12_1$, $a = 4.063(2)$, $b = 9.901(4)$, $c = 18.808(15)$ Å, $V = 756.6$ Å^3, $D_m = 2.88(1)$ (by flotation), $Z = 4$, $D_c = 2.867$ g cm^{-3}. Systematic absences: $h00$, $h = 2n + 1$; $0k0$, $k = 2n + 1$; $00l$, $l = 2n + 1$. μ(Mo Kα) = 209 cm^{-1}; λ(Mo Kα) = 0.7107 Å.

The crystal used was approximately a cube with edges of 0.15 mm. Intensities were measured with Zr-filtered Mo Kα

Can. J. Chem. Downloaded from www.nrcresearchpress.com by 210.87.254.5 on 09/05/12
For personal use only.

Can. J. Chem. Downloaded from www.nrcresearchpress.com by 210.87.254.5 on 09/05/12
For personal use only.

radiation on a G.E. XRD-6 card-controlled diffractometer. A θ–2θ scan method at 2° m^{-1} over a range of (1.80 + 0.86 tan θ) degrees in 2θ was employed. Backgrounds were measured at both limits of scan for 10 s. Among 819 reflections ($2\theta < 60°$) measured, 605 (74%) had net intensities greater than $3\sigma(I)$; these reflections were used throughout the structural analysis.

The Patterson map had three intense peaks at (0, 0.094, 0.5), (0.5, 0.5, 0.163), and (0.5, 0.407, 0.337). This is in agreement with the space group assignment of $P2_12_12_1$. With mercury atom alone, the agreement between calculated and measured structure factors was good, $R = 0.18$ ($\Sigma||F_o| - |F_c||/\Sigma|F_o|$). Including the sulfur in the calculation lowered R to 0.15. Poorly resolved peaks due to other atoms were not very intense in the Fourier map based on the phase from Hg and S atoms. Atoms in the pyrimidine ring were put in where both electron density and bonding appeared reasonable. Refinement based on data before absorption correction gave an R of 0.09. After this correction, according to ref. 7, the R became 0.073 with anisotropic temperature factors for all atoms. However, the bond lengths and angles from the two refinements were similar. At the final stage, a weighting function $w^{-1} = 40.0 - F_o + 0.01\,F_o^2$ was introduced. The atomic scattering factors (8) with an anomalous scattering correction for the mercury atom (9) were used. The final R and $R_w = (\Sigma w^2(|F_o| - |F_c|)^2/\Sigma w^2|F_o|^2)^{1/2}$ were 0.069 and 0.082 respectively. The final atomic coordinates are given in Table 1.[1]

TABLE 1. Final atomic coordinates with standard deviations x, y, z; $0.5 - x, \bar{y}, 0.5 + z$; $0.5 + x, 0.5 - y, \bar{z}$; $\bar{x}, 0.5 + y, 0.5 - z$

Atom	x	y	z
Hg	0.2382(7)	0.0470(1)	0.33283(7)
S	0.5190(41)	0.2181(11)	0.2656(6)
N(1)	0.841(6)	0.2870(27)	0.3991(16)
N(2)	0.716(13)	0.4447(34)	0.3084(18)
C(1)	0.751(15)	0.3739(54)	0.4515(21)
C(2)	0.599(14)	0.4924(32)	0.4324(20)
C(3)	0.541(19)	0.5286(38)	0.3518(21)
C(4)	0.829(7)	0.3216(33)	0.3359(18)
C(5)	0.025(13)	−0.1022(52)	0.3994(33)

Results and Discussion

The Molecule

The crystal consists of individual molecules. The important bond distances and angles are given in Fig. 1, which is also a packing diagram. The methylmercury group is on one side of the ring plane with a dihedral angle ∠HgSCN(2) of 14.8°. This arrangement gives rise to the chirality of the molecule.

The mercury is 1.4 Å from the least-squares plane of the ring. The equation of the plane is

$$0.8877X + 0.4572Y + 0.0539Z = 4.8$$

(X, Y, and Z are coordinates in Å referred to a, b, and c axes) and the maximum displacement of the atoms from the plane is 0.10 Å. The distances are normal when compared to those in 2,4-dimercaptopyrimidine (10) within experimental error.

The Hg—N(2) distance of 2.83(3) Å indicates a rather strong interaction because the sum of the van der Waals radii for the two atoms is 3.00 Å. The ∠HgSC(4) and ∠SC(4)N(2) angles are 107.7(8) and 114(1)° respectively, whereas the corresponding angles are 109.8(1) and 125.8(3)° in dichlorobis(6-mercaptopurine)mercury(II) (11). In the latter compound, there is no Hg—N coordination; but the mercury(II) ion is coordinated to two sulfur and two chlorine atoms. Therefore, it can be concluded that the short distance is due to the affinity between the N and Hg atoms and is not a consequence of intramolecular stress. However, the coordination is very weak. The Hg—N distances are 2.13(3) and 2.06(4) Å in μ-DL-penicillaminatobis(methylmercury(II)) (12) and (DL-methioninato)methylmercury(II) (13) respectively. For both compounds, the methylmercury groups are bonded to the amino groups.

The nmr spectrum of the hydrogen attached to C(2) (see Fig. 1) is a triplet. The hydrogen atoms attached to C(1) and C(3) are equivalent for 2-mercaptopyrimidine and methyl,2-mercaptopyrimidinatomercury(II) in DMSO or chloroform solutions; the spectrum is a doublet. Since the two hydrogens at the *meta* positions are equivalent in both $CDCl_3$ and DMSO solutions, the Hg...N interaction must be labile. The chemical shifts are listed in Table 2. As expected, the bonding of CH_3Hg— to the sulfur causes a downfield shift. The net shifts are larger for the *para* than for the *meta* hydrogens. The ^{1}H nmr spectra using DMSO-d_6 as solvent indicated the presence of a small quantity of bis(2-mercaptopyrimidinato)mercury(II) in the product as described in the Experimental section. The net downfield shifts for this compound are larger than for those of methyl(2-mercaptopyrimidinato)mercury(II). However, the spectrum of bis(2-mercaptopyrimidinato)-mercury(II) was not observed when using $CDCl_3$ as a solvent, probably due to its limited solubility.

The Packing

Historically, Louis Pasteur investigated the molecular asymmetry and crystallization before crystallography was developed (14). Optically pure compounds crystallize in assymmetric space groups. The enantiomers of some synthetic compounds may grow separately in different crystals resulting in asymmetric space groups: among them, $P2_12_12_1$ is the most common with $P2_1$ being next (15). As an

[1]Tables of anisotropic temperature parameters and structure factors are available, at a nominal charge, from the Depository of Unpublished Data, CISTI, National Research Council of Canada, Ottawa, Ont., Canada K1A 0S2.

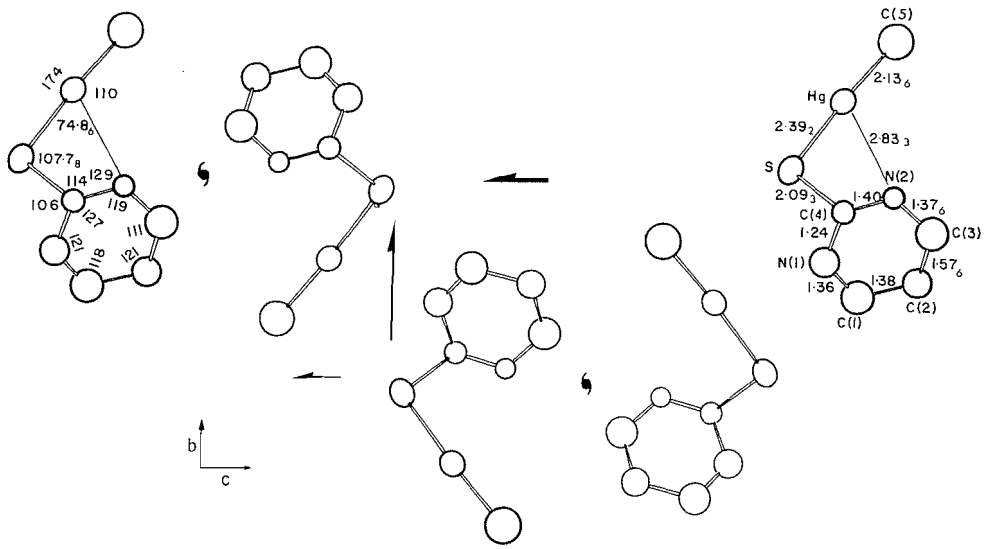

FIG. 1. The packing diagram for methyl,2-mercaptopyrimidinatomercury(II). The screw axes along the three mutually perpendicular directions are indicated by 𝄞 and arrows. Standard deviations are indicated by small numbers referring to the last digit.

TABLE 2. ^{1}H chemical shifts (τ(TMS) = 10) for 2-mercaptopyrimidine and its mercury complexes

Compound	Solvent	CCHC	Δ	CCHN	Δ	$HgCH_3$
2-Mercaptopyrimidine	DMSO	3.13	—	1.68	—	
Methyl,2-mercaptopyrimidinatomercury(II)	DMSO	2.90	0.23	1.59	0.09	9.27
Bis(2-mercaptopyrimidinato)mercury(II)	DMSO	2.67	0.46	8.60	0.18	
Methyl,2-mercaptopyrimidinatomercury(II)	$CDCl_3$	3.03	—	1.64		9.03

example, the racemic form of (4*aRS*,4*bSR*,13*bRS*)-12-bromo-1-(*p*-brophenyl)-1,4*a*,4*b*,5,6,13*b*-hexahydro-4*H*-dipyridazino-[1,6-*a*:4,3-*c*]quinoline crystallizes in $P2_1/c$, whereas the optical pure substance crystallizes in $P2_12_12_1$ (16). There are slight but significant differences in intramolecular non-bonding distances and bonding angles in the two crystal structures. Another similar example is provided by the crystallization study of 3-benzylamino-4-hydroxypent-2-enoic acid lactone hydrobromide. This compound crystallizes from methanol solution in space group $P2_1$ and solutions of a single crystal showed positive or negative rotation of polarized light. However, the hydrochloride analog crystallizes in $P2_1/c$ (17).

Due to the very high absorption coefficient, μ, and the low accuracy of the intensities, the absolute configuration was not determined. However, neither solutions of 2-mercaptopyrimidine or methyl,2-mercaptopyrimidinatomercury(II) were optically active.

If the crystals are recognizable by hemihedry, resolution of the enantiomers may then be achieved by separating the crystals through optical observation (17). A number of heterohelicenes were obtained in optically active forms by crystal picking (18, 19). These compounds were found to show very high optical rotations due to the presence of an inherently dissymmetric chromophore. However, resolution of optical isomers is usually achieved by diastereomer formation (20).

The molecules in this structure, Fig. 1, pack in a normal way and are similar to many molecular structures such as diphenyl ditelluride and *p*-tolylsulfide do (21, 22). Only van der Waal intermolecular contacts were observed.

Acknowledgement

This work was supported by the National Research Council of Canada.

1. E. SLETTEN, J. SLETTEN, and L. H. JENSEN. Acta Crystallogr. **25B**, 1330 (1969).
2. H. PLANT. *In* Organic sulfur compounds. Vol. 1. *Edited by* N. Kharasch. Pergamon Press. 1961. Chapt. 40.

Can. J. Chem. Downloaded from www.nrcresearchpress.com by 210.87.254.5 on 09/05/12
For personal use only.

3. S. M. SKINNER and R. W. LEWIS. Res. Commun. Chem. Pathol. Pharmacol. **16**, 183 (1977).
4. C. CHIEH. Can. J. Chem. **55**, 1115 (1977).
5. D. J. BROWN. The Pyrimidines, Supplement I. Wiley-Interscience. 1970. Chapt. 4.
6. J. M. WOOD. Adv. Environ. Sci. Technol. **2**, 39 (1971).
7. P. COPPENS, L. LEISEROWITZ, and D. ROBINOVICH. Acta Crystallogr. **18**, 1035 (1965).
8. D. T. CROMER and J. T. WABER. Acta Crystallogr. **18**, 104 (1965).
9. D. T. CROMER. Acta Crystallogr. **18**, 17 (1965).
10. E. SHEFTER and H. G. MANTER. J. Am. Chem. Soc. **89**, 1249 (1967).
11. P. LAVERTUE, J. HUBERT, and A. L. BEAUCHAMP. Inorg. Chem. **15**, 322 (1976).
12. Y. S. WONG, A. J. CARTY, and C. CHIEH. J. Chem. Soc. Dalton. In press.
13. Y. S. WONG, A. J. CARTY, and C. CHIEH. J. Chem. Soc. Dalton, 1157 (1977).
14. L. PASTEUR. Research on the molecular asymmetry of natural organic products. Published for the Alembic Club by Livingstone Ltd. 1948.
15. A. I. KITAIGORODSKII. Organic Chemical Crystallography. Authorized translation from Russian, Consultants Bureau, New York. 1961.
16. I. K. LARSEN. Acta Crystallogr. Sec. B, **28**, 1136 (1972).
17. P. T. CHENG, C. H. KOO, I. P. MELLOR, S. C. NYBURG, and J. M. YOUNG. Acta Crystallogr. **26**, Sect. B, 1339 (1970); S. C. NYBURG and I. A. POTWOROWSKI. Acta Crystallogr. **29**, Sect. B, 347 (1973).
18. M. B. GROEN and H. WYNBERG. J. Am. Chem. Soc. **93**, 2968 (1971).
19. D. A. LIGHTER, D. T. HEFELFINGER, T. W. POWERS, G. W. FRANK, and K. N. TRUEBLOOD. J. Am. Chem. Soc. **94**, 3492 (1972).
20. A. BROOMHEAD, F. P. DWYER, and J. W. HOGARTH. Inorg. Synth. Vol. 6. McGraw-Hill, NY. 1960. pp. 183 and 186; G. B. KAUFFMAN and E. V. LINDLEY, JR. Inorg. Synth. Vol. 16. 1976.
21. W. R. BLACKMORE and S. C. ABRAHAMS. Acta Crystallogr. **8**, 317 (1955).
22. G. LLABRES, O. DIDEBERG, and L. PUPONT. Acta Crystallogr. **28**, Sect. B, 2438 (1972).

Can. J. Chem. Downloaded from www.nrcresearchpress.com by 210.87.254.5 on 09/05/12
For personal use only.

Crystal structure of mercury(II) bromide dithiocarbamate, $[HgBr_2(S_2CNEt_2)Hg(S_2CNEt_2)]_n$, an inorganic polymer

CHUNG CHIEH

Guelph–Waterloo Centre for Graduate Work in Chemistry, University of Waterloo, Waterloo, Ont., Canada N2M 3G1

Received September 8, 1977

CHUNG CHIEH. Can. J. Chem. **56**, 564 (1978).

A pale yellow crystal obtained from reaction of $HgBr_2$ and tetraethylthiuram disulfide (TETD) has the composition of $HgBr_2{\cdot}Hg[S_2CN(C_2H_5)_2]_2$. TETD was reduced to dithiocarbamate. The molecules are polymeric chains with $HgBr_2$ and Hg^{2+} alternately bridging to dithiocarbamate ions and vice versa. The crystal is monoclinic: a = 10.421(7), b = 15.244(13), c = 14.649(8) Å, β = 113.3(1)°; space group $P2_1/c$. The final R factor for 2085 observed reflections is 0.083. There are two types of coordination geometries for the mercury(II) ions in the crystal: the coordination for one is digonal with two short Hg—S distances of 2.385(11) and 2.365(10) Å. The coordination for the other is tetrahedral with two Hg—S, 2.552(10) and 2.569(10) Å, and two Hg—Br, 2.640(4) and 2.552(7) Å, bonds. The average C=S distance is 1.72(4) Å.

CHUNG CHIEH. Can. J. Chem. **56**, 564 (1978).

Un cristal jaune pâle obtenu par réaction de $HgBr_2$ avec le disulfure de tétraéthylthiurame (TETD) a la composition $HgBr_2{\cdot}Hg[S_2CN(C_2H_5)_2]_2$; le TETD a été réduit en dithiocarbamate lors de la réaction. Les molécules existent alors sous forme de chaînes de polymères contenant en alternance $HgBr_2$ et Hg^{2+} qui servent de pont aux ions dithiocarbamates et vice versa. Le cristal est monoclinique a = 10.421(7), b = 15.244(13), c = 14.649(8) Å, β = 113.3(1)°; groupe d'espace $P2_1/c$. Le facteur d'accord R pour 2085 réflexions observées est de 0.083. Il y a deux types de géométrie de coordination pour les ions mercure(II) dans le cristal: la coordination dans l'un est digonale avec deux distances Hg—S courtes de 2.385(11) et 2.365(10) Å. La coordination de l'autre est tétraédrique avec deux Hg—S, 2.552(10) et 2.569(10) Å, et deux Hg—Br, 2.640(4) et 2.552(7) Å. La distance moyenne C=S est de 1.72(4) Å.

[Traduit par le journal]

Introduction

The conversion of tetraethylthiuram disulfide, $R_2NCS_2S_2CNR_2$, and dithiocarbamate, $R_2NCS_2^-$, is relatively easy according to the equation: $2R_2NCS_2^- \rightarrow R_2NCS_2S_2CNR_2 + 2e$. Oxidation of dithiocarbamato complexes of mercury with halogen results in the oxidation of the ligand yielding thiuram disulfide complexes (1). However, the reactions of mercury(II) halides with tetraethylthiuram disulfide (TETD) often yield dithiocarbamato complexes (2, 3). The reaction of mercury(II) bromide and TETD yielded colorless and pale-yellow crystals. The former is $HgBr_2{\cdot}$TETD which is isostructural with $HgI_2{\cdot}$TETD. The orthorhombic cell constants for $HgBr_2{\cdot}$TETD are: a = 13.050, b = 13.593, c = 22.373 Å.

Crystallographic results indicated that the pale-yellow crystal is a compound of composition $Hg_2Br_2[S_2CN(C_2H_5)_2]_2$. This paper reports the crystal structure.

Experimental

When two ethanolic solutions of $HgBr_2$ and TETD were mixed at 25°C, a white precipitate was obtained. Recrystallization of the precipitate in ethanol–chloroform (1:1 by volume) gave two kinds of crystals. One was colorless and the other pale yellow. The latter were subjected to crystallographic studies. The space group was determined from preliminary photographs. Cell constants were estimated from the same, and then refined by least-squares methods from the 2θ values of 38 reflections measured on a G.E. XRD-6 diffractometer, which was used to measure the intensities of the reflections. Crystal data are as follows.

$Br_2C_{10}H_{20}Hg_2N_2S_4$ fw = 857.4

Monoclinic, a = 10.421(7), b = 15.244(13), c = 14.649(8) Å, β = 113.3(1)°, V = 2137.3 Å^3. D_o = 2.65 (by flotation), Z = 4, D_c = 2.664 g cm^{-3}. Systematic absences: $h0l$, $l = 2n + 1$; $0k0$, $k = 2n + 1$; space group $P2_1/c$ (C_{2h}^5, No. 14). μ(MoKα) = 189.8 cm^{-1}. λ(MoKα) = 0.7107 Å.

The crystal used for intensity measurements was a thin square plate with dimensions of 0.18 × 0.20 × 0.06 mm along a, b, and c directions. It was mounted with b^* along the ϕ axis of the goniometer. The faces developed were {110} and {001}. These data were used for absorption corrections (4). The range of μR is 1.1 to 3.9. There were 2085 observed among 3744 reflections with 2θ(Zr-filtered MoKα) < 50° measured. The scan rate was 2° per min with a range of $\pm(0.95 + 0.85 \tan\theta)$. The majority of unobserved reflections, $I < 3\sigma(I)$, had 2θ > 40°. The structure was solved by the heavy atom method; refinement procedures were similar to those described recently (5). The weighting scheme was $w^{-1} = 60 - F_o + 0.001F_o^2$. The final R ($= \Sigma||F_o| - |F_c||/\Sigma F_o$) and R_w were 0.083 and 0.108, respectively, on refinement of F. The difference Fourier map showed no other atoms. In the final cycle of refinement, the maximum parameter shifts were 0.5σ. Atomic coordinates are given in Table 1. Structure and temperature factors were deposited.[1]

[1]Photocopies may be obtained, upon request, at a nominal charge, from Depository of Unpublished Data, CISTI, National Research Council of Canada, Ottawa, Ont., Canada K1A 0S2.

Can. J. Chem. Downloaded from www.nrcresearchpress.com by 210.87.254.40 on 09/05/12
For personal use only.

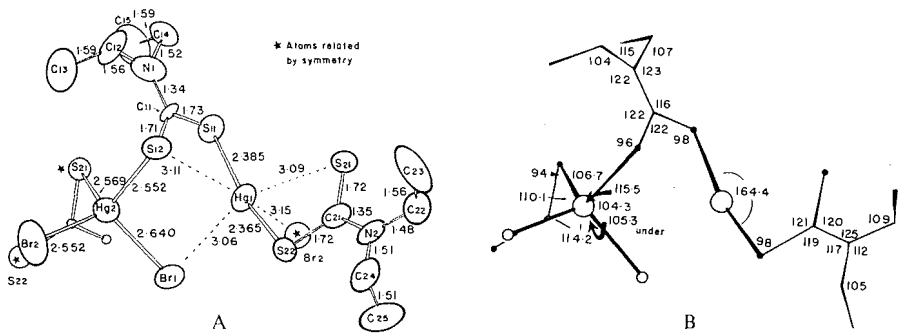

FIG. 1. Bond distances and angles for $[HgBr_2(S_2CNEt_2)Hg(S_2CNEt_2)]_n$. Estimated standard deviations: Hg—Br, 0.005; Hg—S, 0.010; C—S, 0.04; C—N or C—C, 0.05 Å. ∠BrHgBr, 0.1; ∠BrHgS, 0.2; ∠SHgS, 0.3; ∠SCS, 1.0; ∠CNC etc., 2.0°.

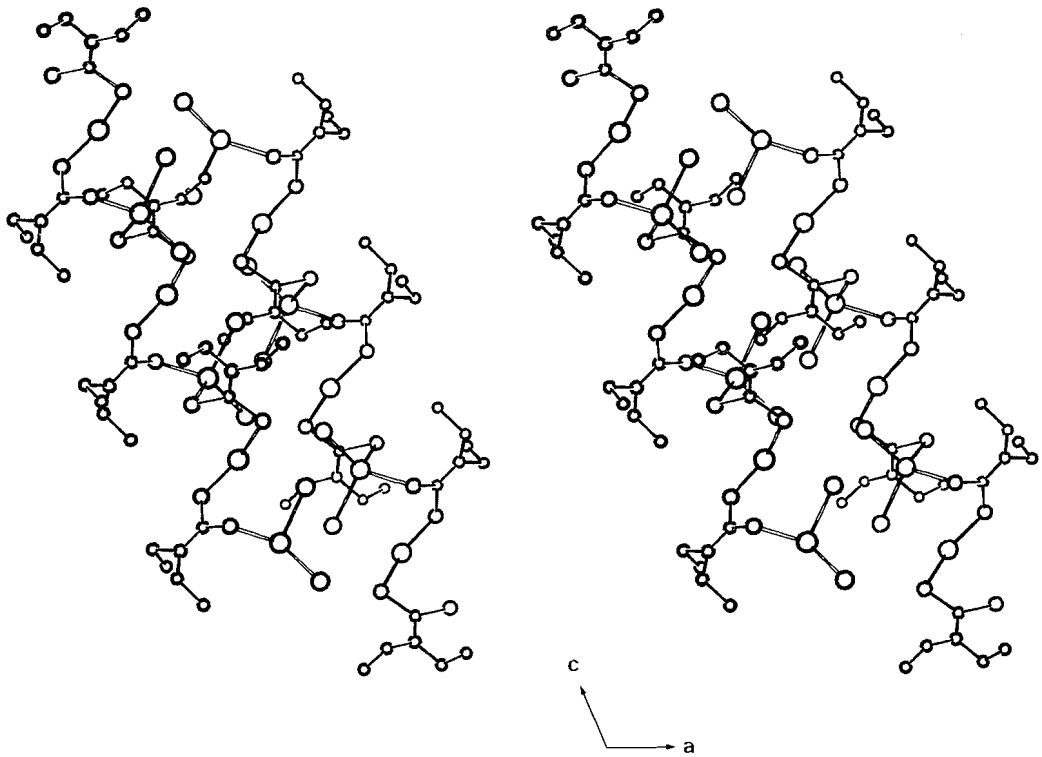

FIG. 2. Stereo pair for the chains looking along the *b*-direction. Two chains are antiparallel. They are related to each other via a centre of symmetry. Sizes of atoms increase with atomic numbers.

Results and Discussion

The compound can be formulated as $[HgBr_2(S_2CNEt_2)Hg(S_2CNEt_2)]_n$. There are two mercury(II), two bromide, and two dithiocarbamate ions per asymmetric unit, which repeats itself by a *c*-glide plane forming a chain. The important bond distances and angles for the basic unit are given in Fig. 1.

A unique and interesting feature in the structure is the existence of two coordination geometries for mercury(II) in one crystal. The coordination for one, Hg_1, is digonal with two short almost linear Hg—S bonds of 2.385(11) and 2.365(10) Å; the angle ∠SHgS is 164.4(3)°. For Hg_1, additional contacts of Hg...S or Hg...Br are of the order of 3.1 Å. The coordination for the other, Hg_2, is tetrahedral with 2 Hg—S (2.552(10) and 2.569(10) Å) and 2 Hg—Br (2.552(7) and 2.640(4) Å) bonds. The bond angles around this ion range from 104.3 to 115.5°. For both mercury ions, the bond lengths and angles are in good agreement with those in the literature (6). Two Hg—Br distances are significantly different resulting from the secondary Hg...Br interactions.

Each dithiocarbamate ion is bonded to one Hg^{2+}

Can. J. Chem. Downloaded from www.nrcresearchpress.com by 210.87.254.40 on 09/05/12
For personal use only.

TABLE 1. Atomic coordinates with standard deviations

Atom	x	y	z
Hg_1	0.2367(2)	0.2113(1)	0.3902(1)
Hg_2	0.2611(2)	0.2023(1)	0.1376(1)
Br_1	0.4595(4)	0.2492(3)	0.3087(3)
Br_2	0.3498(7)	0.1204(4)	0.0220(4)
S_{11}	0.0349(9)	0.2852(8)	0.2768(7)
S_{12}	0.0857(9)	0.1188(7)	0.1866(7)
S_{21}	0.1417(8)	0.1541(7)	0.5559(7)
S_{22}	0.3904(9)	0.1134(7)	0.5082(7)
C_{11}	−0.016(3)	0.208(3)	0.183(2)
N_1	−0.144(4)	0.218(3)	0.111(3)
C_{12}	−0.207(5)	0.149(5)	0.027(3)
C_{13}	−0.146(8)	0.176(7)	−0.053(5)
C_{14}	−0.244(4)	0.288(4)	0.114(3)
C_{15}	−0.212(6)	0.373(4)	0.064(4)
C_{21}	0.297(3)	0.100(2)	0.582(2)
N_2	0.346(3)	0.044(2)	0.660(2)
C_{22}	0.278(5)	0.027(4)	0.729(3)
C_{23}	0.168(9)	−0.048(9)	0.691(7)
C_{24}	0.471(5)	−0.014(3)	0.681(3)
C_{25}	0.595(5)	0.040(4)	0.746(4)

and one $HgBr_2$ via the sulfur. Chains are formed through the mutual bridging between dithiocarbamates and $HgBr_2$ or Hg^{2+} units. In contrast, molecules of the stoichiometric iodo analogue, $[1Hg(S_2CN(C_2H_5)_2]_2$, pack as dimers in the crystal (3). The bridging of the dithiocarbamate is more symmetric in the title compound than in the iodo analogue. Although the Hg—S distances around the two mercury(II) ions are different because the coordination geometries are not the same, the C—S bond lengths are indistinguishable. The average value is 1.72(4) Å. Similar values appeared for one of the dithiocarbamates in the structure of α-mercury(II) dithiocarbamate (7). The configurations for the dithiocarbamate ions are normal with respect to other complexes (1–3).

The packing of this compound presents a typical model for linear polymers. The *c*-glide plane is responsible for extending the chains. Figure 2 is a stereo pair of the chains looking along the *b*-direction. The chains are antiparallel. Parallel chains form layers which stack up along the *b* axis as shown in Fig. 3. The crystals grown from ethanol are thin square plates with a general thickness of 0.06 mm, which is approximately the length of the chains. In this case, the chains contain 9×10^5 basic units and have a molecular weight of 7×10^8.

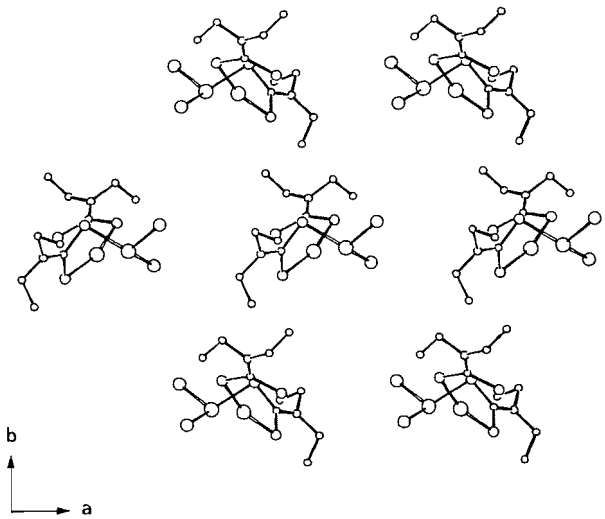

FIG. 3. Packing of the chains looking along *c**-direction.

Because of the polymeric nature of dithiocarbamato mercury(II) complexes, their solubilities are usually low, especially in water.

Acknowledgement

This work was supported by the National Research Council of Canada.

1. J. WILLEMSE, J. A. CRAS, J. J. STEGGERDA, and C. P. KEIJZERS. Struct. Bonding Berlin, **28**, 83 (1976).
2. C. CHIEH and L. P. C. LEUNG. Can. J. Chem. **54**, 3077 (1976).
3. C. CHIEH. Can. J. Chem. **55**, 65 (1977); **55**, 1115 (1977).
4. P. COPPENS, L. LEISEROWITZ, and D. ROBINOVICH. Acta Crystallogr. **18**, 1035 (1965).
5. C. CHIEH and H. D. COWELL. Can. J. Chem. **55**, 3898 (1977).
6. D. GRDENIC. Q. Rev. **19**, 303 (1965).
7. H. IWASAKI. Acta Crystallogr. B**29**, 2115 (1973).

Can. J. Chem. Downloaded from www.nrcresearchpress.com by 210.87.254.40 on 09/05/12
For personal use only.

Dielectric relaxation in 2-acetylnaphthalene and related compounds

J. CROSSLEY, M. A. MAZID, C. K. MCLELLAN,
P. F. MOUNTAIN, AND S. WALKER
Chemistry Department, Lakehead University, Thunder Bay, Ont., Canada P7B 5E1

Received August 29, 1977

J. CROSSLEY, M. A. MAZID, C. K. MCLELLAN, P. F. MOUNTAIN, and S. WALKER. Can. J. Chem. **56**, 567 (1978).

The dielectric absorption of 2-acetylnaphthalene and 2- and 3-acetylphenanthrene has been studied in *p*-xylene solution at several microwave frequencies and in a polystyrene matrix at low frequencies. Acetyl group relaxation has been established from both sets of data. A clear separation of the dielectric absorption of the molecule and the group has been achieved for both 2- and 3-acetylphenanthrene in the matrix. The Eyring activation parameters have been established for acetyl relaxation in these molecules in the matrix. The free energy of activation values for group relaxation increase in the sequence acetophenone < 2-acetylphenanthrene < 3-acetylphenanthrene < 2-acetylnaphthalene. For the *p*-xylene solution data the weight factor for group relaxation, C_2, is appreciably lower than the theoretical value, so that $C_2 < C_1$, bearing out the findings of Fong and Smyth for 2-acetylnaphthalene. In polystyrene matrices, the data for 2- and 3-acetylphenanthrene also indicated that $C_2 < C_1$. The enthalpy of activation for acetyl relaxation in 2- and 3-acetylphenanthrene is similar to that for acetophenone and 1,4-diacetylbenzene whereas that for 2-acetylnaphthalene would seem somewhat larger.

J. CROSSLEY, M. A. MAZID, C. K. MCLELLAN, P. F. MOUNTAIN et S. WALKER. Can. J. Chem. **56**, 567 (1978).

On a étudié l'absorption diélectrique de l'acétyl-2 naphtalène et des acétyl-2 et acétyl-3 phénanthrènes en solution dans le *p*-xylène à plusieurs fréquences de microondes et dans une matrice de polystyrène à de basses fréquences. On a établi la relaxation du groupe acétyle à partir des deux groupes de données. On a pu obtenir une séparation nette de l'absorption diélectrique de la molécule d'une part et du groupe d'autre part pour chacun des acétyl-2 et acétyl-3 phénanthrènes dans la matrice. On a évalué les paramètres d'activation de Eyring pour la relaxation du groupe acétyle dans ces molécules dans la matrice. Les valeurs d'énergies libres d'activation pour la relaxation du groupe augmentent lorsque l'on passe de l'acétophénone < acétyl-2 phénanthrène < acétyl-3 phénanthrène < acétyl-2 naphtalène. Pour les données en solution dans le *p*-xylène, le facteur de poids pour la relaxation du groupe, C_2, est beaucoup plus faible que la valeur théorique; C_2 est donc plus faible que C_1 et ce résultat est en accord avec les conclusions de Fong et Smyth pour l'acétyl-2 naphtalène. Dans des matrices de polystyrène, des données pour les acétyl-2 et acétyl-3 phénanthrènes indiquent aussi que $C_2 < C_1$. L'enthalpie d'activation pour la relaxation du groupement dans les acétyl-2 et acétyl-3 phénanthrènes est semblable à celle observée pour l'acétophénone et le diacétyl-1,4 benzène alors que celle pour l'acétyl-2 naphtalène semblerait plus élevée.
[Traduit par le journal]

Introduction

Dielectric relaxation in 2-acetylnaphthalene, 4-acetylbiphenyl, and 4-acetyl-*o*-terphenyl has been studied by Fong and Smyth (1–3) in benzene solution. Their data analyses in terms of two relaxation times consistently yielded a weight factor $C_2 \simeq 0.14$ for the acetyl group relaxation process. This value is markedly less than the C_2 of 0.6 ± 0.1 reported by Farmer *et al.* (4) for acetophenone. Theoretical calculations for acetophenone based on group moments or bond moments yield expected C_2 values of 0.67 and 0.49, respectively.

Dipole moments of 2-substituted naphthalenes tend to be slightly greater than those of their substituted benzene analogues (e.g., 2-bromonaphthalene, 1.70 D, and bromobenzene, 1.57 D (5)), but this effect is much too small to account for such a large difference in C_2 values between 2-acetylnaphthalene and acetophenone. Moreover, it could not explain the low C_2 values for 4-acetylbiphenyl and 4-acetyl-*o*-terphenyl.

In order to examine these findings further we have measured the dielectric properties of *p*-xylene solutions of 2-acetylnaphthalene and of 2- and 3-acetylphenanthrene, employing a greater number of microwave frequencies than was available in the Fong and Smyth work. In this way we should obtain improved analyses of the data, which ought to give a better indication as to the validity of the low C_2 values.

Fong and Smyth suggested that the reduced contribution (i.e., smaller C_2 value) from acetyl group rotation might be linked to an increased energy barrier to such motion in 2-acetylnaphthalene as compared to acetophenone. At room temperature,

Can. J. Chem. Downloaded from www.nrcresearchpress.com by 210.87.254.40 on 09/05/12
For personal use only.

Can. J. Chem. Downloaded from www.nrcresearchpress.com by 210.87.254.40 on 09/05/12
For personal use only.

the molecular (τ_1) and group (τ_2) relaxation times of these acetyl compounds in benzene solutions differ by less than one order of magnitude. In such cases where C_2 is small, the error in τ_2 is considerable (6), and it is not possible to obtain reliable activation energies from Eyring plots of log ($T\tau$) vs. ($1/T$). Recent work (7–12) has indicated that intramolecular relaxation may be well separated from that of the molecule if the compound is examined in a polystyrene matrix at low temperatures (7–13). The energy barriers to substituent group rotations obtained by this technique have compared favourably with estimates based on other methods (10–13). Therefore we have undertaken such a study of 2-acetylnaphthalene and of 2- and 3-acetylphenanthrene to determine whether the acetyl group definitely relaxes in such compounds, and, if it does, to determine the Eyring activation parameters. Of particular interest is the enthalpy of activation for group relaxation since, as Fong and Smyth (1) have pointed out, this is related to the resonance energy which governs the group rotation. Thus any appreciable enhanced conjugation of the acetyl group with the ring in 2-acetylnaphthalene and 2- and 3-acetylphenanthrene (which may be looked upon as substituted 2-acetylnaphthalenes) ought to be reflected in enhanced ΔH_E values over that found in acetophenone.

Experimental

The apparatus and techniques used to obtain dielectric constant (ε') and loss (ε'') data at up to nine microwave frequencies between 0.8 and 35 GHz for the acetyl compounds in liquid solutions have been described previously (14, 15). Low-frequency dielectric constants (ε_0) were measured at 2 MHz on a WTW Dipolmeter.

Dielectric measurements of solutes in polystyrene matrices and subsequent data analyses in terms of the Fuoss–Kirkwood and Eyring equations were carried out as before (9, 11). The solute concentration in the matrices was approximately 5% (weight), which is sufficiently low to avoid solute concentration effects (8, 16).

Experimental Results

The microwave data from solutions generally gave a smooth, depressed-centre Cole–Cole plot and were computer-fitted (17) to the Cole–Cole equation (18) to obtain mean relaxation times (τ_0), distribution parameters (α), and high-frequency dielectric constants (ε_∞). In addition, the same data were fitted (6, 19) to the Budó equation (20) to obtain discrete relaxation times, τ_1 and τ_2, together with their respective weight factors, C_1 and $C_2 = 1 - C_1$. Table 1 shows the results of these analyses along with the dipole moments obtained in *p*-xylene solutions. The results compare well with the Fong and Smyth (1) results for 2-acetylnaphthalene in benzene.

As an alternative to the Budó analysis technique, rough estimates of the two relaxation times may be obtained sometimes from the equation:

$$[1] \qquad \varepsilon' = \varepsilon_0 - \tau(\varepsilon''\omega)$$

Figure 1*a* shows a plot based on [1] for 3-acetylphenanthrene in *p*-xylene at 298 K, yielding the results shown in Table 1. Figure 1*b* shows the data for a solution containing Nujol mineral oil to increase the macroscopic viscosity to 9.0 cP.

The dielectric loss data from the polystyrene matrices were analyzed via the Fuoss–Kirkwood equation (21). The Cole–Cole distribution parameter, α, was estimated from the Fuoss–Kirkwood β value (22), and the matrix dielectric constants (ε') were analyzed via the Cole–Cole equation (18) to yield ε_∞.

The mean relaxation time, $\tau = 1/2\pi f_{max}$, from Fuoss–Kirkwood analyses of data gathered over a wide range of temperatures was analyzed via Eyring plots of log ($T\tau$) vs. ($1/T$) to yield activation enthalpies and entropies as described previously (9, 11, 12), and these results are summarized in Table 2.

Figure 2 shows plots of dielectric loss factor (ε'') vs. the logarithm of frequency for 3-acetylphenanthrene in a polystyrene matrix at four temperatures. A General Radio bridge was used at the two lower temperatures and a Hewlett-Packard Q-meter at the two higher temperatures. It may be noted that each curve appears symmetric. A second completely separate set of absorption curves was observed above room temperature. This may be contrasted with the data for 2-acetylnaphthalene in polystyrene for which Fig. 3 shows the curves at four temperatures. In these latter cases it would appear that the overall dielectric loss curve is composed of two overlapping contributions. Preliminary attempts were made to analyze such curves in terms of two separate curves each described by the Fuoss–Kirkwood formulation, eq. 2, employed previously (7, 12).

$$[2] \qquad \cosh^{-1}(\varepsilon''_{max}/\varepsilon'') = \beta \ln(f_{max}/f)$$

However, this necessitates the evaluation of six parameters at each temperature, three (ε''_{max}, β, and f_{max}) for each of the two peaks. The results of such attempts were inadequate. A more approximate type of approach is to analyze the data at each temperature in terms of a single absorption of the Fuoss–Kirkwood type. The resultant data are shown in the Eyring graph of Fig. 4 fitted to the two solid lines. This bears out that the overall absorption is dominated by different processes in the limits of lower and higher temperatures. For comparison, Fig. 4 also contains a dotted line fitted to the data for the lower-temperature absorption for 3-acetyl-

TABLE 1. Dielectric relaxation parameters and dipole moments of four aromatic acetyl compounds in *p*-xylene solution

Compound	N*	T (K)	$10^{12}\tau_0$ (s)	α	C_1	$10^{12}\tau_1$ (s)	$10^{12}\tau_2$ (s)	μ (D)
2-Acetylnaphthalene	7	288	34.9	0.08	0.8_0	44.2	13.1	3.04
	7	298	30.3	0.05	0.7_8	37.0	14.8	3.03
	5	313	23.1	0.04	0.7_3	29.2	12.8	3.00
	5	323	20.7	0.04	0.7_8	25.2	10.8	2.98
2-Acetylphenanthrene	6	333	30.7	0.09	0.8_0	40.2	10.0	3.08
3-Acetylphenanthrene	8	298	49.2	0.07	0.8_5	57.1	13.5	3.01
	8	298				49†	17†	
	7	298				123†,‡	18†,‡	3.00
Acetophenone	10	298	65.0§	0.19§		85†,§	8.5†,§	2.82

*N is the number of measurement frequencies.
†τ_1 and τ_2 derived from ε' vs. $\varepsilon''\omega$ plot.
‡Nujol added, viscosity 9.0 cP.
§In pure Nujol, viscosity 166 cP.

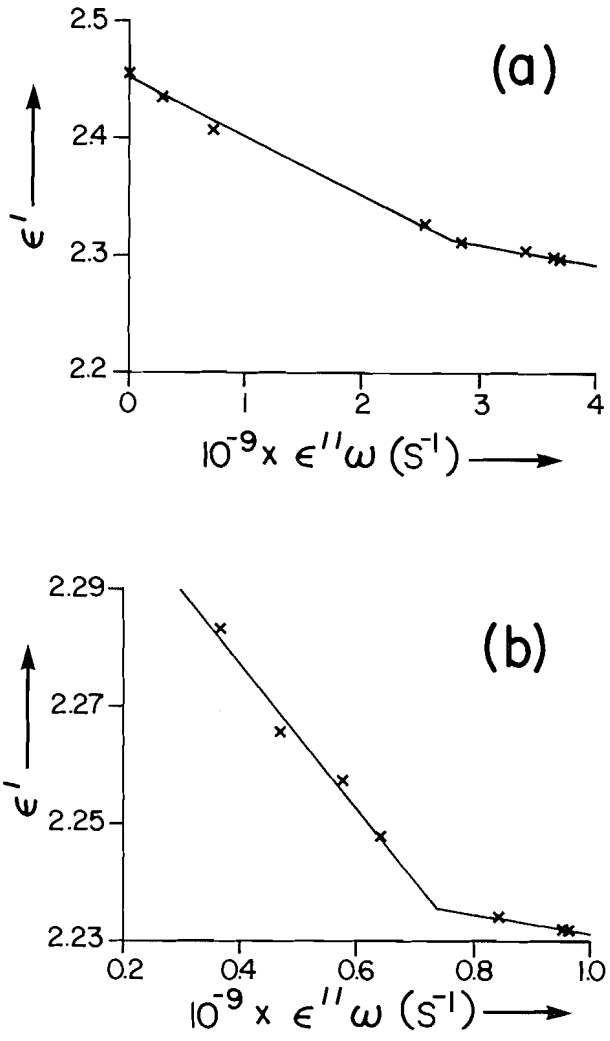

FIG. 1. ε' vs. $\varepsilon''\omega$ plots for 3-acetylphenanthrene at 298 K in (*a*) *p*-xylene, (*b*) *p*-xylene and Nujol (solution viscosity 9.0 cP).

phenanthrene, for which the loss curves were symmetric.

Discussion

Figure 1 shows clearly that there are two distinct relaxation processes for 3-acetylphenanthrene, the shorter relaxation time being relatively insensitive to the macroscopic viscosity of the solution. This would appear to justify the use of Budó analyses of the data in liquid solutions in terms of two relaxation times. Further, there is reasonable agreement in Table 1 between the τ_2 values from Budó analyses and those obtained graphically by means of [1]. The graphical $\tau_2 = 8.5 \times 10^{-12}$ s for acetophenone in pure Nujol is also in agreement with the value of $\tau_2 = 7.8 \times 10^{-12}$ s in cyclohexane at 298 K (4).

Clearly, the acetyl group in 3-acetylphenanthrene does rotate and is characterized by a relaxation time appreciably longer than in acetophenone. Similarly longer τ_2 values resulted from Budó analyses of the microwave data for 2-acetylphenanthrene and 2-acetylnaphthalene. Further, the results in Table 1 agree with those of Fong and Smyth (1–3) with respect to the low values of C_2, the weighting factor associated with the group relaxation process. This suggests that acetyl group rotation in these compounds is somewhat modified, and Fong and Smyth (1) have suggested enhanced resonance of the keto group with the conjugated ring in comparison with acetophenone may be responsible.

Molecular and intramolecular relaxation energy barriers may be obtained with reasonable accuracy from dielectric measurements of solutes in polystyrene matrices (10–13). Table 2 shows such results for 2-acetylnaphthalene, 2- and 3-acetylphenanthrene, and 2-acetyl-1-tetralone, along with some previously published results included for purposes of comparison. In acetophenone, 1,4-diacetylbenzene, and 4-acetylbiphenyl, acetyl group relaxation was

Can. J. Chem. Downloaded from www.nrcresearchpress.com by 210.87.254.40 on 09/05/12
For personal use only.

TABLE 2. Eyring analysis results for eight compounds in polystyrene matrices

Compound	T(K) range	N*	ΔH_E (kJ mol^{-1})	ΔS_E (J K^{-1} mol^{-1})	ΔG_E (kJ mol^{-1}) 200 K	ΔG_E (kJ mol^{-1}) 300 K	τ (s) 200 K	τ (s) 300 K
Acetophenone† (0.265 M)	143–213	12	29.6±0.6	26±3	24.4	21.8	5.6×10^{-7}	9.8×10^{-10}
1,4-Diacetylbenzene† (0.193 M)	133–169	5	28.7±3.0	36±20	21.5	17.8	9.7×10^{-8}	2.0×10^{-10}
4-Acetylbiphenyl† (0.162 M)	146–172	6	29.9±4.2	35±27	23.0	19.5	2.4×10^{-7}	4.0×10^{-10}
	311–331	7	68.0±5.0	33±16	61.5	58.2	2.7×10^{3}	2.2×10^{-3}
4-Nitrobiphenyl† (0.538 M)	294–313	7	85.5±8.9	106±29	64.3	53.8	1.5×10^{4}	3.7×10^{-4}
2-Acetylphenanthrene (0.242 M)	157–187	7	28.3±3.7	4±22	27.4	27.0	3.5×10^{-6}	8.0×10^{-9}
	304–333	7	85.5±5.4	97±17	66.2	56.5	4.6×10^{4}	1.1×10^{-3}
3-Acetylphenanthrene (0.248 M)	169–268	15	28.4±1.2	−4±6	29.3	29.7	1.1×10^{-5}	2.4×10^{-8}
	294–323	8	86.6±9.3	106±30	65.5	55.0	3.1×10^{4}	5.9×10^{-4}
2-Acetylnaphthalene (0.375 M)	202–232	8	33.5±4.3	−24±20	38.3	40.6	2.4×10^{-3}	1.9×10^{-6}
2-Acetyl-1-tetralone (0.424 M)	244–275	7	60.5±2.4	74±9	45.7	38.3	2.1×10^{-1}	7.6×10^{-7}

*N is the number of points on the Eyring plot. Error estimates for ΔH_E and ΔS_E are 95% confidence intervals for (N − 2) degrees of freedom.
†References 11 and 13.

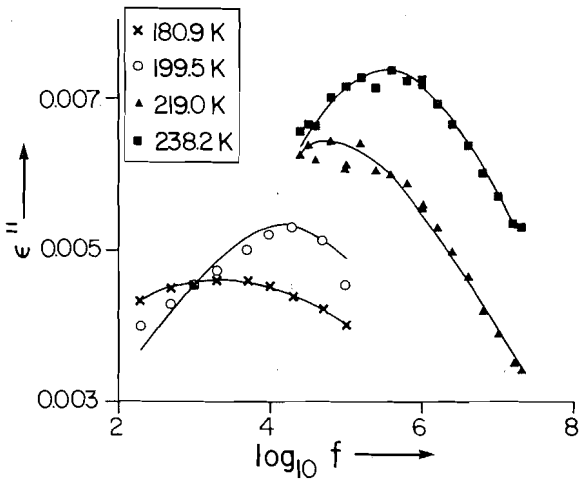

FIG. 2. Dielectric loss factor (ε″) vs. logarithmic frequency for 0.248 M 3-acetylphenanthrene in atactic polystyrene at four temperatures as indicated. The solid lines represent the best fit to the data via the Fuoss–Kirkwood equation.

characterized by $\Delta H_E \simeq 29$ kJ mol^{-1} and $\Delta S_E \simeq 30$ J K^{-1} mol^{-1} while ΔG_E at 200 K was ~23 kJ mol^{-1}. Further, molecular relaxations of 4-acetylbiphenyl and 4-nitrobiphenyl gave much larger values for both ΔH_E and ΔG_E. This would appear to establish a set of reference values for the activation parameters of acetyl group relaxation in aromatic compounds in the absence of appreciable enhanced conjugation.

For 4-acetylbiphenyl both the group and molecular relaxation processes were detected; the latter process is characterized by the Eyring parameters $\Delta H_E = 68$ kJ mol^{-1} and $\Delta G_{E(200)} = 62$ kJ mol^{-1}. 2- and 3-acetylphenanthrenes also exhibit two relaxation processes (see Table 2), and the higher temperature process yields Eyring parameters significantly greater ($\Delta H_E \sim 85$ kJ mol^{-1}) than those for 4-acetylbiphenyl but of the order to be anticipated for these somewhat larger molecules. Certainly, the lower temperature process with a ΔH_E of 28 kJ mol^{-1}, which is, in fact, a typical value for acetyl group relaxation in aromatic ketones, could not be ascribed to the molecular relaxation process. There-

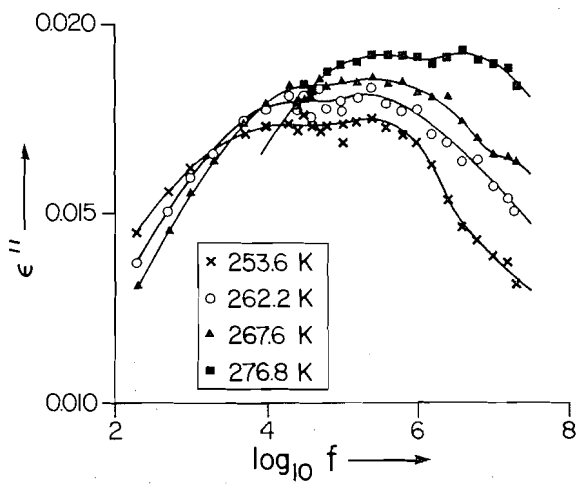

FIG. 3. Dielectric loss factor (ε″) vs. logarithmic frequency for 0.375 M 2-acetylnaphthalene in atactic polystyrene at four temperatures as indicated.

Can. J. Chem. Downloaded from www.nrcresearchpress.com by 210.87.254.40 on 09/05/12
For personal use only.

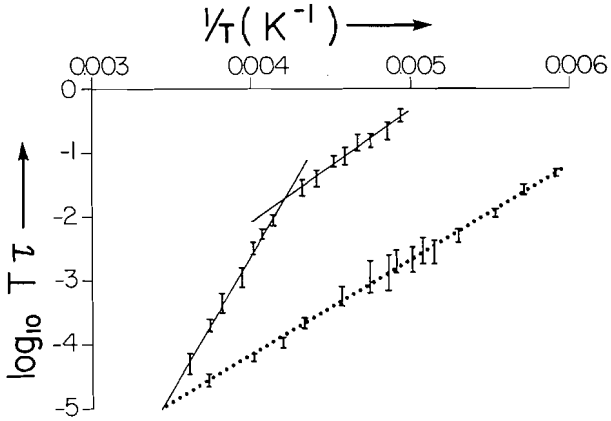

FIG. 4. Eyring graph of log ($T\tau$) vs. ($1/T$) for 0.375 M 2-acetylnaphthalene (solid lines) and for 0.248 M 3-acetylphenanthrene (dotted line) in atactic polystyrene. The vertical bars represent 95% confidence intervals on log ($T\tau$) values.

fore we allot the higher temperature data to the molecular process and the lower one to group relaxation. It must be stressed that the absorption of relaxation. It must be stressed that the absorption of the group and molecule has been separated completely for both the 2- and 3-acetylphenanthrenes in a polystyrene matrix.

Only one relaxation process has been detected for 2-acetyl-1-tetralone, with $\Delta H_E = 61$ kJ mol^{-1} and $\Delta G_{E(200)} = 46$ kJ mol^{-1}, and this corresponds fairly closely with the data for 2-cyanonaphthalene ($\Delta H_E = 54$ kJ mol^{-1} and $\Delta G_{E(200)} = 45$ kJ mol^{-1}), a molecule closely similar in shape and size.[1] Further, the temperature range of observation is higher than that found for the other acetyl group relaxation processes. It is concluded for 2-acetyl-1-tetralone that either the process is totally molecular or is a mixture of group and molecular with the latter predominating.

Although acetyl group relaxation in the two phenanthrenes yielded ΔH_E values similar to the three reference compounds, the ΔS_E values were appreciably lower, with the result that at 200 K ΔG_E values were considerably greater than in the first three compounds. For 2-acetylnaphthalene the trend in ΔS_E was continued, and ΔH_E appeared to be greater, resulting in a very much larger ΔG_E of 38.3 kJ mol^{-1} at 200 K. The higher-temperature data for this compound yielded $\Delta H_E = 82 \pm 8$ kJ mol^{-1} and $\Delta S_E = 180 \pm 30$ kJ^{-1} mol^{-1}, yielding $\Delta G_{E(200)} = 46$ kJ mol^{-1}, in excellent agreement with the value of 45.7 kJ mol^{-1} for 2-acetyl-1-tetralone for which mainly molecular relaxation appears to have been observed, as discussed earlier. These data indicate clearly that, at these temperatures, the dielectric absorption of 2-acetylnaphthalene is dominated by molecular relaxation.

The sequence of increasing ΔG_E values at 200 K for acetyl group rotation in acetophenone, 2- and 3-acetylphenanthrene, and 2-acetylnaphthalene was 24.4, 27.4, 29.3, and 38.3 kJ mol^{-1}, respectively. This sequence is reflected in the stretching frequencies of the carbonyl group ($\bar{\nu}_{C=O}$) shown in Table 3 for these compounds in CCl_4, being 1691, 1689, 1688, and 1678 cm^{-1}, respectively. A decrease in the $\bar{\nu}_{C=O}$ value is in harmony with greater conjugation of the carbonyl group with the ring. Thus, both $\Delta G_{E(200)}$ and $\bar{\nu}_{C=O}$ suggest appreciably enhanced conjugation of the C=O group in 2-acetylnaphthalene in comparison with acetophenone.

Davies and Swain (8) employed Debye and Fuoss–Kirkwood relationships to estimate from their polystyrene matrix data the effective dipole moment, μ, associated with the relaxation process observed. While these were low at the measurement temperatures, they found that a linear extrapolation of μ vs. temperature yielded, on the whole, values comparable to liquid solution results at temperatures between 300 to 320 K. We have followed their procedures for our matrix data for 4-acetylbiphenyl and 2- and 3-acetylphenanthrene. In each of these molecular and acetyl group relaxations were observed to be well separated, and we have evaluated the two dipole moments separately, the data being shown in Table 4. From these data we have calculated the total dipole moment from [3] and the weight factor for molecular relaxation, C_1, from [4] and [5].

$$[3] \qquad (\mu_{tot})^2 = (\mu_{\parallel})^2 + (\mu_{\perp})^2$$

$$[4] \qquad C_1/C_2 = (\mu_{\parallel}/\mu_{\perp})^2$$

$$[5] \qquad C_1 + C_2 = 1$$

Table 4 also includes the extrapolated μ_{tot} for 2-acetylnaphthalene for which the overlap of the two absorption processes prevented separate evaluation of $\mu_{\parallel}$ and $\mu_{\perp}$.

TABLE 3. Infra-red carbonyl stretching frequencies for six compounds

Compound	$\bar{\nu}$ (cm^{-1})	Solvent
Acetylcyclohexane*	1713	CCl_4
Acetophenone	1691	CCl_4
	1689	C_6H_6
2-Acetylphenanthrene	1689	CCl_4
	1688	C_6H_6
3-Acetylphenanthrene	1688	CCl_4
	1687	C_6H_6
2-Acetylnaphthalene*	1678	CCl_4
1-Acetylcyclohexene	1670	CCl_4

*Reference 23.

[1]S. P. Tay. Private communication.

Can. J. Chem. Downloaded from www.nrcresearchpress.com by 210.87.254.40 on 09/05/12
For personal use only.

TABLE 4. Effective dipole moments extrapolated to 320 K for molecular ($\mu_{\parallel}$) and acetyl group ($\mu_{\perp}$) relaxation, with resultant total (μ_{tot}), literature values (μ_{lit}), and molecular relaxation weight factor (C_1)

Compound	$\mu_{\parallel}$ (D)	$\mu_{\perp}$ (D)	μ_{tot} (D)	μ_{lit}* (D)	C_1
4-Acetylbiphenyl	1.95	2.47	3.15	3.10	0.38
2-Acetylphenanthrene	2.02	1.91	2.78		0.53
3-Acetylphenanthrene	2.20	1.70	2.78		0.63
2-Acetylnaphthalene			3.10	3.13	

*Reference 5.

For 4-acetylbiphenyl and 2-acetylnaphthalene the μ_{tot} values are in good agreement with literature data (5). One may expect similar values (~ 3 D) for the two phenanthrenes, and the experimental extrapolated results are in reasonable agreement, bearing in mind that at best the error is of the order of $\pm 10\%$. Such agreement suggests that the component dipole moments so obtained are reasonably reliable, and hence that the C_1 values derived are similarly meaningful. Therefore, it is noteworthy that 2- and 3-acetylphenanthrene which contain the 2-acetylnaphthalene unit yielded C_1 values significantly greater than that of acetophenone ($C_1 \sim 0.33$) (4) while 4-acetylbiphenyl, which has more structural similarity with the latter molecule, gave a C_1 (0.38) similar to that of acetophenone. These results bear out the solution studies in the microwave region; hence, there can be little doubt that some factor is at play which diminishes the value of C_2 in these compounds which contain the 2-acetylnaphthalene unit. The actual values of C_2 by both approaches are prone to considerable error. However, both the matrix and the solution studies being taken into account, it would seem that for the three molecules the C_2 value is something of the order of 0.3 ± 0.15.

The ΔH_E value for acetyl group relaxation in 2-acetylnaphthalene would seem about 6 kJ mol^{-1} greater than that for the other aromatic ketones in Table 2. However, the possibility exists that the ΔH_E value for 2-acetylnaphthalene is in greater error since in this case there may be some overlap of the dielectric absorptions of the group and molecular processes. From the magnitude of the weight factor, though, the main point would appear to be that, although the C_2 values for acetophenone and 2- and 3-acetylphenanthrene differ significantly, the cause of the discrepancy is not to be sought in terms of ΔH_E values. It is possible that the sequence of ΔG_E values for group relaxation offers a more promising lead. It is also to be noted for the microwave data in Table 1 that the τ_2 values for 2-acetylnaphthalene and the 2- and 3-acetylphenanthrenes are all appreciably longer than those for acetophenone; this, of course, again is in line with a lower free energy of activation for group relaxation in acetophenone than in the other three acetyl compounds.

Conclusions

Group relaxation has been established for the acetyl group in dilute solution in nonpolar solvents and in a polystyrene matrix for 2-acetylnaphthalene and 2- and 3-acetylphenanthrene. Both in the liquid solutions and in the matrices we have found that $C_2 < C_1$. The Eyring activation parameters have been determined for these group relaxations in a polystyrene matrix.

It would seem possible that there is enhanced conjugation of the acetyl group in 2-acetylnaphthalene compared with that in acetophenone as Fong and Smyth (1) postulated, and that this is borne out by the ΔH_E values and the carbonyl stretching frequency. However, this enhanced conjugation alone does not account for the low weight factor for group relaxation in 2-acetylnaphthalene since 2- and 3-acetylphenanthrene have similar weight factors but exhibit no sign of an enhanced enthalpy of activation for group relaxation. The ΔG_E values at 200 K for acetyl relaxation follow the sequence: acetophenone < 2-acetylphenanthrene < 3-acetylphenanthrene < 2-acetylnaphthalene, and this is the order of increased conjugation as assessed by the carbonyl stretching frequency. However, the variation in $\bar{\nu}_{C=O}$ amongst the first three is only ~ 3 cm^{-1} whereas between acetophenone and 2-acetylnaphthalene the shift is 13 cm^{-1}.

Acknowledgements

We wish to thank the National Research Council of Canada for financial support and to express our appreciation to Mr. B. K. Morgan for his technical assistance.

1. F. K. FONG and C. P. SMYTH. J. Am. Chem. Soc. **85**, 548 (1963).
2. F. K. FONG and C. P. SMYTH. J. Am. Chem. Soc. **85**, 1565 (1963).
3. F. K. FONG and C. P. SMYTH. J. Chem. Phys. **40**, 2404 (1964).
4. D. B. FARMER, P. F. MOUNTAIN, and S. WALKER. J. Phys. Chem. **77**, 714 (1973).

Can. J. Chem. Downloaded from www.nrcresearchpress.com by 210.87.254.40 on 09/05/12
For personal use only.

5. A. L. McCLELLAN. Table of experimental dipole moments. Vol. 2. Rahara Enterprises, El. Cerrito, CA, U.S.A. 1974.
6. J. CROSSLEY, S. P. TAY, and S. WALKER. Adv. Mol. Relaxation Processes, **6**, 79 (1974).
7. M. DAVIES and A. E. EDWARDS. Trans. Faraday Soc. **63**, 2163 (1967).
8. M. DAVIES and J. SWAIN. Trans. Faraday Soc. **67**, 1637 (1971).
9. S. P. TAY and S. WALKER. J. Chem. Phys. **63**, 1634 (1975).
10. S. P. TAY, J. KRAFT, and S. WALKER. J. Phys. Chem. **80**, 303 (1976).
11. C. K. McLELLAN and S. WALKER. Can. J. Chem. **55**, 583 (1977).
12. S. P. TAY, S. WALKER, and E. WYN-JONES. Adv. Mol. Relaxation Processes. In press.
13. C. K. McLELLAN. Ph.D. Thesis, The University of Manitoba, Winnipeg, Man., Canada. 1977.
14. W. F. HASSELL, M. D. MAGEE, S. W. TUCKER, and S. WALKER. Tetrahedron, **20**, 2137 (1964).
15. E. H. GRANT and S. E. KEEFE. Rev. Sci. Instrum. **39**, 1800 (1968).
16. T. I. BORISOVA and V. N. CHIRKOV. Russ. J. Phys. Chem. **47**, 949 (1973).
17. J. CROSSLEY, S. P. TAY, and S. WALKER. Adv. Mol. Relaxation Processes, **6**, 69 (1974).
18. K. S. COLE and R. H. COLE. J. Chem. Phys. **9**, 341 (1941).
19. M. D. MAGEE and S. WALKER. Trans. Faraday Soc. **62**, 3093 (1966).
20. A. BUDÓ. Z. Phys. **39**, 706 (1938).
21. R. M. FUOSS and J. G. KIRKWOOD. J. Am. Chem. Soc. **63**, 385 (1941).
22. N. E. HILL, W. E. VAUGHAN, A. H. PRICE, and M. DAVIES. Dielectric properties and molecular behaviour. Van Nostrand Reinhold Co., London, England. 1969. p. 292.
23. D. B. FARMER. Ph.D. Thesis, University of Aston in Birmingham, Birmingham, England. 1967.

Can. J. Chem. Downloaded from www.nrcresearchpress.com by 210.87.254.40 on 09/05/12
For personal use only.

Diffusion coefficients and viscosities in glycol and glycerol solutions

JOHN E. EVANOFF AND WALTER E. HARRIS

Department of Chemistry, University of Alberta, Edmonton, Alta., Canada T6G 2G2

Received September 6, 1977

JOHN E. EVANOFF and WALTER E. HARRIS. Can. J. Chem. **56**, 574 (1978).

Diffusion coefficients have been measured polarographically in media with a wide range of viscosities. The range covers five orders of magnitude up to the limits of high viscosity possible by normal polarographic means. The diffusion coefficients obtained are nearly inversely proportional to the viscosity. The diffusion coefficients are in the range of interest to chromatography theory.

JOHN E. EVANOFF et WALTER E. HARRIS. Can. J. Chem. **56**, 574 (1978).

On a mesuré les coefficients de diffusion, d'une façon polarographique, dans des milieux de viscosité très variable. Les écarts de viscosité couvrent cinq ordres de grandeur jusqu'aux limites supérieures de viscosité possibles par les méthodes polarographiques normales. Les coefficients de diffusion obtenus sont, à toutes fins pratiques, inversement proportionnels à la viscosité. Les coefficients de diffusion sont dans les écarts d'intérêt de la théorie de chromatographie.

[Traduit par le journal]

Can. J. Chem. Downloaded from www.nrcresearchpress.com by 210.87.254.6 on 09/05/12
For personal use only.

Rates of diffusion of small solute molecules in viscous solvents are important in gas chromatography because of their influence on resistance to mass transfer and hence on plate height and column efficiency. In van Deemter curves (1) of plate height against carrier-gas velocity, the band broadening at high flow rates is attributed largely to resistance to mass transfer, particularly in the stationary phase. The slow rates of mass transfer to and from the liquid and moving-gas phases is caused mainly by a low rate of diffusion of solute molecules in the liquid phase. Accordingly, a knowledge of diffusion coefficients in viscous liquids should contribute to the quantitative understanding of the factors involved in column efficiency.

In this study diffusion coefficients in viscous media were measured polarographically. The polarographic method is one of the simplest methods and is applicable to dilute solutions. Since measurements of diffusion coefficients by any method are likely to require experimental finesse, it would be convenient if a generally applicable relation could be established between diffusion coefficients and a more simply measurable property such as viscosity.

Several nitro compounds were chosen for the study because of their well established polarographic behaviour and their well defined current–voltage curves (2). Their polarographic reduction proceeds through a four-electron step to form a corresponding hydroxylamine.

Experimental

Fisher reagent-grade ethylene glycol and glycerol were used as solvents with 0.1 *M* lithium chloride as indifferent electrolyte. Several difficulties arising from the high viscosities, particularly of glycerol, had to be overcome. First of all, it was found best to prepare the solutions by weight to give dilute solutions of known concentration about 10^{-3} *M*. Removal of dissolved oxygen took more time (30 min) than for aqueous solutions. Loss of solute during removal was minimized by presaturating the purified nitrogen with a part of the solution to be examined, before passing it into the electrolytic cell, and also by using a low temperature (0°C for glycol, 25°C for glycerol). After treatment the solutions, particularly of glycerol, were milky in appearance from the many small bubbles of nitrogen. The procedure adopted for removal of these bubbles involved storage for up to 12 h in a nitrogen atmosphere prior to making measurements. At the lowest temperature, especially again in glycerol-based solutions, the viscosity is beyond the limit at which normal polarographic measurements can be made. The mercury drops would not fall free from the electrode and would sometimes merge with the next drop to form. A slight extension of the viscosity limit was possible by grinding the electrode tip as shown in Fig. 1. With such a tip the individual drops no longer interfered with each other though they fell extremely slowly, as can be seen from the figure. At temperatures in excess of about 40°C erratic drop formation was observed, which appeared to result from retreat of the mercury column up the capillary after a drop had broken free. This effect disappeared after the inside of the capillary was coated with silicone (3).

The reference electrode used in the polarographic cell was silver – silver chloride, and the electrolytic cell a 29- × 75-mm tube. Viscosities were determined with routine Cannon–Fenske calibrated viscometers; they were chosen so that the efflux time was between 200 and 600 s. The viscometers were charged with the sample solutions, and five efflux time determinations were carried out on each solution and at each temperature. Densities at the various temperatures of the 0.1 *M* lithium chloride – glycol or – glycerol solutions were determined by the pycnometer technique. Capillary constants were measured over the temperature range used. Diffusion coefficients were computed from the Ilkovic equation and the measured diffusion currents.

Results and Discussion

The current–voltage curves obtained for the various nitro compounds were well formed and

Can. J. Chem. Downloaded from www.nrcresearchpress.com by 210.87.254.6 on 09/05/12
For personal use only.

FIG. 1. Instantaneous photograph showing ten consecutive mercury drops in 0.1 *M* LiCl – glycerol at 1°C. Drop time 4.5 s; viscosity approximately 107 P.

symmetrical in both ethylene glycol and glycerol at high and at low temperatures (Fig. 2). All the nitro compounds tested showed a linear relation between diffusion current and concentration in the millimolar range and in the temperature range from 0 to 100°C. The capillary constant over the temperature range of 100°C was relatively constant. It varied from 1.54 to 1.50 $mg^{2/3}\ s^{-1/2}$ in 0.1 *M* LiCl – ethylene glycol and from 1.62 to 1.74 $mg^{2/3}\ s^{-1/2}$ in 0.1 *M* LiCl – glycerol. Diffusion coefficients were calculated from the Ilkovic expression ($I_d = 607nD^{1/2}Cm^{2/3}t^{1/6}$); the results are summarized in Table 1. It is evident from the table that diffusion coefficients were measured that cover the range from values typical of ions in aqueous solution (with glycol at 100°C) to values about five orders of magnitude smaller (with glycerol at 0°C).

Since the measurement of diffusion coefficients by polarographic means is experimentally tedious, an attempt was made to correlate the coefficients to the more simply measurable properties of viscosity and the molecular characteristics. If the viscosities and diffusion coefficients in Table 1 are plotted as a function of each other, we can see a nearly (but not exactly) inverse relation between the two, over several orders of magnitude (Fig. 3).

For the diffusion of spherical macromolecules or particles in a solvent, the Stokes–Einstein relation (4) is valid, that is, the diffusion coefficient is equal to $kT/6\pi\eta r$, where k is Boltzmann's constant, T is absolute temperature, η is viscosity, and r is the radius of the diffusing species. The factor 6π is

TABLE 1. Polarographic diffusion coefficients of nitro compounds in 0.1 *M* LiCl – ethylene glycol (top) or 0.1 *M* LiCl – glycerol (bottom) at temperatures from 0 to 100°C

Temp. (°C)	Viscosity (P)	Diffusion coefficients ($cm^2/s \times 10^7$)								
		Nitroethane	1-Nitropropane	2-Nitropropane	1-Nitrobutane	2-Nitrobutane	Nitrobenzene	*o*-Nitrotoluene	2-Nitro-*p*-xylene	3-Nitro-*o*-xylene
0	0.620	3.4	2.85	2.18	1.93	2.45	2.59	2.18	1.95	2.00
20	0.223	9.8	8.1	6.1	5.1	6.4	7.2	6.4	6.0	5.6
40	0.102	19.6	16.8	13.2	11.0	14.7	18.3	14.8	13.8	13.7
60	0.0546				19 0	28.1	36	31	27.5	28.5
80	0.0328						54	50	47	46
100	0.0215						87	70	65	62
0	130.3	0.0033	0.0032	0.0029	0.0021	0.0009	0.0054	0.0049	0.0044	0.0063
20	15.4	0.031	0.031	0.029	0.0206	0.0054	0.060	0.048	0.042	0.060
40	3.16	0.184	0.178	0.162	0.138	0.0310	0.34	0.296	0.266	0.38
60	0.880				0.49	0.105	1.38	1.07	1.91	1.31
80	0.338						3.35	2.84	2.6	3.5
100	0.157						8.1	5.7	5.5	7.1

Can. J. Chem. Downloaded from www.nrcresearchpress.com by 210.87.254.6 on 09/05/12
For personal use only.

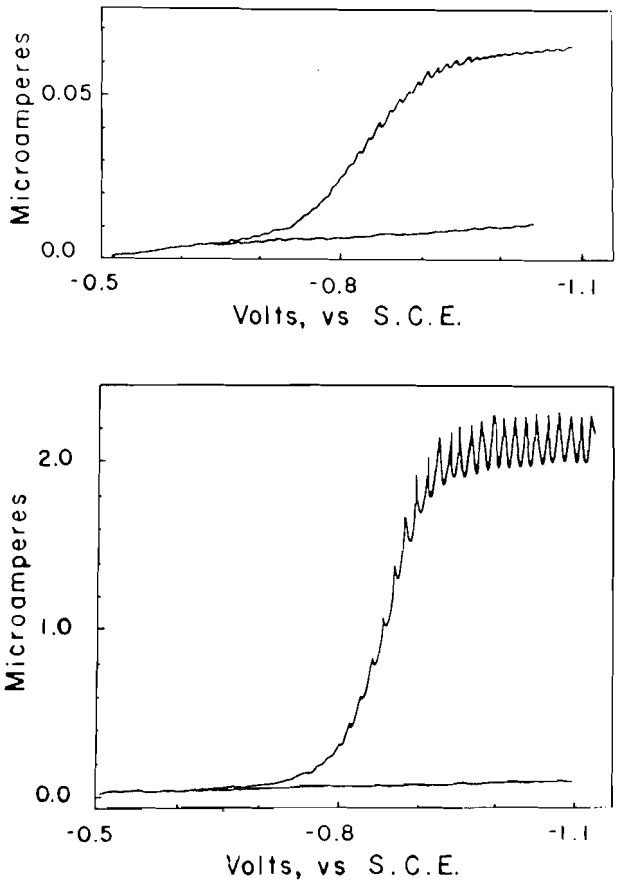

FIG. 2. Polarograms of 5.5×10^{-4} *M* nitrobenzene in 0.1 *M* LiCl – glycerol at 0°C (top) and 100°C (bottom).

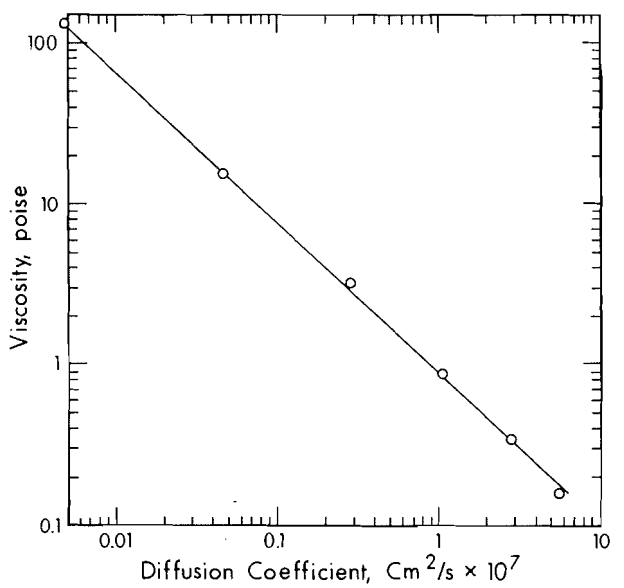

FIG. 3. Relation between viscosity and diffusion coefficient for nitrobenzene in glycerol. Data from Table 1.

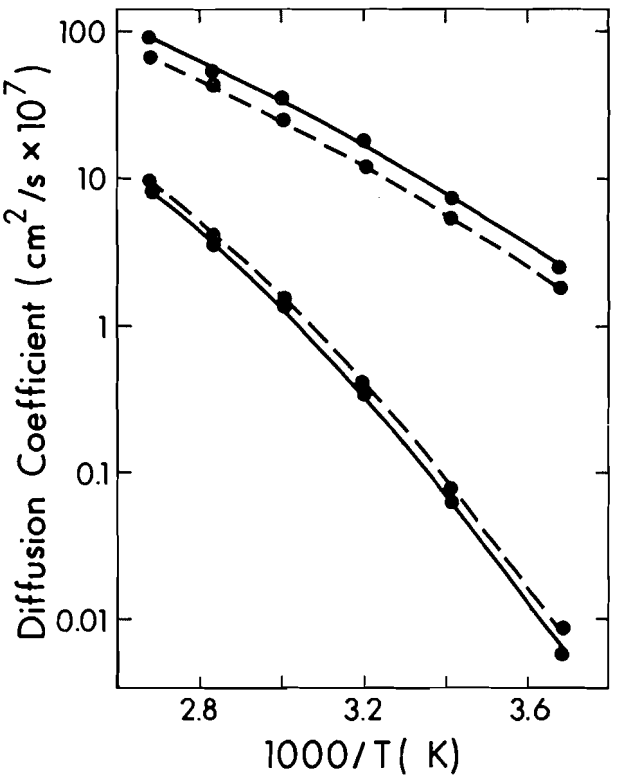

FIG. 4. Comparison of diffusion coefficients calculated from viscosity (dotted lines) for nitrobenzene in 0.1 *M* LiCl – ethylene glycol (top) and in 0.1 *M* LiCl – glycerol (bottom) with those measured polarographically (solid lines).

based on the assumption that the medium can be regarded as homogeneous.

For self-diffusion, that is, diffusion of solvent within itself, hydrodynamic theory (5) indicates that the 6π is replaced by 4π. For spherical, nonsolvated molecules the radius can be expressed in terms of molar volume of the substance, and the Stokes–Einstein relation is modified to

$$[1] \qquad D_{\text{liq}} = \frac{k}{2\pi}\left(\frac{N}{V}\right)^{1/3}\frac{T}{\eta}$$

where N is Avogadro's number and V is the molar volume. Experimentally, the values corresponding to the constant 2π (6.3) were found by Li and Chang to vary between 5.4 and 8.3 (5).

It would not be surprising should a relation similar to that shown in eq. 1 be found to apply for the diffusion of small molecules in a solvent consisting of larger molecules, but with an adjustment of the factor 2π. It seems reasonable, from our knowledge of the diffusion rates of particulates and of self-diffusion, that the factor 2π should be somewhat smaller. Figure 4 compares the diffusion co-

efficients of nitrobenzene measured polarographically and those calculated from eq. 1, with 2π replaced by 1.4π. The trends and general agreement are such that useful estimates of diffusion coefficients could be expected from viscosity information. Even though the agreement is not perfect, the results obtained should be applicable to a range of typical solutes and solvents of interest to gas chromatography.

Acknowledgement

The authors, particularly J.E.E., thank the National Research Council of Canada for support of this research.

1. J. J. VANDEEMTER, F. J. ZUIDERWEG, and A. KLINKENBERG. Chem. Eng. Sci. **5**, 271 (1956).
2. N. RADIN and T. DEVRIES. Anal. Chem. **24**, 971 (1952).
3. J. JORDAN, E. ACKERMAN, and R. L. BERGER. J. Am. Chem. Soc. **78**, 2979 (1956).
4. G. M. BARROW. Physical chemistry. McGraw Hill, New York. 1966. p. 792.
5. J. C. M. LI and P. CHANG. J. Chem. Phys. **23**, 518 (1955).

Can. J. Chem. Downloaded from www.nrcresearchpress.com by 210.87.254.6 on 09/05/12
For personal use only.

Substituent effect on the carbon-13 nuclear magnetic resonance spectra of 2-substituted tropones. Troponoid-I

J. F. BAGLI

Department of Chemistry, Ayerst Research Laboratories, Montréal, P.Q., Canada H3C 3J1

AND

M. ST-JACQUES

Departement de chimie, Université de Montréal, Montréal. P.Q., Canada H3C 3V1

Received September 14, 1977

J. F. BAGLI and M. ST-JACQUES. Can. J. Chem. **56**, 578 (1978).

The ^{13}Cmr spectra of a series of 2-substituted tropones were analysed using a combination of methods including specific deuteration, multiplicities in coupled ^{13}Cmr spectra and proton off-resonance decoupling techniques. The published ^{13}C assignment for tropolone acetate was proven wrong and was corrected. Substituent parameters were defined and shown to exhibit two linear relationships with the corresponding substituent parameters for analogous monosubstituted benzenes. The significance of the results is discussed.

J. F. BAGLI et M. ST-JACQUES. Can. J. Chem. **56**, 578 (1978).

On a analysé le spectre rmn ^{13}C d'une série de tropones substituées en position 2 en faisant appel à une combinaison de méthodes comprenant la deutération spécifique, les multiplicités des spectres rmn ^{13}C couplés et des techniques de découplage du proton. On a démontré que les attributions publiées pour le ^{13}C de l'acétate de tropolone sont incorrectes et on les a corrigées. On a défini des paramètres de substituants et on a montré qu'ils présentent deux relations linéaires avec les paramètres de substituants correspondants pour les benzènes monosubstitués analogues. On discute de la signification de ces résultats.

[Traduit par le journal]

Tropone derivatives constitute a class of naturally occurring nonbenzenoid aromatic substances, several of which could be of potential pharmaceutical interest (1). Structural assignment and isomer characterization of synthetic derivatives are often difficult by proton magnetic resonance (^{1}Hmr) spectroscopy owing to the small chemical shift range for the various strongly coupled nonequivalent ring protons; these often exhibit second-order multiplets (2, 3) which are tedious to analyse completely.

By contrast, because of the larger chemical shifts and greater spectral simplicity, proton decoupled carbon-13 magnetic resonance (^{13}Cmr) spectroscopy appears to be a more promising tool of structure elucidation. Because of our interest in tropone chemistry, it became important for us to determine the advantages and limitations of ^{13}Cmr spectroscopy in this area.

Although the ^{13}Cmr spectra of tropone (**1**) (4), thiotropone (4), and of a few simple derivatives (5) have been reported, very little information exists on the effect of substituents on the ^{13}Cmr parameters of tropone derivatives. This paper describes the analysis of the ^{13}Cmr spectra of a series of 2-substituted tropones (**2**-X, where X denotes the nature of the substituent). All of the compounds studied were prepared using published procedures or modifications thereof as described in the experimental section. By providing a description of the substituent effect on each ring carbon, our investigation has enabled us to reassign unequivocally the carbon signals of tropolone acetate (**2**-$OCOCH_3$) (*5a*).

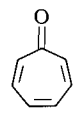

1

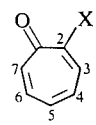

2

X = OH, OCH_3, $OCOCH_3$, NH_2, $NHCH_3$, $NHCOCH_3$, Cl, CH_3, SCH_3

Results and Discussion

Spectral Assignments

The published assignment (4) of the spectral lines of tropone (**1**), the reference compound in our study, has been confirmed by our work (*vide infra*) and the carbon shifts are reported in Table 1.

The spectral analysis of the various 2-substituted tropones (**2**-X) required a combination of arguments: intensity differences owing to relaxation effects, specific deuteration, carbon–hydrogen coupling constants, and proton off-resonance decoupling techniques (6).

Excluding the substituent signals, which are readily assignable, two groups of lines are easily distinguished in the proton decoupled ^{13}Cmr

Can. J. Chem. Downloaded from www.nrcresearchpress.com by 210.87.254.40 on 09/05/12
For personal use only.

TABLE 1. Carbon-13 chemical shifts for the ring carbons of various 2-substituted tropones[a]

Substituent	δ						
	C-1	C-2	C-3	C-4	C-5	C-6	C-7
H	187.7	141.7	135.8	134.4	134.4	135.8	141.7
OCH_3	180.1	165.0	112.2	132.4	127.6	136.3[b]	136.3[b]
$OCOCH_3$[c]	178.3	157.5	128.1	132.1	134.1	137.5	139.5
NH_2	176.2	157.4	112.7	129.9	123.5	136.2[d]	136.7[d]
$NHCH_3$	176.4	156.2	107.9	128.0	121.6	136.0[d]	136.9[d]
$NHCOCH_3$	178.9	146.6	120.6	135.6	130.4	136.0[d]	137.6[d]
Cl	179.9	148.7	135.3	131.2	133.9	138.3	135.6
CH_3	186.9	152.0	134.8[d]	133.5	132.2	139.4	135.2[d]
SCH_3	182.8	159.8	126.4	132.1	129.1	133.8[d]	135.8[d]

[a]In ppm from TMS using $CDCl_3$ as solvent and internal reference with $\delta_C = 76.9$ ppm, unless otherwise indicated.
[b]These two carbons gave lines separated by 0.4 ppm in DMSO-d_6.
[c]Data reported in ref. 5*a* for a DMF solution at −70°C; reassigned (*vide infra*).
[d]The assignment of the pair of labelled lines has not been firmly established and could be reversed for some of the compounds.

spectra: two less intense lines associated with the nonprotonated C-1 and C-2 and five more intense lines associated with the five protonated ring carbons. It is for this latter group that special assignment techniques were required including the preparation of 3,5,7-trideuterio-2-methoxytropone (**3**), 3,5,7-trideuteriotropolone (**4**) and its acetyl derivative **6**.

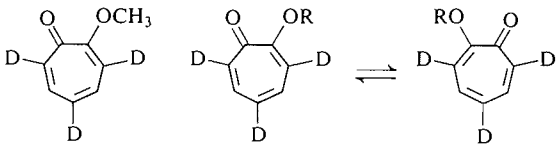

3 **4** (R = H) **6** (R = $COCH_3$) **5** (R = H) **7** (R = $COCH_3$)

Tropolone-d_3 (**4**), which is known to undergo rapid tautomerization (**4** ⇌ **5**) at room temperature, gave a ^{13}Cmr spectrum showing only one protonated carbon line whose chemical shift is in accord with the published (7) value for the signal of the equivalent C-4 and C-6 of tropolone. This observation therefore confirms the assignment based on charge density calculations.

The comparison of the proton decoupled ^{13}Cmr spectra of **2**-OCH_3 (Fig. 1A) and its deuterated derivative **3** (Fig. 1B) allowed the partial assignment of the protonated carbon lines by identifying two sub-groups of lines, namely those arising from C-3, C-5, and C-7 now appearing as weak triplets (because of coupling with the directly bonded deuterium atom) and those arising from C-4 and C-6 still observed as intense singlets.

Charge density arguments similar to those used for tropolone (7) are much less conclusive when used to assign C-4 and C-6. Consequently we proceeded to make an unequivocal assignment through a combination of the following techniques: the analysis of

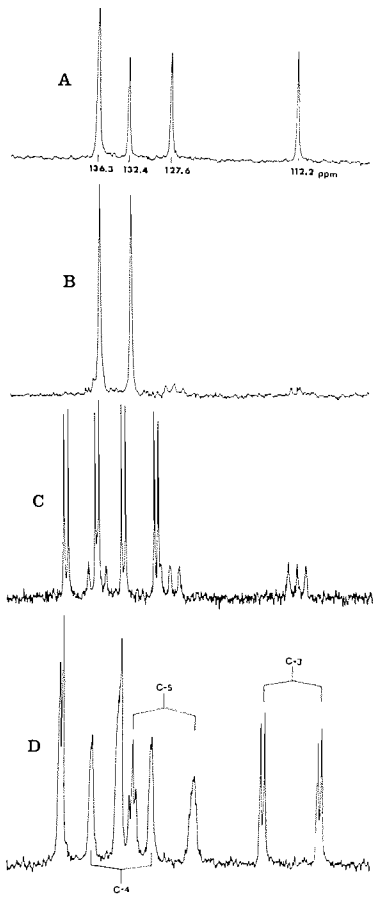

FIG. 1. Proton decoupled and coupled ^{13}Cmr spectra of **2**-OCH_3 (A and D, respectively) and of **3** (B and C).

coupled (i.e. non-proton-decoupled) spectra, the determination of residual splitting in off-resonance decoupled spectra, and selective proton decoupling (6).

The coupled ^{13}Cmr spectrum of **3** (Fig. 1C) shows

Can. J. Chem. Downloaded from www.nrcresearchpress.com by 210.87.254.40 on 09/05/12
For personal use only.

Can. J. Chem. Downloaded from www.nrcresearchpress.com by 210.87.254.40 on 09/05/12
For personal use only.

that both the C-4 and C-6 signals consist of two doublets arising from a large $^1J_{CH}$ and a smaller $^3J_{CH}$. Three signals (C-3, C-5, and C-7) are clearly seen as triplets in accord with one bond C–D couplings and small (unresolved) two-bond carbon–hydrogen couplings as in benzene (8). The pertinent carbon–hydrogen coupling constants obtained from a first-order analysis are reported in Table 2.

Proton decoupling experiments (9–11) with a stepwise variation of the irradiating field frequency provided evidence for the unambiguous assignment of the C-4 and C-6 signals from the analysis of the residual splitting (J_r) arising from coupling only to directly bonded protons (i.e. $^3J_{CH}$ effects are eliminated) as described next.

Bertelli *et al.* (3) reported that the computer simulation of the second-order proton spectrum of **2**-OCH_3 in C_6D_6 revealed a chemical shift difference of 14.8 Hz (100 MHz; $^4J_{HH}$ 1.1 Hz) for H-4 and H-6 whereas our analysis of the first-order 100 MHz deuterium decoupled ^{1}Hmr spectrum of **3** in $CDCl_3$ gave 13.8 Hz ($^4J_{HH}$ = 1.0 Hz). The agreement thus supports the authors' conclusion (3) that H-4 absorbs at higher field than H-6.

The off-resonance proton decoupled spectrum of **3** showed two doublets with J_r larger for the lower field ^{13}C signal when the irradiating field was located upfield from both the H-4 and H-6 resonances whereas the larger splitting was observed for the upfield ^{13}C doublet when the decoupling field was placed downfield from both H-4 and H-6. It is therefore evident that the upfield ^{13}C signal relates with the upfield proton line (and vice versa) and it follows (9) that C-4 is upfield from C-6 in **3** and in **2**-OCH_3 as reported in Table 1.

The coupled ^{13}Cmr spectrum of **2**-OCH_3 is shown in Fig. 1D. First-order patterns arising mainly from $^1J_{CH}$ and $^3J_{CH}$ couplings are not always observed because of the small proton chemical shifts (6). Although second-order effects complicate the spectral analysis, it is nevertheless possible to identify the C-5 multiplet because it is the only carbon atom expected to show multiplicity arising from two relatively large (between 10 and 13 Hz) but not necessarily equal $^3J_{CH}$ couplings. The lowfield component of the C-5 multiplet is sufficiently first order to give a triplet (such is not the case for the upfield component) and thus allow clearcut identification of the C-5 signal. The C-1 signal also gives a triplet because of similarly large three-bond couplings with H-3 and H-6. All the $^1J_{CH}$ values of the protonated carbon atom are given in Table 2.

TABLE 2. Carbon–proton coupling constants[a] for **2**-OCH_3

	J_{CH}				
Nuclei	H-3	H-4	H-5	H-6	H-7
C-3	~153				
C-4		158.9		10.3	
C-5			~162		
C-6		11.8		155.8	
C-7					~160

[a]The $^1J_{CH}$ and $^3J_{CH}$ values (in Hz) obtained from the spectral analysis of **3** are reported with a decimal point. The other $^1J_{CH}$ values were obtained from measurements on the coupled spectrum of 2-OCH_3 and are believed to be accurate within 2 Hz. Furthermore, $^3J_{C\text{-}1,H\text{-}6}$ = 12.5 was obtained from the analysis of **3**.

Proton decoupled off-resonance spectra with variable irradiating field frequency (9) was used to confirm the assignment of the C-3 and C-7 signals by relating these two signals with the assigned (3) proton resonances of H-3 (upfield) and H-7 (downfield). By setting the proton decoupling field upfield from H-3 and then downfield from H-7, the appreciable difference in J_r observed for the appropriate ^{13}C doublets confirmed that C-3 is the most upfield ring carbon. Selective irradiation (11) at the H-3 frequency collapsed the most upfield ring carbon signal and thus confirmed the above assignment.

The coupled ^{13}Cmr spectrum of tropone also revealed that the upfield component of the signal centered at 134.4 ppm (Table 1) is a triplet in accord with the existence of two large $^3J_{CH}$ values for the equivalent C-4 and C-5 atoms responsible for that signal (4).

It has been reported (*5a*) that **2**-$OCOCH_3$ (tropolone acetate) undergoes rapid intramolecular acetyl exchange at room temperature for which $\Delta G^{\neq}$ is 10.8 kcal/mol. Consequently a nonaveraging spectrum can be recorded below −60°C. The protonated ring carbon line in the ^{13}Cmr spectrum of **6** (δ_C = 133.7 in $CDCl_3$ at room temperature) splits into a doublet with components at 136.8 and 131.5 ppm at −72°C in accord with the slowing down of the acetyl exchange **6** ⇌ **7**. This observation demonstrates that the published assignment for the C-3, C-7, and C-4, C-6 pairs is wrong and should be reversed. The correct line assignment is given in Table 1.

The identification of the C-5 signal from the coupled spectra of **2**-NH_2, **2**-$NHCH_3$, and **2**-$NHCOCH_3$ together with the expectation that C-3 should have the smallest methine chemical shift allowed the assignment of the ring carbon signals as reported in Table 1.

Because the spectral lines of the five methine carbons of **2**-Cl and **2**-CH_3 are closely spaced (e.g. 138.3, 135.6, 135.3, 133.9, 131.2 ppm for **2**-Cl), their assignment is less straightforward. The off-resonance doublets for the lines at 138.3, 133.9, and 131.2 ppm were easy to recognize so that J_r could be measured with the proton irradiating field at the higher and at

Can. J. Chem. Downloaded from www.nrcresearchpress.com by 210.87.254.40 on 09/05/12
For personal use only.

the lower field sides of all the methine proton resonances. But because of the closeness of the lines at 135.6 and 135.3 ppm it was impossible to make an unambiguous assignment from J_r values alone. From the knowledge (3) that the proton chemical shifts of **2**-Cl follow the order: H-3 > H-7 > H-6 > H-5 > H-4 it was easy to selectively decouple H-3 and H-7 and show that the chemical shifts of C-3 and C-7 are 135.3 and 135.6 ppm, respectively. The combined use of J_r values, selective decoupling and the analysis of the coupled spectrum of **2**-Cl led to the complete assignment given in Table 1.

The C-5 line of **2**-CH_3 was identified from the coupled ^{13}Cmr spectrum and the other lines were assigned to the various carbons as shown in Table 1 from an analogy with the spectrum of **2**-Cl.

Analysis of the coupled and decoupled spectra of **2**-SCH_3 together with the expectation that C-3 should be upfield (C-5 cannot because it is identified in the coupled spectrum) led to the probable assignment given in Table 1.

The chemical shifts (not reported in Table 1) of the carbon atoms of the various substituents were readily assigned from simple model compounds (12) as follows: OCH_3 (55.9), $OCOCH_3$ (168.0, 19.7), $NHCH_3$ (29.2), $NHCOCH_3$ (169.3, 25.3), CH_3 (22.4), SCH_3 (14.8).

Substituent Effects

The shielding changes observed for the ring carbon nuclei along a series of substituted aromatic compounds are believed to be primarily related to a redistribution of electron density brought about by the substituent change (13). Although charge density correlations in monosubstituted benzenes have been more successful for *para* carbons (14), it is now widely accepted that the empirically obtained substituent chemical shift parameters for all ring carbons are very useful for spectral and structural assignment purposes (6).

Consequently, as a prelude to any correlation with calculated π- and σ-electron densities (as well as bond orders) (14), we first sought to characterize substituent effects in tropone derivatives by a comparison to the known effects for analogous benzene derivatives through an approach somewhat similar to that used previously (15) for pyridine derivatives.

Using the tropone carbon chemical shifts as reference, a set of substituent parameters was derived from the data in Table 1 as summarized in Table 3.

The C-2 shift parameters of the tropone derivatives were then plotted against the substituted carbon (C-X) shift parameter of each corresponding monosubstituted benzene in Fig. 2. A similar plot of the C-5 parameters (tropones) against the *para*-carbon

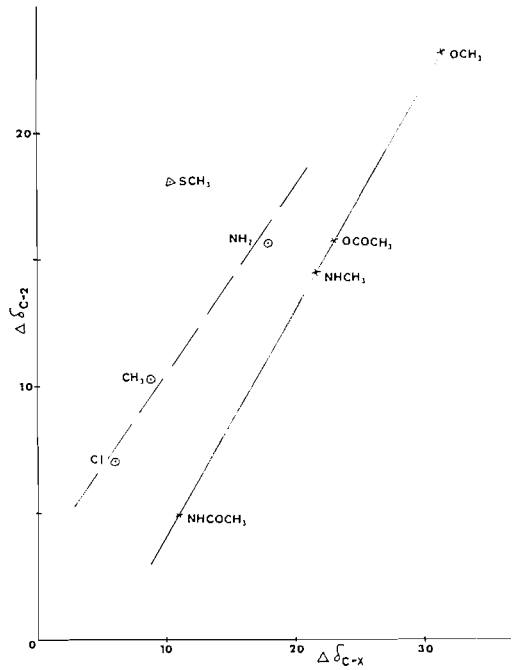

FIG. 2. Substituent parameters of the substituted carbons (C-2 vs. C-X) in 2-substituted tropones and monosubstituted benzenes.

parameters (benzenes) is shown in Fig. 3 while Fig. 4 illustrates the plot of the C-3 parameters versus the *ortho*-carbon parameters. Owing to the very small chemical shift spread of the *meta* carbons for the substituents investigated in our work, a plot against C-4 is not reproduced. It was not possible to obtain data for the non averaging tropolone and consequently the OH group does not appear in our analysis.

Figure 2 (substituted carbons) reveals a very interesting feature which suggests that the substituents (except SCH_3) fall into two categories each appearing to exhibit a linear relationship i.e. OCH_3, $OCOCH_3$, $NHCH_3$, and $NHCOCH_3$ (that is -X-Y type) as the first group and NH_2, CH_3, and Cl (that is -X type) as the second group; SCH_3 evidently behaves differently. Figure 3 (C-5 vs. C-*p*), on the other hand, appears to show a reasonably good single line correlation for all substituents except SCH_3. It is interesting to note, however, that the points for the two categories fall on the same side of the line as they did in Fig. 2. Finally, Fig. 4 (C-3 vs. C-*o*) shows an intermediate behaviour whereby the two groups of substituents each exhibit a characteristic correlation line slightly separated one from the other.

Attention is now drawn to the two major features revealed from our analysis of the data: (*i*) The existence of significant differences in the substituent

Can. J. Chem. Downloaded from www.nrcresearchpress.com by 210.87.254.40 on 09/05/12
For personal use only.

TABLE 3. Carbon-13 substituent effects[a] for carbons 1–5 in 2-substituted tropones

Substituent	δ				
	C-1	C-2 (C-X)[b]	C-3 (C-*o*)	C-4 (C-*m*)	C-5 (C-*p*)
OCH_3	−7.6	+23.3 (+31.4)	−23.6 (−14.4)	−2.0 (+1.0)	−6.8 (−7.7)
$OCOCH_3$	−9.4	+15.8 (+23.0)	−7.7 (−6.4)	−2.3 (+1.3)	−0.3 (−2.3)
NH_2	−11.5	+15.7 (+18.0)	−23.1 (−13.3)	−4.5 (+0.9)	−10.9 (−9.8)
$NHCH_3$	−11.3	+14.5 (+21.7)[c]	−27.9 (−16.2)	−6.4 (+0.7)	−12.8 (−11.8)
$NHCOCH_3$	−8.8	+4.9 (+11)	−15.2 (−9.9)	+1.2 (+0.2)	−4.0 (−6.5)
Cl	−7.8	+7.0 (+6.2)	+2.5 (+0.4)	−3.2 (+1.3)	−0.5 (−1.9)
CH_3	−0.8	+10.3 (+8.9)	+3.6 (+0.7)	−0.9 (−0.1)	−2.2 (−2.9)

[a]In ppm, calculated from Table 1 relative to the resonances of tropone taken as reference.
[b]The values given in parentheses are the well known substituent effects of the four carbons (X, *o*, *m*, and *p*) of monosubstituted benzenes. Taken from ref. 13, p. 244.
[c]Taken from ref. 26. Data converted using δ_C 128.5 for benzene.

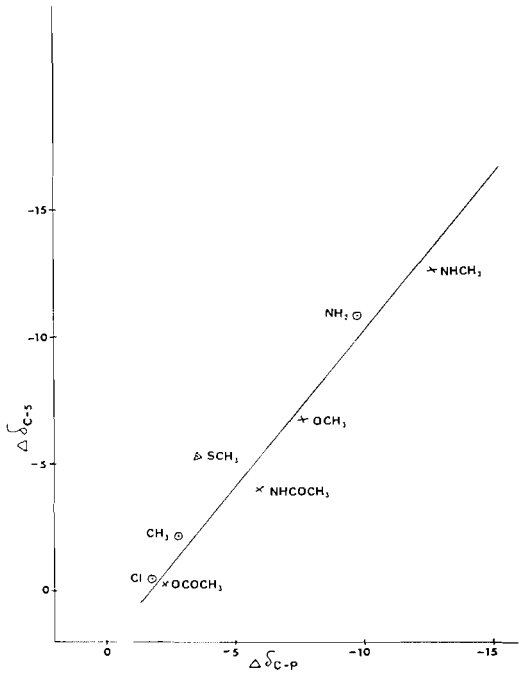

FIG. 3. Substituent parameters of C-5 in 2-substituted tropones and *para* carbons in monosubstituted benzenes.

parameters of the tropones compared to analogous substituted benzenes. (*ii*) The apparent existence of two categories of substituents each characterized by parameters exhibiting a linear relationship with those of benzene derivatives.

The magnitude of substituent effects is usually a composite of several factors whose relative importance is very difficult to establish quantitatively (16). The realization that tropones actually exhibit bond alternation characteristic of polyenones (3) could easily account for the differences in the magnitude of substituent parameters relative to benzenes. In fact the presence of the carbonyl group and the possibility of 'through' conjugation with the electron donating substituents (i.e. **8** ↔ **9**) could account for some of the differences involved, notably for C-4 whose parameters encompass a much larger range than for the corresponding *meta* parameters.

8 **9**

It is now fairly well recognized that π-electron redistribution through mesomeric effects is very important for substituted benzenes (14) and the linear relationships observed for tropones suggest that this mechanism is also very important. But other factors must contribute appreciably as evidenced by the two categories of substituents and the apparent abnormality of SCH_3.

The difference between the two lines representing the two categories of substituents (i.e. -X vs. -X-Y) appears to decrease with distance from the site of substitution. Because C-2 is β to Y and C-3 is γ to it, one would expect some difference if the proximity of the carbonyl group modified the conformational properties of the -X-Y substituents compared to the situation in substituted benzenes. Because of the vastly different nature of the substituents it is difficult to identify clearly the origin (steric or electrostatic) of the rotational conformational perturbation. It is nevertheless clear that this modification causes changes in electron densities by a mechanism other than (although not necessarily exclusively) resonance but which we are unable to identify unambiguously at this time (17).

The apparent abnormality of the SCH_3 substituent together with the realization that no strongly electron attracting substituent has been investigated suggest some caution in extrapolations from the available data although it is hoped that our observations will be a useful starting point for the utilization of ^{13}Cmr spectroscopy for the structure elucidation of more complex substituted tropones.

Can. J. Chem. Downloaded from www.nrcresearchpress.com by 210.87.254.40 on 09/05/12
For personal use only.

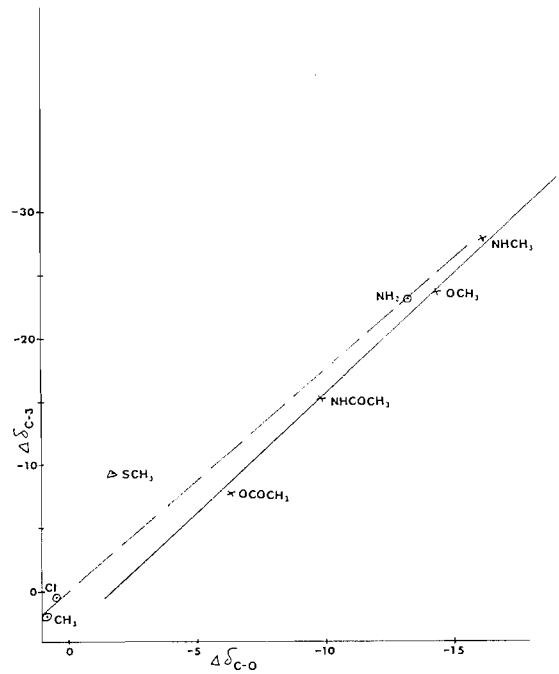

FIG. 4. Substituent parameters of C-3 in 2-substituted tropones and *ortho* carbons in monosubstituted benzenes.

Experimental

The 100 MHz ^{1}Hmr spectra were recorded on a JEOL JNM-4H-100 spectrometer (Université de Montréal) equipped with a JEOL Hetero Spin Decoupler model JNM-SD-HC. The ^{13}Cmr spectra were recorded at 22.63 MHz with a Bruker WH-90 spectrometer (Université de Montréal) equipped with the standard Bruker variable temperature accessories. Heteronuclear ^{1}H–^{13}C double-resonance experiments were carried out using the standard proton decoupler of the WH-90.

All ^{13}C spectra were obtained in the Fourier transform mode using 10 mm diameter sample tubes. The field–frequency lock was provided by the deuterium resonance of the solvent $CDCl_3$. The decoupler power was calibrated by proton off-resonance decoupling of a methanol sample (6). The flip angle was set at about 45° (6 μsec) and the number of accumulations depended on the concentration of the samples which varied according to the amount available. The coupled spectra were obtained through the gated decoupling technique (6) using the standard procedure for WH-90 spectrometers equipped with the Nicolet model 293 I/O Controller.

Synthesis of the 2-Substituted Tropones

The tropolone required for this work was prepared by the method reported by Steven *et al.* (18). The derivatives **2**-OCH_3 (19), **2**-$OCOCH_3$ (20), **2**-$NHCOCH_3$ (21), **2**-Cl (22), and **2**-SCH_3 (23) were prepared essentially as reported. We succeeded in preparing **2**-NH_2 with an 84% yield, much better than previous reports (21) through a modification of Doering and Knox's (20) procedure. Using milder conditions we were able to substantially increase the yield of **2**-$NHCH_3$ over that previously obtained (21) as described below.

*2-Aminotropone (**2**-NH_2)*

2-Methoxytropone (4.0 g) was dissolved in methanol (20 ml) and cooled to −30°C in a pressure bottle. Ammonia was passed into it for 5 min. The bottle was closed, and heated to 90°C for 2 h. The reaction mixture was then cooled and the resulting solution evaporated to dryness. The residue was taken in methanol, treated with charcoal and filtered through Celite to yield 2-aminotropone (2.9 g) mp 94–96°C (lit. (20) mp 100–101°C). All the spectroscopic data, (ir, uv, ms) were in agreement with the structure.

*2-Methylaminotropone (**2**-$NHCH_3$)*

A solution of 2-methoxytropone (3.77 g) in methanol (10 ml) was cooled to −50°C and methylamine was bubbled through it for about 10 min. The reaction mixture was then brought to room temperature, the solvent was removed under vacuum, and it was flushed twice with methanol. The residue was crystallized with ether to yield pure product (3.5 g) mp 80–82°C (lit. (21) mp 83°C).

*2-Methyltropone (**2**-CH_3)*

2-Methyltropone was synthesized by a modification of a previously described procedure (24).

Deuterations

3,5,7-Trideuteriotropolone (**4**) was prepared using the procedure described by Forbes (25). Compounds **3** and **6** were prepared from **4** by the same procedures as used for the non deuterated **2**-OCH_3 and **2**-$OCOCH_3$.

Acknowledgements

We wish to acknowledge the technical (nmr) contribution of Mr. Robert Mayer, the preparation of 2-methyltropone by Dr. B. Palameta, and the financial contribution of the National Research Council of Canada for the purchase of the Bruker WH-90 spectrometer.

1. D. LLOYD. Carbocylic non-benzenoid aromatic compounds. Elsevier Publishing Co., New York, NY. 1966. p. 118.
2. (*a*) H. SUGIYAMA. Sci. Rep. Res. Inst. Tohoku Univ. **20**, 34 (1968); Chem. Abstr. **70**, 15855b (1969); (*b*) A. VERCINI and F. PIETRA. J. Chem. Soc. Chem. Commun. 1262 (1972).
3. D. J. BERTELLI, T. A. ANDREWS, JR., and P. O. CREWS, J. Am. Chem. Soc. **91**, 5286 (1969).
4. T. MACHIGUCHI, Y. INAGAKI, M. HOSHINO, and Y. KITAHARA. Chem. Lett. 497 (1974).
5. (*a*) S. MASAMUNE, A. U. KEMP-JONES, J. GREEN, D. L. RABENSTEIN, M. YASUNAMI, K. TAKASE, and T. NOZOE. J. Chem. Soc. Chem. Commun. 283 (1973); (*b*) H. J. REICH and D. A. MURCIA. J. Am. Chem. Soc. **95**, 3418 (1973).
6. F. W. WEHRLI and T. WIRTHLIN. Interpretation of carbon-13 NMR spectra. Heyden, New York, NY. 1976.
7. L. WEÏLER. Can. J. Chem. **50**, 1975 (1972).
8. F. J. WEIGERT and J. D. ROBERTS. J. Am. Chem. Soc. **89**, 2967 (1967).
9. (*a*) B. BIRDSALL, N. J. M. BIRDSALL, and J. FEENEY. J. Chem. Soc. Chem. Commun. 316 (1972); (*b*) B. BIRDSALL and J. FEENEY. J. Chem. Soc. Perkin Trans. II, 1644 (1972).
10. J. W. EMSLEY, J. C. LINDON, and D. SHAW. J. Magn. Reson. **10**, 100 (1973).
11. A. J. JONES, T. D. ALGER, D. M. GRANT, and W. M. LITCHMAN. J. Am. Chem. Soc. **92**, 2386 (1970).
12. J. B. STOTHERS. Carbon-13 NMR spectroscopy. Academic Press, New York, NY. 1972.
13. G. L. NELSON and E. A. WILLIAMS. *In* Progress in physical organic chemistry. Vol. 12. *Edited by* R. W. Taft. Interscience, New York, NY. 1976. p. 229.
14. W. J. HEHRE, R. W. TAFT, and R. D. TOPSOM. *In* Progress in physical organic chemistry. Vol. 12. *Edited by* R. W. Taft. Interscience, New York, NY. 1976. p. 159.

15. H. L. RETCOFSKY and R. A. FRIEDEL. J. Phys. Chem. **72**, 2619 (1968) and previous papers in this series.
16. G. E. MACIEL. *In* Topics in carbon-13 NMR spectroscopy. Vol. 1. *Edited by* F. C. Levy. Wiley-Interscience, New York, NY. 1974. p. 53.
17. (*a*) K. SEIDMAN and G. E. MACIEL. J. Am. Chem. Soc. **99**, 659 (1977); (*b*) D. G. GORENSTEIN. J. Am. Chem. Soc. **99**, 2254 (1977); (*c*) H. BEIERBECK and J. K. SAUNDERS. Can. J. Chem. **53**, 1307 (1975).
18. H. C. STEVEN, J. K. REIVHENT, J. M. LAVANISH, and G. M. FRENTA. J. Org. Chem. **36**, 2780 (1971).
20. D. H. EVANS. U.S. Patent No. 3,833,657 (1974).
21. W. VON E. DOERING and L. H. KNOX. J. Am. Chem. Soc. **73**, 828 (1951).
22. T. NOZOE, S. SETO, H. TAKEDA, S. MOROSAWA, and K. MATSUMOTO. Sci. Rep. Tohoku Univ. **36**, 126 (1952); Chem. Abstr. **48**, 4497 (1954).
23. W. VON E. DOERING and L. H. KNOX. J. Am. Chem. Soc. **74**, 5686 (1952).
24. T. NOZOE, M. SATO, and K. MATSUI. Proc. Jpn. Acad. **29**, 22 (1953).
25. S. SETO. Sci. Rep. Tohoku Univ. **37**, 367 (1953); Chem. Abstr. **49**, 82348 (1955).
26. E. J. FORBES. J. Chem. Soc. (C), 1693 (1967).
27. L. F. JOHNSON and W. C. JANKOWSKI. Carbon-13 NMR spectra. Wiley-Interscience, Toronto, Ont. 1972.

Can. J. Chem. Downloaded from www.nrcresearchpress.com by 210.87.254.40 on 09/05/12
For personal use only.

Chemical behavior of charge-transfer complexes. VII. Solvolysis of alkyl arenesulfonate donors in the presence of aromatic acceptors[1]

ALLAN K. COLTER[2] AND ROBERT E. C. TURKOS

Department of Chemistry, Carnegie-Mellon University, Pittsburgh, PA 15213, U.S.A. and Guelph-Waterloo Centre for Graduate Work in Chemistry, University of Guelph, Guelph, Ont., Canada N1G 2W1

Received August 19, 1977

ALLAN K. COLTER and ROBERT E. C. TURKOS. Can. J. Chem. **56**, 585 (1978).

Rates of solvolysis of several ethyl and 2-propyl arenesulfonates having π donor leaving groups were measured in the absence of acceptor and in the presence of the π acceptors 1,3,5-trinitrobenzene (TNB) and 2,4,7-trinitrofluorenone (TNF). With four of the nine combinations investigated, added acceptor produced small but measurable rate enhancements. Ester–TNF 1:1 association constants were measured spectrophotometrically at 20, 30, and 40°C in acetic acid for 2-propyl 4-methoxy-1-naphthalenesulfonate (**3***b*), 4,8-dimethoxy-1-naphthalenesulfonate (**4**), 3,7-dimethyl-1-naphthalenesulfonate (**5**), and 1-pyrenesulfonate (**6**). From the equilibrium and kinetic data, the reactivity of the 1:1 ester–TNF complex relative to that of the uncomplexed ester (k_c/k_u) in acetolysis at 85.73°C was estimated to be *less than* 4.2 and 1.4 for **3***b* and **4**, respectively, 4.4 ± 2.0 for **5**, and 2.8 ± 0.4 for **6**. The value of k_c/k_u for **6** determined from analysis of the kinetic data alone is 2.7 ± 0.8.

ALLAN K. COLTER et ROBERT E. C. TURKOS. Can. J. Chem. **56**, 585 (1978).

On a mesuré les vitesses de solvolyse de plusieurs arènesulfonates d'éthyle et de propyle-2 possédant des nucléofuges donneurs d'électrons π; ces mesures ont été effectuées en l'absence d'accepteur et en présence des accepteurs d'électrons π trinitro-1,3,5 benzène (TNB) et trinitro-2,4,7 fluorénone (TNF). Dans quatre des neuf combinaisons étudiées, l'addition d'un accepteur à provoquée des augmentations faibles mais mesurables des vitesses. On a mesuré d'une façon spectroscopique les constantes d'association 1:1 ester–TNF; on a effectué ces mesures à 20, 30 et 40°C dans de l'acide acétique pour les sulfonates suivants: méthoxy-4 naphtalènesulfonate-1 (**3***b*), diméthoxy-4,8 naphtalènesulfonate-1 (**4**), diméthyl-3,7 naphtalènesulfonate-1 (**5**) et pyrènesulfonate-1 (**6**) de propyle-2. En se basant sur les équilibres et les données cinétiques, on a évalué que la réactivité du complexe 1:1 ester–TNF par rapport à celle de l'ester non complexé (k_c/k_u) lors de l'acétolyse à 85.73°C est respectivement plus faible que 4.2 et 1.4 pour **3***b* et **4**, 4.4 ± 2.0 pour **5** et 2.8 ± 0.4 pour **6**. La valeur de k_c/k_u pour **6**, déterminée uniquement à partir d'une analyse de données cinétiques, est de 2.7 ± 0.8.

[Traduit par le journal]

There are three main classes of reactions where catalysis by molecular complexing as a consequence of enhanced charge-transfer interaction in the transition state should be observable (1). A reaction of a π acceptor in which the transition state (or at least that portion of the structure responsible for its acceptor properties) is more electron-deficient than the reactant should be facilitated by complexation with a nonreacting donor. This type of catalysis by π donors has been amply demonstrated in solvolytic reactions of 2,4,7-trinitro-9-fluorenyl *p*-toluenesulfonate and related compounds (2). Reactions involving extension of a conjugated system in the transition state should be catalyzed by either π donors or π acceptors, depending on the reactant. This prediction has again been confirmed by catalysis of racemization of biaryl donors by π acceptors (3).

The third class is reactions of π donors having an electron-rich transition state, where catalysis by a nonreacting π acceptor might be anticipated. For several reasons, attempts to observe catalysis of this kind have been less successful. For example, rates of basic hydrolysis of *N*-(3-indoleacryloyl)imidazole, *p*-nitrophenyl 3-indoleacrylate, and *p*-nitrophenyl 3-indoleacetate in aqueous solution were decreased by complexation with 3,5-dinitrobenzoate ion (4), possibly owing to electrostatic repulsion of the approaching hydroxide or to steric hindrance to the nucleophilic attack. While aromatic nucleophilic substitution is strongly facilitated by electron-withdrawal on the aryl halide, it is difficult to design a substrate having appreciable π donor properties which will undergo nucleophilic substitution under conditions where any of the common strong π acceptors will survive (5). Furthermore, electronic effects due to complexing are likely to be outweighed by unfavorable steric effects. The clearest examples of catalysis due to electron-withdrawal by complexation are the small rate enhancements produced by 1,3,5-trinitrobenzene and other π

[1]For Part VI of this series, see ref. 2.

[2]Present address: Department of Chemistry, University of Guelph, Guelph, Ontario.

Can. J. Chem. Downloaded from www.nrcresearchpress.com by 210.87.254.6 on 09/05/12
For personal use only.

Can. J. Chem. Downloaded from www.nrcresearchpress.com by 210.87.254.6 on 09/05/12
For personal use only.

acceptors in the reaction of several π donor acids with 4-chlorodiphenyldiazomethane (6). Any steric effects in these reactions are apparently of minor importance.

As part of our continuing investigation of the chemical effects of charge-transfer complexing, we have sought additional evidence for appreciable electron transfer in weak π–π donor–acceptor complexes. We have therefore investigated the influence of π acceptors on the rates of solvolysis of several alkyl arenesulfonates having π donor leaving groups. Any rate enhancements in such reactions are expected to be very small since the π donor properties of the arenesulfonate ion (and hence the partially-developed arenesulfonate ion in the transition state) are expected to be only slightly enhanced over those of the ester itself. Nevertheless, even very small rate enhancements would have qualitative significance since the reaction should be free from complicating steric effects and side reactions of the acceptors.

Results

The arenesulfonate esters **1–6** were synthesized by standard methods. Rates of ethanolysis of esters **1***a*,

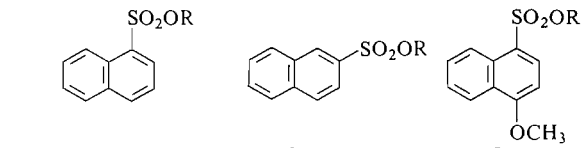

1
a R = C_2H_5
b R = $CH(CH_3)_2$

2
a R = C_2H_5
b R = $CH(CH_3)_2$

3
a R = C_2H_5
b R = $CH(CH_3)_2$

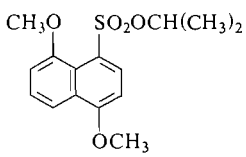

4

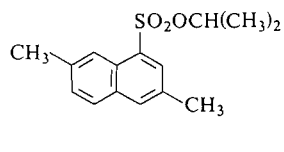

5

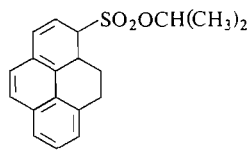

6

2*a*, and **3***a* at 70.1°C, with and without added 1,3,5-trinitrobenzene (TNB) are listed in Table 1. Although the color resulting from addition of TNB decreased the accuracy of the visual end points somewhat, significant rate enhancements were observed with **1***a* and **3***a*. Rates of acetolysis of esters **1***b*, **2***b*, **3***b*, **4**, **5**, and **6** at 85.73°C, with and without added 2,4,7-trinitrofluorenone (TNF) are listed in Table 2. Significant rate enhancements were observed with **5** and **6** only.

TABLE 1. Rates of ethanolysis of ethyl arenesulfonates at 70.1°C

Ester[a]	$10^2 \times$ [TNB] (M)[b]	$10^5 \times k_{obs}$ (s^{-1})	k_{obs}/k_u
1*a*	0	3.17±0.06	
	6.67	3.42±0.08	1.08±0.03
2*a*	0	3.12±0.07	
	4.60	3.15±0.01	1.01±0.02
3*a*	0	1.20±0.02	
	6.25	1.37±0.04	1.14±0.04

[a]Concentrations of esters at 70.1°C: **1***a* 0.0193 M, **2***a* 0.0122 M, **3***a* 0.0131 M.
[b]At 70.1°C.

TABLE 2. Rates of acetolysis of 2-propylarenesulfonates at 85.73°C[a]

Ester[a]	$10^2 \times$ [TNF] (M)[b]	$10^5 \times k_{obs}$ (s^{-1})	k_{obs}/k_u
1*a*	0	13.6±0.2	
	4.21	13.5±0.1	0.99±0.02
2*b*	0	15.9±0.4	
	3.27	16.3±0.3	1.03±0.03
3*b*	0	5.69±0.07	
	4.68	5.75±0.04	1.01±0.01
4	0	2.81±0.07	
	4.68	2.79±0.04	0.99±0.02
5	0	10.7±0.1	
	4.68	11.4±0.1	1.07±0.01
6	0	12.0±0.1	
	1.87	13.1±0.1	1.09±0.01
	2.33	13.4±0.1	1.12±0.01
	2.80	13.6±0.1	1.13±0.01
	3.74	14.1±0.2	1.18±0.02

[a]Concentrations of esters at 85.73°C: 9.4×10^{-3} M.
[b]At 85.73°C.

By analogy with earlier work (2), the simplest mechanism for catalysis by added acceptor, A, is as represented by [1], where RX is the arenesulfonate

[1]
$$\begin{array}{ccc} RX + A & \overset{K}{\rightleftharpoons} & RX\cdot A \\ \downarrow k_u & & \downarrow k_c \\ \text{Products} & & \text{Products} \end{array}$$

ester donor, k_u and k_c are rate constants for acetolysis of uncomplexed ester and 1:1 ester–acceptor complex, respectively, and K is the 1:1 ester–acceptor association constant. Under conditions where the stoichiometric concentration of acceptor, c_A, is much greater than the concentration of 1:1 complex, RX·A, this mechanism leads to [2] (1), where k_{obs} is the observed rate constant in the presence of c_A M

[2] $$1/(k_{obs} - k_u) = 1/(k_c - k_u) + 1/K(k_c - k_u)c_A$$

acceptor. In theory, therefore, both k_c and K can be obtained by measurement of k_{obs} at two or more acceptor concentrations and analysis of a plot of $1/(k_{obs} - k_u)$ vs. $1/c_A$. In practice, however, such an analysis requires substantial rate enhancements over

TABLE 3. Equilibrium constants for molecular complex formation with TNF in acetic acid

Ester	K (ℓ mol^{-1})			
	20°C	30°C	40°C	85.73°C[a]
3*b*	7.85±0.44	4.62±0.93	2.70±0.42	0.37±0.17
4*b*	4.49±0.25	4.25±0.13	3.51±0.20	2.28±0.44
5	4.41±0.81	2.54±0.37	1.97±0.30	0.42±0.23
6	48.6 ±1.4	28.5 ±3.3	18.4 ±1.5	2.94±0.71

[a]Extrapolated from data at 20, 30, and 40°C.

a range of acceptor concentrations corresponding to a substantial variation in the fraction of ester which is complexed, and in the present work was marginally possible only for acetolysis of **6** in the presence of TNF. The analysis leads to $K = 3.1 \pm 1.4$ ℓ mol^{-1}, $k_c = 3.3 \pm 1.0 \times 10^{-4}$ s^{-1}, and $k_c/k_u = 2.7 \pm 0.8$.

To confirm this result, and to gain further information about the effects of complexation with the other systems, ester–TNF association constants were measured spectrophotometrically for esters **3***b*, **4**, **5**, and **6** in acetic acid at 20, 30 and 40°C. The results are summarized in Table 3, together with an estimate of the complexation constants at 85.73°C, obtained by extrapolation. The associated thermodynamic quantities ΔH^0 and ΔS^0 (30°C) are, respectively: **3***b* -9.7 ± 1.5 kcal mol^{-1}, -29.1 ± 5.0 cal deg^{-1} mol^{-1}; **4** -2.2 ± 0.7 kcal mol^{-1}, -4.5 ± 2.4 cal deg^{-1} mol^{-1}; **5** -7.4 ± 2.2 kcal mol^{-1}, -22.5 ± 7.2 cal deg^{-1} mol^{-1}; **6** -8.9 ± 0.8 kcal mol^{-1}, -22.7 ± 2.6 cal deg^{-1} mol^{-1}. The extrapolated value of K for **6** (2.9 ± 0.7 ℓ mol^{-1}) is in good agreement with the value (3.1 ± 1.4 ℓ mol^{-1}) obtained by analysis of the kinetic data alone.

From [1], k_{obs} at a particular set of ester and acceptor concentrations is given by [3], where F_c is the fraction of ester which is complexed and F_u

$$[3] \quad k_{obs} = k_u F_u + k_c F_c = k_u + (k_c - k_u)F_c$$

($= 1 - F_c$) is the fraction uncomplexed. Under conditions where the acceptor is in large excess over the ester and/or the complexation constants for the ester and arenesulfonate ion product do not differ greatly, F_c will be very nearly constant over the course of the reaction and strict first order kinetics are expected. In the present work, no deviations from first-order behavior were detectable over two half lives.

Rearrangement of [3] yields an expression for k_c/k_u [4]. Using the values of K at 85.73°C obtained

$$[4] \quad k_c/k_u = \frac{k_{obs} - k_u + k_u F_c}{k_u F_c}$$

by extrapolation (Table 3), c_A, and initial ester concentration (Table 2), values of F_c were calculated for the conditions of each rate measurement in the presence of TNF. These values of F_c were then combined with the appropriate values of k_{obs} and k_u (Table 2) to calculate k_c/k_u using [4]. The values of k_c/k_u so obtained are 4.4 ± 2.0 for **5** and 2.8 ± 0.4 for **6**. Values of k_c/k_u for **6** calculated from the rate data at four different TNF concentrations were 2.8 ± 0.5, 2.9 ± 0.5, 2.8 ± 0.4, and 2.8 ± 0.4 for 0.0187, 0.0233, 0.0280, and 0.0374 M TNF, respectively. This agreement and the close agreement with k_c/k_u obtained from analysis of the kinetic data alone (2.7 ± 0.8) supports the reliability of the results for **6**.

Using the standard deviations in k_u, k_{obs} and K, minimum and maximum values of k_c/k_u were estimated from minimum and maximum values of $(k_{obs} - k_u)$ and maximum and minimum values of K, respectively. In this way, we estimate for **3***b*, $k_c/k_u = 1.6$ (maximum range, 0.6 to 4.2) and for **4**, $k_c/k_u = 0.9$ (maximum range 0.6 to 1.4). Thus it is possible that the chemical effect of complexation by TNF in acetolysis of **3***b* is similar to that estimated for **5** and **6**, but that measurable rate enhancements were not observed because of the very small extent of complexation. In contrast, the behavior of **4**, where k_c/k_u is *less than* 1.4, appears to be distinctly different.

Discussion

With four of the nine solvolyses of π donor – alkyl arenesulfonates investigated, added TNB or TNF produced measurable rate enhancements. We have interpreted the rate increases in terms of a mechanism involving complexation between donor ester and acceptor to form a 1:1 complex which is more reactive than uncomplexed ester. The most plausible explanation for the increased reactivity of the 1:1 complex is electron withdrawal by the complexed acceptor, and we consider the results to provide further evidence for significant charge transfer in weak π–π donor–acceptor complexes.

The absence of measurable rate enhancements in several systems where the extent of complexation is expected to be very small (particularly acetolysis of **1***b* and **2***b* in the presence of TNF) argues strongly against some general more specific medium effect not involving complexing. For the acetolysis of **3***b* in the presence of TNF, we estimate from independent

Can. J. Chem. Downloaded from www.nrcresearchpress.com by 210.87.254.6 on 09/05/12
For personal use only.

Can. J. Chem. Downloaded from www.nrcresearchpress.com by 210.87.254.6 on 09/05/12
For personal use only.

spectrophotometric measurements that an increase in ester reactivity due to complexation (k_c/k_u) less than 4.2 would not lead to a significant rate enhancement under the conditions of our experiments. The extent of complexation is almost certainly smaller for esters **1***b* and **2***b* + TNF in acetic acid.

The increase in ester reactivity due to complexation by TNF (k_c/k_u) estimated for esters **5** and **6** is small as expected. In the absence of rate data for acetolysis of a series of substituted 2-propyl 1-naphthalenesulfonates and 1-pyrenesulfonates, only a very approximate comparison between the electron-withdrawing effect of a complexed TNF and those of typical electron-withdrawing substituents can be made. In the 1-naphthalenesulfonate series the rate-retarding effect of a 4-methoxy group (i.e., **3***b* vs. **1***b*) is very close to that of a *p*-methoxy group in acetolysis of cyclohexyl benzenesulfonates at 70°C (7). If the influence of a 3-substituent in the 1-naphthalenesulfonate series is similar to that of a *meta* substituent in the benzenesulfonates, the rate enhancing effect of a complexed TNF in acetolysis of 2-propyl 1-naphthalenesulfonates (4.4) is between that expected for 3-Cl (~3.0) and 3-CN (~5.3) substituents. Measured in this way, this effect is very similar in magnitude to that of a complexed TNB on the acidities of several donor carboxylic acids (6).

The results for ester **4** are unusual in two ways. The association constant determined spectrophotometrically is unusually insensitive to temperature changes, both the enthalpy decrease ($-\Delta H^0$) and entropy decrease ($-\Delta S^0$) accompanying complexation being unusually small. We have previously observed unexpectedly small complexation constants for dimethoxynaphthalene donors and 2,4,7-trinitro-9-fluorenyl *p*-toluenesulfonate in acetic acid (8). It is possible that a methoxy group may sterically hinder complexation in the same way that an ethyl group does (9). It is interesting that *both* $-\Delta H^0$ and $-\Delta S^0$ are smaller for complexation of I_2 (10) and ICl (11) with hexaethylbenzene than with hexamethylbenzene. The smaller $-\Delta H^0$ and $-\Delta S^0$ values measured for **4** may therefore reflect a looser complex, possibly as a result of steric hindrance from the two methoxy groups and the alkoxysulfonate group. The second unusual result with **4** is the absence of any increase in reactivity on complexation with TNF. This result could also be a consequence of a looser complex. Alternatively, complexation may sterically hinder solvation of the developing sulfonate anion in the transition state.

Experimental

All melting points are corrected. Microanalyses were performed by Galbraith Laboratories, Knoxville, Tennessee, U.S.A. Infrared spectra were measured using a Perkin-Elmer model 137B spectrophotometer, and nuclear magnetic resonance spectra with a Varian A-60 spectrometer.

Reagents and Solvents

1,3,5-Trinitrobenzene was Fisher highest purity, used without further purification. 2,4,7-Trinitrofluorenone was prepared as described by Woolfolk and Orchin (12) and had mp 175.5–176°C (lit. (12) mp 175.2–176°C). Anhydrous ethanol was prepared by heating reagent grade absolute ethanol for 12 h at reflux over magnesium ethoxide, followed by distillation under anhydrous conditions. Anhydrous acetic acid, and standard (0.01 *M*) sodium acetate in acetic acid were prepared as previously described (13). Standard alcoholic sodium hydroxide (0.02 *M*) was prepared by dilution of 0.2 ml of a filtered solution of reagent grade sodium hydroxide in 7 ml of distilled water, to 1 ℓ with absolute ethanol, and standardization using a potassium hydrogen phthalate primary standard.

Synthesis of Esters

The esters were synthesized by reaction of ethanol or 2-propanol with the appropriate acid chloride, either commercially available (1- and 2-naphthalenesulfonyl chlorides) or obtained by reaction of the corresponding potassium arenesulfonate with thionyl chloride. The arenesulfonate salts were prepared by sulfonation of pyrene or the appropriate substituted naphthalene.

Arenesulfonate Salts

Sulfonation of 1-methoxynaphthalene, 1,5-dimethoxynaphthalene (8), and 2,6-dimethylnaphthalene is illustrated by the following procedure. To a cooled (0°C), stirred, solution of 0.20 mol of substituted naphthalene in 500–700 ml of CH_2Cl_2 was slowly added 0.22 mol of distilled chlorosulfonic acid. After complete addition the solution was stirred for an additional 6–9 h at 0–5°C. Cold water (200–250 ml) was added and stirring continued for 1 h. The aqueous layer was separated and the CH_2Cl_2 solution extracted with water. The aqueous extracts were combined and K_2CO_3 carefully added until the solution was slightly basic. The resulting suspension was heated on a steam cone until solution was complete. The salt which separated on cooling was filtered, dried, washed with ether or methylene chloride, and dried again at 120°C. Potassium 4-methoxy-1-naphthalenesulfonate was obtained in 94% yield; ir (Nujol): 1198, 1182, 1059, 687 cm^{-1} ($—SO_3^-$); *p*-toluidide mp 211–212°C. Potassium 4,8-dimethoxy-1-naphthalenesulfonate was obtained in 86% yield, ir (Nujol): 1199, 1176, 1059, 701 cm^{-1} ($—SO_3^-$); *p*-toluidide mp 198.5–199.5°C. Potassium 3,7-dimethyl-1-naphthalenesulfonate was obtained in 86% yield; ir (Nujol): 1205, 1183, 1058, 705 cm^{-1} ($—SO_3^-$); *p*-toluidide mp 268–269°C (lit. (14) mp 279°C).

Sodium 1-pyrenesulfonate was obtained in 98% yield by sulfonation of pyrene following the procedure of Tietze and Bayer (15) using CH_2Cl_2 as the solvent; ir (Nujol): 1198, 1181, 1062, 706 cm^{-1} ($—SO_3^-$); *p*-toluidide mp 234–236°C.

Sulfonyl Chlorides

The procedure was adapted from that of Bosshard *et al.* (16). To a stirred suspension of 0.10 mol of dry sulfonate salt in 100 ml of distilled DMF was added 36 ml (0.5 mol) of thionyl chloride over a period of 5–10 min. After stirring for an additional 10–45 min, the mixture was poured onto 800 ml of ice-water and the precipitate filtered and washed with water. The precipitate was dissolved in CH_2Cl_2, the solution dried over $MgSO_4$, and filtered. The product was isolated by evaporation and crystallization from CH_2Cl_2 – petroleum ether (bp 60–110°C). 4-Methoxy-1-naphthalenesulfonyl chloride was obtained in 85% yield, mp 98–99.5°C (lit. (17) mp 98.5°C); ir (CH_2Cl_2): 1361, 1161 cm^{-1} (SO_2). 4,8-Dimethoxy-1-naphthalenesulfonyl chloride was obtained in 86% yield, mp

Can. J. Chem. Downloaded from www.nrcresearchpress.com by 210.87.254.6 on 09/05/12
For personal use only.

118.5–119.5°C; ir (CH_2Cl_2): 1351, 1159 cm^{-1} (SO_2), nmr ($CDCl_3$) τ: 5.95 (s, 6H, methoxy), 3.20 (d, J = 9 Hz, 1H, H-3), 2.85 (doublet of doublets, J = 8 Hz, 1.5 Hz, 1H, H-7), 2.43 (t, J = 8 Hz, 1H, H-6), 2.02 (doublet of doublets, J = 8 Hz, 1.5 Hz, 1H, H-5), 1.48 (d, J = 9 Hz, 1H, H-2). *Anal.* calcd. for $C_{12}H_{11}O_4SCl$: C 50.26, H 3.86, S 11.18, Cl 12.38; found: C 50.47, H 4.08, S 11.16, Cl 12.20. 3,7-Dimethyl-1-naphthalenesulfonyl chloride was obtained in 79% yield, mp 107–108.5°C (lit. (18) mp 105–107°C); ir (CH_2Cl_2): 1361, 1176 cm^{-1} (SO_2). 1-Pyrenesulfonyl chloride was obtained in 82% yield, mp 175–176°C (lit. (19) mp 120°C); ir (KBr): 1355, 1170 cm^{-1} (SO_2); nmr ($CDCl_3$) τ: 1.78 (m, 7H, aromatic), 1.27 (d, J = 8 Hz, 1H, H-2), 0.90 (d, J = 9.5 Hz, H-10). *Anal.* calcd. for $C_{16}H_9O_2SCl$: C 63.89, H 3.01, S 10.66, Cl 11.78; found: C 63.79, H 2.93, S 10.85, Cl 11.82.

Esters

Ethyl 1-naphthalenesulfonate (**1***a*) and 2-naphthalenesulfonate (**2***a*) were prepared from the corresponding acid chlorides (Eastman Kodak, highest purity) using the method of Rodionow (20). A 74% yield of **1***a* was obtained as an oil, ir (CH_2Cl_2) 1342, 1171 cm^{-1} (SO_2). *Anal.* calcd. for $C_{12}H_{12}SO_3$: C 60.99, H 5.12; found: C 60.77, H 4.97. A 76% yield of **2***a* was obtained as an oil, ir (CH_2Cl_2) 1344, 1168 cm^{-1} (SO_2). *Anal.* calcd. for $C_{12}H_{12}SO_3$: C 60.99, H 5.12; found: C 61.10, H 5.30.

Ethyl 4-methoxy-1-naphthalenesulfonate (**3***a*) and the 2-propyl-1-naphthalenesulfonates (**1***b*, **2***b*, **3***b*, **4**, and **5**) were prepared by the usual method (21) using a 4- to 10-fold molar ratio of alcohol to acid chloride and reaction times of 2 to 3 days. Unreacted acid chloride was destroyed before work-up using aqueous NaOH (22). With the preparation of **1***b* and **2***b* the solvent was 3:10 (v/v) pyridine–benzene. The esters were crystallized from Skellysolve B (**3***a*), CH_2Cl_2 – petroleum ether (60–110°C), or $CHCl_3$ – petroleum ether (60–110°C). The 2-propyl esters were further purified before use by chromatography on Fluorosil using benzene or benzene – 1% ethyl acetate eluent. Ethyl 4-methoxy-1-naphthalenesulfonate was obtained in 27% yield, mp 118.5–119.5°C, ir (CH_2Cl_2): 1344, 1170 cm^{-1} (SO_2); nmr ($CDCl_3$) τ: 8.80 (t, J = 7 Hz, 3H, ethyl CH_3), 5.97 (quartet, J = 7 Hz, 2H, ethyl CH_2), 5.97 (s, 3H, methoxy), 3.18 (d, J = 8 Hz, 1H, H-3), 2.37 (m, 2H, H-6 and H-7), 1.77 (d, J = 8 Hz, 1H, H-2), 1.48 (m, 2H, H-5 and H-8). *Anal.* calcd. for $C_{13}H_{14}SO_4$: C 58.62, H 5.29, S 12.04; found: C 58.48, H 5.40, S 11.88. 2-Propyl-1-naphthalenesulfonate was obtained in 66% yield, mp 59–60°C, ir (CH_2Cl_2): 1340, 1171 cm^{-1} (SO_2). *Anal.* calcd. for $C_{13}H_{14}O_3S$: C 62.37, H 5.64, S 12.81; found: C 62.23, H 5.59, S 12.69. 2-Propyl 2-naphthalenesulfonate was obtained in 51% yield, mp 55–56°C; ir (CH_2Cl_2): 1333, 1168 cm^{-1} (SO_2). *Anal.* calcd. for $C_{13}H_{14}SO_3$: C 62.37, H 5.64, S 12.81; found: C 62.25, H 5.65, S 12.77. 2-Propyl 4-methoxy-1-naphthalenesulfonate was obtained in 59% yield, mp 107.5–108.5°C; ir (CH_2Cl_2): 1353, 1167 cm^{-1} (SO_2), nmr ($CDCl_3$) τ: 8.79 (d, J = 6.5 Hz, 6H, isopropyl CH_3), 5.90 (s, 3H, methoxy), 5.25 (sept., J = 6.5 Hz, 1H, isopropyl CH), 3.10 (d, J = 8 Hz, 1H, H-3), 2.26 (m, 2H, H-6 and H-7), 1.63 (d, J = 8 Hz, 1H, H-2), 1.52 (doublet of doublets, J_{ortho} = 8 Hz, J_{meta} = 2 Hz, 1H, H-5), 1.28 (doublet of doublets, J_{ortho} = 8.5 Hz, J_{meta} = 2 Hz, 1H, H-8). *Anal.* calcd. for $C_{14}H_{16}O_4S$: C 59.98, H 5.75, S 11.44; found: C 59.81, H 5.60, S 11.44. 2-Propyl 4,8-dimethoxy-1-naphthalenesulfonate was obtained in 67% yield, mp 119–120°C, ir (KBr): 1351, 1160 cm^{-1} (SO_2); nmr ($CDCl_3$) τ: 8.73 (d, J = 6 Hz, 6H, isopropyl CH_3), 5.99 (s, 6H, methoxy), 5.08 (sept., J = 6 Hz, 1H, isopropyl CH), 3.18 (d, J = 8 Hz, 1H, H-3), 2.88 (doublet of doublets, J_{ortho} = 8 Hz, J_{meta} = 1.5–2 Hz, 1H, H-7), 2.47 (t, J = 8 Hz, 1H, H-6), 2.03 (doublet of doublets, J_{ortho} = 8 Hz, J_{meta} = 1.5–2 Hz, 1H, H-5), 1.53 (d, J = 8 Hz, 1H, H-2). *Anal.* calcd. for $C_{15}H_{18}O_5S$: C 58.05, H 5.84, S 10.33; found: C 57.86, H 5.92, S 10.34. 2-Propyl 3,7-dimethyl-1-naphthalenesulfonate was obtained in 55% yield, mp 80–81°C; ir (CH_2Cl_2): 1337, 1174 cm^{-1} (SO_2); nmr ($CDCl_3$) τ: 8.78 (d, J = 6 Hz, 6H, isopropyl CH_3), 7.45 (s, 6H, aryl CH_3), 5.28 (sept., J = 6 Hz, 1H, isopropyl CH), 2.62 (doublet of doublets, J_{ortho} = 9 Hz, J_{meta} = 1.5 Hz, 1H, H-6), 2.25 (d, J = 9 Hz, 1H, H-5), 2.17 (broad s, 1H, 8-H), 1.87 (d, J = 1.5 Hz, 1H, H-2), 1.65 (broad s, 1H, H-4). These assignments are based on the paper of Garbutt *et al.* (23). *Anal.* calcd. for $C_{15}H_{18}O_3S$: C 64.72, H 6.52, S 11.52; found: C 64.58, H 6.37, S 11.53.

2-Propyl 1-pyrenesulfonate was prepared as follows. To a solution of 10.5 g (0.035 mol) of 1-pyrenesulfonyl chloride in 125 ml of dry pyridine was added 10 ml of triethylamine and 25 ml of dry 2-propanol. After shaking at room temperature for 10 min, the mixture was kept at 10°C for 20 h and then added to a separatory funnel containing 600 ml of 10% HCl and 250 ml of $CHCl_3$. After separating the $CHCl_3$ layer, the aqueous layer was extracted again with $CHCl_3$ and the combined $CHCl_3$ extracts washed with 10% HCl, water, dried over $MgSO_4$, boiled with decolorizing charcoal, and filtered. After removal of the solvent under vacuum, the ester was purified by chromatography on Fluorosil (benzene eluent) followed by crystallization from 50:50 (v/v) benzene – Skellysolve B, to yield 4.27 g (37.8%), mp 133.5–134°C; ir (KBr): 1342, 1176 cm^{-1} (SO_2); nmr ($CDCl_3$) τ: 8.80 (d, J = 6 Hz, isopropyl CH_3), 5.22 (sept., J = 6 Hz, 1H, isopropyl CH), 1.88 (m, 7H, aromatic), 1.37 (d, J = 8.5 Hz, 1H, H-2), 1.05 (d, J = 8.5–9 Hz, 1H, H-10). *Anal.* calcd. for $C_{19}H_{16}O_3S$: C 70.35, H 4.97, S 9.89; found: C 70.22, H 4.85, S 9.79.

Kinetic Measurements

Weighed amounts of ester (approximately 0.002 mol in ethanolyses, 0.001 mol in acetolyses) and acceptor were dissolved in anhydrous ethanol or acetic acid and adjusted to 100 ml in a volumetric flask. Aliquots of 6–7 ml were sealed under nitrogen in 6 in. Pyrex test tubes and placed in a constant temperature bath. After thermal equilibration ampoules were withdrawn at appropriate intervals of time, quenched thermally, and an accurately-measured aliquot (5 ml, 25°C) analyzed. In the ethanolyses, the 5 ml aliquot was dissolved in 25 ml of ethanol and titrated with standard 0.02 M ethanolic sodium hydroxide solution using Lacmoid indicator. In the presence of high concentrations of TNB, accurate determination of the end point was difficult because the solutions were already highly colored. The extent of acetolysis was determined by titration with standard 0.01 M sodium acetate in acetic acid. End points were determined potentiometrically using a Beckman model 76004 expanded scale pH meter equipped with a combination Ag/AgCl–glass electrode, estimated accuracy ±0.005 ml. Infinity determinations were carried out in triplicate after 10 half lives. Rate constants were calculated using the integrated first order rate expression, using individual titers and times (together with zero and infinity titers), and are reported as averages with standard deviations of the mean. Infinity titers were generally 97–99% of theory.

Determination of Association Constants

Optical density measurements utilized a Guilford model 200 spectrophotometer equipped with a thermostatted cell compartment. The temperature in the cell compartment was maintained to within ±0.05°C of the stated temperature by circulation of water. Four stock solutions containing close to equimolar amounts of ester and TNF in dry acetic acid were prepared, and an additional three or four solutions prepared by dilution. Concentration ranges were 5×10^{-3} to 4×10^{-2}

Can. J. Chem. Downloaded from www.nrcresearchpress.com by 210.87.254.6 on 09/05/12
For personal use only.

M for **3***a*, **4***a*, and **5**, and 4×10^{-3} to 1.25×10^{-2} M for **6**. Measurements were made at 10 nm intervals from 440–460 nm with **3***b*, 430–460 nm with **4***b* and **5**, and 430–470 nm with **6**. The experimental data were analyzed by computer using an adaptation of the iterative method of de Maine and Seawright (24), described by Dewar and Thompson (25). The reported association constants are averages of the values obtained at 3 to 5 wavelengths, with standard deviations of the means.

Calculations and Error Estimates

Analysis of the kinetic data for acetolysis of **6** in the presence of TNF using [2] is based on the approximation $c_A \approx [A]$, which is only marginally valid in this case. However, stoichiometric acceptor concentrations, c_A, can be used to obtain an initial estimate of K (intercept ÷ slope), this value used to calculate initial values of [A] for the conditions of each rate measurement, and the process repeated using these values of [A] in place of c_A to obtain a second estimate of K. Values of K and k_c obtained in this way converged after two cycles.

The reported values of ΔH^0, ΔS^0, and K(85.73°C, extrapolated) were obtained by least squares analysis of a plot of ln K vs. $1/T$. Standard deviations (s) in ΔH^0, ΔS^0, and K(ext) were calculated as follows. Analytical expressions for these quantities in terms of the values of K at 20 and 40°C (and the temperatures) were derived. These were differentiated with respect to K(20°C) and K(40°C) to obtain expressions for $s_{\Delta H^0}$, $s_{\Delta S^0}$, and $s_{K(\text{ext})}$ in terms of $s_{K(20°C)}$ and $s_{K(40°C)}$. The standard deviations so obtained were larger in every case than those calculated in the usual way from least-squares analysis of the ln K vs. $1/T$ plot. The latter reflect only the degree of scatter from a perfect straight line and, for only three points, are considered less realistic.

The equilibrium expression 5 for 1:1 complexation was used

$$[5] \qquad K = \frac{[D{\cdot}A]}{\{c_A - [D{\cdot}A]\}\{c_D - [D{\cdot}A]\}}$$

to obtain an expression for F_c ($= [D{\cdot}A]/c_D$) in terms of K, c_A, and c_D. Standard deviations in F_c were then calculated in the usual way (26) from $s_{K(\text{ext})}$ by differentiation of this expression. Finally, standard deviations in k_c/k_u were obtained in the same way from $s_{k_{obs}}$, s_{k_u}, and s_{F_c} by differentiation of [4].

Acknowledgements

This work was supported by the National Science Foundation (Grant GP-6380) and by the National Research Council of Canada.

1. A. K. COLTER and M. R. J. DACK. *In* Molecular complexes. Vol. 1. *Edited by* R. Foster. Elek Science, London. 1973. p. 301.
2. A. K. COLTER, ARTHUR L. MCKENNA III, and M. A. KASEM. Can. J. Chem. **52**, 3748 (1974).
3. (*a*) B. M. GRAYBILL and J. E. LEFFLER. J. Phys. Chem. **63**, 1461 (1959); (*b*) A. K. COLTER and L. M. CLEMENS. J. Am. Chem. Soc. **87**, 847 (1965).
4. F. M. MENGER and M. L. BENDER. J. Am. Chem. Soc. **90**, 4387 (1968).
5. R. E. C. TURKOS. Ph.D. thesis, Carnegie-Mellon University, Pittsburgh, Pennsylvania. 1969.
6. A. K. COLTER and R. J. KERSTING. Can. J. Chem. **55**, 1028 (1977).
7. D. N. KEVILL, K. C. KOLWYCK, D. M. SHOLD, and C. KIM. J. Am. Chem. Soc. **95**, 6022 (1973).
8. A. K. COLTER and S. HUI. J. Org. Chem. **33**, 1935 (1968).
9. R. FOSTER. Organic charge-transfer complexes. Academic Press, New York, NY. 1969. p. 195.
10. R. M. KEEFER and L. J. ANDREWS. J. Am. Chem. Soc. **77**, 2164 (1955).
11. N. OGIMACHI, L. J. ANDREWS, and R. M. KEEFER. J. Am. Chem. Soc. **77**, 4202 (1955).
12. E. O. WOOLFOLK and M. ORCHIN. Org. Synth. Coll. Vol. III, 837 (1955).
13. A. K. COLTER, S. S. WANG, G. H. MEGERLE, and P. S. OSSIP. J. Am. Chem. Soc. **86**, 3106 (1964).
14. L. F. FIESER. J. Am. Chem. Soc. **55**, 4977 (1933).
15. E. TIETZE and O. BAYER. Ann. **540**, 189 (1939).
16. H. H. BOSSHARD, R. MORY, M. SCHMID, and H. ZOLLINGER. Helv. Chim. Acta, **42**, 1653 (1959).
17. E. KNÜSLI. Thesis, Eidgen. Tech. Hochschule Zurich, 1948. *Cited in* Elsevier's encyclopedia of organic chemistry. Ser. III. Vol. 12B. Elsevier Publishing Co., Amsterdam. 1955. p. 5274.
18. R. WEISSGERBER and O. KRUBER. Ber. **52**, 346 (1919).
19. H. VOLLMANN, H. BECKER, M. CORELL, and H. STREECK. Ann. **531**, 1 (1937).
20. W. M. RODIONOW. Bull. Soc. Chim. Fr. Ser. 4, **45**, 109 (1929).
21. R. S. TIPSON. J. Org. Chem. **9**, 235 (1944).
22. A. K. COLTER and R. D. JOHNSON. J. Am. Chem. Soc. **84**, 3289 (1962).
23. D. C. F. GARBUTT, K. G. R. PACHLER, and J. R. PARRISH. J. Chem. Soc. 2324 (1965).
24. P. A. D. DE MAINE and R. D. SEAWRIGHT. Digital computer programs for physical chemistry. Vol. 1. MacMillan, New York, NY. 1962. Chapt. IV.
25. M. J. S. DEWAR and C. C. THOMPSON, JR. Tetrahedron Suppl. **7**, 97 (1966).
26. L. G. PARRATT. Probability and experimental errors in science. John Wiley and Sons, Inc., New York, NY. 1961.

Canadian Journal of Chemistry

Published by
THE NATIONAL RESEARCH COUNCIL OF CANADA

Journal canadien de chimie

Publié par
LE CONSEIL NATIONAL DE RECHERCHES DU CANADA

Volume 56 Number 5 March 1, 1978

Volume 56 numéro 5 1 mars 1978

Can. J. Chem. Downloaded from www.nrcresearchpress.com by 210.87.254.6 on 09/05/12
For personal use only.

An interferometric study of a convectionless steady state of concentration polarization

ROBERT N. O'BRIEN AND HENRYK KOLNY[1]

Department of Chemistry, University of Victoria, Victoria, B.C., Canada V8W 2Y2

Received September 15, 1977

ROBERT N. O'BRIEN and HENRYK KOLNY. Can. J. Chem. **56**, 591 (1978).

The use of interferometry to make visible concentration gradients at working electrodes has progressed to video tape recording of interferograms. Rapid accurate analysis should be able to gain sufficient data from experimental runs where migration effects are just balanced by diffusion effects to help evolve a better mathematical formula with which to predict concentration changes at working convectionless electrodes. Data are presented showing a quasi-steady state polarization in a low current density electrolysis run with Fe^{2+} the electroactive species.

ROBERT N. O'BRIEN et HENRYK KOLNY. Can. J. Chem. **56**, 591 (1978).

L'utilisation de l'interférométrie pour rendre visible des gradients de concentrations à des électrodes en opération peut maintenant être effectuée à l'aide d'un enregistrement vidéo des interférogrammes. Une analyse précise et rapide devrait permettre d'obtenir assez de données, à partir de résultats expérimentaux où les effets de migrations sont exactement contrebalancés par des effets de diffusion, pour permettre l'élaboration d'une meilleure expression mathématique avec laquelle on pourrait prédire les changements de concentration au niveau d'électrodes opérant sans convection. On présente des données montrant un état de polarisation pratiquement statique lors d'une électrolyse à basse densité de courant impliquant du Fe^{2+} comme espèce électroactive.

[Traduit par le journal]

The idea of observing concentration gradients at working electrodes and thereby studying electrochemical transport is not of recent origin. Samarcev (1) in 1934 used a two-beam interferometer to view the diffusion layer at solid electrode and in 1938 Antweiler (2) published his classic work on the polarographic maximum in which he used a form of interferometry. In 1955 Ibl and Muller (3) published the first good two-beam interferograms of a diffusion layer at one working electrode. In 1957 O'Brien and Axon published the first multiple-beam interferogram of a complete cell showing concentration gradients from electrode to electrode (4). In the following years diffusion constants were measured (5) and also the effects of natural convection in limiting diffusion layers (6).

A first attempt to fit observed concentration gradients to theoretical curves generated for convectionless transport was reasonably successful for short times, moderate concentrations, low current densities, and electrode separations that could be considered to be semi-infinite (7). A further attempt at lower concentrations, but the same current densities, electrode separation, and electrolysis times showed much worse agreement (8). Meanwhile Tobias' group (9, 10) have shown conclusively that errors inherent in the optical set-up for interferometry are too large for its use for high current density, thick electrodes (cells), poor focussing, and long times. It is clear, however, that for low current densities (<2 mA cm^{-2}), thin cells (<0.5 cm), and hence low refractive index changes, that optical errors are smaller than other experimental errors (10).

Muller (9) has summarized progress in two-beam interferometry to 1973 (essentially to the present) and

[1]Permanent address: Akademia Garniczo-Hutnicza, al. Mickiewicza 30, bl. A-2, 30-057 Krakow, Poland.

Can. J. Chem. Downloaded from www.nrcresearchpress.com by 210.87.254.6 on 09/05/12
For personal use only.

Srivansan (11) has summarized holographic interferometry to the same date. The concentration gradient across an electrodialysis membrane by holographic interferometry has been published since Srivansan's summary (12).

In most galvanostatic studies it is assumed that steady state has been achieved at about 60 s because the potential usually has ceased to vary. This is correct if forced convection is present or at vertical (actually non-horizontal) electrodes where natural convection will limit the diffusion layer thickness and bring about a constant concentration gradient (6*c*). The exception is for horizontal electrodes where although the potential may not be perceptibly changing, the concentration contour is (7). This work was done to investigate the galvanostatic case where in the absence of convection a steady state is attained both in potential and the concentration contour, a situation at variance with mathematical solutions (8, 13). Some recent work in which the effect of a Teflon electret immersed in a KI solution was studied, where the solution was observed interferometrically, was the immediate stimulus to this work. A straight line gradient as expected in migration was first observed then the usual error function-type diffusion gradient developed and decayed (14).

Experimental

A Micro electrolysis cell which was also a Fabry-Perot interferometer giving Fizeau-type multiple beam wedge fringes similar in design to cells previously described (7, 15, 16) was used. The system in which the work was done was the $Fe/Fe(NH_4)_2(SO_4)_2/Fe$ system. The cell was 3.18 mm thick with the electrodes 8 mm apart, the solution was 0.1 *M* in $Fe(NH_4)_2(SO_4)_2$ (Mohr's Salt) and 0.1 *M* in sodium citrate at p*H* 5.1. The electrodes were Armco iron of high purity. The current density was 0.25 mA cm^{-2}.

A further series of runs was done in the system $Cu/CuSO_4/Cu$. The cathode was polycrystalline but the anode area consisted of two pieces of a single crystal with the 110 and the 111 faces exposed. The $CuSO_4$ concentration was 0.5 *M* at p*H* 4.1 at 25°C and the current density was 0.05 mA cm^{-2}. Further results with this system will be reported elsewhere.

Many runs were also done with the $Zn/ZnSO_4/Zn$ system at 0.10 *M* $ZnSO_4$ (p*H* 4.7) at 0.50 mA cm^{-2} and 0.25 mA cm^{-2}. Approximately 30 h of experiments were recorded on video tape, each experiment required about 4 min (3 min continuous taping from inception then approximately 10 s bursts for up to 1 h of electrolysis) constituting about 10^5 fields (frames) of which about 100 were analysed in detail. The data were recorded by voice on the video tape to mark times, events of experimental importance, and to record immediate impressions and values from ancillary instrumentation. The recording system consisted of a Spectra-Physics Model 122 He-Ne single mode laser as light source, a Sony Model AVC-3210 video camera, a Sony AV-3650 half-inch video recorder, and a 26 in. monitor.

Hand analysis was done by photographing the monitor with a 35 mm Nikon camera projecting the negative onto a plotting table and plotting the fringes on 30 × 50 cm transparent graph paper. Points in the drawn fringes were then converted to concentration. The conversion factor is obtained from refractive index data obtained separately with an Abbé precision refractometer or a locally designed and built interferometer using the formula:

$$[1] \qquad 2nt \cos\theta = N\lambda$$

The thickness of the interferometric cell is *t*, *n* is the refractive index of the electrolyte, θ is the angle between perpendicular incidence and the actual angle which must be so close that $\cos\theta = 1$ for good fringes, and *N* is the order of interference or twice the number of wavelengths λ in the thickness of the cell. Since *n*, *t*, and λ are known, *N* can be found and for each change of one unit (*N* is about 10^4 for the cell used) called one fringe shift, a refractive index change and hence a concentration change can be found as previously reported in detail (15, 16).

Results and Discussion

A case of steady state electrolysis for galvanostatic conditions where both the potential and the concentration contour is constant has been found and is reported here for the first time to the best of the authors' knowledge. Previously all such results occurred only when some limitation to concentration polarization such as natural or forced convection was present. It is considered that since three systems have shown this effect, two of them simple and one complex, that the effect is likely to be universal.

Figure 1 gives a plot of concentration change vs. time for the iron system typical of these 'steady-state' conditions which are achieved at about 90–120 s. Data for 3 min of the run only are shown since the remainder of the run showed only the expected experimental scatter. It is significant that constant concentration begins simultaneously (as closely as can be measured) at the electrode surface and 0.005 cm out from it. Figure 2 shows a similar plot for $Cu/CuSO_4/Cu$. The rate of anodic dissolution of the 111 plane is faster than that of the 110 plane. The effect is transferred to the part of the cathode opposite the 111 plane anode as well. Steady state is

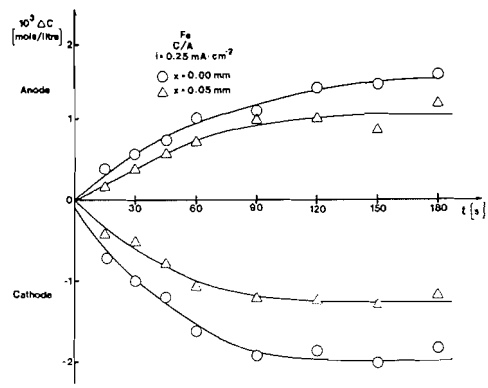

FIG. 1. The change in concentration of Fe^{2+} ion at two distances from each electrode with time of electrolysis.

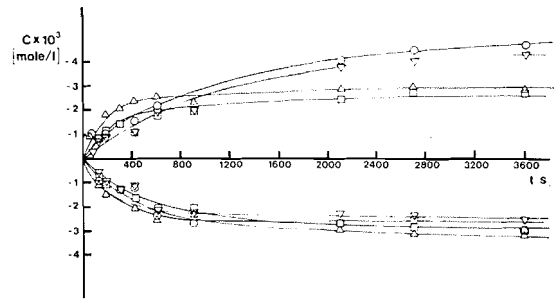

FIG. 2. The change in concentration of $CuSO_4$ at the electrode surface and 7.8×10^{-3} cm measured perpendicularly from it with time in the system $Cu/CuSO_4/Cu$. Concentration at the electrode face of the 111 and the 110 phase denoted by ○ and ▽ and at 7.8×10^{-3} cm by △ and □ respectively. The polycrystalline cathode values opposite the two anodes are marked the same way and show similar variations. The solution was 0.05 *M* $CuSO_4$, p*H* 4.1 at 25°C, and cd 0.05 mA cm^{-2}.

achieved at approximately 2000 s. The $Zn/ZnSO_4/Zn$ system showed analogous results.

The expression most commonly used to describe a non-convecting system is a solution of the differential equation (Fick's second law)

$$[2] \qquad \frac{\partial C}{\partial t} = D\frac{\partial^2 C}{\partial x^2}$$

for the boundary conditions that initially at $t = 0$ (s), $C = C_0$ the bulk concentration (mol cm^{-3}) at all x from 0 to l where $2l$ is the distance between the two electrodes (cm) and that $\Delta C = 0$, at $x = l$ for all $t > 0$ and $\partial\Delta C/\partial t$ is constant at $x = 0$ and $t > 0$. Either electrode can be taken as $x = 0$ but the case studied was the anode. When solved for these conditions by Laplace transform the expression obtained is

$$[3] \qquad \Delta C_{(x,t)} = \frac{2I\sqrt{t}}{nF\sqrt{D}}\left[\text{ierfc}\left(\frac{(2l-x)}{2\sqrt{Dt}}\right) - \text{ierfc}\left(\frac{x}{2\sqrt{Dt}}\right)\right]$$

where I is current density (A cm^{-2}), t is time (s), F is the faraday (coulombs mol^{-1}), D is the diffusion constant of the electrolyte molecule ($cm^2\ s^{-1}$), n is the number of electrons transferred in the reaction, and ierfc is the integrated error function complement tabulated by Carslaw and Yaeger (17). These are the first two terms of a series. It is usual to take into account the effect of migration by multiplying by the transport number (t_-) of the negative ion if the cation is the electroactive species as in the systems studied here. The reasoning for this procedure has been summarized by Wilke, Eisenberg, and Tobias (17). If the interest is in short times (less than 150 s) of electrolysis, the expression then becomes (8)

$$[4] \qquad \Delta C_{(x,t)} = \frac{-2It_-}{nF}\sqrt{\frac{t}{D}}\,\text{ierfc}\frac{x}{2\sqrt{Dt}}$$

It is suggested that simply multiplying by the appropriate transport number cannot give the correct concentration gradient. A solution should be sought from general transport considerations. The flux of the ith ion can be represented by

$$[5] \qquad \boldsymbol{J}_i = -D_i\left(\frac{\partial C_i}{\partial x}\right) + \mu_i v_i C_i \boldsymbol{E}$$

where all symbols have their previous meaning and μ_i is the mobility ($cm\ s^{-1}\ V^{-1}$), v_i is the charge on the ion, and $\boldsymbol{E}$ is the electric field ($V\ cm^{-1}$). When the concentration at the electrodes is constant in time at constant current density, the equation to be solved is

$$[6] \qquad \frac{\partial C_i}{\partial t} = D_i\frac{\partial^2 C_i}{\partial x^2} - \mu_i v_i \boldsymbol{E}\left(\frac{\partial C_i}{\partial x}\right) = 0$$

or

$$D_i\left(\frac{\partial^2 C_i}{\partial x^2}\right) = \mu_i v_i \frac{\partial(\boldsymbol{E}C_i)}{\partial x}$$

The statement means that rate of diffusion of ions down the concentration gradient formed by migration (the effect of the electrode field on the ion) is equal at all points to the rate of migration of ions or a steady state is reached. However, when, as is required, activities of the ions are used the solution of eq. 6 becomes very difficult.

Conclusions

The powerful method of analysis of interferometric concentration polarization data should be used to follow the onset of steady state polarization where the effects of migration are just offset by diffusion down the migration-established concentration gradient. Exact knowledge of the form of the concentration gradient should help in setting up suitable solutions to eq. 6. Clearly multiplying by the transport number does not allow eq. 4 to fit the concentration gradients observed. Intuitively, one would expect the anion transport number to approach zero as the electrode surface or more exactly the outer Helmholtz plane is approached. A mathematical solution is presently being sought.

The data and the mathematical formulations were given at the International Symposium in Ottawa July, 1976.

Acknowledgements

The work was supported mainly by Paint Research Institute Grant No. 59 Co. and in part by the National

Can. J. Chem. Downloaded from www.nrcresearchpress.com by 210.87.254.6 on 09/05/12
For personal use only.

Research Council of Canada and the University of Victoria.

1. A. G. SAMARCEV. Z. Phys. Chem. A**168**, 45 (1934).
2. H. J. ANTWEILER. Z. Electrochem. **44**, 719 (1938).
3. N. IBL and R. H. MULLER. Z. Elektrochem. **59**, 671 (1955).
4. R. N. O'BRIEN and H. J. AXON. Trans. Inst. Met. Finish. **34**, 41 (1957).
5. (*a*) R. N. O'BRIEN and C. ROSENFIELD. J. Phys. Chem. **67**, 643 (1963); (*b*) R. N. O'BRIEN, D. QUON, and C. R. DARSI. J. Electrochem. Soc. **117**, 888 (1970).
6. (*a*) R. N. O'BRIEN, W. F. YAKYMYSHYN, and J. LEJA. J. Electrochem. Soc. **110**, 820 (1963); (*b*) A. TVARUSKO and L. S. WATKINS. Electrochim. Acta, **13**, 891 (1968); (*c*) R. N. O'BRIEN. J. Electrochem. Soc. **119**, 489 (1972).
7. R. N. O'BRIEN. J. Electrochem. Soc. **113**, 289 (1966).
8. R. N. O'BRIEN, J. LEJA, and E. A. BEER. J. Electrochem. Soc. **121**, 370 (1974).
9. ROLF MULLER. Double beam interferometry for electrochemical studies. *In* Advances in electrochemistry and electrochemical engineering. Vol. 9. *Edited by* Paul Delahay and Charles Tobias. Wiley, New York, NY. 1973.
10. F. R. MCLARNON, R. H. MULLER, and C. W. TOBIAS. J. Electrochem. Soc. **122**, 59 (1975).
11. VAKULA SRIVANSAN. Holography and holographic interferometry. *In* Advances in electrochemistry and electrochemical engineering. Vol. 9. *Edited by* Paul Delahay and Charles Tobias. Wiley, New York, NY. 1973.
12. R. N. O'BRIEN. Electrochim. Acta, **20**, 447 (1975).
13. R. N. O'BRIEN and K. J. LUSHINGTON. Nature (London), Phys. Sci. **243**, 117 (1973).
14. R. N. O'BRIEN. Rev. Sci. Instrum. **35**, 803 (1964).
15. R. N. O'BRIEN. Interferometry in techniques of chemistry. Physical Methods. Vol. I. Part IIIA. *Edited by* A. Weissberger and B. Rossiter. Wiley-Interscience, New York, NY. 1972. Chapt. I.
16. H. S. CARSLOW and J. C. YAEGER. Conduction of heat in solids. 2nd ed. Oxford University Press. 1959. p. 485.
17. (*a*) C. W. TOBIAS, M. EISENBERG, and C. R. WILKE. J. Electrochem. Soc. **98**, 359c (1952); (*b*) JOHN NEWMAN. Transport processes. *In* Advances in electrochemistry and electrochemical Engineering. Vol. 5. *Edited by* Paul Delahay and C. W. Tobias. Wiley, New York, NY. 1967. p. 96.

Can. J. Chem. Downloaded from www.nrcresearchpress.com by 210.87.254.6 on 09/05/12
For personal use only.

Transition layer model of the oxide–electrolyte interface

MICHAEL J. DIGNAM

Department of Chemistry, University of Toronto, Toronto, Ont., Canada M5S 1A1

Received June 9, 1977

MICHAEL J. DIGNAM. Can. J. Chem. **56**, 595 (1978).

A model of the oxide–electrolyte interface is proposed which accounts both for the Nernstian behaviour of the oxide (glass) electrode and the anomalous capacitance values of some oxides defined in terms of the change in surface charge with p*H*. The essential feature of the model is the existence of a transition layer of atomic dimensions in thickness within which is established an equilibrium between oxide and aqueous ionic species. The Nernstian behaviour of the oxide (glass) electrode is independent of the model chosen for the oxide–electrolyte double layer but requires that the oxide be conducting; the capacitance of the system, of course, is dependent on the detailed structure of the interface.

MICHAEL J. DIGNAM. Can. J. Chem. **56**, 595 (1978).

On propose un modèle pour l'interface oxyde-électrolyte qui tient compte à la fois du comportement Nernstien de l'oxyde (verre) électrode et des valeurs anormales de la capacité de quelques oxydes; ce modèle est défini en termes de changements, en fonction du p*H*, dans la charge superficielle. La caractéristique principale du modèle est l'existence d'une couche de transition dont l'épaisseur possède des dimensions atomiques et dans laquelle il s'établit un équilibre entre l'oxyde et les espèces ioniques aqueuses. Le comportement Nernstien de l'oxyde (verre) électrode ne dépend pas du modèle choisi pour la double couche oxyde–électrolyte; elle nécessite toutefois que l'oxyde soit conducteur. Il est entendu que la capacité du système dépend de la structure détaillée de l'interface.

[Traduit par le journal]

Introduction

The behaviour of the oxide/electrolyte system has for some time posed a problem, which has been tackled by many researchers who have offered as many interpretations. Ahmed (1) has recently presented a review of some of these, in addition to presenting his own. A brief summary of the situation follows.

A large number of oxide electrodes (1) that are conducting obey the Nernst equation

$$[1] \quad \psi_M - \psi_{aq} = 2.303(kT/e)(\mathrm{p}H_{zpc}{}^{(M)} - \mathrm{p}H)$$

where ψ_M is the potential of the metal in contact with the oxide, ψ_{aq} that of the aqueous electrolyte, $\mathrm{p}H_{zpc}{}^{(M)}$ the p*H* of the electrolyte for which $\psi_M - \psi_{aq} = 0$, with the other symbols having their usual meaning. Furthermore, the potential drop across a conducting glass (vitreous metal oxide) membrane follows a Nernstian relation,

$$[2] \quad \psi_2 - \psi_1 = 2.303(kT/e)(\mathrm{p}H_1 - \mathrm{p}H_2)$$

where the subscripts designate the properties of the solution on the two sides of the membrane.

On the other hand, Levine and Smith (2) have developed a detailed model of the oxide–electrolyte interface from which they deduce that the potential drop from the oxide surface to the bulk electrolyte only obeys the Nernst equation under certain limiting conditions which relate to the equilibrium constants for adsorption of H_3O^+ (henceforth H^+) and OH^- on the oxide surface. On the basis of these relations they are able to account for certain anomalies in the double layer capacitance of oxides determined from acid/base titration of high surface area oxide powders in conjunction with the Nernst equation. The acid/base titration readily yields a plot of surface charge density, σ_s^e, of H^+/OH^- as a function of solution p*H*. The total apparent or effective differential capacitance C_t^e of the oxide–solution interface is then calculated from:

$$[3] \quad C_t^e = -\frac{e}{2.303kT}\frac{d\sigma_s^e}{d(\mathrm{p}H)}$$

The 'true' total differential capacitance of the interface, defined as

$$[4] \quad C_t = d\sigma_s/d(\psi_s - \psi_{aq})$$

will equal C_t^e if and only if both the Nernst equation applies to the total double layer potential, $\psi_s - \psi_{aq}$, and the net surface charge is due solely to H^+/OH^-. Levine and Smith's approach accounts for anomalously low values of C_t^e since, for their model, the Nernst equation is not invariably obeyed. Ahmed, on the other hand, accounts for anomalously high values for $d\sigma_s^e/d(\mathrm{p}H)$ by invoking a partially compensating desorption/adsorption of the counter ions.

In this paper we outline a model which preserves the Nernst relation for all situations in which it can be tested directly, while at the same time supporting

Can. J. Chem. Downloaded from www.nrcresearchpress.com by 210.87.254.42 on 09/05/12
For personal use only.

Can. J. Chem. Downloaded from www.nrcresearchpress.com by 210.87.254.42 on 09/05/12
For personal use only.

the essential ideas advanced by both Levine and Smith and by Ahmed to account for experimental capacitance values.

Transition Layer Model – Thermodynamic Properties

Basic Concept

The basic concept behind the transition layer model is very simple, involving no more than a layer of thickness of the order of atomic dimensions between the oxide and the electrolyte, within which an equilibrium between ions originating from the oxide and from the electrolyte can be established. We examine first how such a model leads to Nernstian behaviour for the two situations in which it can be tested; a metal in contact with the oxide, and an oxide membrane separating electrolytes of different pH. We then consider in detail the molecular processes by which equilibrium (and hence Nernstian behaviour) can be established for soluble oxides, then for insoluble oxides which are respectively cationic, anionic, and electronic conductors.

The Nernst Equation

The model shown diagramatically in Fig. 1 relates to the system metal/(oxide of the metal)/electrolyte and in Fig. 2 to the system electrolyte(*1*)/oxide/electrolyte(*2*) for the case of cationic conducting oxides.

Treating the system represented in Fig. 1 by equating electrochemical potentials gives:

$$[5] \quad \frac{1}{z}\bar{\mu}(M_M^{z+}) = \frac{1}{z}\bar{\mu}(M_t^{z+}),\ K_a$$

$$[6] \quad \frac{1}{z}\bar{\mu}(M_t^{z+}) = \bar{\mu}(H_t^{+}) + \Delta\mu_b^0,\ K_b$$

$$[7] \quad \bar{\mu}(H_t^{+}) = \bar{\mu}(H_{aq}^{+}),\ K_c$$

Taking the usual approximate form for the electrochemical potential, e.g.:

$$[8] \quad \bar{\mu}(M_t^{z+}) = \mu^0(M_t^{z+}) + kT \ln [a(M_t^{z+})] + ze\psi_s$$

where ψ_s is the potential appropriate for the species in the transition layer (i.e., the potential of the oxide surface), eqs. 5 to 7 give, respectively:

$$[9] \quad [a(M_t^{z+})]^{1/2} = K_a \exp [e(\psi_M - \psi_s)/kT]$$

$$[10] \quad a(H_t^{+}) = K_b[a(M_t^{z+})]^{1/2}$$

$$[11] \quad a(H_{aq}^{+}) = K_c a(H_t^{+}) \times \exp [e(\psi_s - \psi_{aq})/kT]$$

where

$$K_a = \exp [\{\mu^0(M_M^{z+}) - \mu^0(M_t^{z+})\}/zkT]$$

$$K_b = \exp [\{1/z)\mu^0(M_t^{z+}) - \mu^0(H_t^{+}) + \Delta\mu_b^0\}/kT]$$

$$K_c = \exp [\{\mu^0(H_t^{+}) - \mu^0(H_{aq}^{+})\}/kT]$$

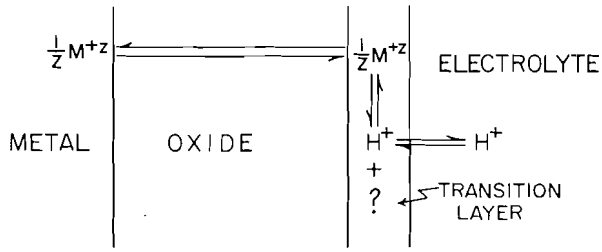

FIG. 1. Schematic diagram of the transition layer model for the system metal/metal oxide/electrolyte, showing the essential features of the equilibrium processes.

Elimination of $a(M_t^{z+})$ and $a(H_t^{+})$ from eqs. 9 to 11 gives, on taking logarithms,

$$[12] \quad \psi_M - \psi_{aq} = (2.303kT/e)[pH_{zpc}^{(M)} - pH]$$

where $pH \equiv -\log [a(H_{aq}^{+})]$ and $pH_{zpc}^{(M)} \equiv -\log (K_aK_bK_c)$.

In practice, a counter electrode must be used, whose electrostatic potential with respect to the solution is independent of pH, to give for the overall cell potential,

$$[13] \quad \psi_M - \psi'_{ref} = \text{const} - (2.303kT/e)pH$$

where ψ'_{ref} is defined to include the difference in Fermi level for the electrons in the two metals so that the $\psi_M - \psi'_{ref}$ is an observable. Note that this result, which represents Nernstian behaviour, is independent of the model chosen for the double layer. It rests, however, on being able to construct a transition region having the desired properties.

In precisely the same way, the equilibria depicted in Fig. 2 lead to

$$[14] \quad \psi_2 - \psi_1 = -(2.303kT/e)(pH_2 - pH_1)$$

Molecular Processes For A Soluble Ionic Conducting Oxide

We now set up a particular model for the transition layer and the molecular processes involved. For oxides which are ionic, rather than electronic, conductors, there will be only one oxidation state which need be considered. If more than one were involved, the oxide would presumably be a semiconductor. We therefore choose a model of the transition layer consisting of an approximately two-dimensional lattice or net of cation and anion sites, occupied by M^{z+}, O^{2-}, H^+, OH^-, as well as H_2O and other ions present in the electrolyte. The presence of these other ions has no effect on the Nernstian behaviour of the system but will influence the distribution of potential across the oxide, and the oxide–electrolyte double layer.

It is instructive to begin by considering the case of a soluble oxide. For equilibrium conditions to be established, the electrolyte must be saturated with

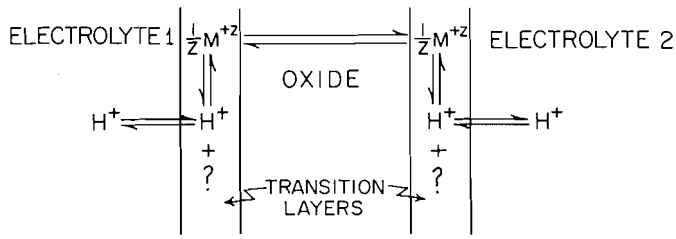

FIG. 2. Schematic diagram of the transition layer model for the system electrolyte(*1*)/metal oxide/electrolyte(*2*), showing the essential features of the equilibrium process.

respect to the oxide, so that for an acidic electrolyte

[15] $(1/2z)M_2O_z + H_{aq}^+ \rightleftharpoons (1/z)M_{aq}^{z+} + \frac{1}{2}H_2O_{(l)}$, K_s

The various molecular processes involving transition layer species presumably can be represented by the following:

[16] $(1/z)M_{aq}^{z+} \rightleftharpoons (1/z)M_{t+}^{z+}$, K_z

[17] $H_{aq}^+ \rightleftharpoons H_{t+}^+$, K_{1+}

[18] $H_2O_{(l)} \rightleftharpoons OH_{t-}^- + H_{aq}^+$, K_{1-}

[19] $OH_{t-}^- \rightleftharpoons O_{t-}^{2-} + H_{aq}^+$, K_{2-}/K_{1-}

where the subscripts t+ and t− denote species occupying cation and anion sites respectively of the transition layer.

Processes 15 to 17 lead to the following equilibrium statement

[20] $(1/2z)M_2O_z + H_{t+}^+ \rightleftharpoons (1/z)M_{t+}^{z+} + \frac{1}{2}H_2O_{(l)}$, $K_t/K_{2-}^{1/2}$ or $K_sK_zK_{1+}$

which is of the desired form, since the electrochemical potentials of M_2O_z and $H_2O_{(l)}$ are constant, or nearly so, at fixed temperature and pressure. Proceeding from Fig. 1, therefore, we obtain eq. 12, with $K_b = K_{2-}^{1/2}/K_t$, $K_c = 1/K_{1+}$ so that

[21] $pH_{zpc}^{(M)} = \log (K_{1+}K_t/K_aK_{2-}^{1/2})$

Molecular Processes For Insoluble Cationic Conducting Oxide

Equations 15, 16, 18, and 19 lead to the following equilibrium statement:

[22] $(1/2z)M_2O_z \rightleftharpoons (1/z)M_{t+}^{z+} + \frac{1}{2}O_{t-}^{2-}$, $K_t = K_sK_zK_{2-}^{1/2}$

The molecular processes represented by eqs. 17 to 19 and 22 are thermodynamically equivalent to those represented by eqs. 15 to 19, but the former processes remain viable for oxides of vanishingly low solubility, provided that a mechanism exists of sufficiently low activation energy ($\gtrsim$0.7 eV for room temperature), for transforming bulk oxide into transition layer ions at the oxide – transition layer boundary, and vice versa. This will ensure that the equilibrium represented by eq. 22 can be established in a reasonable time ($\gtrsim$1 s). We imagine this to occur via surface diffusion of M^{z+} and O^{2-} to and from lattice steps on the oxide surface, processes which would be expected to have activation energies substantially lower than that for transfer of the ions to the electrolyte phase. The high concentration of surface lattice steps existing for all but very carefully equilibrated oxide surfaces will require that ions move no more than a few lattice distances across the surface (see Fig. 3), while processes 18 and 19 combined, effectively lead to movement of O^{2-} from one site in the transition layer to another, through the aqueous phase. Processes 17 to 19 and 22 again give eqs. 20 and 21.

Molecular Processes For Insoluble Anionic Conducting Oxide

The same result is obtained for the case of an oxide which is an anionic conductor, provided again that some movement of ions at the oxide interfaces is possible so that both process 22 and an analogous process in the oxide layer at the metal–oxide interface can proceed to equilibrium. The latter process would involve the equivalent of grain boundary

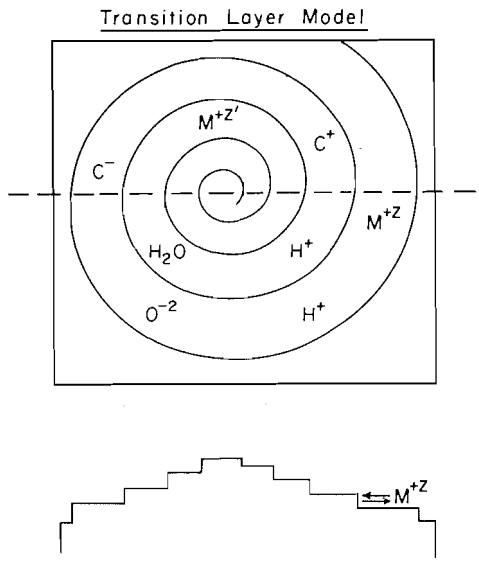

FIG. 3. Schematic diagram of a surface showing how surface steps aid in establishing the equilibrium concentration of M^{z+} in the transition layer. (C^+ and C^- represent counter ions in the transition layer.)

Can. J. Chem. Downloaded from www.nrcresearchpress.com by 210.87.254.42 on 09/05/12
For personal use only.

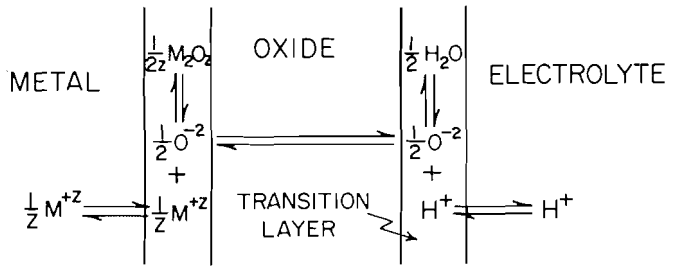

FIG. 4. Schematic diagram of the transition layer model for the system metal/metal oxide/electrolyte for an anionic conducting oxide.

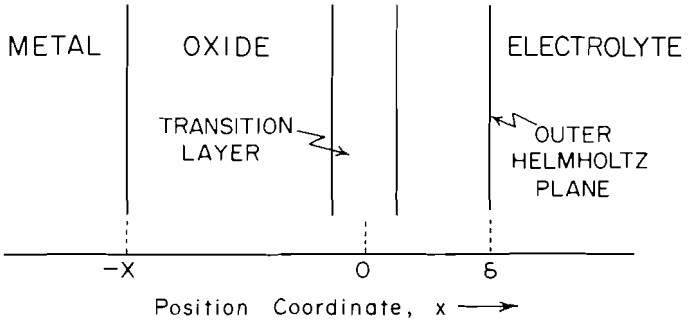

FIG. 5. Illustration of the coordinate system chosen for determining the distribution of charge and potential.

ionic diffusion, and once again, most likely low activation energies. This case is depicted in Fig. 3, and clearly leads to Nernstian behaviour. The appropriate equilibrium in the oxide–electrolyte transition layer is obtained from [17] to [19]

[23] $$H_2O_{(l)} = O_{t-}^{2-} + 2H_{t+}^{+},\ K_{1+}K_{2-}$$

to which we add the molecular processes

[24] $$(1/z)M_M^{z+} \rightleftharpoons (1/z)M_m^{z+},\ K_d$$

[25] $$\tfrac{1}{2}O_m^{2-} \rightleftharpoons \tfrac{1}{2}O_{t-}^{2-},\ K_a'$$

[26] $$(1/2z)M_2O_z \rightleftharpoons \tfrac{1}{2}M_m^{z+} + (1/z)O_m^{2-},\ K_m$$

where the subscript m designates the oxide layer next to the metal. However, [24] to [26], with [22], give

[27] $$\frac{1}{z}M_M^{z+} = \frac{1}{z}M_{t+}^{z+},\ \frac{K_mK_a'}{K_dK_t} \equiv K_a$$

which leads to eq. 5 so that eq. 21 is obtained for this case as well. Thus the final expression is independent of the molecular processes by which overall equilibrium is established, which of course must be the case if the situation being considered is a true equilibrium one. The boundary layer postulate simply provides a mechanism for the establishment of equilibrium in the case of oxides of negligible solubility. It also provides, however, a model for determining the distribution of potential across the oxide and its interfaces, which is a non-thermodynamic property (it cannot be measured) as is $\psi_M - \psi_{aq}$, though not $\psi_M - \psi'_{ref}$.

Molecular Processes For Insoluble Electronic Conducting Oxide

We next look at the case of a semiconducting oxide. Most such oxides depend for their conductivity upon the existence of two oxidation states of the metal separated by a relatively small oxidation potential. A number of different conduction mechanisms based on dual oxidation states can arise, which need not concern us, except to note that they all depend on having a significant representation of both metal oxidation states in the oxide lattice, hence presumably in the transition layer as well. We assume, therefore, the establishment throughout the oxide and the transition layer of the following equilibrium

[28] $$M^{z+} \rightleftharpoons M^{z'+} + (z' - z)e$$

Furthermore, we assume the composition of the non-stoichiometric oxide to be uniform in the vicinity of the oxide–electrolyte interface. This is most easily represented by treating the oxide as a solution of M_2O_z and $M_2O_{z'}$, the chemical potentials of M_2O_z and $M_2O_{z'}$ being constant near the transition layer. Thus equilibrium processes of the form of [22] in the transition layer lead to:

[29] $$\bar{\mu}(M_{t+}^{z+}) + (z/2)\bar{\mu}(O_{t-}^{2-}) = \tfrac{1}{2}\mu(M_2O_z)$$

Can. J. Chem. Downloaded from www.nrcresearchpress.com by 210.87.254.42 on 09/05/12
For personal use only.

Can. J. Chem. Downloaded from www.nrcresearchpress.com by 210.87.254.42 on 09/05/12
For personal use only.

[30] $\bar{\mu}(M_{t+}^{z'+}) + (z'/2)\bar{\mu}(O_{t-}^{2-}) = \frac{1}{2}\mu(M_2O_{z'})$

so that

[31] $\bar{\mu}(M_{t+}^{z+}) - \bar{\mu}(M_{t+}^{z'+}) = \frac{1}{2}(z' - z)\bar{\mu}(O_{t-}^{2-}) + \frac{1}{2}[\mu(M_2O_z) - \mu(M_2O_{z'})]$

However, since process 28 applies to the transition region, and electronic equilibrium is assumed throughout the system,

[32] $\bar{\mu}(M_{t+}^{z+}) - \bar{\mu}(M_{t+}^{z'+}) = (z' - z)\bar{\mu}(e_t) = (z' - z)\bar{\mu}(e_M)$

Equations 31 and 32 now give

[33] $\frac{1}{2}\bar{\mu}(O_{t-}^{2-}) = \bar{\mu}(e_M) + \frac{\mu(M_2O_z) - \mu(M_2O_{z'})}{2(z - z')}$

However

[34] $\frac{1}{2}\bar{\mu}(O_{t-}^{2-}) + \bar{\mu}(H_{aq}^{+}) = \frac{1}{2}\mu(H_2O_l)$

so that

[35] $\bar{\mu}(e_M) + \bar{\mu}(H_{aq}^{+}) = -\frac{\mu(M_2O_z) - \mu(M_2O_{z'})}{2(z - z')} + \frac{1}{2}\mu(H_2O_{(l)})$

which again leads to eq. 12 with

[36] $pH_{zpc}^{(M)} = \frac{1}{2.303kT} \times \left[\chi + \frac{\mu(M_2O_z) - \mu(M_2O_{z'})}{2(z - z')} + \mu^0(H_{aq}^{+}) - \frac{1}{2}\mu(H_2O_{(l)})\right]$

where $\chi \equiv \mu(e_M)$ is the Fermi level of the metal.

Drift of ZPC

We examine next the consequence of making the contact to the oxide using a metal not belonging to the oxide. It is apparent that in the case of ionic conducting oxides, once the metal and the oxide in contact with it establish equilibrium concentrations with respect to the two cations, the transition layer treatment of the system again leads to the Nernst equation, as long as the foreign metal ion does not reach the oxide–electrolyte interface. One would predict, therefore, a drift in the value of $pH_{zpc}^{(M)}$ with time following formation of the contact, the value ultimately stabilizing for all practical purposes. The predicted drift arises from the dependence of $pH_{zpc}^{(M)}$ on the distribution of metal ions through the metal–oxide contact. Note, however, that no such dependence exists in the case of an electronic conductor, since the only equilibrium process involving the metal–oxide interface is an electronic equilibrium between the bulk metal and the transition layer. On the other hand the value of $pH_{zpc}^{(M)}$ for an electronic conducting oxide depends directly on the composition of the oxide near the oxide–electrolyte interface, and might well be subject to drift on that account. Thus from eq. 36

[37] $pH_{zpc}^{(M)} = \frac{1}{2(z - z')} \log \frac{a(M_2O_z)}{a(M_2O_{z'})} + \text{const}$

For true thermodynamic equilibrium to be established in the case of the electronic conducting oxide, not only must the metal belonging to the oxide be used in the contact, but the oxide composition near the oxide–electrolyte interface must be that corresponding to equilibration with the metal.

Summary of Thermodynamic Properties

Conducting metal oxide systems should satisfy the Nernst equation provided that a transition layer is established, and that equilibrium between oxide and aqueous ions can be effected through the good offices of the transition layer, so to speak. We see no problem in this respect if both oxide and aqueous ionic species make significant contributions to the composition of the transition layer. If this condition is not met, we are faced with precisely the same problem we started with, which was to find a medium for effecting equilibration of oxide and aqueous ions for insoluble oxides.

The novelty of the transition layer model lies in the introduction of an interphase whose composition is variable with respect to both species resident in the aqueous phase as well as the oxide phase. Levine and Smith (2) allow only for the former while Ahmed (1) assumes, without theoretical justification, that the Nernst equation applies to the potential drop from the oxide surface to the bulk electrolyte. The transition layer model leads to exact adherence to the Nernst equation, in part in accord with Ahmed's assumption, but as we shall show shortly, it is a potential drop across the entire system, not just the electrolyte double layers, that satisfies the Nernst equation. Only under certain limiting conditions does the electrolyte double layer potential satisfy the Nernst equation, in qualitative agreement with the results of Levine and Smith.

Transition Layer Model – Charge Distribution

Surface Charge Neglecting Counter Ion Absorption

For purposes of illustrating the main features of the distribution of charge and potential across the systems metal/oxide/electrolyte and electrolyte(*1*)/

Can. J. Chem. Downloaded from www.nrcresearchpress.com by 210.87.254.42 on 09/05/12
For personal use only.

oxide/electrolyte(*2*), we assume that only the following ionic species in the transition layer need to be considered, M^{2+}, O^{2-}, H^+, OH^-. We choose the stoichiometry MO, and shall neglect discreteness-of-charge effects (2) and other second order energy corrections, in the interest of algebraic simplicity.

No matter which conduction mechanism is assumed, or indeed in the absence of any oxide conductivity, processes 17 to 19 and 22 are presumably operative. They lead, for the case $z = 2$, to the following

$$[38] \quad MO + 2H_{aq}^{+} \rightleftharpoons M_{t+}^{2+} + H_2O_{(l)}, \; K_{2+}$$

$$[39] \quad H_{aq}^{+} \rightleftharpoons H_{t+}^{+}, \; K_{1+}$$

$$[40] \quad H_2O_{(l)} \rightleftharpoons OH_{t-}^{-} + H_{aq}^{+}, \; K_{1-}$$

$$[41] \quad H_2O_{(l)} \rightleftharpoons O_{t-}^{2-} + 2H_{aq}^{+}, \; K_{2-}$$

If the oxide is a conductor, then we add to the above either that $\psi_M - \psi_{aq}$ is given by eq. 12, or that $\psi_1 - \psi_2$ is given by eq. 14, whichever is appropriate. That is, for a conducting oxide, the potential drop across the entire system is fixed for electrolyte(s) of fixed p*H*, being independent of the details of the double layer structure and hence of the distribution of charge throughout the system.

We next assume ideal thermodynamic behaviour for the species in the transition layer, so that for example

$$[42] \quad \bar{\mu}(M_{t+}^{z+}) = \mu^0(M_{t+}^{z+}) + kT \ln \left[\frac{\theta_{2+}}{1 - \theta_{1+} - \theta_{2+}} \right] + 2e\psi_s$$

where θ_{2+} and θ_{1+} are the fractions of the cation sites occupied by M^{2+} and H^+ respectively, and ψ_s is the potential at the oxide surface, which we define to coincide with the plane of net charge[1] in the transition layer. The form of the activity used in eq. 42 is that appropriate for species obeying a Langmuir adsorption isotherm, and can be derived from elementary statistical mechanics (2). Equations 38 to 41 now give:

$$[43] \quad \frac{\theta_{2+}}{1 - \theta_{1+} - \theta_{2+}} = K_{2+}[a(H_{aq}^{+})]^2 \exp[-2(p_s - p_{aq})]$$

$$[44] \quad \frac{\theta_{1+}}{1 - \theta_{1+} - \theta_{2+}} = K_{1+}[a(H_{aq}^{+})] \exp[-(p_s - p_{aq})]$$

$$[45] \quad \frac{\theta_{1-}}{1 - \theta_{1-} - \theta_{2-}} = K_{1-}[a(H_{aq}^{+})]^{-1} \exp[(p_s - p_{aq})]$$

$$[46] \quad \frac{\theta_{2-}}{1 - \theta_{1-} - \theta_{2-}} = K_{2-}[a(H_{aq}^{+})]^{-2} \exp[2(p_s - p_{aq})]$$

where $p \equiv e\psi/kT$ is a dimensionless potential, and θ_{2-} and θ_{1-} are the fractions of anion sites occupied by O^{2-} and OH^- respectively. Assuming that the number of lattice sites per unit area, N_s, is the same for cations and anions, and that virtually every site is occupied by an ion rather than H_2O say (i.e., $(\theta_{1+} + \theta_{2+})/(1 - \theta_{1+} - \theta_{2+}) \gg 1$ and $(\theta_{1-} + \theta_{2-})/(1 - \theta_{1-} - \theta_{2-}) \gg 1$), we obtain

$$[47] \quad \frac{\sigma_s}{eN_s} = (2\theta_{2+} + \theta_{1+}) - (\theta_{1-} + 2\theta_{2-}) \simeq \frac{1 + 2(K_{2+}a_H/K_{1+})l^{-\Delta p_s}}{1 + (K_{2+}a_H/K_{1+})l^{-\Delta p_s}} - \frac{2 + (K_{1-}a_H/K_{2-})l^{-\Delta p_s}}{1 + (K_{1-}a_H/K_{2-})l^{-\Delta p_s}}$$

where σ_s is the net charge per unit area on the oxide surface, $a_H \equiv a(H_{aq}^{+})$, and $\Delta p_s = p_s - p_{aq}$. Defining p^* and b according to:

$$[48] \quad p^* - p_{aq} = \tfrac{1}{2} \ln [K_{2+}K_{1-}/K_{2-}K_{1+}] + \ln a_H$$

$$[49] \quad b = (K_{2+}K_{2-}/K_{1+}K_{1-})^{1/2}$$

upon eliminating $(K_{2+}a_H/K_{1+})$ and $(K_{1-}a_H/K_{2-})$ from eq. 47 using eqs. 48 and 49, the result can be expressed as follows:

$$[50] \quad \frac{\sigma_s}{eN_s} = \frac{2 \sinh (p_s - p^*)}{b + b^{-1} + 2 \cosh (p_s - p^*)}$$

Now since $N_s \simeq 10^{15}$ cm^{-2}, it follows that $\sigma_s/eN_s \ll 1$. Thus if $|p_s - p^*| \gtrsim 1$ then $b + b^{-1} \gg 2 \cosh (p_s - p^*)$, while if $|p_s - p^*| \ll 1$, $2 \cosh (p_s - p^*) \simeq 2$.

Thus for all possible cases, we may approximate eq. 50 by:

$$[51] \quad \sigma_s/eN_s = \tfrac{1}{2}\alpha \sinh (p_s - p^*)$$

where $\alpha = 4/(b + b^{-1} + 2)$, or from eq. 49:

$$[52] \quad \alpha = 4\left[\left(\frac{K_{2+}K_{2-}}{K_{1+}K_{1-}} \right)^{1/4} + \left(\frac{K_{1+}K_{1-}}{K_{2+}K_{2-}} \right)^{1/4} \right]^{-2}$$

and is restricted to the range $1 \gtrsim \alpha > 0$.

Three limiting cases may be distinguished. For $b \gg 1$, the transition layer is populated almost en-

[1]That plane chosen so that the first moment of the charge displacements from the plane is zero.

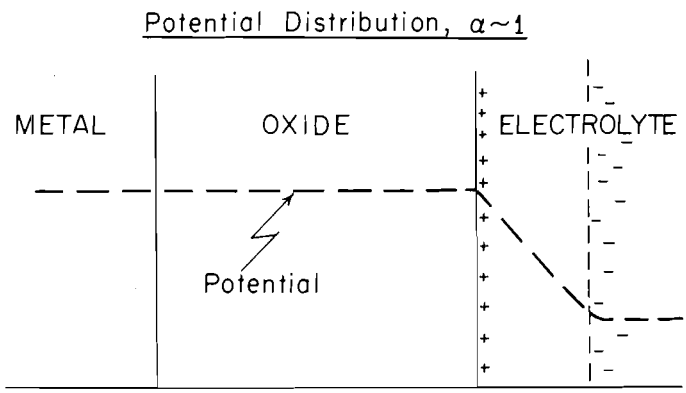

FIG. 6. Schematic representation of the potential and charge distribution for $\alpha \sim 1$.

tirely by M^{2+} and O^{2-}, while for $b \ll 1$ almost entirely by H^+ and OH^-. For $b \sim 1$, all four species occupy a substantial fraction of the available sites.

The ZPC For Free Oxide

Inverting eq. 51 and substituting for p^* from eq. 48 gives

$$[53] \quad \psi_s - \psi_{aq} = 2.303(kT/e)[pH_{zpc}^{(ox)} - pH] + (kT/e)\sinh^{-1}(2\sigma_s/eN_s\alpha)$$

where

$$[54] \quad pH_{zpc}^{(ox)} = \tfrac{1}{2}\log[K_{2+}K_{1-}/K_{2-}K_{1+}]$$

Applying eq. 53 to nonconducting free oxide particles immersed in an aqueous solution, if $\sigma_s = 0$, one must also have $\psi_s - \psi_{aq} = 0$. (In keeping with our intent to minimize algebraic complexity, we neglect the contribution of oriented water molecules to the double layer potential.) For this case, therefore, $pH_{zpc}^{(ox)}$ is the pH corresponding to the zpc for the free oxide. For sufficiently small oxide particles, even if they are conducting, the total charge within them may be neglected. We therefore regard $pH_{zpc}^{(ox)}$, given by eq. 54, as characterizing the zpc for the free oxide, whether or not it is conducting.

Distribution of Potential Across Oxide and Double Layers

We are now in a position to determine the distribution of potential for various cases. A quantitative though simplified treatment of the problem is presented in the Appendix, the conclusions being in accord with the following more qualitative treatment.

The total potential drop from metal to electrolyte is given by eq. 12 and is a property of the metal and the electrolyte pH only, being independent of the energetics of the equilibrium processes involving the transition layer species. We shall hold this potential constant, therefore, and consider the variation in the distribution of potential on varying α and the ratio of the oxide thickness, X, to the characteristic space charge length in the oxide, X_o. Three cases are illustrated in Figs. 6 to 8.

For $\alpha \sim 1$, eq. 53 leads to $\psi_s - \psi_{aq} \simeq 2.303(kT/e)[pH_{zpc}^{(ox)} - pH]$ while for all possible values of α we have from eq. 12,

$$\psi_M - \psi_{aq} = 2.303(kT/e)[pH_{zpc}^{(M)} - pH]$$

Thus for $\alpha \sim 1$, $\psi_s - \psi_{aq}$ satisfies the Nernst equation, while $\psi_M - \psi_s$ is independent of pH, oxide thickness, and so on. Since $\psi_M - \psi_s$ itself is not an observable but only changes in $\psi_M - \psi_s$, and since it does not change, we have set it to zero in sketching the behaviour in Fig. 6. In effect we have chosen the zero of electrostatic potential for each phase to be that corresponding to the zpc for the oxide covered metal.

For α sufficiently small, on the other hand, from eq. 53 we deduce that σ_s will be essentially zero, giving rise, therefore, to potential distributions qualitatively of the forms shown in Figs. 7 and 8. For a sufficiently thick oxide having a large X_o, virtually all of the pH dependent potential will appear across the oxide, not the double layers. These conclusions can be further justified by considering analytical solutions to the charge distribution problem (see Appendix) but they are almost self evident.

The case of an oxide membrane separating solutions of different pH can be treated in the same way. For α sufficiently large, the potential drop across the oxide is essentially zero, while each double layer potential satisfies a Nernst equation, whereas for α very small and for a thick membrane of sufficiently large characteristic space charge length, X_0, the double layer potentials are nearly zero, while the potential drop across the oxide satisfies the Nernst equation. Again for intermediate conditions, neither

Can. J. Chem. Downloaded from www.nrcresearchpress.com by 210.87.254.42 on 09/05/12
For personal use only.

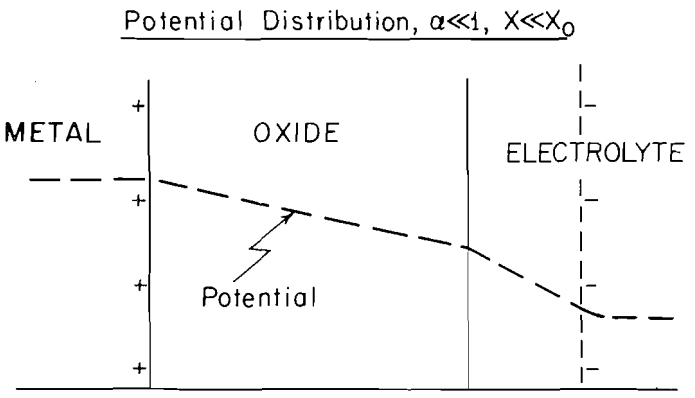

FIG. 7. Schematic representation of the potential and charge distribution for $\alpha \ll 1$ and the film thickness, X, small compared to the characteristic space charge length, X_0.

individually satisfy the Nernst equation, while their sum does.

We treat finally the case of particles of conducting oxide in the two limits, $R \ll X_0$ and $R \gg X_0$, when R is the particle radius. For $R \ll X_0$, space charge in the oxide can be neglected so that the field in the oxide particle is everywhere essentially zero. The only potential drop in this case is across the double layer which is again given by eq. 53.

For α large, $\psi_s - \psi_{aq}$ satisfies the Nernst equation, while for α very small, $\psi_s - \psi_{aq} \simeq 0$.

For $R \gg X_0$, space charge must be taken into account. But, once again, for α large, ψ_s satisfies the Nernst equation, while $\psi_{in} - \psi_s = \psi^* - \psi^* = 0$. For α very small and X_0 sufficiently large, $\psi_{in} - \psi_s$ satisfies the Nernst equation and $\psi_s \simeq 0$.

Double Layer Capacitance

The relationship between the true and apparent total differential capacitance of the double layer can be seen as follows: Differentiating eq. 53 with respect to pH, and substituting for $d(\psi_s - \psi_{aq})/d(pH)$ and $d\sigma_s/d(pH)$ using eqs. 3 and 4 gives the following result:

$$[55] \quad \frac{1}{C_t} = \frac{1}{C_t^e} + \left[\left(\frac{2\sigma_s}{eN_s}\right)^2 + \alpha^2\right]^{-1/2} \frac{1}{C_0}$$

where $C_0 = N_s e^2/2kT$ and is $\sim 3 \times 10^3$ μF at room temperature for $N \sim 10^{15}$ cm^{-2}. From eq. 55 it follows that $C_t^e > C_t$. Several realms of behaviour may now be distinguished. For $\alpha^2 \gg (2\sigma_s/eN_s)^2$, eq. 55 reduces to

$$[56] \quad \frac{1}{C_t} \simeq \frac{1}{C_t^e} + \frac{1}{\alpha C_0}$$

which in turn has two limits, $C_t \simeq C_t^e$ and $C_t \simeq \alpha C_0$ depending on the value of α. For $\alpha^2 \ll (2\sigma_s/eN_s)^2$, eq. 55 reduces to

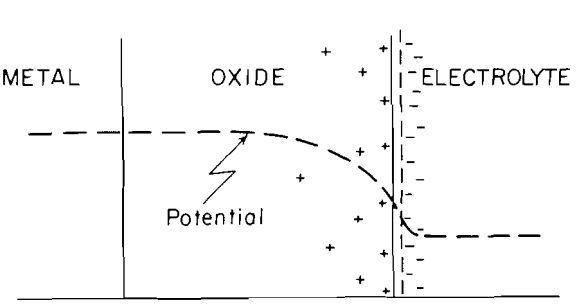

FIG. 8. Schematic representation of the potential and charge distribution for $\alpha \ll 1$ and the film thickness, X, larger than the characteristic space charge length, X_0.

$$[57] \quad \frac{1}{C_t} \simeq \frac{1}{C_t^e} + \frac{eN_s}{2\sigma_s} \frac{1}{C_0}$$

Equation 57 cannot apply, of course, close to the zpc. We see, therefore, that there are two situations in which C_t may be calculated from the results of acid/base titration of high surface area oxides and a knowledge of the zpc. When the competition between the two sets of ions for places in the transition layer is an even one (i.e., $\alpha \sim 1$) then $C_t \simeq C_t^e$, while if the competition is extremely uneven (i.e., α very small) C_t will be given by eq. 57 away from the zpc. This only applies, however, if the anion of the acid and cation of the base (i.e., the counterions) do not occupy a significant number of sites in the transition layer. If this is not the case, the calculated change in surface charge density based on H^+/OH^- titration, $\Delta\sigma_s^e$, will be in error. In particular, for a change in pH at essentially constant counter ion activities, $|\Delta\sigma_s^e| > |\Delta\sigma_s|$. Thus on decreasing the pH, some of the H^+ absorption will take place by replacing absorbed counterions, and conversely for the de-

Can. J. Chem. Downloaded from www.nrcresearchpress.com by 210.87.254.42 on 09/05/12
For personal use only.

Can. J. Chem. Downloaded from www.nrcresearchpress.com by 210.87.254.42 on 09/05/12
For personal use only.

sorbed OH^- ions. Since in practice, C_t^e is calculated from $d\sigma_s^e/d(pH)$, this effect also leads to values of C_t^e which are too large. There is an important difference, however, between the two effects. In the absence of counter ion absorption, the maximum possible value of C_t^e occurs for $\alpha = 1$ when $C_t^e = C_t = C_t^m$ where C_t^m is expected to be of the order of the capacitance of the Hg–electrolyte interface, i.e., 20 $\mu F/cm^2$. The first effect, although it gives $C_t^e > C_t$, always gives $C_t^e < C_t^m$, while the effect of counter ion adsorption will give $C_t^e > C_t^m$ for $\alpha \sim 1$ so that anomalously high values of C_t^e can result.

The above discussion is in some respects a composite of those offered by Levine and Smith (2) and Ahmed (1), except that the model of ion adsorption at the interface used here differs from their models in subtle but important ways as already noted. We will not pursue the question of surface capacitance further, however, since for this to be a worthwhile exercise would require introducing refinements and including an extensive review of relevant data, such being beyond the scope of the present paper.

Summary and Conclusions

In this paper, the consequence of assuming the existence of a transition layer of ions between the oxide and the electrolyte, such ions conforming to the oxide lattice structure, has been examined. If the oxide is a conductor, with both the ions of the oxide and those of the electrolyte (H^+ and OH^-) present in the transition layer to a significant extent at equilibrium, and if further the activation energy for surface migration of metal and oxygen ions at one or both of the oxide interfaces is $\gtrsim 0.7$ eV, then equilibrium or quasi-equilibrium conditions can be established within a few seconds for systems metal/oxide/electrolyte and electrolyte(*1*)/oxide/electrolyte(*2*) in the absence of significant oxide solubility. The transition layer acts essentially as a two dimensional medium within which equilibrium among the ions M^{z+}, O^{2-}, H^+, OH^- can be established. Equilibrium conditions for these systems lead to Nernstian behaviour with respect to the p*H* dependence of the total potential drop across the oxide and double layer(s). The double layer potential itself, however, only satisfies the Nernst equation to a good approximation if the concentrations of (M^{z+}, O^{2-}) and (H^+, OH^-) in the transition layer are comparable at equilibrium.

Use of the Nernst equation to calculate double layer capacitances from measurements of H^+/OH^- adsorbed per unit change in p*H* leads to values above the true value whenever the above condition is not satisfied. The values themselves, however, will be smaller than for the Hg–electrolyte system say. Counter ion adsorption within the transition layer, on the other hand, can lead to anomalously high capacities for H^+/OH^- adsorption. These two effects are essentially those discussed by Levine and Smith (2) and Ahmed (1) respectively. The transition layer postulate, however, effectively reconciles the apparently contradictory approaches taken by these researchers.

1. S. M. Ahmed. *In* Symposium on oxide–electrolyte interfaces. *Edited by* R. S. Alwitt. The Electrochemical Society Inc., Princeton, NJ. 1973. pp. 1–30.
2. S. Levine and A. L. Smith. Discuss. Faraday Soc. **52**, 290 (1971).
3. Yu. V. Pleskov. *In* Progress in surface and membrane science. Vol. 7. *Edited by* J. F. Danielli, M. D. Rosenberg, and D. A. Cadenhead. Academic Press Inc., New York, NY. 1973. pp. 57–93.

Appendix

Potential Distribution for a Simplified Model

The general features of the distribution of charge and potential arising from the transition layer model are determined here for a particularly simple model, but are not effected materially by model refinement.

We exclude the influence of counter ion absorption into the transition layer and employ the Gouy–Chapman model for 1:1 electrolytes, ignoring any net orientation of water dipoles adjacent to the transition layer. Apart from the inclusion of σ_s as given by the transition layer model, the treatment to follow does not differ from numerous already published treatments (see e.g., ref. 3).

We examine the system metal/oxide/electrolyte first (see Fig. 5). Charge neutrality requires that:

$$[A1] \qquad \sigma_M + \sigma_s + \sigma_{aq} + \int_{-X}^{0} \rho \, dx = 0$$

where σ_M and σ_{aq} are the net charge per unit area on the metal and aqueous phases respectively and ρ the space charge concentration within the oxide. Gauss' theorem then gives

$$[A2] \qquad \varepsilon\left(\frac{d\psi_{ox}}{dx}\right)_{x=0} = 4\pi(\sigma_s + \sigma_{aq})$$

$$[A3] \qquad \varepsilon\left(\frac{d\psi_{ox}}{dx}\right)_{x=-X} = -4\pi\sigma_M$$

$$[A4] \qquad \varepsilon_d(\psi_s - \psi_\delta)/\delta = -4\pi\sigma_{aq}$$

while the continuity condition on the electric displacement at the plane $x = \delta$ yields

$$[A5] \qquad \varepsilon_d(\psi_s - \psi_\delta)/\delta = -\varepsilon_{aq}\left(\frac{d\psi_{dif}}{dx}\right)_{x=\delta}$$

Can. J. Chem. Downloaded from www.nrcresearchpress.com by 210.87.254.42 on 09/05/12
For personal use only.

where ε, ε_d, and ε_{aq} are the integral dielectric constants of: the oxide phase of thickness X, the Helmholtz double-layer of thickness δ, and the diffuse layer respectively, and ψ_{dif} is the potential in the diffuse layer. The model of the diffuse layer developed by Gouy leads to the following expression for a 1:1 electrolyte:

$$[A6] \quad -\left(\frac{dp_{dif}}{dx}\right) = \frac{2}{X_{aq}} \sinh [(p_{dif} - p_{aq})/2]$$

where X_{aq} is the Debye–Hückel length for the electrolyte given by

$$[A7] \quad X_{aq} = \sqrt{\frac{\varepsilon_{aq} kT}{8\pi n_{aq} e^2}}$$

and n_{aq} is the bulk electrolyte concentration. The Debye–Hückel length is about 10 Å for a 0.1 M solution at room temperature.

Equations A5 and A6 now yield

$$[A8] \quad \frac{\varepsilon_d X_{aq}}{\varepsilon_{aq} \delta}(p_s - p_\delta) = 2 \sinh [(p_\delta - p_{aq})/2]$$

while eqs. A2 and A4 give:

$$[A9] \quad \frac{\sigma_s}{eN_s} = X_s\left(\frac{dp_{ox}}{dx}\right)_{x=0} + \frac{\varepsilon_d X_s}{\delta}(p_s - p_\delta)$$

where X_s is a characteristic length associated with the transition layer, and is given by

$$[A10] \quad X_s = \frac{\varepsilon kT}{4\pi N_s e^2}$$

at room temperature, for $N_s = 10^{15}$ cm^{-2} and $\varepsilon = 10$, $X_s = 0.014$ Å.

The Poisson–Boltzmann equation for the ionic or electronic current carriers in the oxide and the compensating immobile charged species is given by:

$$[A11] \quad \frac{d^2\psi_{ox}}{dx^2} = -\frac{4\pi n_0 z_c e}{\varepsilon}\{\exp [ez_c(\psi_z - \psi_{ox})/kT] - 1\}$$

where $-n_0 z_c e$ is the charge per unit volume due to the compensating immobile charged species, $z_c e$ the charge on the current carriers, and ψ_z the potential for which the net space charge is zero. Equation A11 may be written

$$[A12] \quad \frac{d^2y}{dx^2} = \frac{1}{X_o^2}\{1 - e^{-y}\}$$

where

$$[A13] \quad y = z_c(p_{ox} - p_z) = \frac{z_c e}{kT}(\psi_{ox} - \psi_z)$$

and

$$[A14] \quad X_o = \sqrt{\frac{\varepsilon kT}{4\pi n_0 z_c^2 e^2}}$$

Analytic solutions to [A12] are not available. Solutions can easily be found, however, for the following three limiting cases: $|y| \ll 1$, $y \gg 1$, and $-y \gg 1$. We shall pursue only the first case, however, which places a severe restriction on the quantitative applicability of the resulting expressions, but not on their qualitative applicability. Following the same procedures, more general expressions can be obtained at the expense of an enormous increase in complexity.

Expanding e^{-y} to first order eq. A13 is readily integrated to give:

$$[A15] \quad y = c \sinh\left(\frac{x - x_0}{X_o}\right)$$

where c and x_0 are the integration constants. Differentiation of eq. A15 once, then setting $x = 0$ gives

$$[A16] \quad z_c\left(\frac{dp_{ox}}{dx}\right)_{x=0} = \frac{c}{X_o} \cosh \frac{x_0}{X_o}$$

while differentiation of eq. A15 twice then setting $x = -X$ gives

$$[A17] \quad c \sinh\left(\frac{X + x_0}{X_o}\right) = \left(\frac{n_{-X}}{n_0} - 1\right)$$

where n_{-X} is the concentrate of carriers at the metal–oxide interface, which we assume to be a constant. Finally, application of eq. A16 at the two boundaries gives

$$[A18] \quad z_c(p_M - p_s) = c\left[-\sinh\left(\frac{X + x_0}{X_o}\right) + \sinh\left(\frac{x_0}{X_o}\right)\right]$$

Elimination of c and x_0 from eqs. A16 to A18 gives

$$[A19] \quad \left(\frac{dp_{ox}}{dx}\right)_{x=0} = \left[p_M - p_s + p_I\left(1 - \operatorname{sech}\frac{X}{X_o}\right)\right]\frac{\coth (X/X_o)}{X_o}$$

where $p_I \equiv (n_{-X}/n_0 - 1)/z_c$ and is a system constant. For $X \ll X_o$ this reduces to

$$[A20] \quad \left(\frac{dp_{ox}}{dx}\right)_{x=0} = -\frac{(p_M - p_s)}{X}$$

while for $X \gg X_o$ it reduces to

$$[A21] \quad \left(\frac{dp_{ox}}{dx}\right)_{x=0} = -\frac{(p_M - p_s + p_I)}{X_o}$$

Combining eqs. 51, A9, and A20 gives for $X \ll X_o$

[A22] $$\frac{\sigma_s}{eN_s} = -\frac{X_s}{X}(p_M - p_s) + \frac{\varepsilon_d X_s}{\varepsilon\delta}(p_s - p_\delta) = \tfrac{1}{2}\alpha \sinh(p_s - p^*)$$

while eqs. 51, A9, and A21 give for $X \gg X_o$

[A23] $$\frac{\sigma_s}{eN_s} = -\frac{X_s}{X_o}(p_M - p_s - p_I) + \frac{\varepsilon_d X_s}{\varepsilon\delta}(p_s - p_\delta) = \tfrac{1}{2}\alpha \sinh(p_s - p^*)$$

For moderately concentrated solutions $\varepsilon_d X_{aq} \ll \varepsilon_{aq}\delta$ so from eq. A8, $p_\delta \simeq p_{aq}$. Setting $p_\delta = p_{aq} = 0$, eqs. A22 and A23 can be written

[A24] $$\frac{\sigma_s}{eN_s} = -\frac{X_s}{X}p_M + \left(\frac{X_s}{X} + \frac{\varepsilon_d X_s}{\varepsilon\delta}\right)p_s = \tfrac{1}{2}\alpha \sinh(p_s - p^*)$$

[A25] $$\frac{\sigma_s}{eN_s} = -\frac{X_s}{X_o}(p_M + p_I) + \left(\frac{X_s}{X_o} + \frac{\varepsilon_d X_s}{\varepsilon\delta}\right)p_s = \tfrac{1}{2}\alpha \sinh(p_s - p^*)$$

while eq. 12 and eq. 48 plus eq. 54 give respectively

[A26] $$p_M = 2.303(pH_{zpc}^{(M)} - pH)$$

[A27] $$p^* = 2.303(pH_{zpc}^{(ox)} - pH)$$

For α of the order of unity, $p_s \simeq p^*$ as already noted, so that

[A28] $$\psi_s \simeq 2.303(kT/e)(pH_{zpc}^{(ox)} - pH)$$

and

[A29] $$(\psi_M - \psi_s) \simeq 2.303(kT/e) \times (pH_{zpc}^{(M)} - pH_{zpc}^{(ox)})$$

For α vanishingly small, on the other hand, we have for $X \ll X_o$

[A30] $$\psi_s = 2.303(kT/e)\left(1 + \frac{\varepsilon_d X}{\varepsilon\delta}\right)^{-1} \times (pH_{zpc}^{(M)} - pH)$$

[A31] $$(\psi_M - \psi_s) = 2.303(kT/e)\left(1 + \frac{\varepsilon\delta}{\varepsilon_d X}\right)^{-1} \times (pH_{zpc}^{(M)} - pH)$$

while for $X \gg X_o$

[A32] $$\psi_s = 2.303(kT/e)\left(1 + \frac{\varepsilon_d X_s}{\varepsilon\delta}\right)^{-1} \times (pH_{zpc}^{(M)} + pH^{(I)} - pH)$$

[A33] $$\psi_M - \psi_s = 2.303(kT/e)\left(1 + \frac{\varepsilon\delta}{\varepsilon_d X_o}\right)^{-1} \times (pH_{zpc}^{(M)} + pH^{(I)} - pH)$$

where

[A34] $$pH^{(I)} = p_I/2.303 = (n_{-X}/n_0 - 1)/2.303z_c$$

For α sufficiently large (specifically for $\frac{1}{2}\alpha \gg X_s/X$, $\varepsilon_d X_s/\varepsilon\delta$, X_s/X_o) the double layer potential, ψ_s, satisfies the Nernst equation, while the potential drop across the oxide ($\psi_M - \psi_s$) is independent of pH. For the opposite extreme in which α is so small that the final terms in eqs. A24 and A25 may be set to zero, and the oxide sufficiently thick and with a sufficiently low concentration of conducting species so that $\varepsilon\delta \ll \varepsilon_d X$, $\varepsilon_d X_o$, the potential drop across the oxide satisfies the Nernst equation while that across the double layer is independent of pH. For intermediate conditions, neither satisfies the Nernst equation, but their sum does. Three limiting cases are illustrated in Figs. 6 to 8 and have been discussed in the main body of the paper.

Can. J. Chem. Downloaded from www.nrcresearchpress.com by 210.87.254.42 on 09/05/12
For personal use only.

The effect of the variation of potential on progressive three-dimensional nucleation and growth

STEPHEN FLETCHER
Department of Chemistry, Carleton University, Ottawa, Ont., Canada K1S 5B6
AND
ARTHUR SMITH
Department of Mathematics, Carleton University, Ottawa, Ont., Canada K1S 5B6

Received June 13, 1977

STEPHEN FLETCHER and ARTHUR SMITH. Can. J. Chem. **56**, 606 (1978).

The effect of varying the applied potential during progressive three-dimensional nucleation and growth is described. The assumed model is that due to Armstrong, Fleischmann, and Thirsk in which expanding nuclei are considered to be right circular cones distributed at random on the electrode surface. The present work extends the previous potentiostatic approach by considering that the electrode surface coverage function responds instantaneously to small changes of applied potential. Under these circumstances we show that it is possible to calculate in an exact way the theoretical response of the model to various applied potential waveforms. In particular, the linear potential sweep and the staircase potential ramp are considered, as well as feedback loops generated by uncompensated ohmic overpotential. Certain limiting cases are derived which may be tested by experiment.

STEPHEN FLETCHER et ARTHUR SMITH. Can. J. Chem. **56**, 606 (1978).

On décrit l'effet qui résulte de la variation du potentiel appliqué sur le cours de la croissance et d'une nucléation tridimentionnelle. Le modèle utilisé comme hypothèse est celui proposé par Armstrong, Fleischmann et Thirsk dans lequel on considère que les noyaux qui croissent sont des cônes circulaires droits distribués au hasard sur la surface de l'électrode. Le présent travail suggère des extensions à l'approche potentiostatique antérieure; ces extensions sont basées sur des considérations à l'effet que la fonction qui décrit la couverture de la surface de l'électrode répond instantanément à des petits changements du potentiel appliqué. Dans de telles circonstances, on montre qu'il est possible de calculer d'une manière exacte la réponse théorique du modèle à diverses formes d'onde de potentiel appliqué. On considère en particulier le balayage potentiel linéaire et la rampe de potentiel en escalier de même que des circuits de réponse qui sont générés par des surpotentiels ohmiques non compensés. On a dérivé certains cas limites pour lesquels des vérifications expérimentales peuvent être faites.

[Traduit par le journal]

Introduction

The electrochemical formation of thick (i.e., three-dimensional) anodic films is of fundamental importance in the study of the kinetics of corrosion and passivation (1). In many cases it has been shown that reaction proceeds via a nucleation and growth mechanism, in which nuclei of the new phase appear at the electrode–solution interface under the influence of the applied electrode potential (2). Such nuclei form either instantaneously or progressively in time, and the slow step in the overall mechanism occurs at the edge of the expanding crystal lattice. This slow step, for each individual crystal face, is characterized by a potential-dependent rate constant for lattice growth (2, 3).

In order for a complete model to be described, however, assumptions have to be made regarding the geometry of the growing nuclei. Also account must be taken of the overlap of individual nuclei as they expand into each other. Avrami has shown how this may be accomplished (4–6). Provided overlap is completely random then the true surface coverage of the electrode is given by the expression

$$[0.1] \qquad s = 1 - \exp(-s_{1;ex})$$

where $s_{1;ex}$ is the fractional surface coverage calculated neglecting overlap. Application of this equation to a given geometry then allows the calculation of the current–time response expected at a given potential.

(1) The Basic Model

The model of progressive three-dimensional nucleation and growth used here is based on the work of Armstrong, Fleischmann, and Thirsk (7). Growing nuclei are considered to be right circular cones distributed at random on the electrode surface. At constant potential, following the application of a potential step, it is possible to formulate the transient current response of such a system as a function of

Can. J. Chem. Downloaded from www.nrcresearchpress.com by 210.87.254.105 on 09/05/12
For personal use only.

Can. J. Chem. Downloaded from www.nrcresearchpress.com by 210.87.254.105 on 09/05/12
For personal use only.

time. The result is

$$[1.1] \quad i = nFk_2[1 - \exp(-\pi M^2 k_1^2 A t^3/3\rho^2)] \times \exp(-\pi M^2 k_1^2 A t^3/3\rho^2)$$

where i is current density (mA cm^{-2}), F is the faraday (96 500 C mol^{-1}), n is number of electrons, k_1 is the rate constant for lattice growth parallel to the surface (mol cm^{-2} s^{-1}), k_2 is the rate constant for lattice growth perpendicular to the surface (mol cm^{-2} s^{-1}), M is gram molecular weight (g), t is time (s), ρ is density of 3-dimensional layer (g cm^{-3}), and A is a time-independent nucleation rate constant (nuclei cm^{-2} s^{-1}). Note that the growth of each individual nucleus is assumed to follow a deterministic law, whilst strictly speaking the nucleation rate constant is a stochastic quantity (8). Therefore the electrode must be sufficiently large to ensure that the current takes on its expectation value. The fractional surface coverage function corresponding to [1.1] is

$$[1.2] \quad s = 1 - \exp(-\pi M^2 k_1^2 A t^3/3\rho^2)$$

which may be calculated directly via Avrami's theorem.

A convenient form of analysis of experimental transients expected for growth of this type is in terms of the current maximum of [1.1] and the time at which the maximum occurs. Thus

$$[1.3] \quad i_m = nFk_2/4$$

$$[1.4] \quad t_m = (3\rho^2 \ln(2)/\pi M^2 k_1^2 A)^{1/3}$$

where i_m (mA cm^{-2}) is current maximum in potentiostatic transient and t_m (s) is the time taken to achieve i_m. Definition of these parameters allows the expression of [1.1] in the more convenient reduced-variable form

$$[1.5] \quad \frac{i}{i_m} = 4[1 - (\tfrac{1}{2})^{(t/t_m)^3}](\tfrac{1}{2})^{(t/t_m)^3}$$

Transients of this shape are therefore always to be expected at constant step potential. If, however, it is desired to describe the experimental response to time-varying potential waveforms then it is necessary to make some assumptions regarding the potential dependences of k_1, k_2, and A. Experimental data have indicated that these quantities are exponential functions of the applied potential (7, 9) and hence

$$[1.6] \quad i_m = 10^{(a_1 E + b_1)}$$

$$[1.7] \quad t_m = 10^{(a_2 E + b_2)}$$

where a_1, a_2, b_1, and b_2 are experimentally determined constants free of ohmic effects. Combination of eqs. [1.1] to [1.7] therefore allows the theoretical description of the effect of varying the applied potential.

The current–time responses at various constant potentials are illustrated in Fig. 1.

(2) General Considerations Regarding the Time Variation of E

It is clear that if E varies in time, then the functional forms of i and s as given in [1.1] and [1.2] will change. In order to obtain these forms a new assumption is required. Suppose [1.2] is written $s = f(t, E)$ and $S = F(t, E(t))$ when E varies in time. Then at some time t_1, $S = F(t_1, E(t_1))$. Furthermore there is a transient of identical potential E corresponding to the fixed potential $E(t_1)$ for which $s = f(t - t_1 + \tau(t_1), E)$, where s is zero at time $\tau(t_1)$ and $f(\tau(t_1), E) = F(t_1, E(t_1))$. Thus the assumption is that the gradients of $f(t - t_1 + \tau(t_1), E)$ and $F(t, E(t))$ match at time $t = t_1$. *This implies that the fractional surface coverage function S responds instantaneously to any instantaneous change in applied E.* This is only possible if there is no relaxation of nucleation i.e., the steady state values of A are always observed at given potentials. Consequently

$$[2.1] \quad f(\tau(t_1), E(t_1)) = F(t_1, E(t_1))$$

and

$$[2.2] \quad \left.\frac{df}{dt}\right|_{t=t_1} = \left.\frac{dF}{dt}\right|_{t=t_1}$$

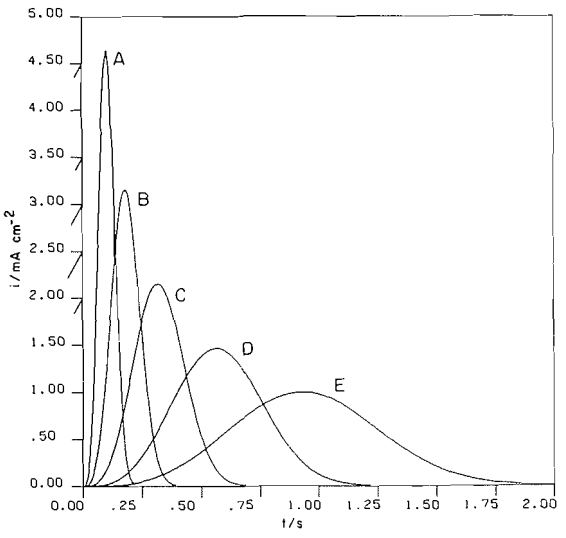

FIG. 1. Current–time transients expected for progressive 3-dimensional nucleation and growth at constant step potential. Constants are; $a_1 = 1/3$, $a_2 = -1/2$, $b_1 = b_2 = 0$, $R = 0$. (*A*) $E = 2.0$ mV, (*B*) $E = 1.5$ mV, (*C*) $E = 1.0$ mV, (*D*) $E = 0.5$ mV, (*E*) $E = 0.0$ mV.

Can. J. Chem. Downloaded from www.nrcresearchpress.com by 210.87.254.105 on 09/05/12
For personal use only.

Note that t_1 is any point in time; in general therefore

[2.3] $$f(\tau(t), E(t)) = F(t, E(t))$$

so that

$$\left.\frac{df}{dt}\right|_{t=t_1} = \frac{df}{d\xi}\cdot\frac{d\xi}{dt}$$

$$= \left.\frac{df}{d\xi}\right|_{t=t_1} = \left.\frac{\partial f(\tau(t), E(t))}{\partial \tau}\right|_{t=t_1}$$

where $\xi = t - t_1 + \tau(t_1)$ and by virtue of [2.3], [2.2] becomes

[2.4] $$\frac{\partial f}{\partial \tau} = \frac{dF}{dt} = \frac{df}{dt} = \frac{\partial f}{\partial \tau}\cdot\frac{d\tau}{dt} + \frac{\partial f}{\partial E}\cdot\frac{dE}{dt}$$

Hence

[2.5] $$\frac{d\tau}{dt} = 1 - \frac{\partial f}{\partial E}\cdot\frac{dE}{dt}\Big/\frac{\partial f}{\partial \tau}$$

Equation [2.5] may be regarded as a differential equation determining $\tau(t)$ and F via [2.3]. In the particular case that f has the functional form $f(\tau, E) = f(\tau g(E))$ for some function g then [2.5] reduces to

$$\frac{d\tau}{dt} = 1 - \tau g'(E) f'(\tau g(E))\cdot\frac{dE}{dt}\Big/ g(E)\cdot f'(\tau g(E))$$

$$= 1 - \tau\frac{dg}{dt}\Big/ g(E)$$

That is $(d/dt)(\tau g) = g$ so that

[2.6] $$f(\tau, E) = f(\tau g(E))$$

$$= f\left(\int_0^t g(E(t'))\cdot dt' + C\right)$$

The constant of integration C is given by $f(C) = f_0$ where f_0 is the value of f at time $t = 0$. The particular form of [2.6] is sufficient, for example, to find the form of S when E varies as the result of an ohmic potential drop at the electrode surface. This is an important case to consider because of the rapid rise of current as implied by [1.1].

(3) Behaviour of the Model in the Presence of Uncompensated Ohmic Potential Drop

Uncompensated ohmic potential drop is an experimental artifact which arises because of the presence of a finite resistance R (Ω cm^2) between the tip of the luggin reference probe and the working electrode (10). It may also arise in the working electrode lead. Although R may be evaluated by high frequency ac methods, exact compensation is not easy under potentiostatic conditions because its influence on the experimental data acquisition is complex. Its presence not only distorts the observed current response but also changes the applied potential waveform. Partial compensation has recently become possible by utilizing feedback circuitry incorporated into the analog potentiostat design; however, complete compensation is not usually attempted because it can result in oscillations in the operational amplifiers. Consequently there is always some residual ohmic component in the applied electrode potential. Unfortunately the profound influence of ohmic effects in measurements of electrocrystallization reactions is still not widely appreciated (see the comment of Harrison (2)). Clearly then it is desirable to consider the effect of R on the present theoretical formulation.

Uncompensated ohmic potential drop may be taken into account by the transformation $E \rightarrow E - i(t)R$ where R is a constant resistance, thus rendering E time-varying even in the transient case. The form of s in the basic model is, from [1.2], [1.4], and [1.7]

[3.1] $$s = 1 - \exp\left[-k(t10^{-a_2E})^3\right]$$

where $k = 10^{-3b_2}\ln(2)$. Thus under the transformation [2.6] and allowing for R

[3.2]

$$S = 1 - \exp\left[-k\left(\int_0^t 10^{-a_2(E(t')-i(t')R)}\,dt' + C\right)^3\right]$$

$$= 1 - \exp(-kJ^3)$$

where

[3.3] $$J(t) = \int_0^t Q(t')dt' + C$$

[3.4] $$Q(t) = 10^{-a_2(E(t)-i(t)R)}$$

The function $\tau(t)$ is determined entirely by the basic form of S and so the form of $i(t)$ is, from [1.1] and [1.2],

[3.5] $$i(t) = 4i_m(1 - S)(S)$$

$$= 4 \times 10^{(a_1(E-i(t)R)+b_1)}(1 - S)(S)$$

where S is given by [3.2]. Simplifying again [3.5] may be rewritten

[3.6] $$i(t) = PQ^{\lambda}(1 - S)(S)$$

where $P = 4 \times 10^{b_1}$, and $\lambda = -a_1/a_2$. This equation can now be used to describe the behaviour of the model in response to both linear scans of potential and potential steps, either in the absence or presence of ohmic potential drop.

Generally speaking it is the parameters a_1 and a_2 which one wishes to extract from [3.1] to [3.6]. The value of R is also of some importance. It can be controlled during a given experiment in that an additional resistance can be deliberately intro-

Can. J. Chem. Downloaded from www.nrcresearchpress.com by 210.87.254.105 on 09/05/12
For personal use only.

duced into the circuit. Mathematically it is possible to use all available data on S, i, and E to solve [3.1]–[3.6] in some way that determines the above parameters. There are, however, considerable experimental constraints. In particular deviations from the model are encountered at small values of observed current because of the presence of background reactions such as dissolution etc. Therefore the most reliable data available are the values of the peak current and the time (or when $E = \nu t$, the potential) at which this current occurs. Furthermore the asymptotic behaviour of the various parameters is worthy of investigation because simplifications occur in the mathematical analysis.

(4) Evaluation of Maximum Parameters

The description of $i(t)$ as an explicit function of time would allow the analytical prediction of the general shape of the i–t curve for a given applied potential waveform. Then from [3.6] it would be easy to solve for the maximum current simply by evaluating $\mathrm{d}i/\mathrm{d}t = 0$. The result of such an analysis is

$$[4.1] \qquad \gamma S \, \mathrm{d}E/\mathrm{d}t = (2S - 1) \cdot J^2 Q$$

Here, $\gamma = a_1 \ln (10)/3k$. It is conventional to label the current maximum as i_m in the transient case and as i_p in the voltammogram case ($E = \nu t$, where ν (mV s^{-1}) is the potential scan rate). Note that in theory it is possible to deal with the case of E being any function of time; however only the situations E = const. and $E = \nu t$ are considered here.

(5) The Case $R = 0$, $E = \nu t$

The case of $R = 0$ is simpler to deal with than $R > 0$, because the equations for S and i are not coupled. It is, however, a singular case because there is no feedback effect on the applied potential via the transformation $E \rightarrow E - i(t)R$. As a result the asymptotic forms of i_p and E_p, the potential (mV) at which i_p occurs, as $\nu \rightarrow \infty$ are entirely different from the $R > 0$ case. For $R = 0$

$$[5.1] \qquad E = \nu t$$

$$[5.2] \qquad S = 1 - \exp(-kJ^3)$$

$$[5.3] \qquad J(E) = [-(1/\nu) a_2 \ln 10][e^{-a_2 E \ln 10} - 1] + C$$

$$[5.4] \qquad Q(E) = 10^{-a_2 E}$$

so that

$$[5.5] \qquad J(E) = [-(1/\nu) a_2 \ln 10](Q - 1) + C$$

From [4.1], and denoting the parameters at the current maximum by the subscript p

$$[5.6] \qquad \gamma S_p \nu = (2S_p - 1) J_p^2 Q_p$$

Recalling [3.6] and taking logarithms

$$[5.7] \qquad \log (i) = \log (P) + a_1 E + \log (S) + \log (1 - S)$$

and hence

$$[5.8] \qquad \frac{\mathrm{d} \log (i)}{\mathrm{d}E} = a_1 + (1 - 2S) 3kJ^2 Q/S\nu$$

If $C \neq 0$ then as $\nu \rightarrow \infty$ both J and $1/S$ remain bounded and the second term of [5.8] approaches 0. Therefore

$$[5.9] \qquad \lim_{\nu \rightarrow \infty} \frac{\mathrm{d} \log i}{\mathrm{d}E} = a_1$$

In practice a_1 can be evaluated by plotting log i vs. E at high scan rates. This phenomenon is similar to Tafel-like behaviour exhibited by various reaction schemes and consequently some confusion may have arisen in practical applications in the past. However, an important diagnostic criterion of the present model is the variation of i_p with ν. From [5.5]

$$[5.10] \qquad Q/\nu = -a_2(J - C) \ln (10) + 1/\nu$$

Substituting in [5.6] when $Q \rightarrow Q_p$ and $J \rightarrow J_p$ yields

$$[5.11] \qquad \gamma S_p = (2S_p - 1) J_p^2 [-a_2 (J_p - C) \times \ln (10) + 1/\nu]$$

As $\nu \rightarrow \infty$, $J_p \rightarrow J_p^*$, $S_p \rightarrow 1 - \exp(-kJ_p^{*3}) = S_p^*$ where

$$[5.12] \qquad \gamma S_p^* = J_p^{*2} (2S_p^* - 1)(-a_2 (J_p^* - C) \ln 10)$$

The important points to note are that $S_p^* < 1$ and $Q_p/\nu \rightarrow$ a definite limit L as $\nu \rightarrow \infty$ as is clear from [5.10]. Therefore, from [3.6]

$$[5.13] \qquad i_p = P(Q_p/\nu)^\lambda S_p (1 - S_p) \nu^\lambda$$

so that

$$i_p \sim PL^\lambda S_p^* (1 - S_p^*) \nu^\lambda \qquad \text{as} \qquad \nu \rightarrow \infty$$

Therefore

$$[5.14] \qquad \log i_p \sim \lambda \log \nu + \text{constant}$$

Hence a graph of log i_p vs. log ν is asymptotically a straight line with slope $-a_1/a_2$. In a similar way it is possible to show that a plot of log E_p vs. log ν is asymptotically a straight line with slope $-1/a_2$.

The plot of log i_p vs. log ν is of particular significance in the present work because it provides a clear distinction between three-dimensional nucleation and growth, two-dimensional nucleation and growth, and diffusion-controlled reactions (in particular the dissolution–precipitation mechanism). Nicholson and Shain (11) have shown that for diffusion-controlled reactions at a stationary laminar electrode, log i_p vs.

Can. J. Chem. Downloaded from www.nrcresearchpress.com by 210.87.254.105 on 09/05/12
For personal use only.

log v should usually have a gradient of 0.50; in the present case it is expected that $0.5 < -a_1/a_2 < 1.0$. For two-dimensional nucleation and growth the gradient of the plot should be unity, at the high scan rate, because of the constant charge required in the formation of a monolayer. It is clear therefore that 2-dimensional growth, 3-dimensional growth, and diffusion control can be simply distinguished by observing the effect of varying v on the peak parameters.

(6) The Case $R > 0, E =$ constant

In this instance [4.1] reduces to $S_m = 1/2$ so that from [3.5]

$$[6.1] \qquad i_m = 10^{(a_1(E - i_m R) + b_1)}$$

which expresses i_m implicitly as a function of E. From [6.1] it is possible to extract information about a_1 and R in various ways. Note that

$$i_m 10^{a_1 i_m R} = 10^{(a_1 E + b_1)}$$

showing that $i_m \to \infty$ as $E \to \infty$ and that

$$[6.2] \qquad R = \lim_{E \to \infty} (E/i_m)$$

Also from [6.1]

$$[6.3] \qquad \frac{dE}{d \log i_m} = 1/a_1 + \ln (10) i_m R$$

Thus a graph of $dE/d \log i_m$ vs. i_m yields a straight line, the intercept and gradient yielding a_1 and R. Note the linearity of this function even in the presence of uncompensated resistance. This is a very good experimental test provided that $dE/d \log i_m$ can be evaluated accurately. To obtain t_m (and hence a_2) is somewhat more difficult because of the coupling between the equations for i and S, and requires obtaining i as an explicit function of t. In the transient case $C = 0$ so that [3.2] becomes

$$[6.4] \quad S = 1 - \exp\left[-k 10^{-3 a_2 E} \times \left(\int_0^t 10^{a_2 i(t') R} \, dt' \right)^3 \right]$$

and from [3.6]

$$[6.5] \qquad S^2 - S + [i(t) Q^{-\lambda}/P] = 0$$

where

$$[6.6] \qquad Q = 10^{-a_2 (E - iR)}$$

From [6.4]

$$[6.7] \quad \int_0^t Q(t') \, dt' = \left[\frac{\ln (1 - S)}{k} \right]^{1/3} = h(i)$$

say, where S is obtained as a function of i via [6.5]. Then $h'(i) = Q \, dt/di$ and

$$[6.8] \quad t = \int_0^i Q^{-1} h'(i) \, di = h(i) Q^{-1} + a_2 R \ln 10 \int_0^i Q^{-1} h(i) \, di$$

When $i = i_m$, $S_m = 1/2$ so $h(i_m) = 10^{b_2}$ and

$$[6.9] \quad t_m = [10^{a_2 (E - i_m R) + b_2}] + a_2 R \ln (10) \int_0^{i_m} Q^{-1} h(i) \, di$$

To obtain $h(i)$ suppose $i \leq i_m$. Under these circumstances [6.5] can be solved uniquely for S giving

$$[6.10] \quad h(i) = 10^{b_2} \times \left[1 - \frac{\ln (1 + \sqrt{1 - Q^{-\lambda} 4i/P})}{\ln 2} \right]^{1/3}$$

From here $i(t)$ may be obtained by numerical integration. A typical result is illustrated in Fig. 2. By expansion of [6.9] and consideration of [6.1] it can also be shown, over the experimental range of i_m, that

$$[6.11] \qquad d \log (t_m)/d (E - i_m R) \simeq a_2$$

whilst from [6.1]

$$[6.12] \qquad d \log (i_m)/d (E - i_m R) = a_1$$

Thus a graph of $\log t_m$ vs. $\log i_m$ is very insensitive to the effects of R, approximating the exact relation

$$[6.13] \qquad \log t_m = (a_2/a_1) \log i_m$$

Comparison of this plot with [5.14] should therefore provide an excellent experimental value for a_2/a_1.

(7) The Case $R > 0, E = vt$

First it is necessary to show that [6.3] holds asymptotically as $v \to \infty$. Here i has the form of [5.7] and hence

$$\log i = \log P + a_1 (E - iR) + \log S + \log (1 - S)$$

giving

$$[7.1] \quad \frac{d \log i}{dE} = \left[a_1 + \frac{(1 - 2S) 3k J^2 Q}{Sv} \right] \Big/ (1 + a_1 R i)$$

As in section 5, when $v \to \infty$ the second term in the numerator $\to 0$ so

$$[7.2] \qquad \lim_{v \to \infty} \frac{dE}{d \log i} = 1/a_1 + Ri$$

which is a direct generalization of [5.9]. This equation makes a_1 and R accessible to experimental evaluation.

Can. J. Chem. Downloaded from www.nrcresearchpress.com by 210.87.254.105 on 09/05/12
For personal use only.

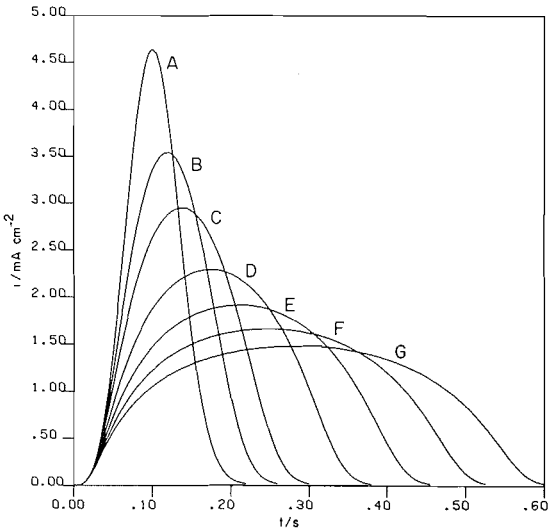

FIG. 2. Effect of uncompensated ohmic overpotential on a single, progressive 3-dimensional nucleation and growth transient. Constants are; $a_1 = 1/3$, $a_2 = -1/2$, $b_1 = b_2 = 0$, $E = 2.0$ mV. (*A*) $R = 0\ \Omega\ cm^2$, (*B*) $R = 0.1\ \Omega\ cm^2$, (*C*) $R = 0.2\ \Omega\ cm^2$, (*D*) $0.4\ \Omega\ cm^2$, (*E*) $0.6\ \Omega\ cm^2$, (*F*) $0.8\ \Omega\ cm^2$, (*G*) $1.0\ \Omega\ cm^2$.

Next to be examined is the behaviour of i_p and E_p as a function of ν and R. When $R > 0$ it is possible to deal only with asymptotic behaviour, although this is interesting in its own right. For example i_p behaves differently in the limit $\nu \to \infty$ for $R = 0$ and $R > 0$, no matter how small R may be. This is because i_p and E_p become linked through R, as $i_pR \sim E_p$. This is not the case when $R = 0$.

The analysis of the cases where R is fixed > 0, $\nu \to \infty$, and ν is fixed > 0, $R \to \infty$ is possible by rearranging the equations of section 3 and attacking the cases in conjunction. Equations 3.2 to 3.6 plus the relation $E = \nu t$ can be regarded as being five equations in S, J, Q, E, t, i, and may be considered as giving the first five quantities as functions of i. Thus

$$[7.3] \qquad Q(i) = 10^{-a_2(\nu t(i) - iR)}$$

$$[7.4] \qquad J(i) = \int_0^{t(i)} Q(t')\,dt' + C$$

so that

$$\frac{dQ}{di} = -a_2 \ln(10) Q\left(\nu \frac{dt}{di} - R\right)$$

and

$$dJ/di = Q\,dt/di$$

Thus

$$[7.5] \qquad \frac{dQ}{di}\frac{1}{\nu} = -a_2 \ln(10)\left(\frac{dJ}{di} - \frac{QR}{\nu}\right)$$

Solving for Q from [3.6] gives

$$[7.6] \qquad \frac{1}{\nu}(S(1-S))^{1/\lambda}\frac{dQ}{dt} = -a_2 \ln(10) \times \left[(S(1-S))^{1/\lambda}\frac{dJ}{di} - \left[\frac{i}{P}\right]^{1/\lambda}\frac{R}{\nu}\right]$$

Integrating [7.5] with respect to i yields

$$J = \frac{R}{\nu}\int_0^i Q\,di - (Q^{-1}/\nu a_2 \ln 10)$$

and from [3.6]

$$i = PQ^{\lambda}S(1-S) \le PQ^{\lambda}/4$$

Hence

$$[7.7] \qquad Q \ge (4i/P)^{1/\lambda}$$

Then from [7.6] and [7.7]

$$[7.8] \qquad J \ge \frac{R}{\nu}(4/P)^{1/\lambda}\frac{i^{(1+1/\lambda)}}{1+1/\lambda} - (Q-1)/(\nu a_2 \ln 10)$$

This inequality is valid at all times and in particular when $J = J_p$, $Q = Q_p$, and $i = i_p$. It allows us to show, using [4.1], that $J_p \to \infty$ as $\nu \to \infty$ unlike the $R = 0$ case. Integration of [7.6] with respect to i between the limits 0 and i_p leads to

$$[7.9] \qquad \log i_p \sim \frac{\lambda}{1+\lambda}\log \nu$$

which should be compared with [5.14]. In a similar way it is possible to estimate the effect of the variation of R at constant ν. The results are

$$[7.10] \qquad \lim_{R\to\infty}\frac{d\log i_p}{d\log R} = -\frac{\lambda}{1+\lambda}$$

$$[7.11] \qquad \lim_{R\to\infty}\frac{d\log E_p}{d\log R} = \frac{1}{1+\lambda}$$

Employing [7.10] and [7.11] in conjunction therefore allows the estimation of a_1 and a_2.

(8) The Case $R = 0$, Staircase Voltammogram

The idea of replacing the linear potential sweep with a potential staircase is due to Barker (12). The benefit of such a technique lies in the fact that it produces (at long times) a purely Faradaic response and hence eliminates the contribution of the double layer charging current to the overall observed current. This is particularly advantageous at high scan rates. The applied potential behaves according to

$$[8.1] \qquad E_n = n\nu\Delta t \qquad n = 0, 1, 2, 3 \ldots$$

where both ν and Δt are specified. Several features of this technique are of interest. In particular it is necessary to investigate the current response as $\Delta E\ (= \nu\Delta t) \to 0$. From [3.1] it is clear that

[8.2] $$S_n = 1 - \exp(-k\tau_n^3\, 10^{-3a_2E_n}) \qquad n = 0, 1, 2, 3 \ldots$$

and

[8.3] $$S_{n+1} = 1 - \exp(-k(\tau_n + \Delta t)^3 10^{-3a_2E_n})$$

which when differenced with [8.2] becomes the approximation to [2.2]. To obtain S_n note from [8.2] that

[8.4] $$S_{n+1} = 1 - \exp(-k\tau_{n+1}^3 10^{-3a_2E_{n+1}})$$

so that

$$\tau_{n+1}^3 10^{-3a_2E_{n+1}} = (\tau_n + \Delta t)^3 10^{-3a_2E_n}$$

giving

[8.5] $$\tau_{n+1} = (\tau_n + \Delta t)10^{a_2\nu\Delta t}$$

Equation 8.5 is a linear difference equation which may be solved to yield

[8.6] $$\tau_n = 10^{a_2 n\nu\Delta t}\tau_0 + \Delta t(10^{-a_2 n\nu\Delta t} - 1)/(10^{-a_2\nu\Delta t} - 1)$$

Substituting back into [8.2] gives

[8.7] $$S_E = 1 - \exp[-k(\tau_0 + \Delta t(10^{-a_2 n\nu\Delta t} - 1)/(10^{-a_2\nu\Delta t} - 1))^3]$$

where

[8.8] $$S_0 = 1 - \exp(-k\tau_0^3)$$

When $R = 0$ and $E = \nu t$ [3.2] may be solved to give S as an explicit function of time. Thus

[8.9] $$S(E) = 1 - \exp[-k((10^{-a_2\nu t} - 1)/(-a_2\nu \ln 10) + \tau_0)^3]$$

Setting $n\nu\Delta t = E$ and $\nu\Delta t = \Delta E$ shows that the finite approximation S_E given in [8.7] differs from the exact solution only in the fact that $\Delta E/(10^{-a_2\Delta E} - 1)$ replaces $1/(-a_2 \ln 10)$. But as $\Delta E \to 0$:

[8.10] $$\lim_{\Delta E \to 0} \Delta E/(10^{-a_2\Delta E} - 1) = -1/a_2 \ln 10$$

thus proving convergence of the finite approximation.[1]

When R is not zero it is not possible to obtain explicit formulae for S_n, but it is expected that convergence will still occur since the general effect of R on S (and hence $i(t)$) is to decrease gradients due to the feedback effect on the applied potential.

Conclusion

The effect of varying the applied potential on progressive three-dimensional nucleation and growth has been described. Various limiting cases have been considered on the assumption that the electrode surface coverage responds instantaneously to any instantaneous change in applied potential. A number of results are presented which may be tested by experiment.

1. D. A. VERMILYEA. Adv. Electrochem. Electrochem. Eng. **3**, 211 (1963).
2. J. A. HARRISON and H. R. THIRSK. Electroanal. Chem. **5**, 67 (1971).
3. E. B. BUDEVSKI. Prog. Surf. Membr. Sci. **11**, 71 (1976).
4. M. AVRAMI. J. Chem. Phys. **7**, 1103 (1939).
5. M. AVRAMI. J. Chem. Phys. **8**, 212 (1940).
6. M. AVRAMI. J. Chem. Phys. **9**, 177 (1941).
7. R. D. ARMSTRONG, M. FLEISCHMANN, and H. R. THIRSK. J. Electroanal. Chem. **11**, 208 (1966).
8. S. K. RANGARAJAN. J. Electroanal. Chem. **46**, 119 (1973).
9. R. G. BARRADAS, S. FLETCHER, and J. D. PORTER. J. Electroanal. Chem. **80**, 295 (1977).
10. R. PIONTELLI, G. BIANCHI, U. BERTOCCI, C. GUERCI, and B. RIVOLTA. Z. Elektrochem. **58**, 54 (1954).
11. R. S. NICHOLSON and I. SHAIN. Anal. Chem. **36**, 706 (1964).
12. G. C. BARKER. Adv. Polarography, **1**, 144 (1960).

[1]It may also be proved that the relative error $|(S(E) - S_E)/S(E)|$ is bounded by $D.\Delta E$, where D is a constant of order unity.

Can. J. Chem. Downloaded from www.nrcresearchpress.com by 210.87.254.105 on 09/05/12
For personal use only.

The chemistry of some 6-methyl-4-hydroxy-2-pyridones

JOHN A. FINDLAY, WAH HUNG JOHN TAM, AND JIRI KREPINSKY
Department of Chemistry, University of New Brunswick, Fredericton, N.B., Canada E3B 5A3

Received August 16, 1977

JOHN A. FINDLAY, WAH HUNG JOHN TAM, and JIRI KREPINSKY. Can. J. Chem. **56**, 613 (1978).

Some oxidations and reductions of 4-hydroxy-6-methyl-2-pyridones are discussed. A remarkable reduction–cyclization of 4-hydroxy-3-(1′-hydroxy-2′-oxopropyl-)-6-methyl-2-pyridone (**2***b*) produces the novel system **10***a*.

JOHN A. FINDLAY, WAH HUNG JOHN TAM et JIRI KREPINSKY. Can. J. Chem. **56**, 613 (1978).

On discute de quelques oxydations et de quelques réductions d'hydroxy-4 méthyl-6 pyridones-2. Une réaction remarquable de réduction–cyclisation de l'hydroxy-4 (hydroxy-1′ oxo-2′ propyl)-3 méthyl-6 pyridone-2 (**2***b*) conduit au nouveau système **10***a*.

[Traduit par le journal]

Can. J. Chem. Downloaded from www.nrcresearchpress.com by 210.87.254.6 on 09/05/12
For personal use only.

In the course of studies successfully directed at the total synthesis of the antibiotic flavipucine **1** (1) we have studied the chemistry of some 4-hydroxy-2-pyridones and now report our findings.

Of central focus has been compound **2***a*, the product of the novel condensation of 6-methyl-4-hydroxy-2-pyridone with isobutylglyoxal (2), which was eventually transformed into (±)-flavipucine **1** by the agency of *tert*-butylhydroperoxide. Initial attempts to achieve this transformation were directed by the observation of Becker *et al.* (3) that 2,4-di-*tert*-butyl-6-hydroxymethyl phenol affords the corresponding spiroepoxy-2,4-di-*tert*-butyl cyclohexadienone when treated with sodium metaperiodate in methanol at room temperature. Treatment of **2***a* and **2***b* under similar conditions resulted in cleavage at the α-hydroxy ketone site of the side chain in preference to the 1,3-enediol system and gave the aldehyde **3**. Attempts to prepare the dithioketal of **2***b* were unsuccessful and treatment with ethylene glycol in boiling benzene in the presence of paratoluene sulfonic acid gave only the tricyclic ether **4**. In support of formulation **4** the ir spectrum shows only a single carbonyl band at 1650 cm^{-1} (conjugated lactam) while mass spectral (*m/e* 223) and microanalytical data are consistent with composition $C_{11}H_{13}NO_4$ and the uv spectrum resembles those of other 3-substituted 6-methyl-4-hydroxy-2-pyridones. Further corroboration is provided by the nmr spectrum (*vide infra*).

Oxidation of **2***b* with a variety of other oxidizing agents usually gave complex mixtures; however, manganese dioxide on charcoal oxidized **2***a* and **2***b* to the corresponding α-diketones **5***a* and **5***b*, respectively, in moderate yields.

Reduction of the system **2***b* was also explored and conditions were found to achieve various degrees of reduction of both side chain and nucleus. Thus,

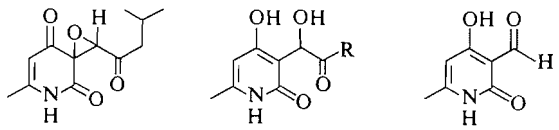

1 **2** **3**

a R = $CH_2CH(CH_3)_2$
b R = CH_3

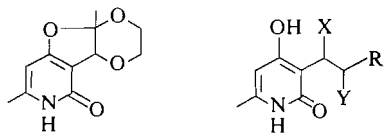

4 **5**

a X, Y = O; R = $CH_2CH(CH_3)_2$
b X, Y = O; R = CH_3
c X, Y = OH; R = CH_3
d X = H; Y = O; R = CH_3
e X = H; Y = OH; R = CH_3

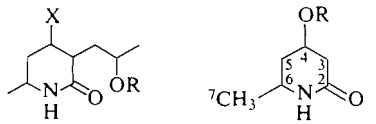

6 **7**

a X, R = H
b X = OH; R = H
c X = OAc; R = Ac

a R = H
b R = $\overset{8}{C}(=O)\text{—}\overset{9}{C}H_3$

sodium borohydride in water smoothly converted **2***b* to the corresponding triol **5***c* in near quantitative yield, while catalytic reduction using palladium-on-charcoal at 25°C and 85 psi caused hydrogenolysis of the side-chain hydroxyl of **2***b* to furnish **5***d* in 60% yield. More vigorous catalytic reduction employing a nickel catalyst at 125°C and 1400 psi resulted in a mixture of products among which the major component (14%) was identified as 3-(2′-hydroxypropyl)-5-methyl-2-piperidone **6***a*. Reduction of the 2-pyridone nucleus has previously been achieved using

Can. J. Chem. Downloaded from www.nrcresearchpress.com by 210.87.254.6 on 09/05/12
For personal use only.

Raney nickel in ethanol at room temperature to yield 2-piperidones (4) and using nickel carbonate – copper carbonate at high temperatures catalyses the hydrogenation of 2-pyridones to 2-piperidones (5). In most cases *N*-substituted substrates were employed.

We have also subjected 6-methyl-4-hydroxy-2-pyridone to catalytic hydrogenation using ruthenium-on-charcoal in ethanol at 65°C and 700 psi. The crystalline product 6-methyl-4-hydroxy-2-piperidone (**7***a*) was obtained in 60% yield and further characterized as the acetate **7***b*. Assuming that in the catalytic reduction the hydrogen is added from only one side, then the product **7***a* should have the *cis* configuration. This conclusion is consistent with the 100 MHz nmr data; however, the alternate configuration cannot be completely excluded. Attempts to oxidize the piperidone **7***a* to the corresponding ketone (or enol) were remarkably unsuccessful suggesting that the anticipated β-dicarbonyl product is highly unstable under the various conditions employed.

Ruthenium–charcoal catalyzed hydrogenation of **2***b* at elevated temperature and high pressure gave, as major product, the crystalline diol pyridone **5***e* or diol piperidone **6***b* when a large excess of catalyst was employed. The latter was transformed into the crystalline diacetate **6***c* by treatment with acetic anhydride in pyridine.

Numerous attempts to prepare an ene-trione by dehydration of **2***b* were remarkably unsuccessful and only under forcing conditions could any type of dehydration be induced and then it was accompanied by an unusual reduction and ring formation. Thus, when **2***b* was treated with *p*-toluenesulfonic acid in refluxing ethylene glycol in the presence of molecular sieve the product **10***a* was obtained whose structure is fully supported by high resolution mass spectral, ^{1}H nmr, and ^{13}C nmr data. Furthermore, the compound **10***a* has also been prepared from the more logical precursor **5***d* by treatment under the same extreme dehydrating conditions and presumably proceeding via the dehydration of the hemiacetal form **9***a*. A rationalization of the remarkable transformation **2***b* → **10***a* is portrayed in Scheme 1 in which the ether formation to give **8**, a reaction type well precedented for this system (1), is first envisaged. A reductive cyclodecomposition of **8** could lead to the ejection of glycoaldehyde and the formation of the necessary hemiacetal **9***a*. Mild catalytic hydrogenation of **10***a* gave the crystalline dihydro derivative **9***b* while treatment with sodium hypochlorite in dioxane afforded the monochlorination product **10***b*. The placement of the chlorine atom at C5 follows from a comparison of chemical shifts, coupling constants and multiplicities in the ^{13}C nmr spectra of **10***a* and **10***b*.

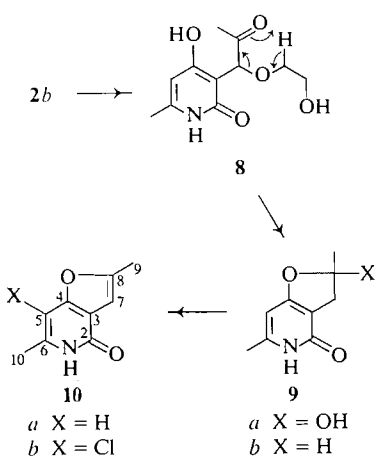

SCHEME 1

Experimental

Melting points were determined on a Kofler hot stage apparatus and are uncorrected. Mass spectra were recorded with an Hitachi-Perkin-Elmer RMU-6D spectrometer. High resolution mass spectra were recorded with a Consolidated Electrodynamics Corporation R6-1 instrument. The nmr spectra were recorded with a Varian T-60 instrument (unless otherwise noted) using tetramethylsilane as internal standard. Line positions are reported in ppm from this standard. ^{13}C nmr spectra were obtained with a Varian XL-100-15 equipped with S1-124 Fourier transform accessory. Ultraviolet spectra were obtained with a Perkin-Elmer model 467 spectrophotometer and infrared spectra with a Perkin-Elmer model 457 grating instrument. Preparative tlc plates were of 1-mm silica gel G.

Preparation of 4-Hydroxy-6-methyl-3-carboxaldehyde-2-pyridone 3 from 2b

To pyridone **2***b* (1.97 g) in methanol (50 ml) a suspension of sodium metaperiodate (2.3 g) in water (33 ml) was added. After stirring at room temperature overnight the mixture was filtered and the filtrate evaporated yielding a white crystalline solid (1.06 g, 69%), mp 232–238°C; nmr δ_{TMS}(DMSO-d_6): 2.20 (s, 3H, CH_3—C=C) 3.2–3.8 (broad, 1H, O*H*), 5.85 (s, 1H, HC=C—), 9.15 (s, 1H, —CHO) and 11.95 (s, 1H, NH); ir ν_{max}(KBr): 1620 (conjugated lactam/dienamine), 1670 cm^{-1} (conjugated aldehyde); uv λ_{max}(ethanol): 232, 272, 337 (ε 6200, 1200, 5200); ms *m/e* 153 (M^+). *Anal.* calcd. for $C_7H_7NO_3$: C 54.90, H 4.61, O 31.35, N 9.15; found: C 54.70, H 4.65, O 31.51, N 9.02.

Preparation of 4 from 2b

A mixture of **2***b* (1 g) and *p*-toluenesulfonic acid (0.32 g) in dry ethylene glycol (20 ml) and benzene (50 ml) was refluxed for 14 h. After cooling and neutralizing with 5% sodium bicarbonate solution to p*H* 8–9 the mixture was extracted with chloroform and this extract was washed with water and evaporated giving a foam (0.99 g). Purification by preparative tlc on silica gel (chloroform–methanol 93:7) afforded white solid **4** (0.43 g, 38%), mp 183–185°C; nmr δ_{TMS}($CDCl_3$): 1.50 (s, 3H, CH_3—C—O), 2.30 (s, 3H, CH_3C=C), 3.7 (bm, 4H,

TABLE 1. ^{13}C nmr chemical shift data (δ_{TMS} ppm)

Compound	C2	C3	C4	C5	C6	C7	C8	C9	C10
10*a**	161.8†	114	161.3†	94.8	140.6	102.2	153.0	13.7	19.2
10*b**	157.8	115.1	155.3	97.5	137.5	103.2	153.9	13.2	15.7
7*b*‡	170.6	36.9†	67.2	36.3†	45.4	22.2	170.2	21.1	

*Solvent DMSO-d_6.
†Assignments may be interchanged. The assignment of ^{13}C resonances to the individual carbon atoms are based on standard Fourier transform ^{13}C nmr techniques, selective ^{13}C-{^1H}decoupling experiments, spectral comparison, and known substituent effects.
‡Solvent $CDCl_3$.

TABLE 2. Nuclear magnetic resonance data for compound **7***b**

H	δ (ppm)	*J* (Hz)
3a	2.34	$J_{3e,3a} = -17.0$, $J_{3a,4a} = 10.0$, $J_{3a,5a} = J_{3a,5e} = J_{3a,6a} = 0$
3e	2.76	$J_{3e,4a} = 6.2$, $J_{3e,5e} = 1.8$, $J_{3e,5a} = J_{3e,6a} = 0$
4a	5.06	$J_{4a,5a} = 11.0$, $J_{4a,5e} = 4.0$, $J_{4a,6a} = 0$
5a	1.46	$J_{5a,5e} = -12.5$, $J_{5a,6a} = 11.0$
5e	2.23	$J_{5e,6a} = 4.0$, $J_{6a,CH_3} = 6.4$
6a	3.55	

*100 MHz, $CDCl_3$, TMS.

—OCH_2CH_2O—), 4.60 (s, 1H, C=C—CH—O—), 5.85 (s, 1H, CH=C), and 12.8 (bs, 1H, NH); ir ν_{max}($CHCl_3$): 1650 cm^{-1} (conjugated lactam); uv λ_{max}(ethanol): 215, 290 (ε 26 300, 6500); ms *m/e* 223 (M^+). *Anal.* calcd. for $C_{11}H_{13}NO_4$: C 59.18, H 5.87, O 28.67; found: C 59.34, H 5.77, O 28.72.

Preparation of 5a from 2a

Compound **2***a* (0.5 g) in pyridine (15 ml) was stirred with manganese dioxide on charcoal (5.59 g) at room temperature for 18 h. After filtration through Celite and evaporation of the filtrate, a yellow solid was obtained which was purified by preparative tlc on silica gel (methanol–chloroform 3:97) to furnish **5***a* (0.1126 g, 12%) as a yellow solid mp 174–180°C; nmr δ_{TMS}(Py-d_5): 1.10 (d, 6H, J = 6.5 Hz, $(CH_3)_2CH$—), 2.18 (s, 3H, CH_3—C=C—), 2.38 (m, 2H, —CH_2—CO—), 5.28 (bs, 2H, NH/OH – deuterium exchangeable), 5.92 (s, 1H, HC=C—); ir ν_{max}(KBr): 1720 (ketones), 1650, 1620 cm^{-1} (conjugated lactam); uv λ_{max}(ethanol) 207, 230, 317 (ε 8500, 8000, 8900); ms *m/e* 237 (M^+). *Anal.* calcd. for $C_{12}H_{15}O_4N$: C 60.75, H 6.37, O 26.98; found: C 60.54, H 6.28, O 27.04.

Preparation of Compound 5b from 2b

A mixture of **2***b* (0.2 g) in pyridine (10 ml) and manganese-dioxide-on-charcoal (2 g) was stirred at room temperature for 3 days. After filtration and evaporation a yellow solid was obtained which was purified by preparative tlc on silica gel (methanol–chloroform 1:9) and afforded yellow crystalline **5***b* (0.82 g, 41%), mp 128–130°C; nmr δ_{TMS}(DMSO-d_6): 1.55 (s, 3H, CH_3C=C), 2.20 (s, 3H, CH_3CO—), 5.87 (s, 1H, CH=C); ir ν_{max}(KBr): 1725 (ketones), 1640, 1610 cm^{-1} (conjugated lactam); uv λ_{max}(ethanol): 207, 230, 318 (ε 12 300, 11 900, 13 500); ms *m/e* 195 (M^+). *Anal.* calcd. for $C_9H_9O_4N$: C 55.38, H 4.68, O 32.79; found: C 55.52, H 4.41, O 32.84.

Sodium Borohydride Reduction of 2b to 5c

Sodium borohydride (0.62 g) was added to a suspension of **2***b* (2.0 g) in water (92 ml) and the mixture was stirred at room temperature for 18 h then filtered and evaporated to give a white solid (1.79 g, 88%), mp 298°C (dec.); nmr δ_{TMS}(D_2O): 1.05 (d, 3H, J = 7 Hz, CH_3—CH), 2.30 (s, 3H, CH_3C=C<), 4.3 (bm, 1H, —CHOHCH_3), 4.90 (m, 1H, >C=C—CHOH), 5.96 (s, 1H, —CH=C<); ir ν_{max}(KBr): 1630 cm^{-1} (conjugated amide); uv λ_{max}(ethanol): 218, 280 (ε 15 100, 3600); ms *m/e* 181 ($M^+ - H_2O$). *Anal.* calcd. for $C_9H_{13}NO_4$: C 54.25, H 6.58, O 32.13; found: C 54.12, H 6.49, O 32.28.

Catalytic Reduction of 2b to 5d

A mixture of compound **2***b* (2.66 g) in suspension in ethanol (210 ml) and palladium-on-charcoal (0.84 g, 10%) was hydrogenated at 85 psi and 25°C for 3 h. After filtration through Celite and evaporation, a white solid (2.2 g) was obtained which after recrystallization from ethanol yielded compound **5***d* (1.45 g, 60%), mp 209–212°C; nmr δ_{TMS}(DMSO-d_6): 2.15 (s, 3H, CH_3—), 2.28 (s, 3H, CH_3—), 4.08 (s, 2H, =C—CH_2—CO—), 6.04 (s, 1H, —CH=C); ir ν_{max}(KBr): 1720 (ketone), 1645, 1620 cm^{-1} (conjugated amide); uv λ_{max}(ethanol): 215, 280 (ε 13 300, 4500); ms *m/e* 181. *Anal.* calcd. for $C_9H_{11}NO_3$: C 59.66, H 6.12, O 7.73; found: C 59.48, H 6.01, O 7.89.

Catalytic Reduction of 2b to 6a

A suspension of **2***b* (0.49 g) and nickel catalyst (#28)* (2.16 g) in water (20 ml) was hydrogenated at 1250–1400 psi at 125°C for 40 h. After cooling, filtration through Celite, and evaporation an oil (0.38 g) was obtained which was purified by preparative tlc on silica gel (chloroform–methanol 9:1) giving **6***a* as a homogeneous oil (0.06 g, 14%); nmr δ_{TMS}($CDCl_3$ + D_2O): 1.12 (d, 6H, J = 7 Hz, $2CH_3$—CH—), 1.7 (bm, 5H), 2.4 (bm, 1H, —CH—CONH—), 3.5 (bm, 1H, —CH—NHCO—), 3.9 (bm, 1H, —CHOH—); ir ν_{max}($CHCl_3$) 3400 (hydroxyl), 1640 cm^{-1} (amide); ms *m/e* 171 (M^+).

Reduction of 4-Hydroxy-6-methyl-2-pyridone to 7a

A mixture of 4-hydroxy-6-methyl-2-pyridone (2.6 g) and ruthenium-on-charcoal (0.94 g, 5%) in ethanol (84 ml, 95%) was hydrogenated at 300–1000 psi at 58°C for 19 h. After cooling, filtration through Celite, and evaporation a white solid (2.58 g) was obtained which on recrystallization from ethanol afforded white crystalline **7***a* (1.55 g, 57%), mp 204–206°C; ir ν_{max}(KBr); 1660 cm^{-1} (amide); ms *m/e* 129 (M^+).

Can. J. Chem. Downloaded from www.nrcresearchpress.com by 210.87.254.6 on 09/05/12
For personal use only.

Can. J. Chem. Downloaded from www.nrcresearchpress.com by 210.87.254.6 on 09/05/12
For personal use only.

Anal. calcd. for $C_6H_{11}NO_2$: C 55.81, H 8.52, O 24.80, N 10.85; found: C 55.81, H 8.55, O 25.09, N 10.99.

Esterification of 7a to 7b

A mixture of **7***a* (1.02 g), acetic anhydride (14.01 g), and dry pyridine (36 ml) was stirred at room temperature for 20 h. After evaporation a yellow solid (1.37 g) was obtained which was purified by preparative tlc on silica gel (chloroform–methanol 93:7) yielding white crystalline acetate **7***b* (0.6 g, 44%), mp 138–141°C; nmr, 100 MHz, spectrum, $\delta_{TMS}(CDCl_3)$; see Table 2; ms *m/e* 171 (M^+). *Anal.* calcd. for $C_8H_{13}NO_3$: C 56.12, H 7.65, O 8.18; found: C 55.92, H 7.58, O 8.35.

Ruthenium Catalyzed Hydrogenation of 2b to 5e

A mixture of **2***b* (5 g) and ruthenium-on-charcoal (1.15 g, 5%) in ethanol (150 ml, 95%) was hydrogenated at 500–1000 psi and 85°C for 20 h. After cooling and filtration through Celite, evaporation of the filtrate yielded a white solid which was recrystallized from ethanol to give **5***e* (1.8 g, 56%), mp 273–275°C; nmr δ_{TMS}(Py-d_5): 1.50 (d, 3H, CH_3—CHOH), 2.15 (s, 3H, CH_3—C=C—), 3.35 (m, 2H, —CH_2—CHOH), 4.55 (m, 1H, —CHOH), 6.10 (s, 1H, HC=C—); uv ν_{max}(KBr): 1625 cm^{-1} (conjugated lactam); uv λ_{max}(ethanol): 215, 288 (ε 14 000, 5600); ms *m/e* 183 (M^+). *Anal.* calcd. for $C_9H_{13}NO_3$: C 59.00, H 7.15, O 26.20; found: C 58.88, H 7.20, O 26.10.

Ruthenium Catalyzed Reduction of 2b to 6b

A mixture of **2***b* (0.51 g) and ruthenium-on-charcoal (0.76 g, 5%) in ethanol (60 ml, 95%) was hydrogenated at 600–1200 psi at 80°C for 21 h. After cooling, filtering, and evaporating an oil (0.32 g) was obtained which was purified by preparative tlc on silica gel (chloroform–methanol 9:1) giving the oil **6***b* (0.08 g, 17%) which was characterized by acetylation (acetic anhydride – pyridine at room temperature for 16 h) to give the crystalline acetate **6***c*, mp 96–98°C; nmr $\delta_{TMS}(CDCl_3)$: 1.20 (d, 6H, J = 7 Hz, 2× CH_3—CH—), 2.08 (s, 3H, CH_3COO), 2.10 (s, 3H, CH_3COO) superimposed on 1.4–2.8 (multiplets, 4H, 2× —CH_2—), 3.6 (m, 1H, —CH—NHCO), 5.2 (m, 2H, —CHOAc), 6.6 (bm, 1H, deuterium exchangeable, NH); ir $\nu_{max}(CHCl_3)$: 1735 (esters), 1660 cm^{-1} (amide); ms *m/e* 171 (M^+). *Anal.* calcd. for $C_{13}H_{21}NO_5$: C 57.55, H 7.80, O 5.16; found: C 57.66, H 7.71, O 5.04.

Preparation of 10a from 2b

A mixture of **2***b* (9.0 g), *p*-toluenesulfonic acid (8.8 g) and molecular sieve (39 g, type 5Å) under dry nitrogen in dry ethylene glycol (1.59 ℓ) was refluxed for 40 h, cooled and diluted with water (1 ℓ) and filtered through Celite. The filtrate was cooled to 6°C and treated with sodium bicarbonate (50 g). Extraction with chloroform afforded a yellow solid which was chromatographed on a silica gel (155 g) column. Elution with chloroform–methanol (~200 ml) (93:3.5) gave a yellow solid which on recrystallization from chloroform–ether (1:1) gave white crystalline **10***a* (0.35 g, 5%), mp 227–229°C; nmr $\delta_{TMS}(CDCl_3)$: 2.22 (s, 3H, CH_3—C=C<), 2.32 (s, 3H, CH_3—C=C<), 6.38 (s, 1H, CH=C<), 6.77 (s, 1H, CH=C<), 12.9 (bs, 1H, deuterium exchangeable, NH); ir ν_{max}(KBr): 1670 cm^{-1} (lactam); uv λ_{max}(95% ethanol) 254, 262, 295 (ε 12 900, 12 300, 8700). *Mol. Wt.* calcd. for $C_9H_9O_2N_2$: 163.0633; found (ms) 163.0633 (100), 162.0559 (74, M^+ −H), 134.0604 (41, M^+ −H−CO).

Preparation of 10a from 5d

A mixture of **5***d* (0.5 g), *p*-toluenesulfonic acid (0.53 g), molecular sieve (4.56 g, type 5Å), and ethylene glycol (100 ml) under nitrogen was refluxed for 40 h. After cooling and filtering through Celite, the solution was cooled to 3°C and sodium bicarbonate solution (100 ml of 5%) was added. Extraction with chloroform afforded a yellow solid (0.58 g) which yielded white crystalline **10***a* (0.16 g, 23%), mp 227–229°C after preparative tlc on silica gel, identical in all respects with **10***a* obtained from **2***b* (*vide supra*).

Reduction of 10a to 9b

A solution of **10***a* (0.15 g) in ethanol (38 ml, 95%) was hydrogenated over palladium-on-charcoal (240 mg, 10%) at 27 psi for 45 h. The mixture was filtered through Celite and evaporated yielding a white solid (0.14 g) which was purified by preparative tlc using silica gel (chloroform–methanol 7:3) to give a white crystalline solid (0.07 g, 43%), mp 187–201°C. The mass spectrum *m/e* 165 (M^+). The nmr spectrum δ_{TMS} ($CDCl_3$–D_2O): 1.38 (d, 3H, J = 7 Hz, CH_3CHO—), 2.25 (s, 3H, CH_3—C=CH—), 2.2–3.4 (multiplets, 2H, —CH_2—), 4.95 (multiplet, 1H, —CHO—), 5.70 (s, 1H, —CH=C). The ir spectrum ν_{max}(KBr) 1630 cm^{-1} (v broad, conjugated lactam). The uv spectrum λ_{max}(ethanol) 223, 237(s), 294 (ε 6600, 3400, 6900).

Preparation of 10b from 10a

Sodium hypochlorite solution (3.9 g, 5% aqueous) was added to a suspension of **10***a* (0.2 g) in dioxane (4 ml) at 17°C. After stirring at ~23°C for 68 h, water (6.6 ml) was added and the white precipitate which formed was filtered off. Purification of this white solid (0.21 g) by preparative tlc on silica gel (chloroform–methanol 98:2) afforded white crystalline **10***b* (0.13 g, 53%), mp 210–232°C; nmr $\delta_{TMS}(CDCl_3)$: 2.48 (s, 3H, CH_3—C=CH), 2.54 (s, 3H, CH_3—C=C—), 6.65 (s, 1H, —CH=C—), ~9.0 (v. broad, 1H, NH); ir ν_{max}: 1680, 1600 cm^{-1}; uv λ_{max}(ethanol): 256, 264, 305 (ε 12 400, 11 400, 7400); ms *m/e* 197 (M^+). *Anal.* calcd. for $C_9H_8NO_2Cl$: C 54.68, H 4.05, O 16.20, N 7.08, Cl 17.97; found: C 54.43, H 4.13, O 16.47, N 7.00, Cl 17.51.

Acknowledgements

The authors are grateful to the National Research Council of Canada for financial support. Thanks are due to D. G. Smith (Atlantic Regional Laboratory, Halifax, Nova Scotia) for providing and analyzing the ^{13}C nmr spectra of compounds **7***b*, **10***a*, and **10***b* and the 100 MHz spectrum of **7***b*.

1. J. A. Findlay, W. H. J. Tam, and J. Krepinsky. Synth. Commun. **7**, 149 (1977).
2. J. A. Findlay and F. Y. Shum. Synth. Commun. **3**, 355 (1973).
3. H. D. Becker, T. Bremholt, and E. Adler. Tetrahedron Lett. 4205 (1972).
4. J.-A. Gautier. Compt. Rend. **205**, 614 (1937).
5. C. Räth. Ann. **489**, 107 (1931).

Intermediates in the cycloanhydrotetramerization of furan with aliphatic and alicyclic ketones

WILLIAM HAMILTON BROWN AND BRUCE JAMES HUTCHINSON[1,2]

Department of Chemistry, University of Guelph, Guelph, Ont., Canada N1G 2W1

Received August 4, 1977

WILLIAM HAMILTON BROWN and BRUCE JAMES HUTCHINSON. Can. J. Chem. **56**, 617 (1978).

The acid-catalysed reaction of furan with acetone has been investigated for the presence of intermediates by vapour phase chromatography of the reaction mixture. It has been shown that 2-furyl-2-propene is a component of the furan–acetone reaction mixture. Other possible intermediates have been prepared and their reactions investigated. It is our conclusion that the alcohol, 2-furyl-2-propanol, is the initial intermediate in the condensation reaction. We have also reexamined some reactions between furan and cyclohexanone reported by other investigators.

WILLIAM HAMILTON BROWN et BRUCE JAMES HUTCHINSON. Can. J. Chem. **56**, 617 (1978).

On a étudié la réaction acido-catalysée du furanne avec l'acétone afin de déterminer la présence d'intermédiaires. Ces études ont été effectuées par chromatographie en phase gazeuse de mélanges réactionnels. On a montré que le furyl-2 propène-2 est un constituant du mélange réactionnel furanne–acétone. On a aussi préparé d'autres intermédiaires possibles et on a étudié leurs réactions. On conclut que l'alcool, furyl-2 propanol-2, est l'intermédiaire initial dans la réaction de condensation. On a aussi réétudié quelques réactions entre le furanne et la cyclohexanone qui avaient été rapportées par d'autres chercheurs.

[Traduit par le journal]

Introduction

In view of the recent interest in the preparation of cycloanhydropolymers formed by the acid-catalysed condensation of carbonyl compounds with furan, we wish to report on our investigation of the intermediates involved in such reactions.

The acid-catalysed condensation of furan with methyl ketones was first reported by Ackman *et al.* (1). The reaction leads to the formation of porphyrinogen-like cyclic products which have been given the trivial name 'tetroxaquaterenes' (2). Brown and co-workers (3–5), extended the investigation of these reactions, using pyrrole as well as furan. Yields in most of these reactions are inherently low. However Chastrette and Chastrette (6) have reported that the yield of the tetroxaquaterene formed from furan and acetone can be raised from 18 to 45% by introducing a metallic cation such as lithium perchlorate into the reaction mixture.

Kobuke *et al.* (7) have extended the synthesis of cyclic anhydropolymers. Utilizing furan and various carbonyl compounds they have succeeded in preparing macrocyclic compounds containing six furan and six carbonyl compound residues. Hydrogenation of these macrocycles renders them capable of binding metal cations.

Interest in these cyclic compounds appears to be high. Thus, for example, compound **5**, is being produced and marketed under the name octamethylcyclotetrafurylene (8).

Results and Discussion

When furan **1** in excess is treated with acetone and concentrated hydrochloric acid, the intermediates, compounds **2**, **3**, and **4** are readily obtained. If acetone is present in excess the product is mainly the tetroxaquaterene, **5**.

The initial compound formed in the furan-acetone reaction is probably 2-furyl-2-propanol **6**, although none was detected in the reaction mixture using vpc. Brown and co-workers (1) and Katritzky and Lagowski (9) have proposed the mechanism shown in Scheme 1 for the formation of **6** and the corresponding alkene, **8**. The same reactions occur with all other simple aldehydes and ketones except chloral, where the alcohol analogous to **6** has been isolated by Willard and Hamilton (10). This result is not surprising since three electronegative chlorine atoms are on the α-carbon. To gain more information on the mechanism of this condensation reaction we prepared four possible 'alcohol' intermediates, **6**, **9**, **10**, and **11**, as well as the proposed 'alkene' intermediate, 2-furyl-2-propene, **8**. The products obtained by treating these compounds with furan or appropriate intermediates and hydrochloric acid catalyst are shown in Table 1.

Brown *et al.* (11) have reported on the acid catalysed reactions of cyclohexanone with furan and

[1]Taken in part from the M.Sc. Thesis of B. J. Hutchinson.

[2]Present address: Lambton College of Applied Arts and Technology, Box 969, Sarnia, Ont., Canada N7T 7K4.

Can. J. Chem. Downloaded from www.nrcresearchpress.com by 210.87.254.105 on 09/05/12
For personal use only.

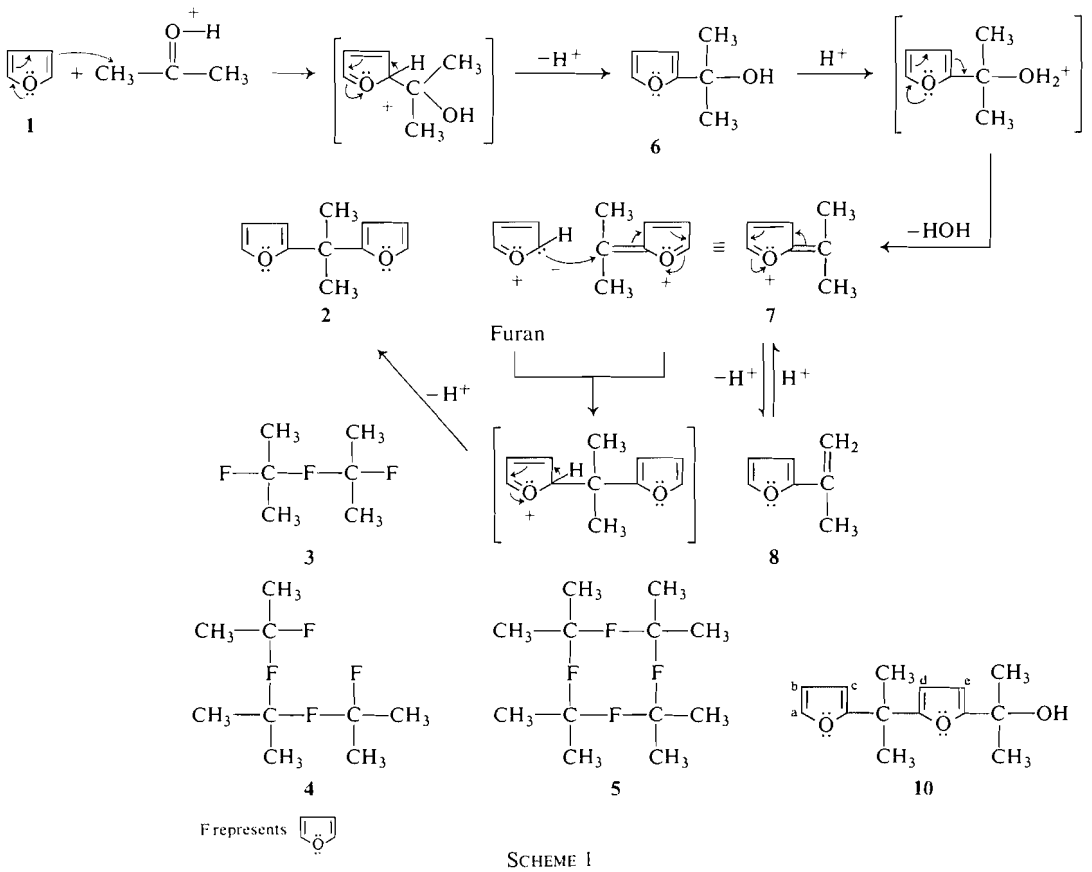

SCHEME 1

pyrrole. Some intermediates, which they isolated, were treated with the appropriate 'missing link' unit to yield the expected cycloanhydrotetramer, **14** (Scheme 2). Casy *et al.* (12) have reported the preparation of 1-(2′-furyl)cyclohexanol, **12** from furyllithium and cyclohexanone. They dehydrated by treating with acetyl chloride to form what they claimed to be 1-(2′-furyl)cyclohexene, **13**. We have repeated their synthesis and found that their chemistry is correct. However, Casy *et al.* did not determine the molecular weight of the supposed alkene **13** which we find to be 592. This value is exactly *four* times the molecular weight, 148, of the monomer 1-(2′-furyl)cyclohexene, $C_{10}H_{12}O$, **13**. Their combustion analysis results for the cyclic tetramer, **14**, of course, are correct for either the monomer $C_{10}H_{12}O$ *or* the tetramer $C_{40}H_{48}O_4$.[3]

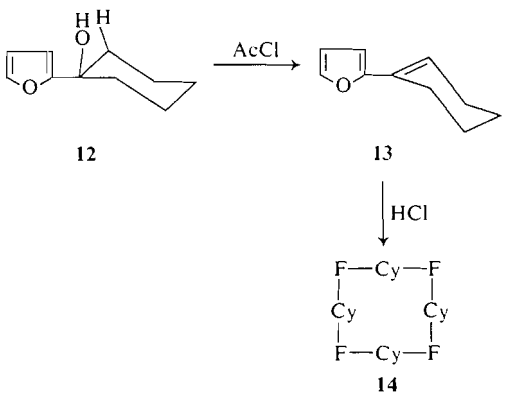

SCHEME 2

Williams (13) cites essentially the same procedure as used by Casy *et al.* (12) for the synthesis of 2-(1′-cyclohexenyl)furan, which, if followed, would also lead to the formation of the cyclic tetramer **14**. We have also prepared authentic 1-(2′-furyl)cyclohexene **13** by following an alternate procedure also described by Casy *et al.* (12). The above alkene when catalysed by acid forms the cyclic tetramer **14** much more rapidly than the corresponding alcohol, which would support our proposal that in the case of the condensation reaction between furan and acetone, the alcohol, 2-furyl-2-propanol, **6**, is the first intermediate in this reaction.

[3]We have communicated with Dr. A. F. Casy and he has given us his kind permission to point out this oversight on their part.

Can. J. Chem. Downloaded from www.nrcresearchpress.com by 210.87.254.105 on 09/05/12
For personal use only.

TABLE 1. Products from the reactions of synthesized possible intermediates*

Intermediate	Reactant	Product(s)	Method of identification	Reference
F-C-OH **6**	Furan **1**	F-C-F **2**, F-C-F-C-F **3**	vpc	17
F-C-OH	F-C-F **2**	F-C-F-C-F **3**	vpc	17
F-C(=CH_2)-CH_3 **8**	Furan **1**	F-C-F **2**, F-C-F-C-F **3**	vpc	18
	F-C-F **2**	F-C-F-C-F **3**	vpc	18
HO-C-F-C-OH **9**	Furan **1**	F-C-F-C-F **3**	vpc	1
F-C-F-C-OH **10**	F-C-F **2**	F-C-F-C-F-C-F **4**	Distillation and characterisation by ir. Reaction with acetone to give tetroxaquaterene compound.	
F-C-F-C-OH	F-C-F-C-OH **10**	Tetroxaquaterene **5**	ir, mixture melting point	
F-C-F-C-OH	Furan **1**	F-C-F-C-F **3**	vpc	
HO-C-F-C-F-C-OH **11**	F-C-F- **2**	Tetroxaquaterene **5**	ir, mixture melting point	15
HO-C-F-C-F-C-OH **11**	Furan **1**	F-C-F-C-F-C-F **4**	Reaction with acetone to give tetroxaquaterene compound.	

*F-C- represents 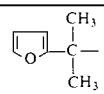

Experimental

Nuclear magnetic resonance spectra were obtained on a Varian A-60-A high resolution spectrometer. For vpc analyses the gas chromatograph used was F and M model 810 with thermal conductivity detector using 1.8 m by 0.64 cm stainless steel columns. Infrared spectra were run on a Beckman IR5A instrument. Some molecular weights were determined by the Rast method while for others a Varian MAT, CH7 mass spectrometer (MS) was employed.

Vapour Phase Chromatographic Analysis of Furan–Acetone Reaction Mixture

In a three-necked 500 ml flask, fitted with reflux condenser and magnetic stirrer, were placed 34 g (0.5 mol) of furan, 29 g (0.5 mol) of acetone, and 30 ml of absolute ethanol. While this mixture was being vigorously stirred, 35 ml of 37% aqueous hydrochloric acid solution was added all at once. After 90 s reaction time stirring was stopped. A 25 ml sample of the organic (upper) layer was quenched with an excess of solid sodium bicarbonate, after which the sample was decanted and dried over anhydrous magnesium sulfate. The volume of the sample was reduced to one-half by removal of unreacted furan and acetone under diminished pressure.

The sample was then chromatographed on three different columns: (*a*) Diisodecyl phthalate; (*b*) Carbowax 20M; (*c*) SE-30 column.

On column (*a*) (Chromatographic conditions: He flow rate 40 ml/min; column temperature programmed 110–160°C at 6° per minute, injector 190°C, detector 310°C) 2-furyl-2-propene, **8**, was retained for 5.2 min. A peak in the reaction mixture sample also had a retention time of 5.2 min. The chromatogram of the sample also showed a peak at 15.2 min which is the retention time for a sample of difurylpropane, **2**.

All other vpc runs were carried out in a similar manner. The results are given in Table 2. All other reactions of the furylpropanols and 2-furyl-2-propene, **6**, **8**, **9**, **10**, and **11**, leading to the formation of compounds **2**, **3**, **4**, and **5**, were carried out as outlined above and were identified as indicated in Table 1 (14).

TABLE 2

Column	Retention time (min)	Compound identified
(*a*)	5.2	2-Furyl-2-propene **8**
	15.2	Difurylpropane **2**
(*b*)	1.8	2-Furyl-2-propene **8**
	5.6	Difurylpropane **2**
	40	2,5-bis(α,α-Dimethylfurfuryl) furan **3**
(*c*)	3.25	Difurylpropane **2**
	11.1	**3**

*Synthesis of 2-{2-[5-(α,α-Dimethyl)furfuryl]-furyl}-2-2-propanol (F-C-F-C-OH) **10**, Table 1*

An ethereal solution of methyl magnesium iodide was prepared by the reaction of 0.975 g (0.04 mol) of magnesium turnings and 5.6 g (0.04 mol) of methyl iodide in 12.5 ml of dry ether. The solution was cooled in an ice-bath, and while being stirred vigorously 8.0 g (0.0367 mol) of 2-furyl-2-(5-acetylfuryl)propane, prepared according to the method of Brown and French (15), was added dropwise over a period of 20 min. Stirring was continued for 2 h at room temperature. The complex was decomposed according to the method of Fieser (16), using saturated cold aqueous ammonium chloride. The ether solution was decanted and the solid salt in the reaction flask was washed twice with ether. The combined ether solutions were dried over anhydrous magnesium sulfate. Removal of ether yielded 7.69 g (89%) of pale yellow oil which crystallized; mp 23–27°C, bp 98.0–98.5°C (0.5 Torr); ir λ_{max} (μ): 3.0, 3.38, 6.62, 7.22, 7.85, 8.60, 9.88, 10.4, 10.72, 12.70, 13.65, (b); ^{1}Hmr 60 MHz (CCl_4) δ: 7.25 (H_a, bd, J_{obs} = 1.2 Hz), 6.20 (H_b, dd, J_{obs} = 3.2 and 1.2 Hz), 5.94 (ab q, J_{obs} = 3.5 Hz) (resonance due to H_c obscured by ab q), 2.75 (s, H on OH), 1.60 (s, 6H), 1.45 (s, 6H). Shaking with D_2O eliminated the 2.75 s. Integration accounts for 18 hydrogen atoms. Mass determined on a V.G. Micromass 7070 F using peak matching unit (6000 resolving power), calcd. for $C_{14}H_{18}O_3$: 234.1256:

Can. J. Chem. Downloaded from www.nrcresearchpress.com by 210.87.254.105 on 09/05/12
For personal use only.

Can. J. Chem. Downloaded from www.nrcresearchpress.com by 210.87.254.105 on 09/05/12
For personal use only.

found: 234.1259. *Anal.* calcd. for $C_{14}H_{18}O_3$: C 71.80, H 7.69; found: C 71.83, H 7.76.

*Reactions of 2-{2-[5-(α,α-Dimethyl)furfuryl]-furyl}-2-propanol (F-C-F-C-OH) **10**, Table 1*

(a) With Difurylpropane (F-C-F)

A solution of 1.0 g (0.0043 mol) of **10**, 7.55 g (0.043 mol) of F-C-F, and 10 ml of absolute ethanol was chilled in an ice-bath. To the stirred solution was added all at once 2 ml of 37% aqueous hydrochloric acid solution. The mixture was stirred at room temperature for 24 h and then was treated with 25 ml water and extracted with 50 ml ether. The extract was neutralized with 5% aqueous sodium bicarbonate solution and dried over anhydrous magnesium sulphate. The product was distilled after flashing off the ether. The starting material (5.43 g) boiled at 55–60°C/1 Torr. A fraction (0.47 g) boiled at 165–170°C/1 Torr. The ir spectrum of this fraction is identical with that for 2,2-isopropylidenebis(5-(dimethylfurfuryl)furan) **4**.

The product from the reaction was treated with 1.58 g (0.027 mol) of acetone, 5 ml of absolute ethanol, and saturated with dry hydrogen chloride gas. After standing for 24 h the product was removed by filtration and washed with ethanol. The white crystals melted at 220–237°C. Crystallization from benzene yielded white crystals mp 238–241°C. The melting point was not depressed on admixture with **5**, and the ir spectra of the product and **5** were identical.

(b) With Itself (F-C-F-C-OH)

This reaction was anticipated by Ackman *et al.* (1). To a stirred solution of 0.5 g (0.0002 mol) of **10** and 5 ml of absolute ethanol were added dropwise 0.5 ml of 37% aqueous hydrochloric acid solution. The mixture was stirred for 24 h at room temperature. The aqueous phase was decanted and the sticky solid washed with water. The product was washed with acetone and 0.020 g of a white solid collected mp 229.0–237.4°C. Crystallization from benzene yielded 0.01 g of product mp 238–241°C. The melting point was not depressed on admixture with **5**. The ir spectra of the product and **5** were identical.

(c) With Furan (F)

To a 25 ml Erlenmeyer flask were added 6 drops of **10**, 15 drops of furan, 0.5 ml of absolute ethanol, and 4 drops of 37% aqueous hydrochloric acid solution. The mixture was stoppered and shaken for 5 min at room temperature. The reaction was quenched with 5% aqueous sodium bicarbonate solution, extracted with ether and the extract dried over anhydrous magnesium sulphate. The sample was analysed by vpc.

(*i*) Column (*b*). Chromatographic conditions: He flow rate 70 ml/min, column isothermal 202°C, injector 250°C, detector 318°C. A peak for compound **3** occurs at a retention time of 13.2 min. (*ii*) Column (*c*). Chromatographic conditions: He flow rate 50 ml/min, column isothermal 202°C, injector 250°C, detector 318°C. A peak for 2,5-bis(α,α-dimethylfurfuryl)furan **3** was observed at a retention time of 4.6 min.

*Reactions of 2,2-bis-(1-Hydroxy-1-methylethyl-2 furyl)-2-propane (HO-C-F-C-F-C-OH) **11**, Table 1*

(a) With Difurylpropane (F-C-F)

A solution of 1.0 g (0.0034 mol) of (HO-C-F-C-F-C-OH), prepared according to the method of Brown and French (15), 0.605 g (0.0034 mol) of (F-C-F) and 10 ml of absolute ethanol in a 50 ml Erlenmeyer flask was cooled in an ice-bath. To this solution was added dropwise 0.5 ml 35% aqueous hydrochloric acid solution while swirling. The mixture was agitated for 6 h at room temperature. The product was removed by filtration and washed with 10 ml of acetone. The yield of crude white crystals was 0.16 g (10.75%) mp 235.3–239.4°C. Crystallization from benzene gave 0.090 g of white crystals mp 241–242°C. The melting point was not depressed on admixture with **5**. The ir spectra of the product and **5** were identical.

(b) With Furan (F)

To a 50 ml flask fitted with a stirrer and a condenser was added 1.0 g (0.0034 mol) of (HO-C-F-C-F-C-OH) **11**, 2.31 g (0.034 mol) of furan, 10 ml of absolute ethanol, and 2 ml of 37% aqueous hydrochloric acid solution. The mixture was stirred at room temperature for 10 h. At this time the residual furan was removed in a current of air over a period of 45 min. The residue containing **4** (F-C-F-C-F-C-F), already reported by Ackman *et al.* (1), was treated with 5 ml of acetone and stirred for 14 h at room temperature. The solid produce was removed by filtration and washed with 10 ml of cold acetone. The yield of crude product was 0.20 g. Crystallization from benzene gave 0.06 g of white crystals mp 240–242°C. The melting point was not depressed on admixture with **5**. The ir spectra of the product and **5** were identical.

*Reaction of Acetyl Chloride with 1-(2'-Furyl)cyclohexanol **12***

The preparation of 1-(2'-furyl)cyclohexanol **12** was carried out following the procedure of Casy *et al.* (12); mp 30.5°C. When 1.66 g (0.01 mol) of **12**, dissolved in 10 ml of methylene chloride in a 50 ml flask, was treated with 3.9 g (0.05 mol) of freshly distilled acetyl chloride a heat reaction set in after 5 min and at the same time a white solid began to form. When the heat reaction subsided the reaction mixture was refluxed for 1.5 h and then allowed to stand at room temperature overnight.

The resulting solid product was removed by filtration on a Hirsch funnel, then washed with a small amount of methylene chloride. The initial yield of crude solid was 1.0 g (68%). Removal of some of the methylene chloride solvent and unreacted acetyl chloride from the filtrate gave a further yield of crude solid. Overall yield of crude was 1.25 g (84%). Crystallization of the crude product from hexane gave a white substance, mp 268°C. A mixture melting point with the quaterene reported by Brown *et al.* (11) showed no depression. *Anal.* calcd. for $C_{10}H_{48}O_4$ (mol wt. 592): C 81.08, H 8.11; found (ms 592): C 81.09, H 8.44.

Acknowledgment

B.J.H. is indebted to the National Research Council of Canada for financial assistance.

1. R. G. Ackman, W. H. Brown, and G. F Wright. J. Org. Chem. **20**, 1147 (1955).
2. A. Patterson, L. Capel, and D. Walker. The ring index. 2nd ed. 1959. p. 756.
3. R. E. Beals and W. H. Brown. J. Org. Chem. **21**, 447 (1956).
4. W. H. Brown and W. Sawatzky. Can. J. Chem. **34**, 1147 (1956).
5. W. H. Brown and W. N. French. Can. J. Chem. **36**, 537 (1958).
6. M. Chastrette and F. Chastrette. J. Chem. Soc. Chem. Commun. 534 (1973).
7. Y. Kobuke, K. Hanji, K. Horiguchi, M. Asada, Y. Nakayama, and J. Furukawa. J. Am. Chem. Soc. **98**, 7414 (1976).
8. Parish Chemical Company, 815 West Columbia Lane, Provo, UT 84601.
9. A. R. Katritzky and J. M. Lagowski. The principles of

heterocyclic chemistry. Methuen and Company Limited, London. 1967.
10. J. R. WILLARD and C. S. HAMILTON. J. Am. Chem. Soc. **73**, 4805 (1951).
11. W. H. BROWN, B. J. HUTCHINSON, and M. H. MACKINNON. Can. J. Chem. **49**, 4017 (1971).
12. A. F. CASY, A. H. BECKETT, and N. A. ARMSTRONG. Tetrahedron **16**, 85 (1961).
13. ALEC WILLIAMS (*Editor*). Furans synthesis and applications. Noyes Data Corporation, Park Ridge, NJ. 1973. p. 53; U.S. Patent 3 449 368, June 10, 1969.
14. B. J. HUTCHINSON. M.Sc. Thesis, University of Guelph, Guelph, Ont. 1966.
15. W. H. BROWN and W. N. FRENCH. Can. J. Chem. **36**, 371 (1958).
16. L. F. FIESER. Experiments in organic chemistry. 3rd ed. D. C. Heath and Company, Boston, MA. 1957. p. 270.
17. T. REICHSTEIN, H. ZSCHOKKE, R. GEHRING, and G. RONA. Helv. Chim. Acta, **15**, 1118 (1932).
18. G. B. BACHMAN and L. V. HEISEY. J. Am. Chem. Soc. **71**, 1985 (1949).

Can. J. Chem. Downloaded from www.nrcresearchpress.com by 210.87.254.105 on 09/05/12
For personal use only.

Synthesis and study of the conformational stability of sequential polypeptides containing δ-benzyloxycarbonyl-L-ornithine and benzyl esters of L-aspartic and L-glutamic acids

NGA HO-DUC AND HUBERT DAOUST[1]

Département de Chimie, Université de Montréal, Montréal (Qué.), Canada H3C 3V1

AND

SERGE ST-PIERRE

Département de Pharmacologie, Faculté de Médecine, Université de Sherbrooke, Sherbrooke (Qué.), Canada J1H 5N4

Received July 29, 1977

NGA HO-DUC, HUBERT DAOUST, and SERGE ST-PIERRE. Can. J. Chem. **56**, 622 (1978).

The synthesis of the sequential polypeptides $(N\text{-}\delta\text{-}Z\text{-}L\text{-}Orn\text{-}\gamma\text{-}Bzl\text{-}L\text{-}Glu)_n$ and $(N\text{-}\delta\text{-}Z\text{-}L\text{-}Orn\text{-}\beta\text{-}Bzl\text{-}L\text{-}Asp)_n$ by solution methods is described. Both polypeptides are α helical in chloroform as shown by circular dichroism. However, the conformation in this solvent is rather fragile, since small additions of TFA to a dilute solution of the polypeptides in chloroform is sufficient to cause the helix-to-coil transition, as demonstrated by cd and nmr. It is postulated that the low stability of the helical conformation is attributed, in this case, to a cooperative collapse of the ordered conformation.

NGA HO-DUC, HUBERT DAOUST et SERGE ST-PIERRE. Can. J. Chem. **56**, 622 (1978).

La synthèse en solution des polypeptides séquencés $(N\text{-}\delta\text{-}Z\text{-}L\text{-}Orn\text{-}\gamma\text{-}Bzl\text{-}L\text{-}Glu)_n$ et $(N\text{-}\delta\text{-}Z\text{-}L\text{-}Orn\text{-}\beta\text{-}Bzl\text{-}L\text{-}Asp)_n$ est décrite. Les deux polypeptides forment des hélices α comme l'indiquent les spectres de dichroïsme circulaire (dc) dans le chloroforme. Cependant, la conformation dans ce solvant est plutôt fragile car de petites additions d'acide trifluoroacétique à des solutions diluées des polypeptides dans le chloroforme suffisent pour produire la transition hélice–pelote statistique comme le montrent les spectres dc et rmn. La faible stabilité de la conformation hélicoïdale est probablement due, dans le cas présent, à l'effondrement coopératif de cette conformation.

Introduction

The synthesis (1) of sequential polypeptides with the repeating units *N*-ε-*Z*-L-Lys-β-Bzl-L-Asp (PLA) and *N*-ε-*Z*-L-Lys-γ-Bzl-L-Glu (PLG) and a study of their conformational stability (2) have been reported in two previous articles.[2] It has been shown that both copolypeptides assume the α-helical conformation in helicogenic solvents. However, this helical structure is relatively weak as compared with other helices formed by homopolypeptides and some other copolypeptides. In fact, both PLA and PLG in solution in $CDCl_3$ proceed to an helix-to-coil transition at rather low percentages of TFA (3–5%), as shown by nmr spectroscopy (2). This phenomenon has been attributed to a cooperative collapse of the ordered conformation; it is the case when the probability of H-bonding between side chains having different chemical structures is larger for the coiled than for the helical conformation. Then, the collapse of an ordered section of the main chain induces the breaking down of other sections of the chain more easily than for other types of polypeptides.

We have synthesized poly(*N*-δ-*Z*-L-Orn-β-Bzl-L-Asp) (POA) and poly(*N*-δ-*Z*-L-Orn-γ-Bzl-L-Glu) (POG) in order to keep on with our previous study on the importance of the interaction between chemically different neighboring side chains and between side chains and backbone. We have also studied the helix-to-coil transition in dilute solution of both copolymers in chloroform by nmr and cd.

Results and Discussion

The protected, activated monomers γ-benzyl-L-glutamyl-*N*-δ-carbobenzoxy-L-ornithyl *N*-succinimidyl ester and β-benzyl-L-aspartyl-*N*-δ-carbobenzoxy-L-ornithyl *N*-succinimidyl ester were prepared via a modification (3) of Goodman and Steuben's 'backing-off' procedure (4), as described in Fig. 1. The *N*-hydroxysuccinimide-activated, free-amine ornithine moiety was coupled with the amine-protected, free-carboxyl glutamyl or aspartyl residue through a mixed carbonic anhydride reaction. Isobutyl chloroformate and *N*-methyl morpholine were used for the formation of the mixed anhydride, as recommended by Anderson *et al.* (5), to minimize racemization

[1]To whom all correspondence should be sent.

[2]Abbreviations used are those recommended by the IUPAC–IUB Commission on Biochemical Nomenclature. Other abbreviations used are: TFA, trifluoroacetic acid; DCC, *N*,*N*-dicyclohexylcarbodiimide; DMF, *N*,*N*-dimethylformamide; DCHU, dicyclohexylurea; THF, tetrahydrofuran; TMS, tetramethylsilane.

Can. J. Chem. Downloaded from www.nrcresearchpress.com by 210.87.254.42 on 09/05/12
For personal use only.

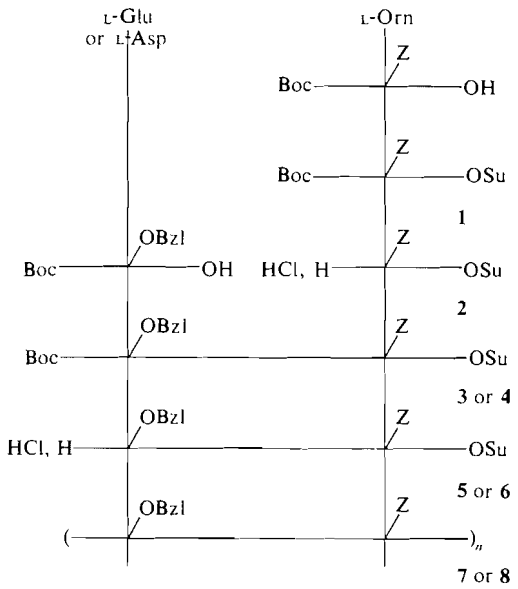

FIG. 1. Schematic description of the synthesis of sequential polydipeptide (L-glutamyl-L-ornithyl)$_n$ and (L-aspartyl-L-ornithyl)$_n$ using solution techniques for the synthesis of the monomer and *N*-succinimide group as an active ester for its polymerization.

during the coupling. This methodology had been shown adequate and very convenient for the preparation of activated peptide monomers in previous work (6, 7). The 'backing-off' method makes it possible to purify the Boc dipeptide ester via simple extraction procedures with dilute aqueous base and acid while the separation of dipeptide ester from a free-carboxyl dipeptide contaminant is much more difficult, the latter being less soluble in water. Moreover, it is safer to activate a single *N*-protected amino acid residue than a dipeptide to avoid possible racemization of the *C*-terminal residue. In a recent work on the preparation of polyheptapeptide models of muscle protein (20), it has been shown that this aforementioned series of procedures gives rise to polymeric material that is virtually free from racemization (<2%).

On the other hand, the yields of protected polydipeptides are kept below 50% because of the important formation of diketopiperazine by-product, which competes strongly with the intermolecular polymerization reaction of activated dipeptides. Fortunately, the cyclic material is easily separated from the polypeptide by washing with hot methanol (21).

The conformational stability of the two polypeptides in chloroform has been studied by both nmr and cd. Figure 2 shows the qualitative cd spectra of POA and POG in chloroform, using cells with a pathlength shorter than 0.01 cm. Cells with short path lengths were used in order to obtain spectral information down to 205 nm where the first π–π^* transition of the amide chromophore occurs. These spectra are qualitative since the thickness of the spacers between the quartz windows is not exactly known (0.001–0.005 cm). In this case, $\Delta\varepsilon$ represents the sign of the ellipticity. The qualitative spectra show that troughs around 220 and 208 nm represent, respectively, the n–π^* and the parallel π–π^* transitions of the amide chromophore indicating that both polypeptides adopt the α-helix structure in this solvent (19). When longer path lengths are used with chloroform as a solvent, the scanning has to be stopped at 215 nm because of strong noise due to the absorbance of chloroform in the uv.

The quantitative spectra of POA and POG in pure chloroform (l = 0.01 cm, c = 2 mg/ml) show the trough corresponding to the n–π^* transition at 222 nm with respective ellipticities of $-16\,000$ and $-28\,000$ deg cm^2 dmol^{-1}. The n–π^* transition of the amide chromophore allows one to follow the variation of the intensity of the trough as a function of the composition of the solvent. As in the case of PLA, the chirality of the helix is not reversed by the regular insertion of β-benzyl-aspartyl residues in the chain.

Figure 3 shows the ellipticity ratio at 220 nm of POA and POG solutions in $CHCl_3$–TFA as a function of the TFA content. The helix-to-coil transition is complete at 9% TFA for POA and at 13% for POG. A parallel study of the effect of TFA on the conformation of the chain has been made by nmr spectroscopy. Figure 4 shows the nmr spectrum of POG in $CDCl_3$; the peak at 3.96 ppm which is assigned to the α-CH proton is typical of the helical conformation of poly-γ-benzyl-glutamate (PBLG) and is reported to be 3.95 ppm (8). Unfortunately, no nmr study of poly-*N*-δ-carbobenzoxy-L-ornithine (PCLO) is reported; however, its nmr spectrum

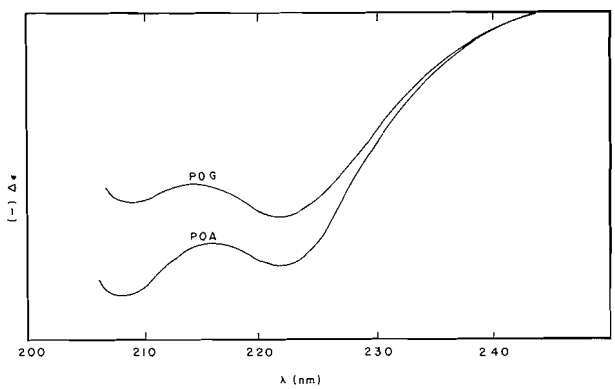

FIG. 2. Qualitative cd spectra of POA and POG in chloroform solution: $c \simeq$ 5–8 mg/ml; $l \simeq$ 0.001–0.005 mm.

Can. J. Chem. Downloaded from www.nrcresearchpress.com by 210.87.254.42 on 09/05/12
For personal use only.

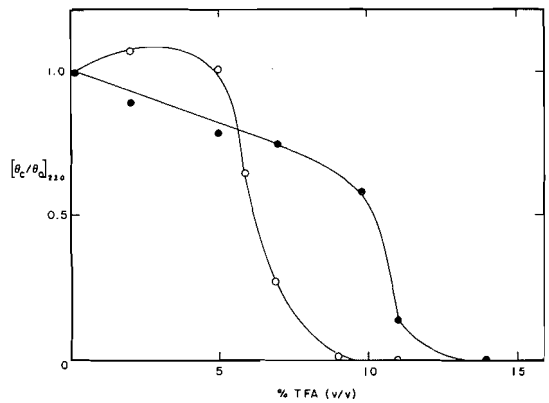

FIG. 3. The helix-to-coil transition of POA (○) and POG (●) in mixtures of chloroform: TFA as measured by circular dichroism at 220 nm; $[\theta_c/\theta_0]_{220}$ represents the ellipticity ratio at 220 nm of a peptide solution in $CHCl_3$–TFA containing respectively c and 0% (v/v) of TFA; c = 2 mg/ml; l = 0.01 cm.

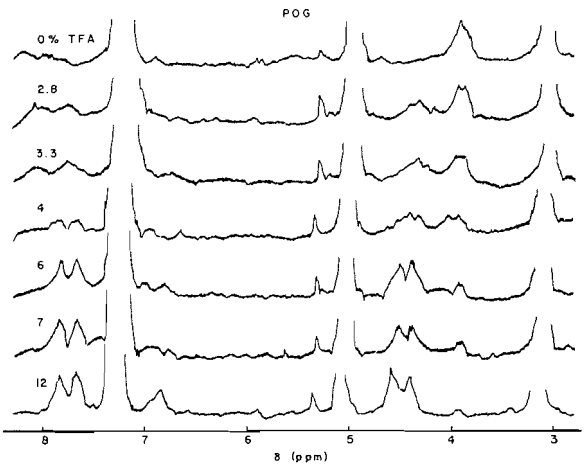

FIG. 4. The 220 MHz nmr spectra of POG in $CDCl_3$ (1% TMS) with increasing amount of TFA at 25°C.

should be very similar to the one of poly-*N*-ε-carbobenzoxy-L-lysine (PCLL); the latter shows a peak at 3.90 for the α-CH proton (8): this peak is hidden on the spectrum. Two broad peaks around 8.2 and 7.6 ppm should appear for the NH proton of the glutamyl and the ornithyl moieties, respectively. This broadening of the peak is well known and is due to molecular association or formation of liquid crystals (9). When 2.8% TFA is added, the position of the glutamyl α-CH peak remains unchanged but the peak of the ornithyl residue is shifted to 4.35 ppm. The NH peaks appear at 8.15 and 7.7 ppm, respectively, for the two residues. The pattern of the nmr spectra changes gradually as more TFA is added, up to 7% v/v: the NH proton peaks appear at 7.84 and 7.6 ppm whereas the α-CH proton peaks appear at 4.5 and 4.4 ppm for the two amino acid residues. Those chemical shifts are characteristic of the random coil conformation of most homopolypeptides (8). The helix–coil transition is complete at 7% TFA since no more changes occur in the spectrum by further addition of TFA.

Figure 5 shows a similar nmr study done with POA. This time, the transition is considered complete at 4–5% TFA. The NH proton peak moves upfield from 8.7 to 7.9 ppm and the α-CH peak is shifted downfield from 4.3 to 4.8 ppm for the aspartyl residue when the TFA content of the solution is increased from less than 1% up to 5%. The hypothesis of many authors (22), that the two peaks observed for α-CH for a given residue might come from acid solvated and unsolvated random coil residues (23) has not been retained, neither has the hypothesis that the low field resonance of α-CH might be due to protonated states of the random coil (24).

It is difficult to discuss the effect of polydispersity of the copolypeptides described here on the α-proton resonance at the transition midpoint (22) since a very small quantity of TFA is needed to complete the transition. However, in the case of POG at 3.3 and 4% TFA, as compared to 0 and 13%, a double peak which might be due to polydispersity appears.

Results obtained in the present work agree with those obtained previously (2) and indicate that the stability of helical conformation of sequential copolypeptides is lower when compared to the helical structure formed by corresponding statistical and block copolypeptides and homopolypeptides (10, 11). It has been shown that the average molecular weight of the polypeptide is an important factor that contributes to the stability of the secondary structure, in organic as well as in aqueous solutions (12). Fortunately, it can be safely assumed that this effect levels off when the chains reach a certain length, which could place the high molecular weight homo- and random copolypeptides obtained by the polymerization of their corresponding *N*-carboxyanhydrides (NCA) in a similar situation as the sequential polypeptides having comparable molecular weights.

The major difference between the four copolypeptides that have been investigated so far in this laboratory lies in the length of the side chains of their monomers. Let us now compare PLG with POG: their amino side chains differ only by one CH_2 unit. It has been shown that PCLO has a slightly more stable helical conformation than PCLL (13). Their initiation parameter, σ, which measures the difficulty of nucleating a helical region, is 1.9×10^{-5} and 1.2×10^{-5}, respectively (14, 15), indicating that destruction of PCLO helix is less cooperative. Moreover, H-bonding between two neighboring side chains in POG should be more important than for

Can. J. Chem. Downloaded from www.nrcresearchpress.com by 210.87.254.42 on 09/05/12
For personal use only.

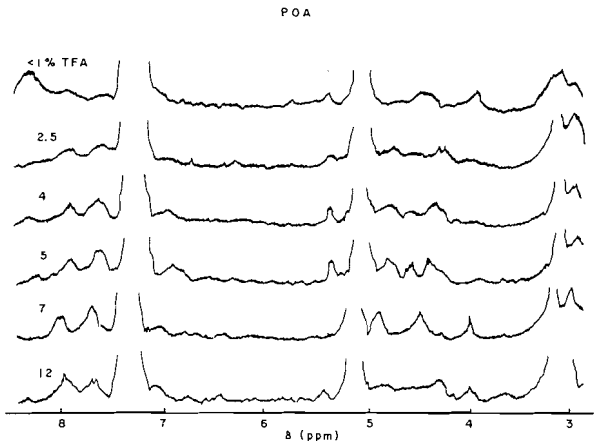

FIG. 5. The 220 MHz nmr spectra of POA in $CDCl_3$ (1% TMS) with increasing amount of TFA at 25°C.

PLG since the NH group in the ornithyl side chain faces more favorably the carbonyl group in the glutamyl side chain. Consequently, the helical conformation of POG should be reinforced by side chain – side chain interactions. However, the nmr results previously obtained for PLG (2) are very similar to those for POG, indicating that this stabilizing effect is counterbalanced by the cooperative collapsing effect due to the higher probability of forming H-bonding in the disordered conformation. The same conclusions apply when PLA and POA are compared.

In addition to side chain – side chain interactions that could increase the stability of the POG helix, we believe that POG can form stronger helices than POA because, in the latter case, of the competition that exists for hydrogen bonding between the backbone carbonyl groups and those from the aspartyl side chains. This phenomenon, which is already well known (12), tends to weaken the helical structure of POA and other aspartyl-containing polypeptides. A similar explanation can be given for the weaker stability of the helical conformation of poly (β-benzyl-L-aspartate) (PBLA) when compared to PBLG (14).

Experimental

N-α-Boc-*N*-δ-*Z*-L-Ornithine, β-Bzl-L-aspartic acid, and γ-Bzl-L-glutamic acid were purchased from Bachem Fine Chemicals (Marina del Rey, California) and were used without further purification. DCC (Aldrich Chemicals) was purified as described in a previous publication (1). *N*-Hydroxysuccinimide (Aldrich) was used without further purification. Dioxane, DMF, and triethylamine were purified according to the procedure used before (1). HCl (4 *N*) in dioxane in 10 ml ampoules was obtained from Pierce Chemical Company and diluted to 2 *N* with anhydrous dioxane. All the other solvents and reagents were of Analytical Reagent quality and used without further purification.

Melting points were determined on a Uni-Melt melting point apparatus and are uncorrected. Optical rotations were measured with a Perkin-Elmer Model 141 polarimeter at 589 nm, using a 1-dm path length microcell (0.9 ml volume). Infrared spectra of the intermediate products were recorded from KBr pellets, using a Perkin-Elmer model 621 spectrophotometer. Proton magnetic resonance spectra were taken with a Varian model T-60 spectrometer in $CDCl_3$, using TMS as an internal reference. Elemental analysis were performed by Galbraith Laboratories (Knoxville, TN). Thin-layer chromatography was carried out on precoated silica gel plates (Kodak 246 F), in the following solvent systems: 1-butanol – acetic acid – water in a ratio 4:1:5 (top phase) (BAW5) and in a ratio 4:1:1 (BAW1); chloroform – acetic acid in a ratio 95:5 (CA) and acetone – acetic acid in a ratio 98:2 (AA). Peptide spots were visualized directly under uv light or by treatment with ninhydrin spray (0.2% in acetone) and heating (free amine) or treating the plates with HCl vapors (15 min), spraying with ninhydrin, and heating (*t*-Boc amines).

N-α-*Boc*-N-δ-Z-L-*Ornithine* N-*Succinimidyl Ester (1)*

A mixture of *N*-α-Boc-*N*-δ-*Z*-L-ornithine (5 g, 0.013 mol) and *N*-hydroxysuccinimide (1.57 g, 0.013 mol) was dissolved in ethyl acetate (100 ml) and dioxane (40 ml). The solution was cooled down to 0°C and DCC (3.09 g, 0.015 mol) in ethyl acetate (5 ml) was added. The reaction was stirred at 0°C for 2 h and at 4°C for 48 h. Glacial acetic acid (5 drops) was added and after 2 h at 4°C, the DCHU was filtered off and the filtrate evaporated to an oil which was dissolved in ethyl acetate (60 ml). After standing overnight at 4°C, more DCHU was filtered, 100 ml of ethyl acetate added to the filtrate, and the organic solution was extracted, at 0°C, with 0.5 *M* $NaHCO_3$ (3 × 50 ml), washed with water, dried over $MgSO_4$, filtered, and evaporated to an oil, which was redissolved in ether and evaporated again. After repeating this operation one more time, a solid residue remained which was recrystallized in ether–hexane (5:1) to give 5.18 g (82%) of pure compound **1**, as shown by analysis: mp 80–82°C; $[\alpha]_D^{25}$ −18.44° (*c* 2, ethyl acetate); R_F^{AA} 0.82, R_F^{CA} 0.78, R_F^{BAW5} 0.65; $\bar{\nu}$ (KBr): 1805, 1780, 1685 cm^{-1}; τ ($CDCl_3$): 2.70 (5 H, phenyl singlet), 4.60 (1 H, NH), 4.72 (1 H, NH), 7.05 (4 H, singlet, CH_2 succinimido), 8.50 (13 H, multiplet, CH_2's and CH_3's). *Anal.* calcd. for $C_{22}H_{29}N_3O_8$: C 57.02, H 6.26, N 9.07; found: C 56.98, H 6.19, N 9.09.

N-*Boc*-γ-*Bzl*-L-*Glutamyl*-N-δ-Z-L-*ornithine* N-*Succinimidyl Ester (3)*

N-α-Boc-*N*-δ-*Z*-L-Ornithine *N*-succinimidyl ester (6 g, 13 mmol) was reacted with 2 *N* HCl in dioxane for 1 h. After evaporation, trituration of the residue with ether, filtration, and drying *in vacuo*, 5.2 g of hydrochloride **2** was obtained (quantitative yield). The white, hygroscopic powder was shown homogeneous by tlc (R_F^{BAW1} 0.69). Boc-γ-Bzl-L-Glutamic acid (1.72 g, 5.1 mmol) was dissolved in THF and the solution was cooled to −20°C. *N*-Methylmorpholine (0.52 g, 5.1 mmol) and isobutyl chloroformate (0.7 g, 5.1 mmol) were added and after 1 min, a cold solution containing compound **2** (2.05 g, 5.1 mmol) in DMF (4 ml) was added. Triethylamine (0.52 g, 5.1 mmol) was added dropwise to the suspension over a period of 5 min. The reaction was then stirred at −20°C for 10 min, at 0°C for 30 min, and at room temperature for 1 h. The solvents were evaporated *in vacuo*, ethyl acetate (100 ml) was added, and the insoluble salts were filtered and washed with more ethyl acetate (25 ml). The filtrate was cooled to 0°C and washed successively with 0.01 *N* HCl (3 × 25 ml), water, 0.5 *M* $NaHCO_3$ (3 × 25 ml), and with water, was dried over anhydrous $MgSO_4$ and the ethyl acetate evaporated to an oil, which was redissolved in ether and evaporated. After repeating

Can. J. Chem. Downloaded from www.nrcresearchpress.com by 210.87.254.42 on 09/05/12
For personal use only.

Can. J. Chem. Downloaded from www.nrcresearchpress.com by 210.87.254.42 on 09/05/12
For personal use only.

the last operation, a white powder was obtained which was recrystallized from acetone – petroleum ether (30–60°C); yield, 2.25 g (64%); mp 57–59°C; $[\alpha]_D^{25}$ −22.84° (*c* 2, dioxane); R_F^{CA} 0.90, R_F^{AA} 0.67. *Anal.* calcd. for $C_{34}H_{42}N_4O_{11}$: C 59.82, H 6.16, N 8.21; found: C 59.77, H 6.21, N 8.19.

N-*Boc*-β-*Bzl*-L-*Aspartyl*-N-δ-Z-L-*ornithine* N-*Succinimidyl Ester (4)*

Boc-β-Bzl-L-Aspartic acid, (1.41 g, 4.37 mmol), *N*-methylmorpholine, (0.44 g, 4.37 mmol), isobutyl chloroformate, (0.6 g, 4.37 mmol), compound **2** (1.75 g, 4.37 mmol), and triethylamine (0.44 g, 4.37 mmol) were reacted as described previously to give 1.94 g (66% yield) of compound **4**: mp 58–59°C; $[\alpha]_D^{25}$ −21.05° (*c* 2, dioxane); R_F^{CA} 0.91, R_F^{AA} 0.65. *Anal.* calcd. for $C_{33}H_{40}N_4O_{11}$: C 59.28, H 5.99, N 8.38; found: C 59.36, H 6.04, N 8.36.

γ-*Bzl*-L-*Glutamyl*-N-δ-Z-L-*ornithine* N-*Succinimidyl Ester Hydrochloride (5)*

Compound **3** (2 g, 2.9 mmol) was dissolved in 2 *N* HCl in dioxane (20 ml). After 1 h at room temperature, the solution was evaporated to an oil, under vacuum with exclusion of moisture. The oil was triturated with anhydrous ether to give a white solid, which was filtered, washed with more ether and dried *in vacuo* over KOH. Compound **5** (1.8 g) was found to be homogeneous by tlc: R_F^{BAW1} 0.68; mp 65–67°C; $[\alpha]_D^{25}$ −7.81° (*c* 2, DMF); amino acid analysis: orn/glu = 0.95. *Anal.* calcd. for $C_{29}H_{35}N_4O_9Cl$: C 56.27, H 5.66, N 9.05, Cl 5.74; found: C 56.27, H 5.70, N 9.01, Cl 5.65.

β-*Benzyl*-L-*aspartyl*-N-δ-Z-L-*ornithine* N-*Succinimidyl Ester Hydrochloride (6)*

Compound **4** (1.75, 2.6 mmol) was deprotected with 2 *N* HCl in dioxane as described above: yield, 1.58 g (quantitative): mp 75–77°C; $[\alpha]_D^{25}$ −12.76° (*c* 2, DMF); R_F^{BAW1} 0.61; amino acid analysis: orn/asp = 0.97. *Anal.* calcd. for $C_{28}H_{33}N_4O_9Cl$: C 55.58, H 5.46, N 9.26, Cl 5.67; found: C 55.50, H 5.49, N 9.23, Cl 5.80.

Poly(γ-*Bzl*-L-*glutamyl*-N-δ-Z-L-*ornithyl*) *(7)*

Compound **5** (1.5 g, 2.4 mmol) was dissolved in purified DMF (2 ml), the solution cooled to 0°C, and triethylamine (0.25 g, 2.4 mmol) in DMF (1 ml), was added. The reaction mixture solidified immediately and additional DMF (2 ml) was added. The thick suspension was kept under vigorous stirring at 4°C for 2 days. After further dilution with DMF (2 ml), the suspension was stirred at room temperature for 7 days, DMF (2 ml) being added every day. The mixture was then evaporated down to a paste on a rotary evaporator, water added, and the solid centrifuged. The water was decanted and the washing repeated several times with water; the solid was then filtered, washed with hot methanol and with ether and dried at 50°C *in vacuo* for 48 h to give 509 mg of polypeptide **7**, which was found satisfactory by infrared spectroscopy: ν (KBr pellet): 3280, 1725, 1655 and 1540 cm^{-1}. *Anal.* calcd. for $C_{25}H_{29}N_3O_6$: C 64.24, H 6.21, N 8.99; found: C 64.12, H 6.33, N 8.95.

Poly(β-*Bzl*-L-*aspartyl*-N-δ-L-*ornithyl*) *(8)*

Hydrochloride **6** (1.24 g 2.05 mmol) was used with triethylamine (0.207 g, 2.05 mmol) and the reaction carried out as described above for compound **7**: yield 0.45 g. *Anal.* calcd. for $C_{24}H_{27}N_3O_6$: C 63.58, H 5.96, N 9.27; found: C 63.40, H 6.07, N 9.21.

Characterization and Conformational Analysis of the Polypeptides

Molecular Weight Determination

The molecular weights were estimated from the intrinsic viscosity – molecular weight calibration curve of Doty *et al.* (16). Intrinsic viscosities were determined in dichloroacetic acid at 25°C with a Hewlett-Packard automatic viscometer equipped with a Cannon semimicro Ubbelhode-type viscometer. The average viscosity molecular weights are 12500 for POG and 10000 for POA.

Amino Acid Analysis

The amino acid compositions were evaluated with a Beckman 120 automatic analyser, using the procedure of Spackman *et al.* (17), after hydrolysis with 6 *N* hydrochloric acid in evacuated sealed tubes at 110°C for 22 h.

Circular Dichroism Measurements

Circular dichroism measurements were made with a Cary 60 spectropolarimeter (cd attachment Cary 6002) using 0.01-cm quartz cuvettes and quartz plates. During the measurements, the instrument was purged with nitrogen at a rate of 40 ft^3 min^{-1}. The spectropolarimeter had been previously calibrated with (+)-camphor-10-sulphonic acid (18). The mean residue ellipticity, $[\theta_\lambda]$(in deg cm^2 $dmol^{-1}$), was calculated according to the relationship $[\theta_\lambda] = \theta_\lambda$ (MRW)/10 *lc*, where θ_λ is the observed ellipticity in degrees at the wavelength λ, MRW is the average molecular weight of a residue (226.5 for POA and 233.5 for POG), *l* is the path length of the cell (cm) and *c* the concentration (g cm^{-3}).

Nuclear Magnetic Resonance Spectroscopy

The nmr spectra were obtained with a HR 220 MHz spectrometer, property of the Department of Medical Genetics, University of Toronto, Toronto, Ontario. Solvents used were $CDCl_3$ 99.8% deuterated (Merck, Sharp and Dohme, Canada Limited), and TFA (J. T. Baker). Polypeptide concentration was approximately 2% w/v and 1% TMS was added as internal reference.

Acknowledgements

We acknowledge support of this project by a grant from the Department of Education of the Province of Quebec. We also wish to thank Dr. A. Grey for recording the nmr 220 MHz spectra.

1. H. Daoust and S. St-Pierre. J. Chem. Soc. Perkin I, **5**, 1453 (1976).
2. H. Daoust, J. Prud'homme, and N. Ho-Duc. Eur. Polym. J. **12**, 147 (1976).
3. D. Nissen, C. Gilon, and M. Goodman. Makromol. Chem. **176**, 23 (1975).
4. M. Goodman and K. C. Steuben. J. Am. Chem. Soc. **81**, 3980 (1959).
5. G. W. Anderson, J. E. Zimmerman, and F. M. Callahan. J. Am. Chem. Soc. **89**, 5012 (1967).
6. S. St-Pierre, R. T. Ingwall, and M. Goodman. Biopolymers. In press.
7. S. St-Pierre and R. S. Hodges. Can. J. Biochem. **55**, 636 (1977).
8. E. M. Bradbury, P. D. Cary, C. Crane-Robinson, and P. G. Hartman. Pure Appl. Chem. **36**, 53 (1973).
9. F. A. Bovey. Pure Appl. Chem. **16**, 417 (1968).
10. L. Paolillo, D. Temussi, E. Trivellone, A. M. Bradbury, and C. Crane-Robinson. Biopolymers, **10**, 2555 (1971).
11. L. Paolillo, D. Temussi, E. M. Bradbury, and C. Crane-Robinson. Biopolymers, **11**, 2043 (1972).
12. G. D. Fasman. *In* Poly-α-amino acids. Vol. I. *Edited by* G. D. Fasman. Marcel Dekker, Inc., New York, NY. 1967. Chapt. 11.

13. M. HATANO, M. YONEYAMA, I. ITO, T. NOGAWA, and M. NAKAI. J. Am. Chem. Soc. **91**, 2165 (1969).
14. T. GASKIN and J. T. YANG. Biopolymers, **10**, 631 (1971).
15. F. E. KARASZ, J. M. O'REILLY, and H. E. BAIR. Biopolymers, **3**, 241 (1965).
16. P. DOTY, J. H. BRADBURY, and A. M. HOLTZER. J. Am. Chem. Soc. **78**, 747 (1956).
17. D. H. SPACKMAN, W. H. STEIN, and S. MOORE. Anal. Chem. **30**, 1190 (1958).
18. H. DAOUST and S. ST-PIERRE. Can. J. Chem. **53**, 1861 (1975).
19. A. J. ADLER, N. J. GREENFIELD, and G. D. FASMAN. *In* Methods in enzymology. Vol. XXVII. *Edited by* C. H. W. Hirs and S. N. Timasheff. Academic Press Inc., New York, NY. 1973. pp. 675–735.
20. F. S. TJOENG, S. ST-PIERRE, and R. S. HODGES. 5th Am. Peptide Symp. San Diego, CA, June 1977.
21. P. M. HARDY, H. N. RYDON, and R. C. THOMPSON. J. Chem. Soc. Perkin I, **1**, 5 (1972).
22. I. A. BOVEY. J. Polymer Sci. Macromol. Rev. **9**, 1 (1974).
23. I. J. JOUBERT, N. LOTAN, and H. A. SCHERAGA. Biochemistry, **9**, 2197 (1970).
24. J. W. O. TAM and I. M. KLOTZ. J. Am. Chem. Soc. **93**, 1313 (1971).

Can. J. Chem. Downloaded from www.nrcresearchpress.com by 210.87.254.42 on 09/05/12
For personal use only.

Studies in decarboxylation. XI.[1] The gas phase pyrolysis of some arylacetic acids

DAVID B. BIGLEY AND RICHARD H. WEATHERHEAD
University Chemical Laboratory, Canterbury, Kent, CT2 7NH, England

Received August 5, 1977

DAVID B. BIGLEY and RICHARD H. WEATHERHEAD. Can. J. Chem. **56**, 628 (1978).

The gas phase decarboxylations of 1-naphthyl-, 2-naphthyl-, and 9-phenanthrylacetic acids all proceed through a homolytic pathway. There is no evidence for the concerted 1,5-hydrogen shift usually encountered in the decarboxylation of β,γ-unsaturated acids.

DAVID B. BIGLEY et RICHARD H. WEATHERHEAD. Can. J. Chem. **56**, 628 (1978).

La décarboxylation en phase gazeuse des acides naphtyl-1, naphtyl-2 et phénantryl-9 acétiques se produit par un mécanisme homolytique. On n'a trouvé aucune indication suggérant la présence du déplacement 1,5 d'hydrogène que l'on rencontre généralement dans la décarboxylation des acides β,γ non-saturés.

[Traduit par le journal]

Can. J. Chem. Downloaded from www.nrcresearchpress.com by 210.87.254.40 on 09/05/12
For personal use only.

In previous papers of this series we have shown that the pyrolysis of β,γ-unsaturated aliphatic acids is a unimolecular concerted process involving a 1,5-hydrogen shift, yielding carbon dioxide and the respective alkene (2). More recently we have explored the scope and limitations of the reaction by variation of the environment of the β,γ-double bond of the acid. We have shown that β,γ-acetylenic (3), α,β,γ- and β,γ,δ-allenic (4), α,β-γ,δ-dienoic (4), and cyclopropylacetic acids (5) are all subject to a mechanistically similar decomposition. We now report our observations on the pyrolysis of some acids in which the unsaturation forms part of an aromatic system.

Experimental

The 1- and 2-naphthylacetic acid were commercial samples (Koch-Light) and were purified by sublimation; (mp 133 and 141°C, respectively (lit. (6, 7) mp 131.5 and 138°C, respectively).

We experienced considerable difficulty in the preparation of 9-phenanthrylacetic acid and in our hands the literature routes were unreliable. We were eventually successful by the oxidation of 9-phenanthrylethanol. This compound was prepared by the unusual route of Bergmann and Blum-Bergmann (8), distilled at 200°C/1 Torr and solidified in the condenser. This alcohol (7 g) was dissolved in acetone (33 ml), was cooled in an ice bath under nitrogen, and was oxidised by the dropwise addition of a cooled solution of chromium trioxide (7.5 g) in aqueous (38 ml) sulphuric acid (12 ml concentrated). The mixture was stirred at < 20°C for 45 min when it was extracted with ether (3 × 100 ml). The usual base (1 *N* NaOH) acid procedure then gave the acid as a brown powder. This was purified by vacuum sublimation to give a white crystalline powder (1 g), mp 227°C (lit. (9) mp 225°C).

Deuterium Exchange

The naphthylacetic acids were each shaken in ether solution with several portions of D_2O (99.9%) until, on evaporation of the ether, the nmr spectrum showed total loss of the carboxyl hydrogen. 9-Phenanthrylacetic acid proved to be insoluble in most of the common water immiscible solvents, but was soluble in dioxan. It was therefore precipitated from purified dry dioxan with D_2O several times, and filtered under a dry atmosphere. We could not estimate the exchange level since on removal of solvents in vacuum we found that the acid was insoluble in the normal nmr solvents.

Stoichiometry

The 1- and 2-naphthylacetic acids were pyrolysed at 300–310°C at 150 Torr pressure in break-seal tubes. The volatile products were measured in a vacuum line; in both cases CO_2 was obtained in 100% yield (absorption on soda asbestos) together with material which did not condense at liquid nitrogen temperature. Removal of the latter by a Toeppler pump showed that it constituted about 10% yield by volume. The residual involatile product in the break-seal tube was investigated by glc and was shown to comprise two major fractions, together with several minor products. Larger samples of the involatile products were obtained by flash vacuum pyrolysis (3) of the acid at 700°C and 0.01 Torr. The pyrolysis tube was found to be coated with soot after the reaction but clean products were isolated in traps in liquid nitrogen. The products from 2-naphthylacetic acid were left to stand overnight during which time a white crystalline material deposited; this was recrystallised from benzene and found to have a sharp melting point (184°C) (10) and parent ion (*m/e*) 282. This and other spectroscopic data showed the solid to be 1,2-bis-2-naphthylethane. The residual liquid was shown to be mostly 2-methylnaphthalene, with small traces of other compounds not further identified. For 1-naphthylacetic acid, the pyrolysis products were separated by preparative tlc. Two major components were similarly identified as 1-methylnaphthalene and 1,2-bis-1-naphthylethane. The amounts of involatile compounds were estimated by glc after prior standardisation of peak heights with authentic samples. 1-Naphthylacetic acid yielded 50% 1-methylnaphthalene; 20% 1,2-bis-1-naphthylethane. 2-Naphthylacetic acid yielded 65% 2-methylnaphthalene; 15% 1,2-bis-2-naphthylethane.

9-Phenanthrylacetic acid was pyrolysed in an evacuated break-seal tube at 240°C for 24 h to give a quantitative yield of carbon dioxide and no noncondensible products. The residue in the tube was vacuum sublimed and shown to be 9-methylphenanthrene $> 90\%$ yield. A small amount of dark material ($\sim 5\%$) left in the tube was not investigated further.

Kinetics

An attempt was made to measure the rates of decarboxyla-

[1]For Part X, see ref. 1.

Can. J. Chem. Downloaded from www.nrcresearchpress.com by 210.87.254.40 on 09/05/12
For personal use only.

tion of the three acids by the pyrolysis of known weights of each acid in a series of evacuated break-seal tubes in a well thermostatted salt bath by following the amount of carbon dioxide liberated. It was shown that decarboxylation appeared to follow first-order kinetics initially but the rate slowed appreciably over the second 50% reaction. Dilution of the sample by the usual radical inhibitors, cyclohexene or toluene, had little effect on this behaviour, nor was it affected by inclusion of an inert acid, 2-ethylhexanoic acid. The reaction rate was somewhat dependent on the initial pressure but it was not possible to obtain reliable rate constants in our simple apparatus. However, approximate rate constants were estimated at several temperatures from initial slopes, to permit extrapolation to 500 K. For comparison, phenylacetic acid (range 860–995 K), $k_{500} = 5 \times 10^{-11}$ s^{-1} (relative rate 1) (12); 1- and 2-naphthylacetic acid (530–600 K), k_{500} = ca. 1×10^{-7} s^{-1} (relative rate 2×10^3); 9-phenanthrylacetic acid (500–550 K), k_{500} = ca. 1×10^{-6} s^{-1} (relative rate 2×10^4).

Nuclear Magnetic Resonance

^{13}C nmr spectra were recorded using a JEOL PS-100 spectrometer operating in Fourier transform mode and employing an internal deuterium lock. The results obtained for the various naphthalene derivatives are shown in Table 1, using the assignments of Doddrell and Welles (11). The deuterium magnetic resonance spectra of 1-methylphenanthrene showed only one peak at 204.0 Hz relative to deuteriochloroform (266.7 Hz) though peaks of less than 10% of that observed could be hidden in base-line noise.

Discussion

Our previous work had indicated that β,γ-unsaturated acids decarboxylate by a concerted 1,5-hydrogen shift to yield carbon dioxide and the α,β-unsaturated olefin. On the other hand phenylacetic (12) and diphenylacetic (13) acids, both formally β,γ-unsaturated acids, had been shown to decarboxylate by a radical mechanism. The difference probably results from the aromaticity of the latter acids. For these acids to lose carbon dioxide via the normal concerted 1,5-hydrogen shift, the activation energy would have to be sufficient to overcome the loss of aromaticity in the intermediate (114 kJ mol^{-1})[2] in addition to that for the activation of the normal β,γ-substituted-β,γ-unsaturated acid (142 kJ mol^{-1}) (14). These together would be greater than the normal bond dissociation energy, ϕCH_2—COOH (230 kJ mol^{-1}) (12). In addition the *A*-factor for dissociation into radicals will be more favourable than that for a concerted process; the homolytic mechanism shown in Scheme 1 is thus well understood.

Polycyclic aromatic compounds all contain bonds intermediate in order between the 1.5 of benzene and the full 2 of a double bond. We chose the 1,2 bond of naphthalene and the 9,10 of phenanthrene as possible candidates to show the changeover between mechanisms. There is, of course, considerable evidence for bond fixation in naphthalene: a particularly pertinent comparison is between simple *N*-alkylaniline derivatives which are recovered unchanged after thermal treatment (15) or undergo fragmentation at higher temperatures (16), and *N*-allylnaphthylamine which pyrolyses via a Claisen type of reaction (17). By analogy phenyl- and naphthylacetic acids might decarboxylate through different mechanisms. The following features of the

[2]Calculated as the difference between the resonance energies of benzene (151 kJ mol^{-1}) and hexa-1,3,5-triene (37 kJ mol^{-1}).

TABLE 1. ^{13}C chemical shifts (relative to TMS) and assignments to individual carbon atoms of the pyrolysis of undeuteriated and carboxyl-*D*-arylacetic acids

Chemical shift of 1-methylnaphthalene	Assignment (11)	Chemical shift of deuteriated-1-methylnaphthalene
19.2	1-Me	18.87 ($^1J_{CD}$ = 19.5 Hz) 19.2 (residual peak)
123.9	8	123.9
125.4	3, 6, 7	125.4
126.4	4	125.6
	2	126.4
128.4	5	128.4
132.6	8a	132.6
133.6	1	133.6
134.0	4a	134.0

Chemical shift of 2-methylnaphthalene	Assignment (11)	Chemical shift of deuteriated-2-methylnaphthalene
21.5	2-Me	21.3 ($^1J_{CD}$ = 19.5 Hz) 21.5 (residual peak)
124.9	6	124.9
125.7	7	125.7
126.8	1	126.8
127.2	8	127.2
127.6	4, 5	127.5
128.0	3	127.9
131.8	4a	131.7
133.7	8a	133.6
135.2	2	135.2

Chemical shifts of 9-methylphenanthrene	Assignment	Chemical shifts of 9-deuteriomethylphenanthrene
20.0	9-Me	19.9 ($^1J_{CD}$ = 10.0 Hz) 20.0 (residual peak)
122.5	Aromatics	122.4
123.0		123.0
124.6		124.6
125.4		125.7
125.8		
126.2		126.2
126.5		126.4
126.7		
127.8		127.8
130.6		129.6
130.9		130.3
132.0		132.0
132.5		132.4

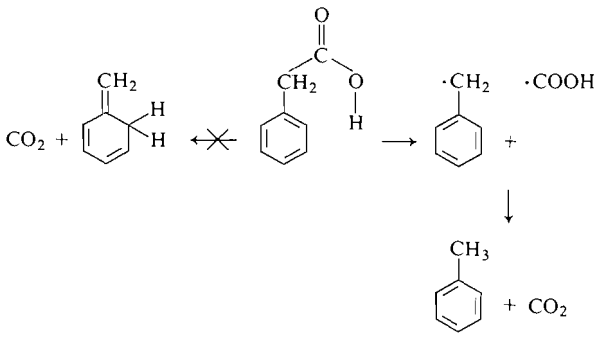

SCHEME 1

decarboxylation of both 1- and 2-naphthylacetic acids imply radical pathways: (*i*) kinetics which are not of the first order; (*ii*) appearance of noncondensible gases; (*iii*) observation of dimeric products. However the two mechanistic pathways are now closer in energy and none of the above features excludes the coexistence of both. We therefore examined the pyrolysis of the carboxyl deuteriated acids. The concerted six-centre mechanism would give rise to an intermediate (**1**), which would require a 1,3-hydrogen shift to give rise to the observed product. However for the deuteriated acid, a kinetic isotope effect would favour the transfer of a hydrogen atom rather than a deuteron and **2** would be favoured over **3** (Scheme 2).

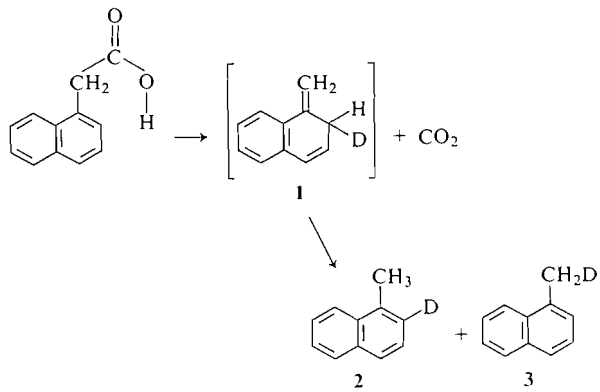

SCHEME 2

A radical process would involve initial cleavage of the ϕCH_2—COOH bond and would be followed by abstraction by or recombination of the arylmethyl radical, and dedeuteriation of the carboxyl radical to yield carbon dioxide. Thus only **3** should be formed, although as not all products are accounted for, and the decarboxylation pathway is unlikely to be simple, it may be possible for the arylmethyl radical to obtain a hydrogen atom either from the walls of the reaction vessel or other product to give completely undeuteriated material. The ^{13}C nmr spectra of deuterio-1-methylnaphthalene obtained from the pyrolysis of carboxyl-*D*-1-naphthylacetic acid (Table 1) shows that the signal at 18.9 ppm due to the methyl group is split into a 1:1:1 triplet as expected for a —CH_2D fragment, the proton coupling being removed by noise decoupling. The value $^1J_{CD}$ = 19.5 Hz is of the expected magnitude (18). Some undeuteriated methyl group is also present in the sample as evidenced by a residual signal at 19.2 ppm. The C-2 atom of the naphthalene ring gives rise to a signal at 126.4 ppm which in the undeuteriated sample is superimposed with the signal from C-4 but is separated in the deuteriated sample. No evidence of any splitting of this signal could be obtained and it is thus unlikely that any considerable amount of **2**, the expected major component of a concerted reaction, was present in the sample. Thus the major product of the pyrolysis of carboxyl-*D*-1-naphthylacetic acid is **3** together with some undeuteriated material. This result is entirely consistent with the radical pathway but precludes, within the limits of nmr detection, the concerted mechanism.

Similarly, the ^{13}C nmr spectrum obtained from the pyrolysis product of carboxyl-*D*-2-naphthylacetic acid (Table 1) shows that the signal at 21.3 ppm due to the 2-methyl group of 2-methylnaphthalene is split into a 1:1:1 triplet with $^1J_{CD}$ = 19.5 Hz, again implying a CH_2D fragment. A residual peak due to an undeuteriated methyl group was also noted at 21.5 ppm. According to a possible concerted mechanism, it would be expected that some deuterium should appear at the C-1 position (**4**) (Scheme 3) but examination of the signal at 126.8 ppm due to the C-1 carbon shows it to be unsplit in the deuteriated sample; thus it is unlikely that the concerted reaction plays any part in the decarboxylation of this acid.

It has been estimated that the C9—C10 bond of the phenanthrene nucleus has about 90% double bond character (19). This has been demonstrated chemically by the ease of addition rather than substitution at these positions. Thus, it was hoped that the 9,10 bond in 9-phenanthrylacetic acid would act sufficiently like an isolated double bond to allow the concerted decarboxylation mechanism to proceed. No evidence for the formation of any dimer or effect of radical traps was noted on pyrolysis and high

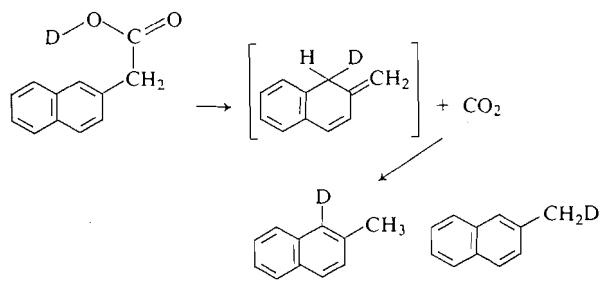

SCHEME 3

Can. J. Chem. Downloaded from www.nrcresearchpress.com by 210.87.254.40 on 09/05/12
For personal use only.

Can. J. Chem. Downloaded from www.nrcresearchpress.com by 210.87.254.40 on 09/05/12
For personal use only.

yields of 9-methylphenanthrene (>90%) were obtained. The ^{13}C nmr spectrum of the deuteriated 9-methylphenanthrene obtained from the pyrolysis of a carboxyl-*D*-9-phenanthrylacetic acid is reported in Table 1, along with ordinary 9-methylphenanthrene. It is clear from the signal at about 20 ppm that there is considerable deuteriation at the methyl group. Without allowing for an unfavourable T_1 and nuclear Overhauser effect decreasing the intensity of 1:1:1 triplet signal for the deuteriated carbon atom as compared to the singlet for the residual undeuteriated methyl group, it may be estimated that at least 60% of deuterium from the original carboxyl-*D*-labelled acid has transferred to the 9-methyl group. Unfortunately, the various signals for the phenanthrene nucleus have not been identified with individual carbon atoms and it is not known which of the aromatic signals is due specifically to the carbon atom in the 10-position. Although the aromatic region of the ^{13}C nmr spectra is complex, there do not appear to be any extra signals characteristic of a deuterium triplet of splitting 20 Hz centred on one of the existing peaks.

To confirm the lack of deuteriation of the aromatic phenanthrene nucleus, a 13.8 MHz deuterium magnetic resonance spectrum was obtained of the deuteriated 9-methylphenanthrene. This showed only two singlet signals (204.0 and 266.7 Hz), the latter due to the deuteriochloroform solvent, and the former, calculated from the proton magnetic resonance spectrum, due to a deuterium atom in the 9-methyl group. No signals for a deuterium atom attached to the C-10 was noted, although a signal of less than 10% of that of the 9-methyl group might have been lost in the baseline noise.

It is concluded that the concerted 1,5-hydrogen shift mechanism is not significantly (<10%) involved in the decarboxylation of this acid. It will be borne in mind that had an intermediate with deuterium at C-10 been formed, a deuterium kinetic isotope effect would have favoured its retention there in place of its tautomerisation to the methyl group.

Accordingly, although no dimer is found in the product, we are bound to conclude that 9-phenanthrylacetic acid also decarboxylates via a homolytic mechanism, as integration of the ^{1}Hmr spectrum of the deuteriomethylphenanthrene showed that the methyl group was ca. 90% deuteriated.

The same general mechanism of decarboxylation may therefore be written for all five arylacetic acids investigated to date:

$$ArCH_2—COOH \rightarrow ArCH_2\cdot + \cdot COOH \rightarrow ArCH_3 + CO_2$$

The sequence of approximate rates of decarboxylation for these acids is 9-phenanthryl- > 2-naphthyl- and 1-naphthyl- > diphenyl- > phenyl-. A similar order is followed in decreasing bond order, except that the last two acids are identical in this respect. Thus although concerted mechanism would predict a fall in rates in the same general sense, it must also predict an identity of rate for the last two. Back and Sehon (12, 13) have shown this to be far from true. On the other hand the observed sequence is precisely that to be expected from decreasing stability of the substituted benzyl radical (20), further support for the homolytic mechanism.

Finally, the evidence we have presented does not rule out the thermally forbidden 1,3-hydrogen shift (Scheme 4). With the naphthylacetic acids the

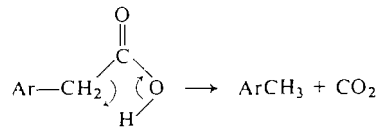

SCHEME 4

reaction products indicate that such a mechanism could be at best only a contributor.

Acknowledgements

We wish to thank Dr. C. Brown, of this Laboratory, for discussions concerning the ^{13}C nmr spectra and Professor E. W. Randall, of Queen Mary College, London, for the deuterium nmr spectrum. We thank the Science Research Council for a maintenance grant to one of us (R.H.W.).

1. D. B. BIGLEY, R. H. WEATHERHEAD, and R. W. MAY. J. Chem. Soc. Perkin Trans. II, 745 (1977).
2. D. B. BIGLEY. J. Chem. Soc. 3897 (1964).
3. D. B. BIGLEY and R. H. WEATHERHEAD. J. Chem. Soc. Perkin Trans. II, 592 (1976).
4. D. B. BIGLEY and R. H. WEATHERHEAD. J. Chem. Soc. Perkin Trans. II, 704 (1976).
5. C. L. FETTER. Ph.D. Thesis, University of Kent. 1977.
6. A. CAMBRON. Can. J. Res. **17**, 10 (1939).
7. H. GILMAN and J. E. KIRBY. J. Am. Chem. Soc. **51**, 3475 (1929).
8. E. BERGMANN and O. BLUM-BERGMANN. J. Am. Chem. Soc. **58**, 1678 (1936).
9. E. MOSETTIG and J. VAN DE KAMP. J. Am. Chem. Soc. **55**, 3442 (1933).
10. P. SCHORIGEN. Ber. **59**, 2510 (1926).
11. D. DODDRELL and P. R. WELLS. J. Chem. Soc. Perkin Trans. II, 1333 (1973).
12. M. H. BACK and A. H. SEHON. Can. J. Chem. **38**, 1261 (1960).
13. M. H. BACK and A. H. SEHON. Can. J. Chem. **38**, 1271 (1960).
14. D. B. BIGLEY and R. W. MAY. J. Chem. Soc. B, 557 (1967).
15. M. ELLIOT and N. F. JAMES. J. Chem. Soc. B, 1780 (1967).
16. D. S. TARBELL. Org. React. **2**, 2 (1944).
17. S. MARCINKIEWICZ, J. GREEN, and P. MAMALIS. Tetrahedron, **14**, 208 (1961).
18. J. B. STOTHERS. *In* Topics in carbon-13 NMR spectroscopy. *Edited by* G. C. Levy. Wiley-Interscience, New York, NY. 1974.
19. L. PAULING. The nature of the chemical bond. 3rd ed. Cornell University Press, Ithaca, NY. 1960.
20. H. C. LONGUET HIGGINS. J. Chem. Phys. **18**, 265 (1950).

1,2-Dihydroquinolines: preparation and isolation as intermediates in the synthesis of quinolines

G. A. DAUPHINEE AND T. P. FORREST

Chemistry Department, Dalhousie University, Halifax, N. S., Canada B3H 4J3

Received August 19, 1977

G. A. DAUPHINEE and T. P. FORREST. Can. J. Chem. **56**, 632 (1978).

2,6-Dimethyl-1,2-dihydroquinoline has been isolated as an intermediate in the Doebner-Miller synthesis of 2,6-dimethylquinoline. Dihydroquinolines may be efficiently prepared by the acid catalysed elimination of water from a 4-hydroxy-1,2,3,4-tetrahydroquinoline. The analogous 4-phenylamino derivatives also undergo facile elimination of the benzylic amino group under similar conditions.

G. A. DAUPHINEE et T. P. FORREST. Can. J. Chem. **56**, 632 (1978).

On a isolé la diméthyl-2,6 dihydro-1,2 quinoléine comme intermédiaire dans la synthèse de Doebner-Miller de la diméthyl-2,6 quinoléine. Les dihydroquinoléines peuvent être préparées d'une façon efficace par l'élimination acido-catalysée d'eau d'une hydroxy-4 tétrahydro-1,2,3,4 quinoléine. Les dérivés analogues phénylamino-4 subissent aussi une élimination facile du groupe benzylique amino dans des conditions semblables.

[Traduit par le journal]

1,2-Dihydroquinolines which are unsubstituted at the nitrogen, and have at least one hydrogen on carbon-2 are very unstable. They are rapidly oxidized by air to the quinoline, or disproportionated by trace acids to a mixture of the quinoline and the tetrahydroquinoline (1). Although difficulties have been encountered in the preparation of some 1,2-dihydroquinolines (2, 3), some have been prepared by the reduction of the corresponding quinoline with lithium aluminium hydride (2) or sodium borohydride (4), and in the case of some 2-substituted quinolines which did not respond to lithium aluminium hydride, by reduction with dialkyl aluminium hydrides (5). Reduction of quinoline by sodium in liquid ammonia was reported (6) to form 1,2-dihydroquinoline but it has recently been shown that the product is in fact 1,4-dihydroquinoline (7). The preparation of 2-alkyl-1,2-dihydroquinolines by addition of Grignard reagents to quinoline is illustrated in a recent paper (8) which also describes some facile rearrangements of 2-alkenyl-1,2-dihydroquinolines.

1,2-Dihydroquinolines are generally assumed to be intermediates in the Doebner-Miller preparation of quinolines (9) but no 1,2-dihydroquinoline has ever been isolated from this reaction, and a recent report concludes that they are not intermediates (10). We have now succeeded in isolating a 1,2-dihydroquinoline in high yield from a Doebner-Miller reaction, thus providing evidence for this intermediate and leading to a convenient method for the preparation of 1,2-dihydroquinolines.

In the normal Doebner-Miller reaction acetaldehyde and an aromatic amine are added to an aqueous acid solution and after about an hour at room temperature the mixture is heated under reflux for several hours. We have found that, if the reaction mixture is allowed to remain at room temperature for a longer period of time and the acid concentration is increased prior to heating, an excellent yield of the 1,2-dihydroquinoline is obtained after a very short reflux period. The dihydroquinoline may also be obtained by treating the aminoalcohol (**2**) or the diamine (**3**) with refluxing 6 *M* HCl for a short time.

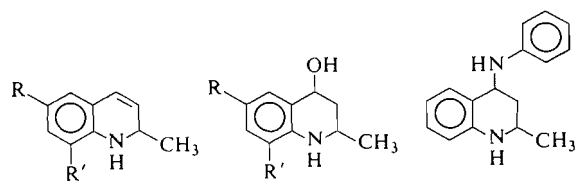

1 **2** **3**

a R = R′ = H; *b* R = CH_3, R′ = H; *c* R = R′ = CH_3

As a method of preparation of 1,2-dihydroquinolines, the aminoalcohol provides the most convenient starting material since it may be readily prepared, can be stored indefinitely, and produces only water as the by-product of elimination. The diamine produces an equivalent amount of an aromatic amine which may be separated chromatographically. Handling of the 1,2-dihydroquinolines should be kept to a minimum since they are very sensitive to oxygen and to dilute acids; although they may be relatively stable in strongly acidic solutions, they disproportionate rapidly in dilute acid. The purity of the product from a typical preparation from the aminoalcohol may be judged from the nmr spectrum of 2,6-dimethyl-1,2-dihydroquinoline (Fig. 1), ob-

Can. J. Chem. Downloaded from www.nrcresearchpress.com by 210.87.254.105 on 09/05/12
For personal use only.

Can. J. Chem. Downloaded from www.nrcresearchpress.com by 210.87.254.105 on 09/05/12
For personal use only.

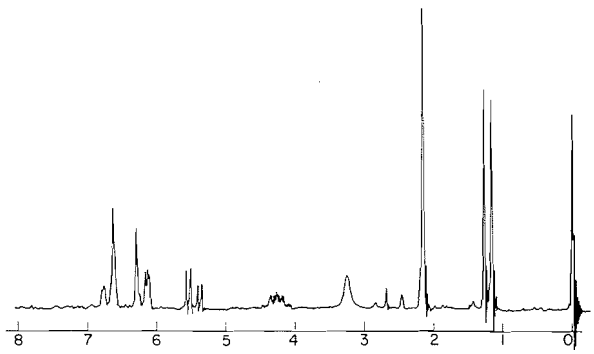

FIG. 1. Nuclear magnetic resonance spectrum of 2,6-dimethyl-1,2-dihydroquinaldine (**1***b*) from a typical preparation without further purification.

tained from a sample prepared without taking any precautions to exclude oxygen, and isolated by simple extraction of the product with ether, and removal of the solvent without further purification. The presence of a small amount of 2,6-dimethylquinoline is indicated by the peaks at δ 2.47 and 2.68 but this impurity may be kept below the detectable level (nmr) by using peroxide-free ether in the extraction and by avoiding heating the product while removing the solvent.

Experimental

Nuclear magnetic resonance spectra were determined on either of a Varian T60 or CFT20 spectrometer from solutions of about 10% solute in deuteriochloroform. Chemical shifts are reported in ppm relative to tetramethylsilane and coupling constants in Hz as line separations as measured directly from the spectra. Mass spectra were determined on a Dupont 21-220 mass spectrometer at 70 eV, infrared spectra on a Perkin-Elmer 237B spectrometer, and melting points on a Fisher-Johns apparatus.

*2,6-Dimethyl-1,2-dihydroquinoline (**1***b*) *from a Doebner-Miller Reaction*

To a solution of *p*-toluidine (1.08 g, 0.01 mol) in 2 *M* HCl (20 ml) at 5°C was added acetaldehyde (1.1 g, 0.025 mol) and the reaction mixture was stored at room temperature for 24 h. Activated charcoal (1 g) was added, the solution stirred for 5 min, and then filtered. Hydrochloric acid (14 ml of 12 *M*) was added, the solution heated under reflux for 15 min, and then poured into a cold sodium hydroxide solution (150 ml of 2 *M*). The reaction mixture was then extracted with three 50-ml portions of peroxide-free ether and the combined ether extracts stirred with activated charcoal (0.5 g), filtered, dried with anhydrous sodium sulfate, and the solvent removed *in vacuo* to yield 1.56 g of a pale yellow crystalline solid. An nmr spectrum of the product indicated that it was mainly **1***b*, contaminated by a small amount of 2,6-dimethylquinaldine and some aliphatic polymeric impurities. A portion of the product was oxidized as described below to 2,6-dimethylquinoline.

The yellow solid (0.75 g) in 75 ml of ether was vigorously stirred with 50 ml of water at room temperature while a solution of iodine in aqueous potassium iodide (0.1 *M*) was added dropwise until a brown color remained in the ether layer. With continued stirring, solid sodium thiosulfate was added until the brown color disappeared and then sodium hydroxide solution (20 ml of 2 *M*) was added. The ether layer was removed, the ether evaporated *in vacuo* and the residue steam distilled. The distillate was extracted with ether and after drying the ether was removed to yield 2,6-dimethylquinoline (83% yield based on *p*-toluidine), identical in nmr, ir, and uv spectra with an authentic sample.

*2,6,8-Trimethyl-1,2-dihydroquinoline (**1***c*) *from* cis*-2,6,8-Trimethyl-4-hydroxy-1,2,3,4-tetrahydroquinoline (**2***c*)

cis-2,6,8-Trimethyl-4-hydroxy-1,2,3,4-tetrahydroquinoline (11) (designated as the β isomer in this reference), (1 g, 5 mmol) was added to refluxing hydrochloric acid (20 ml of 6 *M*). After refluxing for 5 min the reaction mixture was poured into cold sodium hydroxide solution (100 ml of 2 *M*) and the product extracted with two 30-ml portions of peroxide-free ether. After drying with anhydrous sodium sulfate the ether was removed *in vacuo* to yield a relatively pure sample of **1***c*. Extension of the reflux time causes increasing amounts of disproportionation in this case although this was not so for 1,2-dihydroquinaldine (**1***a*) and 2,6-dimethyl-1,2-dihydroquinoline (**1***b*) in their preparation by this method. The *cis* or *trans* isomer of the starting material may be used in this reaction.

2,6,8-Trimethyl-1,2-dihydroquinoline (**1***c*), yield 96%; colorless oil; nmr δ: 1.25 (d, J = 6.5, CH_3), 1.99 (s, CH_3), 2.14 (s, CH_3), 3.71 (bs, NH), 4.28 (m, J = 6.5, 3.7, 1.6, H-2), 5.47 (dd, J = 9.7, 3.7, H-3), 6.22 (dd, J = 9.7, 1.6, H-4), 6.54 (bs, H_{arom}), 6.65 (bs, H_{arom}); ir (neat): 3440, 1640 cm^{-1}; ms: 173(18), 172(26), 171(100), 158(56).

2,6-Dimethyl-1,2-dihydroquinoline (**1***b*), prepared from *cis*-2,6-dimethyl-4-hydroxy-1,2,3,4-tetrahydroquinoline (**2***b*) (12); yield 96%; pale yellow crystals mp 60–63°C; nmr δ: 1.18 (d, J = 6.5, CH_3), 2.14 (s, CH_3), 3.61 (bs, NH), 4.22 (m, J = 6.4, 3.6, 1.6, H-2), 5.41 (dd, J = 10.0, 3.6, H-3), 6.15 (dd, J = 10.0, 1.6, H-4), 6.1–6.7 (m, H_{arom}); ir ($CHCl_3$): 3440, 1640 cm^{-1}; ms: 159(27), 158(33), 157(100), 144(87).

1,2-Dihydroquinaldine (**1***a*) (5), prepared from *cis*-2-methyl-4-hydroxy-1,2,3,4-tetrahydroquinoline (**2***a*) (11); yield 94%; colorless oil; nmr δ: 1.18 (d, J = 6.5, CH_3), 3.50 (bs, NH), 4.30 (m, J = 6.5, 3.5, 1.5, H-2), 5.43 (dd, J = 9.8, 3.5, H-3), 6.23 (dd, J = 9.8, 1.5, H-4), 6.1–7.2 (m, H_{arom}); ir (neat): 3440, 1640 cm^{-1}; ms: 145(23), 144(33), 143(97), 130(100).

*1,2-Dihydroquinaldine (**1***a*) *from* cis*-2-Methyl-4-anilino-1,2,3,4-tetrahydroquinoline (**3**)*

cis-2-Methyl-4-anilino-1,2,3,4-tetrahydroquinoline (**3**) (13), (1 g, 4.2 mmol) was added to refluxing 6 *M* HCl (20 ml) and after 10 min the reaction mixture was poured into 2 *M* NaOH solution (100 ml). After extraction with two 30-ml portions of peroxide-free ether and evaporation of the solvent, the residue, an equimolar mixture of aniline and **1***a* (by nmr), was subjected to column chromatography on silica gel (Merck G) using petroleum ether (bp 30–60°C) – benzene (50:50) as eluant. (tlc, Eastman pre-coated silica sheets using the same solvent system gave R_f values of 0.70, 0.37, and 0.05 for dihydroquinaldine, aniline, and quinaldine, respectively.) A yield of 41% (0.25 g) of 1,2-dihydroquinaldine was obtained from the column with very little quinaldine present, in spite of the fact that the column was not run under nitrogen.

Acknowledgements

The financial assistance of the National Research Council of Canada and the technical assistance of Dr. J. Kim are gratefully acknowledged.

1. Y. OGATA, A. KAWASAKI, and S. SUYAMA. Tetrahedron, **25**, 1369 (1969).
2. K. W. ROSENMUND, F. ZYMALKOWSKI, and N. SCHWARTE. Chem. Ber. **87**, 81 (1954).
3. G. M. BADGER, H. P. CROCKER, B. C. ENNIS, J. A. GAYLER, W. E. MATTHEWS, W. G. C. RAPER, E. L. SAMUEL, and T. M. SPOTWOOD. Aust. J. Chem. **16**, 814 (1963).
4. K. V. RAO and D. JACKMAN. J. Heterocycl. Chem. **10**, 213 (1973).
5. W. P. NEUMANN. Ann. **618**, 90 (1958).
6. W. HUCKEL and L. HAGEDORN. Chem. Ber. **90**, 752 (1954).
7. A. J. BIRCH and P. G. LEHMAN. Tetrahedron Lett. 2395 (1974).
8. J. J. EISCH and D. R. COMFORT. J. Org. Chem. **40**, 2288 (1975).
9. R. C. ELDERFIELD. Heterocyclic compounds. Vol. 4. Wiley, New York, NY. 1952. p. 10.
10. Y. OGATA, A. KAWASAKI, and S. SUYAMA. J. Chem. Soc. (B), 805 (1969).
11. H. O. JONES and E. J. WHITE. J. Chem. Soc. **97**, 632 (1910).
12. T. P. FORREST, G. A. DAUPHINEE, and W. F. MILES. Can. J. Chem. **52**, 884 (1974).
13. T. P. FORREST, G. A. DAUPHINEE, and W. F. MILES. Can. J. Chem. **47**, 2121 (1969).

Can. J. Chem. Downloaded from www.nrcresearchpress.com by 210.87.254.105 on 09/05/12
For personal use only.

Vapour pressures of aqueous solutions of (Ag,Tl,Cd)NO_3 at 98.5°C. II. Henry's law and excess free energy

MARIE-CHRISTINE ABRAHAM AND MAURICE ABRAHAM

Département de Chimie, Université de Montréal, Case postale 6210, Succursale A, Montréal (Qué.), Canada H3C 3V1

AND

JAMES MALCOLM SANGSTER[1]

Département de Génie Chimique, Ecole Polytechnique, Campus de l'Université de Montréal, Case postale 6079, Succursale A, Montréal (Qué.), Canada H3C 3A7

Received October 13, 1977

MARIE-CHRISTINE ABRAHAM, MAURICE ABRAHAM, and JAMES MALCOLM SANGSTER. Can. J. Chem. **56**, 635 (1978).

Curves of the water activity coefficient γ_w have been obtained as a function of water mole fraction in the mixtures $AgNO_3 + TlNO_3 + Cd(NO_3)_2 + H_2O$ at 98.5°C. It has been shown, in this study, from the BET equation itself and verified experimentally, that γ_w may pass through an extremum value for certain systems. The position of such an extremum near the fused salt end of the concentration scale can explain the appearance of a 'practical' Henry's law in a finite concentration range. The curves of the excess free energy of the system undergo rather unusual changes of shape as the cadmium content of the melt is varied.

MARIE-CHRISTINE ABRAHAM, MAURICE ABRAHAM et JAMES MALCOLM SANGSTER. Can. J. Chem. **56**, 635 (1978).

On a étudié les courbes du coefficient d'activité de l'eau γ_w en fonction de sa fraction molaire pour des mélanges $AgNO_3 + TlNO_3 + Cd(NO_3)_2 + H_2O$ à 98.5°C. On a démontré théoriquement à partir de l'équation BET, et vérifié expérimentalement, que γ_w peut passer par une valeur extremum pour certains systèmes. La position d'un tel extremum dans le domaine des solutions pauvres en eau peut expliquer l'apparition d'une loi de Henri pratique dans un intervalle fini de concentration. Les courbes de l'enthalpie libre de mélange d'excès des sels avec l'eau subissent des modifications inhabituelles quand on fait varier la concentration en $Cd(NO_3)_2$.

Introduction

In a previous article (1*b*) we presented and discussed the BET isotherm constants for the system $AgNO_3 + TlNO_3 + Cd(NO_3)_2 + H_2O$ at 98.5°C, at mole ratio Ag/Tl = 1.06 and for five Cd mole fractions in the melt, viz., 0, 0.05, 0.075, 0.1, and 0.125. The BET equation, modified for aqueous solutions (2), was found to represent the data over an unexpectedly wide water concentration range. We showed that some of these systems exhibited 'cross-over points' in their Raoult's law behaviour, and that the BET constants uniquely specified these points. The BET constants were found to follow simple additivity rules. In the present article the data are discussed in terms of the water activity coefficient, Henry's law, and the excess free energy. The symbolism and conventions used here are the same as those used previously (1).

Water Activity Coefficient

Figure 1 presents curves of the activity coefficient of water γ_w as a function of its mole fraction in each of the five melt mixtures studied, S_0, S_5, $S_{7.5}$, S_{10}, and $S_{12.5}$. The first four of these curves show maxima; this is unusual behaviour for electrolyte solutions, which generally (3) give a rising asymptote much like the one for $S_{12.5}$. The maxima are displaced toward the water end as the Cd content of the melt is increased.

Just as in the preceding article (1*b*) the rather complex Raoult's law behaviour of these systems was better understood by consideration of the BET equation, so here this equation can help to clarify Fig. 1. The equation (1*a*) can be written as

$$[1] \qquad a_w(1 - x_w)/x_w(1 - a_w) = A + Ba_w$$

where $A = 1/cr$ and $B = (c - 1)/cr$, c and r being the BET constants described previously. Insofar as the a_w data of a system can adequately be represented by an equation such as eq. 1 the maximum value of γ_w (if there is one) can be specified by the BET constants, as follows. Rearrangement of eq. 1 gives

$$[2] \quad Ax_w/a_w - Ba_wx_w + x_w(1 - A + B) - 1 = 0$$

Introducing $a_w = \gamma_w x_w$ into eq. 2 yields

$$[3] \quad A + x_w\gamma_w(1 + B - A) - B(x_w\gamma_w)^2 - \gamma_w = 0$$

[1]To whom correspondence should be addressed.

Can. J. Chem. Downloaded from www.nrcresearchpress.com by 210.87.254.42 on 09/05/12
For personal use only.

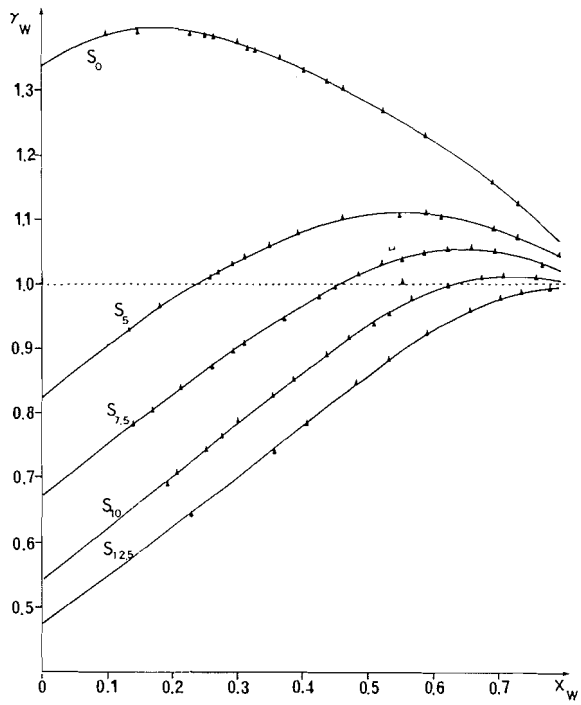

FIG. 1. Curves of γ_w vs. x_w for the system $(Ag,Tl,Cd)NO_3 + H_2O$ at 98.5°C, for five cadmium contents in the melt.

Differentiating eq. 3 with respect to x_w and remembering that, at an extremum, $d\gamma_w/dx_w = 0$, we obtain

$$[4] \qquad 1 + B - A - 2Ba_{wm} = 0$$

where a_{wm} is the water activity of the solution whose water activity coefficient is a maximum, γ_{wm}. From eq. 4 then

$$[5] \qquad a_{wm} = (1 + B - A)/2B$$

Substituting eq. 5 in eq. 2 and solving for x_w, we obtain

$$[6] \quad x_{wm} = [2AB/(1 + B - A) + (1 + B - A)/2]^{-1}$$

and thus, from eqs. 5 and 6

$$[7] \qquad \gamma_{wm} = A + (1 + B - A)^2/4B$$

where $a_{wm} = x_{wm}\gamma_{wm}$.

Experimental values of A and B for all five systems are given in Table 1, and also the derived values for x_{wm} and γ_{wm}. The x_{wm} and γ_{wm} values for S_{10} and $S_{12.5}$ are placed in parentheses since in these cases x_{wm} lies beyond the range of applicability of the BET equation (1*b*), and hence these values are not strictly valid. The values themselves are, however, of reasonable magnitude.

TABLE 1. The intercepts (A) and slopes (B) of the BET plots, with the derived extrema (γ_{wm}, x_{wm}) and Henry's law constants (γ_w^∞, K_H^∞)*

System	$A = \gamma_w^\infty$	B	x_{wm}	γ_{wm}	K_H^∞, atm
S_0	1.34	0.722	0.193	1.39	1.25
S_5	0.824	0.741	0.559	1.11	0.770
$S_{7.5}$	0.666	0.733	0.691	1.05	0.622
S_{10}	0.550	0.699	(0.804)	(1.02)	0.514
$S_{12.5}$	0.474	0.610	(0.928)	(1.00)	0.442

*Values in this table are given to three significant figures, of which the third is uncertain.

Henry's Law

The intercept A (eq. 1) of a BET isotherm plot may be equated (1*a*) to the limiting activity coefficient γ_w^∞ of water dissolved in molten salt. The corresponding Henry's law constants K_H^∞ may be calculated directly from γ_w^∞ through the relations (1*a*)

$$[8] \quad f_w = f_w^0 a_w = [f_w^0 \gamma_w^\infty x_w]_{x_w \to 0} = [K_H^\infty x_w]_{x_w \to 0}$$

where f_w is the fugacity of dissolved water and f_w^0 the fugacity of pure water. Values of K_H^∞ are also included in Table 1. It is seen that K_H^∞ decreases steadily as cadmium is added to the melt. This is what would be expected if a strongly hydrated ion such as Cd^{2+} is added to solutions of weakly-hydrated ions like Ag^+ and Tl^+. This effect has already been noted (1*a*) in the cases of Li^+ and Ca^{2+}.

Henry's law is strictly valid only at infinite dilution. There are cases, however, where the ratio f_w/x_w varies little over a finite concentration range. Depending on the error which can be tolerated and the range of concentration of interest, a 'practical' Henry's law constant K_H may be used

$$[9] \qquad f_w = K_H x_w$$

which must be distinguished from K_H^∞. The activity coefficient data (1*b*) of the series S_0 show that γ_w varies a few percent in the interval $0 < x_w < 0.3$. As Cd is progressively added to the melt, however, this interval becomes smaller. Another way of seeing this is to compare the ratio $\gamma_w(x_w = 0.3)/\gamma_w^\infty$ for all five systems: S_0, 1.03; S_5, 1.25; $S_{7.5}$, 1.35; S_{10}, 1.42; $S_{12.5}$, 1.45. What distinguishes the S_0 curve (Fig. 1) from the others is the situation of the maximum close to $x_w = 0$. Since, in the region of an extremum, a function changes little, we deduce a criterion for the existence of a practical Henry's law constant, viz., the presence of a maximum or minimum in γ in the dilute solution region of the solute of interest.

Excess Free Energy

Values of G^E were calculated for the systems S_0 to

Can. J. Chem. Downloaded from www.nrcresearchpress.com by 210.87.254.42 on 09/05/12
For personal use only.

Can. J. Chem. Downloaded from www.nrcresearchpress.com by 210.87.254.42 on 09/05/12
For personal use only.

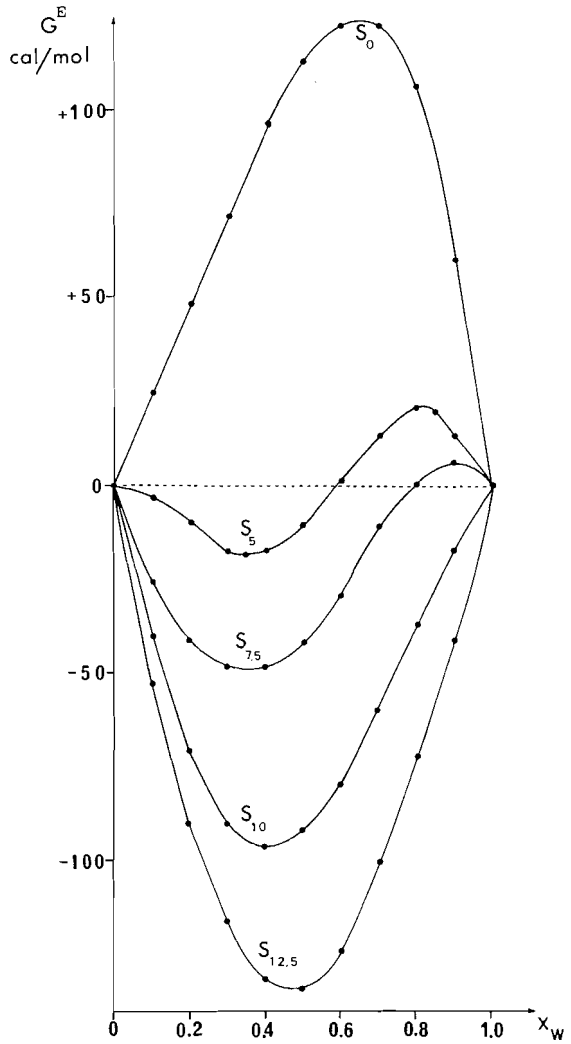

FIG. 2. Curves of G^E vs. x_w for the system (Ag,Tl,Cd)NO_3 + H_2O at 98.5°C, for five cadmium contents in the melt.

$S_{12.5}$ in the same way as previously described (1*a*). The results are given in Fig. 2. The change in orientation and shape of these curves as the Cd content of the melt changes is unusual and merits some comment. First, the presence of 'cross-over points' in the Raoult's law curves of these systems (1*b*) leads one to expect some unusual results in related thermodynamic properties. Second, the general behaviour shown in Fig. 2 is very similar to that in the following two cases: (*1*) variation of H^E at 25°C for mixtures of water and simple alcohols $C_nH_{2n+1}OH$, $n = 1$ to 3 (4); (*2*) variation of H^E for water + ethanol mixtures in the temperature range 25–110°C (5). In water + alcohol mixtures, the addition of one component to the other changes the local structure in both liquids in noticeable ways; this kind of explanation is sometimes invoked in case (*1*). As the temperature increases, the local structure in the pure components decreases, and hence their interaction also changes; this is sometimes mentioned in instances like case (*2*). Since, in the present work, water is preferentially hydrated to Cd^{2+} over Tl^+ and Ag^+, it is probable that the behaviour shown in Fig. 2 could be interpreted in terms of changes in solvent–solute interaction through the series S_0 to $S_{12.5}$.

Acknowledgment

We thank the Ministère de l'Education de la Province de Québec for financial aid.

1. M.-C. TRUDELLE, M. ABRAHAM, and J. SANGSTER. Can. J. Chem. (*a*) **55**, 1713 (1977); (*b*) In press.
2. R. H. STOKES and R. A. ROBINSON. J. Am. Chem. Soc. **70**, 1870 (1948).
3. H. BRAUNSTEIN and J. BRAUNSTEIN. J. Chem. Thermodyn. **3**, 419 (1971).
4. R. F. LAMA and B. C. Y. LU. J. Chem. Eng. Data, **10**, 216 (1965).
5. J. A. LARKIN. J. Chem. Thermodyn. **7**, 137 (1975).

The total synthesis of 4-deoxy-D,L-daunosamine

HING-KWOK HUNG, HING-YAT LAM, WALTER NIEMCZURA, MEI-CHING WANG, AND CHIU-MING WONG

Department of Chemistry, University of Manitoba, Winnipeg, Man., Canada R3T 2N2

Received July 12, 1977

HING-KWOK HUNG, HING-YAT LAM, WALTER NIEMCZURA, MEI-CHING WANG, and CHIU-MING WONG. Can. J. Chem. **56**, 638 (1978).

The aminosugar 4-deoxy-D,L-daunosamine and its derivatives were synthesized starting with 2,4-pentanedione which was converted to the key intermediate oxazolino-α-pyrone (**19**) by enamine formation with morpholine, oxidation with benzoyl peroxide, condensation with ammonium acetate, bromination with *N*-bromosuccinimide, nitrile formation, acid hydrolysis, and cyclization with thionyl chloride. Hydrogenation of **19** gave the δ-lactone **22** which was converted to 4-deoxy-D,L-daunosamine derivatives by reducing the lactone ring to the corresponding hemiacetal **26**.

HING-KWOK HUNG, HING-YAT LAM, WALTER NIEMCZURA, MEI-CHING WANG et CHIU-MING WONG. Can. J. Chem. **56**, 638 (1978).

On a synthétisé le sucre aminé déoxy-4-D,L-daunosamine et ses dérivés à partir de la pentanedione-2,4 que l'on a transformée en oxazolino-α-pyrone (**19**), un intermédiaire clé, grâce à une formation d'énamine avec la morpholine, une oxydation par le peroxyde de benzoyle, une condensation avec l'acétate d'ammonium, une bromation avec la *N*-bromosuccinimide, la formation d'un nitrile, une hydrolyse acide et une cyclisation par le chlorure de thionyle. L'hydrogénation de **19** fournit la δ-lactone **22** que l'on a transformée en dérivés de la déoxy-4-D,L-daunosamine par réduction du cycle de lactone en hémiacétal correspondant **26**.

[Traduit par le journal]

Introduction

The anthracycline antibiotics daunorubicin (**1**), adriamycin (**2**), and carminomycin (**3**) have attracted much attention because of their very promising antitumor properties (1, 2). Clinical tests have clearly established their values as broad spectrum chemotherapeutic antitumor agents (3). One of their common, yet very undesirable side effects is their dose-related and progressive cardiomyopathy which is responsible for patients' death or discontinuation of chemotherapy with this group of drugs. The nature of cardiotoxicity has not been established, although morphological changes of affected heart cells indicated that interference with protein synthesis (4) and uncoupling of oxidative phosphorylation (5) could be some of the reasons. Metabolic studies of daunorubicin showed that daunorubicinol (**4**) and daunomycinone (**6**) were among the metabolites.

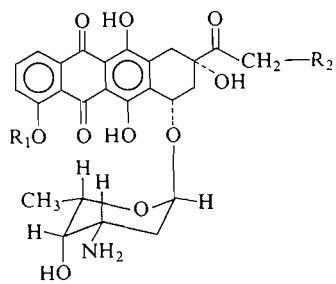

1 $R_1 = CH_3$, $R_2 = H$
2 $R_1 = CH_3$, $R_2 = OH$
3 $R_1 = R_2 = H$

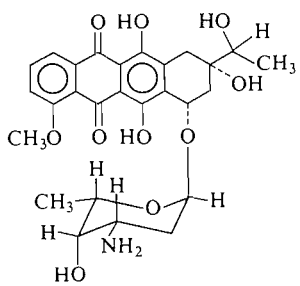

4

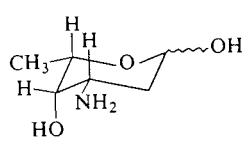

5

The fate of the aminosugar portion, daunosamine (**5**), has not been well established but daunomycinone (**6**) does not seem to be responsible for the observed cardiomyopathy (6). Many aminosugars and related antibiotics interfere with protein synthesis (7) and their bacterial toxicities could be greatly modified by manipulating the stereochemistry or removing only one hydroxyl group in the molecule (8). Furthermore, the reported reduced toxicity to cultured heart cells of 4′-epiadriamycin (9) pointed to the importance of the aminosugar 4-deoxydaunosamine (**7**) in attempts to reduce cardiotoxicity of this group of drugs.

Results and Discussion

Our synthetic scheme of aminosugars is based on the early concept of relationship between aminosugars and oxazolines or pyrrolines in the Morgan–Elson test (10). The oxazolines could be considered as having amino groups in latent forms. Thus an oxazolino-α-pyrone such as **19** would be a suitable

Can. J. Chem. Downloaded from www.nrcresearchpress.com by 210.87.254.40 on 09/05/12
For personal use only.

Can. J. Chem. Downloaded from www.nrcresearchpress.com by 210.87.254.40 on 09/05/12
For personal use only.

intermediate in the synthesis of some 3-deoxy-3-aminohexopyranoses like daunosamine (11*a*), acosamine (11*b*), ristosamine (11*c*), and other related highly deoxygenated deoxyaminosugars, for example, 4-deoxydaunosamine (**7**).

The oxazolino-α-pyrone (19) was prepared in high yield in five steps starting with 3-benzoyloxy-2,4-pentanedione (**8**) (12). Refluxing **8** with ammonium acetate in glacial acetic acid gave the 2-phenyl-4-methyl-5-acetyl-1,3-oxazole (**9**) and the 1,3-diazole (**10**). The relative yield of **9** and **10** could be controlled from one extreme of forming only the oxazole **9** to the other extreme of forming only the diazole **10**, by adjusting the amount of ammonium acetate and glacial acetic acid. Photocatalyzed bromination of **9** by *N*-bromosuccinimide in carbon tetrachloride solution gave exclusively the 2-phenyl-4-bromomethyl-5-acetyl-1,3-oxazole (**11**) which was converted to the corresponding cyano compound **12** by potassium cyanide in liquid hydrogen cyanide solution. The bromo compound **11** was very unstable in basic solution and only under the hydrogen cyanide buffered condition could it be converted to the cyano compound **12** in acceptable yield. Acid hydrolysis of **12** to the corresponding carboxylic acid **13** was carried out at room temperature in aqueous acetic acid solution saturated with hydrogen chloride. This acid decarboxylated easily back to the oxazole **9** and thus only its methyl ester **14** was fully characterized. This ester was prepared in almost quantitative yield by methanolysis of **12** in anhydrous methanol solution saturated with hydrogen chloride and then converted to the acid **13** in hydrogen chloride-saturated aqueous acetic acid solution.

The crucial point at this stage was to ascertain the structure of the carboxylic acid **13**, because there was no concrete evidence to exclude the possibility of structures **16**, **17**, and **18** in the sequence of reactions described previously. The only rigorous proof came as a result of the cyclization of **13** to form the oxazolino-α-pyrone (**19**) in anhydrous alcohol-free chloroform solution containing thionyl chloride. The nmr spectrum of **19** showed a methyl doublet at 251.63 Hz, with a coupling constant of 0.80 Hz and an olefinic proton quartet at 615.76 Hz with a coupling constant of 0.80 Hz (HA-100 spectrum). This result eliminated the likelihood of structures **16**, **17**, and **18**.

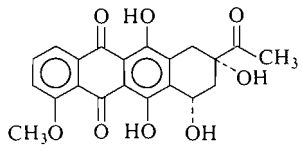

6

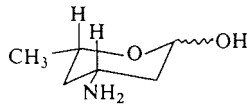

7

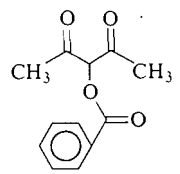

8

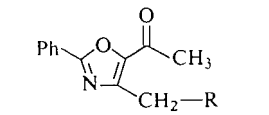

9 R = H **11** R = Br
12 R = CN **13** R = COOH
14 R = $COOCH_3$
15 R = $COOC_2H_5$

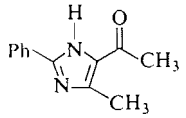

10

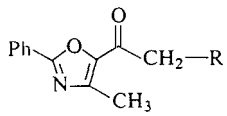

16 R = Br
17 R = CN
18 R = COOH

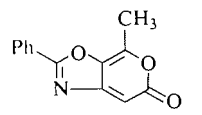

19

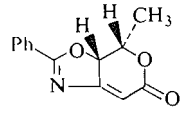

20

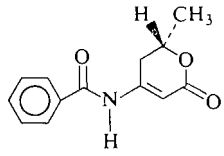

21

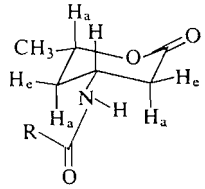

22 R = Ph
23 R =

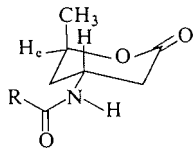

24 R = Ph
25 R =

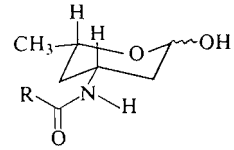

26 R = Ph
27 R =

Catalytic hydrogenation of **19** in the presence of Adam's catalyst in ethyl acetate solution yielded the 3-benzamido-5-hydroxyhexanoic acid lactone (**22**) and 3-cyclohexylcarbonylamino-5-hydroxyhexanoic acid lactone (**23**). Separation of these two from each other was very tedious but prolonged hydrogenation of **19** gave **23** exclusively. A small amount of hydrogenation by-product was identified as the ethyl ester **15** the quantity of which varied according to the activity of the catalyst. Very active Adam's catalyst gave good yield of **23** whereas less active catalyst such as platinum black gave a mixture of **15**, **22**, and **23**. Since the ethyl acetate had been rigorously purified, it was very likely that small amount of ethanol which opened the α-pyrone ring of **19** to form **15**, was slowly generated by hydrogenation of the solvent.

Formation of **22** and **23** involved hydrogenolysis which would indicate that the first hydrogenation

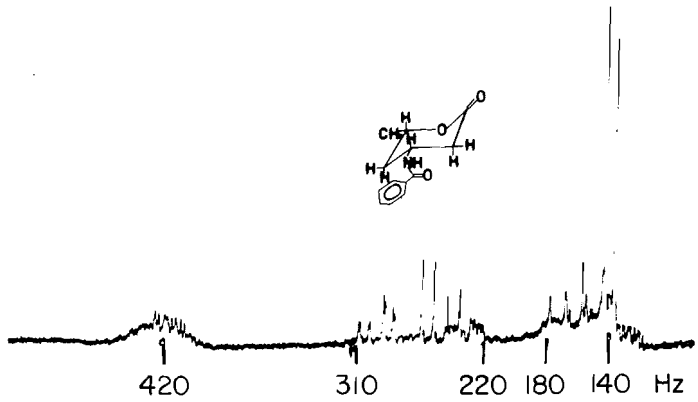

FIG. 1. The HA-100 spectrum of compound **22** (aromatic areas omitted).

product could be the oxazolinodihydropyrone (**20**) (11*a*). When hydrogenation was prematurely discontinued, a small amount of by-product presumably the dihydropyrone **21**, (m^+/e 231; ir: 3420, 1703, 1695, 1637 cm^{-1}) was isolated which because of its transient character, was not further characterized. But further hydrogenation of this compound with Adam's catalyst gave exclusively **23**.

The stereochemistry of the δ-lactone ring of **22** or **23** needed further clarification. Hydrogenation of **20** could lead to both the *cis*-1,3-disubstituted (**22**, **23**) or the *trans*-1,3-disubstituted (**24**, **25**) products. The nmr spectrum of the fully saturated lactone **23** (or **25**) was too complicated to be fully analyzed owing to the overlap of the cyclohexane ring protons over the C_4 protons of the lactone ring. However, detailed analyses of the nmr spectrum of **22** (or **24**) was possible (Fig. 1).

Conformation analysis predicts that for a *trans*-1,3-disubstituted α-lactone like **24**, the benzamido group should preferably occupy the equatorial position. Likewise, *cis*-1,3-disubstituted δ-lactone such as **22** would have both the methyl and the benzamido groups in equatorial position. This means H_5 will be in the axial position.

Table 1 gives the chemical shifts and coupling constants of the protons considered as determined from an iterative fit of the simulated spectrum against the observed line positions. Figures 2–4 show a comparison between the observed spectrum and the computer simulation using the values in Table 1. A complete simulation of the H_5, H_3 region was impractical because of the overlap of the two resonances and the inability of the program to reproduce the broad signals of H_3 because of the ^{14}N coupling and N–H proton exchange.

H_{2a} and H_{2e} were identified by the large coupling constant (17.2 Hz) usually observed between geminal protons next to a carbonyl group (13). The signals

TABLE 1. Chemical shifts and coupling constants of **22**

Chemical shifts (δ) (ppm from TMS)		Coupling constants (Hz)	
H_{2a}	2.54±0.005	$J_{2a\text{-}2e}$	−17.2±0.2
H_{2e}	2.96±0.005	$J_{2a\text{-}3a}$	8.5±0.2
H_{3a}	4.47±0.005	$J_{2e\text{-}3a}$	6.9±0.2
H_{4a}	1.60±0.005	$J_{4a\text{-}4e}$	−13.9±0.2
H_{4e}	2.34±0.005	$J_{3a\text{-}4a}$	11.3±0.2
H_{5a}	4.42±0.005	$J_{3a\text{-}4e}$	5.7±0.2
CH_3	1.36±0.005	$J_{4a\text{-}5a}$	11.7±0.2
		$J_{4e\text{-}5a}$	2.6±0.2
		$J_{5a\text{-}CH_3}$	6.5±0.2
		$J_{4e\text{-}2e}$	1.2±0.2

at δ 2.54 ppm (Fig. 2) were assigned to H_{2a} (14) which is further coupled by 8.5 Hz to H_3, indicating that the latter proton is in the axial position. The H_{2e} signals at δ 2.96 ppm in the AB pattern of Fig. 3 is also coupled to H_{3a} by the unusually large coupling constant of 6.9 Hz. This indicates that the lactone group is causing ring flattening at the C-1 end of the molecule, making H_{2a} and H_{2e} almost equivalent with respect to H_3. This is further substantiated by the additional coupling observed in the H_{2e} multiplet. Each of the four lines is further split by 1.18 Hz, apparently by H_{4e}, in agreement with an estimation based on Karplus relationships (15). This coupling establishes the resonance at δ = 2.34 ppm as belonging to H_{4e} which is further split by 13.9 Hz by H_{4a}, 5.7 Hz by H_{3a}, and 2.6 Hz by H_5. The latter value tentatively indicates that H_5 is axially oriented. H_{4a} was identified as that at δ 1.60 ppm with splittings, other than to H_{4e}, of 11.3 and 11.7 Hz attributed to H_{3a} and H_{5a}, respectively. These large values are typical of axial–axial couplings, confirming the orientation of H_3 and H_5 as axial. Using values obtained from the other protons, the H_{5a} resonance at δ 4.42 ppm was confirmed by the use of a stick diagram. Working with first-order rules

Can. J. Chem. Downloaded from www.nrcresearchpress.com by 210.87.254.40 on 09/05/12
For personal use only.

Can. J. Chem. Downloaded from www.nrcresearchpress.com by 210.87.254.40 on 09/05/12
For personal use only.

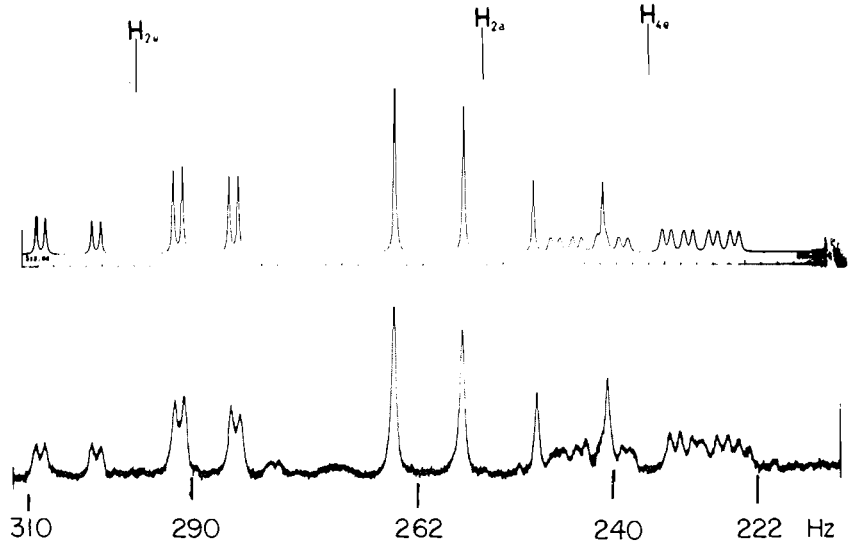

FIG. 2. The simulated (top) and recorded spectrum of H_{2a}, H_{2e}, and H_{4e} of compound **22**.

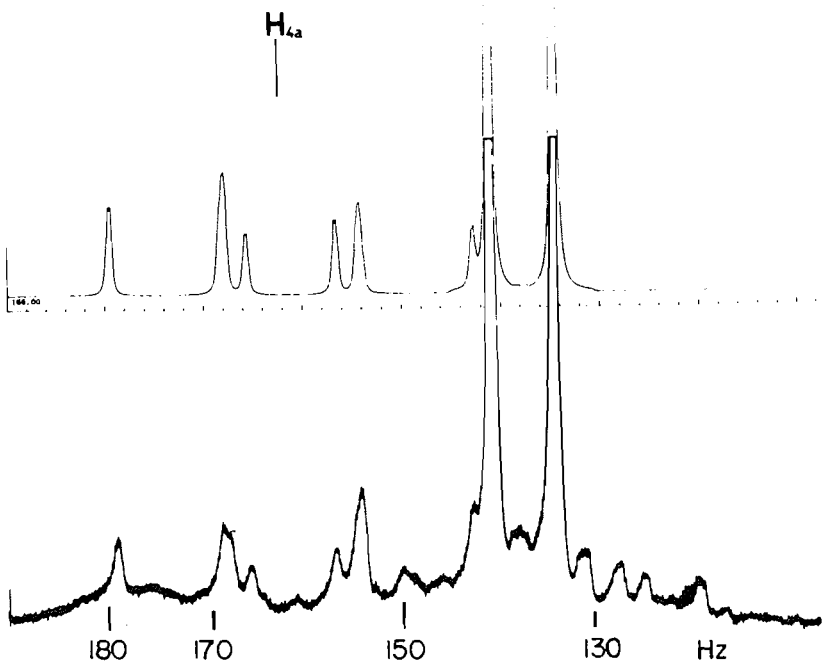

FIG. 3. The simulated (top) and recorded spectrum of H_{4a} and CH_3 of compound **22**.

and the 6.5 Hz coupling observed in the methyl resonance, the apparent splitting pattern could be very well reproduced (Fig. 4).

Having established the stereochemistry of **22**, the δ-lactone ring was then reduced to the hemiacetal **26** by the modified Red-al (*vide infra*) reagent. In large scale preparation, **19** was exhaustively hydrogenated to give exclusively **23** which was then reduced to the hemiacetal **27** as before. This operation was necessary, because **22** was always contaminated with **23** and the condition that favoured the formation of **22** always led to the formation of **15**. Hydrolysis of **26** or **27** in acetic–hydrobromic acid solution gave the hydrobromide of 4-deoxy-D,L-daunosamine (**7**).

Experimental

Most of the nmr spectra were recorded on a Varian A56/60A spectrometer using deuterated chloroform as solvent and

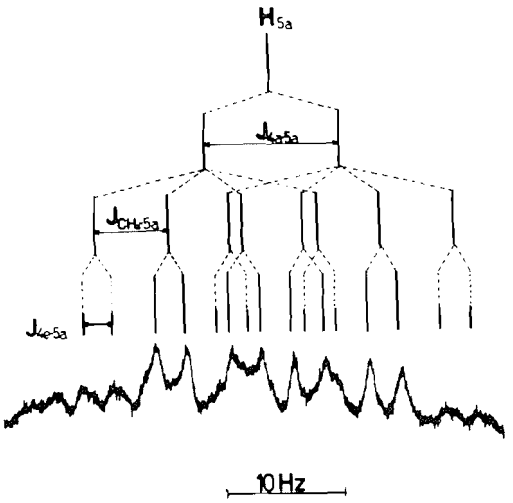

FIG. 4. The expanded spectrum of H_{5a} of compound **22**.

tetramethylsilane as internal standard. Other nmr spectra for high resolution studies were recorded on a Varian HA-100 spectrometer operating in the internal lock frequency sweep mode at a probe temperature of 31.5 ± 0.5°C. Line positions were estimated from a single calibration by periodically placing frequency markers and measuring the distance to the line positions. The analysis was performed using LAME-8 (16) (LAOCOON for eight-spins with magnetic equivalence) program.

Infrared spectra were recorded on a Perkin-Elmer infracord Model 710A spectrophotometer using methylene chloride as solvent or otherwise specified. Routine mass spectra were recorded on a Finnigan quadrupole 1015 mass spectrometer and high resolution spectra were recorded on an A.E.I. MS-9 mass-spectrometer. Microanalyses were performed by Dr. Daessle of Montreal and melting points were taken on a Fisher–Johns apparatus.

*Preparation of 2-Phenyl-4-methyl-5-acetyl-1,3-oxazole (**9**) and 1,3-Diazole (**10**)*

Acetylacetone (100 g), morpholine (90 g), and benzene (350 ml) in a 3-ℓ flask equipped with a Dean-Stark water separator and condenser was refluxed for 17 h under nitrogen. The water was removed and the solution was concentrated by removing the benzene through the Dean-Stark separator. Benzoyl peroxide (245 g) dissolved in $CHCl_3$ (1½ ℓ) was added slowly to the cooled benzene solution in 2 h keeping the temperature of the reaction mixture between 10–15°C. After stirring for 6 h at 15°C, the mixture was then warmed up to room temperature and stirring was continued for another 2 h keeping the temperature below 25°C. Water (200 ml) was added and the reaction mixture was stirred for 3 h in a 60°C hot water bath. The chloroform layer was separated, washed with water (2 × 200 ml), dried over magnesium sulfate, filtered, and evaporated under reduced pressure to give a heavy dark brown syrupy residue from which a sample was purified and the properties were comparable with those reported in the literature. To the residue was added ammonium acetate (230 g) and glacial acetic acid (1.7 ℓ) and the solution was heated to a gentle reflux for 10 h. Acetic acid (~900 ml) was removed by low pressure distillation and the residue was then diluted with water and extracted exhaustively with ether. The ether solution was washed with water (3 × 300 ml), potassium carbonate solution (10%), dried over magnesium sulfate, and evaporated to dryness to give the crude crystalline oxazole (69 g) which was purified by distillation at 115°C/0.5 Torr or recrystallization from cold ether, mp 62–63°C; ir: 1680 (ketone), 1600 (oxazole and phenyl) 1395, 1370 (methyl groups) cm^{-1}; ms m^+/e: 201; nmr δ: 2.48 (s, CH_3), 2.51 (s, CH_3), 7.45 (m, 3H phenyl), 8.03 ppm (m, 2H phenyl). *Anal.* calcd. for $C_{12}H_{11}O_2N$: C 71.64, H 5.47, N 6.96; found: C 71.72, H 5.58, N 6.70.

In another experiment, the amount of acetic acid was reduced to 500 ml and ammonium acetate was increased to 380 g. The above procedure led to the isolation of mainly 2-phenyl-4-methyl-5-acetyl-1,3-diazole (**10**) (22 g) which could be purified by recrystallization from benzene, mp 172–173°C; ir: 3420 (NH), 1665 (vinylogous amide), 1640 cm^{-1} (diazole ring); ms m^+/e: 200; nmr δ: 2.57 (s, CH_3), 2.60 (s, CH_3), 7.42 (m, 3H phenyl), 7.98 ppm (m, 2H, phenyl).

*Preparation of 2-Phenyl-4-bromomethyl-5-acetyl-1,3-oxazole (**11**)*

N-Bromosuccinimide (15 g) was added to a freshly distilled carbon tetrachloride (500 ml) solution containing **9** (16 g) in a 1-ℓ flask equipped with condenser, drying tube, and a magnetic stirring bar. The solution was heated to a gentle reflux while being irradiated for 6 h by a Hanovia Utility quartz lamp. About half of the carbon tetrachloride was removed by distillation under reduced pressure and the residual solution was cooled in cold water for 2 h. The white solid of succinimide was then removed by filtration and the solution was evaporated under reduced pressure to give a crystalline residue. Recrystallization from cold ether gave 2-phenyl-4-bromomethyl-5-acetyl-1,3-oxazole (**11**) (16 g). The mother liquor in ether solution (100 ml) was stirred with zinc dust (5 g) in the presence of acetic acid for 10 min, then filtered and washed with water and dried over magnesium sulfate. Evaporation of the ether solution to dryness as usual gave the starting oxazole **9** (3.4 g). A sample of **11** was further purified by recrystallization from ether (3×), mp 108–109°C; ms m^+/e calcd.: 280.9891; found: 280.9872; ir: 1680 (ketone), 1595 (oxazole and phenyl), 1370 cm^{-1} (—CH_3); nmr δ: 2.58 (s, —CH_3), 4.73 (s, —CH_2—Br), 7.48 (m, 3H, phenyl), 8.12 ppm (m, 2H, phenyl).

*Preparation of 2-Phenyl-4-cyanomethyl-5-acetyl-1,3-oxazole (**12**)*

Liquid hydrogen cyanide (200 ml), *N*,*N*-dimethylformamide (100 ml), and pulverized potassium cyanide (20 g) were added in sequence to a flask containing 2-phenyl-4-bromomethyl-5-acetyl-1,3-oxazole (20 g) in an ice bath. The flask was then securely stoppered and the mixture was stirred at room temperature for 4 h. The hydrogen cyanide (~100 ml) was then recovered by low pressure distillation with Dry-Ice trap. Water (200 ml) was added to the residue and the aqueous mixture was extracted with benzene (4 × 200 ml). The combined benzene solution was washed with water, dried over anhydrous magnesium sulfate, and worked up as usual to yield the crystalline 2-phenyl-4-cyanomethyl-5-acetyl-1,3-oxazole (11.8 g) a sample of which was purified by recrystallization from chloroform–ether (3×), mp 126–127°C; ir: 2300 (—CN), 1680 (ketone), 1600 (oxazole and phenyl), 1375 cm^{-1} (—CH_3); nmr δ: 2.58 (s, —CH_3), 4.10 (s, 2H, —CH_2—CN), 7.58 (m, 3H, phenyl), 8.17 ppm (m, 2H, phenyl); ms m^+/e calcd.: 226.0742; found: 226.0740.

*Preparation of 2-Phenyl-4-carbomethoxymethyl-5-acetyl-1,3-oxazole (**14**)*

To an ice-cooled anhydrous methanolic solution (500 ml) in a 1-ℓ flask containing 2-phenyl-4-cyanomethyl-5-acetyl-1,3-oxazole (19 g) was introduced anhydrous hydrogen chloride

Can. J. Chem. Downloaded from www.nrcresearchpress.com by 210.87.254.40 on 09/05/12
For personal use only.

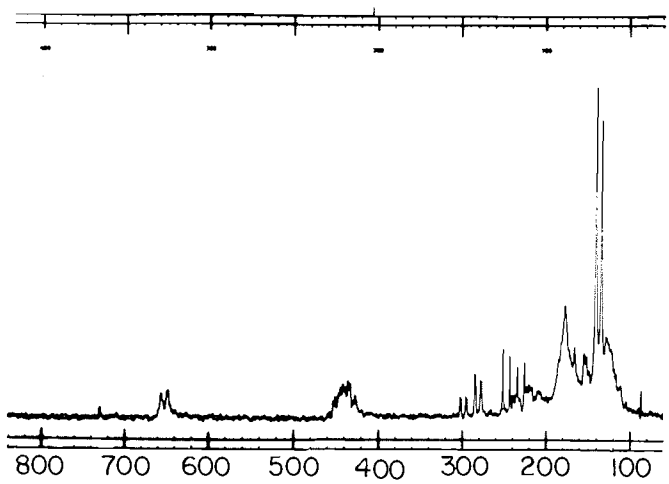

FIG. 5. The HA-100 spectrum of compound **23**.

until no absorption was visible. The flask was then securely stoppered and the solution stirred at room temperature for 24 h. The methanolic solution was evaporated under reduced pressure to give a light brown residue which was digested by chloroform (200 ml) and washed with water and bicarbonate solution (2%). The chloroform layer, dried over magnesium sulfate, was worked up as usual to give the crystalline 2-phenyl-4-carbomethoxymethyl-5-acetyl-1,3-oxazole (21 g), a sample of which was purified by recrystallization from ether, mp 98–99°C; ir: 1740 (ester), 1682 (ketone), 1600 (oxazole and phenyl), 1380 cm^{-1} (—CH_3); ms m^+/e: 259; nmr δ: 2.58 (s, —CH_3), 3.73 (s, —OCH_3), 4.05 ppm (s, 2H, —CH_2—). *Anal.* calcd. for $C_{14}H_{13}O_4N$: C 64.86, H 5.02, N 5.41; found: C 64.85, H 5.18, N 5.35.

*Preparation of 2-Phenyl-4-carboxymethyl-5-acetyl-1,3-oxazole (**13**)*

The methylester **14** (6.5 g) was dissolved in a mixture of glacial acetic acid (150 ml) and concentrated hydrochloric acid (50 ml). This solution was then saturated with hydrogen chloride and stirred for 90 h at room temperature. Under reduced pressure and at room temperature, most of the acetic acid was removed by evaporation and the residue was further diluted with water and extracted exhaustively by ethyl acetate. The ethyl acetate solution was treated as usual and evaporated to dryness at room temperature under reduced pressure to give a white solid residue (5 g) which was further purified by recrystallization from ethyl acetate, mp 194°C (dec. fast heating), ir (Nujol): 3200–2700 broad (—OH), 1735 (ester), 1690 (ketone), 1600 cm^{-1} (oxazole and phenyl). This compound was converted back to **14** by diazomethane for identification.

*Preparation of Oxazolino-α-pyrone (**19**)*

To a 2-ℓ flask was added the carboxylic acid **13** (5 g), chloroform (1-ℓ), and then thionyl chloride (25 ml). The solution was stirred at room temperature for 6 h under anhydrous conditions and evacuated occasionally to remove hydrogen chloride. The chloroform solution was then evaporated to dryness under reduced pressure and the solid residue was recrystallized from methylene chloride (3.8 g), mp 185–187°C (dec.); ir: 1730 (pyrone), 1680 and 1540 cm^{-1}; nmr δ: 2.51 (d, J = 0.8 Hz, 3H, —CH_3), 6.157 (q, J = 0.8 Hz, 1H, vinylic); ms m^+/e calcd. for $C_{13}H_9O_3N$: 227.0582; found: 227.0579.

*Preparation of 3-Benzamido-5-hydroxyhexanoic Acid Lactone (**22**) and 3-Cyclohexylcarbonylamino-5-hydroxyhexanoic Acid Lactone (**23**)*

Oxazolino-α-pyrone (**19**) (750 mg) in freshly distilled anhydrous ethyl acetone (150 ml) was hydrogenated in the presence of Adam's catalyst (400 mg) under atmospheric pressure for 4 h. After the catalyst was removed by filtration and the filtrate evaporated to dryness as usual, the clear oily residue was subjected to preparative tlc separation on silica plates developed by ethyl acetate. The top fraction at R_F 0.8 was identified as 2-phenyl-4-carbethoxymethyl-5-acetyl-1,3-oxazole (**15**) (48 mg), mp 52–53°C; ir: 1740 (ester), 1680 (ketone), 1600 cm^{-1} (oxazole and phenyl); ms m^+/e: 273; nmr δ: 1.33 (t, $3H_s$, —CH_2—CH_3), 2.58 (s, $3H_s$, CH_3), 4.04 (s, $2H_s$, —CH_2—), 4.30 (q, —CH_2—CH_3), 7.50 (m, $3H_s$, phenyl), 8.18 ppm (m, $2H_2$ phenyl). This compound is identical to the product obtained by dissolving the oxazolino-α-pyrone (**19**) in ethanol.

The second fraction at R_F about 0.5 was identified as 3-benzamido-5-hydroxyhexanoic acid lactone (**22**) overlapped with 3-cyclohexylcarbonylamino-5-hydroxyhexanoic acid (**23**). Purification by repeated separation and multiple development on silica plates with chloroform – ethyl acetate 15% and recrystallization from benzene–ether gave the lactone **22** (38 mg), mp 88–91°C; ir: 3450 (—NH), 1740 (lactone), 1675 (amide), 1610, 1590 cm^{-1} (phenyl of benzoyl compounds); nmr: Table 1 and Fig. 1; ms m^+/e calcd.: 233.1052; found: 233.1046.

From the area immediately below the fraction containing **22** was isolated the lactone **23** (270 mg) which was invisible under uv light. This compound was recrystallized from methylene chloride – ether mp 128–130°C; ir: 3450 (—NH), 1740 (lactone), 1680 cm^{-1} (amide); ms m^+/e: 239; nmr (Fig. 5) (HA-100) δ: 1.37 (d, $J_{CH_3-5_a}$ 6.2 Hz —CH_3), 2.37 (q, H_{2a}, J_{2a-2e} = 17.3 Hz, J_{2a-3a} = 8.4 Hz), 2.92 (d of q, H_{2e}, J_{2a-2e} = 17.3 Hz, J_{2e-3a} = 6.7 Hz, J_{2e-4e} = 1.2 Hz), 4.40 (m, H_{5a}) 6.52 ppm (broad d, —NH); ms m^+/e: 239. *Anal.* calcd. for $C_{13}H_{21}O_3N$: C 65.12, H 8.78, N 5.86; found: C 65.33, H 8.71, N 5.69.

Preparation of N-*Benzoyl-4-deoxy-*D,L-*daunosamine (3-Benzamido-2,3,4,6-tetradeoxy-*D,L-*threohexose) (**26**)*

To a benzene solution (20 ml) containing 3-benzamido-5-hydroxyhexanoic acid lactone (46 mg) was injected 0.4 ml of modified Red-al reagent prepared by adding isopropyl

Can. J. Chem. Downloaded from www.nrcresearchpress.com by 210.87.254.40 on 09/05/12
For personal use only.

alcohol (7 ml) slowly into a benzene solution (75 ml) containing the Red-al reagent (28 ml). The reaction mixture was stirred at room temperature for $1\frac{3}{4}$ h, washed with water and dilute hydrochloric acid, dried over magnesium sulfate, and evaporated to dryness yielding a semicrystalline residue which upon purification by tlc on silica plate developed by ethyl acetate, gave the *N*-benzoyl-4-deoxy-D,L-daunosamine (**26**) (28 mg), mp 104–109°C; ir: 3580 (—OH), 3430 (—NH), 1670 (amide), 1615 and 1590 cm^{-1} (phenyl ring of benzoyl group); ms m^+/e calcd.: 235.1208; found: 235.1213.

Similarly **23** (270 mg) was converted to the *N*-cyclohexanecarbonyl-4-deoxy-D,L-daunosamine (**27**) (180 mg) which could be purified by recrystallization from methylene chloride – ether, mp 172–176°C; ir: 3560 (—OH), 3430 (—NH), 1675 cm^{-1} (amide); ms m^+/e: 241. *Anal.* calcd. for $C_{13}H_{23}O_3N$: C 64.73, H 9.54, N 5.81; found: C 64.83, H 9.41, N 5.69.

Preparation of 4-Deoxy-D,L-daunosamine Hydrobromide

N-Cyclohexanecarbonyl-4-deoxy-D,L-daunosamine (70 mg) was heated at 100°C in a solution of acetic acid (5 ml) and hydrobromic acid (5 ml) for $1\frac{1}{2}$ h. The solution was evaporated to dryness under reduced pressure and the residue was digested with chloroform. The insoluble crystalline compound was filtered and could be recrystallized from methanol–chloroform; mp 199–210°C (slowly decomposing). This compound was converted back to *N*-benzoyl-4-deoxy-D,L-daunosamine (**26**) by reacting with benzoyl chloride and pyridine, followed by mild acid hydrolysis.

Acknowledgement

We would like to thank the National Research Council of Canada for financial support.

1. 2nd Int. Symp. Adriamycin. European Press Medikon, Belgium. 1975.
2. 1st Int. Symp. Adriamycin. Springer-Verlag, New York, NY. 1972.
3. S. K. CARTER. J. Natl. Cancer Inst. **55**, 1265 (1975).
4. R. S. JAENKE. Cancer Res. **36**, 2958 (1976).
5. K. MAILER and D. H. PETERING. Biochem. Pharmacol. **25**, 2085 (1976).
6. D. H. HUFFMAN, R. S. BENJAMIN, and N. R. BACHUR. Clin. Pharmacol. Thera. **13**, 895 (1972).
7. (*a*) J. DAVIES, L. GORINI, and B. D. DAVIS. Mol. Pharmacol. **1**, 93 (1965); (*b*) N. TANAKA, Y. YOSHIDA, K. SASHIKATE, H. YAMAGUCHI, and H. UMEZAWA. J. Antibiot. **19**, 65 (1966); (*c*) J. DAVIES, P. ANDERSON, and B. D. DAVIS. Science, **149**, 1096 (1965).
8. (*a*) S. UNIZAWA, T. TSUCHIYA, R. MUTO, and Y. NISHIMURA. J. Antibiot. **24**, 274 (1971); (*b*) H. MASUKAWA and N. TANAKA. J. Antibiot. **21**, 70 (1968); (*c*) B. BANNISTER. J. Antibiot. **25**, 377 (1972); (*d*) W. T. SHIER, K. L. RINEHART, JR., and D. GOTTLIEB. J. Antibiot. **23**, 51 (1970).
9. F. ARCAMONE, S. PENCO, A. VIGEVANI, S. RADAELLI, and G. FRANCHI. J. Med. Chem. **18**, 703 (1975).
10. P. W. KENT and M. W. WHITEHOUSE. Biochemistry of the aminosugars. Butterworth's, London. 1955.
11. (*a*) C. M. WONG, T. L. HO, and W. P. NIEMCZURA. Can. J. Chem. **53**, 3144 (1975); (*b*) W. LEE, H. Y. WU, J. J. MARSH, JR., C. W. MOSHER, E. M. ACTON, L. GOODMAN, and D. W. HENRY. J. Med. Chem. **18**, 767 (1975); (*c*) W. LEE, H. Y. WU, J. E. CHRISTENSEN, L. GOODMAN, and D. W. HENRY. J. Med. Chem. **18**, 768 (1975).
12. H. J. JAKOBSEN, E. H. LARSEN, P. MADSEN, and S. O. LAWESSON. Ark. Kemi, **24**, 519 (1965).
13. A. A. BOTHNER-BY. Adv. Magn. Reson. **1**, 195 (1965).
14. R. U. LEMIEUX and J. D. STEVENS. Can. J. Chem. **43**, 2059 (1965).
15. (*a*) P. R. CAREY and R. DITCHFIELD. Mol. Phys. **15**, 515 (1968); (*b*) M. BARFIELD. J. Am. Chem. Soc. **93**, 1066 (1971).
16. C. W. HAIGH and J. M. WILLIAMS. J. Mol. Spectrosc. **32**, 398 (1969).

Can. J. Chem. Downloaded from www.nrcresearchpress.com by 210.87.254.40 on 09/05/12
For personal use only.

Biosynthetic studies of stress metabolites from potatoes: incorporation of sodium acetate-$^{13}C_2$ into 10 sesquiterpenes[1,2]

A. STOESSL, J. B. STOTHERS, AND E. W. B. WARD

Agriculture Canada Research Institute and the Department of Chemistry, University of Western Ontario, London, Ont., Canada N6A 5B7

Received October 12, 1977

A. STOESSL, J. B. STOTHERS, and E. W. B. WARD. Can. J. Chem. **56**, 645 (1978).

The results of incorporation studies of doubly-labelled sodium acetate-$^{13}C_2$ into the stress metabolites produced by fungal invasion of potato tubers are presented. The ^{13}C-labelling patterns for 10 sesquiterpenes have been determined by ^{13}C nmr. Two of these products have not been described previously and their structural elucidation is discussed. The biosynthetic interrelationships of these compounds are considered in detail.

A. STOESSL, J. B. STOTHERS et E. W. B. WARD. Can. J. Chem. **56**, 645 (1978).

On rapporte les résultats d'études d'incorporation d'acétate de sodium $^{13}C_2$ doublement marqué dans des métabolites de tension qui se forment sous l'effet d'une invasion fongique des rhizomes de patates. On a déterminé, grâce à la rmn ^{13}C, les types de marquage ^{13}C de dix sesquiterpènes. Deux de ces produits n'avaient pas été décrits antérieurement et on discute de l'élucidation de leurs structures. On considère en détail les rapports mutuels biosynthétiques de ces composés.

[Traduit par le journal]

Recently we reported in preliminary form, the results of incorporation of doubly-labelled acetate-$^{13}C_2$ into six sesquiterpenoidal stress metabolites of potatoes (1). Their biosynthetic mode of formation is of interest and the labelling studies provide information bearing on this question. In this paper we wish to present the full results for 10 sesquiterpenes isolated in these experiments, including 2 compounds which have not been described previously.[3]

The known compounds for which incorporation data were obtained are rishitin (**1**) (2), lubimin (**2**) (3–5), hydroxylubimin (**3**) (5, 6), phytuberin (**4**) (7, 8), desacetylphytuberin (phytuberol) (**5**) (9), solavetivone (katahdinone) (**6**) (10, 11), 15-dihydrolubimin (**7**) (4, 5), and isolubimin (**8**) (11). In general these compounds are generated by an incompatible fungus–potato interaction but other means of inducing their formation in potato tissue have been reported from several laboratories (12). The compounds are not found in any but minute traces in normal healthy potato tissue. In the present experiments, their synthesis was induced by inoculating potato tuber slices with either *Monilinia fructicola* or *Glomerella cingulata*. Sodium acetate, equally enriched to approximately 90% ^{13}C at both C-1 and C-2, was added 1 day after inoculation and the lipophilic metabolites which had been produced were extracted one day thereafter. The individual metabolites were isolated by careful chromatography on silica gel.

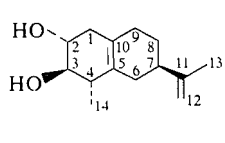

1

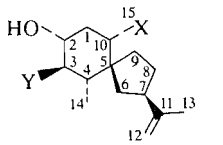

2 X = CHO, Y = H
3 X = CHO, Y = OH
7 X = CH_2OH, Y = H

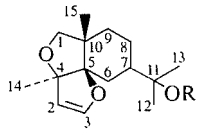

4 R = Ac
5 R = H

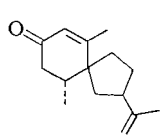

6

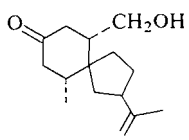

8

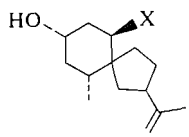

9 X = CHO
10 X = CH_2OH

Rishitin (**1**) was obtained in comparable amounts from both interactions but significant differences in quantity were found for the other sesquiterpenes. The *M. fructicola* interaction gave only a very small amount of **4** while **5** was probably produced in traces

[1]Part 76 of ^{13}C nmr studies. For Part 75 see ref. 25.

[2]Part XXIX in the series, "Post infectional inhibitors from plants." For Part XXVIII see ref. 14. Contribution No. 703 from the Agriculture Canada Research Institute.

[3]During the preparation of this manuscript, the isolation of epilubimin and its reduction to dihydroepilubimin was reported (24).

Can. J. Chem. Downloaded from www.nrcresearchpress.com by 210.87.254.105 on 09/05/12
For personal use only.

Can. J. Chem. Downloaded from www.nrcresearchpress.com by 210.87.254.105 on 09/05/12
For personal use only.

TABLE 1. ^{13}C parameters[a] for sesquiterpenes **1–10**

Compound	C-1	C-2	C-3	C-4	C-5	C-6	C-7	C-8	C-9	C-10	C-11	C-12	C-13	C-14	C-15
1	38.4	71.5	79.2	41.7	129.1	31.2	40.5	26.6	29.7	124.9	148.9	109.0	21.1	16.5	
	(37)	(37)		(36)	(42)	(42)	(32)	(32)			(72)	(72)		(36)	
2	41.8	69.3	40.3	41.0	46.9	33.3	47.4	32.6	25.9	58.4	147.3	108.8	21.2	16.4	205.0
	(36)	(36)		(37)	(36)	(36)	(33)	(33)		(40)	(72)	(72)		(37)	(40)
9	42.4	66.6	39.9	36.9	46.3	32.9	48.0	30.8	30.7	58.6	147.6	108.5	21.4	17.0	205.5
	(36)	(36)		(36)	(35)	(35)	(33)	(33)		(39)	(72)	(72)		(36)	(39)
3	42.2	74.1	76.8	47.1	48.3	32.7	47.3	30.5	26.8	57.6	147.0	109.0	21.2	11.2	204.3
	(36)	(36)		(38)	(36)	(36)	(33)	(33)		(41)	(72)	(72)		(38)	(41)
4	74.0	146.7	105.3	93.5	95.1	29.6	44.1	22.1	34.8	45.4	83.7	23.7	23.1	23.7	16.7
				(44)	(40)	(40)	(34)	(34)		(38)	(40)	(40)		(44)	(38)
5	73.8	146.9	104.6	93.4	95.0	29.6	46.3	21.7	34.6	45.1	72.4	26.7	27.3	23.3	16.6
				(45)	(41)	(41)	(34)	(34)		(38)	(40)	(40)		(45)	(38)
6	125.6	198.9	43.0	39.3	50.2	40.9	46.6	32.8	34.4	166.5	147.2	109.1	21.3	15.9	20.9
	(52)	(52)		(36)	(33)	(33)	(32)	(32)		(42)	(72)	(72)		(36)	(42)
7	40.6	69.9	40.8	41.2	46.7	36.7	47.4	32.7	25.4	48.5	148.1	108.2	21.5	16.7	64.1
	(37)	(37)		(37)	(35)	(35)	(33)	(33)		(38)	(72)	(72)		(37)	(38)
10	42.1	66.6	40.4	35.4	46.4	34.0	47.9	31.2	31.3	49.1	148.4	108.2	21.5	17.2	62.1
	(37)	(37)		(37)	(35)	(35)	(33)	(33)		(38)	(72)	(72)		(37)	(38)
8	50.1	211.6	46.7	43.0	46.8	40.0	47.2	32.5	25.0	42.4	147.6	108.6	21.5	16.7	64.3
	(38)	(38)		(37)	(35)	(35)	(32)	(32)		(38)	(72)	(72)		(37)	(38)

[a]Data obtained for $CDCl_3$ solutions; shieldings in ppm from internal TMS and ^{13}C–^{13}C coupling constants (in parentheses) in Hz for directly bonded ^{13}C nuclei arising from a common acetate-$^{13}C_2$ unit.

but was not isolated; **6** was not detected. Two new compounds were isolated in very small amounts and were characterized as 10-epilubimin (**9**) and 15-dihydro-10-epilubimin (**10**) from the following results.

Compound **9** proved difficult to separate from **2** but was isolated as a syrup by multiple chromatography. An exact mass determination showed **9** to have the composition $C_{15}H_{24}O_2$. Its mass spectrum was strikingly similar to that of **2**. The infrared spectrum revealed the presence of a hydroxyl group, an aldehyde, and a terminal double bond. These features were all confirmed by the proton spectrum which contained absorptions for a formyl proton at 9.84 ppm as a triplet with spacings of $\sim$1 Hz, olefinic methylene protons at 4.68 ppm as a multiplet, and a carbinyl proton, 3.69 ppm, also as a multiplet. Of these patterns that for the formyl proton differs from the corresponding absorption for **2** by 0.06 ppm and in multiplicity since the latter is a doublet. The other absorptions are essentially identical for **2** and **9** and, further, a methyl doublet, 0.94 ppm, $J \sim 7$ Hz, and a broadened methyl singlet, 1.70 ppm, appear for both compounds. These data suggested that **9** is a stereoisomer of **2**, a conclusion which was strongly supported by a comparison of their ^{13}C spectra. Of the 15 signals in the decoupled spectrum of **9** those for an aldehydic carbonyl, 205.5 ppm, an isopropenyl group, 147.6, 108.5, and 21.4 ppm, a carbinyl carbon, 66.6 ppm, a secondary methyl, 17.0 ppm, and a second quaternary carbon, 46.3 ppm, were readily identified. These shieldings correspond closely with those for **2** (Table 1). From the ^{13}C spectrum of **9**-$^{13}C_x$, isolated from the enriched acetate feeding experiment, the immediate neighbors for the individual signals noted were readily identified and it was apparent that three carbons arose from C-2 of the mevalonate units since these lacked the ^{13}C satellites found for the pairs of carbons arising from intact acetate units in mevalonate. By comparison of the shieldings for **9**, with those for **2**, assignments were straightforward. The increased shieldings for the methine carbon bearing the secondary methyl group and for the carbinyl carbon, combined with the decreased shielding for C-9, constitute good evidence that **9** and **2** differ only in orientation of the aldehyde function. It is equatorial in **2** and would exert a shielding γ *gauche* effect at C-9, but if axial, the carbinyl and methine carbons (C-2 and -4, respectively) would be shielded by γ *gauche* interactions with the formyl group while C-9 would be expected to be less shielded. The remaining carbons should be little affected as is observed with the exception of C-8. The 1.9 ppm shift for this carbon is not readily explained but may reflect an alteration in the preferred conformation of the isopropenyl group. The

Can. J. Chem. Downloaded from www.nrcresearchpress.com by 210.87.254.105 on 09/05/12
For personal use only.

ord curves for **2** and **9** confirmed the conclusion regarding the aldehyde orientation since **9** exhibited a distinctly negative Cotton effect while the Cotton effect for **2** was strongly positive (4).

On treatment with sodium borohydride **9** furnished a diol as the major product which was found to be identical to **10** isolated from the products obtained from the *M. fructicola* interaction. Diol **10** is a crystalline compound whose mass spectrum was almost superimposable on that of **7** of which it is an isomer since an exact mass determination showed its molecular formula to be $C_{15}H_{26}O_2$. Although the two compounds are not separable by preparative tlc, pure **10** was isolated by preferential crystallization with mp 138–140°C which was depressed to 106–120°C upon admixture with **7**, mp 126–128°C. The proton spectrum of **10** was very similar to that of **7** with characteristic absorptions for olefinic methylene protons at 4.68 ppm, a vinyl methyl group at 1.70 ppm and a secondary methyl at 0.85 ppm, $J \sim 7$ Hz. A three-proton multiplet centred near 3.7 ppm could be ascribed to a single carbinyl proton and the methylene absorption of an hydroxymethyl group. The AB pattern for the hydroxymethyl group was revealed by spin decoupling at 1.65 ppm. The chemical shift difference of 0.15 ppm for these methylene protons is much smaller than that found for **7**, 0.6 ppm, and the pattern obscured the absorption of the carbinyl methine centre in contrast to the spectrum for **7**. The ^{13}C spectrum of **10** was also similar to that of **7** (Table 1). Readily identified signals included those for a carbinyl methine and hydroxymethyl group at 66.6 and 62.1 ppm, respectively, an isopropenyl group, 148.4, 108.2, and 21.5 ppm, a secondary methyl carbon, 17.2 ppm, and a second quaternary carbon at 46.4 ppm. The ^{13}C-labelled material, from the acetate-$^{13}C_2$ feeding experiment, gave a ^{13}C spectrum from which it was apparent that three signals arose from C-2 of mevalonate units and that the product contained six intact acetate units. Significant upfield shifts for C-2 and -4, as well as the hydroxymethyl carbon, together with the downfield shift for C-9, all relative to the corresponding shieldings for **7**, establish the orientation of the 15-hydroxymethyl group as axial. The formation of **10** from **9**, by analogy with the **2** → **7** reduction, confirmed the relationship between the compounds. Their absolute stereochemistries follow from the correlation with **2** which, in turn, has been related by its ord curve (6) to **3** whose full stereochemistry is known (13).

The potato – *G. cingulata* interaction gave considerably more extractable material than that with *M. fructicola* and the extract appeared to be more complex. Numerous metabolites accrued in very small amounts but **1**, **4**, **5**, and **6** were found in relatively large and readily isolable quantities. Although there was evidence of the presence of **3**, the amount was too small to allow its isolation. Lubimin (**2**) was obtained only in admixture with **8** and **9** as was readily apparent from the ^{13}C spectrum which contained three carbonyl absorptions, as well as three carbinyl carbon signals, one of which arose from a methylene carbon, and three secondary methyl signals. In addition, the appearance of signals at 50.0 and 36.9 ppm with relative intensities corresponding to those of the absorptions noted above for **8** and **9**, respectively, confirmed the presence of these compounds in the mixture since these absorptions are well separated from other peaks in the spectra of the three compounds. The remaining signals coincided with those listed for **2**, **8**, and **9** in Table 1.

These assignments were substantiated by the eventual isolation of essentially pure isolubimin (**8**) from an adjacent fraction. Compound **8** has been described previously (11) but its ^{13}C spectrum has not been reported, nor has the hydroxymethyl absorption in its proton spectrum been fully described. The latter is informative by comparison with that for **7** since the two patterns are very similar. This AB portion of an ABX pattern has $\delta_{AB} = 0.5$ ppm (cf. 0.6 ppm for **7**) suggesting the same stereochemistry for this group in both compounds since $\delta_{AB} = 0.15$ ppm for **10** having an axial CH_2OH. The ^{13}C shieldings for **8** are listed in Table 1 and the spectrum established that the material arose from six intact acetate units with three carbons from C-2 of mevalonate units.

Somewhat surprisingly, **7** was produced in the largest amount in the *G. cingulata* – potato interaction and was accompanied by only traces of its epimer **10**. The latter were revealed by the nmr spectra of mother liquors from which **7** had crystallized. There is little doubt that **7** arose primarily from fungal reduction of **2** since it is known that this process occurs readily in pure culture (14). However, it seems likely that at least a portion of **7** was formed by the action of host rather than fungal enzymes. This suggestion follows from the fact that a careful search revealed a very small quantity of **7** in *M. fructicola* – potato extracts, although this fungus does not appear to effect the reduction of **2** in pure culture (14). Biosynthetically, **7** is as likely to stand in a precursor as in a product relationship to **2**, although it may then only occur in an enzyme bound form. Of course, the two compounds may be in an equilibrium relation. A similar situation obtains for **9** and **10** and it is conceivable that the four terpenes may be dynamically related as shown in Scheme 1. These possibilities are receiving further attention.

We can now turn to a consideration of the biosynthetic information provided by this study. The

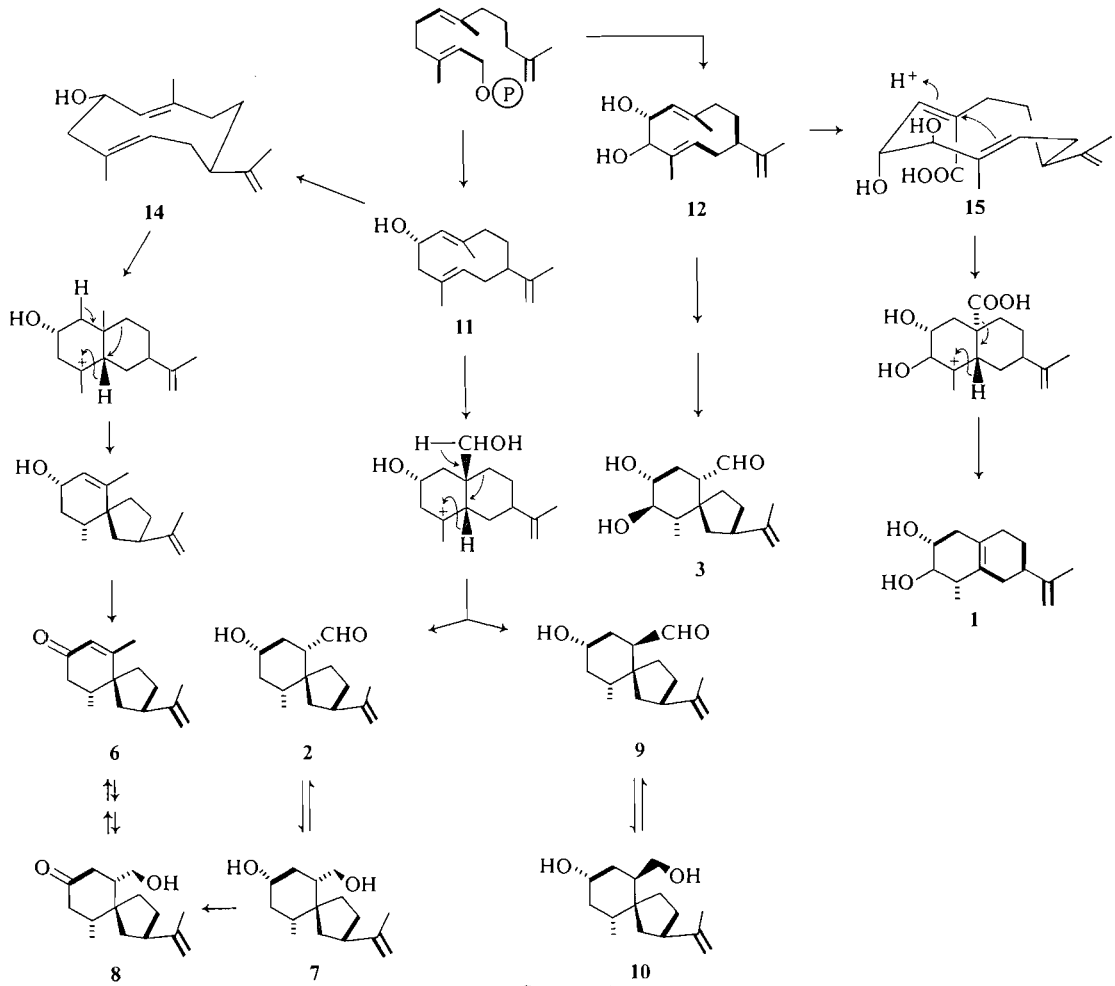

SCHEME 1

use of acetate doubly-labelled with ^{13}C and ^{13}C spectroscopy of the isolated metabolites proved to be both convenient and highly informative. A major disadvantage associated with biosynthetic studies of higher plants is that frequently only low levels of incorporation are achieved. Fortunately, this problem did not arise in these studies, nor in earlier experiments by Brooks and his associates (15) because the production of metabolites under stress conditions assured their *de novo* synthesis and, consequently, relatively high levels of incorporation. The lowest levels encountered in the present work were of the order of 0.7% enrichment and at this level useful ^{13}C spectra can be obtained on as little as 0.004 mmol of substance. The advantages of utilizing doubly-labelled acetate-^{13}C for biosynthetic studies with ^{13}C nmr techniques have been illustrated by several workers and we need only note that for terpenes the incorporation of acetate-$^{13}C_2$ into mevalonate units yields mevalonate with two intact acetate units and one carbon (C-2) which has lost its original neighbor. For sesquiterpenes formed without rearrangement or cleavage of the farnesyl chain, the ^{13}C spectrum of an enriched product contains six pairs of signals having ^{13}C satellites for each of the six intact acetate units, and three enhanced signals lacking prominent satellites which arise from C-2 of the mevalonate units. The spacing of the satellites is the ^{13}C–^{13}C coupling constant across a specific C—C bond and pairwise matching of the spacings permits unequivocal assignments of specific signals in many cases. For each of the metabolites isolated in this study, the ^{13}C shieldings and ^{13}C–^{13}C one-bond couplings have been collected in Table 1. Although the majority of these data had been reported previously it seemed worthwhile to gather these together for ease of comparison with the results for the new compounds. A few of the earlier assignments have been revised on the basis of the spectra of the enriched products. For example, the allylic methyl

Can. J. Chem. Downloaded from www.nrcresearchpress.com by 210.87.254.105 on 09/05/12
For personal use only.

Can. J. Chem. Downloaded from www.nrcresearchpress.com by 210.87.254.105 on 09/05/12
For personal use only.

TABLE 2. Incorporation data[a] for metabolites **1–10**

	M. fructicola interaction			*G. cingulata* interaction	
Compound	Yield (mg)	^{13}C enrichment(%)	Compound	Yield (mg)[b]	^{13}C enrichment(%)
1	69	4.0	**1**	53	1.5
2	15	2.9	**2**	(16)[c]	1.3
3	8	3.0	**4**	39	0.7
4	<1	—	**5**	11	0.8
9	3	3.5	**6**	19	1.4
10	4	4.4	**7**	79(10)[d]	1.8
			8	12(8)[c]	1.8
			9	(3)[c]	1.3
			10	(5)[d]	1.6

[a]From the relative intensities of the ^{13}C satellites and central signals (see text), ±0.2%.
[b]Amounts in parentheses obtained in the mixtures noted.
[c]In a mixture of **2**, **8**, and **9**.
[d]In a mixture of **7** and **10** from the mother liquors of **7**.

carbons in **6** arise from different carbons in the mevalonate precursor with C-13 from C-2 and C-15 from C-3′. Thus the latter will give rise to an absorption pattern with readily observable satellites, while the former appears as a singlet, clearly distinguishing the two and providing unequivocal assignments. In addition to revealing the biosynthetic mode of formation of the metabolites the ^{13}C spectrum of the enriched products provides a direct measure of the incorporation level from the relative intensities of the satellites and the central signal. A detailed analysis of the quantitative dependence of the intensities of multiplet lines produced by ^{13}C–^{13}C coupling as a function of ^{13}C enrichment has been published (16). In the present series, the signals for C-12, -14, and -15 readily provided the requisite data while the carbinyl patterns for a number of the examples were also analyzed. The enrichment levels determined from these absorption patterns are listed in Table 2.

With the exception of **1**, **4**, and **5**, these metabolites contained six intact acetate units (see Table 1) since prominent ^{13}C satellites were observed for 12 of the 15 signals which corresponded to the 15 singlets found for samples containing ^{13}C in natural abundance. This observation limits the possible modes of formation of the spirovetivane skeleton from a farnesyl chain, which is almost assuredly the primary C_{15} precursor. A plausible scheme to account for the genesis of **1–3** and **6–10** is illustrated in Scheme 1 in which intact acetate units are indicated by heavy bonds. On the basis of the available data for the stress metabolites of the *Solanaceae* the product of a most reasonable initial cyclization is the germacrenol **11**. Earlier we established the formation of the more highly oxidized analog **12** in *M. fructicola* – *Datura stramonium* interactions (13*a*) and preliminary tracer experiments in these laboratories indicate that **12** is not involved in the generation of **2** but does lead to **3**. The cyclodecadiene ring of **11** (and **12**) may adopt a variety of conformations and consideration of these possibilities led us to propose a scheme which accounts for the known stereochemistries of **1**, **2**, and **3** as well as that for an additional metabolite, aubergenone (**13**), formed in *Solanum melongena* (4). The question of preferred conformation and stereoselectivity in the cyclization of *E,E*-1,5-cyclodecadienes has been considered in detail by Sutherland (17). Laboratory studies support the contention that the CC conformation, in Sutherland's terminology, is highly preferred for the transition state leading to the *trans*-decalin skeleton as the major product. Such a conformation is required for our proposed route to **13** but generation of the spirovetivane skeleton appears to require the TT conformation **14** while the

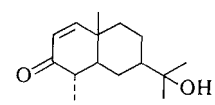

13

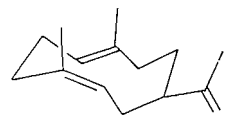

16

CT conformation **15** nicely accounts for a cyclization which can lead readily to rishitin. Although **14** and **15** are disfavored in laboratory studies it is not unreasonable to suggest their intermediacy in living systems involving enzymic processes, as has been noted by Coates (18). An alternative pathway, not included in Scheme 1, can be suggested, namely, isomerization to the 1*E*,5*Z* configuration followed by cyclization. In this case the CT conformation **16** would be expected to form a *cis*-decalin skeleton on

Can. J. Chem. Downloaded from www.nrcresearchpress.com by 210.87.254.105 on 09/05/12
For personal use only.

cyclization from which the generation of the spirovetivane system is readily envisaged. It has been shown that the CT conformation is favored for the parent diene (19) in the solid state. Since **11**, however, can adopt the suitable conformation **14** it seems unnecessary to include an additional step, the isomerization, at this stage of investigation.

Cyclization of **14** to a *cis*-decalin, followed by proton loss and ring contraction as shown in Scheme 1 requires only oxidation of the allylic alcohol to the conjugated ketone to afford **6**. Analogous transformations have been discussed for closely related systems (18, 20). A corresponding cyclization of **11**, after allylic oxidation at the methyl carbon, would lead to **2** (and **9**). Proton loss from the hydroxymethyl group furnishes the enol form of the aldehyde function which upon tautomerization would be expected to produce a mixture of epimeric aldehydes **2** and **9**, with the former favored. Ring contraction by cleavage of the 9,10 carbon–carbon bond with formation of a 5,9 linkage does not rupture an intact acetate unit since C-9 originates from C-2 of mevalonate. Reduction of the aldehyde to a hydroxymethyl group gives **7** and **10** which, as suggested above, may undergo selective oxidation back to **2** and **9**, respectively. No evidence on this point is yet available. Oxidation of the secondary hydroxyl of **7**, however, provides **8** directly from which **6** could conceivably arise by dehydration and facile double bond isomerization. The reverse interconversion, **6** → **8** → **2** has been reported to occur in vivo (11) but without evidence from tracer studies. Allylic oxidation of **12** forms **15**, shown in a CT conformation, which can cyclize to a *trans*-decalin skeleton, decarboxylation of which with a hydride shift furnishes **1**. The loss of carbon dioxide cleaves a C—C bond of an intact acetate unit and four signals in the ^{13}C spectrum of **1**-$^{13}C_x$ were found to lack prominent ^{13}C satellites, as expected.

In contrast to the foregoing examples the ^{13}C spectra of the enriched samples of **4** and **5** clearly revealed only five intact acetate units. A feasible sequence leading to the phytuberin skeleton is outlined in Scheme 2 in which **11** is envisaged as the initial cyclization product in common with many of the co-occurring metabolites. Upon epoxidation of the 1,10 double bond and adoption of the CT conformation indicated the second cyclization can lead to *cis*-decalin **17**. Allylic oxidation to furnish the tertiary allylic alcohol **18** seems reasonable and has analogy in a closely related system since a *cis*-decalol derivative, β-rotunol, has been isolated from nutgrass (20*a*). It may be noted that β-rotunol readily undergoes dehydration to furnish a spirovetivone derivative (20*a*). Although hydration of the 11,12 double

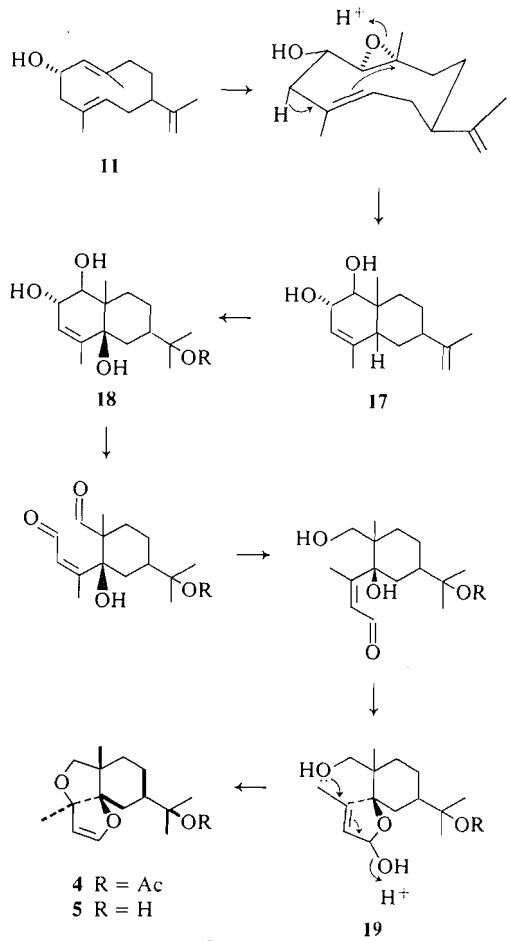

SCHEME 2

bond is also included in Scheme 2 at this point, there is no evidence of the precise stage at which this occurs. It is indicated here merely to simplify the scheme but may well occur at another stage. Cleavage of the vicinal diol **18** followed by hemiacetal formation to afford **19** accounts nicely for the generation of the dihydrofuran ring having the correct stereochemistry at C-5. Furthermore, the orientation of this ring in **19** leads directly to the correct product from the final cyclization, which is essentially an S_N2' process with water as the leaving group. This sequence accounts for the formation of **4** (**5**) in a more complete fashion than our earlier proposals.

It is interesting that the level of enrichment found for **4** and **5** is distinctly lower than that observed for the other metabolites isolated from the *G. cingulata* interaction. While this may be an indication that the generation of **4** and **5** involves a sequence significantly different from that proposed with a precursor other than **11**, no other evidence is currently available. It is also remarkable that the metabolites from the *Monilinia* experiment are enriched to nearly the same

TABLE 3. Basic fractionation of metabolites from fungus–potato interactions

Fungus	Fraction	Weight (mg)	Compounds (isolated and/or characterized)	1st refractionation[b] solvent
M. fructicola[a]	13–17	8	**4**	B (tlc)
	18–25	45	**9, 2**	C
	29–32	24	**2, 1**	A
	33–44	84	**1, 3**	A
	45–54	29	**1, 3, 10**	D
	55–64	11	**10**	D
G. cingulata[c]	35–40	39	**4**	—
	41–45	17	**4, 6**	B (tlc)
	59–67	51	**5**	Acetone–hexane (1:4)
	69–72	19	**8**	
	73–82	49	**2, 8, 9**	A
	91–95	113	**1**	A
	111–124	117	**7**	Recrystallized

[a]On silica with solvent A [b] as described in the text.
[b]Columns of silica gel (Camag DF5, unactivated, ca. 1 g/mg substrate) were used unless tlc is specified. In the latter case, plates were activated at 120°C. Solvents were: A, MeOH–$CHCl_3$ (5:95); B, Et_2O – light petroleum (1:1); C, Et_2O; D, *sec*-BuOH–EtOAc (5:95).
[c]On silica with a succession of solvents as described in the text.

degree. It could be argued that this implies sequential elaboration of one compound from another but concurrent elaboration of the individual compounds from a common precursor cannot be dismissed. Further investigations of both of these points are clearly required. The essentially equal labelling at all sites found for each compound, as is readily seen in the previously published spectra (1), implies the nonintervention of preformed metabolic pools such as geranyl pyrophosphate and almost certainly requires an uninterrupted sequence of synthesis of farnesyl pyrophosphate on the same enzyme (21). The intensity of labelling in the isopropenyl side chains confirms the absence of allylic shifts in agreement with the earlier findings for capsidiol (22).

Experimental

General

Melting points were determined on a Kofler hot stage and are uncorrected. The spectrometers employed included a Varian MAT 311A for mass spectra, a Varian XL-100-12 for ^{1}Hmr, a Varian XL-100-15 for ^{13}Cmr and a Beckman IR20A for ir spectra. A Jasco ORD-UV5 instrument was used to obtain ord curves (path length, 0.1 dm). Solvents were redistilled before use; light petrol was of bp 30–60°C and EtOH refers to 96% EtOH.

Nuclear Magnetic Resonance Spectra

Fourier transform methods were used to obtain ^{13}C spectra with square wave modulated proton decoupling for completely decoupled spectra or with single frequency proton irradiation for off-resonance decoupled spectra. Shielding data (±0.05 ppm) are reported for $CDCl_3$ solutions (5–10%, w/v) with TMS as internal reference; coupling constants (±0.5 Hz) were measured from expanded spectra. Smaller samples of enriched material (0.5–2 mg) were examined as CD_2Cl_2 solutions in 50 µl microcells. Proton spectra were recorded for the $CDCl_3$ solutions.

Feeding Experiments

Potato tubers, 54 kg, cultivar Kennebec, grown and purchased locally and kept at 4°C until used, were scrubbed with tap water, briefly surface-sterilized with 70% ethanol and cut into ca. ½ in. slices. These were inoculated by the method of Metlitskii *et al.* (3), by scooping out several hemispherical wells (diameter, ca. 2 cm) from one surface of each slice with a melon baller. After charging the wells with a spore suspension of *Monilinia fructicola* (Wint.) Honey (2×10^5 spores/ml; 2 ml per well; ca. 4 ℓ total), the slices were incubated for 18 h at room temperature in glass-covered trays lined with moist filter paper. A solution containing sodium acetate-1,2-$^{13}C_2$ (0.984 g; 90 at.% ^{13}C) in 400 ml of water was then added (0.20 ml/well; 393 ml total). After incubating the slices for another 30 h, the liquid (the 'diffusate') was collected and the wells were rinsed with a little water. Diffusate and washings were combined (4.2 ℓ) and extracted with three successive half-volumes of ether. The ether layers were washed in turn with two small portions of water, combined, dried (Na_2SO_4), filtered, and evaporated to furnish 213 mg of crude extract.

In a similar experiment *Glomerella cingulata* (Stonem) Spauld and Schrenk (5×10^5 spores/ml; total 3 ℓ) was used to inoculate Kennebec potatoes (29 kg) 24 h before treatment with sodium acetate-1,2-$^{13}C_2$ (90 at.%; 0.714 g). Extraction of the diffusates and washings with methylene chloride after another 30 h gave 742 mg of crude extract.

Isolation and Characterization of Metabolites from the M. fructicola Interaction

The crude extract was chromatographed over a column of silica gel (Camag DF5; not activated, 350 g) in solvent A (Table 3); 64 25-ml fractions were collected. Fractions of similar composition as shown by tlc were combined (Table 3) and rechromatographed in one or more of the indicated systems. The compounds isolated in this experiment were characterized as follows.

(*a*) Phytuberin (**4**) required no purification beyond that indicated in Table 3. Except for isotope peak intensities, its mass spectrum substantially matched that of an authentic specimen kindly supplied by Professor J. Kuć. The amount of material isolated (< 1 mg) precluded a precise determination of ^{13}C enrichment by ^{13}Cmr.

Can. J. Chem. Downloaded from www.nrcresearchpress.com by 210.87.254.105 on 09/05/12
For personal use only.

Can. J. Chem. Downloaded from www.nrcresearchpress.com by 210.87.254.105 on 09/05/12
For personal use only.

(*b*) Epilubimin (**9**) still containing a trace of **2** (tlc) had ν_{max} (CCl_4): 3410 (br), 3060 (w), 2940, 2865, 2730 (w), 1645 and 892 cm^{-1}. *Exact mass* calcd. for $C_{15}H_{24}O_2$: 236.1776; found (high resolution ms): 236.1777. A dilute solution of **9** in EtOH exhibited a pronounced negative Cotton effect (λ_{min} 336, 324, λ_{max} 300 nm; for **2** λ_{max} 323, λ_0 300 nm) but insufficient material was available to permit quantitative measurements.

A small quantity (ca. 1 mg) of the substance in MeOH (1 ml) was treated with sodium borohydride (4 mg) at room temperature. Reduction was complete after 2 min (tlc). The main product, extracted with ether and purified by preparative tlc and sublimation (85°C/20 Torr) was identical with naturally occurring **10** by tlc, mp, and mixture mp.

A mixture (21 mg) of 9 and **2** in a ratio of 1:2 was also obtained by column chromatography of the crude extract (181 mg) from the interaction of potatoes (34 kg) with a *M. fructicola* suspension (3.8 ℓ) without added sodium acetate. Rechromatography (solvent D, 40 g SiO_2) afforded **9** (2.6 mg) containing only traces of **2**. This material was employed to confirm the assignments in the ^{13}C spectrum. The ord curve of this specimen did not differ in any significant aspect from that described above for enriched **9**.

(*c*) Lubimin (**2**) was purified by further preparative tlc (solvent C). Its identity was confirmed by ms comparison with authentic specimens (4, 6).

(*d*) Rishitin (**1**) was obtained as a syrup (34 mg) from fractions 33–44 by one refractionation (Table 3). More of the compound (35 mg) was isolated by rechromatography of other fractions.

(*e*) Hydroxylubimin (**3**) crystallized after preparative tlc (solvent A) of enriched fractions. Two recrystallizations from ether gave pure material, mp 95–97.5°C (6).

(*f*) 15-Dihydro-10-epilubimin (**10**) crystallized after preparative tlc (solvent D) of enriched fractions and was recrystallized from $CHCl_3$ at −10°C, mp 138–140°C. *Exact mass* calcd. for $C_{15}H_{26}O_2$: 238.1933; found (high resolution ms): 238.1936.

Compounds **7** and **10** had almost identical R_f values in most tlc solvents examined but were partially separated in *i*-PrOH–EtOAc, 1:9 (solvent E) with R_f values, ca. 0.32 and 0.30, respectively. The two materials could be further distinguished by their slightly different color reactions with a vanillin–phosphoric acid spray reagent (23) (**7**, purple fading to olive-brown; **9**, purple, fading to mauve).

The mother liquors from which **10** had crystallized contained a small amount of **7**, in addition to **10** and other compounds, as shown by tlc. Compounds **7** and **10** were also detectable in other impure fractions obtained during rechromatography of initial fractions 33–54 (Table 3). Column chromatography of the combined material (8.5 mg) in solvent E afforded a fraction (2.6 mg) which consisted of **7** and **10** in a ratio of ca. 1:2.5, to judge from the ^1Hmr and ^{13}Cmr spectra.

Isolation and Characterization of Metabolites from the G. cingulata *Interaction*

The crude extract was chromatographed over a column of silica (Camag DF5, 350 g) with solvent B (fractions 1–20), solvent C (fractions 21–50), MeOH–Et_2O, 5:95 (solvent F, fractions 51–115), and finally MeOH–Et_2O, 1:9 (fractions 116–130). Fractions (25 ml each) were combined as indicated in Table 3 and refractionated as necessary. Incorporation data for the characterized materials are listed in Table 2.

(*a*) Phytuberin (**4**) was obtained pure from the initial chromatogram and was identical with Professor Kuć's specimen by tlc, ^1Hmr, ^{13}Cmr, mass, and ir spectra.

(*b*) Solavetivone (**6**), $[\alpha]_D$ −96° (*c* 0.5, EtOH), was found to be identical with a sample provided by Dr. D. T. Coxon by tlc, uv, ir, and mass spectra.

(*c*) Desacetylphytuberin (**5**) was identified by its ^1H and ^{13}C spectra but the sample decomposed before further characterization was done.

(*d*) Isolubimin (**8**) was isolated as a syrup, ν_{max} (CCl_4): 3400 (br), 3050 (w), 2940, 2860, 1710 (s), 1640 (m), and 885 cm^{-1}. Its nmr spectral data were discussed above. *Exact mass* calcd. for $C_{15}H_{24}O_2$: 236.1776; found (high resolution ms): 236.1779.

(*e*) Lubimin (**2**) was obtained in admixture (27 mg) with **8** and **9**; these compounds were present in the ratio of 6:3:1 to judge from the ^{13}C spectrum.

(*f*) Rishitin (**1**) required further chromatography (solvent E) for final purification.

(*g*) 15-Dihydrolubimin (**7**), after recrystallization from Et_2O, was identical with material prepared by the sodium borohydride reduction of **2** (4) by mp, mixture mp, tlc, nmr, and mass spectra. The mother liquors from the recrystallization were repeatedly refractionated by tlc (solvent D and MeOH–$CHCl_3$, 1:9) to give a mixture (15 mg) which was shown to contain **7** and **10** in a ratio of 2:1 by the ^{13}Cmr spectrum.

Acknowledgements

We are grateful for financial support by the National Research Council of Canada. We thank Professor J. Kuć and D. T. Coxon for generously supplying samples for comparisons and we wish to acknowledge the skillful technical assistance of Marlene Brown, Barbara Ollerenshaw, Heather Shroeder, D. Hairsine, A. M. Jevnikar, G. Rock, and C. H. Unwin.

1. A. Stoessl, E. W. B. Ward, and J. B. Stothers. Tetrahedron Lett. 3271 (1976).
2. N. Katsui, A. Murai, M. Takasugi, M. Imaizumi, T. Masamune, and K. Tomiyama. J. Chem. Soc. Chem. Commun. 43 (1968); N. Harada and K. Nakanishi. J. Am. Chem. Soc. **91**, 3989 (1969); T. Masamune, A. Murai, M. Takasugi, A. Matsunaga, N. Katsui, N. Sato, and K. Tomiyama. Bull. Chem. Soc. Jpn. **50**, 1201 (1977).
3. L. V. Metlitskii, O. L. Ozeretskovskaya, N. S. Vul'fson, and L. I. Chalova. Dokl. Biochem. **200**, 301 (1971).
4. A. Stoessl, J. B. Stothers, and E. W. B. Ward. Can. J. Chem. **53**, 3351 (1975).
5. N. Katsui, A. Matsunaga, and T. Masamune. Tetrahedron Lett. 4483 (1974); N. Katsui, A. Matsunaga, H. Kitahara, F. Yagihashi, A. Murai, T. Masamune, and N. Sato. Bull. Chem. Soc. Jpn. **50**, 1217 (1977).
6. A. Stoessl, J. B. Stothers, and E. W. B. Ward. J. Chem. Soc. Chem. Commun. 431 (1975).
7. J. L. Varns, J. Kuc, and E. W. Williams. Phytopathology, **61**, 174 (1971).
8. D. T. Coxon, K. R. Price, B. Howard, and R. F. Curtis. J. Chem. Soc. Perkin I, 53 (1977).
9. W. W. Currier. Diss. Abstr. Int. B, **36**, 685 (1975); K. R. Price, B. Howard, and D. T. Coxon. Physiol. Plant Pathol. **9**, 189 (1976).
10. D. T. Coxon, K. R. Price, B. Howard, S. F. Osman, E. B. Kalan, and R. M. Zacharius. Tetrahedron Lett. 2921 (1974); D. L. Hughes and D. T. Coxon. J. Chem. Soc. Chem. Commun. 822 (1974).
11. E. B. Kalan and S. F. Osman. Phytochemistry, **15**, 775 (1976).

12. A. STOESSL, J. B. STOTHERS, and E. W. B. WARD. Phytochemistry, **15**, 855 (1976).
13. (*a*) G. I. BIRNBAUM, C. P. HUBER, M. L. POST, J. B. STOTHERS, J. R. ROBINSON, A. STOESSL, and E. W. B. WARD. J. Chem. Soc. Chem. Commun. 330 (1976); (*b*) N. KATSUI, H. KITAHARA, F. YAGIHASHI, A. MATSUNAGA, and T. MASAMUNE. Chem. Lett. 861 (1976).
14. E. W. B. WARD and A. STOESSL. Phytopathology, **67**, 468 (1977).
15. F. C. BAKER and C. J. W. BROOKS. Phytochemistry, **15**, 689 (1976).
16. R. E. LONDON, V. H. KOLLMAN, and N. A. MATWIYOFF. J. Am. Chem. Soc. **97**, 3565 (1975).
17. J. K. SUTHERLAND. Tetrahedron, **30**, 1651 (1974).
18. R. M. COATES. Fortschr. Chem. Org. Naturst. **33**, 73 (1976).
19. D. ROGERS and M. L. SMART. Acta Crystallogr. Congr. Abstr. S149, XIII-2 (1969).
20. (*a*) H. HIKINO, K. AOTA, D. KUWANO, and T. TAKEMOTO. Tetrahedron, **27**, 4831 (1971); (*b*) N. H. ANDERSON, M. S. FALCONE, and D. D. SYRDAL. Tetrahedron Lett. 1759 (1970).
21. J. W. CORNFORTH. Angew. Chem. Int. Ed. Engl. **7**, 903 (1968).
22. F. C. BAKER, C. J. W. BROOKS, and S. A. HUTCHINSON. J. Chem. Soc. Chem. Commun. 293 (1975).
23. K. G. KREBS, D. HEUSSER, and H. WIMMER. *In* Thin-layer chromatography. *Edited by* E. Stah. Springer-Verlag, New York, NY. 1969. p. 854.
24. N. KATSUI, F. YAGIHASHI, A. MATSUNAGA, K. ORITO, A. MURAI, and T. MASAMUNE. Chem. Lett. 723 (1977).
25. R. M. CORY and J. B. STOTHERS. Org. Magn. Reson. In press.

Can. J. Chem. Downloaded from www.nrcresearchpress.com by 210.87.254.105 on 09/05/12
For personal use only.

Pyrrole chemistry. XIX. Reactions of 2-pyrrolecarbonitrile and its 4-substituted derivatives

HUGH J. ANDERSON, CYRIL R. RICHE, THOMAS G. COSTELLO, CHARLES E. LOADER, AND GRAHAM H. BARNETT

Department of Chemistry, Memorial University of Newfoundland, St. John's, Nfld., Canada A1B 3X7

Received October 17, 1977

HUGH J. ANDERSON, CYRIL R. RICHE, THOMAS G. COSTELLO, CHARLES E. LOADER, and GRAHAM H. BARNETT. Can. J. Chem. **56**, 654 (1978).

2-Pyrrolecarbonitrile has been acylated to its 4-formyl, trichloroacetyl, ester, and thiolester derivatives. Further reactions gave other 2,4-difunctionalized compounds. These included conversion of the 2-nitriles to the corresponding 2-aldehydes. Subsequent removal of the aldehyde group afforded several 3-substituted pyrroles in good yield.

HUGH J. ANDERSON, CYRIL R. RICHE, THOMAS G. COSTELLO, CHARLES E. LOADER et GRAHAM H. BARNETT. Can. J. Chem. **56**, 654 (1978).

On a acétylé le pyrrolecarbonitrile-2 et on a ainsi obtenu ses dérivés formyle, trichloroacétyle, ester et thioester en position 4. Des réactions subséquentes permettent d'obtenir d'autres composés difonctionnalisés en 2,4. Parmi ceux-ci, on en a obtenus qui correspondent à la transformation de nitriles-2 en aldéhydes-2 correspondants. L'élimination subséquente du groupe aldéhyde permet d'obtenir, avec de bons rendements, plusieurs pyrroles substitués en position 3.
[Traduit par le journal]

Selective Friedel–Crafts 4-acylation of 2-substituted pyrroles is an essential step in the preparation of 3-acylpyrroles by the currently available methods. In an effort to improve the route to 3-substituted pyrroles we have investigated in more detail the Friedel–Crafts acylation of 2-pyrrolecarbonitrile which had been found to undergo acylation almost exclusively in the 4-position and in excellent yield (1). Recently we reported an improved synthesis of 2-pyrrolecarbonitrile (2) avoiding the rather tedious earlier synthesis (3). The newer nitrile synthesis has now been carried out on a molar scale without decrease in yield. The cyano group offers the possibilities of hydrolysis to the acid, partial reduction with aldehyde formation, as well as complete reduction to the aminomethyl group. Therefore, we decided to explore the synthesis from the 2-nitrile of 2,4-disubstituted pyrroles which were either not known or not readily available. Among the useful carbon functional groups we wished to introduce in the 4-position were the formyl, ester, and the thiol ester as well as a second nitrile group.

Treibs and Kreuzer (4) have shown that pyrrole may be trichloroacetylated easily and that a haloform type reaction then gives the carboxylic acid. The recent modification by Harbuck and Rapoport (5) affords the more useful ester group. 2-Pyrrolecarbonitrile neither reacted with trichloroacetyl chloride using the literature method nor did it undergo a mild Friedel–Crafts acylation using the aluminum chloride – nitromethane complex as catalyst. However, a normal Friedel–Crafts acylation in methylene chloride using aluminum chloride catalyst gave about 40–45% yield of 4-trichloroacetyl-2-pyrrolecarbonitrile. This compound was converted in excellent yield to the desired methyl 2-cyano-4-pyrrolecarboxylate. The same reaction sequence when applied to methyl 2-pyrrolecarboxylate gave an excellent overall yield of methyl 2,4-pyrroledicarboxylate.

Oxalyl chloride acylation was also used by Treibs (4) and the oxalyl group has found some use in earlier pyrrole chemistry (6). We expected that a regular Friedel–Crafts acylation followed by work-up with cold methanol might produce methyl 2-cyano-4-pyrroleglyoxylate. However, instead we obtained methyl 2-cyano-4-pyrrolecarboxylate in a 'one-pot' operation. This loss of carbon monoxide from oxalyl chloride in Friedel–Crafts acylation is common (7), although glyoxylic derivatives may be formed as well. Indeed, the infrared and mass spectra of the crude product indicated the probable presence of a small amount of methyl 2-cyano-4-pyrroleglyoxylate.

The thiol ester group offers the possibility of conversion to aldehyde, hydroxymethyl, and methyl (8) as well as to other acid derivatives. Alkyl chlorothiolformates have been used as Friedel–Crafts acylating agents for benzene and a number of benzene derivatives (9). We were successful in using ethyl chlorothiolformate with aluminum chloride catalyst to obtain a very good yield of ethyl 2-cyano-4-pyrrolethiolcarboxylate. If the work-up was slow, some hydrolysis to the 4-acid-2-nitrile was observed.

Friedel–Crafts type formylation using dichloromethyl butyl ether with $AlCl_3$ catalyst gave 4-formyl-2-pyrrolecarbonitrile in good yield although the reaction required carefully controlled conditions. Attempts to acylate the 2-nitrile using ethyl malonyl

Can. J. Chem. Downloaded from www.nrcresearchpress.com by 210.87.254.105 on 09/05/12
For personal use only.

Can. J. Chem. Downloaded from www.nrcresearchpress.com by 210.87.254.105 on 09/05/12
For personal use only.

chloride and aluminum chloride were unsuccessful and the nitrile was recovered unchanged. Similarly, cyanogen bromide and aluminum chloride failed to produce the 2,4-dinitrile from 2-pyrrolecarbonitrile.

We have demonstrated (10) that the 2-nitrile can be alkylated with *tert*-butyl chloride in the presence of aluminum or gallium chloride as catalyst; the latter giving the least rearrangement of 4-*tert*-butyl to 5-*tert*-butyl-2-nitrile. So this method, together with reduction of the acylated derivatives, may be used to obtain 4-alkylated 2-nitriles.

It has been reported that neither the 2-ester-4-nitrile nor the 3-nitrile itself undergo Stephen type reduction (11). We have now determined that modified Stephen type reductions will convert 4-substituted 2-pyrrolecarbonitriles to the corresponding 2-aldehydes. Of the methods tried, Raney nickel alloy in formic acid (12) was the most reliable and gave the required aldehydes in good yields. In particular, this method cleanly converted ethyl 2-cyano-4-pyrrolethiolcarboxylate to ethyl 2-formyl-4-pyrrolethiolcarboxylate without desulfurization of the thiolcarboxylate group. This provides a convenient route to 4-substituted 2-pyrrolecarboxaldehydes which are not easily obtained from 2-pyrrolecarboxaldehyde itself (1).

In our earlier work involving the replacement of the thiolester group by hydrogen, using W5 Raney nickel catalyst in a catalytic decarbonylation reaction (13) we had also observed that pyrrolecarboxaldehydes were decarbonylated under very mild conditions. Using this method, 4-acetyl-2-pyrrolecarboxaldehyde and methyl 2-formyl-4-pyrrolecarboxylate were readily decarbonylated to give 3-acetyl pyrrole and methyl 3-pyrrolecarboxylate respectively. Although catalytic decarbonylation reactions of this type are not unusual (14), in the presence of Raney nickel, 2-pyrrolecarboxaldehydes decarbonylate remarkably easily.

Thus, 2-pyrrolecarbonitrile may be converted in good yield to a number of 2,4-disubstituted pyrroles possessing useful functional group combinations. It may also be used to synthesize certain 3-substituted pyrroles.

Experimental

Melting points are uncorrected. Elemental analyses were by Alfred Bernhardt, West Germany, Atlantic Microlabs, GA, U.S.A., or by Memorial University Water Analysis Facility. The ir spectra were recorded on a Perkin-Elmer 237B grating spectrophotometer using potassium chloride discs. The ^{1}Hmr spectra were determined using a Varian EM 360 instrument. Values are given on the δ scale using tetramethylsilane as internal reference. Mass spectra were recorded on a Hitachi-Perkin-Elmer RMU-6E spectrometer using a direct inlet system.

2-Pyrrolecarbonitrile

This compound was prepared on a 1-mol scale in 50% yield using methyl thiocyanate instead of ethyl thiocyanate (2). Much of the unreacted pyrrole could be recovered.

Trichloroacetylation of 2-Pyrrolecarbonitrile

This reaction was carried out by normal Friedel–Crafts procedures (13) using 2-pyrrolecarbonitrile (10.0 g, 0.11 mol), trichloroacetyl chloride (25.0 g, 0.14 mol) and aluminum chloride (35 g, 0.25 mol) in methylene chloride for 2.5 h at reflux. The bright yellow reaction mixture was poured onto a mixture of ice and 6 *M* HCl and then extracted with chloroform three times. The organic layer was washed with cold water, dried ($MgSO_4$), and the solvent removed under vacuum to give a light brown solid. The solid was washed with a little cold carbon tetrachloride to remove color and unreacted 2-pyrrolecarbonitrile. The product, 4-trichloroacetyl-2-pyrrolecarbonitrile, (12.5 g, 48%) had (after sublimation) mp 138–139°C; ir ν: 1680 (CO), 2245 cm^{-1} (CN); nmr (DMSO-d_6) δ: 7.45 (m, 1H), 8.02 (m, 1H), ~13.2 (b, 1H), $J_{3,5}$ = 1.6 Hz; *m/e* 236 ($^{35}Cl_3$), 238 ($^{35}Cl_2{}^{37}Cl$). *Anal.* calcd. for $C_7H_3Cl_3N_2O$: C 35.41, H 1.27; found: C 35.55, H 1.36.

Methanolysis of 4-Trichloroacetyl-2-pyrrolecarbonitrile

Following the literature method (5) 4-trichloroacetyl-2-pyrrolecarbonitrile (0.68 g, 2.9 mmol) was added all at once to a stirred solution of sodium methoxide from sodium (0.6 g, 25 mmol) dissolved in absolute methanol (120 ml). After 30 min the methanol was evaporated to give a light brown solid which was taken up in water and extracted with ether. The water solution was acidified and saturated with salt and extracted with ether. The combined ether extracts were washed with water, dried (Na_2SO_4) and after removal of the solvent, gave a nearly white solid (0.38 g, 87%) which was sublimed to give methyl 2-cyano-4-pyrrolecarboxylate; mp 174–175°C; ir ν: 1675 (CO), 2220 cm^{-1} (CN); nmr (DMSO-d_6) δ: 3.72 (s, 3H), 7.22 (m, 1H), 7.70 (m, 1H), $J_{3,5}$ = 1.4 Hz; *m/e* 150. *Anal.* calcd. for $C_7H_6N_2O_2$: C 56.01, H 4.03; found: C 55.78, H 4.03.

Methyl 4-Trichloroacetyl-2-pyrrolecarboxylate

Following the trichloroacetylation procedure above, methyl 2-pyrrolecarboxylate (1.0 g, 8 mmol) was converted into methyl 4-trichloroacetyl-2-pyrrolecarboxylate (1.7 g, 78%), recrystallized from benzene–hexane and sublimed, mp 118–119°C; ir ν: 1700 and 1710 cm^{-1}; nmr ($CDCl_3$) δ: 3.90 (s, 3H), 7.50 (m, 1H), 7.83 (m, 1H), ~10.2 (b, 1H); *m/e* 269 ($^{35}Cl_3$), 271 ($^{35}Cl_2{}^{37}Cl$). *Anal.* calcd. for $C_8H_6Cl_3NO_3$: C 35.52, H 2.24; found: C 35.43, H 2.26.

Methyl 2,4-Pyrroledicarboxylate

The methanolysis procedure described above was used to convert methyl 4-trichloroacetyl-2-pyrrolecarboxylate (1.0 g, 3.6 mmol) to methyl 2,4-pyrroledicarboxylate (0.5 g, 75%), mp 125.5–127°C, (lit. (14) mp 126–127°C). Spectra were in agreement with those recorded earlier (15).

Methyl 2-Cyano-4-pyrrolecarboxylate

Following the trichloroacetylation procedure above a stirred mixture of 2-pyrrolecarbonitrile (1.0 g, 11 mmol), aluminum chloride (3 g, 22 mmol) in methylene chloride (40 ml) was treated with oxalyl chloride (1.4 g, 11 mmol) at room temperature. The bright orange product was refluxed for 1 h and cooled in ice. Methanol was added dropwise until the vigorous reaction ceased and the mixture was poured onto ice. Extraction with chloroform, drying ($MgSO_4$) and evaporation gave a pale brown solid (1.4 g, 84% crude). The crude material was shown by nmr, ir, and mass spectra to be almost entirely methyl 2-cyano-4-pyrrolecarboxylate, but its ir and mass spectra indicated that a trace of methyl 4-pyrroleglyoxylate-2-carboxylate was present. Recrystallization gave pure methyl 2-cyano-4-pyrrolecarboxylate identical to that reported above.

Can. J. Chem. Downloaded from www.nrcresearchpress.com by 210.87.254.105 on 09/05/12
For personal use only.

Ethyl 2-Cyano-4-pyrrolethiolcarboxylate

Ethyl chlorothiolformate (1.4 g, 11 mmol) was added slowly to a stirred mixture of 2-pyrrolecarbonitrile (1.0 g, 11 mmol) and aluminum chloride (3.0 g, 22 mmol) in methylene chloride (40 ml) at such a rate that the reaction mixture refluxed gently (about 25 min). The deep green reaction mixture was refluxed for a further 30 min and poured onto ice – 6 *M* hydrochloric acid (about 100 g). After 1 h the layers were separated and the water layer was extracted three times with chloroform. The combined extracts were washed with water, dried ($MgSO_4$) and the solvent was removed under vacuum. The light brown solid was recrystallized from benzene to give ethyl 2-cyano-4-pyrrolethiolcarboxylate (1.4 g, 71%), mp 111–111.5°C; ir ν: 1610 (CO), 2225 cm^{-1} (CN); nmr ($CDCl_3$) δ: 1.32 (t, 3H), 3.05 (q, 2H), 7.21 (m, 1H), 7.51 (m, 1H), ~10.4 (b, 1H), $J_{3,5}$ 1.6 Hz; *m/e* 180. *Anal.* calcd. for $C_8H_8N_2OS$: C 53.32, H 4.47; found: C 53.32, H 4.47.

4-Formyl-2-pyrrolecarbonitrile

A solution of 2-pyrrolecarbonitrile (9.2 g, 0.1 mol) in dry CH_2Cl_2 (60 ml) and a solution of nitromethane (4.8 ml, 0.079 mol) in CH_2Cl_2 (20 ml) was added to a (mechanically) stirred suspension of $AlCl_3$ (23.6 g, 0.177 mol) in CH_2Cl_2 (60 ml), under N_2 at about −78°C. Dichloromethyl *n*-butyl ether (16) (21.1 g, 0.13 mol) in CH_2Cl_2 (50 ml) was then added dropwise during about 3 h in which the bath temperature was allowed to rise slowly to about −10°C. Thin-layer chromatography indicated that reaction had ceased after a further 1 h during which the bath temperature had risen to about +10°C. The reaction mixture was poured carefully with vigorous stirring onto ice-cold solid NH_4Cl. A yellow solid precipitated from the solution and after about 15 min it was collected by vacuum filtration and washed briefly with ice-cold water. The dichloromethane layer was separated from the filtrate, the yellow aqueous layer saturated with NaCl and extracted thoroughly with ethyl acetate. The ethyl acetate and CH_2Cl_2 extracts were combined, dried (Na_2SO_4) and the solvent was removed giving a yellow solid residue which was combined with the yellow precipitate collected above and recrystallized from hot water (as brown needles) to remove inorganic salts. The solid residue left after evaporation of the aqueous mother liquor was extracted continuously with petroleum (bp 100–120°C) to give more of the required pyrrole. Sublimation of the crude products gave pure 4-formyl-2-pyrrolecarbonitrile (8.9 g, 74%)[1] as a white powder, mp 173–175°C; ν (Nujol): 2235 (CN), 1660 cm^{-1} (CO); nmr (acetone-d_6) δ: 7.29 (d, 1H), 7.88 (d, 1H), 9.78 (s, 1H), $J_{3,5}$ = 1.5 Hz; *m/e* 120. *Anal.* calcd. for $C_6H_4N_2O$: C 60.00, H 3.36, N 23.32; found: C 60.16, H 3.53, N 23.35.

5-tert-Butyl-2-pyrrolecarbonitrile

This product crystallized from the mixture obtained by the $AlCl_3$ catalyzed Friedel–Crafts acylation of 2-pyrrolecarbonitrile (10). The 5-*tert*-butyl-2-pyrrolecarbonitrile was sublimed for analysis, mp 115–116°C; ir (Nujol mull) ν: 3286 (N—H), 2216 cm^{-1} (C≡N); nmr ($CDCl_3$) δ: 1.26 (s, 9H), 5.86 (m, 1H), 6.64 (m, 1H), 9.32 (b, 1H), $J_{3,4}$ 3.6 Hz, $J_{1,3}$ and $J_{1,4}$ 2.7 Hz. *Anal.* calcd. for $C_9H_{12}N_2$: C 72.94, H 8.16, N 18.90; found: C 73.36, H 8.15, N 18.98.

Conversion of the 2-Pyrrolecarbonitriles to 2-Pyrrolecarboxaldehydes

4-Acetyl-2-pyrrolecarboxaldehyde

Raney nickel alloy (2.0 g) and formic acid (75% aq, 60 ml) were mixed in a 100 ml flask. The mixture was stirred using a magnetic stirrer and heated until the mixture just began to reflux and the evolution of gas was brisk. 4-Acetyl-2-pyrrolecarbonitrile (1.00 g) was then added and the heating and stirring was maintained so that the mixture did not quite reflux but gas evolution continued. After 1 h the mixture, while still being warmed and stirred, was extracted continuously with toluene for 24 h. The toluene extract was collected and the solvent was removed to leave a brownish residue of the crude product (1.01 g). Recrystallization from ethyl acetate – petroleum mixture gave 4-acetyl-2-pyrrolecarboxaldehyde (0.84 g, 82%), mp 141.5–142°C (lit. (1) mp 136–137°C). Mixture mp with authentic material was undepressed.

Using the same procedure the following aldehydes were obtained:

Ethyl 2-Formyl-4-pyrrolethiolcarboxylate

Ethyl 2-cyano-4-pyrrolethiolcarboxylate gave ethyl 2-formyl-4-pyrrolethiolcarboxylate which was crystallized from a benzene–petroleum mixture and then sublimed to give prisms, mp 72.5–74°C, in 62% yield; nmr ($CDCl_3$) δ: 1.31 (t, 3H), 3.04 (q, 2H), 7.75 (m, 2H), 9.50 (d, 1H); *m/e* 183. *Anal.* calcd. for $C_8H_9NO_2S$: C 52.44, H 4.95; found: C 52.48, H 4.98.

Methyl 2-Formyl-4-pyrrolecarboxylate

The *product* was obtained from methyl 2-cyano-4-pyrrolecarboxylate and recrystallized from toluene–petroleum mixture as fluffy needles, (71%) mp 127–128°C after sublimation; ir (Nujol mull) ν: 1660 (CO), 1720 cm^{-1} (CO); nmr ($CDCl_3$) δ: 3.80 (s, 3H), 7.34 (m, 1H), 7.65 (m, 1H), 9.48 (d, 1H), $J_{3,5}$ 1.4 Hz, J_{CHO-5} 1.0 Hz; *m/e* 153. *Anal.* calcd. for $C_7H_7NO_3$: C 54.90, H 4.61; found: C 55.04, H 4.62.

2,4-Pyrroledicarboxaldehyde

4-Formyl-2-pyrrolecarbonitrile gave the product which was crystallized from water as brown needles (68%) mp 148–151°C after sublimation (lit. (13) mp 151.5–152°C).

4-tert-Butyl-2-pyrrolecarboxaldehyde

The *product* was extracted continuously with petroleum (bp 40–60°C) rather than with toluene, and finally sublimed (89%), mp 86.5–87.5°C; ir (Nujol mull) ν: 3227 (N—H), 1664 cm^{-1} (C=O); nmr ($CDCl_3$) δ: 1.24 (s, 9H), 6.80 (m, 1H), 6.89 (m, 1H), 9.31 (s, 1H), $J_{3,4}$ 3.84 Hz, $J_{1,3}$ 2.4 Hz, $J_{1,4}$ 2.5 Hz. *Anal.* calcd. for $C_9H_{13}NO$: C 71.49, H 8.66, N 9.26; found: C 71.74, H 8.51, N 8.95.

5-tert-Butyl-2-pyrrolecarbaldehyde was obtained similarly (70%), mp 66–67°C; ir (Nujol mull) ν: 3281 (N—H), 1646 cm^{-1} (CO); nmr ($CDCl_3$) δ: 1.32 (s, 9H), 6.03 (m, 1H), 6.80 (m, 1H), 9.23 (s, 1H), 9.81 (b, 1H); *m/e* 151. *Anal.* calcd. for $C_9H_{13}NO$: C 71.49, H 8.66, N 9.26; found: C 71.72, H 8.49, N 9.02.

Decarbonylation of the 4-Substituted 2-Pyrrolecarboxaldehydes

Methyl 3-Pyrrolecarboxylate

A stirred mixture of methyl 2-formyl-4-pyrrolecarboxylate (500 mg), toluene (20 ml) and W5 Raney nickel (17) (about 1 g) was refluxed for 4½ h. The mixture was then cooled at room temperature and filtered through a Celite pad to remove the nickel. The nickel and pad were washed with acetone and the filtrates were combined. The solvent was then removed and the solid residue was recrystallized from chloroform–petroleum mixture (342 mg, 84%), mp 87–87.5°C (lit. (18) mp 88°C); ($CDCl_3$) δ: 3.69 (s, 3H), 6.57 (m, 2H), 7.31 (m, 1H), 9.89 (b, 1H).

3-Acetylpyrrole

Decarbonylation of 4-acetyl-2-pyrrolecarboxaldehyde (1) gave 3-acetylpyrrole in 87% yield, mp 115–116°C (lit. (1) mp 115–116°C); the mixture mp with authentic material was undepressed.

[1]Less mild conditions gave lower yields and were less selective, significant amounts of a second formylation product (nmr) being formed, presumably the result of attack at the C-5 position.

Acknowledgements

The authors gratefully acknowledge the continued financial support of the National Research Council of Canada and the Memorial University of Newfoundland.

1. H. J. ANDERSON and C. W. HUANG. Can. J. Chem. **45**, 897 (1967).
2. C. E. LOADER and H. J. ANDERSON. Can. J. Chem. **49**, 45 (1971).
3. H. J. ANDERSON. Can. J. Chem. **46**, 798 (1968).
4. A. TREIBS and F. H. KREUZER. Justus Liebigs Ann. Chem. **721**, 105 (1969).
5. J. W. HARBUCK and H. RAPOPORT. J. Org. Chem. **37**, 3618 (1972).
6. H. FISCHER and H. ORTH. Die chemie des Pyrrols. Vol. I. Akademische Verlagsgesellschaft M.B.H., Leipzig. 1934, p. 305.
7. A. H. PETO. *In* Friedel–Crafts and related reactions. Vol. III. *Edited by* G. A. Olah. Wiley-Interscience, New York, NY. 1964. p. 608.
8. E. BULLOCK, T.-S. CHEN, and C. E. LOADER. Can. J. Chem. **44**, 1007 (1966); E. BULLOCK, T.-S. CHEN, C. E. LOADER, and A. E. WELLS. Can. J. Chem. **48**, 1651 (1970).
9. G. A. OLAH and P. SCHILLING. Justus Liebigs Ann. Chem. **761**, 77 (1972).
10. J. K. GROVES, H. J. ANDERSON, and H. NAGY. Can. J. Chem. **49**, 2427 (1971).
11. M. K. A. KHAN, K. J. MORGAN, and D. P. MORREY. Tetrahedron, **22**, 2095 (1966).
12. T. S. VAN ES and B. STASKUN. J. Chem. Soc. 5775 (1965).
13. C. E. LOADER and H. J. ANDERSON. Tetrahedron, **25**, 3879 (1969).
14. R. A. NICOLAUS and L. MANGONI. Gazz. Chim. Ital. **86**, 757 (1956); Chem. Abstr. **52**, 2833 (1958).
15. S.-F. LIU. M.Sc. Thesis. Memorial University of Newfoundland, St. John's, Nfld. 1965.
16. A. RIECHE, H. GROSS, and E. HÄFT. Chem. Ber. **93**, 88 (1960).
17. R. MOZINGO. Org. Synth. Coll. Vol. 3. *Edited by* E. C. Horning. J. Wiley and Sons, Inc., New York, NY. 1947. p. 176.
18. I. J. RINKES. Recl. Trav. Chim. **57**, 423 (1938).

Can. J. Chem. Downloaded from www.nrcresearchpress.com by 210.87.254.105 on 09/05/12
For personal use only.

Protonated cyclopropanes. X. Studies on the deamination of *n*-butylamine-1-^{14}C and the decomposition of 3-(*n*-butyl-1-^{14}C)-1-phenyltriazene

CHOI CHUCK LEE, RANDY REICHLE, AND URSULA WEBER

Department of Chemistry and Chemical Engineering, University of Saskatchewan, Saskatoon, Sask., Canada S7N 0W0

Received August 12, 1977

CHOI CHUCK LEE, RANDY REICHLE, and URSULA WEBER. Can. J. Chem. **56**, 658 (1978).

The HNO_2 deamination of *n*-butylamine-1-^{14}C (**1**-NH_2-1-^{14}C) in aqueous $HClO_4$ gave a *n*-butyl-^{14}C alcohol (**1**-OH-^{14}C) with about 0.7% scrambling of the label from C-1 to C-2, and a *sec*-butyl-^{14}C alcohol (**2**-OH-^{14}C) which showed extensive scrambling between C-1 and C-4, as well as small amounts of rearrangement of the label into C-2 and C-3. Analysis of the data suggested that about 2.5% of the **2**-OH-^{14}C product could be derived from equilibrating protonated methylcyclopropane intermediates. The $HClO_4$ catalyzed decomposition of 3-(*n*-butyl-1-^{14}C)-1-phenyltriazene (**1**-NNNHPh-1-^{14}C) gave the unrearranged **1**-OH-1-^{14}C and a **2**-OH-^{14}C which showed only about 17–18% scrambling from C-1 to C-4. It is suggested that the different results observed in the deamination and the triazene decomposition may be due to a more ready initial formation of an ion pair in the triazene decomposition.

CHOI CHUCK LEE, RANDY REICHLE et URSULA WEBER. Can. J. Chem. **56**, 658 (1978).

La désamination nitreuse de la butylamine ^{14}C-1 (**1**-NH_2-1-^{14}C) dans de l'acide perchlorique aqueux conduit à de l'alcool butylique ^{14}C (**1**-OH-^{14}C) contenant environ 0.7% d'échange du marqueur du C-1 vers C-2 et un alcool butylique secondaire ^{14}C (**2**-OH-^{14}C) qui présente beaucoup d'échange entre les C-1 et C-4 de même que de petites quantités de réarrangement du marqueur vers les positions C-2 et C-3. Une analyse des données suggère qu'environ 2.5% du produit de **2**-OH-^{14}C pourrait provenir de l'équilibration de méthylcyclopropanes intermédiaires. La décomposition catalysée par $HClO_4$ du (butyl ^{14}C-1)-3 phényl-1 triazène (**1**-NNNHPh-1-^{14}C) conduit à du **1**-OH-^{14}C qui n'est pas réarrangé et à un **2**-OH-^{14}C qui ne présente qu'environ 17–18% d'échange entre les carbones 1 et 4. On suggère que les résultats différents observés lors de la désamination et de la décomposition du triazène peuvent être dus à une formation initiale plus facile d'une paire d'ions lors de la décomposition du triazène.

[Traduit par le journal]

The HNO_2 deamination of various D-labeled *n*-butylamines, coupled with mass spectral analysis, carried out in HOAc by Streitwieser and Schaeffer (1) and in aqueous $HClO_4$ by Karabatsos *et al.* (2), showed no detectable scrambling in the *n*-butyl product (1, 2) and scrambling in the *sec*-butyl product resulted only from reversible 1,2-hydride shifts in the *sec*-butyl cation (2). Such results indicated that protonated methylcyclopropanes are not important intermediates in these reactions. However, the scrambling data did not exclude a minor amount of involvement of such intermediates since small extents of rearrangements might be within the experimental errors of the method of measurement. Karabatsos *et al.* (2) estimated that there may be about 0.6% methylcyclopropane among the hydrocarbon products in the deamination and concluded that the only evidence for the intermediacy of protonated methylcyclopropanes in the aqueous acid deamination of *n*-butylamine was the formation of methylcyclopropane. Recently, we have shown that in the trifluoroacetolysis of *n*-butyl-1-^{14}C tosylate (3) and of *n*-butyl-1-^{14}C-mercuric perchlorate (4), the scramblings in the *sec*-butyl products can be explained only by invoking some contribution from equilibrating protonated methylcyclopropanes as intermediates. Since reinvestigations of the early work of Roberts and Halmann (5) on the HNO_2 deamination of *n*-propylamine-1-^{14}C in aqueous $HClO_4$ gave evidence in support of equilibrating protonated cyclopropanes (6, 7), we decided to carry out a study on the deamination of *n*-butylamine-1-^{14}C in order to ascertain more quantitatively the involvement of protonated methylcyclopropane intermediates. In conjunction with this work, the acid catalyzed decomposition of 3-(*n*-butyl-1-^{14}C)-1-phenyltriazene was investigated since this reaction, as in the deamination, might proceed via the alkyldiazonium ion (8).

n-Butylamine-1-^{14}C (**1**-NH_2-1-^{14}C) was prepared by the $LiAlH_4$ reduction of $CH_3CH_2CH_2{}^{14}CN$ (2, 5). That all of the ^{14}C label was located at C-1 was shown by oxidation of **1**-NH_2-1-^{14}C to CH_3CH_2-$CH_2{}^{14}COOH$ (10) followed by a Schmidt reaction to give inactive CH_3CH_2COOH. The deamination of **1**-NH_2-1-^{14}C in aqueous $HClO_4$ was carried out under the conditions used by previous workers (2, 5). The yields of the isomeric *n*-butyl, *sec*-butyl, isobutyl, and *tert*-butyl alcohols (**1**-OH, **2**-OH, **3**-OH, and **4**-OH, respectively) were determined by isotopic

Can. J. Chem. Downloaded from www.nrcresearchpress.com by 210.87.254.40 on 09/05/12
For personal use only.

Can. J. Chem. Downloaded from www.nrcresearchpress.com by 210.87.254.40 on 09/05/12
For personal use only.

TABLE 1. Yields (%) of isomeric butyl alcohols calculated from isotopic dilution in the HNO_2 deamination of *n*-butylamine-1-^{14}C in aqueous $HClO_4$

	n-BuOH	*sec*-BuOH	*iso*-BuOH	*tert*-BuOH
Run 1	22.9	9.5	Trace	0.2
Run 2	25.7	8.8	Trace	0.2
Run 3	23.3	10.2	Trace	0.2

TABLE 2. ^{14}C distributions in the *n*-butyl-^{14}C alcohol (**1**-OH-^{14}C) derived from the deamination of *n*-butylamine-1-^{14}C (**1**-NH_2-1-^{14}C)

	Specific activity (dpm/mmol)*			^{14}C distributions (%)			
	1-OH†	CH_3CH_2COOH‡	CH_3COOH‡	C-1	C-2	C-3	C-4
Run 1	241 000	1680	0	99.3	0.7	0	0
Run 2	830 000	5830	0	99.3	0.7	0	0
Run 3	744 000	5960	0	99.2	0.8	0	0

*^{14}C activities in this and other tables were measured by a liquid scintillation counter. Statistical counting errors were ± 1% or less.
†Assayed as the α-naphthylurethane.
‡Assayed as the *S*-benzylisothiouronium salt.

TABLE 3. ^{14}C distributions in the *sec*-butyl-^{14}C alcohol (**2**-OH-^{14}C) derived from the deamination of *n*-butylamine-1-^{14}C (**1**-NH_2-1-^{14}C) and from the decomposition of 3-(*n*-butyl-1-^{14}C)-1-phenyltriazene (**1**-NNNHPh-1-^{14}C)

	Specific activity (dpm/mmol)					^{14}C distribution (%)			
Reaction	**2**-OH*	CBr_4	CH_3CH_2COOH†	CH_3COOH†	CH_3NH_2‡	C-1	C-2	C-3	C-4
Deamination									
Run 1	754 000	380 000	—	—	—	50.4	—	—	—
Run 2	1 250 000	632 000	620 000	616 000	604 000	50.6	0.3	1.0	48.3
Run 3	1 390 000	703 000	587 000	683 000	669 000	50.6	0.3	1.0	48.1
Triazene decomposition									
Run 1	52 400	43 100	9 300	9 400	9 360	82.3	0	0	17.8
Run 2	31 800	26 400	5 500	5 500	5 500	83.0	0	0	17.5
Triazene decomposition with added DPPH									
Run 1	57 800	47 400	10 000	—	—	82.0	—	—	17.3
Run 2	53 100	44 000	9 100	—	—	82.9	—	—	17.1

*Assayed as the α-naphthylurethane.
†Assayed as the *S*-benzylisothiouronium salt.
‡Assayed as the *p*-toluenesulfonamide.

dilution (4, 9) and the results are given in Table 1. The main products, **1**-OH-^{14}C and **2**-OH-^{14}C, were degraded as described previously (4, 9) to give the ^{14}C distributions. The results are summarized in Tables 2 and 3.

n-Butyl-1-^{14}C chloride (9) was converted to the Grignard reagent and treated with phenyl azide to give 3-(*n*-butyl-1-^{14}C)-1-phenyltriazene (**1**-NNNHPh-1-^{14}C) (11). The acid catalyzed decomposition of **1**-NNNHPh-1-^{14}C was effected at room temperature with 0.1% $HClO_4$ in 90% acetone – 10% H_2O, which was one set of conditions that was used to generate triarylvinyl cations from triarylvinylphenyltriazenes (12). While the decomposition of alkylphenyltriazenes in HX–H_2O proceeds by an ionic mechanism (11, 13), it has been reported that in the absence of HX, decomposition in media such as H_2O–CH_3OH or H_2O–C_6H_6 emulsions may follow a radical process (13). To ascertain whether radicals were involved under the present conditions, the $HClO_4$ catalyzed decomposition of **1**-NNNHPh-1-^{14}C in aqueous acetone was also carried out in the presence of the radical scavenger, diphenylpicrylhydrazyl (DPPH). It was found that the added DPPH had no effect on either the yields of butyl alcohols or on the extents of isotopic scrambling. In both the presence and absence of DPPH, the decomposition of **1**-NNNHPh-1-^{14}C gave yields of 43–44% **1**-OH-^{14}C and 16–17% **2**-OH-^{14}C as determined by isotopic dilution. There were no detectable amounts of **3**-OH-^{14}C or **4**-OH-^{14}C. Degradation of **1**-OH-^{14}C showed that there was no isotopic scrambling, and this product was unrearranged **1**-OH-1-^{14}C. Degradation of the **2**-OH-^{14}C product showed that

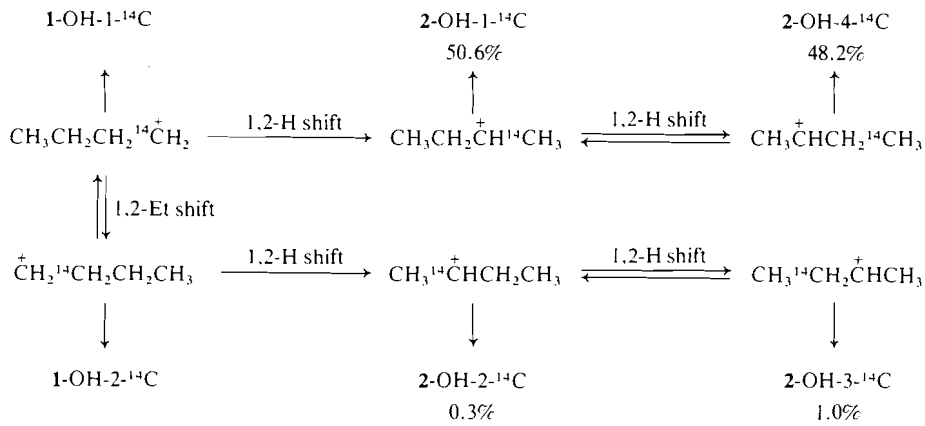

SCHEME 1

scramblings occurred only between C-1 and C-4, and the results are included in Table 3.

For the deamination of **1**-NH_2-1-^{14}C, the scrambling data may be interpreted in the same way as in the interpretation of the results from the trifluoroacetolysis of **1**-OTs-1-^{14}C (3) and **1**-$HgClO_4$-1-^{14}C (4). Consider, firstly, the ^{14}C distribution in the **2**-OH-^{14}C (Table 3). The extensive scramblings between C-1 and C-4 indicate that a major process is a degenerate 1,2-hydride shift interconverting the *sec*-butyl-1-^{14}C and *sec*-butyl-4-^{14}C cations. To account for the small amounts of ^{14}C activity at C-2 and C-3, a mechanism involving a 1,2-ethyl shift as depicted in Scheme 1 may be suggested. Since the *sec*-butyl-1-^{14}C and *sec*-butyl-2-^{14}C cations differ only in the position of the label, one would expect these ions to undergo essentially the same subsequent reactions. Thus according to Scheme 1, the ratio of **2**-OH-4-^{14}C to **2**-OH-1-^{14}C should be equal to the ratio of **2**-OH-3-^{14}C to **2**-OH-2-^{14}C. Clearly this expectation does not agree with the experimental data since 48.2:50.6 is far from equalling 1.0:0.3. The mechanism in Scheme 1, therefore, is inadequate to account for the observed results.

To account for the small amounts of scrambling into C-2 and C-3 of the *sec*-butyl product, an alternative mechanism could involve a contribution from equilibrating protonated methylcyclopropanes (3, 4). Utilizing corner-protonated methylcyclopropanes **5***a–c*, Scheme 2 shows the partitioning of the various routes leading to the ^{14}C distribution in **2**-OH-^{14}C. As suggested previously (3, 4), it is proposed that **5***b* and **5***c* could give the *sec*-butyl product directly or give rise to the more stable *sec*-butyl cation which subsequently would undergo degenerate hydride shifts. In this scheme, the equality of the product ratios derived from equilibrating *sec*-butyl cations is also maintained (47.2:50.2 $\simeq$ 0.3:0.3). The net ^{14}C contents would be 50.2 + 0.3, 0.3, 0.7 + 0.3, and 47.2 + 0.7 + 0.3 or 50.5, 0.3, 1.0, and 48.2%, respectively, for C-1, C-2, C-3, and C-4. These calculated values agree completely with the averaged, observed ^{14}C distribution in **2**-OH-^{14}C derived from the deamination of **1**-NH_2-1-^{14}C (Table 3). These results are in general accord with the conclusion of Karabatsos *et al.* (2) that there is only a minor involvement of protonated methylcyclopropane intermediates in the aqueous acid deamination of *n*-butylamine; the present work using the sensitive radioactive tracer technique has shown more quantitatively that about 2.5% of the *sec*-butyl product was derived from equilibrating protonated methylcyclopropanes.

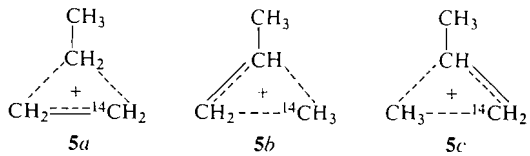

In the *n*-butyl product, **1**-OH-^{14}C, there is about 0.7% rearrangement of the label from C-1 to C-2 (Table 2). This scrambling can be attributed to product formation from protonated methylcyclopropane **5***a*. Moreover, **5***b* and **5***c* can also give rise to the isobutyl product and a facile rearrangement of the isobutyl to the *tert*-butyl cation would account for the small amount of *tert*-BuOH among the products as recorded in Table 1.

The decomposition of RNNNHPh in aqueous acids is known to give ROH, N_2, and $PhNH_2$ as products (11, 13). If the alcohol were formed via RN_2^+ and R^+, there is an apparent similarity between the decomposition of alkylphenyltriazenes and the deamination of primary amines. As can be seen from Table 3, **2**-OH-^{14}C derived from the deamination of **1**-NH_2-1-^{14}C and from the decomposition of **1**-NNNHPh-1-^{14}C showed entirely different extents of isotopic scrambling. In the

Can. J. Chem. Downloaded from www.nrcresearchpress.com by 210.87.254.40 on 09/05/12
For personal use only.

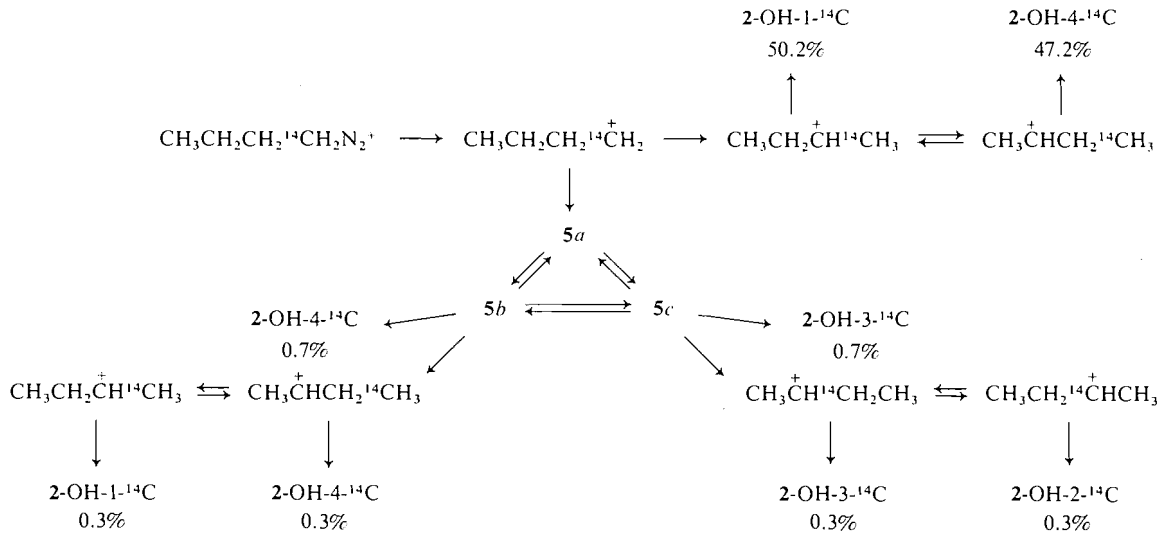

SCHEME 2

2-OH-^{14}C from the triazene decomposition, there was only 17–18% rearrangement of the label from C-1 to C-4, with no detectable amount of scrambling into C-2 and C-3. The possibility that the lesser extent of rearrangement may be due to a contribution from radical processes was eliminated since the presence of DPPH did not influence the results.

To explain the different results obtained in the deamination and triazene decomposition, it is of interest to note that Collins (14) has pointed out that ion-pairing exerts a pronounced effect on product formation in carbocationic reactions including deamination. In the present work, although there are differences in the reaction media for the deamination and the triazene decomposition, both reactions were carried out in the presence of H_2O. Any coordination or ion-pairing involving the same nucleophilic solvent is not likely to exert a sufficiently large effect to account for the differences in isotopic scrambling observed in these two reactions as recorded in Table 3. Kawanisi *et al.* (15) have reported a novel decomposition of RNNNHPh in benzene catalyzed by silica gel. Besides the usual products of ROH, N_2, and $PhNH_2$, PhNHR was also obtained and the recombination of the R group with the anilino group was found to occur with retention of configuration at the α-carbon of the R group. While the precise function of the silica gel was not known, it was proposed that the reaction mechanism involved an intimate ion-pair formed between the carbocation and the anilino ion. In the decomposition of **1**-NNNHPh-1-^{14}C in aqueous acid, possibly, there may also be an initial formation of an ion-pair between the butyl and anilino ions which could rapidly react with solvent without rearrangement. Upon further dissociation to give solvated butyl cations, more scrambling through degenerate 1,2-hydride shifts can occur. In the deamination of **1**-NH_2-1-^{14}C, there is no analogous ion-pairing with the anilino group and the net result is the occurrence of more extensive scrambling as was observed.

Experimental

Deamination of n-*Butylamine-1-*^{14}*C (1-*NH_2*-1-*^{14}*C)*

Butyronitrile-1-^{14}C, prepared from $CH_3CH_2CH_2Cl$ and $Na^{14}CN$, was reduced with $LiAlH_4$ and treated with $HClO_4$ to give **1**-$NH_2 \cdot HClO_4$-1-^{14}C using procedures similar to those reported for the preparation of $CH_3CH_2{}^{14}CH_2NH_2 \cdot HClO_4$ (5) and **1**-$NH_2 \cdot HClO_4$-1,1-d_2 (2). The deamination was carried out as described by previous workers (**1**-$NH_2 \cdot HClO_4$-1-^{14}C in 35% $HClO_4$ treated with aqueous $NaNO_2$ at 30°C) (2, 5). The reaction mixture was distilled to dryness. The distillate was acidified with HCl and distilled again to dryness. The latter distillate was saturated with KF and the organic layer was separated. The yields of the four isomeric alcohols were determined by isotopic dilution with added carriers, with purification by preparative vpc as described previously (4, 9). The major products, *n*-butyl-^{14}C and *sec*-butyl-^{14}C alcohols (**1**-OH-^{14}C and **2**-OH-^{14}C), with more carriers added if necessary, were degraded using procedures that have also been described in the previous work (4, 9).

*3-(*n*-Butyl-1* ^{14}*C)-1-phenyltriazene (1-NNNHPh-1-*^{14}*C)*

The triazene was prepared from the reaction of **1**-MgCl-1-^{14}C and phenyl azide (11, 12). The Grignard reagent, prepared from 12.5 g (13.5 mmol) of **1**-Cl-1-^{14}C in 35 ml of ether, was cooled in an ice bath. An equivalent of freshly prepared phenyl azide (16) in 35 ml of ether was added. The reaction mixture was stirred at room temperature for 2 h, treated with a solution of 10% NH_4OH – 10% NHCl, and then extracted with ether. The extract was washed with H_2O and dried over $MgSO_4$. After removal of the ether, 14.4 g (60%) of **1**-NNNHPh-1-^{14}C was recovered as a yellow oil, which was crystallized in petroleum ether in a cold room, mp 18°C (lit (17), mp 17–18°C).

Decomposition of 1-NNNHPh-1-^{14}*C*

To 3.0 g (17 mmol) of **1**-NNNHPh-1-^{14}C was added 20 ml of 90% acetone – 10% H_2O (by volume) containing 0.1%

Can. J. Chem. Downloaded from www.nrcresearchpress.com by 210.87.254.40 on 09/05/12
For personal use only.

$HClO_4$. Evolution of N_2 occurred immediately and apparently ceased within about 1 min. The reaction mixture was stirred at room temperature for 1 h and then ordinary **1**-OH, **2**-OH, **3**-OH, and **4**-OH were added as carriers. After drying over $MgSO_4$ (about 2 g), the resulting solution was filtered, the acetone removed by distillation, and the residual alcohols were purified by preparative vpc. The yields of butyl alcohols were calculated from isotopic dilution and the **1**-OH-^{14}C and **2**-OH-^{14}C were degraded as before (4, 9).

When the decomposition was carried out in the presence of DPPH, the same procedure was used except that the solvent, 90% acetone – 10% H_2O, was saturated with DPPH (about 0.1%).

Acknowledgement

The financial support given by the National Research Council of Canada is gratefully acknowledged.

1. A. STREITWIESER, JR. and W. D. SCHAEFFER. J. Am. Chem. Soc. **79**, 2888 (1957).
2. G. J. KARABATSOS, R. A. MOUNT, D. O. RICKTER, and S. MEYERSON. J. Am. Chem. Soc. **92**, 1248 (1970).
3. C. C. LEE, A. J. CESSNA, E. C. F. KO, and S. VASSIE. J. Am. Chem. Soc. **95**, 5688 (1973).
4. C. C. LEE and R. REICHLE. J. Org. Chem. **42**, 2058 (1977).
5. J. D. ROBERTS and M. HALMANN. J. Am. Chem. Soc. **75**, 5759 (1953).
6. C. C. LEE and J. E. KRUGER. Tetrahedron, **23**, 2539 (1967).
7. C. C. LEE. Progr. Phys. Org. Chem. **7**, 129 (1970).
8. H. ZOLLINGER. Azo and diazo chemistry. Interscience Publishers, New York, NY. 1961. Chapt. 8.
9. C. C. LEE and I. Y. ZEA PONCE. Can. J. Chem. **50**, 3179 (1972).
10. E. G. MOSBACH, E. F. PHARES, and S. F. CARSON. Arch. Biochem. Biophys. **33**, 179 (1951).
11. O. DIMROTH. Ber. **38**, 670 (1905).
12. C. C. LEE and E. C. F. KO. Can. J. Chem. **54**, 3041 (1976).
13. V. YA. ANDAKUSHKIN, B. A. DOLGOPLOSK, and I. I. RADCHENKO. Zhur. Obshchei Khim. **26**, 2972 (1956) (J. Gen. Chem. USSR, **26**, 3307 (1956)).
14. C. J. COLLINS. Chem. Soc. Rev. **4**, 251 (1975).
15. M. KAWANISI, I. OTANI, and H. NOZAKI. Tetrahedron Lett. 5575 (1968).
16. R. O. LINDSAY and C. F. H. ALLEN. Organic syntheses. Coll. Vol. III. John Wiley and Sons, New York, NY. 1955. p. 710.
17. B. A. DOLGOPLOSK, B. L. ERUSALIMSKY, V. A. KROL, and L. M. ROMANOV. Zhur. Obshchei Khim. **24**, 1775 (1954) (J. Gen. Chem. USSR, **24**, 1745 (1954)).

Can. J. Chem. Downloaded from www.nrcresearchpress.com by 210.87.254.40 on 09/05/12
For personal use only.

Analyse des spectres de vibration de la β-alanine, de la taurine et de la ciliatine-β

CHANTAL GARRIGOU-LAGRANGE

Centre de Recherche Paul Pascal, Domaine Universitaire, 33405 - Talence, France

Reçu le 5 octobre 1977

CHANTAL GARRIGOU-LAGRANGE. Can. J. Chem. **56**, 663 (1978).

Les spectres de vibration de la β-alanine, de la taurine et de la ciliatine (forme β) à l'état solide sont analysés. Un calcul de modes normaux est effectué. Les champs de force de valence obtenus pour ces trois molécules à l'état cristallin sont très voisins et montrent que le radical $N—C_\alpha H_2—C_\beta H_2—$ est électroniquement équivalent dans les trois molécules.

CHANTAL GARRIGOU-LAGRANGE. Can. J. Chem. **56**, 663 (1978).

Infrared and Raman spectra of solid β-alanine, taurine and ciliatine (β form) are analysed. A normal mode calculation is made. The given valence force fields of the three crystalline molecules are very similar. It shows the $N—C_\alpha H_2—C_\beta H_2—$ radical is electronically equivalent in the three molecules.

Can. J. Chem. Downloaded from www.nrcresearchpress.com by 210.87.254.105 on 09/05/12
For personal use only.

La ciliatine ou acide 2-amino-éthyl phosphonique et la taurine ou acide 2-amino-éthyl sulfonique sont largement représentées dans les organismes vivants, des protozoaires aux vertébrés et à l'homme (1–4). Leur grand intérêt biologique nous a amenés à étudier leurs spectres de vibration, en liaison avec leur structure. A la suite des travaux que nous avons déjà effectués sur des acides α aminés (5, 6) et des peptides (7–10), nous avons fait un calcul des modes normaux de ces molécules. Pour comparaison, nous avons inclus dans cette étude la β-alanine ou acide 2 amino-éthyl carboxylique.

La ciliatine possède deux variétés allotropiques α et β caractérisées par leurs spectres infrarouges (11). La structure cristalline de la forme β est connue (12). On connaît également celles de la β-alanine (13) et de la taurine (14).

Une interprétation des spectres de vibration infrarouges et Raman de la β-alanine hydrogénée (15), de la taurine hydrogénée et *N* deutériée (16) à l'état solide a déjà été proposée. Par contre, aucune attribution détaillée des spectres de la ciliatine n'a, à notre connaissance, été publiée.

Dans ce travail, après avoir discuté l'interprétation des spectres de vibration de ces trois acides aminés, nous exposerons les résultats du calcul de modes normaux que nous avons effectué.

Les vibrations NH et ν OH ne sont pas envisagées dans ce mémoire: elles ne peuvent pas être localisées, les groupements NH_3^+ et OH étant très auto-associés. Quant aux vibrations ν CH, elles n'entrent pas en interaction avec les autres modes de vibration; nous n'avons donc pas cherché à les attribuer ni, a fortiori, à préciser les constantes de force correspondantes.

Analyse des spectres de vibration

Nous avons enregistré les spectres infrarouges et Raman jusqu'à 200 cm^{-1} de la β-alanine, de la taurine et de la ciliatine forme β et de leurs homologues deutériés sur l'azote et (pour la ciliatine) sur l'oxygène, à l'état solide.[1]

β-*Alanine*

L'attribution des spectres de vibration de la β-alanine hydrogénée que nous proposons sur le tableau 1 est basée sur les résultats que nous avons obtenus pour les trois variétés allotropiques de la glycine (5). Elle est en assez bon accord avec celle des auteurs précédents (15). La comparaison des spectres infrarouges des dérivés hydrogéné et *N* deutérié nous a cependant amenés à intervertir les fréquences des vibrations δ_d NH_3 et ν_a COO. En outre, nous faisons correspondre la bande observée à 1261 cm^{-1} à une vibration de torsion *t* CH_2, les vibrations de balancement *w* CH_2 étant habituellement situées à fréquence plus élevée.

Pour le dérivé *N* deutérié, la comparaison avec les glycines ND_3 (5) conduit aux attributions du tableau 1. Nous n'avons pas donné d'interprétation pour les bandes relevées entre 800 et 1100 cm^{-1}, les modes observés dans cette région dans le cas de la glycine étant très complexes.

Taurine

A l'exception de la faible raie Raman à 420 cm^{-1} relevée par Stahlberg et Steger (16) et que nous n'avons pas observée, nos résultats expérimentaux concordent avec ceux de ces auteurs. L'interprétation que nous proposons, basée sur la comparaison avec la β-alanine et indiquée sur le tableau 2, est très proche de celle donnée par les auteurs précédents (16), sauf en ce qui concerne certaines vibrations des groupements NH_3 et ND_3. Ces auteurs, en effet, attribuent quatre fréquences: 891, 961, 1103 et 1388 cm^{-1} aux deux vibrations de balancement *r* NH_3.

[1]Les spectres pourront être obtenus sur demande.

TABLEAU 1. Nombres d'onde (cm^{-1}) et distribution d'énergie potentielle de la β-alanine (*a*) et de son homologue *N* deutérié (*b*)

Attributions (PT)	ν obs Infrarouge	ν obs Raman	ν calc	Distribution d'énergie potentielle* $100(L_{ti}^2F_{ti}/\lambda k)$
			(*a*) $H_3\overset{+}{N}C_\alpha H_2C_\beta H_2COO^-$	
δ_d NH_3†	1650 1632		1653.5 1652	92 δ_s' NH_3 93 δ_a NH_3
ν_a COO†	1572		1578.5	100 ν_a COO, 14 *r* COO
δ_s NH_3	1507		1501	84 δ_s NH_3
δ CH_2	1466 1448	1467 1453	1464 1438	19 δ $C_\alpha H_2$, 45 δ $C_\beta H_2$, 12 *w* $C_\beta H_2$ 53 δ $C_\alpha H_2$, 14 *w* $C_\beta H_2$
	1413	1427 1410	1411	22 δ $C_\beta H_2$, 10 *w* $C_\alpha H_2$, 33 *w* $C_\beta H_2$
ν_s COO	1403 1388	1401 1388	1379	15 ν $C_\beta C$, 63 ν_s COO, 15 δ COO
w CH_2	1333	1332	1336	14 δ $C_\beta H_2$, 62 *w* $C_\alpha H_2$, 11 *w* $C_\beta H_2$
t CH_2	1293	1294	1283	82 *t* $C_\beta H_2$
t CH_2†	1261	1264	1260	86 *t* $C_\alpha H_2$
	1157	1161	1145	11 $r_{\|}$ NH_3, 41 $r_\perp$ NH_3, 17 *r* $C_\alpha H_2$
r NH_3	1128	1134	1116	49 $r_{\|}$ NH_3, 19 $r_\perp$ NH_3
ν NC_α	1060	1063	1032	47 ν NC_α, 20 ν $C_\alpha C_\beta$
r CH_2	991	993	982	15 $r_{\|}$ NH_3, 19 $r_\perp$ NH_3, 10 *r* $C_\alpha H_2$, 17 *r* $C_\beta H_2$, 12 ν $C_\alpha C_\beta$
	945	941	958	29 ν $C_\beta C$, 15 ν_s COO
ν $C_\alpha C_\beta$	886	888	891.5	17 *t* NH_3, 29 *r* $C_\alpha H_2$, 11 ν $C_\beta C$
	846	848	842.5	43 *r* $C_\beta H_2$, 29 ν NC_α
δ COO	653	654.5	662	11 *t* NH_3, 14 δ $C_\alpha C_\beta C$, 36 δ COO, 16 *r* COO
w COO	575	582	565.5	83 *w* COO
r COO et *t* NH_3	538 530	536	536	11 ν $C_\beta C$, 15 δ $NC_\alpha C_\beta$, 17 δ COO, 35 *r* COO
			475	51 *t* NH_3, 16 *r* $C_\alpha H_2$, 13 ν $C_\beta C$, 12 δ COO
	401	388	395.5	12 ν $C_\alpha C_\beta$, 52 δ $NC_\alpha C_\beta$, 13 *r* COO
δ $NC_\alpha C_\beta$†	322	323		
	228	247 221	248	56 δ $C_\alpha C_\beta C$, 15 τ $C_\alpha C_\beta$, 15 *r* COO
			130.5	14 *r* $C_\beta H_2$, 10 δ $C_\alpha C_\beta C$, 29 τ $C_\alpha C_\beta$, 29 *t* COO
			100	36 τ $C_\alpha C_\beta$, 54 *t* COO
			(*b*) $D_3\overset{+}{N}C_\alpha H_2C_\beta H_2COO^-$	
ν_a COO	1571		1578.5	100 ν_a COO, 14 *r* COO
δ CH_2	1470 1450	1469 1449	1467 1442	37 δ $C_\alpha H_2$, 37 δ $C_\beta H_2$, 11 *w* $C_\beta H_2$ 56 δ $C_\alpha H_2$, 20 δ $C_\beta H_2$, 11 *w* $C_\beta H_2$
	1414	1430.5	1412	20 δ $C_\beta H_2$, 14 *w* $C_\alpha H_2$, 37 *w* $C_\beta H_2$, 12 ν $C_\alpha C_\beta$
ν_s COO	1399 1383	1400 1384.5	1379	15 ν $C_\beta C$, 63 ν_s COO, 15 δ COO
w CH_2	1315	1318 1310.5	1338	14 δ $C_\beta H_2$, 68 *w* $C_\alpha H_2$, 10 *w* $C_\beta H_2$
t CH_2	1279	1294 1281	1283	83 *t* $C_\beta H_2$
t CH_2	1231	1233	1259	84 *t* $C_\alpha H_2$
δ ND_3	1202 1187 1160	1205 1162	1188 1183 1164.5	92 δ_s' ND_3 90 δ_a ND_3 74 δ_s ND_3, 33 ν NC_α
	1092	1094.5	1077.5	24 *r* $C_\alpha H_2$, 24 ν $C_\alpha C_\beta$
	1027	1032	1010	26 *r* $C_\alpha H_2$, 14 ν $C_\alpha C_\beta$, 10 ν $C_\beta C$
	1015	1022	976	17 δ_s ND_3, 22 *r* $C_\beta H_2$, 24 ν NC_α
	897	900	918	32 ν $C_\beta C$, 15 ν_s COO, 12 δ COO
	862 839	853 847.5	841	22 $r_{\|}$ ND_3, 40 *r* $C_\beta H_2$, 14 ν NC_α
r ND_3	805 767	777.5 764	802 776.5	39 $r_{\|}$ ND_3, 21 ν NC_α, 12 *r* COO 67 $r_\perp$ ND_3, 13 *r* $C_\alpha H_2$
δ COO	647	649	645	12 δ $C_\alpha C_\beta C$, 41 δ COO, 14 *r* COO
w COO	575	585.5	565	83 *w* COO

Can. J. Chem. Downloaded from www.nrcresearchpress.com by 210.87.254.105 on 09/05/12
For personal use only.

TABLEAU 1 (*Suite et fin*)

Attributions (PT)	ν obs Infrarouge	ν obs Raman	ν calc	Distribution d'énergie potentielle* $100(L_{ii}^2F_{ii}/\lambda k)$
r COO	529	522.5	517.5	16 ν $C_\beta C$, 11 δ $NC_\alpha C_\beta$, 21 δ COO, 34 *r* COO
		422.5		
			385.5	28 *t* ND_3, 30 δ $NC_\alpha C_\beta$, 16 *r* COO
	379	371.5	370	31 *t* ND_3, 26 δ $NC_\alpha C_\beta$
	316	314.5		
		206	228	13 *t* ND_3, 51 δ $C_\alpha C_\beta C$, 12 τ $C_\alpha C_\beta$, 12 *r* COO
			124	14 *r* $C_\beta H_2$, 11 δ $NC_\alpha C_\beta$, 24 τ $C_\alpha C_\beta$, 34 *t* COO
			95	42 τ $C_\alpha C_\beta$, 48 *t* COO

*Seules sont indiquées les répartitions supérieures à 10.
†Attribution différentes de celles données par réf. 15.

Ciliatine forme β

L'attribution présentée sur le tableau 3 a été faite par comparaison avec l'acide amino méthyl phosphonique (6, 17), la β-alanine et la taurine.

Calcul du champ de force et des modes normaux

Géométrie des ions

La géométrie utilisée est celle donnée par les rayons X (12–14). Pour les distances XH, nous avons pris les valeurs généralement admises: λ N—H = 1.03 Å, λ C—H = 1.08 Å, λ O—H = 0.97 Å.[2] Les angles autour des atomes d'azote ont été pris tétraédriques.

Coordonnées

Les coordonnées choisies sont des combinaisons linéaires de coordonnées internes correspondant aux vibrations de groupe utilisées pour interpréter les spectres. Nous les avons définies comme dans la glycine (5) et l'acide amino-méthylphosphonique (AMPh) (6), sauf pour les vibrations de torsion pour lesquelles nous avons adopté la définition utilisée dans le cas de l'acide glycylaminométhylphosphonique (Gly AMPh) (9).

Méthode de calcul

Le calcul est effectué en supposant l'ion isolé dans le réseau cristallin. Ne disposant pas de nombreuses molécules isotopiques, nous n'avons pas raffiné nos résultats, mais nous avons cherché à obtenir des champs de force aussi voisins que possible pour les trois molécules étudiées. Pour la β-alanine et la ciliatine, le champ de force de départ a été basé respectivement sur ceux de la glycine (5) et de l'AMPh (6). Pour la taurine, nous avons recherché par tâtonnements un champ de force rendant compte des fréquences du groupement SO_3 et l'avons choisi proche de celui du groupement PO_3. La comparaison avec un calcul de modes normaux effectué simultanément sur la glycyl taurine (10) nous a permis d'améliorer nos résultats. Les champs de force que nous avons finalement obtenus pour les trois molécules sont reportés sur le tableau 4.[3]

Discussion

Les fréquences calculées, accompagnées de la répartition d'énergie potentielle s'y rapportant, sont rassemblées sur les tableaux 1–3. On note que, dans l'ensemble, il y a un assez bon accord entre les fréquences calculées et les fréquences observées. Un certain nombre de bandes, non expliquées par le calcul, semblent dues à des démultiplications par interaction des différents ions dans la maille cristalline. Cette observation est contraire à l'hypothèse faite pour effectuer le calcul, mais la fréquence calculée est toujours relativement proche de celles relevées sur les spectres.

Dans le cas de la β-alanine, il a été impossible de calculer la vibration ν $C_\alpha C_\beta$ vers 850 cm^{-1} comme le laisse supposer l'aspect des spectres infrarouges et Raman et comme l'attribuent Krishnan et Katiyar (15). A cette fréquence est calculé un mode mettant particulièrement en jeu le mouvement de balancement *r* $C_\beta H_2$, mais il y a aussi une contribution importante de la vibration ν NC_α qui peut expliquer l'intensité de la raie Raman. Aucune fréquence n'a été calculée vers 320 cm^{-1} où Krishnan et Katiyar (15) situent la vibration δ $NC_\alpha C_\beta$. Cette bande pourrait être due à une vibration harmonique ou de combinaison.

Dans le cas de la taurine, on note que le groupement SO_3 se comporte pratiquement comme s'il possédait une symétrie ternaire: les deux bandes attribuées à ν_a et ν_s' SO_3 d'une part, à δ_a et δ_s' SO_3 d'autre part, pourraient également être dues à un

[2]Notons que, dans le cas de la glycine (5) et de l'AMPh (6), nous avions choisi de prendre λ N—H = 1.0 Å, λ C—H = 1.09 Å, λ O—H = 0.8 Å, ce qui peut expliquer certaines variations relevées dans les constantes de force.

[3]On peut obtenir le tableau 4, à un prix nominal, en s'adressant au Dépôt de données non publiées, ICIST, Conseil national de recherches du Canada, Ottawa (Ont.) Canada K1A 0S2.

Can. J. Chem. Downloaded from www.nrcresearchpress.com by 210.87.254.105 on 09/05/12
For personal use only.

TABLEAU 2. Nombres d'onde (cm^{-1}) et distribution d'énergie potentielle de la taurine et de son homologue deutérié

Attributions (PT)	ν obs Infrarouge	ν obs Raman	ν calc	Distribution d'énergie potentielle* $100(L_{ii}^2F_{ii}/\lambda k)$
			(*a*) $H_3\overset{+}{N}C_\alpha H_2C_\beta H_2SO_3^-$	
δ_d NH_3	1615		1613	91 δ_a NH_3
	1585		1588.5	91 δ_s' NH_3
	1524		1518	91 δ_s NH_3
δ_s NH_3	1511	1508		
δ CH_2	1467	1454	1468	70 δ $C_\beta H_2$, 21 *w* $C_\beta H_2$
	1425	1422	1414	90 δ $C_\alpha H_2$
w CH_2†	1387	1385	1380	70 *w* $C_\alpha H_2$, 15 *w* $C_\beta H_2$, 17 ν $C_\alpha C_\beta$
	1344	1340	1344	24 δ $C_\beta H_2$, 17 *w* $C_\alpha H_2$, 44 *w* $C_\beta H_2$
	1304	1303	1279	21 *t* $C_\alpha H_2$, 57 *t* $C_\beta H_2$
	1249	1256	1267.5	59 *t* $C_\alpha H_2$, 16 *t* $C_\beta H_2$
		1246		
ν_d SO_3	1215	1218	1213	12 *t* $C_\beta H_2$, 69 ν_a SO_3
	1182	1173	1185.5	80 ν_s' SO_3
r NH_3†	1111	1107	1112	44 $r_\parallel$ NH_3, 10 $r_\perp$ NH_3, 10ν $C_\alpha C_\beta$
	1102	1096	1102	12 $r_\parallel$ NH_3, 57 $r_\perp$ NH_3
	1046	1048	1044	40 ν NC_α, 17 ν $C_\alpha C_\beta$, 13 ν_s SO_3
ν_s SO_3	1038	1031	1024	10 ν NC_α, 73 ν_s SO_3
†	959	963	953	24 $r_\parallel$ NH_3, 14 *r* $C_\alpha H_2$, 30 *r* $C_\beta H_2$, 10 ν $C_\alpha C_\beta$
	892	895	904.5	12 $r_\perp NH_3$, 28 *r* $C_\alpha H_2$, 13 ν $C_\alpha C_\beta$, 10 ν $C_\beta S$
r CH_2 + Sq	846	846	837.5	36 *r* $C_\beta H_2$, 29 ν NC_α, 10 ν $C_\alpha C_\beta$
ν $C_\beta S$	740	736	756	14 *t* NH_3, 54 ν $C_\beta S$, 12 δ $C_\alpha C_\beta S$
	735			
δ_d SO_3	596	592	591	79 δ_s' SO_3, 10 δ_a SO_3
	594		590	82 δ_a SO_3
δ_s SO_3	528	528	531	11 ν $C_\beta S$, 10 δ $NC_\alpha C_\beta$, 10 δ $C_\alpha C_\beta S$, 61 δ_s SO_3
	522			
	464	474	475	37 δ $NC_\alpha C_\beta$, 19 δ_s SO_3
		465		
			436.5	49 *t* NH_3, 12 *r* $C_\alpha H_2$, 17 δ_s SO_3
	372	365	367.5	21 $r_\parallel$ SO_3, 44 $r_\perp$ SO_3
	324	326	289.5	23 δ $NC_\alpha C_\beta$, 38 $r_\parallel$ SO_3, 28 $r_\perp$ SO_3
	303			
	237	234	230.5	40 δ $C_\alpha C_\beta S$, 14 τ $C_\alpha C_\beta$, 19 $r_\parallel$ SO_3
			118	14 *r* $C_\beta H_2$, 10 δ $NC_\alpha C_\beta$, 13 δ $C_\alpha C_\beta S$, 26 τ $C_\alpha C_\beta$, 26 *t* SO_3
			92	38 τ $C_\alpha C_\beta$, 51 *t* SO_3
			(*b*) $D_3\overset{+}{N}C_\alpha H_2C_\beta H_2SO_3^-$	
δ CH_2	1458	1456	1468	70 δ $C_\beta H_2$, 22 *w* $C_\beta H_2$
	1425	1420	1425.5	89 δ $C_\alpha H_2$
w CH_2	1395		1377	72 *w* $C_\alpha H_2$, 15 *w* $C_\beta H_2$, 17 ν $C_\alpha C_\beta$
	1335	1329	1345	24 δ $C_\beta H_2$, 16 *w* $C_\alpha H_2$, 43 *w* $C_\beta H_2$, 10 *t* $C_\alpha H_2$
	1277	1281	1280	15 *t* $C_\alpha H_2$, 61 *t* $C_\beta H_2$
		1243	1267	64 *t* $C_\alpha H_2$, 11 *t* $C_\beta H_2$
ν_a SO_3	1227	1211	1215	68 ν_a SO_3
	1216		1185	75 ν_s' SO_3
	1185			
δ ND_3		1162	1172.5	62 δ_s ND_3, 23 ν NC_α
	1151		1156	91 δ_a ND_3
	1135		1137	92 δ_s' ND_3
†	1068	1069	1045.5	35 ν $C_\alpha C_\beta$, 14 ν_s SO_3
ν_s SO_3	1045	1031	1029	14 *r* $C_\alpha H_2$, 60 ν_s SO_3
	1039			
	1022			
	1006	1014	990	10 δ_s ND_3, 14 *r* $C_\alpha H_2$, 17 *r* $C_\beta H_2$, 14 ν NC_α, 10 ν $C_\alpha C_\beta$
			968	19 $r_\perp$ ND_3, 20 *r* $C_\alpha H_2$, 10 ν NC_α, 10 δ $NC_\alpha C_\beta$
r CH_2 + Sq	838	842	845	17 $r_\parallel$ ND_3, 40 *r* $C_\beta H_2$, 21 ν NC_α
	829			
r ND_3	773	775	792	54 $r_\perp$ ND_3, 27 ν $C_\beta S$
			762	59 $r_\parallel$ ND_3, 11 ν NC_α
ν $C_\beta S$	733	727	740	13 *t* ND_3, 12 *r* $C_\alpha H_2$, 38 ν $C_\beta S$, 10 δ $C_\alpha C_\beta S$
	724	720		

Can. J. Chem. Downloaded from www.nrcresearchpress.com by 210.87.254.105 on 09/05/12
For personal use only.

TABLEAU 2 (*Suite et fin*)

Attributions (PT)	ν obs Infrarouge	ν obs Raman	ν calc	Distribution d'énergie potentielle* $100(L_{ii}^2F_{ii}/\lambda k)$
δ_d SO_3	592	590	591	78 δ_s' SO_3, 11 δ_a SO_3
			590	11 δ_s' SO_3, 80 δ_a SO_3
δ_s SO_3 1	530	528	520	76 δ_s SO_3
	522			
	444	445	457.5	35 δ $NC_\alpha C_\beta$, 15 δ_s SO_3, 12 $r_\perp$ SO_3
	369	365	386	13 *t* ND_3, 10 δ $C_\alpha C_\beta S$, 28 $r_\perp$ SO_3
	315		327	47 *t* ND_3, 22 $r_\parallel$ SO_3, 17 $r_\perp$ SO_3
			281	25 δ $NC_\alpha C_\beta$, 35 $r_\parallel$ SO_3, 28 $r_\perp$ SO_3
			210.5	16 *t* ND_3, 38 δ $C_\alpha C_\beta S$, 12 τ $C_\alpha C_\beta$, 13 $r_\parallel$ SO_3
			111	14 *r* $C_\beta H_2$, 12 δ $NC_\alpha C_\beta$, 12 δ $C_\alpha C_\beta S$, 21 τ $C_\alpha C_\beta$, 32 *t* SO_3
			86	44 τ $C_\alpha C_\beta$, 45 *t* SO_3

*Seules sont indiquées les répartitions supérieures à 10.
†Attribution différente de celles données par réf. 16.

TABLEAU 3. Nombres d'onde (cm^{-1}) et distribution d'énergie potentielle de la ciliatine (*a*) et de son homologue N et O deutérié (*b*) dans la variété cristallographique β

Attributions (PT)	ν obs Infrarouge	ν obs Raman	ν calc	Distribution d'énergie potentielle* $100\,(L_{ii}^2F_{ii}/\lambda k)$
			(*a*) $H_3\overset{+}{N}C_\alpha H_2C_\beta H_2PO_3H^-$ variété β	
δ_d NH_3	1635	1628	1628.5	91 δ_a NH_3
			1627	91 δ_s' NH_3
δ_s NH_3	1475		1488	80 δ_s NH_3, 13 δ $C_\alpha H_2$
δ CH_2	1465	1465	1467	14 δ $C_\alpha H_2$, 52 δ $C_\beta H_2$, 17 *w* $C_\beta H_2$
	1426	1431	1431	34 δ $C_\alpha H_2$, 31 *w* $C_\alpha H_2$, 24 *w* $C_\beta H_2$, 12 ν $C_\alpha C_\beta$
w CH_2	1385	1387	1399	14 δ_s NH_3, 37 δ $C_\alpha H_2$, 15 δ $C_\beta H_2$, 28 *w* $C_\alpha H_2$
	1340	1350	1324	26 δ $C_\beta H_2$, 30 *w* $C_\alpha H_2$, 38 *w* $C_\beta H_2$
t CH_2		1275	1275	87 *t* $C_\alpha H_2$
	1265		1258	77 *t* $C_\beta H_2$
δ OH	1215		1214	26 ν_a PO_3, 54 δ OH
		1161	1176	19 $r_\perp$ NH_3, 19 ν_a PO_3, 23 δ OH
ν_a PO_3	1135	1131	1144	27 $r_\perp$ NH_3, 37 ν_a PO_3
		1089	1108	65 $r_\parallel$ NH_3, 12 *r* $C_\alpha H_2$
ν_s' PO_3	1070	1063	1054	64 ν_s' PO_3
	1055			
	1025	1028	1021	62 ν NC_α, 12 ν $C_\alpha C_\beta$
	998	991		
	952	957	962	31 $r_\perp$ NH_3, 41 ν $C_\alpha C_\beta$
ν_s PO_3	928	937	934	15 ν $C_\beta P$, 61 ν_s PO_3, 12 δ_s PO_3, 16 γ OH
γ OH	900	910	888	33 *r* $C_\alpha H_2$, 34 γ OH
			884	27 *r* $C_\alpha H_2$, 46 γ OH
ν $C_\beta P$	775	778	780	13 ν NC_α, 44 ν $C_\beta P$, 17 ν_s PO_3
	755	756	751	63 *r* $C_\beta H_2$, 10 τ $C_\alpha C_\beta$
δ_s PO_3	570	574	558.5	81 δ_s PO_3
	547			
	538	540		
δ_d PO_3	482		498	90 δ_a PO_3
	477	478	474.5	85 δ_s' PO_3
	456	448	456	74 *t* NH_3, 12 *r* $C_\alpha H_2$
	436			
r PO_3		379	382.5	34 δ N $C_\alpha C_\beta$, 15 δ $C_\alpha C_\beta P$, 33 $r_\perp$ PO_3
	350	347	348	63 $r_\parallel$ PO_3, 16 $r_\perp$ PO_3
		316	299	15 ν $C_\alpha C_\beta$, 28 ν $C_\beta P$, 27 δ $NC_\alpha C_\beta$
		217		
		187	192	10 δ $NC_\alpha C_\beta$, 38 δ $C_\alpha C_\beta P$, 13 $r_\parallel$ PO_3, 34 $r_\perp$ PO_3
			119	73 τ $C_\alpha C_\beta$
			83	86 τ $C_\beta P$

Can. J. Chem. Downloaded from www.nrcresearchpress.com by 210.87.254.105 on 09/05/12
For personal use only.

TABLEAU 3 (*Suite et fin*)

Attributions (PT)	ν obs Infrarouge	ν obs Raman	ν calc	Distribution d'énergie potentielle* 100 ($L_{ii}^2F_{ii}/\lambda k$)
			(*b*) $D_3\overset{+}{N}C_\alpha H_2C_\beta H_2PO_3D^-$ variété β	
	1467	1463	1468	24 δ $C_\alpha H_2$, 51 δ $C_\beta H_2$, 19 *w* $C_\beta H_2$
δ CH_2	1433	1431	1430	50 δ $C_\alpha H_2$, 17 *w* $C_\alpha H_2$, 21 *w* $C_\beta H_2$, 10 ν $C_\alpha C_\beta$
w CH_2	1407		1412	24 δ $C_\alpha H_2$, 13 δ $C_\beta H_2$, 51 *w* $C_\alpha H_2$
	1382			
	1377			
w CH_2		1322	1327	28 δ $C_\beta H_2$, 29 *w* $C_\alpha H_2$, 38 *w* $C_\beta H_2$
t CH_2	1249		1273.5	91 *t* $C_\alpha H_2$
	1234		1255	86 *t* $C_\beta H_2$
	1195		1188	67 ν_a PO_3
δ ND_3 et	1184		1169.5	84 δ_a ND_3
ν_a PO_3	1165		1165	84 δ_s' ND_3
	1151	1150	1152	65 δ_s ND_3, 32 ν NC_α, 10 ν_a PO_3
	1130	1130		
		1080	1097	18 ν $C_\alpha C_\beta$, 45 ν_s' PO_3
ν_s' PO_3	1070		1063	27 ν $C_\alpha C_\beta$, 36 ν_s' PO_3
	1020	1016		
	1004	1000	974.5	13 δ_s ND_3, 19 *r* $C_\alpha H_2$, 18 ν NC_α, 11 ν $C_\alpha C_\beta$
	961	962	967	17 $r_\parallel$ ND_3, 37 *r* $C_\alpha H_2$
ν_s PO_3	924	917	921	10 ν NC_α, 12 ν $C_\beta P$, 70 ν_s PO_3, 10 δ_s PO_3
	888	892		
δ OD	876		865	81 δ OD
	847	845		
	805	800	792	62 $r_\perp$ ND_3, 13 ν $C_\alpha C_\beta$
			772	24 $r_\parallel$ ND_3, 12 *r* $C_\alpha H_2$, 10 *r* $C_\beta H_2$, 14 ν $C_\beta P$
	752	754	762.5	33 $r_\parallel$ ND_3, 27 ν $C_\beta P$
	740	740	746	57 *r* $C_\beta H_2$
γ OD	660		680	10 δ_s PO_3, 80 γ OD
δ_s PO_3	551			
	542	542	544.5	67 δ_s PO_3, 11 δ_s' PO_3, 11 γ OD
	474			
	470	466	481	12 δ_s' PO_3, 75 δ_a PO_3
δ_d PO_3	457			
	438	440	465	67 δ_s' PO_3, 12 ν_a PO_3
	397	401		
r PO_3	366	369	376	27 *t* ND_3, 12 δ $NC_\alpha C_\beta$, 35 $r_\perp$ PO_3
	360		363	12 *t* ND_3, 14 δ $NC_\alpha C_\beta$, 12 δ $C_\alpha C_\beta P$, 37 $r_\parallel$ PO_3
	326	326	319	42 *t* ND_3, 10 *r* $C_\alpha H_2$, 27 $r_\parallel$ PO_3, 11 $r_\perp$ PO_3
	303	303		
		284	282.5	13 ν $C_\alpha C_\beta$, 26 ν $C_\beta P$, 32 δ $NC_\alpha C_\beta$
			183	12 δ $NC_\alpha C_\beta$, 38 δ $C_\alpha C_\beta P$, 13 $r_\parallel$ PO_3, 31 $r_\perp$ PO_3
			110	10 *r* $C_\beta H_2$, 73 τ $C_\alpha C_\beta$
			79.5	87 τ $C_\beta P$

*Seules sont indiquées les repartitions supérieures à 10.

effet Davydov. Un phénomène analogue a été observé dans le cas de la glycyl taurine (10).

Les champs de force obtenus pour la partie $NC_\alpha H_2C_\beta H_2$— des trois molécules sont très proches, ce qui permet de penser que la structure électronique de ces groupements est pratiquement la même dans ces trois composés. Rappelons la valeur des angles dièdres autour de la liaison $C_\alpha C_\beta$, observés à l'état solide: β-alanine, 84°; taurine, —70.5°; ciliatine, 174°. Ainsi donc, la différence de conformation de ces trois ions n'influe pas sur le champ de force calculé, non plus que la chélation qui a été observée dans le cas de la taurine (14) entre les groupements SO_3^- et NH_3^+. Notons, enfin, que les champs de force donnés sur le tableau 4 sont très proches de ceux des molécules modèles (5, 6, 8, 9).

Certaines constantes de force d'interaction (*t* $C_\alpha H_2$, $r_\perp$ NH_3; *r* $C_\alpha H_2$, $r_\perp$ NH_3; *w* $C_\alpha H_2$, $r_\parallel$ NH_3) ont cependant pu être posées égales à zéro sans que les fréquences calculées et la répartition d'énergie potentielle soient perturbées de façon notable. En outre, dans le cas de la taurine, nous avons du annuler la constante ν $C_\beta S$, ν_s SO_3 pour pouvoir expliquer les spectres observés.

Can. J. Chem. Downloaded from www.nrcresearchpress.com by 210.87.254.105 on 09/05/12
For personal use only.

Can. J. Chem. Downloaded from www.nrcresearchpress.com by 210.87.254.105 on 09/05/12
For personal use only.

Conclusion

Ce travail donne un bon exemple de la transférabilité des champs de force entre molécules de formule voisine.

Le manque de molécules isotopiques ne nous a pas permis de raffiner les champs de force que nous avons obtenus ni de dégager les relations qui doivent exister entre les fréquences des vibrations et la conformation. Nos résultats doivent cependant pouvoir être utilisés, en particulier pour faciliter l'interprétation de molécules à liaison amide, formées à partir des acides aminés étudiés dans ce mémoire et qui font l'objet de recherches entreprises conjointement d'un point de vue conformationnel (10, 18)[4] et biochimique (19–28).

Partie expérimentale

La β-alanine est un produit Fluka, la taurine un produit Merck. La ciliatine a été synthétisée par la méthode de Kosolapoff (29). Les composés deutériés sur les atomes d'azote et (pour la ciliatine) l'oxygène ont été préparés par échanges répétés avec de l'eau lourde en excès, l'eau résiduelle étant ensuite éliminée par évaporation sous vide. La variété β de la ciliatine a été identifiée par comparaison de ses spectres infrarouges avec ceux publiés par Horiguchi et Kandatsu (11). On a vérifié, avant et après enregistrement du spectre Raman, que l'échantillon irradié par le laser était resté sous forme β. Les échantillons solides ont été examinés par spectrométrie infrarouge suivant la région spectrale considérée, en suspension dans le Nujol ou le fluorolube. Pour les spectres Raman, la poudre cristalline a été placée dans de petits tubes cylindriques en verre. Les spectres infrarouges ont été enregistrés sur un appareil à réseaux Perkin Elmer 225. Les fréquences d'absorption des bandes fines sont lues à ± 1 cm^{-1}, dans tout le domaine spectral. Les spectres Raman ont été obtenus sur un appareil Coderg PH 1, éclairé par un laser 'Spectra Physics' à Argon ionisé ($\lambda = 4880$ Å). Les lectures ont été faites à ± 3 cm^{-1}. Les calculs ont été faits sur un ordinateur CII Iris 80, en utilisant un champ de force de valence et la méthode décrite par Wilson *et al.* (30). L'énergie potentielle a été écrite dans la même approximation que la matrice d'énergie cinétique G, c'est-à-dire en posant nulles les constantes de force d'interaction entre vibrateurs sans atome commun.

Remerciements

Nous remercions Mme E. Dupart qui a préparé la ciliatine, et Mme M. Rey qui a relu et discuté ce manuscrit.

[4]C. Garrigou-Lagrange. Travaux en cours.

1. H. A. Cassaigne. Thèse Médecine, No. 159, Bordeaux, 1967; Imp. E. Drouillard, 1968.
2. J. A. Alhadeff et G. D. Davies. Biochemistry, **9**, 4866 (1970).
3. J. A. Alhadeff et G. D. Davies. Biochim. Biophys. Acta, **244**, 211 (1971).
4. A. Laporte. Thèse Médecine, No. 403, Bordeaux. 1975.
5. C. Destrade, C. Garrigou-Lagrange et M. T. Forel. J. Mol. Struct. **10**, 203 (1971).
6. C. Garrigou-Lagrange et C. Destrade. C. R. Acad. Sci. Ser. C, **280**, 969 (1975).
7. C. Destrade, E. Dupart, M. Joussot-Dubien et C. Garrigou-Lagrange. Can. J. Chem. **52**, 2590 (1974).
8. C. Destrade et C. Garrigou-Lagrange. J. Mol. Struct. **31**, 301 (1976).
9. M. Cotrait, M. Avignon, J. Prigent et C. Garrigou-Lagrange. J. Mol. Struct. **32**, 45 (1976).
10. C. Garrigou-Lagrange, H. Jensen et M. Cotrait. J. Mol. Struct. **36**, 275 (1977).
11. M. Horiguchi et M. Kandatsu. Agr. Biol. Chem. **28**, 408 (1964).
12. Y. Okaya. Acta Crystallogr. **20**, 712 (1966).
13. P. Jose et L. M. Pant. Acta Crystallogr. **18**, 806 (1965).
14. Y. Okaya. Acta Crystallogr. **21**, 726 (1966).
15. R. S. Krishnan et R. S. Katiyar. Bull. Chem. Soc. Jpn. **42**, 2098 (1969).
16. U. Stahlberg et E. Steger. Spectrochim. Acta, **23A**, 475 (1967).
17. C. Garrigou-Lagrange et C. Destrade. J. Chim. Phys. **67**, 1646 (1970).
18. J. Prigent. Thèse Docteur Ingénieur, Bordeaux, 1976.
19. A. M. Lacoste et E. Neuzil. C.R. Acad. Sci. **269**, 254 (1969).
20. E. Neuzil, H. Jensen et J. Le Pogam. J. Chromatogr. **39**, 238 (1969).
21. A. Cassaigne, A. M. Lacoste et E. Neuzil. Biochim. Biophys. Acta, **252**, 506 (1971).
22. M. Tamari, A. Cassaigne, A. M. Lacoste et E. Neuzil. Biochimie, **57**, 97 (1975).
23. A. M. Lacoste, A. Cassaigne et E. Neuzil. C.R. Acad. Sci. Ser. D, **280**, 1173 (1975).
24. E. Moreaud, A. M. Lacoste et E. Neuzil. C.R. Acad. Sci. Ser. D, **280**, 1309 (1975).
25. A. Cassaigne, A. M. Lacoste, M. Tamari et E. Neuzil. FEBS, 10ième Conf. Ann. Abstr. No. 1172 (1975).
26. J. Fourche, H. Jensen et E. Neuzil. Anal. Chem. **48**, 155 (1976).
27. A. Cassaigne, A. M. Lacoste et E. Neuzil. C.R. Acad. Sci. Ser. D, **282**, 1637 (1976).
28. A. M. Lacoste, A. Cassaigne, M. Tamari et E. Neuzil. Biochimie, **58**, 703 (1976).
29. G. M. Kosolapoff. J. Am. Chem. Soc. **69**, 2112 (1947).
30. E. B. Wilson, J. C. Decius et P. Cross. Molecular vibrations. McGraw Hill, New York, NY. 1955.

Gas phase acidic solvolysis reactions of acyl halides by ion cyclotron resonance spectroscopy

T. B. McMAHON

Department of Chemistry, University of New Brunswick, Fredericton, N.B., Canada E3B 5A3

Received September 22, 1977

T. B. McMAHON. Can. J. Chem. **56**, 670 (1978).

A number of gas phase ion molecule reactions of protonated species with acyl halides have been examined by ion cyclotron resonance spectroscopy. A number of these reactions are found to involve an addition–elimination reaction having the character of an acidic solvolysis process. Observation of the occurrence or non-occurrence of such reactions and a consideration of appropriate thermochemical data allow a set of criteria to be formulated governing the feasibility of observing the acidic solvolysis reaction. In addition a number of mechanistic inferences are made concerning intermediates involved in the various reactions.

T. B. McMAHON. Can. J. Chem. **56**, 670 (1978).

On a étudié un certain nombre de réactions ion–molécule en phase gazeuse d'espèces protonées avec des halogénures d'acyle en faisant appel à la spectroscopie à trajectoire cycloïdale résonante. On a trouvé qu'un certain nombre de ces réactions implique une réaction addition–élimination possédant un caractère de processus de solvolyse acide. L'observation de l'existence de telles réactions et la considération de données thermodynamiques appropriées permettent de formuler un ensemble de critère concernant la possibilité d'observer la réaction de solvolyse acide. On peut de plus déduire un certain nombre d'implications mécanistiques concernant les intermédiaires intervenant dans les diverses réactions.

[Traduit par le journal]

Introduction

The detailed mechanisms of organic reactions in solution have preoccupied physical organic chemists for several decades. Of particular interest have been the reactions of carboxylic acids and carboxylic acid derivatives because of the great synthetic utility of these compounds, the variety of reactions which they undergo and the pronounced effects of acid and base catalysis on their reactions (1–3). Of the carboxylic acid derivatives the acyl halides have been the least extensively characterized due to their extremely high reactivity (1). It has recently been shown, however, that in the case of solution reactions which proceed via ionic mechanisms a great deal of mechanistic information may be derived from the study of appropriate analogous ion molecule reactions in the gas phase (4–6). Using a variety of techniques it is possible to obtain both qualitative and quantitative information concerning the nature of the intermolecular interaction between the reacting species. In addition since in the gas phase complicating solvation phenomena are eliminated the intrinsic reactivity and stability of the ionic species of interest may be ascertained. Further, by contrasting analogous solution and gas phase reactions, it is frequently possible to elucidate the role of the solvent in the reaction.

The present work describes an ion cyclotron resonance (ICR) study of the reactions of a series of protonated molecules with several acyl halides. The observed reactions can be placed in three general categories: (*i*) proton transfer yielding protonated acyl halide, (*ii*) halide abstraction to give acylium ion, and (*iii*) addition–elimination producing a new protonated carboxylic acid derivative plus hydrogen halide. This reaction has the character of an acidic solvolysis process. A number of requirements have been formulated which allow an a priori prediction of which of the possible reaction channels may be expected. These requirements also suggest mechanistic details concerning the course of reaction and allow probable reaction intermediates to be postulated.

Experimental

The experiments described in this work were performed on a Varian V-5900 ICR spectrometer modified by Dynaspec Inc. to allow for operation in both conventional and trapped-ion modes (7). The timing and sequence of pulses to the ICR plates in trapped-ion experiments was generated by a DCC Model D-116 Minicomputer. All other ICR instrumentation and techniques were identical to those described in detail elsewhere (8, 9). Typical operating conditions are: drift voltages, 0.2 V/cm; trapping voltage, 0.2 V/cm; electron emission current, 0.01 to 1 μA; total ion current, 10^{-10} to 10^{-12} A; magnetic field sweep, 0 to 14 kG. Ion kinetic energies are all near thermal energy (less than 0.1 eV).

Approximate pressures only could be read from the ion-pump current and may be in error by a factor of two. Consequently rate constant determinations are quite approximate. In favorable cases more accurate rate constants may be inferred when a reaction is observed whose rate constant is well known. In such cases a more nearly exact pressure can be calculated from the observed experimental ion intensities.

Can. J. Chem. Downloaded from www.nrcresearchpress.com by 210.87.254.6 on 09/05/12
For personal use only.

Can. J. Chem. Downloaded from www.nrcresearchpress.com by 210.87.254.6 on 09/05/12
For personal use only.

Binary gas mixtures were prepared directly in the instrument by admitting the two reagents through separate vacuum inlet systems. Mixture ratios were determined from changes in ion pump current on introduction of each gas and again may be in error due to different ion pump response to different gases and due to modification of the flow of the gas initially admitted by the addition of flow of the second gas. Attempts to prepare binary mixtures of acyl halides with other materials in a single vessel frequently led to direct neutral–neutral reaction in the sample vessel (1). For example mixtures of methanol and acetyl fluoride always produced methyl acetate in a very short time. Since protonated methyl acetate is the species of interest in this mixture, the resulting impurity obviously invalidates the results. Thus it is imperative to use separate inlets for these experiments.

Acetyl fluoride was obtained from PCR Inc., benzoyl fluoride, acetyl chloride, and benzoyl chloride from Aldrich and methane, ammonia, methylamine, and dimethylamine from Matheson. All other materials were commercially available reagent grade chemicals.

Results

The reactions of acyl halides, RCOX, with protonated species $R'MH^+$ can be divided into three general categories as illustrated by reactions 1–3.

[1] $RCOX + R'MH^+ \rightarrow RCOXH^+ + R'M$

[2] $RCOX + R'MH^+ \rightarrow RCO^+ + R'M + HX$

(or $R'X + MH$)

[3] $RCOX + R'MH^+ \rightarrow RCOMR'^+ + HX$

Reaction 1 is simple proton transfer and can be expected to occur whenever the proton affinity of the acyl halide is greater than that of the base, R'M. Reaction 2 produces acylium ion and a pair of neutral products which may be either hydrogen halide, HX, plus base, R'M, or alkyl halide, R'X, plus a hydride, MH. In some cases both pairs of neutral products are thermodynamically possible but in others only the latter pair may be exothermically produced. Reaction 3 is an addition–elimination reaction yielding a new protonated carboxylic acid derivative plus hydrogen halide which bears a strong resemblance in many cases to observed solvolysis reactions of acyl halides in acidic solution.

The possible reactions for each of the acyl halides with protonated substrates studied are summarized in Table 1. Included are the enthalpy change for each reaction, the total observed reaction rate constant for protonated substrate with acyl halide, and the experimentally determined product distribution.

(1) Reactions of H_3O^+ and H_3S^+

From Table 1 it may be seen that the dominant reaction path for H_3O^+ and H_3S^+ with acetyl halides is acetyl cation formation. Data for a mixture of H_2S and acetyl fluoride are shown in Fig. 1 and

[4] $H_2S^+ + H_2S \rightarrow H_3S^+ + SH$

[5] $H_2S^+ + CH_3COF \rightarrow CH_3COSH^+ + HF$

[6] $H_3S^+ + CH_3COF \rightarrow CH_3CO^+ + HF + H_2S$

[7] $H_3S^+ + CH_3COF \rightarrow CH_3COFH^+ + H_2S$

[8] $CH_3COFH^+ + H_2S \rightarrow (CH_3COSH)H^+ + HF$

are typical of reactions between these species. The observed reactions occurring in this mixture confirmed by double resonance experiments are summarized below. Similar reactions are observed for H_3O^+ with acetyl fluoride and acetyl chloride and for H_3S^+ with acetyl chloride. These results establish the proton affinities of both acetyl halides to be above that of H_2S, 172 kcal/mol.

In the reactions of H_3O^+ and H_3S^+ with benzoyl fluoride no protonated benzoyl fluoride is observed even though the proton affinity of benzoyl fluoride is established to be greater than that of H_2S. It may be seen from Table 1 that the decomposition of protonated benzoyl fluoride to benzoyl cation and HF is 3 kcal/mol exothermic. Thus it is likely that no protonated benzoyl fluoride is observed since exothermic proton transfer is immediately followed by unimolecular elimination of HF to produce the abundantly observed benzoyl cation, reaction 9.

[9] $H_3S^+ + \phi COF \rightarrow H_2S + [\phi CFOH^+]^* \rightarrow \phi CO^+ + HF$

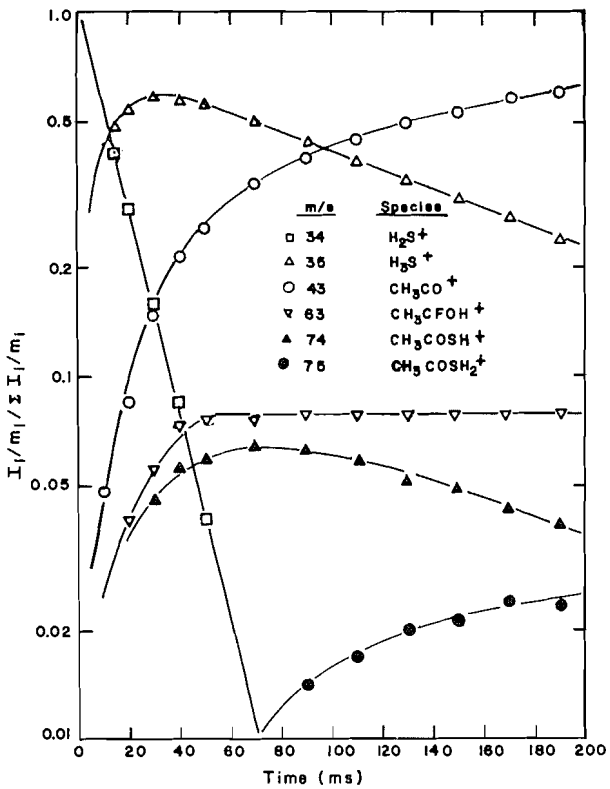

FIG. 1. Variation of relative ion abundances with reaction time in a 3:1 mixture of H_2S and acetyl fluoride at 15 eV and a total pressure of 1.0×10^{-6} Torr.

TABLE 1. Kinetics and thermochemistry of acyl halide reactions

Reactants	Products	ΔH^a (kcal/mol)	Product distribution	Total rate constant (cm^3 $molecule^{-1}$ s^{-1})
$H_3O^+ + CH_3COF$	$CH_3CFOH^+ + H_2O$	−6	0.5	
	$CH_3CO^+ + FH + H_2O$	−5	0.5	3.0×10^{-9}
	$CH_3CO_2H_2^+ + HF$	−24	—	
$H_3O^+ + CH_3COCl$	$CH_3CClOH^+ + H_2O$	−11	—	
	$CH_3CO^+ + HCl + H_2O$	−8	1.0	3.0×10^{-9}
	$CH_3CO_2H_2^+ + HCl$	−27	—	
$H_3O^+ + \phi COF$	$\phi CFOH^+ + H_2O$	−16	0.5	
	$\phi CO^+ + HF + H_2O$	−15	0.5	3.2×10^{-9}
	$\phi CO_2H_2^+ + HF$	−31[b]	—	
$H_3S^+ + CH_3COF$	$CH_3CFOH^+ + H_2S$	−3	0.2	
	$CH_3CO^+ + HF + H_2S$	−2	0.8	8×10^{-10}
	$CH_3C(OH)(SH)^+ + HF$	−23[b]	—	
H_3S^+ CH_3COCl	$CH_3CClOH^+ + H_2S$	−8	—	
	$CH_3CO^+ + HCl + H_2S$	−5	1.0	1×10^{-9}
	$CH_3C(OH)(SH)^+ + HCl$	−26[b]	—	
$H_3S^+ + \phi COF$	$\phi CFOH^+ + H_2S$	−13	0.4	
	$\phi CO^+ + HF + H_2S$	−12	0.6	2×10^{-9}
	$\phi C(OH)(SH)^+ + HF$	−30[b]	—	
$HCO_2H_2^+ + CH_3COF$	$CH_3CFOH^+ + HCO_2H$	+3	—	
	$CH_3CO^+ + HF + HCO_2H$	+4	—	1.9×10^{-9}
	$(CH_3CO_2COH)H^+ + HF$	−18[b]	1.0	
$HCO_2H_2^+ + CH_3COCl$	$CH_3CClOH^+ + HCO_2H$	−2	—	
	$CH_3CO^+ + HCl + HCO_2H$	+1	—	1.9×10^{-9}[c]
	$(CH_3CO_2COH)H^+ + HCl$	−21[b]	—	
$HCO_2H_2^+ + \phi COF$	$\phi CFOH^+ + HCO_2H$	−7	—	
	$\phi CO^+ + HF + HCO_2H$	−6	—	
	$(\phi CO_2COH)H^+ + HF$	−28[b]	—	
$CH_3OH_2^+ + CH_3COF$	$CH_3CFOH^+ + CH_3OH$	+7	—	
	$CH_3CO^+ + CH_3F + H_2O$	−4	0.4	1.2×10^{-9}
	$(CH_3CO_2CH_3)H^+ + HF$	−25	0.6	
$CH_3OH_2^+ + CH_3COCl$	$CH_3CClOH^+ + CH_3OH$	+2	—	
	$CH_3CO^+ + CH_3Cl + H_2O$	−2	0.3	1.5×10^{-9}
	$(CH_3CO_2CH_3)H^+ + HCl$	−28	0.7	
$CH_3OH_2^+ + \phi COF$	$\phi CFOH^+ + CH_3OH$	−3	—	
	$\phi CO^+ + HF + CH_3OH$	−2	1.0	2.0×10^{-9}
	$(\phi CO_2CH_3)H^+ + HF$	−31[b]	—	
$C_2H_5OH_2^+ + CH_3COF$	$CH_3CFOH^+ + C_2H_5OH$	+12	—	
	$CH_3CO^+ + HF + C_2H_5OH$	+13(+16)	—	1.5×10^{-9}
	$(CH_3CO_2C_2H_5)H^+ + HF$	−23	1.0	
$C_2H_5OH_2^+ + CH_3COCl$	$CH_3ClOH^+ + C_2H_5OH$	+7	—	
	$CH_3CO^+ + HCl + C_2H_5OH$	+10(+3)	—	8.3×10^{-10}
	$(CH_3CO_2C_2H_5)H^+ + HCl$	−26	1.0	
$C_2H_5OH_2^+ + \phi COF$	$\phi CFOH^+ + C_2H_5OH$	+2	—	
	$\phi CO^+ + HF + C_2H_5OH$	+3(+6)	—	2.3×10^{-9}
	$(\phi CO_2C_2H_5)H^+ + HF$	−29[b]	1.0	
$CH_3CO_2H_2^+ + CH_3COF$	$CH_3CFOH^+ + CH_3CO_2H$	+12	—	
	$CH_3CO^+ + HF + CH_3CO_2H$	+13	—	2×10^{-9}
	$(CH_3CO_2COCH_3)H^+ + HF$	−17[b]	1.0	
$CH_3CO_2H_2^+ + CH_3COCl$	$CH_3CClOH^+ + CH_3CO_2H$	+7	—	
	$CH_3CO^+ + HCl + CH_3CO_2H$	+10	—	2×10^{-9}
	$(CH_3CO_2COCH_3)H^+ + HCl$	−20[b]	1.0	
$NH_4^+ + CH_3COF$	$CH_3CFOH^+ + NH_3$	+26	—	
	$CH_3CO^+ + HF + NH_3$	+27	—	NR[a]
	$(CH_3CONH_2)H^+ + HF$	−7[b]	—	
$NH_4^+ + CH_3COCl$	$CH_3CClOH^+ + NH_3$	+21	—	NR
	$CH_3CO^+ + HCl + NH_3$	+24	—	
	$(CH_3CONH_2)H^+ + HCl$	−4[b]	—	
$NH_4^+ + \phi COF$	$\phi CFOH^+ + NH_3$	+16	—	NR
	$\phi CO^+ + HF + NH_3$	+17	—	
	$(\phi CONH_2)H^+ + HF$	−10[b]	—	

[a]Proton affinity data taken from Kebarle *et al.* (29), all other thermochemical data from ref. 30, or estimated on basis of group equivalent methods, ref. 11.
[b]In cases where proton affinities have not been determined they are estimated on the basis of substituent effects in similar systems.
[c]See text.

Can. J. Chem. Downloaded from www.nrcresearchpress.com by 210.87.254.6 on 09/05/12
For personal use only.

Can. J. Chem. Downloaded from www.nrcresearchpress.com by 210.87.254.6 on 09/05/12
For personal use only.

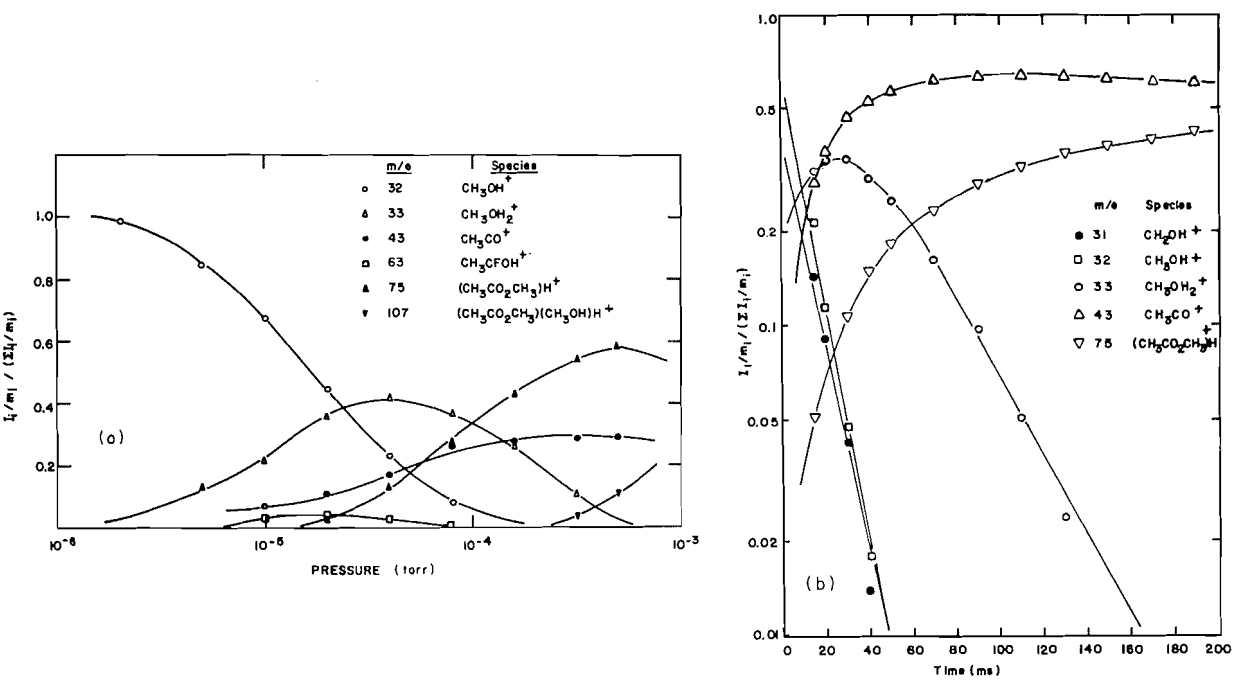

FIG. 2. (*a*) Variation of relative ion abundances with pressure in a 4.4:1 mixture of methanol and acetyl fluoride at 13 eV. (*b*) Variation of relative ion abundances with reaction time in a 2:1 mixture of methanol and acetyl fluoride at 14 eV and a total pressure of 2.4×10^{-6} Torr.

(2) Reactions of Protonated Alcohols

Protonated alcohols were found to react with acetyl fluoride and acetyl chloride to produce the corresponding protonated esters. The reactions observed in a mixture of acetyl fluoride and methanol are shown in Fig. 2 both as a function of increasing pressure and increasing reaction time to show the similarity of results from both types of experiment. Reactions observed are summarized in [10]–[14].

[10] $CH_3OH^+ + CH_3OH \rightarrow CH_3OH_2^+ + CH_3O$

[11] $CH_2OH^+ + CH_3OH \rightarrow CH_3OH_2^+ + CH_2O$

[12] $CH_2OH^+ + CH_3COF \rightarrow CH_3CO^+ + HF + CH_2O$

[13] $CH_3OH_2^+ + CH_3COF \rightarrow CH_3CO^+ + CH_3F + H_2O$

[14] $CH_3OH_2^+ + CH_3COF \rightarrow [CH_3CO_2CH_3]H^+ + HF$

Reaction 13 is of particular interest since the neutral products have been inferred on the basis of thermochemical arguments and leads to important mechanistic considerations.

Similar results are observed in a mixture of ethanol with acetyl fluoride or acetyl chloride and methanol with acetyl chloride. In the case of ethanol and acetyl fluoride, however, another interesting product at *m/e* 87 is observed as a result of reaction of *m/e* 45, protonated acetaldehyde with the acetyl fluoride. This reaction is in principle similar to the acidic solvolysis reactions of protonated alcohols to yield protonated esters and the assumed product from protonated acetaldehyde is protonated biacetyl. This product does not appear in ethanol – acetyl chloride mixtures presumably because it does not compete favorably with acetyl cation formation. Typical data for ethanol – acetyl chloride mixtures is shown in Fig. 3.

In each of the cases where the presumed acidic solvolysis reaction is observed an alternative explanation of the reaction products is possible. In gas phase reactions of Li^+ with acetyl bromide reaction 14′ was observed which has the character of an acid induced elimination reaction producing

[14′] $Li^+ + CH_3COBr \rightarrow Li \cdots {}^+O{=}C{=}CH_2 + HBr$

an Li^+ bound to ketene (10). In analogy to this reaction it was considered possible that an alternative explanation of reactions such as [14] might be [14*a*] where the ionic product now is a proton bound

[14*a*] $CH_3OH_2^+ + CH_3COF \rightarrow$

$$CH_2{=}C{=}O \cdots \overset{+}{H}(HOCH_3) + HF$$

dimer of methanol and ketene. Since the elimination of HF from acetyl fluoride is only about 27 kcal/mol endothermic if the binding energy of protonated methanol to acetyl fluoride were in excess of 27 kcal/mol an elimination of HF such as in [14*a*] might be induced. In order to investigate this possibility

Can. J. Chem. Downloaded from www.nrcresearchpress.com by 210.87.254.6 on 09/05/12
For personal use only.

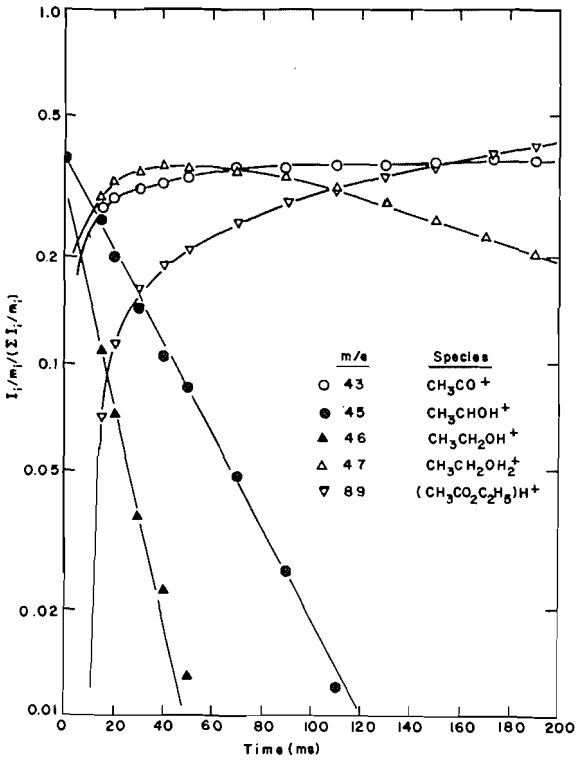

FIG. 3. Variation of relative ion abundances with reaction time in a 4:1 mixture of ethanol and acetyl chloride at 13 eV and a total pressure of 1.0×10^{-6} Torr.

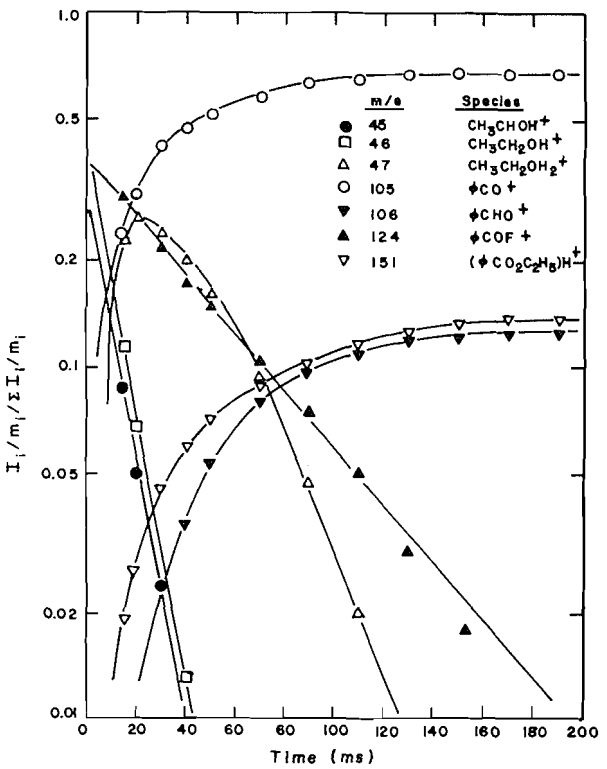

FIG. 4. Variation of relative ion abundances with reaction time in a 3.4:1 mixture of ethanol and benzoyl fluoride at 14 eV and a total pressure of 2.2×10^{-6} Torr.

the reactions occurring in a mixture of CD_3OD and CH_3COF was examined. In this case only reaction 14*b* was observed and not [14*c*].

[14*b*] $CD_3OD_2^+ + CH_3COF \rightarrow (CH_3CO_2CD_3)D^+ + DF$

[14*c*] $CD_3OD_2^+ + CH_3COF \not\rightarrow$

$CH_2{=}C{=}O \cdots D \therefore (DOCD_3) + HF$

With benzoyl fluoride protonated methanol exhibited significantly different behaviour than the other protonated alcohols. Protonated methanol was found to react with benzoyl fluoride to produce only benzoyl cation while each of the other protonated aliphatic alcohols also yielded protonated alkyl benzoates. Competitive proton transfer experiments established that the proton affinity of benzoyl fluoride was intermediate between methanol and ethanol and can be assigned a value of 184 ± 2 kcal/mol. Typical data for alcohol – benzoyl fluoride systems where acidic solvolysis occurs are shown in Fig. 4 for a mixture of ethanol and benzoyl fluoride. In addition to reactions similar to those previously observed a rather novel reaction product at *m/e* 106 was found to arise from reaction of the benzoyl fluoride molecular ion, *m/e* 124, with ethanol. A feasible explanation of this product is reaction 15.

[15] $\phi COF^+ + CH_3CH_2OH \rightarrow \phi CHO^+ + CH_3F + CH_2O$ (or $HF + CH_3CHO$)

(3) Reactions of Protonated Ammonia and Amines

Ammonium ion and all alkyl ammonium ions were observed to be unreactive towards each of the acyl halides studied. The ion molecule reactions occurring in a mixture of ammonia and acetyl chloride are shown in Fig. 5. The only reaction of interest is proton transfer from the acyl cation to ammonia, reaction 16, in agreement with recent determinations of the proton affinity of ketene from thermochemical data which establish it to be less than ammonia.[1]

[16] $CH_3CO^+ + NH_3 \rightarrow NH_4^+ + CH_2CO$

Additional interesting results were obtained in mixtures of ammonia and amines with benzoyl fluoride. Since the ionization potential of benzoyl

[1]Proton affinity of ketene calculated from $\Delta H_f^0(CH_3CO^+) = 153$ kcal/mol (30) and $\Delta H_f^0(CH_2CO) = -14.6$ kcal/mol (30).

Can. J. Chem. Downloaded from www.nrcresearchpress.com by 210.87.254.6 on 09/05/12
For personal use only.

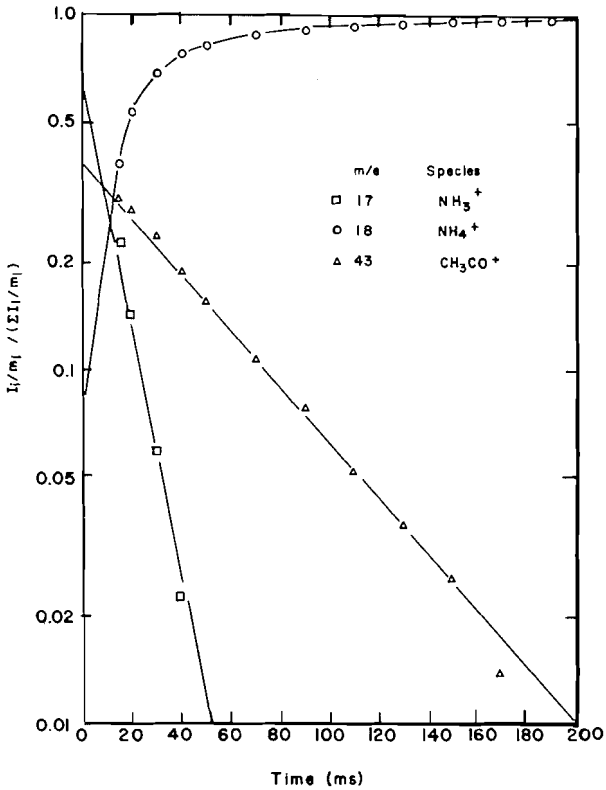

FIG. 5. Variation of relative ion abundances with reaction time in a 3:1 mixture of ammonia and acetyl chloride at 15 eV and a total pressure 2.0×10^{-6} Torr.

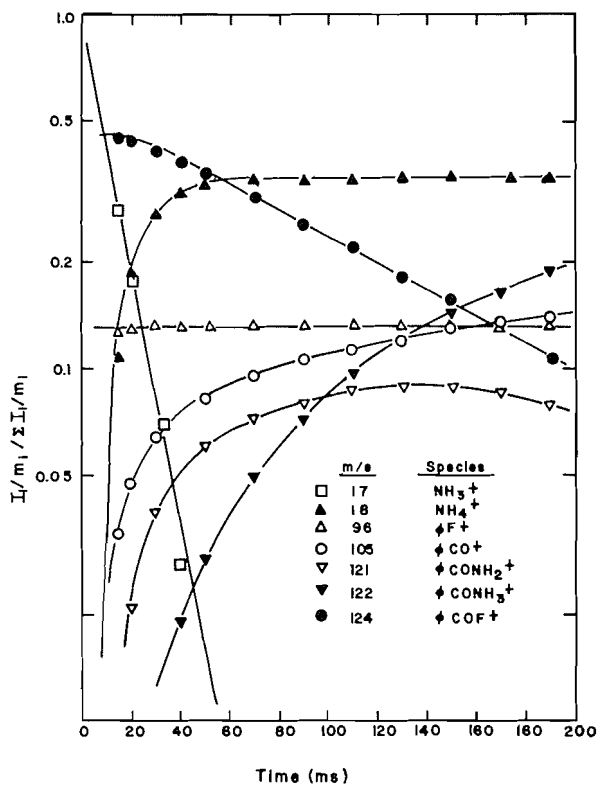

FIG. 6. Variation of relative ion abundances with reaction in a 4:1 mixture of ammonia and benzoyl fluoride at 14 eV and a total pressure of 2.0×10^{-6} Torr.

fluoride is comparable to ammonia it is necessary to operate under conditions where benzoyl fluoride molecular ion is also present. This ion initiates the sequence of reactions 17 and 18. In addition reactions 19 and 20 also occur.

[17] $\phi CFO^+ + NH_3 \rightarrow \phi CONH_2^+ + HF$

[18] $\phi CONH_2^+ + NH_3 \rightarrow \phi CONH_3^+ + NH_2$

[19] $NH_3^+ + \phi COF \rightarrow \phi CFO^+ + NH_3$

[20] $NH_3^+ + \phi COF \rightarrow \phi CO^+ + HF + NH_2$

These reactions are illustrated in Fig. 6. Analogous behaviour is observed for methyl amine – benzoyl fluoride mixtures.

(4) Reactions of Protonated Carboxylic Acids

The reactions of protonated formic acid with acetyl fluoride, Fig. 7, and acetyl chloride, Fig. 8, are noteworthy in that radically different products are formed in each case. With acetyl fluoride protonated formic acid reacts to produce a new ion at *m/e* 89 corresponding to protonated formic acetic anhydride, reaction 21. This reaction is analogous to the acidic solvolysis reactions observed above.

[21] $HCO_2H_2^+ + CH_3COF \rightarrow (CH_3CO_2COH)H^+ + HF$

In addition products also appear at *m/e* 105, 103, and 61 which may be explained by the sequence of reactions 22–24 respectively.

[22] $(HCO_2COCH_3)H^+ + CH_3COF \rightarrow (CH_3CO)_2F^+ + HCO_2H$

[23] $(HCO_2COCH_3)H^+ + CH_3COF \rightarrow ((CH_3CO)_2O)H^+ + HF + CO$

[24] $(CH_3CO)_2F^+ + HCO_2H \rightarrow CH_3CO_2H_2^+ + CH_3COF + CO$

It is interesting to note that reactions 22 and 24 constitute a chain reaction leading to the overall decomposition of protonated acetic anhydride to protonated acetic acid plus carbon monoxide, reaction 25.

[25] $(HCO_2COCH_3)H^+ \rightarrow CH_3CO_2H_2^+ + CO$

In the reactions of protonated formic acid with acetyl chloride no protonated mixed anhydride is formed. Instead the immediate product of reaction is *m/e* 61

Can. J. Chem. Downloaded from www.nrcresearchpress.com by 210.87.254.6 on 09/05/12
For personal use only.

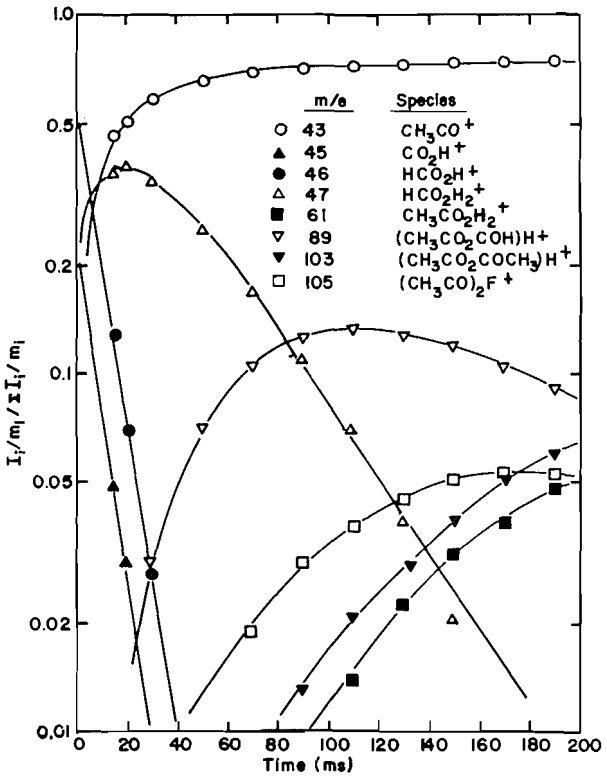

FIG. 7. Variation of relative ion abundances with reaction time in a 4:1 mixture of formic acid and acetyl fluoride at 17 eV and a total pressure of 2.0×10^{-6} Torr.

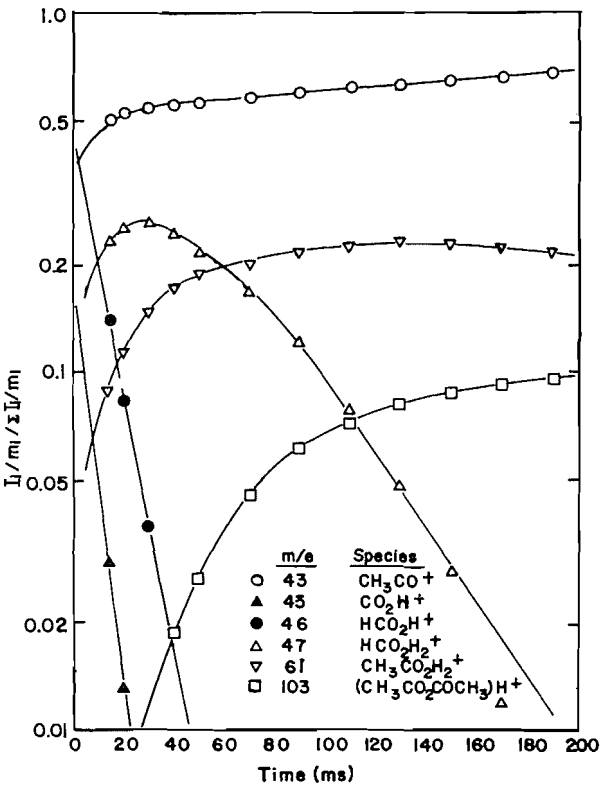

FIG. 8. Variation of relative ion abundances with reaction time in a 3:1 mixture of formic acid and acetyl chloride at 15 eV and a total pressure of 1.6×10^{-6} Torr.

protonated acetic acid, reaction 26, followed by further reaction with acetyl chloride to produce the protonated symmetric anhydride, reaction 27.

[26] $HCO_2H_2^+ + CH_3COCl \rightarrow CH_3CO_2H_2^+ + HCl + CO$

[27] $CH_3CO_2H_2^+ + CH_3COCl \rightarrow ((CH_3CO)_2O)H^+ + HCl$

Thus although protonated acetic acid leads to anhydride formation as expected from the acetyl fluoride results protonated formic acid does not, contrary to expectation. Competitive proton transfer experiments established the proton affinity of acetyl fluoride as intermediate between H_2S and formic acid and of acetyl chloride as intermediate between formic acid and methanol. These results have important mechanistic implications to be discussed below.

(5) Reactions of Other Protonated Species

In order to test the generality of the addition–elimination reaction, [1], a number of other protonated species were reacted with the acyl halides. CH_5^+, H_2Cl^+, and CH_3ClH^+ reacted only via proton transfer or acyl cation formation. Protonated alkyl ethers and ketones were completely unreactive toward the acyl halides. In addition as seen from the data presented above protonated esters and anhydrides underwent no addition–elimination reactions with the acyl halides.

Discussion

From the above data it is evident that not all protonated species will undergo the addition–elimination reaction with acyl halides. However, careful examination reveals that when the following criteria are met the acidic solvolysis reaction may be expected to occur.

(1) The reaction must be exothermic. This is a general requirement of all thermal energy ion molecule reactions (12).

(2) Proton transfer from the protonated 'solvent' molecule to the acyl halide must be endothermic. This requirement is similar to that observed for gas phase nucleophilic displacement reactions (4). For example although reactions 28 and 29 are both exothermic, [28] occurs while [29] does not since the competing reaction 30 is also exothermic. This situation does not arise in the ethylchloride case since the proton affinity of ethyl chloride is greater than that of water.

[28] $C_2H_5ClH^+ + H_2O \rightarrow C_2H_5OH_2^+ + HCl$

[29] $CH_3ClH^+ + H_2O \not\rightarrow CH_3OH_2^+ + HCl$

[30] $CH_3ClH^+ + H_2O \rightarrow H_3O^+ + CH_3Cl$

An exactly analogous situation may be seen for the

Can. J. Chem. Downloaded from www.nrcresearchpress.com by 210.87.254.6 on 09/05/12
For personal use only.

acidic solvolysis reactions observed here. Thus although both [31] and [32] are very exothermic only [31] is observed since [33] dominates in reactions of protonated methanol with benzoyl fluoride.

[31] $CH_3CH_2OH_2^+ + \phi COF \rightarrow (\phi CO_2C_2H_5)H^+ + HF$

[32] $CH_3OH_2^+ + \phi COF \not\rightarrow (\phi CO_2CH_3)H^+ + HF$

[33] $CH_3OH_2^+ + \phi COF \rightarrow \phi CFOH^+ + CH_3OH$

$\rightarrow \phi CO^+ + HF + CH_3OH$

In this situation where two exothermic reaction channels are available from a common intermediate the channel involving the more extensive molecular rearrangement is less favorable. For similar reasons protonated formic acid undergoes addition–elimination with acetyl fluoride but not with acetyl chloride; H_3O^+ and H_3S^+ react only by proton transfer and ethanol and higher alcohols all undergo the acidic solvolysis reaction.

(3) The protonated solvent molecule must have at least two labile protons. This requirement arises from the observation that although reaction of protonated alcohols with acyl halides yield the corresponding protonated esters (for example reaction 14), protonated ethers are unreactive toward acyl halides. For example reaction 34 is not observed even though

[34] $(CH_3)_2OH^+ + CH_3COF \not\rightarrow$

$(CH_3CO_2CH_3)H^+ + CH_3F$

it is 20 kcal/mol exothermic. Similarly no acidic solvolysis was ever observed from protonated species with less than two labile protons. It is important to note that the two labile protons need not be bound to the same atom and need not be equivalent. For example protonated formic acid reacts with acetyl fluoride to give protonated formic acetic anhydride, reaction 21, even though the requisite two protons are on different but equivalent oxygens. In addition protonated acetaldehyde is observed to react with acetyl chloride to produce protonated biacetyl, reaction 35, even though one of the labile protons is bound to oxygen and the other to carbon. *Ab initio* calculations indicate that the hydrogen bound to

[35] $CH_3CHOH^+ + CH_3COF \rightarrow [(CH_3CO)_2]H^+ + HF$

oxygen has a formal positive charge of +0.412 while the hydrogen bound to the carbonyl carbon has a charge of +0.289 (13). It is therefore reasonable to expect a certain degree of lability from this second hydrogen.

(4) The protonated solvent must have at least one additional lone pair of electrons to participate in new bond formation. This requirement is indicated by the inability of protonated ammonia and amines to react with acyl halides to produce protonated amides even though the reactions are quite exothermic and in the case of the acetyl halides no other exothermic competing reaction channel of any kind exists. This criterion again has precedent if the ion molecule reactions of alkyl halides (14, 15), alcohols (16–18), and amines (19–21) are compared. While reactions 36 and 37 occur readily for protonated alcohols and alkyl halides the analogous reaction 38 of protonated amines is not observed at all even though it is exothermic.

[36] $ROH_2^+ + ROH \rightarrow R_2OH^+ + H_2O$

[37] $RXH^+ + RX \rightarrow RXR^+ + HX$

[38] $RNH_3^+ + RHH_2 \not\rightarrow R_2NH_2^+ + NH_3$

This result is attributable to the lack of an available electron pair on nitrogen in the proton bound dimer intermediate for the reaction. In the alcohols and halides simultaneous bond breakage and formation can occur in the intermediate since in these cases the heteroatoms have one or two nonbonding electron pairs available to participate in formation of new bonds.

On the basis of the evidence presented above the probability is high that if all four of these criteria are met an addition–elimination reaction having the character of an acidic solvolysis will occur to an observable extent. If other reaction channels are available the fraction of protonated species reacting with acyl halide via this pathway may be appreciably less than unity. In the cases examined above however wherever the suggested criteria are met some acidic solvolysis is observed.

Consideration of the above criteria and appropriate thermochemical data provides several clues to the details of the mechanisms of several of the reactions observed. On the basis of observation of reactions of protonated molecules with n-donor bases the most likely initially formed intermediate in the acidic solvolysis reaction is a linear proton bound dimer (22, 23). This geometry is supported by several *ab initio* calculations of model systems (24–26). This intermediate is typified by structure **1** for the

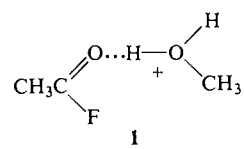

1

methanol acetyl fluoride system. In order to eliminate HF to produce protonated methyl acetate or to produce acetyl cation two further reaction intermediates are possible. The first of these, structure **2**, is a tetrahedral structure, postulated by solution organic chemists as the intermediate involved in the solvolysis of acyl halides. Structure **3** is a bent proton bound dimer which is in general considered to be less stable than a linear proton bound dimer. How-

Can. J. Chem. Downloaded from www.nrcresearchpress.com by 210.87.254.6 on 09/05/12
For personal use only.

ever, Del Bene has recently carried out calculations of hydrogen bonded dimers of bifunctional carbonyl compounds and has shown that in several systems such as the dimer of urea and water two bent O—H...O and N—H...O bonds may be formed (27). This system is conceptually similar since a second weaker hydrogen bond may form to the fluorine. Both **2** and **3** are adequate to explain the formation of protonated methyl acetate. However,

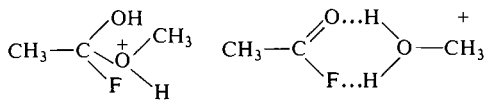

2 **3**

an analysis of additional reactions which do and do not occur provides a useful indication of which of **2** and **3** is more plausible. In addition to protonated ester formation it is observed that protonated methanol reacts with acetyl fluoride to produce acyl cation. The corresponding neutral products of this reaction may be either methanol and HF or methyl fluoride and water. An analysis of thermochemical data reveals however that only reaction associated with the latter pair of neutral products is exothermic. Elimination of CH_3F from **2** suggests that formation of protonated acetic acid would also be a feasible reaction product since this reaction is exothermic by 22 kcal/mol. Since this product is in fact not observed structure **3** seems to be the more reasonable intermediate. Elimination of HF simultaneous with carbonyl carbon to alcohol oxygen bond formation facilely leads to the protonated ester. In addition rotation about the O—H...O bond allows for elimination of CH_3F and H_2O to yield acetyl cation.

The above conjecture is supported by mechanistic studies of esterification of acetic acid using deuterium and ^{18}O labelling carried out by Beauchamp (28). In this case esterification occurs for all alcohols and acetic acids but by different mechanisms depending upon the relative proton affinities of the alcohol and the acid. The mechanistic conclusions drawn are outlined in Scheme 1. In this system the proton affinities of methanol and ethanol are less than acetic acid so that the mechanism involves proton transfer to the acid and formation of a tetrahedral intermediate followed by loss of H_2O. For isopropanol and *tert*-butanol the alcohol proton affinities are greater than acetic acid and the mechanism involves intramolecular R^+ transfer within the intermediate with loss of H_2O. This latter mechanism is exactly analogous to that proposed here for protonated species with acyl halides. The proton affinity of the acyl halide is less than the protonated species and a tetrahedral intermediate need not be formed. Using the methanol – acetyl fluoride case as an example the mechanism can be illustrated by Scheme

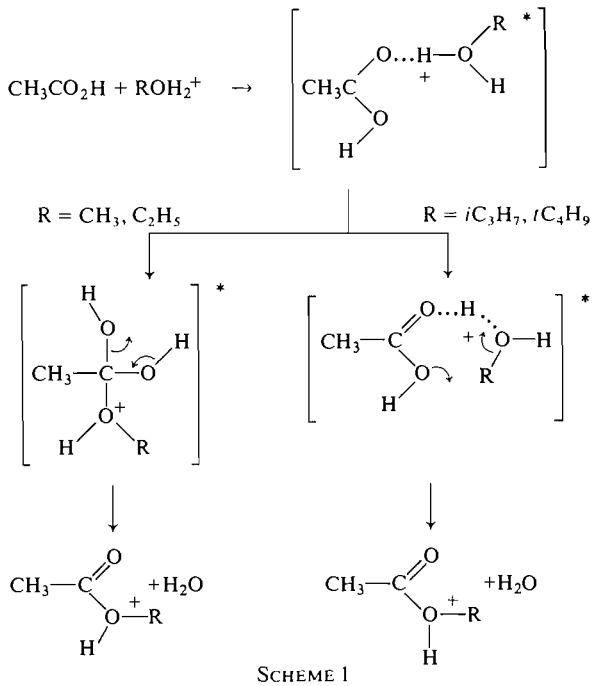

SCHEME 1

2. The evidence and precedents all tend to support this as the most reasonable mechanism for acyl halide acidic solvolysis reactions.

It is also of interest to note that in certain cases where proton transfer from the protonated species to acyl halide is exothermic reactions may occur which can be assumed to arise from a tetrahedral intermediate. For example the reactions of protonated formic acid with acetyl fluoride and acetyl chloride are markedly different. In the case of acetyl

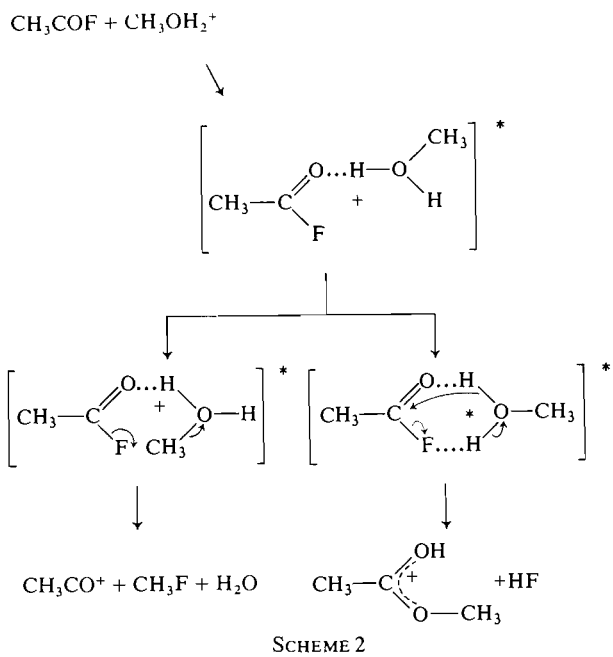

SCHEME 2

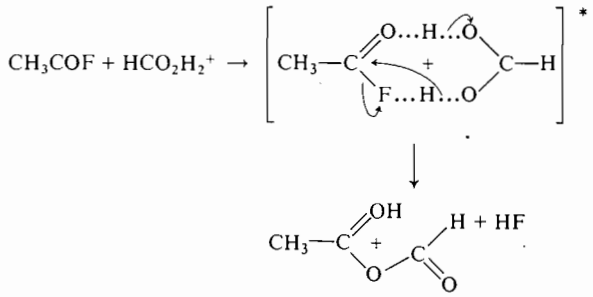

SCHEME 3

fluoride the proton affinity is less than formic acid and the acidic solvolysis product, protonated acetic-formic anhydride is formed. This reaction is illustrated by Scheme 3. However, the proton affinity of acetyl chloride is greater than that of formic acid and the observed reaction product, protonated acetic acid must arise from a different mechanism. Two reasonable mechanisms represented by Scheme 4*a* and *b* are possible. By analogy with the reactions of

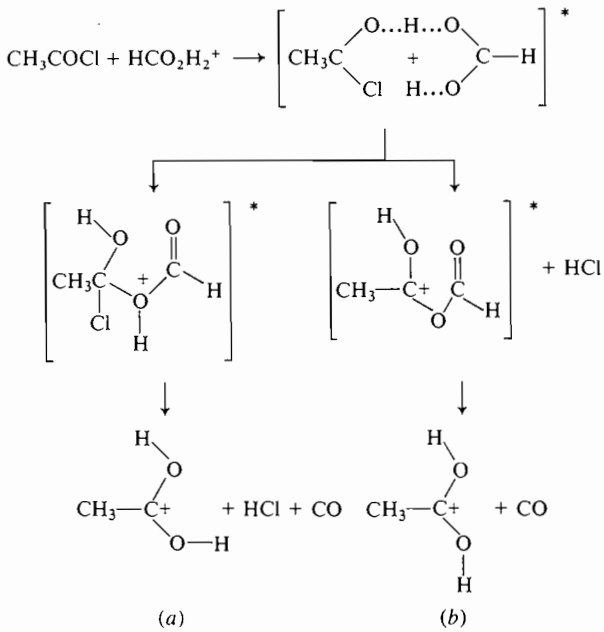

SCHEME 4

protonated methanol and ethanol with acetic acid where proton transfer is accompanied by tetrahedral intermediate formation it is likely that Scheme 4*a* is the actual reaction mechanism. Although similar reaction of protonated formic acid with acetyl fluoride leading to protonated acetic acid is exothermic it is not observed, presumably because the initial proton transfer and tetrahedral intermediate formation do not occur.

Conclusions

The results and arguments presented above provide a rational basis for the general understanding of ion molecule reactions of protonated species with acyl halides. The competition between various reaction channels may be understood given the criteria described for acidic solvolysis to occur and in cases of new reactants prediction of dominant reaction pathways should be possible. In addition the gas phase ion molecule mechanism provides a first approximation for understanding the much more complex solvolysis reaction in solution.

1. A. KIVINEN. *In* The chemistry of acyl halides. *Edited by* S. Patai. Interscience, London. 1972.
2. R. J. E. TALBOT. *In* Comprehensive chemical kinetics. Vol. 10. *Edited by* C. H. Bamford and D. F. H. Tippen. Elsevier, Amsterdam. 1972.
3. M. L. BENDER. Chem. Rev. **60**, 153 (1960).
4. D. HOLTZ, J. L. BEAUCHAMP, and S. D. WOODGAGE. J. Am. Chem. Soc. **92**, 7484 (1970).
5. C. A. LIEDER and J. I. BRAUMAN. J. Am. Chem. Soc. **96**, 4028 (1974).
6. S. BENEZRA, M. K. HOFFMAN, and M. M. BURSEY. J. Am. Chem. Soc. **92**, 7501 (1970).
7. T. B. MCMAHON and J. L. BEAUCHAMP. Rev. Sci. Instrum. **43**, 509 (1972).
8. J. L. BEAUCHAMP. Ann. Rev. Phys. Chem. **22**, 517 (1971).
9. J. M. S. HENIS. *In* Ion molecule reactions. *Edited by* J. L. Franklin. Plenum Press, New York. 1972. Chapt. 9.
10. R. D. WIETING, R. H. STALEY, and J. L. BEAUCHAMP. J. Am. Chem. Soc. **97**, 924 (1975).
11. S. W. BENSON and H. E. O'NEAL. Kinetic data on gas phase unimolecular reactions. NSRDS-NBS 21, U.S. Govt. Printing Office, Washington, DC. 1970.
12. J. L. FRANKLIN. J. Chem. Ed. **40**, 284 (1963).
13. A. C. HOPKINSON and I. G. CSIZMADIA. Can. J. Chem. **52**, 546 (1974).
14. J. L. BEAUCHAMP, D. HOLTZ, S. D. WOODGATE, and S. L. PATT. J. Am. Chem. Soc. **94**, 2798 (1972).
15. R. J. BLINT, T. B. MCMAHON, and J. L. BEAUCHAMP. J. Am. Chem. Soc. **96**, 1269 (1974).
16. M. S. B. MUNSON. J. Am. Chem. Soc. **87**, 5313 (1965).
17. L. W. SIECK, F. P. ABRAMSON, and J. H. FUTRELL. J. Chem. Phys. **45**, 2859 (1966).
18. J. M. S. HENIS. J. Am. Chem. Soc. **90**, 844 (1968).
19. M. S. B. MUNSON. J. Phys. Chem. **70**, 2034 (1966).
20. L. HELLNER and L. W. SIECK. Int. J. Chem. Kinet. **5**, 177 (1973).
21. J. M. BRUPBACHER, C. J. EAGLE, and E. TSCHUIKOW ROUX. J. Phys. Chem. **79**, 671 (1975).
22. A. J. CUNNINGHAM, J. D. PAYZANT, and P. KEBARLE. J. Am. Chem. Soc. **94**, 7627 (1972).
23. P. KEBARLE. *In* Ion molecule reactions. *Edited by* J. L. FRANKLIN. Plenum Press, New York. 1972.
24. P. A. KOLLMAN and L. C. ALLEN. J. Am. Chem. Soc. **92**, 6101 (1970).
25. M. D. NEWTON and S. EHRENSON. J. Am. Chem. Soc. **93**, 4971 (1971).
26. P. LERLET, S. D. PEYERIMHOFF, and R. J. BUENKER. J. Am. Chem. Soc. **94**, 8301 (1972).
27. J. E. DEL BENE. J. Chem. Phys. **63**, 4666 (1975).
28. J. L. BEAUCHAMP. *In* Interactions between ions and molecules. *Edited by* P. Ausloos. Plenum Press, New York. 1975.
29. R. YAMDAGNI and P. KEBARLE. J. Am. Chem. Soc. **98**, 1320 (1976).
30. H. M. ROSENSTOCK, K. KRAXL, B. W. STEINER, and J. T. HERRON. J. Phys. Chem. Ref. Data, **6**, suppl. 1 (1977).

Can. J. Chem. Downloaded from www.nrcresearchpress.com by 210.87.254.6 on 09/05/12
For personal use only.

The formation of hex-5-enopyranosides and their selective hydrolysis in methylated polysaccharides[1]

GERALD OLIVER ASPINALL[2] AND KARL-GUNNAR ROSELL

Department of Chemistry, York University, Downsview, Toronto, Ont., Canada M3J 1P3

Received October 14, 1977

GERALD OLIVER ASPINALL and KARL-GUNNAR ROSELL. Can. J. Chem. **56**, 680 (1978).

The introduction of hex-5-enopyranoside residues into methylated acidic polysaccharides is effected by reduction of uronic acid residues, followed by reaction with triphenyl phosphite methiodide, and dehydroiodination. The selective hydrolysis of hex-5-enopyranosidic linkages with characterization of the 6-deoxyglycos-5-uloses thus formed and location of the aglyconic hydroxyl groups thus exposed has been demonstrated for methylated derivatives of birch xylan and gum arabic. The reaction sequence provides a new method for linkage analysis of acidic polysaccharides.

GERALD OLIVER ASPINALL et KARL-GUNNAR ROSELL. Can. J. Chem. **56**, 680 (1978).

On effectue l'introduction de résidus hexéno-5 pyrannosides dans des polysaccharides méthylés acides en faisant appel à la réduction de résidus d'acide uronique, suivie par une réaction avec de l'iodométhylate de triphénylphosphite et une déhydroiodation. On a pu mettre en évidence l'hydrolyse sélective des liens hexéno-5 pyrannosides accompagnée d'une caractérisation des déoxy-6 glycosuloses-5 ainsi formés et de la détermination de la position des groupes hydroxyles aglyconiques ainsi exposés dans le cas de dérivés méthylés de xylanes de bouleau et de la gomme arabique. La série de réactions fournit une nouvelle méthode pour analyser la nature des liens de polysaccharides acides.

[Traduit par le journal]

In connection with the development of procedures for the selective fragmentation of polysaccharides (1, 2) we have shown that the introduction of acid-sensitive hex-5-enopyranoside units may be achieved from primary hydroxyl groups by reaction with triphenylphosphite methiodide followed by dehydroiodination with (1,5-diazabicyclo [5.4.0] undec-5-ene (DBU) (3). The hydrolysis of hex-5-enopyranosides proceeds under extremely mild conditions with no detectable hydrolysis of normal glycosidic linkages. The characterization of the 6-deoxyglycos-5-uloses thus formed by reduction with sodium borohydride and further *O*-alkylation (or *O*-acylation) has now been carried out for disaccharide derivatives. Methyl 2,2′,3,3′,4′,6′-hexa-*O*-methyl-β-maltoside (**1**) was converted into the corresponding hex-5-enopyranoside (**2**) which was hydrolyzed, reduced with sodium borodeuteride (**3**), and trideuteriomethylated. Despite the formation of products (**4**), which were epimeric at C-5, the two derivatives were separable by gas chromatography and gave identical mass spectra (Scheme 1), in which the main fragment ions indicated the site of attachment of the *O*-glycosyl substituent to the 6-deoxyhexitol unit. Furthermore, the ^{1}H nmr spectrum of the mixture of epimers (**4**) gave confirmatory evidence for the configuration of the intact glycosidic linkage.

The formation of hexopyranose residues in polysaccharides, which are substituted other than at O-6, by selective blocking and deblocking is cumbersome. However, primary hydroxyl groups are readily introduced into methylated uronic acid-containing polysaccharides by reduction with lithium aluminum hydride. We have now examined the formation of hex-5-enopyranose residues from carboxy-reduced uronic acid residues in two methylated polysaccharides and have characterized, as products of selective hydrolysis, both the liberated 'reducing'

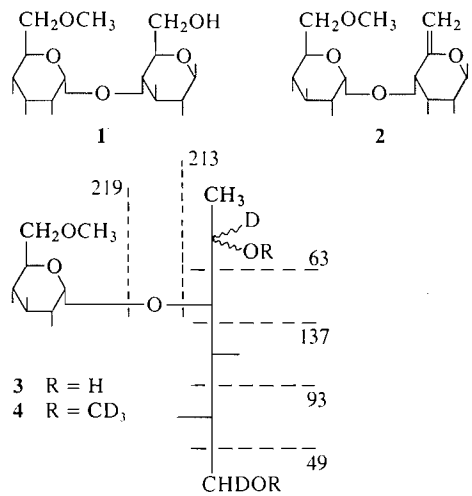

SCHEME 1. Mass spectral fragmentation of epimeric 6-deoxy-1,5-dideuterio-2,3-di-*O*-methyl-1,5-di-*O*-trideuteriomethyl-4-*O*-(2,3,4,6-tetra-*O*-methyl-α-D-glucopyranosyl)hexitols (**4**). Unless otherwise specified substituents are OCH_3.

[1]Presented in part at the joint American Chemical Society – Chemical Institute of Canada Conference, Montreal, Quebec, May 30 – June 3, 1977.

[2]Author to whom enquiries should be directed.

Can. J. Chem. Downloaded from www.nrcresearchpress.com by 210.87.254.42 on 09/05/12
For personal use only.

TABLE 1. Methylation analyses of neutral sugar components of native and modified birch xylan

Polysaccharide	Mol (%)				
	2,3,4-Xyl[a] $T = 0.68$[c]	2-Et-3-Me-Xyl[b] $T = 1.38$	2,3-Xyl $T = 1.54$	2,3,4-Glc $T = 2.50$	3-Xyl $T = 2.92$
Native	1		93		6
Native, reduced[d]	1		82	8[e]	9
Modified from hex-5-enopyranose degradation, ethylated	1	7	91		1

[a]2,3,4-Xyl = 2,3,4-tri-*O*-methyl-D-xylose etc.
[b]2-Et-3-Me-Xyl = 2-*O*-ethyl-3-*O*-methyl-D-xylose.
[c]Retention time of the derived alditol acetate relative to 1,5-di-*O*-acetyl-2,3,4,6-tetra-*O*-methyl-D-glucitol on an ECNSS-M column at 170°C.
[d]Carboxy-reduced ($LiAlD_4$) after methylation.
[e]Deuterium labelling at C-6.

sugars and the exposed aglyconic hydroxyl groups (see Scheme 2).

The methylated polysaccharide (**5**) from birch 4-*O*-methylglucuronoxylan (4) was reduced with lithium aluminum hydride, and then treated successively with triphenylphosphite methiodide and DBU. Mild acid hydrolysis of the modified polysaccharide (**6**) gave a degraded polysaccharide and a syrupy 6-deoxyglycos-5-ulose. Reduction of the syrup with sodium borodeuteride followed by acetylation gave epimeric 1,6-di-*O*-acetyl-6-deoxy-1,5-dideuterio-2,3,4-tri-*O*-methylhexitols (**7**) which were separated by gas chromatography and gave identical mass spectra. The degraded methylated polysaccharide was then *O*-ethylated to label positions from which the modified uronic acid residues had been removed. The sugar composition of the ethylated degraded methylated polysaccharide was determined by glc analysis of the partially alkylated alditol acetates obtained from sugars formed on hydrolysis by reduction and acetylation. The compositions of the parent methylated polysaccharide, its carboxy-reduced derivative, and the ethylated degraded methylated polysaccharide are shown in Table 1. The point of attachment of glucuronic acid residues at O-2 of xylose residues in the main chain is clearly shown by the formation of 2-*O*-ethyl-3-*O*-methylxylitol triacetate, and the quantitative data indicates that the overall conversions proceeded in high yield (Scheme 3).

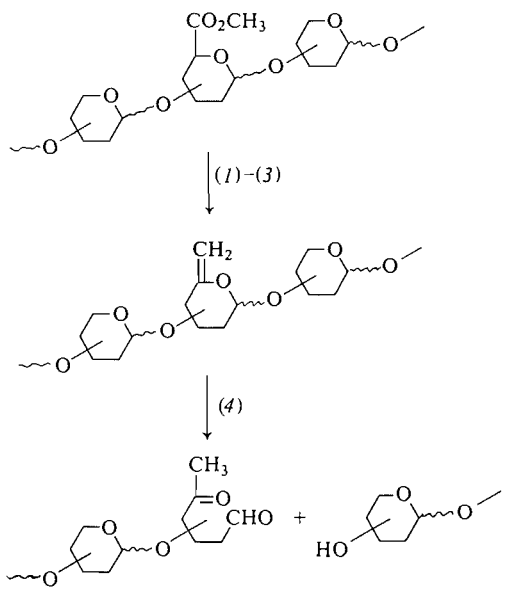

SCHEME 2. Formation and selective hydrolysis of hex-5-enopyranosides in methylated polysaccharides. (*1*) $LiAlH_4$; (*2*) $(C_6H_5O)_3PCH_3^+ I^-$; (*3*) DBU; (*4*) H_3O^+.

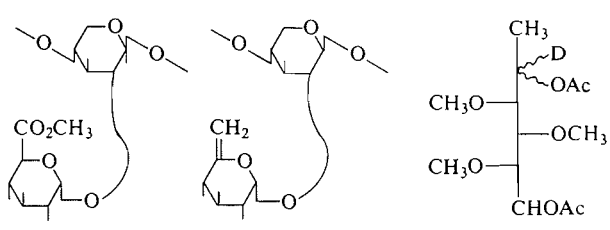

SCHEME 3. Regions of branching in methylated xylan.

A similar series of reactions was then carried out on methylated gum arabic. This polysaccharide contains a small proportion of D-glucuronic acid end groups but the majority of glucuronic acid residues are in non-terminal positions and carry α-L-rhamnopyranose residues at O-4 (**8**). Direct evidence for this linkage was obtained earlier by the isolation of rhamnose-containing oligosaccharides on partial acetolysis of the carboxy-reduced polysaccharide (5). The characterization of such partial fragmentation products from a degradation of adequate but low selectivity requires relatively large quantities of polysaccharide. Modified methylated gum arabic carrying hex-5-enopyranose residues was hydrolyzed, the reaction mixture was treated directly with sodium borohydride, and products of low molecular weight were separated from degraded polysaccharide. The nmr spectra of the mixture of alditols was consistent with the presence therein of α-L-rhamnopyranose residues (in **9**) showing signals at δ 5.10 in the ^1H spectrum assignable to H-1 (6) and at δ 99.6 in the

Can. J. Chem. Downloaded from www.nrcresearchpress.com by 210.87.254.42 on 09/05/12
For personal use only.

Can. J. Chem. Downloaded from www.nrcresearchpress.com by 210.87.254.42 on 09/05/12
For personal use only.

^{13}C spectrum assignable to the anomeric carbon (C-1) (7). Acetylated derivatives from the mixture of alditols were examined by glc – mass spectrometry. A pair of epimeric alditols had the same retention times and identical mass spectra as the derivatives formed from methylated birch xylan. A further pair of components were separated from each other, and their identical mass spectra were consistent with their formulation as 1,5-di-*O*-acetyl-6-deoxy-2,3-di-*O*-methyl-4-*O*-(2,3,4-tri-*O*-methyl-α-L-rhamnopyranosyl)hexitols (**10**). In similar manner *O*-trideuteriomethylation of the alditol mixture furnished *inter alia* a pair of methylated disaccharide alditols which were separable on glc and whose identical mass spectra supported their structural formulation (as **11**) (Scheme 4).

α-L-Rha*p*-(1 → 4)-β-D-Glc*p*A-(1 → 6)-β-D-Gal*p*-(1-
(3)
(**8**)

The degraded methylated polysaccharide from the above series of reactions was further alkylated with trideuteriomethyl iodide. The fully alkylated polysaccharide was analyzed for constituent sugars by

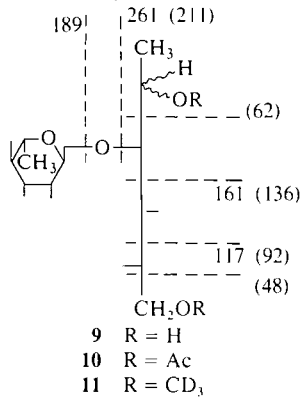

9 R = H
10 R = Ac
11 R = CD_3

SCHEME 4. Mass spectral fragmentations of derivatives of 6-deoxy-2,3-di-*O*-methyl-4-*O*-(2,3,4-tri-*O*-methyl-α-L-rhamnopyranosyl)hexitols; *m/e* values are for ions from derivatives **10** and **11** (in parentheses where different).

conversion into methylated alditol acetates and Table 2 shows the sugar analyses for this polysaccharide derivative, the parent methylated gum arabic and its carboxy-reduced derivative. The following observations are of particular significance: (*i*) the loss of the majority of rhamnopyranose end groups; (*ii*) the absence of detectable glucose derivatives; (*iii*) no change in the overall relative proportions of arabinose and galactose methyl ethers; and (*iv*) the incorporation of trideuteriomethyl groups only at O-6 of galactose residues. These results imply that the majority of rhamnopyranose end groups in gum arabic are linked to glucuronic acid residues and are lost as fragments of low molecular weight during the selective hydrolysis of the modified sugar residues. Since base-catalyzed degradation of methylated gum

TABLE 2. Methylation analyses of neutral sugar components of native and modified gum arabic

Sugar	T^a	Mol (%) of derived alditol acetates[b] (A)	(B)	(C)	(D)	(E)
2,3,4-Me_3 Rha[c]	0.42	13	11	11	3	2
2,3,5-Me_3 Ara[c]	0.42	15	12	12	19	14
2,3,4-Me_3 Ara	0.52	2	2	2	2	2
2,5-Me_2 Ara	0.88	18	15	15	16	12
2,3,4,6-Me_4 Gal	1.19	10	8	8	12[e]	9
2,4,6-Me_3 Gal	2.03	2	2	2	7[e]	5
2,3,4-Me_3 Gal	2.89	1	1	1	1	1
2,6-Me_2 Gal	3.14	2	2	2	10[e]	7
2,4-Me_2 Gal	5.1	20	16	17	23	17
2-Me Gal	6.3	16	13	13	7	5
2,3,4-Me_3 Glc	2.22			4[d]		
2,3-Me_2 Glc	4.50			13[d]		

[a]Retention times of partially acetylated alditol acetates relative to that of 1,5-di-*O*-acetyl-2,3,4,6-tetra-*O*-methyl-D-glucitol on column *c*.
[b](A) Neutral sugar constituents only from methylated gum arabic; (B) calculated from (A) allowing for 19% of uronic acid residues; (C) from carboxyl-reduced methylated polysaccharide; (D) from modified methylated gum arabic after hydrolysis of hex-5-enopyranoside residues and trideuteriomethylation; (E) calculated from (D) allowing for loss of ~80% of the uronic acid and rhamnose residues originally present.
[c]The relative proportions of these two sugars were estimated separately by glc of the methyl glycosides formed on methanolysis of the methylated polysaccharides.
[d]Deuterium at C-6 (from mass spectra).
[e]These constituents contained OCD_3 at C-6 (from mass spectra).

arabic results in complete loss of rhamnose end groups (8) it is known from independent evidence that all the rhamnose residues are linked to glucuronic acid. The presence of a small proportion of residual rhamnose residues in the degraded polysaccharide indicates incomplete modification of glucose residues during the overall sequence, probably from an undetected side reaction. The results of realkylation of the degraded methylated polysaccharide must be treated with some reserve. Judged by the slight excess of apparent branch points over end groups in methylated gum arabic it is not easily possible to achieve complete methylation of the interior galactose residues (for a fuller discussion on this point see the accompanying paper (9)). Consequently further alkylation of the degraded methylated polysaccharide would lead to the introduction of trideuteriomethyl groups at sites of initial incomplete methylation and at liberated hydroxyl groups exposed during the degradation. Nevertheless the detection of labelled alkyl groups only at O-6 of galactose residues is in accord with well documented evidence that glucuronic acid residues in gum arabic are linked (1 → 6) to galactose residues (10).

The experiments now reported show that uronic acid residues in methylated polysaccharides may be converted into hex-5-enopyranose residues which may be selectively hydrolyzed with the formation of 6-deoxyglycos-5-uloses. The characterization of these derivatives provides useful new structural information, especially, as in the case of gum arabic, where

Can. J. Chem. Downloaded from www.nrcresearchpress.com by 210.87.254.42 on 09/05/12
For personal use only.

the cleavage of non-terminal residues gives derivatives carrying glycosyl substituents. In particular the characterization of such oligosaccharide derivatives provides information on the anomeric configuration of the intact glycosidic linkages which may otherwise be difficult to obtain unambiguously.

Experimental

Evaporations were carried out under diminished pressure at bath temperatures of 40°C or less. Optical rotations were measured with a Perkin-Elmer model 141 polarimeter at 20 ± 2°. The ir spectra were measured on a Unicam SP 200 spectrophotometer. ^{1}H nmr spectra were recorded on Varian A-60, EM-360 and HA-100 spectrophotometers in deuteriochloroform with tetramethylsilane as internal standard. ^{13}C nmr spectra were recorded on a Varian CFT-20 FT spectrometer operating at 20 MHz with an 8K 620L-100 computer. Chemical shifts were internally referenced to deuteriochloroform and are reported corrected to tetramethylsilane. Gas–liquid chromatography was performed with Hewlett-Packard model 5750 and Perkin-Elmer 990 chromatographs using columns of Gas-Chrom Q coated with (*a*) 5% of neopentylglycol adipate polyester (operating temperature 130–160°C), (*b*) 3% of silicone–polyester copolymer ECNSS-M (170–190°C), (*c*) 3% of silicone gum OV-225 (170–200°C), and (*d*) 5% of silicone gum XE-60 (160°C), and (*e*) an OV-225 S.C.O.T. column. For glc – mass spectrometry columns were attached to a Perkin-Elmer–Hitachi RMU-6 spectrometer, operated with an inlet temperature of 250°C, an ionization potential of 70 eV, and an ion-source temperature of ~250°C. Thin-layer chromatography was performed with Polygram SilG/UV$_{254}$ as the adsorbent and plates were sprayed with ethanol containing 5% sulfuric acid and heated at about 150°C. Column chromatography was carried out on MN silica gel (0.05–0.2 mm/70–270 mesh ASTM). Light petroleum refers to the fraction of bp 30–60°C.

Examination of Polysaccharides

Polysaccharides were dissolved in water, the solutions were shaken with Amberlite resin IR-120(H) to ensure complete removal of metal ions, and the solutions were filtered, concentrated, and freeze-dried. Hydrolyses of polysaccharides (including reduction of uronic acid components as their trimethylsilyl derivatives) were carried out as described by Lindberg *et al.* (11). Sugar analyses of polysaccharide hydrolyzates were carried out by reduction with sodium borohydride, followed by acetylation and glc of the resulting alditol acetates (12) on column *a*. Birch 4-*O*-methylglucuronoxylan was isolated as described previously (4) and contained 8% of uronic acid residues. The batch of gum arabic (from *Acacia senegal*) was that used in earlier studies (5), and had the composition rhamnose (14%), arabinose (28%), galactose (39%), and glucuronic acid (19%).

Preparation and Analysis of Methylated Polysaccharides

Methylation of polysaccharides was performed by the Hakomori procedure (12) as described by Lindberg *et al.* (11). Methylated polysaccharides and their derivatives were purified by chromatography on columns (15 × 1 cm) of Sephadex LH20 using chloroform–acetone (2:1) as eluant. The sugar components of methylated polysaccharides were analyzed as partially methylated alditol acetates formed on hydrolysis, followed by reduction with sodium borohydride and acetylation (13), by glc alone or glc–ms on columns *b*, *c*, or *e*. The identities of all components of different retention times (Tables 1 and 2) were confirmed by the presence of diagnostic fragment ions in their mass spectra. For separation of derivatives of 2,3,4-tri-*O*-methylrhamnose and 2,3,5-tri-*O*-methylarabinose, methylated polysaccharides were heated under reflux in methanolic 5% hydrogen chloride for 16 h, followed by neutralization with silver carbonate and examination of the resulting methyl glycosides by glc on column *a*.

Reduction of methylated acidic polysaccharides was performed by heating under reflux the sample (10 mg) in tetrahydrofuran (5 ml) containing lithium aluminum deuteride (50 mg) for 4 h. Excess reagent was destroyed by the addition of water, the mixture was acidified to p*H* 4, and reduced methylated polysaccharide was isolated by extraction into chloroform.

Preparation and Hydrolysis of Methyl 6-Deoxy-4-O-(2,3,4,6-tetra-O-methyl-α-D-glucopyranosyl)-2,3-di-O-methyl-β-D-xylo-hex-5-enopyranoside

Methyl 2,2′,3,3′,4′,6′-hexa-*O*-methyl-β-maltoside (100 mg) was kept in tetrahydrofuran (4 ml) containing triphenylphosphite methiodide (250 mg) for 18 h with continuous stirring. Thin-layer chromatography (chloroform–acetone, 7:3) showed that reaction had gone to completion, and the solution was poured into ice-water (10 ml) and extracted with chloroform (3 × 10 ml). Concentration of the dried chloroform extract afforded syrupy methyl 6-deoxy-6-iodo-4-*O*-(2,3,4,6-tetra-*O*-methyl-α-D-glucopyranosyl)-2,3-di-*O*-methyl-β-D-glucopyranoside (105 mg) (**1**); ir no absorption at 3600 cm^{-1}; ms *m/e* (% relative abundance): 550 (0.8) (M$^+$), 375 (37) (abJ_1)[3], 315 (28) (bA$_1$), 219 (32) (aA$_1$), 187 (41) (aA$_2$), 101 (92), 88 (100), and 45 (39). The iodo compound (100 mg) was kept in DBU (1 ml) at room temperature for 24 h. Thin-layer chromatography (light petroleum – acetone, 5:1) showed that reaction was complete and ice-water (10 ml) was added to the reaction mixture and the resulting suspension was extracted with ether (3 × 10 ml). The combined ether extracts were washed with water to remove DBU, dried and concentrated to give syrupy methyl 6-deoxy-4-*O*-(2,3,4,6-tetra-*O*-methyl-α-D-glucopyranosyl)-2,3-di-*O*-methyl-β-D-*xylo*-hex-5-enopyranoside (**2**) (70 mg); ν_{max} (film): 1640 cm^{-1} (C=C).

The unsaturated disaccharide **2** (60 mg) in acetone–water (1:1, 5 ml) was stirred overnight with Dowex 50(H) resin. Thin-layer chromatography (chloroform–acetone, 7:3) showed that reaction was complete with the formation of a single product, resin was removed by filtration, and concentration of the filtrate gave syrupy glycos-5-ulose (52 mg). A portion (10 mg) of the syrup in methanol–water (2:1, 5 ml) was treated with sodium borodeuteride (30 mg) for 3 h. Amberlite resin IR-120(H) was added to destroy excess reagent and to remove sodium ions, and the filtered solution was repeatedly concentrated with methanol to remove boric acid to give diastereomeric diols (**3**); ^{1}H nmr ($CDCl_3$) δ: 5.19 (d, $J_{1',2'}$ = 4 Hz, H-1′). The residue was alkylated with trideuteriomethyl iodide and sodium methylsulfinylmethanide in methyl sulfoxide (11), and analysis of the product by glc – mass spectrometry using column *e* showed the presence of two components (**4**) which were clearly separated but gave identical mass spectra with prominent fragment ions at *m/e* (% relative abundance) 273 (19), 219 (28), 213 (53), 187 (94), 137 (20), 111 (77), 101 (91), 93 (20), 88 (100), 63 (79), and 49 (17).

Modification of Methylated Birch Xylan

Methylated birch xylan (400 mg) in tetrahydrofuran (50 ml) containing lithium aluminum hydride (200 mg) was heated under reflux for 4 h, and the reduced methylated xylan (320 mg) was isolated in the usual way. Completeness of reaction was established in the ir spectrum by appearance of a band at 3600 cm^{-1} (OH) and disappearance of the band at 1735 cm^{-1} (ester C=O), and by glc examination of the methanolysis

[3]The nomenclature of fragment ions is that developed by Kochetkov *et al.* (14).

Can. J. Chem. Downloaded from www.nrcresearchpress.com by 210.87.254.42 on 09/05/12
For personal use only.

products on column *a* which showed the formation of methyl glycosides of 2,3,4-tri-*O*-methylglucose and the absence of those of 2,3,4-tri-*O*-methylglucuronic acid. A sample of the reduced methylated xylan was also analyzed in the usual way (Table 1).

Reduced methylated xylan (300 mg) was treated with triphenylphosphite methiodide (500 mg) in tetrahydrofuran at room temperature for 20 h. Methanol (1 ml) was added to ensure complete reaction of reagent, the solution was concentrated to a syrup which was dissolved in chloroform (50 ml), and the resulting solution was washed successively with *M* sodium hydroxide, aqueous sodium thiosulfate, and dried. The chloroform solution was concentrated (5 ml) and chromatographed on a column (50 × 5.5 cm) of Sephadex LH20. Elution of the column with chloroform–acetone (1:1) afforded modified methylated polysaccharide (340 mg) which was isolated by precipitation with light petroleum and showed no hydroxyl absorption in the ir spectrum. Completeness of reaction was also shown by glc examination of the methanolysis products in which methyl glycosides of 2,3,4-tri-*O*-methylglucose were absent.

The methylated 6-deoxy-6-iodopolysaccharide (110 mg) in tetrahydrofuran (2 ml) containing DBU (2 ml) was heated on a boiling water bath for 1 h and the solution was stirred overnight at room temperature. The solution was dialyzed to remove organic solvent and reagent, and the modified polysaccharide was isolated by extraction into chloroform. The dried chloroform solution was chromatographed on Sephadex LH20 (as above) and furnished unsaturated methylated xylan (90 mg); ν_{max} (film): 1640 cm^{-1} (C=C). Unsaturated methylated xylan (90 mg) in acetone–water (1:1, 5 ml) was stirred overnight with Dowex 50(H) resin. The filtered solution was concentrated to dryness, the residue was dissolved in chloroform, addition of light petroleum afforded a precipitate of degraded methylated xylan (75 mg) (ir spectrum showed absorption at 3600 cm^{-1} (OH) but none at 1640 cm^{-1} (C=C)) and concentration of the supernatant liquid gave syrupy glycos-5-ulose. The glycos-5-ulose was reduced with sodium borodeuteride (20 mg) in methanol–water (3:1, 5 ml), and the product was acetylated. Examination of the resulting partially methylated alditols by glc – mass spectrometry on column *e* showed the presence of two compounds whose identical mass spectra showed prominent fragment ions at *m/e* 176 (19), 162 (29), 132 (72), 118 (89), 102 (89) and 43 (100), which were characteristic of 1,5-di-*O*-acetyl-6-deoxy-2,3,4-tri-*O*-methylhexitols. The degraded methylated xylan was alkylated with ethyl iodide and the resulting polysaccharide derivative was analyzed in the usual way (Table 1).

Modification of Methylated Gum Arabic

Methylated gum arabic (1 g) was successively converted into reduced methylated gum arabic (840 mg) (for analysis see Table 2), the methylated 6-deoxy-6-iodopolysaccharide (640 mg) (*Anal.* calcd. for modified methylated gum arabic: I 10.82; found: I 11.35), and unsaturated methylated gum arabic (380 mg) (ν_{max} (film): 1640 cm^{-1} (C=C)), as described for derivatives of methylated birch xylan. Unsaturated methylated gum arabic (380 mg) in acetone–water (1:1, 20 ml) was stirred overnight with Amberlite resin IR-120(H). The filtered solution was concentrated and the residue in methanol–water (3:1, 20 ml) was treated with sodium borohydride (100 mg) for 3 h. The solution was treated with Amberlite resin IR-120(H) to destroy excess of hydride and remove sodium ions, and the filtrate was repeatedly concentrated with methanol to remove boric acid. The residue was dissolved in chloroform, addition of light petroleum furnished a precipitate of degraded methylated gum arabic (270 mg) (ν_{max} (film): 3600 cm^{-1} (OH)), and concentration of the supernatant liquid gave a syrup which was purified by chromatography on a column (15 × 1.5 cm) of silica gel. Elution of the column with dichloromethane–methanol (10:1) afforded a mixture of partially methylated alditols (80 mg); ^1H nmr ($CDCl_3$) δ: 5.10 (d, 1H, $J_{1',2'}$ = 2Hz, H-1′); ^{13}C nmr ($CDCl_3$) δ: 99.6 (C-1′). The degraded methylated gum arabic was alkylated with trideuteriomethyl iodide and the resulting polysaccharide derivative was analyzed in the usual way (Table 2).

A portion of the mixture of partially methylated alditols was acetylated and examination of the resulting acetates by glc – mass spectrometry showed the presence of two pairs of diastereomeric compounds. The first pair of compounds showed identical mass spectra with prominent fragment ions at *m/e* 175 (31), 161 (41), 131 (88), 117 (89), 101 (89) and 43 (100) characteristic of 1,5-di-*O*-acetyl-6-deoxy-2,3,4-tri-*O*-methylhexitols. The second pair of compounds showed identical mass spectra with prominent fragment ions at *m/e* 321 (15), 261 (19), 189 (62), 161 (16), 117 (74), 101 (87), 88 (100), 87 (69) and 43 (88) characteristic of 1,5-di-*O*-acetyl-6-deoxy-2,3-di-*O*-methyl-4-*O*-(6-deoxy-2,3,4-*O*-methylhexopyranosyl)hexitols. A further portion of the mixture of partially methylated alditols was trideuteriomethylated and examination of the products by glc – mass spectrometry on column *e* showed two major components whose identical mass spectra contained prominent fragment ions at *m/e* 271 (8), 211 (64), 189 (88), 136 (28), 92 (29), 88 (100), 62 (87) and 48 (48) characteristic of isotopically labelled permethylated 6-deoxy-4-*O*-(6-deoxyhexopyranosyl)-hexitols.

Acknowledgements

The authors thank the National Research Council of Canada for financial support, and Drs. B. H. Khouw and C. E. Holloway respectively for recording mass and ^{13}C nmr spectra.

1. B. Lindberg, J. Lönngren, and S. Svensson. Adv. Carbohydr. Chem. Biochem. **31**, 185 (1975).
2. G. O. Aspinall. Pure Appl. Chem. **49**, 1105 (1977).
3. G. O. Aspinall, O. Igarashi, T. N. Krishnamurthy, W. Mitura, and M. Funabashi. Can. J. Chem. **54**, 1708 (1976).
4. K.-G. Rosell and S. Svensson. Carbohydr. Res. **42**, 297 (1975).
5. G. O. Aspinall, A. J. Charlson, E. L. Hirst, and R. Young. J. Chem. Soc. 1696 (1963); G. O. Aspinall and R. Young. J. Chem. Soc. 3003 (1965).
6. G. G. S. Dutton and K. L. Mackie. Carbohydr. Res. **55**, 49 (1977).
7. J. Haverkamp, M. J. A. de Bie, and J. F. G. Vliegenthart. Carbohydr. Res. **37**, 111 (1974); **39**, 201 (1975).
8. G. O. Aspinall and K.-G. Rosell. Carbohydr. Res. **57**, C23 (1977).
9. G. O. Aspinall and K.-G. Rosell. Can. J. Chem. This issue.
10. S. W. Challinor, W. N. Haworth, and E. L. Hirst. J. Chem. Soc. 258 (1931).
11. B. Lindberg, J. Lönngren, J. L. Thompson, and W. Nimmich. Carbohydr. Res. **25**, 49 (1972).
12. S. Hakomori. J. Biochem. (Tokyo), **55**, 205 (1964).
13. J. S. Sawardeker, J. H. Sloneker, and A. R. Jeanes. Anal. Chem. **37**, 1602 (1965).
14. N. K. Kochetkov and O. S. Chizhov. Adv. Carbohydr. Chem. **21**, 39 (1966); N. K. Kochetkov, O. S. Chizhov, and A. F. Bochkov. MTP International review of science, organic chemistry series 1. Vol. 7. *Edited by* G. O. Aspinall. Butterworths, London, and University Park Press, Baltimore. 1973.

The selective cleavage of glycopyranosiduronamide linkages in methylated polysaccharides[1]

GERALD OLIVER ASPINALL[2] AND KARL-GUNNAR ROSELL

Department of Chemistry, York University, Downsview, Toronto, Ont., Canada M3J 1P3

Received October 14, 1977

GERALD OLIVER ASPINALL and KARL-GUNNAR ROSELL. Can. J. Chem. **56**, 685 (1978).

Hofmann degradation of glycosiduronamide linkages in methylated polysaccharides furnishes pentodialdose derivatives to which any sugar residues external to uronic acid residues remain attached together with degraded methylated polysaccharides carrying aglyconic hydroxyl groups. The selective degradation has been carried out on methylated derivatives of birch xylan, gum arabic, and the capsular polysaccharide from *Klebsiella* type 47. Procedures for the degradation of methylated polysaccharides in the vicinity of uronic acid residues are assessed.

GERALD OLIVER ASPINALL et KARL-GUNNAR ROSELL. Can. J. Chem. **56**, 685 (1978).

La dégradation d'Hofmann de liens glycosiduronamides dans des polysaccharides méthylés fournit des dérivés pentodialdoses auxquels reste attachée toute portion de sucre externe aux résidus de l'acide uronique ainsi que tous les polysaccharides méthylés dégradés portant des groupes hydroxyles aglyconiques. On a effectué la dégradation sélective sur des dérivés méthylés de xylanes de bouleau, sur de la gomme arabique et sur des polysaccharides capsulaires provenant de *Klebsiella* type 47. On a évalué les procédés pour la dégradation de polysaccharides méthylés dans l'environnement de résidus d'acide uronique.

[Traduit par le journal]

Kochetkov *et al.* (1) have shown that Hofmann degradation of glycosiduronamides proceeds in high yield with cleavage of the glycosidic linkage and liberation of a pentodialdose from the uronic acid residues. In an application to a polysaccharide, reaction of birch xylan amide was shown to result in removal of 93% of the 4-*O*-methylglucuronic acid side chains. Selective bond cleavage in methylated polysaccharides (2) liberates only a limited number of reducing sugars or derivatives of known origin, and simultaneously exposes only those hydroxyl groups to which the cleaved glycosyl substituents were attached. Since more structural information is obtained from the characterization of these cleavage products than of the corresponding products from the parent polysaccharide, we have now extended the glycosiduronamide degradation to methylated polysaccharides. Two of the three methylated polysaccharides chosen for study were those resulting in the liberation of a disaccharide which was suitable for conversion into volatile derivatives, many of whose structural features could be determined using glc – mass spectrometry. Methylated birch xylan (3) was converted into the amide which was treated with sodium hypochlorite at p*H* 12.5, followed by hydrolysis at p*H* 5, to give a degraded methylated polysaccharide and a syrupy residue. The syrup was reduced with sodium borohydride and acetylated to give a single volatile component originating from cleaved glucuronic acid residues, which was characterized by glc – mass spectrometry as 2,3,4-tri-*O*-methylxylitol diacetate. The degraded polysaccharide contained no residual amide groups, and exposed hydroxyl groups were further alkylated with ethyl iodide. Sugar analysis of the alkylated polysaccharide showed that the 2-hydroxyl group of xylose was the only site of labelling and that ~90% of the branch points to which uronic acid residues were previously attached had been ethylated (see Table 1).

Methylated gum arabic amide (**1**) was similarly degraded on treatment with sodium hypochlorite, the reaction mixture was treated directly with sodium borohydride and separated to give a mixture of partially methylated alditols and a degraded methylated polysaccharide. The ^{1}H nmr spectrum of the mixture of alditols showed one signal assignable to the anomeric proton of the intact rhamnosidic linkage (in **2**) at δ 5.08 ($J_{1,2}$ 1 Hz) (4). The ^{13}C nmr spectrum likewise showed only one signal in the anomeric region whose chemical shift at 96.4 ppm, corresponded to that of a methylated α-L-rhamnopyranoside (5). Acetylation of the alditols gave two components, one with the retention time and mass spectrum of 2,3,4-tri-*O*-methylxylitol diacetate, and the other whose mass spectrum showed primary fragment ions (Scheme 1) which were consistent with the structure, 1,5-di-*O*-acetyl-2,3-di-*O*-methyl-4-*O*-(2,3,4-tri-*O*-methylrhamnopyranosyl) xylitol (**3**). Trideuteriomethylation of the alditols similarly gave a single disaccharide alditol derivative (**4**) which was

[1]Presented in part at the joint American Chemical Society – Chemical Institute of Canada Conference, Montreal, Quebec, May 30–June 3, 1977.

[2]Author to whom enquiries should be addressed.

Can. J. Chem. Downloaded from www.nrcresearchpress.com by 210.87.254.5 on 09/05/12
For personal use only.

TABLE 1. Methylation analyses of neutral sugar components of native and modified birch xylan

Polysaccharide	Mol% 2,3,4-Xyl[a] $T = 0.68$[c]	2-Et-3-Me-Xyl[b] $T = 1.38$	2,3-Xyl $T = 1.54$	2,3,4-Glc $T = 2.50$	3-Xyl $T = 2.92$
Native	1		93		6
Native, reduced[d]	1		82	8[e]	9
Modified from glycosiduronamide degradation, ethylated	1	7	91		1

[a]2,3,4-Xyl = 2,3,4-tri-*O*-methyl-D-xylose etc.
[b]2-Et-3-Me-Xyl = 2-*O*-ethyl-3-*O*-methyl-D-xylose.
[c]Retention time of the derived alditol acetate relative to 1,5-di-*O*-acetyl-2,3,4,6-tetra-*O*-methyl-D-glucitol on an ECNSS-M column at 170°C.
[d]Carboxy-reduced ($LiAlD_4$) after methylation.
[e]Deuterium labelling at C-6.

analyzed by glc – mass spectrometry. The degraded methylated polysaccharide (**5**) was realkylated with trideuteriomethyl iodide and sugar analysis of the polysaccharide derivative, before and after realkylation, showed that loss of rhamnose residues had accompanied glycosiduronamide cleavage and trideuteriomethyl groups were only detected at O-6 of some galactopyranose units, in accord with the known site of attachment of glucuronic acid residues (6). It is important, however, to consider in greater detail the significance of methylation analysis of acidic polysaccharides and their derivatives and Table 2 summarises such analyses for several derivatives of methylated gum arabic.

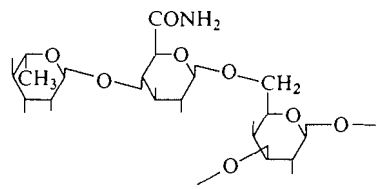

1

Terminal residues in methylated gum arabic amide; unless otherwise specified substituents are OCH_3.

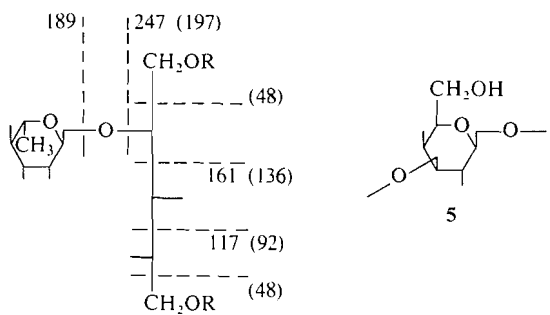

2 R = H
3 R = Ac
4 R = CD_3

SCHEME 1. Mass spectral fragmentations of derivatives of 2,3-di-*O*-methyl-4-*O*-(2,3,4-tri-*O*-methyl-α-L-rhamnopyranosyl)-D-xylitol; *m/e* values are for ions from derivatives **3** and **4** (in parentheses where different).

Methylation of polysaccharides is most effectively performed in methyl sulfoxide using sodium methylsulfinylmethanide as base (7). Lindberg *et al.* (8) have reported many examples of the successful use of this method for the methylation of uronic acid-containing polysaccharides provided that etherification is achieved *in a single operation*. Repetition of the procedure using fresh base results in base-catalyzed degradation initiated by β-elimination from 4-*O*-substituted hexuronate residues (9, 10). Presumably in the methylation the presence of strong base ensures complete ionization of hydroxyl groups so that the weakly nucleophilic carboxylate ions fail to compete effectively with the strongly nucleophilic alkoxide ions for methyl iodide. Consequently esterification of uronic acid residues will be slow and by the time reaction is reasonably complete the diminution of base concentration is such that base-catalyzed degradation is not a significant competing reaction. However, as noted in the accompanying publication (11) it is not easily possible to achieve complete methylation of the interior galactose residues in gum arabic. It follows, therefore, that further alkylation of the exposed hydroxyl groups in the degraded methylated polysaccharide may be accompanied by alkylation of hydroxyl groups which had escaped initial methylation. In the event, however, trideuteriomethyl groups were only detected at O-6 of galactose residues.

Treatment of methylated gum arabic with sodium methylsulfinylmethanide in sulfoxide followed by direct alkylation (10) results in complete loss of uronic acid units and of sugar residues attached thereto together with alkylation of sites to which uronic acid residues were attached. The complete loss of rhamnose residues taken together with unaltered relative overall proportions of galactose and arabinose methyl ethers implies that rhamnose residues are linked only to glucuronic acid residues. It may be noted that similar base-catalyzed degradation of methylated gum arabic amide results in complete removal of rhamnose units. Analysis of the

Can. J. Chem. Downloaded from www.nrcresearchpress.com by 210.87.254.5 on 09/05/12
For personal use only.

TABLE 2. Methylation analyses of neutral sugar components of native and modified gum arabic

		Mol% of derived alditol acetates[b]										
	T^a	(A)[c]	(B)[c]	(C)[c]	(D)	(E)	(F)	(G)	(H)	(I)	(J)	(K)
2,3,4-Me_3 Rha[d]	0.42	13	11	11	0	0	0	0	3	2	3	2
2,3,5-Me_3 Ara[d]	0.42	15	12	12	18	12	18	12	19	14	18	13
2,3,4-Me_3 Ara	0.52	2	2	2	2	1	2	1	2	2	2	2
2,5-Me_2 Ara	0.88	18	15	15	18	12	17	11	20	15	14	10
2,3,4,6-Me_4 Gal	1.19	10	8	8	13[f]	9	13[f]	9	11	8	12[f]	9
2,4,6-Me_3 Gal	2.03	2	2	2	9[f]	6	8[f]	5	2	2	2[f]	6
2,3,4-Me_3 Gal	2.89	1	1	1	1	1	1	1	1	1	1	1
2,6-Me_2 Gal	3.14	2	2	2	15[f]	10	16[f]	11	2	2	14[f]	10
2,4-Me_2 Gal	5.1	20	16	17	20	13	21	14	22	16	22	17
2-Me Gal	6.3	16	13	13	4	3	4	3	17	12	6	4
2,3,4-Me_3 Glc	2.22			4[e]								
2,3-Me_2 Glc	4.50			13[e]								

[a]Retention times of partially acetylated alditol acetates relative to that of 1,5-di-*O*-acetyl-2,3,4,6-tetra-*O*-methyl-D-glucitol on column *c*.
[b](A) Neutral sugar constituents only from methylated gum arabic; (B) calculated from (A) allowing for 19% of uronic acid residues; (C) from carboxyl-reduced methylated polysaccharide; (D) base-degraded methylated gum arabic after trideuteriomethylation; (E) calculated from (D) as proportions of the parent methylated polysaccharide allowing for loss of uronic acid (19%) and rhamnose (14%) residues; (F) base-degraded methylated gum arabic amide after trideuteriomethylation; (G) calculated from (F) as proportions of the parent methylated polysaccharide allowing for loss of uronic acid and rhamnose residues; (H) degraded methylated gum arabic after glycosiduronamide degradation; (I) calculated from (H) as proportions of parent methylated polysaccharide allowing for loss of ~80% of the original uronic acid and rhamnose residues; (J) degraded methylated gum arabic after glycosiduronamide degradation followed by trideuteriomethylation; (K) calculated from (J) as proportions of parent methylated polysaccharide allowing for loss of ~80% of the original uronic acid and rhamnose residues.
[c]Data from accompanying paper.
[d]The relative proportions of these two sugars were estimated separately by glc of the methyl glycosides formed on methanolysis of the methylated polysaccharide.
[e]Deuterium at C-6 (from mass spectra).
[f]These constituents contained OCD_3 at C-6 (from mass spectra).

TABLE 3. Methylation analyses of neutral sugar components of native and modified capsular polysaccharide from *Klebsiella* type 47

Polysaccharide	2,3,4-Rha[a] $T = 0.42$[b]	2-Rha $T = 1.37$	2,4,6-Gal $T = 2.03$	2,3-Glc $T = 4.50$
Native	24	37	39	
Native, reduced[c]	23	27	26	24[d]
Modified from glycosiduronamide degradation	4	48	52	

[a]2,3,4-Rha = 2,3,4-tri-*O*-methyl-L-rhamnose, etc.
[b]Retention time of the derived alditol acetate relative to 1,5-di-*O*-acetyl-2,3,4,6-tetra-*O*-methyl-D-glucitol on an ECNSS-M column at 170°C.
[c]Carboxy-reduced ($LiAlD_4$) after methylation.
[d]Deuterium at C-6 (from mass spectrum).

degraded methylated polysaccharide from the Hofmann degradation showed that ~80% of the rhamnose residues had been removed. The incomplete loss of rhamnose residues during the glycosiduronamide degradation is probably accounted for by incomplete amidation or by some amide hydrolysis during the Hofmann reaction.

The capsular polysaccharide from *Klebsiella* type 47 (12) is of an entirely different structural type (**6**) but the same terminal sequence in side chains, α-L-Rha*p*-(1 → 4)-D-Glc*p*A-(1- , as in gum arabic has been proposed on the basis of various experiments including a base-catalyzed degradation which results in β-elimination of the rhamnose unit from the uronic acid residue followed by further reaction and loss of the modified uronic acid residues (9). Application of the glycosiduronamide degradation to the methylated polysaccharide amide has now provided direct evidence on this point. Treatment of the methylated polysaccharide amide with sodium hypochlorite, followed by reduction of the pentodialdose derivative and acetylation gave a disaccharide alditol, which was shown by glc – mass spectrometry to be identical to the compound (**3**) derived from gum arabic. Insufficient material was obtained to provide nmr spectroscopic evidence for the configuration of the intact rhamnosidic linkage which had been assigned as α-L- on the basis of optical rotatory data (12). Sugar analysis of the degraded methylated polysaccharide (Table 3)

→ 3)-β-D-Gal*p*-(1 → 4)-α-L-Rha*p*-(1-
3
↑
1
β-D-Glc*p*A
4
↑
1
6 α-L-Rha*p*

Can. J. Chem. Downloaded from www.nrcresearchpress.com by 210.87.254.5 on 09/05/12
For personal use only.

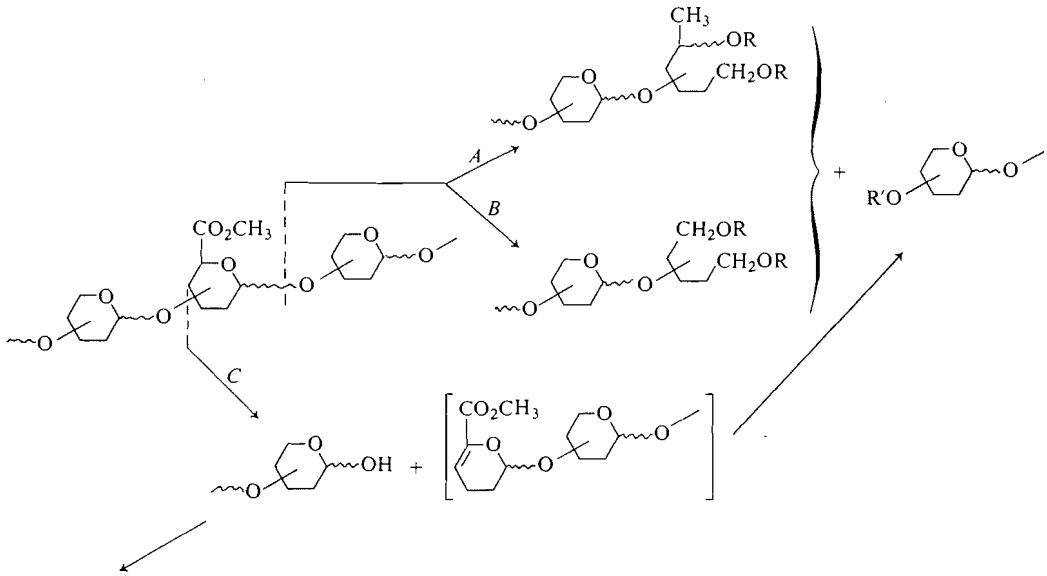

SCHEME 2. Degradations of methylated acidic polysaccharides in the vicinity of uronic acid residues. *A*, hex-5-enopyranoside degradation: $—CO_2CH_3 \rightarrow —CH_2OH \rightarrow —CH_2I \rightarrow =CH_2$: H^+; $NaBH_4$; derivatization (R). *B*, glycosiduronamide degradation: $—CO_2CH_3 \rightarrow —CONH_2$; NaOCl: H^+; $NaBH_4$; derivatization (R). *C*, base-catalyzed β-elimination: $^-CH_2SOCH_3$; derivatization (R').

showed that only a small proportion of rhamnose-terminated side chains were not removed.

The glycosiduronamide degradation and the preferential hydrolysis of hex-5-enopyranosides (11) are alternative reaction sequences which may be applied to the selective cleavage of glycosiduronic acid linkages in methylated polysaccharides (Scheme 2, *A* and *B*). Both procedures after subsequent reduction yield alditols or *O*-glycosylalditols. Despite the formation of epimeric pairs of 6-deoxyhexitols from the hex-5-enopyranose degradation, derivatives suitable for glc analysis whether separable or not, give mass spectra which provide unambiguous evidence for the site of attachment of *O*-glycosyl substituents. In contrast, the glycosiduronamide degradation yields structurally symmetrical pentitols for which independent evidence would be required to distinguish between 2-*O*- and 4-*O*-substitution. The glycosiduronamide degradation involves a much simpler reaction sequence and may be performed on much smaller quantities of methylated polysaccharide than are required for the hex-5-enopyranoside degradation. Furthermore the latter degradation has been performed so far only on glucuronic acid-containing polysaccharides. The necessary transformations may prove more difficult to achieve satisfactorily for galacturonic acid-containing polysaccharides. Displacements at C-6 of galactopyranose derivatives are well known to proceed with difficulty (13) and the dehydroiodination of a 6-deoxy-6-iodogalactose derivative has been shown to occur much more slowly than for *gluco* derivatives (14). In comparison with the base-catalyzed β-elimination from 4-*O*-substituted hexuronate residues, both degradations provide more structural information since sugar residues external to uronic acid units in polysaccharide chains are isolated intact and still attached to a stub recognizably derived from the uronic acid. In base-catalyzed β-eliminations the glycosidic linkage initially broken is external to the uronic acid, and the reducing sugar unit liberated, unless protected (15), will be further degraded in the basic medium and may be entirely lost (Scheme 2, *C*) In such cases sugar analyses of the parent and degraded methylated polysaccharides indicate which sugar residues have been removed during the degradation. However, the β-elimination reaction with attendant analyses may be performed on only milligram quantities of material. Although both glycosiduronamide and hex-5-enopyranoside degradations proceed in high yield, the β-elimination reaction achieves more complete removal of uronic acid and attached glycosyl residues and the exposed aglyconic group(s) may be less ambiguously recog-

Can. J. Chem. Downloaded from www.nrcresearchpress.com by 210.87.254.5 on 09/05/12
For personal use only.

Can. J. Chem. Downloaded from www.nrcresearchpress.com by 210.87.254.5 on 09/05/12
For personal use only.

nized after further alkylation. Indeed, as recently reported, base-catalyzed degradation and further alkylation may be carried out in a single operation without intermediate isolation of the degraded methylated polysaccharide (10).

Experimental

Unless otherwise stated general experimental methods and the procedures for the preparation and examination of methylated polysaccharides were as described in the accompanying paper (11). For the conversion of esters into amides dry ammonia was bubbled through solutions of methylated polysaccharides in methanol or methanol–tetrahydrofuran (1:1) at 0°C for 0.5 h and the solutions were left overnight. Methylated polysaccharide amides were recovered by concentration, dissolution of the residue in chloroform and precipitation by the addition of light petroleum. To ensure complete amidation, methylated polysaccharide in methanol–water (1:2) was treated with Amberlite resin IR-120(H), carboxylic acid residues were esterified by treatment with diazomethane, and treatment with ammonia was repeated. Completeness of amidation was checked by disappearance of ester C=O absorption in the ir spectrum. Base-catalyzed degradations of methylated polysaccharides were performed by treatment of the methylated derivative (10 mg) in *M* sodium methylsulfinylmethanide in methyl sulfoxide (4 ml) in an atmosphere of argon for 16 h. Further alkylation was carried out by direct dropwise addition of trideuteriomethyl (or ethyl) iodide (2 ml) with stirring of the resulting solution for 0.5 h. The fully alkylated degraded polysaccharide was isolated in the usual way.

Degradation of Methylated Birch Xylan Amide

Treatment of methylated birch xylan (400 mg) with ammonia furnished methylated birch xylan amide (360 mg). Sodium hypochlorite (1.5 *M*) was added with stirring (to p*H* 12.5) to the polysaccharide amide (160 mg) in tetrahydrofuran (5 ml) under an argon atmosphere at 0°C, and the solution was kept at room temperature for 2 h and then placed in a boiling-water bath for 5 min. The cooled solution was acidified with acetic acid (to p*H* 5) and left overnight at room temperature. The solution was concentrated and the residue was extracted with boiling chloroform. Concentration of the chloroform extract to small volume followed by addition of light petroleum gave a precipitate (125 mg) of degraded methylated xylan whose ir spectrum showed absorption at 3600 cm^{-1} (OH) but none at 1650 cm^{-1} (amide C=O). The degraded polysaccharide was further alkylated with ethyl iodide and the product was analyzed in the usual way (Table 1). The supernatant liquid from the above precipitation was concentrated, the residue was reduced with sodium borohydride and then acetylated, and examination of the product by glc – mass spectrometry showed the formation of 1,5-di-*O*-acetyl-2,3,4-tri-*O*-methylxylitol as the sole volatile product.

Degradation of Methylated Gum Arabic Amide

Treatment of methylated gum arabic (800 mg) with ammonia gave methylated gum arabic amide (620 mg) (*Anal.* calcd. for modified methylated gum arabic: N 1.30; found: N 1.63). A sample of the methylated polysaccharide amide was treated with base as described above and alkylated directly with trideuteriomethyl iodide, and the product was analyzed (Table 2). Methylated gum arabic amide (600 mg) in methanol–water (2:1, 30 ml) was treated with sodium hypochlorite, as described for methylated birch xylan amide, and the product was hydrolyzed at p*H* 5. Concentration of the reaction mixture gave a residue which was extracted with boiling chloroform, and the chloroform extract afforded a product which showed no amide absorption in the ir spectrum. The reaction product in methanol–water (3:2, 20 ml) was treated with sodium borohydride (200 mg) for 16 h, Amberlite resin IR-120(H) was added to destroy excess hydride and to remove sodium ions, and the filtered solution was repeatedly concentrated with methanol. Addition of light petroleum to the residue in chloroform furnished degraded methylated gum arabic (500 mg) and from the supernatant liquid a syrupy mixture (180 mg) of partially methylated alditols was recovered; ^1H nmr ($CDCl_3$) δ: 5.08 (d, 1H, $J_{1',2'}$ = 2 Hz, H-1′), 1.25 (d, 3H, $J_{5',6'}$ = 5 Hz, H-6′); ^{13}C nmr ($CDCl_3$) δ: 96.4 (C-1′). Samples of degraded methylated gum and of the polysaccharide after further alkylation with trideuteriomethyl iodide were analyzed in the usual way (Table 2).

A portion of the mixture of partially methylated alditols was acetylated and examination of the resulting acetates by glc – mass spectrometry on column *e* showed two components. The minor product was indistinguishable (retention time and mass spectrum) from 1,5-di-*O*-acetyl-2,3,4-tri-*O*-methylxylitol, and the major product gave a mass spectrum which was characteristic of a 1,5-di-*O*-acetyl-2,3-di-*O*-methyl-4-*O*-(6-deoxy-2,3,4-tri-*O*-methylhexopyranosyl)pentitol with prominent fragment ions at *m/e* (% relative abundance) 307 (13), 247 (32), 189 (32), 157 (11), 117 (42), 101 (84), 88 (100), and 43 (72). A further portion of the partially methylated alditols was alkylated with trideuteriomethyl iodide and examination of the product by glc and mass spectrometry on column *e* showed a single methylated disaccharide alditol whose mass spectrum contained prominent fragment ions at *m/e* 257 (2), 197 (65), 189 (35), 157 (10), 136 (6), 101 (56), 92 (17), 88 (100), and 48 (30) which were characteristic of an isotopically labelled permethylated 4-*O*-(6-deoxyhexopyranosyl)pentitol.

Degradation of Methylated Klebsiella *Type 47 Polysaccharide Amide*

Methylated *Klebsiella* 47 polysaccharide (50 mg) was treated with ammonia and the methylated polysaccharide amide was degraded with sodium hypochlorite, as described for methylated birch xylan amide, and the product was hydrolyzed at p*H* 5. Work-up of the reaction mixture followed by reduction with sodium borohydride, as above, afforded degraded methylated polysaccharide (15 mg) (for analysis see Table 3) and a syrupy residue. The syrup was acetylated and examination of the product by glc – mass spectrometry showed a single component which was indistinguishable (retention time and mass spectrum) from the partially methylated disaccharide alditol acetate formed from methylated gum arabic acid amide.

Acknowledgements

The authors thank the National Research Council of Canada for financial support, Dr. J. Lönngren for a sample of *Klebsiella* type 47 polysaccharide, and Drs. B. H. Khouw and C. E. Holloway respectively for recording mass and ^{13}C nmr spectra.

1. N. K. Kochetkov, O. S. Chizhov, and A. F. Sviridov. Carbohydr. Res. **14**, 277 (1970).
2. G. O. Aspinall. Pure Appl. Chem. **49**, 1105 (1977).
3. K.-G. Rosell and S. Svensson. Carbohydr. Res. **42**, 297 (1975).
4. G. G. S. Dutton and K. L. Mackie. Carbohydr. Res. **55**, 49 (1977).

5. J. HAVERKAMP, M. J. A. DE BIE, and J. F. G. VLIEGENTHART. Carbohydr. Res. **37**, 111 (1974); **39**, 201 (1975).
6. S. W. CHALLINOR, W. N. HAWORTH, and E. L. HIRST. J. Chem. Soc. 258 (1931).
7. S. HAKOMORI. J. Biochem. (Tokyo), **55**, 205 (1964).
8. B. LINDBERG, J. LÖNNGREN, and S. SVENSSON. Adv. Carbohydr. Chem. Biochem. **31**, 185 (1975).
9. B. LINDBERG, J. LÖNNGREN, and J. L. THOMPSON. Carbohydr. Res. **28**, 351 (1973).
10. G. O. ASPINALL and K.-G. ROSELL. Carbohydr. Res. **57**, C23 (1977).
11. G. O. ASPINALL and K.-G. ROSELL. Can. J. Chem. This issue.
12. H. BJÖRNDAL, B. LINDBERG, J. LÖNNGREN, K.-G. ROSELL, and W. NIMMICH. Carbohydr. Res. **27**, 373 (1973).
13. A. C. RICHARDSON. Carbohydr. Res. **10**, 395 (1969).
14. G. O. ASPINALL, O. IGARASHI, T. N. KRISHNAMURTHY, W. MITURA, and M. FUNABASHI. Can. J. Chem. **54**, 1708 (1976).
15. G. O. ASPINALL and A. S. CHAUDHARI. Can. J. Chem. **53**, 2189 (1975).

Can. J. Chem. Downloaded from www.nrcresearchpress.com by 210.87.254.5 on 09/05/12
For personal use only.

A synthesis of 3-acetamido-3-deoxy-D-*glycero*-D-*gulo*-heptose and 3-acetamido-3-deoxy-D-*glycero*-D-*ido*-heptose from 2-acetamido-2-deoxy-D-glucose[1]

LAURE BENZING AND MALCOLM B. PERRY

Division of Biological Sciences, National Research Council of Canada, Ottawa, Ont., Canada K1A 0R6

Received August 26, 1977

LAURE BENZING and MALCOLM B. PERRY. Can. J. Chem. **56**, 691 (1978).

The reluctance of 2-acetamido-2-deoxy-D-glucose to undergo base catalyzed addition with nitromethane was overcome by using the acetamidoglycose in the form of a substituted acyclic aldehydo derivative. 2-Acetamido-2-deoxy-D-glucose diethyl dithioacetal was isopropylidenated to yield 2-acetamido-2-deoxy-3,4:5,6-di-*O*-isopropylidene-D-glucose diethyl dithioacetal which on demercaptalation afforded 2-acetamido-2-deoxy-3,4:5,6-di-*O*-isopropylidene-*aldehydo*-D-glucose. The aldehydo derivative readily underwent base catalyzed addition of nitromethane to give the expected epimers 3-acetamido 1,3-dideoxy-4,5:6,7-di *O*-isopropylidene-1-nitro-D-*glycero*-D-*gulo*-heptitol and 3-acetamido-1,3-dideoxy-4,5:6,7-di-*O*-isopropylidene-1-nitro-D-*glycero*-D-*ido*-heptitol which, after deisopropylidenation by mild acid treatment, were converted under modified Nef reaction conditions to give 3-acetamido-3-deoxy-D-*glycero*-D-*gulo*-heptose and 3-acetamido-3-deoxy-D-*glycero*-D-*ido*-heptose, respectively.

LAURE BENZING et MALCOLM B. PERRY. Can. J. Chem. **56**, 691 (1978).

L'acétamido-2 déoxy-2 D-glucose réagit difficilement avec le nitrométhane en milieu basique; on a surmonté cette résistance en faisant appel à l'acétamidoglycose sous forme de dérivé aldéhydo acyclique. On a transformé l'acétamido-2 déoxy-2 D-glucose diéthyldithioacétal en son dérivé isopropylidène pour obtenir l'acétamido-2 déoxy-2 di-*O*-isopropylidène-3,4:5,6 D-glucose diéthyldithioacétal qui, par élimination des mercaptans, fournit l'acétamido-2 déoxy-2 di-*O*-isopropylidène-3,4:5,6 aldéhydo D-glucose. Le dérivé aldéhydo subit facilement une addition catalysée par les bases du nitrométhane pour conduire aux épimères attendus, acétamido-3 didéoxy-1,3 di-*O*-isopropylidène-4,5:6,7 nitro-1 D-*glycéro*-D-*gulo*-heptitol et acétamido-3 didéoxy-1,3 di-*O*-isopropylidène-4,5:6,7 nitro-1 D-*glycéro*-D-*ido*-heptitol qui, après élimination des groupements isopropylidènes par traitement en milieu acide dilué, ont pu être transformés respectivement en acétamido-3 déoxy-3 D-*glycéro*-D-*gulo*-heptose et en acétamido-3 déoxy-3 D-*glycéro*-D-*ido*-heptose grâce à une réaction de Nef modifiée.

[Traduit par le journal]

The base catalyzed addition of nitromethane to aldoses to produce 1-deoxy-1-nitroglycitols (1–3) which may be converted under Nef (4) reaction conditions to give aldoses provides an important method for the ascension of the glycose chain which is often of greater utility than the Fischer-Kiliani (5) cyanohydrin route to higher glycoses.

Although the nitromethane addition method can be applied to most aldoses, in some cases the addition does not proceed to a practical extent under the usual experimental conditions. Attempts to use the nitromethane addition method to effect the stepwise synthesis of *N*-acetylneuraminic acid (6) and its analogues, starting from 2-acetamido-2-deoxyhexoses, were initially hindered by the reluctance of some hexoses and synthesized higher aldose derivatives to undergo nitromethane addition. It was found for example, that 2-acetamido-2-deoxy-D-glucose and 2-acetamido-2-deoxy-D-galactose did not undergo base catalyzed addition of nitromethane. Subsequent experiments revealed that these glycoses in the form of substituted acyclic *aldehydo* derivatives underwent satisfactory addition of nitromethane. Demercaptalation of ketal substituted dialkyl dithioacetal glycoses provided a suitable method for preparing the *aldehydo*-glycoses and this note records the successful application of this approach to the addition of nitromethane to 2-acetamido-2-deoxy-D-glucose and the subsequent conversion of the resulting 1-deoxy-1-nitroheptitol derivatives to 3-acetamido-3-deoxyglycoses.

2-Acetamido-2-deoxy-D-glucose diethyl dithioacetal on acid catalyzed isopropylidenation in 2,2-dimethoxypropane–acetone mixture afforded crystalline 2-acetamido-2-deoxy-3,4:5,6-di-*O*-isopropylidene-D-glucose diethyl dithioacetal (**1**) (7) in almost quantitative yield. Demercaptalation of **1** with mercuric chloride and mercuric oxide in aqueous acetone afforded 2-acetamido-2-deoxy-3,4:5,6-di-*O*-isopropylidene-*aldehydo*-D-glucose (**2**) whose pmr and ir spectra gave peaks consistent with the presence of the *aldehydo* function. The *aldehydo*-glucose (**2**) on treatment with nitromethane in the presence of sodium methoxide afforded approx-

[1]NRCC No. 16402.

Can. J. Chem. Downloaded from www.nrcresearchpress.com by 210.87.254.42 on 09/05/12
For personal use only.

Can. J. Chem. Downloaded from www.nrcresearchpress.com by 210.87.254.42 on 09/05/12
For personal use only.

imately equal amounts of the expected epimeric heptitol derivatives 3-acetamido-1,3-dideoxy-4,5:6,7-di-*O*-isopropylidene-l-nitro-D-*glycero*-D-*gulo*-heptitol (**3**) and 3-acetamido-1,3-dideoxy-4,5:6,7-di-*O*-isopropylidene-1-nitro-D-*glycero*-D-*ido*-heptitol (**4**) which were each obtained crystalline by fractional crystallization of their mixture from methanol. The assigned configurations of **3** and **4** were based on the positive Cotton effect observed in the ord spectrum at 342 nm for **3** and the negative Cotton effect at 346 nm for **4** (8) and the assignments were further verified by the identification of the 3-acetamido-3-deoxyheptoses subsequently obtained from the respective 1-deoxy-1-nitroheptitols. Compounds **3** and **4** were deisopropylidenated by treatment with hot dilute sulfuric acid to yield crystalline 3-acetamido-1,3-dideoxy-1-nitro-D-*glycero*-D-*gulo*-heptitol (**5**) and 3-acetamido-1,3-dideoxy-1-nitro-D-*glycero*-D-*ido*-heptitol (**6**), respectively. The 1-deoxy-1-nitroheptitols **5** and **6** underwent a modified Nef reaction (9) to yield crystalline 3-acetamido-3-deoxy-D-*glycero*-D-*gulo*-heptose (**7**) and 3-acetamido-3-deoxy-D-*glycero*-D-*ido*-heptose (**8**) which had physical and chromatographic characteristics in agreement with those previously recorded for these compounds which were made by a route involving the addition of hydrogen cyanide to 2-acetamido-2-deoxy-D-glucose (10). Improved yields of the 3-acetamido-3-deoxyheptoses **7** and **8** were obtained by omitting the isolation of crystalline intermediates. The mixture of the nitromethane addition products **3** and **4** were hydrolyzed to yield **5** and **6** and treatment of this mixture under modified Nef reaction conditions afforded the final products **7** and **8** which were obtained in a pure crystalline form following their separation by cellulose column chromatography.

Experimental

Evaporations were performed under reduced pressure and below 40°C. Melting points were determined on a Fisher-Johns apparatus and are corrected. Optical rotations were determined at 20°C using a Perkin-Elmer Model 141 polarimeter. Optical rotary dispersion measurements (ord) were made using a JASCO model ORD/UV-5 spectrometer. Infrared (ir) spectra were obtained by the KBr disc technique using a Perkin-Elmer 237B Infracord.

Proton magnetic resonance (pmr) spectra were recorded using a Varian EM 360 spectrometer at 60 MHz with tetramethylsilane as an internal standard.

Paper chromatography was performed by the descending method on Whatman No. 1 filter paper using pyridine – ethyl acetate – water (2:5:5 v/v, top layer) as the mobile phase and sugars were detected by the dip procedure using 2% (w/v) silver nitrate in acetone followed by 3% (w/v) sodium hydroxide in ethanol (11). The mobilities of glycoses are quoted relative to 2-acetamido-2-deoxy-D-glucose (R_{GN}). Thin-layer chromatography (tlc) was done on precoated 0.25 mm silica gel 60 plates (E. Merck) using (*A*) benzene–methanol (9:1 v/v) or (*B*) butan-1-ol–acetone–water (4:5:1 v/v) mixtures as the mobile phases. Compounds were detected by spraying the plates with 10% sulfuric acid in ethanol and heating at 120°C and mobilities are quoted relative to the solvent front (R_f).

Gas–liquid chromatography (glc) was done using a Hewlett-Packard 402 gas chromatograph with a hydrogen flame detector fitted with glass U-tubes (4 ft × 6 mm × 3 mm id) packed with 3% (w/w) ECNSS-M on 100–120 mesh Gas Chrom Q and retention times are quoted relative to penta-*O*-acetyl-2-acetamido-2-deoxy-D-glucitol (T_{GN}).

*2-Acetamido-2-deoxy-3,4:5,6-di-*O*-isopropylidene-D-glucose Diethyl Dithioacetal (1)*

2-Acetamido-2-deoxy-D-glucose diethyl dithioacetal (12) (15 g) was added to a stirred solution prepared by adding 2,2-dimethoxypropane (60 ml) to dry acetone (22 ml) containing sulfuric acid (0.37 ml) and the mixture was kept stirred at 20°C for 90 min. The mixture was neutralized with saturated aqueous barium hydroxide and, following the addition of barium carbonate (0.2 g), it was filtered through a bed of Celite. The filtrate and water washings were treated with 2 drops of pyridine and were concentrated under reduced pressure to yield **1** (17.4 g, 93%) as a solid which gave a single spot on tlc (solvent *A*) with R_f 0.49 and it was used without purification in the next synthetic step.

An analytical sample of **1** obtained crystalline from hexane solution had mp 65–66°C and $[\alpha]_D$ −35.7° (*c* 2.1, methanol) (lit. (7) mp 66–67°C and $[\alpha]_D$ −36° (methanol)) and gave a single spot on tlc (solvent *A*) with R_f 0.49; pmr ($CDCl_3$) τ: 3.82 (1H, d, NH), 7.22 (4H, q, CH_2 of SEt), 7.92 (3H, s, $COCH_3$), and 8.65 ppm (18H, m).

*2-Acetamido-2-deoxy-3,4:5,6-di-*O*-isopropylidene-aldehydo-D-glucose (2)*

To a stirred solution of **1** (13.7 g) in acetone (230 ml) and water (12 ml) was added mercuric oxide (23 g) followed by mercuric chloride (23 g) and the mixture was kept stirred at 20°C for 48 h. The mixture was filtered and the filtrate was concentrated in the presence of mercuric oxide (1 g) and the residue was extracted with chloroform (2 × 150 ml). The chloroform extract was washed with 17% aqueous potassium iodide (150 ml) followed by water (3 × 50 ml) and the dried (anhydrous Na_2SO_4) solution was concentrated to yield **2** (5.8 g, 57%) as a syrup which gave a single spot on tlc (solvent *A*) having R_f 0.14. The product was used without further purification in the next synthetic step.

An analytical sample of **2** obtained by column chromatography on silica gel using benzene–methanol (9:1 v/v) as the mobile phase had $[\alpha]_D$ 0° (*c* 2.1, chloroform); pmr ($CDCl_3$) τ: 0.25 (1H, s, CHO), 3.65 (1H, m, NH), 7.80 (3H, s, $COCH_3$), 8.62 ppm (12H, m); ir: 1730 (CHO), 1660 (NH*CO*CH_3), and 1510 cm^{-1} (*NH*$COCH_3$).

*3-Acetamido-1,3-dideoxy-4,5:6,7-di-*O*-isopropylidene-1-nitro-D-glycero-D-gulo-heptitol (3) and 3-Acetamido-1,3-dideoxy-4,5:6,7-di-*O*-isopropylidene-1-nitro-D-glycero-D-ido-heptitol (4)*

To a stirred solution of **2** (5.8 g) in nitromethane (220 ml) was added 1.7 *N* sodium methoxide in methanol (18.6 ml) followed by methanol (120 ml), to dissolve precipitated material, and the mixture was further stirred at 20°C for 70 h. The reaction mixture was saturated with carbon dioxide and, following concentration under reduced pressure, the residue was extracted with warm chloroform (400 ml). Concentration of the chloroform extract gave a mixture of **3** and **4** (6.2 g, 89%) as a solid which on tlc (solvent *A*) gave two spots of equal visual intensity having R_f values of 0.23 and 0.28.

The mixture of **3** and **4** (4.3 g) was dissolved in hot methanol and the solution on cooling gave pure crystalline **3** (1.8 g)

Can. J. Chem. Downloaded from www.nrcresearchpress.com by 210.87.254.42 on 09/05/12
For personal use only.

which had mp 194–195°C, $[\alpha]_D$ 0° (*c* 2.0, methanol), $[\phi]_{342}$ +219° (*c* 0.09, water) and on tlc gave a single spot (solvent *A*) having R_f 0.23. *Anal.* calcd. for $C_{15}H_{26}N_2O_8$: C 49.71, H 7.23, N 7.73; found: C 49.78, H 7.29, N 7.72.

On concentration of the methanol solution it first afforded a mixture of **3** and **4** (0.2 g) followed by pure crystalline **4** (0.11 g) which, after crystallization from a mixture of chloroform and hexane, had mp 143–144°C, $[\alpha]_D$ +31.9° (*c* 0.78, methanol), $[\phi]_{346}$ −54° (*c* 0.10, water) and gave a single spot on tlc (solvent *A*) having R_f 0.28. *Anal.* calcd. for $C_{15}H_{26}N_2O_8$: C 49.71, H 7.23, N 7.73; found: C 49.53, H 7.35, N 7.71.

3-Acetamido-1,3-dideoxy-1-nitro-D-glycero-D-gulo-*heptitol (5)*

A stirred suspension of **3** (0.2 g) in 0.02 *N* sulfuric acid (10 ml) was heated on a boiling water bath for 15 min and following neutralization with barium carbonate and subsequent filtration, the filtrate was passed down a column of mixed Rexyn 101 (H^+) and Duolite A4 (OH^-) ion exchange resins (2 ml). The eluate and washings were concentrated under reduced pressure and the residue was taken up in hot ethanol from which was obtained crystalline **5** (0.15 g, 96%) which had mp 158–160°C, $[\alpha]_D$ −16.2° (*c* 2.1, water), $[\phi]_{342}$ +120° (*c* 0.11, water) and gave single spots on tlc (solvent *B*, R_f 0.64) and paper chromatography (R_{GN} 2.30). *Anal.* calcd. for $C_9H_{18}N_2O_8$: C 38.30, H 6.43, N 9.92; found: C 38.49, H 6.60, N 9.76.

3-Acetamido-1,3-dideoxy-1-nitro-D-glycero-D-ido-*heptitol (8)*

Compound **4** (50 mg) was hydrolyzed under the same conditions as those described for the preparation of **5** to yield pure crystalline **6** (40 mg), from ethanol solution, which had mp 133–134°C, $[\alpha]_D$ +38.1° (*c* 2.19, water), $[\phi]_{347}$ −41° (*c* 0.10, water) and gave a single spot on tlc (solvent *B*, R_f 0.64) and on paper chromatography (R_{GN} 2.30). *Anal.* calcd. for $C_9H_{18}N_2O_8$: C 38.30, H 6.43, N 9.92; found: C 38.12, H 6.41, N 9.87.

3-Acetamido-3-deoxy-D-glycero-D-gulo-*heptose (7)*

Compound **5** (0.28 g) dissolved in a solution of $Ba(OH)_2 \cdot 8H_2O$ (0.35 g) in water (6 ml) was added dropwise to a cooled solution of sulfuric acid (0.6 ml) in water (3.2 ml) and the mixture was then kept stirred for 18 h at 20°C. The neutralized ($BaCO_3$) reaction mixture was filtered and the filtrate was passed down a column of mixed Rexyn 101 (H^+) and Duolite A4 (OH^-) ion exchange resins (1 ml). The eluate and water washings were concentrated to a solid (0.15 g) which was taken up in a minimum of hot ethanol. On cooling, the ethanol solution afforded crystalline **7** (0.11 g, 44%) which had mp 192–194°C and $[\alpha]_D$ −7.4° (*c* 1.34, water) (lit. (10) mp 196°C and $[\alpha]_D$ −4.9° (water)) and on paper chromatography it gave a single spot with R_{GN} 0.92. Gas chromatography (225°C) of the reduced ($NaBH_4$) and acetylated **7** (13) gave a single peak having T_{GN} 2.03. *Anal.* calcd. for $C_9H_{17}NO_7$: C 43.02, H 6.82, N 5.58; found: C 43.24, H 6.96, N 5.53.

3-Acetamido-3-deoxy-D-glycero-D-ido-*heptose (8)*

Compound **6** (0.2 g) was treated in the same way as that described above for the conversion of **5** to **7** to yield **8** (0.1 g, 56%) which after recrystallization from ethanol had mp 185–187°C and $[\alpha]_D$ −77° (*c* 0.1, water) (lit. (10) mp 186–189°C and $[\alpha]_D$ −87.2° (water)) which gave a single spot on paper chromatography having R_{GN} 1.18 and the reduced ($NaBH_4$) and acetylated product on glc (225°C) gave a single peak with T_{GN} 1.63. *Anal.* calcd. for $C_9H_{17}NO_7$: C 43.02, H 6.82, N 5.58; found: C 43.10, H 6.95, N 5.52.

Direct Synthesis of 7 and 8

The crude mixture of 1-deoxy-1-nitroheptitols **3** and **4** (1 g) resulting from the addition of nitromethane to compound **2**, were deisopropylidenated by heating their solution in 0.02 *N* sulfuric acid (50 ml) for 15 min on a boiling water bath and, following neutralization ($BaCO_3$), were concentrated to yield a mixture of **5** and **6** (0.72 g, 92%). The mixture of **5** and **6** (0.72 g) dissolved in a solution of $Ba(OH)_2.8H_2O$ (0.9 g) in water (14 ml) was added dropwise to a solution of sulfuric acid (1.55 ml) in water (8 ml) and the stirred mixture was kept at 20°C for 18 h. The mixture was neutralized ($BaCO_3$), filtered, and the filtrate was concentrated to yield a mixture of **7** and **8** (0.46 g, 72%) which was fractionated by cellulose column (3 × 40 cm) chromatography using butan-1-ol–water (10:1 v/v) as the mobile phase. The first compound eluted was concentrated to yield crystalline **7** (0.15 g) from ethanol solution, and the second compound eluted yielded crystalline **8** (0.11 g), both compounds having identical chromatographic and physical properties with those recorded for their individual preparation.

1. J. C. SOWDEN and H. O. L. FISCHER. J. Am. Chem. Soc. **66**, 1312 (1944).
2. J. C. SOWDEN. Adv. Carbohydr. Chem. **6**, 291 (1951).
3. H. H. BAER. Adv. Carbohydr. Chem. Biochem. **24**, 64 (1969).
4. J. U. NEF. Ann. **280**, 263 (1894).
5. C. S. HUDSON. Adv. Carbohydr. Chem. **1**, 1 (1946).
6. L. BENZING-NGUYEN and M. B. PERRY. J. Org. Chem. In press.
7. J. YOSHIMURA and T. SATO. Nippon Kagaku Zasshi, **80**, 1479 (1959); Chem. Abstr. **55**, 5355 (1961).
8. C. SATOH and A. KIYOMOTO. Carbohydr. Res. **3**, 248 (1966).
9. C. SATOH and A. KIYOMOTO. Chem. Pharm. Bull. Tokyo, **12**, 615 (1964).
10. R. KUHN and G. BASCHANG. Ann. Chem. **636**, 164 (1960).
11. W. E. TREVELYAN, D. P. PROCTER, and J. S. HARRISON. Nature (London), **166**, 444 (1950).
12. M. L. WOLFROM and K. ANNO. J. Am. Chem. Soc. **74**, 6150 (1952).
13. M. B. PERRY and A. C. WEBB. Can. J. Biochem. **46**, 1163 (1968).

The mechanism of the microbial hydroxylation of steroids. Part 4. The C-6 β hydroxylation of androst-4-ene-3,17-dione and related compounds by *Rhizopus arrhizus* ATCC 11145

HERBERT L. HOLLAND AND PETER R. P. DIAKOW

Department of Chemistry, Brock University, St. Catharines, Ont., Canada L2S 3A1

Received September 26, 1977

HERBERT L. HOLLAND and PETER R. P. DIAKOW. Can. J. Chem. **56**, 694 (1978).

The steroid analogue 4,4a,5,6,7,8-hexahydro-2(3*H*)-naphthalenone was hydroxylated at C-8α, C-8β, and C-4a by *Rhizopus arrhizus*. Similar products were obtained by peracid oxidation of the corresponding enol ethers: hydroxylation of estr-4-ene-3,17-dione by the same fungus occurred at the analogous C-6 and C-10 positions. These results are consistent with a mechanism of microbial hydroxylation involving the enol form of the Δ^4-3-ketone. Data from the incubations with *R. arrhizus* of androst-4-ene-3,17-dione specifically labelled with deuterium at C-4, C-6α, or C-6β and from those of other deuterium labelled substrates have been interpreted in terms of a mechanism of C-6β hydroxylation involving a rate-determining step before enolization of the ketone, followed by rapid enolization and oxidation of the enol to give the 6β-hydroxy-Δ^4-3-ketone. The kinetic isotope effect, k_H/k_D, for the hydroxylation of androst-4-ene-3,17-dione at C-6β has been found to be 1.2 ± 0.1.

HERBERT L. HOLLAND et PETER R. P. DIAKOW. Can. J. Chem. **56**, 694 (1978).

L'hydroxylation, par le *Rhizopus arrhizus*, de l'analogue stéroïdal hexahydro-4,4a,5,6,7,8 (3*H*)-naphtalène-2-one s'effectue dans les positions 8α, 8β et 4a. On obtient des produits semblables par l'oxydation à l'aide de peracides des éthers énoliques correspondants; l'hydroxylation de l'estrène-4 dione-3,17 par le même champignon se produit dans les positions analogues 6 et 10. Ces résultats sont en accord avec un mécanisme d'hydroxylation microbiologique impliquant la forme énolique de la Δ^4 cétone-3. On a interprété des données d'incubation avec *R. arrhizus* de l'androstène-4 dione-3,17 marqué spécifiquement avec du deutérium dans les positions 4, 6α ou 6β, et à partir d'autres substrats marqués avec du deutérium, en termes d'un mécanisme d'hydroxylation en 6β impliquant une étape déterminant la vitesse antérieure à l'énolisation de la cétone, suivie par une énolisation rapide et une oxydation de l'énol pour conduire à l'hydroxy-6β Δ^4 cétone-3. On a trouvé que l'effet isotopique cinétique k_H/k_D pour l'hydroxylation de l'androstène-4 dione-3,17 en 6β est 1.2 ± 0.1.

[Traduit par le journal]

Introduction

The microbial C-6β hydroxylation of Δ^4-3-ketosteroids may involve the intermediacy of the $\Delta^{3,5}$ enol (1). Circumstantial evidence for this was obtained (2) by incubation of 4a-methyl-4,4a,5,6,7,8-hexahydro-2(3*H*)-naphthalenone (**1***a*) with *Rhizopus arrhizus*, a microorganism known to hydroxylate Δ^4-3-ketosteroids at C-6β (3). Both C-8β and C-8α substituted products (**2***a* and **3***a*, respectively) were obtained, and their formation rationalized by stereoelectronically controlled electrophilic addition of oxygen to the *s-trans* enol **4***a*.

The observation (4) that androst-4-ene-3,17-dione-6α-T (**5***b*) was hydroxylated at C-6β by *R. arrhizus* without loss of label has been interpreted (4) in terms of a direct hydroxylation with retention of configuration, following the pattern for enzymic hydroxylation at saturated carbon (5–8), but since subsequent investigation of the enolization of Δ^4-3-ketosteroids (9–12) has established that formation of the $\Delta^{3,5}$ enol occurs with stereoelectronically controlled preference for the loss of the C-6β hydrogen relative to that at C-6α of 53:1 (2), data such as that obtained from hydroxylation of **5***b* at C-6β are not amenable to unambiguous mechanistic interpretation. This paper describes the synthesis and incubation with *R. arrhizus* of a series of specifically deuterated androst-4-ene-3,17-diones (**5***c*–**5***g*) and of the 19-norsteroid analogue **1***b* and estr-4-ene-3,17-dione (**6***a*).

19-Nor-Δ^4-3-ketosteroids are commonly hydroxylated at C-6β (13–23), C-10β (13, 14, 16, 23–26), and C-11α (13, 15, 17, 19–21, 23, 24) by microorganisms. In many cases (13–16, 20, 22, 23, 26) hydroxylations at C-6β and C-10β are concurrent or occur with the same species, and there is only one reported instance (25) of C-10β hydroxylation of a 19-nor-Δ^4-3-ketosteroid in which C-6β hydroxylation by a fungus of the same genus is unknown. The possibility therefore exists that hydroxylation at

Can. J. Chem. Downloaded from www.nrcresearchpress.com by 210.87.254.40 on 09/05/12
For personal use only.

Can. J. Chem. Downloaded from www.nrcresearchpress.com by 210.87.254.40 on 09/05/12
For personal use only.

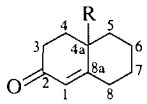

1

a R = CH_3
b R = H
c R = OH

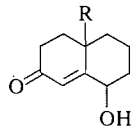

2

a R = CH_3
b R = H

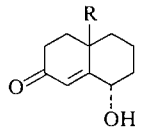

3

a R = CH_3
b R = H

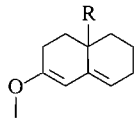

4

a R = CH_3
b R = H

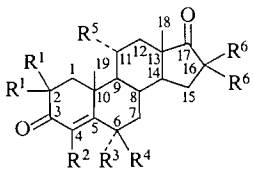

5

a $R^1 = R^2 = R^3 = R^4 = R^5 = R^6 = H$
b $R^1 = R^2 = R^4 = R^5 = R^6 = H, R^3 = T$
c $R^1 = R^2 = R^3 = R^4 = R^6 = D, R^5 = H$
d $R^1 = R^2 = R^4 = R^5 = R^6 = H, R^3 = D$
e $R^1 = R^3 = R^4 = R^5 = R^6 = H, R^2 = D$
f $R^1 = R^2 = R^3 = R^5 = R^6 = H, R^4 = D$
g $R^1 = R^2 = R^3 = R^4 = R^5 = H, R^6 = D$
h $R^1 = R^2 = R^5 = R^6 = H, R^3 = D, R^4 = OH$
i $R^1 = R^2 = R^4 = R^6 = H, R^3 = D, R^5 = OH$
j $R^1 = R^2 = R^3 = R^5 = H, R^6 = D, R^4 = OH$
k $R^1 = R^2 = R^3 = R^4 = H, R^6 = D, R^5 = OH$

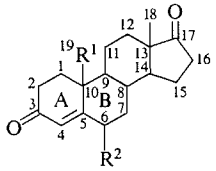

6

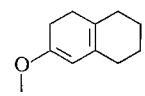

7

a $R^1 = R^2 = H$
b $R^1 = H, R^2 = OH$
c $R^1 = OH, R^2 = H$

C-10β of a 19-nor-Δ^4-3-ketosteroid is a function of the C-6β hydroxylating system, operating on the *s-cis* enol analogous to **7**.

Synthesis of Labelled Substrates

Androst-4-ene-3,17-dione-2,2,4,6,6,16,16-d_7 (**5***c*), androst-4-ene-3,17-dione-4-*d* (**5***e*), and the -16,16-d_2 compound **5***g* were synthesized by standard procedures. The C-6β deuterated compound **5***f* was prepared by two routes. The existing method (10), as noted by others (27), produced considerable amounts of di- and trideuterated products; modification of this procedure gave **5***f* which was at best 14% dideuterated but which had one atom of deuterium at C-6β (d_0 content = 0%, ^{1}Hmr analysis (10, 11)). Compound **5***f* was also synthesized (Scheme 1) from epoxide **9** of established configuration. The product contained 6% undeuterated species, indicating that some dehydration of **11** to C-6 with loss of deuterium had occurred. Since thionyl chloride – pyridine dehydration takes place with stereospecific loss of hydrogen antiperiplanar to the hydroxyl (in this case C-4β or C-6β) in an E2 manner (28), any dehydration of **11** giving Δ^5 olefin with subsequent pyridine-catalysed rearrangement to the Δ^4 isomer (11, 29, 30) must involve loss of deuterium.

Androst-4-ene-3,17-dione-6α-*d* (**5***d*) was synthesized (Scheme 2) from the (5,6)β epoxide **14**, which gave (31) the **5**β alcohol **15**, oxidation of which afforded **16** which was dehydrated to give **5***d*. The latter reaction was accompanied by loss of 30% of the label. The loss of label in this step may be rationalized as follows. The C-5β alcohol of **16** is antiperiplanar only to the highly hindered C-4α hydrogen, so that elimination from **16** is E1-like (28). Accordingly, C-6α or C-6β may be lost in forming a Δ^5 olefin, or loss from C-4 occur to form

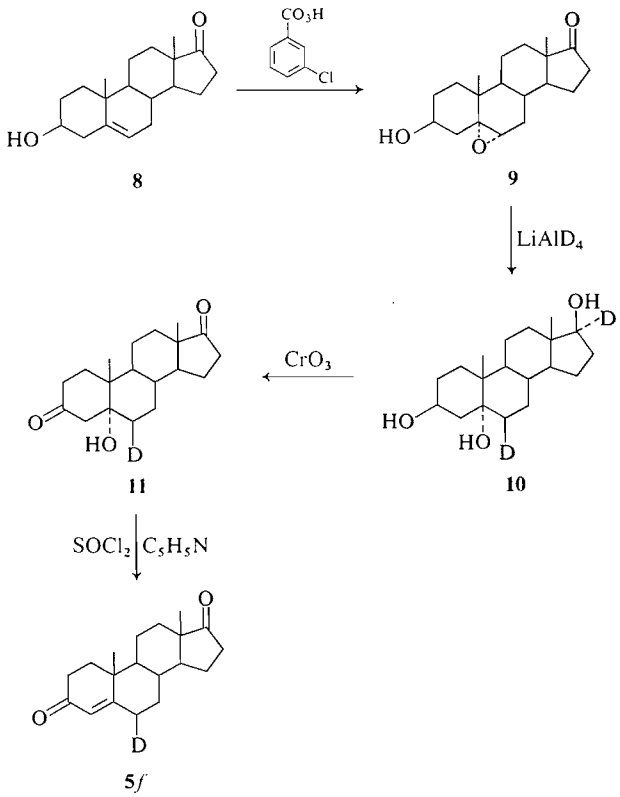

SCHEME 1. Synthesis of androst-4-ene-3,17-dione-6β-*d* (**5***f*).

Can. J. Chem. Downloaded from www.nrcresearchpress.com by 210.87.254.40 on 09/05/12
For personal use only.

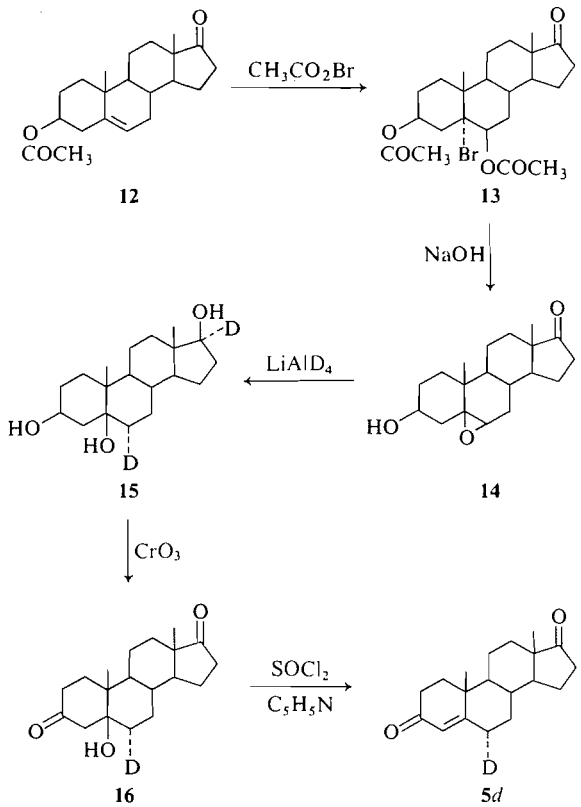

SCHEME 2. Synthesis of androst-4-ene-3,17-dione-6α-*d* (**5***d*).

5*d* directly. In the former case, subsequent base-catalyzed rearrangement (29, 30) to **5***d* must involve protonation at C-6β (11), so that any label at C-6 will ultimately occupy the α position.

Results

Incubation of **1***b* with *R. arrhizus* gave rise to three transformation products, identified as 4a-hydroxy-4,4a,5,6,7,8-hexahydro-2(3*H*)-naphthalenone (**1***c*), 8β-hydroxy-4,4a-5,6,7,8-hexahydro-2(3*H*)-naphthalenone (**2***b*), and 8α-hydroxy-4,4a,5,6,7,8-hexahydro-2(3*H*)-naphthalenone (**3***b*), in the ratio 11:11:1. The structure of **1***c* follows from spectral data and comparison of physical data with published values. Mass spectra of **2***b* and **3***b* indicated the introduction of one hydroxyl group in each case, the location of which was determined by ^{1}Hmr. Signals for the methine hydrogen geminal to oxygen indicate the structures shown (2). Both **2***b* and **3***b* gave the enedione **17** on oxidation. Location of a carbonyl function at C-8 of **17** is confirmed by the downfield

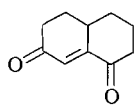

17

shift (relative to **1***b*) of 0.7 ppm for the resonance due to the olefinic C-1H. The relative stereochemistry of substitution at C-8 in **2***b* and **3***b* then follows from analysis of the olefinic C-1 proton absorption in both cases. In **2***b*, this appears as a narrow doublet (J = 2 Hz, $w_{\frac{1}{2}}$ = 3.4 Hz) coupled only to the methine hydrogen at C-4a (32), and in **3***b* as a broad singlet ($w_{\frac{1}{2}}$ = 4.5 Hz), with allylic couplings to both the C-4a and C-8β hydrogens.

A parallel to the microbial hydroxylation of **1***b* was observed in the peracid oxidation of the mixture of enol ethers **18** and **19** (Scheme 3). Treatment of **1***b* with ethyl orthoformate gave the unstable enol ether mixture **18** + **19** (33), oxidation of which (2) gave **2***b*, **3***b*, and **1***c* in the ratio 4:1:2.

Incubations were also performed with the monocyclic steroid analogues (**20***a*–**20***d*) and the bicyclic βγ unsaturated ketone **21**: no transformation products were observed. The failure of *R. arrhizus* to hydroxylate or even rearrange **21** is of interest in view of the observation that estr-5(10)-ene-3,17-dione (**22**) is hydroxylated only at C-11α by *R. arrhizus* and several other fungi (34, 35).

Incubation of the 19-norsteroid estr-4-ene-3,17-dione (**6***a*) with *R. arrhizus* gave the C-6β and C-10β monohydroxylated products **6***b* and **6***c*, respectively: trace amounts of 10β,17β-dihydroxyestr-4-ene-3,17-dione (**23***a*) were also formed.

The results of the incubations of the labelled substrates are summarized in Table 1. In confirmation of earlier work (4) the C-6α labelled substrate **5***d* is hydroxylated at C-6β (to give **5***h*) and C-11α (to give **5***i*) without loss of label. ^{1}Hmr analysis indicated that the position of label was unchanged. The same

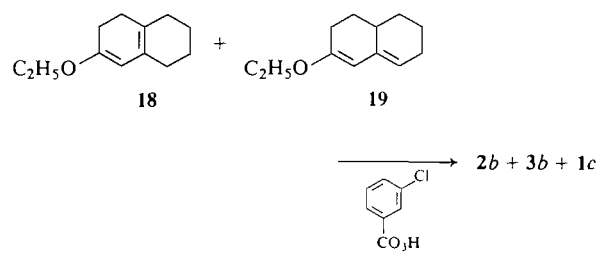

SCHEME 3. Oxidation of **18** and **19** by *m*-chloroperbenzoic acid.

result was observed for C-6β and C-11α hydroxylation of substrates labelled at C-4 (**5***e*) and C-16 (**5***g*). Substrate **5***c*, with label at C-2, -4, -6, and -16, lost one atom of deuterium on hydroxylation at C-6β and none on C-11α hydroxylation.

The C-6β labelled substrate **5***f* retained ca. 12–15% of the label on C-6β hydroxylation; location of the remaining deuterium at C-6α was confirmed by

TABLE 1. Incubation of deuterium labelled androst-4-ene-3,17-dione with *R. arrhizus*

Substrate	Position of label	Deuterium content (%)				
		Substrate		Recovered substrate	6β-Alcohol	11α-Alcohol
5*d*	6α	d_1	69	70	70	69
		d_0	31	30	30	31
5*f*	6β	d_3	1	1	0	1
		d_2	14	13	2	13
		d_1	85	86	26	86
		d_0	0	0	70	0
5*f* (from **11**)	6β	d_1	94	95	15	94
		d_0	6	5	85	6
5*e*	4	d_1	45	44	43	43
		d_0	55	55	56	56
5*c*	2α, 2β, 4	d_7	82	81	1	83
	6α, 6β,	d_6	15	17	82	15
	16α, 16β	d_5	2	1	15	1
		d_4	0	0	3	0
5*g*	16α, 16β	d_2	78	77	76	76
		d_1	16	15	16	17
		d_0	5	7	6	7
5*g* + **24***a*	16α, 16β	d_2	78[a]	60[b]	29	62
		d_1	16[a]	13[b]	6	14
		d_0	5[a]	27[b]	64	23
5*g* + **5***f*	16α, 16β	d_3	1[c]	2	0	2
	+	d_2	48[c]	47	51	48
	6β	d_1	47[c]	46	24	46
		d_0	3[c]	3	24	3

[a]Values for 5g only.
[b]Values for recovered androst-4-ene-3,17-dione.
[c]Combined values for 5g + 5f.

oxidation to the corresponding ketone, with loss of label.

The kinetic isotope effect for hydroxylation at C-6β was determined from co-incubation of **5***f* and **5***g*. Analysis of the results by the modified method of

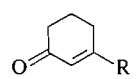

20
a R = CH_3
b R = C_2H_5
c R = n-C_3H_7
d R = n-C_4H_9

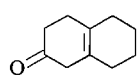

21

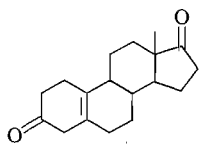

22

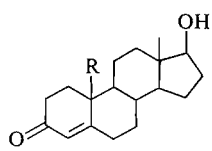

23
a R = OH
b R = CH_3
c R = H

Collins and Lietzke (36, 37) gave a value of $K_H/K_D = 1.2 \pm 0.1$.

To gain information about the rate-determining step in the hydroxylation process, the metabolism of the $\Delta^{3,5}$ enol acetate **24***a* was also investigated. Incubation of **24***a* with *R. arrhizus* gave both Δ^4-3-ketone (**5***a*) and the C-6β hydroxylated product (38), although the corresponding enol ether (**24***b*) was recovered unchanged from *R. arrhizus*. Co-incubation of equimolar amounts of **24***a* and **5***g* (Table 1) suggested that **24***a* can be transformed directly to 6β-hydroxy-Δ^4-3-ketone **5***j* *without* prior conversion to **5***a*. The deuterium content of **5***j* so

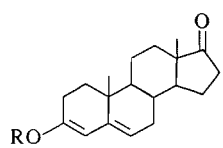

24
a R = Ac
b R = Et

obtained differs substantially from the limiting value expected (d_2 39%, d_1 8%, d_0 52%) if the pathway **24***a* → **5***a* → **5***j* were mandatory.

Discussion

The concurrent formation of **2***b* and **3***b* from **1***b* in both enzymic and chemical oxidation may be rationalized by a mechanism analogous to that proposed for the hydroxylation of **1***a* (2) (*vide supra*) and formation of **1***c* in terms of electrophilic addition

Can. J. Chem. Downloaded from www.nrcresearchpress.com by 210.87.254.40 on 09/05/12
For personal use only.

Can. J. Chem. Downloaded from www.nrcresearchpress.com by 210.87.254.40 on 09/05/12
For personal use only.

of oxygen to the *s-cis* enol **7** (cf. 39, 40). The observation that **2***b*, **3***b*, and **1***c* are produced concurrently by the fungus militates against a mechanism of enzymic hydroxylation of **1***b* in which the regio- and stereospecificity of hydroxylation is determined solely by the three-dimensional relationship between the substrate and the enzyme active site, although such a mechanism operates in the case of hydroxylation at saturated carbon remote from oxygen functionality (21, 41).

Enzymic hydroxylation of **6***a* via the *s-trans* and *s-cis* enols analogous to **4***b* and **7**, respectively, would also produce, by a stereoelectronically controlled axial addition of electrophilic oxygen, the observed products **6***b* and **6***c* (39, 40). The formation of a C-6α hydroxylated product analogous to **3***b* is prevented by the rigid conformation of ring B precluding C-6α becoming axial in a nonchair conformation (2).

The failure of *R. arrhizus* to metabolise **21** together with the observation that recovered starting material showed no loss or scrambling of label in any of the incubations performed with labelled substrates, confirm the observation (42) that nonenzymic reversible enolization with exchange of hydrogens with the medium does not occur in microbial hydroxylation of ketosteroids. The formation of both *s-cis* and *s-trans* enols from **1***b* and **6***a* implies that, although the enolization is an enzymic process, the regiospecificity of enol formation may not be under strict enzymic control.

The retention of some label at C-6α upon C-6β hydroxylation of **5***f* is inconsistent with direct hydroxylation with retention of configuration. Base-catalysed enolization of **5***f* occurs with loss of 83% of label (12), the preference for loss of the axial β deuteron being counteracted by a primary kinetic isotope effect (12). The similarity between the 17% retention observed for chemical enolization of **5***f* and the 12–15% retention observed during its microbial hydroxylation at C-6β strongly indicates that the latter process involves formation of the $\Delta^{3,5}$ enol.

Since the retention of label from C-6β at C-6 during enolization is dependent upon the existence of a primary kinetic isotope effect (chemically $k_{6\beta H}/k_{6\beta D} = 9$ (12)), the value determined for the C-6β hydroxylation (12) indicates that enolization cannot be rate determining in the enzymic process.

Since **22***a* is hydroxylated at C-6β more rapidly than **5***g*, a mechanism involving rate-determining oxidation of enol can be discounted. The mechanism proposed for C-6β hydroxylation (Scheme 4) thus involves a rate-determining step prior to enolization, such as binding of substrate to enzyme, k_B. The primary isotope effect $k_{EH6\beta}/k_{ED6\beta}$, necessary to account for the retention of some deuterium from C-6β in the product, is thus masked and direct binding of **24***a* to the enzyme bypasses the slow step.

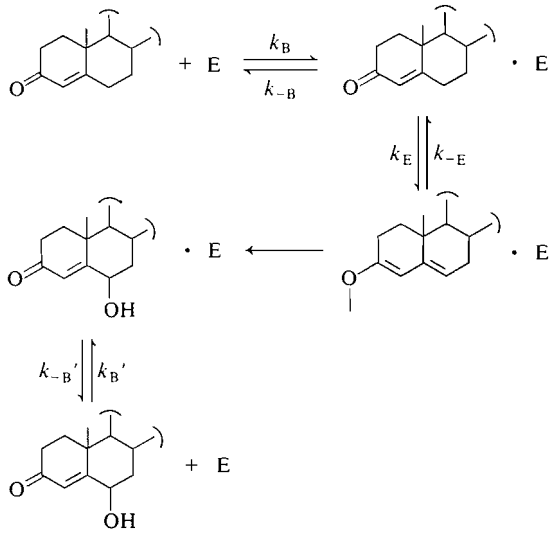

SCHEME 4. Proposed mechanism of C-6β hydroxylation of androst-4-ene-3,17-dione by *R. arrhizus*.

An irreversible oxidation of enol to product is in accord with chemical analogies (2, 39, 43) and need not occur under enzymic control (2, 39). The detailed mechanism of this step and the existence of possible intermediates such as Δ^5-3-ketone are currently under investigation.

Experimental

Apparatus, Materials, and Methods

Melting points were determined on a Kofler heating stage and are uncorrected. Infrared spectra were recorded with a Perkin-Elmer 237B, ^{1}Hmr spectra with a Bruker WP-60 or Varian A-60, using $CDCl_3$ as solvent and TMS as internal standard, and mass spectra were obtained with an AEI MS30. Deuterium content was estimated by repeated scanning of the relevant ions and application of the appropriate corrections for ^{13}C; values are accurate to ±1%. Column chromatography was performed on silica gel (60–200 mesh) or alumina (basic, activity 1), thin-layer chromatography on Merck silica gel 60 F-254 or alumina F-254 type E, and preparative-layer chromatography on Merck silica gel PF-254 (containing calcium sulfate) or alumina F-254.

Microanalyses were carried out by the Pascher microanalytical Laboratory, Bonn, W. Germany.

Rhizopus arrhizus ATCC 11145 was maintained on 4.5% malt agar slopes.

Preparation of Substrates

3-Methylcyclohex-2-enone (**20***a*) was a commercial sample. Estr-4-ene-3,17-dione (**6***a*) was prepared by Jones' oxidation (44) of estr-4-ene-17β-ol-3-one (**23***c*) and gave satisfactory analytical and spectral data. The following compounds were prepared by established procedures and gave satisfactory analytical and spectral data: 3-ethylcyclohex-2-enone (**20***b*) (45), 3-*n*-propylcyclohex-2-enone (**20***c*) (45), 3-*n*-butylcyclohex-2-enone (**20***d*) (45), 4,4a,5,6,7,8-hexahydro-2(3*H*)-naphthalenone (**1***b*) (46, 47), 3,4,5,6,7,8-hexahydro-2(1*H*)-naphthal-

Can. J. Chem. Downloaded from www.nrcresearchpress.com by 210.87.254.40 on 09/05/12
For personal use only.

enone (**21**) (48), 3-acetoxyandrosta-3,5-diene-17-one (**24***a*) (49), and 3-ethoxyandrosta-3,5-diene-17-one (**24***b*) (50).

*5-Bromo-3β,6β-dihydroxy-5α-androstan-17-one 3,6-Diacetate (**13**)*

A solution of acetyl hypobromite (51) in dry carbon tetrachloride (160 ml, 0.1 *M*) at 0°C was added to a solution of 3β-hydroxyandrost-5-ene-17-one, 3-acetate (**12**) (5 g) in dry carbon tetrachloride (50 ml) at 0°C. The resulting solution was stirred at 0°C for 5 min, 5% sodium metabisulphite (5 ml) then added, and after a further 5 min the solution was washed with water (2 × 100 ml), dried over anhydrous sodium sulphate, and evaporated without heating over 40°C. Methanol (30 ml) was added to the residue and the resulting slurry filtered. The product was then recrystallized from methanol to give 4.8 g (63%) (**13**), mp 214–216°C $[\alpha]_D^{20}$ −38° (*c* 1.0, $CHCl_3$); ^{1}Hmr δ: 0.88 (3H, s, C-18 H), 1.32 (3H, s, C-19 H), 2.0, 2.08 (each 3H, s, OAc), 5.2–5.6 (2H, m, C-3α and C-6α H's). *Anal.* calcd. for $C_{23}H_{33}BrO_5$: C 58.85, H 7.09, Br 17.02; found: C 58.83, H 7.09, Br 17.06.

*(5,6β)-Epoxy-3β-hydroxy-5β-androstan-17-one (**14**)*

Sodium hydroxide (4 g) was added to a solution of **13** (4.5 g) in methanol (80 ml) and the solution then heated under reflux for 1 h. The solution was then cooled, neutralised (acetic acid), and poured onto water (300 ml). The resulting solution was extracted (chloroform) and the extract washed with water and then dried and evaporated. Crystallization from aqueous methanol afforded the product (2.4 g, 82%), mp 166–168°C (lit. (52) mp 166–167°C); ^{1}Hmr δ: 0.85 (3H, s, C-18 H), 1.03 (3H, s, C-19 H), 3.11 (1H, d, J = 2.6 Hz, C-6α H), 3.35–3.95 (1H, m, C-3α H).

*3β,5,17β-Trihydroxy-5β-androstane-6α,17α-d_2 (**15**)*

A solution of the epoxide **14** (1.5 g) in benzene–ether (80 ml, 50%) was added over 15 min to a solution of lithium aluminum deuteride (1 g) in dry ether (100 ml). The mixture was refluxed for 36 h, a mixture of ether (20 ml) and acetone (5 ml) added, the solution washed with 5% sulphuric acid (3 × 200 ml), and the washings re-extracted with ether (3 × 200 ml). The combined ethereal extract was washed with water (2 × 500 ml), dried, and evaporated. Crystallization of the residue from acetone–hexane gave the title compound (1.16 g, 78%), mp 194–197°C, (lit. (53) mp 196–198°C); ^{1}Hmr δ: 0.74 (3H, s, C-18 H), 0.98 (3H, s, C-19 H); ms isotopic composition: d_2 99%.

*5-Hydroxy-5β-androstane-3,17-dione-6α-d (**16**)*

A solution of **15** (0.75 g) in acetone (50 ml) at 0°C was oxidized with standard chromic acid reagent (44). After the usual work-up, recrystallization from acetone–hexane gave the product (0.59 g, 80%), mp 182–184°C (lit. (54) mp 183–186°C); ms isotopic composition: d_1 99%.

*Androst-4-ene-3,17-dione-6α-d (**5d**)*

Thionyl chloride (0.2 ml) was added to a solution of **16** (0.5 g) in pyridine (10 ml) at 0°C. The mixture was allowed to stand at 0°C for 5 min, poured onto water (150 ml), and extracted with ether (3 × 100 ml). The ether extract was washed (5% sulphuric acid, water), dried, and evaporated to give a residue which crystallized from ether to give **5***d* (0.42 g, 88%), identical in spectral, mp, and tlc comparisons with an authentic sample of unlabelled material; ^{1}Hmr δ: 0.93 (3H, s, C-18 H), 1.22 (3H, s, C-19 H), 5.74 (1H, br s, $w_{\frac{1}{2}}$ = 3 Hz, C-4 H); ms isotopic composition: d_1 69%, d_0 31%.

*(5,6α)-Epoxy-3β-hydroxy-5α-androstan-17-one (**9**)*

A solution of *m*-chloroperbenzoic acid (2.45 g) in dichloromethane (50 ml) was added over 1 h to a stirred solution of 3β-hydroxyandrost-5-ene-17-one (**8**) (2.45 g) in dichloromethane (50 ml) at 0°C and the resulting solution allowed to stand at 0°C for 12 h. The solution was then washed (5% sodium sulphite, 2 *N* sodium bicarbonate, and water), dried, and evaporated. The residue was crystallized twice from methanol to give **9** (2.1 g, 77%), mp 225–228°C (lit. (55) mp 227–229°C); ^{1}Hmr δ: 0.82 (3H, s, C-18 H), 1.08 (3H, s, C-19 H), 2.92 (1H, d, J = 3.6 Hz, C-6β H), 3.54–4.14 (1H, m, C-3α H).

*3β,5,17β-Trihydroxy-5α-androstane-6β,17α-d_2 (**10**)*

Reduction of **9** (1.5 g) by lithium aluminum deuteride (1 g) using the procedure described for the reduction of **14** gave the title compound (1.14 g, 76%), mp 192–195°C (diisopropyl ether) (lit. (54) mp 193–196°C); ^{1}Hmr δ: 0.74 (3H, s, C-18 H), 1.02 (3H, s, C-19 H); ms isotopic composition: d_2 99%.

*5-Hydroxy-5α-androstane-3,17-dione-6β-d (**11**)*

A solution of **10** (0.75 g) in acetone (50 ml) was oxidized by standard chromic acid reagent (44) and gave, after recrystallization from aqueous methanol, 0.67 g **11** (89%), mp 218–221°C, $[\alpha]_D^{22}$ +105° (*c* 0.8, $CHCl_3$) (lit. (54) mp 217–222°C, $[\alpha]_D$ +106°); ms isotopic composition: d_1 99%.

*Androst-4-ene-3,17-dione-6β-d (**5f**) from (**11**)*

Dehydration of **11** (0.7 g) by the procedure described above gave **5***f* (0.52 g, 79%), from ether, identified by spectral, mp, and tlc comparisons with an authentic sample of unlabelled material; ^{1}Hmr δ: 0.93 (3H, s, C-18 H), 1.22 (3H, s, C-19 H), and 5.74 (1H, s, $w_{\frac{1}{2}}$ = 1.6 Hz, C-4 H); ms isotopic composition: d_1 94%, d_0 6%.

*17β-Hydroxyandrost-4-ene-3-one-6β-d (**23b**, 6β-d)*

This was prepared from 3-ethoxy-17β-hydroxyandrosta-3,5-diene (50) by a modification of previous methods (10, 27). The enol ether (3.6 g) was added to a mixture of acetic acid-OD (20 ml) and deuterium oxide (50 ml), the suspension heated under reflux for 10 min, and the resulting clear solution stirred at 50–60°C for 3 h. The solution was then cooled to room temperature, water (300 ml) added and the mixture extracted with ether. The extract was washed (2 *N* sodium bicarbonate, water), dried, and evaporated. The resulting residue (2.8 g) was free of starting material (tlc) and was used without subsequent purification.

*Androst-4-ene-3,17-dione-6β-d (**5f**)*

17β-Hydroxyandrost-4-ene-3-one-6β-*d* (2.5 g) was dissolved in acetone (100 ml) and oxidized with standard chromic acid reagent (44) at −10°C. After the usual work-up, the product (2.2 g, 88% from ether) was identified by mp, tlc, and spectral comparisons with an authentic sample of unlabelled material; ^{1}Hmr δ: 0.93 (3H, s, C-18 H), 1.22 (3H, s, C-19 H), and 5.74 (1H, s, $w_{\frac{1}{2}}$ = 1.6 Hz, C-4 H); ms isotopic composition: d_3 1%, d_2 14%, d_1 85%.

*Androst-4-ene-3,17-dione-4-d (**5e**)*

Androst-5-ene-3,17-dione-4,4-d_2 (30) (d_2 60%, d_1 30%, d_0 10%), (1 g) was dissolved in a mixture of diglyme (200 ml) and 1 *N* HCl (20 ml). The solution was stirred at room temperature for 2 h, water (400 ml) added, and the resulting mixture extracted with ether (4 × 150 ml). The extract was washed with water (4 × 100 ml), dried, and evaporated. The residue was crystallized from ether to give **5***e* (0.6 g, 60%), identified by mp, tlc, and spectral comparisons with an authentic sample of unlabelled material; ^{1}Hmr δ: 0.93 (3H, s, C-18 H), 1.22 (3H, s, C-19 H), and 5.74 (0.5 H, br s, C-4 H); ms isotopic composition: d_1 45%, d_0 55%.

3β-Hydroxyandrost-5-ene-17-one-16,16-d_2

Tetra-*n*-butyl ammonium bromide (5 g) was added to a solution of sodium deuteroxide in deuterium oxide (100 ml,

Can. J. Chem. Downloaded from www.nrcresearchpress.com by 210.87.254.40 on 09/05/12
For personal use only.

5%) and the resulting solution added to a solution of 3β-hydroxyandrost-5-ene-17-one (5 g) (**8**) in dry benzene (100 ml). The mixture was stirred and heated under reflux for 12 h, then cooled, and the organic layer separated and evaporated. Crystallization of the residue from ether gave the title compound, 4.6 g (92%), identified by comparison with an authentic sample of unlabelled material; ms isotopic composition: d_2 90%, d_1 10%.

Androst-4-ene-3,17-dione-16,16-d_2 *(5g)*

A solution of the above ketone (3 g) in dry toluene (80 ml) was heated and 20 ml of toluene allowed to distil from the flask. Cyclohexanone (15 ml) and freshly distilled aluminum isopropoxide (1.5 g) were then added to the flask and the mixture heated under reflux for 30 min. The solution was then cooled, water (200 ml) added, and the mixture acidified to p*H* 4 (5% hydrochloric acid). The organic layer was separated and the remaining aqueous layer extracted with ether. The combined organic extract was washed (2 *N* sodium bicarbonate, water), dried, and evaporated (rotary evaporator). Residual cyclohexanone was removed by the addition of water (100 ml) followed by steam distillation to dryness. The residue was crystallized from ether to give **5***g* (1.8 g, 60%), identified by comparison with an authentic sample of unlabelled material; ms isotopic composition: d_2 78%, d_1 16%, d_0 5%.

Androst-4-ene-3,17-dione-2,2,4,6,6,16,16-d_7 *(5c)*

This was prepared from androst-4-ene-3,17-dione (**5***a*) (1 g) by the exchange procedure described above. The product (0.78 g, 77% from ether) showed the following isotopic composition: d_7 82%, d_6 15%, d_5 2%.

*Oxidation of 4,4a,5,6,7,8-Hexahydro-2(3*H*)-naphthalenone Enol Ethers (18 + 19)*

A mixture of the enol ethers **18** and **19** (33) (3.8 g) was oxidized by *m*-chloroperbenzoic acid using the procedure described for the oxidation of 2-ethoxy-4a-methyl-3,4,4a,5,6,7-hexahydronaphthalene (2). The resulting oil (3.0 g) was applied to a column of silica gel and the column eluted with 20% ether–benzene to give **1***b* (0.21 g, 7%). Elution with ether gave a fraction (2.7 g) which by ^{1}Hmr analysis was shown to consist of a mixture of **3***b*, **2***b*, and **1***c* (1:4:2). This mixture was rechromatographed on silica gel (elution from ether to 2% methanol–ether) to give two components. The less polar material (R_f 0.26, 1% methanol–ether, silica gel) consisted of a mixture of **2***b* and **1***c*; the other (R_f 0.19) afforded *8α-hydroxy-4,4a,5,6,7,8-hexahydro-2(3*H*)-naphthalenone* (**3***b*), 0.12 g (4%) on crystallization from hexane. Recrystallization gave pure **3***b*, mp 98–100°C; ir (KBr) ν_{max}: 1675, 3400 cm^{-1}; ^{1}Hmr δ: 0.9–2.5 (11H, C-3–C-7 H's), 3.3 (1H, br s, exchanges D_2O, OH), 3.9–4.3 (1H, m, C-8βH), 6.23 (1H, br s, $w_{\frac{1}{2}}$ = 4.5 Hz, C-1H); ms *m/e* (%): 166 (M$^+$, 93), 148 (16), 138 (91), 137 (45), 122 (43), 110 (100), 109 (93). *Anal.* calcd. for $C_{10}H_{14}O_2$: C 72.26, H 8.49; found: C 72.20, H 8.35. 2,4-DNP mp 206–208°C (EtOH).

The mixture of **2***b* and **1***c* was rechromatographed on alumina (elution from chloroform to ethyl acetate, increments of 10% ethyl acetate) to give *4a-hydroxy-4,4a,5,6,7,8-hexahydro-2(3*H*)-naphthalenone* (**1***c*) (0.42 g, 13%), mp 66–68°C from hexane (lit. (56) mp 67–68°C); ir (KBr) ν_{max}: 1675, 3400 cm^{-1}; ^{1}Hmr δ: 1.0–2.8 (11H, C-3–C-8 H's), 3.05 (1H, br s, exchanges D_2O, OH), 5.77 (1H, d, *J* = 1.8 Hz, $w_{\frac{1}{2}}$ = 3.2 Hz, C-1 H). 2,4-DNP mp 163–166°C (EtOH), followed by *8β-hydroxy-4,4a,5,6,7,8-hexahydro-2(3*H*)-naphthalenone* (**2***b*), (0.82 g, 25%), bp 140–145°C/0.15 Torr; ir (film) ν_{max}: 1675, 3400 cm^{-1}; ^{1}Hmr δ: 1.0–3.0 (11H, C-3–C-7 H's), 3.86 (1H, br s, exchanges D_2O, OH), 4.36 (1H, m, C-8α H), 5.85 (1H, d, *J* = 2 Hz, $w_{\frac{1}{2}}$ = 3.4 Hz, C-1 H); ms *m/e* (%): 166 (M$^+$, 90), 148 (20), 138 (92), 137 (40), 122 (42), 110 (100), 109 (85). *Anal.* calcd. for $C_{10}H_{14}O_2$: C 72.26, H 8.49; found: C 72.37, H 8.49.

Some epimerization of **2***b* to give **3***b* occurred during chromatography on alumina. Submission of **2***b* to the above reaction conditions resulted in near quantitative recovery of starting material, no epimerization occurring other than during chromatography.

*4,4a,5,6-Tetrahydro-2,8(3*H*,7*H*)-naphthalenedione (17)*

Oxidation of either **2***b* or **3***b* by the standard chromic acid procedure (44) gave 4,4a,5,6-tetrahydro-2,8(3*H*,7*H*)-naphthalenedione (85% from **2***b*, 80% from **3***b*), bp 135–140°C/0.15 Torr; ir (film) ν_{max}: 1700, 1675 cm^{-1}; ^{1}Hmr δ: 1.2–2.8 (11H, C-3–C-7 H's), 6.52 (1H, d, *J* = 3 Hz, C-1 H); ms *m/e* (%): 164 (M$^+$, 80), 136 (100), 108 (80). *Anal.* calcd. for $C_{10}H_{12}O_2$: C 73.15, H 7.37; found: C 73.26, H 7.18.

Incubations with Rhizopus arrhizus *ATCC 11145*

All incubations were performed as previously described (2).

*4,4a,5,6,7,8-Hexahydro-2(3*H*)-naphthalenone (1b)*

Incubation of 3.5 g gave an extract (3.1 g) which was chromatographed as described above for the oxidation products of **18** + **19** and gave **1***b* (2.6 g) and a fraction (0.13 g) which by ^{1}Hmr analysis was determined to consist of a mixture of **2***b*, **1***c*, and **3***b* in the ratio 11:11:1. Separation of this mixture was achieved as described for the analogous fraction from the oxidation of **18** + **19**.

Final purification was carried out by preparative-layer chromatography. The compounds thus obtained proved identical in spectral and analytical properties with the corresponding alcohols prepared as outlined above.

Estr-4-ene-3,17-dione (6a)

Incubation of 1 g gave an extract (1.3 g) which was chromatographed on silica gel by stepwise elution from benzene to ether (increments of 5% ether) to give *estr-4-ene-3,17-dione* (0.031 g) identical with authentic material, *10β-hydroxyestr-4-ene-3,17-dione* (**6***c*) (0.31 g from ethyl acetate – hexane), mp 197–199°C (lit. (57) mp 198–201°C, lit. (58) mp 198–211°C); ^{1}Hmr δ: 0.95 (3H, s, C-18 H), 5.80 (1H, d, *J* = 1.8 Hz, C-4 H); ms *m/e* (%): 288 (100), 270 (60), *6β-hydroxyestr-4-ene-3,17-dione* (**6***b*) (0.19 g from ethyl acetate – hexane), mp 162–164°C (lit. (17) mp 161–163°C); ^{1}Hmr δ: 0.96 (3H, s, C-18 H), 4.44 (1H, m, C-6α H), 5.91 (1H, d, *J* = 1.8 Hz, C-4 H); ms *m/e* (%): 288 (100), 273 (9), 270 (15), 259 (27), and *10β,17β-dihydroxyestr-4-ene-3-one* (**23***a*) (0.017 g from ethyl acetate – hexane), mp 208–210°C (lit. (58) mp 204–210°C); ^{1}Hmr δ: 0.82 (3H, s, C-18 H), 3.70 (1H, m, C-17α H), 5.77 (1H, d, *J* = 1.8 Hz, C-4 H); ms *m/e* (%): 290 (100), 272 (34), 262 (80). A total of 0.01 g of more polar material eluted from the column with 1% methanol–ether was not investigated further.

Androst-4-ene-3,17-dione

In all experiments described below, products were separated, purified, and identified as described for the incubation of unlabelled androst-4-ene-3,17-dione (**5***a*). Isotopic compositions are listed in the table. Although trace quantities of 11α,-17β-dihydroxyandrost-4-ene-3-one were detected (tlc) in all the following incubations, this compound was isolated only from the incubation of unlabelled material as described below.

Incubation of 1.2 g **5***a* gave an extract (0.96 g) which was applied to a column of silica gel in benzene. The column was eluted with ether–benzene (increments of 10% ether) to give in order of elution, *androst-4-ene-3,17-dione* (0.16 g from ether), identical in all respects with starting material, *11α,17β-dihydroxyandrost-4-ene-3-one* (0.014 g from ether), mp 180–182°C (lit. (3) mp 181–184°C); ^{1}Hmr δ: 0.80 (3H, s, C-18 H), 1.35 (3H, s, C-19 H), 3.5–4.0 (2H, m, C-11β and C-17α H's),

Can. J. Chem. Downloaded from www.nrcresearchpress.com by 210.87.254.40 on 09/05/12
For personal use only.

5.80 (1H, br s, C-4 H), *6β-hydroxyandrost-4-ene-3,17-dione* (0.184 g from ethyl acetate – hexane), mp 190–192°C (lit. (3) mp 191–194°C); ^{1}Hmr included signals at δ 0.95 (3H, s, C-18 H), 1.42 (3H, s, C-19 H), 4.42 (1H, m, C-6α H), 5.84 (1H, s, $w_{\frac{1}{2}}$ = 1.8 Hz, C-4 H), and *11α-hydroxyandrost-4-ene-3,17-dione* (0.37 g from ether), mp 222–224°C (lit. (3) mp 225–227°C); ^{1}Hmr δ: 0.94 (3H, s, C-18 H), 1.36 (3H, s, C-19 H), 3.6–4.3 (1H, m, C-11β H), and 5.77 (1H, br s, C-4 H). Separation of fractions containing mixtures was achieved by preparative-layer chromatography on silica gel, 1% methanol–ether.

*Androst-4-ene-3,17-dione-6α-*d *(**5d**)*

Incubation of 0.5 g gave an extract (0.53 g) which afforded *androst-4-ene-3,17-dione-6α-*d (0.082 g), *6β-hydroxyandrost-4-ene-3,17-dione-6α-*d (0.073 g), and *11α-hydroxyandrost-4-ene-3,17-dione-6α-*d (0.17 g).

*Androst-4-ene-3,17-dione-6β-*d *(**5f** from **11**)*

Incubation of 0.5 g gave an extract (0.55 g) which afforded *androst-4-ene-3,17-dione-6β-*d (0.052 g), *6β-hydroxyandrost-4-ene-3,17-dione* (0.036 g) oxidation of which by chromic acid (44) gave androst-4-ene-3,6,17-trione free from label, and *11α-hydroxyandrost-4-ene-3,17-dione-6β-*d (0.104 g), ^{1}Hmr analysis of which (10, 11, 32) indicated the presence of deuterium at C-6β.

*Androst-4-ene-3,17-dione-6β-*d *(**5f**)*

Incubation of 0.46 g gave an extract (0.5 g) which afforded *androst-4-ene-3,17-dione-6β-*d (0.033 g), *6β-hydroxyandrost-4-ene-3,17-dione* (0.038 g), chromic acid oxidation of which (44) gave androst-4-ene-3,6,17-trione of isotopic composition d_2 1%, d_1 11%, d_0 89%, and *11α-hydroxyandrost-4-ene-3,17-dione-6β-*d (0.184 g); ^{1}Hmr analysis of which indicated the presence of deuterium at C-6β (10, 11, 32).

*Androst-4-ene-3,17-dione-4-*d *(**5e**)*

Incubation of 0.45 g gave an extract (0.42 g) which afforded *androst-4-ene-3,17-dione-4-*d (0.047 g), *6β-hydroxyandrost-4-ene-3,17-dione-4-*d (0.058 g), and *11α-hydroxyandrost-4-ene-3,17-dione-4-*d (0.094 g). ^{1}Hmr analysis of the above samples indicated ca. 0.5 H present at C-4.

Androst-4-ene-3,17-dione-16,16-d_2 *(**5g**)*

Incubation of 0.45 g gave an extract (0.51 g) which afforded *androst-4-ene-3,17-dione-16,16-*d_2 (0.12 g), *6β-hydroxyandrost-4-ene-3,17-dione-16,16-*d_2 (0.024 g), and *11α-hydroxyandrost-4-ene-3,17-dione-16,16-*d_2 (0.088 g).

Androst-4-ene-3,17-dione-2,2,4,6,6,16,16-d_7 *(**5c**)*

Incubation of 0.6 g gave an extract (0.65 g) which afforded *androst-4-ene-3,17-dione-2,2,4,6,6,16,16-*d_7 (0.125 g), *6β-hydroxyandrost-4-ene-3,17-dione-2,2,4,6α,16,16-*d_6 (0.052 g) and *11α-hydroxyandrost-4-ene-3,17-dione-2,2,4,6,6,16,16-*d_7 (0.21 g).

Androst-4-ene-3,17-dione-16,16-d_2 *(**5g**)* + *3-Acetoxyandrosta-3,5-diene-17-one (**24a**)*

Incubation of 0.288 g **5*g*** + 0.328 g **24*a*** gave an extract (0.66 g) which afforded *androst-4-ene-3,17-dione-16,16-*d_2 (0.27 g), *6β-hydroxyandrost-4-ene-3,17-dione-16,16-*d_2 (0.18 g), and *11α-hydroxyandrost-4-ene-3,17-dione-16,16-*d_2 (0.043 g).

*3-Acetoxyandrosta-3,5-diene-17-one (**24a**)*

Incubation of 0.3 g gave an extract (0.25 g) which afforded *androst-4-ene-3,17-dione* (0.12 g), *6β-hydroxyandrost-4-ene-3,17-dione* (0.07 g), and *11α-hydroxyandrost-4-ene-3,17-dione* (0.015 g).

*Androst-4-ene-3,17-dione-6β-*d *(**5f**)* + *Androst-4-ene-3,17-dione-16,16-*d_2 *(**5g**)*

Incubation of a mixture of **5*g*** (0.576 g) and **5*f*** (0.488 g) gave an extract (1.1 g) which afforded *androst-4-ene-3,17-dione* (0.13 g), *6β-hydroxyandrost-4-ene-3,17-dione* (0.102 g), and *11α-hydroxyandrost-4-ene-3,17-dione* (0.174 g).

*3-Ethoxyandrosta-3,5-diene-17-one (**24b**)*

Incubation of 0.5 g gave 0.45 g of extract; tlc analysis indicated the absence of transformation products. Purification afforded only **24*b*** (0.5 g), identical with starting material.

Acknowledgement

Financial support from the National Research Council of Canada is gratefully acknowledged.

1. W. Charney and H. L. Herzog. Microbial transformations of steroids: a handbook. Academic Press, New York, NY. 1967. p. 25.
2. H. L. Holland and B. J. Auret. Can. J. Chem. **53**, 2041 (1975).
3. S. H. Eppstein, P. D. Meister, H. M. Leigh, D. H. Peterson, H. C. Murray, L. M. Reineke, and A. Weintraub. J. Am. Chem. Soc. **76**, 3174 (1954).
4. S. Baba, H. J. Brodie, M. Hayano, D. H. Peterson, and O. K. Sebek. Steroids, **1**, 153 (1963).
5. M. Hayano, M. Gut, R. I. Dorfman, O. K. Sebek, and D. H. Peterson. J. Am. Chem. Soc. **80**, 2336 (1958).
6. E. J. Corey, G. A. Gregoriou, and D. H. Peterson. J. Am. Chem. Soc. **80**, 2338 (1958).
7. M. Hayano, M. Gut, R. I. Dorfman, A. Schubert, and R. Siebert. Biochim. Biophys. Acta, **32**, 269 (1959).
8. Y. Sato, T. Oda, and H. Saitô. J. Chem. Soc. Chem. Commun. 415 (1977).
9. S. K. Malhotra and H. J. Ringold. J. Am. Chem. Soc. **85**, 1538 (1963).
10. S. K. Malhotra and H. J. Ringold. J. Am. Chem. Soc. **86**, 1997 (1964).
11. S. K. Malhotra and H. J. Ringold. J. Am. Chem. Soc. **87**, 3228 (1965).
12. G. Subrahmanyam, S. K. Malhotra, and H. J. Ringold. J. Am. Chem. Soc. **88**, 1332 (1966).
13. R. L. Pederson, J. A. Campbell, J. C. Babcock, S. H. Eppstein, H. C. Murray, A. Weintraub, R. C. Meeks, P. D. Meister, L. M. Reineke, and D. H. Peterson. J. Am. Chem. Soc. **78**, 1512 (1956).
14. H. C. Murray and D. H. Peterson. U.S. Patent No. 2,888,384 (May 26, 1959).
15. H. C. Murray and D. H. Peterson. U.S. Patent No. 2,683,725 (July 13, 1954).
16. J. de Flines, W. F. van der Waard, W. J. Mijs, L. A. van Dijck, and S. A. Szpilfogel. Recl. Trav. Chim. **82**, 149 (1963).
17. H. J. Brodie, C. E. Hay, and J. D. Townsley. Biochim. Biophys. Acta, **239**, 103 (1971).
18. H. J. Brodie and C. E. Hay. Biochem. J. **120**, 667 (1970).
19. I. Kim, C. E. Hay, and H. J. Brodie. J. Biol. Chem. **248**, 2134 (1973).
20. A. M. Bell, J. W. Browne, W. A. Denny, E. R. H. Jones, A. Kasal, and G. D. Meakins. J. Chem. Soc. Perkin I, 2930 (1972).
21. A. M. Bell, P. C. Cherry, I. M. Clark, W. A. Denny, E. R. H. Jones, G. D. Meakins, and P. D. Woodgate. J. Chem. Soc. Perkin I, 2081 (1972).
22. Y. Y. Lin, M. Shibahara, and L. L. Smith. J. Org. Chem. **34**, 3530 (1969).
23. L. L. Smith, G. Greenspan, R. Rees, and T. Foell. J. Am. Chem. Soc. **88**, 3120 (1966).
24. J. de Flines, W. F. van der Waard, W. J. Mijs, and S. A. Szpilfogel. Recl. Trav. Chim. **82**, 129 (1963).

25. S. C. PAN, J. SEMAR, B. JUNTA, and P. A. PRINCIPE. Biotechnol. Bioeng. **11**, 1183 (1969).
26. K. SCHUBERT, G. ROSE, and C. HÖRHOLD. J. Steroid Biochem. **4**, 283 (1973).
27. A. VIGER, A. MARQUET, and J.-C. TABET. Org. Mass Spectrom. **11**, 1063 (1976).
28. D. N. KIRK and M. P. HARTSHORN. Steroid reaction mechanisms. Elsevier, New York, NY. 1968. p. 102.
29. J. B. JONES and D. C. WIGFIELD. J. Am. Chem. Soc. **89**, 5294 (1967).
30. J. B. JONES and D. C. WIGFIELD. Can. J. Chem. **47**, 4459 (1969).
31. A. S. HALLSWORTH and H. B. HENBEST. J. Chem. Soc. 3571 (1960).
32. T. A. WITTSTRUCK, S. K. MALHOTRA, and H. J. RINGOLD. J. Am. Chem. Soc. **85**, 1699 (1963).
33. E. E. VAN TAMELEN and W. C. PROOST. J. Am. Chem. Soc. **76**, 3632 (1954).
34. MERCK & Co. Neth. Patent Appl. No. 6,409,039 (February 7, 1966); Chem. Abstr. **65**, 6263b (1966).
35. A. E. OBERSTER, R. E. BEYLER, L. H. SARETT, T. S. BRY, and J. FRIED. Brit. Patent No. 1,127,603 (September 18, 1960).
36. C. COLLINS and M. H. LIETZKE. J. Am. Chem. Soc. **81**, 5379 (1959).
37. I. BJÖRKHEM. Eur. J. Biochem. **18**, 299 (1971).
38. H. L. HOLLAND and B. J. AURET. Tetrahedron Lett. 3787 (1975).
39. D. N. KIRK and J. M. WILES. J. Chem. Soc. Chem. Commun. 518 (1970).
40. F. B. COLTON. U.S. Patent No. 2,729,654 (January 3, 1956).
41. V. E. M. CHAMBERS, W. A. DENNY, J. M. EVANS, E. R. H. JONES, A. KASAL, G. D. MEAKINS, and J. H. PRAGNELL. J. Chem. Soc. Perkin I, 1500 (1973).
42. H. L. HOLLAND and B. J. AURET. Can. J. Chem. **53**, 845 (1975).
43. P. B. D. DE LA MARE and B. N. B. HANNAN. J. Chem. Soc. Perkin II, 1086 (1973).
44. C. DJERASSI, R. R. ENGLE, and A. BOWERS. J. Org. Chem. **21**, 1547 (1956).
45. G. F. WOODS, P. H. GRISWOLD, B. H. ARMBRECHT, D. I. BLUMENTHAL, and R. PLAPINGER. J. Am. Chem. Soc. **71**, 2028 (1949).
46. G. STORK, A. BRIZZOLARA, H. LANDESMAN, J. SZMUSZKOVICZ, and R. TERRELL. J. Am. Chem. Soc. **85**, 207 (1963).
47. D. I. SCHUSTER and D. F. BRIZZOLARA. J. Am. Chem. Soc. **92**, 4357 (1970).
48. J. S. FASSNACHT and N. A. NELSON. J. Org. Chem. **27**, 1885 (1962).
49. B. E. EDWARDS and P. NARASHIMA. J. Org. Chem. **31**, 324 (1966).
50. A. ERCOLI and P. DE RUGGIERI. J. Am. Chem. Soc. **75**, 650 (1953).
51. S. K. LEVINE and M. E. WALL. J. Am. Chem. Soc. **81**, 2826 (1959).
52. M. DAVIS and V. PETROW. J. Chem. Soc. 2536 (1949).
53. T. NAMBARA, M. ITO, M. ITO, J. MOHRI, J. GOTO, and H. HOSADA. Chem. Pharm. Bull. **21**, 2452 (1973).
54. B. CAMERINO and D. CATTAPAN. Farmaco Ed. Sci. **13**, 39 (1958).
55. K. I. H. WILLIAMS, R. S. ROSENFELD, M. SMULOVITZ, and D. K. FUKUSHIMA. Steroids, **1**, 377 (1963).
56. G. F. BURKINSHAW, B. R. DAVIS, E. G. HUTCHINSON, P. D. WOODGATE, and R. HODGES. J. Chem. Soc. C, 3002 (1971).
57. R. L. PEDERSON and J. C. BABCOCK. U.S. Patent No. 2,806,862 (September 17, 1957); Chem. Abstr. **52**, 10225e (1958).
58. A. v. WARTBURG. Helv. Chim. Acta, **46**, 591 (1963).

Can. J. Chem. Downloaded from www.nrcresearchpress.com by 210.87.254.40 on 09/05/12
For personal use only.

Etude polarographique de l'antimoine(III) et (V) dans le fluorure d'hydrogène anhydre et dans ses mélanges avec l'eau[1]

JACQUES DEVYNCK ET BERNARD TREMILLON

Laboratoire d'Electrochimie Analytique et Appliquée, Ecole Nationale Supérieure de chimie de Paris, Université Pierre et Marie Curie, Paris, France

ET

HUGUES MENARD

Faculté des Sciences, Université de Sherbrooke, Sherbrooke (Qué.), Canada J1K 2R1

ET

GERMAIN COMARMOND

Laboratoire de chimie, Institut National des Sciences et Techniques Nucléaires, Saclay, France

Reçu le 11 novembre 1977

JACQUES DEVYNCK, BERNARD TREMILLON, HUGUES MENARD et GERMAIN COMARMOND. Can. J. Chem. **56**, 703 (1978).

On décrit le comportement électrochimique de Sb(III) et Sb(V) dans les mélanges eau–HF et dans HF anhydre. Une électrode à gouttes de mercure à capillaire de Teflon permettant la mise en œuvre des techniques polarographiques directement dans les mélanges eau–HF et dans HF anhydre est proposée. L'étude a montré, par polarographie classique et par polarographie à impulsions, que Sb(III) est réductible à l'état de Sb(0) comme en milieu acide non-fluoré, la réaction n'étant reversible qu'en présence d'ions Cl^- ou Br^-, I^-. Sb(V) n'est pas électroactif dans les différents milieux considérés sauf s'il est ajouté sous la forme $SbCl_5$; il présente alors deux vagues de réduction, qui disparaissent au cours du temps par suite de la formation de SbF_6^-. On discute les possibilités d'applications au dosage de Sb(III) en milieu eau–HF et dans HF anhydre.

JACQUES DEVYNCK, BERNARD TREMILLON, HUGUES MENARD, and GERMAIN COMARMOND. Can. J. Chem. **56**, 703 (1978).

The electrochemical behaviour of Sb(III) and Sb(V) in water–HF mixtures (2.5 to 50% HF) and in anhydrous HF is described. A Teflon capillary dropping mercury electrode is proposed for polarographic investigations in these fluorinated media. It is shown, by classical or pulse polarography, that Sb(III) can be reduced to Sb(0), as in acidic non-fluorinated media. The electrochemical reaction becomes reversible by addition of Cl^-, Br^- or I^-. Sb(V) is not electroactive in the various HF-media, except when it is introduced as the $SbCl_5$. In this case, the two polarographic waves of Sb(V) disappear with time because of SbF_6^- formation. Analytical applications to the determination of Sb(III) in water–HF and in anhydrous HF are discussed.

Introduction

Le fluorure d'hydrogène anhydre et ses mélanges avec l'eau sont connus comme étant de bons milieux d'attaque de minerais et de verres, et l'analyse des éléments métalliques dans ces matériaux passe très souvent par une attaque en milieu eau – fluorure d'hydrogène (1).

En raison du caractère corrosif de HF, l'analyse des éléments n'est pas effectuée directement dans le mélange eau–HF: quelle que soit la technique d'analyse employée, il est préconisé de chasser HF, opération qui peut conduire à des pertes des éléments à doser par suite d'une évaporation ou d'un entraînement par la vapeur. Des pertes de cette nature ont été évoquées notamment lors de l'analyse de l'antimoine (2).

Une application des méthodes électrochimiques directement dans les solutions d'attaque permet d'éviter ces pertes, mais elle n'est possible que si l'on dispose d'électrodes et de cellules résistant au fluorure d'hydrogène. La polarographie, en particulier, nécessite l'utilisation d'un capillaire de Teflon dont la fabrication a longtemps été reconnue comme difficile et le fonctionnement délicat (3).

Nous avons, pour notre part, réalisé un capillaire de fabrication simple et nous l'avons utilisé dans ce travail pour analyser le comportement électrochimique de Sb(III) et Sb(V) dans les mélanges eau–HF de teneur en HF supérieure à 20% (en poids) et dans HF anhydre.

L'antimoine aux degrés d'oxydation (III) et (V) a donné lieu a de très nombreuses études polarographiques (4). Il est connu que Sb(III) est réduit irréversiblement dans les milieux acides non complexants, comme les solutions de $HClO_4$ (5), et il a été montré que l'addition d'ions halogénures, Cl^- notamment,

[1]Adresser la correspondance à: Jacques Devynck, Laboratoire d'Electrochimie Analytique et Appliquée, ENSCP, 11 rue Pierre et Marie Curie, 75231 Paris Cedex 05, France.

Can. J. Chem. Downloaded from www.nrcresearchpress.com by 210.87.254.5 on 09/05/12
For personal use only.

Can. J. Chem. Downloaded from www.nrcresearchpress.com by 210.87.254.5 on 09/05/12
For personal use only.

rend le système réversible (6). L'antimoine(V) n'est, quant à lui, pas électroactif en milieu acide, sauf sous la forme de complexe $SbCl_6^-$ en milieu HCl très concentré (7). La non-électroactivité de Sb(V) est particulièrement intéressante lorsqu'il est nécessaire de doser Sb(III) à très faible concentration en présence de Sb(V) concentré: c'est précisément le cas des phases catalytiques à base de SbF_5 utilisées dans la chimie des milieux superacides (8–10).

Etant donné l'intérêt des mélanges eau–HF sur le plan analytique et les possibilités offertes par l'application directe des méthodes dérivées de la polarographie, nous avons étudié le comportement électrochimique de Sb(III) et Sb(V) dans le but de mettre au point des méthodes de dosage de l'antimoine(III).

Partie expérimentale

Cellule

Le matériel utilisé pour cette étude dérive de celui qui a été décrit pour des études du fluorure d'hydrogène anhydre et des mélanges eau – fluorure d'hydrogène (11, 13). La cellule est en voltalef (contenance: 30 ml). HF anhydre et les mélanges eau–HF très concentrés en HF sont manipulés au moyen d'une rampe spéciale (12). Les mélanges de teneur inférieure ou égale à 50% de HF sont manipulés dans un simple récipient cylindrique, en voltalef, muni d'un couvercle de Teflon dans lequel sont percées les ouvertures pour les électrodes.

Electrodes-référence

Pour l'étude des mélanges de teneur inférieure à 70% de HF, l'électrode de référence était une électrode au calomel en solution aqueuse (Tacussel, type C10) placée dans un compartiment de Teflon et séparée de la solution fluorhydrique par du Teflon poreux (11). Pour éviter la diffusion d'ions chlorure, le compartiment intermédiaire contenait une solution aqueuse de $NaNO_3$ 0.1 *M*.

Dans HF anhydre et dans les mélanges de teneur supérieure à 70% de HF, l'électrode de référence était réalisée à partir du système Cu, CuF_2, KF 0.2 *M* (14).

Electrodes à gouttes de mercure

Les capillaires de verre utilisés en polarographie sont inutilisables en présence de HF. Certaines techniques, comme l'utilisation d'une goutte fixe placée sur un support adéquat (13) ou l'utilisation d'une électrode amalgamée (or ou argent) (15) permettent de s'en affranchir. Cependant, les résultats n'ont pas la reproductibilité de ceux obtenus à l'aide d'un capillaire ou d'une électrode à goutte pendante et présentent donc peu d'intérêt analytique. Différents types de capillaires utilisables dans les mélanges eau–HF et dans HF anhydre ont été décrits, par Clifford (16), Raeen (17) et Headrige (18) puis, plus récemment, par Bond, O'Donnell et coll. (3, 19). Une mise au point sur ce sujet a été publiée par Bond et O'Donnell (3). A partir des modèles de capillaires inattaquables proposés, nous avons réalisé une électrode à gouttes différente, dont le schéma est représenté sur la fig. 1. L'électrode est composée d'un petit cylindre de Teflon dans lequel un canal de 0.1 à 0.2 mm de diamètre est réalisé par surmoulage à chaud d'un fil métallique (capillaire PFA 9705, SAIMAP, Issy-les Moulineaux). Ce cylindre de Teflon est inséré et collé dans un capillaire de verre classique (Capillaire METROHM EA671). L'espace compris entre le capillaire de verre et le cylindre de Teflon est partiellement rempli de paraffine (aspiré à l'état fondu à travers le tube de Teflon), de façon à ménager une chambre de forme sensiblement sphérique qui se remplit de mercure sans retenir de bulles d'air. L'ensemble capillaire de verre et tube de Teflon est gainé d'un tube de polyoléfine thermorétractable (gaine TTR, Compagnie française des Isolants Paris). L'électrode ainsi réalisée a été utilisée avec un dispositif de stillation forcée Tacussel, type MP03.

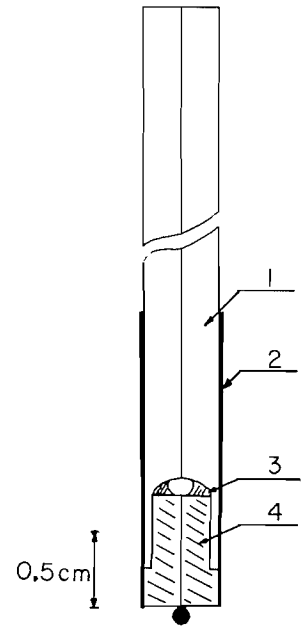

FIG. 1. Vue en coupe du capillaire de l'électrode à gouttes de mercure. (*1*) Capillaire de verre (METROHM-EA671); (*2*) gaine de polyoléfine thermorétractable; (*3*) paraffine; (*4*) tube capillaire en voltalef (ϕ intérieur: 100 à 200 μm).

L'électrode auxiliaire était un fil de platine.

Appareillage

Les courbes voltampérométriques ont été obtenues à l'aide d'un polarographe Tacussel type PRG5 et enregistrées sur table traçante Sefram type Luxytrace.

Produits

Fluorure d'hydrogène: les mélanges eau–HF de teneur inférieure à 50% ont été réalisés à partir des solutions commerciales (Merck). Cependant, ces solutions contenaient des traces d'ions chlorure qui se sont avérées gênantes pour certaines études; les mélanges ont été alors préparés par addition d'eau au fluorure d'hydrogène de haute pureté (Comhurex, Pierrelatte).

Les solutions d'antimoine (Anachemia, Reagent Grade) ont été préparées, à partir de produits purs pour analyse, dans des fioles jaugées en polypropylène (Nalgene) dont la résistance aux mélanges eau–HF s'est révélée excellente aux concentrations de HF inférieures à 50%.

Résultats

(1) Comportement électrochimique de l'antimoine(III)

(a) Dans le mélange à 40% de HF

Les solutions de Sb(III) (sous forme d'oxyde ou de fluorure) présentent une vague polarographique bien définie ($E_{1/2} = -0.540$ V/ECS) dont la hauteur

Can. J. Chem. Downloaded from www.nrcresearchpress.com by 210.87.254.5 on 09/05/12
For personal use only.

est proportionnelle à la concentration, mais irréversible (fig. 2). Par polarographie à impulsions (fig. 3), la proportionnalité de la hauteur du pic à la concentration est bien vérifiée dans le domaine: 10^{-7} M < Sb(III) < 10^{-2} M.

L'addition d'ions chlorure (sous forme de HCl ou de KCl) provoque, comme dans d'autres solutions aqueuses acides (20), un déplacement de la vague vers les potentiels positifs. A partir d'une concentration d'ions Cl^- environ 1 M, la réduction de Sb(III) à l'état d'amalgame est devenue réversible (fig. 2). Le potentiel de demi-vague est alors $E_{1/2} = -0.358$ V/ECS. La présence d'ions Cl^- provoque simultanément l'apparition d'une vague d'oxydation du mercure. L'évolution du système Sb(III)/Sb(0) vers la réversibilité lors de l'addition de Cl^- peut également être constatée par polarographie à impulsions (fig. 3). La largeur du pic à mi-hauteur est alors de 75 mV (valeur théorique pour des impulsions de 50 mV: 54 mV d'après Parry et Osteryoung (21)).

Remarque: Les solutions d'antimoine(III) dans les mélanges eau–HF présentent, lorsqu'elles sont fraîchement préparées en l'absence d'ions Cl^- une prévague qui disparaît au cours du temps. Une telle prévague a également été observé en milieu $HClO_4$ (22) et a été attribuée à la réduction de SbO^+ formé par hydrolyse partielle de Sb^{3+}, selon la réaction:

$$SbO^+ + 2H^+ + 3e \rightarrow Sb(Hg) + H_2O$$

(b) Dans HF anhydre (+ KF 0.2 M)

Les phénomènes observés dans les mélanges eau – fluorure d'hydrogène sont un peu modifiés dans le fluorure d'hydrogène anhydre. Le polarogramme

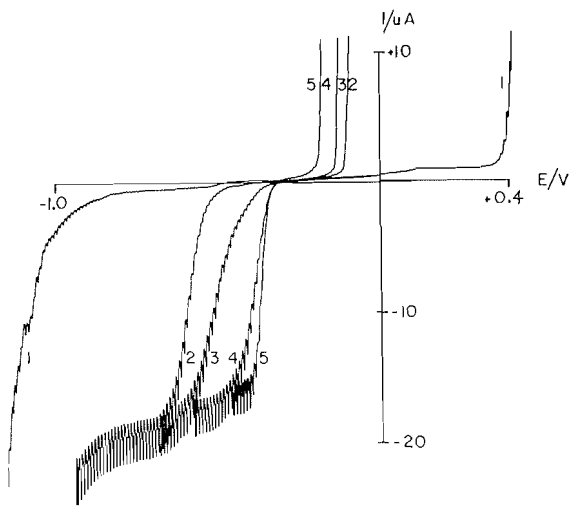

FIG. 2. Polarogrammes d'une solution de Sb_2O_3 dans un mélange eau – HF contenant 40% de HF (en poids), + KCl. (*1*) Courant résiduel; (*2*) Sb_2O_3 5 × 10^{-4} M; après addition de KCl: (*3*) 3 × 10^{-2} M; (*4*) 7 × 10^{-2} M; (*5*) 1 M.

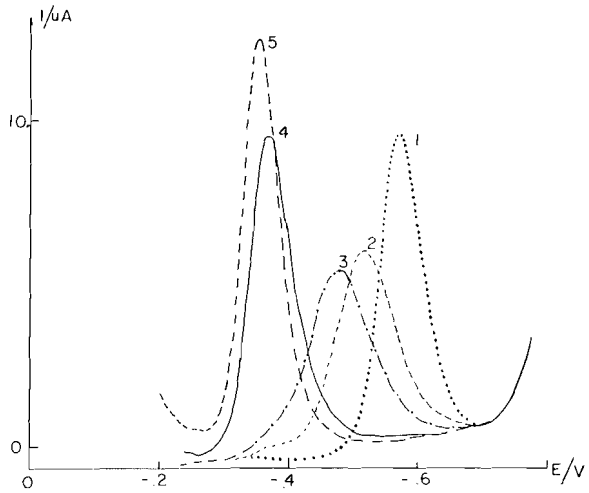

FIG. 3. Polarographie à impulsions de Sb_2O_3 3 × 10^{-5} M dans un mélange eau – HF contenant 40% de HF: influence des ions chlorure. (*1*) Sb_2O_3 seul; après addition de KCl: (*2*) 10^{-2} M; (*3*) 2 × 10^{-1} M; (*4*) 5 × 10^{-1} M; (*5*) 1.3 M. Impulsions: 50 mV, temps de goutte: 1 s.

d'une solution de Sb(III) présente également une vague de réduction non-réversible ($E_{1/2} = -0.770$ V/Cu, CuF_2). L'addition d'ions chlorure rend le système réversible, le potentiel de demi-vague est alors $E_{1/2} = -0.660$ V (fig. 4). Notons cependant que, du fait de la basicité de Cl^- et de la faible solubilité de HCl dans HF anhydre, on observe, au cours du temps, la disparition progressive de la vague réversible au profit de la vague irréversible.

(2) Comportement électrochimique de l'antimoine(V)

(a) Dans les mélanges eau–HF

Les sels de Sb(V) (Sb_2O_5 ou SbF_5) ne sont pas électroactifs dans les mélanges eau–HF. Seul le chlorure d'antimoine(V) présente une double vague de réduction (fig. 5). Les hauteurs relatives des deux vagues sont compatibles avec la mise en jeu, respectivement, de deux électrons (système Sb(V)/Sb(III) et trois électrons (système Sb(III)/Sb(0)). La dissolution de chlorure d'antimoine(V) fait immédiatement apparaître une vague d'oxydation, correspondant à l'oxydation du mercure en présence d'ions chlorure et, comme dans d'autres milieux, la réduction de Sb(V) a lieu pratiquement au même potentiel que l'oxydation du mercure; la détermination du potentiel de demi-vague de la première vague est donc impossible. Le potentiel de demi-vague correspondant à la seconde étape de réduction est: $E_{1/2} = -0.460$ V. Au cours du temps, la double vague de réduction de Sb(V) diminue, tandis que la vague d'oxydation du mercure en présence de chlorure augmente. Lorsque la vague de Sb(V) a complète-

Can. J. Chem. Downloaded from www.nrcresearchpress.com by 210.87.254.5 on 09/05/12
For personal use only.

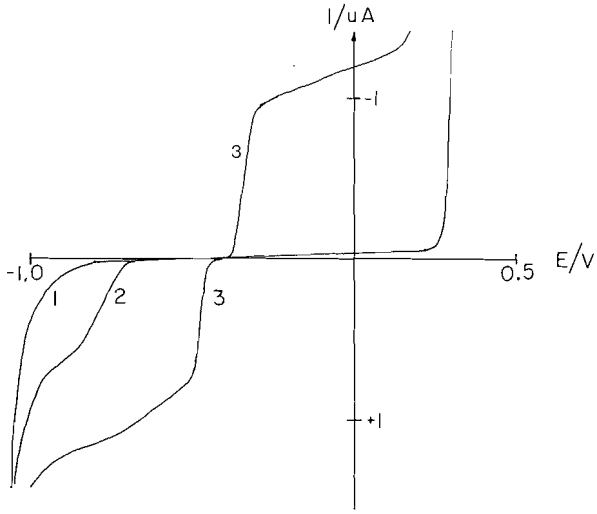

FIG. 4. Polarogramme d'une solution de Sb_2O_3 2.5×10^{-4} *M* dans HF anhydre (+KF 0.2 *M*). Influence de la concentration des ions chlorures. (*1*) Courant résiduel; (*2*) solution de Sb_2O_3 seul; (*3*) après addition de KCl 10^{-1} *M*.

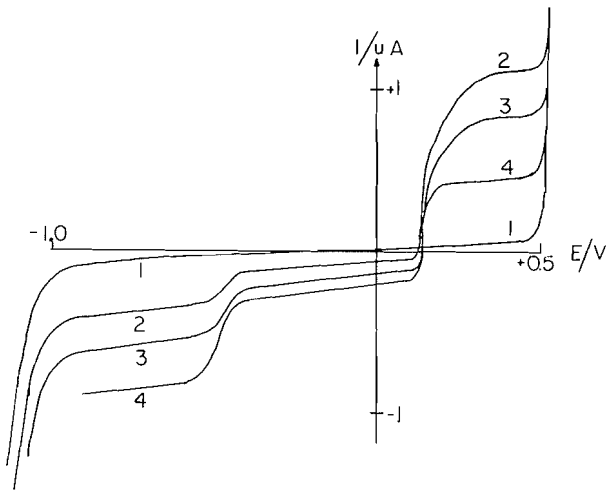

FIG. 5. Polarogramme d'une solution de $SbCl_5$ 5×10^{-4} *M* dans un mélange eau – HF contenant 40% de HF: évolution en fonction du temps *t*. (*1*) Courant résiduel; (*2*) après addition de $SbCl_5$, $t = 1$ h; (*3*) $t = 4$ jours; (*4*) $t = 6$ jours.

ment disparu, la vague d'oxydation du mercure a alors une hauteur sensiblement égale à la hauteur totale des vagues de réduction de Sb(V) en Sb(0) (fig. 5, courbe 2).

(b) Dans HF anhydre

Comme dans le cas de Sb(III), le comportement de Sb(V) diffère peu dans les mélanges eau–HF et dans HF anhydre basique. Lorsque Sb(V) est dissous sous la forme de fluorure, il n'est pas électroactif; seules les solutions de $SbCl_5$ présentent une double vague en réduction. Cette vague disparaît lentement au cours du temps (fig. 6) en même temps que la vague anodique due aux ions chlorure, du fait de la faible solubilité de HCl. Le phénomène est accéléré par un barbotage d'un gaz inerte qui entraine HCl. On obtient finalement la courbe correspondant au courant résiduel.

Discussion

Le comportement électrochimique de l'antimoine(III) dans les mélanges eau–HF de concentration en HF variable, jusqu'à HF anhydre (basique) est tout à fait comparable à celui qui avait été précédemment observé en milieu acide non fluoré. Les méthodes électrochimiques d'analyse de Sb(III) sont donc directement transposables aux mélanges eau–HF, avec des électrodes à gouttes de mercure réalisées à l'aide de matériaux résistant au fluorure d'hydrogène. Les techniques polarographiques très sensibles (polarographie à impulsions ou redissolution anodique) permettent ainsi un dosage de traces de Sb(III) directement dans les solutions d'attaque des matériaux, ce qui présente un avantage par rapport aux procédés précédemment décrits (1, 23) nécessitant l'élimination de HF.

Dans tous les mélanges eau–HF, Sb(III) présente une vague de réduction irréversible, mais l'addition d'ions Cl^- déplace cette vague de réduction vers les potentiels positifs et rend le système réversible. Outre l'intérêt qu'elle présente sur le plan analytique (meilleure "résolution" de Sb(III) en polarographie à impulsions, par exemple), cette évolution apporte quelques indications sur le comportement de Sb(III)

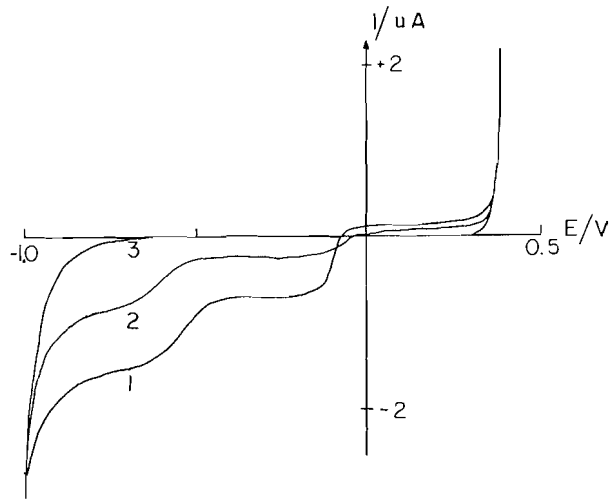

FIG. 6. Polarogramme d'une solution de $SbCl_5$ dans HF anhydre (+KF 0.2 *M*); évolution en fonction du temps. (*1*) Solution de $SbCl_5$ 3×10^{-4} *M*; $t = 1$ h; (*2*) $t = 24$ h; (*3*) courant résiduel.

Can. J. Chem. Downloaded from www.nrcresearchpress.com by 210.87.254.5 on 09/05/12
For personal use only.

en milieu HF et sur la réactivité de ce milieu. Notons tout d'abord que les complexes chlorure de Sb(III) sont vraisemblablement peu stables dans les mélanges eau–HF: l'addition de $SbCl_3$ conduit à la libération quantitative des ions Cl^-, identifiables par la vague d'oxydation du mercure. On peut supposer que les ions halogénures X^- (Cl^-, Br^- ou I^-) sont déplacés des complexes SbX_3 par HF du fait de la stabilité des complexes fluorure et de la basicité de l'ion X^-, selon la réaction:

$$SbCl_3 + 3\ HF \leftrightarrows SbF_3 + 3HCl$$

Il n'y a donc probablement pas lieu d'invoquer la formation de complexes chlorure en solution (complexes dont on sait que la réduction est réversible pour expliquer les modifications de la cinétique de la réduction électrochimique. On observe d'ailleurs que l'addition supplémentaire d'ions halogènure au-delà de la concentration minimale nécessaire pour rendre le système réversible est sans effet sur la vague polarographique; pas de déplacement de la vague de réduction qui pourrait être attribué à la formation de complexes en solution.

Il a, en effet, été montré que des complexes fluorure de Sb(III) peuvent se former en milieu HF dilué (18–22). Cependant, il convient de noter que l'activité des ions fluorures diminue lorsque la concentration de HF augmente dans les mélanges eau–HF, du fait de la très forte solvatation de l'ion F^- par HF (24). Les complexes fluorures, s'ils existent, sont vraisemblablement de moins en moins stables quand la concentration de HF augmente et les mélanges couramment utilisés (comme le mélange à 40% de HF) sont, en fait, très peu "complexants" (25).

L'origine du phénomène responsable de la variation de la cinétique de réduction de Sb(III) lors de l'addition d'ions halogènure a donné lieu à de très nombreux travaux. Si la formation de complexes halogènures en solution a été fréquemment invoquée (4), des effets catalytiques ont aussi été avancés pour justifier l'effet des ions I^- (26), SCN^- (27), ou encore $S_2O_3^{2-}$ (28). Il apparaît ici vraisemblable que la réduction réversible de Sb(III) nécessite l'adsorption des ions halogènure X^- (ou de HX quand l'halogènure est protoné) (29). On peut, en effet, observer que la charge de la double-couche est positive dans le domaine de potentiel ou Sb(III) est réduit (par exemple, dans un mélange à 22% de HF (17)) et que la concentration nécessaire pour observer la réversibilité dans un milieu donné est d'autant plus faible que l'halogénure est plus fortement adsorbé; cette adsorption des ions halogénure en milieu eau–HF est actuellement en cours d'étude (30).

L'antimoine(V) est électroactif sous la forme de complexe chlorure ($SbCl_5$ ou $SbCl_6^-$) et présente alors dans les milieux eau–HF le même comportement qu'en milieu HCl concentré. Cependant, du fait de la très grande stabilité des complexes fluorure, l'équilibre

$$[1] \qquad SbCl_5 + 7HF \leftrightarrows SbF_6^- + 5HCl\uparrow + H_2F^+$$

est fortement déplacé vers la formation de SbF_6^-, complexe non-électroactif. On ne forme pas les complexes mixtes du type $SbCl_xF_y$ mis en évidence par Dove (31) (dans des conditions expérimentales toutefois très différentes). La réaction 1 a été mise a profit pour préparer le fluorure d'antimoine à partir du chlorure correspondant (32). Du fait du caractère non-électroactif de SbF_5 en milieu eau–HF comme dans HF anhydre, le dosage de Sb(V) n'y est pas possible par polarographie. Ce caractère peut être mis à profit pour doser Sb(III) en présence de grandes quantités de Sb(V), comme cela a été proposé pour l'analyse des produits de réduction des milieux superacides contenant SbF_5 (33).

Remerciements

Les auteurs remercient la sous-commission Franco-Québécoise qui a attribué une bourse post-doctorale (H.M.) et le commissariat à l'Energie Atomique qui a financé ces recherches.

1. D. G. JEFFERY. Chemical methods of rock analysis. Pergamon, Oxford. 1975.
2. Bulletin de la Commission International du Verre, Institut International du Verre, Charleroi (Belgique). 1970.
3. A. M. BOND, T. A. O'DONNELL et A. B. WAUGH. J. Electroanal. Chem. **39**, 137 (1972).
4. V. PAST. *Dans* Encyclopedia of electrochemistry of the elements. Tome IV. M. Dekker, New York. 1975.
5. J. J. LINGANE. Ind. Eng. Chem., Anal. Ed. **15**, 585 (1963).
6. I. M. KOLTHOFF et J. J. LINGANE. Polarographie. Tome II. Wiley Interscience, NY. 1952.
7. G. P. HAIGHT. J. Anal. Chem. **26**, 593 (1954).
8. R. J. GILLESPIE. Endeavour, **32**, 3 (1973).
9. J. LUKAS, P. A. KRAMER et A. P. KOUWENHOVEN. Recueil Trav. Chim. Pays-Bas, **92**, 44 (1973).
10. J. W. LARSEN. J. Am. Chem. Soc. **99**, 4379 (1977).
11. J. P. MASSON. Thèse, A010717, Paris. 1974.
12. J. P. MASSON, J. DEVYNCK et B. TREMILLON. J. Electroanal. Chem. **64**, 175 (1975).
13. A. VAILLANT. Thèse, Paris. 1974.
14. R. BURROWS et R. JASINSKI. J. Electrochem. Soc. **115**, 348 (1968).
15. R. THIEBAULT et M. MERLEM. J. Electroanal. Chem. A paraître.
16. A. F. CLIFFORD et G. BALOG. Nucl. Sci. Abstr. **5**, 694 (1951).
17. H. P. RAAEN. Anal. Chem. **34**, 1714 (1962).
18. J. B. HEADRIDGE, A. M. HAMZA, D. P. HUBBARD et M. S. TAYLOR. *Dans* Polarography 1964. *Rédigé par* G. J. Hills. McMillan, Londres. 1966.
19. A. M. BOND et T. A. O'DONNELL. Anal. Chem. **44**, 590 (1972).

20. B. BREYER, F. GUTMAN et S. HACOBIAN. Aust. J. Sci. Res. A, **4**, 595 (1951).
21. E. P. PARRY et R. A. OSTERYOUNG. Anal. Chem. **37**, 1634 (1965).
22. A. M. BOND. J. Electrochem. Soc. **117**, 1145 (1970).
23. P. J. WILLIAMS et T. A. SCHWENKLER. J. Am. Ceramic Soc. **38**, 367 (1955).
24. H. MENARD, J. P. MASSON, J. DEVYNCK et B. TREMILLON. J. Electroanal. Chem. **63**, 163 (1975).
25. A. VAILLANT, F. LEBLOND, H. MENARD, J. DEVYNCK et B. TREMILLON. A paraître.
26. L. R. TAYLOR, R. J. DAVENPORT et D. C. JOHNSON. Talanta, **20**, 947 (1973).
27. E. JACOBSEN et T. ROJOHN. Anal. Chim. Acta, **54**, 261 (1971).
28. E. D. MORHEAD et S. LIPCSEY. Anal. Lett. **6**, 821 (1973).
29. D. M. MOHILNER. *Dans* Electroanalytical chemistry. *Rédigé par* A. J. Bard. M. Dekker, New York. 1966.
30. H. MENARD, F. LEBLOND et J. DEVYNCK. En cours.
31. M. F. A. DOVE et O. ALI. J. Inorg. Nucl. Chem. Suppl. 77 (1976).
32. P. PASCAL. Nouveau traité de chimie minérale. Tome XI. Masson et Cie, Paris. 1958. p. 559.
33. J. DEVYNCK et G. COMARMOND. Anal. Lett. A paraître.

Can. J. Chem. Downloaded from www.nrcresearchpress.com by 210.87.254.5 on 09/05/12
For personal use only.

Kinetics and mechanism of the base hydrolysis of some *trans*-dihalogeno(cyclam)rhodium(III) complexes

H. L. CHUNG[1] AND E. J. BOUNSALL

Department of Chemistry, University of Windsor, Windsor, Ont., Canada N9B 3P4

Received June 22, 1977

H. L. CHUNG and E. J. BOUNSALL. Can. J. Chem. **56**, 709 (1978).

The base hydrolysis of *trans*-[Rh(cyclam)XY]$^+$ (cyclam = 1,4,8,11-tetraazacyclotetradecane; X^- and Y^- = Cl^-, Br^-, and I^-) are studied in aqueous solution over a range of OH^- concentration and at various temperatures. The kinetics are done at a constant ionic strength with excess of [OH^-] (smallest ratio = 200:1) so that pseudo first order rate constants are obtained for all the determinations. All of the reactions proceed with complete retention of configuration, and no *trans*-to-*cis* isomerization is found. The kinetic *trans* effect of these complexes is $I^- > Br^- > Cl^-$ on a rate basis, but based on ΔH^*, $I^- > Br^- = Cl^-$. These Rh(III) complexes exhibit kinetic class (*b*) character on the ΔH^* basis. The results of the rate constants and the activation parameters are interpreted in terms of an S_N1CB mechanism. The behavior of these complexes is compared to that of the other analogous complexes.

H. L. CHUNG et E. J. BOUNSALL. Can. J. Chem. **56**, 709 (1978).

On a étudié l'hydrolyse basique du [Rh(cyclam)XY]$^+$ *trans* (cyclam = tétraaza-1,4,8,11 cyclotétradécane, X^- et Y^- = Cl^-, Br^- et I^-); ces études ont été effectuées en solution aqueuse à des concentrations de OH^- variables et à diverses températures. On a déterminé les cinétiques à une force ionique constante avec un excès de concentration de OH^- (plus petit rapport = 200:1) de façon à obtenir des constantes de vitesse de pseudo premier ordre pour toutes les déterminations. Toutes les réactions se produisent avec une rétention de configuration et on ne trouve aucune isomérisation *trans* vers *cis*. L'effet cinétique *trans* de ces complexes, tel que déterminé à partir des vitesses, correspond à $I^- > Br^- > Cl^-$ alors que l'ordre est $I^- > Br^- = Cl^-$ si l'on utilise le ΔH^* comme base. En se basant sur les ΔH^*, ces complexes Rh(III) présentent un caractère de cinétique de classe (*b*). Ces résultats concernant les constantes de vitesse et les paramètres d'activation peuvent être interprétés en termes d'un méchanisme S_N1CB. On compare le comportement de ces complexes avec celui d'autres complexes analogues.

[Traduit par le journal]

Introduction

The kinetics of substitution reactions in octahedral six-coordinate transition metal complexes have been extensively investigated and reviewed (1). In general, these octahedral complexes undergo acid hydrolysis and substitution reactions with other ligands at rates which are of the same magnitude and which are independent of the nature and concentration of the incoming group. Only first order kinetics are observed. In marked contrast, the hydroxide ion exhibits distinctly different behavior. Its substitution (base hydrolysis) takes place at a rate that is many orders of magnitude faster than other substitution reactions of these complexes. The base hydrolysis reactions are second order overall, first order with respect to the concentration of the complex and the hydroxide ion.

The rate of base hydrolyses of some octahedral ammine and amine complexes of Rh(III) has been reported (2). Surprisingly the hydroxide ion had little or no effect on the rate of reaction and acted like any other nucleophiles, and all reacted with complete retention of configuration.[2]

Bounsall and Koprich (4) have successfully synthesized some *trans*-[Rh(cyclam)XY]$^+$ complexes. They found that substitution reactions took place with strict retention of configuration and were independent of the nature and concentration of the incoming ligand. They also reported that these complexes were sensitive to base hydrolysis. This observation was unexpected in view of the other ammine and amine complexes of Rh(III) but identical to that found for Co(III). In view of this anomaly, it became important to study the base hydrolysis of these cyclam complexes of Rh(III).[3]

Experimental

Materials

Complexes of *trans*-[Rh(cyclam)XY]$^+$ used in this study were prepared as described previously (4). For all kinetic runs,

[1]Present address: Department of Chemistry, Michigan Cancer Foundation, Detroit, MI 48201.

[2]During the course of this work, Poe and Vuik (3) reported the base hydrolysis of *trans*-[Rh(en)$_2$X$_2$]$^+$ (en = ethylenediamine, X^- = Cl^-, Br^-, and I^-) complexes by using sufficiently high hydroxide ion concentration.

[3]The base hydrolysis of *trans*-[Rh(cyclam)Cl$_2$]$^+$ has been mentioned (5) during the course of this work.

Can. J. Chem. Downloaded from www.nrcresearchpress.com by 210.87.254.40 on 09/05/12
For personal use only.

Can. J. Chem. Downloaded from www.nrcresearchpress.com by 210.87.254.40 on 09/05/12
For personal use only.

deionized water was rendered carbon dioxide free by boiling and cooling under nitrogen atmosphere. Sodium hydroxide solutions were standardized before use. The deuterio *trans*-[Rh(D_4-cyclam)X_2]X (X^- = Cl^- and I^-) were prepared by dissolving the corresponding *trans*-[Rh(cyclam)X_2]X in hydroxide solution using D_2O as a solvent. The compounds were heated and then precipitated by adding the corresponding sodium salt.

Instruments

The electronic spectra were recorded with a Bausch and Lomb Spectronic 505 Recording Spectrophotometer. The reaction solutions were thermostatted in an oil bath with a Sargent thermo-regulator. The infrared spectra were taken on a Beckmann 10 Infrared Spectrophotometer.

Kinetics

A known quantity of the compound and the appropriate concentration of sodium hydroxide solution were prepared separately in equal volumes of water. The two solutions were previously brought to reaction temperature in a thermostatted oil bath and then mixed in a volumetric flask. Sufficient sodium nitrate was added to the sodium hydroxide solution before dilution to ensure a final ionic strength of 0.30 *M* in the reaction mixture. For the *trans*-[Rh(cyclam)I_2]$^+$ complex at 40°C, with the ionic strength adjusted to 3.00 *M*, there was a direct first order dependence on the concentration of hydroxide ion up to 2.00 *M*. (Sodium perchlorate could not be used due to the insufficient solubility of the complexes under investigation.) The final concentrations of the complexes varied from 3×10^{-5} *M* for the diiodo to 3×10^{-4} *M* for the dibromo complexes, with the lowest ratio of [OH^-] to [complex] throughout being 200 to 1, and therefore quite sufficient to ensure pseudo first order kinetics. At appropriate time intervals, aliquots were withdrawn and quenched in cold water and brought to room temperature. The reaction mixtures were analyzed immediately at suitable wavelengths for which the difference between the absorbance of the reactant and product was large.

Hydrogen–Deuterium Exchange Reactions

The reactions were done on the *trans*-[Rh(cyclam)Cl_2]$^+$ and *trans*-[Rh(cyclam)I_2]$^+$ complexes. (These two complexes were chosen because they represent the two extremes in rates, the former being the slowest and the latter the fastest in the base hydrolysis series studied.) An appropriate amount of the complex was dissolved in a solution of sodium hydroxide. The reaction mixture was heated at different times and temperatures, and the complex precipitated by addition of $NaClO_4$ and was analyzed by an infrared spectrum.

Results

Kinetics

The kinetic study of the base hydrolysis of the *trans*-[Rh(cyclam)X_2]$^+$ and *trans*-[Rh(cyclam)XY]$^+$ complexes was carried out spectrophotometrically. The reactions were studied over a temperature range of 25 to 85°C. Each complex was studied at three temperatures over 30°C to permit calculation of the activation parameters. Six different concentrations of hydroxide were employed. The reaction rate was followed for at least one half-life and usually for two or three half-lives. The rate of disappearance of the complex always followed the first order kinetic law. The pseudo first order rate constants for the reactions were determined graphically from the relationship:

$$k_{obsd} = \frac{2.30}{t} \log \frac{a}{a - x} = \frac{2.30}{t} \log \frac{A_0 - A_\infty}{A_t - A_\infty}$$

where t is the time in seconds, A_0 is the absorbance of the initial reading, A_t is the absorbance at time t, and A_∞ is the absorbance calculated from the known extinction coefficient of the product being formed. Isosbestic points were obtained in some systems in the wavelength range studied. Good first order rate plots were obtained throughout. Second order rate constants were calculated from the following expression:

$$k = \frac{k_{obsd}}{[OH^-]}$$

Excellent straight line plots of k_{obsd} vs. [OH^-] were obtained throughout over the range of [OH^-] used. No evidence of *trans*-to-*cis* isomerization was found in this study. This fact was found in the preparative work and the substitution and anation studies (6).

The activation parameters were calculated from the equation (7):

$$k = \frac{KT}{h} e^{\Delta S^\ddagger/R} e^{-\Delta H^\ddagger/RT}$$

where k is the second order rate constant at T(K), R is the gas constant, K is the Boltzmann constant, and h is the Planck constant.

The rate data were evaluated statistically using the methods of pooled variances (8). The kinetic results are given in Tables 1 and 2.

Hydrogen–Deuterium Exchange Reactions

The infrared spectra of the reaction products after the hydrogen–deuterium exchange reactions showed that the deuterium of the amine group in the complexes exchanged with hydrogen in hydroxide solution. All the four amine deuterium atoms contained in the complex could be interchanged with hydrogen. The extent of exchange depended on the concentration of the hydroxide, the temperature, and the time of the reaction. These hydrogen–deuterium exchanges were found to be faster than even the dissociative reaction step of the complex. But this was not the case in neutral and acidic solution, in which the hydrogen–deuterium exchanges were by comparison much less under the same conditions.

Discussion

The distinctive features of the base hydrolysis reactions of the cyclam complexes of Rh(III) in comparison with other substitution reactions (6*a*) are the fast rates, the large enthalpies of activation, and the large positive entropies of activation which are found

Can. J. Chem. Downloaded from www.nrcresearchpress.com by 210.87.254.40 on 09/05/12
For personal use only.

TABLE 1. Summary of second order rate constants for base hydrolysis of *trans*-[Rh(cyclam)XY]$^+$ complexes

Complex X	Complex Y	T (°C)	$10^5\,k$ ($M^{-1}\,s^{-1}$)
I	I	25	3.64±0.06
		40	55.5±1.0
		55	753±13
I	Br	25	1.95±0.03
		40	26.1±0.4
		55	256±4
I	Cl	25	1.21±0.50
		40	13.2±0.5
		55	121±4
Br	Br	40	0.958±0.030
		55	13.8±0.4
		70	152±4
Br	Cl	55	3.59±0.04
		70	41.8±0.5
		85	365±4
Cl	Cl	55	0.750±0.004
		70	7.90±0.04
		85	75.7±0.4

TABLE 2. Activation parameters for base hydrolysis of *trans*-[Rh(cyclam)XY]$^+$ complexes

Complex X	Complex Y	$\Delta H^\ddagger$ (kcal mol^{-1})	$\Delta S^\ddagger$ (cal deg^{-1} mol^{-1})	$10^5\,k_{55°C}$ ($M^{-1}\,s^{-1}$)
I	I	33.9±0.1	34.9±0.2	753±13
I	Br	30.8±0.2	23.2±0.4	256±4
I	Cl	29.2±0.3	17.0±0.5	121±4
Br	Br	35.4±0.2	31.5±0.4	13.8±0.4
Br	Cl	35.3±0.1	28.5±0.2	3.59±0.04
Cl	Cl	35.3±0.2	25.1±0.7	0.750±0.004

throughout the series of complexes studied. An unique feature is the high relative rate constants paralleled by high enthalpies of activation. This was a little unexpected, even though the relative rates are temperature dependent. Given a different range of temperatures the order of rate constants could be reversed.

The rate constants and activation parameters for the base hydrolysis reactions of the *trans*-[Rh(cyclam)XY]$^+$ complexes can be used to compare the kinetic *trans* effects (9) of the halogen ligands quantitatively, to classify the complexes as kinetically class (*a*) or (*b*) character (10), and to propose a reaction mechanism.

Kinetic trans *Effect*

A *trans* effect order can be found for the group *trans* to the leaving group. For the *trans*-[Rh(cyclam)XCl]$^+$ complexes with Cl^- as the leaving group, the rate constants are 121, 3.59, and 0.750 × 10^{-5} M^{-1} s^{-1} (in the ratio of 161:5:1) at 55°C for $X^- = I^-$, Br^-, and Cl^- respectively, and the values of $\Delta H^\ddagger$ are 29.2, 35.3, and 35.3 kcal mol^{-1} respectively. It is clear the *trans* effect in the *trans*-[Rh(cyclam)XCl]$^+$ complexes is $I^- > Br^- > Cl^-$, in terms of rate constants. On the $\Delta H^\ddagger$ basis, the *trans* effect is $I^- > Br^- = Cl^-$, I^- being 6.1 kcal mol^{-1} greater than Br^- and Cl^-, which are identical. With Br^- as the leaving group, with $X^- = I^-$ and Br^-, these rate constants are in the ratio of 19:1 and I^- has a $\Delta H^\ddagger$ value of 4.6 kcal mol^{-1} lower than Br^-. In other studies on octahedral complexes, on the basis of rate constants, Br^- has been found a better *trans* activator than Cl^- (10*b*).

*Kinetic Class (*a*) and (*b*) Character*

A systematic trend occurs in the case of releasing Y^- from the *trans*-[Rh(cyclam)IY]$^+$ complexes. At 55°C the rate constants for $Y^- = Cl^-$, Br^-, and I^- are 121, 256, and 753 × 10^{-5} M^{-1} s^{-1} (the ratio is 1:2:3), respectively. Based on rate constants, the complexes appear kinetically more labile as Y^- changes from Cl^- to Br^- and to I^-, and therefore of class (*a*). However, the values of $\Delta H^\ddagger$ are 29.2, 30.8, and 33.8 kcal mol^{-1} respectively and the complexes become kinetically more inert as Y^- changes from Cl^- to Br^- and to I^- by 1.6 and 3.1 kcal mol^{-1} differences which indicates class (*b*) behavior. Since the relative rate constant effect is dependent upon the temperature chosen for comparison, the $\Delta H^\ddagger$ is much more reliable. It can be concluded that the *trans*-[Rh(cyclam)IY]$^+$ complexes are kinetically of class (*b*). With $X^- = Br^-$ in the *trans* position, and Br^- and Cl^- the leaving groups Y^-, the same effect is observed: Br^- is released two times as quickly as Cl^-, but the $\Delta H^\ddagger$ of Br^- is greater than Cl^-, though only slightly (0.1 kcal mol^{-1}).

The kinetic class (*b*) character of the Rh(III) in the *trans*-[Rh(cyclam)IY]$^+$ complexes agrees with the substitution and anation results for the same complexes (6). Kinetic class (*b*) character of Rh(III) metal is common in some other Rh(III) systems, such as $[Rh(NH_3)_5X]^{2+}$ (11) and $[Rh(en_2)XY]^+$ (10*b*).

Mechanism

The mechanism of basis hydrolysis of octahedral complexes has been the subject of much discussion. Several different mechanisms have been proposed to explain the rapid base hydrolysis (12). It is normal for reactions whose rates depend on hydroxide catalysis to involve acid–base equilibria before reaction. The hydroxide ion produces an active intermediate which then reacts faster than the original substrate (13). Based on hydrogen–deuterium exchange evidence,

Can. J. Chem. Downloaded from www.nrcresearchpress.com by 210.87.254.40 on 09/05/12
For personal use only.

a conjugate base mechanism in which the hydroxide ion is involved initially in a rapid acid–base equilibrium as in this study, is consistent with Poon and Tobe's (14) base hydrolysis result of *trans*-[Co(D_4-cyclam)X_2]$^+$ (X^- = Cl^- and Br^-). Thus, the mechanism of base hydrolysis of these *trans*-[Rh(cyclam)XY]$^+$ complexes, following the S_N1CB mechanism as it is now widely accepted, can be outlined as follows:

[1] *trans*-[Rh(cyclam)XY]$^+$ + $OH^- \underset{\text{fast}}{\overset{K}{\rightleftharpoons}}$ *trans*-[Rh(cyclam-H)XY]^0 + H_2O

[2] *trans*-[Rh(cyclam-H)XY]^0 $\xrightarrow[\text{slow}]{k_{cb}}$ *trans*-[Rh(cyclam-H)X]$^+$ + Y^-

[3] *trans*-[Rh(cyclam-H)X]$^+$ + H_2O $\xrightarrow{\text{fast}}$ *trans*-[Rh(cyclam-H)X(H_2O)]$^+$

[4] *trans*-[Rh(cyclam-H)X(H_2O)]$^+$ $\xrightarrow{\text{fast}}$ *trans*-[Rh(cyclam)X(OH)]$^+$

The first step is the fast deprotonation of the amine group in the *trans*-[Rh(cyclam)XY]$^+$ to form its conjugate base. The second step is the rate-determining step of the dissociation of the leaving group. The third and the fourth steps are very fast processes. The water molecule bonds to the Rh(III) in the *trans*-[Rh(cyclam-H)X]$^+$ complex and the water proton rearranges to the amido group to form the hydroxo complex.

The normal mechanism for the base hydrolysis of octahedral ammine and amine complexes of Co(III) involves an S_N1CB mechanism in which the five coordinated intermediate takes on trigonal bipyramidal geometry. This is due to the observation that base hydrolysis is often accompanied by stereochemical change and that *cis* and *trans* isomers do not differ enormously in their reactivity. This can be understood if the main labilizing effect occurs in the transition state since, in a trigonal bipyramide, the symmetry distinction between ligands that were originally *trans* or *cis* to the leaving group is lost (5). Since stereochemical change is not observed in these Rh(III) complexes as was the case in Co(III), it suggests that any five-coordinated intermediate is square pyramide (15). The crystal field stabilization energy for the square pyramidal structure is greater in a low spin d^6 system than for the trigonal bipyramidal structure. Because of the greater crystal field strength of Rh(III) relative to Co(III), the greater loss in crystal field stabilization energy would make it easier to produce a square pyramidal structure in these Rh(III) systems.

TABLE 3. Second order rate constants, $\Delta H^{\ddagger}$ and $\Delta S^{\ddagger}$, for the base hydrolysis of *trans*-dichloro(cyclam) complexes of Co(III), Cr(III), and Rh(III) in aqueous solution (various ionic strengths) at 25°C

trans-[M(cyclam)Cl_2]$^+$	$\Delta H^{\ddagger}$ (kcal mol^{-1})	$\Delta S^{\ddagger}$ (cal deg^{-1} mol^{-1})	k (M^{-1} s^{-1})
Co	13.7	12	6.7×10^{4}[a]
Cr	—	—	1.3[b]
Rh	35.3	25.1	3.8×10^{-8}[c]

[a]Reference 16*a*.
[b]Reference 17.
[c]This work (extrapolated).

Comparisons

The base hydrolysis data for the analogous cyclam complexes of Co(III) have been reported (14, 16). The base hydrolysis of these *trans* isomers studied in buffer solutions was a fast, two stage reaction. Campi *et al.* (17) have studied the base hydrolysis of *trans*- and *cis*-[Cr(cyclam)Cl_2]$^+$ complexes. They reported that a typical second order rate law was observed.

The only available data for comparison of the rates for base hydrolysis are the *trans*-dichloro(cyclam) complexes of Rh(III), Co(III), and Cr(III) and are given in Table 3. For the cyclam complexes of all three metals no steric change was observed in the course of reactions. This is not surprising as the increased rigidity of the cyclam chelate resists rearrangement in the transition state.

Based on the rates at 25°C, the sensitivity to base hydrolysis of the analogous cyclam complexes is in the order Co(III) > Cr(III) > Rh(III). The order of acidity is Cr(III) > Co(III) > Rh(III) for the amine complexes; it can be expected to be in the same order for cyclam. The electron affinity gives the order Co(III) > Rh(III) > Cr(III) and the crystal field activation energy decreases in the order Cr(III) > Co(III) > Rh(III) irrespective of the intermediate structures (18). Thus, the lowest rate for Rh(III) can be explained on the basis of a low acidity and a large crystal field activation energy, which counteracts a reasonable high electron affinity.

A greater reactivity of the cyclam complexes to hydroxide ion, compared with the tetraammine and bis(ethylenediamine) complexes of Rh(III) (2, 3), is found in this study. The tetraammine complexes have little effect on the rate of base hydrolysis. The base hydrolysis of the bis(ethylenediamine) complexes is found that the [OH^-]-dependent path leads to *trans* → *cis* isomerization and has an S_N1CB–S_N1IP mechanism. As Poon (19) concludes for the Co(III) complexes, the nephelauxetic effect is only one of

many factors, which can be explained satisfactorily in terms of the faster rate of the base hydrolysis of the cyclam complex than the analogous tetraammine and bis(ethylenediamine) complexes.

Acknowledgment

The authors wish to thank the National Research Council of Canada for financial support of this work.

1. (*a*) F. Basolo and R. G. Pearson. Mechanisms of inorganic reactions. 2nd ed. John Wiley and Sons, Inc., New York, NY. 1967. Chapt. 3; (*b*) C. H. Langford and H. B. Gray. Ligand substitution processes. W. A. Benjamin, New York, NY. 1965. Chapt. 3; (*c*) J. O. Edwards. Inorganic reaction mechanism. W. A. Benjamin, New York, NY. 1964. Chapt. 6.
2. S. A. Johnson, F. Basolo, and R. G. Pearson. J. Am. Chem. Soc. **85**, 1741 (1963).
3. A. Poe and C. Vuik. J. Chem. Soc. Dalton Trans. 661 (1976).
4. E. J. Bounsall and S. R. Koprich. Can. J. Chem. **48**, 1481 (1970).
5. M. L. Tobe. Acc. Chem. Res. **3**, 377 (1970).
6. (*a*) S. R. Koprich. Ph.D. thesis, University of Windsor, Windsor, Ontario. 1970; (*b*) P. J. Dunn. M.Sc. thesis, University of Windsor, Windsor, Ontario. 1971.
7. A. A. Frost and R. G. Pearson. Kinetics and mechanism. 2nd ed. Wiley, New York, NY. 1961. Chapt. 7.
8. J. Mandel. The statistical analysis of experimental data. Wiley-Interscience, New York, NY. 1964. Chapts. 4 and 7.
9. F. Basolo and R. G. Pearson. Prog. Inorg. Chem. **4**, 381 (1962).
10. (*a*) S. Ahrland, J. Chatt, and N. R. Davies. Q. Rev. **12**, 265 (1958); (*b*) H. L. Bott, E. J. Bounsall, and A. J. Poe. J. Chem. Soc. A, 1275 (1966).
11. G. W. Bushnell, G. C. Lalor, and E. A. Moelwyn-Hughes. J. Chem. Soc. A, 719 (1966).
12. (*a*) D. D. Brown, C. K. Ingold, and R. S. Nyholm. J. Chem. Soc. 2696 (1953); (*b*) F. Basolo. Chem. Rev. **52**, 459 (1953); (*c*) S. C. Chan and O. W. Lau. Aust. J. Chem. **22**, 1851 (1969); (*d*) R. D. Gillard. J. Chem. Soc. A, 917 (1967).
13. J. March. Advanced organic chemistry: reactions, mechanism and structures. McGraw-Hill, New York. 1968. p. 217.
14. C. K. Poon and M. L. Tobe. Chem. Commun. 156 (1968).
15. A. Panunzi and F. Basolo. Inorg. Chem. Acta, **1**, 223 (1967).
16. (*a*) C. K. Poon and M. L. Tobe. J. Chem. Soc. A, 2069 (1967); (*b*) C. K. Lui and C. K. Poon. J. Chem. Soc. Dalton Trans. 216 (1972); (*c*) K. S. Mok, C. K. Poon, and H. W. Tong. J. Chem. Soc. Dalton Trans. 1701 (1972); (*d*) P. W. Mak and C. K. Poon. Inorg. Chem. **15**, 1949 (1976).
17. E. Campi, J. Ferguson, and M. L. Tobe. Inorg. Chem. **9**, 1781 (1970).
18. J. A. Broomhead, F. Basolo, and R. G. Pearson. Inorg. Chem. **3**, 826 (1964).
19. C. K. Poon. J. Am. Chem. Soc. **92**, 4467 (1970).

Can. J. Chem. Downloaded from www.nrcresearchpress.com by 210.87.254.40 on 09/05/12
For personal use only.

Reorientation of thiophene molecules in a benzene lattice[1]

WILLIAM E. SANFORD AND ROBERT K. BOYD

Guelph-Waterloo Centre for Graduate Work in Chemistry (Guelph Campus), University of Guelph, Guelph, Ont. Canada N1G 2W1

AND

JOHN A. RIPMEESTER

Division of Chemistry, National Research Council of Canada, Ottawa, Ont., Canada K1A 0R6

Received August 8, 1977

WILLIAM E. SANFORD, ROBERT K. BOYD, and JOHN A. RIPMEESTER. Can. J. Chem. **56**, 714 (1978).

Benzene and thiophene are known to form solid solutions over the entire composition range; the present work demonstrates the orientational freedom of thiophene molecules in solid solution with excess perdeuterobenzene, through measurements of spin–lattice relaxation times. In addition, the atom–atom approximation to intermolecular forces yielded a potential energy profile for in-plane rotation of a thiophene molecule, embedded in a benzene lattice, which is consistent with the experimental activation energy for the relaxation. The second moment of the absorption signal for thiophene in perdeuterobenzene at 80 K was determined to be 0.66 G^2, compared with a value of 0.42 G^2 computed as the intramolecular contribution only for in-plane rotation.

WILLIAM E. SANFORD, ROBERT K. BOYD et JOHN A. RIPMEESTER. Can. J. Chem. **56**, 714 (1978).

On sait que le benzène et le thiophène forment des solutions solides à toutes les compositions; dans le présent travail, on démontre la liberté d'orientation des molécules de thiophène dans une solution solide de perdeutérobenzène en excès en faisant appel à des mesures de temps de relaxation spin–réseau. De plus, l'approximation atome–atome des forces intermoléculaires conduit à un profil d'énergie potentielle pour la rotation dans le plan d'une molécule de thiophène, incluse dans un réseau de benzène, qui est en accord avec l'énergie d'activation expérimentale pour la relaxation. On a déterminé que le second moment du signal d'absorption pour le thiophène dans le perdeutérobenzène à 80 K est de 0.66 G^2 comparé avec une valeur de 0.42 G^2 calculée comme contribution intramoléculaire uniquement pour la rotation dans le plan.
[Traduit par le journal]

Can. J. Chem. Downloaded from www.nrcresearchpress.com by 210.87.254.42 on 09/05/12
For personal use only.

It is well known that benzene and thiophene form a continuous series of solid solutions, over the entire composition range (1). In addition, it was shown by Anderson (2) using pulse nmr techniques that thiophene molecules, in solid solution with perdeuterobenzene, possess considerable rotational freedom over considerable ranges of both composition and temperature. More recently it was shown (3) that Anderson's original measurements of spin–lattice relaxation times (T_1), for pure crystalline thiophene, were suspect below 172 K; at this temperature, adiabatic calorimetry experiments (4) indicate a phase transition. Both the calorimetry (4) and the more recent (3) T_1 experiments suggest that thiophene may be readily supercooled through this transition, and that the earlier T_1 data (2) pertain to a metastable phase.

Accordingly, it was felt worthwhile to reinvestigate the motion of thiophene in solid solution with perdeuterobenzene. The thiophene was purified as described previously (3); measurements of T_1 for the protons in solid solution containing 10.1 mol% of thiophene in perdeuterobenzene were made at 60 MHz using a Bruker SXP variable frequency spectrometer. (This concentration was chosen as the lowest at which reasonable signal-to-noise ratios could be readily attained; this was done in order to approximate as closely as possible to the case where each thiophene molecule would have only benzene molecules as nearest neighbours.) The resulting T_1 values are shown as a function of temperature between 77 K and 160 K in Fig. 1. The results obtained below about 140 K are consistent with a rapid motion of the thiophene molecules; this motion is characterised by an activation energy of 4–5 kJ mol^{-1}. The decrease in T_1, observed at temperatures above about 140 K, is presumably due to the onset of appreciable motion of the benzene-d_6 molecules; by extrapolation from the work of Anderson (2), who also studied the motions of benzene in solid solution with perdeuterothiophene, it can be inferred that the motional behaviour of benzene molecules in our solid solution was little different from that in pure benzene. The

[1]NRCC No. 16430. Taken in part from the M.Sc. Thesis of W.E.S., University of Guelph, 1975.

Can. J. Chem. Downloaded from www.nrcresearchpress.com by 210.87.254.42 on 09/05/12
For personal use only.

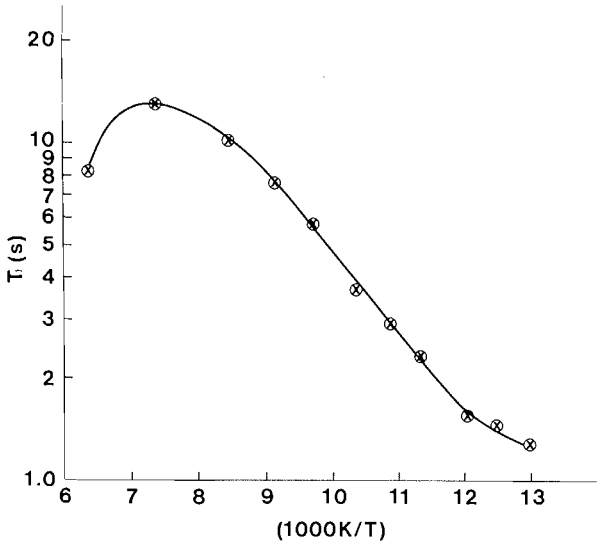

FIG. 1. Proton spin–lattice relaxation times (T_1), measured at 60 MHz, for thiophene in perdeuterobenzene; 10.1 mol% thiophene.

latter is well characterized (7), and seems consistent with the observed fall-off in T_1 at about 140 K. The mechanism could involve either ^1H–^2H (thiophene–benzene) cross-relaxation, or might be dominated by the residual protons in the sample of perdeuterobenzene. (In the solid solution used, assuming 99.5 at.% deuteration of benzene, the ratio of thiophene to benzene protons was 13:1.) No evidence of supercooling through phase transitions was detected in the present work.

For those planar aromatic molecules which display rapid spin–lattice relaxation in the solid state the molecular motion providing the mechanism for the relaxation is usually an in-plane jump between potential wells. Second-moment studies can yield useful information in this regard, and a value of 0.66 G^2 was presently obtained at 80 K for the second moment of the same solid solution as was used for the T_1 studies. This may be compared with values calculated, for the intramolecular contribution only, of 1.68 G^2 for a rigid thiophene molecule, and of 0.42 G^2 for a thiophene molecule undergoing in-plane reorientation between n potential wells, with $n > 3$. The temperature used for the experimental determination was such that the T_1 data (Fig. 1) predict that the second moment should have its high-temperature limiting value; the intermolecular contribution could not be calculated, since no crystal structure is available, so the agreement between the experimental value and the calculated value for fast motion, while reasonable and supportive of the proposed character of the motion, requires some additional evidence. Accordingly, calculations of the potential energy profile for in-plane rotation of a thiophene molecule substituted into a benzene crystal lattice, were undertaken; the general procedure, as applied to pure thiophene, was described previously (3). The present calculation considered a thiophene molecule at the origin of a unit cell, which in turn was centrally located in a 3 × 3 × 3 block of 27 unit cells of the benzene structure characterised (5) at 138 K. The thiophene molecule was substituted into this structure in such a way that the molecular plane coincided with that of the substituted benzene molecule; in addition, the centre of repulsion of the thiophene molecule was placed at the centre of symmetry of the benzene (also the crystallographic origin). The determination of this 'centre of repulsion' was described previously (3).

The computed profile thus obtained is shown in Fig. 2; the orientation corresponding to 0° rotation was arbitrarily chosen such that the sulfur atom of the thiophene molecule lay on a carbon–hydrogen vector of the substituted benzene molecule. The profile is again characterized by six potential wells, as found previously (3, 6) for pure thiophene, with energy barriers of about the correct size.

One final check was made; for one pair of nuclear spins, moving relative to one another in a plane, with a discrete number n of available sites ($n \geq 3$), T_1 may be computed by a formula due to Woessner (8):

$$(T_1)^{-1} = \left(\frac{9}{40}\right)\gamma^4\hbar^2 r^{-6} g(\omega_0, \tau_c)$$

At the minimum of the T_1 curve, $g(\omega_0, \tau_c) = (1.425/\omega_0)$; also, for more than two nuclei, the result may be obtained by summing over all pairwise interactions in the crystal:

$$(T_1)^{-1} = (1.425/\omega_0)\left[(9/40)(\gamma^4\hbar^2/N_A)\left(\sum_{i>j} r_{ij}^{-6}\right)\right]$$

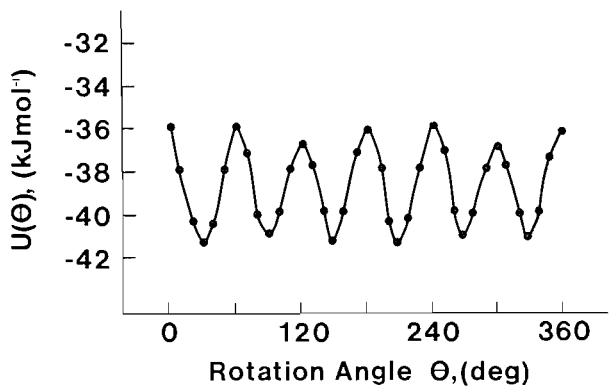

FIG. 2. Calculated potential energy profile for in-plane rotation of a thiophene molecule in a benzene lattice at 138 K.

If this is evaluated for thiophene, again including intramolecular contributions only (i.e. assuming all nearest neighbours to be perdeuterobenzene), $(T_1)_{min} = 0.44$ s at $\omega_0/2\pi = 60$ MHz; the experimental value is probably about 1 s from an extrapolation of Fig. 1. This agreement is reasonable; the discrepancy may be partly due to a distribution of correlation times τ_c, rather than a single unique value, in the sample used. For such a 10% solution, some thiophene molecules must have at least one other thiophene molecule as a nearest neighbour; this not only introduces an appreciable intermolecular contribution, but also affects τ_c.

The present work thus confirms the earlier conclusion of Anderson (2) concerning the motional freedom of thiophene in solid solutions with benzene. The question of why thiophene, a five-membered ring, should substitute for a hexagonal benzene molecule so readily, is closely related to the question discussed previously (3) as to why the potential energy profile for in-plane rotation of a thiophene molecule, in its own crystal structure, should display six rather than five potential wells. As pointed out previously (3), the general shape of such a profile is dominated by the interactions of the peripheral hydrogen atoms; the molecular geometry of thiophene is such that the four vectors, each of which is defined by the centre of repulsion and one of the four hydrogen atoms, make angles with one another all three of which are very close to 60°. Thus, rotation by 60° from an orientation corresponding to a potential energy minimum will result in three of the four hydrogen atoms occupying positions formerly occupied by hydrogen atoms prior to the rotation; this new orientation should therefore also correspond to a potential minimum though not necessarily of the same depth as the original.

Acknowledgements

We are grateful to the National Research Council of Canada for financial support of this research, and for the award of an NRCC Scholarship to W.E.S.

1. F. S. Fawcett and H. E. Rasmussen. J. Am. Chem. Soc. **67**, 1705 (1945).
2. J. E. Anderson. Mol. Cryst. Liq. Cryst. **11**, 343 (1970).
3. W. E. Sanford and R. K. Boyd. Can. J. Chem. **54**, 2773 (1976).
4. G. B. Guthrie, D. W. Scott, W. N. Hubbard, C. Katz, J. P. McCullough, M. E. Gross, K. D. Williamson, and G. Waddington. J. Am. Chem. Soc. **74**, 4662 (1952).
5. D. E. Bacon, N. A. Curry, and S. A. Wilson. Proc. R. Soc. **279**A, 98 (1964).
6. A. Gavezzotti and M. Simonetta. Acta Crystallogr. A**31**, 645 (1975).
7. R. Van Steenwinkel. Naturforsch. **24**a, 1526 (1969).
8. D. E. Woessner. J. Chem. Phys. **36**, 1 (1962).

Can. J. Chem. Downloaded from www.nrcresearchpress.com by 210.87.254.42 on 09/05/12
For personal use only.

Metabolites of bird's nest fungi. Part 8.[1] Some minor metabolites of *Cyathus helenae* and some correlations among the cyathins

WILLIAM A. AYER, LOIS M. BROWNE, JOHN R. MERCER, DAVID R. TAYLOR, AND DALE E. WARD

Department of Chemistry, University of Alberta, Edmonton, Alta., Canada T6G 2G2

Received October 21, 1977

WILLIAM A. AYER, LOIS M. BROWNE, JOHN R. MERCER, DAVID R. TAYLOR, and DALE E. WARD. Can. J. Chem. **56**, 717 (1978).

The isolation and structure determination of neoallocyathin A_4 (**10***a*) is described. Structures are proposed for cyathin A_4 (**11**) and cyathin C_5 (**15**). Methods for the transformation of cyathin A_3 into cyathin B_3, allocyathin B_3, and cyathin C_3 are reported. The isolation of glochidone (**22**) and ergosterol from the mycelium of *Cyathus helenae* is reported.

WILLIAM A. AYER, LOIS M. BROWNE, JOHN R. MERCER, DAVID R. TAYLOR et DALE E. WARD. Can. J. Chem. **56**, 717 (1978).

On décrit l'isolement et la détermination de structure de la néoallocyathine A_4 (**10***a*). On propose des structures pour la cyathine A_4 (**11**) et la cyathine C_5 (**15**). On rapporte aussi les méthodes permettant de transformer la cyathine A_3 en cyathine B_3, en allocyathine B_3 et en cyathine C_3. On rapporte finalement l'isolement de glochidone (**22**) et d'ergostérol à partir du mycélium de *Cyathus helenae*.

[Traduit par le journal]

Can. J. Chem. Downloaded from www.nrcresearchpress.com by 210.87.254.105 on 09/05/12
For personal use only.

In Part 1 of this series (2) we reported the isolation of six new diterpenoids (cyathin A_3, cyathin A_4, cyathin B_3, cyathin B_4, allocyathin A_4, and cyathin C_5) produced when the bird's nest fungus *Cyathus helenae* Brodie (strain Brodie 1500) is grown in liquid culture. The structures of two of these six, cyathin A_3 (**1**), and cyathin B_3 (**2**), and those of allocyathin B_3 (**3**) and cyathin C_3 (**4**), compounds which were not detected in our initial isolation, have previously been reported (3, 4). In this paper we wish to: (*i*) report the isolation and structure determination of another cyathin, neoallocyathin A_4; (*ii*) comment on the structures of cyathin A_4 and cyathin C_5; (*iii*) describe some interconversions of these compounds; (*iv*) report on the antibacterial and antifungal activity of some of the cyathins; (*v*) report the isolation of the triterpene glochidone as well as ergosterol from extracts of the mycelium of *C. helenae*.

Neoallocyathin A_4,[2] $C_{20}H_{30}O_4$, was first detected by mass spectrometry as an impurity present in some samples of cyathin A_3 (**1**) which had been purified (3) by silicic acid chromatography followed by preparative thin-layer chromatography (ptlc) over 10% silver nitrate – silica gel. The mass spectrum of these samples showed, in addition to the peaks for cyathin A_3 (mol. wt. 318), peaks at *m/e* 334 ($C_{20}H_{30}O_4$) and 319 ($C_{19}H_{27}O_4$). This material showed a single spot on tlc using several different solvent systems. Acetylation provided material which again could not be separated by chromatography but the mass spectrum of which showed a peak at *m/e* 418 in addition to the *O,O*-diacetylcyathin A_3 parent peak at *m/e* 402. Alternatively, treatment of the mixture with 2,2-dimethoxypropane under acid catalysis yielded a mixture of acetonides which was separable by ptlc into cyathin A_3 acetonide (**5**) and neoallocyathin A_4 acetonide, shown (*vide infra*) to possess structure **6**.

The ^{1}Hmr, ir, and uv spectra of neoallocyathin A_4 acetonide (see Experimental) are very similar to those of cyathin A_3 acetonide (**5**). Comparison of these spectra indicates the absence of hydroxyl or extra carbonyl functions in neoallocyathin A_4 acetonide and since the ^{1}Hmr spectrum does not show extra absorption associated with hydrogens geminal to oxygen, the 'extra' oxygen is present as a fully substituted ether. The absence of absorption in the δ 2.6–3.1 region of the ^{1}Hmr spectrum (in **5** the protons at C-2, C-5, and C-18 absorb in this region (2)) indicates that the C-3,C-4 double bond is not present. The fully substituted ether must thus be between C-3 and C-4, C-3 and C-5, or C-4 and C-5. Treatment of cyathin A_3 acetonide (**5**) with *one equivalent* of *m*-chloroperbenzoic acid in chloroform gave neoallocyathin A_4 acetonide (**6**) in quantitative yield, proving the presence of the C-3,C-4 oxide. The β-stereochemistry of the oxide depicted in **6** is assigned on the following basis: (*i*) examination of Drieding models indicates that the β-face of **5** is much less hindered than the α-face and, in the absence of proximate oxygen functions, peracid

[1]For Part 7, see ref. 1.

[2]For the system of trivial nomenclature adopted for the cyathins see ref. 2.

Can. J. Chem. Downloaded from www.nrcresearchpress.com by 210.87.254.105 on 09/05/12
For personal use only.

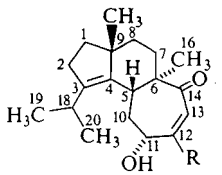

1 R = CH_2OH(C-15)
2 R = CHO(C-15)

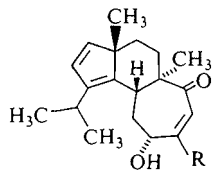

3 R = CH_2OH(C-15)
4 R = CHO(C-15)

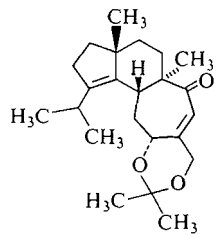

5

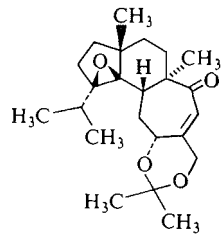

6

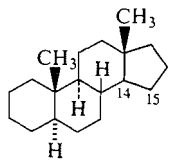

7 14β,15β-Oxide
8 14α,15α-Oxide
9 Δ^{14}

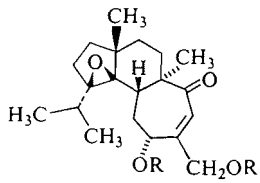

10*a* R = H
10*b* R = Ac

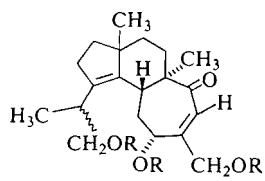

11 R = H
12 R = Ac
13 R = —CO—C$_6$H$_4$—Br

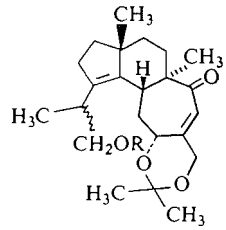

14 R = H

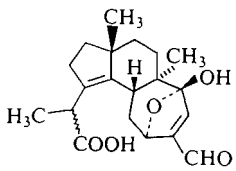

15

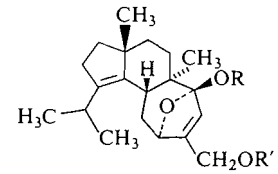

16 R = H, R′ = H
17 R = CH_3, R′ = Ac

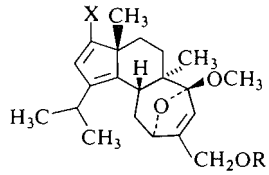

18 X = H, R = Ac
19 X = Br, R = Ac
20 X = H, R = H

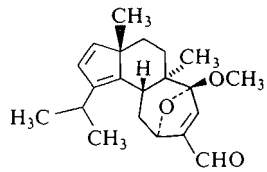

21

oxidation usually occurs from the less hindered side (5); (*ii*) the chemical shift of the C-9 methyl protons in **6** (δ 1.24) is considerably downfield from the same methyl in **5** (δ 1.10). In the androstane series, the C-18 methyl is deshielded (δ 1.14) in the 14β,15β-oxide (**7**) and shielded (δ 0.87) in the 14α,15α-oxide (**8**) relative to androst-14-ene (**9**, δ 0.94) (6). Neoallocyathin A_4, isolated as its acetonide **6** but detected by mass spectrometry as $C_{20}H_{30}O_4$, is thus the epoxy diol **10***a*. Although **10***a* has not been isolated directly from the crude metabolites, a sample of neoallocyathin A_4 (**10***a*) has been obtained by peracid oxidation of *0,0*-diacetylcyathin A_3 (diacetyl derivative of **1**) followed by deacetylation (K_2CO_3–MeOH) of the resulting *O,O*-diacetylneoallocyathin A_4 (**10***b*).

In our earlier publication (2) we reported the isolation of two other $C_{20}H_{30}O_4$ compounds, cyathin A_4 and allocyathin A_4, of which cyathin A_4 was the more fully characterized. More recent liquid cultures of *C. helenae* Brodie (strain Brodie 1500) have failed to produce isolable amounts of these two metabolites. However, the data obtained earlier for cyathin A_4, when considered in the light of the structures since established for cyathins **1**–**4**, allow the assignment of structure **11** to cyathin A_4. Cyathin A_4 forms a triacetyl derivative **12** (2), a crystalline tri-*p*-bromobenzoate **13** (2), and an acetonide **14** (2) which on acetylation affords a monoacetyl derivative. The ^{1}Hmr spectra of the derivatives of cyathin A_4 are very similar to those of the corresponding cyathin A_3 derivatives with the exception that the signals for the isopropyl group in cyathin A_3 are replaced in cyathin A_4 derivatives by signals for the grouping $CH_3—\underset{|}{C}H—CH_2OR$. In *O,O,O*-triacetylcyathin A_4 (**12**) for example, this group appears as a doublet (J = 7 Hz) at δ 0.96 (CH_3 group), a multiplet centered at δ 3.08 (allylic methine), and an eight line signal centered at δ 3.90 for the diastereotopic methylene protons (J = 10.5 Hz) coupled (J = 7.5 Hz) to the methine proton. Simultaneous irradiation at δ 3.08 caused the methyl signal to collapse to a singlet and the methylene signal to collapse to a doublet of doublets (splitting 10.5 Hz). Since all other structural features appear to be the same as those in cyathin A_3 (**1**), cyathin A_4 is assigned structure **11**, with the stereochemistry at C-18 unspecified. Efforts to directly correlate cyathin A_4 with A_3, e.g., via the acetonide **14**, had to be abandoned when we were unable to obtain further quantities of cyathin A_4.

Cyathin C_5, another metabolite which has not been isolated from recent cultures of *C. helenae* but

Can. J. Chem. Downloaded from www.nrcresearchpress.com by 210.87.254.105 on 09/05/12
For personal use only.

which was well characterized (mp, ir, ^{1}Hmr, CHO analysis) in our initial paper (2), appears on the basis of its spectral characteristics to possess structure **15**. The α,β-unsaturated aldehyde system gives rise to singlets at δ 9.89 (C*H*O) and 7.27 (β-proton) in the ^{1}Hmr. The two *tertiary* methyls appear at δ 0.92 and 0.81, but the isopropyl group is not present. Instead a secondary methyl at δ 1.08 which is coupled to a quartet at δ 3.69 indicates the grouping CH_3—CH(COOH)— attached to a double bond. The presence of only two carbonyl peaks in the solid phase ir (1700 carboxylic acid, 1675 cm^{-1}, unsaturated aldehyde) indicates that cyathin C_5 crystallizes in the hemiacetal form and leads to the tentative assignment of structure **15**.

We have previously reported on the antimicrobial activity of the total crude metabolites of *C. helenae* (2). Further testing has revealed that the components which are mainly responsible for this activity are the α,β-unsaturated aldehydes cyathin B_3 and cyathin C_3.[3] Since cyathin A_3 (**1**) is the major component of the crude metabolites, it was desirable to develop methods for the transformation of cyathin A_3 (**1**) to cyathin B_3 (**2**) and to cyathin C_3 (**4**). In solution cyathin A_3 exists as a mixture of the hydroxyketone form **1** and the tautomeric internal hemiacetal **16**. Selective oxidation of the primary allylic alcohol at C-15 should be possible if the secondary allylic alcohol at C-11 is 'protected' as the hemiacetal **16**. Infrared spectra determined in $CHCl_3$ and CH_2Cl_2 indicate the presence of a considerable amount of the hydroxyketone tautomer **1** but spectra determined in ether showed essentially no carbonyl absorption. Whereas oxidation with manganese dioxide in the former solvents led to a mixture of products, oxidation of cyathin A_3 with activated manganese dioxide (7) *in ether* gave cyathin B_3 (**2**) as the only product in better than 80% yield.

The transformation of cyathin A_3 (**1**) into cyathin C_3 (**4**) involves the introduction of a double bond into ring A as well as oxidation of the primary alcohol to the corresponding aldehyde. Because of the sensitivity of the unsaturated aldehyde function to both oxidation and Michael-type additions (4) we chose first to form the cyclopentadiene system, then perform the oxidation, i.e. to proceed via allocyathin B_3 (**3**) rather than via cyathin B_3 (**2**). To protect the ring C functionality, the starting material

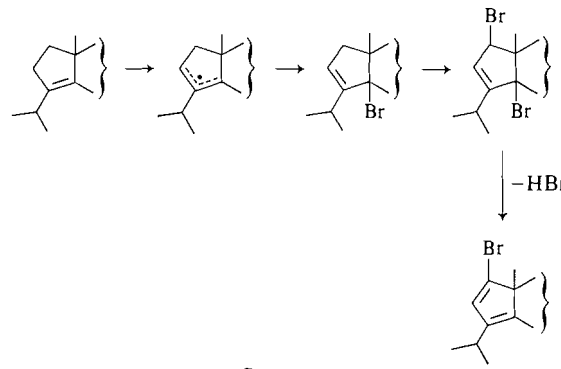

SCHEME 1

chosen was *O*-acetylcyathin A_3 methyl acetal (**17**) (3). Treatment of **17** with *N*-bromosuccinimide (1 equiv.) in refluxing carbon tetrachloride in the presence of a catalytic amount of benzoyl peroxide gave a mixture of two products along with recovered starting material in a ratio of ca. 1:1:1. The two products, which could be separated from starting material using $AgNO_3$ – silica gel, but which could not be separated from one another, proved to be a mixture of the desired **18** and its bromo derivative **19**. All attempts to stop the reaction at the monobromination stage were unsuccessful. However, treatment of **17** with just over 2 equiv. of *N*-bromosuccinimide led to the formation of the bromo compound **19**,[4] in good yield. The formation of the bromo diene, for which there is ample precedent (8), may involve double allylic bromination and elimination of HBr as illustrated in Scheme 1.

Treatment of **19** with an excess of the reagent prepared from $LiAlH(OCH_3)_3$ and CuI in THF (9) gave allocyathin B_3 methyl acetal (**20**) in 76% yield. Acid catalyzed hydrolysis of the methyl acetal **20** gave allocyathin B_3 (**3**). Oxidation of **20** with MnO_2 in ether gave cyathin C_3 methyl acetal (**21**) which on hydrolysis afforded cyathin C_3 (**4**). Cyathin C_3 (**4**) was also obtained by MnO_2 oxidation of allocyathin B_3 (**3**).

The cyathins are isolated by extraction of the culture broth of *C. helenae* after removal of the mycelium by filtration. Soxhlet extraction of the mycelium with ethyl acetate does not yield detectable amounts of cyathins but does give after chromatography a small amount of ergosterol along with larger quantities of a triterpenoid $C_{30}H_{46}O$, mp 158–160.5°C, identified from its melting point and

[3]Details of the in vitro antimicrobial activity of these compounds, determined by the Smith, Kline, French Laboratories, Philadelphia, are submitted as Appendix 1, which is available, at a nominal charge, from the Depository of Unpublished Data, CISTI, National Council of Canada, Ottawa, Ont., Canada K1A 0S2. Recent results show that the activity of these compounds is not retained in vivo.

[4]Our preference for the location of the bromine at C-1 rather than at C-2 is based on ^{13}Cmr studies which reveal that the carbon carrying the bromine resonates at δ 134.5. Chemical shift assignments for the ^{13}Cmr spectra of the various cyathins and derivatives have been made and will be detailed in a separate paper. The assignment of the position of the bromine (C-1 or C-2) is not crucial for present purposes.

spectral characteristics as glochidone, **22** (10). Identity was confirmed by comparison with an authentic sample.[5]

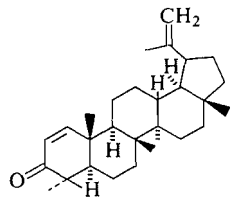

22

Experimental

Mass spectra were recorded on an A.E.I. model MS-50, MS-9, or MS-12 mass spectrometer and are reported as *m/e* (relative intensity). Unless diagnostically significant only peaks at least 20% as intense as the base peak are reported. Infrared spectra were recorded on a Unicam SP1000 or Perkin-Elmer model 421 dual grating spectrophotometer, uv spectra on a Cary model 14M spectrophotometer, cd spectra on a Jasco model SS-20-2 spectropolarimeter, and optical rotations on a Perkin-Elmer Model 141 automatic polarimeter. Proton magnetic resonance spectra were measured using a Varian HA-100 spectrometer with tetramethylsilane as internal standard. Melting points were recorded on a Fisher-Johns melting point apparatus and are uncorrected.

Silica gel tlc plates were 0.5 mm silica gel G (E. Merck, Darmstadt) containing 1% electronic phosphor (General Electric, Cleveland); materials were detected by spraying with 30% sulfuric acid and charring. All solvents were reagent grade and were distilled before use. Skellysolve B refers to Skelly Oil Company light petroleum, bp 62–70°C.

Isolation of Neoallocyathin A_4 Acetonide

The crude metabolites (1.01 g) of *C. helenae*, isolated as previously described (2), were chromatographed over silicic acid (Mallinckrodt, 100 mesh, 68 g) using 1.5% CH_3OH in $CHCl_3$ as eluant. Eighteen 125 ml fractions were collected. Fractions 9, 10, and 11 all showed peaks at *m/e* 334 in the mass spectrum and were combined (215 mg) and subjected to ptlc (20 × 100 cm plate, 0.5 mm layer of silica gel G (E. Merck) containing 5% added inorganic phosphor) using acetone – Skellysolve B (7:3) as the solvent system. The band centered at R_f 0.66 was removed and eluted with ether to give a clear oil (57 mg). This latter material was again subjected to ptlc (20 × 20 cm plate, 0.5 mm silica gel G impregnated with 10% $AgNO_3$) using acetone – Skellysolve B (7:3). After drying, the plate was sprayed lightly with 2′,7′-dichlorofluorescein and observed under long wave uv light. Two bands were observed, one at R_f 0.59 and one at R_f 0.50. The band at R_f 0.59 gave a clear oil (15 mg) when eluted with ether. Mass spectrometry of this fraction indicated a mixture of compounds $C_{20}H_{30}O_4$ and $C_{20}H_{30}O_3$. The material at R_f 0.50 (18 mg) was shown (ir, ms) to be allocyathin B_3 (**3**). The material of R_f 0.59 was dissolved in 2,2-dimethoxypropane (2 ml) and *p*-toluenesulfonic acid (~1 mg) added. After standing 30 min at room temperature the solution was concentrated and then applied to a ptlc plate (silica gel G) which was developed with benzene – acetone – acetic acid (75:25:1). The major fraction (R_f 0.57, 9 mg) was subjected to further ptlc (silica gel G) using Skellysolve B – acetone (4:1) as developing solvent. Bands were observed at R_f 0.59 and 0.49. Elution of the band at higher R_f gave cyathin A_3 acetonide (**5**, 5 mg) and elution of the lower R_f material gave neoallocyathin A_4 acetonide (**6**, 3 mg), mp 144.5–146°C (from ether–pentane). Mass spectrum: *m/e* 374 (45, M^+), 359 (11), 189 (26), 149 (21), 79 (25), 61 (30), 43 (100); cd (*C* 0.001 *M*, CH_3OH) $\Delta\varepsilon_{300}$ −0.18, $\Delta\varepsilon_{270}$ −0.23; ir ($CHCl_3$): 1685 (sh), 1635 (s); ^{1}Hmr ($CDCl_3$) δ: 1.03 (s, 3H, C-16 CH_3), 1.08 (apparent t, 6H, isopropyl CH_3's), 1.24 (s, 3H, C-17 CH_3), 1.40, 1.50 (each 3H singlets, acetonide methyls), 4.15–4.35 (m, 3H, C-15 and C-11 H's), 7.25 (bs, 1H, C-13 H); uv (CH_3OH) λ_{max} (ε): 232 (12 000), 322 (100). *Exact mass* calcd. for $C_{23}H_{34}O_4$: 374.2457; found: 374.2452.

Cyathin A_3 Acetonide (5)

Cyathin A_3 (**1**, 18 mg) was dissolved in 2,2-dimethoxypropane (5 ml) and a small crystal of *p*-toluenesulfonic acid added. The reaction was complete in 15 min as judged by tlc. The solvent was reduced in volume (ca. 0.5 ml) and the reaction mixture was applied directly to a 20 × 20 cm silica gel tlc plate and developed with Skellysolve B – acetone (7:3), R_f 0.51. Elution gave cyathin A_3 acetonide (**5**, 14 mg) as a crystalline solid. Mass spectrum: *m/e* 358 (100, M^+), 343 (49), 315 (25), 300 (22), 285 (88), 257 (52), 203 (40), 189 (37), 149 (30), 123 (32), 121 (31), 119 (31), 107 (30), 105 (37), 96 (50), 91 (31), 55 (45); ir ($CHCl_3$): 1660 (α,β-unsaturated ketone): ^{1}Hmr ($CDCl_3$): δ 0.98 and 1.01 (each 3H doublets, isopropyl methyls), 1.04 (s, 3H), 1.09 (s, 3H), 1.38 and 1.45 (each 3H's, acetonide methyls), 2.90 (septet, 1H, C-18 H), 4.30 (m, 2H, C-15 H's), 5.69 (bs, 1H, C-11 H).

Neoallocyathin A_4 Acetonide from Cyathin A_3 Acetonide

Cyathin A_3 acetonide (**5**, 13.5 mg) was dissolved in $CHCl_3$ (5 ml) and a solution of *m*-chlorobenzoic acid (6.5 mg) in $CHCl_3$ (6.5 ml) was added. The solution was stirred at room temperature for 5 min, then the $CHCl_3$ solution was washed with aqueous $NaHCO_3$, H_2O, and brine. Evaporation of the solvent gave a clear oil (13.6 mg) which was crystallized from ether–pentane to give colorless crystals (8 mg), mp 144.5–146°C, identical (ir, ^{1}Hmr, tlc) with neoallocyathin A_4 acetonide described above.

O,O-*Diacetylneoallocyathin A_4 (10b)*

O,O-Diacetylcyathin A_3 (3) (100 mg) in CH_2Cl_2 (5 ml) was treated with *m*-chloroperbenzoic acid (55 mg) at room temperature for 30 min, then the solution was washed (aqueous $NaHCO_3$, H_2O) and evaporated to give *O,O*-diacetylneoallocyathin A_4 (**10***b*) as an oil (93 mg); ir (neat): 1748, 1660 cm^{-1}; ^{1}Hmr ($CDCl_3$) δ: 1.05 (s, 3H, C-16 CH_3), 1.06 (d, 3H, J = 7 Hz), and 1.07 (d, 3H, J = 7 Hz, isopropyl methyls), 1.28 (s, 3H, C-17 CH_3), 2.02 and 2.11 (acetyl methyls), 4.65 (m, 2H, C-15 H's), 5.39 (m, 1H, C-11 H), 6.13 (bs, 1H, C-13 H). *Exact mass* calcd. for $C_{24}H_{34}O_6$: 418.2355; found: 418.2355.

Neoallocyathin A_4 (10a)

O,O-Diacetylneoallocyathin A_4 (40 mg) was dissolved in CH_3OH (4 ml) and K_2CO_3 (20 mg) was added. After 30 min tlc indicated that the reaction was complete. The mixture was diluted with H_2O and extracted with $CHCl_3$ to give neoallocyathin A_4 (**10***a*) as an oil; ir (neat): 3400 br, 1642 br; ^{1}Hmr ($CDCl_3$) δ: 1.01 (s, 3H, C-16 CH_3), 1.06 (d, 3H, J = 7 Hz) and 1.10 (d, 3H, J = 7 Hz, isopropyl methyls), 1.24 (s, 3H, C-17 CH_3), 4.0–4.5 (m, 3H, C-11 and C-15 H's), 6.03 (bs, 1H, C-13 H). *Exact mass* calcd. for $C_{20}H_{30}O_4$: 334.2144; found: 334.2138.

Cyathin A_4 (11) and Cyathin C_5 (15)

These compounds and their derivatives have been described earlier (2). To further characterize cyathin A_4, the infrared

[5]We wish to thank W. H. Hui (10*b*) for a sample of glochidone.

Can. J. Chem. Downloaded from www.nrcresearchpress.com by 210.87.254.105 on 09/05/12
For personal use only.

Can. J. Chem. Downloaded from www.nrcresearchpress.com by 210.87.254.105 on 09/05/12
For personal use only.

spectrum of the tribromobenzoate, and the ^{1}Hmr spectrum of the triacetyl derivative are submitted as Appendix 2. The infrared spectrum of cyathin C_5 is also included in Appendix 2. These spectra are available from the Depository of Unpublished Data.[6]

Cyathin B_3 (2) from Cyathin A_3 (1 ⇄ 16)

Cyathin A_3 (103 mg) was dissolved in ether (40 ml) and activated (7) manganese dioxide (750 mg) was added. The mixture was stirred at room temperature for 2 h, then filtered and the filtrate evaporated to yield a colorless oil (80 mg) which solidified on standing. The product was identified as cyathin B_3 by comparison (ir, ms, tlc) with an authentic sample.

O-Acetyl-1-bromoallocyathin B_3 Methyl Acetal (19)

O-Acetylcyathin A_3 methyl acetal (**17**, 75 mg) was dissolved in CCl_4 (8 ml) and *N*-bromosuccinimide (75 mg) and a trace of benzoyl peroxide (~1 mg) was added. The mixture was stirred under reflux for 3 h, then filtered, evaporated, and the residue subjected to ptlc (silica gel, Skellysolve B – acetone (3:1)) to give **19** (75 mg) as an oil which was used in the next step without further purification; ^{1}Hmr ($CDCl_3$) δ: 0.82 (s, 3H) and 0.97 (s, 3H) (C-16 and C-17 methyls), 1.04 (d, J = 7 Hz, 3H) and 1.10 (d, J = 7 Hz, 3H) isopropyl methyls, 2.09 (s, 3H, acetyl methyl), 3.21 (s, 3H, ketal methyl), 4.77 (m, 3H, C-11 and C-15 H's), 6.14 (m, 1H, C-13 H), 6.35 (s, 1H, C-2 H). *Exact mass* calcd. for $C_{23}H_{31}O_4{}^{79}Br$: 450.1405; found: 450.1399; calcd. for $C_{23}H_{31}O_4{}^{81}Br$: 452.1385; found: 452.1389.

Allocyathin B_3 Methyl Acetal 20 from 19

Lithium trimethoxyaluminum hydride (3 ml, 1.04 *M*) in tetrahydrofuran (THF) was added dropwise to cuprous iodide (290 mg) in THF (0.6 ml) at 0°C under nitrogen. After a few drops had been added, the mixture became yellowish-brown and viscous. Further THF (~0.5 ml) was added to allow efficient stirring. This process was repeated until all of the $Li(OCH_3)_3AlH$ solution had been added. The mixture was then stirred at 0°C for 15 min to give a dark brown solution. The bromodiene **19** (80 mg) in THF (0.5 ml) was added. After stirring for 5 min at 0°C the solution was allowed to warm to room temperature and was stirred for 8 h, then CH_3OH (1 ml) was added dropwise, followed by H_2O (0.1 ml). The solution was diluted with ether, filtered through Celite, and washed successively with saturated NH_4Cl solution and brine. Drying ($MgSO_4$) and evaporation of the solvents left an oil which was purified by ptlc (silica gel, Skellysolve B – acetone (3:1)) to give allocyathin B_3 methyl acetal (**20**, 45 mg), identical (tlc, ir, ms) with an authentic sample.

Cyathin C_3 Methyl Acetal (21) from (20)

Allocyathin B_3 methyl acetal (**20**, 20 mg) in ether (2 ml) was stirred with activated manganese dioxide (100 mg) at room temperature for 30 h. Filtration and evaporation of solvent gave cyathin C_3 methyl ketal (**21**, 18 mg), identical with an authentic sample.

Allocyathin B_3 (3) from 20

The ketal **20** (40 mg) was dissolved in THF (4 ml) and 1 *N* aqueous perchloric acid (0.5 ml) was added and the solution was stirred at room temperature for 5 days after which time tlc showed only the desired **3**. The solution was diluted with saturated aqueous $NaHCO_3$ and extracted with $CHCl_3$. Evaporation of the solvent gave allocyathin B_3 (**3**, 32 mg) as an oil, identical (tlc, ir, ms) with authentic material. Oxidation of **3** with MnO_2–ether as described above yielded cyathin C_3 (**4**).

Isolation of Glochidone and Ergosterol

The mycelium from 6 ℓ of culture broth, grown as previously described (2), was placed in a Soxhlet thimble and extracted for 3 days with ethyl acetate. The ethyl acetate extract was washed with water, dried ($MgSO_4$), and concentrated to give a brown oil (6.6 g). A portion (2 g) of the crude extract was chromatographed over silica gel (Woelm, < 0.063 mm). Elution with CH_2Cl_2 (1 ℓ) gave glochidone (**22**, 1.0 g), mp 158–160.5°C, (lit. (10*a*) mp 164°C), identical (mmp, tlc, ir) with an authentic sample. Further elution with methylene chloride (1 ℓ) gave ergosterol (0.03 g), identical (tlc, ir), with an authentic sample.

[6]Photocopies may be obtained at a nominal charge from the Depository of Unpublished Data, CISTI, National Research Council of Canada, Ottawa, Ont., Canada K1A 0S2.

Acknowledgements

The financial assistance of the National Research Council of Canada is gratefully acknowledged. One of us (D.E.W.) thanks the National Research Council of Canada for a postgraduate scholarship.

1. W. A. AYER and S. FUNG. Tetrahedron, **33**, 2771 (1977).
2. A. D. ALLBUTT, W. A. AYER, H. J. BRODIE, B. N. JOHRI, and H. TAUBE. Can. J. Microbiol. **17**, 1401 (1971).
3. W. A. AYER and H. TAUBE. Can. J. Chem. **51**, 3842 (1973).
4. W. A. AYER and L. L. CARSTENS. Can. J. Chem. **51**, 3157 (1973).
5. H. O. HOUSE. Modern synthetic reactions. 2 ed. W. A. Benjamin, Inc., Menlo Park, CA. 1972. pp. 302–306.
6. N. S. BHACCA and D. H. WILLIAMS. Application of NMR spectroscopy in organic chemistry. Illustrations from the steroid field. Holden-Day, Inc., San Francisco, CA. 1964. Chapt. 2.
7. I. M. GOLDMAN. J. Org. Chem. **34**, 1979 (1969).
8. L. HORNER and E. H. WINKELMANN. *In* Newer methods of preparative organic chemistry. Vol. 3. *Edited by* W. Foerst. Academic Press, New York, NY. 1964. pp. 151–198.
9. S. MASAMUNE, P. A. ROSSY, and G. S. BATES. J. Am. Chem. Soc. **95**, 6452 (1973).
10. (*a*) A. K. GANGULY, T. R. GOVINDACHARI, P. A. MOHAMED, A. D. RAMIMTULLA, and N. VISWANATHAM. Tetrahedron, **22**, 1513 (1966); (*b*) W. H. HUI and M. L. FUNG. J. Chem. Soc. (C), 1710 (1969).

Preparation of two acidic metabolites of timolol

PATRICE C. BÉLANGER

Department of Medicinal Chemistry, Merck Frosst Laboratories, P.O. Box 1005, Pointe Claire – Dorval, P.Q., Canada H9R 4P8

Received October 17, 1977

PATRICE C. BÉLANGER. Can. J. Chem. **56**, 722 (1978).

The preparation of two acidic metabolites of timolol, 2-[4-(4-morpholinyl)-1,2,5-thiadiazol-3-yloxy]acetic acid and *d,l*-3-[4-(4-morpholinyl)-1,2,5-thiadiazol-3-yloxy]lactic acid is reported using 3-chloro-4-(4-morpholinyl)-1,2,5-thiadiazol as starting material.

PATRICE C. BÉLANGER. Can. J. Chem. **56**, 722 (1978).

La préparation de deux métabolites acides de timolol, l'acide [(morpholinyl-4)-4-thiadiazol-1,2,5-yl-3-oxy]-2-acétique et l'acide *d,l*-[(morpholinyl-4)-4-thiadiazol-1,2,5-yl-3-oxy]-3-lactique y est rapporté en employant comme produit de départ le chloro-3-(morpholinyl-4)-4-thiadiazole-1,2,5.

Introduction

Timolol **1**, (*S*)-1[(1,1-dimethylethyl)amino]-3-{[4-(4-morpholinyl)-1,2,5-thiadiazol-3-yl]oxy}-2-propanol is a β-adrenergic blocking agent (1, 2) with antihypertensive (3) and antianginal properties (4). It is rapidly absorbed, metabolized, and excreted in man, rats, and dogs (5). The two most important sites of metabolic attack are the amine side chain and the morpholinyl group, respectively. Degradation of the (1,1-dimethylethyl)amino-2-hydroxypropoxy chain leads to the acidic metabolites **2** and **3**. Structural assignment for the metabolites was based primarily on mass spectral evidence (5) and on electrophoresis.

In this paper, syntheses of the two acidic metabolites formed by the degradation of the amine side chain, 2-[4-(4-morpholinyl)-1,2,5-thiadiazol-3-yloxy]-acetic acid **2** and 3-[(4-morpholinyl)-1,2,5-thiadiazol-3-yloxy]lactic acid **3** are reported. The latter, while presumably an optically active metabolite, was prepared as the racemate.

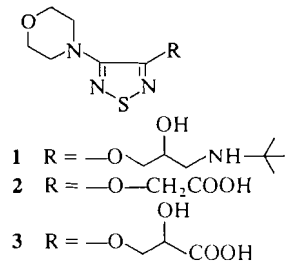

Results and Discussion

Initially for the preparation of **2** and **3**, condensation of the anion of 3-hydroxy-4-(4-morpholinyl)-1,2,5-thiadiazole **4** with either chloroacetic **5***a* or β-chlorolactic acid **5***b* was attempted, using procedures previously reported for substituted phenols (6) or for metabolites of propanolol (7). The best conditions were found to be heating equimolar amounts of **4** with the corresponding halo acid **5** and 2 equiv. of aqueous sodium hydroxide for several days. Reaction (as monitored by disappearance of starting material **4**) was slow and extensive decomposition occurred. Yields of the corresponding acidic metabolites **2** and **3** were only 2 and 4%, respectively.

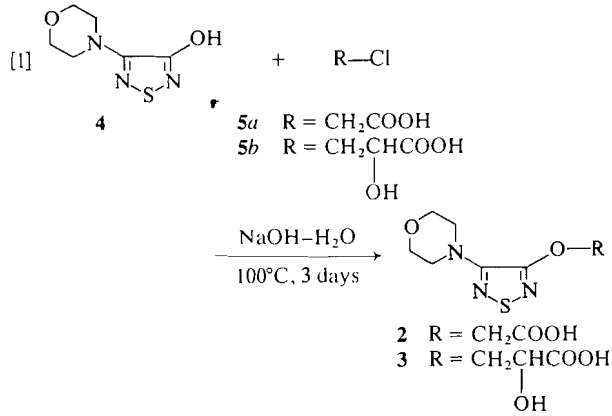

The low yields are probably explicable based on the reduced reactivity of the chloro substituted carboxylic acids in the anion form and on the tautomeric nature of the 4-(4-morpholinyl)-1,2,5-thiadiazol-3(2*H*)one which permits alkylation to occur on either the oxygen or the nitrogen atom. Other examples of low yields on alkylation of a hydroxy-1,2,5-thiadiazole are known.[1]

In an alternative approach, treatment of 3-chloro-4-(4-morpholinyl)-1,2,5-thiadiazole **6** with 2,2-dimethyl-1,3-dioxolane-4-methanol in DMF with potassium *tert*-butoxide as base at 110°C for 6 h led to good yields of **7**. Hydrolysis of the resulting acetonide **7** in dilute hydrochloric acid gave crystalline diol **8** in nearly quantitative yield. Cleavage of the diol **8** to the aldehyde **9** was achieved with lead tetraacetate in benzene at room temperature (8) in nearly quantitative yield. Sodium metaperiodate was

[1]Merck Frosst Laboratories. Unpublished results.

Can. J. Chem. Downloaded from www.nrcresearchpress.com by 210.87.254.105 on 09/05/12
For personal use only.

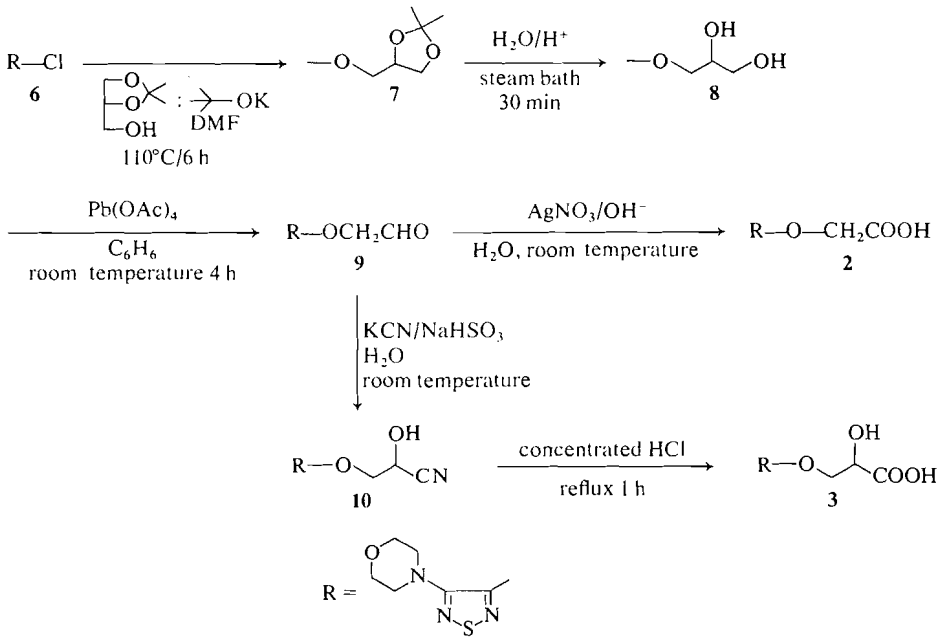

SCHEME I

also effective for the cleavage but the yields were much lower and less reproducible. The conversion of **9** to metabolite **2** occurred smoothly in 47% yield by silver oxide oxidation (9). Transformation of **9** to the racemic metabolite **3** was done through the cyanohydrin reaction followed by hydrochloric acid hydrolysis. These reactions are summarized in Scheme I; the mass spectra of synthetic **2** and **3** and the electrophoretic behavior were identical with those of metabolites **2** and **3**.

The synthetic compounds **2** and **3** were found to be inactive as β-adrenergic blocking agents or antihypertensive agents.

Experimental

Melting points were taken on a Thomas Hoover apparatus and are uncorrected. Infrared spectra were determined on a Perkin-Elmer 257 grating spectrophotometer. A Varian EM-360 instrument was used to record nmr spectra in deuteriochloroform using tetramethylsilane as an internal standard. Elemental analyses were performed by Dr. C. Daesslé. The low resolution mass spectral analyses were performed on a AEI MS 902 mass spectrometer and on an LKB 900 gc–ms spectrometer.

All reactions as well as column chromatography were monitored by tlc using precoated 0.25 mm silica gel plates (Eastman Kodak) with visualization of spots either by uv or by exposure to iodine vapors.

2-[4-(4-Morpholinyl)-1,2,5-thiadiazol-3-yloxy]acetic Acid (2)

3-Hydroxy-4-(4-morpholinyl)-1,2,5-thiadiazole **4** (6.2 g, 33 mmol) and chloroacetic acid (3.2 g, 34 mmol) in 40 ml 1 *N* sodium hydroxide were heated for 3 days on a steam bath. The reaction mixture was acidified and unreacted **4** (1.7 g), mp 190°C, was recovered. On evaporation of the filtrate to half volume, crude **2** was obtained which on recrystallization from water afforded 70 mg, mp 174–176°C, homogeneous by tlc, R_f: 0.6 (chloroform–methanol–ammonia 8:4:0.5 by volume); ir: COOH 1765 cm^{-1}; ^1H nmr δ: 4.95 (2, s, CH_2CO), 3.68 (4H, m, CH_2—N—CH_2), 3.80 (4H, m, CH_2—O—CH_2); ms: M^+ 245. *Anal.* calcd. for $C_8H_{11}N_3O_4S$: C 39.18, H 4.52, N 17.14, S 13.07; found: C 39.27, H 4.74, N 17.01, S 12.93.

d,l-*3-[4-(4-Morpholinyl)-1,2,5-thiadiazol-3-yloxy]lactic Acid (3)*

Similarly, the reaction of **4** with β-chlorolactic acid led to 3.0 g of unreacted **4** and to a residue after evaporation of the filtrate to dryness. This residue was dissolved in ethanolic HCl and refluxed 3 h. On evaporation to dryness, 2.4 g of an oil was obtained and tlc analysis showed it to be a mixture of seven components. Silica gel chromatography with chloroform elution was performed, taking fractions of 10 ml. The desired ester was found to be between tubes 41 and 61. These fractions were combined and 342 mg of an oil was obtained. This ester was hydrolysed with sodium hydroxide in methanol. The residue after evaporation was acidified with aqueous HCl and the mixture extracted several times with chloroform to yield 196 mg of **3**, mp 134–135°C after crystallization from chloroform–hexane (1:5 v/v); tlc, R_f: 0.5 (chloroform–methanol–ammonia 8:4:0.5 by volume); ir: COOH, 1732 cm^{-1}; ^1H nmr δ: 3.52 (4H, m, CH_2NCH_2), 3.72 (4H, m, CH_2OCH_2), 4.60 (3H, m, CHO and CH_2O); ms: M^+ 275. *Anal.* calcd. for $C_9H_{13}N_3O_5S$: C 39.27, H 4.76, N 15.26, S 11.65; found: C 39.63, H 5.01, N 15.13, S 11.91.

4-[4-(2,2-Dimethyl-1,3-dioxolan-4-yl)methoxy]-3-(4-morpholinyl)-1,2,5-thiadiazole (7)

3-Chloro-4-(4-morpholinyl)-1,2,5-thiadiazole (10) (41 g, 0.21 mol), 2,2-dimethyl-1,3-dioxolan-4-ylmethanol (11) (28 g, 0.21 mol), and potassium *tert*-butoxide (30 g, 0.26 mol) in 200 ml dimethyl formamide were heated in an oil bath at 110°C for 6 h. The mixture was poured into water (1000 ml) and extracted twice with ethyl acetate (2 × 1000 ml). The extract after washing with water, drying over magnesium sulfate was concentrated under vacuum to give 39.6 g (66%) of **7** as an oil

Can. J. Chem. Downloaded from www.nrcresearchpress.com by 210.87.254.105 on 09/05/12
For personal use only.

Can. J. Chem. Downloaded from www.nrcresearchpress.com by 210.87.254.105 on 09/05/12
For personal use only.

that distilled at 165–170°C/1 Torr; tlc, R_f: 0.7 (ethyl acetate); ^{1}H nmr δ: 1.37 and 1.43 (6H, s, CH_3), 3.60 (4H, m, CH_2NCH_2), 3.72 (4H, m, CH_2OCH_2), 4.50 (5H, m, CH_2O, CHO); ms: M^+ 301. *Anal.* calcd. for $C_{12}H_{19}N_3O_4S$: C 47.83, H 6.37, N 13.94, S 10.64; found: C 47.41, H 6.67, N 14.08, S 10.54.

3-[4-(4-Morpholinyl)-1,2,5-thiadiazol-3-yloxy]-1,2-propanediol (8)

4-[4-(2,2-Dimethyl-1,3-dioxolan-4-yl)methoxy]-3-(4-morpholinyl)-1,2,5-thiadiazole (**7**) (37.3 g, 0.125 mol), water (100 ml), and concentrated hydrochloric acid (3 ml) were heated on a steam bath for 30 min until a one-phase system was obtained. The water was removed under vacuum and the yellow solid residue after trituration in 200 ml benzene gave compound **8** (31.1 g, 95.6%), mp 95–96°C; tlc, R_f: 0.2 (ethyl acetate); ir:—OH, 3380 cm^{-1}; ^{1}H nmr (DMSO-d_6) δ: 3.50 (4H, m, CH_2NCH_2), 3.70 (4H, m, CH_2OCH_2), 4.40 (5H, m, CHO— and CH_2O—); ms: M^+ 261. *Anal.* calcd. for $C_9H_{15}N_3O_4S$: C 41.37, H 5.79, N 16.08, S 12.27; found: C 41.19, H 5.95, N 15.99, S 12.02.

2-[4-(4-Morpholinyl)-1,2,5-thiadiazol-3-yloxy]acetaldehyde (9)

3-[4-(4-Morpholinyl)-1,2,5-thiadiazol-3-yloxy]-1,2-propanediol (**8**) (8.7 g, 33 mmol) and lead tetraacetate (15.5 g, 35 mmol) in 200 ml benzene were stirred at room temperature for 4 h. The solids were filtered and the filtrate washed with water, dried over magnesium sulfate, and concentrated under vacuum to yield 7.5 g of **9** as a yellow oil, homogeneous by tlc, R_f: 0.2 (ethyl acetate); ir: C=O, 1735 cm^{-1}; ^{1}H nmr ($CDCl_3$) δ: 3.57 (4H, m, CH_2NCH_2), 3.75 (4H, m, CH_2OCH_2), 5.00 (2H, s, CH_2O), 9.80 (1H, s, CHO); ms: M^+ 229. *Anal.* calcd. for $C_{14}H_{15}N_7O_6S$: C 41.08, H 3.69, N 23.95, S 7.83; found: C 40.88, H 3.90, N 23.84, S 7.63.

2-[4-(4-Morpholinyl)-1,2,5-thiadiazol-3-yloxy]acetic Acid (2)

2-[4-(4-Morpholinyl)-1,2,5-thiadiazol-3-yloxy]acetaldehyde **9** (6.7 g, 29 mmol) was suspended in 100 ml water and freshly made silver oxide, prepared from 25 g silver nitrate and 100 ml 2 *N* sodium hydroxide, was added. After stirring for 20 min, the solids were removed by filtration and the filtrate evaporated to 75 ml. Following refiltration and acidification with 6 *N* HCl, compound **4** was obtained, which after washing with water and air drying, weighed 3.2 g (47%), mp 180–181°C.

(D,L)-*3-[4-(4-Morpholinyl)-1,2,5-thiadiazol-3-yloxy]lactonitrile (10)*

2-[4-(4-Morpholinyl)-1,2,5-thiadiazol-3-yloxy]-acetaldehyde **9** (7.9 g, 34.5 mmol) was suspended in 100 ml water. Potassium cyanide (3 g, 45 mmol) was added, followed by sodium bisulfite (5 g, 48 mmol). After stirring 10 min at room temperature, a solid precipitated, which was filtered, washed with cold water, and air dried. 3-[4-(4-Morpholinyl)-1,2,5-thiadiazol-3-yloxy]lactonitrile **12**, (5.7 g, 65%), mp 70–71°C, was obtained. This was probably a hydrate as a dried sample melted at 101°C; tlc, R_f: 0.5 (ethyl acetate – benzene 1:1); ir: OH, 3190 cm^{-1}, CN not detected; ^{1}H nmr ($CDCl_3$) δ: 3.50 (4H, m, CH_2NCH_2), 3.82 (4H, m, CH_2OCH_2), 4.60 (2H, m, CH_2O), 4.85 (1H, m, CHO); ms: M^+ 256, base peak 229 (loss of HCN). *Anal.* calcd. for $C_9H_{12}N_4O_3S$: C 42.18, H 4.72, N 21.86, S 12.51; found: C 42.11, H 5.04, N 22.32, S 12.89.

(D,L)-*3-[4-(4-Morpholinyl)-1,2,5-thiadiazol-3-yloxy]lactic Acid (3)*

(D,L)-3-[4-(4-Morpholinyl)-1,2,5-thiadiazol-3-yloxy]lactonitrile **12** (4.1 g, 16 mmol) in concentrated hydrochloric acid (25 ml) was refluxed for a period of 1 h. The solution was poured into water (50 ml) and extracted twice with ethyl acetate (75 ml). The ethyl acetate extract was washed with water, dried over magnesium sulfate, and concentrated under vacuum to yield an oil that crystallized when triturated in petroleum ether. On filtration compound **3** was obtained (2.7 g, 61%), mp 137–138°C.

Acknowledgements

The author extends his appreciation to Mr. R. E. Rhodes of Merck Sharp & Dohme Research Laboratories, West Point, PA and to Dr. W. J. A. Vanden Heuvel for the mass spectra measurements, to Dr. D. Mulvey, Merck Sharp & Dohme Research Laboratories, Rahway, NJ, and to Dr. C. S. Rooney, Merck Frosst Laboratories for useful discussions on thiadiazole chemistry. The author is also grateful to Dr. A. Scriabine and his colleagues of Merck Sharp & Dohme Research Laboratories, West Point, PA for the biological testing of the metabolites.

1. B. K. Wasson, W. K. Gibson, R. S. Stuart, H. W. R. Williams, and C. H. Yates. J. Med. Chem. **15**, 651 (1972).
2. M. Ulryck, J. A. Franciosa, and J. F. Conway. Clin. Res. **19**, 343 (1971).
3. M. Ulryck, J. A. Franciosa, and J. F. Conway. Clin. Pharmacol. Ther. **13**, 232 (1972).
4. D. Brailovsky. *In* Beta-adrenergic blocking agents in the management of hypertension and angina pectoris. *Edited by* B. Magnani. Raven Press, New York, NY. 1974. p. 117.
5. D. J. Tocco, A. E. W. Duncan, F. A. Deluna, H. B. Hucker, V. F. Gruber, and W. J. A. Vanden Heuvel. Drug Metab. Dispos. **3**, 361 (1975).
6. I. Csiba, L. Krasmed, and M. Stuchlik. Cesk. Farm. **17**, 28 (1968); Chem. Abstr. **69**, 67041g (1968).
7. P. A. Bond. Nature, **213**, 721 (1967).
8. F. J. Walf and J. Weijland. Org. Synth. Coll. **4**, 124 (1963).
9. E. Campaigne and W. M. LeSuer. Org. Synth. Coll. **4**, 919 (1963).
10. L. M. Weinstock, P. Davis, B. Handelsman, and R. Tull. J. Org. Chem. **32**, 2823 (1967).

Carbon-13 nuclear magnetic resonance spectra of *N*-, *O*-, and *S*-methylated uracil and thiouracil derivatives

IAN W. J. STILL[1] AND NICK PLAVAC
Department of Chemistry, University of Toronto, Toronto, Ont., Canada M5S 1A1
AND
DAVID M. MCKINNON AND MOHINDER S. CHAUHAN
Department of Chemistry, University of Manitoba, Winnipeg, Man., Canada R3T 2N2
Received August 26, 1977

IAN W. J. STILL, NICK PLAVAC, DAVID M. MCKINNON, and MOHINDER S. CHAUHAN. Can. J. Chem. **56**, 725 (1978).

^{13}C nmr chemical shifts have been recorded for a number of uracil, thiouracil, and pyrimidine derivatives. These data are discussed in relation to what is known of the lactam–lactim tautomerism in such systems and possible correlations of chemical shifts with normal aromatic substituent chemical shift parameters. The chemical shifts for the CH_3 groups in simple methylated derivatives of uracil are very characteristic of the site of methylation and should prove useful as a tool for assigning structures to alkylated derivatives of this general type.

IAN W. J. STILL, NICK PLAVAC, DAVID M. MCKINNON et MOHINDER S. CHAUHAN. Can. J. Chem. **56**, 725 (1978).

On a enregistré les déplacements chimiques en rmn ^{13}C d'un certain nombre de dérivés de l'uracile, du thiouracile et de la pyrimidine. On discute de ces données par rapport à ce qui est connu pour le tautomérisme lactame–lactime dans de tels systèmes et pour des corrélations possibles de déplacements chimiques avec les paramètres de déplacements chimiques normaux pour des substituants aromatiques. Les déplacements chimiques des groupes CH_3 dans des dérivés méthylés simples de l'uracile sont très caractéristiques du site de méthylation et devraient s'avérer utiles dans l'attribution de structures pour des dérivés alkylés de ce type général.
[Traduit par le journal]

Introduction

As part of our continuing investigation of the ^{13}C nmr spectra of heterocyclic systems with sulfur-containing functional groups (1–4), we wish to report a study of the ^{13}C chemical shifts in a number of methylated derivatives of uracil, 2- and 4-thiouracil, and 2,4-dithiouracil. In the interests of clarity, we have categorized these compounds as uracils (*N*-methyl), pyrimidines (*O*- or *S*-methyl), or dihydropyrimidinones (methyl derivatives with only *one* formal C=O or C=S group).

Since the early pioneering work of Lauterbur (5) there have been a number of investigations of the ^{13}C nmr spectra of both pyrimidines (6–8) and uracils (9–11), as well as related ^{13}C nmr studies on both pyrimidine (12, 13) and purine nucleosides (14). In our work, in addition to a study of the effects of methyl substitution at various sites in the uracil **1** structure on ^{13}C chemical shifts, we have attempted to show the utility of these effects for structural assignment purposes. As earlier workers had already noted in the purine series (14), we have observed little difference between the chemical shifts for the ring carbon atoms (with the notable exception of C-6) in the *N*(1)-methyl-substituted uracils, compared to the analogously substituted nucleoside derivatives, and hence our conclusions are likely to be valid for any similar series of alkyl-substituted uracils or uridines.

There has been widespread interest in recent years in the tautomeric stuctures of uracil and the thiouracils (15) and other biological pyrimidines and the subject has been comprehensively reviewed recently (16, 17). The structures of the major tautomeric forms are now well established by a variety of physical methods. We believe that additional evidence in support of the tautomeric structures of uracil and the thiouracils is provided by the present work. The nature of the methylation products of uracil and related nucleic acid constituents with diazomethane has also attracted attention recently, particularly with regard to a possible relationship between the mechanisms of metagenesis and carcinogenesis (18). As we hope to demonstrate in the subsequent discussion, ^{13}C nmr chemical shifts of the CH_3 groups in methylated uracils provide a very effective way of establishing whether methylation has occurred on O-, S-, or N-sites and, in the latter case, whether at N-1 or N-3.

All our ^{13}C nmr spectra were recorded in solution in dimethyl sulfoxide. Previous workers, however,

[1]Author to whom correspondence should be addressed.

Can. J. Chem. Downloaded from www.nrcresearchpress.com by 210.87.254.105 on 09/05/12
For personal use only.

Can. J. Chem. Downloaded from www.nrcresearchpress.com by 210.87.254.105 on 09/05/12
For personal use only.

have studied the effects of solvent on chemical shifts in uridine (19). Although these effects are not large at neutral p*H* for the series of solvents water, pyridine, dimethyl sulfoxide, the C-2 and C-4 carbonyl carbons appear farthest upfield in dimethyl sulfoxide, presumably because of decreased hydrogen bonding effects.

Experimental

Natural abundance proton decoupled ^{13}C nmr spectra were obtained on a Varian XL-100-15 spectrometer at 25.16 MHz, in the pulsed Fourier transform mode. All spectra were recorded in DMSO-d_6 solution and partially coupled spectra were also recorded in all cases. Operating temperature of the probe was 32 ± 3°C. Spectral widths of 6000 Hz were used routinely, with acquisition times of 0.666 s and pulse widths of 12 μs. (A 90° flip angle is equivalent to ca. 55 μs.)

With the exceptions noted below, compounds used in this study were available from the suppliers indicated in the tables: (Aldrich (A), Eastman (EK), Vega-Fox Biochemicals (V-F), or Sigma Chemical Co. (S)), or were synthesized following the literature procedures, also cited in the tables.

2-Chloro-4-methylthiopyrimidine

2,4-Dichloropyrimidine (2.98 g, 0.02 mol) in dimethylformamide (10 ml) and triethylamine (10 ml) was treated with excess methanethiol (~10 ml) with stirring. After 5 min the solution became turbid and a solid deposited. After 4 h the mixture was filtered under strong vacuum to remove excess mercaptan, and poured on ice. A colorless precipitate was collected and recrystallized from petroleum ether (bp 60–80°C) as colorless prisms, mp 60°C (72%); nmr ($CDCl_3$) δ:2.54 (3H, s), 7.08 (1H, d, J = 6.0 Hz, C-5 proton), 8.14 ppm (1H, d, J = 6.0 Hz, C-6 proton); *Anal.* calcd. for $C_5H_5ClN_2S$: C 37.38, H 3.12, Cl 22.12, N 17.67, S 19.94; found: C 37.45, H 3.26, Cl 21.96, N 17.61, S 20.13.

2-Methoxy-4-methylthiopyrimidine

2-Chloro-4-methylthiopyrimidine (0.4 g, 2.5 mmol) was added to a solution of sodium (0.067 g, 2.5 mmol) in methanol (10 ml) and the solution refluxed 1.5 h. The mixture was cooled, diluted with an equal amount of water, and extracted with chloroform (2 × 25 ml). The united extracts were dried over magnesium sulfate and evaporated to give a pale yellow, odoriferous oil. This was not analysed but was sufficiently pure (83%) for nmr studies; nmr ($CDCl_3$) δ:2.50 (3H, s), 3.89 (3H, s), 6.79 (1H, d, J = 6.0 Hz, C-5 proton), 8.12 ppm (1H, d, J = 6.0 Hz, C-6 proton).

Spectral assignments have been based largely on multiplicity and chemical shift correlation arguments, although where necessary fully coupled spectra were obtained to remove any remaining ambiguity (7).

Results and Discussion

^{13}C nmr chemical shifts for a series of 14 uracil and thiouracil derivatives are listed in Table 1. This series includes the four parent uracils and thiouracils, seven of the eight possible mono-*N*-methylated derivatives, and three of the four di-*N*-methylated compounds.

Within any one of the sub-series in Table 1 (uracil, 2-thiouracil, 4-thiouracil, 2,4-dithiouracil) the changes in chemical shift of the ring carbons accompanying *N*-methylation are generally small and, with one exception, less than 2 ppm for C-2, C-4, and C-5. For the uracil derivatives these small chemical shifts were invariably to higher field, but in the various thiouracils no consistent pattern is apparent, with an apparently random distribution of small shielding and deshielding effects observed, probably as the result of competing electronic and steric strain factors.

The C-6 signal in this series of compounds, however, shows a markedly greater sensitivity towards *N*-methylation. Methylation at N-1, in uracil as well as the thiouracils, produces deshielding effects at C-6 ranging between +3.4 and +4.6 ppm. These can be attributed to the β-effect of the methyl group and are in excellent agreement with similar effects observed for *N*-methyl-2-pyridone and its 2-thione analogue (3). In contrast, methylation at N-3 produces shielding effects at C-6 ranging between −1.5 and −2.8 ppm. These may arise from a small *p*-substituent effect of the methyl group in the canonical form **1***a*.

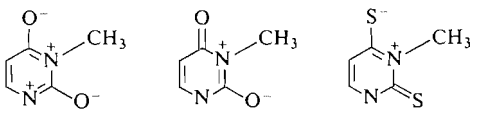

1*a* **1***b* **1***c*

As expected, in the *N*,*N*-dimethylated derivatives the C-6 signal shows only small deshielding effects (+0.9 to +1.6 ppm), reflecting the operation of a combination of the two effects described above.

Undoubtedly the most dramatic effects in Table 1 are those observed for the *N*-methyl carbon signals and these have been summarized in Table 2. Most notably, the position of the N-3 methyl signal appears to be a very sensitive indicator of the presence of one, or two, thiocarbonyl groups at C-2/C-4 since the chemical shift ranges from a maximum of 41.2 ppm in 3-methyl-2,4-dithiouracil to a minimum of 26.4 ppm in 3-methyluracil, with 3-methyl-2-thiouracil showing an intermediate value of 32.9 ppm. Indeed, in the case of 1,3-dimethyl-2,4-dithiouracil the position of this signal reaches a value of 45.9 ppm. This astonishing range of chemical shifts, in such marked contrast to the relative insensitivity of the O—CH_3 and S—CH_3 chemical shifts (see Table 2), likely arises from a combination of the operation of steric strain factors and the anisotropies of the C=O and C=S bonds at C-2/C-4.

In the case of 3-methyluracil the very shielded position observed for this signal is probably due to the importance of canonical forms such as **1***a* and **1***b*, resulting in abnormal shielding of the *N*-methyl

TABLE 1. ^{13}C Chemical shifts[a,b] of uracils and thiouracils, **1**

Compound	C-2	C-4	C-5	C-6	Methyl carbons	Reference No. (source)
Uracil (U)	152.7	165.2	100.9	143.0	—	(EK)
1-Methyl-U	151.2	163.9	100.5	146.4	35.1	(V-F)
3-Methyl-U	151.7	163.4	99.6	140.3	26.4	(V-F)
1,3-Dimethyl-U	151.5[c]	162.8[c]	99.6[c]	144.6[c]	27.1(N-3)[c] 36.3(N-1)[c]	23
2-Thiouracil	175.9	160.9	105.2	142.0	—	(A)
1-Methyl-2-thio-U	176.4	160.4	105.9	146.6	42.0	24
3-Methyl-2-thio-U	176.6	160.4	103.8	140.5	32.9	24
4-Thiouracil	148.6	191.3	111.6	138.3	—	25
1-Methyl-4-thio-U	148.8	190.1	111.7	142.4	36.0	26
1,3-Dimethyl-4-thio-U	149.7	189.8	112.3	139.2	34.7(N-3) 37.4(N-1)	27
2,4-Dithiouracil	172.7	187.6	117.0	136.4	—	(A)
1-Methyl-2,4-dithio-U	173.4	186.4	117.3	140.7	42.8	28
3-Methyl-2,4-dithio-U	174.2	188.2	118.0	133.6	41.2	29
1,3-Dimethyl-2,4-dithio-U	174.7	186.8	117.1	138.0	42.8(N-3) 45.9(N-1)	27

[a]In ppm from TMS.
[b]In dimethyl sulfoxide-d_6.
[c]These data differ significantly from the values reported in ref. 21 (Spectrum No. 170) for 1,3-dimethyluracil in $CDCl_3$. In addition, the assignments of the N—CH_3 signals in that spectrum should be reversed.

TABLE 2. Relation between site of methylation in uracils and ^{13}C chemical shift of CH_3-groups

Compound	δOCH_3[a]	δSCH_3[a]	$\delta N(1)—CH_3$[a]	$\delta N(3)—CH_3$[a]
Uracil	53.7–54.5	—	35.1–36.3	26.4–27.1
2-Thiouracil	—	—	42.0	32.9
4-Thiouracil	54.4	12.0	36.0–37.4	34.7
2,4-Dithiouracil	—	12.1–13.6	42.8–45.9	41.2–42.8

[a]A range of values is quoted (ppm) where data for more than one compound with this structural feature have been obtained.

group. The *N*-methyl carbon signal in *N*-methyl-2 pyridone, for example, appears at 41.8 ppm (3). To explore this point a little farther we examined the model system, *N*-methylmaleimide **2** and found the *N*-methyl signal to occur at 23.3 ppm, in a situation where steric strain effects should be less important than in the six-membered ring case. Turning to the 2,4-dithiouracil case, because of the greater steric bulk of the sulfur atoms, or because of the lesser importance of canonical forms such as **1***c*, the nitrogen at N-3 may prefer to adopt an sp^3 pyramidal configuration. With respect to the latter, it is interesting that the chemical shift of the N-1 methyl signal in *N*-methyl-2-pyridinethione (3) at 46.0 ppm is very close to the chemical shift observed for the methyl signal in *N*-methylpiperidine, 47.9 ppm (20). Of course, since the C=S is significantly longer than the C=O bond, the much greater chemical shift observed for the N-3 methyl signal in the thiouracils may also arise from the location of the N—CH_3 (whether in a planar or a pyramidal configuration) in a deshielding, rather than a shielding, zone of the anisotropic functionality.

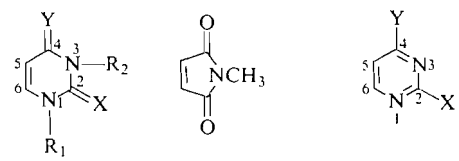

1
X, Y = O or S
R_1, R_2 = H or CH_3

2

3
X, Y = H, OCH_3, SCH_3, Cl

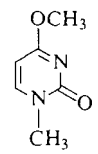

4

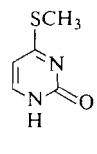

5

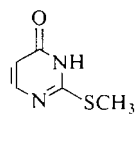

6

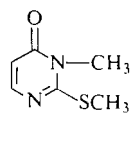

7

As indicated in the introduction, there has been considerable interest in the question of the tautomerism of uracil and related pyrimidines. Inspection of the data in Tables 1 and 3 adds further support to the large body of physical data which already exists (16, 17) in favor of the di-lactam formulation **1**. The positions of the C-2 and C-4 signals in 1,3-dimethyluracil, for example, are much closer to those in the parent compound than are the corresponding signals in 2,4-dimethoxypyrimidine (Table

Can. J. Chem. Downloaded from www.nrcresearchpress.com by 210.87.254.105 on 09/05/12
For personal use only.

TABLE 3. ^{13}C Chemical shifts[a,b] of 2,4-disubstituted pyrimidines, **3**

Substituents							
C-2	C-4	C-2	C-4	C-5	C-6	Methyl carbons	Reference No. (source)
H	H	158.6[c]	157.1[c]	122.1[c]	157.1[c]		(S)
Cl	Cl	161.7	159.5	121.3	162.0		30
OCH_3	OCH_3	165.4	171.3	101.9	159.1	53.7(C-4) 54.5(C-2)	31
SCH_3	SCH_3	170.4	171.1	113.7	154.9	12.1(C-4) 13.6(C-2)	27
OCH_3	SCH_3	164.4	172.5	112.1	157.1	12.0(S—CH_3) 54.4(O—CH_3)	This work
Cl	OCH_3	159.2	170.6	107.5	159.8	54.7	32
Cl	SCH_3	159.5	174.2	117.3	157.4	12.4	This work

[a]In ppm from TMS.
[b]In dimethyl sulfoxide-d_6.
[c]These values are in good agreement (within 2 ppm) with those cited in ref. 6.

TABLE 4. ^{13}C Chemical shifts of dihydropyrimidinones **4–7**

Compound	C-2	C-4	C-5	C-6	Methyl carbons	Reference No. (source)
1-Methyl-4-methoxy-1,2-dihydropyrimidin-2-one(**4**)	155.9	171.1	93.7	149.7	37.0(N—CH_3) 53.5(O—CH_3)	31
4-Methylthio-1,2-dihydropyrimidin-2-one(**5**)	154.3	177.5	101.8	143.1	11.9	33
2-Methylthio-3,4-dihydropyrimidin-4-one(**6**)	167.8	166.0	108.3	153.5	13.0	34
3-methyl-2-methylthio-3,4-dihydropyrimidin-4-one(7)	160.0	163.5	109.2	151.8	14.7(S—CH_3) 29.9(N—CH_3)	35

3). If a correctional factor for *O*-methylation of approximately 5 ppm (based on the data for C-1 in phenol and anisole, (21)) is applied, however, the distinction between the lactam and lactim tautomers at C-4 in uracil becomes rather difficult to determine on the basis of the chemical shifts. The unavailability of further model systems such as 4-methoxy-2-methylthiopyrimidine and 3-methyl-4-thiouracil also make rigorous conclusions regarding the tautomerism of the various thiouracils unwarranted, although again one can generally conclude that the thione and not the thiol tautomers appear to be favored from the data in Tables 1 and 3.

^{13}C nmr data for a number of C-2 and C-4 methoxy- and methylthio-substituted pyrimidines **3** are found in Table 3. These compounds may also be considered to be *O*-methyl or *S*-methyl substituted uracil derivatives. The chemical shift assignments were in most cases obvious from an application of shift effects and signal multiplicities. The C-2 carbon bearing an OCH_3 substituent is generally found at ca. 165 ppm but at lower field when the substituent was SCH_3. The C-4 carbon bearing either OCH_3 or SCH_3 on the other hand is consistently found at $\delta > 170$ ppm. The signal due to C-5 in this series is much more variable than that of C-6. Indeed, the C-5 chemical shifts can be predicted, with a surprising degree of accuracy (± 2.7 ppm), by using the *o*- and *p*-substituent effect parameters from the benzene series for —Cl, —OCH_3(22) and —SCH_3(2) groups at C-2 and C-4. For the other ring carbon atoms in these compounds, however, no simple correlations of this sort can be applied.

As discussed earlier, the OCH_3 and SCH_3 δ values are remarkably constant compared to those for their NCH_3 analogues. In both cases, the C-2 methyl signal is generally found slightly downfield from that at C-4, perhaps as a result of the proximity to both the ring nitrogen atoms. In either case, however, the total range encompassed is little more than 1 ppm.

Data for four compounds **4**, **5**, **6**, and **7**, whose tautomeric structures fall best into the intermediate category of dihydropyrimidinones are included in Table 4. These data require little further comment except to note in passing a relatively deshielded δ value of 14.7 ppm for the S—CH_3 group in **7** and an exceptionally large shielding effect at C-2 (-7.8 ppm), which is probably partly steric in origin, on converting **6** into its 3-methyl derivative. The δ value of 29.9 ppm for the N-3 methyl group in **7** is intermediate between the values of 26.4 and 32.9 in the

Can. J. Chem. Downloaded from www.nrcresearchpress.com by 210.87.254.105 on 09/05/12
For personal use only.

analogous monomethyl derivatives of uracil and 2-thiouracil, respectively.

Our data have demonstrated the large variation in chemical shifts of the *N*-methyl signals in uracil and the thiouracils and the way in which these shifts can be correlated with the site of methylation, at N-1 or N-3. When taken in conjunction with the well documented chemical shift parameters for *O*-methyl and *S*-methyl compounds these data provide a reliable method for identifying the site of methylation in these multifunctional compounds.

Acknowledgement

We are grateful to the National Research Council of Canada for financial support.

1. N. PLAVAC, I. W. J. STILL, M. S. CHAUHAN, and D. M. MCKINNON. Can. J. Chem. **53**, 836 (1975).
2. M. S. CHAUHAN and I. W. J. STILL. Can. J. Chem. **53**, 2880 (1975).
3. I. W. J. STILL, N. PLAVAC, D. M. MCKINNON, and M. S. CHAUHAN. Can. J. Chem. **54**, 280 (1976).
4. I. W. J. STILL, N. PLAVAC, D. M. MCKINNON, and M. S. CHAUHAN. Can. J. Chem. **54**, 1660 (1976).
5. P. C. LAUTERBUR. J. Chem. Phys. **43**, 360 (1965).
6. J. RIAND, M.-T. CHENON, and N. LUMBROSO-BADER. Tetrahedron Lett. 3123 (1974).
7. C. J. TURNER and G. W. H. CHEESEMAN. Org. Magn. Reson. **8**, 357 (1976).
8. P. VAN DE WEIJER and C. MOHAN. Org. Magn. Reson. **9**, 53 (1977).
9. A. J. JONES, D. M. GRANT, M. W. WINKLEY, and R. K. ROBINS. J. Am. Chem. Soc. **92**, 4079 (1970).
10. A. R. TARPLEY, JR. and J. H. GOLDSTEIN. J. Am. Chem. Soc. **93**, 3573 (1971).
11. M. DRAMIŃSKI and E. FRASS. Bull. Acad. Pol. Sci. (Sér. Sci. Chim.), **24**, 37 (1976).
12. A. J. JONES, D. M. GRANT, M. W. WINKLEY, and R. K. ROBBINS. J. Phys. Chem. **74**, 2684 (1970).
13. A. A. AKHREM, G. V. ZAITSEVA, I. A. MIKHAILOPULO, and A. F. ABRAMOV. J. Carbohydr. Nucleosides, Nucleotides, **4**, 43 (1977).
14. M.-T. CHENON, R. J. PUGMIRE, D. M. GRANT, R. P. PANZICA, and L. B. TOWNSEND. J. Am. Chem. Soc. **97**, 4627 (1975); **97**, 4636 (1975).
15. A. PSODA, Z. KAZIMIERCZUK, and D. SHUGAR. J. Am. Chem. Soc. **96**, 6832 (1974).
16. J. S. KWIATKOWSKY and B. PULLMAN. Adv. Heterocycl. Chem. **18**, 199 (1975).
17. J. ELGUERO, C. MARZIN, A. R. KATRITZKY, and P. LINDA. The tautomerism of heterocycles. (Advances in heterocyclic chemistry Supplement I.), Academic Press, New York, NY. 1976. pp. 129, 148, 158.
18. J. L. WONG and D. S. FUCHS. J. Org. Chem. **36**, 848 (1971).
19. H. H. MANTSCH and I. C. P. SMITH. Can. J. Chem. **51**, 1384 (1973).
20. J. B. STOTHERS. Carbon-13 NMR spectroscopy. Academic Press, New York, NY. 1972. p. 270.
21. L. F. JOHNSON and W. G. JANKOWSKI. Carbon-13 nmr spectra. Wiley-Interscience, New York, NY. 1972.
22. G. C. LEVY and G. L. NELSON. Carbon-13 nuclear magnetic resonance for organic chemists. Wiley-Interscience, New York, NY. 1972. p. 81.
23. D. DAVIDSON and O. BAUDISCH. J. Am. Chem. Soc. **48**, 2379 (1926).
24. R. N. WARRENER and E. N. CAIN. Austr. J. Chem. **24**, 785 (1971).
25. Y. MIZUNO, M. IKEHARA, and K. A. WATANABE. Chem. Pharm. Bull. **10**, 647 (1962).
26. J. J. FOX, D. VAN PRAAG, I. WEMPEN, I. R. DOERR, L. CHEONG, J. E. KNOLL, M. L. EIDINOFF, A. BENDICH, and G. B. BROWN. J. Am. Chem. Soc. **81**, 178 (1959).
27. D. J. BROWN and J. S. HARPER. J. Chem. Soc. 1298 (1961).
28. B. CHATAMRA and A. S. JONES. J. Chem. Soc. 811 (1963).
29. D. J. BROWN. J. Appl. Chem. **9**, 203 (1959).
30. S. GABRIEL. Chem. Ber. **38**, 1689 (1905).
31. G. E. HILBERT and T. B. JOHNSON. J. Am. Chem. Soc. **52**, 2001 (1930).
32. H. YAMANAKA. Chem. Pharm. Bull. **7**, 297 (1959).
33. T. J. DELIA, M. J. OLSEN, and G. B. BROWN. J. Org. Chem. **30**, 2766 (1965).
34. H. W. BARRETT, I. GOODMAN, and K. DITTMER. J. Am. Chem. Soc. **70**, 1753 (1948).
35. D. J. BROWN, E. HOERGER, and S. F. MASON. J. Chem. Soc. 211 (1955).

Can. J. Chem. Downloaded from www.nrcresearchpress.com by 210.87.254.105 on 09/05/12
For personal use only.

The Darzens glycidic ester condensation of indan-1-ones. A reinvestigation of the reaction

GERRY KAVADIAS[1] AND STEPHAN VELKOF

Bristol Laboratories of Canada, 100 Industrial Boulevard, Candiac, P.Q., Canada J5R 1J1

Received October 6, 1977

GERRY KAVADIAS and STEPHAN VELKOF. Can. J. Chem. **56**, 730 (1978).

The Darzens glycidic ester condensation of indan-1-one (**1***a*) with ethyl chloroacetate was reinvestigated. Contrary to previous reports, the reaction proceeded normally yielding the glycidic ester **2***a* in high yield. Similarly, 5-cyclohexylindan-1-one (**1***b*) produced the glycidic ester **2***b*. The glycidic esters **2***a,b* were converted to the corresponding aldehydes **4***a,b* by hydrolysis and decarboxylation. Oxidation of **4***b* yielded (±)-5-cyclohexylindan-1-carboxylic acid (3), a potent anti-inflammatory agent.

GERRY KAVADIAS et STEPHAN VELKOF. Can. J. Chem. **56**, 730 (1978).

On a réexaminé la réaction de condensation de Darzens entre l'indanone-1 (**1***a*) et le chloroacétate d'éthyle. Contrairement à des résultats antérieurs, la réaction se produit d'une façon normale pour conduire à l'ester glycidique **2***a* avec un très bon rendement. De la même manière, la cyclohexyl-5 indanone-1 (**1***b*) conduit à l'ester glycidique **2***b*. On a pu transformer les esters glycidiques **2***a,b* en aldéhydes correspondants **4***a,b* par hydrolyse et décarboxylation. L'oxydation de **4***b* fournit l'acide (±)-cyclohexyl-5 indancarboxylique-1, un produit anti-inflammatoire très puissant.

[Traduit par le journal]

The potency of (1*S*)-(−)-5-cyclohexylindan-1-carboxylic acid as an anti-inflammatory agent (3) led us to investigate an alternative synthesis for this valuable compound.

The present paper describes the synthesis of (±)-5-cyclohexylindan-1-carboxylic acid (**5**) via the glycidic ester **2***b*, the derived aldehyde **4***b* followed by oxidation (Scheme 1). It has been reported (2) that the Darzens glycidic ester condensation of indan-1-one (**1***a*) with ethyl chloroacetate in the presence of potassium *tert*-butoxide as the condensing agent yields the olefinic esters **6** and **7** instead of the expected glycidic ester **2***a*. It was concluded that this reaction with indan-1-one is of very limited practicality.

Upon repeating the above condensation reaction, a product was obtained in 94% yield which contained about 90% of the glycidic ester **2***a* as ascertained by nmr. The spectrum of this product showed a singlet at δ 3.90 for the hydrogen on the epoxide ring but no signals in the olefinic region thus establishing that the crude glycidic ester was free of olefinic esters **6** and **7**.

After completion of the reaction, it was necessary to neutralize the mixture with carbon dioxide prior to isolation of the glycidic ester **2***a*. Compound **2***a* was found to be sensitive to strong acids and bases and even when an ethereal solution was washed with dilute aqueous sodium hydroxide or hydrochloric acid, it was partly converted to the olefinic ester **6**. It was also sensitive to prolonged heating. Thus, although a small sample of crude **2***a* (8.0 g) could be distilled from a short column (Claisen head) without structural change (nmr), a larger sample (31.0 g) subjected to the same distillation gave a product (58%) which contained **2***a* and about 10% of the olefin **6** (nmr). Apparently, the partial conversion of **2***a* to **6** was the result of the longer heating period required for the larger scale experiment. When the above distillate was redistilled from a spinning band column a product was obtained (33%) which on nmr showed

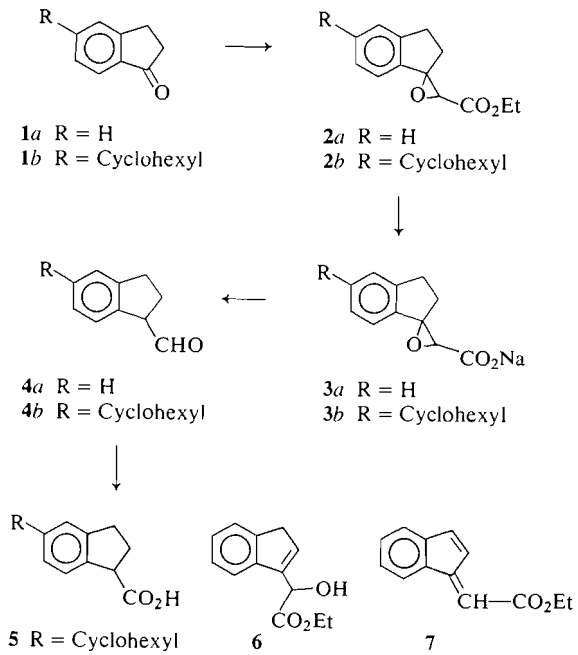

1*a* R = H
1*b* R = Cyclohexyl

2*a* R = H
2*b* R = Cyclohexyl

3*a* R = H
3*b* R = Cyclohexyl

4*a* R = H
4*b* R = Cyclohexyl

5 R = Cyclohexyl

6

7

SCHEME 1

[1]Author to whom correspondence concerning this paper may be addressed.

Can. J. Chem. Downloaded from www.nrcresearchpress.com by 210.87.254.5 on 09/05/12
For personal use only.

Can. J. Chem. Downloaded from www.nrcresearchpress.com by 210.87.254.5 on 09/05/12
For personal use only.

the complete absence of the glycidic ester **2***a*. The major component of the distillate was the olefinic ester **6** which was separated by column chromatography and identified. In all distillations, an appreciable quantity of residue was formed. A mechanism for the thermal conversion of **2***a* to **6** has been discussed (*2a*). Pure crystalline **2***a*, mp 56–58°C, was obtained by crystallization from ethanol.

From the above discussion, it is evident that the Darzens reaction proceeds normally in this case but care should be exercised in the isolation of the product.

The glycidic ester **2***a* was hydrolyzed by the Claisen method (4) to give the sodium salt **3***a*. Treatment of the salt **3***a* with glacial acetic acid was accompanied by a vigorous gas evolution and led to the aldehyde **4***a* (5). The above results demonstrate the usefulness of the process for the synthesis of 1-formylindanes.

Condensation of 5-cyclohexylindan-1-one (3) (**1***b*) with ethyl chloroacetate produced the glycidic ester **2***b*. The nmr spectrum of this product confirmed the structural assignment and showed no evidence of olefinic protons. Hydrolysis of **2***b* by the Claisen procedure (4) gave the sodium salt **3***b* which on treatment with glacial acetic acid yielded (±)-5-cyclohexyl-1-formylindane (**4***b*) in 52–55% yield based on the indanone **1***b*. Oxidation of the aldehyde **4***b* with the Jones' reagent in acetone (6) produced (±)-5-cyclohexylindan-1-carboxylic acid (3).

Experimental

The melting points were determined on a Mel-Temp melting point apparatus and are uncorrected. The ir spectra were recorded on a Unicam SP.200G grating ir spectrometer. The nmr spectra were recorded on a Varian A-60A spectrometer using deuteriochloroform as the solvent. The chemical shifts are expressed in δ values using tetramethylsilane as internal reference. Microanalysis were performed by Micro-Tech Laboratories Inc., Skokie, Illinois, U.S.A.

Ethyl Indane-1-spiro-2′-oxiran-3′-carboxylate (2a)

The general procedure described by Johnson *et al.* (7) was followed. In a flame-dried and nitrogen-purged 500 ml three-neck flask fitted with a mechanical stirrer, dropping funnel, and nitrogen inlet tube was added 20.0 g (151 mmol) of indan-1-one and 27.0 g (220 mmol) of freshly distilled ethyl chloroacetate. The mixture was kept under nitrogen, cooled in an ice-bath, and stirred. A solution of 24.6 g (220 mmol) of potassium *tert*-butoxide (Aldrich Chemical Co.) in 250 ml dry *tert*-butanol (7) was added dropwise over 1.5 h while stirring and maintaining the temperature below 10°C. After completion of the addition, stirring at the ice-bath temperature was continued for an additional 1.5 h. The excess potassium *tert*-butoxide was decomposed by passing CO_2 through the reaction mixture and the solvent was removed *in vacuo* at 35–40°C. Ether (250 ml) was added to the residue and the mixture filtered through a bed of Celite. The Celite bed was washed with ether and the washings were combined with the filtrate and evaporated to dryness to give 31.0 g (94%) of a dark-brown oil which crystallized on standing. The nmr spectrum showed the bands required for **2***a* (see below) and in addition two extraneous single bands at δ 1.50 and 3.82 belonging to an impurity which is assumed to be *tert*-butyl indane-1-spiro-2′-oxirane-3′-carboxylate. No absorption bands for olefinic protons were observed. The crude product contained about 90% of **2***a* as estimated by nmr from the relative intensities of the bands at δ 1.30 (methyl group of **2***a*) and δ 1.50 (impurity). This material was used without further purification in the next reaction. A sample (8.0 g) was crystallized from ethanol (15 ml) to give 4.0 g of crystalline **2***a* mp 51–55°C. After one recrystallization from the same solvent, it melted at 56–58°C; ir (Nujol): 1745 cm^{-1}; nmr δ: 1.30 and 4.28 (t and q for OCH_2CH_3), 2.35 (m, 2, C-2H), 3.0 (m, 2, C-3H), 3.90 (s, 1, epoxyproton), 6.9–7.3 (m, 4, ArH). *Anal.* calcd. for $C_{13}H_{14}O_3$: C 71.56, H 6.46; found: C 71.70, H 6.50. In another experiment, the crude product (8.0 g) was distilled from a Claisen head to give 6.0 g of oil, bp 106–108°C/0.1 Torr. The ir and nmr spectra showed that no change in structure had occurred.

In another experiment, crude **2***a* (31 g) (which on nmr showed no olefinic protons) was distilled from a Claisen head to give 18 g bp 120–122°C/0.2 Torr and a high boiling residue. The nmr spectrum of the distillate showed, in addition to the bands for **2***a*, a small band at δ 6.55 for the olefinic proton of **6**. The distillate contained about 10% of **6** as estimated by nmr. This distillate was redistilled using a spinning band column to give 6.0 g (33%) bp 118–122°C/0.1–0.05 Torr and a high boiling residue.

The nmr spectrum showed that conversion to **6** had occurred (olefinic proton and no absorption band for the epoxyproton). Thin-layer chromatography on silica with 5% ethyl acetate – benzene as the solvent (two immersions) showed one major spot with R_f 0.36 (**6**) and two minor ones with R_f 0.50 and 0.78. Compound **6** was separated by column chromatography on silica using 5% ethyl acetate – benzene as the eluent; ir (neat): 3450, 1740 cm^{-1}; nmr δ: 1.22 and 4.25 (t and q for OCH_2CH_3), 3.35 (m, 2, benzylic), 5.25 (s, 1, O—CH), 6.55 (m, 1, olefinic), 7.15–7.70 (m, 4, ArH). *Anal.* calcd. for $C_{13}H_{14}O_3$: C 71.54, H 6.46; found: C 71.56, H 6.52.

A sample of crude **2***a* (1.0 g) was dissolved in ether (30 ml) and the solution washed with 5% sodium hydroxide (2 × 30 ml). After drying and removal of the solvent by evaporation, the residue was examined by nmr. The spectrum showed, in addition to the bands for **2***a*, bands at δ 3.35, 5.25, and 6.55 indicating that **2***a* was partly (20–30%) converted to **6**.

Ethyl 5-Cyclohexylindan-1-spiro-2′-oxiran-3′-carboxylate (2b)

The procedure described above was followed. To a mixture of 5-cyclohexylindan-1-one (3) (21.4 g, 100 mmol) and 18.3 g (150 mmol) ethyl chloroacetate was added dropwise (1.5 h) a solution of 16.8 g (150 mmol) potassium *tert*-butoxide in *tert*-butanol (200 ml). After the addition, the ice-bath was removed and the reaction mixture stirred at room temperature for 2.5 h. The product was isolated as above to give 27.0 g of crude **2***b*. The nmr spectrum showed a band for the epoxy proton at δ 3.90 and was consistent with the expected structure **2***b*. The crude product was used without further purification in the next step.

(±)-1-Formylindane (4a)

Hydrolysis of the Glycidic Ester 2a

This step was carried out according to the procedure of Claisen (4) and was as follows: To a solution of 1.69 g (0.0735 g-at.) of sodium in 30 ml absolute ethanol was added 1.32 ml (73.5 mmol) of water and the solution cooled in an ice-bath. To this was added a solution of 16.2 g (74.5 mmol) of crude **2***a* in absolute ethanol (8 ml) and the mixture stirred in the cold for 15 min and then at room temperature for 3.5 h. The solids were filtered and washed with ice-cold ethanol (10 ml) and

with ether (2 × 50 ml) to give 14.1 g (90%) of **3***a*; ir (Nujol): 1610 cm^{-1} (CO).

Conversion of 3a to 4a

Compound **3***a* (13.67 g, 64.5 mmol) was placed in a flask and 25 ml glacial acetic acid was added. A vigorous evolution of carbon dioxide occurred and after stirring at room temperature for 15 min, the reaction had subsided. The reaction mixture was then heated on a steam-bath until the evolution of gases ceased (15 min). The reaction mixture was cooled to room temperature, diluted with water (150 ml) and extracted with ether (3 × 60 ml). The combined extracts were washed with water (2 × 100 ml) and with 10% sodium bicarbonate solution (100 ml) and dried. Evaporation of the solvent gave 8.2 g of crude **4***a*. Thin-layer chromatography on silica with benzene as solvent showed one major spot R_f 0.53 and two minor ones with R_f 0.23 and 0. The ir and nmr spectra were in agreement with the expected structure **4***a*. The crude product was distilled to give 6.6 g (70%) of **4***a* bp 122–124°C/20 Torr, (lit. (5) bp 135°C/30 Torr); ir (neat): 1725 cm^{-1}; nmr δ: 2.25 (m, 2, CH_2), 2.95 (m, 2, benzylic), 3.84 (dt, 1, C-1H, J_1 = 3.0, J_2 = 7.0 Hz), 7.20 (m, 4, ArH) 9.60 (d, 1, CHO, J = 3.0 Hz).

(±)-5-Cyclohexyl-1-formylindane (4b)

Hydrolysis of the Glycidic Ester 2b

The procedure described above for the hydrolysis of **2***a* was followed. To an ice-cold solution of 2.04 g (0.089 g-at.) of sodium in 35 ml absolute ethanol was added 1.62 ml (90 mmol) of water followed by a solution of 27.0 g (90 mmol) of crude **2***b* in 10 ml ethanol. The product was separated as above to give 23.3 g (88%) of **3***b*; ir (Nujol): 1610 cm^{-1}.

Conversion of 3b to 4b

Compound **3***b* (23.3 g, 78 mmol) was treated with 30 ml glacial acetic acid and the product was isolated as above to give 14.7 g (82.5%) of crude **4***b*. This product was used as such in the next step. Thin-layer chromatography on silica with 5% ether–benzene as solvent showed one major spot and some impurities with R_f 0. A sample of 2.2 g, was chromatographed on a silica column (14 cm × 3.2 cm ID) with chloroform as the eluent and the fraction containing **4***b* (70–120 ml) was evaporated to dryness to give 1.7 g of **4***b*. This indicated that the crude product contained 78–80% of **4***a*; ir (neat):1725 cm^{-1}; nmr δ: 3.90 (dt, 1, C-1H, J_1 = 3.0 Hz; J_2 = 7.0 Hz), 9.65 (d, 1, CHO, J = 3.0 Hz). *Anal.* calcd. for $C_{16}H_{20}O$: C 84.17, H 8.83; found: C 84.00, H 8.79.

(±)-5-Cyclohexylindan-1-carboxylic Acid (5)

The Jones' reagent was prepared as described by Djerassi *et al.* (8). Chromium trioxide, 26.72 g (267.2 mmol) in 23 ml concentrated sulfuric acid was cooled in ice and diluted by careful addition of water to a volume of 100 ml. A solution of the crude aldehyde **4***b* (14.7 g, 64.5 mmol) in 100 ml of acetone was cooled in an ice-bath while stirring. When the temperature reached 4°C, 17.0 ml of Jones' reagent was added dropwise to maintain the temperature at 20–25°C. After completion of the addition (3–4 min), the mixture was stirred in the cold for 5 min, diluted with water (300 ml), and the crystalline precipitate collected by filtration and washed with water. The pale yellow crystals were dissolved in ether, the solution dried ($MgSO_4$) and evaporated to dryness to give 14.0 g of crystalline **5**. The aqueous phase after extraction with ether gave an additional 390 mg of product. The crystalline product (14.0 g) was recrystallized from petroleum ether (bp 65–75°C) to give 10.0 g of product, mp 142–145°C. The product of the extraction (390 mg) was added to the mother liquor and the solution evaporated to dryness. Recrystallization of the residue from petroleum ether gave 1.0 g of product, mp 140–145°C. This fraction was combined with the first fractions to give a total of 11.0 g of product. Recrystallization from benzene (20 ml) – petroleum ether (200 ml) gave 10.2 g of product **5** (64.5%), mp 144–146°C (lit. (3) mp 145–146°C).

1. M. Balester. Chem. Rev. **55**, 283 (1955); M. S. Newman and B. J. Magerlein. Org. React. **5**, 413 (1949).
2. (*a*) A. H. Bone and L. A. Cort. Chem. Ind. 22 (1961); (*b*) A. H. Bone and L. A. Cort. J. Chem. Soc. 1986 (1962).
3. P. F. Juby, W. R. Goodwin, T. W. Hudyma, and R. A. Partyka. J. Med. Chem. **15**, 1297 (1972).
4. L. Claisen. Ber. **38**, 693 (1905).
5. M. Tiffeneau and A. Orekhoff. Bull. Soc. Chim. **27**, 782 (1920); Chem. Abstr. **15**, 236 (1921).
6. L. F. Fieser and M. Fieser. Reagents for organic synthesis. Vol. 1. John Wiley and Sons, Inc., New York, NY. p. 142, and references therein.
7. W. S. Johnson, J. S. Belew, L. J. Chinn, and R. H. Hunt. J. Am. Chem. Soc. **75**, 4995 (1953).
8. C. C. Djerassi, R. R. Engle, and A. Bowers. J. Org. Chem. **21**, 1547 (1956).

Can. J. Chem. Downloaded from www.nrcresearchpress.com by 210.87.254.5 on 09/05/12
For personal use only.

Photolysis of diterpenoid quinones[1,2]

OLIVER E. EDWARDS AND PAK-TSUN HO[3]

Division of Biological Sciences, National Research Council of Canada, Ottawa, Ont., Canada K1A 0R6

Received August 30, 1977

OLIVER E. EDWARDS and PAK-TSUN HO. Can. J. Chem. **56**, 733 (1978).

Photolysis of the diterpene quinone royleanone in benzene gave predominantly products resulting from both side-chain rearrangement and formation of an ether bridge to C-1. It is proposed that these arose by very specific transfer of two hydrogen atoms in a highly oriented complex between ground state royleanone and photo-excited royleanone. In contrast 7α-acetoxyroyleanone gave products of simple side chain rearrangement, with or without loss of acetic acid, probably via a spirocyclopropyl intermediate.

Royleanone methyl ether gave mainly an oxetanol in benzene but a methylenedioxy compound and an acetoxymethoxy compound in acetic acid. It is suggested that these arise from diradical and zwitterionic intermediates.

OLIVER E. EDWARDS et PAK-TSUN HO. Can. J. Chem. **56**, 733 (1978).

La photolyse de la quinone diterpénique royléanone dans le benzène conduit d'une façon prédominante à des produits provenant tant d'une transposition de la chaîne latérale que de la formation d'un pont éther vers le C-1. On suggère que ces produits proviennent d'un transfert très spécifique de deux atomes d'hydrogène dans le complexe hautement orienté entre l'état fondamental de la royléanone et de la royléanone photoexcitée. Par opposition, l'acétoxy-7α royléanone conduit uniquement à des produits provenant d'une transposition simple de la chaîne latérale accompagnée ou non d'une perte d'acide acétique probablement par l'intermédiaire spirocyclopropyle.

L'éther méthylique de la royléanone conduit principalement à un oxétanol dans le benzène alors que dans l'acide acétique il y a formation d'un composé méthylènedioxy et d'un composé acétoxyméthoxy. On suggère que ces composés proviennent d'intermédiaires diradicalaire et zwittérionique.

[Traduit par le journal]

Introduction

Royleanone **1** (R = H) is a naturally-occurring diterpenoid quinone with a structure (1) derived from the parent tricyclic diterpene abietane. Rüedi and Eugster (2) have established the presence in nature of related diterpenes coleons E and F **2** in which the side chain is a modified *n*-propyl group. Zelnik and co-workers (3) isolated and established the structure of barbatusin (**3**) in which the common isopropyl side chain now appears as a spirocyclopropyl unit. The same unit was later found (4) in cyclobutatusin **4**, and Eugster and co-workers (5) determined the structure of a series of compounds (coleons G, J, M, N, O, P, Q, and R) all of which contain this feature. Although the modified side chains of these compounds could be formed in the plants by completely ionic processes (2*a*) our interest was aroused by the possibility that they resulted from photochemical transformation of royleanone-like precursors. Indeed it was recognized by Zelnik and co-workers (4) that the cyclobutanol unit of cyclobutatusin could have a photochemical origin, and recent work (6) has shown that irradiation of barbatusin does give a product containing this feature.

In the hope that products related to the coleons and barbatusin could be obtained we undertook a study of the photolysis of royleanone **1**, 7α-acetoxy-royleanone **5** (1, 5*b*), and royleanone methyl ether **6**.

Results

Royleanone

Irradiation of a benzene solution of royleanone **1** (R = H) with light from a medium pressure mercury lamp through Pyrex, followed by acetylation (all under argon) gave a number of unusual products (in 84% yield).[4] The only predictable one isolated was the hydroquinone triacetate **7**. The other three products characterized were the cyclic ethers **8** (or **9**), **10**, and **11**. Their structures were deduced on the basis of their ^{1}H nmr spectra (see Experimental for values) and reactions.

Substance **8** (or **9**) was clearly a phenolic acetate (ν_{max} 1760 cm^{-1}) containing two aryl-alkyl ether oxygens (^{13}C nmr signals at 80.79 and 80.55 ppm) and no longer containing the isopropyl side chain. A

[1]NRCC No. 16422.

[2]Presented in part at the Chemical Institute of Canada – American Chemical Society meeting, Montreal, Quebec, May 30 – June 2, 1977.

[3]NRCC Research Associate.

[4]All cited yields are based on starting material consumed.

Can. J. Chem. Downloaded from www.nrcresearchpress.com by 210.87.254.40 on 09/05/12
For personal use only.

Can. J. Chem. Downloaded from www.nrcresearchpress.com by 210.87.254.40 on 09/05/12
For personal use only.

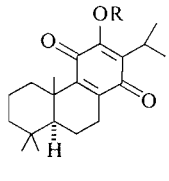

1

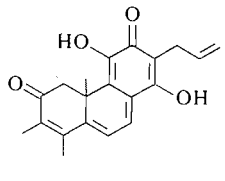

2

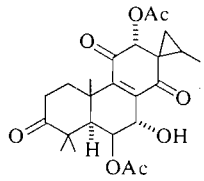

3

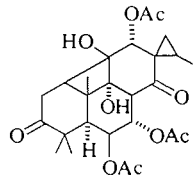

4

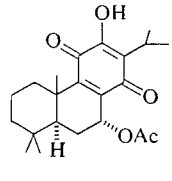

5

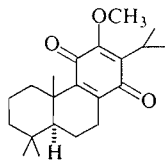

6

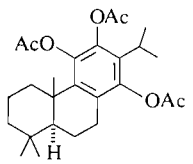

7

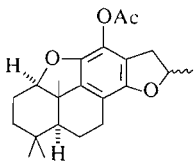

8

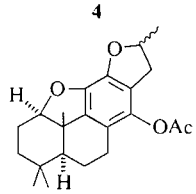

9

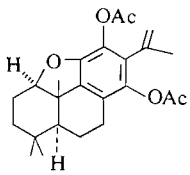

10

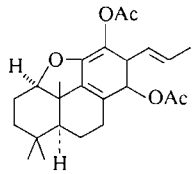

11

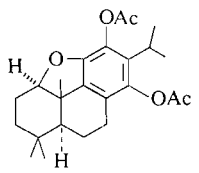

12

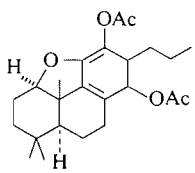

13

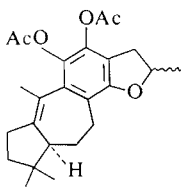

14

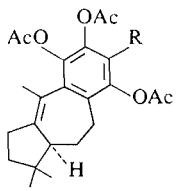

15 R = isopropyl
16 R = *n*-propyl

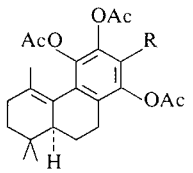

17

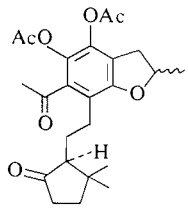

18

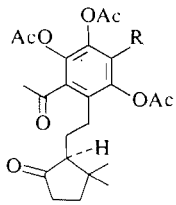

19 R = isopropyl
20 R = *n*-propyl

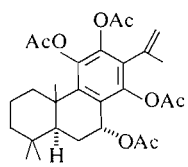

21

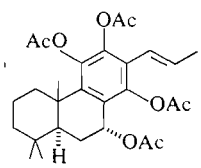

22

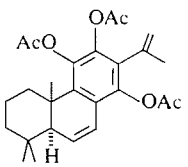

23

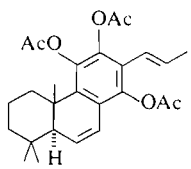

24

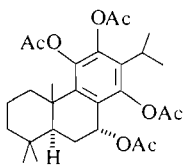

25

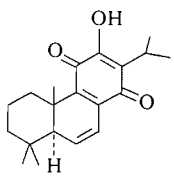

26

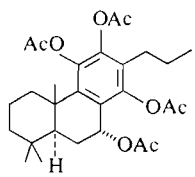

27

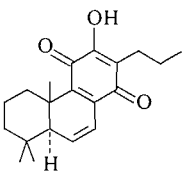

28

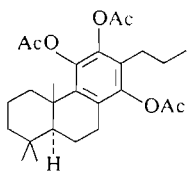

29

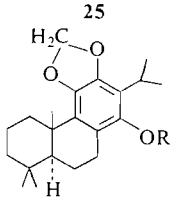

30

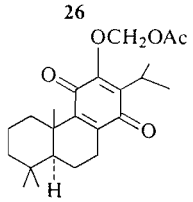

31

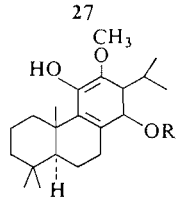

32

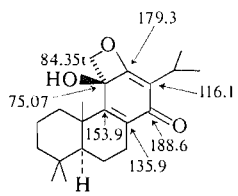

33

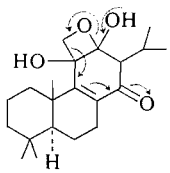

34

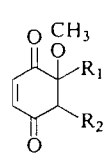

35

Can. J. Chem. Downloaded from www.nrcresearchpress.com by 210.87.254.40 on 09/05/12
For personal use only.

pair of methyl doublets at δ 1.45 and 1.5, and the related low field multiplet (δ 4.80) were readily reconciled with transformation of the original isopropyl side chain into a pair of isomers containing a methyldihydrofuran ring. The fact that the acetoxy carbonyl gave a single ^{13}C nmr signal at δ 168.13 and a single ^{1}H nmr signal (δ 2.30) makes it probable that the isomers were methyl epimers rather than having the two different ether locations (**8** or **9**). A choice as to which structure is correct would be arbitrary with the available evidence but mechanistic considerations (see Discussion) lead us to favour **8**.

Catalytic hydrogenation converted **10** into **12** which now had the ^{1}H nmr spectral characteristics of an isopropyl derivative (see Experimental for values). Similar reduction of **11** gave **13** whose ^{1}H nmr spectrum fitted the presence of a *n*-propyl group. The characteristic common feature of **8-11** was a ^{1}H quartet near δ 3.9, the magnitude of the couplings was consistent with their origin being an α hydrogen on C-1 with a 1β–11 ether bridge.[5] The gross structures of **8**, **12**, and **13** were shown to be as depicted by the action of boron trifluoride etherate in acetic anhydride leading to rearrangement to the styrene derivatives **14–16**. However, since these had an allylic methyl group (δ near 1.9) they could also have been products of methyl migration, e.g. **17**. The correct structure was established by ruthenium tetroxide oxidation of **14–16** to **18–20**, respectively. The cyclopentanone moiety was in each case evident from the infrared spectrum (ν_{max} 1740 cm^{-1}) and the acetophenone unit from the peaks near 1700 cm^{-1} and extra CH_3CO signals in the ^{1}H nmr spectra.

The irradiation of royleanone under identical conditions to the above experiments but using dimethoxyethane as solvent, led to a complex mixture with much incorporation of the solvent into products.

7α-Acetoxyroyleanone

The behavior of 7α-acetoxyroyleanone **5** on irradiation was in striking contrast to that of royleanone. The same main products were produced in benzene as in dimethoxyethane, but the conversion was more rapid in the latter solvent and the products cleaner. No significant incorporation of the ether into products was noted. The four major products after acetylation under argon were **21** (30%), **22** (34%), **23** (8.5%), and **24** (10%). It was clear from the empirical formulae and ^{1}H nmr spectra that these consisted of two pairs of compounds, one pair with the original 7-acetoxy group and the other in which this had been eliminated to give a 6,7-ene. One member of each pair had an isopropenyl side chain and the other a *trans*-1-propenyl side chain. The structure assigned to **21** was confirmed by hydrogenation to **25**, which now had an isopropyl side chain, followed by acid catalysed hydrolysis and elimination, then air oxidation to the known 6-dehydroroyleanone **26** (1). Comparable treatment of **22** gave **27** and **28** with spectral characteristics parallel to those of **25** and **26**. Accompanying the simple hydrogenation products **25** and **27** were the products **7** and **29** of hydrogenolysis of the 7-acetoxy group, a not unexpected event. Compound **7** was identical to an authentic sample prepared by reductive acetylation of royleanone.

The structures of **23** and **24** were evident from their ^{1}H nmr spectra (see Experimental for values). Confirmation was provided by hydrogenation to **7** and **29**, respectively.

Royleanone Methyl Ether

Photolysis of royleanone methyl ether **6** in a 2.5:1 acetic acid – acetic anhydride mixture under argon using radiation peaked at 254 nm gave quite rapid (2 h) conversion into products. These mainly involved the methoxyl group. After air oxidation the products isolated (yields based on unrecovered starting material) were the methylenedioxy acetate **30** (R = Ac) (17%), the acetoxymethoxyquinone **31** (10%), and a monoacetate of the hydroquinone **32** (R = H) (9%) which was tentatively assigned the 14-acetoxy structure **32** (R = Ac). The structural assignments followed from the ^{1}H nmr spectra and the following physical and chemical evidence.

The ^{13}C nmr signal at δ 99.9, the ^{1}H nmr signal at δ 5.9 and the absence of the methoxyl group made the presence of a methylenedioxy group in **30** certain. The unchanged isopropyl group (^{1}H nmr) and the phenolic acetate (ν_{max} 1750 cm^{-1}) were only compatible with the assigned structure.

The compound to which we assign structure **31** was a yellow gum with ν_{max} 1650 (quinone) and 1755 cm^{-1} (acetate). The OCH_2O group gave rise to a quartet in its ^{1}H nmr spectrum and to a ^{13}C nmr signal at 87 ppm. The characteristic ^{1}H nmr signals for the isopropyl group were present. Mild basic hydrolysis to royleanone confirmed the structure.

Compound **32** (R = Ac) was a nearly colorless oil which had an exchangeable proton (δ 5.9 in $CDCl_3$) and was a phenolic acetate (ν_{max} 1755 cm^{-1}) with an intact isopropyl group (^{1}H nmr). Treatment of the hydroquinone **32** (R = H), derived from royleanone methyl ether, at room temperature with 1:1 acetic

[5]A half-chair conformation of ring A would permit formation of a 1α–11 ether bridge, giving the same coupling constants but the all-chair product seems more probable.

Can. J. Chem. Downloaded from www.nrcresearchpress.com by 210.87.254.40 on 09/05/12
For personal use only.

acid – acetic anhydride mixture for 22 h resulted in very little acetylation. However acetic anhydride – pyridine at room temperature converted it into a mixture of mono- and diacetates. The former proved to be identical with **32** (R = Ac). The location of the acetate is made to correspond with what we consider to be the least hindered hydroxyl group.

When royleanone methyl ether was irradiated in acetic acid alone the major identifiable products were **30** (R = H) (16%) and **31** (22%). The presence of **30** (R = H) was at first missed since it had an unexpectedly high R_f on silica gel (nearly the same as **6** in C_6H_6), and the expected sharp singlet near δ 5.9 was absent in deuteriochloroform although a broad multiplet was present with this chemical shift. However addition of deuterium oxide transformed this signal into a sharp 2H singlet while a 1H singlet at δ 4.3 disappeared. In addition a complex set of signals between δ 1.5 and 3.6 resolved into the characteristic multiplet for the CH (δ 3.3) and doublet for the methyl groups (δ 1.37) of the isopropyl group. This phenomenon was reversible. The acetylation of **30** (R = H) in acetic acid – acetic anhydride or acetic anhydride alone was very slow but acetic anhydride – pyridine converted it into the **30** (R = Ac) described above. Under none of these conditions was **31** produced from **30** (R = H).

The photolysis of **6** in benzene was attempted with radiation peaked at either 350 or 300 nm. The starting material was recovered essentially unchanged. Using radiation peaked at 254 nm the quinone was slowly transformed (ca. 50% in 6 h). The products were strikingly different from those produced in acetic acid.

The major product (47% based on unrecovered **6**) was a colorless crystalline compound which has been assigned the oxetanol structure **33**. The only other product identified was royleanone (13% based on unrecovered **6**).[6] The structure of **33** was deduced on the basis of its formula, $C_{21}H_{30}O_3$, spectra, and reactions. The infrared spectrum (ν_{max} 3570, 3360, 1710, and 1622 cm^{-1}) suggested the presence of a hydroxyl group and an enone. It was inert to all but vigorous acetylation conditions, hence the hydroxyl was tertiary. The enone character was substantiated by its ultraviolet absorption (λ_{max} 248, ε 11 700 and 316 nm, ε 1770). The ^1H nmr spectrum showed the absence of a methoxyl group but the presence of a $—CH_2—O$ group (2H, dd, δ 4.90 and 5.16, J = 5 Hz) and the isopropyl group. Possible ^{13}C nmr assignments based on off-resonance decoupling and analogy (7) are indicated on structure **33**. All this evidence is consistent with the assigned structure. It was reasoned that good nucleophiles might open the oxetane ring. Action of hydroxide ion under argon on **33** did open it as illustrated in **34**. The reaction mixture was neutralized then allowed to oxidize in the air. Royleanone was produced, giving final confirmation of the structure.[7]

Discussion

The fact that the photolysis of royleanone was much faster using lamps with peak emission at 254 nm as compared with those giving longer wavelengths indicates that the 270 nm absorption band of the quinones is involved in the reactions we have observed. This is consistent with the marked slowing of the photolysis of the methyl ether when benzene was used as solvent compared to acetic acid. Finally the fact that, although acetoxyroyleanone **5** was photolysed more slowly in benzene than in dimethoxyethane, the major products were the same indicates that the photoexcited states were the same in both solvents.

The observations on royleanone methyl ether in benzene seem best interpreted as major (eq. 1) and minor (eq. 2) homolytic processes. Clearly the

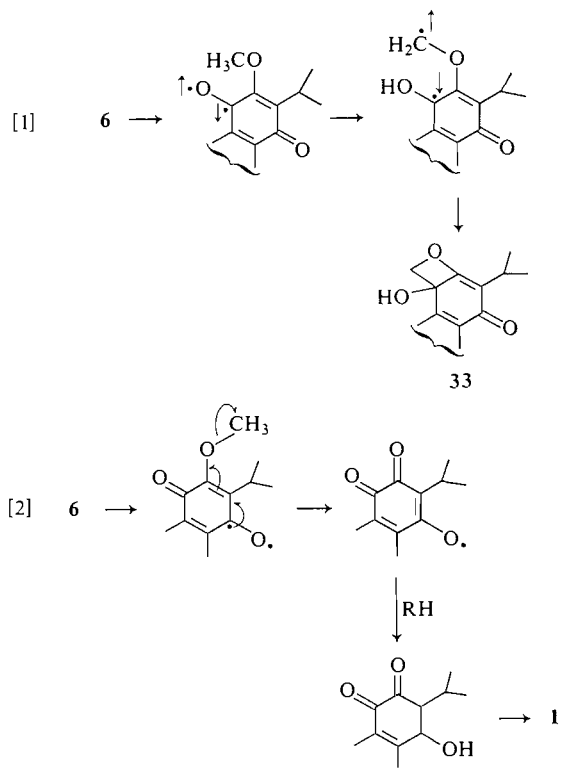

[6]Care was taken to ensure that no royleanone was present in the starting material. The benzene used had been dried over sodium wire.

[7]The structure has been confirmed and stereochemistry determined using X-ray crystallography by Drs. M. Przybylska and F. R. Ahmed.

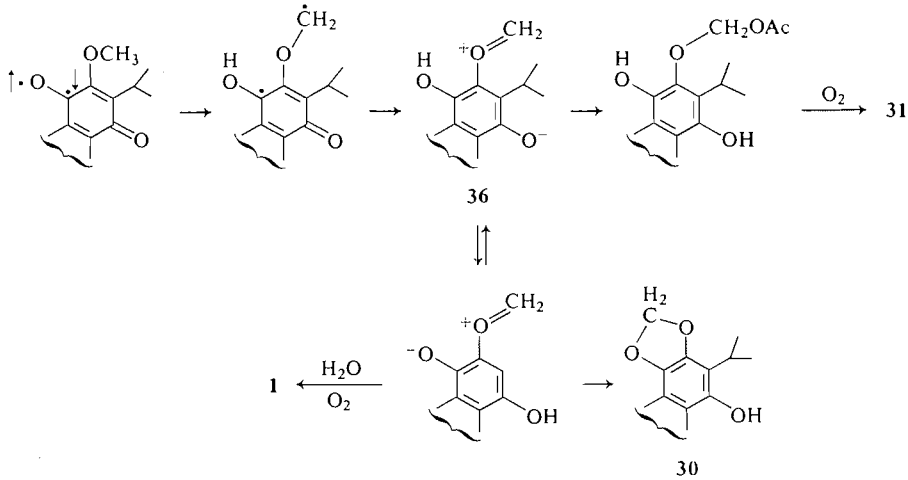

SCHEME 1

methoxyl group is the most reactive function for radical type processes. Comparable ether cleavage has been observed previously (8). Although oxetanol formation has been observed several times for methoxycyclohexenediones of type **35** (9, 10) the formation of the much more strained oxetane ring of **33** seems to be unique. A striking feature of its infrared spectrum was a peak of medium intensity at 1710 cm^{-1}. The Raman spectrum of **33** had similar peaks at 1717 (medium) and 1631 (strong) cm^{-1}. A preliminary study of the Raman spectrum in polar and nonpolar solvents indicated that the bands were of complex olefinic and carbonyl origin.[8]

The photochemical behavior of royleanone methyl ether in acetic acid or acetic acid – acetic anhydride mixtures is in striking contrast to that in benzene. If we are correct in assuming that the same excited state is involved in both solvents, the difference in reaction seems best interpreted as a rapid transition to ionic pathways as in Scheme 1 in the more polar solvents. The electron transfer could be intramolecular (analogous to Zimmerman's electron demotions) (11) or an intermolecular charge-transfer-type of electron migration. Both the formation of acetoxymethoxy and methylenedioxy groups in photolysis of a methoxy quinone in acetic anhydride were discovered recently by Baldwin and Brown (12), and the above type of ionic mechanism invoked to account for their production. Their work showed that protons are not needed to induce the ionic state, whereas ours shows that no acetylating agent is needed. It is surprising that no oxetanol is formed, i.e. that the transition to a zwitterion is so rapid and complete. The formation of the monoacetate of the methylenedioxy compound in the 1:1 acetic acid – acetic anhydride mixture seems revealing. The methylenedioxy phenol does not acetylate under these conditions, hence the reaction would seem to be capture of the phenoxide ion of **36** by acetic anhydride.

The course of photolysis of 7α-acetoxyroyleanone fits in part well-established patterns. The side-chain rearrangement and olefin formation could be readily accounted for in terms of the initial diradical formation, electron transfer to give a zwitterion, then proton abstraction to give the olefins (with or without prior methyl migration). However, the unimportance of electron transfer in benzene in the case of the methyl ether (see above), and the failure to detect dihydrofuran products, incline us to favor side-chain rearrangement via spirocyclopropyl ketones (Schemes 2 and 3). This type of intermediate was postulated by Orlando and co-workers (13) to account for side-chain rearrangement in simple quinones. Work of Farid (14) supported this con-

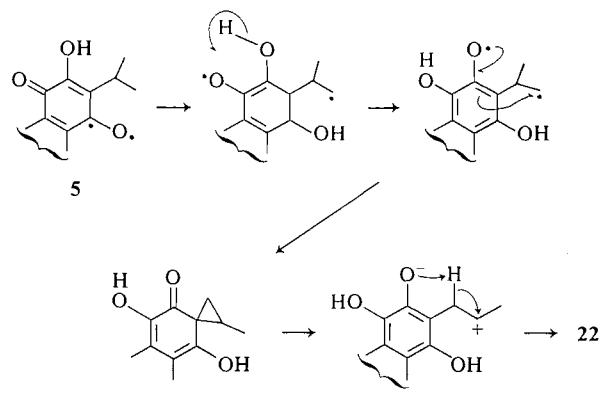

SCHEME 2

[8]We are grateful to Dr. P. Carey for obtaining the Raman spectrum and for advice on its significance.

Can. J. Chem. Downloaded from www.nrcresearchpress.com by 210.87.254.40 on 09/05/12
For personal use only.

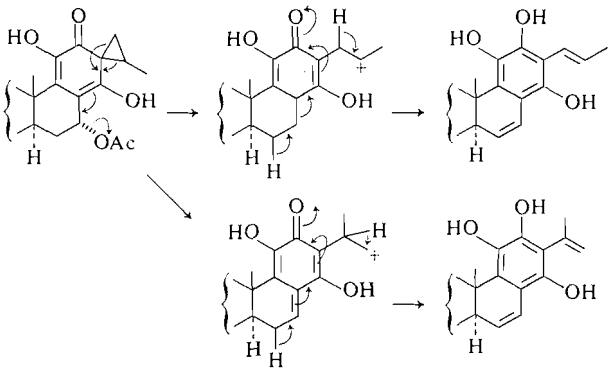

SCHEME 3

ception. But thermal [1,5] sigmatropic rearrangement of spirocyclopropyl dienones to olefins leads in all known cases (15) to *nonconjugated* olefin.[9] Hence if these are intermediates in our case, the observed opening to *conjugated* olefins would have to be by a second photolytic process[10] or by an ionic process during work-up.

Whatever the detail of mechanism, we observed none of the hoped-for spirocyclopropanes in the products of the photolysis and subsequent acetylation.

The elimination of the 7α-acetoxy group can be formulated as an alternative mode of reaction of the spirocyclopropane (Scheme 3).

The important products from photolysis of royleanone, aside from the hydroquinone, cannot arise from a simple one-photon process. In previous work on the photolysis of simple quinones (16) only minor products of similar character have been encountered and in the case of 7α-acetoxyroyleanone no comparable products were obtained.

Two interpretations of this unusual behavior seem worthy of discussion.

(*i*) A hydroquinone with a dihydrofuran ring (e.g. **38**) or unsaturated side chain could be produced in a first photochemical step. This could then be reoxidized to quinone (e.g. **39**) by parent quinone. A second photolysis of **39** could give the diradical **40** (16). This could be transformed into one of the products via a spirocyclopropane **41** and the zwitterion **42**. We discount this sequence on the following grounds. (*a*) It is not evident why more than fractional amounts of the hydroquinones such as **38** should be reoxidized by residual parent quinone. In simple models (13, 16) this is clearly a minor process. (*b*) The diradical **40** is most likely to give a cyclobutanol if hydrogen is abstracted from C-1. Indeed Zelnik *et al.* (17) have recently shown that barbatusin (**3**) does give such a cyclobutanol when irradiated. (*c*) If the cation in **42** had significant lifetime, methyl migration or ring-A contraction to give benzylic cations would have been expected. No such products were observed. (*d*) Internal oxygen radical addition to the unsaturated side chains produced in the first photolysis step should have occurred in the second (18). No products obviously derived from such events were obtained.

(*ii*) The apparent molecular weight of royleanone in 7.6×10^{-2} *M* solution in benzene was normal and no charge-transfer band was evident in its absorption spectrum. However the photoexcited state may be

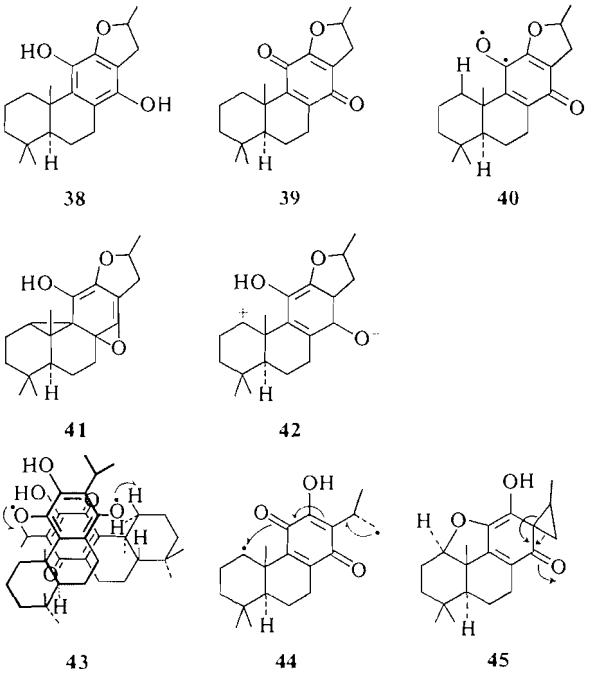

38 **39** **40**

41 **42**

43 **44** **45**

more polar. We hence postulate that loose but highly oriented complexes form between photoexcited molecules and ones in the ground state (excimers). Such a complex, with minimal nonbonded interactions and stabilization by hydrogen bonding is illustrated in **43**. This is ideally oriented for double hydrogen atom abstraction leading to 1 molecule of hydroquinone and a transient diradical **44**. The latter would probably collapse rapidly to the spirocyclopropyl ether **45** (fishhooks) especially since the methylene radical of the side chain, when formed, would be orthogonal to the enone system. The spirocyclopropane **45** would give zwitterions leading to the three types of product observed (arrows).

Not only does explanation **2** account for the observations on royleanone, it can explain the fact

[9]This led Eugster and co-workers (2*a*) to postulate that spirocyclopropyl derivatives were intermediates in the biosynthesis of coleons such as **2**.

[10]Shorter wavelength light than that in the work of Orlando and Farid (13, 16) was used.

Can. J. Chem. Downloaded from www.nrcresearchpress.com by 210.87.254.40 on 09/05/12
For personal use only.

Can. J. Chem. Downloaded from www.nrcresearchpress.com by 210.87.254.40 on 09/05/12
For personal use only.

that 7α-acetoxyroyleanone, in which the axial acetoxy group would preclude the association shown in **43**, gave products accountable for on the basis of isolated photoexcited molecules.

Summary

Despite a high probability that spirocyclopropyl intermediates are involved in the photochemistry of royleanone and acetoxyroyleanone we were unable to isolate one. Hence the hoped-for route to barbatusin was not realized. However we still consider that this class of compounds may well be formed in vivo by irradiation of royleanones in the oil glands in the leaves of the appropriate plants.

Diradical states, zwitterionic states and a complex between molecules in the ground and excited states are invoked to explain the formation of the observed products.

Experimental

Infrared spectra were of chloroform solutions, ultraviolet spectra of solutions in 95% ethanol, and ^{1}H nmr and ^{13}C nmr spectra in deuteriochloroform solutions with TMS as internal reference. Thin-layer and preparative-layer chromatography was done using silica gel containing a fluorescent indicator (G_{254}).

Materials

Royleanone 1 (R = H)

This was recrystallized from methylene chloride – ethanol giving flat needles with mp 181°C; ^{1}H nmr δ: 7.3 (1Hs, OH), 3.2 (1H, m), 1.27 (9H, s), 1.16 (3H, s), and 0.93 (6H, s); λ_{max} (benzene; 1.3×10^{-3} *M*): 409 nm, ε 380. *Mol. Wt.* calcd. for $C_{20}H_{28}O_3$: 316; found (thermistor drop method, in benzene): 313.

Royleanone Methyl Ether 6

This crystallized from methylene chloride – methanol, mp 120°C; ^{1}H nmr δ: 3.90 (3H, s), 3.2 (1H, m), 1.32 (3H, s), 1.21 (6H, d, J = 7 Hz), 0.94 (6H, s).

Royleanone Acetate 1 (R = Ac)

This compound was prepared by a standard procedure for acetylation and recrystallized from ether–methanol to a constant melting point 78°C; ^{1}H nmr δ: 2.35 (3H, s), 1.30 (3H, s), 1.21 (6H, d, J = 8 Hz), 0.93 (3H, s), 0.91 (3H, s).

Royleanone

Photolysis of Royleanone 1 (R = H)

A solution of royleanone **1** (R = H) (250 mg) in anhydrous benzene (120 ml) was irradiated by a 200 W medium pressure Hanovia mercury lamp with a Pyrex filter under argon at about 10°C for 8 h, after which acetic anhydride (5 ml) and pyridine (10 ml) were added to the reaction mixture and the solution was left overnight. Evaporation of the solvent *in vacuo* resulted in a brown residue which showed four components on tlc (silica gel, 5% ether in benzene), besides the starting material as its acetate. Chromatography by preparative tlc on silica gel afforded 56 mg of the reduction product **7**, 30 mg of compound **8** (or **9**), 22 mg of compound **10**, and 23 mg of compound **11**. The photolysis gave 48% conversion to the products with 44% recovery of royleanone as its acetate (118 mg) and the total yield was 84%. The reduction product **7** was recrystallized from ethanol with mp 128°C and identified by comparison with authentic sample in all respects (mp, ir, nmr, and tlc). The other three components **8** (or **9**), **10**, and **11** were thick oils homogeneous by tlc in several solvent systems.

Compound (8 or 9)—ir ($CHCl_3$): 1760 cm^{-1} (phenolic acetate); ^{1}H nmr ($CDCl_3$) δ: 4.80 (m, 1H, —CH—O—), 3.89 (q, J = 10 Hz, J = 4 Hz, 1H, —CH—O—), 2.30 (s, 3H, —$OCOCH_3$), 1.50 and 1.45 (two d, J = 6 Hz, 3H, isomeric methyl), 1.10 (s, 3H, —CH_3), 1.03 (s, 3H, —CH_3), 0.98 ppm (s, 3H, —CH_3); ^{13}C nmr ($CDCl_3$) δ: 168.13 (—$OCOCH_3$) 142.50, 142.30, 142.21, 128.41, 116.53 and 111.33 (aromatic carbons), 80.79 and 80.55 ppm (two —O—C—). *Mol. Wt.* calcd. for $C_{22}H_{28}O_4$: 356.1991; found (high resolution mass spectroscopy): 356.1991.

Compound 10—ir ($CHCl_3$): 1760 cm^{-1} (phenolic acetate); ^{1}H nmr ($CDCl_3$) δ: 5.21 and 4.84 (two broad s, 2H, two vinylic protons), 3.95 (q, J = 11 Hz, J = 5 Hz, 1H, —CH—O—), 2.23 (s, 3H, —$OCOCH_3$), 2.20 (s, 3H, —$OCOCH_3$), 1.94 (broad s, 3H, C=C—CH_3), 1.14 (s, 3H, —CH_3), 1.03 (s, 3H, —CH_3), 0.97 ppm (s, 3H, —CH_3). *Mol. Wt.* calcd. for $C_{24}H_{30}O_5$: 398.2105; found (high resolution mass spectroscopy): 398.2096.

Compound 11—ir ($CHCl_3$): 1760 cm^{-1} (phenolic acetate); ^{1}H nmr ($CDCl_3$) δ: 6.03 (d, J = 11 Hz, 1H, —C=CH—), 5.90 (m, 1H, —C=C*H*CH_3), 3.92 (q, J = 11 Hz, J = 5 Hz, 1H, —CH—O—), 2.30 (s, 6H, two —$OCOCH_3$), 1.84 (d, J = 5 Hz, 3H, —C=CCH_3), 1.12 (s, 3H, —CH_3), 1.02 (s, 3H, —CH_3), 0.95 ppm (s, 3H, —CH_3). *Mol. Wt.* calcd. for $C_{24}H_{30}O_5$: 398.2105; found (high resolution mass spectroscopy): 398.2104.

Hydrogenation of Compound 10

Compound **10** (40 mg) was subjected to an atmospheric pressure hydrogenation in methanol (8 ml) with 10% palladium-on-charcoal (29 mg). After 3 h, the palladium-on-charcoal was removed by filtration and the solvent was evaporated to afford quantitatively crystalline dihydro derivative **12** (40 mg). An analytical sample was prepared by recrystallization from ether–*n*-hexane with mp 135–136°C; ir ($CHCl_3$): 1760 cm^{-1} (phenolic acetate); ^{1}H nmr ($CDCl_3$) δ: 3.94 (q, J = 10 Hz, J = 5 Hz, 1H, —CH—O—), 2.32 (s, 6H, two —$OCOCH_3$), 1.22 (d, J = 5 Hz, 6H, isopropyl), 1.14 (s, 3H, —CH_3), 103 (s, 3H, —CH_3), 0.94 ppm (s, 3H, —CH_3). *Anal.* calcd. for $C_{24}H_{32}O_5$: C 71.91, H 8.05; found: C 71.88, H 7.98.

Hydrogenation of Compound 11

Compound **11** (38 mg) was hydrogenated as described above for compound **10** to yield quantitatively compound **13** which was a waxy material homogeneous by tlc in several solvent systems; ir ($CHCl_3$): 1760 cm^{-1} (phenolic acetate); ^{1}H nmr ($CDCl_3$) δ: 3.95 (q, J = 11 Hz, J = 5 Hz, 1H, —CH—O—), 2.31 (s, 6H, two —$OCOCH_3$), 1.13 (s, 3H, —CH_3), 1.04 (s, 3H, —CH_3), 0.97 ppm (s, 3H, —CH_3). *Mol. Wt.* calcd. for $C_{24}H_{32}O_5$: 400.2256; found (high resolution mass spectroscopy): 400.2257.

Preparation of Compound 15

To a stirred solution of compound **12** (30 mg) in acetic anhydride (2 ml) precooled to −10°C was added freshly distilled boron trifluoride etherate (0.4 ml). The mixture was kept at −10°C with stirring for ½ h, after which it was poured into water and extracted with ether several times. The residue obtained after the combined extracts had been dried over anhydrous magnesium sulfate and evaporated in vacuo was purified by preparative tlc on silica gel. 22 mg (67%) of compound **15** was obtained as an oil homogeneous by tlc; ir ($CHCl_3$): 1760 cm^{-1} (phenolic acetate); ^{1}H nmr ($CDCl_3$) δ: 2.36 (s, 3H, —$OCOCH_3$), 2.32 (s, 3H, —$OCOCH_3$), 2.23 (s, 3H, —$OCOCH_3$), 1.90 (broad s, 3H, —C=C—CH_3), 1.26 and 1.21 (two d, J = 6 Hz, 6H, isopropyl), 0.93 (s, 3H, —CH_3), 0.86 ppm (s, 3H, —CH_3); uv (EtOH) λ_{max}: 252 nm (ε 1.1 ×

Can. J. Chem. Downloaded from www.nrcresearchpress.com by 210.87.254.40 on 09/05/12
For personal use only.

10^4). *Mol. Wt.* calcd. for $C_{26}H_{34}O_6$: 442.2355; found (high resolution mass spectroscopy): 442.2355.

Preparation of Compound ***16***

Compound **16** was prepared from compound **13** by the same method described above for compound **15**. The yield was 69% and **16** was an oil homogeneous by tlc; ir ($CHCl_3$): 1760 cm^{-1} (phenolic acetate); ^1H nmr ($CDCl_3$) δ: 2.36 (s, 3H, $-OCOCH_3$), 2.31 (s, 3H, $-OCOCH_3$), 2.23 (s, 3H, $-OCOCH_3$), 1.92 (broad s, 3H, $-C{=}C-CH_3$), 0.98 (t, 3H, $-CH_2CH_3$), 0.94 (s, 3H, $-CH_3$), 0.83 ppm (s, 3H, $-CH_3$); uv (EtOH) λ_{max}: 254 nm (ε 1.2×10^4). *Mol .Wt.* calcd. for $C_{26}H_{34}O_6$: 442.2355; found (high resolution mass spectroscopy): 442.2349.

Formation of Compound ***14***

Compound **14** was prepared from compound **8** under the same conditions as described above for the preparation of **15**. The yield was 70% and the oily compound **14** behaved homogeneously by tlc in several solvent systems; ir ($CHCl_3$): 1760 cm^{-1} (phenolic acetate); ^1H nmr ($CDCl_3$) δ: 4.81 (m, 1H, —CH—O—), 2.26 (s, 6H, two $-OCOCH_3$), 1.87 (broad s, 3H, $-C{=}C-CH_3$), 1.43 and 1.37 (two d, J = 6 Hz, 3H, $-CH-CH_3$), 0.87 (s, 3H, $-CH_3$), 0.80 ppm (s, 3H, $-CH_3$); uv (EtOH) λ_{max}: 251 (ε 8140), 298 nm (ε 3880). *Mol. Wt.* calcd. for $C_{24}H_{30}O_5$: 398.2099; found (high resolution mass spectroscopy): 398.2098.

Cleavage of Olefin ***15*** *to Diketone* ***19***

To a stirred solution of compound **15** (40 mg) in carbon tetrachloride (5 ml) precooled to −10°C was added dropwise a solution of ruthenium tetroxide prepared from 58% ruthenium dioxide (56 mg) in carbon tetrachloride (10 ml) and sodium metaperiodate (400 mg) in water (10 ml). The solution was stirred for 5 min, after which the black precipitate was removed by filtration. Evaporation of the filtrate to dryness resulted in a residue which was purified by preparative tlc on silica gel to give 28 mg (65%) of diketone **19** as a waxy material homogeneous by tlc; ir ($CHCl_3$): 1760 (phenolic acetate), 1740 (five-membered ring ketone), 1700 cm^{-1} (acyl ketone); ^1H nmr ($CDCl_3$) δ: 2.50 (s, 3H, $-COCH_3$), 2.46 (s, 3H, $-OCOCH_3$), 2.33 (s, 3H, $-OCOCH_3$), 2.27 (s, 3H, $-OCOCH_3$), 1.25 (d, J = 6 Hz, 6H, isopropyl), 1.18 (s, 3H, $-CH_3$), 0.80 ppm (s, 3H, $-CH_3$). *Mol. Wt.* calcd. for $C_{26}H_{34}O_8$: 474; found (mass spectroscopy): 474.

Preparation of Diketone ***20***

Olefin **16** (21 mg) was oxidized with ruthenium tetroxide under the same conditions as described above for compound **15** to give 13 mg (59%) of diketone **20** as a thick oil; ir ($CHCl_3$): 1760 (phenolic acetate), 1740 (five-membered ring ketone), 1700 cm^{-1} (acyl ketone); ^1H nmr ($CDCl_3$) δ: 2.50 (s, 3H, $-COCH_3$), 2.44 (s, 3H, $-OCOCH_3$), 2.31 (s, 3H, $-OCOCH_3$), 2.25 (s, 3H, $-OCOCH_3$), 1.13 (s, 3H, $-CH_3$), 0.94 (t, 3H, $-CH_2CH_3$), 0.83 ppm (s, 3H, $-CH_3$). *Mol. Wt.* calcd. for $C_{26}H_{34}O_8$: 474; found (mass spectroscopy): 474.

Preparation of Diketone ***18***

Olefin **14** (24 mg) was oxidized using the same method described above for compound **15** to yield 14 mg (54%) of ketone **18** as an oil which behaved homogeneously by tlc; ir ($CHCl_3$): 1760 (phenolic acetate), 1740 (five-membered ring ketone), 1705 cm^{-1} (acyl ketone); ^1H nmr ($CDCl_3$) δ: 4.92 (m, 1H, —CH—O), 2.47 (s, 3H, $-COCH_3$), 2.26 (s, 6H, two $-OCOCH_3$), 1.45 (d, J = 6 Hz, 3H, $-CH-CH_3$), 1.13 (s, 3H, $-CH_3$), 0.80 ppm (s, 3H, $-CH_3$). *Mol. Wt.* calcd. for $C_{24}H_{30}O_7$: 430; found (mass spectroscopy): 430.

Acetoxyroyleanone

Photolysis of 7-Acetoxyroyleanone ***5***

A solution of 7-acetoxyroyleanone **5** (300 mg) in anhydrous dimethoxyethane (150 ml) was irradiated using a 200 W medium pressure Hanovia mercury lamp with a Pyrex filter under argon at about −10°C for 7 h. Acetic anhydride (5 ml) and pyridine (10 ml) were immediately added to the reaction mixture and the solution was left overnight under argon. Removal of the solvent and usual work-up gave 320 mg of residue. Analysis of the residue by tlc on silica gel using 15% ether in benzene as developing solvent indicated that it consisted of two major products **21** and **22**, and two minor components **23** and **24**. Chromatography by preparative tlc on silica gel effected separation of the products. There was obtained 124 mg of starting material as its acetate, 92 mg of compound **21**, 102 mg of compound **22**, 26 mg of compound **23**, and 31 mg of compound **24** as thick oils. They behaved homogeneously by tlc in several solvent systems. The total yield was 65%.

Compound ***21***—ir ($CHCl_3$): 1770 (phenolic acetate), 1730 cm^{-1} (acetate); ^1H nmr ($CDCl_3$) δ: 6.03 (broad s, 1H, proton deshielded by acetoxyl), 5.27 and 4.92 (two broad s, 2H, vinylic protons), 2.32 (s, 6H, two acetoxy methyls), 2.23 (s, 3H, acetoxy methyl), 1.92 (broad s, 3H, vinylic methyl), 1.26 (s, 3H, tertiary methyl), 0.91 ppm (s, 6H, two tertiary methyls). *Mol. Wt.* calcd. for $C_{28}H_{36}O_8$: 500.2410; found (high resolution mass spectroscopy): 500.2412.

Compound ***22***—ir ($CHCl_3$): 1770 (phenolic acetate), 1728 cm^{-1} (acetate); ^1H nmr ($CDCl_3$) δ: 6.03 (broad s, 9H, proton deshielded by acetoxyl), 5.97 (d, J = 9 Hz, 1H, vinylic proton), 5.76 (m, 1H, vinylic proton), 2.30 (s, 3H, acetoxy methyl), 2.16 (s, 6H, two acetoxy methyls), 2.05 (s, 3H, acetoxy methyl), 1.83 (d, 3H, vinylic methyl), 1.25 (s, 3H, tertiary methyl), 0.90 ppm (s, 6H, two tertiary methyls). *Mol. Wt.* calcd. for $C_{28}H_{36}O_8$: 500.2410; found (high resolution mass spectroscopy): 500.2413.

Compound ***23***—ir ($CHCl_3$): 1772 cm^{-1} (phenolic acetate); uv (EtOH) λ_{max}: 225 (ε 11 600), 362 nm (ε 4650); ^1H nmr ($CDCl_3$) δ: 6.31 (m, 2H, vinylic protons), 5.25 and 4.90 (two broad s, 2H, vinylic protons), 2.36 (s, 3H, acetoxy methyl), 2.30 (s, 6H, two acetoxy methyls), 1.98 (broad s, 3H, vinylic methyl), 1.15 (s, 3H, tertiary methyl), 1.03 (s, 3H, tertiary methyl), 0.98 ppm (s, 3H, tertiary methyl). *Mol. Wt.* calcd. for $C_{26}H_{32}O_6$: 440.2198; found (high resolution mass spectroscopy): 440.2197.

Compound ***24***—ir ($CHCl_3$): 1792 cm^{-1} (phenolic acetate); uv (EtOH) λ_{max}: 234 (ε 11 100), 365 nm (ε 3407); ^1H nmr ($CDCl_3$) δ: 6.28 (m, 2H, vinylic protons), 6.13 (d, J = 12 Hz, 1H, vinylic proton), 5.93 (m, 1H, vinylic proton), 2.36 (s, 6H, two acetoxy methyls), 2.23 (s, 3H, acetoxy methyl), 1.83 (d, 3H, vinylic methyl), 1.16 (s, 3H, tertiary methyl), 1.02 (s, 3H, tertiary methyl), 0.98 ppm (s, 3H, tertiary methyl). *Mol. Wt.* calcd. for $C_{26}H_{32}O_6$: 440.2198; found (high resolution mass spectroscopy): 440.2193.

Hydrogenation of Compound ***23*** *to the Tetrahydroderivative* ***7***

Compound **23** (30 mg) was hydrogenated in methanol (10 ml) with 10% palladium-on-charcoal (30 mg) for 4 h. The palladium-on-charcoal was filtered off and the methanolic solution was evaporated to dryness. The product **7** was crystallized from ethanol and melted at 129°C. The yield was quantitative. Identity was established by comparison with an authentic sample in all respects (mp, ir, nmr); ir ($CHCl_3$): 1770 cm^{-1} (phenolic acetate); ^1H nmr ($CDCl_3$) δ: 2.34 (s, 3H, acetoxy methyl), 2.30 (s, 6H, two acetoxy methyls), 1.26 (s, 3H, tertiary methyl), 1.15 (d, J = 5 Hz, 6H, isopropyl), 0.93 ppm (s, 6H, two tertiary methyls). *Anal.* calcd. for $C_{26}H_{36}O_6$: C 70.24, H 8.19; found: C 70.15, H 8.24.

Hydrogenation of Compound ***24*** *to the Tetrahydroderivative* ***29***

Compound **24** (20 mg) was hydrogenated under the same

Can. J. Chem. Downloaded from www.nrcresearchpress.com by 210.87.254.40 on 09/05/12
For personal use only.

conditions used in the preparation of **7**. Crystallization from ethanol–water yielded **29**, mp 94°C, in a quantitative yield; ir ($CHCl_3$): 1770 cm^{-1} (phenolic acetate); ^1H nmr ($CDCl_3$) δ: 2.36 (s, 3H, acetoxy methyl), 2.26 (s, 6H, two acetoxy methyls), 1.24 (s, 3H, tertiary methyl), 0.91 (s, 6H, two tertiary methyls), 0.89 ppm (t, 3H, methyl). *Anal.* calcd. for $C_{26}H_{36}O_6$: C 70.24, H 8.19; found: C 70.36, H 8.24.

Hydrogenation of Compound 21

Compound **21** (100 mg) was hydrogenated in methanol (15 mg) with 10% palladium-on-charcoal overnight. The product was a mixture of two compounds which could be separated by preparative tlc on silica gel to yield the crystalline compound **7** (11 mg, 13%) and compound **25** (82 mg, 80%). Compound **25** was recrystallized from ethanol and showed mp 172°C.

Compound 25—ir ($CHCl_3$): 1770 (phenolic acetate), 1730 cm^{-1} (acetate); ^1H nmr ($CDCl_3$) δ: 5.97 (broad s, 1H, proton deshielded by acetoxyl), 2.30 (s, 9H, three acetoxy methyls), 2.03 (s, 3H, acetoxy methyl), 1.24 (s, 3H, tertiary methyl), 1.13 (d, J = 6 Hz, 6H, isopropyl), 0.89 ppm (s, 6H, two tertiary methyls). *Anal.* calcd. for $C_{28}H_{38}O_8$: C 66.99, H 7.63; found: C 67.06, H 7.70.

Hydrogenation of Compound 22

Compound **22** (48 mg) which was hydrogenated under the same conditions used for **21** yielded a mixture of two compounds. Preparative tlc on silica gel resulted in separation of the mixture to give 6 mg (14%) of crystalline compound **29** and 38 mg (80%) of compound **27**. Crystallization of **27** from ethanol–water gave an analytical sample, mp 144–146°C.

Compound 27—ir ($CHCl_3$): 1770 (phenolic acetate), 1730 cm^{-1} (acetate); ^1H nmr ($CDCl_3$) δ: 5.89 (broad s, 9H, proton deshielded by acetoxyl), 2.20 (s, 9H, three acetoxy methyls), 1.99 (s, 3H, acetoxy methyl), 1.21 (s, 3H, tertiary methyl), 0.92 (s, 6H, two tertiary methyls), 0.90 ppm (t, 3H, methyl). *Anal.* calcd. for $C_{28}H_{38}O_8$: C 66.99, H 7.63; found: C 67.12, H 7.74.

Conversion of Compound 25 to 7-Dehydroroyleanone 26

A mixture of compound **25** (40 mg) and *p*-toluenesulfonic acid (140 mg) in aqueous methanol (10 ml) was heated under reflux and under nitrogen for 2 days. The reaction mixture was diluted with water and extracted with chloroform three times. The combined extracts were washed with water and dried over anhydrous magnesium sulfate. Removal of the solvent gave a reddish brown residue. Purification by preparative tlc on silica gel and recrystallization from ethanol–water yielded the product **26** (11 mg, 48%), mp 168°C, and unchanged on admixture with an authentic sample. Identity was also established by comparison of ir, nmr, and tlc.

Conversion of Compound 27 to the Quinone Derivative 28

Compound **27** (38 mg) was converted to compound **28** under the same conditions used in the preparation of **26**. There was obtained after purification and recrystallization from ethanol–water 12 mg (54%) of the quinone **28** as red needles, mp 93°C; ir ($CHCl_3$): 3380 (hydroxyl), 1640 cm^{-1} (carbonyl); uv (EtOH) λ_{max}: 214 (ε 15 300), 247 (ε 7344), 330 nm (ε 6579); ^1H nmr ($CDCl_3$) δ: 7.28 (s, 1H, hydroxyl, exchanged with D_2O), 6.70 (m, 2H, vinylic protons), 1.03 (s, 9H, three tertiary methyls), 0.96 ppm (t, 3H, methyl). *Anal.* calcd. for $C_{20}H_{26}O_3$: C 76.46, H 8.34; found: C 76.58, H 8.41.

Royleanone Ether

Royleanone Methyl Ether (6) in Benzene

A solution of 316 mg of royleanone methyl ether **6** in 80 ml of dry benzene was flushed with argon, then irradiated at ca. 15°C for 6 h in a Rayonet apparatus using lamps with radiation peaked at 254 nm in a Corex vessel. After evaporation of the solvent the residue crystallized from methanol solution. The material from the mother liquor was separated on a 1000 μ, 20 × 20 cm plate using benzene for development. The crystals from methanol and the fastest moving yellow zone were recovered **6** (153 mg). A fast moving mauve zone was shown by mp and ^1H nmr spectrum to be royleanone (28 mg, 18%). The zone with lowest R_f was faintly colored but visible under uv light. It was rich in oxetanol **33** (82 mg, 50%). No other products could be characterized.

A comparable run was made using 207 mg of royleanone ether **6** under argon (7 h), then the products were acetylated by addition of 5 ml of acetic anhydride and 5 ml of pyridine followed by standing overnight at room temperature under argon. Unchanged ether (55 mg) was recovered, and 6 mg of royleanone acetate **1** (R = Ac) and 52 mg of oxetanol **33** isolated following preparative tlc. The photolysis rate was slower but the products identical when lamps peaked at 300 nm were used.

Oxetanol 33

This was purified by preparative tlc separation using 5% methanol in chloroform for development. It crystallized from hexane, mp 162–163°C, $[\alpha]_D$ +80° (*c*, 1.77, ethanol); ν_{max} 3570, 3360, 1710 and 1622 cm^{-1}; λ_{max} 248 (ε 11 700) and 316 nm (ε 1800); Raman spectrum ($CHCl_3$) ν_{max}: 1717 (m) and 1631 (s) cm^{-1}; ^1H nmr δ: 4.88 (1H, d, J = 5 Hz) and 5.15 (1H, d, J = 5 Hz), 4.3 (1H, s, OH), 2.7 (1H, m, —C*H*$(CH_3)_2$), 1.45 (3H, s), 1.18 (6H, d, J = 8 Hz), 0.95 (6H, s); ^{13}C nmr δ: 188.6 (s), 179.3 (s), 153.9 (s), 135.9 (s), 116.1 (s), 84.35 (t), 75.07 (s), 49.5 (m), 41.7 (m), 38.6, 36.7 (m), 33.4 (s + q), 24.5, 21.9, 21.35, 21.1, 20.65, 18.6, 18.0; ms *m/e*: 330 (M^+), 315, 298, 297, 288, 287, 219, and 193. *Anal.* calcd. for $C_{21}H_{30}O_3$: C 76.32, H 9.15; found: C 76.41, H 9.25. The compound was inert to acetic anhydride – pyridine (1:1) at room temperature. When quite pure **33** was purified by separation on a SiO_2 plate using benzene, no royleanone was produced.

Forty-eight milligrams of **33** was added under argon to a mixture of 2 ml of pure dioxane, 1 ml of water, and 100 mg of potassium hydroxide (two phases). The mixture was maintained at 60°C under argon for 1 h. The dioxane-rich phase became purple. The mixture was cooled, acidified, then evaporated to small volume under reduced pressure. Water was added then the products extracted into methylene chloride. After a wash with sodium bicarbonate solution the methylene chloride solution was dried and distilled. The residue was placed on a 500 μ, 20 × 20 cm plate and developed with benzene. The fastest moving zone (brownish-mauve, R_f 0.5) gave 14 mg of yellow material which gave crystals from methanol, mp 165°C. This was recrystallized from acetone–hexane as thin plates recrystallizing to laths at around 150°C, mp 173°C. This gave no mp depression with but gave identical ir and ^1H nmr spectra to those of royleanone.

Royleanone Methyl Ether 6 in Acetic Acid

Royleanone methyl ether (397 mg) in 160 ml of dry acetic acid flushed with argon was irradiated in a Rayonet apparatus with lamps peaked at 254 nm for 2.25 h. The solution was then evaporated to dryness at 40°C on a rotating evaporator. The solution of the residue in 20 ml of methylene chloride was stirred vigorously in air for 45 min. It was then washed with sodium bicarbonate solution, dried and distilled. The nmr spectrum of the products showed the presence of methylenedioxy phenol **30** (R = H) but the acetoxymethoxy compound was not clearly evident. The total product was acetylated overnight at room temperature using 2 ml of acetic anhydride and 2 ml of pyridine. The resulting brown gum was adsorbed on a column of 30 g of tlc silica gel and developed with methylene chloride. Fifteen 15-ml fractions were collected. The first five fractions contained 210 mg, including all the recognizable products. These were purified further by preparative tlc (CH_2Cl_2) giving in decreasing order of R_f 104 mg of methy-

Can. J. Chem. Downloaded from www.nrcresearchpress.com by 210.87.254.40 on 09/05/12
For personal use only.

lenedioxy acetate **30** (R = Ac), 20 mg of royleanone acetate (5%), and 43 mg of acetoxymethoxy quinone **31** (10%).

In a photolysis experiment similar to the above, 125 mg of methyl ether **6** in 40 ml of dry acetic acid was irradiated for 2 h. The product was worked up *without* acetylation, giving 27 mg of the methylenedioxyphenol **30** (R = H) (21%) and 29 mg of the acetoxymethoxyquinone **31** (20%).

Royleanone Methyl Ether in Acetic Acid – Acetic Anhydride

A solution of 224 mg of methyl ether **6** in 50 ml of acetic acid and 20 ml of acetic anhydride was irradiated using 254 nm lamps for 65 min under argon. The solvents were evaporated at 45°C under reduced pressure, then the residue dissolved in methylene chloride and washed with sodium bicarbonate. The resulting mixture was separated on a 1000 μ, 20 × 20 cm plate giving in order of decreasing R_f 80 mg of starting material, 43 mg (26%) of methylenedioxy acetate **30** (R = Ac), 36 mg of acetoxymethoxy quinone **31** (25%), and 15 mg (9%) of the monoacetate of dihydroroyleanone methyl ether **32** (R = Ac).

*Methylenedioxy Acetate **30** (R = Ac)*—This was only obtained as a glass, distilling over a short path at 120°C, 5×10^{-4} Torr; ν_{max} 1750 cm^{-1}; ^1H nmr δ: 5.9 (2H, s), 2.45–3.2 (4H), 2.3 (3H, s), 1.32 (3H, s), 1.23 (6H, d, J = 8 Hz), 0.92 (6H, s); ^{13}C nmr δ: 169.6, 143.7, 142.3, 140.4, 130.3, 121.6, 120.7, 99.9, 51.2, 41.6, 38.2, 36.8, 33.5, 26.2, 21.8, 21.0, 20.5, 19.1, and 18.5 ppm. *Anal.* calcd. for $C_{23}H_{32}O_4$: C 74.16, H 8.66; found: C 73.96, H 8.73. The acetate was recovered unchanged from 19 h in solution in 3 ml of methanol containing 0.1 ml of 70% perchloric acid.

*Methylenedioxy Phenol **30** (R = H)*—Potassium carbonate (200 mg) was added to a solution of 100 mg of methylenedioxy acetate **30** (R = Ac) in 5 ml of methanol containing 0.2 ml of water under argon. The mixture was stirred for 2 h under argon, then evaporated to small volume under reduced pressure. The residue was taken up in water, nearly neutralized, then extracted with methylene chloride. The 86 mg of orange gum recovered was a complex mixture by tlc. It was separated on a 20 × 20 cm, 1000 μ plate using double development with benzene. A yellow front zone gave 43 mg of quite pure **30** (R = H). It was followed by a mauve zone (19 mg) which crystallized and had the same R_f and ^1H nmr spectrum as royleanone; ν_{max}: 3600, 1420, 1065, 967, and 875 cm^{-1}; ^1H nmr δ: 6.85 (broad singlet, sharpening when D_2O added), 4.4 (broad s, OH), 3.3 (1H, m), 1.42 (3H, s), 1.30 (6H, s), 1.00 (3H, s), 0.97 (3H, s). The phenol was not appreciably acetylated after 40 h at room temperature in 1:1 acetic acid – acetic anhydride.

*Acetoxymethoxy Quinone **31***—This was obtained as a yellow glass, distilling at 120°C over a short path under 5×10^{-4} Torr; ν_{max}: 1755 and 1650 cm^{-1}; λ_{max}: 273 (ε 1.41×10^4) and 363 nm (ε 330); ^1H nmr δ: 5.9 (1H, d, J = 6 Hz), 5.6 (1H, d, J = 6 Hz), 3.2 (1H, m), 2.12 (3H, s), 1.33 (3H, s), 1.19 (6H, d, J = 7 Hz), 0.93 (6H, s); ^{13}C nmr spectrum had signals at 142.9, 135.8, 87, 51.5, 41.5, 38.7, 36.2, 33.5, 25.7, 24.9, 21.9, 20.7, 20.5, 20.35, 19.0, 17.5 ppm (carbonyl and some olefinic carbons not recorded due to slow relaxation). *Anal.* calcd. for $C_{23}H_{32}O_5$: C 71.10, H 8.30; found: C 71.15, H 8.30.

When 27 mg of **31** was added to 3 ml of methanol and 0.5 ml of water containing 100 mg of potassium hydroxide under argon an immediate purple color developed. After 1 h at room temperature the solution was evaporated, water added followed by dilute sulfuric acid to neutralize the base. The yellow product extracted by methylene chloride (25 mg) crystallized spontaneously. After one recrystallization from aqueous methanol it had mp 179°C. This had the same R_f (C_6H_6) as royleanone and gave no mp depression when mixed with it.

*Dihydroroyleanone Methyl Ether Monoacetate **32** (R = Ac)* This was a nearly colorless glass; ν_{max}: 3515 and 1755 cm^{-1}; ^1H nmr δ: 5.9 (1H, s, OH), 3.77 (3H, s), 3.0–3.6 (2H, m), 2.32 (3H, s), 1.35 (3?H, s), 0.94 (6H, s). The signals for the isopropyl methyl groups seemed to be split into a pair of doublets due to restricted rotation. The monoacetate **32** (R = Ac) was only partially converted to a diacetate in acetic anhydride – pyridine at room temperature in 18 h.

A solution of 75 mg of royleanone methyl ether **6** in 3 ml of acetic anhydride containing 30 mg of Adams' platinum oxide catalyst was shaken in a hydrogen atmosphere until colorless. The solution and apparatus was flushed with argon then 0.5 ml of pyridine added. After 19.5 h at room temperature the solution was filtered and evaporated. A solution of the residue in methylene chloride was washed with sodium bicarbonate solution, dried and distilled. The products were separated on a 1000 μ, 20 × 20 cm plate using chloroform. Methyl ether diacetate (δ: 3.73 (3H, s) and 2.37 (6H, s)) (48 mg) and methyl ether monoacetate (28 mg) were obtained. The latter gave a ^1H nmr spectrum identical to the photolysis product described above.

Acknowledgements

We thank Mr. H. Seguin for the microanalyses and nominal mass spectra and Mr. L. Turner for the ^{13}C nmr spectra. We are grateful to Dr. K. Haque for preliminary experiments on the photolysis of 7-acetoxyroyleanone.

1. O. E. Edwards, G. Feniak, and M. Los. Can. J. Chem. **40**, 1540 (1962).
2. (*a*) P. Rüedi and C. H. Eugster. Helv. Chim. Acta, **55**, 1994 (1972); (*b*) P. Rüedi and C. H. Eugster. Helv. Chim. Acta, **56**, 1129 (1973).
3. A. H.-J. Wang, I. C. Paul, R. Zelnik, K. Mizuta, and D. Lavie. J. Am. Chem. Soc. **95**, 598 (1973).
4. A. H.-J. Wang, I. C. Paul, R. Zelnik, D. Lavie, and E. C. Levy. J. Am. Chem. Soc. **95**, 580 (1974).
5. (*a*) M. Moir, P. Rüedi, and C. H. Eugster. Helv. Chim. Acta, **56**, 2539 (1973); (*b*) S. Arihara, P. Rüedi, and C. H. Eugster. Helv. Chim. Acta, **58**, 343 (1975).
6. R. Zelnik, J. A. McMillan, I. C. Paul, D. Lavie, N. G. Toscano, and R. R. DaSilva. J. Org. Chem. **42**, 923 (1977).
7. C. Huber, W. A. Court, J. P. Devlin, O. E. Edwards, and P. M. Scott. Tetrahedron Lett. 2545 (1974).
8. H. W. Moore and K. Folkers. J. Am. Chem. Soc. **88**, 564 (1966); A. Eckert. Ber. **58**, 313 (1925).
9. F. A. L. Anet and D. P. Mullis. Tetrahedron Lett. 737 (1969).
10. T. Otsuki. Bull. Chem. Soc. Jpn. **49**, 2596 (1976).
11. H. E. Zimmerman. Angew. Chem. Int. Ed. **8**, 1 (1969).
12. J. E. Baldwin and J. E. Brown. Chem. Commun. 167 (1969).
13. C. M. Orlando, Jr., H. Mark, A. K. Bose, and M. S. Manhas. J. Org. Chem. **33**, 2512 (1968).
14. S. Farid. Chem. Commun. 303 (1970); 73 (1971).
15. H.-J. Hansen. *In* Mechanism of molecular migrations. Vol. 3. *Edited by* B. S. Thyagarajan. Wiley-Interscience, New York, NY. 1971. pp. 177–236.
16. C. M. Orlando, Jr., H. Mark, A. K. Bose, and M. S. Manhas. J. Am. Chem. Soc. **89**, 6527 (1967).
17. R. Zelnik, J. A. McMillan, I. C. Paul, D. Lavie, V. G. Toscano, and R. R. DaSilva. J. Org. Chem. **42**, 923 (1977).
18. J. M. Bruce. *In* The chemistry of the quinonoid compounds. *Edited by* S. Patai. Wiley-Interscience, New York, NY. 1974. Chapt. 9, pp. 514–520.

Can. J. Chem. Downloaded from www.nrcresearchpress.com by 210.87.254.5 on 09/05/12
For personal use only.

Time resolved fluorescence of aqueous tryptophan[1]

D. M. RAYNER AND A. G. SZABO

Division of Biological Sciences, National Research Council of Canada, Ottawa, Ont., Canada K1A 0R6

Received December 1, 1977

D. M. RAYNER and A. G. SZABO. Can. J. Chem. **56**, 743 (1978).

The fluorescence decay of aqueous tryptophan is shown to be described by a two exponential decay function whose components have life-times of 3.14 ns and 0.51 ns. These components are assigned as the solvent equilibrated ^1L_a and ^1L_b states respectively. The time-resolved emission spectra are presented and can be resolved into two spectra with λ_{max} at 350 nm and 335 nm corresponding to these two states.

D. M. RAYNER et A. G. SZABO. Can. J. Chem. **56**, 743 (1978).

La décroissance de la fluorescence du tryptophane en solution aqueuse peut être décrite par une fonction de décroissance à deux exponentielles dont les composantes possèdent des temps de vie de 3.14 ns et 0.51 ns. On attribue respectivement ces composantes aux états ^1L_a et ^1L_b en équilibre avec le solvant. On présente les spectres d'émission résolus dans le temps et on peut les résoudre en deux spectres avec des λ_{max} à 350 nm et 335 nm correspondants à ces deux états.

[Traduit par le journal]

The fluorescence properties of the amino acid L-tryptophan and its parent indole ring system have been widely investigated both because of their intrinsic interest and their importance in the interpretation of the fluorescence properties of peptides and proteins.

The fluorescence lifetime of tryptophan in neutral aqueous solution has been reported by workers using instruments of varying degrees of sophistication, to exhibit single exponential decay with a lifetime of $\sim$3 ns (1–6). We have recently developed a fluorescence lifetime system and technique with the express purpose of obtaining data accurate enough to allow the confident determination of multi-exponential decay parameters (7, 8). We can now show that the fluorescence of L-tryptophan in neutral aqueous solution decays by a double exponential process.

The lifetime system was identical to that described previously (7) except a thermostated sample block was used. Solutions were deoxygenated by bubbling with nitrogen. The ratio correction technique developed to correct for the variation of the instrumental time-response function with wavelength (8) was used in all the experiments. Deconvolution was carried out using a non-linear least-squares fitting procedure (9). The quality of fit, and hence our confidence in the decay model and parameters found, was judged primarily by the inspection of weighted residual plots (7, 8). Our instrument and techniques were tested by measuring the fluorescence decay of the scintilator PPD in ethanol for which our confidence criteria were well met, as required, by a single exponential model ($\tau = 1.35 \pm 0.04$).

When we measured the fluorescence decay of L-tryptophan in cacodylate buffer, pH = 7, at 20°C, with $\lambda_{ex} = 280$ nm we found that our confidence criteria required a double exponential function for an adequate fit in the emission wavelength range 310–370 nm. Our results show that the lifetimes are similar at all wavelengths but the ratio of pre-exponentials increases with wavelength and is always positive until at 380 nm only single exponential behaviour is found (Table 1). The recurrence of the same two lifetimes with changing emission wavelength allows us to state that the double exponential decay represents a physical model for the decay process and is not arbitrary mathematical curve fitting. While our experience with the instrument and with the correction and deconvolution procedures gave us a high degree of confidence in these results, the significance of our observations demanded that artifactual explanations be eliminated. We found that similar results were obtained using L-tryptophan from several sources; using samples without prior purification; using samples after several recrystallizations from either water or water–ethanol solutions; and using samples in phosphate rather than cacodylate buffer. Sample decomposition was imperceptible using spectrophotometric and fluorimetric measurements. We confirmed that there was negligible scattered light.

The mean lifetime of the long-lived component is

[1]NRCC No. 16507.

Can. J. Chem. Downloaded from www.nrcresearchpress.com by 210.87.254.5 on 09/05/12
For personal use only.

TABLE 1. Fluorescence lifetimes and ratio of pre-exponentials for double exponential decay behaviour of aqueous tryptophan[a]

$\lambda_{em} \times nm^{-1}$	$\tau_1 \times ns^{-1}$	$\tau_2 \times ns^{-1}$	α_1/α_2
310	3.08±0.15	0.46±0.16	0.96±0.15
315	3.18±0.08	0.54±0.11	1.15±0.10
320	3.13±0.05	0.48±0.07	1.41±0.11
320	3.20±0.19	0.85±0.27	1.68±0.30
325	3.10±0.03	0.31±0.07	1.63±0.24
325	3.31±0.04	0.58±0.07	1.72±0.20
330	2.91±0.06	0.88±0.14	2.40±0.23
330	3.32±0.03	0.44±0.07	1.82±0.16
335	3.30±0.03	0.44±0.08	1.89±0.21
340	3.17±0.04	0.67±0.12	2.88±0.18
350	3.15±0.05	0.65±0.23	4.52±0.54
350	2.97±0.02	0.37±0.13	3.76±0.82
350	3.16±0.04	0.94±0.15	4.11±0.37
360	3.25±0.03	0.65±0.14	4.32±0.31
370	3.17±0.05	0.78±0.36	7.3 ±1.2
370	3.20±0.05	0.54±0.11	7.4 ±1.1
380	3.10±0.01	—	—

[a]20°C, pH 7; $\lambda_{ex} = 280$ nm; weighted mean $\tau_1 = 3.13 \pm 0.02$, $\tau_2 = 0.51 \pm 0.04$.

3.13 ± 0.2 ns, the same as the single exponential lifetime found at 380 nm. The mean lifetime of the short-lived component is 0.51 ± 0.04 ns. The fluorescence decay was also measured with $\lambda_{em} = 330$ nm at two other excitation wavelengths, 265 nm and 300 nm. Double exponential decay with the same kinetic parameters as at $\lambda_{ex} = 280$ nm were found in both cases showing that the decay is independent of excitation wavelength. Time resolved spectra have been generated from the decay curves and show a shift to lower energy with time (Fig. 1).

Several physical models which include two excited states or species have been suggested earlier to explain the steady state fluorescence properties of indoles. The concept of a solvent exiplex (10, 11) has been presented to explain the large Stokes shift observed for indole in water ($\lambda_{max} = 350$ nm) compared with non-polar solvents ($\lambda_{max} = 305$ nm). The emission observed at 350 nm in water where none is seen in non-polar solvents is assumed to be due to the exiplex. However, such a system requires that in the spectral region where the exiplex fluorescence predominates the pre-exponentials must be equal but opposite. This is not the case. We favour a physical model based on concepts suggested by other workers (12–16) involving two separate solvent stabilized states. We suggest excitation of tryptophan to its manifold of excited singlet states results in rapid partitioning between the coupled ^1L_a and ^1L_b states which initially have a solvent environment similar to the ground state. While both states have dipole moments which differ from the ground state, the dipole moment change of the ^1L_a state is substantial and solvent relaxation results in the solvent relaxed ^1L_a state being below the ^1L_b state. The population

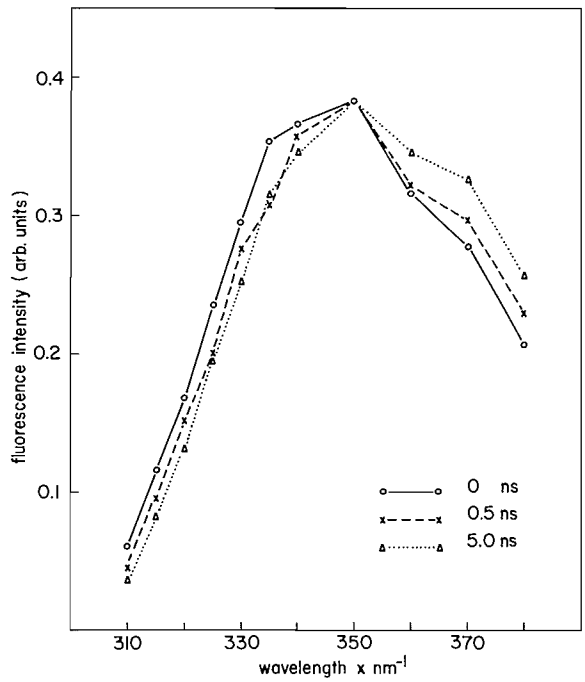

FIG. 1. Time-resolved emission spectra at $t = 0$, 0.5, and 5 ns of aqueous tryptophan normalized to the peak at 350 nm.

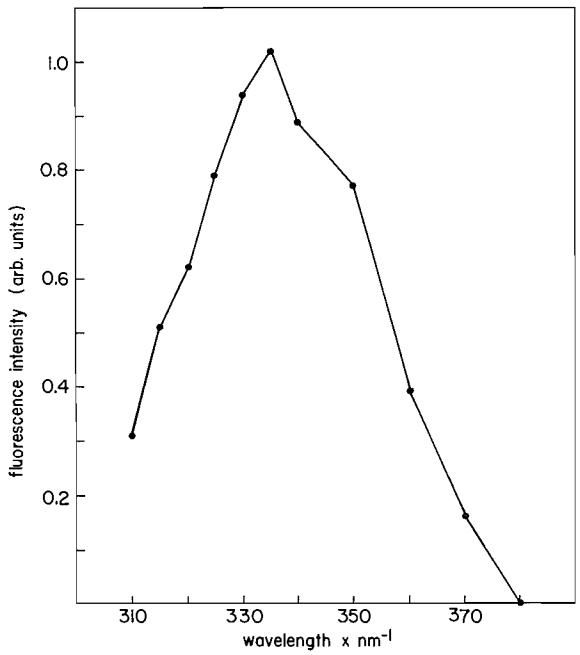

FIG. 2. Calculated (see text) emission spectrum of the fast decay component ($\tau = 0.51$ ns) at $t = 0$ ns.

distribution of the two states is dependent on the initial distribution prior to solvent reorientation after which the two states are no longer readily interconvertible. Hence double exponential decay is observed with the pre-exponentials depending on the overlap of the emission bands of the two solvent re-

laxed states. We can generate the spectrum of the short-lived component from the time resolved spectra assuming only the long-lived component emits at 380 nm (Fig. 2). We find the short-lived component has $\lambda_{max} = 335$ nm. This short-lived component we assign to the solvent equilibrated ^1L_b state. The long-lived component with $\lambda_{max} = 350$ nm we assign to the ^1L_a state.

In conclusion we have demonstrated the double exponential decay of tryptophan fluorescence in aqueous solution. This result can be explained most simply by a model involving two non-interconvertible states which we suggest are the solvent relaxed ^1L_a and ^1L_b states. To confirm or reject this proposal we are currently investigating the effect of temperature and solvent on the fluorescence decay of tryptophan and other indoles. On the other hand our results have implications in the interpretation of protein fluorescence. Current interest in the heterogeneity of protein fluorescence (17) makes the observations of double exponential decay from tryptophan in solution especially important.

1. I. WEINRYB and R. F. STEINER. *In* Excited states of proteins and nucleic acids. *Edited by* R. F. Steiner and I. Weinryb. Plenum Press, New York. 1971. p. 277.
2. R. W. RICCI. Photochem. Photobiol. **12**, 67 (1970).
3. R. MCGUIRE and I. FELDMAN. Photochem. Photobiol. **18**, 119 (1973).
4. R. F. STEINER and E. P. KIRBY. J. Phys. Chem. **74**, 4480 (1969).
5. W. B. DELAUDER and P. WAHL. C. R. Acad. Sci. Paris, **270***b*, 1115 (1970).
6. G. WEBER and J. R. LAKOWICZ. Chem. Phys. Lett. **22**, 419 (1973).
7. D. M. RAYNER, A. E. MCKINNON, A. G. SZABO, and P. A. HACKETT. Can. J. Chem. **54**, 3246 (1976).
8. D. M. RAYNER, A. E. MCKINNON, and A. G. SZABO. Rev. Sci. Instrum. **48**, 1050 (1977).
9. A. E. MCKINNON, A. G. SZABO, and D. MILLER. J. Phys. Chem. **81**, 1564 (1977).
10. T. R. HOPKINS and R. LUMRY. Photochem. Photobiol. **15**, 555 (1972).
11. M. S. WALKER, T. W. DEDRAR, and R. LUMRY. J. Chem. Phys. **47**, 1020 (1967).
12. S. V. KONEV. Fluorescence and phosphorescence of proteins and nucleic acids. Plenum Press, New York. 1967.
13. A. KAWSKI and I. GRYCZYNSKI. Bull. Acad. Polon. Sci. **21**, 1061 (1973).
14. M. SUN and P. S. SONG. Photochem. Photobiol. **25**, 3 (1977).
15. G. WEBER. Biochem. J. **75**, 335 (1960).
16. N. KAKASHIMA, H. INOUE, N. MATAGA, and C. YAMANAKA. Bull. Chem. Soc. Jpn. **46**, 2288 (1973).
17. A. GRINVALD and I. Z. STEINBERG. Biophys. J. **19**, 74 (1977).

Can. J. Chem. Downloaded from www.nrcresearchpress.com by 210.87.254.5 on 09/05/12
For personal use only.

Canadian Journal of Chemistry

Published by
THE NATIONAL RESEARCH COUNCIL OF CANADA

Volume 56 Number 6 March 15, 1978

Journal canadien de chimie

Publié par
LE CONSEIL NATIONAL DE RECHERCHES DU CANADA

Volume 56 numéro 6 15 mars 1978

Relationship between Taft and Kirkwood–Westheimer equations

BO-LONG POH

School of Chemical Sciences, Universiti Sains Malaysia, Penang, Malaysia

Received July 29, 1977

BO-LONG POH. Can. J. Chem. **56**, 747 (1978).

The relationship between Taft and Kirkwood–Westheimer equations has been derived with the use of the modified MacInnes equation.

BO-LONG POH. Can. J. Chem. **56**, 747 (1978).

Faisant appel à une équation modifiée de MacInnes, on a déduit la relation qui existe entre les équations de Taft et de Kirkwood–Westheimer.

[Traduit par le journal]

Introduction

Two approaches have been used by chemists to correlate the reactivities of molecules with their structures, one based upon fundamental theory and the other purely empirical. The Kirkwood–Westheimer cavity model (1) represents the first approach and Taft equation (2) the second approach, in the correlation of substituent effects upon the ionizations of organic acids in which polar effect is the only contribution. Attempts have been made to give theoretical interpretations (3, 4) to the empirical Taft equation to understand its successes and failures, but the relationships between the parameters of Taft equation (eq. 2) and those of Kirkwood-Westheimer equations (eqs. 5, 6) still remain unsolved. We report in this paper the relationships between them.

Results and Discussion

In an earlier paper (5) we have shown the relationship between our modified MacInnes equation (eq. 1) and Taft equation. The parameter S is related to σ^* in the form of eq. 3 and l_1^2/l^2 related to ρ^* in the form of eq. 4 (S is an empirical constant, l is the distance between the substituent and the ionizing proton, and l_1 refers to this distance in XCH_2-COOH). Equation 1 is also related to Kirkwood–Westheimer eqns. (e refers to the electronic charge, μ is the dipole moment, θ is the angle between the dipole axis and the line joining the reaction site to the dipole, D_e is the effective dielectric constant, k is Boltzmann constant, and T is the absolute temperature). For charged substituents the relationship is

$$[1] \quad pK_a - pK_0 = Sl_1^2/l^2$$

$$[2] \quad pK_a - pK_0 = -\sigma^* \rho^*$$

$$[3] \quad \sigma^* = -0.58S$$

$$[4] \quad \rho^* = 1.72l_1^2/l^2$$

$$[5] \quad pK_a - pK_0 = -e^2/(2.3kTD_e l)$$

for charged substituents

$$[6] \quad pK_a - pK_0 = -e\mu \cos\theta/(2.3kTD_e l^2)$$

for dipolar substituents

$$[7] \quad S = -e^2 l/(2.3kTD_e l_1^2)$$

for charged substituents

$$[8] \quad S = -e\mu \cos\theta/(2.3kTD_e l_1^2)$$

for dipolar substituents

given by eq. 7 which implies that for a given series of acids with the same charged substituent the factor l/D_e is a constant for a given medium and temperature. The results in Table 1 for some ω-substituted amino acids support this prediction. For dipolar substituents the relationship is given by eq. 8 which implies that $\cos\theta/D_e$ is a constant for a given series of acids with the same substituent in a given medium and temperature. The results in Table 2 for some

Can. J. Chem. Downloaded from www.nrcresearchpress.com by 210.87.254.42 on 09/05/12
For personal use only.

TABLE 1. l/D_e values for $\overset{+}{N}H_3(CH_2)_nCOOH$ in water at 25°C

n	l* (Å)	D_e†	l/D_e
1	3.97	30.2	0.13
2	5.54	46.0	0.12
3	6.55	52.5	0.12
4	8.00	58.0	0.14
5	9.09	60.3	0.15

*Calculated for fully extended conformation, the positive charge at 0.33 Å beyond the nitrogen atom and the carboxyl proton at 1.45 Å beyond the carboxyl carbon atom (ref. 12).
†Calculated using Tanford method (ref. 10) and data of D_e from ref. 11; the positive charge is placed at 1.0 Å below the cavity.

TABLE 2. $\cos\theta/D_e$ values* for $X(CH_2)_nCOOH$ in water at 25°C

	n	1	2	3	4
X = Cl	$\cos\theta$	0.559	0.951	0.669	0.906
	D_e	3.1	5.3	7.3	10.0
	$\cos\theta/D_e$	0.18	0.18	0.09	0.09
X = Br	$\cos\theta$	0.574	0.956	0.676	0.924
	D_e	3.7	5.5	7.8	12.0
	$\cos\theta/D_e$	0.16	0.17	0.09	0.08
X = I	$\cos\theta$	0.595	0.959	0.682	0.927
	D_e	3.8	5.5	7.8	12.5
	$\cos\theta/D_e$	0.16	0.17	0.09	0.07
X = OH	$\cos\theta$	0.500	0.946	0.656	0.906
	D_e	3.5	5.0	7.2	11.4
	$\cos\theta/D_e$	0.14	0.19	0.09	0.08

*θ was calculated for fully extended conformation; D_e calculated using Tanford method (ref. 10) and data of D_e from ref. 11; the dipole is placed at 1.5 Å below the cavity.

substituted carboxylic acids show qualitative agreement. The lack of better agreement is probably due to the fact that eqs. 1, 5, and 6 are not exact equations.

A comparison of eqs. 3, 7, and 8 suggests that it would be more consistent with Kirkwood–Westheimer's cavity model if Hammett (6) had originally defined the parameter σ (therefore σ*) as dependent on all the factors characterizing the reaction series instead of as a constant characteristic of the substituent only because eqs. 7 and 8 show the inverse proportionality between S (therefore σ*) and T and D_e. It would also be more consistent if the parameter ρ* were defined as independent of all the factors characterizing the reaction series instead of dependent on them because eq. 4 shows that ρ* could be expressed as inversely proportional to l^2 only. However, owing to Hammett's original arbitrary definitions of σ and ρ, the terms T and D_e for σ* (eqs. 7 and 8) refer to 25°C and water as the solvent respectively, and the inverse proportionality to T and D_e is transferred to the parameter ρ*. Similar conclusions regarding the inverse proportionality between ρ* and T and D_e have also been reported by several workers (4, 7–9). It is hoped that the relationship between Taft and Kirkwood–Westheimer equations given above will lead to better understanding and improvement of these equations and the Hammett equation as well.

Acknowledgement

The author wishes to thank the Universiti Sains Malaysia for a Short Term Research Project Grant.

1. J. G. KIRKWOOD and F. H. WESTHEIMER. J. Chem. Phys. **6**, 506 (1938); **6**, 513 (1938).
2. R. W. TAFT, JR. and I. C. LEWIS. J. Am. Chem. Soc. **81**, 5343 (1959).
3. S. EHRENSON. *In* Progress in physical organic chemistry. Vol. 2. Interscience, New York. 1964.
4. O. EXNER. *In* Advances in linear free energy relationships. Plenum Press, London. 1972.
5. B. L. POH. Can. J. Chem. In press.
6. L. P. HAMMETT. Physical organic chemistry. McGraw-Hill, New York. 1940.
7. L. P. HAMMETT. J. Am. Chem. Soc. **59**, 96 (1937).
8. I. A. KOPPEL and V. A. PALM. *In* Advances in linear free energy relationships. Plenum Press, London. 1972.
9. H. H. JAFFE. Chem. Rev. **53**, 191 (1953).
10. C. TANFORD. J. Am. Chem. Soc. **79**, 5348 (1957).
11. J. T. EDWARD, P. G. FARRELL, and J. L. JOB. J. Chem. Phys. **57**, 5251 (1972).
12. F. H. WESTHEIMER and M. W. SHOOKHOOF. J. Am. Chem. Soc. **61**, 555 (1939).

Can. J. Chem. Downloaded from www.nrcresearchpress.com by 210.87.254.42 on 09/05/12
For personal use only.

Effect of hydrocarbon solutes on electron ranges and free ion yields in liquid xenon[1]

TOYOAKI KIMURA[2] AND GORDON R. FREEMAN

Chemistry Department, University of Alberta, Edmonton, Alta., Canada T6G 2G2

Received August 4, 1977

TOYOAKI KIMURA and GORDON R. FREEMAN. Can. J. Chem. **56**, 749 (1978).

The energy transfer efficiency ratio, ETE = $(\sigma_h \Delta E_h / \sigma_x \Delta E_x)$, for hydrocarbons dissolved in liquid xenon has the following values: ethane, 96; propane, 180; *n*-butane, 485; ethylene, 193; propylene, 255; *cis*-butene-2, 425; *trans*-butene-2, 665. The large increase on going from propane to butane is attributed to the energy absorption capability of the C_2H_5 groups through rotation about the central bond in butane. The presence of a double bond in the molecule enhances ETE, presumably through the participation of transient negative ion states in the energy transfer process. The *cis–trans* effect in butene-2 is still not understood.

TOYOAKI KIMURA et GORDON R. FREEMAN. Can. J. Chem. **56**, 749 (1978).

Les valeurs des rapports d'efficacité de transfert d'énergie ETE = $(\sigma_h \Delta E_h / \sigma_x \Delta E_x)$, pour des hydrocarbures dissous dans le xénon liquide sont les suivantes: éthane, 96; propane, 180; *n*-butane, 485; éthylène, 193; propylène, 255; butène-2 *cis*, 425; butène-2 *trans*, 665. On a attribué l'augmentation rapide qui se produit lorsque l'on passe du propane au butane à une capacité d'absorption de l'énergie des groupes C_2H_5 par l'intermédiaire d'une rotation autours du lien central du butane. La présence d'une double liaison dans la molécule augmente la valeur du rapport ETE probablement à cause d'une participation d'états ioniques négatifs de transition dans le processus de transfert d'énergie. On ne comprend toujours pas l'effet *cis–trans* dans le butène-2.

[Traduit par le journal]

Introduction

It has long been known that electrons move more freely in liquid argon than in liquid nitrogen or hydrocarbons (1–4). For many nonpolar substances the freedom of electron motion correlates approximately with the degree of sphericity of the molecules (5). Exceptions are helium (1, 6, 7) and neon (8–10), which have low polarizabilities, and substrates that capture electrons (1).

As a result of the relative freedom of motion, the penetration ranges of low energy electrons into the liquids argon, krypton, and xenon are an order of magnitude greater than those into nonspherical hydrocarbons (11, 12). It is of interest to study the rate at which addition of nonspherical hydrocarbons to a noble liquid decreases the electron penetration range. In this way information can be obtained about electron scattering by individual molecules in the liquid phase. Xenon is a convenient solvent to use for such measurements, because its normal boiling point (165 K) is sufficiently high that simple alkanes will not freeze in it.

Experimental

Materials and Sample Preparation

The hydrocarbons were Phillips research grade and the xenon was Linde research grade from Union Carbide Co. The materials were purified by techniques similar to those reported earlier (11, 12). Potassium mirrors were used for the final treatment of xenon, ethane, ethylene, and propylene, while liquid Na/K alloy (1/4 by weight) was used for the other compounds. The treatments with metal lasted one week, the mirrors being renewed under vacuum twelve times during that period.

The amounts of xenon and hydrocarbons used to make a solution were measured by PVT. They were mixed in the gas phase and condensed together into the conductance cell.

The cell used for xenon and the solutions is shown in Fig. 1*b* of ref. 11*a*, and that for the pure hydrocarbons is described in ref. 13.

The low temperature baths and the method of temperature control were similar to those described in ref. 14.

Determination of the Free Ion Yields

The free ion yields were measured by the charge clearing technique (12, 15). The pulse length was usually 100 ns, but was 1 μs for the pure hydrocarbons and the 70% hydrocarbon solutions. The respective pulse doses were 2×10^{10} and 1×10^{11} eV/g. Thermoluminescent dosimetry was normalized to a more accurate technique (12) that employed solid cesium iodide powder as "dummy xenon" in the cell, because it has an average atomic number equal and a density similar to that of liquid xenon.

Physical Properties of the Liquids

The densities and dielectric constants of the pure compounds were taken from refs. 11*b* and 13. These properties were assumed to be additive in the solutions.

Results

Free ion yields were measured at 168 and 192 K in xenon, in solutions containing 1, 2, 4, 10, 20, 40, and 70 mol% hydrocarbon, and in pure hydrocarbon. The

[1]Assisted financially by the National Research Council of Canada.

[2]Postdoctoral fellow 1972–1974. Present address: Department of Synthetic Chemistry, Nagoya University, Nagoya, Japan.

Can. J. Chem. Downloaded from www.nrcresearchpress.com by 210.87.254.105 on 09/05/12
For personal use only.

Can. J. Chem. Downloaded from www.nrcresearchpress.com by 210.87.254.105 on 09/05/12
For personal use only.

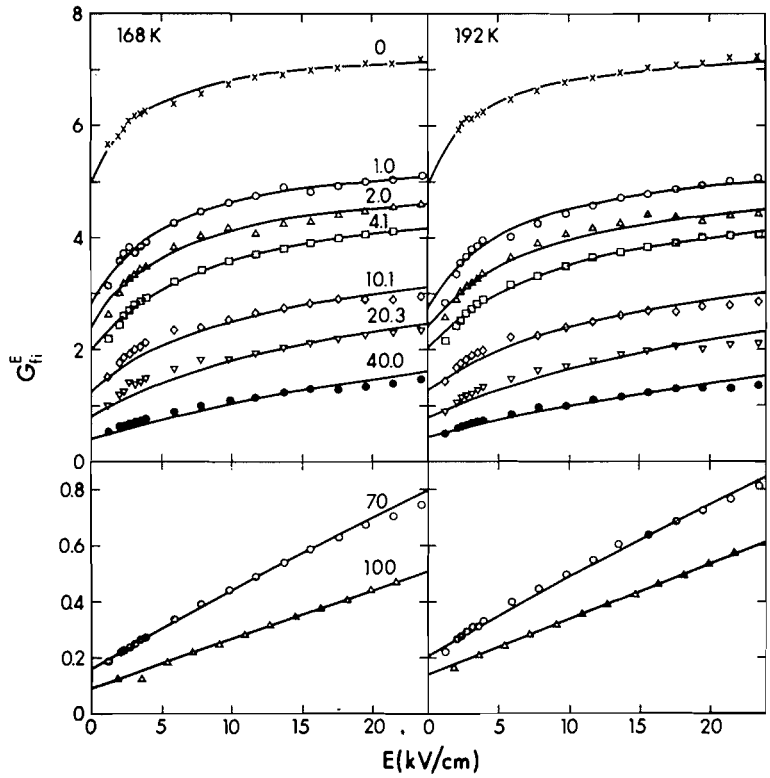

FIG. 1. Free ion yields in xenon/ethane solutions at 168 and 192 K. The numbers labelling the curves are mol% ethane. The solid curves were calculated from the model.

alkanes and olefins used were ethane, propane, *n*-butane, ethylene, propylene, *cis*-butene-2, and *trans*-butene-2.

Addition of 1 mol% of ethane to xenon caused the free ion yield to drop by about 35% (Fig. 1). Further additions decreased the yield monotonically. The yield extrapolated to zero applied field, G_{fi}^{0}, in pure ethane at 168 K was only 2% of that in pure xenon.

The behaviour was similar at 168 and 192 K (Fig. 1). The temperature was changed mainly in an attempt to detect phase separation in the solutions, if it should occur, because the sample in the thermostated box could not be monitored visually. No evidence of phase separation was obtained in any of the solutions.

Propane (Fig. 2) decreased the ion yields somewhat more than did ethane, and butane decreased it still further. To save space, the butane data are not displayed.

The effect of ethylene (Fig. 3) at low concentrations was similar to that of ethane. At higher concentrations ethylene caused a greater lowering of the free ion yield than did ethane, culminating in a tenfold difference between the yields in the pure olefin and alkane (Figs. 1 and 3).

Propylene (data not shown) behaved similarly to propane at low concentrations. The relative effect of propylene increased with concentration. In the pure liquids, G_{fi}^{0}(propane)/G_{fi}^{0}(propylene) = 3.8, in agreement with earlier work (11*b*).

There is a surprisingly large difference between the free ion yields in the *cis* and *trans* isomers of butene-2 (13). These compounds were therefore of particular interest to study in the xenon solutions. In accord with the preceding descriptions, the behavior of the two isomers was similar at low concentrations, but the *trans* compound caused progressively greater decreases of the free ion yields at high concentrations (Figs. 4 and 5).

Model

The most probable distance that the secondary electrons penetrate the liquid away from their geminate ions is denoted b_{GP} (13). Values of b_{GP} were estimated for each solution by fitting the results in Figs. 1–5, and those from the *n*-butane and propylene solutions, to the Onsager model (13, 16). The field dependence of the electron mobility in xenon (17) indicates that the geminate electrons would have energies greater than thermal at the ion–

Can. J. Chem. Downloaded from www.nrcresearchpress.com by 210.87.254.105 on 09/05/12
For personal use only.

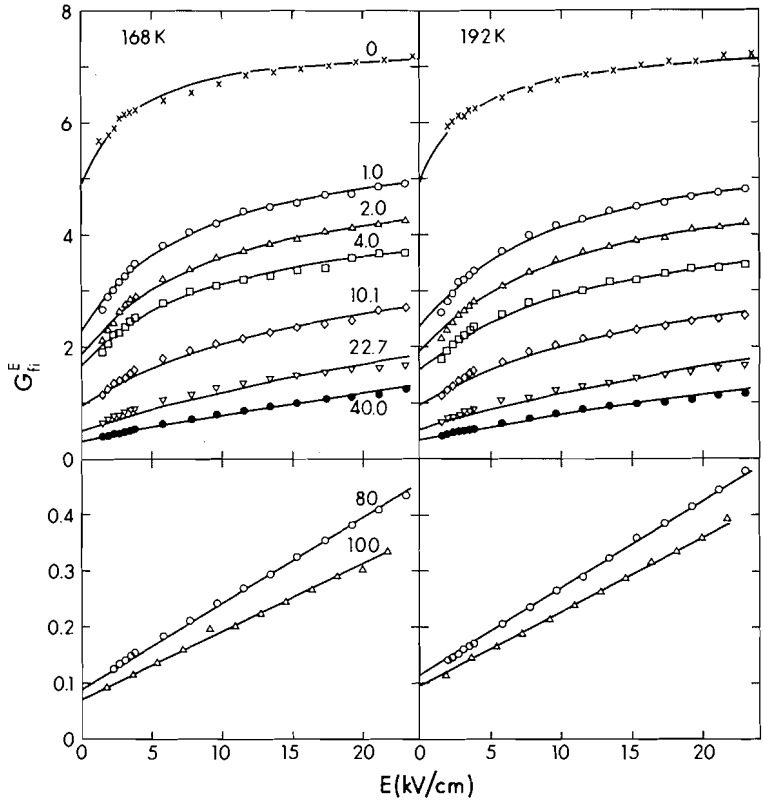

FIG. 2. Free ion yields in xenon/propane solutions at 168 and 192 K. The numbers labelling the curves are mol% propane. The solid curves were calculated from the model.

electron separation distances of major concern to us. However, the effect that the field-heating of the electrons has upon their escape probabilities depends upon the degree of anisotropy of the scattering, which is not known. Isotropic scattering would enhance the escape probability, whereas skew in the field direction would tend to favor recombination. For the lack of better knowledge, we assume that the field-heating effect does not greatly alter the escape probability that would be obtained in its absence.

Assumed values of G_{tot} varied from 3.9 for ethylene and 4.3 for *n*-butane (11*b*) to 7.4 for xenon (positive applied voltage (12)), with intermediate values for the solutions. The values obtained for b_{GP} are given in Fig. 6.

To simplify the following analysis of the secondary electron ranges b_{GP}, the parameter values that depend upon the solution composition, or on the electron energy and scattering angle, are assumed to be averages.

The first attempt was to use the model from ref. 15. However, it was found that it did not fit the results from the xenon/hydrocarbon solutions. The following analysis proved satisfactory.

During the thermalization of a secondary electron of initial energy E_0 it undergoes N_x collisions with xenon, losing energy ΔE_x per collision, and N_h collisions with the hydrocarbon, losing ΔE_h per collision. One can write:

$$[1] \qquad E_0 = N_x\Delta E_x + N_h\Delta E_h + 1.5kT \approx N_x\Delta E_x + N_h\Delta E_h$$

We represent the respective values of b_{GP} in pure xenon, pure hydrocarbon, and a solution as b_x, b_h, and b_s. Then assuming isotropic scattering (18):

$$[2] \qquad b_x \approx \sqrt{2N_x^0}/n_x^0\sigma_x$$

$$[3] \qquad b_h \approx \sqrt{2N_h^0}/n_h^0\sigma_h$$

$$[4] \qquad b_s \approx \sqrt{2N_s}/(n_x\sigma_x + n_h\sigma_h)$$

where n_x^0 and n_h^0 represent the respective numbers of molecules/cm^3, the superscript zeros indicate pure compounds, and

$$[5] \qquad N_s = N_x + N_h$$

Furthermore, the ratio N_x/N_h in a solution is related

Can. J. Chem. Downloaded from www.nrcresearchpress.com by 210.87.254.105 on 09/05/12
For personal use only.

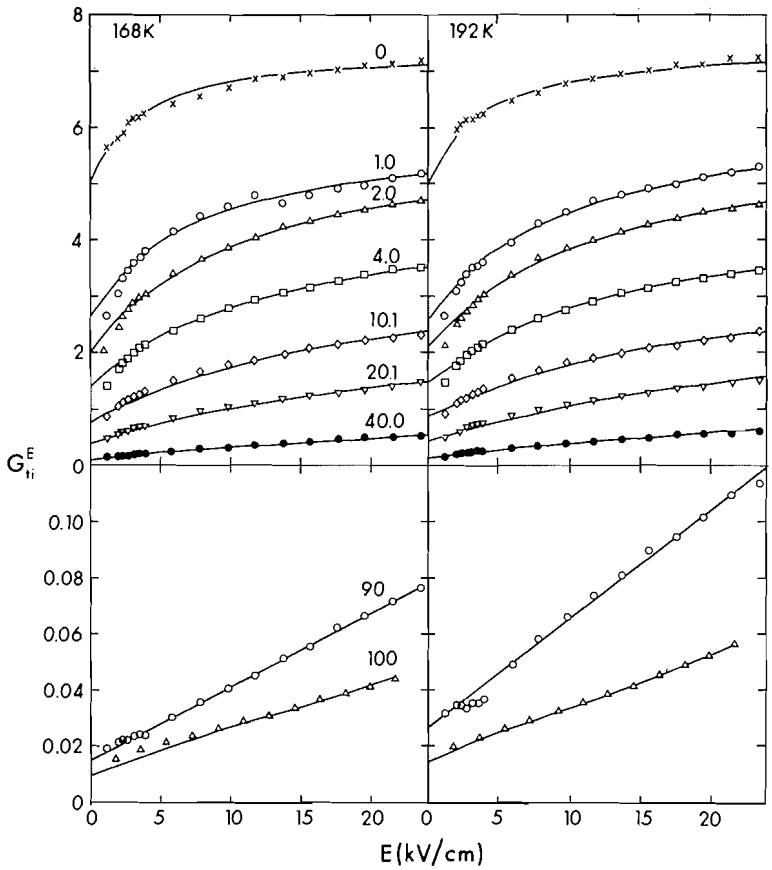

FIG. 3. Free ion yields in xenon/ethylene solutions at 162 and 192 K. The numbers labelling the curves are mol% ethylene. The solid curves were calculated from the model.

to the ratio of collision cross sections σ_x/σ_h through [6].

$$[6] \qquad N_x/N_h = n_x\sigma_x/n_h\sigma_h$$

From [1] and [6] one obtains

$$[7] \qquad N_h = \left(\frac{n_x\sigma_x}{n_h\sigma_h}\frac{\Delta E_x}{E_0} + \frac{\Delta E_h}{E_0}\right)^{-1}$$

and from [5]–[7]

$$[8] \qquad N_s = \left(\frac{n_x\sigma_x}{n_h\sigma_h} + 1\right)\Big/\left(\frac{n_x\sigma_x}{n_h\sigma_h}\frac{\Delta E_x}{E_0} + \frac{\Delta E_h}{E_0}\right)$$

Putting [8] in [4] gives

$$[9] \qquad b_s = \left[2\left(\frac{n_x\sigma_x}{n_h\sigma_h} + 1\right)\Big/\left(\frac{n_x\sigma_x}{n_h\sigma_h}\frac{\Delta E_x}{E_0} + \frac{\Delta E_h}{E_0}\right)\right]^{0.5} \times (n_x\sigma_x + n_h\sigma_h)^{-1}$$

To examine the behavior of [9] we make the gross assumptions that E_0, σ_x, and σ_h have similar values in the solutions and pure components. Then one may write

$$[10] \qquad \Delta E_x/E_0 = 1/N_x^0 = 2/(b_x n_x^0\sigma_x)^2$$

$$[11] \qquad \Delta E_h/E_0 = 1/N_h^0 = 2/(b_h n_h^0\sigma_h)^2$$

and

$$[12] \qquad b_s = \frac{[(n_r\sigma_r + 1)/(n_r\sigma_r E_x + E_h)]^{0.5}}{n_x\sigma_x + n_h\sigma_h}$$

where $n_r = n_x/n_h$, $\sigma_r = \sigma_x/\sigma_h$, $E_x = \Delta E_x/E_0$, and $E_h = \Delta E_h/E_0$.

Discussion

Iterative calculations were done with [12] by assigning values to σ_x and σ_r, and comparing calculated values of b_s with those obtained experimentally. The results were sensitive to the value of σ_r, but not to that of σ_x over a wide range. We therefore arbitrarily took $\sigma_x = 0.1$ Å^2, which is small due to diffraction effects. The 'best fit' values of $\sigma_r^{-1} = \sigma_h/\sigma_x$ are listed in Table 1 and the corresponding curves are displayed in Fig. 6.

Can. J. Chem. Downloaded from www.nrcresearchpress.com by 210.87.254.105 on 09/05/12
For personal use only.

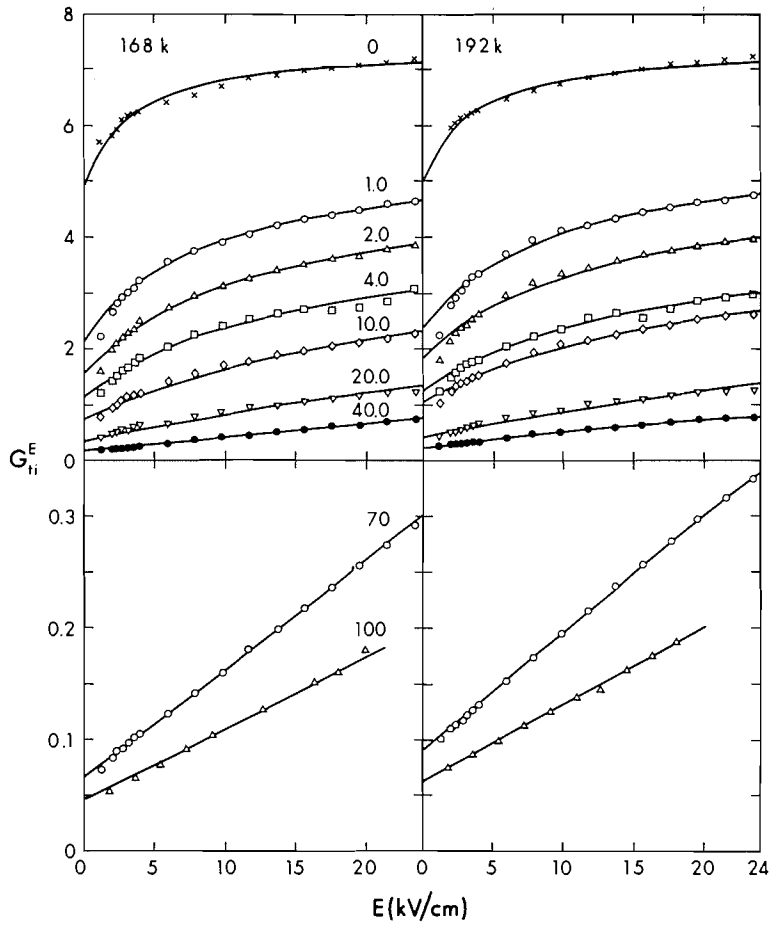

FIG. 4. Free ion yields in xenon/*cis*-butene-2 solutions at 162 and 192 K. The numbers labelling the curves are mol% *cis*-butene-2. The solid curves were calculated from the model.

TABLE 1. Electron range and energy transfer parameters

	168 K					192 K					
	b_x or b_h (Å)	n_x^0 or n_h^0 (10^{20}/cm^3)	σ_h/σ_x	$\Delta E_h/\Delta E_x$	ETE*	b_x or b_h (Å)	n_x^0 or n_h^0 (10^{20}/cm^3)	σ_h/σ_x	$\Delta E_h/\Delta E_x$	ETE*	ETE$_{av}$§
Xe	1100	139	1	1	1	1100	131	1	1	1	1
C_2H_6	100	114	2.1	41	86	106	109	1.5	70	105	96
C_3H_8	84	90	2.4	72	170	86	86	2.0	96	190	180
n-C_4H_{10}	59	72	2.6	190	490	62	70	2.3	210	480	485
C_2H_4	42	123	5.0	35	175	45	115	3.8	54	210	193
C_3H_6	41	97	6.0	40	240	45	93	4.4	62	270	255
cis-C_4H_8-2	59	82	2.4	178	430	59	79	2.3	182	420	425
trans-C_4H_8-2	38	80	4.1	151	620	40	77	3.0	238	710	665

*ETE = $(\sigma_h \Delta E_h/\sigma_x \Delta E_x)$.
§Average of the values at 168 and 192 K.

Can. J. Chem. Downloaded from www.nrcresearchpress.com by 210.87.254.105 on 09/05/12
For personal use only.

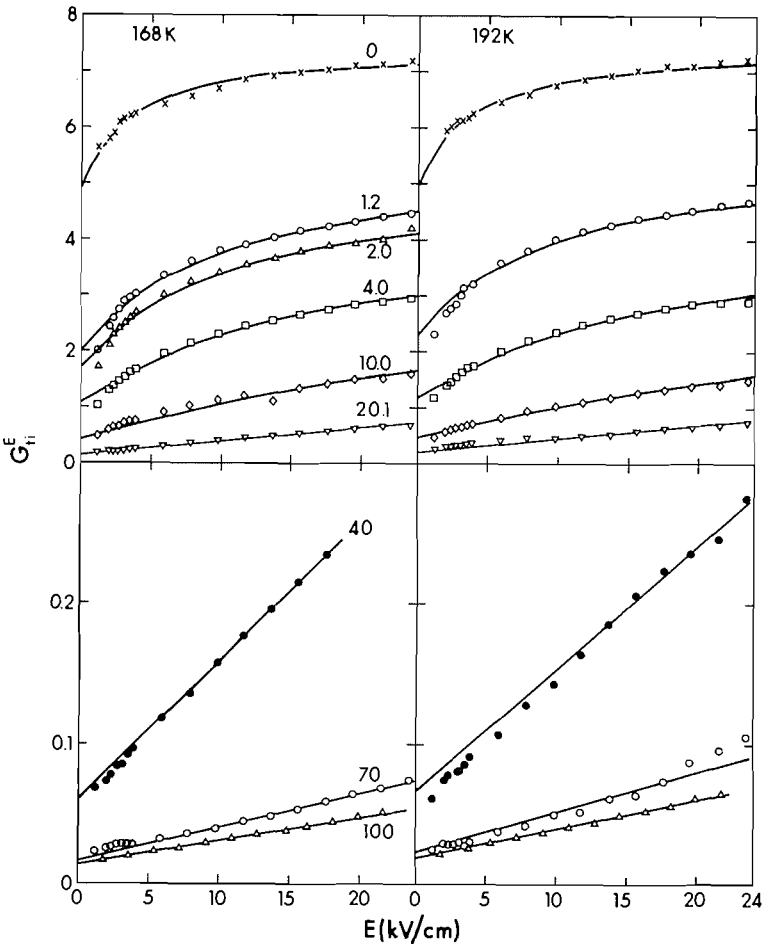

FIG. 5. Free ion yields in xenon/*trans*-butene-2 solutions at 162 and 192 K. The numbers labelling the curves are mol% *trans*-butene-2. The solid curves were calculated from the model.

Values of the energy transfer ratio $\Delta E_h/\Delta E_x$ were calculated from [13].

$$[13] \qquad \Delta E_h/\Delta E_x = (b_x n_x \sigma_x / b_h n_h \sigma_h)^2$$

This ratio is one to two orders of magnitude larger than the cross section ratio σ_h/σ_x (Table 1). However, there are variations within the series that may be associated with shortcomings of the model. At the present state of development a more dependable parameter is the over-all energy transfer efficiency ratio ETE, the product of the cross section and energy transfer ratios:

$$[14] \qquad \mathrm{ETE} = \frac{\sigma_h \Delta E_h}{\sigma_x \Delta E_x} = \frac{\sigma_x}{\sigma_h}\left(\frac{b_x n_x}{b_h n_h}\right)^2$$

Values of ETE range from about 100 in ethane to about 700 in *trans*-butene-2 (Table 1). The large values are related to the energy absorption capability of the vibrational and rotational modes of the polyatomic molecules.

The energy transfer efficiency doubles on going from ethane to propane, and more than doubles again on going to butane. The large increase between propane and butane is attributed to the rotation of the C_2H_5 groups about the central bond in butane.

Addition of a double bond to the molecule doubles ETE in the C_2 compounds and has smaller proportionate effects in the larger molecules (Table 1). The enhancement is attributed to energy transfer by way of transient negative ion states. The value of ETE for *cis*-butene-2 is *smaller* than that for *n*-butane, while that in *trans*-butene-2 is larger. This *cis–trans* effect was noted earlier (13, 19), but is still not understood. It seems to be related to the ease of rotation of the molecules in the liquid.

Can. J. Chem. Downloaded from www.nrcresearchpress.com by 210.87.254.105 on 09/05/12
For personal use only.

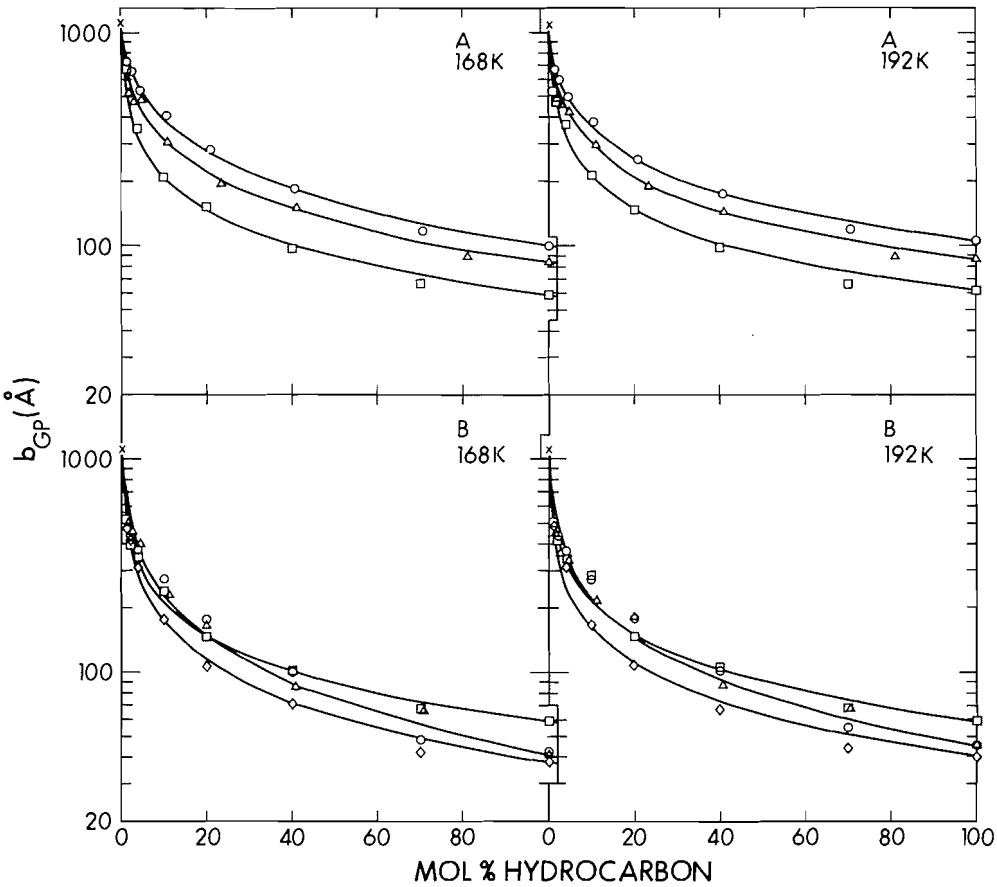

FIG. 6. Most probable ranges b_{GP} of secondary electrons in xenon/hydrocarbon solutions. ×, Pure xenon. *A*: ○, ethane; △, propane; □, *n*-butane. *B*: ○, ethylene; △, propylene; □, *cis*-butene-2; ◇, *trans*-butene-2. The curves were calculated from [12], using parameter values from Table 1. The curves for ethylene and propylene are the same, within the thickness of the line.

1. A. N. GERRITSEN. Physica, **14**, 407 (1948).
2. N. DAVIDSON and A. E. LARSH. Phys.Rev. **74**, 220 (1948); 77, 706 (1950).
3. R. L. WILLIAMS. Can. J. Phys. **35**, 134 (1957).
4. P. H. TEWARI and G. R. FREEMAN. J. Chem. Phys. **51**, 1276 (1969).
5. P. H. TEWARI and G. R. FREEMAN. J. Chem. Phys. **49**, 4394 (1968).
6. L. MEYER, H. T. DAVIS, S. A. RICE, and R. J. DONNELLY. Phys. Rev. **126**, 1927 (1962).
7. J. JORTNER, N. R. KESTNER, S. A. RICE, and M. H. COHEN. J. Chem. Phys. **43**, 2614 (1965).
8. G. R. FREEMAN. Gordon Conference on Radiation Chemistry, New Hampton, NH. July, 1966.
9. L. BRUSCHI, G. MAZZI, and M. SANTINI. Phys. Rev. Lett. **28**, 1504 (1972).
10. R. J. LOVELAND, P. G. LECOMBER, and W. E. SPEAR. Phys. Lett. A, **39**, 225 (1972).
11. M. G. ROBINSON and G. R. FREEMAN. Can. J. Chem. (*a*) **51**, 641 (1973); (*b*) **52**, 440 (1974).
12. S. S.-S. HUANG and G. R. FREEMAN. Can. J. Chem. **55**, 1838 (1977).
13. J.-P. DODELET, K. SHINSAKA, U. KORTSCH, and G. R. FREEMAN. J. Chem. Phys. **59**, 2376 (1973).
14. J.-P. DODELET and G. R. FREEMAN. Can. J. Chem. **55**, 2893 (1977).
15. W. F. SCHMIDT and A. O. ALLEN. J. Phys. Chem. **72**, 3730 (1968).
16. L. ONSAGER. Phys. Rev. **54**, 554 (1938).
17. J. S. MILLER, S. HOWE, and W. E. SPEAR. Phys. Rev. **166**, 871 (1968).
18. E. W. MCDANIEL. Collision phenomena in ionized gases. Wiley, New York, NY. 1964. pp. 49, 492.
19. J.-P. DODELET, K. SHINSAKA, and G. R. FREEMAN. J. Chem. Phys. **59**, 1293 (1973).

Effect of hydrocarbon solutes on electron mobilities in liquid xenon[1]

TOYOAKI KIMURA[2] AND GORDON R. FREEMAN

Chemistry Department, University of Alberta, Edmonton, Alta., Canada T6G 2G2

Received August 16, 1977

TOYOAKI KIMURA and GORDON R. FREEMAN. Can. J. Chem. **56**, 756 (1978).

Ethylene, propylene, *cis*-butene-2, *trans*-butene-2, ethane, propane, and *n*-butane were added to xenon at 168 and 192 K. At concentrations up to 4 mol%, electrons were scattered by one hydrocarbon molecule at a time and a gas phase model was used to estimate the scattering cross sections. The values for thermal electrons were, in Å^2: ethane, 2.7; propane, 4.6; *n*-butane, 7.2; ethylene, 4.7; propylene, 5.4; *cis*-butene-2, 7.4; *trans*-butene-2, 9.4. The scattering cross sections of the hydrocarbons dissolved in liquid xenon were about half of those in the gas phase, where comparisons could be made.

The mobility of electrons in pure xenon decreases with increasing electric field strength, due to heating of the electrons by the field. Addition of a small amount of hydrocarbon increases the mobility at high fields, eightfold by 4% of ethylene, propylene, or *cis*-butene-2 at 23.4 kV/cm and 192 K. The scattering cross sections of the hydrocarbons are two orders of magnitude larger than the effective cross section of liquid xenon, and the collisions with the hydrocarbons tend to prevent the electrons from becoming heated.

Electrons begin to form localized states in solutions containing 10 mol% hydrocarbon, or 20 mol% in the case of ethane. The mobility decreases approximately exponentially with concentration above these thresholds. The values of μ_0 for these exponential regions reflect the different scattering coefficients of the hydrocarbons: $\mu = \mu_0 \exp(-E_\mu/RT)$. The values of E_μ increase with molecular size in a series, and are greater for olefins than for alkanes. For the C_2 and C_3 hydrocarbons E_μ increases linearly with the mol fraction of hydrocarbon. *cis*-Butene-2 shows anomalous behaviour, as found earlier for electrons in the pure compound.

TOYOAKI KIMURA et GORDON R. FREEMAN. Can. J. Chem. **56**, 756 (1978).

On a ajouté de l'éthylène, du propylène, du butène-2 *cis*, du butène-2 *trans*, de l'éthane, du propane et du butane à du xénon à 168 et à 192 K. A des concentrations allant jusqu'à 4 mol%, les électrons sont dispersés par une molécule à la fois et on peut utiliser un modèle de phase gazeuse pour évaluer la section efficace de dispersion. Les valeurs pour les électrons thermiques sont, en Å^2: éthane, 2.7; propane, 4.6; butane, 7.2; éthylène, 4.7; propylène, 5.4; butène-2 *cis*, 7.4; butène-2 *trans*, 9.4. Dans le cas où il est possible de faire une comparaison, les valeurs des sections efficaces de dispersion des hydrocarbures dissous dans le xénon liquide correspondent à environ la moitié de celles en phase gazeuse.

La mobilité des électrons dans le xénon pur diminue avec une augmentation de l'intensité du champs électrique; ce résultat est dû à un échauffement des électrons par le champs. L'addition de petites quantités d'hydrocarbures augmente la mobilité à des hauts champs, environ 8 fois par l'addition de 4% d'éthylène, de propylène ou de butène-2 *cis* à 23.4 kV/cm et 192 K. Les sections efficaces de dispersion des hydrocarbures sont environ 100 fois plus grandes que la section efficace du xénon liquide et les collisions avec les hydrocarbures ont tendance à empêcher l'échauffement des électrons.

Les électrons commencent à former des états localisés dans des solutions contenant environ 10 mol% d'hydrocarbure, ou 20% dans le cas de l'éthane. La mobilité diminue presque exponentiellement avec la concentration au dessus de ces seuils. Ces valeurs de μ_0 pour ces régions exponentielles sont un reflet des différents coefficients de dispersion des hydrocarbures: $\mu = \mu_0 \times \exp(-E_\mu/RT)$. Les valeurs de E_μ augmentent avec la grosseur moléculaire dans les séries et sont plus grandes pour les oléfines que pour les alcanes. Dans le cas des hydrocarbures en C_2 et C_3, E_μ augmente d'une façon linéaire avec la fraction molaire de l'hydrocarbure. Le butène-2 *cis* présente un comportement anormal tel que trouvé antérieurement pour les électrons dans le liquide pur.

[Traduit par le journal]

Introduction

The mobility of electrons in liquid xenon (1, 2) is several orders of magnitude greater than that in most hydrocarbons (2–4). The high mobility is associated with the spherical shape and high polarizability of the molecules (3). The ability of small hydrocarbon molecules to scatter low energy electrons in the liquid is attributed to the electron interaction with rotational motions through the anisotropy of polarizability of the molecules.

In a continuing attempt to understand the behavior of electrons in liquids, we have added a series of hydrocarbons to xenon and measured their effects

[1]Assisted financially by the National Research Council of Canada.

[2]Postdoctoral fellow 1972–1974. Present address: Department of Synthetic Chemistry, Nagoya University, Nagoya, Japan.

Can. J. Chem. Downloaded from www.nrcresearchpress.com by 210.87.254.5 on 09/05/12
For personal use only.

Can. J. Chem. Downloaded from www.nrcresearchpress.com by 210.87.254.5 on 09/05/12
For personal use only.

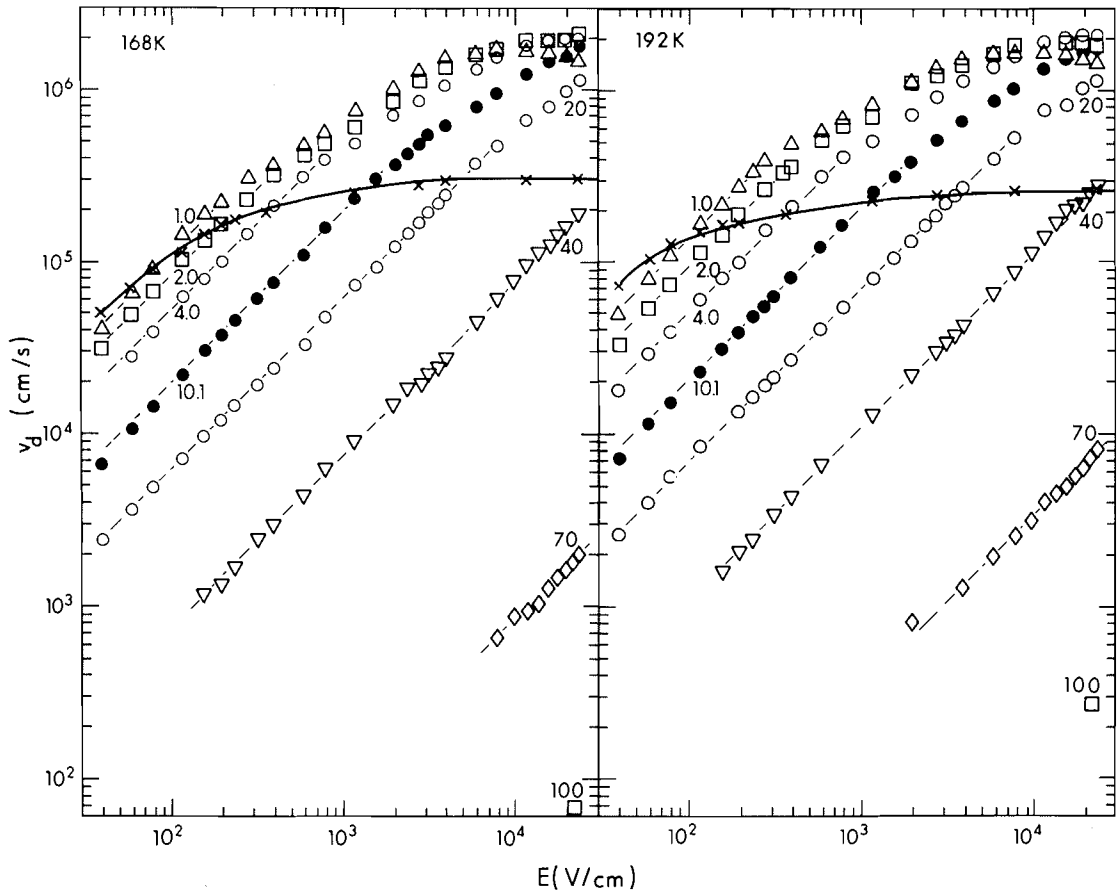

FIG. 1. Electron drift velocities in pure liquid xenon (×) and in xenon/ethylene solutions at 168 and 192 K, as functions of the applied field strength E. The numbers labelling the curves represent mol% ethylene. The dashed lines have slopes of unity.

upon the electron mobility. The concentrations were varied from pure xenon to pure hydrocarbon.

Experimental

The materials and the method of preparation of the samples were the same as those described in ref. 5.

The mobilities, μ, were measured by time-of-flight (6) and conductance (2) methods. The former is based upon [1] and the latter upon [2].

$$[1] \qquad \mu = l^2/Vt_d$$

where l is the distance between the parallel plate electrodes, V is the applied voltage, and t_d is the time required for the electrons to drift from the cathode to the anode.

$$[2] \qquad \mu = G_{fi}{}^E \mu/G_{fi}{}^E$$

where the value of the product of the free ion yield $G_{fi}{}^E$ and the mobility is obtained from the height of the conductance transient after a pulse of radiation, and the free ion yield is measured in a separate, charge clearing experiment. The two methods gave results the same within 15% under conditions where both could be used. The time-of-flight method is preferred because it is more direct and quicker. However, the conductance method is sometimes more dependable at low field strengths.

The radiation pulse length was usually 100 ns, but was 1 μs for the pure hydrocarbons and the 70% hydrocarbon solutions. The respective pulse doses were $\sim 2 \times 10^{10}$ and 1×10^{11} eV/g.

Physical Properties of the Liquids

The densities and dielectric constants of the pure compounds were taken from refs. 2 and 7. These properties were assumed to be additive in the solutions.

Results

The mobility of electrons in xenon is strongly field dependent (1). It is more instructive in this case to discuss the velocity of drift v_d in the direction of the applied electric field E.

$$[3] \qquad v_d = \mu E$$

The drift velocity tends to become independent of field strength at high fields (Fig. 1).

Increasing the liquid temperature from 168 to 192 K increases the drift velocity at low fields, but decreases the plateau value at high fields (compare Figs. 1 and 2). The plateau values are 2.6 km/s at

Can. J. Chem. Downloaded from www.nrcresearchpress.com by 210.87.254.5 on 09/05/12
For personal use only.

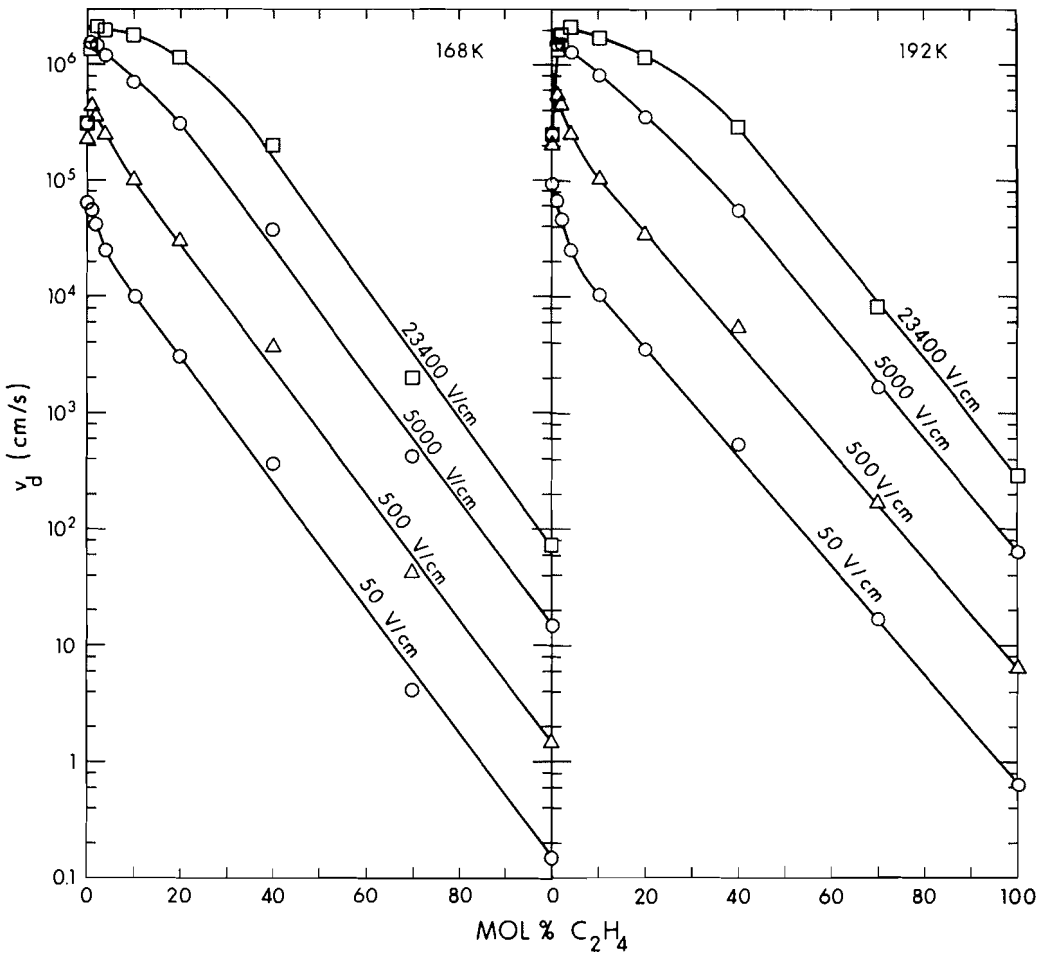

FIG. 2. Effect of ethylene concentration upon the electron drift velocity at constant field stengths in xenon/ethylene solutions at 168 and 192 K.

192 K and 3.1 km/s at 168 K, compared to 2.9 km/s at 163 K reported earlier (1).

Xenon/Ethylene Solutions

Addition of 1 mol% of ethylene to xenon lowers the value of v_d slightly at low fields, but increases it greatly at high fields (Fig. 1). The drift velocity passes through a maximum of 17 km/s at $E = 10$ kV/cm at 168 K.

Further additions of ethylene continue to lower v_d at low fields. However, at the highest field used, 23.4 kV/cm, v_d increases to 21 km/s at 2% ethylene, then decreases monotonically as the ethylene concentration is increased (Fig. 1).

The behavior is similar at 192 K, except for the crossover of the 2% and 4% curves at high fields (Fig. 1). The 1% crosses to below the 2, 4, and 10% curves at both temperatures, at $\sim 10^4$ V/cm.

The effect of ethylene concentration upon the drift velocity at fixed applied field strengths at 168 K is shown in Fig. 2. At 50 V/cm there is an initial relatively rapid decrease in v_d as the first 5% of ethylene is added, followed by a slower but approximately exponential decrease at higher concentrations. Similar behavior is observed at 500 V/cm, except that the first 1% of ethylene causes v_d to increase by a factor of two. At 5000 V/cm, addition of the first 1% of ethylene increases v_d fivefold, while the next 3% have relatively little effect. Further additions cause an exponential decrease in v_d, as at lower fields. At 23 400 V/cm the peak in the v_d/concentration curve is higher and broader than at lower fields. The maximum occurs at 2 mol% ethylene, with a sevenfold increase in v_d over the value in pure xenon (Fig. 2).

The behavior at 192 K is similar to that at 168 K, with small differences in detail (Fig. 2). For example, at 23 400 V/cm the maximum v_d is eightfold the value in pure xenon, and it occurs at 4 mol% ethylene.

Effects of Other Olefins

The effects of ethylene, propylene, and *cis*- and

Can. J. Chem. Downloaded from www.nrcresearchpress.com by 210.87.254.5 on 09/05/12
For personal use only.

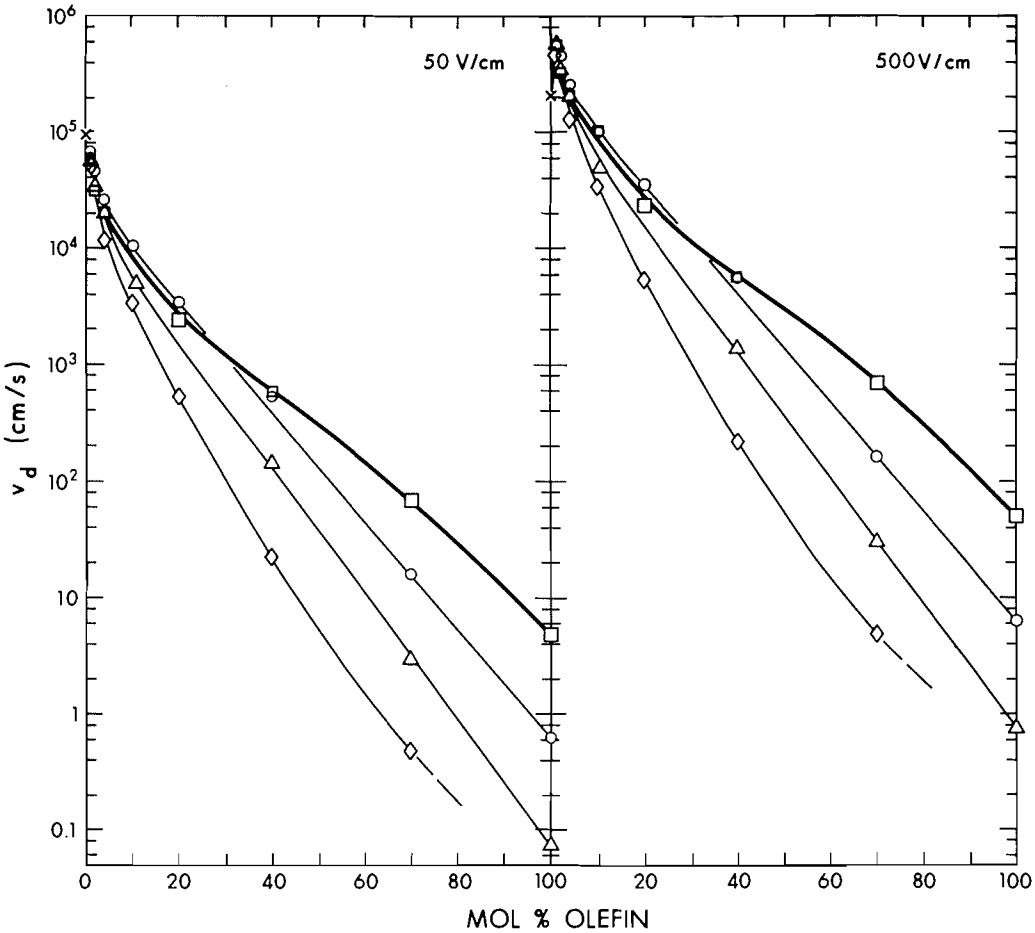

FIG. 3. Effect of olefin concentration upon the electron drift velocity in xenon/olefin solutions at 50 and 500 V/cm, 192 K. ○, Ethylene; △, propylene; □, *cis*-butene-2; ◇, *trans*-butene-2.

trans-butene-2 are compared at each of four different field strengths in Figs. 3 and 4. Similar behavior was observed at 168 and 192 K. To conserve space only the latter are displayed.

At 50 V/cm all the olefins cause a rapid decrease in v_d at low concentrations, followed by a more gradual decrease at high concentrations. The magnitudes of the effects are in the order ethylene < propylene < *trans*-butene-2 (Fig. 3). *cis*-Butene-2 behaves similar to propylene at low concentrations, but is even less effective than ethylene at high concentrations. The crossover of the *cis*-butene-2 and ethylene curves occurs at about 30 mol% olefin, where the mobility is about 30 cm^2/V s.

At 500, 5000, and 23 400 V/cm the addition of 1% olefin causes a large increase in v_d (Figs. 3 and 4). The effects of small concentrations of olefins at 50 and 23 400 V/cm are contrasted in Fig. 5. At 1% concentration all of the olefins are equally effective in increasing v_d at the high field strength. In the subsequent lowering of v_d by higher concentrations, the olefins have relative effectivenesses similar to those observed at 50 V/cm (Figs. 3 and 4). The crossover of the *cis*-butene-2 and ethylene curves shifts slightly at high field strengths. At 23.4 kV/cm the crossover occurs at 40 mol% olefin and $\mu = 12$ cm^2/V s (Fig. 4).

Effects of Alkanes

Data analogous to those in Fig. 1 were also obtained for ethane, propane, and *n*-butane solutions. The trends were the same at 168 and 192 K. The data for 192 K are summarized in Figs. 6 and 7.

Each alkane was less effective than its corresponding olefin in lowering v_d. *n*-Butane is compared here with *trans*-butene-2, because the behavior of the *cis* isomer is anomalous.

At high field strengths v_d increased with the addition of the first percent of alkane (Figs. 6 and 7), as it did with the olefins.

Discussion

Extra electrons in liquid xenon reside in a con-

Can. J. Chem. Downloaded from www.nrcresearchpress.com by 210.87.254.5 on 09/05/12
For personal use only.

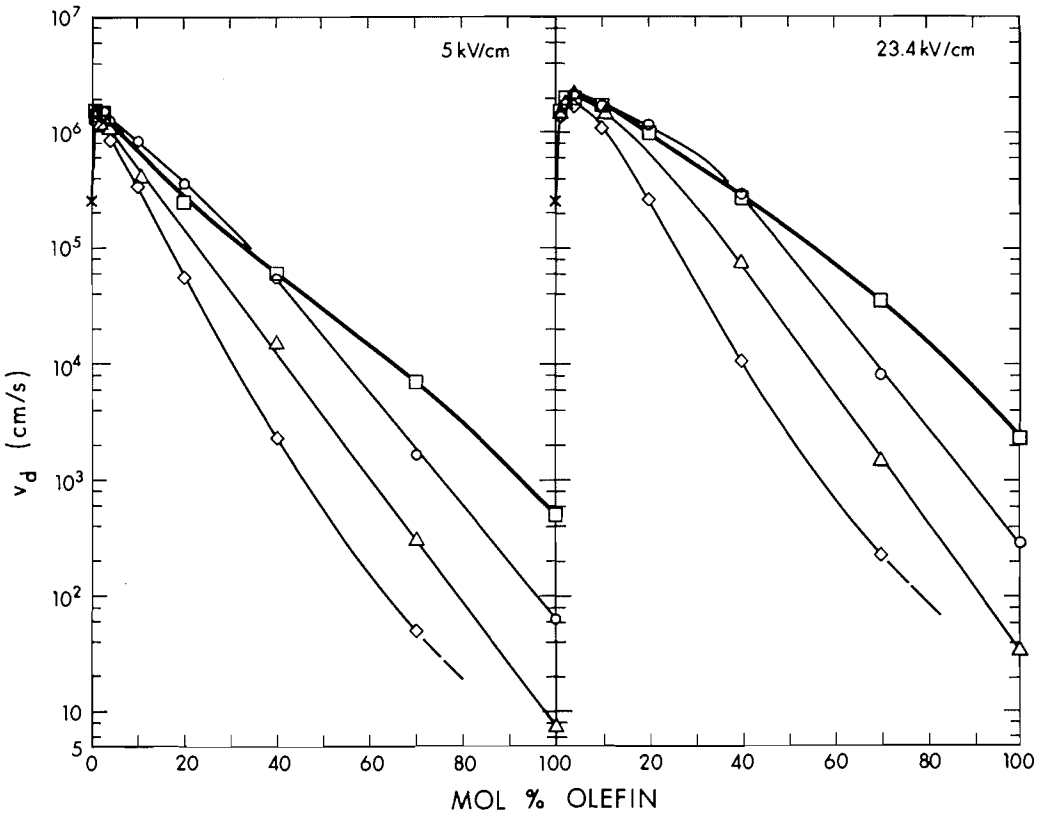

FIG. 4. Effect of olefin concentration upon the electron drift velocity at 5000 and 23 400 V/cm, 192 K. ○, Ethylene; △, propylene; □, *cis*-butene-2; ◇, *trans*-butene-2.

duction band. When the electrons remain in thermal equilibrium with the medium, their drift velocity is directly proportional to the applied field strength. In terms of [3] this means that μ is independent of E. However, at sufficiently large fields the electrons gain more energy from the field than they lose by collisions with the medium, and the mobility becomes a function of the field strength.

The mobility μ_0 of an electron in a conduction band or in a gas is directly proportional to the time between collisions. Thus, μ_0 is directly proportional to the mean free path Λ_v between collisions, and inversely proportional to the relative velocity v of the electrons with respect to the molecules (8, 9).

$$\mu_0 \propto \Lambda_v/v \qquad [4]$$

where Λ_v is a function of v. In the solutions the mean free path may be represented approximately by [5].

$$\Lambda_v = (n_x\sigma_x + n_h\sigma_h)^{-1} \qquad [5]$$

where n_x and n_h are the numbers of xenon and hydrocarbon molecules/cm^3, respectively, while σ_x and σ_h are the corresponding scattering cross sections. In [5], diffraction effects due to multiple interactions in the dense fluid (9) are included for simplicity in the σ's. They are also functions of v.

The variations of μ with E, temperature, and composition in the dilute solutions reflect changes in v and Λ_v. In pure xenon v_d increases less than linearly with field at $E \geq 40$ V/cm (Fig. 1), which means that μ_0 decreases with increasing E. This is due to increases in v and σ_x.

At a given field strength, under steady state conditions the electrons have certain average values of v_d and v, and the medium has a certain average value of σ. The energy gained by the electron from acceleration in the field is removed by collision with the medium

$$eE\Lambda_v = \Delta\varepsilon_v \qquad [6]$$

where $\Delta\varepsilon_v$ is the average amount of energy lost per collision when the average velocity of the electron relative to the molecules is v. In a solution $\Delta\varepsilon_v$ is given by [7].

$$\Delta\varepsilon_v = \frac{n_x\sigma_x\Delta\varepsilon_x + n_h\sigma_h\Delta\varepsilon_h}{n_x\sigma_x + n_h\sigma_h} \qquad [7]$$

where $\Delta\varepsilon_x$ and $\Delta\varepsilon_h$ are the average amounts of energy

Can. J. Chem. Downloaded from www.nrcresearchpress.com by 210.87.254.5 on 09/05/12
For personal use only.

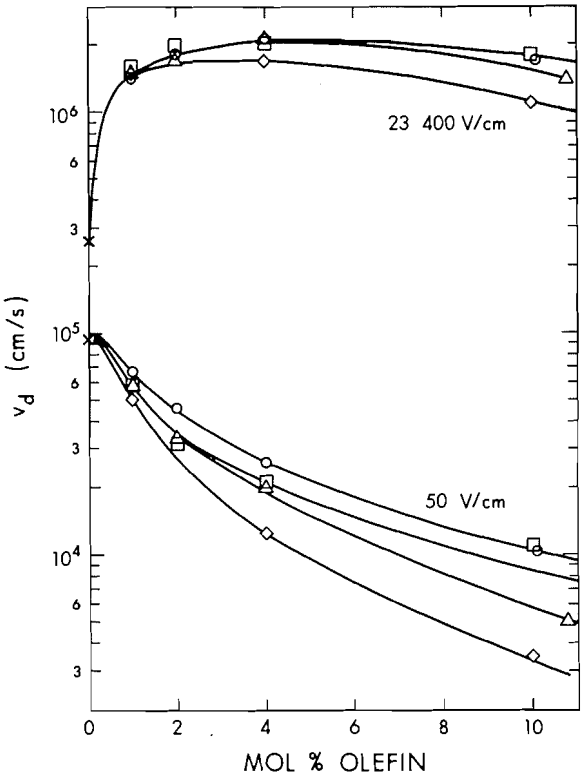

FIG. 5. Effects of low concentrations of olefins on the electron drift velocity at 50 and 23 400 V/cm. Temperature = 192 K. ○, Ethylene; △, propylene; □, *cis*-butene-2; ◇, *trans*-butene-2.

lost per collision with xenon and a hydrocarbon, respectively. The fact that 1 mol% of a hydrocarbon has such a large effect on v_d (Fig. 1) means that $\sigma_h \Delta\varepsilon_h \gg \sigma_x \Delta\varepsilon_x$. Equations 5–7 then imply that the minimum field required to cause electron 'heating' should increase linearly with the hydrocarbon concentration at low concentrations. Such is the case (Fig. 8).

Molecular Scattering Cross Sections for Thermal Electrons in Xenon Solvent

The thermal electron mobilities in the dilute solutions were analysed to determine the electron scattering cross sections of the hydrocarbon molecules dissolved in xenon. The scattering properties of the xenon were assumed to be unaffected by the presence of up to 4 mol% hydrocarbon. The results indicated that collective effects of the hydrocarbon molecules were negligible up to this concentration. The electrons remain in a delocalized state and the drift velocity is given by [8] (9).

$$[8] \qquad v_d = \frac{2}{3}\left(\frac{2}{\pi m k T}\right)^{1/2} eE\Lambda_v$$

where m and e are the electron mass and charge, respectively, k is Boltzmann's constant, and T is the absolute temperature. The values of $\mu = v_d/E$ in pure xenon were taken to be 2000 $cm^2/V\ s$ at 168 K and 2800 $cm^2/V\ s$ at 192 K (10), which gave values of $(n_x\sigma_x)^{-1}$ equal to 1080 and 1610 Å, respectively. Analysis of the mobilities in solutions of up to 4 mol% hydrocarbon, using [5] and [8], gave the values of σ_h listed in Table 1.

In general the scattering cross section of an olefin is greater than that of the corresponding alkane (Table 1). The values for the alkanes are only about half those in the gas phase (11). The reduction could be attributed to dielectric screening by the liquid xenon, which has a dielectric constant of ~1.9 in this temperature region. There might also be a structure factor contribution, but more systems need to be studied in the gas and solution phases to determine it.

The effective value of σ_x is two orders of magnitude

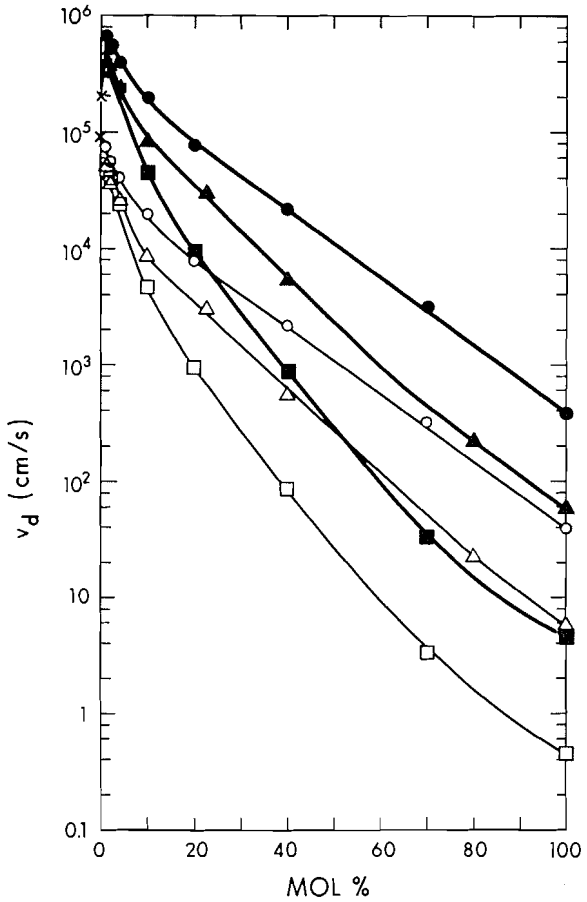

FIG. 6. Effect of alkane concentration upon the electron drift velocity in xenon/alkane solutions at 50 (open points) and 500 V/cm (black points), 192 K. ○, Ethane; △, propane; □, *n*-butane.

Can. J. Chem. Downloaded from www.nrcresearchpress.com by 210.87.254.5 on 09/05/12
For personal use only.

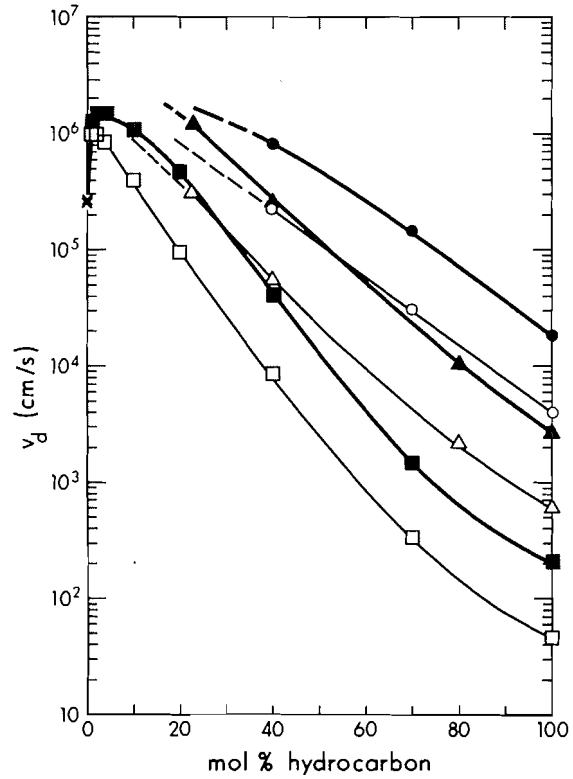

FIG. 7. Effect of alkane concentration upon the electron drift velocity in xenon/alkane solutions at 5000 (open points) and 23 400 V/cm (black points), 192 K. ○, Ethane; △, propane; □, *n*-butane.

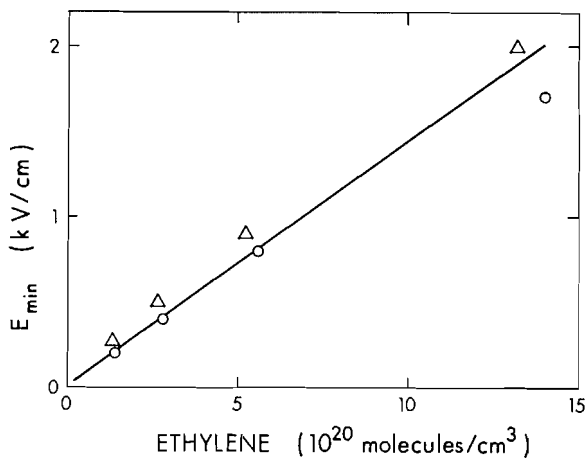

FIG. 8. The minimum field E_{min} required to raise the electron energy above thermal, plotted against the ethylene concentration in xenon. ○, 168 K; △, 192 K.

smaller than those of σ_h, due partly to the small value of the structure factor (1, 9), that is, to diffraction effects. Another reason is that the 'atomic' scattering cross section of xenon at these densities appears to be only a small factor greater than that at

TABLE 1. Thermal electron scattering cross sections of hydrocarbons dissolved in liquid xenon

Hydrocarbon	σ_h (Å^2)*	σ_h/σ_x*	ETEσ_x/σ_h†
Ethane	2.7	47	2.0
Propane	4.6	81	2.2
n-Butane	7.2	126	3.9
Ethylene	4.7	83	2.3
Propylene	5.4	95	2.7
cis-Butene-2	7.4	130	3.3
trans-Butene-2	9.4	165	4.0

*Average of the values at 168 and 192 K.
†ETE = energy transfer efficiency ratio, hydrocarbon/xenon, determined from the secondary electron ranges in the solutions (5).

the gas phase Ramsauer–Townsend minimum (10). The low energy limit of the structure factor $S(0)$ is given by [9] (1).

$$[9] \qquad S(0) = nkT\chi_T$$

where χ_T is the isothermal compressibility (12). The values of $S(0)$ are 0.058 at 168 K and 0.085 at 192 K.

Addition of a hydrocarbon to xenon reduced the penetration ranges of the secondary electrons into the liquid away from their parent positive ions (5). An energy transfer efficiency ratio, hydrocarbon/xenon, was estimated from the results. The energy transfer efficiency ratio for the slowing down of secondary electrons was 2–4 times larger than the corresponding cross section ratios for thermal electrons (Table 1). It is reasonable to assume that the slowing down of secondary electrons is governed by inelastic scattering. The strong correlation between the scattering cross sections determined from the mobilities and the energy transfer efficiency ratios determined from the ranges seems to imply that inelastic scattering makes an important contribution to limiting the mobilities of thermal electrons in these systems.

Collective Effects of the Hydrocarbons

The breakdown of the isolated molecule model for hydrocarbon concentrations ≥ 10 mol% indicates that interactions of an electron with more than one hydrocarbon molecule at a time are important at these concentrations. The average center-to-center distance between hydrocarbon molecules at 10 mol% is $n_h^{-0.33} = 9$ Å. This is about half the distance (15 Å) between xenon atoms where multibody interactions become important in high density xenon gas (10).

The approximately exponential decrease of v_d with increasing ethylene concentration beyond the threshold (Fig. 2) indicates that the decrease is caused by the formation of electron localized states. The straight lines at >9 mol% ethylene for $E = 50$ and 500 V/cm in Fig. 2 follow [10].

Can. J. Chem. Downloaded from www.nrcresearchpress.com by 210.87.254.5 on 09/05/12
For personal use only.

$$[10] \quad v_d = \mu E = \mu_0 \exp(-E_\mu/RT)E = 250 \exp\left(\frac{-4200[\mathrm{MF}-0.09]}{RT}\right)E$$

where E_μ is the activation energy, MF is the mol fraction of hydrocarbon, and 0.09 is the threshold value. The pre-exponential factor μ_0 must also be affected by MF, although the differences in the shapes of the curves in Figs. 3 and 6 indicate that the manner is not simple. For ethylene, if one took $\mu_0 = 113\ \mathrm{MF}^{-0.33}$ cm^2/V s and $E_\mu = 3800[\mathrm{MF} - 0.09]$ cal/mol K, [10] would follow within a few percent of the 50 V/cm lines in Fig. 2, at all concentrations from 1 to 100 mol%. The significance of that is not known, and is dubious below 9 mol% where the exponential term exceeds unity.

The analogous equation to [10] for propylene is

$$[11] \quad v_d = 120 \exp\left(\frac{-4700[\mathrm{MF}-0.09]}{RT}\right)E$$

The lower pre-exponential factor reflects the greater scattering cross section of propylene (Table 1). The curve is in Fig. 3.

The lower curve for *trans*-butene-2 (Fig. 3) reflects the still larger scattering cross section of that molecule and the deeper traps formed. The approximately linear portion between 10 and 40 mol% corresponds to $\mu_0 = 72$ cm^2/V s and $E_\mu = 6300[\mathrm{MF} - 0.09]$ cal/mol K. The more gentle slope at the lower end is due to a gradual transition to an ion-like transport mechanism, as observed at low temperature in pure *trans*-butene-2 (13).

In dilute solutions *cis*-butene-2 scatters electrons much more strongly than does ethylene (Table 1), but at high concentrations collective interactions of the butene reduce its scattering efficiency. The *cis*-butene-2 curve in Fig. 3 crosses to above the ethylene curve at about 30 mol%. This peculiar behavior of *cis*-butene-2 compared to other olefins was noted some time ago (4), but is not yet understood. It seems to be related to the ease of rotation of the molecules in the liquid. The fact that the permanent dipole of the molecule is perpendicular to the major axis of polarizability might also reduce the net charge – dipole interaction.

Ethane has about double the threshold concentration of ethylene for the formation of localized electron states. The linear portion of the curve in Fig. 6 corresponds to [12].

$$[12] \quad v_d = 194 \exp\left(\frac{-2550[\mathrm{MF}-0.17]}{RT}\right)E$$

The threshold concentrations of propane and *n*-butane to begin to localize electrons are similar to those for the olefins. The approximately linear portion of the propane curve between 10 and 80 mol% in Fig. 6 is satisfactorily described by [13].

$$[13] \quad v_d = 168 \exp\left(\frac{-3300[\mathrm{MF}-0.10]}{RT}\right)E$$

The portion of the *n*-butane curve between 10 and 40 mol% corresponds approximately to $\mu_0 = 88$ cm^2/V s and $E_\mu = 5200[\mathrm{MF} - 0.10]$ cal/mol K. It is not known whether the more gentle slopes towards the bottoms of the propane and butane curves are due to a change from mechanism [10] to small polaron hopping (14), or to interference effects of the type that raised the *cis*-butene-2 curve (Fig. 3).

Field Effect in the Hydrocarbon Solutions

The more gentle negative slopes at the tops of the curves in Figs. 4 and 7 are due to electron heating. This is illustrated by the fact that the slopes at the tops of the 10 and 20 mol% curves in Fig. 1 are less than unity. The heating of the electrons would also inhibit their localization, as observed in dense xenon gas (10). The treatment of the mobilities in this region would therefore be complex.

1. L. S. Miller, S. Howe, and W. E. Spear. Phys. Rev. **166**, 871 (1968).
2. M. G. Robinson and G. R. Freeman. Can. J. Chem. **52**, 440 (1974).
3. J.-P. Dodelet and G. R. Freeman. Can. J. Chem. **50**, 2667 (1972).
4. J.-P. Dodelet, K. Shinsaka, and G. R. Freeman. J. Chem. Phys. **59**, 1293 (1973).
5. T. Kimura and G. R. Freeman. Can. J. Chem. This issue.
6. J.-P. Dodelet and G. R. Freeman. Can. J. Chem. **53**, 1263 (1975).
7. J.-P. Dodelet, K. Shinsaka, V. Kortsch, and G. R. Freeman. J. Chem. Phys. **59**, 2376 (1973).
8. W. P. Allis. *In* Hanbuch der physik. Vol. 21. *Edited by* S. Flügge. Springer-Verlag, Berlin. 1956. p. 413.
9. M. H. Cohen and J. Lekner. Phys. Rev. **158**, 305 (1967).
10. S. S.-S. Huang and G. R. Freeman. J. Chem. Phys. To be published.
11. L. G. Christoporou, M. W. Grant, and D. Pittman. Chem. Phys. Lett. **38**, 100 (1976).
12. J. Rouch, C. Vaucamps, J. P. Chabrat, and L. Letamendia. Chem. Phys. Lett. **24**, 608 (1974).
13. J.-P. Dodelet and G. R. Freeman. Can. J. Chem. **55**, 2893 (1977).
14. J.-P. Dodelet and G. R. Freeman. Can. J. Chem. **55**, 2264 (1977).

X-Ray, Raman, infrared, and nuclear magnetic resonance studies of the crystal structure of ammonium tetrachloroaluminate, NH_4AlCl_4

GAËTAN MAIRESSE, PIERRE BARBIER, AND JEAN-PIERRE WIGNACOURT

Laboratoire de Chimie Minérale I, Université des Sciences et Techniques de Lille, 59650 Villeneuve d'Ascq, France

AND

ANNICK RUBBENS AND FRANCIS WALLART

Laboratoire de Spectrochimie Infrarouge et Raman, C.N.R.S., Université des Sciences et Techniques de Lille, 59650 Villeneuve d'Ascq, France

Received May 13, 1977

GAËTAN MAIRESSE, PIERRE BARBIER, JEAN-PIERRE WIGNACOURT, ANNICK RUBBENS, and FRANCIS WALLART. Can. J. Chem. **56**, 764 (1978).

Ammonium tetrachloroaluminate crystallizes in the orthorhombic system $a = 11.022(6)$ Å, $b = 7.072(3)$ Å, $c = 9.257(5)$ Å, $Z = 4$, space group *Pnma*. The structure was determined by direct methods from diffractometer data and refined by full-matrix least-squares procedures to final R and R_ω values of 0.053 and 0.069 respectively, for 596 reflections with $I > 2\sigma(I)$. Hydrogen atoms were not observed. Al—Cl bond lengths are similar to those of other alkaline chloroaluminate salts (Li^+, Na^+, NO^+). The salt is isostructural with NH_4ClO_4.

Crystals and polycrystalline samples of this compound have been studied by Raman scattering above 10 K, and infrared spectra of specimens of a polycrystalline sample have been recorded in Nujol and a fluorolube above 80 K. Both methods enabled us to observe the bands corresponding to the $\nu_1(A_2)$, ν_3, and $\nu_4(F_2)$ vibration modes of the ammonium ion but the infrared spectra contain no band due to combination modes involving the librations of this ion. Nuclear magnetic second moment remains equal to 4 G^2 over the range 298–80 K. These spectroscopic results, compared to those of other ammonium salts, indicate that the ammonium ion seems to be freely rotating.

The four characteristic bands of the $AlCl_4^-$ tetrahedral anion have been studied by Raman scattering in the 298–10 K temperature range.

GAËTAN MAIRESSE, PIERRE BARBIER, JEAN-PIERRE WIGNACOURT, ANNICK RUBBENS et FRANCIS WALLART. Can. J. Chem. **56**, 764 (1978).

Le tétrachloroaluminate d'ammonium cristallise dans le système orthorhombique $a = 11.022(6)$ Å, $b = 7.072(3)$ Å, $c = 9.257(5)$ Å, $Z = 4$, groupe d'espace *Pnma*. La structure a été résolue par les méthodes directes et affinée par celle des moindres carrés (matrice complète) jusqu'à des facteurs d'accord R et R_ω de 0.053 et 0.069, avec 596 réflexions telles que $I > 2\sigma(I)$ enregistrées au diffractomètre. Les atomes d'hydrogène n'ont pas été observés. Les distances Al—Cl sont comparables à celles d'autres sels alcalins (Li^+, Na^+, NO^+). Le sel est isostructural de NH_4ClO_4.

Des échantillons monocristallins et polycristallins du composé ont été analysés par diffusion Raman jusqu'à une température de 10 K ainsi que des suspensions dans le Nujol et le fluorolube par spectrométrie ir jusqu'à 80 K. Les bandes relatives aux fréquences ν_1 d'espèce A_1, ν_3 et ν_4 d'espèce F_2, de l'ion NH_4^+, ont été observées par ces deux techniques. Aucune bande de combinaison due à des modes de libration du cation n'a été mise en évidence sur les spectres d'absorption infrarouge. En rmn du proton, le second moment magnétique nucléaire garde la même valeur (~ 4 G^2) entre 298 et 80 K. Ces résultats spectroscopiques comparés à ceux d'autres sels d'ammonium indiquent que l'ion ammonium semble être en "libre rotation".

Les quatre bandes caractéristiques de l'anion tétraédrique $AlCl_4^-$ ont été étudiées par diffusion Raman dans l'intervalle de température 298–10 K.

Introduction

It seemed worthwhile to extend our structural knowledge of the compounds formed between aluminum trichloride and alkaline chlorides, to the pseudoalkaline salts $NOAlCl_4$ and NH_4AlCl_4, owing to the polyatomic nature of their cations. We have recently shown that in nitrosyl tetrachloroaluminate the nitrosyl ion occupied two different positions at room temperature (1), but seemingly only one at 210 K (2). The present paper reports a similar study of the ammonium salt, using X-ray diffraction, vibration spectrometry, and proton nmr techniques. The results obtained are compared with those of other tetrachloroaluminate alkaline salts and other previously reported data about ammonium salts.

Experimental

Preparation

The reagent-grade aluminum trichloride, contaminated by iron trichloride, was purified through successive sublimations

Can. J. Chem. Downloaded from www.nrcresearchpress.com by 210.87.254.5 on 09/05/12
For personal use only.

Can. J. Chem. Downloaded from www.nrcresearchpress.com by 210.87.254.5 on 09/05/12
For personal use only.

under hydrogen chloride gas and then dynamic vacuum. Ammonium chloride was dried over phosphorus pentoxide under vacuum. Stoichiometric amounts of $AlCl_3$ and NH_4Cl were inserted in a U-shaped glass apparatus with $SOCl_2$, and then liquid SO_2 was condensed. The reactor was then sealed off and the $AlCl_3$ solution in the mixed solvent reacted with NH_4Cl at room temperature to give a NH_4AlCl_4 solution (3). A difference of temperature between the two parts of the reactor produced a slow distillation of SO_2, giving single crystals of the salt insoluble in $SOCl_2$. These crystals were separated from the remaining solution and then isolated by sealing off the tube. This process enabled us to obtain crystals suitable for both X-ray diffraction or Raman scattering and nmr. These crystals were very hygroscopic and had a fragile texture. They were handled in a glove-box (filled with dry nitrogen) and washed in previously dried carbon tetrachloride.

Crystallographic Study

The irregular shaped crystal selected was coated with dried paraffin, and then sealed off in a quartz capillary. It had the approximate dimensions of ca. 0.25 × 0.35 × 0.20 mm. Preliminary Weissenberg and precession photographs gave the conditions for diffraction as $hk0$ ($h = 2n$) and $0kl$ ($k + l = 2n$) which indicated either $Pnma$ (D_{2h}^{16}) or $Pn2_1a$ (C_{2v}^{9}) as possible space groups. $Pnma$ was ultimately chosen as correct for reasons referred to later in the text.

The unit cell parameters were obtained from a least-squares refinement of the setting angles of 25 reflections which had been carefully centered on a four circle Philips PW 1100 automatic diffractometer using the MoK_α radiation with a graphite monochromator. Crystal data are:

NH_4AlCl_4 fw = 186.83
Orthorhombic, $a = 11.022(6)$ Å, $b = 7.072(3)$ Å, $c = 9.257(5)$ Å, $V = 721.60$ Å^3, $\rho_o = 1.68$, $Z = 4$, $\rho_c = 1.72$ (20°C, MoK_α, $\lambda = 0.7107$ Å, $\mu = 16$ cm^{-1}).

Intensities were collected on the diffractometer by the ω–2θ technique with a ω scan speed of 0.03° s^{-1} and a variable scan width (0.90 + 0.40 tan θ) deg over the $4° < 2\theta < 60°$ range. The weak reflection intensities were measured several times (with a maximum of 5) in order to obtain more precision. Weak reflections with $I_{peak} - 2\sqrt{I_{peak}} < I_{background}$ after the first scan were discarded as being unobserved. The background measurement time t_b was adapted to the strength of the reflection as $t_b = t_s\sqrt{I_b/I_s}$ (with t_s = scanning time, I_b = average intensity per second of the background, I_s = average intensity per second during scanning), this giving the minimum of $(t_s + t_b)\sigma^2(I_{net})$, $(\sigma^2(I_{net}) = I_s/t_s + I_b/t_b$ with $I_{net} = I_s - I_b)$. Three standard reflections $\bar{2}12$, 212, 008 were monitored every 60 reflections throughout the data collection to check crystal stability. No trends were observed in the standards. We collected the intensities in the two octants, hkl and $\bar{h}kl$, and corrected them for Lorentz and polarization effects. No absorption correction was applied because of the irregularities of the crystal surface and the low value of the linear absorption coefficient. After averaging the equivalent reflections we obtained 596 unique reflections with $I > 2\sigma(I)$.

NH_4AlCl_4 seemed to be isostructural to $CsAlCl_4$ and the $NOAlCl_4$ room temperature phase ($BaSO_4$ type centrosymmetric structure) but on account of the previous controversy about the choice of the $Pnma$ or $Pn2_1a$ space group in the NH_4ClO_4 crystal study (4, 5), we solved the structure by direct methods, independently of all a priori considerations, using the multisolution MULTAN computer program (6). The distribution of the normalized structure factors E did not enable us to choose either a centric or acentric distribution.

	Experimental	Theoretical	
		Centrosymmetric	Noncentrosymmetric
E^2	0.999	1.000	1.000
$\lvert E^2 - 1\rvert$	0.825	0.968	0.736
$\lvert E\rvert$	0.856	0.798	0.886

So we tried to resolve the structure in both cases. In each of them, the E map corresponding to the best 'figure of merit' showed the $AlCl_4$ anion atoms. After two cycles of refinement of the positional and isotropic thermal parameters of these atoms, a difference Fourier map revealed the position of the N atom. The full-matrix least-squares refinement of the positional and isotropic, then anisotropic thermal parameters of the Al, Cl, and N atoms, converged smoothly to $R = 0.053$ and $R_\omega = 0.069$ in the space group $Pnma$, and to $R = 0.060$ and $R_\omega = 0.066$ in $Pn2_1a$. At this stage a final difference Fourier map showed no significant residual electronic density in the region of the ammonium group. The maximum residual density (0.3 e Å^{-3} in $Pnma$ and 0.9 e Å^{-3} in $Pn2_1a$) occurred in the regions of the chlorine atoms in the tetrachloroaluminate anion. Attempts to include disordered ammonium groups by using rigid-body constrained refinement techniques (7) were made but gave no significant results. The refinements in both space groups give almost identical results for the geometry of the $AlCl_4^-$ ion as well as for the thermal parameters. Thus, the ambiguity related to the space group was removed through a study of the compound by Raman scattering, which led us, as later explained in this paper, to choose the $Pnma$ centrosymmetric space group.

The least-squares refinement was based on the minimization of $\Sigma\omega(|F_o| - |F_c|)^2$, the weighting scheme used being $\omega = 1/\sigma^2(F)$ where ω is derived from $\sigma^2(I)$ according to $\sigma(I) = [P + 0.25(B_1 + B_2)(T_p/T_b)^2 + (pI)^2]^{1/2}$ where P is the scan count, B_1 and B_2 are the background counts, T_p and T_b are the count times on the peak and background respectively, I is the resulting intensity, and p is the 'ignorance factor' included to avoid overweighting very strong reflections. A value of 0.04 was used for p. The scattering factors for N, Al, and Cl atoms were those calculated by Cromer and Waber (8). The effects of anomalous dispersion were not taken into account.

On the final cycle of refinement the mean parameter shift was 0.43 of its estimated standard deviation (in the centrosymmetric space group).

The final positional and thermal parameters of the atoms are given in Table 1, the intraionic distances and angles in Table 2. Measured and calculated structure factors have been placed in the Depository of Unpublished Data.[1]

Raman, Infrared, and nmr Studies

For Raman and nmr techniques we used crystals of about 1 cm^3 size, sealed off under dry nitrogen in glass tubes. Polycrystalline fluorescent samples were purified by zone melting. For infrared absorption, the compound was mulled in Nujol or fluorolube and placed between caesium iodide, calcium fluoride, or polythene cell windows.

To record the Raman spectra, we used double and triple monochromator spectrometers built in our laboratory (9, 10). These spectra were excited by the 530.9 nm line of an ionized

[1]A complete set of data is available, at a nominal charge, from the Depository of Unpublished Data, CISTI, National Research Council of Canada, Ottawa, Ont., Canada K1A 0S2.

Can. J. Chem. Downloaded from www.nrcresearchpress.com by 210.87.254.5 on 09/05/12
For personal use only.

TABLE 1. Final positional parameters ($\times 10^5$), isotropic,[a] and anisotropic[b] thermal parameters ($\times 10^4$) with estimated standard deviations in parentheses

Atom	x/a	y/b	z/c	B_{eq}	β_{11}	β_{22}	β_{33}	β_{12}	β_{13}	β_{23}
Al	56652(13)	25000	68838(14)	2.99	068(1)	150(3)	078(1)	000	002(1)	000
Cl(1)	71891(18)	25000	54944(19)	6.74	151(2)	368(5)	161(2)	000	097(2)	000
Cl(2)	40057(21)	25000	57645(28)	8.84	133(2)	579(8)	247(4)	000	−111(3)	000
Cl(3)	57686(10)	00746(14)	82357(12)	5.33	116(1)	220(3)	173(2)	009(1)	017(1)	084(2)
N	68464(50)	25000	17485(66)	6.32	077(4)	435(17)	190(9)	000	−003(5)	000

[a]B_{eq} is the equivalent isotropic thermal parameter calculated from β_{ij}: $B_{eq} = (4/3)\Sigma_i\Sigma_j\beta_{ij}a_ia_j$.
[b]Anisotropic thermal parameter is of the form: $\exp -(\beta_{11}h^2 + \beta_{22}k^2 + \beta_{33}l^2 + 2\beta_{12}hk + 2\beta_{13}hl + 2\beta_{23}kl)$.

TABLE 2. Intraionic lengths and angles

Bond	Length (Å)	Bonds	Angle (deg)	Bond	Length (Å)
Al—Cl(1)	2.116(2)	Cl(1)—Al—Cl(2)	113.03(9)	Cl(1)—Cl(2)	3.518(3)
Al—Cl(2)	2.102(3)	Cl(1)—Al—Cl(3)	108.38(7)	Cl(1)—Cl(3)	3.440(2)
Al—Cl(3)	2.126(1)	Cl(2)—Al—Cl(3)	109.68(8)	Cl(2)—Cl(3)	3.457(2)
		Cl(3)—Al—Cl(3′)[a]	107.54(6)	Cl(3)—Cl(3′)	3.431(1)

[a]Cl(3′) is related to Cl(3) by the mirror at $y = 1/4$.

krypton laser and the 514.5 nm line of an ionized argon laser (Spectra-Physics). The double monochromator spectrometer was equipped with a fast-scanning system and spectra accumulation fittings (9). Above 80 K, we used cryostats with continuous gaseous nitrogen flux and for lower temperatures cryostats with liquid helium. To record ir and nmr spectra, we used respectively Perkin-Elmer 180 and Varian DP 60 spectrometers.

Results and Discussion

Crystallographic Results

NH_4AlCl_4 belongs to the alkaline tetrachloroaluminate family characterized by: orthorhombic system, space group *Pnma* (D_{2h}^{16}). It is isostructural to $RbAlCl_4$ (11), $CsAlCl_4$ (12), and the $NOAlCl_4$ room temperature phase (1) but different from $KAlCl_4$ (11) that crystallizes in the monoclinic system, space group $P2_1$ (C_2^2). Figure 1 shows the ionic packing of the NH_4AlCl_4 crystal structure (29). The anionic tetrahedron look slightly distorted. The Al—Cl distances and Cl—Al—Cl angles are very close to those found in $NOAlCl_4$. In both NH_4AlCl_4 and $NOAlCl_4$, the chlorine atoms thermal motions are important when compared to those occurring in $LiAlCl_4$ (13) and $NaAlCl_4$ (11). As a comparison, we reported in Table 3, from results obtained in our laboratory, the Cl—Cl and Al—Cl average distances in the $AlCl_4^-$ anions associated with different cations. The $NaAlCl_4$ data resulted from a new refinement with 1160 reflections ($I > 2\sigma(I)$) of those previously reported by Baenziger (14). We obtained final $R = 0.027$ and $R_\omega = 0.039$. (While writing this paper, Scheinert and Weiss (15) published a similar refinement of the $NaAlCl_4$ structure leading to $R_\omega = 0.079$.) There would seem to be a correlation between the slight shortening of the average distances and the increasing of the cation size. In fact, if we go on examining the chlorine atoms and their average equivalent isotropic temperature factors $\langle B_{eq}\rangle$ calculated from the β_{ij} coefficients, it is obvious that the apparent decrease in distances is due to increasing thermal motion (16). A close study of the thermal motion parameters of the $AlCl_4^-$ anion atoms (Table 1) made it clear that the aluminum atom motion is less important than those of the chlorine atoms. From Busing and Levy's work, it can be assumed that the chlorine atoms "ride" upon the

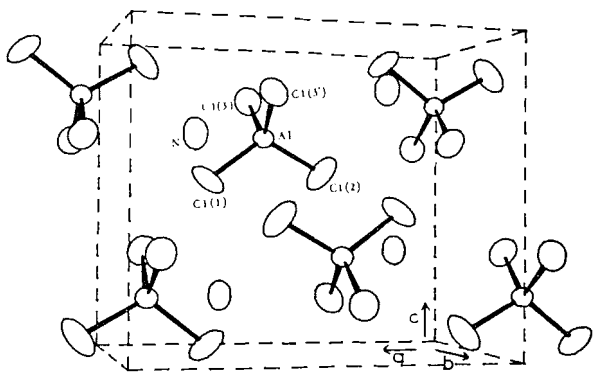

FIG. 1. Computer-drawn model in perspective of the NH_4AlCl_4 unit cell.

TABLE 3. Average distances and isotropic thermal coefficients in some tetrachloroaluminate salts

	Li^+	Na^+	NO^+	NH_4^+
⟨Al—Cl⟩	2.137	2.135	2.119	2.117
⟨Cl—Cl⟩	3.49	3.49	3.46	3.46
$\langle B_{eq}\rangle$	3.01	3.30	5.78	6.56

Can. J. Chem. Downloaded from www.nrcresearchpress.com by 210.87.254.5 on 09/05/12
For personal use only.

aluminum one. Using the anisotropic thermal parameters, we corrected the bond lengths from the riding motion theory. Thus we obtained: Al—Cl (1): 2.150, Al—Cl (2): 2.155, Al—Cl (3): 2.147, and ⟨Al—Cl⟩: 2.150 Å. This correction greatly reduced the differences in the same $AlCl_4^-$ anion distances. Furthermore, the same correction applied to the other salts brought back all the average Al—Cl distances to 2.14 and 2.15 Å. The Al—Cl distance fluctuations seem to be due to the different thermal motions of the chlorine atoms and not to different interactions between the anionic chlorine atoms and the associated cation. The main distortions of the $AlCl_4^-$ tetrahedron essentially concern the angles but remain relatively weak.

The nitrogen atom of the ammonium ion is surrounded by six chlorine atoms situated between 3.328 and 3.488 Å, four other chlorine being at 3.864 (×2) and 3.871 (×2) Å (Table 4). These 10 atoms belong to 7 anionic tetrahedrons. Some of them form, with the nitrogen atom, Cl—N—Cl angles of about 109°, but they are not enough to constitute a tetrahedral packing around the nitrogen atom. The sole knowledge of the chlorine–nitrogen distances and angles in NH_4AlCl_4 does not appear sufficient to deduce the presence in the crystal of preferential orientations for the ammonium ion by straight H bonds. Referring to the isostructural compound NH_4ClO_4, Choi, Prask, and Prince (17) have proved by neutron diffraction that at 10 K the ammonium ion is stabilized in the lattice owing to a network of four hydrogen bonds with N—H···O angles of 159, 180, and 138° (×2). This equilibrium position already appeared at room temperature but the refinement of the hydrogen atomic positions did not converge on account of their excessively important thermal displacements. These results corroborated Peyronel and Pignedoli's (4) similar observations about this same equilibrium position (done by X-ray diffraction at room temperature).

Molecular Spectroscopy

To make the following chapter more easily understandable, we decided to represent the $AlCl_4^-$ anion frequencies by ν^- and the NH_4^+ cation ones by ν^+.

Choice of the Space Group

The ambiguity related to the space group was removed through a study of the Raman scattering spectra for the $AlCl_4^-$ anion. As a matter of fact, let us consider the $Pn2_1a$ group, and we shall notice four active components ($A_1 + A_2 + B_1 + B_2$) for the ν_1^- band and eight components ($2A_1 + 2A_2 + 2B_1 + 2B_2$) for the ν_2^- band. On the other hand, let us consider *Pnma* as the correct space group and then we shall notice respectively two ($A_g + B_{2g}$) and four ($A_g + B_{1g} + B_{2g} + B_{3g}$) components for these bands.

TABLE 4. Coordination about the nitrogen atom[a]

N ...	Cl(2)	4/000	3.328(6)	N ... Cl(1)	1/000 3.488(6)
	Cl(3)	3/101	3.409(5)	Cl(3)	1/00$\bar{1}$ 3.864(6)
	Cl(3′)	3/1$\bar{1}$1	3.409(5)	Cl(3′)	1/00$\bar{1}$ 3.864(6)
	Cl(3)	2/10$\bar{1}$	3.481(5)	Cl(1)	2/10$\bar{1}$ 3.871(3)
	Cl(3′)	2/1$\bar{1}\bar{1}$	3.481(5)	Cl(1)	2/1$\bar{1}\bar{1}$ 3.871(3)

[a]Coding of equivalent positions: 1: x, y, z; 2: $1/2 - x, 1/2 + y, 1/2 + z$; 3: $\bar{x}, 1/2 + y, \bar{z}$; 4: $1/2 + x, y, 1/2 - z$. N is in position 1. Cl(3) 3/101 means that Cl(3) atom is in position 3 translated by 1*a*, 0*b*, and 1*c*.

With orientated single crystals we could obtain, in the $X(ZY)Z$ and $X(YX)Z$ orientations (18), ν_1^- bands with nearly the same but very low intensity. In the $X(ZX)Z$ orientation the intensity of the ν_1^- band increases; in the last one $X(YY)Z$ we notice a very high intensity. These observations are consistent with the existence of the A_g and B_{2g} modes. Moreover, at temperatures lower than 30 K in the spectral region of the ν_2^- (E) vibration, four maxima appeared at 133 cm^{-1} (B_{3g}), 128 cm^{-1} (B_{1g}), 125 cm^{-1} (A_g), and 120 cm^{-1} (B_{2g}) respectively. That is why we decided to describe the structure in the *Pnma* centrosymmetric space group.

$AlCl_4^-$ Anionic Region

At room temperature, in the low frequency range corresponding to the $AlCl_4^-$ anion vibrations and to the external modes (frequencies lower than 500 cm^{-1}) we observed on the Raman spectrum the four characteristic bands of the anionic tetrahedron with frequency values close to those of the other alkaline salts (19). Nevertheless we noticed that the ammonium salt spectrum was resolved better than the nitrosyl one. On the other hand, during the cooling process from room temperature to liquid nitrogen, there was no change in the NH_4AlCl_4 Raman spectrum contrary to the nitrosyl one (Figs. 2 and 3).

At room temperature, with orientated single crystals, broad bands could be observed and the signal/noise ratio was weak, except for the band related to the symmetric stretching mode. Thus the positions of the components in the above mentioned orientations could not be easily defined and we only reported the values obtained with polycrystalline samples (Table 5). Only at temperatures close to liquid helium could we begin to notice the site and the intermolecular coupling effects. In the $X(YY)Z$ orientation the components assigned to the A_g mode appeared at: 125 cm^{-1} for ν_2^-, 178 and 181 for ν_4^-, 356 cm^{-1} for ν_1^-. The other orientations enabled us to observe components of the B_{1g}, B_{2g}, and B_{3g} species. As for the broad band related to the ν_3^- (F_2) vibration, its intensity at 10 K was too low to enable us to notice its components clearly. But as soon as we reach 80 K,

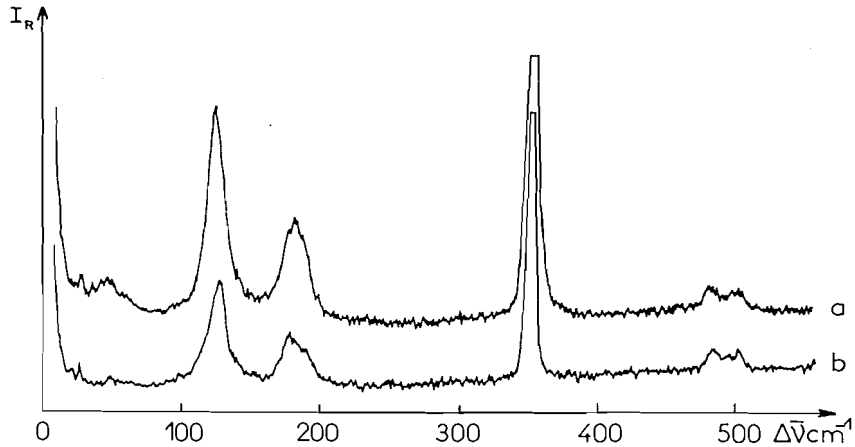

FIG. 2. Raman spectra of NH_4AlCl_4: (*a*) at room temperature, (*b*) at liquid nitrogen temperature.

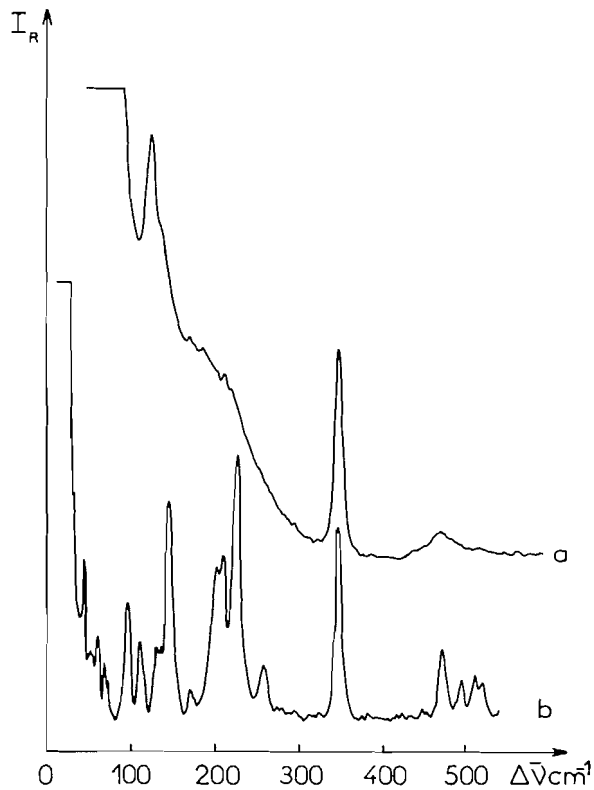

FIG. 3. Raman spectra of $NOAlCl_4$: (*a*) at room temperature, (*b*) at liquid nitrogen temperature.

we observe a splitting corresponding to the site effect (Table 5).

As for the other tetrachloroaluminates, infrared absorption spectra in this frequency range gave no further information on account of the very low intensity of the bands.

NH_4^+ Cationic Region

In Raman spectroscopy, the NH_4^+ ion does not scatter very well, and at room temperature the only band observed on the four ones expected was the ν_1^+ (A_1) band at 3176 cm^{-1}. Its intensity was weak when compared to those of the anion bands, which compelled us to use very wide spectrometer slits. The band width at half-height was about 30 cm^{-1}. During the cooling process, we noticed a slight shape refinement but the band remained wide and asymmetric. At 80 K, using the conventional recording conditions the ν_1^+ band remains the only one observed with a maximum intensity at 3161 cm^{-1}, the very important shift showing its high sensitivity to surroundings. The accumulation of 20 spectra then revealed (Fig. 4) an additional broad weak band (its maximum intensity being 3250 cm^{-1}) that we assigned to ν_3^+ (F_2), the ν_2^+ (E), and ν_4^+ (F_2) bands remaining unobserved. At 10 K, not only the 3161 and 3250 cm^{-1} bands appeared but also the ν_4^+ (F_2) band at 1411 cm^{-1}.

To complete our study in this frequency range, we used infrared spectrometry, for the ammonium ion absorption bands ν_3^+ and ν_4^+ showed a higher intensity than the Raman ones. At room temperature, we observed a broad band centered on 3240 cm^{-1}, with a shoulder at 3160 cm^{-1}, and another one at 1414 cm^{-1} (Fig. 5).

At 80 K, the same lines appeared at 3250, 3158, and 1414 cm^{-1}, respectively, and remained broad and weak. As in the Raman spectrum, we could not see any band in the spectral region of ν_2^+ near 1700 cm^{-1}, whereas this mode is active in the solid state. This band is often missing in spectra of ammonium salts.

The spectra of the deuterated salt were analogous to those of the normal compound. We only studied it above 80 K. The observed frequencies are reported in Table 5.

Numerous authors have tried to characterize hy-

Can. J. Chem. Downloaded from www.nrcresearchpress.com by 210.87.254.5 on 09/05/12
For personal use only.

TABLE 5. Vibrational assignment of NH_4AlCl_4 and ND_4AlCl_4

Raman				Infrared				
NH_4AlCl_4		ND_4AlCl_4		NH_4AlCl_4		ND_4AlCl_4		
293 K	10 K	293 K	80 K	293 K	80 K	293 K	80 K	Assignment
				3327	3320		2452	ν_3^+
	3250	2414			3250	2432		ν_3^+
				3242			2426	ν_3^+
					3230			ν_3^+
3176	3161	2282		3160	3158		2280	ν_1^+
				3060	3060		2250	$\nu_4^+ + \nu_2^+$
					2818	2140	2140	$2\nu_4^+$
	1411			1412	1414	1072	1073	ν_4^+
						1020	1028	ν_4^+
					514			
503	506[a]		506					B_{1g}–B_{3g}
					501			
	499[a]	499	500					A_g–B_{2g} ν_3^-
485	488[a]	483	488					A_g–B_{2g}
				485	486			
356	356	355	355					ν_1^- A_g
	351							ν_1^- B_{2g}?
	193		195					B_{1g}–B_{3g}
	185		186					B_{2g}
184	181	181	182					A_g ν_4^-
	178							A_g
	174							B_{2g}
	133							B_{3g}
126	128							B_{1g} ν_2^-
	125	126	126					A_g
	120							B_{2g}

[a]Values at 80 K.

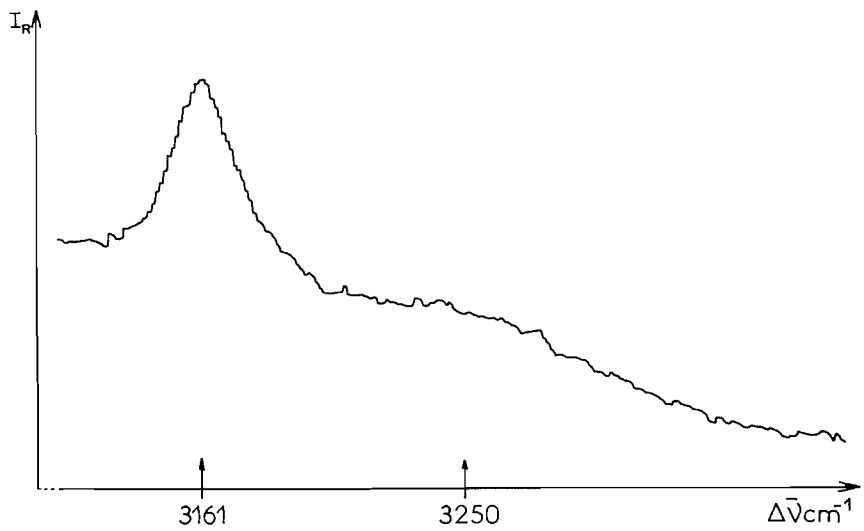

FIG. 4. Raman spectrum of NH_4AlCl_4, 3100–3400 cm^{-1} range.

drogen bonds in crystalline ammonium salts using molecular spectroscopy (Raman scattering and, mainly, infrared absorption) e.g.: Waddington (20), Mathieu and Poulet (21), Dunsmuir and Lane (22). Studying Dunsmuir and Lane's work on complex halides was particularly interesting for us. According to them, three criteria could prove the existence of such H bonds: (*i*) the observation of both $\nu_4 + \nu_6$ and $\nu_2 + \nu_6$ in the infrared spectrum (ν_6 being the torsional mode of the ammonium ion resulting from

Can. J. Chem. Downloaded from www.nrcresearchpress.com by 210.87.254.5 on 09/05/12
For personal use only.

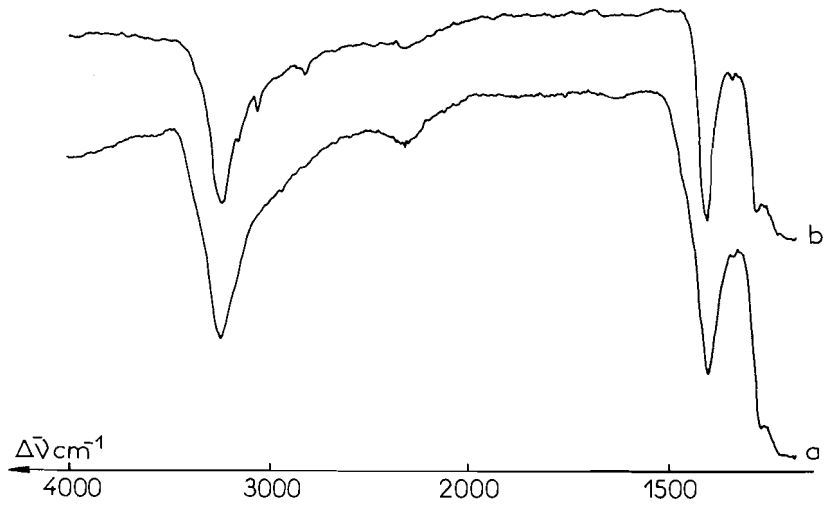

FIG. 5. Infrared spectra of NH_4AlCl_4: (*a*) at room temperature, (*b*) at liquid nitrogen temperature.

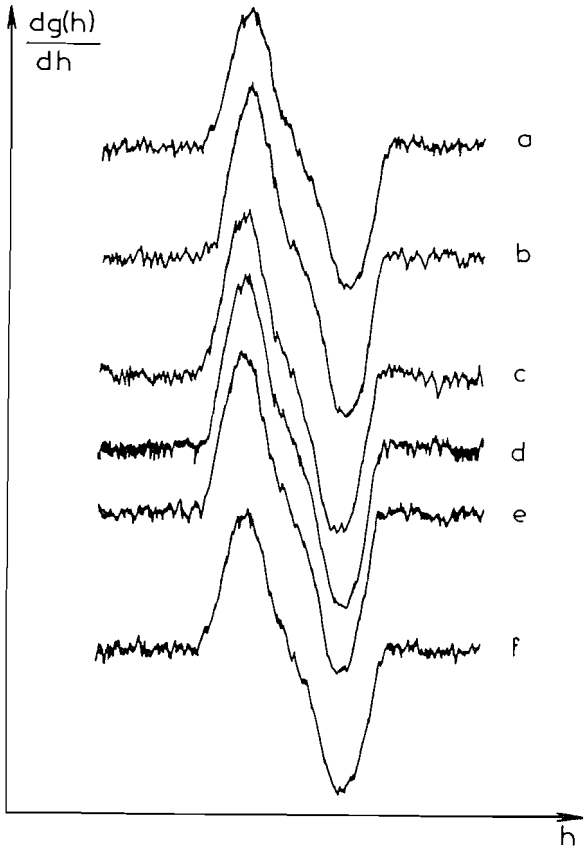

FIG. 6. Proton nmr spectra of NH_4AlCl_4: (*a*) powder at 298 K, (*b*) single crystal at 298 K, (*c*) single crystal at 298 K turned 90° in the field, (*d*) single crystal at 298 K turned 180° in the field, (*e*) single crystal at 298 K turned 270° in the field, (*f*) powder at 77 K.

restricted rotation of the cation caused by hydrogen bonding); (*ii*) the broadening of the lattice bands in the far infrared region; (*iii*) the ν_4 frequency. Although we did not, for NH_4AlCl_4, observe any absorption in the 1600–2000 cm^{-1} frequency range, where we should find combination modes (1993 and 1755 cm^{-1} for $\nu_4 + \nu_6$ and $\nu_2 + \nu_6$ respectively, in $(NH_4)_3ZnCl_5$ (21)), the high ν_4 value, 1414 cm^{-1}, compared with the values of the other chlorinated complexes (between 1393 and 1400 cm^{-1} according to ref. 22) should characterize the existence of H bonds. This criterion cannot be sufficient because, in $(NH_4)_2PtCl_6$ and $(NH_4)_2TeCl_6$, H bonds did not seem to exist although the ν_4 values were greater than 1400 cm^{-1}: 1402.8 cm^{-1} and 1409.0 cm^{-1} respectively (23).

Proton nmr

The proton nmr enables one, in the best cases, to evaluate the proton–proton distances and the group orientations, studying the general outline of the band obtained (24). We collected the proton resonance spectra at room temperature on polycrystalline samples and single crystals. The nuclear magnetic second moment value, which represents the mean quadratic value of the resonance line (Fig. 6), is small: 4 G^2. It is much smaller than the theoretical value, 43 G^2, associated with a regular and immobile tetrahedral ammonium ion (25). Moreover the spectrum did not change either by rotating the crystal by 90° in the magnetic field or by cooling the sample down to liquid nitrogen temperature.

This small value of the second moment is often found in ammonium salts at room temperature (26).

Can. J. Chem. Downloaded from www.nrcresearchpress.com by 210.87.254.5 on 09/05/12
For personal use only.

Can. J. Chem. Downloaded from www.nrcresearchpress.com by 210.87.254.5 on 09/05/12
For personal use only.

Its stability during the cooling process from room temperature to 80 K is similar to the NH_4ClO_4 example given by Ibers (27) and Hennel and Lalowicz (28). According to them this small value of the second moment resulted from reorientation about random axes of the ammonium ion, the dipole interactions within the ion then being averaged to zero by isotropic reorientation, only the weak intermolecular H—H contributions remaining.

Conclusions

NH_4AlCl_4 can be said to be isostructural with the nitrosyl (at room temperature), rubidium, and caesium tetrachloroaluminate salts.

As for the ammonium ion we remark that the hydrogen atoms are invisible on the difference Fourier synthesis. Moreover the Raman scattering bands are broad with low intensities whereas the infrared absorption spectra reveal no $\nu_2 + \nu_6$ or $\nu_4 + \nu_6$ combination bands. And last we observe the very small value of the nuclear magnetic second moment. A comparison between these results and those obtained for other ammonium salts enables us to deduce that the ammonium ion behaves as a 'spherical ion' without any apparent restricting motion.

Acknowledgments

We are grateful to Dr. F. Baert of Equipe de Dynamique des Cristaux Moléculaires E.R.A. No. 465 for the use of his crystallographic program chain. We thank Dr. Touillaux of Laboratoire de Chimie Physique et de Cristallographie (C.R.I.S.), Université de Louvain-la-Neuve, Belgique, for running the proton nmr spectra.

1. P. Barbier, G. Mairesse, J. P. Wignacourt, and F. Baert. Cryst. Struct. Commun. **5**, 633 (1976).
2. P. Barbier. Thèse de Doctorat d'Etat, Université de Lille. October 1976.
3. P. Barbier and G. Mairesse. C. R. Acad. Sci. Paris, Ser. C, **272**, 66 (1971).
4. G. Peyronel and A. Pignedoli. Acta Crystallogr. Sect. B, **31**, 2052 (1975).
5. C. S. Choi, H. J. Prask, and E. Prince. Acta Crystallogr. Sect. B, **32**, 2919 (1976).
6. G. Germain, P. Main, and H. Woolfson. Multan a computer program for the automatic solution of crystal structures. 1972.
7. D. Andre, R. Fourme, and M. Renaud. Acta Crystallogr. Sect. B, **27**, 2375 (1971).
8. D. T. Cromer and J. T. Waber. Acta Crystallogr. **18**, 104 (1965).
9. F. Wallart. Thèse de Doctorat d'Etat, Université de Lille. 1970.
10. R. Demol. D.E.S. Lille (1973).
11. G. Mairesse. Unpublished results.
12. R. C. Gearhart, Jr. Ph.D. Thesis, University of Delaware, Newark, DE. June 1972.
13. G. Mairesse, P. Barbier, J. P. Wignacourt, and F. Baert. Cryst. Struct. Commun. **6**, 15 (1977).
14. N. C. Baenziger. Acta Crystallogr. **4**, 216 (1951).
15. W. Scheinert and A. Weiss. Z. Naturforsch. **31**a, 1354 (1976).
16. W. R. Busing and H. A. Levy. Acta Crystallogr. **17**, 142 (1964).
17. C. S. Choi, H. J. Prask, and E. Prince. J. Chem. Phys. **61**, 3523 (1974).
18. S. P. Porto, P. A. Fleury, and T. C. Damen. Phys. Rev. **154**, 522 (1967).
19. P. Barbier, G. Mairesse, J. P. Wignacourt, F. Wallart, and A. Rubbens. Proceedings of the Fifth International Conference on Raman Spectroscopy, University of Freiburg, September 1–8 1976. *Edited by* E. D. Schmid (Freiburg in Breisgau, F. R. G.). p. 672.
20. T. C. Waddington. J. Chem. Soc. 4340 (1958).
21. J. P. Mathieu and H. Poulet. Spectrochim. Acta, **16**, 696 (1960).
22. J. T. R. Dunsmuir and A. P. Lane. Spectrochim. Acta Part A, **28**, 45 (1972).
23. I. A. Oxton, O. Knop, and M. Falk. Can. J. Chem. **53**, 2675 (1975).
24. R. Touillaux. Thèse, Université Catholique de Louvain, Belgique. 1964.
25. D. Pendred and R. E. Richards. Trans. Faraday Soc. **51**, 468 (1955).
26. R. E. Richards and T. Schaefer. Trans. Faraday Soc. **57**, 210 (1961).
27. J. A. Ibers. J. Chem. Phys. **32**, 1448 (1960).
28. J. W. Hennel and Z. T. Lalowicz. Acta Phys. Pol. A, **38**, 675 (1970).
29. G. Nowogrocki. Unpublished program from ORTEP (C. K. Johnson) written for Hewlett Packard 9825 computer.

Microwave spectrum of methylthioacetonitrile

R. KEWLEY

Department of Chemistry, Queen's University, Kingston, Ont., Canada K7L 3N6

Received August 25, 1977

R. KEWLEY. Can. J. Chem. **56**, 772 (1978).

The microwave rotational spectrum of methylthioacetonitrile has been studied in the frequency range 18–37 GHz. The spectrum found is that of the *gauche* conformer. The non-observation of the spectrum of the *trans* conformer indicates that its abundance is less than about 5%. The rotational and centrifugal distortion constants for the ground vibrational state of the *gauche* conformer are: $A = 7715.123$ MHz, $B = 2641.756$ MHz, $C = 2174.538$ MHz, $D_K = 0.6824$ MHz, $D_{JK} = -2.52$ kHz, and $D_J = 1.96$ kHz. The observed rotational constants are compatible with a dihedral angle of 66 ± 5° and a CSC angle of 104 ± 2°. The dipole moment of the *gauche* conformer has been determined as 3.02 D. Vibrational satellites due to S—CH_2 torsion have been observed and a torsional frequency of 101 cm^{-1} has been estimated from relative intensity measurements.

R. KEWLEY. Can. J. Chem. **56**, 772 (1978).

On a étudié le spectre de microonde de rotation du méthylthioacétonitrile à des fréquences allant de 18–37 GHz. Le spectre trouvé correspond à celui du conformère *gauche*. Le fait que l'on n'a pas observé le spectre de l'isomère *trans* indique que sa quantité présente ne dépasse pas 5%. Les constantes de distortions rotationnelle et centrifuge pour l'état fondamental de vibration du conformère *gauche* sont $A = 7715.123$ MHz, $B = 2641.756$ MHz, $C = 2174.538$ MHz, $D_K = 0.6824$ MHz, $D_{JK} = -2.52$ kHz et $D_J = 1.96$ kHz. Les constantes de rotation observées sont en accord avec un angle dièdre de 66 ± 5° et un angle CSC de 104 ± 2°. On a déterminé que le moment dipolaire du conformère *gauche* est de 3.02 D. On a observé les satellites de vibration dus à la torsion S—CH_2 et on a évalué, à partir de mesures d'intensité relative, que la fréquence de torsion est de 101 cm^{-1}.

[Traduit par le journal]

Introduction

The present investigation represents an extension of our recent interest in straight chain methoxy derivatives. The first microwave spectroscopy study of a molecule closely related to methylthioacetonitrile, CH_3SCH_2CN, was Hirota's (1) work on butyronitrile, $CH_3CH_2CH_2CN$, which was found to be present in the gas phase as both *gauche* and *trans* conformers, related by rotation around the CH_2—CH_2 bond. In addition Hirota concluded that the energy difference between the two conformers is less than 1 kcal mol^{-1}. In our laboratory it was determined that methoxyacetonitrile, CH_3OCH_2CN, is predominantly in the *gauche* form with a small amount of higher energy (by about 1.4 kcal mol^{-1}) *trans* form also present (2). By contrast we found that 3-methoxypropionitrile, $CH_3OCH_2CH_2CN$, exists almost entirely as a fully *trans* conformer (3). Recent microwave studies of molecules of the type CH_3OCH_2X, X = F, Cl, Br, and C≡CH, each resulted in the detection of a sole conformer, the *gauche* (4–7). The Raman and infrared spectra of methyl propargyl ether, $CH_3OCH_2C{\equiv}CH$, are explicable in terms of a predominant *gauche* conformer in the solid, liquid, and vapor states (8). The infrared spectrum of methylthioacetonitrile in the liquid, solid, and dissolved states has been investigated recently by Owen and co-workers (9). They were unable to obtain the gas phase infrared spectrum because of the low vapor pressure of CH_3SCH_2CN at room temperature. Solution infrared spectra were interpreted as showing no evidence of rotational isomerism. On the other hand spectral changes during warming and cooling between the solid and liquid phases did indicate that rotational isomerization was taking place. They also measured the dipole moment of CH_3SCH_2CN in solution in toluene. The observed value of 3.10 D is below the values of 3.2 and 5.0 D which they predicted from bond moments for the *gauche* and *trans* conformers, respectively. This indicates that the proportion of *gauche* conformer is close to 100%.

In view of the ambiguous nature of the results of the infrared and dipole moment study a microwave investigation should be of value since both conformers should be detectable if present in significant amounts, as for methoxyacetonitrile (2). Also a microwave study provides an independent check on the value of dipole moment, which in Owen's study might have been an average over more than one conformer.

Experimental

The sample of methylthioacetonitrile was supplied by the Aldrich Chemical Company and was used without further purification.

Frequency measurements were carried out at room tem-

Can. J. Chem. Downloaded from www.nrcresearchpress.com by 210.87.254.6 on 09/05/12
For personal use only.

Can. J. Chem. Downloaded from www.nrcresearchpress.com by 210.87.254.6 on 09/05/12
For personal use only.

perature, because of the fairly low vapor pressure of the substance, and at sample pressures in the range 5–50 micron. The frequencies are considered to be accurate to 0.1 MHz or better. However, the lines were all rather broad, about 1 MHz at 30 micron typically, due to unresolved quadrupole structure, so that the frequency accuracy of some of the weaker excited state lines is in the range 0.2 to 0.5 MHz.

Initially scans and frequency measurements were made in the 26.5 to 37 GHz region using the Rice University Hewlett-Packard 8460A MRR spectrometer. Additional frequencies and the Stark shifts were measured at Queen's University with a 100 kHz Hughes-Wilson Stark modulation spectrometer, described earlier (10). Computations were done using the Queen's University Burroughs 6700 computer.

Rotational Spectrum

Predictions, Assignment

Predictions for the normal (^{32}S) species of CH_3SCH_2CN, based on structural parameters taken from the molecules $(CH_3)_2S$ (11) and CH_3CN (12), were that the *gauche* conformer should have $\kappa \simeq -0.88$ with the higher K_{-1} lines of the $J = 6 \leftarrow 5$ and $7 \leftarrow 6$ transitions falling near 29 250 and 34 100 MHz respectively, while the *trans* conformer should have $\kappa \simeq -0.98$ with the $J = 8 \leftarrow 7$ transition near 30 550 MHz and the $J = 9 \leftarrow 8$ transition near 34 350 MHz.

A scan at 150 micron pressure and 100 V cm^{-1} Stark voltage contained the expected transitions of the *gauche* conformer. However scans at low Stark voltages, ~20 V cm^{-1}, failed to reveal any absorption peaks assignable as the *trans* conformer high K_{-1} groups. Under similar conditions the *trans* conformer of methoxyacetonitrile (2) gave easily recognizable lines of about the same intensity as those due to the corresponding *gauche* conformer. Since in methoxyacetonitrile the proportion of *trans* conformer was estimated as about 5% and since the dipole moment components of CH_3OCH_2CN (2) and CH_3SCH_2CN (see below) are rather similar it can be concluded that in methylthioacetonitrile the proportion of *trans* conformer is appreciably less than 5%.

The frequencies in the *a*-type $J = 6 \leftarrow 5$ and $7 \leftarrow 6$ transitions and the *b*-type transitions of the *gauche* conformer were measured with the Hewlett-Packard instrument, those in the *a*-type $J = 4 \leftarrow 3$ and $5 \leftarrow 4$ transitions with the 100 kHz modulation spectrometer. The observed frequencies for the ground vibrational state are given in Table 1. The derived rotational constants and the three symmetric rotor centrifugal distortion constants are shown in Table 2. These constants were obtained from a least-squares fit which employed derivatives of frequency with respect to *A*, *B* and *C*, calculated with the aid of a rigid rotor frequency prediction program (ROTSPE), and the known derivatives with respect to D_K, D_{JK}, and D_J. Compared to *gauche* methoxyacetonitrile, which has $D_J = 2.93$ kHz and $D_{JK} = -23.3$ kHz, for methylthioacetonitrile D_J is similar in magnitude while D_{JK} is a factor of about 10 lower.

The ground vibrational state transition frequencies were also fitted with the computer program CDANAL, originally written by Dr. W. H. Kirchhoff. The resulting parameters are given in the lower part of Table 2. The last three centrifugal distortion coefficients are strongly correlated with correlation matrix elements of about 0.9. These three distortion coefficients are all negative in sign. This appears to be normal since a literature survey of some recently studied substances showed that for widely differing molecules these coefficients were always negative, for example sulfur dichloride (13), 3-chloropyridine (14), and *n*-propyl isocyanide, *trans* and *gauche* conformers (15). It may also be noted that the relationship:

$$[1] \qquad D_{JK} = -D_J - D_K - \tfrac{1}{4}\tau_{aaaa}\hbar^4$$

should be obeyed (16), where $\tau_{aaaa}\hbar^4 = \tau''_{aaaa}$. The calculated value of τ''_{aaaa} from eq. 1, using the *D* values from Table 2, is -2.75 ± 0.02 MHz which is fairly close to the τ''_{aaaa} value from the CDANAL fit of -2.89 ± 0.08 MHz. Better agreement would probably be obtained if a much larger number of transition frequencies were measured, including those of some *c*-type transitions.

Dipole Moment

The electric dipole moment components of *gauche* methylthioacetonitrile were determined from a least-squares fit to the four observed Stark shifts in Table 3. Linear plots of $\Delta\nu$ vs. E^2 were obtained for the four lobes, using Stark voltages in the range 350–4700 V cm^{-1}. The effect of ^{14}N nuclear quadrupole interaction was ignored. The Stark cell was calibrated using the value of $\mu_{OCS} = 0.71512 \pm 0.00003$ D (17). The dipole moment components are given in Table 3. For comparison the corresponding values for *gauche* methoxyacetonitrile are $\mu_a = 2.40$, $\mu_b = 1.37$, $\mu_c = 1.11$, and $\mu = 2.98$ D. The total dipole moment of 3.02 ± 0.03 D for *gauche* methylthioacetonitrile is close to Owen's value in toluene solution of 3.10 D (9) and serves to confirm the conclusion that the amount of *trans* conformer present must be very small.

Torsional Satellites

In addition to the rotational spectrum of the ground vibrational state of the *gauche* conformer two sets of vibrational satellites have been observed to lower frequency. These satellites are assigned as the first and second excited states (*T*1 and *T*2) of the S—CH_2 torsional mode. Transition frequencies for the *T*1 and *T*2 states are given in Table 1 and the derived constants in Table 2.

Can. J. Chem. Downloaded from www.nrcresearchpress.com by 210.87.254.6 on 09/05/12
For personal use only.

TABLE 1. Observed transition frequencies, in MHz, of *gauche* methylthioacetonitrile, ground, and two torsionally excited states

Transition	Ground	$T1$	$T2$
		a-type	
4(0,4) ← 3(0,3)	18 964.57(+0.20)[a]		
4(1,4) ← 3(1,3)	18 272.39(+0.10)	18 221.04(+0.02)	
4(1,3) ← 3(1,2)	20 133.73(+0.18)	20 065.38(+0.05)	20 002.89(+0.06)
4(2,3) ← 3(2,2)	19 240.84(+0.04)	19 180.38(+0.34)	
4(2,2) ← 3(2,1)	19 541.39(+0.36)	19 472.84(+0.21)	19 409.48(−0.20)
5(0,5) ← 4(0,4)	23 500.48(−0.62)	23 437.96(−0.55)	23 383.20(+0.15)
5(1,5) ← 4(1,4)	22 790.41(+0.02)	22 727.35(−0.10)	
5(1,4) ← 4(1,3)	25 099.68(−0.30)		24 940.18(−0.13)
5(2,4) ← 4(2,3)	24 012.50(+0.34)		
5(2,3) ← 4(2,2)	24 591.10(−0.09)		
5(3,3) ← 4(3,2)	24 174.16(+0.30)	24 095.12(+0.22)	
5(3,2) ← 4(3,1)	24 200.36(+0.01)		
5(4,2) ← 4(4,1)	24 149.16(−0.17)	24 070.72(−0.12)	
6(0,6) ← 5(0,5)	27 939.79(−0.10)	27 869.47(−0.10)	
6(1,5) ← 5(1,4)	30 014.97(+0.22)		29 829.24(+0.05)
6(2,5) ← 5(2,4)	28 758.11(+0.12)		
6(2,4) ← 5(2,3)		29 602.09(−0.31)	29 500.01(+0.04)
6(3,4) ← 5(3,3)	29 032.21(−0.09)	28 937.35(+0.20)	28 850.18(+0.04)
6(3,3) ← 5(3,2)	29 102.10(−0.07)		
6(4,3) ← 5(4,2)			28 819.82(+0.39)
6(5,2) ← 5(5,1)	28 973.74(−0.25)		28 793.87(−0.30)
7(0,7) ← 6(0,6)	32 302.70(+0.01)	32 224.80(+0.29)	
7(2,6) ← 6(2,5)	33 473.90(+0.02)		33 280.26(−0.31)
7(3,5) ← 6(3,4)	33 894.27(−0.04)	33 783.03(−0.08)	33 681.70(+0.43)
7(3,4) ← 6(3,3)	34 048.47(−0.14)	33 931.07(+0.13)	
7(4,4) ← 6(4,3)	33 863.20(−0.11)		
7(4,3) ← 6(4,2)	33 868.24(−0.25)		33 654.37(−0.17)
7(5,3) ← 6(5,2)	33 821.66(−0.12)	33 711.30(−0.19)	33 609.88(−0.34)
7(6,2) ← 6(6,1)	33 799.39(+0.33)	33 689.51(+0.07)	33 589.71(+0.27)
		b-type	
4(2,3) ← 3(2,1)	33 769.71(−0.12)		
5(1,5) ← 4(0,4)	26 137.37(−0.09)		
6(1,6) ← 5(0,5)	29 917.96(+0.27)		
10(2,9) ← 10(1,10)	29 310.50(+0.03)		
12(4,8) ← 12(3,9)	33 037.10(+0.04)		
Standard deviation of fit	0.23	0.28	0.30

[a](Observed frequency − calculated frequency) is given in parentheses.

Measurements of intensity relative to the ground state absorption spectrum was carried out for a total of thirteen $T1$ satellite peaks in the $J = 6 \leftarrow 5$ and $7 \leftarrow 6$ transitions. These measurements yielded an average relative intensity of $0.61_4 \pm 0.07_6$ at 25°C, which corresponds to a torsional frequency of $101 \pm 30\ cm^{-1}$. This frequency is similar to those found in closely related molecules of $93\ cm^{-1}$ in CH_3OCH_2CN (2), and of $105\ cm^{-1}$ in CH_3OCH_2-$C{\equiv}CH$ (7).

Neither methyl torsion satellites nor any splitting of ground vibrational state lines by methyl torsion has been observed. If some high J c-type Q branch lines could be assigned then it should be possible to determine the height of the barrier, V_3, from the A–E splitting of the ground state. This has been done by Karlsson (18) for methoxyacetonitrile, giving a V_3 value of 2280 cal mol^{-1}. It might be expected that the value in methylthioacetonitrile would be somewhat lower than this figure in view of the barriers 2720 cal mol^{-1} in $(CH_3)_2O$ (19) and 2132 cal mol^{-1} in $(CH_3)_2S$ (11).

Molecular Structure

Estimates of up to three structural parameters can be made from the three observed rotational constants of the *gauche* conformer if assumptions are made concerning the values of the remaining parameters.

Three angles upon which the rotational constants are fairly strongly dependent are $\angle C_1SC_2$, the dihedral angle between the C_1SC_2 and SC_2C_3 planes, and the angle of tilt which the axis of each

Can. J. Chem. Downloaded from www.nrcresearchpress.com by 210.87.254.6 on 09/05/12
For personal use only.

TABLE 2. Rotational and centrifugal distortion constants of *gauche* methylthioacetonitrile

Constant[a]	Ground state	*T*1 state	*T*2 state
A (MHz)	7715.123±0.072	7751.14±2.20	7795.11±2.46
B (MHz)	2641.756±0.008	2631.93±0.04	2622.83±0.04
C (MHz)	2174.538±0.007	2169.03±0.04	2164.18±0.07
κ	−0.831347	−0.834148	−0.837096
D_K (MHz)	0.6824±0.0055		
D_{JK} (kHz)	−2.52 ±0.44	−2.93±0.68	−3.93±0.74
D_J (kHz)	1.96 ±0.07	2.11±0.28	2.63±0.41
Kirchhoff parameters (in MHz)			
A''	7715.324 ±0.175		
B''	2641.821 ±0.029		
C''	2174.500 ±0.032		
τ_1	−0.009121±0.002707		
τ_2	−0.000322±0.001393		
τ_3	1.056 ±0.162 (assumed)		
τ''_{aaaa}	−2.888 ±0.084		
τ''_{bbbb}	−0.01512 ±0.00242		
τ''_{cccc}	−0.006584±0.001448		
	(Standard deviation 0.21)		

[a]The uncertainty quoted represents one standard error in the corresponding constant.

TABLE 3. Stark effect coefficients and dipole moment components of *gauche* methylthioacetonitrile

		$10^6 \times \Delta\nu/E^2$ (MHz cm² V⁻²)	
Transition	$\|M\|$	Observed	Calculated
4(1,4) ← 3(1,3)	1	24.70	24.63
5(1,5) ← 4(1,4)	1	−14.52	−14.56
5(0,5) ← 4(0,4)	2	4.094	4.088
6(1,6) ← 5(1,5)	1	−1.259	−1.263

Dipole component	Value (D)
μ_a	2.37±0.02
μ_b	1.63±0.02
μ_c	0.93±0.03
μ	3.02±0.03

attached group, CH_3 or CH_2CN, makes with the corresponding SC bond. Both attached groups were taken to have the same tilt angle, a positive tilt angle being defined as one that causes a decrease of the $H_{13}C_1S$ and SC_2C_3 angles from the value at zero tilt.

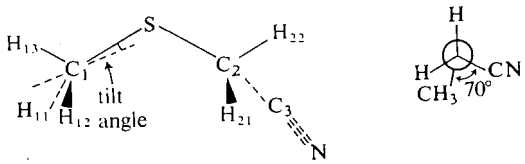

In dimethyl sulfide the methyl groups are tilted at 2.75° so that their axes are at an angle of 104.37° while the CSC angle is 98.87° (11). Including a 2.75° tilt angle for each of the CH_3 and CH_2CN groups the following initial structure was assumed, based on the known r_s structures of $(CH_3)_2S$ (11) and CH_3CN (12).

$C_1S = C_2S$	= 1.802 Å	$\angle H_{13}\,C_1S$	= 106.63°
C_2C_3	= 1.458 Å	HC_1H angles	= 109.57°
C_3N	= 1.157 Å	$\angle C_1SC_2$	= 98.87°
C_1H distances	= 1.091 Å	$\angle SC_2C_3$	= 106.92°
C_2H distances	= 1.12 Å	$\angle C_2C_3N$	= 180°
Dihedral angle	= 70°	$\angle H_{21}C_2H_{22}$	= 109.27°
Tilt angle	= 2.75°	$\angle C_3C_2H_{21}$ = $\angle C_3C_2H_{22}$	= 109.67°

This structure gave calculated rotational constants (in MHz): A = 7686.07, B = 2681.84, and C = 2270.74.

Two procedures were tried in fitting the observed A, B, and C values. First a least-squares fit was performed by allowing the C_1SC_2 angle and the dihedral angle to vary with all the remaining parameters fixed. The best fit occurred at a C_1SC_2 angle of 104.69° and a dihedral angle of 69.02° and yielded calculated rotational constants (in MHz) A = 7700.70, B = 2615.06, and C = 2196.16. In the second procedure the tilt angle was considered as a third variable and the new values of the angles were obtained by solving three simultaneous equations involving the observed rotational constants, those calculated from the initial structure, and the derivatives of A, B, and C with respect to the three angles. The observed rotational constants were reproduced at $\angle C_1SC_2$ = 102.94°, dihedral angle = 63.04°, and tilt angle = −0.32°. On the basis of these calculations reasonable estimates of the two angles of main interest are $\angle C_1SC_2$ = 104 ± 2° and dihedral angle = 66 ± 5°.

The dihedral angle estimate is slightly lower than the one of 69° estimated in methoxyacetonitrile (2). For that molecule the solution (in carbon tetra-

chloride) dipole moment of 2.99 D has been interpreted by Ritchie and co-workers (20) in terms of a single conformer, the *gauche*, with dihedral angle 70°. In this case the microwave study showed the *gauche* form to be present in 95% abundance and to have a dipole moment of 2.98 D. Ritchie has also made some corresponding predictions, which include the effect of bond polarizability, of the dipole moment of *gauche* methylthioacetonitrile for various dihedral angles: 60°, 2.88 D; 65°, 2.98 D; 70°, 3.09 D; and 75°, 3.19 D. The observed dipole moment of 3.02 D in the present study together with an estimated dihedral angle near 66° are in good agreement with Ritchie's predictions.[1]

Acknowledgements

The author is most grateful to Professor R. F. Curl of Rice University, Houston, Texas, for the use of his Hewlett-Packard spectrometer at the beginning of this study. Much patient assistance in overcoming computer difficulties was provided by Mr. D. E. Farmiloe of Computing Services, Queen's University. Support of the project by grant number A-2046 from the National Research Council of Canada is gratefully acknowledged.

[1]N. L. Owen, private communication (copy of letter from G. L. D. Ritchie), 1977.

1. E. Hirota. J. Chem. Phys. **37**, 2918 (1962).
2. R. Kewley. Can. J. Chem. **52**, 509 (1974).
3. R. S. Lowe and R. Kewley. J. Mol. Spectrosc. **63**, 216 (1976).
4. J. Nakagawa and M. Hayashi. Chem. Lett. 349 (1976).
5. T. Ikeda, R. F. Curl, and H. Karlsson. J. Mol. Spectrosc. **53**, 101 (1974).
6. M. Hayashi, K. Kuwada, and H. Imaishi. Chem. Lett. 913 (1974).
7. K.-M. Marstokk and H. Møllendal. J. Mol. Struct. **32**, 191 (1976).
8. A. Bjorseth and J. Gustavsen. J. Mol. Struct. **23**, 301 (1974).
9. S. W. Charles, F. C. Cullen, and N. L. Owen. J. Mol. Struct. **34**, 219 (1976).
10. R. Kewley. Can. J. Chem. **50**, 1690 (1972).
11. L. Pierce and M. Hayashi. J. Chem. Phys. **35**, 479 (1961).
12. L. F. Thomas, E. I. Sherrard, and J. Sheridan. Trans. Faraday Soc. **51**, 619 (1955).
13. R. W. Davies and M. C. L. Gerry. J. Mol. Spectrosc. **65**, 455 (1977).
14. S. D. Sharma and S. Doraiswamy. J. Mol. Spectrosc. **57**, 377 (1975).
15. M. J. Fuller and E. B. Wilson. J. Mol. Spectrosc. **58**, 414 (1975).
16. W. Gordy and R. L. Cook. Microwave molecular spectra. Vol. 9, Part 2. *Edited by* W. West. Interscience, New York, NY. 1970. Chapt. 8, Table 8.6, p. 222.
17. F. H. De Leeuw and A. Dymanus. Chem. Phys. Lett. **7**, 288 (1970).
18. H. Karlsson. J. Mol. Struct. **33**, 319 (1976).
19. P. H. Kasai and R. J. Myers. J. Chem. Phys. **30**, 1096 (1959).
20. R. J. W. Le Fèvre, G. L. D. Ritchie, and P. J. Stiles. J. Chem. Soc. B, 819 (1967).

Can. J. Chem. Downloaded from www.nrcresearchpress.com by 210.87.254.6 on 09/05/12
For personal use only.

Application de la spectrométrie ir et Raman à l'étude des complexes en solution aqueuse – $Be^{2+} - H_2C_2O_4$

M. JABER,[1] F. BERTIN ET G. THOMAS-DAVID

Laboratoire de Chimie Analytique II, Université Claude Bernard, Lyon I, 43 boulevard du 11 Novembre 1918, 69621 Villeurbanne, France

Reçu le 28 juin 1977

M. JABER, F. BERTIN et G. THOMAS-DAVID. Can. J. Chem. **56**, 777 (1978).

L'étude des solutions d'oxalate complexe de béryllium, par spectrométrie ir et Raman, a montré la formation des trois espèces complexes: BeC_2O_4, $Be(C_2O_4)_2^{2-}$ et $Be_3(OH)_3(C_2O_4)_3^{3-}$ quel que soit le rapport étudié. Chaque complexe est caractérisé par des fréquences de vibration spécifiques indépendantes du p*H* de la solution. La mesure des hauteurs de certaines bandes de diffusion Raman caractéristiques des complexes nous a permis de calculer la concentration de chaque espèce en fonction du p*H*, ainsi que leurs constantes de stabilité.

M. JABER, F. BERTIN, and G. THOMAS-DAVID. Can. J. Chem. **56**, 777 (1978).

A study of solutions of the oxalate complexes of berylium by ir and Raman spectrometry has demonstrated the formation of three complexed species: BeC_2O_4, $Be(C_2O_4)_2^{2-}$, and $Be_3(OH)_3(C_2O_4)_3^{3-}$ regardless of the ratio used. Each complex is characterized by specific vibrational frequencies which are independent of the p*H* of the solution. It was possible to determine the concentration of each species as a function of p*H*, as well as its stability constant, by measuring the intensities of certain characteristic bands in the Raman scattering spectrum.

[Journal translation]

Introduction

Les complexes du béryllium avec l'acide oxalique ont fait l'objet de plusieurs recherches (1–18) qui conduisent, pour la plupart, à l'existence, tant en solution qu'à l'état cristallisé, de deux espèces BeC_2O_4 et $Be(C_2O_4)_2^{2-}$.

Dragulescu a découvert qu'une espèce hydroxydée polynucléaire $Be_3(OH)_3(C_2O_4)_3^{3-}$ (19) pouvait se former à côté du complexe BeC_2O_4 en dépit d'un excès d'ions oxalate. Dans ce travail l'auteur ne mentionne à aucun moment la formation de $Be(C_2O_4)_2^{2-}$ dont il avait pourtant admis la présence en faible proportion dans une publication antérieure (18).

Plus récemment Faucherre (20) a pu conclure à l'existence à côté de BeC_2O_4 et $Be(C_2O_4)_2^{2-}$ d'une espèce hydroxydée différente de celle de Dragulescu: $Be_2(OH)_2(C_2O_4)_2^{2-}$. Les valeurs des constantes de stabilité données par les auteurs pour les mêmes espèces sont assez différentes.

Ce mémoire présente les résultats obtenus dans l'étude systématique du système Be^{2+}–$C_2O_4^{2-}$ en solution aqueuse par spectrométrie ir et Raman, en suivant l'évolution des spectres en fonction du p*H* pour différents rapports t = [métal]/[coordinat]: mise en évidence des espèces formées et par analogie avec les systèmes H^+–$C_2O_4^{2-}$ et Al^{3+}–$C_2O_4^{2-}$ (22) détermination des concentrations des complexes et calcul de leurs constantes de formation.

[1]Bousier C.N.R.S. Libanais.

Conditions expérimentales

Les solutions étudiées sont de concentrations 0.30, 0.32 et 0.225 *M* en acide oxalique pour des rapports t = [métal]/[coordinat] respectivement $\frac{1}{3}$, $\frac{1}{2}$ et 1. Elles sont obtenues à partir de solutions mères préparées en dissolvant du chlorure de béryllium anhydre $BeCl_2$ et de l'acide oxalique $H_2C_2O_4 \cdot 2H_2O$, produits Merck. Le p*H* des solutions est fixé par addition de soude 13 *N* ou d'acide chlorhydrique PROLABO RP (la soude a été préférée à la potasse pour une question de solubilité). Le p*H* est mesuré au moyen de la chaîne suivante: electrode en verre/solution titrée/NaCl saturé/Hg_2Cl_2–Hg par l'intermédiaire d'un potentiomètre Metrohm E 388. La précision sur la mesure de la concentration en ion H^+ est faible compte tenu de la valeur élevée et variable de la force ionique.

Quant aux solutions dans l'eau deutériée elles sont préparées à partir du chlorure de béryllium anhydre et de l'oxalate neutre de sodium $Na_2C_2O_4$, produits Merck, dans D_2O 99.75%. L'acidité des solutions examinées est fixée par addition de DCl ~ 7.8 *N* dont la teneur en D_2O est 99.5%.

Les spectres Raman sont enregistrés à la température ordinaire (20°C) dans une région de fréquences comprise entre 1800 et 150 cm^{-1} avec un appareil CODERG PHO. La raie excitatrice est la raie 488 nm d'un laser à argon ionisé Spectra Physics. Les conditions d'enregistrement des spectres sont les suivantes: la puissance du laser est 900 mW, la tension d'alimentation du photomultiplicateur refroidi est de l'ordre de 1200 V, les fentes ont une largeur spectrale constante de 6 cm^{-1} et la vitesse de défilement du réseau V = 25 cm^{-1}/mn; l'échantillon à examiner est contenu dans une petite cuve en verre de 1 ml.

Les spectres ir sont réalisés à la température ordinaire entre 2000 et 650 cm^{-1} sur un spectromètre à double faisceau: Perkin-Elmer 457. La cellule est constituée de deux fenêtres d'Irtran II d'épaisseur 27 μm.

Résultats de la spectrométrie Raman

Evolution des spectres Raman en fonction du

Can. J. Chem. Downloaded from www.nrcresearchpress.com by 210.87.254.105 on 09/05/12
For personal use only.

TABLEAU 1. Fréquences et intensités des bandes Raman des oxalates complexes de Be^{2+} pour un rapport $t = \frac{1}{2}$ à différentes acidités

pH = 0.7		pH = 1.3		pH = 2.2		pH = 2.8		pH = 4.1		pH = 5.0		pH = 7.3	
F	h_v	F	h_v	F	h_v	F	h_v	F	h_v	F	h_v	F	h_v
365	0.03	365	0.05	368	0.13	368	0.17	368	0.17	368	0.15	368	0.05
454	0.50	454	0.44	450	0.29	450	0.20	449	0.16	449	0.19	449	0.27
								498		498		498	
553	0.04	533											
		558											
				583	0.18	583	0.26	583	0.25	583	0.37	583	0.34
601	0.19	601	0.46	601	0.49	601	0.44	601	0.26				
				614	0.48	614	0.63	614	0.56	614	0.46	614	0.05
725	0.05	725	0.04	725	0.03								
		793		793		793?							
				833		833		833		838	0.08	838	0.09
848	0.64	848	0.35										
		857		857		857		857		857		857	
868	0.51	868	0.53	868	0.31	868	0.16						
												903	
910	0.09	910	0.24	911	0.61	911	0.80	911	1.02	911	0.98	911	0.78
1093		1093		1093		1093		1093		1093		1103	
1283		1283		1283		1283		1283		1283		1283	
1305		1305		1305									
						1308	0.04	1308	0.10	1308	0.21	1308	0.37
1380		1380		1380									
1410	0.37	1410	0.71	1415	1.29	1415	1.63	1417	1.71	1419	1.48	1428	1.08
1444		1444		1444									
						1452		1452		1452		1452	
						1486	0.08	1486	0.25	1486	0.43	1486	0.76
										1683		1683	
1698		1698		1698		1698		1698		1698			
										1708		1708	
1730	1.03	1730	1.10	1730	1.04	1730	0.95	1730?	0.70	1727	0.74	1727	0.71
				1743	0.99	1743	1.19	1743	1.08	1743	0.84	1743	0.22
1750	0.87	1750	0.50										

rapport [métal]/[coordinat] et du pH des solutions: les modifications spectrales qui se produisent pour les rapports $t = 1$ et $t = \frac{1}{2}$ quand le pH augmente sont données dans les tableaux 1 et 2. Les spectres les plus caractéristiques ont été choisis; h_v représente pour une fréquence $\bar{\nu}$, l'intensité relative des maxima des bandes par rapport à l'intensité de la bande de l'eau à 1640 cm^{-1} prise comme référence (22). Des spectres ont été enregistrés en solution deutériée à différents pH et pour les différents rapports afin de suivre l'évolution des bandes dans la région de fréquences 1400–1800 cm^{-1}. Les différentes observations sont les suivantes.

Spectres Raman des complexes dans un rapport $t = \frac{1}{2}$ *(tableau 1)*

Le domaine de pH: $0.4 \leq$ p$H \leq 7.3$ s'étend du début de formation des complexes à la précipitation de l'hydroxyde de béryllium. Les spectres à p$H < 0.4$ comportent essentiellement les bandes, précédemment attribuées aux espèces $H_2C_2O_4$ et $HC_2O_4^-$ en solution (22) et une bande à 533 cm^{-1} due à l'espèce $Be(H_2O)_4^{2+}$ en solution (21). La neutralisation de la solution nous permet de distinguer trois étapes.

Dans un domaine de pH: $0.4 <$ p$H < 1.6$ il apparait de nouvelles bandes, dues aux complexes dont l'intensité augmente régulièrement avec le pH; ces raies ont une fréquence constante sur toute la gamme définie de pH et se situent à 365, 558, 601, 793, 857, 910, 1093, 1283, 1410, 1698 et 1730 cm^{-1}. Simultanément il y a une diminution d'intensité des bandes dues au coordinat.

A p$H \sim 1.6$ d'autres raies commencent à apparaître aux fréquences 583, 614, 833 et 1743 cm^{-1}. Dans l'intervalle $1.6 <$ p$H < 4.2$ leur position en fréquence reste constante et leurs intensités augmentent régulièrement, tandis qu'on assiste à une diminution d'intensité des raies 601, 793 et 1730 cm^{-1} qui disparaissent complètement à p$H \sim 4.2$, et à un glissement de deux fréquences 365 → 368 et 1410 → 1417 cm^{-1}; de plus l'intensité des bandes 911 et 1417 cm^{-1} augmente considérablement comme nous

Can. J. Chem. Downloaded from www.nrcresearchpress.com by 210.87.254.105 on 09/05/12
For personal use only.

TABLEAU 2. Fréquences et intensités des bandes Raman des oxalates complexes de Be^{2+} dans un rapport $t = 1$ à différentes acidités

pH = 0.8		pH = 1.9		pH = 3.7		pH = 4.1		pH = 5.1		pH = 6.6	
F	h_v	F	h_v	F	h_v	F	h_v	F	h_v	F	h_v
365	0.03	365	0.13	365	0.16	368	0.14	368	0.12	368	0.10
455	0.36	448	0.26	446	0.09	448	0.09	448	0.07	448	0.05
						498		498	0.06	498	0.05
533	0.07	533?	0.02								
		558		558							
						583		583	0.47	583	0.45
601	0.28	601	0.67	601	0.56	597	0.43				
				614	0.35	614	0.29	614	0.16	614	0.07
725											
793		793	0.10	793	0.10	793	0.08	793			
						833		833	0.13		
										838	0.09
848	0.40										
		857		857		857		857		857	
868	0.35	868	0.14								
910	0.13	910	0.36	911	0.46	911	0.45	911	0.39	911	0.33
		1093		1093		1093		1093		1103?	
1283		1283		1283		1283		1283		1283	
				1308	0.02	1308	0.02	1308	0.05	1308	0.07
1380		1380									
1409	0.36	1410	0.88	1416	1.17	1419	1.16	1426	1.31	1428	1.32
1444		1444									
				1452		1452		1452		1452	
				1486	0.05	1486	0.08	1486	0.09	1486	0.25
								1683		1683	
1698		1698		1698		1698					
								1708		1708	
								1727	0.84	1727	0.81
1730	0.86	1730	1.08	1730	1.05	1730	0.94				
				1743	0.66	1743	0.60	1743	0.35	1743	0.21
1750	0.50										

montre le tableau 1. A p$H \sim 4.1$ les bandes du coordinat existant sur le spectre sont celles attribuées à $C_2O_4^{2-}$ en solution; la concentration de ce dernier, calculée sur les bandes situées à 1308 et 1486 cm^{-1} en utilisant les coefficients de diffusion calculés antérieurement (22), représente 16% de la concentration analytique en coordinat.

A p$H > 4.5$ quatre bandes apparaissent à 498, 1683, 1708 et 1727 cm^{-1}, pendant que disparaissent celles situées à 614, 1698 et 1743 cm^{-1} et que l'intensité des bandes attribuées à $C_2O_4^{2-}$ augmente. L'augmentation du pH entraîne un déplacement progressif important de la fréquence de vibration située à 1417 cm^{-1} suivi d'une diminution d'intensité; en même temps l'intensité de la bande à 368 cm^{-1} diminue.

A p$H \sim 7.3$ les fréquences de vibration des complexes se trouvent ainsi à: 368, 449, 498, 583, 838, 857, 911, 1103, 1283, 1428, 1683, 1708 et 1727 cm^{-1}. Les résidus de deux bandes 614 et 1743 cm^{-1}, très intenses dans l'étape précédente, se présentent ici sous forme d'épaules à peine marquées; en outre la concentration de l'ion $C_2O_4^{2-}$ non engagé constitue presque la moitié de la concentration analytique du coordinat.

Spectres Raman des complexes dans un rapport $t = \frac{1}{3}$

Nous pouvons distinguer aussi trois régions principales analogues à celles que nous avons observées pour un rapport $t = \frac{1}{2}$. Les bandes des complexes de la première étape apparaissent dès p$H \sim 0.3$. Les raies aperçues à p$H \sim 1.6$ dans un rapport $t = \frac{1}{2}$ commencent à apparaître à p$H \sim 1.4$ pour $t = \frac{1}{3}$.

Le spectre des solutions dans l'intervalle $1.4 <$ pH < 4.7 est analogue à la deuxième étape du rapport $t = \frac{1}{2}$, on remarque cependant la présence de bandes caractéristiques du coordinat libre et le déplacement progressif de la fréquence $446 \rightarrow 450$ cm^{-1}. Ce déplacement provient de l'interférence de deux bandes larges dues l'une au coordinat, l'autre aux complexes. Il en résulte une bande de fréquence intermédiaire. Parmi les spectres de cet intervalle

Can. J. Chem. Downloaded from www.nrcresearchpress.com by 210.87.254.105 on 09/05/12
For personal use only.

Can. J. Chem. Downloaded from www.nrcresearchpress.com by 210.87.254.105 on 09/05/12
For personal use only.

trois ont été enregistrés aux pH: 3.4, 3.8 et 4.5, dans lesquels nous observons seulement les douze raies à 368, 450, 583, 614, 833, 857, 911, 1093, 1283, 1417, 1693 et 1743 cm^{-1} d'intensité relative constante, et les diverses bandes déjà attribuées au coordinat libre. A ces pH la concentration du coordinat non engagé représente exactement le tiers de la concentration analytique.

Au delà de pH 4.9 on assiste à une diminution d'intensité des bandes observées dans l'étape précédente et en même temps à une apparition des raies nouvelles déjà observée pour $t = \frac{1}{2}$ à p$H > 4.5$. On constate la même évolution dans le rapport $t = \frac{1}{2}$, avec une augmentation d'intensité des raies dues à $C_2O_4^{2-}$ en solution. Les deux fréquences situées à 614 et 1743 cm^{-1} subsistent avec une faible intensité même à p$H \sim 7$, et la quantité de $C_2O_4^{2-}$ en solution représente les $\frac{2}{3}$ de la concentration analytique à cette valeur du pH.

Spectres Raman des complexes dans un rapport t = *1 (tableau 2)*

L'étape intermédiaire observée pour $t = \frac{1}{2}$ et $t = \frac{1}{3}$ est moins claire ici. En effet, les spectres des solutions dans l'intervalle de pH 0.5 < pH < 2.6 comprennent les mêmes fréquences observées dans la première étape des rapports $t = \frac{1}{2}$ et $\frac{1}{3}$, ainsi que celles dues au coordinat libre et $Be(H_2O)_4^{2+}$. Ces dernières disparaissent à p$H \sim 2.6$. Quant à la bande 456 cm^{-1} primitivement attribuée aux trois espèces $H_2C_2O_4$, $HC_2O_4^-$ et $C_2O_4^{2-}$ (22) elle subit une diminution irrégulière d'intensité et un déplacement progressif de 456 à 446 cm^{-1} lorsque le pH augmente. Toutefois son intensité reste importante malgré la disparition complète de toutes les autres raies caractéristiques du coordinat, il y a donc certainement une bande de diffusion due aux complexes dans ce domaine de fréquence, en interférence avec la bande du coordinat.

Sur les spectres des solutions de 2.6 < pH < 4.1 en plus des bandes déjà observées, il apparait d'autres épaulements à 583, 614, 833 et 1743 cm^{-1} correspondant à des bandes intenses pour $t = \frac{1}{2}$ et $t = \frac{1}{3}$ dans le même domaine du pH. La diminution d'intensité des bandes 446, 601 et 793 cm^{-1} et le déplacement progressif de deux fréquences 365 → 368 cm^{-1} et 1410 → 1417 cm^{-1} sont remarqués lorsque le pH augmente.

Les mêmes phénomènes observés précédemment pour $t = \frac{1}{2}$ et $t = \frac{1}{3}$ à p$H > 4.5$ et 4.9 respectivement, sont constatés ici à p$H > 4.1$; cependant la bande située à 601 cm^{-1} se déplace progressivement dans l'intervalle 4.1 < pH < 4.6 pour atteindre 583 cm^{-1}. Enfin l'intensité des bandes très faibles à 1308 et 1486 cm^{-1} dues à $C_2O_4^{2-}$ (22) et apparues à p$H \sim 3.7$ subit une légère augmentation.

Discussion

Identification des différentes espèces complexes

L'observation globale des spectres Raman montre la présence de trois espèces caractérisées par des fréquences assez différentes, quel que soit le rapport étudié. Pour le rapport $t = \frac{1}{3}$, l'espèce intermédiaire caractérisée par les fréquences 368, 450, 583, 614, 833, 857, 911, 1093, 1283, 1417, 1698 et 1743 cm^{-1} est prépondérante dans l'intervalle 3.5 < pH < 4.5; toutes ces bandes conservent une intensité maximum et constante dans ce domaine de pH en présence d'un excès de coordinat libre en solution représentant le $\frac{1}{3}$ de la concentration analytique du coordinat. Si on admet que la quasitotalité du béryllium est complexée ces bandes sont à attribuer au composé $Be(C_2O_4)_2^{2-}$ déjà signalé par d'autres auteurs (3, 10, 11, 18, 20). Ceci est en bon accord avec les résultats obtenus pour $t = \frac{1}{2}$ et explique la faible intensité des bandes de ce composé pour $t = 1$.

Quant à la première étape commune aussi pour tous les rapports, elle correspond à la formation d'un composé possédant les fréquences de vibrations situées à 365, 445, 558, 601, 793, 857, 910, 1093, 1283, 1410, 1698 et 1730 cm^{-1} qui restent fixes quelle que soit l'intensité des bandes. Ce composé précède l'apparition du complexe $Be(C_2O_4)_2^{2-}$. Sa composition, calculée pour $t = 1$, donne une valeur du rapport $[Be]/[C_2O_4]$ très proche de l'unité, il s'agit donc incontestablement de BeC_2O_4.

La dernière étape commune pour tous les rapports, doit correspondre à la constitution d'une espèce hydroxyée caractérisée par les bandes de diffusion: 368, 449, 498, 583, 838, 857, 911, 1103, 1283, 1428, 1683, 1708 et 1727 cm^{-1}. En effet, dans cette étape le béryllium non engagé, pour $t = \frac{1}{2}$ et $t = \frac{1}{3}$ peut être considéré comme nul; la quantité de coordinat complexé indique que ce complexe possède un rapport stoechiométrique $[Be]/[C_2O_4] \sim 1$.

Dans un travail effectué au laboratoire (23), Duc a observé par potentiométrie dans ce domaine de pH la formation du complexe $Be_3(OH)_3(C_2O_4)_3^{3-}$, déjà signalé par Dragulescu (19). Cette espèce qui correspond bien à une stoechiométrie 1/1 en métal/coordinat est probablement celle que nous observons par spectrométrie et nous retenons cette hypothèse.

La fig. 1 représente les spectres des trois complexes BeC_2O_4, $Be(C_2O_4)_2^{2-}$ et $Be_3(OH)_3(C_2O_4)_3^{3-}$, enregistrés dans des conditions telles que chacun d'eux est seul en solution. Sur ces spectres on retrouve les modifications de fréquence et d'intensité mises en

Can. J. Chem. Downloaded from www.nrcresearchpress.com by 210.87.254.105 on 09/05/12
For personal use only.

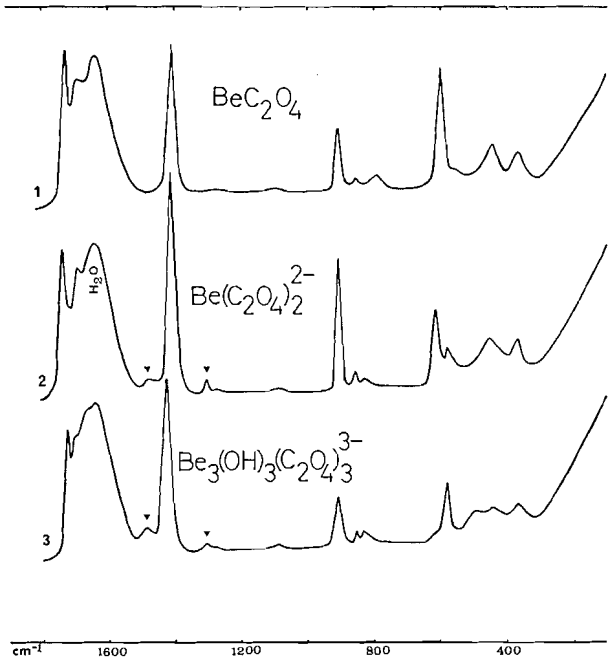

FIG. 1. Spectres Raman des oxalatobéryllates en solution aqueuse. ▶ Bandes Raman de $C_2O_4^{2-}$ libre. (*1*) $t = 1$, p$H = 2.6$, soit $[BeC_2O_4] = 0.15\ M$; (*2*) $t = \frac{1}{2}$, p$H = 3.6$, soit $[Be(C_2O_4)_2^{2-}] = 0.10\ M$; (*3*) $t = 1$, p$H = 6.6$, soit $[Be_3(OH)_3(C_2O_4)_3^{3-}] = 0.06\ M$.

évidence lors de l'étude systématique à t et pH variables.

Confirmation apportée par spectrométrie infrarouge

Grâce à l'existence de certaines bandes très intenses caractéristiques des espèces $HC_2O_4^-$ (1635 cm^{-1}) et $C_2O_4^{2-}$ (1310 et 1570 cm^{-1}) (22), l'étude des oxalatobéryllates dans H_2O et D_2O par spectrométrie ir nous a permis de repérer les différentes raies dues aux complexes sans difficultés majeures.

Pour un rapport $t = \frac{1}{2}$, le déplacement plus ou moins important des fréquences des bandes, les variations d'intensité et l'apparition ou la disparition de nouvelles bandes, en fonction du pH, montrent trois étapes successives en bon accord avec les spectres Raman. La première caractérise une espèce individuelle à p$H < 1.6$. Puis à partir de pH 1.6 un deuxième composé complexe commence à se former dont les bandes apparaissent seules à p$H \sim 4$ environ, après la disparition quasicomplète des bandes du coordinat. A des p$H > 4.5$ une dernière série de bandes est observée, ainsi que toutes les bandes du $C_2O_4^{2-}$ en solution. L'intensité des bandes de $C_2O_4^{2-}$ augmente, dans cet intervalle d'acidité, quand le pH augmente.

Pour $t = 1$ les bandes de la première étape persistent seules jusqu'à p$H \sim 3$. Celles de la dernière apparaissent à p$H > 4$, et simultanément on aperçoit les bandes du coordinat sous faible intensité. Par contre certaines bandes caractéristiques du complexe intermédiaire sont observées comme épaules; cette étape est beaucoup moins nette que les autres pour ce rapport.

Ces observations en fonction du t et du pH recoupent celles que nous avons observées par spectrométrie Raman concernant la formation de trois composés complexes en solution. On donne dans le tableau 3 les fréquences que nous attribuons aux trois complexes en question.

Méthode de détermination des concentrations par spectrométrie Raman des différents complexes formés

Choix des bandes

L'évolution des spectres Raman des oxalatobéryllates, en fonction du pH et du rapport [métal]/[coordinat], montre l'existence des bandes intenses caractéristiques de chaque espèce, surtout dans le domaine de fréquence situé vers 600 cm^{-1}, mais qui ne sont pas sans interférences entre elles. Pour cela notre calcul des coefficients de diffusion aux différentes fréquences est fait en procédant par étapes. La bande de l'eau située à 1640 cm^{-1} est utilisée comme étalon interne (22).

La concentration du coordinat non engagé en complexe est calculée sur les bandes 848 et 868 cm^{-1} dues aux espèces $H_2C_2O_4$ et $HC_2O_4^-$ et 1308, 1486 cm^{-1} caractéristiques de l'espèce $C_2O_4^{2-}$ en solution. Les deux premières ne sont pratiquement pas influencées par la bande très faible des complexes située à 857 cm^{-1}. Les coefficients de diffusion trouvés antérieurement (22) sont utilisés ici pour les quatres fréquences.

Pour déterminer la concentration des trois espèces: BeC_2O_4, $Be(C_2O_4)_2^{2-}$ et $Be_3(OH)_3(C_2O_4)_3^{3-}$ on a pu utiliser l'intensité des bandes aux fréquences

TABLEAU 3. Fréquences des bandes ir des oxalates complexes de béryllium

BeC_2O_4		$Be(C_2O_4)_2^{2-}$		$Be_3(OH)_3(C_2O_4)_3^{3-}$	
820	tf	820	m	820	f
855	tf	855	f	—	
920	F	930	F	935	F
—		1040	f	—	
1280	F	1280	F	1290	F
1400	F	1390	F	1420	F
1460	f	1460	m	1460	f
1550?		—		1550?	
1705	F	1695	TF	1695	TF
1725	TF	1720	TF	1718	F

Can. J. Chem. Downloaded from www.nrcresearchpress.com by 210.87.254.105 on 09/05/12
For personal use only.

situées à 368, 583, 601, 614, 1417 et 1428 cm^{-1}, indépendantes des bandes du coordinat sous toutes les formes à l'exception des deux dernières; celles-ci sont influencées d'une part par les bandes du triplet 1380–1410–1444 cm^{-1} dû à $HC_2O_4^-$ et la bande située à 1452 cm^{-1} attribuée à $C_2O_4^{2-}$ non engagé d'autre part. Pour cette raison la relation générale exprimant l'intensité à ces deux fréquences tient compte de la contribution de ces deux espèces dont les coefficients de diffusion utilisés B_v et C_v sont calculés sur les spectres de l'acide oxalique en fonction du pH (22) dans des intervalles convenables; les moyennes de dix valeurs reproductibles sont $B_{1417} = 1.34$ et $B_{1428} = 1.10$ pour $HC_2O_4^-$, $C_{1417} = 0.15$ et $C_{1428} = 0.30$ pour $C_2O_4^{2-}$.

Principe de la méthode de calcul des concentrations

Les symboles utilisés dans ce calcul ont toujours la même signification que précédemment (22). De plus, P, Q et R représentent les concentrations de BeC_2O_4, $Be(C_2O_4)_2^{2-}$ et $Be_3(OH)_3(C_2O_4)_3^{3-}$, et D_v, E_v et F_v leurs coefficients de diffusion.

Le principe de la méthode de calcul, peut être résumé de la façon suivante.

Les bandes 848, 868, 1308 et 1486 cm^{-1} permettent de calculer la concentration du coordinat libre selon les relations:

$$[1] \qquad h_{848} = A_{848}X + B_{848}Y$$

$$[2] \qquad h_{868} = A_{868}X + B_{868}Y$$

$$[3] \qquad h_{1308} = C_{1308}Z, \quad h_{1486} = C_{1486}Z$$

Les relations de bilan entrainent:

$$[4] \qquad CL = (X + Y + Z) + P + 2Q + 3R$$

$$[5] \qquad CM = [Be^{2+}] + P + Q + 3R$$

Etant donné l'interférence possible des bandes des différentes espèces complexes et l'interférence des bandes du coordinat aux fréquences 1417 et 1428 cm^{-1}, les relations aux six fréquences observées sont exprimées sous la forme générale:

$$[6] \qquad h_v = B_vY + C_vZ + D_vP + E_vQ + F_vR$$

Enfin à partir des différents coefficients de diffusion (voir ci dessous) et de la concentration du coordinat libre en solution, le programme SPECTRAL (22) permet de déterminer par moindres carrés les concentrations optimales de trois espèces P, Q et R.

Calculs des coefficients de diffusion D_v, E_v *et* F_v *à différentes fréquences*

Pour tous les rapports étudiés, les spectres enregistrés à faible pH nous permettent de calculer la concentration du coordinat libre $(X + Y + Z)$ par les relations [1], [2] et [3] et par conséquent d'obtenir le coefficient D_v, en appliquant les relations [4] et [6] dans un intervalle de pH précédant le début de l'apparition des bandes intenses attribuées à $Be(C_2O_4)_2^{2-}$, Q et R étant nulles. Quinze spectres ont été utilisés pour ce type de calcul.

Sur les spectres des solutions à p$H > 6.5$ pour tous les rapports nous n'observons pratiquement que les bandes attribuées à l'espèce $Be_3(OH)_3(C_2O_4)_3^{3-}$; le résidu très faible de la bande intense à 614 cm^{-1} due à l'espèce $Be(C_2O_4)_2^{2-}$ (et qui ne disparait à aucun moment) est négligé dans notre calcul. Dans ce cas la quantité du coordinat non engagé est calculée par la relation [3] et par suite la relation [6] donne les coefficients F_v, P et Q sont négligeables. Sept spectres enregistrés dans ce domaine de pH donnent des valeurs assez reproductibles de F_v quel que soit le rapport t.

Enfin étant donnée l'interférence des bandes des trois espèces à toutes les fréquences sélectionnées, le calcul des coefficients de diffusion E_v est réalisé indirectement sur les spectres de deux rapports $t = \frac{1}{2}$ et $\frac{1}{3}$ suivant deux voies différentes utilisant les valeurs moyennes des coefficients de diffusion D_v et F_v déjà déterminés.

La première méthode consiste à se placer dans un intervalle $2.8 <$ p$H < 4$ où l'on peut supposer les ions Be^{2+} entièrement complexés et la concentration en espèce $Be_3(OH)_3(C_2O_4)_3^{3-}$ absolument nulle. Dans ces conditions les relations [1], [2] et [3] permettent de déterminer le facteur $(X + Y + Z)$, les relations [4] et [5] les valeurs de P et Q; nous en déduisons E_v d'après la relation [6].

Après la disparition complète des bandes attribuées à BeC_2O_4, les deux espèces $Be(C_2O_4)_2^{2-}$ et $Be_3(OH)_3(C_2O_4)_3^{3-}$ coexistent à des $4.6 <$ p$H < 5.5$. Les relations [2] et [3] nous permettent de connaître $(Y + Z)$, P et X étant nulles à ces pH; par suite Q et R sont données par les relations [4] et [5], et permettent de calculer les coefficients E_v, par la relation [6].

Dans tous nos calculs nous avons supposé que les espèces hydroxydées simples du béryllium étaient absentes ou en quantité négligeable; ceci est confirmé par le fait que les bandes de $Be_3(OH)_3^{3+}$ (21) ne sont observées à aucun moment.

Le tableau 4 donne quelques exemples parmi les 21 spectres enregistrés suivant les deux voies différentes. Il montre que ces valeurs, à l'exemple de celles de D_v et F_v sont reproductibles.

On rassemble dans le tableau 5 les moyennes des différentes valeurs trouvées pour D_v, E_v et F_v aux six fréquences signalées.

Répartition des différentes espèces en fonction du pH

A partir des valeurs moyennes des coefficients de

TABLEAU 4. Coefficients de diffusion E_v

Rapport t	pH	$X+Y+Z$	P	Q	E_{368}	E_{583}	E_{601}	E_{614}	E_{1417}	E_{1428}
$\frac{1}{2}$	3.6	0.058	0.580	0.094	1.60	1.65	1.16	5.32	13.02	7.55
$\frac{1}{2}$	4.1	0.049	0.049	0.103	1.40	2.40	1.00	5.37	14.44	8.60
$\frac{1}{3}$	3.0	0.117	0.022	0.074	1.10	2.13	1.37	5.51	13.71	8.38
$\frac{1}{3}$	3.4	0.108	0.012	0.083	1.27	2.33	1.61	5.89	14.45	8.92
			R	Q						
$\frac{1}{2}$	5.0	0.081	0.027	0.070	1.61	2.14	2.26	6.05	14.04	8.32
$\frac{1}{2}$	5.4	0.099	0.033	0.053	1.31	1.84	2.24	5.93	12.72	7.78
$\frac{1}{3}$	4.8	0.103	0.002	0.089	1.19	2.06	1.75	4.96	13.39	7.89
$\frac{1}{3}$	5.2	0.122	0.009	0.067	1.13	2.25	1.71	4.99	12.61	9.13

TABLEAU 5. Valeurs moyennes des coefficients de diffusion des trois espèces complexes aux différentes fréquences

	Valeur à $\bar{\nu}$ (cm^{-1})					
Coefficients	368	583	601	614	1417	1428
D_v	0.7±0.1	0.7±0.2	4.6±0.2	2.0±0.2	4.3±0.3	2.0±0.2
E_v	1.3±0.3	2.1±0.4	1.6±0.6	5.4±0.6	13.7±0.9	8.2±0.9
F_v	1.3±0.4	7.4±0.2	1.4±0.2	0.4±0.1	14.6±0.9	21 ±1

diffusion, des hauteurs relatives des bandes aux différentes fréquences et de la concentration du coordinat non engagé, nous avons à l'aide du programme SPECTRAL dont le principe a été décrit dans un travail antérieur (22), calculé les concentrations P, Q et R des différentes espèces présentes en solution en fonction du degré d'acidité pour tous les rapports étudiés.

Ces valeurs des concentrations en complexes sont utilisées pour déterminer les valeurs optimales des constantes des équilibres de formation des complexes:

$$Be^{2+} + C_2O_4^{2-} \rightleftarrows BeC_2O_4 \qquad \beta_1$$

$$Be^{2+} + 2C_2O_4^{2-} \rightleftarrows Be(C_2O_4)_2^{2-} \qquad \beta_2$$

$$3Be^{2+} + 3OH^- + 3C_2O_4^{2-} \rightleftarrows Be_3(OH)_3(C_2O_4)_3^{3-} \qquad \beta_{333}$$

L'affinement par moindres carrés est réalisé à l'aide du programme AFFIBETA à partir de 50 points expérimentaux situés dans un domaine de pH: $0.5 < pH < 7.4$. Sont introduites également les constantes des espèces hydroxydées simples du béryllium (24). Les valeurs obtenues sont:

$$\beta_1 = 1.82 \times 10^3$$

$$\beta_2 = 2.11 \times 10^5$$

$$\beta_{333} = 8.75 \times 10^{39}$$

Nous les avons utilisées pour obtenir la courbe de répartition des complexes à l'aide du programme CALCON. Les figs 2 et 3 représentent cette répartition calculée pour les deux rapports $t = \frac{1}{2}$ et $\frac{1}{3}$. Nous représentons sur ces mêmes figures la répartition obtenue en utilisant les valeurs des constantes

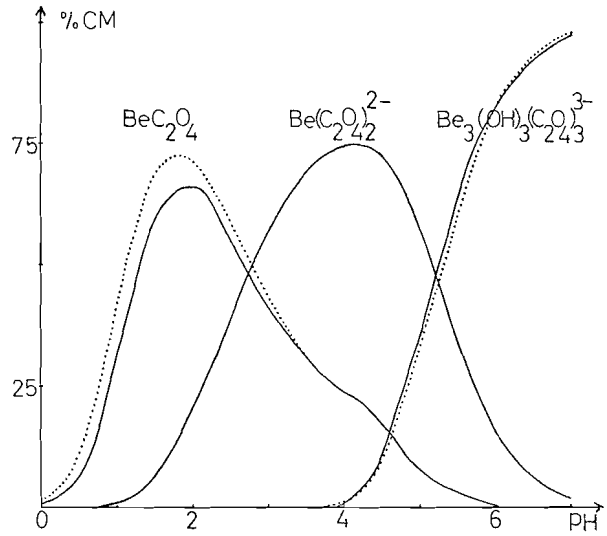

FIG. 2. Courbe de répartition des oxalatobéryllates représentant le pourcentage de la concentration de béryllium engagé dans chaque complexe par rapport à la concentration analytique CM pour $t = \frac{1}{2}$. — Constantes déduites des spectres Raman; ··· constantes obtenues par Duc par la méthode de pH. Pour $Be(C_2O_4)_2^{2-}$ les deux courbes sont confondues.

trouvées par Duc (23) par la méthode de pH pour la concentration 10^{-2} M en coordinat en milieu perchlorate 0.5 M.

Conclusion

L'étude systématique des spectres Raman des oxalatobéryllates en solution aqueuse, en fonction du rapport t = [métal]/[coordinat] et du pH, montre très clairement quel que soit le rapport, la formation

Can. J. Chem. Downloaded from www.nrcresearchpress.com by 210.87.254.105 on 09/05/12
For personal use only.

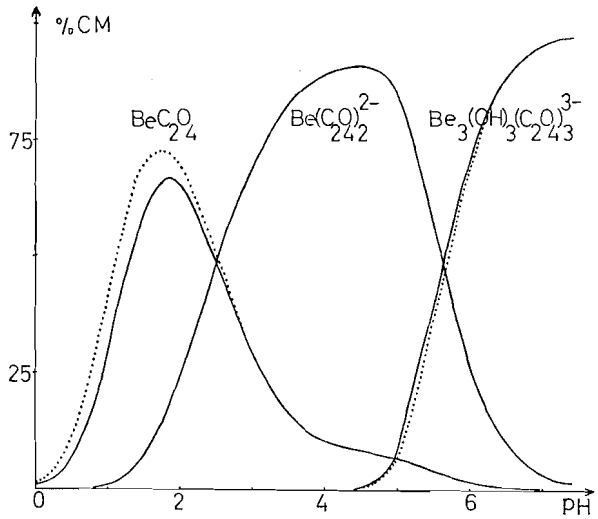

FIG. 3. Courbes de répartition des oxalatobéryllates représentant le pourcentage de la concentration de béryllium engagé dans chaque complexe par rapport à la concentration analytique CM pour $t = \frac{1}{3}$. — Constantes déduites des spectres Raman; ··· constantes obtenues par Duc par la méthode de pH. Pour $Be(C_2O_4)_2^{2-}$ les deux courbes sont confondues.

de trois espèces complexes caractérisées par des fréquences de vibration Raman et infrarouge spécifiques. A partir des spectres des différentes espèces, dont les bandes sont séparées de certaines bandes du coordinat libre, nous avons déterminé le rapport stoechiométrique [métal]/[coordinat] pour chaque complexe et identifié ainsi BeC_2O_4, $Be(C_2O_4)_2^{2-}$ et $Be_3(OH)_3(C_2O_4)_3^{3-}$. Leurs constantes de stabilité sont déduites de la concentration des espèces déterminées sur la hauteur des bandes.

Ces résultats sont en bon accord avec ceux obtenus par Duc (23) pour $t = \frac{1}{2}$ et $\frac{1}{3}$ tant en ce qui concerne la nature des espèces que leur stabilité; comme le montre la comparaison des courbes de répartition sur les figs 2 et 3. Par contre, pour le rapport $t = 1$, cet auteur interprète les résultats potentiométriques obtenus, par la présence d'une seconde espèce hydroxydée $Be_3(OH)_3(C_2O_4)^+$ à côté de $Be_3(OH)_3(C_2O_4)_3^{3-}$. Dans notre étude quel que soit le rapport, les spectres à p$H > 4.5$ montrent une série de bandes de fréquences constantes à l'exception d'un léger déplacement, déjà cité pour $t = 1$ de la bande à 601 cm^{-1} dans l'intervalle $4.1 <$ p$H < 4.6$. Des spectres enregistrés dans ce domaine de pH pour un rapport $t = 1.5$ qui devrait favoriser la formation de l'espèce $Be_3(OH)_3(C_2O_4)^+$ par rapport à $Be_3(OH)_3(C_2O_4)_3^{3-}$ n'ont pas modifié les résultats. La formation du complexe $Be_3(OH)_3(C_2O_4)_3^{3-}$ est donc la plus probable à la concentration étudiée même pour le rapport $t = 1$; de plus, si l'espèce hydroxydée $Be_3(OH)_3(C_2O_4)^+$ existait en possédant les mêmes fréquences de vibration que l'autre, la quantité toujours très faible d'oxalate libre en solution pour $t = 1$ et la valeur constante des coefficients F_v (voir ci dessus) pour tous les rapports, rejettent sa présence, au moins en quantité importante. Le déplacement observé dans les deux rapports $t = 1$ et 1.5 peut s'expliquer par interférence des deux bandes intenses 601 et 583 cm^{-1} dues respectivement à BeC_2O_4 et $Be_3(OH)_3(C_2O_4)_3^{3-}$ (le complexe $Be(C_2O_4)_2^{2-}$ est toujours en faible quantité). Cette interférence est inexistante pour les rapports $t = \frac{1}{2}$ et $\frac{1}{3}$ car la bande à 583 cm^{-1} caractéristique de $Be_3(OH)_3(C_2O_4)_3^{3-}$ n'apparait qu'après la disparition du complexe BeC_2O_4 (bandes à 601 cm^{-1}) et ne peut que renforcer celle du complexe intermédiaire $Be(C_2O_4)_2^{2-}$ à 583 cm^{-1}.

L'examen des solutions d'oxalatobéryllate à p$H >$ 5 (où seuls existent les complexes hydroxydés pour $t = 1$ et 1.5) par la résonance magnétique nucléaire du noyau ^{13}C nous a apporté une confirmation supplémentaire. En effet, pour le rapport $t = \frac{1}{3}$ à p$H \sim 6.5$ un seul signal apparait à 1008 Hz par rapport à C_6D_6 utilisé comme référence externe. Pour $t = 1$ et 1.5 à p$H > 5$ les spectres montrent la présence d'un seul signal situé à 1008 Hz de la référence utilisée. Ceci est en bon accord avec les interprétations que nous avons présentées à propos des spectres Raman et le signal observé pour tous les rapports est dû au complexe $Be_3(OH)_3(C_2O_4)_3^{3-}$ en solution.

La différence que l'on peut noter entre les courbes de répartition déduite des résultats spectrométrique et potentiométrique (figs 2 et 3) peut s'expliquer principalement par l'erreur commise sur la mesure de pH pour les valeurs très acides.

1. F. DOUVILLE, M. DUVAL et J. LECOMTE. Bull. Soc. Chim. **9**, 548 (1942).
2. N. V. SIDGWICK et N. B. LEWIS. J. Chem. Soc. 1287 (1926); 2538 (1926).
3. A. K. SEN GUPTA et G. CHATTOPADHYAY. J. Indian Chem. Soc. **46**, 1126 (1969).
4. C. DRAGULESCU, P. TRIBUNESCU et I. MENESSY. Stud. Cercet. Sti. Chim. Trimisoara, **9**, 197 (1962).
5. J. STARY. Anal. Chim. Acta, **28**, 132 (1963).
6. C. DRAGULESCU, P. TRIBUNESCU et I. MENESSY. Rev. Roum. Chim. **12**, 389 (1967).
7. C. DRAGULESCU, P. TRIBUNESCU et I. MENESSY. Stud. Cercet. Chim. Acad. Rep. Pop. Roum. **13**, 639 (1965).
8. L. KOLDITZ et K. BAUER. Z. Chem. **3**, 312 (1963); Z. Anorg. Allg. Chem. **325**, 196 (1963).
9. D. GRADDON. Chem. Ind. 80 (1956); 81 (1956).
10. D. GRADDON. J. Inorg. Nucl. Chem. **3**, 308 (1956).
11. J. P. MATHIEU et J. POULET. J. Chem. Phys. **59**, 369 (1962).
12. R. BELDIE et V. E. SAHINI. Rev. Roum. Chim. **14**, 419 (1969).
13. L. G. SILLEN et A. E. MARTELL. Stability constants of metal–ion complexes. The Chemical Society, London. 1964.

Can. J. Chem. Downloaded from www.nrcresearchpress.com by 210.87.254.105 on 09/05/12
For personal use only.

14. A. K. BHATTACHARYA et G. S. RAO. J. Univ. Saugar, Part 2, Sect. A, **8**, 21 (1959).
15. H. J. DE BRUIN, D. KAIRAITIS et R. B. TEMPLE. Austr. J. Chem. **15**, 457 (1962).
16. H. J. DE BRUIN et R. B. TEMPLE. U.S. At. Energy Comm. A. AEC/E.68.
17. T. SEKINE et M. SAKAIRI. Bull. Chem. Soc. Jpn. **40**, 261 (1967).
18. C. DRAGULESCU, P. TRIBUNESCU et I. MENESSY. Rev. Roum. Chim. **10**, 407 (1965).
19. C. DRAGULESCU, P. TRIBUNESCU et I. MENESSY. Rev. Roum. Chim. **12**, 31 (1967).
20. Y. COUTURIER et J. FAUCHERRE. Bull. Soc. Chim. Fr. **4**, 1323 (1970).
21. F. BERTIN et J. DEROUAULT. C.R. Acad. Sci. Paris 280, 21 Avril. Ser. C. 973–975 (1975).
22. M. JABER. Thèse Lyon. 1975. n° 475.
23. G. DUC, F. BERTIN et G. THOMAS-DAVID. Bull. Soc. Chim. Fr. 196 (1977).
24. F. BERTIN. Thèse Lyon. 1970. n° 647.

Can. J. Chem. Downloaded from www.nrcresearchpress.com by 210.87.254.105 on 09/05/12
For personal use only.

Mechanism of borohydride reductions. Evidence for lack of disproportionation in the reduction of ketones

DONALD C. WIGFIELD AND FREDERICK W. GOWLAND
Department of Chemistry, Carleton University, Ottawa, Ont., Canada K1S 5B6

Received September 26, 1977

DONALD C. WIGFIELD and FREDERICK W. GOWLAND. Can. J. Chem. **56**, 786 (1978).

Examination of unreacted sodium borohydride after reduction of ketones by mixtures of $NaBH_4$ and $NaBD_4$ shows that it is still isotopically pure and that no detectable species $NaBH_nD_{4-n}$ have been formed. Disproportionation of intermediates back to $NaBH_4$ therefore plays no significant role in the reduction.

DONALD C. WIGFIELD et FREDERICK W. GOWLAND. Can. J. Chem. **56**, 786 (1978).

Un examen du borohydrure de sodium qui n'a pas réagit lors de la réduction de cétones par des mélanges de $NaBH_4$ et de $NaBD_4$ indique que ce dernier est encore isotopiquement pur et l'on n'a pas détecté la formation d'entités $NaBH_nD_{4-n}$. La dismutation d'intermédiaires pour reconduire à $NaBH_4$ ne joue donc aucun rôle important.

[Traduit par le journal]

Can. J. Chem. Downloaded from www.nrcresearchpress.com by 210.87.254.5 on 09/05/12
For personal use only.

Little is known about the mechanism of borohydride reductions of ketones. Three major questions, of increasing level of molecular detail, exist. Firstly, given the 4:1 stoichiometry, what are the structures of the reducing agents for reduction of each of the four ketone molecules? Secondly, given the structure of the reducing agent(s), what is the mechanism of reduction: is it cyclic or acyclic; does it differ for each reducing species; what role, if any, do the metal cation and the solvent play? Thirdly, given the reducing agent and the mechanism for each reducing species, where on the reaction coordinate do the transition states occur: are they reactant-like, product-like, or somewhere in between? Finally, if one knew the answers to the above questions, presumably the problem of understanding the striking stereoselectivity of the reactions could at least be approached on a rational basis.

With several notable exceptions (see for example refs. 1–3), investigations in this area seem to be a persistent case of the cart before the horse. Speculations concerning the cause of stereoselectivity have been discussed for over twenty years. Speculators do not seem to have been greatly troubled by the almost total lack of knowledge of the reaction mechanism. Similarly, a good deal of effort has been expended to define the degree of hydride transfer in the transition state but the answer to this question is still unsettled. In contrast, little attention has been paid to the first two, rather more fundamental, questions posed above. The questions are not intangible and this communication is aimed at the first of these: what is(are) the structure(s) of the reducing agent(s)?

Results and Discussion

The Problem

All four hydrides of sodium borohydride are available for reduction of simple ketones.[1] While there is not much doubt that the reduction is initiated by reaction of $NaBH_4$ itself with a molecule of ketone, considerable uncertainty exists about what happens then. We have recently shown that the hydroxylic solvent plays a crucial role in this first step (5, 6) and it may therefore be represented as shown in [1], with the alkoxyl group from the solvent, and not from the product alcohol, becoming attached to boron. The question whether this monoalkoxyborohydride species acts directly as a reducing agent in the second stage of the reaction or if it disproportionates back to sodium borohydride now arises. The stepwise (nondisproportionation) mechanism proposed by Garrett and Lyttle (1) and later by Brown *et al.* (2) is shown in eq. 2.[2]

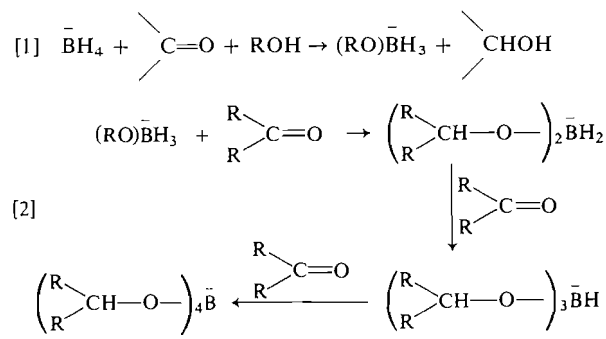

[1] $\bar{B}H_4 + \text{C=O} + ROH \rightarrow (RO)\bar{B}H_3 + \text{CHOH}$

[2] $(RO)\bar{B}H_3 + \text{C=O} \rightarrow \left(\text{CH—O—}\right)_2\bar{B}H_2 \xrightarrow{\text{C=O}} \left(\text{CH—O—}\right)_3\bar{B}H \xrightarrow{\text{C=O}} \left(\text{CH—O—}\right)_4\bar{B}$

[1] At least for simple ketones (4). The identity of the ketones actually used to form the basis of this statement is not stated. A systematic investigation on the generality of the 4:1 stoichiometry does not seem to have been carried out and is presently under investigation.

[2] These equations should now also be modified to take into account the incorporation of solvent alkoxy group (5, 6). However [2] is left unaltered for the sake of simplicity and of emphasizing the important difference between it and the disproportionation equations.

Can. J. Chem. Downloaded from www.nrcresearchpress.com by 210.87.254.5 on 09/05/12
For personal use only.

In contrast to this stepwise mechanism, the disproportionation mechanism is shown in eqs. 3–5.[3]

[3] $$(RO)\bar{B}H_3 \rightarrow \bar{B}H_4 + (RO)_2\bar{B}H_2$$

[4] $$(RO)_2\bar{B}H_2 \rightarrow \bar{B}H_4 + (RO)_3\bar{B}H$$

[5] $$(RO)_3\bar{B}H \rightarrow \bar{B}H_4 + (RO)_4\bar{B}$$

In this way exactly the same products are eventually formed as with [2] and all four hydrides are available for reduction. The crucial difference, however, is that in the stepwise [2] mechanism there are four different reducing agents of increasing steric bulk involved in reducing ketone molecules, whereas in the disproportionation mechanism all the *reduction* steps are done by $NaBH_4$ itself.

The Existing Evidence

Three pieces of evidence bear on this problem.

(i) The Reaction Kinetics

The kinetics of reduction of ketones by sodium borohydride are known to be second order, first order in both ketone and borohydride (1–3, 7). This observation led Garrett and Lyttle (1) to propose the stepwise (nondisproportionation) mechanism, in which transfer of the first hydride is rate determining. The reduction of the other three ketone molecules then occurs in fast, kinetically, unobservable steps.

This evidence, however, does not rule out disproportionation. If complete disproportionation were to occur, the initial step would give second order kinetics, followed by disproportionation regenerating three out of four sodium borohydride molecules that had reacted. Thus, once again, provided the rate of disproportionation exceeded that of reduction, the observed result would be second order kinetics with a 4:1 stoichiometry.

(ii) Disproportionation of Intermediates

Of the intermediates postulated in the stepwise mechanism [2], i.e. the mono-, di-, and trialkoxyborohydrides, only the latter appear to possess reasonable stability, and only in THF solution (8). Experiments that might be expected to yield mono- or dialkoxyborohydrides (3, 9) (e.g. [6]), give disproportionation products instead.

[6] $$2B_2H_6 + 3NaOCH_3 \rightarrow 3NaBH_4 + B(OCH_3)_3$$

While this evidence does not establish that disproportionation occurs in the reduction reaction, it certainly confirms the tendency of these intermediates toward disproportionation.

(iii) Change of Stereochemistry

If disproportionation did not occur and several different reducing agents of increasing steric bulk (e.g. [2]) were involved in ketone reductions one might expect the reaction to change its stereoselectivity as the reaction proceeded. Rickborn and Wuesthoff (3) showed that detectable, although modest, such changes do occur. This evidence tends to exclude complete disproportionation, but does not rule out mechanisms involving less than complete disproportionation.

Mechanism Distinction. Exchange of Hydrogen Isotopes in $NaBH_4$

If the stepwise mechanism [2] occurs, then any sodium borohydride reisolated after reaction is simply unreacted sodium borohydride. On the other hand, if disproportionation back to sodium borohydride occurs, then sodium borohydride is continually being reformed by the disproportionation interaction between two or more different alkoxyborohydride molecules (eqs. 3–5). This difference becomes experimentally tangible if reduction is carried out using a mixture of sodium borohydride and sodium borodeuteride; reisolated reducing agent must still be $NaBH_4$ and $NaBD_4$ if the mechanism is stepwise reduction; on the other hand the disproportionation equations 3–5 demand that isotopically mixed borohydrides $NaBH_nD_{4-n}$ must be produced. Detection of such mixed isotopic species may be made by the deuterium coupling, and isotope shift of the proton nmr signals of $NaBH_4$ (10).

Accordingly, we have carried out reductions of cyclohexanone with mixtures of $NaBH_4$ and $NaBD_4$. The ketone to borohydride ratio was maintained at approximately 2.0 (i.e. ketone to available hydride ratio 0.5) and reaction taken to completion to ensure that remaining borohydride would have had maximum opportunity for isotopic exchange via the disproportionation mechanism. Ratios of borohydride–borodeuteride were varied with either one in predominance. Spectra of authentic isotopically mixed borohydrides were obtained by hydrolysis of mixtures of sodium borohydride and sodium borodeuteride (10), and the spectral difference between $NaBH_4$ and $NaBH_nD_{4-n}$ is shown in Fig. 1. Results are shown in Table 1. In contrast to borohydride hydrolysis (10), under no circumstances is there any evidence of the formation of isotopically mixed borohydrides. These results are consistent only with the sequential [2] mechanism for borohydride reduction of cyclohexanone and appear to rule out disproportionation back to $NaBH_4$ occurring to any significant extent.

Cyclohexanone, however, is one of the least likely ketones to cause isotopic scrambling of sodium borohydride. Since solvent alkoxy groups become attached to boron in the reduction (5), the rate of disproportionation of intermediates is presumably

[3]For the sake of simplicity these equations are left unbalanced.

TABLE 1. Results of exchange experiments

Ketone	BH_4/BD_4	Hydride/ketone	Nuclear magnetic resonance results
Cyclohexanone	0.429	2.01	No exchange
	0.529	2.00	No exchange
	1.59	1.98	No exchange
3,3,5,5-Tetramethylcyclohexanone	0.550	2.02	No exchange
	0.916	1.97	No exchange

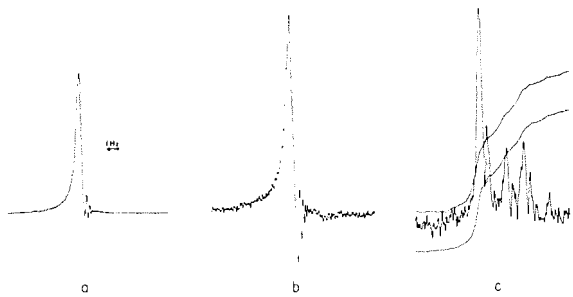

FIG. 1. Proton nmr spectra of (*a*) $NaBH_4$ in the presence of $NaBD_4$, after reduction of cyclohexanone; (*b*) $NaBH_4$ in the presence of $NaBD_4$ after reduction of 3,3,5,5-tetramethylcyclohexanone; (*c*) $NaBH_nD_{(4-n)}$ species prepared by hydrolysis of $NaBH_4$ in D_2O.

All spectra are the second lowest field portion of the borohydride quartet. This avoids the problem of isopropoxide, from hydrolyzed $NaB(OPr\text{-}i)_4$, interference in the spectrum. All spectra were deuterium decoupled.

essentially independent of the ketone being reduced. In contrast, the rate of ketone reduction varies widely. 3,3,5,5-Tetramethylcyclohexanone is reduced more slowly than cyclohexanone by a factor of almost 400 (11, 12), and thus the possibility of disproportionation playing a role is greatly enhanced. The results of Table 1 show that even in this case there is no evidence for the formation of isotopically mixed borohydrides.

Conclusions

Because of the lack of formation of isotopically mixed borohydrides, it is concluded that there is essentially no disproportionation back to $NaBH_4$ during reduction of ketones by $NaBH_4$ in 2-propanol. Disproportionation of the monoalkoxyborohydride [3] therefore does not occur during the reduction process, and this species cleanly reduces the second molecule of ketone to yield a dialkoxyborohydride [2]. The possibility that the dialkoxyborohydride and trialkoxyborohydride intermediates may disproportionate incompletely (i.e. back to monoalkoxyborohydride but not as far as $\overline{B}H_4$) can not at present be ruled out; this is a more difficult problem that is currently under investigation. The present results, however, rule out the complete disproportionation mechanism in which $NaBH_4$ itself reduces all or most of the ketone molecules; since no detectable disproportionation back to $NaBH_4$ occurs, it follows that only 25% of the ketone molecules are reduced by $NaBH_4$ and 75% by intermediate alkoxyborohydrides. This result is clearly of direct relevance to ideas on the stereoselectivity of this reaction.

Experimental

$NaBD_4$ (0.750 g, 0.0179 mol) (Merck, Sharp & Dohme) and $NaBH_4$ (0.250 g, 0.0066 mol) (British Drug House) were stirred magnetically, overnight in 25 ml of 2-propanol (Fisher). These solutions were gravity filtered and standardized using the iodate–thiosulphate standardization procedure (11, 12). Appropriate volumes of the two species were combined and to this solution was added a 1 ml solution of ketone whose concentration would give 50% oxidation of the borohydride species present in the solution. This solution was stirred magnetically for 1–2 h in the case of cyclohexanone and 3 days for 3,3,5,5-tetramethylcyclohexanone to ensure that reduction was complete. The solvent was rotary evaporated and the solid residue dissolved in D_2O. The proton magnetic resonance spectra were obtained in D_2O on a Varian T-60 instrument or a Varian HA-100.

Acknowledgements

We are very grateful to Professor M. M. Kreevoy, University of Minnesota, for furnishing some details of the borohydride hydrolysis and to Professor R. R. Fraser, University of Ottawa, for assistance with the nmr spectra. We thank the National Research Council of Canada for financial support.

1. E. R. GARRETT and D. A. LYTTLE. J. Am. Chem. Soc. **75**, 6051 (1953).
2. H. C. BROWN, O. H. WHEELER, and K. ICHIKAWA. Tetrahedron, **1**, 214 (1957).
3. B. RICKBORN and M. T. WUESTHOFF. J. Am. Chem. Soc. **92**, 6894 (1970).
4. S. W. CHAIKIN and W. G. BROWN. J. Am. Chem. Soc. **71**, 122 (1949).
5. D. C. WIGFIELD and F. W. GOWLAND. Tetrahedron Lett. 3373 (1976).
6. D. C. WIGFIELD and F. W. GOWLAND. J. Org. Chem. **42**, 1108 (1977).
7. D. C. WIGFIELD and D. J. PHELPS. J. Chem. Soc. Perkin Trans. II, 680 (1972).
8. H. C. BROWN, E. J. MEAD, and C. J. SHOAF. J. Am. Chem. Soc. **78**, 3616 (1956).
9. H. I. SCHLESINGER, H. C. BROWN, H. R. HOEKSTRA, and L. R. RAPP. J. Am. Chem. Soc. **75**, 199 (1953).
10. M. M. KREEVOY and J. E. C. HUTCHINS. J. Am. Chem. Soc. **94**, 6371 (1972).
11. D. C. WIGFIELD and D. J. PHELPS. J. Am. Chem. Soc. **96**, 543 (1974).
12. D. C. WIGFIELD and D. J. PHELPS. J. Org. Chem. **41**, 2396 (1976).

Can. J. Chem. Downloaded from www.nrcresearchpress.com by 210.87.254.5 on 09/05/12
For personal use only.

The chemistry of 2-methyltetrahydropyran-4-one: An L-Selectride reaction that gives predominantly the equatorial alcohol

DONALD C. WIGFIELD AND STEVE FEINER

Department of Chemistry, Carleton University, Ottawa, Ont., Canada K1S 5B6

Received August 16, 1977

DONALD C. WIGFIELD and STEVE FEINER. Can. J. Chem. **56**, 789 (1978).

The stereoisomers of 2-methyltetrahydropyran-4-ol have been separated and identified by carbon-13 and proton nmr analysis of the trideuteriomethyl-2,6,6-trideuterio analogue. Stereoisomeric product ratios of reduction of 2-methyltetrahydropyran-4-one (**1**) by $NaBH_4$, KBH_4, L-Selectride, K-Selectride, and $LiBH(n\text{Bu})_3$ have been determined and compared with reductions of 3-methylcyclohexanone. Product ratios in the reduction of the two substrates by the borohydride reducing agents are similar but are quite different in the reduction by the Selectride reducing agents, **1** being reduced by Selectride to give 73% *equatorial alcohol*. Two possible mechanisms of reduction of **1** are proposed, involving intramolecular assistance by the cyclic ether oxygen.

DONALD C. WIGFIELD et STEVE FEINER. Can. J. Chem. **56**, 789 (1978).

On a séparé les stéréoisomères du méthyl-2 tétrahydropyrannol-4 et on les a identifiés par rmn ^{13}C et rmn ^1H de l'analogue trideutériométhyl trideutério-2,6,6. On a déterminé le rapport des produits stéréoisomères lors de la réduction de la méthyl-2 tétrahydropyrannnone-4 (**1**) par $NaBH_4$, KBH_4, L-Sélectride, K-Sélectride et $LiBH(n\text{Bu})_3$ et on les a comparés avec ceux observés lors des réductions de la méthyl-3 cyclohexanone. Les rapports de produit dans la réduction de ces deux substrats par des agents réducteurs du borohydrure sont semblables mais ils sont très différents lors de la réduction par des agents réducteurs Sélectride; le composé I est réduit par le Sélectride pour conduire à 73% *d'alcool équatorial*. On propose deux mécanismes possibles pour la réduction du produit **1** impliquant chacun une aide intramoléculaire par un oxygène éther cyclique.

[Traduit par le journal]

Recently, in an investigation to study the kinetic role of hydroxylic solvent in the borohydride reduction of ketones, an acylic mechanism was proposed involving two molecules of solvent (1). Consideration of other factors led to the suggestion that the axial hydrogen at C-4 of a cyclohexanone might be playing a part in controlling the stereochemistry of these reactions. To pursue this idea further it was of interest to examine the stereochemistry of reduction of a similar substrate lacking an axial hydrogen at C-4. For this purpose 2-methyltetrahydropyran-4-one (**1**) was selected. This communication reports our

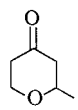

1

findings on the reduction of this compound by a variety of reducing agents.

Results and Discussion

Synthesis of Substrate

2-Methyltetrahydropyran-4-one is not commercially available. A mixture of stereoisomers of 2-methyltetrahydropyran-4-ol, **2**, was obtained by the Prins reaction of 3-buten-1-ol with acetaldehyde according to the method of Hanschke (2). This mixture of stereoisomers was oxidized to 2-methyltetrahydropyran-4-one using the Brown oxidation (3) (Scheme 1).

Stereoisomer Purification

The stereochemistry of the reaction between homoallylic alcohols and carbonyl compounds has only recently been studied (4). Berti *et al.* (5) have reported that the reaction between 3-buten-1-ol and acetaldehyde gave the *cis*-4-ol (*cis*-**2**) as the main product, this conclusion based on nmr analysis. From the proton nmr spectrum of the mixture of stereoisomers of **2** obtained in our hands, however, we were unable to conclude anything; the crucial methine signal due to the proton at C-4 was completely obliterated by the signals of the three protons at C-2 and C-6. We therefore undertook the task of obtaining pure samples and positive identification of each stereoisomer.

Gas–liquid chromatographic analysis of the stereoisomeric mixture of alcohols **2** obtained from

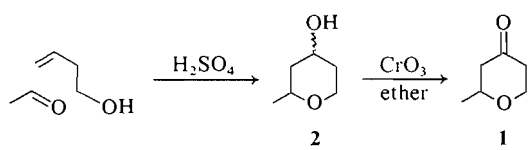

2 **1**

SCHEME 1

Can. J. Chem. Downloaded from www.nrcresearchpress.com by 210.87.254.5 on 09/05/12
For personal use only.

Can. J. Chem. Downloaded from www.nrcresearchpress.com by 210.87.254.5 on 09/05/12
For personal use only.

the Prins reaction indicated two products in the ratio 96:4. This glc analysis, however, gave a great deal of difficulty. Previous investigations of similar stereoisomers in this laboratory have used a SCOT-TCEP column; the resolution of this column, and indeed of similar packed columns, was completely ruined by two or three injections of this mixture. This problem was not overcome in this investigation and final stereochemical product ratios arising from reduction of **1** were obtained not by glc but by proton nmr analysis of specifically deuterated samples (*vide infra*). The two stereoisomers were referred to as **2***A* (shorter retention time on glc) and **2***B* (longer retention time on glc). The 96% component in the mixture was **2***B*.

Preparative separation of the stereoisomers **2***A* and **2***B* was achieved on an alumina column, eluted with benzene containing 10% ether. In this way pure samples of **2***B* could be obtained from the crude 96:4 stereoisomeric mixture. Samples of **2***A* were obtained by catalytic hydrogenation of ketone **1** over PtO_2 (giving a 60:40 mixture of **2***A* and **2***B*) followed by column chromatography referred to above.

Stereoisomer Identification

Axial–equatorial stereoisomer identifications previously in this series have been made by nmr examination of the methine proton on the hydroxyl-bearing carbon and by Raney Nickel equilibrations of the pair, the predominant one in the equilibrium mixture being assumed to have the hydroxyl group equatorial. Both methods failed in the present case. We have already mentioned that the methine proton signal at C-4 is masked by those at C-2 and C-6. In the Raney Nickel equilibrations, although the treatment tended to produce **2***B* at the expense of **2***A* when carried out on a mixture, treatment of a pure sample of **2***A* failed to give any conversion. This latter result remains an anomaly. Two somewhat less than conclusive pieces of evidence indicated that stereoisomer **2***B* was the equatorial alcohol: (*i*) **2***B* was the predominant isomer formed in the Prins reaction, (*ii*) **2***A* has a shorter retention time on glc and this seems to be characteristic of the axial isomer of an axial–equatorial pair, not only in our own work but in others' also (6).

In view of this situation, conclusive evidence was sought from carbon-13 and proton nmr spectroscopy. Both of these confirmed that stereoisomer **2***A* was the axial alcohol and stereoisomer **2***B* the equatorial. Carbon-13 nmr spectroscopy of **2***A* showed signals for C-2 and C-6 at δ 67.9 and 62.4, respectively. These signals in stereoisomer **2***B* occurred at δ 72.4 and 65.9, respectively. This upfield shift of approximately 4 ppm of the γ carbons in comparing **2***A* with **2***B* is

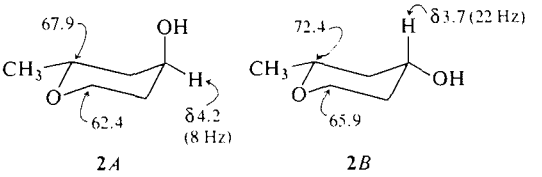

2*A* **2***B*

consistent with C-4 bearing an axial substituent in stereoisomer **2***A* (7).

Proton magnetic resonance distinction between **2***A* and **2***B* was achieved by examination of the stereoisomeric 2-trideuteriomethyl-2,6,6-trideuteriotetrahydropyran-4-ols, synthesized as indicated in Fig. 1. Again a 96:4 ratio of stereoisomers **2***B* and **2***A* was obtained; the amount of **2***A* was enhanced again by Brown oxidation and PtO_2 reduction and the stereoisomers separated by column chromatography on alumina. The spectra of these deuterated compounds are shown in Fig. 2. In stereoisomer **2***A* the C-4 methine proton gives a signal at δ 4.20, of half width 8 Hz; in stereoisomer **2***B* the corresponding signal is at δ 3.70 and a half width 22 Hz. These values (8) leave no doubt that the methine hydrogen at C-4 is equatorial in stereoisomer **2***A* and is axial in stereoisomer **2***B*.

Stereochemistry of Reduction of 1

Having established conclusively the stereoisomeric identity of alcohols **2***A* and **2***B*, the stereoselectivity of reduction of **1** by sodium borohydride was studied. In view of the glc difficulties already mentioned, product ratios were determined by nmr integration of the hexadeuterio species, the C-4 methine signals of the stereoisomers being completely separated from each other and from any other signals. The result (Table 1) that 19% axial alcohol is formed in the reduction of **1** is a result that is not markedly different to the stereoselectivity of reduction of 3-methylcyclohexanone (Table 1), despite the absence of any hydrogens at C-4. Consideration of this result, which can be rationalized in a number of ways, led to one possible suggestion involving intra-

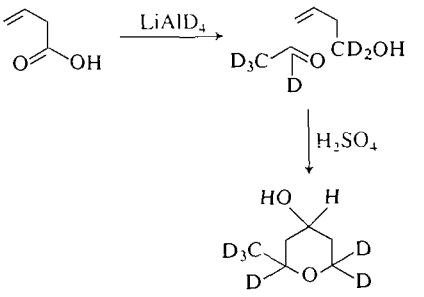

FIG. 1. Preparation of 2-trideuteriomethyl-2,6,6-trideuteriotetrahydropyran-4-ol.

TABLE 1. Stereoselectivities of reduction

Ketone	Reducing agent (solvent)	Stereoselectivity[a] % *cis* (equatorial OH)	% *trans* (axial OH)
1	$NaBH_4$ (*i*PrOH)	81	19
	KBH_4 (*i*PrOH)	77	23
	L-Selectride (Et_2O)	73	27
	K-Selectride (Et_2O)	68	32
	$LiB(nBu)_3H(Et_2O)$	83	17
3-Methylcyclohexanone	$NaBH_4$ (*i*PrOH)	86	14[b]
	KBH_4 (*i*PrOH)	86	14
	L-Selectride (Et_2O)	12	88
	K-Selectride (Et_2O)	10	90
	$LiB(nBu)_3H(Et_2O)$	60	40

[a]Determinations at least in duplicate. Reproducibility ± 3%.
[b]Data from ref. 9.

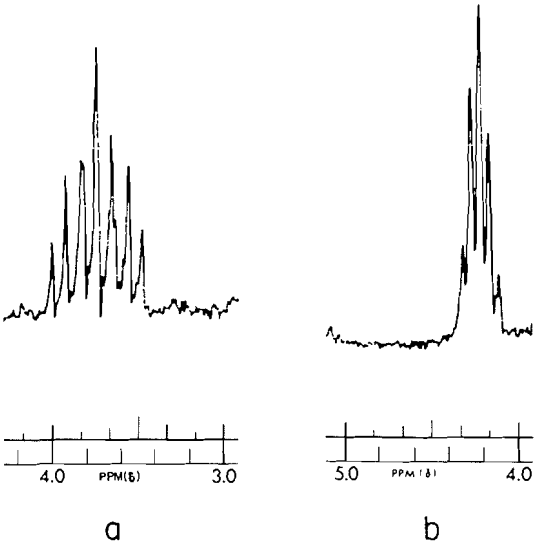

FIG. 2. Proton magnetic resonance signals of the C-4 methine in (*a*) *cis*- and (*b*) *trans*-2-trideuteriomethyl-2,6,6-trideuteriotetrahydropyran-4-ol.

molecular assistance to the formation of *cis*-**2**-methyltetrahydropyran-4-ol. This mechanism, shown in Fig. 3, in which the ether bridge flips up and reduction takes place through a temporary boat conformation, is consistent with the apparent need for boron to maintain tetravalency throughout the reduction (1) and here achieving this end intramolecularly rather than, as usually, intermolecularly. It should be noted that reduction through the other boat conformation, in which the carbonyl group flips instead of the ether oxygen, would result in formation of the *trans* alcohol. Molecular models of this situation, however, indicate considerable interference of the C-2 methyl group with borohydride.

If this mechanism of borohydride reduction of **1**

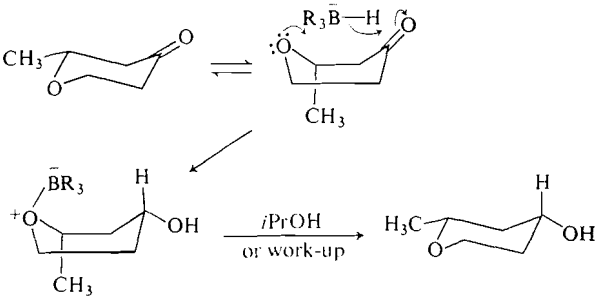

FIG. 3. Proposed mechanism of reduction of 2-methyltetrahydropyran-4-one to yield the *cis*-ol.

were correct, it would have one highly unexpected and unprecedented corollary. While the stereochemical result in the reduction of **1** by $NaBH_4$ is of no great surprise and can be rationalized in several ways, presumably[1] this pathway would also be available to reductions by the very bulky reducing agents, such as L-Selectride (10), and thus L-Selectride would also be predicted to reduce **1** to give predominantly the *equatorial alcohol*. Table 1 reports the stereoselectivity of reduction of **1** and of 3-methylcyclohexanone by three bulky reducing agents; clearly the prediction that these two substrates should be reduced with markedly differing stereoselectivities based on the boat mechanism for **1** is upheld and *the reduction of 1 by L-Selectride gives predominantly the equatorial alcohol*. Whether or not the explanation is correct, this is a somewhat striking result, the first instance, to our knowledge, that L-Selectride has failed to give predominantly the axial alcohol.

Other possible explanations for the dramatic change in stereoselectivity of L-Selectride are worth

[1]Nothing is known of the mechanism of Selectride reductions.

Can. J. Chem. Downloaded from www.nrcresearchpress.com by 210.87.254.5 on 09/05/12
For personal use only.

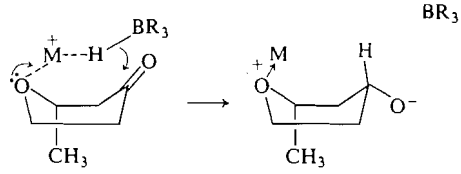

FIG. 4. Alternative mechanism involving the boat conformation of 2-methyltetrahydropyran-4-one.

considering. Any rationalization based on some general effect of having an oxygen in the ring can be discarded since L-Selectride reduction of 2-methyltetrahydropyran-3-one (i.e. ether oxygen in the 3-, rather than 4-position relative to the carbonyl) gives 99% *cis* alcohol (axial OH) (5). The specific effect of the oxygen in the 4-position relative to the carbonyl is consistent with the idea of a boat conformation during reduction. The other main possibility is whether reduction could occur through the alternative *chair* conformation (i.e. methyl group axial), since the methyl group is in an anomeric position. Two factors render this possibility rather unlikely. Firstly the anomeric effect is not known to be marked for nonelectronegative groups (11 and refs. therein), and secondly, in order to account for the results one would need to postulate this alternative chair conformation predominating for Selectride reductions and the normal (equatorial methyl) conformation predominating for sodium borohydride reductions.

Since the original writing of this manuscript, Professor H. C. Brown has pointed out to us that no ether–BR_3 complexes of the type proposed in Fig. 3 have ever been isolated. Professor Brown has suggested to us an alternative mechanism, again involving the same boat conformation, but involving an ether ---M ---H—BR_3 interaction, for which he has recently provided evidence (12, 13). This alternative mechanism is shown in Fig. 4. While one might have expected that this mechanism would have resulted in differing stereoselectivities depending on the nature of the cation, it is clear that the present evidence does not offer firm distinction between the two mechanisms (Figs. 3 and 4). One crucial difference between the two mechanisms is the question of whether boron maintains tetracovalency during the reaction. In this regard it is worth noting that although the mechanism in Fig. 3 achieves this, it does so in a 6-*endo-tet* manner, disfavoured by the Baldwin Rules (14).

In summary, the stereochemical results seem best accounted for by reaction through a boat conformation with involvement of the ether oxygen. Whether the ether oxygen interacts with boron or the metal cation remains uncertain, although the nature of the latter has little effect on the stereochemical outcome.

Experimental

Infrared spectra were obtained on a Perkin-Elmer Model 237-B spectrophotometer and ^{1}Hmr spectra in $CDCl_3$, with TMS as internal standard, on a Varian T-60 instrument. ^{13}C nmr spectra (natural abundance) were obtained on a Varian XL-100-12 nmr spectrometer equipped with a Nicolet Technology Corporation Fourier transform data system. Gas–liquid chromatography was performed on a Hewlett-Packard F and M Model 402 gas chromatograph using 6 ft packed columns or on a Perkin-Elmer 990 gas chromatograph using 50 ft support-coated open tubular columns, both instruments attached to an Infotronics CRS-208 integrator.

1,1-Dideuterio-3-buten-1-ol

A 500 ml three-necked round bottom flask fitted with a dropping funnel, reflux condenser, gas inlet tube, drying tubes, and magnetic stirring bar was charged with a suspension of lithium aluminum deuteride (4.0 g, 9.5×10^{-2} mol) in anhydrous ether (150 ml). The funnel was charged with a solution of vinylacetic acid (8.2 g, 9.5×10^{-2} mol) in anhydrous ether (100 ml). The system was flushed with dry nitrogen for 15 min and the acid solution added dropwise at such a rate as to maintain a gentle reflux. After addition was complete the reaction was stirred at room temperature for 1 h. Water (4 ml), 15% aqueous sodium hydroxide solution (4 ml), and water (4 ml) were added dropwise in that order to the stirred reaction mixture. The white precipitate was removed by suction filtration through a medium sintered glass filter funnel and washed with ether (4 × 20 ml). The combined ether solutions were washed with water (2 × 5 ml) and the combined washings back-extracted with ether (3 × 10 ml). The combined ether solutions were dried (Na_2SO_4), rotary evaporated, taken up in chloroform (25 ml), dried (Na_2SO_4), and evaporated to give a pale yellow liquid (5.1 g, 73%) which was purified by bulb-to-bulb distillation at water aspirator pressure (63% recovery); ν_{max} (neat): 2110, 2220 cm^{-1}; δ: 2.30 (2H, d, J = 6 Hz, CH_2), 3.33 (1H, s, OH), and 4.9 to 6.4 (3H, m, vinyl hydrogens); other properties identical to a nondeuterated commercial sample.

2-Trideuteriomethyl-2,6,6-trideuteriotetrahydropyran-4-ol (Mixture of Stereoisomers)

The procedure of Hanschke (2) for the preparation of the nondeuterated analogue was followed, using 1,1-dideuterio-3-buten-1-ol and acetaldehyde-d_4. Because of the water solubility of the product, neutralization in work-up was done with ammonia gas instead of aqueous sodium hydroxide solution. Water washings were all back-extracted with ether, and the ether solution evaporated, taken up in chloroform, dried, and re-evaporated; 80% yield was obtained; δ: 1.0–2.2 (4H, m, C-3 and C-5 H's), 2.30 (1H, s, OH), and 3.0–4.3 (axial and equatorial C-4 H), other properties identical with a *nondeuterated sample* (**2***A* and **2***B*) prepared in the same way; bp 73–74°C/5 Torr (lit. (2) bp 99°C/20 Torr), n_D^{21} 1.4548 (lit. (2) n_D^{20} 1.4543).

2-Trideuteriomethyl-2,6,6-trideuteriotetrahydropyran-4-one

A 100 ml three-necked round bottom flask fitted with a dropping funnel, thermometer, condenser, and stirring bar was charged with a solution of 2-trideuteriomethyl-2,6,6-trideuteriotetrahydropyran-4-ol (mixture of stereoisomers) (4.1 g, 3.1×10^{-2} mol) in ether (20 ml). Brown's solution (10) (16 ml) was added dropwise at such a rate as to maintain a temperature of 30°C. The mixture was stirred overnight at room temperature, the layers separated, and the aqueous layer extracted with ether (5 × 30 ml). The combined ether extracts were washed with water (2 × 5 ml) and these washings back-extracted with ether (3 × 10 ml). The total ether solution was

Can. J. Chem. Downloaded from www.nrcresearchpress.com by 210.87.254.5 on 09/05/12
For personal use only.

Can. J. Chem. Downloaded from www.nrcresearchpress.com by 210.87.254.5 on 09/05/12
For personal use only.

dried (Na_2SO_4), concentrated, taken up in $CHCl_3$ (30 ml), dried (Na_2SO_4), and evaporated to give 3.7 g (90%) of a clear yellow liquid. On occasions when glc indicated incomplete oxidation, re-oxidation was performed using the appropriate amount of oxidant. Bulb-to-bulb distillation gave a clear colourless liquid; ν_{max} (neat): 1720 (C=O), 2110, 2240 (C—D) cm^{-1}; δ: 2.0–2.6 (m, C-3, C-5 H's): other properties identical with a *nondeuterated sample* (**1**) prepared in the same way, bp 30°C/8 Torr (lit. (2) bp 70°C/20 Torr); n_D^{23} 1.4450 (lit. (2) n_D^{20} 1.4469).

Platinum Oxide Catalysed Hydrogenation of Hexadeuterated Ketone ***1***

A 100 ml round bottom flask was charged with platinum oxide (0.16 g) and 95% ethanol (50 ml), equipped with a magnetic stirring bar and a gas inlet tube. The flask was attached to a hydrogenation apparatus and flushed with hydrogen five times. The catalyst was stirred overnight at room temperature under 1.1 atm of hydrogen. The deuterated ketone **1** was then added and hydrogenated overnight at room temperature under 1.1 atm of hydrogen. The flask was then stirred open to the air for 30 min. Aqueous ferrous sulfate (0.25 ml, 0.1 *M*) and further platinum oxide (0.4 g) were then added (15) and the mixture again hydrogenated overnight as before. The reaction mixture was then suction filtered through medium (once) and fine (three times) sintered glass filter funnels, gravity filtered (Whatman No. 42), and dried (Na_2SO_4) to give a clear light green solution with no particulate matter. The solution was rotary evaporated, the residue taken up in ether (30 ml), and the ether solution washed with water (2 × 2 ml). The combined washings were back-extracted with ether (3 × 10 ml) and the combined ether solutions dried (Na_2SO_4), evaporated, the residue taken up in chloroform (25 ml), dried (Na_2SO_4), and evaporated. The glc and nmr analyses of the resulting alcohol mixture showed it to be 60% axial alcohol (*trans*) and 40% equatorial (*cis*).

Separation of cis- *and* trans-*2-Methyltetrahydropyran-4-ol*

The mixture of alcohols (0.48 g) was chromatographed on alumina (Woelm neutral, Activity III, 100 g), fractions of 25 ml being taken. Sixteen fractions of benzene were taken, followed by elution with 10% ether – 90% benzene. The *trans* isomer was contained in fractions 17–64 (^{13}C nmr δ: 21.7 (CH_3), 32.9 (C-5), 40.6 (C-3), 62.4 (C-6), 63.8 (C-4), and 67.9 (C-2); ^{1}Hmr of hexadeuterated sample, δ: 4.20, half width 8 Hz (C-4 H)); the *cis* isomer in fractions 76–170 (^{13}C nmr δ: 21.8 (CH_3), 35.4 (C-5), 43.2 (C-3), 65.9 (C-6), 67.5 (C-4), and 72.4 (C-2); ^{1}Hmr of hexadeuterated sample, δ: 3.70, half width 22 Hz (C-4 H)).

Raney Nickel Equilibration of Stereoisomeric Alcohols ***2***

Raney Nickel equilibrations were carried out as described previously (16) using the procedure of Eliel and Schroeter (17).

Stereoisomeric Product Ratio Determinations

(a) Borohydride Reductions

Reductions were carried out in 2-propanol using a two-fold excess of reductant over hexadeuterated **1**, at room temperature overnight. Concentrated hydrochloric acid was then added until gas evolution ceased. The solution was evaporated, taken up in ether (30 ml), washed with water (1 × 2 ml), the washings back-extracted with ether (3 × 10 ml), and the combined ether solutions dried (Na_2SO_4), the residue taken up in chloroform (25 ml), dried (Na_2SO_4), and evaporated. Product ratios were determined by nmr integration at δ 3.7 (axial C-4 H) and δ 4.2 (equatorial C-4 H).

(b) Selectride Reductions

A 100 ml round bottom three-necked flask fitted with a dropping funnel, stirring bar, gas inlet tube, and drying tube was flushed with nitrogen and charged with anhydrous ether (10 ml) and the reducing agent (4×10^{-3} mol). The flask was cooled (ice-water bath) and the ketone (0.26 g, 2×10^{-3} mol) in anhydrous ether (15 ml) added dropwise with stirring. The reaction was stirred at room temperature for 1 h. Aqueous sodium hydroxide (3 *M*, 1.0 ml) and 30% hydrogen peroxide (5 ml) were then added, the aqueous layer saturated with K_2CO_3, extracted with ether and the washings back-extracted, transferred to chloroform, and product ratios determined as for the borohydride reductions.

Acknowledgements

We wish to acknowledge stimulating discussion with Professor H. C. Brown on the mechanistic implications of this work and for his suggestion of the mechanism shown in Fig. 4.

The financial support of the National Research Council of Canada is also gratefully acknowledged.

1. D. C. Wigfield and F. W. Gowland. J. Org. Chem. **42**, 1108 (1977).
2. E. Hanschke. Chem. Ber. **88**, 1053 (1955).
3. H. C. Brown, C. P. Garg, and K.-T. Liu. J. Org. Chem. **36**, 387 (1971).
4. D. Tavernier, M. Anteunis, and N. Hosten. Bull. Soc. Chim. Belg. **85**, 151 (1976).
5. G. Berti, G. Catelani, M. Ferretti, and L. Monti. Tetrahedron, **30**, 4013 (1974).
6. D. C. Ayres, D. N. Kirk, and R. Sawdaye. J. Chem. Soc. B, 505 (1970).
7. J. B. Stothers. Carbon-13 nmr spectroscopy. Academic Press, New York, NY. 1972. pp. 112–118, 404–414.
8. R. U. Lemieux, R. K. Kullnig, H. J. Bernstein, and W. G. Schneider. J. Am. Chem. Soc. **80**, 6098 (1958).
9. D. C. Wigfield and D. J. Phelps. J. Org. Chem. **41**, 2396 (1976).
10. H. C. Brown and S. Krishnamurthy. J. Am. Chem. Soc. **94**, 7159 (1972).
11. E. L. Eliel, N. L. Allinger, S. J. Angyal, and G. A. Morrison. Conformational analysis. Interscience Publishers, New York, NY. 1965. pp. 376–377.
12. H. C. Brown, A. Khuri, and S. Krishnamurthy. J. Am. Chem. Soc. **99**, 6237 (1977).
13. H. C. Brown, A. Khuri, and S. C. Kim. Inorg. Chem. **16**, 2229 (1977).
14. J. E. Baldwin. J. Chem. Soc. Chem. Commun. 734 (1976).
15. R. L. Augustine. Catalytic hydrogenation. Marcel Dekker, Inc., New York, NY. 1965. p. 81.
16. D. C. Wigfield, G. W. Buchanan, C. M. E. Ashley, and S. Feiner. Can. J. Chem. **54**, 3536 (1976).
17. E. L. Eliel and S. H. Schroeter. J. Am. Chem. Soc. **87**, 5031 (1965).

Addition of pseudohalogens to unsaturated carbohydrates. VI.[1] Synthesis of 4′-thiocordycepin[2]

R. GEORGE S. RITCHIE, DOLATRAI M. VYAS, AND WALTER A. SZAREK[3]

Department of Chemistry, Queen's University, Kingston, Ont., Canada K7L 3N6

Received July 28, 1977

R. GEORGE S. RITCHIE, DOLATRAI M. VYAS, and WALTER A. SZAREK. Can. J. Chem. **56**, 794 (1978).

The addition of the pseudohalogen iodine nitrate ($IONO_2$) to the endocyclic alkenic bond in benzyl 2-*O*-benzyl-3,4-dideoxy-α-D-*glycero*-pent-3-enopyranoside (**3**) is described. The stereochemistry and regiochemistry of addition were elucidated by chemical degradation, ^{1}Hmr spectroscopy, mass-spectral analysis, and polarimetry. A synthetic route to 4′-thiocordycepin (**20**) from compound **3**, by way of the intermediacy of the preponderant iodine nitrate adduct of **3**, namely, benzyl 2-*O*-benzyl-3-deoxy-3-iodo-4-*O*-nitro-β-L-lyxopyranoside (**4**), is also described.

R. GEORGE S. RITCHIE, DOLATRAI M. VYAS et WALTER A. SZAREK. Can. J. Chem. **56**, 794 (1978).

On décrit l'addition du pseudohalogène nitrate d'iode ($IONO_2$) à la double liaison endocyclique du *O*-benzyl-2 didéoxy-3,4 α-D-glycéropenténo-3 pyrannoside de benzyle (**3**). On a étudié la stéréochimie et la régiochimie de l'addition par dégradation chimique, par spectroscopie rmn ^{1}H, par spectrométrie de masse et par polarimétrie. On décrit aussi une méthode de synthèse permettant de transformer le composé **3** en thio-4′ cordycépine (**20**) par l'intermédiaire de l'*O*-benzyl-2 déoxy-3 iodo-3 *O*-nitro-4 β-L-lyxopyrannoside de benzyle (**4**), l'adduit formé de façon prépondérante lors de l'addition du nitrate d'iode sur **3**.

[Traduit par le journal]

Introduction

A continuing area of research in this laboratory is the investigation of addition reactions of unsaturated carbohydrates. One particular project is concerned with the addition to these substrates of reagents that have been referred to as pseudohalogens. Many of these reagents are conveniently prepared *in situ* by the reaction of the appropriate silver salts with iodine. The present article describes the reaction of the pseudohalogen iodine nitrate ($IONO_2$) with a pyranoid derivative possessing an endocyclic double bond, namely, benzyl 2-*O*-benzyl-3,4-dideoxy-α-D-*glycero*-pent-3-enopyranoside (**3**). The reaction has led to a facile synthesis of 4′-thiocordycepin (**20**), an analog of the nucleoside antibiotic cordycepin in which the ring oxygen of the carbohydrate moiety is replaced by sulfur.

The addition of iodine nitrate to a furanoid derivative having an exocyclic double bond has already been reported (3); also, reactions with steroidal (4) and other noncarbohydrate olefins (5) have been studied. The pseudohalogen has been prepared by a variety of methods. Birckenbach and Goubeau (6) originally used mercury(II) nitrate, or silver nitrate, and iodine in ether; the reagent has also been generated by the reaction of silver nitrate with iodine in acetonitrile (3), from iodine – dinitrogen tetroxide (4), or by the reaction of iodine chloride with silver nitrate in chloroform–pyridine solution (5).

Results and Discussion

The unsaturated sugar **3** (Scheme 1) was originally prepared (7) by heating benzyl 2-*O*-benzyl-β-L-arabinopyranoside 3,4-thionocarbonate in trimethyl phosphite. In the present work, **3** was more conveniently obtained in high yield from benzyl 2-*O*-benzyl-3,4-di-*O*-(methylsulfonyl)-β-L-arabinopyranoside (**2**) (prepared in almost quantitative yield from the diol **1**) by treatment with a large excess of sodium iodide in refluxing *N*,*N*-dimethylformamide in the

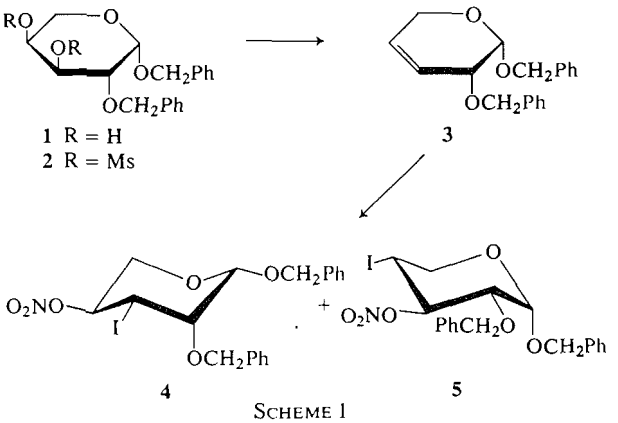

SCHEME 1

[1]For Part V in this series, see ref. 1.
[2]For a preliminary communication, see ref. 2.
[3]Author to whom inquiries should be addressed.

Can. J. Chem. Downloaded from www.nrcresearchpress.com by 210.87.254.105 on 09/05/12
For personal use only.

Can. J. Chem. Downloaded from www.nrcresearchpress.com by 210.87.254.105 on 09/05/12
For personal use only.

presence of zinc dust (Tipson–Cohen procedure (8)). The reaction of silver nitrate and iodine with **3** in ether was found to be very slow; even after 9 days, only a partial consumption of **3** had been observed. However, the use of acetonitrile, in which silver nitrate is very soluble, resulted in a rapid reaction with **3**; thus, with a solution containing 1.1 equiv. of iodine nitrate, the reaction was complete in 60 min, and in a solution containing 1.25 equiv., all of the unsaturated sugar **3** was consumed within 5 min to give a major component, namely benzyl 2-*O*-benzyl-3-deoxy-3-iodo-4-*O*-nitro-β-L-lyxopyranoside (**4**), and also benzyl 2-*O*-benzyl-4-deoxy-4-iodo-3-*O*-nitro-α-D-xylopyranoside (**5**). The mixture gave a positive spot test for a nitrate, namely, an intense blue coloration on addition of diphenylamine – sulfuric acid (9). The elemental analysis was consistent with an adduct of iodine nitrate and **3**. The proton magnetic resonance (^{1}Hmr) spectrum of the mixture of adducts showed an isolated multiplet, containing at least seven lines centered at τ 4.70, attributable to H-4 with a band width of 15 Hz (2 $J_{ax,ax} + J_{ax,eq}$);[4] the signals of all of the other sugar-ring protons were observed at higher field. It has been reported (11) with a large number of iodine nitrate adducts (5*b*) that the signal for the proton on the carbon bearing the nitrate group occurs at lower field (~ 1 ppm) than that for the proton on the carbon bearing the iodo group. In the present case, the nitrate group in the preponderant adduct is thus assigned to C-4. The band width of the H-4 signal implies the *trans*-diequatorial arrangement of the groups at C-3 and C-4. This observed stereochemistry is consistent with the stereospecific *trans* addition of iodine nitrate reported (4–6) with numerous other cyclic alkenes. Presumably, the iodo and nitrate groups in the minor adduct are also *trans* to each other.

The structures assigned to the two iodine nitrate adducts (**4** and **5**) were elucidated by a chemical degradation procedure (Scheme 2). The first step involved a reductive denitration. A variety of reagents and methods have been employed for selective *O*-denitration; these include acid- or base-catalyzed acetolysis (12), reductive electrolysis (5*b*), hydrazine (13), sodium nitrite (14), lithium aluminum hydride (15), metal (iron/zinc) dusts in boiling acetic acid (16), zinc-copper couple (5*b*), and high pressure catalytic hydrogenolysis over palladium (17). In this laboratory hydrogenolysis using Raney nickel catalyst has been employed effectively for both *O*-denitration (18) and reductive dehalogenation (1, 19).

[4]In the case of a ^{1}Hmr spectral pattern that is amenable to a first-order analysis, the band width may be considered as a measure of the sum of the coupling constants (10).

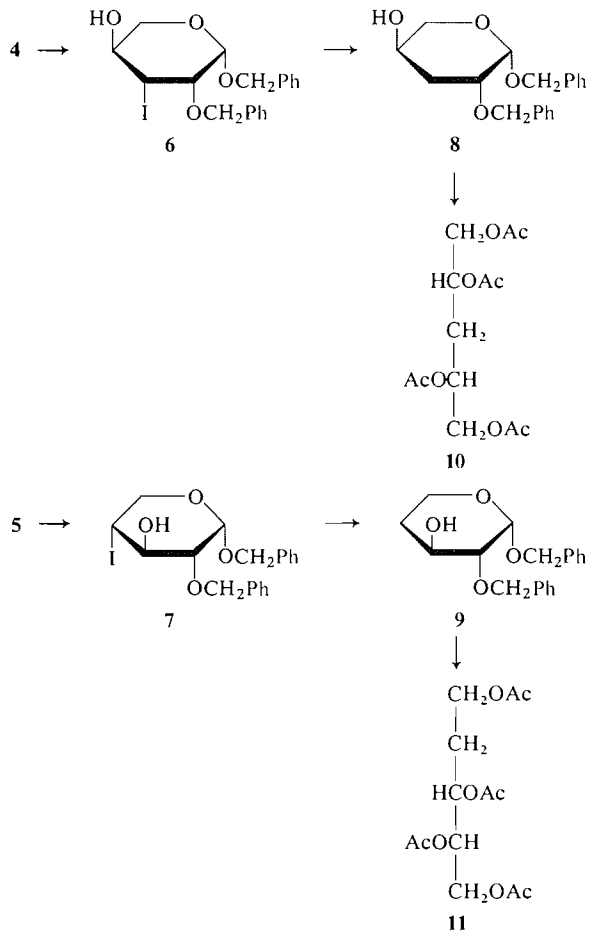

SCHEME 2

Thus, when a solution of a syrupy mixture of adducts **4** and **5** in ethanol and triethylamine containing Raney nickel was subjected to a hydrogen pressure, there was an initial conversion into three compounds, which were isolated by column chromatography, namely, the unsaturated sugar **3** (11%), the syrupy 3-iodo glycoside **6** (68%), and crystalline benzyl 2-*O*-benzyl-4-deoxy-4-iodo-α-D-*xylo*-pentopyranoside (**7**) (10%). Further hydrogenation of **6** and **7** over Raney nickel afforded the deoxypentopyranoside derivatives **8** and **9**, respectively. The structures assigned to compounds **8** and **9** were corroborated by their conversions into 1,2,4,5-tetra-*O*-acetyl-3-deoxy- and 1,3,4,5-tetra-*O*-acetyl-2-deoxy-L-*threo*-pentitols **10** and **11**, respectively, on *O*-debenzylation with sodium in liquid ammonia, followed by reduction of the resultant free sugars with sodium borohydride, and finally acetylation of the pentitols with acetic anhydride – pyridine. The syrupy tetraacetates **10** and **11**, when subjected to gas–liquid chromatography appeared to be homogeneous products, an observation which supports the contention that no epimeri-

Can. J. Chem. Downloaded from www.nrcresearchpress.com by 210.87.254.105 on 09/05/12
For personal use only.

zation at C-2 had occurred during *O*-debenzylation of benzyl glycosides **8** and **9** with sodium in liquid ammonia. The alditol acetates **10** and **11** were unequivocally characterized as 1,2,4,5-tetra-*O*-acetyl-3-deoxy-L-*threo*-pentitol and 1,3,4,5-tetra-*O*-acetyl-2-deoxy-L-*threo*-pentitol, respectively, on the basis of their specific rotations, mass spectra, and glc retention times. For glc analysis, authentic samples of monodeoxypentitol tetraacetates **12–15** were prepared. Examination of the glc retention times (see Table 1) of tetraacetates **10–15** relative to those of erythritol tetraacetate (R_{Ery}) and ribitol pentaacetate (R_{Rib}), indicated that compound **10** was a 3-deoxy-*threo*-pentitol isomer. Such an unequivocal assignment to alditol acetate **11** was not feasible, based on the comparison of the glc retention times; however, in this respect the mass spectra of **10** and **11** were very useful. According to the mass-spectral investigations of polyol acetates reported by Golovkina *et al.* (20), the peaks at *m/e* 231 in the spectrum of **10**, and at *m/e* 231, 159, and 145 in the spectrum of **11** were consistent with the pertinent fragmentations (see Scheme 3). It was noteworthy that in the spectrum of compound **10**, there were no peaks corresponding to *m/e* 159 and 145; this indicated that compound **11** was the 2-deoxy-*threo* isomer.

Finally, the assignment of the L-configuration to the pentitol acetates **10** and **11** was based on a comparison of their specific rotations in chloroform (see Experimental) with those of the authentic monodeoxypentitol tetraacetates **13** and **14**, respectively. Thus, in light of the above discussion the formation of the L-*lyxo*- and D-*xylo*-iodonitrate adducts **4** and **5**, respectively, from the unsaturated sugar **3**, by pseudohalogen ($IONO_2$) addition could be rationalized in terms of more preferred *trans*-diaxial opening of the initially formed equilibrating iodonium ions by the nitrate anion (see Scheme 4).

In the quest for potent anticancer and antibiotic

TABLE 1. Gas–liquid chromatographic[a] mobilities of monodeoxypentitol tetraacetates relative to erythritol tetraacetate (R_{Ery}) and ribitol pentaacetate (R_{Rib})

Compound	R_{Ery}	R_{Rib}
1,3,4,5-Tetra-*O*-acetyl-2-deoxy-D-*erythro*-pentitol (**12**)	1.90	0.47
1,2,4,5-Tetra-*O*-acetyl-3-deoxy-L-*threo*-pentitol (**13**)	2.19	0.54
1,3,4,5-Tetra-*O*-acetyl-2-deoxy-D-*threo*-pentitol (**14**)	2.48	0.61
1,2,4,5-Tetra-*O*-acetyl-3-deoxy-D-*erythro*-pentitol (**15**)	2.56	0.62
10	2.19	0.54
11	2.50	0.61

[a]On 3% (w/w) ECNSS-M on Gas-Chrom Q (100–120 mesh) column at 150°C.

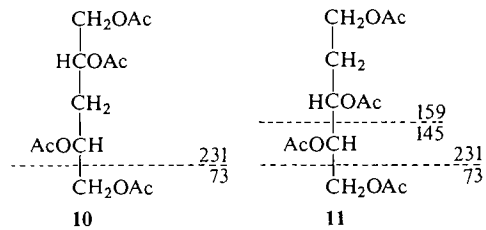

SCHEME 3

agents a number of 4′-thio analogs of naturally occurring and biologically active synthetic nucleosides have been reported (21). These purine and pyrimidine 4′-thio nucleosides have exhibited activity against certain bacteria and tumor cells (21). The effect of substitution of sulfur for the ribofuranosyl-ring oxygen on the biological activity of these nucleosides has been briefly reviewed (21*a*). In the present work, hydration of the readily available unsaturated sugar **3**, by way of the addition of the pseudohalogen iodine nitrate, has provided a viable synthetic route to 4′-thiocordycepin (Scheme 5). The synthesis of the nucleoside antibiotic cordycepin (3′-deoxyadenosine) (22) itself was achieved independently by Moffatt and co-workers (23) and Robins *et al.* (24) from adenosine and adenosine 2′,3′-orthoesters, respectively.

Thus, tosylation of the key intermediate alcohol **8** with *p*-toluenesulfonyl chloride in pyridine afforded the crystalline 4-*O*-*p*-tolylsulfonyl derivative (**16**) in 76% yield. The observation of the ^{1}Hmr signal for H-4 in compound **16** at τ 5.30 as a narrow band (width ~8 Hz) was consistent (10) with the axial orientation of the *p*-tolylsulfonyloxy group and **16** being in the *C*1(L) conformation. Heating the *p*-toluenesulfonate **16** for 48 h at reflux temperature in methanol containing benzyl thiol and sodium methoxide afforded, almost in quantitative yield, the 4-*S*-benzylglycoside (**17**). In the ^{1}Hmr spectrum of **17** the H-4 signal at τ 7.31 appeared as a seven-line multiplet ($J_{4,5ax}$ = 10.0 Hz, $J_{3ax,4}$ = 10.5 Hz, $J_{3eq,4}$ = $J_{4,5eq}$ = 5.0 Hz) indicating the equatorial orientation for the *S*-benzyl group and the *C*1(D) conformation for compound **17**.

All of the benzyl groups in compound **17** were removed with sodium in liquid ammonia, and the resultant free sugar was converted, on treatment with benzoyl chloride – pyridine, into a 1:3 mixture of the α- and β-anomers, respectively, of the 4-thio sugar (**18**). In the ^{1}Hmr spectra of the α- and β-anomers the signals for H-1 at τ 3.39 (doublet, $J_{1,2}$ = 4.3 Hz) and 3.58 (broad singlet, $J_{1,2}$ ~0.5 Hz), respectively, are in agreement with the assigned anomeric configurations. The presence of the thiofuranoid rings in the above anomers was confirmed by the

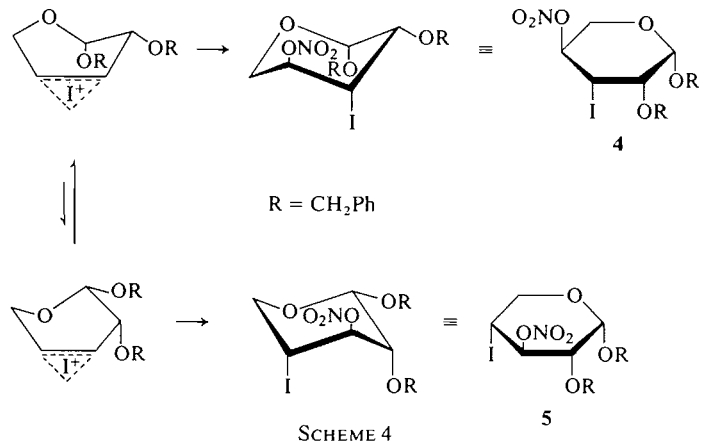

4

5

SCHEME 4

absence of *S*-benzoyl carbonyl bands in their ir spectra.

Each anomer of the tribenzoate (**18**) was separately treated, in 1,2-dichloroethane for 7 h at reflux temperature, with 6-benzamido-9-chloromercuripurine,

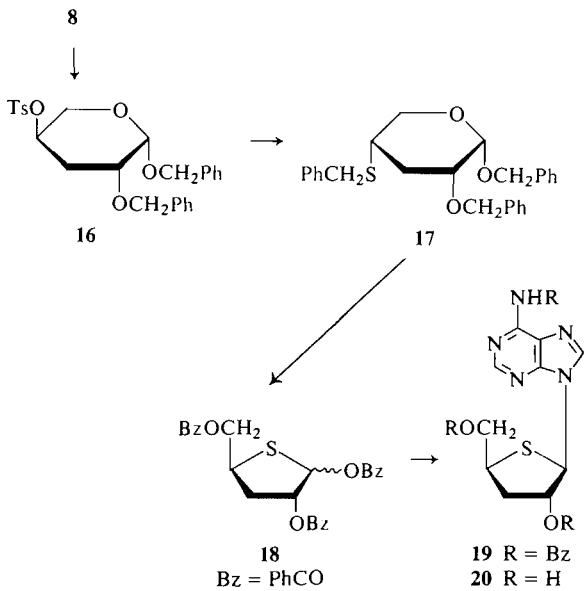

16 17

18 Bz = PhCO

19 R = Bz

20 R = H

SCHEME 5

in the presence of titanium tetrachloride (25), to give, after column chromatography, the protected nucleoside (**19**) (82 and 78% yields from the α- and β-anomers, respectively). The assignment of the β-anomeric configuration to **19** was based on the splitting pattern observed for the H-2′ and H-5′,H-5″ signals in the ^{1}Hmr spectra of **19** and the α- and β-anomers of **18**. Thus, the observation of the ^{1}Hmr signal for H-2′ in compound **19** and the β-anomer of **18** as a narrow multiplet was consistent with the assigned β-anomeric configuration to **19**. This assignment was further substantiated by the fact that the two H-5′ nuclei were observed as the A_2 portion of an apparent A_2B spin system in the spectrum of the α-anomer of **18**, and as the AB portion of an ABX system in the spectra of **19** and the β-anomer of **18**.

Treatment of the fully benzoylated nucleoside **19** with methanolic sodium methoxide for 2 h at reflux temperature afforded 9-(3-deoxy-4-thio-β-D-*erythro*-pentofuranosyl)adenine (**20**, 4′-thiocordycepin) as white needles in 75% yield. After hydrogen–deuterium exchange in deuterium oxide the ^{1}Hmr spectrum of **20** in methyl sulfoxide-d_6 exhibited the H-1′ signal at τ 4.11 as a doublet with $J_{1',2'} = 3.4$ Hz. Montgomery and Hewson (26) have observed, in the ^{1}Hmr spectra of a number of 9-β-ribofuranosylpurines in methyl sulfoxide-d_6, the chemical shift of H-1′ to be characteristic (τ 4.0–4.2). In contrast, the marked chemical-shift differences expected in the sugar-ring carbon signals in the Cmr spectra of ribofuranosyl and 4′-thioribofuranosyl nucleosides are typified by the chemical-shift data of thiocordycepin (**20**) and cordycepin (**21**) (Table 2). The presence of different hetero atoms in the sugar rings is clearly reflected in the C-1′ and C-4′ chemical shifts. The signal assignments in the above two nucleosides, especially for the purine-ring carbons, was facilitated by the availability of ^{13}Cmr data (27) for adenosine (in methyl sulfoxide) and 2-deoxyadenosine (in *N*,*N*-dimethylformamide). The deshielding (~3.5 ppm) of C-2′ and C-3′ in the spectrum of **20** with respect to the corresponding carbons in the spectrum of **21** is consistent with the observed deshielding of C-3 and C-4 in the spectrum of thiacyclopentane with respect to C-3 and C-4 in tetrahydrofuran (28). The effect of substitution of sulfur for oxygen, in the above compounds, on the shielding of the γ carbons has also been reported previously (29). The origin of this effect has been discussed by Perlin *et al.* (30) in connection with carbohydrates. Similar effects in

Can. J. Chem. Downloaded from www.nrcresearchpress.com by 210.87.254.105 on 09/05/12
For personal use only.

TABLE 2. Carbon-13 chemical shifts for cordycepin (**21**) and thiocordycepin (**20**)[a]

Compound	Carbon[b] 1′	2′	3′	4′	5′	2	4	5	6	8
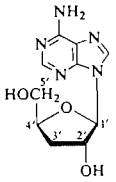 **21**	92.2	75.5	34.5	81.4	63.6	152.4	149.1	119.3	156.5	139.6
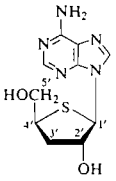 **20**	68.3	79.0	37.9	50.2	65.1	152.8	149.8	119.7	156.5	139.7

[a]In ppm from tetramethylsilane (TMS) in *N,N*-dimethylformamide and benzene-d_6 (20% solution).
[b]Chemical shifts obtained for the purine ring carbons of adenosine (**27**) measured in methyl sulfoxide are as follows: 153.5 (C-2), 150.1 (C-4), 120.4 (C-5), 157.1 (C-6), 141.2 (C-8).

trans-fused bicyclic hexopyranoside derivatives (31) and dioxanes (32) have been reported. The magnitude of the chemical-shift difference for C-2′ in **20** and **21** further corroborates the assigned β-anomeric configuration in **20**; an α-anomeric configuration in **20** would have resulted in the shielding of C-2′ due to *cis* C-1′,C-2′ substituent interactions (33).

Experimental

Melting points were determined on a Fisher–Johns melting-point apparatus and are uncorrected. Optical rotations were measured with Perkin-Elmer model 141 automatic polarimeter at 26 ± 3°. Infrared spectra were recorded with a Unicam SP 1000 spectrophotometer. The ^{1}Hmr spectra were recorded at 60 MHz in chloroform-*d* with tetramethylsilane as the internal standard, unless otherwise stated. The Cmr spectra were recorded in *N,N*-dimethylformamide–benzene-d_6 on a Bruker HX-90E Fourier transform spectrometer with tetramethylsilane as external or internal standard. Thin-layer chromatography was performed on silica gel G, containing 1–3% of indicator Lumilux Green ZS (Brinkmann Instruments (Canada) Ltd., Rexdale, Ont.), as the adsorbent in the following solvent systems (v/v): (*A*) 3:2 petroleum ether (bp 60–80°C) – ethyl acetate; (*B*) 3:1, (*C*) 5:1; (*D*) 2:3; (*E*) 1,2-dichloroethane; (*F*) 2:1 carbon tetrachloride – ethyl acetate; (*G*) 1:1 acetone – ethyl acetate; (*H*) ethanol; (*I*) ethyl acetate; (*J*) 2:1 toluene–acetone; (*K*) 3:1 chloroform–ethanol. The developed plates were air dried and the detection of components consisted of three stages: irradiation with a short-wavelength uv lamp (UVS-54) to detect benzoates, tosylates, purines, and benzyl ethers; spraying with dilute aqueous permanganate to test for isolated double bonds and divalent sulfur groups; and finally spraying with a solution of 1% cerium sulfate and 1.5% molybdic acid in 10% sulfuric acid and heating the plates at about 150°C. Paper chromatography was performed on Whatman No. 1 paper by the descending method, using aqueous 5% disodium hydrogen phosphate (*L*) and water-saturated *n*-butanol (*M*) as eluants. Detection was by a short-wavelength uv lamp for nucleosides. The term R_{Ad} refers to mobility relative to adenine. Gas–liquid chromatography (glc) was performed on an F & M, model 402, high-efficiency chromatograph employing a flame ionization detector and helium as the carrier gas. The column (U shaped, 120 cm long, 3.8 mm diameter) was packed using 3% (w/w) ECNSS-M on Gas-Chrom Q (100–120 mesh). A carrier-gas flow rate of about 90 ml/min was used, and the oven temperature was kept at 150°C. High resolution mass spectra were determined with a JEOLCO double focusing spectrometer, model JMS-OSIC, equipped with a heated, direct sample-injection system operated at 83°C, and fitted to record data by a photoplate; ionizing potential 75 eV.

Benzyl 2-O-Benzyl-3,4-di-O-(methylsulfonyl)-β-L-arabino-pyranoside (2, R = Ms)

To a solution of benzyl 2-*O*-benzyl-β-L-arabinopyranoside (1, R = H) (34) (68.3 g, 48.3 mmol, R_F (*A*) = 0.09) in pyridine (150 ml), cooled in an ice-water bath, was added in portions methanesulfonyl chloride (55 g) and the mixture was allowed to react overnight at room temperature. Isolation of the product in the usual fashion afforded the crude mesylate (**2**, R = Ms) (94.8 g, 97%). After recrystallization from methanol (on seeding), the compound had mp 97–98°C, $[\alpha]_D$ +140° (*c* 3.20, chloroform); R_F (*A*) = 0.43; ν_{max} (film): 770, 710 (OCH_2Ph), 1370, 1190 cm^{-1} (OMs); ^{1}Hmr τ: 4.90–5.10 (3H, H-1, H-3, H-4) 5.20–5.65 (4H, —OCH_2Ph), 6.00–6.25 (3H, H-2, H-6,6′), 6.93 and 7.09 (two 3H s's, —OSO_2CH_3). *Anal.* calcd. for $C_{21}H_{26}O_9S_2$: C 51.8, H 5.4, S 13.2; found: C 51.9, H 5.5, S 13.0.

Benzyl 2-O-Benzyl-3,4-dideoxy-α-D-glycero-pent-3-eno-pyranoside (3)

A vigorously stirred suspension of a solution of dimesylate (**2**, R = Ms) (88.5 g, 182 mmol, R_F (*A*) = 0.58, R_F (*B*) = 0.16) in *N,N*-dimethylformamide (200 ml), sodium iodide (100 g) and zinc dust (30 g) was refluxed for 2 h. The solids were removed by filtration, and the filtrate was concentrated; the residue was partitioned between chloroform and water.

Can. J. Chem. Downloaded from www.nrcresearchpress.com by 210.87.254.105 on 09/05/12
For personal use only.

Can. J. Chem. Downloaded from www.nrcresearchpress.com by 210.87.254.105 on 09/05/12
For personal use only.

The chloroform solution was washed several times with water, dried (Na_2SO_4), and then evaporated to give a crude syrup (49.9 g), which, on dissolution in ethanol and cooling, precipitated unreacted dimesylate (5.0 g). The residual syrup (36 g) afforded crystalline material on washing through a short column of alumina (80 g) with carbon tetrachloride (500 ml), concentration to dryness, and cooling. Recrystallization from ethanol afforded pure olefin **3** (24.2 g, 60%) as colorless needles, mp 31–33°C, $[\alpha]_D$ +111° (*c* 3.30, chloroform) (lit. (7) mp 32–35°C, $[\alpha]_D$ +115° (*c* 1.19, chloroform)); R_F (*A*) = 0.85, R_F (*B*) = 0.55; ν_{max} (film): 1640 (HC=CH *cis*), 1605 cm^{-1} (aromatic); ^{1}Hmr τ: 2.54–2.65 (10H, aromatic H's), 4.15 (s, 2H, H-3, H-4), 4.98 (1H, H-1), 5.09, 5.30 (2H AB pattern, anomeric —O*CH*$_2$Ph), 5.39 (s, 2H, —O*CH*$_2$Ph), 5.75–5.92 (3H, H-2, H-5,5′). This olefin is unstable to storage at room temperature.

*Reaction of Benzyl 2-*O*-Benzyl-3,4-dideoxy-*α*-*D*-*glycero*-pent-3-enopyranoside (**3**) with Silver Nitrate and Iodine*

Olefin **3** (7.2 g, 24.3 mmol, R_F (*C*) = 0.45) and silver nitrate (4.5 g, 1.12 equiv.) in dry acetonitrile (150 ml) were added, in one portion, to a stirred solution of iodine (7.0 g, 1.13 equiv.) in dry acetonitrile (150 ml) in a flask covered with aluminum foil. After 60 min,[5] the reaction mixture was filtered, and the filtrate was concentrated to a dark red syrup. The syrupy residue was extracted with carbon tetrachloride, and the extract was washed with aqueous sodium thiosulfate solution, dried over anhydrous magnesium sulfate, and decolorized. The solution was concentrated to a pale yellow oil (11.2 g, 94%). Thin-layer chromatography (solvent *E*) showed that all of the starting olefin had been consumed and revealed the presence of two new components, one as a major spot (R_F = 0.85) the other as a minor component (R_F = 0.88). Attempted distillation of the oil resulted in decomposition. The ir spectrum (film) showed absorptions at 1655, 1648, 1642, 1630, 1276 cm^{-1} (ONO_2); partial ^{1}Hmr of the preponderant compound **4** τ: 4.70 (7-line m, band width = 15 Hz, H-4), 5.32 (d, $J_{1,2}$ = 3.5 Hz, H-1), 5.21, 5.50 (AB pattern, anomeric —O*CH*$_2$Ph), 5.36 (s, —O*CH*$_2$Ph). *Anal.* calcd. for $C_{19}H_{20}INO_6$: C 47.0, H 4.1, I 26.2, N 2.9; found: C 47.2, H 3.8, I 26.7, N 3.1.

*Hydrogenolysis of the Iodine Nitrate Adducts from Olefin **3***

A solution of the mixture of the iodine nitrate adducts **4** and **5** (13.0 g, freshly prepared from 8.2 g of **3** in 90% yield) in ethanol (120 ml) containing triethylamine (25 ml) was hydrogenated over Raney nickel (#28) at 60 psig. The catalyst was removed and the solution was concentrated to dryness; the resultant residue (12.5 g) was partitioned between carbon tetrachloride and water. The carbon tetrachloride solution was washed once with water, dried (Na_2SO_4), and evaporated to afford a crude syrup (9.5 g). Thin-layer chromatography (solvent *B*) indicated the presence of three components having R_F's = 0.60, 0.44 and 0.36. The syrup was chromatographed on silica gel (800 g) and sequentially eluted as follows.

Elution with 1:1 (v/v) petroleum ether (bp 60–80°C) – ethyl acetate afforded olefin **3** (0.8 g, 11%, R_F (*B*) = 0.60), identical in all respects with an authentic sample.

Elution with 3:1 (v/v) carbon tetrachloride – ethyl acetate gave benzyl 2-*O*-benzyl-4-deoxy-4-iodo-α-D-xylopyranoside (**7**) (1.1 g, 10%) as fine needles after crystallization from chloroform – petroleum ether (bp 60–80°C), mp 89–91°C, $[\alpha]_D$ +130° (*c* 1.34, chloroform); R_F (*B*) = 0.44; ν_{max} (KBr): 3480 cm^{-1} (OH), no absorption attributable to ONO_2; ^{1}Hmr τ: 2.70–2.73 (10H, aromatic H's), 5.20–5.82 (6H, H-1, H-4, —O*CH*$_2$Ph), 6.05–6.70 (4H, H-2, H-3, H-5,5′), 6.95 (1H, OH).

[5]This reaction was complete in 5 min (tlc) when 1.25 equiv. of reagents were used.

Anal. calcd. for $C_{19}H_{21}IO_4$: C 52.9, H 4.8, I 28.8; found: C 53.1, H 4.9, I 28.3.

Elution with 2:1 (v/v) carbon tetrachloride – ethyl acetate yielded benzyl 2-*O*-benzyl-3-deoxy-3-iodo-β-L-lyxopyranoside (**6**) as a syrup (7.4 g, 68%), $[\alpha]_D$ +110° (*c* 1.25, chloroform); R_F (*B*) = 0.36; ν_{max} (film): 3480 cm^{-1} (OH), no absorption attributable to ONO_2; ^{1}Hmr τ: 2.60–2.80 (10H, aromatic H's), 5.00–6.40 (10H,) 7.00 (1H, OH).

*Benzyl 2-*O*-Benzyl-3-deoxy-*β*-L-*threo*-pentopyranoside (**8**) and Benzyl 2-*O*-Benzyl-4-deoxy-*β*-L-*threo*-pentopyranoside (**9**)*

Further hydrogenolysis of the products, obtained from the hydrogenation of a mixture of the iodine nitrate adducts (**4** and **5**) (3.8 g, 7.9 mmol), in the usual fashion in ethanol containing triethylamine and a fresh batch of Raney nickel catalyst, afforded a crude syrup (2.4 g). Upon column chromatography on silica gel using 3:2 (v/v) petroleum ether (bp 60–80°C) – ethyl acetate as eluant, the 4-deoxy isomer **9** (0.2 g, 9%) having R_F = 0.36 and $[\alpha]_D$ +137° (*c* 1.1, chloroform), and the 3-deoxy isomer **8** (1.5 g, 55% from **3**) having R_F = 0.20 and $[\alpha]_D$ +135° (*c* 1.8, chloroform) were isolated as syrups. The latter recrystallized from ether – petroleum ether (bp 60–80°C); the crystals had mp 121–123°C and their ir spectrum was virtually identical to that of **6**; ^{1}Hmr τ: 2.50–2.83 (10H, aromatic H's), 5.12 (d, 1H, $J_{1,2}$ = 3.2 Hz, H-1), 5.26, 5.48 (AB q, J_{AB} = 12.5 Hz, anomeric—O*CH*$_2$Ph), 5.55 (s, 2H, —O*CH*$_2$Ph), 5.97–6.80 (5H, H-2, H-5,5′, OH), 7.90–8.20 (narrow m, 2H, H-3,3′).

Compound **9** was characterized as its 4-*O*-trifluoroacetyl derivative, which was an oil, bp 142–149°C/0.1 Torr, $[\alpha]_D$ +114° (chloroform); ν_{max} (film): 1785 cm^{-1} (CF_3C=O), no absorption attributable to OH; ^{1}Hmr τ: 2.50–2.80 (10H, aromatic H's), 4.90 (m, 1H, H-4), 5.07 (d, 1H, $J_{1,2}$ = 3.2 Hz, H-1), 5.31, 5.51 (AB q, anomeric—O*CH*$_2$Ph), 5.53 (s, 2H, —O*CH*$_2$Ph), 6.00–6.60 (3H, H-2, H-5,5′), 7.70–8.00 (m, 2H, H-3,3′). *Anal.* calcd. for $C_{21}H_{21}F_3O_5$: C 61.5, H 5.2; found: C 61.5, H 5.2.

*1,2,4,5-Tetra-*O*-acetyl-3-deoxy-*L*-threo-pentitol (**10**)*

To a stirred suspension of alcohol **8** (1.30 g, 4.1 mmol) in liquid ammonia (120 ml), was added sodium metal (6–8 equiv.) in small portions until the intense blue color persisted. The basic solution, obtained on destroying the excess of sodium with aqueous ammonium chloride and evaporation of ammonia, was diluted with water (100 ml) and then immediately neutralized with strong-acid ion-exchange resin. The solids were removed, and the aqueous solution was extracted with chloroform; the organic solution was decolorized (charcoal), filtered through Celite, and the filtrate was evaporated to give a clear syrup (494 mg, 89%). The major component having R_F (*G*) = 0.40 was recovered by column chromatography on silica gel using 1:1 (v/v) acetone – ethyl acetate as eluant. The ir spectrum of the resulting syrup exhibited a strong band at 3500–3250 cm^{-1} attributable to OH.

The reduction of the above free sugar (125 mg, 0.9 mmol, R_F (*H*) = 0.85) with sodium borohydride (~100 mg) in water (5 ml) in the usual fashion afforded in quantitative yield the deoxypentitol as a yellow syrup (127 mg), $[\alpha]_D$ +25° (*c* 12.7, ethanol); R_F (*H*) = 0.45–0.60.

Acetylation of the above deoxypentitol in acetic anhydride – pyridine afforded **10** as a homogeneous syrup (238 mg, 83%), bp 99–103°C/0.07 Torr, $[\alpha]_D$ +12° (*c* 3.45, chloroform); ν_{max} (film): 1755, 1740 (C=O), 1070–1030 cm^{-1} (C—O), no absorption attributable to OH; ^{1}Hmr τ: 4.83 (2H, H-2, H-4, $J_{1,2} = J_{4,5}$ = 3.9 Hz, $J_{1',2} = J_{4,5'}$ = 6.0 Hz, $J_{2,3} = J_{3,4}$ = 6.1 Hz, $J_{2,3'} = J_{3',4}$ = 7.9 Hz), 5.72 (2H, H-1, H-5, $J_{1,1'} = J_{5,5'}$ = 12.5 Hz), 5.97 (2H, H-1′, H-5′), 7.95 (12H, OCO*CH*$_3$),

Can. J. Chem. Downloaded from www.nrcresearchpress.com by 210.87.254.105 on 09/05/12
For personal use only.

8.10 (2H, H-3,3′); for glc mobilities, see Table 1. *Anal.* calcd. for $C_{13}H_{20}O_8$: C 51.3, H 6.6; found: C 51.5, H 6.6.

1,3,4,5-Tetra-O-*acetyl-2-deoxy*-L-threo-*pentitol* (**11**)

Treatment of benzyl 2-*O*-benzyl-4-deoxy-β-L-*threo*-pentopyranoside (**9**) (0.2 g) in exactly the same sequential fashion as for compound **8** afforded the title compound **11** in low yield as a clear, colorless syrup (10 mg), bp 100–110°C/0.07 Torr, $[\alpha]_D$ −23° (*c* 0.2, chloroform); for glc mobilities, see Table 1.

1,3,4,5-Tetra-O-*acetyl-2-deoxy*-D-erythro-*pentitol* (**12**)

Commercially available 2-deoxy-D-*erythro*-pentose (4 mg), on reduction with sodium borohydride in the usual fashion and followed by acetylation (acetic anhydride – pyridine) of the resulting deoxypentitol, afforded compound **12** as a homogeneous product, $[\alpha]_D$ +20° (*c* 1.65, chloroform); for glc mobilities, see Table 1.

1,2,4,5-Tetra-O-*acetyl-3-deoxy*-L-threo-*pentitol* (**13**)

Acid-catalyzed hydrolysis of 3-deoxy-1,2-*O*-isopropylidene-β-L-*threo*-pentofuranose, (484 mg, 2.78 mmol, R_F (*I*) = 0.54) prepared from D-glucose according to the published procedures of Prokop and Murray (35), with strong-acid ion-exchange resin (2 g) in 50% methanol (40 ml) at reflux temperature for ~3 h afforded 3-deoxy-L-*threo*-pentose (320 mg, 86%); R_F (*I*) = 0.15.

3-Deoxy-L-*threo*-pentose, on reduction with sodium borohydride and followed by acetylation in the usual fashion of the resulting deoxypentitol, gave **13** as a colorless syrup, bp 98–104°C/0.07 Torr, $[\alpha]_D$ +13° (*c* 2.0, chloroform); R_F (*A*) = 0.40; the ir and ^{1}Hmr spectra of this material were identical to those of compound **10**; for glc mobilities, see Table 1.

1,3,4,5-Tetra-O-*acetyl-2-deoxy*-D-threo-*pentitol* (**14**)

To a solution of 3-deoxy-D-*xylo*-hexose (prepared by the acid-catalyzed hydrolysis of 3-deoxy-1,2:5,6-di-*O*-isopropylidene-α-D-*xylo*-hexofuranose (35)) in water (15 ml) was added with stirring sodium metaperiodate (0.75 g). After 18 h, 2-deoxy-D-*threo*-pentose was obtained as a syrup, on removal by filtration of the iodates and periodates (precipitated by adding barium chloride), followed by evaporation of the filtrate to dryness, extraction of the resulting residue with ethanol, and finally solvent removal.

2-Deoxy-D-*threo*-pentose, on reduction with sodium borohydride (0.4 g) in water (5 ml) and followed by acetylation in the usual manner of the resulting deoxypentitol, afforded **14** as a syrup, $[\alpha]_D$ +20° (*c* 1.65, chloroform). Gas–liquid chromatographic analysis suggested that, in addition to **14**, there was present a minor component.

1,2,4,5-Tetra-O-*acetyl-3-deoxy*-D-erythro-*pentitol* (**15**)

Treatment of methyl 2,3-anhydro-β-L-ribopyranoside (36) (1.2 g, 8.3 mmol) with lithium aluminum hydride (~1 g) in dry tetrahydrofuran (30 ml) afforded methyl 3-deoxy-β-L-*erythro*-pentopyranoside (37). Acid-catalyzed hydrolysis of this product under the conditions reported by Kent *et al.* (38), followed by reduction with sodium borohydride and acetylation in the usual fashion, afforded compound **15** as a clear, colorless syrup, bp 122–128°C/0.1 Torr; ^{1}Hmr τ: 4.65–5.03 (4H, H-2, H-4), 5.73 (2H, H-1, H-5, $J_{1,2} = J_{4,5} = 4.0$ Hz, $J_{1',2} = J_{4,5'} = 6.0$ Hz, $J_{1,1'} = J_{5,5'} = 12.5$ Hz), 5.93 (2H, H-1′, H-5′), 7.95 (12H, OCOCH_3), 8.01 (2H, H-3,3′); for glc mobilities, see Table 1.

Benzyl 2-O-*Benzyl-3-deoxy-4*-O-p-*tolylsulfonyl*-β-L-threo-*pentofuranoside* (**16**)

A solution of alcohol **8** (627 mg, 2.0 mmol R_F (*A*) = 0.20) and *p*-toluenesulfonyl chloride (689 mg, 1.75 equiv.) in pyridine (5 ml) was kept for 2 days at 40°C. Isolation of the product in the usual fashion afforded a crude syrup (855 mg, 91%), which was chromatographed on silica gel, using 3:1 (v/v) carbon tetrachloride – ethyl acetate as eluant, to remove unreacted starting material. The tosylate **16** was obtained as fine, white needles (760 mg, 76%) on cooling of its solution in methanol, mp 57–58°C, $[\alpha]_D$ +99° (*c* 1.33, chloroform); R_F (*A*) = 0.70; ν_{max} (film): 3070, 3040 (aromatic C—H), 2950 aliphatic C—H), 1370–1360, 1095 cm^{-1} (—SO_2OR); ^{1}Hmr τ: 2.60–2.85 (12H, aromatic H's), 5.11 (d, 1H, $J_{1,2} = 3.2$ Hz, H-1), 5.30 (m, 1H, H-4, band width = 8–9 Hz), 5.31, 5.50 (AB q, $J_{AB} = 12.5$ Hz, anomeric —OCH_2Ph), 5.62 (s, 2H, —OCH_2Ph), 6.05–6.66 (3H, H-2, H-5,5′), 7.67 (s, 3H, —OSO_2PhCH_3), 7.60–8.15 (m, 2H, H-3,3′). *Anal.* calcd. for $C_{26}H_{28}O_6S$: C 66.6, H 6.0, S 6.8; found: C 66.7, H 5.7, S 6.7.

Benzyl 2-O-*Benzyl-4*-S-*benzyl-3-deoxy-4-thio*-α-D-erythro-*pentopyranoside* (**17**)

To a well purged (with nitrogen) solution of crystalline tosylate **16** (6.7 g, 14.3 mmol, R_F (*C*) = 0.55) in methanol (150 ml) was added a solution of benzyl thiol (5.0 ml, 3 equiv.) in methanolic sodium methoxide (54 ml, 1.06 *N*, 4 equiv.) and the mixture was refluxed under nitrogen for 30 h. The solution was cooled and concentrated to dryness, and the resulting residue was partitioned between water and ether. The combined ether extract was washed with concentrated aqueous sodium hydroxide (twice) and aqueous sodium chloride (twice), dried (Na_2SO_4), and concentrated to a syrup (5.74 g, 95%). From the crude syrup, **17** was obtained by distillation, bp 168–173°C/0.10 Torr, $[\alpha]_D$ +62° (*c* 1.08, chloroform); R_F (*C*) = 0.45; ^{1}Hmr τ: 2.76 (m, 5H), 2.81 (s, 10H, aromatic H's), 5.22 (d, 1H, $J_{1,2} = 3.2$ Hz, H-1), 5.29, 5.52 (AB q, $J_{AB} = 12.5$ Hz, anomeric —OCH_2Ph), 5.61 (s, 2H, —OCH_2Ph), 6.35 (s, 2H, —SCH_2Ph), 6.22–6.76 (5H, —SCH_2Ph, H-2, H-5,5′), 7.31 (1H, 7-line m, $J_{3eq,4} = J_{4,5eq} = 5.0$ Hz, $J_{3ax,4} = 10.5$ Hz, $J_{4,5ax} = 10.0$ Hz, H-4), 7.80–8.40 (m, 2H, H-3,3′). *Anal.* calcd. for $C_{26}H_{28}O_3S$: C 74.3, H 6.7, S 7.6; found: C 74.3, H 6.7, S 7.5.

1,2,5-Tri-O-*benzoyl-3-deoxy-4-thio*-D-erythro-*pentofuranose* (**18**)

A solution of **17** (5.74 g, 13.7 mmol) in ether (10 ml) was added with vigorous stirring to liquid ammonia (300 ml); sodium metal (2.8 g, 120 mmol) was added to this in small portions over a period of 1 h. Stirring was continued for an additional 30 min and the ammonia and solvent were evaporated then under a stream of nitrogen; the excess of sodium was destroyed by careful addition of water (50 ml) and the resulting aqueous solution extracted with ether. The aqueous solution, on neutralization with strong-acid ion-exchange resin and concentration to dryness, gave a black syrup (2.08 g); pyridine (30 ml) was added, and a black material (0.2 g) was removed by filtration. To the chilled, pyridine filtrate was added, dropwise, benzoyl chloride (5.5 ml, 41 mmol), and the reaction was allowed to proceed for 12 h. The usual processing of the reaction mixture and solvent removal gave a syrup (5.5 g); tlc (solvent *B*) indicated the presence of two major components, having R_F = 0.5 and 0.17, a minor component having R_F = 0.3 (not characterized), and benzoic anhydride. The latter contaminant was separated from the sugar components by column chromatography on silica gel using benzene as eluant. This initial separation afforded pure sugar components (2.0 g, 32%), which on further column chromatography on silica gel with 5:1 (v/v) petroleum ether (bp 60–80°C) – ethyl acetate as eluant yielded the two major benzoylated products.

The first component (R_F (*B*) = 0.5) isolated, upon trituration with methanol containing a little ether, afforded a crystalline solid. Recrystallization from chloroform – petroleum ether (bp 60–80°C) gave 1,2,5-tri-*O*-benzoyl-3-deoxy-4-

Can. J. Chem. Downloaded from www.nrcresearchpress.com by 210.87.254.105 on 09/05/12
For personal use only.

thio-α-D-*erythro*-pentofuranose (596 mg, 9.4%), mp 140–141°C, $[\alpha]_D$ +249° (*c* 1.08, chloroform); ν_{max} (KBr): 1745, 1730, 1710 cm^{-1} (C=O, benzoate); ^{1}Hmr τ: 1.83–2.60 (15H, aromatic H's), 3.37 (d, 1H, $J_{1,2}$ = 4.3 Hz, H-1), 4.21 (1H, 6-line m, $J_{2,3} = J_{2,3'}$ = 8.3 Hz, H-2), 5.56 (2H, 3 lines, an apparent A_2 portion of an A_2B spin system, H-5,5′),5.78-6.22 (m, 1H, H-4), 7.20–7.47 (m, 2H, H-3,3′). *Anal.* calcd. for $C_{26}H_{22}O_6S$: C 67.5, H 4.8, S 6.9; found: C 67.3, H 4.9, S 6.9.

Removal of solvent from the mother liquor of the α-anomer afforded syrupy 1,2,5-tri-*O*-benzoyl-3-deoxy-4-thio-β-D-*erythro*-pentofuranose (769 mg, 12.1%), $[\alpha]_D$ −110° (*c* 1.30, chloroform); R_F (*B*) = 0.52; ir spectrum essentially identical to that of the α-anomer; ^{1}Hmr τ: 1.85–2.92 (15H, aromatic H's), 3.58 (s, 1H, bandwidth = 2 Hz, H-1), 4.10 (m, 1H, bandwidth = 6 Hz, H-2), 5.42, 5.56, 5.83 (m, 3H, $J_{4,5}$ = 7.2 Hz, $J_{5,5'}$ = 11.0 Hz, $J_{4,5'}$ = 5.3 Hz, H-5,5′ and H-4, respectively), 7.34, 7.64 (m, 2H, $J_{3,3'}$ = 14.0 Hz, $J_{3,4}$ = 6.0 Hz, $J_{3',4}$ = 9.0 Hz, H-3,3′).

The second major component (R_F (*B*) = 0.17) isolated was 1,5-di-*O*-benzoyl-3-deoxy-4-thio-β-D-*erythro*-pentofuranose (870 mg, 17.7%), mp 93–96°C (not recrystallized); ^{1}Hmr τ: 1.80–2.80 (10H, aromatic H's), 3.62 (s, 1H, H-1), 5.00–6.25 (5H, H-2, H-5,5′, OH), 5.15 (m, 1H, band width = 6 Hz), 6.12 (1H, OH), 7.20–8.10 (m, 2H, H-3,3′). Benzoylation of this dibenzoate in pyridine (10 ml) and benzoyl chloride (0.3 ml) overnight afforded the α-anomer of the tribenzoate (914 mg, 82%).

*4′-Thiocordycepin (**20**)*

From a mixture of 1,2,5-tri-*O*-benzoyl-3-deoxy-4-thio-α-D-*erythro*-pentofuranose (518 mg, 1.20 mmol, R_F (*A*) = 0.75), 6-benzamido-9-chloromercuripurine (687 mg, 1.25 equiv.), Celite (0.5 g), and 1,2-dichloroethane (80 ml) was distilled 25 ml of the solvent to exclude moisture from the reaction mixture. Titanium tetrachloride (0.15 ml, 1.25 equiv.) in dry 1,2-dichloroethane (2 ml) was added, dropwise, and the reaction mixture was stirred while being heated at reflux temperature. The progress of the reaction was monitored by tlc (solvent *A*) which revealed that all of the starting material (R_F = 0.75) had been consumed after 7 h and a new component (R_F = 0.07) had been formed. Saturated, aqueous sodium hydrogen carbonate (25 ml) was added to the reaction mixture, and after being stirred for 30 min, the mixture was filtered through Celite and the filter cake washed twice with chloroform. The organic solution was sequentially washed with water, 30% aqueous potassium iodide, and water, and dried over anhydrous sodium sulfate. Evaporation of the solvent afforded crude, blocked nucleoside **19** as a white foam (720 mg), which was further purified by column chromatography on silica gel using 1:2 (v/v) carbon tetrachloride – ethyl acetate as eluant. Pure **19** was obtained as a brittle, white foam (554 mg, 82%), mp 134–135°C, $[\alpha]_D$ −25° (*c* 1.05, chloroform); R_F (*I*) = 0.6–0.8; ν_{max} (KBr): 3250 (NH), 1730 (C=O, benzoate), 1700, 1610, 1590 cm^{-1} (aromatic, purine); ^{1}Hmr (50°C) τ: 0.72 (1H, N-H), 1.30 (s, 1H, H-2), 1.60 (s, 1H, H-8), 1.83–2.83 (15H, aromatic H's), 3.62 (d, 1H, $J_{1',2'}$ = 2.5 Hz, H-1′), 3.97 (1H, 4-line m, $J_{2',3'} + J_{2',3''}$ = 7.0 Hz, H-2′), 5.22, 5.34 (AB portion of an ABX system, $J_{4',5'}$ = 6.7 Hz, $J_{4',5''}$ = 6.0 Hz, $J_{5',5''}$ = 11.0 Hz, H-5′,5″, respectively), 5.72 (m, 1H, $J_{3',4'} + J_{3'',4'}$ = 13.3 Hz, H-4′), ~7.37 (m, 2H, H-3′,3″).

Condensation of 1,2,5-tri-*O*-benzoyl-3-deoxy-4-thio-β-D-*erythro*-pentofuranose (1.55 g, 3.6 mmol) with 6-benzamido-9-chloromercuripurine (2.06 g) and titanium tetrachloride (0.45 ml) in 1,2-dichloroethane (250 ml) in the same manner as described above afforded **19** (1.56 g, 78%).

A solution of pure, blocked nucleoside **19** (1.15 g, 2.0 mmol) in methanol (50 ml) containing sodium methoxide (0.5 ml, 1.06 *M* in MeOH) was refluxed for 2 h; tlc (solvents *J* and *K*) revealed that all of **19** was deacylated. The cooled solution was neutralized by adding Rexyn-102 (H^+ form), filtered, and concentrated to dryness with ethanol several times. The residual white powder (441 mg, 82%), on recrystallization from methanol, gave 9-(3-deoxy-4-thio-β-D-*erythro*-pentofuranosyl)adenine (**20**) (4′-thiocordycepin) as white needles (398 mg, 75%), mp 257–260°C (dec.), $[\alpha]_D$ −55° (*c* 0.09, methanol), $[\alpha]_D$ −34° (*c* 1.09, methyl sulfoxide); R_{Ad} = 1.30 (solvent *L*), R_{Ad} = 1.07 (solvent *M*); λ_{max} (MeOH) 260 nm (ε 14 870); ν_{max} (KBr): 3400 (OH), 3270–3160 (NH), 1690, 1615, 1575, 1475 (purine ring), 1425 (C—CH_2), 1060 cm^{-1} (C—O); ^{1}Hmr (methyl sulfoxide-d_6, 60°C)[6] τ: 1.58 (s, 1H, H-2), 1.80 (s, 1H, H-8), 2.88 (unexchanged NH), 4.11 (d, 1H, $J_{1',2'}$ = 3.4 Hz, H-1′), 4.43, 4.92 (unexchanged OH and HOD), 5.33 (m, 1H, band width ~13 Hz, H-2′), 6.10–6.50 (3H, H-4′, H-5′,5″), 7.80–8.00 (m, 2H, H-3′,3″). *Anal.* calcd. for $C_{10}H_{13}N_5O_2S$: C 44.9, H 4.9, N 26.2, S 12.0; found: C 44.8, H 4.9, N 26.4, S 11.9.

Acknowledgements

The authors thank the National Research Council of Canada for financial support of this work and Dr. G. Lukacs, Institut de Chimie des Substances Naturelles, C.N.R.S., Gif-sur-Yvette, France, for recording the ^{13}Cmr spectra.

1. R. G. S. RITCHIE and W. A. SZAREK. Can. J. Chem. **50**, 507 (1972).
2. R. G. S. RITCHIE and W. A. SZAREK. Chem. Commun. 686 (1973).
3. (*a*) D. H. BALL, A. E. FLOOD, and J. K. N. JONES. Can. J. Chem. **37**, 1018 (1959); (*b*) I. SZCZEREK, J. S. JEWELL, R. G. S. RITCHIE, W. A. SZAREK, and J. K. N. JONES. Carbohydr. Res. **22**, 163 (1972).
4. J. E. KROPP, A. HASSNER, and G. J. KENT. Chem. Commun. 906 (1968).
5. (*a*) U. E. DINER and J. W. LOWN. Chem. Commun. 333 (1970); (*b*) U. E. DINER and J. W. LOWN. Can. J. Chem. **49**, 403 (1971); (*c*) U. E. DINER, M. WORSLEY, and J. W. LOWN. J. Chem. Soc. C, 3131 (1971); (*d*) J. W. LOWN and A. V. JOSHUA. J. Chem. Soc. Perkin Trans. 1, 2680 (1973).
6. L. BIRCKENBACH and J. GOUBEAU. Chem. Ber. **67**, 1420 (1934).
7. A. H. HAINES. Carbohydr. Res. **1**, 214 (1965).
8. R. S. TIPSON and A. COHEN. Carbohydr. Res. **1**, 338 (1965).
9. F. FEIGEL. Spot tests in organic analysis. 7th ed. Elsevier, New York, NY. 1966. p. 300.
10. N. C. FRANKLIN and H. FELTKAMP. Angew. Chem. Int. Ed. **4**, 774 (1965).
11. J. W. EMSLEY, J. FEENEY, and L. H. SUTCLIFFE. High resolution nuclear magnetic resonance spectroscopy. Vol. 2. Pergamon Press, London. 1966. p. 672.
12. M. L. WOLFROM, R. S. BOWER, and G. G. MAHER. J. Am. Chem. Soc. **73**, 874 (1951).
13. K. S. ENNOR, T. C. STENNING, and J. HONEYMAN. Chem. Ind. (London), 1308 (1956).
14. J. HONEYMAN and J. W. W. MORGAN. J. Chem. Soc. 3660 (1955).
15. E. G. ANSELL and J. HONEYMAN. J. Chem. Soc. 2778 (1952).
16. J. W. H. OLDHAM and J. K. RUTHERFORD. J. Am. Chem. Soc. **54**, 366 (1932).

[6]The nucleoside was boiled in deuterium oxide and freeze dried at least three times prior to dissolving it in methyl sulfoxide-d_6.

17. (*a*) L. P. KUHN. J. Am. Chem. Soc. **68**, 1761 (1946); (*b*) I. G. WRIGHT and L. D. HAYWARD. Can. J. Chem. **38**, 316 (1960).
18. J. S. JEWELL. Ph.D. Thesis, Queen's University, Kingston, Ont. 1971.
19. W. A. SZAREK, A. ZAMOJSKI, A. R. GIBSON, D. M. VYAS, and J. K. N. JONES. Can. J. Chem. **54**, 3783 (1976).
20. L. S. GOLOVKINA, O. S. CHIZHOV, and N. F. VUL'FSON. Bull. Acad. Sci. USSR, 1853 (1966).
21. (*a*) A. BLOCH. *In* Drug design. Vol. IV. *Edited by* E. J. Ariens. Academic Press, New York, NY. 1973. Chapt. 8, p. 328, and references cited therein; (*b*) N. OTOTANI and R. L. WHISTLER. J. Med. Chem. **17**, 535 (1974); (*c*) M. BOBEK, A. BLOCH, R. PARTHASARATHY, and R. L. WHISTLER. J. Med. Chem. **18**, 784 (1975); (*d*) M. V. PICKERING, J. T. WITKOWSKI, and R. K. ROBINS. J. Med. Chem. **19**, 841 (1976).
22. R. J. SUHADOLNIK. Nucleoside antibiotics. Wiley-Interscience, New York, NY. 1970. p. 50.
23. A. F. RUSSELL, S. GREENBERG, and J. G. MOFFATT. J. Am. Chem. Soc. **95**, 4025 (1973).
24. M. J. ROBINS, R. MENGEL, and R. A. JONES. J. Am. Chem. Soc. **95**, 4074 (1973).
25. (*a*) E. M. ACTON, K. J. RYAN, and L. GOODMAN. J. Am. Chem. Soc. **89**, 467 (1967); (*b*) E. J. REIST, L. V. FISHER, and L. GOODMAN. J. Org. Chem. **33**, 189 (1968).
26. J. A. MONTGOMERY and K. HEWSON. J. Med. Chem. **9**, 234 (1966).
27. A. J. JONES, D. M. GRANT, M. W. WINKLEY, and R. K. ROBINS. J. Am. Chem. Soc. **92**, 4079 (1970).
28. J. B. STOTHERS. Carbon-13 NMR spectroscopy. Academic Press, New York, NY. 1972.
29. W. A. SZAREK, D. M. VYAS, A.-M. SEPULCHRE, S. D. GERO, and G. LUKACS. Can. J. Chem. **52**, 2041 (1974).
30. A. S. PERLIN, B. CASU, and H. J. KOCH. Can. J. Chem. **48**, 2596 (1970).
31. E. CONWAY, R. D. GUTHRIE, S. D. GERO, G. LUKACS, A.-M. SEPULCHRE, E. W. HAGMAN, and E. WENKERT. Tetrahedron Lett. 4879 (1972).
32. (*a*) A. J. JONES, E. L. ELIEL, D. M. GRANT, M. C. KNOEBER, and W. F. BAILEY. J. Am. Chem. Soc. **93**, 4772 (1971); (*b*) F. G. RIDDELL. J. Chem. Soc. B, 331 (1970); (*c*) G. M. KELLIE and F. G. RIDDELL. J. Chem. Soc. B, 1030 (1971).
33. M. C. DEPEW. Ph.D. Thesis, Queen's University, Kingston, Ont. 1976.
34. F. WOLD. J. Org. Chem. **26**, 198 (1961).
35. J. PROKOP and D. H. MURRAY. J. Pharm. Sci. **54**, 359 (1965).
36. (*a*) W. G. OVEREND and M. STACEY. J. Chem. Soc. 1234 (1949); (*b*) L. HOUGH and J. K. N. JONES. J. Chem. Soc. 4349 (1952).
37. R. D. GUTHRIE. *In* The carbohydrates. 2nd ed. Vol. 1A. *Edited by* W. Pigman and D. Horton. Academic Press, New York, NY. 1972. p. 423.
38. P. W. KENT, M. STACEY, and L. F. WIGGINS. J. Chem. Soc. 1232 (1949).

Can. J. Chem. Downloaded from www.nrcresearchpress.com by 210.87.254.105 on 09/05/12
For personal use only.

Competitive thermal and photochemical processes in cyclopropylketone rearrangements. I. Photolysis of spiro[*n*.2]alkan-2-ones

EDWARD LEE-RUFF AND PRABHAKAR GOVIND KHAZANIE
Department of Chemistry, York University, Downsview, Ont., Canada M3J 1P3

Received July 22, 1977

EDWARD LEE-RUFF and PRABHAKAR GOVIND KHAZANIE. Can. J. Chem. **56**, 803 (1978).

The series of cyclopropyl ketones **1–6** was irradiated in methanol. Cyclopentanones **1** and **2** gave mainly products of type I reaction whereas ketones **3**, **5**, and **6** gave type II products. Formation of type II products can arise by two different mechanisms. One involves the intermediacy of a dienol which can be trapped with methanol-OD. Photochemical degradation of the cyclopentanones was slower than the corresponding cyclohexanones.

EDWARD LEE-RUFF et PRABHAKAR GOVIND KHAZANIE. Can. J. Chem. **56**, 803 (1978).

On a effectué l'irradiation d'une série de cyclopropyles cétones **1–6** dans le méthanol. Les cyclopentanones **1** et **2** conduisent principalement aux produits de réaction du type I alors que les cétones **3**, **5** et **6** donnent les produits du type II. La formation des produits de type II peut provenir de deux mécanismes différents. L'un implique un diénol comme intermédiaire qui peut être piégé avec du méthanol-OD. La dégradation photochimique des cyclopentanones est plus lente que celle des cyclohexanones correspondantes.

[Traduit par le journal]

Can. J. Chem. Downloaded from www.nrcresearchpress.com by 210.87.254.105 on 09/05/12
For personal use only.

Introduction

The photochemistry of cyclopropyl ketones has been extensively investigated (1–3). Much of the photochemistry of such systems bears close analogy with the thermal reactions for related compounds. Thus, for instance, Norrish type II ring opening of methyl substituted cyclopropyl ketones (4) resembles the thermal 'ene' rearrangement of the same system (5). The oxovinylcyclopropane to dihydrofuran rearrangement occurs both photochemically (6) and thermally (7). It is conceivable that intermediates such as vibrationally excited ground states and diradicals are common to both processes (8). To evaluate the extent to which thermal chemistry overlaps photodeactivation processes we undertook a comparative photochemical and pyrolytic study of a series of spiro[*n*.2]alkan-2-ones. This series was chosen because the favourable bisected conformation of cyclopropyl ketones required for maximum conjugation (9) is incorporated in these compounds. In this part we report the photochemical results.

Results

The syntheses of ketones **1–6** have been described elsewhere (10). Irradiation of ketone **1** in methanol

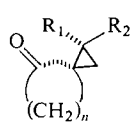

1 $R_1 = H; R_2 = CH_3; n = 3$
2 $R_1 = CH_3; R_2 = H; n = 3$
3 $R_1 = R_2 = CH_3; n = 3$
4 $R_1 = H; R_2 = CH_3; n = 4$
5 $R_1 = CH_3; R_2 = H; n = 4$
6 $R_1 = R_2 = CH_3; n = 4$

using a Vycor filter resulted in the exclusive formation of cyclopropanecarboxaldehyde **7** in the early stages of the reaction. The yield of **7** reached a maximum of 40%[1] after 90 min irradiation and subsequently decreased with concomitant formation of a more complex mixture. Under the photolytic conditions **7** was found to be photolabile and secondary products ensued upon prolonged irradiations. The structure of **7** was assigned based on the spectral and

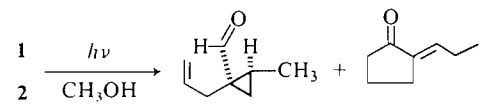

7 **8**

analytical data. The assignment of the stereochemistry of **7** is based on the nmr chemical shift of the methyl group at δ 1.21 ppm and comparison with the reported value of 1.20 for the methyl signal of *trans*-1-acetyl-2-methylcyclopropane (5). The corresponding value for the *cis*-isomer is slightly higher (δ 1.30).

Irradiation of the *syn*-isomer **2** in methanol resulted in a mixture of ketone **1**, 2-propylidenecyclopentanone (**8**), and cyclopropanecarboxaldehyde **7**. The relative yields of photoproducts was a function of irradiation time. Furthermore, **7** appeared to be a secondary photoproduct as was evident from monitoring the photoreaction. The structure of **8** was established from its spectral and analytical data as well as its independent synthesis by condensation of cyclopentanone and propanal. Such reactions generate the thermodynamically more stable *anti*-

[1]All reported yields are based on vpc peak integrations (using internal standards) unless otherwise specified.

Can. J. Chem. Downloaded from www.nrcresearchpress.com by 210.87.254.105 on 09/05/12
For personal use only.

isomer. The aldehyde **7** obtained from the *syn*-ketone **2** was identical in all respects with the product obtained from the *anti*-isomer **1**.

Irradiation of **3** in methanol resulted in the production of enone **9** and ketal **10** in 19 and 58% yields, respectively, based on unreacted starting material. The photoenone **9** was found to be labile under these conditions and in a separate experiment was shown to be transformed to the cyclic ketal **10** in 80% yield. The identity of **10** was established by its independent synthesis from methyl (2-oxocyclopentyl)acetate according to Scheme 1 (11). The identity of enone **9** was deduced from its spectral and analytical data as well as its hydrogenation to **11** which was independently synthesized.

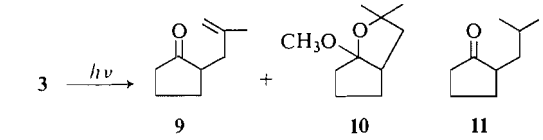

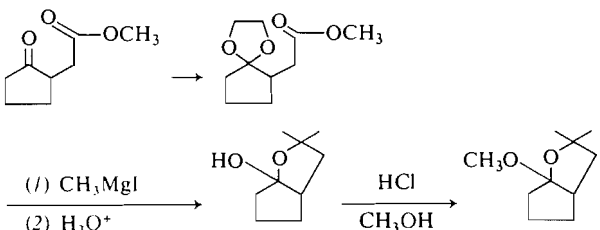

SCHEME 1

Irradiation of spiroketone **4** gave three products, **12**, **13**, and **14** in 41, 25, and 16% yields, respectively. Upon prolonged irradiation, the yield of cyclobutanol **14** increased at the expense of **12**. The structural assignments of **12** and **14** are based on characteristic group frequency assignments of their ir and nmr spectra as well as elemental analysis. The structure of 2-allylcyclohexanone (**13**) was unambiguously established by its independent synthesis. Irradiation of the isomeric ketone **5** gave a 70% yield of 2-allylcyclohexanone (**13**) and irradiation of ketone **6** resulted in 80% conversion to ketone **15**, the structure of which was assigned from analysis of spectral and analytical data and its hydrogenation to **16** which was independently synthesized.

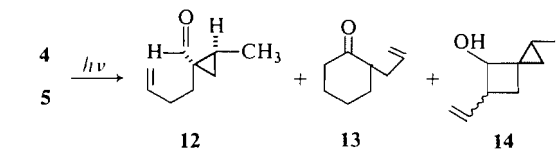

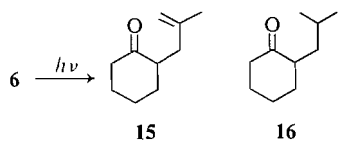

Discussion

The following trends are observed for the photodecomposition of spiro[*n*.2]alkan-2-ones. Norrish type I fragmentation appears to be the dominant pathway in the absence of a suitably disposed γ-hydrogen for type II process. Products from cyclopropane ring opening arise only for *syn*-2-methylcyclopropylketones, and in such cases not all products are derived from type II reaction. For the spiroketones **5** and **6** at least 70% of cyclopropane ring opening can be rationalized as resulting from type II rearrangement from deuterium labelling studies. When the irradiation of **5** and **6** was carried out in CH_3OD, ketones **13** and **15** were obtained

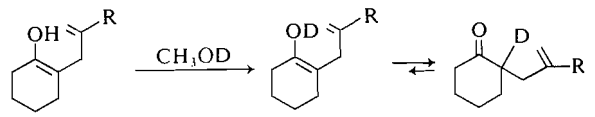

with about 70% deuterium incorporation. Under the same conditions, neither ketones **13** and **15** nor starting materials **5** and **6** underwent deuterium exchange. Type II rearrangement would be expected to yield dienols **17** which would undergo deuterium exchange under these conditions. That *complete* deuterium exchange did not occur can be rationalized in terms of (*A*) keto–enol tautomerism occurring as efficiently as exchange of D with CH_3OD and/or (*B*) ketones **13** and **15** being formed by a pathway not involving dienols **17**. A diradical of type **18** could conceivably also result in the formation of ketones **13** and **15** without proceeding through dienol **17**. That keto–enol tautomerism is not a unimolecular process is indicated by the relatively long lifetime ($\tau_{\frac{1}{2}}$ = 167 s) reported for a similar dienol **19** in the gas phase (8). It is unlikely that under our conditions a sufficient concentration of dienols **19** would be obtained such that bimolecular enol–keto tautomerism competes with proton exchange in methanol. It is noteworthy that no deuterium incorporation accompanied the formation of enones **8** and **9** from

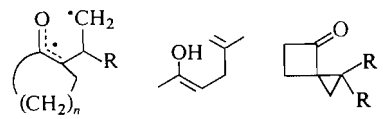

Can. J. Chem. Downloaded from www.nrcresearchpress.com by 210.87.254.105 on 09/05/12
For personal use only.

2 and **3**, respectively, when irradiations were carried out in CH_3OD. Thus cyclopropane ring opening takes place in these systems by a process other than type II rearrangement and enol formation. For type II reactions to occur, certain stereochemical constraints have to be met, namely that the γ-hydrogen has to lie in close proximity to the vacant n orbital in the n–π* state (12). Model studies show that the methyl hydrogens in the more stable conformations of **5** and **6** are in closer proximity to the carbonyl plane than in the case of **2** and **3**. Thus cyclopropane ring opening in **2** and **3** is expected to proceed by a mechanism other than type II. This is also substantiated by a significant amount of photoisomerization of the *syn*-ketone **2**.

Relative efficiencies of decomposition of these ketones were found in the order **6** ~ **5** > **4** > **3** ~ **2** > **1**. This data is in contrast to the reported greater efficiency of cyclopentanones over cyclohexanones to undergo α-cleavage reactions (13). Extension of the relative decomposition rate studies to include spiroketones **20***a* and *b* (14) showed that these were even slower than ketones **1** and **3**. This is in contrast to the more efficient photodecomposition of other cyclobutanones (14). Further, no type II or other products resulting from cyclopropane ring opening were observed from either **20***a* or *b*. These results point to a stabilizing effect of conjugated cyclopropane in carbonyl photodecompositions. Such effects appear to be maximized when the conjugating effects of cyclopropane are favourable such as in the case of spiroketones **20***a* and *b* where the carbonyl group is oriented in the bisected conformation relative to the cyclopropane ring. Similar effects of conjugated double bonds on carbonyl inertness to photochemistry have been observed for 2-alkylidenecycloalkanones (14).

Also in contrast to 2-alkylcyclohexanones possessing a primary γ-hydrogen (12), type II rearrangement in spirohexanones **5** and **6** is more efficient than type I cleavage. This can be attributed to the greater conformational rigidity of the γ-hydrogens in the latter case.

The anomalous photolytic transformation of **9** to

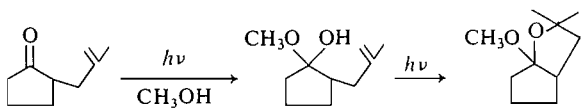

9 **21** **10**

10 does not appear to be general for 2-allylcycloalkanones. Such a process is formally analogous to cyclization of γ,δ-unsaturated carboxylic acids to δ-lactones (15) and may involve the intermediacy of hemiketal **21**.

Experimental

Melting points were uncorrected. The ir spectra were recorded with a Unicam SP 1000 instrument. The nmr spectra were measured on Varian A-60, HA-100, and EM-360 spectrometers. Samples were dissolved in CCl_4 or $CDCl_3$ solvents using TMS as the internal standard. Vapour phase chromatographic analyses and collections were performed on a Varian Aerograph Series 1700 instrument using a 6 ft glass column (0.25 in. od) packed with 6% SE-30 + 4% QF-1 on Chromosorb W AW, DMCS treated. Microanalyses were performed by Gygli Microanalytical Labs, Toronto. All of the starting materials were prepared according to procedures described in refs. 16 and 17.

General Photolysis Procedure

All irradiations were carried out in quartz tubes (od 1.7 cm) with a 450 W Hanovia high-pressure quartz mercury vapour lamp (679A-36), using a water cooled quartz immersion well containing a Vycor filter. The concentration of all solutions was 10–20 mg/ml. The solutions were purged with nitrogen for 5–10 min preceding photolysis and stoppered. Spectrograde methanol and cyclohexane were obtained from J. T. Baker Chemical Company and from Matheson Coleman & Bell, respectively. The progress of the reaction was followed by withdrawing small portions after every 10 min and injecting a constant volume of the irradiated sample into a vpc instrument. The percentage formation of the products was thus calculated. The photolysis of every sample was repeated at least thrice and the results were reproducible to within 3–9%. At the end of the irradiation, the solution was carefully concentrated, and the residual liquid was subjected to preparative scale vpc. Methanolic solutions of all cyclopropylketones were stirred in the dark to ensure that no dark reaction occurred.

Photolysis of syn-*6-Methylspiro[2.4]heptan-2-one (2)*

A solution of 160 mg of the title compound in 8 ml methanol was photolyzed for ½–1½ hours; vpc (He flow 55 cc/min, 100°C) of the photomixture showed the following components.

Aldehyde **7** (13–24%, retention time 6 min 12 s): ir (CCl_4): 875, 920, 1045, 1430, 1450, 1638, 1712, 2715, 2820, 3070 cm^{-1}; nmr δ; 8.8 (1H, CHO), 4.98 (2H, m), 5.75 (1H, m), 0.8–2.5 (7H, m with a broad singlet at 1.21), 0.5 (1H, m). *Anal.* calcd. for $C_8H_{12}O$: C 77.41, H 9.67; found: C 77.40, H 9.52.

Ketone **8** (5–8%, retention time 12 min 4 s): ir (CCl_4): 1033, 1132, 1204, 1286, 1410, 1462, 1650, 1720, 2875, 2960 cm^{-1}; nmr (CCl_4) δ: 1.06 (3H, t, J = 7 Hz) 1.45–2.84 (8H, m), 6.36 (1H, m).

Ketone **1** (28–34%) identical with a previously synthesized sample (10).

Preparation of anti-*2-Propylidenecyclopentanone (8)*

A mixture of cyclopentanone (16.8 g, 0.2 mol), propionaldehyde (11.6 g, 0.2 mol), and 0.5% KOH (20 ml) was stirred at 0°C for 30 min and then at room temperature for 15 h Work-up of the reaction mixture in ether gave 11.2 g of a fraction, bp 70–100°C/1.2 Torr. This fraction was then treated with orthophosphoric acid to give 6.9 g (27%) of *anti*-2-propylidenecyclopentanone, bp 63–64°C/1.5 mm (lit. (18) bp 81–82°C/11 Torr), mp of 2,4-dinitrophenylhydrazone 203–205°C (lit. (18) 204–205°C).

Photolysis of anti-*6-Methylspiro[2.4]heptan-2-one (1)*

A solution of 200 mg of the title compound in 10 ml methanol was photolyzed as described for ketone **2**; vpc showed only one peak apart from the starting peak. After 90 min of irradiation the solution was concentrated and sub-

Can. J. Chem. Downloaded from www.nrcresearchpress.com by 210.87.254.105 on 09/05/12
For personal use only.

jected to preparative vpc separation to give 52 mg (26%) of starting ketone **1** and 80 mg of aldehyde **7** identical in all respects with a sample obtained from the photolysis of ketone **2**.

*Photolysis of 6,6-Dimethylspiro[2.4]heptan-2-one (**3**)*

A solution of 120 mg of the title compound in 12 ml spectrograde methanol was irradiated for different time periods. After 21 min irradiation, vpc of the irradiation mixture (temperature 100°C, He flow 55 cc/min) showed two photoproducts and 64% of the starting ketone. The products were shown to be compound **10** (21%, retention time 5.47 min) and **9** (7%, retention time 9.37 min), respectively. The structure of compound **10** is based on its characteristic spectral properties and its independent synthesis (see below): ir (CCl_4): 870, 1018, 1097, 1148, 1185, 1366, 1380, 2825, 2865, 2965 cm^{-1}; nmr (CCl_4) δ: 1.1–2.82 (15H, m, 1.25 s). The enone **9** displayed the following spectral data: ir (CCl_4): 898, 1155, 1375, 1417, 1453, 1648, 1740, 2965, 3080 cm^{-1}; nmr (CCl_4) δ: 1.65–2.7 (12H, m, 1.715), 4.7 (2H, a broad singlet). The structure of this compound was confirmed by hydrogenation to a product which was independently synthesized (see below).

When the photolysis was allowed to continue for a longer period, increased amounts of **10** were observed. Compound **10** was shown to be a secondary photoproduct by photolyzing **9** independently under the above conditions.

*Photolysis of **9***

A solution of 80 mg of **9** in 8-ml methanol was irradiated as above; vpc of the 20-min irradiated sample showed complete disappearance of the starting material yielding 79% of **10**, plus three other unidentified products. The ir and nmr spectra of **10** were identical with those of the compound obtained by direct photolysis of **3**.

*Synthesis of Mixed Ketal **10***

The mixed ketal was prepared by the following steps.

A. Preparation of Ethylene Ketal of Methyl (2-Oxocyclopentyl)acetate

A solution of methyl (2-oxocyclopentyl)acetate (7.8 g, 0.05 mol), ethylene glycol (3.6 g, 0.055 mol), and *p*-toluenesulfonic acid (25 ml) in 75 ml dry benzene was refluxed with a Dean Stark trap until no more water was collected. The reaction mixture was neutralized with sodium methoxide and worked up with additional 75 ml benzene to give 8 g (86%) of the title ketal; ir (neat) 950, 1028, 1438, 1738 cm^{-1}; nmr (CCl_4) δ: 1.3–2.67 (9H, m), 3.6 (3H, s), 3.83 (4H, s).

B. Reaction of Ketal from A with Methylmagnesium Iodide

To a solution of methylmagnesium iodide (0.045 mol) in 40 ml diethyl ether was added to the above ketal (4 g, 0.021 mol) in 15 ml ether at room temperature. The mixture was refluxed for 1 h, cooled, decomposed with saturated aqueous solution of ammonium chloride, and worked up in the usual way to give 3.3 g (77%) of 2-(6,9-dioxaspiro[4.4]nonyl)-2′-methyl-2′-propanol. This compound was purified by vacuum transfer at 125°C and 1 Torr pressure; ir (neat): 905, 946, 1023, 1148, 1338, 1470, 3430 cm^{-1}; nmr (CCl_4): 1–2.1 (15H, with a sharp singlet at 1.15), 2.9 (1H, a broad singlet, disappeared with D_2O), 3.85 (4H, s).

C. Hydrolysis of 2-(6,9-Dioxaspiro[4.4]nonyl)-2′-methyl-2′-propanol

The title compound was dissolved in 30 ml acetone and 8 ml water containing 30 mg of *p*-toluenesulfonic acid. The solution was heated to reflux on an oil bath for 1 h. The mixture was cooled, excess acetone removed under reduced pressure, and extracted with ether to give a hemiketal in equilibrium with a small amount of 2-(2′-methyl-2′-hydroxypropyl)cyclopentanone. The hemiketal (64%) was purified by vacuum transfer at 100°C and 5 Torr pressure; ir (neat): 988, 1010, 1075, 1150, 1260, 1313, 1368, 1382, 1454, 1468, 3400 cm^{-1}; nmr (CCl_4) δ: 1.05–2.8 (15H, m, a sharp singlet at 1.23), 4.53 (1H, s).

*D. Preparation of the Mixed Ketal **10***

To 2 ml of an ice cold solution of 1% methanolic HCl was added 100 mg of the hemiketal, while stirring. After stirring for 3 h, the solution was treated with $NaHCO_3$, extracted with 20 ml ether, and ether extract washed with brine until neutral. The extract was dried over anhydrous magnesium sulfate and ether removed under reduced pressure to give the mixed ketal in quantitative yield. The ir and nmr spectra of this compound were identical with those of the compound obtained by photolysis of **3**; ir (CCl_4): 870, 1018, 1097, 1148, 1185, 1366, 1380, 2825, 2865, 2965 cm^{-1}; nmr (CCl_4) δ: 1.1–2.82 (15 H, m, with a broad singlet at 1.25), 3.17 (3H, m). *Anal.* calcd. for $C_{10}H_{18}O_2$: C 70.59, H 10.60; found: C 70.56, H 10.55.

Preparation of anti-*2-Isobutylidenecyclopentanone*

A mixture of 16.8 g (0.2 mol) of cyclopentanone, 14.4 g (0.2 mol) of isobutyraldehyde, and 20 ml of 0.5% KOH was stirred at 0°C for 30 min and then at room temperature for 12 h. The reaction mixture was worked up to give 12.4 g of a fraction, bp 80–100°C/1.2 Torr, which was then treated with orthophosphoric acid as described for *anti*-2-propylidenecyclopentanone; yield of the product: 7.7 g (28%), bp 62–63°C/1.5 Torr (lit. (19) bp 86°C/11 Torr); ir (CCl_4): 945, 1142, 1178, 1205, 1290, 1410, 1466, 1653, 1722, 2960 cm^{-1}; nmr (CCl_4) δ: 1.02 (6H, d), 1.62–2.8 (7H, m), 6.23 (1H, a doublet of triplets); λ_{max} (EtOH) 246 nm (ε 8004).

Hydrogenation of anti-*2-Isobutylidenecyclopentanone*

The title ketone (58 mg), was hydrogenated at atmospheric pressure with 8 mg of platinum oxide in 6 ml of ethylacetate. One equivalent of hydrogen was taken up whereupon the hydrogen uptake ceased. The solution was filtered and the solvent removed under reduced pressure to give 53 mg of essentially pure product (analyzed by vpc): ir (neat): 1183, 1392, 1410, 1432, 1480, 1492, 1765 (C=O stretch)cm^{-1}; nmr (CCl_4) δ: 0.77–1.1 (6H, two doublets centered at 0.83, J = 1.5 Hz, J = 1.5 Hz), 1.15–2.4 (10H, m).

*Hydrogenation of **9***

A solution of 25 ml of the title compound in 6 ml ethyl acetate was hydrogenated over 5 mg of platinum oxide Work-up and isolation gave 2-isobutylcyclopentanone in almost quantitative yield. This ketone, had ir and nmr spectra identical with those of a sample prepared by hydrogenation of *anti*-2-isobutylidenecyclopentanone.

Photolysis of anti-*7-Methylspiro[2.5]octan-2-one (**4**) in Methanol*

A solution of 200 mg of *anti*-7-methylspiro[2.5]octan-2-one in 10 ml spectrograde methanol (Baker analyzed reagent) was flushed with nitrogen and irradiated at 25°C using a Vycor filter. After 16 min irradiation, vpc of the irradiated sample (100°C, rate of He flow 55 cc/min) showed two products and 52% of the starting material (retention time 12.44 min). The two products were shown to be compounds **12** (26%, retention time 7 min 40 s) and **13** (15%, retention time 10 min), respectively. The spectrum of compound **12** rests on its characteristic properties and analysis: ir (neat liquid) 765, 860, 712, 995, 1394, 1450, 1635, 1708, 2720, 3065 cm^{-1}; nmr (CCl_4) δ: 5.67 (1H, m), 4.95 (2H, m), 0.85–2.35 (9H, m, broad singlet at 1.22), 0.55 (1H, m), 8.68 (1H, s); M^+: *m/e* 138. *Anal.* calcd. for $C_9H_{14}O$: C 78.26, H 10.15; found: C 78.04, H, 10.27.

2-Allylcyclohexanone (**13**) (20) was synthesized independently from ethyl 2-cyclohexanonecarboxylate and allyl bromide, and its spectral properties were compared with those of the synthesized sample. When the photolysis was allowed to

Can. J. Chem. Downloaded from www.nrcresearchpress.com by 210.87.254.105 on 09/05/12
For personal use only.

continue for an additional 14 min, vpc of the mixture showed compound **12** (41%), **13** (25%), starting ketone (16%), and the initially minor peak (**14**, retention time 6 min 2 s) increased in intensity. On prolonged photolysis the peak at 6 min and 2 s increased considerably in size with a subsequent loss of **12**. The ir, nmr, and mass spectra of this compound indicated the structure **14**: ir (CCl_4): 920, 1070, 1108, 1398, 1450, 1635, 3070, 3630 cm^{-1}; nmr (CCl_4, external TMS) δ: 6 (1H, m), 5.25 (2H, m), 4 (1H, d, J = 7 Hz), 2.48 (1H, OH, disappeared with D_2O), 2.72 (1H, m), 1.9 (2H, d, J = 9 Hz), 1.14 (3H, d), 0.05 (1H, m), 0.75 (2H, m); M^+: *m/e* 138.

Photolysis of syn-*7-Methylspiro[2.5]octan-2-one (5) in Methanol*

A solution of 200 mg of the title compound in 10 ml methanol was photolyzed under the same conditions as mentioned in the photolysis of **4**: vpc analysis of the photomixture after 16 min of photolysis showed **13** (58%), starting material 19%), and four other unidentified products totalling 23%. After 30 min of photolysis the mixture was found to contain **13** (69%), starting ketone (3%), and other products totalling 28%. The ir and nmr spectra of the major product were identical with those of the compound obtained by the photolysis of *anti*-7-methylspiro[2.5]octan-2-one.

Photolysis of 7,7-Dimethylspiro[5.2]octan-2-one (6)

A solution of 100 mg of **6** in 10 ml spectrograde methanol was irradiated as described earlier. After 15 min irradiation vpc of the irradiation mixture (85°C, He flow 50 cc/min) showed 47% of a major product (retention time 18 min), 16% of starting ketone (retention time 14 min), and four other minor peaks. The major product was identified as compound **15** on the basis of its spectral data: ir (CCl_4): 890, 1048, 1130, 1450, 1645, 1710, 3060 cm^{-1}; nmr (CCl_4) δ: 1.68 (3H, s), 1.72–2.5 (11H, m). The structure of **15** was confirmed by comparing spectra of its hydrogenated product with those of the synthesized sample (see below).

When the photolysis was continued for a longer period, increased amounts of unidentified products were observed at the expense of **15**. In a separate experiment a solution of **6** (100 mg) in cyclohexane (5 ml) was irradiated for 15 min; vpc of the mixture showed 79% **15** and 10% unreacted ketone **6**.

Preparation of anti-*2-Isobutylidenecyclohexanone*

A mixture of cyclohexanone (19.6 g, 0.2 mol), isobutyraldehyde (14.4 g, 0.2 mol), and 1.5% KOH (50 ml) was stirred at 0°C for 20 min and then at room temperature for 12 h. The mixture was worked up to give 14.5 g of a fraction, bp 93–103°C/1.2 Torr, which was then treated with orthophosphoric acid. Yield of the product was 9.5 g (31%), bp 68–69°C/1.5 Torr (lit. (21) bp 96–98°C/7 Torr); ir (CCl_4): 1140, 1303, 1465, 1620, 1690 (C=O stretch) cm^{-1}; nmr (CCl_4) δ: 0.93 (3H, s), 10.5 (3H, s), 1.5–2 (4H, m), 2.15–2.7 (5H, m), 6.28 (1H, a doublet of triplets).

Hydrogenation of 15

Unsaturated ketone **15** (82 mg) was hydrogenated over 8 mg of platinum oxide in 10 ml methanol. When 1 equiv. of hydrogen was taken up, the solution was filtered and the solvent removed under reduced pressure at room temperature to give 78 mg of essentially pure product **16** (as analyzed by vpc): ir (CCl_4): 883, 1122, 1313, 1368, 1387, 1430, 1450, 1468, 1712 (C=O stretch) cm^{-1}; nmr (CCl_4) δ: 0.82 (3H, s), 0.9 (3H), 1.25–2.6 (12H, m).

Hydrogenation of anti-*2-Isobutylidenecyclohexanone*

This compound was hydrogenated as ketone **15** and gave **16** in quantitative yield. The ir and nmr spectra of this compound were identical with those of a sample prepared by hydrogenation of **15**.

Photolysis in CH_3OD

Solutions of spiroketones **2–6** in CH_3OD (distributed by EM Reagent Division, Brinkmann Instruments, Inc., Westbury, NY) were prepared and irradiated under identical conditions. Enones **8**, **9**, **13**, and **15** were isolated by vpc and the extent of deuterium incorporation determined by the relative intensities of M + 1 and M peaks in their mass spectra (correcting for M − 1 fragmentation). Reinjection of deuterated **13** and **15** through the vpc showed no decrease of deuterium. In the same runs ketones **3**, **4**, and **6** were isolated and shown not to be enriched with deuterium. Nondeuterated ketones **13** and **15** were subjected to identical irradiation conditions and shown not to undergo deuterium exchange in CH_3OD.

Relative Rate Studies

Methanolic solutions (10 ml, 0.05 m) in standard quartz tubes were placed in a merry-go-round apparatus and irradiated with the same photochemical assembly described above. Samples were withdrawn after certain time intervals and the starting ketone concentration monitored by vpc.

1. W. G. Dauben, L. Schutte, G. W. Shaffer, and R. B. Gagosian. J. Am. Chem. Soc. **95**, 468 (1973).
2. W. G. Dauben, G. W. Shaffer, and E. J. Deviny. J. Am. Chem. Soc. **92**, 6273 (1970).
3. J. K. Crandall and R. J. Seidewald. J. Org. Chem. **35**, 697 (1970).
4. W. G. Dauben, L. Schutte, and R. E. Wolf. J. Org. Chem. **34**, 1849 (1969).
5. R. M. Roberts, R. G. Landolt, R. N. Greene, and E. W. Heyer. J. Am. Chem. Soc. **89**, 1404 (1967).
6. W. G. Dauben and G. W. Schaffer. J. Org. Chem. **34**, 2301 (1969).
7. D. E. McGreer and J. W. McKinley. Can. J. Chem. **51**, 1487 (1973).
8. D. G. Marsh, J. N. Pitts, Jr., K. Schaffner, and A. Tuinman. J. Am. Chem. Soc. **93**, 333 (1971).
9. J. A. Al Khafaji and M. Shanshal. Z. Naturforsch. **30a**, 1023 (1975).
10. E. Lee-Ruff and P. Khazanie. Can. J. Chem. **53**, 1708 (1975).
11. E. D. Bergman and R. Ikan. J. Am. Chem. Soc. **78**, 1482 (1956).
12. N. J. Turro and D. S. Weiss. J. Am. Chem. Soc. **90**, 2185 (1968).
13. J. C. Dalton, K. Dawes, N. J. Turro, D. S. Weiss, J. A. Barltrop, and J. D. Coyle. J. Am. Chem. Soc. **93**, 7213 (1971).
14. D. R. Morton, E. Lee-Ruff, R. M. Southam, and N. J. Turro. J. Am. Chem. Soc. **92**, 4349 (1970).
15. E. Lee-Ruff, N. J. Turro, P. Amice, and J. M. Conia. Can. J. Chem. **47**, 2798 (1969).
16. P. G. Khazanie and E. Lee-Ruff. Can. J. Chem. **51**, 3173 (1973).
17. P. Khazanie. Ph.D. Thesis, York University, Toronto, Ont. 1974.
18. G. Lardelli, V. Lamberti, W. T. Weller, and A. P. de Jonge. Recl. Trav. Chim. Pays-Bas, **86**, 481 (1967).
19. L. Birkofer, S. M. Kim, and H. D. Engels. Chem. Ber. **95**, 1495 (1962).
20. G. Stork, A. Brizzolara, H. Laudesuman, J. Szmuszkovicz, and R. Terrell. J. Am. Chem. Soc. **85**, 207 (1963).
21. N. Barbulescu and A. Quilco. Gazz. Chim. Ital. **91**, 326 (1961).

Competitive thermal and photochemical processes in cyclopropylketone rearrangements. II. Thermal isomerization of spiro[*n*.2]alkan-2-ones

PRABHAKER G. KHAZANIE AND EDWARD LEE-RUFF

Department of Chemistry, York University, Downsview, Ont., Canada M3J 1P3

Received July 22, 1977

PRABHAKER G. KHAZANIE and EDWARD LEE-RUFF. Can. J. Chem. **56**, 808 (1978).

Conformationally-rigid methyl-substituted cyclopropyl ketones with a suitably disposed γ-hydrogen undergo thermal type II reactions efficiently. Comparison of yields of these rearrangements with their photochemical analogs suggest that photochemical type II reactions arise from excited vibrational states. In the absence of a suitably disposed γ-hydrogen, and if strain factors permit, such systems undergo oxovinylcyclopropane to dihydrofuran rearrangement. The inertness of these systems to undergo such thermal rearrangement increased on going from cyclohexanone to the cyclopentanone series.

PRABHAKER G. KHAZANIE et EDWARD LEE-RUFF. Can. J. Chem. **56**, 808 (1978).

Les cyclopropyl-cétones conformationnellement rigides substitués par des groupes méthyles et comportant un hydrogène en γ orienté convenablement subissent des réactions thermiques du type II d'une manière efficace. Une comparaison des rendements de telles transpositions avec celles obtenues dans les réactions analogues photochimiques suggère que les réactions photochimiques de type II proviennent d'état vibrationnel excité. Lorsqu'il n'y a pas d'hydrogène γ orienté convenablement et si les facteurs stériques le permettent, de tels systèmes subissent la transposition oxovinylcyclopropane → dihydrofuranne. L'inertie des transpositions thermique augmente lorsque l'on passe des dérivés de la cyclohexanone à ceux de la cyclopentanone.

[Traduit par le journal]

Can. J. Chem. Downloaded from www.nrcresearchpress.com by 210.87.254.105 on 09/05/12
For personal use only.

Cyclopropanes and ethylenes exhibit similar electronic properties as far as affecting the chemical nature of neighbouring activated sites. Both show π-releasing and σ-electron-withdrawing behaviour in solvolyses of conjugated sulphonate esters (1, 2). Furthermore the stereochemical orientation of the conjugating group relative to that of the carbonium ion is critical in establishing the amount of π-electron release by these groups. We have shown that ring size and cyclopropyl substitution in spiro[*n*.2]alkan-2-ones play an important role in the photochemistry of cyclopropyl ketones (3). The more rigidly confined the cyclopropyl group is to a bisected geometry with respect to the carbonyl group the greater the inertness towards photochemical degradation. The same pattern is observed in α,β-unsaturated ketones, the decrease in reactivity of such systems attributed to a change in the nature of the lowest excited state (from n-π* to π-π*) and competitive nonchemical deactivation processes (16, 17). The similarity of photoproducts from the spiro[*n*.2]alkan-2-ones with products obtained from the thermal isomerization of acyclic cyclopropylketones prompted us to investigate the thermal reactions of these to evaluate the extent to which excited vibrational states are possibly involved in these photochemical transformations. In addition we were also interested if such 'resonance stabilization' would be reflected in their ground state reactions.

In 1968, Dauben reported (10) that the irradiation of bicyclo[4.1.0]heptan-2-one (**1**) resulted in a 31% conversion to cyclohexanone **2**. The stereoselectivity

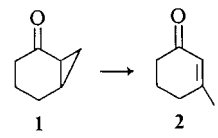

1 **2**

of the cyclopropane ring opening was attributed to the bond-weakening of the bond with optimum overlap with respect to the carbonyl group in the excited state. We report that such stereoselectivity of cyclopropane ring opening is also a ground state phenomenon and that the same transformation of **1** to **2** occurs thermally (270°C)[1] with greater efficiency (78%)[2]. Thus, photochemical transformations of cyclopropyl ketones involving cyclopropane ring opening may involve radiationless deactivation to vibrationally excited states. In the first part of this study (3) we reported the results of the photochemistry of a series of spiro[*n*.2]alkan-2-ones. In this paper we report on the thermal labilities of the same series.

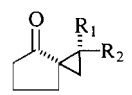

3 $R_1 = R_2 = H$
4 $R_1 = CH_3; R_2 = H$
5 $R_1 = H; R_2 = CH_3$
6 $R_1 = R_2 = CH_3$

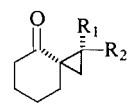

7 $R_1 = R_2 = H$
8 $R_1 = CH_3; R_2 = H$
9 $R_1 = H; R_2 = CH_3$
10 $R_1 = R_2 = CH_3$

[1]All pyrolyses were carried out at the indicated temperatures with neat samples.

[2]Percentage yields are based on unrecovered starting material.

Can. J. Chem. Downloaded from www.nrcresearchpress.com by 210.87.254.105 on 09/05/12
For personal use only.

Ketones **3** and **7** were stable up to 400°C above which both compounds started to char. In the case of **7** a 32% yield of *o*-ethylphenol was isolated and characterized by comparison with an authentic sample. Pyrolysis of **4** at 260°C gave a 90% conversion to 2-allylcyclopentanone (**11**) and a trace of

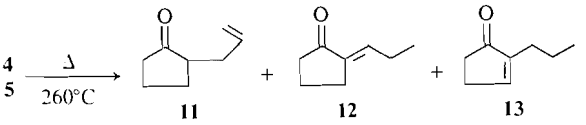

conjugated ketone **12**. Similarly the *anti*-isomer **5** gave **11** as the major product (71%) along with a significantly larger amount of **12** (16%) and cyclopentenone **13** (9%). All products were stable under the pyrolysis conditions. The structures of the products were established by comparison with authentic samples.

Ketone **6** was found to be most thermally labile in this series and was transformed in 87% yield to enone **14**. In addition to **14**, small amounts of **15** and **16**

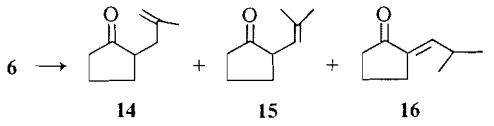

were also detected. Upon prolonged reaction times the amounts of **15** and **16** increased at the expense of **14**. In a separate experiment, **14** was shown to be thermally transformed to a mixture of **15** and **16**, and **15** isomerized to **16** and **14** under identical conditions. The structure of enone **16** was assigned unequivocally by comparison with the product obtained from the condensation of cyclopentanone and isobutyraldehyde. The identity of enones **14** and **15** was elucidated from their spectral data and comparison with products obtained from the photolysis of **6** (3).

The series of spiro[5.2]octanones **8–10** was shown to be more thermally labile than the corresponding spiro[4.2]heptanones and significant oxovinylcyclopropane to dihydrofuran rearrangements were observed. Ketone **8** was transformed to allylcyclohexanone (**17**) in 82% yield along with a 10% (1:1) mixture of the dihydrofurans **18** and **19**. The isomeric

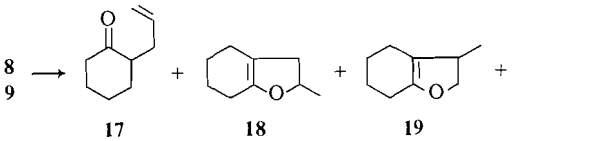

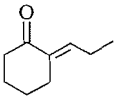

anti-isomer **9** gave the same mixture; however, the amount of dihydrofurans **18** and **19** (54%) exceeded that of 2-allylcyclohexanone (**17**) (30%). In addition a small amount (8%) of 2-propylidenecyclohexanone (**20**) was isolated from the reaction mixture. Under the same conditions all pyrolysis products were found to be stable and the structures of these were established by independent syntheses (see Experimental).

The thermal rearrangement of **10** at 200°C proceeded to give a mixture of isomers **21**, **22**, **23**, and **24**. The major products were **21** (84%) and **24** (12%),

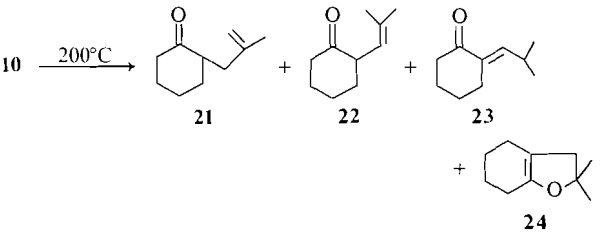

whereas enones **22** and **23** were formed as secondary products from subsequent thermal rearrangement of **21**.

Discussion

Comparison of the photochemical and pyrolysis data indicates a close similarity in the yields of type II products for the spiro[5.2]octan-2-ones (Table 1), however the extent of such reactions in the corresponding spiro[4.2]heptan-2-ones was significantly greater in the thermolysis of these as compared to their photolyses. The absence of any type II products in the photolysis of **4** and **5** and the absence of deuterium incorporation of enone **14** from the photolysis of **6** has been attributed to the inability of such systems to obtain the stereochemical conformation required for such type II reactions. The propensity of type II products in the thermolysis of **4** to **6** suggest that 'type II' products can arise from pathways other than cyclic six-centered transition states and concerted dienol **25** formation. A 1,3 diradical of type **26** may lead to the same products and would not have to meet the same stereochemical

TABLE 1. Thermal and photoproducts from spiro[*n*.2]alkan-2-ones

Compounds	% type II products *hν*	% type II products Δ	% DHF's from Δ
4	0	90	0
5	0	71	0
6	76	87	0
8	72	82	10
9	30	30	54
10	85	84	12

NOTE: DHF, dihydrofurans; *hν*, photolysis; Δ, thermolysis.

Can. J. Chem. Downloaded from www.nrcresearchpress.com by 210.87.254.105 on 09/05/12
For personal use only.

constraints as the type II reaction. The large amount of 2-allylcyclopentanone **11** from the thermolysis of the *anti*-spiroketone **5** bears on this point. Based on our data one cannot, however, rule out the occurrence of an enol intermediate in these thermal conversions.

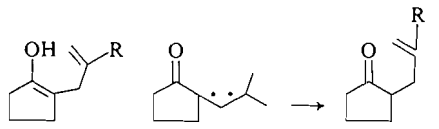

25 **26** **11** R = H; **14** R = CH_3

Another significant deactivation process of cyclopropyl carbonyl ring-opening reaction is formation of dihydrofurans (DHF). One such thermal reaction has been reported by McGreer and McKinley (4) and their studies support a diradical mechanism.

It is of interest to note that the yields of dihydrofurans show an increase of from 10% for ketone **8** to 54% for ketone **9**. If a 1,3 diradical were common to both **8** and **9** and that DHF's as well as 2-allylcyclohexanone (**17**) were derived from it then the relative yields of enone **17** to DHF's would be expected to be identical in both cases. The larger amount of 2-allylcyclohexanone (**17**) from *syn*-ketone **8** *suggests that most of 17 is derived from a concerted mechanism.* Furthermore if the 30:54 dichotomy of 2-allylcyclohexanone to DHF is used as a measure of 1,3 diradical present the amount of **17** obtained from *syn*-ketone **8** derived from a diradical is calculated as 6%. It follows then, where a γ-hydrogen is predisposed for a type II reaction to be possible such thermal analogs follow a concerted mechanism. The similarity of product distribution from ketone **10** supports this concept.

The absence of DHF's in the spiro[4.2]heptanones can be attributed to the strain of such 5,5 fused bicyclics. Attempts to prepare these by methods similar to the preparation of **18**, **19**, and **24** were unsuccessful.

Relative rates of decomposition of these ketones were determined to follow the order **10** > **6** ~ **8** > **9** ~ **4** > **5** ≫ **7** > **3**. From these results it is apparent that in spite of the larger strain in cyclopentanones (5), the spiro[5.2]octan-2-ones are more labile than the corresponding spiro[4.2]heptan-2-ones. This can be attributed to the greater coplanarity of the cyclopentanone ring compared to cyclohexanone (6) and the possibility of the former to adopt a bisected conformation of the cyclopropylcarbonyl group permitting greater resonance stabilization.

Experimental

Melting points were uncorrected. The ir spectra were recorded with a Unicam SP 1000 instrument. The nmr spectra were measured on Varian A-60, HA-100, and EM-360 spectrometers. Samples were dissolved in CCl_4 or $CDCl_3$ solvents using TMS as the internal standard. Vapour phase chromatographic analyses and collections were performed on a Varian Aerograph Series 1700 instrument using the following column: a 6 ft glass column (0.25 in. od) packed with 6% SE-30 + 4% QF-1 on Chromosorb W AW, DMCS treated. Microanalyses were performed by Gygli Microanalytical Labs, Toronto. All of the starting materials were prepared according to procedures described in refs. 7–9.

General Thermolyses Procedures

Thermolyses were conducted in a muffle furnace with operating temperatures of 200–500°C. The temperature gauge of the oven was calibrated using a thermocouple. Samples were placed in Pyrex tubes, 1 cm diameter, 1 mm thick, and 6–8 cm long. The samples were degassed by five to six freeze-pump-thaw cycles at 10^{-3} Torr pressure, sealed, wrapped in an aluminum foil, and heated for varying lengths of time. The ampules were cooled, opened, and the mixtures analyzed by tlc, vpc, ir, nmr, and mass spectroscopy. The products were then confirmed by their independent synthesis. Known amounts of authentic samples were injected in vpc and the peaks compared with those of the product mixtures. The percentage yield of the products was thus calculated. Negligible amounts of high boiling products or polymers were observed at temperatures below 260°C but above this temperature polymer formation increased substantially. Polymer formation also increased if the sample tubes were not properly degassed.

Pyrolysis of Bicyclo[4.1.0]heptan-2-one (1)

A sample of the title ketone (100 mg) was heated at 270°C for 45 min. The pyrolysate was subjected to preparative vpc which resulted in separations of two volatile products. The more volatile material (36 mg) was identified as 3-methyl-2-cyclohexenone (**2**) based on the spectral data: ir (neat): 1679, 1640, 1380; nmr (CCl_4) δ: 1.60–2.50 (9 H, m with broad singlet δ 1.92), 5.70 (1 H, q); *m/e* 110. This was identical to a commercial sample (Aldrich). The less volatile material was identified as starting ketone **1**. A second pyrolysis was carried out at the same temperature for 95 min and the product yields tabulated (Table 2).

Attempted Pyrolysis of Spiro[2.4]heptan-2-one (3) at Different Temperatures

Four ampules, each containing **3** (100 mg) were thermolyzed at different temperatures for different time intervals. The results are summarized in Table 2. Compound **3**, unlike other

TABLE 2. Thermolyses of ketones **1**, **3**, and **7**

Compound	Temperature of thermolysis (°C)	Time of thermolysis (min)	% product	% unreacted starting material
1	270	45	36	57
	270	95	49	21
3	260	150	—	100
	350	90	—	100
	400	15	—	88
	400	90	Charred	0
7	200	150	—	100
	300	150	—	100
	350	60	—	100
	400	90	32	7
	500	90	Charred	0

Can. J. Chem. Downloaded from www.nrcresearchpress.com by 210.87.254.105 on 09/05/12
For personal use only.

members of the series was very stable up to 360°C and any attempt to carry out thermolysis at higher temperatures resulted in complete charring of the starting material.

Pyrolysis of Spiro[2.5]octan-2-one (7) at Different Temperatures

Five ampules, each containing **7** (125 mg) were degassed and thermolyzed between 200–500°C for different time intervals. The results are summarized in Table 2. The compound was stable up to 360°C for 1 h. However, unlike compound **3**, **7** pyrolyzed at 400°C during 90 mins to give 2-ethylphenol (32%): ir (CCl_4): 1112, 1170, 1325, 1455, 3020, 3630 cm^{-1}; nmr (CCl_4) δ: 1.2 (3H, t, J = 7 Hz), 2.72 (2H, q, J = 7 Hz), 4.56 (1H, OH, disappeared with D_2O), 6.5–7.2 (4H, m); starting ketone **7** (7%); nine minor peaks; and polymeric material. This phenol was synthesized from phenol and absolute ethanol in the presence of anhydrous aluminum chloride. The ir and nmr spectra of this compound were identical with those of the sample obtained by thermolysis of **7**.

Thermolysis of syn-*6-Methylspiro[2.4]heptan-2-one (4) at 260°C*

A sample of the spiroketone **4** (100 mg) was heated at 260°C for different periods of time; vpc analysis (He flow rate 50 cc/min, 100°C) of the sample which was thermolyzed for 15 min, showed 24% conversion to 2-allylcyclopentanone **11** and 68% of the starting ketone (retention time 5 min 5 s). Upon heating for an additional hour, compound **4** gave a mixture containing **11** (90%), **12** (1%), and **5** (4%) as analyzed by vpc and ir. The results are summarized in Table 3. Structural identification for **11** was based on its spectral data: ir (CCl_4): 923, 1160, 1408, 1442, 1455, 1640, 1745, 2960, 3080 cm^{-1}; nmr (CCl_4) δ: 1.3–2.7 (9H, m), 4.8–5.18 (2H, m), 5.42–6.1 (1H, m). An identical material was synthesized (see below) by an alternate method. Compound **12** was identical in all respects with a product obtained from the photolysis of **4** (3).

Thermolysis of anti-*6-Methylspiro[2.4]heptan-2-one (5) at 260°C*

A sample of spiroketone **5** (100 mg) was heated at 260°C initially for 15 min; vpc monitoring (He flow rate 50 cc/min, 100°C) of the thermolyzed sample showed only 8% conversion to 2-allylcyclopentanone (**11**) (retention time 5 min 48 s) and starting ketone (89%, retention time 7 min 5 s). Upon heating for an additional hour, compound **5** gave a mixture containing **11** (55%), *anti*-2-propylidenecyclopentanone (**12**) (12%, retention time 8 min 35 s), ketone **13** (retention time 9 min 20 s), and the starting material (23%). The results are summarized in Table 3. Compounds **11**, **12**, and **13** were collected on vpc and their spectra compared with those obtained by an alternate synthesis (see below).

Preparation of 2-Allylcyclopentanone (11)

A solution of sodium ethoxide (0.80 g Na, 30 ml absolute ethanol) was cooled to 5°C. To this, ethyl 2-cyclopentanonecarboxylate containing 45% methyl ester (5.3 g, 0.035 mol) was added dropwise with stirring over 15 min. The solution was stirred for an additional 15 min, allyl bromide (5 g, 0.042 mol) was added and heated to boiling for 30 min. The solution was cooled, diluted with 100 ml water, and the ester extracted with three 75-ml portions of ether. The combined ether extracts were dried over anhydrous magnesium sulfate and ether removed under reduced pressure. The residue after distillation gave 4.9 g (74%) of allyl derivative of ethyl 2-cyclopentanonecarboxylate, bp 80°C/0.1 Torr; nmr (CCl_4) δ: 1.22 (3H, t, 7 Hz), 1.67–2.82 (8H, m), 3.67 (3H, s), 4.1 (2H, q, J = 7 Hz), 4.83–5.25 (2H, m), 5.32–6.1 (1H, m). The allyl ester was refluxed with 5% aqueous KOH (50 ml) between 80–90°C for 12 h to give 2-allylcyclopentanone in 27% yield, bp 45°C/1.4 Torr (lit. (11) bp 55–57°C/18 Torr); ir (CCl_4): 923, 1160, 1408, 1442, 1445, 1640, 1745, 2960, 3080 cm^{-1}; nmr (CCl_4) δ: 1.3–2.7 (9H, m), 4.8–5.18 (2H, m), 5.42–6.1 (1H, m).

*Preparation of 2-*n*-Propyl-2-cyclopentenone (13)*

A mixture of *anti*-2-propylidenecyclopentanone (1.0 g) (3) and polyphosphoric acid (1:1 mixture of P_2O_5 and H_3PO_4 aged for 10 h at 100°C) was heated at 100°C for 30 min in a flask equipped with a condenser. Water (7 ml) was added to the cooled mixture and 50 ml ether was added for extraction. The ether layer was washed with brine, dried over anhydrous magnesium sulfate, and evaporated to give 0.85 g of a crude liquid which was purified by distillation, bp 59–60°C/1.3 Torr; yield, 0.51 g (51%); ir (CCl_4): 930, 1060, 1105, 1355, 1380, 1405, 1455, 1630, 1715, 2960, 3040 cm^{-1}; nmr (CCl_4) δ: 0.92 (3H, t, J = 7 Hz), 1.12–2.70 (8H, m), 7.2 (1H, m); M^+ m/e 124.

Thermolysis of 6,6-Dimethylspiro[2.4]heptan-2-one (6) at 200°C

Samples of spiroketone **6** (200 mg of each) in two sealed ampules were placed in an oven at 200°C. The tubes were removed from the oven after 17 and 37 min, respectively, and cooled. After opening each tube, the contents were analyzed by vpc (He flow 48 cc/min, 100°C); compound **6** was unstable above 120°C column temperature and a pure sample when injected in vpc at 128°C showed about 3% conversion to **14**. The first compound to elute was identified as **14** (71%, retention time 11 min 40 s) by comparison of its spectra with those of the sample obtained via photolysis of **6** (3). The second compound (4%, retention time 13 min 55 s) was identified as **15** by its characteristic spectral properties: ir (CCl_4): 955, 1380, 1408, 1455, 1745, 2960 cm^{-1}; nmr (CCl_4) δ: 1.56–3.0 (13H, m, a doublet centered at 1.68, J = 5 Hz), 4.88 (1H, m). This compound was hydrogenated to the previously characterized 2-isobutylcyclopentanone (3).

The contents of the second ampule (37 min pyrolysis) under the vpc conditions mentioned above showed three peaks. The peak due to **14** decreased in area, that due to **15** increased in area (30%) and a new peak due to compound **16** (11%, retention time 16 min 30 s) appeared. The spectra of **16** were identical with those of a synthesized sample (3).

Compounds **15** and **16** were suspected to be secondary products of thermolysis, and hence **14**, **15** were thermolyzed separately under the above conditions.

Thermal Rearrangement of 14

Thermolysis of 50 mg of compound **14** was carried out as in the case of spiroketone **6** at 200°C for 37 min. By vpc analysis the product mixture was found to consist of starting ketone **14** (27%), **15** (41%), **16** (28%), and few other minor products totalling 4%. These ketones displayed ir and nmr spectra identical with those of the products obtained by the thermolysis of **6**. The thermolysis results are summarized in Table 4.

Thermal Rearrangement of 15

A 60 mg sample of pure **15** was thermolyzed as above at

TABLE 3. Pyrolysis of ketones **4** and **5** at 260°C

Compound	Time of thermolysis (min)	% product			% unreacted starting material
		11	**12**	**13**	
4	15	24	—	—	68
	75	90	1	—	(4% **5**)
5	15	8	—	—	89
	75	55	12	7	23

Can. J. Chem. Downloaded from www.nrcresearchpress.com by 210.87.254.105 on 09/05/12
For personal use only.

TABLE 4. Thermolyses of ketones **6**, **14**, **15**, and **16** at 200°C

Compound	Time of thermolysis (min)	% product **14**	% product **15**	% product **16**	% starting material
6	17	71	4	—	18
	37	50	30	11	1
14	37	27	41	28	27 (**14**)
15	37	8	46	40	46 (**15**)
16	37	—	—	100	Unchanged

200°C for 37 min. The product mixture was separated by vpc. The results are summarized in Table 4. Enones **14** and **16** were identified by their spectral properties and by their comparison with the spectra of the products obtained in the pyrolysate mixture of **6**.

Attempted Thermal Rearrangement of ***16***

In an attempt to check if **16** isomerized to **14** and/or **15**, a sample of **16** (49 mg) was thermolyzed under the above conditions. The product mixture when analyzed by vpc showed unreacted starting material.

Thermolysis of syn-*7-Methylspiro*[*2.5*]*octan-2-one* (***8***) *at 260°C*

The title compound when pyrolyzed at 260°C for 45 min gave 82% **17**, 5% **18**, 4% **19**, and three other minor products totalling 9% by preparative vpc. These results are summarized in Table 5. The ir and nmr spectra of the ketone and the enol ethers were identical with those of synthesized samples (see below) (12, 13).

Synthesis of 3-Methyl-2,3,4,5,6,7-hexahydrobenzofuran (***19***)

The title compound was synthesized by the following steps.

A. Preparation of Ethyl 2-(2-Cyclohexanone)propionate

To a refluxing solution of 1-(1′-cyclohexenyl)pyrrolidene (14) (7.555 g, 0.05 mol) in 75 ml benzene, ethyl α-bromopropionate (10.86 g, 0.06 mol) was added over a period of 1 h. Upon refluxing for 2 h, the solution was cooled, and excess bromoester and solvent removed under reduced pressure. The residue was then refluxed in 50 ml methanol and 10 ml water for 1 h. The solution was concentrated once again, extracted with ether, and worked up in the usual way to give 1.8 g (18%) of ethyl 2-(2-cyclohexanone)propionate: ir (neat): 1050, 1178, 1253, 1312, 1340, 1378, 1450, 1710 (C=O stretch of the ring), 1730 (C=O stretch of the ester); nmr (CCl_4) δ: 0.9–2.85 (16H, m, with a triplet centered at 1.21, J = 7 Hz), 4.06 (2H, q, J = 7 Hz). This reaction would require more than 2 h reflux period since a lot of cyclohexanone was recovered.

B. Ethylene Ketal of Ethyl 2-(2-Cyclohexanone)propionate

A solution of ethyl 2-(2-cyclohexanone)propionate (*A*) 0.9 g, 0.0045 mol), ethylene glycol (0.28 g, 0.0045 mol), and *p*-toluenesulfonic acid (8 mg) in 25 ml dry benzene was refluxed using a Dean Stark trap until the theoretical amount of water had been collected in the trap. The cooled solution was washed with 7% sodium bicarbonate, then with brine, dried over anhydrous sodium sulfate and the solvent removed under reduced pressure. The compound thus obtained was sufficiently pure to be used in the next step: ir (neat): 808, 865, 927, 950, 1040, 1098, 1170, 1258, 1333, 1376, 1446, 1730 (ester carbonyl); nmr (CCl_4) δ: 0.92–2.82 (16H, m, with a triplet centered at 1.2, J = 7 Hz, and a doublet at 1.05, J = 7 Hz), 3.85 (4H, s), 4.05 (2H, q, J = 7 Hz).

C. Preparation of Ketal Alcohol

To a stirred slurry of lithium aluminum hydride (0.228 g, 0.006 mol) in 20 ml of anhydrous ether, was added the ketal ester *B* (1 g, 0.0041 mol) in 10 ml ether over a period of 20 min. After the addition was complete, the solution was refluxed for 1 h, the work-up gave 0.7 g (85%) of the ketal alcohol: ir (neat): 924, 950, 1030, 1096, 1165, 1220, 1260, 1280, 1340, 1352, 1445, 2935, 3430 cm^{-1}; nmr (CCl_4) δ: 0.83 (3H, d, J = 7 Hz), 1.05–2.2 (10H, m), 3.1–3.8 (3H, m), 3.9 (4H, s).

D. Hydrolysis of the Ketal Alcohol C

Compound *C* (0.7 g, 0.0035 mol) was hydrolyzed by heating for 1 h on an oil bath with 15 ml acetone and 5 ml water containing 15 mg of *p*-toluenesulfonic acid. Work-up of the reaction mixture gave 0.52 g of hemiketal in equilibrium with a minor fraction of γ-hydroxyketone: ir (neat): 810, 950, 1015, 1090, 1260, 1448, 1720 (weak), 3410 cm^{-1}; nmr (CCl_4) δ: 0.7–2.9 (13H, m, with four sharp peaks at 0.78, 0.88, 0.98, and 1.1), 3.05–3.6 (2H, m), 3.3–3.7 (1H, m).

Preparation of 3-Methyl-2,3,4,5,6,7-hexahydrobenzofuran (***19***)

The hemiketal *D* was heated to 130°C and distilled between 35–40 Torr to give the title compound in quantitative yield: ir (neat): 873, 950, 968, 1083, 1140, 1205, 1283, 1388, 1450, 1710 (enol ether C=C), 2880, 2940 cm^{-1}; nmr (CCl_4) δ: 0.9–2.33 (11H, m, with a doublet centered at 1), 2.5–3.17 (1H, m), 4.22 (1H, q, J = 9 Hz), 3.58 (1H, q, J = 9 Hz); M^+ *m/e* 138. These spectra were identical with those of the compound obtained by pyrolysis of spiroketone **8**.

Preparation of 2-Methyl-2,3,4,5,6,7-hexahydrobenzofuran (***18***)

This compound was prepared as described in the literature (13).

Thermolysis of anti-*7-Methylspiro*[*2.5*]*octan-2-one* (***9***) *at 260°C*

A sample of 150 mg of compound **9** was thermolyzed at 260°C for 45 min; vpc analysis (55 cc/min, 100°C) of the thermolyzed mixture showed 28% 2-allylcyclohexanone (**17**) (retention time 10 min 45 s), 9% *anti*-2-propylidenecyclohexanone (**20**) (retention time 20 min), 28% 2-methyl-2,3,4,5,6,7-hexahydrobenzofuran (**18**) (retention time 5 min, 55 s), 23% 3-methyl-2,3,4,5,6,7-hexahydrobenzofuran (**19**) (retention time 6 min, 37 s), 6% starting ketone (12 min, 43 s), and small amounts of volatile fractions. These results are summarized in Table 5. The nmr and ir spectra of ketone **17** and the enol ethers were identical with those of the synthesized samples. The structures of ketone **20** was based on comparison of this sample with a sample synthesized by an alternate route (see below).

Preparation of anti-*2-Propylidenecyclohexanone* (***20***)

Following the procedure described for the preparation of 2-isobutylidenecyclohexanone (3), compound **20** was obtained in 40% yield, bp 56–57°C/1.6 Torr (lit. (15) bp 80–82°C/4 Torr): ir (neat): 820, 1145, 1305, 1615, 1690, 2870, 2940 cm^{-1}; nmr (CCl_4) δ: 1.04 (3H, t, J = 7 Hz), 1.6–2.67 (10H, m), 6.28–6.7 (1H, m).

Thermolysis of 7,7-Dimethylspiro[*2.5*]*octan-2-one* ***10***

Three sealed ampules each containing 240 mg of **10** were placed in an oven at 200°C. The ampules were removed from

TABLE 5. Thermolyses of ketones **8** and **9** at 260°C

Compound	Time of thermolysis (min)	% product **17**	% product **20**	% product **18**	% product **19**	% starting material
8	45	82	—	5	4	0
9	12	7	2	6	5	72 (3% **8**)
	45	28	8	28	23	6

Can. J. Chem. Downloaded from www.nrcresearchpress.com by 210.87.254.105 on 09/05/12
For personal use only.

TABLE 6. Thermolyses of ketones **10**, **21**, and **22** at 200°C

Compound	Time of thermolysis (min)	% product				% starting material
		21	**22**	**23**	**24**	
10	17	80	—	—	11	5
	60	74	8	—	12	0
	150	22	37	14	12	0
21	150	17	52	23	—	17 (**21**)
22	150	5	35	48	—	35 (**22**)
23	150	—	—	—	—	Unchanged

the oven after 17, 60, and 150 min; vpc analysis (He flow 50 cc/min, 85°C) of the 17-min thermolyzed sample showed three peaks. The major component (80%, retention time 18 min 15 s) was identified as **21** by its characteristic spectral data. These spectra were identical with those of the product obtained via photolysis of **10** (3). The minor product (11%, retention time 5 min 30 s) was identified as 2,2-dimethyl-2,3,4,5,6,7-hexahydrobenzofuran (**24**) and had spectral properties identical with those of the synthesized sample (14).

Ketone **10** on thermolysis for 60 min, showed in addition to **21** and **24**, a new compound **22** (8%, retention time 22 min 11 s). The structure of **22** was based on its spectral data: ir (CCl_4): 1130, 1305, 1380, 1450, 1715 cm^{-1}; nmr (CCl_4) δ: 1.5–2.5 (14H, m, with two singlets at 1.58 and 1.73), 3.05 (1H, m), 5.25 (1H, broad doublet, $J = 8$ Hz). The structure of **22** was confirmed by hydrogenation to the known 2-isobutylcyclohexanone (3).

The sample which was thermolyzed for 150 min, showed in addition to **21**, **24**, and **22**, another new compound **23** (14%, retention time 26 min 42 s), the structure of which was established by independent synthesis. Compounds **22** and **23** were suspected to be secondary thermal products since decrease in the size of the peak due to **21** was observed.

*Thermal Isomerization of **21** at 200°C*

A sample of 42 mg of **21** was heated at 200°C for 2½ hours; vpc of the product mixture showed **22** (52%), **23** (23%), starting ketone **21** (17%), and several other unidentified fractions totalling 8%. The nmr and ir spectra of these ketones were identical with those of the products obtained by the thermolysis of **10**. The thermolysis results are summarized in Table 6.

*Thermal Isomerization of **22** at 200°C*

A sample of 53 mg of **22** was thermolyzed as before at 200°C for 2½ h; vpc analysis of the mixture showed **21** (5%), starting ketone **22** (35%), **23** (48%), and other unidentified products totalling 12%. The results are summarized in Table 6.

*Attempted Thermal Rearrangement of **23** at 200°C*

In an attempt to check if **23** isomerized thermally to **21** and/or **22**, a sample of **23** (120 mg) was thermolyzed at 200°C for 2½ h. The vpc analysis of the product mixture showed 94% of the starting ketone and no other peak.

1. T. TSUJI, I. MORITANI, and S. NISHIDA. Bull. Chem. Soc. Jpn. **40**, 2338 (1967).
2. B. R. REE and J. C. MARTIN. J. Am. Chem. Soc. **92**, 1660 (1970).
3. E. LEE-RUFF and P. G. KHAZANIE. Can. J. Chem. This issue.
4. D. E. MCGREER and J. W. MCKINLEY. Can. J. Chem. **51**, 1487 (1973).
5. G. WOLF. Helv. Chim. Acta, **55**, 1446 (1972).
6. H. J. KOEHLER and M. SCHOLZ. J. Prakt. Chem. **312**, 165 (1970).
7. E. LEE-RUFF and P. G. KHAZANIE. Can. J. Chem. **53**, 1708 (1975).
8. W. G. DAUBEN and G. H. BEREZIN. J. Am. Chem. Soc. **89**, 3449 (1967).
9. P. G. KHAZANIE. Ph.D. Thesis, York University, Toronto, Ont. 1974.
10. W. G. DAUBEN, G. W. SHAFFER, and E. J. DEVINY. J. Am. Chem. Soc. **92**, 6273 (1970).
11. G. J. KARABATSOS and N. HSI. J. Am. Chem. Soc. **87**, 2864 (1965).
12. G. STORK, A. BRIZZOLARA, H. LANDESMAN, J. SZMUSZKOVICZ, and R. TERRELL. J. Am. Chem. Soc. **85**, 207 (1963).
13. W. E. HARVEY and D. S. TARBELL. J. Org. Chem. **32**, 1579 (1967).
14. A. SEGRE, R. VITERBO, and G. PARISI. J. Am. Chem. Soc. **79**, 3503 (1957).
15. N. BARBULESCU and A. QUILCO. Gazz. Chim. Ital. **91**, 326 (1961).
16. J. J. MCCULLOUGH, H. OHORODNYK, and D. P. SANTRY. Chem. Commun. 570 (1969).
17. B. FURTH, J. P. MORIZUR, and J. KOSSANYI. Compt. Rend. **271C**, 691 (1970).

Reduction of Co(II) with $NaBH_4$ in the presence of triphenylphosphine

D. G. HOLAH, A. N. HUGHES, B. C. HUI, AND C. T. KAN

Department of Chemistry, Lakehead University, Thunder Bay, Ont., Canada P7B 5E1

Received July 15, 1977

D. G. HOLAH, A. N. HUGHES, B. C. HUI, and C. T. KAN. Can. J. Chem. **56**, 814 (1978).

The reactions of $NaBH_4$ with Co(II) compounds in the presence of triphenylphosphine (P) have been studied in ethanol and benzene solutions. The conditions for the isolation of the Co(I) complexes, $Co(BH_4)P_n$ (n = 2, 3), have been established and the structures of these species are discussed in the light of various physical measurements.

D. G. HOLAH, A. N. HUGHES, B. C. HUI et C. T. KAN. Can. J. Chem. **56**, 814 (1978).

On a étudié les réactions de $NaBH_4$ avec les composés Co(II) en présence de triphénylphosphine (P) dans des solutions dans l'éthanol et le benzène. On a déterminé les conditions permettant d'isoler les complexes Co(I), $Co(BH_4)P_n$ (n = 2, 3) et on discute des structures de ces espèces à la lumière de diverses mesures physiques.

[Traduit par le journal]

Can. J. Chem. Downloaded from www.nrcresearchpress.com by 210.87.254.40 on 09/05/12
For personal use only.

Introduction

This paper is an extension of work we have already published dealing with the reactions of $NaBH_4$ with first row transition metal salts in the presence of tertiary phosphines (1). We present here results of an extensive study of reactions of the Co(II)/P/$NaBH_4$ (P = triphenylphosphine) system in a variety of solvents in an attempt to understand more fully the mechanism of the reduction which has previously been presented in outline form and which is known to lead to a variety of Co(I), (II), and (III) complexes (1, 2).

Results and Discussion

Tetrahydroboratobis(triphenylphosphine)cobalt(I), $Co(BH_4)P_2$

There are a number of reactions which lead to the formation of this highly crystalline air sensitive green Co(I) complex. For example, it is formed from the reaction between $NaBH_4$, Co(II) chloride, and P (~8:1:6) in toluene/ethanol (2:1) or benzene ethanol (2:1). It is interesting to note that when tricyclohexylphosphine (PCy_3) is used instead of P in analogous reactions, only the Co(II) complex $HCo(BH_4)(PCy_3)_2$ is formed (3). This is reasonable since P is a better π-acceptor than PCy_3 (4) and the bulky tertiary phosphines such as PCy_3, PPr_3^i and PBu_3^t etc. have been shown to stabilize BH_4 complexes of transition metals in higher oxidation states (5). The above green complex is also the product when a 10 M excess of $NaBH_4$ (suspension in ethanol) is added to a suspension of $CoClP_3$ in benzene. Also, the reaction between Co(II) perchlorate, P, and $NaBH_4$ (~1:6:10) in ethanol produces the same compound. (As will be seen later, Co(II) chloride behaves quite differently under these conditions, producing a mixture of Co(I) chloride and hydride complexes.) Finally, the complex was made during attempts to recrystallize $Co(BH_4)P_3$ (see later) from benzene or THF in the presence of free P.

Excellent chemical analyses (Co, C, H) for $Co(BH_4)P_2$, together with identical X-ray powder patterns and ir spectra, have been obtained for samples from each of the above preparations including those obtained from the crude crystalline reaction products and samples after either one or two recrystallizations from THF/ethanol solutions. Magnetic moment measurements, however, varied between a maximum value of 6.0 B.M. decreasing to an 'equilibrium value' of ~1.2 B.M. after two recrystallizations. It appears therefore that some decomposition of $Co(BH_4)P_2$ is occurring during crystallization from solution and it became necessary to wash the recrystallized samples with 10% aqueous HNO_3 to remove all traces of the ferromagnetic impurity (thought to be Co metal or boride since these products, which are readily soluble in dilute HNO_3, are readily formed in Co(II)/$NaBH_4$ reactions (2)) leaving the pure diamagnetic $Co(BH_4)P_2$. Chemical analyses, ir spectra, and X-ray powder patterns on samples before and after HNO_3 washings are identical and show that, surprisingly, no decomposition of the BH_4 complex occurs during such washings. The only observable change is that a faint pink coloration appears in the initial wash liquid as the trace amounts of boride are removed. Decomposition of a BH_4–phosphine complex to the metal boride has not been observed before, although it occurs readily in some amine complexes (6). In air, $Co(BH_4)P_2$ is oxidized to a mixture of the phosphine oxide and the borane adduct P–BH_3. The latter is also formed when the complex is dissolved in CH_3CN or CH_3NO_2.

The reflectance spectrum of $Co(BH_4)P_2$ shows a

Can. J. Chem. Downloaded from www.nrcresearchpress.com by 210.87.254.40 on 09/05/12
For personal use only.

band at 14 700 cm^{-1} and an intense charge-transfer maximum at 24 390 cm^{-1}. In THF solution the lower energy band appears at 15 400 cm^{-1} ($\varepsilon \sim 380$) and both the position and intensity of this band are consistent with that found for diamagnetic square planar d^8 systems (especially Ni(II)) and would suggest that the BH_4 group is acting as a bidentate ligand. The ir spectrum shows B—H_t stretches at 2450(s) and 2390(w,sh) cm^{-1} and what could be the symmetric and antisymmetric bridging stretches at 2040 and 1970 cm^{-1}. There appears to be an additional weak band at 1830 cm^{-1}. This part of the spectrum is very similar to that of $Cu(BH_4)P_2$ which is known to contain the bidentate BH_4 group (7). The other expected bands for this type of coordination (8) are the ν_{B-H_b} at 1300–1500 cm^{-1} and the δ_{B-H} at ~1100–1200 cm^{-1} which are not seen and could be hidden under Nujol or ligand bands (the complex decomposes to $CoCl_2P_2$ in hexachlorobutadiene and in other chlorinated hydrocarbon solvents such as $CHCl_3$, CH_2Cl_2, and CCl_4). The ir spectrum of $Co(BD_4)P_2$ shows the terminal ν_{B-D_t} stretching frequency at 1830 cm^{-1} ($\nu_D/\nu_H = 0.747$, consistent with that observed in $DCo(BD_4)(PCy_3)_2$ (3)) although other B—D vibrational modes could not be found. However, the ir data could also be accounted for if the BH_4 group is acting as a tridentate ligand with expected and observed bands at (8) 2600–2450 cm^{-1} (ν_{B-H_t}, singlet), 2200–2100 cm^{-1} (ν_{B-H_b}, doublet), and 1250–1150 cm^{-1}. It is impossible to distinguish between these without X-ray data. (See later discussion.) As expected, the powder pattern of $Co(BH_4)P_2$ is quite different from that of the tetrahedral $Cu(BH_4)P_2$ (7).

Tetrahydroboratotris(triphenylphosphine)cobalt(I), $Co(BH_4)P_3$

In our previous study (1) we reported the preparation of this complex by the reaction of an excess of $NaBH_4$ on $CoXP_3$ (X = Cl, Br, I, prepared *in situ*) in ethanol for 3 h. Further investigation has revealed that this method is unreliable and, in general, leads to complex mixtures. Thus, the products from the Co(II) chloride/P/$NaBH_4$ (1:3:5 to 1:10:20) reactions in ethanol depend mostly on the *rate* of addition of the $NaBH_4$ suspension and less so on the reaction time and the molar ratios of the reactants. If all the $NaBH_4$ suspension is added to the Co(II)/P mixture within ~3 min, a mixture of H_3CoP_3 (9), $HCo(N_2)P_3$ (9), and P–BH_3 is obtained, even though the reaction time may vary from 30 min to 18 h. The formation of these products may be rationalized as follows.

The low solubility of P in ethanol at room temperature (compared with that of Co(II) chloride) means that if the $NaBH_4$ is added too quickly, not enough P is in solution to protect the Co(II) from rapid reduction to the boride. The latter would catalyse the decomposition of $NaBH_4$ to release H_2 (2) thus accounting for the formation of the Co-hydride complexes. The P–BH_3 complex is formed by oxidation of the Co(I)–BH_4–P complexes which are undoubtedly present in the mixture. (In recording X-ray patterns of $Co(BH_4)P_3$, lines of P–BH_3 appear if the capillary is improperly sealed or if the tip is broken during its mounting in the camera.)

If the $NaBH_4$ suspension is added to the Co(II)–P mixture more slowly, e.g., over a period of 30 min, or if 1 mol (per mole of Co(II)) of $NaBH_4$ is first added followed by a large excess, then the major product is the yellow-brown impure $CoClP_3$, While this can be recrystallized from benzene in the presence of P to yield the pure green $CoClP_3$, it appears that the crude material does not undergo further reaction with $NaBH_4$ in ethanol even if the mixture is stirred for up to 3 days.

We have reproducibly prepared the pure green air-sensitive $Co(BH_4)P_3$ in two ways. The complex is formed when $CoClP_3$ and P (1:3) are stirred with an ethanolic suspension of $NaBH_4$ (Co:$NaBH_4$, 1:10) in ethanol for a minimum of 4 days. The greater the excess of P the more easily the conversion takes place. Alternatively $Co(BH_4)P_2$ can be converted to $Co(BH_4)P_3$ by a curious reaction in which a small amount of cobalt boride is added to a mixture of $Co(BH_4)P_2$ and P in ethanol, when conversion occurs over a 4 day period. Similarly, crude samples of $Co(BH_4)P_2$, particularly those prepared from $CoClP_3$ (which contain significant amounts of what is presumably cobalt boride as discussed earlier), when stirred with a 3–6 *M* excess of P in ethanol for 4 days are converted into $Co(BH_4)P_3$ which must then be washed with water, 10% HNO_3, water, ethanol, and ether. The addition of $NaBH_4$ to the reaction mixture speeds up the reaction and $Co(BH_4)P_3$ is produced in 1 day. Pure $Co(BH_4)P_2$ or recrystallized samples prior to HNO_3 washings and which contain only small quantities of boride will not react further with P. All attempts to recrystallize $Co(BH_4)P_3$ from benzene or THF, even in the presence of an excess of P, result in its rapid conversion to $Co(BH_4)P_2$ and not to the N_2 adduct previously reported (1).

The complex is paramagnetic (μ_{eff} = 3.40 B.M.) and is isomorphous with the tetrahedral $CoClP_3$. Its electronic reflectance spectrum is also similar to that of $CoClP_3$ (10) with bands at 6250 ($^3T_1 \rightarrow {}^3T_2$), 7407 ($^3T_1 \rightarrow {}^3A_2$), and 16 390 cm^{-1} ($^3T_1 \rightarrow {}^3T_1$(P)). The complex is closely related to the paramagnetic $Co(p_3)(BH_4)$ (p_3 is the tridentate tripod ligand 1,1,1-tris(diphenylphosphinomethyl)ethane) which is also

Can. J. Chem. Downloaded from www.nrcresearchpress.com by 210.87.254.40 on 09/05/12
For personal use only.

isomorphous with and has similar electronic properties to the corresponding tetrahedral $Co(p_3)Cl$ (11). In $Co(p_3)(BH_4)$, the BH_4 group is a bidentate ligand as shown by X-ray crystallographic studies. The ir spectrum (Fig. 1) of $Co(BH_4)P_3$ shows bands at 2415(s), 2320(s), 2075(sh,m), 2045(m), and 1104 cm^{-1} consistent both with monodentate (8, 12) or bidentate (8) BH_4 coordination. It seems that as more BH_4 complexes are synthesized, the less useful does ir spectroscopy become in distinguishing between the possible coordination modes.

Sacconi and co-workers (11) have described the $M–BH_4$ link in such species in terms of a spherical BH_4 anion with a largely ionic bond to the metal instead of the conventional covalent $M—BH_4$ description. The fact that $Co(BH_4)P_n$ do not react with ($n = 2$) or are decomposed by ($n = 3$) an excess of $NaPF_6$ or $NaBPh_4$ (unlike $NiL_2(BH_4)$, L = 1,10-phenanthroline (13), and $Ni(BH_4)P_3$ (14) where the BH_4 groups are exchanged for PF_6^- and BPh_4^- anions) implies a $Co—BH_4$ bond which is more covalent than ionic. Clearly the bonding between metal ions and BH_4 needs further attention.

The ir spectrum previously reported (1) for $Co(BH_4)P_3$ (1060, 1105, 2340(sh), 2390(s)) is almost certainly that of an oxidized sample as these bands are very close to those of $P–BH_3$ (1060, 1105, 2340(sh), 2388(s)).

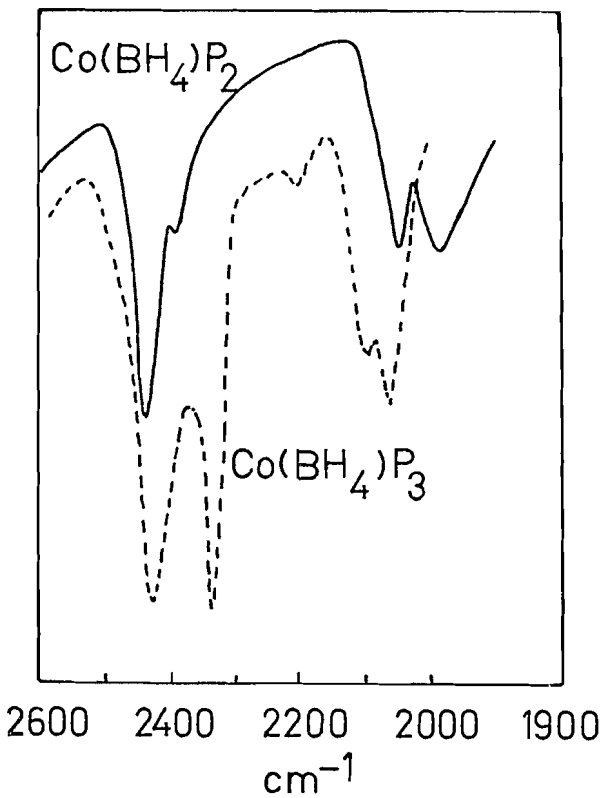

FIG. 1. Infrared spectra of $Co(BH_4)P_2$ and $Co(BH_4)P_3$ in the 1900–2600 cm^{-1} region.

$Co(BH_4)P_3$ cannot be converted to $Co(BH_4)P_2$ in ethanol probably due to the low solubility of the former in this solvent. Like $Co(BH_4)P_2$, $Co(BH_4)P_3$ decomposes to $CoCl_2P_2$ in chlorinated hydrocarbon solvents and to $P–BH_3$ in CH_3CN and CH_3NO_2.

When $Co(BH_4)P_n$ ($n = 2, 3$) is heated under reflux with P in ethanol for several hours, decomposition occurs to give a dark green paramagnetic hydride ($\nu_{Co–H}$ 1920 cm^{-1}). Although this is soluble in both polar and nonpolar solvents (including *n*-hexane and petroleum ether) repeated recrystallizations failed to yield a pure identifiable product.

Mechanism

While only two solvents have been studied in these reductions it is apparent that the solvent does play an important role in determining the nature of the product(s). For example, the reaction of $CoClP_3$ with $NaBH_4$ in ethanol in the presence of P slowly gives $Co(BH_4)P_3$ in 4 days but in a benzene/ethanol mixture, the reaction proceeds much faster and in less than 30 min produces $Co(BH_4)P_2$. If $CoClP_3$ dissociates in benzene, as has been shown to occur extensively with $NiClP_3$ (15), then the following reaction sequence may take place.

$$CoClP_3 \rightleftharpoons [CoClP_2] \rightleftharpoons \underset{\text{(monodentate)}}{[Co(BH_4)P_2]} \begin{matrix} \rightleftharpoons Co(BH_4)P_2 \\ \rightleftharpoons Co(BH_4)P_3 \end{matrix}$$

In this case, no $Co(BH_4)P_3$ is obtained since, as shown earlier, it is rapidly converted to $Co(BH_4)P_2$ in benzene. In pure ethanol, however, $CoClP_3$ is much less soluble, dissociation is repressed, especially in the presence of free P, and therefore $Co(BH_4)P_3$ is probably formed by a direct substitution reaction. On the other hand, the Co(II) perchlorate/P/$NaBH_4$ reaction in ethanol results *only* in the formation of $Co(BH_4)P_2$ probably via an intermediate such as $[CoP_x]^+$.

In summary, this work has established the conditions, in Co(II)—P—$NaBH_4$ reactions, for the isolation of two of the many possible products, the formation of which depends essentially on three factors: (*i*) the rate of addition of $NaBH_4$, (*ii*) the presence of free ligand, and (*iii*) the solvent. The overall reaction sequence remains as outlined previously (2).

Experimental

Materials

All chemicals were reagent grade and were used without purification. Solvents were purified in the usual way, degassed, and stored over molecular sieves (4A).

Can. J. Chem. Downloaded from www.nrcresearchpress.com by 210.87.254.40 on 09/05/12
For personal use only.

Physical Measurements

Physical measurements were carried out as previously described (1). Samples were suitably protected from atmospheric oxidation.

Syntheses

All syntheses were carried out under pure N_2 in a glove box, and complexes were produced in high yields (~70–80%).

1. $CoClP_3$

This compound was synthesized by a slight modification to Sacco's method (10). A suspension of $NaBH_4$ (0.14 g, 3.7 m*M*) in ethanol (~8 ml) was added dropwise over a period of ~½ h to a stirred mixture of $CoCl_2 \cdot 6H_2O$ (0.79 g, 3.34 m*M*) and P (3.79 g, 14.4 m*M*) in ethanol (50 ml) at room temperature.

The yellow mixture was stirred for 2 h before the crude product was filtered off, washed with ethanol, water, ethanol, and ether before drying under reduced pressure.

The crude product was dissolved in benzene (~150 ml) containing P (~2 g), stoppered, and allowed to stand for ~½ h. The brownish-green solution was filtered and the residual green solid was extracted into more benzene and filtered again. The filtrates were combined and the volume was reduced by ~⅓ under reduced pressure to yield green crystals of $CoClP_3$.

d-*Spacings* (relative intensities 0–10)—9.60(5), 8.89(10), 5.40(2), 4.94(2), 4.35(2), 3.85(5), 3.57(5), 3.41(3), 2.86(1).

2. $Co(BH_4)P_2$

(a) From Co(II) chloride – P in benzene/ethanol and $NaBH_4$/ethanol—A suspension of $NaBH_4$ (~0.2 g, 5.2 m*M*) in ethanol (~10 ml) was added dropwise to the stirred suspension of $CoCl_2 \cdot 6H_2O$ (0.15 g, 0.63 m*M*) and P (~1 g, 3.8 m*M*) in benzene, toluene, benzene/ethanol (2:1), or toluene/ethanol (2:1) (~10 ml). A gas (presumably H_2) was generated during the initial stages of the $NaBH_4$ addition and the blue suspension changed immediately to green and then brownish-green (within 10 min). After the addition of all the $NaBH_4$ suspension, dark green crystals were produced which were filtered off, washed with ethanol, water, ethanol, and ether, and dried under reduced pressure.

The product was recrystallized from THF, dark green crystals appearing on addition of ethanol. After washing with ethanol, ether, and drying, the product was finally washed with 10% HNO_3 (3 × 10 ml), water (6 × 10 ml), ethanol, and ether. *Anal.* calcd. for $Co(BH_4)P_2$: C 72.3, H 5.7, Co 9.8; found: C 71.7, H 6.0, Co 9.7.

d-*Spacings* (relative intensities)—13.52(8), 9.62(1), 8.70(10), 7.85(2), 6.30(1), 5.77(1), 4.95(1), 4.71(5), 4.37(7), 3.86(3), 3.35(1).

(b) From $CoClP_3$ in benzene and $NaBH_4$ in ethanol—A suspension of $NaBH_4$ (0.2 g, 5.2 m*M*) in ethanol (~10 ml) was added dropwise into a stirred solution of $CoClP_3$ (~0.4 g, 0.45 m*M*) in benzene (~15 ml). The green solution became brownish-green and quickly precipitated dark green crystals which were isolated and purified as described above.

(c) From Co(II) perchlorate/P in ethanol and $NaBH_4$ in ethanol—A suspension of $NaBH_4$ (~0.2 g, 5.2 m*M*) in ethanol (~10 ml) was added dropwise to a suspension of Co(II) perchlorate (~0.15 g, 0.4 m*M*) and P (0.7 g, 2.7 m*M*) in ethanol (15 ml). A gas (presumably H_2) was generated in the initial stages of the addition of the $NaBH_4$ suspension and the color of the solution turned from pink to greenish-yellow. The mixture was stirred for 3 h after which the yellow-green product was filtered off and purified as described above.

(d) From $Co(BH_4)P_3$ in benzene—Co $(BH_4)P_3$ (~0.3 g) was dissolved in benzene (~30 ml) either in the absence of P or with additional P (Co:P up to 1:10). The solution was then filtered and concentrated under vacuum at room temperature until the total volume was reduced to ~15 ml. The dark green product was precipitated by the addition of ether (~20 ml), filtered off, and purified as described above.

3. $Co(BH_4)P_3$

(a) From $CoClP_3$/P/$NaBH_4$ in ethanol—Solid $NaBH_4$ (~0.2 g, 5.2 m*M*) was added in small amounts to a stirred suspension of finally powdered $CoClP_3$ (~0.4 g, 0.45 m*M*) and P (~0.4 g, 1.5 m*M*) in ethanol (~20 ml). After the addition of all the $NaBH_4$, the mixture was stirred for 4 days. The resulting light green precipitate was filtered off, washed with ethanol, water, ethanol, and *n*-hexane, and finally dried under high vacuum for 3 h. *Anal.* calcd. for $Co(BH_4)P_3$: C 75.4, H 5.7, Co 6.8; found: C 74.9, H 5.8, Co 6.8.

d-*Spacings* (relative intensities)—9.67(5), 8.99(10), 5.41(2), 4.91(2), 4.36(2), 3.85(5), 3.58(5), 3.42(2), 2.86(1).

(b) From impure $Co(BH_4)P_2$—Finely powdered $Co(BH_4)P_2$ (~0.3 g, 0.5 m*M*) (prepared as in 2(*b*), but *not* purified) and P (~0.3 g, 1.1 m*M*) were stirred in ethanol (~20 ml) for 4 days during which the color slowly changed from dark to light green. The product was separated, washed, and dried as in 3(*a*) and finally washed with 10% HNO_3 (3 × 10 ml), water (6 × 10 ml), ethanol, and *n*-hexane.

(c) From $Co(BH_4)P_2$ with added boride—Pure $Co(BH_4)P_2$ was treated with P as described in 3(*b*) except that a small amount of cobalt boride (~10 mg) was added. (The latter was prepared by adding ethanol to a Catgen pellet, supplied by Ventron Corporation and consisting of a mixture of $CoCl_2$/$NaBH_4$ in a 1:4 molar ratio. When the effervescence subsided, the dark colored solid was separated, washed with ethanol, water, ethanol, and ether, and dried under vacuum.) The product was isolated and washed as in 3(*b*).

Acknowledgements

The authors thank the National Research Council of Canada and the Ventron Corporation, Beverly, Massachusetts, for the generous financial support of this work.

1. D. G. Holah, A. N. Hughes, B. C. Hui, and K. Wright. Can. J. Chem. **52**, 2990 (1974).
2. R. Wade, D. G. Holah, A. N. Hughes, and B. C. Hui. Catal. Rev. Sci. Eng. **14**, 211 (1976).
3. M. Nakajima, H. Moriyama, A. Kobayashi, T. Saito, and Y. Sasake. Chem. Commun. 80 (1975).
4. C. A. Tolman. J. Am. Chem. Soc. **92**, 2953 (1970).
5. H. D. Empsall, E. Mentzer, and B. L. Shaw. Chem. Commun. 861 (1975).
6. B. D. James and M. G. H. Wallbridge. Prog. Inorg. Chem. **11**, 99 (1970).
7. S. J. Lippard and K. M. Melmed. Inorg. Chem. **6**, 2223 (1967); S. J. Lippard and D. A. Ucko. Inorg. Chem. **7**, 1051 (1968).
8. T. J. Marks and J. R. Kolb. Chem. Rev. **77**, 263 (1977).
9. A. Sacco and M. Rossi. Inorg. Chim. Acta, **3**, 127 (1968).
10. M. Aresta, M. Rossi, and A. Sacco. Inorg. Chim. Acta, **3**, 227 (1969).
11. P. Dapporto, S. Midollini, A. Orlandini, and L. Sacconi. Inorg. Chem. **15**, 2768 (1976).
12. J. C. Bommer and K. W. Morse. Chem. Commun. 137 (1977).
13. D. G. Holah, A. N. Hughes, and B. C. Hui. Can. J. Chem. **55**, 4048 (1977).
14. D. G. Holah, A. N. Hughes, B. C. Hui, and C. T. Kan. Can. J. Chem. To be published.
15. M. J. Nilges, E. K. Barefield, R. L. Belford, and P. H. Davis. J. Am. Chem. Soc. **99**, 755 (1977).

Sphere tensiometry: wall effects and correction factors

E. BAYRAMLI, C. HUH, AND S. G. MASON

Pulp and Paper Research Institute of Canada, McGill University, Department of Chemistry, Montreal, P.Q., Canada H3A 2A7

Received June 20, 1977

E. BAYRAMLI, C. HUH, and S. G. MASON. Can. J. Chem. **56**, 818 (1978).

This paper is a supplement to an earlier one on the new absolute gravimetric method of measuring surface and interfacial tension which takes into account the effect of the wall in circular containers of finite radius which causes the liquid surface to dimple instead of remaining flat as in an unbounded system as assumed earlier.

Using conventional capillarity theory, the basic principles for correcting force–displacement curves, called sphere-tensiograms, are derived. Numerical correction factors calculated from the theory for systems with perfect wetting (zero contact angle) for an experimentally realistic range of parameters, and corroborative experimental data are presented.

E. BAYRAMLI, C. HUH et S. G. MASON. Can. J. Chem. **56**, 818 (1978).

Ce travail s'ajoute à une publication antérieure sur une nouvelle méthode gravimétrique absolue de mesurer les tensions superficielles et interfaciales qui tient compte du fait que la paroi de contenant circulaire de rayons finis provoquent une ondulation de la surface alors que l'on avait fait l'hypothèse antérieurement que cette surface devait demeurer plane dans des systèmes non-entourés.

Faisant appel à la théorie de capilarité conventionnelle, on peut dériver les principes de base permettant de corriger les courbes force-déplacement que l'on appelle tensiogrammes de sphère. On présente des facteurs de corrections numériques calculés à partir de la théorie pour des systèmes avec des mouillages parfaits (angle de contact zéro) pour une variation réaliste au point de vue expérimental des paramètres et on présente des données expérimentales permettant de corroborer la théorie.

[Traduit par le journal]

Introduction

Sphere tensiometry has recently been proposed (1, 2) as an alternative to the (du Nouy) ring and (Wilhelmy) plate gravimetric methods for measuring fluid interfacial (or surface) tensions. It has a number of potential advantages over other absolute methods, especially when the interface is not visible. In making full use of the method, the vertical force – displacement curve of the sphere (which we term the sphere-tensiogram) as it penetrates the interface is determined from which various quantities in addition to the interfacial tension can be calculated (2).

The numerical calculations used to analyze the tensiograms were made for infinite interfaces. This is a restriction which can introduce errors from wall effects of the vessels containing the liquid(s) (2). In this paper we consider these effects in circular cylindrical containers as a function of B/R where B and R are the respective radii of the vertical container and the axially located sphere, as an extension of similar calculations of an infinite horizontal cylinder located midway between two vertical parallel plates (3).

As illustrated in Fig. 1, a container of finite radius introduces an error in the earlier calculations of the interfacial tension γ_{23}, since one of the boundary conditions for solving the Young–Laplace equation was that the slope of the interface at a horizontal radial distance r from the center of the sphere becomes zero at $r = \infty$; instead, the interface now assumes some slope angle $\phi_B \neq 0$ at $r = B$. Also, if the experiment is performed with a constant volume of liquid, as the sphere is pulled vertically along the

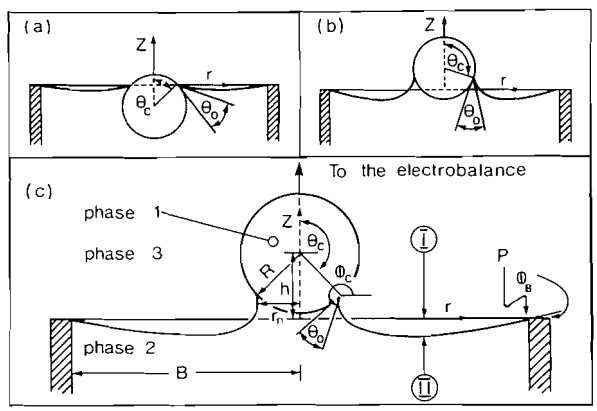

FIG. 1. Sketches showing the three different positions of the sphere used in deriving [4*d*]. In (*a*) $\theta_c < \pi/2$; in (*b*) $\pi/2 \leq \theta_c < \pi$ and $(\theta_c - \pi/2) \leq \theta_0$; and in (*c*) $\pi/2 \leq \theta_c < \pi$ and $(\theta_c - \pi/2) > \theta_0$ the latter being the geometric condition for forming a meniscus neck of $\bar{r} = \bar{r}_n$. In this treatment the 23 interface is made initially flat (interface I) with the sphere (phase 1) completely submerged in phase 2. The sphere is pulled vertically along the axis of the cylindrical container whose upper rim is polished flat so that the 23 interface sticks to the sharp inner edge P(4); on raising the sphere to h the interface assumes shape II.

Can. J. Chem. Downloaded from www.nrcresearchpress.com by 210.87.254.42 on 09/05/12
For personal use only.

Can. J. Chem. Downloaded from www.nrcresearchpress.com by 210.87.254.42 on 09/05/12
For personal use only.

axis of the cylindrical container, the interface will dimple from shape I into shape II in Fig. 1. The tensiogram obtained will thus differ from that for $B/R = \infty$.

In this paper we outline the method of solving theoretically for the case where the equilibrium contact angle at the sphere surface has all possible values, i.e., $0 \leq \theta_0 < \pi$ and give numerical[1] and experimental results for the particular case $\theta_0 = 0$. We calculate numerically for a range of the nondimensional[2] radius $\bar{R}$ between 0.8 and 1.6, the maximum nondimensional force D, and the maximum nondimensional height $\bar{h}$ (2) as functions of $\bar{R}$ and $\bar{B}$, where

$$[1] \qquad D = 3F/4\pi(\rho_2 - \rho_3)gR^3$$

g being gravity and ρ_2, ρ_3 the densities of phases 2 and 3, respectively (Fig. 1); F is the equilibrium vertical force on a thin thread attached to the sphere, arbitrarily taken (without loss of generality (2)) as zero when the sphere is entirely immersed in phase 2; h is the height of the sphere centre above the initial level of the fluid/fluid interface which for both theoretical and experimental convenience is initially flat and is made to adhere to the sharp edge P of the container (Fig. 1) by utilizing the sharp edge effect which permits the meniscus to rotate about P (4).

Quantitative experiments were performed for $B/R = \bar{B}/\bar{R}$ between 2.5 to 5.0 and $\bar{R}$ between 0.8 to 1.6. On raising the sphere center to h the interface assumed shape II as shown in Fig. 1. The measured D_{mB} gave generally good agreement with the theory, and under certain circumstances yielded values of γ_{23} which were significantly different from uncorrected values based on $B/R = \infty$. As an independent measurement of γ_{23} the standard pendant drop method was used which yielded values very similar to those from sphere tensiometry.

Theoretical Part

(a) General

When the liquid interface is confined in a vertical cylindrical container of finite B, and the sphere moves along its axis, the equilibrium relation between F and H will depend on B and the condition of the interface at the container wall. In this analysis we restrict consideration to the case where the interface is initially flat and remains fixed at the sharp-edged rim of the container as h is increased. As established experimentally by Oliver *et al.* (4), the Gibbs inequality condition holds on such an edge so that it is safe to assume that ϕ_B, the slope angle of the meniscus at $r = B$ can pivot freely between $0 \leq \theta_B \leq \pi/2$.

The interface shape is governed by the classical Young–Laplace equation,

$$[2] \qquad \frac{1}{\bar{r}}\frac{d}{d\bar{r}}(r \sin\phi) = \bar{z} + \bar{z}'$$

The initially flat level of the interface corresponds to a vertical coordinate $\bar{z} = 0$, and $\bar{z}' = 0$ if $B = \infty$; but for finite $\bar{B}$, $\bar{z}' > 0$. In the following force equation $\bar{z}'$ is an additional term to that for $B = \infty$ (2), due to the wall:

$$[3] \quad 2D = 1 - \cos^3\theta_c + \frac{3}{\bar{R}^2}\sin\theta_c \sin\phi_c + \frac{3}{2\bar{R}}\sin^2\theta_c(\bar{h} + \bar{z}')$$

where θ_c, ϕ_c are angles defined with reference to the contact line in Fig. 1. Because the liquid interface will dimple downwards to fill in the volume displaced by the sphere, the following conservation of volume requirement must be met for the three possible states of immersion when $\theta_0 \leq \pi/2$ illustrated in Fig. 1.

1. $0 < \theta_c < \pi/2$ (Fig. 4*a*):

$$[4a] \quad 2\pi\int_0^{\bar{r}_c}[\bar{h} + \sqrt{\bar{R}^2 - \bar{r}^2}]\bar{r}\,d\bar{r} + 2\pi\int_{\bar{r}_c}^{\bar{B}}\bar{z}\bar{r}\,d\bar{r} = 0$$

2. $\pi > \theta_c \geq \pi/2$; $\theta_c - \pi/2 \leq \theta_0$ (Fig. 4*b*):

$$[4b] \quad 2\pi\int_0^{\bar{R}}(\bar{h} + \sqrt{\bar{R}^2 - \bar{r}^2})\bar{r}\,d\bar{r} + 2\pi\int_{\bar{R}}^{\bar{r}_c}(\bar{h} - \sqrt{\bar{R}^2 - \bar{r}^2})\bar{r}\,d\bar{r} + 2\pi\int_{\bar{r}_c}^{\bar{B}}\bar{z}\bar{r}\,d\bar{r} = 0$$

3. $\pi > \theta_c \geq \pi/2$; $\theta_c - \pi/2 > \theta_0$ (Fig. 4*c*):

$$[4c] \quad 2\pi\int_0^{\bar{R}}(\bar{h} + \sqrt{\bar{R}^2 - \bar{r}^2})\bar{r}\,d\bar{r} + 2\pi\int_{\bar{R}}^{\bar{r}_c}(\bar{h} - \sqrt{\bar{R}^2 - \bar{r}^2})\bar{r}\,d\bar{r} + 2\pi\int_{\bar{r}_n}^{\bar{B}}\bar{z}\bar{r}\,d\bar{r} + 2\pi\int_{\bar{r}_c}^{\bar{r}_n}\bar{z}\bar{r}\,d\bar{r} = 0$$

where $\bar{r}_c$ is the contact line radius, $\bar{r}_n$ is the radius of the meniscus neck which forms when $(\theta_c - \pi/2) >$

[1]Photocopies of these tabulations are available upon request, at a nominal charge, from the Depository of Unpublished Data, CISTI, National Research Council of Canada, Ottawa, Ont., Canada K1A 0S2. They are also deposited at PPRIC Library, Pointe Claire, Montreal, Quebec.

[2]Nondimensional linear dimensions, e.g., $\bar{R}$, $\bar{B}$, $\bar{h}$ are given by multiplying the corresponding scalar quantities by $\sqrt{C_{23}} = [(\rho_2 - \rho_3)g/\gamma_{23}]^{1/2}$.

Can. J. Chem. Downloaded from www.nrcresearchpress.com by 210.87.254.42 on 09/05/12
For personal use only.

θ_0, and $\bar{z}$ represents the meniscus profile defined by [2]. Inserting [2] into [4*a*, *b*, *c*] we obtain on reduction the identical result for all three cases:

$$[4d] \quad \frac{\bar{R}^2}{2}\sin^2\theta_c(\bar{h}+\bar{z}') + \frac{\bar{R}^3}{3}(1-\cos^3\theta_c) + \bar{B}\sin\phi_B - \frac{\bar{z}'}{2}\bar{B}^2 - \bar{R}\sin\phi_c\sin\theta_c = 0$$

It is readily shown that [4*d*] also applies to $\pi/2 \leq \theta_0 < \pi$ when F can become negative, i.e., the sphere must be pushed downwards through the interface (5).

The values of $\bar{r}_c$, $\bar{z}_c$, and ϕ_c ($\equiv 2\pi - \theta_c + \theta_0$) for the meniscus shape at the contact line should now obey [4*d*] in addition to condition [3] and the following geometric relations:

$$[5a] \quad \bar{r}_c = \bar{R}\sin\theta_c$$

$$[5b] \quad \bar{z}_c = \bar{h} + \bar{R}\cos\theta_c$$

(b) Numerical Calculations

To obtain the values of $\bar{r}_c$, $\bar{z}_c$, and θ_c, we transform [2] into its parametric forms

$$[6a] \quad \frac{d\bar{r}}{d\phi} = \frac{\cos\phi}{\bar{y} - \frac{\sin\phi}{\bar{r}}}$$

$$[6b] \quad \frac{d\bar{y}}{d\phi} = \frac{\sin\phi}{\bar{y} - \frac{\sin\phi}{\bar{r}}}$$

where $\bar{y} \equiv \bar{z} + \bar{z}'$. We then integrate [6] numerically, employing the Runge–Kutta method. The initial conditions employed are

$$[7a] \quad \phi = \phi_c$$

$$[7b] \quad \bar{r} = \bar{R}\sin\theta_c$$

$$[7c] \quad \bar{y} = (\bar{h} + \bar{z}') + \bar{R}\cos\theta_c$$

where $(\bar{h} + \bar{z}')$ is the adjustable parameter which we vary for given $\bar{R}$ and θ_c. The earlier calculations (2) give a unique $\bar{h}$ for various values of $\bar{R}$ and θ_c when $\bar{B} = \infty$, $\bar{z}' = 0$. For finite $\bar{B}$, $(\bar{h} + \bar{z}')$ is larger than that for $\bar{B} = \infty$, and for $\theta_0 = 0°$, we employ 30 values of $(\bar{h} + \bar{z}')$ which are increased from the value at $\bar{B} = \infty$ in increments of 0.0001. Equations 6*a*, *b* are then integrated numerically at increasing ϕ until at a certain set of $(\phi, \bar{r}, \bar{y})$, [4*d*] is satisfied and thus the set assumes the values of $\phi = \phi_B$, $\bar{r} = \bar{B}$, and $\bar{y} = \bar{z}'$. D and $\bar{h}$ can subsequently be calculated from [3] and [5*b*]. The values of $\bar{B}$ obtained generally fall between 1.5 and 10.0 from which we interpolate D and $\bar{h}$ at regularly spaced intervals of $\bar{B}$. Between $\bar{B} = 2.5$ and 5.0, $\bar{R}$ is varied from 0.8 to 1.6 at intervals of 0.2; θ_c from 10° to 90° and from 90° to 160° at intervals of 10° and 2° respectively.

Figure 2 shows the D–$\bar{h}$ curves obtained by numerical calculation for different $\bar{B}$'s for $\bar{R} = 1.0$ and $\theta_0 = 0°$ the only contact angle which is reproducible and thermodynamically significant. From such D–$\bar{h}$ curves we obtained D_{mB} and $\bar{h}_{mB}$ as functions of $\bar{R}$ and $\bar{B}/\bar{R}$ by the Aitken–Lagrange interpolation scheme. Figure 3 shows $(D_{mB} - D_{m\infty})/D_{m\infty}$ as a function of $\bar{R}$ and $\bar{B}/\bar{R}$ where D_{mB} and $D_{m\infty}$ are D maxima at finite $\bar{B}$ and infinite $\bar{B}$, respectively. We see that D_{mB} exceeds $D_{m\infty}$ by more than 1.0% when $\bar{B}/\bar{R} < 5.0$ and $\bar{R} < 0.8$. The wall effect is not as significant for $\bar{R} > 0.8$ in the range of $\bar{B}/\bar{R}$ investigated. For example, when $\bar{R} = 1.6$ and $\bar{B}/\bar{R} = 4.3$, D_{mB} is larger than $D_{m\infty}$ by only 0.1%. To illustrate the wall effect by a practical example, e.g., water/air interface at 25°C, when $\bar{R} = 1.0$ ($R = 2.7$ mm) the minimum ratio, $\bar{B}/\bar{R}$ for an error of less than 1% when the numerical data for $\bar{B} = \infty$ are used is $\bar{B}/\bar{R} = 4.0$.

If the interfacial tension is to be calculated, the $\bar{R}$ value corresponding to the measured D_{mB} is found from the numerical tabulation by linear interpolation among the four closest values with respect to B/R and D_{mB}; since $\bar{R} = R\sqrt{C_{23}}$, where $C_{23} = (\rho_2 - \rho_3)g/\gamma_{23}$, the interfacial tension is given by

$$[8] \quad \gamma_{23} = (\rho_2 - \rho_3)g\left(\frac{R}{\bar{R}}\right)^2$$

Knowing $(\rho_2 - \rho_3)$, g, and R, as we do in the experiment described below, in determining γ_{23} it is un-

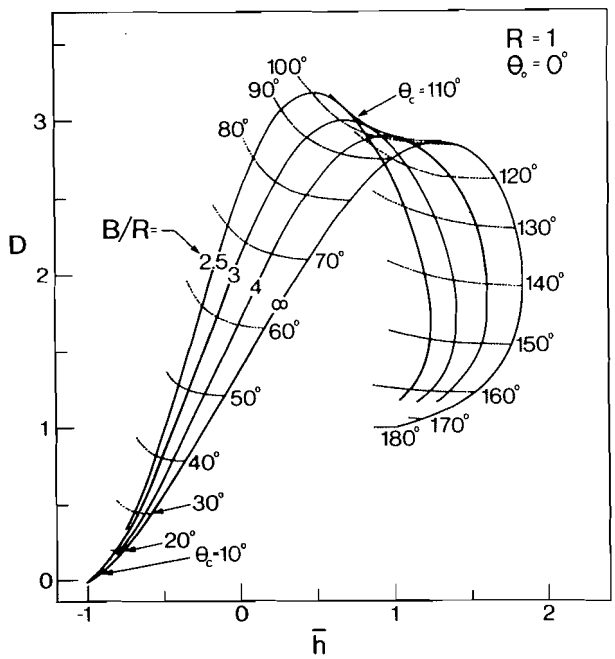

FIG. 2. Numerically calculated equilibrium D–$\bar{h}$ curves for $\bar{R} = 1.0$, $\theta_0 = 0°$ at different $\bar{B}/\bar{R}$. The broken lines indicate loci at fixed values of θ_c.

Can. J. Chem. Downloaded from www.nrcresearchpress.com by 210.87.254.42 on 09/05/12
For personal use only.

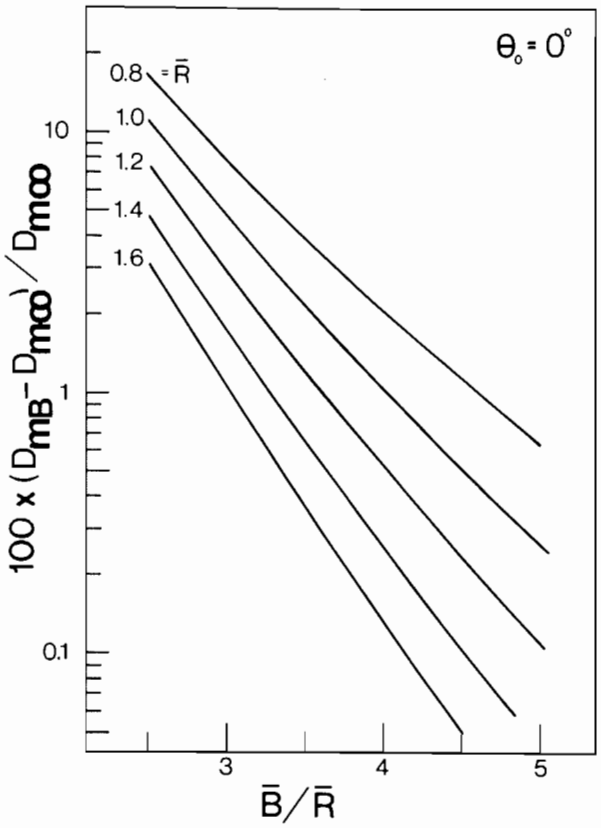

FIG. 3. Variation of maximum force, F_m expressed as $100 \times (D_{mB} - D_{m\infty})/D_{m\infty}$ with $\bar{B}/\bar{R}$ and $\bar{R}$ for $\theta_0 = 0°$.

necessary to use the whole tensiogram (2) but only the maximum force F_m or, less practicably, h_m.

Figure 4 shows $\bar{h}_{mB}/\bar{h}_{m\infty}$ as a function of $\bar{R}$ and $\bar{B}/\bar{R}$, where $\bar{h}_{mB}$ and $\bar{h}_{m\infty}$ at finite $\bar{B}$ and at $\bar{B} = \infty$, respectively. We see that the wall effect is much larger on $\bar{h}_{mB}$ than on D_{mB}; in the range of $\bar{R}$ studied, as much as 10.0% difference occurs in $\bar{h}_m$ when $\bar{B}/\bar{R} = 5$.

Figure 5 shows $\bar{h}_{DB}/\bar{h}_{D\infty}$ as functions of $\bar{B}/\bar{R}$ and $\bar{R}$, where $\bar{h}_{DB}$ and $\bar{h}_{D\infty}$ correspond to D_{mB} and $D_{m\infty}$ respectively. The influence of finite $\bar{B}$ is again quite significant. The large deviation is caused by dimpling of the horizontal interface due to the displacement of the sphere volume when it comes out of phase 2; the value of $\bar{h}$ measured from the base of the dimpled interface rather than the initial flat level, in fact is closer to the value of $\bar{h}_m$ at $\bar{B} = \infty$.

Experimental Part

(a) Methods

The experimental arrangement was basically the same as described earlier (2), with the following additional refinements:

1. The drive system for the platform on which the liquid container rested was hydraulically driven, employing a plunger-type micrometer attached to a variable speed motor and reduction gear with the motor speed controlled by a feedback mechanism to yield stage velocities from 0.1 to 1.0 mm/min, constant to ±0.2%.

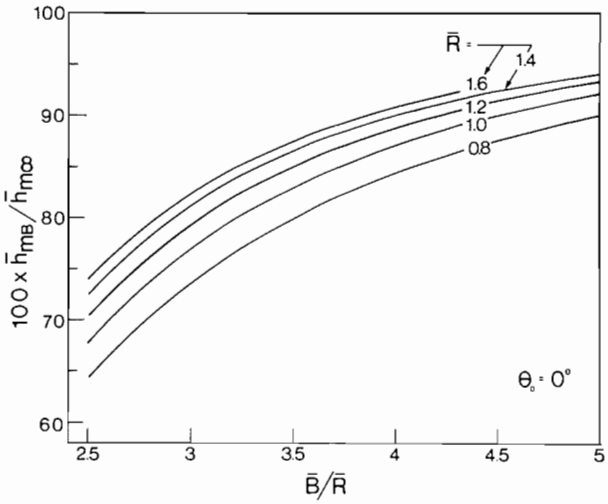

FIG. 4. Variation of maximum height h_m expressed as $100 \times h_{mB}/h_{m\infty}$ with $\bar{B}/\bar{R}$ and $\bar{R}$ for $\theta_0 = 0°$.

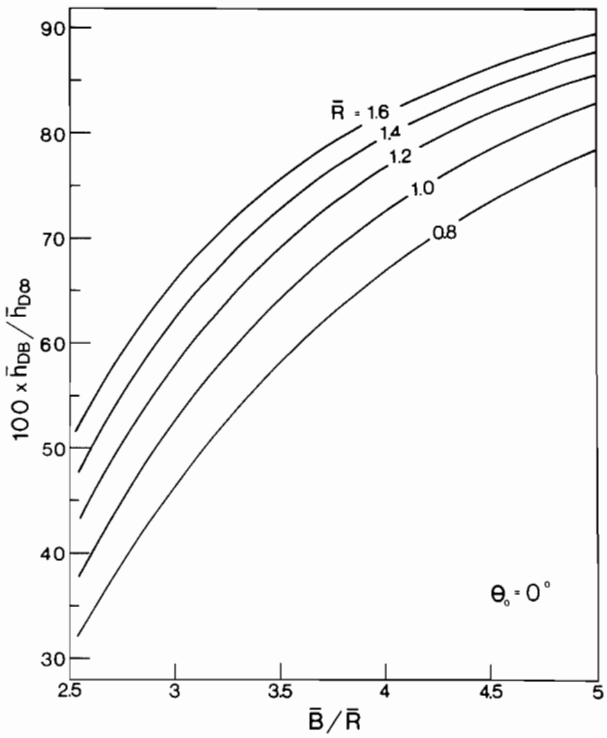

FIG. 5. Equilibrium relation between height h expressed as $100 \times \bar{h}_{DB}/\bar{h}_{D\infty}$ and $\bar{B}/\bar{R}$ at various $\bar{R}$ where $\bar{h}_{DB}$ and $\bar{h}_{D\infty}$ are the height at the maximum force state for container radii B and ∞ respectively.

2. Force–displacement (F vs. h) curves were recorded using a Hewlett-Packard X-Y Recorder (Model HP 7044A); a Hewlett-Packard displacement transducer (Model HP 7DDT-500) attached to the stage and calibrated using a dial type micrometer yielded height displacements accurate to better than 10 μm.

The cylindrical containers were made of Pyrex tubing with

Can. J. Chem. Downloaded from www.nrcresearchpress.com by 210.87.254.42 on 09/05/12
For personal use only.

TABLE 1. Comparison of experimental data with theory. *System* Silicone Oil/air; $\rho_2 = 0.815$ (g/cm^3); $\rho_3 = 0.0$; $g = 980.7$ (cm s^{-2}); average of $(C_{23})^{1/2} = 6.87$ cm^{-1} (experiments 1, 5, and 8)

Experiment No.	$\frac{B}{R}$	D_{mB} Measured	D_{mB} Theory	$\bar{R}$(exp) (corrected for B/R)	γ_{23} (dyn/cm) a*	γ_{23} (dyn/cm) b†	$\frac{(a-b)}{a} \times 100$	$\bar{h}_{mB}$ Exp.	$\bar{h}_{mB}$ Theory	$\frac{(\bar{h}_{m\infty} - \bar{h}_{mB})}{\bar{h}_{mB}} \times 100$
					$R = 0.1185$ cm					
1	39.98	3.719	3.719	0.815	16.89	16.89	0.0	1.63	1.60	0.0
2	5.30	3.808	—	—	—	17.32	2.55	1.46	—	10.32
3	4.20	3.817	3.800	0.809	17.08	17.51	3.67	1.40	1.36	14.13
4	3.38	3.887	3.888	0.815	16.88	18.07	6.97	1.34	1.34	18.05
					$R = 0.1600$ cm					
5	29.61	2.570	2.570	1.099	16.94	16.94	0.0	1.99	1.97	0.0
6	4.53	2.594	2.579	1.093	17.10	17.17	1.36	1.75	1.78	11.98
7	3.92	2.604	2.591	1.094	17.08	17.27	1.95	1.71	1.71	14.10
					$R = 0.2388$ cm					
8	19.04	1.762	1.762	1.639	16.96	16.96	0.0	2.63	2.63	0.0
9	3.04	1.850	—	—	—	19.14	12.80	2.16	—	17.80

*From measured D_m, corrected for wall effect. Mean value of 7 measurements, $\bar{\gamma}_{23} = 17.00 \pm 0.10$ dyn/cm.
†From measured D_m, not corrected for wall effect.

sharply polished edges, with their bottoms cemented to flat microscope slides. They were cleaned ultrasonically in detergent solution and then washed with copious amounts of distilled water and oven dried before use.

(b) Materials

Dow Corning Silicone Oil (200 Fluid, 1cs) was used as the liquid without further purification; its density (0.815 g/cc at 25°C) was determined by a pycnometer. Precision-grade hard nylon spheres (Industrial Tetronics, Inc., Ann Arbor, MI) were used. They were thoroughly cleaned in acetone and hexane, oven heated at 80°C, and rinsed in distilled water 10 times. After evaporating the water by air-drying the spheres were stored in Silicone Oil overnight. The sphere radii R were measured to $\pm 10^{-4}$ cm by Nikon Shadograph; the deviation from sphericity $(R_{max} - R_{min})/R_m$, was always less than 0.1%.

(c) Procedures

The measurements were made at 25 ± 0.5°C. The container was filled by dropwise addition at the tube wall until the sphere was submerged and the liquid/air interface located at the sharp edge was flat. The sphere was connected to the Cahn recording electrobalance arm (2) by a 0.1 mm steel wire which passed through a small hole drilled through the center of the sphere. Since F is taken as zero when the sphere is just below the 23 interface, no buoyancy correction is needed for the hole or the steel thread; the latter may cause an uncertainty of about 0.05 cm in h but this can be eliminated by extrapolating the F–h curve to the base-line at the starting point of the tensiogram.

A tensiogram was obtained by pulling the sphere slowly (0.2 mm/min) from the liquid until the meniscus ruptured. In some experiments the motion of the stage was reversed to check for any contact angle hysteresis; in all such cases the tensiograms were reversible whether or not the meniscus was allowed to rupture, from which we conclude that the contact angle was always 0° (2), as can also be seen from the photograph in Fig. 6*d*. The surface tension of the Silicone Oil was measured independently by the pendant drop technique, using the Nikon Shadowgraph to analyze the photographs of the drop and the numerical tables of Roe *et al.* (6).

Results and Discussion

Figure 7 shows some typical D–$\bar{h}$ curves constructed from the tensiograms; Table 1 summarizes the experimental results and their comparison with numerical calculations. Experiment Nos. 1 and 3–8 fell within the range of the present tabulations on wall effect or the earlier tabulations for $\bar{B} = \infty$ (2). One can see from Fig. 7 (which is similar to Fig. 2) for experiments 5–7 that for a constant θ_c (see Fig. 2) the D(exp) increased and $\bar{h}$(exp) decreased as $\bar{B}/\bar{R}$ diminished. The arrows indicate D_{mB}(theory) and $\bar{h}_{mB}$(theory). Without the use of wall corrections, γ_{23} calculated would have been significantly larger than the true value.

For example, for experiment 9 (Table 1): the measured uncorrected value for γ_{23} was 12.8% greater than the mean corrected γ_{23}'s. The mean corrected interfacial tension values were 17.00 ± 0.10 dyn/cm; γ_{23} determined independently by the pendant drop method was 17.02 dyn/cm. These small differences can be a result of slight fluctuations in chamber temperature (25 ± 0.5°C), deviations from sphericity which is a critical parameter in the calculations, small

Can. J. Chem. Downloaded from www.nrcresearchpress.com by 210.87.254.42 on 09/05/12
For personal use only.

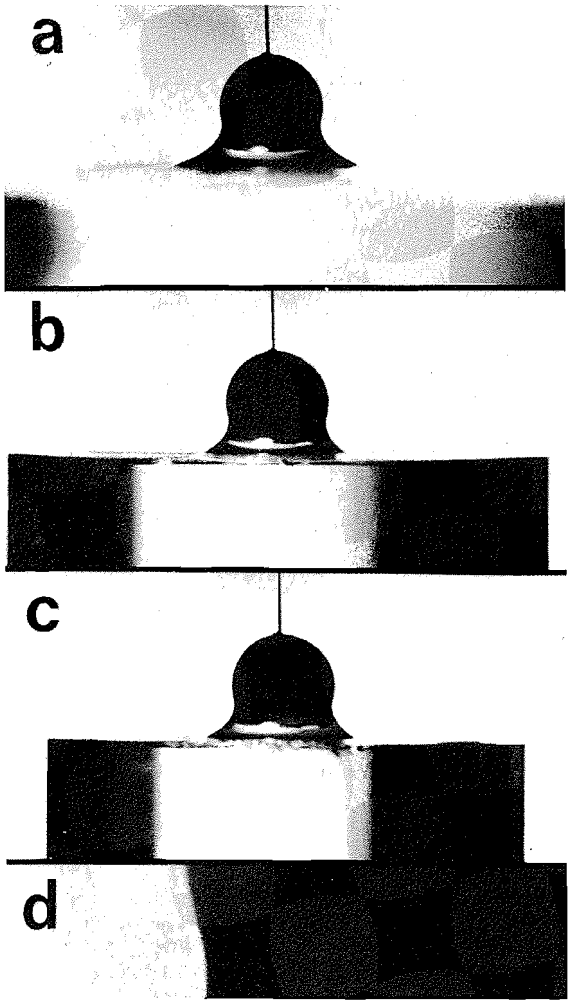

FIG. 6. Photograph of a nylon sphere ($R = 0.1600$ cm) at the Silicone Oil interface in the maximum force state, for values of $\bar{B}/\bar{R} = 29.61$, 4.53, and 3.92 in parts *a*, *b*, and *c*. Due to nonsymmetrical illumination it is not obvious from these photographs that the contact angle θ_0 was zero. At higher magnification (part *d*), however, no discontinuity can be seen at the contact line from which (plus the observation that *F–h* curves were reversible) it is concluded that $\theta_0 = 0$ for this system.

errors in density, and the fact the measurements were made at different times on different aliquots of liquid. Considering all these factors it can be said that excellent agreement exists between experiments and the theory.

The experimental force maximum, D_{mB}(exp), in Table 1 was calculated from experimental F vs. h curves and $\bar{R}$(exp) was found by linear interpolation among the 4 closest values of the B/R and D_{mB}(exp) in numerical tabulations. The theoretical maximum, D_{mB}(theory), was calculated using the average γ_{23} value which was found from runs 1, 5, and 8 all of which had large B/R values, hence it was assumed

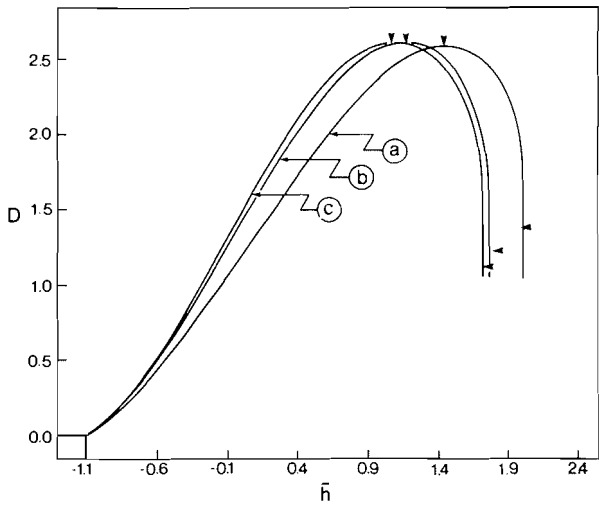

FIG. 7. Typical D–$\bar{h}$ curves (Experiments 5–7, Table 1) constructed from experimental F–h tensiograms for $R = 0.1600$ cm. The vertical arrows indicate D_m(theory) and horizontal arrows are $\bar{h}_m$(theory). The tensiograms *a*, *b*, *c* indicate the cases where container radius to sphere radius ratio, $\bar{B}/\bar{R}$, are equal to 29.61, 4.53, and 3.92 respectively. Note that they are similar in shape to the theoretical curves in Fig. 2 where lines of constant θ_c are also shown.

that they needed no correction due to wall effects. The corrected γ_{23}'s were calculated from [8] using the numerical tabulations which are corrected for wall effects while the uncorrected γ_{23} values were calculated assuming an unbounded interface and using the numerical tables with $\bar{B} = \infty$. The experimental maximum height $\bar{h}_{mB}$(exp) was found from the tensiogram by making use of $\bar{R}$(exp) and C_{23} values for each experiment; $\bar{h}_{mB}$(theory) is the maximum height corresponding to the particular D_{mB}(exp) in the tables.

We can conclude that if D_m alone is to be used to measure γ_{23} (when $\theta_0 = 0°$ is reasonably assured or θ_0 is known), the wall effect is not significant if $\bar{B}/\bar{R} > 5$, but one must recognize that as $\bar{R}$ decreases the wall effect increases for a constant $\bar{B}/\bar{R}$. If $\bar{h}_m$ or other parameters of the tensiogram (2) are to be used, care should be taken to assure a sufficiently large $\bar{B}/\bar{R}$, to avoid the wall effect; it should be noted however that the maximum force, F_m is much more easily measured than the maximum height h_m before rupture.

1. A. D. SCHELUDKO and A. D. NIKOLOV. Colloid Polymer Sci. **253**, 396 (1975).
2. C. HUH and S. G. MASON. Can. J. Chem. **54**, 969 (1976).
3. C. HUH and S. G. MASON. Colloid Polymer Sci. **255**, 460 (1977).
4. J. F. OLIVER, C. HUH, and S. G. MASON. J. Colloid Interface Sci. **59**, 568 (1977).
5. E. BAYRAMLI. Thesis. McGill University, Montreal. In preparation.
6. R. J. ROE, Y. L. BACCHETTAN, and P. M. G. WONG. J. Phys. Chem. **71**, 18 (1967).

Structure and properties of a *trans–anti* photodimer of 5-methylorotate[1]

CAROL P. HUBER,[2] GEORGE I. BIRNBAUM, AND MICHAEL L. POST

Division of Biological Sciences, National Research Council of Canada, Ottawa, Ont., Canada K1A 0R6

AND

EWA KULIKOWSKA, LUCYNA GAJEWSKA, AND DAVID SHUGAR

Department of Biophysics, Institute of Experimental Physics, University of Warsaw, 02-089 Warszawa, Poland

Received September 19, 1977

CAROL P. HUBER, GEORGE I. BIRNBAUM, MICHAEL L. POST, EWA KULIKOWSKA, LUCYNA GAJEWSKA, and DAVID SHUGAR. Can. J. Chem. **56**, 824 (1978).

5-Methylorotate is relatively radiation resistant in aqueous fluid medium, but readily photodimerizes in an ice matrix. Rapid formation of such a matrix made possible the preparative isolation of the photodimer in good yield. The potassium salt of the photodimer crystallizes as the hexahydrate, $C_{12}H_{10}N_4O_8K_2 \cdot 6H_2O$. The crystals are triclinic with space group $P\bar{1}$, $a = 8.139(3)$, $b = 9.759(3)$, $c = 7.398(3)$ Å, $\alpha = 100.28(7)$, $\beta = 74.22(5)$, $\gamma = 108.67(7)°$, and $V = 533.0$ Å^3, $Z = 1$. The structure was solved by Patterson and direct methods; refinement by block-diagonal least-squares converged at $R = 0.041$ for all 1671 observed reflections. The pyrimidine rings of the centrosymmetric photodimer are arranged in *trans–anti* configuration across the planar cyclobutane ring. The potassium ion is seven-coordinated. In aqueous medium the photodimer exhibits a pK_a of 12.8 due to dissociation of the ring N(3) hydrogen. Irradiation in aqueous medium at 254 nm leads to quantitative regeneration of the monomer with a quantum yield of 0.8. Thermal regeneration of the monomer also occurs in neutral and acid aqueous media, but at a slower rate than for the *trans–syn* orotate photodimer. In contrast to the orotate photodimer, which undergoes alkali-catalyzed opening of the 3,4 bonds of the pyrimidine rings, the 5-methylorotate photodimer under these conditions dissociates to the parent monomer.

CAROL P. HUBER, GEORGE I. BIRNBAUM, MICHAEL L. POST, EWA KULIKOWSKA, LUCYNA GAJEWSKA et DAVID SHUGAR. Can. J. Chem. **56**, 824 (1978).

Dans l'eau liquide, le méthyl-5 orotate est assez résistant aux radiations; toutefois il subit facilement une photodimérisation dans une matrice de glace. La formation rapide d'une telle matrice permet d'isoler le photodimère avec de bons rendements à l'échelle préparative. Le sel du potassium du photodimère cristallise sous forme d'hexahydrate, $C_{12}H_{10}N_4O_8K_2 \cdot 6H_2O$. Les cristaux sont tricliniques avec un groupe d'espace $P\bar{1}$, $a = 8.139(3)$, $b = 9.759(3)$, $c = 7.398(3)$ Å, $\alpha = 100.28(7)$, $\beta = 74.22(5)$, $\gamma = 108.67(7)°$ et $V = 533.0$ Å^3, $Z = 1$. On a résolu la structure par les méthodes directes et de Patterson; un affinement par la méthode des moindres carrés (bloc diagonal) converge vers une valeur de R de 0.041 pour les 1671 réflexions observées. Les cycles de pyrimidine du photodimère centrosymétrique sont orientés dans une configuration *trans–anti* à travers le cycle planaire du cyclobutane. L'ion potassium est heptacoordonné. En solution aqueuse, le photodimère présente un pK_a de 12.8 qui est dû à une dissociation à l'hydrogène attaché en position N(3) du cycle. L'irradiation d'une solution aqueuse à 254 nm conduit à une regénération quantitative du monomère avec un rendement quantique de 0.8. La regénération thermique du monomère se produit aussi en milieu aqueux acide et neutre mais à une vitesse plus lente que pour le photodimère orotate *trans–syn*. Par opposition avec le photodimère orotate qui subit une ouverture catalysée par les bases des liens 3 et 4 du cycle pyrimidine, le photodimère du méthyl-5 orotate se dissocie, dans ces conditions, pour régénérer le monomère de base.

[Traduit par le journal]

Introduction

Various cyclobutane photodimers of 2,4-diketopyrimidines are involved in the lethal and mutagenic effects of ultraviolet irradiation, and orotic acid analogues have been extensively used as model systems in studies of the photodimerization reactions. Whereas orotic acid (I), in aqueous medium over the concentration range 10^{-2} *M* to 10^{-4} *M*, readily photodimerizes via a triplet state (1) to yield almost exclusively the *trans–syn* cyclobutane photodimer (2, 3), 5-methylorotate under these conditions is only slightly susceptible to photodimerization at

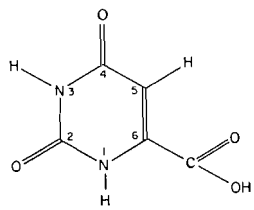

I

[1]NRCC No. 16389.

[2]Author to whom correspondence should be addressed.

Can. J. Chem. Downloaded from www.nrcresearchpress.com by 210.87.254.5 on 09/05/12
For personal use only.

Can. J. Chem. Downloaded from www.nrcresearchpress.com by 210.87.254.5 on 09/05/12
For personal use only.

irradiation wavelengths to the red of 270 nm, and virtually fully resistant when irradiated at 254 nm (4). This situation is reversed in aqueous frozen medium, or in a KBr matrix. In the latter case (5) the quantum yields for photodimer formation from orotate and 5-methylorotate are 0.12 and 0.90, and probably depend on the extent of base stacking in the matrix. We have now found that the degree of photodimerization of 5-methylorotate in an ice matrix may be considerably enhanced by increasing the rate of formation of the matrix from the liquid phase. This has, in turn, made it possible to isolate the main photoproduct in adequate yield for crystallization on a preparative scale, and to examine some of its additional properties in solution, as well as to determine its structure by X-ray diffraction. A different (*cis–anti*) photodimer of 5-methylorotate has also been isolated, in very low yield, from frozen aqueous medium and analyzed crystallographically (6).

Experimental

5-Methylorotic acid was a product of Sigma Chemical Co. The photodimer of orotic acid was prepared as previously described (4).

Ultraviolet absorption spectra and spectral titrations made use of Zeiss (Jena, GDR) and Hilger UVISPEK instruments with 10-mm pathlength quartz cuvettes. ^{1}H nmr spectra were run on Varian 60 and 220 MHz instruments, using solutions in D_2O with sodium 2,2′-dimethyl-2-silapentane-5-sulphonate as internal standard. Infrared spectra were recorded on a Zeiss (Jena, GDR) UR-10 spectrophotometer, using variable pathlength cuvettes fitted with CaF_2 windows. Thin-layer chromatography made use of Merck cellulose F plates with the following solvent systems: (*A*) MeOH – conc. NH_4OH – H_2O (7:1:2), (*B*) *i*-ProOH – MeOH – conc. NH_4OH – H_2O (3:4:1:2), (*C*) *n*-BuOH – acetone – ether – H_2O (8:4.5:4.5:8), (*D*) EtOH – 1 *M* ammonium acetate (4:3). Quantum yields for photodimer dissociation were estimated by chemical actinometry, with the aid of the photohydration reaction of uridine, for which the quantum yield is 0.021.

Preparation of 5-Methylorotate Photodimer

A 10^{-2} *M* solution of 5-methylorotate in 0.01 *N* HCl was gently sprayed onto the surface of a 70 cm × 15 cm glass plate, the lower surface of which was in contact with finely powdered dry ice. Spraying was continued until an approximately 1-mm thick layer of frozen solution had been formed. This layer was then irradiated for a total of about 10–12 min with a Westinghouse 40-W germicidal lamp supported about 2 cm from the surface of the layer; at intervals of 2–3 min during irradiation, the surface of the layer was gently brushed to remove the opaque film formed by condensation from the atmosphere. Upon subsequent thawing of the irradiated frozen solution, a precipitate formed, due to the low solubility of the dimer photoproduct. The precipitate was collected by centrifugation, and the supernatant (the optical density of which was reduced to half of its initial level) concentrated twofold under reduced pressure and further irradiated as above. The final pooled product was extracted several times with small volumes of cold water to remove traces of monomer, dissolved in the minimum volume of 0.02 *N* NH_4OH and centrifuged to remove dust and other impurities. The clear solution was then brought to dryness and the ammonium salt of the 5-methylorotic acid dimer crystallized from water in the form of colourless needles (overall yield 30–35%). The ammonium salt was soluble in water, less so in ethanol and methanol. Suitable crystals for X-ray diffraction could not be obtained with this product, and it was therefore converted to the potassium salt by passage through a column of Dowex 50W-X8. Exposure of an aqueous solution of the potassium salt to ethanol vapour in a desiccator at atmospheric pressure led to precipitation of satisfactory crystals.

Neither the ammonium nor potassium salts exhibited clearly defined melting points, both undergoing initial thermal conversion to the parent 5-methylorotate. For the potassium salt, 20 min heating at 305°C, followed by thin-layer chromatography, showed 90% conversion to monomer, which included some thymine resulting from decarboxylation of the 5-methylorotate. Attempts to thermally decarboxylate the product to thymine photodimer were unsuccessful.

Thin-layer chromatography of the crude ammonium and potassium salts of 5-methylorotate photodimer with solvent systems *A*, *B*, *C*, and *D* showed one major component with R_f values of 0.44, 0.10, 0.08, and 0.21, respectively. The corresponding R_f values for the parent 5-methylorotate were 0.56, 0.37, 0.24, and 0.50. In addition, there were up to three minor spots, amounting to less than 10% of the total, presumably photodimer isomers. Attempts to isolate these by gas chromatography of the trimethylsilylated derivatives were unsuccessful. However, all four isomers in aqueous medium exhibited similar spectral and photochemical characteristics (see below).

Collection and Reduction of X-Ray Data

Preliminary precession photographs indicated triclinic symmetry. The crystal used for data collection was a prism with approximately hexagonal cross section, 0.25 mm across, was 0.57 mm long, and was mounted with b^* as rotation axis; the direction of elongation was parallel to (101). Cell-parameter and intensity measurements were made with a card-controlled Picker four-circle diffractometer equipped with a scintillation counter and pulse-height analyser, using Ni-filtered Cu radiation. Cell dimensions were calculated from 2θ values of high-angle reflections.

$[C_{12}H_{10}N_4O_8]^{2-}\cdot 2K^+\cdot 6H_2O$ fw = 524.5

$P\bar{1}$ (confirmed by the structure analysis), a = 8.139(5), b = 9.759(5), c = 7.398(5) Å, α = 100.28(7), β = 74.22(5), γ = 108.67(7)°. (Delaunay reduced cell: a = 9.393, b = 10.518, c = 7.398 Å, α = 92.57, β = 123.50, γ = 112.20°.) V = 533.0 Å^3, ρ_o = 1.632(5), Z = 1, ρ_c = 1.634 g cm^{-3}. (Cu Kα_1, λ = 1.54051, Cu Kα_2, λ = 1.54433 Å; 20°C.)

One asymmetric unit contains half a dimer anion, one K^+ ion, and three water molecules.

Moving-crystal moving-counter (θ/2θ) scans were used for the intensity measurements; a 10-s background count was accumulated at the end of each scan. All 1818 independent reflections accessible to the diffractometer (2θ ≤ 130°) were measured, and of these, 1671 had net counts above a threshold level which was determined as 20 (deca) counts or 10% of the total background count, whichever was greater. The 147 reflections considered as 'unobservably weak' were excluded from the structure determination and refinement, but included in the final structure-factor calculation. The intensities of two check reflections were monitored periodically during the data collection; fluctuations were less than 2% and appeared to be random. Absorption corrections were applied using a Gaussian integration formula; maximum and minimum transmission factors were 0.428 and 0.136 respectively for μ(Cu Kα) = 46.2 cm^{-1}. The usual Lorentz and polarization corrections were also applied to obtain structure-factor amplitudes.

Determination and Refinement of the Crystal Structure

Positions for eight atoms were deduced from a sharpened

Can. J. Chem. Downloaded from www.nrcresearchpress.com by 210.87.254.5 on 09/05/12
For personal use only.

Patterson synthesis. Extension from this partial structure by tangent refinement (7) gave 17 more atom sites, and a difference synthesis revealed the rest of the structure. Intensity statistics had been inconclusive regarding the presence or absence of a centre of symmetry, and therefore the analysis was carried out in space group $P1$ until the existence of the symmetry centres became obvious. Refinement by block-diagonal least-squares converged at a final R value of 0.041 for all observed reflections. Scattering factors for K^+, O, N, and $C_{valence}$ were taken from International Tables for X-ray Crystallography, Vol. IV (8), and the real part ($\Delta f' = 0.365$) of the anomalous dispersion correction was applied to the K^+ curve. Scattering factor values for bonded H were taken from Stewart *et al.* (9). Non-hydrogen atoms were refined anisotropically and hydrogen atoms, which were all located on difference maps, were refined with isotropic thermal parameters. The function minimized was $\Sigma w(|F_o| - |F_c|)^2$, and the final weighting scheme used was

$$w = w_1 w_2$$

where

$$w_1 = 1 \Big/ \left(1 + \left[\frac{F_o - 10.0}{10.0}\right]^2\right)$$

$$1.25 \leq F_o \leq 73.25$$

and

$$w_2 = (\sin^2 \theta / 0.65)^2$$

if $\sin^2 \theta < 0.65$, otherwise $w_2 = 1.0$. An extinction correction (10) was applied near the end of the refinement. The largest (shift/estimated standard deviation) ratio in the final least-squares cycle was 0.30, and the mean (shift/σ) was less than 0.10. A difference synthesis computed[3] from the final structure factors[4] showed two small peaks and a trough (maximum height ± 0.45 e/Å^3) near the K^+ ion site plus a peak (0.38 e/Å^3) near the mid-point of the C(6)—C(5)′ bond, the latter possibly attributable to bonding electron density.

Results

Properties of 5-Methylorotate Photodimer

In neutral aqueous medium the photodimer exhibited only end absorption in the ultraviolet. Spectral titration in alkaline medium, accompanied by the appearance of a clearly defined band at 240 nm, demonstrated the existence of a pK_a of 12.8, corresponding to the known dissociation of the N(3) hydrogen of 2,4-diketopyrimidines with a saturated 5,6 bond (12, 13).

The infrared spectrum of the photodimer in a KBr matrix in the 1600–1700 cm^{-1} region showed two intense bands at 1690 and 1710 cm^{-1}. Similar carbonyl bands were exhibited by the orotate photodimer.

The 60 MHz ^{1}H nmr spectrum of 5-methylorotate in D_2O showed a single sharp singlet at 2.00 ppm, ascribed to the 5-methyl protons. The 220 MHz spectrum of the photodimer in D_2O showed a unique singlet at 1.44 ppm. This shift to higher field is similar to that observed for the 5-methyl protons in thymine photodimers (14) and is consistent, as are the other spectral properties, with a cyclobutane photodimer structure. However, the only noncrystallographic evidence regarding the nature of the isomer present comes from the titration in acid medium of the photodimers of orotate and of 5-methylorotate against the corresponding parent monomers as controls. Each photodimer gave a single titration curve, indicating that each photodimer must have the *trans* configuration.[5]

Lability in Aqueous Medium

Irradiation of a 10^{-4} M solution at 254 nm led to quantitative photodissociation to the parent monomer with a quantum yield of 0.8, as observed for other 2,4-diketopyrimidine cyclobutane photodimers (4). At neutral pH the photoproduct underwent thermal dissociation to the parent monomer. Heating for 15 h at 100°C, at a concentration of 10^{-4} M, led to 8% conversion to monomer at pH 6.5, and 22% conversion in 1 N HCl. Under analogous conditions the *trans–syn* orotate photodimer proved more labile; conversion to the monomer was 24% and 85% in neutral and acid media respectively. In strongly alkaline medium the 5-methylorotate photodimer was slowly converted to the parent monomer. In 1 N NaOH at 60°C the rate constant for this reaction was 6.3×10^{-2} min^{-1}, so that the $t_{1/2}$ was about 11 min. Under such conditions orotate photodimer is more reactive, but its reactivity is manifested by disappearance of the uv absorption band at about 240 nm (4), as in the case of 5,6-dihydro-2,4-diketopyrimidines (12), and appears to be due to opening of the 3,4 bonds in the pyrimidine rings, with retention of the cyclobutane ring as in the case of a thymine photodimer (15).

X-Ray Analysis Results

Final fractional coordinates and thermal parammeters are listed with their esd's in Table 1. Bond lengths and bond angles are shown for the organic anion in Fig. 1, and interatomic distances and angles for the coordination polyhedron around the potassium ion have been deposited.[4] The anisotropic thermal vibrations of the atoms comprising the anion were analysed (16) for rigid-body motion, and the translational and librational motion of the group was found to be very small. Bond length corrections

[3]Unless otherwise indicated, all computations were made with the NRCC set of Crystallographic Programs for the IBM/360 system (11).

[4]Copies of tables of observed and calculated structure factors and of interatomic distances and angles in the K—O coordination polyhedron are available, at a nominal charge, from the Depository of Unpublished Data, CISTI, National Research Council of Canada, Ottawa, Ont., Canada K1A 0S2.

[5]A *cis* configuration would have led to the known splitting of the pK values for neighbouring carboxyl groups in dicarboxylic acids.

Can. J. Chem. Downloaded from www.nrcresearchpress.com by 210.87.254.5 on 09/05/12
For personal use only.

TABLE 1. Final parameters and their standard deviations

(*a*) Nonhydrogen atoms[a]

Atom	x	y	z	U_{11}	U_{22}	U_{33}	$2U_{23}$	$2U_{13}$	$2U_{12}$
$K^+(1)$	6890(1)	3733(0)	−5723(1)	318(2)	298(2)	378(2)	113(3)	−73(4)	137(3)
N(1)	1797(2)	1464(2)	−2268(2)	222(7)	234(7)	204(7)	142(12)	48(12)	214(12)
C(2)	3187(2)	1011(2)	−3245(2)	187(8)	203(8)	211(8)	9(13)	−40(13)	81(13)
O(2)	4086(2)	1439(1)	−4781(2)	242(6)	294(7)	206(6)	135(10)	116(10)	194(10)
N(3)	3628(2)	9(2)	−2509(2)	201(7)	310(8)	273(8)	160(13)	112(12)	276(13)
C(4)	2660(2)	−709(2)	−977(3)	204(8)	252(9)	242(8)	81(14)	−40(14)	163(14)
O(4)	3081(2)	−1700(2)	−618(2)	335(7)	354(8)	373(8)	265(12)	60(12)	410(13)
C(5)	1199(2)	−116(2)	347(2)	193(8)	219(8)	183(8)	43(13)	−29(13)	128(13)
C(6)	773(2)	1121(2)	−394(2)	178(7)	217(8)	180(8)	42(13)	−3(12)	130(13)
C(7)	1705(3)	264(2)	2258(3)	321(10)	311(10)	225(9)	37(15)	−201(15)	150(16)
C(8)	964(2)	2529(2)	997(3)	221(8)	233(8)	253(9)	−3(14)	−69(14)	169(14)
O(9)	−194(2)	2492(2)	2491(2)	296(7)	359(8)	260(7)	−143(11)	24(11)	230(12)
O(10)	2320(2)	3564(2)	536(2)	361(8)	262(7)	397(8)	−57(12)	−46(13)	−40(12)
O(11)	7661(3)	3624(2)	−2145(2)	645(11)	395(9)	357(8)	108(14)	−22(16)	498(16)
O(12)	9049(2)	6526(2)	−5906(2)	413(8)	349(8)	350(8)	32(13)	−212(13)	251(13)
O(13)	4780(2)	5129(2)	−2490(3)	387(9)	503(10)	443(9)	233(15)	−234(15)	163(15)

(*b*) Hydrogen atoms[b]

Atom	x	y	z	B	Atom	x	y	z	B
H(11)	162(3)	207(3)	−272(3)	0.0(0.4)	H(111)	765(6)	446(5)	−149(6)	3.3(0.8)
H(31)	446(4)	−30(3)	−319(4)	0.5(0.5)	H(112)	733(6)	310(5)	−139(6)	3.4(0.8)
H(71)	85(4)	62(3)	323(4)	0.8(0.5)	H(121)	924(5)	683(4)	−489(5)	2.0(0.6)
H(72)	283(4)	94(4)	210(5)	1.6(0.6)	H(122)	1011(5)	651(4)	−658(5)	2.2(0.6)
H(73)	187(4)	−56(3)	258(4)	0.9(0.5)	H(131)	558(5)	556(4)	−198(6)	2.8(0.7)
					H(132)	411(6)	447(5)	−174(6)	3.5(0.8)

[a]These parameters were multiplied by 10^4. The thermal parameters are expressed as $\exp[-2\pi^2(U_{11}h^2a^{*2} + U_{22}k^2b^2 + U_{33}l^2c^{*2} + 2U_{23}klb^*c^* + 2U_{13}hla^*c^* + 2U_{12}hka^*b^*)]$.
[b]The number of the atom to which the hydrogen is bonded is obtained by dropping the least significant digit of the hydrogen atom number. The coordinates were multiplied by 10^3.

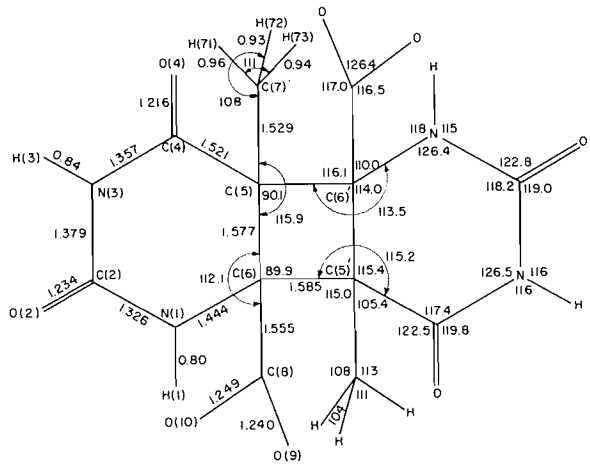

FIG. 1. Bond distances and angles in the 5-methylorotate photodimer anion. The esd's for the distances involving only nonhydrogen atoms are 0.002–0.003 Å; esd's for the corresponding angles are 0.13–0.19°. When hydrogen atoms are involved the esd's are about 10 times larger.

derived from the libration tensor were less than the individual esd's and were therefore not applied.

Discussion of the Crystal Structure

In this photodimer a crystallographic centre of symmetry lies in the centre of the cyclobutane ring, constraining it to be planar. The two pyrimidine rings are fused to the cyclobutane ring in *trans–anti* configuration and the dihedral angle between the cyclobutane ring and the mean pyrimidine ring plane is 121.6°. Each pyrimidine ring is significantly nonplanar, and the endocyclic torsional angles, given in Table 2, indicate that the distortions from planarity are in the direction of a slight twist-boat shape (17). Of the six atoms, C(4) deviates most (0.088 Å) from the mean pyrimidine ring plane, carrying O(4) 0.181 Å out of the plane, thereby increasing the separation between O(4) and C(7) which is, even so, only 2.84 Å. The C(7)···C(8) and C(7)···N(1)′ nonbonded distances, 2.83 and 2.81 Å respectively, are also rather short, indicating the severe overcrowding caused by the full substitution of C(5), C(6), C(5)′, C(6)′.

The bond lengths and angles in this structure are, in general, equal within experimental error to those in the *cis–anti* photodimer of 5-methylorotate (6). The few significant deviations are shown in Table 3, and it is interesting to note that where parameters involving only pyrimidine ring atoms differ, i.e. the N(1)—C(2) bond length and C(6)—N(1)—C(2), C(5)—C(6)—N(1) bond angles, the values found in the present *trans–anti* structure compare rather better with the values in the thymine *trans–anti* photodimer (18). Other significant deviations, involving the

TABLE 2. Torsional angles in the photodimer

(*a*) Endocyclic torsional angles in the pyrimidine ring

N(1)—C(2)—N(3)—C(4)	8.4
C(2)—N(3)—C(4)—C(5)	−16.0
N(3)—C(4)—C(5)—C(6)	9.5
C(4)—C(5)—C(6)—N(1)	2.4
C(5)—C(6)—N(1)—C(2)	−10.9
C(6)—N(1)—C(2)—N(3)	6.5

(*b*) Other torsional angles

C(7)—C(5)—C(6)—C(8)	0.3
C(8)—C(6)—C(5)′—C(4)′	3.6
N(1)—C(6)—C(5)′—C(7)′	2.5
N(1)—C(6)—C(8)—O(10)	−23.2
C(5)—C(6)—C(8)—O(9)	−71.8
C(5)—C(6)—C(8)—O(10)	104.9
C(5)′—C(6)—C(8)—O(9)	29.5

C(4)—C(5)—C(7), N(1)—C(6)—C(8), and C(5)′—C(6)—C(8) angles, probably can be explained as the result of the different distortions necessary to minimize interatomic repulsion in the two isomers.

Partial relief of these forces of interatomic repulsion is also achieved by the lengthening of the C(5)—C(6) and C(6)—C(8) bonds. The C(5)—C(6) bond length in the present structure (1.577 Å), while essentially equal to the corresponding value (1.57 Å) in the *cis–anti* isomer, is significantly longer than in most other pyrimidine photodimers (3, 18–21). The C(6)—C(8) bond lengths in this structure (1.555 Å) and the *cis–anti* isomer (1.56 Å) are significantly longer than corresponding values in the orotic acid monohydrate structure (22) (1.498 Å) and in the *trans–syn* photodimer of methylorotate (3) (1.522 Å).

Differences in the interpyrimidine bond lengths in the present structure and in the *trans–syn* orotate photodimer help partially to explain the differences in lability of the two dimers. In the *trans–syn* crystal structure (3), the C(6)—C(6)′ bond, to which both carboxyl groups are bonded, is abnormally lengthened to 1.628 Å, while the C(5)—C(5)′ bond, 1.556 Å, is close to normal length, as are the intrapyrimidine bonds, 1.544 Å. In the present structure the strain induced by overcrowding is distributed more equally; the interpyrimidine bonds (1.585 Å) are essentially the same length as the intrapyrimidine bonds (1.577 Å). If we assume that the C(6)—C(6)′ bond in (nonesterified) *trans–syn* orotate photodimer has a fairly similar length to that observed in the crystal structure of the methyl ester (and the configurations of the dimer acid and ester have been shown to be identical (2)), then the increased lability in neutral and acid media of the orotate photodimer relative to the 5-methylorotate dimer

Can. J. Chem. Downloaded from www.nrcresearchpress.com by 210.87.254.5 on 09/05/12
For personal use only.

TABLE 3. Comparison of molecular geometry in the *trans–anti* (*A*) and *cis–anti* (*B*) photodimers of 5-methylorotate. Bond length and bond angle values given here are those showing significant differences in the two structures. Comparable values are shown also from the *trans–anti* thymine photodimer (*C*)

	A	*B*[a]	*C*[b]
N(1)—C(2)	1.326(3) Å	1.36(1) Å	1.334(3) Å
C(2)—N(1)—C(6)	126.4(2)°	122.9(7)°	125.7(2)°
N(1)—C(6)—C(5)	114.0(1)°	111.7(6)°	116.0(2)°
C(4)—C(5)—C(7)	105.4(2)°	108.6(5)°	110.5(2)°
N(1)—C(6)—C(8)	110.0(1)°	104.9(6)°	—
C(5)′—C(6)—C(8)	116.1(1)°	122.1(6)°	—

[a]From ref. 6.
[b]From ref. 18.

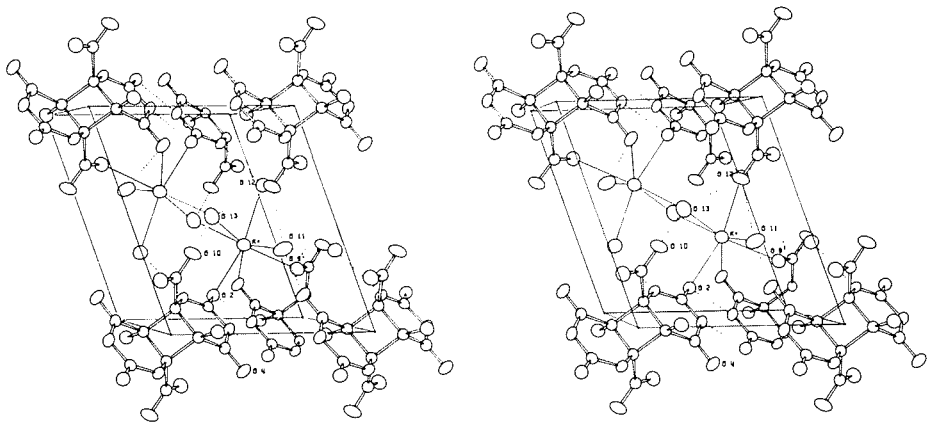

FIG. 2. Stereoscopic view of the packing arrangement drawn by the ORTEP program (23). $K^+\cdots O$ contacts are indicated by single solid lines, hydrogen bonds by dotted lines. Axial directions: $x\rightarrow$, $y\uparrow$, z pointing out of the plane toward the reader.

can be correlated with this longer bond. It is not so easy to understand why, in alkaline solution, the cyclobutane ring is preserved in the case of orotate photodimer (and also a *cis–syn* thymine photodimer (15)), and cleaved in the case of 5-methylorotate photodimer.

The carboxyl groups in the present dimer are both ionized, balancing the two K^+ ions per unit cell, and one would therefore expect delocalization to make the C—O bond lengths equal. The small difference, 0.009 Å, between the observed C(8)—O(9) and C(8)—O(10) bond lengths is possibly not significant, but could be ascribed to different hydrogen bonding patterns at O(9) and O(10) (see below).

The potassium ion is seven-coordinated, by three oxygen atoms from the dimer and by four contacts to water-molecule oxygens. Six of the $K^+\cdots O$ distances are in the range 2.67–2.94 Å, while the seventh is 3.057 Å. There are no other $K^+\cdots O$ distances less than 3.50 Å, and no short contacts to nonoxygen atoms. The six closer oxygens can be described as forming a distorted octahedron, with the seventh oxygen accommodated outside the largest octahedral face. Both the sevenfold coordination of the K^+ ion and the range of $K^+\cdots O$ distances are unexceptional.

Figure 2 gives a stereoscopic view of the packing arrangement and hydrogen bonding, and further geometrical details about the hydrogen bonds are listed in Table 4. All of the available hydrogen atoms are involved in hydrogen bond formation.

The dimer anions are linked into infinite chains along [10$\bar{1}$] by pairs of hydrogen bonds joining N(3) and O(2) of one dimer to O(2) and N(3) respectively of an adjacent dimer. The pairs of pyrimidine rings joined by hydrogen bonds are coplanar within 0.2 Å. Dimer anions within a chain are also linked through participation of O(2), O(4), and O(9), from adjacent dimers, in each potassium coordination polyhedron.

The coordination polyhedra occur in pairs, sharing an edge of which the mid-point is a centre of symmetry. The only linkage of one dimer chain to another by the potassium coordination polyhedron is indirect, via centrosymmetrically related O(2), O(4), and O(9) atoms at opposite ends of each coordination pair.

Can. J. Chem. Downloaded from www.nrcresearchpress.com by 210.87.254.5 on 09/05/12
For personal use only.

TABLE 4. Geometrical details of the hydrogen bonds, *D*—H···*A*

D	*H*	*A*	*D*···*A* (Å)	*D*—H (Å)	H···*A* (Å)	*D*—H···*A* (deg)
N(1)	H(1)	O(12)	2.909	0.80	2.11	173
N(3)	H(3)	O(2)	2.849	0.84	2.04	163
O(11)	H(111)	O(10)	2.786	0.87	1.93	168
O(11)	H(112)	O(4)	2.835	0.76	2.08	169
O(12)	H(121)	O(9)	2.832	0.79	2.05	169
O(12)	H(122)	O(11)	2.711	0.88	1.83	176
O(13)	H(131)	O(10)	2.925	0.80	2.13	172
O(13)	H(132)	O(10)	2.859	0.87	2.03	160

Other cohesive forces are provided by the hydrogen bonds involving water molecules. Adjacent dimer chains in the *xz* plane are linked via O(12), while connections in the *y* direction are via O(11) and O(13).

The appearance of the report (6) on the *cis–anti* photodimer of 5-methylorotate, which followed completion of the present analysis, raises the question of why two different isomers were obtained under apparently very similar experimental conditions. (Both photodimers were prepared by irradiation of frozen aqueous solutions of 5-methylorotic acid, and then converted to the particular salts.) It seems possible that the different dimer may have resulted from differences in the procedure employed for preparation of the ice matrix, or that crystallization of the barium salt led to preferential isolation of one of the minor isomers referred to above. Unfortunately, Cheng *et al.* (6) give no quantitative data on yields or chromatographic behaviour of the crude photodimer solution prior to crystallization.

Acknowledgments

We thank Dr. R. W. Dabeka and H. Seguin for chemical analyses.

1. M. CHARLIER, C. HÉLÈNE, and M. DOURLENT. J. Chim. Phys. Phys.-Chim. Biol. **66**, 700 (1969).
2. G. I. BIRNBAUM, J. M. DUNSTON, and A. G. SZABO. Tetrahedron Lett. 947 (1971).
3. G. I. BIRNBAUM. Acta Crystallogr. Sect. B, **28**, 1248 (1972).
4. E. SZTUMPF and D. SHUGAR. Photochem. Photobiol. **4**, 719 (1965).
5. R. LISEWSKI and K. L. WIERZCHOWSKI. Photochem. Photobiol. **11**, 327 (1970).
6. P.-T. CHENG, V. HORNBY, W. WONG-NG, S. C. NYBURG, and D. WEINBLUM. Acta Crystallogr. Sect. B, **32**, 2251 (1976).
7. J. KARLE. Acta Crystallogr. Sect. B, **24**, 182 (1968).
8. International Tables for X-ray Crystallography. Vol. IV. Kynoch Press, Birmingham, England. 1974. p. 72.
9. R. F. STEWART, E. R. DAVIDSON, and W. T. SIMPSON. J. Chem. Phys. **42**, 3175 (1965).
10. P. R. PINNOCK, C. A. TAYLOR, and H. LIPSON. Acta Crystallogr. **9**, 173 (1956).
11. F. R. AHMED, S. R. HALL, M. E. PIPPY, and C. P. HUBER. J. Appl. Crystallogr. **6**, 309 (1973).
12. C. JANION and D. SHUGAR. Acta Biochim. Pol. **7**, 309 (1960).
13. K. L. WIERZCHOWSKI, E. LITOŃSKA, and D. SHUGAR. J. Am. Chem. Soc. **87**, 4621 (1965).
14. D. L. WULFF and G. FRAENKEL. Biochim. Biophys. Acta, **51**, 332 (1961).
15. G. M. BLACKBURN and R. J. H. DAVIES. J. Chem. Soc. C, 2239 (1966).
16. V. SCHOMAKER and K. N. TRUEBLOOD. Acta Crystallogr. Sect. B, **24**, 63 (1968).
17. R. BUCOURT and D. HAINAUT. Bull. Soc. Chim. Fr. 1366 (1965).
18. N. CAMERMAN and S. C. NYBURG. Acta Crystallogr. Sect. B, **25**, 388 (1969).
19. N. CAMERMAN, D. WEINBLUM, and S. C. NYBURG. J. Am. Chem. Soc. **91**, 982 (1969).
20. E. ADMAN and L. H. JENSEN. Acta Crystallogr. Sect. B, **26**, 1326 (1970).
21. J. KONNERT and I. L. KARLE. J. Cryst. Mol. Struct. **1**, 107 (1971).
22. F. TAKUSAGAWA and A. SHIMADA. Bull. Chem. Soc. Jpn. **46**, 2011 (1973).
23. C. K. JOHNSON. ORTEP, Report ORNL-3794. 2nd rev. Oak Ridge National Laboratory, Oak Ridge, Tennessee. 1970.

Can. J. Chem. Downloaded from www.nrcresearchpress.com by 210.87.254.5 on 09/05/12
For personal use only.

Studies on nucleation phenomena occurring in aqueous solutions supersaturated with calcium sulfate

D. M. KELLER, RONALD E. MASSEY, AND O. E. HILEMAN, JR.
Department of Chemistry, McMaster University, Hamilton, Ont., Canada L8S 4M1

Received July 8, 1977

D. M. KELLER, RONALD E. MASSEY, and O. E. HILEMAN, JR. Can. J. Chem. **56**, 831 (1978).

The results of a set of experiments designed to delineate the nucleation rate, supersaturation, temperature surface for the system $CaSO_4 \cdot 2H_2O/H_2O$ are reported. The data were obtained using the droplet technique coupled with *in situ* generation of SO_4^{2-} under the conditions that dS/dt was large during the early part of the induction period and it was zero during the actual nucleation events. The observed shape of the surface is compared with that suggested by the classical theory of nucleation and differences are commented on. The critical parameters important in classical nucleation theory are reported.

D. M. KELLER, RONALD E. MASSEY et O. E. HILEMAN, JR. Can. J. Chem. **56**, 831 (1978).

On rapporte les résultats d'un ensemble d'expériences ayant pour but de délimiter la vitesse de nucléation, la sursaturation et la surface de température du système $CaSO_4 \cdot 2H_2O/H_2O$. On a obtenu les données en utilisant la technique des goutellettes de concert avec la formation *in situ* de SO_4^{2-} dans des conditions telles que la valeur dS/dt est plus grande durant la partie initiale de la période d'induction et qu'elle est égale à zéro lorsque la nucléation s'effectue. On a comparé la forme observée pour la surface avec celle qui est suggérée par la théorie classique de la nucléation et on présente des commentaires au sujet des différences. On rapporte les paramètres critiques importants dans la théorie de nucléation classique.
[Traduit par le journal]

Introduction

The classical theory of nucleation arose out of recognition that the observation of supercooling or supersaturation in a system undergoing a phase transformation represents a barrier to that transformation and, additionally, that the description of such a process is a problem in kinetics. Equation 1 summarizes the essence of the theory.

$$[1] \qquad J = A \exp(-\Delta G^*/kT)$$

where J is the rate of nucleation, A is some collection of constant and exponential terms assumed to be constant, ΔG^* represents the free energy barrier to the transformation, and k and T have their usual meanings.

The free energy change accompanying a phase transformation is thought to be composed of two parts: one related to the work of formation of a surface between the new and the mother phase and one related to the difference in chemical potential between a monomer in the new phase and one in the mother phase. If one assumes spherical embryos, the expression for the magnitude of this free energy change has the following form.

$$[2] \qquad \Delta G = \frac{4}{3}\frac{\pi r^3}{\bar{v}}(\phi_n - \phi_m) + 4\pi r^2\sigma$$

where r is the radius of the newly forming phase and ϕ_n is the chemical potential of one of its interior monomers, ϕ_m is the chemical potential of a monomer in the mother phase, σ is the surface tension between the mother phase and the newly forming phase, and $\bar{v}$ is the molecular volume in the new phase.

Because the two terms in eq. 2 are of opposite signs and are of different power dependencies upon r, a maximum occurs in the ΔG, $\phi_n - \phi_m$, r surface. For systems undergoing homogeneous crystal nucleation from a supersaturated solution, the expression for the free energy values along this maximum is given by eq. 3.

$$[3] \qquad \Delta G_{max} = \frac{16\pi\sigma^3\bar{v}^2}{3(kT \ln S)^2} = \frac{4\pi\sigma r_{max}^2}{3}$$

where $(\phi_n - \phi_m)$ has been replaced by $kT \ln S$, S being the level of supersaturation being experienced by the system at the point of nucleation.

In 1926, Volmer and Weber recognized the connection between ΔG^* of eq. 1 and ΔG_{max} of eq. 3; i.e., that the frequency of formation of nuclei by spontaneous fluctuations in solution is proportional to $\exp[-\Delta G_{max}/kT]$ (1). Thus, ΔG_{max} appears to be analogous to the activation free energy of reaction rate theory and could be substituted for it in eq. 1 yielding eq. 4.

$$[4] \qquad J = A \exp\left[-\frac{16\pi\sigma^3\bar{v}^2}{3(kT)^3(\ln S)^2}\right]$$

Outside of the identification of the various components of A, little has been added to the classical theory for 40 or so years (2–7). It is used currently as a guide in the experimental design of and as a

Can. J. Chem. Downloaded from www.nrcresearchpress.com by 210.87.254.105 on 09/05/12
For personal use only.

Can. J. Chem. Downloaded from www.nrcresearchpress.com by 210.87.254.105 on 09/05/12
For personal use only.

basis for data analysis and interpretation of the results of studies on homogeneous crystal nucleation from supersaturated solutions.

Testing of the classical theory as applied to homogeneous crystal nucleation from solution has been confounded by the catalytic effect of preformed surfaces in solution. Vonnegut was the first to recognize that miniaturization of a macroscopic sample of a condensed phase via subdivision into many non-communicating micro samples sequestered the effect of such surfaces and, thus, allowed the study of homogeneous phase transformations in melts (8). White and Frost extended the technique to homogeneous crystal nucleation from solution (9). Each, however, was limited to those materials that could be caused to nucleate under a driving force created by narrow temperature change ranges. Through research in our laboratories we have extended the applicability of the droplet technique to a rather wide variety of materials by coupling it with either *in situ* generation of the insoluble substance from very soluble precursors or selective extraction of solvent from the droplet population into a surrounding medium (10–16). Recent results from our studies on $CaSO_4$ nucleation have shown that additional problems in testing the theory arise during the reduction of raw 'number–time' data obtained from droplet experiments to nucleation rates if the complications of time dependent supersaturation levels and supersaturation dependent time lags are present. Two of the authors have discussed the former problem in an earlier paper (16).

The purpose of this paper is to describe a set of experiments designed to delineate the response surface of J with respect to S and T. The shape of this response surface suggests an empirical relationship between the observable and the two experimental variables and this may be compared with theory.

Experimental Details

A droplet experiment can be divided into a series of steps, namely, preparation of an aqueous solution containing the precursors for generation of the supersaturation, dispersion of a small, known amount of this solution in an immiscible oil, selection and subsequent preparation of a population of droplets for microscopic observation, generation of the supersaturation, notation of 'number–time' data and then data analysis and interpretation. Additionally, the rate of formation of the supersaturation and the equilibrium solubility of the crystalline product in aqueous medium must be measured.

The reaction between $S_2O_8^{2-}$ and I^- was used to generate SO_4^{2-} *in situ*, in the presence of Ca^{2+}. Supersaturation data for a droplet population were inferred from results of 'beaker' experiments carried out in parallel. The appearance of crystals within the droplet population was recorded photomicrographically. For subsequent analysis, the 'number-time' data were separated on the basis of narrow droplet volume ranges.

Reagents and Apparatus

All salts ($Ca(NO_3)_2 \cdot 4H_2O$ (Baker), $K_2S_2O_8$ (Allied), NH_4I (Baker), and EDTA (Fisher)) were of Reagent Grade quality. Solutions prepared from them were pressure filtered (N_2) through a 0.3 μ PCV filter (Sartorius). Solution A was prepared by mixing, just before use, equal volumes of the $Ca(NO_3)_2 \cdot 4H_2O$ and the $K_2S_2O_8$ solutions. Solution B contained NH_4I. Light and heavy mineral oils (BDH) were used as supplied. The apparatus used has been described elsewhere (16).

Solubility of $CaSO_4 \cdot 2H_2O$

A synthetic matrix was prepared that contained KNO_3 (0.204 *M*), NH_4NO_3 (0.204 *M*), NH_4I (0.146 *M*), and an excess of freshly prepared $CaSO_4 \cdot 2H_2O$. The suspension was stirred for 24 h at the desired temperature and then pressure filtered (N_2). The Ca^{2+} content of the resulting filtrate was determined by an EDTA/Mg^{2+} back titration.

Determination of Supersaturation Data

The change in concentration of I_3^- in solution as a function of time was determined by $S_2O_3^{2-}$ titration. Aliquots of the reaction mixture were removed at increasing reaction time intervals, the reaction was quenched by dilution, and the I_3^- was titrated with standard $S_2O_3^{2-}$ to a starch end point. The reaction was also monitored spectrophotometrically at 610 nm. The transmittance range was set with deionized H_2O (100% T) and an equilibrated reaction mixture (0% T).

Temperature Rise-time

Measurements of temperature rise-times after start-up of the supply of circulating, thermostatted water to the cell holder and the resulting equilibrium temperatures of mineral oil samples contained in the nessler cup put in place on the microscope stage were carried out using a fine wire (iron–constantan) thermocouple and a potentiometer (Leeds–Northrup).

Droplet Experiments

The usual procedure was used to prepared a large population of non-communicating droplets of narrow volume range and situated on an optically flat surface ready for photomicroscopic observation (16). Equal volumes of freshly pressure filtered solutions of A and B were mixed just immediately prior to the experiment. The solution compositions studied are shown in Table 1. 'Number–time' data were collected from the 35 mm slides in the usual manner (16).

Results

From the data obtained during preliminary experiments it was established that $CaSO_4 \cdot 2H_2O$ is the sparingly soluble product formed during the reaction between I^- and $S_2O_8^{2-}$ in the presence of Ca^{2+}. The measured values of the solubility of gypsum were found to be invariant, within experimental error, over the narrow range of ionic strengths encountered in the experiments. The effect of temperature on its solubility is noted in Fig. 1 and, together with calculated or interpolated K_{sp} values, in Table 2.

The result of the spectrophotometric determination of the times required for the generation reaction ($S_2O_8^{2-} + I^-$) to reach equilibrium as a function of various initial I^- concentrations are shown in Fig. 2. Approximately 12 min overall are required for mixing of reagents, droplet preparation and selection and initial microscopic observations. During the

Can. J. Chem. Downloaded from www.nrcresearchpress.com by 210.87.254.105 on 09/05/12
For personal use only.

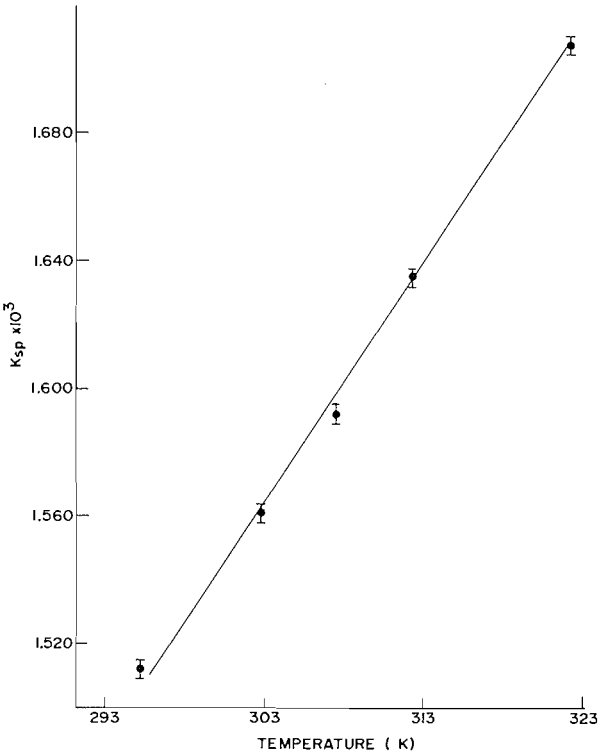

FIG. 1. A plot of the K_{sp} of $CaSO_4 \cdot 2H_2O$ in the matrix solution at various temperatures.

latter part of this time interval, the reaction should reach chemical equilibrium. Additionally, the equilibrium temperature of the reaction mixture must be increased from $\sim 15°C$ to the temperature of interest during this time interval. The results of temperature rise-time studies are shown in Fig. 3. In addition to reaction time considerations enough unreacted I^- must remain at equilibrium to solubilize the I_2 formed (as I_3^-). Taken together, these factors led to use of an initial I^- concentration of 0.350 *M* for each of the nucleation experiments.

'Number–time' data resulting from analysis of the photomicrographic record of nucleation events occurring with each droplet population were fitted to eq. 5 with the aid of a non-linear least squares program 'Gaushaus'.

$$[5] \qquad n_{t,v} = N(1 - \exp[-J_f' v(t_e - \tau)])$$

where $n_{t,v}$ is the count of the number of droplets in a population of volume v in which a crystal has been detected at experimental time t_e, N is the total number of droplets in a population of volume v, J_f' is the best fit nucleation rate, and τ is the lag time. The fit was optimized by adjustment of the two parameters, N and J_f'. Final estimates of τ were found by iteration. The results are shown in Table 3.

TABLE 1. Experimental variables used in the constant driving force experiments

Variables[a]	E_4	E_5	E_6	E_7	E_8	E_9	E_{10}	E_{11}	E_{12}	E_{13}	E_{14}	E_{15}
$T(\pm 1)$ K	295.0	301.3	307.5	313.6	295.0	301.3	307.5	313.6	295.0	301.3	307.5	313.6
$[Ca^{2+}]_i$	0.175	0.175	0.175	0.175	0.204	0.204	0.204	0.204	0.233	0.233	0.233	0.233
$[SO_4^{2-}]_f$	0.175	0.175	0.175	0.175	0.204	0.204	0.204	0.204	0.233	0.233	0.233	0.233
$[S_2O_8^{2-}]_i$	0.0875	0.0875	0.0875	0.0875	0.102	0.102	0.102	0.102	0.117	0.117	0.117	0.117
$[K^+]$	0.175	0.175	0.175	0.175	0.204	0.204	0.204	0.204	0.233	0.233	0.233	0.233
$[NO_3^-]$	0.350	0.350	0.350	0.350	0.408	0.408	0.408	0.408	0.466	0.466	0.466	0.466
μ_f	1.23	1.23	1.23	1.23	1.37	1.37	1.37	1.37	1.52	1.52	1.52	1.52

[a] $[SO_4^{2-}]_f$ = final sulfate concentration; μ_f = final ionic strength, $pH = 3.23$; $[NH_4] = 0.350$ *M*. $[Ca^{2+}]/[SO_4^{2-}] = 1.00$.

TABLE 2. Determination of K_{sp} of $CaSO_4 \cdot 2H_2O$ at four temperature levels

Constant temperature bath (K)	Beaker temperature (K)	$[Ca^{2+}] \times 10^2$	$K_{sp} \times 10^{3a}$	Nessler cup temperature (K)	$K_{sp} \times 10^{3b}$
293.16±0.05	293.16±0.05	3.888±0.008	1.512±0.003	295.0±1.0	1.518±0.003
303.16±0.05	302.76±0.05	3.951±0.008	1.561±0.003	301.3±1.0	1.553±0.003
313.16±0.05	312.26±0.05	4.044±0.008	1.635±0.003	307.5±1.0	1.598±0.003
323.16±0.05	322.16±0.05	4.133±0.008	1.708±0.003	313.6±1.0	1.644±0.003

[a]Calculated at the corresponding beaker temperature; used in preparation of Fig. 1.
[b]Obtained by interpolation in Fig. 1 for the corresponding Nessler cup temperature.

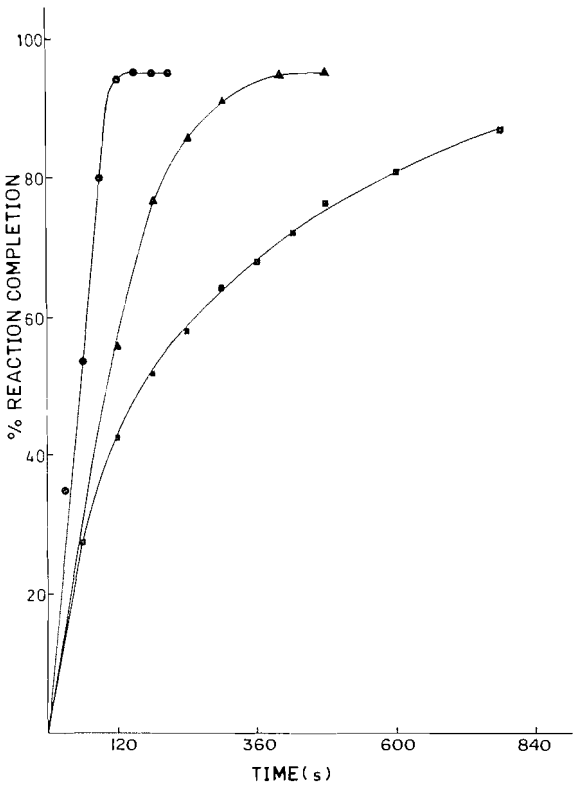

FIG. 2. A plot of percent reaction completion vs. time at various initial iodide concentrations. $[S_2O_8^{2-}] = 0.102$; $T = 295.0 \pm 1.0$ K; initial $[I^-]$: ●, 0.500; ▲, 0.400; and ■, 0.250.

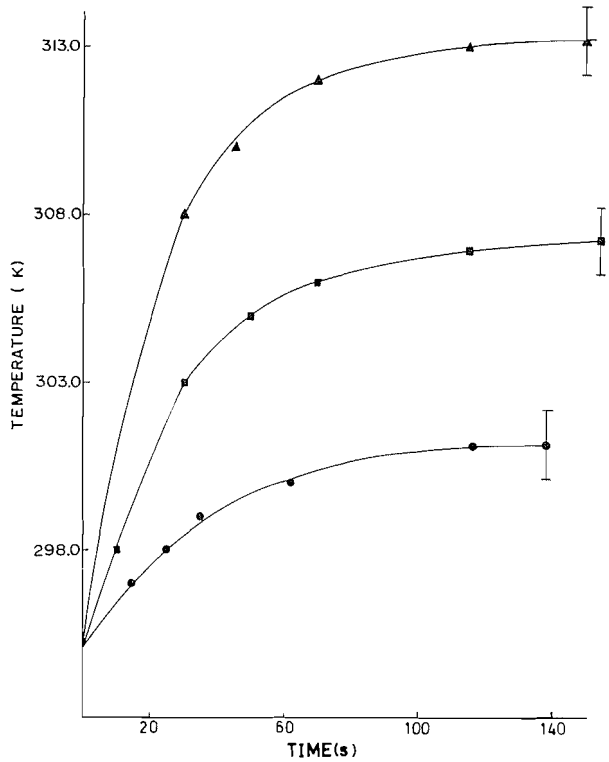

FIG. 3. Plots of temperature rise times in the observation cup. Constant temperature bath temperature ●, 303.2 K; ■, 313.2 K; and ▲, 323.2 K.

Discussion

Difficulties surrounding the interpretation of results obtained from nucleation studies with a time dependent driving force were presented in a previous publication (15). In this study, an attempt was made to produce a 'step function' change in the driving force and then to follow the subsequent nucleation events; thus, eliminating these difficulties. To this end, a stoichiometric excess of iodide was used to reduce peroxydisulfate. The iodine formed was held in solution by the remaining iodide ion as I_3^-. Thus, $CaSO_4 \cdot 2H_2O$ was the only sparingly soluble species present in solution and its analytical concentration was effectively invariant with time during the experiment. This invariance was negated somewhat at higher levels of the temperature and/or the ion product.

Estimates of J_f', τ, and N values were obtained from the 'number–time' data using eq. 5. Large uncertainties in the values were noted if a particular volume sub-class within the droplet population numbered less than 100. To decrease this uncertainty, data from equivalent volume sub-classes but different populations were combined before analysis. A high degree of negative correlation between the parameters N and J_f' was noted if the maximum $n_{t,v}/N$ ratio was much less than one. Initial estimates

Can. J. Chem. Downloaded from www.nrcresearchpress.com by 210.87.254.105 on 09/05/12
For personal use only.

TABLE 3. A summary of J_f' and τ values of four temperature and three ion product levels

Ion product	Parameter	Value at 295.0 K	301.3 K	307.5 K	313.6 K
0.03063	J_f' (s^{-1} cm^3)	5.80×10^3	4.67×10^4	2.22×10^6	3.67×10^6
	τ (s)	1.56×10^4	5.40×10^3	9.80×10^2	4.2×10^1
0.04162	J_f' (s^{-1} cm^3)	1.90×10^5	4.27×10^6	3.25×10^7	5.77×10^7
	τ (s)	6.40×10^3	7.03×10^2	1.00×10^2	2.1×10^1
0.05429	J_f' (s^{-1} cm^3)	5.27×10^6	1.36×10^7	1.23×10^8	3.14×10^8
	τ (s)	1.85×10^3	2.30×10^2	2.7×10^1	1.3×10^1

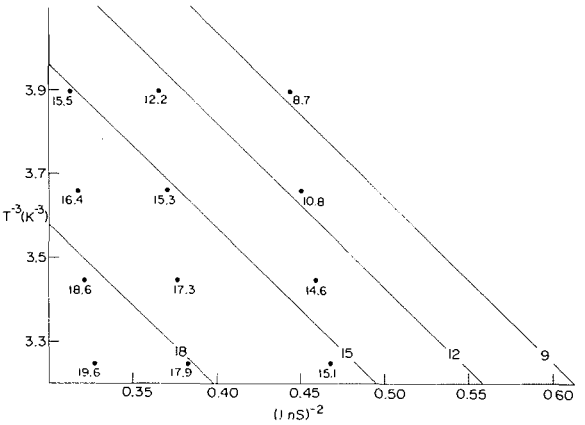

FIG. 4. A contour diagram showing ln J as a function of T^{-3} and $(\ln S)^{-2}$.

of τ were obtained by extrapolation of the steeply rising and nearly linear section of the $n_{t,v}$ vs. time curve to meet the time axis. Improved estimates of it were obtained by plotting ln $(1 - n_{t,v}/N)$ vs. t_c. The resulting straight line intersected the time axis at a value of $t_c = \tau$. Values of the three parameters were not determined simultaneously using 'Gaushaus' because of the large correlations noted among their values. A subsequent paper in this series will focus on the lag time problem in $CaSO_4 \cdot 2H_2O$ nucleation.

To note the effects of temperature and ion product on the rate of $CaSO_4 \cdot 2H_2O$ nucleation studies were carried out over the ranges 295.0 ± 1 to 313.6 ± 1 K and 0.03063 ± 0.00012 to 0.05429 ± 0.00012 respectively. Combinations were selected from these ranges that produced nucleation rate levels such that $n_{t,v}/N > 0.5$ within a 12-h period and also that produced a reasonable number of photomicrographs distributed over the whole of the experimental time interval. Advantage was taken of the rather long lag times observed at low temperature compared with those within the experimental range in that the samples were prepared for observation at low temperature then brought to the desired temperature quickly by start-up of the thermostatted water supplied to the cell holder. Careful attention to the design and fabrication of the observation cup and its holder resulted in a low thermal inertia for the system. The results of these experiments are shown as the dependency of ln J on both the variables $(\ln S)^{-2}$ and T^{-3} in the contour diagram of Fig. 4 as suggested by eq. 4.

Several iso-ln J contour lines have been drawn on the diagram and these accent the shape of the response surface. The curve resulting from the intersection of the response surface and a plane perpen-

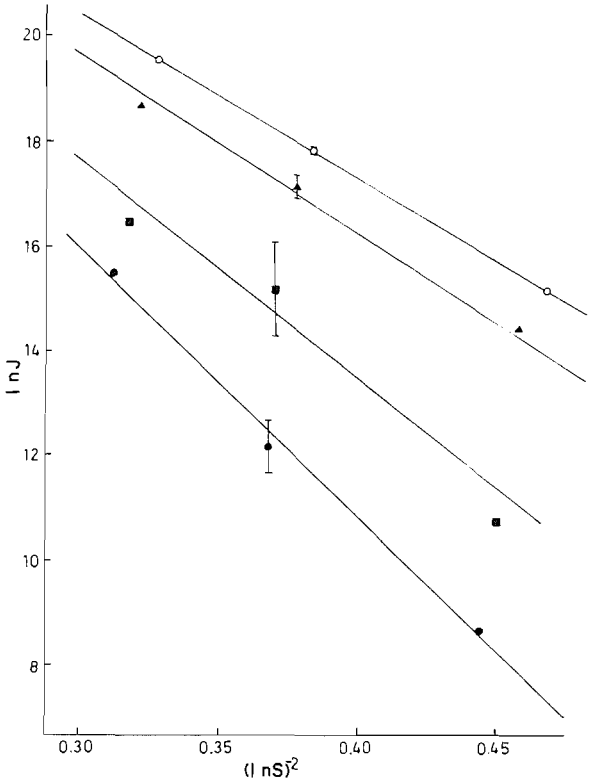

FIG. 5. Plots of ln J vs. $(\ln S)^{-2}$ at various temperatures: ●, 295.0 K; ■, 301.3 K; ▲, 307.5 K; and ○, 313.6 K.

Can. J. Chem. Downloaded from www.nrcresearchpress.com by 210.87.254.105 on 09/05/12
For personal use only.

TABLE 4*a*. A summary of various parameters calculated from the data of Figs. 5 and 6

Parameter[a]	Value at 295.0 K	301.3 K	307.5 K	313.6 K
Slope (Fig. 5)	-51.6 ± 5.2	-43.8 ± 9.5	-29.7 ± 2.3	-31.58 ± 0.60
ln A (intercept of Fig. 5)	31.4 ± 2.0	30.7 ± 3.7	28.29 ± 0.90	29.91 ± 0.24
σ (erg cm^{-2})	23.9 ± 1.4	23.1 ± 2.9	20.73 ± 0.94	21.59 ± 0.25
S^* (Fig. 5)	3.61 ± 0.41	3.30 ± 0.77	2.79 ± 0.18	2.794 ± 0.042
n^{*b}	49.0 ± 5.2	51 ± 11	55.2 ± 3.7	58.3 ± 1.0
r^* (nm)[b]	1.130 ± 0.69	1.15 ± 0.14	1.176 ± 0.046	1.197 ± 0.012
ΔG_S^* (erg) $\times 10^{12}$[b]	1.278 ± 0.081	1.28 ± 0.15	1.200 ± 0.039	1.296 ± 0.011
S_b^* (Fig. 6)	3.13 ± 0.18	2.5 ± 1.9	1.54 ± 0.46	1.62 ± 0.28
n_b^{*c}	69.7 ± 9.2	108 ± 115	734 ± 764	567 ± 327
r_b^* (nm)[c]	1.270 ± 0.096	1.47 ± 0.90	2.8 ± 1.7	2.56 ± 0.85
$\Delta G_{S_b}^*$(erg) $\times 10^{12}$[c]	1.62 ± 0.20	2.1 ± 1.8	6.7 ± 5.7	5.9 ± 2.8

[a] $\pm$ are standard deviations.
[b] Calculated from S^* values.
[c] Calculated from S_b^* values.

TABLE 4*b*. Levels at which values of the parameters shown in Table 4*a* are significantly different at 1 degree of freedom

Parameter	Comparison[a] A–B	B–C	C–D	A–C	B–D	A–D
Slope (Fig. 5)	30%	50%	30%	70%	50%	80%
ln A (intercept of Fig. 5)	<10%	30%	60%	50%	10%	30%
σ	10%	30%	30%	50%	20%	60%
S^* (Fig. 5)	10%	30%	<10%	60%	30%	60%
n^{*b}	<10%	10%	30%	30%	10%	60%
r^{*b}	<10%	<10%	20%	20%	10%	40%
ΔG_S^{*b}	0%	20%	60%	30%	<10%	10%
S_b^* (Fig. 6)	10%	20%	<10%	70%	20%	80%
n_b^{*c}	10%	30%	<10%	40%	50%	60%
r_b^{*c}	10%	30%	<10%	40%	30%	50%
$\Delta G_{S_b}^{*c}$	10%	30%	<10%	40%	40%	60%

[a] A = 295.0 K; B = 301.3 K; C = 307.5 K; D = 313.6 K.
[b] Calculated from S^* values.
[c] Calculated from S_b^* values.

dicular to these contour lines is not linear but bends downward (i.e., the observed J values are lower than expected) at increasing levels of T and S. This trend reflects, most likely, limitations to the experimental technique used and not limitations to the theory of nucleation as expressed by eq. 4. The data of Table 3 and Figs. 2 and 3 suggest that temperature rise times in the observation cup become of the same order of magnitude as the measured lag times as S and T mutually increase and that dS/dt effects become important also. These effects, taken together, result in measured J values that are too low.

Estimates of the values of the parameters in eq. 4 obtained from the slopes and intercepts (least-square fit) of the ln J vs. $(\ln S)^{-2}$ curves shown in Fig. 5 are listed in Table 4*a*. For ease of comparison with other data in the literature estimates of n^*, r^*, and ΔG^* were calculated from each S^* value using eqs. 6, 7, and 8.

$$\Delta G^* = \frac{16\pi\sigma^3\bar{v}^2}{3(kT\ln S^*)^2} \quad [6]$$

$$n^* = \frac{32\pi\sigma^3\bar{v}^2}{3(kT\ln S^*)^3} \quad [7]$$

$$r^* = \frac{2\sigma\bar{v}}{kT\ln S^*} \quad [8]$$

where S^* is the value of S found by extrapolation of the ln J vs. $(\ln S)^{-2}$ plot to the point where $J = 1$, n^* is the number of monomers in the critical embryo, and r^* is the radius of the critical embryo assuming it to be spherically shaped. These results along with values of the same parameters calculated from in-

Can. J. Chem. Downloaded from www.nrcresearchpress.com by 210.87.254.105 on 09/05/12
For personal use only.

Can. J. Chem. Downloaded from www.nrcresearchpress.com by 210.87.254.105 on 09/05/12
For personal use only.

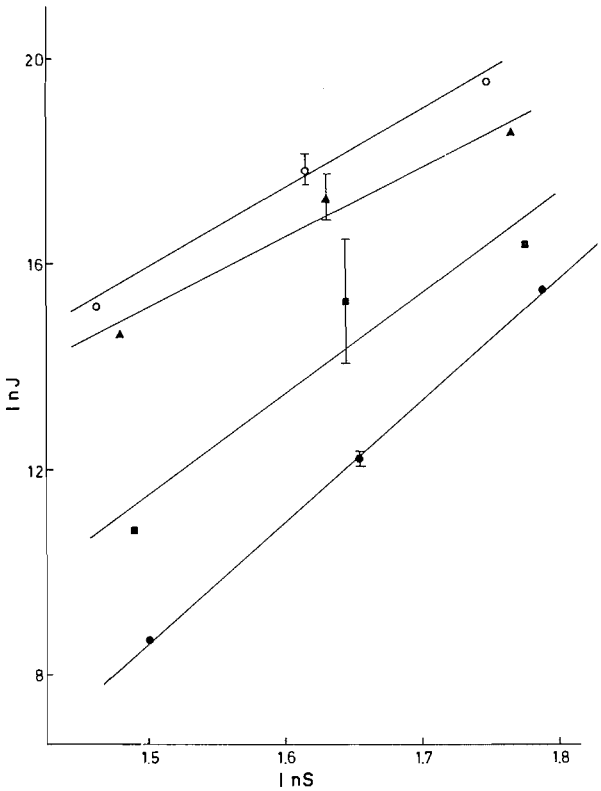

FIG. 6. Plots of ln J vs. ln S at various temperatures: ●, 295.0 K; ■, 301.3 K; ▲, 307.5 K; and ○, 313.6 K.

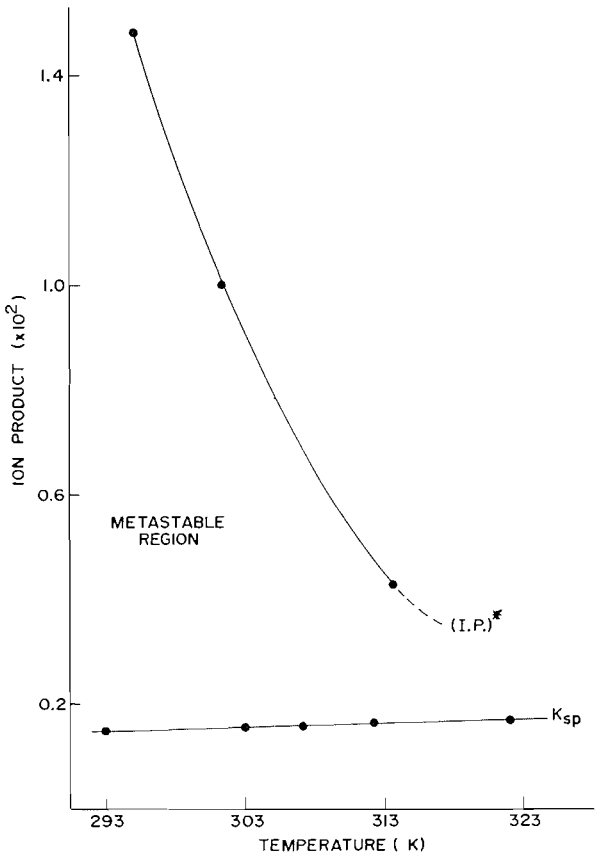

FIG. 7. The Ostwald diagram for $CaSO_4 \cdot 2H_2O$ over the temperature range 295.0 through 313.6 K.

dividual S_b* values obtained by extrapolation to the point where $J = 1$ of the ln J vs. ln S data shown in Fig. 6 and the last mentioned three equations are included in Table 4*a*. Critical ion product values for $CaSO_4 \cdot 2H_2O$ at each temperature were calculated from the tabular S_b* values using eq. 9.

$$[9] \qquad IP^* = (S_b^*)^2 K_{sp}$$

Both IP* and K_{sp} are plotted vs. temperature in Fig. 7 producing an Ostwald diagram for gypsum covering the temperature range 295.0 through 313.6 K.

Trends in the derived data over the temperature range studied can be seen from the results of an investigation into the confidence levels at which the tabular values of each of the parameters are significantly different from each other. This is shown in Table 4*b*. In general comparisons of nearest neighbour tabular values fall below the 50% confidence level while nearest neighbour but two comparisons are above this level. Thus, we can conclude that σ, S^*, and S_b* values tend to decrease with increasing temperature. The same trend in ln A values can be noted but not with the same level of confidence. Each of ΔG^*, n^*, and r^* tend to increase in value as the temperature increases. Large uncertainties, however, erode confidence in the trend when S^* is used in the calculation.

The data obtained in this study tend to confirm the form of the classical theory of nucleation as expressed by eq. 4. Deviations in the observed dependency of J on S and T at combinations of higher values of each are attributed to limitations of the experimental technique used to obtain the data and not to limitations of the theory.

Acknowledgements

The authors acknowledge the financial assistance provided by the National Advisory Committee on Water Resources Research of the Department of Energy, Mines and Resources and the National Research Council of Canada.

1. M. VOLMER and A. WEBER. Z. Phys. Chem. Leipzig, **119**, 277 (1926).
2. L. FARKAS. Z. Phys. Chem. Leipzig, A**125**, 236 (1927).

3. R. BECKER and W. DÖRING. Ann. Phys. **24**, 719 (1935).
4. M. VOLMER. Kinetic der Phasenbildung. Steinkopff, Dresden. 1939.
5. J. B. ZELDOVICH. Acta Physicochim. URSS, **18**, 1 (1943).
6. J. FRENKEL. Kinetic theory of liquids. Clarendon, Oxford. 1946.
7. D. TURNBULL and J. C. FISHER. J. Chem. Phys. **17**, 71 (1949).
8. B. VONNEGUT. J. Colloid Sci. **3**, 563 (1948).
9. M. L. WHITE and A. A. FROST. J. Colloid Sci. **14**, 247 (1959).
10. O. E. HILEMAN, JR. Talanta, **14**, 139 (1967).
11. J. A. VELAZQUEZ and O. E. HILEMAN, JR. Talanta, **15**, 1060 (1968).
12. J. A. VELAZQUEZ and O. E. HILEMAN, JR. Talanta, **17**, 623 (1970).
13. J. A. VELAZQUEZ and O. E. HILEMAN, JR. Can. J. Chem. **48**, 2896 (1970).
14. O. A. BEMPAH and O. E. HILEMAN, JR. Can. J. Chem. **51**, 3435 (1973).
15. O. A. BEMPAH and O. E. HILEMAN, JR. J. Colloid Sci. **51**, 380 (1975).
16. R. E. MASSEY and O. E. HILEMAN, JR. Can. J. Chem. **55**, 1285 (1977).

Can. J. Chem. Downloaded from www.nrcresearchpress.com by 210.87.254.105 on 09/05/12
For personal use only.

The effect of temperature on the optical spectra and the yields of solvated electrons and ion-pairs in amines[1]

WILLIAM ARTHUR SEDDON, JOHN WALLACE FLETCHER, AND FRED CHARLES SOPCHYSHYN

Physical Chemistry Branch, Atomic Energy of Canada Limited, Chalk River Nuclear Laboratories, Chalk River, Ont., Canada K0J 1J0

Received September 13, 1977

WILLIAM ARTHUR SEDDON, JOHN WALLACE FLETCHER, and FRED CHARLES SOPCHYSHYN. Can. J. Chem. **56**, 839 (1978).

Optical absorption spectra for the solvated electron, e_s^-, and ion-pairs, (Na^+, e_s^-), have been observed in methylamine (MA), ethylamine (EA), and isopropylamine (IPA), at temperatures ranging from 184 to 338 K. Changes in the (Na^+, e_s^-) spectra, relative to e_s^-, are consistent with a gradual transition in the ion-pair structure toward a more 'electron-like' entity with decreasing temperature and increasing solvent polarity. Extinction coefficients, $\varepsilon_{max}(e_s^-) = 3.3 \pm 0.2, 3.2 \pm 0.5$, and $3.2 \pm 0.5 \times 10^4\ M^{-1}\ cm^{-1}$ in MA, EA, and IPA respectively. Corresponding values for the ion-pairs, $\varepsilon_{max}(Na^+, e_s^-) = 2.5 \pm 0.2, 2.1 \pm 0.2$, and $1.9 \pm 0.2 \times 10^4\ M^{-1}\ cm^{-1}$.

In EA and IPA, the yield $G_{e_s^-}$ (molecules/100 eV) shows a marked solute concentration dependence. This is consistent with an empirical scavenging model from which the escaped solvated $G(e_s^-)_{esc}$ and spur $G(e_s^-)_{spur}$ electrons are estimated as $G(e_s^-)_{esc} = 0.5$ and 0.4, $G(e_s^-)_{spur} = 1.8$ and 1.4, giving $G(e_s^-)_{total} = 2.3$ and 1.8 in EA and IPA, respectively. In MA, $G_{e_s^-} = G(e_s^-)_{esc} = 2.2_5 \pm 0.2$, independent of solute concentration.

WILLIAM ARTHUR SEDDON, JOHN WALLACE FLETCHER et FRED CHARLES SOPCHYSHYN. Can. J. Chem. **56**, 839 (1978).

On a observé les spectres d'absorption optique d'électrons solvatés, e_s^-, et de paires d'ion (Na^+, e_s^-) dans la méthylamine (MA), l'éthylamine (EA) et l'isopropylamine (IPA) à des températures allant de 184 à 338 K. Les changements dans les spectres (Na^+, e_s^-) par rapport à e_s^- sont en accord avec une transition progressive d'une structure de paire d'ions vers une structure qui ressemble plus aux électrons au fur et à mesure que la température diminue et que la polarité du solvant augmente. Les coefficients d'extinctions $\varepsilon_{max}(e_s^-)$ sont respectivement $3.3 \pm 0.2, 3.2 \pm 0.5$ et $3.2 \pm 0.5 \times 10^4\ M^{-1}\ cm^{-1}$ dans MA, EA et IPA. Les valeurs correspondantes pour les paires d'ions $\varepsilon_{max}(Na^+, e_s^-)$ sont $2.5 \pm 0.2, 2.1 \pm 0.2$ et $1.9 \pm 0.2 \times 10^4\ M^{-1}\ cm^{-1}$.

Dans EA et IPA, le rendement $G_{e_s^-}$ (molécules/100 eV) varie considérablement avec la concentration du soluté. Ce résultat est en accord avec un modèle empirique de piégeage à partir duquel on peut évaluer que les valeurs de $G(e_s^-)_{esc}$ sont 0.5 et 0.4 et les valeurs $G(e_s^-)_{spur}$ sont 1.8 et 1.4 conduisant à des valeurs respectives de $G(e_s^-)_{totale}$ de 2.3 et 1.8 pour EA et IPA. Dans MA, la valeur de $G_{e_s^-} = 2.2_5 \pm 0.2$ et cette valeur est indépendante de la concentration du soluté.

[Traduit par le journal]

Introduction

The absorption spectra of solvated electrons, e_s^-, and species considered to be alkali metal cation–electron pairs, (M^+, e_s^-), have been observed by pulse radiolysis in several amines at room temperature (1 and references therein). In general, the band maxima for (M^+, e_s^-) show a shift towards higher energies from those found for the corresponding e_s^- absorptions (1–3). The magnitude of this shift is, however, dependent on solvent polarity and for the series methylamine (MA), ethylamine (EA), and isopropylamine (IPA) is in the order MA < EA < IPA. Such shifts show a good correlation with the hyperfine splitting constants obtained for the species of stoichiometry M in alkali metal – amine solutions suggesting that the transient species produced by pulse radiolysis are the same as those studied in steady state metal solutions by electron spin resonance (esr). Depending on the solvating ability of the solvent such species have been considered to range from "tight" (contact) to "loose" (solvent separated) ion-pairs (4, 5).

This interpretation has implications with respect to the "static" and "dynamic" models which have been put forward to explain the effect of temperature on the esr hyperfine spectra. In the former model, a single species is proposed whose structure is markedly affected by temperature (6, 7), whereas the latter visualizes a rapid temperature dependent equilibrium between two (or more) distinct species

[1]AECL No. 6074.

Can. J. Chem. Downloaded from www.nrcresearchpress.com by 210.87.254.42 on 09/05/12
For personal use only.

Can. J. Chem. Downloaded from www.nrcresearchpress.com by 210.87.254.42 on 09/05/12
For personal use only.

whose structures are relatively independent of temperature (8, 9).

This paper describes the effect of temperature on the spectra of e_s^- and (Na^+, e_s^-) in MA, EA, and IPA. Spectral properties are listed and discussed with respect to the nature of ion-pairs in these amines. In addition differences in the yield, $G(e_s^-)$ (molecules/100 eV), as a function of solute concentration, are discussed in terms of an empirical scavenging model (10–12) and are compared with previous values deduced at low temperature (13).

Experimental

Details of the experimental techniques and methods of solvent purification have been described previously (14, 15). In this work all solutions were irradiated in the absence of solvent base using 1.0 cm quartz cells and 0.3 μs pulses of 2.25 MeV electrons. Yields and/or extinction coefficients were deduced from linear plots of optical density against energy absorbed per pulse using doses $\leq 1 \times 10^{20}$ eV ℓ^{-1}.

Sodium tetraphenylboron ($NaB\phi_4$) was used as received.

Results

Solvated Electron Spectra

Figure 1 shows the optical absorption spectra observed at the end of the pulse for e_s^- in pure MA from 184 to 241 K (fp 179 K). The inset displays the shift in band maximum, ν_{max} (cm^{-1}) as a function of temperature, giving the coefficient $d\nu_{max}/dT = -28.1 \pm 2\ cm^{-1}\ K^{-1}$. Extrapolating to room temperature (294 K) indicates a ν_{max} of 5215 ± 100 cm^{-1}. Within experimental error the width of the absorption band at half height, $\Delta\nu_{1/2} = 4800 \pm 100$ cm^{-1}, is independent of temperature.

Similar results were observed for pure EA and IPA over the range 193–294 K (fp 189 K) and 176–294 K (fp 172 K), respectively. In IPA the spectrum appears to narrow ($\sim$300–500 cm^{-1}) with decrease in temperature. Examples of their spectra are given in Fig. 2.

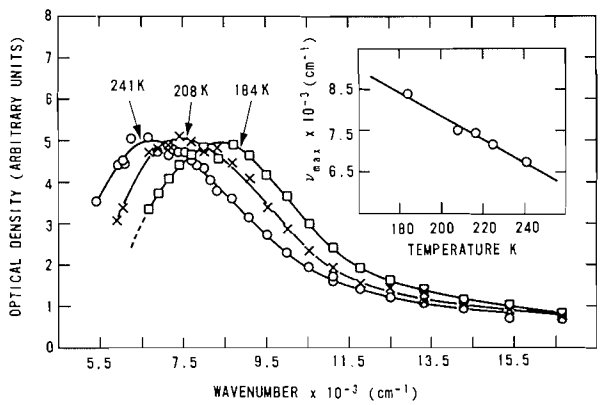

FIG. 1. Optical absorption spectra and band maxima of e_s^- in MA as a function of temperature.

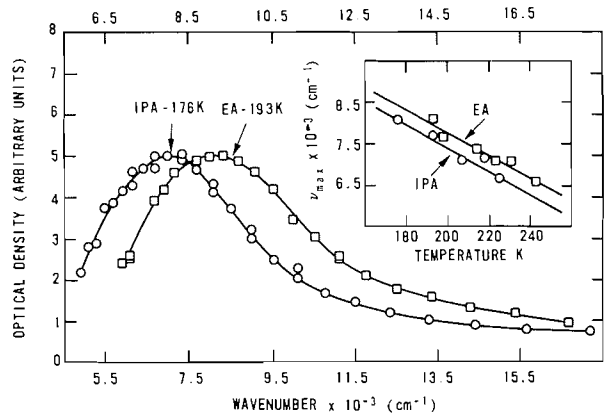

FIG. 2. Optical absorption spectra and band maxima of e_s^- in EA and IPA at low temperatures.

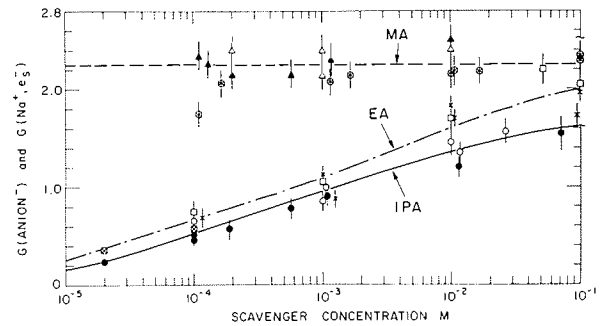

FIG. 3. Anion and ion-pair yields in MA, EA, and IPA as a function of solute concentration. ●, ▲, ⊠, biphenyl (this work); ×, ⊛, biphenyl and pyrene (16); □, ○, △, $NaB\phi_4$.

Yield, Extinction Coefficient, and Oscillator Strength

Yields and extinction coefficients, $\varepsilon_{max}(e_s^-)$ at the band maximum, were deduced at room temperature by comparison with Gε (anion) formed in the presence of biphenyl (B) as an electron scavenger (16). To minimize errors due to solvent absorptions, optical densities for e_s^- were measured at 1400 nm (7140 cm^{-1}) and then corrected to ν_{max} using the overall band shape observed at low temperatures. Figure 3 shows the anion yields as a function of concentration assuming the extinction coefficients $\varepsilon_{B^-} = 4 \times 10^4$ and $1.25 \times 10^4\ M^{-1}\ cm^{-1}$ at 407.5 and 630 nm, respectively (17). Also shown are previous results obtained in MA[2] and EA using B and pyrene (16), or $NaB\phi_4$ (see below), as e_s^- scavengers. The marked solute dependence observed in EA and IPA indicates that the rate of decay of solvated electrons escaping spur recombination must be significant with respect to the scavenging process. Therefore in order to ascertain $G(e_s^-)$ (in the absence

[2]In rechecking these data we found a systematic error which resulted in the previously reported yields for MA being 5% low. The data given in Fig. 3 have been corrected accordingly.

Can. J. Chem. Downloaded from www.nrcresearchpress.com by 210.87.254.42 on 09/05/12
For personal use only.

TABLE 1. Spectral properties of e_s^- in MA, EA, and IPA. Values for liquid ammonia (15, 20–24) are shown for comparison

Solvent	Temp. (K)	$\nu_{max} \pm 100^a$ (cm^{-1})	$d\nu_{max}/dK \pm 2.0$ ($cm^{-1}\ K^{-1}$)	$\Delta\nu_{1/2} \pm 100$ (cm^{-1})	$\varepsilon_{max} \times 10^{-4}$ ($M^{-1}\ cm^{-1}$)	f
MA	184	8300	−28.1	4800	3.3±0.2	≥0.68
	294	5215				
EA	193	7950	−27.9	5100	3.2±0.5	≥0.70
	294	5130				
IPA	176	8100	−28.5	4500	3.2±0.5	≥0.62
	294	4715				
NH_3	294	5500	−20.0[b]	3500	4.9±0.1	≥0.74

[a]Values at 294 K are interpolated from $d\nu_{max}/dK$.
[b]Reference 30.

of solute) and hence $\varepsilon_{max}(e_s^-)$, use is made of an empirical scavenging model originally proposed for hydrocarbons and extended to alcohols (10–12). This procedure is amplified in the discussion.

Table 1 summarizes the spectral properties for e_s^- in the three amines along with those in liquid ammonia for comparison. Lower limits for the oscillator strengths, f, for the absorption bands were estimated from the approximation (18)

$$f \sim 4.32 \times 10^{-9}\ \varepsilon_{max}\Delta\nu_{1/2}$$

Ion-pair Spectra

Figure 4 shows the optical absorption spectra at the end of the pulse in $\sim 10^{-2}$ *M* $NaB\phi_4$ solutions in MA from 185.5 to 243 K. The inset shows the effect of temperature on ν_{max}. Figure 5 shows examples of the corresponding spectra in EA at 194 and 294 K and IPA at 294 K. Since $NaB\phi_4$ precipitated from IPA solutions at 238 K a similar low temperature study was not possible in this solvent. However, in IPA solutions a slight ($\sim 700\ cm^{-1}$) shift to higher energies and broadening ($\sim 300\ cm^{-1}$) was observed in the ion-pair spectrum at 338 K.

Yield, Extinction Coefficient, and Oscillator Strength

Ion-pair yields and extinction coefficients at 294 K were determined by comparison of the optical density of (Na^+, e_s^-) with that of (Na^+, B^-) produced in reaction 1 (19).

[1] $$(Na^+, e_s^-) + B \rightarrow (Na^+, B^-)$$

The procedure is more direct than for e_s^- since for comparable doses per pulse the natural ion-pair decay process is about an order of magnitude slower than observed for e_s^-. Using solutions containing 10^{-3} to 10^{-2} *M* $NaB\phi_4$ and from 10^{-4} to 5×10^{-4} B, the experimental conditions were adjusted such

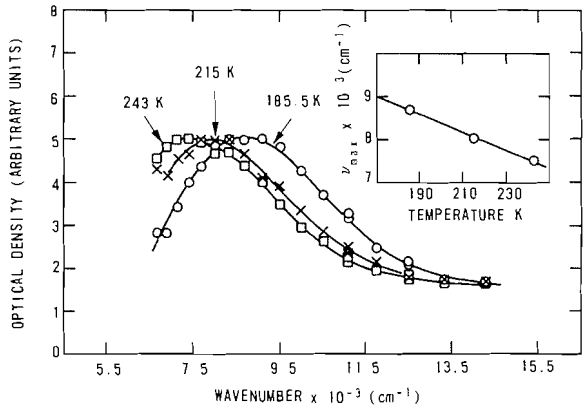

FIG. 4. Optical absorption spectra and band maxima of (Na^+, e_s^-) in MA as a function of temperature.

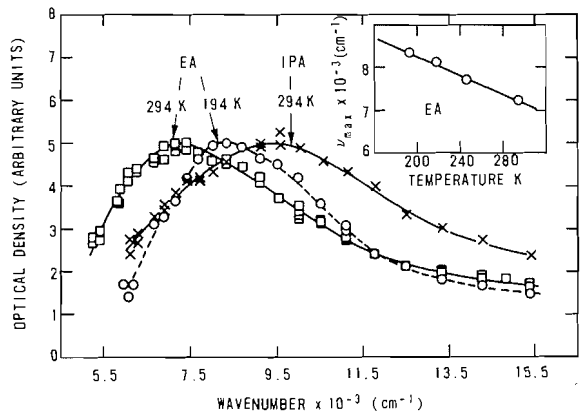

FIG. 5. Optical absorption spectra of (Na^+, e_s^-) in EA and IPA.

that the rate of formation of (Na^+, B^-) was $\geq 10\times$ the rate of decay of (Na^+, e_s^-) in the absence of B. Taking $G(Na^+, B^-) = G(Na^+, e_s^-)$ then $\varepsilon_{max}(Na^+, e_s^-)$ can be calculated. Because of solvent absorp-

TABLE 2. Spectral properties of (Na^+, e_s^-) in MA, EA, and IPA

Solvent	Temp. (K)	ν_{max} (cm^{-1})	$d\nu_{max}/dK$ (cm^{-1} K^{-1})	$\Delta\nu_{1/2}$ (cm^{-1})	$\varepsilon_{max} \times 10^{-4}$ (M^{-1} cm^{-1})	f
MA	185.5	8 700 $\pm$100	-21.0 ± 2	5200$\pm$100	2.5$\pm$0.2	$\geq$0.56
	294	6 420[a]				
EA	194	8 330 $\pm$100	-11.2 ± 2	5300 $\pm$100	2.1$\pm$0.2	
	294	7 210		6300		$\geq$0.57
IPA	294	9 300$\pm$200		8800$\pm$200	1.9$\pm$0.2	$\geq$0.72
	338	10 000$\pm$500		9000$\pm$300		

[a]Interpolated from $d\nu_{max}/dK$.

tions optical densities for the ion-pair in MA were measured at 1400 nm and then corrected to ν_{max} on the basis of the band shape observed at lower temperatures. In EA and IPA comparisons were made at the appropriate band maxima of 1400 and 1100 nm, respectively.

Values for $G(Na^+, e_s^-) = G(e_s^-)$ as a function of $NaB\phi_4$ concentration are given in Fig. 3 and the spectral properties are summarized in Table 2. Using 10^{-2} M $NaB\phi_4$ solutions, ion-pair yields, as a function of temperature from 185–245 K, were found to be independent of temperature with $G\varepsilon_{max}(Na^+, e_s^-) = 5.3 \pm 0.3 \times 10^4$ and $4.5 \pm 0.3 \times 10^4$ in MA and EA, respectively.

Discussion

Optical Spectra

The spectral properties of e_s^- in each of the three amines are very similar but do show a slight decrease in ν_{max} from MA to IPA (Table 1). These values are also slightly red shifted with respect to liquid ammonia, e_{am}^- (15, 20–24), and follow a trend toward lower energies with decreasing dielectric constant of the solvent. Whereas the band widths and temperature coefficients are greater than for e_{am}^-, values for ε_{max}(amine) are significantly less than $\varepsilon_{max}(NH_3)$ resulting in comparable oscillator strengths throughout the series.

The ion-pair spectra are broadened with respect to e_s^- the extent of which increases markedly in the order MA < EA < IPA. However, in EA the band width also decreases slightly with decreasing temperature. Extinction coefficients are less than those measured for the corresponding e_s^- spectra and tend to decrease from MA to IPA resulting in a relatively constant oscillator strength throughout the series. The ion-pair spectra also have a lower temperature coefficient than is found for e_s^-. Blue shifts in $\nu_{max}(Na^+, e_s^-)$ relative to $\nu_{max}(e_s^-)$ increase markedly from MA to IPA.

These observations are consistent with the blue shift being due to an interaction between e_s^- and Na^+ in the ion-pair, the magnitude of which increases with decreasing dielectric character of the solvent and decreases with decreasing temperature. This is in accord with the marked changes in hyperfine splitting with changes in solvent and temperature (25–27). In each case the data are consistent with the "static" model and a trend toward a more "atom-like" structure or greater M^+–e_s^- interaction (and vice versa) as the temperature is raised or the solvent polarity decreased (4, 5). This situation should be contrasted with ether solutions where we concluded that a combination of both the "static" and "dynamic" model was applicable, either one of which could predominate depending on the coordinating power of the solvent (28).

In common with ether solutions (28) a relatively weak long-lived absorption, peaking at 900 nm and thought to result from reactions involving $B\phi_4^-$, is observed to grow in after the decay of the initial ion-pair absorption. Neither this absorption nor that arising from the formation of small amounts of Na^- give any significant contribution to the ion-pair spectra observed immediately after the pulse.

Yields of e_s^-

The yields of e_s^- escaping spur recombination processes show a marked temperature (13) and solute concentration dependence for EA and IPA but not for MA. As in the case of hydrocarbons (10), the solute concentration dependence for EA and IPA may be described by an empirical equation of the form

$$[2] \quad G_{e_s^-} = G(e_s^-)_{esc} + G(e_s^-)_{spur} \times (\alpha S)^{1/2}/[1 + (\alpha S)^{1/2}]$$

where $G(e_s^-)_{esc}$ and $G(e_s^-)_{spur}$ represent the yields of the solvated escaped and spur electrons, respectively; S is the concentration of the scavenger, and α is a parameter which represents the reactivity of electrons towards the solute relative to their recombination with geminate positive ions or radicals (29). The value of α was estimated experimentally at a constant

Can. J. Chem. Downloaded from www.nrcresearchpress.com by 210.87.254.42 on 09/05/12
For personal use only.

Can. J. Chem. Downloaded from www.nrcresearchpress.com by 210.87.254.42 on 09/05/12
For personal use only.

dose per pulse. By choosing acceptable values for $G(e_s^-)_{esc} \sim 0.6$ and $G(e_s^-)_{spur}$ 1.2–1.6 (13), [2] only fits the data reasonably well above 10^{-4} M scavenger concentration. Since there is a competition between the homogeneous decay of $(e_s^-)_{esc}$ and the scavenging process, [2] can be modified (11, 12) to give

$$[3] \quad G_{e_s^-} = G(e_s^-)_{esc}\,[\delta S/1 + \delta S] + G(e_s^-)_{spur}(\alpha S)^{1/2}/[1 + (\alpha S)^{1/2}]$$

In this equation, $\delta = k/k_d$ where k_d represents the first order rate constant for the homogeneous decay of $(e_s^-)_{esc}$ and k is the second order rate constant for its scavenging by solute. The solid curves drawn through the points in Fig. 3 represent the best fit of [3] using for EA and IPA, $G(e_s^-)_{total} = 2.3$ and 1.8 with $G(e_s^-)_{esc} = 0.5$ and 0.4; $G(e_s^-)_{spur} = 1.8$ and 1.4; $\alpha = 5 \times 10^4$ and 2.5×10^4 and $\delta = 261$ and 417 M^{-1}, respectively. In turn the values for $G(e_s^-)_{esc}$ were then used to deduce $\varepsilon_{max}(e_s^-)$ at 294 K from the measured values of $G_{e_s^-}\varepsilon_{max}(e_s^-) = 1.61 \times 10^4$ and 1.28×10^4 for EA and IPA, respectively, in the absence of solute.

For MA, $G_{e_s^-} = G(e_s^-)_{esc} = 2.25 \pm 0.2$ (dotted line in Fig. 3).

The above results can be compared with previous values deduced at low temperatures in the pure amines (13). To evaluate $G_{e_s^-}$ the latter study assumed $\varepsilon_{max}(e_s^-) = 3 \times 10^4\ M^{-1}\ cm^{-1}$. Correcting the low temperature results on the basis of $\varepsilon_{max}(e_s^-)$ measured in this work gives $G(e_s^-)_{total} = 2.0 \pm 0.2$, 1.7 ± 0.3, and 1.7 ± 0.3 in MA, EA, and IPA, respectively. These values can also be compared with the low temperature yields obtained in this work in the presence of 10^{-2} M $NaB\phi_4$ as an electron scavenger. Using values of $\varepsilon_{max}(Na^+, e_s^-)$ from Table 2, then $G(e_s^-)_{total} = 2.1_5 \pm 0.2$ and 2.1 ± 0.2 for MA and EA, respectively. The good agreement between the three sets of data provides a self-consistent picture for the quoted extinction coefficients and spectral properties of e_s^- and (Na^+, e_s^-) in these amines. We believe that the lack of both a solute and temperature dependence on $G(e_s^-)$ in MA reflects a much higher mobility of e_s^- relative to the competing spur decay processes than is the case for EA and IPA (13).

Finally it should be noted that $G(e_s^-)_{total}$ is not to be confused with G(total ionization) = 4.8 (13). Thus, as in the case of methanol (29), there is a yield of electrons with $G \geq 2.5$ which presumably recombine in the spur prior to solvation. The product of this recombination appears to be easily scavenged by the solvent base (13), but as yet this mechanism is not understood.

1. J. W. Fletcher and W. A. Seddon. J. Phys. Chem. **79**, 3055 (1975).
2. M. T. Lok, F. J. Tehan, and J. L. Dye. J. Phys. Chem. **76**, 2975 (1972).
3. W. A. Seddon, J. W. Fletcher, and F. C. Sopchyshyn. Chem. Phys. **15**, 377 (1976).
4. W. A. Seddon, J. W. Fletcher, and R. Catterall. Can. J. Chem. **55**, 2017 (1977).
5. J. L. Dye. Pure Appl. Chem. **49**, 3 (1977).
6. K. Bar-Eli and T. R. Tuttle, Jr. J. Chem. Phys. **40**, 2508 (1964).
7. K. Bar-Eli and T. R. Tuttle, Jr. J. Chem. Phys. **44**, 114 (1966).
8. L. R. Dalton, J. D. Rynbrandt, E. M. Hansen, and J. L. Dye. J. Chem. Phys. **44**, 3969 (1966).
9. R. Catterall and P. P. Edwards. J. Phys. Chem. **79**, 3010 (1975).
10. J. M. Warman, K.-D. Asmus, and R. H. Schuler. Adv. Chem. Ser. **82**, 25 (1968).
11. S. J. Rzad and J. H. Fendler. J. Chem. Phys. **52**, 5395 (1970).
12. K. M. Bansal and S. J. Rzad. J. Phys. Chem. **74**, 2888 (1970).
13. J. W. Fletcher and W. A. Seddon. Discuss. Faraday Soc. **63**, 18 (1977).
14. J. W. Fletcher, W. A. Seddon, and F. C. Sopchyshyn. Can. J. Chem. **51**, 2975 (1973).
15. W. A. Seddon, J. W. Fletcher, J. Jevcak, and F. C. Sopchyshyn. Can. J. Chem. **51**, 3653 (1973).
16. W. A. Seddon, J. W. Fletcher, F. C. Sopchyshyn, and J. Jevcak. Can. J. Chem. **52**, 3269 (1974).
17. J. Jagur-Grodzinski, M. Feld, S. L. Yang, and M. Szwarc. J. Phys. Chem. **69**, 628 (1965).
18. J. G. Calvert and J. N. Pitts, Jr. Photochemistry. John Wiley and Sons, Inc., New York, NY. 1966. p. 172.
19. G. A. Salmon, W. A. Seddon, and J. W. Fletcher. Can. J. Chem. **52**, 3259 (1974).
20. R. C. Douthit and J. L. Dye. J. Am. Chem. Soc. **82**, 4472 (1960).
21. J. Corset and G. Lepoutre. Metal–ammonia solutions. Colloque Weyl I. *Edited by* G. Lepoutre and M. J. Sienko. W. A. Benjamin, Inc., New York, NY. 1964. p. 186.
22. D. F. Burow and J. J. Lagowski. Adv. Chem. Ser. **50**, 125 (1965).
23. I. Hurley, T. R. Tuttle, Jr., and S. Golden. Metal–ammonia solutions, I.U.P.A.C., Colloque Weyl II. *Edited by* J. J. Lagowski and M. J. Sienko. Butterworths, London, 1970, p. 503.
24. J. F. de la Renaudière and J. Belloni. Int. J. Radiat. Phys. Chem. **5**, 31 (1973).
25. J. L. Dye and L. R. Dalton. J. Phys. Chem. **71**, 184 (1967).
26. R. Catterall, J. Slater, and M. C. R. Symons. Metal–ammonia solutions, I.U.P.A.C., Colloque Weyl II. *Edited by* J. J. Lagowski and M. J. Sienko. Butterworths, London. 1970, p. 329.
27. J. L. Dye. Electrons in fluids. *Edited by* J. Jortner and N. R. Kestner. Springer-Verlag, Berlin. 1973. p. 77.
28. W. A. Seddon, J. W. Fletcher, F. C. Sopchyshyn, and R. Catterall. Can. J. Chem. **55**, 3356 (1977).
29. D. W. Johnson and G. A. Salmon. Can. J. Chem. **55**, 2030 (1977).
30. G. Rubinstein, T. R. Tuttle, Jr., and S. Golden. J. Phys. Chem. **77**, 2872 (1973).

A vapor pressure method for the simultaneous determination of standard thermodynamic functions of both solutes in a ternary dilute solution

CLAUDE TREINER,[1] PIERRE TZIAS, AND MARIUS CHEMLA

Laboratoire d'Electrochimie, Université Pierre et Marie Curie - 4, Place Jussieu, 75230 Paris Cedex 05, E.R.A. 310, France

Received July 21, 1977

CLAUDE TREINER, PIERRE TZIAS, and MARIUS CHEMLA. Can. J. Chem. **56**, 844 (1978).

It is shown that from vapor pressure measurements on dilute solutions of ternary mixtures with one nonvolatile component, the standard free energy of transfer (ΔG_t^0) of both solutes from water to aqueous binary solvents can be determined simultaneously. The method is most useful in the case of volatile components. ΔG_t^0 values are discussed in particular in the case of the transfer of tetrahydrofuran, acetone, and acetonitrile from water to aqueous tetrabutylammonium bromide and urea solutions and compared to the case of the transfer of nonpolar solutes to the same aqueous solution. In each case, the free energy of transfer from water to an aqueous solution of a nonpolar molecule was negative, and introduction in that molecule of a polar group caused the free energy of transfer to be considerably less negative.

CLAUDE TREINER, PIERRE TZIAS et MARIUS CHEMLA. Can. J. Chem. **56**, 844 (1978).

On montre que l'on peut déterminer l'enthalpie libre de transfert ΔG_t^0 de deux solutés d'un mélange ternaire aqueux de l'eau à la solution binaire correspondante à partir d'une même série de mesures de pression de vapeur sur le mélange ternaire. La méthode est surtout utile dans le cas où l'un des solutés est très volatil. Les valeurs de ΔG_t^0 sont discutées en particulier dans le cas du transfert du tetrahydrofurane, de l'acétone et de l'acétonitrile de l'eau à des solutions aqueuses de bromure de tétrabutylammonium et d'urée et comparées au transfert de solutés non polaires aux mêmes solutions aqueuses. Dans chaque cas l'introduction d'un groupe polaire dans une molécule non polaire augmente considérablement l'enthalpie libre standard de transfert de l'eau aux solutions aqueuses considérées.

Introduction

The determination of standard thermodynamic quantities of transfer of solutes between two solvents has been an active field of interest for many years. In the case of ternary solutions, the standard free energy of transfer ΔG_t^0 of a nonvolatile electrolytic solute from water (usually) to a mixture of water and a co-solvent may be obtained from emf, solubility, or vapor pressure measurements (1); in the case of a volatile solute, only the solubility or the distribution method (2) have been used extensively in the limited case of sparingly soluble compounds; an interesting freezing point method has been proposed recently (3) but, of course, enthalpy and heat capacity measurements with the same accuracy are needed in order to obtain ΔG_t^0 values at temperatures different from that of the freezing point.

We propose in this paper the use of a vapor pressure method which, besides being a direct and general method, enables the determination from the same experiments on the vapor pressure variation of a solvent mixture with the addition of a nonvolatile solute, both ΔG_t^0 of the nonvolatile solute from water to the mixture of solvents and the ΔG_t^0 of the co-solvent from water to the mixture with the nonvolatile solute (which may, of course, be an electrolyte). Grunwald and Bacarella (4) have given a thermodynamic derivation which permits the determination $(\partial \bar{G}_3^0/\partial Z_1)$, the rate of change of the standard chemical potential of a nonvolatile solute with respect to solvent composition Z_1 (1 refers to water, 2 to the volatile co-solvent, and 3 to the nonvolatile component). If this quantity is obtained for several Z_1 values and the resulting curve integrated from water to the solvent mole fraction Z_1, then one obtains the quantity ΔG_t^0 $(w \rightarrow w + 2)$ (5). We shall show now how ΔG_t^0 $(w \rightarrow w + 3)$ may be computed from the same experimental data.

[1]To whom correspondence should be addressed.

Theory

The chemical potential of a volatile solute may be written as:

$$[1] \qquad \bar{G}_2 = G_2^{0*} + RT \ln P_2$$

where G_2^{0*} is the chemical potential of pure gaseous 2 in its standard state, and P_2 the partial pressure of 2. In an ideal case, one has:

$$[2] \qquad \bar{G}_2 = \bar{G}_2^{0*} + RT \ln X_2 + RT \ln K_2$$

where K_2 is Henry's law constant. We may put

$$[3] \qquad \bar{G}_2^0 = \bar{G}_2^{0*} + RT \ln K_2$$

where $\bar{G}_2^0$ is the chemical potential of 2 in the infinitely dilute reference state. In water

Can. J. Chem. Downloaded from www.nrcresearchpress.com by 210.87.254.42 on 09/05/12
For personal use only.

TABLE 1. Sample calculation for the standard free energy of transfer of a volatile component (acetone) in a ternary mixture: *n*-Bu_4NBr/water/acetone*

System	$m_3(w, 2)$† (m kg^{-1})	P (Torr)	y	10^3X_3	$m_3(w)$‡ (m kg^{-1})	$-\Delta G_t^0(w \rightarrow w + 3)$ (cal mol^{-1})
n-Bu_4NBr +	0	48.91	0.52167	0	0	0
4.910 wt%	0.01166	48.84	0.52111	0.22	0.01226	1.35
acetone	0.02401	48.75	0.52049	0.45	0.02525	3.02
	0.03424	48.69	0.51998	0.64	0.03601	4.21
	0.04707	48.60	0.51931	0.88	0.04950	5.93
					(0.1)	(12.2)
n-Bu_4NBr +	0	62.75	0.61330	0	0	0
7.941 wt%	0.00614	62.68	0.61299	0.12	0.00667	0.89
acetone	0.01299	62.62	0.61265	0.25	0.01411	1.71
	0.01819	62.56	0.61234	0.35	0.01976	2.52
	0.02373	62.51	0.61209	0.45	0.02578	3.17
					(0.1)	(12.1)

*The variations of P and y with electrolyte concentration have been obtained for each run by adding successive amounts of *n*-Bu_4NBr to a mixture of acetone and water (Z_1 = cte) (5).
†Electrolyte molality in binary solvent.
‡Electrolyte molality in water.

[4] $$\bar{G}_2^0(w) = \bar{G}_2^{0*} + RT \ln K_2(w)$$

In a mixture of water and 3

$$\bar{G}_2^0(w + 3) = G_2^{0*} + RT \ln K_2(w, 3)$$

Thus

[5] $$\Delta G_t^0(w \rightarrow w + 3) = RT \ln \frac{K_2(w, 3)}{K_2(w)}$$

In a dilute solution, Henry's law may be applied, then

[6] $$\Delta G_t^0(w \rightarrow w + 3) = RT \ln \frac{PYX_2^0}{p_2^0 y^0 X_2}$$

where P, y, X_2, and p_2^0, y^0, X_2^0 are respectively the total pressure, the vapor phase composition, and the mole fraction of 2 with and without (indicated by superscript zero) the nonvolatile component 3. Finally, eq. 6 may be rewritten as:

[7] $$\Delta G_t^0(w \rightarrow w + 3) = RT \ln \frac{Py}{p^0 y^0} - RT \ln (1 - X_3)$$

where X_3 is the mole fraction of the nonvolatile component.

The precise measurement of the total pressure P above a multi-component solution is easier to obtain experimentally than the vapor-phase composition y. It has been shown previously (5) that from the variation of the total pressure of a binary volatile solvent with solute concentration X_3 it was possible to calculate the vapor-phase composition by making use of the Gibbs–Duhem equation provided the nonvolatile solute was sufficiently diluted (see ref. 5 for details of the procedure). ΔG_t^0 for the volatile solute from water to mixtures of water and the nonvolatile component (considered now as part of the solvent) can thus be calculated using eq. 7.

In order to show that our procedure is essentially correct we give the following example. In the case of a ternary solution of tetrabutylammonium bromide (*n*-Bu_4NBr)/acetone/water (6), ΔG_t^0 $(w \rightarrow w + 2)$ had been calculated for several composition Z_1 of the solvent using Grünwald's thermodynamic derivation; ΔG_t^0 $(w \rightarrow w + 3)$ has now been obtained using eq. 7 from water to a mixture of 0.1 *m* of *n*-Bu_4NBr in water using the results corresponding to the two most diluted acetone solutions, i.e. 4.910 and 7.941 wt% of acetone. ΔG_t^0 $(w \rightarrow w + 3)$ is equal to -12.2 and -12.1 cal mol^{-1} (see Table 1). This example shows that Henry's law does apply up to these acetone concentrations ($Z_2 = 0.0261$ mole fraction) in water.

A further comment is worthwhile. It can be shown by making use of the cross-differentiation identity:

[8] $$\frac{\partial^2 G}{\partial n_2 \partial n_3} = \frac{\partial^2 G}{\partial n_3 \partial n_2}$$

that in a ternary solution one has (4)

[9] $$\frac{1000}{M_{12}} \left(\frac{\partial \bar{G}_2}{\partial m_3}\right)_{Z_1} = -Z_1 \left(\frac{\partial \bar{G}_3}{\partial Z_1}\right)_{m_3} - \left(\frac{\partial \bar{G}_3}{\partial m_3}\right)_{Z_1} \frac{m_3 M_2}{M_{12}}$$

where $M_{12} = Z_1 M_1 + Z_2 M_2$ (M_1 and M_2 are the molecular weights of the two solvents), m_3 is the nonvolatile component molality. When Z_1 goes to 1 (pure water) and m_3 goes to zero, eq. 9 reduces, on the mole fraction scale, to:

[10] $$\frac{1000}{M_1} \left(\frac{\partial \bar{G}_2^0}{\partial m_3}\right)_{Z_1} = -\left(\frac{\partial \bar{G}_3^0}{\partial Z_1}\right)_{m_3} - \nu RT$$

Can. J. Chem. Downloaded from www.nrcresearchpress.com by 210.87.254.42 on 09/05/12
For personal use only.

Can. J. Chem. Downloaded from www.nrcresearchpress.com by 210.87.254.42 on 09/05/12
For personal use only.

TABLE 2. Standard free energy of transfer (on mole fraction scale) of organic molecules from water to 0.1 *m* aqueous solutions at 298.15 K

Solute	$\Delta G_t^0(w \rightarrow w+3)$ (cal mol^{-1})	$(\partial \bar{G}_3^0/\partial Z_1)_{Z_1 \rightarrow 1}$ (kcal mol^{-1})	Solvent
THF	−14.9 ± 1.1	7.1 ± 0.6	Water + 0.1 *m* *n*-Bu_4NBr
Acetone	−12.2 ± 0.2	5.6 ± 0.1	—
Acetonitrile	−0.2 ± 0.2	−1.1 ± 0.1	—
Methane	−30.9		—
Ethane	−38.9		—
Propane	−51.3		—
Butane	−56.8		—
n-Butanol	−24.1		—
n-Butanol	11.2		Water + 0.1 *m* NaCl
THF	20 ± 2	−12.3 ± 1.1	—
Acetone	−20.1 ± 0.15	10.0 ± 0.3	Water + 0.1 *m* *n*-DTMABr*
—	−21.1 ± 0.4	10.5 ± 0.3	Water + 0.1 *m* SDS‡
—	11.77 ± 0.05	−7.75 ± 0.03	Water + 0.1 *m* CH_3OSO_3Na†
—	−0.22 ± 0.08	1.05 ± 0.05	Water + 0.1 *m* Me_4NBr†
THF	−9.4 ± 0.1	4.0 ± 0.2	Water + 0.1 *m* Thiourea
— (288.15)	−0.50 ± 0.24	−0.32 ± 0.12	Water + 0.1 *m* Urea
— (298.15)	−1.32 ± 0.15	0.14 ± 0.08	—
— (308.15)	−1.72 ± 0.07	0.36 ± 0.04	—
Propane (288.15)	−4.0		—
— (298.15)	−5.9		—
— (308.15)	−6.8		—

n-Decyltrimethylammonium bromide.
†C. Treiner and A. Le Besnerais, to be published.
‡Sodium decylsulfate.

(v = 2 in the case of a 1-1 elctrolyte and 1 for a nonelectrolyte).

Equation 10 presents a special advantage which concerns the use of the vapor pressure method for the evaluation of ΔG_t^0 $(w \rightarrow w+2)$ of a solute between two volatile solvents: $(\partial \bar{G}_3^0/\partial Z_1)$ which is the quantity defined by Grunwald and Bacarella often changes drastically near pure water (7) (Fig. 1) and the integration process used to obtain $\Delta G_t^0(w \rightarrow w+2)$ is difficult leading to relatively large errors on the integrated values; $(\partial \bar{G}_2^0/\partial m_3)_{Z_1}$ is easier to obtain through eq. 7 and can then be used to calculate $\partial \bar{G}_3^0/\partial Z_1$ for $Z_1 = 1$, which will then be used for the integration process of $\partial \bar{G}_3^0/\partial Z_1$ with respect to Z_1.

Equation 10 also shows that when both the solute and the co-solvent are very diluted with respect to water than the energy of interaction of 2 with water and 3 is equal to the energy of interaction of 3 with water and 2. This conclusion is equivalent to that deduced experimentally by Desnoyers *et al.* (8, 9) for enthalpies, volumes, and heat capacities, and theoretically by the same authors using pair interaction parameters of the McMillan–Mayer formalism (10).

Results and Discussion

We have used previously published vapor pressure data of *n*-Bu_4NBr, urea, NaCl, and thiourea in water–tetrahydrofuran, water–acetone, and water–acetonitrile mixtures (5–7, 11). $\Delta G_t^0(w \rightarrow w+3)$ has been calculated for acetone, tetrahydrofuran, and acetonitrile from water to 0.1 *m* *n*-Bu_4NBr, urea, NaCl, and thiourea as some literature values are available for related compounds for the transfer to the same solvent molality. Note that in the case of the electrolyte solutions $\Delta G_t^0(w \rightarrow w+3)$ was assumed to be linear with electrolyte concentration up to 0.1 *m* (2). The results are presented in Table 2 together with some pertinent literature values (2, 12).

Comparison of $\Delta G_t^0(w \rightarrow w+3)$ for the nonpolar alkanes and the polar molecules shows that the transfer to the aqueous *n*-Bu_4NBr solutions becomes less favorable in the latter case. The effect of a CH_2 group is to decrease $\Delta G_t^0(w \rightarrow w+3)$ by about 8 cal mol^{-1}, whereas introduction of a polar group increases $\Delta G_t^0(w \rightarrow w+3)$ by about 30 cal mol^{-1}. Obviously a repulsion term predominates in the interaction energy between a polar and a nonpolar group.

In the case of the transfer of THF and *n*-propane to aqueous urea solutions, the same behavior is observed; however, for such small differences to be discussed, the shape of the molecules should also be taken into account as was shown convincingly by Jolicoeur and Lacroix (13) for the transfer of branched and linear ketones from light to heavy water. Also it is noteworthy that the dependence of $\Delta G_t^0(w \rightarrow w+3)$ on temperature is the same for the polar and the nonpolar molecule for the transfer to the same 0.1 *m* aqueous urea solution; $\Delta H_t^0(w \rightarrow$

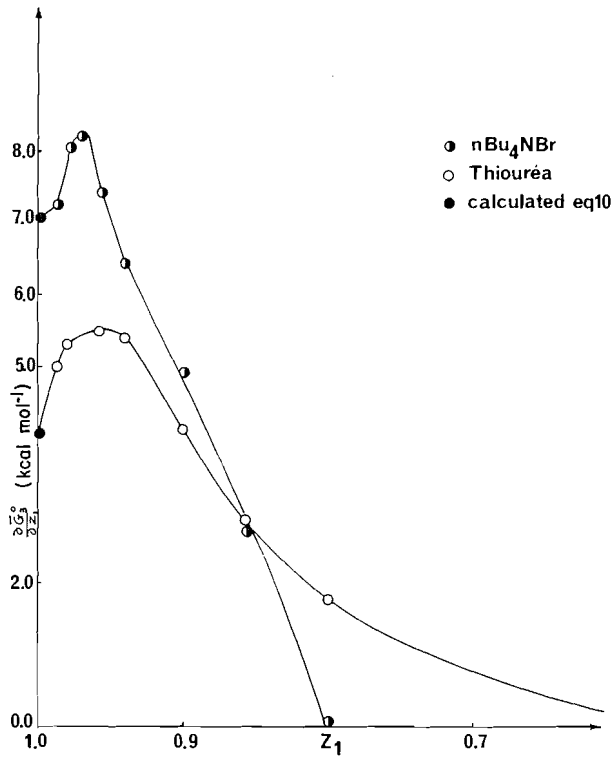

FIG. 1. Rate of change of the standard chemical potential of a solute with solvent composition: n-Bu_4NBr (6) and thiourea (11) in water–tetrahydrofuran mixtures at 298.15K.

$w + 3$) is positive in both cases and of the same order of magnitude, i.e. $+35$ cal mol^{-1} for n-propane and $+20$ cal mol^{-1} for THF.

In conclusion the proposed method for the determination of accurate standard free energy of transfer of polar, soluble molecules in aqueous media should be especially useful in the case of the study of quite volatile solvents.

1. H. SCHNEIDER. *In* Topics in current chemistry. Springer-Verlag, **68**, 103 (1976).
2. R. AVEYARD and R. HESELDEN. J. Chem. Soc. Faraday Trans. I, **70**, 1953 (1974).
3. J. E. DESNOYERS, M. BILLON, S. LEGER, G. PERRON, and J. P. MOREL. J. Soln. Chem. **5**, 681 (1976).
4. E. GRUNWALD and A. L. BACARELLA. J. Am. Chem. Soc. **80**, 3840 (1958).
5. C. TREINER. J. Chim. Phys. **70**, 1183 (1973).
6. C. TREINER and P. TZIAS. Adv. Chem. Ser. **155**, 301 (1976).
7. C. TREINER, P. TZIAS, M. CHEMLA, and G. M. POLTORATSKI. J. Chem. Soc. Faraday Trans. I, **72**, 2007 (1976).
8. J. E. DESNOYERS, G. PERRON, J. P. MOREL, and L. AVEDIKIAN. *In* Chemistry and physics of aqueous gas solutions. *Edited by* W. A. Adams. Electrochemical Society, Princeton. 1975. p. 172.
9. J. E. DESNOYERS, G. PERRON, L. AVEDIKIAN, and J. P. MOREL. J. Soln. Chem. **5**, 631 (1975).
10. J. J. KOZAK, W. S. KNIGHT, and W. KAUZMANN. J. Chem. Phys. **48**, 675 (1968).
11. C. TREINER and P. TZIAS. J. Soln. Chem. **4**, 471 (1975).
12. W. Y. WEN and J. H. HUNG. J. Phys. Chem. **74**, 170 (1970).
13. C. JOLICOEUR and G. LACROIX. Can. J. Chem. **51**, 3051, (1973).

Can. J. Chem. Downloaded from www.nrcresearchpress.com by 210.87.254.42 on 09/05/12
For personal use only.

Polyol–protein interactions. Thermodynamical evidence for a selective solvation of glycerol and hexitols by aqueous β-lactoglobulin

GIUSEPPA DIPAOLA[1] AND BERNARD BELLEAU[2]

Department of Chemistry, McGill University, Montreal, P.Q., Canada H3A 2K6

Received July 29, 1977

GIUSEPPA DIPAOLA and BERNARD BELLEAU. Can. J. Chem. **56**, 848 (1978).

Apparent specific heat capacities and volumes of the protein β-lactoglobulin have been determined under a variety of solute–solvent and solvent–cosolvent compositions. These quantities were derived from measurements of volumetric specific heats and densities with a flow microcalorimeter and flow densimeter. The effect of homologous polyols on the isothermal denaturation of the protein by urea at 25°C was investigated. The results suggest that polyol binding on the protein is sensitive to structural effects, maximum discrimination being exerted in favor of glycerol and its doubles, the hexitols.

GIUSEPPA DIPAOLA et BERNARD BELLEAU. Can. J. Chem. **56**, 848 (1978).

On détermine les volumes et les capacités calorifiques spécifiques apparentes de la protéine β lactoglobuline dans diverses compositions de soluté–solvant et de solvant–cosolvant. On a calculé ces quantités à partir de mesures de chaleur spécifique volumétrique et de densité faisant appel à un microcalorimètre à écoulement et à un densimètre à écoulement. On a étudié l'effet de polyols homologues sur la dénaturation isotherme de la protéine par l'urée à 25°C. Les résultats suggèrent que les capacités de liaison du polyol sur la protéine sont sensibles à des effets de structures et qu'une discrimination maximale est excercée en faveur du glycérol et de ses analogues doubles, les hexitols.

[Traduit par le journal]

Introduction

It is well known that urea, a statistical structure breaker in water, causes proteins to unfold (1). In marked contrast, aqueous glycerol, which like aqueous urea displays virtually ideal behavior, has a strong stabilizing effect on many proteins (2, 3). Other polyols share to some extent this remarkable property of glycerol and it has been proposed that the stabilizing effects may be mediated through alteration of the water structure (4) and/or the induction of small conformational changes (5). However, we have recently shown that glycerol behaves as a weak structure breaker in water, as judged from the sign of the heat capacities of transfer of a variety of hydrophobic probes (from water to aqueous glycerol) (6). On that basis, we suggested that binding of glycerol on protein nucleation sites for unfolding would account best for the stabilization effects on the native conformation (6). Accordingly, one may expect the nucleation binding sites to be 'guest' selective (through selective solvation) in view of the widespread structural discriminatory capabilities of protein binding domains. Available information is not inconsistent with this expectation (7).

The present work provides evidence that polyol binding on the model protein, β-lactoglobulin (bovine) is indeed markedly sensitive to structural effects, maximum discrimination being exerted in favor of glycerol and its doubles, the hexitols.

Experimental

Heat capacities were measured with a flow microcalorimeter (8) which can detect differences between the volumetric specific heat of a solution (6) and that of a reference solvent (σ_0) to $\pm 3 \times 10^{-5}$ J K^{-1} cm^{-3}, during a temperature rise of 2°C and a liquid flow rate of 0.80 cm^3 min^{-1}. The overall precision on $\Delta\sigma/\sigma_0$ is 0.3% (9). Densities were determined with a flow digital densimeter (10) sensitive to $\pm 3 \times 10^{-6}$ g cm^{-3}, connected in series with the microcalorimeter. Thermostatic control of the instrument was achieved with a closed-loop bath (11) whose stability was better than 0.001°C. Weight specific heats (C_p and C_p^0) (J K^{-1} g^{-1}) were calculated from the volumetric specific heats (σ and σ_0), thus

$$[1] \qquad C_p/C_p^0 = (\sigma/\sigma_0)\,(d_0/d)$$

All experimental measurements of σ/σ_0 were determined at least in duplicate. All heat capacity measurements were made at 25°C. Because of the experimental setup, density measurements were obtained at 24.00°C. The values for C_p and d_0 of pure water were taken as 4.1793 J K^{-1} g^{-1} (12) and 0.997299 g cm^{-3} (13). The error introduced by taking the ratio of densities at 24 rather than 25°C is negligible.

By analogy with apparent molal quantities of simple solutes in solution, an apparent specific heat capacity $\bar{C}_p$ (J K^{-1} g^{-1})[3] and apparent specific volume $\bar{V}$ (cm^3 g^{-1}) (14) can be defined for macromolecular solutes (such as proteins) as follows:

$$[2] \qquad \bar{C}_p = [(1000 + W_p)C_p - 1000\,C_p^0]/W_p$$

[1]Holder of a Centennial Predoctoral Scholarship of the National Research Council of Canada. Present address: Department of Chemistry, University of Toronto, Toronto, Ont. M5S 1A1.

[2]To whom correspondence may be addressed.

[3]C. Jolicoeur. Personal communication.

TABLE 1. Effects of polyols on $\bar{C}_p$ of unfolded β-lactoglobulin monomers (0.2 g/100 ml solution) in 9.2–9.6 m urea at 25°C, p*H* 7.0[a]

Polyol[b]	*m*	$\bar{C}_p$ (±0.01) (J K^{-1} g^{-1}) Control	+polyol	$\Delta\bar{C}_p$ (±0.02)	% decrease (±3%)
Glycol (C-2)	0.58	2.16	2.15	−0.01	2
Glycerol (C-3)	0.58	2.29	2.10	−0.19	32
	2.41	2.25	1.96	−0.29	48
meso-Erythritol (C-4)	0.60	2.23	2.08	−0.15	25
D-Arabitol (C-5)	0.57	2.25	2.05	−0.20	33
D-Xylitol (C-5)	0.57	2.20	2.05	−0.15	25
D-Mannitol (C-6)	0.57	2.28	1.97	−0.31	52
D-Sorbitol (C-6)	0.57	2.30	1.97	−0.33	55
	1.20	2.27	1.93	−0.34	57
myo-Inositol (C-6)	0.61	2.23	1.91	−0.32	53

[a]Measured in CO_2-free doubled distilled water with a Picker flow-microcalorimeter; the instrument detects differences between volumetric heat of a solution and reference solvent down to 3×10^{-5} J K^{-1} cm^{-3} for ΔT of 2°C.
[b]Reagent grade reagents from Sigma and Aldrich Chemical Co.; urea of ultra pure grade was used; the β-lactoglobulin was from Sigma, lot. No. 15C-0188.

and

$$[3] \qquad \bar{V} = [1 - (d - d_0/C_2]d_0$$

where W_p is the number of grams of protein per kilogram solvent and C_2 is the number of grams of protein per millilitre of solution. All other symbols have their usual meaning (6).

All solutions were prepared by weight with doubly-distilled deionized water, and used the same day. Unless otherwise specified, the protein concentration was 0.2% (g/100 ml). All data reported here were obtained after a 10-min exposure of the protein to solvent. Salt-free solutions were used after it was ascertained that the presence of 0.15 *m* NaCl had no effect on the $\Delta\bar{C}_p$ values for isothermal denaturation.

Crystalline β-lactoglobulin was from Sigma (lot No. 15C-0188). The other reagents which met acceptable standards of purity were urea (Schwarz-Mann, Ultra Pure) and D-sorbitol (Sigma). The source of the other polyols has been reported previously (15).

Results and Discussion

Pace and co-workers have shown (16, 17) that urea-induced unfolding of β-lactoglobulin is completely reversible and best represented by a two-state model. The observed $\Delta\bar{C}_p$ for the transition is consistent with the involvement of hydrophobic hydration, as is the case for other proteins (18). We have examined the effects of the polyols listed in Table 1 on this urea-induced transition by measuring the heat capacity changes ($\Delta\bar{C}_p$) accompanying the shift from the folded to the unfolded form of β-lactoglobulin (25°C, p*H* 7).

A typical curve for isothermal unfolding of β-lactoglobulin in the presence of urea is shown in Fig. 1 where dimer dissociation at about 2 *m* urea (plateau at 1.80 ± 0.2 J K^{-1} g^{-1}) gives rise to a minor transition, as previously shown by Pace and co-workers (16, 17); in 10 *m* urea, unfolding virtually reaches a maximum (16, 17). The desired $\Delta\bar{C}_p$ value for unfolding was obtained by subtracting $\bar{C}_p$ in 3 *m* urea from $\bar{C}_p$ in 12 *m* urea.[4] In pure water, the observed $\Delta\bar{C}_p$ (unfolding) in the presence of urea amounted to 10.80 ± 0.36 kJ K^{-1} mol^{-1}, a value in good agreement with the van't Hoff quantity of 9 kJ K^{-1} mol^{-1} reported by Pace and co-workers (16, 17).

The effects of various polyols on $\Delta\bar{C}_p$ (unfolding) (in 10 *m* urea) are summarized in Table 1.

Apart from ethylene glycol, all the polyols examined decrease $\Delta\bar{C}_p$ (unfolding) (by as much as 48% with 2.4 *m* glycerol).[5] Viscosity effects cannot explain the variations in $\Delta\bar{C}_p$ (unfolding) because equimolal concentrations of glycerol and ethylene glycol are essentially equiviscous (19, 20) (ratio of 1.056) at 25°C, yet the former is from four to five times more effective in lowering $\Delta\bar{C}_p$ (unfolding). Specific interactions between urea and the polyols were also ruled out as a possible contributing factor because in 9 *m* urea, the heat capacities of 0.5 *m* polyols are a perfect linear function of the number of hydroxyl groups (or chain length) (21).

When the percentage decrease in $\Delta\bar{C}_p$ (unfolding) caused by low polyol concentrations (0.6 *m*) is plotted against the number of hydroxyl groups (Fig. 2), one observes that glycerol and its doubles, the hexitols, form a separate group displaying enhanced activity against unfolding, glycerol being the most effective on a weight basis.

A complete understanding of the mechanisms underlying the above phenomena is impossible at this time because of the limited amount of work that has been done with polyhydric alcohols – water mixtures. Nevertheless, a number of observations should be kept in mind if one hopes to rationalize

[4]Complete set of tabular data for d_0/d, σ/σ_0, $\bar{C}_p$, and $\bar{V}$ is available, at a nominal charge, from the Depository of Unpublished Data, CISTI, National Research Council of Canada, Ottawa, Ont., Canada K1A 0S2.

[5]These changes in $\Delta\bar{C}_p$ originate only from a lowering of the apparent specific heat capacity of the unfolded state, the native state values being unaffected by the polyols.

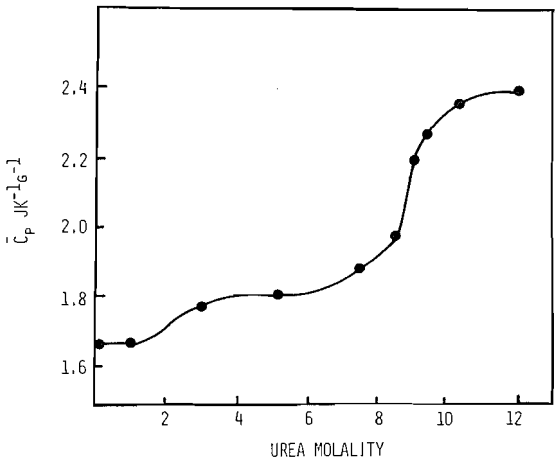

FIG. 1. Isothermal unfolding at 25°C, p*H* 7.0, of β-lactoglobulin (0.2 g% aqueous solution) as measured by the change in heat capacity vs. urea concentration. The $\bar{C}_p$ values are accurate to ± 0.02 J K^{-1} g^{-1}. The minor transition reflects dissociation into monomers.

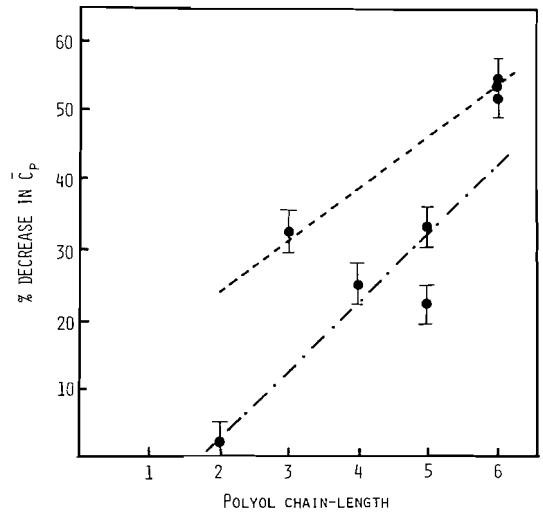

FIG. 2. Percentage decrease in heat capacity of unfolded β-lactoglobulin vs. polyol chain length at 0.57–0.61 *m* (~5–10% by weight) concentrations of polyols. The broken lines represent visual fits.

the results in the future. The idea that the widespread occurrence of glycerol solvation sites on proteins (3) might have fundamental structural significance is worth retaining. In this connection, it may be useful to examine the possible relevance of Warner's models for water–polyol and water–peptide complementation (22). This author has pointed out that glycerol can adopt a conformation where the 1,3-oxygens are spaced by 4.8 Å (parallel projections). This spacing is thus compatible with the second nearest neighbor distance between the oxygens of liquid water (in a hypothetical ice lattice). A similar complementarity was shown to exist for peptide–water interactions, the bonding distances between the C=O and —NH— groups also corresponding to the second nearest neighbor oxygen distance in water. The above results with β-lactoglobulin may be partly relevant to Warner's theory as far as the 'locking' effect of glycerol on the conformation of strategic peptide bonds (or nucleation sites for unfolding) is concerned. It is pertinent to note that among several solvents of extreme polarities, water is uniquely the most efficient in 'freezing' rotation about the amide bond (23), a property which is magnified by the addition of glycerol (24).

1. C. TANFORD. The hydrophobic effect. Wiley-Interscience, New York, NY. 1973.
2. L. J. LANGER and L. L. ENGEL. J. Biol. Chem. **233**, 583 (1958); J. JARABAK, J. A. ADAMS, H. C. WILLIAMS-ASHMAN, and P. TALALAY. J. Biol. Chem. **237**, 345 (1962); J. JARABAK, A. E. SEEDS, JR., and P. TALALAY. Biochemistry, **5**, 1269 (1966); S. L. BRADBURY and W. B. JAKOBY. Proc. Natl. Acad. Sci. (USA), **69**, 2373 (1972).
3. J. S. MYERS and W. B. JAKOBY. Biochem. Biophys. Res. Commun. **51**, 631 (1973).
4. I. FRIDOVICH. J. Biol. Chem. **238**, 592 (1963); M. A. LAUFFER and C. L. STEVENS. *In* Advances in virus research. Vol. 3. *Edited by* K. M. Smith and M. A. Lauffer. Academic Press, New York, NY. 1968. p. 1; M. L. SHELANSKY, F. GASKIN, and C. R. CANTOR. Proc. Natl. Acad. Sci. (USA), **70**, 765 (1973).
5. J. S. MYERS and W. B. JAKOBY. J. Biol. Chem. **250**, 3785 (1975).
6. G. DIPAOLA and B. BELLEAU. Can. J. Chem. **53**, 3452 (1975); G. DIPAOLA and B. BELLEAU. *In* L'eau et les systèmes biologiques. *Edited by* A. Alfsen and A. J. Berteaud. Editions du Centre National de la Recherche Scientifique, Paris. 1976. p. 255.
7. S. Y. GERLSMA. J. Biol. Chem. **243**, 957 (1968); S. Y. GERLSMA. Eur. J. Biochem. **14**, 150 (1970).
8. P. PICKER, P.-A. LEDUC, P. R. PHILIP, and J. E. DESNOYERS. J. Chem. Thermodyn. **3**, 631 (1971).
9. J.-L. FORTIER, P.-A. LEDUC, and J. E. DESNOYERS. J. Solution Chem. **3**, 323 (1974).
10. P. PICKER, E. TREMBLAY, and C. JOLICOEUR. J. Solution Chem. **3**, 377 (1974).
11. P. PICKER, C. JOLICOEUR, and J. E. DESNOYERS. J. Chem. Educ. **45**, 614 (1968).
12. H. F. STIMSON. Am. J. Phys. **23**, 614 (1955).
13. G. S. KELL. J. Chem. Eng. Data, **12**, 66 (1967).
14. D. W. KUPKE. *In* Molecular biology: physical techniques of protein chemistry. Part C. *Edited by* S. J. Leach. Academic Press, New York, NY. 1973. pp. 1–75.
15. G. DIPAOLA and B. BELLEAU. Can. J. Chem. Submitted.
16. N. C. PACE and C. TANFORD. Biochemistry, **7**, 198 (1968).
17. R. F. GREENE, JR. and C. N. PACE. J. Biol. Chem. **249**, 5388 (1974).
18. D. EAGLAND. *In* Water: a comprehensive treatise. *Edited by* F. Franks. Plenum Press, New York, NY. 1975. p. 339.
19. C. S. MINES and N. N. DALTON. Glycerol. Reinhold Publishing Corporation, New York, NY. 1953.
20. W. P. JENCKS. Fed. Proc. Suppl. **15**, S-50 (1965).
21. G. DIPAOLA. Ph.D. Thesis, McGill University, Montreal, P.Q. 1976; G. DIPAOLA and B. BELLEAU. To be published.
22. D. T. WARNER. J. Theor. Biol. **1**, 514 (1961); D. T. WARNER. Nature, **196**, 1055 (1962).
23. F. SCHUBER and B. BELLEAU. Bioorg. Chem. **2**, 111 (1973).
24. F. SCHUBER and B. BELLEAU. To be published.

Phlegmarine, a likely key intermediate in the biosynthesis of the Lycopodium alkaloids

LOUIS NYEMBO, ANDRÉ GOFFIN, CLAUDE HOOTELÉ,[1] AND JEAN-CLAUDE BRAEKMAN[1]

Service de Chimie Organique, Faculté des Sciences, Université Libre de Bruxelles, 1050 Bruxelles, Belgium

LOUIS NYEMBO, ANDRÉ GOFFIN, CLAUDE HOOTELÉ, and JEAN-CLAUDE BRAEKMAN. Can. J. Chem. **56**, 851 (1978).

The isolation and structure determination of four novel bases (**6**, **7**, **8**, **9**), representative of a new type of Lycopodium alkaloids, are reported. The phlegmarine skeleton is proposed to be a key intermediate in the biosynthesis of the Lycopodium alkaloids.

LOUIS NYEMBO, ANDRÉ GOFFIN, CLAUDE HOOTELÉ et JEAN-CLAUDE BRAEKMAN. Can. J. Chem. **56**, 851 (1978).

Dans le présent travail nous décrivons l'isolement et la détermination de structure de quatre alcaloïdes tricycliques (**6**, **7**, **8**, **9**) représentatifs d'un type nouveau d'alcaloïdes des Lycopodium. Le squelette phlegmarine est proposé comme intermédiaire clé dans la biosynthèse des alcaloides des Lycopodium.

Lycopodane (**1**), lycodane (**2**), and cernuane (**3**) are the three main skeletons from which the structure of most of the Lycopodium alkaloids can be derived (1, 2). During the study of the biosynthesis of these alkaloids, it was found that acetate, malonate, lysine, cadaverine, Δ^1-piperideine, and pelletierine serve as precursors of lycopodine (**4**) (3–8) and cernuine (**5**) (9, 10). Radioactivity from all except pelletierine is incorporated in such a manner that each of the two 'halves' of lycopodine and cernuine (i.e. C-1 to C-8 and C-9 to C-16) contains 50% of the label. Unexpectedly, pelletierine does not enter the C-1 to C-8 chain while it enters the other one. To explain this apparent anomaly, a biogenetic model has been outlined (7, 10). This model is depicted in Scheme 1. Nevertheless, it could not be corroborated experimentally (8), thus implying that modifications are required.

In this paper, we wish to report the isolation and structure determination of four novel alkaloids, representative of a new type of Lycopodium alkaloids. The structure of these compounds led us to reconsider the problem of the biosynthesis of the Lycopodium alkaloids and to propose a new scheme

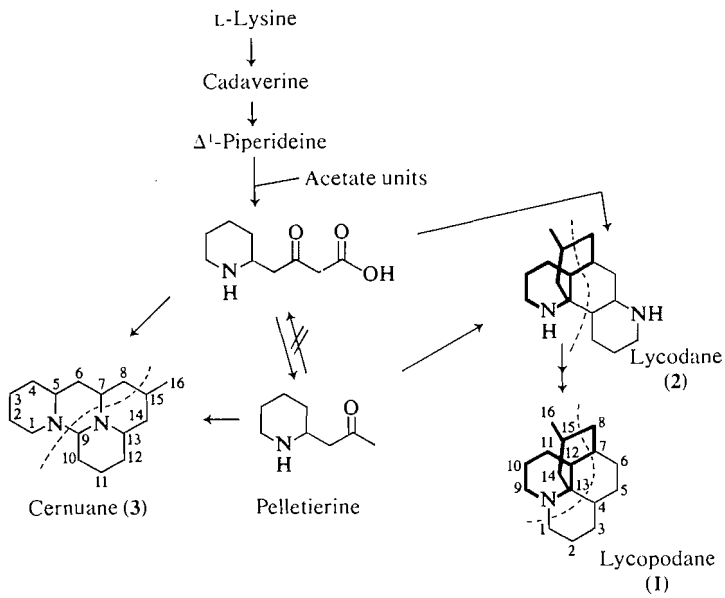

SCHEME 1. The biosynthesis of lycopodine and cernuine. A synthesis of the hypothetical pathways proposed in refs. 7 and 10.

[1]Chercheur qualifié du Fonds National de la Recherche Scientifique.

Can. J. Chem. Downloaded from www.nrcresearchpress.com by 210.87.254.105 on 09/05/12
For personal use only.

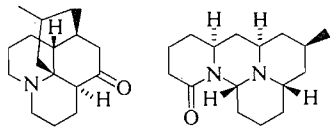

4 5

to explain the asymmetrical incorporation of pelletierine.

Together with lycopodine,[2] anhydrolycodoline,[2] β-dihydrolycopodine,[2] acetyl-β-dihydrolycopodine,[2] lycodoline,[2] and lycoflexine (11), we have isolated from *L. clavatum* var. *borbonicum* the minor base **6** ($C_{19}H_{34}N_2O$ by hrms). The ir and nmr spectra of **6** suggest the presence of an *N*-acetyl, an *N*-methyl, and a secondary methyl group.

On the other hand, we have isolated from *L. phlegmaria*, together with lycodoline,[2] anhydrolycodoline,[2] lycoflexine (11), lycopodine,[2] and gnidioidine (12), two minor alkaloids, compounds **7** and **8**, structurally related to **6**. Indeed by acetylation, compound **7** yields a monoacetyl derivative identical with compound **6**; by methylation, following the Eschweiler-Clarke procedure (15), the *N,N*-dimethyl derivative **10** is obtained. This latter compound is also obtained by methylation of **8** which could also be acetylated to the *N,N*-diacetyl derivative **11**.

Finally, from *L. cernuum*, we have isolated a fourth minor base, compound **9**, isomeric with **7**. When submitted to an acetylation reaction, **9** yields the monoacetyl derivative **12** isomeric with **6**. By treatment with formaldehyde in the presence of formic acid, **9** is transformed into the *N,N*-dimethyl derivative **10**.

All these facts can be rationalized by considering that the four naturally occurring compounds **6–9** all possess the same skeleton **8**, for which the name phlegmarine was coined and differ only by their nitrogen atom substituents (Scheme 2). The molecular formula of phlegmarine (**8**, $C_{16}H_{30}N_2$) implies three points of unsaturation. Since there is no evidence for the presence of multiple bonds, compounds **6–9** must be tricyclic.

The elementary composition of the more characteristic fragment ions of **6** has been determined by high resolution mass spectrometry and the genetic relationship existing between these fragment ions established by mass analyzed ion kinetic energy (mike) spectrometry (13, 14) as summarized in Scheme 3.

From these data it follows that the two fragment ions appearing at *m/e* 166 and 180 both originate from the molecular ion by an unimolecular decomposition and differ from each other only by a methylene group. Moreover, the fragment ions at *m/e* 180 and 126 account for all the atoms present in the molecular ion. A way to rationalize these facts is to consider that **6** is constituted of a $C_7H_{12}NO$ unit attached to a $C_{11}H_{20}N$ unit through a methylene bridge as depicted in Scheme 4. In such a case, rupture *a* would generate the fragments 180 and 126 whereas rupture *b* would explain the fragment 166.

The composition of the $C_{10}H_{17}NCH_3$ unit is reminiscent of 7-methyl-*N*-methyldecahydroquinoline, a partial structure frequently encountered in the Lycopodium alkaloids (see Scheme 1), while the $C_5H_9NCOCH_3$ unit is compatible with *N*-acetylpiperidine.

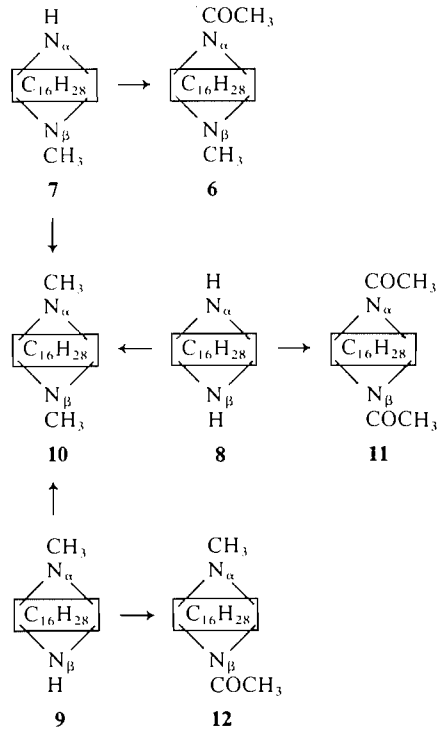

SCHEME 2. Chemical intercorrelations between compounds **6–9**.

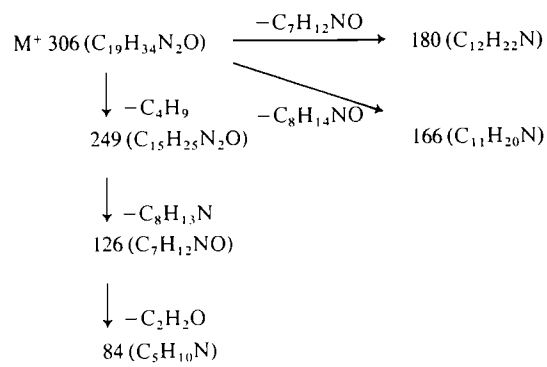

SCHEME 3. Genetic relationship between the characteristic fragment ions of **6**, obtained by mike spectrometry.

[2]Information about the structure, chemistry, and origin of these alkaloids may be found in refs. 1 and 2.

Can. J. Chem. Downloaded from www.nrcresearchpress.com by 210.87.254.105 on 09/05/12
For personal use only.

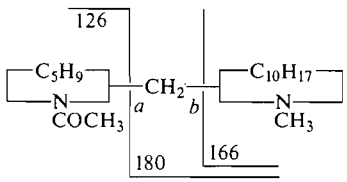

SCHEME 4. Partial structure of **6**.

When bringing together all these assumptions and taking into account the biosynthetic origin of the Lycopodium alkaloids, the attractive structures **6–9** may be proposed for phlegmarine (**8**) and its con-

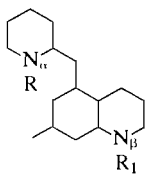

6	R = $COCH_3$, R_1 = CH_3	N_α-Acetyl-N_β-methylphlegmarine
7	R = H, R_1 = CH_3	N_β-Methylphlegmarine
8	R = H, R_1 = H	Phlegmarine
9	R = CH_3, R_1 = H	N_α-Methylphlegmarine

geners. To validate this hypothesis we decided to synthesize compound **6**, or at least a stereoisomer of **6**, following the reactional pathway depicted in Scheme 5.

The starting compound **13** was prepared according to the procedure described by Dugas *et al.* (15) for the synthesis of 12-epilycopodine. Owing to the

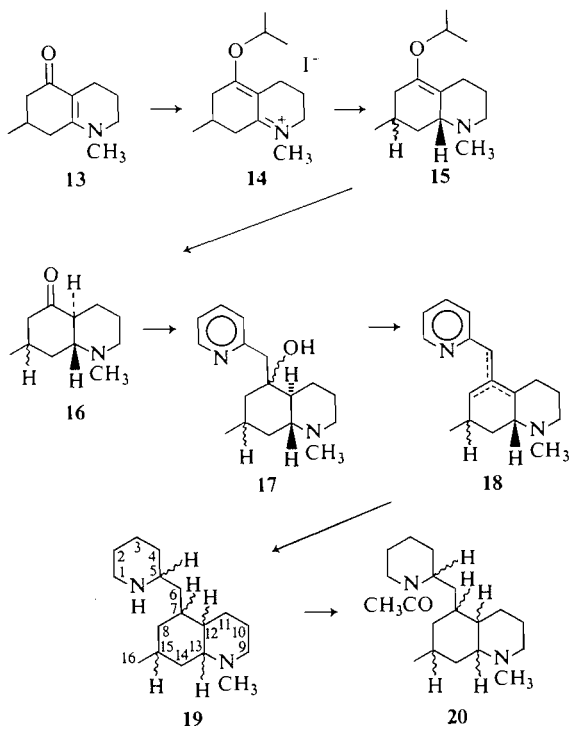

SCHEME 5. Scheme of synthesis of **20**.

failure of the direct reduction of **13** into **16** by catalytic hydrogenation, sodium in ammonia or hydride reduction, this conversion was achieved by borohydride reduction of the immonium salt **14**, followed by acidic hydrolysis. This afforded the homogeneous (tlc and gc) aminoketone **16** which could be isolated as its crystalline hydrochloride with an overall yield of 55%. The *trans*-ring fusion attributed to **16** follows finding that it did not epimerize under strongly basic conditions (16). The stereochemistry of the methyl group was not established.

Treatment of **16** with 2-picolyllithium furnished a mixture of two alcohols as observed by gc and tlc. The more polar derivative in tlc crystallized out of a pentane solution and its spectral properties are in good agreement with the structure **17** (see Experimental). By gc–ms it was found that the less polar constituent had the same mass spectrum, suggesting that these two alcohols are epimeric at C-7.

Dehydration of the mixture of the two alcohols with $SOCl_2$ yielded a mixture of three new compounds in the ratio of 29:10:61, as determined by gc. Moreover, it was found by gc–ms that each of these derivatives presents a molecular ion at *m/e* 256 suggesting that they are isomeric anhydro derivatives of **17**. This mixture was without further purification hydrogenated to a new mixture of two perhydro compounds (M^+ 294) which was directly treated with acetic anhydride in pyridine to obtain the corresponding acetates. The gc of these acetates shows two peaks, in the approximate ratio of 50:50, which were subsequently separated using preparative gc. The spectral properties of the acetate having the shorter retention time are in good agreement with structure **20** (see Experimental). The mass spectrum of the second peak was found to be identical with that of the former one, but the nmr spectrum indicates that it is still a mixture, probably of two or more stereoisomers of **20**.

These synthetic compounds were found to be different by tlc and gc from the natural compound **6**. However, the conventional mass spectra of all of them, as well as the mike (13, 14) and collision induced decomposition (cid) spectra (17) of their respective ions at *m/e* 306, 249, 180, 166, and 126 are superimposable. This clearly suggests that they have the same skeleton and that they are diastereoisomers.

In the introduction we pointed out that the biogenetic model outlined in Scheme 1 to explain the asymmetrical incorporation of pelletierine into the Lycopodium alkaloids, could not be corroborated experimentally. The discovery of compounds whose structure derives from the phlegmarine skeleton, leads us to suggest an alternative model in which this entity appears as a key intermediate.

Indeed, it is tempting to assume that the phleg-

Can. J. Chem. Downloaded from www.nrcresearchpress.com by 210.87.254.105 on 09/05/12
For personal use only.

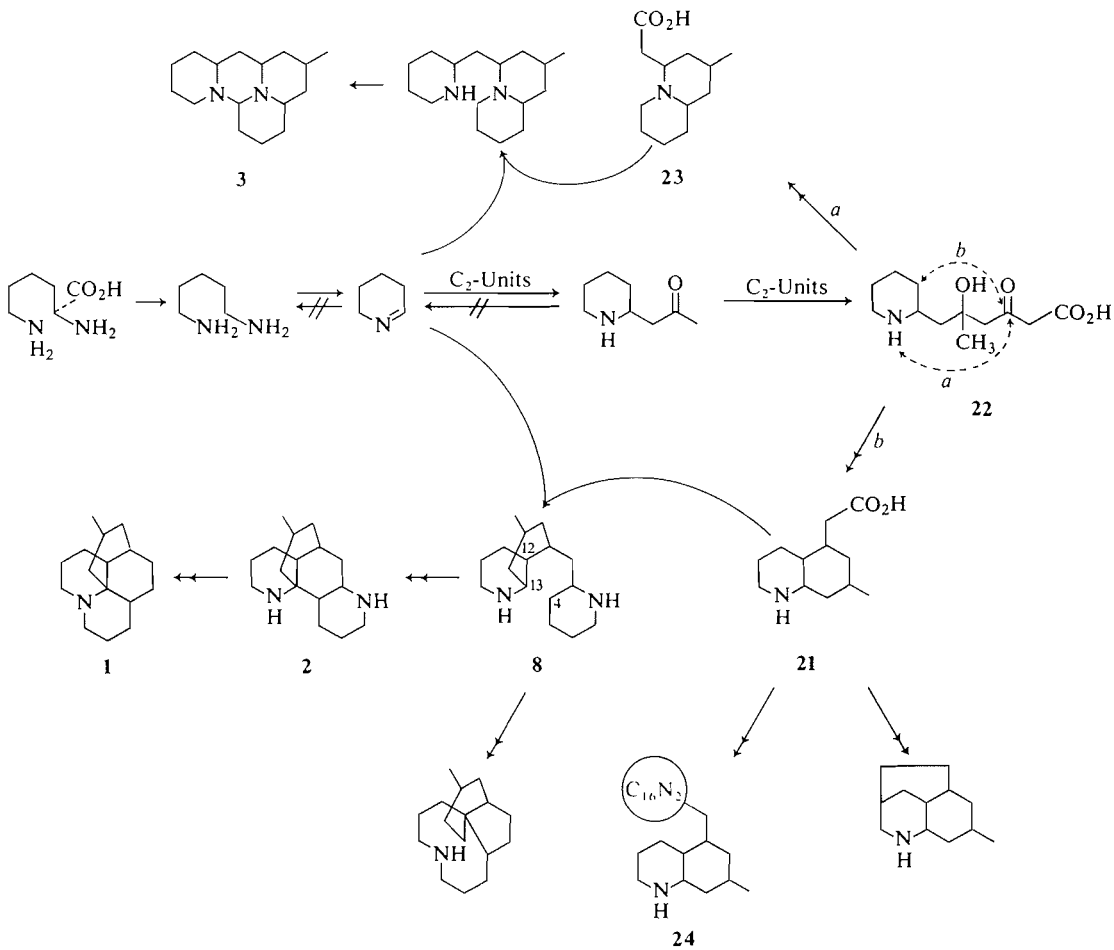

SCHEME 6. The biogenesis of the Lycopodium alkaloids. A new scheme.

marine type alkaloids derive from the condensation of Δ^1-piperideine with intermediate **21**, this latter arising from the condensation of two C_2-units with pelletierine followed by an internal cyclization (Scheme 6, path *b*). From the key intermediate **8** it is easy, by formation of a bond between C-4 and C-13, to build up the closely related lycodane and lycopodane skeletons, while the fawcettimane skeleton is readily obtained by formation of a bond between C-4 and C-12 and rupture of the C-13—N bond.

Furthermore: (*i*) the formation of cernuane can be imagined to be issued from the substituted quinolizidine **23**, this latter intermediate resulting from the alternative internal cyclization of **22** (Scheme 6, path *a*); (*ii*) it is also possible to derive the lucidulane skeleton as well as the partial structure **24** of the $C_{27}N_3$ Lycopodium alkaloids (18)[3] from the key intermediate **8**.

It is obvious, that the pathway proposed here is, for the clearness of the scheme, only a coarse description of a possible biosynthetic pathway for the Lycopodium alkaloids, and that the represented intermediates are not necessarily on the main route, for instance intermediates having other states of oxidation are also conceivable.

[3]A. Goffin, C. Hootelé, and J.-C. Braekman. Unpublished results.

Experimental

The general experimental details are the same as those previously described (19).

Isolation of the Alkaloids

The procedure described in ref. 20 was used for all the extractions. The extraction of 1.25 kg of powdered *L. clavatum* var. *borbonicum* collected on the Biano plateau, Shaba, Zaïre, yielded 4.5 g (0.36%) of a crude alkaloid mixture. This mixture was fractionated by dry column chromatography (alumina, activity III, 1.60 m; eluent: ethyl acetate); the column was cut up into 10 fractions and the constituents were eluted from the support with MeOH. The numbering of the fractions starts from the front of the solvent. Fractions 1 + 2 yielded 95 mg of anhydrolycodoline (ir, R_f, gc, ms, and nmr). Fractions 3 + 4 (1.33 g) were submitted to a counter-current distribution ($CHCl_3$ – McIlvaine buffer p*H* 6.1; 23 transfers); tubes 7–17 yielded, after crystallization from acetone, 0.85 g of pure lycopodine (ir, R_f, gc, ms, nmr). Fractions 5 + 6 + 7

Can. J. Chem. Downloaded from www.nrcresearchpress.com by 210.87.254.105 on 09/05/12
For personal use only.

Can. J. Chem. Downloaded from www.nrcresearchpress.com by 210.87.254.105 on 09/05/12
For personal use only.

TABLE 1. High resolution mass spectrometry of compound **6**

Composition	Mass		Relative intensity
	Calculated	Measured	
$C_{19}H_{34}N_2O$ (M^+)	306.2670	306.2674	9
$C_{15}H_{24}N_2O$	249.1966	249.1967	12
$C_{12}H_{22}N$	180.1751	180.1750	20
$C_{11}H_{20}N$	166.1595	166.1593	100
$C_7H_{12}NO$	126.0918	126.0921	37
$C_5H_{10}N$	84.0813	84.0810	27

(0.622 g) were chromatographed over alumina. Elution with increasing amounts of ethyl acetate in benzene furnished lycopodine (145 mg), lycoflexine (20 mg; ir, ms, gc, nmr, R_f) and β-acetyldihydrolycopodine (150 mg; ir, ms, gc, nmr, R_f). Fractions 8 + 9 (0.67 g) were submitted to a counter-current distribution ($CHCl_3$ – McIlvaine buffer p*H* 7.45; 23 transfers). Tubes 7–15 yielded, after crystallization from acetone, 80 mg of pure lycodoline (mp, ir, ms, R_f, gc, nmr), tubes 16–23 β-dihydrolycopodine (145 mg; mp, R_f, gc, ir, ms, nmr), and tubes 1–14, 43 mg of N_α-acetyl-N_β-methyl-phlegmarine (**6**)[4] further purified by chromatography over alumina (oil $[\alpha]_D$-($CHCl_3$) −11° (*c* 0.7); ir (film) $\nu_{C=O}$: 1640 cm^{-1}; nmr δ: 0.90 (d, 3H, 0.90 *J* = 7 Hz), 2.06 (s, 3H), 2.45 ppm (s, 3H); ms: see Table 1.

The extraction of 425 g of powdered *L. phlegmaria* L., collected at Yangambi, Zaïre, yielded 1.12 g (0.25%) of a crude alkaloid mixture. This mixture was dissolved in 100 ml of $CHCl_3$ and the solution extracted twice with 200 ml of McIlvaine buffer p*H* 6.0. The organic layer furnished after evaporation 420 mg of a brownish residue (F_1). The aqueous layer was made basic with aqueous ammonia and extracted with $CHCl_3$; evaporation of the $CHCl_3$ solution gave 650 mg of a brownish residue (F_2).

From fraction F_1 were isolated, after counter-current distribution ($CHCl_3$ – McIlvaine buffer p*H* 5.3, 23 transfers) and chromatography over alumina, 7 mg of anhydrolycodoline (ir, gc, ms, R_f) and 64 mg of lycoflexine (ir, R_f, nmr, gc, ms).

Fraction F_2 was submitted to a counter-current distribution ($CHCl_3$ – McIlvaine buffer p*H* 7.2, 23 transfers); tubes 2–16 yielded 323 mg of a mixture which was chromatographed over alumina. Elution with $CHCl_3$ yielded 22 mg of gnidioidine (ir, R_f, gc, ms) and 72 mg of crystalline lycodoline (ir, R_f, gc, mp, ms). The mass spectrum of the crude contents of tubes 17–23 (330 mg) showed the presence of at least two products (M^+ at 250 and 264 mu). A 150 mg portion of this mixture was acetylated (acetic anhydride – pyridine) and after several chromatographies over alumina furnished 15 mg of N_α-acetyl-N_β-methylphlegmarine (**6**) identical (ir, R_f, nmr, ms, gc) with the sample isolated from *L. clavatum* and 40 mg of *N,N*-diacetylphlegmarine (**11**)[4] (oil, ir: $\nu_{C=O}$ at 1640 cm^{-1}; nmr δ: 0.9 (d, 3H, *J* = 6 Hz), 2.05 (s, 3H), and 2.06 ppm (s, 3H); ms: 334 (M^+, 11), 292 (3), 291 (17), 209 (11), 208 (29), 195 (5), 194 (7), 166 (3), 152 (6), 150 (6), 140 (3), 138 (25), 127 (28), 126 (100), 112 (4), 98 (5), 97 (4), 96 (5), 85 (7), 84 (92), 83 (8), 82 (6), 81 (5).

A 180 mg portion of the same mixture was methylated using the procedure of Eschweiler-Clarke (15). After the usual work-up and chromatography on alumina, 110 mg of *N,N*-dimethylphlegmarine (**10**)[4] was obtained (oil; $[\alpha]_D(CHCl_3)$ −21° (*c* 1.3); ir ν_{N-CH_3}: 2780 cm^{-1}; nmr δ: 0.93 (d, 3H, *J* = 7 Hz), 2.26 ppm (s, 6H); ms: 278 (M^+, 30), 277 (4), 264 (3), 263 (9), 221 (8), 181 (10), 180 (34), 167 (5), 166 (16), 99 (75), 98 (100), 97 (26), 96 (24).

The crude alkaloid mixture from a sample of *L. cernuum* collected on the Biano plateau, Shaba, Zaïre, was dissolved in $CHCl_3$ and extracted with McIlvaine buffer of p*H* 7. A part of the extract (90 mg) which showed in the ms a molecular ion at 264 mu was acetylated. The residue obtained after the usual work-up furnished after chromatography on alumina 43 mg of N_α-methyl-N_β-acetylphlegmarine (**12**)[4] (oil; $[\alpha]_D(CHCl_3)$ −60° (*c* 0.41)); ir ν_{N-CH_3}: 1640 cm^{-1}; nmr δ: 0.9 (d, 3H), 2.07 (s, 3H), 2.27 ppm (s, 3H); ms: 306 (M^+, 3), 291 (2), 264 (2), 263 (5), 250 (2), 249 (12), 206 (3), 181 (4), 180 (20), 167 (15), 166 (100), 164 (6), 127 (4), 126 (37), 124 (5), 123 (6), 98 (19), 97 (14), 85 (2), 84 (27).

After methylation and fractionation by chromatography on alumina 100 mg of the same extract gave 50 mg of *N,N*-dimethylphlegmarine (**10**).

Synthesis of Compounds ***20***

Compound **14** was prepared according to the procedure described (15).

Ketone ***16*** *from the Immonium Salt* ***14***

A 1.37 g portion of immonium salt **14** was dissolved in 20 ml of methanol and treated with 0.2 g of $NaBH_4$. The reduction is instantaneous. After usual work-up, 1.1 g of the crude vinyl ether **15** was obtained and left for 12 h at room temperature in 100 ml of 10% aqueous HCl. The solution was made basic by addition of aqueous ammonia and extracted with chloroform. Evaporation of the solvent yielded 470 mg of a yellowish oil which was dissolved in anhydrous ether and treated with gaseous HCl. The precipitate was crystallized twice from acetone–ether: **16**·HCl; mp 181°C; ir $\nu_{C=O}$: 1710 cm^{-1}; nmr δ: 1.14 (d, 3H, *J* = 6 Hz), 2.88 (d, 3H, *J* = 5 Hz), 3.49 ppm (m, 1H); ms: 181 (M^+, 12), 139 (40), 124 (42), 97 (100), 82 (13). *Anal.* calcd. for $C_{11}H_{20}NOCl$: C 60.68, H 9.26, Cl 16.28; found: C 60.81, H 9.25, Cl 16.65.

The ketone **16** is recovered unchanged (tlc, gc) after treatment in equilibrating conditions: reflux in MeONa–MeOH for 4 h.

Condensation of Ketone ***16*** *with 2-Picolyllithium*

To 233 mg of finely divided lithium was added dropwise and under nitrogen a solution of 5.03 g of bromobenzene in 50 ml of anhydrous ether. The mixture was stirred until the disappearance of lithium was complete; 4.8 g of 2-picoline was then introduced slowly. Stirring was maintained for 30 min after addition. The resulting solution was added dropwise to an ethereal solution (30 ml) of **16** (520 mg). After stirring (30 min), the mixture was poured on crushed ice and extracted with ether. Evaporation of the solvent yielded 663 mg of a brownish oil which was chromatographed over alumina (eluent: ether–MeOH 9:1). The fractions containing the two epimeric alcohols **17** were combined, evaporated to dryness (568 mg), and dissolved in pentane. Crystals of one isomer separate on standing (mp 128°C; ir (KBr) ν_{OH}: 3300 cm^{-1}, ν_{N-CH_3}: at 2780 cm^{-1}, $\nu_{C=C}$: 1600 cm^{-1}; δ: 0.82 (d, 3H, *J* = 6 Hz) 2.30 (s, 3H), 2.48 (d, 1H, *J* = 14 Hz), 2.82 (d, 1H, *J* = 8 Hz), 5.23 (s, 1H, disappearing on treatment with D_2O), 7.14–8.47 ppm (m, 4H); ms: 274 (M^+, 13), 255 (7), 241 (10), 217 (15), 182 (100), 164 (98).

The mother liquors were constituted of a mixture of the two epimeric alcohols **17** (identical mass spectra by gc and ms).

Dehydration of the Alcohols ***17***

To a solution of 50 mg of the epimeric alcohols **17** in anhydrous pyridine was added 36 mg of $SOCl_2$. The solution was stirred for 1 h at room temperature. The excess of reagent was destroyed by water and the solution evaporated to dryness under reduced pressure. After filtration over alumina, an oily

[4]Compounds **6**, **10**, **11**, and **12** were found to be homogeneous by gc on three different columns: 10% SP2330 (235°C), 1% SP 1000 (190°C), and 4% OVI (185°C).

residue was obtained which was found to contain three isomeric compounds (**18***a*, **18***b*, **18***c*) in the ratio of 29:10:61 (gc 10% SP2330 at 200°C): gc–ms: **18***a*: M^+ 256 (32), 241 (12), 213 (22), 199 (14), 198 (19), 184 (24) 178 (24), 164 (100), 97 (72); **18***b*: M^+ 256 (7), 214 (12), 213 (14), 199 (12), 198 (8), 164 (100); **18***c*: M^+ 256 (18), 241 (9), 213 (14), 212 (18), 199 (24), 198 (32), 184 (70), 171 (46), 170 (42), 164 (100).

After chromatography on alumina (eluent: ethyl acetate – MeOH 9:1) a 40:60 mixture of **18***a* and **18***b* was separated; uv (CH_3OH) λ_{max} 264 nm; nmr δ: 0.92 and 1.01 (d, 2 secondary methyls, J = 7 Hz), 2.31 and 2.34, respectively (s, 2 N—CH_3's); 5.25 (1 multiplet of 0.4H) 7.15–8.50 ppm (aromatic protons); ir (film): 2775, 1650, 1590, and 1470 cm^{-1}.

Catalytic Hydrogenation of Compounds ***18***

Catalytic hydrogenation of compounds **18** was performed at room temperature in acetic acid (Pt, 4 kg/cm^2) for 48 h. After the usual work-up and filtration over alumina, an oily residue was obtained. It shows two peaks by gc (SP 2330 10%, 175°C); ms: M^+ 264 (39), 249 (13), 207 (20), 181 (34), 166 (78) 164 (46), 124 (56), 98 (42), 97 (55), 84 (100); ir ν_{N-CH_3}: at 2760 cm^{-1}, no more aromatic bands; nmr: 2.24 and 2.28 (2 s, N—CH_3), no signals beyond 3.5 ppm.

Without further purification the mixture was acetylated (acetic anhydride – pyridine 24 h at room temperature). The oily residue obtained after the usual work-up presents two peaks by gc (10% SP 2330, 220°C) which were separated by preparative gc. The compound having the shorter retention time was found to be homogeneous on three different columns (10% SP 2330, 235°C; 1% SP 1000, 190°C; 4% OVI, 185°C) and by tlc. Its mass spectrum was superimposable with that of compound **6**; nmr δ: 0.9 (d, 3H, J = 7 Hz), 2.07 and 2.28 ppm (s, 3H); ir (film): 2780, 1640, 1430, and 1270 cm^{-1}. The mass spectrum of the second peak was also superimposable with that of compound **6** but it was found to be still a mixture (tlc, nmr). The R_f value and retention time of the synthetic derivatives **20** were found to be different from those of the natural derivative **6**; however, all compounds had identical mass spectra and identical mike and cid spectra for the peaks at *m/e* 306 (15), 249 (20), 180 (27), 166 (100), 126 (57), 84 (52).

Acknowledgements

We wish to thank Professor A. Maquestiau and Dr. R. Flamang (Université de Mons) for the cid and mike spectrometry measurements, and Professor D. B. MacLean for valuable discussions. Two of us wish to thank the Institut pour l'Encouragement de la Recherche Scientifique dans l'Industrie et l'Agriculture (A.G.) and the A.G.C.D. (L.N.) for the award of fellowships.

1. D. B. MacLean. *In* The alkaloids. Vol. X. *Edited by* R. H. F. Manske. Academic Press, New York, London. 1968. p. 305.
2. D. B. MacLean. *In* The alkaloids. Vol. XIV. *Edited by* R. H. F. Manske. Academic Press, New York, London. 1973. p. 347.
3. R. N. Gupta, M. Castillo, D. B. MacLean, I. D. Spenser, and J. T. Wrobel. J. Am. Chem. Soc. **90**, 1360 (1968).
4. M. Castillo, R. N. Gupta, D. B. MacLean, and I. D. Spenser. Can. J. Chem. **48**, 1893 (1970).
5. M. Castillo, R. N. Gupta, Y. K. Ho, D. B. MacLean, and I. D. Spenser. J. Am. Chem. Soc. **92**, 1074 (1970).
6. M. Castillo, R. N. Gupta, Y. K. Ho, D. B. MacLean, and I. D. Spenser. Can. J. Chem. **48**, 2911 (1970).
7. J.-C. Braekman, R. N. Gupta, D. B. MacLean, and I. D. Spenser. Can. J. Chem. **50**, 2591 (1972).
8. W. D. Marshall, T. T. Nguyen, D. B. MacLean, and I. D. Spenser. Can. J. Chem. **53**, 41 (1975).
9. R. N. Gupta, Y. K. Ho, D. B. MacLean, and I. D. Spenser. Chem. Commun. 409 (1970).
10. Y. K. Ho, R. N. Gupta, D. B. MacLean, and I. D. Spenser. Can. J. Chem. **49**, 3352 (1971).
11. W. A. Ayer, Y. Fukazawa, P. P. Singer, and B. Altenkirk. Tetrahedron Lett. 5045 (1973).
12. L. Nyembo, N. Kahindo, J.-C. Braekman, and C. Hootelé. Bull. Soc. Chim. Belg. **85**, 595 (1976).
13. T. Wachs, P. F. Bente, and F. W. McLafferty. Int. J. Mass Spectr. Ion Phys. **9**, 333 (1972).
14. J. H. Beynon, R. G. Cooks, J. W. Amy, W. E. Baitinger, and T. Y. Ridley. Anal. Chem. **45**, 1023 A (1973).
15. H. Dugas, R. A. Ellison, Z. Valenta, K. Wiesner, and C. M. Wong. Tetrahedron Lett. 1279 (1965).
16. E. L. Eliel. *In* Stereochemistry of carbon compounds. New York. 1962. p. 280.
17. K. Levsen and H. Schwarz. Angew. Chem. Int. Ed. **15**, 509 (1976).
18. D. S. Nkunika. Ph.D. Thesis. University of Alberta, Edmonton, Alta. 1967.
19. J. C. Braekman, C. Hootelé, and W. A. Ayer. Bull. Soc. Chim. Belg. **80**, 83 (1971).
20. J. C. Braekman, L. Nyembo, P. Bourdoux, N. Kahindo, and C. Hootelé. Phytochemistry, **13**, 2519 (1974).

Can. J. Chem. Downloaded from www.nrcresearchpress.com by 210.87.254.105 on 09/05/12
For personal use only.

Basicité des composés $(R_2N)_{3-n}(RO)_nP$ vis-à-vis de BH_3. Etude comparée par résonance magnétique nucléaire et enthalpies de réaction

LUCIEN ELEGANT ET JEAN-FRANÇOIS GAL

Laboratoire de Chimie Physique Organique, Université de Nice, Parc Valrose, 06034 Nice Cedex – France

ET

CLAUDE JOUANY ET GÉRARD JUGIE[1]

Laboratoire de Chimie de Coordination du CNRS, B.P. 4142, 31030 Toulouse Cedex – France

Reçu le 8 juin 1977

LUCIEN ELEGANT, JEAN-FRANÇOIS GAL, CLAUDE JOUANY et GÉRARD JUGIE. Can. J. Chem. **56**, 857 (1978).

Les composés d'addition $(Me_2N)_{3-n}(t\text{BuO})_nP \rightarrow BH_3$ (avec $n = 1$, 2 et 3) ont été préparés et caractérisés pour la première fois. L'évolution des paramètres provenant de l'analyse des spectres de rmn (^1H, ^{11}B et ^{31}P) est confrontée avec celle des enthalpies de réaction entre les phosphines libres et le borane et avec les données issues des réactions de déplacement. Il ne semble pas y avoir de corrélation entre $^1J_{BP}$ et la stabilité des complexes.

LUCIEN ELEGANT, JEAN-FRANÇOIS GAL, CLAUDE JOUANY, and GÉRARD JUGIE. Can. J. Chem. **56**, 857 (1978).

The equimolecular adducts between aminoalkoxyphosphines $(Me_2N)_{3-n}(t\text{BuO})_nP$ with $n = 1$, 2, and 3) and borane BH_3 have been prepared and characterised. The nmr study has been undertaken to compare some parameters ($^1J_{BH}$, $^1J_{BP}$, $\delta^{11}B$ etc.) with both those derived from the enthalpies of reaction of diborane with the parent phosphines and from the displacement reactions. No overall correlations between the $^1J_{BP}$ coupling constants and the complex stabilities seem evident.

Les composés d'addition $X_3P \rightarrow BY_3$ constituent des exemples de choix pour une étude de l'évolution des valeurs des déplacements chimiques et des constantes de couplage relatifs tant au donneur qu'à l'accepteur, en fonction de la nature des substituants X et Y fixés sur les deux pôles de la liaison de coordination. En fait, de nombreux travaux (cf. réfs. (1–7)) ont tenté de dégager des relations entre les grandeurs issues des analyses par résonance magnétique nucléaire et la stabilité relative des complexes. C'est dans ce cadre général que se situent nos travaux antérieurs (8); ils revêtent cependant un caractère particulier dans la mesure où nous nous efforçons de prendre en considération les enthalpies de réactions (9) et les réactions de déplacement ce qui nous amène à remettre en cause l'utilisation de certains paramètres rmn comme critère de stabilité des complexes $X_3P \rightarrow BY_3$.

Après avoir considéré, à ce point de vue, les composés d'addition de BH_3 avec les bases phosphorées du type $Me_{3-n}(MeO)_nP$ et $Me_{3-n}(Me_2N)_nP$ ($0 \leq n \leq 3$) (9), nous envisageons ici la série $(Me_2N)_{3-n}(RO)_nP \rightarrow BH_3$ dont les trois termes ont pu être isolés dans un état de pureté convenable en utilisant un reste alcoxylé particulier: le reste tertiobutoxy.

Partie Expérimentale

Obtention des bases phosphorées

Les deux diméthylaminotertiobutoxyphosphines $(Me_2N)_2(t\text{BuO})P$ (**2**) et $(Me_2N)(t\text{BuO})_2P$ (**3**) ont été préparées selon le procédé décrit par Burgada *et al.* (10), qui repose sur une alcoolyse contrôlée de $(Me_2N)_3P$ (**1**) par le tertiobutanol. Les constantes physiques de nos échantillons sont très proches de celles de la littérature. Pour ce qui est du terme extrême de la série constitué par $(t\text{BuO})_3P$ (**4**), il est bien connu qu'il n'est pas possible de le préparer par la méthode envisagée ci-dessus. Mark et Van Wazer (11) ont obtenu ce composé par la méthode générale de préparation des phosphites c'est-à-dire par action de PCl_3 sur l'alcool correspondant, mais la pureté du produit ainsi atteint reste inférieure à 90% en raison de la forte propension de (**4**) à se transformer en phosphonate $(t\text{BuO})_2P(O)H$. Pour notre part, nous sommes parvenus à améliorer notablement le procédé de Mark et Van Wazer (11), sans toutefois parvenir à éliminer totalement le phosphonate, en utilisant le mode opératoire suivant: la réaction

$$3t\text{BuOH} + PCl_3 + 3Et_3N \rightarrow (t\text{BuO})_3P + 3Et_3N, HCl$$

est effectuée dans un filtre muni d'une jaquette thermostatée et dont le couvercle à trois tubulures reçoit une ampoule à brome, un agitateur et une gaine thermométrique et dont la base est constituée par un verre fritté (de porosité G_4). Grâce à la circulation d'un fluide thermostatique (méthanol) dans la jaquette, la température de l'ensemble est très rigoureusement maintenue en dessous de 5°C. Toutes les opérations sont conduites en atmosphère inerte strictement contrôlée; 65 g (0.5 mol) dichlorure de phosphore en solution dans 150 cm^3 d'éther sont ajoutés goutte à goutte à 112 g (1.5 mol) de tertiobutanol et 170 g (1.68 mol) de triéthylamine en solution dans 500 cm^3 d'éther.

Après maintien d'une agitation vigoureuse pendant 48 h, et toujours à 5°C, la solution éthérée est filtrée puis le solvant extrait lentement sous vide; 120 g d'un liquide visqueux légèrement opalescent sont ainsi obtenus, correspondant à un rendement voisin de 95%. Ce liquide, filtré une seconde fois pour le rendre parfaitement limpide, cristallise bien à 0°C et possède un indice de réfraction n_D^{20} 1.426_5. La rmn du

[1]Auteur à qui doit être envoyée la correspondance.

Can. J. Chem. Downloaded from www.nrcresearchpress.com by 210.87.254.105 on 09/05/12
For personal use only.

Can. J. Chem. Downloaded from www.nrcresearchpress.com by 210.87.254.105 on 09/05/12
For personal use only.

TABLEAU 1. Principales caractéristiques physiques des complexes $(R_2N)_{3-n}(RO)_nP \rightarrow BH_3$[a]

Composes	Abréviation	Point d'ébullition (°C/Torr)	n_D^{20}	d_4^{20}	%C		%H		%B		%N		%P	
					Théor.	Exp.	Théor.	Exp.	Théor.	Exp.	Théor.	Exp.	Théor.	Exp.
$(Me_2N)_2(tBuO)P \rightarrow BH_3$	**2**·BH_3	50/0.2	1.452	0.898_2	46.60	46.41	11.74	11.49	5.24	5.56	13.59	13.58	15.03	15.07
$(Me_2N)(tBuO)_2P \rightarrow BH_3$	**3**·BH_3	61/0.2	1.442	0.897_6	51.06	51.15	11.50	11.49	4.60	4.94	5.95	6.09	13.17	13.18
$(tBuO)_3P \rightarrow BH_3$	**4**·BH_3	75/0.05	—	—	54.56	54.79	11.45	11.34	4.10	4.19	—	—	11.73	11.63
$(nBuO)_3P \rightarrow BH_3$	**4′**·BH_3	89/0.1	1.435	0.908_6	54.56	54.60	11.45	11.48	4.10	4.17	—	—	11.73	11.80

[a]Les déterminations analytiques ont été effectuées par le Centre National de Microanalyse du CNRS.

proton a permis de constater que cet échantillon ne contenait au plus que 2% de ditertiobutylphosphonate.

Obtention des composés d'addition avec BH_3

Pour **1**·BH_3, **2**·BH_3 et **3**·BH_3, nous avons utilisé le procédé de préparation de Reetz (12) et isolé les composés d'addition par distillation fractionnée. Par contre, pour **4**·BH_3 nous avons dû prendre en compte l'instabilité thermique de la tritertiobutoxyphosphine: ainsi, nous avons fait réagir directement le diborane gazeux sur une solution benzénique de **4** dont la température était rigoureusement maintenue en dessous de 10°C. La fin de la réaction est observée lorsque B_2H_6 n'est plus absorbé. Après élimination du solvant, on obtient un liquide visqueux qui est purifié par distillation fractionnée et conduit à de beaux cristaux blancs (p.f. 46°C).

Les trois composés **2**·BH_3, **3**·BH_3 et **4**·BH_3 n'ont fait l'objet, à notre connaissance, d'aucune description dans la littérature; leurs principales caractéristiques sont rassemblées dans le tableau 1, dans lequel nous avons également mentionné, à titre de comparaison, quelques données relatives au complexe de la *n*-tributoxyphosphine.

Les spectres de résonance magnétique nucléaire

Les différents spectres rmn ont été enregistrés dans les conditions habituelles au laboratoire (9): les principaux paramètres issus de leur analyse sont rassemblés dans le tableau 2.

Les déterminations calorimétriques

Elles ont été effectuées selon le mode opératoire décrit précédemment (9). Les valeurs obtenues apparaissent dans le tableau 3.

Les réactions de déplacement

Chacun des quatre composés d'addition a été mis en présence, en quantités sensiblement équimoléculaires, des trois autres ligands phosphorés de la série; ainsi, 12 mélanges initiaux ont été réalisés, correspondant deux à deux aux six systèmes suivants:

[1] $(tBuO)_3P + (tBuO)_2(Me_2N)P \rightarrow BH_3 \leftrightarrows (tBuO)_3P \rightarrow BH_3 + (tBuO)_2(Me_2N)P$

[2] $(tBuO)_3P + (tBuO)(Me_2N)_2P \rightarrow BH_3 \leftrightarrows (tBuO)_3P \rightarrow BH_3 + (tBuO)(Me_2N)_2P$

[3] $(tBuO)_3P + (Me_2N)_3P \rightarrow BH_3 \leftrightarrows (tBuO)_3P \rightarrow BH_3 + (Me_2N)_3P$

[4] $(tBuO)_2(Me_2N)P + (tBuO)(Me_2N)_2P \rightarrow BH_3 \leftrightarrows (tBuO)_2(Me_2N)P \rightarrow BH_3 + (tBuO)(Me_2N)_2P$

[5] $(tBuO)_2(Me_2N)P + (Me_2N)_3P \rightarrow BH_3 \leftrightarrows (tBuO)_2(Me_2N)P \rightarrow BH_3 + (Me_2N)_3P$

[6] $(tBuO)(Me_2N)_2P + (Me_2N)_3P \rightarrow BH_3 \leftrightarrows (tBuO)(Me_2N)_2P \rightarrow BH_3 + (Me_2N)_3P$

A la température ambiante, l'évolution des mélanges est faible ou nulle en raison, sans doute, de l'encombrement stérique important des restes tertiobutoxy, et diméthylamino, portés par le phosphore. En conséquence, les systèmes ont été maintenus à une température de 65°C pendant 5 jours. On a pu ainsi atteindre des états finaux bien définis, dont la composition a pu être établie sans ambiguïté par analyse des spectres ^{11}B et ^{31}P. Les proportions relatives des espèces présentes à

Can. J. Chem. Downloaded from www.nrcresearchpress.com by 210.87.254.105 on 09/05/12
For personal use only.

l'équilibre ont été évaluées par intégration des signaux de résonance magnétique du noyau ^{31}P: pour le système [1] on aboutit à un équilibre entre les quatre espèces, déplacé vers la gauche ~75%, pour 25% à droite; pour toutes les autres équations, que le mélange initial soit celui de gauche ou de droite, on parvient toujours au système totalement déplacé vers la gauche.

Discussion des résultats

En raison du caractère original de trois des composés étudiés dans cet article, il convenait avant tout de s'assurer de leur identité en vérifiant que la fixation de l'accepteur BH_3 avait bien lieu sur l'atome central de phosphore et qu'il n'apparaissait pas de réactions de redistribution (composés **2**·BH_3 et **3**·BH_3) ou de dégradation (composé **4**·BH_3) des restes fixés sur l'atome de phosphore. Ainsi, parmi les caractéristiques structurales des spectres rmn (^{11}B, ^{31}P et ^{1}H) nous retiendrons:

(*i*) l'allure de la figure de résonance du noyau ^{11}B qui apparaît dans tous les cas sous forme d'un quintuplet déformé traduisant la combinaison des couplages $^{1}J_{BH}$ et $^{1}J_{BP}$ dont les valeurs absolues sont voisines. Le découplage sélectif des protons a cependant permis d'atteindre les valeurs de $^{1}J_{BP}$ figurant dans le tableau 2 avec une précision convenable; (*ii*) l'importante évolution aussi bien sur le plan des déplacements chimiques que sur l'allure de la raie de résonance du noyau ^{31}P après complexation. Dans tous les cas en effet, nous avons observé que la fixation de BH_3 se traduisait par un déplacement important du massif de résonance vers les champs forts avec apparition plus ou moins marquée de l'éclatement du signal de ^{31}P sous la forme d'un quadruplet ($^{1}J_{BP}$); (*iii*) l'apparition, en résonance de ^{1}H, de quatre doublets B—*H* de pics largement étalés sur la zone spectrale (~300 Hz) et résultant de la combinaison des couplages $^{1}J_{BH}$ et $^{2}J_{PBH}$. Pour **2**·BH_3 et **3**·BH_3 nous avons vérifié, par intégration des massifs de résonance, la bonne répartition des signaux protoniques entre CH_3—N et $(CH_3)_3C$ tandis que pour **4**·BH_3, nous avons pu constater la disparition de tout pic attribuable à $(t\text{BuO})_2\text{P(O)H}$ après distillation du composé d'addition.

Ayant clairement identifié le site donneur de ces ligands, il paraît intéressant, comme il a été déjà fait précédemment, de confronter les échelles de basicité issues des données calorimétriques et des réactions de déplacement, à l'évolution de certains paramètres rmn.

Ainsi, en considérant que les variations d'enthalpies sont essentiellement liées à la rupture et au rétablissement de la liaison de coordination P → B et qu'en première approximation, (13–16), les variations d'entropie sont négligeables puisqu'elles con-

TABLEAU 2. Paramètres rmn (^{1}H, ^{11}B et ^{31}P) caractérisant les phosphines libres et leurs complexes avec BH_3

Composés	Abréviations	$\delta^{31}P$	$\delta^{11}B$	δCH_3—C—O	δCH_3—N	δB—*H*	$^{4}J_{HCCOP}$	$^{3}J_{HCNP}$	$^{2}J_{HPB}$	$^{1}J_{BH}$	$^{1}J_{BP}$[a]
$(Me_2N)_3P$	**1**	9	—	—	2.4$_7$	—	—	9	—	—	—
$(Me_2N)_3P \rightarrow BH_3$	**1**·BH_3	−8	−43	—	2.5$_7$	0.3$_6$	—	10	18	94	<98
$(Me_2N)_2(t\text{BuO})P$	**2**	16	—	1.3$_3$	2.5$_1$	—	~0.5	9.5	—	—	—
$(Me_2N)_2(t\text{BuO})P \rightarrow BH_3$	**2**·BH_3	−1	−42	1.4$_5$	2.6$_5$	0.4$_8$	~0.5	10	18	95	95
$(Me_2N)(t\text{BuO})_2P$	**3**	22	—	1.3$_3$	2.5$_8$	—	~0.5	9.5	—	—	—
$(Me_2N)(t\text{BuO})_2P \rightarrow BH_3$	**3**·BH_3	−5	−39	1.4$_4$	2.6$_0$	0.5$_8$	~0.5	10	18	95	99
$(t\text{BuO})_3P$	**4**	25	—	1.3$_0$	—	—	0.5	—	—	—	—
$(t\text{BuO})_3P \rightarrow BH_3$	**4**·BH_3	−14	−35	1.4$_8$	—	0.6$_0$	n.o.	—	~17	95	105
$(n\text{BuO})_3P$	**4′**	25	—	—	—	—	—	—	—	—	—
$(n\text{BuO})_3P \rightarrow BH_3$	**4′**·BH_3	3	−45	—	—	—	—	—	n.o.	~95	105

NOTE: Les spectres ont été enregistrés pour des composés en solution dans CH_2Cl_2 à une concentration égale à 10% en volume. Les déplacements chimiques (δ) sont comptés positivement lorsque le signal de résonance du noyau considéré est situé à champ faible par rapport au signal de la référence $(CH_3)_4Si$ interne, $(C_2H_5)_2O \rightarrow BF_3$ et P_4O_6 externes.
[a]Valeurs des spectres à partir du noyau ^{11}B après découplage sélectif des protons, sur spectromètre Brücker WH90.

Can. J. Chem. Downloaded from www.nrcresearchpress.com by 210.87.254.105 on 09/05/12
For personal use only.

TABLEAU 3. Paramètres issus de l'analyse des déterminations calorimétriques

Composés	$-\Delta H_1$[a] (kcal/mol)	$-\Delta H_2$[a] (kcal/mol)	σ_m[b]	ic_{95}[c]
1 + BH_3	49.53	42.27	0.16	0.41
2 + BH_3	45.63	40.31	0.22	0.62
3 + BH_3	42.19	38.72	0.22	0.57
4 + BH_3	47.27	41.13	0.25	0.57
4′ + BH_3	41.58	38.23	0.09	0.40

[a]Comparez avec réf. 9; ΔH_1 correspond à la valeur expérimentale de l'enthalpie liée à la réaction:

$2(Me_2N)_{3-n}(tBuO)_nP(sol.) + B_2H_6(gaz) \rightarrow 2(Me_2N)_{3-n}(tBuO)_nP \rightarrow BH_3(sol.)$

Connaissant l'enthalpie de dissociation du diborane (35 kcal/mol), on atteint ΔH_2 qui correspond alors à la réaction:

$(Me_2N)_{3-n}(tBuO)_nP(sol.) + BH_3(gaz) \rightarrow (Me_2N)_{3-n}(tBuO)_nP \rightarrow BH_3(sol.)$

[b]σ_m = écart moyen.
[c]ic_{95} = intervalle de confiance à 95%.

cernent des ligands appartenant à une même famille, l'évolution des systèmes [1] à [6] permet d'établir vis-à-vis de BH_3 la séquence suivante:

$$(Me_2N)_3P > (Me_2N)_2(tBuO)P > (Me_2N)(tBuO)_2P \sim (tBuO)_3P$$

Les mesures calorimétriques (cf. tableau 3) conduisent à une séquence identique à l'exception de la tritertiobutoxyphosphine qui occupe une place particulière. Si on fait abstraction de ce dernier composé, cette échelle peut être confrontée à l'évolution de la constante de couplage $^1J_{BP}$ retenue par certains auteurs (4) comme une mesure directe de la basicité des phosphines vis-à-vis du borane; pour la série étudiée présentement, $^1J_{BP}$ passe par un minimum pour le composé d'addition $(Me_2N)_2(tBuO)P \rightarrow BH_3$ et ne rend pas compte de l'échelle de basicité établie. Ce désaccord n'est pas surprenant dans la mesure où de nombreuses restrictions au domaine de validité du critère $^1J_{BP}$ ont déjà pu être relevées (3*b*, 17).

En ce qui concerne le couplage direct $^1J_{BH}$, en retenant le traitement de Pople et Santry (18) l'accroissement de sa valeur absolue devrait traduire un accroissement du caractère *s* de la liaison B—H et donc une diminution de la basicité du dérivé phosphoré entrant en jeu. Dans la limite de la précision de nos déterminations, $^1J_{BH}$ reste constant et traduirait donc des basicités voisines pour ces quatre ligands.

Enfin pour $\delta^{11}B$, son évolution bien que faible, permet de retrouver la même séquence que celle déduite des réactions de déplacement et vient donc s'ajouter aux résultats obtenus par Mooney et coll. (19). Cet accord, cependant ne constitue pas à nos yeux une preuve irréfutable puisque, dans d'autres séries (8*b*) ce critère a pu être mis en défaut.

Conclusions

En définitive, dans la série $(Me_2N)_{3-n}(tBuO)_nP \rightarrow BH_3$ il n'apparaît pas de corrélation évidente entre les critères de basicité habituellement retenus (tels que $^1J_{BP}$ ou $^1J_{BH}$) et la stabilité des complexes telle qu'elle peut être évaluée à partir des données calorimétriques ou des réactions de déplacement. Cette difficulté peut trouver son origine dans la complexité des ligands envisagés (qui possèdent des substituants à fort encombrement stérique et porteurs de doublets électroniques libres) et dans la différence relativement faible de leur affinité pour BH_3.

1. J. G. VERKADE, R. W. KING et C. W. HEITSCH. Inorg. Chem. **3**, 884 (1964).
2. E. MUYLLE et G. P. VAN DER KELEN. Spectrochim. Acta, **32**A, 599 (1976); E. MUYLLE, G. P. VAN DER KELEN et E. G. CLAEYS. Spectrochim. Acta, **32**A, 1149 (1976).
3. (*a*) R. W. RUDOLPH et R. W. PARRY. J. Am. Chem. Soc. **89**, 1621 (1967); (*b*) R. W. RUDOLPH et C. W. SCHULTZ. J. Am. Chem. Soc. **93**, 6821 (1971).
4. A. H. COWLEY et M. C. DAMASCO. J. Am. Chem. Soc. **93**, 6815 (1971).
5. J. S. HARTMAN et J. M. MILLER. Inorg. Chem. **13**, 1467 (1974); M. J. BULA, J. S. HARTMAN et C. V. RAMAN. Can. J. Chem. **53**, 326 (1975).
6. M. L. DENNISTON, M. A. CHIUSANO et D. R. MARTIN. J. Inorg. Nucl. Chem. **38**, 979 (1976).
7. J. E. DRAKE et B. RAPP. J. Chem. Soc. Dalton Trans. 2341 (1972); Inorg. Chem. **12**, 2868 (1973).
8. (*a*) C. JOUANY, G. JUGIE et J. P. LAURENT. Bull. Soc. Chim. Fr. 880 (1972); (*b*) C. JOUANY, G. JUGIE, J. P. LAURENT, R. SCHMUTZLER et O. STELZER. J. Chim. Phys. **3**, 395 (1974).
9. G. JUGIE, C. JOUANY, L. ELEGANT, J. F. GAL et M. AZZARO. Bull. Soc. Chim. Fr. 1 (1976).
10. R. BURGADA, G. MARTIN et G. MAVEL. Bull. Soc. Chim. Fr. 2154 (1963).
11. V. MARK et J. R. VAN WAZER. J. Org. Chem. **29**, 1006 (1964).
12. T. REETZ et B. KATLAFSKY. J. Am. Chem. Soc. **82**, 5036 (1960); T. REETZ. J. Am. Chem. Soc. **82**, 5039 (1960).
13. F. FOESTER et K. COHN. Inorg. Chem. **11**, 2590 (1972).
14. D. E. YOUNG, G. E. ACHRAN et S. G. SHORE. J. Am. Chem. Soc. **88**, 4390 (1966).
15. W. A. G. GRAHAM et F. G. A. STONE. J. Inorg. Nucl. Chem. **3**, 164 (1956).
16. E. NIOBOER et W. A. E. MCBRYDE. Can. J. Chem. **48**, 2565 (1970).
17. E. L. LINES et L. F. CENTOFANTI. Inorg. Chem. **12**, 2111 (1973); **13**, 2796 (1974).
18. J. A. POPLE et D. P. SANTRY. Mol. Phys. **8**, 1 (1964).
19. P. N. GATES, E. J. MCLAUCHLAN et E. F. MOONEY. Spectrochim. Acta, **21**, 1445 (1965).

A Poisson–Boltzmann treatment of the capacitance of a layer of symmetrical spherical dipoles

PENNY DALRYMPLE-ALFORD AND KEITH B. OLDHAM
Department of Chemistry, Trent University, Peterborough, Ont., Canada K9J 7B8

Received September 12, 1977

PENNY DALRYMPLE-ALFORD and KEITH B. OLDHAM. Can. J. Chem. **56**, 861 (1978).

The capacitance of a layer of spherical orientable dipoles has been determined. The properties attributed to each dipole are those of two point charges on a diameter of the sphere and equidistant from its centre. A one-dimensional potential distribution is assumed to exist normal to the layer and to be coupled to the charge distribution via Poisson's law. The orientation of the dipoles is random in the absence of polarization, but is taken as governed by Boltzmannian statistics when an applied field is present. The treatment predicts that the capacitance will display a pronounced hump at the point of zero charge. Though this study was motivated by a wish to interpret the inner-layer capacitance at a mercury/aqueous electrolyte solution interface, the treatment is shown to be inapplicable quantitatively to such a system.

PENNY DALRYMPLE-ALFORD et KEITH B. OLDHAM. Can. J. Chem. **56**, 861 (1978).

On a déterminé la capacité d'une couche de dipoles sphériques pouvant être orientés. Les propriétés attribuées à chaque dipole correspondent à celles de charges ponctuelles sur un diamètre de la sphère et équidistantes de son centre. On fait l'hypothèse qu'il existe une distribution de potentiel unidimensionnelle perpendiculaire à la couche et couplée à la distribution de charge par la loi de Poisson. L'orientation des dipoles se fait au hasard en l'absence de polarisation mais on considère qu'elle est gouvernée par des statistiques de Boltzmann lorsqu'on applique un champ. La théorie prédit que la capacité présentera une courbe prononcée au point de la charge zéro. Quoique cette étude ait été motivée par un désir d'interpréter la capacité de la couche interne à l'interface mercure/solution électrolytique aqueuse, on démontre que le traitement ne peut être appliqué quantitativement à de tels systèmes.

[Traduit par le journal]

Can. J. Chem. Downloaded from www.nrcresearchpress.com by 210.87.254.105 on 09/05/12
For personal use only.

Many of the theories proposed in explanation of the so-called inner layer capacity of a mercury/solution interface in the absence of specific adsorption attribute the 'hump' in the graph of capacitance vs. charge density to the orientability of the dipolar molecules that constitute the innermost layer of solvent (see refs. 1–4 for reviews). In this article we evaluate the capacitance of a model system that bears a similarity to some authors' concepts of the inner region of the electrical double layer. This article is a development of an earlier article (5) and uses ideas that have proved very successful in explaining the behaviour of the *diffuse* double layer (6, 7).

Consider the situation depicted cross-sectionally in Fig. 1, in which a layer of spheres is located between two conducting plates. The plates are parallel planes bearing equal and opposite charge densities σ and $-\sigma$. The spheres are close-packed and therefore their number density is $2/3^{1/2}\delta^2$ where δ, the spheres' diameter, equals the distance between the plates. Each sphere contains two point charges of magnitudes $\mu/2Y$ and $-\mu/2Y$ located on a diameter of the sphere at distances Y from the centre. Thus μ is the dipole moment of the sphere. The entire space between the conducting plates has a uniform and constant permittivity ε.

A distance coordinate y is erected as diagrammed, with its origin at the plane occupied by the centres of the spheres. Whatever the orientation of the spheres, their charges cannot penetrate the regions $Y < y < \frac{1}{2}\delta$ and $-\frac{1}{2}\delta < y < -Y$ and therefore the field in these outer regions is given simply by

$$[1] \qquad \frac{d\phi}{dy} = \frac{\sigma}{\varepsilon} \qquad Y \leq |y| \leq \tfrac{1}{2}\delta$$

where ϕ represents the local potential. If $y = 0$ is chosen as the point of zero potential, considerations of symmetry dictate that ϕ be an odd function of y, as depicted in Fig. 2; that is

$$[2] \qquad \phi(-y) = -\phi(y)$$

Likewise,

$$[3] \qquad \phi(Y) = -\phi(-Y) = \Phi$$

where the potentials $\phi = \pm\Phi$ correspond to the extremities of the dipolar influence: ϕ is linear beyond these extremes as indicated in [1]. The total potential between the conducting plates is

$$[4] \quad \phi\left(\frac{\delta}{2}\right) - \phi\left(\frac{-\delta}{2}\right) = 2\phi\left(\frac{\delta}{2}\right) = 2\left[\Phi + \left(\frac{\delta}{2} - Y\right)\frac{\sigma}{\varepsilon}\right]$$

Can. J. Chem. Downloaded from www.nrcresearchpress.com by 210.87.254.105 on 09/05/12
For personal use only.

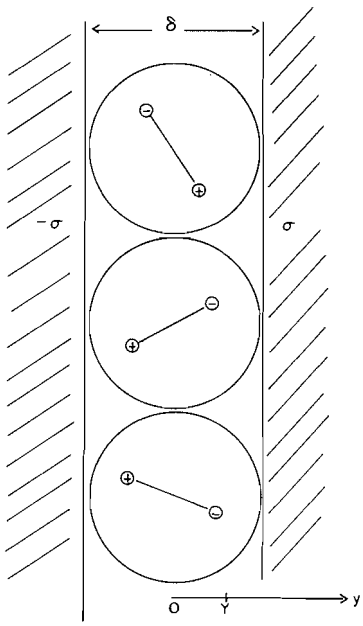

FIG. 1. The model system: a layer of spherical dipoles located between two charged plates. The interaction between dipoles is treated as being solely via an average electric potential ϕ, the magnitude of which depends on y and reflects the degree of dipolar orientation.

and, accordingly, the differential capacitance has a reciprocal given by

$$[5]\quad \frac{1}{C} = \frac{\mathrm{d}}{\mathrm{d}\sigma}\left[\phi\left(\frac{\delta}{2}\right) - \phi\left(\frac{-\delta}{2}\right)\right] = \frac{\delta - 2Y}{\varepsilon} + 2\frac{\mathrm{d}\Phi}{\mathrm{d}\sigma}$$

On account of its two charges being located in regions of different potential, the electrostatic energy of a dipole is

$$[6]\quad U(y) = \left(\frac{-\mu}{2Y}\right)\phi(y) + \left(\frac{\mu}{2Y}\right)\phi(-y) = \frac{-\mu\phi(y)}{Y}$$

where y is the coordinate of its negative pole. Now imagine all the spheres to be superimposed so that the poles come to lie on a smaller sphere of radius Y. The number $\mathrm{d}N$ of negative poles that are aligned at angles between θ and $\mathrm{d}\theta$ to the y-axis is given by the Boltzmann proportionality

$$[7]\quad \mathrm{d}N(\theta) \propto \exp\{-U(\theta)/kT\}(2\pi \sin\theta\, \mathrm{d}\theta)$$

where k is Boltzmann's constant and T the thermodynamic temperature. The $2\pi \sin\theta\, \mathrm{d}\theta$ term is the element of solid angle inclined between θ and $\theta + \mathrm{d}\theta$ to the y-axis. However, $Y\cos\theta = y$ and therefore $-Y\sin\theta\, \mathrm{d}\theta = \mathrm{d}y$, so that [7] becomes

$$[8]\quad \mathrm{d}N \propto -\frac{2\pi}{Y}\exp\left\{\frac{-U}{kT}\right\}\mathrm{d}y$$

or

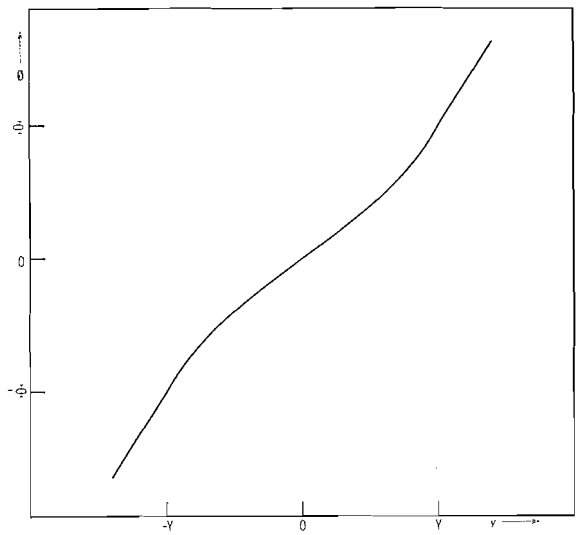

FIG. 2. The potential profile. Beyond $y = Y$ the profile is linear, corresponding to the constant field $(\mathrm{d}\phi/\mathrm{d}y) = \sigma/\varepsilon$. In the central region, $-Y < y < Y$, the profile shape has been accurately drawn for the parameter choices $\Lambda = 2.000$, $m = 0.000$ (see Appendix A).

$$[9]\quad \mathrm{d}N(y) = \frac{n}{Y}\exp\left\{\frac{-U(y)}{kT}\right\}\mathrm{d}y$$

where n is a proportionality factor the value of which will depend on σ. Combination of [6] and [9] produces the equation

$$[10]\quad \mathrm{d}N(y) = \frac{n}{Y}\exp\left\{\frac{\mu\phi(y)}{YkT}\right\}\mathrm{d}y$$

which demonstrates preference for an orientation of negative poles towards the positively charged plate.

The value of the proportionality factor n may be related to the total number density of spheres by the integral

$$[11]\quad \frac{2}{3^{1/2}\delta^2} = \int_{y=-Y}^{y=Y}\mathrm{d}N(y) = \frac{n}{Y}\int_{-Y}^{Y}\exp\left\{\frac{\mu\phi(y)}{YkT}\right\}\mathrm{d}y = \frac{n}{Y}\int_{0}^{Y}\left[\exp\left\{\frac{\mu\phi(y)}{YkT}\right\} + \exp\left\{\frac{\mu\phi(-y)}{YkT}\right\}\right]\mathrm{d}y = \frac{2n}{Y}\int_{0}^{Y}\cosh\left\{\frac{\mu\phi}{YkT}\right\}\mathrm{d}y$$

The last step in [11] is a consequence of property [2].

To this point our treatment parallels that originated by Debye (8) to explain the temperature dependence of the polarizability of polar liquids. To

Can. J. Chem. Downloaded from www.nrcresearchpress.com by 210.87.254.105 on 09/05/12
For personal use only.

continue in that vein one would ignore the restriction on [1] and substitute it into [10] and [11], a procedure that leads ultimately to a Langevin function. In so doing, however, one is ignoring the effect of the partially oriented dipoles in opposing the applied field σ/ε in the central region. One method of allowing for this is to assume, despite the partially random orientations of the dipoles, that ϕ is an unique function of y. This function, which reflects the average of all the dipolar orientations, will be determined by considering the relationship, expressed by Poisson's law, between the potential and the spatial charge density that arises from the preferred orientation of the spheres. A similar procedure was adopted by Gouy (6) and by Chapman (7) in their successful theory of the diffuse double layer at metal/aqueous solution interface.

Consult Fig. 3 and note that, when y and σ are positive, the charge density $s(y)$ between the planes y and $y + dy$ is due to a number $dN(y)$ of negative charges lying in this zone, together with a smaller number of positive charges there. The latter number, however, equals the number $dN(-y)$ of negative charges lying between planes $-y$ and $-y - dy$. Hence, the local charge density is

$$[12]\quad s(y) = \left(\frac{-\mu}{2Y}\right)\frac{dN(y)}{dy} + \left(\frac{\mu}{2Y}\right)\frac{dN(-y)}{dy}$$

$$= \frac{-\mu n}{2Y^2}\exp\left\{\frac{\mu\phi(y)}{YkT}\right\} + \frac{\mu n}{2Y^2}\exp\left\{\frac{\mu\phi(-y)}{YkT}\right\}$$

$$= \frac{-\mu n}{Y^2}\sinh\left\{\frac{\mu\phi(y)}{YkT}\right\}$$

When Poisson's law

$$[13]\qquad \frac{-s(y)}{\varepsilon} = \frac{d^2\phi}{dy^2} = \frac{1}{2}\frac{d}{d\phi}\left(\frac{d\phi}{dy}\right)^2$$

is invoked, we obtain

$$[14]\qquad \int d\left(\frac{d\phi}{dy}\right)^2 = \frac{2\mu n}{\varepsilon Y^2}\int \sinh\left\{\frac{\mu\phi}{YkT}\right\} d\phi$$

after formal integration. Keeping the lower integration limit indefinite but choosing as the upper limit $y = Y$ (where, by [1] and [3], $\phi = \Phi$ and $(d\phi/dy) = \sigma/\varepsilon$) leads to

$$[15]\quad \left(\frac{d\phi}{dy}\right)^2 = \frac{2nkT}{\varepsilon Y}\cosh\left\{\frac{\mu\sigma}{YkT}\right\} + \frac{\sigma^2}{\varepsilon^2} - \frac{2nkT}{\varepsilon Y}\cosh\left\{\frac{\mu\Phi}{YkT}\right\}$$

after some algebra.

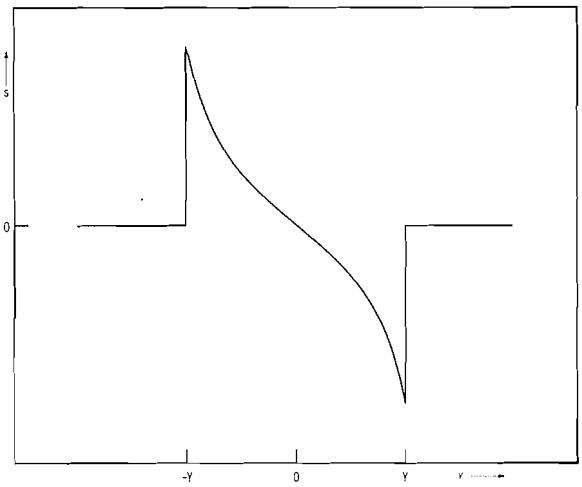

FIG. 3. Charge density as a function of distance. The charge density is zero outside the central region. The same parameter choices as for Fig. 2 were made in drawing the curve, which is accurately shaped.

Extraction of the square root of [15] followed by a further integration with lower limits at $y = 0$ (where $\phi = 0$ by definition) yields a relationship of form $\phi = f(y,n,\sigma)$. This relationship permits integral [11] to be evaluated so that n becomes a known function of σ. In turn, this may be inserted back into $\phi = f(y,n,\sigma)$ to give an expression which, on specialization to $y = Y$, yields a relation between Φ and σ. The mathematics involved is complicated and has been relegated to Appendix A, only the results being presented here. The final result, interrelating Φ and σ, cannot be written explicitly, but only as the equation pair

$$[16]\qquad \frac{\mu\Phi}{YkT} = 2\,\mathrm{arccosh\ dc}\,(\lambda|m)$$

$$[17]\qquad \frac{\mu\sigma}{\varepsilon kT} = 2\lambda(1-m)^{1/2}\,\mathrm{nc}\,(\lambda|m)$$

where λ and m are parameters interrelated by

$$[18]\quad \lambda^2 - 2\lambda E(\lambda|m) + 2\lambda\,\mathrm{sn}\,(\lambda|m)\,\mathrm{dc}\,(\lambda|m) = \Lambda^2$$

Λ being the constant defined by

$$[19]\qquad \Lambda \equiv \frac{\mu}{\delta(3^{1/2}Y\varepsilon kT)^{1/2}}$$

Moreover, [16]–[18] are useful only if m is positive and less than unity. An m value in excess of unity has no physical meaning but m may well be less than zero. When m is negative, the above results are to be replaced by

$$[20]\qquad \frac{\mu\Phi}{YkT} = 2\,\mathrm{arccosh\ nc}\,(\lambda_2|m_2)$$

Can. J. Chem. Downloaded from www.nrcresearchpress.com by 210.87.254.105 on 09/05/12
For personal use only.

TABLE 1. Computation results for Φ, σ, and $d\sigma/d\Phi$ for $\Lambda = 2.000$

m	λ	m_2	λ_2	$\frac{\mu\Phi}{YkT}$	$\frac{\mu\sigma}{\varepsilon kT}$	$\frac{Y}{\varepsilon}\frac{d\sigma}{d\Phi} = \frac{C^c}{C_\infty{}^c}$
1.000	2.000			0.000	0.000	2.075
0.999	1.994			0.228	0.473	2.072
0.990	1.948			0.692	1.429	2.045
0.950	1.804			1.357	2.762	1.951
0.900	1.692			1.727	3.468	1.868
0.800	1.551			2.129	4.199	1.759
0.700	1.458			2.376	4.623	1.686
0.600	1.389			2.554	4.920	1.632
0.500	1.334			2.694	5.146	1.591
0.400	1.289			2.811	5.328	1.559
0.300	1.251			2.910	5.482	1.530
0.200	1.217			2.997	5.613	1.507
0.100	1.188			3.074	5.728	1.495
0.000	1.161	0.000	1.161	3.143	5.831	1.467
		0.100	1.196	3.213	5.932	1.449
		0.200	1.236	3.291	6.045	1.430
		0.300	1.282	3.380	6.172	1.409
		0.400	1.335	3.484	6.317	1.386
		0.500	1.400	3.608	6.487	1.360
		0.600	1.481	3.762	6.694	1.330
		0.700	1.588	3.963	6.957	1.294
		0.800	1.744	4.251	7.324	1.251
		0.900	2.020	4.759	7.943	1.193
		0.950	2.307	5.284	8.558	1.150
		0.990	3.002	6.564	9.988	1.091
		0.999	4.033	8.507	12.064	1.052
		1.000	∞	∞	∞	1.000

NOTE: Though Λ, m, λ, m_2, and λ_2 are cited in this table to three or four significant figures only, far greater precision than this is needed to ensure four-figure accuracy in Φ, σ, and C^c. Our calculations used ten significant digits.

$$[21] \qquad \frac{\mu\sigma}{\varepsilon kT} = 2\lambda_2 \, \mathrm{dc}\,(\lambda_2|m_2)$$

and

$$[22] \quad (1 - m_2)\lambda_2{}^2 - 2\lambda_2 E(\lambda_2|m_2) + 2\lambda_2 \, \mathrm{sn}\,(\lambda_2|m_2) \, \mathrm{dc}\,(\lambda_2|m_2) = \Lambda^2$$

where λ_2 and m_2 are related to λ and m as explained in Appendix A. The bivariate function $E(\,|\,)$ is an incomplete elliptic function of the second kind, while dc(|), nc(|), and sn(|) are three of the twelve Jacobian elliptic functions; see Appendix B for a description of these functions and some of their properties.

To utilize results [16] through [22] one proceeds as follows. First, choose a value for the right-hand member of [18]. Second, using the computational techniques described in Appendix B, find pairs of λ,m values that satisfy [18]. (For negative m, switch over to [22] and find λ_2,m_2 pairs.) Third, use [16] and [17] (or [20] and [21] for negative m) to calcalculate Φ and σ. Table 1 lists examples of values computed in this way.

Returning to [5], we note that the capacitance is compounded of two elements in series. The first, of magnitude $\varepsilon/(\delta - 2Y)$, is simply the capacitance of the regions $Y \leqq |y| \leqq \frac{1}{2}\delta$ beyond the dipoles: it is a constant. The second, of magnitude $\frac{1}{2}(d\sigma/d\Phi)$, represents the central region $|y| \leqq Y$ which is subjected to dipolar influence. It is, of course, this second capacitance that is of special interest: we term it the *central capacitance* C^c.

$$[23] \qquad C^c \equiv \frac{1}{2}\frac{d\sigma}{d\Phi} = \left[\frac{1}{C} - \frac{\delta - 2Y}{\varepsilon}\right]^{-1}$$

As we shall see, the value of C^c depends on the extent of polarization of the central capacitor, falling to the saturation value

$$[24] \qquad C_\infty{}^c = \varepsilon/2Y$$

at extreme polarizations. The factor $C/C_\infty{}^c$ represents the enhancement in the central capacitance resulting from dipolar orientation. As was shown earlier (5), the maximum value of this factor occurs at vanishingly small polarizations, being given by

$$[25] \qquad \max\,(C^c/C_\infty{}^c) = C_0{}^c/C_\infty{}^c = \Lambda \coth \Lambda$$

where Λ is the constant defined in [19].

To obtain an analytic expression for the central capacitance, other than at zero or infinite polarization, [16] and [17] (or [20] and [21] for negative m) are differentiated and the ratio of these derivatives

Can. J. Chem. Downloaded from www.nrcresearchpress.com by 210.87.254.105 on 09/05/12
For personal use only.

is taken. After much tedious algebra, there emerge the following results for the $0 < m < 1$ and $m < 0$ cases:

$$[26]\quad \frac{C^c}{C_\infty{}^c} = \frac{Y}{\varepsilon}\frac{d\sigma}{d\Phi}$$

$$= \lambda\, sc(\lambda|m)\, dn(\lambda|m) + \frac{\frac{2m}{\lambda}\frac{d\lambda}{dm} + 1 - \frac{dn^2(\lambda|m)}{1-m}}{\frac{2m}{\lambda}\frac{d\lambda}{dm} + 1 - \frac{E(\lambda|m)}{\lambda(1-m)}}$$

$$= \lambda_2(1-m_2)\, sc(\lambda_2|m_2)\, nd(\lambda_2|m_2) + \frac{\frac{2m_2}{\lambda_2}\frac{d\lambda_2}{dm_2} + 1 - nd^2(\lambda_2|m_2)}{\frac{2m_2}{\lambda_2}\frac{d\lambda_2}{dm_2} + 1 - \frac{Nd(\lambda_2|m_2)}{\lambda_2}}$$

where, from [18] and [22],

$$[27]\quad \frac{\lambda}{2m}\frac{dm}{d\lambda} + 1 = \frac{1 + scd(\lambda|m) - cn^2(\lambda|m)E(\lambda|m)}{1 - \lambda\, dn^2(\lambda|m)}$$

and

$$[28]\quad \frac{\lambda_2}{2m_2}\frac{dm_2}{d\lambda_2} + 1 = \frac{scd(\lambda_2|m_2) - sn^2(\lambda_2|m_2)E(\lambda_2|m_2)}{E(\lambda_2|m_2) - (1-m_2)\lambda_2}$$

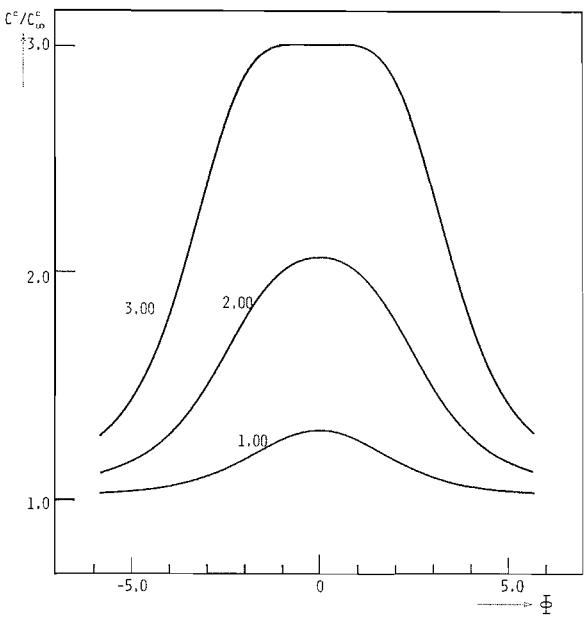

FIG. 4. The central capacitance as a function of applied charge. The units of the abscissa are $\varepsilon kT/\mu$. The value associated with each curve is that of Λ.

respectively. The abbreviations $Nd(\lambda|m) \equiv [E(\lambda|m) - m\, sn(\lambda|m)\, cd(\lambda|m)]/[1-m]$ and $scd(\lambda|m) \equiv sn(\lambda|m)\, cn(\lambda|m)\, dn(\lambda|m)$ have been used in the above.

The equations of the last paragraph were used, for a variety of Λ values, to calculate numerical values of the central capacitance enhancement factor $C^c/C_\infty{}^c$. A convenient procedure is to use the same λ,m pairs (or λ_2,m_2 pairs for negative m) that were previously used to determine Φ and σ. Table 1 contains a column calculated in this way for $\Lambda = 2.000$, while Figs. 4 and 5 show the effect of varying the Λ parameter. It is evident from these results that a Poisson–Boltzmann treatment of orientable dipoles does predict a humped central capacitance, the height and, to a lesser extent, the width of the hump being determined by the constant Λ. The physical significance of this constant (more strictly of Λ^2) is that it assesses the relative magnitudes of the electrostatic energy and the thermal energy of the dipole.

Discussion

There are several ways in which the mathematical treatment of the Fig. 1 model may be criticized. The assumption of a uniform permittivity is a clear oversimplification. Imaging has been ignored, but could be important. We do not know how well the interaction of a particular dipole with its neighbours is simulated by its interaction with the average of all dipoles. One might rather imagine that a clustering of dipoles occurs, in the way proposed by Damaskin and Frumkin (9) and elaborated by Parsons (10).

Still more criticisms can be levelled at any attempt to pass-off the model as a representation of the true state of affairs at the junction between mercury and

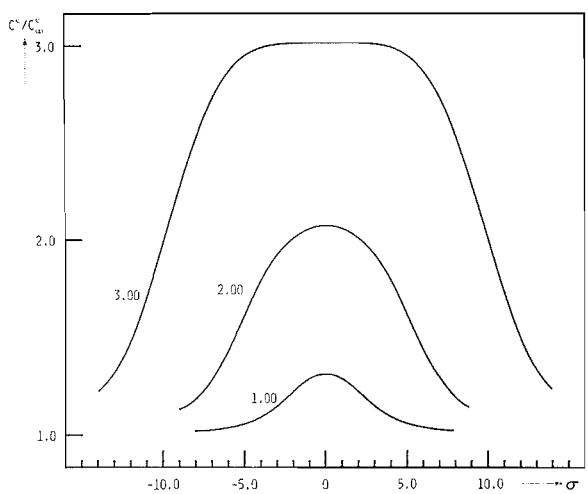

FIG. 5. The central capacitance as a function of the potential Φ. The units of the abscissa are YkT/μ.

Can. J. Chem. Downloaded from www.nrcresearchpress.com by 210.87.254.105 on 09/05/12
For personal use only.

an electrolyte solution. Can dipolar molecules be treated as spheres? What error is introduced by treating their charged regions as point charges? Does Poisson's law hold within molecules? If so, what significance has permittivity? How accurately does Boltzmann's law describe the distribution of orientations? Is the interaction between neighbouring molecules restricted to Coulombic and 'billiard ball' forces, as the model assumes? Can a mercury surface be regarded, on the atomic level, as a uniformly charged, flat, ideal conductor? Is it not even less likely that the bulk electrolyte, and its diffuse layer, will behave as a flat uniformly-charged conductor? Do not the solute ions influence the inner layer of solvent in some way? We have no convincing answers to these, and many other, legitimate questions.

However, there are some encouraging considerations. Foremost is the fact that many of the objections that can be directed against our treatment may also be directed with equal force against the Gouy–Chapman theory (6, 7), which nonetheless appears to hold well: secondly, the treatment does indeed predict a capacity hump at the point of zero charge and of a shape that is not inconsistent with experimental data (3, 10).

We have not sought to compare the theory quantitatively with experimental curves, because no solvent for which capacity data are available can be expected to conform to the *symmetrical* dipole model to which, for mathematical reasons, our treatment is restricted. Water is, of course, the most studied solvent, but structural interpretations (11, 12) of its properties are generally in terms of a tripolar configuration.

In the geometry of the water molecule, according to the model of Lemberg and Stillinger (12), the negative pole is a point charge placed at the centre of mass of the oxygen atom, i.e. very close to the centre of gravity of the molecule as a whole. If the two positive point-charges of the model are resolved into a single pole, then the resulting dipole is 59 pm long, and traverses the centre of the molecule. However, the negative end of the dipole lies only 7 pm from the molecule centre, so that the dipole is extremely asymmetric. The present treatment is therefore inapplicable.

Acknowledgements

The National Research Council of Canada has generously supported this research by means of an operating grant and a travel grant. Sabbatical hospitality and inspiration were kindly accorded to one of the authors by the Department of Mathematics, Claremont Graduate School, California, and by the School of Chemistry, Bristol University, England. A preliminary account of this work was presented at the 173rd national meeting of the American Chemical Society, New Orleans, March 1977.

1. J. R. MacDonald and C. A. Barlow. Proceedings of the first Australian conference on electrochemistry. *Edited by* J. A. Friend and F. Gutman. Pergamon Press, Oxford. 1965. p. 199.
2. R. Payne. Advances in electrochemistry and electrochemical engineering. Vol. 7. *Edited by* P. Delahay and C. W. Tobias. Wiley/Interscience Publishers, New York, NY. 1970. Chapt. 1.
3. R. M. Reeves. Modern aspects of electrochemistry. Vol. 9. *Edited by* J. O'M. Bockris and B. E. Conway. Plenum Press, New York, NY. 1974. Chapt. 4.
4. R. Parsons. Croat. Chem. Acta, **48**, 597 (1976).
5. K. B. Oldham and R. Parsons. Electrokhimiya, **13**, 866 (1977).
6. G. Gouy. J. Phys. **9**, 457 (1910).
7. D. L. Chapman. Philos. Mag. **25**, 475 (1913).
8. P. Debye. Phys. Z. **13**, 97 (1912).
9. B. B. Damaskin and A. N. Frumkin. Electrochim. Acta, **19**, 173 (1974).
10. R. Parsons. J. Electroanal. Chem. **59**, 229 (1975).
11. J. D. Bernal and R. H. Fowler. J. Chem. Phys. **1**, 515 (1933).
12. H. L. Lemberg and F. H. Stillinger. J. Chem. Phys. **62**, 1677 (1975).
13. I. S. Gradshteyn and I. M. Ryzhik. Table of integrals series and products. Academic Press, New York and London. 1965. Sect. 2.464.
14. M. Abramowitz and I. A. Stegun. Handbook of mathematical functions. Dover Publications, New York, NY. 1965. Chapt. 14.
15. C. J. E. Farina and K. B. Oldham. J. Electroanal. Chem. **81**, 21 (1977).
16. E. H. Neville. Jacobian elliptic functions. Clarendon Press, Oxford. 1944.
17. A. Erdelyi, W. Magnus, F. Oberhettinger, and F. G. Tricomi. Higher transcendental functions. Vol. 2. McGraw-Hill Book Company, New York, NY. 1953.
18. I. S. Gradshteyn and I. M. Ryzhik. Table of integrals series and products. Academic Press, New York and London. 1965. Sect. 8.146.

Appendix A

The parameters are defined by

$$[A.1] \quad \cosh^2\left(\frac{\mu\Phi}{2YkT}\right) - \frac{Y\sigma^2}{4n\varepsilon kT} \equiv m \equiv \frac{-m_2}{1-m_2}$$

and

$$[A.2] \quad \mu\sqrt{\frac{n}{Y\varepsilon kT}} \equiv \lambda \equiv (1-m_2)^{1/2}\lambda_2$$

It is also convenient to define the dimensionless variables

$$[A.3] \quad \frac{\mu\phi}{YkT} \equiv \psi$$

and

$$[A.4] \quad \frac{y}{Y} \equiv z$$

Can. J. Chem. Downloaded from www.nrcresearchpress.com by 210.87.254.105 on 09/05/12
For personal use only.

as well as the dimensionless constants

$$[A.5] \qquad \frac{\mu\sigma}{\varepsilon kT} \equiv \chi$$

and

$$[A.6] \qquad \frac{\mu\Phi}{YkT} \equiv \Psi$$

By means of the above definitions, the square root of [15] may be formally integrated in the alternative forms

$$[A.7] \qquad \sqrt{2}\int_0 dz = \frac{1}{\lambda}\int_0 \frac{d\psi}{[\cosh\psi - 2m + 1]^{1/2}} = \frac{1}{\lambda_2}\int_0 \frac{d\psi}{[(1-m_2)\cosh\psi + m_2 + 1]^{1/2}}$$

Standard integrals (13) now permit these integrals to be evaluated as elliptic integrals of the first kind, thus

$$[A.8] \qquad z = \begin{cases} \frac{1}{\lambda}F\left(\arctan\frac{\sinh\{\frac{1}{2}\psi\}}{\sqrt{1-m}}, m\right) & 0 < m < 1 \\ \frac{1}{\lambda_2}F(\arctan\sinh\{\frac{1}{2}\psi\}, m_2) & 0 < m_2 < 1 \end{cases}$$

Inversion gives the alternative expressions

$$[A.9] \qquad \cosh\{\tfrac{1}{2}\psi\} = \begin{cases} \mathrm{dc}(\lambda z|m) & 0 < m < 1 \\ \mathrm{nc}(\lambda_2 z|m_2) & 0 < m_2 < 1 \end{cases}$$

which, on specialization to $z = 1$, are equivalent to [16] and [20] of the text.

Equation A.9 was used to provide data for drawing Fig. 2, the choice $m = m_2 = 0$ being made. Though it reduces [A.9] and [18] to the mathematically simple relations $\phi \propto \mathrm{arcsinh}\tan\{\lambda y/Y\}$ and $\tan\lambda = (\Lambda^2 + \lambda^2)/2\lambda$, the selection of $m = 0$ is typical and has no special physical significance. Equation 12 likewise simplifies when $m = 0$ to $-s \propto \sec\{\lambda y/Y\} \times \tan\{\lambda y/Y\}$, a relationship used in drawing Fig. 3.

From definitions [A.1], [A.2], [A.5], and [A.6], the relationships

$$[A.10] \qquad \frac{\chi^2}{4} = \lambda^2[\cosh^2\{\tfrac{1}{2}\Psi\} - m] = \lambda_2{}^2[(1-m_2)\cosh^2\{\tfrac{1}{2}\Psi\} + m_2]$$

follow. Equation A.9 may then be utilized (after specialization to $z = 1$) to replace the $\cosh\{\frac{1}{2}\Psi\}$ terms. It now requires only the application of standard formulas (14) interrelating the squares of Jacobian elliptic functions to generate expressions that, on restoration of the original variables, become [17] and [21].

In terms of dimensionless variables, [11] can be rewritten

$$[A.11] \qquad \Lambda^2 = -\lambda^2 + 2\lambda^2\int_0^1 \cosh\{\tfrac{1}{2}\psi\}\,dz$$

Substitution from [A.9] now gives

$$[A.12] \qquad \Lambda^2 = \begin{cases} \lambda^2\left[-1 + 2\int_0^1 \mathrm{dc}^2(\lambda z|m)\,dz\right] & 0 < m < 1 \\ (1-m_2)\lambda_2{}^2\left[-1 + 2\int_0^1 \mathrm{nc}^2(\lambda_2 z|m_2)\,dz\right] & 0 < m_2 < 1 \end{cases}$$

These are standard definite integrals (14) and lead directly to [18] and [22].

Appendix B

Incomplete elliptic integrals of the first and second kinds are bivariate functions defined respectively by

$$[B.1] \qquad F(\phi,m) \equiv \int_0^\phi (1 - m\sin^2\theta)^{-1/2}\,d\theta = \lambda$$

and

$$[B.2] \qquad E(\phi,m) \equiv \int_0^\phi (1 - m\sin^2\theta)^{1/2}\,d\theta$$

However, instead of regarding E as a function of ϕ and m, it is often preferable to treat E as a function of λ and m: the symbolism $E(\lambda|m)$ is then used.

In a rather similar way, certain trigonometric functions of ϕ can be regarded as bivariate functions of λ and m. Thus

$$[B.3] \qquad \mathrm{sn}(\lambda|m) \equiv \sin\phi$$

$$[B.4] \qquad \mathrm{nc}(\lambda|m) \equiv \sec\phi$$

and

$$[B.5] \qquad \mathrm{dc}(\lambda|m) \equiv (\sec^2\phi - m\tan^2\phi)^{1/2}$$

are three examples of Jacobian elliptic functions. For definitions of the other nine, and for a geometric interpretation of Jacobian functions, see ref. 15.

In this study, there has been a need to calculate Jacobian and other elliptic functions very frequently. We have found the so-called nome expansions, of which

$$[B.6] \qquad \mathrm{sn}(\lambda|m) = \frac{2\pi}{m^{1/2}F(\frac{1}{2}\pi, m)} \times \sum_{j=1}^{\infty}\frac{q^{j-(1/2)}}{1-q^{2j-1}}\sin\left\{\frac{(2j-1)\pi\lambda}{2F(\frac{1}{2}\pi, m)}\right\}$$

TABLE 2. Partial derivatives of 13 elliptic functions

f	$(\partial f/\partial\lambda)_m$	$(\partial f/\partial m)_\lambda$
sn	cn dn	$-$cn dn $\{E - \lambda + m\lambda - m$ sn cd$\}/2m(1 - m)$
cn	$-$sn dn	sn dn $\{E - \lambda + m\lambda - m$ sn cd$\}/2m(1 - m)$
dn	$-m$ sn cn	sn cn $\{E - \lambda + m\lambda -$ sn dc$\}/2(1 - m)$
sd	cd nd	$-$cd nd $\{E - \lambda + m\lambda - m$ sn dc$\}/2m(1 - m)$
cd	$-(1 - m)$ sd nd	sd nd $\{E - \lambda + m\lambda\}/2m$
nd	m sd cd	$-$sd cd $\{E - \lambda + m\lambda -$ sn dc$\}/2(1 - m)$
sc	dc nc	$-$dc nc $\{E - \lambda + m\lambda - m$ sn cd$\}/2m(1 - m)$
dc	$(1 - m)$ sc nc	$-$sc nc $\{E - \lambda + m\lambda\}/2m$
nc	sc dc	$-$sc dc $\{E - \lambda + m\lambda - m$ sn cd$\}/2m(1 - m)$
cs	$-$ds ns	ds ns $\{E - \lambda + m\lambda - m$ sn cd$\}/2m(1 - m)$
ds	$-$cs ns	cs ns $\{E - \lambda + m\lambda - m$ sn dc$\}/2m(1 - m)$
ns	$-$cs ds	cs ds $\{E - \lambda + m\lambda - m$ sn cd$\}/2m(1 - m)$
E	dn^2	$-$cn$^2\{E - \lambda + \lambda$ dc$^2 -$ sn dc$\}/2(1 - m)$

and

$$[B.7]\quad E(\lambda|m) = \frac{\lambda E(\tfrac{1}{2}\pi, m)}{F(\tfrac{1}{2}\pi, m)} + \frac{2\pi}{F(\tfrac{1}{2}\pi, m)} \times \sum_{j=1}^{\infty} \frac{q^j}{1 - q^{2j}} \sin\left\{\frac{j\pi\lambda}{F(\tfrac{1}{2}\pi, m)}\right\}$$

are examples (see refs. 16–18 for others), to be accurate and efficient for this purpose and to lend themselves well to computer implementation. The nome is defined by

$$[B.8]\quad q \equiv \exp\{-\pi F(\tfrac{1}{2}\pi, m)/F(\tfrac{1}{2}\pi, 1 - m)\}$$

and depends only on the parameter m.

In generating [26] through [28] it was necessary to partially differentiate elliptic functions both with respect to their argument λ and their parameter m. If $f(\lambda|m)$ denotes any one elliptic function, then tables of $(\partial f/\partial\lambda)_m$ are available (14), but corresponding tables of $(\partial f/\partial m)_\lambda$ could not be found in the literature. Accordingly, these partial derivatives had to be determined *ab initio* and, for the benefit of future workers in this area, they are listed in Table 2. For brevity, arguments and parameters are omitted from the tabulation; thus sn means sn$(\lambda|m)$ and E means $E(\lambda|m)$.

Can. J. Chem. Downloaded from www.nrcresearchpress.com by 210.87.254.105 on 09/05/12
For personal use only.

An electron spin resonance and CIDEP study of the photoreduction of *tert*-butyl-*p*-benzoquinones

TERRY FOSTER, A. JOHN ELLIOT, BABATUNDE B. ADELEKE, AND JEFFREY K. S. WAN

Department of Chemistry, Queen's University, Kingston, Ont., Canada K7L 3N6

Received August 4, 1977

TERRY FOSTER, A. JOHN ELLIOT, BABATUNDE B. ADELEKE, and JEFFREY K. S. WAN. Can. J. Chem. **56**, 869 (1978).

The photoreduction of 2-*tert*-butyl-*p*-benzoquinone and 2,5- and 2,6-di-*tert*-butyl-*p*-benzoquinone were studied by esr spectroscopy. In the photolysis of 2,6-di-*tert*-butyl-*p*-benzoquinone, only one semiquinone radical was observed and its decay kinetics were monitored by esr. The reduction of the triplet 2-*tert*-butyl-*p*-benzoqinone leads to the formation of isomeric semiquinone radicals **1** and **2** in the primary photochemical processes, and this is then followed by a chemical equilibrium between the two isomeric radicals. The relative rates of formation of the two radicals cannot be monitored by conventional esr methods but the CIDEP results show that the formation of radical **2** is about five to seven times faster than that of radical **1**. A secondary reaction of the phenoxy radical with a product benzohydrofuran **4** leads to the observation of a polarized radical **3** which derives all its polarization from the primary phenoxy radical.

TERRY FOSTER, A. JOHN ELLIOT, BABATUNDE B. ADELEKE et JEFFREY K. S. WAN. Can. J. Chem. **56**, 869 (1978).

Faisant appel à la rpe, on a étudié la photoréduction de la *tert*-butyl-2 *p*-benzoquinone et des di-*tert*-butyl-2,5 et 2,6 *p*-benzoquinones. Lors de la photolyse de la di-*tert*-butyl-2,6 *p*-benzoquinone, on observe uniquement un radical semiquinone et la cinétique de sa disparition a pu être évaluée par rpe. La réduction du triplet de la *tert* butyl-2 *p*-benzoquinone conduit à la formation des radicaux semiquinones isomères **1** et **2** lors du processes photochimique primaire et celui-ci est alors suivi par un équilibre chimique entre les deux radicaux isomères. On ne peut évaluer les vitesses relatives de formation des deux radicaux par la rpe conventionnelle mais des résultats de CIDEP montrent que la formation du radical **2** est environ cinq à sept fois plus rapide que celle du radical **1**. Une réaction secondaire du radical phénoxy avec un produit benzohydrofuranne **4** conduit à l'observation d'un radical polarisé **3** qui tire sa polarisation du radical phénoxy primaire.

[Traduit par le journal]

Introduction

Electron spin resonance spectroscopy has been commonly used to follow photochemical reactions (1) in solutions because the transient free radicals can be detected and identified, and their decay kinetics easily followed. However, spectra recorded during irradiation often exhibit 'polarizations' which arise from the electron spin states of the radicals being populated in a non-Boltzmann manner. Such 'polarizations' must be accounted for before any meaningful kinetic measurements can be obtained. In general, there are two types of 'polarizations' in photochemically generated radicals (2), the E-A and the initial polarizations. The former arises through the same radical-pair mechanism which generates most of the CIDNP in solution and the latter through the photoexcited triplet mechanism which involves the chemical quenching of a spin polarized triplet state (2). With the coexistence of both types of polarizations well demonstrated, it is now possible to gain information not normally obtained from conventional esr studies for those photochemical reactions which show 'initial polarization' (2, 3) in the CIDEP observations.

In this paper we report the esr results from a kinetic and CIDEP study of the photoreduction of 2-*tert*-butyl-*p*-benzoquinone (*t*BBQ), 2,5- and 2,6-di-*tert*-butyl-*p*-benzoqinones (2,5- and 2,6-d*t*BBQ) by 2-propanol as well as by phenols. Our interest in these systems arose out of our studies of the photoreduction of quinones as model systems in establishing the role of the excited triplet quinones in CIDEP and CIDNP (2). We have found that the primary photoreduction of *t*BBQ leads to the formation of polarized semiquinone radicals in two isomeric forms:

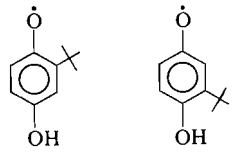

1 **2**

With the CIDEP results, it was also possible to establish that both isomeric radicals **1** and **2** are primary radicals formed by the spin polarized triplet *t*BBQ abstracting from both carbonyl groups. In the previous esr, CIDEP, and CIDNP studies (4, 5) of 2-methyl-*p*-benzoquinone and 2,6-di-*tert*-butyl-*p*-

Can. J. Chem. Downloaded from www.nrcresearchpress.com by 210.87.254.40 on 09/05/12
For personal use only.

Can. J. Chem. Downloaded from www.nrcresearchpress.com by 210.87.254.40 on 09/05/12
For personal use only.

benzoquinone, only one primary semiquinone radical with a structure similar to **1** was observed.

In addition to the semiquinone radicals, we have observed in these systems a polarized secondary radical **3** whose concentration, relative to the semiquinone radicals, depends on the solvent. This radical **3** serves as an interesting example for polarization transfer from a primary radical to a secondary radical, which further demonstrates the usefulness of the CIDEP techniques in mechanistic photochemistry.

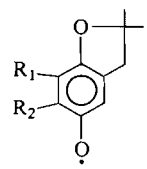

3

3*a* $R_1 = R_2 = H$
3*b* R_1 = *tert*-butyl, $R_2 = H$
3*c* $R_1 = H$, R_2 = *tert*-butyl

Experimental

The chemicals used in these experiments were purchased from one of the following companies: Aldrich, Allied Chemicals, Baker, Canlab, Eastman, Fisher, and Thompson-Packard. 2-*tert*-Butyl-*p*-benzoquinone and 2,5-di-*tert*-butyl-*p*-benzoquinone were synthesized by the oxidation of the corresponding hydroquinones using sodium chlorate and vanadium pentoxide in 2 vol% sulfuric acid (6). Because quinones, hydroquinones, and phenols tend to deteriorate on storage; the hydroquinones were recrystallized from benzene, and the phenols and quinones were purified by vacuum sublimation. All solvents were distilled before use.

Unless otherwise stated, the concentration of quinone in the solution was 0.1 mol dm^{-3} and that of the phenol was 0.5 mol dm^{-3}. These solutions were all deoxygenated by bubbling with nitrogen gas immediately before photolysis. In a few specified experiments, flowing solutions (2–10 ml/min) were photolyzed at room temperature in a quartz flat cell inside the microwave cavity of a Varian E-3 X-band spectrometer. However, in most experiments, static samples were photolyzed in Pyrex cells directly in the cavity of a Bruker ER-420 spectrometer with temperature control accessories. The light source used was either a 200 W or a 1 kW super high pressure mercury lamp. The CIDEP experiments were carried out in the Bruker spectrometer interfaced to a Nicolet 1180 computer. The CIDEP method has been described elsewhere (2, 7). In many cases where spectra from different radicals overlapped substantially in the centre, polarization measurements were restricted to outer lines with minimum overlap. In those cases the E-A polarization from the radical-pair component was removed by the method of averaging (2, 7). The viscosity of the solutions was measured with an Ostwald viscosimeter.

Results and Discussions

The Photolysis of tert-*Butyl*-p-*benzoquinones*

The photolysis of 2-*tert*-butyl-*p*-benzoquinone, 2,5- and 2,6-di-*tert*-butyl-*p*-benzoquinone in 2-propanol or in a 10 vol% 2-propanol–toluene solution (with or without a phenol present) leads to the observation of the semiquinone radicals. In the case of *t*BBQ, two isomeric radicals **1** and **2** were observed, whereas for 2,5-d*t*BBQ and 2,6-d*t*BBQ only one semiquinone was observed. The hyperfine coupling constants of all the observed semiquinone radicals, which varied with solvent and temperature, are summarized in Table 1. The assignment of the hydroxylic proton splittings was confirmed by carrying out the photolysis in fully deuterated solvents. In the case of 2,6-d*t*BBQ in which two isomeric semiquinone radicals were expected by analogy to *t*BBQ, the photoreduction was carried out in the above two solvents and also in acetic acid at temperatures ranging between −50 and 50°C. However, the isomeric equivalent of radical **2** was never detected.

When the photoreduction of *t*BBQ was carried out in the presence of a phenol, such as 2-methylphenol or pentachlorophenol, using toluene as a solvent, another radical was predominantly observed which we have assigned to the substituted benzohydrofuran radical **3***a*. If the solvent toluene was replaced by acetic acid both the semiquinone radicals and the radical **3***a* were observed. A typical esr spectrum consisting of all three radicals is shown in Fig.1. The coupling constants of **3***a* are given in Table 1. The assignment of **3***a* was confirmed by the observation of **3***b* and *c* when the corresponding di-*tert*-butyl-benzoquinones were photolyzed under similar conditions (see Table 1).

Using toluene as a solvent, when *t*BBQ was photoreduced in the presence of 2,6-di-*tert*-butylphenol, radical **3***a* was not observed but the esr spectrum of the phenoxy radical was obtained. Intermediate cases showing both radical **3***a* and phenoxy radicals can be obtained by using less hindered phenols such as 2-methyl-6-*tert*-butylphenol and by varying the temperature. This suggested to us that radical **3***a* may be formed in 'secondary' reactions with photoproducts. To prevent the build up of products, we photolyzed flowing solutions of *t*BBQ – phenol – acetic acid and measured the relative intensities of the radicals **1**, **2**, **3***a*. With no flow, the ratios were 2:1:1 but as the flow rate was increased the intensity of **3***a* relative to the first two decreases, until at 10 ml/min the ratio was 2:1:0.1. This supports the hypothesis that **3***a* was formed through a secondary reaction.

It is known that when *tert*-butylbenzoquinones are photolyzed in benzene or acetic acid a substituted benzohydrofuran **5** is formed but when the photolysis is carried out in the presence of 2-propanol, in addition to the expected hydroquinone, a second hydroquinone **4** with a rearranged side group is produced.

TABLE 1. Proton hyperfine coupling constants (mT) of radicals observed during photolyses of *tert*-butyl-*p*-benzoquinones

Radical	Solvent	$a^{2,6}$	$a^{3,5}$	a^{OH}	a^{CH_2}
1	10% 2-propanol–toluene, −20°C	0.524	0.052 0.02	0.18	—
	Acetic acid – phenol, −12°C	0.50	0.05 0.02	0.02	—
2	10% 2-propanol–toluene, −20°C	0.453 0.524	0.02	0.18	—
	Acetic acid – phenol, −12°C	0.43 0.46	0.02	0.20	—
3*a*	Acetic acid – phenol, −12°C	0.54 0.37	0.02	—	0.21
	Toluene, −20°C	0.574 0.400	0.054	—	0.166
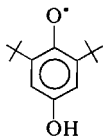	Acetic acid – phenol, −12°C	—	0.054	0.16	—
3*b*	Acetic acid – phenol, −12°C	0.42 0.47	—	—	0.21
	Toluene, −20°C	0.499 0.424	—	—	0.176
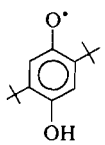	Acetic acid – phenol, −12°C	0.46	0.05	0.18	—
3*c*	Acetic acid – phenol, −12°C	0.40	0.07	—	0.19
	Toluene, −20°C	0.460	0.053	—	0.180

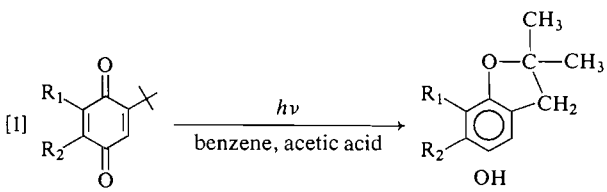

5

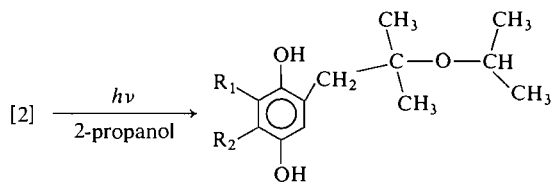

4

Both these reactions are thought to involve internal hydrogen abstractions from the side chain. This species then undergoes a series of reactions depending on the media, but all involve rearrangement of the side group (8). It is almost certainly **5** which is the precursor of radical **3**.

The formation of the semiquinone radicals involves the chemical quenching of the quinone triplet by a hydrogen donor (HD):

[3*a*] $^3(t\text{BBQ}) \xrightarrow{\text{HD}} \mathbf{1, 2}$

[3*b*] $^3(2,6\text{-d}t\text{BBQ}) \xrightarrow{\text{HD}}$ 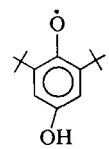

[3*c*] $^3(2,5\text{-d}t\text{BBQ}) \xrightarrow{\text{HD}}$ 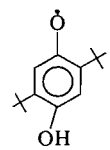

If 2-propanol was the hydrogen donor, the counter radical will reduce a ground state quinone molecule to a semiquinone radical.

[4] $\quad Q + (CH_3)_2\dot{C}OH \rightarrow \dot{Q}H + (CH_3)_2CO$

When the hydrogen donor is a phenol, a phenoxy

Can. J. Chem. Downloaded from www.nrcresearchpress.com by 210.87.254.40 on 09/05/12
For personal use only.

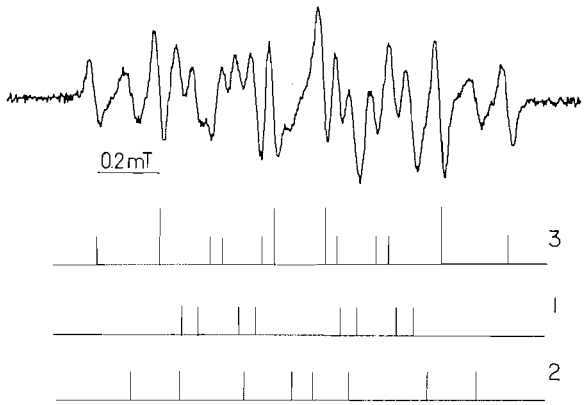

FIG. 1. Electron spin resonance spectrum observed during the photoreduction of *t*BBQ by phenol in acetic acid −12°C.

radical is formed, and its fate is uncertain in solutions containing 2-propanol.

However, as radicals **3***a*, *b*, and *c* are only observed in the absence of 2-propanol, then it is most likely that they are formed by the reaction of the primary phenoxy radical with **5** in reaction 5.

[5] $$\dot{\text{O}}\text{Ph} + \mathbf{5} \rightarrow \mathbf{3} + \text{PhOH}$$

This premise is supported by the fact that when a more stable phenoxy radical (e.g. 2,6-di-*tert*-butylphenoxy) is formed in reaction 3, it is the phenoxy radical that is observed and not radicals **3**. The CIDEP results to be described later also support this reaction.

The low steady state yield of semiquinone radicals in toluene solution is due to a combination of their intensity being reduced by emissive CIDEP and the higher second order termination rate constants found for semiquinones in toluene as opposed to 2-propanol (7, 11).

Kinetic Electron Spin Resonance Study of the Photoreduction of 2,6-dtBBQ

In recent years, Griller and Ingold (9) have demonstrated beautifully the effect of bulky substituents on the persistence of transient radicals. Among the substituted benzoquinones studied in this laboratory, the 2,6-d*t*BBQ is certainly the simplest case for the kinetic esr study of such effects. Although recent CIDEP studies have unequivocally established the excited triplet quinones as the precursors of the polarized semiquinone radicals (2), direct esr detection of the excited triplet quinones remains unattainable. Nevertheless, conventional kinetic esr methods can be applied here to investigate the transfer of the triplet energy from 2,6-d*t*BBQ to naphthalene during the photoreduction.

An alcoholic solution of 2,6-d*t*BBQ containing about 0.02 mol dm^{-3} naphthalene was photolyzed at 77 K within the microwave cavity of an esr spectrometer. A coloured glass filter was used to select light with a wavelength >396 nm so that it would be absorbed only by the quinone. During the irradiation the $\Delta m = 2$ transition belonging to the triplet naphthalene was observed (10). Irradiation with light $\lambda > 396$ nm on naphthalene alone did not produce esr signals. This confirmed the transfer of excitation energy from triplet 2,6-d*t*BBQ to naphthalene.

In a series of photoreduction experiments of 2,6-d*t*BBQ in 2-propanol at room temperature, various concentrations ($4–20 \times 10^{-3}$ mol dm^{-3}) of naphthalene were added to quench the photoreduction. The reactions can be summarized in the following scheme:

[6] $$\text{Q} + h\nu\ (396\ \text{nm}) \xrightarrow{\phi I_a} {}^3\text{Q}$$

[7] $$^3\text{Q} + (\text{CH}_3)_2\text{CHOH} \rightarrow \dot{\text{Q}}\text{H} + (\text{CH}_3)_2\dot{\text{C}}\text{OH}$$

[8] $$(\text{CH}_3)_2\dot{\text{C}}\text{OH} + \text{Q} \rightarrow \dot{\text{Q}}\text{H} + (\text{CH}_3)_2\text{CO}$$

[9] $$^3\text{Q} + \text{C}_{10}\text{H}_8 \rightarrow \text{Q} + {}^3(\text{C}_{10}\text{H}_8)$$

[10] $$\dot{\text{Q}}\text{H} + \dot{\text{Q}}\text{H} \rightarrow \text{Q} + \text{QH}_2$$

Recent CIDEP studies of the photoreduction of quinones in 2-propanol indicate that reaction 8 is an efficient process (7, 11) which accounts for the major fate of the 2-propanol radical. A kinetic analysis of the above scheme yields the following expression for the steady-state concentration of semiquinone radicals $\dot{\text{Q}}\text{H}$ in a continuous photolysis:

[11] $$[\dot{\text{Q}}\text{H}]^{-2} = k_{10}/2\phi I_a\left(1 + \frac{k_9[\text{C}_{10}\text{H}_8]}{k_7[\text{ROH}]}\right)$$

It should be mentioned that for conventional esr kinetic measurements, care must be taken to ensure that the steady-state radical concentration is corrected for any polarization (2). In the present system at room temperature, the semiquinone radical at the steady-state was effectively thermalized as no observable 'initial polarization' was evident in the time profiles of the signal when the light was chopped with the rotating sector.

Figure 2 presents the experimental results by plotting $[\dot{\text{Q}}\text{H}]_0^2/[\dot{\text{Q}}\text{H}]^2$ vs. $[\text{C}_{10}\text{H}_8]$. $[\dot{\text{Q}}\text{H}]_0$ is the steady-state concentration of the semiquinone radicals in the absence of naphthalene. Using an estimated value of 5×10^9 dm^3 mol^{-1} s^{-1} for k_9 (12), the rate constant k_7 for the abstraction reaction by the triplet 2,6-d*t*BBQ can be estimated from the slope and is found to be about 2×10^6 dm^3 mol^{-1} s^{-1}. This value is comparable to the rate constant for the triplet benzophenone abstracting hydrogen from 2-propanol (13), which is found to be 1.3×10^6 dm^3 mol^{-1} s^{-1} by flash photolysis. The abstraction

Can. J. Chem. Downloaded from www.nrcresearchpress.com by 210.87.254.40 on 09/05/12
For personal use only.

Can. J. Chem. Downloaded from www.nrcresearchpress.com by 210.87.254.40 on 09/05/12
For personal use only.

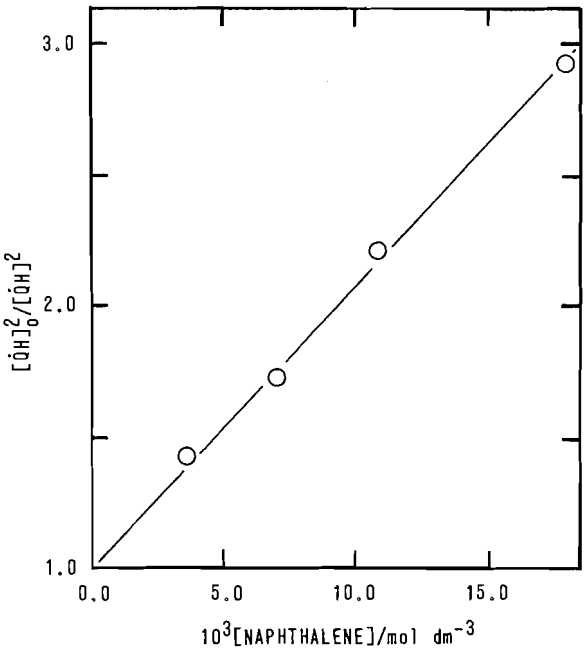

FIG. 2. Variation of steady-state concentration of 2,6-di-*tert*-butylbenzosemiquinone radicals with naphthalene concentration in 2-propanol.

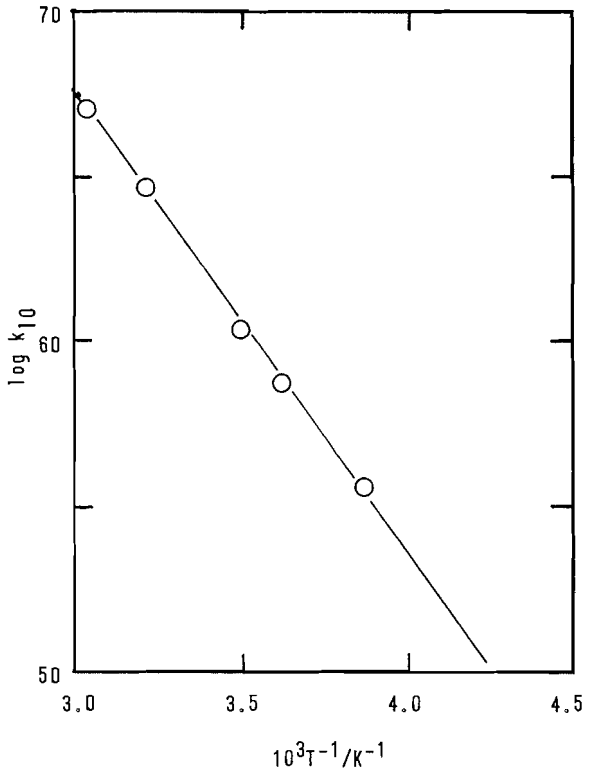

FIG. 3. The Arrhenius plot for the decay of 2,6-di-*tert*-butylbenzosemiquinone radicals in 2-propanol.

reaction between the triplet duroquinone and 2-propanol is, however, much slower (6×10^3 dm^3 mol^{-1} s^{-1}) (14), although the same triplet duroquinone would rapidly react with the durohydroquinone with a rate constant of 2 to 4×10^9 dm^3 mol^{-1} s^{-1} (14–16). In a separate CIDEP study (7) Elliot and Wan have observed that the slow reaction of triplet duroquinone with 2-propanol is rather unique, since most of the other quinones do react with 2-propanol at a reasonable rate to produce 'initial polarization'.

The decay of the transient semiquinone radicals in reaction 10 was also studied by the rotating sector-kinetic esr technique (17) at different temperatures between −20 and 60°C. In all cases the decay curves followed good second order kinetic plots. The Arrhenius parameters of the decay of the 2,6-di-*tert*-butylbenzosemiquinone radicals were obtained from a plot of log k_{10} against $1/T$ K^{-1} as shown in Fig. 3 and summarized in Table 2.

In order to establish the steric effect of the substituents on the kinetic parameters of the semiquinone radicals, a parallel kinetic study of the decay of the 2,6-dimethylbenzosemiquinone radicals was also carried out. The results are given in Table 2, along with those of other semiquinone radicals which have been previously studied in this laboratory (18).

In Table 2 it is seen that the decay of the 2,6-di-*tert*-butylbenzosemiquinone radicals is three orders of magnitude *slower* than that of the other semiquinone radicals. Such a drastic difference parallels the decay of 2,6-di-*tert*-butylphenoxy radicals as compared to the less sterically hindered phenoxy radicals (22). The dramatic steric effect on the persistence of the radicals has been well established by Ingold and coworkers (9).

The comparison between the persistence of 2,6-di-*tert*-butylbenzosemiquinone radicals and that of 2,6-dimethylbenzosemiquinone radicals is rather interesting. It appears that the persistence of the 2,6-di-*tert*-butylbenzosemiquinone radical is a result of a substantial increase in the activation energy of the decay process [12] rather than decrease in the *A*-factor.

[12] 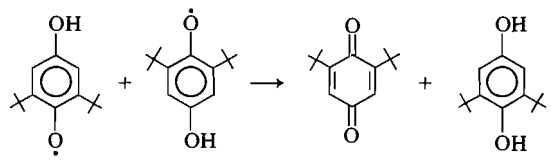

Thus, the steric effect may be associated with the enthalpy of the reaction, instead of the entropy of the reaction. In reaction 12, one 'unhindered' O—H bond is destroyed while a 'hindered' O—H bond is formed. The dissociation energy of that 'hindered'

Can. J. Chem. Downloaded from www.nrcresearchpress.com by 210.87.254.40 on 09/05/12
For personal use only.

TABLE 2. Second-order rate constants and Arrhenius parameters for the self-disproportionation of some semiquinone radicals in 2-propanol (20°C)

Radical	k_{10} (dm^3 mol^{-1} s^{-1})	E_a (kJ mol^{-1})	log A	Reference
2,6-Di-*tert*-butyl-semiquinone	1.7×10^6	26 ± 3	10.9	This work
2,6-Dimethyl-semiquinone	0.3×10^9	14 ± 2	10.9	This work
Durosemiquinone	0.7×10^9	14 ± 2	11.0	18
p-Benzosemiquinone	1.5×10^9	15 ± 2	11.8	18

O—H bond could be as much as 32 kJ less than that of the 'unhindered' O—H bond (20). This may reflect in an increase in activation energy for the process 12. For the decay of 2,6-dimethylbenzosemiquinone radicals, there is not much difference between the two O—H bonds (20), and hence the activation energy of the decay would not be much different from that of the unsubstituted semiquinone radicals.

Since the photoreduction of *t*BBQ in 2-propanol produces two isomeric semiquinone radicals **1** and **2**, it would seem inviting to compare their decay kinetics. The experimental measurements show that there is little difference in their half-lives. However, the CIDEP results given below suggest that there is a very rapid equilibrium between the two semiquinone radicals and our conventional rotating-sector kinetic esr measurements cannot resolve the individual decay versus the rapid equilibrium between them.

CIDEP

In the photoreduction of *t*BBQ in 2-propanol at −20°C, *all* hyperfine lines of the radicals **1** and **2** exhibit emission. In the presence of phenol, the emission magnitude was greatly increased as the abstraction reaction between the triplet quinone and phenol is substantially faster than that with 2-propanol. Such polarization dependence on chemical rates is predicted by the phototriplet mechanism which is now well understood (2). For quantitative CIDEP studies, the photoreduction of *t*BBQ was carried out in a 10% 2-propanol–toluene solution at −20°C in the presence of varying amounts of 2-methylphenol.

The polarization of the radicals **1** and **2** is measured separately from the 'time profile' (Fig. 4) in terms of an enhancement factor, V, which is related to the experimentally measured 'steady-state enhancement factor', V_{ss}, by the following relationship (2);

$$V = V_{ss}t_{1/2}/T_1$$

where $t_{1/2}$ is the radical half-life which can be measured directly from the 'time profile', and T_1 is the spin–lattice relaxation time of the radical. It was

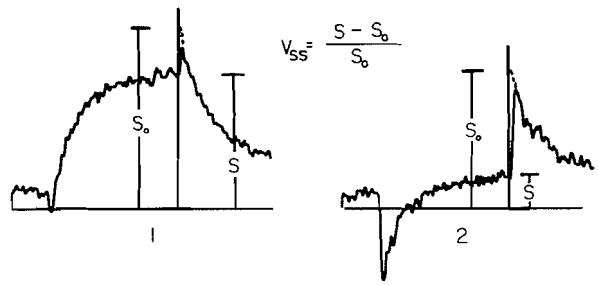

FIG. 4. The time profiles of representative peaks within radicals **1** and **2**, respectively. The downward spike is the 'light on' point and the upward spike is the 'light-off' point. The duration was about 11 ms.

established by a series of power saturation experiments that there is no significant difference in T_1 for radicals **1** and **2**. Since the absolute value of T_1 is not available for radicals **1** and **2**, we used the reported T_1 values for the semiquinone radical anion of *t*BBQ (19) corresponding to the viscosity of the solution containing phenol. The estimation[1] using the semiquinone anion T_1 values has been found to be satisfactory (7). The calculated T_1 increases from 6 μs to 8 μs over the 2-methylphenol concentration range studied.

In the phototriplet mechanism the enhancement value is related to the quencher concentration by the following equation (27)

$$[13] \qquad 1/V = 1/V_0 + 1/(V_0{}^3T_1k_q[\text{phenol}])$$

where V_0 is the enhancement factor at infinite quencher concentration, k_q is the quenching rate constant between the triplet quinone and phenol, and ${}^3T_1$ is the spin–lattice relaxation time for the triplet quinone. A plot of $1/V$ vs. 1/[phenol] is given in Fig. 5 for both radicals **1** and **2**. Equation 13 was applied to the experiments where the concentration of 2-methylphenol was varied from 0 to 2 mol dm^{-3}. However, since V_0 is an intrinsic constant of the quinone triplet, and ${}^3T_1$ tends to increase with viscosity while k_q decreases with increasing viscosity,

[1] T_1 is calculated from the relationship (19) $(T_1)^{-1} = A(T/\eta) + B$ where $A = 6 \times 10^8$ P s^{-1} K^{-1} and $B = 5.4 \times 10^{-10}$ s^{-1}.

Can. J. Chem. Downloaded from www.nrcresearchpress.com by 210.87.254.40 on 09/05/12
For personal use only.

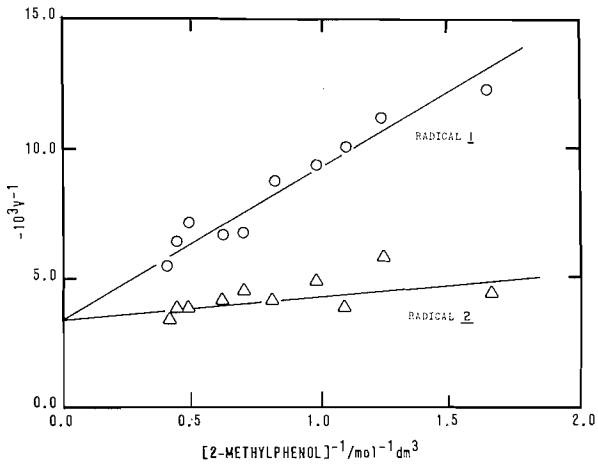

FIG. 5. The plot of reciprocal enhancement factors vs. reciprocal 2-methylphenol concentration for radicals **1** and **2**.

the combination is such that a constant slope may be obtained.

The CIDEP results are consistent with the following phototriplet mechanism:

[14] ^{3}(2-*t*BBQ) + PhOH $\longrightarrow$ PhȮ + **1**

[15] ^{3}(2-*t*BBQ) + PhOH $\longrightarrow$ PhȮ + **2**

In the presence of a phenol, the semiquinone radicals **1** and **2** are produced mainly by reactions 14 and 15. Since both radicals are produced from the primary reactions with the same spin polarized triplet quinone, it is expected that V_0 (a property of the triplet) should have the same value for both radicals **1** and **2**, and this is observed in Fig. 5. The ratio of the two slopes in Fig. 5 suggests that k_{15} is about 5 to 7 times greater than k_{14}. Further examination of the system, however, revealed that the concentration of **1** is always about twice that of radical **2** and that both radicals **1** and **2** appeared to decay with similar half-lives. These results can be explained by an equilibrium between radicals **1** and **2**, probably via the common radical anion intermediate:

[16] 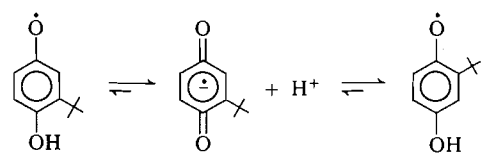

2 **1**

Thus, although **2** is generated faster than **1** in the primary photochemical reactions, the forward and back reactions are sufficiently fast to maintain the equilibrium under the conditions of the experiment.

The rapid equilibrium in [16] was confirmed by further experiments in which radicals **1** and **2** were generated in different ways. Radicals **1** and **2** were generated by reaction of 2-*tert*-butylhydroquinone (0.8 mol dm^{-3}) with di-*tert*-butyl peroxide (5 vol%) in 10 vol% 2-propanol–toluene at −20°C. The radicals observed were not polarized but their relative concentration was again 2:1.

In the photoreduction of 2-methylanthraquinone (0.05 mol dm^{-3}) by *2-tert-butylhydroquinone* (0.8 mol dm^{-3}) in 10 vol% 2-propanol–toluene solvent at −25°C, both radicals **1** and **2** were generated as the counter radicals:

[17] 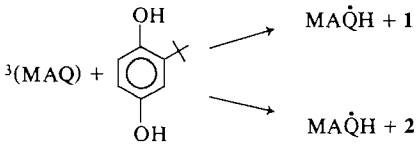

[18]

Both radicals **1** and **2** were totally emissive but the enhancement factor for radical **2** (<0.05) was now actually smaller than radical **1** (V = 0.2). The steady-state concentration of **1**, however, was still about twice as great as radical **2**. The greater V for radical **1** is reasonable since reaction 17 should proceed faster than reaction 18 based on the argument that the two O—H bonds may have different dissociation energy amounting to as much as 32 kJ (20) in favour of forming radical **1**. The relative concentration of **1** and **2** is nevertheless always governed by the equilibrium 16. Finally, when *t*BBQ was used to photoreduce its own 2-*tert*-butylhydroquinone, the enhancement factor of radical **2** was still greater than that of radical **1**. The relative concentration of **1** and **2** remained 2:1.

With the establishment of the equilibrium between **1** and **2**, it is now necessary to consider any possible transfer of polarization from **2** to **1** during the equilibrium. In the extreme case of reactions 14 and 15, **1** may not be formed at all in the primary photochemical reaction, and it would derive the polarization solely from the primary radical **2** via the equilibrium 16. If the rate of approaching equilibrium is greater than the spin–lattice relaxation rate of the polarized radical **2**, the plot in Fig. 5 should have yielded only a single line for both **1** and **2**. If the rate is comparable or smaller than the spin–lattice relaxation rate, the plot in Fig. 5 should have given two *parallel* lines each having an identical slope but with entirely different intercepts. Since the lines are not parallel (Fig. 5), this indicates that radicals **1** and **2** are both produced in the primary photochemical reactions involving the same triplet quinone, with $k_{15} > k_{14}$. Within the experimental errors, there could be some transfer of polarization from **2** to **1** in the equilibrium 16, but the rate of exchange is unlikely to be greater than 10^{-5} s^{-1}, which repre-

Can. J. Chem. Downloaded from www.nrcresearchpress.com by 210.87.254.40 on 09/05/12
For personal use only.

sents a typical spin–lattice relaxation rate for semiquinone radicals.

One might expect that radical **1** would be formed predominantly in the photoreduction of *t*BBQ because of steric hinderance from the *tert*-butyl group. In an earlier paper (14), it was suggested that this was indeed the case for 2-methylbenzoquinone since only the equivalent of radical **1** was observed by esr. However, in the present experiments, although the equilibrium 16 favours **1**, the analysis of the CIDEP results clearly indicates that the formation of **2** in the primary photochemical process was 5 to 7 times faster than that of **1**. Conventional product analysis and kinetic esr would have failed to reveal this fact. Furthermore, it should be remembered that not only was the carbonyl group adjacent to the *tert*-butyl group abstracting hydrogen from the surrounding media, but that internal hydrogen abstraction was also occuring at that center.

CIDEP was observed when 2,6- and 2,5-d*t*BBQ were photoreduced in 10 vol% 2-propanol–toluene solutions containing a phenol but because of the long half-life of 2,6-di-*tert*-butylbenzosemiquinone radicals and the rapid depletion of 2,5-d*t*BBQ, quantitative CIDEP studies could not be made. The 2,5-d*t*BBQ depletes because internal hydrogen abstraction can occur at either end.

While the CIDEP study establishes that the triplet *t*BBQ can abstract from both carbonyl end groups to form semiquinone radicals **1** and **2**, it remains unclear why many of the other unsymmetrical benzoquinones only generate one observable semiquinone radical. For example 2,6-d*t*BBQ only leads to a radical with a structure similar to **1**. Perhaps in this case one may argue that the 2,6-d*t*BBQ semiquinone radical **1** would be more persistent than the isomer **2**, and a similar equilibrium 16 may favour entirely the formation of **1**. Experimental results do point to the greater persistence of the isomer **1** in the photoreduction of 2,6-d*t*BBQ. However, there is no compelling evidence that the 2-methylbenzosemiquinone **1** should be more persistent than the analogous **2**, and in the photoreduction of 2-methyl-*p*-benzoquinone (4) only radical **1** was observed.

In the photoreduction of *t*BBQ by phenol in acetic acid or in toluene, the radical **3***a* was found to have all lines in diminished absorption, i.e. in the emissive mode. Evidence has been presented above that radical **3***a* is generated in a secondary reaction 5, and its polarization therefore must derive solely from the primary phenoxy radical. (It is unlikely to be formed in any photoreduction reaction because its concentration will be at most a thousand-fold less than that of the phenol. Polarization derived from the competitive reaction 4 was also unlikely since Fischer (23) had found that this reaction is very slow ($k = 10^3$).) It is further confirmed that it is not just the observation of radical **3***a* that depends on the reactivity of the phenoxy radicals, but the enhancement factor of radical **3***a* also depends on the 'type' of phenoxy radicals present. Such a transfer of polarization can yield some information on the rate of the chemical reaction. For example, in reaction 5 the rate must compete effectively with the spin–lattice relaxation rate of the polarized phenoxy radicals, which usually is in the order of 10^{-5} s^{-1}. Thus, for radical **3***a* to be polarized by the transfer of polarization from the phenoxy radicals, k_5[**5**] must have the magnitude of 10^{-5} s^{-1}. If the photochemical product **5** has a concentration of about 10^{-4} mol dm^{-3}, it follows that k_5 would be about 10^9 mol^{-1} dm^3 s^{-1}, which is near diffusion-controlled.

The CIDEP observation on the analogous radicals **3** in the photolyses of 2,6-d*t*BBQ and 2,5-d*t*BBQ in the presence of phenol are similar to that of *t*BBQ. Thus, the reaction 5 is another example of polarization transfer in a chemical reaction, which is the basic principle underlying the phototriplet mechanism. McLauchlan and Sealy (21) have demonstrated the polarization transfer from a primary triethylamine radical to biacetyl. Such a polarization transfer can be used not only as a probe in reaction mechanism studies but also as a means to derive some kinetic information of the chemical reaction we have shown above. Furthermore, in a system where the T_1 of the radical undergoing the polarization transfer is unknown, a quantitative polarization transfer study as a function of the quencher concentration would lead to an estimate of the T_1 provided the rate constant for the transfer is known.

Conclusions

The results in this report indicate that the combination of CIDEP and conventional esr studies provides a powerful tool with which to study the mechanisms of the free radical reactions in the photochemistry of *tert*-butyl substituted quinones. This technique has enabled us to show that *t*BBQ is photoreduced to form two isomeric semiquinone radicals **1** and **2**, and that both carbonyl groups are undergoing photochemical reduction. Also from the CIDEP results we are able to estimate the magnitude of k_5 for the hydrogen transfer reaction between **5** and the phenoxy radical.

Acknowledgments

This research is supported by the National Research Council of Canada. B. B. Adeleke wishes to acknowledge the award of a Canadian Common-

wealth Scholarship, and Terry Foster acknowledges the award of an Ontario Graduate Scholarship.

1. J. K. S. WAN. Adv. Photochem. **9**, 1 (1974).
2. J. K. S. WAN and A. J. ELLIOT. Acc. Chem. Res. **10**, 161 (1977) and references therein.
3. J. K. S. WAN, D. A. HUTCHINSON, and S. K. WONG. Acc. Chem. Res. **7**, 58 (1974).
4. H. M. VYAS, B. B. ADELEKE, and J. K. S. WAN. Spectro. Lett. **9**, 663 (1976).
5. B. B. ADELEKE, K. Y. CHOO, and J. K. S. WAN. J. Chem. Phys. **62**, 3822 (1975); B. B. ADELEKE and J. K. S. WAN. J. Chem. Soc. Faraday I, **72**, 1799 (1976); B. B. ADELEKE. Ph.D. Thesis, Queen's University, Kingston, Ont. 1976.
6. A. H. BLATT (*Editor*). Organic synthesis. Vol. 2. John Wiley and Sons, NY. 1943. p. 553.
7. A. J. ELLIOT and J. K. S. WAN. J. Phys. Chem. In press.
8. J. M. BRUCE and A. CHAUDHRY. J. Chem. Soc. Perkin I, 372 (1972); S. FARID. Chem. Commun. 303 (1970); 73 (1971); C. M. ORLANDO, H. MARK, A. K. BOSE, and M. S. MANHAS. J. Am. Chem. Soc. **89**, 6527 (1967).
9. D. GRILLER and K. U. INGOLD. Acc. Chem. Res. **9**, 13 (1976).
10. J. B. FARMER, C. L. GARDNER, and C. A. MCDOWELL. J. Chem. Phys. **34**, 1058 (1961).
11. A. J. ELLIOT and J. K. S. WAN. To be published.
12. P. J. WAGNER and I. KOCHEVAR. J. Am. Chem. Soc. **90**, 2232 (1968).
13. A. BECKETT and G. PORTER. Trans. Faraday Soc. **59**, 2038 (1963).
14. J. NAFISI-MOVAGHAR and F. WILKINSON. Trans. Faraday Soc. **66**, 2257 (1970); **66**, 2268 (1970).
15. E. AYMOSYAL and R. BENSASSON. J. Chem. Soc. Faraday I, **72**, 1274 (1976).
16. D. R. KEMP and G. PORTER. Proc. R. Soc. A**326**, 117 (1970).
17. S. K. WONG, L. FABES, W. J. GREEN, and J. K. S. WAN. J. Chem. Soc. Faraday I, **68**, 2211 (1972).
18. S. K. WONG, W. SYTNK, and J. K. S. WAN. Can. J. Chem. **50**, 3052 (1972).
19. S. K. RENGAN, H. P. KHAKHAR, B. S. PRABHANANDA, and B. VENKATARAMAN. Pramana, **3**, 95 (1974).
20. L. R. MAHONEY, F. C. FERRIS, and M. A. DAROOGE. J. Am. Chem. Soc. **91**, 3883 (1969).
21. K. A. MCLAUCHLAN and R. C. SEALY. Chem. Phys. Lett. **39**, 310 (1976).
22. K. U. INGOLD. Free radicals. Vol. 1. *Edited by* J. K. Kochi. Wiley Interscience, New York. 1973. p. 58.
23. E. J. HAMILTON and H. FISCHER. Helv. Chim. Acta, **56**, 795 (1973).

Can. J. Chem. Downloaded from www.nrcresearchpress.com by 210.87.254.40 on 09/05/12
For personal use only.

The crystal structure of *cis*-chlorobis(triethylphosphine)phthalazineplatinum(II) tetrafluoroborate, $[PtCl(PEt_3)_2(phth)]BF_4$

GORDON W. BUSHNELL AND KEITH R. DIXON

Department of Chemistry, University of Victoria, Victoria, B.C., Canada V8W 2Y2

Received August 31, 1977

GORDON W. BUSHNELL and KEITH R. DIXON. Can. J. Chem. **56**, 878 (1978).

The crystal structure of *cis*-chlorobis(triethylphosphine)phthalazineplatinum(II) tetrafluoroborate has been determined by single crystal X-ray diffraction and refined to an *R*-value of 0.076 for 1935 reflections. The cell dimensions are $a = 1315.7(2)$, $b = 2462.7(4)$, $c = 899.6(3)$ pm, $\beta = 104.99(2)°$. The space group is $P2_1/c$ with 4 molecules per unit cell, $\rho_o = 1.593$, $\rho_c = 1.613$ g cm^{-3}. The structure is a square planar 4-coordinate platinum(II) complex with an angle of 80.0° between the plane of the phthalazine molecule and that of the coordination. Interatomic distances to platinum are Pt—Cl, 235.4(9); Pt—P(1), 225.2(8); Pt—P(2), 226.9(8); Pt—N(1), 208(3); and Pt—N(2), 297(3) pm, the phthalazine ligand being monodentate. The structure is compared to previous results and discussed in relation to variable temperature nmr studies of solutions, which show that the heterocyclic ligand exchanges its point of attachment to and fro between N(1) and N(2) by a dissociative mechanism at elevated temperatures.

GORDON W. BUSHNELL et KEITH R. DIXON. Can. J. Chem. **56**, 878 (1978).

On a déterminé la structure cristalline du tétrafluoroborate du chlorobis(triéthylphosphine)-phtalazineplatine(II) *cis* en faisant appel à la diffraction de rayons-X de monocristaux et on a affiné la structure jusqu'à un facteur d'accord de 0.076 pour 1935 réflexions. Les dimensions de la maille sont $a = 1315.7(2)$, $b = 2462.7(4)$, $c = 899.6(3)$ pm, $\beta = 104.99(2)°$. Le groupe d'espace est $P2_1/c$ pour quatre molécules par maille, $\rho_o = 1.593$, $\rho_c = 1.613$ g cm^{-3}. La structure correspond à un complexe plan carré tétracoordonné du platine(II) avec un angle de 80.0° entre la molécule de phtalazine et celle de la coordination. Les distances interatomiques vers le platine sont Pt—Cl, 235.4(9); Pt—P(1), 225.2(8); Pt—P(2), 226.9(8); Pt—N(1), 208(3) et Pt—N(2), 297(3) pm, et le ligand phtalazine est monodentate. On a comparé cette structure avec des résultats antérieurs et on en discute par rapport aux résultats obtenus lors d'études rmn en solutions qui montrent qu'à haute température le ligand hétérocyclique échange son point d'attache entre les azotes 1 et 2 par un mécanisme dissociatif.

[Traduit par le journal]

Introduction

A nuclear magnetic resonance study (1) and two crystal structure determinations (2, 3) have been completed for a series of compounds *cis*-$[PtCl(PEt_3)_2L]BF_4$, where L is a potentially bidentate heteroaromatic ligand containing two nitrogen atoms. The ligands used have been dipyridyl or *o*-phenanthroline, naphthyridine, and pyridazine or phthalazine. This is the third crystal structure determination of a series in which the interatomic distance between the nitrogen atoms of the ligand is decreasing. The preceding studies for which L = phen (2) and L = naph (3) have shown that in the crystalline state these ligands are monodentate. The structures of the phenanthroline and naphthyridine ligands prevent the second nitrogen atom from being completely removed from the platinum atom, but a survey of M—N(1) and M—N(2) distances in other known structures showed that the ratio of the bond distances Pt—N(2):Pt—N(1) was extremely high for our compounds (2, 3).

The nuclear magnetic resonance results (1) show that the phenanthroline and naphthyridine complexes in solution at room temperature are undergoing a rapid intramolecular fluxional process in which the point of attachment of the ligand to the platinum is exchanging between N(1) and N(2). By lowering the temperature, the rate of naphthyridine exchange can be reduced sufficiently to obtain a low temperature limiting spectrum at −60°C in which the proton resonances for the two aromatic rings are not equivalent. The fluxional process for the phenanthroline complex is faster and the low temperature limiting spectrum cannot be observed even at −85°C, at which point crystallization and viscosity broadening make further cooling unprofitable.

For the pyridazine and phthalazine complexes the nmr spectra indicate that the fluxional process is much slower (1). The room temperature spectrum is the low temperature limiting spectrum. Above 90°C the peaks coalesce but the absence of Pt or P sidebands shows that the fluxional process is dissociative rather than intramolecular (1).

Can. J. Chem. Downloaded from www.nrcresearchpress.com by 210.87.254.6 on 09/05/12
For personal use only.

Can. J. Chem. Downloaded from www.nrcresearchpress.com by 210.87.254.6 on 09/05/12
For personal use only.

We have been able to correlate the solid state structures of the phenanthroline and naphthyridine complexes with the nmr kinetics (3). Consideration of the preferred direction of the N sp^2 sigma bonding seemed important in this regard. It was therefore of interest to obtain a crystal structure of *cis*-[$PtCl(PEt_3)_2L$]BF_4 where L was either pyridazine or phthalazine, and the two preferred bonding directions diverge outwards from the nitrogen atoms. Good crystals of the phthalazine containing compound were obtainable and so we have proceeded on this basis.

No previous crystal structure determinations of phthalazine complexes have been found in the literature, but the crystal structure of phthalazine itself is known (4). The crystal structure of a binuclear Ni(II) complex of 1,4-dihydrazinophthalazine has been determined (5), in which both ring nitrogens and both NH_2 groups are coordinated. The phthalazine part of the ligand plays a bridging role between the nickel centres. The crystal structure of [CuCN·pyridazine] has been determined (6) and contains zigzag CuCN chains linked by the N atoms of the organic ligand, the copper atom being approximately tetrahedral. 3,6-Diphenylpyridazine (dphp) reacts with $Fe_2(CO)_9$ to produce [$Fe_2(CO)_6$(dphp)], a compound containing a bridging (dphp) group and an Fe—Fe bond. Crystal structures have been obtained for two derivatives [$Fe_2(CO)_5P\phi_3$(dphp)] (7) in which the N—N bond of the bridging pyridazine ring is transverse to the Fe—Fe bond and the maleic anhydride adduct [$Fe_2(CO)_6$(dphp)($C_4H_2O_3$)] in which the bridging (dphp) group has its N—N bond approximately parallel to the Fe—Fe bond (8). If the phenyl groups in (dphp) are replaced by 2-pyridyl groups we obtain a ligand (dpyp) which is potentially quadridentate. The crystal structure of [$Mn(dpyp)_2(NO_3)_2$] contains both nitrate and (dpyp) as bidentate ligands making the Mn(II) 8-coordinate (9). The (dpyp) ligand resembles 2,2′-dipyridyl in this structure and only one nitrogen of the pyridazine ring forms a coordinate bond. These data suggest that phthalazine is likely to act as a bridging ligand in many compounds but monodentate structures are also a possibility.

Experimental

The preparation and analysis of the compound have already been reported, together with the spectroscopic results (1). The crystal was grown by a vapour diffusion method (ref. 10, p. 65) using methanol and diethyl ether as solvents. The title compound, $C_{20}H_{36}BClF_4N_2P_2Pt$, is monoclinic, space group $P2_1/c$, molecular weight 683.8, and cell dimensions a = 1.3157(2), b = 2.4627(4), c = 0.8996(3) nm, β = 104.99°. The cell having the volume 2.816(1) nm^3 contains 4 molecules and the density is 1.593 g cm^{-3} (measured) and 1.613 g cm^{-3} (calculated). Mo K_α X-rays, λ = 71.069 pm were used for intensity measurements on a crystal of dimensions 0.424 × 0.058 × 1.33 mm. The absorption coefficient was 54.89 cm^{-1}. The space group $P2_1/c$ was established from Weissenberg and precession photographs using Cu radiation. The shape of the crystal chosen for intensity measurements was like the blade of a pointed knife, the mounting direction being the c-axis, along the length of the blade. Only the pointed tip of the blade was not immersed in the beam. The irradiated material changed from colourless to yellow during data collection. The crystal was put on a Picker 4-circle diffractometer. The cell dimensions were refined by least squares using 31 pairs of positive and negative 2θ measurements. The density was measured by flotation in a solution of carbon tetrachloride and bromoform. The diffractometer matrix was refined from 32 pairs of automatic centering measurements. The scan was by 50 steps of 0.04° in 2θ counting for 1 s per step. The background counts were for 10 s at each end of the scan. A set of three standards 8,0,0; 0,−14,0; and 0,0,4 was measured after every batch of 50 reflections. Measurements were completed up to 45° in 2θ, h positive and negative, $k \geq 0$, $l \geq 0$. Reflections for which $I < 3\sigma(I)$ were not output. The intensities were corrected using the current set of standards and the Lorentz and polarization factors were applied. An instrument instability constant of 0.04 was derived from the standards and used to calculate $\sigma(F)$, (ref. 10, p. 454). Absorption corrections were done by numerical integration using a 10 × 4 × 16 Gaussian grid, the program was that of Coppens, Leiserowitz, and Rabinovich (11) modified for our diffractometer. The measurements were then sorted and merged to give 1935 independent observations.

Structure Determination

The structure was solved by the heavy atom method. The programs used were kindly supplied by Penfold (12), and are considerably modified versions of ORFLS, FORDAP, ORTEP, and ORFFE. The atomic scattering factors for P, Cl, and Pt were from Cromer and Waber (13). Pt was treated as an anomalous scatterer (14). The atomic scattering factors for B, C, N, and F were taken from the International Tables (15). All atoms were assumed to be uncharged. The Pt atom was located using a three dimensional Patterson map, and the first structure factor calculation gave an R-value of 0.25. The other atoms were located using Fourier and difference maps and refinement was by full matrix least squares, minimizing $\Sigma w(|F_o| - |F_c|)^2$. When R = 0.081, a weighting scheme was devised having the form $W = [A + B|F_o| + C|F_o|^2 + D|F_o|^3]^{-1}$ with A = 18.96, B = −0.1283, C = 1.740 × 10^{-3}, D = 5 × 10^{-6}. The heavy atoms were given anisotropic temperature parameters and refinement was completed with several cycles of full matrix least squares. The maximum change/error in the final cycle was 0.15 and the mean value 0.011, the larger changes being associated with the BF_4^- ion. The final conventional R-value was 0.076 and the weighted R-value, $(\Sigma(w\Delta^2/wF_o^2))^{1/2}$ was 0.099. The final difference map gave no indications of any misplaced atoms.

The final positional and temperature parameters are given in Tables 1 and 2. The structure factor table is in the Depository for Unpublished Data.[1]

Results and Discussion

The crystal structure contains separate [$PtCl(PEt_3)_2$(phth)]$^+$ and BF_4^- ions. Figure 1 is the packing diagram of one unit cell. Figure 2 gives a

[1]Copies may be obtained upon request, at a nominal charge, from the Depository of Unpublished Data, CISTI, National Research Council of Canada, Ottawa, Ont., Canada K1A 0S2.

Can. J. Chem. Downloaded from www.nrcresearchpress.com by 210.87.254.6 on 09/05/12
For personal use only.

TABLE 1. Atomic parameters. Fractional atomic coordinates ($\times 10^4$ for Pt—P(2), $\times 10^3$ for N(1)—F(4)) and isotropic temperature parameters

Atom	x	y	z	$U_{iso} \times 10^{-1}$ (pm²)*
Pt	1852(1)	1364(1)	1264(1)	
Cl	1745(7)	1820(5)	−1071(9)	
P(1)	1778(6)	931(4)	3438(8)	
P(2)	3501(7)	1117(4)	1193(9)	
N(1)	34(2)	168(2)	99(3)	76(7)
N(2)	−48(3)	133(2)	27(4)	99(8)
C(1)	19(3)	218(2)	132(4)	84(9)
C(2)	−85(3)	241(2)	102(4)	74(8)
C(3)	−96(3)	296(2)	138(5)	112(12)
C(4)	−207(5)	313(3)	106(7)	176(21)
C(5)	−292(4)	274(2)	50(5)	120(13)
C(6)	−275(3)	224(2)	6(5)	110(12)
C(7)	−170(3)	207(2)	45(4)	99(11)
C(8)	−145(3)	153(2)	1(4)	96(11)
C(11)	185(4)	21(2)	338(5)	117(13)
C(12)	96(4)	−6(2)	203(6)	147(17)
C(13)	54(3)	110(2)	396(4)	91(10)
C(14)	40(3)	78(2)	542(5)	116(12)
C(15)	280(4)	113(2)	519(5)	119(13)
C(16)	277(4)	176(2)	542(6)	133(15)
C(21)	429(3)	177(2)	95(5)	105(11)
C(22)	446(4)	209(2)	253(6)	134(15)
C(23)	436(3)	77(2)	275(4)	91(10)
C(24)	549(4)	67(2)	254(6)	133(15)
C(25)	347(3)	71(2)	−55(4)	101(11)
C(26)	276(4)	25(2)	−81(6)	135(15)
B	418(6)	−102(4)	261(8)	150(21)
F(1)	491(3)	−60(2)	307(4)	164(10)
F(2)	449(4)	−142(2)	332(5)	228(16)
F(3)	323(3)	−83(2)	274(4)	185(11)
F(4)	408(4)	−108(2)	112(6)	252(18)

*$T = \exp(-8\pi^2 U_{iso} \sin^2\theta/\lambda^2)$.

picture of the cation displaying the thermal parameters and the atom labelling scheme. Tables 3 and 4 give interatomic distances and bond angles respectively. The triethylphosphine ligands are normal having mean lengths: P—C, 185 pm; C—C, 156 pm, and mean angles: C—P—C, 105°; P—C—C, 112°. The distances and angles in the ligand phthalazine are not significantly different from those which have been measured more accurately in pure crystalline phthalazine (4).

The results of the mean plane calculations have been deposited.[1] Significant non-planarity of the phthalazine ligand was not observed ($\chi^2 = \sum_i |P_i^2 \div \sigma^2(P_i)| = 12$, where P_i = the perpendicular distance of atom i from the plane). Pt was 7.9(1) pm from this plane. A similar treatment for the phthalazine molecule is available, and the small departures from planarity (≤ 1 pm) are discussed (4). The atoms Pt, Cl, P(1), P(2), and N(1) deviate slightly from the least squares plane through them ($\chi^2 = 31$). The deviations are Pt −0.1(1), Cl 4(1), P(1) 3.0(9), P(2) −0.2(9), N(1) −4(3), and C(7) 3(4), C(6) 19(4). The major contributors to χ^2 are P(1) and Cl rather than N(1). The angle between the mean planes for the Pt(II) coordination and the phthalazine ligand is 80.0°.

The tetrafluoroborate anion is not unusual in having fairly high thermal parameters, a mean B—F length of 132 pm, and angles close to the tetrahedral value.

The platinum coordination geometry is best discussed in relation to that of the two previous structures of the series (2, 3). In Table 5*a* the first three entries show that bond lengths which do not involve the heterocyclic ligand are closely similar in the three compounds. The Pt—N(1) bond may be slightly longer for phen than for the other two compounds, but the significance of this is marginal. The lengths Pt—N(2) and N(1)—N(2) are expected to differ, and the observed values are to be compared with values calculated from idealized models in which the ligands have regular hexagonal rings and all bond angles are 120°. Figure 3 gives the idealized geometry for N(1)—N(2), Pt—N(2), Pt—Pt′ distances in our series of compounds. Pt′ is the position the platinum atom would have if it were bonded to N(2) instead of N(1), the ligand position being fixed. The secondary Pt site is relevant to the nmr results and its distance from the primary site is greatest in the phth complex whereas the Pt—N(2) distance is at a maximum for naph. The greatest discrepancy between the observed and idealized distances in Table 5*a* is that Pt—N(2) in the phen complex is 32 pm greater than the value suggested by the model. This is caused by a tilt of the phenanthroline ligand such that the two observed Pt—N(1)—C angles differ by 8.1°.

TABLE 2. Anisotropic temperature parameters* for the heavy atoms

Atom	U_{11}	U_{22}	U_{33}	U_{12}	U_{13}	U_{23}
Pt	73.0(7)	83.3(9)	48.0(8)	9.7(8)	16.6(5)	0.5(8)
Cl	114(7)	161(10)	70(5)	23(7)	26(5)	39(6)
P(1)	93(6)	81(7)	56(5)	−1(5)	30(4)	−4(5)
P(2)	84(6)	104(8)	65(5)	24(5)	28(4)	10(5)

*Tabulated values should be multiplied by 10 to obtain mean square amplitudes in pm². $T = \exp -2\pi^2(U_{11} h^2a^{*2} + \ldots + 2U_{12} hka^*b^* + \ldots)$. Estimated standard deviations in parentheses.

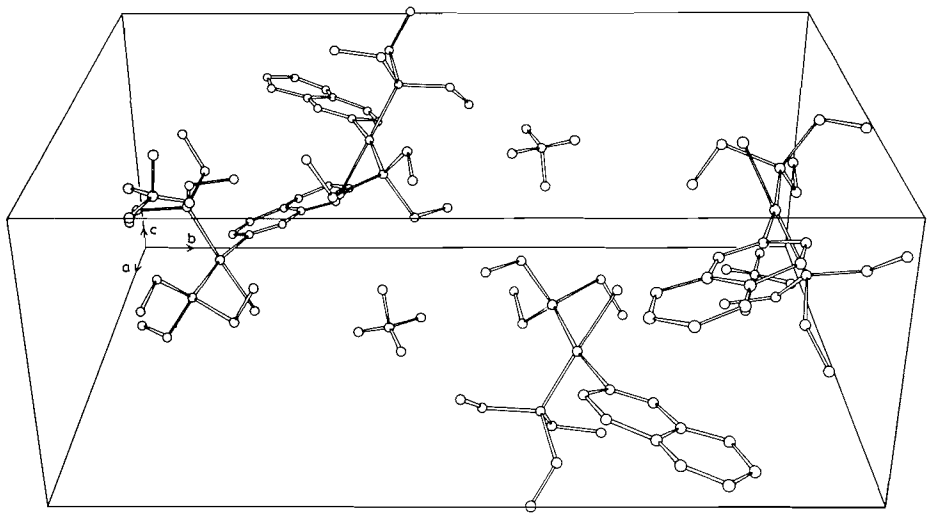

FIG. 1. The packing diagram for $[PtCl(PEt_3)_2(phth)]^+BF_4^-$.

TABLE 3. Interatomic distances (pm)

Atoms	Length	Atoms	Length
	(*a*) The platinum coordination		
Pt—N(1)	208(3)	Pt—N(2)	297(3)
Pt—P(1)	225.2(8)	Pt—P(2)	226.9(8)
Pt—Cl	235.4(9)		
	(*b*) The triethylphosphine ligands		
P(1)—C(11)	177(5)	P(2)—C(21)	196(4)
P(1)—C(13)	186(4)	P(2)—C(23)	178(4)
P(1)—C(15)	185(5)	P(2)—C(25)	186(4)
C(11)—C(12)	160(6)	C(21)—C(22)	159(6)
C(13)—C(14)	158(5)	C(23)—C(24)	156(5)
C(15)—C(16)	157(6)	C(25)—C(26)	144(6)
	(*c*) The phthalazine ligand		
N(1)—C(1)	131(4)	N(2)—C(8)	133(4)
C(1)—C(2)	143(4)	C(8)—C(7)	146(5)
C(2)—C(3)	141(5)	C(7)—C(6)	139(5)
C(3)—C(4)	146(6)	C(6)—C(5)	134(5)
C(4)—C(5)	145(7)	C(2)—C(7)	139(5)
N(1)—N(2)	140(4)		
	(*d*) The tetrafluoroborate ion		
B—F(1)	139(7)	B—F(2)	119(7)
B—F(3)	137(7)	B—F(4)	132(7)

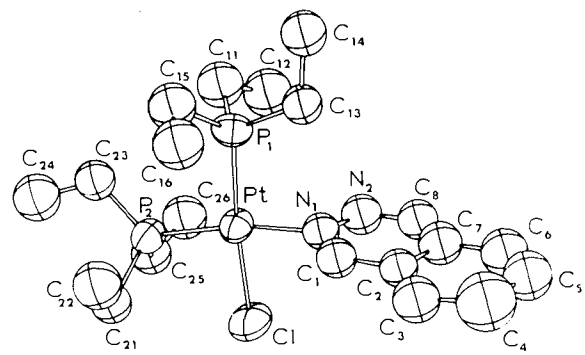

FIG. 2. Molecular structure and atom labelling scheme.

Table 5*b* shows that the bond angles of the platinum coordination are identical for the three complexes except when N(1) is involved. The close agreement shows that these angles are determined by intraionic repulsions, not by the crystal structure which is different for each compound. The conformation of the $Pt(PEt_3)_2$ moiety is identical in the three complexes of the series. The phosphorus atom and the carbon atoms of two of the ethyl groups form a W-shape which runs approximately perpendicular to the coordination plane. The carbon atoms of the third ethyl group of each ligand lie approximately in the coordination plane, avoiding the Cl atom in one ligand, and toward the heterocyclic ligand in the other. When N(1) is involved the angles of the phen complex in Table 5*b* are different from those of the naph and phth complexes, particularly the N(1)—Pt—P(*trans*) angle.

Table 5*c* gives comparable figures from the mean plane calculations for the three complexes. The planes of the ligands are roughly perpendicular to the coordination planes, with the maximum deviation of 10° for the phthalazine ligand which is least hindered for rotation about the Pt—N(1) bond. The decrease in χ^2 for plane 1 in going from phen to phth shows that the planarity is improving. The perpendicular distances of N(1) from the mean planes are given. They show that N(1) is a major contributor to χ^2 for phen and naph, but not for phth. The atoms N(1) and N(2) lie on opposite sides of the mean coordination planes in all cases.

Can. J. Chem. Downloaded from www.nrcresearchpress.com by 210.87.254.6 on 09/05/12
For personal use only.

Can. J. Chem. Downloaded from www.nrcresearchpress.com by 210.87.254.6 on 09/05/12
For personal use only.

TABLE 4. Bond angles (deg)

Bonds	Angle	Bonds	Angle
(a) The platinum coordination			
Cl—Pt—P(1)	174.3(3)	P(2)—Pt—N(1)	169.8(7)
Cl—Pt—P(2)	86.5(4)	Cl—Pt—N(1)	83.4(7)
P(1)—Pt—P(2)	98.9(3)	P(1)—Pt—N(1)	91.3(7)
N(1)—Pt—N(2)	25.2(9)		
(b) The triethylphosphine ligands			
Pt—P(1)—C(11)	116(2)	Pt—P(2)—C(21)	109(2)
Pt—P(1)—C(13)	111(2)	Pt—P(2)—C(23)	122(2)
Pt—P(1)—C(15)	115(2)	Pt—P(2)—C(25)	111(2)
C(11)—P(1)—C(13)	106(2)	C(21)—P(2)—C(23)	104(2)
C(13)—P(1)—C(15)	103(2)	C(23)—P(2)—C(25)	106(2)
C(15)—P(1)—C(11)	105(2)	C(25)—P(2)—C(21)	104(2)
P(1)—C(11)—C(12)	114(3)	P(2)—C(21)—C(22)	105(3)
P(1)—C(13)—C(14)	114(3)	P(2)—C(23)—C(24)	114(3)
P(1)—C(15)—C(16)	109(3)	P(2)—C(25)—C(26)	115(3)
(c) The phthalazine ligand			
N(1)—N(2)—C(8)	117(3)	N(2)—N(1)—C(1)	122(3)
N(2)—C(8)—C(7)	124(4)	N(1)—C(1)—C(2)	122(3)
C(8)—C(7)—C(6)	119(4)	C(1)—C(2)—C(3)	120(3)
C(8)—C(7)—C(2)	116(4)	C(1)—C(2)—C(7)	118(4)
C(6)—C(7)—C(2)	124(4)	C(3)—C(2)—C(7)	123(4)
C(7)—C(6)—C(5)	115(4)	C(2)—C(3)—C(4)	112(4)
C(6)—C(5)—C(4)	122(5)	C(3)—C(4)—C(5)	122(6)
Pt—N(1)—C(1)	122(3)	Pt—N(1)—N(2)	116(2)
(d) The tetrafluoroborate ion			
F(1)—B—F(2)	110(6)	F(2)—B—F(3)	116(7)
F(1)—B—F(3)	106(6)	F(2)—B—F(4)	113(7)
F(1)—B—F(4)	105(6)	F(3)—B—F(4)	106(6)

TABLE 5. Comparison of *cis*-$[PtCl(PEt_3)_2L]^+BF_4^-$ structures, where L = *o*-phenanthroline, 1,8-naphthyridine, and phthalazine

(a) Interatomic distances

Atoms	Distance (pm) phen	naph	phth
Pt—Cl	236.1(6)	236.6(4)	235.4(9)
Pt—P (*trans* to Cl)	224.1(6)	225.2(4)	225.2(8)
Pt—P (*cis* to Cl)	223.9(7)	225.4(4)	226.9(8)
Pt—N(1)	214(2)	208(1)	208(3)
Pt—N(2)	284(2)	305(1)	297(3)
N(1)—N(2)	285(3)	229(3)	140(4)
Pt—N(2)*	252	321	305
N(1)—N(2)*	280	242	140

*Calculated using 120° angles, Pt—N(1) = 210 pm, and hexagons of side 140 pm.

(b) Bond angles

Bonds	Angle (deg) phen	naph	phth
Cl—Pt—P	85.5(2)	86.8(2)	86.5(4)
P—Pt—P	99.5(2)	99.3(1)	98.9(3)
P—Pt—N(1)	93.6(5)	90.6(3)	91.3(7)
N(1)—Pt—Cl	81.2(5)	83.2(3)	83.4(7)
N(1)—Pt—P(*trans*)	162.5(5)	169.7(3)	169.8(7)
Cl—Pt—P(*trans*)	174.8(3)	173.6(1)	174.3(3)

(c) Mean plane results

Parameter	Value phen	naph	phth
Angle between plane *1** and ligand plane	97.5°	92.0°	100.0°
χ^2 for plane *1*	500	136	31
Perpendicular distance, N(1)–plane *1*	37(2) pm	8(1) pm	4(3) pm

*Defined as the coordination plane.

The X-ray structural results are closely related to the kinetics of the fluxional processes in solution. We have already discussed the relationship between the Pt—Pt′ distance and the activation energy for the exchange process (3). The deviation of the atom N(1) from the mean coordination plane is now correlated with the exchange rate. It seems that for these compounds the crystal structure gives a premonition of what will happen intramolecularly in solution. For the phen complex, N(1) is far from the coordination mean plane, in a direction which suggests exchange, and the exchange rate in solution is fast. For the phthalazine complex there is little or no deviation of N(1) from the plane and intramolecular rearrangement does not occur. The napthyridine complex is the intermediate case.

The structural evidence does not support a model in which the ligand phen is a rigid framework with N(2) attracted to the Pt atom with a force which displaces N(1) from the coordination plane. If this were true we would expect the Pt—N(2) distance to be abnormally short, whereas it is found to be longer than expected. A more suitable theory is that in order to exchange its point of attachment from N(1) to N(2) an idealized phen ligand in a perfectly square planar complex would have to rotate through 60° and translate through a distance of about 70 pm, the Pt—Pt′ distance. The extreme ends of this rotational motion are unfavourable energetically because the lone pair of electrons on N(2) repel the Pt(II) d_{z^2} electrons, hence the long Pt—N(2) distance observed. This repulsive force has a turning moment about Pt and N(1), producing the displacement of N(1) from the coordination plane and the inequality of the Pt—N—C angles. These strains result in economies in the actual motion of the ligand necessary to effect exchange, and a lower activation energy. For the naphthyridine ligand the required motion is mainly

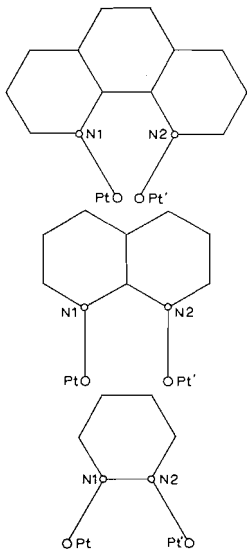

FIG. 3. Idealized structures for the heterocyclic ligands.

translational. The repulsion of the lone pair electrons is less, the resulting strain reduced, and the saving in activation energy is small. In the phthalazine case the orientation of the lone pairs is unsuitable for the five coordinate intermediate required by an intramolecular process and the mechanism of exchange becomes dissociative.

Acknowledgements

Technical assistance by Mrs. Kathy Beveridge is gratefully acknowledged and we thank the University of Victoria and the National Research Council of Canada for research grants.

1. K. R. DIXON. Inorg. Chem. **16**, 2618 (1977).
2. G. W. BUSHNELL, K. R. DIXON, and M. A. KHAN. Can. J. Chem. **52**, 1367 (1974).
3. G. W. BUSHNELL, K. R. DIXON, and M. A. KHAN. Can. J. Chem. **56**, 450 (1978).
4. C. HUISZOON, B. W. VAN DER WAAL, A. B. VAN EGMOND, and S. HARKEMA. Acta Crystallogr. Sect. B, **28**, 3415 (1972).
5. J. E. ANDREW and A. B. BLAKE. J. Chem. Soc. A, 1408 (1969).
6. D. T. CROMER and A. C. LARSON. Acta Crystallogr. Sect. B, **28**, 1052 (1972).
7. L. G. KUZ'MINA, N. G. BOKII, YU. T. STRUCHKOV, A. V. ARUTYUNYAN, L. V. RYBIN, and M. I. RYBINSKAYA. J. Struct. Chem. **12**, 801 (1971).
8. H. A. PATEL, A. J. CARTY, M. MATHEW, and G. J. PALENIK. J. Chem. Soc. Chem. Commun. 810 (1972).
9. J. E. ANDREW, A. B. BLAKE, and L. R. FRAZER. J. Chem. Soc. Dalton Trans. 800 (1975).
10. G. H. STOUT and L. H. JENSEN. X-Ray structure determination. MacMillan, New York, NY. 1968.
11. P. COPPENS, L. LEISEROWITZ, and D. RABINOVICH. Routines for the CDC 1604, Rehovoth, Israel.
12. B. R. PENFOLD. University of Canterbury Crystallographic Programs, Christchurch, New Zealand.
13. D. T. CROMER and J. T. WABER. Acta Crystallogr. **18**, 104 (1965).
14. D. T. CROMER. Acta Crystallogr. **18**, 17 (1965).
15. J. A. IBERS. International tables for X-ray crystallography. Vol. III. Kynoch Press, Birmingham. 1962. Table 3.3.1A, p. 201.

Can. J. Chem. Downloaded from www.nrcresearchpress.com by 210.87.254.6 on 09/05/12
For personal use only.

Variational energies for highly excited states of the helium atom

WAI-TAK MA, MARY KURIYAN, and HUW O. PRITCHARD
Centre for Research in Experimental Space Science, York University, Downsview, Ont., Canada M3J 1P3

Received June 13, 1977

WAI-TAK MA, MARY KURIYAN, and HUW O. PRITCHARD. Can. J. Chem. **56**, 884 (1978).

The efficient correlated variational wave functions used previously to study the higher $1sns$ states of helium have been extended to other states of the helium atom, $1snp$ ($n \leq 23$), $2pnp\ ^1P$ ($n \leq 25$), and $2pnp\ ^3P$ ($n \leq 25$); similar uncorrelated wave functions were used for $1snd$ ($n \leq 21$), $2pnp\ ^1D$ ($n \leq 10$), and $2pnp\ ^3D$ ($n \leq 10$). Attempts to use the same techniques for the $2pnp\ ^{1,3}S$ states appear to converge variationally to the energies of the $2s^2\ ^1S$ and $2s3s\ ^3S$ states respectively. Comparison is made with experimental results where appropriate, and agreement is excellent except in the case of the $1snd$ states above $n = 13$.

A search was made for excited states of H^- in each of these configurations, but no new states were found.

WAI-TAK MA, MARY KURIYAN et HUW O. PRITCHARD. Can. J. Chem. **56**, 884 (1978).

On a étendu les fonctions d'onde variationnelles corrélées efficaces, utilisées antérieurement pour étudier les états $1sns$ élevés de l'hélium, à d'autres états de l'atome d'hélium, $1snp$ ($n \leq 23$), $2pnp\ ^1P$ ($n \leq 25$) et $2pnp\ ^3P$ ($n \leq 25$); on a aussi utilisé des fonctions d'onde non corrélées semblables pour les états $1snd$ ($n \leq 21$), $2pnp\ ^1D$ ($n \leq 10$) et $2pnp\ ^3D$ ($n \leq 10$). Des essais en vue d'utiliser les mêmes techniques pour les états $2pnp\ ^{1,3}S$ semblent converger respectivement d'une façon variationnelle vers les énergies des états $2s^2\ ^1S$ et $2s3s\ ^3S$. On a fait une comparaison avec des résultats expérimentaux lorsque ceux-ci étaient disponibles et on a trouvé une excellente corrélation excepté dans le cas des états $1snd$ où $n > 13$.

On a fait une recherche des états excités de H^- dans chacune de ces configurations mais on n'a trouvé aucun nouvel état.

[Traduit par le journal]

Introduction

We have shown previously (1) that by choosing the trial wave function in a certain way, it is possible to obtain very accurate expectation values of the energy for the higher $1sns$ states of the helium atom using expansion lengths N which are only of the order of $n + 3$. In this paper, we explore the extension of these ideas to non-spherical states of helium, $1snp$, $1snd$, and $2pnp$. However, because of the considerable increase in complexity of the problem, the choice of a generalised product wave function in coordinates r_1, r_2, and r_{12} is inconvenient and two other choices were explored, product wave functions in r_1 and r_2, either uncorrelated or correlated with powers of $\cos\theta_{12}$.

$1snp\ ^1P$ and ^3P States

For the $1snp$ states, we follow the derivation of Breit (2) and use a correlated generalised product wave function of the form

$$[1] \quad \psi = F_2(r_1,r_2,\theta_{12})\cos\theta_2 \pm F_1(r_1,r_2,\theta_{12})\cos\theta_1$$

with the (+) sign corresponding to ^1P states and the (−) sign to ^3P states. In eq. 1

$$[2] \quad F_2(r_1, r_2, \theta_{12}) = \sum_{i=0}^{n}\sum_{j=0}^{n'}\sum_{k=0}^{m} c_{ijk}(\zeta r_1)^i(\zeta r_2)^{j+1} \times \cos^k\theta_{12}e^{-\zeta(ar_1+br_2)}$$

and $F_1(r_1,r_2,\theta_{12})$ is the same expression with the electron subscript indices 1 and 2 interchanged; in future equations the conventional symbol $(1 \pm P_{12})$ will be used to represent this antisymmetrising operation. In eqs. 1 and 2, r_1 and r_2, θ_1, and θ_2 are the polar coordinates of the two electrons and θ_{12} is the angle between the two radius vectors r_1 and r_2. For discussion purposes, we will label functions, as before (1), with a descriptor $\sum(i_{max},j_{max},k_{max})$ which indicates the maximum power of r_1, r_2, and $\cos\theta_{12}$ used in any calculation, but in general not the exact combination of terms. The general features of these calculations are very similar to those reported earlier for the $1sns$ states (1): that for low-lying states ($1s2p\ ^1P$, $1s3p\ ^1P$, and $1s2p\ ^3P$), the optimum combination of terms for a given expansion length N contained powers of r_1, r_2, and $\cos\theta_{12}$, e.g. $\sum(2,2,3)$, $N = 36$; on the other hand, for the higher $1snp$ states, it is always preferable to add terms in r_2 rather than r_1, and for n above about 10, addition of another term in r_2 is always preferable to one in $\cos\theta_{12}$. For any expansion length N, the absolute

Can. J. Chem. Downloaded from www.nrcresearchpress.com by 210.87.254.42 on 09/05/12
For personal use only.

Can. J. Chem. Downloaded from www.nrcresearchpress.com by 210.87.254.42 on 09/05/12
For personal use only.

accuracies of the calculated energy levels are comparable with those for the $1sns$ states given previously, and a table of energy levels using the $\sum(0,25,0)$ approximation for $1snp$, ^1P, and ^3P, ($n \leq 23$) together with the optimum values of the disposable parameter b is available on request.[1] To take just one example, using this approximation, the calculated energies of the $1s20p$ ^1P and ^3P states are both just 0.3 cm^{-1} above the observed values (3).

Previous calculations for $1snp$ states may be divided into two classes. One, these devoted to very accurate treatment of the low-lying ($n \leq 5$) states (4–6); our calculation is not intended to compete with these, but for $1s5p$, our best $N = 26$ results are about 8×10^{-5} au (i.e. 17 cm^{-1}) too high for both singlet and triplet. Two, an exploratory study using 25 hydrogen-like basis functions, by Wang and Weinhold (7) extending up to $1s13p$: in all cases, our $N = 26$ energies are superior to these by (respectively for singlets or triplets) about 37 or 28 cm^{-1} at $1s5p$, 6 or 4 cm^{-1} at $1s9p$, and 2 or 1 cm^{-1} at $1s13p$; the reason for this is that (unlike our eq. 2) Wang and Weinhold use a function with $a = b$.

Following our previous technique (8), we searched for bound $1snp$ states of H^- (and also $1snd$ states), but none was found, in conformity with general expectation (ref. 9, also ref. 5).

$1snd$ ^1D and ^3D States

From the conclusions of the earlier work on $1sns$ and $1snp$ states described above, it would appear that no new principles relating to the efficient choice of wave functions are to be found using our present approach. Consequently, for reasons which will become apparent in the later discussion, we only examined uncorrelated wave functions of the general form

$$[3] \quad \psi = (1 \pm P_{12}) \sum_{i=0}^{n} \sum_{j=0}^{n'} c_{ij}(\zeta r_1)^i(\zeta r_2)^{j+2} \times e^{-\zeta(ar_1+br_2)}(3\cos^2\theta_2 - 1)$$

The agreement of the calculated and observed energy levels for high n is good, as expected, and a table of calculated energies using the $\sum(0,25,0)$ approximation for $1snd$, ^1D, and ^3D, ($n \leq 21$) together with the optimum values of the disposable parameter b is available on request.[1] Earlier configuration–interaction calculations (25) terminated at $1s8d$, where the energies are, understandably, lower than ours by about 1 cm^{-1}.

$2pnp$ ^1P, ^3P, ^1D, and ^3D States

It is possible to choose combinations of two single p-electron wave functions in such a way that the total wave function is ^1P or ^3P, ^1D or ^3D, ^1S or ^3S in character (2, 10): this order of presentation represents the order of increasing difficulty in performing variational calculations.

For the P states of $2pnp$, the following correlated product wave function was used.

$$[4] \quad \psi = (1 \pm P_{12}) \sum_{i=0}^{n} \sum_{j=0}^{n'} \sum_{k=0}^{m} c_{ijk}(\zeta r_1)^{i+1}(\zeta r_2)^{j+1} \times \cos^k\theta_{12} e^{-\zeta(ar_1+br_2)}[(\sin\theta_1 \sin\theta_2 \sin(\phi_1 - \phi_2)]$$

where the (+) sign refers to the ^3P state and the (−) sign to the ^1P state. Calculations were performed up to and including $2p25p$ for both singlets and triplets: the upper limit of n arises, as before (ref. 1, also ref. 7), because of overflow problems in the integrals for $b < 0.025$. The lowest member of each series calculated using our 27th order $\sum(2,2,2)$ wave function is somewhat inferior to those obtained by Drake and Dalgarno (11) and by Doyle, Oppenheimer, and Drake (12) because (see below) $\cos\theta_{12}$ correlation is less efficient than r_{12} correlation: the differences are 22.7 cm^{-1}, 18.8 cm^{-1}, and 2.6 cm^{-1} for the $2p^2$ ^3P, $2p3p$ ^3P, and $2p3p$ ^1P states respectively. A table of these calculated energy levels is available on request.[1] There are, however, no experimental values available for $n > 3$, but judging from the convergence properties for the $1sns$, $1snp$, and $1snd$ energies using these kinds of wave function, it seems likely that these $2pnp$ energies are in general accurate to better than 1 cm^{-1} for n in the range 10–20.

There seems no valid theoretical reason for thinking that these energies represent true upper bounds since there is no guarantee of orthogonality with the $1snp$ manifold below, but it appears empirically that this is the case; likewise for the D states below.

The use of wave functions analogous to [4] to describe the D states of $2pnp$ requires only a straightforward extension (10); however, the calculations would be considerably lengthier because more terms are required in the matrix elements, and we did not explore them for reasons of cost. We did, however, explore the uncorrelated analogue of [4]

[1]Tables similar to Table 3 of ref. 1 are available, at a nominal charge, from the Depository of Unpublished Data, CISTI, National Research Council of Canada, Ottawa, Ont., Canada K1A 0S2. They will also be available in thesis form later (W.-T.M.). However, using eq. 9 and the diagrams reproduced later in this paper, it is possible to reconstruct the computed energies to a very high degree of precision.

Can. J. Chem. Downloaded from www.nrcresearchpress.com by 210.87.254.42 on 09/05/12
For personal use only.

$$[5]\quad \psi = (1 \pm P_{12}) \sum_{i=0}^{n} \sum_{j=0}^{n'} c_{ij}(\zeta r_1)^{i+1}(\zeta r_2)^{j+1} \times e^{-\zeta(ar_1+br_2)} \times [\sin\theta_1 \sin\theta_2 \cos(\phi_1 - \phi_2) - 2\cos\theta_1 \cos\theta_2]$$

where the (+) sign refers to ^1D and the (−) sign to ^3D, on the basis of our accumulated experience that the energies of highly excited states are adequately represented using uncorrelated wave functions. Calculations were performed up to $n = 10$, which should provide sufficient information[1] to make reasonable estimates of the positions of D resonances by interpolation between the calculated values and the low-lying observed values (3); Rydberg plots such as are shown later in this paper should be excellent for this purpose.

S States, 2*sns* and 2*pnp*

Straightforward modification of the wave function [4] to give the combinations of p-electron functions appropriate to an S state leads to

$$[6]\quad \psi = (1 \pm P_{12}) \sum_{i=0}^{n} \sum_{j=0}^{n'} \sum_{k=0}^{m} c_{ijk}(\zeta r_1)^{i+1}(\zeta r_2)^{j+1} \times \cos^k\theta_{12} e^{-\zeta(ar_1+br_2)} \times [\cos\theta_1 \cos\theta_2 + \sin\theta_1 \sin\theta_2 \cos(\phi_2 - \phi_1)]$$

where the (+) sign corresponds to ^1S and the (−) sign to ^3S. Use of this wave function leads immediately to calculated energies below the observed values for both $2p^2\ ^1S$ and $2p3p\ ^3S$ (for example, with a function $\sum(0,12,1)$, $N = 26$, values of −0.723 and −0.579 au, compared with the observed values (3) of −0.620 and −0.558 au respectively). In common parlance, this is because there is strong configurational mixing between 2*pnp* and 2*sns*, and it is hoped that the following numerical experiments will help to shed some more light on the nature of this problem, insofar as the classic variational approach to the description of these states is concerned (13, 14).

(*ia*) In the case of the ^1S state, one can argue that the wave function [6] is not orthogonal to $2s^2\ ^1S$, and therefore not orthogonal to $1s^2\ ^1S$ either. One can therefore follow established procedures (13, 15) and attempt to project out of the calculated solution the $1s^2$, 1*sns* components (represented by a function such as [8] below). Computed energies with uncorrelated wave functions for $2p^2\ ^1S$ in the range −0.633 to −0.635 au are fairly persistent, occurring over quite a wide range of the disposable parameters a and b: the use of these projection techniques on any of these wave functions immediately pushes these eigenvalues up towards, but not quite up to the experimental level.

(*ib*) The same results can be achieved in a more systematic way. It is usual to make use of Green's theorem in calculating the integrals required in two-electron calculations (16): this ensures that the matrix elements of the Hamiltonian are symmetric. However, one can evaluate these integrals for wave functions like [6] in a straightforward fashion without the use of Green's theorem (17) in which case the secular matrix is slightly unsymmetric: it gives, nevertheless, the same eigenvalues. If we now choose a trial wave function

$$[7]\qquad \psi = \alpha\psi(1s^2\ ^1S) + \beta\psi(2p^2\ ^1S)$$

then in this unsymmetric reduction, certain $1s^2$–$2p^2$ matrix elements appear in the secular matrix: there are no cross terms in T and S, but there are in V. If one now observes the behaviour of the eigenvalue near $E = -0.634$ au, it has the following properties. Increasing the expansion length of the $2p^2$ function lowers the energy, or leaves it the same, as expected. Improving the representation of the $1s^2$ function raises the value of this eigenvalue, again as expected. It seems obvious, then, that the solution to the problem of obtaining a quasi-variational energy for the $2p^2\ ^1S$ state is to use a wave function of the form of [7] with this unsymmetric reduction procedure, and simply increase the expansion lengths for both $1s^2$ and $2p^2$ until convergence is achieved. Unfortunately, this does not work because if the expansion length of the $1s^2$ part is made too great, the target eigenvalue again falls below the observed value: we believe this is due to the fact that since the $1s^2$ part of the function is only a variational approximation, it is not strictly orthogonal to all other approximate wave functions; overlap integrals of the order of 10^{-3} have been shown to be typical (18) in these kinds of variational calculations. Since we have been unable to resolve this difficulty, we will not report the details of these calculations, but they will be made available elsewhere (17).

(*ii*) If one wanted to perform a variational calculation for the $2s^2\ ^1S$ or the $2s3s\ ^3S$ state, using these kinds of correlated wave functions, one might choose

$$[8]\quad \psi = (1 \pm P_{12}) \sum_{i=0}^{n} \sum_{j=0}^{n'} \sum_{k=0}^{m} c_{ijk}(\zeta r_1)^{i}(\zeta r_2)^{j} \times \cos^k\theta_{12} e^{-\zeta(ar_1+br_2)}$$

However, the final angular term in eq. 6 is nothing more than $\cos\theta_{12}$, so that the only difference between the two functions [6] and [8] is that [6] excludes the

Can. J. Chem. Downloaded from www.nrcresearchpress.com by 210.87.254.42 on 09/05/12
For personal use only.

configurations including $r_1^0\ r_2^0$ and $\cos^0\theta_{12}$; consequently, there is little distinction between the trial wave functions for the S states of $2sns$ and $2pnp$. Nor, apart from some reduced efficiency (see below), is [8] really any different from eq. 1 of ref. 1, which can be used to describe the whole $1sns$ manifold of states, so it is actually useless for exploring $2sns$ states. What is interesting, however, if one chooses a wave function containing only powers of r_1^1, r_2^1, and $\cos^k\theta_{12}$, k only even up to very high powers of k, viz. eq. 6 $\sum(0,0,33)$ (or eq. 8 $\sum(1,1,34)$ which is the same function), the energy appears to converge variationally to the energy of the $2s^2\ ^1S$ state, for example with $N = 18$, $E = -0.771$ au compared with the observed value (3) of -0.777 au. Likewise, the 26-term wave function eq. 6 $\sum(0,1,31)$ (or $\sum(1,2,32)$ using eq. 8) gives $E = -0.59744$ au for the $2s3s\ ^3S$ state, compared with other theoretical estimates of around -0.6024 to -0.6026 au (15, 19). Convergence for these wave functions is exceedingly slow, as was found a long time ago for the $\cos\theta_{12}$ correlated treatment of the ground state of helium (20). This shows itself up in two ways. One is the extremely small improvement in energy as terms above $\cos^{30}\theta_{12}$ in [8] are added. The other is the extremely poor correspondence between the higher eigenvalues and the energies of other excited states; this despite the fact that each eigenvalue is obviously an approximation to an individual member of a Rydberg series in the sense that for the nth eigenvalue, the optimum value of b is close to $0.5/n$, for both singlet and triplet and up to $n = 25$.

Rydberg Series

These calculations, and the earlier ones for $1sns$ states (1), show that the non-relativistic Schrödinger equation for the helium atom yields an infinite series of solutions for $1sns$, $1snp$, $1snd$, $2sns$, and $2pnp$; on the other hand, it appears that only a very limited number of solutions exists for H^- (5, 8, 9, 15, 21, 22). Experimentally, relatively few $2pnp$ states of the helium atom are known, and comparison between the experimental and calculated energies has been made, where appropriate, in the foregoing two sections. However, many singly excited states of helium are known (3), and in the case of the $1sns$ states, a simple Rydberg formula provides a very accurate way of representing the energies of the states for large n (1). According to the Heisenberg treatment of highly excited states of helium-like atoms (23), the first-order energies can be written in the Rydberg form

$$[9] \qquad E + \frac{1}{2}Z^2 = -\frac{1}{2}\frac{(Z-1)^2}{(n+\delta_c \pm \delta_A)^2}\ \text{au}$$

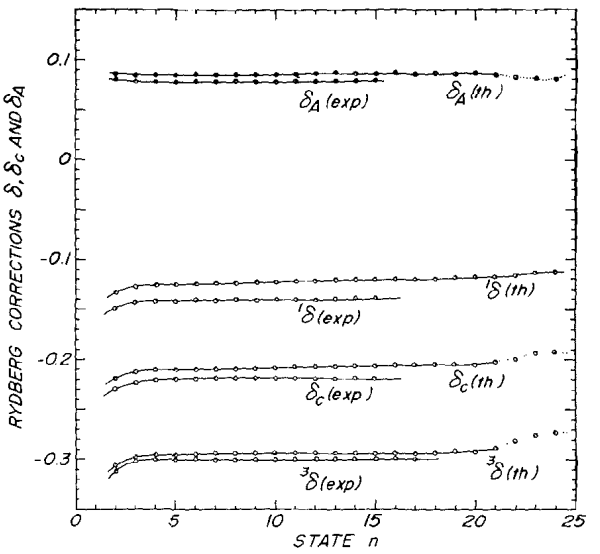

FIG. 1. Plots of the experimental and theoretical values of δ, δ_c, and δ_A for the singlet and triplet $1sns$ states of the helium atom. Note that $\delta_c = \frac{1}{2}(^1\delta + {}^3\delta)$, $\delta_A = \frac{1}{2}(^1\delta - {}^3\delta)$.

or

$$[9a] \qquad E + 2 \simeq \frac{-1}{2(n+\delta_c \pm \delta_A)} \equiv \frac{-1}{2(n+\delta)^2}$$

when $Z = 2$, and for the helium atom, 1 au = 219 444.53 cm^{-1}; δ_c and δ_A are respectively the coulomb and exchange parts of the Rydberg correction term, and $\delta = (\delta_c \pm \delta_A)$ for either singlet or triplet, i.e. $^1\delta$ or $^3\delta$. Figure 1 shows the experimental (3) and theoretical (1) $1sns$ data plotted in this form. Remembering that at $n = 20$, a change in δ of 0.01 corresponds to a change of energy of about 0.25 cm^{-1}, this plot shows that the calculations are properly converged up to $n = 20$, and that both the experimental ($4 \leq n \leq 15$) and theoretical ($4 \leq n \leq 20$) energies can be well represented by eq. 9.

In the $1snp$ case, the theoretical values of $^3\delta$ do not converge to constant values as n increases, but above $n \sim 12$–14, they appear to increase roughly linearly with n, corresponding to a spacing of the upper levels rather greater than predicted by any Rydberg formula; the theoretical values of $^1\delta$ do, however, appear to converge at large n. Figure 2 shows that the experimental results follow the same pattern, and that this curious behaviour does not arise from either the coulomb term or the exchange term alone: both δ_c and δ_A appear to depend on n, but at large n, this dependence cancels for the singlets and reinforces for the triplets.[2]

[2]We are currently investigating (17), along the lines worked out by Ludwig (24), the supposition that this n-dependence of δ_c and δ_A arises within the Heisenberg treatment (23) from neglected second order polarisation terms.

Can. J. Chem. Downloaded from www.nrcresearchpress.com by 210.87.254.42 on 09/05/12
For personal use only.

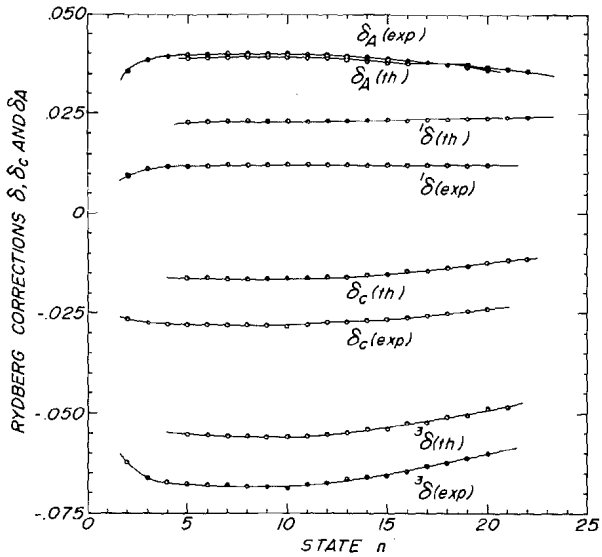

FIG. 2. Plots of the experimental and theoretical values of δ, δ_c, and δ_A for the singlet and triplet 1*snp* states of the helium atom.

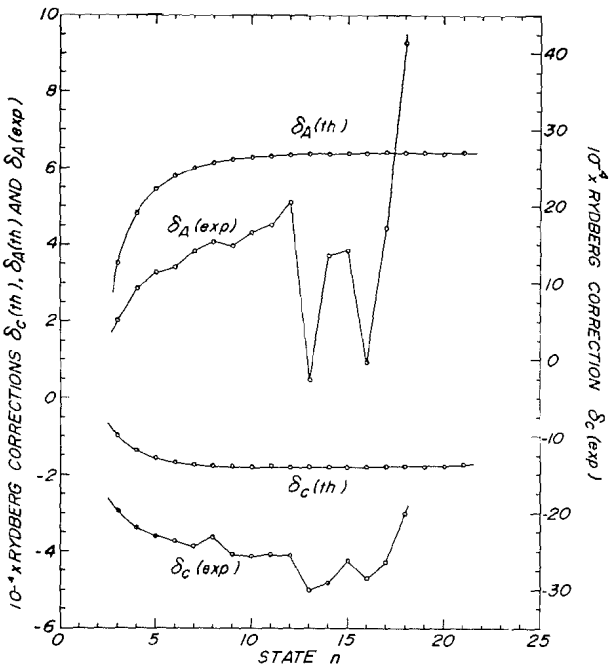

FIG. 3. Plots of the experimental and theoretical values of δ_c and δ_A for the singlet and triplet 1*snd* states of the helium atom; notice the shift of scale between the experimental and theoretical values of δ_c.

In the 1*snd* case, Fig. 3 shows that the theoretical values adhere very closely to the form of eq. 9, and also that the singlet–triplet splitting (δ_A) is much better represented than is the absolute value of the energy (δ_c). However, it is clear that there are significant irregularities in the experimental energies at $n = 8$, and from 13 onwards, although these plots

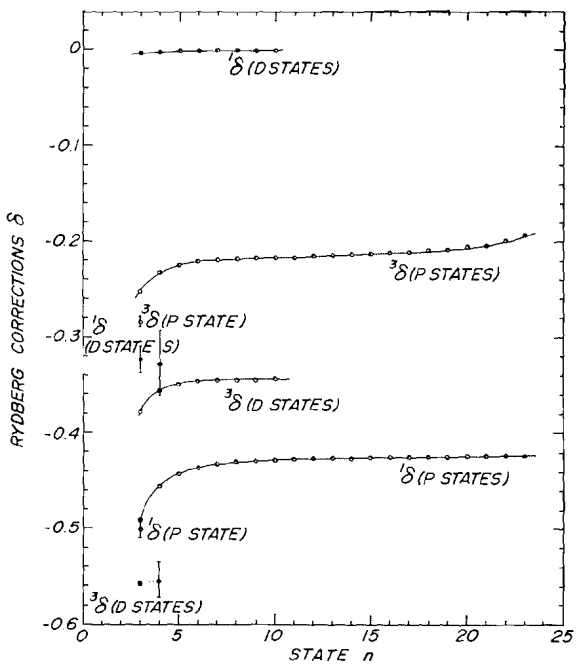

FIG. 4. Plots of the theoretical values of $^1\delta$ and $^3\delta$ for the *P* and *D* 2*pnp* states of the helium atom: experimental points are denoted by open circles with error bars. (For the *P* states, $\delta_A = \frac{1}{2}(^3\delta - {}^1\delta)$, whereas for the *D* states $\delta_A = \frac{1}{2}(^1\delta - {}^3\delta)$ as in Figs. 1–3; this arises because we have avoided the use of the *ortho-* and *para-* designations (23) for these states.)

are extremely sensitive indicators of such irregularities; for example, a change of δ_c of about 0.0002 at $n = 8$ corresponds only to a displacement of about 0.1 cm^{-1}.

Figure 4 shows Rydberg plots of the theoretical values of δ for the *P* and *D* states of 2*pnp*, from which the calculated energies can easily be reconstructed using an appropriately modified form of eq. 9, viz.

$$[9b] \quad E + 0.5 = \frac{-1}{2(n + \delta_c \pm \delta_A)^2} \equiv \frac{-1}{2(n+\delta)^2} \text{ au}$$

The agreement between theory and experiment for the *P* states is good, but for the *D* states, the agreement is less satisfactory.

Acknowledgement

This work was supported by the National Research Council of Canada.

1. M. KURIYAN and H. O. PRITCHARD. Can. J. Chem. **54**, 1543 (1976).
2. G. BREIT. Phys. Rev. **35**, 569 (1930); **36**, 383 (1930).
3. W. C. MARTIN. J. Phys. Chem. Ref. Data, **2**, 257 (1973).
4. Y. ACCAD, C. L. PEKERIS, and B. SCHIFF. Phys. Rev. A**4**, 516 (1971).
5. J. S. SIMS, S. A. HAGSTROM, and J. R. RUMBLE. Int. J. Quant. Chem. **10**, 853 (1976).
6. A. J. THAKKAR and V. H. SMITH. Phys. Rev. A**15**, 16 (1977).

7. P. S. C. WANG and F. WEINHOLD. J. Chem. Phys. **57**, 1738 (1972).
8. A. WALLIS, D. L. S. MCELWAIN, and H. O. PRITCHARD. J. Chem. Phys. **50**, 4543 (1969).
9. R. N. HILL. Phys. Rev. Lett. **38**, 643 (1977).
10. P. M. MORSE and H. FESCHBACH. Methods of theoretical physics. McGraw-Hill Book Co. Inc., New York. 1953. pp. 1719–1728.
11. G. W. F. DRAKE and A. DALGARNO. Phys. Rev. A**1**, 1325 (1970).
12. H. DOYLE, M. OPPENHEIMER, and G. W. F. DRAKE. Phys. Rev. A**5**, 26 (1972).
13. L. LIPSKY and A. RUSSEK. Phys. Rev. **142**, 59 (1966).
14. D. E. RAMAKER and D. M. SCHRADER. Phys. Rev. A**9**, 1980 (1974).
15. A. K. BHATIA, A. TEMKIN, and J. F. PERKINS. Phys. Rev. **153**, 177 (1967).
16. C. C. J. ROOTHAAN and A. W. WEISS. Rev. Mod. Phys. **33**, 194 (1960).
17. W.-T. MA. Ph.D Thesis, York University, Downsview. To be submitted.
18. F. W. BIRSS and P. SENN. J. Chem. Phys. **63**, 1276 (1975).
19. T. F. O'MALLEY and S. GELTMAN. Phys. Rev. **137**A, 1344 (1965).
20. P.-O. LÖWDIN. Adv. Chem. Phys. **2**, 207 (1959).
21. A. K. BHATIA and A. TEMKIN. Phys. Rev. **182**, 15 (1969).
22. A. K. BHATIA. Phys. Rev. A**2**, 1667 (1970); A**6**, 120 (1972).
23. H. A. BETHE and E. E. SALPETER. Quantum mechanics of one- and two-electron atoms. Academic Press, New York. 1957. p. 136.
24. G. LUDWIG. Helv. Phys. Acta, **7**, 273 (1934).
25. L. C. GREEN, E. K. KOLCHIN, and N. C. JOHNSON. Phys. Rev. **139**, A373 (1965).

Can. J. Chem. Downloaded from www.nrcresearchpress.com by 210.87.254.42 on 09/05/12
For personal use only.

Can. J. Chem. Downloaded from www.nrcresearchpress.com by 210.87.254.6 on 09/05/12
For personal use only.

Canadian Journal of Chemistry

Published by
THE NATIONAL RESEARCH COUNCIL OF CANADA

Journal canadien de chimie

Publié par
LE CONSEIL NATIONAL DE RECHERCHES DU CANADA

Volume 56 Number 7 April 1, 1978

Volume 56 numéro 7 1 avril 1978

The crystal and molecular structure of (4-diethylaminophenyl)diazenyltriphenylphosphonium tetrafluoroborate

FREDERICK W. B. EINSTEIN, DEREK SUTTON, AND PETER L. VOGEL

Department of Chemistry, Simon Fraser University, Burnaby, B.C., Canada V5A 1S6

Received September 29, 1977

FREDERICK W. B. EINSTEIN, DEREK SUTTON, and PETER L. VOGEL. Can. J. Chem. **56**, 891 (1978).

The title compound crystallizes in the space group $P2_1/c$ with four formula units in a cell of dimensions $a = 10.146(6)$ Å, $b = 10.593(4)$ Å, $c = 26.31(1)$ Å, $\beta = 103.14(3)°$. Using 1496 observed reflections ($I = 2.3\sigma(I)$) in the range $0° < 2\theta < 40°$ measured on a Picker FACS-1 automatic diffractometer with Mo-Kα radiation, the structure was solved (symbolic addition) and refined (full-matrix least-squares procedure) to $R = 0.062$ ($R_w = 0.058$), with all hydrogen atoms included and all non-hydrogen atoms having anisotropic thermal parameters. The dimensions within the cation are consistent with a delocalized electronic structure which is intermediate between valence formulations involving benzenoid or quinonoid structures for the (4-diethylaminophenyl)diazenyl residue. Some important bond lengths are N3—C22 1.336(7) Å, N2—C19 1.356(7) Å, N1—N2 1.308(6) Å, and P—N1 1.648(5) Å.

FREDERICK W. B. EINSTEIN, DEREK SUTTON et PETER L. VOGEL. Can. J. Chem. **56**, 891 (1978).

Le composé mentionné dans le titre cristallise dans le groupe d'espace $P2_1/c$ avec quatre formules stoechiométriques par maille dont les dimensions: $a = 10.146(6)$ Å, $b = 10.593(4)$ Å, $c = 26.31(1)$ Å, $\beta = 103.14(3)°$. Utilisant 1496 réflexions observées ($I = 2.3\sigma(I)$) à des angles de $0° < 2\theta < 40°$ mesurés à l'aide d'un diffractomètre automatique Picker FACS-1 avec la radiation Mo-Kα, on a résolu la structure (addition symbolique) et on l'a affinée par la méthode des moindres carrés (matrice complète) jusqu'à une valeur finale de $R = 0.062$ ($R_w = 0.058$) en incluant tous les atomes d'hydrogène et tous les atomes qui ne sont pas des hydrogènes possédant des paramètres thermiques anisotropiques. Les dimensions à l'intérieur du cation sont en accord avec une structure électronique délocalisée qui est intermédiaire entre les formulations de valence impliquant des structures benzénoïdes ou quinonoïdes pour le fragment (diméthylamino-4 phényle)diazényle. Parmi les longueurs de liaisons, les plus importantes sont N3—C22 1.336(7) Å, N2—C19 1.356(7) Å, N1—N2 1.308(6) Å et P—N1 1.648(5) Å.

[Traduit par le journal]

Introduction

The reaction of $[p\text{-}Et_2NC_6H_4N_2][BF_4]$ with triphenylphosphine yields bright red crystals of the title complex. Studies by Carroll *et al.* (1) have shown the structural formula $[p\text{-}Et_2NC_6H_4NNPPh_3][BF_4]$ to be consistent with the available spectroscopic evidence. However, the measured values of ν(N=N) and ν(P—N) in the ir and Raman spectra appear to indicate a considerable contribution of the valence-bond formalism **1***b* to the electronic structure of the cation.

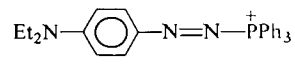

1*a*

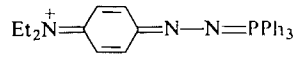

1*b*

The intense red colour of the compound, and its enhanced stability compared with those with substituents other than NEt_2 are probably a result of this delocalization. The purpose of this work was, therefore, to determine whether additional evidence for a delocalized electronic structure could be found in the molecular structure determined by X-ray diffraction.

Can. J. Chem. Downloaded from www.nrcresearchpress.com by 210.87.254.6 on 09/05/12
For personal use only.

Experimental

The deep-red needle shaped crystals of the title compound were elongated along the *b* axis. Photographic information indicated monoclinic Laue symmetry. Systematic absences $h0l$ ($l = 2n + 1$) and $0k0$ ($k = 2n + 1$) unambiguously indicated the space group $P2_1/c$. Cell dimensions were obtained from counter measurement and least-squares refinement of the setting angles of nine reflections with $2\theta > 28°$, using a Picker FACS-1 automatic four-circle diffractometer (λMo-Kα_1 = 0.70962 Å) and a brick-shaped crystal of dimensions 0.11 × 0.15 × 0.51 mm. Intensity measurements for 2576 reflections were recorded in two shells, $0° < 2\theta < 25°$, $25° < 2\theta < 40°$ with beam widths of 1.0° and 0.7° respectively. A total of 1496 reflections were considered observed at the significance level $I/\sigma(I) = 2.3$, where $\sigma(I)$ is the standard deviation derived from counting statistics. A θ–2θ scan technique was employed using Nb-filtered Mo-Kα radiation and a scan speed of 2°/min increased for dispersion. Background measurements of 4 s were taken at the scan limits. Two standard reflections were monitored periodically for the purpose of data scaling. Corrections for Lorentz and polarization effects were applied, but an absorption correction was not considered necessary (μ(Mo-Kα) = 1.57 cm^{-1}).

Symbolic addition techniques followed by a Fourier summation gave coordinates for 30 non-hydrogen atoms. Electron density difference maps interspersed with cycles of full-matrix least-squares refinement gave the positions for the remaining non-hydrogen atoms. With anisotropic temperature factors included for the phosphorus and fluorine atoms, a value of the discrepancy index $R = 0.11$ was obtained, where $R = \Sigma|(|F_o| - |F_c|)|/\Sigma|F_o|$. Including all the hydrogen atoms in calculated positions (with fixed temperature factors $U = 0.076$ Å^2) and with anisotropic thermal motion parameters for all non-hydrogen atoms, the discrepancy index dropped to 0.064. Two final cycles of anisotropic refinement, in which the coordinates of the six methyl hydrogens were also refined, gave a final R value of 0.062 ($R_w = 0.058$).[1]

Unobserved reflections were excluded from all stages of the least-squares refinement. For the initial refinement constant (unit) weights were used, but in the final cycles weights w were used (where $w = 1/\sigma(F_o)^2$). A final electron density difference map showed only two peaks greater than $3\sigma(\rho)$ ($\sigma(\rho)$ = 0.098 e Å^{-3}). These peaks were in the $[BF_4]^-$ region.

Scattering factors for the non-hydrogen atoms, including anomalous dispersion corrections to the phosphorus scattering, were those of Cromer and Waber (2). Hydrogen scattering factors were taken from ref. 3. Crystallographic computer programs used in this work have been cited elsewhere (4).

The crystal data are summarized in Table 1. Final atomic coordinates and thermal motion parameters are listed in Table 2, interatomic distances and angles are given in Table 3, and least-squares planes relevant to the discussion are given in Table 4. Standard deviations in all tables are in parentheses as units in the least significant figure. Tables 2*b* and 4 together with Table 5, a listing of structure factor amplitudes, have been deposited with the Depository of Unpublished Data.[2]

[1]The methyl hydrogen atoms were refined because their positioning was considered to be much more uncertain than that of all the other hydrogen atoms, whose positions could be calculated reliably.

[2]Copies of material on deposit may be obtained, at a nominal charge, from the Depository of Unpublished Data, CISTI, National Research Council of Canada, Ottawa, Ont., Canada K1A 0S2.

Results and Discussion

The structure is composed of $[p\text{-}Et_2NC_6H_4\text{-}NNPPh_3]^+$ cations and tetrafluoroborate anions occupying general positions in the space group $P2_1/c$. Before discussing the geometry of the complex cation (Fig. 1), we note some features which indicate the level of reliability of the dimensions in this determination. The average C—C distance in the triphenylphosphine moiety is 1.372 Å with the greatest and the least observed values deviating by 3–4 σ, at 1.400(8) Å and 1.342(10) Å; the average internal angle is 120.0° with the greatest and the least observed values again differing by 3–4 σ at 121.4(9)° and 117.1(7)°. The three angles subtended at the phosphorus atom by C(1), C(7), and C(13) agree closely and show a maximum deviation of only 1.1(3)° from the mean value of 109.3°. By contrast, the angle enclosed by N(1) and C(1) is only 105.1(3)° whilst the angles N(1)—P—C(7) and N(1)—P—C(13) are 111.4(3)° and 112.6(3)° respectively, and this inequality can be seen to be due to the orientation of the bent diazenyl function away from C(1) and toward C(7) and C(13).

The bond lengths and interbond angles within the C(19)···C(24) cycle follow the pattern which would be expected on the basis of a contribution from **1***b* to the electronic structure. Thus, bonds C(20)—C(21) and C(23)—C(24) are clearly short, at 1.342(8) and 1.351(8) Å compared with the remaining four bonds which range 1.413(8) to 1.429(8); and the angles at C(19) and C(22) are both smaller (117.9(6) and 118.9(6)) than the remainder. Note that whilst this pattern is chemically sensible, individual values are barely outside the extreme variation observed in individual values for the aromatic PPh_3 rings; however, the PPh_3 rings do not display any such systematic bond length or angle variation. It therefore seems that the pattern observed for the C(19)···C(24) ring is probably chemically significant. This view obtains good support from other observations,

TABLE 1. Crystal data for $[p\text{Et}_2NC_6H_4NNPPh_3][BF_4]$, $C_{28}H_{29}N_3F_4B$, fw = 525.0

Monoclinic, space group $P2_1/c$	
a	10.146(6) Å
b	10.593(4) Å
c	26.31(1) Å
β	103.14(3)°
V	2753.6 Å^3
ρ_o	1.29(2) g cm^{-3}
ρ_c	1.27 g cm^{-3}
Z	4
μ(Mo-Kα)	1.57 cm^{-1}
T	23 ± 2°C

Can. J. Chem. Downloaded from www.nrcresearchpress.com by 210.87.254.6 on 09/05/12
For personal use only.

TABLE 2. Fractional atomic coordinates and thermal motion parameters

(*a*) Non-hydrogen atoms: positional parameters and their esd's have been multiplied by 10^4

Atom	*x/a*	*y/b*	*z/c*
P	4574(2)	2117(2)	4283(1)
F(1)	7125(7)	2266(7)	2878(3)
F(2)	7773(10)	3961(6)	3264(3)
F(3)	8701(6)	3258(8)	2687(3)
F(4)	8895(8)	2352(7)	3447(3)
N(1)	3646(5)	1694(5)	4693(2)
N(2)	3388(5)	2657(5)	4967(2)
N(3)	1052(5)	1942(6)	6635(2)
C(1)	4666(6)	740(7)	3898(3)
C(2)	5048(8)	845(7)	3432(3)
C(3)	5082(9)	−196(9)	3131(3)
C(4)	4760(8)	−1357(8)	3299(3)
C(5)	4422(8)	−1482(7)	3769(4)
C(6)	4374(7)	−453(8)	4072(2)
C(7)	6226(7)	2596(6)	4619(3)
C(8)	7358(10)	2269(7)	4446(3)
C(9)	8617(10)	2682(9)	4694(4)
C(10)	8774(9)	3434(10)	5126(5)
C(11)	7682(13)	3770(9)	5302(3)
C(12)	6413(9)	3390(8)	5055(3)
C(13)	3820(8)	3384(6)	3858(2)
C(14)	4637(7)	4190(7)	3662(3)
C(15)	4042(11)	5112(7)	3311(3)
C(16)	2675(12)	5255(8)	3170(3)
C(17)	1868(8)	4423(9)	3365(3)
C(18)	2453(8)	3479(7)	3709(3)
C(19)	2707(8)	2430(7)	5345(3)
C(20)	2213(7)	1242(7)	5460(3)
C(21)	1664(7)	1074(6)	5873(3)
C(22)	1565(6)	2101(8)	6215(3)
C(23)	2035(7)	3312(6)	6094(3)
C(24)	2581(7)	3457(6)	5674(3)
C(25)	970(9)	2981(8)	7009(4)
C(26)	2282(13)	3202(10)	7394(4)
C(27)	599(9)	702(7)	679(3)
C(28)	−839(12)	471(11)	6499(4)
B(1)	8134(19)	3013(16)	3061(5)

(*c*) Hydrogen atoms; positional parameters and their esd's have been multiplied by 10^3; isotropic thermal factors, *U*, are fixed at 0.076 Å^2. Atoms are labelled with the number of the carbon atom to which they are bound

Atom	*x/a*	*y/b*	*z/c*
H(2)	529	165	332
H(3)	533	−12	281
H(4)	477	−208	309
H(5)	421	−229	388
H(6)	415	−55	440
H(8)	727	175	415
H(9)	939	245	457
H(10)	965	372	530
H(11)	779	428	561
H(12)	565	367	518
H(14)	559	412	377

TABLE 2 (*Concluded*)

Atom	*x/a*	*y/b*	*z/c*
H(15)	461	566	317
H(16)	229	592	294
H(17)	91	451	326
H(18)	186	290	384
H(20)	227	55	524
H(21)	134	26	594
H(23)	197	402	631
H(24)	288	427	560
1H(25)	71	375	681
2H(25)	28	277	720
1H(26)	319(6)	328(6)	722(2)
2H(26)	193(6)	389(5)	764(2)
3H(26)	252(7)	260(6)	762(3)
1H(27)	118	5	670
2H(27)	65	69	716
1H(28)	−111(7)	−36(6)	662(2)
2H(28)	−147(6)	80(6)	669(2)
3H(28)	−95(6)	40(5)	606(2)

which we now describe. The bonds N(3)—C(25) and N(3)—C(27) are equal and average 1.482(8) which agrees well with the expected N—C sp^3 single bond length of 1.479(5) (sp^3N) or 1.472(5) (sp^2N) (5), but the N(3)—C(22) bond is only 1.336(7) Å due to partial double bond character, as evidenced by the stereochemistry at N(3) which deviates only slightly

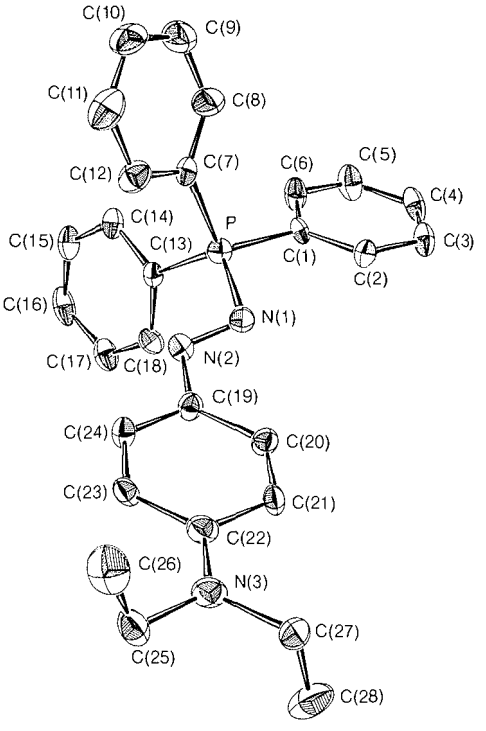

FIG. 1. A perspective view of the cation in [*p*-$Et_2NC_6H_4$-$NNPPh_3$][BF_4].

Can. J. Chem. Downloaded from www.nrcresearchpress.com by 210.87.254.6 on 09/05/12
For personal use only.

TABLE 3. Interatomic distances and angles

(*a*) Distances

Bond	Length (Å)	Bond	Length (Å)
P—N(1)	1.648(5)	N(1)—N(2)	1.308(6)
P—C(1)	1.789(6)	N(2)—C(19)	1.356(7)
P—C(7)	1.782(7)	C(19)—C(20)	1.413(8)
P—C(13)	1.801(6)	C(19)—C(24)	1.415(8)
C(1)—C(2)	1.374(8)	C(20)—C(21)	1.342(8)
C(1)—C(6)	1.399(8)	C(21)—C(22)	1.429(8)
C(2)—C(3)	1.362(9)	C(22)—C(23)	1.429(8)
C(3)—C(4)	1.371(9)	C(23)—C(24)	1.351(8)
C(4)—C(5)	1.362(9)	C(22)—N(3)	1.336(7)
C(5)—C(6)	1.358(8)	N(3)—C(25)	1.490(9)
C(7)—C(8)	1.373(8)	N(3)—C(27)	1.473(8)
C(7)—C(12)	1.400(8)	C(25)—C(26)	1.498(12)
C(8)—C(9)	1.368(10)	C(27)—C(28)	1.502(12)
C(9)—C(10)	1.367(11)	B—F(1)	1.297(12)
C(10)—C(11)	1.342(10)	B—F(2)	1.231(17)
C(11)—C(12)	1.365(10)	B—F(3)	1.273(13)
C(13)—C(14)	1.370(8)	B—F(4)	1.327(15)
C(13)—C(18)	1.384(8)		
C(14)—C(15)	1.386(9)		
C(15)—C(16)	1.360(10)		
C(16)—C(17)	1.379(10)		
C(17)—C(18)	1.381(9)		

(*b*) Angles in degrees

Bonds	Angle	Bonds	Angle
N(1)—P—C(1)	105.1(3)	P—C(1)—C(2)	120.1(6)
N(1)—P—C(7)	111.4(3)	P—C(1)—C(6)	120.6(6)
N(1)—P—C(13)	112.6(3)	C(2)—C(1)—C(6)	119.3(6)
C(1)—P—C(7)	110.4(3)	C(1)—C(2)—C(3)	120.2(7)
C(1)—P—C(13)	109.1(3)	C(2)—C(3)—C(4)	120.1(7)
C(7)—P—C(13)	108.4(3)	C(3)—C(4)—C(5)	120.4(7)
P—N(1)—N(2)	111.4(4)	C(4)—C(5)—C(6)	120.4(7)
N(1)—N(2)—C(19)	117.7(5)	C(5)—C(6)—C(1)	119.6(6)
N(2)—C(19)—C(20)	125.4(7)	P—C(7)—C(8)	121.8(6)
N(2)—C(19)—C(24)	116.4(7)	P—C(7)—C(12)	121.0(7)
C(20)—C(19)—C(24)	117.9(6)	C(8)—C(7)—C(12)	117.1(7)
C(19)—C(20)—C(21)	121.7(6)	C(7)—C(8)—C(9)	121.4(8)
C(20)—C(21)—C(22)	120.7(6)	C(8)—C(9)—C(10)	120.2(9)
C(21)—C(22)—C(23)	117.9(6)	C(9)—C(10)—C(11)	119.4(9)
C(21)—C(22)—N(3)	121.4(7)	C(10)—C(11)—C(12)	121.4(9)
C(23)—C(22)—N(3)	120.7(7)	C(11)—C(12)—C(7)	120.3(8)
C(22)—C(23)—C(24)	120.3(6)	P—C(13)—C(14)	119.3(6)
C(23)—C(24)—C(19)	121.5(6)	P—C(13)—C(18)	119.5(6)
C(22)—N(3)—C(25)	122.9(6)	C(14)—C(13)—C(18)	121.0(6)
C(22)—N(3)—C(27)	122.5(7)	C(13)—C(14)—C(15)	118.8(7)
C(25)—N(3)—C(27)	114.5(6)	C(14)—C(15)—C(16)	121.6(8)
N(3)—C(25)—C(26)	112.7(7)	C(18)—C(16)—C(17)	118.8(8)
N(3)—C(27)—C(28)	109.8(7)	C(16)—C(17)—C(18)	121.2(8)
		C(17)—C(18)—C(13)	118.6(7)
		F(1)—B—F(2)	112(2)
		F(1)—B—F(3)	107(1)
		F(1)—B—F(4)	104(1)
		F(2)—B—F(3)	114(1)
		F(2)—B—F(4)	106(1)
		F(3)—B—F(4)	114(2)

from planar (Table 4*f*). The bond N(2)—C(19) is similarly short (1.356(7)), whilst the N(1)—N(2) bond at 1.308(6) Å is longer than a typical double bond value for N=N (1.24 Å in PhN:NPh and HN:NH (6)). Values of N—N bond lengths in some aryldiazenido–metal complexes, ArNNM, having a *trans*-doubly-bent geometry similar to that observed here, are generally even smaller at 1.17–1.19 Å (7). This alternation of long and short bonds throughout the skeleton includes also the P—N(1) bond. The calculated Pauling covalent radii for P—N single and double bonds are respectively 1.78 Å and 1.64 Å (8). The value of 1.648(5) observed here is similar to the P=N distance of 1.641(2) in $Ph_2FP:NMe$ (9), but is longer than the value in $Ph_3P:NC_6H_4Br$ (1.567(7) Å) (10) or in cyclic phosphonitrilic compounds (11).

All features can be reconciled with a significant contribution from structure **1***b* to the electronic structure of the cation, so that the crystallographic results are in qualitative agreement with the earlier spectroscopic data (1).

Acknowledgement

This work was supported by the National Research Council of Canada through operating grants.

1. J. A. CARROLL, D. R. FISHER, G. W. RAYNER CANHAM, and D. SUTTON. Can. J. Chem. **52**, 1914 (1974).
2. D. T. CROMER and F. T. WABER. International tables for X-ray crystallography. Vol. IV. Kynoch Press, Birmingham, England. 1974.
3. R. F. STEWART, E. F. DAVIDSON, and W. T. SIMPSON. J. Chem. Phys. **42**, 3175 (1965).
4. F. W. B. EINSTEIN and R. D. G. JONES. Inorg. Chem. **11**, 395 (1972).
5. International tables for X-ray crystallography. Vol III. Kynoch Press, Birmingham, England. 1962. p. 276.
6. C. J. BROWN. Acta Crystallogr. **21**, 146 (1966); **21**, 153 (1966); G. C. HEMPSON and J. M. ROBERTSON. J. Chem. Soc. 409 (1941); A. TROMBETTI. Can. J. Phys. **46**, 1005 (1968).
7. R. E. COBBLEDICK, F. W. B. EINSTEIN, N. FARRELL, A. B. GILCHRIST, and D. SUTTON. J. Chem. Soc. Dalton, 373 (1977).
8. L. PAULING. The nature of the chemical bond. 3rd ed. Cornell University Press, Ithaca, NY. 1960.
9. G. W. ADAMSON and J. C. J. BART. J. Chem. Soc. A, 1452 (1970).
10. M. J. E. HEWLINS. J. Chem. Soc. B, 942 (1971).
11. A. W. SCHLUETER and R. A. JACOBSON. J. Chem. Soc. A, 2317 (1968).

Can. J. Chem. Downloaded from www.nrcresearchpress.com by 210.87.254.6 on 09/05/12
For personal use only.

Lignin and related compounds. V. The hydrogenolysis of aspen wood lignin using rhodium-on-charcoal as catalyst

JAMES M. PEPPER AND REGINALD W. FLEMING

Department of Chemistry and Chemical Engineering, University of Saskatchewan, Saskatoon, Sask., Canada S7N 0W0

Received September 6, 1977

JAMES M. PEPPER and REGINALD W. FLEMING. Can. J. Chem. **56**, 896 (1978).

The hydrogenolysis of aspen lignin using rhodium-on-charcoal as catalyst has been studied. The maximum yield of chloroform-soluble lignin degradation products was obtained at a reaction temperature of 195°C. Analysis of this chloroform-soluble fraction revealed that the monomeric fraction was composed essentially of the four compounds, **1–4**, only, and in a total yield representing at least 40% of the original lignin.

Solvent extraction was shown to be preferred over thermal distillation as a preparative procedure for the separation of these phenolic derivatives. The significance of the isolation of these lignin degradation products is discussed.

JAMES M. PEPPER et REGINALD W. FLEMING. Can. J. Chem. **56**, 896 (1978).

On a étudié l'hydrogénolyse de la lignine du tremble utilisant le rhodium sur charbon comme catalyseur. On obtient un rendement maximal de produits de dégradation solubles dans le chloroforme en opérant à une température de réaction de 195°C. L'analyse de cette portion soluble dans le chloroforme révèle que la fraction monomère est formée presqu'entièrement de quatre composés soit **1–4** le rendement global représente au moins 40% de la lignine originale.

On a montré que l'extraction par solvant est préférable à la distillation thermique comme méthode applicable pour la séparation de ces dérivés phénoliques. On a discute de la signification de l'isolement de ces produits de dégradation de la lignine.

[Traduit par le journal]

Introduction

In an earlier publication (1), rhodium-on-charcoal was shown to be an effective catalyst for the low pressure hydrogenolysis of spruce wood lignin. Under the conditions reported (dioxane–water (1:1) medium, initial pressure of hydrogen of 500 psi, 5 h at 195°C) all the lignin was degraded and converted into a chloroform-soluble material. By gas chromatographic analysis of the diethyl ether soluble fraction of this product, a significant amount of the original lignin was found as monomeric (phenylpropanoid) compounds. Of these, two compounds, **1** and **2**, were predominant: together equalling at least 20% of the original lignin.

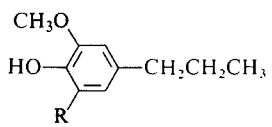

1 R = H
3 R = OCH_3

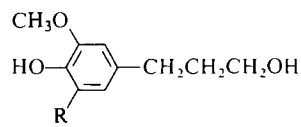

2 R = H
4 R = OCH_3

This paper reports the results of a similar catalytic hydrogenolysis of aspen wood lignin. Initially, experiments were made to determine the optimum temperature for the reaction, with the criteria to be considered being the weights of the chloroform-soluble fraction obtained from the extraction of the filtered hydrogenolysis mixture and the degree of diethyl ether solubility of this fraction. These data are given in Table 1. Since the Klason lignin content of the 10 g aspen wood meal sample was 1.88 g a reaction temperature of 195°C was chosen for subsequent studies. This same temperature had been shown earlier (2) to be preferable for the similar hydrogenolysis of aspen wood meal using Raney nickel as the catalyst.

Using a procedure of hydrogenolysis and extraction similar to that reported for spruce wood (1), a chloroform-soluble fraction was obtained. This was analyzed by gas chromatography. As expected from a hardwood the four monomeric compounds (**1–4**), were detected. The relative abundances of these lignin degradation products for two separate hydrogenolyses are given in Table 2.

TABLE 1. Effect of temperature on yields of hydrogenolysis products*

Temperature (°C)	Yield (g)	
	Chloroform-soluble	Ether-soluble
170	1.48	0.79
180	1.92	1.23
195	2.20	1.89
210	2.17	1.90
230	2.08	1.66

*Preextracted aspen wood meal (10 g), Rh–charcoal (1 g), dioxane–water (1:1, 150 ml) initial hydrogen pressure (500 psig), 5 h.

Can. J. Chem. Downloaded from www.nrcresearchpress.com by 210.87.254.6 on 09/05/12
For personal use only.

Can. J. Chem. Downloaded from www.nrcresearchpress.com by 210.87.254.6 on 09/05/12
For personal use only.

TABLE 2. Gas–liquid chromatographic analyses of aspen lignin hydrogenolysis products

Compound	Relative retention time	Abundance* Run A	Run B	Average
1	1	7.1	5.4	6.3
2	1.7	3.6	3.6	3.6
3	1.9	12.8	9.1	11.0
4	2.6	19.6	24.2	21.9
Total		43.1	42.3	42.8

*Reported as percentage of total chloroform-soluble fraction.

It was of interest to examine procedures for the separation of the combined monomeric compounds, **1** → **4**, from the remainder of the lignin material in the chloroform solution. Such a separation would be important as a preparative procedure for these phenolic lignin derivatives as well as a means of recovering the unknown lignin material for further chemical study. Solvent extraction and thermal distillation were studied.

Sequential extraction of the original organo-aqueous filtrate from a typical hydrogenolysis run was effected with two different combinations of solvents. For one set, A, the order was cyclohexane, benzene, diethyl ether (each by continuous liquid–liquid extraction), and chloroform (separatory funnel), whereas for the second set, B, the order was *n*-hexane, benzene, chloroform, and diethyl ether. The relative abundances of the extracted material are given in Table 3.

Gas chromatographic analysis of the cyclohexane (or *n*-hexane), benzene and diethylether extracts leads to three important observations: (*i*) all the monomeric compounds were removed by either combination of the initial two solvents; (*ii*) the aryl propanes (compounds **1** and **3**) were *selectively* removed by the cyclohexane or *n*-hexane whereas the propanols (compounds **3** and **4**) were extracted subsequently by benzene; and (*iii*) some other higher molecular weight lignin material was associated with the monomers.

TABLE 3. Solvent extraction of filtrate from hydrogenolysis of aspen wood*

Solvent system A	Extract (g)	Solvent system B	Extract (g)
Cyclohexane	0.93	*n*-Hexane	0.75
Benzene	0.80	Benzene	0.74
Diethyl ether	0.37	Chloroform	0.10
Chloroform	0.03	Diethyl ether	0.36
Total	2.13	Total	1.95

*Preextracted aspen wood meal (10 g) Klason lignin (1.88 g), 5% Rh-charcoal (1 g), dioxane–water (1:1, 150 ml), 5 h at 195°C.

Thermal distillation was also examined as a preparative method of separation of the monomeric degradation products. Distillation of the chloroform-soluble fraction up to a vapour temperature of 240°C/1.5 Torr, left none of compounds **1**–**4** in the residue but led to some unwanted degradation as evidenced by the production of low boiling products that were collected in the cold traps. Evidence that these more volatile compounds did not arise from the compounds **1**–**4**, was provided by an initial removal by low temperature distillation of these volatile materials, cleaning of the cold traps and continued distillation of the monomeric substances. No further low boiling products were obtained.

Rehydrogenolysis of the unidentified higher molecular weight lignin residues was examined. Both a residue resulting from a thermal distillation (vapour temperature > 160°C/1.5 Torr) and one remaining after removal of the diethyl-ether-soluble component of an initial chloroform-soluble hydrogenolysis product were studied. The conditions of the rehydrogenolysis were the same as those used initially for the wood meal, keeping the residue–catalyst ratio at 10:1.

The product from the distillation residue, which by gas chromatographic analysis was free of any of compounds **1**–**4** showed a trace of **1** only. Elemental analysis of the rehydrogenolysis product gave: C 66.6, H 6.9, a result which suggests retention of oxygen in the polymer other than that attached to the aromatic rings. A product from the ether-insoluble residue, also initially free of any of the monomeric compounds, **1**–**4**, and analyzing for C 63.9, H 7.2, was obtained which analyzed for C 63.8, H 7.8 and which on chromatographic analysis was shown to contain small amounts of the four monomeric compounds in essentially the same relative abundance as obtained in the original hydrogenolysis. It is apparent that solvent extraction is preferred over distillation as an initial method to separate the monomeric products. In the latter case, the evidence is that internal structural changes have occurred, probably including loss of water (supported by the elemental analysis) and leading to more complex structures which are resistant to further hydrogenolytic breakdown.

This research emphasizes the usefulness of the hydrogenolysis method of lignin degradation in studies involving both the classification and chemical structure of lignins. It is particularly adaptable to a relatively small-scale procedure. The data reported here, if compared with those previously published for the similar hydrogenolysis of spruce wood (1) clearly support the greater ease of liberation of lignin degradation products from hardwoods over softwoods. In

the present case, the combined total yield of the compounds **1–4** represents a significant recovery of over 40% of the original lignin in the aspen wood. Since a large percentage (ca. 60%) of these identified compounds are of the phenylpropanol type (**2** and **4**), it is evident that the γ-oxygen linkages are prevalent in the lignin and readily cleaved under the hydrogenolytic conditions. The ratio of approximately 3.3:1 for the combined syringyl-type compounds (**3** and **4**) to the combined guaiacyl-type compounds (**1** and **2**) is typical of the ratio of these nuclei obtained by other modes of lignin degradation (3).

An indication has been given of a potentially large source of phenolic chemicals of the type illustrated by compounds **1–4**. Their initial separation from the other lignin degradation products, as well as their subsequent separation into the substituted propanes (**1** and **3**) and the substituted propanols (**2** and **4**) has been shown to be possible by simple solvent extraction.

Experimental

Aspen sapwood (*Populus tremuloides*, Michx) was ground to ca. 20 mesh in a Wiley mill, extracted 48 h with ethanol–benzene (1:1), and air dried. Found: Klason lignin 18.8%, moisture 4.57%.

The catalyst, 5% rhodium-charcoal, was obtained from K & K Laboratories, Inc. The dioxane was purified according to Vogel (4). Copies of the gas chromatograms are available from the Depository of Unpublished Data.[1]

General Reaction Procedure

Aspen wood meal (10 g), 5% Rh–C (1 g) and dioxane–water (1:1) (150 ml) were mixed in a 1410 ml capacity bomb of an Aminco hydrogenator. The reactor was flushed twice with hydrogen and then filled to an initial pressure of 500 psig. The temperature was raised (about 120°C/h) and controlled automatically at 195 ± 5°C for 5 h. During the heating period the reactor was rocked continuously.

After cooling, the reactor contents were suction filtered. The residual pulp and catalyst were washed with dioxane–water (1:1). The washings and original filtrate were combined, transferred to a separatory funnel and extracted with chloroform (5 × 100 ml). The extract was dried over anhydrous sodium sulfate, filtered and the solvent removed under reduced pressure keeping the temperature below 40°C. The resulting yellow-brown oil was weighed as the chloroform-soluble fraction. The ether-soluble component of such a chloroform-soluble fraction was obtained by extraction under reflux with anhydrous ether (2 × 200 ml), removal of the ether and drying to constant weight in a vacuum desiccator.

Gas–Liquid Chromatographic Analyses

All analyses were conducted using an F & M Chromatograph, model 5750 with dual flame ionization detectors and temperature programming. The columns (6 ft × ⅛ in.) (purchased from Chromatographic Specialties, Brockville, Ont.) were packed with 10% SE-30 on Chromosorb W (100–120 mesh, AW-DMCS treated). All chromatograms were obtained under similar conditions of helium flow rate of 40 ml/min; temperature programmed from 100–270°C at 4°/min; injection temperature 260°C; detector temperature 280°C; and recorder chart speed 0.5 in./min. Identification of the compounds represented by the peaks was made by comparison of the retention times and mass spectra with those similarly obtained from authentic reference compounds (2).

The quantitative analytical data were obtained using the procedure reported earlier (1) but with 1,2,3-trimethoxybenzene as the internal standard.

[1]Photocopies may be obtained at a nominal charge, upon request, from the Depository of Unpublished Data, CISTI, National Research Council of Canada, Ottawa, Ont., Canada K1A 0S2.

Acknowledgements

For support of this work we thank the National Research Council of Canada for financial assistance and the Saskatchewan Research Council for the award (to R.W.F.) of two Government of Saskatchewan Graduate Research Scholarships.

1. J. M. Pepper and Y. W. Lee. Can. J. Chem. **47**, 723 (1969).
2. J. M. Pepper and W. Steck. Can. J. Chem. **41**, 2867 (1963).
3. K. V. Sarkanen and C. H. Ludwig. Lignins: Occurrence, formation, structure and reactions. Wiley-Interscience, New York, NY. 1971.
4. A. I. Vogel. A textbook of practical organic chemistry. Longmans, Green and Co., London. 1948.

Can. J. Chem. Downloaded from www.nrcresearchpress.com by 210.87.254.6 on 09/05/12
For personal use only.

Lignin and related compounds. VI. A study of variables affecting the hydrogenolysis of spruce wood lignin using a rhodium-on-charcoal catalyst

JAMES M. PEPPER AND PUNSRI SUPATHNA

Department of Chemistry and Chemical Engineering, University of Saskatchewan, Saskatoon, Sask., Canada S7N 0W0

Received September 6, 1977

JAMES M. PEPPER and PUNSRI SUPATHNA. Can. J. Chem. **56**, 899 (1978).

The effect of reaction conditions on the hydrogenolysis of spruce wood lignin over a rhodium-on-charcoal catalyst has been studied and monitored by the yields of the three major degradation products, **1**, **2**, and **5**. Variables included: initial pressure of hydrogen, amount of catalyst, and acidity–basicity of the media. Little variation occurred under moderate acidic or basic conditions with yields of 18–20% of lignin recovered as monomers. Under strongly acidic or basic conditions both yields and relative abundances changed appreciably. Initial hydrogen pressures less than 500 psig resulted in slightly decreased yields in some cases. In strongly alkaline media similar results were obtained with or without added hydrogen provided the catalyst were present.

JAMES M. PEPPER et PUNSRI SUPATHNA. Can. J. Chem. **56**, 899 (1978).

On a étudié l'effet des conditions de la réaction sur l'hydrogénolyse de la lignine de bois d'épinette effectuée en présence d'un catalyseur de rhodium sur charbon et on a évalué ces effets par les rendements des trois produits principaux de dégradation soit **1**, **2** et **5**. Les variables comprennent: la pression initiale d'hydrogène, la quantité de catalyseur et l'acidité–basicité du milieu. Il se produit peu de variations dans des conditions acides ou basiques modérées et l'on récupère 18–20% de la lignine sous forme de monomères. Lorsque des conditions fortement acides ou basiques sont utilisées, les rendements ainsi que les quantités relatives de produits changent d'une façon appréciable. A des pressions initiales d'hydrogène de moins que 500 psig, il se produit, dans quelques cas, une légère diminution des rendements. Lorsque le catalyseur est présent dans un milieu fortement alcalin, on obtient des résultats semblables avec ou sans addition d'hydrogène.

[Traduit par le journal]

Introduction

Previous work in these laboratories has shown that rhodium-on-charcoal is an effective catalyst for the hydrogenolysis of both softwoods (spruce; ref. 1) and hardwoods (aspen; ref. 2) since by such a technique essentially all the lignin may be extracted from the wood as a chloroform-soluble fraction. Furthermore the lignin has been largely degraded into smaller fragments of which a significant percentage has been identified as being of the phenylpropanoid type as illustrated by compounds **1**–**4**.

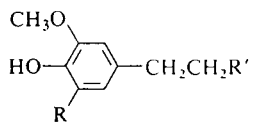

1	R = H, R' = CH_3	**2**	R = H, R' = CH_2OH
3	R = OCH_3, R' = CH_3	**4**	R = OCH_3, R' = CH_2OH
5	R = R' = H	**6**	R = H, R' = OH
7	R = OCH_3, R' = H	**8**	R = OCH_3, R' = OH

From spruce wood, compounds **1** and **2** have been shown to represent together at least 20% and from aspen wood, compounds **1**–**4** represent at least 40% of the original lignin material. The significance of these observations with respect to the protolignin structure and with respect to the potential source of such phenolic chemicals has been discussed (1, 2). The reaction conditions used in these studies were those that had been adopted for similar earlier studies on the hydrogenolysis of aspen but using Raney nickel as the catalyst (3). Although apparently effective if applied to the use of rhodium-on-charcoal, it could not be assumed that such conditions were optimal for production of either the lignin monomeric derivatives (**1**–**4**) or of degradation products of different structure. Of particular interest were the effects of the amount of catalyst and of the initial hydrogen pressure should the process be studied at some later date for possible commercialization; and the effect of the initial 'pH'[1] of the solvent medium.

Several workers had earlier reported (4–7) that the initial 'pH' had a marked effect on the nature of the lignin hydrogenolysis products. In studies involving both spruce and aspen wood (4), using both Raney nickel and palladium-on-charcoal, it was found that the major products using initially neutral conditions were the phenylpropanol derivatives (**2** and **4**). If initially the medium were to be made acidic, the yield of the phenylpropane derivatives increased at

[1]'pH' is used to refer to the reading indicated by a pH meter used to monitor the acidity of the initial dioxane–water (1:1) medium.

Can. J. Chem. Downloaded from www.nrcresearchpress.com by 210.87.254.42 on 09/05/12
For personal use only.

Can. J. Chem. Downloaded from www.nrcresearchpress.com by 210.87.254.42 on 09/05/12
For personal use only.

the expense of the phenylpropanol compounds, and if initially the medium were to be made alkaline, the corresponding phenylethane or phenylethanol type products were predominant. Several other workers (5–7) had noted that under initially alkaline conditions, the catalytic hydrogenolysis of lignin gave rise to essentially phenylethanoid rather than phenylpropanoid fragments.

This paper reports the results of a study of the effect of changing the various conditions of the hydrogenolysis of spruce wood using rhodium-on-charcoal as the catalyst. The hydrogenolyses and subsequent isolation and identification of products were carried out by the procedure reported earlier (1) using 10 g of preextracted woodmeal, the variations being in the deliberate change of one of the reaction conditions at a time. The effect of these changes was monitored by a quantitative gas chromatographic determination of the major monomeric products (**1**, **2**, **5**, **6**) that were produced.

Discussion of Results

The choice of an initial hydrogen pressure of 500 psig had been based on earlier studies (8) but in which Raney nickel was used as a catalyst and the effectiveness of the procedure determined solely by the extent of chloroform solubility of the released lignin products. With the different catalyst (Rh–C) and improved monitoring procedures it was of interest to determine again the effect of initial hydrogen pressure. For runs using an initial hydrogen pressure of 500, 100, 50, and 0 psig, the corresponding yields of 4-*n*-propylguaiacol (**1**) were 8.8, 9.0, 9.2, and 0% and of dihydroconiferyl alcohol (**2**) were 10.2, 8.0, 5.6, and 0%, based on original Klason lignin. These results suggest that the liberation of **1** and **2** involves different types of structures and hence arise from different parts of the original lignin. Support for the hydrogenolyses aspect of the degradation reaction was given by the result of two runs made using nitrogen at 500 psig initial pressure to replace the hydrogen. Under these conditions, both with and without catalyst, no monomeric products were obtained.

The effect of the amount of catalyst was studied as shown in Table 1. Although the yield of the more structurally significant dihydroconiferyl alcohol (**2**) increased with increasing catalyst to woodmeal ratios, the total yield of the monomeric products passed through a maximum following which degradation began to occur as evidenced by the increased yield of (**5**) with a concurrent decrease in **1**. With more than 1 g of catalyst, traces of cyclohexyl derivatives were noted. As the amount of catalyst increases so does the yield of monomeric products even though, at the same time, the yield of the chloroform-soluble fraction decreases. This would clearly indicate that the liberation of the lignin from an original lignin–carbohydrate complex is facilitated by the increase in the catalyst. The choice of 1 g of catalyst (Rh–C) per 10 grams of wood meal was considered optimal and used subsequently.

It was of interest to determine if the initial addition of acid had a similar effect on the nature of the lignin monomeric products, when the rhodium-on-charcoal was used instead of Raney nickel (4). Also under such acidic conditions the effect of change in the initial pressure of hydrogen was studied. These data are recorded in Table 2.

Since lignins are believed to contain no appreciable amount of terminal methyl groups (9) the 4-*n*-propylguaiacol (**1**) obtained in all hydrogenation experiments arises most likely by a propanol–propane conversion. This is strongly supported by the results obtained under acidic conditions, for which the initial acid-catalyzed dehydration of the propanol could be followed by reduction of the resulting propene and thus leading to high relative yields of the phenylpropane (**1**). It is, however, less easy to understand the constancy of the yields of **1** since those of **2** decrease with lower initial pressure. An alternate route to the direct formation of **1** could be the reductive cleavage of γ-ether bonds. As in the case of using initially neutral conditions, hydrogen was required to promote the degradation process.

Since earlier studies using Raney nickel had established that hydrogenolysis under initially alkaline conditions had led to predominantly phenylethanoid fragments (compounds **5**–**8**) it was of interest to examine the effect of rhodium-on-charcoal under similar conditions. The standard procedure was followed except that 4.5 g NaOH were added initially and the cooled bomb contents were acidified with dilute HCl before extraction with chloroform. The results are given in Table 3.

The total yield of phenylpropanoid and ethanoid lignin fragments is markedly less than under initially neutral or acidic conditions and is coupled with extensive loss of side-chain carbon to produce mainly the phenylethanoid type products. There is evidence for the ready loss under alkaline conditions of the hydroxymethyl group from a propanol side chain bearing a β-arylether linkage (10).

In marked contrast to the other conditions, in this case the lack of hydrogen had surprisingly no effect on the yields and nature of the products. However, a similar reaction carried out with *no* initial hydrogen and *no* catalyst produced only a typical alkali lignin and no monomeric degradation products. It is apparent that the catalyst plus alkali is responsible

TABLE 1. Effect of amount of catalyst (Rh–C) on hydrogenolysis of spruce lignin ('neutral' conditions)

Catalyst (g)	$CHCl_3$-soluble fraction (g)	Yield*		
		4-Ethylguaiacol (**5**)	4-*n*-Propyl-guaiacol (**1**)	Dihydroconiferyl alcohol (**2**)
0.1	3.3	Trace	7.0	5.0
0.5	2.5	Trace	6.6	8.8
1.0	2.3	<1.0	8.8	10.2
2.0	2.4	1.6	7.6	11.4
3.0	1.8	1.7	3.6	12.0

*Reported as percentage of original Klason lignin.

TABLE 2. Effect of initial hydrogen pressure on hydrogenolysis of spruce lignin (acidic conditions*)

Initial pressure (psig)	$CHCl_3$-soluble fraction (g)	Yield†		
		4-Ethylguaiacol (**5**)	4-*n*-Propyl-guaiacol (**1**)	Dihydroconiferyl alcohol (**2**)
500	2.6	Trace	12.3	5.3
250	2.7	Trace	13.1	3.1
100	2.6	Trace	13.1	2.2
50	3.0	Trace	13.4	Trace
0	2.6	0	0	0

*HCl (10.3 ml 2 *N*) added initially to the dioxane–water solution.
†Reported as percentage of original Klason lignin.

TABLE 3. Effect of initial hydrogen pressure on hydrogenolysis of spruce lignin (alkaline conditions*)

Initial pressure (psig)	$CHCl_3$-soluble fraction (g)	Yield†		
		4-Ethyl-guaiacol (**5**)	4-*n*-Propyl-guaiacol (**1**)	Dihydroconiferyl alcohol (**2**)
500	2.0	4.8	<1	1.8
50	2.0	5.7	<1	1.1
0	2.0	5.8	<1	1.0

*NaOH (4.5 g) added initially to the dioxane–water solution.
†Reported as percentage of original Klason lignin.

for bond cleavage and subsequent stabilization of the lignin fragments and a further study of this observation may be of importance in the utilization of alkali pulping liquors as a source of chemicals.

These experiments clearly indicated that major changes in the nature of the products of hydrogenolysis occurred as the reaction medium varied from strongly acidic through neutral to strongly alkaline. It was therefore of interest to study these changes as the 'p*H*' was varied by controlled steps from one extreme to the other and to determine if there were definitive 'p*H*' values at which significant changes occurred. The results are given in Table 4.

The markedly reduced total yield of monomeric products obtained under the very low initial 'p*H*' was unexpected. Assuming acid catalysis facilitates lignin–carbohydrate cleavage, it may be that the released lignin either further condenses to a form that resists subsequent hydrogenolysis to monomeric units or if the smaller units are formed they in turn undergo secondary, possibly polymerization, reactions. Of more interest is the recognition that maximum yields (18–20% of original Klason lignin) of the identified monomeric lignin products results over a broad initial 'p*H*' range (ca. 3–10), with little variation in the relative abundance of the propane and propanol derivatives. An earlier conclusion that the propane derivatives may result directly from an initial dehydration of the propanol derivatives followed by hydrogenation must now be questioned since it is unlikely that such a reaction would occur under alkaline conditions. Further work using model compounds is required to permit a better understanding of the structural features of lignin that would lead to these observations.

The approximately 20% of the original lignin of sprucewood that may be recovered as monomeric phenolic compounds using rhodium-on-charcoal as a catalyst is essentially the same, in yields and in chemical structure, as that obtained using Raney

Can. J. Chem. Downloaded from www.nrcresearchpress.com by 210.87.254.42 on 09/05/12
For personal use only.

TABLE 4. Effect of 'pH' on the hydrogenolysis of spruce wood meal*†

Initial 'pH'	Chloroform-soluble fraction (g)	Yield‡ 4-Ethyl-guaiacol	Yield‡ 4-*n*-Propyl-guaiacol	Yield‡ Dihydro-coniferyl alcohol	Yield‡ Total
0.1	2.2	Trace	5.8	2.4	8.2
1.1	2.7	Trace	11.4	6.6	18.0
3.1	2.7	Trace	8.6	10.4	19.0
5.6	2.3	<1	8.5	10.0	18.5
7.2	2.3	<1	8.8	10.2	19.0
10.8	2.6	<1	8.4	11.7	20.1
11.3	1.8	1.0	3.8	10.5	15.3
11.7	1.8	1.7	1.0	6.0	8.7
12.7	1.8	3.4	<1	3.3	6.7
3% NaOH§	2.4	4.7	<1	1.8	6.5

*Addition of hydrochloric acid or sodium hydroxide to produce the 'pH' recorded.
†Results are the averages of duplicate runs.
‡Reported as percentage of original Klason lignin.
§Two layers resulted and no 'pH' measurement was possible.

nickel (4). Added support is thus provided for the belief that only a certain portion of the protolignin is amenable to such hydrogenolysis breakdown to monomeric units and that the remainder is bonded by other linkages (e.g. carbon–carbon) which are resistant to such treatment. Two observations that may have significance with respect to an interest in large scale production of these lignin chemicals are the need for only a relatively low initial hydrogen pressure in initially acidic or neutral conditions and no added hydrogen under strongly alkaline conditions. Indeed the role of the rhodium which is required for the production of monomeric products in this latter case is of interest but as yet not understood.

Experimental[2]

White spruce sapwood (*Picea glauca* Moench (voss)) was ground to ca. 20 mesh in a Wiley mill, extracted 48 h with ethanol–benzene (1:1) and air dried. Found: Klason lignin, 27.3%; moisture, 2.18%. The catalyst, 5% rhodium-on-charcoal, was obtained from K and K Laboratories, Inc. The dioxane was purified according to Vogel (11). The change in initial conditions of 'pH' was effected by the addition of suitable quantities of hydrochloric acid or sodium hydroxide. Copies of the gas chromatograms are available from the Depository of Unpublished Data.[3]

General Reaction Procedure

The procedure was similar to that reported in a previous communication (2). Ten gram samples of spruce wood meal were used and the amounts of catalyst, hydrochloric acid and sodium hydroxide that were added were as designated in Discussion of Results.

Gas–Liquid Chromatographic Analyses

All analyses were conducted using an F & M Chromatograph, Model 5750 with dual flame ionization detectors and temperature programming. The details of the analyses were identical to those reported earlier (2) with the exception that coumarin was used as the initial standard as reported in (1).

Acknowledgements

We are indebted to the National Research Council of Canada and the Canadian Forestry Service for support of this research.

1. J. M. PEPPER and Y. W. LEE. Can. J. Chem. **47**, 723 (1969).
2. J. M. PEPPER and R. W. FLEMING. Can. J. Chem. This issue.
3. J. M. PEPPER and W. STECK. Can. J. Chem. **41**, 2867 (1963).
4. J. M. PEPPER, W. F. STECK, R. SWOBODA, and J. C. KARAPALLY. Adv. Chem. Ser. **59**, 205 (1966).
5. H. HIBBERT and J. M. PEPPER. J. Am. Chem. Soc. **70**, 67 (1948).
6. J. M. PEPPER, C. BROUNSTEIN, and D. SHEARER. J. Am. Chem. Soc. **73**, 3316 (1951).
7. C. SCHUERCH, H. ARLT, and S. GROSS. Tappi, **41** (2), 64 (1958).
8. J. M. PEPPER and D. C. HAGERMAN. Can. J. Chem. **32**, 614 (1954).
9. E. ADLER, J. M. PEPPER, and E. ERIKSOO. Ind. Eng. Chem. **49**, 1391 (1957).
10. J. GIERER and I. NOREN. Acta Chem. Scand. **16**, 1713 (1962).
11. A. I. VOGEL. A textbook of practical organic chemistry. Longmans, Green and Co., London. 1948.

[2]The authors wish to draw attention to the following. The particular reactor used in this study and all preceding studies reported from these laboratories, was one of chrome-steel construction. More recently, it has been found using a stainless steel bomb (Parr Series 4560 Pressure Reactor, 2000 ml capacity) that in attempting to duplicate the experiments reported herein significantly different results were obtained. In particular, although the same compounds were obtained, the relative abundance was different with the major change being that of an increased yield of *n*-propylguaiacol (**1**) and a concurrent decreased yield of dihydroconiferyl alcohol (**2**). A similar result was noted if the chrome-steel reactor was used but the reactants contained in a glass liner. It is apparent that the reaction is sensitive to the catalytic environment and close attention must be given to this fact in future studies.

[3]Photocopies may be obtained, at a nominal charge, upon request, from the Depository of Unpublished Data, CISTI, National Research Council of Canada, Ottawa, Ont., Canada K1A 0S2.

Can. J. Chem. Downloaded from www.nrcresearchpress.com by 210.87.254.42 on 09/05/12
For personal use only.

The photochemistry of benzylic sulfonyl compounds: The preparation of sulfones and sulfinic acids

R. F. LANGLER,[1] Z. A. MARINI, AND J. A. PINCOCK[1]

Department of Chemistry, Dalhousie University, Halifax, N.S., Canada B3H 4J3

Received October 17, 1977

R. F. LANGLER, Z. A. MARINI, and J. A. PINCOCK. Can. J. Chem. **56**, 903 (1978).

The photolysis of benzylic sulfonyl compounds (XSO_2CH_2Ph) gives products which are explained in terms of the chemistry of the benzyl and sulfonyl ($XSO_2^{\cdot}$) radicals. The synthetic applications of this photocleavage have been examined for two general cases: (*i*) preparation of sulfones from disulfone precursors, $R_1SO_2CHR_2SO_2CH_2Ph$ to $R_1SO_2CH_2R_2$ (yields ~ 90%); (*ii*) preparation of sulfinic acids and sulfonyl chlorides from mono sulfone precursors, $R_3SO_2CH_2Ph$ to R_3SO_2H and R_3SO_2Cl (yields ~ 55%).

R. F. LANGLER, Z. A. MARINI et J. A. PINCOCK. Can. J. Chem. **56**, 903 (1978).

La photolyse de composés sulfonyles benzyliques (XSO_2CH_2Ph) conduit à des produits qui peuvent être expliqués en termes de la chimie des radicaux benzyles et sulfonyles ($XSO_2^{\cdot}$). On a étudié la possibilité d'appliquer ce photoclivage en synthèse dans deux cas généraux: (*i*) pour la préparation de sulfones à partir de précurseurs disulfones, $R_1SO_2CHR_2SO_2CH_2Ph$ vers $R_1SO_2CH_2R_2$ (rendement ~90%); (*ii*) pour la préparation d'acides sulfiniques et de chlorures de sulfonyles à partir de précurseurs monosulfones $R_3SO_2CH_2Ph$ vers R_3SO_2H et R_3SO_2Cl (rendements ~55%).

[Traduit par le journal]

Can. J. Chem. Downloaded from www.nrcresearchpress.com by 210.87.254.105 on 09/05/12
For personal use only.

The photochemistry of sulfones has received only limited attention as indicated by the fact that only a few papers are discussed in recent reviews (1, 2). However, benzyl sulfones have been shown to be photoreactive in a variety of systems (1, 3, 4 and refs. therein) and give products which are explained in terms of the chemistry of benzyl and sulfonyl radicals. We wish to report here, results that demonstrate that this is a general phenomenon and that the benzyl sulfonyl group is a synthetically useful, photochemically labile structural unit.

Results and Discussion

Our preliminary experiments were with the benzylic sulfone **1**, in the hope that the excited state would show similar behaviour to that of the radical cation in the mass spectrometer: Ramberg-Bäcklund rearrangement initiated by H abstraction from the benzylic carbon by the phenyl substituted sulfonyl group (5). This would have been analogous to the well-known photochemical Norrish type II reactivity in carbonyl compounds (6). Instead, photolysis of 1.0 g of **1** in 300 ml of methanol for 4 h using a 200 W medium pressure Hanovia mercury lamp gave clean conversion to phenyl methyl sulfone (94%) and 1,2-diphenylethane (36%), eq. 1. By the odour of the reaction mixture, sulfur dioxide was also formed. That no unexpected rearrangements were occurring was confirmed by photolysis in a quartz nmr tube of the deuterated sulfone, **1***a* in 10% CD_3OD–CD_3CN. The methyl group of phenyl methyl sulfone was only derived from the methylene carbon between the two sulfonyl groups. Moreover, nmr analysis of the photolysis mixture without removal of solvent indicated a yield of 1,2-diphenylethane greater than 90%. The lower yield in methanol is a result of the formation of toluene (glc analysis) which is lost because of its volatility during work-up.

[1] $PhCH_2SO_2CX_2SO_2Ph$

1 X = H
1*a* X = D

$$\xrightarrow[MeOH]{h\nu} HX_2CSO_2Ph + PhCH_2CH_2Ph + SO_2$$

The seemingly simple photoreactivity of the disulfone **1** could be explained by several routes as outlined in Scheme 1. Path *a* would be analogous to the well-known β-cleavage that occurs for ketones with substituents on the α-carbon: $R-\overset{\overset{O}{\|}}{C}-CH_2-X$ and $PhSO_2CH_2-SO_2CH_2Ph$ (6). However, results for the photolysis of other sulfone substrates suggest that this is not the case. First, de Mayo and co-workers (7) have examined a related ketone sulfone, where the products obtained are explained in terms of β-cleavage (eq. 5). The benzyl sulfonyl radical ($PhCH_2SO_2^{\cdot}$) formed then partitions between H abstraction from the solvent methanol to form the sulfinic acid and loss of sulfur dioxide to form the benzyl radical and therefore 1,2-diphenylethane. Since we observe no sulfinic acid formation in methanol for photolysis of the disulfone **1**, the benzyl sulfonyl radical is not formed. Second, photolysis of the sulfone sulfide, $PhSO_2CH_2-SCH_2Ph$, gave no

[1]To whom correspondence can be addressed.

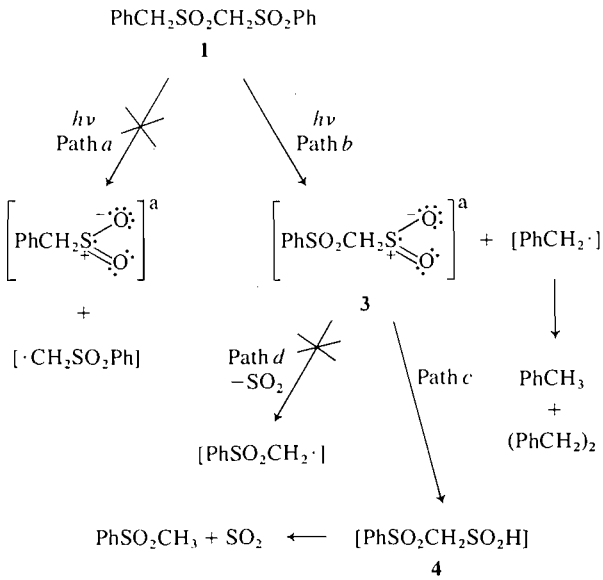

SCHEME 1. Mechanism of the photoreactivity of disulfone **1**.[2]

reaction. Third, photolysis of the disulfone, CH_3SO_2-CH_2—SO_2CH_2Ph (**2**), again gave clean conversion to dimethyl sulfone (91%) and 1,2-diphenylethane,

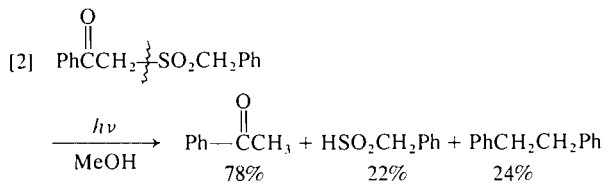

Scheme 2. Unlike the cases in carbonyl photochemistry, simple alkyl sulfones do not absorb under the conditions of these experiments. Therefore, the only chromophore in **2** is the benzene ring of the benzylic sulfone and the photochemistry is the same as that of **1**. Finally, as discussed below, simple benzylic sulfones give products which are only possible by cleavage of the sulfur to benzylic carbon bond. The photolysis of these disulfones must then be occurring from the excited state by path *b* in Scheme 1.

The fate of radical, $PhSO_2CH_2SO_2$·, **3**, can be inferred from the known chemistry of sulfonyl radicals (8). The activation enthalpy for loss of sulfur dioxide from CH_3SO_2· has been estimated to be about 23 kcal/mol (9). Therefore, **3** should have only a short lifetime if the loss of sulfur dioxide is favoured by the sulfone substituent. Note that this substituent effect would have to be very large since even $PhCH_2SO_2$· is apparently long enough lived to react with methanol (eq. 2) although the barrier to loss of sulfur dioxide is estimated to be 12 kcal/mol (9). This can not be the case since results on free radical chlorination of substituted alkanes demonstrate that sulfonyl groups destabilize adjacent radicals, presumably by an electron-withdrawing inductive effect (10). Therefore, the loss of sulfur dioxide from **3**, $PhSO_2CH_2$-SO_2·, to give $PhSO_2CH_2$· must have a barrier greater than 23 kcal/mol and path *c* in Scheme 1 must be preferred to path *d*. The resulting acid **4** is then desulfonylated by the usual ionic mechanism observed for other sulfinic acids with anion stabilizing substituents on carbon 1 (11).

Independent of the mechanism for the photochemistry of these disulfones, the process provides a good method for general sulfone synthesis as outlined in Scheme 2. This route relies on the fact that benzylic disulfones are readily available by reaction of thiols with α-chlorosulfones followed by oxidation (14). The methylene carbon of the disulfone is now activated for proton removal and then reaction with electrophiles. The benzylic sulfonyl group can then be removed under conditions which are mild, neutral and specific. Suitable choice of R_1 and the electrophile determines the resulting sulfone and, as shown in Scheme 2, the yields for the photolyses are, in general, excellent. This method would have particular advantages for the preparation of sulfones where one of the substituents is sensitive to oxidizing agents, since the introduction of R_2 completes the assembly of the sulfone skeleton. We also note that the sequence is reminiscent of the acetoacetic ester synthesis of ketones in carbon chemistry.

According to the mechanism advanced in Scheme 2 photolysis of benzylic sulfones in methanol permits the formation and isolation of sulfinic acids in cases

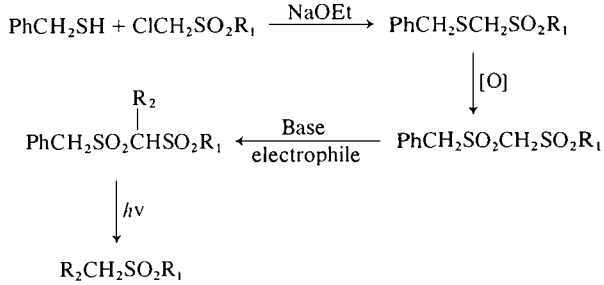

	R_1	R_2	Yield (%)
1	Ph	H	94
2	Me	H	91
5	Me	Me	70
6	Me	$PhCH_2$	97
7	Me	$CH_2CH_2CO_2Me$	94

SCHEME 2. Photochemical cleavage of benzylic sulfones as a general synthesis of sulfones.

[2]The radical site in sulfonyl radicals appears to be mainly centered on sulfur as indicated by the esr study of Waters *et al.* (12) and our own MO calculations (13).

Can. J. Chem. Downloaded from www.nrcresearchpress.com by 210.87.254.105 on 09/05/12
For personal use only.

Can. J. Chem. Downloaded from www.nrcresearchpress.com by 210.87.254.105 on 09/05/12
For personal use only.

where the acids are more resistant to desulfonylation. These expectations were realized by the observation that photolysis in methanol of benzyl methyl sulfone **8** gave a reasonable yield of methane sulfinic acid, **9** (44%), and again diphenylethane (eq. 3). For ease of isolation and determination of structure the sulfinic acid was converted to the corresponding sulfonyl chloride by aqueous chlorination (15). The yield

[3] $\underset{\mathbf{8}}{PhCH_2SO_2CH_3} \xrightarrow[MeOH]{h\nu} PhCH_2CH_2Ph + \underset{\mathbf{9}}{HSO_2CH_3} \xrightarrow[H_2O]{Cl_2} ClSO_2CH_3$

reported for the sulfinic acid is actually in terms of sulfonyl chloride isolated.

The yield of the sulfinic acid could be increased to 63% by photolysis in 2-propanol. The chemistry of the benzyl radical also changed since now 2-methyl-3-phenyl-2-propanol, 53%, as well as 1,2-diphenylethane, 17%, was formed. Later experiments for other sulfones also demonstrated the formation of toluene, 28% (by glc analysis). The increased yield of the sulfinic acid in 2-propanol suggests that there is competition between two processes for the methyl sulfonyl radical formed by the photochemical benzylic cleavage: H atom abstraction or loss of sulfur dioxide. The first, of course, becomes more favorable in 2-propanol. The process involving loss of SO_2 should lead to the formation of hydrocarbon, namely methane from H abstraction by methyl radicals. Volatility, of course, makes methane difficult to detect. However, this possibility was confirmed by photolysis of 2-phenylethyl benzyl sulfone, **7**, in 2-propanol where the yields of 2-phenylethane sulfinic acid, 54%, and phenylethane, 36%, account for 90% of the original sulfone (note eq. 4).

Methods of preparing sulfinic acids, particularly for alkyl cases, are relatively few (11). This photochemical method is quite general as shown for a variety of benzylic sulfones in Table 1. Since the sulfones are readily available by oxidation of the sulfide obtained from a thiol and an alkyl halide, this is effectively a conversion of alkyl halides to alkyl sulfinic acids. This method should also provide a powerful and general route for the synthesis of sophisticated sulfonyl chlorides. Most procedures for preparing sulfonyl chlorides require precursors which are very sensitive to oxidizing agents (as for instance, thiols and sulfides (17, 18)). The storage of a sulfonyl chloride in the form of an oxidant-resistant functionality like the benzylic sulfone in conjunction with the previously published method employing the chlorination of benzylic sulfides (17) provides, as well, the potential to prepare polysulfonyl compounds such as sulfonate ester sulfonamides and mixed sulfonate esters.

TABLE 1. Preparation of sulfinic acids by photolysis of benzylic sulfones in 2-propanol

Sulfone	Sulfinic acid	Yield (%)[a]
1. $CH_3SO_2CH_2Ph$	CH_3SO_2H	63
2. $CH_3CH_2SO_2CH_2Ph$	$CH_3CH_2SO_2H$	59
3. $CH_3CH_2CH_2SO_2CH_2Ph$	$CH_3CH_2CH_2SO_2H$	60
4. $ClCH_2CH_2SO_2CH_2Ph$	$ClCH_2CH_2SO_2H$	40
5. $PhCH_2CH_2SO_2CH_2Ph$	$PhCH_2CH_2SO_2H$	54[b]
6. $PhSO_2CH_2Ph$	$PhSO_2H$	26
7. CH_3SO_2CHPh (CH$_3$)	CH_3SO_2H	50
8. $CH_3CH_2SO_2CHPh$ (CH$_3$)	$CH_3CH_2SO_2H$	60
9. $CH_3CH_2CH_2SO_2CHPh$ (CH$_3$)	$CH_3CH_2CH_2SO_2H$	40

[a]All yields reported are for the corresponding sulfonyl chloride obtained by aqueous chlorination of the acidic fraction from photolysis.
[b]Yield of $PhCH_2CH_3$ 36% in 2-propanol and 33% in methanol.

[4] $\underset{\mathbf{10}}{PhCH_2CH_2SO_2CH_2Ph} \xrightarrow[2\text{-propanol}]{h\nu} [PhCH_2\cdot] + [PhCH_2CH_2SO_2\cdot]$

$[PhCH_2\cdot] \xrightarrow{-SO_2} [PhCH_2CH_2\cdot] \rightarrow PhCH_2CH_3$ (36%)

$[PhCH_2CH_2SO_2\cdot] \rightarrow PhCH_2CH_2SO_2H$ (54%)

[5] $XSO_2CH_2Ph \xrightarrow{h\nu} \cdot CH_2Ph + XSO_2\cdot$

$XSO_2\cdot \xrightarrow{-SO_2} X\cdot \xrightarrow{RH} XH$

$XSO_2\cdot \xrightarrow{RH} XSO_2H \longrightarrow XH + SO_2$

In summary, we have found that the photochemical cleavage of benzylic sulfones to a sulfonyl radical seems general but that the fate of the radical may be variable. As shown in eq. 5, the preferred pathway will depend on the stability of $XSO_2\cdot$ to loss of SO_2, the stability of the sulfinic acid to desulfonylation and the hydrogen donating ability of the reaction medium. We are currently exploring the scope of these processes in other systems.

Can. J. Chem. Downloaded from www.nrcresearchpress.com by 210.87.254.105 on 09/05/12
For personal use only.

Experimental

General

The ir spectra were recorded on a Perkin-Elmer 237B grating spectrophotometer. The nmr spectra were obtained on a Varian T-60 instrument using TMS as the internal standard. The mass spectra were recorded on a Dupont-CEC model 21-104 mass spectrometer. The samples were directly introduced using an all glass probe and the spectra were run at 30 eV with a source temperature of 150°C. Melting points were determined on a Fisher-Johns melting point apparatus and are uncorrected. Gas chromatographic analysis for hydrocarbons was performed on a Hewlett-Packard 5750 instrument with a $\frac{1}{4}$ in. × 9 ft 20% Carbowax 20 M on Chromosorb W column programmed from 60–115°C.

Photolyses: General

The appropriate weight of sample was dissolved in the desired solvent (300 ml). The solution was photolyzed for 4 h in an immersion well (after purging with N_2 for 1 h) using a 200 W medium pressure Hanovia mercury lamp and a VYCOR filter.

Standard Work-up

A volume of water equal to the total volume of the reaction mixture was added to the reaction mixture. The resultant solution was washed with chloroform (five 100-ml aliquots). The combined chloroform layers were base washed with 2.5% NaOH (100 ml aliquots), whenever the solvent for reaction was acetic acid, until the aqueous p*H* remained basic. The chloroform layers were dried ($MgSO_4$), filtered, and the chloroform rotary evaporated, affording a crude residue.

Preparation of $PhSCH_2SCH_2Ph$

Sodium metal (1.479 g) was dissolved in absolute ethanol (100 ml) and benzyl thiol (7.8 ml) was added. Phenyl chloromethyl sulfide (10.040 g) in absolute ethanol (50 ml) was added to the cooled reaction mixture over a period of about 20 min. The reaction was stirred at ambient temperature for 24 h followed by standard work-up. The crude residue (17.307 g) was used directly to obtain the corresponding disulfone.

Preparation of $PhSO_2CH_2SO_2CH_2Ph$ (1)

Reaction of the disulfide (4.996 g) with chromium trioxide (9.146 g) in glacial acetic acid (150 ml) as described previously (5) for the oxidation of the sulfone sulfide furnished β-disulfone (**1**) (3.101 g) identical in all respects with that reported previously (5).

Preparation of $CH_3SO_2CH_2SO_2CH_2Ph$ (2)

The preparation and properties of this compound have been described elsewhere (19).

Preparation of $CH_3SO_2\underset{\displaystyle CH_3}{\underset{|}{C}}HSO_2CH_2Ph$ (5)

Sodium metal (0.1848 g) was dissolved in methanol (100 ml) and the β-disulfone (**2**) (1.9996 g) was added. A solution of methyl iodide (3.4317 g) in methanol (20 ml) was added and the reaction mixture stirred at room temperature for 24 h. Standard work-up furnished a crude product. The crude material was dissolved in chloroform (100 ml) and the resultant solution washed with 2.5% NaOH (four 100-ml aliquots). Concentration of the solution and recrystallization of the residue from 95% ethanol (8 ml) afforded clean disulfone (**5**, 1.4655 g, mp 108–109°C); ir ($CHCl_3$): 1330, 1310, and 1120 cm^{-1}; nmr ($CDCl_3$) δ: 7.33 (5H, s), 4.90 (1H, d, J = 14 Hz), 4.36 (1H, d, J = 14 Hz), 4.06 (1H, q, J = 8 Hz), 3.13 (3H, s), and 1.70 (3H, d, J = 8 Hz); ms *m/e*: 119 (5.9%),[3] 118 (10.5%),[3] 92 (10.2%), and 91 (100%). *Anal.* calcd. for $C_{10}H_{14}O_4S_2$: C 45.78, H 5.37; found: C 45.13, H 5.49.

[3]The significance of these ions has been discussed in detail (5, 20).

Preparation of $CH_3SO_2\underset{\displaystyle CH_2Ph}{\underset{|}{C}}HSO_2CH_2Ph$ (6)

Sodium metal (0.4906 g) was dissolved in methanol (250 ml) and the β-disulfone (**2**) (5.0158 g) added. Benzyl chloride (7.668 g) was added and the reaction mixture refluxed for 24 h. Standard work-up furnished a crude product which was recrystallized from 95% ethanol (20 ml). The crystalline product contained starting material (2.10 g) and the C-3 benzylated disulfone (2.650 g). The product was dissolved in chloroform (500 ml) and the solution washed with 2.5% NaOH (six 500-ml aliquots). The chloroform was removed and the residue recrystallized from 95% ethanol affording clean disulfone (**6**, 1.2655 g, mp 125–126°C); ir ($CHCl_3$): 1340, 1320, and 1123 cm^{-1}; nmr ($CDCl_3$) δ: 7.43 (5H, s), 7.30 (5H, s), 4.80 (1H, d, J = 13 Hz), 4.43 (1H, d, J = 13 Hz), 4.30 (1H, t), 3.50 (2H, d), and 3.06 (3H, s); ms *m/e* 338 (M^+, 1%), 195 (8.3%),[3] 194 (20%),[3] 92 (10%), and 91 (100%). *Anal.* calcd. for $C_{16}H_{18}O_4S_2$: C 56.78, H 5.36; found: C 56.91, H 5.40.

Preparation of $CH_3SO_2\underset{\displaystyle CH_2CH_2CO_2CH_3}{\underset{|}{C}}HSO_2CH_2Ph$ (7)

Sodium metal (0.828 g) was dissolved in methanol (350 ml) and the β-disulfone (**2**) (9.0068 g) added. Methyl acrylate (9.3589 g) was added and the reaction mixture refluxed for 24 h. Standard work-up furnished a crude product which was recrystallized from 95% ethanol (90 ml). The crystals were filtered off, shown to be unchanged disulfone **2** (4.634 g), and the mother liquor concentrated. The mother-liquor concentrate was dissolved in 95% ethanol (9 ml) and a second crop of crystals obtained. The second crop proved to be clean ester disulfone (7, 1.8791 g, mp 87–89°C); ir ($CHCl_3$) 1740, 1355, 1310, and 1115 cm^{-1}; nmr ($CDCl_3$) δ: 7.43 (5H, s), 4.90 (1H, d, J = 13 Hz), 4.50 (1H, d, J = 13 Hz), 4.26 (1H, m), 3.63 (3H, s), 3.20 (3H, s), and 2.57 (4H, m); ms *m/e*: 191 (3.4%),[3] 190 (7.6%),[3] 92 (10%), and 91 (100%). *Anal.* calcd. for $C_{13}H_{18}O_6S_2$: C 46.69, H 5.42; found: C 47.01, H 5.30.

Photolysis of the β-Disulfones 1, 2, 5, 6, and 7

The photolyses of the disulfones were carried out in the same manner as illustrated below for the debenzylsulfonylation of the benzylated β-disulfone **6**.

The benzylated β-disulfone (**6**, 1.0024 g) was photolyzed and the solvent evaporated. The residue was chromatographed on silica gel (100 g) employing chloroform (100 ml fractions) for elution. Fractions 5–7 were combined and concentrated, affording methyl phenethyl sulfone (0.5336 g). The product was recrystallized from 95% ethanol and shown to be identical to authentic material by nmr, ir, and mp.

Preparation of Benzylic Sulfones

The necessary benzylic sulfides were obtained by treating the appropriate alkyl halide with phenylmethanethiol. (17). The corresponding benzylic sulfones were obtained by oxidation of the benzylic sulfide with Fieser's reagent. (20).

Preparation of $PhCH_2SCH_2CH_2Cl$

Benzyl ω-hydroxyethyl sulfide was prepared from mercapto ethanol and benzyl chloride in the standard fashion (17). Benzyl ω-hydroxyethyl sulfide (40.006 g) was added to chloroform (30 ml) and the solution brought to gentle reflux. A solution of thionyl chloride (29.794 g) in chloroform (20 ml) was added dropwise over a period of 45 min. Upon completion of the addition the reaction mixture was refluxed for 1.5 h. The chloroform was evaporated and the residue rectified at reduced pressure affording the chlorosulfide (bp 138–142°C/220 Torr,

33.054 g); nmr ($CDCl_3$) δ: 7.23 (5H, s), 3.70 (2H, s), 3.50 (2H, t), and 2.70 (2H, t); ms *m/e*: 188 (10%) 186 (M^+, 30%), 92 (16%), and 91 (100%).

Preparation of $PhCH_2SO_2CH_2CH_2Cl$

The chlorosulfide (5.007 g) was oxidized with CrO_3 (6.722 g) in glacial acetic acid (100 ml) in the usual way, (5, 20, 21). After recrystallization from 95% ethanol the chlorosulfone (4.296 g) had mp 90–91°C; ir ($CHCl_3$): 1320 and 1120 cm^{-1}; nmr ($CDCl_3$) δ: 7.46 (5H, s), 4.33 (2H, s), 3.83 (2H, t), and 3.30 (2H, t); ms *m/e*: 218 (M^+, 1.8%), 92 (8.8%), and 91 (100%).

CH_3
|

Preparation of $PhCHSH$

α-Mercaptoethylbenzene was prepared from α-chloroethylbenzene following the procedure of Tsung and Chi (21).

CH_3
|

Preparation of $PhCHSO_2R$

These sulfones were prepared by condensing the appropriate alkyl halide with α-mercaptoethylbenzene (17) followed by chromium trioxide oxidation (21).

Photolyses of Simple Sulfones

The photolyses of the sulfones depicted in Table 1 were carried out in the same manner as illustrated below for benzyl methyl sulfone.

Benzyl methyl sulfone (0.458 g) was photolyzed in 2-propanol and the solvent evaporated. The residue was dissolved in chloroform (25 ml) and the resultant solution washed with 2.5% NaOH (two 10-ml aliquots). The *organic layer* was concentrated and stored.

The aqueous layer was acidified with 10% HCl and Cl_2 (ca. 200 ml/min) was bubbled into the solution for 10 min. The reaction mixture was extracted with methylene chloride (three 25-ml aliquots). The combined extracts were dried and concentrated yielding methanesulfonyl chloride (0.193 g).

The organic layer obtained from the photolysis concentrate contained diphenyl ethane (0.041 g) and 2-benzyl-2-propanol (0.214 g). This material was chromatographed on silica gel (30 g) employing chloroform (25 ml aliquots) for elution. Fraction 4 contained pure diphenylethane which was identical to authentic material by mp, ir, nmr, and ms. Fractions 6 and 7 furnished clean 2-benzyl-2-propanol which furnished the expected ir, nmr, and ms.

Acknowledgements

The authors are indebted to Mr. H. O. Fong, Mr. W. R. Hardstaff, and Mr. T. D. J. Dunstan for technical assistance. We thank Dr. J. H. Kim for running the mass spectra. We are grateful for financial support from Dalhousie University and from the National Research Council of Canada.

1. E. Block. Quart. Rep. Sulfur Chem. **4**, 315 (1969).
2. Photochemistry. Vols. 1–6. The Chemical Society, J. Wright & Sons, Bristol. 1970–1975.
3. (*a*) T. Sato, Y. Goto, T. Tohyama, S. Hayahsi, and K. Hata. Bull. Chem. Soc. Jpn. **40**, 2975 (1967); (*b*) Y. Odaira, K. Yamaji, and S. Tsutsumi. Bull. Chem. Soc. Jpn. **37**, 1410 (1964).
4. M. P. Cava, M. V. Lakshmikantham, and M. Behforouz. J. Org. Chem. **39**, 206 (1974).
5. R. F. Langler, W. S. Mantle, and M. J. Newman. Org. Mass Spectrom. **10**, 1135 (1975).
6. N. J. Turro. Energy transfer and organic photochemistry. Interscience, J. Wiley & Sons, New York, NY. 1969. p. 206.
7. C. L. McIntosh, P. de Mayo, and R. W. Yip. Tetrahedron Lett. 37 (1967).
8. J. L. Kice. *In* Free radicals. Vol. II. *Edited by* J. K. Kochi. Wiley & Sons, New York, NY. 1973. p. 731.
9. W. K. Busfield, K. J. Ivin, H. Mackle, and P. A. G. O'Hare. Trans. Faraday Soc. **57**, 1064 (1961).
10. L. Horner and L. Schläfer. Ann. **635**, 31 (1960).
11. C. M. Stirling. Int. J. Sulfur Chem. Part B, **6**, 277 (1971).
12. M. McMillan and W. A. Waters. J. Chem. Soc. B, 422 (1966).
13. R. J. Boyd, A. Gupta, R. F. Langler, and J. A. Pincock. Can. J. Chem. To be submitted.
14. R. F. Langler and J. A. Pincock. Can. J. Chem. **55**, 2316 (1977).
15. J. S. Grossert and R. F. Langler. Chem. Commun. 49 (1973).
16. F. Wudl, D. A. Lightner, and D. J. Cram. J. Am. Chem. Soc. **89**, 4099 (1967).
17. R. F. Langler. Can. J. Chem. **54**, 498 (1976).
18. J. S. Grossert and R. F. Langler. Can. J. Chem. **55**, 407 (1977).
19. W. R. Hardstaff and R. F. Langler. Org. Mass Spectrom. **10**, 215 (1975).
20. W. E. Truce, G. H. Birum, and E. T. McBee. J. Am. Chem. Soc. **74**, 3594 (1952).
21. J. Tsung and J. Chi. Chem. Abstr. **55**, 17635 (1961).

Can. J. Chem. Downloaded from www.nrcresearchpress.com by 210.87.254.105 on 09/05/12
For personal use only.

Galvanostatic transients and crystallization overvoltage

STEPHEN FLETCHER

Department of Chemistry, Carleton University, Colonel By Drive, Ottawa, Ont., Canada K1S 5B6

AND

ARTHUR SMITH

Department of Mathematics, Carleton University, Colonel By Drive, Ottawa, Ont., Canada K1S 5B6

Received September 26, 1977

STEPHEN FLETCHER and ARTHUR SMITH. Can. J. Chem. **56**, 908 (1978).

The theory of galvanostatic transients is extended to include the formation of a three-dimensional crystalline layer. The mechanism of formation of this layer is assumed to be one of nucleation and subsequent growth of randomly distributed nuclei on the electrode surface. The resulting crystallization overvoltage is shown to be a complex function of the applied current density, as well as being related to the potential-dependences of the rate constants for lattice growth and the potential-dependence of the nucleation rate constant. The complete E–t response is calculated numerically and also certain limiting cases are described which have exact analytical solutions. A method of testing the model experimentally is briefly discussed.

STEPHEN FLETCHER et ARTHUR SMITH. Can. J. Chem. **56**, 908 (1978).

On a étudié la théorie des intermédiaires galvanostatiques pour inclure la formation d'une couche cristalline tri-dimensionnelle. On a fait l'hypothèse que le mécanisme de formation de cette couche provient d'une nucléation et d'une croissance subséquente des noyaux distribués au hasard sur la surface de l'électrode. On démontre que le survoltage de cristallisation qui en résulte est une fonction complexe de la densité du courant appliqué de même qu'il est relié avec les dépendances de potentiel des constantes de vitesse pour la croissance du réseau et la dépendance de potentiel de la constante de vitesse de nucléation. On a calculé numériquement les relations complètes E–t et on décrit aussi un certain nombre de cas limites pour lesquels des solutions analytiques exactes existent. On discute brièvement d'une méthode permettant de vérifier le modèle d'une façon expérimentale.

[Traduit par le journal]

Introduction

In recent years the potentiostatic method of investigating electrocrystallization reactions has become increasingly accepted as the technique of choice, to a large extent replacing the earlier galvanostatic methods. The major reason for this development was the inherent complexity of galvanostatic data as compared to potentiostatic data.

In galvanostatic measurements the current density is the controlled parameter and hence the total interfacial rate is maintained constant as a function of time. Each individual reaction which contributes to the overall rate is therefore constrained in such a way that the overall current density is identical to the externally-applied value. In order to maintain this state of affairs the electrode potential responds in a complex way as a function of time. By monitoring the changes in the electrode potential, important information regarding individual processes may, however, be obtained provided that (*a*) an appropriate theoretical model exists and (*b*) sufficient resolution between component processes is achieved.

On the other hand, potentiostatic measurements allow the straightforward manipulation of the independent variable, i.e., the electrode potential, so that the current density is the observed parameter. One consequence of this is that theoretical models of electrocrystallization may easily be described because no assumptions are required regarding the potential-dependences of any rate constants which appear in the overall rate equation. All that is needed is a geometrical model of some description. In general, therefore, the values of individual rate constants and their related potential-dependences have usually been determined by potentiostatic techniques.

Although potentiostatic techniques have been singularly successful in the development of geometrical models of electrocrystallization processes, a certain number of limitations to the basic experimental method have become apparent in recent years. Some of these limitations are caused by (*a*) ohmic effects, in particular iR-drop, (*b*) finite rise-time distortions of potential waveforms, (*c*) concurrent dissolution reactions, (*d*) double-layer charging effects, (*e*) adsorption phenomena, (*f*) finite solubility of growing films (i.e., anodic films), (*g*) irreproducibility of applied potentials (within 0.01 mV, say), and (*h*) poor cell configurations, etc. All of these problems conspire to restrict the range over which experimental data may be usefully accumulated. It is also possible that other problems exist which have remained undiagnosed because of the

Can. J. Chem. Downloaded from www.nrcresearchpress.com by 210.87.254.6 on 09/05/12
For personal use only.

Can. J. Chem. Downloaded from www.nrcresearchpress.com by 210.87.254.6 on 09/05/12
For personal use only.

use of only one experimental approach (i.e., the potentiostatic method). Consequently it seems worthwhile to investigate some new methods of elucidating electrocrystallization mechanisms. This necessarily involves the understanding of the correct mathematical transformations which are required to describe the underlying phenomena. Once these have been evolved, then diverse methods might be used under appropriate circumstances to yield improved experimental results.

In an earlier paper we described the theoretical effects of ohmic overpotential (*iR*-drop), linear potential sweep, and potential staircase waveforms on 3-D progressive nucleation and growth. In the present work we calculate the theoretical response of such a system to a simple galvanostatic step. The solution of this problem is important for several reasons. Firstly, it would allow a very accurate experimental test of the mathematical transformations employed in its derivation, and hence is of general significance for other waveforms derived by similar transformations. Secondly, comparison of potentiostatic and galvanostatic data would provide a bridgehead between the newer and the older literature data. Thirdly, galvanostatic techniques may prove to be superior to potentiostatic techniques in some experimental regions of interest (e.g., at low current densities, where potentiostatic measurement is often difficult). Fourthly, 'cross-fertilization' should be possible such that new techniques involving combinations of potentiostatic and galvanostatic pulses can be developed (31).

The application of galvanostatic techniques to simple charge-transfer processes has been carried out for many years. The method involves stepping the applied current from zero to some known value, whereupon the resulting variation of potential is followed as a function of time. When no current flows it is clear that the equilibrium potential (E_e) for a given reaction is observed. Therefore the potential difference or overvoltage may be recorded directly.

The simplest case, for which concentration polarization was absent, was first studied by Roiter *et al.* (1). The method was much improved by Berzins and Delahay (2, 3) who developed a technique for the evaluation of the entire potential–time curve (for the single-step method) including superposed charge-transfer and diffusion overvoltages. This technique allowed the determination of the exchange current density i_0 and the charge-transfer co-efficient α from a single measurement, provided the double-layer charging had first been extrapolated out (4, 5).

Another technique which was developed was the cyclic galvanostatic method of Wijnen and Smit (6) in which rectangular current pulses of a given frequency were applied to the working electrode. An elegant improvement in this case was proposed by Sluyters (7), who replaced the rectangular pulses with a sinusoidally-varying current. An advantage of both of these methods, besides improved accuracy, was that it was not necessary to know a priori the ohmic resistance of the solution in order to eliminate the ohmic potential drop between the luggin reference probe and the working electrode.

A further interesting development may be found in the work of Gerischer and Krause (8, 9). In order to eliminate some of the difficulties of short-time measurements caused by double-layer charging, a short current pulse (~ 1 μs) was first applied before the final current was switched in. This served to charge the double layer on a time-scale shorter than that used in recording experimental data. The method has also been extended and improved by Matsuda *et al.* (10).

None of the outlined methods have been applied to a theoretical analysis of crystallization overvoltage, however, although a large number of experimental measurements may be found in the literature (11). In particular, large potential 'jumps' have frequently been recorded. Since these corresponded to the supersaturations observed in the formation of three-dimensional nuclei during crystallization in solution (12) they were attributed to this cause (13, 14). This explanation was qualitatively improved following the early potentiostatic investigations of Bewick (15) and Fleischmann and coworkers (16–20). These workers showed that the peaks on the potential–time plots (21–23) corresponded to the initial stages of formation of new phases *at the electrode surface*. The mechanism of formation of such phases under potentiostatic conditions was shown to be the classical mechanism of nucleation and growth, except that the slow step in the overall reaction occurred at the edge of the expanding crystal lattice.

Unfortunately, the galvanostatic model of nucleation and growth was not developed because the solution involved certain differential equations which were difficult to analyse. The purpose of the present work is to show that, given certain simplifying assumptions, the galvanostatic response of electrocrystallization reactions may indeed be theoretically investigated.

Theory

In a previous paper (24) a method was described for the determination of the effect of varying potential during progressive, three-dimensional nucleation and growth. Both the linear potential sweep method and the staircase potential ramp were

Can. J. Chem. Downloaded from www.nrcresearchpress.com by 210.87.254.6 on 09/05/12
For personal use only.

considered, as well as feedback loops generated by uncompensated ohmic overpotential. The model of three-dimensional growth used was that of Armstrong, Fleischmann, and Thirsk (25). At constant potential the current response as a function of time was given by

$$[1] \qquad i(t) = 4i_m(1 - S)S$$

where S is the surface coverage function ($0 < S < 1$) and i_m is the maximum in the current–time transient. In order to take the variation of potential into account it was assumed that i_m and t_m (the time taken to achieve i_m) were exponential functions of potential, viz.

$$[2] \qquad i_m = 10^{a_1E+b_1}$$

$$[3] \qquad t_m = 10^{a_2E+b_2}$$

The validity of these assumptions has been shown for many systems, at least in experimentally accessible regions, e.g., see ref. 25. The corresponding problem in electrolytic nucleation has also been discussed at length by Milchev and co-workers (28, 29). The constants a_1 and a_2 are determined experimentally, where it is evident that a_1 is positive, a_2 negative ($-a_2 > a_1$). The current 10^{b_1} and the time 10^{b_2} depend on the chosen potential scale and as such are unimportant in the present work. This is because experimental values may only be obtained relative to a given reference electrode system. The dependence of i_m on E is built into the potentiostatic model, though with varying E it is clear that i_m no longer represents the current maximum as it does in ref. 25.

To obtain S and hence i when E varies it is assumed that the response of the surface coverage to changing E is essentially instantaneous. This was shown previously (24) to be mathematically equivalent to the transformation

$$f(E,t) \rightarrow F(E(t),t)$$

where $f(E,t)$ is the surface coverage function at constant E and

$$F(E(t),t) = f\left(\int_0^t E(t')\,dt', t\right)$$

This led in ref. 24 to the following equations

$$[4] \qquad S = 1 - e^{-kJ^3}$$

$$[5] \qquad J = \int_0^t Q(t')\,dt'$$

$$[6] \qquad Q = \frac{dJ}{dt} = 10^{-a_2(E(t)-i(t)R)}$$

$$[7] \qquad i(t) = PQ^\lambda S(1 - S) = PQ^\lambda(1 - e^{-kJ^3})e^{-kJ^3}$$

where R is a constant resistance and the constants P, λ, k are related to a_1, a_2, b_1, b_2 by $P = 4 \times 10^{b_1}$, $\lambda = -a_1/a_2$, $k = \ln 2 \times 10^{-3b_2}$.

The Problem

Equation 7 is an integral equation which determines $i(t)$ as a function of the applied potential $E(t)$. What we wish to describe in the present work is the solution $i(t) = i_g$, a constant current for some waveform $E(t)$. To treat this galvanostatic case it is necessary to examine the equation

$$[8] \qquad i_g = PQ^\lambda(1 - e^{-kJ^3})e^{-kJ^3} = PQ^\lambda S(1 - S)$$

as an integral equation that yields E as a function of t. Since Q is now given by $10^{-a_2(E(t) - i_gR)}$ note that the significance of R as a complex feedback parameter (emphasized in ref. 24) between E and i is lost and i_gR becomes a simple constant shift in the experimentally recorded potential.

It is expected on experimental grounds that $E(t)$ in the galvanostatic case will be a U-shaped curve (30). Equation 8 does in fact yield such a curve as is shown in the analysis. However, no explicit solution for $E(t)$ exists in terms of familiar functions. This is no drawback since numerical simulation yields a solution curve while the analytical method is successful in giving $E(t)$ in the regions of interest. The numerical and analytical solutions can then be compared, and the results shown to be consistent.

The Analytical Solution

Taking advantage of the fact that [8] may be regarded as an ordinary differential equation in J and t, since $dJ/dt = Q$, we immediately obtain t as a function J, giving

$$[9] \qquad \left(\frac{i_g}{P}\right)^{1/\lambda} t = \int_0^J \exp(-kx^3/\lambda) \times [1 - \exp(-kx^3)]^{1/\lambda}\,dx$$

Hence t is an increasing bounded function of J with the limit $t = t_{ext}$ given by

$$[10] \qquad \left(\frac{i_g}{P}\right)^{1/\lambda} t_{ext} = \int_0^\infty \exp(-kx^3/\lambda) \times [1 - \exp(-kx^3)]^{1/\lambda}\,dx$$

The right-hand side of [10] may be evaluated numerically for a given k and λ. The transformation $x = k^{-1/3}y$ shows that the integral has the form $k^{-1/3}G(\lambda)$ for some function G. A good approximation to $G(\lambda)$ can be obtained by expressing the integral in the form $\int_0^\infty e^{P(x)/\lambda}\,dx$ and expanding $P(x)$ about the maximum. The result is that the integral in [10] has the approximate value $\sqrt{\pi\lambda}/4^{1/\lambda}3k^{1/3}(\ln 2)^{2/3}$. To obtain a more exact value note that when $k/\lambda \sim 1$, the range of integration in [10] can be reduced to [0, 2] while retaining 4 figure accuracy.

Can. J. Chem. Downloaded from www.nrcresearchpress.com by 210.87.254.6 on 09/05/12
For personal use only.

From [9] and [10] it follows that the inverse function $J(t)$ exists, defined on the domain $[0, t_{ext}]$ on which it increases without bound as $t \to t_{ext}$.

Equation 9 by the transformation $e^{-kx^3} = y$ may be put in the form

$$[11] \qquad 3k^{1/3}\left(\frac{i_g}{P}\right)^{1/\lambda} t = \int_{e^{-kJ^3}}^{1} f(y)\,dy$$

where

$$f(y) = y^{1/\lambda - 1}(1 - y)^{1/\lambda}(-\ln y)^{-2/3}$$

and correspondingly [10] becomes

$$[12] \qquad 3k^{1/3}\left(\frac{i_g}{P}\right)^{1/\lambda} t_{ext} = \int_{0}^{1} f(y)\,dy$$

To obtain the asymptotic behaviour of E as $t \to t_{ext}$, observe that [9] and [10] give

$$[13] \qquad \left(\frac{i_g}{P}\right)^{1/\lambda}(t_{ext} - t) = \int_{J}^{\infty} \exp(-kx^3/\lambda) \times [1 - \exp(-kx^3)]^{1/\lambda}\,dx$$

As $t \to t_{ext}$, $J \to \infty$ and the right-hand side of [13] is asymptotic to

$$I(J) = \int_{J}^{\infty} e^{-kx^3/\lambda}\,dx = \int_{J}^{\infty} \{(-3kx^2/\lambda)\, e^{-kx^3/\lambda}/(-3kx^2/\lambda)\}\,dx$$

Integrating by parts gives

$$[14] \qquad I(J) = \frac{e^{-kJ^3/\lambda}}{3kJ^2/\lambda} - \frac{\lambda}{6k}\int_{J}^{\infty} \frac{e^{-kx^3/\lambda}}{x^3}dx$$

The integral in [14] does not exceed $(\lambda/6kJ^3)I(J)$ showing $I(J)$ is asymptotic to the first term on the right-hand side of [14]. From this observation, and [13], we obtain

$$[15] \qquad (1 - \tau)\left(\frac{i_g}{P}\right)^{1/\lambda} t_{ext} \sim \frac{e^{-kJ^3/\lambda}}{3kJ^2/\lambda}$$

where the dimensionless quantity τ has been introduced and is defined by

$$[16] \qquad \tau = t/t_{ext}$$

Now from [8], as $J \to \infty$

$$[17] \qquad \left(\frac{i_g}{P}\right)^{1/\lambda} \sim Q\, e^{-kJ^3/\lambda}$$

Combining [17] and [15] gives

$$[18] \qquad 3kt_{ext}J^2Q/\lambda \sim \frac{1}{1 - \tau}$$

But $dJ/dt = Q$. Hence [18] may be written

$$k(t_{ext}/\lambda)\frac{dJ^3}{dt} \sim \frac{1}{1 - \tau}$$

and hence

$$[19] \qquad kJ^3/\lambda \sim -\log(1 - \tau)$$

Feeding [19] back into [18] then gives the asymptotic form of Q and taking logs soon yields

$$[20] \qquad a_2(E - i_gR) \sim \log(1 - \tau) + \tfrac{2}{3}\log(-\log(1 - \tau)) + \text{constant}$$

Therefore a plot of $\log(1 - \tau)$ vs. E is asymptotically a straight line whose gradient gives a_2. This was tested by numerical simulation and Fig. 1 gives the result even to the extent of predicting the correct slight deviation from a straight line.[1]

The form of E as $\tau \to 0$ is a little easier to obtain. For [9] gives immediately that, as $\tau \to 0$, the integral in [9] is asymptotic to

$$[21] \qquad J(kJ^3)^{1/\lambda}$$

Hence $J \sim$ constant $\times\, t^{\lambda/(3+\lambda)}$ and so $Q = dJ/dt \sim$ constant $\times\, t^{-3/(3+\lambda)}$. Taking logs using $\lambda = -a_1/a_2$ and [16] gives

$$[22] \qquad E(t) - i_gR \sim \frac{3}{3a_2 - a_1}\log\tau + \text{constant} \quad \text{as } \tau \to 0$$

and [22] gives the value $(3a_2 - a_1)$.

We now show E has a minimum at $S = \frac{1}{2}$. For, from [8] $0 = \lambda Q^{\lambda-1}\,(dQ/dt)S(1 - S) + Q\,(d/dt)S(1 - S)$ so $dQ/dt = 0$ when $(d/dt)S(1 - S) = 0$ which occurs at $S = \frac{1}{2}$. When $S = \frac{1}{2}$, $S(1 - S)$ is maximal and hence Q has a minimum Q_{min}, since $Q^{\lambda}S(1 - S)$ is constant and $\lambda > 0$.

But $dQ/dt = -a_2Q\,(dE/dt)$ so dQ/dt and dE/dt have the same sign (since $a_2 < 0$) and vanish together. Thus E has a minimum E_{min} at $S = \frac{1}{2}$.

Further at $S = \frac{1}{2}$, $\exp(-kJ^3) = \frac{1}{2}$, so E_{min} occurs at a time t_{min}, which from [11] is given by

$$[23] \qquad 3k^{1/3}\left(\frac{i_g}{P}\right)^{1/\lambda} t_{min} = \int_{1/2}^{1} f(y)\,dy$$

From [12] and [23] we see that t_{min}/t_{ext} depends only on λ and is given by

$$[24] \qquad t_{min}/t_{ext} = \int_{1/2}^{1} f(y)\,dy \Big/ \int_{0}^{1} f(y)\,dy$$

[1] In Figs. 1–4 which are obtained from the numerical simulation we cross-check some aspects of the numerical and analytical solutions to the galvanostatic problem. In all cases agreement is excellent. In each case we take $b_1 = b_2 = 0 = R$ for convenience, since these quantities are unimportant in the present work as indicated in the text. We take the typical values $a_1 = \frac{1}{3}$, $a_2 = -\frac{1}{2}$ (so that $\lambda = \frac{2}{3}$).

Can. J. Chem. Downloaded from www.nrcresearchpress.com by 210.87.254.6 on 09/05/12
For personal use only.

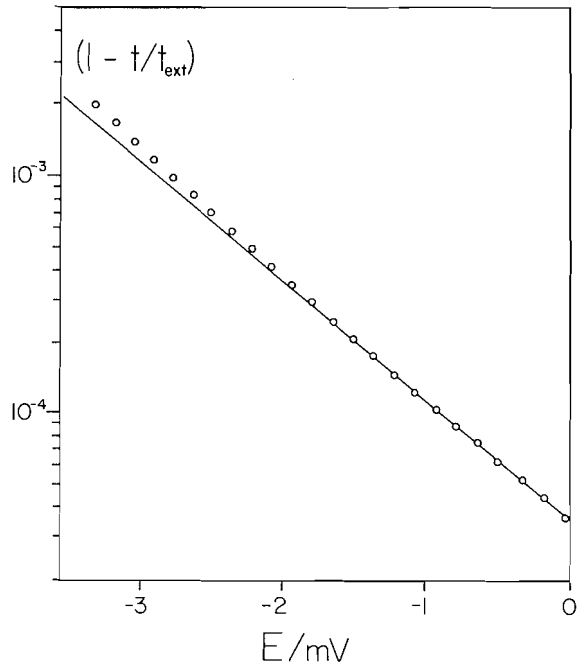

FIG. 1. Plot of log $(1 - \tau)$ vs. E for $1 - \tau \ll 1$. $i_g = 0.005$ mA. This is in agreement with [20].

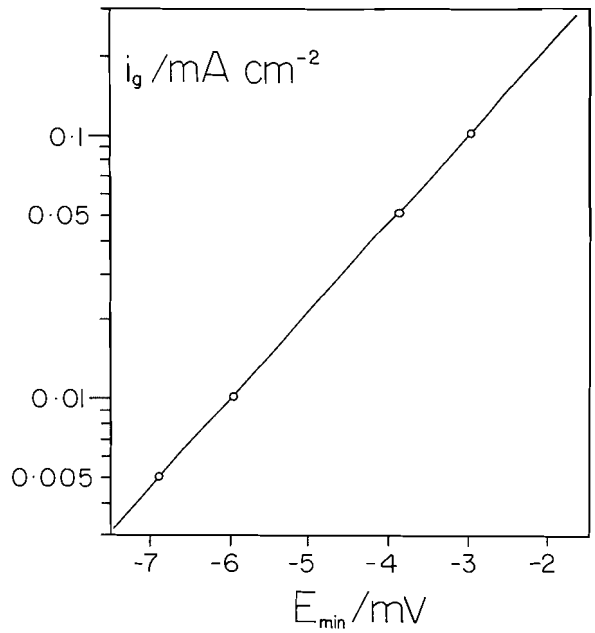

FIG. 2. Galvanostatic current vs. E_{min}. i_g = various. The gradient is 0.33 decade mV^{-1} and should be $a_1 = \frac{1}{3}$ according to [25].

Furthermore, at t_{min}, [8] gives $i_g = (P/4)Q^{\lambda}{}_{min}$ and taking logs gives

$$\log i_g = a_1(E_{min} - i_g R) + b_1 \qquad [25]$$

This is a most important result because of the ease of obtaining i_g, E_{min} experimentally. It is clear that a graph of $E_{min} - i_g R$ vs. log (i_g) should be linear with a gradient of $1/a_1$. This result is compared with that obtained numerically in Fig. 2. Excellent agreement is observed. Equations 14, 25, and 10 allow us to predict accurately the value of E_{min}, t_{min}, and t_{ext} for given i_g, k, λ, R, and P as is illustrated in Fig. 3.

An interesting consequence of [25] relates to the absolute verification of the theory outlined both in the present work and in a previous paper (24). In each case the transformations described by [4]–[7] were calculated on the basis of the instantaneous response of the surface coverage function to small changes in the applied potential. This assumption can now be tested in a very exact way. That is, plots of log (i_g) vs. E_{min} obtained from a series of *galvanostatic* transients should (according to the theory presented above) exactly superimpose on plots of log (i_m) vs. $E_{applied}$ obtained from a series of *potentiostatic* transients. Furthermore, no experimental compensation is required for iR drop because its influence should be identical in both cases. Since the potentiostatic theory is known to be exact (25, 26) the superimposition of the galvanostatic and potentiostatic plots will serve as a diagnostic criterion of the accuracy of the galvanostatic theory.

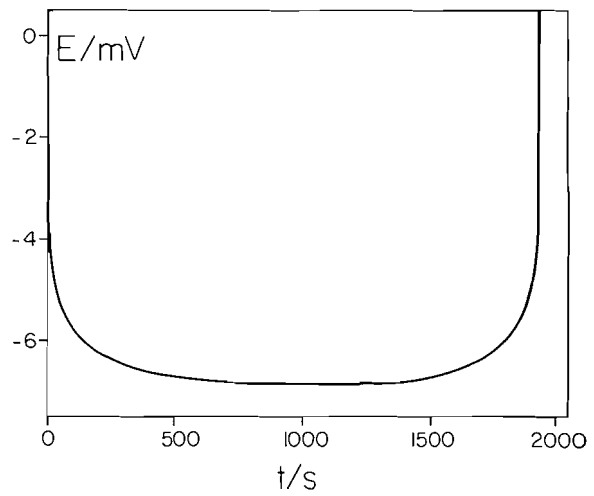

FIG. 3. Complete galvanostatic transient for progressive three-dimensional nucleation and growth. $i_g = 0.005$ mA. The values of E_{min}, t_{ext}, t_{min} are in agreement with the values predicted by [25], [10], [24] respectively. $E_{min} = -6.89$ mV, measured and should be 3 log 0.005 $= -6.903$ according to [25]. $t_{ext} = 1940$ and [10] gives $t_{ext} = 1950$. The values of t_{min} measured and evaluated are consistent but not useful experimentally, due to the shallowness of the E–t graph.

Using the fact that $i_g = (P/4)Q^{\lambda}{}_{min}$ together with [12] gives us $i_g t_{ext}$, the amount of charge consumed in the formation of the three-dimensional layer. We

Can. J. Chem. Downloaded from www.nrcresearchpress.com by 210.87.254.6 on 09/05/12
For personal use only.

obtain $i_g t_{ext} = \text{constant} \times Q^{\lambda-1}{}_{min}$ and hence

[26] $\log(i_g t_{ext}) = (a_1 + a_2)(E_{min} - i_g R) + \text{constant}$

The numerical simulation confirms this gradient of $a_1 + a_2$ in a log $(i_g t_{ext}) - E_{min}$ graph, and is illustrated in Fig. 4.

The Numerical Solution

Instead of solving [8] by standard numerical methods, we instead use a simulation technique which corresponds more closely with the physical situation. It has been shown previously that this technique is exactly equivalent to solving [8], but the starting point here is the family of curves defined by [1]–[3]. The situation is illustrated diagrammatically in Fig. 5. Each curve represents a section of the *i–t* response of progressive, three-dimensional nucleation and growth under potentiostatic conditions. In the interests of clarity only two curves are represented; one of potential E_1 and the other of potential E_2. Each curve is separated individually into elements, the height of which is Δi. Having chosen a fixed current (i_g) and an initial surface coverage ($S_0 < 0.1\%$), an *i–t* transient is located such that the current ($i_g - \Delta i$) corresponds precisely to the surface coverage S_0. This potential is then recorded (E_1). Growth is then allowed to continue on the transient until a current ($i_g + \Delta i$) is reached. At this point the new surface coverage is calculated (S_1). The length of time required to achieve this process is called Δt_1.

The whole process is then repeated. That is, a new *i–t* transient is located (of potential E_2) such that the observed current ($i_g - \Delta i$) corresponds exactly to the surface coverage S_1, and so *ad infinitum*. Should an *i–t* curve pass through a maximum then the logic is inverted to deal with a falling, rather than a rising, transient. In this way the entire potential–time response may be obtained for a given i_g by plotting E_n vs. $\sum_n \Delta t_n$, having shown that the data converges as $\Delta i \to 0$. The rather distinctive result is shown in Fig. 3. As t increases from zero, E decreases from $+\infty$ to E_{min} at a time t_{min} and then rises again to $+\infty$ at a fixed extinction time (t_{ext}).

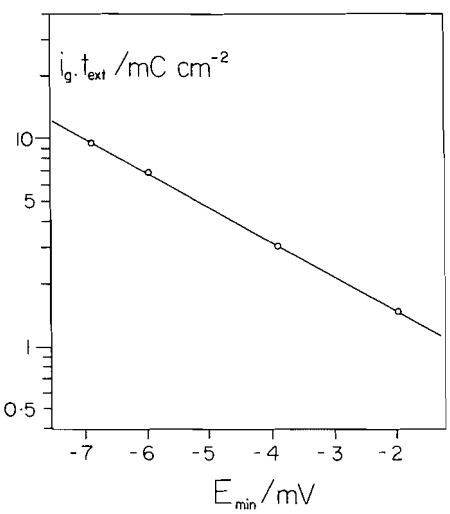

FIG. 4. Charge consumed in the galvanostatic formation of a three-dimensional layer as a function of E_{min}. i_g = various. The gradient is -0.17 and should be $a_1 + a_2 = -\frac{1}{6}$ according to [26].

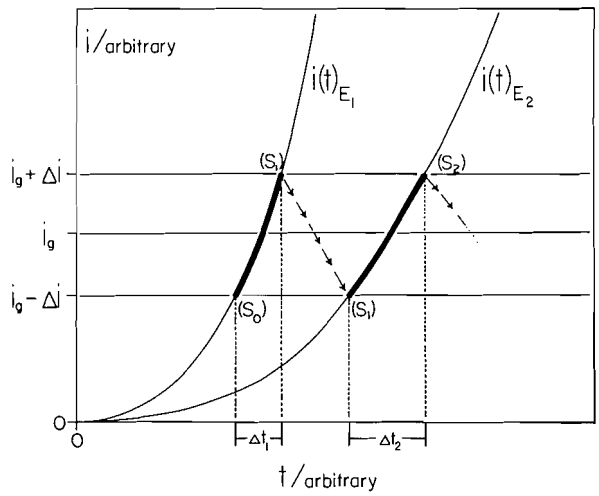

FIG. 5. Basis of the numerical solution.

The physical significance of this is that the rapid fall in potential toward E_{min} is due to the expansion of the emerging interface available for the growth process, once individual nuclei have begun to grow. When the growth centres coalesce, however, the available interface diminishes and so the potential rises back to $+\infty$ again.

Conclusions

The theory of galvanostatic transients has been extended to include crystallization overvoltage. The model chosen was that of progressive, three-dimensional nucleation and growth. It is shown that it is possible to obtain a numerical solution for the entire potential–time plot following the application of a constant current, provided that it is assumed that the electrode surface coverage function responds instantaneously to small changes in potential. Certain limiting cases are also derived which are mathematically exact. A method of testing the model is briefly discussed.

In summary, the present work predicts the following response of the model subsequent to a current step. As t increases from zero, E decreases from $+\infty$ to E_{min} at a time t_{min}. After t_{min}, the potential rises again to $+\infty$ as $t \to t_{ext}$. The minimum occurs at

50% surface coverage and

$$\log (i_g) = \text{constant} + a_1(E_{min} - i_g R)$$

For $\tau \ll 1$

$$\frac{3}{3a_2 - a_1} \log \tau + \text{constant} \sim E - i_g R$$

For $\tau < 1$ and $(1 - \tau) \ll 1$

$$\frac{1}{a_2} \log (1 - \tau) \sim E - i_g R$$

Since fixing i_g is experimentally easy, these equations enable us to evaluate the constants a_1, a_2. Furthermore, the equation of Sand (27) which is widely used in chronopotentiometry for describing diffusion-controlled reactions

$$(\text{transition time})^{1/2} = \frac{\pi^{1/2} n F D^{1/2} C_b^0}{2 i_g}$$

can now be distinguished from the case of three-dimensional nucleation and growth, and so possible confusion can be avoided. This is because, in the present work, (eq. 10)

$$i_g \, t^{\lambda}_{ext} = \text{constant}$$

It also follows that the appropriate experimental plot should be one of $-\log (i_g)$ vs. $\log (t_{ext})$, not i_g vs. $t^{-1/2}_{ext}$.

Finally, it should be noted that the present work can easily be extended to include other models of nucleation and growth, for example the formation of crystalline monolayers. In that case, similar general trends are expected but with some interesting mathematical differences, e.g., the product $i_g t_{ext}$ should be a constant (independent of current) corresponding to the amount of charge consumed in the formation of the surface film. This contrasts with the three-dimensional case which has a variable charge consumption (Fig. 4) and hence variable thickness.

1. V. A. Roiter, V. A. Juza, and E. S. Polujan. Zh. Fiz. Khim. **13**, 605 (1939).
2. T. Berzins and P. Delahay. J. Am. Chem. Soc. **77**, 6448 (1955).
3. T. Berzins and P. Delahay. Z. Elektrochem. **59**, 792 (1955).
4. P. Delahay and C. C. Mattax. J. Am. Chem. Soc. **76**, 874 (1954).
5. P. Delahay, C. C. Mattax, and T. Berzins. J. Am. Chem. Soc. **76**, 5319 (1954).
6. M. D. Wijnen and W. M. Smit. Rec. Trav. Chim. **79**, 203 (1960); **79**, 289 (1960).
7. J. H. Sluyters. Rec. Trav. Chim. **81**, 297 (1962).
8. H. Gerischer and M. Krause. Z. Phys. Chem. **10**, 264 (1957).
9. H. Gerischer and M. Krause. Z. Phys. Chem. **14**, 184 (1958).
10. M. Matsuda, S. Oka, and P. Delahay. J. Am. Chem. Soc. **81**, 5077 (1959).
11. D. A. Vermilyea. *In* Advances in electrochemistry and electrochemical engineering. Vol. 3. *Edited by* P. Delahay. Wiley Interscience, New York, NY. 1963. pp. 211–286.
12. M. Fleischmann and H. R. Thirsk. *In* Advances in electrochemistry and electrochemical engineering. Vol. 3. *Edited by* P. Delahay. Wiley Interscience, New York, NY. 1963. pp. 123–210.
13. T. Erdey-Grüz and H. Wick. Z. Phys. Chem. Abt. A, **162**, 63 (1932).
14. G. Tohmfor and M. Volmer. Ann. Phys. **33**, 109 (1938).
15. A. Bewick. Ph.D. Thesis, University of Durham, Durham, England. 1961.
16. I. Dugdale, M. Fleischmann, and W. F. K. Wynne-Jones. Electrochim. Acta, **5**, 229 (1961).
17. M. Fleischmann and M. Liler. Trans. Faraday Soc. **54**, 1370 (1958).
18. M. Fleischmann and H. R. Thirsk. Trans. Faraday Soc. **51**, 71 (1955).
19. M. Fleischmann and H. R. Thirsk. Electrochim. Acta, **1**, 146 (1959).
20. M. Fleischmann and H. R. Thirsk. Electrochim. Acta, **2**, 22 (1960).
21. W. Beck, R. Lind, and W. F. K. Wynne-Jones. Trans. Faraday Soc. **50**, 147 (1954).
22. H. Lal, H. R. Thirsk, and W. F. K. Wynne-Jones. Trans. Faraday, Soc. **47**, 70 (1951).
23. P. Jones, H. R. Thirsk, and W. F. K. Wynne-Jones. Trans. Faraday Soc. **52**, 1003 (1956).
24. S. Fletcher and A. Smith. Can. J. Chem. In press.
25. R. D. Armstrong, M. Fleischmann, and H. R. Thirsk. J. Electroanal. Chem. **11**, 208 (1966).
26. R. G. Barradas, F. C. Benson, S. Fletcher, and J. D. Porter. J. Electroanal. Chem. **85**, 67 (1977).
27. H. J. S. Sand. Philos. Mag. **1**, 45 (1901).
28. A. Milchev, S. Stoyanov, and R. Kaischev. Thin Solid Films, **22**, 255 (1974); **22**, 267 (1974).
29. A. Milchev and S. Stoyanov. J. Electroanal. Chem. **72**, 33 (1976).
30. V. Ashworth and D. Fairhurst. J. Electrochem. Soc. **124**, 506 (1977).
31. G. A. Gunawardena, G. J. Hills, and I. Montenegro. Discuss. Faraday Soc. To be published.

Can. J. Chem. Downloaded from www.nrcresearchpress.com by 210.87.254.6 on 09/05/12
For personal use only.

Significance of effects of pressure on electrode reactions. Part III. Equilibrium processes at reference electrodes and the volume of H in Pd

BRIAN E. CONWAY AND J. C. CURRIE[1]

Chemistry Department, University of Ottawa, Ottawa, Ont., Canada

Received June 30, 1977

BRIAN E. CONWAY and J. C. CURRIE. Can. J. Chem. **56**, 915 (1978).

For studies on effects of pressure on kinetics of electrode processes (Parts I, II), reversible reference electrodes suitable for use in a completely enclosed high-pressure bomb are required. The electrodes must exhibit reversible behaviour over the pressure range employed in the experiments, i.e., their changes of emf with increasing and decreasing changes of pressure must be reproducible and correspond to the respective volume changes in the reactions.

A series of reversible reference electrodes is examined over a range of pressures up to ca. 2500 bars. The Pd–H/H^+ and Ag,AgCl/Cl^- reference electrodes are found to behave very satisfactorily at elevated pressures; the Pt,H_2/H^+ electrode is, however, less satisfactory, due to problems associated with dissolved H_2.

The results enable the volume of Pd–H and of H sorbed into Pd to be evaluated, together with estimates of the partial molar volume of H_2 in aqueous HCl. These data enable the pressure-coefficients of metal–solution potential differences at individual reference electrodes to be evaluated. Such information is required for interpretation of effects of pressure on kinetics of electrode processes.

BRIAN E. CONWAY et J. C. CURRIE. Can. J. Chem. **56**, 915 (1978).

Dans le cadre de nos études sur l'effet de la pression sur la cinétique des processus aux électrodes (partie I, II), on devait disposer d'électrodes de référence réversibles pouvant être utilisés dans une bombe à haute pression complètement isolée. Les électrodes doivent posséder un comportement réversible à toutes les pressions utilisées au cours des expériences; entre autre on doit être capable de reproduire des changements de force électromotrice avec des augmentations et des diminutions de pression et ces changements doivent correspondre aux changements de volume respectif des réactions.

On a étudié une série d'électrodes de référence réversibles à diverses pressions allant jusqu'à environ 2500 bars. On a trouvé que les électrodes de référence Pd–H/H^+ et Ag,AgCl/Cl^- se comportent d'une façon satisfaisante à des pressions élevées; toutefois l'électrode Pt,H_2/H^+ est moins satisfaisante à cause des problèmes associés avec l'hydrogène dissous.

Les résultats permettent d'évaluer le volume de Pd–H et de H absorbé dans du Pd et d'évaluer les volumes molaires partiels de H_2 dans HCl aqueux. Ces données permettent d'évaluer les coefficients de pression des différences de potentiel métal–solution à des électrodes de référence individuelles. De telles informations sont nécessaires pour interpréter les effets de pression sur les cinétiques des processus aux électrodes.

[Traduit par le journal]

Introduction

In Parts I and II[2] we considered the effect of pressure on the kinetics of cathodic hydrogen evolution and of the $Fe(CN)_6^{3-}/Fe(CN)_6^{4-}$ redox reaction in order to evaluate volumes of activation and examine electrostriction effects in the hydration shell reorganization process. Such studies (1–5) require reference electrodes (1, 2, 4, 5) which (*a*) can be used reliably in an enclosed vessel at high pressure up to say 3000 bars and (*b*) have well-defined and measurable pressure-coefficients of emf when used in appropriate combination with suitable electrolytes. Also, the individual half-cell pressure coefficients of metal/solution potential-difference should be susceptible to evaluation by satisfactory nonthermodynamic means in order that interpretation (3, 6) of pressure effects on the kinetics of electrode processes can be made. Reference electrodes reliable at high pressure (2) are also required for evaluation of battery electrode behaviour at high hydrostatic pressures, e.g. in deep marine environments. There has been little previous work on this kind of problem but the papers of Hills and Kinnibrugh (1) and of Valeriote and Gallop (2) provide an important background for the present work, especially with regard to experimental techniques.

In this paper, we report investigations on the behaviour of three well-known reference electrode systems, Pt,H_2/H^+_{aq}, Pd–H/H^+_{aq}, and Ag,AgCl/Cl^-_{aq}, under conditions of elevated pressure up to ca. 3000 bars. Special attention was given to the Pd–H/H^+ electrode, which has a potential of 0.050 V

[1]Present address: Department of Chemistry, Queen's University, Kingston, Ont.

[2]For Parts I and II, see ref. 3.

Can. J. Chem. Downloaded from www.nrcresearchpress.com by 210.87.254.40 on 09/05/12
For personal use only.

Can. J. Chem. Downloaded from www.nrcresearchpress.com by 210.87.254.40 on 09/05/12
For personal use only.

vs. H_2/H^+ at 1 bar with standard H_2 pressure, as this electrode is particularly suitable for studies of electrode processes at elevated pressures since no added gas is required in the high-pressure cell. Also, the pressure-dependence of the Pd–H/H^+ electrode potential enables the molar volume of H sorbed in Pd, as the β-PdH phase, to be derived.

The pressure dependence of the potential of a reversible electrode reaction is related to the volume change occurring in the half-cell reaction. Thus, the pressure coefficient of emf, E, can be written in terms of the appropriate partial molar volumes V_P of products and V_R of reactants as

$$[1] \qquad \left(\frac{\partial E}{\partial P}\right)_T = -\frac{1}{zF}(\sum V_P - \sum V_R)$$

Since single electrode potentials cannot be experimentally evaluated, the electrochemical cell is comprised of two reversible electrodes, whose emf is measured as a function of pressure. The evaluation of the behaviour of certain reversible electrodes for possible use as reference electrodes in high-pressure electrode kinetic studies was performed by measurements on a combination of two different reversible electrodes (e.g. Ag,AgCl and Pt,H_2) in a single high-pressure cell. If the measured cell emf is reproducible in the modes of compression and decompression of the solution, then the pressure coefficient of emf should be correctly given by $(-1/zF)(\sum V_P - \sum V_R)$. Alternatively, the partial molar volume of one of the components of the reaction can be evaluated if we have precise knowledge of $(\partial E/\partial P)_T$ and the partial molar volumes of the remaining constituents of the cell reaction. If the determination of such a partial molar volume is consistent with the volumes reported in the literature, then it can be assumed that the two reversible electrodes forming the cell are functioning in a thermodynamically well-defined manner and therefore can be used as reference electrodes at high pressures.

Experimental

1. High-pressure System

Details of the high-pressure system, including the thermostatted bomb for containing the electrolytic cells, were given in Part II (3). All measurements in this system were made at 298.06 ± 0.02 K.

2. Electrochemical Cells for Use at High Pressure

Cells consisted of two Pyrex end-pieces joined by 2× heat shrinkable Teflon tubing. The top of the cell contains the electrodes varying in number from 2 to 4, depending on the type of system under examination. All the electrode leads are made of platinum wire of initial diameter 0.025 cm, which is hammered flat and sealed into the Pyrex glass tops of the cells. This type of metal–glass seal was found to withstand repeated elevation of pressure up to 2500 bars without development of any leaks or cracks.

The bottom of the cell is a glass cup with a threaded opening for introducing the electrolyte. A screw cap with a Teflon plug insert and Teflon-covered O-ring was used to make a high-pressure seal. Both the top and bottom of the cell had ridges which allowed a positive Teflon-to-glass seal to be made when the two pieces are joined with the shrinkable Teflon tubing. This type of cell can easily tolerate a 30% volume change without undue strain being generated.

The cell for high-pressure emf measurements consists of 3 reversible electrodes, two of which are of the same type. This provides a reliable check on the behaviour of each electrode while inside the high-pressure bomb. For example, if the cell is Pt,H_2|HCl||Pd–H,Pd, the potential of the palladium–hydrogen electrode can be measured, in turn, against the two Pt,H_2 electrodes. The potential between the two Pt,H_2 reference electrodes was also measured periodically. Thus, three emf measurements are obtained at each pressure. This type of cell is illustrated in Fig. 1.

3. Cell Preparation

All electrochemical cells, including those used at ambient and high pressures, were washed in concentrated sulfuric acid for several hours, followed by thorough rinsing in doubly-distilled H_2O. The cells were then filled with pyro-distilled H_2O and allowed to soak overnight. The electrochemical cells for high-pressure measurements were placed in a glove bag which was under a positive pressure of nitrogen. The solutions were degassed (to remove O_2) with pre-purified N_2 in the glove bag. The cells were then filled with the appropriate solution and allowed to soak for 30 min. The cell was then emptied, rinsed a second time, and filled with the solution required for the experiment. The cell was then sealed with the lower screw cap.

In the case of equilibrium emf measurements involving a Pt,H_2 reference electrode, the electrolyte was presaturated with the H_2 gas at ambient pressure. The cell was then filled with electrolyte and H_2 gas was again passed through it for 15 min. Several small bubbles of H_2 gas were allowed to remain in the cell after the cell had been sealed, in order to ensure that the Pt,H_2 electrode remained in a well-defined state at elevated pressures.

4. Reference Electrodes

The Pt,H_2 (1 bar)/H^+, Ag,AgCl, and Pd,Pd–H reversible electrodes were chosen as being the most convenient for electrochemical studies at high pressures in the present work.

(a) The Pt,H_2 Electrode

The hydrogen electrode was prepared by first cleaning two Pt wires (in the high-pressure cell cap) in warm aqua-regia solution, followed by thorough washing in pyro-distilled water. The wires were then platinized together by the standard procedure with no addition of Pb^{2+} ions. The electrodes were then repeatedly washed with water, followed by several washings in pyro-distilled water.

(b) The Pd,Pd–H Electrode

A palladium electrode was built into the high-pressure cell by welding a piece of palladium wire to a platinum wire. The platinum was then sealed into the high-pressure cell cap with care being taken to expose only the Pd wire. The electrode was cleaned thoroughly with concentrated sulfuric acid and washed with pyro-distilled water. The Pd–H electrode was prepared by constant current cathodic electrolysis in 0.5 M H_2SO_4 for a controlled time. The electrode was oxidized for 1 min, followed by a 90-s reduction, both at a current density of 200 mA cm^{-2}. This cycling procedure was continued for approximately 10 min with termination of the electrolysis in the cathodic direction. The electrode was then washed with pyro-distilled water. This electrode was activated in this

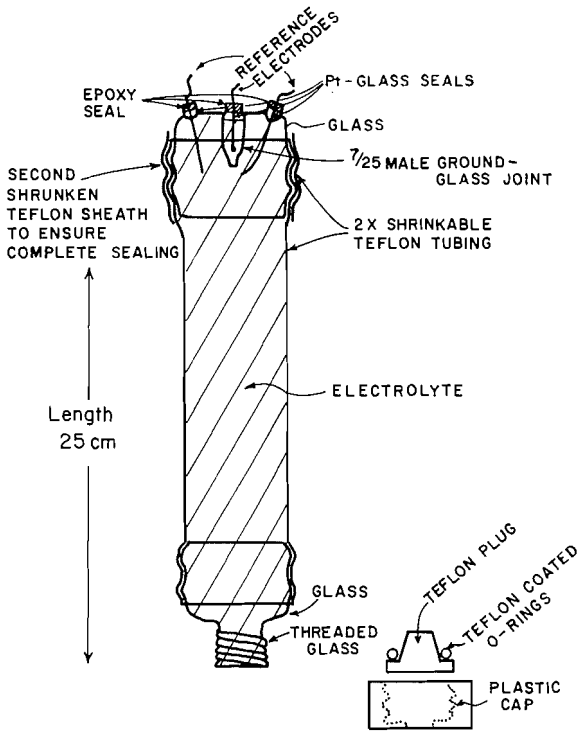

FIG. 1. High-pressure cell for emf measurements. The cell is fabricated from heat-shrinkable Teflon tubing and glass. The cell contains three reversible electrodes of which two are of the same kind.

manner at the beginning of each experiment and gave a reproducible +50 mV potential (17) vs. a Pt,H_2 electrode in the same solution at $P = 1$ bar. This potential corresponds to an equilibrium of H in co-existing α and β phases of PdH with H^+ in solution, and H content < ca. 57 at.%. For convenience, in most of the material which follows, the α + β PdH system will be referred to simply as 'Pd–H'.

(c) The Ag,AgCl Electrode

The silver, silver chloride reference electrode was prepared from a piece of silver wire welded to a platinum wire which was then sealed into the high-pressure cell exposing only the Ag wire. The electrode was cleaned with concentrated sulfuric acid, followed by repeated washings with pyro-distilled water. Anodic deposition of AgCl on the silver wire was carried out (17) by electrolysis from a 1 *M* aqueous HCl solution at a current density of 1.0 mA cm^{-2} for 30 min.

5. Equilibrium EMF Measurements at High Pressures

After the cell had been assembled and connected electrically to the leads in the head of the bomb, it was placed in the high pressure bomb. The cell was then allowed to come to thermal equilibrium before any emf measurements were made. The emf measurements were monitored with a calibrated digital voltmeter (Dana Laboratory, Inc. Model 4300). Elevated pressures were then applied only if the cell emf at ambient pressure had varied less than 100 μV during the last 1 h of the 3 h equilibration period. If this condition was met, the pressure was slowly increased in increments of 276 bars, up to a maximum of 2500 bars. The appreciable heat of compression which is generated was allowed to dissipate for a period of 3 h at each pressure before the emf values were measured. After the maximum pressure had been reached, the system was decompressed in steps of 276 bars, and the emf values were again measured after the normal equilibration period at each pressure.

The pressure coefficient of emf, $(\partial\Delta E/\partial P)_T$, at 1 bar for each pair of reference electrodes was determined graphically from plots of the measured emf values vs. pressure.

Results and Discussion

1. The $Pt,H_2|0.5$ M aq. $H_2SO_4|Pd$–H,Pd Cell

The emf data, ΔE, for this cell as a function of pressure are listed in Table 1. The cell reaction is

$$[2] \qquad Pd + \tfrac{1}{2}H_2 \rightleftarrows PdH$$

As mentioned earlier, 'PdH' is used to represent the 2-phase α + β PdH system at equilibrium which gives (17) the 50 mV potential wrt the Pt,H_2(1 bar)$|H^+$ electrode. The variation of ΔE as a function of pressure is illustrated in Fig. 2. The reversibility of the pressure effects is good with some small degree of hysteresis occurring only with regard to the final readings at low pressure. The slope at 1 bar is $(8.6 \pm 0.5) \times 10^{-6}$ V bar^{-1}. At pressures above 800 bars, the ΔE vs. P plot is linear with a slope of $(6.8 \pm 0.2) \times 10^{-6}$ V bar^{-1}. The hysteresis is probably due to the loss of molecular hydrogen during the course of the run by diffusion through the Teflon walls of the high pressure cell (see below).

The pressure coefficient of emf, $(\partial\Delta E/\partial P)_T$ for the cell reaction 2 is related to the accompanying volume change by

$$[3] \qquad \left(\frac{\partial\Delta E}{\partial P}\right)_T = -\frac{1}{zF}\left(V_{Pd-H} - V_{Pd} - \frac{V_{H_2}}{2}\right)$$

where V_{H_2} is the partial molar volume of H_2, and V_{Pd} and V_{Pd-H} are the molar volumes of Pd and Pd–H, respectively. Therefore, at 1 bar, the volume change for reaction 2 is -8.3 ± 0.5 cm^3 mol^{-1} and at pressures above 800 bars, the volume change tends towards a value of -6.6 ± 0.2 cm^3 mol^{-1}. The increase of the reaction volume as the pressure is enhanced is due to the pressure dependence of the par-

TABLE 1. The emf data for the cell $Pt,H_2|0.5$ *M* aq. $H_2SO_4|$ Pd–H,Pd at 298 K

P (bars)	ΔE(compression) (V)	ΔE(decompression) (V)
1	0.0545	0.0531
280	0.0562	0.0557
560	0.0582	0.0581
840	0.0604	0.0604
1120	0.0622	0.0621
1400	0.0640	0.0642
1680	0.0659	0.0662
1960	0.0677	0.0680
2240	0.0694	0.0700
2520	0.0711	0.0711

Can. J. Chem. Downloaded from www.nrcresearchpress.com by 210.87.254.40 on 09/05/12
For personal use only.

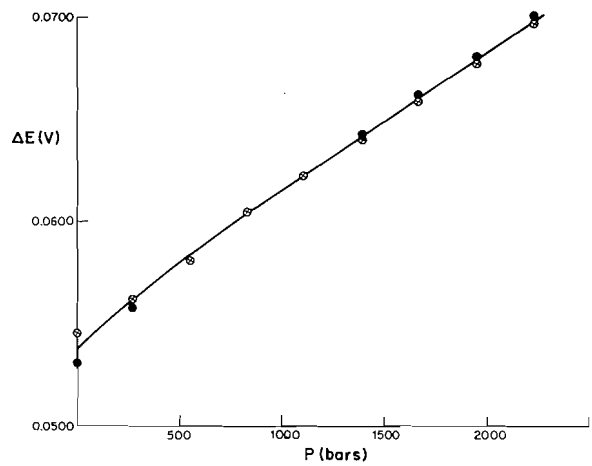

FIG. 2. The variation of emf as a function of pressure at 298.06 K for the cell: $Pt,H_2|0.5\ M\ H_2SO_4|Pd\text{–}H,Pd$.

tial molar volume of H_2 in water. It was found that the $Pd\text{–}H/H^+$ electrode, with Ag,AgCl (see below), provides a stable reference electrode in acid solutions at pressures up to 2500 bars. The Pt,H_2 electrode is stable to within 1 mV during the course of the experiments, but the problems associated with a gaseous reference electrode in a plastic or Teflon cell are always present.

2. The Pt,H_2|1 M HCl|Pd–H,Pd Cell

The behaviour of this cell, with HCl as the electrolyte, was studied in order to provide a basis for use of the $Pd\text{–}H/H^+$ electrode in conjunction with the $Ag,AgCl/Cl^-$ electrode which will be discussed in the following subsection.

The emf data for this $Pt,H_2/Pd\text{–}H$ cell as a function of pressure are listed in Table 2 for two separate experiments. The results are also shown graphically in Fig. 3. The behaviour is, as expected, similar to that of the cell described in subsection 1 above. The slope at 1 bar, $(\partial\Delta E/\partial P)_T$, is $(8.4 \pm 0.5) \times 10^{-6}$ V bar^{-1}; at pressures above 800 bars the pressure coefficient is constant at a value of $(6.9 \pm 0.2) \times 10^{-6}$ V bar^{-1}. The volume change for the reaction 2 is found to be -8.1 ± 0.4 cm^3 mol^{-1} and -6.7 ± 0.2 cm^3 mol^{-1} at 1 bar and above 800 bars, respectively, using the above cell with aq. HCl as electrolyte. The volume data are in quite good agreement with those derived above for the same cell with aq. H_2SO_4 as electrolyte.

The measured cell emf at 1 bar of 0.0502 V is in excellent agreement with the value of 0.0495 V reported by Schuldiner and co-workers (7). The value of ΔE measured after the high-pressure readings, 0.0490 V, is 1 mV less than the initial value at 1 bar. This behaviour is quite similar to that for 0.5 *M* H_2SO_4 and therefore can be rationalized in the same manner, viz. through effects associated with loss of H_2 through the Teflon.

TABLE 2. The emf data for the cell: $Pt,H_2|1\ M$ HCl|Pd–H,Pd at 298 K obtained in two runs

	ΔE (V)	
P (bars)	Run 1	Run 2
1	0.0503	0.0501
276	0.0512	0.0513
552	0.0525	0.0526
828	0.0550	0.0550
1105	0.0571	0.0571
1376	0.0589	0.0590
1656	0.0607	0.0607
1930	0.0625	0.0625
2210	0.0644	0.0644
2480	0.0663	0.0663
1	0.0492	0.0488

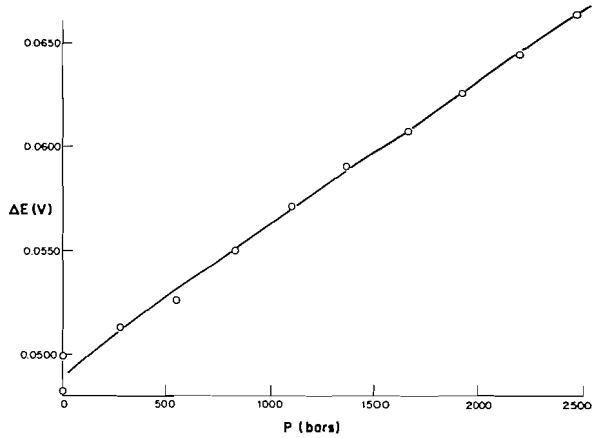

FIG. 3. The variation of emf as a function of pressure at 298.06 K for the cell: $Pt,H_2|1.0\ M$ HCl|Pd–H,Pd.

3. The Pd,Pd–H|M HCl|AgCl,Ag Cell

The pressure coefficient of emf for this cell was measured at a series of HCl concentrations at the following molarities 0.01, 0.25, 0.50, 0.75, and 1.0 (at $P = 1$ bar) in order to evaluate the behaviour of the Pd–H,H^+ and Ag,AgCl reference electrodes as a function of electrolyte concentration over a range of pressures. This cell enables the apparent value of the molar volume of Pd–H to be evaluated at each HCl concentration from the appropriate pressure coefficient of emf and known values of the partial molar volume of aq. HCl, and the molar volumes of AgCl, Ag, and Pd. A true value for V_{Pd-H} can then be obtained for infinite dilution of electrolyte by appropriate extrapolation.

The experimental emf data are listed in Table 3 for each HCl concentration, *C*, and pressure. The emf data as a function of pressure are also illustrated

Can. J. Chem. Downloaded from www.nrcresearchpress.com by 210.87.254.40 on 09/05/12
For personal use only.

TABLE 3. The emf data in volts for the cell Pd,Pd–H|aq. HCl, molarity M|AgCl,Ag at 298 K

Pressure P (bars)	Emf at concentration of HCl (M), C = 0.01	0.25	0.50	0.75	1.0
1	0.40084*	0.24846	0.21301	0.19210	0.17432
276	0.40064	0.24800	0.21238	0.19142	0.17368
552	0.40025	0.24750	0.21180	0.19069	0.17296
828	0.39978	0.24696	0.21118	0.19004	0.17228
1105	0.39937	0.24641	0.21061	0.18935	0.17162
1376	0.39891	0.24583	0.20994	0.18868	0.17089
1656	0.39842	0.24524	0.20931	0.18800	0.17023
1930	0.39796	0.24468	0.20868	0.18731	0.16952
2210	0.39746	0.24412	0.20806	0.18667	0.16884
1	0.40080	0.24865	0.21314	0.19208	0.17449

*Due to the high stability of the emf of this cell a '5½' digit digital voltmeter was used for these measurements.

in Fig. 4, where the differences of emf, $\Delta E_P - \Delta E_1$, at pressures P and 1 bar are plotted against pressure. The slopes are constant with increasing pressure for the three highest concentrations over the complete pressure range. At 0.01 and 0.25 M, the pressure coefficient decreases (becomes more negative) with increasing pressure up to 500 bars; at pressures above 500 bars, the pressure coefficient of the emf becomes independent of P. The values of $(\partial E/\partial P)_T$ at $P = 1$ bar and $P \geq 500$ bars are listed in Table 4. The volume changes at each concentration for the cell reaction

[4] $$\text{Pd–H} + \text{AgCl} \rightleftharpoons \text{Pd} + \text{Ag} + \text{HCl}$$

are also included in Table 4.

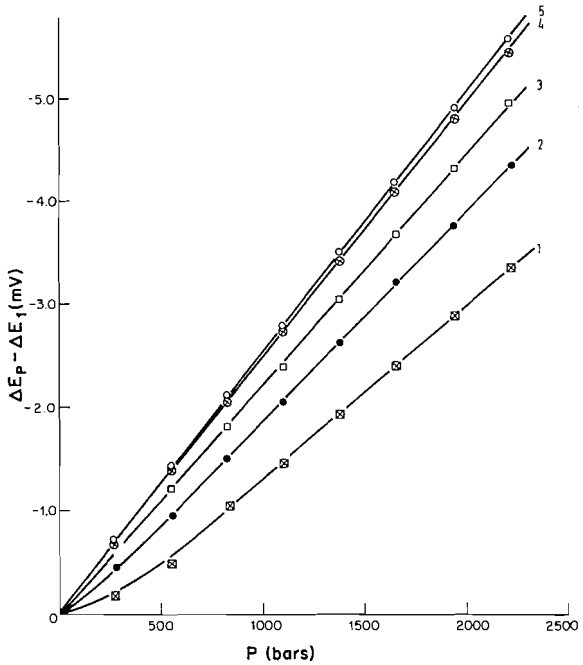

FIG. 4. The variation of emf as a function of pressure at 298.06 K relative to the value at 1 bar for the cell: Pd,Pd–H|HCl|AgCl,Ag at HCl concentrations: (*1*) 0.01 M, (*2*) 0.25 M, (*3*) 0.50 M, (*4*) 0.75 M, (*5*) 1.00 M.

The pressure coefficient is related to the appropriate volume quantities for the cell reaction 4 by the equation

[5] $$\left(\frac{\partial \Delta E}{\partial P}\right)_T = -\frac{1}{F}(V_{Pd} + V_{Ag} + V_{HCl} - V_{Pd-H} - V_{AgCl})$$

where V_{Pd}, V_{Pd-H}, V_{Ag}, and V_{AgCl} are the molar volumes of Pd, Pd–H, Ag, and AgCl, respectively. The molar volumes of Pd, Ag, and AgCl are determined from the appropriate molecular weights and densities of the solid phases in their standard states. V_{HCl} is the partial molar volume of HCl but, for the purpose of this calculation, the partial molal volume of HCl at infinite dilution, V^{∞}_{HCl}, is utilized. From the experimentally determined values of $(\partial \Delta E/\partial P)$, apparent values of the volume V_{Pd-H} can be evaluated from [5] for each concentration of HCl employed. The values of V_{Pd-H} are 'apparent' because V_{HCl} in [5] is concentration-dependent according to the Debye-Hückel law. Inserting the appropriate numerical data (8) in [5] gives

[6] $$\left(\frac{\partial \Delta E}{\partial P}\right)_T = -\frac{1}{F}(9.33 + 10.27 + 17.83 - V_{Pd-H} - 25.78)$$

The apparent values of V_{Pd-H} calculated from the data for each HCl concentration and [6] are listed in Table 5. Apparent values of V_{Pd-H} are then plotted vs. $C^{1/2}$ and extrapolated to zero ionic strength of

Can. J. Chem. Downloaded from www.nrcresearchpress.com by 210.87.254.40 on 09/05/12
For personal use only.

Can. J. Chem. Downloaded from www.nrcresearchpress.com by 210.87.254.40 on 09/05/12
For personal use only.

TABLE 4. Pressure coefficients of emf for the cell: Pd,Pd–H|*M* HCl|AgCl,Ag at 298 K and the corresponding volume changes ΔV, or ΔV_p at pressure = 1 or *P* bars

C(HCl) molarity	*P* = 1 bar		*P* ≥ 500 bars	
	$(\partial\Delta E/\partial P)_T$ (μV bar^{-1})	ΔV_1 (cm^3 mol^{-1})	$(\partial\Delta E/\partial P)_T$ (μV bar^{-1})	ΔV_p (cm^3 mol^{-1})
0.01	−0.50±0.02*	0.50±0.02	−1.70±0.05	1.60±0.05
0.25	−1.50±0.05	1.50±0.05	−2.00±0.1	2.00±0.1
0.50	−2.20±0.1	2.10±0.1	−2.20±0.1	2.10±0.1
0.75	−2.48±0.1	2.40±0.1	−2.48±0.1	2.40±0.1
1.00	−2.55±0.1	2.46±0.1	−2.55±0.1	2.46±0.1

*Estimated errors are evaluated from standard deviations, duplicate emf measurements in the compression and decompression modes and the intrinsic error in the pressure measurement.

TABLE 5. Apparent values of the molar volume of Pd–H* at 298 K

C (*M*) HCl	V_{Pd-H} (cm^3 mol^{-1})
0.01	11.2
0.25	10.2
0.50	9.55
0.75	9.25
1.00	9.19
0 (extrapolated)	11.3±0.1

*The significance of this volume deduced from the emf measurements is examined in section 5.

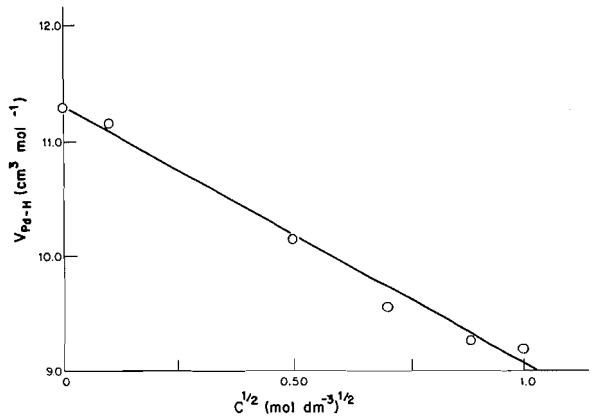

FIG. 5. The variation of the molar volume of Pd–H, V_{Pd-H} with $C_{HCl}^{1/2}$. The best-fit straight line obtained by the method of least squares is shown.

HCl giving a true value of V_{Pd-H} as shown in Fig. 5. The best-fit straight line by the method of the least squares gives an intercept at $C = 0$ of $V_{Pd-H} = 11.3 \pm 0.1$ cm^3 mol^{-1}. The solution compression effect considered in kinetic experiments (3) need not be taken into account here since molalities are employed in the Nernst equation for emf's so that (cf. ref. 2) compression effects are included in the activity coefficients giving a nonideal volume contribution which is eliminated on extrapolation to infinite dilution.

The emf data in Table 4 are satisfactorily reproducible over the pressure range 1 to 2210 bars. The maximum variation of ΔE at 1 bar recorded before and after the high-pressure measurements was 1.7×10^{-4} V ($C = 1.0$ *M* HCl). The minimum variation was 2×10^{-5} V ($C = 0.75$ *M* HCl). Therefore the electrodes Pd–H/H$^+$ and Ag,AgCl/Cl$^-$ can be used as reliable reference electrodes at elevated pressures, with an uncertainty in the measured emf not greater than 1.7×10^{-4} V.

4. The Pt,H_2|1 M HCl|AgCl,Ag Cell

The emf of this cell was found to be relatively unstable in comparison with that of the other cells referred to above. It was initially thought that a time-dependent mixed-potential was set up at the Ag,AgCl electrode in the presence of H_2. Another possible explanation is that reduction of traces of dissolved Ag$^+$ by molecular hydrogen occurs at the Pt,H_2 electrode. A separator between the Ag,AgCl and the Pt,H_2 electrodes was therefore introduced in the cell, but the cell emf again proved to be unstable. Significant diffusion of H_2 through the Teflon walls of the high-pressure cell appears to be a more realistic explanation for the time-dependent emf of this cell. Earlier experiments with the Pt,H_2 vs. Pd–H,Pd system referred to in subsection 1 gave, however, much more stable potentials in the ascending and descending direction of pressure change. In the later experiments, the cells used were made of Teflon from a source different from that employed in the earlier measurements. Therefore, it seems that the two Teflon samples have a different structure, the more recently obtained being permeable to molecular hydrogen.

Heusler and Gaiser (4) also observed instability and systematic errors of about 2 mV for the equilibrium emf of the cell Pt,H_2|HCl, NaCl|AgCl,Ag at atmospheric pressure. The errors were attributed to irreversible reduction of AgCl and to the fact that the H_2 partial pressure became less than 1 bar. The loss of hydrogen was attributed to diffusion through their Teflon cell into the hydraulic oil in the high-pressure vessel. Valeriote and Gallop (2) also observed similar drifts of cell potentials when a

TABLE 6. Pressure coefficients of emf for cells 1, 2, and 3 at 298 K

P (bar)	C (mol dm^{-3} HCl)	$(\partial\Delta E_1/\partial P)_T$ (μV bar^{-1})	$(\partial\Delta E_2/\partial P)_T$	$(\partial\Delta E_3/\partial P)_T$	ΔV_1 (cm^3 mol^{-1})	V_{H_2} (cm^3 mol^{-1})
1	1.0	5.85	8.40	−2.55	−5.65	17.6
>800	1.0	4.35	6.90	−2.55	−4.20	14.1

hydrogen electrode is used in a Teflon, Lexan, or nylon high-pressure cell. The effects were again attributed to diffusion of H_2 through the walls of the cell.

In order to obtain a more reliable estimate of the pressure-dependence of emf of the cell $Pt,H_2|HCl|AgCl,Ag$ (cell 1), an indirect approach must therefore be taken. The two cell systems treated in subsections 2 and 3 are considered:

$$Ag,AgCl|1\ M\ HCl|Pd\text{–}H,Pd \quad \text{(cell 2)}$$

and

$$Pt,H_2|1\ M\ HCl|Pd\text{–}H,Pd \quad \text{(cell 3)}$$

The $(\partial\Delta E_1/\partial P)_T$ for the $Pt,H_2|1\ M$ HCl|AgCl,Ag system, i.e., for the cell reaction

[7] $$\tfrac{1}{2}H_2 + AgCl \rightleftarrows Ag + HCl$$

for which

[8] $$\left(\frac{\partial\Delta E_1}{\partial P}\right)_T = -\frac{1}{F}\left(V_{Ag} + V_{HCl} - \frac{V_{H_2}}{2} - V_{AgCl}\right)$$

is obtained from the pressure dependence of the emf's of cells designated 2 and 3.

The $(\partial\Delta E/\partial P)_T$ values for cells 1, 2, and 3, and the volume change, ΔV_1, for the cell reaction 7 are listed in Table 6. The partial molar volume of H_2 in 1 M HCl at $P = 1$ bar, as calculated from [8], is also given in Table 6.

5. *The Volume of H Sorbed into Pd and the Significance of the Quantity* V_{PdH}

From the data given above, it is seen that evaluation of the pressure coefficient of emf for the cell

[9] $$Pd,Pd\text{–}H|M\ HCl|AgCl,Ag$$

can provide a convenient method for the determination of the molar volume, $V_{Pd\text{–}H}$, of Pd–H. The significance of $V_{Pd\text{–}H}$ can best be visualized if the processes involved in the $Pd\text{–}H,H^+$ reference electrode reaction are considered.

The behaviour of the $Pd\text{–}H,H^+$ reference electrode has been studied by Schuldiner *et al.* (7), Flanagan and Lewis (9), and by Aben and Burgers (10) with varying opinions on the actual mechanisms involved in the functioning of such an electrode. However, the mechanism described below appears to be the most consistent with the experimental facts. It is known that a palladium wire charged with hydrogen electrolytically or under hydrogen atmosphere will achieve a potential of about +0.050 V with respect to a standard Pt,H_2 reference electrode. Hydrogen is absorbed initially by palladium in the α-phase up to a limiting composition of H/Pd = 0.03 at 298 K. Further H absorption produces a second phase, β, with an H/Pd ratio of 0.60. The stable, well defined electrode potential is due to the simultaneous presence at the electrode surface of the two phases in thermodynamic equilibrium, with the H also in equilibrium with H^+_{aq} and electrons. Electrochemical equilibrium thus exists between the α + β Pd–H electrode and the electrolyte as represented formally by the equation

[10*a*] $$Pd + H^+ + e \rightleftarrows Pd\text{–}H$$

More specifically, when the electrode exhibits the '50 mV' potential (7, 9, 10), α and β-PdH phases co-exist with the α-PdH phase saturated (3 at.% H). Reaction 10*a* should hence be written

[10*b*] $$\alpha\text{-PdH (satd.)} + H^+ + e \rightleftarrows (\alpha + \beta)\text{-PdH}$$

The absorption of H into Pd to form, initially, the α-phase is known (10) to occur with very little expansion of the Pd lattice. Hence, in [5] for reaction 4, V_{Pd} strictly refers to $V_{\alpha\text{-PdH (satd)}}$ and is almost equal to this quantity while V_{PdH} refers to the volume of α-PdH + β-PdH formed from the saturated α-phase by reaction 10*b*. On the other hand, the formation of the β-phase occurs with considerable increase of the lattice parameters, *a*. Values of the latter, obtained by Aben and Burgers (10), using X-ray diffraction, are listed in Table 7.

The value of the measured molar volume of 'PdH' in an α + β-PdH system is therefore associated with the production of H in the β-phase, since it is only this phase that forms with a relatively large expansion of the Pd lattice and a corresponding positive volume change. Hence the value $V_{Pd\text{–}H} = 11.3$ cm^3 mol^{-1} given in Table 5 is the molar volume of formation of H in the β-phase. The apparent volume of H itself, V_H, can then be evaluated by taking the difference of '$V_{Pd\text{–}H}$' and the molar volume of α-PdH

TABLE 7. Lattice parameters for the Pd,Pd–H system (10)

α-Phase	α-Phase + H	(α + β) Phase + H
$a = 0.3882$ nm	$a = 0.3886$ nm	$a_\alpha = 0.3886$ nm
		$a_\beta = 0.4017$ nm

Can. J. Chem. Downloaded from www.nrcresearchpress.com by 210.87.254.40 on 09/05/12
For personal use only.

Can. J. Chem. Downloaded from www.nrcresearchpress.com by 210.87.254.40 on 09/05/12
For personal use only.

assuming $V_{\alpha\text{-PdH (satd)}} \doteqdot V_{Pd}$. This approach gives a value for $V_H = 2.0\ cm^3\ mol^{-1}$ which is the net volume change of α-PdH (satd) upon absorption of 1 mol of H atoms to produce β-PdH.

Direct evaluation[3] of the quantities V_{Pd-H} and V_H for H in palladium does not seem to have been previously reported in the literature, although V_H in pure iron and in Pd–Ag alloys has been evaluated by measuring the uptake of H_2 under uni-axial stress. This type of measurement is based on the fact that when a tensile stress is applied to a metal it causes an increase in the solubility of H while a compressive stress decreases the quantity of absorbed H-atoms. The change of solubility of H is related to the applied stress by

$$[11] \qquad \frac{\partial \ln (c/c_0)}{\partial \sigma} = \frac{V_H}{3RT}$$

where c is the solubility of hydrogen (moles of H/cm^3 of substrate) when the applied uniaxial stress is σ and c_0 is the solubility when the applied stress is zero. Utilizing this approach, Bockris and co-workers (11) have determined V_H for H in pure Fe as 2.6 cm^3 mol^{-1}. Wriedt and Oriani (12) have determined the value to be 1.90 cm^3 mol^{-1} in a 75% Pd – 25% Ag alloy which is in good agreement with the value obtained in this work: $V_H = 2.0\ cm^3\ mol^{-1}$. It is of interest that this value is appreciably smaller than the volume of adsorbed H at Pt, which we recently determined (22).

The behaviour of the Pd,Pd–H|*M* HCl|AgCl,Ag cell at pressures up to 2500 bars appears to be sufficiently reliable and reversible with respect to increasing and decreasing changes of pressure, that F times the pressure-coefficient of the cell emf can be equated with certainty to the known molar volume differences of the respective components in the cell reaction. This being the case, the Pd–H,H^+ electrode can be utilized as a satisfactory reference electrode in high-pressure electrochemical studies in acid media, as were described in Part II. The Ag,AgCl electrode can be adopted for use in Cl^- salt solutions at elevated pressures.

6. *The Partial Molar Volume of H_2 in Aqueous Solution*

From measurements at various hydrostatic pressures on cells involving the Pt–H_2/H^+_{aq} electrode, the partial molar volume of H_2 in aqueous solution can be derived. Previous data in the literature for V_{H_2} derived from emf measurements (1, 2) are apparently discrepant and differ from a value obtained by Tiepel and Gubbins (13) using a dilatometric technique. The differences appear to be due to ionic strength effects on the apparent molar volume of H_2.

For the cell Pt,H_2|0.1 *M* HCl|AgCl,Ag, Valeriote and Gallop's (2) results give a partial molar volume of H_2 in 0.1 *M* HCl as 17.9 cm^3 mol^{-1}. Hills and Kinnibrugh (1), using the cell Pt,H_2|0.1 *N* HCl|Hg_2Cl_2,Hg, quote $V_{H_2} = 15\ cm^3\ mol^{-1}$ for 0.1 *M* HCl. Heusler and Gaiser (4), using cell 1 (eq. 8), obtained emf values over a range of HCl concentration and evaluated the infinite dilution volume $V^{\infty}_{H_2} = 24\ cm^3\ mol^{-1}$ from the pressure effect on the emf of this cell.

It has been mentioned in subsection 4 that the pressure-coefficient of emf of the cell Pt,H_2|1 *M* HCl|AgCl,Ag could not, for various possible reasons, be measured experimentally in a reliable manner (cf. ref. 4) but could be satisfactorily derived from emf measurements on the cells Pt,H_2|1 *M* HCl|Pd–H,Pd and Pd,Pd–H|1 *M* HCl|AgCl,Ag. The pressure-coefficient of emf obtained in this manner can be used to determine the partial molar volume of H_2 in 1 *M* HCl.

The partial molar volume of H_2 obtained by this procedure in the present work for 1 *M* HCl is $V_{H_2} = 17.6\ cm^3\ mol^{-1}$ and agrees quite well with the value of Heusler and Gaiser (4): $V_{H_2} = 17.7\ cm^3\ mol^{-1}$ for 0.80 *M* HCl. The V_{H_2} values of Heusler and Gaiser are plotted as a function of $C^{1/2}$ in Fig. 6. The best-fit straight line has a slope of −6.3 and gives an intercept $V^{\infty}_{H_2}$ of 24 cm^3 mol^{-1}. The value of V_{H_2} obtained in the present work is within 0.2 cm^3 mol^{-1} of the corresponding value of Heusler and Gaiser on their V_{H_2}–$C^{1/2}$ plot at $C = 1.0$ *M* HCl. This would give $V^{\infty}_{H_2} = 24\ cm^3\ mol^{-1}$ (using their

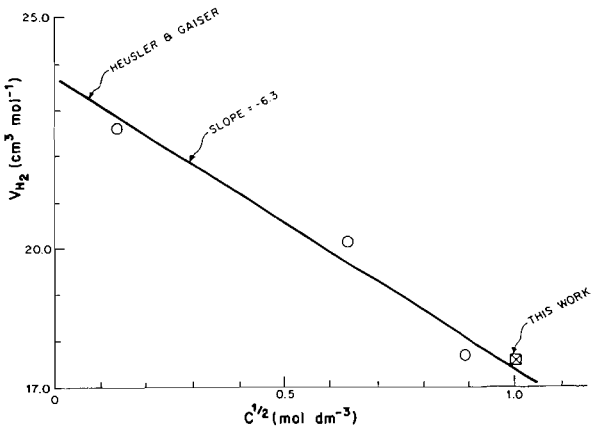

FIG. 6. The variation of the partial molar volume of H_2, V_{H_2}, with $C^{1/2}$ from the data of Heusler and Gaiser (4).

[3]The 'partial molar volume' of H in Pd and various Pd alloys was evaluated by Baranowsky *et al.* (23) from changes of lattice parameters as a function of uptake of H from H_2 at high pressures.

Can. J. Chem. Downloaded from www.nrcresearchpress.com by 210.87.254.40 on 09/05/12
For personal use only.

slope). This value is in good agreement with the previously reported (13) value $V_{H_2}^{\infty} = 25.2$ cm^3 mol^{-1}, based on dilatometric measurements in pure water.

Apparent discrepancies in the literature for V_{H_2} values are evidently due to dependence of the apparent values of V_{H_2} on ionic strength (salting-out effect). Table 8 summarizes the values of V_{H_2} obtained from the literature and from the present work.

It is seen that introduction of a small molecule such as H_2 into an aqueous solution results in a surprisingly large volume increase ($\sim$24 cm^3 mol^{-1}). This observation is consistent with the earlier work of Frank and Evans (14) on the effect of dissolved nonelectrolytes on the structure of water. The introduction of nonpolar gases such as H_2, Ar, He, and Rn into aqueous solutions was found by these authors in a large decrease in entropy of the system (-105–170 J K^{-1} mol^{-1}). This behaviour was related to the ability of these solutes to promote so-called structure building of water around nonpolar solute molecules. The larger solute molecules, such as Rn, promote a greater degree of structure making. The formation of aggregates of structured water will result in expansion of the solvent as reflected in the relatively large values of the observed apparent or partial molar volume of nonpolar solutes.

The partial molar volume of H_2 in 1 *M* aqueous HCl at 1 bar is 17.6 cm^3 mol^{-1}; however, as the pressure is increased, V_{H_2} decreases steadily until about 800 bars. Above this pressure, the value of V_{H_2} becomes constant at 14.1 cm^3 mol^{-1} (Table 6). The decrease of V_{H_2} with pressure is due to the pressure-induced destruction of part of the expanded water structure around the H_2 solute. Above 800 bars, local structure promoted by the introduction of H_2 into the aqueous electrolyte has evidently been 'regelated'. This behaviour is analogous to the observations made by Frank and Evans (14) on the increase of entropy with increasing temperature for nonpolar gases in water. This variation was attributed to the 'melting' of the so-called 'iceberg' structures surrounding the solute molecules.

TABLE 8. Partial molar volumes of H_2 in aq. HCl

C (mol dm^{-3} HCl)	V_{H_2} (cm^3 mol^{-1})				
	Ref. 4*	Ref. 2†	Ref. 1‡	Ref. 13§	This work
0	24	—	—	25.2	$\sim 24 \pm 1$
0.02	22.6	—	—	—	—
0.10	—	17.9	15.0	—	—
0.42	20.2	—	—	—	—
0.80	17.7	—	—	—	—
1.00	—	—	—	—	17.6 ± 0.6

*Pt,H_2|*M* HCl|AgCl,Ag.
†Pt,H_2|0.1 *M* HCl|AgCl,Ag.
‡Pt,H_2|0.1 *M* HCl|Hg_2Cl_2,Hg.
§Dilatometer method in aqueous KOH.

The large concentration dependence of apparent values of V_{H_2} observed in this work and that of Heusler and Gaiser (4) ($S_v = -6.3$) can be explained in terms of the salting-out effect. In solutions of moderate electrolyte concentration (0.01 $\rightarrow$ 1 *M*), increasing mole fractions of the solvent will be involved in solvation of the respective ions as their concentration increases. Therefore, a solute molecule such as H_2 when introduced into an ionic solution sees a smaller volume of 'free' solvent molecules than would be the case in pure water. The activity coefficient of the H_2 gas is therefore increased corresponding to reduction of its solubility (salting-out effect) (15, 16). Therefore the volume change accompanying the dissolution of H_2 will be less than the $V_{H_2}^{\infty}$ value due to the effect of pressure on the activity coefficient associated with the influence of the ions present.

7. *Pressure Coefficients of Individual Electrode – Solution Potential Differences*

In studies of kinetics of electrode processes as a function of pressure, an apparent volume of activation $\Delta V_a^{\ddagger}$ is obtained (3) which differs (6, 18) from the true, kinetically significant value $\Delta V_t^{\ddagger}$ by β times the volume change, ΔV_0, for the same overall electrode process at equilibrium: $\Delta V_t^{\ddagger} = \Delta V_a^{\ddagger} + \beta \Delta V_0$ or $\Delta V^{\ddagger} = \Delta V_a^{\ddagger} - (1 - \beta)\Delta V_0$, where β is the symmetry coefficient for the electron-transfer process. The term $\beta \Delta V_0$ enters (6) into the expression for $\Delta V_t^{\ddagger}$ due to the pressure-dependence of the potential difference at the reversible reference electrode used to make the kinetic measurements at well-defined electrode potentials.

The present results enable the individual pressure coefficients of the metal–solution potential differences for the Pd–H/H$^+$ and Pt–H_2/H$^+$ reference electrodes to be estimated, taking a value for $V_{H^+}^{\infty} = -5.4$ cm^3 mol^{-1} based on (*a*) ultrasonic vibration potentials (19) and (*b*) extrapolation of volumes of R_4N^+ halide salt ions (20), methods which give values for $V_{H^+}^{\infty}$ in very good agreement (21). The individual pressure-coefficients and corresponding volume changes ΔV_0 are given in Table 9. The ΔV_0 values depend on the assignment of a value V_e for the volume of electrons in a metal. The figure of 3 cm^3 Faraday^{-1} from ref. 4 has been used for the data given in Table 9.

The individual pressure coefficients of potential differences in Table 9 do not take account of the (unknown) pressure dependence of surface-potential

TABLE 9. Pressure coefficient of metal–solution potential differences at individual reference electrodes

Electrode	ΔV (cm^3 mol^{-1})	$(dE/dP)_T$ (μV bar^{-1})
$H^+ + e \rightleftharpoons \frac{1}{2} H_2$	14.4	−14.9
$H^+ + e + Pd \rightleftharpoons Pd\,H$	4.4	−4.6
$AgCl + e \rightleftharpoons Ag + Cl^-$	4.7	−4.9

differences, $d\chi/dP$. However, the corresponding effects of varying temperature indicate that $d\chi/dT$ is not appreciable. Hence it is reasonable to assume that any pressure dependence of χ up to ca. 3000 bars will not seriously affect the values of the pressure coefficient of individual electrode potentials evaluated from V data, and hence of the derived true activation volumes in kinetic studies.

Acknowledgements

Grateful acknowledgement is made to the Defence Research Board for support of this work in its early stages and to the National Research Council of Canada for its support over the past two years. We also acknowledge useful discussions with Drs. W. Adams and J. Valeriote.

1. G. J. HILLS and D. R. KINNIBRUGH. J. Electrochem. Soc. **113**, 1111 (1966).
2. E. M. L. VALERIOTE and L. D. GALLOP. J. Electrochem. Soc. **121**, 1245 (1974).
3. B. E. CONWAY and J. C. CURRIE. J. Electrochem. Soc. **125**, 252 (1978); **125**, 257 (1978).
4. K. E. HEUSLER and L. GAISER. Ber. Bunsenges. Phys. Chem. **72**, 1059 (1969).
5. W. R. HAINSWORTH, H. J. ROWLEY, and D. A. MACINNES. J. Am. Chem. Soc. **46**, 1437 (1924).
6. B. E. CONWAY. *In* Chemical physics of ionic solutions. *Edited by* B. E. Conway and R. G. Barradas. John Wiley and Sons Inc., New York, NY. 1966. pp. 577–578.
7. S. SCHULDINER, J. P. HOARE, and G. W. CASTELLAN. J. Chem. Phys. **28**, 16 (1958); **28**, 22 (1958).
8. F. J. MILLERO. *In* Water and aqueous solutions. *Edited by* R. A. Horne. Wiley Interscience, New York, NY. 1972.
9. R. B. FLANAGAN and F. A. LEWIS. Trans. Faraday Soc. **55**, 1409 (1959).
10. P. C. ABEN and W. G. BURGERS. Trans. Faraday Soc. **58**, 1989 (1962).
11. W. BECK, J. O'M. BOCKRIS, J. MCBREEN, and L. NANIS. Proc. R. Soc. London, A, **290**, 220 (1966).
12. H. A. WRIEDT and R. A. ORIANI. Acta Metall. **18**, 753 (1970).
13. E. W. TIEPEL and K. E. GUBBINS. J. Phys. Chem. **76**, 3044 (1972).
14. H. S. FRANK and M. W. EVANS. J. Chem. Phys. **13**, 507 (1945).
15. P. DEBYE and J. MACAULAY. Z. Phys. Chem. **26**, 22 (1925).
16. B. E. CONWAY and D. M. NOVAK. *In* Chemistry and physics of aqueous gas solutions. The Electrochemical Society, Princeton. 1975. p. 115.
17. D. J. G. IVES and G. J. JANZ. Reference electrodes. Academic Press, New York, NY. 1961. pp. 112–115, 203–218.
18. B. E. CONWAY. J. Electrochem. Soc. **113**, 1118 (1966).
19. R. ZANA and E. YEAGER. J. Phys. Chem. **70**, 954 (1966); **71**, 521 (1967).
20. B. E. CONWAY, J. E. DESNOYERS, and R. E. VERRALL. J. Phys. Chem. Trans. Faraday Soc. **62**, 2738 (1966).
21. B. E. CONWAY, J. E. DESNOYERS, and R. E. VERRALL. J. Phys. Chem. **75**, 3031 (1971).
22. B. E. CONWAY and J. C. CURRIE. J. Chem. Soc. Faraday Trans. I. In press.
23. B. BARANOWSKI, S. MAJCHRZAK, and T. B. FLANAGAN. J. Phys. F, **1**, 258 (1971).

Can. J. Chem. Downloaded from www.nrcresearchpress.com by 210.87.254.40 on 09/05/12
For personal use only.

Etude des interactions des oxirannes et thiirannes avec les α,β,γ,δ-tétraphénylporphyrines au cadmium, zinc et magnésium

PHILIPPE DUMAS

Laboratoire de Chimie Macromoléculaire associé au C.N.R.S., Université Pierre et Marie Curie, 4, place Jussieu 75230 Paris Cedex 05, France

ET

PHILIPPE GUERIN

Laboratoire de Chimie de Coordination Organique et Biologique, Ecole Normale Supérieure, 24, rue Lhomond 75231 Paris Cedex 05, France

Reçu le 25 juillet 1977

PHILIPPE DUMAS et PHILIPPE GUERIN. Can. J. Chem. **56**, 925 (1978).

Les α,β,γ,δ-tétraphénylporphyrines au cadmium, zinc et magnésium forment avec les oxirannes et les thiirannes des complexes 1:1. Les valeurs relatives des constantes de complexation sont en accord avec la théorie des acides et bases "durs et mous".

Les α,β,γ,δ-tétraphénylporphyrines au cadmium, zinc et magnésium sont démétallées par les thiols. Celle au cadmium peut réagir avec des hétérocycles soufrés possédant un hydrogène en β du soufre pour donner la porphyrine libre et un thiolate de cadmium. Lorsque cet hétérocycle est le méthylthiiranne, l'organocadmien ainsi formé est susceptible d'amorcer *in situ* la polymérisation stéréospécifique de cet hétérocycle.

PHILIPPE DUMAS and PHILIPPE GUERIN. Can. J. Chem. **56**, 925 (1978).

1/1 adducts from oxiranes or thiiranes and cadmium, zinc, or magnesium α,β,γ,δ-mesotetraphenylporphyrins were obtained in benzene and complexation constants determined. Results agree with the theory of 'hard and soft' acids and bases.

Demetallation of the metaloporphyrins of Cd, Zn, and Mg is achieved with thiols. The cadmium porphyrin reacts with sulfur heterocycles which contain a β hydrogen to yield the free porphyrin and a thiolate of cadmium. If this heterocycle is methylthiirane, the organocadmium compound formed may initiate the subsequent *in situ* stereospecific polymerization of methylthiirane.

Introduction

Les dérivés du cadmium, du zinc et du magnésium amorcent les polymérisations stéréospécifiques des oxirannes et des thiirannes (1, 2). Le mécanisme de ces polymérisations est supposé anionique coordiné. La coordination du soufre (ou de l'oxygène) de l'hétérocycle serait suivie d'une insertion du monomère entre l'extrémité de la chaîne macromoléculaire active et le métal. L'ouverture du cycle oxiranne ou thiiranne se produit dans ce cas presque exclusivement entre le carbone secondaire et l'hétéroatome; elle conserve la configuration absolue du carbone asymétrique de l'hétérocycle. Il est supposé que l'amorceur (le dérivé organométallique) choisit la configuration du monomère à introduire et que par suite de ce contrôle, les chaînes macromoléculaires ne contiennent qu'un seul type d'unités configurationnelles. Le polymère est stéréorégulier et possède une structure isotactique. Cette stéréorégularité proviendrait donc d'effets stériques et de la complexation entre le métal et l'oxygène (ou le soufre).

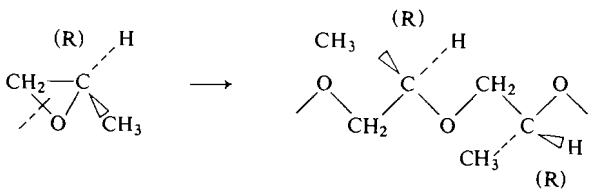

Malheureusement la complexité des espèces organométalliques actives ne permet pas d'étudier directement ces interactions et l'utilisation de modèles s'avère nécessaire (3). Les α,β,γ,δ-tétraphénylporphyrines métallées ne présentent pas de phénomène d'autoassociation, possèdent un spectre d'absorption dans le visible caractéristique (4) et sont donc des composés modèles particulièrement pratiques pour examiner des phénomènes de complexation. Nous avons pu ainsi comparer les différences de comportement entre des hétérocycles contenant du soufre ou de l'oxygène avec le zinc, le cadmium ou le magnésium.

Partie expérimentale

La tétraphénylporphyrine a été préparée selon la méthode décrite par Adler et coll. (5) et purifiée en présence de 2,3 dichloro-5,6 dicyanobenzoquinone pour éliminer la porphine (6). L'insertion des métaux a été effectuée dans la diméthylformamide en utilisant l'acétate de cadmium, l'acétate de zinc et le chlorure de magnésium (7).

Le tertbutylthiiranne, seule base de Lewis non commer-

Can. J. Chem. Downloaded from www.nrcresearchpress.com by 210.87.254.42 on 09/05/12
For personal use only.

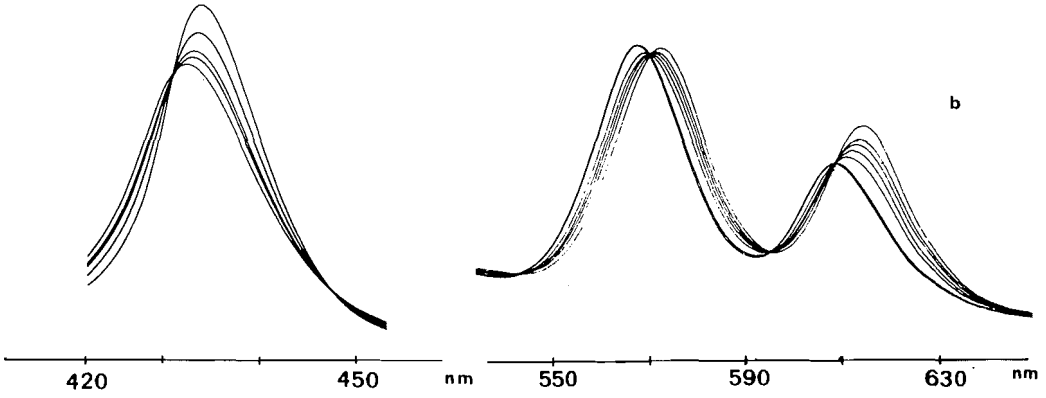

FIG. 1. Etude en spectroscopie visible de la formation du complexe par introductions successives de méthylthiiranne dans une solution benzénique de tétraphénylporphyrine au cadmium, à 20°C. (*a*) Région 400–450 nm, chemin optique de la cuve: 1 mm; (*b*) région 500–650 nm, chemin optique de la cuve: 10 mm.

cialisée utilisée par nous, a été préparé suivant une méthode déjà décrite par l'un d'entre nous (8).

Les déterminations de constantes de complexations ont été effectuées dans le benzène à 617 nm pour la porphyrine au cadmium, 609 nm pour celle au magnésium et 592 nm pour celle au zinc. La concentration de l'hétérocycle variait de 10^{-3} à 1 *M* et celle de la tétraphénylporphyrine était égale à 6.3×10^{-5} *M* (TPPCd), 6.8×10^{-5} *M* (TPPZn), 7.3×10^{-5} *M* (TPPMg).

Etude des complexations

La complexation entre des métalloporphyrines et des bases de Lewis dans des solvants non aqueux est maintenant bien connue (9, 10). En particulier un travail considérable a été fait sur l'interaction entre la mésotétraphénylporphyrine au zinc et des molécules contenant de l'azote (11). Par analogie avec les polymérisations étudiées par ailleurs, nous avons choisi comme bases de Lewis: le méthylthiiranne (sulfure de propylène), le tertbutylthiiranne, le méthyloxiranne (oxyde de propylène) et l'épichlorhydrine. Les changements dans les spectres d'absorption dans le visible (région 500 à 700 nm) accompagnant la formation de complexe ont été utilisés pour étudier quantitativement la réaction de complexation.

Dans tous les cas, les spectres des métalloporphyrines en présence d'une base de Lewis ont la même allure que ceux des métalloporphyrines non complexées. On observe aussi lors de l'addition de l'agent complexant la présence de points isobestiques dans les régions de la bande de Soret (400, 450 nm) et des bandes α et β (500, 700 nm) (exemple fig. 1). Ceci montre que le milieu réactionnel ne contient en quantité appréciable qu'une seule espèce coordinée et la métalloporphyrine libre.

Pour connaître le degré de complexation et déterminer la constante de cette complexation, nous avons utilisé les relations mathématiques dérivées de la loi de Beer (12, 13). Si

$$M + nL \rightleftharpoons ML_n$$

$$K = \frac{[ML_n]}{[M][L]^n}$$

[M] étant la concentration de la métalloporphyrine non complexée, [L] celle de la base de Lewis libre et $[L_t]$ la concentration totale de base ajoutée, *n* le degré de complexation et $[M]_0$ la concentration initiale de la métalloporphyrine:

$$[M]_0 = [M] + [ML_n]$$

et

$$[L] = [L_t] - n[ML_n]$$

Ici [L] peut être assimilée à $[L_t]$ puisque $[M]_0 \ll [L_t]$. Pour [L] = 0: $D = D_0 = \varepsilon_M[M]_0$. *D* étant la densité optique et ε le coefficient d'extinction molaire. Pour [L] quelconque: $D = \varepsilon_M[M] + \varepsilon_{ML_n}[ML_n]$. La densité optique correspondant à la formation du complexe s'écrit donc:

$$D_\infty = \varepsilon_{ML_n}[ML_n]$$

d'où

$$D - D_0 = (\varepsilon_{ML_n} - \varepsilon_M)[ML_n]$$

$$D_\infty - D = (\varepsilon_{ML_n} - \varepsilon_M)[M]$$

$$D_\infty - D_0 = (\varepsilon_{ML_n} - \varepsilon_M)[M]_0$$

d'où

$$\frac{[ML_n]}{[M]} = \frac{D - D_0}{D_\infty - D} = K[L]^n = K[L_t]^n$$

ce qui peut s'écrire sous la forme:

$$\frac{1}{D - D_0} = \frac{1}{D_\infty - D_0} + \frac{1}{D_\infty - D_0}\frac{1}{K[L_t]^n}$$

La linéarité de la représentation

Can. J. Chem. Downloaded from www.nrcresearchpress.com by 210.87.254.42 on 09/05/12
For personal use only.

$$\frac{1}{D - D_0} = f\left(\frac{1}{[L]^n}\right)$$

est testée avec $n = 1$ ou 2, la constante K et D_∞ sont déduits graphiquement. Quel que soit le métal inséré dans la porphyrine (Cd, Mg ou Zn), la linéarité a été vérifiée pour $n = 1$ (exemple fig. 2). Nous sommes donc en présence d'une complexation de type 1:1.

De tels complexes 1:1 ont déjà été observés entre des métalloporphyrines et des dérivés oxygénés et soufrés, notamment entre TPPZn et les 1,1,3,3-tétraméthylurée et thiourée (15). Les constantes K de complexation étant respectivement égales à 26 et 12.

Nous constatons dans le tableau 1 que le comportement du cadmium vis-à-vis du soufre et de l'oxygène est très différent de celui du zinc et du magnésium. En effet les interactions entre le cadmium et le méthylthiiranne sont plus importantes qu'avec le méthyloxiranne, alors que pour le zinc et le magnésium la situation est inversée. Ces résultats sont conformes à la classification de Ahrland et coll. (14*a*) et Pearson (14*b*) sur les acides et bases "durs et mous". Il est admis que le cadmium est un acide "mou", alors que le magnésium est un acide "dur" et le zinc fait partie des métaux qui ne peuvent être classés tout en étant moins "mou" que le cadmium.

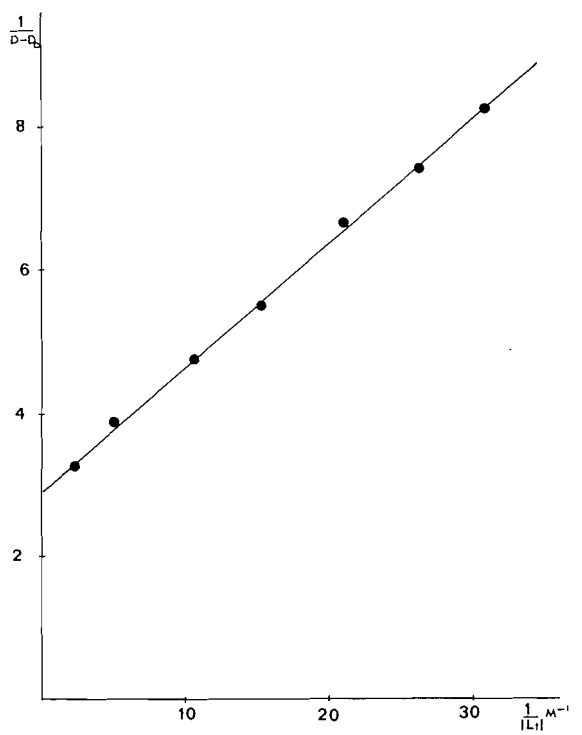

FIG. 2. Représentation des variations de densité optique à 617 nm de TPPCd en fonction de l'inverse de la concentration de méthylthiiranne ajoutée.

TABLEAU 1. Mesure des constantes de complexation (dans le benzène à 20°C)

α,β,γ,δ-Tétraphényl-porphyrine métallée	Base de Lewis	K (M^{-1})
TPPCd	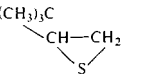	40±5
	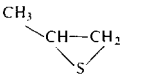	20±2
	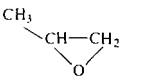	~0.5
	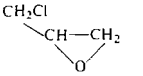	$\ll 10^{-1}$
TPPZn	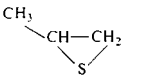	3±0.5
TPPMg	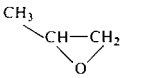	6±0.5
	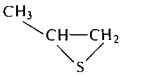	$\ll 10^{-1}$
	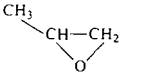	~0.5

Le soufre est une base "molle" et l'oxygène une base "dure".

Ces différences de complexation du zinc et du cadmium vis-à-vis du soufre peuvent expliquer, en partie, les résultats obtenus dans les polymérisations des thiiranes amorcées par des dérivés du zinc et du cadmium: les sels de cadmium (carbonates (16), tartrates (2) ou thiolates (17)) conduisent à des polymères stéréoréguliers de structure isotactique tandis que les sels correspondant du zinc ne permettent d'obtenir que des polymères non réguliers de structure atactique. La situation est plus complexe dans le cas des produits d'hydrolyse ou d'alcoolyse des dérivés organométalliques du zinc et du cadmium (2). A une forte interaction cadmium soufre correspond une stéréosélection élevée (choix spécifique de l'un des antipodes avant l'insertion) tandis qu'une faible interaction zinc soufre voit disparaître cette stéréosélection.

La faible interaction cadmium oxygène est en accord avec le fait que les dérivés du cadmium n'amorcent pas la polymérisation des oxirannes.

Pour un couple métal, hétéroatome, la variation de la constante de complexation est en accord avec les effets inductifs existant dans l'hétérocycle. L'effet inductif plus fortement donneur du groupement

Can. J. Chem. Downloaded from www.nrcresearchpress.com by 210.87.254.42 on 09/05/12
For personal use only.

Can. J. Chem. Downloaded from www.nrcresearchpress.com by 210.87.254.42 on 09/05/12
For personal use only.

tertiobutyle par rapport au méthyle se traduit par une augmentation des interactions soufre cadmium et nous obtenons une valeur double pour la constante de complexation. L'effet inductif attracteur du chlore se traduit par une très forte diminution des interactions oxygène cadmium. Ces résultats sont en accord avec les observations recueillies dans l'étude des polymérisations stéréospécifiques de ces monomères. Pour un même amorceur, nous constatons que les poly(tertbutylthiirannes) sont plus stéréoréguliers que les poly(méthylthiirannes) et que le comportement de ces deux monomères peut même devenir assez différent dans les polymérisations appelées stéréoélectives (18). Ces écarts de comportement peuvent être expliqués par des effets stériques et donc aussi par des interactions monomère métal différentes.

La très faible interaction épichlorhydrine–zinc expliquerait la très faible réactivité de ce monomère en polymérisation anionique coordinée amorcée par des systèmes organozinciques (19).

La complexation TPPMg oxyde de propylène (complexe 1:1) est différente de celle observée entre TPPMg et la pyridine où des complexes 1:2 ont été mis en évidence (10).

Réactions de demétallation des porphyrines métallees

Les métalloporphyrines sont des complexes relativement stables. Elles ne sont ni hydrolysables, ni alcoolysables. L'acide acétique glacial ne décompose pas le complexe TPPZn mais décompose TPPMg et TPPCd (20).

Nous avons fait réagir le *n*-dodécylmercaptan, à température ordinaire, avec ces trois complexes: TPPCd et TPPMg sont immédiatement détruits, TPPZn après quelques heures. Dans les trois cas, en présence d'un excès de thiol, nous obtenons une solution verte avec un spectre caractéristique de la tétraphénylporphyrine protonée-bande de Soret déplacée à 448 nm et deux pics à 650 nm (intense) et 600 nm (faible) (4); le lavage de cette solution par une solution aqueuse de Na_2CO_3 régénère la base libre. L'ordre de réactivité de ces complexes avec un thiol est le même que celui observé avec l'acide acétique glacial.

Le cadmium est légèrement trop volumineux pour l'anneau porphyrine et il a été montré que le métal Cd n'est pas exactement situé dans le plan défini par la porphyrine contrairement au zinc et au magnésium (9). Cette position légèrement excentrée ne correspond pas à des conditions optimales de stabilité; des réactions d'échange sont connues, par exemple (9):

$$TPPCd + ZnR_2 \rightarrow TPPZn + CdR_2$$

Nous avons observé certaines réactions spécifiques de démétallation de ce complexe TPPCd qui pourraient être dûes à sa géométrie particulière. Nous avons fait réagir le méthylthiiranne à 80°C avec les trois complexes. Aucune réaction autre que la complexation déjà décrite n'intervient entre TPPZn ou TPPMg et le méthylthiiranne. Par contre le méthylthiiranne provoque en quelques heures la démétallation de TPPCd. Nous obtenons la base libre et un organocadmien qui est susceptible d'amorcer *in situ* la polymérisation du méthylthiiranne. Les polymères ainsi obtenus sont de faibles masses moléculaires ($M_n \sim 5000$) et ont une structure isotactique. Le pourcentage des diades isotactiques mesuré par résonance magnétique nucléaire du carbone 13 (21) est supérieur à 90% pour les polymérisations effectuées à température ordinaire. Ce taux de tacticité décroît lorsque la température de polymérisation croît. Ces polymères contiennent des insaturations (doubles liaisons éthyléniques) décelées par spectrophotométrie d'absorption infrarouge et ne renferment pas de reste tétraphénylporphyrine.

L'hypothèse la plus raisonnable pour cette réaction de démétallation est:

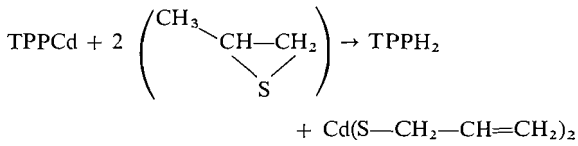

En effet, les thiolates de cadmium amorcent la polymérisation du méthylthiiranne et permettent d'obtenir des produits stéréoréguliers de hautes masses moléculaires (17). La tacticité de ces polymères varie avec la température de polymérisation (22) tout comme nous l'avons observé. De plus, l'amorçage du méthylthiiranne par un allylthiolate de cadmium expliquerait la présence des insaturations observées dans nos polymères. Cet organocadmien n'a pu être isolé; en effet la réaction de démétallation s'effectue en présence d'un excès de méthylthiiranne qui est immédiatement amorcé, cet amorçage consommant l'allylthiolate de cadmium libéré.

Une telle réaction de démétallation de TPPCd est aussi observée (par spectrophotométrie d'absorption) avec le tétrahydrothiophène mais pas avec le tertbutylthiiranne qui est pourtant fortement complexé avec TPPCd. Le tertbutylthiiranne ne possède pas d'hydrogène situé en β par rapport au soufre, contrairement au méthylthiiranne et au tétrahydrothiophène et ne pourrait donc pour cette raison, conduire à la formation d'un allylthiolate de cadmium.

Le mécanisme de la réaction de démétallation pourrait être le suivant (schéma 1):

Can. J. Chem. Downloaded from www.nrcresearchpress.com by 210.87.254.42 on 09/05/12
For personal use only.

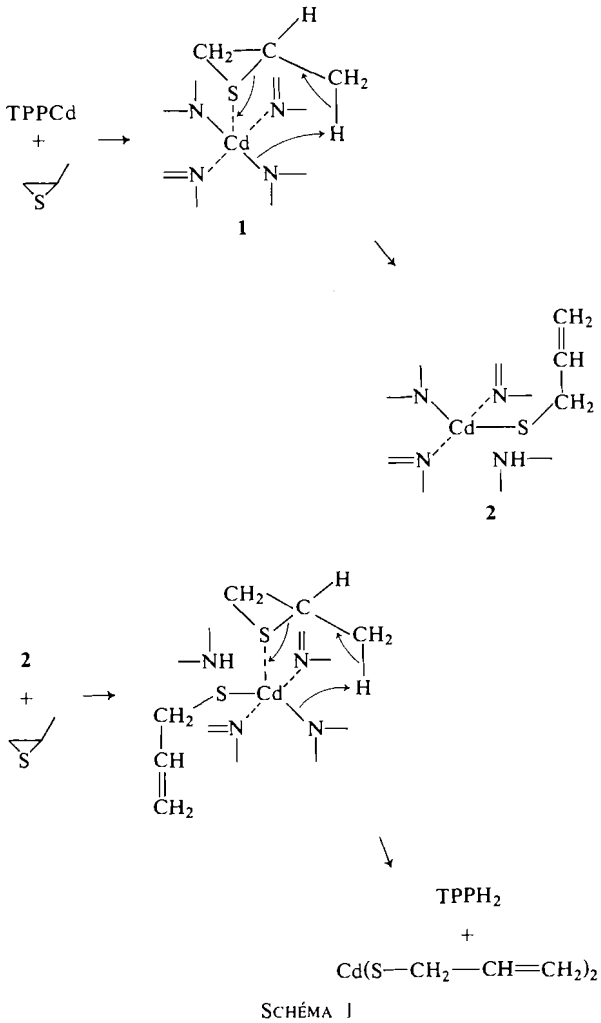

SCHÉMA 1

Pour des raisons graphiques la molécule de TPPCd est uniquement représentée par le métal et les quatre azotes des noyaux pyrroliques. La molécule de méthylthiiranne se positionne au-dessus du plan de la porphyrine (**1**) avant de réagir pour former l'allylthiolate (**2**). La réaction se poursuit par attaque d'une deuxième molécule de méthylthiiranne pour donner la porphyrine libre et le bisallylthiolate de cadmium.

La polymérisation *in situ* du méthylthiiranne est amorcée par l'allylthiolate de cadmium ainsi formé. La tétraphénylporphyrine libérée agirait comme agent de transfert ce qui expliquerait les très faibles masses moléculaires obtenues. Nous avons vérifié l'existence de cette réaction de transfert en amorçant, dans des conditions identiques, la polymérisation du méthylthiiranne par le phényl-2éthanethiolate de cadmium en présence et en absence de tétraphénylporphyrine. En absence de $TPPH_2$ nous obtenons un polymère de masse moléculaire élevée: $M_n \sim 50\,000$. La réaction de transfert pourrait s'écrire (schéma 2) avec formation de l'espèce intermédiaire **2** entrevue dans la réaction de démétallation (schéma 1) qui évolue en présence de méthylthiiranne en $TPPH_2$ et allylthiolate de cadmium. Il a été montré que les thiolates de cadmium sont des amorceurs monofonctionnels (22), c'est-à-dire que la croissance de la macromolécule se fait par insertion du monomère sur un seul groupement allyle de l'organocadmium. La régénération de l'amorceur et de la tétraphénylporphyrine explique les très faibles masses moléculaires obtenues et l'absence de restes tétraphénylporphyrine dans les oligomères.

Conclusions

Les α,β,γ,δ-tétraphénylporphyrines métallées sont des modèles simples permettant d'étudier les interactions entre un métal et le soufre ou l'oxygène. Il se forme des complexes 1:1. Les valeurs relatives des constantes de complexation sont conformes à la théorie des acides et bases "durs et mous", c'est-à-dire forte interaction entre cadmium et soufre et entre zinc et oxygène. Des effets inductifs donneurs augmentent ces interactions et la constante de complexation TPPMe–hétérocycle; des effets inductifs attracteurs diminuent cette interaction.

Les résultats obtenus sont en accord avec les observations faites dans les polymérisations anioniques coordinées de ces hétérocycles, montrant la dépendance étroite entre la stéréorégularité du

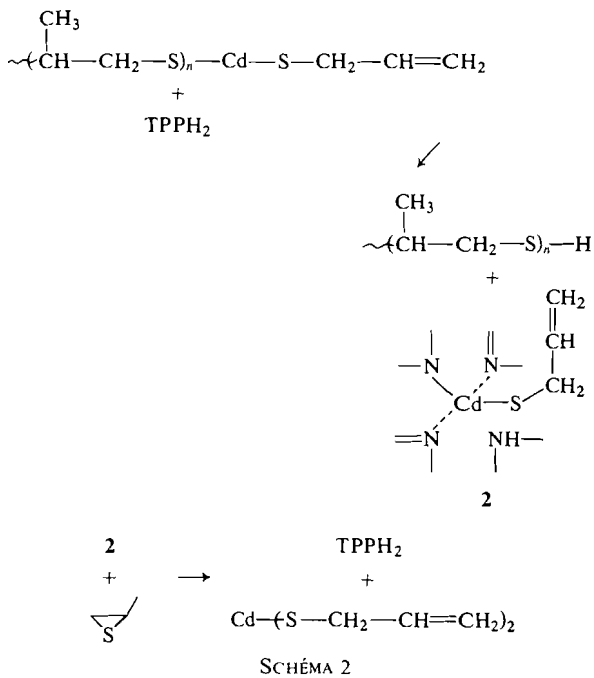

SCHÉMA 2

polymère et les interactions du métal avec le monomère.

Nous avons observé une réaction de démétallation spécifique de TPPCd avec des hétérocycles soufrés possédant un hydrogène en β du soufre conduisant à la tétraphénylporphyrine libre et à un allylthiolate de cadmium susceptible d'amorcer *in situ* la polymérisation stéréospécifique du méthylthiiranne.

Remerciements

Les auteurs remercient vivement le Professeur P. Sigwalt pour ses remarques et pour l'intérêt qu'il a porté à ce travail.

1. T. Tsuruta. J. Polym. Sci. D, 179 (1972).
2. P. Sigwalt. Int. J. Sulfur Chem. Part C, **7**, 83 (1972).
3. Ph. Guerin. Thèse, Université P. et M. Curie, Paris. 1976.
4. G. D. Dorough, J. R. Miller et F. M. Huennekens. J. Am. Chem. Soc. **73**, 4315 (1951).
5. A. D. Adler, F. R. Longo, J. D. Finarelli, J. Goldmacher, J. Assour et T. Korsakoff. J. Org. Chem. **32**, 476 (1967).
6. G. H. Barnett, M. F. Hudson et K. M. Smith. J. Chem. Soc. Perkin Trans. I, 1401 (1975).
7. A. D. Adler, F. R. Longo, F. Kampas et J. Kim. J. Inorg. Nucl. Chem. **32**, 2443 (1970).
8. Ph. Dumas, N. Spassky et P. Sigwalt. Makromol. Chem. **156**, 55 (1972).
9. J. E. Falk. Porphyrins and metalloporphyrins. Elsevier Publishing Co., Amsterdam. 1964.
10. J. R. Miller et G. D. Dorough. J. Am. Chem. Soc. **74**, 3977 (1952).
11. P. Hambright. Coord. Chem. Rev. **6**, 247 (1971).
12. N. J. Rose et R. S. Drago. J. Am. Chem. Soc. **81**, 6138 (1959).
13. M. Rougee et D. Brault. Biochemistry, **14**, 4100 (1975).
14. S. Ahrland, J. Chatt et N. R. Davies. Q. Rev. **12**, 265 (1958); R. G. Pearson. J. Am. Chem. Soc. **85**, 3533 (1963).
15. G. C. Vogel et L. A. Searby. Inorg. Chem. **12**, 926 (1973).
16. S. Adamek, B. B. J. Wood et R. T. Woodhams. Rubber Plast. Age, **46**, 55 (1965).
17. W. Cooper, D. R. Morgan et R. T. Wragg. Eur. Polym. J. **5**, 71 (1969).
18. P. Sigwalt. Pure Appl. Chem. **48**, 257 (1976).
19. A. Pourdjavadi. Thèse 3e cycle, Université P. et M. Curie, Paris. 1975.
20. P. Rothemund et A. R. Menotti. J. Am. Chem. Soc. **70**, 1808 (1948).
21. S. Boileau, H. Cheradame, Ph. Guerin et P. Sigwalt. J. Chem. Phys. **10**, 1420 (1972).
22. Ph. Guerin, S. Boileau et P. Sigwalt. Eur. Polym. J. **10**, 13 (1974).

Can. J. Chem. Downloaded from www.nrcresearchpress.com by 210.87.254.42 on 09/05/12
For personal use only.

Effect of aromatic substituents on the rates of hydrolysis of ethyl thiolbenzoate and ethyl thionbenzoate in aqueous sulfuric acid

JOHN T. EDWARD, SIN CHEONG WONG, AND GRAEME WELCH

Department of Chemistry, McGill University, Montreal, P.Q., Canada H3A 2K6

Received September 28, 1977

JOHN T. EDWARD, SIN CHEONG WONG, and GRAEME WELCH. Can. J. Chem. **56**, 931 (1978).

The rates of hydrolysis of seven *meta*- and *para*-substituted ethyl thiolbenzoates and seven *meta*- and *para*-substituted ethyl thionbenzoates in various concentrations of sulfuric acid above 48% have been determined. The Yates–McClelland r and the Hammett ρ parameters indicate that substituted ethyl thiolbenzoates hydrolyze by an $A_{Ac}1$ mechanism but substituted ethyl thionbenzoates by an $A_{Ac}2$ mechanism.

JOHN T. EDWARD, SIN CHEONG WONG et GRAEME WELCH. Can. J. Chem. **56**, 931 (1978).

On a mesuré les vitesses de l'hydrolyse de sept thiolbenzoates d'éthyle substitués en *meta* et *para* et de sept thionbenzoates d'éthyle substitués en *meta* et *para* dans diverses concentrations d'acide sulfurique supérieures à 48%. Les paramètres r de Yates–McClelland et ρ de Hammett indiquent un mécanisme $A_{Ac}1$ pour l'hydrolyse des thiolbenzoates, mais un mécanisme $A_{Ac}2$ pour l'hydrolyse des thionbenzoates.

Introduction

Recent studies (1) have shown that whereas ethyl thiolbenzoate hydrolyzes by an $A_{Ac}1$ mechanism (Scheme 1) in sulfuric acid concentrations above

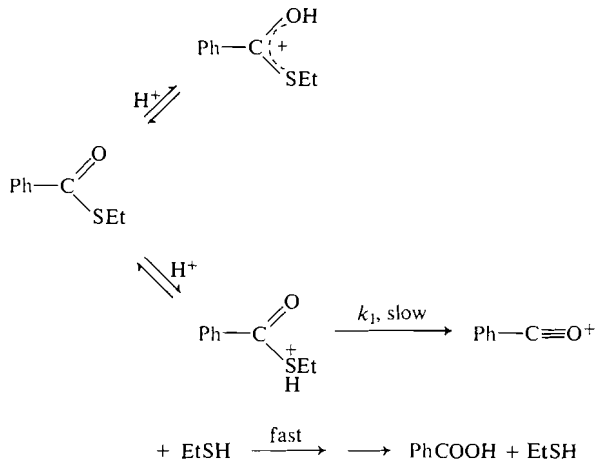

SCHEME 1

65%, ethyl thionbenzoate hydrolyzes by an $A_{Ac}2$ mechanism (Scheme 2) in even the highest concentrations of acid. In this paper, we report kinetic data for the hydrolysis of seven *meta*- and *para*-substituted ethyl thiolbenzoates and seven *meta*- and *para*-substituted ethyl thionbenzoates; these results give further support to the mechanisms of Schemes 1 and 2.

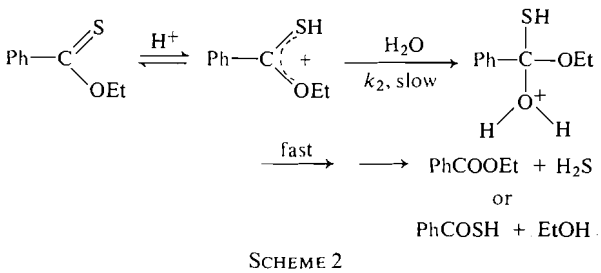

SCHEME 2

Experimental

Materials

p-Methoxy, *p*-methyl, *m*-methyl, *p*-chloro, *p*-bromo, *m*-bromo, and *p*-nitro derivatives of ethyl thionbenzoate were prepared from the appropriate benzonitriles via benzimidate hydrochloride intermediates (2, 3). *p*-Methoxy, *p*-methyl, *m*-methyl, *p*-chloro, *m*-bromo, *m*-nitro, and *p*-nitro derivatives of ethyl thiolbenzoate were prepared by reaction of the corresponding benzoyl chlorides with ethanethiol (cf. ref. 4). Boiling points and elemental analyses of four new ethyl thiolbenzoates are available as supplementary data. Sulfuric acid solutions were made up and standardized by procedures described previously (2).

Determination of Protonation Constants of Thiol Esters

The hydrolysis of ethyl *p*-nitrothiolbenzoate and ethyl *m*-nitrothiolbenzoate in sulfuric acid at 10.0°C was slow. Ionization ratios I (available as supplementary material[1]) and hence protonation constants K_{SH^+} of these compounds could be determined by the conventional spectrophotometric procedure (5). pK_{SH^+} values calculated by both the Yates–McClelland (6) and the Bunnett–Olsen equations (7) are given in Table 1 along with slope parameters m and ϕ.

The *m*-bromo-, *p*-chloro-, and *m*-methyl thiolbenzoates were hydrolyzed more rapidly in concentrated acids, so that extinction coefficients of the compounds at these concentrations were obtained by extrapolating back to the time of preparation of the solution. These extrapolations became unreliable in very concentrated acid solutions when the rates of hydrolysis were extremely fast, making it difficult to obtain the extinction coefficient ε_{SH^+} of the conjugate acid SH^+. Consequently, a value of ε_{SH^+} was chosen by trial-and-error so that the plots

[1]A complete set of tabular data is available, at a nominal charge, from the Depository of Unpublished Data, CISTI, National Research Council of Canada, Ottawa, Ont., Canada K1A 0S2.

Can. J. Chem. Downloaded from www.nrcresearchpress.com by 210.87.254.6 on 09/05/12
For personal use only.

Can. J. Chem. Downloaded from www.nrcresearchpress.com by 210.87.254.6 on 09/05/12
For personal use only.

TABLE 1. Ionization constants of substituted thiolbenzoates at 10°C

Compound	Yates–McClelland eq. m	Yates–McClelland eq. pK_{SH^+}	Bunnett–Olsen eq. ϕ	Bunnett–Olsen eq. pK_{SH^+}
Ethyl *p*-nitrothiolbenzoate	0.74	−6.61	0.27	−6.83
Ethyl *m*-nitrothiolbenzoate	0.74	−6.49	0.27	−6.71
Ethyl *m*-bromothiolbenzoate	0.71	−5.97	0.31	−6.22
Ethyl *p*-chlorothiolbenzoate	0.73	−5.54	0.29	−5.76
Ethyl *m*-methylthiolbenzoate	0.73	−5.26	0.28	−5.47
Ethyl *p*-methylthiolbenzoate	(0.73)[a]	−4.88[b]	(0.29)[a]	−5.10[b]
Ethyl *p*-methoxythiolbenzoate	(0.73)[a]	−4.54[b]	(0.29)[a]	−4.76[b]

[a]Obtained by averaging m or ϕ values above.
[b]Calculated from $p\sigma^+$ relation.

of $\log I$ ($\equiv \log(\varepsilon_S - \varepsilon)/(\varepsilon - \varepsilon_{SH^+})$) against $-H_0$ (6) and of $\log I + H_0$ against $H_0 + \log[H^+]$ (7) would be linear. From such plots were determined the pK_{SH^+} values shown in Table 1. The slopes m and ϕ of these compounds (Table 1) were close to the values found for the more stable nitro compounds.

Kinetic Measurements

Pseudo-first-order hydrolysis rate constants k_ψ of the 14 thio-esters were determined spectrophotometrically at 25.0 ± 0.1°C following standard procedures (8). Triplicate runs agreed to within 4%. Results are plotted in Figs. 1 and 2 and tabulated in the supplementary material.[1]

Results and Discussion

Preequilibrium Protonation

Acid-catalyzed ester hydrolysis is preceded by a preequilibrium protonation step. The seven thionbenzoates are *S*-protonated and follow the h_T acidity function. Their pK_{SH^+} values have been reported (2, 3). However, thiol esters, like other carboxylic acid derivatives which are protonated on the carbonyl oxygen (9), do not follow exactly any of the presently-established acidity functions. The pK_{SH^+} values of five thiolbenzoates were determined above; that of the parent ethyl thiolbenzoate has already been reported (1). It was found that their m and ϕ values (Table 1) are close to those of ethyl benzoate ($m = 0.74$, $\phi = 0.27$ at 25°C (10)), but grossly different from that of sulfides ($\phi \simeq -0.3$ (11)), lending further support to the idea of carbonyl protonation. The pK_{SH^+} values of thiolbenzoates correlated better with σ^+ values (12) (linear regression correlation coefficient 0.999) than with σ (correlation coefficient 0.991) and yielded ρ of +1.58, lying between that for acetophenone (+2.17 (13)) and for benzoic acid (+1.09 (13)). The relatively weak resonance interaction within the protonated thiol ester function indicated by these re-

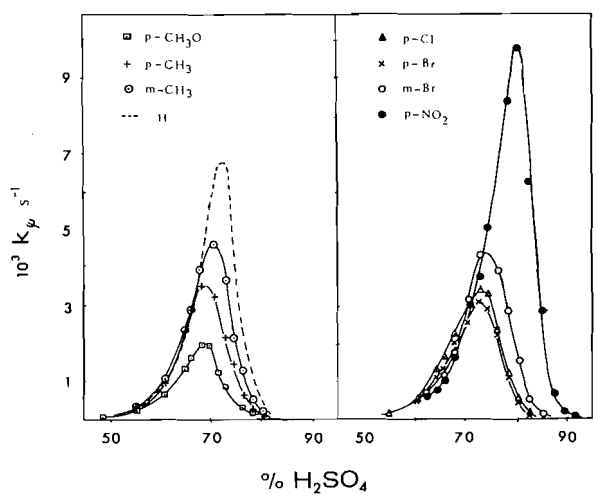

FIG. 1. Rate–acidity profiles for hydrolysis of substituted ethyl thionbenzoates.

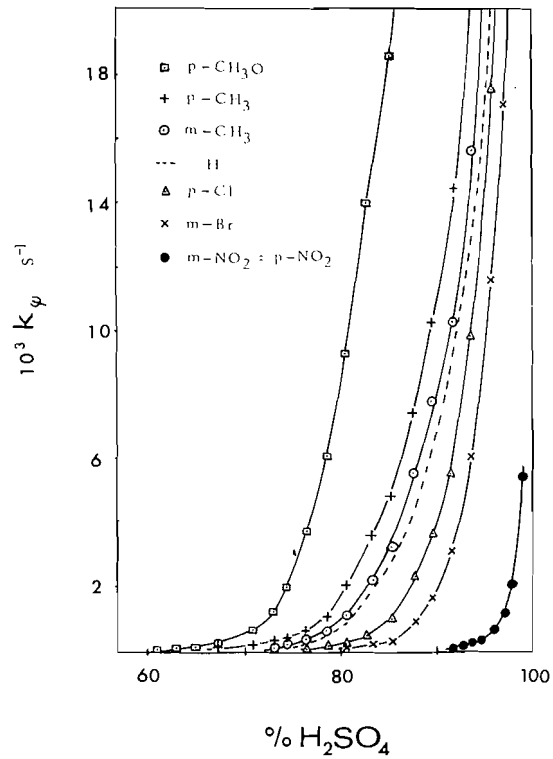

FIG. 2. Rate–acidity profiles for hydrolysis of substituted ethyl thiolbenzoates.

Can. J. Chem. Downloaded from www.nrcresearchpress.com by 210.87.254.6 on 09/05/12
For personal use only.

sults is in line with the reluctance of the sulfur atom to form 3π–2π bonds.

Ethyl *p*-methyl- and *p*-methoxythiolbenzoate hydrolyzed too rapidly for their pK_{SH^+} values to be determined by the conventional spectrophotometric procedure; the values shown in Table 1 were calculated by the $\rho\sigma^+$ relation.

Rate Profiles

The rate–acidity profiles of the seven substituted ethyl thionbenzoates, shown in Fig. 1, all have a single maximum.[2] The positions of maxima confirm the relative basicities of the thion esters (3): the stronger the electron-withdrawing ability of the substituent and the less basic the thion ester, the higher the acidity at which the rate maximum occurs. These profiles are characteristic of $A_{Ac}2$ reactions (6).

The pseudo-first-order hydrolysis rates of the seven substituted ethyl thiolbenzoates are shown in Fig. 2. They all increase sharply with concentration of acid. The fact that electron-withdrawing substituents decrease the rate of hydrolysis and electron-releasing substituents increase it indicates an $A_{Ac}1$ rather than an $A_{Al}1$ mechanism (14).

Quantitative Treatments

Application of the Yates–McClelland treatment (6) to the data for the seven substituted thionbenzoates of Table 2, using pK_{SH^+} and h_T values in the literature (2, 3),[3] gave *r* parameters close to 2. This is the value expected for hydrolysis by the $A_{Ac}2$ mechanism (6).

The intercepts of the Yates–McClelland plots give log k_2 (Scheme 2) for the hydrolysis of the protonated thion esters in pure water. These values, given in Table 2, are considerably greater than those for carboxylate esters (15), in agreement with the generally high reactivity of the thiocarbonyl group (16). A good linear relationship exists between log k_2 values and σ^+ (correlation coefficient 0.996), with a slope of +1.49, about the same as ρ for the similar step in the $A_{Ac}2$ hydrolysis of benzamides (17), and providing further support for an $A_{Ac}2$ mechanism.

Application of the Yates–McClelland treatment to the kinetic data for the thiolbenzoates, using the pK_{SH^+} and *m* values of Table 1[4] gave negative *r* values (Table 3), indicative of an A-1 mechanism. Similarly, the Bunnett–Olsen treatment (7) gave

[2]Ethyl *p*-nitrothionbenzoate shows a rate increase and a departure from pseudo-first-order kinetics in acid concentrations below 62%. We cannot explain this anomalous behaviour.

[3]Application of the Bunnett–Olsen treatment (7) to the same data gave curved plots.

[4]These values were determined at 10°C, although kinetic data refer to 25°C; however, it seems likely that this will not affect results significantly (6).

TABLE 2. Correlation of A-2 rates with acidity for substituted thionbenzoates

Substituent	*r* value	log k_2
p-CH_3O	1.91	−0.06
p-CH_3	2.04	0.67
m-CH_3	1.99	0.90
H	1.95[a]	1.10[a]
p-Cl	1.90	1.15
p-Br	1.94	1.25
m-Br	1.88	1.68
p-NO_2	1.67	2.31

[a]From ref. 1.

TABLE 3. Correlation of A-1 rates with acidity for substituted thiolbenzoates

Substituent	*r* value	ϕ value
p-CH_3O	−0.65	−0.47
p-CH_3	−0.55	−0.51
m-CH_3	−0.51	−0.49
H	−0.46[a]	−0.47[a]
p-Cl	−0.65	−0.68
m-Br	−0.72	−0.81
m-NO_2	−0.87	−1.16
p-NO_2	−0.88	−1.17

[a]From ref. 1.

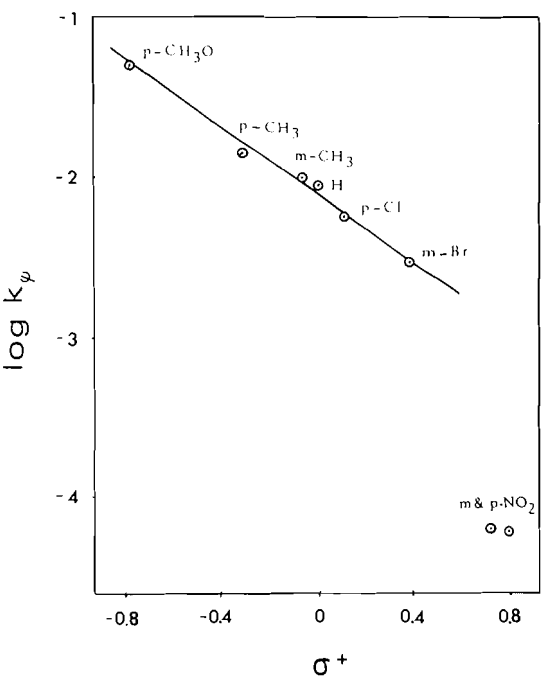

FIG. 3. Correlation of pseudo-first-order rate with σ^+ for some ethyl thiolbenzoates in 91.6% sulfuric acid.

Can. J. Chem. Downloaded from www.nrcresearchpress.com by 210.87.254.6 on 09/05/12
For personal use only.

negative ϕ values (Table 3), again suggesting an A-1 mechanism.

The mode of fission in these hydrolyses is thus established as A-1 but the r and ϕ parameters are equally compatible with an $A_{Ac}1$ and an $A_{Al}1$ mechanism. However, the latter can be rejected, because thioacids are not found as intermediate hydrolysis products (cf. ref. 1); it is also incompatible with the $\rho\sigma$ relation. This was tested in 91.6% acid, the only acid concentration in which the rates of hydrolysis of all seven thiolbenzoates are neither too fast nor too slow to be measured conveniently. The pseudo-first-order rate constants correlate quite well with the σ^+ values of the substituents, as shown in Fig. 3. The slope ρ is -1.04 (correlation coefficient 0.994) if the nitro compounds are excluded. The rate constants for the nitro compounds can be accommodated only if very much enhanced σ^+ values are attributed to the nitro substituents in 91.6% sulfuric acid. This would seem reasonable: many years ago Hammett and Chapman (18) showed that the solubility of nitrobenzene changed very little with sulfuric acid concentration up to 80% but increased very sharply above 80% acid. This indicated the onset of some interaction, perhaps formation of complexes such as

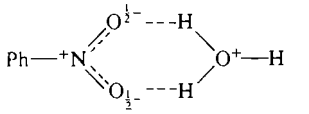

or

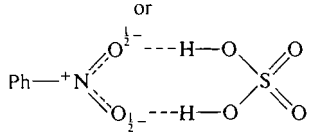

Such complexation would increase the electron-withdrawing ability, and hence σ^+, of the *m*- and *p*-nitro groups in sulfuric acid above 80% in concentration.[5]

The ρ value of -1.04 for the reaction in 91.6% acid is the sum of ρ values for three individual steps:

$$\rho = \rho_1 + \rho_2 + \rho_3$$

where ρ_1 refers to the ionization of the *O*-protonated ester, ρ_2 to that of the *S*-protonated ester (in the reverse direction), and ρ_3 to the rate-determining *S*-acyl fission (see Scheme 1). We have shown above that $\rho_1 = +1.58$. The *S*-protonated ester has a localized charge separated from the benzene ring by one carbon atom and so its protonation may be expected to have $\rho_2 \simeq -0.7$, like the protonation of substituted benzylamines (19). ρ_3 would then be about -1.9. This value has the correct sign but is considerably smaller than the value for rates of formation of cumyl carbonium ion (20); perhaps because delocalization of the charge from carbon to the carbonyl oxygen is much more effective than delocalization towards the aromatic ring.

For the hydrolysis of ethyl *p*-methoxythiolbenzoate in sulfuric acid concentrations below 63%, and of the *p*-methyl and *m*-methyl compounds below 67 and 73%, respectively, r and ϕ values become positive, indicative of a switchover to an A-2 mechanism in dilute acid.

[5]A referee has pointed out that although this explanation is plausible qualitatively, the σ^+ values required by Fig. 3 for the protonated *m*- and *p*-nitro groups seem impossibly large; it is possible that because of experimental errors the straight line of Fig. 3 is sloping less steeply than it should.

Acknowledgment

The continued financial support from the National Research Council of Canada is gratefully acknowledged.

1. J. T. Edward and S. C. Wong. J. Am. Chem. Soc. **99**, 7224 (1977).
2. J. T. Edward, I. Lantos, G. D. Derdall, and S. C. Wong. Can. J. Chem. **55**, 812 (1977).
3. J. T. Edward, G. D. Derdall, and S. C. Wong. Can. J. Chem. **55**, 2331 (1977).
4. M. Renson and J. Bidaine. Bull. Soc. Chim. Belg. **70**, 517 (1961).
5. L. A. Flexser, L. P. Hammett, and A. Dingwall. J. Am. Chem. Soc. **57**, 2103 (1935).
6. K. Yates and R. A. McClelland. J. Am. Chem. Soc. **89**, 2686 (1967).
7. J. F. Bunnett and F. P. Olsen. Can. J. Chem. **44**, 1899, 1917 (1966).
8. W. I. Congdon and J. T. Edward. Can. J. Chem. **50**, 3767 (1972).
9. G. A. Olah, A. T. Ku, and A. M. White. J. Org. Chem. **34**, 1827 (1969).
10. J. T. Edward and S. C. Wong. J. Am. Chem. Soc. **99**, 4229 (1977).
11. P. Bonvicini, A. Levi, V. Lucchini, G. Modena, and G. Scorrano. J. Am. Chem. Soc. **95**, 5960 (1973).
12. L. P. Hammett. Physical organic chemistry. 2nd ed. McGraw Hill, New York, NY. 1970. p. 356.
13. R. Stewart and K. Yates. J. Am. Chem. Soc. **80**, 6355 (1958); **82**, 4059 (1960).
14. D. N. Kershaw and J. A. Leisten. Proc. Chem. Soc. 84 (1960).
15. C. A. Lane, M. F. Cheung, and G. F. Dorsey. J. Am. Chem. Soc. **90**, 6492 (1968).
16. E. Campaigne. *In* The chemistry of the carbonyl group. *Edited by* S. Patai. Interscience, London. 1966. Chapt. 13.
17. J. T. Edward, H. S. Chang, K. Yates, and R. Stewart. Can. J. Chem. **38**, 2271 (1960).
18. L. P. Hammett and R. P. Chapman. J. Am. Chem. Soc. **56**, 1282 (1934).
19. H. H. Jaffe. Chem. Rev. **53**, 191 (1953).
20. H. C. Brown and Y. Okamoto. J. Am. Chem. Soc. **80**, 4979 (1958).

The hydrolysis of thioacetic, thiobenzoic, and three substituted thiobenzoic acids in perchloric and sulfuric acids

JOHN T. EDWARD, GRAEME WELCH, and SIN CHEONG WONG
Department of Chemistry, McGill University, Montreal, P.Q., Canada H3A 2K6

Received October 12, 1977

JOHN T. EDWARD, GRAEME WELCH, and SIN CHEONG WONG. Can. J. Chem. **56**, 935 (1978).

The rates of hydrolysis of thioacetic, thiobenzoic, and three substituted thiobenzoic acids increase with concentration of solvent sulfuric or perchloric acid to a maximum in 30–40% acid and then decrease. Yates–McClelland *r*, Bunnett–Olsen ϕ, and Hammett ρ parameters, and entropies of activation indicate an $A_{Ac}2$ mechanism over this range of acid concentrations. In acid concentrations above 50–60% the rates increase sharply and the same mechanistic criteria now indicate an $A_{Ac}1$ mechanism. The difference between the rate–acidity profile of thiobenzoic acid and that of ethyl thiolbenzoate can be explained by the different response of the activity coefficients of their transition states to increase in sulfuric acid concentration.

JOHN T. EDWARD, GRAEME WELCH et SIN CHEONG WONG. Can. J. Chem. **56**, 935 (1978).

Les vitesses d'hydrolyse d'acides thioacétiques, thiobenzoïques et de trois acides thiobenzoïques substitués augmentent avec la concentration des acides sulfuriques ou perchloriques agissant comme solvant jusqu'à un maximum de 30–40% d'acide; à partir de ces valeurs, les vitesses diminuent. Les paramètres *r* de Yates–McClelland, ϕ de Bunnett–Olsen et ρ de Hammett ainsi que les entropies d'activation suggèrent l'existence d'une mécanisme $A_{Ac}2$ à toutes les concentrations d'acide indiquées dans cet intervalle. A des concentrations d'acide au dessus de 50–60%, les vitesses augmentent rapidement et les mêmes critères mécanistiques indiquent maintenant la présence d'un mécanisme $A_{Ac}1$. On peut expliquer la différence entre le profil de vitesse–acidité de l'acide thiobenzoïque et celui du thiolbenzoate d'éthyle par des réponses différentes des coefficients d'activité de leurs états de transition à une augmentation dans la concentration de l'acide sulfurique.

[Traduit par le journal]

The hydrolysis of thiocarboxylic acids is catalyzed by acid (1).

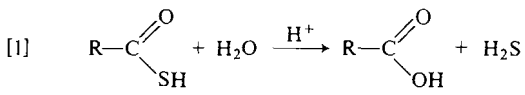

[1]

Hipkin and Satchell (2) investigated the rates of hydrolysis of thioacetic and thiobenzoic acids in varying concentrations of hydrochloric acid, up to 4.80 *M*. The pseudo-first-order rate constants k_ψ followed $[H_3O^+]$ rather than the Hammett acidity function h_0. This was taken to indicate an A-2 rather than A-1 mechanism for the acid-catalyzed hydrolysis. However, we have recently shown that although thiol esters are hydrolyzed by an $A_{Ac}2$ mechanism in 30–60% sulfuric acid, this mechanism is superceded by a very fast $A_{Ac}1$ reaction in higher acid concentrations (3, 4). Consequently, it became of interest to investigate the acid-catalyzed hydrolysis of the thio acids over a wider range of acid concentrations. In this paper we report kinetic studies of the hydrolysis of thioacetic acid, thiobenzoic acid, and three substituted thiobenzoic acids in concentrations of sulfuric acid up to 80% and of perchloric acid up to 67%.

Experimental

Materials

Thioacetic and thiobenzoic acids were commercial products. *p*-Methoxy-, *p*-methyl-, and *p*-chlorothiobenzoic acids were obtained by a standard procedure (5) from the substituted benzoyl chlorides and potassium hydrosulfide. The thioacids were freshly distilled before each kinetic run; titration against standard alkali then indicated them to be approximately 99.9% pure. (On standing several days the titre dropped, presumably because of oxidation to the disulfide.)

Mineral acid solutions were prepared by dilution of reagent grade perchloric acid (70%) or sulfuric acid (96%) with distilled water and their concentrations determined by titration against standard alkali to phenolphthalein end point.

Kinetics

All measurements were made with a Unicam SP 800 uv spectrophotometer having a thermostatted cell compartment. The change in absorbance (A) due to hydrolysis of thiobenzoic acid and thioacetic acid was recorded at 260 and 225 nm, respectively, following procedures described already (3). Pseudo-first-order rate constants k_ψ were calculated from a computer least-squares treatment of log $(A - A_\infty)$ against time. Reproducibility of independent measurements was usually better than $\pm 2\%$, except for the very rapid rates at high acid concentrations. Results at 50.0°C are displayed in Figs. 1 and 2.[1]

[1]The original numerical data may be obtained, at a nominal charge, from the Depository of Unpublished Experimental Data, CISTI, National Research Council of Canada, Ottawa, Ont., Canada K1A 0S2.

Can. J. Chem. Downloaded from www.nrcresearchpress.com by 210.87.254.105 on 09/05/12
For personal use only.

Can. J. Chem. Downloaded from www.nrcresearchpress.com by 210.87.254.105 on 09/05/12
For personal use only.

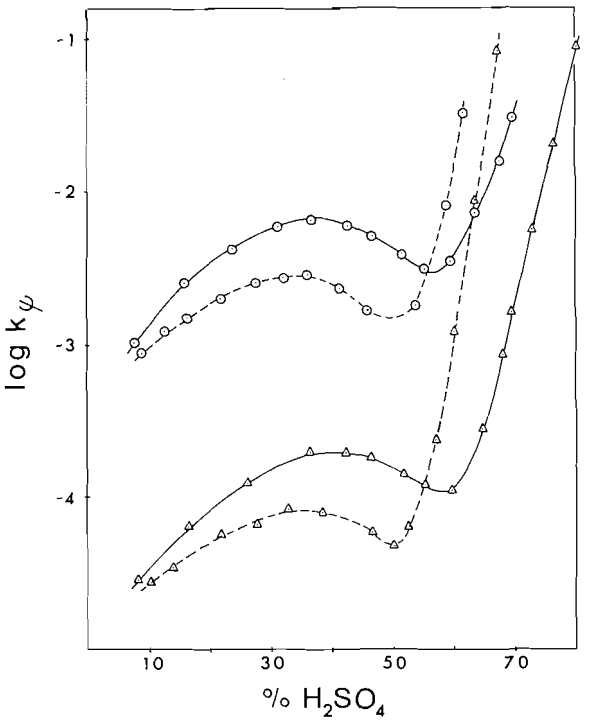

FIG. 1. Rates of hydrolysis of thioacetic acid (⊙) and thiobenzoic acid (△) in varying concentrations of sulfuric (—) and perchloric (---) acids at 50°C.

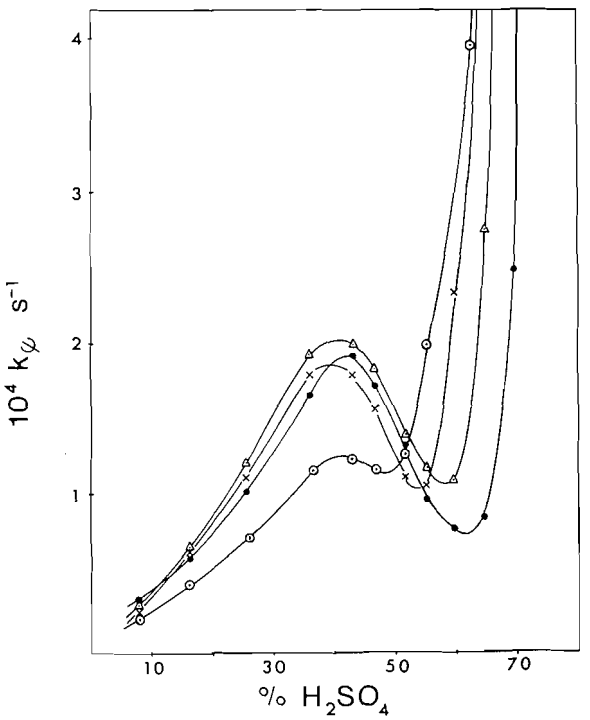

FIG. 2. Rates of hydrolysis in varying concentrations of sulfuric acid of thiobenzoic acid (△) and of *p*-methoxy (⊙), *p*-methyl (×), and *p*-chloro (●) substituted thiobenzoic acids at 50°C.

Protonation Constants of Thiobenzoic Acid and p-Thiotoluic Acid

Because of rapid hydrolysis at high acid concentrations, the protonation constant K_{SH^+} of thiobenzoic acid could not be determined at 25°C, and was determined instead at 10.0°C. Extinction coefficients of the compound in various concentrations of sulfuric acid were obtained by following the change in its absorbance with time at 325 nm (λ_{max} of the protonated thiobenzoic acid) and extrapolating to zero time. Ionization ratios[1] were then calculated according to Hammett's procedure (6) and a pK_{SH^+} value of −6.18 ($m = 0.74$) was obtained by the Yates–McClelland equation (7):

$$[2] \qquad \log\frac{[SH^+]}{[S]} = -mH_0 + pK_{SH^+}$$

and of −6.35 ($\phi = 0.28$) by the Bunnett–Olsen equation (8):

$$[3] \quad \log\frac{[SH^+]}{[S]} + H_0 = \phi(H_0 + \log[H^+]) + pK_{SH^+}$$

Application of the same treatments to data for *p*-thiotoluic acid determined at 5.0°C gave pK_{SH^+} values −6.01 ($m = 0.75$) and −6.21 ($\phi = 0.27$). These values of m and ϕ are close to those found previously for ethyl thiolbenzoate at 10°C (3).

Attempts to measure pK_{SH^+} of thioacetic acid were thwarted by its very fast rates of hydrolysis, even at 0°C.

Results and Discussion

Rate Profiles

The rate profiles shown in Figs. 1[2] and 2 are qualitatively similar to those found for the hydrolysis of ethyl thiolbenzoate in sulfuric acid (3), and indicate an A-2 reaction mechanism in acid concentrations up to 50–60%, where the rate minimum is reached, superceded by an A-1 mechanism in higher acid concentrations, where the rates increase sharply. However, they differ from the profile of the ester in having the rate maxima at lower acid concentrations, and hence better separated from the steep slopes of the A-1 reactions. The reasons for this difference are discussed later.

Catalytic Power of H_2SO_4 vs. $HClO_4$

For the A-2 region, the thioacids are hydrolyzed more rapidly in sulfuric acid than in perchloric acid, whereas the reverse is true for the A-1 region. This agrees with findings of Bunton *et al.* (10) in other hydrolyses that the catalytic order of the two acids is $HClO_4 > H_2SO_4$ for an A-1 mechanism and $H_2SO_4 > HClO_4$ for an A-2 mechanism. These authors attributed the difference in rate to the differing charge densities on bisulfate and perchlorate ions, resulting in differing abilities to stabilize the transition states of A-1 and A-2 hydrolyses.

In perchloric acid or sulfuric acid below 50% in concentration, protonation abilities (11) and water

[2]The data for thioacetic acid in perchloric acid are taken from the thesis of G.D. Derdall (9).

Can. J. Chem. Downloaded from www.nrcresearchpress.com by 210.87.254.105 on 09/05/12
For personal use only.

TABLE 1. Activation parameters for the hydrolysis of thioacetic acid (A) and thiobenzoic acid (B)

Substrate	Medium	$\Delta H^{\ddagger}$ (kcal)	$\Delta S^{\ddagger}$ (eu)
A	22.1% $HClO_4$	+17	−18
A	36.5% H_2SO_4	+16	−20
B	36.9% $HClO_4$	+19	−19
B	36.5% H_2SO_4	+17	−23
A	61.7% $HClO_4$	+21	−2
A	68.1% H_2SO_4	+20	−4
B	60.2% $HClO_4$	+26	+8
B	68.1% H_2SO_4	+24	+1

activities (12) of equal (weight percent) concentration of the two acids are about equal, and the hypothesis of Bunton *et al.* (10) seems plausible. However, in more concentrated solutions protonation abilities and water activities of perchloric and sulfuric acids diverge (13) and these differences also may be important in determining relative rates of hydrolysis. These effects are taken up later.

Activation Parameters $\Delta H^{\ddagger}$ *and* $\Delta S^{\ddagger}$

The A-2 and A-1 mechanistic classification is also supported by activation parameters listed in Table 1.[1] In all cases, log k_{ψ} was found to be linear with respect to $1/T$, and $\Delta H^{\ddagger}$ and $\Delta S^{\ddagger}$ were calculated in the usual way.[3] The large negative values of $\Delta S^{\ddagger}$ found for the hydrolysis of thioacetic and thiobenzoic acids in the more dilute mineral acids are characteristic of A-2 reactions and the small positive or negative values found for the hydrolysis in more concentrated acids are characteristic of A-1 reactions (14).

Rate–Acidity Correlations

Both the Bunnett–Olsen ϕ (8) and the Yates–McClelland r treatments (7) were applied to the thiobenzoic and *p*-thiotoluic acid hydrolysis data, by plotting log k_{ψ} − log $[SH^+]/([SH^+] + [S])$ against H_0 + log $[H^+]$ and against log a_{H_2O}, respectively. The H_0 (15) and a_{H_2O} (16) data for sulfuric acid at 50°C were available and $[H^+]$ was equated with stoichiometric acid concentration (8). The ratio $[SH^+]/([SH^+] + [S])$ was calculated from ionization data measured at 10 or 5°C without correcting for temperature change.[4]

The H_0 and a_{H_2O} data for perchloric acid are not available at 50°C and data at 25°C (11–13) were used. Furthermore, because of the lack of sufficiently

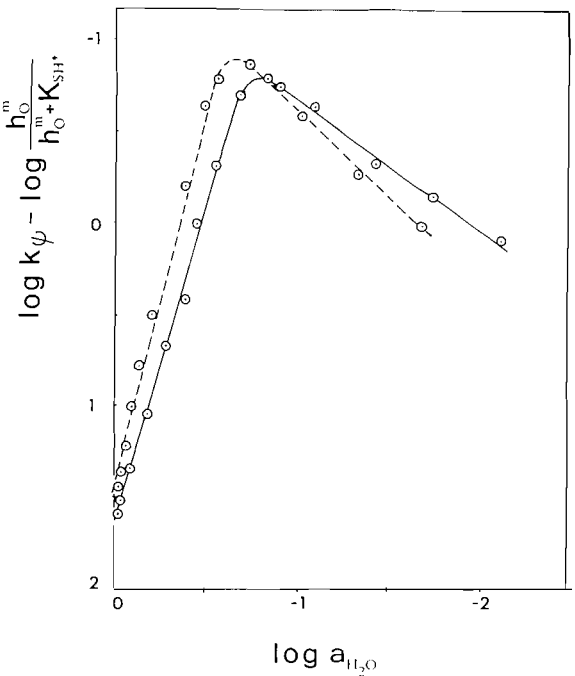

FIG. 3. Yates–McClelland plots for the hydrolysis of thiobenzoic acid in sulfuric (—) and perchloric (---) acids.

concentrated perchloric acid solutions, the pK_{SH^+} of thiobenzoic acid could not be determined in this acid. It was therefore necessary to adopt the pK_{SH^+} determined in sulfuric acid. These approximations should make the slopes r and ϕ of the correlation plots, shown in Figs. 3 and 4, slightly less reliable than those obtained with sulfuric acid solutions.

The r and ϕ values thus obtained from these and other plots are listed in Table 2, and give further support for the classification of the mechanisms as A-2 in more dilute and A-1 in more concentrated acid. However, it should be noted that the r and ϕ values are considerably greater than those found for carboxylate (7) and thiocarboxylate esters (3). We attempt to explain this later.

Hammett $\rho\sigma$ *Relation*

The number of *m*- and *p*-substituted thiobenzoic acids was less than usually considered proper for a Hammett $\rho\sigma$ study (although Dewar (17) has argued forcefully against this view) but qualitatively the evidence is very clear. In 36% sulfuric acid $\rho \simeq 0$, as expected for an A-2 mechanism which involves a preequilibrium protonation (18); in 64.7% sulfuric acid, $\rho \simeq -2$ having the correct sign for an A-1 reaction ($\rho = -1.04$ for the A-1 hydrolysis of ethyl thiolbenzoates in 91.6% sulfuric acid (4); $\rho = -3.21$ for the A-1 hydrolysis of methyl benzoates in 99.9% sulfuric acid (19)).

[3]The rate-determining step in acid hydrolysis is always preceded by a preequilibrium protonation step. The activation parameters are therefore composite of the 'true' activation parameters and a contribution from the preequilibrium protonation. They nevertheless serve as useful empirical parameters to distinguish A-2 reactions from A-1 reactions (14).

[4]Yates and McClelland (7) showed that this would not affect results significantly.

Can. J. Chem. Downloaded from www.nrcresearchpress.com by 210.87.254.105 on 09/05/12
For personal use only.

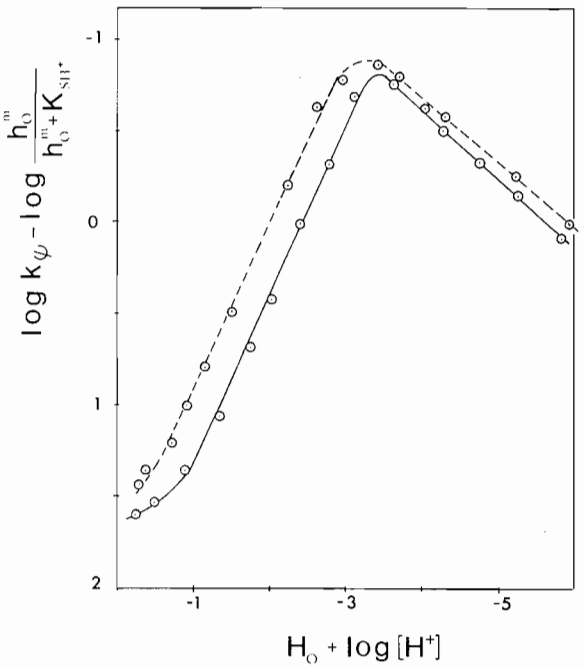

FIG. 4. Bunnett–Olsen plots for the hydrolysis of thiobenzoic acid in sulfuric (—) and perchloric (---) acids.

TABLE 2. Yates–McClelland r and Bunnett–Olsen ϕ parameters for hydrolyses at 50°C

Substrate	Medium	r	ϕ
Thiobenzoic acid	H_2SO_4 0–65%	3.46	0.95
	H_2SO_4 65–85%	−0.69	−0.39
p-Thiotoluic acid	H_2SO_4 0–55%	3.59	0.99
	H_2SO_4 60–75%	−1.13	−0.52
Thiobenzoic acid	$HClO_4$ 0–50%	4.09	0.94
	$HClO_4$ 55–67%	−0.94	−0.35

Differing r *Values for the A-2 Hydrolysis of Thiobenzoic Acid and Ethyl Thiolbenzoate*

We can now address ourselves to the attempt to understand some of the differences pointed out above.

If the A-2 hydrolysis of the thio acid and ester follows the mechanism:

[4] $$S + H^+ \underset{\text{fast}}{\overset{K_{SH^+}}{\rightleftharpoons}} SH^+$$

[5] $$SH^+ + pH_2O \xrightarrow[\text{slow}]{k_2} S^{\ddagger} \rightarrow \text{Products}$$

the Brønsted–Bjerrum rate expression yields

[6] $$\log k_\psi = \log k_2 + \log [SH^+]/([S] + [SH^+]) + p \log a_{H_2O} + \log f_{SH^+} - \log f_{S^\ddagger}$$

where a represents activity and f activity coefficient.

Following an earlier treatment of Bunnett (20), Yates and McClelland (7) assumed $f_{SH^+} \simeq f_{S^\ddagger}$ in all concentrations of mineral acid. This leads to p, the number of molecules of water[5] reacting with SH^+ to give the transition state $S^\ddagger$, being equal to r, the slope of the plot of log k_ψ − log $[SH^+]/([S] + [SH^+])$ against log a_{H_2O}. For the hydrolysis of two such similar compounds as thiobenzoic acid and ethyl thiolbenzate, it is reasonable to expect p values to be identical; in fact, the r values (~4 and ~2) are very different. This suggests that r is made up not only of p but of a factor q measuring the dependence of log $f_{SH^+}/f_{S^\ddagger}$ on the activity of water (and hence the sulfuric acid concentration)

If we assume $p = 1$, the structures of the ionic species in [5] can be represented as follows:

[7] 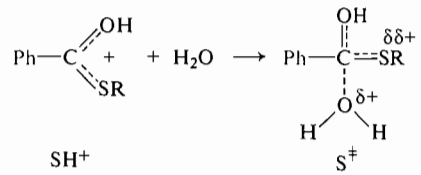

The transition state $S^\ddagger$ has a positive charge largely localized on the oxygen of the attacking water molecule (δ+ ≫ δδ+ (21)), and so will be highly stabilized by hydration. Furthermore, in water, the hydration of $S^\ddagger$ (R = H) can be expected to be considerably greater than that of $S^\ddagger$ (R = Et).[6] As the water activity of the sulfuric acid solution goes down with rising acid concentration, $f_{S^\ddagger}$ of both species will increase but that of $S^\ddagger$ (R = H) more rapidly than that of $S^\ddagger$ (R = Et). On the other hand, the charge on the ions SH^+ (R = H and Et) is more delocalized, so that the hydration of these ions in water should be less extensive, and the increase in f_{SH^+} with rising acid concentration should be much less marked (21, 23). Consequently, the difference between f_{SH^+} for the protonated thio acid and ester will not be important. On these grounds, the greater r parameter for the hydrolysis of thiobenzoic acid arises mainly because $f_{S^\ddagger}$ for this reaction increases more rapidly with sulfuric acid concentration than does $f_{S^\ddagger}$ for the hydrolysis of ethyl thiolbenzoate.[7]

[5]This is the number of molecules of water forming or rupturing covalent bonds in the formation of $S^\ddagger$; there may be additional molecules of water involved in the hydration changes of [5] but these are accounted for in f_{SH^+} and $f_{S^\ddagger}$.

[6]For an example of decreased hydration caused by alkyl substitution fairly remote from the charged centre of an ion, see ref. 22.

[7]The change in $f_{S^\ddagger}$* for the hydrolysis of ethyl thiolbenzoate in rising concentrations of sulfuric acid has been reported (3); an attempt to measure in comparable fashion the change in $f_{S^\ddagger}$* for the hydrolysis of thiobenzoic acid (cf. ref. 21) was abortive because of experimental difficulties in determining the change in $f_{S^\ddagger}$.

Can. J. Chem. Downloaded from www.nrcresearchpress.com by 210.87.254.105 on 09/05/12
For personal use only.

While the decrease in a_{H_2O} with rising concentration of H_2SO_4 or $HClO_4$ is probably the dominant factor in changing f_{SH^+} and $f_{S^\ddagger}$ (21, 23) another factor undoubtedly is the increase in concentration of HSO_4^- and ClO_4^- (10). The more localized charge of HSO_4^- would be expected to make it more effective than ClO_4^- in stabilizing cations, particularly $S^\ddagger$, and hence in reducing $f_{S^\ddagger}$ as the mineral acid concentration goes up. This would account for the greater effectiveness of sulfuric acid as a hydrolyzing agent in acid concentrations below 50% (see Fig. 1), in spite of the fact that at any given concentration below 50% its h_0 and a_{H_2O} values are almost identical with those of perchloric acid.

Different Rate Profiles for the Hydrolysis of Thiobenzoic Acid and Ethyl Thiolbenzoate

Examining [6], we can see that the pseudo-first-order rate constant k_ψ for the hydrolysis of the thioacid or thiol ester will at first increase with rising sulfuric acid concentration, because the increase in the fraction of the substrate protonated ($[SH^+]/([S] + [SH^+])$) and the increase in f_{SH^+} are more important than the drop in a_{H_2O} and the increase in $f_{S^\ddagger}$. However, beyond the maximum the sum of the first two factors becomes less important than the sum of the second two: at a maximum, the two sums are in balance. For a series of related compounds, such as the substituted thiobenzoic acids, the change in f_{SH^+} and $f_{S^\ddagger}$ with sulfuric acid concentration should be about the same, and so the position of the maximum will be determined by the fraction protonated, and hence by the basicity of the substrate S (cf. ref. 24). It can be seen from Fig. 2 that this is the case for the substituted thiobenzoic acids.

On the other hand, the maximum in the rate of the A-2 hydrolysis of thiobenzoic acid occurs in about 40% sulfuric acid and that of the hydrolysis of ethyl thiolbenzoate in about 50% sulfuric acid (where it tends to merge into the rising curve for the A-1 reaction in concentrations above 60%), in spite of the fact that ethyl thiolbenzoate is more basic (3). Evidently the much greater rise in $f_{S^\ddagger}$ of the thioacid as the sulfuric acid concentration rises is more important than the change in fraction protonated in causing k_ψ to reach a maximum.

Difference in the Effectiveness of Sulfuric and Perchloric Acid in the A-1 Hydrolysis of Thioacids

We may now consider why perchloric acid is more effective than sulfuric in hydrolyzing a thio acid by an A-1 mechanism although it is less effective in hydrolyzing it by an A-2 mechanism (Fig. 1).

In concentrations of mineral acid above 60% the major part of the thio acid exists in the *O*-protonated form SH^+; the A-1 reaction requires the formation in minute amounts of the *S*-protonated tautomer TH^+:

[8] $$R{-}C(=OH)(^+SH) \underset{\text{fast}}{\overset{K_{SH^+}}{\rightleftharpoons}} R{-}C(=O){-}SH + H^+$$

(SH^+)

$$R{-}C(=O){-}SH \overset{\text{fast}}{\underset{}{\overset{K_{TH^+}}{\rightleftharpoons}}} R{-}C(=O){-}{}^+SH_2$$

(TH^+)

[9] $$R{-}C(=O){-}{}^+SH_2 \xrightarrow[\text{slow}]{k_1} R{-}C(=O^{\delta+}){\cdots}{}^{\delta\delta+}SH_2 \longrightarrow \text{Products}$$

(TH^+) ($T^\ddagger$)

If the protonation of S to SH^+ is governed by an acidity function h_0^m (7), and the protonation of T to TH^+ by h_0^n, where $n > m$ (25), and if we take account of the fact that the concentration of TH^+ is negligible in comparison with that of SH^+, the Brønsted–Bjerrum equation for the mechanism [8], [9] becomes:

[10] $$k_\psi = \frac{k_1 h_0^{n-m} K_{SH^+} f_{TH^+}}{K_{TH^+} f_{T^\ddagger}}$$

The behaviour of f_{TH^+} and $f_{T^\ddagger}$ with rising concentration of sulfuric or perchloric acid is the inverse of that described above for f_{SH^+} and $f_{S^\ddagger}$: now TH^+ has a concentrated charge and $T^\ddagger$ a delocalized charge. Consequently, the effect of increasing mineral acid concentration (and consequent decreasing a_{H_2O}) is to raise f_{TH^+} greatly, and $f_{T^\ddagger}$ rather little. Hence k_ψ increases with increase in concentration of mineral acid because of the increase both in h_0^{n-m} and in $(f_{TH^+}/f_{T^\ddagger})$. Furthermore, in concentrations above 50%, perchloric should be more effective than sulfuric acid because (*i*) it has a higher h_0 (11); (*ii*) it has a lower a_{H_2O} (13), which should lead to a higher f_{TH^+}; and (*iii*) the more diffuse perchlorate ion should be less effective than bisulfate ion in lowering f_{TH^+}. The total effect is about one order of magnitude (Fig. 1) but it is impossible to say how the different factors *i*, *ii*, and *iii* contribute to this effect.

Acknowledgements

We are grateful to G. D. Derdall for unpublished data, and to the National Research Council of Canada for financial support.

1. J. Summer and I. Wadso. Trans. Faraday Soc. **53**, 455 (1957).
2. J. Hipkin and D. P. N. Satchell. Tetrahedron, **21**, 835 (1965).

3. J. T. EDWARD and S. C. WONG. J. Am. Chem. Soc. **99**, 7224 (1977).
4. J. T. EDWARD, S. C. WONG, and G. WELCH. Can. J. Chem. This issue.
5. P. NOBLE and D. S. TARBELL. Org. Synth. Coll. IV, 924 (1963).
6. L. A. FLEXSER, L. P. HAMMETT, and H. DINGWALL. J. Am. Chem. Soc. **57**, 2103 (1935).
7. K. YATES and R. A. MCCLELLAND. J. Am. Chem. Soc. **89**, 2686 (1967).
8. J. F. BUNNETT and F. P. OLSEN. Can. J. Chem. **44**, 1899, 1917 (1966).
9. G. D. DERDALL. Ph.D. Thesis, McGill University, Montreal, P.Q. 1971.
10. C. A. BUNTON, J. H. CRABTREE, and L. ROBINSON. J. Am. Chem. Soc. **90**, 1258 (1968).
11. K. YATES and H. WAI. J. Am. Chem. Soc. **86**, 5408 (1964).
12. R. A. ROBINSON and O. J. BAKER. Trans. R. Soc. N.Z. **97**, 250 (1946).
13. H. WAI and K. YATES. Can. J. Chem. **47**, 2326 (1969).
14. L. L. SCHALEGER and F. A. LONG. Adv. Phys. Org. Chem. **1**, 1 (1963).
15. C. D. JOHNSON, A. R. KATRITZKY, and S. A. SHAPIRO. J. Am. Chem. Soc. **91**, 6654 (1969).
16. C. R. SMITH and K. YATES. J. Am. Chem. Soc. **93**, 6578 (1971).
17. M. J. S. DEWAR. The molecular orbital theory of organic chemistry. McGraw-Hill, New York, NY. 1969. p. 423.
18. R. W. TAFT. *In* Conformational analysis. *Edited by* M. S. Newman. John Wiley, New York, NY. 1956. p. 556.
19. D. N. KERSHAW and J. A. LEISTEN. Proc. Chem. Soc. 84 (1960).
20. J. F. BUNNETT. J. Am. Chem. Soc. **83**, 4956 (1961); **83**, 4968 (1961); **83**, 4973 (1961).
21. R. A. MCCLELLAND, T. A. MODRO, M. F. GOLDMAN, and K. YATES. J. Am. Chem. Soc. **97**, 5223 (1975).
22. J. T. EDWARD, P. G. FARRELL, J. KIRCHNEROVA, J.-C. HALLE, and R. SCHAAL. Can. J. Chem. **54**, 1899 (1976).
23. K. YATES and R. A. MCCLELLAND. Prog. Phys. Org. Chem. **11**, 323 (1974).
24. J. T. EDWARD and S. C. R. MEACOCK. J. Chem. Soc. 2000 (1957).

Can. J. Chem. Downloaded from www.nrcresearchpress.com by 210.87.254.105 on 09/05/12
For personal use only.

Kinetics of radical reactions in sodium diffusion flames[1,2]

KENNETH J. MINTZ[3] AND DONALD J. LE ROY[4]

Lash Miller Chemical Laboratories, Department of Chemistry, University of Toronto, Toronto, Ont., Canada M5S 1A1

Received September 15, 1977

KENNETH J. MINTZ and DONALD J. LE ROY. Can. J. Chem. **56**, 941 (1978).

The primary reaction in sodium diffusion flames, Na + RX = NaX + R, has been investigated as a possible source of free radicals for kinetic studies. A number of different alkyl halides were investigated as possible radical sources. Optimum conditions were found to minimize wall reactions and hydrogen abstraction from the halide, the two factors which invalidated previous work using this method. Rate constants were derived from product analyses by the numerical solution of simultaneous non-linear differential equations based on a spherical model involving diffusion. Values were obtained for the two modes of decomposition of n-C_3H_7, the abstraction of primary and secondary H atoms from C_3H_8 by CH_3, and the addition of CH_3 to C_2H_4. These are in reasonably good agreement with values determined by more conventional methods.

KENNETH J. MINTZ et DONALD J. LE ROY. Can J. Chem. **56**, 941 (1978).

On a étudié la réaction primaire dans les flammes de diffusion du sodium, Na + RX = NaX + R, comme source possible de radicaux libres pour des études cinétiques. On a examiné un certain nombre d'halogénures d'alkyle différents comme sources possibles de radicaux. On a déterminé les conditions optimales pour minimiser les réactions de paroi et d'enlèvement d'hydrogène à partir des halogénures, deux facteurs qui avaient invalidés les travaux antérieurs faisant appel à cette méthode. On a évalué les constantes de vitesse en faisant appel à des analyses de produits par une solution numérique d'équations différentielles non-linéaires simultanées basées sur un modèle sphérique impliquant de la diffusion. On a obtenu des valeurs pour les deux modes de décomposition de n-C_3H_7, l'enlèvement d'atomes d'hydrogène primaires et secondaires à partir de C_3H_8 par CH_3 et l'addition de CH_3 sur C_2H_4. Ces résultats sont en bon accord avec les valeurs déterminées par des méthodes conventionnelles.

[Traduit par le journal]

Introduction

In a previous paper (1), the primary reaction occurring in sodium diffusion flames, viz., Na + RX → NaX + R, was investigated both experimentally and theoretically. The present paper is concerned with the reactions of the radicals produced and thus with the possibility of using this method of preparation for determining rate constants of radical reactions. Although this method has been used several times in the past (2–8), the results obtained have generally been in serious disagreement with those obtained by other methods.

Theoretical

The theoretical model used in treating the primary process and the calculation of the spatial distributions of the two reactants, Na and RX, have been discussed previously (1). In order to examine the spatial distribution of primary radicals we consider the case of methyl radicals formed by the reaction of sodium with methyl bromide. Assuming that the only means of mass transport is by diffusion, and that the only reaction of CH_3 is combination, then the equation of mass continuity of CH_3 is

$$[\mathrm{i}]\quad d^2[CH_3]/dr^2 + (2/r)d[CH_3]/dr + (k_1/D_R) \times [Na][CH_3Br] - (2k_2/D_R)[CH_3]^2 = 0$$

where r is the radial distance from the nozzle, D_R is the diffusion coefficient of CH_3, k_1 is the rate constant of the primary reaction, and k_2 is the rate constant for methyl radical combination. Since there does not appear to be a closed-form solution of eq. [i], it was solved numerically by the boundary-value finite-difference method (9) utilizing an optimized variable step-size (10). The boundary conditions employed were $[CH_3] = 0$ at both the "effective nozzle radius" (1) and at the walls of the reactor. The latter implies that reaction on the walls is sufficiently fast that $[CH_3]$ in the gas phase next to the walls is depleted to near zero. The values of k_1 and k_2 used were $10^{14} \exp(-2 \times 10^3/RT)$ (1) and $2.4 \pm 0.2 \times 10^{13}$ (11–13) $cm^3\ mol^{-1}\ s^{-1}$, respectively. The diffusion coefficients were calculated as before (1), using a Lennard–Jones parameter σ for CH_3 of 3.50 Å (14).

In Fig. 1 are shown the calculated radial and

[1]NRCC No. 16431.

[2]The authors are grateful to the National Research Council of Canada for financial assistance.

[3]Present address: Explosives Research Laboratories, Canadian Industries Limited, McMasterville, P.Q., Canada.

[4]Present address: Division of Chemistry, National Research Council of Canada, Ottawa, Ont., Canada K1A 0R6.

Can. J. Chem. Downloaded from www.nrcresearchpress.com by 210.87.254.42 on 09/05/12
For personal use only.

Can. J. Chem. Downloaded from www.nrcresearchpress.com by 210.87.254.42 on 09/05/12
For personal use only.

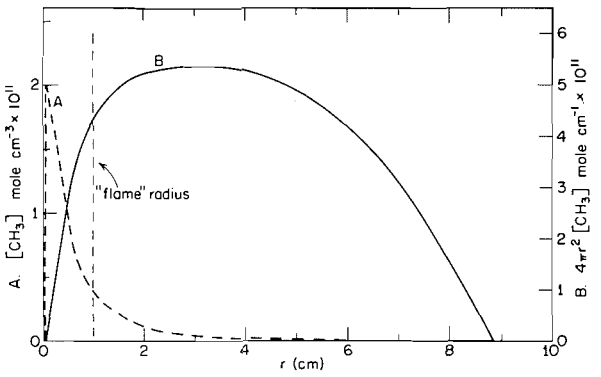

FIG. 1. Calculated radial (*A*) and spherical (*B*) distributions of CH_3 in the reaction Na + CH_3Br = NaBr + CH_3 when CH_3 is removed by combination only, assuming temperature of 300°C, spherical reactor of 8.9 cm radius, 4 Torr of N_2 as carrier gas, initial Na concentration of 4.2×10^{-10} mol cm^{-3}, flame radius of 1.0 cm.

spherical distributions for $[CH_3]$ for typical operating conditions: 300°C, 4 Torr total pressure, 100% saturation of the carrier gas (N_2) with sodium vapour, and a flame radius of 1 cm. The reactor was assumed to have a radius of 8.9 cm. Although the radial distribution peaks well inside the visible flame region, the spherical distribution peaks well beyond it. In the steady state the number of moles of CH_3 in the reactor is given by the area under curve *B*, in this example 3.5×10^{-10} mol. In Fig. 2 the spherical rate of formation of CH_3 is contrasted with its rate of combination. While both curves peak well within the flame radius, the latter goes to zero much less rapidly. The area under curve *A* is equal to the flow rate of sodium into the reactor, in this example 2.3×10^{-8} mol s^{-1}. If all of the methyl radicals produced combined before reaching the wall the area under curve *B* should be equal to that under curve *A*. Actually, it is always found to be less, in this example 1.7×10^{-8} mol s^{-1}. The reason for this is that the radical concentration far from the flame becomes so small that the probability of bimolecular combination is very small relative to diffusion to the walls. Hence, the assumption that all radicals combine before reaching the walls is invalid.

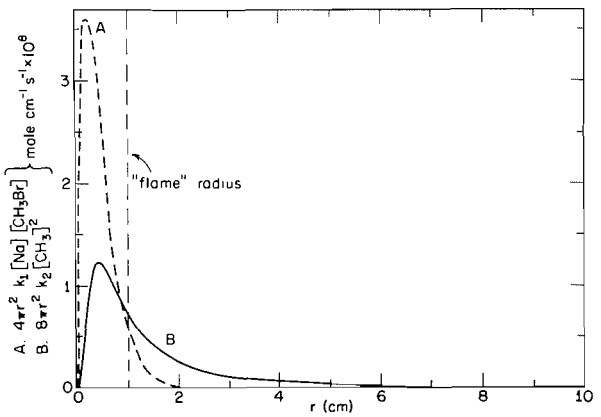

FIG. 2. Rates of formation (*A*) and combination (*B*) of CH_3 under same conditions as in Fig. 1.

Calculations were done for a number of model experimental conditions in order to determine how to minimize the number of radicals reaching the wall. Increasing the total pressure by increasing the partial pressure of carrier gas has the greatest effect, since D_R is approximately inversely proportional to the pressure. However, the use of higher pressure has two drawbacks: (*1*) the system takes a very long time to reach a steady state; (*2*) the yield of products is inversely proportional to the pressure of carrier gas. Another means of decreasing the fraction of radicals reaching the wall would be to utilize a higher molecular weight carrier gas. Nitrogen was taken to be the carrier gas in calculating the distributions shown in Figs. 1 and 2; it was also used in some of the preliminary experiments. However, helium was used in many of the experiments described in this paper because of the ease of separating it from the methane formed. Calculations showed that the pressure of helium required for a certain fraction of radicals to reach the wall was approximately four times as large as that for nitrogen. Increasing the flow rate of sodium into the reactor by increasing the temperature of the saturator decreases the fraction to some extent. However, since the reactor must be at a temperature at least as high as the saturator to prevent condensation of sodium vapour, the rate of thermal decomposition of molecular reactants will also increase. The fraction of radicals reaching the wall was found to be a strong function of reactor size. Under the typical conditions specified above it was calculated to be 46% for a reactor of 3 cm radius, compared to 25% for one of radius 8.9 cm. The former was the size commonly used by previous workers. Increasing the radius to 50 cm only decreases the fraction to 15%. A disadvantage of using very large reactors is that the observer must be farther away from the flame, and thus his detection limit (1), corresponding to the edge of the flame, is increased. Thus, not much advantage could be achieved by using reactors larger than, say, 10 cm in radius.

The reactor used in the present experiments (1) was actually a cylinder of diameter 17.8 cm and length 26.4 cm. The spherical assumption is therefore not strictly valid. The calculated methyl radical concentration far from the walls is not greatly affected by variation of the radius of the reactor, other parameters being kept constant. Hence, under most conditions (viz., when gas-phase reaction is pre-

Can. J. Chem. Downloaded from www.nrcresearchpress.com by 210.87.254.42 on 09/05/12
For personal use only.

dominant) it suffices to bracket a rate constant calculated from the experimental data between the value assuming a radius of 8.9 cm and the value assuming a radius of 13.2 cm.

The calculation of the effect of varying the flame radius on the fraction of radicals reaching the walls indicated that the optimum value is about 0.5 to 1.0 cm, depending on the other parameters. This is the result of two counteracting factors which come into play as the flame radius is increased: (*1*) because they are produced, on the average, farther from the nozzle, the methyl radicals have less time to react before reaching the walls; (*2*) as the methyl radical concentration is increased the rate of combination also increases. As a result, the methyl radical concentration distribution is not very dependent on the sodium concentration distribution. This actually has the advantage that any uncertainty in the measurement of the flame radius has relatively little effect on the $[CH_3]$ distribution.

In summary, high total pressure and high saturator temperature at the optimum flame radius are the conditions required to minimize the number of methyl radicals reaching the wall for a particular reactor and carrier gas. However, use of the maximum practical values of pressure and temperature still results in about 6% of the radicals reaching the wall. This inability to achieve exclusively gas-phase reaction of radicals must be considered as a distinct liability of the sodium diffusion flame method of studying the reactions of primary radicals. It should be emphasized, however, that in the above theoretical treatment the only gas-phase secondary reaction considered was bimolecular combination. If the primary radicals also undergo reaction with another reactant the fraction reaching the wall could be reduced. Such reactions will be considered later in this paper.

Experimental

The apparatus was the same as that described and illustrated previously (1). After the system had been thoroughly evacuated the sodium saturator was heated about 20°C above the desired working temperature for 2 h before final adjustment. The carrier gas was then allowed to flow through the saturator and reactor. With the sodium lamp *on*, the flow rate of the halide was adjusted until a 'flame' of the desired diameter was achieved. The system was then maintained at constant conditions for 2 h before trapping out any products. Non-volatile materials were then trapped over a period of 2 to 3 h. When helium was used as the carrier gas two traps were used, both at liquid nitrogen temperature. The first was empty, and collected everything but helium, methane, and some of the ethylene; the second one was filled with Linde 5A molecular sieve and collected methane and the remaining ethylene. When nitrogen was used as the carrier gas only the first trap was used but it was maintained at −210°C by means of a continuously pumped dewar; while this trapped out all of the ethylene it collected only part of the methane. Several aliquots of the product mixture (which included unreacted halide reagent) were analyzed by glc. A 6-ft column of molecular sieve type 13X (80/100 mesh) with temperature programming was used for analysis of the light hydrocarbons. A 25-ft column of 20% w/w bis-2-(2-methoxyethoxy) diethyl ether (15) on 40/60 mesh chromosorb P was used for the heavier hydrocarbons and a 10-ft column of 25% w/w tri-*m*-tolyl phosphate (16) on 60/80 mesh chromosorb P for halogenated hydrocarbons. For quantitative analysis, calibration curves were constructed for each substance using known quantities.

Experimental Results and Discussion

The purpose behind the experimental measurements was to survey the possibilities of the diffusion flame as a suitable source of radicals, rather than to make in-depth studies of particular radical reactions. In part *A* eight different alkyl halides were tested as primary radical sources per se, i.e. in the absence of any reagent other than the halide: CH_3Br, CH_3Cl, C_2H_5Br, C_2H_5I, n-C_3H_7Br, s-C_3H_7Br, t-C_4H_9Br, and t-C_4H_9Cl. In parts *B* and *C* some experiments were done using C_3H_8 and C_2H_4 as additional reagents in order to study their reactions with methyl radicals produced from CH_3Br or CH_3Cl and to derive relevant rate constants.

A. Alkyl Halides as Radical Sources

CH_3Br

The results are shown in Table 1. The only products detected by gas chromatography were CH_4, C_2H_6, C_2H_4, and C_3H_8, with the last two usually accounting for less than 1% of the total. No gaseous bromides, such as C_2H_5Br or $C_2H_4Br_2$, could be found. Qualitative evidence for HBr was obtained by treating the trapped effluent with $AgNO_3$. After several runs a small amount of a black deposit having the characteristics of amorphous carbon appeared on the end of the nozzle through which the sodium vapour entered the reactor. Carbon, as well as CH_4 and HBr, was also observed by Meisner and Schumacher (17) in their study of the thermal decomposition of CH_3Br.

Although it was not possible to devise a completely satisfactory mechanism to explain the results shown in Table 1, it would appear that the important reactions are

$$[1] \qquad CH_3Br + Na = CH_3 + NaBr$$

$$[2] \qquad 2CH_3 = C_2H_6$$

$$[3] \qquad CH_3 + CH_3Br = CH_4 + CH_2Br$$

The fate of the CH_2Br radicals is not clear. This is basically the same problem that plagued the work of Raal and Steacie (18) and Ridge and Steacie (19) and invalidated the rate constants derived by the former for the reactions of methyl radicals with methyl

TABLE 1. $Na + CH_3X = NaX + CH_3$

Parameter	Value							
	CH_3Br							CH_3Cl
Reactor temp. (°C)	267	294	321	321	336	375	389	389
Total press. (Torr)	98	2.8	3.5	3.3	16.1	18.0	19.9	18.5
He flow (μmol s^{-1})	17.8	14.9	15.3	15.6	21.4	14.2	13.0	13.8
CH_3X flow[a] (nmol s^{-1})	1.34	105	31.5	168	77	89	98	894
Flame diam. (cm)	0.97	1.24	1.00	1.68	0.95	1.19	1.42	0.60
Products:								
CH_4 (nmol s^{-1})	0.111	0.29	0.61	0.70	0.79	21.0	33.7	53.8
C_2H_6 (nmol s^{-1})	0.207	4.54	1.73	15.4	13.5	18.2	21.8	14.2
C_2H_4 (pmol s^{-1})	2.3	<10	<100	<10	<10	108	134	1850
C_3H_8 (pmol s^{-1})	0.58	<10	5	<10	<10	197	290	350
k_3 (cm^3 mol^{-1} s^{-1} × 10^{-9})[b]	4	0.5	11	0.6	6	9	25	3

[a]From product analysis.
[b]Averages for cell radii of 8.9 cm and 13.2 cm.

bromide and methyl chloride. These workers too found no evidence of C_2H_5X. However Ridge and Steacie (19) found that C_2H_4 was comparable to C_2H_6 and that HX was also formed. We suggest that at least some of the CH_2Br formed in [3] is consumed by [4],

[4] $$CH_3 + CH_2Br = C_2H_5Br^{\dagger} = C_2H_4 + HBr$$

The occurrence of this reaction is supported by the observation (19) that the ethylene formed by the photolysis of perdeuteroacetone in the presence of CH_3Cl is $C_2H_2D_2$. However, if this were the only fate of CH_2Br then the concentrations of CH_4 and C_2H_4 should be the same, which is far from being the case.

The absence of any $C_2H_4Br_2$ is surprising, since the chlorine analog has been found as one of the products of the reaction of H atoms with CH_3Cl (20). We can only conclude that the CH_2Br concentration is maintained very much lower than that of CH_3. Consideration of the final observed products suggests that the major gaseous product formed by the reactions consuming CH_2Br would have to be CH_4, presumably through H atom abstraction. Unfortunately, kinetic data on such reactions are lacking and even the thermodynamic data are sparse. The standard heats of formation (in kcal mol^{-1} at 298 K) given for CH_3Br are −8.4 (21) and −9.1 (22); from the estimated C—H bond dissociation energy in CH_3Br (23) these give 41.5 and 40.8 for CH_2Br. The corresponding values listed for CBr are 122 ± 15 (21) and 133 (24). Thus, successive H atom abstractions from CH_2Br by CH_3 to form CBr would appear to be not unreasonable thermodynamically. If this were case the value of k_3 would be given by

[ii] $$k_3 = \tfrac{1}{3}R_f[CH_4]/\int(CH_3)(CH_3Br)d\tau$$

The values of k_3 given in Table 1 were calculated from eq. [ii] using eq. [i] to obtain the spacial distribution of CH_3. The latter equation, of course, neglects removal of CH_3 by reactions other than [2] but, in view of the uncertainty in the validity of eq. [ii], it was not considered worthwhile to use a more elaborate iterative procedure.

Insofar as obtaining a value of k_3 is concerned, the results are far from satisfactory. From the point of view of using reaction [1] as a source of CH_3 radicals for kinetic purposes it is evident that the rate of reaction [3] must be kept small relative to the rates of the reactions of CH_3 being studied.

CH_3Cl

Only one run was done with this halide and the results are included in Table 1. The rate constant of the primary reaction, analogous to [1], is considerably smaller than for CH_3Br (1) and so relatively higher temperatures and CH_3Cl concentrations have to be used. Both factors make CH_3Cl unsuitable as a source of CH_3 for kinetic studies.

C_2H_5Br

Since the disproportionation to combination ratio k_d/k_c for ethyl radicals is generally agreed to be 0.14 ± 0.01, independent of temperature (21, 22), this reaction can be used as a reference point in studying the reactions resulting from the primary reaction of sodium with ethyl bromide. The experiments fall into three groups.

In the first group of experiments a small diameter cell (6 cm) was used with N_2 as the carrier gas, a total pressure of ca. 3 Torr and a temperature of 250°C. It was estimated that under these conditions most of the radicals would have reached the walls before reacting. The ratio $R_f[C_2H_6]/R_f[C_4H_{10}]$ was found to depend on the amount of NaBr on the walls of the reaction vessel. The ratio always started off at approximately 0.1 for a clean reactor but

Can. J. Chem. Downloaded from www.nrcresearchpress.com by 210.87.254.42 on 09/05/12
For personal use only.

Can. J. Chem. Downloaded from www.nrcresearchpress.com by 210.87.254.42 on 09/05/12
For personal use only.

increased with the number of runs made, when the NaBr was allowed to accumulate from run to run, until it levelled off at about 0.45. The final value is very close to the average value of 0.44 found by Kerr, Lissi, and Trotman-Dickenson (8). Evidently the enhancement of the disproportionation reaction arises from a heterogeneous process on NaBr surfaces, possibly due to oriented adsorption of C_2H_5 radicals.

In the second group of experiments the large diameter cell (17.8 cm) was used under otherwise similar conditions. In this case the ratio $R_f[C_2H_6]/R_f[C_4H_{10}]$ averaged approximately 0.16. Although in this case as well most of the radicals reached the walls before reacting, the extent of coverage of the walls by NaBr was much less.

The third group of experiments was done under conditions designed to ensure that most of the radicals reacted in the gas phase before reaching the walls, viz. total pressures 15 to 20 Torr, reaction cell temperature 300 to 350°C (saturator temperature slightly less). A thorough analysis of the products showed that ethane, ethylene, and *n*-butane accounted for over 99% of the products. In addition, 2-bromobutane and vinyl bromide were found, the former to the extent of ca. 0.3% and the latter slightly less. The average ratio $R_f[C_2H_6]/R_f[C_4H_{10}]$ was 1.5; the ratio $R_f[C_2H_6]/R_f[C_2H_4]$ was approximately 2.

We interpret these results on the basis of the following reactions:

[5] $$2C_2H_5 = C_2H_6 + C_2H_4$$

[6] $$2C_2H_5 = C_4H_{10}$$

[7] $$C_2H_5 + C_2H_5Br = C_2H_6 + CH_3CHBr$$

[8] $$C_2H_5 + CH_3CHBr = C_2H_4 + C_2H_5Br$$

[9] $$C_2H_5 + CH_3CHBr = CH_3CH_2CHBrCH_3$$

[10] $$C_2H_5 + CH_3CHBr = C_2H_6 + CH_2CHBr$$

Thus, insofar as gas phase reactions are concerned, we attribute the anomalous k_d/k_c ratio to the abstraction reaction [7] and the disproportionation reaction [8]. The combination reaction [9] and the disproportionation reaction [10] are of minor importance. The fact that some 2-bromobutane was observed, whereas the corresponding reaction [4] between CH_3 and CH_2Br produced only the decomposition products is not surprising since one would expect a larger stabilization/decomposition ratio for the hot combination product in the case of the larger radicals.

C_2H_5I

One experiment was carried out using ethyl iodide (at 249°C and 4 Torr pressure of N_2). The only significant difference, as compared to ethyl bromide, was that no butyl iodide was found (i.e. <0.05% of products) while the vinyl iodide amounted to 1.3%. Thus the disproportionation/combination ratio corresponding to reactions [10] and [9] is greater for the iodide than for the bromide, as one might expect on steric grounds.

n-*C_3H_7Br*

Four experiments were carried out, at temperatures ranging from 309 to 318°C (with the saturator at slightly lower temperatures) and at N_2 pressures from 3.5 to 17 Torr. Methane was not trapped out and no search for brominated hydrocarbons was made except for *n*- and *s*-C_3H_7Br. Only the former was observed.

Since C_2H_6 and C_2H_4 were the most important products (accounting for 36 to 65% of the total), it is evident that the decomposition of *n*-C_3H_7 is very important under these conditions, viz.

[11] $$n\text{-}C_3H_7 = C_2H_4 + CH_3$$

The remaining products were C_3H_8, C_3H_6, *n*-C_4H_{10}, and *n*-C_6H_{14}. The complete absence of isomers of *n*-C_4H_{10} and *n*-C_6H_{14} shows that isomerization of *n*-C_3H_7 is not important relative to reaction [11].

Because of the importance of reaction [11] it would appear that the CH_3 concentration can actually exceed that of *n*-C_3H_7, and so the number of possible reactions is such as to preclude any satisfactory determination of mechanism. It should be noted, however, that the apparent value of k_d/k_c (0.5 to 2.4), whether it was based on C_3H_8 or C_3H_6, was not constant and was always larger than the generally accepted value of 0.14 (25, 26). Thus abstraction from the halide by *n*-C_3H_7 would appear to be important at these temperatures.

s-*C_3H_7Br*

Four experiments were carried out at 309°C and at 4.5 to 5.5 Torr of N_2. The major products, accounting for 93 to 99% of the total, were those expected from the disproportionation and combination of *i*-C_3H_7, namely C_3H_8, C_3H_6, and 2,3-dimethylbutane (2,3-DMB). However, the ratios $R_f[C_3H_6]/R_f$[2,3-DMB] and $R_f[C_3H_8]/R_f$[2,3-DMB] averaged 2.4, several times the probable value of 0.5 to 0.65 for k_d/k_c (25, 27). Thus abstraction from the halide would appear to be important in this case as well.

The minor products (1 to 7%) included 2-methyl pentane (2-MP) and *n*-hexane (considerably more of the former than of the latter), as well as C_2H_6, C_2H_4, and *i*-C_4H_{10}. This would suggest that some *n*-C_3H_7 was present, although its mode of formation is not clear. Isomerization of *i*-C_3H_7 to *n*-C_3H_7 is an unlikely source since this is much slower than the reverse reaction, and that was not observed in the experiments with *n*-C_3H_7Br.

Can. J. Chem. Downloaded from www.nrcresearchpress.com by 210.87.254.42 on 09/05/12
For personal use only.

t-C_4H_9Br *and* t-C_4H_9Cl

Two experiments with the former and one with the latter were sufficient to show that thermal decomposition plays an important role in competition with the primary reaction with sodium. This was particularly evident in the case of the chloride where, because of the smaller value of the rate constant for the primary process, the initial concentration had to be about 30 times as great as for the bromide in order to obtain a 'flame'. Although the expected combination and disproportionation products were found, namely 2,2,3,3-tetramethylbutane, i-C_4H_{10}, and i-C_4H_8, the butene was far in excess of the butane (by a factor of 5.6) as the result of the thermal decomposition reaction

[12] $$t\text{-}C_4H_9Cl = i\text{-}C_4H_8 + HCl$$

A rough value of k_{12} was obtained using the expression

[iii] $$k_{12} = \frac{R_f[i\text{-}C_4H_8] - R_f[i\text{-}C_4H_{10}]}{(t\text{-}C_4H_9Cl)V}$$

where V is the volume of the reaction vessel. The value so obtained, $2.7 \pm 0.3 \times 10^{-3}$ s^{-1}, is about 17 times that derived from the rate constant expression recommended by Benson and O'Neal (28), but this is not surprising because the decomposition is known to be greatly enhanced by wall reaction.

On the assumption that i-C_4H_{10} arose solely from disproportionation, the value of k_d/k_c derived from the three experiments was 5.3 ± 0.5 at an average temperature of 275°C. Literature values range from 2.2 to 7.4 (25, 27).

B. Kinetics of the Reaction $CH_3 + C_3H_8$

By flowing C_3H_8 through the reactor along with CH_3Br or CH_3Cl it was possible to study the kinetics of the abstraction reactions:

[13] $$CH_3 + C_3H_8 = CH_4 + n\text{-}C_3H_7$$

[14] $$CH_3 + C_3H_8 = CH_4 + i\text{-}C_3H_7$$

The results are shown in Table 2. The flow rates listed for the reagents CH_3X and C_3H_8 are the values determined during product analysis. Since the experimental conditions with CH_3Br were such as to make CH_3 the predominating radical, the three hexanes were formed in quite small amounts in comparison with the two butanes, formed by the reactions

[15] $$CH_3 + n\text{-}C_3H_7 = n\text{-}C_4H_{10}$$

[16] $$CH_3 + i\text{-}C_3H_7 = i\text{-}C_4H_{10}$$

The CH_4 is attributed to reaction [3] as well as to the disproportionation reaction corresponding to reactions [15] and [16]:

[17] $$CH_3 + C_3H_7 = CH_4 + C_3H_6$$

It was not possible to measure the C_3H_6 formed in reaction [17] in the presence of the very large excess of C_3H_8. Some decomposition of n-C_3H_7 occurred by reaction [11], giving rise to the C_2H_4. The C_2H_6 is attributed to reaction [2]. Because of their small amounts, the butenes and pentanes were not used in the mathematical analysis of the results.

In order to determine the rate constants k_{11}, k_{13}, and k_{14} the equations of mass continuity for Na, CH_3, n-C_3H_7, and i-C_3H_7 were solved simultaneously. The values of k_d/k_c required were taken from the literature or, where this was not possible, were calculated from simple collision theory based on $k_2 = 2.4 \times 10^{13}$ cm^3 mol^{-1} s^{-1}. The rate constants in Table 2 for CH_3Br as the atmospheric reagent are the averages of the values obtained using cell radii of 8.9 cm and 13.2 cm; the values for CH_3Cl are for the small reactor model only. In the latter case (as shown in Table 1) an appreciable amount of C_2H_4 was formed by the analog of reaction [4], and hence the values of k_{11} and k_{13} are the upper limits; in the runs with CH_3Br all C_2H_4 was assumed to arise from reaction [11]. Aside from this, the uncertainties in the rate constants arise mainly from the problem of taking into account the fate of the CH_3 and i-C_3H_7 radicals that reach the wall. This was not a problem with n-C_3H_7 because almost all of it was consumed in the first order process [11].

In comparing our values of k_{11} with the literature (23) one is struck by the fact that there are variations of as much as two orders of magnitude in previously published data. However, there is a relatively good agreement between our values and those derived from the more recent and thorough investigation of Papic and Laidler (29), viz. 5.0×10^2 at 336°C, 2.5×10^3 at 375°C.

Our over-all rate constants for the abstraction reaction, $k_{13} + k_{14}$, are about 50% greater than found by Jackson, McNesby, and Darwent (30). On the other hand, our values for k_{13}/k_{14} are 1.3 and 1.5 at 336 and 375°C, respectively (runs 1 and 2), whereas the values derived from the work of these authors are 0.52 and 0.56. The values of the ratio derived from our work are virtually independent of the approximation used and so the discrepancy is real.

C. Kinetics of the Reaction $CH_3 + C_2H_4$

A number of experiments were performed in which various amounts of C_2H_4 were added to the reagent stream, along with CH_3Br, with the objective of measuring the rate constant of the addition reaction

[18] $$CH_3 + C_2H_4 = n\text{-}C_3H_7$$

The n-C_3H_7 radicals so formed would be expected to decompose by reaction [11], the reverse of [18], or

Can. J. Chem. Downloaded from www.nrcresearchpress.com by 210.87.254.42 on 09/05/12
For personal use only.

TABLE 2. Na + CH_3X + C_3H_8

Parameter	Value		
	CH_3Br		CH_3Cl
Reactor temp. (°C)	336	375	336
He press. (Torr)	19.2	19.0	16.8
CH_3X flow[a] (nmol s^{-1})	31.8	32.8	441
C_3H_8 flow[a] (nmol s^{-1})	460	769	192
Products:			
CH_4 (nmol s^{-1})	2.6	27.1	12.7
C_2H_6 (nmol s^{-1})	9.6	23.6	9.2
C_2H_4 (nmol s^{-1})	0.73	2.87	1.07
n-C_4H_{10} (nmol s^{-1})	0.0483	0.164	0.021
i-C_4H_{10} (nmol s^{-1})	0.462	1.53	0.146
C_4H_8-1 + i-C_4H_8 (pmol s^{-1})	6	22	18
i-C_5H_{12} (pmol s^{-1})	3	14	3
n-C_5H_{12} (pmol s^{-1})	2	22	<10
C_5H_{10}, n-C_6H_{14} (pmol s^{-1})	<1	<1	<1
2-MP + 2,3-DMB (pmol s^{-1})	50	370	290
Percent gas phase reaction[b]			
n-C_3H_7	99.8	100.0	—
i-C_3H_7	64	73	—
CH_3	77	85	—
Rate constants[b,c]			
k_{13} (cm^3 mol^{-1} s^{-1} × 10^{-8})	2.0±0.4	4.2±0.5	<7.4
k_{14} (cm^3 mol^{-1} s^{-1} × 10^{-8})	1.5±0.3	2.9±0.3	1.2
k_{11} (s^{-1} × 10^{-3})	0.50±0.13	2.0±0.4	<3.0

[a]From product analysis.
[b]Results for CH_3Br are averages of values for cell radii of 8.9 and 13.2 cm.
[c]Results for CH_3Cl are for cell radius of 8.9 cm.

react with CH_3 (the predominant radical) by reactions [15] and [17]. In analysing the results of part *B*, above, it was assumed that the alternative decomposition process [19]

[19] $$n\text{-}C_3H_7 = C_3H_6 + H$$

was of negligible importance. However in the presence of much larger concentrations of C_2H_4, and in the absence of large amounts of C_3H_8, reaction [19] would be easier to detect. Thus, the H atoms formed would rapidly add to C_2H_4 to form C_2H_5 which would give rise to C_3H_8 by combination with CH_3 and to n-C_5H_{12} by reaction [20].

[20] $$C_2H_5 + n\text{-}C_3H_7 = n\text{-}C_5H_{12}$$

The corresponding disproportionation reactions would form CH_4, C_2H_4, C_2H_6, C_3H_8, and C_3H_6.

The results are given in Table 3. The amounts of C_3H_8 formed by the above mechanism can be predicted from the observed rates of formation of C_3H_6, n-C_4H_{10}, and n-C_5H_{12} using available information on disproportionation/combination reactions (25). The amounts predicted in this way were 3.3, 7.5, 6.1, 35, 58, and 350 pmol s^{-1} for runs 1 to 6 respectively, in reasonably good agreement with the measured values of C_3H_8.

In addition to the products listed in Table 3, traces of C_2H_2 were also found (ca. 1 to 5 pmol s^{-1}). This probably arises by H atom abstraction from C_2H_4 followed by the disproportionation of CH_3 and C_2H_3 radicals:

[21] $$CH_3 + C_2H_4 = CH_4 + C_2H_3$$

[22] $$CH_3 + C_2H_3 = CH_4 + C_2H_2$$

The rate of [21] is, of course, much smaller than that of [18] (31, 32).

The rate constants k_{18} and k_{19} were calculated by numerically solving the equations of mass continuity for Na, CH_3Br, and n-C_3H_7, together with those for reactions [18] and [19] based on the above mechanism. The values of k_{11} were those derived in part *B*. The fairly large uncertainty in k_{11} caused only about 10% uncertainty in k_{18} and k_{19}, less than those inherent in allowing for the wall reaction.

Considering the wide range of conditions, particularly with respect to the amount of CH_3 reacting in the gas phase, the values of k_{18} and k_{19} are reasonably consistent, suggesting that the assumed model is reasonable. Literature values of k_{18} were all determined at considerably lower temperatures than those used here. When extrapolated to the temperatures used here they are somewhat smaller than those listed in Table 3; for example, at 336°C the extrapolated values are (in units of 10^8 cm^3 mol^{-1} s^{-1}) 5 (33), 6 (34), 7 (32), 12 (35) compared to our

Can. J. Chem. Downloaded from www.nrcresearchpress.com by 210.87.254.42 on 09/05/12
For personal use only.

TABLE 3. Na + CH_3Br + C_2H_4

Parameter	Value					
	1	2	3	4	5	6
Reactor temp. (°C)	294	308	308	321	321	336
He press. (Torr)	3.5	9.1	3.5	3.6	3.7	18.3
CH_3Br flow[a] (nmol s^{-1})	21.6	22.7	8.8	67	20	67.6
C_2H_4 flow[a] (nmol s^{-1})	82	79	220	270	590	534
Products:						
CH_4 (nmol s^{-1})	0.021	2.2	0.68	1.14	2.5	10.2
C_2H_6 (nmol s^{-1})	2.9	1.9	0.52	10.2	6.2	13.0
C_3H_8 (pmol s^{-1})	4.5	10	6.7	30	40	340
C_3H_6 (pmol s^{-1})	4.5	8.2	6.7	39	62	420
i-C_4H_{10} (pmol s^{-1})	< 3	< 2	< 1	< 2	< 2	< 10
n-C_4H_{10} (pmol s^{-1})	20	12.9	9.8	72.5	76	690
C_4H_8-1 + i-C_4H_8 (pmol s^{-1})	—	—	—	—	—	14
n-C_5H_{12} (pmol s^{-1})	—	—	—	—	—	53
n-C_6H_{14} (pmol s^{-1})	—	—	—	—	—	10
Rate constants:[b]						
k_{18} (cm^3 mol^{-1} s^{-1} × 10^{-8})	12 ± 2	6.5 ± 1.0	15 ± 3	10 ± 2	7 ± 2	14 ± 3
k_{19} (s^{-1})	4 ± 1	9 ± 2	11 ± 3	15 ± 1	13 ± 3	23 ± 4
Percent gas phase reaction:[b]						
CH_3	22	52	7	43	36	81
n-C_3H_7	86	97	92	94	94	99

[a]From product analysis.
[b]Average of values for cell radii of 8.9 and 13.2 cm.

value of 14 ± 3; Kerr and Parsonage have recommended 5.7 (36). Previously determined values of k_{19}, evaluated for 336°C, are 13 s^{-1} (37), 16 s^{-1} (38), and 6.6 s^{-1} (39), compared to our value of 23 ± 4 s^{-1}.

Calculations showed that the rate of isomerization of n-C_3H_7 was less than 2% of its rate of 'slow' decomposition by reaction [19] at the temperatures used.

Summary and Conclusions

The present investigation has shown that the main difficulties associated with the use of sodium diffusion flames as sources of free radicals for kinetic studies arise from wall reactions and hydrogen abstraction from the halide. The former can be minimized by using a large diameter reactor, a relatively high pressure of inert carrier gas (preferably of high molecular weight), a 'flame' radius of from 0.5 to 1.0 cm, and by operating the sodium saturator at a temperature only slightly below that of the reactor.

Abstraction from the halide, being competitive with reactions of the primary radical with other added reagents, can be reduced by using low concentrations of the halide. Since the rate constants of the primary reaction with sodium are in the order iodide > bromide > chloride, the higher atomic weight halogens are more favourable as less halide is required for a given rate of radical production. However, the rates of thermal decomposition of the halides are generally in the same order. In the present work bromides were found to provide the best compromise.

Since the reactant concentrations are spherically symmetrical and controlled by diffusion, rate constants were derived from product analyses by the numerical solution of simultaneous non-linear differential equations. By reacting CH_3Br with Na in the presence of added C_3H_8 and C_2H_4 under more or less optimal conditions rate constants were determined for five different reactions: the two modes of decomposition of n-C_3H_7, the abstraction of primary and secondary H atoms from C_3H_8 by CH_3, and the addition of CH_3 to C_2H_4. The values obtained are in reasonably good agreement with those obtained by more conventional methods.

1. K. J. MINTZ and D. J. LE ROY. Can. J. Chem. **53**, 1726 (1975).
2. J. W. HODGINS, A. W. TICKNER, and D. J. LE ROY. Can. J. Res. Sect. B, **26**, 619 (1948).
3. A. W. TICKNER and D. J. LE ROY. J. Chem. Phys. **19**, 1247 (1951).
4. C. E. H. BAWN and R. F. HUNTER. Trans. Faraday Soc. **34**, 608 (1938).
5. C. E. H. BAWN and J. MILSTEAD. Trans. Faraday Soc. **35**, 889 (1939).
6. C. E. H. BAWN and C. F. H. TIPPER. Discuss. Faraday Soc. **2**, 104 (1937).
7. A. A. COMSTOCK and G. K. ROLLEFSON. J. Chem. Phys. **19**, 441 (1951).

8. J. A. KERR, E. A. LISSI, and A. F. TROTMAN-DICKENSON. J. Chem. Soc. 1673 (1964).
9. L. FOX. The numerical solution of two-point boundary problems in ordinary differential equations. Clarendon Press, Oxford. 1957.
10. K. J. MINTZ. Ph.D. Thesis, University of Toronto, Toronto, Ont. 1972.
11. R. E. MARCH and J. C. POLANYI. Proc. R. Soc. A**273**, 360 (1963).
12. N. BASCO, D. G. L. JAMES, and R. D. SUART. Int. J. Chem. Kinet. **2**, 215 (1970).
13. T. C. CLARK, T. P. J. IZOD, M. A. DI VALENTIN, and J. E. DOVE. J. Chem. Phys. **53**, 2982 (1970).
14. T. L. HILL. J. Chem. Phys. **17**, 1125 (1949).
15. S. SANDLER and J. A. BEECH. Can. J. Chem. **38**, 1455 (1960).
16. P. W. WEST, B. SEN, B. R. SANT, K. L. MALLIK, and J. G. S. GUPTA. J. Chromatogr. **6**, 220 (1961).
17. H. P. MEISNER and H. J. SCHUMACHER. Z. Phys. Chem. **185A**, 435 (1939).
18. F. A. RAAL and E. W. R. STEACIE. J. Chem. Phys. **20**, 578 (1952).
19. M. J. RIDGE and E. W. R. STEACIE. Can. J. Chem. **33**, 396 (1955).
20. G. L. LEE and D. J. LE ROY. Can. J. Res. Sect. B, **28**, 500 (1950).
21. JANAF Thermochemical Tables, NSRDS-NBS 37. National Bureau of Standards, U.S.A. 1971.
22. J. D. COX and G. PILCHER. Thermochemistry of organic and organometallic compounds. Academic Press Inc., London. 1970.
23. S. FURUYAMA, D. M. GOLDEN, and S. W. BENSON. J. Am. Chem. Soc. **91**, 7564 (1969).
24. J. L. FRANKLIN, J. G. DILLARD, H. M. ROSENSTOCK, J. T. HERRON, K. DRAXL, and F. H. FIELD. Ionization potentials, appearance potentials, and heats of formation of gaseous positive ions, NSRDS-NBS 26, National Bureau of Standards, U.S.A. 1969.
25. A. F. TROTMAN-DICKENSON and G. S. MILNE. Tables of bimolecular gas reactions, NSRDS-NBS 9. National Bureau of Standards, U.S.A. 1967.
26. D. G. HOOPER, M. SIMON, and M. H. BACK. Can. J. Chem. **53**, 1237 (1975).
27. G. MCKAY, J. M. C. TURNER, and F. ZARÉ. J. Chem. Soc. Faraday Trans. I, **73**, 803 (1977).
28. S. W. BENSON and H. E. O'NEAL. Kinetic data on gas phase unimolecular reactions, NSRDS-NBS 21. National Bureau of Standards, U.S.A. 1970.
29. M. M. PAPIC and K. J. LAIDLER. Can. J. Chem. **49**, 549 (1971).
30. W. M. JACKSON, J. R. MCNESBY, and B. DE B. DARWENT. J. Chem. Phys. **37**, 1610 (1962).
31. A. F. TROTMAN-DICKENSON and E. W. R. STEACIE. J. Chem. Phys. **19**, 169 (1959).
32. R. J. CVETANOVIĆ and R. S. IRWIN. J. Chem. Phys. **46**, 1694 (1967).
33. L. ENDRENYI and D. J. LE ROY. J. Phys. Chem. **70**, 4081 (1966).
34. A. M. HOGG and P. KEBARLE. J. Am. Chem. Soc. **86**, 4558 (1964).
35. R. K. BRINTON. J. Chem. Phys. **29**, 781 (1958).
36. J. A. KERR and M. J. PARSONAGE. Evaluated kinetic data on gas phase addition reactions. Butterworths, London. 1972.
37. S. BYWATER and E. W. R. STEACIE. J. Chem. Phys. **19**, 319 (1951).
38. J. A. KERR and A. F. TROTMAN-DICKENSON. Trans. Faraday Soc. **55**, 572 (1959).
39. W. M. JACKSON and J. R. MCNESBY. J. Chem. Phys. **36**, 2272 (1962).

Can. J. Chem. Downloaded from www.nrcresearchpress.com by 210.87.254.42 on 09/05/12
For personal use only.

Fluxional behaviour of potentially bidentate phenanthroline, naphthyridine, and phthalazine ligands in palladium complexes

J. BRADLEY BRANDON, MICHAEL COLLINS, AND KEITH R. DIXON[1]

Department of Chemistry, University of Victoria, Victoria, B.C., Canada V8W 2Y2

Received August 31, 1977

J. BRADLEY BRANDON, MICHAEL COLLINS, and KEITH R. DIXON. Can. J. Chem. **56**, 950 (1978).

The synthesis of a series of palladium complexes, *cis*-$[PdCl(PEt_3)_2L][Y]$; L = 1,10-phenanthroline, 1,8-naphthyridine, or phthalazine; Y = BF_4^- or ClO_4^-; is reported. Variable temperature ^1H and ^{31}P nmr spectra are discussed in terms of square planar structures in which the heterocyclic ligands are essentially monodentate and fluxional with the palladium exchanging between the two nitrogen atoms. Above ca. −10°C a dissociative exchange mechanism operates in all three complexes and, when L = 1,10-phenanthroline or 1,8-naphthyridine, exchange continues at lower temperatures by an intramolecular process.

J. BRADLEY BRANDON, MICHAEL COLLINS et KEITH R. DIXON. Can. J. Chem. **56**, 950 (1978).

On rapporte la synthèse d'une série de complexes de palladium $[PdCl(PEt_3)_2L][Y]$ *cis*; L = phénanthroline-1,10, naphthyridine-1,8 ou phtalazine; Y = BF_4^- ou ClO_4^-. On discute des spectres rmn ^1H et ^{31}P à températures variables en terme d'une structure plan carré dans laquelle les ligands hétérocycliques sont essentiellement monodentates et fluxionels par rapport au palladium qui s'échange entre les deux atomes d'azote. Au-dessus de −10°C, un mécanisme d'échange dissociatif opère dans les trois complexes et lorsque L = phénanthroline-1,10 ou naphthyridine-1,8, l'échange continue à des températures plus basses par un processus intramoléculaire.

[Traduit par le journal]

Introduction

We have recently completed studies of a series of platinum complexes, *cis*-$[PtCl(PEt_3)_2L][BF_4]$, in which only one site in the square coordination plane is available to a potentially bidentate ligand, L (1–4). For example, when L = 1,8-naphthyridine (naph), an X-ray diffraction study (3) shows the following structure in which only one nitrogen is strongly bound to the platinum (1).

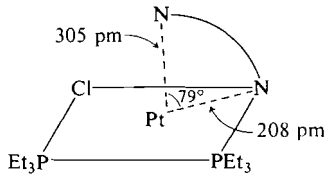

1

Closely related structures for the L = 1,10-phenanthroline (phen) and phthalazine (phth) complexes have also been established by X-ray diffraction (1, 4).

In solution, nmr studies (2) show that these complexes are fluxional with exchange of the coordinated platinum between the two nitrogen sites on the ligands. In the series L = phen, naph, or phth, the rate of this fluxional process decreases rapidly (approximate coalescence temperatures are < −80, −30, and +90°C) as the orientation of the nitrogen lone pairs becomes less suitable for a 5 coordinate intermediate. For L = phth the mechanism is dissociative rather than intramolecular (2). The present

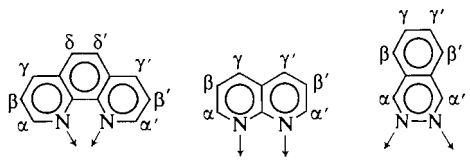

paper reports the results of a similar nmr investigation of the corresponding palladium complexes.

Results and Discussion

(a) Synthesis

The complexes, *cis*-$[PdCl(PEt_3)_2L]^+$, L = 1,10-phenanthroline (phen), 1,8-naphthyridine (naph), or phthalazine (phth), were prepared as both fluoroborate and perchlorate salts by the reactions:

$$[Pd_2Cl_2(PEt_3)_4][BF_4]_2 + 2L \rightarrow \textit{cis}\text{-}[PdCl(PEt_3)_2L][BF_4]$$

$$\textit{trans}\text{-}[PdCl_2(PEt_3)_2] + L + NaClO_4 \xrightarrow{\text{acetone}} \textit{cis}\text{-}[PdCl(PEt_3)_2L][ClO_4] + NaCl$$

[1]To whom correspondence should be addressed.

Can. J. Chem. Downloaded from www.nrcresearchpress.com by 210.87.254.42 on 09/05/12
For personal use only.

Can. J. Chem. Downloaded from www.nrcresearchpress.com by 210.87.254.42 on 09/05/12
For personal use only.

Infrared spectra showed the expected ligand and anion absorptions and were in general almost identical with spectra of corresponding platinum complexes for which X-ray structural data are available (1–4). Molar conductance measurements gave values in the range 75–95 Ω^{-1} cm^2 typical of 1:1 electrolytes in nitromethane (5).

As noted previously (6), the *cis*-$[PdCl(PEt_3)_2(phen)]^+$ cation is very labile and in solution tends to form $[PdCl(PEt_3)(phen)]^+$, a square planar cation containing bidentate phenanthroline. The displaced PEt_3 reacts with $[Pd_2Cl_2(PEt_3)_4]^{2+}$, present during the preparation of *cis*-$[PdCl(PEt_3)_2(phen)]^+$, or with *cis*-$[PdCl(PEt_3)_2(phen)]^+$ itself to form $[PdCl(PEt_3)_3]^+$. ^{31}P nmr spectra showed that preparations of $[PdCl(PEt_3)_2(phen)]^+$ salts were always slightly contaminated by $[PdCl(PEt_3)(phen)]^+$ and $[PdCl(PEt_3)_3]^+$ as a consequence of the above reactions.

(b) ^{31}P nmr Spectra

Spectra of the three *cis*-$[PdCl(PEt_3)_2L]^+$ cations were all basically similar, consisting of two broad absorptions at 30°C. When L = naph or phth, these resonances sharpened to a well resolved AX pattern at 0°C and reduction of temperature below this caused no further change. When L = phen the spectra were of poorer quality due to the impurities discussed above and $J_{AX}(J_{PP})$ was not resolved although the two resonances were much sharper at 0°C. Raising the temperature caused decomposition of the phenanthroline complex but the resonances for the L = naph or phth complexes continued to broaden and coalesced at approximately 50°C. The AX spectra at 0°C are consistent with structures similar to **1** and as the temperature is raised an exchange process occurs in which the phosphorus positions *trans* to Cl and *trans* to N are interchanged.

(c) ^1H nmr Spectra

The spectrum of *cis*-$[PdCl(PEt_3)_2(phth)]^+$ at 35°C was very similar to that of non-coordinated phthalazine except for differences in chemical shifts. In particular the $\alpha\alpha'$ resonance was a sharp singlet with no evidence of coupling to phosphorus. Cooling caused broadening and then splitting into two resonances, the low field component being broader ($W_{1/2} \sim 6$ Hz) than the other ($W_{1/2} \sim 3$ Hz). The coalescence temperature was −5°C. Thus, there is fluxional exchange of palladium between the two coordination sites on phthalazine, the process being fast at 35°C and slow below −5°C. The low field resonance is assigned to the proton (α) adjacent to the coordinated nitrogen and is broadened by coupling to phosphorus. The absence of observable[2] coupling to phosphorus at 35°C suggests that the fluxional process is dissociative, as is expected from our previous results (2) on platinum phthalazine complexes. This was confirmed by the observation of a marked increase in the rate of exchange when small quantities of phthalazine were added to the solution. A dissociative process also accounts for the observed collapse of the ^{31}P spectra if the palladium intermediate permits interchange of phosphorus positions. It is interesting, however, that the coalescence temperature in the ^{31}P spectra is ~50°C whereas in the ^1H spectra it is ~ −5°C. Computer simulation[3] of the spectra shows that the exchange of proton positions is 4–5 times faster than the exchange of phosphorus positions, which is not unexpected if the dissociation leading to the former is prerequisite to the latter. $\Delta G^{\ddagger}$ is ~50 kJ mol^{-1} for both processes.

The *cis*-$[PdCl(PEt_3)_2(naph)]^+$ spectrum was also similar to that of the free heterocyclic ligand. Cooling to −70°C caused no change except that the double doublet assigned to $\alpha\alpha'$ broadened at −10°C so that the multiplicity was no longer resolved. This is evidence for coupling to phosphorus below −10°C and, in conjunction with the ^{31}P spectra, shows a dissociative exchange process above this temperature as in the phthalazine case. Addition of excess naphthyridine accelerated the exchange and signals due to coordinated and non-coordinated naphthyridine were then clearly resolved on further cooling.[4] However, whereas the phthalazine complex is non-fluxional below −10°C, the two heterocyclic rings in the naphthyridine complex remain chemically equivalent down to −70°C, the lowest temperature accessible before crystallization of the complex spoiled the experiment. This suggests that exchange of palladium between the two nitrogen sites continues at low temperature by an intramolecular process similar to that in the corresponding platinum complex (2). The alternate explanation of symmetric chelation cannot be entirely excluded but it seems relatively unlikely in view of the similarity of infrared and nmr evidence to that for platinum complexes.

Solutions of *cis*-$[PdCl(PEt_3)_2(phen)]^+$ contained non-coordinated phenanthroline (~15%) as a result of the lability of the complex and the sequence of reactions (see section *a* above) leading to $[PdCl(PEt_3)_3]^+$. ^1H resonances due to coordinated and non-coordinated phenanthroline were clearly resolved below −20°C but exchange occurred above this temperature. As in the naphthyridine case, the

[2]The line width in the spectra should have permitted observation of coupling constants >1 Hz.

[3]Using the DNMR 3 programme obtainable as No. 165 from the Quantum Chemistry Programme Exchange, University of Indiana.

[4]Coincidences of chemical shift prevented similar resolution in the phthalazine case.

TABLE 1. Nuclear magnetic resonance data

Complex[a]	Temp.[b] (°C)	^{1}H spectrum of heterocycle[c] Chemical shifts (τ) α / α′	β / β′	γ / γ′	δ / δ′	Coupling constants (Hz) αβ / α′β′	αγ / α′γ′	βγ / β′γ′	^{31}P spectrum[d] Chem. shift (ppm)	$J_{P—P}$ (Hz)
1,10-Phenanthroline	35	1.16	2.60	1.92	2.41	4.4	1.6	8.1		
[PdCl(PEt$_3$)(phen)]$^+$[e]	35	0.50 1.04	1.98 1.75	1.26 1.21	1.88 1.88	5.1 5.3	1.4 1.3	8.2 8.3	106.0	
cis-[PdCl(PEt$_3$)$_2$(phen)]$^+$	−20	0.76	2.26	1.61	2.25	4.2	[f]	7.8	105.8 114.7	[f]
1,8-Naphthyridine	35	0.91	2.42	1.61		4.2	2.0	8.0		
cis-[PdCl(PEt$_3$)$_2$(naph)]$^+$	35	0.67	2.08	1.23		4.8	1.7	8.3	105.6 111.3	13
Phthalazine	35	0.67	~2.2	~2.2		~0	~0	8.2		
cis-[PdCl(PEt$_3$)$_2$(phth)]$^+$	35	0.34	~2.0	~2.0		[f]	[f]	[f]	109.1 104.4	16
cis-[PdCl(PEt$_3$)$_2$(phth)]$^+$	−70	0.26 0.55	~2.1	~2.1		[f]	[f]	[f]		
[PdCl(PEt$_3$)$_3$]$^+$									107.8[g] 114.4[h]	19

[a]Complex cations were studied as both BF_4^- and ClO_4^- salts. There were no significant differences.
[b]Temperatures of ^{1}H spectra. All ^{31}P spectra were recorded at 0°C.
[c]α, β, γ, and δ positions were labelled relative to the nitrogen atoms. Where a single entry occurs for primed and unprimed parameters, the two are chemically equivalent. In other cases primes denote positions adjacent to the non-coordinated nitrogen or, in the case of [PdCl(PEt$_3$)(phen)], the ring *trans* to chlorine. Spectra were recorded using CH_2Cl_2 as reference and lock in $(CD_3)_2CO$ solution except for naph and *cis*-[PdCl(PEt$_3$)$_2$(naph)] for which a TMS lock was used and [PdCl(PEt$_3$)(phen)]$^+$ which was in CD_2Cl_2 solution.
[d]Recorded in CD_2Cl_2 solution at 0°C using $P(OCH_3)_3$ as external reference. Chemical shifts are in ppm upfield from the reference.
[e]The α, α′, and β resonances showed doubleting due to ^{31}P, $J_{\alpha P} = 3.9$, $J_{\alpha' P} = 3.1$, $J_{\beta P} = 1.7$ Hz.
[f]Not resolved.
[g]Triplet
[h]Doublet.

two heterocyclic rings of the coordinated ligand remained chemically equivalent down to −70°C. Thus, the fluxional processes in all three complexes are similar to those observed in the platinum analogues (2), except that the rates of both dissociative and intramolecular processes are increased relative to the platinum case. This is expected since palladium complexes are well known to be generally more labile than those of platinum.

Experimental

Our general techniques and instrumentation have been described previously (2). ^{31}P nmr spectra were recorded at 24.288 MHz on a Nicolet TT-14 Fourier transform spectrometer using $P(OMe)_3$ as external reference, C_6D_6 as external lock, and CH_2Cl_2 as solvent. Positive chemical shifts are upfield from the reference. ^{1}H nmr spectra were recorded at 90 MHz on a Perkin-Elmer R32 spectrometer using $(CD_3)_2CO$ as solvent and CH_2Cl_2 as the most usual lock signal (see Table 1). Magnet ambient temperature was 35°C for the ^{1}H spectra and 30°C for the ^{31}P spectra.

1,8-Naphthyridine was prepared as previously described (7) and the other ligands were commercially available. [PdCl(PEt$_3$)$_n$(phen)][BF_4] complexes were prepared as previously described (6) except that conversion of the $n = 2$ complex to the $n = 1$ was achieved rapidly and almost quantitatively by addition of a few drops of H_2O_2 solution to the former complex in methanol under reflux. Preparations of [PdCl(PEt$_3$)$_2$L][BF_4], L = naph, phth, pyridazine, or PEt$_3$, were exactly analogous to the previous method for L = phen (6). The pyridazine complex gave nmr results analogous to those described for the corresponding phthalazine complex.

Perchlorate salts were prepared because of initial analytical difficulties with the fluoroborates which tended to oil rather than crystallize. They were obtained in high yield by use of the appropriate ligand in reactions similar to the following example.

cis-[*PdCl(PEt$_3$)$_2$(phth)*][ClO_4]

A solution of phthalazine (0.049 g, 0.38 mmol) and $NaClO_4 \cdot H_2O$ (0.070 g, 0.50 mmol) in acetone (5 ml) was added dropwise to a stirred solution of *trans*-[$PdCl_2$(PEt$_3$)$_2$] (0.154 g, 0.37 mmol) in acetone (5 ml) under a nitrogen atmosphere at 25°C. After 15 min the mixture was evaporated to dryness under reduced pressure and the residue extracted with dichloromethane to leave NaCl and unreacted $NaClO_4$ as residue. Evaporation of the extract and crystallization of the resulting oil from methanol by the addition of diethyl ether gave *the complex* as white crystals (0.168 g, 0.28 mmol) which were recrystallized by the same procedure.

Analyses

Anal. calcd. for [PdCl(PEt$_3$)(phen)][ClO_4]: C 40.1, H 4.3, N 5.2; found: C 40.2, H 4.4, N 5.1. *Anal.* calcd. for [PdCl(PEt$_3$)$_2$(naph)][BF_4]: C 40.4, H 6.1, N 4.7; found: C 40.7, H 5.7, N 4.2. *Anal.* calcd. for

Can. J. Chem. Downloaded from www.nrcresearchpress.com by 210.87.254.42 on 09/05/12
For personal use only.

$[PdCl(PEt_3)_2(naph)][ClO_4]$: C 39.5, H 6.0, N 4.6; found: C 38.9, H 5.7, N 4.5. *Anal.* calcd. for $[PdCl(PEt_3)_2(phth)][BF_4]$: C 40.4,[5] H 6.1, N 4.7; found: C 42.7, H 6.1, N 4.7. *Anal.* calcd. for $[PdCl(PEt_3)_2(phth)][ClO_4]$: C 39.5, H 6.0, N 4.6; found: C 39.9, H 6.1, N 4.7. *Anal.* calcd. for $[PdCl(PEt_3)_2(pyridazine)][BF_4]$: C 35.3, H 6.3, N 5.1; found: C 35.4, H 6.3, N 4.6. *Anal.* calcd. for $[PdCl(PEt_3)_3][BF_4]$: C 37.1, H 7.8; found: C 36.5, H 7.5.

Acknowledgements

We thank the University of Victoria and the National Research Council of Canada for research grants.

[5]Difficult to crystallize, see Experimental section.

1. G. W. BUSHNELL, K. R. DIXON, and M. A. KHAN. Can. J. Chem. **52**, 1367 (1974).
2. K. R. DIXON. Inorg. Chem. **16**, 2618 (1977).
3. G. W. BUSHNELL, K. R. DIXON, and M. A. KHAN. Can. J. Chem. **56**, 450 (1978).
4. G. W. BUSHNELL and K. R. DIXON. Can. J. Chem. **56**, 878 (1978).
5. W. GEARY. Coord. Chem. Rev. **7**, 81 (1971).
6. K. R. DIXON and A. D. RATTRAY. Can. J. Chem. **51**, 618 (1973).
7. W. W. PAUDLER and T. J. KRESS. J. Org. Chem. **32**, 832 (1967).

Can. J. Chem. Downloaded from www.nrcresearchpress.com by 210.87.254.42 on 09/05/12
For personal use only.

Fonction d'acidité relative aux amines secondaires: un critère de validité du postulat de Hammett

JEAN-MARIE CARPENTIER ET PATRICK LEMETAIS

Laboratoire de Chimie Physique Organique, Faculté des Sciences et Techniques, 76130 Mont Saint Aignan, France et Laboratoire de Chimie Analytique, Faculté de Pharmacie, Université Paris V, 75005 Paris, France

Reçu le 29 juillet 1977

JEAN-MARIE CARPENTIER et PATRICK LEMETAIS. Can. J. Chem. **56**, 954 (1978).

Une fonction d'acidité a été construite par spectrophotométrie, en milieu eau – acide sulfurique, à 298 K, à l'aide de sept amines secondaires comme indicateurs. Cette fonction est la même que celle basée sur les amines primaires et diffère ainsi de celle relative aux amines tertiaires. Les deux premiers types d'amines sont donc les indicateurs de la même fonction d'acidité. On conclut que pour une fonction d'acidité donnée, le postulat de Hammett est seulement vérifié pour tous les composés caractérisés par la valeur identique d'un paramètre structural τ: le taux apparent de solvatation.

JEAN-MARIE CARPENTIER and PATRICK LEMETAIS. Can. J. Chem. **56**, 954 (1978).

An acidity function has been determined spectrophotometrically in aqueous sulphuric acid, at 298 K, by using seven secondary amine indicators. This function is the same as that based on primary amines and so differs from that relative to tertiary amines. Therefore, the first two types of amines are the indicators of the same acidity function. It is concluded that for a given acidity function, the Hammett postulate is only verified for all the compounds characterized by the same value of a τ structural parameter: apparent ratio of solvation.

Can. J. Chem. Downloaded from www.nrcresearchpress.com by 210.87.254.5 on 09/05/12
For personal use only.

Il est maintenant connu qu'à l'unicité de l'échelle pH correspondent plusieurs fonctions d'acidité (1, 2). Si le postulat de Hammett (3) reste vérifié à l'intérieur d'une même série d'indicateurs, cela revient à écrire, à une acidité donnée, la relation [1]:

$$[1] \quad H_X = -\log I + \mathrm{p}K_{XH^+} = -\log I' + \mathrm{p}K_{X'H^+}$$

avec $I = |XH^+|/|X|$; $I' = |X'H^+|/|X'|$; X et X' indicateurs de H_X.

Comme les variations expérimentales de $\log I = f(\log I')$ ne sont pas toujours des droites de pente unitaire, un certain nombre de travaux (parmi lesquels réfs 4–6 et réf. dans réfs 1, 2) ont mis en doute la validité du postulat de Hammett, et donc celle du concept de fonction d'acidité. C'est pourquoi, nous avons entrepris l'étude de différents critères de validité; nous exposons les premiers résultats dans ce mémoire.

Si la pente de la droite $\log I = f(\log I')$ dépend du couple d'indicateurs (X, X'), il existe peu de chances que l'on obtienne des valeurs identiques de fonction d'acidité avec des couples différents. Mais, Yates et Shapiro (7) ont montré qu'en utilisant des anilines primaires non substituées par des groupements nitro, la fonction d'acidité obtenue est la même que celle bâtie uniquement sur des nitro-anilines. Dans ce travail, nous comparons les résultats obtenus *avec deux séries distinctes* d'indicateurs. Dans un précédent mémoire (8), nous avons établi, au moyen d'un procédé graphique, que la protonation des amines secondaires obéissait à la fonction H'_0. Cette obéissance, qui se traduit par une pente sensiblement unitaire de la droite $\log I = f(H'_0)$, ne constitue pas une preuve suffisante. Nous avons donc construit la fonction d'acidité (H''_0) relative à la protonation des amines secondaires.

Résultats et discussion

Ancrage de la fonction H''_0

La nature du premier indicateur et la valeur de son pK conditionnent fortement l'exactitude d'une fonction d'acidité. Pour cette raison, l'ancrage de H''_0 repose sur deux indicateurs. Les pK de la diphénylamine ($+0.77_5$) et de la *N*-éthyl-nitro-2-aniline (-0, 11) ont été déterminés spectrophotométriquement en solution acide diluée (pour les concentrations égales ou inférieures à $0.532\ M \times \ell^{-1}$, l'acide est de l'acide chlorhydrique), selon le procédé classique:

$$[2] \quad -\log |H^+| + \log I = A' |H^+| + \mathrm{p}K_{XH^+}$$

A' étant le produit des constantes de Setschenow ($\log \gamma = A|H^+|$) et $|H^+|$ désignant la molarité de l'acide.

L'extrapolation à dilution infinie d'acide donne la valeur thermodynamique de $\mathrm{p}K_{XH^+}$, (tableau 1). Pour tous les composés, les valeurs du rapport d'ionisation I ont été mesurées à deux longueurs d'onde; aucun effet de milieu n'a été enregistré. La méthode des chevauchements continus (1, 2) a été utilisée pour la détermination du pK des autres composés. La concordance des valeurs de pK du second indicateur déterminées par la méthode des chevauchements continus et par le procédé de l'extrapo-

Can. J. Chem. Downloaded from www.nrcresearchpress.com by 210.87.254.5 on 09/05/12
For personal use only.

TABLEAU 1. Valeurs des pK_{XH^+} des amines secondaires à 298 K

Amines	pK_{XH^+}
(1) Diphénylamine	$+0.775 \pm 0.003^{a,b}$
(2) *N*-Ethyl-nitro-2-diphénylamine	-0.110 ± 0.008^{a} -0.11 ± 0.01^{c}
(3) *N*-Ethyl-chloro-4-nitro-2-aniline	-0.69 ± 0.01^{c}
(4) Nitro-4-diphénylamine	$-2.48 \pm 0.02^{c,d}$
(5) Nitro-2-diphénylamine	-3.28 ± 0.02^{c}
(6) *N*-Ethyl-dinitro-2,4-aniline	-4.40 ± 0.03^{c}
(7) Chloro-5-nitro-2-diphénylamine	-4.69 ± 0.04^{c}

[a]Valeur déterminée par extrapolation à dilution infinie.
[b]pK_{XH^+} (litt.) = 0.78 (9); 0.77 (10).
[c]Valeur déterminée par chevauchements des indicateurs.
[d]pK_{XH^+} (litt.) = −2.50 (2).

lation à dilution infinie d'acide, confirme que l'ancrage de la fonction d'acidité est correct.

Validité du postulat de Hammett

Les pentes de différentes droites $\log I = f(\log I')$ (les valeurs des rapports d'ionisation ont été déposées au Journal où elles peuvent être demandées)[1] ont des valeurs comprises entre 0.99_1 et 1.00_7. A un niveau donné d'acidité, la relation [1] exprimant le postulat de Hammett est donc vérifiée. La fonction H''^0 calculée (tableau 2) est identique à celle obtenue avec les anilines primaires, nitrées (11) ou non (7). Ce résultat démontre que tous ces composés sont des indicateurs de la même fonction d'acidité, indépendante certes de la nature et du nombre des substituants (7), mais également du type de *ses* indicateurs. Ce résultat est généralisable aux autres fonctions d'acidité. En effet, nous avions déjà constaté (15) que les thioamides aliphatiques et les amines tertiaires (mais pas les indoles) étaient les indicateurs de la même fonction d'acidité $|H'''_0$ (16)|.

Le postulat de Hammett est donc vérifié non seulement à l'intérieur d'une série d'indicateurs de structure donnée, mais pour tous les indicateurs d'une fonction d'acidité donnée quel que soit le groupement chimique protonable. Le cas particulier des ions oxonium sera traité ultérieurement.

Comparaison des fonctions H'_0, H''_0 *et* H'''_0

L'existence de fonctions d'acidité différentes pour les amines primaires (H'_0: réfs 7, 11–14) et tertiaires (H'''_0 = réf. 16) a conduit à imaginer une fonction H''_0 relative aux amines secondaires et située entre H'_0 et H'''_0. Cette hypothèse s'appuie sur les travaux de Taft (17). Selon cet auteur, les pentes 3.0 et 4.0 des droites $(H_R - H'_0)$ en fonction de $\log a_{H_2O}$ données par la nitro-4-diphénylamine et la dichloro-2,4-nitro-6-aniline, correspondent respectivement aux équilibres:

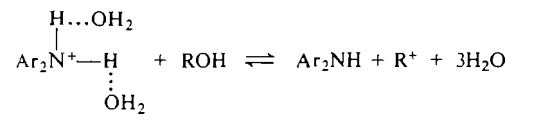

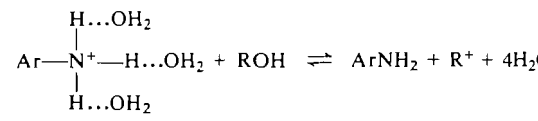

Cette différence d'hydratation impliquerait deux fonctions d'acidité. Cette interprétation nous semble criticable pour les raisons suivantes.

(*a*) Avec les valeurs expérimentales d'ionisation (3) utilisées par Taft, les graphes $\log I = f(H'_0)$,

TABLEAU 2. Valeurs de H''_0 et H'_0 ($\equiv {}^3H$), dans le système H_2O–H_2SO_4 à 298 K

	Indicateurs	
% H_2SO_4	Amines secondaires (Ce travail)	Amines primaires (11)
2	0.53	0.53
4	0.23	0.20
6	0.00	−0.02
8	−0.18	−0.20
10	−0.34	−0.35
12	−0.48	−0.50
14	−0.61	−0.65
16	−0.75	−0.78
18	−0.88	−0.92
20	−1.01	−1.06
22	−1.15	−1.20
24	−1.29	−1.34
26	−1.42	−1.47
28	−1.54	−1.60
30	−1.70	−1.73
32	−1.84	−1.85
34	−1.98	−1.99
36	−2.12	−2.12
38	−2.27	−2.27
40	−2.43	−2.42
42	−2.60	−2.60
44	−2.76	−2.77
46	−2.93	−2.95
48	−3.10	−3.12
50	−3.32	−3.30
52	−3.53	−3.48
54	−3.76	−3.68
56	−3.98	−3.90
58	−4.21	−4.13
60	−4.45	−4.37
62	−4.70	−4.62
64	−4.92	−4.91
66	−5.19	−5.20
68	−5.47	−5.52
70	−5.77[a]	−5.82

[a]Valeur extrapolée.

[1]On peut obtenir les données mises en dépôt à un prix nominal en s'adressant au Dépôt de données non publiées, ICIST, Conseil national de recherches du Canada, Ottawa (Ont.), Canada K1A 0S2.

Can. J. Chem. Downloaded from www.nrcresearchpress.com by 210.87.254.5 on 09/05/12
For personal use only.

$|H'_0$ (réf. 11)|, donnent des droites de pente 1.01 et 0.97 indiquant un comportement similaire de ces deux composés. D'ailleurs, en milieu hydroalcoolique acide à 20% en volume d'éthanol, l'identité des fonctions H''_0 et H'_0 avait été envisagée (4), après correction de l'ancrage de la fonction d'acidité basée sur des diphénylamines (18).

(*b*) Dans l'intervalle d'acidité considéré par Taft, H_R étant le double de H'_0 (1, 2, 15), la différence $(H_R - H'_0)$ est égale à H'_0. On note que le graphe $H'_0 = f(\log a_{H_2O})$ est une droite de pente 3.2 entre 48 et 60% de H_2SO_4 (intervalle où Taft obtient une droite de pente 3.0 pour la nitro-4-diphénylamine) et une droite de pente 4.0 entre 52 et 64% de H_2SO_4 (intervalle où Taft obtient une droite de pente 4.0 pour la dichloro-2,4-nitro-6-aniline).

(*c*) Taft a fait appel au concept du nombre d'hydratation pour expliquer la basicité des différentes classes d'ions ammonium. Or, Arnett et Burke (19) ont démontré plus tard que ce traitement n'était pas applicable en milieu acide.

L'identité des fonctions d'acidité H'_0 et H''_0 ne signifie pas que la solvatation globale des entités soit similaire; ainsi, les coefficients d'activité des ions anilinium et *N*-éthyl-anilinium peuvent être différents (20). Cette identité implique celle des différences des variations des énergies de solvatation (ΔG^0_t) caractéristiques des couples RNH_2/RNH_3^+ et $RR'NH/RR'\overset{+}{N}H_2$ (21). La plus faible solvatation constatée dans le cas du couple $RR'R''N/RR'R''\overset{+}{N}H$ serait due à l'encombrement stérique autour de l'atome d'azote.

Nécessité d'introduire un paramètre structural

Dans la définition classique d'une fonction d'acidité, aucun paramètre ne permet de distinguer les composés de structure différente qui sont les indicateurs de la même fonction d'acidité. Dans les travaux antérieurs (21), nous avons caractérisé chaque fonction d'acidité par la valeur d'un paramètre structural τ appelé "taux apparent de solvatation". Ce coefficient est indépendant de la nature de l'acide, du solvant (22), de la température (23) et varie seulement avec la nature du site porteur de la charge positive. Il traduit la différence énergétique de solvatation entre les formes neutre et ionisée. En ayant posé par référence que cette différence est nulle pour les triarylcarbinols, nous avons caractérisé d'une part, les amines primaires et secondaires (8) par la valeur $\tau = 3$ et d'autre part les thioamides et les amines tertiaires par la valeur $\tau = 2$ du taux apparent de solvatation (15). Selon nous, le critère de validité du postulat de Hammett n'est pas nécessairement l'appartenance d'un composé à une série donnée d'indicateurs. Le postulat de Hammett est vérifié pour tous les composés caractérisés par une valeur identique de τ quelles que soient leur structure, la température, et qu'ils soient chargés ou non.

Les auteurs remercient la Délégation Générale à la Recherche Scientifique et Technique, Action concertée Chimie Analytique n° 75.7.0505 pour son support financier.

Partie expérimentale

Les produits utilisés sont tous d'origine commerciale (Aldrich). Les solutions d'acide sulfurique sont préparées par dilution d'acide à 96% en poids et dosées par détermination de la densité à l'aide d'un microdensimètre Anton Paar digital (DMA 02 D). Quelle que soit l'acidité, l'incertitude sur les molarités est inférieure à ± 0.01. En raison de la faible solubilité dans l'eau de la forme neutre, les solutions-mères d'amines furent réalisées en milieu sulfurique. Les spectres uv furent enregistrés sur un spectrophotomètre Beckman DK 2 A, le compartiment cuves étant thermostaté à 298.0 $\pm$ 0.1 K.

1. M. LILER. Reaction mechanisms in sulphuric acid. Academic Press, New York, NY. 1971.
2. C. H. ROCHESTER. Acidity functions. Academic Press, New York, NY. 1970.
3. L. P. HAMMETT et A. J. DEYRUP. J. Am. Chem. Soc. **54**, 272 (1932).
4. A. J. KRESGE et H. J. CHEN. J. Am. Chem. Soc. **94**, 8192 (1972).
5. M. KREEVOY. J. Am. Chem. Soc. **95**, 8178 (1973).
6. N. MARZIANO, G. CIMINO et R. PASSERINI. J. Chem. Soc. Perkin Trans. II, 1915 (1973); 206 (1977).
7. K. YATES et S. SHAPIRO. Can. J. Chem. **50**, 581 (1972).
8. J. M. CARPENTIER et P. LEMETAIS. Bull. Soc. Chim. Fr. **9–10**, 1399 (1976).
9. M. A. PAUL et F. LONG. Chem. Rev. **57**, 1 (1957).
10. M. I. VINNICK. Russ. Chem. Rev. 802 (1966).
11. M. J. JORGENSON et D. R. HARTTER. J. Am. Chem. Soc. **85**, 878 (1963).
12. P. TICKLE, A. G. BRIGGS et J. M. WILSON. J. Chem. Soc. B, 65 (1970).
13. C. D. JOHNSON, A. R. KATRITZKY et S. A. SHAPIRO. J. Am. Chem. Soc. **91**, 6654 (1969).
14. R. S. RYABOVA, I. M. MEDVETSKAYA et M. I. VINNICK. Russ. J. Phys. Chem. **40**, 182 (1966).
15. J. M. CARPENTIER. Bull. Soc. Chim. Fr. **11**, 2946 (1973).
16. E. M. ARNETT et G. W. MACH. J. Am. Chem. Soc. **86**, 2671 (1964).
17. R. W. TAFT. J. Am. Chem. Soc. **82**, 2965 (1960).
18. D. DOLMANN et R. STEWART. Can. J. Chem. **45**, 903 (1967).
19. E. M. ARNETT et J. J. BURKE. J. Am. Chem. Soc. **88**, 2340 (1966).
20. R. H. BOYD. J. Am. Chem. Soc. **85**, 1555 (1963).
21. J. M. CARPENTIER et M. B. FLEURY. Bull. Soc. Chim. Fr. **7–8**, 1075 (1976).
22. J. M. CARPENTIER. Bull. Soc. Chim. Fr. **9–10**, 1812 (1974); **9–10**, 1817 (1974).
23. P. LEMETAIS et J. M. CARPENTIER. Bull. Soc. Chim. Fr. **1**, 11 (1977).

Crystal structure of aquohydronium hexachloroantimonate(V)

HUGH M. MATHESON AND W. ALEX WHITLA

Department of Chemistry, Mount Allison University, Sackville, N.B., Canada E0A 3C0

Received August 5, 1977

HUGH M. MATHESON and W. ALEX WHITLA. Can. J. Chem. **56**, 957 (1978).

Crystals of the compound, $H_5O_2^+SbCl_6^-$ have been obtained. The structure shows an isolated $H_5O_2^+$ ion with O—O 2.52(1) Å. Crystal data: orthorhombic (*Immm*) $a = 6.96(1)$, $b = 9.15(1)$, $c = 7.91(1)$ Å.

HUGH M. MATHESON et W. ALEX WHITLA. Can. J. Chem. **56**, 957 (1978).

On a obtenu des cristaux du composé $H_5O_2^+SbCl_6^-$. La structure indique la présence d'un ion $H_5O_2^+$ isolé avec une distance O—O 2.52(1) Å. Les données cristallographiques: orthorhombique (*Immm*) $a = 6.96(1)$, $b = 9.15(1)$, $c = 7.91(1)$ Å.

[Traduit par le journal]

Can. J. Chem. Downloaded from www.nrcresearchpress.com by 210.87.254.105 on 09/05/12
For personal use only.

The interest in structures of compounds containing strong hydrogen bonds (ref. 1, and references therein) has shown the importance of the aquohydronium ion, $H_5O_2^+$, in such systems. However, no previous structure contains this ion isolated from other water molecules or from strong hydrogen bonds to adjacent ions.

Crystals of the compound, $H_5O_2^+SbCl_6^-$, were obtained in X-ray capillaries when attempting to grow crystals of an adduct of antimony pentachloride. The structure was solved but did not correspond to any product reported in the literature (2). Recently Ortwein and Schmidt (3) have characterized the products $H_5O_2^+SbCl_6^-$ and $H_7O_3^+$-$SbCl_6^-$. We now report our structural data on the former compound.

The compound formed orthorhombic crystals with $a = 6.96(1)$, $b = 9.15(1)$, $c = 7.91(1)$ Å; $D_c = 2.45$ for $Z = 2$; $M = 371.5$; space group *Immm*.[1] The data crystal was grown by vacuum sublimation in a 0.3 mm quartz X-ray capillary and data were collected on a G.E. XRD-6 manual diffractometer using CuKα radiation. No absorption corrections have been made for the 236 reflections observed. (Crystal dimension: ~0.2 mm cube.) The atomic parameters given in Table 1 gave $R = 0.116$ for 224 observed reflections.[2] The relatively high R value and the large standard deviation of the thermal parameters indicate the need for an absorption correction. The data crystal decomposed and the necessary data for an absorption correction cannot be obtained.

The structure was solved by Patterson techniques and shows an octahedral hexachloroantimonate(V) ion with *mmm* symmetry. The $SbCl_6^-$ ions are packed head to tail along c in the I-centred cell with Cl—Cl contact of 3.206(3) Å. The two Sb—Cl bonds along c are 2.354(3) Å while the remaining four Sb—Cl bonds are 2.348(2) Å. The Cl—Sb—Cl angles are 91.14(5)° facing the $H_5O_2^+$ ion (b-axis) and 88.86(5)° (a-axis).

The environment of the aquohydronium ion is shown in Fig. 1. The O—O distance of 2.52(1) Å is similar to other room temperature hydrogen bond distances in "$H_5O_2^+$" species (1, 4). The shortest non-bonded contact of 3.494(5) Å are with Cl2 subtending an angle of 69.55(8)° with the O—O direction. With Cl1, four interactions of 3.605(3) Å have angles of 95.64(9)° and eight remaining contacts of 3.636(6) Å subtend angles of 137.90(9)°. Only the latter contacts would involve the possibility of some hydrogen bonding. With the high local symmetry the $H_5O_2^+$ ion either has free rotation in the ionic lattice or a disordered distribution of H-bonds to the eight equivalent chlorine atoms.

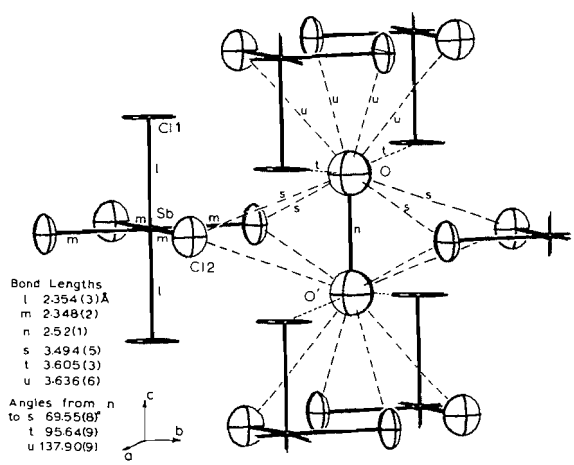

FIG. 1. $H_5O_2^+SbCl_6^-$ – oxygen environment.

[1]Errors estimated from film measurements.

[2]Copies of the structure factors in Table A may be obtained, at a nominal charge, from the Depository of Unpublished Data, CISTI, National Research Council of Canada, Ottawa, Ont., Canada K1A 0S2. Weighting scheme: $W = A^2/[A^2 + (F_o - B)^2]$, $A = 120$, $B = 50$ for full matrix refinement.

TABLE 1. Atom parameters for $H_5O_2^+SbCl_6^-$*

Immm site	Symmetry	x	y	z	U_{11} (U_{iso})	U_{22}	U_{33}	U_{12}
Sb	*a,mmm*	0	0	0	25(3)	19(2)	1(2)	
Cl1	*i,mm*	0	0	2975(17)	79(13)	139(19)	0.3(6)	
Cl2	*n,m*	2411(16)	1796(12)	0	17(7)	9(6)	24(8)	−14(5)
O	*j,m*	5000	0	3409(81)	93(9)			

*$x, y, z, \times 10^4$, U's $\times 10^3$; estimated standard deviations apply to the last figure given.

In this structure the two oxygen atoms lie across a mirror plane but the contribution of the H atom would not allow the distinction between the space groups *Immm* and *Imm*2. However, the environment of the $H_5O_2^+$ ion in this compound is symmetric in all directions (the mid-point between the oxygen positions must have *mmm* symmetry in space group *Immm*) and the angles of the O—O—Cl contacts would indicate weak H-bonds between $H_5O_2^+$ and $SbCl_6^-$. Although these conditions do not require a symmetric hydrogen bond for $H_5O_2^+$, they are essential to this possibility.

1. J. M. WILLIAMS and S. W. PETERSON. Spectrosc. Inorg. Chem. **2**, 1 (1971).
2. F. KLAGES, H. MEURESCH, and W. STEPPICH. Annalen, **592**, 81 (1955).
3. V. R. ORTWEIN and A. SCHMIDT. Z. Anorg. Allg. Chem. **425**, 10 (1976).
4. J. M. WILLIAMS. Inorg. Nucl. Chem. Lett. **3**, 297 (1967).
5. P. A. KOLLMAN and L. C. ALLEN. J. Am. Chem. Soc. **92**, 6101 (1970).
6. M. DEPAZ, S. EHRENSON, and L. FRIEDMAN. J. Chem. Phys. **52**, 3362 (1970).

Can. J. Chem. Downloaded from www.nrcresearchpress.com by 210.87.254.105 on 09/05/12
For personal use only.

Local anisotropic contributions to ^{1}H nuclear magnetic resonance shifts in alkynes

ARVIND AGARWAL AND MICHAEL J. MCGLINCHEY[1]

Department of Chemistry, McMaster University, Hamilton, Ont., Canada L8S 4M1

Received August 25, 1977

ARVIND AGARWAL and MICHAEL J. MCGLINCHEY. Can. J. Chem. **56**, 959 (1978).

Local anisotropic contributions to chemical shifts of protons sited near an alkyne moiety have been calculated using a classical model previously applied to aromatic systems. The results are presented in terms of an isoshielding contour map. The upfield shifts of ethyne and propyne and also the downfield shifts of the γ-protons of cyclooctynes are well accounted for by this theory.

ARVIND AGARWAL et MICHAEL J. MCGLINCHEY. Can. J. Chem. **56**, 959 (1978).

Utilisant un modèle classique appliqué antérieurement à des systèmes aromatiques, on a calculé les contributions anisotropiques locales aux déplacements chimiques des protons situés près d'une portion alcyne. On présente les résultats en terme d'une carte de contour de constantes d'écran égales. Les déplacements vers les hauts champs de l'éthyne et du propyne et aussi les déplacements vers les bas champs des protons γ des cyclooctynes peuvent être expliqués par cette théorie.

[Traduit par le journal]

Introduction

The anomalously high field absorption of the alkyne proton in nmr spectroscopy was rationalised two decades ago by Pople (1) who calculated that the neighbour anisotropy effect would produce a sizeable upfield shift, perhaps of the order of ~10 ppm. This paramagnetic contribution more than compensates for the downfield shift anticipated for a proton bonded to a relatively electronegative *sp*-hybridized carbon atom.

It has recently been demonstrated (2) that local anisotropic contributions to chemical shifts for protons in benzene and condensed aromatic systems are readily calculable by combining classical electromagnetic induction theory with the ^{13}C tensors obtained by Waugh and co-workers (3) using the technique of proton enhanced nuclear induction spectroscopy. This approach has been extended to include all proton positions in the vicinity of the benzene ring (4) and isoshielding contour maps incorporating both local anisotropic and ring current contributions to the chemical shifts of out-of-plane protons have now been calculated (5).

We now present the results of calculations of local anisotropic contributions to protons in the vicinity of the alkyne moiety.

Results and Discussion

Calculation of Local Anisotropic Shifts

Using the analogy of a current circulating in a loop of wire (2) the proton shielding component is given by

$$[1]\quad \sigma_{ii}^{H} = \frac{a}{\pi}\frac{1}{[(a+\rho)^2+z^2]^{1/2}} \times \left[K + \frac{a^2-\rho^2-z^2}{(a-\rho)^2+z^2}E\right]\sigma_{ii}^{C}$$

where σ_{ii}^{H} and σ_{ii}^{C} are the proton and carbon shielding components, respectively, ρ and z are the usual cylindrical coordinates, a is the radius of circulation (taken as 0.47 Å for circulation about a carbon atom (2)), and K and E are complete elliptical integrals of the first and second kind with argument

$$k^2 = \frac{4a\rho}{(a+\rho)^2+z^2}$$

In short, $\sigma_{ii}^{H} = G\sigma_{ii}^{C}$ where G is a geometric factor. The isotropic shielding, as measured in solution, is given by averaging the components:

$$[2]\qquad \langle\sigma^{H}\rangle = 1/3[\sigma_{11}^{H} + \sigma_{22}^{H} + \sigma_{33}^{H}]$$

The ^{13}C tensors for 2-butyne have been obtained by Waugh and co-workers (6) and, as anticipated, revealed considerable anisotropy. Since the ^{13}C isotropic shifts of the alkyne carbons in 2-butyne and acetylene itself are so similar and furthermore σ_{33} (which induces a field along the C—R axis) in substituted benzenes has been shown to be quite insensitive to the nature of the substituent (R = H, CH_3, or C_2H_5), it seems not unreasonable to use the ^{13}C tensors in 2-butyne for calculations on acetylene itself. As noted by Barfield *et al.* (2), it is necessary to convert the shielding tensors to absolute values by adding 71 ppm (ref. 2 note 40) to Waugh's experimental values.

[1] Author to whom correspondence should be addressed.

Can. J. Chem. Downloaded from www.nrcresearchpress.com by 210.87.254.42 on 09/05/12
For personal use only.

Can. J. Chem. Downloaded from www.nrcresearchpress.com by 210.87.254.42 on 09/05/12
For personal use only.

TABLE I

	Proton coordinates[a]			Induced shift[b]
	x	*y*	*z*	H
H—C≡C—H	0	0	1.66	4.439
H—C≡C—CH_3	1.04	0	2.43	0.647
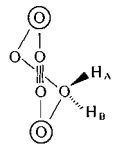	1.39	1.87	0.23	−0.423
	0.98	3.54	0.66	−0.115

[a]Units are Å; the origin is at the centre of the triple bond which lies along the *z* axis.
[b]Units are ppm.

The Chemical Shift of Acetylene

Now using $\sigma_{11}{}^{C} = 244$, and $\sigma_{22}{}^{C} = \sigma_{33}{}^{C} = 42$ and taking into account the contribution of both carbon atoms, we see (Table 1) that an upfield shift of 4.44 ppm is indicated. To evaluate the chemical shift (δ) of the alkyne protons in acetylene, it is necessary to know the inherent shift of an *sp*-carbon-bonded proton to which the local anisotropic incremental shift can be added.

The 'inherent shift' of a —C≡C—H system would have to reflect the inductive pull of the alkyne moiety and this is not a trivial problem since neither Hammett nor Taft values for the H—C≡C— substituent appear to be widely used; however, estimates of the electronegativity of the alkyne moiety have been published (7). Although the values of $^{1}J_{CH}$ for C_2H_6, C_2H_4, and C_2H_2 correlate nicely with the percentage of *s* orbital character or with pK_a values of the hydrocarbons (8), analogous extrapolation of chemical shifts would predict an alkyne proton shift to be in the range 15–16 δ. (This circumstance arises since the observed C_2H_4 resonance is shifted *downfield* owing to the anisotropic nature of the sp^2 carbons.) A somewhat naive, but nevertheless empirically useful, correlation ($\bar{r} = 0.977$) can be drawn between the chemical shifts of X—H and pK_a values of X—CO_2H, where X = CH_2F, CH_2Cl, CH_2Br, and CH_2I. Now, knowing the pK_a value of H·C≡C—CO_2H, this correlation can be extrapolated to predict an 'inherent shift' for C_2H_2 of ~7 δ. In the light of these considerations, the calculated chemical shift of C_2H_2 (allowing for local anisotropy) is ~2.6 δ which is gratifyingly close to the experimental value of 2.88 δ.

Goldstein and Reddy (9, 10) have estimated the anisotropy in the magnetic susceptibility of the alkyne moiety to be -16.5×10^{-6} cm^3 mol^{-1}; this leads to a predicted upfield shift for the directly bonded proton of 4 ± 0.5 ppm, in good agreement with that obtained by the approach presented here.

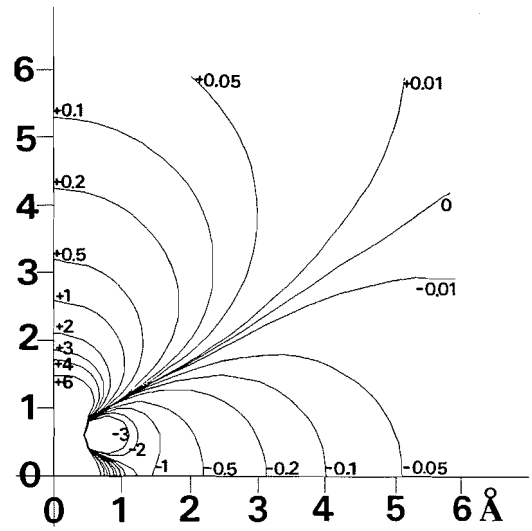

FIG. 1. Incremental shifts (in ppm) of a nucleus positioned near an alkyne linkage. The plot represents one quadrant of a plane containing the C_∞ axis; the origin is at the centre of the triple bond which lies along the ordinate axis. A positive sign corresponds to an upfield shift.

The Chemical Shift of Propyne

A methyl group bonded directly to a triple bond is predicted (Table 1) to exhibit an upfield shift of 0.65 ppm but again one has to determine what the 'inherent shift' of such a methyl group should be. For this purpose, we noted the excellent correlation (9) between $^{1}J_{CH}$ (11) and δ for a series of CH_3X molecules, in which large deviations from the straight line are shown by $CH_3C{\equiv}C{-}H$, CH_3CN, and CH_3—Ph. In the first two cases, the chemical shifts are upfield by ~0.75 ppm as is to be expected for molecules with large anisotropic contributions along the multiple bond axis; in the case of toluene the methyl group is downfield by ~1 ppm and this is nicely accounted for by local anisotropic contributions of the benzene ring (4, 5).

Deshielding by the Triple Bond

It has been noted previously (12) that the triple bond should have a deshielding zone entirely analogous to the situation already well established for benzene. However, attempts to observe this effect have so far been unsuccessful (13). The isoshielding contour map (Fig. 1) derived from our calculations[2] shows that to maximise this effect one needs a proton sited close to the centre of the triple bond. This situation does arise in the small ring cycloalkynes whose spectra have been studied by Krebs (14). In particular, the γ-protons of 4,4,7,7-tetramethylcyclooctyne, which show a singlet at room temperature, are clearly separated upon cooling to −80°C.

[2]Details of the programme available on request.

Since these protons have the same inherent shift, but are experiencing different induced fields when the molecule is no longer free to invert, they provide an ideal test of the theory. Now, using the γ-proton positions provided by the electron-diffraction study of cyclooctyne (15), one can readily evaluate the chemical shift difference between these two protons. The calculated (Table 1) separation of 68 Hz at 220 MHz compares very favorably with the experimental separation of 61 Hz at 220 MHz.

It is of interest to compare the calculated values obtained above for the γ-protons of the tetramethylcyclooctyne system with those predicted using the McConnell relationship (16) in conjunction with the previously quoted (10) value of -16.5×10^{-6} cm^3 mol^{-1} for Δ_χ; H_A and H_B (see Table 1 for coordinates) are predicted to be shifted downfield by 0.692 and 0.170 ppm, respectively. This would lead to a separation of 0.522 ppm, or 115 Hz at 220 MHz. As previously noted by Reddy and Goldstein (10) this extremely useful dipolar approximation must be used with caution for proximate protons.

To conclude, the simple classical model of circulating currents around the alkyne carbon atoms, in conjunction with the experimentally derived ^{13}C tensors of Waugh allows the evaluation of proton shifts in the proximity of a triple bond. These calculated shifts agree remarkably well, both in magnitude and sign, with the experimental spectra.

Acknowledgement

We thank the National Research Council of Canada for financial support.

1. J. A. Pople. Proc. R. Soc. A, **239**, 541 (1957).
2. M. Barfield, D. M. Grant, and D. Ikenberry. J. Am. Chem. Soc. **97**, 6956 (1975).
3. S. Pausak, A. Pines, and J. S. Waugh. J. Chem. Phys. **59**, 591 (1973).
4. A. Agarwal, J. A. Barnes, J. L. Fletcher, M. J. McGlinchey, and B. G. Sayer. Can. J. Chem. **55**, 2575 (1977).
5. A. Agarwal. M.Sc. Thesis, McMaster University, Hamilton, Ont. 1976.
6. A. Pines, M. G. Gibby, and J. S. Waugh. Chem. Phys. Lett. **15**, 373 (1972).
7. W. Zeil and H. Buchert. Z. Phys. Chem. **38**, 47 (1963); J. K. Wilmshurst. J. Chem. Phys. **27**, 1129 (1957).
8. N. Muller and D. E. Pritchard. J. Chem. Phys. **31**, 768 (1959); J. N. Shoolery. J. Chem. Phys. **31**, 1427 (1959).
9. J. H. Goldstein and G. S. Reddy. J. Chem. Phys. **36**, 2644 (1962).
10. G. S. Reddy and J. H. Goldstein. J. Chem. Phys. **39**, 3509 (1963).
11. G. E. Maciel, J. W. McIver, Jr., N. S. Ostlund, and J. A. Pople. J. Am. Chem. Soc. **92**, 1 (1970); **92**, 11 (1970).
12. R. M. Lynden-Bell and R. K. Harris. Nuclear magnetic resonance spectroscopy. Thomas Nelson, London. 1969. p. 89.
13. J. E. Nordlander, J. M. Hanish, J. E. Mollenshot, and L. R. Sheeler. Abstr. 151st Meeting Am. Chem. Soc. Abstr. K112 (1966).
14. A. Krebs. Tetrahedron Lett. 4511 (1968).
15. J. Haase and A. Krebs. Z. Naturforsch. **26A**, 1190 (1971).
16. H. M. McConnell. J. Chem. Phys. **27**, 226 (1957).

Can. J. Chem. Downloaded from www.nrcresearchpress.com by 210.87.254.42 on 09/05/12
For personal use only.

Equilibrium constants for a series of simple aldol condensations, and linear free energy relations with other carbonyl addition reactions

J. PETER GUTHRIE[1]

Department of Chemistry, University of Western Ontario, London, Ont., Canada N6A 5B7

Received July 18, 1977

J. PETER GUTHRIE. Can. J. Chem. **56**, 962 (1978).

A set of equilibrium constants for aldol condensations of acetaldehyde, acetone, acetophenone, and acetic acid as nucleophiles and formaldehyde, acetaldehyde, benzaldehyde, acetone, and acetophenone as carbonyl acceptors has been evaluated. The four values determined, directly or indirectly, by experiment have been augmented by values calculated from thermochemical data and equilibrium constants for enone hydration, and by estimation of free energies of formation of the reaction products by use of hypothetical disproportionation reactions. When the carbonyl nucleophiles are compared to other nucleophiles which can add to carbonyl compounds, it is found that they can be incorporated in the linear free energy relationship of Sander and Jencks, with γ values of 0.45 for acetaldehyde, 0.16 for acetone, 0.05 for acetophenone, and 3.56 for acetic acid. These results make it possible to predict the equilibrium constants for any of a large number of aldol condensations from the equilibrium constant for the addition of any nucleophile to the carbonyl acceptor compound.

J. PETER GUTHRIE. Can. J. Chem. **56**, 962 (1978).

On a évalué une série de constantes d'équilibre pour les condensations aldoliques de l'acétaldéhyde, de l'acétone, de l'acétophénone et de l'acide acétique agissant comme nucléophile alors que la formaldéhyde, l'acétaldéhyde, la benzaldéhyde, l'acétone et l'acétophénone agissent comme accepteur de carbonyle. Aux quatre valeurs déterminées directement ou indirectement à l'aide des expériences on a pu apporter un complément grâce aux valeurs calculées à partir de données thermodynamiques et de constantes d'équilibre pour l'hydratation d'énones et aussi grâce à des évaluations des énergies libres de formation des produits de réaction faites en se basant sur des réactions de dismutations hypothétiques. Lorsque l'on compare les carbonyles nucléophiles avec d'autres nucléophiles qui peuvent s'additionner sur les groupements carbonyles, on trouve qu'ils peuvent être incorporés dans la relation linéaire d'énergies libres de Sander et Jencks avec des valeurs γ de 0.45 pour l'acétaldéhyde, 0.16 pour l'acétone, 0.05 pour l'acétophénone et 3.56 pour l'acide acétique. En se basant sur ces résultats, il est donc possible de prédire les constantes d'équilibre d'un grand nombre de condensations aldoliques en se basant sur la constante d'équilibre pour l'addition de n'importe quel nucléophile sur un composé carbonylé accepteur.

[Traduit par le journal]

Introduction

The aldol reaction is of enormous importance in synthetic organic chemistry, as witness the entire volume of 'Organic Reactions' required to review it (1). Despite this importance and utility, there have been relatively few mechanistic investigations (2–13) and even fewer studies of the equilibrium constants (4, 6, 14) for simple aldol reactions. In part this is the result of the notorious tendency of aldol reactions to yield complex reaction mixtures, with competing reactions, polymerizations and worse confusing the situation. Nonetheless, in view of the utility of this reaction it seemed worthwhile to seek a quantitative understanding of the factors controlling the position of equilibrium for aldol addition reactions. Naturally it would be even more valuable to know the rate constants and the factors controlling them, but that is a more difficult problem, and it seems likely that the equilibrium constants will have to be known if many of the rate constants are to be determined. In any case the aldol reaction is so often determined by thermodynamic rather than kinetic factors that it seems appropriate to report at the present stage, when a set of equilibrium constants have been obtained.

The aldol reaction has been difficult to study in a systematic way because many of the reactions which one would like to investigate are experimentally inaccessible. For instance the reaction of acetaldehyde with acetone in the sense of eq. 1 is not

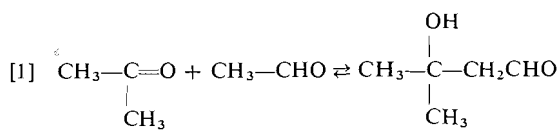

[1] $CH_3-C(=O)(CH_3) + CH_3-CHO \rightleftarrows CH_3-C(OH)(CH_3)-CH_2CHO$

directly accessible because acetone is relatively unreactive toward carbonyl addition while acetaldehyde reacts readily with itself. In fact a cross product

[1]Alfred P. Sloan Fellow, 1975–1979.

Can. J. Chem. Downloaded from www.nrcresearchpress.com by 210.87.254.6 on 09/05/12
For personal use only.

from the reaction of acetone with acetaldehyde can be obtained (15), but it is the product of reaction in the sense of eq. 2. Similar problems render it diffi-

[2] $CH_3-\underset{\underset{CH_3}{|}}{C}=O + CH_3-CHO \rightleftarrows CH_3-\overset{\overset{O}{||}}{C}-CH_2-\overset{\overset{OH}{|}}{CH}-CH_3$

cult if not impossible to measure equilibrium constants for numerous other simple aldol reactions. Yet another problem which can arise, particularly for aromatic carbonyl compounds, is favorable dehydration of the initially formed aldol product, so that the only observable product of reaction is the enone. For these reasons it will be very difficult to augment, by direct measurement of equilibrium position, the very limited set of equilibrium constants presently available.

A number of further values may be determined by making use of thermochemical data for the enones and the corresponding carbonyl precursors, together with experimental values for the dehydration equilibrium constants, measured under conditions where retroaldol reaction is not a problem. This approach was employed for the aldol condensation of acetaldehyde with itself to give an estimate of the equilibrium constant, which turned out to be measurable by indirect experiments (4).

Still more values may be determined by estimating the free energies of formation of the aldol products by a method which is equivalent to Benson's additivity of group contributions (16, 17) procedure but which avoids the problem of cumulative error from a large number of parameters as the molecular size increases.

In these various ways a complete set of equilibrium constants for the reactions of each of four carbonyl compounds acting as nucleophiles adding to each of five carbonyl compounds acting as acceptor could be obtained. This represents the first systematic study of the effects of structure upon equilibrium for the aldol reaction. Possession of these data permits a recognition of the relative importance of structural variation in the carbonyl acceptor and the carbonyl nucleophile upon the equilibrium constant.

Sander and Jencks (18) have introduced a linear free energy relation for additions to carbonyl compounds of alcohols, thiols, amines, hydrogen cyanide, and bisulfite as nucleophiles. I wish to report that this relationship can be extended to the aldol reaction, and that self-consistent values of γ, the parameter describing the tendency for a nucleophile to add to a carbonyl compound, can be evaluated for acetaldehyde (4), acetone, acetophenone, and acetic acid. The approach used here could in principle be extended to other nucleophiles.

Results and Discussion

The equilibrium constants for the aldol formation and dehydration reactions considered here are collected in Table 1. Details concerning the evaluation of these equilibrium constants, where they were not directly obtainable from the literature, are presented in the Experimental section and the Appendix. Although the obtention of these represented a major effort, discussion of the methods here would be needlessly distracting: full details of the calculations are contained in the Appendix. The equilibria are:

[3] $CH_3CO-R_1 + R_2-CO-R_3 \overset{K_1}{\rightleftharpoons} R_2R_3C(OH)-CH_2-CO-R_1 \overset{K_2}{\rightleftharpoons} R_2R_3C=CH-CO-R_1$

where K_1 and K_2 are apparent equilibrium constants expressed in terms of total concentrations of each compound, with no correction for the presence of covalent carbonyl hydrates. This effect is most important for formaldehyde, where the carbonyl form is present in only minor amounts. Values of the K's are given only where they have been measured experimentally. It should be noted that there are only four experimental values for K_1 and that three of these are indirect values, calculated from the rate constants for the forward and reverse reactions. For equilibria where the free energy change was evaluated indirectly from free energies of formation, only the ΔG value is given, with an estimated uncertainty derived from an error analysis of the calculations. For acrylic, crotonic, and senecioic (dimethylacrylic) acids the values reported represent the results of long extrapolations from values at higher temperatures; the uncertainties are accordingly large. For the other experimentally determined values an arbitrary value of 0.1 kcal/mol has been taken as the uncertainty.

It had been hoped that benzophenone, the sixth of the fundamental types of carbonyl compounds, could have been included in the table, but the necessary data were not available. The only relevant equilibrium constant is an indirectly evaluated value for hydration of 3,3-diphenylacrylic acid (19).

In Table 2 are collected equilibrium constants for the addition of nucleophiles to carbonyl compounds. For all but formaldehyde Table 2 is essentially a complete list of the available data. For acetaldehyde a few additional amines have been studied (20) but γ values are not available. For formaldehyde numerous other nucleophiles have been studied; the values are

Can. J. Chem. Downloaded from www.nrcresearchpress.com by 210.87.254.6 on 09/05/12
For personal use only.

Can. J. Chem. Downloaded from www.nrcresearchpress.com by 210.87.254.6 on 09/05/12
For personal use only.

TABLE 1. Equilibrium constants for aldol formation and dehydration[a]

Nucleophile	Carbonyl compound	Aldol formation ΔG_1[b]	Aldol formation K_1[c]	Aldol dehydration ΔG_2[b]	Aldol dehydration K_2[d]
CH_3CHO	CH_2O	−6.32(0.70)[e]		+1.29	0.11[f]
	CH_3CHO	−3.55	400[g]	−0.02	1.03[h]
	PhCHO	−2.18(1.0)[e]		−3.59(1.63)[e]	
	$(CH_3)_2CO$	−0.02(0.72)		−0.56	2.6[i]
	$PhCOCH_3$	+2.31(0.86)[e]		−4.23(1.66)[e]	
$(CH_3)_2CO$	CH_2O	−4.58(0.72)[e]		+1.88	0.043[j,k]
	CH_3CHO	−1.75(0.73)[e]		+0.07	0.88[j,k]
	PhCHO	−1.27	8.5[l]	−2.04	31[l]
	$(CH_3)_2CO$	+1.92	0.039[m]	+1.64	0.063[n]
	$PhCOCH_3$	+4.08(0.89)[e]		−1.86(1.68)[e]	
CH_3COPh	CH_2O	−3.30(1.14)[e]		+0.49(1.97)[e]	
	CH_3CHO	−0.47(1.16)[e]		+1.09(1.99)[e]	
	PhCHO	+0.16	0.76[o]	−2.65	87[o]
	$(CH_3)_2CO$	+3.00(1.17)[e]		+0.85(2.00)[e]	
	$PhCOCH_3$	+5.37(1.26)[e]		−3.18(2.04)[e]	
CH_3COOH	CH_2O	−9.84(1.01)[e]		+3.0(0.6)	0.0059[f,p]
	CH_3CHO	−6.94(1.17)[e]		+1.9(0.4)	0.042[p,q]
	PhCHO	−6.53(2.07)[e]		−1.50	13[s,t]
	$(CH_3)_2CO$	−3.39(1.17)[e]		+2.3(1.5)	0.020[p,r]
	$PhCOCH_3$	−1.14(1.28)[e]		−0.03	1.05[u]
	PhCOPh			−2.53	71[v]

[a]In aqueous solution at 25°C, unless otherwise noted; apparent equilibrium constants and free energies, not corrected for hydration or symmetry.
[b]In kcal/mol; error limits are taken as ±0.1 kcal/mol unless otherwise indicated.
[c]M^{-1}; only experimentally determined values for K_1 are listed.
[d]Dimensionless; only experimentally determined values of K_2 are listed.
[e]Calculated from the free energies of formation of starting materials and products; see Tables 3 and 5.
[f]Reference 46.
[g]Reference 4.
[h]Reference 47.
[i]Reference 48.
[j]Reference 49.
[k]Interpolated from data at other temperatures, and corrected to $a_{H_2O} = 1.0$ (measured in $HClO_4$ solutions (49)).
[l]Calculated from the data of ref. 6.
[m]Reference 14.
[n]Reference 50.
[o]Calculated from the data of refs. 8–10.
[p]Extrapolated from data at higher temperatures.
[q]Reference 51.
[r]Reference 52.
[s]Calculated from an equilibrium constant at 45°C, assuming ΔS is the same as for dehydration of acrylic (51) and crotonic (52) acids.
[t]Calculated from the data of ref. 53.
[u]Reference 54.
[v]Reference 19.

summarized in ref. 18 and will not be repeated here, but will be employed in Fig. 1, and for calculations based upon it.

Equilibrium constants for aldol addition reactions to formaldehyde, acetaldehyde, benzaldehyde, and acetone and acetophenone are taken from Table 1, but have been corrected for symmetry effects, and also for the effects of hydration of reactants and products. There appear to have been no studies of the covalent hydration of the carbonyl group in β-hydroxy aldehydes; the equilibrium constants were estimated using the ρ* value reported by Greenzaid *et al.* (21). Equilibrium constants determined experimentally are given to two significant figures; those derived from thermodynamic calculations are only given to one.

Equilibrium constants[2] for addition reactions other than aldols were fitted to [4] by least squares

$$[4] \qquad \log (K_{HNu}/K_{H_2O}) = \Delta \cdot \Gamma$$

where $\Gamma = \gamma_{HNu} - \gamma_{H_2O}$. This formulation appears to have several advantages over that originally proposed by Sander and Jencks (18). (*a*) It makes addition of water the reference reaction, with water the reference nucleophile; since equilibrium constants for hydration of carbonyl groups can be obtained, either by direct measurement or indirectly by extrathermodynamic calculations (22, 23) for *all* carbonyl compounds, this constitutes a more con-

[2]K_{H_2O} is the equilibrium constant for the reaction $R_2R_2CO + H_2O = R_2R_2C(OH)_2$ and has the dimensions M^{-1}.

Can. J. Chem. Downloaded from www.nrcresearchpress.com by 210.87.254.6 on 09/05/12
For personal use only.

TABLE 2. Equilibrium constants for addition to carbonyl groups, and γ values for nucleophiles[a]

Nucleophile	γ[b]	Equilibrium constant (M^{-1}) for addition to					
		$H_2C{=}O$	CH_3CHO	C_6H_5CHO	CH_3COCH_3	$C_6H_5COCH_3$	$(C_6H_5)_2CO$
H_2O	−3.58[c]	41[c]	0.019[d]	1.5×10^{-4}[c]	2.5×10^{-5}[f]	1.2×10^{-7}[e]	2.1×10^{-9}[e]
$HOCH_3$	−2.22[c]	1.3×10^{3}[c]	0.70[g]	3.6×10^{-3}[h]	1.9×10^{-4}[f]		
NH_2CONH_2	−1.84	5.8×10^{4}[c,i]	1.03[i,j]				
$CH_3CH(COO^-)NH_2$	−1.26	5.5×10^{4}[c]	21.5[k]				
$CH_2(COO^-)NH_2$	−0.75	3.0×10^{5}[c]	39[k]				
H_2O_2	−0.64[c]	1.7×10^{4}[c,l]	48[l,l]		2.7×10^{2}[l,f]		
O⌒NH	−0.43[c]	1.8×10^{6}[c]	20.5[k]	0.27[m]			
$HOCH_2CH_2SH$	+0.35	1.4×10^{6}[c]	32[n]	1.5[m]	<0.2[n]		
$NH_2CONHNH_2$	+0.46[c]	1.4×10^{7}[c]	1.32[o]				
$HONH_2$	+1.24[c]		11.3[p]	1.0[p]			
HCN	+2.44	9.18×10^{8}[q]	3.7×10^{4}[q]	1.95×10^{2}[r,s,t]	14[n]	0.77[s,v]	
HSO_3^-	+4.02[c]			6.4×10^{3}[w,x]	2.3×10^{2}[y]		
CH_3CHO	+0.45(0.29)[z]	6×10^{7}[aa]	2.5×10^{2}[i,ab]	3×10^{1}[aa]	4×10^{-1}[aa]	7×10^{-3}[aa]	1×10^{-5}[ac]
CH_3COCH_3	+0.16(0.90)[z]	3×10^{6}[i,aa]	2×10^{1}[i,aa]	5.5[i,ab]	9.9×10^{-3}[ab,ad]	5×10^{-4}[i,aa]	7×10^{-6}[i,ac]
$CH_3COC_6H_5$	+0.05(0.15)[z]	6×10^{5}[aa]	5[aa]	7.6×10^{-1}[s,ab]	6×10^{-3}[aa]	6×10^{-5}[aa]	5×10^{-6}[ac]
CH_3COOH	+3.56(0.41)[z]	4×10^{10}[aa]	2×10^{5}[aa]	6×10^{4}[aa]	3×10^{2}[aa]	7[aa]	1×10^{-2}[ac]

[a]In aqueous solution at 25°C unless otherwise noted. Equilibria are for addition to the unhydrated carbonyl. For aldol additions equilibria refer to reaction of unhydrated carbonyl starting materials to give products with unhydrated carbonyls; see text.
[b]γ is defined (18) as the logarithm of the equilibrium constant for addition of a nucleophile to pyridine-4-carboxaldehyde relative to the equilibrium constant for methylamine, $\gamma = \log [K_{HX}/K_{CH_3NH_2}]$.
[c]Reference 18.
[d]Reference 55.
[e]Calculated as described in the text.
[f]Values from ref. 56*a* corrected to 25°C as described in ref. 56*b*.
[g]Reference 57.
[h]Reference 58.
[i]Corrected for symmetry by dividing K_{obs} by 2.
[j]Reference 59.
[k]Reference 20.
[l]Reference 60.
[m]Estimated from the value for *p*-chlorobenzaldehyde (18) assuming that the ratio of equilibrium constants is the same as for addition of HCN (18, 61).
[n]Reference 62.
[o]Reference 63.
[p]Reference 64.
[q]Reference 65.
[r]Reference 61.
[s]In ethanol.
[t]At 20°C.
[u]Reference 66.
[v]Reference 67.
[w]Reference 68.
[x]At 21°C.
[y]Calculated from the data in ref. 69.
[z]Calculated from the equilibrium constants for aldol formation and the lines relating log *K* and γ; see text.
[aa]Calculated from ΔG_f^0(aq) values in Tables 3 and 5; see Table 1.
[ab]Experimentally determined value; see Table 1.
[ac]Estimated assuming log *K* is linearly dependent on γ with the same slope as for acetone and acetophenone using the log *K* values for water and values of γ evaluated here.
[ad]Corrected for symmetry by dividing K_{obs} by 4.

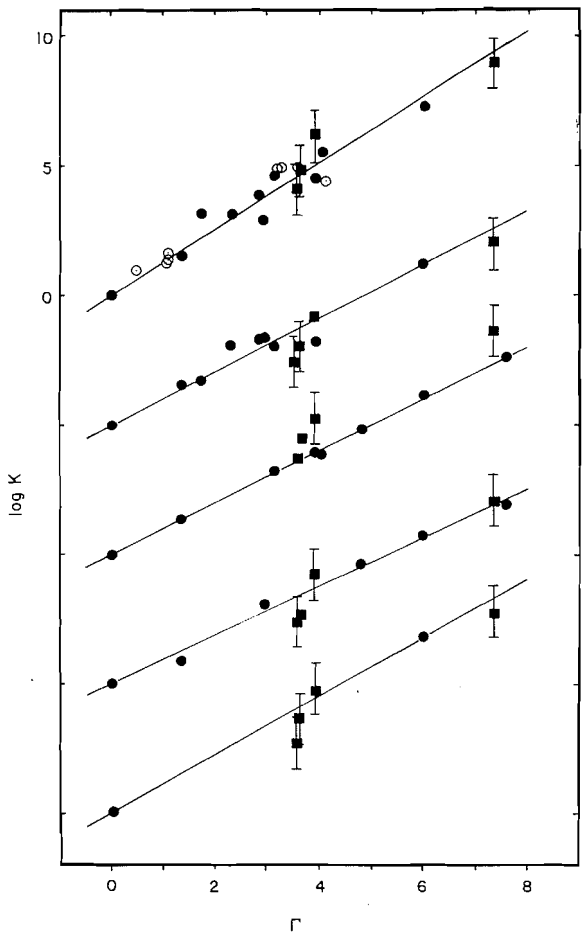

FIG. 1. Relationship between the logarithm of $K_{rel} = K_{HNu}/K_{H_2O}$ and $\Gamma = \gamma_{HNu} - \gamma_{H_2O}$. (●) data from Table 2; (○) data from Table IV of ref. 18; (■) aldol reactions. To avoid overlapping, the data for successive compounds are displaced down by five log units. The carbonyl compounds are, reading down from the top, formaldehyde, acetaldehyde, benzaldehyde, acetone, and acetophenone. Error bars are shown for equilibrium constants derived from thermochemical data.

venient reference point. (*b*) By using relative equilibrium constants, which are in effect equilibrium constants for reaction 5, it focuses attention on the

[5] $R_1R_2C(OH)_2 + HNu \rightleftharpoons R_1R_2C(OH)Nu + H_2O$

fact that obedience to [4] (or the original equation of Sander and Jencks (18)) is *not* dependent upon structural effects in the carbonyl compound, but only upon the effects of the nature of R_1, R_2, and Nu upon the ease of replacement of OH by Nu.

Γ values for the carbonyl compounds as nucleophiles were then calculated from these graphs, with uncertainties related to the error limits in the equilibrium constants for the aldol reactions, and the weighted average values for the Γ values were calculated. These led to the γ values reported in Table 2. Finally equilibrium constants for aldol additions to benzophenone were estimated from the Γ values for the carbon nucleophiles and K_{H_2O}, assuming that the slope for benzophenone was the same for acetone. This led to the values found in Table 2, which are all unfavorable, in agreement with expectation, in view of the normal unreactivity of benzophenone.

The slopes for these lines were respectively 1.22, 1.06, 1.02, and 0.92 for formaldehyde, acetaldehyde, benzaldehyde, and acetone. With data extending over a narrower range (since *K* for HCN was not available then) Sander and Jencks (18) concluded that the formaldehyde data were best represented by two lines of unit slope, one for oxygen and sulfur nucleophiles, the other for nitrogen nucleophiles. To the present author it appears preferable to regard the data as giving a less than ideal fit to a single line.

It is interesting to note that the γ values for $CH_3CO—Z$ increase with increasing electronegativity of Z as measured by σ*. It is also noteworthy that for Z = H, CH_3, or C_6H_5, the variation in γ is very small, and that the variation in equilibrium constant for aldol equilibrium is due almost entirely to variations in the nature of the carbonyl group acting as electrophile.

Equilibrium constants have been derived for acetic acid as nucleophile, because free energies of formation of the aldol addition products were accessible. Esters are much more commonly utilized since base catalyzed reactions are feasible; although no information is available at present, it seems reasonable to expect that the values for methyl or ethyl acetate should be similar to those found for acetic acid.

Conclusions

(*1*) The linear-free energy relationship of Sander and Jencks (18) can be extended to include aldol reactions; thus the equilibrium constant for any unknown aldol reaction can be estimated from that for addition of any nucleophile, such as water or HCN, to the carbonyl acceptor and the γ value of the carbonyl nucleophile; since the latter shows little variation for aldehydes or ketones, it may be possible to estimate it without serious error.

(*2*) Since it appears to be possible in many cases to estimate free energies of formation of the enone products by methods related to Benson's Group Additivity scheme, it should be possible to estimate the equilibrium constant for an overall aldol condensation even where no addition equilibria have been studied, provided that there are no severe steric interactions. Molecular mechanics calculations are rapidly approaching the point (24–26) where this limitation will be overcome.

Can. J. Chem. Downloaded from www.nrcresearchpress.com by 210.87.254.6 on 09/05/12
For personal use only.

Can. J. Chem. Downloaded from www.nrcresearchpress.com by 210.87.254.6 on 09/05/12
For personal use only.

Experimental

Materials

Benzalacetone was recrystallized; mp 37°C; lit (27) mp 42°C. Cinnamaldehyde and acrylic acid were distilled in vacuum before use; 3-penten-2-one was distilled under nitrogen. Acrelein was distilled under nitrogen immediately before use.

Solubility Determinations

3-Penten-2-one was shaken repeatedly with p*H* 7 phosphate buffer ($\mu = 0.1$) containing 0.103 *N tert*-butanol and allowed to stand at 25°C. A sample of the aqueous layer was analyzed by nmr, integrating the signals from the ketone methyl groups relative to the *tert*-butyl groups of the standard; the solubility was 1.15 *M*.

Cinnamaldehyde was stirred with p*H* 7 phosphate buffer at 25°C; a sample of the aqueous layer was diluted 1000-fold with buffer and analyzed by uv spectroscopy. It was important not to stir for too long, or oxidation of the aldehyde would lead to spuriously high absorbances (and a shift of the maximum to lower wavelength). Replicate determinations based on λ_{max} 285, using $\varepsilon = 22\,900$ (28) led to a solubility of 0.015 *M*.

Benzalacetone was stirred several hours with p*H* 7 phosphate buffer, allowed to stand at 25°C, and analyzed as for cinnamaldehyde; based on λ_{max} 287, using $\varepsilon = 20\,900$ (29) the solubility was 0.0091 *M*.

Heat of Solution

Heats of solution were measured using the calorimeter and technique described previously (30), with 0.1 *N* HCl as the solvent. The heats of solution were -1.35 ± 0.04 kcal/mol for acrolein, and $+0.14 \pm 0.03$ kcal/mol for acrylic acid.

Acknowledgements

I wish to thank the National Research Council of Canada and the Alfred P. Sloan Foundation for financial support and Patricia A. Cullimore and Dana Zendrowski for technical assistance.

1. A. T. Nielsen and W. J. Honlikan. Organic reactions. Vol. 16. Wiley, New York, NY. 1968.
2. (*a*) C. C. French. J. Am. Chem. Soc. **51**, 3215 (1929); (*b*) G. M. Murphy. J. Am. Chem. Soc. **53**, 977 (1931); (*c*) V. K. LaMer and M. L. Miller. J. Am. Chem. Soc. **57**, 2674 (1935).
3. (*a*) R. P. Bell. J. Chem. Soc. 1637 (1937); (*b*) K. F. Bonhoeffer and W. D. Walters. Z. Phys. Chem. A, **181**, 441 (1938); (*c*) A. Broche and R. Gilbert. Bull. Soc. Chim. Fr. 131 (1955); (*d*) R. P. Bell and M. J. Smith. J. Chem. Soc. 1691 (1958); (*e*) A. Broche. Colloque national de cinetique. Strasbourg. 1953; (*f*) R. P. Bell and P. T. McTigue. J. Chem. Soc. 2983 (1960).
4. J. P. Guthrie. Can. J. Chem. **52**, 2037 (1974).
5. J. L. Jensen and H. Hashtroudi. J. Org. Chem. **41**, 3299 (1976).
6. D. S. Noyce and W. L. Reed. J. Am. Chem. Soc. **81**, 624 (1959) and references therein.
7. D. S. Noyce and W. A. Pryor. J. Am. Chem. Soc. **77**, 1397 (1955).
8. E. Coombs and D. P. Evans. J. Chem. Soc. 1295 (1940).
9. D. S. Noyce and W. A. Pryor. J. Am. Chem. Soc. **77**, 1397 (1955).
10. E. A. Walker and J. R. Young. J. Chem. Soc. 2045 (1957).
11. J.-E. Vik. Acta Chem. Scand. **27**, 251 (1973).
12. Y. Ogata, A. Kawasaki, and K. Yokoi. J. Chem. Soc. B, **13**, 1013 (1967).
13. P. Carsky, P. Zuman, and V. Horak. Coll. Czech. Chem. Commun. **30**, 4316 (1965).
14. K. Koelichen. Z. Phys. Chem. **33**, 129 (1900); A. A. Frost and R. G. Pearson. Kinetics and mechanism. 2nd ed. Wiley, New York, NY. 1963. p. 340.
15. J. E. Dubois. Bull. Soc. Chim. Fr. 66 (1949).
16. S. W. Benson and J. H. Buss. J. Chem. Phys. **29**, 546 (1958).
17. S. W. Benson. Thermochemical kinetics. 2nd ed. Wiley, New York, NY. 1976.
18. E. G. Sander and W. P. Jencks. J. Am. Chem. Soc. **90**, 6154 (1968).
19. D. S. Noyce, S. K. Brauman, and F. B. Kirby. J. Am. Chem. Soc. **87**, 4335 (1965).
20. B. Gaux and P. LeHenaff. C. R. Acad. Sci. Paris, **271**, 1093 (1970).
21. P. Greenzaid, Z. Luz, and D. Samuel. J. Am. Chem. Soc. **89**, 749 (1967).
22. J. P. Guthrie. J. Am. Chem. Soc. **95**, 6999 (1973).
23. J. P. Guthrie. Can. J. Chem. **53**, 898 (1975).
24. N. L. Allinger and D. Y. Chung. J. Am. Chem. Soc. **98**, 6798 (1976).
25. T. Liljefors and N. L. Allinger. J. Am. Chem. Soc. **98**, 2745 (1976).
26. E. M. Engler, J. D. Andose, and P. v. R. Schleyer. J. Am. Chem. Soc. **95**, 8005 (1973).
27. A. H. Cook, H. M. Bunbury, and D. H. Hey (*Editors*). Dictionary of organic chemistry. 4th ed. Eyre and Spottiswoode, London. 1965.
28. O. H. Wheeler and L. A. Kaplan (*Editors*). Organic electronic spectral data. Vol. 3. Wiley, New York, NY. 1966.
29. J. P. Phillips, R. E. Lyle, and P. R. Jones (*Editors*). Organic electronic spectral data. Vol. 5. Wiley, New York, NY. 1969.
30. J. P. Guthrie. J. Am. Chem. Soc. **96**, 3608 (1974).
31. F. Franks and D. S. Reid. *In* Water, a comprehensive treatise. Vol. 2. *Edited by* F. Franks. Plenum Press, New York, NY. 1973. Chapt. 5.
32. J. P. Guthrie. Can. J. Chem. **55**, 3700 (1977).
33. Landolt-Bornstein. 6th ed. Vol. 2, Part 4. Springer, Berlin. 1961.
34. D. R. Stull, E. F. Westrum, Jr., and G. C. Sinke. The chemical thermodynamics of organic compounds. Wiley, New York, NY. 1969.
35. G. Bauduin, Y. Pietrasanta, and B. Pucci. Tetrahedron Lett. 2889 (1975).
36. J. Hine. Structural effects on equilibria in organic chemistry. Wiley, New York, NY. 1975. p. 11.
37. J. Hine and P. K. Mookerjee. J. Org. Chem. **40**, 292 (1975).
38. J. D. Cox and G. Pilcher. Thermochemistry of organic and organometallic compounds. Academic Press, New York, NY. 1970.
39. N. C. Deno, F. A. Kish, and H. J. Peterson. J. Am. Chem. Soc. **87**, 2157 (1965).
40. H. Adkins and E. W. Adams. J. Am. Chem. Soc. **47**, 1368 (1925).
41. J. M. Bell, D. G. Kubler, P. Sartwell, and R. G. Zapp. J. Org. Chem. **30**, 4284 (1965).
42. P. Greenzaid. J. Org. Chem. **38**, 3164 (1973).
43. G. J. Pfeiffer and H. Adkins. J. Am. Chem. Soc. **53**, 1043 (1931).
44. R. W. Taft. *In* Steric effects in organic chemistry. *Edited by* M. S. Newman. Wiley, New York, NY. 1956.
45. G. B. Barlin and D. D. Perrin. Q. Rev. 75 (1966).

Can. J. Chem. Downloaded from www.nrcresearchpress.com by 210.87.254.6 on 09/05/12
For personal use only.

46. D. PRESSMAN and H. J. LUCAS. J. Am. Chem. Soc. **64**, 1953 (1942).
47. S. WINSTEIN and H. J. LUCAS. J. Am. Chem. Soc. **59**, 1461 (1937).
48. H. J. LUCAS, W. T. STEWART, and D. PRESSMAN. J. Am. Chem. Soc. **66**, 1818 (1944).
49. J. L. JENSEN and D. J. CARRE. J. Org. Chem. **39**, 2103 (1974).
50. D. PRESSMAN, L. BREWER, and H. J. LUCAS. J. Am. Chem. Soc. **64**, 1122 (1942).
51. D. PRESSMAN and H. J. LUCAS. J. Am. Chem. Soc. **61**, 2271 (1939).
52. D. PRESSMAN and H. J. LUCAS. J. Am. Chem. Soc. **62**, 2069 (1940).
53. D. S. NOYCE and C. A. LANE. J. Am. Chem. Soc. **84**, 1635 (1962).
54. D. S. NOYCE and R. A. HELLER. J. Am. Chem. Soc. **87**, 4325 (1965).
55. J. L. KURZ. J. Am. Chem. Soc. **89**, 3524 (1967).
56. (*a*) J. HINE. J. Am. Chem. Soc. **93**, 3701 (1971); (*b*) J. HINE and R. W. REDDING. J. Org. Chem. **35**, 2769 (1970).
57. M. R. CRAMPTON. J. Chem. Soc. Perkin Trans. II, 185 (1975).
58. J. P. GUTHRIE. J. Am. Chem. Soc. **95**, 6999 (1973).
59. Y. OGATA, A. KAWASAKI, and N. OKUMURA. Tetrahedron, **22**, 1731 (1966).
60. P. L. KOOIJMAN and W. L. GHIJSEN. Rec. Trav. Chim. **66**, 205 (1947).
61. J. W. BAKER and M. C. HEMMING. J. Chem. Soc. 191 (1942).
62. G. E. LIENHARD and W. P. JENCKS. J. Am. Chem. Soc. **88**, 3982 (1966).
63. R. WOLFENDEN and W. P. JENCKS. J. Am. Chem. Soc. **83**, 2763 (1961).
64. W. P. JENCKS. J. Am. Chem. Soc. **81**, 475 (1959).
65. G. SCHLESINGER and S. L. MILLER. J. Am. Chem. Soc. **95**, 3729 (1973).
66. D. P. EVANS and J. R. YOUNG. J. Chem. Soc. 1310 (1954).
67. A. P. LAPWORTH and R. H. F. MANSKE. J. Chem. Soc. 1976 (1930).
68. F. C. KOKESH and R. E. HALL. J. Org. Chem. **40**, 1632 (1975).
69. M. A. GUBAREVA. Zh. Obshch. Khim. **17**, 2259 (1947); Chem. Abstr. **42**, 4820b (1948).
70. F. D. ROSSINI, D. D. NAGMAN, W. H. EVANS, S. LEVINE, and I. JAFFE. Nat. Bur. Stand. U.S. Circ. No. 500.
71. E. W. BLAIR and W. LEDBURY. J. Chem. Soc. **127**, 26 (1925); **127**, 2832 (1925).
72. F. WALKER. J. Phys. Chem. **35**, 1104 (1931).
73. S. G. D'AVILA and R. S. F. SILVA. J. Chem. Eng. Data, **15**, 421 (1970).
74. H. K. EIGENMANN, D. M. GOLDEN, and S. W. BENSON. J. Phys. Chem. **77**, 1687 (1973).
75. G. C. WILLIAMS. Am. J. Enol. Vitic. **13**, 169 (1962).
76. A. F. FROLOV, M. A. LOGINOVA, B. F. USTAVSHCHIKOV, and V. A. DMITRICHEVA. Russ. J. Phys. Chem. **41**, 1121 (1967).
77. J. JAKUBICEK. Collect. Czech. Chem. Commun. **28**, 3180 (1963).
78. W. M. SCHUBERT, B. CAMM, and J. R. KEEFER. J. Am. Chem. Soc. **86**, 4727 (1964).
79. R. C. WEAST (*Editor*). Handbook of chemistry and physics. 48th ed. Chemical Rubber Co., Cleveland, Ohio. 1967.
80. D. AMBROSE, J. E. CONNETT, J. H. S. GREEN, J. L. HALES, A. J. HEAD, and J. F. MARTIN. J. Chem. Thermodyn. **7**, 1143 (1975).
81. K. E. COULTER, H. KEHDE, and B. F. HISCOCK. *In* Vinyl and diene monomers. Vol. 24, Part 2. *Edited by* E. C. Leonard. Wiley, New York, NY. 1971. p. 558.
82. Beilsteins Handbuch der organischen Chemie. Vol. 2, 2nd suppl. Springer, Berlin. 1942. p. 391.
83. I. WADSO. Acta Chem. Scand. **20**, 544 (1966).
84. S. W. BENSON and G. D. MENDENHALL. J. Am. Chem. Soc. **98**, 2046 (1976).
85. Beilsteins Handbuch der organischen Chemie. Vol. 1, Part 3, 3rd suppl. Springer, Berlin. 1961. p. 2995.
86. H. STEPHEN and T. STEPHEN (*Editors*). Solubilities of inorganic and organic compounds. Vol. 1. Pergamon Press, Oxford. 1963.
87. A. R. UBBELHOHDE. Q. Rev. **4**, 356 (1950).
88. Beilsteins Handbuch der organischen Chemie. Vol. 7, 3rd suppl. Springer, Berlin. 1968. p. 2052.

Appendix: Thermodynamic Calculations

Free Energies of Transfer, From Activity Coefficients at Higher Temperatures

It frequently happens that activity coefficients, which are equivalent to transfer from dilute solution to the gas phase, are available at the boiling point of the solvent, but not at room temperature. This is a particularly serious problem for small molecules in aqueous solution, because direct determination of the activity coefficient at room temperature is experimentally demanding, and correction of the value at 100 to 25°C is complicated by the fact that the enthalpy of transfer will be a function of temperature. Although for many solvents the variation in the enthalpy of transfer from 100 to 25°C might well be negligible, this is almost certainly not the case for aqueous solutions, because of the well known large changes in partial molar heat capacity upon transfer from gas to water for organic molecules (31). Fortunately it has recently been found (32) that the partial molar heat capacity of organic compounds in aqueous solution can be estimated with useful accuracy by additivity methods, and it has been known for some time that the heat capacity of gaseous compounds can be estimated quite easily (16, 17). Therefore it is possible to calculate $\Delta C_{p_t} = \overline{C_{p_2}} - C_p(g)$. The values so obtained for acrolein, acrylic acid, and methyl vinyl ketone are: $\overline{C_{p_2}}$, $C_p(g)$, ΔC_{p_t}; 58.8 ± 3.3, 16.44 ± 0.5, 42.4 ± 3.5; 45.2 ± 3.3, 19.3 ± 0.5, 25.83 ± 3.5; 85.1 ± 3.3, 28.6 ± 0.5, 56.5 ± 3.5.

The enthalpy of transfer at 25°C can be determined from the heat of solution and the heat of vaporization. The heat of vaporization of acrolein is 6.9 kcal/mol (33); that for acrylic acid is 11.21 kcal/mol (34). The heats of solution were measured in this work and are −1.35 ± 0.04 and +0.14 ± 0.03 kcal/mol, respectively.

The equation used for free energy of transfer as a function of temperature is:

$$\frac{\Delta G_t^T}{RT} = \frac{\Delta G_t^0}{R\theta} - \frac{\Delta H_t^0}{R}\left(\frac{1}{\theta} - \frac{1}{T}\right) - \frac{\Delta C_{p_t}^0}{R}\left(\frac{\theta}{T} - 1 + \ln\frac{T}{\theta}\right)$$

where θ is the reference temperature, here 298 K, ΔG_t^0, ΔH_t^0, and $\Delta C_{p_t}^0$ are the values at the reference temperature, and ΔG_t^T is the observed value at temperature T. This equation can now be solved for ΔG_t^0, the only unknown. This was done for acrolein and acrylic acid starting with activity coefficients at 100°C from refs. 75 and 76 respectively. For methyl vinyl ketone, activity coefficients were available at two temperatures, 325.7 and 358.8 K (77), and no heat of vaporization appears to have been reported. Accordingly it seemed preferable to use the known values of ΔG_t^T and $\Delta C_{p_t}^0$ and solve for ΔG_t^0 and ΔH_t^0: this led to values of -3.07 and -13.48 respectively.

Free Energy of Formation of Methyl Vinyl Ketone

Although no value for the heat of formation has been reported, the free energy of formation may be estimated as follows. The free energy change for the reaction

[6] 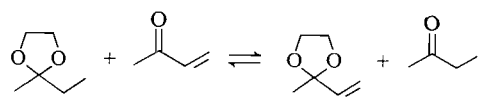

1 2 3 4

was determined in benzene (35), and found to be $\Delta G^0 = -0.45 \pm 0.05$ kcal/mol. Since the functional groups in starting materials and products are very similar, any differences in free energies of transfer from benzene to the gas phase must arise from interactions between functional groups perturbing the solvation forces; for benzene as solvent these perturbations should be small.

The free energy of formation of methyl ethyl ketone is known; -34.91 kcal/mol (34). Free energies of formation for the acetals may be calculated from the group contributions reported by Benson (17). However it is necessary to assume that $[C(C)_2(O)_2]$ is the same as $[C(C)(C_d)(O)_2]$ since the latter value is unknown. This approximation is usually good (36) but may introduce an extra error of 1 kcal/mol in the final value. The values so estimated for **1** and **3** are -48.37 ± 1.57 and -27.18 ± 1.86 kcal/mol respectively. (Errors of 1.5 kcal/mol in ΔH_f^0, 1.5 eu in S^0 and an additional error of 1.0 kcal/mol for the above assumption were used.)

These values lead to a free energy of formation in the gas phase for methyl vinyl ketone of -13.27 ± 2.43 kcal/mol.

No value for the group contribution $[CO(C)(C_d)]$ is available, and this group is not necessarily similar to known groups such as $CO(C)_2$ because there is π overlap between CO and C_d.

Calculation of Free Energies of Formation in Aqueous Solution by Disproportionation

Initially free energies of the enone products of aldol condensations were calculated by straightforward application of Benson's Group Additivity scheme (17), using Hine's group contributions (37) to calculate free energies of transfer. However, it became clear on working with these values that for the larger enones the cumulative effect of small errors in each of the many parameters required to calculate the free energy of formation had led to unacceptably large errors in the final values. It has been possible to overcome this problem, by taking advantage of the central concept of group additivity, but performing calculations which make more direct use of experimental values. If group additivity is correct, then the free energy change for the disproportionation reaction 7 must be zero (provided that

[7] $R_1R_2C{=}CH{-}CO{-}R_3 + R_4R_5C{=}CH_2 \rightleftharpoons R_4R_5C{=}CH{-}CO{-}R_3 + R_1R_2C{=}CH_2$

one has corrected for any change in symmetry number or steric interactions). This can be tested for those cases where free energies for all four components are available; the observed free energy changes are found in Table 6, along with the uncertainties in these free energy changes, based upon the error limits on the free energies of formation of the reactants. Only absolute values of the free energy change are considered, since the direction of the disproportionation is arbitrary. The weighted average value of the free energy change for reaction 7 is taken as the error which would be introduced in a free energy calculated by assuming that the free energy change for any such disproportionation is zero. The value so found is 1.4 kcal/mol which is not much larger than the uncertainty in many experimental free energy values (and is smaller than some). Accordingly, this approach is considered to be valid, and was used to calculate the free energies of formation found in Table 5; error limits were calculated from the errors in the three experimental values, and the error calculated above for the assumption of zero free energy change for disproportionation.

A similar approach was used to calculate the free energies of the hydroxy carbonyl products of aldol addition. In this case there was no possibility of calculating the free energies by direct application of group additivity, because there are no parameters

Can. J. Chem. Downloaded from www.nrcresearchpress.com by 210.87.254.6 on 09/05/12
For personal use only.

Can. J. Chem. Downloaded from www.nrcresearchpress.com by 210.87.254.6 on 09/05/12
For personal use only.

available to account for the interaction between the hydroxyl and the carbonyl. The disproportionation reaction is:

[8] $R_1R_2C(OH)—CH_2CO—R_3 + R_4R_5C(OH)CH_3 \rightleftharpoons$

$R_4R_5C(OH)—CH_2—CO—R_3 + R_1R_2C(OH)CH_3$

The assumption that the free energy change for this hypothetical reaction is zero can be tested as before; the results of applying this test to the available data from Table 3 are found in Table 6. The weighted average value for the deviation from zero is 0.53 kcal/mol. Values for free energies of formation calculated by means of the disproportionation assumption are found in Table 5.

Although the enthalpy of formation of 1,1-diphenylethylene is known (38), and the free energy of formation in aqueous solution can be calculated, examination of space filling models suggested that severe steric interactions would force the phenyl groups to twist out of conjugation to a greater extent in the enones with $R_4 = R_5$ = phenyl than in 1,1-diphenylethylene, and therefore would introduce a large and unknown error if the disproportionation assumption were applied. No value for the equilibrium constant for hydration of 1,1-diphenylethylene is available; under conditions where acid catalyzed equilibration is possible, side reactions intervene (39).

Calculation of Equilibrium Constants for Hydration of Benzaldehyde, Acetophenone, and Benzophenone

Direct measurement of these equilibrium constants has not been possible, even for benzaldehyde, for which hydration should be most favorable. It is possible to calculate values indirectly by taking advantage of an extrathermodynamic relation linking acetal formation and hydration. It has been shown that for reaction 9 the free energy change can be

[9] $R_1R_2R_3C—OR_4 + H_2O \rightleftharpoons R_1R_2R_3C—OH + R_4OH$

calculated, taking account of the electronic effects of the substituents on the central carbon, and any steric or symmetry effects (23). By doing this twice the equilibrium constant for the hypothetical reaction converting acetal to carbonyl hydrate can be calculated, and from this and the equilibrium constant for acetal formation, the equilibrium constant for hydration can be calculated.

For benzaldehyde and acetophenone, the equilibrium constants for dimethyl acetal formation have been reported (40, 41); then by the methods just described it is straightforward to calculate the equilibrium constants for hydration. For benzaldehyde an independent check is available. Greenzaid (42) has measured the equilibrium constant for the addition of hydroxide ion to benzaldehyde, and by estimating

TABLE 3. Experimentally determined thermodynamic quantities for compounds discussed in this paper[a]

Compound	ΔH_f^0(g)[b]	S^0(g)[c]	ΔG_f^0(g)[b]	ΔH_v[b,d]	ΔH_f^0(l)[b]	ΔG_f[b,e]	ΔG_f^0(aq)[b]
H_2O	−57.80[f]	45.11[f]	−54.68[f]		−68.32[f]		−56.69(0.01)[f]
CH_2O	−25.95(0.12)[g]	52.26(0.3)[f]	−24.52(0.16)[h]			−4.99(0.08)[i]	−79.51(0.17)[h]
CH_2=CH_2	12.45(0.10)[g]	52.45(0.3)[j]	16.23(0.13)[h]			3.19(0.10)[k]	19.42(0.16)[h]
CH_3CHO	−39.73(0.12)[g]	63.15(0.3)[j]	−31.86(0.16)[j]			−1.49(0.10)[l]	−33.38(0.18)[h]
CH_3COOH	−103.26(0.12)[g]	67.52(0.3)[j]	−89.36(0.16)[h]			−4.82(0.10)[k]	−94.21(0.19)[h]
CH_3CH_2OH	−56.24(0.07)[g]	67.54(0.3)[j]	−40.34(0.12)[h]			−3.01(0.10)[k]	−43.35(0.16)[h]
CH_3CH=CH_2	4.88(0.16)[g]	63.80(0.3)[j]	14.99(0.19)[h]			3.18(0.10)[k]	18.16(0.21)[h]
CH_2=$CH—CHO$	−17.8(0.5)[m]	70.54(1.5)[p]	−11.70(0.71)[h]			−2.12(0.10)[n]	−13.82(0.71)[h]
CH_2=$CHCOOH$	−80.51(0.55)[h]	75.29(0.3)[j]	−68.52(0.57)[h]	11.21(0.5)[j]	−91.72(0.25)[g]	−4.31(0.1)[n]	−73.83(0.58)[h]
$CH_2(OH)CH_2CHO$							−71.80(0.72)[f]
CH_3COCH_3	−51.90(0.12)[g]	70.49(0.3)[j]	−36.48(0.16)[h]			−1.92(0.1)[k]	
$CH_2(OH)CH_2COOH$							−133.56(0.98)[f]
$CH_3CH(OH)CH_3$	−65.13(0.13)[g]	74.07(0.3)[j]	−41.46(0.16)[h]			−2.86(0.1)[k]	−44.32(0.19)[h]
$(CH_3)_2C$=CH_2	−4.26(0.15)[g]	70.17(0.3)[h]	−13.66(0.18)[j]			3.19(0.1)[k]	16.79(0.21)[h]
CH_3CH=$CHCHO$	−24.03(0.37)[g]	80.35(0.3)[o]	−11.14(0.29)[o]			−2.42(0.1)[o]	−13.56(0.27)[o]
CH_2=$CHCOCH_3$	−27.39(2.63)[h]	76.21(1.5)[p]	−13.27(2.43)[q]			−3.07(1.0)[r]	−16.34(2.63)[h]
CH_3CH=$CHCOOH$	−86.4(5.1)[r]	83.5(1.5)[p]	−67.1(5.1)[h]		−103.1(5.0)[r,s,ab]	−5.11(0.5)[r]	−72.2(5.1)[h]
$CH_3CH(OH)CH_2CHO$							−70.25(0.27)[o]
$CH_2(OH)CH_2COCH_3$							−75.01(2.63)[m]
$CH_3CH(OH)CH_2COOH$							−130.78(5.1)[m]

Can. J. Chem. Downloaded from www.nrcresearchpress.com by 210.87.254.6 on 09/05/12
For personal use only.

TABLE 3 (*Concluded*)

Compound	ΔH_f^o(g)[b]	S^o(g)[c]	ΔG_f^o(g)[b]	ΔH_v[b,d]	ΔH_f^o(l)[b]	ΔG_t[b,e]	ΔG_f^o(aq)[b]
$(CH_3)_3COH$	−74.72(0.21)[g]	77.98(0.3)[j]	−42.51(0.23)[h]			−2.63(0.10)[k]	−45.14(0.25)[h]
$(CH_3)_2C{=}CHCOCH_3$	−44.10(0.59)[h]	94.98(1.5)[p]	−17.08(0.31)[h]			−1.87(0.10)[t]	−18.95(0.29)[v]
$(CH_3)_2C(OH)CH_2COCH_3$							−75.08(0.29)[v]
C_6H_5CHO	−8.80(0.71)[w]	80.28(0.23)[w]	5.35(0.71)[w]			−2.14(0.10)[k]	3.21(0.72)[h]
$C_6H_5CH{=}CH_2$	35.30(0.25)[g]	82.48(0.3)[j]	51.08(0.27)[h]			0.69(0.10)[t]	51.77(0.29)[h]
$C_6H_5CH(OH)CH_3$							−7.12(0.31)[u]
$C_6H_5COCH_3$	−20.71(0.40)[g]	89.12(0.3)[j]	0.49(0.41)[h]			−2.70(0.10)[k]	−2.21(0.42)[h]
$C_6H_5C(CH_3){=}CH_2$	28.27(0.34)[h]	91.7(0.3)[j]	51.11(0.36)[h]	11.43(0.20)[x]	16.84(0.28)[g]	−0.21(0.10)[t]	50.90(0.37)[h]
$C_6H_5(CH_3)_2COH$							−7.34(0.38)[h]
$C_6H_5CH{=}CHCHO$	7.8(5.1)[h]	199.16(1.5)[p]	26.3(5.1)[h]	14.2(0.10)[y]	−6.4(5.0)[j,z]	−3.65(0.10)[t]	22.65(5.1)[h]
$C_6H_5CH{=}CHCOOH$	−60.76(1.10)[aa]	103.55(1.5)[p]	−36.15(1.86)[h]		−78.14(0.43)[g,ab]	−5.58(0.10)[t]	−42.34(1.86)[h]
$C_6H_5CH(OH)CH_2COOH$							−97.53(1.93)[n]
$C_6H_5CH{=}CHCOCH_3$	−11.49(0.91)[h]	107.45(1.5)[p]	14.36(0.76)[h]			−3.58(0.10)[t]	+17.94(0.75)[v]
$C_6H_5CH(OH)CH_2COCH_3$							−36.61(0.75)[v]
$(C_6H_5)_2CO$	14.6(0.7)[g]	113.3(1.5)[p]	39.92(0.86)[h]			−2.91(0.2)[t]	37.01(0.88)[h]
$C_6H_5CH{=}CHCOC_6H_5$							55.33(0.84)[v]
$C_6H_5CH(OH)CH_2COC_6H_5$							1.17(0.84)[v]

[a] At 25°C; standard states are ideal gas at 1 atm, pure liquid and 1 *M* aqueous solution with an infinitely dilute reference state, except that ΔG_f^o(aq) for H_2O is taken as ΔG_f^o(l).
[b] In kcal mol^{-1}.
[c] In cal deg^{-1} mol^{-1}.
[d] Heat of vaporization.
[e] Free energy of transfer from gas to aqueous solution.
[f] Reference 70.
[g] Reference 38.
[h] Calculated from values in this table.
[i] Calculated from the data of refs. 71 and 72.
[j] Reference 34.
[k] Reference 37.
[l] Calculated using activity coefficient data from ref. 73.
[m] Reference 74.
[n] Calculated from activity coefficients at 100°C, using ΔH_i and ΔC_{P_i} estimated as described in the text. Activity coefficients at 100°C were from ref. 75, acrolein; and ref. 76, acrylic acid.
[o] Reference 4.
[p] Estimated using the group contributions reported by Benson (17); where values were not available, the missing groups were approximated by groups with similar atoms attached. The justification for this procedure is the good approximation to additivity of atomic contributions for entropy (16).
[q] Calculated as described in the text.
[r] Calculated from activity data at higher temperatures (77) as described in the text.
[s] The available value for ΔH_f^o(s) is old (34); bearing in mind the warnings of Cox and Pilcher (38) concerning the unreliability of pre-1930 calorimetry, an error limit of ± 5.0 kcal/mol was assigned. ΔH_f^o(g) was calculated using the heat of fusion (3.1 ± 0.1 kcal/mol) (33) and a heat of vaporization derived from the vapor pressure – temperature data of ref. 79 using the Clausius-Clapeyron equation (13.6 ± 1 kcal/mol).
[t] From Table 4.
[u] Calculated from ΔG_f^o(aq) for the enone or alkene and ΔG^o for hydration, using values from Table 1 for enones, and equilibrium constants of 41 for hydration of styrene (78) and 14 for hydration of α-methylstyrene (39).
[v] Calculated from the equilibrium constants for aldol formation and dehydration (Table 1) and free energies of formation in this table.
[w] Reference 80.
[x] Reference 81.
[y] Calculated from vapor pressure data using the Clausius-Clapeyron equation.
[z] Old heat of formation; see footnote [s].
[aa] Calculated from the heat of formation of the solid using the heat of fusion (2.39 ± 0.1 kcal/mol) (33) and a heat of vaporization of the liquid derived from the vapor pressure – temperature data in ref. 79 using the Clausius-Clapeyron equation (17.38 ± 1 kcal/mol).
[ab] Heat of formation of the solid.

Can. J. Chem. Downloaded from www.nrcresearchpress.com by 210.87.254.6 on 09/05/12
For personal use only.

TABLE 4. Free energies of transfer[a]

Compound	Solubility	Vapor pressure	ΔG_t (kcal/mol)
CH_3—CH=CH—COOH	1.09[b]	3.35[c]	−5.11
CH_3CH=CH—CO—CH_3	1.15[d]	13.8[e]	−2.46
$(CH_3)_2C$=CH—CO—CH_3	0.294[f]	10[g]	−1.87
C_6H_5—CH=CH—CHO	0.015[d]	0.024[g]	−3.65
C_6H_5—CH=CH—COOH	0.0041[h]	0.00026[c]	−5.58
C_6H_5—CH=CH=CO—CH	0.0091[d]	0.0165[i]	−3.58
C_6H_5CH=CH_2	0.0031[j]	7.5[g]	+0.69
$C_6H_5C(CH_3)$=CH_2	0.00474[j]	2.52[g]	−0.21
$(C_6H_5)_2CO$	0.00041[k]	0.00145[l]	−3.18

[a]For transfer from the ideal gas at 1 atm to 1 *M* aqueous solution with an infinitely dilute reference state, at 25°C.
[b]Reference 82.
[c]The vapor pressure at the melting point and the heat of vaporization (Clausius-Clapeyron equation) were calculated from the vapor pressure data in ref. 79; the vapor pressure at 25°C was calculated using a heat of sublimation taken as the sum of the heat of vaporization and the heat of fusion (33).
[d]This work.
[e]Estimated from the boiling point using ΔH_{vap} calculated from the boiling point by means of the Wadso equation (83) and ΔC_{pvap} taken as −12 eu (84).
[f]Reference 85.
[g]Calculated from vapor pressure – temperature data in ref. 79.
[h]Reference 86.
[i]Estimated as described in footnote [c], except that the heat of fusion was estimated from the melting point using an assumed value of 9 eu for the entropy of fusion (87).
[j]Reference 81.
[k]Reference 88.
[l]Estimated as described in footnote [c], except that the heat of sublimation given in ref. 38 was used.

TABLE 5. Free energies of formation estimated by disproportionation

Compound	ΔG_f^0(aq)	Compound	ΔG_f^0(aq)
$CH_2(OH)CH_2COCH_3$	−72.49(0.67)	CH_2=$CHCOCH_3$	−16.73(1.46)
$CH_3CH(OH)CH_2COOH$	−134.53(1.14)	CH_3CH=$CHCOOH$	−74.27(1.64)
$(CH_3)_2C(OH)CH_2CHO$	−71.80(0.68)	$(CH_3)_2C$=$CHCHO$	−15.34(1.47)
$CH_3CH(OH)CH_2COCH_3$	−73.53(0.68)	CH_3CH=$CHCOCH_3$	−17.17(1.47)
$(CH_3)_2C(OH)CH_2COOH$	−136.00(1.14)	$(CH_3)_2C$=$CHCOOH$	−76.05(1.64)
$C_6H_5CH(OH)CH_2CHO$	−33.05(0.69)	C_6H_5CH=$CHCHO$	20.05(1.48)
$CH_2(OH)CH_2COC_6H_5$	−35.02(1.05)	CH_2=$CHCOC_6H_5$	22.16(1.67)
$C_6H_5(CH_3)C(OH)CH_2CHO$	−33.28(0.73)	$C_6H_5(CH_3)C$=$CHCHO$	19.18(1.50)
$CH_3CH(OH)CH_2COC_6H_5$	−36.06(1.07)	CH_3CH=$CHCOC_6H_5$	21.72(1.68)
$C_6H_5(CH_3)C(OH)CH_2COOH$	−97.56(1.19)	$C_6H_5(CH_3)C$=$CHCOOH$	−41.53(1.66)
$C_6H_5(CH_3)C(OH)CH_2COCH_3$	−36.53(0.76)	$C_6H_5(CH_3)C$=$CHCOCH_3$	18.30(1.50)
$(CH_3)_2C(OH)CH_2COC_6H_5$	−37.61(1.08)	$(CH_3)_2C$=$CHCOC_6H_5$	19.94(1.68)
$C_6H_5(CH_3)C(OH)CH_2COC_6H_5$	0.95(1.11)	$C_6H_5(CH_3)C$=$CHCOC_6H_5$	54.46(1.71)

TABLE 6. Tests of the disproportionation assumptions[a]

					ΔG^b	
R_1	R_2	R_3	R_4	R_5	Reaction 7	Reaction 8
CH_3	CH_3	H	H	CH_3	0.29(2.66)	2.37(2.66)
CH_3	CH_3	H	Ph	CH_3	1.50(0.88)	0.20(0.90)
H	Ph	H	H	CH_3	1.21(2.35)	2.17(2.76)
H	H	H	Ph	OH	1.68(2.04)	0.20(2.19)
Weighted average					1.41	0.53

[a]For the hypothetical reactions and as discussed in the text, in aqueous solution at 25°C.
[b]Absolute value of the free energy charge, calculated from the free energies of formation in Table 3; kcal/mol.

the acidity of the hydrate, estimated that the equilibrium constant for hydration was $2.0 \times 10^{-4}\ M^{-1}$.

No direct measurement of the equilibrium constant for formation of an acetal from benzophenone has been reported, but Pfeiffer and Adkins (43) have equilibrated both benzophenone and acetophenone with triethyl orthoformate, which permits calculation of the equilibrium constant for formation of the acetal of benzophenone (subject to the approximation that the mole fraction equilibrium constants for the methyl and ethyl acetals will be the same; see ref. 23 for data supporting this assumption). The

equilibrium constant for hydration of benzophenone may then be calculated as above.

Correction of Equilibrium Constants for Aldol Addition Reactions

In order to be simply interpretable, equilibrium constants should refer to a single process; aldol additions involving aldehydes as starting material and products are complicated by covalent hydration of the aldehyde carbonyl groups. For the starting materials the correction is straightforward, since the hydration constants are known. The true equilibrium constant is more favorable by a factor of $1 + K_{\text{hydration}}$. For product aldehydes the correction is less facile, since there appear to have been no studies of the extent of covalent hydration of the aldols considered here. Accordingly it has been necessary to estimate the equilibrium constants for hydration, making use of the linear free energy relation reported by Greenzaid *et al.* (21). Propanal was used as a reference point, and its known hydration constant (21) was corrected using ρ^* (21) and σ^* values estimated as follows. It was assumed that

$$\sigma^*(R_1R_2C(OH)\text{—}CH_2) = \sigma^*(CH_2(OH)\text{—}CH_2) + \sigma^*(R_1CH_2CH_2) + \sigma^*(R_2CH_2CH_2) - 2\sigma^*(CH_3CH_2)$$

Then from the σ^* values reported for CH_3CH_2—, $HOCH_2CH_2$—, $CH_3CH_2CH_2$—, and $PhCH_2CH_2$— (44) (σ^* for $HOCH_2CH_2$ was estimated from the value for $HOCH_2$ using a fall off factor of 0.36 (45)) the necessary values were calculated.

Where necessary symmetry corrections were made to the equilibrium constants reported in Table 2. Since all the carbonyl nucleophiles have a methyl group, the values were not corrected for the number of hydrogens; thus the equilibrium constants are per methyl and not per hydrogen. However it was necessary to correct the values for acetone as nucleophile for the presence of two equivalent methyls. Similarly it was necessary to correct the values for self-condensations by a factor of two.

Can. J. Chem. Downloaded from www.nrcresearchpress.com by 210.87.254.6 on 09/05/12
For personal use only.

Crystal structure of dibromotetraethylthiuramdisulfidemercury(II)

CHUNG CHIEH

Guelph–Waterloo Centre for Graduate Work in Chemistry, University of Waterloo, Waterloo, Ont., Canada N2M 3G1

Received November 24, 1977

CHUNG CHIEH. Can. J. Chem. **56**, 974 (1978).

Dibromotetraethylthiuramdisulfidemercury(II) is one of the products of the reaction between mercury(II) bromide and tetraethylthiuram disulfide (TETD). The crystals are orthorhombic with $a = 13.050(5)$, $b = 13.593(7)$, $c = 22.373(12)$ Å; space group *Pbca*. The compound is isostructural with the iodo analogue. The final R factor using 1421 observed reflections is 0.10. Mean bond lengths are: Hg—Br = 1.504(6) Å, Hg—S = 2.66(1) Å. The coordination geometry for mercury(II) is tetrahedral.

CHUNG CHIEH. Can. J. Chem. **56**, 974 (1978).

Le dibromotétraéthylthiuramdisulfure de mercure(II) est un des produits de la réaction entre le bromure de mercure(II) et le disulfure de tétraéthylthiurame (TETD). Les cristaux sont orthorhombiques avec $a = 13.050(5)$, $b = 13.593(7)$, $c = 22.373(12)$ Å; groupe d'espace *Pbca*. Le composé est isostructural avec l'analogue iodé. Le facteur d'accord R, utilisant 1421 réflexions observées, est de 0.10. Les longueurs moyennes des liaisons sont Hg—Br = 1.504(6) Å, Hg—S = 2.66(1) Å. La géométrie de coordination du mercure(II) est tétraédrique.

[Traduit par le journal]

Introduction

Mercury(II) halides react with tetraethylthiuram disulfide (TETD) in many ways (1, 2). In the reaction between mercury(II) bromide and TETD, both pale yellow and colorless crystals were obtained. TETD was reduced to form a dithiocarbamato complex in the pale yellow crystal (3). Colorless crystals are now confirmed to be dibromotetraethylthiuramdisulfidemercury(II), $HgBr_2$·TETD. This compound is isostructural with diiodotetraethylthiuramdisulfidemercury(II), HgI_2·TETD (4).

Based on nmr results, it was reported that mercury(II) halides form stable complexes with *N,N,N',N'*-tetraalkylthiuram sulfides (5). To date, only the structures of HgI_2·TETD, diiodotetramethylthiuramdisulfidemercury(II) (HgI_2·TMTD) (6), and diiodotetramethylthiurammonosulfidemercury(II) (HgI_2·TMTM) (7) were determined by X-ray methods. This paper reports the first X-ray structural analysis carried out for a complex formed between mercury(II) bromide and a tetraalkylthiuram di- or mono-sulfide.

Experimental

The compound $HgBr_2$·TETD was prepared along with mercury(II) bromide dithiocarbamate $\{HgBr_2(S_2CNEt_2)Hg(S_2CNEt_2)\}_n$ by experimental procedure already published (3). The crystals are colorless plates. The space group was determined from X-ray photographs. Cell constants were refined from the 2θ (Mo-Kα) values of 19 reflections measured on a G.E. XRD-6 diffractometer. Crystal data are as follows.

$C_{10}H_{20}Br_2HgN_2S_4$ fw = 656.9

Orthorhombic, $a = 13.050(5)$, $b = 13.593(7)$, $c = 22.373(12)$ Å; space group *Pbca*. $D_m = 2.20(5)$, $Z = 8$, $D_c = 2.198$ g cm^{-3}. μ(Mo-Kα) = 125 cm^{-1}. Systematic absences: $0kl$, $k = 2n + 1$, $h0l$, $l = 2n + 1$, $hk0$, $h = 2n + 1$. λ(Mo-Kα) = 0.7107 Å.

The crystal used for data collection was approximately a square plate of 0.18 × 0.18 × 0.10 mm^3 along the *a*, *b*, and *c* directions. It was mounted diagonally with [110] parallel to the φ axis. Among 4549 reflections with $2\theta < 55°$ measured by the stationary-crystal stationary-counter method, only 1420 had intensities greater than the background by $3\sigma(I)$. Few of the 2930 reflections with $40° < 2\theta < 55°$ were observed. The intensities of four reflections used for a stability standard decreased by 9% at the end of data collection. X-ray photographs of $HgBr_2$·TETD and HgI_2·TETD were similar and the atomic coordinates of the latter were used as a trial model. Full-matrix least-squares methods were used to refine the structure. Anisotropic temperature factors were given to Hg, Br, and S atoms. At the final stages, a weighting scheme,

TABLE 1. Atomic coordinates with standard deviations

Atom	*x*	*y*	*z*
Hg	0.0051(2)	0.2187(2)	0.13529(7)
Br(1)	−0.0870(4)	0.2003(6)	0.2328(2)
Br(2)	0.0610(4)	0.1029(5)	0.0548(2)
S(1)	−0.0981(8)	0.357(1)	0.0762(4)
S(2)	0.0226(9)	0.513(1)	0.1452(5)
S(3)	0.1129(9)	0.485(1)	0.0762(5)
S(4)	0.1661(9)	0.326(1)	0.1677(5)
N(1)	−0.167(3)	0.459(3)	0.172(2)
N(2)	0.249(2)	0.346(3)	0.060(1)
C(1)	−0.090(4)	0.438(4)	0.130(2)
C(2)	−0.260(4)	0.392(4)	0.169(2)
C(3)	−0.335(4)	0.454(4)	0.131(2)
C(4)	−0.163(4)	0.548(4)	0.217(2)
C(5)	−0.117(5)	0.478(5)	0.273(3)
C(6)	0.184(3)	0.381(3)	0.099(2)
C(7)	0.261(3)	0.386(4)	−0.000(2)
C(8)	0.185(4)	0.337(4)	−0.046(2)
C(9)	0.309(3)	0.250(4)	0.070(2)
C(10)	0.419(4)	0.289(4)	0.096(2)

Can. J. Chem. Downloaded from www.nrcresearchpress.com by 210.87.254.40 on 09/05/12
For personal use only.

TABLE 2. Interatomic distances (Å) and angles (deg) for tetraalkylthiuram mono- and di-sulfide complexes with mercury(II) halides

Parameter	Value			
	HgI_2·TMTD	HgI_2·TMTM	HgI_2·TETD	$HgBr_2$·TETD
Bond (Å)				
Hg—S	2.882(7), 2.651(7)	2.832(5), 2.659(5)	2.737(7), 2.670(7)	2.66(1), 2.66(1)
Hg—X	2.661(2), 2.654(2)	2.672(2), 2.656(2)	2.668(2), 2.668(2)	2.504(6), 2.504(5)
C—S(Hg)	1.84(2), 1.79(2)	1.79(2), 1.78(2)	1.71(3), 1.70(3)	1.72(5), 1.63(5)
C—S(S)	1.72(2), 1.71(2)	1.71(2), 1.69(2)	1.81(3), 1.75(3)	1.82(5), 1.76(5)
C—N	1.32(3), 1.27(3)	1.29(2), 1.27(2)	1.35(3), 1.32(3)	1.41(5), 1.31(5)
Angles (deg)				
∠XHgX	142.1(1)	135.29(5)	134.0(1)	134.9(1)
∠SHgS	93.1(2)	85.8(2)	96.3(2)	98.5(3)
∠XHgS	109.4(2), 104.2(2)	109.5(1), 108.9(1)	105.9(2), 104.5(2)	108.0(3), 105.1(2)
	102.1(2), 93.4(2)	105.4(1), 99.5(1)	103.5(1), 103.3(1)	103.6(2), 101.3(3)
∠HgSC	100.7(8), 93.3(8)	101.0(6), 91.7(7)	95.1(8), 94.9(8)	96(1), 95(2)

$w^{-1} = 70 - F_o + 0.001F_o^2$, was used. The final maximum parameter shifts were 0.5σ. The final R $(= \Sigma||F_o| - |F_c||/\Sigma|F_o|)$ and R_w $((\Sigma w^2(|F_o| - |F_c|)^2/\Sigma w^2 F_o^2)^{1/2})$ for 1420 observed reflections were 0.10 and 0.11 respectively. The final parameters are given in Table 1.[1]

Results and Discussion

The bond distances and angles are given in Fig. 1. The atomic numbering system is the same as that of HgI_2·TETD. A unique feature for $HgBr_2$·TETD is that the two Hg—S distances are equal, 2.66(1) Å. However, in HgI_2·TETD, HgI_2·TMTD, and HgI_2·TMTM, the two Hg—S bonds in each case are significantly different. A comparison of these distances is shown in Table 2. The differences in Hg—I distances for HgI_2·TMTD and HgI_2·TMTM are 0.007 and 0.16 Å respectively, whereas Hg—X values are identical for the two TETD complexes. No trend in the variation of ∠XHgX can be found from Table 2. Aside from HgI_2·TMTM, values are similar. The angles ∠SHgS are limited by the bites of the ligands and $HgBr_2$·TETD has the largest value, 98.5°. Among the four compounds, the coordination geometry for mercury(II) shows the least deviation from tetrahedral in $HgBr_2$·TETD. A satisfactory condition in which to prepare $HgCl_2$·TETD has yet to be found.

Due to the shape of the crystal used in data collection and a slightly higher absorption coefficient in $HgBr_2$·TETD than HgI_2·TETD, the R factor in the present structure was only 0.10. The intensities were collected a year ago. Now, that crystal has become deep brown and some small crystals have grown on the surface at the expense of the original single one.

In all four tetraalkylthiuram sulfide complexes, the structures comprise discrete molecules and van der Waals intermolecular contacts are expected.

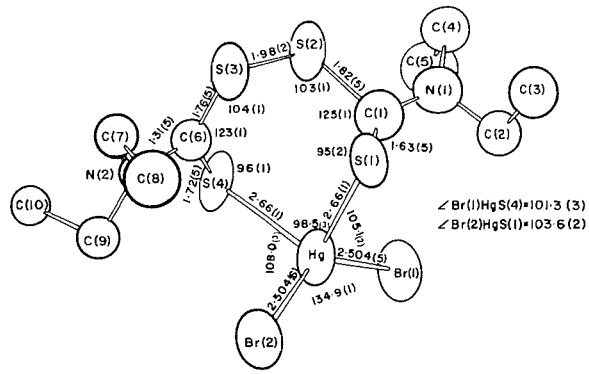

FIG. 1. Important bond distances (Å) and angles (deg) for $HgBr_2$·TETD.

Acknowledgement

This work was supported by the National Research Council of Canada.

[1]The structure factor and temperature parameters are available, at a nominal charge, from the Depository of Unpublished Data, CISTI, National Research Council of Canada, Ottawa, Ont., Canada K1A 0S2.

1. C. CHIEH and L. P. C. LEUNG. Can. J. Chem. **54**, 3077 (1976).
2. C. CHIEH. Can. J. Chem. **55**, 65 (1977).
3. C. CHIEH. Can. J. Chem. **56**, 564 (1978).
4. C. CHIEH. Can. J. Chem. **55**, 1115 (1977).
5. H. C. BRINKHOFF, A. M. GROTENS, and J. J. STEGGERDA. Recl. Trav. Chim. **89**, 11 (1970).
6. P. T. BEURSKENS, J. A. CRAS, J. H. NOORDIK, and A. M. SPRUIJT. Cryst. Mol. Struct. **1**, 93 (1971).
7. B. W. SKELTON and A. H. WHITE. Aust. J. Chem. **30**, 1693 (1977).

Can. J. Chem. Downloaded from www.nrcresearchpress.com by 210.87.254.40 on 09/05/12
For personal use only.

Resonance Raman in platinum phthalocyanine[1]

TZER-HSIANG HUANG, KLAUS E. RIECKHOFF, AND EVA-MARIA VOIGT

Departments of Physics and Chemistry, Simon Fraser University, Burnaby, B.C., Canada V5A 1S6

Received June 27, 1977

TZER-HSIANG HUANG, KLAUS E. RIECKHOFF, and EVA-MARIA VOIGT. Can. J. Chem. **56**, 976 (1978).

The resonance Raman spectra and excitation profiles of platinum phthalocyanine (PtP_c) in α-chloronaphthalene (α-ClN) and in mixtures of α-ClN and *n*-octane were obtained at 295 K with excitation from 660 to 570 nm covering the total lower energy absorption region of PtP_c. Eighteen fundamentals and overtone-combinations were observed. Our data show that the third absorption maximum of PtP_c in the visible region is actually the (0–1), but not the (0–2) as previously interpreted, transition. The (0–1) bands in the excitation profiles of most resonance-enhanced-vibrations were found to be more intense and frequency shifted compared with their counterparts in absorption. Based on the depolarization ratios, we deduced the symmetry of PtP_c in α-ClN in the excited singlets to be D_{2h}, C_{2v}, or D_2; no differences were found in the mixed solvents. The small Stokes loss observed in the absorption spectra, as well as the absence of the (0–2) maxima in the excitation profiles, indicate that the equilibrium position of the first excited singlet is only slightly different from that of the ground state.

TZER-HSIANG HUANG, KLAUS E. RIECKHOFF et EVA-MARIA VOIGT. Can. J. Chem. **56**, 976 (1978).

On a déterminé les spectres de résonance Raman et les profils d'excitation du phtalocyanure de platine (PtP_c) dans α-chloronaphtalène (α-ClN) et dans des mélanges d'α-ClN et d'octane à 295 K avec une excitation allant de 660 à 570 nm couvrant toute la région d'absorption de basse énergie du PtP_c. On a observé 18 bandes fondamentales et de combinaisons harmoniques. Nos données montrent que le troisième maximum d'absorption de PtP_c dans la région visible correspond en fait à la transition (0–1) plutôt que la transition (0–2) qui avait été suggérée antérieurement. On trouve que les bandes (0–1) de la plupart des vibrations qui sont augmentées en intensité par résonance dans les profils d'excitation sont plus intenses et plus déplacés que les bandes d'absorption équivalentes. En se basant sur les rapports de dépolarisation, on a pu déduire que la symétrie de PtP_c dans α-ClN dans des singulets excités est D_{2h}, C_{2v} ou D_2; on n'a pu trouver aucune différence dans les solvants mixtes. La petite perte de Stokes observée dans le spectre d'absorption de même que l'absence de maxima (0–2) dans les profils d'excitation indiquent que la position d'équilibre du premier singulet excité ne diffère que légèrement de l'état fondamentale.

[Traduit par le journal]

Introduction

We present in this paper the first detailed investigation of the Raman spectrum of a metalphthalocyanine (metal P_c) complex in solution. The phthalocyanines (P_c's) are used commercially as dyes and as Q-switches for lasers; they are, as well, molecules related to the biologically important porphyrins. For the reader unfamiliar with these molecules, we show the general structure of a metal P_c in Fig. 1. In our study the central metal is Pt. While the Raman spectra of the porphyrins have been studied extensively, this has not been the case for the P_c's, largely because of their extremely low solubility in all common solvents, and even the few usable solvents (such as α-chloronaphthalene, and quinolene) are far from satisfactory for Raman studies (typically 10^{-4} *M* or less). Therefore it was evident that resonance Raman scattering would be the most favourable experimental method to employ even though a number of the light metal (filled shell) P_c's fluoresce very efficiently. Thus, we chose for our study PtP_c in α-ClN (as well as in mixed solvents) partly because of its very low fluorescence yield. Furthermore, our previous extensive energy transfer studies of the P_c's (1) and especially the low temperature electronic relaxation behaviour of PtP_c (2), together with our

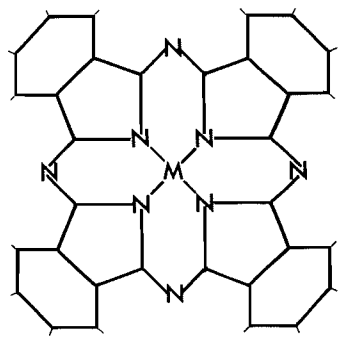

FIG. 1. The structure of metallophthalocyanine.

[1]This research was supported through operating grants from the National Research Council of Canada to K. E. Rieckhoff and E.-M. Voigt.

Can. J. Chem. Downloaded from www.nrcresearchpress.com by 210.87.254.6 on 09/05/12
For personal use only.

Can. J. Chem. Downloaded from www.nrcresearchpress.com by 210.87.254.6 on 09/05/12
For personal use only.

recent observation of the Shpol'skii effect for this molecule in mixed solvents[2] raised the question whether the molecular species in the solid solution of α-ClN and that in mixed matrices of α-ClN and *n*-octane were the same or not.

Moreover, in our theoretical analysis of all known relaxation data on the P_c's (3) it was necessary to assume a crystal field perturbation in the excited electronic state distorting the molecular symmetry from D_{4h}, which so far has been the generally accepted symmetry for the metal P_c's. The resonance Raman data of this study show also that the molecular structure of PtP_c in the excited singlets in solution is not completely D_{4h}, but has a slight distortion to lower symmetry, D_{2h}, C_{2v}, or D_2.

Experimental

The PtP_c used in this work was purified by repeated recrystallization from the commercial product—the main purpose was to remove metal free phthalocyanine (H_2P_c) whose strong fluorescence would otherwise have seriously interfered with the resonance Raman signal. The technical grade α-ClN was distilled before use which was not necessary for the chromotographic grade *n*-octane. Data were obtained in neat α-ClN and mixed solvent (one part α-ClN plus three parts or more *n*-octane). The overall concentrations of PtP_c in both solvent systems were 10^{-4} to 10^{-5} *M*, or sometimes less. The extinction coefficient for the α-ClN solution is $10^{4.86}$ at the main absorption maximum (1), and almost the same in the *n*-octane mixture. Several guidelines helped to show that the samples were pure enough for our purpose: first, the emission spectra of the α-ClN solution at 77 K showed only a single phosphorescence maximum around 940 nm, plus a very weak residual H_2P_c fluorescence. Furthermore, when PtP_c is incorporated in the rigid matrix of the mixed solvent at 77 K, band widths in absorption and emission become less than 8 cm^{-1} (this is called the Shpol'skii effect) and we observed no impurity in fluorescence, except the residual H_2P_c, or phosphorescence. Second, all the excitation profiles (*vide infra*) agree with the PtP_c absorption spectrum. Third, we found that in the Shpol'skii experiments the excitation profiles also agreed with the PtP_c absorption.

Photodecomposition occurred in both solvent systems under strong excitation (greater than 200 mW). This was suppressed significantly but not completely when the sample was placed in a rotating cell. We have paid particular attention to this when we were recording and analyzing the data. Incidentally, removing oxygen from the solutions did not help to any detectable extent.

The resonance Raman data were all obtained with the direction of observation perpendicular to the incident polarization. Light source was the jet stream dye (R6G) laser pumped by Ar^+ laser, both of coherent radiation. Laser power used ranged from 50 to 200 mW. Both the polarized and unpolarized resonance Raman signal were scrambled before entering the Spex Industries ½ m double monochromator. The depolarization ratios (ρ_l's) were measured with a sheet polarizer between the scrambler and the sample. The signal was finally detected by the ITT FW130 (S 20) photomultiplier tube with photon counting electronics. The total uncertainty in the positions of the resonance Raman bands is better than ± 1.5 cm^{-1} if not otherwise indicated. In Figs. 4–6, the error bars represent intensity uncertainties estimated for each measurement and, sometimes, for repeated measurements, whereas in Figs. 7 and 8 they represent the uncertainty estimated for each measurement.

The enhancements of all resonance Raman vibrations were normalized to the 666 cm^{-1} vibration of α-ClN, whose intensity depends insignificantly on the excitation used since α-ClN does not absorb in the visible. No corrections were made for the chromophore absorptions, i.e. the PtP_c absorptions at the individual resonance–Raman–Stokes shifts with respect to that at the 666 cm^{-1} shift, and for the responses of the grating (blazing at 5000 Å) and the photomultiplier whose sensitivity increases continuously towards the blue. The absence of these corrections does not affect our results and conclusions since we are not concerned with the absolute intensities, but the relative intensities only.

Results

The Raman spectra of the solvents used in this study, i.e. α-ClN and a mixture of α-ClN and *n*-octane (one part α-ClN and four parts *n*-octane), are shown in Fig. 2. The vibrational bands arising from *n*-octane are indicated in the top trace (B), and α-ClN in trace A′. The vertical arrows give the positions of the resonance Raman bands of PtP_c (shown in Fig. 3). At first sight, it appears that the solvent Raman bands interfere seriously with the resonance Raman bands of PtP_c. That this is not the case can be seen by making band intensity and sometimes band position and shape comparisons (*vide infra*).

The resonance Raman spectra are listed in Table 1 and shown in Fig. 3. We have scanned the Raman Stokes region, 150 to 3000 cm^{-1}, exciting into the main absorption band, and have found no significant signal of PtP_c above 1600 cm^{-1}. Vertical arrows in Fig. 3 point to where most of the α-ClN Raman bands (Fig. 2) are. α-ClN interference occurs at 225, 1145, 1196, 1343, 1358, 1436, and 1458 cm^{-1}. The 225 cm^{-1} band is distinguished from the 220 cm^{-1} band of α-ClN by not only the shift in position, but also the great intensity gain as excitation approaches the absorption maximum (Fig. 4). The weak resonance band at 1196 cm^{-1} is separated from the extremely weak interfering band at 1200 cm^{-1} by more than experimental uncertainty in band position. Furthermore, the intensity of the 1200 cm^{-1} band should be negligible when the 1372 cm^{-1} band of α-ClN is as intense as shown in trace C of Fig. 3. The 1145, 1343, 1358, and 1458 cm^{-1} bands are much stronger than their respective interfering bands at 1143, 1341, 1361, and 1459 cm^{-1} when compared with the very strong 1372 cm^{-1} of α-ClN. That the 1358 cm^{-1} band belongs to PtP_c is also clear from the fact that the 1361 cm^{-1} band should at most

[2]To be discussed in a forthcoming publication.

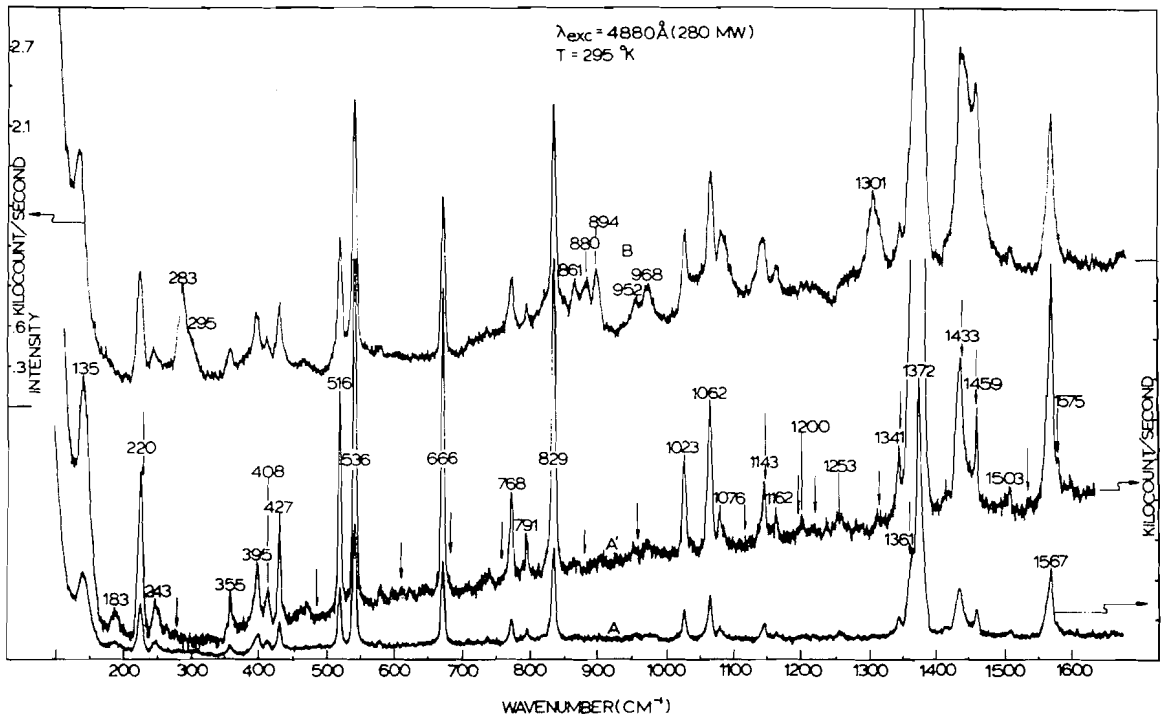

FIG. 2. The Raman spectra of α-ClN (A and A′) and of a mixture of one part α-ClN and four parts *n*-octane (B). The slit widths used for A (full scale 30 kilocount/s), A′ (full scale 3 kilocount/s), and B traces are, respectively, 4, 2.3, and 5.7 cm^{-1}. Vertical arrows indicate the positions of the resonance Raman bands shown in Fig. 3.

appear as the shoulder of the very strong α-ClN band at 1372 cm^{-1}.

Although the 1436 cm^{-1} band has never been completely separated from the interfering 1433 cm^{-1} of α-ClN, we believe it has a PtP_c contribution. First, whenever the peak height ratio of 1433 cm^{-1} to 1372 cm^{-1} becomes larger than 1:5.4 of neat α-ClN (see the bottom spectrum of Fig. 2), the band maximum is shifted towards 1436 cm^{-1} which was observed with 6486 Å excitation. Second, the ratio decreases, although not as rapidly as that of 1458 cm^{-1} to 1372 cm^{-1}, when excitation is moved away from the main absorption maximum (649 nm) of PtP_c. The highest ratio observed with 6486 Å excitation was 1:3.2 when the concentration of the PtP_c was slightly higher than that of trace C, Fig. 3. Third, we have measured the depolarization ratio, in terms of peak height again, of this 1436 cm^{-1} band as a function of excitation in the (0–1) absorption region. It was found to be 0.25 at 5910 Å (approximately the (0–1) absorption maximum), and to decrease slowly to 0.17 (possibly the ρ_l of the polarized 1433 cm^{-1} band of α-ClN) at 5790 Å. Although the difference of these two ratios is not much greater than the experimental uncertainty, it is consistent with the above mentioned two observations.

The weak band at 878 cm^{-1} (trace E, Fig. 3) is attributed to PtP_c for three reasons: one, there is no solvent transition in the vicinity; two, 6190 Å excitation lies near the (0–1) vibronic position for this vibration, and, thus, it should be enhanced; three, the 77 K spectra (which will be reported elsewhere) of the same sample and with the same excitation clearly show this vibration, in addition to several others in the region 1100 to 1300 cm^{-1}.

In Fig. 3 we also show the room temperature fluorescence (broad) and the change in its shift from the excitation line. From traces D and E, along with other excitation, we find its position at 655 ± 1 nm. The strong background in traces A and B is also due to fluorescence which clearly has affected the quality of the resonance Raman spectra and the precision of the data.

The data presented in Figs. 4–6 (excluding the broken traces) were accumulated from many runs. The best curves were drawn through the points by hand. The excitation profile of the 225 cm^{-1} vibration levels off on the short wavelength side as a result of the prevailing 220 cm^{-1} vibration of the solvent. For most of the excitation profiles, there are two maxima corresponding to the (0–0) and the (0–1) transitions. These two transitions are presumably too close to be resolved in the excitation profiles of the 225 and the 275 cm^{-1} vibrations. For

Can. J. Chem. Downloaded from www.nrcresearchpress.com by 210.87.254.6 on 09/05/12
For personal use only.

Can. J. Chem. Downloaded from www.nrcresearchpress.com by 210.87.254.6 on 09/05/12
For personal use only.

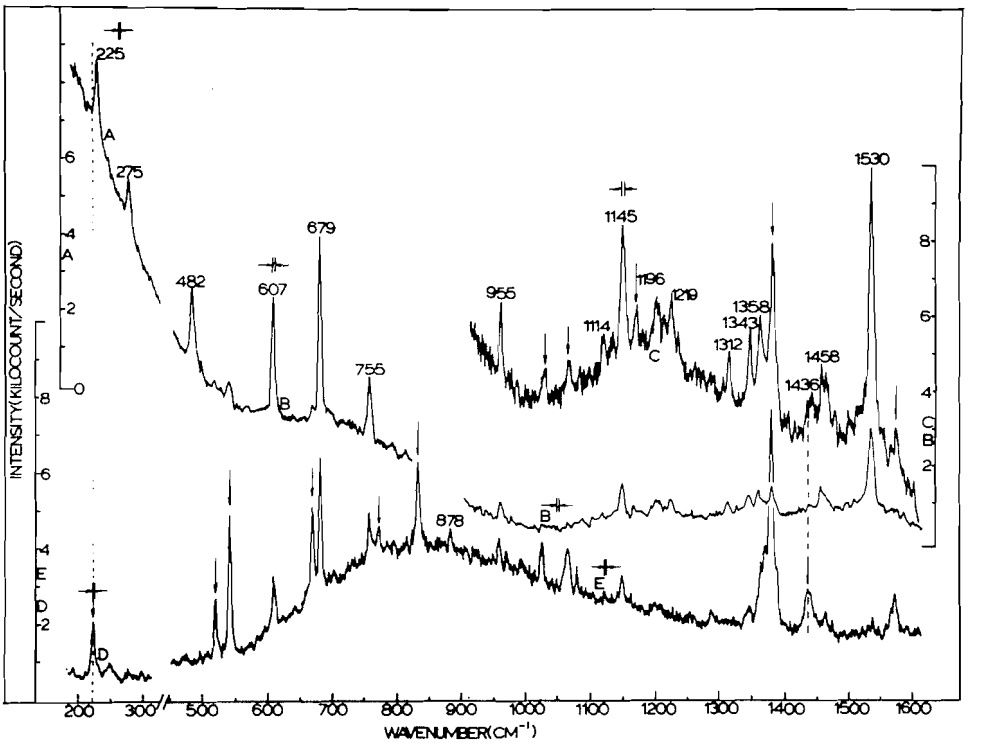

FIG. 3. The resonance Raman spectra of PtP_c in α-ClN at room temperature. Traces A and B were recorded from the same sample, D and E from another sample, C still another. Vertical arrows indicate most of the α-ClN Raman bands shown in Fig. 2. Slit widths used are indicated next to the spectra recorded. The spectrum-recording conditions were, for trace A, λ_{exc} = 6490 Å (100 mW), full scale 3 kilocount/s, slit = 2.6 cm^{-1}; for trace B, λ_{exc} = 6490 Å (100 mW), 3 kilocount/s, slit = 3.7 cm^{-1}; trace C, λ_{exc} = 6486 Å (200 mW), 1 kilocount/s, slit = 3.3 cm^{-1}; trace D, λ_{exc} = 6220 Å (150 mW), 1 kilocount/s, slit = 2.2 cm^{-1}; trace E, λ_{exc} = 6190 Å (150 mW), 1 kilocount/s, slit = 2.2 cm^{-1}.

TABLE 1. Resonance Raman spectra of PtP_c in solution at 295 K

Stokes shift (cm^{-1})	Intensity[a]	Depolarization ratio [ρ_l][b]	Symmetry[e] assignment
225	vs	0.45[c]	$A_g(A_1)$
275	s	0	$A_g(A_1)$
482 [483][d]	s	1.0[1.1][d]	$B_{1g}(A_2)$
607 [608]	vs	0.25[0.3]	$A_g(A_1)$
679 [679]	vs	0.25[0.2]	$A_g(A_1)$
755	s	0.62	$A_g(A_1)$
878 (275+607 = 882)	w		A_g
955	m	0.7	$B_{1g}(A_2)$
1114	w		
1145	m	0.5	$A_g(A_1)$
1196	w	0.5	
1219	w	1.0	$B_{1g}(A_2)$
1312	m	0.9	$B_{1g}(A_2)$
1343	m		
1358 (2×679 = 1358)	m		A_g
1436±4 (679+755 = 1434)	w	0.2	$A_g(A_1)$
1458±4	w	0.4	$A_g(A_1)$
1530±2 [1530±2]	s	0.55[0.6]	$A_g(A_1)$

[a]649 nm excitation; s = strong; m = medium; w = weak; vs = very strong.
[b]Also 649 nm excitation except 1436 and 1458 cm^{-1} (both under 596 nm excitation).
[c]A depolarized Raman band of α-ClN interferes, so the actual value should be less.
[d]The quantities in square brackets refer to the mixed solvent (see text), and were obtained with 642 nm excitation.
[e]The symmetry assignment is based on C_{2v}, in parentheses, and D_{2h} in agreement with the correlation table in the text.

Can. J. Chem. Downloaded from www.nrcresearchpress.com by 210.87.254.6 on 09/05/12
For personal use only.

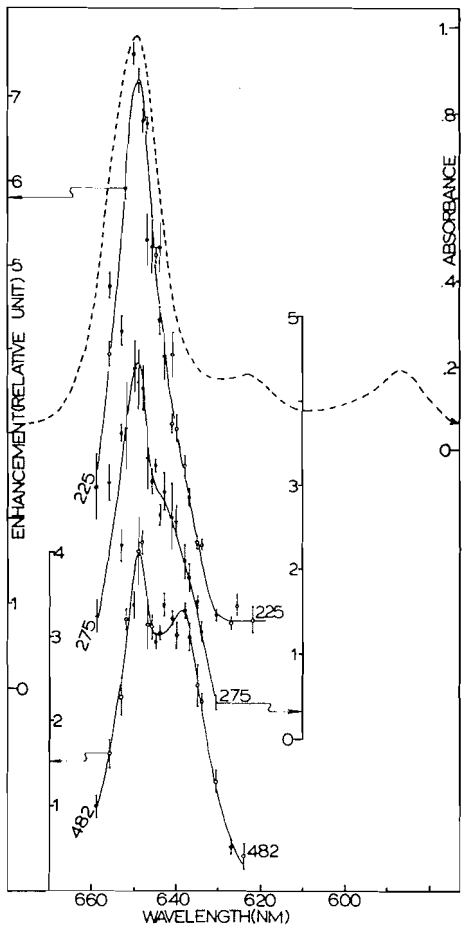

FIG. 4. Intensity enhancements of the resonance Raman bands, top to bottom: 225, 275, and 482 cm^{-1}, of PtP_c in α-ClN at 295 K as a function of excitation. The absorption spectrum (broken) refers to the extreme right ordinate.

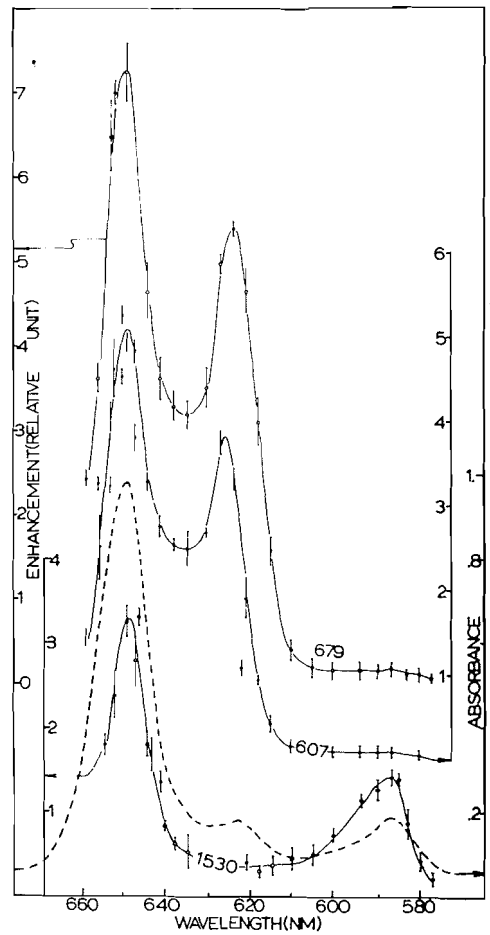

FIG. 5. Intensity enhancements of the resonance Raman bands, top to bottom: 679, 607, and 1530 cm^{-1}, of PtP_c in α-ClN at 295 K as a function of excitation. The absorption spectrum (broken) refers to the extreme right ordinate.

the vibrations whose (0–2) transitions are still in the tunable range of the dye laser, we do not see any corresponding maxima in the excitation profiles. We have also observed small energy differences of about 50 to 100 cm^{-1} between the (0–0)—(0–1) energy difference in absorption and that in the excitation profiles, which may partially result from the interference of two close lying resonances and also from the fact that the resonance Raman signals are not corrected for the instrument response and the chromophore absorptions (see above).

Figure 7 shows the depolarization ratios of most of the resonance Raman bands (indicated in cm^{-1}) in α-ClN at room temperature. In the detectable spectral range, the depolarization ratio of the 275 cm^{-1} vibration is approximately zero, and is not shown in the figure. The depolarization ratio of the 225 cm^{-1} vibration is interfered with the strong depolarized Raman band of the solvent at 220 cm^{-1}, particularly when the excitation wavelength is shifted away from the absorption maximum because of the wide slit needed for the ratio measurement. Thus the ratio may actually be less than 0.44 at the absorption maximum, and should tend to 0.75 as the wavelength becomes shorter. The maximum at 640 nm in the depolarization ratio of the 482 cm^{-1} vibration was carefully investigated, and found to be reproducible. The smaller variation in the depolarization ratios of the other vibrations (except 607 cm^{-1} and 679 cm^{-1}) have not been tested specifically, and, thus, we are not equally sure if they are genuine or not. However, the fluctuations in the 607 and the 679 cm^{-1} ρ_l's are greater than the experimental uncertainty, and are believed to be real. We also point out here that the 482, 1312, 1219, and possibly 955 cm^{-1} vibrations are anomalously, or inversely polarized ($\rho_l > \frac{3}{4}$, see Table 1). A general behaviour of the ρ_l's as a function of excitation

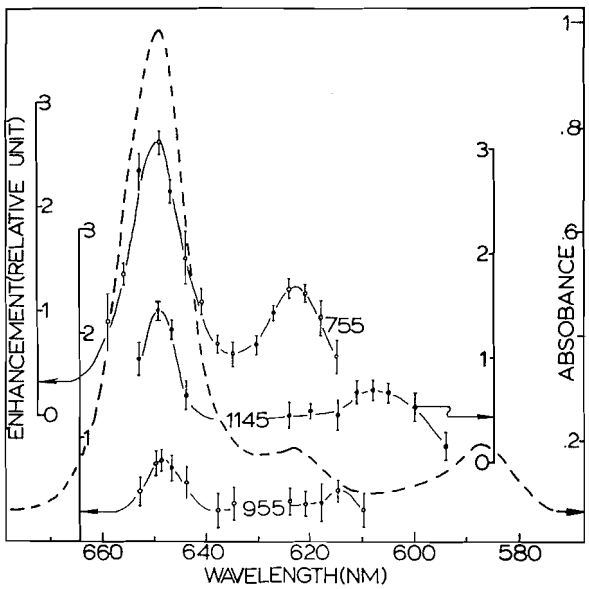

FIG. 6. Intensity enhancements of the resonance Raman bands, top to bottom: 755, 1145, and 955 cm^{-1}, of PtP_c in α-ClN at 295 K as a function of excitation. The absorption spectrum (broken) refers to the extreme right ordinate.

should be noted here, and will be referred to in the next section, namely they are well-behaved, they vary only slightly with excitation, and they are bounded in the spectral region where they are detectably enhanced.

In Fig. 8, we present the results obtained from PtP_c in mixtures of α-ClN and *n*-octane at room temperature. The enhancement and depolarization data in this figure have a greater uncertainty because of lower concentration and greater photodecomposition. Nevertheless, they serve well to prove or disprove, by comparison, if the entity of PtP_c has undergone any change in symmetry going from the neat α-ClN to the mixed solvent as will be shown.

Discussion and Conclusions

We believe that the Raman spectra shown in Fig. 3 are unambiguously resonance enhanced because (*a*) the intensity gain as the excitation wavelength approaches the absorption maxima cannot simply be accounted for by the ν^4 law (see Figs. 4–6 and 8), and (*b*) four vibrations, 482, 955, 1219, and 1312 cm^{-1}, have depolarization ratios $\geq \frac{3}{4}$ (see Figs. 7 and 8).

At least 14 fundamentals and four combinations and overtones (Table 1) are enhanced when excited into the main absorption band (649 and 642 nm, respectively, in α-ClN and the mixed solvent at 295 K). As the excitation is shifted to shorter wavelength, these vibrational modes are all selectively

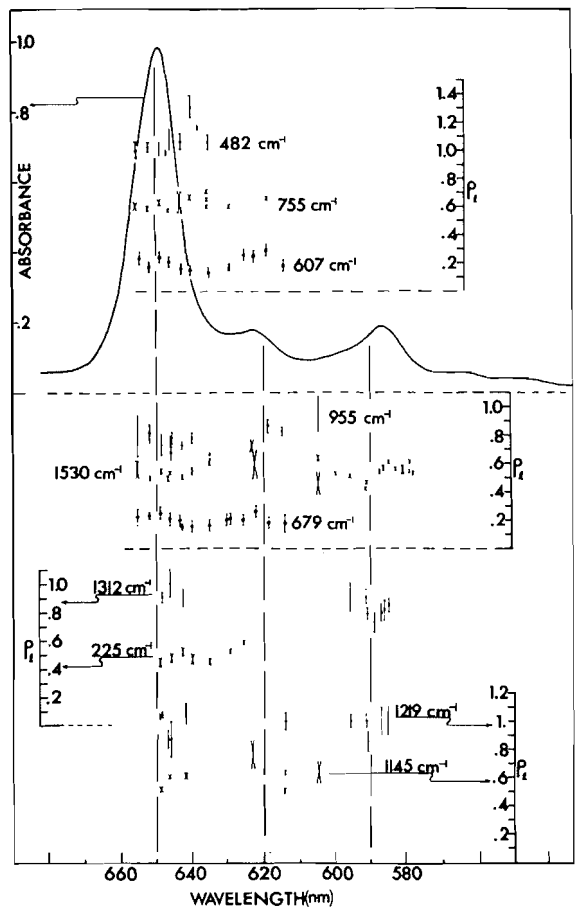

FIG. 7. The depolarization ratios (ρ_l) of the resonance Raman bands (indicated in cm^{-1}) of PtP_c in α-ClN at room temperature as a function of excitation wavelength together with the absorption spectrum.

excited (see Figs. 4–6 and 8). We conclude that the 649 nm (642 nm) absorption in α-ClN (mixed solvent) at 295 K is the pure electronic (0–0) transition, whereas the bands at 622 nm (616 nm) and 587 nm (582 nm) are the (0–1) vibronic transitions. Previously, the additional bands to the red of the main fluorescence (1) and to the blue of the main absorption maximum (4) were considered to be the vibronic progression. While this is qualitatively correct, our data show clearly that the 587 nm (582 nm) band in α-ClN (mixed solvent) at 295 K is the (0–1), and not the (0–2) transition as previously assumed. This conclusion is supported by consideration of the vibrational integrals as follows.

According to Koningstein and Jakubinek (5), based on the vibronic coupling model of Albrecht (6), the resonance Raman scattering intensity is obtained from the expression for the scattering tensor

Can. J. Chem. Downloaded from www.nrcresearchpress.com by 210.87.254.6 on 09/05/12
For personal use only.

$$(\alpha_{\rho\sigma})_{vv'} = \frac{1}{h(\nu_{r,v'';k,v} - \nu_0) + i\gamma_{r,v''}} \times \Big\{ \sum_{r,v''} (M_\rho{}^0)_{rk}(M_\sigma{}^0)_{kr}\langle v|v''\rangle\langle v''|v'\rangle + \sum_{r,t\neq r,v''} h_{tr}{}^Q[(M_\sigma{}^0)_{kt}(M_\rho{}^0)_{rk}\langle v'|v''\rangle\langle v''|Q|v\rangle + (M_\rho{}^0)_{tk}(M_\sigma{}^0)_{kr}\langle v|v''\rangle\langle v''|Q|v'\rangle] + \sum_{r,t\neq k,v''} h_{tk}{}^Q[(M_\rho{}^0)_{rk}(M_\sigma{}^0)_{tr}\langle v'|v''\rangle\langle v''|Q|v\rangle + (M_\sigma{}^0)_{kr}(M_\rho{}^0)_{tr}\langle v|v''\rangle\langle v''|Q|v'\rangle]$$

where

$$h_{tr}{}^Q \equiv \left\langle t^0 \left| \left(\frac{\partial H}{\partial Q}\right)_{Q=0} \right| r^0 \right\rangle \Big/ (E_t{}^0 - E_r{}^0)$$

$\langle t^0|$ is some electronic state coupled to $|r^0\rangle$ by the normal coordinate Q; $|r^0\rangle$ and $|k^0\rangle$ are the first excited and ground electronic states, respectively; H is the electronic Hamiltonian; $|v\rangle$ and $|v'\rangle$, respectively, are the $v = 0$ and 1 vibrational states of $|k^0\rangle$; v'' is the vibrational quantum number in $|r^0\rangle$; (M^0)'s are the electric dipole integrals between electronic states.

The square of the factor, $(M^0)_{kr}\langle v|v''\rangle$, is the intensity for the absorption, $k,v \rightarrow r,v''$. Assuming that $|v\rangle$ and $|v''\rangle$ are harmonic and that the shift in equilibrium position in $|r^0\rangle$ from that in $|k^0\rangle$, R_0, is finite, the transition probability calculated from the overlap integral, $\langle v|v''\rangle$, for $h\nu \gg kT$ is

$$W_{v\rightarrow v''} = (M^0)_{kr}\, e^{-P}\frac{P^{v''}}{v''!}$$

where P is called the Stokes loss for the normal vibration, and is equal to $m\nu^2R_0{}^2/2h\nu$ (7). M is the mass of the oscillator. $(M^0)_{kr}$, as well as h^Q's above, are constants throughout the whole vibronic progression. It is shown in ref. 7 that as P becomes smaller, the transition to smaller v'' becomes more probable than that to larger v''. In particular, when $P = 0.1$, $W_{0\rightarrow 0}$ is nine times $W_{0\rightarrow 1}$, $W_{0\rightarrow 2}$ being negligible. The intensity distributions shown in the absorption spectra (Fig. 4 and, particularly, Fig. 8) suggest that our system has a very small Stokes loss for a given ν (this is confirmed by observations to be published shortly). Thus,

$$W_{0\rightarrow 0} \gg W_{0\rightarrow 1} \quad \text{and} \quad W_{0\rightarrow 2} \sim 0$$

It follows that

$$\langle v = 0|v'' = 0\rangle \approx 1 \gg \langle v = 0|v'' = 1\rangle$$

and

$$\langle v = 0|v'' = 2\rangle \sim 0$$

and also

$$\langle v' = 1|v'' = 0\rangle \ll \langle v' = 1|v'' = 1\rangle \approx 1 \sim \gg \langle v' = 1|v'' = 2\rangle$$

The other intensity factors which vary with v'', i.e. $\langle v''|Q|v\rangle$ and $\langle v''|Q|v'\rangle$, can be calculated from the expressions given in ref. 8. They are

	$v'' = 0$	$v'' = 1$	$v'' = 2$	$v'' = 3, 4, \ldots$
$\langle v''\|Q\|v\rangle$	$= a\langle 1\|0\rangle$,	$= a\langle 1\|1\rangle$	$= a\langle 1\|2\rangle$,	≈ 0
$\langle v''\|Q\|v'\rangle$	$\approx a\langle 0\|0\rangle$,	$= \langle 2\|1\rangle + a\langle 0\|1\rangle$,	$\approx \langle 2\|2\rangle$,	≈ 0

where $a = \sqrt{2}/2$ and $\langle 1|0\rangle \equiv \langle v_k = 1|v'' = 0\rangle$ etc. From these integrals involving the normal coordinate and the above overlap integrals, the observation that the resonance Raman signal of a PtP_c vibration is too weak to be observed as the excitation is tuned to $v'' > 1$ can be easily understood to be a result of very small R_0.

The typical structure of MP_c's has already been shown in Fig. 1. So far, these molecules have been assumed to have D_{4h} symmetry. To deduce the symmetry of PtP_c in both solvent systems at 295 K, we therefore start out with D_{4h} and then distort it, if necessary.

From the evaluation of the integrals above we see that the terms containing the vibronic couplings, i.e. $h_{tr}{}^Q$ and $h_{tk}{}^Q$, in the expression of $(\alpha_{\rho\sigma})_{vv'}$ dominate. Among the two observed electronic transitions, the Soret band is so much stronger than the visible band that only the terms with $h_{tr}{}^Q$ need be considered for our resonance Raman intensity. $(M^0)_{tr}$ is Laporte forbidden given that $|t^0\rangle$ and $|r^0\rangle$ are the E_u electronic states in the Soret and visible regions, respectively. In order that $h_{tr}{}^Q$ is nonvanishing the normal modes must transform as A_{1g}, A_{2g}, B_{1g}, and B_{2g} (9). It is to be noted that ρ_l is expressed in terms of the matrix elements of $(\alpha_{\rho\sigma})_{vv'}$ (10) and is, thus, governed by the same vibronic coupling between $|t^0\rangle$ and $|r^0\rangle$. Therefore, the symmetry deduced in the following from the ρ_l's does not pertain to $|k^0\rangle$, the ground state, but to $|t^0\rangle$ and $|r^0\rangle$, the electronic states in the Soret and visible regions. It will be shown in a forthcoming paper that the ground state symmetry is indeed identical with that of the first excited singlet.

Our depolarization data (Figs. 7 and 8, Table 1) clearly show that the symmetry of PtP_c in α-ClN is not D_{4h}, D_{2d}, D_4, or C_{4v}. In these point groups the ρ_l, calculated from the expressions given in refs. 9 and 11, for representation $A_{2g}(D_{4h})$ or $A_2(D_{2d}, D_4,$ and $C_{4v})$ is infinite which we do not observe.

We next consider the remaining subgroups of

Can. J. Chem. Downloaded from www.nrcresearchpress.com by 210.87.254.6 on 09/05/12
For personal use only.

Can. J. Chem. Downloaded from www.nrcresearchpress.com by 210.87.254.6 on 09/05/12
For personal use only.

D_{4h}, i.e. C_{4h}, C_4, S_4; D_{2h}, C_{2v}, D_2; C_{2h}, C_2, C_s; and C_i. Our observed ρ_l's exclude C_{4h}, C_4, and S_4 because they all contain a resonance Raman active representation with $\rho_l = \frac{3}{4}$ *independent* of excitation. Due to the large numbers of nonzero, independent matrix elements in the resonance Raman tensors (11), the dependences of calculated ρ_l's on excitation in point groups C_{2h}, C_2, C_s, and C_i are very complex, and are not expected to be bounded for *every* resonance Raman mode. Our observed ρ_l's, however, are all bounded by low values. Thus, our data are fully consistent only with D_{2h}, C_{2v}, and D_2. The following correlation is valid also for D_2 so far as ρ_l's go, because it has the same resonance Raman tensors as those of D_{2h} and C_{2v} (11).

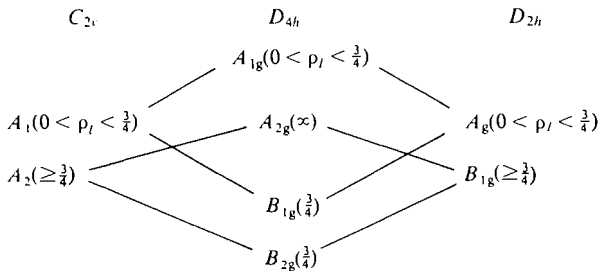

Note that the correlation is not unique (12). There can be two D_{4h}–D_{2h} correlations and four D_{4h}–C_{2v}'s, i.e. two and four ways of distorting D_{4h} to D_{2h} and C_{2v}, respectively. For all the possible distortions, the correlation shown is valid so far as ρ_l is concerned. The ρ_l's are now all bounded, although still excitation dependent. It is obvious that the behaviour of the ρ_l's shown in Figs. 7 and 8 agrees well with the calculated values.

We conclude, therefore, that the molecular symmetry of PtP_c in α-ClN is D_{2h}, C_{2v}, or D_2. The distortion from D_{4h} must be small, otherwise one should observe two main (0–0) absorptions as in metal free P_c (which has D_{2h} symmetry) and we do not. The symmetry assignments of the vibrations in Table 1 are based on D_{2h} and C_{2v}, and on the correlation above. The depolarization ratio of the 1219 cm^{-1} vibration is anomalous and supports the B_{1g} (D_{2h}) assignment, rather than A_g (the first overtone of 607 cm^{-1}). The assignment of A_g (D_{2h}) to the 878 and the 1358 cm^{-1} vibrations is based on the combination and overtone, respectively, of the A_g fundamentals (Table 1).

We next consider the mixed solvent case. Solutions of PtP_c in the mixed solvents show the Shpol'skii effect when frozen suddenly or slowly. In other words, the absorption (solid trace at the bottom of Fig. 8) and phosphorescence become quasiline spectra upon freezing. The individual vibronic bands are then well resolved, important not just for structural analysis but also for comparison with theoretical vibronic

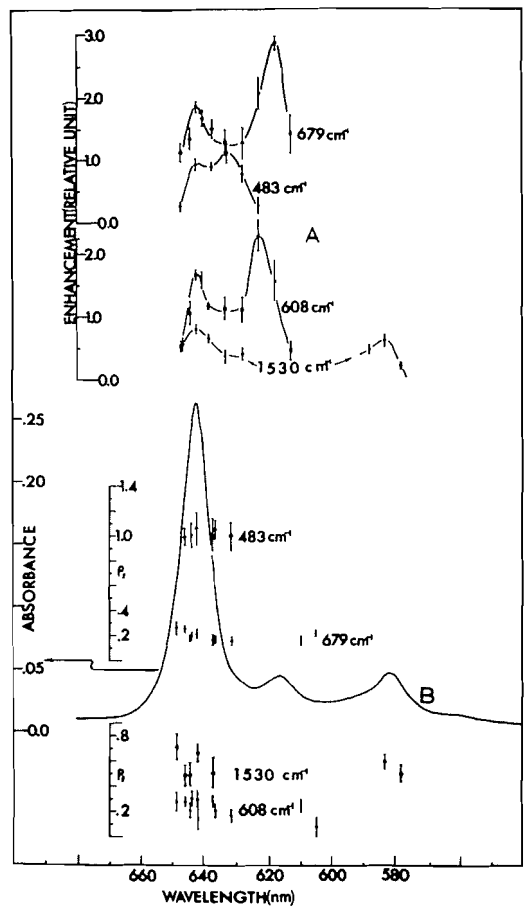

FIG. 8. Intensity enhancements (A) and the depolarization ratios (ρ_l) of the resonance Raman bands (indicated in cm^{-1}) of PtP_c in the mixed solvent as a function of excitation at 295 K together with the absorption spectrum.

coupling. At room temperature the halfwidth of the main absorption band in mixed solvents is 270 cm^{-1} vis-à-vis 340 cm^{-1} (see e.g. Fig. 4) in neat α-ClN. There exists in both solvent systems a common broadening mechanism, e.g. the tumbling and translational motions. But, as these degrees of freedom are frozen in the 340 cm^{-1} width of the neat α-ClN solution decreases insignificantly (the same thing occurs in phosphorescence), whereas the 270 cm^{-1} width of the mixed solvent spectrum becomes smaller than 8 cm^{-1} arising from the homogeneous (intrinsic) and inhomogeneous broadenings (13). Thus there must be another broadening mechanism, namely the interaction between solute and solvent or electron–phonon interaction (14) in solid state terminology. This interaction can also account for the difference between 270 and 340 cm^{-1} at room temperature if we believe that the (π–π^*) optical electron (3) of PtP_c in the mixed solvent couples very weakly to the thermal phonons, or the solvation sheath, whereas that in neat α-ClN couples very

Can. J. Chem. Downloaded from www.nrcresearchpress.com by 210.87.254.6 on 09/05/12
For personal use only.

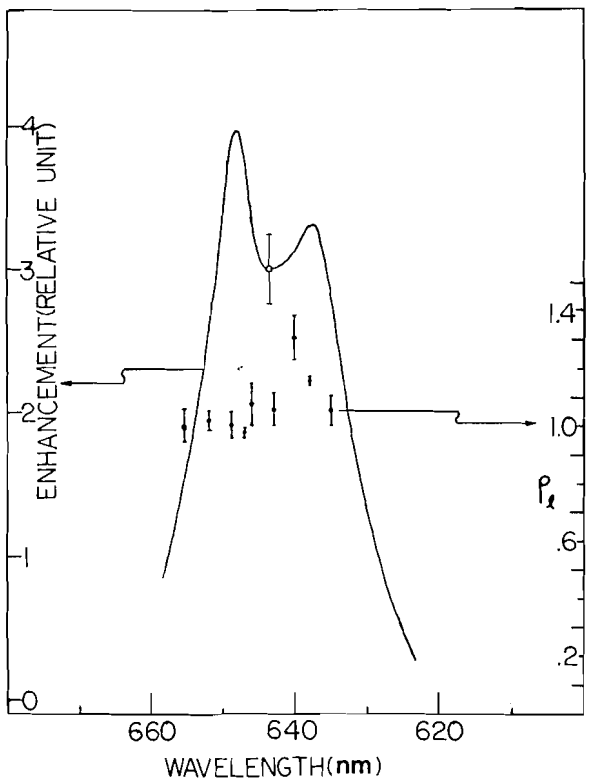

FIG. 9. The excitation profile (with a representative error bar) and the depolarization ratios of the 482 cm^{-1} normal mode as a function of excitation wavelength at room temperature. Reproduced from Figs. 4 and 7.

strongly. This also agrees with our finding that photodecomposition is more efficient in the mixed solvent than in neat α-ClN at room temperature. We, therefore, conclude that the 270 cm^{-1} width is due mainly to the molecular motions only while the 340 cm^{-1} width results mainly from electron–phonon interaction rather than molecular motions.

For the four fundamentals shown in Fig. 8, we see that their band positions, excitation profiles, and particularly, the depolarization ratios are the same as their counterparts in neat α-ClN. We also note that the (0–1) bands in the excitation profiles are stronger than their counterparts in neat α-ClN and that the profiles, except 1530 cm^{-1}, agree with the theoretical works of other authors (15).

For vibrations with anomalous depolarization ratios, theory predicts that the depolarization ratio as a function of excitation should peak midway between the maxima in the excitation profile (15). Among the anomalously polarized resonance Raman bands observed, only the 482 cm^{-1} vibration is intense enough for testing this prediction. The results are shown in Fig. 9 and it can be seen that our data agree qualitatively with this prediction. The depolarization maximum (at 640 nm) occurs much closer to the high energy maximum in the excitation profile. The variation in the depolarization ratio was also determined for the 607 and 679 cm^{-1} vibrations, although there it is less pronounced than in the 482 cm^{-1} vibration (see Fig. 7). The resonance Raman tensor of the $A(D_2)$, the $A_1(C_{2v})$, and the $A_g(D_{2h})$ representations (to which 607 cm^{-1} and 679 cm^{-1} belong) has three different matrix elements (11). Their different variations with wavelength can give rise to the fluctuation in the depolarization ratio, which further supports our conclusion that the molecule has D_{2h}, C_{2v}, or D_2 symmetry.

In summary, we have made the first careful study of the resonance Raman spectrum, their excitation profiles, and their depolarization ratios of a phthalocyanine molecule, namely PtP_c, in α-ClN and in mixed solvents. A judicious analysis of our data including comparisons with absorption spectra has enabled us to make assignments of the vibrations responsible for the observed Raman lines and has led us to the conclusion that the singlets in the Soret and visible regions of PtP_c in solution do not have D_{4h} symmetry but rather D_{2h}, C_{2v}, or D_2 symmetry. This conclusion is of interest and importance since previous work on the lowest excited triplet state of PtP_c by a completely different experimental method has also clearly established a symmetry lower than D_{4h} for that state (3).

1. E. R. MENZEL, K. E. RIECKHOFF, and E.-M. VOIGT. J. Chem. Phys. **58**, 5726 (1973), and previous papers cited therein.
2. T.-H. HUANG, K. E. RIECKHOFF, and E.-M. VOIGT. Can. J. Phys. **54**, 633 (1976).
3. T.-H. HUANG, K. E. RIECKHOFF, E.-M. VOIGT, and E. R. MENZEL. Chem. Phys. **19**, 25 (1977).
4. E. R. MENZEL, K. E. RIECKHOFF, and E.-M. VOIGT. Chem. Phys. Lett. **13**, 604 (1972).
5. J. A. KONINGSTEIN and B. G. JAKUBINEK. J. Raman Spectrosc. **2**, 317 (1974).
6. A. C. ALBRECHT. J. Chem. Phys. **34**, 1476 (1961).
7. K. K. REBANE. Impurity spectra of solids. Plenum Press, New York, NY. 1970. p. 71.
8. A. WARSHEL and P. DAUBER. J. Chem. Phys. **66**, 5477 (1977).
9. R. MENDELSOHN, S. SUNDER, A. L. VERMA, and H. J. BERNSTEIN. J. Chem. Phys. **62**, 37 (1975); S. SUNDER, R. MENDELSOHN, and H. J. BERNSTEIN. J. Chem. Phys. **63**, 573 (1975); A. L. VERMA and H. J. BERNSTEIN. J. Chem. Phys. **61**, 2560 (1974).
10. J. A. SHELNUTT, L. D. CHEUNG, R. C. C. CHANG, N.-T. YU, and R. H. FELTON. J. Chem. Phys. **66**, 3387 (1977).
11. W. M. MCCLAIN. J. Chem. Phys. **55**, 2789 (1971).
12. E. B. WILSON, JR., J. C. DECIUS, and P. C. CROSS. Molecular vibrations. McGraw-Hill, New York, NY. 1955. p. 336.
13. S. VOELKER, R. M. MACFARLANE, A. Z. GENACK, H. P. TROMMSDORFF, and J. H. VAN DER WAALS. J. Chem. Phys. **67**, 1759 (1977).
14. R. BARRIE, I. W. SHARPE, and B. L. JONES. Can. J. Phys. **50**, 231 (1972).
15. B. B. JOHNSON, L. A. NAFIE, and W. L. PETICOLAS. Chem. Phys. **19**, 303 (1971); S. HASSING and O. S. MORTENSEN. Chem. Phys. Lett. **47**, 115 (1977).

Synthesis and structure of 4-methylpyridine complexes of cobalt(II) and nickel(II) hexafluorophosphate and hexafluoroarsenate

RAYMOND M. MORRISON AND ROBERT C. THOMPSON

Department of Chemistry, The University of British Columbia, Vancouver, B.C., Canada V6T 1W5

Received September 19, 1977

RAYMOND M. MORRISON and ROBERT C. THOMPSON. Can. J. Chem. **56**, 985 (1978).

The complexes $M(4mepy)_4A_2$ and $M(H_2O)_2(4mepy)_8A_2$ (where M is Ni or Co and A is PF_6 or AsF_6) have been prepared and their electronic spectra and magnetic properties studied. A preliminary report is made of single crystal X-ray diffraction studies on $Ni(H_2O)_2(4mepy)_8(PF_6)_2$, $Co(H_2O)_2(4mepy)_8(PF_6)_2$, and $Co(4mepy)_4(PF_6)_2$. All of the complexes have structures involving complex cations and non-coordinated anions, consistent with extremely weak ligating abilities for both PF_6^- and AsF_6^-. Cations identified and characterized are the squashed tetrahedral $[Co(4mepy)_4]^{2+}$ ion, the square planar $[Ni(4mepy)_4]^{2+}$ ion, and the tetragonal $[Co(4mepy)_4((4mepy)_2H_2O)_2]^{2+}$ and $[Ni(4mepy)_4((4mepy)_2H_2O)_2]^{2+}$ ions. The ligand field strength of 4-methylpyridine is found to be indistinguishable from that of pyridine in these complexes. Infrared spectra are reported and infrared criteria for establishing the presence of non-coordinated anions in PF_6^- and AsF_6^- complexes are suggested.

RAYMOND M. MORRISON et ROBERT C. THOMPSON. Can. J. Chem. **56**, 985 (1978).

On a préparé les complexes $M(4mépy)_4A_2$ et $M(H_2O)_2(4mépy)_8A_2$ (où M = Ni ou Co et A = PF_6 ou AsF_6) et on a étudié leurs spectres électroniques et leurs propriétés magnétiques. On présente un rapport préliminaire sur des études de diffraction de rayons-X sur des monocristaux de $Ni(H_2O)_2(4mépy)_8(PF_6)_2$, $Co(H_2O)_2(4mépy)_8(PF_6)_2$ et $Co(4mépy)_4(PF_6)_2$. Tous ces complexes ont des structures impliquant des cations complexes et des anions non-coordonnés qui sont en accord avec le fait que PF_6^- et AsF_6^- sont des ligands extrêmement faibles. Les cations identifiés et caractérisés sont l'ion tétraédrique aplati $[Co(4mépy)_4]^{2+}$, l'ion plan carré $[Ni(4mépy)_4]^{2+}$ et l'ion tétragonal dans $[Co(4mépy)_4((4mépy)_2H_2O)_2]^{2+}$ et $[Ni(4mépy)_4((4mépy)_2H_2O)_2]^{2+}$. On a trouvé qu'il est impossible de distinguer entre la force de champ de ligand de la méthyl-4 pyridine et celle de la pyridine dans ces complexes. On rapporte les spectres infrarouges et on suggère des critères infrarouges pour déterminer la présence des anions non-coordonnés dans des complexes PF_6^- et AsF_6^-.

[Traduit par le journal]

Introduction

This work is part of a study involving the synthesis and characterization of transition metal complexes containing anions of strong acids (1–3). The hexafluorophosphate ion exhibits a relatively weak coordinating ability and while some evidence for coordination to metal ions in complexes has been claimed (4), for the most part, complexes of PF_6^- contain non-coordinated anions (3, 5). Such complexes are of interest because they may contain cationic complex ions, such as the tetrakis(pyridine)-cobalt(II) ion, $[Co(py)_4]^{2+}$ (3), which are not obtainable where the counter anion is more strongly coordinating. In addition, it is expected that studies of the electronic and molecular structures of complexes containing the PF_6^- and related anions coordinated to metal ions should, because of the ionic nature of the interactions involved, enhance our understanding of metal–ligand bonding in general.

We reported previously some studies on pyridine complexes of cobalt(II) hexafluorophosphate and hexafluoroarsenate (3) and we describe here the preparation of related 4-methylpyridine complexes and studies of their magnetic and spectral properties. Mayfield and Bull reported (5) the preparation of diamagnetic $Ni(4mepy)_4(PF_6)_2$ and paramagnetic $Ni(py)_4(PF_6)_2$ and this rather significant difference between related pyridine and 4-methylpyridine complexes prompted our further investigations of the latter complexes. Also, we found during the course of this work it is generally easier to obtain crystalline products when the ligand is 4-methylpyridine rather than pyridine. This has provided an opportunity for structure determination by X-ray diffraction techniques and this paper includes a preliminary report of such studies on $M(H_2O)_2(4mepy)_8(PF_6)_2$ (where M = Co or Ni) and $Co(4mepy)_4(PF_6)_2$.

Experimental

All materials were reagent grade; 4-methylpyridine was purified by refluxing over barium oxide overnight followed by distillation at atmospheric pressure.

None of the products are stable indefinitely in air. After drying samples *in vacuo*, all manipulations were performed in an inert atmosphere box. Samples were stored in sealed vials.

Can. J. Chem. Downloaded from www.nrcresearchpress.com by 210.87.254.42 on 09/05/12
For personal use only.

Can. J. Chem. Downloaded from www.nrcresearchpress.com by 210.87.254.42 on 09/05/12
For personal use only.

TABLE 1. Analytical data

Compound	Calculated (%)			Found (%)		
	C	H	N	C	H	N
$Ni(H_2O)_2(C_6H_7N)_8(PF_6)_2$	51.0	5.35	9.92	51.3	5.42	10.1
$Ni(H_2O)_2(C_6H_7N)_8(AsF_6)_2$	47.3	4.96	9.20	47.0	4.99	9.00
$Ni(C_6H_7N)_4(PF_6)_2$	40.0	3.91	7.77	39.8	3.71	7.88
$Ni(C_6H_7N)_4(AsF_6)_2$	35.6	3.49	6.93	35.5	3.53	7.10
$Co(H_2O)_2(C_6H_7N)_8(PF_6)_2$	51.0	5.35	9.92	51.0	5.20	9.89
$Co(H_2O)_2(C_6H_7N)_8(AsF_6)_2$	47.3	4.97	9.20	47.5	4.80	9.10
$Co(C_6H_7N)_4(PF_6)_2$	40.0	3.91	7.77	39.7	3.91	7.87
$Co(C_6H_7N)_4(AsF_6)_2$	35.6	3.49	6.92	35.6	3.66	7.17

Preparations

Diaquooctakis(4-methylpyridine)cobalt(II) and Nickel(II)-hexafluoro-phosphate and -arsenate, $M(H_2O)_2(4mepy)_8A_2$

All four complexes were prepared in the same manner. Metal nitrate (hydrate) (0.02 mol) was dissolved in 100 ml of water containing 39 ml 4-methylpyridine. To this solution was added, with stirring, a filtered solution of 0.04 mol ammonium hexafluorophosphate in 50 ml water (or 0.04 mol potassium hexafluoroarsenate in 250 ml water). Stirring was continued for about 1 h during which time a two-liquid phase system developed consisting of an upper colourless layer and a more dense oily layer which was red in the case of the cobalt system and blue in the case of the nickel system. The oily layer was transferred to an evaporating dish placed over phosphoric oxide in a vacuum desiccator. After a period of one to two weeks, orange-red crystals of the cobalt complexes and blue crystals of the nickel complexes formed. The crystals were washed with a solution of 5 ml 4-methylpyridine in 50 ml water. Since the crystals tend to lose 4-methylpyridine on prolonged exposure to the atmosphere or to a vacuum, they were stored in sealed vials while still 'wet' with the washing liquid. Just prior to use the crystals were dried for about 15 min *in vacuo* at room temperature.

Tetrakis(4-methylpyridine)cobalt(II) and Nickel(II)hexa-fluoro-phosphate and -arsenate, $M(4mepy)_4A_2$

The corresponding $M(H_2O)_2(4mepy)_8A_2$ complex was ground to a fine powder in the inert atmosphere box then heated *in vacuo* for 3–4 h at temperatures of 100–110°C for the nickel complexes and 80–90°C for the cobalt complexes. Both nickel complexes were recrystallized from dichloromethane. The cobalt complexes were not recrystallized except for the sample of $[Co(4mepy)_4](PF_6)_2$ used in the X-ray diffraction studies which was obtained from an equal volume mixture of dichloromethane and chloroform. All four of these complexes were found to be extremely hygroscopic and required handling in an inert atmosphere box and storage in sealed vials.

Analytical Data

C, H, and N analyses were performed by P. Borda of the Department of Chemistry, University of British Columbia. Results are given in Table 1.

Spectral and Magnetic Susceptibility Measurements

Infrared spectra of samples mulled in Nujol and contained between KRS-5 (Harshaw Chemical Co.) plates were obtained using a Perkin-Elmer model 457 spectrophotometer. Electronic spectra at room temperature of powdered samples (diffuse reflectance) were measured over the range 13.5–28.5 kK using a Bausch and Lomb Spectronic 600 spectrophotometer and spectra of samples mulled in Nujol and solution spectra were obtained over the range 5–33 kK using a Cary model 14 spectrophotometer. The solution spectra reported in Table 2 were obtained on a 7.8×10^{-3} *M* solution of $Ni(4mepy)_4(PF_6)_2$, a 3.8×10^{-3} *M* solution of $Ni(4mepy)_4(AsF_6)_2$, a 1.7×10^{-3} *M* solution of $Co(4mepy)_4(PF_6)_2$, and a 4.2×10^{-3} *M* solution of $Co(4mepy)_4(AsF_6)_2$. The solvents used were dichloromethane for the nickel complexes and an equal volume mixture of dichloromethane and chloroform for the cobalt complexes.

Magnetic susceptibilities were determined, over the temperature range 80 to 300 K, on powdered samples at field strengths of approximately 4500 and 7000 G using the Gouy equipment and calibration procedures described previously (2). The samples gave no evidence for dependence of magnetic susceptibilities on field strength. The values used for making corrections for the diamagnetism of the atoms were -12 for Co^{2+} and Ni^{2+}, -61 for C_6H_7N, -97 for AsF_6^-, -67 for PF_6^-, and -13 for H_2O (all values in 10^{-6} cm^3 mol^{-1}).

Results and Discussion

Nickel(II) Complexes

In attempting to obtain 4-methylpyridine analogues of $Ni(py)_6(PF_6)_2$ (5), we obtained instead crystalline compounds with the stoichiometry $Ni(H_2O)_2(4mepy)_8A_2$ (where A is PF_6 or AsF_6). It is clear from the electronic spectral and magnetic properties given in Table 2 that these complexes contain six-coordinate nickel(II). This has been confirmed by a single crystal X-ray diffraction study on the hexafluorophosphate derivative.[1] The structure consists of non-coordinated PF_6^- anions and complex cations which may be formulated as $[Ni(4mepy)_4((4mepy)_2H_2O)_2]^{2+}$. Four 4-methylpyridine ligands are bonded in a square planar arrangement about nickel with Ni—N distances in the narrow range of 2.10 to 2.12 Å. Axial positions are occupied by water molecules, each water molecule bonded via hydrogen bonds to two additional 4-methylpyridine molecules, hence, the formulation of the axial ligands as $((4mepy)_2H_2O)$. The Ni—O bond distances are 2.12 Å and it is interesting to note that all of the Ni—O and Ni—N bond distances are the same to within ± 0.02 Å. Consequently, although the microsymmetry about nickel is D_{4h} the electronic spectrum may be assigned on the basis of octahedral symmetry,

[1] S. J. Rettig and J. Trotter, unpublished results.

Can. J. Chem. Downloaded from www.nrcresearchpress.com by 210.87.254.42 on 09/05/12
For personal use only.

TABLE 2. Electronic spectral data and magnetic properties

Compound	Energies of band maxima (kK)[a,b] (a)	(b)	(c)	Assignments[c]	Dq (cm^{-1})[d]	B (cm^{-1})[d]	μ_{eff}[e]	θ
$Ni(py)_6(PF_6)_2$	26.0 s 16.0 s			$^3A_{2g}(F) \rightarrow {}^3T_{1g}(P)$ $\rightarrow {}^3T_{1g}(F)$	1000	800	3.06	+4.0
$Ni(H_2O)_2(4mepy)_8(PF_6)_2$	26.8 s 16.7 s	27.4 s 16.7 s 11.1 m 9.53 m		$^3A_{2g}(F) \rightarrow {}^3T_{1g}(P)$ $\rightarrow {}^3T_{1g}(F)$ $\rightarrow {}^3T_{2g}(F)$	1055	790	3.15	−6.0
$Ni(H_2O)_2(4mepy)_8(AsF_6)_2$	26.9 s 16.7 s	27.4 s 16.8 s 13.3 w 10.3 m		$^3A_{2g}(F) \rightarrow {}^3T_{1g}(P)$ $\rightarrow {}^3T_{1g}(F)$ — $\rightarrow {}^3T_{2g}(F)$	1050	805	3.14	+1.0
$Ni(4mepy)_4(PF_6)_2$	22.1 s	22.5 s	22.0 (90)				Diamagnetic	
$Ni(4mepy)_4(AsF_6)_2$	22.1 s	22.2 s	22.1(82)				Diamagnetic	
$Co(H_2O)_2(4mepy)_8(PF_6)_2$	21. 1s 20.0 s	20.8 sh 20.0 s 8.77 m		$^4T_{1g}(F) \rightarrow {}^4T_{1g}(P)$ $\rightarrow {}^4T_{2g}(F)$	995	840	4.85	
$Co(H_2O)_2(4mepy)_8(AsF_6)_2$	20.4 s	21.5 sh 20.8 s 8.93 m		$^4T_{1g}(F) \rightarrow {}^4T_{1g}(P)$ $\rightarrow {}^4T_{2g}(F)$	1010	845	4.86	
$Co(4mepy)_4(PF_6)_2$	25.3 w 22.7 w 18.9 s 17.7 s	18.9 sh 18.25 s 9.43 m 5.48 w	18.9 sh (611) 17.9 9.09 (64)	$^4A_2(F) \rightarrow {}^4T_1(P)$ $\rightarrow {}^4T_1(F)$ $\rightarrow {}^4T_2(F)$	555	735	4.33	−7.0
$Co(4mepy)_4(AsF_6)_2$	25.6 w 22.7 w 18.9 s 17.7 s	19.0 sh 18.2 s 9.43 m 5.56 w	18.9 sh (517) 17.9 10.5 sh (83) 9.17	$^4A_2(F) \rightarrow {}^4T_1(P)$ $\rightarrow {}^4T_1(F)$ $\rightarrow {}^4T_2(F)$	555	735	4.36	−5.0

[a] s = strong, m = medium, w = weak, sh = shoulder.
[b] (a) Diffuse reflectance spectra, (b) mull spectra, (c) solution spectra; molar extinction coefficients in parentheses.
[c] Approximate assignment assuming O_h or T_d symmetry. Weak bands and shoulders not assigned are probably due to spin-forbidden transitions.
[d] Calculated as described in text.
[e] For $Co(H_2O)_2(4mepy)_8A_2$ complexes, magnetic moment is the room temperature value calculated from $\mu_{eff} = 2.828[\chi_M T]^{1/2}$ BM. For all other complexes the magnetic moment is calculated from $\mu_{eff} = 2.828[(\chi_M - tip)(T - \theta)]^{1/2}$ BM. χ_M is the molar paramagnetic susceptibility corrected for diagmagnetism of all atoms and tip $= 8N\beta^2/10Dq$ (8) is the temperature independent paramagnetism.

Can. J. Chem. Downloaded from www.nrcresearchpress.com by 210.87.254.42 on 09/05/12
For personal use only.

the only evidence of lower symmetry being the splitting observed in the band assigned to the $^3A_{2g}(F) \rightarrow {}^3T_{2g}(F)$ transition in the hexafluorophosphate derivative. The magnetic properties too are typical of spin-free, octahedral nickel(II). The electronic spectra and magnetic properties of $Ni(H_2O)_2(4mepy)_8(AsF_6)_2$ are virtually identical to those of the hexafluorophosphate derivative suggesting that the two compounds have analogous structures.

The ligand field parameters *Dq* and *B* were calculated (6) using the transition energies obtained from the diffuse reflectance spectra. For comparison, we prepared $[Ni(py)_6](PF_6)_2$ as described previously (5) and examined its room temperature electronic spectrum and its magnetic properties (Table 2). Although water occupies lower positions in both the spectrochemical and nephelauxetic series than nitrogen donor ligands (7), there is little difference in the ligand field parameters of the compounds studied here (containing the NiN_4O_2 chromophore) and the complex $Ni(py)_6(PF_6)_2$ (containing the NiN_6 chromophore). In fact, the small difference which is observed in the *Dq* parameter indicates that it is larger for NiN_4O_2 compared to NiN_6, contrary to expectations based on the spectrochemical series. The difference may be a consequence of greater steric crowding, and hence generally longer and weaker bonds, in the NiN_6 case.

Heating the $Ni(H_2O)_2(4mepy)_8A_2$ complexes *in vacuo* followed by recrystallization from dichloromethane gives complexes of composition $Ni(4mepy)_4A_2$. These complexes are diamagnetic and exhibit single absorption bands in the visible region (Table 2), consistent with both compounds having structures involving square planar $[Ni(4mepy)_4]^{2+}$ cations and non-coordinated anions.

Our findings on these square planar nickel(II) complexes are not entirely consistent with the previous work of Mayfield and Bull (5). These authors reported the preparation of 'diamagnetic' $Ni(4mepy)_4(PF_6)_2$ by a procedure which did not involve recrystallization. We carried out several preparations of both the PF_6^- and AsF_6^- compounds and found unrecrystallized samples contained paramagnetic impurities as evidenced by room temperature paramagnetic susceptibilities of the order of 500 to 600×10^{-6} cm^3 mol^{-1} (increasing to 1200 to 1600 $\times 10^{-6}$ cm^3 mol^{-1} at 100 K). In addition, Mayfield and Bull (5) reported that $Ni(py)_4(PF_6)_2$ has a magnetic moment of 1.98 BM. The paramagnetism in this compound may also arise from paramagnetic impurities since, by stirring suspensions of the $Ni(py)_6(PF_6)_2$ precursor in dichloromethane, and avoiding heating the sample as was done in the earlier work, we have been able to obtain samples of $Ni(py)_4(PF_6)_2$ which, like the 4-methylpyridine derivatives, are diamagnetic at room temperature.

Cobalt(II) Complexes

The reaction of cobalt(II) nitrate with ammonium hexafluorophosphate or potassium hexafluoroarsenate and 4-methylpyridine in aqueous solution gives, as was the case for nickel, crystalline complexes with the general formula $Co(H_2O)_2(4mepy)_8A_2$. A single crystal X-ray diffraction study[1] on the hexafluorophosphate compound shows it to have a structure similar to that of the nickel complex. The hexafluorophosphate ions are not coordinated to cobalt. The complex cation has four 4-methylpyridine ligands forming a square planar array about cobalt with Co—N distances in the range 2.20 to 2.22 Å. Axial positions are occupied by $((4mepy)_2H_2O)$ ligands with Co—O distances of 2.11 Å. In contrast to the nickel case there is a significant difference between the Co—O and Co—N bond lengths; the microsymmetry about Co is approximately D_{4h} with two short Co—O bonds and four longer Co—N bonds. In spite of the obviously lower symmetry ligand environment about cobalt, the electronic spectrum (Table 2) of $Co(H_2O)_2(4mepy)_8(PF_6)_2$ does not differ greatly from that of $Co(py)_6(PF_6)_2$ (3). The ligand field parameters were calculated as before (2) using 8.77 kK for the $^4T_{1g}(F) \rightarrow {}^4T_{2g}(F)$ transition energy and 20.2 kK (estimated from the centre of the visible band) for the $^4T_{1g}(F) \rightarrow {}^4T_{1g}(P)$ energy.

The magnetic properties of $Co(H_2O)_2(4mepy)_8(PF_6)_2$ are particularly interesting in that they show the effects of the low symmetry ligand environment (Fig. 1). The variation of the magnetic moment with temperature shows excellent agreement with theoretical moments calculated using the four parameter approach of Figgis *et al.* (9) for spin-free cobalt(II) in an axially compressed tetragonal environment. The parameter values (accuracy estimated at $\pm 5\%$ for k and λ and ± 2 for ν) indicate a splitting of the octahedral ground $^4T_{1g}(F)$ term by some 750 cm^{-1} as a consequence of the axial compression. This analysis of the magnetic data is consistent with the molecular structure as determined by X-ray diffraction and the general agreement provides support for the use of this theory in interpreting the magnetic data for related complexes. For comparison, the magnetic moments previously reported for $Co(py)_6(PF_6)_2$ and $Co(py)_6(AsF_6)_2$ (3) are reproduced graphically in Fig. 1.

The electronic spectra and magnetic properties of $Co(H_2O)_2(4mepy)_8(AsF_6)_2$ do not differ significantly from those of the hexafluorophosphate compound suggesting analogous structures for the two com-

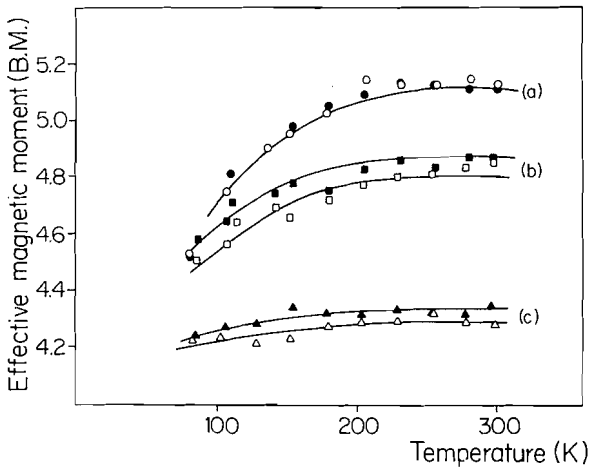

FIG. 1. Magnetic moment data for cobalt complexes. (*a*) ○, $Co(py)_6(PF_6)_2$; ●, $Co(py)_6(AsF_6)_2$. Data taken from ref. 3. Curve is theoretical from ref. 9 for $A = 1.40$, $k = 1.0$, $\nu = 0$, and $\lambda = -145\ cm^{-1}$. (*b*) □, $Co(H_2O)_2(4mepy)_8(PF_6)_2$; ■, $Co(H_2O)_2(4mepy)_8(AsF_6)_2$. Magnetic moments calculated from $\mu_{eff} = 2.828[\chi_M T]^{1/2}$. Upper curve is theoretical from ref. 9 for $A = 1.40$, $k = 0.93$, $\nu = 5$, and $\lambda = -150\ cm^{-1}$. Lower curve is theoretical from ref. 9, for $A = 1.40$, $k = 0.88$, $\nu = 5$, and $\lambda = -150\ cm^{-1}$. (*c*) △, $Co(4mepy)_4(PF_6)_2$; ▲, $Co(4mepy)_4(AsF_6)_2$. Magnetic moments calculated from $\mu_{eff} = 2.828[\chi_M - tip)T]^{1/2}$. Curves show general trend of data and are not theoretical.

pounds. The *Dq* and *B* values given in Table 2 for the hexafluoroarsenate complex were calculated using 8.93 and 20.4 kK for the $^4T_{1g}(F) \rightarrow {}^4T_{2g}(F)$ and $^4T_{1g}(F) \rightarrow {}^4T_{1g}(P)$ transitions respectively. The *Dq* values for these complexes are slightly greater than *Dq* for the $[Co(py)_6]^{2+}$ ion (3) and, as was discussed above for the nickel complexes, this may reflect greater steric crowding in the CoN_6 chromophore compared to CoN_4O_2.

When the $Co(H_2O)_2(4mepy)_8A_2$ complexes are heated to about 80–90°C the corresponding tetrakis-(4-methylpyridine) complexes are obtained. The electronic spectra (Table 2) of $Co(4mepy)_4(PF_6)_2$ and $Co(4mepy)_4(AsF_6)_2$ are virtually identical to those reported previously for the pyridine complexes and are readily assigned assuming a tetrahedral ligand environment about cobalt(II). *Dq* and *B* for these complexes were calculated using 9.43 kK for the $^4A_2 \rightarrow {}^4T_1(F)$ transition energy and 18.3 kK (estimated from the centre of the visible band) for the $^4A_2 \rightarrow {}^4T_1(P)$ energy (6). Unlike the corresponding pyridine complexes, these complexes were sufficiently soluble in an equal volume mixture of dichloromethane and chloroform to obtain solution spectra (Table 2). Changes in the bands assigned to the $^4A_2(F) \rightarrow {}^4T_1(F)$ transition suggest there may be minor changes in geometry on dissolution; however, the structures remain basically tetrahedral as evidenced, in particular, by the large extinction coefficients. The $^4A_2(F) \rightarrow {}^4T_2(F)$ transitions which give rise to weak bands observed only in very thick mulls are too weak to be observed in the solution spectra. The magnetic properties (Table 2 and Fig. 1) obey the Curie–Weiss law with a small Weiss constant, over the temperature range 80–300 K, again consistent with a tetrahedral ligand environment and a $^4A_2$ electronic ground state (8).

The presence of distorted tetrahedral cobalt(II) in these complexes has been shown by a single crystal X-ray diffraction study of $Co(4mepy)_4(PF_6)_2$.[2] This complex has a structure consisting of $[Co(4mepy)_4]^{2+}$ cations and non-coordinated anions. The CoN_4 chromophore is a squashed tetrahedron (D_{2d}) with N—Co—N bond angles of 114 and 101° and Co—N bond lengths of 2.00 Å. It is interesting to note that the Co—N distances in $[Co(4mepy)_4]^{2+}$ are significantly shorter than in $[Co(4mepy)_4((4mepy)_2H_2O)_2]^{2+}$ reflecting less steric crowding in the four-coordinate species.

The coordinating properties of pyridine and 4-methylpyridine appear from the present work to be virtually identical. The differences in *Dq* and *B* for $[Co(4mepy)_4]^{2+}$ and $[Co(py)_4]^{2+}$ (3) cannot be considered significant and the magnetic properties of the two groups of compounds are the same, within experimental error. In addition, as shown above, there appears to be no significant difference in the electronic spectra of $[Ni(4mepy)_4]^{2+}$ and $[Ni(py)_4]^{2+}$ and the difference in the magnetic properties of $Ni(py)_4(PF_6)_2$ and $Ni(4mepy)_4(PF_6)_2$ which was reported previously (5) has not been confirmed here.

In general we find that the electronic and molecular structures of corresponding hexafluorophosphate and hexafluoroarsenate complexes of cobalt(II) and nickel(II) are the same and are consistent with similar, very weak, coordinating abilities for these two ions. A closer examination of the relative coordinating abilities of these anions would require the preparation and study of complexes where there is greater metal–anion interaction.

Vibrational Spectra

Bands arising primarily from anion vibrations and those arising from neutral ligand vibrations were relatively easily distinguished in the infrared spectra of the complexes. Most of the 4-methylpyridine vibrations were found to show small and random shifts in the complexes relative to the free ligand; however, consistent with the results of Goodgame and Hayward (10), the six vibrations listed in Table 3 show increases in energy on coordination. Several

[2]R. M. Morrison, J. Trotter, and R. C. Thompson, unpublished results.

Can. J. Chem. Downloaded from www.nrcresearchpress.com by 210.87.254.42 on 09/05/12
For personal use only.

Can. J. Chem. Downloaded from www.nrcresearchpress.com by 210.87.254.42 on 09/05/12
For personal use only.

TABLE 3. Infrared spectra

Compound	Infrared frequency (cm^{-1})[a]									
	4-Methylpyridine vibrations[b]						Anion vibrations[c]			
	6a	*10b*+12	*1*	*9a*	*19a*	*8a*	$\nu_3(F_{1u})$	$\nu_4(F_{1u})$	$\nu_1(A_{1g})$	$\nu_2(E_g)$
4mepy	515	800	997	1224	1499	1608				
$Ni(H_2O)_2(4mepy)_8(PF_6)_2$	525 m 540 m	818 m 800 m	1024 s 1007 s	1229 m	1509 w	1622 sh 1611 s	840 vs	554 s	739 vw	[g]
$Ni(H_2O)_2(4mepy)_8(AsF_6)_2$	526 m 540 m	816 s 805 s	1026 s 1007 s	1229 m 1235 sh	1506 w	1610 vs	695 vs	392 s	[f]	[g]
$Ni(4mepy)_4(PF_6)_2$	[d]	817 s	1054 w	1250 vw 1240 vw	1513 m	1620 s	847 vs 834 vs	558 s	744 m	575 w
$Ni(4mepy)_4(AsF_6)_2$	565 m	820 s	1053 w	1250 vw 1240 vw	1513 m	1620 s	700 vs	397 s	672 m	575 m
$Co(H_2O)_2(4mepy)_8(PF_6)_2$	526 m 536 sh	[d]	1017 s 1010 s	1230 s	1504 w	1608 s	835 vs	553 s	740 vw	[g]
$Co(H_2O)_2(4mepy)_8(AsF_6)_2$	526 m 538 m	810 vs	1020 s 1007 s	1227 s	1504 w	1610 s	694 vs	394 s	[f]	575 vw
$Co(4mepy)_4(PF_6)_2$	[d]	810 s	[e]	1240 w	1511 m	1622 s	840 vs	557 s	742 w	[g]
$Co(4mepy)_4(AsF_6)_2$	560 m	816 s	[e]	1240 w	1512 m	1622 s	697 vs	392 s	[f]	[g]

[a]s = strong, m = medium, w = weak, v = very.
[b]Assignments from ref. 10.
[c]Assignments (O_h symmetry) from ref. 11.
[d]Obscured by PF_6^- vibrations.
[e]Obscured by $\rho(CH_3)$ at 1040 cm^{-1}.
[f]Not observed; possibly obscured by ν_3.
[g]Not observed.

Can. J. Chem. Downloaded from www.nrcresearchpress.com by 210.87.254.42 on 09/05/12
For personal use only.

of the vibrations in the octahedral complexes are 'doubled', a consequence, presumably, of non-equivalent 4-methylpyridine ligands in these compounds. With the exception of the 800 cm^{-1} band, the ligand vibrations listed seem particularly sensitive to the nature of the complex, shifting to higher energies in the four-coordinate square planar and tetrahedral complexes than in the six-coordinate complexes. Goodgame and Hayward found similar trends to increasing energy with increasing polarizing power and the shifts we observe probably reflect a greater degree of ligand polarization in the four-coordinate species.

The anion bands ν_3 and ν_4, listed in Table 3, have frequencies very close to those reported for KPF_6 and $CsAsF_6$ (11) and for the analogous pyridine complexes (3). Medium to weak bands, assignable to the ν_1 and ν_2 vibrations, are observed in the square planar nickel complexes but are generally absent or appear very weakly in the other complexes.

Recently, there have been a number of reports concerning complex cationic species in which the counter anion is PF_6^- or AsF_6^- (for example, see refs. 12–15). In view of the current use of these anions as non-coordinating species it would be useful to have infrared criteria regarding coordination involving them. The criteria for non-coordinated anions may be obtained from the spectra of the pyridine complexes of cobalt(II) described earlier (3) and the 4-methylpyridine complexes of cobalt(II) described here, where there is little doubt that the anions are not coordinated to metal ions. The spectra all show strong to very strong anion bands assignable to the ν_3 and ν_4 vibrations in O_h symmetry. In addition some of the effects of symmetry lowering described by Bell *et al.* (4) can be seen. These effects are, specifically, a splitting of ν_3 of the order of 10 to 25 cm^{-1}, and the appearance of weak bands corresponding to the formally Raman active ν_1 and ν_2 vibrations. Such effects probably arise from site symmetry lowering or very weak interactions of the anions with other groups such as ligands coordinated to metal ions in a complex. Where PF_6^- and AsF_6^- are more strongly coordinated to other atoms, one would expect to see greater splitting of degenerate modes and greater intensities of bands formally forbidden in O_h symmetry. Some of these effects have been seen in the infrared and Raman spectra of $H_3O^+AsF_6^-$ (16) and $NH_2F_2^+AsF_6^-$ (17) and in the Raman spectrum of $KrF^+AsF_6^-$ (18). In summary, the presence of non-coordinated anions in PF_6^- and AsF_6^- complexes is indicated by spectra which show very strong ν_3 bands (may be split by up to 25 cm^{-1}), strong and unsplit ν_4 bands, and weak or absent ν_1 and ν_2 bands.

The infrared spectra of $Cu(py)_4(PF_6)_2$ (4, 5) and the nickel complexes, $Ni(4mepy)_4(PF_6)_2$ and $Ni(4mepy)_4(AsF_6)_2$, studied here show medium to strong bands assigned to ν_1, weak to medium bands assigned to ν_2 and, in the case of the two hexafluorophosphate compounds, splitting of the ν_3 bands. This suggests that in these complexes the anions are more strongly perturbed than in the corresponding cobalt complexes, a consequence, perhaps, of weak 'semi-coordination' of the anions as was suggested previously for $Cu(py)_4(PF_6)_2$ (4). We plan single crystal X-ray diffraction studies on $Ni(4mepy)_4(PF_6)_2$ and $Cu(4mepy)_4(PF_6)_2$ to help clarify the matter.

Acknowledgements

Financial assistance from the National Research Council of Canada and from the Natural, Applied and Health Sciences Grants Committee of U.B.C. is acknowledged. We also thank J. Trotter and S. J. Rettig of this Department for permitting discussion of X-ray diffraction studies prior to publication.

1. C. S. Alleyne and R. C. Thompson. Can. J. Chem. **52**, 3218 (1974).
2. A. L. Arduini, M. Garnett, R. C. Thompson, and T. C. Wong. Can. J. Chem. **53**, 3812 (1975).
3. R. M. Morrison and R. C. Thompson. Inorg. Nucl. Chem. Lett. **12**, 937 (1976).
4. S. A. Bell, J. C. Lancaster, and W. R. McWhinnie. Inorg. Nucl. Chem. Lett. **7**, 405 (1971).
5. H. G. Mayfield and W. E. Bull. J. Chem. Soc. A, 2779 (1971).
6. A. E. Underhill and D. E. Billing. Nature, **210**, 834 (1966).
7. C. K. Jorgensen. Absorption spectra and chemical bonding in complexes. Pergamon Press, London. 1962.
8. F. E. Mabbs and D. J. Machin. Magnetism and transition metal complexes. Chapman and Hall, London. 1973.
9. B. N. Figgis, M. Gerlock, J. Lewis, F. E. Mabbs, and G. A. Webb. J. Chem. Soc. A, 2086 (1968).
10. M. Goodgame and P. J. Hayward. J. Chem. Soc. A, 632 (1966).
11. G. M. Begun and A. C. Rutenberg. Inorg. Chem. **6**, 2212 (1967).
12. R. J. Restivo, G. Ferguson, D. J. O'Sullivan, and F. J. Lalor. Inorg. Chem. **14**, 3046 (1975).
13. O. A. Serra, M. Perrier, V. K. L. Osorio, and Y. Kawano. Inorg. Chim. Acta, **17**, 135 (1976).
14. M. Nolte, E. Singleton, and M. Laing. J. Chem. Soc. Dalton, 1979 (1976).
15. P. Boldrini, I. D. Brown, R. J. Gillespie, P. R. Ireland, W. Luk, D. R. Slim, and J. E. Vekris. Inorg. Chem. **15**, 765 (1976).
16. K. O. Christe, C. J. Schack, and R. D. Wilson. Inorg. Chem. **14**, 2224 (1975).
17. K. O. Christe. Inorg. Chem. **15**, 2821 (1975).
18. R. J. Gillespie and G. J. Schrobilgen. Inorg. Chem. **15**, 22 (1976).

Synthesis and ^1H and ^{13}C nuclear magnetic resonance spectra of some 4-alkylidene-1-pyrazolines and alkylidenecyclopropanes

ROBERT J. CRAWFORD, HIROKAZU TOKUNAGA, LOUIS M. H. C. SCHRIJVER, JACKY C. GODARD, AND THOMAS NAKASHIMA

Department of Chemistry, The University of Alberta, Edmonton, Alta., Canada T6G 2G2

Received September 28, 1977

ROBERT J. CRAWFORD, HIROKAZU TOKUNAGA, LOUIS M. H. C. SCHRIJVER, JACKY C. GODARD, and THOMAS NAKASHIMA. Can. J. Chem. **56**, 992 (1978).

The ^{1}Hmr and ^{13}Cmr spectra for 15 4-alkylidene-1-pyrazolines and 19 alkylidenecyclopropanes are reported. The assignments of *E* and *Z* isomers are made on the basis of shielding effects about the *exo* cyclic double bonds. The addition of diazomethane-d_2 to 1,2-butadiene is shown to be both regiospecific and stereospecific.

ROBERT J. CRAWFORD, HIROKAZU TOKUNAGA, LOUIS M. H. C. SCHRIJVER, JACKY C. GODARD et THOMAS NAKASHIMA. Can. J. Chem. **56**, 992 (1978).

On rapporte les spectres rmn du ^{1}H et rmn du ^{13}C de 15 alkylidène-4 pyrazolines-1 et de 19 alkylidène cyclopropanes. On a effectué les attributions des configurations *E* et *Z* en se basant sur les effets de blindage autour des doubles liaisons exocycliques. On a montré que l'addition de diazométhane-d_2 au butadiène-1,2 est à la fois régiospécifique et stéréospécifique.

[Traduit par le journal]

We have extended our studies (1) on the mechanism of thermolysis of 4-alkylidene-1-pyrazolines by examining the stereochemistry of the substituents in the alkylidenecyclopropane products, and comparing it with that of the reactant. In this paper we present the syntheses, ^{1}Hmr, and ^{13}Cmr data used to assign the structures of 15 different 4-alkylidene-1-pyrazolines (**1–15**) and 19 different alkylidenecyclopropanes (**15–34**). The thermolysis and mechanistic details are reported in the following paper.

4-Alkylidene-1-pyrazolines

We have used two methods to synthesize the 4-alkylidene-1-pyrazolines: (*a*) the diazoalkane cycloaddition to an allene has been used to prepare all compounds except **7** and **11** whose syntheses have been reported earlier (2) and (*b*) the synthesis of **3** was also achieved from the dibromide **35** and the pyrazolidine **36** (Scheme 1). The product was the same as that obtained by the addition of diazomethane to 1,2-butadiene. The cycloaddition process was regiospecific in that only the addition to the 1,2-double bond was observed.

It was desirable to prepare alkylidene-1-pyrazolines that were different at each of the three methylene groups, particularly those in which substituent effects do not play a major role, and thus a synthesis of **4** and **5** was sought. We had earlier observed that the cycloaddition of diazomethane to 3-methyl-1,2-butadiene reversed the mode of cycloaddition to the 1,2-double bond to produce 3-isopropylidene-1-pyrazoline. Andrews and Day (3) have suggested that steric factors were primarily responsible for this reversal of mode in diazoalkane addition to allenes and thus it seemed reasonable that the addition of diazomethane-d_2 to 1,2-butadiene would produce **4**, whereas the addition of diazomethane to 1,1-dideuterio-1,2-butadiene would produce **5**. The proof of structure of **4** and **5** is derived from the ^{1}Hmr and ^{13}Cmr spectra. As recorded in Table 1, signals arising from C(3) and C(5) of **1** are observed at δ 79.2 whereas for **7** they are displaced upfield to δ 77.5 due to the shielding by the *syn*-methyl group. This is consistent with an average shift of -1.2 ± 0.3 ppm upon the introduction of a *syn*-methyl in alkenes (4). The ^{13}Cmr spectrum of **3** displays two lines in the appropriate region, one at δ 79.1 assigned to the methylene group *anti* to the ethylidene methyl, and the second at δ 76.1 assigned to that *syn* to the methyl group. The ^{13}Cmr spectrum of **4** has only one line at δ 76.1, whereas the product assigned the structure **5** had a spectrum with an intense line at δ 79.1 and no readily observable signal in the higher field region. Comparison of the expanded signals of the ^{1}Hmr methylene protons of **4** and **5** shows that the most intense signal in the methylene spectrum of **4**, at δ 4.910, is absent from the spectrum of **5** and the most intense line for **5** at δ 4.945 is absent from the spectrum of **4**. The proton coupling constant between the vinylic hydrogen and the methylene hydrogens of **4** is 1.95 Hz, whereas the same coupling constant for **5** is 2.3 Hz, supporting the assignment, since *anti* vinylic–allylic coupling constants around a double bond are known to be smaller than those for the *syn* isomer (5). The cycloaddition is thus stereospecific in that the diazomethane adds *anti* to the

Can. J. Chem. Downloaded from www.nrcresearchpress.com by 210.87.254.6 on 09/05/12
For personal use only.

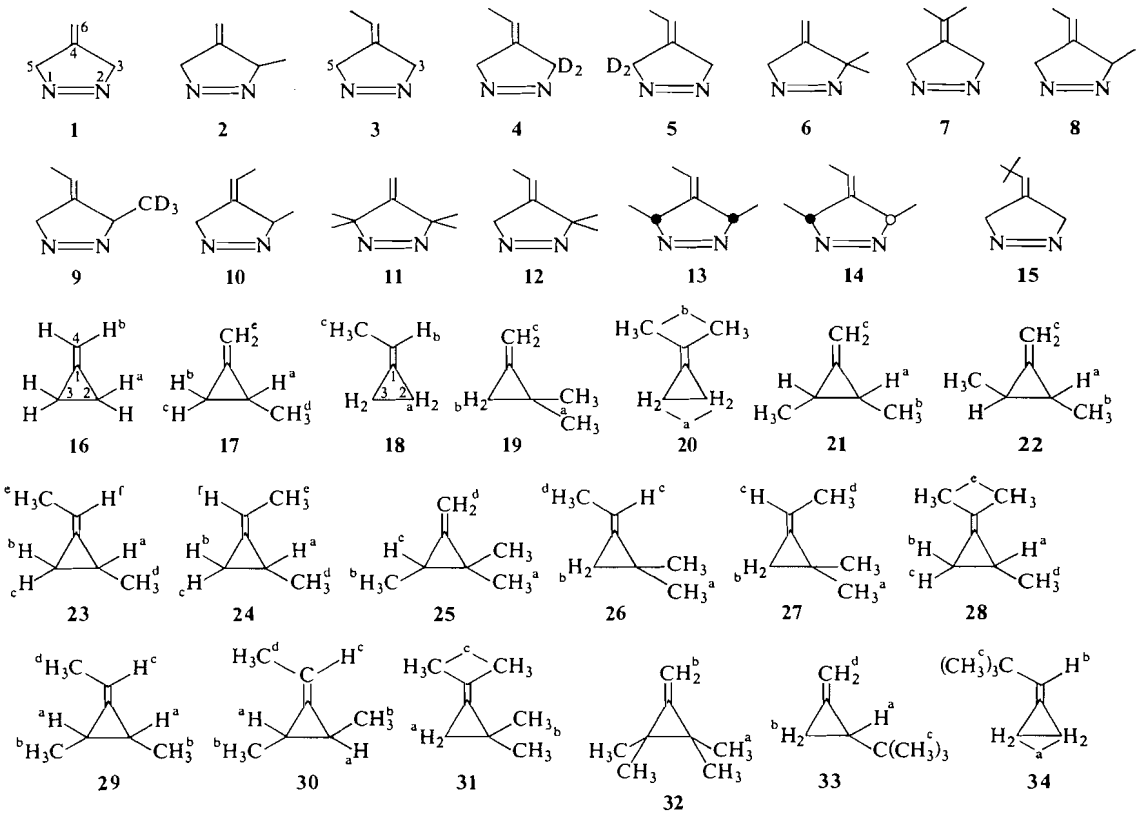

methyl on the allene, and no **4** could be detected in **5** or vice versa.

The addition of diazoethane to 1,2-butadiene gave a cycloadduct whose ^{1}Hmr spectrum differed from that of the adduct of diazomethane to 2,3-pentadiene principally in that the CH_3—C(3) doublet is centered at δ 1.45 in the former and δ 1.37 in the latter. Table 2 lists the ^{1}Hmr spectral characteristics for the 4-alkylidene-1-pyrazolines. The ^{13}Cmr spectrum of the 1,2-butadiene adduct displayed a C(3) resonance at lower field than that of the 2,3-pentadiene adduct. Thus the mode of formation, the ^{13}Cmr shielding, and the proton coupling constants all suggest that the former is the *E* isomer **8** and the latter the *Z* isomer **10**. The methyl resonances of **8** and **10** were assigned by comparison with **9** and by selective proton decoupling, respectively.

The addition of diazoisopropane to 1,2-butadiene gave two isomeric 1:1 adducts, along with acetone azine. The major product, **12**, was assigned the *E* configuration on the basis of the shielding of C(5) by the *syn*-methyl, producing the line at δ 77.1 and the similarity of resonances of C(3) in **12** and **6**, being at δ 87.3 and 87.1, respectively. The isomeric material produced was tentatively assigned the structure 5-ethylidene-3,3-dimethyl-1-pyrazoline (**37**) on the basis of its spectral properties and inertness at temperatures less than 250°C (1).

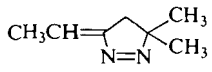

37

The addition of diazoethane to 2,3-pentadiene produced *cis*- (**13**) and *trans*-3,5-dimethyl-4-ethylidene-1-pyrazoline (**14**) in almost equal amounts. One of the isomers undergoes thermolysis at a rate significantly faster than the other thus allowing the isolation of the less reactive isomer. The chemical shift for the C(3) methyl group of the *cis* isomer is calculated from the observed shift of the methyls of **11** by allowing for the δ 7.8 difference observed on going from methyl to *gem*-dimethyl in **2** and **6**, and in **8** and **12**, to give δ Me(3) of 19.5. The Me(5) signal is expected to be an additional 1.4 ppm upfield because of the *syn*-methyl on C(6). The values for the

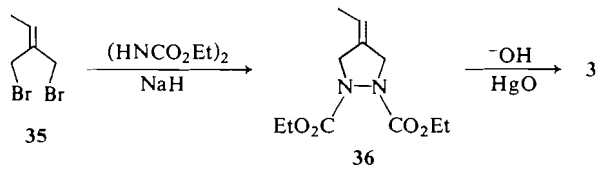

SCHEME 1

Can. J. Chem. Downloaded from www.nrcresearchpress.com by 210.87.254.6 on 09/05/12
For personal use only.

Can. J. Chem. Downloaded from www.nrcresearchpress.com by 210.87.254.6 on 09/05/12
For personal use only.

TABLE 1. Chemical shifts ^{13}Cmr for 4-alkylidene-1-pyrazolines (δ from TMS ±0.1, in dioxane-d_8)

Compound	Position						
	C(3)	C(4)	C(5)	C(6)	Me(3)	Me(5)	Me(6)
1	79.2	140.7	79.2	105.7			
2	84.1	146.4	79.7	105.3	17.9		
3	79.1	131.8	76.1	115.6			16.3
4	*	131.7	76.1	115.7			16.3
5	79.1	131.7	*	115.7			16.3
6	87.1	149.5	79.7	104.2	25.7		
7	77.5	123.2	77.5	124.3			22.2
8	87.0	137.3	76.7	115.5	18.3		16.2
9	83.9	137.4	76.7	115.4	*		16.2
10	81.5	136.6	79.1	115.9	16.9		15.3
11	89.8	159.6	89.8	102.9	27.3	27.3	
12	87.3	141.2	77.1	114.5	26.1		16.1
13	85.9	142.3	82.8	115.9	20.3	18.6	15.3
14	85.9	142.3	82.8	115.8	17.8	16.9	15.1
15	81.8	131.7	74.9	108.4	33.9†	30.0‡	

*Value not determined because of deuteration.
†Quarternary carbon of the *tert*-butyl group.
‡Three methyls of the *tert*-butyl group.

TABLE 2. Chemical shifts ^{1}Hmr for 4-alkylidene-1-pyrazolines (δ from TMS, in $CDCl_3$)

Compound	Position of ^{1}H						Coupling constants (Hz)
	C(3)	C(5)	C(6)	Me(3)	Me(5)	Me(6)	
1	4.88t	—	5.13p	—	—	—	$J_{3,6}$ 2.6
2	4.9m	4.9m	5.1m	1.47d	—	—	
3	4.9m	4.9m	5.6m	—	—	1.65m	
4	—	4.9m	5.52m	—	—	1.63m	$J_{5,6}$ 1.95; $J_{Me,5}$ 2.8
5	4.95p	—	5.55qt	—	—	1.62dt	$J_{3,6}$ 2.25; $J_{Me,3}$ 2.25
6	—	5.05m	5.05m	1.35	—	—	
7	4.90h	4.90h	—	—	—	1.67p	$J_{Me,3}$ 2.5
8	4.80m	4.96m	5.43m	1.46d	—	1.65m	
9	4.80m	4.96m	5.43m	—	—	1.65m	
10	5.14m	4.95dq	5.53m	1.37d	—	1.66m	
11	—	—	5.00	1.42	1.42	—	
12	—	5.02dq	5.35tq	1.37	—	1.62dt	$J_{5,6}$ 2.7; $J_{Me,5}$ 1.8
13	4.92m	5.07m	5.46m	1.42d	1.46d	1.69m	
14	4.79m	5.24m	5.46m	1.49d	1.35d	1.68m	
15	5.03d	5.03d	5.52p	1.07	—	—	$J_{3,6}$ 2.5

NOTE: d doublet, t triplet, q quartet, p pentet, h heptet, m multiplet.

trans isomer are predicted directly from **8** and **10** on the assumption that the introduction of a methyl *trans*, and across the ring, has a minimal effect on the chemical shifts, thus the signals from Me(3) and Me(5) are expected to be at δ 18.3 and 16.9, respectively. The slower reacting isomer with methyl signals at δ 20.3 and 18.6 was thus assigned the *cis* configuration **13** and the faster isomer the *trans* stereochemistry **14**.

Alkylidenecyclopropanes

The ^{13}C and ^{1}H nmr chemical shifts of the alkylidenecyclopropanes **16**–**34** are given in Tables 3 and 4. The alkylidenecyclopropanes were prepared by thermolysis of the 4-alkylidene-1-pyrazolines or by thermal equilibration. The ^{13}Cmr spectra were of greatest use in assigning the *E* and *Z* configurations of **23**, **24**, **26**, and **27**. Gajewski (6) had previously assigned the *E* and *Z* configurations, by synthesis, to the 2-methylethylidenecyclopropanes **23** and **24**. However, in our hands we obtained two isomers whose ^{1}Hmr resonance and relative gc retention times matched those in the literature but the ir spectra were reversed, thus we have used the ^{13}Cmr spectra as confirmation of the earlier ^{1}Hmr assignments. We have also observed that the proton signal at δ 0.65 is enhanced some 16% more than is the signal at δ 1.20, when the allylic methyl at δ 1.82 is irradiated (nuclear Overhauser effect). The ^{13}C resonances of C(2) and C(3) of **23** were assigned on the basis of selective decoupling experiments. The *syn*-methyl of **24** causes a −0.9 ppm shift of the C(2)

Can. J. Chem. Downloaded from www.nrcresearchpress.com by 210.87.254.6 on 09/05/12
For personal use only.

TABLE 3. Chemical shifts ^{13}Cmr for alkylidenecyclopropanes (δ from TMS ±0.1, in $CDCl_3$)

Compound	Positions						
	C(1)	C(2)	C(3)	C(4)	Me(2)	Me(3)	Me(4)
16	131.1	2.8	2.8	103.1			
17	138.2	10.2	10.5	102.2	17.9		
18	121.9	2.7	1.5	112.9			16.9
19	144.2	16.2	17.5	100.8	24.2		
20	115.2	2.4	2.4	120.6			22.3
21	144.5	13.3	13.3	100.5	11.2	11.2	
22	145.2	17.9	17.9	101.4	17.4	17.4	
23	129.2	10.1	9.1	112.0	18.1		16.8
24	128.8	9.3	10.5	112.7	17.7		16.9
25	150.1	18.8	21.2	99.4	18.3*	12.4	
					25.9		
26	135.1	16.1	16.3	110.5	24.4		16.7
27	134.7	15.8	17.7	111.9	23.9		16.9
28	122.4	10.1	10.1	120.5	17.7		22.1, 22.2
29	135.2	13.6	12.6	111.3	11.6	11.2	16.8
30	135.9	18.1	17.2	111.9	17.6	17.2	16.6
31	128.1	16.4	17.2	119.6	24.0		21.9

*Methyl group shielded by *cis*-methyl on C(3).

TABLE 4. Chemical shifts ^{1}Hmr for alkylidenecyclopropanes (δ from TMS, $CDCl_3$)

Compound	Position of ^{1}H						Coupling constants (Hz)
	H_a	H_b	H_c	H_d	H_e	H_f	
16	1.01t	5.10p					J_{ab} 2.1
17	1.46m	1.3m	0.65	1.11	5.36		J_{ac} 2.3; J_{bc} 4.0; J_{ad} 2.6
18	1.01m	5.77	1.78				
19	1.16	0.90t	5.3m				J_{bc} 4.0
20	0.98s	1.80p					J_{ab} 1.6
21	1.45m	1.09d	5.25t				J_{ac} 2
22	1.00m	1.13d	5.29t				J_{ac} 2
23	1.38	1.20	0.65	1.21d	1.82d	5.77	
24	1.30	1.38	0.68	1.21	1.82	5.68	
25	1.08	1.13d	1.5m	5.13m			
26	1.13	0.82	5.74	1.73			J_{bc} 2.5; J_{bd} 1.5
28	1.41m	1.20m	0.59m	1.12d	1.79s		
29	1.48m	1.09d	5.68m	1.78m			J_{ac} 1.8; J_{ad} 2.0
30	0.90m	1.11d	5.77m	1.75m			J_{ac} 1.8; J_{ad} 2.0
31	0.78m	1.14	1.72, 1.74				
32	1.12	5.14					
33	1.42m	~1.0	0.90	5.30q			J_{bd}, J_{ad} 2.0
34	0.9–1.3	5.82	1.11				J_{ab} 2.0

signal relative to that of **17** whereas the shielding at C(3) is essentially unchanged. The *anti*-methyl of **23** has little or no effect on the C(2) resonance and shields C(3) by −1.4 ppm in comparison with **17** (4). These spectra are supportive of the *E* configuration for **23** and the *Z* configuration for **24**. The assignment of *E* and *Z* configurations to **26** and **27** was similarly achieved on the basis of shielding of the ring carbons C(2) and C(3) by the exocyclic *syn*-methyl.

The introduction of a *syn*-methyl group in the pyrazoline system causes a shift of −2.6 ppm for the signal of a methylene carbon, e.g., the C(5) carbon atoms of **1**, **2**, **3**, **6**, and **10** have a chemical shift of δ 79.4 ± 0.3, whereas for the C(5) signal of **3**, **7**, **8** and **12** the average is δ 76.8 ± 0.5. The same shielding effect in the alkylidenecyclopropanes is smaller (e.g., the pairs **16,18**; **17,23**; **19,26**; **18,20**; and **24,28**) in each instance the replacement of a vinylic hydrogen by methyl causes a shift to higher field (average −0.92 ppm). A possible explanation for this is that the smaller cyclopropane bond angle has caused an increase in the distance between the site of the change (methyl for hydrogen) and the cyclopropane ring carbon compared to that of the pyrazoline system or noncyclic alkenes.

Can. J. Chem. Downloaded from www.nrcresearchpress.com by 210.87.254.6 on 09/05/12
For personal use only.

Experimental

All boiling points and melting points are uncorrected. The exact masses were determined on an AEI MS-9 mass spectrometer. Ultraviolet spectra were measured using a Carey Model 14, all wavelengths are reported in nm.

A Varian HA-100 spectrometer was used to obtain ^{1}Hmr spectra and a Bruker HFX 90 system operating in the Fourier transform mode was used for ^{13}Cmr analyses.

Gas chromatographic separations of the products are reported in the accompanying paper on the thermolysis of 4-alkylidene-1-pyrazolines (7).

The syntheses of **1** (1), **6**, **7**, and **11** (2) have been reported previously, as have the syntheses of **16** (1), **17**, **18** (8), **19**, **20**, **31**, **32** (2), and **21–24** (6). The other alkylidenecyclopropanes were prepared under the thermolysis conditions outlined in the following paper.

2-Bromomethyl-1-bromo-2-butene ***35***

2-Hydroxymethyl-2-buten-1-ol (45.5 g, 0.45 mol), dry pyridine (27.5 ml, 0.34 mol), and 450 ml 1:3 dry hexane–ether mixture were placed in a 1-ℓ three-neck flask fitted with reflux condenser, nitrogen inlet, dropping funnel and mechanical stirrer. The flask was cooled to −40°C and phosphorous tribromide (38 ml, 0.40 mol) was slowly added. The mixture was stirred 2 h at −5°C then poured into 350 ml iced bicarbonate solution. The layers were separated and the organic layer dried over sodium sulfate. Removal of the drying agent and solvent gave a residue which upon distillation at reduced pressure gave 16.0 g (17.5%) **7**, bp 65–67°C/4.5 Torr; ^{1}Hmr ($CDCl_3$) δ: 1.8 (d, 3 H), 4.1 (s, 4 H), 5.9 (q, 1 H). *Anal.* calcd. for $C_5H_8Br_2$: C 26.35, H 3.54; found: C 26.33, H 3.41.

1,2-Dicarbethoxy-4-ethylidenepyrazolidine ***36***

syn-Dicarbethoxyhydrazine (13.2 g, 75 mmol) and 300 ml dry 1,2-dimethoxyethane (DME) were placed in a 1-ℓ three-neck flask fitted with reflux condenser, inlet tube, dropping funnel, and magnetic stirrer. A 57% suspension of sodium hydride (3.37 g, 80 mmol NaH) was added in small portions and the reaction mixture stirred for 5 h. A solution of 2-bromomethyl-1-bromo-2-butene **7** (16.0 g, 70 mmol) in DME (50 ml) was added over a period of 4 h. After stirring overnight a solution of sodium ethoxide (75 mmol in 50 ml absolute ethanol) was added and the mixture stirred for an additional 5 h. After concentration on a rotary evaporator 1 ℓ of ice and water was added and the mixture extracted with ether. The extract was dried, the ether removed, and the resulting residue distilled at reduced pressure to give 5.7 g (34%), bp 130–134°C/0.8 Torr, of **36**; ^{1}Hmr ($CDCl_3$) δ: 1.25 (t, 6 H), 1.6 (d, 3 H), 4.2 (q, 8 H), 5.5 (w, 1 H). *Exact mass* calcd. for $C_{11}H_{18}N_2O_4$: 242.1267; found: 242.1273.

*4-Ethylidene-1-pyrazoline (**3**) from **36***

Samples of **36** (19.0 g, 78 mmol), potassium hydroxide (35 g, 625 mmol), ethylene glycol (150 ml), and water (35 ml) were placed in a 500-ml flask fitted with a reflux condenser and nitrogen inlet. The mixture was stirred and heated to 110–120°C for 16 h after which it was distilled under reduced pressure (ca. 100°C/2 Torr) until only a solid residue remained. Concentrated hydrochloric acid (8.3 ml) was added to the distillate and the solvent removed under reduced pressure. On cooling a thick oil resulted, 7.0 g (66%) (^{1}Hmr (D_2O) δ: 1.7 (m, 3 H), 3.9 (s, 4 H), 5.7 (m, 1 H)), along with approximately 5% ethylene glycol.

The pyrazoline **3** was prepared directly from the hydrochloride by the addition of 5 g sample to a slurry of red mercuric oxide (20 g), anhydrous sodium sulfate (20 g), and sodium bicarbonate (10 g) in 100 ml ether. After stirring for 3 h the solid residue was filtered off and the ether carefully removed by distillation. The residue was distilled at reduced pressure, with an oil bath heated to 60°C maximum, to give 1.25 g of a fraction bp 44–45°C/10 Torr; uv (methanol) λ_{max}: 320 (log ε 2.72). The ^{1}Hmr and ^{13}Cmr spectral data are listed in Tables 1 and 2. *Exact mass* calcd. for $C_5H_8N_2$: 96.0688; found: 96.0687.

*4-Ethylidene-1-pyrazoline (**3**) from 1,2-Butadiene*

Diazomethane (in 100 ml ether) prepared from bis(*N*-methyl-*N*-nitroso)terephthalamide (54 g, 150 mmol, 70% in mineral oil) by the procedure of Moore and Reed (9) was placed in a pressure bottle at Dry-Ice temperature and 1,2-butadiene (10.8 g, 193 mmol) was added. The bottle was allowed to warm to room temperature and was left undisturbed until the yellow color disappeared (10 days). The excess butadiene and ether was distilled off at atmospheric pressure and the residue distilled at 10 Torr, bp 50–51°C, to give 5.3 g (36%) of **3** having spectroscopic properties (uv, ir, nmr) identical with those reported above.

E-*3,3-Dideuterio-4-ethylidene-1-pyrazoline (**4**)*

The procedure used was identical to the method of preparation of **2** immediately above, except that diazomethane-d_2 (10) was used. The ^{1}Hmr spectrum displayed a decreased intensity at δ 4.9 equivalent to the substitution of 2 H by 2 D, and a splitting pattern different from that of **3** and **5**.

1,2-Butadiene-1,1-d_2

The procedure of Hurd and Meinert (11) for the debromination of 1,2-dibromo-2-butene was adapted to the preparation of 1,2-butadiene-1,1-d_2 by lithium aluminum deuteride reduction of crotonyl chloride (12) followed by the conversion of the 2-buten-1-ol-1,1-d_2 produced to the corresponding bromide. The bromide was converted to 1,2,3-tribromobutane-1,1-d_2 by the addition of bromine in carbon tetrachloride and the tribromobutane was converted to 1,2-dibromo-2-butene-1,1-d_2 and thence to 1,2-butadiene-1,1-d_2; ^{1}Hmr ($CDCl_3$) δ: 1.65 (d, 3 H), 5.07 (*q*, 1 H). There was no evidence of a proton signal at δ 4.63 corresponding to the vinylic hydrogens of C(1) (estimated < 1%).

Z-*3,3-Dideuterio-4-ethylidene-1-pyrazoline (**5**)*

The procedure used was the same as that described for the preparation of **3** and **4** only that 1,2-butadiene-1,1-d_2 was used. The product **5** had spectral properties analogous to those of **4** except that the splitting pattern at δ 4.9 was different and the ^{13}Cmr spectrum was unique as indicated in the text.

E-*4-Ethylidene-3-methyl-1-pyrazoline (**8**)*

A solution of diazoethane (240 mmol in 240 ml ether) and 1,2-butadiene (18.0 g, 333 mmol) was placed in a pressure bottle at −40°C and upon warming kept at room temperature for 36 h. The unreacted 1,2-butadiene (8.9 g) was then recovered and the ether removed by distillation at atmospheric pressure (taking care not to warm the flask above 50°C). The residue was distilled (bp 30°C/4 Torr) to give 10.7 g (48%) of a colorless liquid; uv (methanol) λ_{max}: 324 (log ε 260); ^{1}Hmr and ^{13}Cmr spectra are described in Tables 1 and 2. *Exact mass* calcd. for $C_6H_{10}N_2$: 110.0844; found: 110.0841.

Z-*4-Ethylidene-3-methyl-1-pyrazoline (**10**)*

A solution of diazomethane (~150 mmol in 100 ml ether) and 2,3-pentadiene (12 g, 176 mmol) was placed in a pressure bottle and maintained at room temperature for 12 days. The unreacted diazomethane and 2,3-pentadiene were removed by passing a stream of nitrogen through the solution and the unreacted diene was recovered (2.4 g). The ether was then removed by careful fractionation and the residue distilled at reduced pressure to give two fractions. Fraction A, bp 30–33°C/3 Torr (7.61 g) and fraction B, bp 35–40°C/1 Torr (6.5 g).

Can. J. Chem. Downloaded from www.nrcresearchpress.com by 210.87.254.6 on 09/05/12
For personal use only.

Fraction A: uv (methanol) λ_{max}: 317 (log ε 2.60); ^{1}Hmr and ^{13}Cmr spectra reported in Tables 1 and 2 confirm the structure **17**. *Exact mass* calcd. for $C_6H_{10}N_2$: 110.0844; found: 110.0846. The higher boiling fraction B was isomeric with A: uv (methanol) λ_{max}: 281 (log ε 3.84); ^{1}Hmr ($CDCl_3$) δ: 1.22 (d, 3 H), 1.77 (d of d, 3 H), 4.37 (m, 1 H), 5.72 (m, 1 H), 8.03 (s, 1 H), broad NH signal removed by D_2O. The spectrum is consistent with the structure of the tautomer of **10**, i.e., Z-4-ethylidene-5-methyl-2-pyrazoline. *Exact mass* found: 110.0846.

E-*4-Ethylidene-3-trideuteriomethyl-1-pyrazoline (9)*

The diazoethane synthesis from ethylamine (13) was modified by using 2,2,2-trideuterioethylamine which had been prepared by the lithium aluminum hydride reduction of trideuterioacetonitrile.

The method described for the preparation of **8** was used except that 2,2,2-trideuteriodiazoethane was used.

The product had a ^{1}Hmr spectrum analogous to that of **8** except for the loss of the doublet at δ 1.46. Mass spectrometric measurements indicated d_0 2.73, d_1 0.00, d_2 2.31, and d_3 94.97%, corresponding to 96.5% deuteration.

E-*4-Ethylidene-3,3-dimethyl-1-pyrazoline (12)*

Dimethyldiazomethane (~34 g, ~480 mmol) and 1,2-butadiene (31 g, 574 mmol) were placed in a pressure bottle and kept for 5 h at room temperature. After the removal of solvent and unreacted 1,2-butadiene the residual material was fractionally distilled using an oil bath temperature of 40°C. Each fraction was identified by uv, ir, and ms. Fractions 1 and 2 at 3.5–10 Torr consisted of 0.8 g acetone azine. Fractions 3 and 4 at 1–2 Torr consisted of 3.2 g of **12** and **37**, and fraction 5 contained 0.2 g of **37** and the tautomer of **12**.

Analysis of fraction 3 indicated it consisted of 67% **12** and 33% **37**; ^{1}H and ^{13}Cmr for **12** are reported in Tables 1 and 2; ^{1}Hmr for **37** ($CDCl_3$) δ: 1.35 (s, 6H), 1.84 (m, 3 H), 2.08 (m, 2 H), 6.63 (m, 1 H). *Exact mass* calcd. for $C_7H_{12}N_2$: 124.1000; found: 124.1002.

cis- *and* trans-*4-Ethylidene-3,5-dimethyl-1-pyrazoline (13 and 14)*

A solution of diazoethane (~13.4 g, ~240 mmol in 200 ml ether) and 2,3-pentadiene (23 g, 338 mmol) was placed in a pressure bottle and maintained at room temperature for 7 days. After recovery of 9.3 g of unreacted diene and the removal of ether the product was distilled at reduced pressure to give 9.2 g (93% yield based on diene used) of **13** and **14**; uv (methanol) λ_{max}: 327 (log ε 2.52) for 49:51 *trans–cis* mixture; ^{1}Hmr and ^{13}Cmr data are listed in Tables 1 and 2. *Exact mass* calcd. for $C_7H_{12}N_2$: 124.1000; found: 124.1003.

4-Neopentylidene-1-pyrazoline (15)

An ethereal solution of diazomethane (0.1 mol in 100 ml) and 4,4-dimethyl-1,2-pentadiene (17.7 g, 184 mmol) was placed in a pressure bottle and kept at room temperature for 2 weeks. The solvent was then carefully removed by fractionation and the residue distilled at 25°C/0.1 Torr to give 5.3 g (40% yield) of product; uv (methanol) λ_{max}: 320 (log ε 2.64); ^{1}Hmr and ^{13}Cmr data are listed in Tables 1 and 2. *Exact mass* calcd. for $C_8H_{14}N_2$: 138.1157; found: 138.1156.

1. R. J. CRAWFORD, D. M. CAMERON, and H. TOKUNAGA. Can. J. Chem. **52**, 4025 (1974).
2. R. J. CRAWFORD and H. TOKUNAGA. Can. J. Chem. **52**, 4033 (1974).
3. S. M. ANDREWS and A. C. DAY. Chem. Commun. 902 (1967).
4. J. B. STOTHERS. Carbon-13 nmr spectroscopy. Academic Press, New York, NY. 1972. pp. 80–82, 406ff.
5. J. W. EMSLEY, J. FEENEY, and L. H. SUTCLIFFE. High resolution nuclear magnetic resonance spectroscopy. Vol. 2. Pergamon Press, Oxford. 1966. p. 728.
6. J. J. GAJEWSKI. J. Am. Chem. Soc. **92**, 2168 (1970).
7. R. J. CRAWFORD, H. TOKUNAGA, L. M. H. C. SCHRIJVER, and J. C. GODARD. Can. J. Chem. This issue.
8. J. P. CHESICK. J. Am. Chem. Soc. **85**, 2720 (1963).
9. J. A. MOORE and D. E. REED. Org. Syn. **41**, 16 (1961).
10. S. M. HECHT and J. W. KOZARICH. Tetrahedron Lett. 1501 (1972).
11. C. D. HURD and R. N. MEINERT. J. Am. Chem. Soc. **53**, 289 (1931).
12. R. D. SCHULTZ and F. W. MILLARD. J. Org. Chem. **24**, 297 (1959).
13. A. L. WILDS and A. L. MEADER, JR. J. Org. Chem. **13**, 763 (1948).

The stereochemistry of thermolysis of 4-alkylidene-1-pyrazolines

ROBERT J. CRAWFORD, HIROKAZU TOKUNAGA,
LOUIS M. H. C. SCHRIJVER, AND JACKY C. GODARD
Department of Chemistry, The University of Alberta, Edmonton, Alta., Canada T6G 2G2

Received September 28, 1977

ROBERT J. CRAWFORD, HIROKAZU TOKUNAGA, LOUIS M. H. C. SCHRIJVER, and JACKY C. GODARD. Can. J. Chem. **56**, 998 (1978).

The products of thermolysis of 11 4-alkylidene-1-pyrazolines were isolated and identified. It is observed that these products cannot be rationalized in terms of a planar singlet trimethylenemethane type of intermediate, nor can they be reconciled in terms of the orthogonal trimethylenemethane singlets. Evidence is presented that for 4-ethylidene-1-pyrazolines the carbon *anti* to the methyl has the greatest propensity to become a cyclopropane carbon, and that which is *syn* is most likely to become the exocyclic methylene.

ROBERT J. CRAWFORD, HIROKAZU TOKUNAGA, LOUIS M. H. C. SCHRIJVER et JACKY C. GODARD. Can. J. Chem. **56**, 998 (1978).

On a isolé et identifié les produits de thermolyse de 11 alkylidène-4 pyrazolines-1. On a observé que ces produits ne peuvent être expliqués en terme d'un intermédiaire singulet planaire de type triméthylèneméthane et qu'ils ne peuvent non plus être réconciliés en terme de singulets orthogonaux triméthylèneméthane. On présente des données à l'effet que, dans l'éthylidène-4 pyrazoline-1, le carbone *anti* par rapport au groupe méthyle possède le plus grand pouvoir de devenir un carbone du cyclopropane et que celui qui se trouve en *syn* a le plus de chance de devenir un méthylène exocyclique.

[Traduit par le journal]

Can. J. Chem. Downloaded from www.nrcresearchpress.com by 210.87.254.5 on 09/05/12
For personal use only.

Over the past decade Dowd (1) has demonstrated that planar trimethylenemethane has a triplet ground state and can be generated either by the photolysis of 3-methylenecyclobutanone or 4-methylene-1-pyrazoline. Structurally modified 4-methylene-1-pyrazolines such as the bicyclic system (**38**) studied by

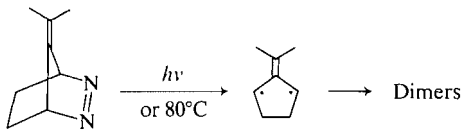

38

Berson and collaborators (2) have been demonstrated to produce both singlet and triplet 1,3-diyls, by both photolysis and thermolysis, as evidenced by trapping experiments and by dimer formation. The kinetics of thermolysis of 4-methylene-1-pyrazoline (**1**) and its deuterium- and ^{13}C-labelled derivatives have implicated a nitrogen free diyl as a possible intermediate (3). Theoretical studies (4) have suggested that for singlet trimethylenemethane the orthogonal diyls are more probable than is the planar species. We have shown that the product proportions from the thermolysis of 4-isopropylidene-1-pyrazoline (**7**)[1] and 3,3-dimethyl-4-methylene-1-pyrazoline (**6**) are easily rationalized in terms of the intermediates **39***a* and **39***b* in Scheme 1. These intermediates were postulated on the basis of the least motion principle and the presumed cleavage of both carbon nitrogen bonds as implicated from the kinetic studies on **1** (3). The product proportions from deuterium labelled **1** cannot be reconciled with a mechanism analogous to Scheme 1. Thus while we had kinetic data for **1** and product data for **6** and **7** we were unable, because of tautomerism, to get sound kinetic data for **6** and **7**, and cannot, because of the possible excess vibrational energy (5), rely upon the product proportions from deuterated **1**. This dilemma prevented us from drawing more definitive conclusions as to the nature of the intermediates involved. In an attempt to define the stereochemistry of the thermolysis process we have examined the methylenecyclopropanes produced from an additional set of 4-alkylidene-1-pyrazolines.

In testing our hypothesis that intermediates analogous to **39***a* and **39***b* could be usefully employed in rationalizing the proportions of methylenecyclopropanes we examined the pair of pyrazolines **2** and **3** and the proportions of methylenecyclopropanes, **17** and **18**, generated by each. The ethylidenecyclopropane and 2-methylmethylenecyclopropane produced on thermolysis of **2** and **3** were identified by their ^1H and ^{13}Cmr spectra and their gc retention times (6,7). That the product proportions are those of kinetic control was demonstrated by the observation that the ratio was not dependent upon reaction time and that the thermodynamic proportion at 175°C,

[1]The structures in this paper retain the numbering used in the preceding paper.

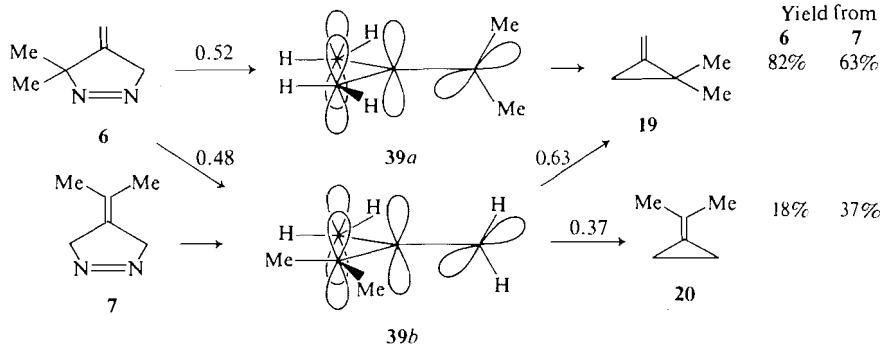

SCHEME 1. Pathways proposed for the thermolysis of **6** and **7**; the fractions over the arrows represent the proportions along each path (3).

extrapolated from the data of Chesick (7), is 36% **17** and 64% **18**; different from that produced by **2** or **3**.

The product proportions from **2** and **3** cannot be

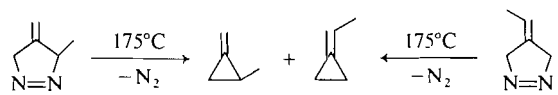

	17	18
From 2	80%	20%
From 3	90%	10%

rationalized in a manner analogous to Scheme 1. The high proportion of **17** produced from **3** suggests that **40** may be the intermediate first produced and that **41** is that which is first derived from **2**. However

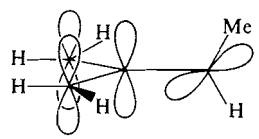

40

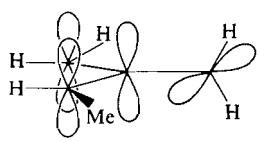

41

such a sequence would not account for the formation of 10% of **18** from **2**, unless there is some interconversion of **40** and **41**. It would also appear to violate the least motion principle but recently Roth and Wegener (8) have observed the racemization of 3-methyl-6-ethylidenebicyclo[3.1.0]hexane at rates competitive with *cis–trans* isomerization and they have suggested that a major component of the reaction involves the rotation of the exocyclic ethylidene group at the same time as the cleavage of the C(1)—C(5) bond. This novel observation implies that the least motion principle cannot always be used in such processes and if extended to the thermolysis of **3** suggests that **40** may indeed be on the reaction path.

To test for this possibility we synthesized the deuterium labelled pyrazolines **4** and **5**. The thermolysis of **4** and **5** was carried out at 160°C and the 2-methylmethylenecyclopropane was purified by preparative gc. The relative proportions of **17** and **18** were unchanged on deuteration. The ratio of **17***a* and **17***b* was determined by both ^{1}Hmr and ^{2}Hmr. The product proportions are listed in Table 1. The structural isomerization of **4** to **5** occurs at measureable rates in the range 200–230°C (7) and

17*a* **17***b*

such an interconversion is not significant under the reaction conditions used here. We were concerned with the possibility of a degenerate rearrangement **17***a* ⇄ **17***b* since Gilbert and Butler (9) had observed

TABLE 1. Deuterium distribution in the 2-methylmethylenecyclopropane produced from the thermolysis of **4** and **5** (160.2°C, 1 atmosphere)

Reactant	Method of analysis	Time (h)	% distribution **17***a*	% distribution **17***b*
4	^{1}Hmr	1	74 ± 1*	26 ± 1
	^{2}Hmr	1	76 ± 1	24 ± 1
5	^{1}Hmr	1	22 ± 1	78 ± 1
	^{2}Hmr	1	19 ± 1	81 ± 1
17*a*:**17***b*†	^{1}Hmr	0	74 ± 1	26 ± 1
17*a*:**17***b*	^{1}Hmr	1	73 ± 1	27 ± 1
17*a*:**17***b*	^{1}Hmr	4	73 ± 1	27 ± 1

*Errors quoted are standard deviations from six samples after separation from ethylidenecyclopropane by preparative gc.
†Sample from the thermolysis of **4** used as a control for the interconversion of **17***a* to **17***b*.

Can. J. Chem. Downloaded from www.nrcresearchpress.com by 210.87.254.5 on 09/05/12
For personal use only.

Can. J. Chem. Downloaded from www.nrcresearchpress.com by 210.87.254.5 on 09/05/12
For personal use only.

that 2,2-diphenyl-1-(dideuteriomethylene)cyclopropane isomerizes at 80°C to 2,2-diphenylmethylenecyclopropane-3,3-d_2. The last two entries in Table 1 demonstrate that such a degenerate rearrangement is not proceeding under the normal reaction conditions. It is possible that **4** produces specifically **17***a* (and **5** produces **17***b*) and that the excess vibrational energy produced in such a unimolecular decomposition is not quenched sufficiently rapidly to prevent the formation of either **17***b* or **18** from **4** (and **17***a* or **18** from **5**). Nevertheless the results do allow us to conclude that **42** cannot be an intermediate on the principal product determining pathway.

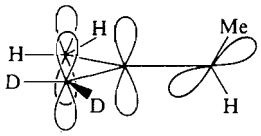

42

The ethylidenecyclopropane from **4** and **5** was examined for the *E* and *Z* isomers (**18***a* and **18***b*). The signals for the methyl and ring hydrogens for the samples obtained from the thermolysis of **4** and **5**

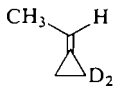

18*a*

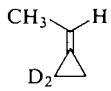

18*b*

were different. In the case of the sample derived from **4** the signal of the ring methylene protons displays two lines flanking the central line separated by 3.7 Hz, whereas for that produced from **5** the separation is 2.1 Hz. It is interesting to compare our data with those reported by Gajewski (10) for *E*- and *Z*-2-methylethylidenecyclopropane. In the case of the *E* isomer Gajewski describes the signal of the methyl group on the double bond as a doublet with fine structure which is similar to that observed in the sample derived from **11**. For the *Z* isomer he describes the methyl signal as a doublet of quartets of 6.5 and 2 Hz, respectively; our sample derived from the thermolysis of **5** displayed a doublet of triplets of 6.5 and 1.9 Hz. These data suggest that the principal isomer of ethylidenecyclopropane produced from **4** is **18***a* and that from **5** is **18***b*. Nevertheless we cannot exclude the possibility of up to 20% of **18***a* in **18***b* and vice versa but they are not the same as the mixture of isomers from **4** and **5**.

There is the possibility that **3**, **4**, and **5** may be producing one product stereospecifically but because of chemical activation we observe a mixture analogous to that observed by Farneth *et al.* (11) and Andrews and Baldwin (12) for the thermal isomerization of 5-methylbicyclo[2.1.0]pent-2-ene. The heat of formation of 4-methylene-1-pyrazoline (**11**) may be calculated using group contributions taken from the compilation of Benson and O'Neal (13) and using the revised data for [—N=N—] of Engel *et al.* (14). Thus ΔH_f for **1** consists of 2[C(C) (H_2)N] + [—N=N—] + $[C_d(C)_2]$ + $[C_d(H_2)]$ = 59.0 kcal mol^{-1} and allowing for cyclopentene ring strain (13) gives ΔH_f of 65 kcal mol^{-1}. The activation energy for **1** is 33 kcal mol^{-1} (3) and thus ΔH_f for the thermolysis transition state is 98 kcal mol^{-1}, which is only 9 kcal mol^{-1} in excess of the energy barrier estimated for the degenerate rearrangement of methylenecyclopropane (1, 7). Even if all of the excess energy is in the hydrocarbon fragment and none in the nitrogen, collisional deactivation should be effective. The deuterium labelled methylenecyclopropanes examined in our earlier studies were (*a*) not at thermodynamic equilibrium and (*b*) gave the same result in solution as at 100 Torr (3). Consequently, we feel that we have generally not been working with the products of chemically activated rearrangements. This concern could be assessed by two methods: (*a*) we could carry out an extensive study upon the pressure dependence of the product distribution or (*b*) we could increase the number of vibronic degrees of freedom within the molecule with the expectation that the internal randomization of energy would suppress the rearrangement. We were also concerned with the implied steric factor in the thermolysis of **4** and **5** and were led to speculate that the carbon-nitrogen bond *syn* to a methyl group of an exocyclic double bond may be lagging in the bond breaking process. Support for this comes from the comparison of the thermolysis rates of **1** and **7**, the latter being $\frac{1}{3}$ the rate of the former (15) and **11** is 32 times faster than 4-isopropylidene-3,3,5,5-tetramethyl-1-pyrazoline (15, 16). A normal mode for the reaction coordinate would be expected to consist of the C—N stretching and consequently the possibility of steric compression being an important factor led us to study the thermolysis of 4-neopentylidene-1-pyrazoline (**15**). Subsequently Rabinovitch *et al.* (17)

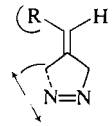

have demonstrated that the internal randomization is not a satisfactory method for quenching hot molecules but the results of the thermolysis of **15** are nevertheless of interest in that the products are 4.2% neopentylidenecyclopropane (**34**) and 95.8% 2-*tert*-butylmethylenecyclopropane (**33**), and are clearly those of kinetic control.[2]

[2]An equilibrium mixture of 42.5% **33** and 57.5% **34** is obtained upon heating a sample of **14** for more than 5 days at 221°C.

Can. J. Chem. Downloaded from www.nrcresearchpress.com by 210.87.254.5 on 09/05/12
For personal use only.

A sample of **15**-d_2 was prepared by the cycloaddition of diazomethane-d_2 to 4,4-dimethyl-1,2-pentadiene. The thermolysis results were analogous to those of **4** in that 70% of the **33** produced had deuterium on the cyclopropane ring (**33***a*) and 30% had it on the exocyclic methylene (**33***b*). Not enough **34**-d_2 was obtained to carry out a positional analysis. These data clearly indicate that the *syn-anti* relationship of the alkyl group and the methylene group of the ring is important and that there is a preference for the carbon *anti* to the alkyl group to become incorporated in the cyclopropane ring along with the exocyclic methylene of the product.

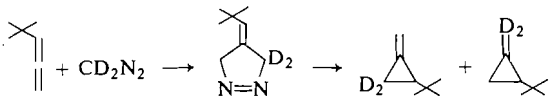

15-d_2 **33***a* **33***b*

E- *and* Z-3-*Methyl-4-ethylidene-1-pyrazoline (8 and 10)*

Taking advantage of the regioselective cycloaddition of diazoalkanes allowed us to synthesize stereospecifically **8** and **10**, and thus we could investigate further this preferential incorporation of the *anti*-methylene in the reactant into the cyclopropane ring of the product.

There are four products produced by thermolysis of **8**. The same four products are produced during the thermolysis of **10**. Some of these isomerize slowly under the thermolysis conditions and consequently we studied a series at various thermolysis times (see Table 2). Zero-time values were obtained by graphical extrapolation and are recorded in Table 2.

TABLE 2. Percentage of isomeric products from the thermolysis of **8** and **10** at 170.0°C (0.5 atmospheres)

		Product			
Reactant	Time	**22**	**23**	**24**	**25**
8	5 min	23.3	53.0	21.2	2.5
	10 min	23.6	51.3	22.1	2.9
	20 min	24.6	47.9	24.2	3.3
	45 min	26.7	40.8	28.5	4.0
	6 days	8.8	2.7	58.3	30.1
	0 time*	23.1	54.5	20.0	2.4
10	5 min	19.3	12.7	32.3	35.7
	10 min	19.1	12.0	32.7	36.2
	20 min	18.8	10.7	33.6	37.0
	30 min	18.6	10.1	34.1	37.2
	0*	19.5	13.5	31.5	35.5
	∞†	6.2	2.5	47.8	43.8

*Zero-time value obtained by extrapolation.
†Equilibrium value, see ref. 10.

We have identified the point of origin of the *exo*-ethylidene in the thermolysis of **8** by preparation of **9**. Isolation of the *E*-2-methylethylidenecyclopropane by preparative gc and subsequent ^{1}Hmr revealed that the deuterium labelling was distributed in both methyls, i.e., from Table 2 and the deuterium

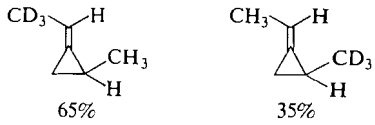

distribution from the thermolysis of **9** it is clear that the C(3) carbon of **8** becomes a cyclopropane ring carbon in at least 84% of the product. The exocyclic carbon becomes a cyclopropyl carbon in 90% of the product and the C(5) methylene in less than 23% of the total. The thermolysis of **10** results in an incorporation to 63%, i.e., approximately to the statistical level, for the incorporation of the methylene group into the cyclopropane ring of the products.

Recently Cichra *et al.* (18) have observed an allylic rearrangement of the pyrazoline like system suggestive of a one-bond azo cleavage mechanism. We have carried out controls on the previously studied 4-methylene-1-pyrazoline (**1**) (3) and on **2**, **6**, **8**, **9**, and **10** in this study, and in no case have we

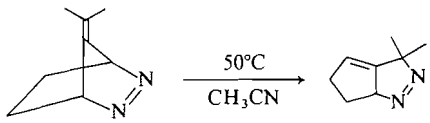

38 **43**

been able to observe the analogous rearrangement, each sample was recovered essentially unchanged. Not all of our pyrazolines have been amenable to heating and reisolation experiments, and control experiments with **3**, **4**, **5**, **7**, **12**, and **15** have been frustrating in that tautomerism has prevented a definitive statement. In no case, however, have we been able to observe evidence for such a rearrangement. It is possible that in the more planar monocyclic system that the second carbon–nitrogen bond is broken more readily than rotation and rebonding to the exocyclic methylene can occur. In the bicyclic system **38** the exocyclic isopropylidene group because

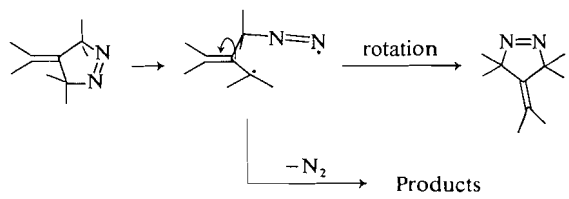

of folding, is much closer to the diazenyl nitrogen and so recombination to **43** is facilitated. The fact that there is so little of **25** present in the thermolysis

Can. J. Chem. Downloaded from www.nrcresearchpress.com by 210.87.254.5 on 09/05/12
For personal use only.

of **8** strongly implies that **8** cannot be isomerizing to **10**, and that in these dimethyl derivatives we may have escaped some of the problems of hot molecule chemistry. The control with **9**, wherein no high field methyl (CH_3) is observed in the recovered product implies that a degenerate rearrangement is not occurring, and in all probability no rearrangement to *cis*- or *trans*-3,5-dimethyl-4-methylene-1-pyrazoline is occurring since using the ^{1}Hmr spectra of **13** and **14** as a guide a high field doublet in the region of δ 1.30 to 1.50 would be expected to appear. We have observed that the thermolysis rates of **8** and **10** are comparable (approximately 1.4 to 1) and thus we would expect to see either isomer accumulating in the ^{1}Hmr spectrum of the other if they were interconverting.

The thermolysis of **12**, see Table 3, gives in excess of 70% of the thermodynamically least stable product again with over 84% of C(3) of the reactant becoming a cyclopropane carbon in the products, and the exocyclic ethylidene C(6) is implicated as a cyclopropyl carbon in greater than 81% of the products. It is interesting to note that the concentration of **26** proceeds through a maximum during the equilibration, implying that the process **25** → **26** is favoured for **25**.

cis- *and* trans-*4-Ethylidene-3,5-dimethyl-1-pyrazoline (13 and 14)*

The addition of diazoethane to 2,3-pentadiene results in the formation of *cis*- (**13**) and *trans*-4-ethylidene-3,5-dimethyl-1-pyrazoline (**14**) in almost equal amounts. One of the isomers undergoes thermolysis at a rate significantly faster than the other thus allowing the isolation of the less reactive isomer[3]. On the basis of ^{1}H- and ^{13}Cmr spectra the slower isomer has been assigned the *cis* configuration (**13**). Thermolysis products of the mixture of **13** and **14** along with the thermolysis of **13** alone are recorded in Table 4 along with equilibration data of the methylenecyclopropanes. The structure of the trimethylmethylenecyclopropanes **29** and **30** are assigned on the basis of chemical shift and ^{1}H coupling constants (6) and on the observation that the equilibrium constant $K = [trans]/[cis] = 2.71$ at 195°C is very similar to the value of 2.65 observed by Gajewski (10) for the ratio of *trans*:*cis* 2,3-dimethylmethylenecyclopropane upon equilibration at 190°C.

In view of these experiments, and the recent observations by Cichra and Berson (18), and those of Clarke *et al.* (19) on 1-pyrazolines, we feel that it is very probable that the sequence in which the carbon-nitrogen bonds are broken plays an important role in the stereochemistry of the products, and we are currently studying some chiral 4-alkylidene-1-pyrazolines in an attempt to define this sequence.

We have in this and in earlier papers attempted with limited success to use both the planar trimethylenemethane singlet and orthogonal diradicals such as **38**–**42**. Failure to develop a consistent pattern has led us to the conclusion that nitrogen is implicated in the stereochemistry of the formation of the products.

[3]Kinetic studies, by interruption and ^{1}Hmr measurements on the recovered reactants, showed that the *trans* isomer underwent thermolysis, at 169.8°C, with a first-order rate constant $k_2 = 7.61 \times 10^{-4}$ s^{-1}, whereas the *cis* isomer had a rate constant $k^2 = 2.66 \times 10^{-4}$ s^{-1}, i.e. differing by a factor of 2.86.

TABLE 3. Percentage of isomeric products from the thermolysis of *E*-4-ethylidene-3,3-dimethyl-1-pyrazoline (**12**) at 170°C (0.5 atmospheres)

	Product			
Time	**25**	**28**	**26**	**27**
5 min	69.4	16.3	14.3	0.0
10 min	67.8	17.6	15.4	0.1
20 min*	63.8	18.3	17.6	0.3
30 min	60.7	18.9	20.1	0.4
24 h	7.6	41.5	46.8	4.1
15 days	1.9	75.5	11.9	10.7
0†	71.5	16.0	12.5	0.0

*The thermolysis of **12** is essentially complete in 20 min.
†By graphical extrapolation.

TABLE 4. Percentage yields of *cis*- (**29**) and *trans*-2,3-dimethylethylidenecyclopropane (**30**) from the thermolysis of *cis*- (**13**) and *trans*-3,5-dimethyl-4-ethylidene-1-pyrazoline (**14**) at 169.7°C

		Product composition	
Sample	Time	**29**	**30**
A 51% **13** and 49% **14**	5 min	37.8	63.2
	15 min	38.3	61.7
	30 min	38.3	61.7
	60 min*	38.1	61.9
B† 94.6% **13** and 5.4% **14**	30 min	44.7	55.3
	60 min	44.2	55.8
	120 min	43.1	56.9
C‡ 34% **29** and 61% **30**	10 min	38.9	61.1
	1 h	34.6	65.4
	2h	30.2	69.8
	4h	27.8	72.2
	4 days	27.1	72.9
	16 days	27.0	73.0

*Recovered reactant consisted of 86.1% **13** and 13.9% **14**.
†Extrapolation to zero time gives a 37:63 mixture of **29** and **30** from pure **13** and a 45:55 mixture from pure **14**.
‡Equilibrium studies at 190°C.

Can. J. Chem. Downloaded from www.nrcresearchpress.com by 210.87.254.5 on 09/05/12
For personal use only.

Experimental

The ^{1}Hmr and ^{13}Cmr of the alkylidenecyclopropanes produced in thermolysis processes reported herein are described in the accompanying paper (6). The ^{2}Hmr were obtained using a Bruker HFX 90 spectrometer in the Fourier transform mode. Gas chromatographic separations on a preparative scale were achieved on a Nestor Faust Prepkromat using bi-wall columns. Exact masses were determined on an A.E.I. MS-9 mass spectrometer.

Thermolysis of ***2***, ***3***, ***4***, *and* ***5***

Pyrex break-seals (18 mm diameter and 70 mm long) were attached to a vacuum line and evacuated and flamed before filling. A sample of the pyrazoline (25–30 mg), such as to give 300 Torr at 160°C, was degassed and transferred to the break-seal. The break-seal was then removed from the vacuum line and immersed in a well-stirred, thermostatted, silicone oil bath for the appropriate length of time. Upon removal and cooling the tubes were reattached to the vacuum line and the contents transferred to a sample vial (5 mm in diameter, total length 45 mm) attached to the vacuum line by a carefully ground 5/20 joint. Each sample was analyzed in triplicate using a 150 ft × 0.01 in. diameter column of SE-30 at 50°C.

The products, **17** and **18**, are known to be stable under the reaction conditions (7). The deuterated 2-methylmethylenecyclopropanes, **17***a* and **17***b*, were shown not to be undergoing a degenerate rearrangement by taking a nonequilibrated sample and putting it back in the constant temperature bath (see Table 1) under the reaction conditions.

Samples of **2** and **3** were reisolated after removing to 50% completion and their ^{1}Hmr examined for possible interconversion. No evidence for an interconversion was detected; however the quality of this control for the isomerization of **3** → **2** is limited by the tendency of **3** to tautomerize during isolation and thus complicate the ^{1}Hmr spectrum; (estimated excess of 10% of **2** in **3** could be detected).

Thermolysis of ***15*** *and* ***15***-d_2

Samples of **15** and **15**-d_2 were degassed, transferred in the vacuum line, and handled in a manner analogous to that of **2**. The product ratio, for thermolysis at 160°C, did not change during the course of thermolysis.

The two hydrocarbon products were prepared for identification by carrying out the thermolysis of a 200 μl sample in an 86 ml tube for 1 h at 199°C and then heating to 220°C for 2 days before subjecting to preparative gc. For purification of the products a 10 ft × 0.25 in. 20% SF-96 Chromosorb-W column was used at 50°C and a flow rate of 60 ml/min. The 2-*tert*-butylmethylenecyclopropane (**33**) had a retention time of 10 min and the neopentylidenecyclopropane (**34**) 14 min. The ^{1}H and ^{13}Cmr assignments are listed in the accompanying paper (6). *Exact Mass* calcd. for C_8H_{14}: 110.1096; found: 110.1093 for **14**, 110.1092 for **15**.

Thermolysis of ***8***, ***9***, *and* ***10***

A 20 μl sample of the pyrazoline to be examined was degassed and transferred to a 13-ml break-seal on a vacuum line. The sealed tubes were then placed in a constant temperature bath for a specific period. The products were then transferred to a sample tube and 80 μl of toluene was added before analysis by gc. A 40 ft × 0.25 in. 20% DMS on Chromosorb WAW column was used at 45°C and a flow rate of 30 ml/min giving retention times for **22**, **21**, **23**, and **24** of 15, 21, 24, and 29 min, respectively. The product proportions listed in Table 3 were obtained by extrapolation to zero time since the products were slowly isomerizing under the reaction conditions (10). The ^{1}Hmr, ^{13}Cmr, and ir are discussed in the accompanying paper (6).

Control Experiments on ***8***, ***9***, *and* ***10***

A sample of pyrazoline (150 μl) was transferred to a reaction vessel (~60 ml), degassed and placed in a well-stirred oil bath for 10 min at 165.7°C. The sample tube was reattached to the vacuum line, the nitrogen removed at −80°C, then warmed to 0°C and the hydrocarbons removed. The recovered pyrazoline was vacuum transferred to a nmr sample tube, dissolved in $CDCl_3$, and examined at 100 MHz. For **8** and **9** approximately 30 μl of sample was recovered, whereas 80 μl of **10** was recovered.

For **9** the recovered sample had, if anything, a decrease in intensity of ^{1}H at the C(3) methyl as implicated by the doublet at δ 1.42 and 1.49. The mass spectrum of the ethylamine-d_3 used to prepare the diazoethane-d_3 indicated 96.5% deuterium substitution.

The sample recovered from the partial thermolysis **8** failed to indicate the presence of any **10** as judged by the absence, in the ^{1}Hmr spectrum, of the outside line of the ethylidene's CH_3 multiplet at δ 1.70, and the lack of increased absorption at δ 1.34 and 1.41; (this latter criterion was less rigorous since the presence of tautomer in both reactant and recovered material displayed absorption very close to this position).

The sample recovered from the partial thermolysis of **10** failed to indicate the presence of any **8** as determined by the absence of increase at δ 1.49 in the ^{1}Hmr spectrum.

In most of the ^{1}Hmr samples small peaks at δ 1.18 and 1.25 were apparent, these have been tentatively assigned to the higher boiling 4-methyl-5-alkylidene-1-pyrazoline which is produced in small amounts during the synthesis. All of the spectra of recovered samples were complicated by the existence of tautomeric materials, but in each case we believe that an increase of 2.3% of the isomeric material would have caused signal enhancement detectable in our experiments.

Thermolysis of ***12***

The sample preparation and thermolysis procedures were the same as those described for **8** and **10**. A series of samples was run to determine if the presence of **37** altered the product proportions but varying amounts of **37** failed to change the proportions of **25**, **26**, and **28**.

A sample of the products was heated at 190°C for 24 h to increase the amount of **27** present and the isomers were separated by preparative gc using a 20 ft × 0.25 in. column of 20% SF 96 on Chromosorb WAW at a flow rate of 60 ml/min at 55°C. The retention times were 14.0, 17.0, and 25 min for **25**, **26**, and **27**, respectively. Isomer **28** produced by product thermolysis came at 19.0 min. The ^{1}Hmr and ^{13}Cmr are reported in the accompanying paper and are the basis of the structural assignments. *Exact Mass* calcd. for C_7H_{12}: 96.0939; found: 96.0952 for **25**, 96.0938 for **26**, and 96.0936 for **27**.

Samples of **23** recovered from the reaction showed little or no isomerization, however a conclusive statement cannot be made since we do not have the isomeric compounds for comparison.

Thermolysis of ***13*** *and* ***14***

Samples of **13** and **14** (48.7 and 51.3%, 150 μl) were transferred to a reaction vessel (86 ml) under vacuum. The vessels were heated at 169.75°C for 20, 40, 60, and 80 min. The hydrocarbon was removed under vacuum at 0°C and the remaining 1-pyrazoline was transferred to an nmr tube. The *cis–trans* ratio was measured by ^{1}Hmr. Data plotted as two separate compounds undergoing first-order thermolysis, without interconversion, gave good first-order rate plots, $k_{13} = 2.66 \times 10^{-4}$ s^{-1} and $k_{14} = 7.61 \times 10^{-4}$ s^{-1}.

The two isomeric hydrocarbons produced were separated on a 10 ft × 0.25 in. 20% dimethylsulfane column at 45°C using a flow rate of 39 m/min; retention times: **30**, 16 min; **29**, 22 min. The ^1H and ^{13}Cmr spectra of **29** and **30** are reported in the accompanying paper (6). *Exact Mass* calcd. for C_7H_{12}: 96.0939; found: 96.0938 for **31** and 96.0938 for **32**.

Acknowledgements

The authors wish to thank the National Research Council of Canada and the University of Alberta for grants in support of this work. One of us, J.C.G., wishes to thank the Canada Council for a grant while on cooperant status from France.

1. P. Dowd and M. Chow. J. Am. Chem. Soc. **99**, 6438 (1977); P. Dowd. Acc. Chem. Res. **5**, 242 (1972); P. Dowd, G. Sengupta, and K. Sachdev. J. Am. Chem. Soc. **92**, 5726 (1970); P. Dowd and K. Sachdev. J. Am. Chem. Soc. **89**, 715 (1967); P. Dowd. J. Am. Chem. Soc. **88**, 2587 (1966).
2. J. A. Berson, R. A. Bushby, J. M. McBride, and M. Tremelling. J. Am. Chem. Soc. **93**, 1544 (1971).
3. R. J. Crawford, D. M. Cameron, and H. Tokunaga. Can. J. Chem. **52**, 4025 (1974).
4. M. J. S. Dewar and J. S. Wasson. J. Am. Chem. Soc. **93**, 3081 (1971); D. R. Yarkony and H. F. Schaefer, II. J. Am. Chem. Soc. **96**, 3754 (1974); J. H. Davis and W. A. Goddard, III. J. Am. Chem. Soc. **98**, 303 (1976); W. J. Hehre, L. Salem, and M. R. Willcott, III. J. Am. Chem. Soc. **96**, 4328 (1974); W. T. Borden. J. Am. Chem. Soc. **98**, 2695 (1976).
5. M. C. Flowers and H. M. Frey. J. Am. Chem. Soc. **94**, 8636 (1972).
6. R. J. Crawford, H. Tokunaga, L. M. H. C. Schrijver, and J. C. Godard. Can. J. Chem. This issue.
7. J. P. Chesick. J. Am. Chem. Soc. **85**, 2720 (1963).
8. W. R. Roth and G. Wegener. Angew. Chem. Int. Ed. **14**, 758 (1975).
9. J. C. Gilbert and J. R. Butler. J. Am. Chem. Soc. **92**, 2168 (1970).
10. J. J. Gajewski. J. Am. Chem. Soc. **93**, 4450 (1971).
11. W. E. Farneth, M. B. D'Amore, and J. T. Brauman. J. Am. Chem. Soc. **98**, 5546 (1976).
12. G. D. Andrews and J. E. Baldwin. J. Am. Chem. Soc. **49**, 4854 (1977); S. McLean, C. J. Webster, and R. J. D. Rutherford. Can. J. Chem. **47**, 1555 (1969).
13. S. W. Benson and H. E. O'Neal. Natl. Stand. Ref. Data Ser. Natl. Bur. Stand. No. 21, 271 (1970).
14. P. S. Engel, J. L. Wood, J. A. Sweet, and J. L. Margrave. J. Am. Chem. Soc. **96**, 238 (1974).
15. R. J. Crawford and H. Tokunaga. Can. J. Chem. **52**, 4033 (1974).
16. P. S. Engel and L. Shen. Can. J. Chem. **52**, 4040 (1974).
17. B. S. Rabinovitch, J. F. Meaghan, K. J. Chao, and J. R. Barker. J. Chem. Phys. **60**, 2932 (1974).
18. D. Cichra, M. S. Platz, and J. A. Berson. J. Am. Chem. Soc. **99**, 8509 (1977).
19. T. C. Clarke, L. A. Wendling, and R. G. Bergman. J. Am. Chem. Soc. **99**, 2740 (1977).

Can. J. Chem. Downloaded from www.nrcresearchpress.com by 210.87.254.5 on 09/05/12
For personal use only.

Rearrangements of vanadium(III) β diketonate complexes

A. J. C. NIXON AND D. R. EATON

Department of Chemistry, McMaster University, Hamilton, Ont., Canada L8S 4M1

Received August 15, 1977

A. J. C. NIXON and D. R. EATON. Can. J. Chem. **56**, 1005 (1978).

The rearrangement reactions of a number of V(III) β diketonate complexes have been studied by nmr. All reactions proceed by an intramolecular rather than an intermolecular process. The use of a complex with diastereotopic groups on the ligand allowed enantiomerization to be observed. Linkage isomerization was shown to be slow in triacetylmethanato V(III) complexes. Activation parameters are reported for five different complexes in a number of different solvents. Permutational analysis did not unambiguously distinguish between possible twisting and bond rupture mechanisms. The data are consistent either with a rhombic twist ($C_3(i)$) mechanism or with a bond breaking mechanism involving square pyramidal intermediates. The possibility that none of the usual simple intramolecular mechanisms provide a valid description of the rearrangement process is discussed. The rates of rearrangement of these V(III) complexes are consistently somewhat greater than those of analogous Al(III) complexes.

A. J. C. NIXON et D. R. EATON. Can. J. Chem. **56**, 1005 (1978).

On a étudié par rmn les réactions de transposition d'un certain nombre de complexes de β dicétonates de V(III). Toutes les réactions se produisent par un processus intramoléculaire plutôt qu'intermoléculaire. L'utilisation d'un complexe avec des groupes diastéréotopes sur le ligand permet d'observer l'énantiométrisation. On a montré que l'isomérisation des liens se produit lentement dans les complexes de triacétylméthano de V(III). On rapporte les paramètres d'activation de cinq complexes différents dans un certain nombre de solvants différents. L'analyse des permutations ne permet pas de distinguer d'une façon non-ambiguë entre les divers mécanismes possibles pour la rotation et la rupture des liens. Les données sont en accord soit avec un mécanisme de rotation rhombique ($C_3(i)$) ou un mécanisme de bris de lien impliquant des intermédiaires pyramidaux carrés. On discute de la possibilité qu'aucun des mécanismes intermoléculaires habituels simples pourrait fournir une description valide du processus de transposition. Les vitesses de transposition de ces complexes de V(III) sont d'une façon systématique un peu plus grandes que celles des complexes analogues de l'aluminium(III).

[Traduit par le journal]

Introduction

The rearrangement reactions of octahedral complexes have been extensively studied. As early as 1912 Werner (1) proposed an intramolecular mechanism for the isomerization of bidentate chelate complexes. There are recent reviews of the area by Serpone and Bickley (2) and by Fortman and Sievers (3). In 1964 Fay and Piper (4) demonstrated the utility of nmr in studies of this kind in an examination of the isomerization of trifluoroacetylacetonates of Al(III), Ga(III), In(III), Co(III), and Rh(III). This has been followed by a considerable number of other papers (5–7) the majority dealing with diamagnetic complexes. Gordon, O'Connor, and Holm (8) have studied some β diketonate complexes of Ru(III), Mn(III), Fe(III), and V(III). They found the Mn and Fe compounds rearranged rapidly, the Ru compounds rearranged slowly, and did not observe any changes in the nmr spectrum of the V(III) trifluoroacetylacetonate below 100°C. This latter result seems anomalous.

The present paper will report studies of the rearrangements of a number of V(III) diketonate complexes. The reactions occur at rates suitable for nmr experiments. The objectives are to identify, as far as possible, the mechanisms of rearrangement and to examine the effect of substituents on the rates and activation parameters. It was hoped to correlate the results with previous nmr studies of substituent effects in V(III) β diketonates (9).

Results

The rates of the reactions under consideration were found to be suitable for nmr studies. There are two possible nmr techniques. Spin saturation transfer (10) experiments have the advantage that they can yield data on exchange rates between individual sites. Unfortunately there are experimental difficulties in using the technique with paramagnetic complexes. The results of the line shape analysis method are less easy to interpret but the large chemical shifts make the method readily applicable to paramagnetic complexes.

V(III) has two unpaired electrons. The very short electron spin relaxation time leads to relatively sharp (20–80 Hz line width at half height) nmr

Can. J. Chem. Downloaded from www.nrcresearchpress.com by 210.87.254.40 on 09/05/12
For personal use only.

Can. J. Chem. Downloaded from www.nrcresearchpress.com by 210.87.254.40 on 09/05/12
For personal use only.

TABLE 1. β-Diketonate ligands

Systematic name	Trivial name	Abbreviation
Pentane-2,4-dionato	Acetylacetonato	$acac^-$
1,1,1,5,5,5-Hexafluoro-pentane-2,4-dionato	Hexafluoroacetyl-acetonato	$hfac^-$
1,1,1,-Trifluoropentane-2,4-dionato	Trifluoroacetyl-acetonato	$tfac^-$
3-Acetylpentane-2,4-dionato	Triacetylmethanato	$triac^-$
2,6-Dimethylheptane-3,5-dionato	Diisobutyrylmethanato	$dibm^-$

resonances. The ligands used in the present study are listed in Table 1 together with the abbreviations used throughout this paper. Figure 1 shows a set of ^{19}F nmr spectra for $V(tfac)_3$ obtained at different temperatures. $V(tfac)_3$ can exist as two isomers, *cis* and *trans*. All three CF_3 groups in the *cis* isomer are equivalent leading to a single nmr line. Each of the CF_3 groups in *trans* $V(tfac)_3$ has a different environment leading to a three line spectrum. In Fig. 1 the *cis* resonance is partly overlapped by the central line of the *trans* spectrum. The proton spectrum is slightly more complex due to the presence of CH as well as CH_3 resonances. The temperature dependence of the spectrum clearly indicates exchange of the non-equivalent CF_3 groups.

Line shape analysis of the spectra in Fig. 1 requires a knowledge of: (*a*) The temperature dependence of the chemical shifts. (*b*) The temperature dependence of the line width of each line. (*c*) The relative intensities of the peaks. (*d*) An exchange matrix which expresses the probability of the transfer of an ^{19}F nucleus from one site to a different site. Given the above information a suitable computer programme (11) may be used to calculate simulated spectra for different rate constants. The simulated spectra may then be fitted to the observed spectra at different temperatures. A comparison between a set of simulated and observed spectra is shown in Fig. 1. Different exchange mechanisms may lead to different exchange matrices. The strategy of the experiment is therefore to find the appropriate exchange matrix by trying the matrices predicted for a variety of mechanisms and to then obtain the activation parameters from the temperature dependence of the rate constants.

The temperature dependences of the chemical shifts follow rather accurately a Curie–Weiss law (12), i.e.:

$$\Delta\nu = a + \frac{b}{T}$$

The constants *a* and *b* may be readily obtained from measurements below the temperature at which exchange broadening commences. These constants *a* and *b* are solvent dependent and must be measured for each line in each solvent. It is not considered that uncertainties in the chemical shifts contribute significantly to the errors in the present experiments.

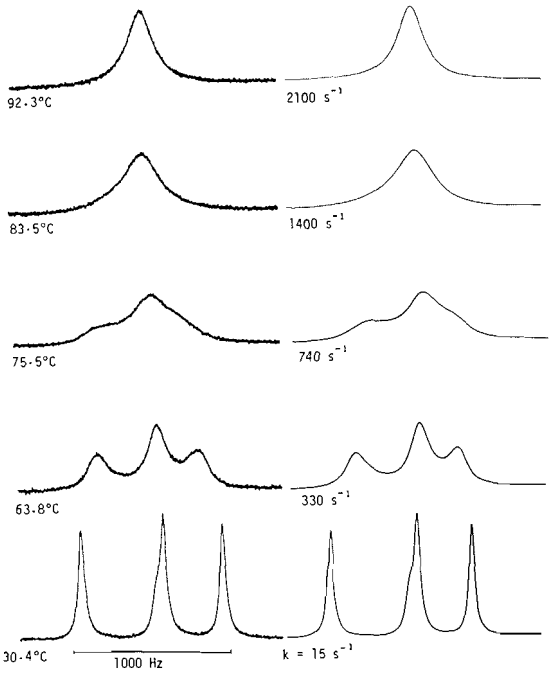

FIG. 1. Comparison of experimental and simulated nmr spectra of $V(tfac)_3$ at various temperatures. ^{19}F at 58.3 MHz in chlorobenzene (equal lifetimes at all sites).

The temperature dependence of the line width of the CH_3 resonance of $V(acac)_3$ has been measured. There can be no exchange broadening in this compound. The line width shows little variation in the temperature range 0–80°C. For these complexes the line width is determined by T_{1e}, the electron spin relaxation time. The electronic relaxation mechanism is most probably dominated by coupling of the molecular motion with the zero-field splitting. LaMar (13) has derived an appropriate expression for T_{1e}. The temperature dependence of T_{1e} arises from the temperature dependence of τ_c, the rotational correlation time of the molecule, which is reflected in the temperature dependence of the viscosity of the solution. However the dependence on τ_c is reversed depending on whether $\omega_s\tau_c \gg 1$ or $\omega_s\tau_c \ll 1$ (ω_s is the electronic Larmor frequency). From the viscosity of $CHCl_3$ $\tau_c \sim 5.7 \times 10^{-11}$ s (25°C) and from ^{13}C nmr measurements on $Co(acac)_3$ (14) $\tau_c = 7.3 \times 10^{-11}$ s (25°C). The latter value gives $\omega_s\tau_c = 2.1$ which is close to unity leading to the conclusion that there will be no pronounced line width temperature dependence around room

Can. J. Chem. Downloaded from www.nrcresearchpress.com by 210.87.254.40 on 09/05/12
For personal use only.

temperature as is confirmed by the results obtained. Small changes in line width will not significantly affect the kinetic data if the chemical shift differences are large. A temperature independent line width has therefore been assumed for $V(tfac)_3$, $V(tfac)(hfac)_2$, and $V(triac)_2(acac)$ all of which have large chemical shift differences. For complexes such as $V(hfac)_2(acac)$, $V(acac)_2(hfac)$, and $V(dibm)_3$ we have assumed that the change in line width with temperature is proportional to the change in line width of a non-exchanging line, e.g. from $V(acac)_3$. Such changes are quite small over the temperature ranges involved but become significant if the chemical shift differences are small.

The relative intensities of the peaks involved can be readily obtained from statistical considerations (e.g. the three lines from *trans* $V(tfac)_3$ are of equal intensity) or by integration (e.g. *cis* and *trans* $V(tfac)_3$).

The relationship between the exchange matrix and the possible mechanisms for exchange is complex. It is usual to proceed by a permutational analysis following the treatment introduced by Longuet-Higgins (15). A detailed analysis of the specific cases of interest in the present paper has been given by Eaton and Eaton (16). The results of this paper have been used to calculate exchange matrices and simulated spectra for the permutation sets corresponding to the proposed mechanisms. A comparison of experimental and simulated spectra for several cases is shown in Fig. 2. The results of these calculations can be summarized quite briefly. In every case the best fit is given by an exchange matrix which corresponds to the situation in which a group has an equal lifetime at each possible site. The implications of this result will be discussed below.

It has been suggested that comparison of the activation parameters for rearrangement reactions in

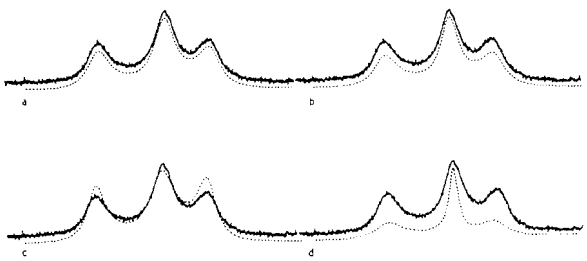

FIG. 2. Comparison of experimental and simulated spectra of $V(tfac)_3$ at an intermediate rate of exchange. (*a*) Equal lifetimes at all sites, ($RC_3(i)$) or SP primary and secondary or TBP with pseudorotation; (*b*) SP primary assuming all bonds rupture and reform with equal probability; (*c*) and (*d*) two cases for TBP mechanisms with lifetimes at downfield and upfield sites equal. The base lines for the simulated spectra have been lowered for clarity. Solvent chlorobenzene $T = 63.8°C$, rate 330 s^{-1}.

TABLE 2. Activation parameters of rearrangement processes of vanadium β-diketonate complexes in various solvents

Complex	Solvent	k^* (s^{-1})	$\Delta H^{\ddagger}$ (kcal)	$\Delta S^{\ddagger}$ (eu)
$V(tfac)_3$	$CDCl_3$	8.9	18.0	6.3
	C_6H_5Cl	9.2	16.5	1.3
	CCl_4	10.9	16.4	1.3
	Acetone	13.3	15.9	−0.1
$V(hfac)_2(tfac)$	$CDCl_3$	103	12.7	−6.7
$V(hfac)_2(acac)$	$CDCl_3$	86	11.8	−10.0
	C_6H_5Cl	105	11.8	−9.6
	CCl_4	110	11.3	−11.2
	Acetone	790	7.2	−21.0
	CH_3CN	565	5.3	−28.1
	CH_2Cl_2	~30	—	—
	Benzene	~40	—	—
$V(acac)_2(hfac)$	$CDCl_3$	40	—	—
	C_6H_5Cl	23	—	—
$V(triac)_2(acac)$	$CDCl_3$	28	10.1	−18.0
$V(dibm)_3$	$CDCl_3$	19	14.9	−2.7

*At 25°C.

different solvents may provide mechanistic information (4). The rearrangement of $V(tfac)_3$ has been studied in four solvents. The resulting activation parameters are given in Table 2. The complex $V(tfac)(hfac)_2$ has five chemically distinct CF_3 groups but two have very similar chemical shifts. Four will be exchanged by rearrangement reactions and one (from the tfac) will not. The spectra obtained by adding $V(tfac)_3$ to $V(hfac)_3$ always contain lines from other complexes but these can be minimized by using excess $V(hfac)_3$ due to the equilibrium

$$V(tfac)_2(hfac) + V(hfac)_3 \rightleftharpoons 2V(tfac)(hfac)_2$$

The single additional line from $V(hfac)_3$ causes relatively little problem in the analysis. Figure 3 shows a set of experimental and simulated spectra for this system. The complexes $V(acac)_2(hfac)$ and $V(acac)(hfac)_2$ present similar problems. Rearrangement of the former can only be studied using the proton spectra and overlap of CH_3 and CH resonances causes problems. $V(acac)(hfac)_2$ can be easily studied using ^{19}F nmr and the exchange has been observed in seven different solvents. In this case the rate is markedly solvent dependent. Activation parameters and rates are given in Table 2.

The complex $V(triac)_3$ offers the possibility of "linkage isomerization" (17). Each ligand has three acetyl groups, two bonded to the metal ion and one not bonded to the metal ion. "Linkage isomerization" involves exchange between the bonded and non-bonded acetyl groups. If rearrangement reactions proceed by a bond breaking rather than a twist mechanism, one might expect to observe linkage isomerization. In the complex $V(triac)_2(acac)$ it should be possible to observe both rearrangement

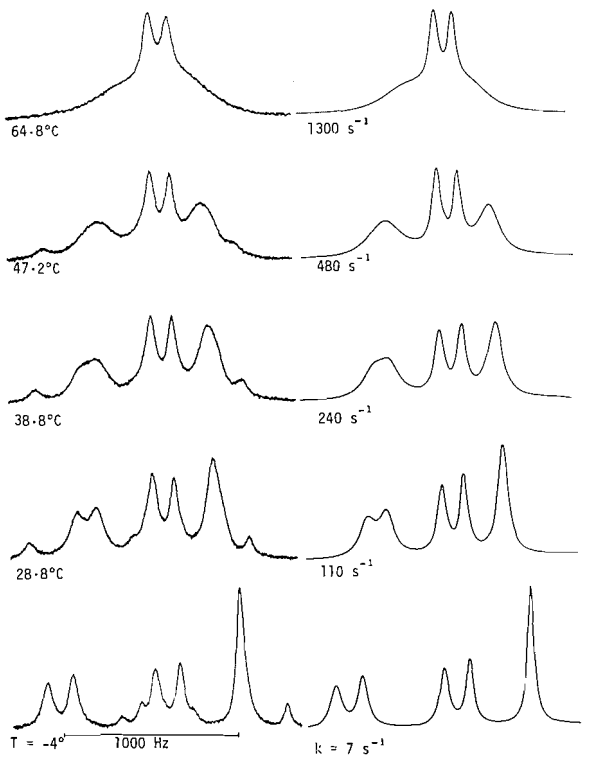

FIG. 3. Comparison of experimental and simulated nmr spectra of $V(hfac)_2(tfac)$ at various temperatures. ^{19}F 58.3 MHz in $CDCl_3$ (equal lifetimes at all sites). The central line of the five strong peaks is assigned to $V(hfac)_3$, and the remaining four lines to $V(hfac)_2(hfac)$. The weaker resonances arise from V(hfac) $(hfac)_2$.

and linkage isomerization. The CH_3 group of the non-bonded acetyl group is observed in an essentially diamagnetic position indicating little spin delocalization to this group. This is consistent with previous observations on acetyl groups attached to the π system of a paramagnetic complex. $V(triac)_2(acac)$ showed rearrangement at a rate corresponding to activation parameters closely similar to the compounds previously examined (see Table 2). There was no evidence for linkage isomerization for either $V(triac)_3$ or $V(triac)_2(acac)$ in solutions of these compounds at 200°C in *o*-dichlorobenzene. Even if rearrangement proceeds by bond breaking we would expect linkage isomerization to be slower, since additional activation energy will be required to rotate the incoming acetyl group about the C—C partially double bond. Thus Serpone and Bickley (2) quote activation enthalpies and entropies of 30.6 kcal/mol and 16 eu for the inversion of $Co(triac)_3$ and 38.9 kcal/mol and 28 eu for linkage isomerization. If it is assumed that this difference represents the barrier to rotation about the C—C bond and that this barrier is the same for the V complex as for the Co complex we may calculate a line broadening of 450 Hz at 200°C for an acetyl group undergoing linkage isomerization. The observed line width is 12 Hz and this is attributed to instrumental broadening due to the difficulty in tuning the spectrometer at high temperatures. It must be concluded therefore either that rearrangement occurs by a twist mechanism or that the additional energy required to rotate the ligand has been considerably underestimated.

In addition to geometric isomers such as *cis* and *trans* $V(tfac)_3$ these chelates also exist as optical isomers. In general, the process of enantiomerization is not observable by nmr techniques. It is, however, desirable to study enantiomerization along with the other rearrangement processes since some mechanisms proceed with retention of configuration and some with inversion. This can be accomplished by including a diastereotopic group on the ligand. The isopropyl group of the ligand dibm serves this function and enables the enantiomerization of the complex to be studied by nmr. Jurado and Springer (18) demonstrated that the coalescence of the isopropyl methyl resonances of $Al(dibm)_3$ was a measure of the enantiomerization of the complex and their arguments are equally applicable to $V(dibm)_3$. In the latter compound at ambient temperatures there is a 40 Hz splitting (at 100 MHz) of the diastereotopic CH_3 groups which coalesce around 43°C. The temperature dependence of the chemical shifts obtained in the temperature range +25°C to −25°C allowed extrapolation of the chemical shifts to higher temperatures. The activation parameters obtained for the enantiomerization process are included in Table 2. The methyl group chemical shifts of $V(dibm)_2(hfac)$ were unfortunately too small to allow a direct comparison of the rearrangement and enantiomerization processes.

Figure 4 shows a plot of $\Delta H^{\ddagger}$ vs. $\Delta S^{\ddagger}$ for the data of Table 2. A good linear relationship is observed. Such an isokinetic relationship indicates a common mechanism for all the reactions (19). Some caution is necessary in reaching a conclusion of this type since the errors in $\Delta H^{\ddagger}$ and $\Delta S^{\ddagger}$ tend to be highly correlated. However the σ values from least-squares treatment of the Arrhenius plots indicate that the correlation of $\Delta H^{\ddagger}$ and $\Delta S^{\ddagger}$ is significant. The systematic errors for the different complexes are likely to be very similar, and it is considered that Fig. 4 demonstrates a genuine isokinetic relationship.

The ligand exchange reactions of V(III) β diketonates are strongly acid catalysed (20). If the catalysis occurs during the breaking of the first chelate bond and if rearrangement proceeds by a

Can. J. Chem. Downloaded from www.nrcresearchpress.com by 210.87.254.40 on 09/05/12
For personal use only.

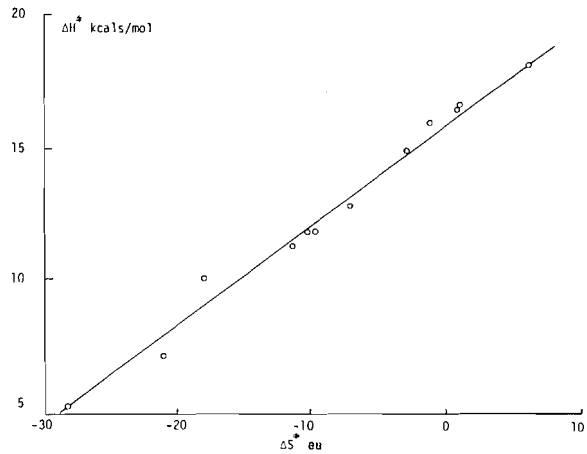

FIG. 4. Linear relationship between $\Delta H^{\ddagger}$ and $\Delta S^{\ddagger}$ for rearrangement of vanadium β-diketonate complexes.

bond breaking mechanism it follows that rearrangement should also be acid catalysed. To investigate this possibility the ^{19}F nmr spectra of $V(tfac)_3$ and $V(hfac)_2(acac)$ were examined at temperatures corresponding to intermediate exchange rates. Such spectra are most sensitive to small changes in rate. No measurable rate change was produced by concentrations of trifluoroacetic acid up to 0.1 *M*. Such a concentration produces a manyfold change in the rate of ligand exchange (20). A similar negative result was observed on addition of the base triethylamine.

Discussion

The review of Serpone and Bickley (2) deals in some detail with the possible rearrangement mechanisms of octahedral chelate complexes. It is usual to make an initial distinction between intermolecular and intramolecular mechanisms. Intermolecular mechanisms involve complete dissociation of one ligand. Intermolecular mechanisms can be unambiguously eliminated in the present case since: (*a*) an independent study (20) showed that the rates of ligand exchange were much slower than the rates of rearrangement; (*b*) in the present study the nmr resonances for free ligand molecules remained sharp at conditions under which the complexed ligands were clearly exchanging. Intramolecular mechanisms may be subdivided into twist and bond breaking mechanisms. Serpone and Bickley (2) showed that all twist mechanisms are basically similar, differing only in the axis about which the twist occurs. Bond breaking mechanisms may involve either a trigonal bipyramid (TBP) or square pyramid (SP) intermediate. The TBP intermediate may have the dangling ligand in either an axial or an equatorial position. Rapid rearrangement of the TBP by pseudorotation must also be considered. Gordon and Holm (6) have distinguished "primary" and "secondary" mechanisms for rearrangements proceeding through an SP intermediate.

Application of the analysis of Eaton and Eaton (16) to the results for $V(tfac)_3$ rules out the trigonal twist, $C_3(p)$, and TBP axial and equatorial pathways. The data can be interpreted either with a rhombic twist, $C_3(i)$, mechanism or with a bond rupture mechanism involving SP intermediates produced either directly or by rapid rearrangement of a TBP intermediate. The data for the other complexes are consistent with this result but do not unambiguously exclude other alternatives. The observation that enantiomerization of $V(dibm)_3$ occurs at a similar rate to the rearrangements is compatible with all but the TBP equatorial mode. The observation of an isokinetic relationship is taken to indicate that all rearrangements proceed by similar mechanisms.

The failure to observe linkage isomerization in $V(triac)_3$ favours, but does not prove, a twist mechanism. The lack of acid catalysis favours, but does not prove, a twist mechanism.

It has been suggested (21) that negative entropies of activation should be associated with twist mechanisms. However a recent compilation (22) shows that the range of observed entropies of activation is very similar for reactions thought to involve a twist mechanism and for those thought to involve bond rupture mechanisms.

It has been suggested (4) that the intermediate in a bond rupture mechanism will be more polar than that of a twist mechanism and hence that if bond rupture is involved the rearrangement will proceed faster in polar than in non-polar solvents. On this basis the data on $V(hfac)_2(acac)$ would favour a bond breaking mechanism but this is not supported by the data on $V(tfac)_3$.

It is concluded therefore that the present study does not provide an unambiguous distinction between twist and bond rupture mechanisms for the rearrangement of these chelate complexes. In this respect it resembles studies of β diketonate complexes of other metals (4, 6, 17, 22). It could be argued that attempts to make such distinctions on the basis of permutational analysis are of dubious value. There is a clear experimental method for differentiating between an intermolecular and an intramolecular process. Different intramolecular mechanisms are much less easily distinguished. For an intramolecular process the energy of the molecule will be a complex function of many bond lengths and bond angles. The activation energy must reside in the normal vibrations of the molecule which in turn are likely to be complex mixtures of bond stretches and bends

Can. J. Chem. Downloaded from www.nrcresearchpress.com by 210.87.254.40 on 09/05/12
For personal use only.

Can. J. Chem. Downloaded from www.nrcresearchpress.com by 210.87.254.40 on 09/05/12
For personal use only.

TABLE 3. Comparison of rates and activation energies of rearrangement of some tris β-diketonate complexes

Metal	Ligands $(tfac)_3$	k (s^{-1})	Temperature (°C)	E_a (kcal/mol)	Reference
Fe		36	−57	<14	8
In					4
Mn		10^3	70	—	8
V		330	64	18.7	This work
Ga		38	62	21	4
Al		34	103	24	4
Co		5×10^{-8}	25	31	4
Ru		2×10^{-12}	25	33	8
Rh		10^{-8}	163	>42	4
	$(dibm)_3$				
V		76	42	15.5	This work
Al		2.5	120	19	18
	$(acac)_2(hfac)$				
Ga		8×10^2	25	15	5
Al		80	25	18	5
V		42	25	—	
	$(hfac)_2(acac)$				
V		82.5	25	12.5	This work
Al		0.86	25	21.3	5

rather than simple group vibrations. There seems no good reason to suppose, therefore, that the lowest energy pathway will result from the accumulation of all the activation energy in the stretching of a single bond or in a single twisting motion as is implied in the various suggested mechanisms. The transition state could rather be a configuration of the molecule in which some angles have been distorted, some bonds have been stretched, and other internuclear distances have become short enough for incipient bond formation. If this were the case, even the most comprehensive data and the most sophisticated permutational analysis will not definitively identify a transition state with simple geometry since none exists.

Finally in Table 3 we compare the rates and activation energies for the rearrangements of β diketonate complexes of a number of molecules. Eaton, Eaton, Holm, and Muetterties (23) have given comparisons for a variety of ligands but note the lack of data on β diketonate complexes. It is seen that contrary to the earlier observation of ref. 8 the V complexes tend to rearrange significantly faster than Al and at rates comparable to Mn and Ga.

Experimental

The ligands acetylacetone, hexafluoroacetylacetone, and trifluoroacetylacetone were obtained from Eastman Kodak Co. Diisobutyrylmethane was obtained from Fisher Scientific Co. and triacetylmethane from Aldrich Chemical Co. Vanadium(III) trichloride and acetylacetonate were purchased from Research Organic/Inorganic Co.

V(III) β diketonate complexes were prepared by the method of Morris *et al.* (24). In the case of $V(dibm)_3$ a small amount of zinc dust effectively retarded oxidation. This method was unsuccessful for $V(triac)_3$ due to hydrolysis of the ligand. The following procedure yielded a mixture of $V(triac)_3$ and $V(triac)_2(acac)$ suitable for nmr experiments. Attempted separations by chromatography failed.

Triacetylmethane (1.1 g) was added to a solution of VCl_3 (0.4 g) in 1:1 acetone water mixture which was flushed with nitrogen. Triethylamine (0.79 g) was added dropwise under nitrogen and the reaction mixture left for 16 h. The product was extracted with CH_2Cl_2, dried with anhydrous $MgSO_4$, and evaporated almost to dryness under nitrogen. Cold petroleum ether (30–60°C) was added and the product separated as a brown oil which eventually crystallized. Recrystallization was from CCl_4.

The nmr spectra were obtained with a Varian DP 60 spectrometer operating at 58.3 MHz for both ^1H or ^{19}F or with a Varian HA 100 spectrometer. In cases where a wide field was scanned the instrument was operated in the field sweep mode to avoid dispersion effects. Simulated spectra were calculated using a Saunders (11) many site line shape programme. The input to the plotting routine was adjusted to conform to the same horizontal scale as the experimental spectrum. The overall rate parameter was adjusted to give the best visual fit.

Random errors in the activation parameters may be estimated from least-squares fits of the Arrhenius plots. At the 2σ level they are not more than 1 kcal in ΔH^* and not more than 3.2 eu in ΔS^*. Systematic errors are more difficult to evaluate. Errors in chemical shifts are considered negligible. Errors in assumed line widths are probably insignificant for $V(tfac)_3$, $V(tfac)(hfac)_2$, and for $V(triac)_2(acac)$ but may be significant for $V(hfac)_2(acac)$ and $V(dibm)_3$. This point was investigated by making Arrhenius plots using data deliberately based on 'incorrect' line widths. It was concluded that an error of 10% in the line width would be readily apparent as a curvature in the Arrhenius plot and would lead to a 15% error in ΔH^*. All such plots were linear within experimental error. Temperature measurements were made by means of a thermocouple in the nmr probe. Relative measurements are accurate to within ±0.5°C but there may be larger errors in the absolute temperatures. Overall the uncertainties in ΔH^* are estimated at ±2 kcal and in ΔS^* at ±7 eu. Results for the same complex in different solvents probably have a higher relative precision since most of the systematic errors are the same.

Acknowledgement

We are indebted to the National Research Council of Canada for financial support of this research.

1. A. WERNER. Ber. **45**, 3061 (1912).
2. N. SERPONE and D. G. BICKLEY. Prog. Inorg. Chem. **17**, 391 (1972).
3. J. J. FORTMAN and R. E. SIEVERS. Coord. Chem. Rev. **6**, 331 (1971).
4. R. C. FAY and T. S. PIPER. Inorg. Chem. **3**, 348 (1964).
5. D. A. CASE and T. J. PINNAVAIA. Inorg. Chem. **10**, 482 (1971).
6. J. G. GORDON and R. H. HOLM. J. Am. Chem. Soc. **92**, 5319 (1970).
7. A. Y. GIRGIS and R. C. FAY. J. Am. Chem. Soc. **92**, 7061 (1970).
8. J. G. GORDON, M. J. O'CONNOR, and R. H. HOLM. Inorg. Chim. Acta, **5**, 381 (1971).

9. D. R. EATON and K. L. CHUA. Can. J. Chem. **51**, 2260 (1973).
10. S. FORSEN and R. A. HOFFMAN. J. Chem. Phys. **39**, 2892 (1963); **40**, 1189 (1964).
11. M. SAUNDERS. Tetrahedron Lett. 1699 (1963).
12. D. R. EATON and K. L. CHUA. Can. J. Chem. **49**, 56 (1971); W. D. PERRY and R. S. DRAGO. J. Am. Chem. Soc. **93**, 2183 (1971).
13. G. N. LAMAR. J. Am. Chem. Soc. **87**, 3568 (1965).
14. S. O. CHAN and D. R. EATON. Can. J. Chem. **54**, 1332 (1976).
15. H. C. LONGUET-HIGGINS. Mol. Phys. **6**, 445 (1963).
16. S. S. EATON and G. R. EATON. J. Am. Chem. Soc. **95**, 1825 (1973).
17. J. R. HUTCHINSON, J. G. GORDON, and R. H. HOLM. Inorg. Chem. **10**, 1004 (1971).
18. (*a*) B. JURADO and C. S. SPRINGER. Chem. Commun. 85 (1971); (*b*) M. PICKERING, A. JURADO, and C. S. SPRINGER. J. Am. Chem. Soc. **98**, 4503 (1976).
19. J. E. LEFFLER and E. GRUNWALD. Rates and equilibria of organic reactions. John Wiley, New York, NY. 1963.
20. A. C. NIXON and D. R. EATON. Can. J. Chem. This issue.
21. P. C. RAY and N. K. DUTT. J. Indian Chem. Soc. **20**, 81 (1943).
22. D. G. BICKLEY and N. SERPONE. Inorg. Chem. **13**, 2908 (1974).
23. S. S. EATON, G. R. EATON, R. H. HOLM, and E. L. MUETTERTIES. J. Am. Chem. Soc. **95**, 1116 (1973).
24. M. L. MORRIS, R. W. MOSHIER, and R. E. SIEVERS. Inorg. Synth. **9**, 28 (1967).

Can. J. Chem. Downloaded from www.nrcresearchpress.com by 210.87.254.40 on 09/05/12
For personal use only.

Ligand exchange reactions of vanadium(III) β diketonate complexes

A. J. C. NIXON AND D. R. EATON

Department of Chemistry, McMaster University, Hamilton, Ont., Canada L8S 4M1

Received August 15, 1977

A. J. C. NIXON and D. R. EATON. Can. J. Chem. **56**, 1012 (1978).

The kinetics of ligand exchange reactions of V(III) β diketonates have been studied. The replacement of acetylacetone by hexafluoroacetylacetone involves a rate law with both first- and second-order terms in the incoming ligand. The replacement of acetylacetone by deuteroacetylacetone involves terms zero-order and first-order in the incoming ligand. Both reactions are markedly catalyzed by acids and inhibited by bases. A mechanism involving a dangling ligand intermediate is suggested. The rates of ligand exchange are much less than the rates of isomerization.

A. J. C. NIXON et D. R. EATON. Can. J. Chem. **56**, 1012 (1978).

On a étudié la cinétique des réactions d'échange de ligands de β dicétonates de V(III). Le remplacement d'un groupe acétylacétone par un hexafluoroacétylacétone implique une loi de vitesse incluant à la fois des termes du premier et du second ordre par rapport au groupe ligand qui arrive. Le remplacement de l'acétylacétone par du deutéroacétylacétone implique des termes d'ordre zéro et du premier ordre relatif au ligand qui arrive. Les deux réactions sont catalysées d'une façon remarquable par les acides et inhibées par les bases. On suggère un mécanisme impliquant un ligand intermédiaire en balance. Les vitesses d'échange de ligand sont beaucoup plus faibles que les vitesses d'isomérisation.

[Traduit par le journal]

Introduction

Although β diketonate ligands form an extensive and well characterized series of chelate complexes with both transition and non-transition metal ions the mechanisms of ligand exchange reactions involving these complexes have been relatively little explored. The subject is of inherent interest since the results may be compared with the much better understood mechanisms of exchange of unidentate ligands. The information obtained may also prove useful in the interpretation of data concerning the isomerization of chelate complexes. The latter area has aroused considerable interest (1, 2). If isomerization is either an intermolecular process or an intramolecular process involving metal–ligand bond breaking a close relationship with ligand exchange is to be anticipated.

The initial study in this area was carried out by Adams and Larsen (3) who investigated the kinetics of ligand exchange of acetylacetone and trifluoroacetylacetone complexes of Zr, Hf, and Th. These proved to be facile reactions which could be conveniently studied by nmr line broadening techniques. They proposed a mechanism which has formed the basis for most of the subsequent discussion. Subsequently Saito and Takahashi (4) have studied the ligand exchange reactions of Pd(II) acetylacetonate and Saito and Masuda (5) those of Al(III) acetylacetonate. The reactions involved in both of these cases are considerably slower than those studied by Adams and Larsen and radio-chemical methods were used. The results with aluminum acetylacetonate differed from those obtained with Zr, Hf, and Th in that the rates were independent of ligand concentration. There are further reports of ligand exchange studies of $Be(acac)_2$ (6), of organometallic acetylacetone complexes of Sn(IV), Au(III), Ga(III), and Tl(III) (7), of (In)III β diketonate complexes (8) and of Sn(IV) alkyl and aryl acetylacetonate compounds (9).

We have undertaken a study of ligand exchange of V(III) β diketonate complexes. There have been no previously reported kinetic studies on these systems or indeed on any of the paramagnetic first row transition metal β diketonate complexes. Concurrently isomerization reactions of the same complexes have been examined (10) and the results reported in the present paper proved useful in the interpretation of the isomerization reactions. The ligand exchange rates are too slow to allow use of nmr line broadening techniques but can be measured by observing the growth of the nmr lines of the products.

Equilibria

The ligand exchange reactions of V(III) acetylacetonate with hexafluoroacetylacetonate and with fully deuterated acetylacetone have been examined. In order to establish suitable experimental conditions for carrying out kinetic studies it is necessary to know the equilibrium concentrations of the various complexes in different mixtures. Equilibrium constants for the reactions:

$$V(acac)_3 + V(hfac)_2(acac) \rightleftharpoons 2V(acac)_2(hfac) \qquad K_1$$

$$V(hfac)_3 + V(acac)_2(hfac) \rightleftharpoons 2V(hfac)_2(acac) \qquad K_2$$

Can. J. Chem. Downloaded from www.nrcresearchpress.com by 210.87.254.5 on 09/05/12
For personal use only.

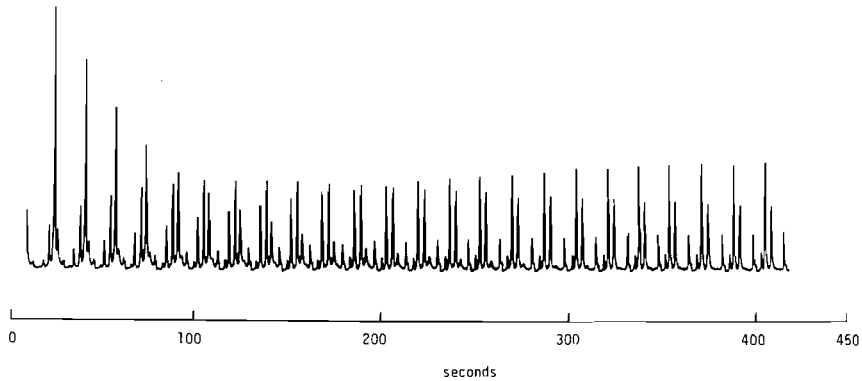

FIG. 1. Intensity of ^1H methyl resonances of $V(acac)_3$, $V(acac)_2(hfac)$, and $V(hfac)_2(acac)$ during a typical ligand exchange reaction of $V(acac)_3$ with Hhfac. Initial concentration of $V(acac)_3$ = 0.178 *M* and of Hhfac = 0.468 *M*. *T* = 27°C. Solvent $CDCl_3$.

can be readily obtained from the nmr spectra of mixtures of $V(acac)_3$ and $V(hfac)_3$. They show large deviations from the statistical values. Similar deviations have been noted by Pinnavaia and co-workers (11) for β diketone complexes with other metal ions. Integration of the resonances of the various complexes gives $K_1 = 1.7 \pm 0.1 \times 10^2$ and $K_2 = 2.8 \pm 0.2 \times 10^3$. If the equilibria were determined by statistical considerations both equilibrium constants would be equal to 3. The mixed complexes are clearly more stable than would be expected from purely statistical considerations. The analogous equilibrium constants for aluminum complexes (12) are $K_1 = 46$ and $K_2 = 725$. The ratio of K_2/K_1 is very similar in both cases (Al, $K_2/K_1 = 16$; V, $K_2/K_1 = 17$).

The enhanced stability of mixed complexes relative to simple complexes has been attributed to a reduction of the average ligand repulsion energy in mixed complexes (13, 14). Using the simple electrostatic model of Kida (13) it may be calculated that a difference of approximately 0.12 units in the negative charge of the oxygens of $acac^-$ and $hfac^-$ would produce the observed equilibrium constants. This model, though, would suggest a greater effect for the smaller Al^{3+} complexes which is contrary to the above results.

Rates of Ligand Exchange

The ligand exchange reactions were followed by repeatedly scanning the methyl region of the nmr spectrum after the addition of a ligand to a V(III) β diketonate complex. A typical trace is shown in Fig. 1. For the reaction between $V(acac)_3$ and Hhfac the initial rate of loss of $V(acac)_3$ was measured as a function of ligand concentration. The results are illustrated in Fig. 2. It is apparent that the rate increases as a function of Hhfac concentration with an order greater than one. The data of Fig. 2 can be fitted to the rate expression:

$$[1] \quad \text{Rate}/[V(acac)_3] = k_1[\text{Hhfac}] + k_2[\text{Hhfac}]^2$$

with $k_1 = 9.8 \times 10^{-3}$ ℓ mol^{-1} s^{-1} and $k_2 = 5.1 \times 10^{-2}$ ℓ^2 mol^{-2} s^{-1}. The reaction is markedly catalyzed by acid and inhibited by base. Figures 3 and 4 illustrate these effects for trifluoroacetic acid and triethylamine respectively. In the presence of base a limiting rate is reached which is directly proportional to Hhfac concentration. A rate constant of 5.4×10^{-3} ℓ mol^{-1} s^{-1} is obtained for the reaction represented by this limiting rate. This rate constant is similar to the k_1 of [1]. It may also be noted that the limiting rate is reached at a concentration of base much less than the Hhfac concentrations used. These observations suggest that the second-order term in [1] represents an acid catalyzed reaction. The acid involved may be Hhfac itself or an impurity, e.g.

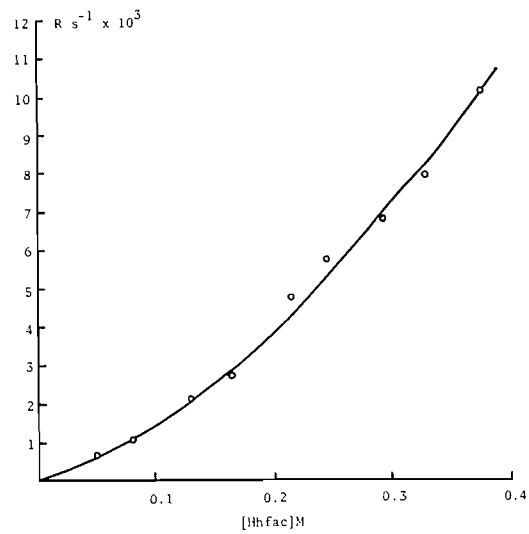

FIG. 2. Initial rate of exchange of $V(acac)_3$ with Hhfac as a function of Hhfac concentration. Solvent $CDCl_3$. $[V(acac)_3]$ at t_0 = 0.178 *M*. *T* = 27°C.

Can. J. Chem. Downloaded from www.nrcresearchpress.com by 210.87.254.5 on 09/05/12
For personal use only.

Can. J. Chem. Downloaded from www.nrcresearchpress.com by 210.87.254.5 on 09/05/12
For personal use only.

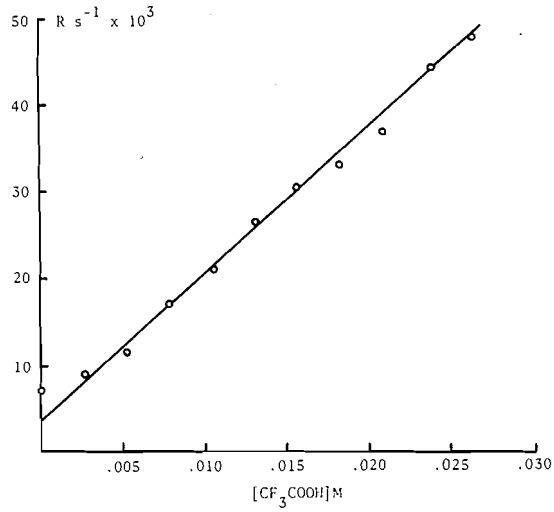

FIG. 3. Initial rate of exchange of $V(acac)_3$ with Hhfac as a function of trifluoroacetic acid concentration. Solvent $CDCl_3$. $[V(acac)_3]$ at $t_0 = 0.178$ *M*. $T = 27°C$.

trifluoroacetic acid arising from hydrolysis of Hhfac. Attempts to eliminate the possible impurity or to determine its concentration by potentiometric titration were unsuccessful.

The exchange of $V(acac)_3$ with deuterated acetylacetone was studied in a similar manner. In this case since we are dealing with an isotopic exchange reaction the data can be most conveniently analysed using McKay's (15) formula:

$$\text{Rate} = \frac{-3ab}{3a + b} \frac{\ln(1 - f)}{t}$$

where a and b are the initial concentrations of complex and ligand respectively and f is the fraction of the reaction which has occurred in time t. The rate again depends on ligand concentration but in this case the form of the expression is:

$$\text{Rate}/[V(acac)_3] = k_0 + k_1[\text{Hacac}]$$

with $k_0 = 1.7 \times 10^{-3}$ s^{-1} and $k_1 = 2.7 \times 10^{-3}$ ℓ mol^{-1} s^{-1}. As with the reaction with Hhfac, acid increases the rate and base decreases the rate. The limiting rate of 0.66×10^{-3} ℓ mol^{-1} s^{-1} is reached at a very low concentration of triethylamine. Water also shows a small catalytic effect.

Discussion

The results described above are qualitatively quite similar to results reported by Adams and Larsen (3) for ligand exchange reactions of other metal acetylacetonates. The mechanisms are complex; acid catalysis is observed and the rate of the non-catalyzed reaction depends on free ligand concentration. Perhaps the most important qualitative result is that the

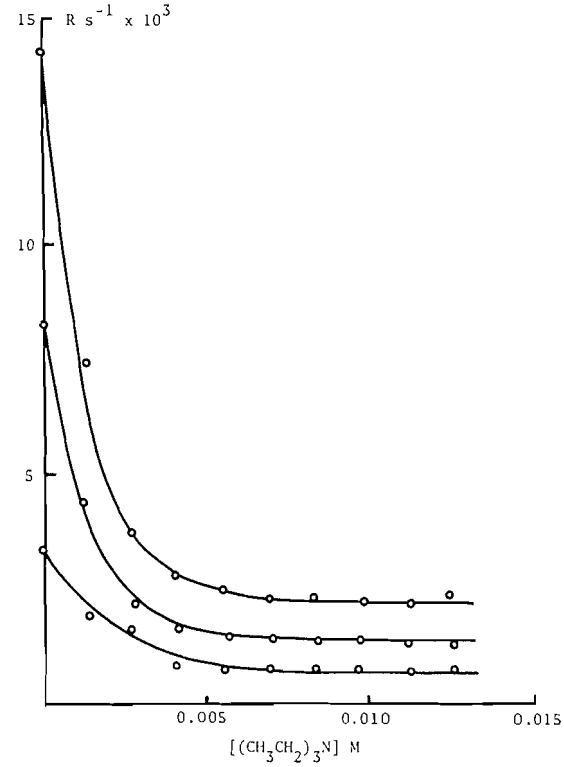

FIG. 4. Initial rate of exchange of $V(acac)_3$ with Hhfac as a function of triethylamine concentration. $[V(acac)_3]$ at $t_0 = 0.142$ *M*. $T = 27°C$. [Hhfac] = (*a*) 0.131 *M*; (*b*) 0.261 *M*; (*c*) 0.392 *M*.

rate of ligand exchange of V(III) β diketonates is much less than the rate of isomerization (10) which eliminates the intermolecular mechanism for the latter process. It is of some interest to compare the absolute rates of ligand exchange for a series of metal acetylacetones—Th(IV)(10^3) (3) > Zr(IV)(10^2) (3) ~ Hf(IV)(10^2) (3) > V(III)(10^{-3}) > Pd(II)($10^{-4} - 10^{-5}$) (4) > Be(II)(10^{-5}) (6) > Al(III)(10^{-6}) (5) > Cr(III) > Co(III). The numbers refer to the ligand dependent pathway and are in 1 mol^{-1} s^{-1} at 25°C (except Al(III)).

Most detailed discussions of the non-acid catalyzed reaction have been based on the reaction scheme of Adams and Larsen (3). This can be represented as

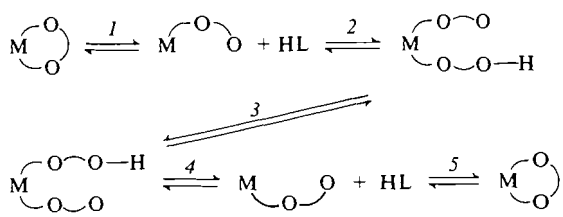

This mechanism will lead to a first-order dependence on free ligand unless step *1*, the formation of the

Can. J. Chem. Downloaded from www.nrcresearchpress.com by 210.87.254.5 on 09/05/12
For personal use only.

dangling ligand intermediate, is rate determining. Steps *1*, *2*, *3*, and *4* have all been suggested as rate determining. In the present case *1* is clearly not rate determining for exchange with Hfac, but may be responsible for the term zero-order in Hacac. Since hexafluoroacetone is a stronger acid than acetylacetone it might be expected that a proton would be transferred more rapidly from Hhfac to $acac^-$ than from Hacac to $hfac^-$. The observation that $V(acac)_3$ exchanges more rapidly with Hhfac than with Hacac therefore suggests that *3* may be the rate determining step for the process which is first-order in ligand. However the kinetic results do not eliminate either steps *2* or *4* from being rate determining.

Saito and Masuda (5) have suggested that acid catalysis is accomplished by protonation of the dangling ligand intermediate which enhances its stability. This would be equally plausible in the present case although direct catalysis of step *3* is also possible. Two aspects of the acid catalyzed reaction remain somewhat puzzling. The small amount of base needed to inhibit the reaction suggests that an acid impurity is present, but this could not be confirmed directly. On the other hand, the dependence of the rate on the square of the hexafluoroacetylacetone concentration is more readily rationalized if the ligand itself is the acid needed for catalysis. The pk_D of hexafluoroacetylacetone is sufficiently low to make this plausible (16). Further speculation on the mechanism does not seem warranted with the present data.

Experimental

The ligands acetylacetone and hexafluoroacetylacetone were obtained from Eastman Kodak Co. Vanadium trichloride and vanadium acetylacetonate were purchased from the Research Organic/Inorganic Co. Vanadium hexafluoroacetylacetonate was prepared by the method of Morris *et al.* (17).

Deuterated acetylacetone was prepared by refluxing a mixture of 20 ml (0.194 *M*) of acetylacetone, 100 g (5 mol) of D_2O, and a small amount of Na_2CO_3 for 24 h. The product was extracted with diethyl ether, dried over Na_2SO_4 for 24 h, and distilled. The distillate was further dried with K_2CO_3 and redistilled collecting the fraction 128–130°C. By nmr the product was 84% deuterated which sufficed for the exchange experiments. $CDCl_3$ was used as a solvent throughout.

Samples for the nmr equilibrium experiments were prepared by the following procedure. The appropriate complex was recrystallized and stored overnight in an evacuated dessicator containing P_2O_5. Solutions were prepared in a glove bag under dry N_2. After degassing on a vacuum line the sample tubes were evacuated and sealed. The sealed samples appear to be indefinitely stable. For kinetic runs the tubes were sealed with serum caps to allow introduction of the ligand. Evidence for decomposition become visible only after several days. The nmr tubes were allowed to thermally equilibrate in the probe before adding free ligand. The initial time was estimated from the time of mixing. The tube must be removed from the probe for about 30 s for ligand addition.

The nmr spectra were obtained with a Varian HA 100 instrument with probe temperature 27°C. The region of interest was repetitively scanned using a simple switching device. Coefficients relating the observed peak heights to the concentrations of the species may be readily obtained. Concentrations were then plotted against time and the initial rates found from the slopes at t_0.

Acknowledgement

We are indebted to the National Research Council of Canada for financial support of this research.

1. N. Serpone and D. G. Bickley. Prog. Inorg. Chem. **17**, 391 (1972).
2. J. J. Fortman and R. E. Sievers. Coord. Chem. Rev. **6**, 331 (1971).
3. A. C. Adams and E. M. Larsen. Inorg. Chem. **5**, 814 (1966).
4. K. Saito and M. Takahashi. Bull. Chem. Soc. Jpn. **42**, 3462 (1969).
5. K. Saito and K. Masuda. Bull. Chem. Soc. Jpn. **41**, 384 (1968); **43**, 119 (1970).
6. A. Barabas. Inorg. Nucl. Chem. Lett. **6**, 775 (1970).
7. G. E. Glass and R. S. Tobias. J. Organomet. Chem. **15**, 481 (1968).
8. G. M. Tanner, D. G. Tuck, and E. G. Wells. Can. J. Chem. **50**, 3950 (1972).
9. N. Serpone and R. Ishayek. Inorg. Chem. **13**, 52 (1974).
10. A. J. C. Nixon and D. R. Eaton. Can. J. Chem. This issue.
11. (*a*) T. J. Pinnavaia and R. C. Fay. Inorg. Chem. **5**, 233 (1966); (*b*) T. J. Pinnavaia, M. T. Mocella, B. A. Averill, and J. T. Woodard. Inorg. Chem. **12**, 763 (1973).
12. J. J. Fortman and R. Sievers. Inorg. Chem. **6**, 2022 (1967).
13. S. Kida. Bull. Chem. Soc. Jpn. **34**, 962 (1961).
14. Y. Marcus and I. Eliezer. J. Phys. Chem. **66**, 1661 (1962).
15. H. A. McKay. Nature, **142**, 997 (1939).
16. L. G. Van Uitert, W. C. Fernelius, and B. E. Douglas. J. Am. Chem. Soc. **75**, 457 (1953).
17. M. L. Morris, R. W. Moshier, and R. E. Sievers. Inorg. Synth. **9**, 28 (1967).

Gas phase dissociation of protonated acetic acid to the acyl cation and water. Heat of formation of CH_3CO^+ and proton affinity of ketene

WILLIAM R. DAVIDSON, YAN K. LAU, AND PAUL KEBARLE
Chemistry Department, University of Alberta, Edmonton, Alta., Canada T6G 2G2

Received October 26, 1977

WILLIAM R. DAVIDSON, YAN K. LAU, and PAUL KEBARLE. Can. J. Chem. **56**, 1016 (1978).

Pulsed electron beam high pressure mass spectrometry was used to measure the enthalpy and entropy of the dehydration of protonated acetic acid, and the proton affinity of ketene in the gas phase. The variation of the equilibrium constant with temperature from 515 to 615 K led to ΔH^0 of 24.6 kcal/mol and a ΔS^0 of 33.1 cal/deg for the dehydration of protonated acetic acid. Proton transfer equilibria measurements of reactions: $BH^+ + CH_2CO = B + CH_3CO^+$ at 600 K with reference bases of known proton affinity led to a proton affinity of 195 kcal/mol for ketene. The heat of formation of the acetyl cation ($\Delta H_f^0(CH_3CO^+) = 160$) was obtained from both the proton affinity of ketene, and from the dehydration enthalpy of protonated acetic acid combined with the proton affinity of acetic acid. The energetics for the dehydration reaction in the gas phase and in solution are compared.

WILLIAM R. DAVIDSON, YAN K. LAU et PAUL KEBARLE. Can. J. Chem. **56**, 1016 (1978).

On a utilisé la spectrométrie de masse à haute pression avec des rayons d'électrons pulsés pour mesurer l'enthalpie et l'entropie de déshydration de l'acide acétique protoné et l'affinité pour les protons du cétène en phase gazeuse. La variation de la constante d'équilibre avec la température de 515 à 615 K conduit à un ΔH^0 de 24.6 kcal/mol et à un ΔS^0 de 33.1 cal/deg pour la déshydratation de l'acide acétique protoné. Des mesures d'équilibre de transfert de proton pour la réaction $BH^+ + CH_2CO = B + CH_3CO^+$ à 600 K avec des bases de référence d'affinité protonique connue conduit à une affinité protonique de 195 kcal/mol pour le cétène. On a obtenu la chaleur de formation du cation acétyle ($\Delta H_f^0(CH_3CO^+) = 160$) à partir de l'affinité protonique du cétène ainsi que de l'enthalpie de déshydratation de l'acide acétique protoné combiné avec l'affinité de l'acide acétique. On compare les données énergétiques pour la réaction de déshydratation en phase gazeuse et en solution.

[Traduit par le journal]

Introduction

Recent reports from this laboratory (1–3) described studies of gas phase equilibria 1 involving the carbocations R^+ ($C_2H_5^+$, $C_3H_7^+$, $t\text{-}C_4H_9^+$) with B (H_2 (1), CH_4 (1), OH_2 and CO (2, 3)). Process 1 may be considered as a Lewis acid–base reaction between the Lewis acid R^+ and the σ (H_2, CH_4), π (CO), and n (OH_2) donor bases.

[1] $$R^+ + B = (RB)^+$$

The present work describes a determination of the temperature dependence of reaction 2 which falls in the class of reactions 1. The hydration of the acylium ion CH_3CO^+ leads to protonated acetic acid (3). The heat of formation of CH_3CO^+ in the gas phase is not well established. ΔH_2 obtained from a van't Hoff plot of the equilibrium constant K_2 permits the evaluation of the above heat of formation since the proton affinity of acetic acid is known. The heat of formation of CH_3CO^+ can be also obtained from the proton affinity of ketene as shown in reaction 3.

[2] $$CH_3CO^+ + OH_2 = CH_3C(OH)_2^+$$

[3] $$CH_3CO^+ = CH_2CO + H^+$$
$$\Delta H_3 = PA(CH_2CO)$$

The present work gives the results of proton affinity measurements for ketene.

The reverse of reaction 2 has been observed (5) by nmr techniques in the condensed phase HSO_3F, SbF_5, SO_2. Olah and White (5) were able to study the temperature dependence of this dehydration reaction and obtain the activation energy. A comparison of the energetics of the dehydration [−2] in the gas phase and in solution proves interesting.

Experimental

The equilibrium [2] was studied with one of the pulsed electron beam high ion source pressure mass spectrometers (6) available in our laboratory. Water vapor at a selected pressure between 1.5–3 Torr containing ~0.1% acetic acid was passed in slow flow through the thermostated ion source. The positive ions produced by electron impact and subsequent ion molecule reactions in water are (6) the protonated water clusters $H^+(H_2O)_n$. The proton transfer [4] to acetic acid is exothermic for low n.

[4] $$H^+(H_2O)_n + CH_3COOH = CH_3C(OH)_2(OH_2)_k^+ + (n - k)OH_2$$

Below 515 K, the major ions observed were: $H^+(H_2O)_n$, $CH_3C(OH)_2(OH_2)_k^+$, and $(CH_3CO_2H)_2H^+$, the latter being formed by addition of acetic acid to protonated acetic acid. Above 515 K the equilibrium [2] becomes observable. At temperatures above 615 K the CH_3CO^+ becomes the dominant

Can. J. Chem. Downloaded from www.nrcresearchpress.com by 210.87.254.5 on 09/05/12
For personal use only.

Can. J. Chem. Downloaded from www.nrcresearchpress.com by 210.87.254.5 on 09/05/12
For personal use only.

ion. Pure water, rather than the usual mixture (6) of carrier gas CH_4 and solvent (H_2O), was used since the establishment of the equilibrium [2] was too slow at low water concentrations.

The proton affinity of ketene was obtained from proton transfer equilbria measurements at 600 K. The equiiibrium

[5] $$BH^+ + CH_2CO = B + CH_3CO^+$$

constant K_5 was used to obtain $\Delta G_5^0 = -RT \ln K_5$ at 600 K. The procedure used in these measurements has been described previously (4).

Results and Discussion

The van't Hoff plot of the equilibrium constant K_2 for reaction 2, $CH_3CO^+ + OH_2 = CH_3C(OH)_2^+$, is shown in Fig. 1. The slope leads to $\Delta H_2^0 = -24.6$ kcal/mol. The resulting $\Delta S_2^0 = -33.1$ cal/deg. The data are summarized in Table 1.

The results from the proton transfer equilibria [5] used for the determination of the proton affinity of ketene are summarized in Fig. 2. The measured ΔG_5^0 when combined with the known (7–9) ΔG_6^0 for the reference bases B lead to $\Delta G_6^0 = 6.3$ kcal/mol for reaction 6 involving ketene at 600 K.

[6] $$NH_4^+ + B = NH_3 + BH^+$$

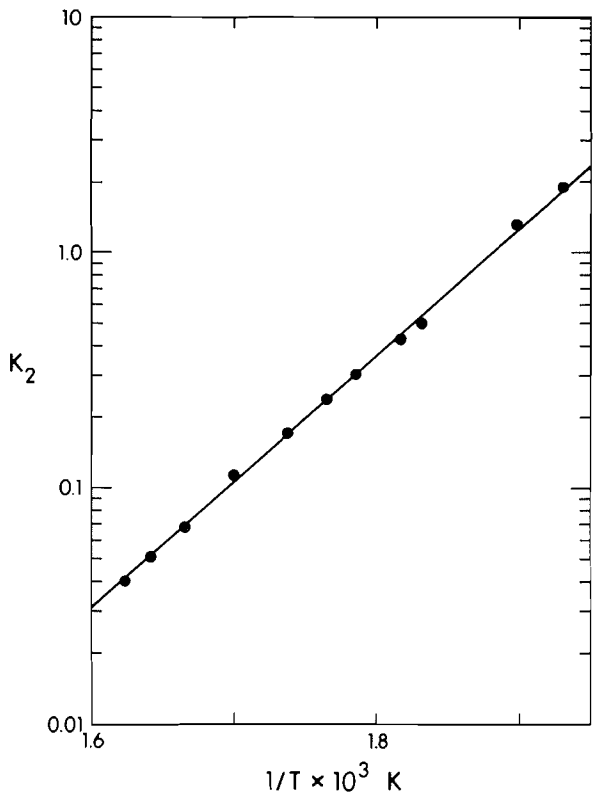

FIG. 1. van't Hoff plot of equilibrium constant K_2 for reaction 2, $CH_3CO^+ + OH_2 = CH_3C(OH)_2^+$ measured in the gas phase. Equilibrium constant calculated with reactant pressures in Torr units.

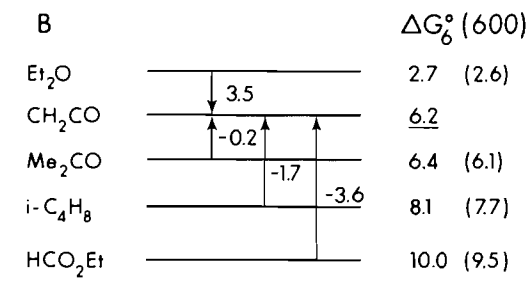

FIG. 2. Summary of proton transfer equilibria used to determine proton affinity of ketene. Numbers beside arrows correspond to $\Delta G_5^0 = -RT \ln K_5$ for the proton transfer equilibrium [5] $BH^+ + CH_2CO = B + CH_3CO^+$ measured at 600 K. The ΔG_6^0 given on the right hand side correspond to the standard free energy changes for proton transfer from the ammonium ion: $NH_4^+ + B = NH_3 + BH^+$ at 600 K. The ΔG_6^0 in parentheses are those from the earlier determination of Yamdagni and Kebarle (4). The ΔG_6^0 without parentheses are more recent values (7). $\Delta G_6^0 = +6.3$ is deduced from the present data for proton transfer to ketene. All values in kcal/mol.

From Fig. 2 it can be seen that the four independent determinations of the ΔG_6^0(ketene) are generally consistent to ~0.2 kcal/mol. Using ΔG_6^0(ketene) = 6.2 kcal/mol and an estimated $T\Delta S_6 = 1$ kcal/mol at 600 K for ketene, obtained from considering rotational symmetry number changes, one obtains ΔH_6^0(ketene) = 7.2 kcal/mol and using the known (8, 9) proton affinity of ammonia PA(NH_3) = 202.3 ± 1 kcal/mol one obtains PA(ketene) = 195 ± 1.5 kcal/mol. Since the proton affinity of acetic acid PA(CH_3COOH) = 186.5 kcal/mol was determined previously (4, 7) from proton transfer equilibria measurements, the thermodynamic consistency of the ion equilibria measurements can be checked through the cycle shown below:

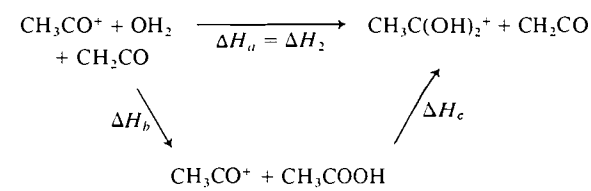

where $\Delta H_a = \Delta H_2 = -24.6$ kcal/mol, $\Delta H_b = \Delta H_f(CH_3OOH) - \Delta H_f(OH_2) - \Delta H_f(CH_2CO) = -34.1$ kcal/mol and ΔH_c = PA(CH_2CO) − PA(CH_3COOH) = 8.5 kcal/mol. Therefore $\Delta H_b + \Delta H_c = -25.6$ kcal/mol while $\Delta H_2 = -24.6$ kcal/mol, which means that the cycle is consistent to within 1 kcal/mol which is as good as could be expected.

The proton affinity of ketene PA(CH_2CO^+) = 195 kcal/mol when combined with $\Delta H_f(H^+) = 367.1$ kcal/mol leads to $\Delta H_f(CH_3CO^+) = 160.7$ kcal/mol while ΔH_2 and PA(CH_3COOH) lead to $\Delta H_f(CH_3CO^+) = 159.7$. The average of these is

Can. J. Chem. Downloaded from www.nrcresearchpress.com by 210.87.254.5 on 09/05/12
For personal use only.

TABLE 1. Summary of thermochemical information for observed reactions

Reaction	ΔH^0 (kcal/mol)	ΔS^0 (cal/deg)	$\Delta H_f^0(CH_3CO^+)$ (kcal/mol)
$CH_3C(OH)_2^+ = CH_3CO^+ + H_2O$	24.6	33.1	
$CH_3C(OH)_2^+ = CH_3COOH + H^+$	186.5[a]		
$H^+ + CH_3COOH = CH_3CO^+ + H_2O$	−161.9[b]		159.7[c]
$CH_3CO^+ = CH_2CO + H^+$	195		160.7[d]

[a]From refs. 4 and 9.
[b]Calculated from the enthalpy of dehydration of protonated acetic acid and the proton affinity of acetic acid.
[c]Calculated from the heats of formation of water ($\Delta H_f^0 = -57.8$ kcal/mol) (10), acetic acid ($\Delta H_f^0 = -103.3$ kcal/mol) (10), and the proton ($\Delta H_f^0 = 367.1$ kcal/mol) (14), and the enthalpy of the reaction.
[d]Calculated from the heats of formation of ketene ($\Delta H_f^0 = -11.4$ kcal/mol) (15), and the proton, and the enthalpy of the reaction.

$\Delta H_f(CH_3CO^+) = 160$ kcal/mol. These data are summarized in Table 1.

Previous determinations of $\Delta H_f(CH_3CO^+)$ were based on appearance potentials. The recommended (10) value $\Delta H_f(CH_3CO^+) = 152$ kcal/mol was based on the appearance potential $A_p(CH_3CO^+,CH_3COCH_3)$ determined by photoionization (11). On the other hand the appearance potential from acetaldehyde $A_p(CH_3CO^+,CH_3COH)$ leads (11) to a higher value $\Delta H_f(CH_3CO^+) = 158$ kcal/mol. Beauchamp and co-workers (12), in a recent publication which appeared while the present work was being completed, reported a redetermination of the above photoionization appearance potentials which confirmed the earlier work (11). On the basis of an ordering of the stabilities of carbonium ions R^+ based on ion molecule reaction studies, Beauchamp and co-workers (12) were able to select the higher heat of formation $\Delta H_f(CH_3CO^+) = 158$ kcal/mol as the only one consistent with the ion molecule results. Furthermore they quoted an as yet unpublished proton affinity determination of ketene PA = 196.4 kcal/mol from their laboratory which leads to $\Delta H_f(CH_3CO^+) = 159.2 \pm 2$ kcal/mol. The present results of 160.7 and 159.7 kcal/mol with an estimated error of ± 2 kcal/mol are thus in good agreement with their heat of formation results.

It is interesting to note that the measured $-\Delta S_2^0 = 33.1$ cal/deg for the hydration of CH_3CO^+ is larger by a few cal/deg than the average $-\Delta S^0$ values observed in association reactions. The latter values are generally below 30 cal/deg (9). The larger loss of entropy in reaction 2 may be associated with the restricted rotation in the protonated acetic acid which is due to internal hydrogen bonding as shown in structure **1**.

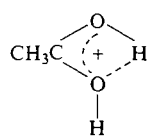

1

Structure **1** has been suggested by nmr experiments. At low temperature **1** is sufficiently rigid such that the two protons become nonequivalent (5, 13).

Olah and White (5) determined the activation energy $\Delta H_{-2}^{\ddagger} = 16.3$ kcal/mol and activation entropy $\Delta S_{-2}^{\ddagger} = -13.1$ cal/deg for the dissociation of protonated acetic acid to the acetyl cation and water, occurring in FSO_3H–SbF_5 solution. In the gas phase, since reaction 2 should have no activation energy, $\Delta H_{-2}^{\ddagger}$(gas phase) may be expected to be close to $\Delta H_{-2} = 24.6$ kcal/mol. The gas phase activation entropy $\Delta S_{-2}^{\ddagger}$ should be positive but smaller than $\Delta S_{-2}^0 = 33$ cal/deg. Comparing the solution with the gas phase data we notice that the activation energy in solution is only half of that in the gas phase and that the entropy in solution is (strongly) negative while that in the gas phase is (strongly) positive. This result is consistent with strong solvent participation in the activated complex. We may consider that an important stabilization of the 'free' CH_3CO^+ in solution is obtained through the interaction of the (Lewis acid) cation with a lone pair on one solvent molecule S1. This means that the essential features of the transition state in solution should be represented by structure **2**. Such a complex is consistent with a low activation energy and a negative activation entropy.

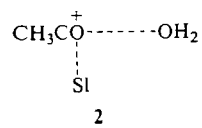

2

1. K. HIRAOKA and P. KEBARLE. J. Am. Chem. Soc. **98**, 6119 (1976).
2. K. HIRAOKA and P. KEBARLE. J. Am. Chem. Soc. **99**, 360 (1977).
3. K. HIRAOKA and P. KEBARLE. J. Am. Chem. Soc. **99**, 366 (1977).
4. R. YAMDAGNI and P. KEBARLE. J. Am. Chem. Soc. **98**, 1320 (1976).
5. G. A. OLAH and A. M. WHITE. J. Am. Chem. Soc. **89**, 3591 (1967); **89**, 7072 (1967).

6. A. J. CUNNINGHAM, J. D. PAYZANT, and P. KEBARLE. J. Am. Chem. Soc. **94**, 2627 (1972).
7. Y. K. LAU and P. KEBARLE. To be published.
8. J. F. WOLF, R. H. STALEY, I. KOPPEL, M. TAAGEPERA, R. T. MCIVER, JR., J. L. BEAUCHAMP, and R. W. TAFT. J. Am. Chem. Soc. **99**, 5417 (1977).
9. P. KEBARLE. Ann. Rev. Phys. Chem. **28**, 445 (1977).
10. J. L. FRANKLIN *et al.* NSRDS-NBS26 National Bureau of Standards. 1969.
11. E. MURAD and M. G. INGHRAM. J. Chem. Phys. **40**, 3263 (1964); **41**, 404 (1964).
12. R. M. STALEY, R. D. WEITING, and J. L. BEAUCHAMP. J. Am. Chem. Soc. **99**, 5964 (1977).
13. M. BROOKHART, G. C. LEVY, and S. WINSTEIN. J. Am. Chem. Soc. **89**, 1735 (1967).
14. D. R. STULL and H. PROPHET. JANAF Thermochemical Tables. 2nd ed. NSRDS-NBS37 National Bureau of Standards. 1971.
15. R. L. NUTTALL, A. H. LAUFEN, and M. V. KILDAY. J. Chem. Thermodyn. **3**, 167 (1971).

Can. J. Chem. Downloaded from www.nrcresearchpress.com by 210.87.254.5 on 09/05/12
For personal use only.

7α-Acetoxydihydronomilin: isolation, spectra, and crystal structure[1]

FARID R. AHMED[2]
Division of Biological Sciences, National Research Council of Canada, Ottawa, Ont., Canada K1A 0R6
AND
ANG S. NG
Department of Chemistry, Nanyang University, Singapore 22
AND
ALEX G. FALLIS
Department of Chemistry, Memorial University of Newfoundland, St. John's, Nfld., Canada A1C 5S7

Received November 21, 1977

FARID R. AHMED, ANG S. NG, and ALEX G. FALLIS. Can. J. Chem. **56**, 1020 (1978).

Methanol extraction of the ground seeds of *Uncaria Gambier Roxb.* followed by chromatography afforded a crystalline $C_{30}H_{38}O_{10}$ terpene. This has been shown by X-ray analysis to be 7α-acetoxydihydronomilin. The crystals are orthorhombic, $P2_12_12_1$, $a = 13.158(2)$, $b = 17.092(2)$, $c = 12.689(2)$ Å, $Z = 4$, $d_x = 1.300$, $d_o = 1.300$ g cm^{-3}. The structure has been determined by the direct method and Fourier syntheses, and refined by block-diagonal least-squares to $R = 0.042$ for 2621 observed reflexions. The molecule contains a seven-membered lactone ring *A*, three six-membered rings *B*, *C*, *D*, a three-membered ring *E*, a furan ring *F*, and two acetate groups. *A* and *B* are chair, *C* is twist-boat, *D* is 1,3-diplanar, while *E* and *F* are planar. The *A*/*B*, *B*/*C*, *C*/*D* junctions are *trans*, *D*/*E* is *cis*, and *F* is linked to *D* by an equatorial C—C bond. The two acetate groups are in axial positions on *A* and *B* and are *cis* to each other. The O atom forming the apex of the three-membered ring is wedged between two H atoms and their parent C atoms at short intramolecular distances O...H = 2.28(2) and 2.28(3), and O...C = 2.623(3) and 2.668(4) Å. No intermolecular hydrogen bonding is indicated.

FARID R. AHMED, ANG S. NG et ALEX G. FALLIS. Can. J. Chem. **56**, 1020 (1978).

L'extraction par le méthanol de grains concassés de *Uncaria Gambier Roxb.* suivie par une chromatographie fournit un terpène cristallin de formule moléculaire $C_{30}H_{38}O_{10}$. On a montré par diffraction de rayon-X qu'il s'agit de l'acétoxy-7 dihydronomoline. Les cristaux sont orthorhombiques $P2_12_12_1$, $a = 13.158(2)$, $b = 17.092(2)$, $c = 12.689(2)$ Å, $Z = 4$, $d_x = 1.300$, $d_o = 1.300$ g cm^{-3}. On a déterminé la structure par une méthode directe et des synthèses de Fourier et on l'a affinée par la méthode des moindres carrés (blocs diagonaux) jusqu'à une valeur de R de 0.042 pour 2621 réflexions observées. La molécule contient un cycle lactonique à sept chaînons (*A*), trois cycles à six chaînons (*B*, *C* et *D*), un cycle à trois chaînons (*E*), un cycle furannique (*F*) et deux groupes acétates. Les cycles *A* et *B* sont dans la conformation chaise, le cycle *C* est dans une conformation bateau déformé, le cycle *D* est diplanaire-1,3 alors que *E* et *F* sont plans. Les jonctions *A*/*B*, *B*/*C* et *C*/*D* sont *trans*, *D*/*E* est *cis* et *F* est lié à *D* par un lien équatorial C—C. Les deux groupes acétates sont en positions axiales sur *A* et *B* et sont *cis* l'un par rapport à l'autre. L'atome d'oxygène formant le sommet du cycle à trois chaînons est calé entre deux atomes d'hydrogène et leurs atomes de carbone à des distances intramoléculaires courtes O...H = 2.28(2) et 2.28(3), et O...C = 2.623(3) et 2.668(4) Å. Il ne semble pas exister de liaison hydrogène intermoléculaire.

[Traduit par le journal]

Introduction

The plant, *Uncaria Gambia Roxb.*, a member of the Rubiaceae family is common to Singapore and Malaysia, where the concentrated aqueous extract of the leaves and stems has been used as a tanning material called Gambir. A few alkaloids (1) have been isolated from these plant extracts but the other chemical components have received little attention. We report herein the results of methanol extraction of seeds of *Uncaria Gambier Roxb.* which after a combination of column and thin-layer chromatography afforded crystalline material, mp 265–266°C.

Results and Discussion

This material was very sensitive to treatment with aqueous base or acid, and simple degradation products could not be isolated in pure form. The molecular ion peak at *m/e* 558 in the mass spectrum and elemental analysis were consistent with the molecular formula $C_{30}H_{38}O_{10}$. A strong, broad infrared absorption at 1720–1740 cm^{-1} indicated the presence of several carbonyl functions; possibly esters and/or lactones. Two methyl carbonyl signals, probably due

[1]NRCC No. 16494.
[2]To whom all correspondence should be addressed.

Can. J. Chem. Downloaded from www.nrcresearchpress.com by 210.87.254.105 on 09/05/12
For personal use only.

Can. J. Chem. Downloaded from www.nrcresearchpress.com by 210.87.254.105 on 09/05/12
For personal use only.

to acetates, could be clearly identified at δ 2.06 and δ 2.16 ppm in the ^{1}Hmr spectrum. This was further supported by the loss of two acetic acid units in the mass spectrum which gave rise to a signal at *m/e* 438.

Weak absorptions at 1630 cm^{-1} and 3140 cm^{-1} in the ir spectrum indicated that some of the 12 double bond equivalents in the molecule are due to double bonds. The nature of this unsaturation was consistent with a furan moiety, the two α hydrogens giving rise to a signal at δ 7.40 ppm (J = 2 Hz) in the ^{1}Hmr spectrum, with the remaining β proton appearing as a doublet (J = 2 Hz) at δ 6.32 ppm. Another singlet at δ 5.60 ppm could arise from a single proton attached to a trisubstituted double bond but in view of the X-ray analysis (*vide infra*) must be assigned to a hydrogen attached to the epoxide ring α to a lactone carbonyl function. Similarly the single proton adjacent to the furan ring attached to the carbon bearing the lactone oxygen appeared as a singlet at δ 3.51 ppm. The secondary hydrogens on the carbons bearing the acetate functions appear as broad single proton multiplets at δ 4.84 and δ 4.50 ppm while the broadened doublet at δ 3.15 (J = 4 Hz) is due to the two protons α to the carbonyl group.

Concurrent with further chemical studies the X-ray analysis was undertaken and permitted the assignment of structure **1** (7α-acetoxydihydronomilin) to this material. The closely related parent terpene nomilin (**2**) has been identified by Dreyer (2) in grapefruit after being isolated earlier by Emerson (3). These molecules are members of a large family of limonoid bitter principles and structure **1** is consistent with the spectral data reported above. The ^{13}Cmr spectrum is presented in Table 1. These assignments are made by analogy with similar limonoids which have been reported in the literature and the data for khivorin (**3**) are included for comparison (4).

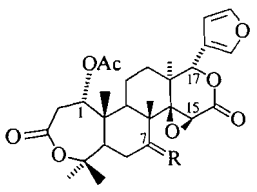

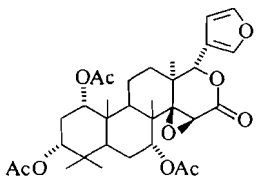

1 R = H, OAc

2 R = O

3

Relatively few X-ray studies of these natural products have appeared (5) and stereochemical assignments have been based on spectral interpretation. The X-ray analysis clearly establishes the stereochemistry of the furan substituent at C(17) and the C(1) acetoxy function, both of which are α. Thus, it is highly likely that the parent nomilin system possesses the same stereochemical features and the original assignment (6) of the C(1) acetoxy group to the β position, based on an ^{1}Hmr argument, is in error and should be reversed.

TABLE 1. ^{13}Cmr chemical shifts ($CDCl_3$; δ_c ppm; Me_4Si standard)

Carbon atom	δ_c 7α-Acetoxydihydronomilin	δ_c Khivorin
1 or 7	73.1	72.3
2	42.0	
3 or 16	169.6	167.6
4	85.1	
5	44.0	37.0
6	34.9	
7 or 1	70.7	73.8
8	44.7	42.2
9	36.8	36.3
10	38.7	40.7
11	25.9	
12	25.7	
13	34.4	38.8
14	69.7	69.7
15	56.8	56.4
16 or 3	167.3	167.6
17	78.1	78.4
20	120.4	120.5
22	109.9	109.9
21	141.1	143.0
23	143.2	141.1
Acetate C=O	169.8, 169.8	
Acetate Me	21.0, 20.9	
Methyl Signals	23.6, 18.4, 16.7, 15.8, 15.0	27.4, 21.6, 18.3, 17.3, 16.4

Crystal Structure

A side-view of the molecule showing its conformation and the numbering system is presented in Fig. 1. The molecule contains three six-membered rings forming the triterpene skeleton to which a three- and a seven-membered ring are fused. A furan ring is linked to the triterpene through a C—C bond in an equatorial position. Five of the rings form a slightly corrugated ribbon that is shaped approximately into a circular arc as shown in Fig. 1, with the three-membered ring in an axial position on the outside surface of the ribbon and the two acetate groups in axial positions on the inside surface. The *A/B*, *B/C*, *C/D* junctions are all *trans*, while the *D/E* is *cis*, as shown by the torsion angles given in Table 2. The absolute configuration has not been determined, and

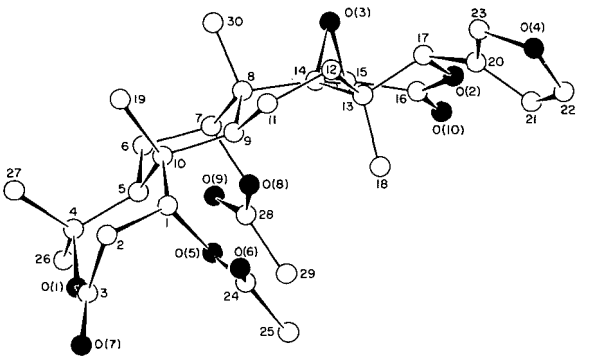

FIG. 1. A side-view of the molecular structure of 7α-acetoxydihydronomilin, $C_{30}H_{38}O_{10}$, showing its conformation and the numbering scheme. The absolute configuration may correspond to this figure or its enantiomorph.

may correspond to the drawing in Fig. 1 or its enantiomorph.

The molecular formula, bond lengths, valency angles, and the rings' torsion angles are given in Fig. 2. Some of the valency angles and torsion angles which could not be fitted in Fig. 2 are compiled in Table 2. These measurements have not been corrected for atomic thermal vibration. The 21 C(sp^3)—C(sp^3) bonds are in the range 1.471–1.588(4) Å and their mean is 1.540 Å. The longest are those in the bond sequence C(4)—C(5)—C(10)—C(9)—C(8)—C(14) of lengths 1.556, 1.563, 1.588, 1.553, 1.570 (4) Å, respectively, and the shortest is C(14)—C(15), 1.471 Å, which is common to rings *D* and *E*. Four of the C(sp^3)—C(sp^2) have normal lengths 1.488–1.506(5) Å, mean = 1.499 Å, but the C(24)—C(25) which is observed as 1.459(5) Å is rather short and may be severely affected by thermal motion. All the other bond lengths are fairly close to their expected values. The C—H are of lengths 0.84–1.12(4) Å, mean = 0.98 Å.

The mean valency angles in the six-membered rings *B*, *C*, *D* are 110.7, 112.2, 114.8°, respectively, with the largest C—C—C angles being C(8)—C(14)—C(13) = 119.2(2)° and C(14)—C(15)—C(16) = 119.3(2)° which appear to result from the fusion of rings *D* and *E* at C(14)—C(15). The mean angle in the lactone ring *A* is 117.7° with the largest being C(3)—O(1)—C(4) = 129.0(2)°, while the mean for the furan ring is 108.0°.

The view of the molecule shown in Fig. 1 and the torsion angles listed in Fig. 2(*c*) indicate clearly the conformation of the rings as: *A* chair, *B* chair, *C* twist-boat, *D* 1,3-diplanar, *E* planar, and *F* planar ($\chi^2 = 0.9$). The C_2O_2 atoms of each acetate group are coplanar, with $\chi^2 = 0.02$ and 0.05 for the two groups. While C(1) is in the plane of its adjacent acetate group, C(7) is 0.055 Å away from the plane

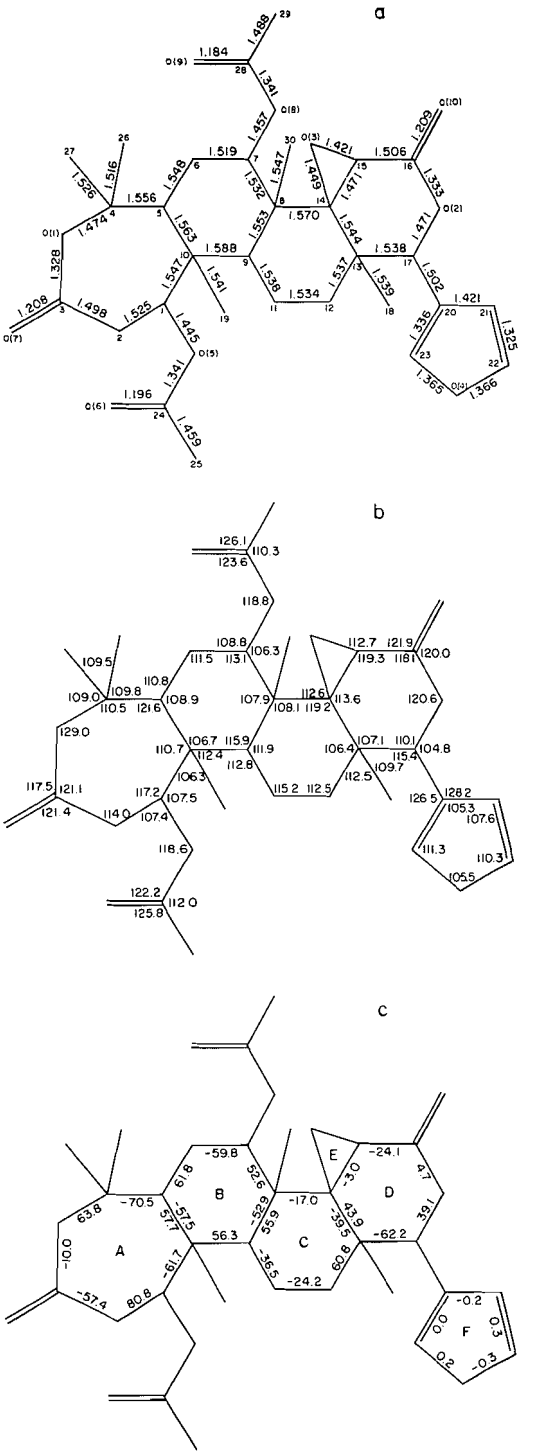

FIG. 2. Schematic drawings of the molecule showing: (*a*) bond lengths (Å), (*b*) valency angles (deg), and (*c*) torsion angles (deg) within the rings. The estimated standard deviations are 0.003–0.005 Å for the bonds and 0.2–0.3° for the angles, excluding the contribution of the parameters' covariance.

Can. J. Chem. Downloaded from www.nrcresearchpress.com by 210.87.254.105 on 09/05/12
For personal use only.

Can. J. Chem. Downloaded from www.nrcresearchpress.com by 210.87.254.105 on 09/05/12
For personal use only.

TABLE 2. Some valency and torsion angles (deg) not listed in Fig. 2

(*a*) Valency angles

Valency angles	Value	Valency angles involving H	Value
O(1)—C(4)—C(26)	99.4	C(17)—H(17)...O(3)	98
C(5)—C(4)—C(27)	117.2	C(30)—H(30)...O(3)	102
C(7)—C(8)—C(14)	110.9	H(17)...O(3)...H(30)	130
C(7)—C(8)—C(30)	108.7	H(17)...O(3)—C(14)	87
C(9)—C(8)—C(30)	114.8	H(17)...O(3)—C(15)	102
C(14)—C(8)—C(30)	106.4	H(30)...O(3)—C(14)	87
C(1)—C(10)—C(9)	105.4	H(30)...O(3)—C(15)	118
C(5)—C(10)—C(19)	115.0	O(3)...C(17)—H(17)	59
C(12)—C(13)—C(17)	109.4	O(3)...C(30)—H(30)	57
C(14)—C(13)—C(18)	111.6		
C(8)—C(14)—C(15)	123.7		
C(13)—C(14)—O(3)	113.5		
O(3)—C(14)—C(15)	58.2		
O(3)—C(15)—C(14)	60.1		
C(14)—O(3)—C(15)	61.7		

(*b*) Torsional angles

Bonds	Angle
C(19)—C(10)—C(5)—H(5)	179.5
C(30)—C(8)—C(9)—H(9)	−178.6
C(18)—C(13)—C(14)—O(3)	−140.2
C(8)—C(14)—C(15)—H(15)	−6.4

of the second acetate group. Also, C(17) lies in the plane of its adjacent furan ring.

The equations of the mean planes of the rings and acetate groups, and some of the dihedral angles between them are summarized in Table 3. The curvature of the molecule is almost uniform as shown by the dihedral angles *A–B*, *B–C*, *C–D* of 18.7, 18.5, and 13.4°, respectively, which add up to 50.6° while *A–D* is 49.9°.

TABLE 3. Mean planes and dihedral angles (deg). The planes are in the form $lX + mY + nZ - p = 0$, where X, Y, Z, p are in Å. The planes are identified in Fig. 2(*c*); Ac(1) and Ac(7) are the substituent groups at C(1) and C(7)

(*a*) Planes

Plane	*l*	*m*	*n*	*p*
A	−0.6136	0.5288	−0.5864	1.2788
B	−0.3295	0.6061	−0.7239	1.3278
C	−0.0140	0.6159	−0.7877	1.9900
D	0.1935	0.5198	−0.8321	2.1507
E	−0.7735	−0.3665	−0.5171	−6.4905
F	0.7650	0.0807	−0.6389	3.5316
Ac(1)	0.8875	0.3203	−0.3315	0.7061
Ac(7)	0.9395	0.0410	−0.3400	1.6886

(*b*) Dihedral angles

Planes	Angle	Planes	Angle
A–B	18.7	*D–E*	84.8
B–C	18.5	*D–F*	43.8
C–D	13.4	*A*–Ac(1)	79.6
A–D	49.9	*B*–Ac(7)	87.8
		Ac(1)–Ac(7)	16.3

O(3), the apex of the three-membered ring, has four close intramolecular neighbours: C(17) and C(30) at distances 2.623(3) and 2.668(4) Å, and their associated H atoms at 2.28(2) and 2.28(3) Å from O(3). The angles associated with these short contacts are listed in Table 2, and the corresponding C—H are 1.03(2) and 1.01(3) Å. Also, it should be stated that H(17) is only 0.56 Å from the mean plane of O(3), C(14), C(13), C(17); and H(30, 1) is 0.45 Å from the mean plane of O(3), C(14), C(8), and C(30). This information is provided for the benefit of those interested in the study of C—H...O hydrogen bonds which may be present in this structure. However, for the lack of a proper analysis of the electron charge distribution in the molecule, the true nature of these contacts cannot be stated at present.

All the other intramolecular O...H contacts are ≥2.33 Å, and the H...H contacts are ≥1.88 Å. There are no unusually short intermolecular van der Waals contacts which might be indicative of hydrogen bonding, and the molecules are therefore held together by electrostatic forces.

Experimental

Melting points were determined on a Fisher-Johns melting point apparatus and are uncorrected. Elemental microanalyses

Can. J. Chem. Downloaded from www.nrcresearchpress.com by 210.87.254.105 on 09/05/12
For personal use only.

TABLE 4. Atomic fractional coordinates ($\times 10^4$ for C and O, $\times 10^3$ for H)

Atom	x/a	y/b	z/c	Atom	x/a	y/b	z/c
C(1)	−6(2)	4071(2)	3610(2)	H(1)	25(2)	461(1)	379(2)
C(2)	−1133(2)	4060(2)	3887(2)	H(2, 1)	−117(2)	435(2)	451(2)
C(3)	−1537(2)	3262(2)	4137(2)	H(2, 2)	−149(3)	428(2)	334(3)
C(4)	−1159(2)	2708(2)	2331(2)	H(5)	34(2)	268(1)	275(2)
C(5)	−34(2)	2980(2)	2230(2)	H(6, 1)	23(2)	215(2)	102(2)
C(6)	415(2)	2734(2)	1152(2)	H(6, 2)	17(2)	307(2)	67(2)
C(7)	1570(2)	2754(2)	1164(2)	H(7)	184(2)	255(1)	51(2)
C(8)	2000(2)	3567(2)	1411(2)	H(9)	173(2)	342(1)	298(2)
C(9)	1497(2)	3859(1)	2446(2)	H(11, 1)	154(3)	509(2)	256(3)
C(10)	291(2)	3841(2)	2471(2)	H(11, 2)	182(2)	474(2)	359(2)
C(11)	1938(2)	4649(2)	2805(3)	H(12, 1)	319(2)	505(2)	194(2)
C(12)	3080(2)	4756(1)	2609(2)	H(12, 2)	343(3)	505(2)	323(3)
C(13)	3648(2)	3973(1)	2533(2)	H(15)	355(2)	244(1)	84(2)
C(14)	3179(2)	3528(1)	1592(2)	H(17)	483(2)	440(1)	154(2)
C(15)	3831(2)	2898(2)	1183(2)	H(18, 1)	367(3)	381(2)	417(3)
C(16)	4869(2)	2776(2)	1657(2)	H(18, 2)	403(4)	307(3)	354(4)
C(17)	4770(2)	4126(1)	2261(2)	H(18, 3)	296(4)	324(2)	370(4)
C(18)	3580(2)	3495(2)	3558(2)	H(19, 1)	23(3)	497(2)	165(3)
C(19)	−185(2)	4464(2)	1745(3)	H(19, 2)	−91(3)	460(2)	192(4)
C(20)	5364(2)	4565(2)	3080(2)	H(19, 3)	−28(3)	431(2)	101(3)
C(21)	6031(2)	4259(2)	3859(3)	H(21)	617(2)	374(2)	402(2)
C(22)	6393(2)	4858(2)	4406(3)	H(22)	685(3)	488(2)	495(3)
C(23)	5374(3)	5340(2)	3224(3)	H(23)	503(2)	579(2)	287(2)
C(24)	737(2)	3781(2)	5290(2)	H(25, 1)	124(4)	324(3)	656(4)
C(25)	1244(3)	3173(3)	5904(3)	H(25, 2)	177(4)	288(3)	547(4)
C(26)	−1240(3)	1846(2)	2065(3)	H(25, 3)	69(4)	267(3)	584(4)
C(27)	−1954(3)	3165(3)	1708(3)	H(26, 1)	−73(3)	152(2)	245(3)
C(28)	1920(2)	1461(2)	1828(3)	H(26, 2)	−182(3)	163(2)	232(3)
C(29)	2279(3)	1039(2)	2784(3)	H(26, 3)	−122(3)	177(2)	131(3)
C(30)	1832(2)	4103(2)	444(2)	H(27, 1)	−259(3)	288(2)	179(3)
O(1)	−1466(2)	2681(1)	3447(2)	H(27, 2)	−177(3)	329(2)	105(3)
O(2)	5314(1)	3381(1)	2132(2)	H(27, 3)	−205(2)	376(2)	195(2)
O(3)	3750(1)	3615(1)	623(1)	H(29, 1)	243(4)	47(2)	264(3)
O(4)	5999(2)	5544(1)	4037(2)	H(29, 2)	171(5)	108(3)	339(5)
O(5)	502(1)	3535(1)	4316(1)	H(29, 3)	292(5)	132(3)	314(5)
O(6)	542(3)	4428(2)	5589(2)	H(30, 1)	224(3)	391(2)	−17(3)
O(7)	−1927(2)	3119(1)	4977(2)	H(30, 2)	120(3)	414(2)	23(3)
O(8)	1935(1)	2236(1)	1994(1)	H(30, 3)	200(3)	464(2)	60(3)
O(9)	1658(2)	1170(1)	1026(2)				
O(10)	5303(2)	2154(1)	1604(2)				

were performed by Beller Microanalytical Laboratory, West Germany.

Infrared spectra were recorded as KBr pellets on a Perkin-Elmer 567 or 710A grating spectrometer and were calibrated against the 2850 and 1601 cm^{-1} bands of polystyrene film. ^{1}Hmr spectra were determined in $CDCl_3$ with a Perkin-Elmer R-12B or Varian HA 100 spectrometer; band positions are reported in parts per million downfield from tetramethylsilane as an internal standard; ^{13}Cmr spectra were recorded on a Varian XL 100 instrument. Mass spectra were recorded by Morgan-Schaeffer, Montreal.

Extraction and Isolation

Fresh seeds of *Uncaria Gambier Roxb.* collected in the botanical garden in Singapore were separated from their nut husks and crushed using a blender. The ground seeds (1500 g) were stirred mechanically in methanol (3000 ml) for 48 h at room temperature. The mixture was filtered and the residue re-extracted with fresh methanol. The combined brownish red extracts were concentrated to approximately half the original volume under reduced pressure on a rotary evaporator and further extracted with petroleum ether followed by benzene (700 ml portions in a separatory funnel).

The concentrated benzene fraction was chromatographed on silica gel. The column was eluted with petroleum ether followed by petroleum ether – diethylether and fractions (~50 ml) were combined on the basis of similar R_f values on tlc slides. Crystalline material was obtained from the more polar fractions and was recrystallized with difficulty from methanol, mp 265–266°C. The 7α-acetoxydihydronomilin had the following spectral properties: ir (KBr) 3140 (CH=C), 1720–1740 (C=O), 1630 (C=C), 875 (furan) cm^{-1}; ^{1}Hmr ($CDCl_3$) 7.40 (2H, d, J = 2 Hz, furan), 6.32 (1H, d, J = 2 Hz, furan), 5.60 (1H, s, H—C—O), 4.84 (1H, m, HCOAc), 4.50 (1H, m, HCOAc), 3.51 (1H, s, H—C—O), 3.15 (2H, d, J = 4 Hz, —CH_2CO) ppm; ms: M* *m/e* 558, calcd. 558. *Anal.* calcd. for $C_{30}H_{38}O_{10}$: C 64.50, H 6.86, O 28.64; found: C 64.30, H 7.12, O 28.58.

Crystal Data

$C_{30}H_{38}O_{10}$ fw = 558.63

Unit cell: orthorhombic, $P2_12_12_1$, a = 13.158(2), b = 17.092(2), c = 12.689(2) Å, V = 2853.7 Å^3, Z = 4, D_c = 1.300, D_o = 1.300 g cm^{-3}, $F(000)$ = 1192, μ(Cu Kα) = 7.68 cm^{-1}, λ(Cu Kα$_1$) = 1.54050, λ(Cu Kα$_2$) = 1.54434 Å.

Can. J. Chem. Downloaded from www.nrcresearchpress.com by 210.87.254.105 on 09/05/12
For personal use only.

The space group was uniquely determined from the systematic absences on precession photographs. The unit-cell parameters were derived from the 2θ values of some high-order axial reflexions. The crystal density was measured by flotation in aqueous KI solution at 26°C.

Intensities

The intensity data were collected on a Picker diffractometer with the θ–2θ scan method, using a prismatic crystal (0.4 × 0.6 × 0.3 mm) and Cu(Kα) radiation to ($\sin\theta/\lambda$) limit of 0.588. The 2θ scans covered 2° for 2θ = 0–100°, and 3° for 2θ = 100–130°. The background corrections were derived from an empirical curve expressed as a function of 2θ. The (006) was used as a monitor reflexion for scaling purposes, and its intensity showed a small random variation of ±2% throughout the experiment. The net intensities were corrected for the Lorentz-polarization effect, but not for absorption. The total number of reflexions scanned was 2740, of which 2621 reflexions (95.8%) were observed above background.

Structure Determination

The positions of the 40 non-hydrogen atoms were determined from an *E* map and two Fourier syntheses. The *E* map, calculated from 328 reflexions with $|E| \geq 1.40$, showed two images of the molecule separated by a prominent C—C bond vector parallel to ***a***. This map was interpreted as described by Huber (7) by placing the molecule halfway between the two images. Twenty of the atomic positions were accepted from this map, and the other 20 positions were derived from two successive Fourier syntheses. At the start, C atoms were placed at most of the atomic positions and their parameters including the occupancies and isotropic temperature factors were refined by three cycles of block-diagonal least-squares calculations. The possible O positions were then identified on the basis of their occupancies and bond lengths. At that stage, the occupancies were 0.91–1.25 for the C sites and 1.23–1.44 for the O sites, with estimated standard deviations of 0.04–0.05. The occupancies were then fixed at 1.00 for all atoms and the parameters were refined anisotropically. Finally the H atoms were located from three difference maps calculated at later stages, and were refined isotropically. The refined atomic positions are listed in Table 4.[3]

The quantity minimized in the least-squares refinement was $\Sigma w(|F_o| - |F_c|)^2$, where $w = 1/\{1 + [(|F_o| - 15)/40]^4\}$ and $1.53 \leq |F_o| \leq 154.1$. All the unobserved reflexions, as well as eight very strong reflexions showing extinction effect, and one weak reflexion were excluded from the refinement. In the final cycle, the mean $(\Delta/\sigma) = 0.22$, maximum $(\Delta/\sigma) = 0.77$ for C and O (= 2.1 for H); $R = 0.037$ and $R_w = 0.039$ for the observed reflexions excluding those omitted from the refinement ($R = 0.042$ for all observed reflexions), $[\Sigma(w\Delta^2)/(m - n)]^{1/2} = 0.70$. There were no outstanding discrepancies in the calculated structure amplitudes of the unobserved reflexions. The residual electron density in the final difference map was randomly distributed within −0.15 and 0.17 e Å^{-3}.

The scattering factor curves were those of ref. 8 for C and O, and of ref. 9 for H. All computations were performed with the NRCC set of crystallographic computer programs (10).

[3]The atomic thermal parameters and the structure amplitudes are available, at a nominal charge, from the Depository of Unpublished Data, CISTI, National Research Council of Canada, Ottawa, Ont., Canada K1A 0S2.

Acknowledgements

The authors are grateful to Dr. A. W. Hanson for measuring the cell parameters and intensity data, to Mrs. M. E. Pippy for assistance with the computations, to Dr. J. Walter for ^{13}Cmr spectra, to the Department of Chemistry, Nanyang University for assistance (to A.S.N.), and to Memorial University of Newfoundland and the National Research Council of Canada for financial support (to A.G.F.) of this research.

1. L. MERLINI, R. MONDELLI, and G. NASINI. Tetrahedron, **23**, 3129 (1967); Tetrahedron Lett. 1571 (1967); Tetrahedron, **26**, 2259 (1970).
2. D. L. DREYER. Phytochem. **5**, 367 (1966); see also D. ARIGONI, D. H. R. BARTON, E. J. COREY, O. JEGER, L. CAGLIOTI, S. DEV, P. G. FERRINI, E. R. GLAZIER, A. MELERA, S. K. PRADHAN, K. SCHAFFNER, S. STERNHELL, J. F. TEMPLETON, and S. TOBINAGA. Experientia, **16**, 41 (1960).
3. O. H. EMERSON. J. Am. Chem. Soc. **70**, 545 (1948); **73**, 2621 (1951).
4. D. A. H. TAYLOR. J. Chem. Soc. Perkin I, 437 (1974).
5. H. R. HARRISON, O. HODDER, C. W. L. BEVAN, D. A. H. TAYLOR, and T. G. HALSALL. Chem. Commun. 1388 (1970); S. ARNOTT, A. W. DAVIE, J. M. ROBERTSON, G. A. SIM, and D. G. WATSON. Experientia, **16**, 49 (1960).
6. D. L. DREYER. Tetrahedron, **21**, 75 (1965).
7. C. S. HUBER. Acta Crystallogr. B**31**, 108 (1975).
8. H. P. HANSON, F. HERMAN, J. D. LEA, and S. SKILLMAN. Acta Crystallogr. **17**, 1040 (1964).
9. R. F. STEWART, E. R. DAVIDSON, and W. T. SIMPSON. J. Chem. Phys. **42**, 3175 (1965).
10. F. R. AHMED, M. E. PIPPY, and C. S. HUBER. J. Appl. Crystallogr. **6**, 309 (1973).

Some reactions of *N*-substituted-1,2-dihydropyridines with cyanogen azide. Synthesis of 1,2,3,4-tetrahydropyridylidene-4-cyanamides

THEODORE A. ONDRUS AND EDWARD E. KNAUS

Faculty of Pharmacy and Pharmaceutical Sciences, University of Alberta, Edmonton, Alta., Canada T6G 2N8

AND

C. S. GIAM

Department of Chemistry, Texas A&M University, College Station, TX 77843, U.S.A.

Received October 21, 1977

THEODORE A. ONDRUS, EDWARD E. KNAUS, and C. S. GIAM. Can. J. Chem. **56**, 1026 (1978).

The reaction of cyanogen azide (**2**) with several *N*-substituted-1,2-dihydropyridines (**1**) has been investigated. Reaction of 1,2-dihydropyridines (**1***a–d*) possessing a *N*-methoxycarbonyl or *N*-methanesulfonyl substituent with **2** afford a 1:1 mixture of stereoisomers *E*- and *Z*-1,2,3,4-tetrahydropyridylidene-4-cyanamides (**3** and **4**). In contrast, reaction of *N*-acetyl-2-butyl-1,2-dihydropyridine (**1***e*) with **2** gave rise to the unexpected 2,7-diazabicyclo[4.1.0]hept-4-ene (**7**) and 2-diazo-1,2,3,6-tetrahydropyridylidene-3-cyanamide (**9**) together with a 1:1 isomeric mixture of **3***e* and **4***e*. Mechanisms for the formation of **3**, **4**, **7**, and **9** are discussed.

THEODORE A. ONDRUS, EDWARD E. KNAUS et C. S. GIAM. Can. J. Chem. **56**, 1026 (1978).

On a étudié la réaction de l'azoture de cyanogène (**2**) avec plusieurs dihydro-1,2 pyridines substituées sur l'azote (**1**). La réaction des dihydro-1,2 pyridines (**1***a–d*) possédant un substituant *N*-méthoxycarbonyle ou *N*-méthanesulfonyle avec **2** conduit à un mélange 1:1 des stéréoisomères *E*- et *Z*-tétrahydro-1,2,3,4 pyridylidènecyanamide-4 (**3** et **4**). Par ailleurs, la réaction de la *N*-acétylbutyl-2 dihydro-1,2 pyridine (**1***e*) avec **2** conduit au diaza-2,7 bicyclo[4.1.0]heptène-4 (**7**) et au diazo-2 tétrahydro-1,2,3,6 pyridylidènecyanamide-3 (**9**) qui sont innattendus de même qu'à un mélange 1:1 des isomères **3***e* et **4***e*. On discute des mécanismes de formation des composés **3**, **4**, **7** et **9**.

[Traduit par le journal]

The 1,3-dipolar cycloaddition reaction of cyanogen azide with cyclic dienamines is an attractive method for the synthesis of pharmacologically interesting heterocycles. Since the synthesis of cyanogen azide was first reported (1) several studies which demonstrate its usefulness have appeared. Reaction with olefins (2) afforded alkylidenecyanamides and *N*-cyanoaziridines and with acetylenes (3) gave rise to 1-cyanotriazoles which are in equilibrium with the tautomeric α-diazo-*N*-cyanoimines. Other reported reactions of molecular cyanogen azide include addition to norbornadiene (4), the ring contraction of enamines of cyclic ketones (5), and ring expansion of alkylidenecycloalkanes (6). It was therefore of interest to develop methods for the preparation of bicyclic ring structures in which 1,2,3-triazoline or aziridine is fused to a tetrahydropyridine ring.

In earlier studies we showed that reaction of pyridine with organolithium reagents afford *N*-lithio-1,2-dihydropyridines (7) which on reaction with acid chlorides or esters (8) gave *N*-substituted-1,2-dyhydropyridines (**1***b*, **1***c*, and **1***e*) whereas the sodium borohydride reduction of *N*-methoxycarbonyl (methanesulfonyl) pyridinium chloride yields **1***a* (9) and **1***d* (10). The reaction of dienamines **1** with cyanogen azide **2** now provides a convenient route to *E*- and *Z*-1,2,3,4-tetrahydropyridylidene-4-cyanamides **3** and **4** and 3-*n*-butyl-7-cyano-2,7-diazabicyclo[4.1.0]hept-4-ene (**7**).

Reaction of *N*-methoxycarbonyl-1,2-dihydropyridine (**1***a*) with a fourfold excess of **2** at 25°C for 18 h afforded a 1:1 mixture (52.1%) of stereoisomers *E*- (**3***a*) and *Z*-1-methoxycarbonyl-1,2,3,4-tetrahydropyridylidene-4-cyanamide (**4***a*) which could not be separated by fractional crystallization or thin-layer chromatography. The mechanism proposed involves the 1,3-dipolar cycloaddition of molecular cyanogen azide to the C(3)—C(4) olefinic bond of **1***a*. Loss of nitrogen and C(4) hydrogen migration from the unstable triazoline intermediate would afford both **3***a* and **4***a*. If the intermediate triazoline adduct is the product of electronic control, the nitrogen atom bearing the cyano group should be directed to the C(4) position of the ring (11). The absence of steric effects at the C(3) and C(5) positions of **3***a* and **4***a* results in a *E*/*Z* ratio of 1:1 (2). A ^{1}H nmr temperature study effected on the mixture of stereoisomers **3***a* and **4***a* in DMSO-d_6 indicated the coalescence temperature to be approximately 90°C which is similar to that reported for simple acyclic alkylidene cyanamides (12). Upon cooling to 25°C the ratio of **3***a*:**4***a* returned to 1:1. (See Fig. 1).

Can. J. Chem. Downloaded from www.nrcresearchpress.com by 210.87.254.105 on 09/05/12
For personal use only.

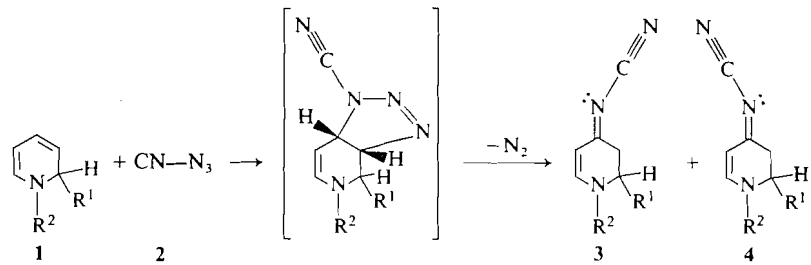

1 2 3 4

a R^1 = H, R^2 = CO_2Me; *b* R^1 = Ph, R^2 = CO_2Me; *c* R^1 = *n*Bu, R^2 = CO_2Me
d R^1 = H, R^2 = SO_2Me; *e* R^1 = *n*Bu, R^2 = COMe

The structures assigned to **3***a* and **4***a* are consistent with the spectral data obtained. The uv spectrum exhibited one band at 333 nm which corresponds well to the λ_{max} expected for the N—C=C—C=N system (13), while the ir spectrum displayed peaks at 2180 (C≡N), 1730 (CO), 1590 (C=N), and 1560 (C=C) cm^{-1}. The ^1H nmr spectrum (δ) of **3***a* and **4***a* exhibited a 2H triplet ($J_{2,3}$ = 7.5) at 2.74 (**4***a*) and 2.95 (**3***a*) attributed to the C(3)H which collapses to two single peaks upon irradiation of the C(2)H at 3.9. The two triplets due to the C(3)H also coalesce to one triplet ($J_{2,3}$ = 7.5) at 2.82 upon heating to 130°C. Other absorptions include a 3H singlet at 3.81 due to the methoxyl methyl, a 2H triplet ($J_{2,3}$ = 7.5) at 3.9 due to the C(2)H and a 1H doublet ($J_{5,6}$ = 8) at 5.59 (**3***a*) and 5.85 (**4***a*) due to the C(5)H which collapse to two single peaks upon irradiation of the C(6)H at 7.93. The two doublets at 5.59 and 5.85 coalesce to one doublet ($J_{5,6}$ = 8) at 5.68 upon heating to 130°C. The 1H doublets ($J_{5,6}$ = 8) at 7.9 (**4***a*) and 7.95 (**3***a*) due to the C(6)H selectively collapse to singlets upon irradiation of the absorption at 5.85 attributed to the C(5)H of **4***a* and the absorption at 5.59 due to the C(5)H of **3***a*, respectively, thereby providing further evidence for the presence of two isomers. The cyano group (**3***a*) is expected (2) to deshield the C(3)H (**3***a*) whereas the cyano group (**4***a*) is expected to deshield the C(5)H (**4***a*). The mass spectrum of **3***a* and **4***a* exhibited a molecular ion at *m/e* 179 (*Exact Mass* calcd. for $C_8H_9N_3O_2$: 179.0694; found (high resolution ms): 179.0694). Similar reactions of **1***b–d* with **2** afforded low to moderate yields of 1:1 mixtures of stereoisomers **3** and **4***b–d*, along with considerable amounts of unreacted **1** (see Table 1).

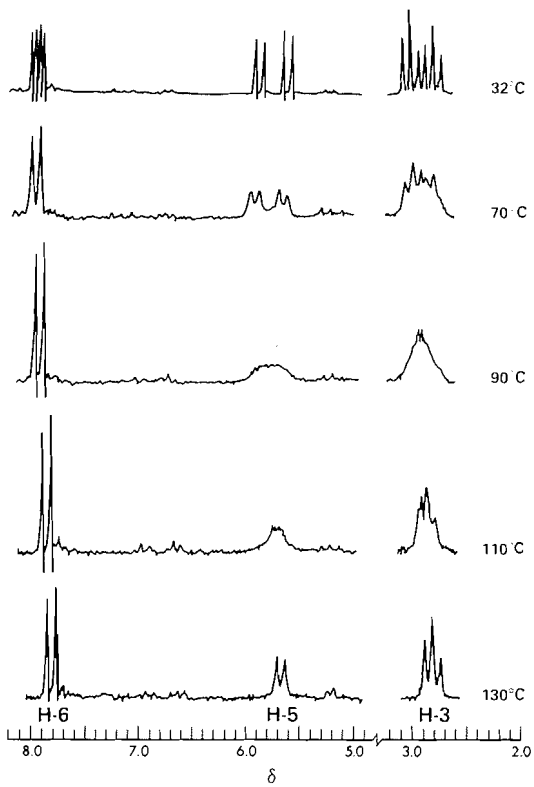

FIG. 1. ^1H nuclear magnetic resonance temperature study of a 1:1 stereoisomeric mixture of *E*- (**3***a*) and *Z*-1-methoxycarbonyl-1,2,3,4-tetrahydropyridylidene-4-cyanamide (**4***a*).

The reaction of *N*-acetyl-2-butyl-1,2-dihydropyridine (**1***e*) with a 4 molar excess of **2** gave rise to a 1:1 mixture of **3***e* and **4***e* (36.5%), 3-*n*-butyl-7-cyano-2,7-diazabicyclo[4.1.0]hept-4-ene (**7**) (19.7%), and *N*-acetyl-6-*n*-butyl-2-diazo-1,2,3,6-tetrahydropyridylidene-3-cyanamide (**9**) (19.4%) as well as unreacted **1***e* (3.9%). The isolation of **3***e* and **4***e* as well as **7** and **9** suggests that a 1,3-dipolar cycloaddition reaction occurred at both the C(3)—C(4) and C(5)—C(6) olefinic bonds. One plausible mechanism for the formation of **7** involves addition of **2** across the C5—C6 olefinic bond of **1***e* to give a triazoline adduct **5**. Attack by azide anion on the carbonyl carbon atom and elimination of acetylazide and nitrogen to afford anion **6** which on cyclization and protonation would give **7**. All of the cyanogen azide solutions contain free azide since a 4 molar excess of sodium azide was used in their preparation.

Alternatively elimination of a molecule of hydrogen from the triazoline adduct **5** would give the more aromatic 1,2-dihydropyridine derivative **8**. Ring

Can. J. Chem. Downloaded from www.nrcresearchpress.com by 210.87.254.105 on 09/05/12
For personal use only.

Can. J. Chem. Downloaded from www.nrcresearchpress.com by 210.87.254.105 on 09/05/12
For personal use only.

TABLE 1. Reactions of 1,2-dihydropyridines with cyanogen azide

Compound	Reaction time (h)	Ratio 1:2	Yield (%) 3 and 4	7	9	Recovered 1
1*a*	18	1:5	52.1[a]			1.3
	20	4:5	20.8[a]			24.3
1*b*	72	1:1	14.6[a]			66.3
1*c*	8	2:3	41.6[a]			21.7
1*d*	20	1:3	14.5[a]			40.1
1*e*	1	4:5	7.2[b,c]	25.3[c]	3.9	44.7
	1	1:5	36.5[b,c]	19.7[c]	19.4	3.9

[a]The ratio of products 3:4 as determined from the integrals of the C(5)H was 1:1.
[b]The ratio of products 3:4 as determined from the integrals of the C(2)H was 1:1.
[c]The yield of 3*e* and 4*e* was calculated from the integral of the C(2)H while the yield of 7 was calculated from the integral of the C(3)H.

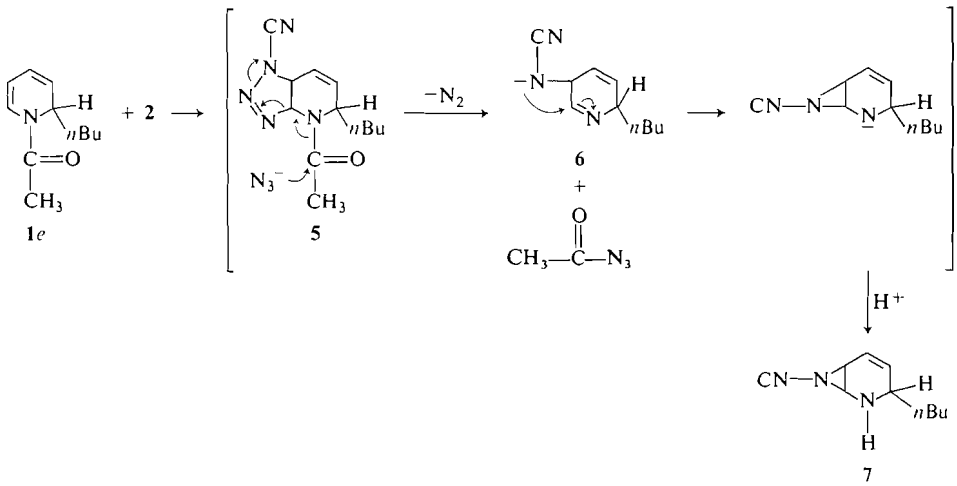

opening of **8**, by a mechanism similar to that proposed for the adduct obtained from acetylene and cyanogen azide (3), would give rise to **9**.

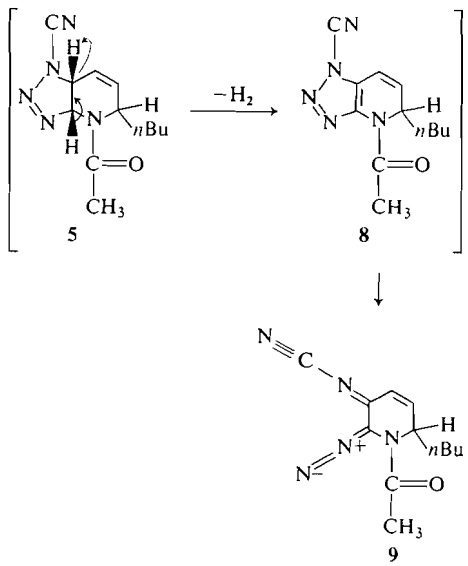

It is interesting to note that addition occurred at both C(3)—C(4) and C(5)—C(6) olefinic bonds of **1***e* suggesting that steric effects of the R^2-substituent may also play a role in determining the site of addition since the acetyl group exhibits a smaller steric effect than methanesulfonyl and methoxycarbonyl (14).

The reacting species in all of these reactions is molecular cyanogen azide since loss of nitrogen to give cyanonitrene occurs above 40°C (15). It is expected that the yield of **3** and **4** could be increased significantly by using larger molar amounts of **2** since a significant percentage of **1** is often recovered (see Table 1).

The reaction of other organic azides and other 1,3-dipoles with both 1,2- and 1,4-dihydropyridine are now in progress to broaden the scope of this reaction.

Experimental

Melting points are determined with a Büchi capillary apparatus and are uncorrected. ^{1}H Nuclear magnetic resonance spectra were determined for solutions in deuterio-

Can. J. Chem. Downloaded from www.nrcresearchpress.com by 210.87.254.105 on 09/05/12
For personal use only.

chloroform unless otherwise noted with TMS as internal standard with a Varian EM-360A, HA-100 or HA-220 spectrometer. Infrared spectra were recorded on a Perkin Elmer 267 spectrometer. Mass spectra were measured with an AEI-MS-9 or MS-50 mass spectrometer and these exact mass measurements are used in lieu of elemental analysis. *Warning*: Cyanogen azide is a hazardous material. It should be handled only in solution. Concentration to pure material will result in violent detonation by heat or shock (2).

Cyanogen Azide (2)

General Procedure A

Cyanogen azide was prepared *in situ* using the procedure of Hermes and Marsh (2). Cyanogen bromide (2.65 g, 25 mmol) in acetonitrile (25 ml) was added slowly with vigorous stirring to a suspension of sodium azide (8.12 g, 0.125 mol) in 75 ml dry acetonitrile at 0°C under a nitrogen atmosphere. After 1 h at 0°C the reaction mixture was warmed slowly to 25°C over a 2-h period. The mixture was maintained at 25°C for 1 h after which the desired 1,2-dihydropyridine (**1**) was added.

E-*1-Methoxycarbonyl-1,2,3,4-tetrahydropyridylidene-4-cyanamide(3*a*) and Z-1-Methoxycarbonyl-1,2,3,4-tetrahydropyridylidene-4-cyanamide(4*a*)*

General Procedure B

A solution of **1***a* (2.78 g, 20 mmol) in 50 ml dry ether was added with stirring to a solution of **2** prepared from cyanogen bromide (2.65 g, 25 mmol) and sodium azide (8.12 g, 125 mmol) in 100 ml dry acetonitrile under a nitrogen atmosphere at 25°C. The reaction was allowed to proceed for 20 h at 25°C. Filtration and removal of the solvent *in vacuo* gave a black semisolid which was partitioned between chloroform (100 ml) and water (100 ml). The chloroform fraction was washed with water (50 ml) and the combined water fractions extracted with chloroform (2 × 75 ml). The chloroform extracts were dried (Na_2SO_4) and solvent removed *in vacuo* to yield a black semisolid which was subjected to preparative tlc on 10 8 in. × 8 in. silica gel G plates, 0.75 mm in thickness, using benzene – ethyl acetate (2:1 v/v) as development solvent. Extraction with 50 ml warm methanol of the fraction having R_f 0.95 gave **1***a* (0.676 g, 24.3%). Extraction of the band having R_f 0.47 afforded a 1:1 mixture of **3***a* and **4***a* (0.744 g, 20.8%).

When the reaction was carried out as above using a 4 molar excess of **2** for 18 h at 25°C **3***a* and **4***a* (52.1%) and **1***a* (1.3%) were obtained. (Spectral data are presented in Discussion.)

E-*1-Methoxycarbonyl-2-phenyl-1,2,3,4-tetrahydropyridylidene-4-cyanamide(3*b*) and Z-1-Methoxycarbonyl-2-phenyl-1,2,3,4-tetrahydropyridylidene-4-cyanamide(4*b*)*

A solution of **1***b* (1.53 g, 7.2 mmol) in 25 ml dry ether was added to a solution of **2** prepared from a solution of cyanogen bromide (0.795 g, 7.5 mmol) and sodium azide (2.44 g, 37.5 mmol) in 50 ml acetonitrile. The reaction was allowed to proceed at 25°C for 72 h as described under Procedure B to give a reddish-black semisolid. Preparative tlc was effected on eight 8 in. × 8 in. silica gel G plates, 0.75 mm in thickness, using benzene – ethyl acetate (9:1 v/v) as development solvent. Extraction of the fraction having R_f 0.78 with 50 ml warm methanol gave **1***b* (1.03 g, 66.3%). Extraction of the band having R_f 0.27 afforded a 1:1 mixture of **3***b* and **4***b* (0.27 g, 14.6%); ir (film): 2180 (s, C≡N), 1730 (s, CO), 1590 (s, C=N), and 1560 cm^{-1} (s, C=C); ^1H nmr δ: 3.07 (**4***b*) and 3.53 (**3***b*) (m, 1H, H-3[1]), 3.26 (**4***b*) and 3.35 (**3***b*) (m, 1H, H-3), 3.9 (s, 3H, OCH_3), 5.72 (m, 1H, H-2), 5.73 (**3***b*) and 6.1 (**4***b*) (d, $J_{5,6}$ = 8 Hz, 1H, H-5), 7.3 (m, 5H, phenyl), 7.98 (d, $J_{5,6}$ = 8 Hz, 1H, H-6); *Exact Mass* calcd. for $C_{14}H_{13}N_3O_2$: 255.1008; found (high resolution ms): 255.1008.

E-*1-Methoxycarbonyl-2-*n*-butyl-1,2,3,4-tetrahydropyridylidene-4-cyanamide(3c) and Z-1-Methoxycarbonyl-2-*n*-butyl-1,2,3,4-tetrahydropyridylidene-4-cyanamide(4c)*

A solution of **1***c* (0.663 g, 3.4 mmol) in 25 ml dry ether was added to a solution of **2** prepared from cyanogen bromide (0.53 g, 5 mmol) and sodium azide (1.62 g, 25 mmol) in 50 ml acetonitrile. The reaction was allowed to proceed at 25°C for 8 h as described under Procedure B to give a reddish-black semisolid. Preparative tlc was effected on nine 8 in. × 8 in. silica gel G plates, 0.75 mm in thickness, using benzene – ethyl acetate (9:1 v/v) as development solvent. Extraction of the fraction having R_f 0.81 with 50 ml warm methanol gave **1***c* (0.144 g, 21.7% recovery). Extraction of the fraction having R_f 0.46 afforded a 1:1 mixture of **3***c* and **4***c* (0.322 g, 41.6%); uv (95% C_2H_5OH, 25°C) λ_{max}; 338 (N̈—C=C—C=N); ir (film): 2180 (s, C≡N), 1730 (s, CO), 1580 (s, C=N) and 1560 cm^{-1} (s, C=C); ^1H nmr δ: 0.88 (t, J = 7 Hz, 3H, —$CH_2CH_2CH_2$-CH_3), 1.1–1.8 (m, 6H, —$CH_2CH_2CH_2CH_3$), 2.72 (**4***c*) and 3.16 (**3***c*) (m, 1H, H-3[1]), 2.83 (**4***c*) and 2.93 (**3***c*) (m, 1H, H-3), 3.89 (s, 3H, OCH_3), 4.5 (m, 1H, H-2), 5.68 (**3***c*) and 5.97 (**4***c*) (d, $J_{5,6}$ = 8 Hz of d, $J_{3,5}$ = 1.25 Hz, 1H, H-5), 7.72 (d, $J_{5,6}$ = 8 Hz of d, $J_{2,6}$ = 1.0 Hz, 1H, H-6); *Exact Mass* calcd. for $C_{12}H_{17}N_3O_2$: 235.1321; found (high resolution ms): 235.1317.

E-*1-Methanesulfonyl-1,2,3,4-tetrahydropyridylidene-4-cyanamide(3*d*) and Z-1-Methanesulfonyl-1,2,3,4-tetrahydropyridylidene-4-cyanamide(4*d*)*

A solution of **1***d* (1.43 g, 9 mmol) in 50 ml dry ether was added to a solution of cyanogen azide prepared from cyanogen bromide (2.65 g, 25 mmol) and sodium azide (8.12 g, 125 mmol) in 100 ml dry acetonitrile. The reaction was allowed to proceed for 20 h at 25°C as described under Procedure B to give a red oil. Preparative tlc was effected on 10 8 in. × 8 in. silica gel G plates, 0.75 mm in thickness, using benzene – ethyl acetate (2:1 v/v) as development solvent. Extraction of the band having R_f 0.91 with 50 ml warm methanol gave unreacted **1***d* (0.575 g, 40.1%). Extraction of the band with R_f 0.34 afforded a 1:1 mixture of **3***d* and **4***d* (0.259 g, 14.5%); ir (film): 2180 (s, C≡N), 1580 (s, C=N), and 1550 (s, C=C) cm^{-1}; ^1H nmr δ: 2.91 (**4***d*) and 3.05 (**3***d*) (m, 2H, H-3), 3.14 (s, 3H, SO_2CH_3), 3.93 (t, $J_{2,3}$ = 7.5 Hz, 2H, H-2), 5.67 (**3***d*) and 5.96 (**4***d*) (d, $J_{5,6}$ = 8 Hz, 1H, H-5), 7.57 (d, $J_{5,6}$ = 8 Hz, 1H, H-6); *Exact Mass* calcd. for $C_7H_9N_3O_2{}^{32}S$: 199.0415; found (high resolution ms): 199.0414.

E-*1-Acetyl-2-*n*-butyl-1,2,3,4-tetrahydropyridylidene-4-cyanamide(3*e*), Z-1-Acetyl-2-*n*-butyl-1,2,3,4-tetrahydropyridylidene-4-cyanamide(4*e*), 3-*n*-Butyl-7-cyano-2,7-diazabicyclo[4.1.0]hept-4-ene(7) and 1-Acetyl-6-*n*-butyl-2-diazo-1,2,3,6-tetrahydropyridylidene-3-cyanamide(9)*

A solution of **1***e* (3.58 g, 20 mmol) in 50 ml dry ether was added dropwise with stirring at 25°C under a nitrogen atmosphere to a solution of **2** prepared from cyanogen bromide (2.65 g, 25 mmol) and sodium azide (8.12 g, 125 mmol) in 100 ml dry acetonitrile. The reaction was allowed to proceed for 1 h at 25°C and completed as described under Procedure B to give a red semisolid. Preparative tlc was effected on six 8 in. × 8 in. silica gel G plates, 0.75 mm in thickness, using benzene–ether (1:2 v/v) as development solvent. Extraction of the band having R_f 0.86 with 50 ml warm methanol gave unreacted **1***e* (1.6 g, 44.7%). Similar extractions of the band with R_f 0.58 yielded **9** (0.192 g, 3.9%); ir (film); 2180 (s, C≡N), 2090 (s, N_2=C), 1700 (s, CO), 1555 (s, C=N), and 1545 cm^{-1} (s, C=C); ^1H nmr δ: 0.9 (t, J = 7 Hz), 3H, —CH_2-

$CH_2CH_2CH_3$), 1.1–1.9 (m, 6H, —$CH_2CH_2CH_2CH_3$), 2.5 (s, 3H, $COCH_3$), 5.11 (m, 1H, H-6), 5.7–6.25 (m, 2H, H-4); *Exact Mass* calcd. for $C_{12}H_{15}N_5O$: 245.1276; found (high resolution ms): 245.1271. Similar extraction of the fraction having R_f 0.47 afforded a 3:1 mixture of **7** and the isomeric **3***e* and **4***e*. The yields were calculated using the ^1H nmr integrals for the H-3 of **7** and H-2 of the **3***e*–**4***e* mixture and were found to be **7** (0.894 g, 25.3%) and **3***e* and **4***e* (0.298 g, 7.2%). This mixture contained all signals present in the ir and ^1H nmr spectra of a pure sample of **7** prepared from the reaction of 2-butyl-1,2-dihydropyridine and cyanogen azide;[1] mp 75°C; ir (KBr): 3225 (m, NH), 2180 (s, C≡N), and 1605 cm^{-1} (s, C=C); ^1H nmr δ: 0.9 (t, J = 7 Hz, 3H, —CH_2CH_2-CH_2CH_3), 1.1–1.9 (m, 6H, —$CH_2CH_2CH_2CH_3$), 3.21 (m, 1H, H-6), 3.3 (m, 1H, H-1), 4.17 (m, 1H, H-3), 5.8 (m, 2H, H-4, H-5), 8.63 (bs, 1H, NH, exchanges with deuterium oxide); *Exact Mass* calcd. for $C_{10}H_{15}N_3$: 177.1266; found (high resolution ms): 177.1265. The mixture also contained those absorptions present in the ir and ^1H nmr spectra of **3***e* and **4***e* described below.

Reaction of **1***e* (3.58 g, 20 mmol) with **2** prepared from equimolar quantities of cyanogen bromide (2.65 g, 25 mmol) and sodium azide (1.625 g, 25 mmol) as described under Procedure A gave a reaction mixture from which a pure sample of the 1:1 isomeric mixture of **3***e* and **4***e* was isolated after a combined series of column and tlc; mp 71°C; ir (KBr): 2180 (s, C≡N), 1700 (s, CO), 1580 (s, C=N), and 1560 cm^{-1} (s, C=C); ^1H nmr δ: 0.9 (t, J = 7 Hz, 3H, $CH_2CH_2CH_2CH_3$), 1.1–1.8 (m, 6H, —$CH_2CH_2CH_2CH_3$), 2.4 (s, 3H, $COCH_3$), 2.58 (**4***e*) and 3.16 (**3***e*) (d, $J_{3,3'}$ = 16 Hz, 1H, H-3[1]), 2.7 (**4***e*) and 2.81 (**3***e*) (d, $J_{3,3'}$ = 16 Hz of d, $J_{2,3}$ = 7.5 Hz, 1H, H-3), 4.76 (m, 1H, H-2), 5.49 (**3***e*) and 5.78 (**4***e*) (d, $J_{5,6}$ = 8 Hz, 1H, H-5), 7.33 (d, $J_{5,6}$ = 8 Hz, 1H, H-6); *Exact Mass* calcd. for $C_{12}H_{17}N_3O$: 219.1372; found (high resolution ms): 219.1372.

[1]E. E. Knaus and T. A. Ondrus. Unpublished results.

Reaction of **1***e* (1.79 g, 10 mmol) with **2** prepared from cyanogen bromide (5.3 g, 50 mmol) and sodium azide (9.75 g, 150 mmol) as described above afforded **1***e* (3.9%), **3***e* and **4***e* (0.755 g, 36.5%), **7** (0.348 g, 19.7%), and **9** (0.47 g, 19.4%).

Acknowledgement

We are grateful to the Medical Research Council of Canada (MA-4888) for financial support of this work.

1. F. D. Marsh and M. E. Hermes. J. Am. Chem. Soc. **86**, 4506 (1964).
2. M. E. Hermes and F. D. Marsh. J. Org. Chem. **37**, 2969 (1972).
3. M. E. Hermes and F. D. Marsh. J. Am. Chem. Soc. **89**, 4760 (1967).
4. A. G. Anastassiou. J. Org. Chem. **31**, 1131 (1966).
5. R. M. Scribner. Tetrahedron Lett. 4737 (1967).
6. J. E. McMurry and A. P. Coppolino. J. Org. Chem. **38**, 2821 (1973).
7. C. S. Giam and J. L. Stout. Chem. Commun. 142 (1969).
8. C. S. Giam, E. E. Knaus, and F. M. Pasutto. J. Org. Chem. **39**, 3565 (1974).
9. F. W. Fowler. J. Org. Chem. **37**, 1321 (1972).
10. E. E. Knaus and K. Redda. Can. J. Chem. **55**, 1788 (1977).
11. G. L'Abbé. Chem. Rev. **69**, 345 (1963).
12. C. G. McCarty and D. M. Wieland. Tetrahedron Lett. 1787 (1969).
13. N. C. Cook and J. E. Lyons. J. Am. Chem. Soc. **88**, 3396 (1966).
14. E. E. Knaus, F. M. Pasutto, and C. S. Giam. J. Heterocycl. Chem. **13**, 481 (1976).
15. A. G. Anastassiou and H. E. Simmons. J. Am. Chem. Soc. **89**, 3177 (1976).

Can. J. Chem. Downloaded from www.nrcresearchpress.com by 210.87.254.105 on 09/05/12
For personal use only.

Bifunctionalized resins. Applications to the synthesis of insect sex attractants[1,2]

THOMAS M. FYLES[3] AND CLIFFORD C. LEZNOFF
Department of Chemistry, York University, Downsview, Ont., Canada M3J 1P3
AND
JOHN WEATHERSTON
Forest Pest Management Institute, Sault Ste. Marie, Ont., Canada P6A 5M7
Received July 28, 1977

THOMAS M. FYLES, CLIFFORD C. LEZNOFF, and JOHN WEATHERSTON. Can. J. Chem. **56**, 1031 (1978).

A 2% crosslinked divinylbenzene–styrene copolymer, incorporating benzoyl chloride groups, was used to monoprotect the symmetrical diol 1,10-decanediol. The corresponding monotrityl ether and *cis*-10-tetradecen-1-ol were prepared by this system, the latter by a Wittig reaction of a polymer-bound ylide with an aldehyde in the solution phase. A series of bifunctionalized resins containing proximally located trityl alcohol and benzoic acid groups was prepared in an attempt to prepare diol linked to the polymer via both a trityl ether and a benzoate linkage. It was established that these polymers bound 1,10-decanediol exclusively at one end only. Polymers, containing both trityl alcohol and benzoic acid groups in a random array or polymers containing proximally located trityl alcohol groups, gave mixtures of both monoprotected and doubly protected diol.

THOMAS M. FYLES, CLIFFORD C. LEZNOFF et JOHN WEATHERSTON. Can. J. Chem. **56**, 1031 (1978).

On a utilisé un copolymère divinylbenzène–styrène réticulé à 2% et incorporant des groupes chlorure de benzoyle pour protéger un seul des hydroxyles du diol symétrique décanediol-1,10. On a préparé l'éther monotritylé correspondant et le tétradécène-10 ol-1 *cis* grâce à ce système; ce dernier composé résulte d'une réaction de Wittig entre un ylure lié au polymère et un aldéhyde en solution. On a préparé une série de résines bifonctionnalisées contenant des alcools trityliques situés à proximité de groupes acides benzoïques, ces résines spéciales ont été préparées en vue de synthétiser des diols liés au polymère à la fois par un lien éther tritylique ainsi qu'à un lien benzoate. On a établi que ces polymères lient exclusivement qu'une extrimité du décanediol-1,10. Les polymères, contenant à la fois des groupes alcool tritylique et acide benzoïque au hasard et les polymères contenant des groupes alcool tritylique situé, à proximité, conduisent à des mélanges de diols mono et doublement protégés.

[Traduit par le journal]

Introduction

Soluble bifunctional polymers have been shown to be capable of mimicking enzymatic reactions (2) by intramolecular cooperation of the two different functional groups. Insoluble bifunctional resins may even more closely approximate enzymatic systems and the studies reported herein may spur development in this area of research. Our own interest in preparing insoluble bifunctional resins lies in another sphere, namely organic synthesis on insoluble polymer supports. Our recently described syntheses of insect sex attractants on solid phases (3–5) still suffer from one minor but persistent problem. In the first step of the synthesis a 2% divinylbenzene (DVB)–styrene copolymer, incorporating trityl chloride groups (**1**) reacts with symmetrical diols, such as 1,10-decanediol (**2**) to give a monoprotected symmetrical diol (**3**), the free end of which can be elaborated to insect sex attractants (3–5). Unfortunately, about 40% of the diol is actually bound to the polymer at both ends (double bound) and although this doubly-bound material does not interfere in the chemical synthesis, its presence means that it is liberated in the final cleavage step from the polymer and must be separated from the desired product.

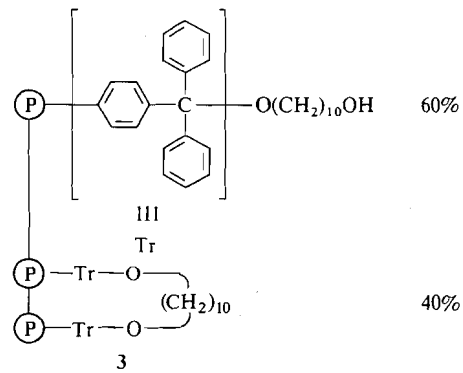

3

[1]The use of polymer supports in organic synthesis. Part XV. For part XIV see ref. 1.
[2]Taken in part from the Ph.D. Thesis of T.M. Fyles.
[3]Holder of NRCC fellowships, 1974–1977.

Can. J. Chem. Downloaded from www.nrcresearchpress.com by 210.87.254.42 on 09/05/12
For personal use only.

Can. J. Chem. Downloaded from www.nrcresearchpress.com by 210.87.254.42 on 09/05/12
For personal use only.

Elimination of this problem would give a clean product without purification and would be more efficient in starting diol. If it were possible to actually *promote* double binding in such a way that the doubly-bound diol is bound to the polymer by two different functional groups, then the diol could be selectively cleaved from one of the functional groups liberating diol solely monoprotected by the insoluble resin. We envisioned that a polymer containing both trityl chloride and benzoyl chloride functional groups in close proximity could serve such a function. Before attempting to synthesize such a bifunctional polymer, we wished to see if it were possible to synthesize an insect sex attractant on a polymer-bound benzoyl chloride so that an attractant could be synthesized simultaneously from both functional groups of the bifunctional resin.

Leznoff and Wong (6) have described the preparation of monoethers of symmetrical diols using a polymer-bound phenylacetyl chloride as a blocking group. This polymer was not suitable for the synthesis of insect sex attractants because of the low loadings of diol previously obtained, the presence of acidic protons α to the carbonyl and the inability of the polymer to be recycled. Hence a polymer-bound benzoyl chloride was sought.

Results and Discussion

Polymer-bound Benzoyl Chloride as a Blocking Group in Synthesis

Polymer-bound phenyllithium (**4**) (7) was quenched with CO_2 and protonated (7,8) or treated with diethyl carbonate, followed by treatment with base and protonation to give the desired polymer-bound benzoic acid (**5**) (7,8).

Treatment of **5** (1.0–1.5 mmol acid/g of **5**) with thionyl chloride in benzene (6) gave the polymer-bound benzoyl chloride (**6**). The infrared (ir) spectrum of this polymer showed strong absorptions at 1810 and 1780 cm^{-1} due to the acid chloride group. Polymer **6** reacted with 1,10-decanediol (**2**) in pyridine to give the monoprotected diol polymer **7**.

The ester linkage of **7** proved to be considerably more inert to base-catalysed hydrolysis than diols bound to the previously described polymer-bound phenylacetyl chloride (6, 9).

Treatment of polymer **7**, however, with 0.2 *M* $(n\text{Bu})_4\text{NOH}$ (10) in THF for 48 h at room temperature resulted in a polymer whose ir spectrum showed no trace of residual ester absorptions. The solution phase contained 0.8–1.0 mmol of diol **2**/g of polymer **7**. The recovered diol was easily separated from impurities introduced by the cleavage reagent by preparative thin-layer chromatography (tlc). Although not as clean as the HCl in dioxane mixture used to cleave trityl resins, $(n\text{Bu})_4\text{NOH}$ is more suitable for the cleavage of benzoate resins than other bases investigated.

Attempts to oxidize polymer-bound diol **7** to a polymer-bound aldehyde using di-*tert*-butyl chromate (4,11) resulted in no observable additional bands in the ir spectrum of the product. Furthermore, attempts to elaborate this polymer-bound aldehyde to insect sex attractants by a previously described Wittig route (4) failed and yielded only starting diol **2**, indicating that the initial oxidation failed.

Because of our experience with trityl resins, we initially suspected that the diol bound to **7** was bound entirely as the diester, i.e. entirely 'doubly-bound.' Conversion of **7** to the polymer-bound monotrityl ether **8** as described by Wong and Leznoff (6) followed by base cleavage gave a mixture of unreacted diol **2** and the expected monotrityl ether of 1,10-decanediol (**9**) as shown in Scheme 1. The yield of **9** might in fact reflect the total amount of monoprotected diol bound to **7**. However, subsequent investigation (see below) showed that this was not the case. Thus this experiment showed only that **7** contained *not less than* 0.24 mmol/g of free alcohol groups of **7**.

Numerous examples of a Wittig reaction in the presence of an ester have been reported (12). This, together with the complete absence of products from base catalysed decomposition of aldehydes suggested that the oxidation of **7** to a polymer-bound aldehyde had not occurred. The benzoate linkage of **7** is relatively acid insensitive and hence a large number of other (acidic) methods were tested for the oxidation of **7** to a polymer-bound aldehyde. Some reagents tested were chromium trioxide in HMPT (13), dimethylsulfoxide and dicyclohexylcarbodiimide (14), dimethylsulfoxide and trifluoroacetic anhydride (15), and even sodium dichromate in acidic HMPT (16). In no case were any products other than unreacted diol recovered upon cleavage of the polymers.

On the basis of observations made of polymers containing both trityl alcohol and benzoate groups (see below), it is likely that the failure of the oxidation of **7** to polymer-bound aldehyde is due to a combination of two factors, namely, the poor swelling properties of polymer-bound diol **7**, especially in some of the solvents used for the oxidations tested, and the presence of by-products from the thionyl chloride reaction which inhibit oxidation by di-*tert*-butyl chromate (11). Indeed, a polymer-bound trityl alcohol, converted to a polymer-bound trityl chloride **1** using *thionyl chloride*, instead of *acetyl chloride*, when loaded with diol to give a

Can. J. Chem. Downloaded from www.nrcresearchpress.com by 210.87.254.42 on 09/05/12
For personal use only.

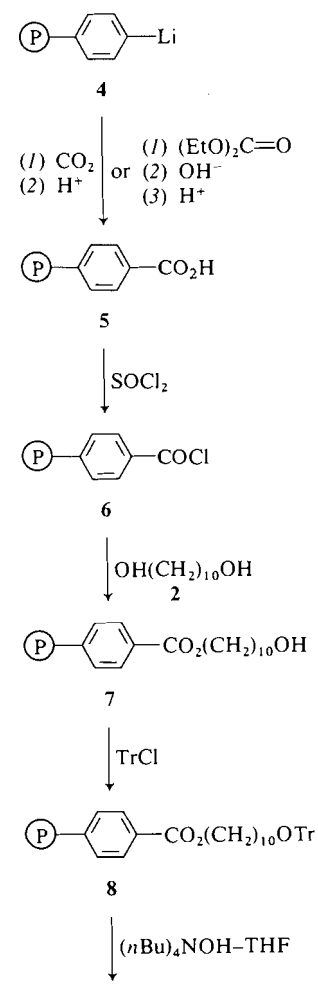

SCHEME 1

polymer-bound diol is sufficiently contaminated with this by-product to completely prevent the oxidation and subsequent 'normal' Wittig reaction. The deleterious effects of thionyl chloride on functionalized resins has been previously noted (17).

Since lithio alkynes are incompatible with the ester blocking group, the remaining 'reverse' Wittig route (4) was investigated with this system as shown in Scheme 2. Polymer-bound diol **7** was converted to the mesylate **10** in the same manner as was used with trityl resins (4). The ir spectrum of **10** showed strong absorptions at 1180 and 1360 cm^{-1} due to the presence of mesylate groups. The free diol monomesylate could not be isolated by base cleavage due to its base lability. Conversion of **10** to the phosphonium salt **11** by treatment of **10** with molten triphenylphosphine for 48 h at 140°C succeeded as shown by the absence of the 1360 cm^{-1} band (unreacted mesylate groups) and the presence of the 1210 cm^{-1} band (phosphonium salt formation) in the ir spectrum of the product polymer.

Treatment of the benzoate-bound phosphonium salt **11** with trityllithium or *tert*-butyllithium followed by treatment for 4 h with butyraldehyde gave polymer-bound alken-l-ol **12**. Base cleavage of **12** as described above produced the expected 10-tetradecen-l-ol (**13**) together with unreacted diol (Table 1). Acetylation of **13** gave **14**, the sex attractant for the oak leaf roller, *Archips semiferamus* Walker (18). The overall yield of attractant was comparable to previously obtained results with trityl resins (4) (Table 1). The stereoselectivity of the process was also quite high as in the previous trityl case (4), providing 85% of the *cis* isomer.

We were hoping that polymer-bound benzoic acid (**5**) prepared via diethyl carbonate would have less functional groups at adjacent sites due to quenching of adjacent phenyllithium sites with diethyl carbonate to give polymer-bound benzophenone. Although the ir spectrum of **5** indeed

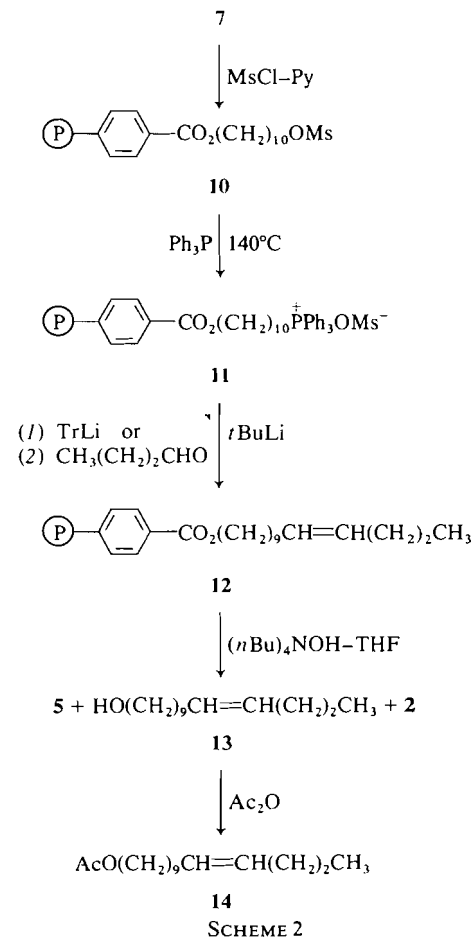

SCHEME 2

TABLE 1. Yields of monotrityl ethers (Scheme 1) and insect sex attractants (Scheme 2) prepared on benzoate polymers

Polymer	Initial quantity of diol[a] (mmol/g)	Quantity of monotrityl ether **9**[b] (recovered diol)[b] (mmol/g)	Overall yield[c] (conversion)[d] (%)	Quantity of alken-1-ol **13**[e] (recovered diol)[e] (mmol/g)	*Cis* isomer[f] (%)	Overall yield[c] (conversion)[d] (%)
5[g]	0.60	0.24(0.36)	40(100)	0.24(0.27)	85	40(70)
5[h,i]	0.41	—	—	0.15(0.19)	91	37(68)
5[i,j]	0.46	0.13(0.31)	27(87)	0.17(0.24)	90	41(70)

[a]Recovered from cleavage of **7**.
[b]Recovered from cleavage of **8**.
[c]Based on quantity of diol initially bound to polymer.
[d]Yield if recovered diol is recycled.
[e]Recovered from cleavage of **12**.
[f]As a percentage of total alken-1-ol.
[g]Third time used **5**, ylide produced using TrLi. Freshly prepared **5** loaded 0.80 mmol of 2/g.
[h]Fifth time used **5**.
[i]Ylide produced using *tert*-butyllithium.
[j]This entry **5** was prepared via diethyl carbonate, while the previous entries were made from CO_2.

showed an additional absorption band at 1680 cm^{-1}, the additional crosslinking of **5** and quenching of adjacent sites did not decrease the eventual amount of double-binding. Syntheses on **5** prepared via diethyl carbonate, were similar to syntheses on **5**, prepared via carbon dioxide (Tables 1 and 2).

In general, benzoate polymers are not as suitable for the monoprotection of symmetrical diols as the corresponding trityl polymers for a variety of reasons. (*a*) Benzoate polymers swell less readily than trityl polymers and hence more forcing conditions are required to drive the desired reaction. (*b*) Benzoate polymers contain by-products resulting from treatment with thionyl chloride. These by-products interfere with the oxidation of alcohols to aldehydes (and possibly other reactions). (*c*) Benzoate polymers cannot be as efficiently recycled as trityl resins. While trityl alcohol polymers remain very little degraded after more than 20 times of reuse, the capacities of used benzoate polymers are much diminished from the initial capacities (Table 1). This problem may be related to the by-products mentioned in point *b*.

Bifunctional Polymers

Addition of a saturated solution of *p*-benzoylphenyl ethyl carbonate (**15**), prepared from 4-hydroxybenzophenone and ethyl chloroformate, in tetrahydrofuran (THF) to polymer-bound phenyllithium (**4**), prepared from a *sec*-butyllithium-TMEDA complex to provide a large proportion of proximally lithiated sites (19), gave a dark green mixture which was decolorized on the addition of water. The ir spectrum of this polymer showed absorptions at 1770 cm^{-1} (carbonate, due to **15** reacted only at the benzophenone), 1740 cm^{-1} (ester, due to mono-reaction at the carbonate of **15** with either ethoxy or phenoxy as leaving group), and 1680 cm^{-1} (benzophenone, due to double reaction at the carbonate of **15** plus reaction at the carbonate of **15** only). Base cleavage of this polymer produced a second product whose ir spectrum contained no residual bands at 1770 and 1740 cm^{-1} but did show a band at 1680 cm^{-1} apparently unaltered by base treatment. Only trace quantities of 4-hydroxybenzophenone could be recovered from the base cleavage mixture and thus the amount of reaction at the carbonate functional group only is minimal. Protonation of the second polymer resulted in production of **16** whose ir spectrum showed an absorption at 1725 cm^{-1} (free carboxylic acid) and again a band at 1680 cm^{-1} (benzophenone). From the above sequence of changes in the ir spectra on reaction with base and acid it was likely that both trityl and benzoate groups had been produced and that the number of trityl groups probably exceeded the number of benzoate groups. This is the expected result since nucleophilic attack on benzophenone would be faster than on carbonate and some of the first formed esters would further react with adjacent lithiated sites.

Treatment of polymer **16** with diazomethane in methylene chloride at low temperature for 16 h, gave polymer **17**. The phenol of **16** had been protected as the methyl ether with concomitant protection of benzoate as the methyl ester. Before proceeding with the synthesis of attractant **14** via bifunctional polymer **17**, as outlined in Scheme 3, the nature of diol bound only to the trityl group of **17** was determined.

Conversion of **17** to the trityl chloride **18** using acetyl chloride in benzene as previously described (7) gave a polymer containing 0.45 mequiv. of chloride/g of resin. Treatment of **18** with 1,10-decanediol (**2**) gave the polymer-bound diol **19**. A polymer-bound diol monoacetate was prepared in the manner previously described (7) which upon cleavage in dilute acid (7) liberated 0.27 mmol of 1,10-decanediol monoacetate (**20**) and no recovered

Can. J. Chem. Downloaded from www.nrcresearchpress.com by 210.87.254.42 on 09/05/12
For personal use only.

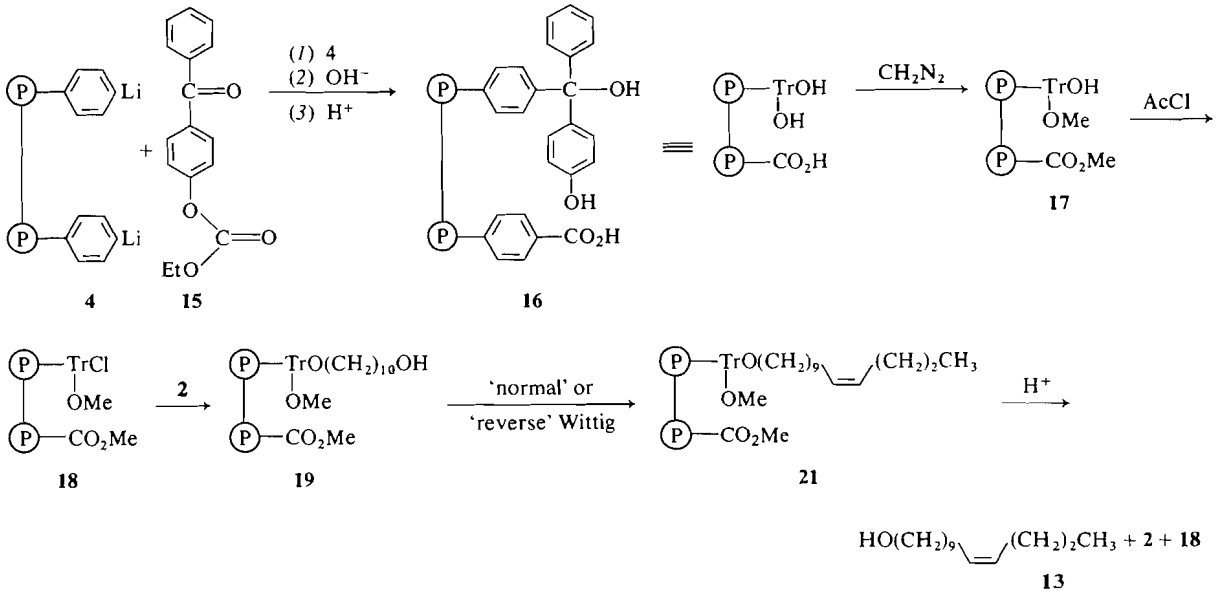

SCHEME 3

diol showing that **2** had been bound to **19** exclusively as the monoprotected trityl ether (Table 2).

Polymer-bound diol **19** could be elaborated by either the 'normal' or 'reverse' Wittig routes to give polymer-bound alken-l-ol **21**. Standard dilute acid cleavage of **21** gave 10-tetradecen-l-ol (**13**) which on acetylation gave **14** the attractant for the oak leaf roller moth (18). The overall yields of attractant **14** by both routes are given in Table 3. It is interesting to note that although **19** led to complete conversion to **20**, showing that acetylation of **19** is complete, **19** leads only to partial conversion to **13** by both the 'normal' and 'reverse' Wittig routes. Diol **2** is recovered in both sequences showing that both oxidation and mesylation of **19** is incomplete. These reactions were also probably incomplete on the simple monofunctionalized resins (4). We then attempted to attach **2** *simultaneously* to both the

TABLE 2. Modes of binding of 1,10-decanediol and yields of monoderivatives of diol bound to bifunctionalized polymers in Schemes 3–6

Polymer	z^a (mmol/g)	x^b (mmol/g)	y^c (mmol/g)	q^d (mmol/g)	Quantity of diol monoacetate (**20**) (recovered diol)^e (mmol/g)	Overall yield^f (conversion)^g (%)
19	0.30	0.30	—	—	0.27(0)	90(90)
24	0.23	0.16	0.07[h]	0	0.16(0)	100
19[i]	0.17	0.17	—	—	0.15(0)	89(89)
24[i]	0.22	0.15	0.05[j]	0.02	0.15(0)	100
29	0.20	0.20	—	—	0.20(0)	100
30	0.24	0.24	—	—	0.15(0.09)	63(100)
32	0.26	0.26	—	—	0.17(0.08)	65(100)
34	0.31	0.27	0.04[k]	0	0.19(0.07)	68(95)
32[l]	0.10	0.10	—	—	0.06(0.04)	60(100)
34[l]	0.19	0.11	0.08[m]	0	0.07(0.04)	64(100)

[a]Total quantity of diol bound to polymer, recovered by acid cleavage and where required by subsequent base cleavage.
[b]**2** recovered by acid cleavage only.
[c]**2** recovered by base cleavage only.
[d]$q = z - x - y$, quantity of diol bound to polymer through both ester and ether linkages.
[e]Recovered by cleavage of polymer-bound diol monoacetate.
[f]Yield based on diol initially bound to polymer.
[g]Yield if recovered diol is recycled.
[h]0.05 mmol/g of **9** + 0.01 mmol/g of **2** prepared on this polymer via Scheme 1.
[i]Prepared from an 0.5 *M* solution of **15** in THF.
[j]0.04 mmol/g of **9** + 0.01 mmol/g of **2** prepared on this polymer via Scheme 1.
[k]0.03 mmol/g of **9** + trace of **2** prepared on this polymer.
[l]Prepared via a 1:10 mixture of benzophenone and diethyl carbonate.
[m]0.06 mmol/g of **9** + 0.02 mmol/g of **2** prepared on this polymer via Scheme 1.

Can. J. Chem. Downloaded from www.nrcresearchpress.com by 210.87.254.42 on 09/05/12
For personal use only.

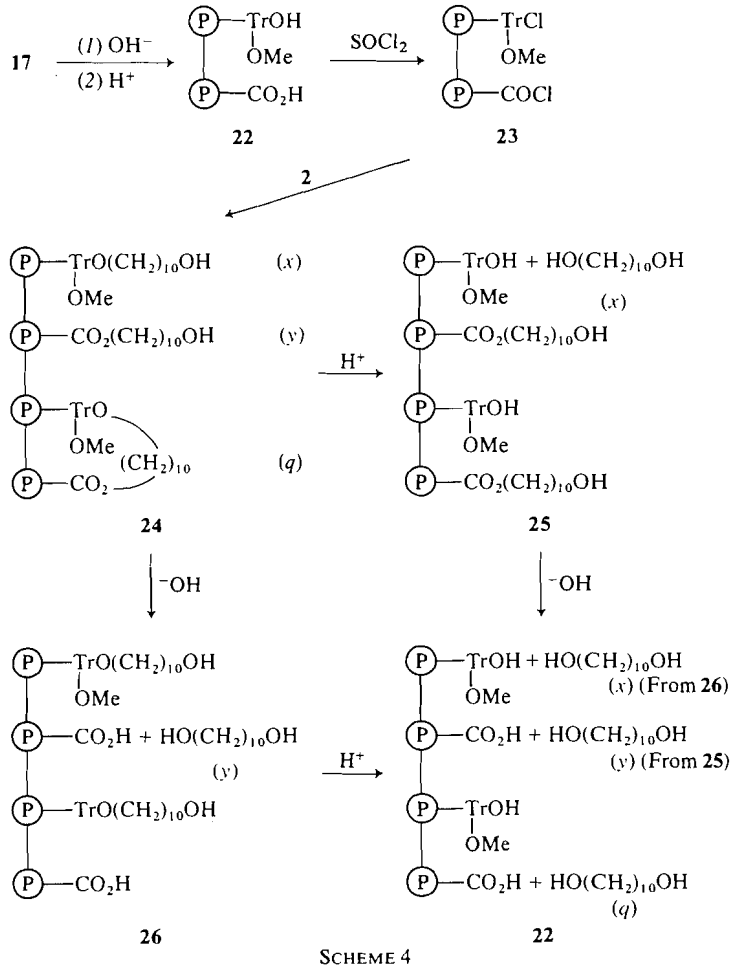

SCHEME 4

trityl and carboxy groups. Base cleavage of **17** as described above followed by protonation gave polymer **22**. Thionyl chloride treatment of **22** gave the mixed trityl – acid chloride polymer **23** containing 0.55 mmol of chloride/g of **23**. Treatment of **23** with 1,10-decanediol (**2**) in pyridine gave polymer **24** containing diol bound in at least three fashions: (*a*) as the monotrityl ether (*x*), (*b*) as the monobenzoate (*y*), and (*c*) as the trityl ether – benzoate intraresin crosslinkage shown (*q*). The proportions of these three modes of diol binding were assessed as outlined in Scheme 4.

Successive treatment of **24** with acid (to give **25**) followed by base cleavage liberates the total quantity of diol bound to polymer **24** (*z*). The amount of diol liberated in the first acid cleavage step must be bound to **24** only via trityl groups (*x*). The amount of diol liberated in the second base cleavage step is then the sum of the amount bound only as benzoates (*y*) plus any doubly-bound diol held as the mixed trityl ether – benzoate (*q*). Alternatively, base cleavage of **24** gives polymer **26** and liberates only diol bound as the benzoate (*y*). Subsequent acid cleavage of **26** gives the sum of doubly-bound (as the trityl ether – benzoate) and trityl only bound diols ($q+x$). The maximum amount of diol bound as the mixed trityl ether – benzoate (q) is thus given by $q=z-x-y$. A check is provided by the two values of the total amount of diol bound to **24** (z and z') obtained from the two independent cleavage sequences.

In any event, x was found to be 0.16 mmol/g of **24**, y to be 0.07 mmol/g of **24** and $z=z'=0.23$ mmol/g of **24**. Thus the maximum amount of diol bound by the mixed trityl ether – benzoate was found to be $q=0.0$ mmol/g of **24** (Table 2). Conversion of **24** to the acetate and acid cleavage as previously described (7) showed complete monoprotection of diol bound to the trityl groups of **24** (Table 2). Similarly conversion of **24** to the monotrityl ether (6) and base cleavage as described above showed at least 83% of the diol bound to the benzoate of **24** was monoprotected (Table 2). These results

Can. J. Chem. Downloaded from www.nrcresearchpress.com by 210.87.254.42 on 09/05/12
For personal use only.

TABLE 3. Yields of insect attractant **14** prepared by the "normal" and "reverse" Wittig routes on bifunctionalized polymers

Polymer	z^a (mmol/g)	Quantity of **13**[b] (mmol/g)	Quantity of recovered diol[b] (mmol/g)	Overall yield of **13**[c] (conversion)[d] (%)	*Cis* isomer[e] (%)
21[f]	0.30	0.16	0.09	53(73)	72
21[g]	0.30	0.19	0.07	63(83)	88
24[f,h]	0.22	0	0.21	0	—
24[g,h]	0.22	0.11	0.10	50(92)	88
29[f]	0.20	0.10	0.10	50(100)	68
30[g]	0.24	0.12	0.12	50(100)	85

[a]Total quantity of 2 bound to polymer, recovered from acid cleavage and where required subsequent base cleavage.
[b]Total quantity recovered from acid cleavage and where required subsequent base cleavage.
[c]Based on initial quantity of diol bound to polymer.
[d]Yield if recovered diol is recycled.
[e]As a per cent of total alken-l-ol.
[f]'Normal' Wittig.
[g]'Reverse' Wittig.
[h]Polymer prepared from 0.5 *M* **15** in THF.

indicated that polymer **24** behaved as if it were a mixture of two separate and independently functionalized polymers. Thus the goal of obtaining a polymer-bound diol doubly-bound through a trityl group at one end and a benzoate group at the other was not achieved. However, exclusive monoprotection of diol bound to trityl groups was obtained although the loading (Table 2) was not sufficiently high nor better than a previously described trityl polymer from the controlled addition of methyl benzoate (7). Since **23** was prepared using $SOCl_2$, attempts to oxidize **24** to an aldehyde failed and the elaboration of **24** to **14** simultaneously on two functional groups by the 'normal' Wittig route failed. Polymer **24** could be elaborated to attractant **14** by the 'reverse' Wittig route (7), however, in modest yield (Table 3).

Attempts to produce higher levels of functionalization by varying the conditions of the quenching reaction of **4** with **15** did give us a polymer capable of double-binding diol through two different functional groups. Thus quenching **4** with a 0.5 *M* solution of **15** in THF did yield a sample (Scheme 4) of **24** which was found by the double cleavage sequence described above to contain 0.02 mmol of **2**/g of **24** doubly-bound as the mixed trityl ether – benzoate (Table 2) but the level of this loading was too low to be useful.

Treatment of **4** with a *dilute* solution of carbonate **15** resulted in complete reaction of the carbonate group to give polymer **27** as shown in Scheme 5. The ir spectrum of **27** exhibited only one carbonyl absorption at 1680 cm^{-1} due to the newly-formed benzophenone group. Polymer **27** was treated with excess phenyllithium to give a new polymer **28**, containing two types of trityl alcohol groups. The two different kinds of trityl alcohol groups are likely constrained to be near each other as they are both derived from **15**. This constraint is borne out by the following reactions. Treatment of **27** with acetyl chloride to form a polymer-bound trityl chloride, followed by the addition of excess 1,10-decanediol (**2**) gave the polymer diol **29**. Acetylation of **29** and acid cleavage yielded exclusively 1,10-decanediol monoacetate (**20**) and no unreacted **2**. Polymer **28**, however, in the same sequence, yielded a polymer diol **30**, which on acetylation and cleavage from **30**, gave **20** *and unreacted 2* (Table 2). Although the quantity of diol bound to **30** is only 0.04 mmol/g of polymer more than the amount bound to **29** (Table 2), greater than half of the trityl groups of **30** are involved in double binding of diol! Diol bound to polymer **29**, however, is bound entirely as the monotrityl ether. Clearly the proximity of functional groups is an important factor in the selective monoprotection of symmetrical diols. We believe that the recovered **2** was obtained because **2** was doubly bound to **28** likely through the two different types of trityl groups. *These key experiments outlined in Scheme 5 strongly support our original hypothesis that polymer-bound phenylithium **4** can be quenched with carbonate **15** at adjacent or conformationally proximal sites.*

For the purposes of comparison with polymer **22**, **4** was quenched with a 1:1 mixture of benzophenone and diethylcarbonate to produce a bifunctionalized polymer **31** in which the trityl groups are not constrained to be in the vicinity of the benzoate groups. Treatment of **31** with acetyl chloride and reaction with **2** gave polymer-bound diol **32**. Base cleavage of **31** and protonation yielded **33**, which reacted with $SOCl_2$ and then **2** to give the polymer-bound diol **34** as outlined in Scheme 6. The amounts of monoprotection of diol were assessed by the methods

Can. J. Chem. Downloaded from www.nrcresearchpress.com by 210.87.254.42 on 09/05/12
For personal use only.

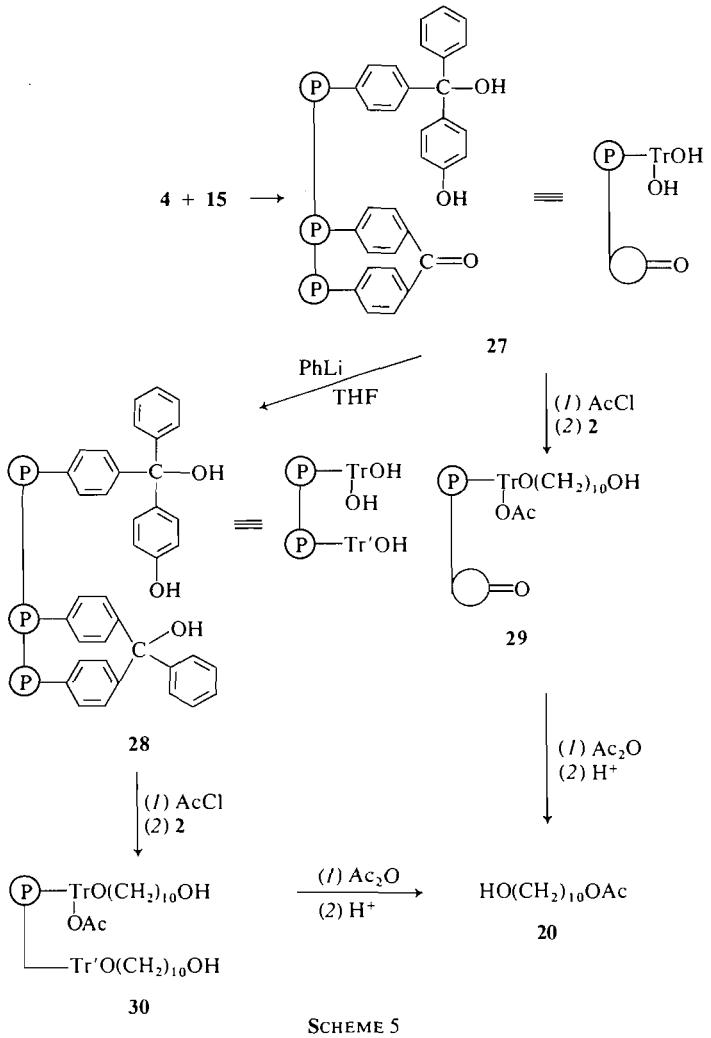

SCHEME 5

described above and gave the data in Table 2. As anticipated, trityl groups were produced in a large excess over benzoate groups due to the differences in the rates of nucleophilic attack (20) on benzophenone versus carbonate. Thus in a subsequent experiment, **4** was quenched with a 1:10 mixture of benzophenone and diethyl carbonate to give a new polymer **31** which contained relatively more carboxy groups. Identical types of experiments carried out on this 'new' **31** are recorded in Table 2. The values of x, y, z, and q for both **31** and 'new' **31** were determined (Table 2) by the methods described above and illustrated in Scheme 4. As a consequence the amount of diol doubly-bound to **34** (or 'new' **34**) as the mixed trityl ether – benzoate was zero. What was not anticipated was the relatively high amounts of double binding of diols bound only to trityl groups even at the low level of loading observed. The possibility that double binding of diol is in part a 'concentration' effect; the higher the degree of functionalization, the higher the double binding of diol is not necessarily the case. The total loading of diol to **32** and **34** was roughly one half the amounts obtained early in experiments on normal polymer-bound trityl chloride (7) but the proportions of double-bound diol was roughly the same.

This result is consistent with those reported previously (7) for the preparation of the monoacetates of 1,4-butanediol and 1,10-decanediol (**2**) and with studies done by Crowley *et al.* (21). Despite the fact that the carbon chain length of 1,4-butanediol is less than half the chain length of **2**, the extent of double binding of these diols is roughly the same (7). The observation that the amount of doubly-bound diol is insensitive to both the degree of functionalization of the polymer backbone and the carbon chain length suggests that the first formed monoblocked diol is not held in an isolated site but

Can. J. Chem. Downloaded from www.nrcresearchpress.com by 210.87.254.42 on 09/05/12
For personal use only.

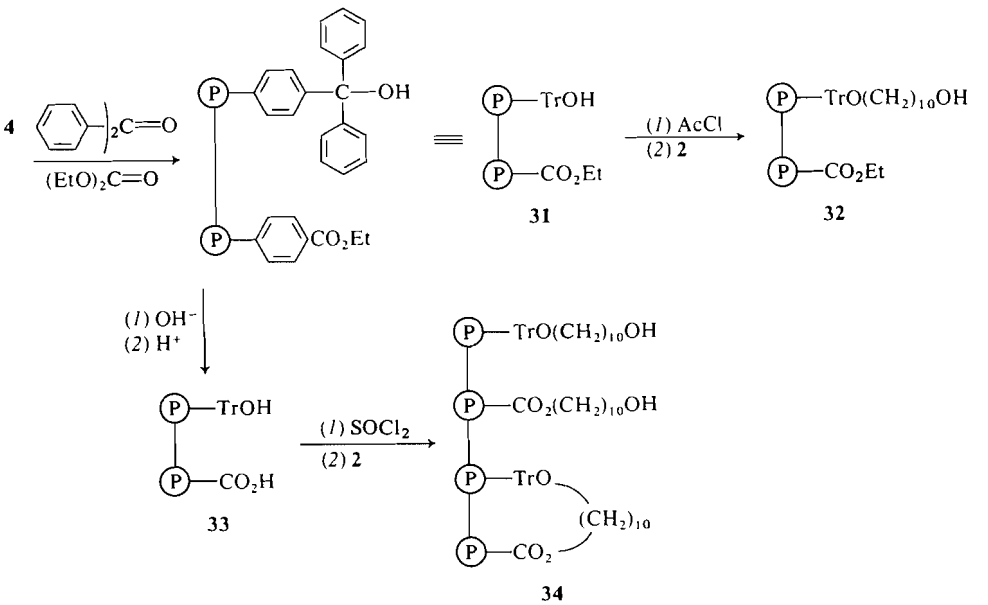

SCHEME 6

is relatively free to move within the polymer matrix. The unreacted end of the monoprotected diol must be sufficiently mobile to allow it to compete effectively with solution phase diol for unreacted functional groups on the polymer.

In summary, bifunctionalized resins, having spatially defined geometries, have been prepared and are expected to find wide applications in (*a*) studies directed towards the elucidation of intraresin interactions, (*b*) organic synthesis on polymer supports,[4] and (*c*) the construction of model systems capable of mimicking enzymatic systems. This study has shown how bifunctional resins can be used to restrict intraresin reactions and examined the scope of synthesizing an insect sex attractant bound to two different functional groups of a single resin.

Experimental

Infrared spectra were recorded on a Unicam SP1000 ir spectrophotometer as neat films between NaCl discs unless otherwise specified. Nuclear magnetic resonance spectra were recorded on a Varian EM360 spectrometer using deuteriochloroform as solvent and tetramethylsilane as internal standard. Mass spectra were recorded on a Perkin-Elmer-Hitachi RMU6E mass spectrometer. Silica gel was used for all thin- and preparative-layer chromatography. Fractions were extracted with ether in a Soxhlet extractor. Filtration was done under vacuum through sintered glass Buchner funnels. Filtration under an inert atmosphere was done as previously described (7). Microanalyses were performed by G. Gygli of Toronto.

[4]A bifunctional resin, containing both nickel and rhodium in a *random* array has been synthesized and used as a catalyst in sequential reactions of oligomerization and hydrogenation (22).

Preparation of Polymer-bound 'Benzoic Acid' 5 via Diethyl Carbonate

To a suspension of 5 g of polymer-bound phenyllithium (**4**) in 100 ml of dry THF under an argon atmosphere was added 10 g of diethyl carbonate in 100 ml of dry THF dropwise over 0.5 h. The mixture was stirred a further 2 h, filtered, washed twice with ethanol (50 ml), and twice with water (50 ml). The polymer was suspended with 50 ml of THF and treated with 25 ml of a 0.5 *M* tetra-*n*-butylammonium hydroxide solution in THF. The mixture was stirred at reflux overnight, filtered, and washed twice with ethanol (50 ml). The polymer was then protonated, filtered, washed, and dried as previously described (7) in the preparation of **5** via CO_2; ir: 1725 (C=O, acid), 1680 cm^{-1} (C=O, benzophenone).

Preparation of Polymer-bound Acid Chloride 6

In a manner similar to that previously described (6–8), 5 g of 'benzoic acid' polymer **5** (1.0–1.5 mmol of acid/g), 10 ml of freshly distilled thionyl chloride, and 80 ml of dry benzene were stirred at reflux under argon overnight. The mixture was filtered, washed with dry benzene (50 ml), twice with dry ether (50 ml), and immediately pumped dry at high vacuum. Treatment of a standard sample of **6** with dioxane–water (1:1) liberated 0.6–1.5 mmol of chloride/g of resin.

Preparation of Polymer-bound Diol 7

By the method of Wong and Leznoff (6), 5 g of **6** and 5 g of 1,10-decanediol (**2**) gave **7**; ir: 1740 cm^{-1} (C=O).

*Preparation of Tetra-*n*-butylammonium Hydroxide in THF Solution (23)*

To a suspension of tetra-*n*-butylammonium iodide (18.5 g, 50 mmol) in 100 ml of distilled water at 90°C was added freshly prepared 'silver hydroxide' (60 mmol, from 10 g of silver nitrate and 2.4 g of sodium hydroxide). The resultant slurry was vigorously stirred at reflux for 0.5 h, cooled in ice, and filtered while cold. The filtrate was evaporated to an oil under reduced pressure, traces of water were removed as the benzene azeotrope and the oil was made to 100 ml in dry THF. Acid–base titration showed the solution to be 0.45–0.48 *M* in hydroxide (90–96% yield).

Can. J. Chem. Downloaded from www.nrcresearchpress.com by 210.87.254.42 on 09/05/12
For personal use only.

Can. J. Chem. Downloaded from www.nrcresearchpress.com by 210.87.254.42 on 09/05/12
For personal use only.

General Base Cleavage of Polymer-bound Benzoate Diols and Derivatives

In a typical procedure to liberate diol and derivatives from benzoate polymers, 1.0 g of polymer was suspended in 20 ml of THF and treated with 10 ml of a 0.5 *M* solution of tetra-*n*-butylammonium hydroxide. The mixture was stirred at room temperature for 48 h, filtered, and the polymer was washed twice with ethanol (10 ml), four times with water (20 ml), twice with ethanol (10 ml), twice with ether (15 ml), and air dried. The ir showed no bands above 1650 cm^{-1} (C=O).

The filtrate was extracted with ether, washed with water, dilute acid, dried ($MgSO_4$), and evaporated to yield the crude product.

Preparation of Polymer-bound Benzoate Diol Monotrityl Ether ***8***

Polymer **8** was prepared from **7** and triphenylmethyl chloride as described by Wong and Leznoff (6). The ir was uninformative.

Isolation of 1-O-Trityl-1,10-decanediol (***9***)

Standard base cleavage of 1 g of **8** and purification of the crude product by preparative tlc (eluant, ether–benzene, 2:3) gave only 1,10-decanediol **2** (R_f 0.2), 63 mg, 0.36 mmol/g of **8**; and 1-*O*-trityl-1,10-decanediol (**9**) (R_f 0.55), 101 mg, 0.24 mmol/g of **8**; ir (neat): 3400 (OH), 2950 (CH_2), 1604 (aromatic C—H), 1050 cm^{-1} (C—O); nmr: 7.4–7.3 (br s, 15H, OTr), 3.6 (t, 8, 2H, CH_2OH), 3.2 (t, 8, 2H, CH_2OTr), 3 var (s, 1H, O*H*), 1.6–1.2 (m, 16H, —CH_2—). The yield data for the preparation of **9** are given in Table 1.

Preparation of Polymer-bound Diol Monomesylate ***10***

Polymer-bound mesylate **10** was prepared from **7** and methanesulfonyl chloride exactly as previously described (7); ir: 1360 (CH_3SO_2), 1180 cm^{-1} (CH_3SO_2).

Preparation of Polymer-bound Phosphonium Salt ***11***

In a manner similar to, but not identical to a previously described procedure (4), 2 g of **10** were added to 25 ml of molten triphenylphosphine and the mixture was heated to 140°C under an argon atmosphere for 48 h. The product polymer **11** was recovered as previously described; ir: 1210 (salt?), 1180 cm^{-1} (CH_3SO_2).

Preparation of Polymer-bound Alken-1-ol ***12*** *('Reverse' Wittig)*

(*a*) *Using Trityllithium*

To a solution of 1 g of triphenylmethane (ca. 5 mmol) in 30 ml of THF at −10°C under an argon atmosphere was added 2.2 ml of methyllithium (1.36 *M*, 3.9 mequiv.). The solution was stirred at 0°C overnight and 1.5 g of **11** was added. The slurry was stirred at 0°C for 3 h, quenched with 5 ml of butyraldehyde, and stirred a further 4 h. The polymer was filtered, washed and air dried as previously described (4).

(*b*) *Using* tert-*Butyllithium*

Polymer **11** (1.5 g) in 30 ml of dry THF was cooled to 0°C under an argon atmosphere and treated with 2 ml of *tert*-butyllithium (2 *M*, 4 mequiv.). The mixture was allowed to warm to room temperature over 1 h, quenched with 5 ml of butyraldehyde, and stirred a further 4 h. The polymer was filtered, washed and air dried as previously described (4). The ir (either method) was uninformative.

Isolation of 10-Tetradecen-1-ol (***13***)

Standard base cleavage of **12** and purification of the crude product by preparative tlc (eluant, ether–benzene, 2:3) gave 1,10-decanediol (**2**) (R_f 0.2), 47 mg, 0.27 mmol/g of **12**; and 10-tetradecen-1-ol (**13**) (R_f 0.6), 51 mg, 0.24 mmol/g of **2**. Acetylation of **13** gave 10-tetradecen-1-ol acetate (**14**). Compounds **13** and **14** were identical to previously prepared samples (4) and the overall yields and isomeric composition, determined by vapour phase chromatography (vpc) and high pressure liquid chromatography (hplc) as previously described (4), of the products are given in Table 1.

Preparation of p-*Benzoylphenyl Ethyl Carbonate* ***15***

To a solution of 4-hydroxybenzophenone (25 g, 0.12 mol) and triethylamine (30 ml, ca. 0.25 mol) in 150 ml of THF was added dropwise 12 ml of ethyl chloroformate (0.15 mol) over 0.5 h. The mixture was heated to reflux for 1 h, cooled, poured into ice, and extracted with methylene chloride. The extract was washed with dilute base and water, dried ($MgSO_4$) and evaporated. The crystalline mass was recrystallized from methanol (mp 118–121°C) and the recrystallized material was further purified by sublimation (115°C/0.05 Torr) to give 20.6 g of *p*-benzoylphenyl ethyl carbonate (**15**) as white needles, mp 123–123.5°C, in 61% yield; ir (KBr): 3020 (CH), 2950 (CH_2), 1770 (OCO_2), 1660 (C=O), 1600 (aromatic C—H), 1470 cm^{-1} (CH_2); nmr: 8.1–7.3 (m, 9H, Ph—*H*), 4.5 (q, 8, 2H, O—CH_2—), 1.4 (t, 8, 3H, CH_3); ms (70 eV *m/e* (relative intensity): C=O 270 (25) (M^+), 225 (31), 197 (72), 149 (70), 121 (100), 105 (80). *Anal.* calcd. for $C_{16}H_{14}O_4$: C 71.10, H 5.22; found: C 70.93, H 5.02.

Preparation of Bifunctionalized Polymer ***16***

To a suspension of 10 g of polymer-bound phenyllithium **4** in 100 ml of dry THF under an argon atmosphere was added 5 g of **15** in approximately 100 ml of THF (saturated solution) dropwise over 15 min. The resultant mixture was stirred a further 2 h at room temperature, filtered and the polymer washed and air dried; ir: 1760 (OCO_2), 1735 (CO_2R), 1680 cm^{-1} (C=O). Base cleavage of this product as described in the preparation of **5** followed by protonation, washing, and drying gave **16**; ir: 1725 (CO_2H), 1680 cm^{-1} (C=O, benzophenone).

Preparation of Methylated Bifunctionalized Polymer ***17***

To a solution of diazomethane (7.0 mmol) in 75 ml of methylene chloride was added 10 g of polymer **17** in portions. The mixture was stirred at −10°C overnight, filtered, and the polymer washed twice with methylene chloride (50 ml) and three times with ether (25 ml); ir: 1730 (CO_2R), 1680 cm^{-1} (C=O, benzophenone).

Preparation of Polymers ***18***, ***19***, *and* ***21***

These polymers were prepared by methods previously described (4, 7).

Preparation of Bifunctional Polymers ***22***, ***23*** *and Polymer-bound Diol* ***24***

Polymer **22** was prepared by the method outlined for the base cleavage/protonation sequence leading to **16**; ir: 1725 (CO_2H), 1680 cm^{-1} (C=O). Polymer **23** was prepared as described for the preparation of **6**; ir: 1810 and 1760 (COCl), 1680 cm^{-1} (C=O). Halide analysis (22) showed 0.55 mmol of chloride/g of **23**. Treatment of **23** with 1,10-decanediol (**2**) in pyridine as previously described (7) gave **24**; ir: 1740 (CO), 1680 cm^{-1} (C=O).

Liberation of 1,10-Decanediol (**2**) *from* ***24***: *Determination of* x, y, z, *and* q

Standard acid cleavage of 1.0 g of **24** and purification of the crude product by preparative tlc (eluant, ether–benzene, 1:1) gave 1,10-decanediol (**2**) (R_f 0.3), 28 mg, 0.16 mmol/g of **24** (*x*). The resultant polymer **25** was treated with base under the standard cleavage conditions to yield on work-up and purification on preparative tlc 1,10-decanediol (**2**), 12 mg, 0.07 mmol/g of **25**. For this sequence $z = 0.07 + 0.16 = 0.23$ mmol of **2**/g of **24**.

Standard base cleavage of a second 1.0 g sample of **24**

followed by purification of the crude product on preparative tlc gave **2**, 12 mg, 0.07 mmol/g of **24** (y). The resultant polymer **26** was treated with acid under the standard conditions to yield on work-up and purification as above, **2**, 28 mg, 0.16 mmol/g of **26**. For this sequence $z' = 0.23$ mmol of **2**/g of **24**. Therefore $q = 0.23 - 0.16 - 0.07 = 0.0$ mmol/g of **24**.

Preparation of Bisfunctionalized Polymer 27

To a suspension of 10 g of polymer-bound phenyllithium **4** in 200 ml of dry THF under an argon atmosphere was added a total of 6 g of **15** in 200 ml of dry THF dropwise over 2 h. The mixture was stirred an additional 2 h, filtered, and the polymer was washed and dried as outlined in the general procedure; ir: 1680 (C=O), no bands between 1700–1900 cm^{-1}.

Preparation of the Mixed Trityl Polymer 28

A mixture of 5 g of **27** in 100 ml of dry THF and 40 ml of phenyllithium (1.5 M in benzene, 60 mmol) was stirred at reflux under an argon atmosphere overnight. The mixture was cooled, poured into a rapidly stirring mixture of 10% acid in ice cold dioxane and the polymer was filtered, washed, and Soxhlet dried as outlined in the general procedure. The ir was uninformative with no bands between 1650 and 1800 cm^{-1}.

Preparation of Bifunctionalized Polymer 31

To a suspension of 10 g of polymer-bound phenyllithium **4** in 100 ml of dry THF under an argon atmosphere was added a mixture of benzophenone (9.1 g, 50 mmol) and diethyl carbonate (5.9 g, 50 mmol) or a mixture of benzophenone (5 mmol) and diethyl carbonate (50 mmol) in 100 ml of dry THF dropwise over 0.5 h. The mixture was stirred a further 2 h at room temperature, filtered, and the polymer was washed and dried as described before (4, 7) to give polymer **31** or new polymer **31** (1:10); ir: 1740 (CO_2Et), 1680 cm^{-1} (C=O).

Preparation of Bifunctionalized Polymers 32, 33, and 34

Polymers **32**, **33**, and **34** were prepared by methods identical to those for **19**, **23**, and **24**.

Acknowledgements

This research was supported by grants from the National Research Council of Canada and the Canadian Forestry Service of Environment Canada, and the Atkinson Charitable Foundation.

1. D. M. Dixit and C. C. Leznoff. J. Chem. Soc. Chem. Commun. 798 (1977).
2. T. Kunitake and Y. Okahata. J. Am. Chem. Soc. **98**, 7793 (1976).
3. C. C. Leznoff and T. M. Fyles. J. Chem. Soc. Chem. Commun. 251 (1976).
4. C. C. Leznoff, T. M. Fyles, and J. Weatherston. Can. J. Chem. **55**, 1143 (1977).
5. T. M. Fyles, C. C. Leznoff, and J. Weatherston. J. Chem. Ecol. **4**, 109 (1978); T. M. Fyles, C. C. Leznoff, and J. Weatherston. Can. J. Chem. **55**, 4135 (1977).
6. C. C. Leznoff and J. Y. Wong. Can. J. Chem. **50**, 2892 (1972); J. Y. Wong and C. C. Leznoff. Can. J. Chem. **51**, 2452 (1973).
7. T. M. Fyles and C. C. Leznoff. Can. J. Chem. **54**, 935 (1976).
8. M. J. Farrall and J. M. J. Fréchet. J. Org. Chem. **41**, 3877 (1976).
9. T. Kusama and H. Hayatsu. Chem. Pharm. Bull. **18**, 319 (1970).
10. J. Dockx. Synthesis, 441 (1973); E. V. Dehmlow. Angew. Chem. Int. Ed. Engl. **13**, 170 (1974).
11. K. B. Sharpless and K. Akashi. J. Am. Chem. Soc. **97**, 5927 (1975).
12. H. J. Bestmann, P. Lange, and R. Kunstmann. Chem. Ber. **104**, 65 (1971).
13. G. Cardillo, M. Orena, and S. Sandri. Synthesis, 394 (1976).
14. K. E. Pfitzner and J. G. Moffatt. J. Am. Chem. Soc. **87**, 5661 (1965).
15. J. R. Parikh and W. von Doering. J. Am. Chem. Soc. **89**, 5505 (1967).
16. Y. S. Rao and R. Filler. J. Org. Chem. **39**, 3304 (1974).
17. G. L. Southard, G. S. Brooke, and J. M. Pettee. Tetrahedron, **27**, 2701 (1971).
18. L. B. Hendry, J. J. Jugovich, L. Roman, M. E. Anderson, and R. O. Mumma. Experientia, **36**, 886 (1974).
19. A. W. Langer, Jr. *In* Polyamine-chelated alkali metal complexes. *Edited by* A. W. Langer. Advances in chemistry series. No. 130. American Chemical Society, Washington, DC. 1974. pp. 6–11.
20. J. March. Advanced organic chemistry: reactions, mechanisms, and structure. McGraw-Hill, New York, NY. 1968. p. 653.
21. J. I. Crowley, T. B. Harvey, III, and H. Rapoport. J. Macromol. Sci. Chem. **7**, 1118 (1973); J. I. Crowley and H. Rapoport. Acc. Chem. Res. **9**, 135 (1976).
22. C. U. Pitman, Jr. and L. R. Smith. J. Am. Chem. Soc. **97**, 1749 (1975).
23. D. L. Fowler, W. V. Loebenstein, D. B. Pall, and C. R. Kraus. J. Am. Chem. Soc. **62**, 1140 (1940).

Can. J. Chem. Downloaded from www.nrcresearchpress.com by 210.87.254.42 on 09/05/12
For personal use only.

Erratum: The pyridinium–dihydropyridine system. I. Synthesis of a series of substituted pyridinium ions and their 1,4-dihydro reduction products and a determination of their stabilities in aqueous buffers

DONALD J. NORRIS AND ROSS STEWART
Department of Chemistry, University of British Columbia, Vancouver, B.C., Canada V6T 1W5
Received February 15, 1978
(Ref.: Can. J. Chem. **55**, 1687 (1977))

The captions for Tables 4 and 5 should include the following: $T = 25°C$.

Erratum: General base catalysis in acidic solutions. Acceleration of intramolecular phosphonate-assisted amide hydrolysis

RONALD KLUGER AND C.-H. LAM
Department of Chemistry, University of Toronto, Toronto, Ont., Canada M5S 1A1
Received February 15, 1978
(Ref.: Can. J. Chem. **55**, 640 (1977))

Some derived values in Table 1 for '$10^4\ k_{corr}$' contain computational errors. Proper values are: cyanoacetate pH 2.7: 2.55; chloroacetate pH 3.1: 6.60; dichloroacetate pH 1.6: 0.270. These values give '$10^4\ k_B$' for cyanoacetate: 3.55; chloroacetate: 9.03; dichloroacetate: 0.35. The statistically corrected Brønsted plot has a slope of 0.9 ($r = 0.999$). These changes do not affect any conclusions or discussion.

Can. J. Chem. Downloaded from www.nrcresearchpress.com by 210.87.254.6 on 09/05/12
For personal use only.

Can. J. Chem. Downloaded from www.nrcresearchpress.com by 210.87.254.42 on 09/05/12
For personal use only.

Canadian Journal of Chemistry

Published by
THE NATIONAL RESEARCH COUNCIL OF CANADA

Journal canadien de chimie

Publié par
LE CONSEIL NATIONAL DE RECHERCHES DU CANADA

Volume 56 Number 8 April 15, 1978

Volume 56 numéro 8 15 avril 1978

An investigation of discrepancies in the reported properties of tetraphenyl-*p*-dioxin

BILLY J. YAGER AND WILFORD L. WOOTAN, JR.
Southwest Texas State University, San Marcos, TX 78666, U.S.A.

Received December 13, 1977

BILLY J. YAGER and WILFORD L. WOOTAN, JR. Can. J. Chem. **56**, 1043 (1978).

A compound prepared by refluxing methyl benzoate with boron sulfide (B_2S_3) and previously identified as tetraphenyl-*p*-dioxin has been identified in this investigation as tetraphenylthiophene.

BILLY J. YAGER et WILFORD L. WOOTAN, JR. Can. J. Chem. **56**, 1043 (1978).

On a démontré que le composé préparé par reflux de benzoate de méthyle avec le sulfure de bore (B_2S_3) et qui avait été identifié antérieurement comme étant la tétraphényl-*p*-dioxinne est plutôt la tétraphénylthiophène.

[Traduit par le journal]

Consideration of the two functional groups of the benzoin molecule (**1**), led to the speculation that an acid catalyzed condensation reaction between two of these molecules and subsequent dehydration should result in the formation of tetraphenyl-*p*-dioxin (**2**). Reactions of this type, using benzene as solvent and *p*-toluenesulfonic acid as a catalyst, were carried out in these laboratories, but were only partially successful. No tetraphenyl-*p*-dioxin was obtained but tetraphenylfuran (**3**) was isolated and identified by its infrared spectrum (1) and physical properties (2).

At this point, a review of the literature revealed that Berger and Summerbell (3) had successfully prepared tetraphenyl-*p*-dioxin by the method described above using hexane as the solvent. It was also discovered, however, that Jerumanis and Lalancette (4) reported properties for tetraphenyl-*p*-dioxin which were in conflict with those reported earlier. While Berger and Summerbell reported that tetraphenyl-*p*-dioxin consisted of bright yellow crystals melting at 218–219°C, Jerumanis and Lalancette reported white crystals melting at 184–185°C. There were also significant differences in the reported infrared spectra, which indicated that two different compounds were being described.

To determine the true identities of the two compounds described above, both were prepared by their reported methods and subjected to the usual analyses. The results have indicated that the compound of Berger and Summerbell was indeed tetraphenyl-*p*-dioxin, but that the compound reported by Jerumanis and Lalancette was tetraphenylthiophene (**4**). The error on the part of Jerumanis and Lalancette was attributed to an incorrect elemental analysis.

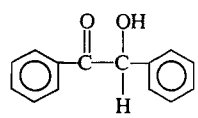

1

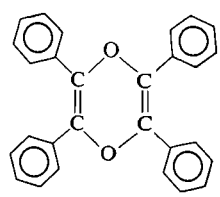

2

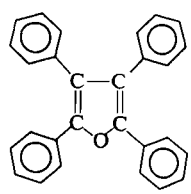

3

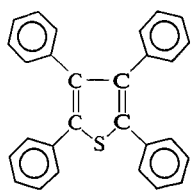

4

Can. J. Chem. Downloaded from www.nrcresearchpress.com by 210.87.254.42 on 09/05/12
For personal use only.

Experimental

Infrared spectra were measured in KBr on a Beckman IR-10 infrared spectrophotometer and the absorption maxima are quoted in wavenumbers (cm^{-1}). Ultraviolet spectra were measured on a Perkin Elmer Double Beam spectrophotometer in absolute ethanol solution, and the absorption maxima are reported in nm. Nuclear magnetic resonance spectra were measured in CCl_4 solution on a Perkin Elmer R 12 A nuclear magnetic resonance spectrometer. Line positions are given in the δ (ppm) scale using tetramethylsilane (TMS) as internal standard. Mass spectra were run by, or under the direction of, Jack Maseles of the University of Texas at Austin, on a Bell and Howell mass spectrometer (model 21-491). All elemental analyses were performed by Galbraith Laboratories Inc., Knoxville, Tennessee.

*The Compound (Tetraphenyl-*p*-dioxin) Reported by Berger and Summerbell (3)*

Benzoin (3 g, recrystallized from ethanol to a melting point of 133–134°C) was refluxed in dry hexane (100 ml) with a catalytic amount (0.1 g) of *p*-toluenesulfonic acid. Reflux was continued for 48 h using an azeotropic trap for removal of water. The hexane was distilled off and to the remaining yellow liquid, 175 ml of ethanol was added. The yellow crystalline product was obtained from this mixture on cooling. The crude product melted at 197–201°C but after recrystallization from acetic anhydride the bright yellow needles melted at 215–217°C (lit. (3) mp 218–219°C); 0.22 g, 8%; ir ν_{max}: 3020, 3060, 3080 (aromatic C—H stretch), 1660 (C=C stretch), 1595, 1495, 1440 (aromatic ring stretching), 1260, 1060–1070 (C—O stretching), 750, 680 (C—H out of plane vibrations of monosubstituted benzene); nmr (CCl_4) δ_{TMS}: 7.25 (sym d, aromatic protons); ms *m/e*: 388 (M^+, base peak), 311, 283, 267, 255, 194, 178, 165, 152, 139, 105, 77. *Anal.* calcd. for $C_{28}H_{20}O_2$: C 86.57, H 5.19, O 8.24; found: C 86.69, H 5.26, O 8.05.

The Compound (Tetraphenylthiophene) Reported by Jerumanis and Lalancette (4)

Methyl benzoate was prepared by a standard method (5) from benzoic acid and methanol. Boron sulfide (B_2S_3) was commercial reagent grade (from Ventron of Danvers, MA) and was used without further purification.

Methyl benzoate (8.9 g) and boron sulfide (2.5 g) were refluxed under nitrogen for about 28 h. As the reaction began, a rapid evolution of gas was observed and during the course of the reaction a fine white powder was deposited on the upper part of the reflux condenser (and the beaker covering it). The reaction mixture was filtered hot and the residue was washed with 5–10 ml of boiling methyl benzoate. Addition of 125 ml of ethanol to the filtrate caused precipitation of dark yellow-brown crystals, which redissolved upon heating the solution.

Two methods of purification[1] were developed. The first method, which may be compared to a fractional crystallization, first involved filtration of the hot ethanolic solution to remove a dark colored powder. The filtrate was then treated with activated charcoal, cooled, and a small crop of mustard-yellow powder was discarded. The filtrate was concentrated to 50 ml and the resulting yellow crystals were treated twice with charcoal in ethanol. White needles (0.26 g) melting at 184–185°C were obtained from this solution.

The second method, which produced higher yields, utilized mercury in the purification process. The 140 ml of ethanolic solution was first concentrated to 100 ml. The concentrated solution was then cooled to effect crystallization, the crystals were dissolved in carbon disulfide, and mercury was added to this solution. Vigorous shaking (at room temperature) of the solution produced a black precipitate of HgS. The solution was decanted periodically and fresh mercury added until no additional HgS was formed. The solution was then filtered, and the carbon disulfide was evaporated. When the residue was recrystallized from ethanol, 0.56 g of off-white needles melting at 185–186°C were produced. The white needles melting at 184–185°C and the off-white needles melting at 185–186°C were shown to be the same substance (lit. (7) mp 184–185°C); ir ν_{max}: 3015, 3060, 3090 (aromatic C—H stretch), 1600, 1495, 1480, 1440 (aromatic ring stretch), 1025, 1065 (in-plane C—H bending), 740, 690 (C—H out-of-plane vibrations of monosubstituted benzene); uv λ_{max} (log ε): 239 (4.401), 309 (4.173) in absolute ethanol, (lit. (8) 238 (4.352), 310 (4.124) in methanol); nmr (CCl_4) δ_{TMS}: 7.10 (s, aromatic protons), 7.05 (small multiplet, aromatic protons); ms *m/e*: 388 (M^+, base peak), 372, 370, 354, 311, 310, 295, 278, 267, 265, 178, 165, 156, 150, 121, 77. *Anal.* calcd. for $C_{28}H_{20}S$: C 86.57, H 5.19, S 8.24; found: C 86.53, H 5.00, S 8.59 (reported by Jerumanis and Lalancette (4) C 87.08, H 5.16, O 8.31).

[1]Early attempts at purification of the crude product from this reaction resulted in the formation of substances melting sharply around 165°C that were indicated to be pure by thin-layer chromatography but were found (by mass spectrum) to be mixtures of tetraphenylthiophene and S_8. These substances (similar to those reported by Bulmer and Mann (6)) resisted purification by repeated recrystallization from ethanol. Preliminary ultraviolet absorption and X-ray diffraction studies have indicated that the formation of a complex, while not likely, is a possibility.

1. Standard grating spectra. Sadtler Research Laboratories Inc., Philadelphia, PA. Vol. 37, No. 36169. 1975.
2. G. Harris (*Editor*). Dictionary of organic compounds. Vol 4. Oxford University Press, New York, NY. 1965. p. 2007.
3. D. R. Berger and R. K. Summerbell. J. Org. Chem. **24**, 1881 (1959).
4. S. Jerumanis and J. M. Lalancette. Can. J. Chem. **42**, 1929 (1964).
5. A. I. Vogel. Elementary practical organic chemistry. Part I: small scale preparations. John Wiley and Sons, New York, NY. 1966. pp. 348–349.
6. G. Bulmer and F. G. Mann. J. Chem. Soc. 678 (1945).
7. G. Harris (*Editor*). Dictionary of organic compounds. Vol 5. Oxford University Press, New York, NY. 1965. p. 3035.
8. J. G. Grasseli (*Editor*). Atlas of spectral data and physical constants for organic compounds. CRC Press, Cleveland, OH. 1973. p. B-938.

Paramagnetic effects in flavin spectroscopy. A ^{13}C nuclear magnetic resonance study

DONALD DAVID MACMURCHIE AND ROBERT JOHN CUSHLEY
Department of Chemistry, Simon Fraser University, Burnaby, B.C., Canada V5A 1S6

Received October 14, 1977

DONALD DAVID MACMURCHIE and ROBERT JOHN CUSHLEY. Can. J. Chem. **56,** 1045 (1978).

Experiments are described whose results indicate that semiquinones produced by intramolecular photoreduction of FMN in basic solution are responsible for specific line broadening observed in the ^{13}C nmr spectrum. Tests with oxidizing agents as well as singlet and triplet quenchers are shown to support this theory rather than the proposition that the paramagnetic species effective in relaxation enhancement is a flavin triplet state. A mechanism for the production of semiquinones and their interaction with the FMN population is discussed.

DONALD DAVID MACMURCHIE et ROBERT JOHN CUSHLEY. Can. J. Chem. **56,** 1045 (1978).

On décrit des expériences dont les résultats indiquent que les semiquinones produites par la photoréduction intramoléculaire de FMN en solution basique sont responsables pour les élargissements de bandes spécifiques observés dans les spectres rmn de ^{13}C. Des essais avec des agents d'oxydation ainsi qu'avec des pièges à singulet et triplet démontrent que cette hypothèse est plus plausible que la proposition à l'effet que l'espèce paramagnétique efficace dans l'augmentation de la relaxation est un état triplet de la flavine. On discute d'un mécanisme de production de semiquinones et de leur interaction avec la population de FMN.

[Traduit par le journal]

The purpose of the research described in this report has been to test, primarily by ^{13}C nmr, various hypotheses concerning the broadening phenomenon observed in ^{1}H nmr spectra of FMN (flavin mononucleotide) (1) and to arrive at an accurate description of the chemical events that lead to resonance broadening. In addition, we have investigated further the assignment of the ^{13}C resonances of FMN.

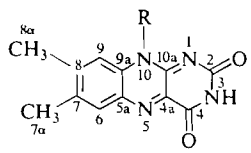

Rfn: R = —$CH_2(CHOH)_3CH_2OH$
FMN (disodium salt): R = —$CH_2(CHOH)_3CH_2OPO_3Na_2$
Lcm: R = —H
Lfn: R = —CH_3
Dfn: R = —CH_2CHO

The use of ^{13}C nmr is particularly appropriate in studying flavins as the number of magnetically distinct protons is small and many of these undergo solvent exchange. Observation of the ^{13}C resonances allows study of all parts of the molecule and the large range of ^{13}C chemical shifts permits resolution of the ^{1}H-decoupled spectrum into individual lines. Both the ^{1}H (2) and the ^{13}C (3) nmr spectra of FMN have been described and definite assignments have been made for some of the ^{13}C resonances on the basis of specific isotopic enrichment (4*a* and *b*).

In alkaline D_2O ($pD > 10$) the resonances associated with the ring protons have been observed to broaden with time to the point of vanishing from the spectrum, whereas the resonances of the ribityl side chain displayed a lessened and unequal broadening (l*a* and *b*). This broadening was observed to commence after a certain induction period and to be abolished by shaking the sample under air but not under nitrogen. These observations led to the suggestion that the broadening results from enhanced relaxation of the ^{1}H nuclei by the paramagnetic flavin triplet state. The possibility was discounted that a flavin semiquinone was responsible for the broadening effect but it has been shown (5*a* and *b*) that production of flavin semiquinone may proceed from the triplet state of the fully oxidized molecule and it is necessary to postulate unusual longevity of a triplet state or its continuous regeneration from an unknown source for a triplet state to be responsible for this effect. We wish to give more serious consideration to mechanisms involving reduced species as the principal broadening agent.

Experimental

Flavin mononucleotide (FMN), lumiflavin (Lfn), and reduced nicotinamide adenine dinucleotide (NADH) were obtained from Sigma Chemical Co. Commercial grade (95–97%) FMN was used without further purification for routine work while 'Grade I' material (99%) was used in experiments to ascertain the effect of the additional impurities. Lumichrome (Lcm) was obtained from Aldrich Chemical Co. and caffeine from British Drug Houses; both were used without further purification. TEMPONE (2,2,6,6-tetramethyl-4-piperidone-l-oxyl) came from Syva. All other chemicals used were reagent grade from standard suppliers except for 2,3-butadione and 2,4-pentadione, which were purified by distillation from practical grade material. Tris(2,4-penta-

Can. J. Chem. Downloaded from www.nrcresearchpress.com by 210.87.254.105 on 09/05/12
For personal use only.

Can. J. Chem. Downloaded from www.nrcresearchpress.com by 210.87.254.105 on 09/05/12
For personal use only.

dionato)Fe^{III} was prepared by addition of the ligand to aqueous $FeCl_3$.

Proton, ^{13}C, and ^{31}P nmr spectra were recorded using a Varian XL-100-15 nmr spectrometer at ambient temperature (~32°C), controlled by a Transform Technology Inc., Fourier transform accessory. Electron spin resonance spectra were recorded using a Varian E-4 spectrometer with signal averaging employing a TTI nmr accessory. Values for p*H* were taken from a Radiometer PHM64 meter and in the case of D_2O solutions are reported as 0.4 units greater than the meter reading, i.e., p*D* = indicated p*H* + 0.40 (6).

Experiments described as 'dark' were performed in minimal room light, using brown glassware where possible. Solution transfers were performed in a darkroom using a low level of red light and opaque cloth was generally used to guard against unwanted illumination. When illumination of samples was called for it was performed with a 300-W tungsten lamp at a distance of approximately 30 cm. Exchange of dissolved gases was carried out by bubbling O_2 or N_2, as required, through the solutions from a Pasteur pipette for a period of approximately 1 h.

In experiments testing the efficacy of various reagents in producing sharp ^{13}C resonances, the samples were subjected to flushing with N_2 and illumination in the nmr tube, followed by injection of a previously deoxygenated reagent solution through the hole in the vortex plug. The solution was then mixed briefly and the N_2 above it expelled as the vortex plug was brought into contact with the liquid surface; the space above the plug was then re-flushed with N_2, the tube capped and the spectrum recorded promptly. For esr spectroscopy, samples were prepared and outgassed in the dark, spectra recorded, the sample illuminated in the esr cavity, and further spectra recorded.

Results

The effects of illumination and oxygenation of FMN solutions at two representative p*D* values are shown in Fig. 1. Spectra of dark, deoxygenated FMN samples displayed sharp resonances identical with those of the same samples after oxygenation, shown for p*D* 10.5 in Fig. 1*a* and p*D* 6.5 in Fig. 1*b*. Upon illumination of the deoxygenated samples, however, the resonances of FMN at p*D* 10.5 were all broadened, Fig. 1*c*, some to the extent of complete disappearance from the spectrum. The resonances of the ring carbons were almost completely obscured and those of the two methyl carbons reduced to a single broad envelope. The effect on the ribityl carbons varied according to their proximity to the ring system. The resonances of C-1′ and C-2′ were no longer discernible whereas those of C-3′ and C-4′ were broadened almost to the point of coalescence and that of C-5′ remained moderately sharp, with a width at half-height of approximately 7 Hz. Oxygenation of the illuminated sample regenerated the sharp-line spectrum (Fig. 1*a*). When we recorded ^{31}P spectra of FMN under the same conditions we observed a slight decrease in line width, from 10 to 8 Hz, on oxygenation.

In contrast to the observations at p*D* 10.5, the nmr lines at p*D* 6.5 remained sharp under all conditions, the spectra before and after illumination being identical to that recorded after oxygenation as shown in Figs. 1*b* and *d*. These spectra were recorded after exponentially weighting the free induction decay to enhance the signal to noise ratio ($S_t' = S_t e^{-t/0.16}$, *t* in seconds); thus the slight paramagnetic broadening by O_2 is not obvious.

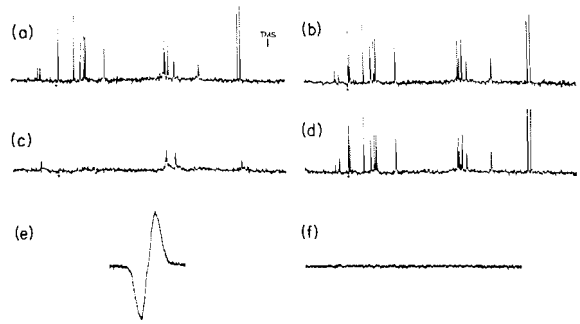

FIG. 1. Proton noise-decoupled ^{13}C nmr spectra (*a*–*d*) and esr spectra (*e* and *f*) of ca. 0.1 *M* FMN solutions in D_2O: Figs. 1*a* and *b*, after dark deoxygenation at p*D* 10.5 and 6.5, respectively; Figs. 1*c* and *d*, after illumination at p*D* 10.5 and 6.5; Figs. 1*e* and *f*, esr spectra of illuminated FMN solutions at p*D* 10.5, before and after oxygenation, respectively. Solutions were buffered with phosphate or borax as required. Spectra at 23.5 kG were averaged over 4000 accumulations of 8192 100-μs data points (spectral width 5 kHz) after a 15-μs (60°) pulse. A delay of 1 s separated the acquisitions. An instrument artifact was removed from the spectra at the positions marked 'X'. Electron spin resonance spectra were recorded at 3380 G, 9.47 GHz, 18 mW, with 100-MHz modulation at 3 G. Sweep parameters were: time 16 min; gain 2×10^4; time constant 1 s.

The esr spectra of a p*D* 10.5 solution of FMN after illumination (Fig. 1*e*) and after illumination followed by oxygenation (Fig. 1*f*) demonstrate the abolition of a paramagnetic species by oxygen corresponding to the sharpening of the ^{13}C nmr spectrum. The esr signal produced by illumination was not measurably diminished after a period of 16 h in the dark when oxygen was excluded from the system. As was the case with the nmr spectra, the esr spectrum of alkaline FMN before illumination was identical to that after oxygenation, i.e., no esr signal was observed. The esr spectrum at p*D* 6.5 (not illustrated), under which conditions the nmr lines remained sharp, consisted of no signal in the dark but showed a transient signal on illumination. In contrast to the persistent esr signal produced on illumination at p*D* 10.5, that at the lower p*D* value was less intense and diminished with time, having a half-life of approximately 20 min, although further illumination regenerated the signal. The signal at p*D* 6.5 also differed in having a line width of approximately 23 G in comparison to approximately 14 G for the alkaline signal. Spectra recorded at concentrations appropriate for ^{13}C nmr study, i.e., 0.1 *M*,

Can. J. Chem. Downloaded from www.nrcresearchpress.com by 210.87.254.105 on 09/05/12
For personal use only.

did not exhibit the line structure reported previously (7) but, in agreement with those earlier observations, more dilute solutions (10^{-3} *M*) produced spectra in which the hyperfine splittings were better resolved (Fig. 2).

The nature of the paramagnetic species was investigated by deoxygenation and illumination of a sample at p*D* 10.5 followed by addition of deoxygenated solutions of various reagents. Table 1 shows the results of these experiments. As substitutes for O_2 in regenerating the sharp-line ^{13}C spectrum, a variety of triplet quenchers, when added after illumination was complete, were not effective but various oxidizing agents were able to eliminate the broadening as had O_2. Although deoxygenated caffeine solutions were not effective in restoring sharpness, FMN solutions which had been made 0.1 *M* in caffeine before deoxygenation required illumination periods more than three times longer than those for caffeine-free FMN solutions for the generation of a comparable paramagnetic interaction among the flavin molecules.

No significant broadening of the caffeine resonances was observed in these flavin solutions, even when the FMN lines were practically obscured (Fig. 3*a*). In a converse experiment the nitroxide TEMPONE was added to neutral FMN solutions in concentrations up to 10^{-2} *M* and the effect on the flavin nmr resonances observed. No significant broadening was found. The esr spectra of illuminated alkaline FMN solutions (0.01 *M*) containing 0.1 *M* caffeine, on the other hand, were characterized by markedly enhanced resolution of the hyperfine structure as well as the necessity for longer illumination to generate an observable concentration of unpaired electron spins. The reduced yield of paramagnetic species on photolysis in the presence of caffeine allows comparison of ^{13}C spectra obtained in the presence of dilute electron spin concentrations produced photochemically with spectra obtained on partial chemical reduction or oxidation, as shown in Fig. 3*b* and *c*. In these experiments neutral solutions of FMN were reduced with $Na_2S_2O_4$ and subsequently reoxidized. The use of flavin solutions at the lower p*H* values eliminates the possibility of species produced by photoreduction contributing to the spectra. When NADH was used as the reducing agent, the results were identical. When lumichrome was substituted for FMN in deoxygenated experi-

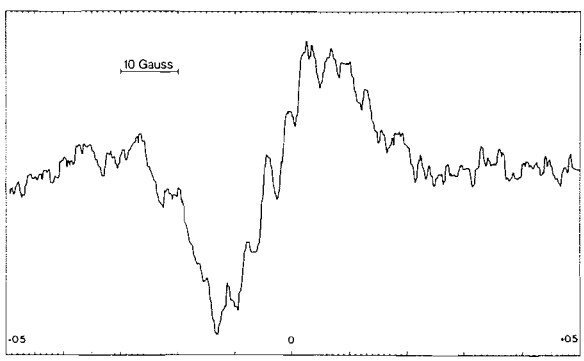

FIG. 2. Electron spin resonance spectrum of 0.001 *M* FMN, p*H* 10.2, fully deoxygenated and illuminated. Spectrum is signal averaged for 641 scans. Electron spin resonance spectra recorded at 3370 G, 20 mW with modulation of 1.25 × 10°. Sweep parameters: time 1 min; gain 5 × 10^4; time constant 0.3 s.

TABLE 1. Effect of various reagents in eliminating broadening

Reagent	Oxidation potential $E°(V)^a$	Triplet energy (kcal mol^{-1})^b	O_2 effect
$(NH_4)_2S_2O_8$	2.0		+
H_2O_2	1.7		+
O_2	1.2		+
$NaClO_4$	1.2		+
KNO_3	0.9		−
2,3-Butadione		55	−
Eosin Y		43	−
(2,4-Butadione)$_3Fe^{III}$		<43	−
Crystal violet		39	−
KI		N/A	−

[a]From ref. 18.
[b]From J. T. Baker Chemical Company.

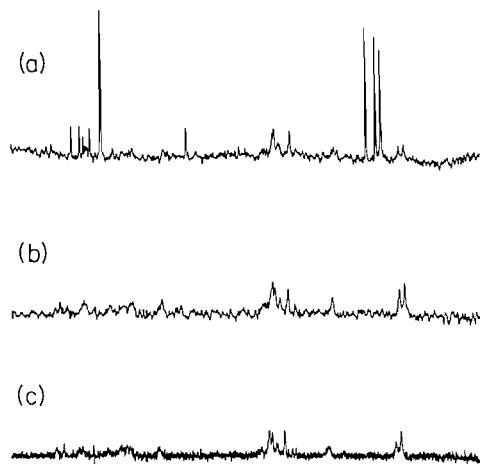

FIG. 3. Proton noise-decoupled ^{13}C nmr spectra of (*a*) 0.05 *M* FMN containing 0.1 *M* caffeine illuminated 2 min, p*D* 10.5; 5939 accumulations; 4096 data points; 5 kHz spectral width; pulse width 15 μs; pulse delay 2 s. The caffeine resonances remain undiminished. (*b*) 0.1 *M* FMN containing 0.01 *M* $Na_2S_2O_4$, p*D* 6.5 which has been partially reoxygenated; 4000 accumulations; 8192 data points; 5 kHz spectral width; pulse width 15 μs; pulse delay 1 s. (*c*) Fully oxygenated 0.1 *M* FMN containing 0.005 *M* $Na_2S_2O_4$, p*D* 6.5; 20 000 accumulations; 8192 data points; 5 kHz spectral width; pulse width 15 μs; pulse delay 1 s.

Can. J. Chem. Downloaded from www.nrcresearchpress.com by 210.87.254.105 on 09/05/12
For personal use only.

TABLE 2. ^{13}C chemical shifts of 0.1 *M* FMN in D_2O (0.1 *M* phosphate buffer, p*D* 7.69); ^1H noise decoupled[a]

Peak No.	Chemical shift	Assignment
1	162.14	C-4
2	159.17	C-2
3	152.33	C-8
4	151.20	C-10a
5	140.97	C-5a[b]
6	135.52	C-7[b]
7	135.15	C-4a[b]
8	133.01	C-9a[b]
9	131.74	C-6
10	118.58	C-9
11	74.20	C-3′
12	73.36	C-4′[c]
13	70.98	C-2′
14	66.80	C-5′[c]
15	49.10	C-1′
16	22.30	C-8α
17	20.18	C-7α

[a]Chemical shifts measured from external TMS and corrected for bulk diamagnetic susceptibility differences: $\delta_{corr} = \sigma_{obs} - \frac{2}{3}\pi(\chi_{TMS} - \chi_{H_2O}) = \delta_{obs} - 0.37$ ppm.
[b]Tentative assignment.
[c]Doublet.

ments at p*D* 10.5, no esr signal was observed on illumination, nor did illumination produce broadening of the ^{13}C nmr resonances.

In addition to these experiments concerning the broadening phenomenon, we also wish to report some observations relating to the assignments of the FMN ^{13}C spectrum. The chemical shifts which we have measured for these resonances, are listed in order of increasing shielding in Table 2, along with assignments on the basis of various arguments (see Discussion). The ^{13}C spectrum of FMN deuterated in the 8α-methyl group by the method of Bullock and Jardetzky (2) reveals the lower field methyl resonance (line No. 16) to be diminished and broadened to a marked degree and the spectrum of the aromatic resonances was also altered. Upon deuteration resonance, line No. 3 was observed to be broadened from 3.8 to 4.5 Hz as well as shifted 0.05 ppm to higher field. This increased shielding was unique to that resonance, all other resonances being consistent with their chemical shifts before deuterium exchange. These changes in the ^{13}C spectrum were not observed with samples heated for an equivalent period in H_2O.

The spectrum of 95–97% pure FMN (Sigma, Grade II, various lots) differed from that of 99% pure FMN (Sigma, Grade I, lot 43C-7010) only by the appearance of a weak resonance at 133.06 ppm in the spectrum of the less pure sample and of three small peaks in the sugar region. Otherwise the nmr and esr spectral characteristics of the two preparations were identical.

Discussion

The assignments of the ^{13}C spectrum of FMN given in Table 2 agree in many cases with those of Breitmaier and Voelter (3), which were made by qualitative comparison of the environments of FMN carbon nuclei with those of nuclei in other compounds, and have been confirmed in the cases of C-2 and C-4 by ^{13}C enrichment (4).

Substitution of ^2H for ^1H on C-8α causes a broadening and diminution of that ^{13}C methyl resonance, resulting from coupling to the ^2H nuclei and loss of the nuclear Overhauser effect. In addition to this, however, one may expect to find the shieldings of nearby carbons somewhat altered (8–10) and the effect observed on line No. 3 reflects this. The shift to higher field which accompanies the broadening of this resonance is consistent with those observed for various deuterated aliphatic and aromatic compounds (9) and we conclude that this resonance is that of C-8, rather than of C-4*a* as suggested previously (3).

Fortunately, the complete assignment of the ^{13}C resonances, while desirable, is not essential to a discussion of the broadening phenomenon. Our chief concern in this communication is to understand the broadening of the FMN ^1H resonances noted in earlier reports (1*a* and *b*) and in our work, and of the ^{13}C and ^{31}P resonances reported here. As the ^1H, ^{13}C, and ^{31}P nmr spectra exhibit the same behaviour in this respect, we take it that the effects in all these spectra have the same underlying cause. The fact that the saturated ribityl moiety is less strongly affected than the unsaturated isoalloxazine ring system and that the resonance of the chain-terminating ^{31}P is least affected of all implicates a paramagnetic centre associated specifically with the ring system, and a considerable population of the flavin triplet state, albeit generated by unknown means, has been suggested by Andrews and Fenn (1*a* and *b*). However, the possibility that the species responsible for shortening the nuclear relaxation times may be the flavin semiquinone, discounted in their report, deserves more serious consideration.

It has been reported that the level of illumination has no effect on the broadening phenomenon, but that deoxygenation leads to immediate loss of flavin signals. Our experiments indicate that p*H*, amount of illumination and the presence of oxidizing agents are critically interrelated in the generation and longevity of paramagnetic species, as evidenced by their effects on both the esr and nmr spectra. Therefore, correct interpretation depends on a precise definition of experimental conditions. For example, with samples thoroughly deoxygenated at p*D* 10.5, the slightest exposure to light is sufficient

Can. J. Chem. Downloaded from www.nrcresearchpress.com by 210.87.254.105 on 09/05/12
For personal use only.

to produce a broad-line condition, whereas in samples that have been poorly degassed, ordinary precautions to ensure darkness suffice to produce sharp spectra. This is clearly a titration of residual O_2 by stray photons, corresponding to the induction time for broadening (1*a* and *b*) and the number of induction flashes required in the photobleaching of FMN with traces of O_2 (5*a*). At p*D* 6.5, we find that illumination of an FMN sample does not yield a persistent esr signal but that the signal is relatively weak, decays with a half-life of approximately 20 min, and has a somewhat shorter relaxation time, T_2. Correspondingly, the ^{13}C nmr spectrum at p*D* 6.5 remains sharp under all circumstances, as shown in Fig. 1*b* and *d*.

The observation of a transient esr signal upon illumination of FMN solutions at neutral or near-neutral p*H* is well established and identified with the semiquinone formed under those conditions (5, 7, 11, 12). Our results are in agreement with these. The esr signal which we have observed on illumination at p*D* > 9 is somewhat more intense and of much longer duration however, indicating a more stable species and accounting for the persistent broadening of the nmr lines. It is significant here that different types of semiquinone radical, whose relative populations are p*H* dependent, have been detected in flavoprotein systems (7, 13), and that the form predominant above p*H* 9 has esr characteristics distinct from those of the radical formed at p*H* 6 (13). The deprotonation of N-3 has a p*K* of 8.4 in the semiquinone radical as opposed to approximately 10 in the fully oxidized species, indicating an increased stability of the anionic semiquinone at higher p*H* values. Furthermore, higher relative concentrations of radicals have also been found at elevated p*H* (15). Although we have discussed the p*H* dependence of these effects in terms of the difference between p*D* 6 and 10 to be consistent with other reports (1, 14), it should be pointed out that the broadening effect on the ^{13}C nmr spectrum arises over a much narrower range of p*H* values, little or no broadening being observed at p*D* 8.7 while the full effect is observed at p*D* 9.4 (Fig. 4) which is reasonably consistent with the p*K* of 8.4 noted earlier for the semiquinone ionization, i.e., the increased stability of the radical anion at higher p*H* value.

The circumstances leading to the production of flavin semiquinones have been studied for some time with the conclusion that, in the case of riboflavin and FMN, a triplet state has indeed been found to be populated on illumination, and that this species may proceed through an intramolecular reduction to a semiquinone radical. Subsequent exposure to O_2, light or basic conditions leads to cleavage of the oxidized side chain and a variety of photolysis products (5*a* and *b*, 12). It is reasonable to suppose that flavin adenine dinucleotide (FAD) reacts similarly. Given the duration of the broadening effect and the esr signal in our experiments, up to 16 h at p*D* 10.5, the theory that a triplet state is responsible seems less likely than one postulating a semiquinone radical as the paramagnetic species. We have tested this by adding a variety of quenchers to FMN test solutions both before and after illumination and observing the ^{13}C spectra, and by testing various oxidizing agents in the same way.

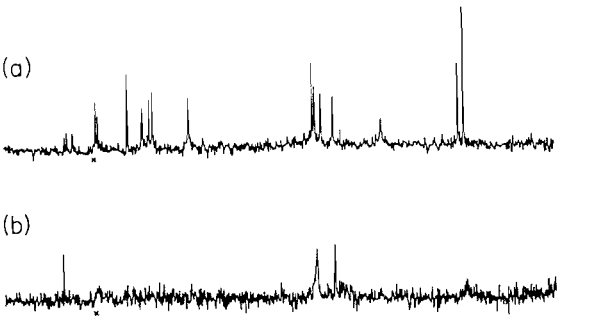

FIG. 4. Proton noise-decoupled ^{13}C nmr spectra of deoxygenated solutions of FMN after illumination at p*D* 8.7 (Fig. 4*a*) and p*D* 9.4 (Fig. 4*b*). Parameters were as described for Fig. 1.

The results of these experiments, Table 1, clearly demonstrate that the species responsible for the broadening of the ^{13}C nmr lines and the generation of the esr signal is removed by reagents of sufficient oxidizing potential but not by common triplet quenchers. The failure of NO_3^- to eliminate the broadening at high p*H* would be explained by a requirement of an oxidation potential of approximately 1 V in this process. We conclude that the species responsible for broadening is the flavin semiquinone and not as suggested previously a long-lived triplet state. It is unlikely that a system of the type

[1] $\text{FMN}^-(\text{triplet}) + \underline{\underline{\text{FMN}}}^-(\text{ground state}) \rightleftharpoons \text{FMN}^-(\text{ground state}) + \underline{\underline{\text{FMN}}}^-(\text{triplet})$

would have a sufficiently long triplet lifetime in the absence of a known energy source to be responsible for the observations. On the other hand, in the absence of other oxidizing or reducing agents, a redox exchange system of the type

[2] $\text{FMNH}^{\cdot} + \underline{\underline{\text{FMN}}}^- \rightleftharpoons \underline{\underline{\text{FMNH}}}^{\cdot} + \text{FMN}^-$

where $\underline{\underline{\text{FMNH}}}^{\cdot}$ is flavin mononucleotide semiquinone,

Can. J. Chem. Downloaded from www.nrcresearchpress.com by 210.87.254.105 on 09/05/12
For personal use only.

could be expected to persist. Although the reduced species initially produced is not in fact $FMN\dot{H}$ but leucodeuterioflavin, $DfnH_2$, redox exchange of this species with FMN (5*a*) followed by subsequent disproportionation of $FMNH_2$ provides a reasonable mechanism for delocalization of the unpaired electron spins throughout the entire FMN population. Thus

$$[3a] \qquad FMN \xrightarrow{h\nu} DfnH_2$$

$$[3b] \qquad DfnH_2^{\cdot} + FMN \rightleftharpoons FMNH_2^{\cdot} + Dfn^{\cdot}$$

$$[3c] \qquad FMNH_2^{\cdot} + FMN \underset{k_d}{\overset{k_a}{\rightleftharpoons}} 2\,FMN\dot{H}^{\cdot}$$

If one considers the parameters which have been determined for the following processes

$$2\,Dfn\dot{H} \xrightarrow{k_f} Dfn + DfnH_2, k_f \simeq 4 \times 10^8\, M^{-1}\, s^{-1} \quad \text{(ref. 5)}$$

and

$$(FMN\dot{H})_2 \rightleftharpoons FMN + FMNH_2, K = 4.5 \times 10^{-4}\, M \quad \text{(ref. 16)}$$

and assumes that the rates for steps 3*a–c* above are of the same order of magnitude an estimate may be made for the two rates in step 3*c*, placing them at approximately $10^5\ M^{-1}\ s^{-1}$ and $10^{13}\ M^{-2}\ s^{-1}$ for the forward and backward steps, respectively. Exchange of the type shown in [2] could be expected to be at least as fast as it does not require collisions between two of the relatively dilute semiquinones. Although these processes would be sufficiently rapid to distribute the unpaired electron spin among a large number of flavin molecules during a nuclear relaxation time, we do not exclude the possibility of an even faster process such as electron exchange which is not accompanied by proton transfer, for example:

$$[4] \qquad FMN\dot{H}^{-} + \underline{FMN}^{-} \rightleftharpoons FMNH + \underline{FMN}^{2-}$$

Although this latter type of process offers a more rapid exchange of electron density, the creation of a dianion and a neutral molecule from the two singly ionized species is unattractive. In either scheme however the central aspect, exchange of paramagnetic electron density among the entire flavin population, remains unaltered.

The fate of the deuterioflavin, whether it remains as such or loses a side-chain fragment, is not central to the broadening phenomenon, although the difference in hydrolysis products as a function of p*H* may be a reflection of the differing natures of the semiquinone radicals at neutral and alkaline p*H* values.

Our finding that lumichrome, which lacks the ribityl side chain, does not exhibit the broadening phenomenon supports the proposition of intramolecular radical formation which may then be followed by redox exchange.

In addition to the redox exchange mechanisms just discussed we have also considered the possibility that a stacking interaction between $FMN\dot{H}$ and FMN could give rise to the observed broadening. It is conceivable that a complex which brought oxidized and half reduced ring systems into close proximity but which did not associate the side chains of the oxidized molecules with the paramagnetic centre could lead to elimination of the signals from the ring system and retention of observable resonances from the aliphatic carbons. The fact that we have not observed significant broadening of the resonances of caffeine in solutions in which the FMN signals have been fully broadened argues against this model, however, and in fact against any model which does not include, on the nmr time scale, some paramagnetic character for all of the molecules affected. Since caffeine is known to form an FMN complex whose dissociation constant, $10^{-2}\ M$ (17) is the same as that of FMN with itself (16) one would expect to observe broadening of its resonances corresponding to that of the oxidized FMN resonances if a stacking interaction were important and might expect to find decreased broadening of the FMN resonances resulting from disruption of any FMN stacking interaction by caffeine. No effect of this type was observed and stacking mechanisms are therefore not considered to be important in the broadening process.

Although the persistent sharpness of the caffeine resonances demonstrates the inefficiency of general intermolecular relaxation enhancement by paramagnetic flavins, the lack of effect on the FMN ^{13}C spectrum of large concentrations, up to $10^{-2}\ M$, of the nitroxide radical TEMPONE indicates the converse, namely that the flavin nuclei are not efficiently relaxed by general paramagnetic species. Thus, flavin semiquinones are not unusually effective as nonspecific relaxation enhancers, nor are diamagnetic flavins particularly susceptible to nonspecific relaxation enhancement and the processes leading to the FMN line broadening must incorporate steps which place unpaired electron spin density on all of the molecules.

The increased illumination time required to produce paramagnetic flavins in the presence of caffeine is consistent with its properties as a quencher of FMN fluorescence (17), thus decreasing the overall yield of semiquinones. Comparably small semiquinone populations may be generated either by addition of small amounts of reducing agent to oxidized FMN or by admittance of traces of oxygen to reduced solutions and spectra obtained under

these conditions have the same characteristics as those of partially photolysed FMN, indicating that the relaxation enhancement depends upon the total number of unpaired spins and, as intermediate spectra are observed, that the unpaired electron density is indeed being distributed throughout the entire flavin system.

Although we do not eliminate the possibility of direct electron exchange among the flavin molecules we feel that the chemical processes described above [3*a*–*c*] which are based on established work in flavin chemistry, and entirely consistent with our results, provide the most probable basis for the observed spectral behaviour of FMN.

Acknowledgement

This work was supported by the National Research Council of Canada (Grant A9709).

1. (*a*) P. R. ANDREWS and M. D. FENN. Proc. Aust. Biochem. Soc. **7**, 55 (1974); (*b*) P. R. ANDREWS and M. D. FENN. Aust. J. Chem. **28**, 1609 (1975).
2. F. J. BULLOCK and O. JARDETZKY. J. Org. Chem. **30**, 2056 (1965).
3. E. BREITMAIER and W. VOELTER. Eur. J. Biochem. **31**, 234 (1972).
4. (*a*) K. YAGI, N. OHISHI, A. TAKAI, K. KAWANO, and Y. KYOGOKU. *In* Flavins Flavoproteins Proc. Int. Symp. 5th. San Francisco, March 31 – April 3, 1975. *Edited by* T. P. Singer. p. 775; (*b*) K. YAGI, N. OHISHI, A. TAKAI, K. KAWANO, and Y. KYOGOKU. Biochemistry, **15**, 2877 (1976).
5. (*a*) B. HOLMSTRÖM. Ark. Kemi, **22**, 281 (1964); (*b*) B. HOLMSTRÖM. Ark. Kemi, **22**, 329 (1964).
6. P. K. GLASOE and F. A. LONG. J. Phys. Chem. **64**, 188 (1960).
7. B. COMMONER and B. B. LIPPINCOTT. Proc. Natl. Acad. Sci. U.S.A. **44**, 1110 (1958).
8. G. E. MACIEL, P. D. ELLIS, and D. C. HOFER. J. Phys. Chem. **71**, 2160 (1967).
9. YU. K. GRISHIN, N. M. SERGEYEV, and YU. A. USTYNYUK. Mol. Phys. **22**, 711 (1971).
10. P. A. J. Gorin. Can. J. Chem. **52**, 458 (1974).
11. W. E. KURTIN, M. A. LATINO, and P.-S. SONG. Photochem. Photobiol. **6**, 247 (1966).
12. P.-S. SONG and D. D. METZLER. Photochem. Photobiol. **6**, 691 (1967).
13. V. MASSEY and G. PALMER. Biochemistry, **5**, 3181 (1966).
14. W. R. WEIMAR and A. H. NEIMS. *In* Riboflavin. *Edited by* R. S. Rivlin. Plenum Press, New York, NY. 1975. p. 7.
15. A. EHRENBERG, G. ERIKSSON, and P. HEMMERICH. *In* Oxidases and related redox systems. Vol. I. *Edited by* T. E. King, H. S. Mason, and M. Morrison. John Wiley and Sons, Inc., New York, NY. 1965. p. 179.
16. Q. H. GIBSON, V. MASSEY, and N. M. ATHERTON. Biochem. J. **85**, 369 (1962).
17. G. WEBER. Biochem. J. **47**, 114 (1950).
18. H. A. SOBER (*Editor*). The handbook of biochemistry. The Chemical Rubber Co., Cleveland, OH. 1969.

Can. J. Chem. Downloaded from www.nrcresearchpress.com by 210.87.254.105 on 09/05/12
For personal use only.

The oxidation of haplophytine

PETER YATES, FREDERICK N. MACLACHLAN, AND IAN D. RAE
Lash Miller Chemical Laboratories, University of Toronto, Toronto, Ont., Canada M5S 1A1

Received November 8, 1977

PETER YATES, FREDERICK N. MACLACHLAN, and IAN D. RAE. Can. J. Chem. **56**, 1052 (1978).

Oxidation of haplophytine (**1**) with alkaline potassium permanganate has been shown to give the seco product **16**. This assignment is based on spectroscopic data and comparison of these with spectroscopic data for the analogous seco product **8** formed on similar oxidation of aspidophytine (**3**), an acid cleavage product of haplophytine. The course of these oxidations contrasts with that of the oxidation of haplophytine and aspidophytine with alkaline hydrogen peroxide, which gives **4** and **6**, respectively, without carbon–carbon bond cleavage.

PETER YATES, FREDERICK N. MACLACHLAN et IAN D. RAE. Can. J. Chem. **56**, 1052 (1978).

On a montré que l'oxydation de l'haplophytine (**1**) avec du permanganate de potassium en milieu alcalin conduit au produit séco **16**. Cette attribution est basée sur des données spectroscopiques et sur une comparaison de ces données avec des données spectroscopiques pour le composé séco analogue **8** formé par une oxydation semblable de l'aspidophytine (**3**), un produit de clivage acide de l'haplophytine. Le cours de ces oxydations est en opposition avec celui de l'oxydation de l'haplophytine et de l'aspidophytine par le peroxyde d'hydrogène en milieu alcalin qui conduit respectivement aux composés **4** et **6** sans coupure du lien carbone–carbone.
[Traduit par le journal]

The binuclear alkaloid haplophytine has been shown to have structure **1** (1, 2). During the course

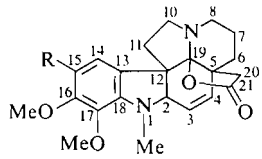

1 R = **2**
3 R = H

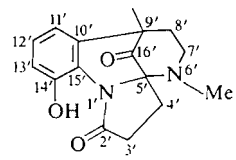

2

of the determination of this structure, the structure of the product formed from **1** on reaction with alkaline hydrogen peroxide was shown to be 10-oxohaplophytine (**4**). Analogous products, **6** and **7**, respectively, were obtained on similar oxidation of aspidophytine (**3**), an acid cleavage product of **1** (1), and of cimicine (**5**), an alkaloid that accompanies **1** in *Haplophyton cimicidum* (Apocynaceae) (3).

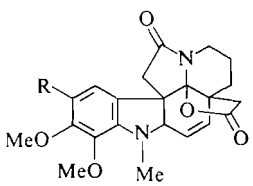

4 R = **2**
6 R = H

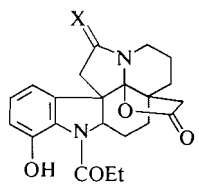

5 X = H_2
7 X = O

In early work on the chemistry of haplophytine, Snyder and co-workers (4) found that oxidation of haplophytine with alkaline potassium permanganate gives a product different from that formed with alkaline hydrogen peroxide. We discuss here the determination of the structure of the permanganate oxidation product.

Elemental and mass spectrometric analysis of this oxidation product and of its methylation product, formed on treatment with diazomethane, showed that the molecular formula of the former is $C_{37}H_{40}N_4O_8$ and that the latter is a dimethyl derivative, $C_{37}H_{38}N_4O_6(OCH_3)_2$. The formula of haplophytine itself is $C_{37}H_{40}N_4O_7$ and thus the formation of the permanganate product formally involves the addition of an oxygen atom; we have therefore dubbed the oxidation product haplophytine oxide.

Although it was not found possible to isolate a pure product from the acid cleavage of haplophytine oxide, alkaline permanganate oxidation of aspidophytine (**3**), $C_{22}H_{26}N_2O_4$, the acid cleavage product obtained from haplophytine itself, gave a product, albeit amorphous, that was shown to have the molecular formula $C_{22}H_{26}N_2O_5$. On treatment with diazomethane this product, which we refer to as aspidophytine oxide, gave a monomethyl derivative, $C_{22}H_{25}N_2O_4(OCH_3)$. The formation of aspidophytine oxide is clearly related to the formation of haplophytine oxide and the determination of the structure of the latter was initiated by the determination of that of the former.

Ultraviolet (uv), infrared (ir), and ^1H nuclear magnetic resonance (^1Hmr) data for aspidophytine oxide are given in Table 1 together with corresponding data for aspidophytine (**3**). The uv spectrum of aspidophytine oxide differs significantly from that of **3** and suggests that the indoline system of **3** has

Can. J. Chem. Downloaded from www.nrcresearchpress.com by 210.87.254.40 on 09/05/12
For personal use only.

TABLE 1. The uv, ir, and ^{1}Hmr spectra of aspidophytine oxide (**8**) and aspidophytine (**3**)

Spectrum	**8**	**3**
λ_{max}(EtOH) (nm) (ε)	228 (24 600) 296 (4600)	222 (28 700) 256 (5900) 304 (2400)
λ_{max}($CHCl_3$) (μ)	3.3–4.5 5.79 6.27	5.73
δ ($CDCl_3$)	3.85 (s, 3H) 3.93 (s, 6H) 4.2–4.65 (m, 1H) 5.99 (d, J = 12 Hz, 1H) 6.53 (d, J = 12 Hz, 1H) 6.82 (d, J = 8 Hz, 1H) 7.20 (d, J = 8 Hz, 1H) 11.6–12.4 (v br s, 1H)	3.15 (s, 3H) 3.73 (m, 1H) 3.75 (s, 3H) 3.80 (s, 3H) 5.53 (dd, J = 10, 1 Hz, 1H) 5.87 (dd, J = 10, 2 Hz, 1H) 6.18 (d, J = 8 Hz, 1H) 6.97 (d, J = 8 Hz, 1H)

been converted to an indole system (5). The strong, broad band at 3–4.5 μ in its ir spectrum together with the strong band at 5.79 μ show the presence of a carboxylic acid group. The strong ir band at 6.27 μ suggested the presence of a second carbonyl group with its stretching band superimposed on an aromatic band, although the environment of this carbonyl group would have to be unusual to account for the exceptionally long wavelength; the presence of this second carbonyl group was subsequently confirmed by ^{13}C nuclear magnetic resonance (^{13}Cmr) spectroscopy (*vide infra*).

The ^{1}Hmr spectrum of aspidophytine oxide confirmed the presence of a carboxylic acid in that a very broad one-proton singlet is present at δ ~ 12. The two doublets in this spectrum at δ 6.82 and 7.20 (J = 8 Hz) can be assigned to two aromatic protons (cf. the ^{1}Hmr spectrum of **3**), and the two doublets at δ 5.99 and 6.53 (J = 12 Hz) can be interpreted as showing the retention of the C3—C4 ethylenic system of **3**. Unlike the case of **3**, however, the vinylic proton doublets of aspidophytine oxide show no additional splitting. The additional splitting in the spectrum of **3** is attributable to coupling of the C3 and C4 protons with the proton at C2, which gives rise to a one-proton multiplet at δ 3.73. The absence of this additional splitting in the spectrum of aspidophytine oxide and of a signal corresponding to the C2 proton signal of **3** clearly indicates that C2 bears no hydrogen atom in aspidophytine oxide. Retention of the two aromatic methoxyl groups of **3** in aspidophytine oxide is demonstrated by the signals at δ 3.85 and 3.93. Since they correspond to nine protons, these signals must also include the signal corresponding to the *N*-methyl group that is present in **3**. Moreover, in accord with the earlier conclusion that the indoline system of **3** has been converted to an indole system in aspidophytine oxide, the *N*-methyl signal for the latter is at considerably lower field than that for the former (δ 3.15) (6).

These spectroscopic data taken together with the molecular formula and source of aspidophytine oxide lead to the assignment to it of structure **8**. This structure incorporates the features previously deduced to be present but further consideration of some of these in terms of **8** is necessary. It might have been expected that the 2-vinylindole system in **8**

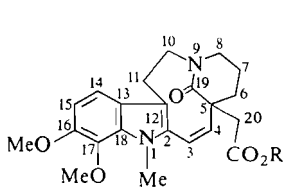

8 R = H
10 R = Me

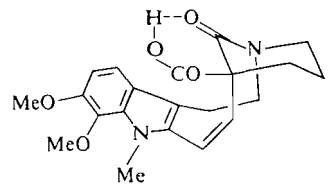

9

would give rise to an uv spectrum different from that of a simple indole system. However, examination of molecular models shows that the plane of the ethylenic double bond is essentially orthogonal to the plane of the indole ring, as illustrated in **9**, which is considered to be the preferred conformation of **8**. This geometrical relationship accounts for the absence of extended indole conjugation in aspidophytine oxide. Ziegler and co-workers (7) have previously advanced a similar interpretation of their observation that the uv spectrum of 3,4-dehydroquebrachamine (**11**) shows the presence of a typical 2,3-dialkylindole chromophore rather than an extended indole chromophore. The unusually long wavelength of the lactam carbonyl-stretching band in the ir spectrum of **8** can be interpreted as being due to strong hydrogen bonding with the carboxylic acid hydrogen. Such hydrogen bonding can also account

Can. J. Chem. Downloaded from www.nrcresearchpress.com by 210.87.254.40 on 09/05/12
For personal use only.

Can. J. Chem. Downloaded from www.nrcresearchpress.com by 210.87.254.40 on 09/05/12
For personal use only.

for the fact that the carbonyl-stretching band of the carboxylic acid group appears at 5.79 μ, a wavelength shorter than normal for a carboxylic acid, if it is assumed that the intramolecular hydrogen bonding with the lactam carbonyl group disrupts the customary intermolecularly hydrogen-bonded dimeric form of the carboxylic acid. An analogous effect has been postulated (8) to account for the observation that the carbonyl-stretching band of *o*-methoxybenzoic acid (**12**) occurs at 0.12 μ to shorter wavelength than that of *p*-methoxybenzoic acid (**13**).[1]

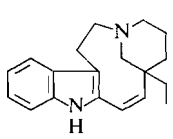

11

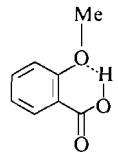

12

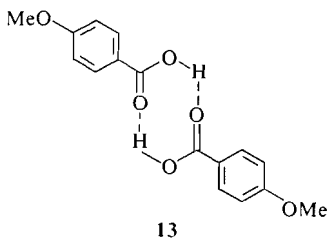

13

This interpretation of the ir spectrum of **8** is in accord with the ir spectrum of the monomethyl derivative of **8**, formed with diazomethane and now assigned structure **10**. The latter spectrum shows bands at 5.79 and 6.15 μ; the position of the lower wavelength band is normal for a carboxylic ester whereas the lactam band, in the absence of hydrogen bonding, appears at considerably shorter wavelength than in the case of **8**. As expected **10** shows in its ^{1}Hmr spectrum four three-proton signals in the region δ 3.7–3.9. An interesting effect of methylation is to bring about the elision of the two vinyl proton signals in the ^{1}Hmr spectrum of **10**, where they appear as a slightly broadened singlet ($w_{\frac{1}{2}}$ = 3 Hz) at δ 6.33. This change with respect to **8** could result from changes brought about in the relative shielding of the vinylic protons when the acetic acid side chain in **8** is freed from its fixed orientation upon removal of hydrogen bonding to the lactam carbonyl group. A one-proton multiplet that appears in the ^{1}Hmr spectra of both **8** and **10** cannot be assigned with certainty, but must be associated with one of the C10 or C11 hydrogen atoms that is deshielded by being held in the plane of the amide or indole systems, respectively.

The ^{13}Cmr spectrum of aspidophytine oxide and its relationship to that of aspidophytine (Table 2) corroborates the structural assignment **8**. Two signals that are attributable to carbonyl carbons are observed at δ 171 and 177 and can be assigned to the lactam and carboxylic acid carbonyl carbons, respectively. Ten signals in the δ 100–150 region, two more than in the case of **3**, can be assigned to the eight indole and two vinyl carbons. It may be noted the signals assigned to the benzene carbons of the indole system appear at higher field than do the corresponding signals of **3**. This implies increased electron density and is in concordance with the electron-rich indole nucleus. It may be noted that, due to the orthogonality of the ethylenic double bond and the indole ring, the latter acts only inductively as an electron-withdrawing group and shifts one of the vinyl carbon signals to significantly lower field than the C3 and C4 signals in the spectrum of **3**. In the region δ < 100 no signal corresponding to that of C2 in **3** (δ 71.8 (d)) is present in the spectrum of **8**. The singlet at δ 47.1 in the spectrum of **8** can be assigned to C5; it is shifted by ~5 ppm relative to the signal assigned to C5 in the spectrum of **3**, an effect attributable to replacement of the sp^3 carbon at C19 in **3** by a carbonyl carbon in **8**. All but one of the remaining high field signals in the spectrum of **8** are analogous to those in the spectrum of **3**. An egregious exception is the signal at δ 19.4 assigned to C11; this carbon in **3** is considered to give rise to a signal at δ–35. Such a large chemical shift difference between a methylene carbon attached to the C3 position of an indole vs. an indoline system has precedent. The signal for the C6 carbon in cuanzine (**14**) appears at δ 17.4 (10) whereas that for the C6 carbon in vindoline (**15**) occurs at δ 43.9 (11).[2]

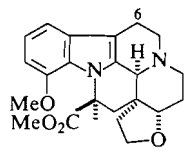

14

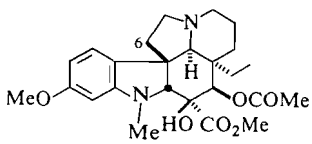

15

With structure **8** established for aspidophytine oxide, it was now possible to assign structure **16** to haplophytine oxide, in which the aspidophytine moiety has undergone a transformation analogous to that in the permanganate oxidation of aspidophytine itself, while the other moiety, the canthiphytine moiety, remains unchanged.

[1]Compare with ref. 9.

[2]It should be noted that C11 and C6 in the indoles **8** and **14**, respectively, both have fewer β substituents than the corresponding carbons of the indoline system **3** and **15**, respectively.

TABLE 2. The ^{13}Cmr spectra of aspidophytine oxide (**8**) and aspidophytine (**3**)

	^{13}Cmr δ	
Carbon	**8**	**3**
2	130.2 (s)	71.8 (d)
3, 4	124.1 (d), 141.3 (d)	125.6 (d), 130.5 (d)
5	47.1 (s)	41.4 (s)
6	34.4 (t)[a]	34.6 (t)[b]
7	23.5 (t)[a]	21.5 (t)
8, 10, 20	44.1 (t), 46.5 (t)[a] 52.1 (t)	43.3 (t), 47.3 (t), 47.8 (t)
11	19.4 (t)	35.4 (t)[b,c]
12	109.8 (s)	57.3 (t)
13	124.3 (s)	133.8 (s)
14	112.9 (d)	120.2 (d)
15	107.6 (d)	102.3 (d)
16	135.6 (s)	153.9 (s)
17	148.5 (s)	143.6 (s)[d]
18	131.5 (s)	149.4 (s)[d]
19	171.3 (s)	107.2 (s)
21	177.2 (s)	175.7 (s)
OCH_3	57.4 (q), 61.9 (q)	55.8 (q), 61.1 (q)
NCH_3	32.6 (q)	35.4 (q)[c]

[a]The multiplicities of these signals could only be defined as either triplet or singlet.
[b]The C6 and C11 signals of **3** could not be individually assigned.
[c]Superimposed signals.
[d]The C17 and C18 signals of **3** could not be individually assigned.

This assignment is based on a comparison of the spectra of haplophytine oxide (Tables 3 and 4) with those of aspidophytine oxide and of haplophytine. The uv spectrum of haplophytine oxide again indicates the presence of an indole system; furthermore, the intensity differences between the spectra of the

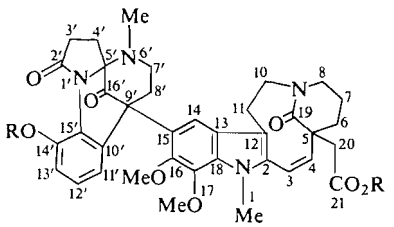

16 R = H
17 R = Me

oxides correspond to those between the spectra of haplophytine and aspidophytine themselves. The ir spectrum of haplophytine oxide shows bands that correspond to those in the spectrum of aspidophytine oxide and in addition bands at 5.71 and 6.03 μ that are similar in position to bands previously assigned to the ketone and lactam carbonyl groups, respectively, of the canthiphytine moiety of haplophytine. This relationship is further evidenced in the ir spectrum of the dimethyl derivative of haplophytine oxide, formed with diazomethane and now assigned structure **17**. This spectrum shows bands at 5.73, 5.86, and 6.1 (br) μ and no hydroxyl band. The band at 6.1 μ can be assigned to the lactam carbonyl of the aspidophytine moiety, shifted to lower wavelength as in the case of **10** as a result of removal of hydrogen bonding on esterification of the carboxylic acid group. The ester carbonyl is not visible as a distinct maximum, but the shallowness of the trough between the 5.73 and 5.86 μ bands is indicative of its presence. The 5.73 and 5.86 μ bands correspond to the ketone and lactam carbonyl groups, respectively, of the canthiphytine moiety with the latter shifted to lower wavelength relative to the lactam band in **16** as a result of removal of hydrogen bonding an etherification of the phenolic hydroxyl group (cf. the lactam carbonyl band for haplophytine methyl ether: 5.88 μ).

The relationship of the ^{1}Hmr spectrum of haplophytine oxide to that of aspidophytine oxide (**8**) is also indicative of the conversion of the aspidophytine moiety of haplophytine to a moiety corresponding to **8** with the retention of the canthiphytine moiety unchanged. A notable exception is the absence of a signal assignable to a carboxylic acid proton. This is attributed to further broadening of the already very broad signal of the carboxylic proton of **8**. The presence of the carboxylic acid group is not in doubt, both by virtue of the presence of a broad strong band in the ir spectrum of haplophytine oxide at 2.8–4.3 μ and of the ^{1}Hmr spectrum of its dimethyl derivative which shows that methylation leads to esterification of the carboxylic group in addition to etherification of the phenolic hydroxyl group in the canthiphytine moiety.

Can. J. Chem. Downloaded from www.nrcresearchpress.com by 210.87.254.40 on 09/05/12
For personal use only.

Can. J. Chem. Downloaded from www.nrcresearchpress.com by 210.87.254.40 on 09/05/12
For personal use only.

TABLE 3. The uv, ir, and ^{1}Hmr spectra of haplophytine oxide (**16**) and haplophytine (**1**)

Spectrum	**16**	**1**
λ_{max}(EtOH) (nm) (ε)	231 (37 150) 292 (8900)	220 (48 500) 265 (14 300) 305 (4500)
λ_{max}($CHCl_3$) (μ)	2.8–4.3 5.71 5.79 6.03 6.27	3–4[a] 5.73 6.06
δ($CDCl_3$)	2.48 (s, 3H) 2.97 (s, 3H) 3.83 (s, 6H) 4.2–4.8 (m, 1H) 5.8–6.3 (m, 2H)[b] 6.52 (d, J = 12 Hz, 1H) 6.8–7.3 (m, 3H) 8.93 (s, 1H)[c]	2.40 (s, 3H) 3.00 (s, 3H) 3.17 (s, 3H) 3.65 (s, 3H) 3.72 (m, 1H) 5.55 (dd, J = 10, 1 Hz, 1H) 5.85 (dd, J = 10, 2 Hz, 1H) 6.27 (dd, J = 7, 2.5 Hz, 1H) 6.9–7.2 (m, 3H) 9.04 (s, 1H)[c]

[a]This broad band is much shallower than the broad band in this region of the spectrum of **16**.
[b]Multiplet with superimposed doublet (J = 12 Hz) at δ 5.98.
[c]Absent after D_2O treatment.

TABLE 4. The ^{13}Cmr spectra of haplophytine oxide (**16**) and haplophytine (**1**)

	δ ($CDCl_3$)	
Carbon	**16**	**1**
2	129.7 (s)	72.0 (s)
3, 4	123.7 (d), 141.3 (d)	125.5 (d), 130.6 (d)
5	47.0 (s)	41.5 (s)
6	34.4 (t)	34.7 (t)[a]
7	23.4 (t)[b]	21.6 (t)
8, 10, 20	44.2 (t),[b] 46.2 (t),[b] 52.0 (t)	43.5 (t), 47.4 (t), 48.9 (t)
11	19.4 (t)	35.3 (t)[a,c]
12	110.2 (s)	57.3 (s)
13	124.2 (s)	126.4 (s)
14	110.7 (d)	118.8 (d)
15	126.5 (s)	124.1 (s)
16	146.3 (s)	151.7 (s)
17	149.0 (s)	143.9 (s)[d]
18	131.6 (s)	149.1 (s)[d]
19	171.4 (s)	107.2 (s)
21	177.1 (s)	175.6 (s)
2′	175.3 (s)	175.1 (s)
3′	38.8 (t)[b]	38.5 (t)
4′	22.3 (t)	22.5 (t)
5′	87.3 (s)	87.5 (s)
7′	48.8 (t)[b]	47.9 (t)
8′	29.8 (t)[b]	29.9 (t)
9′	55.4 (s)	55.1 (s)
10′	124.8 (s)	124.8 (s)
11′	127.9 (d)	128.0 (d)
12′, 13′	118.8 (d), 118.9 (d)	117.9 (d), 118.3 (d)
14′, 15′	138.1 (s), 139.8 (s)	138.6 (s), 139.0 (s)
16′	197.3 (s)	197.2 (s)
OCH_3	58.8 (q), 61.2 (q)	58.5 (q), 60.9 (q)
N(1)CH_3	32.6 (q)	35.3 (q)[c]
N(6′)CH_3	36.7 (q)	36.6 (q)

[a]The C6 and C11 signals of **1** could not be individually assigned.
[b]The multiplicities of these signals could only be defined as either triplet or singlet.
[c]Superimposed signals.
[d]The C17 and C18 signals of **1** could not be individually assigned.

Can. J. Chem. Downloaded from www.nrcresearchpress.com by 210.87.254.40 on 09/05/12
For personal use only.

Further, the ^{13}Cmr spectrum of haplophytine oxide and its relationship to the ^{13}Cmr spectra of haplophytine (Table 4) and of aspidophytine oxide (Table 2) can be interpreted in terms of structure **16** for haplophytine oxide.

It remains to consider the mechanism of formation and stereochemistry of aspidophytine and haplophytine oxides. We proposed the route depicted in Scheme 1, which is related to that proposed earlier

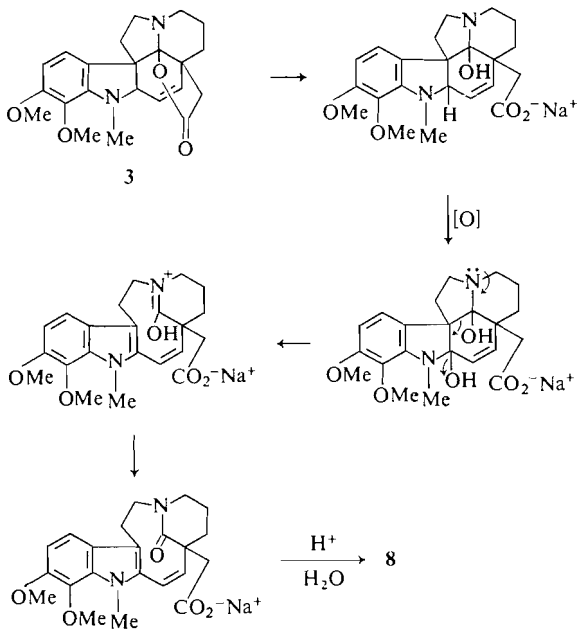

SCHEME 1

by Biemann and Spiteller (12) for the conversion of deacetylaspidospermine to 17-methoxyquebrachamine. Scheme 1 implies that the stereochemistry of aspidophytine oxide and of the corresponding moiety of haplophytine oxide is that in **18**, since the chiral centre at C5 would retain the same absolute configuration as in aspidophytine and haplophytine (**19**) (1, 13).

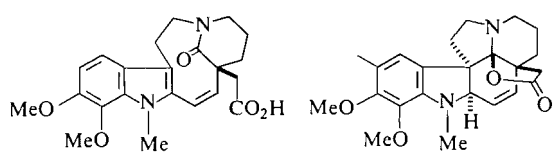

18 **19**

Experimental

*Oxidation of Haplophytine with Potassium Permanganate: Formation of Haplophytine Oxide (19-Oxosecohaplophytine; **16**)*

A stirred solution of haplophytine (100 mg, 0.15 mmol) in aqueous 1% sodium hydroxide (7.5 ml) was cooled in an ice bath. A solution of potassium permanganate (45 mg, 0.28 mmol) in water (15 ml) was added dropwise during 30 min. After an additional 30 min the mixture was saturated with sulfur dioxide, the white precipitate (63 mg) was separated by filtration, and the filtrate was extracted with ether (3 × 15 ml). The extract was dried (Na_2SO_4) and evaporated leaving a white solid foam (10 mg). The combined solids were crystallized from anhydrous ethanol to give microcrystalline **16** (60 mg, 60%): mp 309–318°C (dec.) (sealed tube) (lit. (4) mp 304–306°C (dec.)); the spectra of this compound are listed in Tables 3 and 4; *m/e* 668. *Anal.* calcd. for $C_{37}H_{40}N_4O_8 \cdot C_2H_5OH$: C 65.53, H 6.49, N 7.84; found: C 65.71, H 6.35, N 7.89.

O,O-*Dimethylhaplophytine Oxide (*O,O-*Dimethyl-19-oxosecohaplophytine*; ***17)***

A solution of haplophytine oxide (100 mg) in methanol (20 ml) was cooled in an ice bath. An excess of ethereal diazomethane was added. After 16 h at room temperature the solvents were removed and the residue was crystallized from ethanol to give colorless blades: mp 315–320°C (dec.) (sealed tube); λ_{max}(CHCl$_3$): 5.73, 5.86, 6.1 (br) μ; ^{1}Hmr (CDCl$_3$) δ: 2.52 (s, 3H), 3.08 (s, 3H), 3.70 (s, 3H), 3.82 (s, 3H) 3.85 (s, 3H), 3.97 (s, 3H), 4.2–4.6 (m, 1H), 6.0–6.4 (m, 3H), 6.65–7.3 (m, 3H); *m/e* 696. *Anal.* calcd. for $C_{39}H_{44}N_4O_8$: C 67.22, H 6.37, N 8.04; found: C 67.10, H 6.46, N 7.98.

*Oxidation of Aspidophytine with Potassium Permanganate: Formation of Aspidophytine Oxide (19-Oxosecoaspidophytine; **8**)*

A stirred solution of aspidophytine (222 mg, 0.58 mmol) in aqueous 0.1 *N* sodium hydroxide (34 ml) was cooled in an ice bath. A solution of potassium permanganate (111 mg, 0.70 mmol) in water (12 ml) was added. After 20 min the mixture was saturated with sulfur dioxide, the cream-colored precipitate (121 mg) was separated by filtration, and the filtrate was extracted with dichloromethane (4 × 20 ml). The extract was dried (Na_2SO_4) and evaporated leaving a cream-colored solid foam (47 mg). Neither the precipitate nor the foam could be crystallized (total 168 mg, 73%): molecular distillation gave a glass with unchanged ir and ^{1}Hmr spectra; the spectra of **8** are listed in Tables 1 and 2; *m/e* 398.1866 (M^+ 398.1841).

O-*Methylaspidophytine Oxide (*O-*Methyl-19-oxosecoaspidophytine*; ***10)***

A solution of aspidophytine oxide (50 mg) in methanol (5 ml) was cooled in an ice bath. An excess of ethereal diazomethane was added. After 16 h at room temperature the solvents were evaporated leaving **10** as an oil that could not be crystallized; molecular distillation gave an oil with unchanged ir and ^{1}Hmr spectra: λ_{max}(CHCl$_3$): 5.79, 6.15 (br) μ; ^{1}Hmr (CDCl$_3$) δ: 3.70 (s, 3H), 3.85 (s, 3H), 3.92 (s, 3H), 3.94 (s, 3H), 4.15–4.65 (m, 1H), 6.33 (br s, $w_{1/2}$ = 3 Hz, 2H), 6.78 (d, J = 8 Hz, 1H), 7.18 (d, J = 8 Hz, 1H); *m/e* 412 (100).

Acknowledgement

We thank the National Research Council of Canada for support of this work.

1. P. YATES, F. N. MACLACHLAN, I. D. RAE, M. ROSENBERGER, A. G. SZABO, C. R. WILLIS, M. P. CAVA, M. BEHFOROUZ, M. V. LAKSHMIKANTHAM, and W. ZEIGER. J. Am. Chem. Soc. **95**, 7842 (1973).
2. P.-T. CHENG, S. C. NYBURG, F. N. MACLACHLAN, and P. YATES. Can. J. Chem. **54**, 726 (1976).
3. M. P. CAVA, M. V. LAKSHMIKANTHAM, S. K. TALAPATRA, P. YATES, I. D. RAE, M. ROSENBERGER, A. G. SZABO, B. DOUGLAS, and J. A. WEISBACH. Can. J. Chem. **51**, 3102 (1973).
4. H. R. SNYDER, R. F. FISCHER, J. F. WALKER, H. E. ELS,

and G. A. NUSSBERGER. J. Am. Chem. Soc. **76**, 2819 (1954).
5. A. W. SANGSTER and K. L. STUART. Chem. Rev. **65**, 69 (1965).
6. J. C. N. MA and E. W. WARNHOFF. Can. J. Chem. **43**, 1849 (1965).
7. F. E. ZIEGLER and G. B. BENNETT. J. Am. Chem. Soc. **95**, 7458 (1973).
8. S. MARBURG. Ph.D. Thesis, Harvard University, Cambridge, MA. 1960.
9. D. H. WILLIAMS and I. FLEMING. Spectroscopic methods in organic chemistry. 2nd ed. McGraw-Hill, London. 1973. p. 58.
10. E. BOMBARDELLI, A. BONATI, E. M. MARTINELLI, G. MUSTICH, and B. DANIELI. Tetrahedron, **30**, 4141 (1974).
11. E. WENKERT, D. W. COCHRAN, E. W. HAGAMAN, F. M. SCHELL, N. NEUSS, A. S. KATNER, P. POTIER, C. KAN, M. PLAT, M. KOCH, H. MEHRI, J. POISSON, N. KUNESCH, and Y. ROLLAND. J. Am. Chem. Soc. **95**, 4990 (1973).
12. K. BIEMANN and G. SPITELLER. J. Am. Chem. Soc. **84**, 4578 (1962).
13. D. E. ZACHARIAS. Acta Crystallogr. B, **26**, 1455 (1970).

Can. J. Chem. Downloaded from www.nrcresearchpress.com by 210.87.254.40 on 09/05/12
For personal use only.

Chemistry of chelocardin. IV.[1] *C*(2)-acylation and alkylation of 2-deacetylchelocardin

DANIEL T. W. CHU, EDITH BERNSTEIN, AND STUART N. HUCKIN
Abbott Laboratories, Limited, P.O. Box 6150, Montreal, P.Q., Canada H3C 3K6

Received November 30, 1977

DANIEL T. W. CHU, EDITH BERNSTEIN, and STUART N. HUCKIN. Can. J. Chem. **56**, 1059 (1978).

The properties of the 1,3-cyclohexanedione system in 2-deacetylchelocardin (**2**) and *N*-carbobenzoxy-2-deacetylchelocardin (**3**) are found to be significantly different from those of ordinary 1,3-cyclohexanediones. Acylation and alkylation of (**2**) or (**3**) generally gives *O*-acylation or *O*-alkylation products. However, reaction of *N*-carbobenzoxy-2-deacetylchelocardin (**3**) with methyl orthoformate or *N*,*N*-dimethylformamide dimethyl acetal leads exclusively to *C*-acylation products.

DANIEL T. W. CHU, EDITH BERNSTEIN et STUART N. HUCKIN. Can. J. Chem. **56**, 1059 (1978).

On a trouvé que les propriétés du système cyclohexanedione-1,3 de la déacétyl-2 chélocardine (**2**) et *N*-carbobenzoxydéacétyl-2 chélocardine (**3**) sont assez différentes de celles des cyclohexanediones-1,3 ordinaires. L'acylation et alkylation de **2** ou **3** conduit généralement à des produits de *O*-acylation ou *O*-alkylation. Toutefois la réaction de la *N*-carbobenzoxydéacétyl-2 chélocardine (**3**) avec l'orthoformiate de méthyle ou le diméthylacétal de la *N*,*N*-diméthylformamide conduit uniquement à des produits de *C*-acylation.

[Traduit par le journal]

Chelocardin (**1**) is not only structurally similar to the tetracycline antibiotics but also appears to possess an identical antibacterial mode of action. Both appear to inhibit protein synthesis at the ribosomal level, with the chelation of magnesium being implicated in the mechanism of inhibition (1, 2).

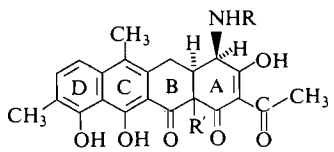

1 R = H R′ = α-OH
4 R = $CO_2CH_2C_6H_5$ R′ = α-OH
5 R = $CO_2CH_2C_6H_5$ R′ = H

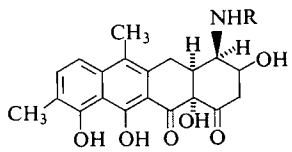

2 R = H
3 R = $CO_2CH_2C_6H_5$

A proton nuclear magnetic resonance study of the site of metal binding in tetracycline seemed to indicate that ring A is the binding site (3). Hence, the presence of the tricarbonyl system seems essential for antibacterial activity.

Partial confirmation of this hypothesis was provided by the lack of antibacterial activity of 2-deacetylchelocardin (**2**), which is produced by the deacylation of chelocardin under ketalization conditions and subsequent hydrolysis of the intermediate diketal (4). Initial attempts to reacylate **2** were not successful (4). We now wish to report the results of an extensive study directed towards the reacylation of **2** at C(2), the purpose of which was the generation of analogues of chelocardin bearing different acyl groups on C(2).

Discussion

Upon reaction with acyl halides or anhydrides, 2-deacetylchelocardin (**2**) undergoes initial substitution at nitrogen (4). To facilitate regeneration of the amine (as well as to minimize epimerization of this functionality) **2** was converted to its *N*-carbobenzoxy derivative **3** which was employed for most of this investigation. However, *N*-carbobenzoxy-2-deacetylchelocardin (**3**) gave only *O*-substitution when treated with acyl halides or anhydrides under a wide variety of conditions, in an identical manner to the reaction of 2-deacetylchelocardin.

The strong chelating powers of chelocardin precluded the use of Lewis acid catalysts as the recovery of the organic portion from chelocardin metal complex is very difficult and frequently impossible.

The ring A β-diketone system of **2** appears to be much modified by the presence of the 12a-hydroxyl group, as other six-membered ring β-diketone compounds, such as dimedone and cyclohexane-1,3-dione, may be acylated at the α position (5).[2]

[1]For Part III, see ref. 16.

[2]It was assumed that conversion of the amino group to either an amide or urethane would render it less anchimeric.

Can. J. Chem. Downloaded from www.nrcresearchpress.com by 210.87.254.40 on 09/05/12
For personal use only.

Can. J. Chem. Downloaded from www.nrcresearchpress.com by 210.87.254.40 on 09/05/12
For personal use only.

Accordingly attempts were made to remove or block this hydroxyl group. The 12a-hydroxyl group can be reduced in *N*-carbobenzoxychelocardin (**4**) (6) but attempts to remove the 2-acetyl group from *N*-carbobenzoxy-12a-deoxychelocardin (**5**) led only to extensive degradation and attempts to reduce the 12a-hydroxyl group of *N*-carbobenzoxy-2-deacetylchelocardin (**3**) failed. Blockade of the 12a-hydroxyl group was only achieved by further reaction of 2-deacetylchelocardin (**2**) with benzyl chloroformate to give the *N,O*-12a-dicarbobenzoxy-2-deacetylchelocardin in very low yield, accompanied by substantial amounts of polysubstitution products: a process not amenable to large scale preparation. Accordingly, our efforts were directed to other reactions of *N*-carbobenzoxy-2-deacetylchelocardin (**3**) which might give carbonyl substituents at C(2).

One of the analogues which we greatly desired to synthesize was 2-carboxamido-2-deacetylchelocardin which would resemble the tetracycline structure very closely. It has been known for a considerable time that the β-dicarbonyl compounds react with organic isocyanates to give *N*-substituted 2-carboxamido-1,3-diketones (7). For instance, dimedone (**6**) reacts with acetyl isocyanate at room temperature in 1 h to give imide **7** (8).

However, *N*-carbobenzoxy-2-deacetylchelocardin (**3**) did not react with methyl, isopropyl, phenyl, or

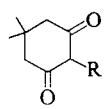

6 R = H

7 R = —C(=O)—NHCOCH$_3$

chlorosulfonyl isocyanates at room temperature. At elevated temperatures it gave only intractable mixtures from which small quantities of polymethane derivatives could be isolated. The procedure of Muxfeldt *et al.* (9) for direct carboxamidation using potassium cyanate was also attempted but again only starting material was recovered.

It has long been known that β-diketones undergo aldol condensation with aldehydes to give a variety of products. The reaction of dimedone with aldehydes to give the 2:1 dimedone adducts is a commonly used derivatization procedure (10). A more recent investigation of the reaction between dimedone and aldehydes (11) has shown that it is possible to produce a dehydrated 1:1 adduct by employing the sodium salt of the dimedone.

Accordingly attempts were made to condense *N*-carbobenzoxy-2-deacetylchelocardin with aldehydes in an aldol manner and it was found that **3** underwent smooth reaction with benzaldehyde merely by refluxing in benzene for 16 h. The structure of the product was shown to be 2-benzylidene-*N*-carbobenzoxy-2-deacetylchelocardin (**8***a*) primarily by its mass spectral behaviour.

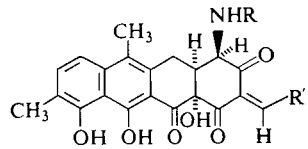

8*a* R = $CO_2CH_2C_6H_5$ R′ = —ϕ
8*b* R = H·HBr R′ = —ϕ
8*c* R = $CO_2CH_2C_6H_5$ R′ = —COϕ
8*d* R = H·HBr R′ = —COϕ

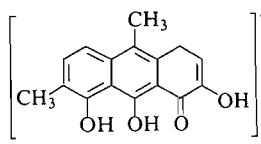

9

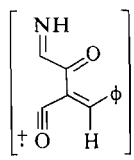

10

Chelocardin (**1**) shows a mass spectral fragmentation pattern analogous to that of the tetracyclines. The most significant fragment ion **9** occurs at *m/e* 270 (12). The aldol product from *N*-carbobenzoxy-2-deacetylchelocardin and benzaldehyde also shows a strong fragment ion at *m/e* 270 implying that substitution had not occurred in the B, C, or D rings. The presence of a fragment at *m/e* 186 which can be assigned to the deprotected residual fragment **10** further established the structure as **8***a*.

Compound **8***a* and its deprotected derivative **8***b* (formed upon treatment of **8***a* with hydrogen bromide in glacial acetic acid) were essentially devoid of antibacterial activity. This further confirmed our postulate of the necessity of the tricarbonyl system for antibacterial activity.

Conversion of the exocyclic double bond to a carbonyl functionality was precluded by the extreme sensitivity of chelocardin to oxidation and the previously mentioned inability to use transition metal containing reagents. A vinylogous tricarbonyl containing analogue **8***c* was generated by an aldol condensation of phenylglyoxal with **3** but neither **8***c* nor the free amine from **8***d* showed any antibacterial activity.

The success of the aldol reaction, in that condensation occurred at C(2), encouraged us to continue the

Can. J. Chem. Downloaded from www.nrcresearchpress.com by 210.87.254.40 on 09/05/12
For personal use only.

search for a method of reintroducing an acyl group. It is known that orthoformate esters are effective formylating agents. For example, dimedone may be converted cleanly to its 2-formyl derivative by reaction with ethyl orthoformate in acetic anhydride (13). Reaction of *N*-carbobenzoxy-2-deacetylchelocardin (**3**) under similar conditions gave only enol acetate derivatives. However, treatment of *N*-carbobenzoxy-2-deacetylchelocardin (**3**) with methyl orthoformate in the presence of *p*-toluenesulfonic acid in benzene under carefully controlled conditions (see Experimental) produced a new product which was subsequently shown to be **11**.

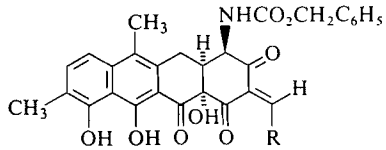

11 R = OH

13 R = $N(CH_3)_2$

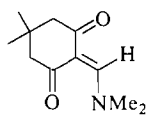

12

The structure of the product was established by elemental analysis and by nmr spectroscopy; its proton spectra showed a new resonance at δ 9.62 ppm and lacked the signal at δ 3.46 ppm assigned to C(2)-H. Its ^{13}C nmr spectrum had a new resonance at δ 186.7 ppm which appeared as a doublet in an off-resonance single frequency decoupling experiment. The spectral data are consistent only with reaction at C(2) particularly the ^{13}C nmr showing no significant shifts for any carbon resonance except those in the A ring. The biological activity of **11** was also consistent with reaction at C(2) in that like *N*-carbobenzoxychelocardin it showed antibacterial activity towards Gram positive bacteria in vitro. However, attempts to cleave the carbobenzoxy group of **11** to produce the unprotected formyl analogue of chelocardin gave only material that appeared to be polymeric, presumably arising from intermolecular condensations of the C(4)-amino group and the aldehyde. This condensation occurs with chelocardin itself but stops at the dimer stage forming isochelocardin.[1] With the more reactive formyl group this reaction would be expected to take place even more readily.

Attempts to generalize the reaction of ortho esters with deacetylchelocardin were unsuccessful. Reaction with either orthoacetic or orthobenzoic esters yielded only enol ethers of 2-deacetylchelocardin, under a wide range of experimental conditions. Even with dimedone, triethyl orthoacetate failed to yield the expected 2-acetyldimedone. Accordingly, a more reactive derivative of ortho esters was sought. Amide acetals fit this category very well, being known to undergo acylation reactions very easily (14), and *N*,*N*-dimethylformamide dimethyl acetal has been reported to react completely with dimedone in only 1 min in refluxing benzene (15).

Treatment of *N*-carbobenzoxy-2-deacetylchelocardin with *N*,*N*-dimethylformamide dimethyl acetal gave the formyl enamine (**13**). The nmr spectrum possesses two additional singlets at δ 3.07 and 3.32 corresponding to the two *N*-methyl groups. The presence of a new resonance singlet for the C(2a) olefinic proton at δ 8.10 together with the loss of signal at δ 3.46 assigned to C(2)-H further confirmed the structure.

As in the case of ortho esters, attempts to generalize the reaction of amide acetals with deacetylchelocardin failed. Enol ether formation was the major complication when amide acetals other than formamide acetal were used.

In summary, we have been able to acylate deacetylchelocardin at the C(2) position with limited success by the use of an ortho ester and an amide acetal. The presence of the 12a-hydroxyl and 4-amino groups in deacetylchelocardin markedly alters the general behaviour of the β-diketone system.

Experimental

The ir spectra were recorded on a Perkin-Elmer model 710A infrared spectrophotometer. The nmr spectra were recorded on Varian Associates A-60 and HA-100 spectrometers in deuterated solvents; resonance positions are given on the δ scale (ppm) relative to internal tetramethylsilane. The nmr peaks were designated as follows: s, singlet; d, doublet; t, triplet; q, quartet; m, multiplet; b, broad. The high resolution mass spectra were determined on Associated Electrical Industries MS-902 Double Focussing mass spectrometer and were processed on an IBM 1800 computer. The ^{13}C nmr spectra were recorded on a Varian Associates XL-100-15/TT-100 spectrometer system in DMSO; resonance positions are given in ppm relative to internal tetramethylsilane. Parameters used were pulse width (30°) 3.5 μs, pulse delay 0.5–1.0 s and sweep width 6K and 8K data table.

Since the ir absorption spectra of the various derivatives reported here have a β-hydroxy- or β-amino-α,β-unsaturated carbonyl function which would have similar absorption to the β-diketone system, very little change in the carbonyl absorption region (1580–1680 cm^{-1}) was observed. However, the change in relative intensity of the carbonyl absorptions correlated with the structural changes. Thus, only the relevant difference in absorption bands will be mentioned.

*2-Benzylidene-*N*-carbobenzoxy-2-deacetylchelocardin (**8**a)*

N-Carbobenzoxy-2-deacetylchelocardin (**3**, 110 mg, 0.22 mmol) was dissolved in benzene (50 ml). After the addition of

Can. J. Chem. Downloaded from www.nrcresearchpress.com by 210.87.254.40 on 09/05/12
For personal use only.

benzaldehyde (400 mg, 3.7 mmol), the mixture was refluxed, under a nitrogen atmosphere, for 24 h with vigorous stirring and azeotropic removal of water. Evaporation to 10 ml and filtration gave a residue which after drying yielded 125 mg (97%) of compound **8***a*; ^{1}Hmr ($CDCl_3$) δ: 2.20 (bm, 6H, C(6)-CH_3, C(9)-CH_3), 2.90 (bm, 3H, C(4a)-*H*, C(5)-CH_2), 4.91 (bm, 4H, O—C$H_2C_6H_5$, C(12a)-O*H*, N*H*), 7.23 (bm, 13H, 2C$_6H_5$, C(7)-*H*, C(8)-H, C(2′)-*H*), 9.81 (m, 1H, C(10)-O*H*), and 14.62 (m, 1H, C(11)-O*H*); ms (*m/e*): 591, 503, 399, 270, 255, 227, 186, 108, 91. *Mol. wt.* calcd. for $C_{35}H_{29}NO_8$: 591.1893; found (high resolution mass spectrometry): 591.1867.

*2-Phenylglyoxilidene-*N*-carbobenzoxy-2-deacetylchelocardin (8c)*

N-Carbobenzoxy-2-deacetylchelocardin (**3**, 100 mg, 0.2 mmol) and phenylglyoxal monohydrate (110 mg, 0.72 mmol) were dissolved in hot benzene (40 ml). The reaction mixture was refluxed under a nitrogen atmosphere for 2 h with vigorous stirring and azeotropic removal of water. After evaporation to dryness, ether (8 ml) was added, giving a light yellow solid. Filtration gave a residue which after drying yielded 94 mg (76%) of compound (**8***c*), mp 210–215°C; ^{1}Hmr ($CDCl_3$) δ: 2.23 (d, 3H, C(6)-CH_3), 2.41 (d, 3H, C(9)-CH_3), 3.10 (bm 3H, C(4a)-H; C(5)-CH_2), 4.40 (bd, 1H, N*H*), 5.0 (bm, 3H, OCH_2—C$_6H_5$, C(12a)-O*H*), 5.68 (m, 1H, C(2′)-*H*), 5.92 (m, 1H, C(4)-*H*), 7.21 (m, 12H, 2C$_6H_5$, C(7)-*H*, C(8)-*H*), 9.61 (m, 1H, C(10)-O*H*), 12.8 (s, ½H, C(11)-O*H*), 14.7 (s, ½H, C(11)-O*H*). Mass spectrum (*m/e*): 619, 502, 394, 270, 255, 227, 108, 91. *Mol. wt.* calcd. for $C_{36}H_{29}NO_9$: 619.1843; found (high resolution mass spectrometry): 619.1846.

*2-Formyl-*N*-carbobenzoxy-2-deacetylchelocardin (11)*

p-Toluenesulfonic acid monohydrate (20 mg, 0.1 mmol) was added to a solution of *N*-carbobenzoxy-2-deacetylchelocardin (**3**, 100 mg, 0.2 mmol) and trimethylorthoformate (127 mg, 1.2 mmol) in benzene (5 ml). The reaction mixture was heated at 90°C for 5 h during which the methanol was allowed to distill from the reaction flask and was trapped by absorption on molecular sieves. After evaporation to dryness, the residue was dissolved in ethyl acetate (1.2 ml). Ether (4 ml) was added yielding a dark orange solid; mp 210–215°C (dec.), 72 mg (68%). ^{13}C nmr showed the presence of a new carbonyl carbon resonance at δ 182.7 ppm which appeared as a doublet in an ORSFD experiment. Mass spectrum possesses the correct molecular ion at *m/e* 531. ^{1}Hmr shows the appearance of a new resonance at δ 9.62 with the disappearance of resonance at δ 3.46 corresponding to the C(2)-H protons. All the other signals are consistent with the assigned structure. *Anal.* calcd. for $C_{29}H_{25}NO_9$: C 66.51, H 4.74, N 2.63, O 27.09; found: C 65.21, H 4.79, N 2.75, O 27.23.

*2-Dimethylaminomethylene-*N*-carbobenzoxy-2-deacetylchelocardin (13)*

N,N-Dimethylformamide dimethyl acetal (72 mg, 0.6 mmol) was added to a refluxing solution of *N*-carbobenzoxy-2-deacetylchelocardin (100 mg, 0.2 mmol) in benzene (15 ml). After 3 min, the reaction was cooled by ice-bath and the product was precipitated with hexane. Filtration gave a residue which after drying yielded 80 mg (73%) of compound **13**; mp 140–159°C (dec.); ^{1}Hmr ($CDCl_3$) δ: 2.20 (s, 3H, C$_6$-CH_3), 2.65 (s, 3H, C(9)-CH_3), 2.85 (m, 3H, C(4a)-*H*, C(5)-CH_2), 3.07 (s, 3H, N-CH_3), 3.32 (s, 3H, N-CH_3), 5.20 (m, 3H, OC$H_2C_6H_5$, C(12a)-O*H*), 6.02 (m, 2H, C(4)-*H*, N*H*), 7.35 (m, 8H, C$_6H_5$, C(7)-*H*, C(8)-*H*, C(10)-O*H*), 8.10 (s, 1H, C(2)-*H*). *Mol. wt.* calcd. for $C_{35}H_{29}NO_8$: 558.2002; found (high resolution mass spectrometry): 558.2009.

Acknowledgements

We thank G. Nettleship, Ms. R. Stanaszek, and Ms. S. Mueller of Abbott Laboratories for ^{1}Hmr, ^{13}C nmr, and mass spectra respectively and the staff of the microanalytical department of Abbott Laboratories for elemental analyses. We also thank D. L. Garmaise for his interest and encouragement throughout the course of this work.

1. J. P. White and C. R. Cantor. J. Mol. Biol. **58**, 397 (1971).
2. J. C.-H. Mao and E. E. Robishaw. Biochim. Biophys. Acta, **238**, 157 (1971).
3. (*a*) J. Gulbis and G. W. Everett, Jr. Tetrahedron, **32**, 913 (1976); (*b*) J. Gulbis and G. W. Everett, Jr. J. Am. Chem. Soc. **97**, 6248 (1975).
4. D. T. W. Chu, D. L. Garmaise, and E. Bernstein. Can. J. Chem. **53**, 1434 (1975).
5. (*a*) W. Dieckmann and R. Stein. Ber. **37**, 3370 (1904); (*b*) H. Smith. J. Chem. Soc. 803 (1953); (*c*) J. M. McIntock and P. M. Beaumier. Can. J. Chem. **51**, 843 (1973).
6. D. T. W. Chu, S. Huckin, and E. Bernstein. Can. J. Chem. **55**, 3341 (1977).
7. W. Dieckmann, J. Hoppe, and R. Stein. Ber. **37**, 4621 (1907).
8. M. M. Shemyakin, Y. A. Arbuzon, M. N. Kalosov, G. A. Shatenshteyn, V. V. Oropienko, and Y. V. Konnova. Zh. Obshch. Khim. **30**, 542 (1960); Chem. Abstr. **54**, 24575i (1960).
9. H. Muxfeldt, G. Grethe, and W. Rogalski. J. Org. Chem. **31**, 2429 (1966).
10. G. Klein and H. Linser. Microchemie, Pregl, Festscht, 204 (1929); D. Vorlander. Fresenius Z. Anal. Chem. **77**, 245 (1929); W. Weinberger. Ind. Eng. Chem. Anal. Ed. **3**, 365 (1931); E. C. Horning and M. G. Horning. J. Org. Chem. **11**, 951 (1946).
11. P. Margarether and O. Polansky. Monatsh. Chem. **101**, 824 (1970).
12. L. A. Mitscher, W. Rosenbrook, Jr., W. W. Andres, R. S. Egan, J. Schenck, and J. V. Juvarkar. Antimicrob. Agents Chemother. 38 (1970).
13. B. D. Akehurst and J. R. Bartels-Keith. J. Chem. Soc. 4798 (1957).
14. R. H. de Wolfe (*Editor*). Carboxylic ortho acid derivatives. Academic Press, New York, NY. 1970. p. 489.
15. Z. Arnold and M. Kornilov. Coll. Czech. Chem. Commun. **29**, 645 (1964).
16. E. Bernstein, Daniel T. W. Chu, Stuart N. Huckin, D. L. Garmaise, R. S. Egan, T. J. Perun, Wm. Rosenbrook, Jr., and R. Carney. J. Org. Chem. Submitted.

Nitration of 1-chloro-2,3-dimethylbenzene in acetic anhydride. Formation and rearomatization of adducts[1]

ALFRED FISCHER AND COLIN CAMPBELL GREIG
Department of Chemistry, University of Victoria, Victoria, B.C., Canada V8W 2Y2

Received November 2, 1977

ALFRED FISCHER and COLIN CAMPBELL GREIG. Can. J. Chem. **56**, 1063 (1978).

Nitration of 1-chloro-2,3-dimethylbenzene in acetic anhydride gives the *cis* and *trans* isomers of 3-chloro-4,5-dimethyl-4-nitrocyclohexa-2,5-dienyl acetate (29%) and 1-chloro-2,3-dimethyl-4-nitro- (46%), -5-nitro- (5%), and -6-nitrobenzene (20%). In formic acid and acidified methanol, exchange of acetate for formate and methoxyl, respectively, occurs and the diastereoisomers of 3-chloro-4,5-dimethyl-4-nitrocyclohexa-2,5-dienyl formate and methyl ether, respectively, are formed. Rearomatization of each isomer of 3-chloro-4,5-dimethyl-4-nitrocyclohexa-2,5-dienyl acetate in acetic acid results in initial isomerization to form the pair of diastereoisomers and subsequent elimination of nitrous acid to form 3-chloro-4,5-dimethylphenyl acetate. In 25% trifluoroacetic acid in deuteriochloroform elimination of acetic acid and migration of the nitro group to form 1-chloro-2,3-dimethyl-4-nitro-benzene and a lesser amount of its 6-nitro isomer is the dominant reaction. In the presence of mesitylene the formation of the nitro derivatives is suppressed and 3′-chloro-2,4,4′,5′,6-pentamethylbiphenyl is obtained. It is proposed that cyclohexadienyl cations are significant intermediates in all of the reactions. Pyrolysis of the adducts gives 1-chloro-2,3-dimethylbenzene as the major product.

ALFRED FISCHER et COLIN CAMPBELL GREIG. Can. J. Chem. **56**, 1063 (1978).

La nitration du chloro-1 diméthyl-2,3 benzène dans l'anhydride acétique conduit aux isomères *cis* et *trans* de l'acétate du chloro-3 diméthyl-4,5 nitro-4 cyclohexadiène-2,5 yle (29%) et aux chloro-1 diméthyl-2,3 nitro-4 (46%), nitro-5 (5%) et nitro-6 benzènes (20%). Dans l'acide formique et le méthanol acidulé, il se produit respectivement des échanges du groupe acétate pour des groupes formiates et méthoxyles et il y a formation des diastéréoisomères des formiates et les éthers de méthyle du chloro-3 diméthyl-4,5 nitro-4 cyclohexadiène-2,5 yle. Une réaromatisation de chaque isomère de l'acétate du chloro-3 diméthyl-4,5 nitro-4 cyclohexadiène-2,5 yle dans l'acide acétique conduit à une isomérisation initiale avec formation de la paire de diastéréoisomères et une élimination subséquente de l'acide nitreux pour conduire à l'acétate du chloro-3 diméthyl-4,5 phényle. Dans de l'acide trifluoroacétique à 25% dans le deutériochloroforme, l'élimination de l'acide acétique et la migration du groupe nitro pour former le chloro-1 diméthyl-2,3 nitro-4 benzène et à des niveaux moindres, de son isomère nitro-6, correspond à la réaction principale. En présence de mésitylène, on supprime la formation des dérivés nitrés et on obtient le chloro-3′ pentaméthyl-2,4,4′,5′,6 biphényle. On suggère que les cations cyclohexadiényles sont des intermédiaires importants dans toutes les réactions. La pyrolyse des adduits conduit au chloro-1 diméthyl-2,3 benzène comme produit principal.

[Traduit par le journal]

Introduction

The importance of *ipso* attack in electrophilic nitration is now widely recognised (2–7). For nitration in acetic anhydride addition of the nitronium ion at an *ipso* position results in the eventual formation of nitronium acetate adducts (8). Most commonly a pair of diastereoisomeric 1,4 adducts is formed (9), although in two instances 1,2 adducts have also been obtained (10, 11). The present study of 1-chloro-2,3-dimethylbenzene (3-chloro-*o*-xylene) was undertaken to determine the substituent effect of a chlorine on *ipso* attack and on the reactions of the adducts so formed. In the nitration of 2,3-dimethylbenzonitrile the position of *ipso* attack is that *meta* to the electron-withdrawing cyano group (12). The chlorine atom is *ortho,para* directing, although deactivating, hence the methyl-substituted site *ortho* to the chlorine should be the preferred position for *ipso* attack.

Results and Discussion

Nitration and Formation of Adducts

Nitration of 1-chloro-2,3-dimethylbenzene in acetic anhydride gave 29% of diene adducts (**1**)[2] and the 4- (46%), 5- (5%), and 6-nitro (20%) substitution products. The products were separated by low-temperature chromatography on alumina. The

[1]Reported in preliminary form in ref. 1.

[2]Individual members of a pair of diastereoisomeric adducts are designated *a* and *b*.

Can. J. Chem. Downloaded from www.nrcresearchpress.com by 210.87.254.40 on 09/05/12
For personal use only.

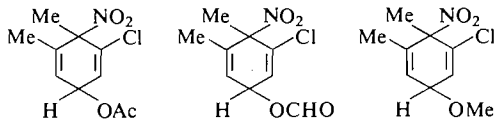

1 2 3

presence of the nitro and acetate groups in the diastereoisomeric adducts is established by the appropriate infrared (ir) absorptions and confirmed by elemental analyses and molecular weight determinations. The absence of ultraviolet (uv) absorption in the region expected for conjugated cyclohexadienes (253 nm or greater (13)) indicates that the dienes are 1,4 and not 1,2 adducts. The nuclear magnetic resonance (nmr) spectra show that no adjacent vinyl protons, which would have $J \approx 8$ Hz, are present since the largest coupling is ca. 4 Hz. Moreover, the two 4-Hz couplings to a common proton show that there are protons on three adjacent carbon atoms which are joined by two single bonds. The double bonds must therefore be located between C-1 and C-6 and between C-3 and C-4, using the enumeration of the parent aromatic. Thus the nitro and acetate groups must be at C-2 and C-5, respectively, or vice versa. Addition of the shift reagent tris(1,1,1,2,2,3,3-heptafluoro-7,7-[$^2H_6$]dimethyl-4,6-[$^2H_3$]octanedionato)europium(III) {Eu([$^2H_9$]fod)$_3$} moved the allylic proton more rapidly downfield than the vinylic protons. The allylic proton must therefore be closer to the acetate group and thus the acetate must be attached to a secondary carbon atom, i.e. C-5, with the nitro group at C-2. The alternative arrangement, with the nitro group at the secondary carbon atom, is chemically unlikely since elimination of acetic acid from such an adduct to form 1-chloro-2,3-dimethyl-5-nitrobenzene would be extremely facile. Thus it is clear that the adducts do have the structure 3-chloro-4,5-dimethyl-4-nitro-1,4-dihydrophenyl acetate.

Addition of the nitronium ion to the *ipso* position adjacent to the halogen substituent is in accord with expectation based on the directing effect of the substituent for electrophilic substitution. Furthermore, the observed product distribution is in semi-quantitative agreement with that predicted from the nitration of chlorobenzene and *o*-xylene in acetic anhydride, assuming additivity of substituent effects. From the data of Roberts *et al.* (14) for chlorobenzene together with the observation of Perrin and Skinner (2) that the reactivity of the position *ipso* to chlorine is similar to that of the *meta* position, and the data of Fischer *et al.* (15) for *o*-xylene,[3] the relative reactivities of the nuclear positions of 1-chloro-2,3-dimethylbenzene are calculated to be, in order from C-1 to C-6: 0, 38, 1, 42, 1, 18. The observed yields of products resulting from attack at these sites are: 0, 29, 0, 46, 5, 20. Clearly, for nitration in acetic anhydride, such calculations give a useful, if not exact (3, 16), indication of the amounts of the various products, including adducts. Such results also support the view that acetic anhydride is effective in trapping the cation formed by addition of nitronium ion to an *ipso* position.

Reactions of the Adducts

Solution reactions of diene adducts (4-nitro-2,5-cyclohexadienyl acetates) involve the formation (or reformation) of cyclohexadienyl cations. Two such cations can be formed. Ionization of the nitro group as nitrite leads to an acetoxycyclohexadienyl cation (3) and protonation of the acetate group followed by loss of acetic acid leads to the nitrocyclohexadienyl cation (17). The outcome of the competition between these two pathways is determined by the other substituents present and by the acidity: formation of the nitrocyclohexadienyl cation is favoured in more acidic media. However, an additional factor has also to be considered. Formation of the nitrocyclohexadienyl cation is reversible in the sense that the cation can recombine with acetic acid or other nucleophile to regenerate the adduct or an analog. Formation of the acetoxycyclohexadienyl cation appears to be irreversible. Thus it is conceivable that the nitrocyclohexadienyl cation is formed more rapidly than the acetoxycyclohexadienyl cation yet the rearomatization products are those formed through the latter (or an analog). An example of this is provided by the observations of Myhre and co-workers (3) on the solvolysis of the adduct of 1,2,3-trimethylbenzene. They noted that 3,4,5-trimethylphenol was obtained as a product under conditions under which the acetate group was stable to hydrolysis. The adduct underwent rapid exchange of acetate for hydroxyl via the nitrocyclohexadienyl cation and the resulting hydroxynitrocyclohexadiene then reacted via the slower ionization of the nitro group to form the hydroxycyclohexadienyl cation which was deprotonated to the phenol. Thus the energetics of processes after the formation of the nitrocyclohexadienyl cation (but not of those after the formation of the acetoxy-

[3]The extent of *ipso* attack in *o*-xylene is given by the proportion of aryl acetate, formed by decomposition of the initially formed adduct, as reported in ref. 15.

Can. J. Chem. Downloaded from www.nrcresearchpress.com by 210.87.254.40 on 09/05/12
For personal use only.

Can. J. Chem. Downloaded from www.nrcresearchpress.com by 210.87.254.40 on 09/05/12
For personal use only.

cyclohexadienyl cation) may be important in determining the outcome of the competition between the rearomatization pathways which involve as intermediates the acetoxycyclohexadienyl cation, on the one hand, and the nitrocyclohexadienyl cation, on the other.[4]

Reaction of the adducts of 1-chloro-2,3-dimethylbenzene in neat acetic acid resulted in the elimination of nitrous acid and the formation of 3-chloro-4,5-dimethylphenyl acetate. Isomerization of **1***a* to **1***b* and of **1***b* to **1***a* was observed in the course of the reaction. In the more acidic formic acid rapid exchange of formate for acetate occurred giving rise to a pair of diastereoisomeric formates **2**. In the still more acidic trifluoroacetic acid (20% in deuteriochloroform) rapid isomerization, or exchange of acetate, was followed by rearomatization to yield 1-chloro-2,3-dimethyl-4-nitrobenzene (78%), 1-chloro-2,3-dimethyl-6-nitrobenzene (7%), and 3-chloro-4,5-dimethylphenyl acetate (15%). Rather more acetate was formed in more dilute (5%) formic acid. Reaction in acidified methanol resulted in the exchange of acetate for methoxyl and the formation of diastereoisomeric ethers **3**.

Rearomatization of secondary acetate adducts, of which **1** is an example, are relatively uncomplicated. Both the nitrocyclohexadienyl cation, **6** from **1**, and the acetoxycyclohexadienyl cation, **4** from **1**, each undergo only one rearomatization reaction. The nitro group of the nitrocyclohexadienyl cation migrates to an unsubstituted position to form an isomeric secondary nitrocyclohexadienyl cation which is rapidly deprotonated to the nitroarene. The acetoxycyclohexadienyl cation is rapidly deprotonated to the aryl acetate. These reactions are depicted for **1** in Scheme 1.[5] In acetic acid the rate of formation of the nitrocyclohexadienyl cation **6** is greater than that of the acetoxycyclohexadienyl cation **4**, as shown by the fact that diastereoisomer **1***a* isomerizes to **1***b* and **1***b* isomerizes to **1***a* before rearomatization. However, the rearomatization product, the aryl acetate, is formed via **4** and no significant amount of nitro derivative is formed via **6**. Thus there is a significant energy barrier to the nitro shift processes such that although the transition states between **1** and **5** and **5** and **6** are of lower energy than that between **1** and **4**, that between **6** and **7** (and **8**) is of higher energy. The adducts of *o*-xylene do not isomerize prior to rearomatization to aryl acetate under the same conditions. In this case the nitrocyclohexadienyl cation is not formed more rapidly than the acetoxycyclohexadienyl cation. This difference between the *o*-xylene and 3-chloro-*o*-xylene adducts can be understood in terms of the substituent effect of the chlorine on the energies of the transition states leading to **4** and **6** and thus on the energies of the cations **4** and **6**. Introduction of the chlorine substituent reduces the stability of both **4** and **6** relative to the unsubstituted case (Scheme 1, Cl replaced by H) and thus reduces the rates of formation of both cations, a consequence of the net electron-withdrawing (deactivating) effect of chlorine. However, in **6** the chlorine is located at a formal cationic centre and thus its electron-donating resonance effect can be fully operative whereas this is not so in **4**.[6] Thus the chlorine destabilizes **6** less than **4** and correspondingly the transition states leading to these cations, the effect being sufficient to reverse the order of stability of the transition states from that obtaining in the case of the *o*-xylene adduct.

As the acidity of the medium is increased **6** is formed more rapidly since the rate of formation of

[4]For the solvolysis of the 1,2,3-trimethylbenzene adduct in aqueous ethanol external return from the acetoxycyclohexadienyl cation has been detected (3). In the acidic media studied in the present work the nitrite ion will be extensively protonated and thus external return is much less likely. Furthermore, Myhre and co-workers (3) reported that the major part of the return was to a diene nitrite ester and not the nitrodiene. It seems unlikely that the nitrite ester could give rise to nitroarene in significant amount and thus formation of the nitrite ester is, in effect, a reversible side-reaction on the pathway between the acetoxycyclohexadienyl cation and product and has essentially no effect on the competition between formation of products via the nitrocyclohexadienyl cation and via the acetoxycyclohexadienyl cation.

[5]In Scheme 1 the isomerization (epimerization) of **1** and in the text the epimerization and exchange reactions of **1** are depicted as S_N1 reactions involving an intermediate nitrocyclohexadienyl cation. There is only one earlier report of exchange (epimerization) of a secondary acetate adduct (18), although tertiary acetate adducts undergo exchange readily. No mechanistic studies of these reactions in the secondary systems have yet been made and it is possible, although it seems unlikely, that the S_N2 mechanism is followed. Exchange reactions of secondary acetate adducts have been proposed as a key part of reaction sequences for the acidolysis, in ~50% aqueous sulfuric acid, of 3,4-dimethyl-4-nitrocyclohexa-2,5-dienyl acetate (19) and 3,4,5-trimethyl-4-nitrocyclohexa-2,5-dienyl acetate (3) and arguments have been adduced in support of the S_N1 ($A_{AL}1$ ester hydrolysis) mechanism. As in the case of 3,4-dimethyl-4-nitrocyclohexa-2,5-dienyl acetate no exchange was detected for 3,4,5-trimethyl-4-nitrocyclohexa-2,5-dienyl acetate at the low acidities in which 3-chloro-4,5-dimethyl-4-nitrocyclohexa-2,5-dienyl acetate undergoes exchange.

[6]This is an exact parallel to the situation in electrophilic substitution of chlorobenzene and to the explanation for chlorine being *ortho,para* directing, although deactivating.

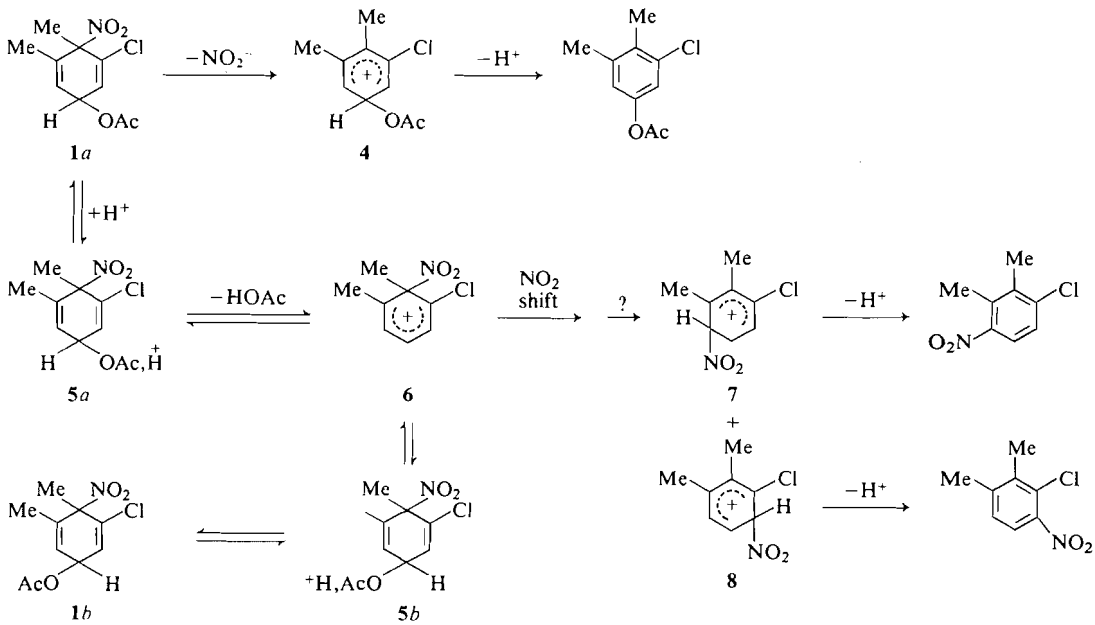

SCHEME 1. Competitive reactions of adducts of 1-chloro-2,3-dimethylbenzene.

6 is determined not only by the energy difference between the **5,6** transition state and **1** but also by the energy difference between the catalytic acid and its conjugate base. Expressed alternatively, the rate of formation of the transition state **5,6** is proportional to the concentration of **5** which is in turn a function of the acid strength of the catalysing acid. It is assumed that this factor outweighs any medium effects on the relative stabilities of the **1,4** and **5,6** transition states. At some particular level of acidity the concentration of **6** will have risen to a level such that the nitro-shift processes occur at a rate that is competitive with the rate of formation of **4**. Apparently this is the situation in 20% trifluoroacetic acid where 85% of the aromatic product arises via **6** and 15% via **4**. The ratio of 4-nitro to 6-nitro derivative formed is 11:1. Both of these are products of formal 1,3-nitro shifts although such shifts could be the result of successive 1,2-nitro shifts. For a direct 1,3-nitro shift the extent to which each isomer is formed should be related to the relative stabilities of the 4-nitro- and 6-nitrocyclohexadienyl cations, **7** and **8** respectively. This ratio should in turn be related to the relative extents of attack by nitronium ion at these positions during nitration of 1-chloro-2,3-dimethylbenzene, calculated to be 2.3:1, as outlined above. Alternatively, if two successive 1,2 shifts occur then both the relative stabilities of the 3-nitro- and 1-nitro ions (related to the calculated relative extents of attack by nitronium ion at these positions of 4.4:1) and that of the 4-nitro- and 6-nitro ions would be significant in determining the relative migratory ratio. Since migration to the 6 position is disfavoured at both steps the discrimination in favour of the 4-isomer should be greater than in the single shift mechanism. Both sets of calculations predict that the 4-nitro isomer should be the predominant product, as observed.

When the reaction with trifluoroacetic acid was carried out in the presence of mesitylene the chloronitroarenes were not formed and 3′-chloro-2,4,4′,5′,6-

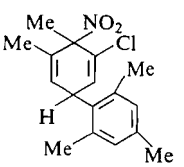

9

pentamethylbiphenyl was obtained instead. Evidently the nitrocyclohexadienyl cation **6** is captured by mesitylene prior to migration of the nitro group to form adduct **9**, i.e. there is electrophilic substitution of mesitylene by **6**. Under the reaction conditions the adduct undergoes rearomatization in the diene ring through ionization of the nitro group as nitrite, to form mesitylcyclohexadienyl cation which is rapidly deprotonated to the biphenyl in a sequence which is a parallel of that for the formation of aryl acetate from **1**.

The reactions of adduct **1** with formic acid and with acidified methanol lead to exchange of acetate for formate and methoxyl, respectively and the formation of diastereoisomers of **2** and **3**. Obviously

Can. J. Chem. Downloaded from www.nrcresearchpress.com by 210.87.254.40 on 09/05/12
For personal use only.

Can. J. Chem. Downloaded from www.nrcresearchpress.com by 210.87.254.40 on 09/05/12
For personal use only.

these reactions occur through the intermediate formation of cation **6** and are indicative of the more rapid formation of **6** than **4** under these conditions.

Pyrolysis of the adducts results in the elimination of the elements of acetyl nitrate and reversion to 1-chloro-2,3-dimethylbenzene. Some aryl acetate and nitro derivatives are also formed.

Experimental

General experimental methods have been described previously (12).

Nitration of 1-Chloro-2,3-dimethylbenzene in Acetic Anhydride

A solution of freshly distilled nitric acid (15 cm^3, 0.36 mol) in acetic anhydride (50 cm^3) was prepared at 0°C, cooled to −30°C, and added slowly with stirring to a solution of 1-chloro-2,3-dimethylbenzene (20 g, 0.14 mol) in acetic anhydride (70 cm^3) also at −30°C. The solution was allowed to warm to 0°C in an ice bath and maintained at that temperature for 15 min, after which time nmr showed the complete disappearance of the chlorodimethylbenzene and absorption in the τ 3.5–4.5 ppm region which represented ca. 30% of the product. The reaction mixture was cooled to −40°C, ether (300 cm^3) was added and the mixture was quenched with ammonia and worked up in the manner previously described (11) to yield 27 g of a yellow oil. The nmr spectrum of the reaction product and of chromatography fractions indicated that the 4-nitro (46%), 5-nitro (5%), and 6-nitro (20%) substitution products were present in addition to diene adducts (29%). Chromatography on alumina at −30°C and elution with ether–pentane mixtures gave in the 0–10% ether fractions, 1-chloro-2,3-dimethyl-4-nitrobenzene, mp 62–63°C (lit. (20) mp 62°C); ir (Nujol): 1540 cm^{-1} (NO_2); nmr ($CDCl_3$) τ: 2.50 (d, 1, J = 8.4 Hz, 5-*H*), 2.70 (d, 1, J = 8.4 Hz, 6-*H*), 7.59 (s, 6, 2-CH_3 and 3-CH_3); mass spectrum (70 eV) *m/e* (relative intensity): 187 (4) and 185 (11, M), 170 (14) and 168 (43, $M-OH$), 142 (4) and 140 (13), 141 (4) and 139 (9, $M-NO_2$), 113 (14), 105 (13), 104 (38), 103 (45), 77 (100). *Anal.* calcd. for $C_8H_8ClNO_2$: C 51.76, H 4.34, N 7.54; found: C 51.62, H 4.18, N 7.40.

The loss of OH from the molecular ion confirms that the nitro and methyl groups are adjacent (21) and thus the identification as the 4-nitro isomer. The nmr spectrum which reveals the *ortho* relationship between the aromatic protons is consistent with this.

The 15 and 20% ether fractions contained a mixture of the three isomeric 1-chloro-2,3-dimethylnitrobenzenes from which, after further chromatography on alumina and recrystallization from ethanol, was isolated 1-chloro-2,3-dimethyl-6-nitrobenzene, mp 45.5–46.5°C (lit. (22) mp 46°C); ir (Nujol): 1545 cm^{-1} (NO_2); nmr ($CDCl_3$) τ: 2.58 (d, 1, J = 8.5 Hz, 5-*H*), 2.92 (d, 1, J = 8.5 Hz, 4-*H*), 7.64 (s, 6, 2-CH_3 and 3-CH_3); mass spectrum (70 eV) *m/e* (relative intensity): 187 (26) and 185 (80, M), 157 (22) and 155 (60, $M-NO$), 141 (8) and 139 (24, $M-NO_2$), 127 (17), 104 (23), 103 (45), 91 (57), 77 (100). The absence of the $M-OH$ peak in the mass spectrum together with the *ortho* protons indicated by the nmr spectrum confirms the identification as the 6-nitro isomer. 1-Chloro-2,3-dimethyl-5-nitrobenzene was present in the residue from recrystallization of the 6-nitro isomer as shown by nmr absorption at τ 1.96 (d, J = 2.5 Hz, 6-*H*) and 2.12 (d, J = 2.5 Hz, 4-*H*) but was not further separated.

The 25–100% ether fractions contained a mixture of two isomeric dienes in varying proportions. The residues from these fractions were combined (9.1 g, 37 mmol) and rechromatographed at −30°C. Recrystallization from ether–pentane of the residue obtained on removal of the solvent from the new 10–20% ether fractions gave 3-chloro-4,5-dimethyl-4-nitrocyclohexa-2,5-dienyl acetate (**1***a*), mp 56.5 – 57.5°C; uv (CH_3OH): 199.5 nm (ε 1450 m^2 mol^{-1}); ir: (Nujol): 1750, 1270, 1250 ($OCOCH_3$), 1570 cm^{-1} (NO_2); nmr ($CDCl_3$, 220 MHz) τ: 3.65 (q, 1, 2-*H*), 4.10 (m, 1, 6-*H*), 4.16 (m, 1, 1-*H*), 7.90 (s, 3, $OCOCH_3$), 8.05 (s, 3, 4-CH_3), 8.16 (t, 3, 5-CH_3), J_{12} = 4.08 Hz, $J_{1,5\text{-}CH_3}$ = 1.32 Hz, J_{16} = 3.94 Hz, J_{26} = 1.45 Hz, $J_{6,5\text{-}CH_3}$ = 1.40 Hz; irradiation of the methyl resonance at τ 8.16 collapsed the 6-H multiplet to a quartet and the 1-H multiplet to a triplet; in the 60 MHz spectrum the multiplets from 1-H and 6-H overlapped but addition of the shift reagent Eu([$^2H_9$]fod)$_3$ shifted the 1-H to lowest field and on decoupling from the 5-CH_3 the 1-H and 6-H appeared as the expected triplet (over-lapping doublets) and quartet, respectively. *Anal.* calcd. for $C_{10}H_{12}ClNO_4$ (M_r 245.5): C 48.89, H 4.89, N 5.70; found (245): C 48.95, H 4.93, N 5.53. **p** 14.2 × 10^{-30} C m (4.26 D).

The 30–40% ether fractions from the second column gave a residue which, on recrystallization from either carbon tetrachloride or ether–pentane, afforded colourless crystals of 3-chloro-4,5-dimethyl-4-nitrocyclohexa-2,5-dienyl acetate (**1***b*), mp 86.5–88°C; uv (CH_3OH): 201 nm (ε 1250 m^2 mol^{-1}); ir (Nujol): 1765 and 1240 ($OCOCH_3$), 1585 cm^{-1} (NO_2); nmr ($CDCl_3$, 220 MHz) τ: 3.69 (q, 1, 2-*H*), 4.13 (m, 1, 6-*H*), 4.25 (m, 1, 1-*H*), 7.85 (s, 3, $OCOCH_3$), 8.11 (s, 3, 4-CH_3), 8.18 (t, 3, 5-CH_3), J_{12} = 3.78 Hz, $J_{1,5\text{-}CH_3}$ = 1.51 Hz, J_{16} = 3.19 Hz, J_{26} = 1.50 Hz, $J_{6,5\text{-}CH_3}$ = 1.51 Hz; irradiation of the methyl resonance at τ 8.18 collapsed the 6-H multiplet to a quartet and the 1-H multiplet to a triplet. *Anal.* calcd. for $C_{10}H_{12}ClNO_4$ (M_r 245.5): C 48.89, H 4.89, N 5.70; found (244): C 48.85, H 4.77, N 5.55. **p** 10.1 × 10^{-30} C m (3.03 D).

Thermolysis of Dienes **1**a *and* **1**b

Pyrolysis of diene **1***a* in the inlet of vapour phase chromatograph at 240°C gave 1-chloro-2,3-dimethylbenzene (82%), 3-chloro-4,5-dimethylphenyl acetate (~17%) and 1-chloro-2,3-dimethyl-4-nitro- and 1-chloro-2,3-dimethyl-6-nitrobenzene (~1%). Pyrolysis of diene **1***b* gave the same products in yields of 95, 3, and ~1%, respectively. The products were identified by comparison of their retention times with those of authentic samples.

Reaction of Dienes **1**a *and* **1**b *in Acetic Acid*

Diene **1***b* (0.1 g) was dissolved in acetic acid (0.4 cm^3) and heated at 50°C. Epimerization to form the **1***a*,**1***b* mixture which contained a preponderance of **1***a* occurred and was detected by the appearance of peaks characteristic of **1***a* in the nmr spectrum. After 1 week the diene peaks had disappeared and had been replaced by a pair of doublets, centred at τ 3.02 and 3.20, J = 2.5 Hz. In a similar experiment **1***a* epimerized and then rearomatized. The combined reaction mixtures were diluted with methylene chloride, cooled to −78°C and excess liquid ammonia was condensed into the solution. After evaporation of the ammonia the solution was worked up to yield a yellow oil which was chromatographed on alumina at −30°C. Elution with pentane gave 3-chloro-4,5-dimethylphenyl acetate as a colourless oil; ir (film): 1775 and 1210 cm^{-1} ($OCOCH_3$); nmr ($CDCl_3$) τ: 3.05 (d, 1, J = 2.4 Hz, 2-*H*), 3.14 (d, 1, J = 2.4 Hz, 6-*H*), 7.73 (overlapping s, 9, 4-CH_3, 5-CH_3, and $OCOCH_3$); mass spectrum (70 eV) *m/e* (relative intensity): 200 (8) and 198

Can. J. Chem. Downloaded from www.nrcresearchpress.com by 210.87.254.40 on 09/05/12
For personal use only.

(26, M), 158 (42) and 156 (100, $M-C_2H_2O$), 143 (15) and 141 (45), 121 (75, $M-C_2H_2OCl$), 91 (19).

The acetate was heated under reflux with sulfuric acid (40 mm^3) in methanol (1 cm^3) for 10 min. After work-up the residue obtained was dissolved in chloroform and filtered through a column of silica gel. Evaporation of the eluate to dryness and recrystallization from pentane gave colourless needles of 3-chloro-4,5-dimethylphenol, mp 97–98°C (lit. (23) mp 98°C); nmr ($CDCl_3$) τ: 3.30 (d, 1, $J = 3$ Hz, 2-*H*), 3.46 (d, 1, $J = 3$ Hz, 6-*H*), 7.78 (s, 6, 4-C*H*$_3$ and 5-C*H*$_3$); mass spectrum (70 eV) *m/e* (relative intensity): 158 (36) and 156 (91, M), 143 (24) and 141 (69, $M-CH_3$), 121 (100, $M-Cl$).

Reaction of Diene **1**a *with Formic Acid*

Formic acid (1.5 cm^3) was added to a solution of diene **1***a* (0.4 g) in deuterochloroform (0.5 ml) at −78°C. The reaction mixture was allowed to warm to 37°C and after 15 min nmr indicated that significant changes had occurred in the diene region. The solution was diluted with chloroform and cooled to −78°C and quenched with liquid ammonia. After work-up the product was chromatographed on alumina and eluted with pentane and ether–pentane mixtures. The formyloxydienes **2** were incompletely separated from each other but sufficiently so for nmr assignments to be made. One diastereoisomer of 3-chloro-4,5-dimethyl-4-nitrocyclohexa-2,5-dienyl formate (**2***a*) was the predominant component (80%) of the 50% ether fraction; ir (film): 1740 and 1160 (OCOH), 1565 cm^{-1} (NO_2); nmr ($CDCl_3$) τ: 1.95 (d, 1, $J = 1$ Hz, OCO*H*), 3.70 (m, 1, 2-*H*) 4.14 (m, 2, 1-*H* and 6-*H*), 8.07 (3, C*H*$_3$), and 8.17 (3, C*H*$_3$). The other diastereoisomer **2***b* was the predominant component (80%) of the 70% ether fraction; ir (film): 1740 and 1164 (OCOH), 1565 cm^{-1} (NO_2); nmr ($CDCl_3$) τ: 1.90 (d, 1, $J = 1$ Hz, OCO*H*), 3.72 (m, 1, 2-*H*), 4.16 (m, 2, 1-*H* and 6-*H*), 8.12 (3, C*H*$_3$) and 8.18 (3, C*H*$_3$).

Reaction of Dienes **1**a *and* **1**b *with Trifluoroacetic Acid*

Trifluoroacetic acid (0.1 cm^3) was added to a solution of diene **1***a* (0.1 g) in deuteriochloroform (0.4 cm^3) at 35°C. The reaction was followed by nmr. The appearance of new peaks in the diene region (τ 3.65) indicated that epimerization and/or exchange to form the trifluoroacetoxy diene occurred concurrently with rearomatization. Rearomatization was complete after 1 h and 1-chloro-2,3-dimethyl-4-nitrobenzene (78%), 1-chloro-2,3-dimethyl-6-nitrobenzene (7%), and 3-chloro-4,5-dimethylphenyl acetate (15%) were formed. In a similar experiment **1***b* gave the same products. When the reaction was repeated using a solution of 5% trifluoroacetic acid in carbon tetrachloride the acetate was the major product.

3′-Chloro-2,4,4′,5′,6,-pentamethylbiphenyl

Trifluoroacetic acid (0.1 cm^3) was added to a solution of diene **1** (0.1 g) and mesitylene (0.1 cm^3) in deuteriochloroform (0.4 cm^3). The solution turned red-brown indicating the presence of nitrogen dioxide and the release of nitrous acid. The nmr spectrum of the mixture did not exhibit any resonances below τ 3.0 showing that no nitro compounds had been formed. The mixture was cooled to −78°C and neutralized with liquid ammonia. The residue obtained after work-up was chromatographed on alumina. Elution with pentane removed excess mesitylene. Elution with ether and chromatography of the residue from the eluate on silica gel, and elution with pentane, gave a clear oil which did not crystallize; ir (film): 2970, 2940, 2910, 2860, 2730, 1630, 1555, 1470, 1445, 1385, 1270, 875, 850, 825, 745, 715, 695, and 600 cm^{-1}; nmr ($CDCl_3$) τ: 3.1 (m, 4, 2′-*H*, 3-H, 5-H, and 6′-H), 7.64 and 7.69 (9, 4-C*H*$_3$, 4′-C*H*$_3$, and 5′-C*H*$_3$), 8.00 (s, 6, 2-C*H*$_3$ and 6-C*H*$_3$); mass spectrum (70 eV) *m/e* (relative intensity): 260 (42), 258.1166 (100, M_r ($^{12}C_{14}$ $^{1}H_{19}$ ^{35}Cl) 258.1175), 245 (17) and 243 (44, $M-CH_3$), 223 (69, $M-Cl$), 209 (16), 208 (81), 207 (32), 193 (50), 192 (22), 191 (17), 178 (17), 174 (39), 159 (30).

Reaction of Diene **1** *with Sulfuric Acid in Methanol*

Diene **1** (0.14 g) was dissolved in a solution of sulfuric acid (5 mm^3) in methanol (0.5 cm^3) and allowed to react for 18 h. The nmr indicated that 40% of the original diene had been converted to 3-chloro-4,5-dimethylphenol or its methyl ether. After neutralization and work-up the product was chromatographed. Elution with the pentane and ether–pentane mixtures gave in the 50% ether fractions a mixture of dienes containing as a major constituent, the methoxydienes **3** (nmr 6.70 and 6.73, OC*H*$_3$ of each diastereoisomer).

1. A. Fischer and C. C. Greig. J. Chem. Soc. Chem. Commun. 50 (1974).
2. C. L. Perrin and G. A. Skinner. J. Am. Chem. Soc. **93**, 3389 (1971).
3. T. Banwell, C. S. Morse, P. C. Myhre, and A. Vollmar. J. Am. Chem. Soc. **99**, 3042 (1977).
4. K. Fugiwara, J. C. Giffney, and J. H. Ridd. J. Chem. Soc. Chem. Commun. 301 (1977).
5. R. B. Moodie and K. Schofield. Acc. Chem. Res. **9**, 287 (1976).
6. R. C. Hahn and M. B. Groen. J. Am. Chem. Soc. **95**, 6128 (1973).
7. H. Suzuki. Synthesis, 217 (1977).
8. D. J. Blackstock, A. Fischer, K. E. Richards, J. Vaughan, and G. J. Wright. Chem. Commun. 641 (1970).
9. D. J. Blackstock, J. Cretney, A. Fischer, M. P. Hartshorn, K. E. Richards, J. Vaughan, and G. J. Wright. Tetrahedron Lett. 2793 (1970).
10. A. Fischer and R. Röderer. Can. J. Chem. **54**, 3978 (1976).
11. A. Fischer and K. C. Teo. Can. J. Chem. **56**, 258 (1978).
12. A. Fischer and C. C. Greig. Can. J. Chem. **52**, 1231 (1974).
13. A. I. Scott. Interpretation of the ultraviolet spectra of natural products. Pergamon Press, Oxford. 1964. Chapt. 2.
14. J. D. Roberts, J. K. Sanford, F. L. J. Sixma, H. Cerfontain, and R. Zagt. J. Am. Chem. Soc. **76**, 4525 (1954).
15. A. Fischer, J. Vaughan, and G. J. Wright. J. Chem. Soc. B, 368 (1967).
16. J. W. Barnett, R. B. Moodie, K. Schofield, and J. B. Weston. J. Chem. Soc. Perkin Trans. II, 648 (1975).
17. P. C. Myhre. J. Am. Chem. Soc. **94**, 7921 (1972).
18. D. J. Blackstock. Ph.D. Thesis, University of Canterbury, Christchurch, New Zealand. 1970.
19. H. W. Gibbs, R. B. Moodie, and K. Schofield. J. Chem. Soc. Chem. Commun. 492 (1976).
20. L. E. Hinkel, W. T. Collins, and E. E. Ayling. J. Chem. Soc. 2972 (1923).
21. H. Budzikiewicz, C. Djerassi, and D. H. Williams. Mass spectrometry of organic compounds. Holden-Day Inc., San Francisco. 1967. p. 516.
22. L. E. Hinkel, E. E. Ayling, and T. M. Waters. J. Chem. Soc. 287 (1934).
23. L. E. Hinkel. J. Chem. Soc. 1853 (1924).

The fluoroformate ion, FCO_2^-. An ion cyclotron resonance study of the gas phase Lewis acidity of carbon dioxide and related isoelectronic species

TERRANCE BRIAN MCMAHON AND COLLEEN JOAN NORTHCOTT

Department of Chemistry, University of New Brunswick, P.O. Box 4400, Fredericton, N.B., Canada E3B 5A3

Received October 18, 1977

TERRANCE BRIAN MCMAHON and COLLEEN JOAN NORTHCOTT. Can. J. Chem. **56**, 1069 (1978).

The gas phase ion molecule reactions of a number of potential fluoride donors with carbon dioxide and carbonyl fluoride have been studied. By determination of preferential directions of fluoride transfer the fluoride affinities of carbon dioxide and carbonyl fluoride have been bracketed and found to be 33 ± 3 kcal/mol and 35 ± 3 kcal/mol respectively. In addition, from gas phase acidity studies of acetyl fluoride and 2-fluoropropene the fluoride affinities of ketene and allene have been calculated to be 38 ± 2 kcal/mol and 15 ± 2 kcal/mol respectively. The order of fluoride affinities (Lewis acidities) of carbon dioxide, ketene, and allene have been examined and explained in terms of the electron affinities of the F—C(A)(B) species (A,B=O,CH_2) and the C—F bond dissociation energies. These quantities have been estimated and the latter interpreted on the basis of the π bond energies of the three compounds.

TERRANCE BRIAN MCMAHON et COLLEEN JOAN NORTHCOTT. Can. J. Chem. **56**, 1069 (1978).

On a étudié les réactions ion-molécule en phase gazeuse d'un certain nombre de donneurs potentiels de fluor avec le dioxyde de carbone et le fluorure de carbonyle. A l'aide de la détermination des directions préférentielles des transferts de fluor, on a pu évaluer les affinités pour le fluorure du dioxyde de carbone et du fluorure de carbonyle et on a trouvé que ces valeurs sont respectivement de 33 ± 3 kcal/mol et de 35 ± 3 kcal/mol. De plus, en se basant sur des études d'acidité en phase gazeuse du fluorure d'acétyle et du fluoro-2 propène, on a pu calculer les affinités pour les fluorures du cétène et de l'allène qui sont évaluées respectivement à 38 ± 2 kcal/mol et 15 ± 2 kcal/mol. On a examiné l'ordre des affinités pour les fluorures (acidités de Lewis) du dioxyde de carbone, du cétène et de l'allène et on les exprime en termes d'affinités électroniques des espèces F—C(A)(B) (A,B=O,CH_2) et des énergies de dissociation des liens C—F. On a évalué ces quantités et on les a interprétées en se basant sur les énergies de liaisons π des trois composés.

[Traduit par le journal]

Introduction

The examination of isoelectronic species has been extensively used in the development of theories of structure and bonding in main group chemistry. Of general interest is the observation that to a large extent molecular geometry is determined by the number of valence electrons in the system (1–8) and a good deal of synthetic and structural chemistry has been directed toward the preparation and examination of molecules to test this postulate. An especially useful group of compounds to test the hypothesis are the oxides, fluorides, and oxofluorides of boron, carbon, and nitrogen. For example it is found that the isoelectronic borate, BO_3^{3-}, carbonate, CO_3^{2-}, and nitrate, NO_3^-, ions are each planar species of D_{3h} symmetry (9). Similarly the isoelectronic tetrafluorides, BF_4^-, CF_4, and NF_4^+ each have a tetrahedral form (10) and the isoelectronic pairs of oxofluorides CF_2O—NF_2O^+ and CF_3O^-—F_3NO are also isostructural (11). A novel carbon oxofluoride which has received some attention recently is the fluoroformate ion, FCO_2^- (12). The isoelectronic, 24 valence electron systems BF_3, CO_3^{2-}, NO_3^-, FNO_2, and CF_3^+ all exhibit planar geometries (8) and thus it would be expected that FCO_2^- will be similarly planar. A preliminary report has suggested that cesium fluoroformate, $CsFCO_2$, is formed at high CO_2 pressure above acetonitrile solutions of CsF (12). More recent attempts to reproduce this result appear to have failed, however.[1] The inability to prepare seemingly stable entities such as FCO_2^- is usually indicative of either a highly reactive nature (particularly toward the solvent medium), a large activation barrier to formation, or in the case of ionic species a low crystal lattice energy associated with salt formation with the chosen counterion. Studies of ionic species in the gas phase such as under the normal operating conditions of an ion cyclotron resonance spectrometer avoid each of the above deterrents to the formation of stable ionic species. Since the ions are formed in the absence of solvent and may be observed for times less than the time between collisions highly reactive species will still be detected. In addition gas phase ion molecule reactions usually proceed with zero activation energy (14) thus allowing formation of a desired ion by any appro-

[1]L. Lawlor and J. Passmore, private communication.

Can. J. Chem. Downloaded from www.nrcresearchpress.com by 210.87.254.6 on 09/05/12
For personal use only.

priate exothermic reaction. Therefore it was deemed feasible that if FCO_2^- is bound with respect to F^- and CO_2 it should be possible to observe the fluoroformate ion by ion cyclotron resonance (ICR) experiments.

The technique of using molecular fluoride anions as gas phase fluoride donors has been described by Haartz and McDaniel (15). Thus reactions such as [1] between MF_n^- and CO_2 can conceivably yield the desired fluoroformate ion whenever the binding energy of F^- to CO_2 is greater than that of F^- to MF_{n-1}.

$$[1] \qquad MF_n^- + CO_2 \rightarrow FCO_2^- + MF_{n-1}$$

The present study describes the details of various reactions in which fluoride ion is donated to carbon dioxide and also of several reactions in which FCO_2^- donates fluoride ion to other molecules. Using available thermochemical information on fluoride binding energies it is possible to assign an accurate limit to the fluoride binding energy of CO_2. In addition the isoelectronic species, acetyl fluoride enolate, CH_2COF^-, and 2-fluoroallyl anion, $(CH_2)_2CF^-$, have been generated and fluoride binding energies determined for comparison with that of FCO_2^-.

Experimental

All experiments were carried out on a Varian Instruments V-5900 ICR spectrometer. The techniques and instrumentation associated with ICR have been described in detail previously (16, 17).

Fluoride donors were generated either by electron attachment processes to a variety of inorganic fluorides or by proton abstraction from a fluorine-containing molecule by F^- generated from NF_3 or CH_3O^- generated from CH_3ONO. For example electron impact at 4.4 eV on SO_2F_2 generates both F_2^- (13%) and SO_2F^- (12%) which may each serve as fluoride donors to appropriate species. Details of electron attachment to molecular fluorides are described by Dillard (18).

SF_6, SO_2F_2, COF_2, and CO_2 were obtained from Matheson of Canada, Ltd. CF_3OF, CH_3COF, and CH_3CFCH_2 were purchased from PCR Inc. and NF_3 from Air Products and Chemicals Inc. Methanol, acetic acid, and formic acid were commercially available reagent grade chemicals.

Results

Fluoride donation from a number of anionic fluorides to carbon dioxide and from FCO_2^- to a variety of neutrals has been examined by the variation of pressure of a mixture of neutral reactants in the range 10^{-6} to 10^{-3} Torr in the ICR spectrometer. The exothermic direction of fluoride transfer was confirmed in each case using ICR double resonance techniques. The fluoride binding energies or fluoride affinities of a number of anions used as reference standards are summarized in Table 1.

TABLE 1. Fluoride affinities of reference fluoride donors

Species – MF^-	Fluoride affinity $D(M—F^-)$ (kcal/mol)	Reference
SF_6^-	11 ± 8	13
SF_5^-	54 ± 12	13
F_2^-	29 ± 2	21*a*, *b*, *c*
SO_2F^-	40 ± 2	21*a*
CH_2COF^-	38 ± 2	*a*
$(CH_2)_2CF^-$	15 ± 2	*a*
CH_3OHF^-	29 ± 4	*b*
$CH_3CO_2HF^-$	44 ± 4	*b*

[a]T.B. McMahon, unpublished results.
[b]Interpolated from the data of Yamdagni and Kebarle (26).

1. SF_6 and CO_2

Electron impact at 70 eV on SF_6 produces SF_6^- and SF_5^- in a ratio of 20:1 (19). When CO_2 was added to the system neither reaction 2 nor 3 was observed to occur. Failure to observe fluoride transfer from SF_6^- to CO_2 might be taken as evidence that the

$$[2] \qquad SF_6^- + CO_2 \not\rightarrow FCO_2^- + SF_5$$

$$[3] \qquad SF_5^- + CO_2 \not\rightarrow FCO_2^- + SF_4$$

fluoride affinity of CO_2 is less than that of SF_5 (11 ± 8 kcal/mol). However recent studies have shown that even when fluoride transfer from SF_6^- is known to be exothermic it has frequently not been observed (20), particularly in the case of transfer to weakly acidic species. Thus no firm conclusion may be drawn from the SF_6^- result. On the basis of failure of reaction 3 to occur a value of $D(F^-—CO_2)$ less than 54 ± 12 kcal/mol may be inferred.

2. SO_2F_2 and CO_2

Dissociative electron attachment at 4.4 eV to SO_2F_2 produces F^- (75%), F_2^- (12%), and SO_2F^- (13%). SO_2F^- was observed to be unreactive toward CO_2 implying a fluoride affinity of CO_2 of less than 40 kcal/mol. Fluoride transfer from F_2^- to CO_2, eq. 4, proceeded efficiently however to produce the

$$[4] \qquad F_2^- + CO_2 \rightarrow FCO_2^- + F$$

fluoroformate ion, FCO_2^-. Determinations of the electron affinity of molecular fluorine place it at 3.0 ± 0.1 eV (21) which, taken with the electron affinity of fluorine atom of 3.40 eV (22) and $\Delta H_f^0{}_{298}(F)$ of 18.88 kcal/mol, allows a calculation of $D(F^-—F)$ of 29 kcal/mol. Therefore the fluoride affinity of CO_2 is established as greater than this value.

3. CH_3ONO and F_2CO

An efficient means of producing fluoroformate was also found in the reaction of methoxide ion generated

Can. J. Chem. Downloaded from www.nrcresearchpress.com by 210.87.254.6 on 09/05/12
For personal use only.

Can. J. Chem. Downloaded from www.nrcresearchpress.com by 210.87.254.6 on 09/05/12
For personal use only.

from methyl nitrite with carbonyl fluoride. Riveros has previously shown that the reaction of methoxide ion with 1,1-difluoroethylene leads to facile production of fluoroenolate ions, eq. 5 (23). It was thus

[5] $CH_3O^- + \underset{F}{\overset{F}{\diagdown}}C{=}C\underset{H}{\overset{H}{\diagup}} \rightarrow \underset{F}{\overset{O^-}{\diagdown}}C{=}CH_2 + CH_3F$

anticipated that reaction of methoxide ion with the isoelectronic carbonyl fluoride might yield the desired fluoroformate ion, eq. 6. The expected result was in

[6] $CH_3O^- + \underset{F}{\overset{F}{\diagdown}}C{=}O \rightarrow \underset{F}{\overset{O^-}{\diagdown}}C{=}O + CH_3F$

fact found as demonstrated by the variation of relative ionic abundances with pressure shown in Fig. 1. In addition reactions 7–9 were also observed.

[7] $CH_3O^- + CH_3ONO \rightarrow CH_2ONO^- + CH_3OH$

[8] $CH_2ONO^- + F_2CO \rightarrow CHFONO + HF + CO$

[9] $FCO_2^- + F_2CO \rightarrow F_3CO^- + CO_2$

The last reaction, eq. 9, establishes the fluoride affinity of CO_2 as being less than that of carbonyl fluoride. Due to a lack of accurate thermochemical data for F_3CO^- experiments were also carried out to establish the fluoride affinity of F_2CO and establish an upper limit for the fluoride affinity of carbon dioxide.

4. CF_3OF and CO_2

Thynne and MacNeil (24) have assigned a value of greater than 1.9 eV for the electron affinity of F_3CO radical based on the production of F_3CO^- by dissociative attachment of zero energy electrons to trifluoromethyl hypofluorite, CF_3OF. At all electron energies they observed F^- to be the most abundant ion formed. In contrast to this in the ICR spectrometer we observe CF_3O^- to be the most abundant species formed by electron attachment to CF_3OF. This result implies that the electron affinity of F_3CO should be greater than the electron affinity of fluorine atom, 3.40 eV (22). This value, taken with $\Delta H_f^0{}_{298}(F_2CO)$ of -152 kcal/mol yields a value of $D(F^-—F_2CO)$ of greater than 24 kcal/mol, consistent with our data for relative fluoride affinities of CO_2 and F_2CO reported above.

When CO_2 was added to the system with CF_3OF no fluoride transfer was observed confirming the exothermic direction of fluoride transfer of eq. 9.

5. CF_3OF and SO_2

Trifluoromethoxide ion generated from CF_3OF was found to react with SO_2 to generate SO_2F^-, eq. 10. This result is consistent with the failure to

[10] $CF_3O^- + SO_2 \rightarrow SO_2F^- + CF_2O$

observe fluoride transfer from SO_2F^- to CO_2 in the SO_2F_2, CO_2 mixture and establishes the fluoride affinity of CF_2O as less than that of SO_2, 40 kcal/mol (21).

6. CF_3OF and Acetic Acid

Trifluoromethoxide generated from CF_3OF underwent fluoride transfer to acetic acid, eq. 11. The acid

[11] $F_3CO^- + CH_3CO_2H \rightarrow CH_3CO_2HF^- + F_2CO$

[12] $CH_3CO_2HF^- + CH_3CO_2H \rightarrow (CH_3CO_2)_2H^- + HF$

solvated fluoride ion reacted further with acetic acid producing the proton bound dimer of acetate ion, eq. 12, by displacement of HF. This latter reaction provides a convenient bimolecular route to dimer anions permitting further studies of anion–solvent binding energies (25).

Based on the data of Yamdagni and Kebarle (26) for solvation of halide ions by a variety of protic solvents a value of $D(F^-—CH_3CO_2H)$ of 44 kcal/mol may be interpolated establishing the fluoride affinity of F_2CO as less than this value.

7. NF_3, CH_3COF, and CO_2

Fluoride ion generated from NF_3 reacted with acetyl fluoride via proton transfer to generate the acetyl fluoride enolate ion eq. 13. This ion may also

[13] $F^- + CH_3COF \rightarrow \underset{F}{\overset{O^-}{\diagdown}}C{=}CH_2 + HF$

be formally regarded as F^- bound to ketene which is isoelectronic with carbon dioxide. The acetyl

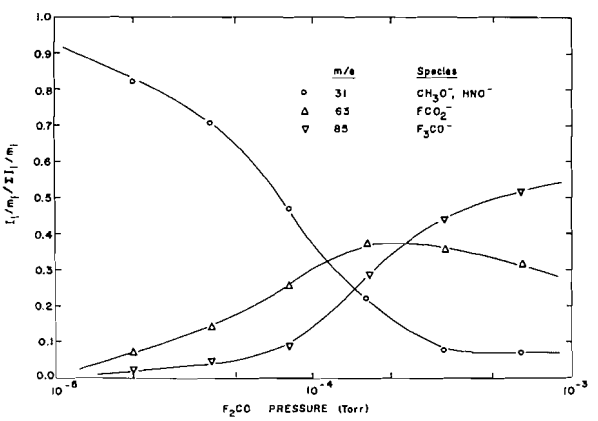

FIG. 1. Variation of relative anionic abundances with pressure in a 10:1 mixture of carbonyl fluoride:methyl nitrite at 70 eV electron energy.

Can. J. Chem. Downloaded from www.nrcresearchpress.com by 210.87.254.6 on 09/05/12
For personal use only.

fluoride enolate did not undergo fluoride transfer to CO_2, eq. 14, indicating that carbon dioxide has a fluoride affinity less than ketene.

[14] 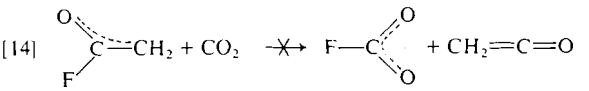

Studies of the acidity of acetyl fluoride have established a proton affinity of the fluoro enolate ion of 357 kcal/mol (27). This value allows a calculation of the fluoride affinity of ketene of 38 kcal/mol. Further work showed the fluoride affinity of ketene to be greater than carbonyl fluoride.

8. CH_3ONO, $CH_2{=}CFCH_3$, and CO_2

Reaction of methoxide generated from methyl nitrite with 2-fluoropropene yields the 2-fluoropropenyl anion, eq. 15, and CH_3OHF^-, eq. 16. Both of

[15] 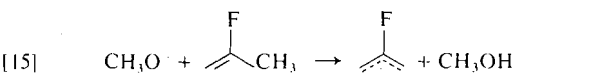

[16] 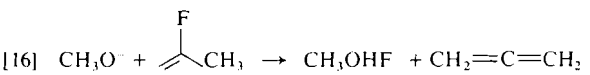

these ions thus generated react further with carbon dioxide to give the fluoroformate ion, eqs. 17 and 18

[17] 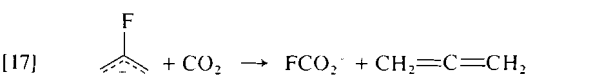

[18] $$CH_3OHF^- + CO_2 \rightarrow FCO_2^- + CH_3OH$$

respectively. The variation of relative ionic abundances with pressure observed for this reaction mixture is shown schematically in Fig. 2.

The acidity of 2-fluoropropene has also been studied and a proton affinity of 376 kcal/mol assigned for the 2-fluoropropenyl anion (27). This

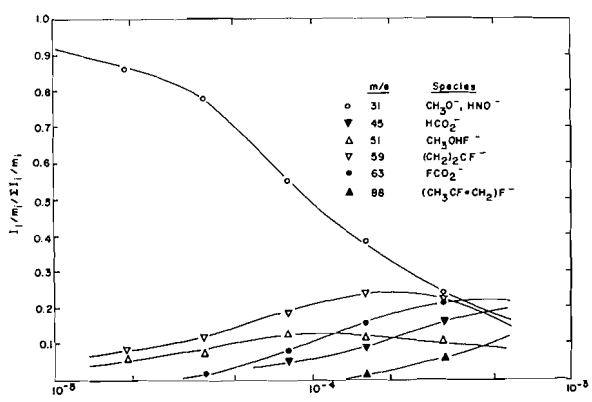

FIG. 2. Variation of relative anionic abundances with pressure in a 20:10:1 mixture of 2-fluoropropene:carbon dioxide:methyl nitrite at 1.5 eV electron energy.

result establishes a fluoride affinity of 15 kcal/mol for allene.

The fluoride affinity of methanol interpolated from Kebarle's data (26) is roughly 29 kcal/mol. Reaction 18 denoting the fluoride affinity of carbon dioxide greater than methanol is thus consistent with reaction 4 which also establishes a CO_2 fluoride affinity greater than 29 kcal/mol.

Discussion

The results presented above together with the thermochemical data summarized in Table 1 provide a basis for assignment of a reasonably accurate fluoride affinity of carbon dioxide. The observation of fluoride transfer from F_2^- to CO_2 provides a lower limit of 29 kcal/mol for $D(F^-{-}CO_2)$. On the basis of failure to observe fluoride transfer from SO_2F^- and CH_2COF^- to CO_2 a fluoride affinity of less than 38 kcal/mol is inferred. Further it is found that FCO_2^- undergoes fluoride transfer to F_2CO and that carbonyl fluoride has a fluoride affinity less than ketene, 38 kcal/mol. Thus, from these observations it is possible to assign fluoride affinities of 35 ± 3 kcal/mol to carbonyl fluoride and 33 ± 3 kcal/mol to carbon dioxide. These assignments allow calculations of $\Delta H_f^0{}_{298}$ for F_3CO^- of -247 kcal/mol and for FCO_2^- of -187 kcal/mol to be made.

It is noteworthy that the value of $\Delta H_f^0{}_{298}$ obtained for fluoroformate ion and the associated fluoride affinity of carbon dioxide are very close to values for these quantities obtained by estimating the gas phase acidity of the hypothetical fluoroformic acid molecule. The proton affinity of the fluoroformate ion may be estimated from the known acidity of trifluoroacetic acid (28) and from a comparison of the relative effects of CF_3 and F substitution on acidities of carbonyl compounds. A comparison of the acidities of 1,1,1-trifluoroacetone (29) and acetyl fluoride (27) reveals that relative to acetone CF_3 substituted for CH_3 lowers the anion proton affinity by 17 kcal/mol (29) while F substituted for CH_3 lowers the proton affinity by some 10 kcal/mol (27). Noting that the trifluoroacetone enolate is isoelectronic with trifluoroacetate and acetyl fluoride enolate isoelectronic with fluoroformate proportionate reductions in proton affinities of enolates and carboxylates might be expected. Therefore on the basis of a 25 kcal/mol reduction in proton affinity of trifluoroacetate relative to acetate ion a proton affinity for the fluoroformate ion of 330 kcal/mol is estimated. Combining this with a value of -153 kcal/mol estimated for $\Delta H_f^0{}_{298}(FCO_2H)$ by group equivalent methods a fluoride affinity of 35 kcal/mol is obtained for CO_2 in good agreement with the results presented above.

Can. J. Chem. Downloaded from www.nrcresearchpress.com by 210.87.254.6 on 09/05/12
For personal use only.

TABLE 2. Thermochemical data related to fluoride affinities of allene, ketene, and carbon dioxide

M	FA(M)[a]	EA(MF)[a,b]	D(M—F)[a]	Eπ(M)[a,c]
O=C=O	33	87	24[d]	183
CH_2=C=O	38	51	65[e]	132
CH_2=C=CH_2	15	22	71[f]	106

[a]All values in kcal/mol.
[b]Electron affinity calculated from the estimated bond energy, D(M—F), the experimental fluoride affinity, and electron affinity of F (3.40 eV).
[c]π Bond energy calculated by the method of Benson (30).
[d]$\Delta H_f°_{298}(FCO_2)$ calculated from estimated $\Delta H_f(FCO_2H) = -153$ kcal/mol and an assumed D(H—OCOF) of 106 kcal/mol.
[e]$\Delta H_f°_{298}(CH_2COF\cdot)$ calculated from $\Delta H_f°_{298}(CH_3COF) = -104$ kcal/mol and an assumed D(H—CH_2COF) of 95 kcal/mol.
[f]$\Delta H_f°_{298}((CH_2)_2CF\cdot)$ calculated from estimated $\Delta H_f°_{298}(CH_3CF{=}CH_2) = -39$ kcal/mol and an assumed D(H—$CH_2CF{=}CH_2$) = 85 kcal/mol.

Further, it is of interest to compare the fluoride affinities of the isoelectronic series of compounds with cumulative double bonds: allene, ketene, and carbon dioxide. On the basis of standard concepts of stability of anions it might have been expected that carbon dioxide would have the highest fluoride affinity of the three compounds since the resulting fluoroformate ion should be more stable than either the fluoroenolate or 2-fluoropropenyl anions. However the fluoride affinities found, which are summarized in Table 2 do not reflect this intuitive ordering. Instead, fluoride affinities increase in the order allene < carbon dioxide < ketene. In order to better understand the reason for this order it is useful to express the fluoride affinity in terms of other thermochemical quantities as shown in Scheme 1. Since the electron affinity of F is constant for the series of molecules differences in fluoride affinity result from differences in electron affinities of the MF radicals and the M—F bond dissociation energies. Estimates of the M—F bond energies are also summarized in Table 2 as well as the radical electron affinities calculated from the estimated MF heat of formation. The electron affinities show the expected trend in anionic stabilities, that is fluoroformate is more stable than fluoroenolate which in turn is more stable than 2-fluoropropenyl anion with respect to electron detachment. The reason the fluoride affinities do not follow the order of electron affinities is found in the greatly reduced F—CO_2 bond energy relative to that in the CH_2COF and $(CH_2)_2$CF radicals. Further, the F—CO_2 bond energy is much lower

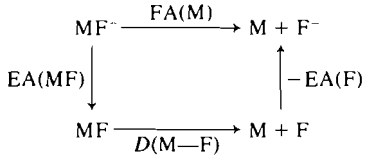

$$FA(M) = EA(MF) + D(M—F) - EA(F)$$

SCHEME 1

than the corresponding C—F bond energies in the other two compounds because of the very high π bond energy of CO_2. For comparison the π bond energies calculated by Benson's (30) method are also included in Table 2. Thus in forming a new C—F bond as F^- approaches the double bond system roughly one half of the π bond energy of the compound is lost. Since this quantity is so much greater for CO_2 than either ketene or allene a much lower fluoride affinity results.

The above analysis demonstrates that although fluoride binding energies are a good measure of Lewis acidity in the gas phase they are not necessarily a good means of assessing relative intrinsic anionic stabilities. A much better measure of the latter quantity is the electron affinity of the corresponding free radical. The approximate values of electron affinity shown in Table 2 dramatically demonstrate the expected stability of the fluoroformate ion.

Conclusions

The present study demonstrates that using a variety of gas phase ion molecule reactions novel anionic species may be observed and characterized. The results obtained for F^-—CO_2 binding energy coupled with an estimated crystal lattice energy for $CsFCO_2$ and the crystal lattice energy for CsF (31) indicate that reaction 19 for the formation of

[19] $$CsF + CO_2 \rightarrow CsFCO_2$$

$CsFCO_2$ should be somewhat exothermic (10 kcal/mol) and that preparation of the material by this route is feasible. Similar demonstrations for fluorine containing anions may prove to be of further aid to synthetic chemists in assessing feasibility of various routes to ionic compounds.

In addition the above data show that experiments of the type carried out in this work can be extremely valuable in providing thermochemistry of unusual anionic species. Further studies of fluoride binding energies are currently in progress.

Acknowledgements

The generous financial support of the New Brunswick Higher Education Commission and the National Research Council of Canada is gratefully acknowledged. Miss C. Northcott performed several of the initial experiments in partial fulfillment of requirements for the B.Sc. degree at U.N.B. Useful discussions with Professor J. Passmore and L. Lawlor are gratefully acknowledged.

1. R. S. MULLIKEN. Rev. Mod. Phys. **14**, 204 (1942).
2. A. D. WALSH. J. Chem. Soc. 2260 (1953), and following articles.
3. J. CASSIE. Nature (London), **131**, 438 (1933).

4. W. G. PENNEY and G. B. SUTHERLAND. Proc. R. Soc. Ser. A, **156**, 654 (1936).
5. N. V. SIDGWICK and H. M. POWELL. Proc. R. Soc. Ser. A, **176**, 153 (1940).
6. G. KIMBALL. J. Chem. Phys. **8**, 188 (1940).
7. L. PAULING. The nature of the chemical bond. Cornell University Press, Ithaca, NY. 1960.
8. R. J. BUENKER and S. D. PEYERIMHOFF. Chem. Rev. **74**, 127 (1974).
9. A. D. WALSH. J. Chem. Soc. 2301 (1953).
10. K. O. CHRISTIE, J. P. GUERTIN, A. E. PAVLETH, and W. SAWODNY. Inorg. Chem. **6**, 533 (1967).
11. F. A. COTTON and G. WILKINSON. Advanced inorganic chemistry. 3rd ed. Wiley-Interscience, New York, NY. 1972.
12. E. MARTINEAU and J. B. MILNE. Chem. Commun. 1327 (1971).
13. R. N. COMPTON and C. P. COOPER. J. Chem. Phys. **59**, 4140 (1973).
14. D. P. STEVENSON and D. O. SCHISSLER. J. Chem. Phys. **29**, 282 (1958).
15. J. C. HAARTZ and D. H. MCDANIEL. J. Am. Chem. Soc. **95**, 8302 (1973).
16. J. L. BEAUCHAMP. Ann. Rev. Phys. Chem. **22**, 517 (1971).
17. J. M. HENIS. *In* Ion molecule reactions. *Edited by* J. L. Franklin. Plenum, New York, NY. 1972.
18. J. G. DILLARD. Chem. Rev. **73**, 589 (1973).
19. L. G. CHRISTOPHOROU, D. L. MCCORKLE, and J. G. CARTER. J. Chem. Phys. **54**, 253 (1971).
20. M. S. FOSTER and J. L. BEAUCHAMP. Chem. Phys. Lett. **31**, 479 (1975).
21. (*a*) R. M. REESE, V. H. DIBELER, and J. L. FRANKLIN. J. Chem. Phys. **29**, 880 (1958); (*b*) W. A. CHUPKA, J. BERKOWITZ, and D. GUTMAN. J. Chem. Phys. **55**, 2724 (1971); (*c*) J. J. DECORPO and J. L. FRANKLIN. J. Chem. Phys. **54**, 1885 (1971).
22. W. A. CHUPKA and J. BERKOWITZ. J. Chem. Phys. **54**, 5126 (1971); J. BERKOWITZ, W. A. CHUPKA, P. M. GUYON, J. H. HOLLOWAY, and R. SPOHR. J. Chem. Phys. **54**, 5165 (1971).
23. J. M. RIVEROS and K. TAKASHIMA. Can. J. Chem. **54**, 1839 (1976).
24. J. C. J. THYNNE and K. A. G. MACNEIL. Int. J. Mass Spectrom. Ion Phys. **5**, 95 (1970).
25. R. CLAIR and T. B. MCMAHON. To be published.
26. R. YAMDAGNI and P. KEBARLE. J. Am. Chem. Soc. **93**, 7139 (1971).
27. T. B. MCMAHON. To be published.
28. K. HIRAOKA, R. YAMDAGNI, and P. KEBARLE. J. Am. Chem. Soc. **95**, 6833 (1973).
29. T. B. MCMAHON and P. KEBARLE. J. Am. Chem. Soc. **98**, 3399 (1976).
30. S. W. BENSON. Thermochemical kinetics. Wiley, New York, NY. 1968.
31. R. M. ROSENBERG. Principles of physical chemistry. Oxford University Press, New York, NY. 1977.

Can. J. Chem. Downloaded from www.nrcresearchpress.com by 210.87.254.6 on 09/05/12
For personal use only.

The radiation chemistry of nitric oxide[1]

A. W. BOYD AND O. A. MILLER

Atomic Energy of Canada Limited, Chalk River Nuclear Laboratories, Physical Chemistry Branch, Chalk River, Ont., Canada K0J 1J0

Received October 11, 1977

A. W. BOYD and O. A. MILLER. Can. J. Chem. **56**, 1075 (1978).

The yield of nitrogen from the radiolysis of nitric oxide is $G(N_2) = 4.5 \pm 0.3$ at doses from 0.1 to 1.0×10^{20} eV g^{-1} and at dose rates of 2.5×10^{16} and 2×10^{27} eV g^{-1} s^{-1}. The addition of SF_6 to NO does not change this yield but in mixtures of NO with 90% Xe the addition of SF_6 reduces $G(N_2)$ by an amount close to $G(Xe^+)$. These results are consistent with suppression of dissociative neutralisation in NO by clustering of the positive ion. Good agreement is obtained between the total energy absorbed and the amounts required for ionization, neutral dissociative excitation, and formation of subexcitation electrons. The neutral dissociative excitation yield is estimated to be $G(NO \rightarrow N + O) = 3.6 \pm 0.3$.

A. W. BOYD et O. A. MILLER. Can. J. Chem. **56**, 1075 (1978).

Le rendement d'azote provenant de la radiolyse de l'oxyde nitrique est $G(N_2) = 4.5 \pm 0.3$ à des doses allant de 0.1 à 1.0×10^{20} eV g^{-1} et à des taux de dose de 2.5×10^{16} et 2×10^{27} eV g^{-1} s^{-1}. L'addition de SF_6 au NO ne change pas ce rendement mais dans des mélanges de NO avec 90% de Xe, l'addition de SF_6 réduit $G(N_2)$ par une quantité proche de $G(Xe^+)$. Ces résultats sont en accord avec la suppression de la neutralisation dissociative dans NO par l'aggrégation d'ions positifs. Une bonne concordance a pu être obtenue entre l'énergie totale absorbée et les quantités requises pour l'ionisation, l'excitation dissociative neutre et la formation d'électrons sous-excités. On a évalué que le rendement d'excitation dissociative neutre est $G(NO \rightarrow N + O) = 3.6 \pm 0.3$.

[Traduit par le journal]

Introduction

Over the past ten years a good understanding of the radiolysis of most of the simple inorganic gases has been obtained by combining primary ion yields, reaction rate constants, and stable product yields (1).

The contribution of ionic processes to the stable products is derived from the ion yields and reaction rate values. The major uncertainty in these data is the identity of the products of neutralisation reactions. This can usually be resolved by measurement of the stable products with and without an electron scavenger, such as SF_6, which suppresses dissociative neutralisation of the positive ion. The charge transfer from the primary positive ions to products or impurities, that may occur before neutralisation with ^{60}Co sources has been eliminated by the use of high intensity pulsed electron accelerators.

The yields of primary neutral species are usually determined from the differences between the ionic contributions and the total product yields but in a few cases these have also been obtained from electron cross section measurements and degradation spectra. In these cases there is reasonable agreement between the physical and chemical values.

It has also been possible for most gases to obtain a balance between the total energy absorbed and that required for ionization, excitation, and formation of subexcitation electrons.

The stable products from the radiolysis of nitric oxide are N_2 and NO_2 (2) (in equilibrium with N_2O_4 and N_2O_3) and $G(NO_2) = 2G(N_2)$. As will be discussed the available data on ion yields and reactions lead to $G(N_2) = 4.7$ from ionic processes. From energy balance calculations the yield from neutral processes is $G(N_2) \approx 3.8$ giving a total of $G(N_2) \approx 8.5$.

There are only two reports of radiolytic yield measurements. The first by Harteck and Dondes (2) gives total disappearance yields of NO at ~64 kPa in fission fragment irradiations with a dose rate of $\sim 10^{19}$ eV g^{-1} s^{-1}. The yield decreased from $G(-NO) = 13.8$ at 6×10^{21} eV g^{-1} to $G(-NO) = 9.5$ at 1.2×10^{23} eV g^{-1}. The maximum yield of N_2 calculated from these is $G(N_2) = 3.45 \pm 0.35$. The second by Hochanadel, Ghormley, and Ogren (3) gives the yields of NO_2 and N_2O_3 from the Febetron radiolysis of NO at 100 kPa. The value obtained was $G(NO_2 + N_2O_3) = 10.6$ over dose rates between 10^{26} and 10^{27} eV g^{-1} s^{-1} and doses between 6×10^{18} and 6×10^{19} eV g^{-1}. This value indicates a nitrogen yield of $G(N_2) = 5.3$.

The contribution of ion neutralisation, in the above estimate, to the nitrogen yield is $G(N_2) = 3.6$. If this neutralisation is not dissociative this would

[1]AECL No. 6105.

Can. J. Chem. Downloaded from www.nrcresearchpress.com by 210.87.254.5 on 09/05/12
For personal use only.

Can. J. Chem. Downloaded from www.nrcresearchpress.com by 210.87.254.5 on 09/05/12
For personal use only.

account for a large part of the disagreement between the predicted and measured values. It is thus of interest not only to determine the effect of an electron scavenger on the yields but also to investigate further their dependence on dose and dose rate.

Experimental

Irradiations and Dosimetry

In the high dose rate irradiations both a Febetron 705 and a Febetron 706 were used. The samples were contained in quartz cells (4 cm diameter × 7 cm long for the 705 and 2.5 cm diameter × 2 cm long for the 706) with 0.05 cm thick windows. The maximum absorbed doses in these cells from nitrous oxide dosimetry ($G(N_2) = 12.4$ (4–6)) were 1×10^{20} eV g^{-1} per pulse ($\sim 2 \times 10^{27}$ eV g^{-1} s^{-1}) and 7.2×10^{19} eV g^{-1} per pulse ($\sim 2 \times 10^{28}$ eV g^{-1} s^{-1}) for the 705 and 706 respectively.

The low dose rate irradiations were done with a Gammacell 220. The absorbed dose rate, determined using a mixture of N_2O with 1 mol% SF_6 and taking $G(N_2) = 8.0$ (4, 7), was 2.5×10^{16} eV g^{-1} s^{-1}. The samples were contained in 90 cm^3 Pyrex cells.

Materials and Analyses

All gases were obtained from the Matheson Co. The nitric oxide was subjected to freeze–pump–thaw cycles to remove permanent gases and low temperature distillation to remove NO_2 and N_2O_3. The removal of the latter two was verified by measurement of the spectrum in the region 200–500 nm with a Cary 17 spectrophotometer. Nitrous oxide was removed by passing the nitric oxide through 3A molecular sieve.

The sulfur hexafluoride and nitrous oxide were freed from permanent gases as described above. The xenon was used directly.

The nitrogen produced by irradiation was measured by freezing the samples with solid nitrogen, collecting the gas remaining in a McLeod gauge, and analyzing this by mass spectrometry.

Results

The amounts of nitrogen from both the Febetron 705 and the Gammacell irradiations as a function of dose are shown in Fig. 1. The standard deviations in these values are in general less than ±5% and thus the uncertainties are in most cases less than those indicated by the dimensions of the symbols.

The yields from these results $G(N_2) = 4.5$ at doses from 0.1×10^{20} to $\sim 2 \times 10^{20}$ eV g^{-1} and $G(N_2) = 3.6$ at doses from $\sim 3 \times 10^{20}$ to 7×10^{20} eV g^{-1} are estimated to have an uncertainty of ±8%. The high dose value is in good agreement with that of Harteck and Dondes (2) $G(N_2) = 3.45 \pm 0.35$ at doses from 6×10^{20} to 6×10^{21} eV g^{-1}. The value of Hochanadel *et al.* (3) can be corrected to $G(N_2) = 0.5$, $G(NO_2 + N_2O_3) = 4.90 \pm 0.25$ by using our value of $G(O_3) = 12.8$ (8) instead of their value of $G(O_3) = 13.8$ (9).

The yields in irradiations with the Febetron 706 varied depending on whether a quartz or an aluminum cell was used and were in the range $G(N_2) = 5$ to $G(N_2) = 7$. They were not changed in the addition of SF_6. Similar anomalously high yields have been previously discussed (10).

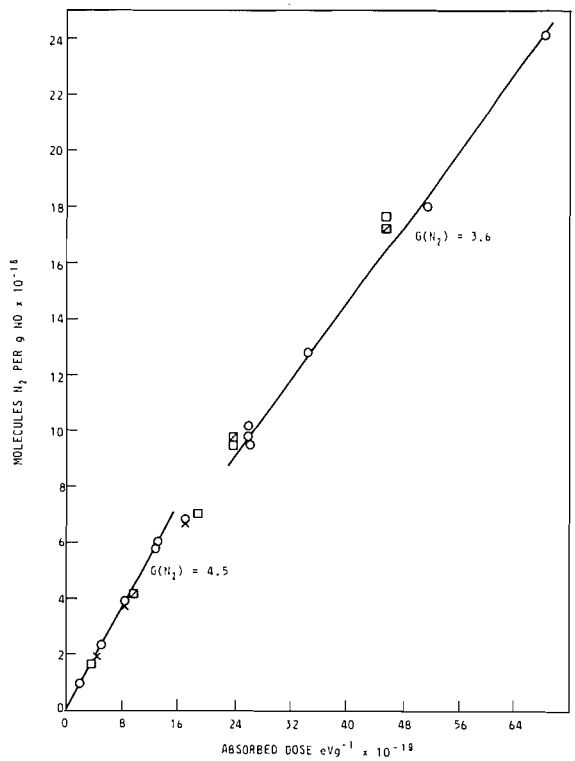

FIG. 1. Amount of N_2 per g of NO as a function of the absorbed dose, Febetron 705 dose rate 2×10^{27} eV g^{-1} s^{-1}: □, 100 kPa NO; ▨, 100 kPa NO 1 kPa SF_6. Gammacell dose rate 2.5×10^{16} eV g^{-1} s^{-1}: ○, 100 kPa NO; ×, 100 kPa NO 1 kPa SF_6.

The results of Febetron 705 irradiations of mixtures of xenon and NO with and without SF_6 are given in Table 1. As will be discussed these were carried out to confirm the explanation proposed for the lack of effect of SF_6 on the yields presented in Fig. 1.

Discussion

Neutralisation Reactions in NO

The data in Fig. 1 and the results obtained with the Febetron 706 show that the addition of 1 mol% SF_6 does not significantly change the values of $G(N_2)$ at dose rates from 2.5×10^{16} to 2×10^{28} eV

TABLE 1. Nitrogen yields from the Febetron 705 radiolysis of Xe–NO mixtures[a]

Sample composition	$G(N_2)$[b]
10 kPa NO + 90 kPa Xe	5.3 ± 0.4
10 kPa NO + 90 kPa Xe + 1 kPa SF_6	1.45 ± 0.1

[a]Dose rate = 5×10^{26} eV g^{-1} s^{-1}; absorbed dose = 2.7×10^{19} eV g^{-1}.
[b]These are the yields based on the energy absorbed by the Xe.

TABLE 2. Ionic and neutral reactions in irradiated nitric oxide

	Reaction	Rate constant (cm^3 $molecule^{-1}$ s^{-1})	Reference
[1]	$N^+ + NO \rightarrow NO^+ + N$	8×10^{-10}	11
[2]	$O^+ + NO \rightarrow NO^+ + O$	$<1.3\times10^{-12}$	12
[3]	$O^+ + N_2 \rightarrow NO^+ + N$	1.2×10^{-12}	13
[4]	$O^+ + NO_2 \rightarrow NO_2^+ + O$	1.6×10^{-9}	13
[5]	$NO_2^+ + NO \rightarrow NO^+ + NO_2$	2.9×10^{-10}	14
[6]	$NO^+ + 2NO \rightarrow (NO)_2^+ + NO$	5×10^{-30}[a]	15
[7]	$e + 2NO \rightarrow NO^- + NO$	8×10^{-31}[a]	16
[8]	$NO^- + NO_2 \rightarrow NO_2^- + NO$	7.4×10^{-10}	17
[9]	$NO^+ + e \rightarrow N + O$	3.1×10^{-7}	18, 19
[10][b]	$(NO)_2^+ + e \rightarrow$ no N or N_2	1.7×10^{-6}	19
[11]	$e + SF_6 \rightarrow SF_6^-$	2.2×10^{-7}	20
[12]	$NO_2^- + NO_2 \rightarrow NO_3^- + NO$	4×10^{-12}	21
[12a]	$NO_3^- + NO \rightarrow NO_2^- + NO_2$	3×10^{-15}	16
[13]	$N + NO \rightarrow N_2 + O$	2.2×10^{-11}	22
[14]	$O + NO + M \rightarrow NO_2 + M$	7×10^{-32}[a]	23
[15]	$O + NO_2 \rightarrow NO + O_2$	9×10^{-12}	24
[16]	$O + NO_2 + M \rightarrow NO_3 + M$	8×10^{-32}[a]	25
[17]	$N + NO_2 \rightarrow N_2O + O$	7.7×10^{-12}	26
[18]	$N + NO_2 \rightarrow NO + NO$	5.9×10^{-12}	26
[19]	$N + NO_2 \rightarrow N_2 + O + O$	2.3×10^{-12}	26
[20]	$N + NO_2 \rightarrow N_2 + O_2$	1.8×10^{-12}	26

[a]Three body rate constant, in cm^6 $molecule^{-2}$ s^{-1}.
[b]The product is presumably 2NO. A similar rate constant has been obtained for $(Kr)_2^+ + e$ (27). If the negative species is NO^- or $(NO)_2^-$ NO is again expected to be the only product.

TABLE 3. Ion lifetimes in irradiated nitric oxide at 100 kPa

Ion	Reaction	Dose rate (eV g^{-1} s^{-1})	Mean lifetime (s)
N^+	$N^+ + NO \rightarrow NO^+ + N$		5×10^{-11}
NO^+	$NO^+ + 2NO \rightarrow (NO)_2^+ + NO$		3.2×10^{-10}
NO^+	$NO^+ + e \rightarrow N + O$	2×10^{27}	$\sim5\times10^{-9}$
		2×10^{28}	$\sim1\times10^{-9}$
e	$e + 2NO \rightarrow NO^- + NO$		2×10^{-9}
$(NO)_2^+$	$(NO)_2^+ + NO^- \rightarrow 3NO$?	2×10^{27}	$\sim2\times10^{-9}$
		2.5×10^{16}	7×10^{-4}
NO^-	$NO^- + NO_2 \rightarrow NO_2^- + NO$	(Dose = 1×10^{19} eV g^{-1})	1.3×10^{-6}

g^{-1} s^{-1}. As all previous studies in many systems (1) have shown that the addition of SF_6 suppresses dissociative neutralisation of the positive ion these results support the suggestion in the Introduction that under the above conditions there is no contribution from neutralisation in pure NO.

To provide a basis for the discussion of this and other features of the radiation behaviour of NO the reactions and lifetimes of ions and radicals that are formed in the radiolysis of NO are listed in Tables 2 and 3. From these tables it can be seen that while the neutralisation of NO^+, reaction 9, is dissociative the positive ion that is neutralised at any dose rate below 10^{29} eV g^{-1} s^{-1} at 100 kPa will be $(NO)_2^+$. The binding energy of the positive ion dimer is 0.59 eV (28) and this will then reduce the available energy released by neutralisation from 9.26 to 8.67 eV. Although this provides an excess of 2 eV over the threshold energy of 6.5 eV it is apparently not enough and this is supported by results obtained in the radiolysis of CO. In CO where the dissociation threshold is 11.16 eV and addition of CO to CO^+ reduces the available neutralisation energy from 14.1 to 13.3 eV (29) there is no decomposition attributable to neutralisation (1). At 10^{26}–10^{27} eV g^{-1} s^{-1} the electron will probably be attached to NO and this ion also may be clustered (17). The electron affinity of NO is small, 0.024 eV (17), but the binding energy of the dimer negative ion is estimated to be 0.5 eV (17). At the Gammacell dose rates the ion lifetime increases to ~1 ms. The positive ion should still be $(NO)_2^+$ but the negative ions will be NO_2^- and NO_3^-. The ratio of these will be dose dependent but as the electron affinity of NO_2 is 2.3 eV (30) and that

Can. J. Chem. Downloaded from www.nrcresearchpress.com by 210.87.254.5 on 09/05/12
For personal use only.

TABLE 4. Energy balance in the radiolysis of nitric oxide

Process	Threshold energy (eV)	Average energy (eV)	Yield	Energy used (eV)[a]
$NO \rightsquigarrow NO^+ + e$	9.25	12.4[b]	2.6[c]	32.2
$NO \rightsquigarrow N^+ + O + e$	19.9 (37)	22[d]	1.04[c]	22.9
$NO \rightsquigarrow N + O^+ + e$	20.6 (37)			
$NO \rightsquigarrow N + O$	6.5	9.8[e]	3.5[f]	34.3
Subexcitation electrons				7.8[g]
			Total energy used	97.2

[a]Per 100 eV of energy absorbed.
[b]Calculated from the second differential ionization efficiency curves for NO (34).
[c]Calculated from the ion pair yield (35) and the relative ionization cross sections for 100 eV electrons (36).
[d]Taken arbitrarily as 2 eV above threshold.
[e]Calculated from the relative dissociation cross sections for 100 eV electrons for the various electronic states (38).
[f]G(obs) − G(dissociative ionization).
[g]Minimum excitation energy × G(ion pair)/3 (1).

of NO_3 3.7 eV (17), in neither case will there be enough neutralisation energy available for the dissociation of NO. Thus our N_2 yields, the lifetimes of NO^+ and the electron, and the above energy considerations are all consistent with no dissociation of NO in reaction 10.

The irradiations with Xe were done to provide further support for this mechanism. If charge transfer from Xe to NO is assumed then as the ion pair yield in Xe is 4.5 (31) and its density is higher the amount of NO^+ formed in a 90 mol% Xe, 10 mol% NO mixture will be about four times that in pure NO. The lifetimes of NO^+ and the electron with respect to addition to NO should be increased by a factor of 100. The values in Table 3 show that NO^+ and the electron should then be neutralised before adding to NO. The difference between the yield of nitrogen due to energy absorbed by the Xe in the mixtures without and with SF_6, $\Delta G(N_2)_{Xe} = 5.3 - 1.45 = 3.8 \pm 0.5$, confirms that reaction 9 is dissociative and this dissociation is suppressed by the addition of SF_6 or by the formation of dimer ions.

The results of Hatano and Shimamori (32) suggest a large reduction in the effective rate constant for electron attachment to SF_6 from that for thermal electrons in the irradiation of N_2O–Xe mixtures. We have found, however, that in Febetron irradiations of O_2 with the rare gases (33) that 1 mol% SF_6 appears to scavenge all the electrons in O_2–Xe mixtures containing as little as 6 mol% O_2. We should expect similar behaviour in NO–Xe mixtures.

Dose Dependence

Our yields give $G(N_2) = 3.6 \pm 0.3$ between $\sim 3 \times 10^{20}$ and 7×10^{20} eV g^{-1} and those of ref. 2 give $G(N_2) = 3.45 \pm 0.35$ between 6×10^{20} and 6×10^{21} eV g^{-1}. The reason for this decrease from the initial yield of $G(N_2) = 4.5$ is not clear.

Taking $G(NO_2) = 10$ the ratio of NO_2 to NO at 6×10^{20} eV g^{-1} is only 0.003. This does not appear to be high enough to reduce the yield of N_2 from reaction 13 nor to affect the yield of N atoms from ionic processes. It is possible that NO_2 suppresses the dissociation of excited NO but the efficiency of this quenching would have to be very high.

Energy Balance

The energy balance estimates are given in Table 4. The ion yields are quite precisely known from W value measurements and mass spectra. Assuming that the neutral dissociative excitation yield obtained from the radiation chemical yields is accurate the major problems are the calculations of the average energies in ionization and excitation. We have previously (1) arbitrarily taken the former as 2 eV above the threshold but the data in ref. 34 appear to give a much more reliable value than this. The absolute values of the cross sections in ref. 38 when taken in conjunction with the absolute cross sections for ionization (36) and G(ion pair) = 3.64 give $G(NO \rightarrow N + O) = 1.4$. Although this is apparently 2.5 times smaller than the correct value the error in the relative cross sections should be much less.

Conclusions

The neutralisation of the dimer ion $(NO)_2^+$ by an electron, NO^-, or NO_2^- does not result in the formation of N_2. In agreement with previous work the neutralisation of NO^+ by an electron is dissociative. This dissociation is suppressed when the negative ion is SF_6^-.

The total energy absorbed in the radiolysis of NO can be accounted for by the ion pair yields and radiation chemical yields, the average energies of ionization and neutral excitation and the energy of formation of subexcitation electrons.

1. C. WILLIS and A. W. BOYD. Int. J. Radiat. Phys. Chem. **8**, 71 (1976) and references therein.
2. P. HARTECK and S. DONDES. J. Chem. Phys. **27**, 546 (1957).
3. C. J. HOCHANADEL, J. A. GHORMLEY, and P. J. OGREN. J. Chem. Phys. **50**, 3075 (1969).

Can. J. Chem. Downloaded from www.nrcresearchpress.com by 210.87.254.5 on 09/05/12
For personal use only.

4. C. WILLIS, A. W. BOYD, and D. A. ARMSTRONG. Can. J. Chem. **47**, 3783 (1969).
5. C. WILLIS, O. A. MILLER, A. E. ROTHWELL, and A. W. BOYD. Adv. Chem. Ser. **81**, 539 (1968).
6. C. WILLIS, A. W. BOYD, and O. A. MILLER. Radiat. Res. **46**, 428 (1971).
7. S. TAKAO, S. SHIDA, Y. HATANO, and H. YAMAZAKI. Bull. Chem. Soc. Jpn. **41**, 2221 (1968).
8. C. WILLIS, A. W. BOYD, M. J. YOUNG, and D. A. ARMSTRONG. Can. J. Chem. **48**, 1505 (1970).
9. J. A. GHORMLEY, C. J. HOCHANADEL, and J. W. BOYLE. J. Chem. Phys. **50**, 419 (1969).
10. A. W. BOYD, D. A. ARMSTRONG, C. WILLIS, and O. A. MILLER. Radiat. Res. **40**, 255 (1969).
11. P. D. GOLDAN, A. L. SCHMELTEKOPF, F. C. FEHSENFELD, H. I. SCHIFF, and E. E. FERGUSON. J. Chem. Phys. **44**, 4095 (1966).
12. D. B. DUNKIN, M. MCFARLAND, F. C. FEHSENFELD, and E. E. FERGUSON. J. Geophys. Res. **76**, 3820 (1971).
13. D. B. DUNKIN, F. C. FEHSENFELD, A. L. SCHMELTEKOPF, and E. E. FERGUSON. J. Chem. Phys. **49**, 1365 (1968).
14. F. C. FEHSENFELD, E. E. FERGUSON, and M. MOSESMAN. Chem. Phys. Lett. **4**, 73 (1969).
15. L. J. PUCKETT and M. W. TEAGUE. J. Chem. Phys. **54**, 2564 (1971).
16. D. A. PARKES and T. M. SUGDEN. J. Chem. Soc. Faraday Trans. II, **68**, 600 (1972).
17. M. MCFARLAND, D. B. DUNKIN, F. C. FEHSENFELD, A. L. SCHMELTEKOPF, and E. E. FERGUSON. J. Chem. Phys. **56**, 2358 (1972).
18. J. P. DOERING and B. H. MAHAN. J. Chem. Phys. **36**, 669 (1962).
19. C. S. WELLER and M. A. BIONDI. Phys. Rev. **172**, 198 (1968).
20. F. C. FEHSENFELD. J. Chem. Phys. **53**, 2000 (1970).
21. F. C. FEHSENFELD, E. E. FERGUSON, and D. K. BOHME. Planet. Space Sci. **17**, 1759 (1969).
22. L. F. PHILLIPS and H. I. SCHIFF. J. Chem. Phys. **36**, 1509 (1962).
23. K. H. BECKER, W. GROTH, and D. THRAN. Chem. Phys. Lett. **15**, 215 (1972).
24. A. A. WESTENBERG and N. DEHAAS. J. Chem. Phys. **50**, 707 (1969).
25. A. B. HARKER and H. S. JOHNSTON. J. Phys. Chem. **77**, 1153 (1973).
26. L. F. PHILLIPS and H. I. SCHIFF. J. Chem. Phys. **42**, 3171 (1965).
27. Y.-J. SHIU and M. A. BIONDI. Phys. Rev. A**16**, 1817 (1977).
28. C. Y. NG, P. W. TIEDEMANN, B. H. MAHAN, and Y. T. LEE. J. Chem. Phys. **66**, 3985 (1977).
29. M. SAPOROSCHENKO. J. Chem. Phys. **49**, 768 (1968).
30. E. HERBST, T. A. PATTERSON, and W. C. LINEBERGER. J. Chem. Phys. **61**, 1300 (1974).
31. I. T. MYERS. Radiation dosimetry. Vol. 1. Fundamentals. *Edited by* F. H. Attix and W. C. Roesch. Academic Press, New York. 1968. Chapt. 7.
32. Y. HATANO and H. SHIMAMORI. J. Phys. Chem. **78**, 954 (1974).
33. A. W. BOYD, O. A. MILLER, and E. B. SELKIRK. Can. J. Chem. **55**, 203 (1977).
34. J. D. MORRISON. J. Chem. Phys. **22**, 1219 (1954).
35. G. G. MEISELS. J. Chem. Phys. **41**, 51 (1964).
36. L. J. KIEFFER and G. H. DUNN. Rev. Mod. Phys. **38**, 1 (1966) and references therein.
37. H. D. HAGSTRUM. Rev. Mod. Phys. **23**, 185 (1951).
38. L. S. POLAK and D. I. SLOVETSKY. Int. J. Radiat. Phys. Chem. **8**, 257 (1976).

Can. J. Chem. Downloaded from www.nrcresearchpress.com by 210.87.254.5 on 09/05/12
For personal use only.

Formation and reactivity of the aminothiyl and iminothiyl radicals by means of flash photolysis

OSAMU ITO AND MINORU MATSUDA

Chemical Research Institute of Non-aqueous Solutions, Tohoku University, Katahira, Sendai 980, Japan

Received October 14, 1977

OSAMU ITO and MINORU MATSUDA. Can. J. Chem. **56**, 1080 (1978).

Flash photolysis of bis[piperidyl-1] disulfide gave a clear transient band at 340 nm and a weak band around 525 nm, which were assigned to the piperidyl-1-thiyl radical. In a similar manner, bis[diphenylimino] disulfide gave a transient band at 420 nm, which could be assigned to the diphenyliminothiyl radical. These radicals disappeared in various solvents according to second-order kinetics with rate constant 0.8–7.2 × 10^9 M^{-1} s^{-1} showing that the radicals decay predominantly by recombination with diffusion controlled rates. These radicals were not reactive toward oxygen, olefins, organophosphorous compounds, and hydrogen donors in agreement with the results given by the kinetic epr study reported by Maillard and Ingold.

OSAMU ITO et MINORU MATSUDA. Can. J. Chem. **56**, 1080 (1978).

La photolyse éclair du bis[pipéridyl-1] disulfure conduit à une bande transitoire claire à 340 nm et à une bande faible autour de 525 nm qui ont été attribuées au radical pipéridyl-1 thiyle. D'une façon semblable, le bis[diphénylimino] disulfure conduit à une bande transitoire à 420 nm qui peut être attribuée au radical diphényliminothiyle. Ces radicaux disparaissent dans divers solvants d'après une cinétique du second ordre avec une constante de vitesse allant de 0.8–7.2 × 10^9 M^{-1} s^{-1} montrant que les radicaux disparaissent principalement par une recombinaison avec des vitesses contrôlées par la diffusion. Ces radicaux ne sont pas réactifs vis-à-vis l'oxygène, les doubles liaisons, les composés organophosphoriques et les donneurs d'hydrogène en accord avec les résultats rapportés pour l'étude cinétique rpe de Maillard et Ingold.

[Traduit par le journal]

Introduction

Dialkylaminothiyl radicals, $R_2NS\cdot$, the sulfur analogues of the dialkylnitroxide radical, have been detected by epr spectroscopy during the thermolysis (1, 2) or photolysis (3) of the corresponding disulfides. From the observed hyperfine coupling constants on nitrogen, the spin distributions were compared with those of nitroxide radical. Using kinetic epr spectroscopy, a useful technique for the kinetic study of radicals, Maillard and Ingold (3) investigated the kinetic behavior of dialkylaminothiyl radicals. The purpose of this study was to obtain the electronic absorption spectra of the aminothiyl radical for comparison with those of nitroxide radical and to estimate their reactivity by means of the flash kinetic spectroscopy. The diphenyliminothiyl radical ($(Ph)_2C{=}N{-}S\cdot$) was also studied.

Experimental

Bis[piperidyl-1] disulfide (ASSA) and bis[diphenylimino] disulfide (ISSI) were prepared by literature methods (3). All the solvents used were spectrophotometric grade. The solutions were degassed, when it was necessary, up to 10^{-5} Torr. A flash photolysis apparatus of standard design (4) delivered a flash with an energy of up to 100 J from xenon-filled flash lamps which exhibited a half-peak duration of 20 μs. The quartz irradiation vessel was 10 cm long and 1 cm in diameter and had optically flat quartz windows at both ends.

Results and Discussion

In Fig. 1, the electronic absorption spectra of disulfides, ASSA and ISSI, are shown. Flash photolyses were made with a band pass filter, which transmits the light between 240 and 400 nm, and appropriate cut-off filters were used so as to avoid the excitation of the solvents and substrates when they were added.

Flash photolysis of ASSA gave a transient absorption spectrum as shown in Fig. 2*a* in which a clear peak was seen at 340 nm and a weak one around 525 nm. Both bands could be observed in both polar and nonpolar solvents. This indicates that the transient species in Fig. 2*a* were not due to the cationic species such as $ASSA^{\ddagger}$ and $AS^{\ddagger}$ which may be formed by the photoejection of an electron from disulfide. The bathochromic shift of the absorption maximum around 340 nm was observed in polar solvents. The slight increase in intensity of this band in polar solvents was also observed. This will be discussed later.

Triplet–triplet transitions also could be ruled out, since these bands were observed even in aerated solutions. Therefore, it is permissible to assign the entity appearing at 340 nm to a free radical species. As possible transient species other than AS· the

Can. J. Chem. Downloaded from www.nrcresearchpress.com by 210.87.254.42 on 09/05/12
For personal use only.

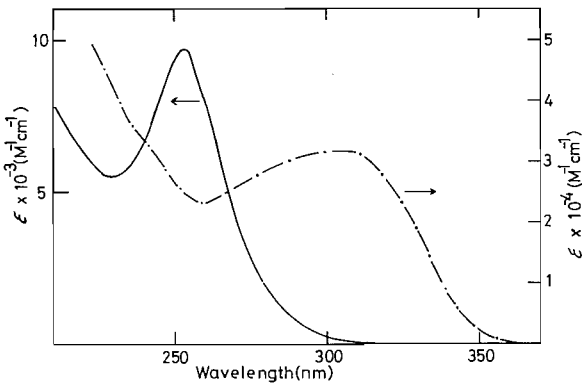

FIG. 1. Absorption spectra of disulfides: bis[piperidyl-1] disulfide (—) and bis[diphenylimino] disulfide (---).

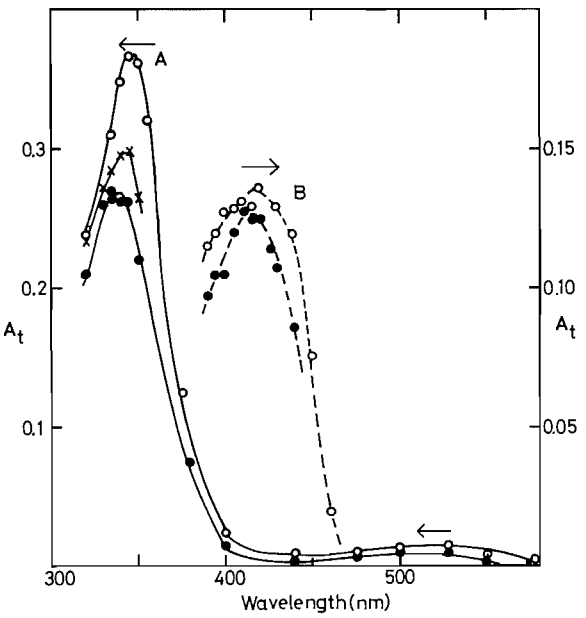

FIG. 2. Transient absorption spectra obtained by the flash photolysis of disulfides plotted at 50 μs after flash. (*a*) Bis-[piperidyl-1] disulfide (2.2×10^{-4} *M*) in aerated methylene chloride (—○—), degassed ethanol (—×—), and aerated *n*-hexane (—●—). (*b*) Bis[diphenylimino] disulfide (7.5×10^{-5} *M*) in aerated methylene chloride (--○--) and cyclohexane (--●--).

unsymmetrical homolytic scission products, A· or ASS·, must also be taken into consideration.

The transient which was tentatively identified as the piperidino radical, A·, produced from *N*-chloropiperidine in neutral aqueous solution was studied recently with the flash photolysis technique by Cessna *et al.* (5). They reported a weakly absorbing transient which decayed by second-order kinetics with $k/\varepsilon_{330\ nm} = 5.1 \times 10^6$ cm s^{-1}. In our study each transient band which appeared at 340 nm in the ASSA solutions also decayed according to the second-order kinetics as shown in Fig. 3, but the slope in the plot for 1/absorbance at 330 nm against time in ethanol gave $k/\varepsilon_{330\ nm}$ of $5.0 \pm 0.7 \times 10^5$ cm s^{-1}, which is one order of magnitude smaller than that for A·. Thus, A· could not be attributed to the transient bands in Fig. 2*a*. As for ASS·, this was not detected in the epr study by Maillard and Ingold of the photolysis of the solution. In the case of dialkyl disulfide (RSSR), it is shown that RSS· could be formed only by the direct (not sensitized) photolysis with short wavelength light such as 195 nm (6). Absorption maxima of RS· having amino acid group on the side chains were reported around 330 nm by means of pulse radiolysis (7, 8), which are in a region similar to the band given in Fig. 2*a*. Furthermore, since the kinetic behavior of the 340 nm band, as described later, agrees with that of AS· given by kinetic epr study, the band at 340 nm can be assigned safely to AS·. Thus, in the photolysis of ASSA reaction 1 may be the main process and other reactions 2–4 could be ruled out in our flash photolysis experiments.

$$[1] \quad \text{ASSA} \overset{h\nu}{\rightleftharpoons} 2\text{AS}\cdot$$

$$[2] \quad \text{ASSA} \overset{h\nu}{\rightharpoonup} \text{ASSA}^{T}$$

$$[3] \quad \text{ASSA} \overset{h\nu}{\rightharpoonup} \text{ASSA}^{+} \text{ (or } \text{AS}^{+} + \text{AS}\cdot) + e^{-}_{solv}$$

$$[4] \quad \text{ASSA} \overset{h\nu}{\rightharpoonup} \text{A}\cdot + \text{ASS}\cdot$$

Maillard and Ingold reported that the rate constant for the recombination (k_r) of AS· in a viscous solvent, *tert*-butylbenzene (η = 38.13 cP at 20°C) is 8.2×10^8 M^{-1} s^{-1} at 23°C with kinetic epr measurements (3). From the flash photolysis technique, only k_r/ε could be observed for the second-order process. In liquid paraffin (η = 21.78 cP), $k_r/\varepsilon_{335\ nm}$ was given as $1.1 \pm 0.1 \times 10^5$ cm s^{-1}. Assuming k_r in liquid paraffin is equal to the value in *tert*-butylbenzene given by epr, ε at absorption maximum (λ_{max}) could be calculated as 7500 ± 800 M^{-1} cm^{-1}. For the dialkylnitroxide radical, two absorption bands have been reported; a strong band at 230–240 nm (ε = 2000–3000 M^{-1} cm^{-1}) and a weak band at 430–450 nm (ε = 5 M^{-1} cm^{-1}) (9). Although the absorption band around 525 nm shown in Fig. 2*a* was not subjected to kinetic analysis because of low intensity, it may be expected that the absorption spectra of AS· and nitroxide radical resemble each other. Supposing that the weak 525 nm band, which may correspond to the weak band at 430–450 nm of nitroxide radical, was due to AS·, ε at this region was calculated from the relative absorbance as less

Can. J. Chem. Downloaded from www.nrcresearchpress.com by 210.87.254.42 on 09/05/12
For personal use only.

Can. J. Chem. Downloaded from www.nrcresearchpress.com by 210.87.254.42 on 09/05/12
For personal use only.

TABLE 1. Second-order rate constants for recombination reaction of the piperidyl-1-thiyl radical in various solvents

Solvent	η^a (cP)	$\lambda_{max}{}^b$ (nm)	$k_r/\varepsilon_{max} \times 10^{-5}$ [c] (cm s^{-1})	$k_r \times 10^{-9}$ [d] (M^{-1} s^{-1})	$k_D \times 10^{-9}$ [e] (M^{-1} s^{-1})
1. Diethyl ether	0.242	340	9.6	7.2	26.9
2. *n*-Hexane	0.313	335	8.1	6.1	20.8
3. Acetonitrile	0.345	345	6.7	5.0	18.9
4. Methylene chloride	0.449	347	5.0	2.2	14.4
5. Methanol	0.551	345	5.7	3.8	11.8
6. Cyclohexane	0.980	330	4.2	3.2	6.8
7. Ethanol	1.078	345	4.6	3.5	5.6
8. Liquid paraffin	21.78	335	1.1	0.8	3.2

[a]Viscosity at 23°C.
[b]Estimated error is within ±3 nm.
[c]Estimated error is within ±10%.
[d]Calculated using $\varepsilon_{max} = 7500\ M^{-1}\ cm^{-1}$.
[e]Calculated second-order diffusion rate constant.

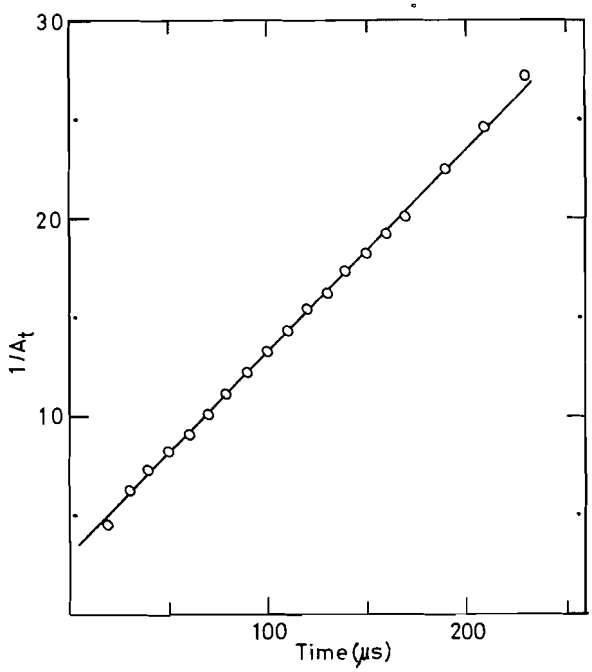

FIG. 3. Second-order plot of the decay at 350 nm of AS· obtained by the flash photolysis of ASSA in aerated cyclohexane: A_t is absorbance at 350 nm.

than 300 M^{-1} cm^{-1}. These comparisons may indicate that by replacement of oxygen in nitroxide radical by sulfur, absorption maxima shift to longer wavelength and intensities increase. This similarity of spectra also supports the assignment of the transient spectra to AS·.

In a similar manner, the transient spectra were given by the flash photolysis of ISSI as shown in Fig. 2*b*. This transient band was observed even in aerated solution and in nonpolar solvent. Thus, this transient band can be attributed to IS· with the same reasons described in the section of AS·. The second-order plot was a straight line giving k_r/ε. Although the absorption spectrum of IS· should be compared with that of the diphenylmethylenenitroxide radical, $(Ph)_2C{=}N{-}O\cdot$, the spectrum of this radical has not been reported. The fact that the absorption maximum of IS· is longer wavelength than the main band of AS· (340 nm) may suggest that an unpaired electron in IS· is delocalized onto π-orbitals.

Both radicals, AS· and IS·, do not react with oxygen dissolved in the solvents (ca. 10^{-3} *M*) (10). With olefins such as hexene-1 (<1 *M*), no promoted decay of the radicals was observed. In the presence of styrene (0.05 *M*), since the absorption of ASSA overlapped with that of styrene, formation of AS· was suppressed. On the other hand, IS· was formed even in the system containing styrene and the decay rate was not affected. Organophosphorous compounds (<0.1 *M*) such as trimethylphosphite and triethylphosphate which are known as effective radical scavengers also did not exhibit any influence on the decay curves of both radicals. Hydrogen donors (ca. 1 *M*) such as toluene, cumene, and tri-*n*-butyltin hydride also did not have any effect on the decay rates. These observations are in agreement with the results obtained by the kinetic epr study by Maillard and Ingold (3).

AS· and IS· are not reactive toward various substrates and decay with recombination reactions as was suggested from Fig. 3. Plotting of k_r/ε_{max} against 1/viscosity gave straight lines as shown in Fig. 4. This linear relationship suggests that the recombination reaction is diffusion controlled and that ε was not affected much by solvent properties such as viscosity and polarity. Thus, k_r for AS· could be calculated using $\varepsilon = 7500\ M^{-1}\ cm^{-1}$ estimated in liquid paraffin, which were summarized in Table 1. In the last column in the table, the calculated rate constants (k_D) from the Debye equation for second-order diffusion controlled reaction (11), $k_D = 8RT/3000\eta$, are listed. As usually indicated, the

TABLE 2. Second-order rate constants for the recombination reaction of the diphenyliminothiyl radical in various solvents

Solvent	λ_{max}[a] (nm)	$k_r/\varepsilon_{max} \times 10^{-5}$[b] (cm s^{-1})	$k_r \times 10^{-9}$[c] (M^{-1} s^{-1})	$k_D \times 10^{-9}$ (M^{-1} s^{-1})
Methylene chloride	420	8.9	4.5	14.4
Cyclohexane	415	5.5	2.8	6.8
Liquid paraffin[d]	415	1.6	0.8	3.2

[a]Estimated error is within ±3 nm.
[b]Estimated error is within ±10%.
[c]Calculated using $\varepsilon_{max} = 5000\ M^{-1}\ cm^{-1}$.
[d]Methylene chloride (2%) was added.

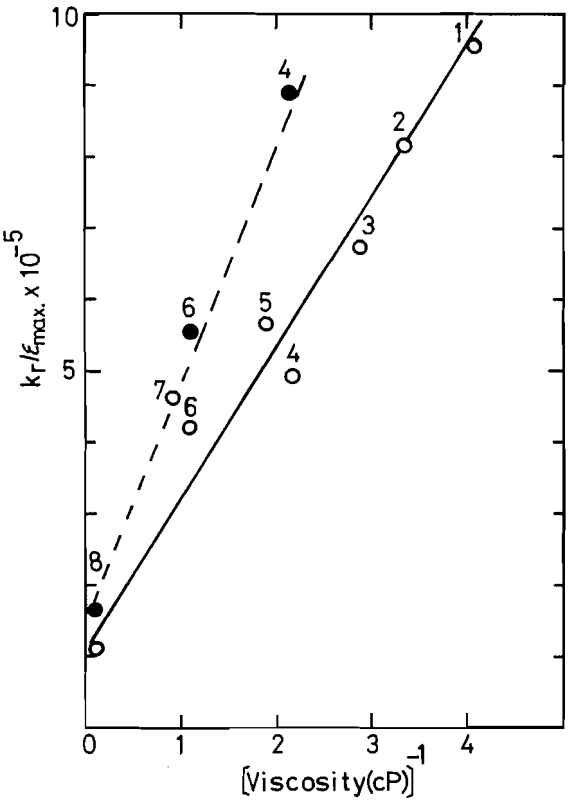

FIG. 4. Plots of k_r/ε_{max} against 1/[viscosity (cP)]. Solvents 1–8 refer to Table 1.

calculated rate constants are about 4 times larger than experimentally obtained ones. As was seen in Fig. 2*a*, intensities of the band of AS· around 340 nm observed in polar solvents such as methylene chloride were considerably larger than those in nonpolar solvents such as *n*-hexane and cyclohexane. The following three factors must be taken into consideration for this reason: high quantum yield for the formation of AS·, large ε value of AS· by the specific interaction with polar solvents, and slow recombination rate in polar solvents. Since this tendency is not dependent both on the deviation of k_r/ε_{max} from the straight line of Fig. 4 and on the k_r value in Table 1, the latter two factors may be discarded.

For IS·, although k_r has not been estimated by the kinetic epr spectroscopy, it may be expected that reactivity is very similar to that of AS· including recombination reaction rate. Assuming that the rate constant for recombination of IS· in paraffin is nearly equal to that of AS·, $k_r \approx 0.8 \times 10^9\ M^{-1}\ s^{-1}$, ε at 415 nm of IS· could be calculated as $5000\ M^{-1}\ cm^{-1}$ and the values of k_r in other solvents are given in Table 2. Since it is well known that the thiyl radicals recombine with diffusion controlled rate (7, 8), it is likely that AS· and IS· resemble RS· rather than the nitroxide radicals.

Acknowledgements

We are grateful to Dr. M. Iino and Mr. S. Shioya of Tohoku University for their useful suggestions and discussions.

1. J. E. BENNETT, H. SPIEPER, and P. TAVS. Tetrahedron, **23**, 1697 (1967).
2. W. C. DANEN and D. D. NEWKIRK. J. Am. Chem. Soc. **98**, 516 (1976).
3. B. MAILLARD and K. U. INGOLD. J. Am. Chem. Soc. **98**, 520 (1976).
4. G. PORTER and M. A. WEST. *In* Techniques of chemistry. Vol. 4. *Edited by* A. Weissberger. John Wiley and Sons, New York, NY. 1974. p. 367.
5. A. J. CESSNA, S. E. SUGAMORI, R. W. YIP, M. P. LAU, R. S. SNYDER, and Y. L. CHOW. J. Am. Chem. Soc. **99**, 4044 (1977).
6. A. B. CALLEAR and D. R. DICKSON. Trans. Faraday Soc. **66**, 1987 (1970).
7. M. Z. HOFFMAN and E. HAYON. J. Am. Chem. Soc. **94**, 7950 (1972).
8. J. W. PURDIE, H. A. GILLIS, and N. V. KLASSEN. Can. J. Chem. **51**, 3132 (1973).
9. T. KAWAMURA, S. MATSUNAMI, and T. YONEZAWA. Bull. Chem. Soc. Jpn. **40**, 1111 (1967).
10. S. L. MUROV. Handbook of photochemistry. Marcel Dekker, New York. NY. 1973. p. 89.
11. K. U. INGOLD. *In* Free radicals. Vol. 1. *Edited by* J. K. Kochi. John Wiley and Sons, New York, NY. 1973. p. 37.

Can. J. Chem. Downloaded from www.nrcresearchpress.com by 210.87.254.42 on 09/05/12
For personal use only.

Heterogeneous metal-insertion: a novel reaction with porphyrins

OTTO HERRMANN, S. HUSAIN MEHDI, AND ALFIO CORSINI
Department of Chemistry, McMaster University, Hamilton, Ont., Canada L8S 4M1
Received December 16, 1977

OTTO HERRMANN, S. HUSAIN MEHDI, and ALFIO CORSINI. Can. J. Chem. **56**, 1084 (1978).

Metal complexes of water-soluble and other porphyrins have been prepared by a heterogeneous reaction with the metal reactant present in an insoluble form. The oxidation state of the metal is important in the reactions. Metal reactants in the lower oxidation states (0, I, II) react with porphyrins but those in the higher oxidation states (III, IV) do not. Metalloporphyrins of high purity may be conveniently prepared by this method.

OTTO HERRMANN, S. HUSAIN MEHDI et ALFIO CORSINI. Can. J. Chem. **56**, 1084 (1978).

On a préparé, par une réaction hétérogène avec le métal réactif présent sous une forme insoluble, des complexes métalliques de porphyrines dont quelques uns sont solubles dans l'eau. L'état d'oxydation du métal est important dans les réactions. Les métaux réactifs dans des états d'oxydation peu élevés (0, I, II) réagissent avec les porphyrines alors que ceux qui existent dans des états d'excitation plus élevés (III, IV) ne réagissent pas. On peut facilement préparé des métalloporphyrines de grande pureté par cette méthode.

[Traduit par le journal]

Introduction

The biological importance of certain metalloporphyrins (1) and the variety of interesting and useful properties that they exhibit (2, 3) make metalloporphyrins a widely studied class of compounds. To date, complexes of porphyrins with over fifty metals and semi-metals have been prepared (3). The methods for preparing metalloporphyrins depend upon the nature of the metal to be inserted and, to a lesser extent, upon the type of porphyrin to be used. In general, however, these preparative procedures involve refluxing the porphyrin with a suitable soluble metal salt or metal complex in an appropriate solvent (4*a*, *b*, 5). We wish to report on a novel heterogeneous reaction for the formation of metalloporphyrins in which the metal to be inserted is present in an insoluble form rather than in solution with the porphyrin.

The heterogeneous metal insertion reaction can be carried out using metal oxides, free metals, metal sulphides, and other insoluble metal salts (e.g., Cu_2Cl_2) in water or in non-aqueous solvents. The method has been used successfully to prepare metal complexes of *meso*-tetra(*p*-sulphophenyl) porphine ($TPPS_4$), hematoporphyrin (HP), protoporphyrin IX dimethyl ester (PPDME), octaethylporphine (OEP), and *meso*-tetraphenylporphine (TPP). This type of metalloporphyrin formation reaction has the immediate advantage over the more conventional methods in that the excess metal reactant can be removed from the product by simple filtration of the solid phase rather than by the tedious methods, often in combination, of extraction, precipitation, dialysis, and chromatography.

Experimental

TPP was prepared as described by Adler *et al.* (6) and sulphonated by the method of Fleischer *et al.* (7). The ammonium salt obtained was purified and converted to the sodium salt by cation exchange. $HP(HCl)_2$, PPDME (both Fluka 'purum'), and OEP (Strem) were used as obtained except that the dihydrochloride was neutralized by dilute alkali before use. Metals and metal oxides of high purity were obtained from Alfa-Ventron, or Fisher Scientific and used as such.

The metallation reaction was carried out as follows. About 50 mg of $TPPS_4$ was added to 100 ml of refluxing distilled, deionized water containing 0.5–1 g of metal oxide or metal. The metal oxide was usually in the form of finely divided powder and the free metal in the form of powder, lumps, turnings, or pellets. In general, since the metals were not as finely divided as the oxides, larger quantities of the former were used. Before the metal was used, its surface was etched with a small amount of dilute hydrochloric acid to dissolve any oxide layer that may have formed and then washed thoroughly with water to remove the acid. Ag and Pb were etched with dilute nitric acid. The mixture was refluxed and kept well stirred for up to 3 days during which time small aliquots were withdrawn to monitor the progress of the reaction spectrophotometrically. Most reactions were complete within 1 h as judged from the change from the four-band visible-range spectrum of the free porphyrin to a two-band spectrum of the metalloporphyrin, and also from the non-appearance of the intense Soret absorption peak at 434 nm corresponding to the porphyrin diacid on addition of acid to the reaction mixture. The latter test is not applicable to the less stable Mg and Ca complexes. The slowest of the successful metallation reactions was with SnO and took about 48 h to reach completion. Collection of the excess solid phase on a 0.22 μ Millipore filter and evaporation of the aqueous filtrate under reduced pressure yielded the metalloporphyrin which was subsequently dried at 120°C *in vacuo*. In the preparation of the $AgTPPS_4$ complex, the mixture of Ag_2O and $TPPS_4$ in water was simply stirred for 2 h at room temperature as refluxing the mixture caused the oxide to peptize, thus rendering it difficult to filter.

A similar procedure was applied to the synthesis of metallo-

Can. J. Chem. Downloaded from www.nrcresearchpress.com by 210.87.254.5 on 09/05/12
For personal use only.

TABLE 1. Elemental analyses of $TPPS_4$ and its metal complexes

Compound	Formula	Calculated (%)					Found (%)				
		C	H	N	S	M	C	H	N	S	M
$TPPS_4$	$C_{44}H_{26}N_4S_4O_{12}Na_4$	51.66	2.56	5.48	12.54	8.99 (Na)	51.61	2.54	5.51	12.37	8.83 (Na)
$CuTPPS_4$	$C_{44}H_{24}N_4S_4O_{12}Na_4Cu$	48.73	2.23	5.17	11.83	5.86 (Cu)	48.27	2.73	5.12	11.35	5.72 (Cu)
$ZnTPPS_4$	$C_{44}H_{24}N_4S_4O_{12}Na_4Zn$	48.65	2.23	5.16	11.81	6.02 (Zn)	48.15	2.53	5.18	11.31	6.50 (Zn)
$CoTPPS_4$	$C_{44}H_{24}N_4S_4O_{12}Na_4Co$	48.94	2.24	5.19	11.88	—	48.51	2.45	5.25	11.37	—
$NiTPPS_4$	$C_{44}H_{24}N_4S_4O_{12}Na_4Ni$	48.95	2.24	5.19	11.88	—	48.56	2.71	5.33	9.17	—
$CdTPPS_4$	$C_{44}H_{24}N_4S_4O_{12}Na_4Cd$	46.63	2.13	4.94	11.32	—	46.70	2.63	5.06	11.11	—

porphyrins in organic solvents. For HP, methanol, DMF, or an aqueous alkaline solution were found suitable as solvents for the metallation although the reaction in methanol took somewhat longer to reach completion (e.g., 24 h for CuO), presumably because of the lower reflux temperature. DMF was also used as a solvent for PPDME reactions and mixtures of DMF and chloroform containing 50–75% v/v DMF were found to be suitable for TPP and OEP.

Elemental analyses were performed on selected metal complexes of $TPPS_4$. The highly hygroscopic nature of these complexes and our inability to isolate definite crystalline hydrates made the conventional handling of these compounds for analysis difficult. Thermograms of these complexes were taken (on a Stanton Redcroft TG-750 thermobalance) to determine their water content and their thermal stability. The results showed that the water content varied with the ambient conditions. For example, the $ZnTPPS_4$ complex was found to contain as much as 27.5% H_2O, corresponding to 16.6 mol of water per mole of complex. Gradual weight loss occurred in all the complexes up to about 220°C. Between 220–400°C, an almost constant-weight region was observed. Above 400°C, rapid decomposition occurred. Metal complex samples for analysis were therefore weighed on the thermobalance at 250°C. In addition to analyses for C, H, N, and S, metal determinations were made on the Cu and Zn complexes of $TPPS_4$. About 10 mg of sample was wet-ashed with a 3:1:1 mixture of H_2SO_4, HNO_3, and $HClO_4$ and the metal ion then titrated with standard EDTA. The results of the elemental analyses are presented in Table 1.

Results and Discussion

The high values for % H in the elemental analyses (Table 1) are due to the rapid adsorption of moisture by the complexes after removal from the thermobalance. The values of % C, S, and N remain unaffected by the adsorption of varying amounts of moisture after the samples have been pre-weighed on a thermobalance. Elemental analyses of the other metalloporphyrins prepared in this work were not carried out but evidence of metallation was obtained as described earlier and also by comparison of the visible-region spectrum of the metalloporphyrins with those reported in the literature (4*c*, 9).

Nearly 50 metals or metal oxides were tested for reactivity with $TPPS_4$. The results are summarized in Tables 2 and 3.

As shown by Table 2, primarily only divalent metal oxides reacted with the porphyrin. (Ag_2O, Cu_2Cl_2, CuS, and $PdBr_2$ were also found to react.) None of the trivalent, tetravalent, or mixed M(II)–M(III) oxides (e.g., Fe_3O_4, Ni_3O_4) were reactive. Although certain M(III) species are known to react with porphyrins in solution (10), these reactions are extremely slow because of the high activation energy required to desolvate the metal ion. The higher lattice energy of the M(III) and higher oxides (~2000–4000 kcal/mol vs. ~1000 kcal/mol for the divalent metal oxides (11)) is probably the reason for their lack of reactivity with $TPPS_4$ in the heterogeneous reaction. It appears, however, that such thermodynamic criteria as the lattice energy of the metal oxide and the stability of the metalloporphyrin are

TABLE 2. Reactivity of metal oxides with $TPPS_4$

Metalloporphyrin formed		No observed reaction*		
MgO	ZnO	BeO	Mn_2O_3	RuO_2
CaO	CdO	BaO	MnO_2	In_2O_3
MnO	HgO	TiO	Fe_2O_3	La_2O_3
CoO	PbO	PdO	Fe_3O_4	Bi_2O_3
NiO	SnO	Sc_2O_3	Ni_3O_4	
CuO	Ag_2O	Cr_2O_3	ZrO_2	

*For 72 h at 100°C.

TABLE 3. Reactivity of metal with $TPPS_4$

Metalloporphyrin formed		No observed reaction*	
Cr	Zn	Ti	Ag
Mn	Cd	V	Sb
Fe	Hg	Ni	W
Co	Sn	Nb	Bi
Cu	Pb	Ru	Au

*For 72 h at 100°C.

Can. J. Chem. Downloaded from www.nrcresearchpress.com by 210.87.254.5 on 09/05/12
For personal use only.

Can. J. Chem. Downloaded from www.nrcresearchpress.com by 210.87.254.5 on 09/05/12
For personal use only.

not the only factors that govern the reactivity of the metal oxide with the porphyrin. It is curious that neither PdO (which has a structure similar to that of CuO (12)) nor PdS reacted even though $PdTPPS_4$ is known to be among the most stable of the metalloporphyrins and is readily formed from $PdBr_2$. Perhaps kinetic considerations, governed by the surface properties of the solid, are also involved.

The reactivities of the metallic elements (Table 3) are even more capricious and do not correlate with standard reduction potentials. For example, Ni and Ag did not react (their oxides did) but several elements whose standard electrode potentials are between those of Ni and Ag did react. Ni and Ag were non-reactive even when present in large quantities as a fine powder with a surface area at least as great as in some of the other cases where metalloporphyrin formation was observed.

In spite of prior etching of the metal surface to remove any oxide layers, it is still possible, for at least some of the metals tested, that the reactive species is not the free metal but some other species formed on the metal surface, such as a hydrous oxide. This is certainly true for the reactions of Fe and Mn in which a coating was immediately formed on the metal surface upon the addition of water. With Mn, the formation of the reactive green oxide was readily observed and reaction with the porphyrin followed. In the case of Fe, the reactive species is probably the transitory hydrated ferrous oxide since the higher oxide was found to be unreactive with the porphyrin (Table 2). Thus, the only way to prepare the iron porphyrin heterogeneously is through reaction with the metal. Certain oxide films render the metal unreactive. Cr metal reacted with the porphyrin only after treatment with dilute hydrochloric acid. Use of sulphuric acid rendered the metal unreactive.

Spectral properties of metalloporphyrins formed by the heterogeneous reaction showed that the oxidation state of the metal in the complex is that which is usually stabilized by the porphyrin (13). Thus, Ag(II), Fe(III), Cr(III), and Mn(III) are all cases where the higher oxidation state is stabilized. The oxidation state of Sn in $SnTPPS_4$ is not certain. Its stability to 1 *M* hydrochloric acid suggests that it is a Sn(IV) complex (13). In the remaining complexes, including that of Co, the metal was in the divalent state.

With HgO, PbO, Pb, MgO, and CaO, adsorption of the porphyrin on the surface of the metal or the metal oxide was found to be a serious problem and substantial amounts of porphyrin were lost. Other metal oxides also adsorbed the porphyrin but usually in much smaller amounts.

An interesting reaction of $TPPS_4$ is the direct extraction of copper from certain ores (e.g., chalcopyrites), from copper-rich alloys such as brasses and from a Cu–Ag–Be alloy. The possibility exists that the heterogeneous reaction may be useful in the selective extraction of certain metals, notably Cu because of its facile reaction, from ores and alloys. However, the non-reactivity of silicate-containing ores and the surface adsorption of the porphyrin may limit the usefulness of such an approach.

The stoichiometry of the heterogeneous oxide reaction is:

$$[1] \quad M(II)O(s) + H_2TPPS_4(aq) \rightleftharpoons M(II)TPPS_4(aq) + H_2O$$

where H_2TPPS_4 designates the hydrogens in the porphyrin centre. For the zero-valent metals, two possible reactions exist. One possibility is that, as in the case of Fe and Mn, surface oxidation by dissolved oxygen in the solvent occurs; the metal-insertion would then occur as by reaction 1.[1] The second possibility is:

$$[2] \quad M^0(s) + H_2TPPS_4(aq) \rightleftharpoons M(II)TPPS_4(aq) + H_2$$

When low concentrations of the porphyrin are used (as under our conditions), the amount of hydrogen gas evolved would be very small and thus difficult to detect. Ostfeld and Tsutsui (3) have represented the reaction of zero-valent metal complexes with porphyrins by a similar equation.

The most useful aspect of the heterogeneous metallation of porphyrins lies in the simplicity of the preparation of metalloporphyrins, particularly those of water-soluble porphyrins. In the conventional procedures with $TPPS_4$ and other water-soluble porphyrins, the excess metal salt is usually separated from the product by repeated precipitation from aqueous methanol (7) or by dialysis (8) and high purity of the metalloporphyrin is difficult to achieve. As the stoichiometry of the heterogeneous reactions shows (reactions 1 and 2), the product is not contaminated by counter-ions, excess metal, or acid provided that the solid phase is highly insoluble. In cases where the metal oxide is slightly soluble (MgO, CaO, ZnO, Ag_2O, HgO, PbO), simple reduction in the volume of the reaction mixture and refiltration through the 0.22 μ Millipore filter result in an appreciable reduction in contamination.

With the water-insoluble porphyrins, representa-

[1]Controlled experiments for the formation of $CuTPPS_4$ from the metal were carried out in two stoppered cuvettes at room temperature. Oxygen gas was bubbled through one and nitrogen through the other. Reaction occurred in both cases but was faster in the presence of excess O_2, indicating that the oxide mechanism [1] is likely significant in the reaction of metals with $TPPS_4$ but that reaction [2] cannot be ruled out.

tive reactions with Cu, CuO, and NiO only were carried out. In general, the reactions in non-aqueous solvents were slower. NiO, for example, which reacted with $TPPS_4$ in less than 2 h, took about 2 days to completely react with OEP in DMF/chloroform. The choice of the non-aqueous solvent is important, especially for OEP and TPP. In both chloroform and DMF, TPP failed to react with CuO. However, in mixtures containing 50–75% v/v DMF with chloroform, reaction readily occurred. These solvent mixtures provided both a suitably high refluxing temperature and sufficient solubility of the porphyrins and metalloporphyrins. Also, these mixtures optimized the surface adsorption/desorption effects of the porphyrins. Such factors explain why some solvents are more suitable than others in the heterogeneous reaction.

Acknowledgements

The authors gratefully acknowledge financial assistance from the National Research Council of Canada.

1. A. D. ADLER (*Editor*). Biological roles of porphyrins and related structures. Ann. N.Y. Acad. Sci. **244** (1975).
2. A. D. ADLER, V. VARADI, and N. WILSON. Ann. N.Y. Acad. Sci. **244**, 685 (1975).
3. D. OSTFELD and M. TSUTSUI. Acc. Chem. Res. **7**, 52 (1974).
4. K. M. SMITH (*Editor*). Porphyrins and metalloporphyrins. Elsevier Scientific Publishing Company, New York. 1975. (*a*) pp. 177–187; (*b*) pp. 195–200; (*c*) pp. 884–885.
5. A. D. ADLER, F. R. LONGO, F. KAMPAS, and J. KIM. J. Inorg. Nucl. Chem. **32**, 2443 (1970).
6. A. D. ADLER, F. R. LONGO, J. D. FINARELLI, J. GOLDMACHER, J. ASSOUR, and L. KORSAKOFF. J. Org. Chem. **32**, 476 (1967).
7. E. B. FLEISCHER, J. M. PALMER, T. S. SRIVASTAVA, and A. CHATTERJEE. J. Am. Chem. Soc. **93**, 3162 (1971).
8. C. A. BUSBY, R. K. DINELLO, and D. DOLPHIN. Can. J. Chem. **53**, 1554 (1975).
9. J. E. FALK. Porphyrins and metalloporphyrins. Elsevier Scientific Publishing Company, New York. 1964. pp. 243–246.
10. W. SCHNEIDER. Struct. Bond. **23**, 123 (1975).
11. M. F. C. LADD and W. H. LEE. *In* Progress in solid state chemistry. Vol. 37. Part 1. *Edited by* H. Reiss. Pergamon Press, London. 1964. pp. 54–56.
12. A. F. WELLS. Structural inorganic chemistry. 2nd. ed. Oxford University Press, London. 1950. p. 362.
13. J.-H. FUHRHOP. Struct. Bond. **18**, 1 (1974).

Can. J. Chem. Downloaded from www.nrcresearchpress.com by 210.87.254.5 on 09/05/12
For personal use only.

A study of the adsorption of formic acid and related molecules onto evaporated copper films, both clean and oxide-covered, by infrared ellipsometric spectroscopy

ROBERT WILLIAM STOBIE AND MICHAEL JOHN DIGNAM

Department of Chemistry, University of Toronto, Toronto, Ont., Canada M5S 1A1

Received October 28, 1977

ROBERT WILLIAM STOBIE and MICHAEL JOHN DIGNAM. Can. J. Chem. **56**, 1088 (1978).

Species formed on evaporated copper surfaces, both clean and oxide-covered, were examined using ir ellipsometric spectroscopy (IRES). Spectra were obtained for CO adsorbed on both bare and oxide-covered copper, the spectra being in accord with published data. No spectra were observed for formic acid adsorption unless free oxygen was present, in which case a spectrum characteristic of a carbonate species was found. Supporting data were obtained to show that the carbonate species was formed by reaction of formic acid and oxygen on the oxide-covered surface. These data illustrate some of the unique advantages of IRES for studying molecular processes on surfaces.

ROBERT WILLIAM STOBIE et MICHAEL JOHN DIGNAM. Can J. Chem. **56**, 1088 (1978).

Faisant appel à la spectrométrie ir ellipsométrique (IRES), on a étudié les espèces qui se forment sur des surfaces de cuivre évaporé, soit propre ou couverte d'oxyde. On a obtenu le spectre du CO adsorbé soit sur du cuivre nu ou couvert d'oxyde; le spectre est en accord avec les données publiées. On n'a observé aucun spectre lors de l'adsorption d'acide formique à moins d'avoir de l'oxygène libre présent; dans ce cas, on a trouvé un spectre caractéristique d'un carbonate. On a obtenu des données permettant de montrer que les carbonates se forment par une réaction de l'acide formique et de l'oxygène sur la surface couverte d'oxyde. Ces données permettent d'illustrer quelques-uns des avantages uniques de l'IRES pour étudier les processus moléculaires sur les surfaces.

[Traduit par le journal]

Introduction

In a previously reported investigation (1) ir ellipsometric spectroscopy (IRES) was used to study the adsorption of CO on evaporated Cu films. This paper represents a continuation of those studies and is concerned with the adsorption of formic acid and related molecules, CO and CO_2, onto evaporated Cu films and oxide-coated Cu films.

Hiroto *et al.* (2) studied adsorption of formic acid on samples of copper, nickel, and zinc dispersed in silica with the dispersions formed by decomposition of the appropriate formate salt. They found that it chemisorbed strongly on Zn and Ni, and the spectra showed clearly the presence of formate bands. With copper the formate bands were much weaker and they disappeared as the free formic acid was pumped out of the cell. Unfortunately the authors were not very quantitative about the pressure dependence of the bands, but it seems that the formic acid desorbed fairly easily. In addition, Tamaru (3) measured the adsorption and decomposition of formic acid on copper powders at temperatures as low as 65°C.

A number of absorption bands have been observed by Amerikov and Katsatkina (4) for adsorption of CO_2 on CuO which were attributed to both carbonate and carboxylate species. No similar results have been reported for Cu_2O.

Tompkins and Greenler (5) found bands at 2113 and 2135 cm^{-1} for CO adsorbed onto 'heavily oxidized' copper surfaces (thickness unknown). They found that the area of the low frequency band decreased as the high frequency band appeared.

Experimental

A description of our instrument, as well as an analysis of the ellipsometric technique employed, has been presented elsewhere (6, 7). The results reported here were obtained using a LN_2 cooled HgCdTe detector and 150 lines/mm grating blazed at 6 m in a 0.5 m monochromator with a slit width of 1.5 mm. The primary digital data, appearing on paper tape, were computer processed and graphed. In addition to carrying out the algebraic manipulations, the processing involved a sliding polynomial fitting procedure for data smoothing, the parameters in this process being chosen so as not to degrade the resolution.

The ultra-high vacuum and gas handling systems are described in our earlier investigation (1).

The reflection cell was fitted with two tungsten electrical feedthroughs each supporting a tantalum filament for depositing the copper films onto the optical flats (see Fig. 1). The copper was deposited from 99.99% pure wire stock to form opaque films within 5 to 10 s. The pressure rose to above 10^{-8} Torr during evaporation, falling to about 10^{-9} Torr within 30 s.

The gases, O_2 (99.99%), H_2 (99.99%), CO (99.5%), and CO_2 (99.5%) were passed through LN_2 traps when introduced into the gas handling system. The formic acid was Analar grade, and was dried by a vacuum distillation from a dispersion with anhydrous copper sulfate in the manner of Kishi, Ogawa, and Hiroto (8).

Can. J. Chem. Downloaded from www.nrcresearchpress.com by 210.87.254.6 on 09/05/12
For personal use only.

Can. J. Chem. Downloaded from www.nrcresearchpress.com by 210.87.254.6 on 09/05/12
For personal use only.

In a typical experimental run, the copper films were evaporated, then following 1 to 2 min to allow time for cooling, a blank or reference state ellipsometric scan was performed. This generally took about 10 min, following which the gas was introduced into the cell and another scan was performed.

Results and Discussion

The ellipsometric absorbance and dispersion spectra (Re(ΔL) and Im(ΔL) respectively vs. wave number) were calculated from the measured ellipsometric parameters, Δ and Ψ, using the relation (1)

$$[1] \qquad L = -[\ln(\tan\Psi) + i\Delta]$$

where $i = \sqrt{-1}$, ΔL is the change in L brought about by absorption, and Re and Im stand for 'the real part of' and 'the imaginary part of' respectively. As noted earlier (1), (2/2.303)Re(ΔL) is indistinguishable within experimental error from the conventional base 10 reflectance absorbance for p-polarizer light. For further details see ref. 1.

When formic acid was introduced into the cell no absorption bands due to adsorbed species were observed either in the C—H region or between 2000 and 1200 cm^{-1} where the carbonyl and formate bands are found. The very intense gas phase absorption limits the pressure that can be used while maintaining a reasonable signal level, so that it was not possible to study 'physically adsorbed' formic acid without going to low temperatures or a very short cell. Nevertheless, the region between the gas phase peaks at 1740 and 1380 cm^{-1} was scanned with a background pressure of 15 Torr (about 0.37 relative pressure) but no formate bands were observed. Finally the cell was filled with formic acid at about 20 Torr, heated to 150°C, allowed to cool, and then pumped out. Still no spectrum was observed although the increase in transmission during the heating phase indicated that approximately 75% of the formic acid had decomposed.

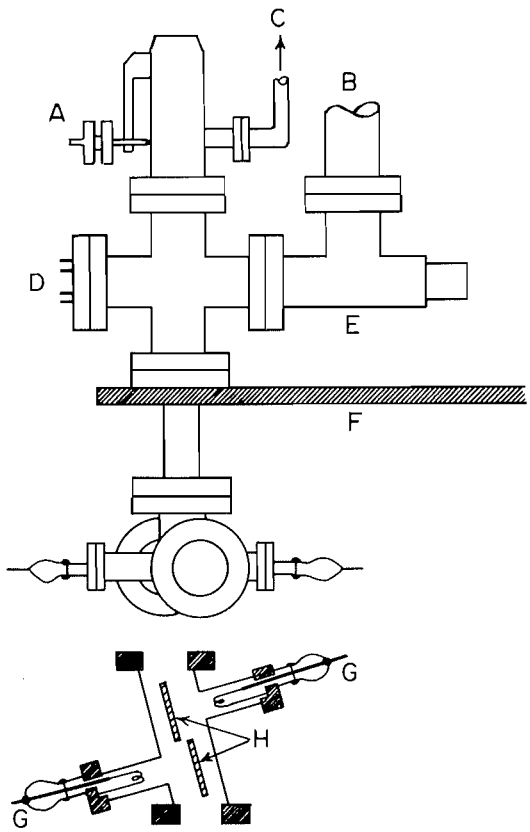

FIG. 1. Ultra-high vacuum reflection cell with leak valve A, ionization gauge head D, and isolation valve E.

Adsorption of acetic acid was tried with similar negative results.

Since oxides of copper are moderately active catalytically, the effect of oxidizing the surface before adsorption was investigated. This provided an opportunity to illustrate the versatility of the ellipsometric spectrometer since it was used without modification to monitor the oxide film growth. For films which are not strongly absorbing, the changes in Im(L) are much larger than those in Re(L), so that ellipsometry is much more sensitive to the presence of the film than is photometry (9).

The oxidation was carried out by admitting 1–10 Torr of O_2 to the cell after evaporation of the copper film. The thickness was then calculated from Im(ΔL) using O'Keefe's (10) value of 6.46 for the dielectric constant of the film and the thin film high reflectivity approximation which simplified the calculations while introducing negligible error. The film thicknesses determined in this way varied between 0.8 and 1.2 nm from film to film.

In one case the film growth was followed as a function of time with the instrument set at a fixed wavelength and at an averaging time of 8 s. The results are shown in Fig. 2 where they have been fitted to a logarithmic equation of the form

$$[2] \qquad d = A + B\ln(\alpha t + 1)$$

Equation 2 is frequently used to describe oxide film growth, particularly on copper, although its theoretical foundation is rather shaky (11). However, it gives very similar curves to the theoretically more sound Mott–Cabrera model (12).

Optical determinations of the thickness of thin oxide films have been criticized on the grounds that the early stages of the film growth often involve nucleation followed by lateral growth (13). However, Dignam and Moskovits (14) have shown that for submonolayer island films the simple optical

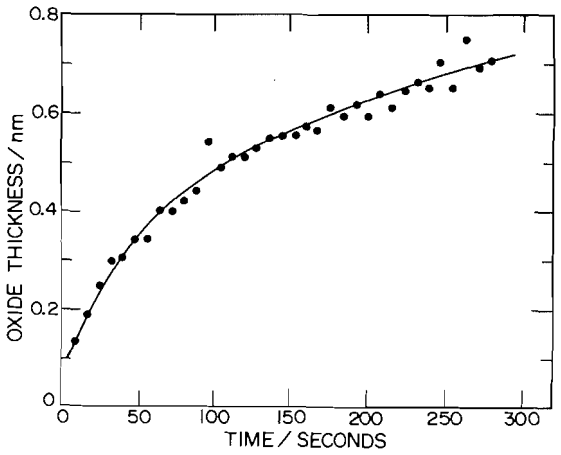

FIG. 2. Oxide film thickness vs. time obtained by ir ellipsometry (O_2 pressure = 2.7 Torr, T = 20°C).

model is valid: the dielectric constant is predicted to be independent of coverage while the calculated film thickness is proportional to it.

Although the oxidation of copper has been studied extensively as a classis example of corrosion (see a review by Ronnquist and Fischmeister (15)), most studies have either been of anodic oxidation (e.g. Dignam and Gibbs (16)) or else gas phase oxidation at high temperature or in unusually corrosive atmospheres. Below 150°C Cu_2O is formed almost exclusively, while above that CuO predominates. The work done at room temperature has shown that very thin oxide films are characteristic of the reaction. From measurements of oxygen uptake on evaporated copper Allen and Mitchell (17) calculated that films of 2.4 nm were formed at 20°C. Rhodin (18) carried out a detailed kinetic study on single crystal surfaces at several temperatures up to 50°C. His gravimetric measurements showed that layers of 0.8 to 1.4 nm thick (depending on the crystal face) were formed at 25°C in a matter of 10 to 20 s independent of pressure in the region 10–100 Torr and that continued exposure for up to a month did not result in significant further growth. The rate observed here is somewhat less than Rhodin's, although comparable to that of Allen and Mitchell. Induction times in accord with those of Heineman *et al.* (19) were observed at low pressures.

After the copper had been oxidized, the O_2 was pumped out of the cell before introducing formic acid. The cell was only pumped down to about 100 microns, however, to reduce the possibility of contamination by backstreaming from the fore pump. Instead of formate bands in the region of 1650 to 1410 cm^{-1}, the spectrum shown in Fig. 3 was observed. The band peaks fall at 1625 and 1380 cm^{-1}. As this spectrum was obtained with a HgCdTe

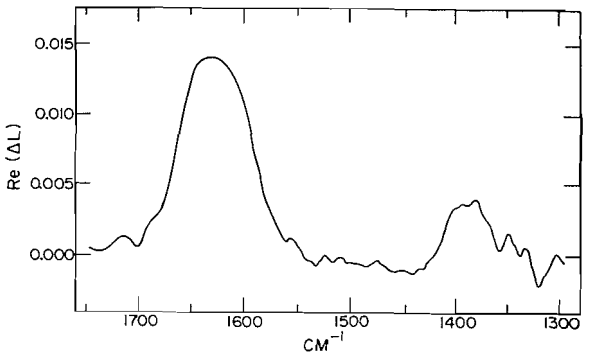

FIG. 3. Absorption spectra of species formed on copper in the presence of formic acid and free oxygen.

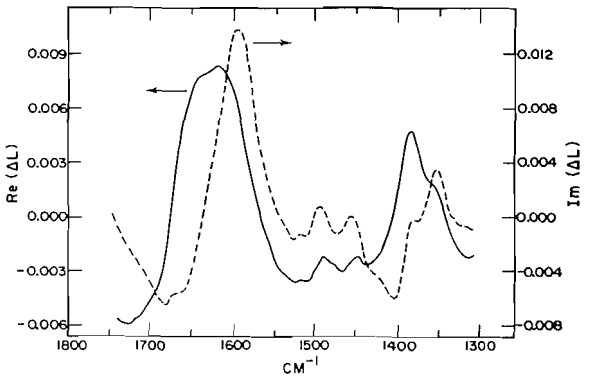

FIG. 4. Absorption and dispersion spectrum of species formed as for Fig. 3, obtained without use of a background or 'bare surface' ellipsometric scan.

detector, rather than the higher detectivity InSb detector used for the previously reported CO studies (1), somewhat poorer quality spectra were obtained. A drop in quality was also caused by absorption due to atmospheric water whose bands intrude into this spectral region.[1] Both Re(ΔL) and Im(ΔL) are shown again in Fig. 4 with the difference that they were obtained without using a bare metal scan. The background spectrum was fitted to a straight line then subtracted from L to produce the spectra (1). It should be noted that although the atmospheric absorption bands have a good deal of structure in this region, they make no detectable contribution to the ellipsometric absorption spectrum, as expected (1).

This species was found to be strongly adsorbed; pumping for up to an hour (down to 10^{-7} Torr) did not cause a measurable reduction in the strength

[1]Dry air was flushed constantly through the box containing the 'input' optics but it was impossible to eliminate all the water vapour bands. This was largely because it was necessary to open the box to remove the polarizers every time the cell had to be aligned.

Can. J. Chem. Downloaded from www.nrcresearchpress.com by 210.87.254.6 on 09/05/12
For personal use only.

Can. J. Chem. Downloaded from www.nrcresearchpress.com by 210.87.254.6 on 09/05/12
For personal use only.

of the absorption bands. Introduction of H_2 into the cell also had no measurable effect on the spectra.

The spectrum is almost certainly due to a carbonate species. Little (20) has summarized the bands due to CO_2 or CO plus O_2 adsorbed onto various substrates. By analogy with the solution spectra of various carbonate species of known structure he ascribes them to different forms. Evidently the species that is being formed here has the structure

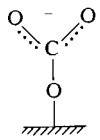

The conditions under which it can be formed are also of interest. If the formic acid is admitted first, nothing is observed until the O_2 is also admitted, as would be expected from the earlier experiments. If the formic acid is admitted in doses (up to 3000 *L*) and then pumped off, nothing is observed even after admission of the oxygen. This supports the contention that the formic acid did not chemisorb on the bare copper. If the oxygen is admitted first and then the formic acid, the spectrum obtained is identical to the first case. If the oxygen is admitted and then pumped off, nothing is observed on admitting the formic acid. This indicates that formic acid does not react with chemisorbed oxygen or very thin oxide layers to form a surface carbonate, but it does not necessarily show that it would not react with bulk cuprous oxide. Cu_2O is known to absorb large amounts of oxygen (21) so that there would be a substantial amount of free O_2 available for reaction. Formic acid adsorbed on powdered Cu_2O might easily show carbonate bands.

To investigate this further, CO and CO_2 were also adsorbed on the oxidized copper. None of the procedures followed with the formic acid lead to carbonate bands with CO_2, or indeed, to any bands at all. London and Bell (22) observed a broad band at 2350 cm^{-1} from physically adsorbed CO_2, but the intense atmospheric absorption from the asymmetric stretch in the present study attenuated the signal too strongly to permit any experiments in this frequency range.

Carbon monoxide also gave rise to no carbonate bands on oxidized copper even in the presence of oxygen. It did, however, give two broad bands at 2115 and 2160 cm^{-1}, as shown in Fig. 5, in general agreement with those found by Tompkins and Greenler (5) at 2113 and 2135 cm^{-1} on their most heavily oxidized surfaces. The low resolution makes it difficult to pinpoint the location of these bands

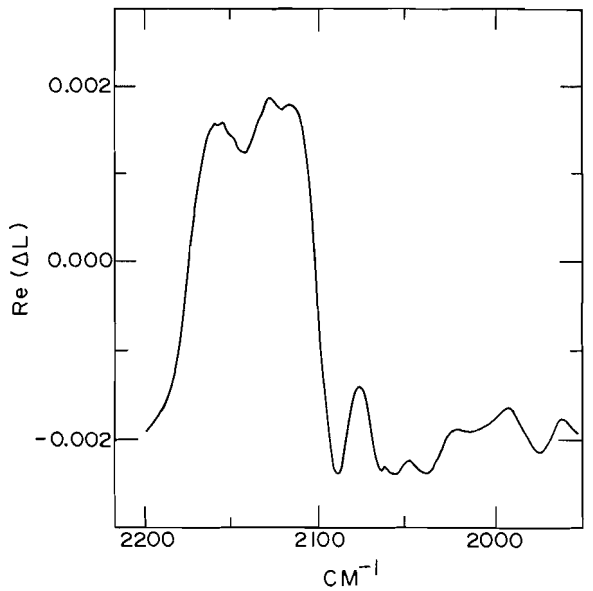

FIG. 5. Absorption spectrum for CO on oxide-covered copper.

exactly, but on dispersed samples peak positions have been reported to depend on the precise method of sample preparation (for example, see Seanor and Amberg (23), or Eischens and Pliskin (24)).

Smith (25) studied the oxidation of carbon monoxide on copper and copper oxide at low temperatures. In addition to the CO band he observed weak bands at 1520 and 1375 cm^{-1} which he felt were due to carbonate species. However, these were formed only after prolonged oxidation and they partially desorbed with pumping.

The data strongly support a model in which the species is formed by the direct interaction of formic acid and oxygen on the surface rather than involving gaseous intermediates. Thus although formic acid could have decomposed or been oxidized on the cell walls or in the gas phase to give either CO or CO_2, and undoubtedly this did occur to some extent, no carbonate bands were observed with either of these gases.

When the carbonate band at 1625 cm^{-1} was first observed, it was felt that it might be due to adsorbed water, since the water bending mode falls at 1595 cm^{-1} in the gas phase. Water was admitted to the cell over both bare and oxidized copper, with and without gaseous O_2, but no bands were detected. While water would almost certainly adsorb under these conditions, the molecules may very well be oriented with the transition dipole parallel to the surface, in which case the band would not be observable (1).

Attempts were also made to obtain spectra for

nitric oxide adsorbed on bare copper. No spectra have ever been reported for adsorption on copper, and none were observed in this work, even with pressures as high as 30 Torr.

Summary and Conclusions

The work reported herein was conducted in part to explore the capabilities of IRES for investigating molecular processes on well defined metal surfaces. Our current studies are on single crystal surfaces for which the technique was developed, but the results reported herein illustrate a number of the unique advantages of IRES for such studies. These include: (*1*) structural information achieved much more readily than through LEED or ARUPS say; (*2*) high sensitivity to surface species coupled with vanishingly low sensitivity to species in the gas phase, in contrast to conventional reflectance or transmittance photometric spectroscopy; (*3*) speed of data collection compared to electron loss spectroscopy, ARUPS, or a complete LEED analysis; (*4*) non-destructive nature of the measurement compared with electron spectroscopies, LEED and ARUPS; (*5*) ability to function in the presence of moderate ambient pressures in contrast to all techniques involving electron emission or absorption.

In the present study it was shown for the first time that oxygen and formic acid react on Cu_2O covered copper to form a chemisorbed carbonate species with a symmetric stretch at 1380 cm^{-1} and an asymmetric stretch at 1625 cm^{-1}. Both these modes correspond to transition dipole moments along the symmetry axis of the molecular species, and hence presumably normal to the metal surface. If this were not the case, then other stretching modes (corresponding to degenerate modes for CO_3^-) should be present since they would correspond to transition dipole moments with components normal to the surface. Parallel components are for all practical purposes infrared inactive.

The weakness of this argument lies of course in the fact that there may be overlapping bands. Isotopic substitutions would be required to test that possibility. The fact remains that orientational information is available in the ir spectrum of molecular species adsorbed onto metal surfaces.

1. R. W. Stobie, B. Rao, and M. J. Dignam. Surf. Sci. **56**, 334 (1976).
2. K. Hiroto, K. Kumata, and Y. Nakai. Bull. Chem. Soc. Jpn. **31**, 861 (1958).
3. K. Tamaru. Trans. Faraday Soc. **55**, 1191 (1959).
4. V. G. Amerikov and L. A. Katsatkina. Kinet. Catal. **12**, 137 (1971).
5. H. G. Tompkins and R. G. Greenler. Surf. Sci. **28**, 194 (1971).
6. R. W. Stobie, B. Rao, and M. J. Dignam. Appl. Opt. **14**, 999 (1975).
7. M. J. Dignam, B. Rao, and R. W. Stobie. J. Opt. Soc. Am. **65**, 25 (1975).
8. K. Kishi, T. Ogawa, and K. Hiroto. J. Catal. **5**, 464 (1966).
9. M. J. Dignam, M. Moskovits, and R. W. Stobie. Trans. Faraday Soc. **67**, 3306 (1971).
10. M. O'Keefe. J. Chem. Phys. **39**, 1789 (1963).
11. D. J. Young and M. J. Dignam. Oxid. Met. **5**, 241 (1972).
12. D. J. Young and M. J. Dignam. J. Phys. Chem. Solids, **34**, 1235 (1973).
13. F. Gronlund and P. E. Hojlund-Nielsen. Surf. Sci. **33**, 399 (1972).
14. M. J. Dignam and M. Moskovits. J. Chem. Soc. Faraday Trans. II, **69**, 56 (1973); **69**, 65 (1973).
15. A. Ronnquist and H. Fischmeister. J. Inst. Met. **89**, 65 (1960).
16. M. J. Dignam and D. B. Gibbs. Can. J. Chem. **48**, 1242 (1970).
17. J. A. Allen and J. W. Mitchell. Discuss. Faraday Soc. **8**, 309 (1950).
18. T. N. Rhodin. J. Am. Chem. Soc. **73**, 3143 (1951).
19. K. Heineman, D. B. Rao, and D. L. Douglass. Oxid. Metals, **9**, 379 (1975).
20. L. H. Little. Infrared spectra of adsorbed species. Academic Press, London and New York. 1966. p. 78.
21. T. J. Jennings and F. S. Stone. Adv. Catal. **9**, 441 (1957).
22. J. London and A. T. Bell. J. Catal. **31**, 32 (1973).
23. D. A. Seanor and C. H. Amberg. Rev. Sci. Instrum. **34**, 917 (1963).
24. R. P. Eischens and W. A. Pliskin. *In* Advances in catalysis. Vol. 10. *Edited by* D. D. Eley, W. G. Frankenburg, and V. I. Komarewsky. Academic Press, London and New York. 1958.
25. A. W. Smith. J. Catal. **11**, 172 (1965).

Can. J. Chem. Downloaded from www.nrcresearchpress.com by 210.87.254.6 on 09/05/12
For personal use only.

Valence-bond studies of 4-electron 3-centre bonding units. I. The π-electrons of O_3, NO_2^-, and CH_2N_2

RICHARD D. HARCOURT AND WALTER ROSO

School of Chemistry, University of Melbourne, Parkville, Victoria 3052, Australia

Received May 26, 1977

RICHARD D. HARCOURT and WALTER ROSO. Can. J. Chem. **56**, 1093 (1978).

Some *ab-initio* valence-bond wave-functions are reported for the π-electrons of the ground-states of O_3, NO_2^-, and CH_2N_2. Examination of these wave-functions provides further support for the hypothesis that, for the ground-states of many electron-excess molecules, important valence-bond structures are those that are compatible with the electroneutrality principle, i.e. they carry either small or zero formal charges on each of the atoms. For O_3 and CH_2N_2, the important valence-bond structures with zero atomic formal charges are

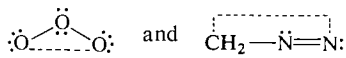

Each of these structures has a 'long-bond' between non-adjacent atoms. The significance of 'long-bond' (or spin-paired diradical) structures for the electronic mechanism of 1,3-dipolar cycloaddition reactions is discussed and 'increased-valence' descriptions of the electronic structure of each molecule are presented. Some comments on the utility of 'increased-valence' structures are provided.

RICHARD D. HARCOURT et WALTER ROSO. Can. J. Chem. **56**, 1093 (1978).

On rapporte quelques fonctions d'onde valence-liaison calculées par des méthodes *ab initio* pour des électrons π des états fondamentaux de O_3, NO_2^- et CH_2N_2. Un examen de ces fonctions d'onde fournit un support additionnel à l'hypothèse selon laquelle pour les états fondamentaux de plusieurs molécules possédant des électrons en excès, les structures importantes de liaison de valence sont celles qui sont compatibles avec le principe de l'électroneutralité c'est-à-dire celles où les charges formelles portées par chaque atome sont ou très faibles ou égales à zéro. Pour O_3 et CH_2N_2, les structures importantes de liaison de valence avec des charges formelles atomiques de zéro sont

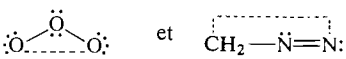

Chacune de ces structures possèdent une liaison longue entre deux atomes non-adjacents. On discute de la signification des structures à liaisons longues (ou du diradical à spin pairé) pour le mécanisme électronique des réactions de cycloadditions dipolaire-1,3 et on présente des descriptions d'augmentation de valence de la structure électronique de chaque molécule. On fournit quelques commentaires sur l'utilité des structures d'augmentation de valence.

[Traduit par le journal]

Introduction

For electron-excess molecular systems, a very important type of triatomic bonding unit involves four electrons distributed amongst three overlapping atomic orbitals located on three atoms (1–4). The resulting 4-electron 3-centre bonding is usually described qualitatively by means of either delocalized 3-centre molecular orbital theory or by valence-bond resonance theory (1–4). The simplest type of valence-bond description involves resonance between the standard valence-bond structures **1** and **2**, each of which has an electron-pair bond between adjacent atoms and a lone-pair of electrons on the third atom. This valence-bond representation shows perhaps more immediately than does a molecular orbital description that 4-electron 3-centre bonding must be an extremely widespread phenomenon; it is possible to write down Lewis–Langmuir valence-bond structures for thousands of molecular systems in which the valence-bond arrangements of **1** and **2** pertain for one or more sets of four electrons (1, 3, 4). Further, these bonding units may be either intra- or intermolecular. Larger *n*-centre bonding units (for example, 6-electron 4-centre) with additional atoms, overlapping atomic orbitals and electrons, represent elaborations of the basic 4-electron 3-centre bonding unit. The purpose of this and subsequent papers is to report the results of some non-empirical valence-bond calculations for a number of molecules that involve either or both of these types of bonding units.

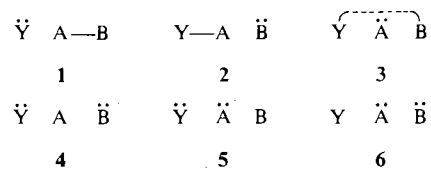

Can. J. Chem. Downloaded from www.nrcresearchpress.com by 210.87.254.42 on 09/05/12
For personal use only.

Can. J. Chem. Downloaded from www.nrcresearchpress.com by 210.87.254.42 on 09/05/12
For personal use only.

In contrast to what is the case for molecular orbital theory, few valence-bond wave-functions have been reported for the ground-states of systems with 4-electron 3-centre bonding units. Of those that have been reported (4–19) (and they range from semi-empirical to *ab-initio*), most show up what we consider to be an important (but much-ignored) result, namely that the bond-eigenfunction coefficient for the 'long-bond' structure **3** can have appreciable magnitude. Indeed, its magnitude is sometimes calculated to be larger than those for either of the standard valence-bond structures **1** and **2**. This is particularly the case when **1** and **2** carry atomic formal charges as in

$$\overset{(-)}{\dot{Y}}\ \overset{(+)}{A}\text{—}B \quad \text{and} \quad Y\text{—}\overset{(+)}{A}\ \overset{(-)}{\dot{B}}$$

and **3** does not. The ramifications of this result for qualitative valence-bond theories of structure and reactivity are very considerable (see for example, refs. 14, 20, 21). Very often, it is not sufficient to write down valence-bond structures of types **1** and **2**, and then hope to obtain a realistic representation for the electronic structure of the molecule. Where appropriate, **3** must be included also. In numerous papers, this has been done (1, 3, 4, 14, 20, 21), and new types of valence formulae (namely, the 'increased-valence' formulae of the next paragraph) have been generated that summarize resonance between the standard and 'long-bond' (or spin-paired diradical) structures **1**, **2**, and **3**. (Of course, valence-bond structures of types **4**–**6** are also needed to form a complete valence-bond basis set for a singlet-spin state involving 4-electron 3-centre bonding.) One purpose of the present series of papers is to provide further quantitative evidence that important valence-bond structures for the ground-states of electron-excess molecules carry either small or zero atomic formal charges, and that such structures may often be of type **3**. The formal charge requirement is compatible with the electroneutrality principle (22).

It may be noted that resonance between all valence-bond structures that do not involve 'long-bonds' may be summarized by using 2-centre bond orbitals instead of Heitler–London wave-functions as the wave-functions for the electron-pair bonds that occur in the standard valence-bond structures **1** and **2** (*1*, 3*b*, 4–10). To include the 'long-bond' structure also, another type of valence formula is needed. For this purpose, the 'increased-valence' formulae **7** and **8** have been devised (1, 3, 4, 14, 20, 21). These formulae have one more bonding electron than have any of **1**–**3** and may be easily generated from the standard valence-bond structures **1** and **2** by delocalizing a non-bonding Y or B electron into a bonding YA or AB orbital, as is shown in **9** and **10**. Because the 1-electron bond A·B summarizes resonance between the valence formulae A $\dot{\dot{B}}$ and $\dot{A}$ B, it is easy to demonstrate that **7** and **8** summarize resonance between **1** and **3**, and **2** and **3**, respectively if Heitler–London type wave-functions are used to describe the A—B and Y—A bonds of **7** and **8**. Alternatively, if localized molecular orbitals (or bond-orbitals) are used to describe these bonds in **7** and **8**, resonance between these 'increased-valence' formulae is equivalent to invoking resonance between all of the valence-bond structures **1**–**6** when Heitler–London type wave-functions are used to describe the electron-pair bonds of **1**–**3** (1, 3*b*, 4, 14*c*). Linnett's non-paired spatial orbital formulae **11** (2, 5–10) may also be used to summarize resonance between the standard and 'long-bond' valence-bond structures **1**–**3**, as well as **4**. Both 'increased-valence' and non-paired spatial orbital formulae will be used in the discussions for this series of papers.

$$\dot{Y} \cdot A\text{—}B \qquad Y\text{—}A \cdot \dot{B}$$

7 **8**

$$\dot{Y}\!\curvearrowright\ A\text{—}B \qquad Y\text{—}A\!\curvearrowright\!\ddot{B} \qquad \dot{Y} \cdot A \cdot \dot{B}$$

9 **10** **11**

Because of limitations to our computing facilities (we have used a CYBER 72, CDC 6400 computer, with a store capacity of 64K words of central memory), it has not been possible to perform all-electron calculations on many of the triatomic and polyatomic systems that we have selected to study. Therefore, we have restricted our attention to a consideration of the different types of valence-bond structures that arise from variations in the distributions of only some of the electrons, namely, those that could delocalize appreciably. For non-linear planar molecules, these electrons were usually either some or all of (*a*) the π-electrons, and (*b*) the lone-pair π′-electrons occupying atomic orbitals that overlap appreciably with the orbitals of σ-bonds. On occasions, we have also allowed for the polarization of certain localized σ- or π-bonds, and when this was done, additional valence-bond structures were introduced into the calculations. For a calculation, it was possible to take account of 6 atoms, 20 atomic orbitals, 20 electrons, and 25 valence-bond structures. When the number of structures that we could write down exceeded 25, we have used chemical intuition and the electroneutrality principle to decide which structures should be included in the treatment.

In the present paper, we shall report the results of valence-bond calculations for the π-electrons of O_3, NO_2^-, and CH_2N_2. We are currently preparing for publication other papers that describe the results of similar types of valence-bond calculations for the

Can. J. Chem. Downloaded from www.nrcresearchpress.com by 210.87.254.42 on 09/05/12
For personal use only.

σ-electrons of HF_2^-, and the π- and π′-electrons for a number of nitroso and nitro compounds, and the oxalate anion.

Method of Calculation

Since completing this work, Gerratt (23) has published a review of valence-bond theory. We shall briefly summarize the procedure that we have used to construct the Hamiltonian and overlap matrix elements for the valence-bond secular equations of [2]. These equations pertain to the linear combination of [1], in which the ψ_i represent the normalized bond-eigenfunctions for the different canonical valence-bond structures.

$$[1] \qquad \Psi = \sum_{j=1}^{N} C_j \psi_j$$

$$[2] \qquad \sum_{j=1}^{N} (H_{ij} - ES_{ij})C_j = 0$$

(*a*) As basis atomic orbitals, we have used single-zeta Slater-type orbitals (STO's) with the 'best atom' orbital exponents of Clementi and Raimondi (24). For the hydrogen 1*s* exponent, Hehre and Pople's value of 1.3 (25) was used. The optimization of exponents in valence-bond calculations makes heavy demands on computer time, and we have not attempted to do this for the polyatomic systems.

(*b*) The bond-eigenfunction for a valence-bond structure involves a linear combination of Slater determinants. Numerous procedures are available for the construction of the appropriate spin eigenstates (23, 26). Because we have been concerned only with singlet ($S = 0$) and doublet ($S = \frac{1}{2}$) spin-states, it is possible to use the simple rule described by Kauzmann (27) to construct the spin eigenfunctions. The branching diagram indicates the existence of spin-degeneracy for systems that involve three or more singly-occupied orbitals (23, 26). The procedure that we have used generates the spin-eigenfunction that is appropriate for the electron-pairing scheme of a given valence-bond structure. The ground-state eigenvectors for [1] that we shall report pertain when both Ψ and the ψ_i bond-eigenfunctions are normalized to unity.

(*c*) To evaluate the Hamiltonian and overlap matrix elements (H_{ij} and S_{ij}) of [2], we have used Löwdin's cofactor method (28).

(*d*) To calculate the 1-electron and 2-electron integrals over atomic orbitals for the H_{ij} and S_{ij}, the STO's were expressed as linear combinations of cartesian Gaussian functions (CGF's), γ_i^{CG}, as in [3] (29). The optimum linear combination of CGF's was determined by Stewart (29) for STO exponents (ξ) of unity. Non-unity values for the exponents are used by scaling (30, 31) the CGF exponents of [3], i.e. by writing $\alpha_i = \alpha_i'\xi^2$. Equation 3 may then be expressed as eq. 4. To avoid using spherical harmonics, the CGF's in [4] were replaced by the simpler lobe Gaussian functions using $R = 0.03\alpha^{-1/2}$, in which R is the distance of the lobe centre from the nucleus (30). The resulting STO is given by [5].

$$[3] \qquad \psi_{STO}(\zeta = 1, r) = \sum_{i=1}^{N} a_i \gamma_i^{CG}(\alpha_i, r)$$

$$[4] \qquad \psi_{STO}(\zeta, r) = \sum_{i=1}^{N} a_i \gamma_i^{CG}(\alpha_i'\zeta^2, r)$$

$$[5] \qquad = \sum_{i=1}^{N} a_i \gamma_i^{LG}(\alpha_i'\zeta^2, R, r)$$

The number of Gaussian components, N, used in all calculations was five (30). When testing the valence-bond procedure, we found that this number is the minimum required to give valence-bond wavefunctions that agree closely with some published STO calculations for LiH (31).

(*e*)With the current valence-bond program, which was prepared by one of us (W.R.), it is possible to perform one or more of the following types of calculations. (*i*) *All-electron calculations*: For certain diatomic and small polyatomic molecules, the program permits all of the electrons to be included specifically in the construction of the Slater determinants to form the bond-eigenfunctions. Minimal atomic orbital basis sets were used in calculations of this type for LiH, HF, CO, and HNO. (*ii*) *All-valence-electron calculations*: For larger molecules, we were unable to treat explicitly all of the electrons, and therefore we have invoked the approximations described here and (*iii*) below. For all-valence electron calculations, only the valence-shell electrons and orbitals are included in the construction of the bond-eigenfunctions. Inner-shell electrons are treated as part of the core, whose charge is equal to the nuclear charge minus the number of inner-shell electrons. We have tested the validity of this approximation by comparing the results of valence-bond calculations for HNO when procedures (*i*) and (*ii*) are both used. These calculations will be described in the second paper of this series. (*iii*) *Hamilton's approximation*: Many of the molecules that we have examined have rather more than 20 valence-shell electrons and orbitals. For them, it was necessary to invoke Hamilton's approximation (11, 32), and include only some of the valence-shell orbitals in the Slater determinants. The remaining electrons are assigned to the core, and are considered only in the calculation of penetration integrals. When this is done, Hamilton's approximation involves the neglect of all electron exchange, except for that which occurs between the

Can. J. Chem. Downloaded from www.nrcresearchpress.com by 210.87.254.42 on 09/05/12
For personal use only.

electrons explicitly included in the Slater determinants. In Part II of this series, we shall compare calculations for FNO and HF_2^- using Hamilton's approximation and either all-valence electron or all-electron procedures.

(*f*) In our discussions of the valence-bond wave-functions, we shall follow Maclagan and co-workers (33) by assuming that the bond-eigenfunction ψ_i whose coefficient has the largest magnitude in the ground-state valence-bond wave-function of [1] represents the most important valence-bond structure. Because the ψ_i are not orthogonal, the weights for the valence-bond structures are not equal to C_i^2. However, an inspection of the structural weights and coefficients for an *ab-initio* study of C_6H_6 (34) indicates that the magnitudes for these two quantities correlate approximately (but *not* exactly) with each other, in so far as if a coefficient C_i has a large magnitude, then the valence-bond weight (or occupation number (34)) is also large.

To ensure correct functioning of the program, valence-bond wave-functions were calculated for a number of systems for which such wave-functions have been reported previously by other workers. Our results for an all-electron calculation for LiH are reported in Table 1, where they are compared with those of Miller *et al.* (31). The calculation of Linnett and co-workers (9) for the formate anion, with Hamilton's approximation, was repeated. Exact agreement between our calculations and those of Linnett *et al.* was not expected, because the latter workers approximated some of the molecular integrals, whereas we have evaluated them accurately. The two wave-functions are the following, for which the bond-eigenfunctions are defined in ref. 9.

Linnett and co-workers (9)

$$\Psi = 0.273\psi_1 + 0.415\psi_2 + 0.168\psi_3 + 0.078\psi_4$$

This work

$$\Psi = 0.278\psi_1 + 0.404\psi_2 + 0.178\psi_3 + 0.075\psi_4$$

Experimental bond-lengths (35) have been assumed for all calculations. The bond-angles for O_3 and NO_2^- were approximated to 120° and 116° respectively.

TABLE 1. Valence-bond wave-functions for LiH

Structure	Li configuration	C_J This work	C_J Ref. 31
Li—H	$1s^2 2s^1$	0.6665	0.6916
Li—H	$1s^2 2p^1$	0.3943	0.4251
$Li^+ H^-$	$1s^2$	0.2390	0.2248
$Li^- H^+$	$1s^2 2s^2$	−0.0554	−0.0696
$Li^- H^+$	$1s^2 2p^2$	−0.0169	−0.0317
$Li^- H^+$	$1s^2 2s^1 2p^1$	−0.0347	−0.0583
Electronic energy (eV)		−216.946	−217.01
Dipole moment (D)		6.039	6.04

Randomly selected integrals*	Value (au) This work	Value (au) Ref. 31
$[a\|b]$	0.1658	0.1663
$[c\|d]$	0.5546	0.5545
$[a\|\hat{H}^0\|a]$	−4.7824	−4.7869
$[a\|\hat{H}^0\|b]$	−0.7174	−0.7169
$[c\|\hat{H}^0\|d]$	−0.8225	−0.8226
$[aa\|aa]$	1.6875	1.6875
$[ab\|ab]$	0.0212	0.0212
$[aa\|ab]$	0.1658	0.1656
$[bd\|cd]$	0.1117	0.1117

*$a = 1s_{Li}$, $b = 2s_{Li}$, $c = 2p_{Li}$, $d = 1s_H$.

Results

(a) Ozone and Nitrite

The ground-states of O_3 and NO_2^- each have four π-electrons distributed amongst three overlapping atomic orbitals. Linnett and co-workers (6, 10) have calculated valence-bond wave-functions for these systems, using Hamilton's approximation. Our results for this type of calculation, and also those for all-valence electron calculations, are reported in Tables 2 and 3. For comparison, eigenvectors obtained by other workers (4, 6, 10) are also reported in these tables.

Each calculation indicates that the bond-eigenfunction ψ_3 for the valence-bond structure with a 'long' OO π-bond has a coefficient with a large magnitude. This is particularly the case for O_3, and is in accord with the electroneutrality principle in so far as the valence-bond structure carries zero formal charges on all atoms. On the basis of their generalized valence-bond calculations, Goddard and co-workers (17) have concluded that O_3 is primarily a diradical rather than a zwitterion, and that the 'long' OO π-bond structure best represents the electronic structure of this molecule. They have used this valence-bond structure to discuss the Criegee mechanism of ozonolysis of olefins (17).

For O_3 and NO_2^-, the standard valence-bond structures that are most usually displayed are the Lewis–Langmuir octet structures 1 and 2 of Tables 2 and 3. However, because the bond-eigenfunction for the 'long-bond' octet structure 3 of either table is also calculated to be important, it is necessary to include this type of structure in the valence-bond representation for the ground-state. This may be done either by writing down the 'long-bond' structure together with the other structures, or by devising valence formulae that summarize resonance between all of these structures. These latter formulae may be

Can. J. Chem. Downloaded from www.nrcresearchpress.com by 210.87.254.42 on 09/05/12
For personal use only.

TABLE 2. π-Electron valence-bond structures and bond-eigenfunction coefficients (C_i) for O_3 ground-state

Type	Structure	C_i A*	C_i B†	Ref. 4*
1	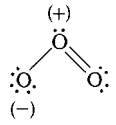	0.2411	0.3084	0.337
2	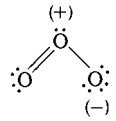	0.2411	0.3084	0.337
3	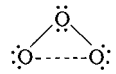	0.8619	0.7934	0.859
4	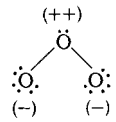	0.0391	0.0670	0.110
5	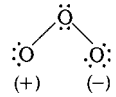	0.0571	0.0674	0.108
6	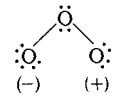	0.0571	0.0674	0.108

*Hamilton's approximation for the four π-electrons.
†All valence electrons in Slater determinants. Gould and Linnett (6) have calculated $\Psi = 0.351(\psi_1' + \psi_2') + 0.390\psi_3' + 0.124\psi_4' + 0.028(\psi_5' + \psi_6')$, in which the ψ_i' are non-normalized bond-eigenfunctions.

either of the 'increased-valence' (1, 3, 4, 14, 20, 21) or non-paired spatial orbital type (2, 5–10). For O_3, these valence formulae are either **12** + **13** (3*a*, 4, 14*b*) or **14** (3, 4, 6). We may generate the 'increased-valence' formulae **12** and **13** from the standard valence-bond formulae by delocalizing a non-bonding π-electron from a terminal oxygen atom into a bonding OO π-orbital, as is shown in **15** and **16** (1, 4, 20, 21).

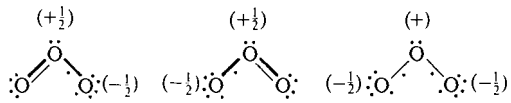

12 **13** **14**

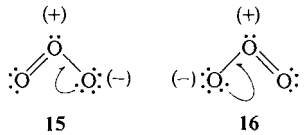

15 **16**

For O_3, 'increased-valence' formulae **17** and **18** may also be generated which carry zero formal charges on all atoms (3*a*, 20*b*, 36). These are obtained by delocalizing an in-plane π′-electron as well as a π-electron from the (−ve) oxygen atom. In the calculations of the present paper, no delocalization of the π′-electrons has been taken account of for either O_3 or NO_2^-. For each of these systems, and for CH_2N_2, we have also not allowed for any polarization of OO, NO, CN, or NN σ-bonds. Therefore, valence-bond structures such as **19**, **20**, and **21** have been omitted from the calculations, even though the absence of formal charges for them might suggest that they may be important structures. However, these structures are not required to interpret reactions of these molecules that involve only the breaking of their π-bonds. The '1,3-dipolar' cycloadditions that are to be discussed in the next section form one such class of reactions.

Electronic mechanisms for reactions such as $X + O_3 \rightarrow XO + O_2$, with X = H or NO, are described in ref. 36. They utilize 'increased-valence' structures **17** and **18** for O_3 and its diradical character.

TABLE 3. π-Electron valence-bond structures and bond-eigenfunction coefficients (C_i) for NO_2^- gound-state

Type	Structure	C_i A*	C_i B†	Ref. 4*
1	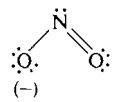	0.4453	0.4642	0.529
2	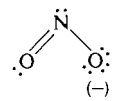	0.4453	0.4642	0.529
3	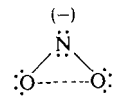	0.4748	0.3019	0.542
4	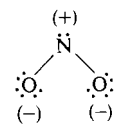	0.2212	0.3501	0.335
5	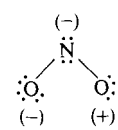	0.0696	0.0544	0.130
6	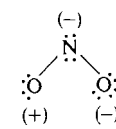	0.0696	0.0544	0.130

*Hamilton's approximation for the four π-electrons.
†All valence electrons in Slater determinants. (For this calculation, the 'best atom' exponents were adjusted for residual formal charges.) Hirst and Linnett (10) have calculated $\Psi = 0.306(\psi_1' + \psi_2') + 0.391\psi_3' + 0.185\psi_4' + 0.070(\psi_5' + \psi_6')$, in which the ψ_i' are non-normalized bond-eigenfunctions.

TABLE 4. π-Electron valence-bond structures and bond-eigenfunction coefficients for CH_2N_2 ground-state

Type	Structure	Coefficients 6 electrons	Coefficients 10 electrons	Type	Structure	Coefficients 6 electrons	Coefficients 10 electrons
1	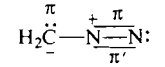	0.3068	0.2822	7	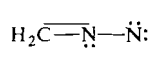	0.2746	0.3140
2	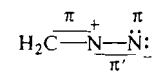	0.2297	0.2385	8	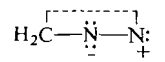	0.1550	0.1820
3	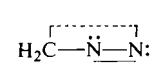	0.3770	0.4038	9	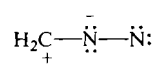	0.0432	—
4	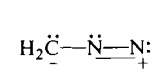	0.1044	0.1100	10	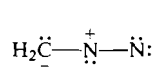	0.1373	0.1393
5	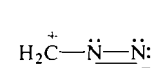	0.0473	—	11	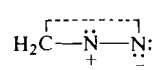	0.0946	—
6	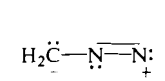	0.1525	0.1636	12	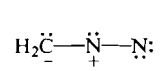	0.0658	—

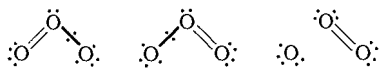

17 18 19

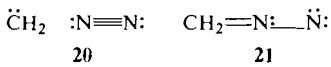

20 21

(b) Diazomethane

Diazomethane has two sets of π-electrons. The standard valence-bond structures are **1** and **2** of Table 4. They each involve four π- and two π′-electrons. Huisgen (37) has classified both O_3 and CH_2N_2 as 1,3-dipolar molecules, and has assumed that the sextet valence-bond structures 5 and 6 of Table 2, and 4 and 5 of Table 4 are the important structures for a concerted mechanism for 1,3-dipolar cycloaddition reactions. An alternative concerted mechanism has been proposed (38) for this class of reaction, which utilizes the 'long-bond' (or spin-paired diradical) structure of type 3 in both Tables 2 and 4 rather than the sextet structures. More recently, Goddard and Walch (18) have also concluded that the spin-paired diradical structure for CH_2N_2 is important for a description of the electronic structure and cycloaddition reactions of this molecule. The results of our valence-bond calculations provide further support for this hypothesis.

We shall report here the results of two valence-bond calculations, each of which utilizes the Hamilton approximation. The first calculation includes explicitly only the six π-electrons in the Slater determinants, whereas the second also includes two CN σ-electrons and two CC σ-electrons. Twelve valence-bond structures were considered that differ in the positions of the six π-electrons. These structures are displayed in Table 4, together with the eigenvectors for the two sets of calculations. The hybridizations for the central nitrogen atom, and the carbon atom, were assumed to be *sp* and sp^2 respectively.

In Table 4, the valence-bond wave-functions have similar sets of coefficients. They indicate that the most important of the bond-eigenfunctions is that which pertains to the 'long-bond' structure 3, with zero formal charges on all atoms. The bond-eigenfunction coefficients for the zwitterionic structures 1 and 2 are smaller than are those for 3. As is the case for O_3, the absence of formal charges in the 'long-bond' structure 3 may be responsible for the importance of its bond-eigenfunction. Structure 7 also carries zero formal charges on all atoms, and the coefficient for its bond-eigenfunction also has appreciable magnitude. Each of these results is in accord with what we would deduce from the electroneutrality principle.

The important valence-bond structures for the Huisgen mechanism of 1,3-dipolar cycloaddition are structures 4 and 5 of Table 4. For the six-electron valence-bond calculation, the coefficients for the bond-eigenfunctions for these structures are 0.1044 and 0.0473. These are much smaller than the 0.3068, 0.2297, and 0.3770 for the bond-eigenfunctions that pertain to the zwitterionic and 'long-bond' structures 1, 2, and 3. Although it is possible that the importance of the sextet structures increases as a 1,3-

Can. J. Chem. Downloaded from www.nrcresearchpress.com by 210.87.254.42 on 09/05/12
For personal use only.

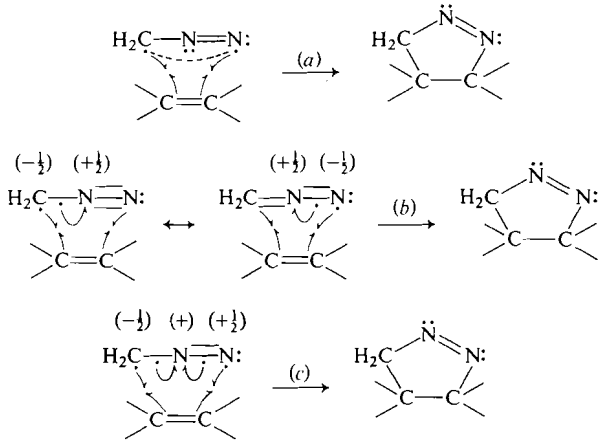

FIG. 1. Electronic mechanisms for 1,3-dipolar cycloaddition reactions.

dipolar cycloaddition reaction proceeds, it may be more favourable energetically to assume that the 'reactive' structures are those that are important for the valence-bond representation of the ground-state of the 1,3-dipolar molecule. Of these latter structures, 3 is calculated to be the most important. If we use structure 3 alone, we may devise a simple mechanism for cycloaddition, namely that of *a* of Fig. 1. This mechanism has also been postulated recently by Goddard and Walch (18). It does not involve a reorganization of the atomic formal charge distribution as the reaction proceeds, and therefore it is compatible with the observed lack of solvent dependency on the rate of cycloaddition (37, 39).

The 'increased-valence'formulae **22** and **23** for CH_2N_2 (38) may be generated from the zwitterionic structures 1 and 2 of Table 4, by delocalizing a carbon and a (terminal) nitrogen non-bonding π-electron into a bonding CN or NN π-orbital. Resonance between these 'increased-valence' structures summarizes resonance between the valence-bond structures 1, 2, and 3 of Table 4. If we use **22** and **23** to represent the electronic structure of CH_2N_2, the mechanism for 1,3-dipolar cycloaddition becomes that of *b* of Fig. 1 (38). Alternatively, use of the Linnett non-paired spatial orbital formula **24** gives the cycloaddition mechanism (*c*) of Fig. 1.[1] Each of these electronic mechanisms depends on the contribution of the spin-paired diradical structure 3 of Table 4 to the description of the electronic diazomethane.

The wave-functions of Table 4 generate the atomic formal charges of **25** and **26**. Both calculations locate a small formal positive charge on the terminal nitrogen atom, and rather larger negative and positive formal charges on the carbon atom and the central nitrogen atom. A comparison of these formal charges with those of **22** and **23** might lead to the conclusion that **22** is the more important of the two 'increased-valence' formulae.

[1]Firestone has formulated mechanism (*c*) as a two-step mechanism (39). See ref. 38 for some comments on the electronic aspects of this procedure.

Some Comments on the Utility of Increased-valence Formulae

When Heitler–London procedures are used to construct wave-functions for the A—B and Y—A bonds of 'increased-valence' formulae **7** and **8**, these structures provide an economical (and easily-derived) method for summarizing resonance between the standard and 'long-bond' structures **1–3**.[2]

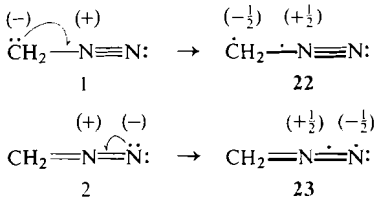

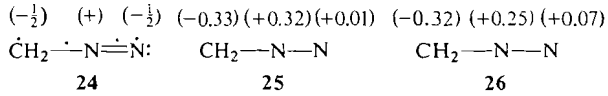

For O_3 and CH_2N_2, the economy gained by using 'increased-valence' formulae **12**, **13**, **22**, and **23** instead of the standard and 'long-bond' structures of Tables 2 and 4 is obviously not great. But if a molecule has two or more sets of 4-electron 3-centre bonding units, as has O_3 with standard valence-bond structures **15** and **16**, then the economy that is obtained by using 'increased-valence' formulae **17** and **18** is rather more considerable. Resonance between these latter structures is equivalent to invoking resonance between the standard structures **15** and **16** and the 'long-bond' structures **27–31**.

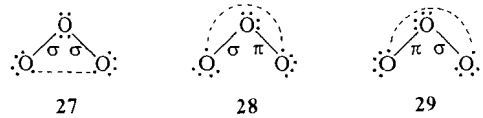

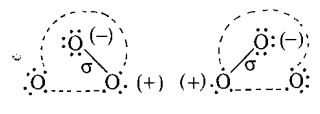

[2]The $S = 0$ wave-function for **7** is $|y\bar{\psi}_{ya}a\bar{b}| + |\psi_{ya}\bar{y}b\bar{a}|$, with $\psi_{ya} = ky + a$ and $k > 0$ (1, 3, 4, 14*b*). This wave-function may be expressed as $k(|y\bar{y}a\bar{b}| + |y\bar{y}b\bar{a}|) + |y\bar{a}a\bar{b}| + |a\bar{y}b\bar{a}|$, which is a linear combination of the bond-eigenfunctions for the standard and 'long-bond' structures **1** and **3**.

Can. J. Chem. Downloaded from www.nrcresearchpress.com by 210.87.254.42 on 09/05/12
For personal use only.

Can. J. Chem. Downloaded from www.nrcresearchpress.com by 210.87.254.42 on 09/05/12
For personal use only.

If at least some of the 'long-bond' structures are required to provide an elementary valence-bond description of certain molecules, it then does not become easy to make deductions about bond properties when these structures are written down together with the standard valence-bond structures. For example by writing down the 'long-bond' structures **27–29** with zero formal charges as well as the standard valence-bond structures **15** and **16**, one does not obtain an obvious understanding of why the OO bond-lengths of 1.28 Å for O_3 are closer to the OO double-bond length (1.21 Å) than to the single-bond length (1.48 Å). This is because although **15** and **16** alone imply some double-bond character for the OO bonds, each of **27–29** has only OO single bonds. Although inclusion of the 'long-bond' structures in the resonance description must lower the energy, the nearest-neighbour bond-orders (or bond-numbers) *seem* to be reduced in value. Inclusion of additional 'long-bond' structures such as **30** and **31** must lead to a further lowering of the energy. However, because each of these latter structures has only one (nearest-neighbour) OO single-bond, a further reduction in the (nearest-neighbour) OO bond-order might be deduced. Therefore we *seem* to obtain a paradoxical situation when 'long-bond' structures as well as standard valence-bond structures are used to represent the electronic structure of a molecule, namely, that inclusion of the 'long-bond' structures lowers the energy but *seems* to reduce the nearest neighbour bond-orders. This paradox arises because simply writing down the standard and 'long-bond' structures does not provide an obvious way to show the effect of resonance on nearest-neighbour bond orders. One way to resolve this difficulty is to use 'increased-valence' formulae such as **17** and **18** for O_3 to represent the electronic structure. We have already indicated that **17** and **18** summarize resonance between the standard and 'long-bond' structures **15**, **16**, and **27–31**. But by inspection of **17** and **18**, we can easily make the appropriate deductions about the OO bond properties. Each of these structures has an O_2 ground-state type double-bond (O÷O) and a weakened O_2 excited-state type double-bond (O═O). Therefore by using 'increased-valence' formulae **17** and **18** as a method to summarize resonance between the standard and 'long-bond' structures **15**, **16**, and **27–31**, we ensure that inclusion of the 'long-bond' structures both lowers the energy and increases the OO bond-orders relative to the values that pertain for resonance between the standard structures **15** and **16** alone. The 'increased-valence' formulae take account of the effect of resonance on nearest-neighbour bond-order in a manner which is identical to that which pertains when the valence structure A·B for a 1-electron bond is used to summarize resonance between the structures $\dot{A}$ B and A $\dot{B}$. Neither of the latter two structures alone has an AB bonding electron, but resonance between them generates AB bonding, which is indicated quite clearly by means of the valence structure A·B.

Acknowledgments

One of us (W.R.) acknowledges the award of a Commonwealth Postgraduate Scholarship, which was held throughout the tenure of this work (1971–1973). The manuscript for this paper was completed during study leave by one of us (R.D.H.) at Cornell and Göttingen Universities. Professors R. Hoffmann and W. A. Bingel are thanked for the use of the facilities of their departments at Cornell and Göttingen. We are indebted to Drs. F. R. Burden and B. T. Hart, and the Monash University Chemistry Department for making available their integral evaluation program.

1. R. D. Harcourt and A. G. Harcourt. J. Chem. Soc. Faraday II, **70**, 743 (1974) and references 1-10 therein.
2. J. W. Linnett. Sci. Prog. (Oxford), **60**, 1 (1972).
3. R. D. Harcourt. (*a*) J. Chem. Educ. **45**, 779 (1968); **46**, 856 (1969); (*b*) Aust. J. Chem. **22**, 279 (1969).
4. R. D. Harcourt and J. F. Sillitoe. Aust. J. Chem. **27**, 691 (1974).
5. D. M. Hirst and J. W. Linnett. J. Chem. Soc. 1035 (1962); 3844 (1962); 1068 (1963).
6. R. D. Gould and J. W. Linnett. Trans. Faraday Soc. **59**, 1001 (1963).
7. J. Bilham and J. W. Linnett. Nature, **201**, 1323 (1964) and unpublished results.
8. H. C. Bowen and J. W. Linnett. Trans. Faraday Soc. **60**, 1185 (1964); A. Macias. J. Chem. Phys. **49**, 2198 (1968).
9. W. H. Kirchhoff, J. Farren, and J. W. Linnett. J. Chem. Phys. **42**, 1410 (1965).
10. D. M. Hirst and J. W. Linnett. J. Chem. Phys. **43**, S74 (1965).
11. H. C. Bowen and J. W. Linnett. J. Chem. Soc. A, 1675 (1966).
12. L. C. Allen, R. M. Erdahl, and J. C. Whitten. J. Am. Chem. Soc. **87**, 3769 (1965).
13. J. C. Schug. J. Chem. Phys. **42**, 2547 (1965).
14. R. D. Harcourt. (*a*) Theoret Chim. Acta, **2**, 437 (1964); **4**, 202 (1966); (*b*) Theoret. Chim. Acta, **6**, 131 (1966); (*c*) Int. J. Quant. Chem. **4**, 173 (1970).
15. M. Hasegawa, K. Daiyasu, and S. Yomosa. J. Phys. Soc. Jpn. **27**, 999 (1969).
16. A. P. Mortola and W. A. Goddard III. J. Am. Chem. Soc. **96**, 1 (1974).
17. W. R. Wadt and W. A. Goddard III. J. Am. Chem. Soc. **97**, 3004 (1975) and refs. 10 and 11 therein.
18. S. P. Walch and W. A. Goddard III. J. Am. Chem. Soc. **97**, 5319 (1975).
19. W. A. Goddard III and B. D. Olafson. Proc. Nat. Acad. Sci. **72**, 2335 (1975).
20. R. D. Harcourt. (*a*) Aust. J. Chem. **28**, 881 (1975); (*b*) J. Inorg. Nucl. Chem. **39**, 237 (1977); **39**, 243 (1977); (*c*) Refs. 11*a–i* of ref. 1; (*d*) I.J.Q.C. Quantum Biology Symposium, Sanibel, **4**, 143 (1977).

21. R. D. HARCOURT and D. P. KELLY. Environ. Sci. Technol. **8**, 675 (1974).
22. L. PAULING. J. Chem. Soc. 1461 (1948).
23. J. GERRATT. Chem. Soc. Specialist Periodical Reports: Theoret. Chem. **1**, 60 (1974).
24. E. CLEMENTI and D. L. RAIMONDI. J. Chem. Phys. **38**, 2686 (1973).
25. W. J. HEHRE and J. A. POPLE. J. Am. Chem. Soc. **92**, 2191 (1970).
26. R. MCWEENY and B. T. SUTCLIFFE. Methods of molecular quantum mechanics. Vol. 2. Academic Press Inc., London. 1969.
27. W. KAUZMANN. Quantum chemistry. Academic Press Inc., London. 1957. p. 422.
28. P. O. LÖWDIN. Phys. Rev. **97**, 1474 (1955); **97**, 1490 (1955).
29. R. F. STEWART. J. Chem. Phys. **50**, 2485 (1969); **52**, 431 (1970).
30. (*a*) B. T. HART. Technical Report No. 1, Theoretical and Spectroscopy Group, Monash University, 1971; (*b*) F. R. BURDEN and B. T. HART. Aust. J. Chem. **26**, 1381 (1973).
31. J. MILLER, R. H. FRIEDMAN, R. P. HURST, and F. A. MATSEN. J. Chem. Phys. **27**, 1385 (1957).
32. W. C. HAMILTON. Proc. R. Soc. A**235**, 395 (1956).
33. (*a*) R. G. A. R. MACLAGAN and G. W. SCHNUELLE. J. Chem. Phys. **55**, 5431 (1971); (*b*) R. G. A. R. MACLAGAN and H. D. TODD. Theoret. Chim. Acta, **34**, 19 (1974).
34. J. M. NORBECK and G. A. GALLUP. J. Am. Chem. Soc. **96**, 3386 (1974).
35. L. E. SUTTON. Tables of interatomic distances. Chem. Soc. Special Publication No. 11, 18 (1958, 1965).
36. R. D. HARCOURT. J. Mol. Struct. **11**, 1 (1972); **18**, 515 (1973).
37. R. HUISGEN. (*a*) J. Org. Chem. **33**, 2291 (1968); (*b*) J. Org. Chem. **41**, 403 (1976).
38. R. D. HARCOURT. J. Mol. Struct. **12**, 351 (1972).
39. R. A. FIRESTONE. (*a*) J. Org. Chem. **33**, 2285 (1968); (*b*) J. Chem. Soc. A, 1570 (1970); (*c*) J. Org. Chem. **37**, 2181 (1972).

Can. J. Chem. Downloaded from www.nrcresearchpress.com by 210.87.254.42 on 09/05/12
For personal use only.

On the construction of the C/D ring systems of chasmanine and napelline by diene addition

KARNAIL S. ATWAL, RINALDO MARINI-BETTOLO, IGNACIO H. SANCHEZ, THOMAS Y. R. TSAI, AND KAREL WIESNER

Natural Products Research Center, University of New Brunswick, P.O. Box 4400, Fredericton, N.B., Canada E3B 5A3

Received November 16, 1977

KARNAIL S. ATWAL, RINALDO MARINI-BETTOLO, IGNACIO H. SANCHEZ, THOMAS Y. R. TSAI, and KAREL WIESNER. Can. J. Chem. **56**, 1102 (1978).

The construction of the C/D ring system of the alkaloids chasmanine and napelline by modification and rearrangement of a common intermediate is explored on model compounds.

The phenolic acid **9** was oxidized to the spirolactone **10**. Addition of benzyl vinyl ether to this material gave the adduct **28** in high yield. This central 'nordenudatine' type intermediate was then modified (in a very few stereospecific steps) to the 'napelline' model compound **47** and to the keto acetal **38**. Compound **38** is an intermediate of our photochemical route and we have already described its conversion to a chasmanine model derivative.

The new syntheses of chasmanine and napelline foreshadowed by the present model studies are expected to be completely stereo- and regiospecific, almost 10 steps shorter and an order of magnitude more efficient than the total syntheses of these two alkaloids which we have reported in the recent past.

Incidentally, with these model studies, the methoxy ketone **20** was prepared. The methoxyl in this compound is epimeric to the corresponding (C16) methoxyl of the aconite alkaloids. Some relevant observations on the nmr spectra and allylic rearrangement (pyro–isopyro rearrangement) of this material are also reported.

KARNAIL S. ATWAL, RINALDO MARINI-BETTOLO, IGNACIO H. SANCHEZ, THOMAS Y. R. TSAI et KAREL WIESNER. Can. J. Chem. **56**, 1102 (1978).

On étudie, sur des composés modèles, la possibilité de construire les systèmes des cycles C/D des alcaloïdes chasmanine et napelline par une modification et une transposition d'un intermédiaire commun.

On a oxydé l'acide phénolique **9** en spirolactone **10**. L'addition d'éther benzylvinylique à ce composé conduit à l'adduit **28** avec un bon rendement. On a alors modifié cet intermédiaire central de type "nordénudatine" (à l'aide de quelques étapes très stéréospécifiques) pour conduire au composé modèle **47** "napelline" et au céto-acétal **38**. Le composé **38** est un intermédiaire dans notre voie photochimique et nous avons déjà décrit sa transformation en un dérivé modèle de chasmanine.

On prévoit que les nouvelles synthèses de la chasmanine et de la napelline préconisées par les présentes études modèles seront complètement stéréo- et régiospécifique, qu'elles comporteront dix étapes de moins et seront au moins 10 fois plus efficaces que les synthèses totales de ces deux alcaloïdes qui ont été rapportés récemment.

Incidemment, avec ces études modèles, on a préparé la méthoxy cétone **20**. Le groupe méthoxy de ce composé est en position épimère par rapport au groupement méthoxy correspondant (C16) des alcaloïdes de l'aconite. On rapporte aussi quelques observations appropriées concernant les spectres rmn et la transposition allylique (transposition pyro–isopyro) de ce composé.

[Traduit par le journal]

Introduction

We have shown (1) that a route proceeding via denudatine-type intermediates is very advantageous for the construction of polysubstituted C19 aconite alkaloids and very recently we have successfully completed a stereospecific total synthesis of the alkaloid chasmanine **I** using such a route (2). In this synthesis the denudatine-type intermediate **II** was constructed by a modification (3) of our photochemical method, rearranged to the oxopyrochasmanine derivative **III**, and this compound was simply functionalized to chasmanine **I**.

In another recent publication we have disclosed a shorter and better method (4) for the construction of the C/D ring system of the alkaloid denudatine based on the addition of a dienophile to a masked *o*-quinone system.

In the present communication we wish to discuss model experiments which pave the way to a much more efficient construction of the chasmanine intermediate **II** by this *o*-quinone method. The versatility of the approach will be further demonstrated by a successful model study for a new synthesis of the alkaloid napelline **IV**.

Our first napelline synthesis (5) proceeded via the intermediate **V**. The C/D ring system of this compound was constructed by a method which was quite lengthy in spite of containing novel features.

Can. J. Chem. Downloaded from www.nrcresearchpress.com by 210.87.254.40 on 09/05/12
For personal use only.

Can. J. Chem. Downloaded from www.nrcresearchpress.com by 210.87.254.40 on 09/05/12
For personal use only.

It will be seen in the sequel that a stereospecific synthesis of the C/D ring system of compound **V** may be accomplished with unexpected simplicity by the *o*-quinone route.

Discussion

The starting material for the present study was the *p*-quinone **1** described by Meinwald and Wiley (6). This material was converted to the methoxy derivative **3** which was our 'stand-in' for the chasmanine aromatic intermediate **VI**.

A stereo- and regiospecific synthesis of compound **VI** by our aziridine rearrangement method refined by several improvements is currently underway on a large scale.

Cleavage of the methoxyl in compound **3** by boron tribromide gave the corresponding phenol **4** in a yield of 89%.[1]

The phenol **4** was next converted into the dithiane derivative **5** using the recently published method of Gassman and Amick (7). Compound **5** was alkylated by methyl bromoacetate to the dithiane ester **6** and the dithiane function in this material was cleaved in the presence of mercuric oxide to give the ester aldehyde **7** in high yield. Baeyer–Villiger oxidation of compound **7** proceeded in a yield of 86% and gave the formate methyl ester **8**. Finally, saponification of compound **8** yielded the phenolic acid **9** and the system was set up for oxidation into the spirolactone according to Berney and Deslongchamps (8).[2]

The oxidation of the phenolic acid **9** by *N*-bromosuccinimide yielded a brilliant reddish-brown solution of the spirolactone **10**, which was immediately treated with an excess of methyl vinyl ether at 0°C. The red color faded in 40 h and the adduct **11** was isolated in an overall yield of 79%. It melted over a range of 99–107°C in agreement with the fact that it was a mixture of two epimers.

Saponification of the adduct **11** by methanolic sodium carbonate yielded 91% of the sharply melting diketone **12** (mp 124–125°C). Compound **12** showed in the infrared (ir) spectrum maxima at 1750, 1737, and 1657 cm^{-1} for the diketone and double bond. The nuclear magnetic resonance (nmr) spectrum displayed the typical doublet for the vinylic hydrogen at $\tau = 4.2$ ($J = 6$ Hz), which we have already encountered in our photochemical approach to this system (2,3), and a methoxyl singlet at $\tau = 6.67$.

The diketone **12** was converted to the sharply melting tosylhydrazone **13** and this compound was reduced by lithium borohydride to the alcohol **14** which also melted sharply at 183–184°C.

Compound **14** was then heated under reflux in dilute methanolic hydrochloric acid with acetyl acetone and the crystalline epimeric mixture **15** was obtained in a yield of 85%. The ratio of the epimers was 3:1 and they were separated for spectral charac-

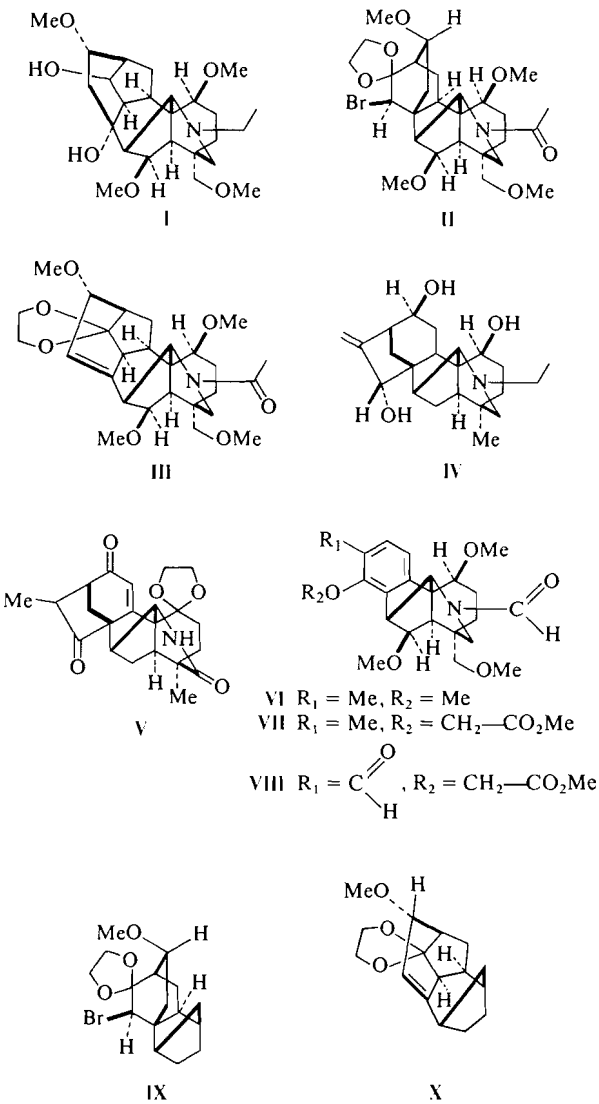

SCHEME 1

[1]This reaction cannot be applied to the polymethoxylated derivative **VI**. However, a selective cleavage of the aromatic methoxyl in this compound has been achieved in a high yield by the thioethoxide ion. Spectral data will be given in the Discussion only in specially relevant cases to conserve space. Full characterization of all compounds may be found in the Experimental.

[2]In the synthesis proper the rather inefficient dithiane method will be replaced by a direct oxidation of the aromatic methyl group in the intermediate **VII** to the aldehyde **VIII**. This reaction has been shown to proceed under controlled conditions in a yield of 90%. The present example is one of many which have convinced us that the progress of total synthesis depends at least as much on strategy as on new methods.

Can. J. Chem. Downloaded from www.nrcresearchpress.com by 210.87.254.40 on 09/05/12
For personal use only.

terization by preparative thin-layer chromatography (tlc). The fact that only a certain amount of epimerization but no α-ketol rearrangement had taken place followed from the subsequent transformations which finally resulted in a connection with our photochemical model series (1). The structures of the photochemical model compounds were in turn supported by an X-ray analysis of the final product.

The ketols **15** were then transformed to the crystalline mixture of the corresponding mesylates **16** and this material was reduced with lithium in liquid ammonia. The resulting alcohol was not characterized, but it was immediately oxidized with the chromium trioxide – pyridine complex and the ketone **17** was obtained in an overall yield of 70%.

Hydrogenation of **17** over rhodium-on-alumina in methanol, followed again by reoxidation with the chromium trioxide – pyridine complex finally gave the saturated ketone **18** in a yield of 89%. The configuration of the newly created chiral centre followed rigorously from the subsequent correlation with our photochemical model series (1).

Bromination of the methoxy ketone **18** with liquid bromine in ether yielded 88% of the bromoketone **19** which melted sharply at 82.5°C. The nmr spectrum of compound **19** showed clearly a narrow doublet at $\tau = 5.78$ ($J = 2.2$ Hz) for the proton unshielded by bromine. However, it was the outcome of the subsequent rearrangement step and its requirement of antiplanarity which enabled us to assign to the bromoketone the configuration **19**.

The bromoketone was heated to 125°C in dimethylsulfoxide (DMSO) and 1,5-diazabicyclo[4.3.0]non-5-ene. The rearrangement product **20** was obtained in a 76% yield as sharply melting colorless plates (mp 77.5°C).

Compound **20** showed in the ir spectrum maxima at 1760 and 1633 cm^{-1} for the ketone and double bond and its ultraviolet (uv) spectrum (λ_{max} 214.5 (log ε 3.5) and 232 nm (log ε 3.2)) was 'anomalous' as a result of orbital overlap. In the nmr spectrum the vinylic proton gave a broad singlet at $\tau = 4.87$.

We prepared for comparison the epimer of compound **20** from one of our photochemical intermediates (*vide infra*). The nmr spectrum of this derivative **21** shows the vinylic hydrogen signal as a doublet ($J = 6$ Hz) at $\tau = 4.51$. It is significant that the vinylic hydrogen signal of **21** resembles very closely the corresponding signal given by the aconite alkaloid pyroderivatives and is very different from the vinylic hydrogen signal of the epimer **20**.

Thus it seems that the nmr signal of the vinylic hydrogen in the pyroderivatives may be used with confidence as evidence for the configuration of the C(16)-methoxyl in delphinine-type alkaloids.

We attempted to achieve a correlation of the unsaturated ketone **20** with our photochemical series (1) by eliminating the methoxyl via an allylic rearrangement. However, this rearrangement (called the pyro–isopyro rearrangement in the corresponding alkaloid derivatives) was unsuccessful in the presence of the keto group, possibly owing to the interaction of this function with the double bond.

Consequently, compound **20** was reduced with sodium borohydride to the alcohol **22** and this material was heated in acetic acid with *p*-toluene sulfonic acid. Under these conditions the desired allylic rearrangement indeed occurred, but the secondary hydroxyl was simultaneously esterified with acetic acid. The product **23** was converted to the known (1) ketone **24** by saponification and oxidation with the chromium trioxide – pyridine complex. As we have already pointed out, the structures in the photochemical model series have been verified by X-ray crystallography.

In spite of the fact that the allylic rearrangement was acid catalyzed and consequently one would not expect it to depend on the configuration of the leaving methoxyl group, the outcome of this reaction was much cleaner and the yield higher with the methoxyl in the epimeric configuration (1). Thus, it seems that the ejection of the protonated methoxyl might be assisted by a concerted attack of a solvent molecule on the double bond, provided the methoxyl and the solvent molecule are sterically correctly disposed (9). However, no firm statement can be made on this aspect of the rearrangement without a careful quantitative study which we are not going to undertake.

The compound **21** was prepared from the known (1) photochemical intermediate **25**. This product was deketalized and the ketone **26** was brominated to the bromo ketone **27**. Rearrangement of the bromo ketone in DMSO with strong base gave the product **21** in a 90% yield.

Before concluding this section we should point out that the rearrangement of the α-bromo ketone had been tried but it failed with the corresponding full fledged chasmanine intermediate (2). When the reaction was allowed to proceed for a very long time, the only observable product was the debrominated ketone. On the other hand the rearrangement of the α-bromo ketal went, in the synthesis proper, smoothly and in high yield (2). This is probably due to the greater ease of the rearrangement in the model system which is lacking two rings. It is clear that the ejection of a leaving group from a position α to a ketone is easier if the keto group is masked.

In principle it might be possible to enter the series of 'natural' C(16) epimers (i.e. compounds with the methoxyl in the same configuration as **21**) via the allylic rearrangement of compound **22** and a sub-

Can. J. Chem. Downloaded from www.nrcresearchpress.com by 210.87.254.40 on 09/05/12
For personal use only.

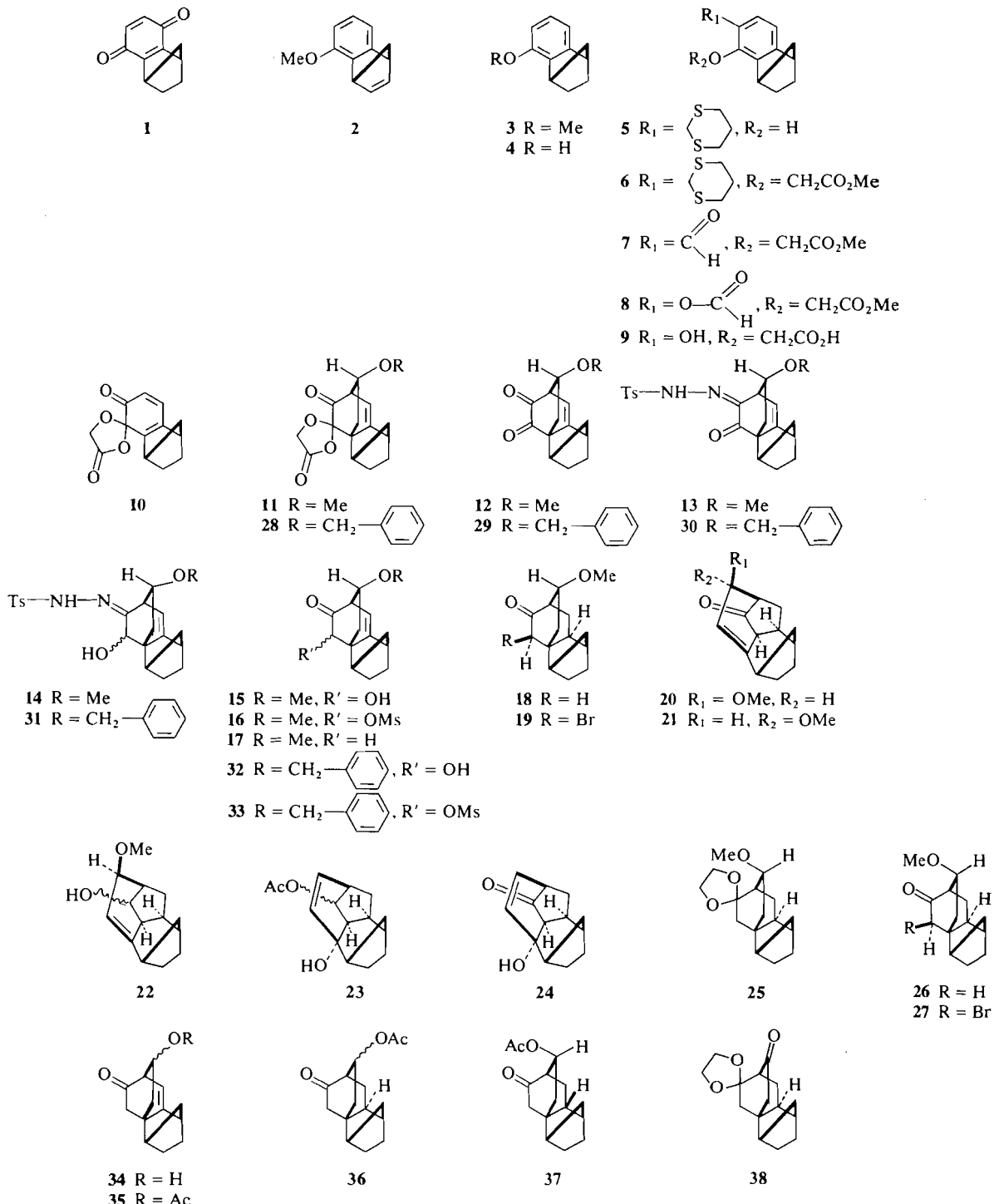

SCHEME 2

sequent transformation of the symmetrical double bond into a methoxyl with the desired configuration. However, in view of the poor yield of the allylic rearrangement in the 'unnatural' series and several other considerations this idea was abandoned. Instead we decided to make a fresh start and use, in the initial diene addition, a dienophile which would enable us to invert the configuration of the substituent destined to become the methoxyl.

The solution of the spirolactone **10** prepared in

Can. J. Chem. Downloaded from www.nrcresearchpress.com by 210.87.254.40 on 09/05/12
For personal use only.

the manner already described was treated with an excess of benzyl vinyl ether and the crystalline mixture of the epimeric adducts **28** was obtained in an overall yield (from compound **9**) of more than 80%. The adducts **28** were now converted (via the intermediates **29**, **30**, **31**, and **32**) to the mixture of the epimeric mesylates **33** using a reaction sequence precisely analogous to the one described above for the adducts **11**. The major and the minor component of the mixture **33** were both crystalline compounds and they were obtained in a ratio of 6:1. The major component was hydrogenated over 10% palladium-on-charcoal and the hydrogenolysis product **34** was obtained in a yield of 87%. Compound **34** is an aldol and it is a mixture of epimers since the hydroxyl is able to equilibrate by a retro aldol reaction – aldol condensation mechanism in the acidic hydrogenation medium and during the isolation process. Moreover, this material proved to be identical with the same mixture which was an intermediate of our photochemical approach (3) and had already been converted (via the compounds **35**, **36**, and **38**) to the bromo acetal **IX** (Scheme **1**) and hence to the rearranged product **X**.

Since the identification of mixtures lacks rigour, we continued the synthesis by the method already described (3) to the keto ketal **38** and proved the identity of this material with the corresponding photochemical intermediate. The details of this work are in the Experimental. It should be pointed out that all steps in this sequence were stereospecific except for the hydrogenation **35** to **36** and **37** which is stereoselective in a ratio 3.2:1. This hydrogenation, however, operates with complete stereospecificity in the synthesis proper as we had opportunity to verify in our recent total synthesis of chasmanine (2).

The minor epimer of the mesylate mixture **33** was resistant to hydrogenation, but both epimers gave the aldol **34** on reduction with calcium in liquid ammonia in a yield of 68%. Thus, the highest yield in the hydrogenolysis step is obtainable if the epimers **33** are separated, the major one is hydrogenated over palladium-on-charcoal and the minor one reduced with calcium in liquid ammonia.

The potential chasmanine synthesis foreshadowed by the model series **28** → **38** would be seven steps shorter than our recent total synthesis of this alkaloid (2) in which the photochemical C/D ring system construction was used.

The only flaw in the process **28** → **38** was the necessity of removing a substituent from the intermediate **33** which had to be subsequently reintroduced. This necessity results from the fact that we have been unable to control the stereochemistry in the reduction **29** → **32**. Moreover, in the rearrangement of the denudatine-type intermediate **IX**, bromine is required as a leaving group and we have been unable to introduce this substituent by displacement. However, even a stereospecific conversion of **30** into the correct epimer of **33** and a displacement of the mesyloxy group in this material by bromide would have saved only one step in comparison with the process which succeeded.

We shall turn now to the discussion of our studies directed toward a facile modification of the adduct **28** to the tetracyclic diketone **47**. This compound is a model for the diketone **V** (Scheme 1) which we have already converted to the alkaloid napelline **IV** (5).

Treatment of the diketone **29** with trimethylsilylmethylmagnesium chloride in tetrahydrofuran (THF) gave 64% of the crystalline epimeric alcohols **39**, which yielded 83% of the oily dienone **40** on warming with methanolic perchloric acid (4).

Reduction of this material with sodium borohydride in methanol gave 76% of compound **41** and 11.4% of a product which was probably the epimeric alcohol. In principle both isomers were potential intermediates for further work; however, to save time and labor we carried on the model synthesis only with the major product. While the configuration of the methyl group in **41** followed from its conversion to the known diketone **47** (*vide infra*), the stereochemistry of the alcoholic group was deduced from the nmr spectrum of the corresponding acetate **42**. The hydrogen deshielded by the acetoxy group in this compound (τ = 5.15, dd, J = 8 and 1 Hz) showed a vicinal coupling constant characteristic of a *cis* coplanar arrangement.

The acetate **42** was then subjected to a hydrogenolysis over palladium-on-charcoal and the resulting crystalline alcohol **43** was converted to the corresponding mesylate **44**.

Thus, in a few simple steps the stage was set for a rearrangement to the 'napelline' system. The mesylate **44** was heated under reflux with glacial acetic acid and the rearranged mixture of the epimers **45** was obtained in a yield of 90%.

The somewhat surprising finding that the rearrangement did not require an antiplanar attack by an acetic acid molecule and consequently gave rise to a mixture of epimeric acetates may be perhaps explained by the intermediacy of a relatively stable allylic carbonium ion. Saponification of the diacetates **45** and oxidation of the resulting diols **46** with the chromium trioxide – pyridine complex finally yielded 80% of the crystalline diketone **47** which melted at 58–59°C.

The diketone **47** was identical by mixture melting point, tlc in several systems, and ir, nmr, and mass

Can. J. Chem. Downloaded from www.nrcresearchpress.com by 210.87.254.40 on 09/05/12
For personal use only.

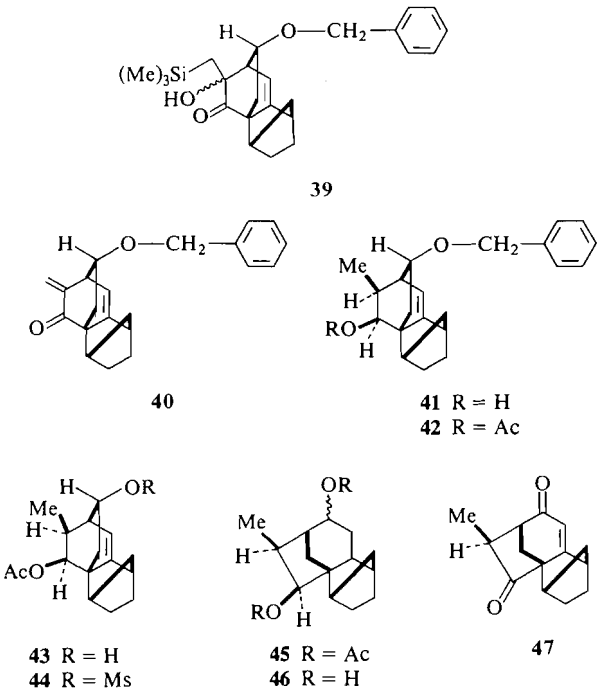

SCHEME 3

spectrometry (ms) with the same compound synthesized by our old method (10)[3] which we employed in our first synthesis of napelline (5).

Experimental

Preparation of Compound 2

A solution of *p*-quinone **1** (6) (25 g) in dry benzene (300 ml) was treated with trimethylphosphite (22 ml) and the resulting mixture heated to reflux under nitrogen overnight. A marked colour change from deep yellow to brown and then to light yellow was observed during the first ½ hour of the reaction. Evaporation of the solvent under reduced pressure produced a brown syrup which was taken up in dry THF (150 ml) and added at −78°C to ammonia (200 ml). Sodium metal (5.5 g) in small pieces was added to the well stirred mixture. A change in colour from dark brown to yellow was observed within the first ½ h of the reaction. After stirring for 1 h, the reaction was quenched with methanol (40 ml). Evaporation of the solvent under reduced pressure produced a reddish residue which was dissolved in water and thoroughly extracted with ether. Extracts were washed with 5% sodium hydroxide solution (until colourless washings were obtained), saturated sodium bicarbonate, water, and brine. After drying over anhydrous sodium sulfate, the solvent was evaporated under reduced pressure and the residue chromatographed on silica gel using ether–hexane (2:98, v/v) to give 14.09 g of the desired product **2** in 70.5% yield as a colourless oil; nmr ($CDCl_3$) τ: 3.15 (m, 4H, two aromatic and two olefinic protons), 3.47 (m, 1H, aromatic proton), 5.83 and 6.13 (b s, 1H each, benzylic bridgehead protons), 6.18 (s, 3H, aromatic methoxyl), 7.80 ppm (m, 2H, methylenic protons). *Mol. Wt.* calcd. for $C_{12}H_{12}O$: 172; found (ms): 172.

[3]C. S. J. Tsai. Unpublished results.

Hydrogenation of Compound 2

A solution of compound **2** (50 g), was hydrogenated at atmospheric pressure over 10% palladium-on-charcoal (5 g) in ethanol (1500 ml). The catalyst was filtered off through a Celite pad and the solvent evaporated under reduced pressure to furnish the dihydro compound **3** in quantitative yield as a colourless oil; nmr ($CDCl_3$) τ: 3.17 (m, 3H, aromatic protons), 6.18 (s, 3H, aromatic methoxyl), 6.37 and 6.68 ppm (b s, 1H each, benzylic bridgehead protons). *Mol. Wt.* calcd. for $C_{12}H_{14}O$: 174; found (ms): 174.

Preparation of Phenol 4

Boron tribromide (50 g) in 300 ml of dry methylene chloride was added to a solution of compound **3** (50 g) in 1000 ml of dry methylene chloride at −78°C. The temperature was raised to 0°C and stirred at this temperature for an additional hour. The reaction was quenched with ice cold water, the organic layer separated, and the aqueous layer re-extracted with methylene chloride. The combined extracts were washed with water and dried over anhydrous sodium sulfate. Evaporation of the solvent gave a light yellow oil which was purified by chromatography on silica gel using ether–hexane (1:4, v/v) to give 41.0 g (89.1%) of phenol **4** as colourless prisms, mp 78–79°C from carbon tetrachloride – hexane; ir ($CHCl_3$): 3675, 3400 cm^{-1} (phenol); nmr ($CDCl_3$) τ: 3.20 (m, 3H, aromatic protons), 5.28 (s, 1H, phenolic proton), 6.48 and 6.65 ppm (b s, 1H each, benzylic bridgehead protons). *Mol. Wt.* calcd. for $C_{11}H_{12}O$: 160; found (ms): 160. *Anal.* calcd. for $C_{11}H_{12}O$: C 82.46, H 7.55; found: C 82.27, H 7.60.

Preparation of the Dithiane Adduct 5 (7)

A solution of *N*-chlorosuccinimide (170 mg) in dry methylene chloride (20 ml) was cooled to 0°C and treated with crystalline 1,3-dithiane (180 mg). After 15 min stirring under nitrogen the temperature was lowered to −20°C (carbon tetrachloride – CO_2 bath) and the recrystallized phenol **4** (200 mg) in dry methylene chloride (3 ml) was added dropwise. Stirring was continued for 30 min and the temperature was then lowered to −78°C (acetone – CO_2 bath). The yellow reaction mixture was treated with triethylamine (145 mg). The resulting red solution was allowed to warm up to room temperature and treated with 1 *N* hydrochloric acid and the colour disappeared. The organic layer was washed to neutrality with water, dried over anhydrous sodium sulfate and evaporated to dryness. The residue was purified by preparative tlc on silica gel using benzene to give 127.4 mg of the dithiane derivative **5** (60.1% yield based on the phenol consumed) as amorphous solid; ir (CCl_4): 3615, 3450 cm^{-1} (phenol); nmr ($CDCl_3$) τ: 3.13 (ABq, J = 7.5 Hz, 2H, aromatic protons), 3.83 (s, 1H,), 4.58 (s, 1H, phenolic proton), 6.43 and 6.72 ppm (broad singlets, 1H each, benzylic bridgehead protons). *Mol. Wt.* calcd. for $C_{15}H_{18}OS_2$: 278; found (ms): 278.

Alkylation of Dithiane Derivative 5

The dithiane derivative **5** (17.0 g) in 300 ml of acetone (potassium carbonate distilled) was stirred at room temperature with 11.0 g of powdered potassium carbonate and 5.5 ml of methyl bromoacetate in the presence of a catalytic amount of crown ether (18-crown-6). After stirring for 3½ h, the inorganic salt was filtered off and the solvent evaporated under reduced pressure to give 20.01 g of the expected product **6** in 93.9% yield as a colourless oil; ir ($CHCl_3$): 1760 cm^{-1} (ester); nmr ($CDCl_3$) τ: 2.83 (ABq, J = 7.5 Hz, 2H, aromatic protons), 4.15 (s, 1H,), 5.32 (s, 2H, methylenic

Can. J. Chem. Downloaded from www.nrcresearchpress.com by 210.87.254.40 on 09/05/12
For personal use only.

protons of the ester side chain), 6.15 ppm (s, 3H, ester methyl). *Mol. Wt.* calcd. for $C_{18}H_{22}O_3S_2$: 350; found (ms): 350.

Preparation of Compound **7**

A solution of compound **6** (20 g) in THF (100 ml) was added to a stirred suspension of mercuric oxide (26 g) and boron trifluoride etherate (15 ml) in 15% aqueous THF (500 ml). After stirring for 30 min, the reaction mixture was diluted with water and the resulting precipitate filtered off. The filtrate was diluted with ether (200 ml), washed with aqueous sodium bicarbonate and brine. Drying over anhydrous magnesium sulfate and evaporation of the solvent furnished 12.7 g of the desired compound **7** in 86.4% yield as a light yellow oil; ir ($CHCl_3$): 1755, 1735 (ester), 1675 cm^{-1} (aromatic aldehyde); nmr ($CDCl_3$) τ: −0.53 (s, 1H, aldehyde proton), 2.66, (ABq, J = 7.5 Hz, 2H, aromatic protons), 5.23 (s, 2H, methylenic protons of ester side chain), 6.17 (s, 3H, ester methyl), 6.33 and 6.60 ppm (b s, 1H each, benzylic bridgehead protons). *Mol. Wt.* calcd. for $C_{15}H_{16}O_4$: 260; found (ms): 260.

Baeyer–Villiger Oxidation of Compound **7**

A solution of compound **7** (9.0 g) in 220 ml of dry dichloromethane was heated under reflux with 9.0 g of *m*-chloroperbenzoic acid for 1 h in a nitrogen atmosphere. The reaction mixture was cooled to room temperature, diluted with 200 ml of dichloromethane and washed thoroughly with aqueous sodium bicarbonate and water. Drying over anhydrous magnesium sulfate and evaporation of the solvent *in vacuo* gave 8.21 g (86%) of the formate ester **8** as a light yellow oil; ir ($CHCl_3$): 1750 cm^{-1} (b, formate and methyl ester); nmr ($CDCl_3$) τ: 1.72 (s, 1H, formate proton), 3.13 (ABq, J = 7 Hz, 2H, aromatic protons), 5.37 (s, 2H, methylenic protons of ester side chain), 6.18 (s, 3H, ester methyl), 6.33 and 6.65 ppm (b s, 1H each, benzylic bridgehead protons). *Mol. Wt.* calcd. for $C_{15}H_{16}O_5$: 276; found (ms): 276.

Preparation of the Diels–Alder Adduct **11**

The formate methyl ester **8** (9.5 g) was heated under reflux with 100 ml of 5% methanolic potassium hydroxide for 1 h. The reaction mixture was cooled to room temperature, diluted with water (50 ml), and acidified with hydrochloric acid. Excess methanol was evaporated under reduced pressure and the residue was extracted with methylene chloride. The combined extracts were washed with water and evaporated to a volume of 300 ml. The resulting solution of the phenolic acid **9** was cooled to 0°C and stirred with 300 ml of aqueous sodium acetate (4.1 g). A solution of 6.23 g of *N*-bromosuccinimide and 4.1 g of sodium acetate in 400 ml of water was added slowly to this two phase reaction mixture. Vigorous stirring was continued for 30 min, the organic layer was separated and the aqueous phase re-extracted with methylene chloride until colourless extracts were obtained. The combined extracts were dried over anhydrous magnesium sulfate and evaporated to a volume of 30 ml. This brilliant reddish-brown solution of the spirolactone **10** was cooled to 0°C and treated with an excess of methyl vinyl ether. The red colour of the quinone faded overnight and the stirring was continued for 40 h at room temperature. The solvent and the excess methyl vinyl ether were evaporated under reduced pressure and the residue was chromatographed on silica gel using ether–hexane (1:2, v/v) to give 8.74 g (78.7%) of adduct **11** as colourless prisms, mp 99–107°C from ether–hexane; ir (CCl_4): 1830 (lactone), 1745 cm^{-1} (six-membered ketone); nmr ($CDCl_3$) τ: 4.43 (d, J = 6 Hz, 1H, vinylic proton), 5.58 (2ABq, 2H, methylenic protons of spirolactone), 6.37 (m, 2H, proton unshielded by methoxyl and bicyclooctane bridgehead proton), 6.72 (s, 3H, methoxyl), 6.98 ppm (b s, 1H, bicycloheptane bridgehead proton). *Mol. Wt.* calcd. for $C_{16}H_{18}O_5$: 290; found (ms): 290. *Anal.* calcd. for $C_{16}H_{18}O_5$: C 66.19, H 6.25; found: C 65.75, H 6.21.

Base Treatment of the Diels–Alder Adduct **11**

The recrystallized adduct **11** (4.0 g) in 200 ml of methanol was stirred at room temperature with 20 ml of 5% aqueous potassium carbonate for 15 min. The reaction mixture was neutralized with dilute hydrochloric acid, diluted with 50 ml of water and most of the methanol was evaporated under reduced pressure. The residue was extracted with ether and the extracts were washed with brine and dried over anhydrous magnesium sulfate. Evaporation of the solvent furnished 2.92 g (91.3%) of the diketone **12** as yellow needles, mp 124–125°C from ether–hexane; ir (CCl_4): 1750, 1737 (cyclic α-diketones), 1657 cm^{-1} (double bond); nmr ($CDCl_3$) τ: 4.2 (d, J = 6 Hz, 1H, vinylic proton), 6.13 (m, 2H, proton unshielded by methoxyl and bicyclooctane bridgehead proton), 6.67 (s, 3H, methoxyl), 6.98 and 7.50 ppm (b s, 1H each, bicycloheptane bridgehead protons). *Mol. Wt.* calcd. for $C_{14}H_{16}O_3$: 232; found (ms): 232. *Anal.* calcd. for $C_{14}H_{16}O_3$: C 72.39, H 6.94; found: C 72.03, H 6.98.

Preparation of the Tosylhydrazone **13**

A solution of the recrystallized diketone **12** (3.0 g) and tosylhydrazine (2.6 g) in 300 ml of methanol was stirred at room temperature for 4 h. The tosylhydrazone crystallized out of the solution as yellow plates which were filtered off and the mother liquor concentrated for a second crop. The two crops furnished 4.55 g (88%) of the tosylhydrazone **13**, mp 166.5–167°C (sintering at 157.5°C) from methanol; ir (CCl_4): 3190 (N—H), 1680 cm^{-1} (six-membered conjugated ketone); nmr ($CDCl_3$) τ: 2.17, 2.68 (2d, J = 8 Hz, 2H each, aromatic protons), 4.17 (d, J = 6 Hz, 1H, vinylic proton), 6.28 (m, 2H, proton unshielded by methoxyl and bicyclooctane bridgehead proton), 6.68 (s, 3H, methoxyl), 7.05 (b s, 1H, bicycloheptane bridgehead proton), 7.55 ppm (s, 4H, aromatic methyl and a bicycloheptane bridgehead proton). *Anal.* calcd. for $C_{21}H_{24}O_4SN_2$: C 62.99, H 6.03, N 7.00; found: C 63.29, H 6.03, N 7.04.

Reduction of Compound **13**

The tosylhydrazone **13** (1.0 g) in dry THF (100 ml) was cooled to 0°C and treated with 100 mg of lithium borohydride. The reaction mixture turned yellow instantaneously but became colourless in about 20 min. It was then poured into ice cold dilute hydrochloric acid and the solvent was evaporated under reduced pressure. The residue was extracted with chloroform and the extracts were washed with water and brine and dried over anhydrous magnesium sulfate. Solvent evaporation under reduced pressure gave 891 mg (89.1%) of the epimeric alcohols **14** as a colourless powder, mp 183–184°C from methylene chloride – hexane; ir ($CHCl_3$): 3425 (hydroxyl), 3100 cm^{-1} (N—H); nmr ($CDCl_3$) τ: 2.13 and 2.97 (2d, J = 8 Hz, 2H each, aromatic protons), 4.43 (d, J = 6 Hz, 1H, vinylic proton), 5.90 (b s, 1H, proton unshielded by hydroxyl), 6.53 (m, 2H, proton unshielded by methoxyl and bicyclooctane bridgehead proton), 6.77 (s, 3H, methoxyl), 7.10 (b s, 1H, bicycloheptane bridgehead proton), 7.53 (s, 3H, aromatic methyl), 7.70 ppm (b s, 1H, bicycloheptane bridgehead proton). *Mol. Wt.* calcd. for $C_{21}H_{26}O_4SN_2$: 402; found (ms): 402.

Preparation of Compound **15**

A solution of compound **14** (6.5 g) in 80% ethanol (150 ml) was heated under reflux with 2 ml of 2 *N* hydrochloric acid and 3.25 g of acetylacetone for 2 h. The reaction mixture was cooled to room temperature and the solvent was evaporated

Can. J. Chem. Downloaded from www.nrcresearchpress.com by 210.87.254.40 on 09/05/12
For personal use only.

in vacuo. The residue was diluted with water (30 ml) and thoroughly extracted with chloroform. The combined extracts were washed with a saturated solution of cupric acetate, water, and brine followed by drying over anhydrous magnesium sulfate. The solvent was evaporated under reduced pressure and the residue was purified by column chromatography on silica gel using chloroform–hexane (1:4, v/v) to yield 3.22 g (85.1%) of the epimeric hydroxy ketones **15** as colourless plates, mp 148.5–154°C from ether. For characterization the mixture was separated by preparative tlc on silica gel using chloroform–hexane (95:5, v/v). The isomers were obtained in an approximate ratio of 3:1.

Major isomer; ir (CCl_4): 3530, 3375 (hydroxyl), 1725 (six-membered ketone), 1662 cm^{-1} (double bond); nmr ($CDCl_3$) τ: 4.45 (d, J = 6 Hz, 1H, vinylic proton), 6.37 (m, 2H, proton unshielded by methoxyl and bicyclooctane bridgehead proton), 6.57 (d, J = 2 Hz, 1H, proton unshielded by hydroxyl), 6.72 (s, 3H, methoxyl), 7.02 and 7.30 ppm (b s, 1H each, bicycloheptane bridgehead protons). *Mol. Wt.* calcd. for $C_{14}H_{18}O_3$: 234; found (ms): 234. *Anal.* calcd. for $C_{14}H_{18}O_3$: C 71.77, H 7.74; found: C 71.39, H 7.67.

Minor isomer; ir (CCl_4): 3515 (hydroxyl), 1725 (six-membered ketone), 1660 cm^{-1} (double bond); nmr ($CDCl_3$) τ: 4.52 (d, J = 6 Hz, 1H, vinylic proton), 6.35 (m, 3H, protons unshielded by methoxyl, hydroxyl and bicyclooctane bridgehead proton), 6.70 ppm (s, 3H, methoxyl). The mass spectra of both epimers were identical. *Mol. Wt.* calcd. for $C_{14}H_{18}O_3$: 234; found (ms): 234.

Preparation of Keto Mesylate ***16***

The hydroxy ketones **15** (1.45 g) in dry pyridine (10 ml) were cooled to 0°C and treated with 850 mg of mesyl chloride. The reaction mixture was stirred at room temperature overnight under nitrogen and then poured into ice cold dilute hydrochloric acid. Exhaustive extraction with chloroform and washing of the extracts with water, sodium bicarbonate, and brine followed by drying over anhydrous magnesium sulfate yielded 1.71 g (88.4%) of the keto mesylates **15** as colourless plates from ether.

Major isomer (β-mesylate; decomposed at 141°C); ir (CCl_4): 1737 cm^{-1} (six-membered ketone); nmr ($CDCl_3$) τ: 4.38 (d, J = 6 Hz, 1H, vinylic proton), 5.48 (d, J = 2 Hz, 1H, proton unshielded by mesylate), 6.30 (m, 2H, proton unshielded by methoxyl and bicyclooctane bridgehead proton), 6.70 (s, 3H, methoxyl), 6.73 ppm (s, 3H, mesylate methyl). *Mol. Wt.* calcd. for $C_{15}H_{20}O_5S$: 312; found (ms): 312. *Anal.* calcd. for $C_{15}H_{20}O_5S$: C 57.69, H 6.46; found: C 58.17, H 6.44.

Minor isomer (α-mesylate); mp 139.5–140°C; the entire mass spectra of both epimers were identical; ir (CCl_4): 1735 cm^{-1} (six-membered ketone); nmr ($CDCl_3$) τ: 4.45 (d, J = 6 Hz, 1H, vinylic proton), 5.40 (s, 1H, proton unshielded by mesylate), 6.35 (m, 2H, proton unshielded by methoxyl and bicyclooctane bridgehead proton), 6.72 (s, 3H, methoxyl), 6.80 ppm (s, 3H, mesylate methyl). *Mol. Wt.* calcd.: 312; found (ms): 312.

Lithium–Ammonia Reduction of Keto Mesylate ***16***

The keto mesylates **16** (700 mg) in anhydrous THF (10 ml) were added dropwise to a stirred solution of lithium metal (250 mg) in liquid ammonia (200 ml). After stirring for 1 h, the reaction mixture was quenched with wet ether and the excess of ammonia was evaporated. The residue was dissolved in water (20 ml), neutralized with dilute hydrochloric acid and extracted with chloroform. The combined extracts were washed with water and dried over anhydrous sodium sulfate. The solvent was evaporated under reduced pressure and the residue was taken up in 20 ml of dry methylene chloride and added to a stirred suspension of the chromium trioxide–dipyridine complex (3.6 g) in dry methylene chloride (100 ml). Stirring was continued for 15 min and the reaction was worked up by the normal procedure. The product was purified by preparative tlc on silica gel using ether–hexane (1:1, v/v) to yield 335 mg (70.3%) of compound **17** as a colourless oil; ir (CCl_4): 1725 cm^{-1} (six-membered ketone); nmr ($CDCl_3$) τ: 4.47 (d, J = 6 Hz, 1H, vinylic proton), 6.25 (m, 1H, proton unshielded by methoxyl), 6.50 (dd, J = 3 and 6 Hz, 1H, bicyclooctane bridgehead proton), 6.70 (s, 3H, methoxyl), 7.05 and 7.77 ppm (b s, 1H each, bicycloheptane bridgehead protons). *Mol. Wt.* calcd. for $C_{14}H_{18}O_2$: 218; found (ms): 218.

Hydrogenation of Compound ***17***

A solution of 310 mg of compound **17** in 20 ml of methanol and 300 mg of 5% rhodium-on-alumina catalyst was hydrogenated at 85 psi for 20 h. The catalyst was filtered off and the solvent was evaporated under reduced pressure. The residue was dissolved in 20 ml of dry dichloromethane and added to a stirred suspension of 2.3 g of the chromium trioxide–dipyridine complex in 100 ml of dry dichloromethane. Standard work-up gave a colourless residue which was purified by preparative tlc on silica gel using ether–hexane (1:1, v/v) to yield 276.4 mg (88.4%) of the single dihydro derivative **18** as a colourless glass; ir (CCl_4): 1720 cm^{-1} (six-membered ketone); nmr ($CDCl_3$) τ: 6.45 (m, 1H, proton unshielded by methoxyl), 6.70 ppm (s, 3H, methoxyl). *Mol. Wt.* calcd. for $C_{14}H_{20}O_2$: 220; found (ms): 220.

Preparation of Bromo Ketone ***19***

The methoxy ketone **18** (200 mg) was dissolved in 20 ml of ether and stirred at room temperature with 10 drops of liquid bromine. After 2½ h, the reaction mixture was diluted with 30 ml of ether and washed with 10% aqueous sodium bisulfite and brine. Drying over anhydrous sodium sulfate and evaporation of the solvent gave a colourless oil which was purified by preparative tlc on silica gel using ether–hexane (1:2, v/v) to yield 238 mg (87.5%) of the single bromo ketone **19** as colourless elongated plates, mp 82.5°C from ether–hexane; ir (CCl_4): 1737 cm^{-1} (six-membered ketone); nmr ($CDCl_3$) τ: 5.78 (d, J = 2.2 Hz, 1H, proton unshielded by bromine atom), 6.10 (m, 1H, proton unshielded by methoxyl), 6.70 ppm (s, 3H, methoxyl). *Mol. Wt.* calcd. for $C_{14}H_{19}O_2Br$: 299; found (ms): 299. *Anal.* calcd. for $C_{14}H_{19}O_2Br$: C 56.20, H 6.40; found: C 56.28, H 6.19.

Rearrangement of Bromo Ketone ***19***

The crystalline bromo ketone **19** (200 mg) in dry DMSO (7 ml) and 1,5-diazabicyclo[4.3.0]non-5-ene (2.5 ml) was heated to 125°C for 75 min under nitrogen. The reaction mixture was cooled to room temperature, poured into 15 ml of water and exhaustively extracted with ether (5 × 20 ml). The combined extracts were washed with 5% acetic acid, water, sodium bicarbonate, and brine and dried over anhydrous magnesium sulfate. Solvent evaporation gave a light yellow oil which was purified by preparative tlc on silica gel using ether–hexane (1:2, v/v) to yield 110 mg (75.4%) of the rearranged compound **20** as colourless plates, mp 77.5°C from hexane; ir (CCl_4): 1760 (five-membered ketone), 1633 cm^{-1} (double bond); nmr ($CDCl_3$) τ: 4.87 (b s, 1H, vinylic proton), 5.60 (d, J = 4 Hz, proton unshielded by methoxyl), 6.67 ppm (s, 3H, methoxyl); uv λ_{max} (CH_3OH): 214.5 (log ε 3.51), 232 nm (log ε 3.15). *Mol. Wt.* calcd. for $C_{14}H_{18}O_2$: 218; found (ms): 218. *Anal.* calcd. for $C_{14}H_{18}O_2$: C 77.03, H 8.31; found: C 77.12, H 8.09.

Preparation of Compound ***22***

A solution of the unsaturated ketone **20** (60 mg) in 10 ml

Can. J. Chem. Downloaded from www.nrcresearchpress.com by 210.87.254.40 on 09/05/12
For personal use only.

of absolute methanol was cooled to 0°C and treated with 12 mg of sodium borohydride. After stirring for 15 min, water (5 ml) was added to the reaction mixture and the excess of methanol was evaporated under reduced pressure. The residue was extracted with ether and the extracts were washed with water and brine and dried over anhydrous magnesium sulfate. Solvent evaporation under reduced pressure and purification of the residue by preparative tlc on silica gel using ether–hexane (3:1, v/v) gave 53 mg (87.5%) of alcohol **22** as a colourless glass; ir (CCl_4): 3600 (hydroxyl), 1650 cm^{-1} (double bond); nmr ($CDCl_3$) τ: 4.77 (b s, 1H, vinylic proton), 5.63 (d, $J = 4$ Hz, 1H, proton unshielded by methoxyl), 5.93 (dd, $J = 4$ and 7 Hz, 1H, proton unshielded by hydroxyl), 6.63 ppm (s, 3H, methoxyl). *Mol. Wt.* calcd. for $C_{14}H_{20}O_2$: 220; found (ms): 220.

Pyro–Isopyro Rearrangement of Compound 22

A solution of compound **22** (60 mg) and *p*-toluenesulfonic acid (20 mg) in glacial acetic acid (10 ml) was heated to 60°C for 30 min. The reaction mixture was cooled to room temperature and the acetic acid was evaporated under reduced pressure. The residue was dissolved in water and extracted with ether (3 × 10 ml). The combined extracts were washed with water, aqueous sodium bicarbonate and brine. Drying over anhydrous sodium sulfate and evaporation of the solvent gave a pale yellow oil which showed the presence of several compounds on tlc. The major product **23** (27 mg, 39.9%) was isolated by preparative tlc on silica gel using ether–hexane (2:1, v/v) as colourless glass; ir (CCl_4): 3600 (tertiary alcohol), 1760, 1740 (acetate), 1640 cm^{-1} (double bond); nmr ($CDCl_3$) τ: 4.13 (dd, $J = 6$ and 10 Hz, 1H, vinylic proton), 4.43 (d, $J = 10$ Hz, 1H, vinylic proton), 5.18 (m, $J = 4$ Hz, 1H, proton unshielded by acetate), 7.97 ppm (s, 3H, acetoxy methyl). *Mol. Wt.* calcd. for $C_{15}H_{20}O_3$: 248; found (ms): 248.

Transformation of Compound 23 to 24

The acetoxy alcohol **23** (25 mg) was heated under reflux with 10 ml of 5% ethanolic potassium hydroxide for 30 min. The reaction mixture was cooled to room temperature, diluted with water (5 ml), neutralized with dilute hydrochloric acid, and the excess ethanol was evaporated under reduced pressure. The residue was extracted with ether, and the extracts were washed with brine and dried over anhydrous magnesium sulfate. The solvent was evaporated, the residue was taken up in 5 ml of dry methylene chloride and added to a stirred suspension of the chromium trioxide – dipyridine complex (220 mg) in methylene chloride (10 ml). After stirring for 15 min, the reaction mixture was quenched with wet ether and worked up by the standard procedure. Solvent evaporation and purification of the residue by preparative tlc on silica gel using ether–hexane (2:1, v/v) gave 16.8 mg of the hydroxy ketone **24**. The identity of this material with a previously synthesized compound (1) was established by all standard spectral and chromatographic techniques.

Preparation of Methoxy Ketone 26

The methoxy ketal **25** (1) (396 mg) was heated to 85°C for 3 h in 30 ml of 80% aqueous acetic acid. The solvent was removed *in vacuo* and the residue was dissolved in ether, washed with water, and aqueous sodium bicarbonate and dried over anhydrous magnesium sulfate. Solvent evaporation under reduced pressure gave 313 mg (95%) of the methoxy ketone **26** which was used without purification for the next step; ir (CCl_4): 1730 cm^{-1} (six-membered ketone); nmr ($CDCl_3$) τ: 6.31 (m, 1H, proton unshielded by methoxyl), 6.73 ppm (s, 3H, methoxyl). *Mol. Wt.* calcd. for $C_{14}H_{20}O_2$: 220; found (ms): 220.

Bromination of Methoxy Ketone 26

Bromination of compound **26** to the bromo ketone **27**, exactly according to the procedure used for the epimer **18**; gave yield of 85%; ir (CCl_4): 1730 cm^{-1} (six-membered ketone); nmr ($CDCl_3$) τ: 5.67 (d, $J = 2.2$ Hz, 1H, proton unshielded by bromine atom), 6.67 ppm (s, 3H, methoxy). *Mol. Wt.* calcd. for $C_{14}H_{19}O_2Br$: 299; found (ms): 299.

Rearrangement of Bromo Ketone 27

A mixture of the bromo ketone **27** (150 mg), tetramethylguanidine (2.5 ml) and DMSO (2.5 ml) was heated to 160°C under nitrogen for 3 h. The reaction mixture was worked up as described for the bromo ketone **19** and the residue was purified by preparative tlc on silica gel using ether–hexane (1:1, v/v) to give 98 mg (90%) of the oily keto olefin **21**; ir (CCl_4): 1761 cm^{-1} (five-membered ketone); nmr ($CDCl_3$) τ: 4.51 (d, $J = 6$ Hz, 1H, vinylic proton), 6.00 (dd, $J = 4$ and 6 Hz, 1H, proton unshielded by methoxy), 6.63 ppm (s, 3H, methoxyl). *Mol. Wt.* calcd. for $C_{14}H_{18}O_2$: 218; found (ms): 218.

Preparation of the Diels–Alder Adduct 28

A solution of the spirolactone **10** (prepared as described above) in methylene chloride was treated with an excess of vinyl benzyl ether and the reaction mixture was stirred at room temperature for 24 h. Solvent evaporation and crystallization of the residue from methanol gave the adduct **28** in a 80.3% yield as colourless needles, mp 138–140°C; ir ($CHCl_3$): 1817 (lactone carbonyl), 1744 cm^{-1} (six-membered ketone); nmr ($CDCl_3$) τ: 2.67 (s, 5H, aromatic protons), 4.40 (d, $J = 6$ Hz, 1H, vinylic proton), 5.52 (s, 2H, benzylic protons), 5.57 (2ABq, 2H, methylenic protons of spirolactone), 6.02 (b m, 1H, proton unshielded by benzyloxy group), 6.43 (m, 1H, bicyclooctane bridgehead proton), 6.97 ppm (b s, 1H, bicycloheptane bridgehead proton). *Mol. Wt.* calcd. for $C_{22}H_{22}O_5$: 366; found (ms): 366. *Anal.* calcd. for $C_{22}H_{22}O_5$: C 72.11, H 6.05; found: C 72.17, H 6.01.

Preparation of Diketone 29

The recrystallized adduct **28** (9.5 g) in 200 ml of a methanol–THF mixture (1:1, v/v) was stirred at room temperature with 20 ml of 5% aqueous potassium carbonate for 30 min. The reaction mixture was diluted with water, neutralized with dilute hydrochloric acid and the excess solvent was evaporated under reduced pressure. The residue was extracted with ether and the extracts were washed with water and brine and dried over anhydrous sodium sulfate. Solvent evaporation gave 7.24 g (90.5%) of diketone **29** as yellow needles, mp 116.5–117.5°C from ether–hexane; ir ($CHCl_3$): 1735, 1750 cm^{-1} (α-diketone); nmr ($CDCl_3$) τ: 2.65 (s, 5H, aromatic protons), 4.15 (d, $J = 6$ Hz, 1H, vinylic proton), 5.47 (s, 2H, benzylic protons), 5.87 (m, 1H, proton unshielded by benzyloxy), 6.22 (m, 1H, bicyclooctane bridgehead proton), 6.95 and 7.50 ppm (b s, 1H each, bicycloheptane bridgehead protons). *Mol. Wt.* calcd. for $C_{20}H_{20}O_3$: 308; found (ms): 308. *Anal.* calcd. for $C_{20}H_{20}O_3$: C 77.92, H 6.49; found: C 77.75, H 6.23.

Preparation of Tosylhydrazone 30

The tosylhydrazone **30** was prepared from the diketone **29** exactly as described above for compound **13**. An analytical sample melted at 129–131°C (methanol); ir ($CHCl_3$): 3200 (N—H), 1683 cm^{-1} (six-membered conjugated carbonyl); nmr ($CDCl_3$) τ: 2.2, 2.27 and 2.72 (9H, aromatic protons), 4.17 (d, $J = 6$ Hz, 1H, vinylic proton), 5.55 (s, 2H, benzylic protons), 6.18 (m, 2H, proton unshielded by benzyloxy and bicyclooctane bridgehead proton), 7.07 (b s, 1H, bicycloheptane bridgehead proton), 7.60 ppm (4H, s, aromatic

Can. J. Chem. Downloaded from www.nrcresearchpress.com by 210.87.254.40 on 09/05/12
For personal use only.

methyl and bicycloheptane bridgehead proton). *Mol. Wt.* calcd. for $C_{27}H_{28}O_4N_2S$: 476; found (ms): 476. *Anal.* calcd. for $C_{27}H_{28}O_4N_2S$: C 68.05, H 5.92, N 5.88; found: C 67.85, H 5.75, N 5.89.

Reduction of Tosylhydrazone 30

The reduction of compound **30** proceeded exactly as described in the case of the methoxy derivative **13** to give the product **31** in an 88% yield as colourless prismatic needles. Several recrystallizations from ether furnished the major isomer which melted at 187.5–188.5°C; ir ($CHCl_3$): 3417 (hydroxyl), 3234 cm^{-1} (N—H); nmr ($CDCl_3$) τ: 2.12 (d, 2H, aromatic protons), 2.73 (s, 7H, aromatic protons of benzyloxy and tosylate groups), 4.45 (d, J = 6 Hz, vinylic proton), 5.60 (s, 2H, benzylic protons), 5.93 (b s, 1H, proton unshielded by hydroxyl), 6.45 (m, 2H, proton unshielded by benzyloxy and bicyclooctane bridgehead proton), 7.10 (b s, 1H, bicycloheptane bridgehead proton), 7.58 ppm (s, 3H, aromatic methyl). *Mol. Wt.* calcd. for $C_{27}H_{30}O_4N_2S$: 478; found (ms): 478. *Anal.* calcd. for $C_{27}H_{30}O_4N_2S$: C 67.76, H 6.32, N 5.85; found: C 68.08, H 6.26, N 5.68.

Preparation of Compound 32

The tosylhydrazone **31** was hydrolyzed to give the hydroxy ketone **32** exactly as described for compound **14**. The ratio of the two isomers was approximately 6:1.

Major isomer (colourless needles); mp 138–139.5°C from ether); ir ($CHCl_3$): 3540, 3450 (hydroxyl), 1725 cm^{-1} (six-membered ketone); nmr ($CDCl_3$) τ: 2.67 (s, 5H, aromatic protons), 4.45 (d, J = 6 Hz, 1H, vinylic proton), 5.53 (s, 2H, benzylic protons), 6.15 (b m, 1H, proton unshielded by benzyloxy group), 6.47 (m, 1H, bicyclooctane bridgehead proton), 6.58 ppm (d, J = 2.2 Hz, 1H, proton unshielded by hydroxyl). *Mol. Wt.* calcd. for $C_{20}H_{22}O_3$: 310; found (ms): 310. *Anal.* calcd. for $C_{20}H_{22}O_3$: C 77.39, H 7.14; found: C 77.30, H 7.10.

Minor isomer (colourless needles); mp 102.5–103.5°C from ether; ir ($CHCl_3$): 3510, 3415 (hydroxyl), 1725 cm^{-1} (six-membered ketone); nmr ($CDCl_3$) τ: 2.68 (s, 5H, aromatic protons), 4.48 (d, J = 6 Hz, 1H, vinylic proton), 5.52 (s, 2H, benzylic protons), 6.12 (b m, 1H, proton unshielded by benzyloxy group), 6.38 (s, 1H, proton unshielded by hydroxyl), 6.47 (m, 1H, bicyclooctane bridgehead proton), 7.07 and 7.37 ppm (b s, 1H each, bicycloheptane bridgehead protons). *Mol. Wt.* calcd. for $C_{20}H_{22}O_3$: 310; found (ms): 310; the entire mass spectra of both epimers were identical.

Mesylation of Hydroxy Ketone 32

The keto mesylate **33** was obtained from compound **32** as described previously for compound **15**. The yield of the reaction was 93.3% and both isomers were obtained as colourless prisms from ether.

Major isomer, mp 108.5–109.5°C; ir ($CHCl_3$): 1737 cm^{-1} (six-membered ketone); nmr ($CDCl_3$) τ: 2.67 (s, 5H, aromatic protons), 4.38 (d, J = 6 Hz, vinylic proton), 5.50 (s, 3H, benzylic protons and a proton unshielded by mesylate), 6.05 (b m, 1H, proton unshielded by benzyloxy group), 6.45 (m, bicyclooctane bridgehead proton), 6.77 (s, 3H, mesylate methyl), 7.00 ppm (b s, 1H, bicycloheptane bridgehead proton). *Mol. Wt.* calcd. for $C_{21}H_{24}O_5S$: 388; found (ms): 388. *Anal.* calcd. for $C_{21}H_{24}O_5S$: C 64.93, H 6.23; found: C 64.98, H 6.31.

Minor isomer, mp 95.5–97.0°C; ir ($CHCl_3$): 1737 cm^{-1} (six-membered ketone); nmr ($CDCl_3$) τ: 2.70 (s, 5H, aromatic protons), 4.45 (d, J = 6 Hz, 1H, vinylic proton), 5.43 (s, 1H, proton unshielded by mesylate), 5.53 (s, 2H, benzylic protons), 6.13 (m, 1H, proton unshielded by benzyloxy), 6.47 (m, 1H, bicyclooctane bridgehead proton), 6.82 (s, 3H, mesylate methyl), 7.03 and 7.57 ppm (b s, 1H each, bicycloheptane bridgehead protons). *Mol. Wt.* calcd. for $C_{21}H_{24}O_5S$: 388; found (ms): 388; the entire mass spectra of both epimers were identical.

Hydrogenation of Keto Mesylate 33 (Major Isomer)

A solution of 170 mg of the crystalline major epimer **33** in 10 ml of dry dioxane was hydrogenated over 35 mg of 10% palladium-on-charcoal at atmospheric pressure for 40 h. The catalyst was filtered off through a Celite pad and the filtering pad was washed with ether. The filtrate was washed with sodium bicarbonate and brine and dried over anhydrous sodium sulfate. Evaporation of the solvent and purification of the residue by preparative tlc using ether–hexane (3:1, v/v) gave 97 mg (86.5%) of the aldol **34** as a colourless glass. This aldol showed spectral properties identical with those displayed by the same material obtained by the photochemical route (3).

Reduction of the Minor Keto Mesylate 33 with Calcium Metal in Liquid Ammonia

The keto mesylate **33** (50 mg) in anhydrous THF (2 ml) was added dropwise to a stirred solution of calcium metal (35 mg) in liquid ammonia (15 ml). Stirring was continued for 5 min after which the excess of the metal was destroyed by adding bromobenzene (0.25 ml). The solvent was evaporated, the residue was dissolved in water, neutralized with dilute hydrochloric acid and extracted with ether (4 × 10 ml). The combined extracts were washed with water and brine and dried over anhydrous magnesium sulfate. Evaporation of the solvent and purification of the residue by preparative tlc using ether–hexane (3:1, v/v) gave 17.8 mg (67.7%) of aldol **34**, identical to the one obtained in the previous experiment.

Acetylation of Aldol 34

Aldol **34** (77 mg) was dissolved in 5 ml of acetic anhydride – pyridine mixture (1:1, v/v) and stirred at room temperature for 1 h. The reaction mixture was then poured into water (10 ml) and extracted with ether (4 × 10 ml). The extracts were washed with water, dilute hydrochloric acid, sodium bicarbonate, and brine. Drying over anhydrous magnesium sulfate and evaporation of the solvent *in vacuo* gave a pale yellow oil which was purified by preparative tlc on silica gel using ether–hexane (1:1, v/v) to give 86 mg (92.5%) of keto acetate **35** as colourless glass; ir ($CHCl_3$): 1730 cm^{-1} (six-membered ketone and acetate); nmr ($CDCl_3$) τ: 4.47 (d, J = 6 Hz, 1H, vinylic proton), 5.08 (m, 1H, proton unshielded by acetate), 6.55 (m, 1H, bicyclooctane bridgehead proton), 7.93 and 7.98 ppm (singlets, 3H, acetoxy methyls). *Mol. Wt.* calcd. for $C_{15}H_{18}O_3$: 246; found (ms): 246.

Hydrogenation of Keto Acetate 35

A solution of keto acetate **35** (65 mg) in absolute methanol (5 ml) and 5% rhodium-on-alumina (65 mg) was hydrogenated at 92 psi for 24 h. The catalyst was filtered off and the filtering pad was washed with methanol. The filtrate was evaporated to dryness and the residue was taken up in dry methylene chloride (5 ml) and added to a suspension of the chromium trioxide – dipyridine complex (400 mg) in the same solvent (20 ml). The reaction was quenched with wet ether and worked up by the normal procedure to give a colourless oil which was purified by preparative tlc on silica gel using ether–hexane (1:1, v/v). The yield was 53 mg (82.8%) of keto acetates **36** and **37** in a ratio of 2.3:1.

Keto acetate **36** (37.2 mg, colourless glass); ir (CCl_4): 1735 cm^{-1} (six-membered ketone, acetate); nmr ($CDCl_3$) τ: 4.93 (m, 1H, proton unshielded by acetate), 7.97 and 8.00 ppm

Can. J. Chem. Downloaded from www.nrcresearchpress.com by 210.87.254.40 on 09/05/12
For personal use only.

(s, 3H, acetoxy methyls). *Mol. Wt.* calcd. for $C_{15}H_{20}O_3$: 248; found (ms): 248.

Keto acetate **37** (16.5 mg, colourless prisms, mp 122.5–123.5°C from ether–hexane); ir (CCl_4): 1737 cm^{-1} (six-membered ketone, acetate); nmr ($CDCl_3$) τ: 4.63 (m, 1H, proton unshielded by acetate), 7.98 ppm (s, 3H, acetoxy methyl). *Mol. Wt.* calcd. for $C_{15}H_{20}O_3$: 248; found (ms): 248.

*Conversion of Keto Acetate **36** into Ketal Ketone **38***

The keto acetate **36** was converted to the homogeneous ketal ketone **38** according to the procedure used in our photochemical model studies (3). Its identity with the previously prepared material (3) was ascertained by tlc, ir, nmr, and ms.

*Preparation of Alcohol **39***

A solution of the diketone **29** (1.0 g) in anhydrous THF (32 ml) was added dropwise to a stirred solution of trimethylsilylmethylmagnesium chloride (8 mmol) in THF (12 ml) at 0°C under nitrogen. The reaction mixture was allowed to stir at room temperature for 30 min, then cooled to 0°C and quenched with wet ether (10 ml). The white precipitate was filtered off through a Celite pad and the filtrate was washed with water and dried over anhydrous magnesium sulfate. The solvent was evaporated *in vacuo* and the residue was chromatographed on silica gel using ether–hexane (1:5, v/v) to give 822 mg (64%) of epimeric alcohols **39**, mp 130–131°C from ether–hexane; ir (CCl_4): 3550 (hydroxyl), 1720 cm^{-1} (six-membered ketone); nmr ($CDCl_3$) τ: 2.67 (s, 5H, aromatic protons), 4.18 (d, J = 6 Hz, 1H, vinylic proton), 5.50 (s, 2H, benzylic protons), 6.80 (m, 1H, bicyclooctane bridgehead proton), 7.04 and 7.60 (b s, 1H each, bicycloheptane bridgehead protons), 9.15 (s, 2H, methylenic protons α to the trimethylsilyl group), 9.90 ppm (3s, 9H, trimethylsilyl group). *Mol. Wt.* calcd. for $C_{24}H_{32}O_3Si$: 396; found (ms): 396. *Anal.* calcd. for $C_{24}H_{32}O_3Si$: C 72.68, H 8.13; found: C 72.52, H 7.75.

*Preparation of α,β-Unsaturated Ketone **39***

The epimeric alcohols **39** (300 mg) in THF (15 ml) were treated with 70% aqueous perchloric acid (1.5 ml) at room temperature. The reaction mixture was heated to 55°C for 2 h, cooled to room temperature and neutralized carefully with sodium bicarbonate. The organic layer was separated and the aqueous layer was extracted with ether. The combined extracts were washed with brine and dried over anhydrous magnesium sulfate. The solvent was evaporated *in vacuo* and the residue was purified by tlc on silica gel using ether–hexane (1:6, v/v) to give 191 mg (82.6%) of the α,β-unsaturated ketone **40** as a colourless oil; ir (CCl_4): 1710 (α,β-unsaturated ketone), 1630 cm^{-1} (conjugated double bond); nmr ($CDCl_3$) τ: 2.64 (s, 5H, aromatic protons), 4.13 (d, J = 6 Hz, 1H, vinylic proton), 4.19 (d, J = 1.75 Hz, 1H, vinylic proton *cis* to carbonyl), 4.87 (d, J = 1.75 Hz, vinylic proton *trans* to carbonyl), 5.47 (s, 2H, benzylic protons), 6.18 (m, 2H, proton unshielded by benzyloxy group and bicyclooctane bridgehead proton), 7.03 and 7.50 ppm (b s, 1H each, bicycloheptane bridgehead protons). *Mol. Wt.* calcd. for $C_{21}H_{22}O_2$: 306; found (ms): 306.

*Reduction of α,β-Unsaturated Ketone **40***

The α,β-unsaturated ketone **40** (180 mg) in absolute methanol (15 ml) was treated with sodium borohydride (560 mg). The reaction mixture was stirred at room temperature for 2 h and then it was neutralized with dilute hydrochloric acid. Excess of methanol was evaporated *in vacuo* and the residue was dissolved in water and extracted with ether. The combined extracts were washed with water and brine and dried over anhydrous magnesium sulfate. The solvent was evaporated and the residue was purified by preparative tlc on silica gel using ether–hexane (1:2, v/v) to give alcohol **41** (133 mg, 76%) as colourless oil; ir (CCl_4): 3630 cm^{-1} (hydroxyl); nmr ($CDCl_3$) τ: 2.67 (s, 5H, aromatic protons), 4.31 (d, J = 6 Hz, 1H, vinylic proton), 5.50 (s, 2H, benzylic protons), 5.90–6.66 (m, 2H, protons unshielded by benzyloxy and hydroxyl groups), 7.14 (b s, 1H, bicycloheptane bridgehead proton), 9.07 ppm (d, J = 8 Hz, 3H, methyl). *Mol. Wt.* calcd. for $C_{21}H_{26}O_2$: 310; found (ms): 310.

*Preparation of Acetate **42***

The alcohol **41** (100 mg) was dissolved in 2 ml of acetic anhydride – pyridine (1:1, v/v) and the reaction mixture was allowed to stir at room temperature overnight. The reaction was worked up by the usual procedure and the residue was purified by preparative tlc on silica gel using ether–hexane (1:5, v/v) to furnish the acetate **42** (92%) as colourless oil; ir (CCl_4): 1725 cm^{-1} (acetate); nmr ($CDCl_3$) τ: 2.67 (s, 5H, aromatic protons), 4.28 (d, J = 6 Hz, 1H, vinylic proton), 5.15 (dd, J = 1 and 8 Hz, 1H, proton unshielded by acetate), 5.50 (s, 2H, benzylic protons), 6.02 (m, 1H, proton unshielded by benzyloxy group), 7.64 (s, 3H, acetoxy methyl), 9.21 ppm (d, J = 8 Hz, 3H, methyl). *Mol. Wt.* calcd. for $C_{23}H_{28}O_3$: 352; found (ms): 352.

*Preparation of Hydroxy Acetate **43***

A solution of compound **42** (130 mg) in methanol (20 ml) was hydrogenolyzed over 10% palladium-on-charcoal (20 mg) at atmospheric pressure. The catalyst was filtered off and the filtrate was evaporated to dryness to give the alcohol **43** (95%), mp 122–124°C from ether–hexane; ir (CCl_4): 3550 (hydroxyl), 1725 cm^{-1} (acetate); nmr ($CDCl_3$) τ: 4.26 (d, J = 6 Hz, 1H, vinylic proton), 5.23 (dd, J = 1 and 8 Hz, 1H, proton unshielded by acetate), 5.83 (b s, 1H, proton unshielded by hydroxyl), 7.90 (s, 3H, acetoxy methyl), 8.88 ppm (d, J = 8 Hz, 3H, methyl). *Mol. Wt.* calcd. for $C_{16}H_{22}O_3$: 262; found (ms): 262.

*Preparation of Mesylate **44***

A solution of the alcohol **43** (48 mg) and triethylamine (27 mg) in dry methylene chloride (10 ml) was cooled to 0°C and treated with methanesulfonyl chloride (25 mg). After stirring for 30 min, the reaction was worked up in the standard manner to yield the expected product **44** (95%) which melted with decomposition at 134°C; ir (CCl_4): 1730 (acetate), 1365, 1330, 1170 cm^{-1} (mesylate); nmr ($CDCl_3$) τ: 4.31 (d, J = 6 Hz, 1H vinylic proton), 4.84 (m, 1H, proton unshielded by mesylate), 5.17 (dd, J = 2 and 10 Hz, 1H, proton unshielded by acetate), 7.04 (s, 3H, mesylate methyl), 7.93 (s, 3H, acetoxy methyl), 9.13 ppm (d, J = 7.5 Hz, 3H, methyl). *Mol. Wt.* calcd. for $C_{17}H_{24}O_5S$: 340; found (ms): 340. *Anal.* calcd. for $C_{17}H_{24}O_5S$: C 59.98, H 7.10; found: C 60.23, H 7.13.

*Rearrangement of Compound **44***

The mesylate **44** (25 mg) in glacial acetic acid (7 ml) was heated under reflux for 20 min. The reaction mixture was cooled to room temperature and the acetic acid was evaporated under reduced pressure. The residue was dissolved in ether, washed with water, brine, and dried over anhydrous magnesium sulfate. The solvent was evaporated and the residue was purified by preparative tlc on silica gel using ether–hexane (1:2, v/v) to yield the rearranged product **45** (90%) as a colourless oil; ir (CCl_4): 1735 cm^{-1} (acetate); nmr ($CDCl_3$) τ: 4.67–5.18 (m, 3H, vinylic proton and protons unshielded by

acetates), 7.93, 7.97 (s, 3H each, acetoxy methyls), 8.93 ppm (d, J = 8 Hz, 3H, methyl). *Mol. Wt.* calcd. for $C_{18}H_{24}O_4$: 304; found (ms): 304.

Preparation of Diol ***46***

A solution of the diacetate **45** (50 mg) in 5 ml of 5% methanolic potassium hydroxide (containing 10% water) was heated under reflux for 12 h. The reaction mixture was cooled to room temperature, neutralized with dilute hydrochloric acid and the excess of the methanol was evaporated under reduced pressure. The residue was dissolved in water (3 ml) and extracted with chloroform (3 × 5 ml). The combined extracts were washed with brine and dried over anhydrous magnesium sulfate. The solvent was evaporated *in vacuo* and the residue was purified by preparative tlc on silica gel using ether–hexane (2:1, v/v) to give diol **46** (34.3 mg, 95%) as a colourless oil; ir (CCl_4): 3620 cm^{-1} (hydroxyl); nmr ($CDCl_3$) τ: 4.87 (b s, 1H, vinylic proton), 6.17 (m, 2H, protons unshielded by hydroxy groups), 9.03 ppm (d, J = 8 Hz, 3H, methyl). *Mol. Wt.* calcd. for $C_{14}H_{20}O_2$: 220; found (ms): 220.

Oxidation of Diol ***46***

The diol **46** (10 mg) in dry methylene chloride (1 ml) was added to a stirred suspension of the chromium trioxide–dipyridine complex (155 mg) in the same solvent (3 ml). The mixture was allowed to stir at room temperature for 10 min and then it was quenched with wet ether (4 ml). Standard work-up and purification by preparative tlc on silica gel using ether–hexane (2:3, v/v) gave the diketone **47** (7.8 mg, 80%) which melted at 58–59°C from ether–hexane. This material was identical with the previously synthesized compound (10) by mixture melting point, tlc, ir, nmr and ms.

Infrared (CCl_4): 1745 (five-membered ketone), 1675 cm^{-1} (six-membered conjugated ketone); nmr ($CDCl_3$) τ: 4.39 (s, 1H, vinylic proton), 7.00 (b s, 1H, bicycloheptane bridgehead allylic proton), 8.72 ppm (d, J = 7 Hz, 3H, methyl). *Mol. Wt.* calcd. for $C_{14}H_{16}O_2$: 216; found (ms): 216. *Anal.* calcd. for $C_{14}H_{16}O_2$: C 77.75, H 7.46; found: C 77.79, H 7.64.

Acknowledgments

We wish to thank the National Research Council of Canada, Hoffmann–La Roche Inc., Vaudreuil, Quebec, and Nutley, New Jersey, and Merck Sharp and Dohme, Pointe Claire, Dorval, Quebec for the financial support of this work. One of us (R.M.-B.) thanks the Centro di studio per la chimica delle sostanze organiche naturali del C.N.R. (Roma, Italy) for a leave of absence.

1. K. Wiesner, P. T. Ho, W. C. Liu, and M. N. Shanbhag. Can. J. Chem. **53**, 2140 (1975).
2. T. Y. R. Tsai, C. S. J. Tsai, W. W. Sy, M. N. Shanbhag, W. C. Liu, S. F. Lee, and K. Wiesner. Heterocycles. Woodward Issue, **7**, 217 (1977).
3. K. Wiesner, I. H. Sanchez, K. S. Atwal, and S. F. Lee. Can. J. Chem. **55**, 1091 (1977).
4. K. Wiesner, T. Y. R. Tsai, G. I. Dmitrienko, and K. P. Nambiar. Can. J. Chem. **54**, 3307 (1976).
5. K. Wiesner, P. T. Ho, and C. S. J. Tsai. Can. J. Chem. **52**, 2353 (1974); K. Wiesner, P. T. Ho, C. S. J. Tsai, and Y. K. Lam. Can. J. Chem. **52**, 2355 (1974).
6. J. Meinwald and G. A. Wiley. J. Am. Chem. Soc. **80**, 3667 (1958).
7. P. G. Gassman and D. R. Amick. Tetrahedron Lett. 889 (1974).
8. D. Berney and P. Deslongchamps. Can. J. Chem. **47**, 515 (1969).
9. G. Stork and W. N. White. J. Am. Chem. Soc. **78**, 4609 (1956).
10. K. Wiesner, A. Deljac, T. Y. R. Tsai, and M. Przybylska. Tetrahedron Lett. 1145 (1970).

Can. J. Chem. Downloaded from www.nrcresearchpress.com by 210.87.254.40 on 09/05/12
For personal use only.

Perepoxide intermediates in the conversion of some β-halohydroperoxides to allylic hydroperoxides by base[1,2]

KARL R. KOPECKY, WAYNE A. SCOTT, PETER A. LOCKWOOD,[3] AND CEDRIC MUMFORD

Department of Chemistry, University of Alberta, Edmonton, Alta., Canada T6G 2E1

Received September 26, 1977

KARL R. KOPECKY, WAYNE A. SCOTT, PETER A. LOCKWOOD, and CEDRIC MUMFORD. Can. J. Chem. **56**, 1114 (1978).

Migration of the hydroperoxy group occurs during the reaction between base and several β-halohydroperoxides to give allylic hydroperoxides. An 86:14 ratio of 3-hydroperoxy-2-(4-methoxyphenyl)-3-methyl-1-butene-3-hydroperoxy-3-(4-methoxyphenyl)-2-methyl-1-butene was formed in 90% yield from 2-bromo-3-hydroperoxy-3-(4-methoxyphenyl)-2-methylbutane. From 1-chloro-, 1-bromo-, and 1-iodo-1-(1-hydroperoxy-1-methylethyl)cyclohexane there were obtained 1-(1-hydroperoxy-1-methylethyl)cyclohexene and 1-hydroperoxy-1-(2-propenyl)-cyclohexane in ratios of 93:7, 94:6, and 94:6, respectively, in 98–100% yield. Isopropylidenecyclohexane was converted with singlet oxygen to these allylic hydroperoxides in a 10:90 ratio. Only the latter allylic hydroperoxide was formed in the reaction between the alkene and triphenyl phosphite ozonide at −70°C. The *p*-nitrobenzoate esters of 1-hydroperoxy(1-chloro-, 1-bromo-, and 1-iodo-1-methylethyl)cyclopentane were converted quantitatively to 1-(1-hydroperoxy-1-methylethyl)cyclopentene and 1-hydroperoxy-1-(2-propenyl)-cyclopentane in 77:23, 73:27, and 70:30 ratios, respectively. Oxidation of isopropylidene-cyclopentane with triphenyl phosphite ozonide at −70°C and singlet oxygen produced the allylic hydroperoxides in 62:38 and 58:42 ratios, respectively. The reactions of the β-halohydroperoxides proceed exclusively via perepoxide intermediates. The reactions between the alkenes and singlet oxygen or triphenyl phosphite ozonide do not involve perepoxide intermediates.

KARL R. KOPECKY, WAYNE A. SCOTT, PETER A. LOCKWOOD et CEDRIC MUMFORD. Can. J. Chem. **56**, 1114 (1978).

La migration du groupe hydroperoxy se produit durant la réaction entre une base et plusieurs β-halohydroperoxydes pour conduire aux hydroperoxydes allyliques. Il se forme l'hydroperoxy-3 (méthoxy-4 phényl)-2 méthyl-3 butène-1 et l'hydroperoxy-3 (méthoxy-4 phényl)-3 méthyl-2 butène-1 dans un rapport de 86:14 et avec un rendement de 90% à partir du bromo-2 hydroperoxy-3 (méthoxy-4 phényl)-3 méthyl-2 butane. A partir des chloro-1 bromo-1 et iodo-1 (hydroperoxy-1 méthyl-1 éthyl)-1 cyclohexane, on obtient les (hydroperoxy-1 méthyl-1 éthyl)-1 cyclohexène et hydroperoxy-1 (propène-2 yl)-1 cyclohexane dans un rapport de 93:7, 94:6 et 94:6, respectivement, avec des rendements de 98–100%. L'isopropylidène-cyclohexane se transforme sous l'influence de l'oxygène singulet dans ces hydroperoxydes allyliques dans un rapport de 10:90. Il ne se forme que le dernier hydroperoxyde allylique dans la réaction de l'alcène et de l'ozonide de triphénylphosphite à −70°C. Il y a une transformation quantitative des esters *p*-nitrobenzoate de l'hydroperoxy-1 (chloro-1, bromo-1 et iodo-1 méthyl-1 éthyl)-1 cyclopentane en (hydroperoxy-1 méthyl-1 éthyl)-1 cyclopentène et l'hydroperoxy-1 (propène-2 yl)-1 cyclopentane dans des rapports respectifs de 77:23, 73:27 et 70:30. L'oxydation de l'isopropylidènecyclopentane avec l'ozonide de triphénylphosphite à −70°C et l'oxygène singulet conduisent à la formation des hydroperoxydes allyliques dans des rapports respectifs de 62:38 et 58:42. Les réactions des β-halohydroperoxydes se produisent exclusivement par l'intermédiaire de perépoxydes. Les réactions entre les alcènes et l'oxygène singulet ou l'ozonide de triphénylphosphite n'impliquent pas d'intermédiaires perépoxydes.

[Traduit par le journal]

Introduction

β-Halohydroperoxides derived from a variety of tetrasubstituted ethylenes are converted in high yield to allylic hydroperoxides on treatment with base (1). This reaction provides an alternate route to the photosensitized oxygenation of such alkenes for the preparation of allylic hydroperoxides.

During a study to compare the product distributions of the two modes of oxidation of an unsymmetrically deuterated 2,3-dimethyl-2-butene it was found that migration of the hydroperoxy group occurred on treatment of the derived mixture of bromohydroperoxides with base (1*b*) (Scheme 1). Both bromohydroperoxides were consumed at the

[1]This research was supported in part by grants from the National Research Council of Canada and the Defense Research Board, Grant Number 9530–99.

[2]Presented in part at the 57th Canadian Chemical Conference of the Chemical Institute of Canada, Regina, Saskatchewan, June 1974, Abstract No. 178.

[3]Holder of a National Research Council of Canada Scholarship 1970–1974.

Can. J. Chem. Downloaded from www.nrcresearchpress.com by 210.87.254.105 on 09/05/12
For personal use only.

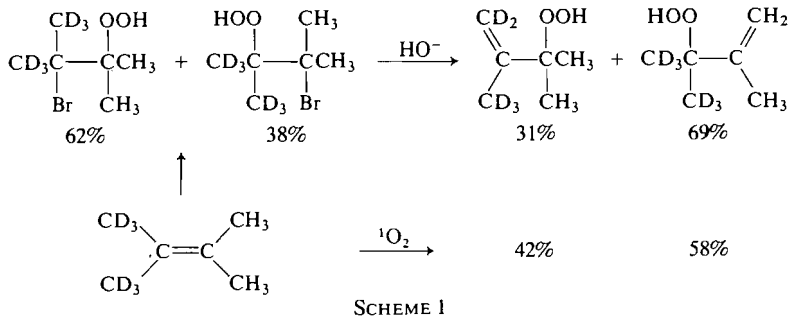

SCHEME 1

same rate. It was concluded that the reaction proceeded exclusively by way of a perepoxide intermediate and that a perepoxide was not an intermediate in the singlet oxygen oxidation of the alkene because of the different product distributions of the two reactions.

The present study was undertaken to search for further examples of hydroperoxy group migration in the reaction between β-halohydroperoxides and base, to determine whether the reaction proceeds exclusively by way of perepoxide intermediates in other systems as well and to obtain further evidence on whether or not perepoxides are formed in the singlet oxygen oxidation of alkenes to allylic hydroperoxides.

Results and Discussion

The reaction between base and 3-bromo-3-hydroperoxy-3-(4-methoxyphenyl)-2-methylbutane produces in 90% yield a mixture of allylic hydroperoxides in which the product of hydroperoxy group migration predominates greatly (Scheme 2). A very similar product distribution is obtained on singlet oxygen oxidation of the corresponding alkene (2). The singlet oxygen oxidation was repeated in the presence of 0.5 *M* sodium hydroxide. The product distribution was nearly the same as in the absence of base.

The product distributions from the oxidation of the unsymmetrical alkenes isopropylidenecyclohexane **1** and isopropylidenecyclopentane **5** by singlet oxygen, by triphenyl phosphite ozonide and those from the reaction between base and the halohydroperoxides derived from these alkenes are shown in Schemes 3 and 4. The three different halohydroperoxides were prepared from each alkene to study the effect of the halogen leaving group on the product distribution.

The halohydroperoxides were prepared by the reaction between the alkene, 1,3-dihalo-5,5-dimethylhydantoin and hydrogen peroxide in ether at −20 to −40°C (1). The reactions with **1** were all regiospecific. Only the isomer with the hydroperoxy group on the carbon bearing the methyl groups appeared to be formed under a variety of conditions. The nmr spectra of the crude reaction mixtures had no signals that could be attributed to the other isomer. Each of the halohydroperoxides derived from **1** was purified by low temperature crystallization from Skelly B to material with >98% active oxygen content. All three compounds were stable at 20°C for at least 10 min.

The degradation shown in Scheme 5 established the structure of the bromohydroperoxide **2**-Br. The nmr signal ($CDCl_3$) of the methyl groups of **2**-Br appeared at τ 8.5. The structures of **2**-Cl and **2**-I followed from their nmr spectra. The methyl groups absorbed at τ 8.6 and 8.4, respectively. The absorptions of the methyl groups of the isomeric halo-

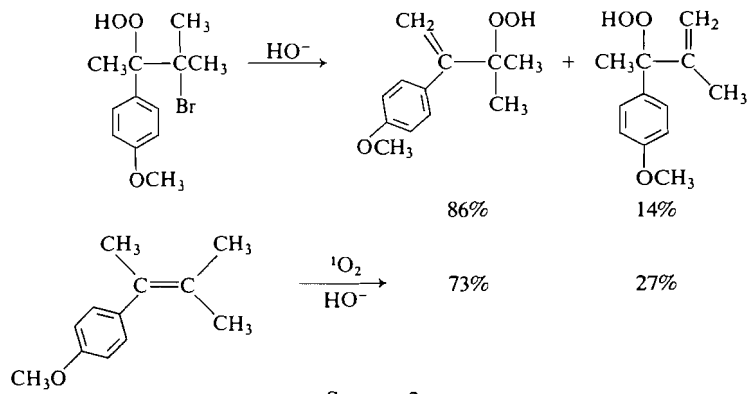

SCHEME 2

Can. J. Chem. Downloaded from www.nrcresearchpress.com by 210.87.254.105 on 09/05/12
For personal use only.

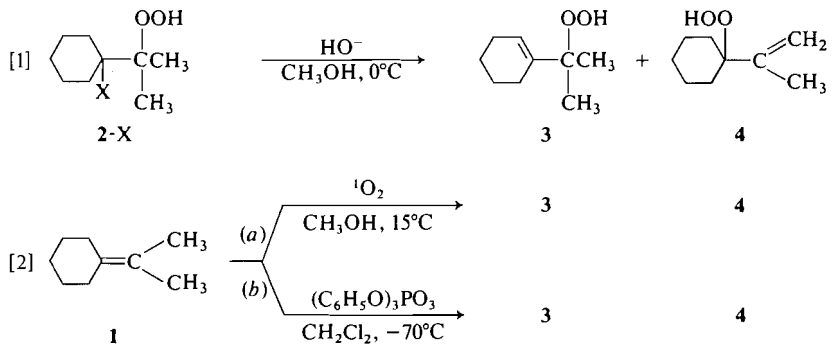

Substrate			Product distribution (%)		
No.	X	Reaction	3	4	Total yield(%)
2	Cl	[1]	93	7	98
2	Br	[1]	94	6	99
2	I	[1]	94	6	100
1		[2*a*]	10	90	—
1		[2*b*]	0	100	99

SCHEME 3

hydroperoxides would be expected to be 0.2 to 0.7 τ units more downfield (1).[4]

The bromo- and iodohydroperoxides **6**-Br and **6**-I of **5** also appear to have been formed regiospecifically with the halogen on the carbon atom bearing the methyl groups. These absorbed at τ 8.12 and 7.94 respectively.[5] A mixture of chlorohydroperoxides **6**-Cl and **9**-Cl was formed from **5**. The isomer with the chlorine atom on the carbon atom bearing the methyl groups predominated by a ratio of ~2:1. It was extremely difficult to separate **6**-Cl and **9**-Cl, which were formed in low yield, from the other products of the reaction. Repetitive chromatography at −30 to −40°C afforded material which had 93% of the theoretical active oxygen content and had sharp singlet absorptions at τ 8.33 and 8.54, assigned to the methyl groups of **6**-Cl and **9**-Cl, respectively. It proved impossible to free **6**-Cl completely from **9**-Cl, but the *p*-nitrobenzoate ester **6**-Cl-PNB could be made pure. It was also necessary to prepare the *p*-nitrobenzoate ester of **6**-I to ensure the purity of this material as **6**-I exploded within a minute after being freed of solvent. At 20°C **6**-I-PNB was stable for some time as were **6**-Cl and **9**-Cl, and **6**-Br.

The base-induced elimination of H-X from **2**-Cl, **2**-Br, and **2**-I produced a quantitative yield (nmr) of the mixture of allylic hydroperoxides **3** and **4** in a ratio that did not vary with the halide ion leaving group. However, the amount of rearrangement of the hydroperoxy group is quite small with **3** greatly predominating in the product mixture. Treatment of the *p*-nitrobenzoate ester of **2**-Cl with base produced the same product ratio as was obtained from **2**-Cl itself.

Pure **3** was isolated readily by low temperature crystallization. The isomeric allylic hydroperoxide **4** is formed almost exclusively on singlet oxygen oxidation of **1** and is the sole product when **1** is treated with triphenyl phosphite ozonide. Thus, either of the two possible allylic hydroperoxides can be prepared from **1**, as has been noted already (3).

Treatment of the halohydroperoxides, or their *p*-nitrobenzoate esters, derived from **5** with base produced a quantitative yield (nmr) of a mixture of allylic hydroperoxides **7** and **8** in which the product of rearrangement of the hydroperoxy group **8** predominates by a ratio of nearly 3:1. The ratio is not quite independent of the leaving halogen ion.

[4]After the work involving **1** and its derivatives had been completed it was reported (3) that both possible bromohydroperoxides were produced from **1** in proportions that depended upon the reaction conditions and that **2**-Br predominated. It was also concluded that there was no migration of the hydroperoxy group when the mixture of bromohydroperoxides was treated with base. The small amount of rearrangement that does occur (Scheme 3 of the present paper) was not detected. No experiments carried out with pure bromohydroperoxide were reported. It was observed, in agreement with the present work, that the reaction between singlet oxygen and **1** produces a product mixture very different from that obtained by treatment of the bromohydroperoxide with base.

[5]The regiospecificities of the addition reactions of **1** and **5** reported here have been noted already in the preparation of the bromohydrins of these alkenes and a rationale has been presented (4).

Can. J. Chem. Downloaded from www.nrcresearchpress.com by 210.87.254.105 on 09/05/12
For personal use only.

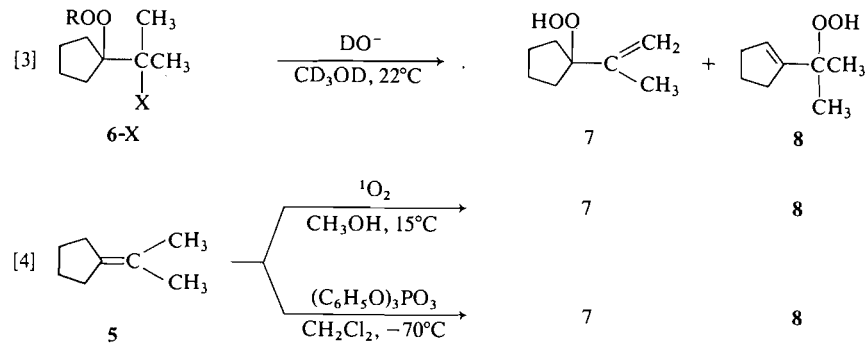

Substrate				Product distribution (%)		
No.	X	R	Reaction	7	8	Total yield (%)
6	Cl	PNB[a]	[3]	23	77	99
6	Br	H	[3]	29	71	101
6	Br	PNB	[3]	26	74	95
6	I	H	[3]	29	71	—
6	I	H	[3]	30	70	99
5			[4*a*]	42	58	84
5			[4*b*]	39	61	80

[a]PNB = *p*-nitrobenzoyl.

SCHEME 4

Slightly more rearrangement occurred with **6**-Cl-PNB than with the bromo or iodo compounds. A 78:22 ratio of **8**:**7**, essentially the same as was obtained from **6**-Cl-PNB, resulted when a mixture of ~80% **6**-Cl and ~20% **9**-Cl, which had 93% of the theoretical active oxygen content, was treated with base. Also, a 79:21 ratio of **8**:**7** was obtained from a mixture, analytically pure, of 75% **6**-Cl-PNB and 25% **9**-Cl-PNB.

An attempt was made to monitor the reaction between **6**-Br and base by nmr spectroscopy at −60°C. A spectrum taken within 30 s after mixing the reactant solutions had signals due only to **7** and **8**, all **6**-Br had already been consumed.

As was observed in the cyclohexyl system oxidation of the alkene **5** with either singlet oxygen or triphenyl phosphite ozonide produced **7** and **8** in ratios significantly different from those in the above reactions.

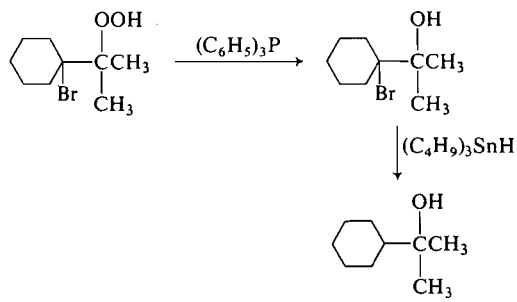

SCHEME 5

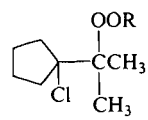

9-Cl, R = H
9-Cl-PNB, R = PNB

Discussion

The formation of **4** from **2**-X and of **8** from **6**-X is direct evidence that migration of a hydroperoxy group occurred in the reaction between the halohydroperoxides and base. The relative insensitivity of the product ratios to the nature of the leaving halide ion is evidence that both rearranged and unrearranged product are produced by only one pathway involving a halogen-free intermediate. These results are in complete agreement with those obtained previously with the bromohydroperoxides of the partially deuterated 2,3-dimethyl-2-butene (1*b*). As was discussed previously (1*b*) the halohydroperoxides must be converted by base to perepoxide intermediates exclusively which then rearrange to allylic hydroperoxides as is shown in Scheme 6 for **6**-X. The fact that mixtures of **6**-Cl or **6**-Cl-PNB containing appreciable amounts of **9**-Cl or **9**-Cl-PNB react to give the same ratio of **7**:**8** as is formed from pure **6**-Cl-PNB means that **9**-Cl and **9**-Cl-PNB also are converted exclusively to the perepoxide. Little, if any, elimination can be occurring by a route that

Can. J. Chem. Downloaded from www.nrcresearchpress.com by 210.87.254.105 on 09/05/12
For personal use only.

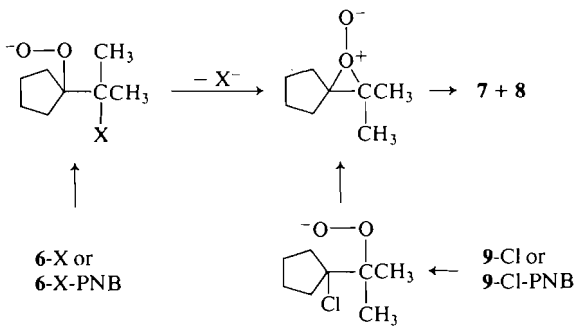

SCHEME 6

does not involve the perepoxide. Thus, it appears that perepoxide formation in the reaction between base and halohydroperoxides of tetrasubstituted ethylenes must be quite general. In principle the rearrangement could also proceed by way of a 1,2-dioxetane but tetramethyl-1,2-dioxetane disappears only after days under the reaction conditions to produce the cleavage product acetone only (1*b*). No allylic hydroperoxide could be detected.

The product ratios obtained on oxidation of the alkenes **1** and **5** with singlet oxygen and triphenyl phosphite ozonide are significantly different from those obtained from the halohydroperoxides. The present work provides further examples to show that singlet oxygen oxidations of tetrasubstituted ethylenes, at least, to allylic hydroperoxides do not proceed by way of perepoxide intermediates. The reaction must be concerted (5).

Recent suggestions, based on experimental evidence and on theoretical calculations, that singlet oxygen reacts to form the perepoxide as the initial product with at least some alkenes have been refuted. Photosensitized oxidation of adamantylideneadamantane in pinacolone produces a mixture of dioxetane and epoxide (6). It was proposed that the epoxide was formed from a perepoxide by transfer of an oxygen atom to pinacolone in a Bayer–Villiger type of reaction and that perepoxide not trapped in this way rearranged to the dioxetane. The suggested oxygen transfer reaction was based on some observations made in ozonolysis reactions (7) which were soon shown to be incorrect (8). Further, there is recent evidence that singlet oxygen is not involved in the formation of adamantylideneadamantane epoxide (9).

The argument has been made that the product distribution from the halohydroperoxide elimination results from a combination of direct elimination plus perepoxide whereas the singlet oxygen oxidation proceeds only through perepoxide (10*a*). However, this cannot be correct since **6**-X gives mainly **8** and more **8** is produced than in the singlet oxygen reaction with **5**.

Several theoretical calculations using empirical methods have been made which show that perepoxides should be readily formed in the reaction between singlet oxygen and alkenes (10), but recent *ab initio* calculations show that perepoxides must be very unstable species (11).

The reaction between triphenyl phosphite ozonide and alkenes to give allylic hydroperoxides must proceed by still a third mechanism since the product distributions are quite different from those of the reactions involving perepoxides and the reagent does not produce singlet oxygen at the temperature where the reactions were carried out (12). The results can be rationalized by an ionic mechanism (13), Scheme 7, in which only one zwitterion is formed from **1** but both possible zwitterions are formed from **2**. This mechanism is consistent with the regioselectivities observed on formation of the halohydroperoxides of **1** and **5**.

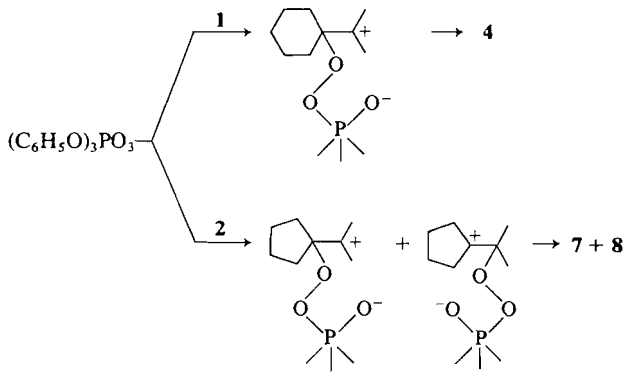

SCHEME 7

Experimental

Microanalyses were performed by Mrs. Darlene Mahlow.

3-(4-Methoxyphenyl)-2-methyl-2-butene

A solution of 51 g (0.5 mol) 3-hydroxy-3-methyl-2-butanone in 100 ml ether was added dropwise to 1.2 mol of 4-methoxyphenylmagnesium bromide in 750 ml ether which was stirred by a high speed stirrer. A glutinous mass formed during the addition. The mixture was heated under reflux for 1 h after the addition was complete and then hydrolyzed with a saturated ammonium chloride solution. The glutinous mass was agitated manually during the hydrolysis and then washed several times with ether. The combined ether layers were dried, concentrated and 40 g methoxybenzene was distilled under reduced pressure from the residual oil. The hot residue was stirred into 100 ml heptane. The solid which formed was recrystallized from carbon tetrachloride to give 79 g (75%) of 2-(4-methoxyphenyl)-3-methyl-2,3-butanediol, mp 76–84°C. A small quantity was recrystallized again to give colorless crystals, mp 82–85°C (lit. (14) mp 87–88°C).

A mixture of 70 g (0.33 mol) of the above diol and 48.8 g (0.33 mol) of triethyl orthoformate was heated at 140°C (15). After 2 h 14.4 g ethanol had distilled and the temperature was then raised to 205°C. After 12 h 12.2 g more ethanol distilled and the temperature was raised to 225°C at which point more

Can. J. Chem. Downloaded from www.nrcresearchpress.com by 210.87.254.105 on 09/05/12
For personal use only.

Can. J. Chem. Downloaded from www.nrcresearchpress.com by 210.87.254.105 on 09/05/12
For personal use only.

ethanol was distilled and carbon dioxide was evolved. Gas evolution ceased after 1 h and the residue was distilled to give 47.3 g (80%) of a colorless oil, bp 239–243°C/702 Torr, n_D^{26} 1.5309 (lit. (16) bp 234°C/760 Torr, n_D^{25} 1.5295).

Photooxygenation of 3-(4-Methoxyphenyl)-2-methyl-2-butene in the Presence of Base

A solution of 2.1 g of the alkene in 30 ml of 0.5 *M* methanolic sodium hydroxide was subjected to Eosin sensitized photooxygenation (1*b*). After 4 h oxygen uptake ceased, the reaction mixture was poured into 100 ml water, and the resulting mixture neutralized with acetic acid and extracted twice with 50 ml ether. After drying the ether solution was added to 1.0 g lithium aluminum hydride in 15 ml ether. After 1 h at reflux the mixture was hydrolyzed with aqueous potassium hydroxide and the ether layer concentrated to give 2.1 g (92%) of a colorless oil; ^{1}H nmr (CCl_4) τ: 2.83 (d, J = 9 Hz, ArH) 3.42 (d, J = 9 Hz, ArH), 4.70 (d, J = 1.7 Hz, =CH*H*), 4.90 (m, =CH*H*), 5.13 (d, J = 1.7 Hz, =C*H*H), 5.13 (m, =C*H*H), 6.27 (s, OCH_3), 8.1 (s, OH), 8.42 (m, =C—CH_3), 8.42 (s, benzylic CH_3), 8.70 (s, $C(CH_3)_2$). The isomer ratio, 2.5:1, was determined from five integrations of the absorptions of the vinyl hydrogens at τ 4.70 and 4.90 which were assigned to 3-hydroperoxy-2-(4-methoxyphenyl)-3-methyl-1-butene and 3-hydroperoxy-3-(4-methoxyphenyl)-2-methyl-1-butene, respectively. The assignments were made on the basis of the relative yields reported for the photooxygenation of the parent alkene in the absence of base (2).

Treatment of 2-Bromo-2-methyl-3-(4-methoxyphenyl)-3-butyl Hydroperoxide with Base

An 8.8 g quantity of 3-(4-methoxyphenyl)-2-methyl-2-butene was treated with 98% hydrogen peroxide and 1,3-dibromo-5,5-dimethylhydantoin in ether using the described procedure for making bromo hydroperoxides (1*a*). Attempts to remove solvent from the reaction mixture after work-up resulted in loss of peroxide content and blackening of the product. Iodometric titration of the ether solution indicated that ~70% of the bromo hydroperoxide had been formed. A portion of the ether solution was added to carbon tetrachloride and the resulting mixture evaporated under reduced pressure until the remaining liquid was ether-free; ^{1}H nmr (CCl_4) τ: 2.32–3.33 (m, ArH), 6.23 (s, OCH_3), 8.11 (s, benzylic CH_3), 8.28 and 8.33 (s, $C(CH_3)_2$); signals due to unreacted starting material were also present.

The remaining ether solution was cooled to 0°C and 100 ml of 0.5 *M* methanolic sodium hydroxide was stirred in over a 15 min period. After stirring for a further 30 min the mixture was poured into 100 ml water and the resulting mixture neutralized with acetic acid. The resulting mixture was extracted twice with 100 ml ether. The combined ether extracts were dried and added to a slurry of 2.5 g lithium aluminum hydride in 60 ml ether. Work-up as above provided a colorless oil which was chromatographed on 300 g basic alumina. Starting alkene, 33%, was eluted with pentane. Elution with 1:1 ether–pentane gave some unidentified solid, and elution with ether removed the mixture of allylic alcohols in 57% yield. The ^{1}H nmr spectrum showed the same peaks as the mixture obtained on photosensitized oxidation. The isomer ratio, determined as before, was 6.3:1.

1-(2-Propenyl)cyclohexanol

This material was prepared from the reaction between 2-propenylmagnesium bromide (17) and cyclohexanone in 66% yield, bp 54°C/2.5 Torr; n_D^{25} 1.4824; ir (CCl_4) 3450 (OH), 1635 (C=C); ^{1}H nmr (CCl_4): 5.05 (s, 1H, =C*H*H), 5.2 (s, 1H, =CH*H*), 7.95 (s, 1H, OH), 8.2 (d, J = 1 Hz, 3H, CH_3), 8.45 (b, 10H, CH_2). *Anal.* calcd. for $C_9H_{16}O$: C 77.14, H 11.42; found: C 77.13, H 11.41.

Isopropylidenecyclohexane (1)

A solution of 28 g (0.2 mol) of the above compound and 10 g ethanol dissolved in 50 ml ether was added to a solution of 10 g (0.4 mol) sodium in 270 ml liquid ammonia at −33°C. A further 10 g ethanol was added and the solution was allowed to reflux for 2 h. Water was added until the blue color just disappeared and the ammonia was allowed to evaporate overnight. Water, 100 ml, was added to the residue and the resulting mixture was extracted with ether three times. The combined ether extracts were washed with water until neutral, dried and concentrated. The residue was distilled to give 17.9 g colorless oil, bp 51–53°C/14 Torr, n_D^{20} 1.4710 (lit. (18) bp 46–48°C/13 Torr, n_D^{20} 1.4714).

1-(2-Propenyl)cyclopentanol

The method used for the preparation of 1-(2-propenyl)-cyclohexanol was used to prepare this material in 50% yield, bp 72–75°C/18 Torr, n_D^{26} 1.4745; ^{1}H nmr (CCl_4) τ: 5.05 (s, 1H, =C*H*H), 5.2 (m, 1H, =CH*H*), 7.1 (b, 1H, OH), 8.2 (d, J = 1Hz, 3H, CH_3), 8.3 (b, 8H, CH_2). *Anal.* calcd. for $C_8H_{14}O$: C 76.19, H 11.11; found: C 75.94, H 10.81.

Isopropylidenecyclopentane (5)

The procedure used for the preparation of **1** was used to make **5** in 50% yield, bp 133–134°C, n_D^{22} 1.4574 (lit. (18) bp 135.5–137.5°C, n_D^{20} 1.4585).

1-(1-Hydroperoxy-1-methylethyl)cyclohexyl Bromide (2-Br)

This material and the halohydroperoxides described below were prepared in the usual way (1*a*). From 12.4 g **1** was obtained 29.7 g of crude product as an oil which contained 76% of the theoretical active oxygen content as determined by iodometric titration (19). Three recrystallizations from Skelly B yielded a white solid, mp 55–56°C, containing 99.7% of the theoretical active oxygen content; ^{1}H nmr ($CDCl_3$) τ: 3.0 (b s, 1H, OOH), 8.3 (b, 10H, CH_2), 8.5 (s, 6H, CH_3).

1-(1-Hydroperoxy-1-methylethyl)cyclohexyl Iodide (2-I)

From 12.4 g **1**, using 1,3-diiodo-5,5-dimethylhydantoin as the halogenating agent, was obtained 35 g yellow solid which had 67% of the theoretical oxygen content. Several recrystallizations from Skelly B gave a white solid, mp 43°C (dec.), with 98% of the theoretical active oxygen content. This material decomposed within several minutes at 25°C; ^{1}H nmr (CCl_4) τ: 2.7 (s, 1H, OOH), 8.2 (b, 10H, CH_2), 8.4 (s, 6H, CH_3).

1-(1-Hydroperoxy-1-methylethyl)cyclohexyl Chloride (2-Cl)

From 1.24 g of compound **1**, using 1,3-dichloro-5,5-dimethylhydantoin as halogenating agent and stirring the reaction mixture an extra 1.5 h at −30°C, was obtained 2.1 g oil. This was added to 10 ml 2-methylbutane and the resulting mixture filtered. The filtrate was cooled to −70°C and the resulting crystals were recrystallized several times from 2-methylbutane at −70°C to yield 0.5 g (26%) of a white solid, mp 46–46.5°C, with 100% of the theoretical oxygen content; ^{1}H nmr (CCl_4) τ: 2.5 (s, 1H, OOH), 8.1–8.3 (b, 10H, CH_2), 8.6 (s, 6H, CH_3).

The *p*-nitrobenzoate ester **2**-Cl-PNB was prepared (20) from 0.5 g **2**-Cl and recrystallized from Skelly B to give 0.27 g (30%) of a white solid, mp 102°C (dec.), containing, 98.5% of the theoretical active oxygen content; ^{1}H nmr ($CDCl_3$) τ: 1.52 (d, J = 8.4 Hz, 2H, ArH), 1.68 (d, J = 8.4 Hz, 2H, ArH), 8.2 (b, 10H, CH_2), 8.4 (s, 6H, CH_3). *Anal.* calcd. for $C_{16}H_{20}ClNO_5$: C 56.23, H 5.90, N 4.10, Cl 10.37; found: C 56.04, H 6.00, N 4.66, Cl 10.59.

1-(1-Bromo-1-methylethyl)cyclopentyl Hydroperoxide (6-Br)

The crude material obtained in the usual way from 5.5 g **5** was recrystallized three times from 2-methylbutane at −70°C

Can. J. Chem. Downloaded from www.nrcresearchpress.com by 210.87.254.105 on 09/05/12
For personal use only.

to give 4.4 g (38%) white crystals, mp −10 to −5°C, which had 99.2% of theoretical oxygen content; ^{1}H nmr ($CDCl_3$) τ: 2.40 (b, 1H, OOH), 8.0 (b, 8H, CH_2), 8.12 (s, 6H, CH_3). The crude product decomposed rapidly above 0°C but the pure product was stable for some time at 20°C.

The *p*-nitrobenzoate ester **6**-Br-PNB had mp 94–96°C (dec.); ^{1}H nmr ($CDCl_3$) τ: 1.66 (d, J = 8.4 Hz, 2H, ArH), 1.88 (d, J = 8.4 Hz, 2H, ArH), 8 (b, 8H, CH_2), 8.04 (s, 6H, CH_3). *Anal.* calcd. for $C_{15}H_{18}BrNO_5$: C 48.40, H 4.87, N 3.76, Br 21.47; found: C 48.14, H 4.81, N 3.70, Br 21.49.

*1-(1-Iodo-1-methylethyl)cyclopentyl Hydroperoxide (**6**-I)*

The crude product prepared in the usual way, using 1,3-diiodo-5,5-dimethylhydantoin as a halogen source and keeping the temperature during the entire workup at 0°C or below, was purified by chromatography on silica gel at −40°C using Skelly B – ether 4:1 as eluent. Removal of solvent under vacuum at −20°C gave a colorless oil which had 98% of the theoretical active oxygen content. This material exploded within less than a minute after being warmed to 0°C; ^{1}H nmr ($CDCl_3$, −30°C) τ: 0.46 (s, 1H, OOH), 7.94 (s, 6H, CH_3), 8.25 (b, 8H, CH_2).

The *p*-nitrobenzoate ester **6**-I-PNB was purified by chromatography on silica gel at −40°C followed by crystallization from ether – Skelly B. The material was applied to the column in toluene. The yellow crystals decomposed without melting at 75–80°C; ^{1}H nmr ($CDCl_3$) τ: 1.68 (d, J = 8.4 Hz, 2H, ArH), 1.87 (d, J = 8.4 Hz, 2H, ArH), 7.86 (s, 6H, CH_3), 8.0 (b, 8H, CH_2). *Anal.* calcd. for $C_{15}H_{18}INO_5$: C 42.97, H 4.33, N 3.34, I 30.27; found: C 43.24, H 4.23, N 3.17, I 30.20.

*1-(1-Chloro-1-methylethyl)cyclopentyl Hydroperoxide (**6**-Cl) and 1-(1-Hydroperoxy-1-methylethyl)cyclopentyl Chloride (**9**-Cl)*

The crude product, prepared in the usual way using 1,3-dichloro-5,5-dimethylhydantoin as a halogen source, was chromatographed on silica gel at −40°C using 10% ether in 2-methylbutane as eluent. The fractions containing chlorohydroperoxide were combined and rechromatographed. This procedure was repeated twice more and then the fraction containing the purest chlorohydroperoxide was crystallized from 2-methylbutane at −70°C. The ^{1}H nmr spectrum of the crystals, which melted well below 0°C, indicated the presence of both **6**-Cl and **9**-Cl in a ratio of ~80:20. Recrystallization produced material with the same isomer ratio that had 93% of the theoretical peroxide content; ^{1}H nmr ($CDCl_3$) τ: 3.10 (s, 1H, OOH), 8.2 (b, 8H, CH_2), 8.33 (s, CH_3 of **6**-Cl), 8.54 (s, CH_3 of **9**-Cl).

A portion of the above material was converted to the *p*-nitrobenzoate esters **6**-Cl-PNB and **9**-Cl-PNB. These were purified by chromatography on silica gel at −40°C and then recrystallization from Skelly B to yellow crystals, mp 73–75°C, that were a mixture of 75% **6**-Cl-PNB and 25% **9**-Cl-PNB as judged from the ^{1}H nmr spectrum ($CDCl_3$) τ: 1.73 (d, J = 8.4 Hz, 2H, ArH), 1.89 (d, J = 8.4 Hz, 2H, ArH), 8.0 (b, 8H, CH_2), 8.21 (s, CH_3 of **6**-Cl-PNB), 8.36 (s, CH_3 of **9**-Cl-PNB). *Anal.* calcd. for $C_{15}H_{18}ClNO_5$: C 54.97, H 5.54, N 4.27, Cl 10.81; found: C 54.96, H 5.61, N 3.98, Cl 11.07.

The chlorohydroperoxide mixture from another preparation which contained 90% **6**-Cl was converted to the *p*-nitrobenzoate esters. Two recrystallizations from Skelly B gave **6**-Cl-PNB, whose ^{1}H nmr spectrum had no trace of the signal due to the methyl hydrogens of **9**-Cl-PNB, mp 87–88°C (dec.). *Anal.* found: C 54.63, H 5.54, N 4.20, Cl 10.88.

*Conversion of 1-(1-Hydroperoxy-1-methylethyl)cyclohexyl Bromide (**2**-Br) to (1-Hydroxy-1-methylethyl)cyclohexane*

To a solution of 2.62 g (0.01 mol) of triphenylphosphine in 50 ml Skelly B was added 2.37 g (0.01 mol) of **2**-Br in 10 ml Skelly B. The reaction mixture was stirred for 1 h and filtered. The filtrate was shaken with 30% hydrogen peroxide, filtered, and the resulting filtrate washed with water, dried, and concentrated. The residue was eluted through a column of silica gel with 25% ether in Skelly B to yield 2 g (90%) of the colorless bromohydrin. This was taken up in 30 ml benzene and 2.9 g (0.01 mol) tributyltin hydride was added. The resulting solution was held at reflux for 12 h and then concentrated. The residue was eluted through a column of silica gel with 25% ether in Skelly B to yield 1.0 g (87%) of a colorless oil that was identical (ir, ^{1}H nmr) with an authentic (21) sample of (1-hydroxy-1-methylethyl)cyclohexane.

*1-(1-Hydroperoxy-1-methylethyl)cyclohexene (**3**)*

A solution of 0.44 g (0.011 mol) sodium hydroxide in 1 ml water and 3 ml methanol was added to 2.37 g (0.01 mol) **2**-Br in 60 ml methanol at 0°C. The resulting solution was stirred at 0°C for 20 min and then poured into a mixture of water and dichloromethane. The aqueous layer was extracted three times with dichloromethane. The combined organic layers were washed with water, dried, and concentrated to give 1.5 g (87%) colorless oil. This was crystallized several times from 2-methylbutane at −78°C to give white crystals, mp 24–26°C, which had 99.7% of the theoretical active oxygen content; ^{1}H nmr (CCl_4) τ: 2.5 (s, 1H, OOH), 4.35 (m, 1H, =CH), 8.0 (b, 4H, allylic CH_2), 8.4 (b, 4H, homoallylic CH_2), 8.75 (s, 6H, CH_3).

*1-(2-Propenyl)cyclohexyl Hydroperoxide (**4**)*

Triphenyl phosphite ozonide was prepared (12) from 3.1 g (0.01 mol) triphenyl phosphine in 40 ml dichloromethane at −70°C. To this solution was added 1.2 g (0.01 mol) **1** and the resulting solution was allowed to stand at −70°C for 12 h and then warmed to 20°C. The solvent was evaporated. A weighed quantity of 1,4-dimethoxybenzene was added. The ^{1}H nmr spectrum indicated that **4** was produced in quantitative yield. No signals due to **3** could be detected. The reaction mixture was then diluted with 50 ml 2-methyl-butane and the resulting mixture stirred and filtered. Solvent was evaporated from the filtrate and the residue chromatographed on silica gel at −40°C using 25% ether in Skelly B as eluent. The fractions containing peroxide were combined and crystallized several times from 2-methylbutane at −70°C to give white crystals, mp 17–19°C, which had 99.5% of the theoretical active oxygen content; ^{1}H nmr (CCl_4) τ: 2.6 (s, 1H, OOH), 5.05 (bs, 2H, =CH_2), 8.25 (d, J = 1 Hz, 3H, CH_3), 8.5 (b, 10H, CH_2).

Reduction of 1.2 g **4** with lithium aluminum hydride produced 0.66 g of 1-(2-propenyl)cyclohexanol which had ir and ^{1}H nmr spectra identical to those of an authentic sample.

1-(1-Hydroxy-1-methylethyl)cyclohexene

A solution of 6.2 g 1-acetylcyclohexene (22) in 10 ml ether was added to a solution of methylmagnesium bromide made from 1.2 g magnesium and 5.0 g bromomethane in 40 ml ether. After 15 min under reflux the reaction mixture was hydrolyzed with saturated ammonium chloride. The usual workup gave 4.3 g (62%) of a colorless oil, bp 85–87°C/14 Torr, n_D^{28} 1.4812; ^{1}H nmr (CCl_4) τ: 4.3 (m, 1H, =CH), 7.5 (s, 1H, OH), 8.05 (m, 4H, allylic CH_2), 8.45 (b, 4H, homoallylic CH_2), 0.75 (s, 6H, CH_3). *Anal.* calcd. for $C_9H_{16}O$: C 77.14, H 11.42; found: C 76.28, H 11.62.

Reduction of 0.78 g of compound **3** with lithium aluminum hydride produced 0.69 g (99%) of an oil which had ir and ^{1}H nmr spectra identical to those of the above material.

*Product Distribution from Reaction of **2**-X and **2**-Cl-PNB with Base*

All the reactions were carried out according to the following procedure. To a solution of 2.37 g (0.01 mol) of **2**-Br in 6 ml

Can. J. Chem. Downloaded from www.nrcresearchpress.com by 210.87.254.105 on 09/05/12
For personal use only.

methanol at 0°C was added 0.60 g (0.011 mol) sodium hydroxide in 1 ml water and 3 ml methanol, dropwise with stirring. The reaction mixture was stirred at 0°C for 1.5 h (it was later found that the reactions were complete in 30 s) and poured into a mixture of 10 ml water and 10 ml dichloromethane. The aqueous layer was shaken with dichloromethane, 3 × 10 ml, the combined organic layers shaken once with water, dried and concentrated. To the residue was added 0.69 g (0.005 mol) 1,4-dimethoxyethane as internal standard. The resulting mixture was taken up in carbon tetrachloride and analyzed by ^{1}H nmr spectroscopy. The relative yields of **3** and **4** were determined by integrating the vinyl protons of each isomer. The yields in Scheme 3 are the average of three integrations. Values were reproducible to within ±0.5%.

The reaction with 2-Cl-PNB was initially heterogeneous and was stirred until the reaction mixture became homogeneous.

Product Distribution from Reaction between Base and 6-X, 6-X-PNB, 9-Cl, and 9-Cl-PNB

All the reactions were based on the following procedure. A solution of 0.0876 g (3.94×10^{-4} mol) of **6**-Br and 0.01097 g (1.40×10^{-4} mol) benzene in methanol-d_4 was made up to 1 ml. A second solution of 0.0397 g (1.73×10^{-3} mol) and deuterium oxide 0.0612 g (3.06×10^{-3} mol) was made up to 2.0 ml with methanol-d_4. Equal volumes of the two solutions were mixed at 20°C in a nmr tube. The ^{1}H nmr spectrum was taken immediately and had signals at τ: 2.68 (s, C_6H_6), 4.44 (t, =CH of **8**), 4.85 (s, HOD), 5.10 (m, $=CH_2$ of **7**), 6.70 (m, H in CD_3OD), 7.66 (b, allylic CH_2 of **8**), 8.2 (b, other CH_2 of **7** and **8** and CH_3 of **7**), 8.68 (s, CH_3 of **8**). The assignments are based on the spectra of **3** and **4**. The relative yields of **7** and **8** were calculated from integration of the vinyl proton signals at τ 4.44 and 5.10. The average of three integrals was taken. These were reproducible to ±2%. The results are presented in Scheme 4.

The reactions using **6**-X-PNB were heterogeneous, and the solid esters were added in four equal portions to a small amount of methanol-d_4 followed by one quarter of the base solution. After each addition the mixture was shaken until it became homogeneous.

Photooxygenation of 1 and 5

A solution of 1.0 g of **1** or **5**, 0.1 g 2,6-di-*tert*-butylphenol, 0.1380 g 1,4-dimethoxybenzene, as internal standard, and 0.05 g methylene blue in 30 ml methanol was irradiated until oxygen uptake ceased and worked up as described (1*b*). The product yield and distribution (Schemes 3 and 4) were determined by ^{1}H nmr.

Treatment of 5 with Triphenyl Phosphite Ozonide

This reaction was carried out as described above for the reaction with **1** using 0.5 g (0.0045 mol) **5** and 1.4 g (0.0045 mol) triphenyl phosphite in 25 ml dichloromethane. After 12 h at −78°C solvent was evaporated at −35°C. The distillate was caught in a −70°C trap and found to contain 0.18 g **5**. The residue was analyzed by ^{1}H nmr spectroscopy. The results are presented in Scheme 4.

1. (*a*) K. R. KOPECKY, J. H. VAN DE SANDE, and C. MUMFORD. Can. J. Chem. **46**, 25 (1968); (*b*) K. R. KOPECKY and J. H. VAN DE SANDE. Can. J. Chem. **50**, 4035 (1972); (*c*) K. R. KOPECKY, J. E. FILBY, C. MUMFORD, P. A. LOCKWOOD, and J.-Y. DING. Can. J. Chem. **53**, 1103 (1975).
2. C. S. FOOTE and R. W. DENNY. J. Am. Chem. Soc. **93**, 5162 (1971).
3. J. E. BALDWIN and O. W. LEVER. J. Chem. Soc. Chem. Commun. 343 (1973).
4. A. J. SISTI. Tetrahedron Lett. 3305 (1970).
5. A. NICKON and J. F. BAGLI. J. Am. Chem. Soc. **83**, 1498 (1961).
6. A. P. SCHAAP and G. R. FALER. J. Am. Chem. Soc. **95**, 3381 (1973).
7. P. R. STORY, E. A. WHITED, and J. ALFORD. J. Am. Chem. Soc. **94**, 2143 (1972).
8. K. R. KOPECKY, P. A. LOCKWOOD, J. E. FILBY, and R. W. REID. Can. J. Chem. **51**, 468 (1973).
9. C. W. JEFFORD and A. F. BOSCHUNG. Tetrahedron Lett. 4771 (1976).
10. (*a*) M. J. S. DEWAR and W. THIEL. J. Am. Chem. Soc. **97**, 3978 (1975); (*b*) M. J. S. DEWAR, A. C. GRIFFIN, W. THIEL, and I. J. TURCHI. J. Am. Chem. Soc. **97**, 4439 (1975); (*c*) S. INAGAKI and K. FUKUI. J. Am. Chem. Soc. **97**, 7480 (1975).
11. L. B. HARDING and W. A. GODDARD III. J. Am. Chem. Soc. **99**, 4520 (1977).
12. P. D. BARTLETT and G. D. MENDENHALL. J. Am. Chem. Soc. **92**, 210 (1970).
13. P. D. BARTLETT and A. P. SCHAAP. J. Am. Chem. Soc. **92**, 6055 (1970).
14. C. G. OVERBERGER and H. GAINER. J. Am. Chem. Soc. **80**, 4556 (1958).
15. G. CRANCK and F. W. EASTWOOD. Aust. J. Chem. **17**, 1392 (1964).
16. G. P. NEWSOROFF and G. STERNHILL. Aust. J. Chem. **19**, 1667 (1966).
17. H. O. HOUSE, R. A. LATHAM, and C. D. SLATER. J. Org. Chem. **31**, 2667 (1966).
18. R. H. SIEGMANN, M. J. BEERS, and H. O. HUISMAN. Recl. Trav. Chim. **83**, 67 (1964).
19. H. B. KNIGHT and D. SWERN. *In* Organic synthesis, Coll. Vol. 4. *Edited by* N. Rabjohn. John Wiley and Sons, Inc. New York. NY. 1963. p. 895.
20. R. L. SHRINER, R. C. FUSON, and D. Y. CURTIN. The systematic identification of organic compounds. 5th ed. John Wiley and Sons, Inc. New York, NY. 1964. p. 235.
21. C. F. WILCOX, JR. and S. S. CHIBBER. J. Org. Chem. **27**, 2332 (1962).
22. E. E. ROYALS and C. M. HENDRY. J. Org. Chem. **15**, 1147 (1950).

Re-examination of the Kirkwood–Westheimer theory of electrostatic effects. II.[1] Possible conformations of α,ω-amino-acids in aqueous solutions, as deduced from dissociation constants

JOHN T. EDWARD, PATRICK G. FARRELL, JOHN L. JOB, AND BO-LONG POH

Department of Chemistry, McGill University, Montreal, P.Q., Canada H3A 2K6

Received August 12, 1977

JOHN T. EDWARD, PATRICK G. FARRELL, JOHN L. JOB, and BO-LONG POH. Can. J. Chem. **56**, 1122 (1978).

The first and second dissociation constants of the ten homologous α,ω-amino-acids $H_3\overset{+}{N}(CH_2)_nCO_2H$ (n = 1–10) have been determined by a potentiometric method at different temperatures, and hence the thermodynamic parameters ΔG^0, ΔH^0, and ΔS^0 were computed. Calculation by Kirkwood–Westheimer theory of $\Delta G_1{}^0$ for the first (carboxyl) dissociation, assuming the conformation of the polymethylene chain to be intermediate between the random-coil and the fully extended conformation, gives results in good agreement with experiment for the longer chains. A similar calculation of $\Delta G_2{}^0$ for the second (ammonium) dissociation gives results in fair agreement with theory for the very long chains (n = 7–10), but in disagreement for shorter chains. A tentative explanation based on electrostatic effects on hydration of the ammonium group is advanced.

JOHN T. EDWARD, PATRICK G. FARRELL, JOHN L. JOB et BO-LONG POH. Can. J. Chem. **56**, 1122 (1978).

On a déterminé les première et deuxième constantes de dissociation de dix acides aminés α,ω homologues $H_3\overset{+}{N}(CH_2)_nCO_2H$ (n = 1–10) par une méthode potentiométrique à différentes températures et on peut donc calculer les paramètres thermodynamiques ΔG^0, ΔH^0 et ΔS^0. Des calculs, par la théorie de Kirkwood–Westheimer, de $\Delta G_1{}^0$ pour la première dissociation (carboxyle), en faisant l'hypothèse que la conformation de la chaîne polyméthylène est intermédiaire entre une pelotte statistique et une conformation complètement étendue, conduit à des résultats qui sont en accord avec les expériences pour les chaînes les plus longues. Un calcul semblable de $\Delta G_2{}^0$ pour la deuxième dissociation (l'ammonium) conduit à des résultats qui sont en bon accord avec la théorie pour les très longues chaînes (n = 7–10), mais qui sont en désaccord pour les chaînes plus courtes. On propose une explication possible basée sur des effets électrostatiques sur l'hydratation du groupe ammonium.

[Traduit par le journal]

Introduction

Following earlier work of Bjerrum (1), Eucken (2), Smallwood (3), and others, Kirkwood and Westheimer (4) in 1938 developed a theory to account for the effect of dipolar or charged substituents on the strengths of carboxylic acids. For example, the effect of the charged ammonium group in promoting the ionization of the carboxyl group of α,ω-amino-acids (**1**):

$$[1] \qquad H_3\overset{+}{N}(CH_2)_nCO_2H \overset{K_1}{\rightleftharpoons} H_3\overset{+}{N}(CH_2)_nCO_2^- + H^+$$

as compared with the ionization of this group in the analogous unsubstituted acid

$$[2] \qquad CH_3(CH_2)_nCO_2H \overset{K_a}{\rightleftharpoons} CH_3(CH_2)_nCO_2^- + H^+$$

can be explained by the stabilization of the zwitterion of [1] by coulombic interactions between positive and negative charges.[2] It can then be shown that ΔpK_1 ($\equiv \log K_a/K_1$) is given by

$$[3] \qquad \Delta pK_1 = e^2/2.3kTRD_{eff}$$

where e is the electronic charge, k Boltzmann's constant, R the distance between charges in the zwitterion, and D_{eff} the effective dielectric constant. Kirkwood and Westheimer showed how the latter could be calculated from the size and shape of the molecule. Thus, for equilibria in water, the lines of force between the positive and negative charges of the zwitterion pass partly through the intervening hydrocarbon chain (dielectric constant assumed to be 2.0) and partly through the surrounding water (assumed to be a continuum having the macroscopic dielectric constant of 78.5 at 25°C). Hence D_{eff} will have some intermediate value, depending upon the

[1]For part I see ref. 7.

[2]This approach differs slightly from conventional Kirkwood–Westheimer treatment, and is justified in this and in subsequent papers.

Can. J. Chem. Downloaded from www.nrcresearchpress.com by 210.87.254.42 on 09/05/12
For personal use only.

Can. J. Chem. Downloaded from www.nrcresearchpress.com by 210.87.254.42 on 09/05/12
For personal use only.

relative amounts of hydrocarbon and of water between the charges, and thus on the shape of the molecule. Assuming for simplicity an ellipsoidal shape with the charges at the foci, Kirkwood and Westheimer were able, by classical electrostatic theory, to relate D_{eff} to λ_0, the ratio of the major axis of the ellipsoid to the interfocal distance R (4).

By the same reasoning, the difference ΔpK_2 ($\equiv \log K_b/K_2$) between the second (ammonium) dissociation constant K_2 of the α,ω-amino-acids:

$$[4] \quad {}^{-}O_2C(CH_2)_nNH_3^{+} \overset{K_2}{\rightleftharpoons} {}^{-}O_2C(CH_2)_nNH_2 + H^{+}$$

and the dissociation contant K_b of the corresponding alkylammonium ion:

$$[5] \quad CH_3(CH_2)_nNH_3^{+} \overset{K_b}{\rightleftharpoons} CH_3(CH_2)_nNH_2 + H^{+}$$

is also given by eq. 3, the negatively charged carboxylate group being acid-weakening.

Application of this equation to the ΔpK_1 values of α,ω-amino-acids available in the literature (5) gave values of the intercharge distance R intermediate between R_{max}, the distance for a fully-extended zwitterion, and R_F, the root-mean-square distance between the ends of the chain, assuming free rotation about the carbon–carbon links (6). These results have been quoted as evidence for a random-coil conformation of α,ω-amino-acids in solution. However, they are in error, because of errors in Kirkwood and Westheimer's D_{eff} values for λ_0 between 1.0 and about 1.8 (i.e., for long, thin molecules). These errors may have arisen because of the approximations required (7).[3] Using different D_{eff} values, we have shown that the ΔpK_1 values for the limited number of α,ω-amino-acids (n = 1–6) reported in the literature yield R values closer to R_{max} than R_F (7).

Such a result can be explained along lines suggested by Everett and Pinsent (9). The strong attraction between the charged groups of the zwitterion and the highly polar water molecules will result in the displacement of the less polar hydrocarbon chain as completely as possible from the vicinity of the charges, so that the chain assumes its most extended conformation.

King and King (10) have claimed that the clustering of water molecules about ionic centres (with consequent stiffening of the hydrocarbon chain) can be expected to extend to a distance of about 5 Å (about four methylene groups) only, and indeed a recent nmr study of n-alkylammonium ions shows progressively greater flexibility of the chain with distance from the charged ammonium group (11). Hence the longer α,ω-amino-acids might be expected to have flexible, random-coil portions at the centres of the polymethylene chains. Furthermore, the end-to-end distances R_F calculated by the earlier random-flight theory of Kuhn (6) are now known to be unrealistically small because of their failure to take account of the excluded volume effect, and of the fact that rotations about carbon–carbon bonds are not free but biased towards certain preferred conformations (12, 13). When these effects are taken into account, the end-to-end distance R_R calculated for a random-coil is greater than R_F. It consequently becomes of interest to see if the R values calculated from [3] agree better with R_{max} or R_R. In this paper we report K_1 and K_2 values for the α,ω-amino-acids from n = 1 to n = 10; the still longer acids (n > 10) could not be studied because they proved to be too insoluble in water at 25°C. The results show that R probably lies between R_{max} and R_R.

[3]These recalculations have recently been discussed in detail by Ehrenson (8).

Experimental

Materials

α,ω-Amino-acids

These were commercial products or prepared in accordance with literature methods. They were recrystallized at least three times from ethanol or ethanol–water mixtures and dried over P_2O_5 at 5 mm Hg for 5 h at 80°C. Their melting or decomposition points agreed with literature values.

Water

Doubly distilled water was passed through a mixed bed ion exchange column (Rexyn I-300; Fisher Scientific) immediately before use.

Buffer Solutions

These were made up according to the specifications described by Bates (14). All salts used were 'Analar' grade, dried at 110°C for several hours before use. The solutions were made up in grade A volumetric flasks.

Titrant Solutions

Solutions of 0.1 *N* HCl and 0.1 *N* NaOH were made up from commercially available concentrates. The HCl solutions were standardized against 'Analar' sodium carbonate (15). These standard HCl solutions were used to standardize those of NaOH.

Measurements

The acid dissociation constants of the amino-acids were determined at concentrations within the range 0.0025-0.01 *M* (the exact value depending upon the solubility of the particular homologue) by potentiometric titration using Sargent-Welch DR S30000 p*H* meters fitted with Sargent combination electrodes (model S-30072-15). The titration vessels were water-jacketed beakers of 150 ml capacity. The titration procedure followed was that described by Albert and Sarjeant (16), the titrant being added by means of Agla micrometer syringes.

The dissociation constants of each compound were determined at 10, 20, 25, 30, and 40°C, each titration being repeated

Can. J. Chem. Downloaded from www.nrcresearchpress.com by 210.87.254.42 on 09/05/12
For personal use only.

at least twice. Temperature control was maintained by circulating water from a constant-temperature bath through the jacketed titration vessel. Temperatures were measured in the titration vessel and fluctuated by no more than ± 0.02°C from the required value.

Data Treatment and Results

The pK values for the equilibria represented by [1] and [4] were evaluated from the pH readings by means of the relationships described by King (17). Since the ratio K_1/K_2 was known to be large (18), overlapping of the dissociations was ignored. Corrections for ion activity coefficients γ were made by means of the Debye–Hückel expression

$$[6] \qquad \log \gamma_{\pm} = (A\sqrt{I})/(1 + \sqrt{I})$$

An additional linear correction term in ionic strength I did not significantly alter the pK values and was therefore not included in the calculations.

In each titration, values deviating from the mean pK value by more than twice the standard deviation of all values were ignored in the calculation of the final mean pK value. (These were usually the first, and last, 3 values.) The mean pK for a given titration was determined by converting the pK values into K values, averaging the K values, and then converting this average to a pK (16). The standard deviation of the K values was determined for each titration, resulting in standard deviations of the pK values within the range ± 0.005–± 0.03 pK units.

The standard enthalpy (ΔH^0) and entropy (ΔS^0) changes were evaluated from [7] using a linear least-squares analysis.

$$[7] \qquad pK = \frac{\Delta H^0}{2.303RT} - \frac{\Delta S^0}{2.303R}$$

The errors in the temperature differences (± 0.04°C) used to determine ΔH^0 and ΔS^0 resulted in pK changes within their quoted experimental errors. Calculated values of ΔH^0 and ΔS^0 were not significantly affected by the experimental errors in the pK data, and the temperature variations of ΔH^0 and ΔS^0 were not significant with respect to the deviations of the pK values.

The pK results at 25°C for equilibria [1] and [4] are given respectively in Tables 1 and 2, together with comparisons with literature data where available, and are plotted in Fig. 1. Also shown in Tables 1 and 2 are ΔH^0 and ΔS^0 values calculated from [7], using the data presented in Table 5. Errors quoted in Tables 1 and 2 are standard deviations from the mean values, obtained directly from the least-squares analysis of the data.

Results and Discussion

The results, displayed in Fig. 1, show that the effects of the positive ammonium group in strengthening the acidity of the carboxyl group, and of the negative carboxylate group in weakening the acidity of the ammonium group,[4] persist to great distances (at the molecular level), the limit not being reached at a separation of ten methylene carbons. In contrast, the effect of a dipolar substituent is attenuated to zero after a separation of about four methylene carbons (20–25).

[4]From the point of view of electrostatic theory, the acid-*strengthening* effect of the carboxylate group at short distances is anomalous, and is discussed below.

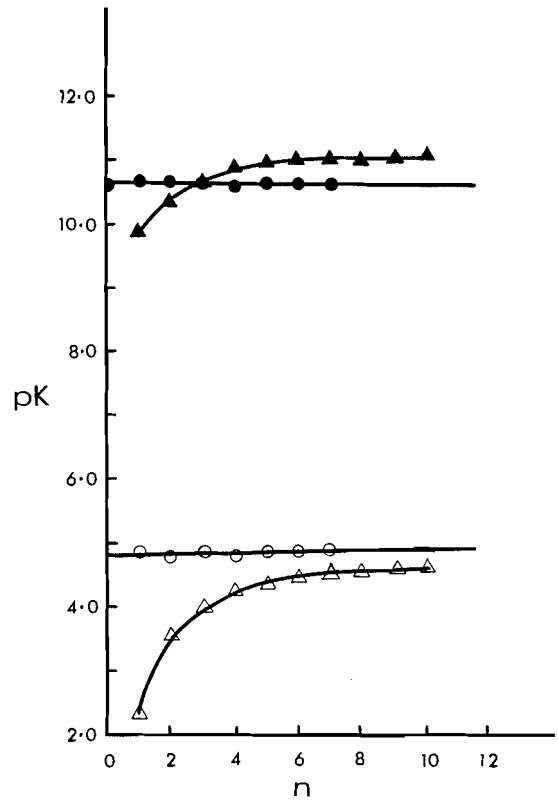

FIG. 1. Plots of pK_1 (△) and pK_2 (▲) of α,ω-amino-acids, of pK_a of *n*-alkyl monocarboxylic acids (○), and of pK_b of *n*-alkylammonium ions (●), against the number *n* of methylene carbon atoms.

In order to calculate ΔpK_1 from [3] for the different amino-acid zwitterions, we must first know the intercharge distance R and the effective dielectric constant D_{eff}. The distances between atoms of the fully extended chain can be calculated by trigonometry using bond lengths and bond angles from the literature (26, 27); however, the distances R_{max} between the terminal charges of the fully extended chains depend on assumptions about the locations of the charges with respect to the atomic centres. We consider the most reasonable location for the positive charge of an ammonium or substituted ammonium group to be the centre of the nitrogen atom, and for the negative charge of the carboxylate group to be the midpoint between the two equivalent oxygen atoms, i.e., 0.65 Å beyond the carboxylate carbon atom on the extension of the C—CO_2^- bond. Kirkwood and Westheimer (4) located the positive charge 0.33 Å beyond the nitrogen atom, on the extension of the C—N bond, and (following Eucken (2)) located the negative charge 1.45 Å beyond the carboxylate carbon atom, on the extension of the C—CO_2^- bond. In this paper we reject these loca-

Can. J. Chem. Downloaded from www.nrcresearchpress.com by 210.87.254.42 on 09/05/12
For personal use only.

TABLE 1. Thermodynamic parameters for first dissociation equilibrium (eq. 1) of α,ω-amino-acids in water at 25°C[a]

n	pK_1	ΔG^0	ΔH^0	ΔS^0
1	2.34	3.21	1.10±0.4	−7.1±1.3
	(2.350)		(0.98)	(−7.5)
2	3.55	4.83	0.84±0.13	−13.4±0.5
	(3.551)		(1.04)	(−12.8)
3	4.04	5.48	0.20±0.16	−17.7±0.5
	(4.031)		(0.39)	(−17.2)
4	4.23	5.75	−0.25±0.11	−20.1±0.4
	(4.20)		(−0.22)	(−19.9)
5	4.37	5.95	−0.98±0.14	−23.1±0.3
	(4.373)		(−0.32)	(−21.1)
6	4.45	6.05	−1.14±0.08	−24.1±0.3
	(4.502)		(−0.47)	(−22.2)
7	4.52	6.13	−0.90±0.15	−23.6±0.5
8	4.54	6.19	−0.80±0.11	−23.5±0.4
9	4.58	6.24	−0.81±0.11	−23.7±0.4
10	4.63	6.29	−1.03±0.16	−24.6±0.6

[a]Literature data from ref. 19 are given in parentheses. In this and the following table, units of ΔG^0 and ΔH^0 are kcal mol^{-1} and units of ΔS^0 are cal deg^{-1} mol^{-1}.

TABLE 2. Thermodynamic parameters for second dissociation equilibrium (eq. 4) of α,ω-amino-acids in water at 25°C

n	pK_2	ΔG^0	ΔH^0	ΔS^0
1	9.84	13.42	10.21±0.17	−10.76±0.58
	9.780[a]		10.57[a]	−9.3[a]
2	10.36	14.12	11.22±0.10	−9.75±0.33
	10.235[a]		11.23[a]	−9.2[a]
3	10.62	14.46	12.12±0.16	−7.86±0.54
	10.556[a]		12.07[a]	−7.8[a]
4	10.85	14.79	13.93±0.05	−2.87±0.17
	10.766[a]			
5	10.94	14.91	13.86±0.21	−3.52±0.70
	10.804[a]		13.56[a]	−4.0[a]
6	10.97	14.93	14.36±0.18	−1.93±0.59
7	10.97	14.96	14.40±0.33	−1.9 ±1.1
8	11.02	15.01	14.86±0.27	−0.5 ±0.9
9	11.02	15.02	14.89±0.10	−0.43±0.35
10	11.07	14.97	14.36±0.67	−2 ±2

[a]Literature data from ref. 21.

tions because they seem to be physically less reasonable, and because their use results in poorer overall agreement between calculated and experimental ΔpK_1 values.

Following our assumptions, the intercharge distances R_{max} were calculated for the fully extended chains of the α,ω-amino-acids $^+H_3N(CH_2)_nCO_2^-$; these are shown in Table 3. Assuming the charges to be located at the foci of ellipsoids having the van der Waals volume V_w (given by addition of atomic increments (28)), the eccentricities λ_0 of the ellipsoids were obtained from the equation

$$[8] \qquad \lambda_0^3 - \lambda_0 = 6V_w/\pi R^3$$

and thence D_{eff} by interpolation from tabulated values (7). The values of ΔpK_1 calculated from R_{max} and D_{eff} are given in column *a* of Table 3.

TABLE 3. Effect of chain length n on the change of acid strength (ΔpK_1) of α,ω-amino-acids

			ΔpK (calcd.)		Exptl.	
n	R_{max} (Å)	ρ	a*	b†	ΔpK_1‡	ΔpK_2§
1	3.00	1.00	5.42	5.42	2.42	−0.86
2	4.43	0.95	1.60	1.96	1.33	−0.32
3	5.57	0.91	0.88	1.17	0.78	−0.01
4	6.93	0.88	0.58	0.76	0.61	0.20
5	8.12	0.85	0.48	0.62	0.49	0.30
6	9.46	0.83	0.39	0.51	0.44	0.31
7	10.67	0.81	0.34	0.45	0.37	0.32
8	11.99	0.79	0.30	0.40	0.35	0.38
9	13.21	0.77	0.27	0.37	0.31	0.38
10	14.53	0.75	0.24	0.34	0.26	0.44

*Calculated using R_{max}.
†Calculated using R_R.
‡K_a values (eq. 2) for n = 1–7 obtained from ref. 24; for n = 8–10 estimated by extrapolation of curve in Fig. 1.
§K_b values (eq. 5) for n = 1–7 obtained from ref. 23; for n = 8–10 estimated by extrapolation of curve in Fig. 1.

In column *b* of Table 3 are given ΔpK_1 values calculated in similar fashion, but using R_R, the intercharge distance for a randomly-coiled chain, in place of R_{max}, still assuming the charges to be at the foci of an ellipsoid. It was assumed that the proportions of the different conformations of H_3N^+-$(CH_2)_nCO_2^-$ were the same as those of $CH_3(CH_2)_n$-CH_3, since the conformational properties of NH_3^+ and CO_2^- groups are not widely different from those of the methyl group (29). The distances R_i between the terminal carbon atoms of the i conformers were found by measurements on a diamond lattice made with Fieser models (see Smith and Mortensen (13) for a discussion), and R_R obtained as the weighted mean of these distances:

$$[9] \qquad R_R = \sum \chi_i R_i$$

where χ_i is the mole fraction of the ith conformer. For example, 66% of *n*-butane at 25°C exists in the *anti*-conformation ($R \equiv R_{max} = 3.90$ Å) and 34% in two enantiomeric *gauche* conformations ($R = 2.95$ Å) (29, 30); consequently $R_R = (0.66 \times 3.90) + (0.34 \times 2.95) = 3.58$. The factor ρ ($\equiv R_R/R_{max}$) by which the end-to-end distance is reduced by coiling is consequently 3.58/3.90 = 0.92. In similar fashion, ρ was calculated for *n*-pentane, *n*-hexane, and *n*-heptane, and is shown plotted against *n* in Fig. 2; ρ for the longer *n*-alkanes was obtained from Tanford (31). The values of ρ in Table 3 were obtained from this curve, and thence R_R ($\equiv \rho R_{max}$), D_{eff}, and ΔpK_1 (*b*) for the zwitterions.

A comparison of ΔpK_1 values thus calculated with the experimental ΔpK_1 values listed in Table 3 shows that for $n \geq 4$ the experimental values lie

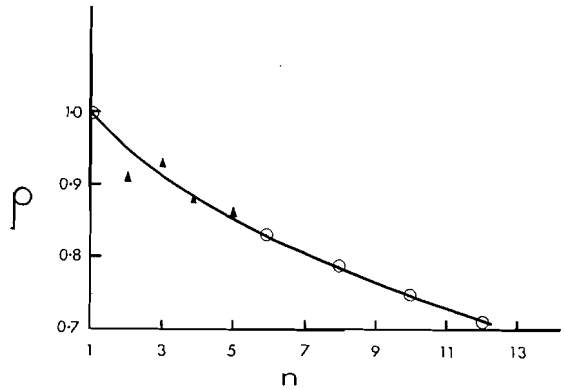

FIG. 2. Ratio ρ of length of the flexible to the fully extended *n*-alkane $CH_3(CH_2)_mCH_3$ of *n* carbon atoms: △, calculated according to Mann (30); ○, from Tanford (31).

between the values calculated for the fully-extended chain (*a*) and the randomly-coiled chain (*b*). For the shorter chains ($n \leq 3$) the Kirkwood–Westheimer treatment, as modified by us, fails increasingly as *n* becomes smaller. The treatment can be salvaged by arbitrarily increasing R_{max} and R_R, by an unrealistic disposition of the charges beyond the ends of the chains, and it is probably for this reason that such alternative locations of charges (discussed above) were adopted when data were available only for comparatively short chains. However, these alternative locations lead to poorer overall agreement with experiment for the larger number of compounds considered here.[5] It seems more reasonable to assume that the Kirkwood–Westheimer treatment breaks down for excessively short intercharge distances *R* because of the intrusion of effects (monopole–dipole, dipole–dipole, solvation: see below) which are negligible for large values of *R*, when only the monopole–monopole effect operates.

An alternative method of obtaining λ_0 and thence D_{eff} is due to Tanford (32): this assumes that the positive ammonium and negative carboxylate charges are at the foci of a prolate ellipsoid, but at a constant depth *d* of 1.0 Å below the ellipsoidal surface. In such a case

$$[10] \qquad \lambda_0 = (R + 2.0)/R$$

The assumption of a constant *d* is physically reasonable, but the location of the charges at the foci of the prolate ellipsoid leads to molecular volumes which become progressively less reasonable as *n* increases. (On the other hand, the use of [8], with a physically reasonable volume (V_w or Traube's molar volume (28)), necessitates a progressive decrease in *d* as *n* increases: again, a physically unrealistic picture.) Fortunately, calculations using the Tanford model give ΔpK values only very slightly greater than those calculated by the conventional Kirkwood–Westheimer approach: the differences for all molecules except the shortest ($n = 1$–3) are less than the experimental errors.

In summary, ΔpK_1 values support the notion that the polymethylene chains of α,ω-amino-acids have some flexibility in their central portions, so that the intercharge distance *R* lies between R_{max} and R_R. This accords with recent studies of dielectric increments of these compounds (33).

The relative success of [3] for ΔpK_1 values of **1** does not extend to ΔpK_2 values, as shown in Table 3. The pronounced failure of [3] for the shorter chains cannot be explained by juxtaposition of the charged ends resulting from extreme coiling of the chain, because a similar failure is observed for calculations of ΔpK_2 (but not ΔpK_1) of 2-(**2**), 3-(**3**), and 4-piperidinecarboxylic acid (**4**) (34), where *R* is fixed by the ring structures. These compounds should exist, to the extent of about 97% (29), in the conformation with an equatorial carboxylate group, as shown in **2**, **3**, and **4**. The intercharge distance in **2** and **3** should be the same as that in **1** ($n = 1$ and 2, respectively); that in **4** (one *gauche*, one *anti* conformation along the bonds marked by heavy lines) should be about R_R for **1** ($n = 3$).

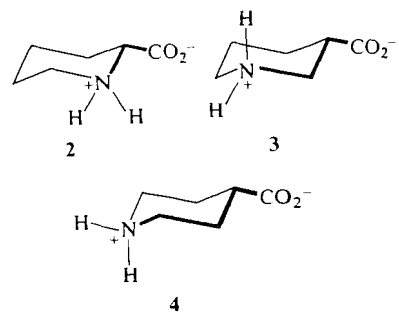

Thermodynamic Parameters for the First and Second Dissociations of α,ω-Amino-acids

The Kirkwood–Westheimer treatment employed above has attempted to explain changes in ΔpK_1 and ΔpK_2, and hence changes in ΔG_1^0 and ΔG_2^0, the standard free energy changes, entirely by changes in the internal energy of molecules resulting from electrostatic interactions. The justification for such an approach goes back many years to Evans and Polanyi (35), but more recent work on substituent effects by Hepler *et al.* (20, 36) has shown that the ionization of acids is determined by both the reaction medium and the polar and steric effects of the

[5]A tabulation of calculations based on the various possible assumptions is available, at a nominal charge, from the Depository of Unpublished Data, CISTI, National Research Council of Canada, Ottawa, Ont., Canada K1A 0R6.

Can. J. Chem. Downloaded from www.nrcresearchpress.com by 210.87.254.42 on 09/05/12
For personal use only.

Can. J. Chem. Downloaded from www.nrcresearchpress.com by 210.87.254.42 on 09/05/12
For personal use only.

[11] $H_3\overset{+}{N}(CH_2)_nCO_2H + CH_3(CH_2)_nCO_2^- \underset{}{\overset{\Delta pK_1}{\rightleftharpoons}} H_3\overset{+}{N}(CH_2)_nCO_2^- + CH_3(CH_2)_nCO_2H$

substituents. To examine substituent effects in the symmetrical reaction shown above, Hepler suggests that the overall effect of a substituent such as the ammonium group can be divided into "internal" and "environmental" contributions. The internal effects are those intrinsic to the molecules or ions, and would be observed if the reaction could be carried out in the absence of solvent. The environmental effects result from the interactions of the molecules or ions with the solvent. For symmetrical reactions such as [11], we can assume that internal contributions to the entropy change are negligible, and that environmental contributions to enthalpy and entropy changes are related by a constant β:

$$[12] \qquad \delta\Delta H_{env} = \beta\delta\Delta S_{env} = \beta\delta\Delta S^0$$

We can then obtain the following equation:

$$[13] \qquad \delta\Delta G^0 = \delta\Delta H_{int} + (\beta - T)\delta\Delta S^0$$

If $\beta \simeq 300$ K, then at 25°C

$$[14] \qquad \delta\Delta G^0 \simeq \delta\Delta H_{int}$$

This equation can be considered justification for the Kirkwood–Westheimer treatment above, which ignored the effects of solvation. Such solvation should affect ΔS^0 and ΔH^0 (cf. eq. 12). The values of $\delta\Delta G^0$, $\delta\Delta H^0$, and $\delta\Delta S^0$, defined as the thermodynamic parameters of [11] and [15]:

[15] $^-O_2C(CH_2)_n\overset{+}{N}H_3 + CH_3(CH_2)_nNH_2 \underset{}{\overset{\Delta pK_2}{\rightleftharpoons}} {}^-O_2C(CH_2)_nNH_2 + CH_3(CH_2)_n\overset{+}{N}H_3$

are given in Table 4, and show that the success of the Kirkwood–Westheimer treatment comes about from the well-known compensation of enthalpy and entropy changes when an isolated ion is transferred from a vacuum into a polar solvent such as water (37). For example, while the introduction of the positive ammonium group into acetic acid to give glycine (**1**; $n = 1$) makes ionization of the carboxyl group intrinsically easier ($\delta\Delta G^0 \simeq \delta\Delta H^0_{int} = -3.40$ kcal mol^{-1}), (Table 4, $n = 1$) it makes the hydration of the carboxylate group less exothermic ($\delta\Delta H_{env} \simeq +5.5$ kcal mol^{-1}), presumably because the nearby positive charge interferes with the binding of water molecules by ion–dipole interactions. Consequently, in water the enthalpic effect of introducing a charged ammonium group into acetic acid is unfavourable to ionization of the carboxyl group. That nonetheless protonated glycine is more acidic than acetic acid

TABLE 4. Changes in ΔG^0, ΔH^0, and ΔS^0 caused by introduction of a charged group at the end of a polymethylene chain, as measured by thermodynamic parameters for the reactions 11 and 15[a]

n	ΔpK	$\delta\Delta G^0$ (kcal mol^{-1})	$\delta\Delta H^0$ (kcal mol^{-1})	$\delta\Delta S^0$ (cal deg^{-1} mol^{-1})
Carboxyl ionization (reaction 11)				
1	−2.52	−3.40	1.26	15.8
2	−1.27	−1.75	1.52	10.9
3	−0.82	−1.13	0.92	6.8
4	−0.65	−0.88	0.35	4.1
5	−0.52	−0.69	(0.39)	1.0
6	−0.44	−0.59	(0.56)	0.1
7	(−0.38)	(−0.52)	(0.34)	(0.6)
8	(−0.37)	(−0.47)	(0.26)	(0.7)
9	(−0.34)	(−0.43)	(0.28)	(0.5)
10	(−0.31)	(−0.40)	(0.52)	(−0.4)
Ammonium ionization (reaction 15)				
1	−0.86	−1.17	−3.4	−7.7
2	−0.34	−0.46	−2.6	−8.1
3	0.05	0.07	−1.9	−6.5
4	0.22	0.30	(−0.2)	(−1.5)
5	0.31	0.42	(−0.2)	(−2.1)
6	0.34	0.46	(0.3)	(−0.5)
7	0.34	0.46	(0.3)	(−0.5)
8	0.38	0.52	(0.8)	(0.9)
9	0.38	0.52	(0.8)	(1.0)
10	0.41	0.56	(0.3)	(−0.6)

[a]Data in parentheses were obtained from estimated values for *n*-alkyl amines and carboxylic acids.

comes about from the more favourable entropy change ($\delta\Delta S^0 = +15.8$ eu), because the CO_2^- of glycine binds fewer water molecules than the CO_2^- of acetate.[6]

For the second step, the competing ionizations of ammonium groups in [15], the enthalpic effect of introducing a CO_2^- group into an alkyl chain explains the otherwise anomalous $\delta\Delta G_2^0$ values for $n = 1$–6 mentioned above. Electrostatic theory would predict that $\delta\Delta H_{int}$ should be positive (the CO_2^- should make the ammonium group a weaker acid). However, $\delta\Delta H^0$ and hence, *a fortiori*, $\delta\Delta H_{env}$ are negative. This can be explained again by electrostatic interference by nearby CO_2^- to the binding of water molecules[7] to the positive ammonium ion, so that [15] is accompanied by a net (exothermic) binding of water molecules, particularly when n is small. This also accounts for $\delta\Delta S^0$ ($\simeq \delta\Delta S_{env}$) of [15] when n is smaller (see Table 4). However, in this case the entropy effect does not compensate the enthalpic effect, so that the ammonium group of **1**

[6]It should be emphasized that this (and any) interpretation of thermodynamic parameters can only be arbitrary, but at least conforms to current orthodoxy (10, 17).

[7]Evidence for the smaller binding of water molecules by the ammonium group of **1** when n is smaller comes from studies of electrostriction (38).

TABLE 5. Temperature variation of pK values for the first and second dissociation equilibria of α,ω-amino-acids in water

n	Parameter	Value				
		10°C	20°C	25°C	30°C	40°C
1	pK_1	2.39±0.01	2.34±0.01	2.34±0.02	2.30±0.005	2.31±0.01
	pK_2	10.23±0.01	9.95±0.01	9.84±0.005	9.74±0.005	9.46±0.01
2	pK_1	3.57±0.01	3.54±0.01	3.55±0.01	3.52±0.015	3.51±0.015
	pK_2	10.79±0.005	10.51±0.01	10.36±0.005	10.21±0.015	9.96±0.015
3	pK_1	4.03±0.02	4.00±0.015	4.04±0.015	4.01±0.01	4.01±0.02
	pK_2	11.07±0.005	10.78±0.005	10.62±0.005	10.45±0.015	10.19±0.015
4	pK_1	4.21±0.015	4.20±0.015	4.23±0.015	4.22±0.02	4.22±0.02
	pK_2	11.38±0.01	11.03±0.01	10.85±0.01	10.67±0.02	10.36±0.02
5	pK_1	4.33±0.03	4.33±0.015	4.37±0.02	4.37±0.02	4.40±0.02
	pK_2	11.48±0.015	11.11±0.01	10.94±0.015	10.74±0.02	10.47±0.02
6	pK_1	4.39±0.02	4.42±0.015	4.45±0.015	4.45±0.02	4.48±0.02
	pK_2	11.51±0.01	11.13±0.01	10.97±0.01	10.75±0.02	10.46±0.02
7	pK_1	4.45±0.025	4.48±0.015	4.52±0.015	4.50±0.015	4.52±0.02
	pK_2	11.52±0.01	11.19±0.01	10.97±0.025	10.75±0.02	10.49±0.015
8	pK_1	4.52±0.02	4.52±0.025	4.54±0.025	4.55±0.03	4.58±0.025
	pK_2	11.56±0.02	11.23±0.005	11.02±0.02	10.83±0.01	10.47±0.01
9	pK_1	4.56±0.02	4.55±0.03	4.58±0.02	4.59±0.02	4.61±0.025
	pK_2	11.59±0.01	11.22±0.005	11.01±0.015	10.82±0.01	10.49±0.015
10	pK_1	4.56±0.02	4.59±0.02	4.63±0.015	4.64±0.01	4.64±0.03
	pK_2	11.50±0.02	11.18±0.005	11.07±0.01	10.75±0.02	10.46±0.02

remains a stronger acid than the ammonium group of RNH_3^+ up to $n = 3$.

This disturbing effect of CO_2^- on the hydration of the ammonium group, depending on a monopole–dipole interaction ($CO_2^- \cdots H_2O$), falls off with distance much more rapidly than monopole–monopole interactions. Consequently, beyond $n = 3$ the effect of CO_2^- on ΔH_{env} and ΔS_{env} becomes less important than its effect on ΔH_{int}, and the zwitterions become stronger acids than the corresponding alkylammonium ions, as predicted by electrostatic theory. It follows that the results of the Kirkwood–Westheimer calculations can be accepted with confidence when the ionizing groups are well separated, but not when they are close together.

Acknowledgment

The financial support of the National Research Council of Canada is gratefully acknowledged.

1. N. BJERRUM. Z. Phys. Chem. **106**, 219 (1923).
2. A. EUCKEN. Z. Angew. Chem. **45**, 203 (1932).
3. H. M. SMALLWOOD. J. Am. Chem. Soc. **54**, 3048 (1932).
4. J. G. KIRKWOOD and F. H. WESTHEIMER. J. Chem. Phys. **6**, 506 (1938); **6**, 513 (1938); **7**, 437 (1939).
5. F. H. WESTHEIMER and M. W. SHOOKHOFF. J. Am. Chem. Soc. **61**, 555 (1939).
6. W. KUHN. Kolloid-Z. **76**, 258 (1936); **87**, 3 (1939); H. EYRING. Phys. Rev. **39**, 746 (1932).
7. J. T. EDWARD, P. G. FARRELL, and J. L. JOB. J. Chem. Phys. **57**, 5251 (1972).
8. S. EHRENSON. J. Am. Chem. Soc. **94**, 7510 (1976).
9. D. H. EVERETT and B. R. W. PINSENT. Proc. R. Soc. (London), A**215**, 416 (1952).
10. E. J. KING and G. W. KING. J. Am. Chem. Soc. **78**, 1089 (1956).
11. G. C. LEVY, R. A. KOMORSKI, and J. HALSTEAD. J. Am. Chem. Soc. **96**, 5456 (1974).
12. P. J. FLORY. Statistical mechanics of chain molecules. Interscience, New York, NY. 1969.
13. R. P. SMITH and E. M. MORTENSEN. J. Chem. Phys. **35**, 714 (1961); R. P. SMITH. J. Chem. Phys. **42**, 1162 (1965).
14. R. G. BATES. The determination of pH. John Wiley, New York, NY. 1964. Chapt. 5.
15. A. I. VOGEL. Quantitative inorganic analysis. 3rd ed. Longmans, London. 1961. pp. 235–238.
16. A. ALBERT and E. P. SARJEANT. Ionisation constants of acids and bases. Methuen, London. 1962. Chapt. 2.
17. E. J. KING. Acid–base equilibria. Pergamon Press, London. 1965. pp. 78–83.
18. J. P. GREENSTEIN and M. WINITZ. Chemistry of the amino acids. Vol. I. John Wiley, New York, NY. 1961. p. 482.
19. J. J. CHRISTENSEN, J. L. OSCARSON, and R. M. IZATT. J. Am. Chem. Soc. **90**, 5949 (1968).
20. P. D. BOLTON and L. G. HEPLER. Q. Rev. **25**, 521 (1971).
21. J. L. LARSON and L. G. HEPLER. *In* Solute–solvent interactions. *Edited by* J. F. Coetzee and C. D. Ritchie. M. Dekker, New York, NY. 1969, and references therein.
22. A. NEUBERGER. Proc. R. Soc. A**158**, 69 (1937).
23. D. D. PERRIN. Dissociation constants of organic bases in aqueous solution. Butterworths, London. 1964.
24. R. P. BELL. The proton in chemistry. 2nd ed. Chapman and Hall, London. 1973.
25. R. P. BELL and G. A. WRIGHT. Trans. Faraday Soc. **57**, 1377 (1961).
26. R. C. WEAST (*Editor*). Handbook of chemistry and physics. 41st ed. The Chemical Rubber Co., Cleveland, OH. 1960.
27. L. E. SUTTON (*Editor*). Tables of interatomic distances and

Can. J. Chem. Downloaded from www.nrcresearchpress.com by 210.87.254.42 on 09/05/12
For personal use only.

configuration of molecules and ions. The Chemical Society, London. 1958.
28. J. T. EDWARD. J. Chem. Educ. **47**, 261 (1970).
29. E. L. ELIEL, N. L. ALLINGER, S. J. ANGYAL, and G. A. MORRISON. Conformational analysis. Academic Press, New York, NY. 1965. p. 44.
30. G. MANN. Tetrahedron, **23**, 3375 (1967).
31. C. TANFORD. J. Phys. Chem. **78**, 2469 (1974).
32. C. TANFORD. J. Am. Chem. Soc. **79**, 5348 (1957).
33. J. KIRCHNEROVA, P. G. FARRELL, and J. T. EDWARD. J. Phys. Chem. **80**, 1974 (1976); J. A. WALDER. J. Phys. Chem. **80**, 2777 (1976).
34. L. D. HANSEN and E. A. LEWIS. J. Phys. Chem. **77**, 286 (1973).
35. M. G. EVANS and M. POLANYI. Trans. Faraday Soc. **32**, 1333 (1936).
36. L. G. HEPLER. J. Am. Chem. Soc. **85**, 3089 (1963).
37. K. J. LAIDLER. Trans. Faraday Soc. **55**, 1725 (1959), and references therein; R. LUMRY and S. RAJENDER. Biopolymers, 1125 (1970), and references therein.
38. F. SHAHIDI. Ph.D. Thesis, McGill University, Montreal, Canada. 1977.

Can. J. Chem. Downloaded from www.nrcresearchpress.com by 210.87.254.42 on 09/05/12
For personal use only.

Re-examination of the Kirkwood–Westheimer theory of electrostatic effects. III. Dissociation constants of *cis*-3- and *trans*-4-substituted cyclohexanecarboxylic acids in water – dimethyl sulfoxide mixtures

JITKA KIRCHNEROVA, PATRICK G. FARRELL, AND JOHN T. EDWARD
Department of Chemistry, McGill University, 801 Sherbooke St. W., Montreal, P.Q., Canada H3A 2K6

AND

JEAN-CLAUDE HALLE AND ROBERT SCHAAL
Laboratoire de Physicochimie des Solutions, LA CNRS 161, ENSCP, Université Pierre-et-Marie Curie, 11 rue Pierre-et-Marie Curie, Paris 5e, France

Received August 12, 1977

JITKA KIRCHNEROVA, PATRICK G. FARRELL, JOHN T. EDWARD, JEAN-CLAUDE HALLE, and ROBERT SCHAAL. Can. J. Chem. **56**, 1130 (1978).

Acid dissociation constants of two *cis*-3- and of four *trans*-4-substituted cyclohexanecarboxylic acids in water – dimethyl sulfoxide mixtures of varying composition were determined by a potentiometric method. Results have been analyzed according to the model of Kirkwood and Westheimer, and shown to differ from calculated values because of certain oversimplifications built into the model. Dissociation constant differences between cyclohexanecarboxylic acid and the compounds studied vary only slightly with changing solvent composition.

JITKA KIRCHNEROVA, PATRICK G. FARRELL, JOHN T. EDWARD, JEAN-CLAUDE HALLE et ROBERT SCHAAL. Can. J. Chem. **56**, 1130 (1978).

On a déterminé, par une méthode potentiométrique, les constantes de dissociation acide d'acides cyclohexanecarboxyliques substitués par des groupements *cis* en position 3 (deux cas) et *trans* en position 4 (quatre cas) dans des mélanges eau–diméthylsulfoxyde de diverses compositions. On a analysé les résultats suivant le modèle de Kirkwood et Westheimer et on a montré qu'ils diffèrent des valeurs calculées à cause d'une simplification outrancière inhérente au modèle. Les différences de constantes de dissociation entre l'acide cyclohexanecarboxylique et les composés étudiés ne varient que légèrement lorsque l'on change la composition du solvant.
[Traduit par le journal]

Introduction

Taking the unsubstituted carboxylic acid as reference, Kirkwood and Westheimer (1) suggested that the pK should be changed by the presence of a positively-charged group (acid-strengthening) or negatively-charged group (acid-weakening) by an amount

$$[1] \qquad \Delta pK = e^2/2.3kTRD_{eff}$$

where e is the electronic charge, k is Boltzmann's constant, T the absolute temperature, R the distance between the charged carboxylate group and the charged substituent,[1] and D_{eff} the effective dielectric constant. Similarly, the introduction of an uncharged substituent having a dipole moment μ should change the pK by

$$[2] \qquad \Delta pK = e\mu \cos\theta/2.3kTR^2D_{eff}$$

where θ is the angle between R, the line joining the centre of the ionizing group to the centre of the dipole, and the axis of the dipole. For the particular case of ellipsoidal molecules having at their foci point charges, or a point charge and a point dipole, Kirkwood and Westheimer calculated D_{eff} as a function of D_e, the dielectric constant of the solvent, and λ_0, the ratio of the major axis to the interfocal distance of the ellipsoid (1, 3, 4).

Recently the superiority of this electrostatic or "field effect" over the widely-accepted "inductive effect" for the explanation of substituent effects has been stressed (5, 6). The inductive mechanism takes no account of orientation of the dipolar substituent, nor of the solvent. Recent researches (7, 8) have amply demonstrated the importance of the orientation of the dipole, but there have been few attempts (9) to test the effect of changing solvent. In the present paper we report the effect of the changing composition of water – dimethyl sulfoxide (DMSO) solvent mixtures on the pK values of some *cis*-3- (**1**; X = CO_2H, CO_2^-) and *trans*-4-substituted cyclohexanecarboxylic acids (**2**; X = NH_3^+, CO_2^-,

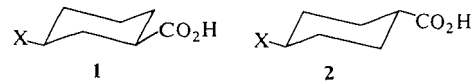

1 **2**

[1]This definition of R differs slightly from that of Kirkwood and Westheimer, and is justified in an earlier paper (2).

Can. J. Chem. Downloaded from www.nrcresearchpress.com by 210.87.254.42 on 09/05/12
For personal use only.

TABLE 1. pK values of *trans*-4-substituted and *cis*-3-substituted cyclohexanecarboxylic acids as a function of water–DMSO composition at 20°C

Substituent	pK values at mol% DMSO =												
	0.0[a]	2.7	5.9	9.6	13.5	19.5	26.6	35.6	48.7	59.3	69.7	83.1	100[b]
4-$\overset{+}{N}H_3$	4.07	4.21	4.42	4.63	4.92	5.32	5.79	6.54	7.66	8.54	9.28	10.40	(11.8)
4-COOH	4.37[c]	4.49	4.67	4.92	5.22	5.62	6.12	6.81	7.87	8.80	9.62	10.70	(12.1)
4-$COOCH_3$	4.69[d]	4.79	4.98	5.24	5.55	5.95	6.45	7.19	8.25	9.12	9.90	10.98	(12.4)
4-COO^-	5.42[e]	5.50	5.69	5.97	6.31	6.75	7.31	8.12	9.16	10.01	10.85	11.96	(13.3)
3-COOH	4.33[f]	4.46	4.61	4.90	5.20	5.57	6.11	6.79	7.86	8.80	[h]	[h]	(12.1)
3-COO^-	5.40[g]	5.47	5.70	5.94	6.31	6.75	7.31	8.19	9.19	10.07	[h]	[h]	(13.4)

[a]1% DMSO (by volume).
[b]Extrapolated values
[c]Reference 11 reports 4.37 at 24.9°C; ref. 16 reports 4.18 at 20°C.
[d]Reference 11 reports 4.69 at 24.9°C.
[e]Reference 11 reports 5.36 at 24.9°C; ref. 16 reports 5.42 at 20°C.
[f]Reference 16 reports 4.10 at 20°C.
[g]Reference 16 reports 5.46 at 20°C.
[h]Solubility too low for pK determination.

CO_2H, CO_2CH_3). These compounds exist essentially completely in the conformation shown in **1** and **2** (10), and the charges or dipoles of the compounds **2** (but not **1**) are close to the foci of the circumscribing ellipsoids. Since not all are very soluble in water, some of them have been studied previously in a single methanol–water or ethanol–water mixture (11). We have chosen to study them in water–DMSO mixtures in the belief that the progressive change from the protic solvent water to the aprotic solvent DMSO represents a more drastic change in solvent character, particularly for anions such as carboxylates, which should be little solvated by dimethyl sulfoxide (12, 13).

Experimental

Materials

cis-1,3-Cyclohexanedicarboxylic acid (**1**; X = CO_2H), *trans*-1,4-cyclohexanedicarboxylic acid (**2**; X = CO_2H), and *trans*-4-aminocyclohexanecarboxylic acid (**2**; X = NH_2) were obtained by hydrogenation of the corresponding aromatic compounds according to known procedures (14). *trans*-4-Methoxycarbonylcyclohexanecarboxylic acid (**2**; X = CO_2Me) was prepared by partial hydrolysis of the diester. Water and dimethyl sulfoxide were purified and their mixtures prepared as described earlier (13).

Procedure

Thermodynamic pK values were determined at 20°C by a procedure already described (12, 13, 15), the calculation of the successive pK's of the dicarboxylic acids being realized by successive approximations. Their accuracy is estimated to be within 0.06 pK units, and the reproducibility to within 0.03 pK units.

Results and Discussion

The results obtained are given in Table 1. Where comparison with results in the literature (11, 16) is possible, agreement is good, as can be seen from the footnotes to Table 1. pK values obtained by extrapolation to 100% DMSO are also given in Table 1, and from previous work (12) seem likely to be reliable.

Taking cyclohexanecarboxylic acid (12) as the standard, we obtain the effect of a 3- or 4-substituent as $\Delta pK_{expt} = pK$(substituted cyclohexanecarboxylic acid) − pK(cyclohexanecarboxylic acid). Such values for 100% water and 100% DMSO are shown in Table 2 (corrected for the statistical effect, where necessary). Also shown in this table are the values (ΔpK_{calcd}) calculated for these solvents from either [1] or [2]. For this calculation the molecular volume V_W was obtained by addition of van der Waals increments (17),[2] and the charge–charge or charge–dipole distance R calculated from standard bond lengths and bond angles by trigonometry; the location of the point charge within the group has already been discussed (2). From V_W and R the eccentricity λ_0 of the ellipsoid may be calculated (2), and thence D_{eff} from the dielectric constants of water and of DMSO (and, if need be, of the water–DMSO mixtures (18)). Values of $\mu \cos \theta$ were taken from ref. 11.

Comparison of ΔpK_{calcd} thus obtained with ΔpK_{expt} shows immediately serious failings in the Kirkwood–Westheimer treatment. Firstly, eq. 1 requires that if the CO_2^- group acts only as a point monopole, its introduction at the 4-position of cyclohexanecarboxylic acid should weaken the acid to roughly the same extent as the 4-NH_3^+ group strengthens it. In fact, the CO_2^- group is only about one quarter as effective as the NH_3^+ group. Secondly, the CO_2H or CO_2Me dipole at the 4-position is about three times *more* effective in strengthening the carboxyl group than calculated by [2].

[2]The molecular volume calculated by Traube's rules (17) is slightly larger, and its use leads to slightly lower D_{eff} values and slightly higher ΔpK values; the differences, however, are small.

Can. J. Chem. Downloaded from www.nrcresearchpress.com by 210.87.254.42 on 09/05/12
For personal use only.

Can. J. Chem. Downloaded from www.nrcresearchpress.com by 210.87.254.42 on 09/05/12
For personal use only.

TABLE 2. Calculated and experimental values of ΔpK of 3- and 4-substituted cyclohexanecarboxylic acids

		H_2O		DMSO	
Substituent	R (Å)	ΔpK_{calcd}	ΔpK_{exptl}	ΔpK_{calcd}	ΔpK_{exptl}
4-NH_3^+	6.74	−0.68	−0.84	−1.08	−0.95
4-CO_2H	7.45	−0.06	−0.24	−0.10	−0.35
4-CO_2^-	7.41	+0.58	+0.21	+0.95	+0.25
4-CO_2CH_3	7.58	−0.07	−0.22	−0.11	−0.35
3-CO_2H	6.04	−0.13	−0.28	−0.18	−0.35
3-CO_2^-	6.04	+0.98	+0.19	+1.40	+0.35

These failings come about because of an over-simple application of [1] and [2] to the compounds in question. The results can be brought into qualitative agreement with the theory if the following assumptions are made:

(*a*) While the NH_3^+ group behaves as a monopole only, the CO_2^- group behaves as a combined monopole and dipole (μ = 3.2 D, according to Wilcox and McIntyre (19), as compared to μ = 1.68 D for CO_2H).

(*b*) The CO_2H and CO_2Me groups are not point dipoles at one focus of an ideal ellipsoid, so that both positive and negative ends are buried equally within the molecular cavity. Instead, the negative oxygen atom is exposed at the surface of the molecule, where it can interact with neutralizing solvent molecules, while the positive carbon atom is buried in the low-dielectric interior of the molecule. Consequently, the ionizing function "feels" the effect of positive carbon more than would be expected from [2].

(*c*) In assessing the effect of a substituent, it is necessary to take account of its effect on *both* the acid and the conjugate base in equilibrium with it.

We may now re-examine the results in Table 2 in the light of these assumptions. What effect should one expect from the presence of the dipolar CO_2H or CO_2Me in **3**/**4** on the acid-strength of the carbonyl group in the equilibrium below?

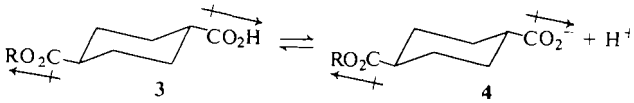

3 **4**

Dipole–dipole interaction in **3** increases its free energy (an acid-strengthening effect); this is more than compensated for by dipole–dipole interaction in **4** (an acid-weakening effect), required by consideration of (*a*) above. However, dipole–dipole interactions $\propto 1/R^3$, and so are unimportant at these distances when compared with the monopole–dipole interaction ($\propto 1/R^2$) found in **4** but not in **3**. This produces a ΔpK of 0.2–0.3, about three times larger than calculated by [2] because of the effect discussed under (*b*) above.

Next, let us consider the effect of introducing the monopole NH_3^+ (assumption *a*) into the 4-position of cyclohexanecarboxylic acid:

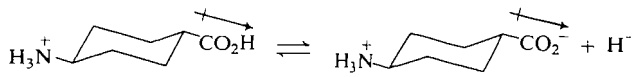

5 **6**

According to Wilcox and McIntyre (19), dipole–monopole interactions in **6** are stronger than dipole–monopole interactions in **5**, and should weaken the acid by 0.2–0.3 pK units; the monopole–monopole interaction, found only in **6**, should strengthen the acid, according to [1], by 1.08 pK units in DMSO and 0.68 pK units in water. The experimental ΔpK is in fair agreement with the ΔpK thus estimated for DMSO (−0.78 to −0.88), taking into account the two effects, but in poorer agreement with that estimated for water (−0.38 to −0.48).

Lastly, consider the effect of the CO_2^- group at the 4-position on the equilibrium:

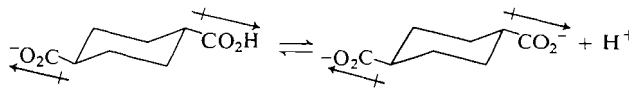

7 **8**

We shall ignore dipole–dipole interactions. There is a monopole–monopole interaction in **8** which should be acid-weakening by 0.58 pK units in water and 0.95 units in DMSO (Table 2). However, this is opposed by the net monopole–dipole interactions: two acid-strengthening interactions in **8**, reduced by one weaker acid-weakening interaction in **7**, so that the net effect should be acid strengthening by about 0.4–0.6 pK units. This brings ΔpK_{calcd} to within fair agreement with ΔpK_{exptl}.

Similar considerations applied to ΔpK_{calcd} of **1** (X = CO_2H and CO_2^-) serve to bring it into better agreement with ΔpK_{exptl}, although for these compounds good agreement should not be expected, because they do not have their charges or dipoles close to the foci of the circumscribing ellipsoid.

In Table 2 we have compared ΔpK_{calcd} with

ΔpK_{expll} only for the two solvents, 100% H_2O and 100% DMSO; a similar comparison for all the other solvent mixtures of Table 1 does not reveal any additional points of interest. While the progressive replacement of water by dimethyl sulfoxide changes only gradually the dielectric constant of the solvent mixtures (18), it changes more drastically the activity coefficient of anions (20). We accordingly expected radically different behaviour in DMSO-rich mixtures. However, it seems that the equations of Kirkwood and Westheimer apply about as well in these mixtures as in water and water–alcohol mixtures studied previously. Their weaknesses arise from the simplifying assumptions (e.g. of point dipoles) necessary for a mathematically-tractable treatment; when these weaknesses can be compensated for (e.g. in the comparative treatment of Wilcox and Leung (6)), the Kirkwood–Westheimer treatment works astonishingly well.

Acknowledgments

We are grateful to Dr. G. E. Langford for preparation of the carboxylic acids, to the National Research Council of Canada for financial support, and to Coopération France–Québec for financing the exchanges between our two laboratories, in particular for the mission of J.K. to Paris where the dissociation constants were measured. We thank Dr. Bo-Long Poh for much help in calculations.

1. J. G. KIRKWOOD and F. H. WESTHEIMER. J. Phys. Chem. **6**, 506 (1938); **6**, 513 (1938).
2. J. T. EDWARD, P. G. FARRELL, J. L. JOB, and B.-L. POH. Can. J. Chem. This issue.
3. J. T. EDWARD, P. G. FARRELL, and J. L. JOB. J. Chem. Phys. **57**, 5251 (1972).
4. S. EHRENSON. J. Am. Chem. Soc. **98**, 7510 (1976).
5. M. J. S. DEWAR. The molecular orbital theory of organic chemistry. McGraw-Hill, New York. 1969. p. 421.
6. C. F. WILCOX and C. LEUNG. J. Am. Chem. Soc. **90**, 336 (1968).
7. C. L. LIOTTA, W. F. FISHER, E. L. SLIGHTON, and C. L. HARRIS. J. Am. Chem. Soc. **94**, 2129 (1972).
8. L. M. STOCK. J. Chem. Educ. **49**, 400 (1972), and references therein; C. T. WANG and E. J. GRUBBS. J. Org. Chem. **42**, 534 (1977).
9. C. D. RITCHIE and E. S. LEWIS. J. Am. Chem. Soc. **84**, 591 (1962).
10. E. L. ELIEL, N. L. ALLINGER, S. J. ANGYAL, and G. A. MORRISON. Conformational analysis. John Wiley and Sons, New York. 1965. p. 44.
11. S. SIEGEL and J. M. KOMARMY. J. Am. Chem. Soc. **82**, 2547 (1960).
12. J. T. EDWARD, P. G. FARRELL, J. KIRCHNEROVA, J.-C. HALLE, and R. SCHAAL. Can. J. Chem. **54**, 1899 (1976).
13. J.-C. HALLE. Thèse, Paris AO 5780 (1971); J.-C. HALLE, R. GABORIAUD, and R. SCHAAL. Bull. Soc. Chim. Fr. 1851 (1969).
14. H. A. SMITH and F. P. BYRNE. J. Am. Chem. Soc. **72**, 4406 (1950); J. P. GREENSTEIN and J. WYMAN. J. Am. Chem. Soc. **60**, 2341 (1938).
15. J.-C. HALLE and R. SCHAAL. Anal. Chim. Acta, **60**, 197 (1972); J.-C. HALLE, R. HARIVEL, and R. GABORIAUD. Can. J. Chem. **52**, 1774 (1974).
16. R. KUHN and A. WASSERMAN. Helv. Chim. Acta, **11**, 50 (1928).
17. J. T. EDWARD. J. Chem. Educ. **47**, 261 (1970).
18. G. DOUHERET. Bull. Soc. Chim. Fr. 3122 (1968).
19. C. F. WILCOX and J. S. MCINTYRE. J. Org. Chem. **30**, 777 (1965).
20. A. J. PARKER. Chem. Rev. **69**, 1 (1969).

Can. J. Chem. Downloaded from www.nrcresearchpress.com by 210.87.254.42 on 09/05/12
For personal use only.

Synthesis of 5- and 6-methylene-2-norbornanones

NICK HENRY WERSTIUK AND ROLAND TAILLEFER

Department of Chemistry, McMaster University, Hamilton, Ont., Canada L8S 4M1

Received July 12, 1977

NICK HENRY WERSTIUK and ROLAND TAILLEFER. Can. J. Chem. **56**, 1134 (1978).

The syntheses of 4,4,6-trimethyl-5-methylene-2-norbornanone (**5***a*), 6,6-dimethyl-2-methylene-2-norbornanone (**5***b*), 5-methylene-2-norbornanone (**5***c*), and 6-methylene-2-norbornanone (**11**) are described. An unusual extended Grob-type cleavage of 6-ethylenedioxy-*exo*-2-methyl-*endo*-2-norbornanol (**13***d*) to 2-chloroethyl (3-methyl-3-cyclopentenyl)acetate (**17**) is documented.

NICK HENRY WERSTIUK et ROLAND TAILLEFER. Can. J. Chem. **56**, 1134 (1978).

On décrit la synthèse des triméthyl-4,4,6 méthylène-5 (**5***a*), diméthyl-6,6 méthylène-2 (**5***b*), méthylène-5 (**5***c*), et un méthylène-6 (**11**) norbornanones-2. On présente des données confirmant l'existence d'une coupure inusitée, du type Grob élargi, de l'éthylènedioxy-6 méthyl-2 *exo* norbornanol-2 *endo* (**13***d*) conduisant à l'acétate du chloro-2 éthyl (méthyl-3 cyclopentène-3 yl) (**17**).

[Traduit par le journal]

Introduction

The chemistry of the carbonyl group recently has been reviewed in two volumes of the series the Chemistry of the Functional Group (1). That there were but three pages devoted to an account of the kinetic and mechanistic aspects of acid- and base-catalyzed enolization and hydrogen isotope exchange of acyclic and monocyclic ketones served to reinforce our view that all the mechanistic intricacies of these ubiquitous reactions had not yet been established. Thus we undertook a detailed study of the kinetic and mechanistic aspects of hydrogen isotope exchange of the diastereotopic protons α to the carbonyl group in a series of bicyclic ketones. For the initial study we required a series of 5- and 6-methylene-2-norbornanones and 2,5-norbornanediones. We report herein, in the first paper of a series which will document our synthetic and mechanistic work, the synthesis of 4,4,6-trimethyl-5-methylene-2-norbornanone (**5***a*), 6,6-dimethyl-2-methylene-2-norbornanone (**5***b*), 5-methylene-2-norbornanone (**5***c*), and 6-methylene-2-norbornanone (**11**). An unusual extended Grob-type cleavage of 6-ethylenedioxy-*exo*-2-methyl-*endo*-2-norbornanol (**13***d*) to 2-chloroethyl (3-methyl-3-cyclopentenyl)acetate (**17**) is documented also.

Results and Discussion

Synthesis

The 2,5-enone substitution pattern in **5***a*, **5***b*, and **5***c* was developed through the use of *endo*-5-ethanoyloxy-4,4,6-trimethyl-2-norbornanone (**6***a*), *endo*-5-ethanoyloxy-6,6-dimethyl-2-norbornanone (**6***b*), and *endo*-5-ethanoyloxy-2-norbornanone (**6***c*), respectively. Compounds **6***a* and **6***b* were prepared from 1,3,3-trimethyl-*endo*-2-norbornyl acetate (fenchyl acetate) (**9***a*) and 3,3-dimethyl-*endo*-2-norbornyl acetate (camphenilyl acetate) (**9***b*) via the methods of Hirsjärvi (2) and Meinwald and co-workers (3, 4), respectively. The acetates **9***a* and **9***b* were prepared from 1,3,3-trimethyl-2-norbornanone (fenchone) (**8***a*) and 3,3-dimethyl-2-norbornanone (camphenilone) (**8***b*) by LAH reduction of the ketones and acetylation of the alcohols. Compound **6***c* was prepared by an acid-catalyzed ring opening of nortricyclanone[1] as described by Meinwald *et al.* (5). Hydrolysis of **6***a* and **6***b* gave *endo*-5-hydroxy-4,6,6-trimethyl-2-norbornanone (**1***a*) and *endo*-5-hydroxy-6,6-dimethyl-2-norbornanone (**1***b*), which were converted to 5-ethylenedioxy-1,3,3-trimethyl-*endo*-2-norbornanol (**2***a*) and 5-ethylenedioxy-3,3-dimethyl-*endo*-2-norbornanol (**2***b*) by ethylene glycol and *p*-toluenesulfonic acid in benzene. Oxidation of the ketalols **2***a* and **2***b* with CrO_3 in pyridine gave 5-ethylenedioxy-1,3,3-trimethyl-2-norbornanone (**3***a*) and 5-ethylenedioxy-3,3-dimethyl-2-norbornanone (**3***b*), which were converted with triphenylphosphonium methide in hexane to 2-ethylenedioxy-4,6,6-trimethyl-5-methylenenorbornane (**4***a*) and 2-ethylenedioxy-6,6-dimethyl-5-methylenenorbornane (**4***b*), respectively. Mild acid-catalyzed hydrolysis of the ketalenes **4***a* and **4***b* gave the enones **5***a* and **5***b*. That the nmr data for **5***a* and **5***b*[2] are consistent with the proposed structures, and **5***a* and **5***b* were converted by periodate–permanganate oxidation to the known compounds 1,3,3-trimethyl-2,5-norbornandione (**10***a*) and 3,3-dimethyl-2,5-norbornandione (**10***a*) and 3,3-di-

[1] Although the mechanism of the ring opening of nortricyclane (*i*) has not been established, it is likely that conversion of $i \rightarrow$ **6***c* proceeds via initial protonation of the carbonyl group rather than the three membered ring.

[2] Photocopies of the nmr spectra are available upon request, at a nominal charge, from the Depository of Unpublished Data, CISTI, National Research Council of Canada, Ottawa, Ont., Canada K1A 0S2.

Can. J. Chem. Downloaded from www.nrcresearchpress.com by 210.87.254.5 on 09/05/12
For personal use only.

Can. J. Chem. Downloaded from www.nrcresearchpress.com by 210.87.254.5 on 09/05/12
For personal use only.

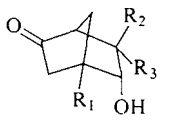

1

a $R_1 = R_2 = R_3 = CH_3$
b $R_1 = H, R_2 = R_3 = CH_3$

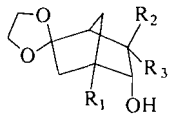

2

a $R_1 = R_2 = R_3 = CH_3$
b $R_1 = H, R_2 = R_3 = CH_3$

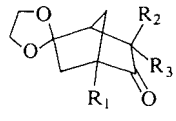

3

a $R_1 = R_2 = R_3 = CH_3$
b $R_1 = H, R_2 = R_3 = CH_3$
c $R_1 = R_2 = R_3 = H$

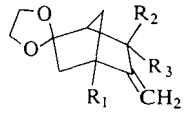

4

a $R_1 = R_2 = R_3 = CH_3$
b $R_1 = H, R_2 = R_3 = CH_3$
c $R_1 = R_2 = R_3 = H$

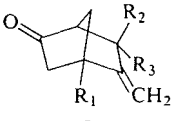

5

a $R_1 = R_2 = R_3 = CH_3$
b $R_1 = H, R_2 = R_3 = CH_3$
c $R_1 = R_2 = R_3 = H$

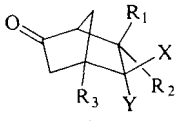

6

a $R_1 = R_2 = R_3 = CH_3, X = H, Y = OAc$
b $R_1 = H, R_2 = R_3 = CH_3, X = H, Y = OAc$
c $R_1 = R_2 = R_3 = H, X = OAc, Y = H$

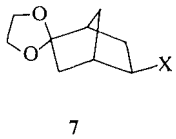

7

a X = OAc
b X = OH

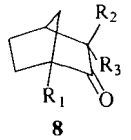

8

a $R_1 = R_2 = R_3 = CH_3$
b $R_1 = H, R_2 = R_3 = CH_3$

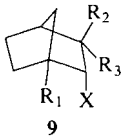

9

a $R_1 = R_2 = R_3 = CH_3, X = OAc$
b $R_1 = H, R_2 = R_3 = CH_3, X = OAc$

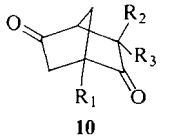

10

a $R_1 = R_2 = R_3 = CH_3$
b $R_1 = H, R_2 = R_3 = CH_3$
c $R_1 = R_2 = R_3 = H$

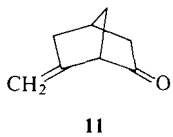

11

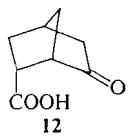

12

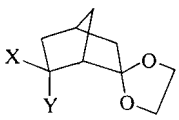

13

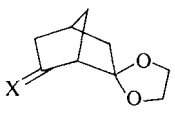

14

a $X = CH_2$
b X = O

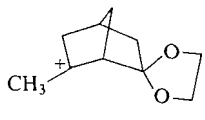

15

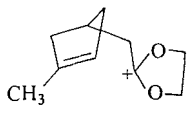

16

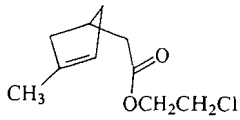

17

a $X = H, Y = CCH_2CH_2OH$ (O)
b $X = H, Y = CH_2OH$
c $X = H, Y = CH_2OAc$
d $X = CH_3, Y = OH$

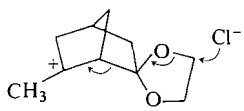

18

methyl-2,5-norbornanedione (**10***b*) (6), respectively, conclusively established the structure of the enones. Also, subsequent to our initial report (7) of **5***b*, Money prepared enone **5***b*[3] via a shorter route. Enone **5***c* was prepared essentially via the same route as **5***a* and **5***b* except that **5***c* was converted into 5-ethylenedioxy-*exo*-2-norbornyl acetate (**7***a*). 5-Ethylenedioxy-*exo*-2-norbornanol (**7***b*), obtained by LAH reduction of **7***a*, was transferred into **5***c* via the usual sequence (*vide supra*). That the nmr spectrum[2] is consistent with the structure of **5***c* and that **5***c* is oxidized to 2,5-norbornanedione (**10***c*) (5) by periodate–permanganate, conclusively establishes the structure of **5***c*.

6-Methylene-2-norbornanone was synthesized by a sequence of reactions which began with the conversion of *endo*-2-norbornene-5-carboxylic acid into 6-oxo-*endo*-2-norbornanecarboxylic acid (**12**) (8). The latter was ketalized and the ketal ester **13***a* was reduced by LAH to 6-ethylenedioxy-*endo*-2-norbornylmethanol (**13***b*). 6-Ethylenedioxy-*endo*-2-norbornylmethyl acetate (**13***c*), obtained by acetylation of **13***b*, was pyrolyzed to yield the ketalene **14***a*. Mild acid-catalyzed hydrolysis of **14***a* gave **11**. The nmr spectrum [2] of **11** is consistent with the proposed structure.

We initially attempted to prepare the ketalene **14***a* from the ketoketal **14***b*[4] by means of a Wittig reaction. Although the ketoketal **14***b* is easily obtained, the addition of triphenylphosphonium meth-

[3]The spectral properties of the independently synthesized enones were identical. Professor T. Money. Personal communication.

[4]Compound **14***b* was prepared from 5-norbornen-2-one via a ketalization (TsOH, $HOCH_2CH_2OH$, benzene) and epoxidation ($PhCO_3H$), a reductive ring opening of the epoxide (LAH, *N*-methylpyrrolidinone), and an oxidation (CrO_3, pyridine).

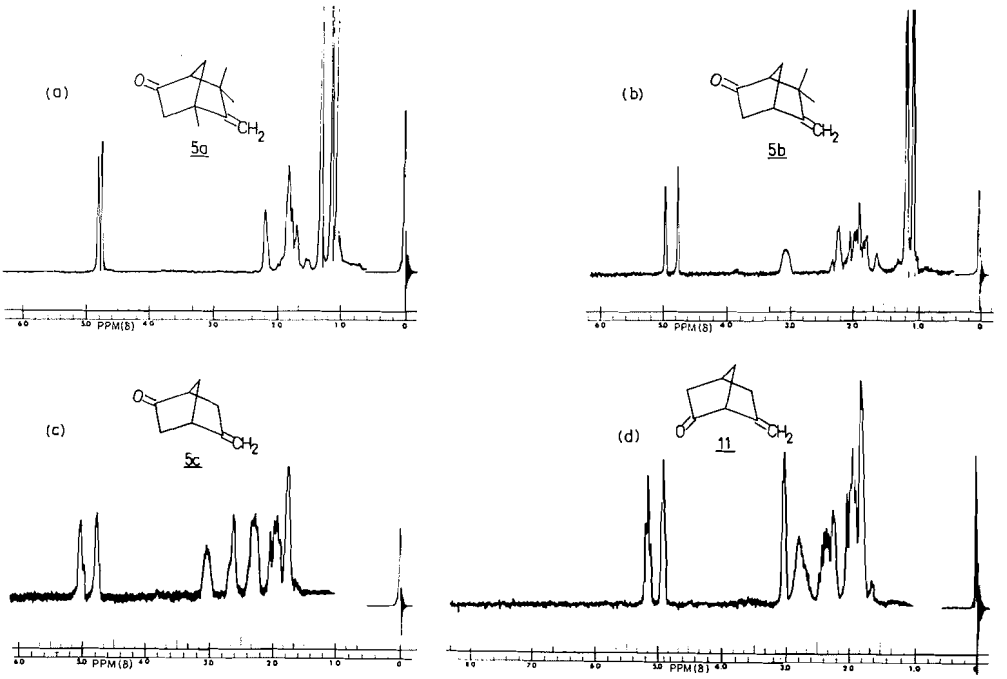

FIG. 1. The nmr (60 MHz) spectra of (*a*) enone **5***a*, (*b*) enone **5***b*, (*c*) enone **5***c*, and (*d*) enone **11**.

ide to the carbonyl group did not occur, perhaps as a consequence of the steric strain that develops between the alkoxide function and *endo* oxygen of the ketal at C (6).

Grob Cleavage

We also attempted to prepare ketalene **14***a* by dehydration of 6-ethylenedioxy-*exo*-2-methyl-*endo*-2-norbornanol (**13***d*) that is prepared from ketoketal **14***b* via a Grignard reaction. When alcohol **13***d* is reacted with $POCl_3$ in pyridine at room temperature, the major product isolated by preparative vpc is **17**. Whether the Grob-type cleavage (9, 10) occurs in a stepwise fashion through cation **15** via attack of Cl^- on a dioxolenium ion **16** or in a synchronous fashion as depicted in **18** can be debated.

Experimental

Melting points were taken on a Kofler block and are uncorrected. Infrared spectra were recorded on a Perkin-Elmer 337 Grating Spectrometer and a Beckman IR5 instrument equipped with NaCl optics. All reported absorptions are obtained from spectra calibrated with a polystyrene film. Nuclear magnetic resonance spectra were obtained on Varian Associates models HA-60 and T-60 spectrometers with tetramethylsilane as an internal standard. Analytical vpcs were obtained on a Varian Associates Model 204 instrument and preparative vpc separations were carried out on a model A-90 P-3 instrument with He as the carrier gas. Mass spectra were obtained on a Perkin-Elmer-Hitachi model RMU 6A spectrometer.

Solutions were dried over anhydrous sodium sulfate or magnesium sulfate.

Microanalyses were performed by A. B. Gygli of 329 St. George Street, Toronto, Ont.

endo-*5-Hydroxy-4,6,6-trimethyl-2-norbornanone* (*1*a)

The ketol **1***a* was prepared from fenchone according to the procedure of Cookson and co-workers (10).

5-Ethylenedioxy-1,3,3-trimethyl-endo-*2-norbornanol* (*2*a)

Ketol **1***a* (5.3 g, 31 mmol) was dissolved in benzene (530 ml, previously distilled from lithium aluminium hydride), and ethylene glycol (8 ml) and *p*-toluenesulfonic acid (0.53 g) were added. The solution was refluxed, with magnetic stirring in a Dean-Stark apparatus, for 20 h. The benzene solution was cooled and quenched with a saturated bicarbonate solution (100 ml), washed with a saturated sodium chloride solution, and dried. Evaporation of the benzene gave 6.6 g of an oil (100%). Purification by preparative vpc on a 5 ft × ¼ in. 20% SE-30 column at 175°C followed by a bulb-to-bulb vacuum distillation gave an analytical sample; nmr (60 MHz, CCl_4) δ: 1.06 (s, 6H, methyl groups), 1.10 (s, 3H, methyl group), 1.10 (s, 3H, methyl group), 3.24 (d, 1H, C(2)-H), 3.85 (m, 4H, ketal); ir (CCl_4): 3620, 3500 cm^{-1}. *Anal.* calcd. for $C_{12}H_{20}O_3$: C 67.92, H 9.43; found: C 67.97, H 9.62.

5-Ethylenedioxy-1,3,3-trimethyl-2-norbornanone (*3*a)

The oxidizing reagent was prepared by adding pyridine (72 ml) to chromium trioxide (7.2 g, 72 mmol) dissolved in water (7.2 ml) which was cooled in an ice bath. The reagent was added to the alcohol (4.4 g, 25 mmol) and the mixture was left standing at room temperature for 17 h. The mixture was diluted with water to 800 ml and extracted with ether (4 × 100 ml). The combined ether extracts were washed with water (6 × 50 ml) to remove as much pyridine as possible and with a saturated sodium chloride solution (50 ml). After drying, the ether was evaporated and the remaining pyridine was distilled under vacuum. There remained 4.1 g of ketone **3***a* (94%). Purification, by preparative vpc on a 5 ft × ¼ in. 20% SE-30

Can. J. Chem. Downloaded from www.nrcresearchpress.com by 210.87.254.5 on 09/05/12
For personal use only.

Can. J. Chem. Downloaded from www.nrcresearchpress.com by 210.87.254.5 on 09/05/12
For personal use only.

column at 175°C followed by bulb-to-bulb distillation, gave an analytical sample; nmr (60 MHz, CCl_4) δ: 3.98 (m, 4H, ketal), 1.08, 1.01, 0.98 (3s, 3H each, methyl groups); ir (CCl_4): 1750 cm^{-1}. *Anal.* calcd. for $C_{12}H_{18}O_3$: C 68.57, H 8.57; found: C 68.49, H 8.88.

*2-Ethylenedioxy-1,3,3-trimethyl-5-methylenenorbornane (**4**a)*

A flow of dry nitrogen was passed through the reaction mixture during the preparation of the ylide. *n*-Butyllithium (2.54 g, in 5 ml hexane, 20 mmol) was added to a mixture of triphenylmethylphosphonium bromide (7.2 g, 20 mmol) in purified hexane; (70 ml of reagent grade hexane were treated with concentrated sulfuric acid, washed with water, then with permanganate; the hexane was washed with water, filtered through a column of alumina, and distilled). The mixture was stirred magnetically for 4 h. Ketoketal **3***a* (4.1 g, 20 mmol) in purified hexane (30 ml) was slowly added and the resulting mixture was refluxed for 24 h. The reaction mixture was cooled, the solids were filtered, and the hexane solution was washed with water until the wash layer was neutral. The solution was dried and the solvent was evaporated to yield 3.3 g (80%) of **4***a*. Purification, by preparative vpc followed by bulb-to-bulb distillation, yielded an analytical sample; nmr (60 MHz, CCl_4) δ: 1.02, 1.12, 1.26 (3s, 3H each, methyl groups), 3.88 (m, 3H, ketal), 4.60 (d, 3H, olefin); ir (neat): 3070, 1650, 880 cm^{-1}. *Anal.* calcd. for $C_{13}H_{20}O_2$: C 75.00, H 9.61; found: C 75.07, H 9.91.

*4,6,6-Trimethyl-5-methylene-2-norbornanone (**5**a)*

The ketol **4***a* was converted, in portions, to the enone **5***a* according to the following procedure. Compound **4***a* (0.3 g, 1.4 mmol) was dissolved in aqueous acetone (90%, 10 ml), which contained 1 drop of concentrated hydrochloric acid. The solution was stirred magnetically at room temperature for 24 h. The reaction mixture was diluted with water to 50 ml and 3–4 drops of sodium hydroxide (10%) were added. The solution was saturated with sodium chloride and extracted twice with ether. The combined ether extracts were washed once with water and once with a saturated sodium chloride solution and dried. Evaporation of the solvent gave 0.1 g of an oil (45%). Purification by preparative vpc on a 5 ft × ¼ in. 20% SE-30 column at 150°C gave 0.040 g of **5***a*; ms *m/e*: 164 (M^+); nmr (60 MHz, CCl_4) δ: 1.02, 1.12, 1.28 (3s, 3H each, methyl groups), 4.72 (1H, olefin), 4.78 (1H, olefin); ir (neat): 3060, 1750, 1640, 880 cm^{-1}.

Confirmation of the Structure of **5**a. *Oxidation to 1,3,3-Trimethyl-2,5-norboranedione (**10**a)*

Compound **5***a* (0.15 g, 0.9 mmol) was dissolved in acetone–water (50%, 10 ml). Potassium periodate (4 g) was added and the mixture was cooled in an ice-water bath. Potassium permanganate (0.2 g) in water (3 ml) was added dropwise over a period of 10 min to the stirred solution. The reaction mixture was stirred for 4 h at room temperature and filtered. The filtrate was diluted to 100 ml with water and extracted with ether (3 × 25 ml). The combined ether extracts were washed with a saturated sodium chloride solution and dried. Evaporation of the solvent gave a solid which was identified as dione **10***a* by comparison of its ir spectrum (1012, 964, 945, 933, 915, and 900 cm^{-1}) to that of an authentic sample (6).

endo-*5-Hydroxy-6,7-dimethyl-2-norbornanone (**1**b)*

Compound **1***b* was prepared by hydrolysis (2) of keto-acetate **6***b* that was obtained from acetate **9***b* via the procedure of Meinwald and co-workers (3).

*5-Ethylenedioxy-3,3-dimethyl-*endo*-2-norbornanol (**2**b)*

Ketol **1***b* (7.5 g) was dissolved in benzene (700 ml, previously distilled from lithium aluminium hydride) and ethylene glycol (10.5 ml) and *p*-toluenesulfonic acid (0.7 g) were added. The mixture was refluxed for 44 h in a Dean-Stark apparatus, cooled, and added to a saturated solution of sodium bicarbonate (200 ml). The benzene solution was washed with water (200 ml), saturated sodium chloride (200 ml) solution, and dried. The solvent was distilled off to give 6.5 g of an oil (76%); nmr (60 MHz, CCl_4) δ: 3.30 (s, 1H, OH), 3.80 (m, 4H, ketal), 1.02 (s, 6H, methyl groups); ir (CCl_4): 3620, 3460 cm^{-1}. Purification, by preparative vpc on a 5 ft × ¼ in. SE-30 column at 175°C followed by bulb-to-bulb vacuum distillation, gave an analytical sample. *Anal.* calcd. for $C_{11}H_{18}O_3$: C 66.67, H 9.09; found: C 66.38, H 9.12.

*5-Ethylenedioxy-**3**,3-dimethyl-2-norbornanone (**3**b)*

The oxidizing reagent was prepared by adding chromium trioxide (9.8 g) in water (9.9 ml) to ice-cold pyridine (98 ml). The reagent was added to the ketalol **2***b* (6.4 g) and resulting solution was left standing at room temperature for 24 h. The reaction mixture was added to ice (500 ml) and the mixture was diluted to 1.5 ℓ with water and extracted with ether (3 × 200 ml). The ether extracts were washed with water (200 ml), dilute hydrochloric acid (200 ml), water (200 ml), saturated sodium bicarbonate solution (200 ml), and water (200 ml). The ether solution was dried and the solvent was taken off under vacuum to give 4.7 g of an oil (72%); nmr (60 MHz, CCl_4) δ: 3.87 (m, 4H, ketal), 1.18, 1.05 (2s, 3H each, methyl groups); ir (neat): 1750 cm^{-1}. Purification, by preparative vpc on a 5 ft × ¼ in. 20% SE-30 column at 195°C followed by a bulb-to-bulb vacuum distillation, yielded an analytical sample. *Anal.* calcd. for $C_{11}H_{16}O_3$: C 67.35, H 8.16; found: C 67.23, H 8.19.

*6,6-Dimethyl-5-methylene-2-norbornanone (**5**b)*

The ketalone **3***b* (4.7 g) in hexane (65 ml) was reacted, as described in the preparation of **4***a*, with the ylide prepared from 13.5 g of phosphonium bromide and 11 ml of 1.5 *M* *n*-butyllithium in hexane (160 ml). After the mixture was refluxed for 24 h, the solids were filtered off and the hexane solution was washed with water until the aqueous layer was neutral. The solvent was distilled off under vacuum and the ketalene **4***b* (2.1 g) was dissolved in 90% aqueous acetone (100 ml) and concentrated hydrochloric acid (0.6 ml) was added. The mixture was stirred at room temperature for 36 h, diluted with water, and extracted with ether (4 × 30 ml). The ether extracts were dried and concentrated by distillation through a 30-cm glass helices column. Compound **5***b* (0.30 g) was isolated from the residue by preparative vpc on a 5 ft × ¼ in. 20% SE-30 column at 125°C; mp 61–63°C; nmr (60 MHz, CCl_4) δ: 4.92 (1H, olefin), 4.73 (1H, olefin), 3.05 (broad s, 1H, bridgehead), 2.4–1.5 (m, 5H), 1.15, 1.06 (2s, 3H each, methyl groups); ir (CCl_4): 3050, 1745, 1650, 890 cm^{-1}; ms *m/e*: 150 (M^+).

Confirmation of the Structure of **5**b. *Oxidation to **3**,3-Dimethyl-2,5-norbornanedione (**10**b)*

Enone **5***b* (0.063 g) was dissolved in aqueous acetone (50%, 7 ml) and KIO_4 (2 g) was added to the solution. To the mixture cooled in ice-water and stirred magnetically, $KMnO_4$ (100 mg) in water (ca. 2 ml) was added dropwise over a period of 10 min. The mixture was warmed to room temperature, stirred for 6 h, diluted to 100 ml with water, and extracted with ether (3 × 25 ml). The ether extracts were washed with water (2 × 25 ml), saturated sodium chloride solution (25 ml), and dried ($MgSO_4$). After evaporation of solvent the oxidation product was isolated by preparative vpc on a 5 ft × ¼ in. 20% SE-30 column at 120°C. Its ir spectrum (1155, 1085, 1058, 960, 926, 896 cm^{-1}) was identical to that of an authentic sample (6) of dione **10***b*.

Can. J. Chem. Downloaded from www.nrcresearchpress.com by 210.87.254.5 on 09/05/12
For personal use only.

endo-*5-Ethanoyloxy-2-norbornanone (**6**c)*

Compound **6***c* was prepared from nortricyclanone via the procedure of Meinwald and co-workers (5).

*5-Ethylenedioxy-*exo*-2-norbornyl Acetate*

Compound **6***c* (10 g, 60 mmol) was dissolved in benzene (500 ml, previously distilled from lithium aluminium hydride), *p*-toluenesulfonic acid (1 g) and ethylene glycol (20 ml) were added and the solution was refluxed for 24 h in a Dean-Stark apparatus. The solution was then quenched with saturated bicarbonate solution (100 ml) and the layers were separated. The benzene solution was dried and the benzene was distilled off to yield 11.0 g (87%) of the ketal. Purification by preparative vpc on a 5 ft × ¼ in. SE-30 column at 160°C followed by bulb-to-bulb vacuum distillation gave an analytical sample of *7a*; nmr (CCl_4) δ: 1.95 (s, 3H, acetate), 3.80 (m, 4H, ketal), 4.60 (q, 1H, *endo*-C(2)H); ir (CCl_4): 1745, 1245 cm^{-1}. *Anal.* calcd. for $C_{11}H_{16}O_4$: C 62.26, H 7.54; found: C 62.25, H 7.66.

*Reduction of the Acetate **7**a*

The glassware was oven dried before use and the ether was distilled from lithium aluminium hydride.

The ketal acetate *7a*, (10 g, 47 mmol) dissolved in ether (150 ml) was added over a period of 1 h at room temperature to a magnetically stirred slurry of lithium aluminium hydride (3.6 g, 94 mmol) in ether (200 ml). The mixture was refluxed for 10 h. The excess lithium aluminium hydride was then destroyed by the addition of water (3.6 ml), 10% NaOH (3.6 ml), and more water (3.6 ml), consecutively, to the vigorously stirred solution. The granular salts were filtered off and the solvent was evaporated to give 5.8 g (73%) of alcohol *7b*; nmr (60 MHz, CCl_4) δ: 3.8 (m, ketal CH_2); ir (neat): 3400 cm^{-1}, no ketonic absorption.

*5-Ethylenedioxy-2-norbornanone (**3**c)*

5-Ethylenedioxy-*exo*-2-norbornanol (*7b*) (5.4 g, 32 mmol) was added to the oxidizing reagent, prepared from chromium trioxide (10 g) dissolved in water (10 ml) and ice-cold pyridine (100 ml), and the solution was left standing at room temperature for 16 h. The solution was diluted to 300 ml with ice-water and the mixture was filtered through Celite. The precipitate was washed with water (30 ml) and methylene chloride (three times for a total of 100 ml). The combined methylene chloride solutions were filtered through Celite. The solvent was concentrated to 100 ml, washed with very dilute sulfuric acid until the wash layer remained acidic, and then with saturated sodium bicarbonate solution. The solution was dried and the solvent was evaporated to give 3.4 g (63%) of **3***c*. Purification by preparative vpc on a 5 ft × ¼ in. 20% SE-30 column at 170°C and a bulb-to-bulb vacuum distillation gave an analytical sample; nmr (CCl_4) δ: 3.8 (m, 4H, ketal), 1.4–2.6 (m, 8H); ir (neat): 1745 cm^{-1}. *Anal.* calcd. for $C_9H_{12}O_3$: C 64.29, H 7.14; found: C 64.27, H 7.30.

*5-Methylene-2-norbornanone (**5**c)*

n-Butyllithium (1.5 *N*, 25 ml, 0.04 mol) was added to a mixture of methyltriphenylphosphonium bromide (10.5 g, 0.04 mol) in ether (150 ml, freshly distilled from lithium aluminium hydride) as a slow flow of dry nitrogen was passed through the reaction mixture. The mixture was stirred magnetically for 4 h at room temperature. 5-Ethylenedioxy-2-norbornanone (3.2 g, 0.04 mol) dissolved in ether (125 ml) was slowly added and the mixture was refluxed for 11 h. The solids were then filtered off and the ether solution was washed until the water layer was neutral. The solvent was distilled through a 2-ft Vigreux column and the oil which remained was dissolved in a mixture of ethanol (75 ml) and water (35 ml). Acetic acid (1 ml) and hydrochloric acid (50%, 5 drops) were added and the mixture was stirred at room temperature for 3 days. It was then diluted to 400 ml with water and extracted with ether (3 × 125 ml). The ether solution was washed with water (100 ml) and saturated sodium bicarbonate solution. The solution was dried and the solvent was distilled through a Vigreux column. Purification of the residue by preparative vpc gave 0.38 g of enone. Bulb-to-bulb vacuum distillation gave an analytical sample; nmr (60 MHz, CCl_4) δ: 5.02 (1H, olefin), 4.78 (1H, olefin), 3.03 (broad s, 1H, bridgehead), 2.65 (broad s, 1H, bridgehead); ir (CCl_4): 3080, 1754, 1660, 890 cm^{-1}. *Anal.* calcd. for $C_8H_{10}O$: C 78.69, H 8.20; found: C 78.65, H 8.25.

*Confirmation of the Structure of 5-Methylene-2-norbornanone. Oxidation to 2,5-Norbornanedione (**10**c)*

The enone **5***b* (0.045 g, 0.37 mmol) was dissolved in aqueous acetone (50%, 7 ml) containing potassium periodate (2 g). The solution was cooled in ice-water and a solution of potassium permanganate (0.1 g in 3 ml of water) was added dropwise over a period of 10 min. The resulting mixture was warmed to room temperature and stirred for 5 h. The solution was filtered through a medium porosity sintered glass funnel, diluted to 100 ml, and extracted with methylene chloride (3 × 50 ml). The combined extracts were washed with water (25 ml), dried, and the solvent was evaporated to yield a compound whose ir spectrum (1180, 1120, 1045, 952, 890 cm^{-1}) was identical to that of an authentic sample of 2,5-norbornanedione (6).

*6-Oxo-2-norbornanecarboxylic acid (**12**)*

The keto acid (37.4 g) was prepared from *endo*-2-norbornene-5-carboxylic acid by the method of Beckman and Geiger (8).

*6-Ethylenedioxy-*endo*-2-norbornylmethanol (**13**b)*

The keto acid **12** (32.3 g, 0.21 mol) was dissolved in benzene (300 ml, freshly distilled from lithium aluminium hydride). Ethylene glycol (100 ml, freshly distilled) and *p*-toluenesulfonic acid (1 g) were added and the mixture was refluxed for 20 h in a Dean-Stark apparatus. After cooling, the layers were separated and the ethylene glycol layer was diluted with saturated sodium bicarbonate solution (100 ml) and extracted with methylene chloride (3 × 75 ml). The extracts were washed with water (50 ml) and dried. The combined organic layers were evaporated to yield 45.5 g of a viscous oil; nmr (60 MHz, $CDCl_3$) δ: 4.2 (m, 2H), 3.7 (m, 4H), 2.7 (broad s, 1H); ir (neat): 3500, 1750, 1200 cm^{-1}. The oil (45 g) which was identified by the spectroscopic data as the ketal ester **13***a*, was dissolved in ether (300 ml) and added to lithium aluminium hydride (10 g) in ether (200 ml) over a period of 2 h. The mixture was refluxed overnight, cooled, and sodium hydroxide (10%, 10 ml) and water (10 ml) were added. After the mixture was stirred for 6 h at room temperature, the inorganic salts were filtered off and the solvent was evaporated to give 36.1 g (93%) of a viscous liquid. Distillation of the oil under reduced pressure gave a colourless liquid; nmr (60 MHz, CCl_4) δ: 3.8 (d, 4H, ketal), 3.7 (m, 7H, CH_2OH, —O—CH_2—CH_2—O—); ir (neat): 3500 cm^{-1}. A sample was further purified by preparative vpc and a bulb-to-bulb vacuum distillation. *Anal.* calcd. for $C_{10}H_{16}O_3$: C 65.22, H 8.70; found: C 65.17, H 8.92.

*6-Ethylenedioxy-*endo*-2-norbornylmethyl Acetate (**13**c)*

The alcohol **13***b* (12 g, 78 mmol) was dissolved in pyridine (40 ml) and acetic anhydride (20 ml). The solution was left standing at room temperature for 20 h, diluted to 400 ml with ice-water, and extracted with ether (3 × 100 ml). The ether solution was washed with water (80 ml), dilute hydrochloric

Can. J. Chem. Downloaded from www.nrcresearchpress.com by 210.87.254.5 on 09/05/12
For personal use only.

acid (5%, 2 × 80 ml), water (80 ml), bicarbonate (80 ml), and water (80 ml). The solution was dried and the solvent was evaporated to yield 13.9 g (81%) of an oil; nmr (60 MHz, CCl_4) δ: 4.2 (m, 2H, CH_2OAc), 3.8 (m, 4H, ketal), 2.0 (s, 3H, acetate); ir (neat): 1745 cm^{-1}. A sample was purified by preparative vpc and a bulb-to-bulb vacuum distillation. *Anal.* calcd. for $C_{12}H_{18}O_4$: C 63.72, H 7.96; found: C 63.72, H 8.16.

6-Methylene-2-norbornanone (11)

A glass column, packed with glass helices, was placed vertically in a pyrolysis oven maintained at 450–500°C. A flow of nitrogen (1 ml min^{-1}) was maintained throughout the experiment to entrain the products. Acetate **13***c* was added very slowly dropwise (3 drops per 5 min) to the top of the column. The products of the reaction were trapped at the end of the column in a flask immersed in a Dry Ice – acetone bath. After the addition was complete the flask was warmed to room temperature and the condensate was dissolved in ether. The ether solution was washed with saturated sodium bicarbonate solution and dried. Evaporation of solvent, and vacuum distillation gave in 5% yield the ketalene **14***a*. The recovered starting material was recycled; nmr (60 MHz, CCl_4) δ: 4.7 (d, 2H, methylene group), 3.9 (narrow m, 4H, ketal), 2.5 (broad s, 1H, bridgehead), 2.3 (m, 1H, bridgehead). Also present were sharp singlets at δ 4.16 and 2.0 of an impurity which comprised 15% of the product isolated by distillation.

Without purification, the ketalene **14***a* was hydrolyzed to the enone. In a typical experiment, the ketalene (0.20 g) was added to water (7 ml) containing 1 drop of concentrated hydrochloric acid. The mixture was stirred at room temperature for 2 h. Solvent extraction and purification by preparative vpc on a 10 ft. × ¼ in. 10% UCON column at 160°C gave 0.055 g of a colourless liquid; nmr (60 MHz, CCl_4) δ: 5.16 (1H, olefin), 4.88 (1H, olefin), 3.03 (s, 1H, C(1)H), 2.80 (unresolved m, 1H, C_4H), 2.6–1.6 (m, 6H); ir (CCl_4): 3080, 1750, 1650, 890 cm^{-1}. A bulb-to-bulb vacuum distillation of a portion gave an analytical sample. *Anal.* calcd. for $C_8H_{10}O$: C 78.69, H 8.20; found: C 78.57, H 8.43.

6-Ethylenedioxy-exo-*2-methyl*-endo-*2-norbornanol* ***13***d

Magnesium metal (220 mg, 10 mmol) and methyl iodide (freshly distilled, 1.4 g, 10 mmol) in ether (ca. 5 ml) were stirred at room temperature for a few minutes. Ketoketal **14***b* (500 mg, 2.7 mmol) in ether (5 ml) was slowly added and the mixture was stirred at room temperature for 24 h. It was added to crushed ice (2 ml) and the aqueous solution was extracted with ether (2 × 10 ml). The combined ether extracts were washed with water, dried, and evaporated. There resulted 440 mg of a viscous oil (81%); nmr (60 MHz, CCl_4) δ: 4.40 (s, 1H, OH), 3.9 (m, 4H, ketal), 1.18 (s, 3H, methyl group); ir (CCl_4): 3500 cm^{-1}.

Dehydration of Alcohol ***13***d

Alcohol **13***d* (440 mg, 2.4 mmol) was dissolved in pyridine (4 ml), phosphoryl chloride (1.4 ml) was added, and the solution was stirred at 40–50°C for 1 h. It was cooled in ice and water (0.5 ml) was slowly added. Sodium hydroxide (10%, 30 ml) was added and the mixture was extracted with ether (2 × 20 ml). The ether extracts were washed with dilute HCl (10 ml), sodium hydroxide (5%, 10 ml), and water (10 ml). The solution was dried and the solvent was evaporated to give an oil. The major product **17** (60%), of longest retention time, was isolated by preparative vpc on a 10 ft × ¼ in. 20% SE-30 column at 195°C; nmr (60 MHz, CCl_4) δ: 5.20 (broad s, 1H, olefin), 4.28 (t, 2H, CH_2Cl), 3.60 (t, 2H, OCH_2), 1.70 (broad s, 3H, methyl group), 2.8–1.8 (m, 8H); ir (CCl_4): 3050, 1750, 1650 cm^{-1}; ms *m/e*: 202 and 204 (M^+ $C_{10}H_{15}O_2Cl$), 123 ($M^+ - ClCH_2CH_2—O$) and 107 ($M^+ - ClCH_2—CH_2—O—\overset{O}{\overset{\|}{C}}$)

Acknowledgement

We thank the National Research Council of Canada for financial support.

1. S. Forsén and M. Nilsson. *In* The chemistry of the carbonyl group. Vols. I and II. *Edited by* S. Patai. John Wiley and Sons, Inc., New York, NY. 1966. 1970.
2. P. Hirsjärvi. Ann. Acad. Sci. Fenn. Ser. A, **84**, 1 (1957).
3. J. Meinwald, P. G. Gassman, and J. J. Hurst. J. Am. Chem. Soc. **84**, 3722 (1962).
4. J. Meinwald, J. C. Shulton, G. L. Buchanan, and A. Courtin. J. Org. Chem. **33**, 99 (1968).
5. J. Meinwald, J. K. Crandall, and P. C. Gassman. Tetrahedron, **18**, 815 (1962).
6. N. H. Werstiuk, R. Taillefer, and Sujit Banerjee. Can. J. Chem. This issue.
7. N. H. Werstiuk, R. Taillefer, R. A. Bell, and B. G. Sayer. Can. J. Chem. **50**, 2146 (1972).
8. S. Beckman and H. Geiger. Chem. Ber. **48**, 94 (1961).
9. C. A. Grob. Angew. Chem. Int. Ed. **8**, 535 (1969).
10. D. E. Bays, G. W. Cannon, and R. C. Cookson. J. Chem. Soc. B, 885 (1966).

Towards a complete account of the exchange chemistry of a diastereotopic proton pair. I. Base-catalyzed enolization–exchange of 2-norbornanones; on the rate controlling factors

NICK HENRY WERSTIUK, ROLAND TAILLEFER, AND SUJIT BANERJEE

Department of Chemistry, McMaster University, Hamilton, Ont., Canada L8S 4M1

Received July 12, 1977

NICK HENRY WERSTIUK, ROLAND TAILLEFER, and SUJIT BANERJEE. Can. J. Chem. **56**, 1140 (1978).

We report the rates of base-catalyzed hydrogen isotope exchange of the *exo* and *endo* protons in a series of 2-norbornanones. The *exo*:*endo* rate ratios for 4-methyl-substituted 2-norbornanones **3** and **6** are less than the rate ratios of the 4-demethyl analogs **2** and **5**. Therefore, a methyl group is not a useful torsional-effect probe. This is supported by an analysis which established that the small difference in the torsional strain (0.45 kcal) between eclipsed vicinal hydrogens and an eclipsed vicinal methyl and hydrogen would only result in a maximum twofold *increase* in the rate ratio. The decrease in the *exo*:*endo* rate ratio is a consequence of the electron-donating effect of a methyl group which affects the *exo* rate to a greater degree. Introduction of a strain-inducing *exo* methylene group at C(5) and C(6) in the norbornyl system does not produce a significant change in the exchange rates. The average increase of 7.9 and 2.6 in the *exo* and *endo* rates, respectively, in enones **4**, **5**, and **6** over the ketones **1**, **2**, and **3**, are explicable by an inductive effect. Thus, homoallylic stabilization of the developing carbanion is not important.

Through application of a new mechanistic criterion which involves a log–log plot of the *exo* and *endo* exchange rate constants, we establish, for the bicyclic ketones, that charge transfer to oxygen is greater in the transition state for *endo* deprotonation.

NICK HENRY WERSTIUK, ROLAND TAILLEFER et SUJIT BANERJEE. Can. J. Chem. **56**, 1140 (1978).

On rapporte les vitesses d'échanges, catalysées par les bases, d'isotope d'hydrogène des protons *exo* et *endo* d'une série de norbornanones-2. Les rapports de vitesse *exo*:*endo* des norbornanones-2 substituées par un méthyle en position 4 (**3**) et (**6**) sont plus faibles que les rapports de vitesse des analogues (**2**) et (**5**) qui ne contiennent pas de méthyle en position 4. On en conclut que le groupe méthyle n'est pas une sonde utile pour mesurer les effets de torsion. Cette conclusion est supportée par une analyse qui a établi que de petites différences dans la tension de torsion (0.45 kcal) entre des hydrogènes vicinaux éclipsés et un groupe méthyle vicinal éclipsé par un hydrogène conduirait à un rapport de vitesse qui ne serait que multiplié par deux. La diminution du rapport des vitesses *exo*:*endo* est une conséquence de l'effet électro-donneur d'un groupe méthyle qui affecte plus la vitesse *exo*. L'introduction en position C(5) et C(6) du système norbornyle d'un groupe méthylène *exo* produisant de la tension ne provoque pas de changements importants dans les vitesses d'échange. L'augmentation moyenne de 7.9 et de 2.6 respectivement pour les vitesses *exo* et *endo* dans les énones **4**, **5** et **6** par rapport aux cétones **1**, **2** et **3** peut être expliquée par un effet inductif. On peut donc en conclure que la stabilisation homoallylique du carbanion que se développe n'est pas importante.

Faisant appel à un nouveau critère mécanistique qui implique une courbe log–log des constantes de vitesse d'échanges *exo* et *endo*, on a établi, pour les cétones bicycliques, que le transfert de charge vers l'oxygène est plus grand dans l'état de transition de la déprotonation *endo*.

[Traduit par le journal]

Can. J. Chem. Downloaded from www.nrcresearchpress.com by 210.87.254.6 on 09/05/12
For personal use only.

Introduction

The chemistry of the carbonyl group has recently been reviewed in two volumes of the series The Chemistry of the Functional Groups (1). Interestingly, only 3 pages (Vol. II, Chapt. 3), of the 1400 which comprise the review, were devoted to an account of the kinetic and mechanistic aspects of acid- and base-catalyzed enolization and hydrogen isotope exchange of ketones. Although the review was not complete by any means, this fact did support our initial conclusion that there indeed was a paucity of kinetic and mechanistic detail about these most ubiquitous reactions. Before 1970 (2–4), there were no accurate rate data for base-catalyzed hydrogen isotope exchange of the diastereotopic protons in polycyclic ketones, even though there were reports (5–8) of the preparation of 80–90% stereochemically pure monodeuterated 2-norbornanones. Thus, at that time we initiated a research program to generate quantitative rate data in an effort to detail the mechanistic intricacies of isotope exchange and enolization of cyclic ketones. We chose to study 2-norbornanones because of their conformational rigidity and the substantial difference in the *exo* and

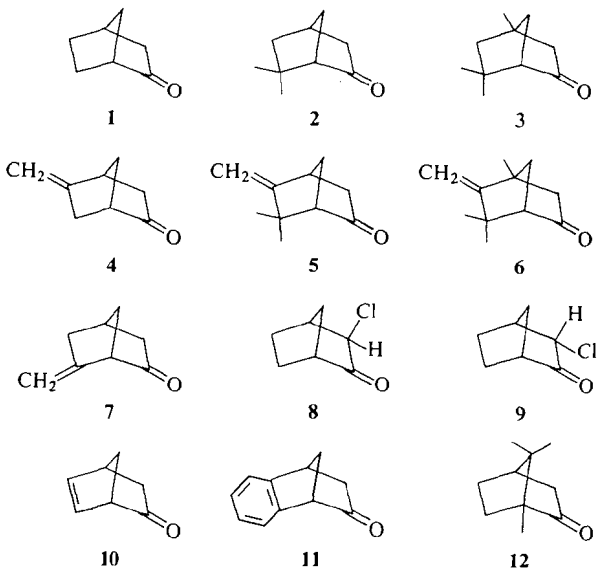

endo exchange rates. We reasoned that the compilation of accurate exchange rate data in a suitable series of ketones would establish (*a*) whether or not torsional strain between hydrogen or methyl at the bridgehead and the hydrogens alpha to the carbonyl group plays an important role in establishing the exo:endo exchange rate ratio, (*b*) the importance of homoallylic and homoenolic assistance to enolization, (*c*) whether the introduction of a strain-inducing exocyclic π system into the [2.2.1] skeleton affects the enolization rates, and (*d*) through the application of a new linear free energy correlation (9), the relative charge development in the transition states for *exo* and *endo* deprotonation.

In this second paper[1] of a series, we describe the mass spectrometric procedure that was developed to accomplish the kinetic study, document the exchange rate data for the bicyclic ketones and enones **1**–**9**, and interpret the results on the basis of the factors listed above.

Results

Exchange (Enolization) of 2-Norbornanones

The rates of NaOD-catalyzed H–D exchange of the protons in the 3-position of substrates **1**–**7** were measured at 25°C in 60% dioxane – 40% D_2O by following the up-take of deuterium by mass spectrometry and are presented in Table 1. The syntheses of **4**, **5**, **6**, and **7** are reported in the preceding paper. Our value of $3.85 \times 10^{-2}\ M^{-1}\ s^{-1}$ for *exo* exchange in 2-norbornanone (**1**) compares well with Tidwell's measurement (4) of $5.58 \times 10^{-2}\ M^{-1}\ s^{-1}$ in 2:1 dioxane–D_2O. That the rate is depressed in the medium containing more water is consistent with Tidwell's findings (4). Figures 1*a* and *b* illustrate, for **3**, the pseudo-first-order plots for *exo* and *endo* exchange, respectively.

Determination of the rates of exchange of the chloroketones **8** and **9** in theory could be complicated since isomerization accompanies exchange and the procedure that was used is outlined below.

Exchange (Enolization) of 3-Chloro-2-norbornanones

The exchange of **8** and **9** leads to a mixture of exchanged and unexchanged species according to the following scheme. The *endo*-3-chloro-2-norbornanone (**9**) is the first formed product of the kinetically favoured *exo* protonation. In deuterated medium **9**-*d* is subsequently isomerized to **8**-*d*.

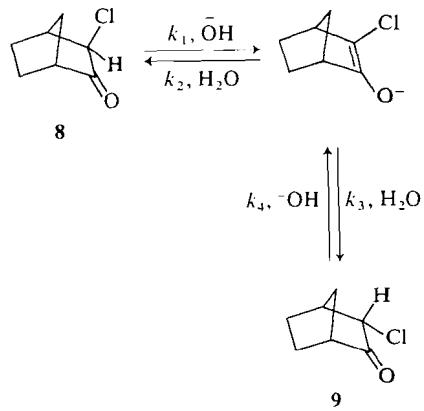

For the isomerization of **8** to **9** the following analysis is appropriate. If the enolate (E) is a steady-state intermediate, and only **8** is present initially, [1] and [2] follow.[2]

$$[1]\quad \ln\frac{k_1k_3[\mathbf{8}]_0}{(k_1k_3 + k_2k_4)[\mathbf{8}] - k_2k_4[\mathbf{8}]_0} = [OH^-]\left(\frac{k_1k_3 + k_2k_4}{k_2 + k_3}\right)t$$

$$[2]\quad \ln\frac{[\mathbf{8}]_0}{(1 + K)[\mathbf{8}] - K[\mathbf{8}]_0} \simeq [^-OH]k_1(1 + K)t$$

Since $k_3 \gg k_2$ and $k_2k_4/k_1k_3 = K$.

In principle, k_1 can be obtained from [2] when the isomerization is carried out in H_2O. However, the equation does not apply in D_2O since ketonization leads to **8**-*d* rather than **8**. Fortunately, $k_3 \gg k_2$ and only very minor amounts of **8**-*d* are formed in the initial stages of the reaction, up to 40% conversion of **8** to **9**-*d*. Hence, k_1 for enolization in nondeuterated and deuterated medium can be determined gas

[1]For a preliminary account, see Ref. 2.

[2]Photocopies of the derivation of [1] are available upon request, at a nominal charge, from the Depository of Unpublished Data, CISTI, National Research Council of Canada, Ottawa, Ont., Canada K1A 0S2.

Can. J. Chem. Downloaded from www.nrcresearchpress.com by 210.87.254.6 on 09/05/12
For personal use only.

Can. J. Chem. Downloaded from www.nrcresearchpress.com by 210.87.254.6 on 09/05/12
For personal use only.

TABLE 1. Rates of base-catalyzed H–D exchange of 2-norbornanones in 60% dioxane – 40% D_2O at 25.0°C

Entry	Substrate	k (M^{-1} s^{-1})*		
		Exo	*Endo*	k_x/k_n
1	2-Norbornanone (**1**)	3.85×10^{-2}	5.90×10^{-5}	650
2	6,6-Dimethyl-**1** (**2**)	1.64×10^{-2}	2.62×10^{-5}	625
3	4,6,6-Trimethyl-**1** (**3**)	9.88×10^{-3}	2.81×10^{-5}	350
4	5-Methylene-**1** (**4**)	3.42×10^{-1}	1.24×10^{-4}	2760
5	6,6-Dimethyl-5-methylene-**1** (**5**)	1.31×10^{-1}	7.48×10^{-5}	1750
6	4,6,6-Trimethyl-5-methylene-**1** (**6**)	6.80×10^{-2}	7.28×10^{-5}	930
7	6-Methylene-**1** (**7**)	6.97×10^{-2}	1.32×10^{-4}	530
8	*exo*-3-Chloro-**1** (**8**)		7.50×10^{-3}	
9	*endo*-3-Chloro-**1** (**9**)	2.48×10^{2}†		33 070‡
10	Norbornen-2-one (**10**)‡	5.36×10^{-4}	4.46×10^{-6}	120
11	Benzonorbornenone (**11**)‡	1.97×10^{-2}	3.31×10^{-5}	595
12	1,7,7-Trimethyl-**1** (**12**)‡	6.99×10^{-4}	3.33×10^{-5}	27

*Average of at least two determinations. Average deviation < 5%.
†The rate constants from entries 2 and 4 in Table 2 have been corrected for a difference in ground state energies and temperature according to footnote 3.
‡These values were obtained from ref. 3 by multiplying the rate constants reported therein by a factor of 0.736 which interrelates the rate constants for 1 in 60:40 dioxane–D_2O and 2:1 dioxane–D_2O.

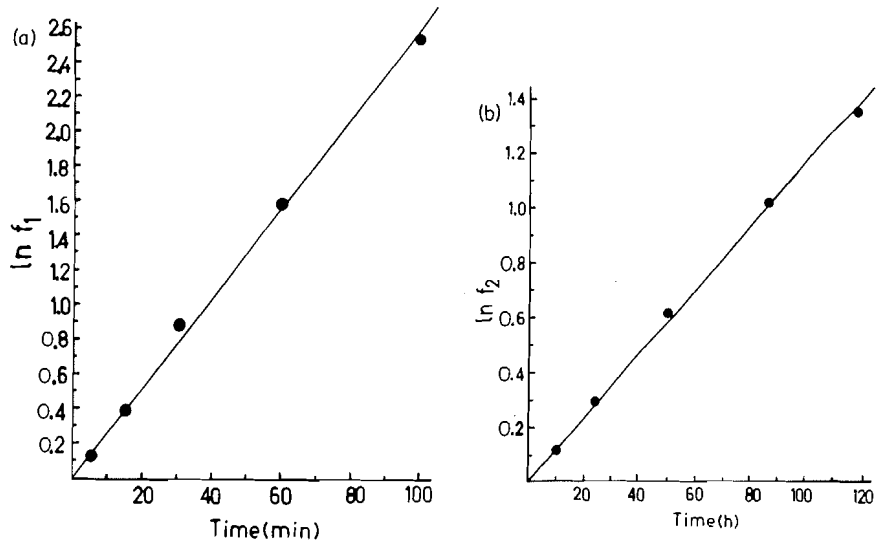

FIG. 1. Pseudo-first-order plot for NaOD-catalyzed H–D *exo* exchange of 4,6,6-trimethyl-2-norbornanone (**3**) at 25°C: (*a*) 0.043 *N* NaOD; (*b*) 0.104 *N* NaOD.

chromatographically by following the conversion of **8** to **9** and **9**-*d*. Thus, the enolization of **8** and **8**-*d* is treated on a pseudo-first-order basis and the rate data are presented in Table 2. Figure 2 illustrates the pseudo-first-order plot for exchange of **8**.

The exchange of **9** in deuterated medium was followed by the mass spectrometric procedure used for the other substrates since no isomerization of **9**-*d* occurred during the period of the kinetic measurement. The reaction was too fast to be followed at the usual base concentrations and a dioxane–buffer solution was utilized as described in the experimental. Figure 3 illustrates the pseudo-first-order plot for deuteration of the *endo*-3-chloroketone **9**. The exchange of the *exo* proton in 2-norbornanone (**1**) was measured in the same dioxane–buffer solution and the second-order rate constant for exchange in **9** was obtained by comparison with this rate as is described in the experimental. The primary isotope effect and the solvent isotope effect for *endo* proton abstraction, available from entries 1–3, are 6.6 and 1.61, respectively. The *endo* isotope effect of 6.6 is compared with Tidwell's value (4) of 5 for *exo* abstraction obtained from base-catalyzed *exo* bromination of 2-norbornanone and 2-norbornanone-3,3-d_2 at 10°C.

Can. J. Chem. Downloaded from www.nrcresearchpress.com by 210.87.254.6 on 09/05/12
For personal use only.

TABLE 2. Rates of base-catalyzed enolization (exchange) of 3-chloro-2-norbornanones at 30.0°C

Entry	Substrate	Medium	k (M^{-1} s^{-1})*
1	**8**	$^-OH/H_2O$	7.08×10^{-3}
2	**8**	$^-OD/D_2O$	1.14×10^{-2}
3	**8**-*d*	$^-OD/D_2O$	1.73×10^{-3}
4	**9**	$^-OD/D_2O$	1.88×10^{2}

*Average of at least two determinations. Average deviation < 5%.

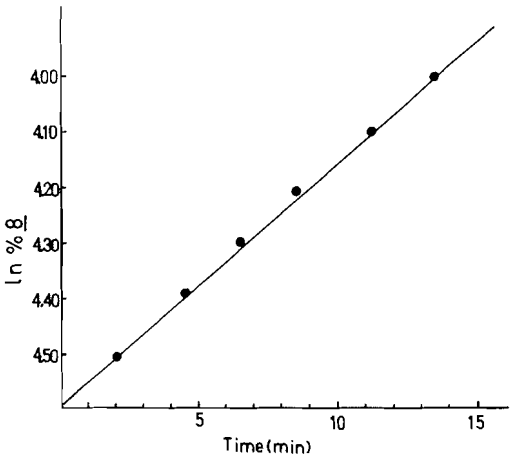

FIG. 2. Pseudo-first-order plot for NaOD (0.0606 *N*)-catalyzed enolization of *exo*-3-chloro-2-norbornanone (**8**) at 30°C.

To allow comparison between the rates of the chloroketones **8** and **9** with those of the substrates listed in Table 1, small corrections for temperature and the ground state energy difference between the two isomers were applied.[3] The final corrected rates are included in Table 1.

Discussion

Before we attempt to interpret the kinetics of exchange of the norbornanones in Table 1, we briefly discuss a potentially complicating factor. In our recent studies (10, 11), which have supported our contention that the mechanistic intricacies of enolization (exchange) of ketones had not been previously established, we demonstrated that ex-

[3]The more reactive *endo*-3-chloro-2-norbornanone (**9**) is also the more stable of the two isomers and therefore the observed rate ratio of 16 940 includes a contribution from the ground state energy difference. To remove this contribution so that the *exo*:*endo* rate ratio for **8** and **9** reflects the difference in transition state free energies measured from a common ground state, the ground state of **9** was raised to that of **8** by means of the equilibrium constant. The rate ratio, after the application of correction, is 33 070.

The chloroketones were run at 30°C, whereas data for the other substrates were acquired at 25°C. A correction for the temperature difference was made by multiplying the data for the chloroketones at 30°C by the rate ratio (0.66) obtained by measuring the exchange of **1** at 25 and 30°C, respectively.

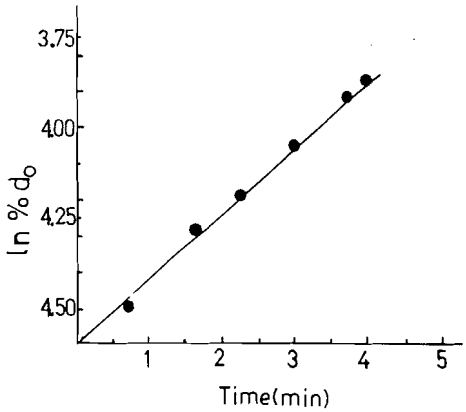

FIG. 3. Pseudo-first-order plot for NaOD-catalyzed (p*D* 10.37) H–D exchange of *endo*-3-chloro-2-norbornanone (**9**) at 30°C.

change (Scheme 1) of the *endo* proton in **1** proceeds via direct proton abstraction (Pathway 1), and epimerization of the initially formed *exo*-D-*endo*-H

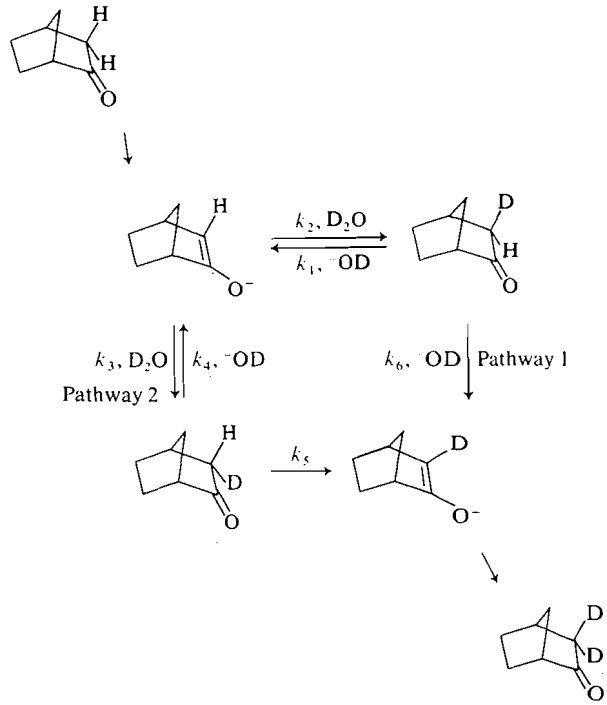

SCHEME I

species to the *exo*-H-*endo*-D material and subsequent exchange of the *exo* proton (Pathway 2). To a first approximation (10, 11), the observed rate ratio is given by $k_x/k_{nH\rightarrow D} = si/(i + 1)$, where s represents the intrinsic selectivity for cleavage of the *exo* and *endo* CH bonds, respectively, and i is the primary kinetic isotope effect at the *exo* site. Hence, if $i = 5$ (*vide*

Can. J. Chem. Downloaded from www.nrcresearchpress.com by 210.87.254.6 on 09/05/12
For personal use only.

supra), then the observed rate ratio for H→D exchange in 2-norbornanone differs from s by about 17%.[4] However, except for the chloroketones **8** and **9**, all the substrates listed in Table 1 are expected to have errors of approximately 17% associated with their rate ratios and thus this effect is not important in a semiquantitative interpretation (*vide infra*).

Torsional Effect

In an attempt to account for the high stereoselectivity observed in reactions involving the norbornyl system, Schleyer (12) postulated that eclipsing interactions between the reacting group and adjacent substrates might be influential in controlling transition state energy. This view gains credence from the observation that torsional effects are responsible for the reactivity differences observed in the base-catalyzed enolization of a series of simple unsubstituted cyclic and bicyclic ketones (11). In the norbornanones, the dihedral angle between $H(3)_x$ and H(4) is about 20°. *Endo* attack by the base at $H(3)_n$ results in a decrease in the $H(3)_x$–H(4) dihedral

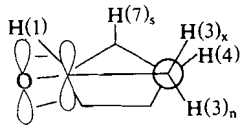

angle, and if the enolate anion is planar, the protons at some point must become fully eclipsed. In the case of *exo* attack at $H(3)_x$, there is a decrease in the $H(3)_n$–H(4) dihedral angle also but the fully eclipsed arrangement is not reached. In the latter case, however, the *release* of torsional strain is greater. Consequently, methyl substitution at C(4) should decrease the *endo* exchange rate and perhaps increase the *exo* exchange rate if the release of torsional strain is the dominant factor. Thus, there would result an overall increase in the *exo*:*endo* rate ratio. Tidwell (13, 14) found that the inclusion of a second bridgehead methyl group in camphor (**12**) led to only minor rate differences and almost no change in the rate ratio for the camphor,**13** pair, whereas an increase in rate ratio is predicted from Schleyer's postulate. Our results, for the **2**,**3** and **5**,**6** pairs, shown below as factors relative to the parent ketones **2** and **5**, respectively, confirm Tidwell's observation to the

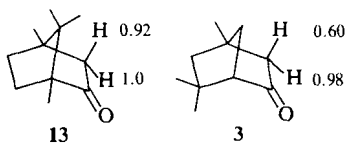

13 **3** **6**

[4]Since $(k_x/k_{n(obs)}) = si/(i+1)$ for **1**, $s = (k_x/k_{n(obs)})\ (6/5) = 780$ when $i = 5$. Therefore, $(k_x/k_{n(obs)})$ (Table 1) differs from s by 17%. The net effect of the dual-channel exchange of the *endo* proton is that $k_{n(obs)} = 1.2\ k_{n(intrinsic)}$.

extent that a decrease in rate ratio rather than an increase results from bridgehead methyl substitution (entries 2,3 and 5,6 in Table 1). Interestingly, the decrease in the rate ratios is a consequence of a small *decrease* in the *exo* exchange rate. Hence, the overall picture appears to be paradoxical, since torsional strain effects appear to account for the reactivity differences in 2-norbornanone and other simple ketones, and yet the predicted consequences of these effects within the [2.2.1] framework are not observed. A possible source of this anomaly likely lies in the invalidity of using bridgehead methyl substituents as a probe for torsional studies in the transition state. A hydrogen–methyl fully eclipsed interaction exceeds that of a hydrogen–hydrogen interaction by approximately 0.45 kcal/mol (15, 16), which translates to a maximum difference in rate of a factor of 2. On the other hand, a linear free energy analysis (*vide infra*) of the rate data establishes that electron-releasing substituents decrease the *exo*:*endo* ratio. Consequently, since full eclipsing is not achieved in the transition state, we conclude that the small rate differences expected on account of torsional effects are easily outweighed by the much larger inductive contributions of the methyl group and that introduction of a methyl group, or a group of equivalent size, at C(4) produces no significant steric retardation to *exo* deprotonation.

Homoallylic Stabilization

From entries 1–6 (Table 1) it is seen that the 5-methylene group exerts a small effect on both rates and on the rate ratios. The rate enhancements over the parent ketone in each case are shown below. The average rate enhancements for $H(3)_x$ and $H(3)_n$ in **4**, **5**, and **6**, over **1**, **2**, and **3**, are 7.9 and 2.6, respec-

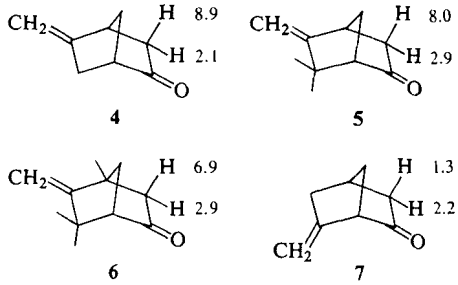

4 **5** **6** **7**

tively, and can be ascribed most economically to the inductive effect of the double bond. Thus, an increase in strain, also present in **7**, and homoallylic stabilization, both possible consequences of the introduction of a remote exocyclic double bond, do not significantly affect the *exo* and *endo* deprotonation rates.

Substituent Effects

It is apparent from inspection of Table 1 that *exo* exchange is more sensitive to a change in substituent.

Can. J. Chem. Downloaded from www.nrcresearchpress.com by 210.87.254.6 on 09/05/12
For personal use only.

This observation is quantified by a linear-free-energy plot[5,6] (Fig. 4) of slope 1.67, and log k_x = 1.67 log k_n = 5.80. In 2-norbornanone even though the C(3)—H_x and C(3)—H_n bonds are expected to exhibit the same thermodynamic acidity (17), cleavage of the endo bond is more difficult because of greater steric hindrance to *endo* approach by the base. That the more difficult *endo* deprotonation is less sensitive to a change in structure or substituent is explicable on the basis that there is a greater degree of delocalization, relative to the *exo* case, of negative charge onto oxygen in the transition state. Thus the more 'delocalized' enolate-like transition state would be expected to be less sensitive to a change either in structure or substituent. We find some support for our contention that the more difficult *endo* proton transfer is assisted to a greater degree by the carbonyl group and results in greater delocalization of charge in the transition state.[7] A parallel basic tenet, in cation chemistry, which states that the more facile the ionization, the smaller the demand the positive charge will make on participating groups for additional participation was introduced by Winstein and co-workers (19). This concept recently has been restated in the tool of increasing electron demand by Gassman (20), Brown (21), and Lambert (22) and their co-workers. A study of the solvolysis of a series of bicyclic tosylates by Wilcox and Jesaitis (23) is a clear example of this effect and relates directly to our study; the rate constants (k (s^{-1})) are shown below.

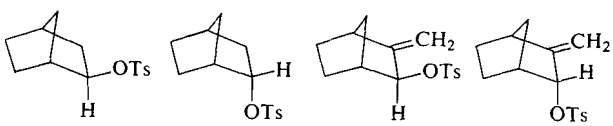

2.36×10^{-5} 8.28×10^{-8} 1.02×10^{-4} 2.62×10^{-5}

[5]The plot differs slightly from the one reported previously (9). The rate constant for endo exchange in **7** is 1.32×10^{-4} and not 1.32×10^{-5} as reported in the earlier paper (9). Also, we have improved the accuracy and precision of the rate constants for **8** and **9**, and log k_x and log k_n now are 2.390 and −2.125, respectively.

[6]As we pointed out in the first part of the discussion, that the *endo* proton in ketones **1**–**7** is exchanged via two channels introduces a potential complicating factor. If, as we have shown in footnote 4, the intrinsic *endo* rate constants are in the order of 17% less than the observed ones, application of the correction to the appropriate *endo* rates in Table 1 does not produce a significant change in the slope of the log–log plot.

[7]That the demand for increased delocalization operates in nitro compounds is indicated by the work of Bordwell and Flanagan (18) who have shown that the rates for *exo* and *endo* deprotonation in *endo*-2-nitro-5-norbornene and *exo*-2-nitro-5-norbornene, relative to the corresponding 2-nitronorbornanes, are 1.7 and 1.1, respectively. Although the effects are small and should be interpreted with caution, the more difficult *endo* proton transfer appears to be least sensitive to introduction of the double bond into the [2.2.1] framework.

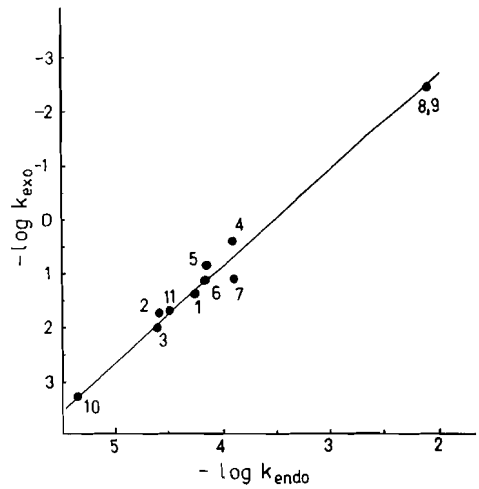

FIG. 4. Plot of $-\log k_x$ vs. $-\log k_n$ for H–D exchange of 2-norbornanones.

Also, Bell (24), in a comparison of carbon and oxygen acids, has predicted through application of simple electrostatic theory that the more difficult the proton transfer, the greater the charge transfer to the electronegative atom.[8]

Since *endo* deprotonation is more difficult because of the steric hindrance to approach by the base, and the difference in charge transfer to oxygen is a manifestation of this, we expect that an increase in steric restraint to ionization of the *exo* proton would equalize both the degree of charge transfer (delocalization) to oxygen and the sensitivity to changes in structure and substituent in the deprotonations.

A study of the enolization of a series of 4-substituted camphors by Casadavell and co-workers (25)

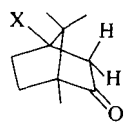

X = H, CH_3, Cl, Br, NO_2

supports this expectation. The slope of the plot of log k_x vs. log k_n for the series is 1.07 (correction coefficient 0.979). Thus, while there is an increase[9] of 10^3 in absolute rate through the series, the *exo*:*endo* rate ratio remains constant. Since $H(3)_x$ and $H(3)_n$ are in essentially identical steric environments, and the activation energies are not significantly different,

[8]Although the prediction was developed from a consideration of different types of pseudo acids, namely nitroalkanes and phenols, it should also hold for pseudo acids of the same type, i.e., a pair of diastereotopic protons α to a carbonyl group.

[9]For X = H, $k_x = 4.83 \times 10^{-4}$, $k_n = 2.55 \times 10^{-5}$, k_x/k_n = 18; for X = CH_3, 3.35×10^{-4}, 3.65×10^{-5}, 9.2; for X = Cl, 3.0×10^{-2}, 1.8×10^{-3}, 16.4; for X = Br, 4.6×10^{-2}, 2.6×10^{-3}, 16.3; for X = NO_2, 3.4×10^{-1}, 2.7×10^{-2}, 13.1 (25).

Can. J. Chem. Downloaded from www.nrcresearchpress.com by 210.87.254.6 on 09/05/12
For personal use only.

the degree of delocalization to the carbonyl group is expected to be comparable in both cases. Thus, both processes exhibit the same sensitivity to a change in structure or substituent. Casadavell's data also support our view that the torsional strain at C(3)—H_x, C(3)—H_n, C(4)—X, and the steric hindrance to *exo* approach of the base are not significantly affected by an increase in the size of X at C(4).

Experimental

2-Norbornanone (**1**) was obtained from Aldrich Chemical Company, and was purified by preparative gas chromatography before use. The syntheses of the 5- and 6-methylene-2-norbornanones **4**–**7** are described in the preceding paper. The ketones **2** (26), **3** (27), and **8** (28) were prepared by literature procedures and were purified by preparative gas chromatography; **8**-*d* was prepared by chlorination of 2-norbornanone-3,3-d_2; **9** was isolated by preparative-gas chromatography from an equilibrium mixture of **8** and **9** that was obtained from **8**. Dioxane was purified by the method of Fieser and Fieser (29).

Kinetic Methods

(*a*) *For Ketones* ***1–7***

A stock solution of sodium deuteroxide in D_2O of convenient normality (0.1–0.4 *N*) was prepared by the addition, under nitrogen, of freshly cleaned sodium metal to D_2O. The solution was standardized before every kinetic run with standard hydrochloric acid using phenolphthalein as the indicator. The ketone solution, typically 0.2 *M*, was prepared by dissolution of the substrate in a 2-ml volumetric flask, previously flushed with dry nitrogen, into sufficient purified dioxane so that it comprised by volume 60% of the run medium. For example, if the total volume of the exchange solution was 2.00 ml, the ketone was dissolved in 1.20 ml of dioxane. Before the start of each run, the NaOD stock solution, the dioxane solution of the ketone, and D_2O were placed, for at least 1 h, in a constant-temperature bath maintained at 25.0 ± 0.05°C. At time 0, the appropriate volume of NaOD solution, usually 0.30–0.50 ml, was accurately transferred to the dioxane solution, the volume was quickly made up to 2.00 ml with D_2O, and the flask was flushed with dry N_2 for 5 s. The NaOD concentration in the studies ranged from 0.0067 to 0.168 *N*. The flask was stoppered with a serum cap and aliquots (0.2–0.3 ml) were removed with a syringe and quenched in 1.5 ml of a dipotassium hydrogen phosphate buffer of p*H* 7.0. The aqueous solution was immediately extracted with ether (2 × 5 ml), saturated with sodium chloride, and extracted with a final portion of ether (1 ml). The combined ether extracts were dried, the solution was concentrated on the rotary evaporator, and the ketone was isolated by preparative vpc on a 5 ft × ¼ in. 20% SE-30 on Chromosorb W column. In some cases, the ether concentrates were introduced directly into the mass spectrometer. The deuterium content of each aliquot was determined mass spectrometrically by scanning the molecular ion 5–10 times at 10 eV. The average intensities were analyzed by standard procedures by computer. Control experiments established that the deuterium content was not altered during the quench-extraction and the mass spectrometric analysis. The *exo* and *endo* rate constants were obtained by monitoring the appearance of d_1 and d_2 species, respectively. For example, the *endo* rate constant for 4,6,6-trimethyl-2-norbornanone (**3**) was obtained by beginning with **3** and following accumulation of d_2 species. With respect to the half-life for *endo* exchange, the period required for build-up of maximum d_1 concentration (≃90%) was considered to be negligible. As a representative example, data for an *endo* exchange of **3**, at a base concentration of 0.104 *N*, is shown below. The plot of ln f_2 vs. time is given in Fig. 1*b*.

Time (h)	$\%d_0$	$\%d_1$	$\%d_2$	ln f_2
0	100.0	0	0	0.000
10	2.4	87.1	10.6	0.113
24	2.1	73.5	24.4	0.286
50	1.3	54.2	44.5	0.603
87	2.0	35.7	62.4	1.009
119	1.3	26.2	72.5	1.340

The pseudo-first-order rate constants were obtained from a plot of ln $f_{(n)}$ (n = 1, 2) vs. time or from a plot of ln $\%d_n$ (n = 0, 1) vs. time for the decay of the appropriate species and

$$f_1 = \frac{100 - \%d_{0(\infty)}}{100 - \%d_{0(\infty)} - \%d_{1(t)}}$$

$$f_2 = \frac{100 - \%d_{0(\infty)}}{100 - \%d_{0(\infty)} - \%d_{2(t)}}$$

the second-order rate constants were obtained by dividing the slope by the base concentrations. Usually the differences between the rate constants obtained by both methods were < 10%. For example, for exchange of **3** from ln f_1 and ln f_2 plots, the *exo* and *endo* rate constants are 9.88 × 10^{-3} M^{-1} s^{-1} (average of 9.82 × 10^{-3} (see Fig. 1*a*) and 9.91 × 10^{-3}) and 2.81 × 10^{-5} M^{-1} s^{-1} (average of 2.59 × 10^{-5} (see Fig. 1*b*) and 3.02 × 10^{-5}), respectively. From the plots of ln $\%d_0$ and ln $\%d_1$ vs. time, the *exo* and *endo* rate constants are 8.39 × 10^{-3} (average of 8.22 and 8.55 × 10^{-3}) and 2.77 × 10^{-5} (average of 2.57 and 2.96 × 10^{-5}). The rate constants for ketones **1** → **7** were obtained by the first method and are listed in Table 1.

(*b*) *For Chloroketones* ***8*** *and* ***9***

The 0.1515 *N* NaOD stock solution was obtained as described above. The 0.0606 *N* NaOH stock solution was prepared by appropriate dilution of a 1 *N* BDH Chemicals concentrated volumetric solution with distilled water. The solutions were standardized against 0.100 *N* HCl using phenolphthalein as the indicator. The exchange rates for **8** and **8**-*d*, in nondeuterated and deuterated media, were obtained by following the rate of isomerization of **8** to **9** gas chromatographically up to 40% conversion. That there is a very minor amount of isomerization of **9**-*d* to **8**-*d* during the course of a kinetic run (up to 40% isomerization) was established when an aliquot (34.5% **9**-*d*, 65.5% **8**) was separated into its components by preparative vpc and each isomer was analyzed for deuterium content by mass spectrometry. While the *endo*-chloroketone **9**-*d* was fully deuterated, the *exo*-chloroketone contained 0.025 excess atoms of deuterium. Typically, 0.030 g of ketone, > 99% pure, purified by gas chromatography, was weighed into a 1 ml volumetric flask that was previously flushed with argon for several minutes. Before the start of a run, the volumetric flasks, the stock NaOD or NaOH solution, and the purified dioxane were equilibrated in the constant temperature bath for at least 1 h at 30.0 ± 0.05°C. Dioxane (0.60 ml) was quickly transferred to the volumetric flask and the solution was equilibrated for at least 15 min. Stock NaOD or NaOH solution (0.40 ml) was quickly added and the flask was stoppered with a serum cap. During the course of a run, five or six aliquots (0.05 ml) were removed with a syringe and each was quenched in a vial which contained 0.2 ml of

Can. J. Chem. Downloaded from www.nrcresearchpress.com by 210.87.254.6 on 09/05/12
For personal use only.

K_2HPO_4 buffer of p*H* 6.5 and 0.5 ml of ether. The resulting solution was 'extracted' by repeatedly drawing in and vigorously forcing out the solution from a rubber-bulb-capped 9-in. Pasteur capillary glass pipette. The ether layer was dried and analyzed gas chromatographically on a Model 560 Tracor gas chromatograph equipped with flame ionization detectors and fitted with 6 ft × 4 mm id 3% OV-1 on Chromosorb W columns. Analysis of a mixture of known amounts of **8** and **9** showed that the flame ionization detector response to both chloroketones was the same.

Temperature programming from 100 to 140°C at 8 deg per minute was utilized and the data were collected on a Varian Model 485 electronic integrator. The percentage of **8** and **8**-*d* was taken as the average of two injections, and the average deviation generally was < 1%. The data, as plots of ln %**8** or ln %**8**-*d*, were analyzed by computer and the correlation coefficients generally exceeded 0.996. The rate constants reported are an average of at least two determinations. The average deviations generally were < 5%. See Fig. 2 for the pseudo-first-order plot for enolization of **8**. Although no other products were detected by gas chromatography during the course of the kinetic runs (15 min for **8** and 70 min for **8**-*d*) there was obtained, after 24 h, in approximately equal amounts, < 10% of two products of much longer retention time.

Because the rate of exchange of *endo*-3-chloro-2-norbornanone was too fast to be measured at the usual $^-$OD concentrations, a $NaDCO_3$–NaOD–D_2O buffer solution was required. However, since it could not be assumed that the measured p*D* of the reaction solution (60% dioxane – 40% buffer) was indeed the correct value, the *exo* exchange rate for 2-norbornanone (**1**) was run in the same buffer solution. Pure **9** (> 99%) was obtained, by preparative gas chromatography on a 5 ft × ¼ in. 10% Carbowax-on-Chromosorb-W column maintained at 140°C, from a mixture of **8** (35%) and **9** (65%) that was obtained from a large scale equilibration of **8**. A solution, of p*D* 10.37, of 60% dioxane and 40% $NaDCO_3$–NaOD–D_2O buffer was prepared and equilibrated in the constant temperature bath. After 1 h, 1.00 ml of the solution was quickly added to 0.020 g of **9** in a stoppered 1-ml volumetric flask. During the course of the kinetic run (4–5 min) aliquots (0.1 ml) were quenched with K_2HPO_4 buffer of p*H* 6.5 and extracted with ether (2 ml). The ether aliquots were dried and concentrated, and the deuterium content was determined mass spectrometrically at 10 eV as was previously described in the Experimental. The pseudo-first-order rate constants were obtained by computer from plots of ln $\%d_0$ vs. time. Correlation coefficients exceeding 0.997 were obtained. The pseudo-first-order rate constant for *exo* exchange in **1** at 30°C in a 60% dioxane – 40% buffer solution of p*D* 10.37, was 9.97×10^{-7} s^{-1}. Since the second-order rate constant for *exo* exchange in **1** at 30°C is 5.85×10^{-2} M^{-1} s^{-1}, division of the pseudo-first-order rate constant (3.20×10^{-3} s^{-1}; average of 3.02 (see Fig. 3) and 3.37×10^{-3} s^{-1}) for exchange of **9** by 1.70×10^{-5} establishes the second-order rate constant as 1.88×10^{2} M^{-1} s^{-1}.

*Determination of K_{eq} for Chloroketones **8** and **9***

The value of K_{eq} for **8** and **9** was determined by analysis of the remaining solution of the kinetic runs in deuterated and nondeuterated media. After at least 24 h, in each case, the solution (0.2 ml) was quenched in K_2HPO_4 buffer (0.4 ml), and extracted with ether. The dried ether extracts were analyzed by gas chromatography as was described previously in this Experimental. Repeated analyses gave $K_{eq} = [\mathbf{8}]/[\mathbf{9}] = 0.54$ with an average deviation of < 5%.

Acknowledgement

We thank the National Research Council of Canada for financial support.

1. S. Forsén and M. Nilsson. *In* The chemistry of the carbonyl group. Vols. I and II. *Edited by* S. Patai. John Wiley and Sons, Inc., New York, NY. 1970.
2. N. H. Werstiuk and R. Taillefer. Can. J. Chem. **48**, 3966 (1970).
3. T. T. Tidwell. J. Am. Chem. Soc. **92**, 1448 (1970).
4. G. A. Abad, S. P. Jindal, and T. T. Tidwell. J. Am. Chem. Soc. **95**, 6326 (1973).
5. A. F. Thomas and B. Willhalm. Tetrahedron Lett. 1309 (1965).
6. J. M. Jerkunica, S. Borčić, and D. E. Sunko. Tetrahedron Lett. 4465 (1965).
7. A. F. Thomas, R. A. Schneider, and J. Meinwald. J. Am. Chem. Soc. **89**, 68 (1967).
8. P. Barraclough and D. W. Young. Tetrahedron Lett. 2293 (1970).
9. S. Banerjee and N. H. Werstiuk. Can. J. Chem. **54**, 678 (1976).
10. S. Banerjee and N. H. Werstiuk. Can. J. Chem. **53**, 1099 (1975).
11. N. H. Werstiuk and S. Banerjee. Can. J. Chem. **55**, 173 (1977).
12. P. von R. Schleyer. J. Am. Chem. Soc. **89**, 701 (1967).
13. S. P. Jindal and T. T. Tidwell. Tetrahedron Lett. 783 (1971).
14. S. P. Jindal, S. S. Sohoni, and T. T. Tidwell. Tetrahedron Lett. 779 (1971).
15. S. Weiss and G. E. Leroi. J. Chem. Phys. **48**, 962 (1968).
16. J. R. Durig, S. M. Craven, and J. Brazin. J. Chem. Phys. **52**, 2046 (1970).
17. W. S. Matthews, J. E. Bares, J. E. Bartmess, F. G. Bordwell, F. J. Cornforth, G. E. Druker, Z. Margolin, R. J. McCallum, G. J. McCollum, and N. R. Vanier. J. Am. Chem. Soc. **97**, 7006 (1975).
18. P. W. K. Flanagan. Diss. Abstr. **18**, 1980 (1958).
19. A. Colter, E. C. Friedrich, N. J. Holness, and S. Winstein. J. Am. Chem. Soc. **87**, 378 (1965).
20. P. G. Gassman and H. F. Fentiman, Jr. J. Am. Chem. Soc. **92**, 2549 (1970).
21. H. C. Brown, K. Takeuchi, and M. Ravindranathan. J. Am. Chem. Soc. **94**, 2684 (1977).
22. J. B. Lambert, H. W. Mark, and E. S. Magyar. J. Am. Chem. Soc. **99**, 3059 (1977).
23. C. F. Wilcox, Jr. and R. G. Jesaitis. Chem. Commun. 1046 (1967).
24. R. P. Bell. The proton in chemistry. Cornell University Press, Ithaca, New York, NY. 1959. pp. 208–212.
25. F. C. Brown, E. Casadevall, P. Metzger, and D. G. Morris. Third IUPAC Conf. Phys. Org. Chem. La Grande Motte, September, 1976. Abstr. p. 83.
26. M. Donaldson. Doctoral Dissertation, Princeton, New Jersey. 1968.
27. H. P. Gervais and A. Rassat. Bull. Soc. Chim. Fr. 743 (1961).
28. E. Tobler, D. E. Battin, and D. J. Foster. J. Org. Chem. **29**, 2834 (1964).
29. L. F. Fieser and M. Fieser. Reagents for organic synthesis. John Wiley and Sons, Inc., New York, NY. 1967. p. 333.

Base-catalyzed enolization of 2,5-norbornanediones. Evidence for homoenolic assistance[1]

NICK HENRY WERSTIUK, ROLAND TAILLEFER, AND SUJIT BANERJEE
Department of Chemistry, McMaster University, Hamilton, Ont., Canada L8S 4M1

Received September 21, 1977

NICK HENRY WERSTIUK, ROLAND TAILLEFER, and SUJIT BANERJEE. Can. J. Chem. **56**, 1148 (1978).

The rate enhancements relative to the monoketones, for base-catalyzed *exo* and *endo* hydrogen isotope exchange in 2,5-norbornanedione (**2**), 3,3-dimethyl-2,5-norbornanedione (**3**), and 1,3,3-trimethyl-2,5-norbornanedione (**4**) have been determined at 25 ± 0.05°C in 60% dioxane – 40% D_2O. After the increase in rate due to the inductive and strain effects of the second carbonyl group is taken into account, the homoenolic-assistance factors are extracted from the overall rate enhancements: for *exo* exchange in **2**, **3**, and **4**, the factors are 13, 39, and 32; for *endo* exchange in **2**, **3**, and **4**, the factors are 26, 64, and 71, respectively.

NICK HENRY WERSTIUK, ROLAND TAILLEFER et SUJIT BANERJEE. Can. J. Chem. **56**, 1148 (1978).

Travaillant à 25 ± 0.05°C dans un mélange contenant 60% de dioxanne et 40% de D_2O, on a déterminé les augmentations de vitesse, relatives au monocétonés, pour les échanges isotopiques d'hydrogènes *exo* et *endo* catalysés par les bases dans la norbornanedione-2,5 (**2**), la diméthyl-3,3 norbornanedione-2,5 (**3**) et la triméthyl-1,3,3 norbornanedione-2,5 (**4**). Après avoir déduit de ces augmentations globales de vitesse les augmentations spécifiques dues aux effets inductifs et stériques du second groupement carbonyle, on peut déduire les facteurs provenant de l'aide homoénolique: pour l'échange *exo* dans **2**, **3** et **4** les facteurs sont respectivement 13, 39 et 32; pour l'échange *endo* dans **2**, **3** et **4**, les facteurs sont 26, 64 et 71.

[Traduit par le journal]

Introduction

As a continuation of our studies (1–4) designed to detail the intricacies of acid- and base-catalyzed enolization, and hydrogen isotope exchange of ketones, we have studied the base-catalyzed hydrogen isotope exchange of 2,5-norbornanedione (**2**), 3,3-dimethyl-2,5-norbornanedione (**3**), and 1,3,3-trimethyl-2,5-norbornanedione (**4**). Specifically, we were interested in establishing whether or not a carbonyl group situated 1,3 from an enolizable site enhances the rate of enolization through homoenolic delocalization (5–10) of the developing negative charge. We chose to study the 2,5-norbornanediones **2**, **3**, and **4** for the following reasons: the compounds are readily available; the required orientation of the carbonyl groups is present; our concomitant studies (4) on the base-catalyzed enolization exchange of 2-norbornanones allowed us to estimate the magnitude of the inductive and strain components of the rate acceleration; and, the results could be compared with the mechanistic details already established for the homoenolization of 2-norbornanones (5–10). Herein, we describe the kinetic methods that were used to determine the rate accelerations and establish the homoenolic-assistance factors for abstraction of the *exo* and *endo* protons in diones **2**, **3**, and **4**.

[1]For a preliminary account, see ref. 1.

Results

Kinetic Methods

Endo *Exchange*

To obtain the *endo* exchange rates for **2**, **3**, and **4**, we used a procedure similar to the one described in the preceding paper (4). However, several modifications were made for two reasons: during the initial stages of the study, exchange of the deuterated diones **2** and **4** occurred in the mass spectrometer inlet system; and, a rate falloff was observed during the course of the kinetic runs.

To overcome the first problem, the deuterated diones **2** and **4** were isolated from the aliquots and reduced by $LiAlH_4$ to the diols which were converted to the corresponding diacetates. Since each diacetate exhibited a molecular ion of low intensity even at 10 eV, the deuterium content was established from an analysis of the $M^+ - CH_3CO$ peaks. To establish that the deuterium content obtained by analysis of a diacetate was equivalent, within experimental error, to the value obtained by analysis of the parent dione, a control experiment was carried out (see Experimental) using **3** that did not show significant exchange in the inlet system.

The rate[2] falloff, due to a decrease in base concen-

[2]The pseudo-first-order rate constants were obtainable from plots of ln $\%d_n$ (n = 0, 1, 2,...) vs. time or from plots of ln

Can. J. Chem. Downloaded from www.nrcresearchpress.com by 210.87.254.6 on 09/05/12
For personal use only.

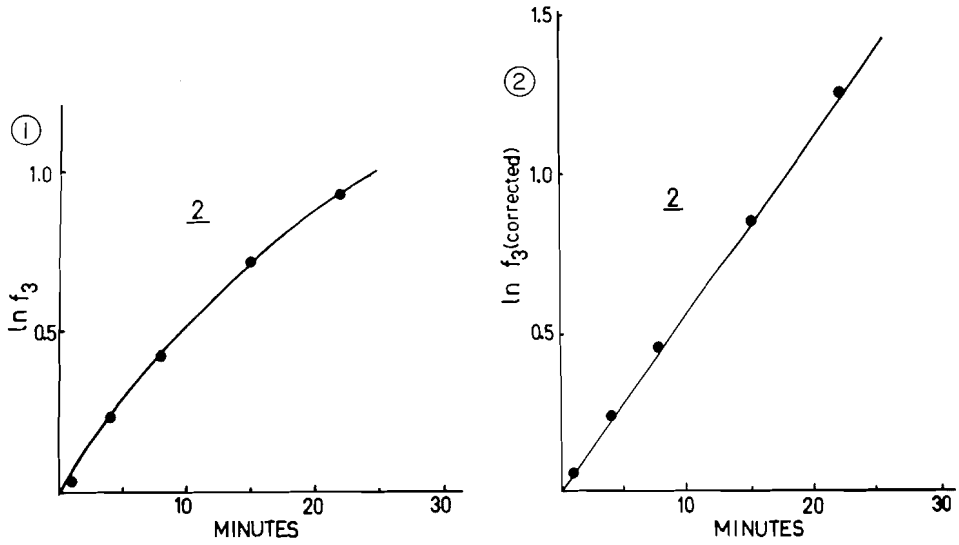

FIG. 1. Plot of ln f_3 vs. time for base-catalyzed (0.0127 *M* NaOD) isotope exchange of the endo hydrogens in **2** at 25.00 ± 0.05°C.

FIG. 2. Plot of ln f_3 (corrected) vs. time for base-catalyzed (0.0127 *M* NaOD) isotope exchange of the endo hydrogens in **2** at 25.00 ± 0.05°C.

tration with time, was most pronounced for 2,5-norbornanedione (**2**) and is illustrated in Fig. 1 as a plot of ln f_3 vs. time. The percentage change in the base concentrations was established by titrating the base in aliquots obtained from a control run for each dione: for dione **2** there was a 16–18% decrease in the base concentration during the kinetic run; for both diones **3** and **4**, a decrease of 8–11% was observed. The observed d_2 (diones **3** and **4**) and $d_3 + d_4$ (dione **2**) abundances, whose appearances were followed to obtain the rate constants, were corrected for the decrease in base concentration as we have described in the Experimental. Figure 2 illustrates the plot of ln f_3 (corrected) vs. time for *endo* exchange in **2**. In Tables 1 and 2 are listed the second-order rate constants and the rate enhancements, respectively. Although the reason for the consumption of the base has not been established, that no significant rate falloff is observed with the monoketones (4) indicates that the reactivity[3] of the 2,5-diones is a contributing factor. Possibly, the base is consumed in an autoxidation reaction (11).

TABLE 1. Second-order rate constants for base-catalyzed isotope exchange of 2,5-norbornanediones at 25.00 ± 0.05°C

Substrate	k (M^{-1} s^{-1})* *Exo*	k (M^{-1} s^{-1})* *Endo*	k_x/k_n†
2	46.1	3.54×10^{-2}	1300
3	57.3	3.89×10^{-2}	1470
4	28.1	4.57×10^{-2}	610

*Averages of at least two determinations with an average deviation of less than 10%.
†Rounded to the nearest 10.

Exo *Exchange*

Because *exo* exchange in **2**, **3**, and **4** is very fast, a $NaDCO_3$–NaOD–D_2O buffer was used as the catalyst to facilitate the measurement of rate constants. Since the p*D* of the 60% dioxane – 40% buffer medium could not be assumed to accurately represent the $^-$OD concentration, the pseudo-first-order rate constants for *exo* exchange in **2**, **3**, **4**, and 2-norbornanone (**1**) were determined in the dioxane–buffer

f_n (n = 1, 2, 3) vs. time. In the latter method, account is taken of the fact that complete deuteration is not achieved due to dilution of the deuterium pool. In the preceding paper (4) we established that the analysis of exchange data by both methods yielded rate constants which differ by 10% or less and that the rate constants obtained from plots of ln f_n are greater than those obtained from plots of ln $\%d_n$.

$$f_1 = \frac{100 - d_{0(\infty)}}{100 - d_{0(\infty)} - d_1}$$

$$f_2 = \frac{100 - d_{0(\infty)}}{100 - d_{0(\infty)} - d_2}$$

$$f_3 = \frac{100 - \frac{1}{2}(d_{0(\infty)} - d_{1(\infty)})}{100 - \frac{1}{2}(d_{0(\infty)} + d_{1(\infty)}) - (d_3 + d_4)}$$

[3]The diones, especially **2**, are much less stable than the parent monoketones. A purified crystalline sample of **2**, left at ambient temperature, is gradually converted into a yellow, oily solid.

Can. J. Chem. Downloaded from www.nrcresearchpress.com by 210.87.254.6 on 09/05/12
For personal use only.

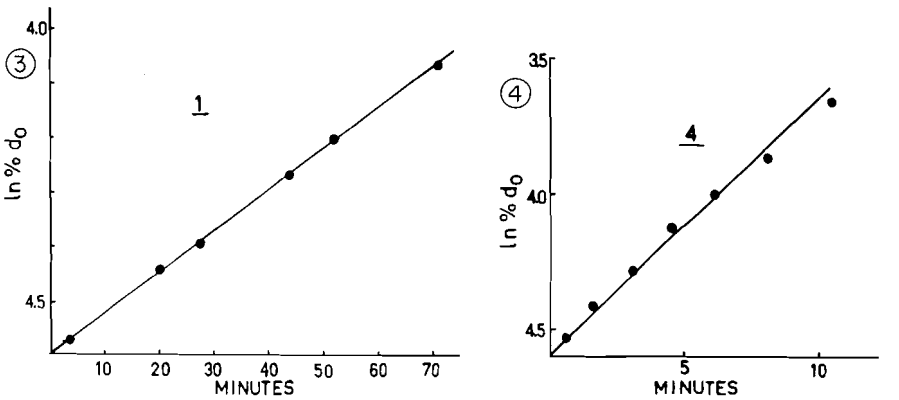

FIG. 3. Plot of ln $\%d_0$ vs. time for base-catalyzed ($NaDCO_3$–NaOD–D_2O buffer, pD 10.84) isotope exchange of the *exo*-C(3)-hydrogen in **1** at 25.00 ± 0.05°C.

FIG. 4. Plot of ln $\%d_0$ vs. time for base-catalyzed ($NaDCO_3$–NaOD–D_2O buffer, pD 10.84) isotope exchange of the *exo*-C(6)-hydrogen in **4** at 25.00 ± 0.05°C.

TABLE 2. Rate enhancements for isotope exchange in 2,5-norbornanedione relative to the corresponding monoketones*

Substrate	*Exo*†	*Endo*†
2	1200	600
3	3490	1480
4	2840	1630

*Relative to the rate for the corresponding protons in the monoketones 2-norbornanone ($k_x = 3.85 \times 10^{-2}$, $k_n = 5.90 \times 10^{-5}$), 6,6-dimethyl-2-norbornanone ($k_x = 1.64 \times 10^{-2}$, $k_n = 2.62 \times 10^{-5}$), 4,6,6-trimethyl-2-norbornanone ($k_x = 9.88 \times 10^{-3}$, $k_n = 2.81 \times 10^{-5}$) ($k$ values in M^{-1} s^{-1}) (4).
†Rounded to the nearest 10.

medium. As representative examples, the first-order plots for *exo* exchange in **1** and **4** in 60% dioxane – 40% buffer (pD 10.84) are given in Figs. 3 and 4, respectively. Since we previously established the second-order rate constant for *exo* exchange in **1**, the second-order rate constants for *exo* exchange are obtained from the following relationship.

$$k_{\text{dione}}(M^{-1}s^{-1}) = \frac{k_{\mathbf{1}}(M^{-1}s^{-1})}{k_{\mathbf{1}}(s^{-1})} k_{\text{dione}}(s^{-1})$$

The rate constants, and the rate enhancements relative to the monoketones, are given in Tables 1 and 2, respectively.

We previously estimated (1) the rate constant for *exo* exchange in **4**, as 2.0 M^{-1} s^{-1}, by considering the extent of $d_0 \rightarrow d_1$ conversion after 1–4 min in three *endo* exchange runs, estimating $t_{\frac{1}{2}}$, using the expression $t_{\frac{1}{2}} = \ln 2/k$, and dividing k by the initial base concentration. That the experimentally determined value is 28.1 M^{-1} s^{-1}, obviates the inaccurate estimate, which stemmed from the fact that *exo* exchange is essentially complete (see Experimental for the data for *endo* exchange in **3**) before the first *endo* exchange aliquot is removed. Consequently, the estimate of $t_{\frac{1}{2}}$ from the percentage of d_0 species remaining (2–5%) is subject to the large error associated with recording and measuring low intensity mass spectral peaks.

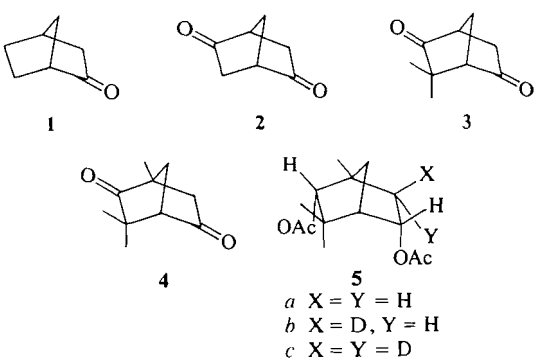

Stereochemistry of Exchange

That abstraction of the *exo*-C(3) hydrogen in 2-norbornanones is preferred over *endo* hydrogen abstraction is well documented (12, 13). To establish that *exo* exchange is also preferred in the diones, we analyzed the 60 MHz nmr spectra of *endo*-2-*endo*-5-diethanoyloxy-1,3,3-trimethylnorbornane (**5***a*), *endo*-2-*endo*-5-diethanoyloxy-1,3,3-trimethylnorbornane-*exo*-6-*d* (**5***b*), and *endo*-2-*endo*-5-diethanoyloxy-1,3,3-trimethylnorbornane-*exo*-6-*endo*-6-d_2 (**5***c*). The partial spectrum of **5***a*, illustrated in Fig. 5*a*, exhibits the *exo*-C(2)-H signal at δ 4.40 (J = 1.3 Hz), and the *exo*-C(5)-H signal as a heptet centered at δ 4.96 with a signal width at half-height of approximately 22 Hz. Dione **4** was monodeuterated and **4**-d_1 was converted into diacetate **5***b*-d_1. Its partial nmr spectrum, illustrated in Fig. 5*b*, shows the *exo*-C(2)-H signal collapsed to a sharp singlet by loss of the W- coupling,

Can. J. Chem. Downloaded from www.nrcresearchpress.com by 210.87.254.6 on 09/05/12
For personal use only.

Can. J. Chem. Downloaded from www.nrcresearchpress.com by 210.87.254.6 on 09/05/12
For personal use only.

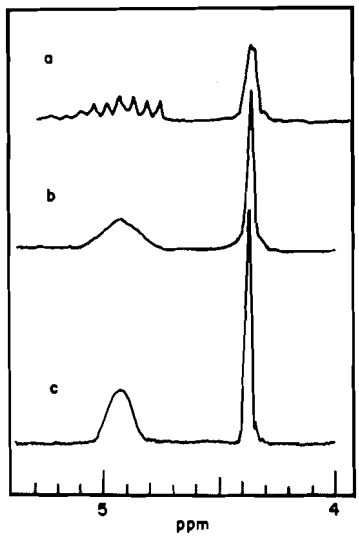

FIG. 5. Partial 60 MHz (CCl_4) spectrum of (*a*) **5***a*; (*b*) **5***b*; and (*c*) **5***c*.

a consequence of the replacement of the *exo*-C(6) proton with deuterium. That the *exo*-C(5)-H signal collapses to a broad peak with a width at half-height of 11 Hz is consistent with the loss of a single coupling in the order of 10–11 Hz, which is expected for removal of an *exo–exo cis* coupling constant (13–15). In the dideuterated diacetate **5***c* (Fig. 5*c*) there is a further sharpening of the *exo*-C(5)-H signal to a width at half-height of 8.5 Hz. This result is consistent with the removal of a 2.5 Hz coupling, which is expected for the loss of a vicinal *exo–endo trans* coupling in the [2.2.1] system (14, 15). Clearly, as in the case of the monoketones, *exo* exchange is preferred.

Discussion

Analysis of Rate Acceleration Data

Before the isotope exchange rates are interpreted, a potentially complicating factor must be considered. In the recent studies (2–4) which support our contention that enolization and isotope exchange of ketones are not simple processes, we demonstrated that exchange of the *endo* hydrogen in 2-norbornanone occurs via two channels: by direct abstraction and by isomerization of first-formed 2-norbornanone-*exo*-3-d_1 to 2-norbornanone-*endo*-3-d_1 that is rapidly converted into 2-norbornanone-*exo*-*endo*-3,3-d_2. Thus, for **1**, the intrinsic selectivity s is 17% larger than the $k_x:k_n$ rate ratio, and $k_{n(obs)} \simeq 1.2\ k_{n(intrinsic)}$ (2–4). Exchange of the *endo* hydrogen in the diones **2**, **3**, and **4** must occur via two channels, also, and the difference between $k_{n(obs)}$ and $k_{n(intrinsic)}$ in each case is expected to be very similar to the difference observed for **1**. Thus the effect of the dual-channel exchange of the *endo* hydrogen is minimized when relative rates for *endo* exchange (Table 2) are considered.

TABLE 3. Homoenolic-assistance factors*

Substrate	*Exo*	*Endo*
2	7	26
3	20	64
4	16	71

*Rounded to the nearest unit.

To establish whether or not the *exo* and *endo* deprotonation rates in **2**, **3**, and **4** are enhanced by homoenolic delocalization of the developing negative charge, we estimated the rate acceleration owing to the inductive and strain effects of the carbonyl group and extracted the homoenolic-assistance factors (Table 3) from the observed rate enhancements.

That the *s* character of a C—H bond in a strained system can control its kinetic acidity, has been established by Streitwieser and co-workers (16), who determined the relative kinetic acidities of the hydrocarbons, cyclohexane (1.00), cyclopentane (5.7), cyclobutane (28.0), and cyclopropane (7.0×10^4).

The increase in strain in diones **2**, **3**, and **4** resulting from the introduction of the second sp^2 centre could enhance the kinetic acidity of the C—H bonds at C(3). We previously established (4) that the rate enhancements, relative to **1**, for *exo* and *endo* exchange in enone **6** are 1.3 and 2.2, respectively. Since

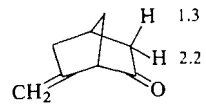

6

the strain in **6** is expected to resemble that in a 2,5-dione system, the increase in rate due to incorporation of the strain-inducing π system, taken as an average of the *exo* and *endo* rate acceleration, is 1.75.

To estimate the rate acceleration due to the inductive effect of the carbonyl group, we correlated Casadevall's rate constants for *endo* exchange (2:1 dioxane–D_2O) in the 4-substituted camphors **7***a*–**7***e*

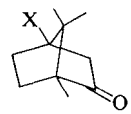

7

a X = H *d* X = Br
b X = CH_3 *e* X = NO_2
c X = Cl *f* X = $C(=O)CH_3$

(17) with σ_I and established that ρ for the process is 4.0. Thus, the *endo* exchange rate for 4-acetylcamphor

Can. J. Chem. Downloaded from www.nrcresearchpress.com by 210.87.254.6 on 09/05/12
For personal use only.

(7*f*) (X = —C(=O)—CH_3, σ_I = 0.28), is estimated to be 13 times the *endo* rate in camphor. Since the *endo* exchange rates for 2-norbornanone (5.90×10^{-5} M^{-1} s^{-1} at 30°C) and camphor (2.55×10^{-5} M^{-1} s^{-1} at 15°C) are nearly identical and should exhibit the same sensitivity to electronic effects, we estimate the *endo* rate constant for 4-acetyl-2-norbornanone to be 7.67×10^{-4} $M^{-1}s^{-1}$. In the preceding publication (4) we established, from a study of a series of 2-norbornanones, that *exo* deprotonation is more sensitive to electronic effects than the *endo* process and we quantified the difference in the form of a linear free energy relationship that is expressed in [1]. From

$$\log k_x = 1.67 \log k_n + 5.80 \quad [1]$$

[1] we estimate the *exo* exchange rate for 4-acetyl-2-norbornanone to be 4.0 M^{-1} s^{-1} and the rate enhancement, relative to *exo* exchange in **1**, is in the region 100.[4] If the C(4)-acetyl group, in which the carbonyl group is situated 1,3 with respect to enolizable hydrogens, approximates the inductive effect

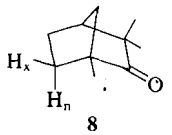

8

of the carbonyl group in the 2,5-diones, the enhancements for *exo* and *endo* exchange, as a combination of the inductive and strain compounds, are 175 and 73, respectively. Thus, the rate enhancements due to homoenolic assistance (Table 3) are obtained from the data in Table 2. That the more difficult *endo* proton transfer is assisted to a greater degree by 1,3 conjugation to the carbonyl group than the *exo* process, is consistent with the hypothesis we presented in the preceding paper re: enolic abstraction. That is, the more difficult *endo* proton transfer at C(3) in 2-norbornanone is assisted to a greater degree by 1,2 conjugation to the carbonyl group than the *exo* process. The *exo* rate in the 2,5-diones, nevertheless, is enhanced to a greater degree (Table 2) than the *endo* rate because the *exo* proton transfer is more sensitive to electronic effects (*vide supra*) than the *endo* process.

In this connection, it is important to note that Stothers (10) has established that the *exo*:*endo* rate ratio for K^+OtBu-catalyzed (185°C) β-enolization at C(6) (homoenolization) in fenchone (8) is 3.5.

We would like to suggest that 1,3 charge transfer from C(6) to the carbonyl group in β-enolization (homoenolization) is greater for *endo* deprotonation than for the *exo* process. Nevertheless, *exo* deprotonation is favoured for two reasons: the inductive effect of the carbonyl group preferentially lowers the activation energy for the *exo* process (*vide supra*) and the *exo* face in the [2.2.1] skeleton, unsubstituted at C(7), is less hindered sterically than the *exo* face.

Effect of a Bridgehead Methyl Group

The rates of *exo* and *endo* deprotonation in **4**, rela-

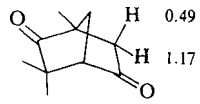

4

tive to the *exo* and *endo* rates in **3**, are given below. That there is a small decrease in the *exo* rate upon replacement of the hydrogen at C(4) by a methyl group is consistent with the results of our study on 2-norbornanones (4): the difference in torsional strain between *exo*-C(3)-H, C(4)-H and *exo*-C(3)-H, C(4)-CH_3 is minimal and a methyl group, or a group of equivalent size, does not sterically hinder *exo* deprotonation.

Experimental

2-Norbornanone (**1**) was obtained from Aldrich Chemical Company. 1,3,3-Trimethyl-2,5-norbornanedione (**4**) was prepared from 1,3,3-trimethyl-2-norbornanone (**3**) by the method of Bays *et al.* (19). 3,3-Dimethyl-2,5-norbornanedione and 2,5-norbornanedione (**2**) were prepared from 3,3-dimethyl-2-norbornanone (20) and nortricyclanone (21), respectively. The substrates **1**, **2**, **3**, and **4** were purified by preparative glpc before each kinetic run.

Kinetic Methods

Purified dioxane and stock NaOD solutions were prepared as described in the preceding paper (4).

Endo *Exchange*

The kinetic method used was essentially the one described in the preceding paper. The exchange solutions, maintained at 25.0 ± 0.05°C, were 0.20–0.25 *M* in ketone and 0.009–0.025 *M* in NaOD. Aliquots of a 2.0 ml exchange solutions contained in a serum cap-stoppered 2-ml volumetric were withdrawn and quenched in deuterated K_2DPO_4 buffer (1.5 ml). The aqueous phase was saturated with NaCl, extracted with ether (3 × 5 ml), and the combined ether extracts were dried. The solvent was distilled through a 1-ft Vigreux column and the dione was isolated by preparative glpc (5 ft × ¼ in. 20% SE-30 on Chromosorb W). A control experiment with **4** and the deuterated

[4]In an alternate approach we utilize the fact that the *exo* exchange rate for *exo*-5-ethoxy-2-norbornanone in 2:1 dioxane–D_2O, as established by Professor Tidwell (T. T. Tidwell, personal communication) is greater than the *exo* rate in 2-norbornanone by a factor of 1.8. From the σ_I for CH_3O—(0.26) we estimate σ_I for CH_3CH_2O—CHR— to be in the region of 0.10 by dividing 0.26 by the CH_2— insulating factor of 2.5. However, in our case the insulating group is CHR and we expect that σ_I for CH_3CH_2O—CHR— lies in the range 0.05–0.10. Thus ρ for *exo* exchange lies in the range 2.6–5.2. When the acetyl group (σ_I = 0.28) is used as a model, the rate acceleration due to the inductive effect of the carbonyl group is in the range of 5–28.

Can. J. Chem. Downloaded from www.nrcresearchpress.com by 210.87.254.6 on 09/05/12
For personal use only.

buffer K_2DPO_4 showed that there was no significant (<2%) exchange during the quench.

Since, in the initial stages of the study, exchange of diones **2** and **4** was observed in the mass spectrometer inlet system, the deuterium analyses were carried out on the corresponding diacetates.

The diol (0.020–0.030 g) obtained from $LiAlH_4$ reduction of the dione was dissolved in acetic anhydride (1.5 ml) and pyridine (2.5 ml). After the mixture was left standing at ambient temperature for 24 h, it was poured onto ice, diluted to 80 ml, and extracted with ether (3 × 25 ml). The combined ether extracts were washed with dilute hydrochloric acid (25 ml), saturated sodium carbonate solution (25 ml), water (25 ml), and finally with a saturated sodium chloride solution (25 ml). After the ether layer was dried and concentrated on the rotatory evaporator, the diacetate was isolated by preparative glpc on a 5 ft × ¼ in. 20% SE-30 on Chromosorb W column. To check that there was no deuterium exchange during the reduction, dione **4** was reduced by $LiAlD_4$ in ether. That there was no experimentally significant (<1%) amount of d_3 species present, established that the reduction proceeds without exchange. Due to the very low relative intensity of the molecular ion of the diacetate derived from **2** and **4**, the $M^+ - CH_3CO$ peaks were used in the deuterium analyses. That the analysis of the diacetate, at low voltage, gives the deuterium content accurately, was established by means of a control experiment on dione **3** that itself did not show significant isotope exchange in the mass spectrometer inlet system. The control experiment involved conversion of the monodeuterated dione to the diacetate: dione **3**, 4.1% d_0, 91.3% d_1, 4.6% d_2; diacetate, 4.5% d_0, 83.7% d_1, and 5.3% d_2.

Correction for Change in Base Concentration

To quantify the change in base concentration during the course of a kinetic run for each ketone, exchange solutions were prepared and 1.0-ml aliquots were titrated with standard 0.100 or 0.010 *N* HCl. For diones **3** and **4** there was an 8–11% change in base concentration during the kinetic runs and for **2** a 16–18% change was observed. In the absence of the diketone the decrease in base concentration was less than 5% during the same interval. The observed abundances were 'corrected' for the decrease in base concentration utilizing the following equation: corrected $\%d_n$ (n = 2, 3 + 4) = observed $\%d_n$ (n = 2, 3 + 4)(100 + % change in base concentration)/100. As an example, the data for *endo* exchange in **3** are given below:

[**3**] = 0.267 *M*, [NaOD] = 0.0114 *M*, $d_{0(\infty)}$ = 1.5%

Time (min)	$\%d_0$	$\%d_1$	$\%d_2$	% change [base]	$\%d_2$ (corr)	ln f_2 Observed	ln f_2 Corrected
0.75	5.4	92.3	2.3	0.4	2.3	0.024	0.024
10.2	3.4	73.5	23.1	2.1	23.6	0.067	0.286
20.0	2.9	58.4	38.7	3.7	40.0	0.499	0.526
30.0	1.7	46.9	51.4	5.7	54.3	0.738	0.801
45.0	1.5	33.9	64.6	8.5	70.1	1.067	1.244
60.0	1.4	26.2	72.3	11.3	80.5	1.324	1.697

Analysis by computer of the data for **3** and **4** as plots of ln f_2 (corrected) vs. time[2] gave the corrected pseudo-first-order rate constants. In the case of **2** the *endo* rate constant was obtained from a plot of ln f_3 (corrected) vs. time.[2] The data for exchange of **2** are given below: [**2**] = 0.204 *M*, [NaOD] = 0.0127 *M*, $d_{0(\infty)}$ = 3.1%, $d_{1(\infty)}$ = 5.7%.

Time (min)	$\%d_0$	$\%d_1$	$\%d_2$	$\%d_3$	$\%d_4$	% change [base]	$\%(d_3 + d_4)$ (corr)	ln f_3 Observed	ln f_3 Corrected
1.0	3.7	5.1	86.0	5.3	0	0.5	5.4	0.057	0.058
4.0	2.9	5.1	72.1	18.6	1.2	3.2	20.4	0.232	0.240
8.0	3.6	5.8	57.6	29.4	3.6	6.6	35.2	0.423	0.458
15.0	2.9	5.0	42.9	39.6	9.1	12.6	54.7	0.712	0.850
22.0	3.0	6.2	33.2	43.2	14.4	18.4	68.2	0.923	1.215

The first-order plots of ln f_3 and ln f_3 (corrected) vs. time are given in Figs. 1 and 2, respectively. Correlation coefficients ≥0.996 were obtained for the plots. The second-order rate constants were obtained by dividing the corrected pseudo-first-order constants by the initial base concentration, and are listed in Table 1.

Exo *Exchange*

The data for *exo* exchange in **2**, **3**, and **4** were obtained by adding the solid ketone (0.020–0.035 g) to 2.0 ml of a solution composed of 60% dioxane and 40% $NaDCO_3$–NaOD buffer (p*D* 10.84) which had been equilibrated in the constant temperature bath. The vial was shaken and aliquots were removed with a rubber-capped 9-in. Pasteur glass pipette and quenched in K_2HPO_4 buffer (1 ml, p*H* 6.5) – ether (2 ml). The aqueous solution was extracted using the pipette by rapidly drawing in and expelling the total solution five or six times. The ether layer was dried, concentrated on the rotatory evaporator, and the concentrate was introduced into the mass spectrometer. The pseudo-first-order rate constants were obtained by computer analysis of the d_0 decay. A representative first-order plot for *exo* exchange in dione **4** is given in Fig. 3. The correlation coefficients were ≥0.996. The first-order plot for *exo* exchange in **1** in the same medium is given in Fig. 4. Since the pseudo-first-order rate constant for *exo* exchange in **1** in the dioxane–buffer medium is 2.15×10^{-6} s^{-1} (average of two determina-

tions 2.09×10^{-6} s^{-1} and 2.21×10^{-6} s^{-1} (see Fig. 4)) and the second-order rate constant is 3.85×10^{-2} M^{-1} s^{-1}, the effective [$^{-}$OD] is established as 5.58×10^{-5}. Division of the pseudo-first-order rate constants, 2.57×10^{-3}, 3.20×10^{-3}, and 1.57×10^{-3} s^{-1} (average of at least two determinations, average deviation $<10\%$) for **2**, **3**, and **4** by 5.58×10^{-5} establishes the second-order rate constants for **2**, **3**, and **4**, as 46.1, 57.3, and 28.1 M^{-1} s^{-1}, respectively.

Acknowledgements

We thank the National Research Council of Canada for financial support and Professor T. T. Tidwell for rate data.

1. N. H. Werstiuk and R. J. Taillefer. Can. J. Chem. **48**, 3966 (1970).
2. S. Banerjee and N. H. Werstiuk. Can. J. Chem. **54**, 678 (1976).
3. N. H. Werstiuk and S. Banerjee. Can. J. Chem. **55**, 173 (1977).
4. N. H. Werstiuk, R. J. Taillefer, and S. Banerjee. Can. J. Chem. This issue.
5. A. Nickon and J. L. Lambert. J. Am. Chem. Soc. **84**, 4664 (1962).
6. A. Nickon, J. L. Lambert, and J. E. Oliver. J. Am. Chem. Soc. **88**, 2287 (1966).
7. A. Nickon, J. Kwasnik, T. Swartz, R. O. Williams, and J. B. DiGiorgio. J. Am. Chem. Soc. **87**, 1615 (1965).
8. D. H. Hunter, A. L. Johnson, J. B. Stothers, A. Nickon, J. L. Lambert, and D. F. Covey. J. Am. Chem. Soc. **94**, 8582 (1972).
9. A. L. Johnson, N. W. Peters, M. B. Rampersad, and J. B. Stothers. Can. J. Chem. **52**, 4143 (1974).
10. A. J. Johnson, J. B. Stothers, and C. T. Tan. Can. J. Chem. **53**, 212 (1975).
11. D. H. R. Barton and N. H. Werstiuk. J. Chem. Soc. C, 148 (1968).
12. A. F. Thomas and B. Willhalm. Tetrahedron Lett. 1309 (1965).
13. A. F. Thomas, R. A. Schneider, and J. Meinwald. J. Am. Chem. Soc. **89**, 68 (1967).
14. T. J. Flautt and W. F. Erman. J. Am. Chem. Soc. **85**, 3212 (1963).
15. K. L. Williamson. J. Am. Chem. Soc. **85**, 516 (1963).
16. A. Streitwieser, Jr., R. A. Caldwell, and W. R. Young. J. Am. Chem. Soc. **91**, 529 (1969).
17. F. C. Brown, E. Casadevall, P. Metzger, and D. G. Morris. Third IUPAC Conf. Phys. Org. Chem., La Grande Motte, September, 1976. Abstr. p. 83.
18. D. E. Bays, G. W. Cannon, and R. C. Cookson. J. Chem. Soc. B, 885 (1966).
19. J. Meinwald, P. G. Gassman, and J. J. Hurst. J. Am. Chem. Soc. **84**, 3722 (1962).
20. J. Meinwald, J. K. Crandall, and P. G. Gassman. Tetrahedron, **18**, 815 (1962).

Can. J. Chem. Downloaded from www.nrcresearchpress.com by 210.87.254.6 on 09/05/12
For personal use only.

Can. J. Chem. Downloaded from www.nrcresearchpress.com by 210.87.254.42 on 09/05/12
For personal use only.

Canadian Journal of Chemistry

Published by
THE NATIONAL RESEARCH COUNCIL OF CANADA

Journal canadien de chimie

Publié par
LE CONSEIL NATIONAL DE RECHERCHES DU CANADA

Volume 56 Number 9 May 1, 1978

Volume 56 numéro 9 1 mai 1978

Biosynthesis of prodiginines. ^{13}C resonance assignments and enrichment patterns in nonyl-, cyclononyl-, methylcyclodecyl-, and butylcycloheptylprodiginine produced by actinomycete cultures supplemented with ^{13}C-labeled acetate and ^{15}N-labeled nitrate[1]

NANCY N. GERBER

Waksman Institute of Microbiology, Rutgers – The State University of New Jersey, New Brunswick, NJ 08903, U.S.A.

A. GAVIN MCINNES, DONALD G. SMITH, JOHN A. WALTER, AND JEFFREY L. C. WRIGHT

Atlantic Regional Laboratory, National Research Council of Canada, Halifax, N.S., Canada B3H 3Z1

AND

LEO C. VINING

Biology Department, Dalhousie University, Halifax, N.S., Canada B3H 4J1

Received August 26, 1977

NANCY N. GERBER, A. GAVIN MCINNES, DONALD G. SMITH, JOHN A. WALTER, JEFFREY L. C. WRIGHT, and LEO C. VINING. Can. J Chem. **56**, 1155 (1978).

Resonances in the ^{13}C nmr spectra of nonylprodiginine, cyclononylprodiginine, methylcyclodecylprodiginine, and butylcycloheptylprodiginine were assigned using information from the literature, from high resolution spectra and double irradiation experiments, and from ^{13}C–^{15}N couplings observed in samples of nonylprodiginine enriched with ^{15}N. Supplementation of cultures with sodium [1-^{13}C]- and [1,2-^{13}C]acetate gave ^{13}C-enriched prodiginines and the labeling patterns were established from ^{13}C nmr spectra. These indicated that rings A and B were formed in a similar manner to rings A and B in prodigiosin and other prodiginine pigments. Ring C and the C2-alkyl substituent were derived in part from acetate units that were condensed in a linear 12- or 14-carbon chain. The same pattern of acetate assembly has been found in all actinomycete prodiginines examined.

NANCY N. GERBER, A. GAVIN MCINNES, DONALD G. SMITH, JOHN A. WALTER, JEFFREY L. C. WRIGHT et LEO C. VINING. Can. J. Chem. **56**, 1155 (1978).

Utilisant des informations provenant de la littérature, des spectres à haute résolution et des expériences d'irradiation double et faisant aussi appel aux couplages ^{13}C–^{15}N observés dans des échantillons de nonylprodiginine enrichies en ^{15}N, on a fait l'attribution des résonances dans le spectre rmn du ^{13}C de la nonylprodiginine, de la cyclononylprodiginine, de la méthylcyclodécylprodiginine et de la butylcycloheptylprodiginine. L'addition de [1-^{13}C]- et de [1,2-^{13}C]-acétate de sodium au milieu de culture conduit à des prodiginines enrichies en ^{13}C et on a établi les distributions de marquages à l'aide des spectres rmn du ^{13}C. Celles-ci indiquent que les modes de formation des cycles A et B sont semblables à ceux des cycles A et B de la prodigiosine et d'autres pigments de la prodiginine. Par ailleurs le cycle C et les substituants alkyles en C2 proviennent en partie d'unités acétates qui se condensent en chaîne linéaire de 12 ou 14 atomes de carbone. On a trouvé la même distribution d'assemblement des acétates dans toutes les prodiginines d'actinomycène examinées.

[Traduit par le journal]

Introduction

Pigments containing the prodiginine skeleton (**1**, $R_1 = R_2 = R_3 = R_4 = H$) are produced by a restricted group of eubacteria and actinomycetes (1). Although prodigiosin (**1**, $R_1 = CH_3$, $R_2 = (CH_2)_4$-CH_3, $R_3 = R_4 = H$), the main biochrome of *Serratia marcescens*, has a long and interesting history (2, 3), its correct chemical structure was deduced only in

[1]Issued as NRCC 16483.

Can. J. Chem. Downloaded from www.nrcresearchpress.com by 210.87.254.42 on 09/05/12
For personal use only.

recent times (4). The formation of a similar class of bright-red pigments by species of *Streptomyces* was first recognized in 1947 (5) but their relationship to prodigiosin was not clarified until later (6–8). Other representatives of the prodiginine family have since been identified among the colored metabolites produced by *Actinomadura* species (9–12). A noteworthy feature of prodiginines from the actinomycetes is the pattern of alkyl substitution in ring C. Whereas prodigiosin and its congeners from eubacteria possess a methyl substituent at C(2) and differ from one another in the length of the alkyl chain attached to C(3) (1, 13), the actinomycete prodiginines are unsubstituted at C(3) but have an extended alkyl chain 9 or 11 carbons long at C(2). Nonylprodiginine (**1**, $R_1 = (CH_2)_8CH_3$, $R_2 = R_3 = R_4 = H$) has been found only in *Actinomadura* species while undecylprodiginine (**1**, $R_1 = (CH_2)_{10}CH_3$, $R_2 = R_3 = R_4 = H$) is present in *Streptomyces*, *Streptoverticillum*, and *Actinomadura* species (14).

Variation is introduced into the structure of actinomycete prodiginines by attachment of the alkyl chain at a second point to the prodiginine skeleton. A series of cycloprodiginines have been discovered, the first of which, metacycloprodigiosin (**1**, R_1R_3 = 1′,9′-cyclo$(CH_2)_8CHCH_2CH_3$, $R_2 = R_4 = H$), was isolated together with undecylprodiginine in *Streptomyces longisporus ruber* (15). *Streptomyces* and *Streptoverticillium* species also produce the related butylcycloheptylprodiginine (**1**, R_1R_3 = 1′,7′-cyclo$(CH_2)_6$-

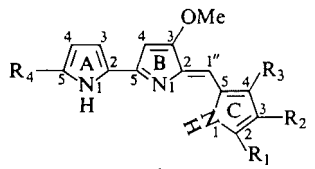

1

$CH(CH_2)_3CH_3$, $R_2 = R_4 = H$), which has hitherto been incorrectly identified as a 2,3-cycloalkyl derivative (1, 14, 16, 17). Neither of these compounds has been observed in *Actinomadura* species, which produce, instead, a series of cyclic derivatives with the alkyl chain attached at C(5) of ring A. These include cyclononylprodiginine (**1**, R_1R_4 = 1′,9′-cyclo$(CH_2)_9$, $R_2 = R_3 = H$) (10), methylcyclooctylprodiginine (**1**, R_1R_4 = 1′,8′-cyclo$(CH_2)_7CHCH_3$, $R_2 = R_3 = H$), ethylcyclononylprodiginine (**1**, R_1R_4 = 1′,9′-cyclo$(CH_2)_8CHCH_2CH_3$, $R_2 = R_3 = H$) (12), and methylcyclodecylprodiginine (**1**, R_1R_4 = 1′,10′-cyclo$(CH_2)_9CH\ CH_3$, $R_2 = R_3 = H$) (11). The latter two have also been found in a *Streptoverticillium* species (14).

Despite a long-standing interest in the biosynthesis of prodigiosin, progress in identifying the biogenetic precursors and their mode of assembly into the unusual pyrryldipyrrylmethene skeleton has been slow. Studies with precursors bearing radioisotope labels showed that proline, glycine, methionine, and acetate were efficiently incorporated into the structure (18) but satisfactory evidence of the labeling pattern was difficult to obtain by chemical dissection. Only with the use of ^{13}C-labeled precursors and development of ^{13}C nmr procedures to analyse their distribution in the metabolite has the biogenesis of prodigiosin been elucidated. Wasserman and his colleagues (19, 20) have shown that proline contributes ring A and carbon B5 of ring B, while acetate supplies carbons B3 and B4 of ring B, as well as C3, C4, C5, and the C3 alkyl substituent of ring C. The methene carbon originates with the hydroxymethyl group of serine, and the adjacent carbon B2 of ring B probably comes from C(2) of this amino acid since C(2) of glycine was a good precursor. In ring C carbon C2 and the adjacent methyl substituent were derived from alanine.

Subsequently Wasserman *et al.* (21) examined the biosynthesis of undecylprodiginine and metacycloprodigiosin in *Streptomyces longisporus ruber*. Whereas rings A and B and the methene carbon were derived from the same precursors as prodigiosin, ring C was formed differently. In the actinomycete pigments carbons C2, C3, C4, and the alkyl substituent came from acetate units, whereas C5 was derived from the methylene group of glycine. In each of the metabolites the incorporation of label from [1-^{13}C]- and [2-^{13}C]acetate suggested that a polyketide chain of 14 carbon atoms contributed to the formation of ring C and its attached alkyl substituent. We have examined the incorporation of singly and doubly ^{13}C-labeled acetate into additional actinomycete prodiginines to ascertain whether ring C was formed with similar participation from acetate units, and whether the acyl chain of representative cyclic and acyclic compounds was formed from acetate units assembled according to a common pattern. The distribution of ^{13}C labels in the prodiginines was determined by ^{13}C nmr spectrometry.

Assignment of Resonances

Assignment of resonances in the natural abundance ^{13}C nmr spectra was based on (*a*) comparison with the ^{13}C chemical shift data for three prodiginines and a number of related pyrrole derivatives reported by Cushley *et al.* (22), (*b*) multiplicities and spacings owing to ^{13}C–H coupling observed in high resolution (hr) spectra (long range couplings were resolved in spectra of cyclononylprodiginine and butylcycloheptylprodiginine only), and (*c*) satellites due to C–N coupling which appeared in proton noise decoupled (pnd) spectra of nonylprodiginine labeled with ^{15}N.

TABLE 1. ^{13}C Chemical shifts (δ_C TMS) and ^{13}C–H coupling constants ($^nJ_{CH}$ Hz, in parentheses) of prodiginines[a]

Carbon	NP[b]	CNP	MCDP	BCHP
A2	128.2[c]	127.4 (7.5, 7.5) (t)	127.3	128.8 (7, 7, 7) (dt)
A3	112.9	112.7 (169.4, 4.2) (dd)	112.8	112.0 (169.4, 4.5, 6.9) (ddd)
A4	110.1	108.9 (170.1, 3.7) (dd)	106.8	109.7 (171.0, 3.7, 7.8) (ddd)
A5	122.9	137.5(m)	142.9	122.3 (184.3, 8.2, 8.2) (dt)
B2	138.5	141.2 (8) (d)	142.9	137.0 (8.1) (d)
B3	169.1	168.1 (1.2, 3.1, 4.3) (ddq)	167.9	168.5(m)
B4	95.7	94.7 (171.8) (d)	95.1	95.2 (171.7) (d)
B5	160.3	158.4 (5.1) (d)	158.8	158.9 (5.0) (d)
C2	144.7	141.0(m)	141.4	145.1 (bm)
C3	108.6	108.5 (170.0, 3.7) (dd)	109.0	114.1 (169.4) (dm)
C4	121.2	118.0 (170.3, 2, 4) (ddd)	118.2	141.7 (bm)
C5	128.4[c]	130.0 (4, 8, 8) (dt)	129.8	126.6 (7.5) (d)
1″	116.0	114.2 (158.4) (d)	114.2	113.0 (153.2) (d)
OCH_3	58.3	58.2 (144.8) (q)	58.2	59.3 (144.8) (q)
1′	27.7	27.9[d]	27.9[d]	25.6[d]
2′	29.3–29.6	27.6[d]	28.3[d]	27.0[d]
3′	29.3–29.6	29.7[d]	29.8[d]	29.2[d]
4′	29.3–29.6	28.2[d]	29.2[d]	30.9[d]
5′	29.3–29.6	26.3[d]	28.3[d]	29.0[d]
6′	29.3–29.6	28.9[d]	26.0[d]	31.4
7′	31.9	28.1[d]	27.3[d]	36.9(d)
8′	22.7	27.2[d]	28.1[d]	38.6
9′	14.1	27.2[d]	37.2	30.5
10′			32.9	23.0(t)
11′			20.2	14.2(q)

[a]Data for the free base in chloroform-*d*; abbreviations are NP = nonylprodiginine, CNP = cyclononylprodiginine, MCDP = methylcyclodecylprodiginine, BCHP = butylcycloheptylprodiginine.
[b]Chemical shifts for carbons 1′ through 9′ in the spectrum of the salt form in dimethylsulfoxide-d_6 were 27.7, 28.3,[d] 28.7,[d] 28.9,[d] 28.7,[d] 28.8, 31.4, 22.2, 14.0.
[c]Assignments may be reversed but were unambiguous in the salt form (A2, δ_C 121.8; C5, δ_C 126.4).
[d]These assignments are tentative only.

Data available on ^{13}C–H and ^{13}C–^{15}N couplings in pyrrole (23, 24) were useful in interpreting the splitting patterns and spacings observed in (*b*) and (*c*). A number of assignments were later confirmed by the direct and long range ^{13}C–^{13}C coupling apparent in spectra of material which had incorporated [1-^{13}C]- and [1,2-^{13}C]acetate. Spectra were obtained for both the free bases and the perchlorate salts. Because the chemical shift trends were similar to those observed by Cushley *et al.* (22), the spectral data for only the free bases are summarized in Table 1.

The ^{13}C signal at lowest field in the spectra of all the prodiginines was assigned to carbon B3, which would be strongly deshielded by the directly bonded methoxyl substituent. In the hr spectrum of cyclononylprodiginine this signal was present as a doublet of doublets of quartets, due to coupling with the B4, 1″, and OCH_3 protons but the corresponding multiplet was not resolved in the spectrum of butylcycloheptylprodiginine. Satellite signals ($^2J_{CN}$ = 5.9 Hz) accompanied this resonance in spectra of ^{15}N-labeled nonylprodigine, consistent with a location β to the pyrrole nitrogen. The signal for B4 appeared at highest field in the aromatic region for all compounds, and was also accompanied by satellites ($^2J_{CN} \approx 6$ Hz) when ^{15}N label was present. The resonances from B2 and B5 displayed a coupling to nitrogen ($J_{CN} \approx 14$ Hz) appropriate to carbons α to a pyrrole nitrogen and these carbons were also long range coupled ($^3J_{CH}$) to single protons by 8 and 5 Hz in cyclononylprodiginine and butylcycloheptylprodiginine. Furthermore, in the spectra of nonylprodigine and cyclononylprodiginine strongly enriched from [1-^{13}C]acetate the extent to which the B3 and B5 lines were resolved permitted a two-bond coupling of 11.0 Hz between these carbons to be observed. When these compounds were derived from doubly labeled acetate B3 and B4 were directly coupled, as were B5 and A2.

Assignments for the carbons in rings A and C in nonylprodiginine, based on those for undecylprodiginine (22), were confirmed by the directly bonded C–H couplings in hr spectra and the C–N satellites ($^1J_{CN}$) observed for the carbons α to nitrogen in the spectrum of the ^{15}N-enriched compound (A2, 14.4; A5, 14.4; C2, 13.5; C5, 13.5 Hz). Further support for the assignments came from the pnd spectrum of material derived from doubly labeled acetate, where direct ^{13}C–^{13}C coupling was observed between the adjacent carbons A4,A5 and C3,C4.

Can. J. Chem. Downloaded from www.nrcresearchpress.com by 210.87.254.42 on 09/05/12
For personal use only.

TABLE 2. Peak height ratios from the mass spectra of labeled prodiginines[a]

Experiment	Prodiginine(P)	Precursor	Observed peak height (%M)					
			$M+1$	$M+2$	$M+3$	$M+4$	$M+5$	$M+6$
1	NP	$Na^{15}NO_3$	156	104	39	—	—	—
	CNP	$Na^{15}NO_3$	121	77	25	—	—	—
2	NP	$CH_3{}^{13}COONa$	39	19	15.5	12	9	—
	CNP	$CH_3{}^{13}COONa$	35	12.5	9.0	7.0	4.5	—
3	NP	DC_3COOD	45.7	16.3	17.9	14.7	7.7	2.8
	CNP	DC_3COOD	45.6	15.2	6.8	3.2	1.0	0
	MCOP	DC_3COOD	41.7	16.9	40	37	19	7.2
4*a*	BCHP[b]	DC_3COOD	35.5	8.2	4.8	3.1	3.3	1.6
4*b*	BCHP[b]	$CH_3{}^{13}COOH$	41.3	23.5	10.2	4.1	1.5	0

[a]The theoretical values of $M+1$ and $M+2$ for the unenriched pigments are: NP, CNP, and MCOP: 26.4, 0.2; BCHP: 28.6, 0.2, respectively.
[b]These two samples were obtained from parallel cultures grown from the same inoculum. MCOP is methylcyclooctylprodiginine; other abbreviations are given in the footnote to Table 1.

The spectra of cyclononylprodiginine and methylcyclodecylprodiginine differed from that of nonylprodiginine mainly in the substantial deshielding of A5 ($\approx$15 ppm for the former and $\approx$20 ppm for the latter) by the alkyl chain. The splittings due to long range coupling in the hr spectrum of cyclononylprodiginine were of the size and multiplicity expected for the pyrrole nucleus (23) with allowance for the substitution patterns in the three rings. Also, in cyclononylprodiginine subsequent labeling experiments with doubly labeled acetate once again supported the assignment of the adjacent pairs A4,A5 and C3,C4.

The chemical shifts for the carbons in the prodiginine skeleton of butylcycloheptylprodiginine were similar in most respects to those reported by Cushley *et al.* for metacycloprodiginine (22), and assignments were supported by the long range couplings observed in the hr spectrum of the free base. Splitting patterns for the carbons in ring A were in agreement with the pyrrole nucleus having a substituent only at position 2. On the other hand, signals for ring C showed that only C3 was directly bonded to a proton, and this proton in turn was long range coupled to C5 by 7.5 Hz.

The signal for the olefinic methene bridge carbon (C-(1″)) was readily identified in each spectrum by the direct C–H coupling value which ranged from 153.2 to 162.2 Hz. In the free base and salt forms of nonylprodiginine, and the salt forms cyclononylprodiginine and methylcyclodecylprodiginine, this signal appeared in the range δ_C 115.9 to 116.6. However, in the free base form of the latter compounds the signal was shifted upfield to δ_C 114.2, and in both forms of butylcycloheptylprodiginine to about δ_C 113.

Adjacent labeling by [1,2-^{13}C]acetate and the labeling of alternate positions by [1-^{13}C]acetate, considered with expected chemical shift trends (25) and signal multiplicities in the hr and off-resonance decoupled spectra, permitted some of the resonances arising from the open or cyclized alkyl side chains of the prodiginines to be assigned (see footnotes to Tables 1 and 2).

Incorporation of Labeled Acetate

Conditions for optimum incorporation of ^{13}C-labeled precursors were developed using [$^2H_4$]acetic acid as the supplement and mass spectrometry for analysis. All of the prodiginines gave strong molecular ions, and a test of the analytical method in which three different samples of unenriched methylcyclodecylprodiginine were repeatedly examined at the highest feasible vacuum to minimize ion-molecule reactions gave average peak heights for $M+1$ of 28.4 $\pm$ 0.5, 28.2 $\pm$ 0.5, and 28.3 $\pm$ 0.9% relative to M. The theoretical value for $C_{25}H_{33}ON_3$ is 28.6%. The ratios of the peak heights of various enriched samples (Table 2) indicates that high incorporations were achieved. Experiments with actinomadurae showed that multiple additions of acetate to cultures gave no better incorporation than one addition after 2–3 days growth, when pigment was first observable. Optimum enrichments were obtained when the cultures were harvested 2 or 3 days after acetate addition, a time well before the maximum yield of pigments was reached. The mass spectral data for the prodiginine pigments in Table 2 showed two kinds of peak height distribution in the $M+1$ to $M+6$ range. All of the pigments labeled with [1-^{13}C]acetate or sodium [^{15}N]nitrate, and cyclononylprodiginine labeled with [$^2H_4$]acetic acid, showed a continuous decrease in peak height at increasing mass values. In contrast nonylprodiginine, methylcyclooctylprodiginine or butylcycloheptylprodiginine labeled by [$^2H_4$]-acetic acid gave an irregular pattern. Since the latter

Can. J. Chem. Downloaded from www.nrcresearchpress.com by 210.87.254.42 on 09/05/12
For personal use only.

Can. J. Chem. Downloaded from www.nrcresearchpress.com by 210.87.254.42 on 09/05/12
For personal use only.

pigments all have a methyl group which is probably derived from the 'starter' unit of a chain biosynthesized from acetate and polymalonate, it seems possible to detect this type of end methyl group by examining the mass spectrum of a pigment which has incorporated [$^2H_4$]acetic acid. This is useful for very minor components such as methylcyclooctylprodiginine, which could not be obtained in sufficient quantity for ^{13}C nmr.

The incorporation of ^{13}C atoms into prodiginines by cultures supplemented with sodium [1-^{13}C]acetate is shown in Table 3 and the results are summarized in Fig. 1. Enrichment of the carbon at B3 parallels the results obtained earlier with prodigiosin, undecylprodiginine and metacycloprodiginine (19–21). Substantial incorporation also occurred at carbon atom A5 of ring A. This can be understood in terms of the formation of ring A from proline via α-ketoglutarate, which is derived from acetate by reactions of the Krebs cycle. The ring-A incorporation is high compared with that reported for prodigiosin (20) but comparable to that obtained for undecylprodiginine and metacycloprodiginine where proline was also shown to be the progenitor of ring A and carbon B5 (21). Differences could be due to distinctive metabolic patterns for acetate in *S. marcescens* and the actinomycetes but it is more likely that they were caused by differences in the proline content of media used. Media containing soy bean meal or a proline supplement, such as were used for the production of butylcycloheptylprodiginine and methylcyclodecylprodiginine, respectively, gave substantially lower incorporation of acetate into ring A carbons.

TABLE 3. Enrichment of ^{13}C in prodiginines from cultures supplemented with sodium [1-^{13}C]acetate[a]

Carbon	NP[b]	CNP[b]	MCDP	BCHP
A5	4.7±1.2	4.4±1.3		
B3	19±4	11±3	7.9±1.2	1.3±0.5
B5	3.2±1.0			
		10±2[c]		
C2	17±4		6.2±1.0	2.2±0.7
C4	9.2±2.3		5.7±1.3	3.4±0.7
2′	8±2	6.7±1.5	4.2±1.0	4.8±0.7
4′	6±1.5	6.3±1.5	3.9±1.0	4.4±0.6
6′	6±1.5	6.3±1.5	4.6±1.1	4.8±0.7
8′	18±4	7.8±2	2.9±0.8	4.3±0.6
10′			5.0±1.2	4.4±0.6

[a]^{13}C concentrations at quaternary carbons A2, A5, B2, B3, B5, C2, C5 estimated from spectrum of salt; concentrations at carbons in aliphatic chain estimated from spectrum of free base (these resonances overlapped in spectrum of salt); remaining enrichments of carbons bonded to ^1H are averages from both salt and free base. The calculation of enrichments and errors followed the procedure discussed in ref. 27. Assignments for carbons 2′,4′-(NP, CNP); 2′,4′,6′(MCDP); and 2′,4′,6′,8′(BCHP) are tentative only, and may be interchanged. Abbreviations for the prodiginines are given in footnote [a], Table 1. Sodium [1-^{13}C]acetate was 90% enriched with ^{13}C.

[b]Couplings ($^2J_{CC}$) of 11.0 Hz were observed between carbons B3 and B5.

[c]Resonances overlap. The spectrum of the free base suggests that only C2 is enriched.

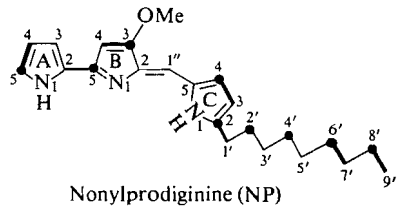

Nonylprodiginine (NP)

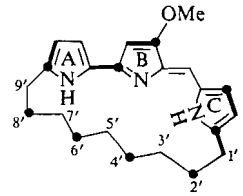

Cyclononylprodiginine (CNP)

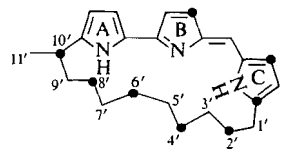

Methylcyclodecylprodiginine (MCDP)

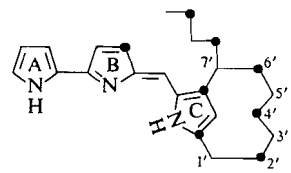

Butylcycloheptylprodiginine (BCHP)

FIG. 1. Incorporation of [1-^{13}C]- and [1,2-^{13}C]acetate into the actinomycete prodiginines. Only those carbon atoms and carbon atom pairs shown to be labeled by ^{13}C nmr spectroscopy are identified.

The pattern of enrichment in the acyl substituents of each prodiginine is similar to that observed by Wasserman and coworkers for the *S. longisporus ruber* pigments and implies that these compounds are made by a common pathway. This conclusion is supported by the results from supplementing a culture of *Actinomadura* strain R39 with [1,2-^{13}C]acetate (Table 4 and Fig. 1). Insofar as the couplings between carbons of the alkyl chain can be distinguished, they show that C2, C3, C4, and the alkyl substituent are assembled as a polyketide chain derived by head-to-tail condensation of acetate units. Besides confirming signal assignments deduced independently, these results also support the expected pattern of acetate incorporation into ring A and carbon B5 via the Krebs cycle and proline, and they establish that an intact acetate unit is involved in the formation of ring B.

Experiments with mutant strains of *S. marcescens* have indicated that the final stage in prodigiosin

Can. J. Chem. Downloaded from www.nrcresearchpress.com by 210.87.254.42 on 09/05/12
For personal use only.

biosynthesis is the coupling of a dipyrrylaldehyde intermediate containing rings A and B and the methene bridge carbon with a monopyrrole derivative consisting of ring C and its substituents (3). Each intermediate is synthesized independently, and it is likely that the pathway leading to the dipyrrylaldehyde in the actinomycetes is the same as that in *S. marcescens*. A plausible mechanism is suggested by the well-known route for sphingosine biosynthesis in which the pyridoxal phosphate- and enzyme-mediated condensation of palmityl coenzyme A and serine is accompanied by loss of the amino acid carboxyl group. The pyrrolidyl-β-keto propionate derivative which would be required in a comparable synthesis of the dipyrrylaldehyde may also be an intermediate in the formation of detoxinine (**2**) which is a component of detoxin D (26).

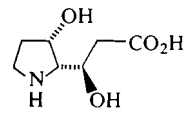

2

The actinomycetes and *S. marcescens* clearly differ in the route by which the monopyrrole intermediate is formed, although here, too, some common elements can be seen. Formation of this intermediate may parallel the route by which δ-aminolevulinate is made from glycine and succinyl coenzyme A in a reaction also catalyzed by a pyridoxal phosphate-requiring enzyme (Fig. 2*a*). Assembly of the monopyrrole derivative of the actinomycete prodiginines would proceed by an initial condensation between C(2) of glycine and the thioester carbonyl of a β-ketoacylcoenzyme A intermediate (Fig. 2*b*) and be

TABLE 4. Incorporation of [1,2-^{13}C]acetate into prodiginines by *Actinomadura* strain R39[a]

Carbon No.	Nonylprodiginine perchlorate		Cyclononylprodiginine perchlorate	
	$^1J_{CC}$	Enrichment	$^1J_{CC}$	Enrichment
A4	60.6	1.07 ± 0.12	61.6	0.71 ± 0.06
A5	60.0	1.12 ± 0.12	61.9	1.18 ± 0.07
A2	76±1	0.28 ± 0.03	75.4	0.34 ± 0.07
B5	76±1	0.30 ± 0.03	75.4	0.38 ± 0.07
B3	68.6	1.93 ± 0.12	69.4	1.63 ± 0.07
B4	68.4	0.74 ± 0.04	69.6	0.87 ± 0.07
C3	54.7	1.16 ± 0.11	54.7	1.21 ± 0.07
C4	55.1	1.26 ± 0.11	54.4	1.26 ± 0.07
C2	47.2	1.58 ± 0.29	47.6	
1′	47.8	0.92 ± 0.05	—	0.80 ± 0.07
6′	34.4	1.34 ± 0.15	—	
7′	34.4		—	
8′	34.7	1.72 ± 0.16	—	
9′	34.7	1.53 ± 0.14	—	

[a]Calculation of enrichments followed the procedure discussed in ref. 27. Enriched (90% ^{13}C) and natural abundance acetate were admixed in the ratio of 1:4 before feeding to cultures.

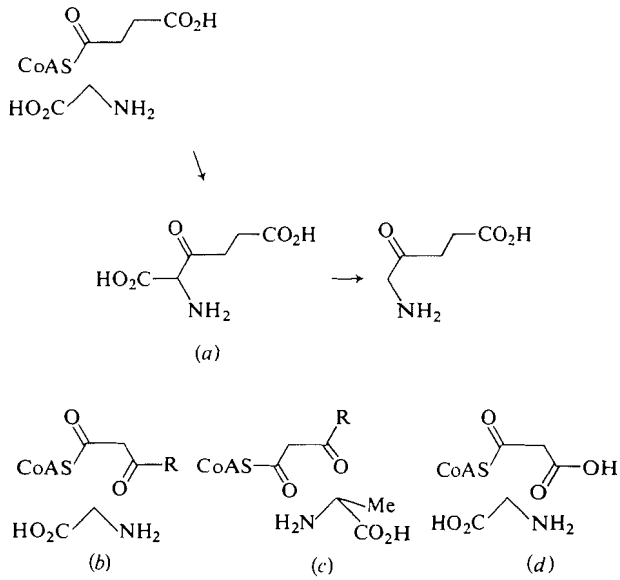

FIG. 2. Levulinic acid biosynthesis (*a*) and possible relationships with the formation of the monopyrrole intermediates of actinomycete prodiginines (*b*) and prodigiosin (*c*), and with pyrrole (*d*).

followed by decarboxylation and cyclization. In *S. marcescens* an initial condensation between C(2) of alanine and the β-carbonyl of a β-ketoacyl coenzyme A intermediate (Fig. 2*c*), followed by decarboxylation and cyclization, would account for the monopyrrole component of prodigiosin. Co-production of this component and pyrrole by mutant 9-3-3 of *S. marcescens* (28) suggests that the enzyme might also accept malonylcoenzyme A as the acylthioester intermediate (Fig. 2*d*).

The evidence from our experiments, together with that already reported for the biosynthesis of undecylprodiginine and metacycloprodiginine indicates that all actinomycete pigments are formed from 12- or 14-carbon chain precursors. Whether these are fatty acid or polyketide derivatives remains to be determined, but it is likely, from their common pattern of biogenesis, that the entire group of open-chain and cyclic metabolites is derived by modification of one biosynthetic sequence. A plausible route is suggested in Fig. 3. Co-production of cyclononylprodiginine and methylcyclooctylprodiginine by *A. madurae*, and of methylcyclodecylprodiginine and ethylcyclononylprodiginine by *A. pelletieri*, favour penultimate unsaturation in the alkyl chain and cyclization to ring A at alternative double-bond carbons as the mechanism by which these compounds are formed. In contrast, the compounds with cyclic alkyl substituents on ring C are not co-produced and the alkyl carbons at the point of attachment would be separated, rather than

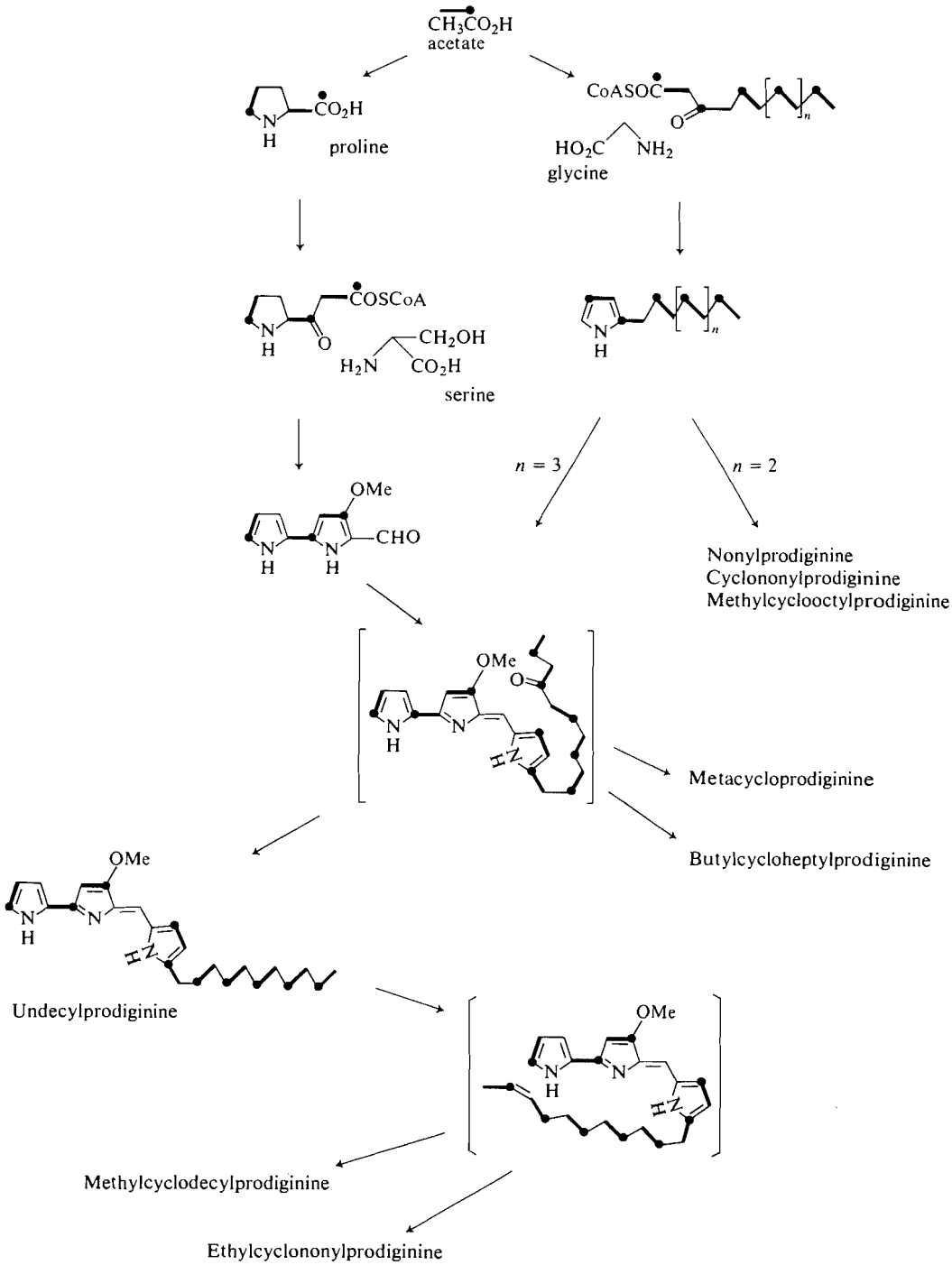

FIG. 3. A possible biogenetic route to the actinomycete prodiginines.

adjacent, in a common precursor. Although they may feasibly be made via unsaturated alkyl intermediates, we suggest here that they are formed by condensation at the alternative methylene groups activated by a residual C(8′) polyketide carbonyl.

Experimental

Cultures and Production of Prodiginines

Nonylprodiginine and cyclononylprodiginine were produced by *Actinomadura madurae* strain R39; methylcyclodecylprodiginine was obtained from *Actinomadura pelletieri*

Can. J. Chem. Downloaded from www.nrcresearchpress.com by 210.87.254.42 on 09/05/12
For personal use only.

Can. J. Chem. Downloaded from www.nrcresearchpress.com by 210.87.254.42 on 09/05/12
For personal use only.

strain 610. The source and methods for cultivation have been reported elsewhere (9, 12). Strain R39 in ref. 12 is the same as strain 953 in refs. 9 and 10. For both actinomadurae the production medium contained Cerelose (a commercial grade of glucose, 1%), yeast extract (Difco, 0.2%), sodium nitrate (0.4%), magnesium sulfate heptahydrate (0.05%), potassium chloride (0.05%), ferrous sulfate heptahydrate (0.001%), and calcium carbonate (0.2%). Seed cultures of the actinomadurae were grown on a medium containing soybean meal (49% solvent extracted soybean meal, Central Soya, Bellevue, Ohio, 1%), Cerelose (2%), peptone (Wilson Co., meat peptone 851C, 1%), sodium chloride (0.5%), and sodium acetate trihydrate (1.36%). Seed cultures were used as soon as they were well grown and pigmented; their age varied from four to seven days.

Butylcycloheptylprodiginine was produced by *Streptoverticillium sp.* 26-1 (1) grown on the soybean medium described above without the sodium acetate. Seed cultures were grown on yeast–dextrose medium (12) and were used when 2 days old.

Isotopic Labeling

Sodium [1-^{13}C]- and [1,2-^{13}C]acetate, each 90% enriched, sodium [^{15}N]nitrate, 95% enriched, and [$^{2}H_4$]acetic acid, 99.5% enriched, were purchased from Merck, Sharp and Dohme, Pointe Claire, Que. They were sterilized as aqueous solutions by autoclaving and added aseptically to cultures when pigment production was first noticed. This was at 2 days for *Actinomadura* R-39 and *Streptoverticillium sp.* 26-1 and at 3 days for *Actinomadura* 610. A total of 1-ℓ culture volume was used for the labeling experiments with the actinomadurae and 200 ml for the streptoverticillium. Labeled acetate was added to a concentration of 500 mg/ℓ. The [1-^{13}C] species was used at 90% enrichment but sodium [1,2-^{13}C]acetate was diluted by a factor of 5 before use. Glycine (1.5 g/ℓ) and proline (2.3 g/ℓ) were added with the acetate to *Actinomadura* sp. 610.

Sodium [^{15}N]nitrate was used in place of the normal unenriched medium component but at a lower concentration (0.1%); unenriched sodium acetate (1.36 g/ℓ) was added to these cultures at 3 days and cultures were harvested at 6 days.

Isolation of Prodiginines

In general the extraction and isolation procedures paralleled those used earlier (1, 12). The actinomadurae cultures were killed after 4–6 days growth by adding chloroform (25 ml) to each flask and shaking for 24 h thereafter. Filter aid (Celite) was added, the mixture filtered and the chloroform layer separated. Pigment remaining in the residual cell material was extracted with acetone and transferred to chloroform after diluting the acetone with water. The combined and evaporated chloroform extracts were dissolved in benzene and chromatographed on a column of previously water-washed and air-dried alumina. The amount of pigment in solution was measured spectrophotometrically (12) and about 1 g of alumina was used for each milligram present. Prodiginine-containing fractions were combined and rechromatographed on silica gel using about 0.5 g of absorbent for each mg of pigment. The column was irrigated with bicarbonate-washed chloroform containing an increasing concentration of ethyl acetate. All eluate fractions were monitored by thin layer chromatography (9, 12) since the separation of components on silica columns was not always clearly visible. The prodiginines were recovered by evaporation and crystallized as perchlorate salts from ethanol by adding a slight excess of 0.7% perchloric acid.

For the streptoverticillium, killing with chloroform and the use of filter aid were omitted. Additional pigment was obtained from cellular material by a second extraction in which acetone – 10% hydrochloric acid (1:1) was used.

Mass Spectrometry

Mass spectra were obtained with a Hitachi model RMU-6 instrument. A small pure sample of pigment in free base form was adsorbed on to a diatomaceous earth gas chromatography support by evaporation of a carbon tetrachloride solution. This sample was placed in the direct inlet of the instrument and the spectrum obtained at the highest vacuum (5.7×10^{-7} Torr) and lowest temperature (usually about 250°C) possible.

^{13}C Nuclear Magnetic Resonance Spectrometry

Spectra were recorded with a Varian Associates XL-100/15 Fourier transform spectrometer under the following conditions: frequency 25.16 MHz, acquisition time 1.6 or 3.2 s (data accuracy ± 0.3 or ± 0.15 Hz), spectral width 5120 Hz, flip angle 40°, internal ^{2}H lock to solvent, temperature about 30°C, internal reference to tetramethylsilane. The procedure for calculation of enrichment and estimation of the error is discussed in ref. 27.

Spectra of cyclononyl-, methylcyclodecyl-, and butylcycloheptylprodiginines were obtained from both the salt (in DMSO-d_6) and free-base (in $CDCl_3$) forms of the materials. More resonances of the aliphatic chain carbons were resolved in spectra of the free bases than in spectra of the salts. However, intensity measurements for resonances of quaternary carbons in the bases were less reliable as their spin–lattice relaxation times were much greater than were those of the salt form. This is almost certainly due to the greater viscosity of the salt solutions in DMSO-d_6. Consequently, the enrichments for quaternary carbons reported in Table 3 were obtained from the salts, those for aliphatic chain carbons from the free bases, and those for other carbons bonded to hydrogen from both salts and free bases. Enrichments for nonylprodiginine were measured from the spectrum of the salt only.

Pigments were prepared in free base form by diluting the dimethyl sulfoxide-d_6 solution of their salt used for nmr analysis with 1 *N* ammonium hydroxide and extracting with methylene chloride. The organic solution was washed with water to remove dimethyl sulfoxide, then in some cases with a 10^{-3} *M* solution of ethylenediamine tetraacetic acid to remove any paramagnetic metal ion impurities.

Acknowledgments

We thank Mrs. E. Fekete for valuable technical assistance. This work was partially supported by a Dalhousie University research associateship (to J.L.C.W.) and by research grants from the National Science Foundation (Grant GB 41631), the National Research Council of Canada (to L.C.V.), and Merck-Frosst Laboratories, Pointe Claire, Quebec (to L.C.V.).

1. N. N. GERBER. Crit. Rev. Microbiol. **3**, 469 (1974).
2. E. R. L. GAUGHRAN. Trans. N.Y. Acad. Sci. Ser. II, **31**, 3 (1969).
3. R. P. WILLIAMS and W. R. HEARN. In Antibiotics. Vol. II. *Edited by* D. Gottlieb and P. D. Shaw. Springer Verlag, New York, NY. 1967. pp. 410 and 449.
4. H. H. WASSERMAN, J. E. MCKEON, L. SMITH, and P. FORGIONE. J. Am. Chem. Soc. **82**, 506 (1960).
5. H. BROCKMANN and H. PINI. Naturwissenschaften, **34**, 190 (1947).

6. F. ARCAMONE, A. DIMARCO, M. GHIONE, and T. SCOTTI. G. Microbiol, **4**, 77 (1957).
7. H. H. WASSERMAN, G. C. RODGERS, JR., and D. D. KEITH. Chem. Commun. 825 (1966).
8. K. HARASHIMA, N. TSUCHIDA, and J. NAGATSU. Agric. Biol. Chem. **30**, 309 (1966).
9. N. N. GERBER. Appl. Microbiol. **18**, 1 (1969).
10. N. N. GERBER. Tetrahedron Lett. 809 (1969).
11. N. N. GERBER. J. Antibiot. **24**, 636 (1971).
12. N. N. GERBER. J. Heterocycl. Chem. **10**, 925 (1973).
13. N. M. GHANDI, J. NAZARETH, P. V. DIVEKAR, H. KOHL, and N. J. DE SOUZA. J. Antibiot. **26**, 797 (1973).
14. N. N. GERBER and M. P. LECHEVALIER. Can. J. Microbiol. **22**, 658 (1976).
15. H. H. WASSERMAN, G. C. RODGERS, and D. D. KEITH. J. Am. Chem. Soc. **91**, 1263 (1969).
16. N. N. GERBER. J. Antibiot. **28**, 194 (1975).
17. N. N. GERBER and D. P. STAHLY. App. Microbiol. **30**, 807 (1975).
18. W. K. TANAKA, L. B. DE MEDINA, and W. R. HEARN. Biochem. Biophys. Res. Commun. **46**, 731 (1972).
19. R. J. CUSHLEY, D. R. ANDERSON, S. R. LIPSKY, R. J. SYKES, and H. H. WASSERMAN. J. Am. Chem. Soc. **93**, 6284 (1971).
20. H. H. WASSERMAN, R. J. SYKES, P. PEVERADA, C. K. SHAW, R. J. CUSHLEY, and S. R. LIPSKY. J. Am. Chem. Soc. **95**, 6874 (1973).
21. H. H. WASSERMAN, C. K. SHAW, R. J. SYKES, and R. J. CUSHLEY. Tetrahedron Lett. 2787 (1974).
22. R. J. CUSHLEY, R. J. SYKES, C. K. SHAW, and H. H. WASSERMAN. Can. J. Chem. **53**, 148 (1975).
23. T. BUNDGAARD, H. J. JAKOBSEN, and E. J. RAHKAMAA. J. Magn. Reson. **19**, 345 (1975).
24. J. M. BRIGGS, E. RAHKAMAA, and E. W. RANDALL. J. Magn. Reson. **11**, 416 (1973).
25. L. P. LINDEMAN and J. Q. ADAMS. Anal. Chem. **43**, 1245 (1971).
26. K. KAKINUMA, N. OTAKE, and H. YONEHARA. Tetrahedron Lett. 2509 (1972).
27. P. CANHAM, L. C. VINING, A. G. MCINNES, J. A. WALTER, and J. L. C. WRIGHT. Can. J. Chem. **55**, 2450 (1977).
28. B. S. DEOL, J. R. ALDEN, and J. L. STILL. Biochem. Biophys. Res. Commun. **47**, 1378 (1972).

Can. J. Chem. Downloaded from www.nrcresearchpress.com by 210.87.254.42 on 09/05/12
For personal use only.

The bromination of 3-arylpropynes: Evidence for phenyl participation at a vinyl cation

JAMES A. PINCOCK AND C. SOMAWARDHANA

Department of Chemistry, Dalhousie University, Halifax, N.S., Canada B3H 4J3

Received August 26, 1977

JAMES A. PINCOCK and C. SOMAWARDHANA. Can. J. Chem. **56**, 1164 (1978).

The bromination of substituted 3-arylpropynes in acetic acid has been examined. The only products obtained are 1,2-dibromo-3-arylpropenes; the stereochemistry of the dibromides is predominantly *trans* except for the 4-methoxy isomer which gives 83% *cis* and 17% *trans*. In the presence of 0.1 *M* lithium bromide all substrates give predominantly *trans* products. Combined with rate studies, these results indicate that these acetylenes react by an unsaturated cyclic bromonium ion except for the 4-methoxy case where phenonium ion stabilization of a vinyl cation is implicated. In the presence of lithium bromide a bromide ion catalyzed addition of molecular bromine (Ad_E3) occurs.

JAMES A. PINCOCK et C. SOMAWARDHANA. Can. J. Chem. **56**, 1164 (1978).

On a étudié la bromation, dans de l'acide acétique, d'aryl-3 propynes substitués. Les seuls produits obtenus sont des dibromo-1,2 aryl-3 propènes; la stéréochimie des dérivés dibromés est principalement *trans* excepté pour l'isomère méthoxy-4 qui donne 83% de *cis* et 17% de *trans*. En présence de bromure de lithium 0.1 *M*, tous les substrats donnent des produits *trans* d'une façon prédominante. Si l'on combine ces résultats avec des études de vitesse, on en déduit que ces acétylènes réagissent par l'intermédiaire d'un ion bromonium cyclique non-saturé excepté dans le cas du méthoxy-4 où il existe une stabilisation d'un radical vinylique par un ion phénomium. En présence de bromure de lithium, il se produit une addition catalysée par l'ion bromure de brome moléculaire (Ad_E3).

[Traduit par le journal]

Introduction

The mechanisms of electrophilic additions to acetylenes have attracted considerable interest in recent years particularly in terms of comparison with the reactions of alkenes (1–3). Much of this work has led to a better understanding of the chemistry of vinyl cations (4, 5). Recent publications by Dubois and co-workers (6, 7) on the addition of molecular bromine to 3-arylpropenes attracted our interest in this respect. Thus as outlined in eq. 1, bromination in chloroform of the unsubstituted isomer gave only 1,2-dibromo-3-phenylpropane whereas the 4-methoxy substrate gave both 1,2-dibromo-3-arylpropane and the rearranged isomer, 1,3-dibromo-2-arylpropane. Moreover, an examination of the kinetics of these reactions revealed rate increases for the resonance electron donating substituents like 4-methoxyl. These results were explained by phenonium ion type participation (**1**) at the developing positive center in the electrophilic addition.

Although rearrangements both across and to the double bond in vinyl cations are now well established

[1] X—$ArCH_2CH{=}CH_2$ $\xrightarrow{Br_2}$ X—$PhCH_2CHBr{-}CH_2Br$ + $CH_2Br{-}CH(X{-}Ph){-}CH_2Br$

X = H	>95%	<5%
X = 4MeO	52%	48%

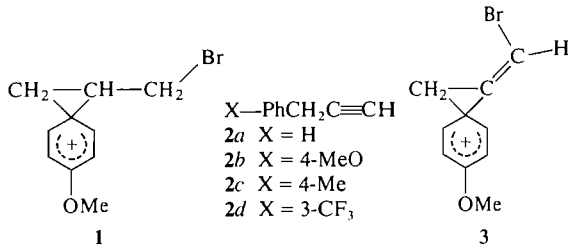

1 **3**

(5, 8–10) phenonium ion participation of this type has never been observed. We wish to report here results for the bromination of 3-arylpropynes (**2***a*–**2***d*) which have yielded excellent evidence for the existence of the ion **3**.

Results and Discussion

Products of the Bromination of 3-Arylpropenes

As outlined in eq. 2 the addition of bromine to the

[2] **2***a*–**2***d* $\xrightarrow[HOAc]{Br_2}$ X—$Ph(Br)C{=}C(H)CH_2Br$ + X—$PhCH_2C(Br){=}C(Br)H$

4*a*–**4***d* **5***a*–**5***d*

four 3-arylacetylenes in acetic acid gave only *cis*- and *trans*-1,2-dibromo-3-arylpropenes (**4***a*–**4***d*, **5***a*–**5***d*). Although solvent incorporated bromoacetates are often obtained in addition to acetylenes (11) none

Can. J. Chem. Downloaded from www.nrcresearchpress.com by 210.87.254.105 on 09/05/12
For personal use only.

Can. J. Chem. Downloaded from www.nrcresearchpress.com by 210.87.254.105 on 09/05/12
For personal use only.

TABLE 1. Product distribution for the bromination of 3-arylpropynes

Substrate		Acetic acid	Acetic acid (0.1 *M* LiBr)
No.	X	*trans–cis*	*trans–cis*
2*b*	4-MeO	17:83	84:16
2*c*	4-Me	91:9	98:2
2*a*	H	99:1	97:3
2*d*	3-CF_3	98:2	98:2

has been detected in these or other simple alkyl acetylenes. The *trans–cis* product distribution as obtained by analytical glc are shown in Table 1. A check of dibromide isomerization under the reaction conditions indicate the products are those of kinetic control.

The structures of the dibromides **4** and **5** were proven in the following way. First they were obviously 1,2-dibromo-3-arylpropenes and not the isomeric 1,3-dibromo-2-arylpropenes as indicated by ultraviolet spectra. In all cases, the absorption maxima and extinction coefficients were similar to substituted toluenes and quite different from that expected for the more highly conjugated arylethene derivatives (see Experimental). The stereochemistry of **4** and **5** was demonstrated by a variety of methods most of which center on the chemistry of the unsubstituted cases, **4***a* and **5***a*. The original difficulty of having only one of the isomers from the bromination reaction was surmounted by the products obtained from the addition of hydrogen bromide to 1-bromo-3-phenylpropyne, eq. 3. Surprisingly, this mixture

[3] $$PhCH_2C{\equiv}CBr \xrightarrow[HOAc]{HBr} 4a(11\%) + 5a(89\%)$$

proved to be much enriched in the *cis* isomer **5***a*. This result is consistent with predominant *anti* addition to the triple bond in both bromination and hydrobromination. Although we have not done any detailed study of the hydrobromination reaction, this result is in agreement with that for other acetylenes (1) and clearly indicates that the two reactions do not proceed via a common cationic intermediate.

With mixtures of the dibromides in hand the two could be easily distinguished without separation. By proton nmr the allylic coupling in the *cis* isomer (1 Hz) was obviously larger than that in the *trans* isomer (<0.5 Hz). This difference has been reported for other dibromo alkene pairs (11, 12). Moreover, the methylene protons of dibromoalkenes appear at higher field for *cis* isomers than for *trans*: 2.50 δ for *cis*-1,2-dibromo-1-hexene vs. 2.60 for *trans* (10); 2.57 δ for *cis*-3,4-dibromo-3-hexene vs. 2.65 for *trans* (10); 4.00 δ for **4***b* (*cis*) vs. 4.20 for **4***a* (*trans*). In the infrared, **4***a* showed a very weak double bond stretch at 1620 cm^{-1} and **4***b* a much stronger one consistent with the higher dipole moment of *cis* isomers. In agreement with this the more polar *cis* isomers always have longer glc retention times. The stereochemistry of the dibromides for the other acetylenes was established by the same reasoning.

The most striking feature of the stereochemistry of the addition products is the change from predominately *anti* addition leading to the *trans* dibromide for **2***a* and **2***d* to predominately *syn* addition for the 4-methoxy isomer **2***b* (note Table 1). Normally additions to simple alkyl acetylenes give exclusively *anti* addition and the suggested intermediate is an unsaturated bromonium ion (11). The results for **2***a* (X = H) and **2***d* (X = 3-CF_3) are in agreement with this proposal as is the observation of the lack of solvent incorporated products. Electrophilic brominations involving bromonium ions in acetic acid are known to give only dibromide products whereas open cations give products resulting from attack by both possible nucleophiles, solvent and the bromide counter ion (11, 13). The observation of both *syn* addition to **2***b*, X = 4-MeO (and to the same extent to **2***c*, X = 4-Me) and lack of solvent containing products logically demands reaction through a mechanism that does not involve an open cation. The cyclic phenonium ion, **3**, seems therefore the best choice, eq. 4. If we assume that

[4] X—Ph—$CH_2C{\equiv}CH$

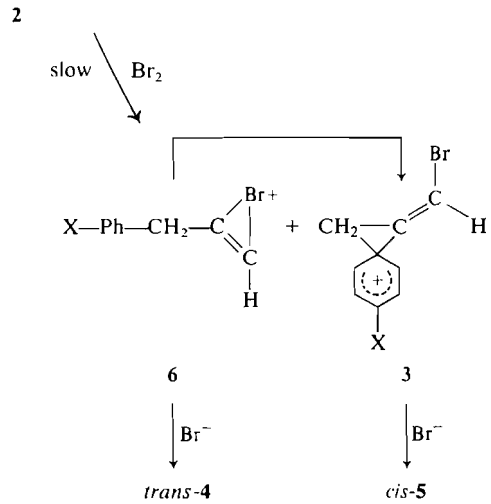

phenonium ion formation occurs *anti* to the original electrophilic attack of bromine, then attack by the nucleophilic bromide ion can give only the *cis* product. The product mixture implies there is a competition between phenonium ion, **3**, and bromonium ion, **6**, bridging as suggested by Dubois for the bromination of the analogous alkenes (6, 7). In contrast to the results for alkenes, attack of bromide ion only

occurs at C(2) to give 1,2-dibromo-3-arylpropenes rather than at both C(2) and C(3). The explanation for this fact must be in terms of kinetic control of product distribution since the conjugated 1,3-dibromo-2-arylpropenes would be expected to be the more stable of the two possibilities. First, these thermodynamic factors will be minimized since the product determining transition state must be an early one for such an exothermic step. Therefore, there should be little development of conjugation in the path leading to the 2-arylpropene from the phenonium ion (**3**) where the aromatic π system is perpendicular to the double bond. Second, bromide ion attack at C(2) (sp^2 hybridized) in **3** should be sterically more favorable than at C(3) (sp^3 hybridized). In the corresponding ion **1** from the bromination of 3-arylpropenes attack at C(3) should be favoured (secondary over tertiary). Finally, the polarizable double bond in **3** with the electron withdrawing bromine atom at C(1) should increase the electrophilicity of C(2) over that of C(3).

If this type of phenonium ion bridging occurs in the rate determining step of the reaction, it should also be revealed by rate increase for the 4-methoxy substrate. The results are discussed in the next section.

Rates of Bromination of 3-Arylpropynes

The kinetics of the addition of molecular bromine to acetylenes in acetic acid are well known to follow the general rate expression, eq. 5 (11). To evaluate the individual rate constants two approaches have been used previously: (*a*) measurement of rates as a function of bromide ion concentration according to

$$[5] \quad -d[Br_2]/dt = (k_2[Br_2] + k_3[Br_2]^2 + k_{Br^-} - [Br_2][Br^-])[\text{acetylene}]$$

[6] where K is the equilibrium constant for tribromide ion formation, eq. 7; (*b*) measurement of rates in the absence of bromide ion and at low bromine

$$[6] \quad k_{obs}(1 + K[Br^-]) = k_2 + k_{Br^-}[Br^-]$$

$$[7] \quad K = [Br_3^-]/[Br^-][Br_2]$$

concentration where only the first term in [5] is kinetically significant. Our first choice was method *a* since this gives information about both the bromide ion catalyzed and the uncatalyzed bromination reactions.

Rates of bromination of the four 3-arylpropynes (**2***a* and **2***d*) were measured in acetic acid with lithium bromide concentrations ranging from 0.10 to 0.02 *M* (ionic strength kept constant at 0.1 with lithium perchlorate). These values are tabulated in Table 2. When these data are plotted according to [6] good straight line plots are obtained (i.e. Fig. 1) giving the rate constants k_{Br^-} from the slope and k_2 from the intercept. These are also listed in Table 2.

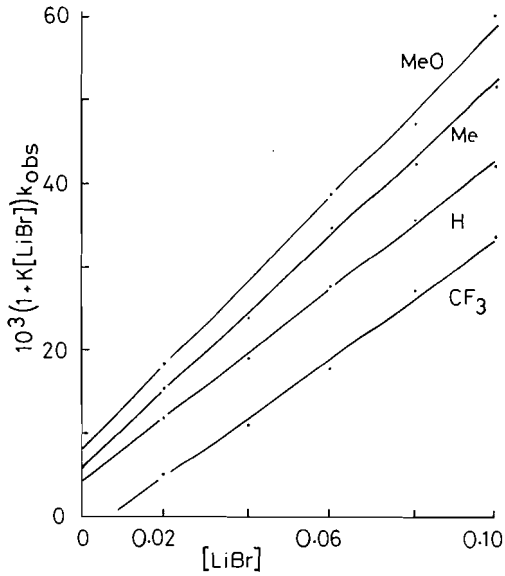

FIG. 1. $(1 + K_t[Br^-])\ k_{obs}$ vs. [LiBr] for the bromination of 3-arylpropynes in acetic acid at 25°C.

The main feature of these results is the large magnitude of the k_{Br^-} process relative to the k_2 molecular bromine process. In fact, the intercepts of the plots used to derive these rate constants are so small relative to the slopes that they are in general unreliable (the 3-CF_3 substituent even gives a negative intercept). This method therefore cannot be used to obtain the rate constants for the uncatalyzed addition of molecular bromine to the acetylenes.

The k_{Br^-} values, however, are of interest because they again demonstrate that for acetylenes this catalyzed process is clearly an Ad_E3 mechanism leading to *anti* addition of bromine via a transition state such as **7** (11, 14). This is most clearly demonstrated for the 4-MeO substrate, **2***b*, where the product ratio changes from 17% *trans* – 83% *cis* for molecular bromination to 84% *trans* – 16% *cis* in the presence of 0.1 *M* lithium bromide. The same effect is present but smaller for the 4-Me case. The other two substrates show almost exclusively *trans* dibromides even in the absence of bromide ion and therefore this change in mechanism can not be detected for these cases by product ratios.

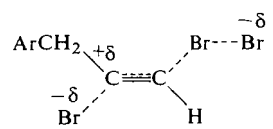

7

Can. J. Chem. Downloaded from www.nrcresearchpress.com by 210.87.254.105 on 09/05/12
For personal use only.

TABLE 2. The rates of bromination of 3-arylpropynes in acetic acid at 25°C in the presence of lithium bromide

Substrate		$k_{obs} \times 10^3$ (M^{-1} s^{-1})						
No.	X	0.10 M LiBr	0.08 M LiBr	0.06 M LiBr	0.04 M LiBr	0.02 M LiBr	$k_2 \times 10^3$[a] (M^{-1} s^{-1})	$k_{Br^-} \times 10^3$[a] (M^{-1} s^{-1})
2*a*	H	4.14	4.20	3.98	3.57	3.54	4.2±0.6	385±10
2*b*	4-OMe	5.92	5.55	5.54	—	5.42	9.5±1.0	470±20
2*c*	4-Me	5.09	5.00	4.99	4.46	4.46	5.8±0.5	461± 8
2*d*	3-CF_3	3.30	3.19	2.56	2.08	1.47	−3.1±1.0	367±15

[a]Errors quoted are the standard deviation of least-squares slope and intercept.

The second feature of these k_{Br^-} values is the very small effect of substituents. Thus the 4-MeO substrate (**2***b*) reacts only 1.3 times as fast as the 3-CF_3 case (**2***d*). This observation is in agreement with the very small positive charge build up on the 2-carbon of the 3-arylpropynes in the transition state **7**. This type of decrease in substituent effects for the bromide ion catalyzed bromination of acetylenes has been observed previously for ethynylbenzenes (11).

Because of the difficulty in obtaining the rate constants, k_2, for the molecular bromination by method *a*, the alternate procedure *b* was used: low bromine and high acetylene concentration, so simple first-order kinetics are obtained according to the first term in [5]. These values are shown in Table 3 along with the σ values required for the Hammett plot in Fig. 2. Also in Table 3 are the rate ratios, k_{Br^-} (0.1)/$k_2 \times 7$ which give the relative amounts of the bromide ion catalyzed versus the uncatalyzed process. The factor of 7 is included in the denominator to correct for the fact that the k_2 values used here were obtained at zero ionic strength. To compare them with the k_{Br^-} values at ionic strength 0.1 they must be multiplied by a factor of approximately 7 (15). We note that for the 4-MeO substrate **2***b* where this *cis–trans* ratio changes drastically in the presence of bromide ion the rate data and product data are consistent. Thus, assuming k_{Br^-} gives entirely *trans* dibromide and k_2 gives a 17:83 *trans–cis* ratio (Table 1), we can estimate the %*trans* expected at 0.1 M lithium bromide: calculated 81%; observed 84% (Table 1).

TABLE 3. Rates of bromination of 3-arylpropynes in acetic acid at 25°C

Substrate		$k_2 \times 10^{-3}$[a]		k_{Br^-} [Br^-][b]
No.	X	(M^{-1} s^{-1})	σ	$7k_2$
2*b*	4-MeO	2.02±0.06	−0.268	3.3
2*c*	4-Me	0.82±0.02	−0.170	8.0
2*a*	H	0.75±0.03	0	7.3
2*d*	3-CF_3	0.64±0.02	+0.430	8.1

[a]Errors are the mean deviation of at least three determinations.
[b]Calculated at 0.10 M LiBr.

The Hammett plot is obviously curved with the 4-MeO substrate **2***b* lying well above the line defined by the other three substrates (Fig. 2). In fact, it reacts about 2.5 times as fast as expected. This observation confirms the formation of large amounts of the *cis* dibromide by a mechanism involving phenonium ion participation in the rate determining electrophilic attack of bromine, eq. 4. Note however, that there may actually be some conversion of **6** to **3** after the rate determining step. The rate increase of 2.5 over that expected for the 4-MeO substrate predicts a product ratio of 60% *cis* and 40% *trans* assuming the phenonium ion rate process leads only to *cis* dibromide and the bromonium ion rate process only to *trans*. The observed ratio is 83% *cis* to 17% *trans*.

The slope of the Hammett plot for the deactivated groups, $\rho \simeq -0.2$ (Fig. 2), is again indicative of very small positive charge build up on the 2-carbon atom of these 3-arylpropynes during bromination. The

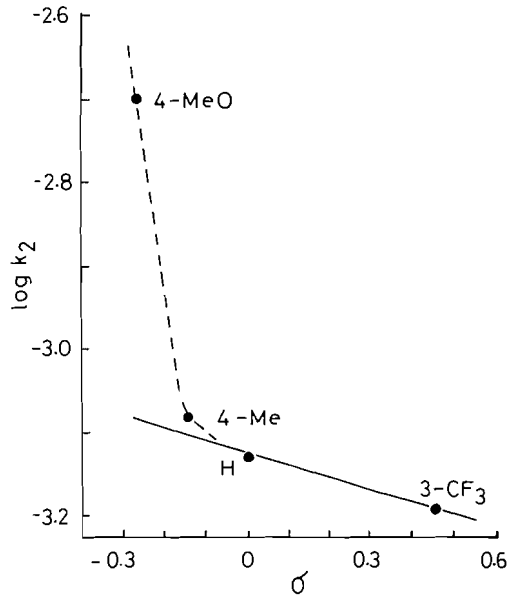

FIG. 2. Hammett plot for the bromination, k_2, of 3-arylpropynes in acetic acid at 25°C.

Can. J. Chem. Downloaded from www.nrcresearchpress.com by 210.87.254.105 on 09/05/12
For personal use only.

Can. J. Chem. Downloaded from www.nrcresearchpress.com by 210.87.254.105 on 09/05/12
For personal use only.

effect of an aryl group β to a cationic center is well known from solvolysis studies of substrates with electron-withdrawing groups ($\rho \simeq -0.7$) (16). Thus the smaller ρ value in the bromination reaction is at least consistent with the intervention of a cyclic unsaturated bromonium ion. However, the explanation may not be as simple as this since ρ values are known to be different in cases where they should be similar. Thus the Taft $\rho^*(k_3) \simeq -1.0$ for the bromination of aliphatic acetylenes in acetic acid (17) is much smaller than that for aliphatic alkenes in methanol, $\rho^* \simeq -3.1$ (18, 7) even though both reactions are presumed to proceed by transition states leading to cyclic bromonium ions. Although this comparison is for two different rate processes in two different solvents, it should still be valid. The selectivity of a series of alkenes to bromine has been shown to be very similar in methanol and acetic acid (19) and substituent effects for bromination of styrenes in acetic acid are nearly identical for both the first-order in bromine process, $k_2(\rho^+ = -4.8)$ and the second-order in bromine process, $k_3(\rho^+ = -4.6)$ (20).

We conclude by emphasizing that these results for the bromination of 3-arylpropynes are consistent with the mechanism outlined in [4] and for the intervention of a vinyl cation stabilized by 4-methoxyphenyl participation in the rate determining transition state and the product determining intermediates. We are planning to look for this type of participation in other vinyl cation systems.

Experimental

Preparation and Purification of Acetylenes

3-Phenylpropyne

This was prepared according to the literature method (21) by isomerization of 1-phenylpropyne with butyllithium; bp 35–36°C/10 Torr (lit. (21) bp 71–73°C/17 Torr). The acetylene was purified by preparation of the silver salt. A 5% silver nitrate in ethanol solution (750 ml) was added to 10.8 g (0.1 mol) of 3-phenylpropyne in 100 ml of ethanol. The white precipitate was collected, air dried, and then refluxed for 30 min with 73 g (0.9 mol) of sodium thiocyanate in 300 ml of water. The free acetylene was extracted with ether and then distilled to give 8.7 g (81% yield) of recovered 3-phenylpropyne; nmr δ: 2.06 (t, J = 3 Hz, 1H), 3.60 (d, J = 3 Hz, 2H), 7.3 (s, 5H).

3-(4-Methoxyphenyl)propyne

To 9.8 g (0.40 mol) of magnesium in 30 ml ether was added 75 g (0.40 mol) of 4-bromoanisole in 150 ml of ether to prepare the Grignard reagent. The mixture was cooled in an ice bath, 35.7 g (0.30 mol) of 3-bromopropyne was slowly added and then stirred for 24 h. Work-up in the usual way gave 35 g (0.24 mol, 80% yield) of a 2:1 mixture of 3-(4-methoxyphenyl)-propyne and 4-methoxyphenylallene as determined by nmr. This mixture was isomerized to the pure acetylene with butyllithium (18) and then purified by column chromatography on silica gel using petroleum ether. Distillation gave pure 3-(4-methoxyphenyl)propyne; bp 80°C/0.3 Torr (lit. (19) bp 76–77°C/0.1 Torr).

3-(4-Methylphenyl)propyne

This compound was prepared in the same way as the 4-methoxy isomer; bp 54–55°C/0.5 Torr; nmr δ: 2.00 (t, J = 3 Hz, 1H), 2.33 (s, 3H), 3.50 (d, J = 3 Hz, 2H), 6.9–7.3 (d of d, 4H).

3-(3-Trifluoromethylphenyl)propyne

This was prepared in the same way as the 4-methoxy isomer; bp 55–56°C/0.3 Torr; nmr δ: 2.13 (t, J = 3 Hz, 1H), 3.63 (d, J = 3 Hz, 2H), 7.5 (m, 4H). *Anal.* calcd. for $C_{10}H_7F_3$: C 65.22, H 3.80, F 30.98; found: C 65.09, H 3.85.

Products of the Bromination of 3-Arylpropynes

3-Phenylpropyne: cis- *and* trans-*1,2-Dibromo-3-phenylpropene*

To 1.00 g (9.0 mmol) of 3-phenylpropyne in 30 ml of acetic acid was added 1.38 g (8.0 mmol) of bromine in 30 ml of acetic acid. The mixture was stirred in the dark for 16 h, poured into 200 ml of water, and extracted with 3 × 30 ml of ether. The ether was washed with 50 ml of 5% sodium bicarbonate, dried over $MgSO_4$, and concentrated to give 2.30 g of a mixture of *trans*-1,2-dibromo-3-phenylpropene (94%) and *cis*-1,2-dibromo-3-phenylpropene (6%) as determined by glc on a $\frac{1}{8}$ in. × 6 ft 20% Carbowax 20 M on Chromosorb W column (200°C, 25 ml/min). The nmr spectrum of the mixture showed principally peaks for the *trans* isomer δ: 4.20 (s, 2H), 6.97 (s, 1H), 7.77 (s, 5H). Other spectral data, ir (film): very weak band, 1620 cm^{-1}; uv (EtOH) λ_{max}: 260 (ε 277). For elemental analysis a sample was purified by column chromatography on silica gel followed by bulb-to-bulb distillation. *Anal.* calcd. for $C_9H_8Br_2$: C 39.15, H 2.92, Br 57.92; found: C 38.96, H 3.10, Br 57.67.

1-Bromo-3-phenylpropyne—To 20 g of sodium hydroxide in 50 ml of water was added 10.7 g (0.13 mol) of bromine. To this mixture with stirring was added 5.80 g (0.05 mol) of 3-phenylpropyne and then left for 60 h at room temperature. The crude oil was extracted with ether and then distilled to give pure 1-bromo-3-phenylpropyne, bp 40–41°C/0.1 Torr; nmr δ: 3.60 (s, 2H), 7.20 (s, 5H).

Hydrobromination of 1-bromo-3-phenylpropyne—Anhydrous hydrogen bromide was passed through 10 ml of acetic acid to obtain a saturated solution, 1.90 g (0.01 mol) of 1-bromo-3-phenylpropyne was added and then the solution stirred at room temperature for 5 days. Extraction in the usual way gave 2.43 g of crude dibromide mixture which by glc analysis consisted of *trans*-1,2-dibromo-3-phenylpropyne (11%) and *cis*-1,2-dibromo-3-phenylpropyne (89%). This mixture, which is principally the *cis* isomer, showed nmr δ: 4.00 (d, J = 1 Hz, 2H), 6.97 (t, J = 1 Hz, 1H), 7.78 (s, 5H); ir: 1618 cm^{-1}.

3-(4-Methoxyphenyl)propyne: cis- *and* trans-*1,2-Dibromo-3-(4-methoxyphenyl)propene*

The procedure followed was the same as for the unsubstituted case; glc analysis of the crude dibromide mixture indicated *trans* 17% and *cis* 83%; nmr δ: 3.67–3.80 (overlapping singlets, 5H), 6.47 (t, J = 1 Hz, 1H) 6.65–7.10 (d of d, 4H) plus smaller peaks for the *trans* isomer the principle one being the methylene singlet at 3.90 δ; uv (EtOH): 278 mm (ε 1970). A sample from the bromination reaction was purified by preparative glc on a $\frac{3}{8}$ in. × 8 ft 5% SE 30 Chromosorb W column (170°C, 160 ml/min). *Anal.* calcd. for $C_{10}H_{10}OBr_2$: C 39.21, H 3.27, Br 52.29; found: C 39.49, H 3.35, Br 52.16.

3-(4-Methylphenyl)propyne: trans-*1,2-Dibromo-3-(4-methylphenyl)propene*

The same bromination procedure for the unsubstituted compound was used; glc analysis of the crude dibromide mixture indicated *trans* (91%) and *cis* (9%); nmr δ: 2.30 (s, 3H), 3.83 (s, 2H), 6.40 (s, 1H), 7.00 (s, 4H); uv (EtOH): 266 (ε 605).

3-(3-Trifluoromethylphenyl)propyne; trans-*1,2-Dibromo-3-(3-trifluoromethylphenyl)propene*

The crude dibromide mixture analyzed for 98% *trans* and 2% *cis*; nmr δ: 4.00 (s, 2H); 6.60 (s, 1H), 7.47 (s, 4H); uv (EtOH): 266 (ε 847). Analytical sample prepared by preparative glc. *Anal.* calcd. for $C_{10}H_7F_3Br_2$: C 34.58, H 2.03, Br 46.11; found: C 34.89, H 2.22, Br 45.89.

Kinetics for Bromination of 3-Arylpropynes

The procedures for obtaining rates of bromination of acetylenes both in the presence and absence of lithium bromide have been described in detail previously (11).

Acknowledgments

We thank the National Research Council of Canada for financial assistance and Dalhousie University Faculty of Graduate Studies for a fellowship to C. Somawardhana.

1. R. C. FAHEY. *In* Topics in stereochemistry. Vol. 3. *Edited by* E. L. Eliel and N. L. Allinger. Wiley-Interscience, New York, NY. 1968. p. 237.
2. P. B. C. DE LA MARE and R. BOLTON. Electrophilic additions to unsaturated systems. Elsevier Publishing Co., Amsterdam. 1966.
3. K. YATES, G. H. SCHMID, T. W. REGULSKI, D. G. GARRATT, H. W. LEUNG, and R. S. MCDONALD. J. Am. Chem. Soc. **95**, 160 (1973).
4. G. MODENA and U. TONELLATO. Adv. Phys. Org. Chem. **9**, 185 (1971).
5. P. J. STANG. Prog. Phys. Org. Chem. **10**, 205 (1973).
6. J. E. DUBOIS, J. TOULLEC, and D. FAIN. Tetrahedron Lett. 4859 (1973).
7. D. FAIN, J. TOULLEC, and J. E. DUBOIS. Tetrahedron Lett. 1725 (1974).
8. Z. RAPPOPORT. Acc. Chem. Res. **9**, 265 (1976).
9. M. HANACK. Acc. Chem. Res. **9**, 364 (1976).
10. P. J. STANG and T. E. DUEBER. J. Am. Chem. Soc. **99**, 2602 (1977).
11. J. A. PINCOCK and K. YATES. Can. J. Chem. **48**, 3332 (1970).
12. R. KÖSTER, K.-H. KRAMER, and R. LIEDTKE. Ann. Chem. 1241 (1973).
13. J. H. ROLSTON and K. YATES. J. Am. Chem. Soc. **91**, 1469 (1969).
14. J. A. PINCOCK and K. YATES. J. Am. Chem. Soc. **90**, 5643 (1968).
15. J. A. PINCOCK and K. YATES. Can. J. Chem. **48**, 2945 (1970).
16. C. J. LANCELOT, D. J. CRAM, and P. VON R. SCHLEYER. *In* Carbonium ions. Vol. III. *Edited by* G. A. Olah and P. von R. Schleyer. Wiley-Interscience, New York, NY. 1972. p. 965.
17. R. GELIN and D. PIGASSE. Bull. Soc. Chim. Fr. 2186 (1971).
18. G. MOUVIER and J. E. DUBOIS. Bull. Soc. Chim. Fr. 1441 (1968).
19. A. MODRO, G. H. SCHMID, and K. YATES. J. Org. Chem. **42**, 3673 (1977).
20. K. YATES, R. S. MCDONALD, and S. A. SHAPIRO. J. Org. Chem. **38**, 2460 (1973).
21. J. W. MULVANEY, T. L. FOLK, and D. J. NEWTON. J. Org. Chem. **32**, 1674 (1967).
22. R. GRAMATICA, D. MONTI, and P. MANITTO. Gazz. Chim. Ital. **104**, 629 (1974).

Can. J. Chem. Downloaded from www.nrcresearchpress.com by 210.87.254.105 on 09/05/12
For personal use only.

Proton magnetic resonance studies of 2′-deoxynucleosides and nucleotides in the *syn* conformation

ARTHUR L. GEORGE AND FRANK E. HRUSKA

Department of Chemistry, University of Manitoba, Winnipeg, Man., Canada R3T 2N2

AND

KELVIN K. OGILVIE

Department of Chemistry, McGill University, Montreal, P.Q., Canada H3C 3G1

AND

ANTONIN HOLY

Institute of Organic Chemistry and Biochemistry, Czechoslovak Academy of Sciences, Praha 5, Czechoslovakia

Received September 14, 1977

ARTHUR L. GEORGE, FRANK E. HRUSKA, KELVIN K. OGILVIE, and ANTONIN HOLY. Can. J. Chem. **56**, 1170 (1978).

Proton magnetic resonance data for 6-methyl-2′-deoxyuridine and its 3′- and 5′-monophosphate derivatives are obtained in aqueous solution and compared with data for corresponding thymine derivatives. The data show that the derivatives of the 6-methyluracil base occupy the *syn* conformation. The presence of the *syn* base leads to a flattening of the sugar ring and destabilization of the g^+ conformer about the C(4′)—C(5′) bond. This destabilization is particularly large at the 5′-nucleotide level and is discussed in terms of a repulsive interaction involving the 2-keto oxygen of the base and the negatively charged 5′-group.

ARTHUR L. GEORGE, FRANK E. HRUSKA, KELVIN K. OGILVIE et ANTONIN HOLY. Can. J. Chem. **56**, 1170 (1978).

Travaillant en solution aqueuse, on a obtenu des données de résonance magnétique du proton pour la méthyl-6 déoxy-2′ uridine et ses dérivés monophosphates en 3′ et 5′ et on a comparé les données avec les valeurs correspondantes pour les dérivés de la thymine. Les données montrent que les dérivés de la base de la méthyl-6 uracile occupent une conformation *syn*. La présence d'une base *syn* conduit à un aplatissement du cycle du sucre et à une déstabilisation du conformère g^+ autour du lien C(4′)—C(5′). Cette déstabilisation est particulièrement importante au niveau du nucléotide 5′ et on la discute en terme d'une interaction répulsive impliquant l'oxygène cétonique 2 de la base et le groupe 5′ chargé négativement.

[Traduit par le journal]

Introduction

An important conformational feature of nucleosides is the sugar–base torsion angle (χ) which defines the relative orientation of the base and sugar moieties.[1] For pyrimidine nucleosides in the *anti* conformation (Fig. 1) the 6-hydrogen of the base is located over the sugar ring whereas in the *syn* conformation it is the more bulky 2-keto oxygen which is so located. For steric reasons then, the *anti* conformation of 'normal' pyrimidine nucleosides (no substitution at the 6-position) has been generally considered predominant though there is increasing evidence (1–3) that in solution the *syn* conformation may contribute significantly to the *syn* ⇄ *anti* balance. Undoubtedly polynucleotides possessing *syn* bases will have altered abilities for base stacking and for complementary complexation. Useful model compounds for the evaluation of the conformational consequences of the presence of *syn* bases are the derivatives possessing 6-methyl substituted pyrimidines since it is certain that nucleosides so substituted are *syn* (4–7). For such an evaluation in the 2′-deoxyribose series we have synthesized 6-methyl-2′-deoxyuridine (m^{6}dU) (Fig. 1), and its 3′- and 5′-monophosphate derivatives, 3′m^{6}dUMP and 5′m^{6}dUMP, respectively.

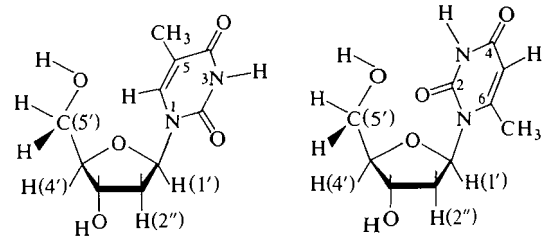

FIG. 1. Structural formulae of 2′-deoxythymidine, dT, (*anti* conformation, left) 6-methyl-2′-deoxyuridine, m^{6}dU, (*syn* conformation, right).

In the present work we report the ^{1}H nmr data for this series of molecules along with data for the analogous thy derivatives, dT, 3′dTMP, and 5′dTMP. The chemical shifts and coupling constants

[1]Abbreviations used: thy, thymine base; m^{6}Ura, 6-methyluracil; dT, 2′-deoxythymidine; m^{6}dU, 6-methyl-2′-deoxyuridine; (3′- or 5′)dTMP and m^{6}dUMP, 3′- or 5′-monophosphate derivatives of dT and m^{6}dU. The familiar notation for the N and S envelope of conformations in the pseudorotational cycle (15), 3′-*endo* and 2′-*endo*, respectively, is retained in the text, except where the conformer equilibrium (N ⇄ S) is indicated.

Can. J. Chem. Downloaded from www.nrcresearchpress.com by 210.87.254.40 on 09/05/12
For personal use only.

Can. J. Chem. Downloaded from www.nrcresearchpress.com by 210.87.254.40 on 09/05/12
For personal use only.

in D_2O and DMSO are discussed in terms of the conformations of the molecules in the two series. An analysis of the ^1H nmr spectrum of aqueous m^6dU has been described by Cadet *et al.* (6). Holy (8*a*) has verified the configuration of m^6dU using uv, cd, and ^1Hmr data.

Experimental

Syntheses

*6-Methyl-2′-deoxyuridine (**1**)*

This compound was prepared according to Holy (8*b*) starting with 2-amino-β-D-arabinofuro(1′,2′:4;5)oxazoline.

*5′-O-Trityl-6-methyl-2′-deoxyuridine (**2**)*

Compound **1** (3 mmol) was allowed to react with triphenylchloromethane (4.5 mmol) at room temperature in pyridine (10 ml) for 20 h. Pyridine was evaporated by codistillation at reduced pressure with ethanol and the residue was applied to silica gel thick-layer plates which were developed first in ether and then in ethyl acetate. In addition to the major product, **2**, mp 191–192°C, 75% crystallized from benzene, there were small amounts of **1** (slower band), and both ditritylated and 3′-tritylated compounds (both moving faster on tlc).

*6-Methyl-2′-deoxyuridine 3′-Phosphate (**3**)*

Compound **2** (0.11 mmol) and β-cyanoethyl phosphate (0.2 mmol) were dried by repeated evaporation of pyridine. Triisopropylbenzenesulfonyl chloride (TPS, 0.4 mmol) was added and the compounds were stirred at room temperature in pyridine (1 ml) for 16 h. Solvents were removed at reduced pressure by coevaporation with ethanol. The residue was dissolved in 80% acetic acid (4 ml) and heated at 90°C for 20 min. Solvents were removed at reduced pressure and the residue was extracted once with ether (10 ml). The residue was dissolved in ethanol (8 ml), 8 ml of concentrated ammonium hydroxide was added, and the solution was heated in a steel bomb for 2 h at 65°C.

The solution was then concentrated at reduced pressure and the residue was applied to Whatman 3 MM chromatography sheets which were developed first in solvent *A* (isopropyl alcohol – ammonium hydroxide – water (7:1:2)) and then in solvent *F* (*n*-propyl alcohol – ammonium hydroxide – water (55:10:35)). The product band separated cleanly; yield 75%, $\lambda_{max}(H_2O)$ 260 nm; R_m^{Tp} 1.0; R_f^F 0.43.

*3′-O-Acetyl-6-methyl-2′-deoxyuridine (**4**)*

Compound **2** (0.25 mmol) was stirred with acetic anhydride (1 ml) in pyridine (2 ml) for 2 h. Ethanol was added and the solvents were removed at reduced pressure. Acetic acid, (80%, 5 ml) was added to the residue and the resulting solution was heated at 90°C for 20 min. The solution was concentrated at reduced pressure and applied to two thick-layer plates which were developed twice in ether. The product band was eluted with ethanol which on evaporation yielded **4**, 66%, mp 153–155°C; $\lambda_{max}(H_2O)$ 260 nm; $R_f^{ET_2O}$ 0.15; R_f^{EtOAc} 0.41.

*6-Methyl-2′-deoxyuridine 5′-Phosphate (**5**)*

Compound **4** (0.3 mmol) and β-cyanoethyl phosphate (0.4 mmol) were dried by repeated evaporation of pyridine. TPS (0.8 mmol) was added and the components were dissolved in pyridine (2 ml) and stirred at room temperature for 6 h. Water (2 ml) was added and the solution stirred at room temperature for an additional 18 h. The solution was concentrated to a gum at reduced pressure, 6 *M* NH_4OH in ethanol (5 ml) was added, and the solution was heated at 100°C for 2 h. The products were isolated by paper chromatography in solvent *A*. The major product was **5**, 78%; $\lambda_{max}(H_2O)$ 260 nm; R_m^{Tp} 1.0. A small amount (10% overall yield) of the β-cyanoethyl derivative of **5** was also obtained; R_m^{Tp} 0.36, $\lambda_{max}(H_2O)$ 260 nm.

Proton Magnetic Resonance Spectra

Proton magnetic resonance spectra were obtained on a variety of spectrometers (Bruker WH-90DS, Manitoba; Bruker HX-360S, Stanford Magnetic Resonance Laboratory; Varian HR-220, Canadian 220 MHz Centre; Varian HA-100, Manitoba) operating in the Fourier transform or continuous-wave mode. Sodium 3-trimethylsilylpropionate-*2,2,3,3-d*$_4$ (TSP) was used as an internal ^1Hmr reference for the studies in D_2O. Solutions (0.1 *M* or less) were freeze-dried three times and dissolved in 100% D_2O. The p*D* of the nucleoside solutions was adjusted to 7.0 while that for the nucleotides was adjusted to 6.4 or less.[2] For the nucleoside studies in DMSO, samples of dT and m^6dU were lyophilized from D_2O to replace the exchangeable hydrogens and then dissolved in fully deuterated DMSO in a dry nitrogen atmosphere. A trace of tetramethylsilane was added for the internal reference. The nucleoside concentration was 0.1 *M* or less.

Spectral analysis was carried out using LAME (9) and computer simulated spectra were generated as a final test of the data. A sample spectrum of 5′m^6dUMP is shown in Fig. 2. The chemical shift (δ) and coupling constant (*J*) data are listed in Table 1. For the sake of comparison data for 3′- and 5′dTMP from ref. 10 are included.

Results and Discussion

Assignment of Proton Spectra

With the aid of spin decoupling experiments the line assignments for m^6dU and its monophosphates were made by analogy to the assignments for dT and its derivatives (10). Following the work of Ritchie and Perlin (11) on selectively deuterated adenosine, the lower-field proton on C(5′) is designated H(5′) for the derivatives of m^6dU as well as those of dT; this is in line with the Remin–Shugar assignment (12) based on chemical shift trends. In cases where the C(2′) protons may be distinguished, their assignment was made on the basis of chemical shift and coupling constant trends. Thus, a characteristic feature of 2′-deoxyriboside spectra appears to be the near equalities, $J_{2'',3'} \simeq J_{3',4'}$ and $J_{1',2''} \simeq J_{2',3'}$ (10, 13). These lead to designating H(2′) as the lower field C(2′) proton for m^6dU and its derivatives. This is the reverse of the situation in 3′dTMP (Table 1).

Conformation about the N-*Glycosyl Linkage*

Schweizer *et al.* (5) have shown that in 6-methylpyrimidine β-ribonucleosides in which the *ortho* 2-keto group on the base is constrained to lie over the sugar ring (e.g. 6-methyluridine) the H(2′) shift is displaced downfield by about 0.6 ppm relative to its resonant position in *anti* nucleosides (e.g. 5-methyluridine). The effect, attributable to the electric fields and magnetic anisotropy of the carbonyl, is a good probe for the presence of the *syn*

[2]At p*D* < 6.4, the monoanionic form of the nucleotides predominates, making more meaningful a comparison with data for dinucleotides (in preparation) which are also monoanionic near neutral p*D*.

TABLE 1. Proton chemical shifts (δ) and coupling constants[a] (*J*) for the 2′-deoxyribonucleoside and its 3′- and 5′-monophosphates of thymine (T) and 6-methyluracil (m^6Ura)[b]

	D_2O			DMSO			D_2O					
	m^6dU		dT	m^6dU		dT	3′m^6dUMP		3′dTMP	5′m^6dUMP		5′dTMP
Parameter	30°C	63°C	30°C	18°C	65°C	30°C	18°C	75°C	30°C	25°C	60°C	30°C
$\delta_{1'}$	6.19[f]	6.18	6.29	6.09	6.11	6.16	6.21	6.18	6.31	6.21	6.20	6.34
$\delta_{2'}$	2.95	2.94	2.37	2.71	2.73	2.10	3.00	2.98	2.41	2.94	2.93	2.37
$\delta_{2''}$	2.27	2.26	2.39	2.05	2.05	2.10	2.42	2.42	2.55	2.27	2.25	2.38
$\delta_{3'}$	4.54	4.53	4.48	4.28	4.31	4.25	4.78	4.79	4.76	4.59	4.57	4.58
$\delta_{4'}$	3.93	3.94	4.03	3.66	3.69	3.78	4.03	4.05	4.18	3.99	3.99	4.17
$\delta_{5'}$	3.86	3.85	3.85	3.61	3.63	3.60	3.91	3.90	3.87	4.03	4.02	4.06
$\delta_{5''}$	3.76	3.77	3.78	3.48	3.52	3.56	3.79	3.79	3.81	3.92	3.92	4.05
δ_5	5.72	5.72	—	5.58	5.54	—	5.72	5.72	—	5.73	5.74	—
δ_6	—	—	7.66	—	—	7.67	—	—	7.68	—	—	7.77
δ_{CH_3}	2.39	2.39	1.90	2.30	2.30	1.79	2.40	2.41	1.91	2.38	2.38	1.93
$J_{1'2'}$	5.3	5.8	6.8	5.7	6.4	6.6	5.6	5.8	7.2	4.7	5.1	[7.0[c]
$J_{1'2''}$	8.4	8.3	6.8	8.0	8.0	7.0	8.2	8.0	6.5	8.5	8.4	[7.0
$J_{2'2''}$	−13.9	−14.0	−14.0[d]	−13.3[d]	−13.2	−14.0[d]	−13.8	−14.2	−14.3	−13.9	−14.1	−13.8[d]
$J_{2'3'}$	8.3	8.2	6.6	7.8	8.0	5.6	8.1	8.0	6.8	8.4	8.5	[4.8[c]
$J_{2''3'}$	5.5	5.6	4.1	5.3	4.8	3.8	5.2	4.8	3.7	6.1	5.7	[4.8
$J_{3'4'}$	5.9	5.6	4.1	5.6	4.9	3.3	5.8	5.2	4.0	6.1	5.9	2.9
$J_{4'5'}$	3.4	3.5	3.6	3.4	3.7	3.4	3.9	3.9	3.5	4.3	4.3	[3.8[c]
$J_{4'5''}$	6.5	6.5	5.0	6.4	5.7	4.4	6.1	6.0	4.8	6.3	6.5	[3.8
Σ^e	9.9	10.0	8.6	9.8	9.4	7.8	10.0	9.9	8.3	10.6	10.8	7.6
$J_{5'5''}$	−12.1	−12.0	−12.4	−11.9	−11.6	−12.2	−12.1	−12.4	−12.5	−11.1	−11.2	−12.1[d]
$J_{P3'}$	—	—	—	—	—	—	7.1	8.3	7.8	—	—	—
$J_{P4'}$	—	—	—	—	—	—	—	—	—	<0.5	<0.5	1.6
$J_{P5'}$	—	—	—	—	—	—	—	—	—	5.8	6.3	[5.0[c]
$J_{P5''}$	—	—	—	—	—	—	—	—	—	5.7	5.7	[5.0
Σ'^e	—	—	—	—	—	—	—	—	—	11.5	12.0	10.0

[a]Chemical shifts in ppm from TSP (D_2O) or tertiary butyl alcohol (DMSO); coupling constants in Hz.
[b]Solutions 0.1 *M* (or less) in solute; monophosphates at p*D* ≃ 6.5 or less.
[c]Due to chemical shift equivalence, only the sum of connected [coupling constants is significant.
[d]Arbitrary. When $\delta_i \simeq \delta_j$ the spectrum is independent of J_{ij}.
[e]$\Sigma = J_{4'5'} + J_{4'5''}$; $\Sigma' = J_{P5'} + J_{P5''}$.
[f]Estimated errors: δ ± 0.004 ppm; *J* = ± 0.2 Hz.

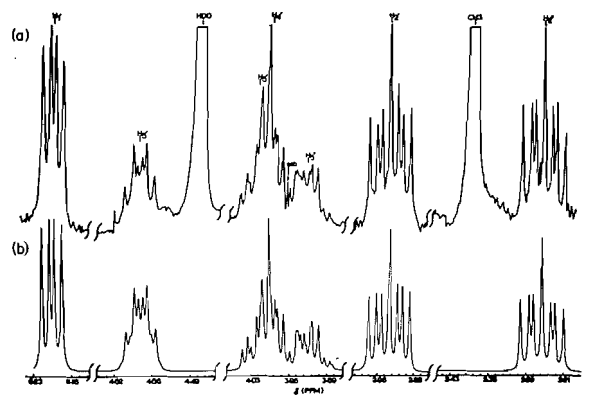

FIG. 2. (*a*) 360 MHz spectrum of 6-methyl-2′-deoxyuridine 5′-monophosphate (5′m^6dUMP) courtesy of the Stanford Magnetic Resonance Laboratory. In D_2O, 60°C, 0.1 *M*, p*D* ≃ 6.4. Shifts in ppm relative to TSP. (*b*) Computer-simulated spectrum.

conformation. The data in Table 1 (aqueous and DMSO solutions) show that H(2′) is displaced downfield by 0.57–0.61 ppm in m^6dU and its monophosphates, relative to the H(2′) resonance position in the corresponding dT derivative. Thus the keto effect on the *endo* C(2′) hydrogen is strikingly similar in the ribose and 2′-deoxyribose series and suggests that a shift towards the *syn* conformation occurs for the m^6Ura derivatives. Furthermore, since the keto group effect on H(2′) in m^6dU (in D_2O and DMSO) and its 3′- and 5′-phosphates are similar (0.57–0.61 ppm), it is reasonable to conclude that the spatial disposition of the 2-keto oxygen and H(2′) is not drastically altered by the solvent change or by phosphorylation. This view is substantiated by the similarity in the 2-keto group effect on the *exo* 2″-hydrogens which are all displaced upfield relative to the H(2″) in the corresponding thy derivative (0.08 to 0.13 ppm for D_2O; 0.05 ppm for the DMSO solution).

H(3′) in the m^6Ura derivatives also experiences a deshielding effect (relative to the dT derivatives) which is, as expected, smaller (0.01–0.06 ppm). Interestingly, this keto group effect on H(3′) is larger for the ribose derivatives studied (0.15–0.19 ppm) (5, 14). This larger effect in the ribosides is probably a consequence of the greater contribution from the 3′-*endo* conformation in this series; in this

Can. J. Chem. Downloaded from www.nrcresearchpress.com by 210.87.254.40 on 09/05/12
For personal use only.

Can. J. Chem. Downloaded from www.nrcresearchpress.com by 210.87.254.40 on 09/05/12
For personal use only.

conformation H(3′) and the 2-keto oxygen are juxtaposed while in the 2′-*endo* conformation, relatively more important in the 2′-deoxy derivatives, these atoms are distant.

Since H(4′) and the base lie on opposite sides of the sugar, it is perhaps surprising that this proton experiences a substantial 'keto group effect' (shielding) of 0.08 to 0.18 ppm. This cannot be due to a direct influence of the 2-keto group, but is, we feel, a consequence of changes in the C(4′)—C(5′) conformer distribution attributable to base–backbone repulsion in the m^{6}Ura derivatives (see below). With one exception (H(5′′) of 5′m^{6}dUMP) the keto group effects on H(5′) and H(5′′) of the m^{6}Ura derivatives are small; these trends are also in line with the C(4′)—C(5′) conformer redistributions (see below).

Sugar Pucker

The conformation of a 2′-deoxyribose ring, described in terms of the pseudorotational parameters (*P*), the amplitude of pucker (τ_m), and the populations of the 2′-*endo* (S) and 3′-*endo* (N) puckers in the N ⇄ S blend (15), can be evaluated from the magnitudes of the vicinal couplings $J_{1'2'}$ through to $J_{3'4'}$ (Table 1). The following general comments about the influence of the *syn* m^{6}Ura base on the sugar conformation may be made. First, for m^{6}Ura derivatives, the corresponding couplings are similar, indicating that the overall conformation is not affected drastically by 3′- or 5′-phosphorylation or by transfer of the nucleoside to a DMSO solution. Furthermore, for the m^{6}Ura series, the magnitudes of the *cis* couplings $J_{1'2''}$ (8.0 – 8.5 Hz) and $J_{2'3'}$ (8.1 – 8.5 Hz) are larger by about 1.5 Hz than the corresponding couplings in the thy series. This means that the dihedral angles τ_1 (about C(1′)—C(2′)) and τ_2 (C(2′)—C(3′)) (15) have been biased, in the m^{6}Ura series relative to the thy series, towards the eclipsed ($\tau_1 = 0°$, $\tau_2 = 0°$) situation. In the Altona–Sundaralingam approach (15) this can be interpreted as a flattening of the ring i.e. a reduction in τ_m. However, a reduction in τ_m should lead to a *decrease* in the sum of the *trans* couplings $J_{1'2'} + J_{3'4'}$ as well as to an increase in the *cis* couplings $J_{1'2''}$ and $J_{2'3'}$ (15). But, from Table 1 we see that these sums, in aqueous solution, lie in the narrow range from 10.8 to 11.4 Hz, with no clear trend between the thy and m^{6}Ura series. The larger *cis* ($J_{1'2''}$ and $J_{2'3'}$) couplings in the m^{6}Ura series coupled with the similarity in the *trans* sum for the two series can be taken as evidence that the sugar ring in the m^{6}Ura series has pseudorotated away from the pure N($P = 0°$) and S($P = 180°$) conformers (15). In the simplest of terms our data indicate that, insofar as relieving strain due to eclipsing of substituents is concerned, rotation about C(2′)—C(3′) (τ_2) has become less important in the m^{6}Ura series.

In their study of 3′,5′-cyclic nucleotides in the 2′-deoxyribo series, Lee and Sarma (16) have observed large increases in $J_{1'2''}$ and $J_{2'3'}$, without concomitant increases in $J_{1'2'} + J_{3'4'}$; these were attributed to a general flattening of the ring. A similar flattening of the sugar ring is evident for *ribosides* in solution where increases in $J_{2'3'}$ of 1.0 to 1.5 Hz are noted upon incorporation of *syn* bases (5, 14, 16, 17). Interestingly, Altona and Sundaralingam (15) have noted that the sugar ring in crystalline 4-thiouridine (18) is not flattened by the *syn* 4-thiouracil base. This discrepancy between the molecule in the crystal and solution states was attributed by these authors to the crystal field packing requirements.

Estimates of the 3′-*endo* and 2′-*endo* contributions to the N ⇄ S balance can be made via [1] based on Davies and Danyluk (19).

$$[1] \qquad \%3'\text{-}endo = 100\,J_{3'4'}/(J_{1'2'} + J_{3'4'})$$

For the thy derivatives the %3′-*endo* contributions lie in the range from 27 to 38%, with 5′dTMP at the lower end and dT at the upper end. For the m^{6}Ura derivatives at the lower temperature in D_2O, the calculated %3′-*endo* contributions lie in the narrow range from 51 to 56%. Thus, the *syn* m^{6}Ura base has induced a substantial shift away from the 2′-*endo* conformation which appears to dominate in *anti*-2′-deoxyribosides in both the crystal (20) and solution (21) states. (Increasing temperature and transfer to a DMSO environment leads to a slight shift towards the 2′-*endo* conformation of the m^{6}Ura derivatives.) In the ribose series of *syn* nucleosides as well, nmr has revealed (5, 14–17) shifts in favor of the 3′-*endo* conformation. These solution results contrast sharply with crystal data; uridine (*anti*,3′-*endo*) (22) and 6-methyluridine (*syn*,2′-*endo*) (7) define a trend for the ribosides which is the reverse of that in solution.

Conformations about the C(4′)—C(5′) (ψ) and C(5′)—O(5′) (ϕ) Bonds

Assuming values of 11.5 and 1.5 Hz for the *trans* and *gauche* vicinal ^{1}H–^{1}H couplings, respectively (10), the following expressions[3] may be used to estimate the g^+, t, g^- conformer populations for the C(4′)—C(5′) (ψ) bond (Fig. 3).

$$[2a] \qquad g^+(\psi) = (13 - \Sigma)/10$$

$$[2b] \qquad t(\psi) = (J_{4'5''} - 1.5)/10$$

where Σ is the observed sum $J_{4'5'} + J_{4'5''}$. Similarly,

[3]From ref. 10; [3] has been modified somewhat by use of what appear (24) to be better choices for the *gauche* and *trans* ^{1}H–^{31}P couplings.

Can. J. Chem. Downloaded from www.nrcresearchpress.com by 210.87.254.40 on 09/05/12
For personal use only.

TABLE 2. Calculated rotamer populations (%) for C(4′)—C(5′) and C(5′)—O(5′)[a]

	C(4′)—C(5′) (ψ)			C(5′)—O(5′) (ϕ)		
	g^+	t	g^-	g^+	t	g^-
m^{6}dU	31	50	19	—	—	—
m^{6}dU (DMSO)	32	49	19	—	—	—
dT	44	35	21	—	—	—
dT (DMSO)	52	29	19	—	—	—
3′m^{6}dUMP	30	46	24	—	—	—
3′dTMP	47	33	20	—	—	—
5′m^{6}dUMP	24	48	28	18	65	17
5′dTMP	54	23	23	14	72	14

[a]Calculated from J data in Table 1 at the lower temperature only. For D_2O solutions except where DMSO indicated. Since *differences* in any pair of J values are accurate to ±0.4 Hz, *differences* in the magnitudes of pairs of conformer populations (which define conformational trends) should be accurate to about ±5%. For further discussion see footnote 7, ref. 10.

assuming 22.9 and 2.1 Hz for *trans* and *gauche* vicinal ^1H–^{31}P couplings (23, 24), respectively, the populations of the g^+, t, g^- conformers of the C(5′)—O(5′) (ϕ) may be estimated from

$$[3a] \qquad g^+(\phi) = (J_{P5''} - 2.1)/20.8$$

$$[3b] \qquad t(\phi) = (25.0 - \Sigma')/20.8$$

where Σ' is the observed sum $J_{P5'} + J_{P5''}$. The populations converted to percentages are listed in Table 2.

For dT values of 44, 35, and 21% are indicated for the $g^+(\psi)$, $t(\psi)$, and $g^-(\psi)$ populations. To within experimental error these are unaffected by 3′-phosphorylation whereas 5′-phosphorylation leads to an increase (10%) in $\%g^+(\psi)$ at the expense of $t(\psi)$. Transfer to a DMSO solution also leads to an increase in $\%g^+(\psi)$. The data reveal further that the m^{6}Ura base has a destabilizing influence upon the $g^+(\psi)$ conformer in the D_2O and DMSO solutions. At the nucleoside and 3′-phosphate levels a decrease (13–17%) is noted for $\%g^+(\psi)$ for the thy-to-m^{6}Ura substitution; simultaneously $\%t(\psi)$ increases (13–15%) whereas $\%g^-(\psi)$ remains essentially constant. At the 5′-phosphate level the effect of the m^{6}Ura base is more pronounced with $\%g^+(\psi)$ decreasing by 30% in 5′m^{6}dUMP relative to 5′dTMP, evident in the 3 Hz increase in Σ upon insertion of the m^{6}Ura base.

Replacement of the thy base by m^{6}Ura leads to a slight decrease in the $t(\phi)$ contribution for the 5′-monophosphates but clearly the C(5′)—O(5′) conformer distribution is much less affected than that of C(4′)—C(5′) at this level. The $t(\phi)$ conformer is dominant in both 5′dTMP and 5′m^{6}dUMP.

In previous studies (25, 26) it has been demonstrated that $^4J_{P4'}$ couplings in 5′-mononucleotides provide information about the C(4′)—C(5′) and C(5′)—O(5′) conformer distributions, with decreases in this coupling correlated with decreases in $\%g^+(\psi)$ and $\%t(\phi)$. In 5′dTMP $^4J_{P4'}$ is 1.6 Hz whereas in 5′m^{6}dUMP it is less than 0.5 Hz. This decrease is further evidence for the destabilizing influence of the m^{6}Ura base on the $g^+(\psi)$ and $t(\phi)$ conformers. Using published correlation plots and equations relating $^4J_{P4'}$ to conformer populations (25), we obtain for 5′dTMP and 5′m^{6}dUMP (in brackets): $\%g^+(\psi)$, 63% (<38%); $\%t(\phi)$ 75% (<67%). In view of the difficulties in measuring small couplings, these populations are deemed in good agreement with those calculated from Σ and Σ′ (Table 2).

The destabilization of the $g^+(\psi)$ rotamer in 5′m^{6}dUMP is reasonably interpreted in terms of a repulsive interaction between the electron pairs on the 2-keto oxygen of the *syn*-oriented m^{6}Ura base and the negatively charged 5′-phosphate. On the other hand, theoretical calculations (27) indicate that the 6-position of a thymine base (which sits over the furanose ring in the *anti*-oriented thy derivatives) is a positive centre and should favor a close approach (i.e. the $g^+(\psi)$ conformer) of the negatively charged 5′-phosphate. Thus, charge considerations form a reasonable basis for discussion of the large (30%) decrease in $\%g^+(\psi)$ in going from 5′dTMP to 5′m^{6}dUMP. Furthermore, on the basis of the charge associated with the 6-carbon and the 2-keto oxygen of the base, we can also understand the *increase* in $\%g^+(\psi)$ for 5′dTMP relative to dT and the *decrease* in $\%g^+(\psi)$ for 5′m^{6}dUMP relative to m^{6}dU. In addition the calculated $\%g^+(\psi)$ values for dT and m^{6}dU reveal a repulsion between the 2-keto oxygen and the polar 5′-hydroxyl but the data indicate that this interaction is attenuated relative to that involving the negatively charged phosphate. Our observation that the $\%g^+(\psi)$ values for dT and 3′dTMP on the one hand and for m^{6}dU and 3′m^{6}dUMP on the other are similar is reasonable since the 3′-phosphate is an *exo* substituent on the sugar whereas the base and 5′-position are *endo*.

The effect of the m^{6}Ura base bears a striking resemblance to that of the 6-azauracil base in that the latter has been shown to destabilize the $g^+(\psi)$ conformation in solution (28) and in the crystal state (29, 30). The 6-aza nitrogen of the 6-azauracil base lies over the ring in the *anti* conformation (29), and since this nitrogen is a negative centre (27), electrostatic repulsion of the 5′-phosphate could account for the reduction in $\%g^+(\psi)$ observed in solution (28) and the absence of $g^+(\psi)$ in the crystal state (29).

It is interesting to note that in the crystal state 5′-nucleotides which are not $g^+(\psi)$ prefer the $t(\psi)$ conformation (20, 29). No known nucleotides have the $g^-(\psi)$ conformation; at the nucleoside level $g^-(\psi)$ is found but less often than $t(\psi)$ (20). This is probably the consequence of unfavorable $O_{3'}$, $O_{5'}$ contacts in the $g^-(\psi)$ conformation, particularly

Can. J. Chem. Downloaded from www.nrcresearchpress.com by 210.87.254.40 on 09/05/12
For personal use only.

when the molecule is 3′*endo*. Our solution data, and nmr results in general, demonstrate that rotation out of $g^+(\psi)$ into $t(\psi)$ is preferred over rotation into $g^-(\psi)$. In this sense a correspondence between the solution and crystal state exists.

The apparent reduction in $\%t(\phi)$ in going from 5′dTMP to 5′m^{6}dUMP (Table 2) is probably not due to a *direct* influence of the polar 2-keto oxygen of the m^{6}Ura base. The reduction in $\%t(\phi)$ in 5′m^{6}dUMP is more likely a secondary phenomenon, i.e., it occurs subsequent to a rotation of the molecule out of $g^+(\psi)$ which was required by the repulsion of the base and backbone in 5′m^{6}dUMP. It is clear from space-filling models that, for steric reasons, $g^+(\phi)$ and $g^-(\phi)$ are unlikely for $g^+(\psi)$ oriented 5′-nucleotides whereas in $g^-(\psi)$ or $t(\psi)$, $g^+(\phi)$ and $g^-(\phi)$ become less sterically hindered. Thus, rotation out of $t(\phi)$ follows logically after rotation out of $g^+(\psi)$. We suggest that our data on the ribose derivatives of uracil and 6-azauracil derivatives (28) and the present data provide evidence that the C(5′)—O(5′) conformer distribution is determined primarily by the C(4′)—C(5′) conformation.

At this point it is useful to comment qualitatively on some of the trends in the H(4′), H(5′), and H(5″) chemical shifts noted for the thy and m^{6}Ura derivatives. It is interesting to note that thy-to-m^{6}Ura change leads to substantial upfield shifts (0.10–0.18 ppm) in H(4′), effects which are larger in absolute magnitude than the effects on H(3′), though H(3′) is closer to the base. These upfield shifts may be rationalized on the basis of the expected (31) shielding effect of a hydroxyl on a *gauche* oriented hydrogen and the deshielding effect expected when the hydrogen is *trans*. Thus, a 5′-hydroxyl should shield H(4′) when the molecule is $t(\psi)$ or $g^-(\psi)$ (Fig. 3). The upfield shifts of H(4′) in the m^{6}Ura series are in line with the increase in the $t(\psi)$ conformation at the expense of $g^+(\psi)$ (Table 2). Interestingly, the largest upfield effect for H(4′) (0.18 ppm) is noted at the 5′-phosphate level where the largest increase in $t(\psi)$ occurs for the thy-to-m^{6}Ura substitution.

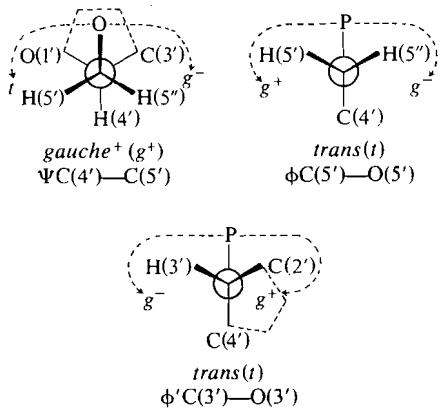

FIG. 3. Newman projections of the dominant conformations viewed along the C(4′)—C(5′) (ψ), C(5′)—O(5′) (ϕ), and C(3′)—O(3′) (ϕ′) bonds.

In aqueous solution the 5′- and 5″-hydrogen are generally insensitive to the thy-to-m^{6}Ura substitution. The exceptional case is H(5″) of 5′m^{6}dUMP which is shifted upfield by 0.13 ppm relative to its resonant position in 5′dTMP. That the H(5″) should be most affected is perhaps reasonable upon consideration of the increase in the $t(\psi)$ conformer population in 5′m^{6}dUMP (48%) relative to 5′dTMP (23%), since rotation into the $t(\psi)$ conformer juxtaposes H(5″) and the magnetically anisotropic 2-keto group of the base.

Conformation about the C(3′)—O(3′) (ϕ′) Bond

The vicinal coupling between H(3′) and the phosphorus atom in a 3′-nucleotide ($^3J_{P3'}$) is a reflection of the $g^+ \rightleftarrows t \rightleftarrows g^-$ blend for the ϕ′ bond (Fig. 3). However, the g^+ conformer may for steric reasons be excluded from consideration (32–34); in no instance does a crystalline 3′-nucleotidyl fragment possess the g^+ conformation (20). However, H(3′) is *gauche* to the phosphorus in both *t* and g^-, and thus $^3J_{P3'}$ values alone can not be used to assess the $t \rightleftarrows g^-$ blend. Some general comments on the ϕ′ conformation of 3′m^{6}dUMP and 3′dTMP may, however, be made.

The $^3J_{P3'}$ couplings (Table 1) lie in the range from 7.1 to 8.3 Hz and are considerably larger than the values expected for truly *gauche* (60° dihedral angle) couplings, that is, about 2 Hz (23). In $g^+(\phi')$ the coupled atoms (H,P) are *trans* and now a large (ca. 23 Hz) $^3J_{P3'}$ is expected (23). But if $g^+(\phi')$ is indeed unimportant, then the observed couplings for the 3′-nucleotides must be reflecting a bias away from the true *gauche* orientations towards the H(3′), P eclipsed conformation ($\phi' = -120°$; Fig. 3). Furthermore, the bias towards the eclipsed conformer must be similar for the pair of 3′-nucleotides at the lower temperature, their $^3J_{P3'}$ values differing by only 0.7 Hz. Interestingly, the increase in $^3J_{P3'}$ (1.2 Hz) with temperature in the 18–75°C range suggests that the bias in 3′m^{6}dUMP is slightly larger at the higher temperature. In contrast $^3J_{P3'}$ in 3′dTMP is independent of temperature in the 30–65°C range (10).

The bias towards the eclipsed conformer is consistent with X-ray data. Thus, in Sundaralingam's review of crystal structure determinations (20), we note that three entries are found in the $g^-(\phi')$ range, with an average ϕ′ value of −103°, while two entries are in the $t(\phi')$ range, with an average ϕ′ value of −144°. These are but 17 and 24°, respec-

tively from the H(3'),P eclipsed situation at $\phi' = -120°$. It is further interesting to point out $^3J_{P3'}$ couplings of 7–8 Hz are consistent[4] with ϕ' angles of about $-82°$ in the g^- range and $-158°$ in the t range.

In summary, the nucleoside 6-methyl-2'-deoxyuridine and its 3'- and 5'-monophosphate derivatives have been synthesized. The ^{1}Hmr data for these molecules are compared with those of the 2'-deoxythymidine and its 3'- and 5'-monophosphates. The data indicate that the 6-methyluracil derivatives are in the *syn* conformation in which the 2-keto oxygen of the base lies above the sugar ring. This leads to alterations in the sugar pucker, in particular, a flattening of the ring, and to a reduction in the g^+ conformation about the C(4')—C(5') bond. Our results for aqueous m^{6}dU are in agreement with those of Cadet *et al.* (6).

NOTE ADDED IN PROOF: Recently C. Giessner-Prettre and B. Pullman (J. Theor. Biol. **65**, 171 (1977)) have calculated the shielding influence of the 2-keto group of the base in pyrimidine nucleosides. They noted that H(2') is strongly deshielded when the molecule is *syn*. They noted also that H(3') should be more strongly deshielded when the sugar is 3'-*endo* than when it is 2'-*endo*. This is consistent with our observations that H(3') shift is more strongly affected by the thy-to-m^{6}Ura substitution in the ribosides than in the 2'-deoxyribosides, since the 3'-*endo* pucker makes a greater contribution in the former series of molecules (see discussion on the *n*-glycosyl linkage).

Acknowledgements

This work was supported by the National Research Council of Canada and by grants from the University of Manitoba and its Faculty of Graduate Studies for the purchase of a Bruker WH-90 spectrometer. We thank Dr. A. A. Grey of the Canadian 220 MHz centre for obtaining 220 MHz spectra and the Stanford Magnetic Resonance Laboratory for the 360 MHz spectra. The work at the SMRL is supported by grants from the NSF (GP23633) and the NIH (RR00711).

1. P. HART and J. DAVIES. J. Am. Chem. Soc. **93**, 753 (1971).
2. R. K. NANDA, R. TEWARI, G. GOVIL, and I. C. P. SMITH. Can. J. Chem. **52**, 371 (1974).
3. C. CHACHATY, T. YOKONO, S. TRAN-DINH, and W. GUSCHLBAUER. Biophys. Chem. **6**, 151 (1977).
4. D. W. MILES, M. J. ROBINS, R. K. ROBINS, M. W. WINKLEY, and H. EYRING. J. Am. Chem. Soc. **91**, 824 (1969); **91**, 831 (1969).
5. M. P. SCHWEIZER, E. B. BANTA, J. T. WITKOWSKI, and R. K. ROBINS. J. Am. Chem. Soc. **95**, 3770 (1973).
6. J. CADET, R. DUCOLOMB, and C. TAIEB. Tetrahedron Lett. 3455 (1975).
7. D. SUCK, W. SAENGER, and H. VORBRUGGEN. Nature, **235**, 333 (1972).
8. (*a*) A. HOLY. Coll. Czech. Chem. Commun. **38**, 3912 (1973); (*b*) A. HOLY. Tetrahedron Lett. 1147 (1973).
9. C. W. HAIGH and J. M. WILLIAMS. J. Mol. Spectrosc. **32**, 398 (1969).
10. D. J. WOOD, F. E. HRUSKA, and K. K. OGILVIE. Can. J. Chem. **52**, 3353 (1974).
11. R. G. S. RITCHIE and A. S. PERLIN. Carbohydr. Res. **55**, 121 (1977).
12. M. REMIN and D. SHUGAR. Biochem. Biophys. Res. Commun. **48**, 636 (1972).
13. D. J. WOOD, K. K. OGILVIE, and F. E. HRUSKA. Can. J. Chem. **53**, 2781 (1975).
14. H. DUGAS, B. J. BLACKBURN, R. K. ROBINS, R. DESLAURIERS, and I. C. P. SMITH. J. Am. Chem. Soc. **93**, 3468 (1971).
15. C. ALTONA and M. SUNDARALINGAM. J. Am. Chem. Soc. **95**, 2333 (1973).
16. C. H. LEE and R. H. SARMA. J. Am. Chem. Soc. **98**, 3541 (1976).
17. F. E. HRUSKA. J. Am. Chem. Soc. **93**, 1795 (1971).
18. W. SAENGER and K. H. SCHEIT. J. Mol. Biol. **50**, 153 (1970).
19. D. B. DAVIES and S. S. DANYLUK. Biochemistry, **14**, 543 (1975).
20. M. SUNDARALINGAM. *In* Proceedings international symposium on the conformation of biological molecules and polymers, symposia on quantum chemistry and biochemistry. Vol. 5. *Edited by* B. Pullman and E. D. Bergmann. Academic Press, Jerusalem. 1973. p. 417.
21. F. E. HRUSKA. *In* Proceedings international symposium on the conformation of biological molecules and polymers, symposia on quantum chemistry and biochemistry. Vol. 5. *Edited by* B. Pullman and E. D. Bergmann. Academic Press, Jerusalem. 1973. p. 345.
22. F. A. GREEN, R. D. ROSENSTEIN, R. SHIONO, D. J. ABRAHAM, B. L. TRUS, and R. E. MARSH. Acta. Crystallogr. **31**, B 102 (1975).
23. B. DONALDSON and L. D. HALL. Can. J. Chem. **50**, 2111 (1972).
24. C. H. LEE and R. H. SARMA. Biochemistry, **15**, 697 (1976).
25. R. H. SARMA, R. J. MYNOTT, D. J. WOOD, and F. E. HRUSKA. J. Am. Chem. Soc. **95**, 6457 (1973).
26. P. J. COZZONE and O. JARDETZKY. Biochemistry, **15**, 4860 (1976).
27. B. PULLMAN and A. PULLMAN. Quantum biochemistry. Interscience, New York, NY. 1963.
28. D. J. WOOD, F. E. HRUSKA, R. J. MYNOTT, and R. H. SARMA. Can. J. Chem. **51**, 2571 (1973).
29. W. SAENGER and D. SUCK. Nature, **242**, 610 (1973).
30. W. SAENGER. Angew. Chem. Int. Ed. **12**, 591 (1973).
31. R. U. LEMIEUX and D. R. LINEBACK. Ann. Rev. Biochem **32**, 155 (1963).
32. B. PULLMAN, D. PERAHIA, and A. SARAN. Biochem Biophys. Acta, **269**, 1 (1972).
33. W. K. OLSON. Biopolymers, **12**, 1787 (1973).
34. S. G. BROYDE, R. M. WARTELL, S. D. STELLMAN, B HINGERTY, and R. LANGRIDGE. Biopolymers, **14**, 159 (1975).

[4]Assuming the applicability of the equation $^3J_{PH}$ (Hz) = 18.1 $\cos^2\theta - 4.08 \cos\theta$ where θ is the dihedral angle in the H—C—O—P fragment (24).

Can. J. Chem. Downloaded from www.nrcresearchpress.com by 210.87.254.40 on 09/05/12
For personal use only.

The reductive denitration of carbohydrate α-nitroepoxides by sodium borohydride[1]

HANS H. BAER AND CHUKWUEMEKA B. MADUMELU

Department of Chemistry, University of Ottawa, Ottawa, Ont., Canada K1N 6N5

Received November 3, 1977

HANS H. BAER and CHUKWUEMEKA B. MADUMELU. Can. J. Chem. **56**, 1177 (1978).

Action of sodium borohydride upon sugar derivatives that contain an α-nitrooxirane grouping leads to reductive denitration producing high yields of α-hydroxy-β-deoxy derivatives. Thus, 5,6-anhydro-1,2-*O*-isopropylidene-6-nitro-α-D-glucofuranose (**2**) gave 5-deoxy-1,2-*O*-isopropylidene-α-D-*xylo*-hexofuranose (**3**). The methyl 2,3-anhydro-4,6-*O*-benzylidene-3-nitrohexopyranosides having the β-D-*talo* (**4**), β-D-*allo* (**5**), and β-D-*manno* (**6**) configurations readily afforded methyl 4,6-*O*-benzylidene-2-deoxy-β-D-*lyxo*-hexopyranoside (**10**; from **4**) and its β-D-*arabino* isomer (**11**; from **5** and **6**). The corresponding nitroepoxy glycoside of α-D-*talo* configuration (**7**) reacted more slowly and gave a mixture of 3-epimeric 2-deoxyglycosides, the analogous α-D-*lyxo* (**13**) and α-D-*xylo* (**14**) compounds. The α-D-*manno* (**8**) and β-D-*gulo* (**9**) nitroepoxides proved unreactive under the same conditions. Stereochemical factors considered to be important in these denitrations are discussed.

HANS H. BAER et CHUKWUEMEKA B. MADUMELU. Can. J. Chem. **56**, 1177 (1978).

L'action du borohydrure de sodium sur des dérivés de sucre contenant les groupes α-nitro-oxiranes conduit à la dénitration réductive produisant avec de bons rendements des dérivés α-hydroxy β-désoxy. Ainsi le 5,6-anhydro-1,2-*O*-isopropylidène-6-nitro-α-D-glucofuranose (**2**) conduit au 5-désoxy-1,2-*O*-isopropylidène-α-D-*xylo*-hexofuranose (**3**). Les méthyl-2,3-anhydro-4,6-*O*-benzylidène-3-nitrohexopyranosides possédant les configurations β-D-*talo* (**4**), β-D-*allo* (**5**) et β-D-*manno* (**6**) fournissent facilement le méthyl-4,6-*O*-benzylidène-2-désoxy-β-D-*lyxo*-hexopyranoside (**10** à partir de **4**) et son isomère β-D-*arabino* (**11** à partir de **5** et **6**). Le nitroépoxy-glycoside correspondant de configuration α-D-*talo* (**7**) réagit plus lentement et conduit à un mélange d'épimères en position 3 de 2-désoxy-glycosides, les analogues α-D-*lyxo* (**13**) et α-D-*xylo* (**14**). On a noté que les nitroépoxydes α-D-*manno* (**8**) et β-D-*gulo* (**9**) ne sont pas réactifs dans ces conditions. On discute des facteurs stéréochimiques que l'on considère être importants dans ces dénitrations.

Carbohydrate derivatives containing an α-nitrooxirane moiety were first obtained some years ago in our laboratory (3–6) and, independently, by Japanese investigators (7), Following the prior use of epoxidized nitrochalcones as intermediates in two special instances of flavonol synthesis (8, 9), the preparation and some chemical transformations of various aliphatic and araliphatic α-nitrooxiranes were studied in more general ways (10–14). Although the available data are still limited in scope, it is already evident that this functionality lends itself to a wide range of reactions with considerable synthetic appeal and mechanistic interest. In the realm of carbohydrate α-nitroepoxides, of which several are now readily available, efforts aimed at exploiting their potential have been disclosed in preliminary communications by the Japanese group (15) and ourselves (2), and we now wish to detail more fully those parts of our results which pertain to the action of sodium borohydride upon these sugar derivatives.

Subjects of our research were one compound that carried an α-nitrooxirane grouping terminally outside the sugar ring, and several compounds in which this moiety was present on the ring itself. The former was 5,6-anhydro-1,2-*O*-isopropylidene-6-nitro-α-D-glucofuranose (**2**), newly prepared for the present work from 3-*O*-acetyl-5,6-dideoxy-1,2-*O*-isopropylidene-6-nitro-α-D-*xylo*-hex-5-enofuranose (**1**) (16) by the method (5) of epoxidation with alkaline hydrogen peroxide.[2] The latter set of substrates

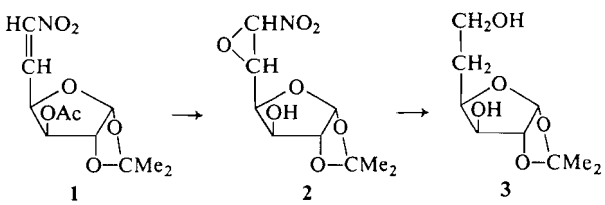

1 **2** **3**

[1]Part 39 in a series on reactions of nitro sugars. For part 38 see ref. 1. The essential features of the research detailed in this article were presented at the 7th International Symposium on Carbohydrate Chemistry, Bratislava, Czechoslovakia, in August 1974. The main body of the work is contained in the Ph.D. thesis submitted in 1976 to this University by C.B.M. For a preliminary communication see ref. 2. The experiments with compound **6** were performed as part of a B.Sc. thesis project (1976–1977) by Mr. Pierre G. Potvin whom the authors thank for his contribution.

[2]Compound **2**, which was isolated crystalline in 64% yield, appeared to be the only product in this epoxidation, as judged from tlc. The D-*gluco* configuration was revealed by catalytic hydrogenation giving (2) the known 6-amino-6-deoxy-1,2-*O*-isopropylidene-α-D-glucofuranose. The configuration at C-6 is not known with certainty; however, a very small coupling constant, $J_{5,6} < 1$ Hz, is suggestive of a H-5,6 *trans* geometry implying the *R* configuration.

Can. J. Chem. Downloaded from www.nrcresearchpress.com by 210.87.254.5 on 09/05/12
For personal use only.

Can. J. Chem. Downloaded from www.nrcresearchpress.com by 210.87.254.5 on 09/05/12
For personal use only.

comprised the previously-described (5, 6), stereoisomeric methyl 2,3-anhydro-4,6-*O*-benzylidene-6-nitrohexopyranosides having the β-D-*talo* (**4**), β-D-*allo* (**5**), β-D-*manno* (**6**), α-D-*talo* (**7**), α-D-*manno* (**8**), and β-D-*gulo* (**9**) configurations.

A majority of these α-nitroepoxides were readily attacked by sodium borohydride at room temperature, to give 60–80% yields of nitrogen-free reduction products. Thus, compound **2** furnished within 15 min a single product (according to tlc) which was isolated crystalline in 60% yield and identified as the known (17) 5-deoxy-1,2-*O*-isopropylidene-α-D-*xylo*-hexofuranose (**3**). Similarly, the pyranosidic, stereoisomeric sugar derivatives **4**, **5**, and **6** reacted smoothly in analogous fashion to afford 2-deoxyglycosides. Evidently, hydride ion causes nucleophilic displacement of the oxirane bond at the carbon atom distal to the nitro group, and this process entails elimination of nitrite ion, with a deoxycarbonyl intermediate so formed being immediately reduced to the carbinol stage by excess reagent (Scheme 1).

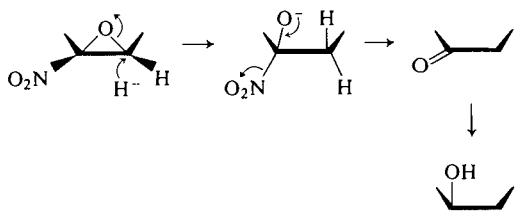

SCHEME 1

The β-D-*talo* glycoside **4** reacted most readily, yielding 76% of crystalline methyl 4,6-*O*-benzylidene-2-deoxy-β-D-*lyxo*-hexopyranoside (**10**) after a reaction of 30 min in ethanolic medium. No second product was detected. The structure of **10** was conclusively deduced from nmr data. There was an octet for H-3 showing a large coupling ($J_{2a,3}$ = 12 Hz), which required H-3 to be axially arranged.

Under the same reaction conditions, the β-D-*allo* glycoside (**5**) reacted somewhat more slowly (1.5–2 h), giving two products that were isolated crystalline in 60 and 20% yields, respectively. The main product proved to be methyl 4,6-*O*-benzylidene-2-deoxy-β-D-*arabino*-hexopyranoside (**11**)[3] in conformity with the preceding example, whereas the minor product (**12**) was found to lack a deoxy function and to possess an *O*-ethyl group instead. This group was evidently incorporated as a result of ethanol competing with the borohydride in attack at C-2 of the nitro epoxide. Indeed, substitution of the alcohol by

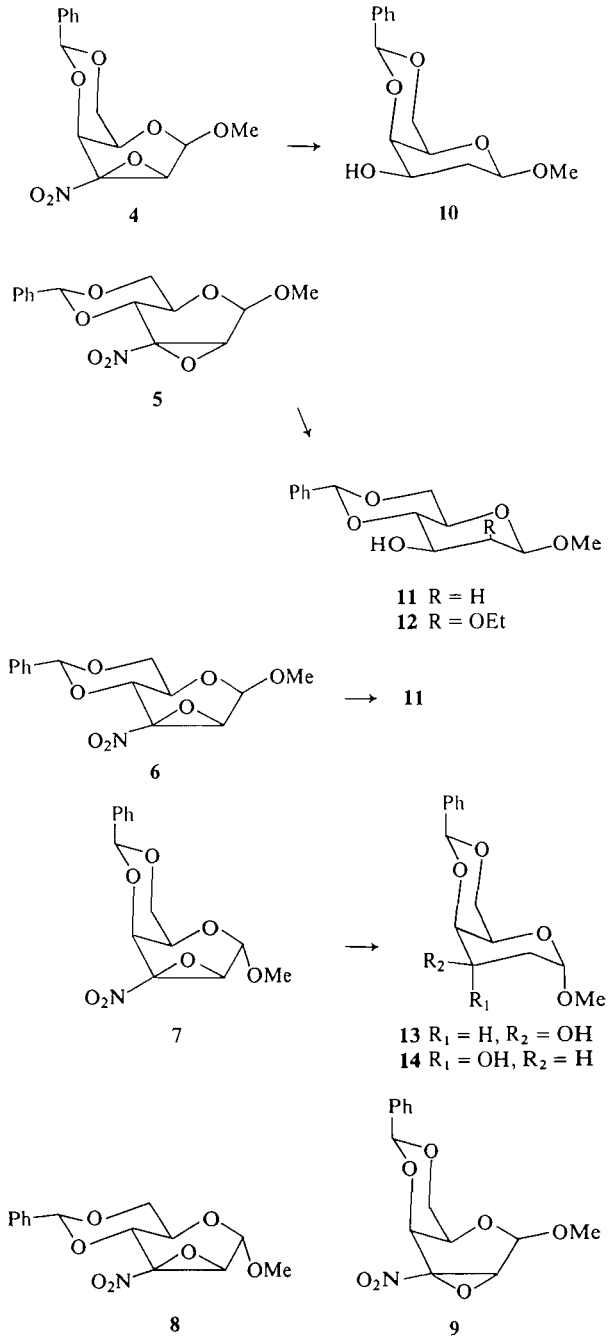

11 R = H
12 R = OEt

13 R_1 = H, R_2 = OH
14 R_1 = OH, R_2 = H

acetonitrile as the solvent led to **11** in better than 90% yield. Similarly, **11** was the only detectable product, isolated crystalline in 72% yield, in the reduction of the β-D-*manno* epoxide **6** in acetonitrile solution.[4]

[3]Compound **11** was first isolated and identified in pilot experiments by Dr. W. Rank in this laboratory. It was also obtained, in noncrystalline condition, by Kumazawa *et al.* (15) who reduced **5** with lithium aluminum hydride in tetrahydrofuran and characterized the product by acetylation.

[4]Small-scale tests indicated that dioxane or 2-propanol may also serve as solvents without giving rise to by-products, although the reactions were somewhat slower than in acetonitrile (3 h vs. 90 min). Ethanol was not tried with **6**, partly because of poor solubility.

Can. J. Chem. Downloaded from www.nrcresearchpress.com by 210.87.254.5 on 09/05/12
For personal use only.

The structure of **11** produced from both **5** and **6** was firmly established by acid hydrolysis to give 2-deoxy-D-*arabino*-hexose, identified as its known (18), crystalline anilide, and by an independent synthesis (19). The axial orientation of H-3 was confirmed by the splitting patterns of the high-field, H-2a and H-2e multiplets in the nmr spectrum. As regards the by-product **12**, its constitution was assigned on the basis of elemental analysis and substituent resonances present in the nmr spectrum. The ethoxy group at C-2 doubtless was axially oriented since a very small coupling of the anomeric proton, the signal of which was an apparent singlet, indicated an equatorial H-2. A decision between the β-D-*manno* and β-D-*altro* configurations was not possible on the basis of the available spectral data, but we tentatively allocated the former since the specific rotation of **12** ($[\alpha]_D$ −126°, in ethanol) resembled more closely those reported (20) for methyl 4,6-*O*-benzylidene-β-D-mannopyranoside and its 2-*O*-benzyl ether ($[\alpha]_D$ −98 and −131°, in chloroform) than those (21) of the corresponding altropyranoside and its 2-*O*-methyl ether ($[\alpha]_D$ −60 and −48°, in ethanol and chloroform, respectively). Moreover, equatorial placement of the hydroxyl group generated at C-3 appeared to be favored in these reductions, at least as far as β-glycosides are concerned.

In contrast to the high reactivity of the aforementioned nitroepoxide isomers, the α-D-talo glycoside **7** did not react under the same, mild conditions. However, in *boiling* ethanol in the presence of an increased proportion of sodium borohydride, it was completely consumed after 50 min and afforded the known, 3-epimeric, α-D-*lyxo* and α-D-*xylo* 2-deoxyglycoside derivatives **13** (22) and **14** (23) in yields of 50 and 40%, respectively. The α-D-*manno* (**8**) and β-D-*gulo* (**9**) nitroepoxides were completely inert towards sodium borohydride at room temperature, even when exposed to the ethanolic reagent for up to 48 h. They did react at reflux temperature but then gave complex mixtures of products that could not be unravelled. Attempted reductions with lithium aluminum hydride in ether at ambient temperature likewise failed to give identifiable products.

Stereochemical Considerations

The presence of the nitro group evidently governs the regioselectivity of nucleophilic attack on the oxirane ring so that the β-carbon atom is always the favored site. This effect may reverse the regioselectivity from what would be predicted for ring opening in the absence of this substituent. Thus, where an epoxide ring occupies a terminal position (as in 5,6-anhydro-1,2-*O*-isopropylidene-α-D-glucofuranose, the non-nitro analog of **2**), almost exclusive nucleophilic attack takes place at the terminal carbon atom (24), whereas **2** was attacked at the penultimate C-5. When an epoxide ring is 2,3-fused to a pyranoside ring which, in turn, bears a cyclic 4,6-acetal blocking group and is thereby rendered conformationally rigid (*trans*-fused acetals) or at least less flexible (*cis*-fused acetals), then a nucleophilic reagent normally gives one preponderant product, namely, according to the Fürst–Plattner rule, that which arises from diaxial ring opening (25). This means that in hydride reductions of non-nitro analogs of **4–9**, the hydride ion enters axially at C-2 when the oxirane ring is below the pyranose plane, but axially at C-3 when it is above that plane (25). Now in those nitro derivatives (**4–7**) which reacted to give identifiable products, attack occurred exclusively at C-2 regardless of the orientation of the ring. Hence, only for the β-D-*allo* epoxide **5** did the pathway conform with the Fürst–Plattner rule. However, this does not necessarily signify an unusual mode of diequatorial ring opening in the cases where the rule is seemingly violated (**4**, **6**, and **7**). At least in the β- and α-D-*talo* compounds **4** and **7** with their more flexible *cis*-fused structures, a transition state involving half-chair inversion could be invoked to allow for diaxial opening, but such an assumption would create problems. Firstly, as shown in Scheme 2 one would expect in this event

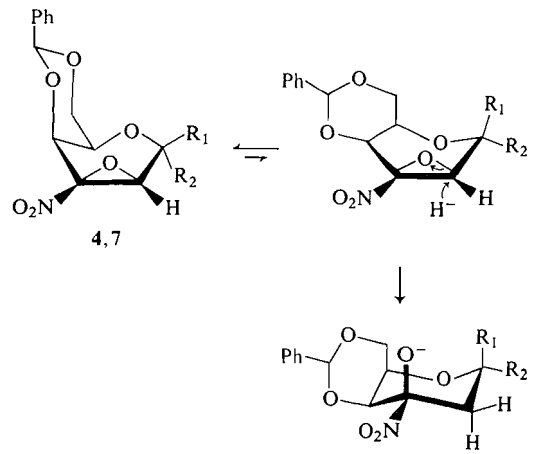

SCHEME 2

the reaction of **4** (R_1 = OMe, R_2 = H) to be more difficult than that of **7** (R_1 = H, R_2 = OMe) because of severe, *syn*-triaxial crowding, which is contrary to the observed relative reactivities of the two compounds. In fact, **4** appears even more reactive than the β-D-*allo* isomer **5** for which diaxial opening does not require a similar conformational inversion. Moreover, the β-D-*manno* epoxide **6** reacts, more readily than **7**, even though it is incapable of assuming the inverted half-chair form because of its *trans*-fused structure. To retain the concept of favored diaxial ring opening one could perhaps

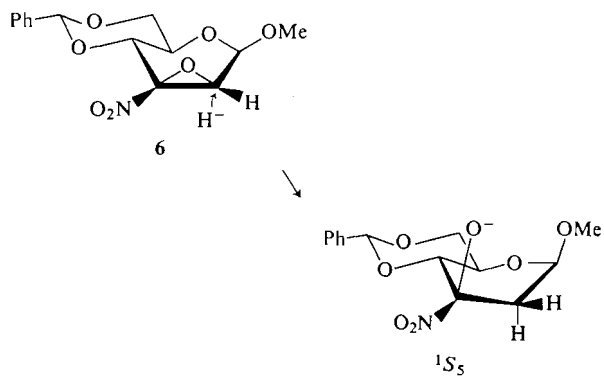

SCHEME 3

consider twist boat-like transition states in which the incoming hydride and displaced oxygen anions are close to being disposed *anti*-diaxially, e.g., the $^1S_5$ conformation of **6** (Scheme 3). A similar form, $^0S_2$, could also apply to **4** and **7** as an alternative to the inverted half-chair discussed above.

However, consideration of conformational changes possible or necessary to attain favorable transition states for ring opening does not account for the differential behavior of all the compounds **4**–**9**. In particular, the striking inertness of the α-D-*manno* isomer **8** and the β-D-*gulo* isomer **9** as compared to **6** and **5**, respectively, as well as the lesser reactivity of **7** as compared to **4** remain unexplained by such reasoning. It is suggested that an essential factor in these reactions is the relative facility of approach of the nucleophile. Thus, backside attack at C-2 appears unhindered in the β-glycosides **4**, **5**, and **6**, whereas in the α-glycosides **7** and **8** it is likely interfered with by the neighboring, pseudoaxial methoxyl group. This interference is severer in the rigid structure **8** than in more flexible[5] **7** which at elevated temperature undergoes a straightforward reaction (albeit without stereoselectivity in the subsequent reduction[6] of the primary product to the alcohol stage). The unreactive β-D-*gulo* isomer **9** requires, like the reactive β-D-*allo* isomer **5**, attack from the upper face of the pyranose ring for facile opening of the oxirane, and it is interesting to observe that the only structural feature distinguishing **9** from **5**, namely the axial oxygen function at C-4, effectively prevents a *syn*-axial approach of hydride ion to C-2.

Catalytic hydrogenations of **4**–**9** also show interesting stereochemical dependencies but furnish altogether different types of products (2). Details will be recorded elsewhere.

Experimental

Melting points were taken with an electrically heated aluminum block apparatus and are uncorrected. Optical rotations were determined at ambient temperature in a Perkin-Elmer 141 automatic polarimeter using a 1-dm cell. Infrared data refer to Nujol mulls. The nmr spectra were recorded from $CDCl_3$, solutions at 100 MHz, with tetramethylsilane added as internal standard, unless otherwise specified. Reactions were routinely monitored by tlc on plates coated with silica gel N/UV_{254} (Macherey & Nagel Co., Germany); the spots were made visible by spraying the plates with 1% ceric sulfate in 10% aqueous sulfuric acid, followed by heating. The following developing systems (v/v) were used: *A*, methanol–chloroform, 1:2; *B*, ethyl acetate – petroleum ether (bp 60–80°C), 1:1; *C*, the same, 2:3; *D*, the same, 1:2; *E*, ethyl acetate – carbon tetrachloride, 2:3; *F*, the same, 1:3.

5,6-Anhydro-1,2-O-isopropylidene-6-nitro-α-D-glucofuranose(2)

To a solution of the nitroolefin **1** (16) (92 mg) in 99% ethanol (10 ml) was added 30% aqueous hydrogen peroxide (0.5 ml), with stirring at room temperature, and the p*H* of the mixture was brought to about 8.5 (indicator paper) by dropwise addition of a saturated aqueous sodium bicarbonate solution. According to tlc (solvent *B*), **1** was completely replaced by a single, more slowly moving product (**2**) after 50 min. The reaction mixture was extracted several times with chloroform, and the extract was washed twice with water, dried ($MgSO_4$), and evaporated to give 65 mg (78%) of syrupy **2**. The syrup crystallized from chloroform – petroleum ether (bp 30–60°C) yielding 53 mg (64%) of needles, mp 127–128°C, raised to 134–135°C by recrystallization from ethyl acetate – petroleum ether; $[\alpha]_D$ −5° (*c*. 0.4, $CHCl_3$); ν_{max} 3400 (OH) and 1560 cm^{-1} (NO_2); nmr τ: 4.06 (d, 1H, $J_{1,2}$ = 3.5 Hz, H-1), 4.48 (s, 1H, H-6), 5.48 (d, 1H, $J_{1,2}$ = 3.5 Hz, H-2), 5.59 (q, collapsing to d on D_2O exchange, 1H, $J_{3,4}$ = 3 Hz, H-3), 5.76 (q, 1H, $J_{3,4}$ = 3, $J_{4,5}$ = 4 Hz, H-4), 6.20 (d, 1H, $J_{4,5}$ = 4 Hz, H-5), 7.48 (d, 1H, removable by D_2O, $J_{3,OH}$ = 4.5 Hz, OH-3), 8.50, 8.66 (s, 2 × 3H, Me_2C). *Anal.* calcd. for $C_9H_{13}NO_7$ (247.2): C 43.73, H 5.30, N 5.67; found: C 43.82, H 5.34, N 5.81.

General Procedure for Borohydride Reductions

Unless otherwise specified, the reactions were performed and the reaction mixtures processed in the following way. The finely divided nitroepoxide was dissolved, under brief and moderate warming if necessary, in the stated volume of solvent, usually 99% ethanol. Cooled to room temperature, the solution or partial suspension was magnetically stirred and a 10-molar excess of solid sodium borohydride was added in portions during a period of several minutes. The flask was then stoppered, and progress of the reaction was checked periodically by tlc. Complete consumption of the starting compound was noted after the periods of time indicated. The solution was deionized with a cation exchange resin which after filtration was washed thoroughly with methanol or ethanol. The filtrate was evaporated at reduced pressure, and 5–6 portions (10 ml each) of methanol were successively added to, and evaporated from, the residue in order to remove boric acid. Typically, a flame test for boric acid was then negative.

[5]Molecular models of **8** and **7** show that a conformational change that would move the glycosidic methoxyl group outwards and out of the way of the approaching nucleophile is associated with a movement of the nitro group that would increase nonbonded interaction (similar to $A^{1,2}$ strain) between the latter and O-4 in **8** but not in **7**.

[6]The loss of stereoselectivity attributable to the presence of an axial substituent at C-1, and the preference for formation of equatorial alcohols in the preceding examples, is in line with expectations based on the stereochemistry of cyclohexanone reductions recently reviewed (26).

Can. J. Chem. Downloaded from www.nrcresearchpress.com by 210.87.254.5 on 09/05/12
For personal use only.

Can. J. Chem. Downloaded from www.nrcresearchpress.com by 210.87.254.5 on 09/05/12
For personal use only.

The resulting, syrupy or solid residue was subsequently crystallized or purified as stated.

5-Deoxy-1,2-O-isopropylidene-α-D-xylo-hexofuranose (3)

The nitroepoxide **2** (40 mg) and sodium borohydride (52 mg) in ethanol (20 ml) reacted within 15 min to give a single product (tlc in solvent *B*). The dried syrup (34 mg) crystallized from ethyl acetate – petroleum ether yielding **3** (20 mg, 63%), mp 92–93°C, $[\alpha]_D$ −8° (*c* 0.4, $CHCl_3$) (lit. (17) mp 94°C, $[\alpha]_D$ −10° ($CHCl_3$)). *Anal.* calcd. for $C_9H_{16}O_5$ (204.2): C 52.93, H 7.90; found: C 52.69, H 7.82.

Methyl 4,6-O-Benzylidene-2-deoxy-β-D-lyxo-hexopyranoside (10)

The reaction between the nitroepoxide **4** (5) (100 mg) and sodium borohydride (130 mg) in ethanol (40 ml) was complete after 30 min and gave a single spot in tlc (solvent *A*). Processing furnished a solid product which was passed through a column (19 cm × 1 cm) of silica gel (40 g) by means of chloroform. Evaporation of the fractions that contained **10** yielded 66 mg (76%) of crystals, mp 200–204°C, $[\alpha]_D$ −40.5° (*c* 0.5, $CHCl_3$); nmr τ: 2.6 (m, 5H, Ph), 4.43 (s, 1H, $PhCHO_2$), 5.65 (q, 1H, $J_{1,2a}$ = 8.7, $J_{1,2e}$ = 2 Hz, H-1), 5.69 (q, narrow, 1H, H-4), 5.9 region (m, 2H, H-6,6′), 6.21 (m, broad, 1H; becomes a clear octet on D_2O exchange, $J_{3,4}$ = 3.5, $J_{2e,3}$ = 5.5, $J_{2a,3}$ = 12 Hz, H-3), 6.51 (s, 3H, OMe), 6.65 (m, narrow, 1H, H-5), 7.7 (broad peak, 1H, removed by D_2O, OH), 7.85–8.35 (m, 2H, H-2e,2a). *Anal.* calcd. for $C_{14}H_{18}O_5$ (266.3): C 63.14, H 6.81; found: C 63.13, H 6.86.

Methyl 4,6-O-Benzylidene-2-deoxy-β-D-arabino-hexopyranoside (11)

(A) From Nitroepoxide 5

A solution of compound **5** (5) (1.0 g) in warm, 99% ethanol (375 ml) was cooled to room temperature, and sodium borohydride (1.0 g) was added in small portions, with stirring. Another 0.3 g of borohydride was added after 1 h and the reaction mixture was worked up after 1.5 h when **5** had been completely replaced by two products that moved more slowly in tlc (solvent *C*). The slower one (**11**) predominated. Crystallization of the syrupy product mixture from chloroform – petroleum ether yielded a first crop of **11** (163 mg, mp 150–151°C). Evaporation of the mother liquor gave a crystalline mixture of **11** and the faster moving by-product (**12**), which was chromatographed on a column (47 cm × 2 cm) of silica gel (110 g) by use of solvent *D* as eluent. The first chromatographically homogeneous fractions were evaporated to give syrupy **12** (182 mg, 20%), further described in a subsequent section. Later fractions furnished a second crop (271 mg) of **11** melting at 148–149°C, undepressed on admixture of the previous crop. The combined amount of **11** (434 mg, 60%) was recrystallized from ethyl acetate – petroleum ether and then had mp 155–156°C and $[\alpha]_D$ −67° (*c* 0.5, $CHCl_3$) (lit. (19) for **11** from an independent synthesis: mp 156–157°C, $[\alpha]_D$ −66.2°). Infrared and nmr spectra were identical; nmr τ: 2.6 (m, 5H, Ph), 4.49 (s, 1H, $PhCHO_2$), 5.54 (q, 1H, $J_{1,2a}$ = 9.5, $J_{1,2e}$ = 2.3 Hz, H-1), 5.7 (m, 1H, probably H-6), 6.2–6.4 and 6.6–6.8 (unresolved m, 4H, H-3,4,5,6′), 6.51 (s, 3H, OMe), 7.22 (broad s, exchangeable by D_2O, OH), 7.78 (o, 1H, $J_{1,2e}$ = 2.3, $J_{2e,3}$ = 5, $J_{2a,2e}$ = 13 Hz, H-2e), 8.36 (o, 1H, $J_{1,2a}$ = 9.5, $J_{2a,3}$ = 11.5, $J_{2a,2e}$ = 13 Hz, H-2a). *Anal.* calcd. for $C_{14}H_{18}O_5$ (266.3): C 63.14, H 6.81; found: C 63.11, H 6.82.

When **5** (31 mg) in acetonitrile (3 ml) was treated with sodium borohydride (38 mg initially, plus 12 mg after 1 h), there was obtained crystalline **11** (26 mg, 97%) showing $[\alpha]_D$ −63.8° (*c* 1.3, $CHCl_3$). It contained a small amount of an unidentified by-product (migrating faster in tlc than both **11** and **12**) which was removed by one recrystallization from ether – petroleum ether; **11** then melted at 158–159°C.

(B) From Nitroepoxide 6

The nitroepoxide **6** (6) (200 mg) in acetonitrile (20 ml) was treated with sodium borohydride (250 mg) at room temperature for 90 min, after which the reaction was nearly complete and **11** was the only product revealed by tlc (solvent *C*). Work-up after deionization with Amberlite IRC-50 (H^+) afforded a crystalline material (171 mg) which was recrystallized from hot methanol by careful addition of water to incipient cloudiness followed by cooling. There was obtained pure **11** (111 mg, 72%) in two crops, mp 157–158 and 159–160°C, $[\alpha]_D$ −69° (*c* 0.5, $CHCl_3$). The infrared spectrum was superimposable on that of **11** from *A*.

(C) Conversion of 11 into 2-Deoxy-β-D-arabino-hexose Anilide

Compound **11** (65 mg) was hydrolyzed in 0.05 *M* hydrochloric acid by stirring for 4 h at 25°C followed by heating on the steam bath for 2 h. The pale yellow hydrolyzate was neutralized using Dowex-1X2 resin (carbonate form) which, after filtration, was washed well with water. Evaporation of the filtrate and drying of the oily residue by several coevaporations with added benzene gave a syrup whose nmr spectrum confirmed the complete removal of the benzylidene and the methoxy group. The product was then heated on a steam bath for 1.5 h with aniline (0.2 ml) in ethanol (2 ml), which led to a single derivative (tlc with solvent *A*). The solution was decolorized with activated charcoal and refrigerated overnight whereby the crystalline *anilide* (20 mg, 74%) was deposited; mp 193–194°C, $[\alpha]_D$ −162.4° → −103° (*c* 1, pyridine, 2 days) (lit. (18) mp 193–194°C, $[\alpha]_D$ −138° → −106° (pyridine, 2 days).

Methyl 4,6-O-Benzylidene-2-O-ethyl-β-D-mannopyranoside (12)

The syrupy **12** isolated by column chromatography (see above) gave crystals (155 mg) from ethyl acetate – petroleum ether; mp 129°C, unchanged on recrystallization; $[\alpha]_D$ −126° (*c* 0.4, ethanol); nmr ($CDCl_3$) τ: 2.6 region (m, 5H, Ph), 4.47 (s, 1H, $PhCHO_2$), 5.59 (s, 1H, $J_{1,2}$ ~ 0 Hz, H-1), 5.69 (q, *J* = 5 and 10 Hz, H-6), 5.8–6.4 (unresolved m, 6H, H-2,3,4,6′, and CH_2 of OEt), 6.49 (s, 3H, OMe), 6.7 (broad m, H-5), 7.5 (broad peak, 1H, removed by D_2O exchange, OH), 8.78 (t, 3H, *J* = 6.5 Hz, CH_3 of OEt). In acetone-d_6, H-1 resonated at τ 5.48, H-6 at 5.80, OMe at 6.57, and CH_3 of OEt at 8.86. *Anal.* calcd. for $C_{16}H_{22}O_6$ (310.3): C 61.92, H 7.15; found: C 61.76, H 7.20.

Methyl 4,6-O-Benzylidene-2-deoxy-α-D-lyxo-hexopyranoside (13) and Methyl 4,6-O-Benzylidene-2-deoxy-α-D-xylo-hexopyranoside (14)

The nitroepoxide **7** (5) (300 mg) in ethanol (66 ml) was treated with sodium borohydride (732 mg) which was added in portions in the course of several hours. No appreciable reaction was observed (tlc in solvent *E*). The mixture was therefore heated at reflux temperature, whereupon two faster-moving products appeared but some **7** was still left after 35 min. Additional borohydride (366 mg) was introduced and heating was continued for another 15 min after which **7** was completely consumed. The product mixture obtained upon work-up was chromatographed on a column (19 cm × 1 cm) of silica gel (40 g) by use of solvent *F*. The faster moving α-D-*xylo* isomer (**14**) was isolated from early fractions as a syrup (93 mg, 40%) that was homogeneous in tlc. The α-D-*lyxo* isomer (**13**) was obtained from subsequent fractions as needles, mp 167–175°C, in a yield of 106 mg (50%).

Recrystallized from ethyl acetate – petroleum ether, **13**

showed mp 186–188°C and $[\alpha]_D$ +117.5° (*c* 0.3, $CHCl_3$) (lit. (22*a*) mp 184–185°C, $[\alpha]_D$ +104° (*c* 0.3, ethanol) and (22*b*) mp 178–179°C, $[\alpha]_D$ +106° (*c* 0.62, $CHCl_3$)); nmr τ: 2.60 (m, 5H, Ph), 4.43 (s, 1H, $PhCHO_2$), 5.09 (t, 1H, $J_{1,2e} = J_{1,2a} = 2.5$ Hz, H-1), 5.73 (q, 1H, $J_{5,6} = 1.8$, $J_{6,6'} = 13$ Hz, H-6), 5.8–6.1 (m, 3H, H-3,4,6′), 6.39 (narrow m, H-5), 6.68 (s, 3H, OMe), 7.85 (broad peak, 1H, exchangeable, OH), 8.0 (overlapping m, 2H, H-2e,2a). *Anal.* calcd. for $C_{14}H_{18}O_5$ (266.3): C 63.14, H 6.81; found: C 63.24, H 6.94.

The syrupy isomer **14** was crystallized from chloroform – petroleum ether; mp 99–101°C, unchanged on recrystallization, $[\alpha]_D$ +78° (*c* 0.5, $CHCl_3$) (lit. (23) mp 102–104°C, $[\alpha]_D$ +79° ($CHCl_3$)). nmr τ: 2.65 (m, 5H, Ph), 4.44 (s, 1H, $PhCHO_2$), 5.24 (narrow q, 1H, $J_{1,2a} = 4$, $J_{1,2e} < 1$ Hz, H-1), 5.82 (center of two AB quartets, $J_{5,6a} = J_{5,6e} = 2$Hz, $J_{6a,6e} = 12$ Hz, H-6,6′), 6.05–6.2 (overlapping narrow m, 3H, H-3,4,5), 6.62 (s, 3H, OMe), 7.74 and 8.16 (2 doublets of narrow triplets, $J_{2a,2e} = 14$ Hz, H-2a,2e). *Anal.* calcd. for $C_{14}H_{18}O_5$ (266.3): C 63.14, H 6.81; found: C 63.31, H 6.91.

Acknowledgement

Support of this research by the National Research Council of Canada is gratefully acknowledged.

1. H. H. Baer and F. F. Z. Georges. Can. J. Chem. **55**, 1348 (1977).
2. H. H. Baer and C. B. Madumelu. Carbohydr. Res. **39**, C8 (1975).
3. H. H. Baer and W. Rank. American Chemical Society and Chemical Institute of Canada Joint Conference, Toronto, Ontario, May 1970. Abstr. CARBO 12.
4. W. Rank. Ph.D. Thesis, University of Ottawa, Ottawa, Ont. 1971.
5. H. H. Baer and W. Rank. Can. J. Chem. **49**, 3192 (1971).
6. H. H. Baer and W. Rank. Can. J. Chem. **51**, 2001 (1973).
7. T. Sakakibara, S. Kumazawa, and T. Nakagawa. Bull. Chem. Soc. Jpn. **43**, 2655 (1970).
8. M. K. Shakhova, Y. Litkei, and G. I. Samokhvalov. Doklady Akad. Nauk SSSR, **151**, 1120 (1963); Engl. Ed. 644 (1963); Chem. Abstr. **59**, 13929 (1963).
9. M. I. Budagyants, M. K. Shakhova, and G. I. Samokhvalov. Zh. Org. Khim. **5**, 1857 (1969); Engl. Ed. 1803 (1969); Chem. Abstr. **72**, 21600 (1970).
10. H. Newman and R. B. Angier. Chem. Commun. 369 (1969); Tetrahedron, **26**, 825 (1970).
11. N. A. Sokolov, Y. G. Chernov, and Y. N. Glazkov. Zh. Org. Khim. **8**, 2325 (1972); Engl. Ed. 2371 (1972); Chem. Abstr. **78**, 58153 (1973).
12. I. Saito, M. Takami, T. Konoike, and T. Matsuura. Bull. Chem. Soc. Jpn. **46**, 3198 (1973).
13. N. A. Sokolov, Y. G. Chernov, and A. A. Michalchuk. Zh. Org. Khim. **10**, 2454 (1974); Engl. Ed. 2466 (1974); Chem. Abstr. **82**, 125193 (1975).
14. R. H. Fischer and H. M. Weitz. Synthesis, 53 (1976).
15. S. Kumazawa, T. Sakakibara, R. Sudoh, and T. Nakagawa. Angew. Chem. **85**, 992 (1973).
16. H. H. Baer and W. Rank. Can. J. Chem. **43**, 3330 (1965); R. L. Whistler and R. E. Pyler. Carbohydr. Res. **12**, 201 (1970).
17. R. E. Gramera, T. R. Ingle, and R. L. Whistler. J. Org. Chem. **29**, 2074 (1964).
18. W. G. Overend, M. Stacey, and J. Staněk. J. Chem. Soc. 2841 (1949).
19. H. H. Baer and F. F. Z. Georges. Carbohydr. Res. **55**, 253 (1977).
20. P. J. Garegg. Arkiv Kemi, **23**, 255 (1964).
21. S. Peat and L. F. Wiggins. J. Chem. Soc. 1088 (1938); 1818 (1938).
22. (*a*) G. B. Howarth, W. A. Szarek, and J. K. N. Jones. Carbohydr. Res. **7**, 284 (1968); (*b*) A. B. Foster, W. G. Overend, and M. Stacey. J. Chem. Soc. 974 (1951).
23. A. C. Meahly and T. Reichstein. Helv. Chim. Acta, **32**, 22 (1949).
24. E. J. Reist, R. R. Spencer, and B. R. Baker. J. Org. Chem. **23**, 1753 (1958); E. J. Hedgley, O. Mérész, and W. G. Overend. J. Chem. Soc. C, 888 (1967).
25. N. R. Williams. Adv. Carbohydr. Chem. Biochem. **25**, 109 (1970).
26. H. O. House. Modern synthetic reactions. 2nd ed. W. A. Benjamin, Inc., London. 1972. pp. 60–63.

Can. J. Chem. Downloaded from www.nrcresearchpress.com by 210.87.254.5 on 09/05/12
For personal use only.

The formation and structure determination of both acyclic and cyclic products in the reaction of sulfene and pyridines

J. STUART GROSSERT,[1] MADAN M. BHARADWAJ, RICHARD F. LANGLER, T. STANLEY CAMERON,[1] AND RUTH E. CORDES

Chemistry Department, Dalhousie University, Halifax, N.S., Canada B3H 4J3

Received October 11, 1977

J. STUART GROSSERT, MADAN M. BHARADWAJ, RICHARD F. LANGLER, T. STANLEY CAMERON, and RUTH E. CORDES. Can. J. Chem. **56**, 1183 (1978).

Sulfene, generated from methanesulfonyl chloride and triethylamine in acetonitrile reacts with itself to form a tetramer which may be isolated as an acyclic crystalline pyridinium sulfonate salt, **1**. When sulfene is generated in tetrahydrofuran in the presence of pyridine, the 1,1,3,3-tetraoxide of 4,4a-dihydropyrido[1,2-*d*][1,5,2]dithiazine, **11**, is formed. Structural evidence (including nmr and mass spectra) for these compounds, for homologs of **11**, and for a series of acyclic polysulfonyl compounds derived from **1** is presented. An X-ray crystal structure determination was carried out on **9**, the 5,7-dimethyl homolog of **11**.

J. STUART GROSSERT, MADAN M. BHARADWAJ, RICHARD F. LANGLER, T. STANLEY CAMERON et RUTH E. CORDES. Can. J. Chem. **56**, 1183 (1978).

Le sulfène, produit à partir du chlorure de méthanesulfonyle et de la triéthylamine dans l'acétonitrile, réagit avec lui-même pour conduire à un tétramère qui peut être isolé sous forme de sel sulfonate de pyridinium cristallin acyclique **1**. Lorsque l'on produit le sulfène dans le tétrahydrofuranne en présence de pyridine, il y a formation du tétraoxyde-1,1,3,3 de la dihydro-4,4a pyrido[1,2-*d*][1,5,2]dithiazine (**11**). On rapporte les preuves de structure (incluant la rmn et les spectres de masse) de ces composés ainsi que des homologues de **11** et d'une série de composés polysulfonyles acycliques, dérivés de **1**. On a effectué une détermination de structure cristalline par diffraction de rayon-X en utilisant le composé **9**, l'homologue diméthylé en 5,7 de **11**.

[Traduit par le journal]

Introduction

The generation of methanesulfonate esters (mesylates) by the reaction between alcohols and methanesulfonyl chloride in pyridine solvent is an old-established process (1). During an attempt to carry out an *in situ* elimination (with triethylamine) of a mesylate formed in this manner, we observed the formation of an unexpected product, which appeared to be a novel cycloadduct (**11**) between the pyridine solvent and a sulfur-containing species. Further work (2) showed the reaction to be characteristic of pyridines even if the 3 or 4 positions were substituted and suggested that the sulfur-containing portion was two sulfene units, presumably generated by reaction between the methanesulfonyl chloride and the triethylamine (ref. 3 and references therein).

Difficulties associated with the purification of **11**, as well as the low yield in which it was formed, suggested that it was not the major product of the reaction and indeed, use of acetonitrile as reaction solvent permitted the isolation of a further new compound which turned out to be the pyridinium salt of the hydrolysis product of a sulfene tetramer (**1**) (4). In this paper we report on the structure determinations and spectroscopic properties of the acyclic product **1** and the novel heterocyclic products **9–11**.

[1]Address communications on crystallography to T.S.C.; other communications and reprint requests to J.S.G.

Results and Discussion

Derivatives from an Acyclic Tetramer of Sulfene

When methanesulfonyl chloride was added to triethylamine and pyridine in acetonitrile, the major product isolated, after addition of the reaction mixture to water, was the crystalline pyridinium salt of a sulfonic acid. Combustion analysis required the formula $C_9H_{15}NO_9S_4$ and titration indicated two acidic protons. The ^1H and ^{13}C nmr spectra were highly informative in that the four carbons of the anionic portion were present as two chemically nonequivalent methyls, a methylene and a methine. Details of these spectra are presented in Tables 1 and 2. In the mass spectrometer, the salt did not show a molecular ion but lost SO_3 very readily and then exhibited the spectrum which would be expected from an acyclic chain of alternating carbons and sulfonyl groups. This information, taken together with the infrared and ultraviolet spectra, required structure **1** to be written for the pyridinium salt of this sulfene tetramer hydrolysis product. Evidence for the structure was further strengthened when long-range ^1H–^1H coupling was noticed between the low-field methyl protons and the methylene protons. The

Can. J. Chem. Downloaded from www.nrcresearchpress.com by 210.87.254.5 on 09/05/12
For personal use only.

TABLE 1. The ^1H nmr spectral parameters of chains with multiple sulfonyl groups

Compound	Resonances			
	Methyl	Methylene	Methine	Other
1*	3.32 (narrow m) 3.38 (s)	5.54 (narrow m)†	6.20 (br)‡	8.5 (5H, m) 10.5 (1H, br)‡
2*	3.30 (t, J = 0.7 Hz) 3.37 (s)	5.50 (q, J = 0.7 Hz)†	6.14 (s)‡	6.8 (1H, s)‡
3§	3.33 (s)	5.53 (s)	—	—
5§	3.73 (s)	—	—	—
6§	3.80 (s)	—	—	—

*Chemical shifts given as δ values with respect to internal TMS in DMSO-d_6 solvent.
†Exchangeable with D_2O.
‡Very rapidly exchangeable with D_2O.
§Chemical shifts given as δ values with respect to internal TMS in acetone-d_6 solvent.

TABLE 2. The ^{13}C nmr spectral parameters* of chains with multiple sulfonyl groups

Compound	Resonances			
	Methyl	Methylene	Methine	Other
1†	43.3, 43.9	72.3	90.3	127.9, 141.8, 147.6 (pyridinium carbons)
2‡	43.5, 44.1	72.0	89.8	—
3§	42.6	69.8	—	—
5§	39.4	—	—	—‖

*All spectra were decoupled for proton noise.
†Chemical shifts were calculated as δ values with respect to TMS from external CS_2 lock, with H_2O solvent.
‡Chemical shifts calculated as δ values with respect to TMS from an internal DSS standard, in D_2O solvent.
§Chemical shifts measured as δ values from internal TMS in acetone-d_6 solvent.
‖Not observable with 1812 transients and 30 s pulse delay.

high-field methyl protons were, however, a sharp singlet. Further investigation, to be described in a subsequent paper (but cf. ref. 4) showed that the presence of pyridine was not required for the formation of the sulfene tetramer.

Our attempts to study the chemistry of **1** were aimed primarily at ester formation, either directly or via the acid chloride. All attempts were frustrated in that either no reaction occurred, or else the molecule lost the elements of sulfur trioxide to form the acyclic tris-sulfone **3**. This was first prepared in an attempt to use Golborn's method for the preparation of sulfonate esters (5) in which the sulfonic acid is heated with a dialkyl acetylphosphonate. When **1** was heated with dimethyl acetylphosphonate (**4**), **3** was isolated in good yield; the same process could also be achieved by simply warming **1** in the presence of a strong mineral acid. Attempts to form a sulfonyl chloride from **1** with PCl_5 led to the tetrachloro derivative (**5**) and it was subsequently found that the same compound or a tetrabromo compound (**6**) could be prepared directly by treating **1** with chlorine or bromine, respectively. This series of reactions is outlined in Scheme 1, along with the fact that **3** and **5** could be interconverted by standard procedures. Both **5** and **6** instantly gave silver halide precipitates with alcoholic silver nitrate, although no clearly defined, homogeneous organic products could be isolated from these reactions. It is perhaps not surprising that the sulfonyl chloride of **2** would be difficult to prepare since **2** itself, being a sulfonic acid adjacent to electron-withdrawing groups, probably readily loses SO_3 (6) under the conditions of chlorination to form **3**, which is then readily chlorinated. Finally, oxidation of the known (7) 2,4,6-trithiaheptane (**7**) unequivocally confirmed the structure of **3**.

Some ^1H and ^{13}C nmr spectral details of the above compounds are presented in Tables 1 and 2. The only feature of interest is the 0.7 Hz long-range ^1H–^1H coupling between methyl and methylene protons in **2**. No long-range ^1H–^{13}C coupling across SO_2 groups was observed in the ^{13}C nmr spectra of **2** or **3** (cf. pyridodithiazine spectra, *vide infra*). The mass spectra of **1**, **2**, and **3** were virtually indistinguishable, apart from some peaks in **1** that were obviously due to pyridine. The mass spectral fragmentations of the tetrachloro compound (**5**) and its tetrabromo analog (**6**) could be followed readily from the isotope peaks due to the different numbers of halogens in each fragment ion. The fragmentation pathways of the

Can. J. Chem. Downloaded from www.nrcresearchpress.com by 210.87.254.5 on 09/05/12
For personal use only.

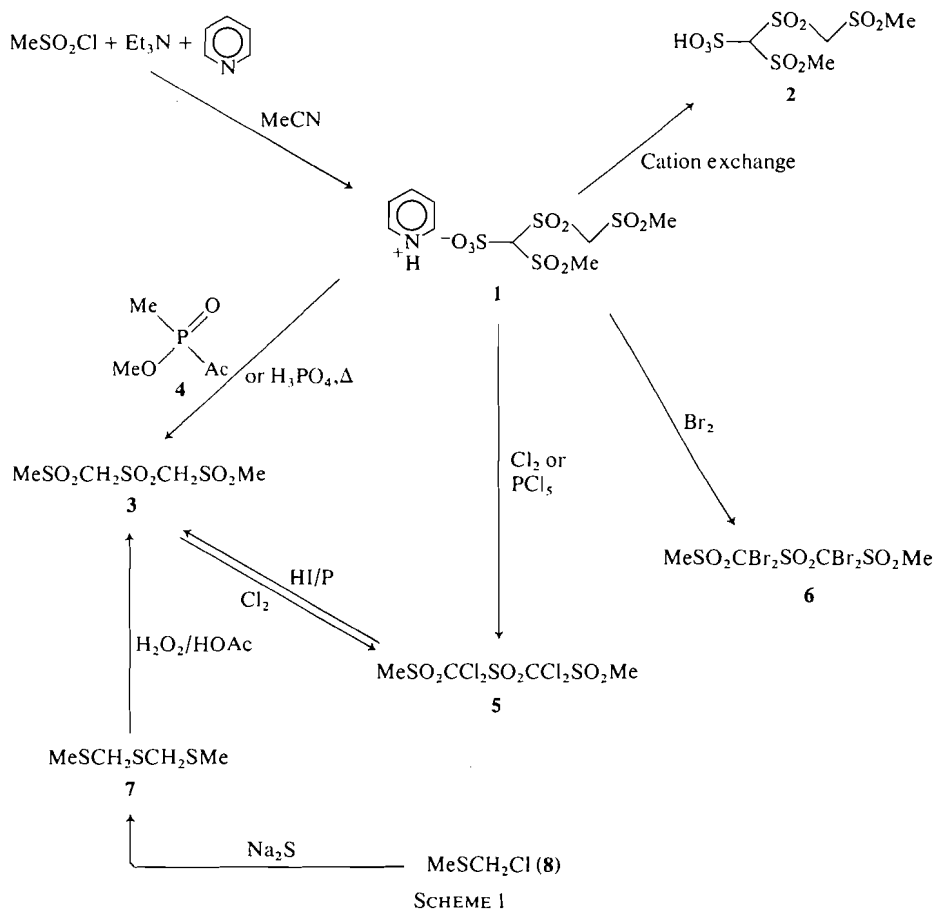

SCHEME 1

two compounds differ, although both exhibit rearrangements which lead to reasonably intense ions of structure CX_3^+, X = Cl or Br.

The Pyridodithiazines (9–11)

When triethylamine was added to a mixture of a pyridine and methanesulfonyl chloride in a less polar solvent such as THF, the major isolable product was a novel heterocycle (**11**) in which two sulfene units had added to a pyridine molecule in a manner similar to the reactions of pyridines with acetylene dicarboxylic esters or with ketenes (2).

Similar reactions of 4-picoline and 3,5-lutidine with sulfene yielded heterocycles **10** and **9**, respectively, which were appropriately similar to the parent compound **11**. On the other hand, α-substitution on the pyridine ring appears to change the course of the reaction and to give rise to different products.[2]

Proof of the structures of heterocycles **9–11** was possible from spectroscopic data. Also, since they form the first examples of a new heterocyclic system, a crystal structure determination was carried out on **9**.

The ultraviolet spectrum of **9** showed an absorption maximum at 287 nm which could be reversibly changed to 303 nm by the addition of base. The position of the maximum was unchanged in acidic medium. An indication of the homocyclic diene system was provided by the double bands at 1666 and 1615 cm^{-1} in the infrared spectrum (8), which also showed appropriate bands for the sulfonyl groups. The ^1H and ^{13}C nmr spectra together provided a wealth of structural information. Details of these spectra and of the ^1H nmr spectra of **10** and **11** are provided in Tables 3 and 4, respectively.

The different chemical shifts of the two methyl groups in **9** attested to their different environments. The proton chemical shifts of both the methyl groups and the olefinic protons showed minimal variations over a 155°C temperature range. Decoupling experiments demonstrated the correct assignments of the resonances corresponding to each carbon and proton in the dimethyl-substituted diene system. These de-

[2]J. S. Grossert and M. M. Bharadwaj. To be published.

Can. J. Chem. Downloaded from www.nrcresearchpress.com by 210.87.254.5 on 09/05/12
For personal use only.

TABLE 3. The ^1H and ^{13}C nmr spectral parameters of compound **9***

C atom No.	^{13}C δ	Off-resonance multiplicity	^1H δ‖ 25°C	25°C, J_{1H-1H} Hz‖ or peak description	^1H δ‖ 100°C	100°C, J_{1H-1H} Hz‖ or peak description
2	68.83	t†	ν_{ax} 5.409±0.003 ν_{eq} 5.528±0.002	J_{gem} 13.8±0.2 $J_{2eq-4eq}$ 2.3±0.4	ν_{ax} ca. 5.17 ν_{eq} ca. 5.20	J_{gem} ca. 14.0
4	45.96	t†	ν_{eq} 3.427±0.004 ν_{ax} 3.516±0.004	J_{gem} 14.2±0.2 J_{4ax-4a} 10.7±0.5 J_{4eq-4a} 2.0±0.5	ν_{eq} 3.213±0.4 ν_{ax} 3.474±0.4	J_{gem} 14.5±0.5 J_{4ax-4a} 11.2±0.5 J_{4eq-4a} 1.7±0.5
4a	52.64	d‡	4.774±0.001	—¶	4.804±0.003	—
5	114.83**	s‡	(C(5)Me, 1.94)	(narrow m)	(C(5)Me, 1.94)	(narrow m)
6	116.98	d‡	5.79	broad s	5.79	broad s
7	127.04**	s§	(C(7)Me, 1.74)	(d, $J \sim 1.5$ Hz)	(C(7)Me, 1.74)	(d, $J \sim 1.5$ Hz)
8	123.27	d‡	6.17	broad s	6.17	broad s

*The ^1H spectrum was recorded in DMF-d_7 at 100 MHz and the ^{13}C spectrum in DMSO-d_6 at 20 MHz.
†With no fine structure (i.e. no observable long-range ^1H-^{13}C coupling).
‡With fine structure, due to long range ^1H–^{13}C coupling.
§Peak not resolved in off-resonance spectrum due to overlapping with C(8) resonance.
‖Precision error limits were calculated as 5 times the standard deviation of the parameter, as given by the LAOCOON IVA program; parameters with no error limits were measured directly from the spectra.
¶A small long-range coupling between H(4a) and the C(5) methyl was demonstrated by decoupling.
**The ^{13}C methyl resonances were observed at 17.14 and 19.22 ppm.

TABLE 4. The ^1H nmr spectral parameters of compounds **10** and **11**

Compound	C atom No.	^1H δ 25°C	Peak description
10*	2	5.60	AB q, with long-range splitting (ca. 2 Hz) on low-field portion; J_{AB} ca. 13.0 Hz; $\Delta\nu_{AB}$ ca. 0.24 ppm.
	4	3.05–3.62	m; to 1st approximation, AB of ABX; long-range splitting on high-field portions (2 triplets); J_{AB} ca. 14.0 Hz.
	4a	4.84–5.08	broad m
	5	5.37 or 5.39	d, J ca. 7.5 Hz
	6	(C(6)Me, 1.73)	narrow m
	7	5.37 or 5.39	d, J ca. 7.5 Hz
	8	6.38	d of ds; J ca. 8.0, 1.5 Hz
11†	2	5.50	as for **10**
	4	3.00–3.75	as for **10**
	4a	4.75–5.15	complex m
	5–8	5.20–6.45	complex m

*Recorded at 100 MHz in DMSO-d_6.
†Recorded at 60 MHz in DMSO-d_6.

coupling experiments also revealed appropriate allylic ^1H–^1H couplings of ca. 1.6 Hz.

The remaining five protons in **9** were bound to sp^3 carbons and formed a complex system that could be reduced to a five-spin system by irradiation of the low-field methyl ^1H resonance. The ^1H chemical shifts of both the methylene pairs varied continuously over a temperature range of +100 to −55°C.

Spectral parameters for the five-spin proton system were obtained by use of a modified LAOCOON IVA computer program (9)[3] on data from the room temperature spectrum. The same program was used to calculate parameters for the protons at C(4) and C(4a) from a spectrum taken at 100°C, while the C(2) proton resonances were irradiated. These parameters showed relatively minor changes with temperature in J_{ae}, J_{aa}, and J_{gem} for the protons on C(4) and C(4a). Long-range coupling between equatorial protons at C(2) and C(4) was significant although comparable to literature values (10 and refs. therein). The value of J_{ae} for the protons on C(4) and C(4a) suggests a dihedral angle of ca. 66°, using Forrest's method (11), which is in good agreement with the X-ray value (*vide infra*). It appears from molecular models that the *cis*-fused conformer of **9** depicted in Fig. 1 has the least number of nonbonded interactions and should be more stable than the other

[3]We thank Dr. T. B. Grindley for making this program available to us.

Can. J. Chem. Downloaded from www.nrcresearchpress.com by 210.87.254.5 on 09/05/12
For personal use only.

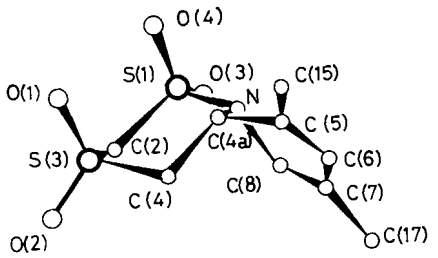

FIG. 1. The molecule **9** viewed at +10° to *b* in the *ab* plane. Atom numbering follows Chemical Abstracts nomenclature. Thus C(4) and C(4a) are independent atoms.

possible *cis*-fused conformer. Inversion at nitrogen produces a *trans*-fused system with somewhat more nonbonded interactions than the conformer in Fig. 1 but which retains the same conformation of the dithiazine ring. It is probable that the changes with temperature in chemical shifts of the methylene protons in **9** reflect solvation changes and possibly a nitrogen inversion process.

The off-resonance ^{13}C nmr spectrum of C(2) and C(4) showed their resonances as sharp triplets, without long-range splitting, an effect no doubt due to the adjacent sulfonyl groups. On the other hand, C(4a) was a doublet with considerable fine structure. All other carbons showed appropriate long-range ^{1}H–^{13}C couplings.

The C(2) methylene protons in **9–11** showed an expected degree of acidity in that they exchanged readily with D_2O in acetone. By use of NaOD in acetone on **10**, a tetradeuterated derivative (**13**) could be produced and by back-exchange the other dideuterated derivative **14** was produced, thereby completing the series of deuterated derivatives, (**12–14**). Mass spectral studies of **10** and **12–14** permitted an unambiguous assignment of the major electron-impact-induced fragmentation pathway in **10**. Comparable spectra were observed for **9** and **11**. Details of the spectra are presented in Table 5,[4] and a typical fragmentation pathway using **14** as an example is outlined in Scheme 2. Loss of SO_2 from ions of type **a** to give ions of type **b** was followed by fragmentations typical of pyridines substituted by an appropriate number of alkyl groups.[5] It is not clear whether loss of sulfene from **9–11** could be induced thermally. The compounds could be sublimed at ca. 160°C, but were not sufficiently volatile to be studied by flash thermolysis.[6]

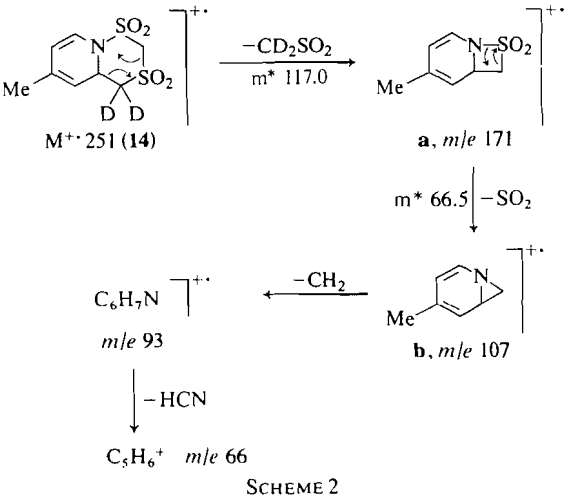

SCHEME 2

Crystal Structure of 9

The crystal (see Experimental for structure data) was found to be constructed from isolated molecules (**9**) which have two six-membered rings fused together at a C—N bond. One ring is the remnant of the pyridine group, the other contains two sulphur atoms bridged by a methylene carbon. The pyridine fragment has a group of four carbon atoms C(5)—C(6)—C(7)—C(8) which are not quite co-planar, the torsional angle between the C(5)—C(6) and C(7)—C(8) bonds about the C(6)—C(7) bond is −16.2° and between S(3)—C(4) and C(4a)—N(9) about the C(4)—C(4a) bond is −65.8°. The torsional angle between the equatorial H(42) and the axial H(4a) in the H(42)—C(4)—C(4a)—H(4a) system is −64.3° which compares with ~66° in solution (nmr). The C(5)—C(6), C(6)—C(7) and C(7)—C(8) bond lengths are 1.316(6), 1.459(7), and 1.334(8) Å, respectively. The

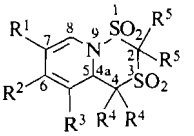

	R¹	R²	R³	R⁴	R⁵
9	Me	H	Me	H	H
10	H	Me	H	H	H
11	H	H	H	H	H
12	H	Me	H	H	D
13	H	Me	H	D	D
14	H	Me	H	D	H

NOTE: Numbering in this structure is dictated by nomenclature conventions which conflict with crystallographic conventions.

bond lengths C(5)—C(6) and C(7)—C(8) are not significantly different but are both significantly shorter than C(6)—C(7). These lengths compare with 1.339, 1.480, and 1.339 Å in buta-1,3-diene (16).

[4]Details of the mass spectra of **9–14** (Table 5) are available at a nominal charge from the Depository of Unpublished Data, CISTI, National Research Council of Canada, Ottawa, Canada K1A 0S2.

[5]J. S. Grossert. Unpublished spectra; see also ref. 12.

[6]Personal communication from Professor P. deMayo, University of Western Ontario.

Can. J. Chem. Downloaded from www.nrcresearchpress.com by 210.87.254.5 on 09/05/12
For personal use only.

Can. J. Chem. Downloaded from www.nrcresearchpress.com by 210.87.254.5 on 09/05/12
For personal use only.

The torsional angle between the C(4a)—C(5) and C(6)—C(7) bonds about C(5)—C(6) is 3.7° and between C(6)—C(7) and C(8)—N(9) about C(7)—C(8) is 0.8°. The C(4a)—C(5) bond length 1.527(8) is an expected (17) value for a single bond between an sp^2 and sp^3 carbon atom. The N(9)—C(4a) bond length (1.492(5) Å) has an acceptable (17) value for an N—C (sp^3) bond though it is slightly longer than the quoted mean length (18) of 1.472(5). The lengthening could be caused by strain within the ring containing the sulphur atoms (see below). The N(9)—C(8) bond length at 1.424(5) compares favourably with the average of 1.426(12) for an N—C (sp^2) single bond (18). Since the shortening of the N—C bond from an sp^3 carbon to an sp^2 is attributed only to the difference in covalent radii of these two types of carbon atoms, it seems unlikely that there is much interaction between the nitrogen lone pair electrons and the conjugated carbon system. This is consistent with the observations in the uv spectrum of **9**. The N(9)—S(1) bond length 1.636(5) compares with 1.522(16) for the formal double bond of the —S=N—S— system (19), with 1.623(9) for the mean length of the formal single bond of the —S=N—S—N=S— system in the same S_3N_3 ring (19), and with 1.635(8) for an isolated S—NH—single bond in a tolylsulphenylamino group that has an sp^3 carbon atom bonded to the third valency at nitrogen (20). The nitrogen atom N(9) is 0.29 Å from the plane of three atoms bonded to it with the sum of interbond angles at N(9) of 349.5°. From the molecular geometry and the bond lengths it seems further unlikely that the π electron system of the butadiene-like group extends, to any great extent, through the nitrogen atom to the sulphonyl group containing S(1).

The six-membered ring containing the two sulphur atoms has the chair conformation (Fig. 1), the four atoms S(3), C(2), N(9), C(4a) have deviations from the least-squares best plane of 0.039–0.048 Å with a mean of 0.045 Å. The plane through C(2)—S(1)—N(9) makes an angle of 129.5° and that through S(3)—C(4)—C(4a) an angle of 125.1° with the four-atom plane. The bond angles N(9)—S(1)—C(2) and C(2)—S(3)—C(4) of 102.6(2) and 103.3(2) compared with a N—S—C angle of about 108° when sulphur is bonded to a nitrogen with essentially three single bonds and 100° when nitrogen forms formally a single bond to sulphur and a double bond to a carbon atom (20). The N—S—C bond angle in this molecule is very similar to the C—S—C bond angle where both carbon atoms are sp^3 hybridized. The small angle therefore is more likely to be required to relieve the steric strain induced in the ring by the long S—C and S—N bonds than to indicate much multiple bonding along the S—N bond.

The angle between the O(3)—S(1)—O(4) and C(2)—S(1)—N(9) planes is 89.4° which is in the range expected (20) for a nitrogen atom that forms these single bonds rather than a double and a single.

In compound **9** there is a *cis* fusion of the two rings which appears to be retained in DMF or DMSO solution. This may be the result of steric interactions between the methyl group C(15) and the adjacent methylene group at C(4) (Fig. 1). In similar compounds, **10** and **11**, without the methyl group, this interaction is absent and the more usual *trans* ring fusion should occur. Attempts are still being made to grow crystals of **10** and **11** which are suitable for X-ray structure analysis.

In summary, it appears to be well established that sulfenes and their amine zwitterions are formed as reactive intermediates when methanesulfonyl chloride is reacted with tertiary amines, such as triethylamine (3). We have communicated a note of the probable formation of **1** (4) and this will be detailed presently.[2] Details on whether the pyridodithiazines form by reaction of pyridine with a sulfene dimer followed by ring closure, or whether sulfene adds to a pyridine–sulfene zwitterion, followed by ring closure, remain to be answered.

Experimental

General

Most experimental details have been described previously (21). Some ^1H and ^{13}C nmr spectra were recorded on a Varian XL-100 spectrometer at the University of Groningen and some microanalyses were performed by the Microanalytical Laboratory at the same University.

Many reactions were carried out using anhydrous conditions under dry N_2. Acetonitrile (Fisher Scientific Co.) was dried by refluxing over and fractionating from CaH_2. Methanesulfonyl chloride was washed successively with cold water, 2.5% $NaHCO_3$ and cold water before being dried over anhydrous $MgSO_4$ and fractionated under vacuum (water aspirator). Amines were fractionated from KOH pellets. THF (Fisher) was distilled from $LiAlH_4$ unless a fresh bottle was available.

Preparation of Pyridinium 2,4,6-Trithiaheptane-3-sulfonate-2,2,4,4,6,6-hexaoxide (1)

Methanesulfonyl chloride (19.5 ml) in CH_3CN (50 ml) was dropped, during 45 min, into a mechanically stirred mixture of pyridine (10 ml) and Et_3N (34.5 ml) in CH_3CN (300 ml) under an N_2 atmosphere. The reaction was maintained at −40°C during the addition, after which the cooling bath was removed. Following stirring for 30 min at room temperature, the reaction mixture was poured in a thin stream into ice-cold water (500 ml). The resulting precipitate was collected, washed (cold water) and recrystallized from water (with charcoal treatment) to give colorless prisms of **1** (18 g, 68%); mp 183–185°C; ir (KBr): 3260, 3200, 3110, 3060, 3000, 2940, 1649, 1622, 1552, 1498, 1350, 1325, 1140, 1050 cm^{-1}; nmr: see Tables 1 and 2; ms (no $M^{+\cdot}$) *m/e*: 250, 171, 157, 108, 94, 79, 77, 63, 48; equiv. wt. (titration vs. NaOH) 205; *Anal.* calcd. for $C_9H_{15}NO_9S_4$: C 26.40, H 3.69, N 3.42, O 35.17, S 31.32, mol. wt. 409.46; found: C 26.38, H 3.45, N 3.66, O 35.52, S 31.08; mol. wt. (cryoscopic) 210.

Can. J. Chem. Downloaded from www.nrcresearchpress.com by 210.87.254.5 on 09/05/12
For personal use only.

Preparation of 2,4,6-Trithiaheptane-2,2,4,4,6,6-hexaoxide-3-sulfonic Acid (2)

An aqueous solution of the pyridinium salt **1** was passed through a cation-exchange column (Dowex 50 W8) in the hydrogen form. The aqueous column eluant was rotary-evaporated to give a thick, colorless syrup which could be rendered anhydrous on keeping *in vacuo* over P_2O_5 for 24 h. The dried white mass of **2** was very hygroscopic and could not be crystallized; for ms, see text; nmr, see Tables 1 and 2.

Conversion of 2 into 2,4,6-Trithiaheptane-2,2,4,4,6,6-hexaoxide (3)

Using Dimethyl Acetylphosphonate (4)

Compound **4** was prepared from acetyl chloride and trimethyl phosphite according to the method of Berlin *et al.* (22) and had bp 50–54°C/0.2 Torr; ^1H nmr ($CDCl_3$) δ: 2.48 (3H, d, J = 5 Hz), 3.88 (6H, d, J = 10 Hz).

A mixture of pyridinium salt **1** (1.0 g) and phosphonate **4** (3.2 g) in pyridine (15 ml) was protected from moisture and was heated in an oil bath at 120°C for 16 h. Gas bubbles were evolved and after the dark mixture was concentrated by rotary evaporation, water (50 ml) was added. The aqueous layer was extracted with ethyl acetate (3 × 25 ml), from which **3** was obtained. Recrystallization (acetone–$CHCl_3$ 1:1) gave **3** (0.57 g, 94%) as colorless prisms, mp 191–192°C; ir (KBr): 1350, 1320, 1175, 1150 cm^{-1}; for ms, see text; nmr, see Tables 1 and 2; *Anal.* calcd. for $C_4H_{10}O_6S_3$: C 19.19, H 4.03, S 38.42; found: C 19.33, H 4.08, S 38.3.

Using Phosphoric Acid

Pyridinium salt **1** (1.0 g) was heated in an oil bath at 105°C in 85% H_3PO_4 (20 ml) for 24 h. The mixture was cooled, diluted with water and extracted with ethyl acetate, from which **3** was obtained in 55% yield.

Preparation of 3,3,5,5-Tetrachloro-2,4,6-trithiaheptane-2,2,4,4,6,6-hexaoxide (5)

Using Phosphorus Pentachloride

Pyridinium salt **1** (1.0 g) and PCl_5 (5 g) were heated at 150–160°C for 4 h. The cooled residue was extracted with ethyl acetate which was filtered, washed with water, dried and concentrated to give **5** as colorless crystals (0.90 g, 95%) that were recrystallized (acetone–$CHCl_3$) and had mp 183–184°C; ir (KBr): 1365, 1355, 1170, 1160, 860, 760 cm^{-1}; ms[7] *m/e*: 386 ($M^{+\cdot}$, 4 Cl), 371 (4 Cl), 307 (4 Cl), 225 (2 Cl), 210 (2 Cl), 117 (3 Cl), 79, 63; nmr, see Tables 1 and 2. *Anal.* calcd. for $C_4H_6Cl_4O_6S_3$: C 12.38, H 1.56, Cl 36.54, O 24.74, S 24.78; found: C 12.45, H 1.51, Cl 36.42, O 24.92, S 24.86.

Using Chlorine

Either an aqueous solution of **1** (1.0 g) *or* a solution of **3** (1.0 g) in MeOH–pyridine (50:1) was saturated with Cl_2. The white precipitate (0.92 g, 97%, in both cases) was collected after cooling and was identical to **5** formed in the previous experiment.

Preparation of 3,3,5,5-Tetrabromo-2,4,6-trithiaheptane-2,2,4,4,6,6-hexaoxide (6)

Bromination of **1** in MeOH–H_2O (5:1) gave a white precipitate of **6**, which was recrystallized (CH_3CN) to give colorless cubes, mp 188–189°C; ir: 1365, 1355, 1345, 1160, 1150 cm^{-1}; ms[7] *m/e*: 404 (4 Br), 340 (3 Br), 261 (2 Br), 249 (3 Br), 198, 182, 170, 158 (all 2 Br), 107 (1 Br), 79, 63; for nmr see Table 1; *Anal.* calcd. for $C_4H_6Br_4O_6S_3$: C 8.49, H 1.07, Br 56.5; found: C 8.46, H 1.00, Br 55.8.

[7]The number of halogens in the fragment ions was determined from the intensities of the halogen isotope peaks.

TABLE 7. Atomic coordinates* (× 10^4) except for the hydrogen atoms (× 10^3) for **9**

	x	y	z
S (1)	3034(1)	3936(1)	4534(2)
S (3)	4617(1)	6096(1)	2582(2)
O (1)	5113(2)	6482(2)	4816(6)
O (2)	5204(2)	6536(2)	472(6)
O (3)	2480(2)	2829(2)	3915(7)
O (4)	3434(2)	4288(2)	6852(5)
N (9)	2310(2)	4329(2)	3996(7)
C (2)	4026(3)	4679(3)	2430(8)
C (4)	3575(3)	6184(3)	2483(8)
C (4a)	2971(3)	5490(3)	4429(7)
C (5)	1950(3)	5651(3)	4385(8)
C (6)	1177(3)	5062(4)	2951(8)
C (7)	1072(3)	4216(3)	1505(8)
C (8)	1627(3)	3862(3)	2051(8)
C (15)	2102(4)	6506(4)	5995(10)
C (17)	308(4)	3704(5)	−489(12)
H (21)	454(4)	457(4)	280(9)
H (22)	374(3)	442(3)	83(9)
H (41)	328(4)	593(4)	85(9)
H (42)	387(3)	693(4)	280(9)
H (4a)	319(3)	569(3)	605(8)
H (6)	62(4)	514(4)	293(10)
H (8)	161(3)	326(4)	118(8)
H(151)	275(4)	717(5)	583(11)
H(152)	208(4)	627(4)	762(10)
H(153)	157(5)	660(5)	578(12)
H(171)	35(5)	157(6)	510(13)
H(172)	−27(5)	191(5)	378(12)
H(173)	−48(4)	77(5)	327(11)

*Atom numbering according to Chemical Abstracts nomenclature; see structure **9**.

Preparation of 2,4,6-Trithiaheptane (7)

The method used was a modification of that due to Fehér and Vogelbruch (7). A suspension of dry, powdered Na_2S (8.09 g; the nonahydrate was ground and dried *in vacuo* over P_2O_5) was stirred in dry MeOH (100 ml) and cooled to −20°C. Chloromethyl methyl sulfide (**8**, 6.0 g) (21) was added dropwise, the mixture was allowed to warm to room temperature overnight and the MeOH was rotary-evaporated. Lixiviation of the resulting sludge with $CHCl_3$, followed by appropriate work-up, gave **7** as a colorless, foul-smelling oil (2.95 g, 30%) which could be distilled, bp 52–54°C/0.1 Torr (lit. (7) 113°C/13 Torr) and had appropriate spectral characteristics.[8]

Oxidation of 7 to give 3

A solution of **7** (2.25 g) was oxidized with 30% H_2O_2 in HOAc in the usual way (23) for 4 days. The oxidation was incomplete and was repeated for 7 days with fresh oxidant. Finally, oxidation was completed using $KMnO_4$ in acetone–HOAc at 60°C for 4 h. The crystalline reaction product (0.98 g) was recrystallized, mp 189–191°C (mixture mp with **3**, 188–191°C) and was identical with **3** by tlc and spectroscopic properties.

Preparation of 4,4a-Dihydro-5,7-dimethylpyrido[1,2-d][1,5,2]dithiazine-1,1,3,3-tetroxide (9)

A mixture of distilled 3,5-lutidine (18.4 ml) and $MeSO_2Cl$ (31.0 ml) in dry THF (100 ml), was cooled by a −70°C bath, with mechanical stirring and protection from moisture. A

[8]J. S. Grossert and W. M. Neaves. To be published.

Can. J. Chem. Downloaded from www.nrcresearchpress.com by 210.87.254.5 on 09/05/12
For personal use only.

TABLE 8. Interatomic distances and interbond angles in **9**

Bond	Distance (Å)	Bond	Distance (Å)
S(1)—O(3)	1.429(3)	N(9)—C(4a)	1.492(6)
S(1)—O(4)	1.423(3)	C(4)—C(4a)	1.545(6)
S(1)—N(9)	1.636(6)	C(4a)—C(5)	1.527(9)
S(1)—C(2)	1.782(4)	C(5)—C(6)	1.316(6)
S(3)—O(1)	1.428(3)	C(5)—C(15)	1.495(9)
S(3)—O(2)	1.428(3)	C(6)—C(7)	1.459(8)
S(3)—C(2)	1.798(5)	C(7)—C(8)	1.334(9)
S(3)—C(4)	1.779(6)	C(7)—C(17)	1.515(9)
N(9)—C(8)	1.424(6)		

Bonds	Angle (deg)	Bonds	Angle (deg)
O(4)—S(1)—O(3)	120.6(2)	C(8)—N(9)—C(4a)	116.2(4)
N(9)—S(1)—O(3)	107.7(2)	S(3)—C(2)—S(1)	112.9(3)
N(9)—S(1)—O(4)	107.4(2)	C(4a)—C(4)—S(3)	114.4(4)
C(2)—S(1)—O(3)	107.8(2)	C(5)—C(4a)—C(4)	109.4(4)
C(2)—S(1)—O(4)	109.2(2)	C(5)—C(4a)—N(9)	107.2(3)
C(2)—S(1)—N(9)	102.6(2)	C(4)—C(4a)—N(9)	110.8(4)
O(2)—S(3)—O(1)	118.9(2)	C(15)—C(5)—C(4a)	115.4(4)
C(2)—S(3)—O(1)	108.6(2)	C(15)—C(5)—C(6)	125.6(6)
C(2)—S(3)—O(2)	105.7(2)	C(4a)—C(5)—C(6)	119.0(5)
C(4)—S(3)—O(1)	109.2(2)	C(7)—C(6)—C(5)	121.8(6)
C(4)—S(3)—O(2)	110.0(2)	C(17)—C(7)—C(6)	120.9(6)
C(4)—S(3)—C(2)	103.3(2)	C(17)—C(7)—C(8)	120.4(6)
C(4a)—N(9)—S(1)	114.9(3)	C(8)—C(7)—C(6)	118.6(5)
C(8)—N(9)—S(1)	118.4(4)	C(7)—C(8)—N(9)	119.2(5)

solution of distilled Et_3N (56 ml) in THF (50 ml) was added dropwise over 140 min and stirring was continued for a further 30 min. The creamy, pale yellow mixture was poured in a fine stream into a well-stirred ice-water mixture which was subsequently filtered and the crude **9** was recrystallized twice from acetone–MeOH (1.38 g (3.3%) after recrystallization). Further recrystallization from acetone gave an analytical sample, mp 217–222°C (dec.); ir (KBr): 2980, 2920, 1666, 1615, 1370, 1320, 1305, 1155, 1045, 895 cm^{-1}; uv (MeOH, neutral or acid): 287 nm (ε 2800), MeOH + NaOH 303 nm; for ms see Table 5; for nmr see Table 3. *Anal.* calcd. for $C_9H_{13}NO_4S_2$: C 41.04, H 4.97, N 5.32, O 24.30, S 24.35; found: C 41.29, H 4.69, N 5.19, O 24.23, S 24.22. See also the preparation of compounds **10** and **11**.

X-Ray Crystal Structure of ***9***

The crystal data are as follows:

$C_9H_{13}NO_4S_2$ fw = 263.3

Monoclinic $P2_1/c$, a = 16.272(5), b = 15.370(5), c = 5.654(2) Å, γ = 125.68 (4)°, V = 1148.6 Å^3, Z = 4, ρ_c = 1.523 g cm^{-3}, (18 ± 2°C; CuK_{α_1}, λ = 1.54051 Å (carbon monochromator) μ = 40.5). $F(000)$ = 536 e.

The cell dimensions (refined from 12 general reflections with 2θ between 70–80°) and intensities of 1455 independent reflections (71% of those observable) with $I > 3\sigma$ were measured on a Picker FACS 1 four-circle diffractometer with an ω-2θ scan and 2θ values between 4 and 120°. The minimum base-width was 2.0°. Three standard reflections were measured every 60 reflections. The intensities of these three reflections decreased steadily throughout the data collection but could be adjusted to a standard scale by a least-squares fit (σ = 0.007) to a first-order decay; from the counting statistics the ratio of esd to reflection of these standards was 0.019. The data were reduced to $|F_o|$ by the routine procedure. No absorption or extinction corrections were applied. The scattering factors for neutral atoms were taken from (13); they were corrected for the real part of the anomalous dispersion. Reflections with $|E| > 1.2$ were used to solve the structure by an application of the tangent formula that examined 256 = 2^8 sets of starting phases and successively eliminated all but the most likely. This program is part of an X-ray system written by Sheldrick (14). The positions of all but the hydrogen atoms were found on the E map with the third lowest Karle R factor (15).

The structure was refined by large block least-squares ($\Sigma(\Delta|F|)^2$ = min) initially with isotropic temperature factors. The hydrogen atoms were located from a difference Fourier synthesis when the conventional R was 0.12. The subsequent refinement with anisotropic temperature factors on all but the hydrogen atoms converged[9] with R 0.045. The least-squares weights were calculated from $w = 1/(\sigma^2|F_o| - 0.00004|F_o|^2)$ where σ is the weight for each reflection derived from the diffractometer counting statistics. The atomic coordinates are given in Table 7,[7] and the interatomic distances and interbond angles are listed in Table 8. Fig. 1 shows a single molecule and Fig. 2 gives its packing within the unit cell.

*Preparation of the 6-Methyl (****10****) and Unmethylated (****10****) Compounds*

Using similar procedures the 6-methyl (**10**) and unmethylated (**11**) compounds were obtained from 4-picoline and pyridine respectively (yields *ca.* 4%). Compound **10** had mp 220–221°C (dec.);[10] ir (KBr): 1664, 1598, 1330, 1345, 1325, 1305,

[9]A list of the structure factors (Table 6) and full details of the atomic parameters (Table 7, including thermal factors) are available at a nominal charge from the Depository of Unpublished Data, CISTI, National Research Council of Canada, Ottawa, Canada K1A 0S2.

[10]When recrystallized from acetone–water, **10** consistently had a melting point of 206–210°C.

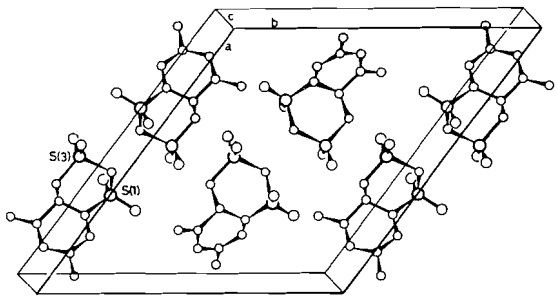

FIG. 2. The unit cell of **9**.

1170, 1130, 885, 760 cm^{-1}; for ms see Table 5; for nmr see Table 4; **11** had mp 205–206°C; ir (KBr): 1650, 1588, 1375, 1355, 1305, 1175, 1130, 880, 695 cm^{-1}; for ms see Table 5; for nmr see Table 4.

Compounds **9–11** were homogeneous on silica gel tlc using benzene–EtOAc (3:2) for elution, and could be sublimed at ca. 160°C/0.01 Torr.

*Deuteration of Methylpyridodithiazine (**10**)*

*(a) Preparation of 2,2-Dideuterated Derivative (**12**)*

A solution of **10** (45 mg) in acetone-d_6 (3 ml) was treated with D_2O (3 drops) and stirred for 18 h at 20°C, after which D_2O (1.5 ml) was added and the mixture was kept at −15°C for 18 h. The solvent was pipetted off to give **12** as colorless needles (30 mg).

*(b) Preparation of 2,2,4,4,-Tetradeuterated Derivative (**13**)*

A solution of **10** (49 mg) in acetone-d_6 was treated with 2% Na in D_2O (3 drops) and handled as in (*a*) above to give **13** (24 mg) as very slightly pink needles.

*(c) Preparation of 4,4-Dideuterated Derivative (**14**)*

Compound **10** (90 mg) was first tetradeuterated as described in (*b*) and the resulting **13** back-exchanged with H_2O-acetone as described under (*a*) to give **14** as colorless needles (31 mg).

The deuterated derivatives **12–14** all showed no depression of the melting point on admixture with **10** and were homogeneous on tlc; for ms see Table 5, and Scheme 2.

Acknowledgements

We thank Dr. A. G. McInnes, Mr. D. G. Smith, and Dr. J. de Wit for nmr spectra, Dr. T. B. Grindley and Dr. H. Kessler for helpful discussions, the National Research Council of Canada for support and for a scholarship (to R.F.L.), and Dalhousie University for support and for an Izaak Walton Killam scholarship (to M.M.B.). Mr. D. B. Embree kindly ran the high-resolution mass spectrum.

1. L. F. FIESER and M. FIESER. Reagents for organic synthesis. Vol. 1. Wiley, New York, NY. 1967. p. 662.
2. J. S. GROSSERT. Chem. Commun. 305 (1970).
3. J. F. KING. Accts. Chem. Res. **8**, 10 (1975).
4. J. S. GROSSERT and M. M. BHARADWAJ. J. Chem. Soc. Chem. Commun. 144 (1974).
5. P. GOLBORN. Synth. Commun. **3**, 273 (1973).
6. W. R. HARDSTAFF, R. F. LANGLER, J. LEAHY, and M. J. NEWMAN. Can. J. Chem. **53**, 2664 (1975).
7. F. FEHÉR and K. VOGELBRUCH. Chem. Ber. **91**, 996 (1958).
8. L. J. BELLAMY. The infra-red spectra of complex molecules. 3rd ed. Chapman and Hall, London, 1975. p. 44–46.
9. J. A. MUSSO and A. ISAIR. Program No. 232, Q.C.P.E. Univ. of Indiana, Bloomington, IN.
10. C. CISTARO, G. FRONZA, R. MONDELLI, S. BRADAMANTE, and G. A. PAGANI. J. Magn. Reson. **15**, 367 (1974); R. GRINTER. *In* Nuclear magnetic resonance. Vol. 1. *Edited by* R. K. Harris. Chem. Soc. London Spec. Report. 1972. p. 100.
11. T. P. FORREST. J. Am. Chem. Soc. **97**, 2628 (1975).
12. Q. N. PORTER and J. BALDAS. Mass spectrometry of heterocyclic compounds. Wiley-Interscience, New York, NY. 1971. pp. 376–380.
13. International tables for X-ray crystallography. Vol. IV. The Kynoch Press, Birmingham, England. 1974.
14. G. SHELDRICK. X-ray system report. University Chemical Laboratory, Lensfield Rd., Cambridge, England. 1976; J. KARLE and H. HAUPTMAN, Acta Crystallogr. **11**, 264 (1958).
15. J. KARLE and I. L. KARLE. Acta Crystallogr. **21**, 849 (1966).
16. B. P. STOICHEFF. *In* Advances in spectroscopy. *Edited by* E. W. Thompson. Interscience, New York, NY. 1959. p. 148.
17. C. A. COULSON. Valence. Oxford University Press, London, England. 1961. p. 210.
18. International tables for X-ray crystallography. Vol. III. The Kynoch Press, Birmingham, England. 1962.
19. E. M. HOLT and S. M. HOLT. J. Chem. Soc. Dalton Trans. 1990 (1974).
20. T. S. CAMERON, C. K. PROUT, B. DENTON, R. SPAGNA, and E. WHITE. J. Chem. Soc. Perkin Trans. II, 176 (1975).
21. J. S. GROSSERT and R. F. LANGLER. Can. J. Chem. **55**, 407 (1977).
22. K. D. BERLIN, D. M. HELLWEGE, and M. NAGABHUSHANAM. J. Org. Chem. **30**, 1265 (1965).
23. A. SCHÖBERL and A. WAGNER. *In* Methoden der organischen Chemie. (Houben-Weyl). 4th ed., Vol. IX. *Edited by* E. Müller. G. Thieme, Stuttgart. 1955. p. 227.

Can. J. Chem. Downloaded from www.nrcresearchpress.com by 210.87.254.5 on 09/05/12
For personal use only.

The crystal structure of $RbCdCl_3$ and the polarized Raman spectra of $RbCdX_3$ (X = Cl, Br)

MAHADEVAN NATARAJAN, HELEN ELAINE HOWARD-LOCK, AND IAN DAVID BROWN

Institute for Materials Research, McMaster University, Hamilton, Ont., Canada L8S 4M1

Received November 30, 1977

MAHADEVAN NATARAJAN, HELEN ELAINE HOWARD-LOCK, and IAN DAVID BROWN. Can. J. Chem. **56**, 1192 (1978).

The polarized Raman spectra of single crystals of $RbCdCl_3$ and $RbCdBr_3$ (isostructural with NH_4CdCl_3) have been measured and analysed by comparison of the frequency shifts. The crystal structure of $RbCdCl_3$ refined by X-ray diffraction is also reported.

MAHADEVAN NATARAJAN, HELEN ELAINE HOWARD-LOCK et IAN DAVID BROWN. Can. J. Chem. **56**, 1192 (1978).

On a mesuré le spectre Raman polarisé de cristaux uniques de $RbCdCl_3$ et $RbCdBr_3$ (isostructuraux avec NH_4CdCl_3) et on les a analysés par une comparaison de leurs déplacements de fréquence. On rapporte aussi la structure cristalline de $RbCdCl_3$ telle qu'affinée par diffraction de rayon-X.

[Traduit par le journal]

Introduction

Studies of the vibrational spectra of mixed halides such as $A^IB^{II}X_3$ have been restricted chiefly to the fluorides, which usually crystallize with the perovoskite structure. The chlorides and bromides with B = Cd crystallize in a different structure containing double $CdCl_3$ or $CdBr_3$ chains. Adams and Newton (1) and Barr and Goldstein (2) have reported the vibrational spectra of some of these compounds. As part of our studies of the $A^IB^{II}X_3$ system we report the polarized Raman spectra of $RbCdBr_3$ and $RbCdCl_3$. We have recently refined the structure of the bromide (3) and since the structure of the chloride has previously only been studied by X-ray powder diffraction (4, 5), we also report a refinement based on X-ray diffraction measurements from a single crystal.

Experimental Details

(a) Preparation of Single Crystals

Single crystals of $RbCdCl_3$ (CAS number = 18532-58-6) and $RbCdBr_3$ (CAS Number = 16593-57-0) were grown by slow evaporation of slightly acidified aqueous solutions containing equimolar proportions of RbX and CdX_2. The reagents were of analytical grade (Alfa or BDH). Colourless needles of $RbCdCl_3$ and $RbCdBr_3$ obtained from solution, were used to grow larger crystals for the Raman spectral studies. A large single crystal of $RbCdBr_3$ was also grown by the Czochralski method. This technique was not attempted with $RbCdCl_3$ because it transforms to a perovoskite related phase above room temperature (4, 5).

(b) Refinement of the $RbCdCl_3$ Structure

Precession photographs of small crystals of $RbCdCl_3$ confirmed the orthorhombic symmetry and indicated the space group *Pnma* or $Pn2_1a$. Since *Pnma*, the space group reported for the isomorphous NH_4CdCl_3, gave a satisfactory refinement, it was assumed to be correct. Lattice parameters (Table 1) were obtained by a least-squares fit to the angular settings of 15 reflections ($9° < 2\theta < 40°$) measured on a Syntex $P2_1$ diffractometer with graphite crystal-monochromated MoKα radiation. Our values are about 0.2% lower than those reported by Swanson *et al.* (4). X-ray intensities of 1713 reflections from a single quadrant ($h \geq 0$, $k \geq 0$) were measured on the diffractometer from a crystal ground into a cylinder of radius 0.05 mm and length (along [010]) 0.25 mm. Cylindrical absorption, Lorentz and polarization corrections were applied and symmetry related reflections were averaged to give 716 unique intensities. The atomic positional parameters found for $RbCdBr_3$ (3) were assumed and these, together with anisotropic temperature factors, a scale factor and an extinction parameter were refined by the locally written full-matrix least-squares program CUDLS (CDC 6400) to yield final agreement indices $R_1 (= \Sigma||F_o| - |F_c||/\Sigma|F_o|) = 0.028$ and $R_2 (= \Sigma\omega(F_o - F_c)^2/\Sigma\omega F_o^2)^{1/2} = 0.030$. In the final round $\omega = [\sigma_c^2 + (0.2F_o^2)]^{-1}$ where σ_c is the standard error based on counting statistics. The final extinction correction applied was $F^* = F(1 + 0.747 \times 10^{-6} \times \beta(2\theta)F^2)^{-1/2}$ (6). The scattering curves for Rb, Cd, and Cl atoms corrected for anomalous dispersion were taken from the International Tables for X-ray Crystallography (7). The final atomic coordinates are given in Table 2 and a table of observed and calculated struc-

TABLE 1. Crystal data for $RbCdCl_3$

Orthorhombic		
Systematic absences	*0kl*	$k + l = 2n + 1$
	hk0	$h = 2n + 1$
Space group	*Pnma*	(D_{2h}^{16})

Parameter	Value: This work	Value: Reference 4
a (Å)	8.949(4)	8.959(1)
b (Å)	4.026(2)	4.0346(4)
c (Å)	14.93(17)	14.976(2)
Z	4	
D_x (g cm^{-3})	3.76	3.73
λ(MoKα) (Å)	0.71069	
μ(MoKα) (mm^{-1})	14.7	

Can. J. Chem. Downloaded from www.nrcresearchpress.com by 210.87.254.6 on 09/05/12
For personal use only.

TABLE 2. Atomic positional and thermal coordinates* for $RbCdCl_3$

Atom	x	z	$U(1,1)$	$U(2,2)$	$U(3,3)$	$U(1,3)$
Rb	0.42731(9)	0.82536(5)	0.0321(1)	0.0236(3)	0.0258(3)	−0.0020(3)
Cd	0.16674(6)	0.05571(3)	0.0263(3)	0.0195(2)	0.0205(2)	−0.0039(2)
Cl(1)	0.2840(2)	0.2067(1)	0.0260(9)	0.0243(9)	0.0198(8)	−0.0021(7)
Cl(2)	0.1710(2)	0.4951(1)	0.0223(8)	0.0200(8)	0.0233(8)	−0.0032(7)
Cl(3)	0.0256(2)	0.9005(1)	0.0238(8)	0.0202(8)	0.0157(7)	−0.0004(6)

*The temperature factor is given by $T = \exp(-2\pi^2 \Sigma_i \Sigma_j U_{ij} H_i H_j A_i^* A_j^*)$. (All atoms at $x, \frac{1}{4}, z$. $U(1,2) = U(2,3) = 0$.)

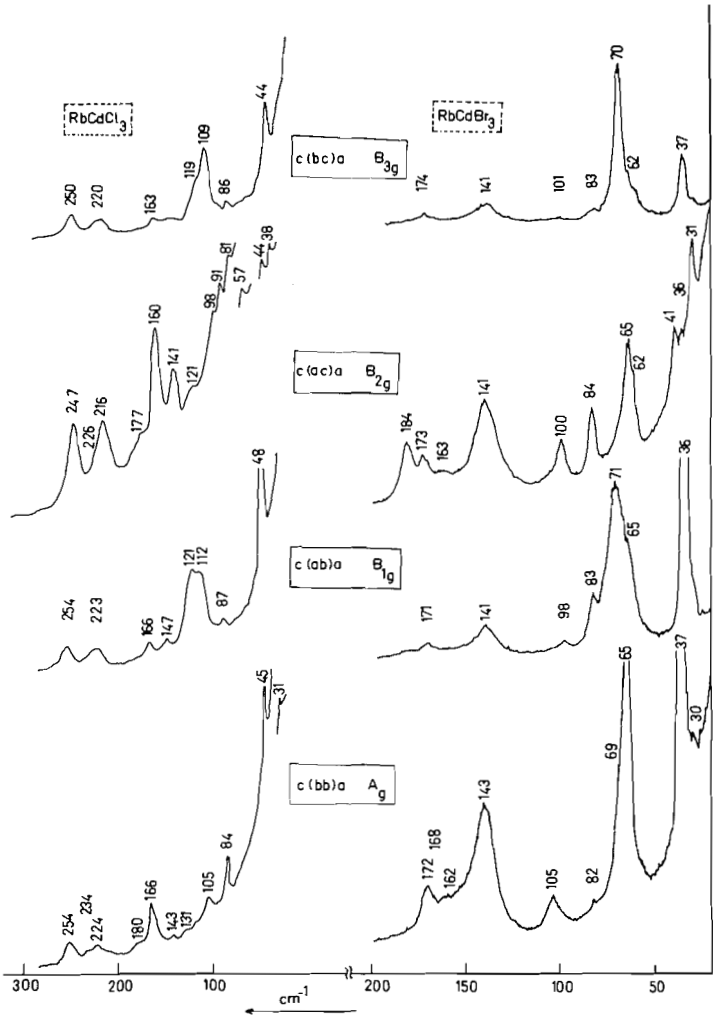

FIG. 1. The polarized Raman spectra of $RbCdX_3$ (X = Cl, Br). The crystal orientation and its relation to beam polarization is given in Porto notation.

ture factors has been placed in the Depository of Unpublished Data.[1]

(c) Polarized Raman Spectra of Crystals

Single crystals 3 × 3 × 6 mm were used for spectral work. They were mounted on an X-ray goniometer and aligned by precession photographs. Faces perpendicular to the crystallographic axes were cut and polished. All spectra were recorded at room temperature. A krypton ion laser (Spectra Physics Model 164) provided plane polarized radiation at 647.1 nm. The laser beam was focussed onto the crystal which had been mounted with one of the axes parallel to the incident laser beam. A broadband polarization rotator (Model 310-21) placed in the path of the beam and a polarizer in the scattered beam permitted the selection of various components of the

[1]Photocopies may be obtained upon request, at a nominal charge, from the Depository of Unpublished Data, CISTI, National Research Council of Canada, Ottawa, Ont., Canada K1A 0S2.

Can. J. Chem. Downloaded from www.nrcresearchpress.com by 210.87.254.6 on 09/05/12
For personal use only.

Can. J. Chem. Downloaded from www.nrcresearchpress.com by 210.87.254.6 on 09/05/12
For personal use only.

TABLE 3. Bond distances and angles in $RbCdCl_3$

Bond	Distance (Å)	Bonds	Angle (deg)
Cd—Cl(1)	2.487(3)	Cl(1)—Cd—Cl(2)	94.5(1) (×2)
Cd—Cl(2)	2.642(1) (×2)	Cl(1)—Cd—Cl(3)′	92.8(1) (×2)
Cd—Cl(3)	2.638(3)	Cl(3)—Cd—Cl(2)	87.9(1) (×2)
Cd—Cl(3)	2.728(1) (×2)	Cl(3)—Cd—Cl(3)′	84.8(1) (×2)
		Cl(2)—Cd—Cl(2)	99.3(1)
Rb—Cl(1)	3.282(2) (×2)	Cl(2)—Cd—Cl(3)′	82.3(1) (×2)
Rb—Cl(1)	3.310(2) (×2)	Cl(3)′—Cd—Cl(3)′	95.1(1)
Rb—Cl(2)	3.355(2) (×2)		
Rb—Cl(2)	3.454(2)		
Rb—Cl(3)	3.486(4)		
Rb—Cl(3)	3.765(2)		

Raman tensor. The spectrum of the scattered light was analysed by means of a Coderg (PHO) Raman spectrometer having an Ebert Fastie grating twin monochromator. The detector was a photomultiplier tube with an S-20 photocathode. The total instrumental width was varied from 0.5 cm^{-1} to 4 cm^{-1}. The Raman spectra of the crystals are shown in Fig. 1 for instrumental widths of 4 cm^{-1} ($RbCdCl_3$) and 2 cm^{-1} ($RbCdBr_3$) and laser power of around 150 mW at the sample.

Discussion

Structure of $RbCdCl_3$

Figure 2 shows the structure of $RbCdCl_3$ (isomorphous with $RbCdBr_3$ (3)) projected down the *b* axis. Bond lengths and angles are given in Table 3. The structure consists of double rutile-like columns of $CdCl_6$ octahedra running along the *b* axis. The columns are linked by nine coordinated Rb atoms (tris-monocapped trigonal prismatic coordination). All atoms lie in the mirror planes. The temperature factors indicate only small thermal anisotropies with rms thermal amplitudes in the range 0.13 to 0.18 Å. The structure was checked by a calculation of bond valences (8). These were summed around each atom to give experimental atomic valences (Table 4), which differ only by 0.02 valence units from the theoretical values. The bond valences, which are identical to those found in $RbCdBr_3$ (3), provide a ready understanding of the large variations found in the lengths of the bonds.

Raman Spectra

The factor group analysis of crystals with the NH_4CdCl_3 structure has been given by Adams and Newton (1) who point out that insofar as the $CdCl_3$ chains can be treated in isolation the A_g and B_{2g} spectra will be similar as will the B_{1g} and B_{3g}. All thirty g modes ($10A_g + 5B_{1g} + 10B_{2g} + 5B_{3g}$) are Raman active (9). Since NH_4CdCl_3, $RbCdCl_3$, and RbCdBr are isostructural and have bonds of similar strengths, the vibrational spectra should be identical except for the shifts resulting from the different masses of the ions. Table 5 lists the bands observed

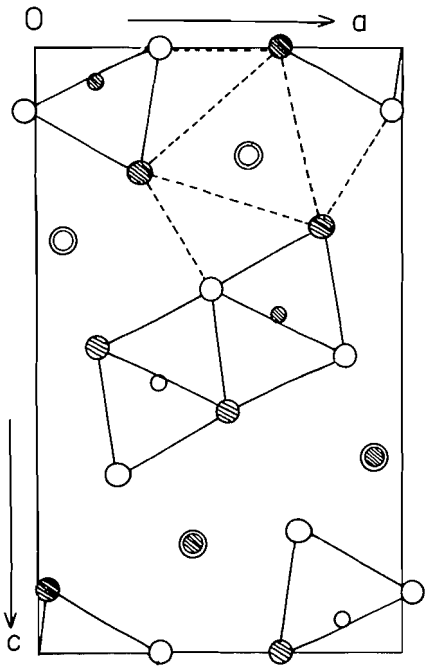

FIG. 2. Projection of the $RbCdCl_3$ structure down the *b* axis. Cadmium atoms are indicated by small circles, chlorine by large single circles, and rubidium by large double circles. Shaded atoms are at $y = 3/4$ and unshaded at $y = 1/4$.

TABLE 4. Bond valence*

	Rb	Cd	Total anion valence
Cl(1)	0.14 (×2) 0.13 (×2)	0.47	1.01
Cl(2)	0.12 (×2) 0.10	0.32 (×2)	0.98
Cl(3)	0.09 0.05	0.28 (×2) 0.33	1.03
Total cation valence	1.02	2.00	

*The valences (*S*) were calculated from the distances (*R*) by means of the expression $S = (R/R_0)^{-N}$ (8) where $R_0 = 2.472$ Å, $N = 7$ for Rb—Cl and $R_0 = 2.19$, $N = 6$ for Cd—Cl.

Can. J. Chem. Downloaded from www.nrcresearchpress.com by 210.87.254.6 on 09/05/12
For personal use only.

TABLE 5. Polarized Raman spectra of $ACdX_3$ crystals (frequencies in cm^{-1})

Mode number	NH_4CdCl_3 (ref. 1)				$RbCdCl_3$					$RbCdBr_3$ (this work)				Ratios of frequencies	
					This work									$\frac{NH_4CdCl_3}{RbCdCl_3}$	$\frac{RbCdCl_3}{RbCdBr_3}$
	A_g	B_{1g}	B_{2g}	B_{3g}	Ref. 2	A_g	B_{1g}	B_{2g}	B_{3g}	A_g	B_{1g}	B_{2g}	B_{3g}	ideal = 2.0	ideal = 1.5
1	244 s	244 w	244 s	244 w	252 s	254 m	254 w	247 s	250 w	172 m	171 w	184 m	174 w	1.0	1.5
2*						†		†		168 m†		173 m†			
3*						234 w†		226 w†		162 w†		163 w†			1.4
4	222 s	222 w	222 s	222 w	222 s	224 m	223 w	216 s	220 w	143 s	141 m	141 s	141 m	1.0	1.6
		(217 w)		(217 w)											
		(184 m)				(180 w)		(177 w)							
5*	161 m		161 m			166 s	(166 w)	160 s	(163 w)	105 m	(98 w)	100 m	(101 w)	1.0	1.6
					(142 m)	(143 w)	(147 w)	(141 m)							
6		121 m		121 m		131 w	121 m	121 w	119 w	82 w	83 m	84 m	83 w	1.0	1.5
7	110 m	107 m	110 m	107 s	100 w	105 m	112 m	98 m	109 m	69 m	71 s	65 s	70 s	1.0	1.5
								(91 w)							
8*			86 m		84 w	84 s	(87 w)	81 w	(86 w)	65 s	(65 m)	62 m	(62 w)	1.0	1.3
					(68 w)			(57 w)				(41 m)			
9	64 s	64 m				45 s	48 s	44 w	44 s	37 s	36 s	36 w	37 m	1.4	1.2
10*				64 m		31 m		38 w		30 w		31 m			1.1

*Modes expected in A_g and B_{2g} only. Frequencies in parentheses are unassignable; s = strong, m = medium, w = weak.
†Region of overlapped peaks, frequencies not accurately measurable.

in the polarized Raman spectra of the three crystals together with Barr and Goldstein's (2) unpolarized spectrum of $RbCdCl_3$. The ratios of the frequencies listed in the right-hand columns show that the motions of the halogen atoms dominate in all the higher frequency modes (numbers 1–8) and those of the alkali metals dominate only in the two lowest (numbers 9 and 10). From the bond valences (10) we estimate the stretching force constants for the Cd—X bonds to lie in the range 0.5 to 1.0 mdyn $Å^{-1}$ (50–100 N m^{-1}), which should give $4A_g + 2B_{1g} + 4B_{2g} + 2B_{3g}$ modes in the region between 180 and 230 cm^{-1} for $RbCdCl_3$ and between 140 and 180 cm^{-1} for $RbCdBr_3$. In other parts of the spectra several unexpected weak bands occur and, while some of these may be caused by imperfect polarization or crystal orientation, others such as the bands at 180 and 142 cm^{-1} observed for the chlorides are more difficult to explain.

Acknowledgement

We wish to thank the National Research Council of Canada for research operating grants.

1. D. M. ADAMS and D. C. NEWTON. J. Chem. Soc. A, 3499 (1971).
2. R. M. BARR and M. GOLDSTEIN. J. Chem. Soc. Dalton, 1180 (1974).
3. M. NATARAJAN IYER, R. FAGGIANI, and I. D. BROWN. Acta Crystallogr. B33, 127 (1977).
4. H. E. SWANSON, H. F. MCMURDIE, M. C. MORRIS, and E. H. EVANS. National Bureau of Standards, Monograph No. 25, Section 5. 1967. p. 41.
5. C. H. MACGILLAVRY, H. NIJVELD, S. DIERDORP, and J. KARSTEN. Recl. Trav. Chim. Pays-Bas, **58**, 193 (1939).
6. A. C. LARSON. Acta Crystallogr. **23**, 664 (1967).
7. International Tables for X-ray Crystallography. Vol. III. Kynoch Press, Birmingham. 1974. pp. 202–216.
8. I. D. BROWN and R. D. SHANNON. Acta Crystallogr. A**29**, 266 (1973).
9. D. M. ADAMS and D. C. NEWTON. Tables for factor group and point group analysis. Beckman, RIIC, Ltd., England. 1970.
10. I. D. BROWN, H. E. HOWARD-LOCK, and M. NATARAJAN. Can. J. Chem. **55**, 1511 (1977).

Methods for the comparison of fulvic acid samples: the effects of origin and concentration on acidic properties[1]

R. Douglas Burch and Cooper H. Langford
Department of Chemistry, Carleton University, Ottawa, Ont., Canada K1S 5B6
and
Donald S. Gamble[2]
Soil Research Institute, Agriculture Canada, Ottawa, Ont., Canada K1A 0C6
Received October 3, 1977

R. Douglas Burch, Cooper H. Langford, and Donald S. Gamble. Can. J. Chem. **56**, 1196 (1978).

The principles according to which the acidic properties of fulvic acid solutions should be compared are demonstrated. An equilibrium function defined and measured for any mixture, including fulvic acid functional groups, will be a weighted average. A concentration change will generally affect this average by changing the relative values of the statistical weights. Concentration corrections are therefore required for the comparison of two fulvic acid solutions. A Chernozem Ah fulvic acid and the previously described Armadale fulvic acid Batch FA1 were examined in this way. They were found to have the same general chemical characteristics, but with somewhat different numerical values. The implications of these results for the definition of fulvic acid are considered.

R. Douglas Burch, Cooper H. Langford et Donald S. Gamble. Can. J. Chem. **56**, 1196 (1978).

On démontre les principes d'après lesquels on devrait comparer les propriétés acides de solutions d'acide fulvique. Une fonction d'équilibre définie et mesurée pour un mélange particulier, incluant des groupes fonctionnels d'acide fulvique, correspond à une moyenne pondérée. Un changement de concentration provoquera généralement un changement de cette moyenne en modifiant les valeurs relatives des poids statistiques. Il est donc nécessaire d'effectuer des corrections de concentration pour comparer deux solutions d'acide fulvique. On a ainsi étudié un acide fulvique Chernosem Ah et le lot FA1 d'acide fulvique Armadale décrit antérieurement. On a trouvé qu'ils ont les mêmes caractéristiques chimiques générales mais qu'ils présentent des valeurs numériques un peu différente. On considère les implications de ces résultats pour la définition de l'acide fulvique.

[Traduit par le journal]

Introduction

Stevenson has recently noted that since humic acids are mixtures, the equilibrium functions for their cation reactions must be averages (1, 2). This point had previously been developed theoretically and demonstrated experimentally for a fulvic acid (3–5). The basis for this is that the structure of fulvic acid is so irregular that no two of its carboxyl groups can be assumed to be chemically identical. They must, therefore, be considered to be a mixture of chemically different carboxyl groups. Such weighted average equilibrium functions will generally depend on solution composition, and in particular a concentration dependence can be anticipated. Stevenson has, in fact, observed such an effect experimentally for a particular humic acid (1). Since fulvic acid solutions may differ either because the dissolved fulvic acids are different or simply because they have different concentrations of the same fulvic acid, this introduces at least two important practical problems. The first is that concentration effects must be accounted for in any quantitative comparison of experimental results for different fulvic acids or from different laboratories. The second is that methods must be available for translating quantitative laboratory results into the field conditions of practical systems. Reported values for organic matter concentrations in soil solutions and surface waters range from about 1.0×10^{-4} g/ℓ to 1.6 g/ℓ (6–9). McKeague *et al.* (10) have postulated that a Podzol leachate might typically have 0.1 g/ℓ. Laboratory investigations, however, are generally restricted to somewhat narrower ranges of concentrations. In addition, there has to date been only one fulvic acid sample for which the weak acid properties have been quantitatively characterized in detail (3–5). It is important, from the agricultural and geological points of view, to know what chemical characteristics, if any, are common to most fulvic acids. In fact, since

[1]SRI Contribution No. 665.
[2]To whom correspondence should be addressed.

Can. J. Chem. Downloaded from www.nrcresearchpress.com by 210.87.254.5 on 09/05/12
For personal use only.

Can. J. Chem. Downloaded from www.nrcresearchpress.com by 210.87.254.5 on 09/05/12
For personal use only.

the term fulvic acid is defined by a separation procedure rather than a molecular constitution, and a given sample contains numerous structural features, some of which may be more or less 'accidental' and unrelated to differences in acidic properties, the question of identifying what chemical factors are common to various preparations is the question of improving the definition of fulvic acid. Schnitzer and co-workers (11, 12) have extensively investigated the organic chemistry from this point of view, but this has not yet been done quantitatively for equilibrium cation reactions. H^+ dissociation is not only the simplest such case, but is also prerequisite to investigations of metal ion binding.

The objectives of this work were, therefore, to characterize the weak acid properties of a second fulvic acid, and to demonstrate concepts according to which fulvic acid solutions differing in either nature of the solute or concentration should be compared.

The fulvic acids used for this purpose were an Alberta Chernozem material, and the previously described Armadale fulvic acid Batch FA1 (3–5).

Type A functional groups, that is, carboxyl groups titrated up to the first titration equivalence point (4, 5), dominate the acidic properties of fulvic acid. In addition, there is evidence of long standing (5, 13–18) which indicates that some of them are in *ortho* positions relative to phenolic OH groups. They are, therefore, important for the bidentate chelation of heavy metal ions. The properties of these type A carboxyl groups are, therefore, assumed to be of central importance to any quantitative comparison of fulvic acids.

Theory

It has previously been shown that for a mixture of type A non-identical carboxyl groups, the acid dissociation equilibrium function is a weighted average of the K_{Ai}'s of the mixture of components (3–5). This is described by [1], in which α_A is the macroscopic degree of ionization for the whole mixture, and $\Delta(1 - \alpha_A)_i$ is the statistical weight of the ith component. ΔG_{Ai}^e is an electrostatic free energy term, and Γ_{Ai} is an activity coefficient term. Each of these terms will generally be a function of α_A. There are at least three possible reasons for the observed dependence of $\bar{K}_A$ on α_A. The first is that a change in α_A implies some change in the composition of the system. The corresponding changes in thermodynamic activities have the result that Γ_{Ai} and K_{Ai}^0 are both functions of α_A. This effect will often be a secondary one, however. A more important point is that for polymeric or aggregated species, electrostatic charge accumulates with increasing α_A, so that $\Delta G_{Ai}^e = f(\alpha_A)$ (4, 19, 20). The third reason, which is implicit in [1], has not previously been considered. It is most important, however, for the comparison of samples having different carboxylate group densities. This point is that $\bar{K}_A$ depends on the behaviour of the statistical weights, $\Delta(1 - \alpha_A)_i$. The nature of this effect may be seen by considering the acid dissociation of the ith small portion of the mixture. Equation 2 describes the equilibrium.

$$[1]\quad \bar{K}_A = \frac{1}{(1-\alpha_A)}\sum_{i=0}^{M} K_{Ai}\Gamma_{Ai} \times \exp(-\Delta G_{Ai}^e/RT)[\Delta(1-\alpha_A)]_i = \frac{m_A m_H}{m_{AH}}$$

$$[2]\quad K_{Ai} = \frac{m_H m_{Ai}}{m_{AiH}}$$

Rearranged, this gives [3];

$$[3]\quad [\Delta(1-\alpha_A)]_i = \frac{(C_{Ai}/C_A)m_H}{(K_{Ai} - m_H)}$$

C_A is the total concentration of the type A mixture of carboxyl groups, and C_{Ai} is the total for the ith portion of this mixture. Assuming that there are no gains or losses of components, then $(C_{Ai}/C_A) = \chi_{Ai}$ = constant. Since

$$\bar{K}_A \equiv \bar{K}_A(\alpha_A) = \left(\frac{\alpha_A}{1-\alpha_A}\right) m_H$$

therefore,

$$[4]\quad m_H \equiv m_H(\alpha_A) = \bar{K}_A(\alpha_A)\left(\frac{1-\alpha_A}{\alpha_A}\right)$$

The ith statistical weight is therefore a decreasing function of α_A, as described by [5] and [6].

$$[5]\quad [\Delta(1-\alpha_A)]_i = \frac{\chi_{Ai} m_H(\alpha_A)}{K_{Ai} + m_H(\alpha_A)} = f_i(\alpha_A)$$

$$[6]\quad \frac{d[\Delta(1-\alpha_A)]_i}{d\alpha_A} = \chi_{Ai}\left[\left(\frac{1}{K_{Ai}+m_H}\right)\frac{dm_H}{d\alpha_A} + m_H\frac{d(K_{Ai}+m_H)^{-1}}{d\alpha_A}\right]$$

For any two components of the mixture, the general case is that

$$[7]\quad \begin{cases} \chi_{Aj} \neq \chi_{Ak} \\ K_{Aj} \neq K_{Ak} \end{cases}$$

$$[8]\quad \frac{d[\Delta(1-\alpha_A)]_j}{d\alpha_A} \neq \frac{d[\Delta(1-\alpha_A)]_k}{d\alpha_A}$$

According to [8], a change in the degree of ionization will change the relative values of the statistical

Can. J. Chem. Downloaded from www.nrcresearchpress.com by 210.87.254.5 on 09/05/12
For personal use only.

TABLE 1. Chernozem Ah fulvic acid. Chemical analyses

Elemental analysis and ash content	Wt.% (±σ)	Metal	Concentration (mmol/g fulvic acid)
			σ = ±1%
Organic carbon	38.4 ±0.8	Al	4.95×10^{-3}
Hydrogen	5.1 ±0.1	Ca	0.175×10^{-3}
Nitrogen	0.95±0.02	Fe	1.00×10^{-3}
Sulphur	1.2 ±0.02	Mg	0.535×10^{-3}
Oxygen (by difference)	46.9 ±0.9	K	0.358×10^{-3}
Ash content	7.50±0.08	Na	17.4×10^{-3}
SiO_2	8.2 ±0.8	Total	24.4×10^{-3}

TABLE 2. Acidic functional groups (mmol/g fulvic acid). A comparison of two fulvic acids

Fulvic acid	Phenolic OH	Total carboxyl	Type A carboxyl	Type B carboxyl
Armadale Bh Batch FA1 (3, 4)	3.3±0.3	7.71 ±0.25	4.99±0.25	2.72±0.34
Alberta Chernozem Ah		4.693±0.032	2.28±0.064	2.41±0.11
Difference		3.0 ±0.28	2.71±0.31	0.31±0.45

weights. This will cause a change in the numerical value of $\bar{K}_A$, the weighted average.

The dependence of $\bar{K}_A$ on concentration and neutralization may now be determined by considering the properties of α_A. From the material balance for total base,

$$[9] \qquad m_A = C_{OH} + m_H - m_{OH}$$

where m_A is the molality of ionized type A carboxyl groups. Equation 10, which is obtained directly from this, may be used together with [4] and an empirical function, [11], for predicting the effects of concentration and neutralization on $\bar{K}_A$.

$$[10] \qquad \alpha_A = y_A + \frac{m_H + K_w/m_H}{C_A}$$

$$[11] \qquad \bar{K}_A = \bar{K}_A(\alpha_A)$$

Y_A is the degree of neutralization, $Y_A = C_{OH}/C_A$.

It is concluded from this that the empirical function, [11], may be obtained from an acid–base titration at one constant concentration, and then used for calculating $\bar{K}_A$ at any other concentration and degree of neutralization. Such a calculation, therefore, requires that the experimental curve of [11] be independent of concentration. An experimental check of this point is important, because any structural changes that might arise from extensive hydrogen bonding or aggregation would be expected to introduce a concentration dependence.

Experimental

Fulvic Acid

The fulvic acid was obtained from the Ah horizon of an Orthic Black Chernozemic soil at a well drained Alberta site (Lat. 50° 11′, Long. 114° 57′). The fulvic acid was extracted and purified according to the previously described methods of Schnitzer and co-workers (3, 4, 17, 21, 22). A Coleman Model 33 C, H Analyser and a Coleman Model 29 N Analyser were both used. S analysis was done by O_2 flask combustion and titration with barium perchlorate. Metal ion analyses were done using nitric–perchloric–HF wet digestion in Teflon beakers, followed by measurements with an atomic absorption spectrophotometer. Table 1 gives the results.

Chemicals

H_2O was redistilled under nitrogen. All other chemicals were certified standards or reagents.

Experimental Methods

The apparatus, techniques, and calculation procedures for acid–base titrations have been described previously (3–5). Six titration curves having a total of about 700 data points were averaged by least-squares fitting. Final calculations of acidic

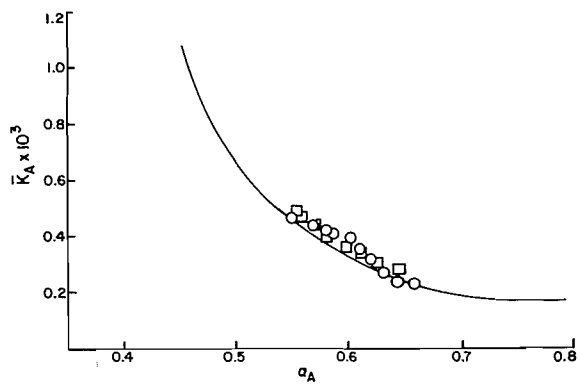

FIG. 1. $\bar{K}_A = f(\alpha_A)$ at different concentraions. Batch FA1 fulvic acid in 0.1 *m* KCl at 25.00°C. ○, 0.01073 g fulvic acid/100 g H_2O. □, 0.01077 g fulvic acid/100.00 g H_2O. —, 0.1000 g fulvic acid/100.00 g H_2O (3, 5).

TABLE 3. H^+ dissociation of Chernozem Ah fulvic acid. Weighted average equilibrium function for type A functional groups. 25.00°C. No inorganic electrolyte

$\bar{K}_A \pm \sigma$	α_A	Y_A $\left(\frac{\text{mol NaOH}}{\text{mol A groups}}\right)$	C_A ($\sigma = \pm 0.064$)
0.490×10^{-3}	0.368	0.0000	2.284×10^{-3}
0.538×10^{-3}	0.399	0.04384	2.282×10^{-3}
0.552×10^{-3}	0.421	0.08768	2.280×10^{-3}
0.536×10^{-3}	0.436	0.1315	2.277×10^{-3}
$0.499 \times 10^{-3} \pm 14.5\%$	0.447	0.1754	2.275×10^{-3}
0.450×10^{-3}	0.456	0.2192	2.273×10^{-3}
0.399×10^{-3}	0.465	0.2630	2.271×10^{-3}
0.352×10^{-3}	0.477	0.3069	2.268×10^{-3}
0.312×10^{-3}	0.492	0.3507	2.266×10^{-3}
0.279×10^{-3}	0.512	0.3946	2.264×10^{-3}
$0.252 \times 10^{-3} \pm 31.7\%$	0.535	0.4384	2.262×10^{-3}
0.224×10^{-3}	0.560	0.4823	2.259×10^{-3}
0.169×10^{-3}	0.617	0.5699	2.255×10^{-3}
0.147×10^{-3}	0.649	0.6138	2.253×10^{-3}
0.136×10^{-3}	0.666	0.6357	2.252×10^{-3}
$0.127 \times 10^{-3} \pm 34\%$	0.684	0.6576	2.251×10^{-3}
0.118×10^{-3}	0.702	0.6795	2.249×10^{-3}
0.111×10^{-3}	0.721	0.7015	2.248×10^{-3}
0.104×10^{-3}	0.740	0.7234	2.247×10^{-3}
0.98×10^{-4}	0.759	0.7453	2.246×10^{-3}
0.94×10^{-4}	0.779	0.7672	2.245×10^{-3}
$0.91 \times 10^{-4} \pm 29.2\%$	0.799	0.7891	2.244×10^{-3}
0.90×10^{-4}	0.820	0.8111	2.243×10^{-3}
0.84×10^{-4}	0.840	0.833	2.242×10^{-3}

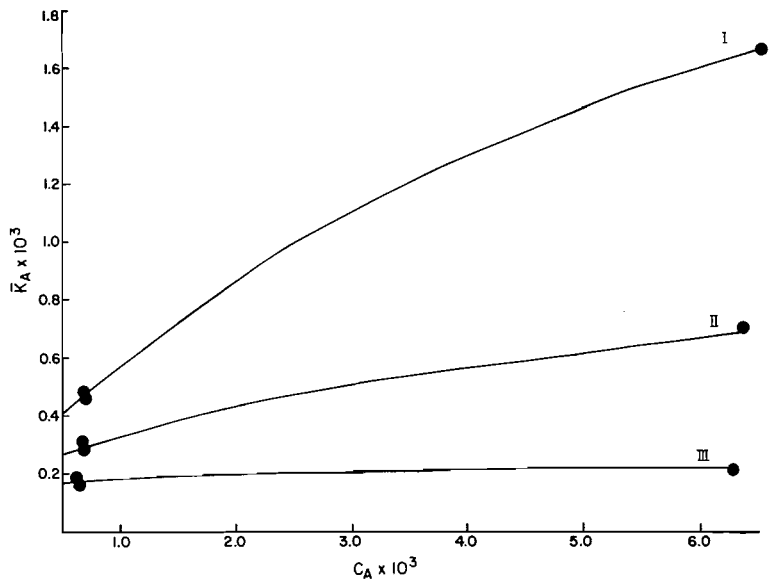

FIG. 2. $\bar{K}_A = f(C_A, Y_A)$. The predicted effects of concentration and neutralization on the weighted average equilibrium function. Batch FA1 fulvic acid in 0.1 *m* KCl at 25.00°C. Y_A: Curve I, 0.0000 (mol NaOH/mol A groups); curve II, 0.3946 (mol NaOH/mol A group); curve III, 0.6533 (mol NaOH/mol A groups). ●, Experimental points.

Can. J. Chem. Downloaded from www.nrcresearchpress.com by 210.87.254.5 on 09/05/12
For personal use only.

Can. J. Chem. Downloaded from www.nrcresearchpress.com by 210.87.254.5 on 09/05/12
For personal use only.

TABLE 4. H^+ dissociation of Chernozem Ah fulvic acid. Equilibrium function for type B functional groups. 25.00°C. No inorganic electrolyte

$\bar{K}_B = 1.82 \times 10^{-10}$
$\sigma = 0.36 \times 10^{-10}$
Standard error $= 0.06 \times 10^{-10}$
No. of data points = 40
$2.750 \leq \left(\frac{\text{mol } 0.1\ N \text{ NaOH}}{0.1 \text{ g fulvic acid}}\right) \leq 4.700$

properties were done with this average titration curve. Titration temperature was 25.00°C ± 0.05.

Results and Discussion

The titration equivalence points in Table 2 were calculated from the averaged titration curve in Fig. 5.[3] The calculation method has been previously described (3). It is evident from Table 2 that the Chernozem Ah and Armadale Bh fulvic acids both have two titration equivalence points. Within the limits of experimental error, they also have approximately the same number of type B carboxyl groups. There is a substantial difference, however, in the type A carboxyl groups. The Chernozem fulvic acid has about 2.7 (mmol/g) fewer than does the Armadale Batch FA1. The chemical analyses in Table 1 indicate that this difference cannot be accounted for by the blocking of functional groups by metal ions. Essentially all of the ash content is SiO_2, which should not block carboxyl groups.

The weighted average equilibrium functions in Tables 3 and 4 are both smaller than the corresponding values published for the Armadale Batch FA1 (3–5). Qualitatively, however, both fulvic acids show the same features. In each case $\bar{K}_A$ is a decreasing function of α_A, while $\bar{K}_B$ is evidently constant to within the experimental errors.

The theoretically predicted concentration dependence of $\bar{K}_A$ has been tested experimentally with Batch FA1 fulvic acid. Figure 1 demonstrates that within the limits of error, the $\bar{K}_A = f_A(\alpha_A)$ curve has the required independence of concentration. The concentration dependence of $\bar{K}_A$ therefore reflects simply the behaviour of $\alpha_A = \alpha_A(C_A, Y_A)$. Figure 2 indicate a close agreement with theory. This result permits a direct comparison of the experimental $\bar{K}_A$ values of the two fulvic acids. This has been done in Fig. 3. It can be seen here that correcting for the difference in carboxyl group concentrations will decrease the apparent difference in $\bar{K}_A$ values. In the greatest case, this accounts for about half of the difference. An important result is that even after this correction, the Chernozem type A carboxyl groups are less acidic than are those of the Armadale Batch FA1. Figure 4 further supports this conclusion with a comparison of K_A curves for the two fulvic acids.

It should be noted in Fig. 4 that qualitatively the two fulvic acids again have some important features in common. In each case, the K_A curve has a steep region I and a flat region II, separated by an inflection point. According to strict logic, a comparison of K_A vs. α_A curves would be more correct since α_A again introduces a concentration dependence. The curves in Fig. 4 were found to be more instructive, however, because the relative stoichiometries of the inflection points and equivalence points are readily seen.

An initial objective of this research was to test alternative criteria according to which fulvic acid could be defined. Molecular structure is not a sufficient criterion for this purpose, since in contrast to monomeric pure compounds, fulvic acid is not characterized by a single and unique structure (11). We, therefore, sought physical chemical parameters that would serve to characterize a particular sample. Since present definitions relate to the method of extraction, and p*H* and ion exchange control are used in extraction, the acid titration curve seemed to be the most promising means of achieving this. As has been noted above, this further requires a proper consideration of the concentration of carboxylates. Successful application of the concentration correction permits one to conclude that essentially the same extraction procedure has produced two fulvic acids

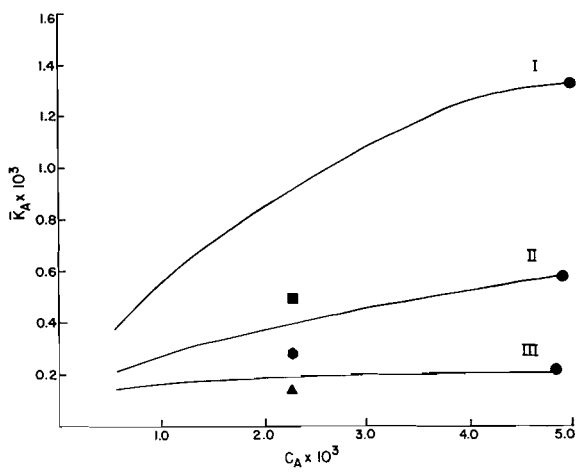

FIG. 3. Comparison of two fulvic acids. Type A functional groups at 25.00°C. No background electrolyte. Predicted curves for Batch FA1 fulvic acid: I, $Y_A = 0.0000$ (mol NaOH/mol A groups); II, $Y_A = 0.4064$ (mol NaOH/mol A group); III, $Y_A = 0.6104$ (mol NaOH/mol A group). ●, Experimental values for Batch FA1 fulvic acid, at the various Y_A values. Experimental values for Chernozem Ah fulvic acid: ■, $Y_A = 0.0000$ (mol NaOH/mol A group); ●, $Y_A = 0.4064$ (mol NaOH/mol A group); ▲, 0.6104 (mol NaOH/mol A group).

[3]Complete set of data may be obtained, at a nominal charge, from the Depository of Unpublished Data, CISTI, National Research Council of Canada, Ottawa, Ont., Canada K1A 0S2.

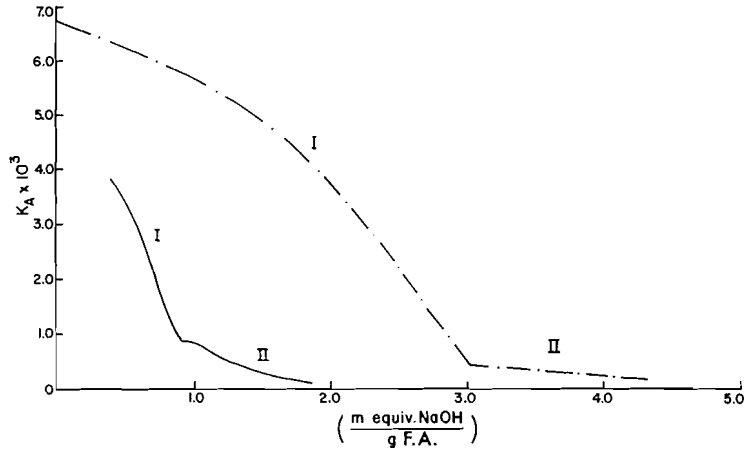

FIG. 4. Differential equilibrium function for type A functional groups. 25.00°C, no background electrolyte. Solid line, Alberta Chernozem Ah fulvic acid. Broken line, Armadale Bh fulvic acid Batch FA1 (3, 5). Steep regions I, $\sigma \approx \pm 1 \times 10^{-3}$. Flat regions II, $\sigma \approx \pm 0.1 \times 10^{-3}$.

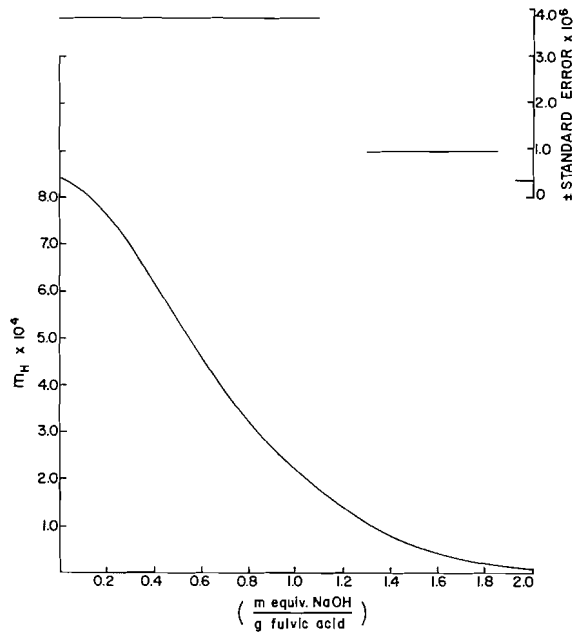

FIG. 5. Average titration curve for Chernozemic Ah Fulvic acid. 25.0°C; 0.1001 g fulvic acid in 100.0000 g distilled H_2O. Complete data may be obtained from the Depository of Unpublished Data.[3]

that represent significantly different examples of the same general type of system.

Acknowledgements

The Chernozem soil sample was collected under the expert direction of Dr. John F. Dormaar of the Agriculture Canada Research Station, Lethbridge, Alberta. Dr. M. Schnitzer and Dr. H. Morita of the Soil Research Institute have provided important advice. Mr. D. A. Hindle assisted with the experimental work.

1. F. J. STEVENSON. Soil Sci. Soc. Am. Proc. **40**, 665 (1976).
2. F. J. STEVENSON. Soil Sci. **123**, 10 (1977).
3. D. S. GAMBLE. Can. J. Chem. **50**, 2680 (1972).
4. D. S. GAMBLE. Can. J. Chem. **48**, 2662 (1970).
5. D. S. GAMBLE and M. SCHNITZER. The chemistry of fulvic acid and its reactions with metal ions. *In* Trace metals and metal–organic interactions in natural waters. *Edited by* P. C. Singer. Ann Arbor Science Publishers, Ann Arbor, MI. 1973. Chapt. 9.
6. W. STUMM and J. J. MORGAN. Aquatic chemistry. Wiley-Interscience, New York, NY. 1970.
7. J. H. SHARP. Limnol. Oceanogr. **18**, 441 (1973).
8. J. H. WEBER and S. A. WILSON. Water Res. **9**, 1079 (1975).
9. M. SCHNITZER and J. G. DESJARDINS. Can. J. Soil. Sci. **49**, 151 (1969).
10. J. A. MCKEAGUE, G. J. ROSS, and D. S. GAMBLE. Properties, criteria of classification, and concepts of genesis of podzolic soils in Canada. Proceedings, Quaternary Soils Symposium, York University, Toronto, Ontario. May 21–23, 1976.
11. M. SCHNITZER. Recent findings of the characterization of humic substances extracted from soils from widely differing climatic zones. International Symposium on soil organic matter studies, Brunswick, Federal Republic of Germany, September 6–10, 1976.
12. M. SCHNITZER. Can. J. Soil Sci. **50**, 119 (1970).
13. D. S. GAMBLE, M. SCHNITZER, and I. HOFFMAN. Can. J. Chem. **48**, 3197 (1970).
14. F. L. HIMES and S. A. BARBER. Soil Sci. Soc. Am. Proc. **21**, 368 (1957).
15. R. S. BECKWITH. Nature, **184**, 745 (1959).
16. S. S. KHANNA and F. J. STEVENSON. Soil Sci. **93**, 298 (1962).
17. M. SCHNITZER and S. I. M. SKINNER. Soil Sci. **96**, 86 (1963).
18. M. SCHNITZER and S. I. M. SKINNER. Soil Sci. **99**, 278 (1965).
19. A. KATCHALSKY and J. GILLIS. Recl. Trav. Chim. **68**, 879 (1949).
20. R. ARNOLD and J. TH. G. OVERBEEK. Recl. Trav. Chim. **69**, 192 (1950).
21. M. SCHNITZER and J. G. DESJARDINS. Soil Sci. Soc. Am. Proc. **26**, 362 (1962).
22. E. H. HANSEN and M. SCHNITZER. Anal. Chim. Acta, **46**, 247 (1969).

Can. J. Chem. Downloaded from www.nrcresearchpress.com by 210.87.254.5 on 09/05/12
For personal use only.

Determination of stability constants by p*H* titrations: a critical examination of data handling

TERRENCE B. FIELD AND W. A. E. MCBRYDE

Department of Chemistry, University of Waterloo, Waterloo, Ont., Canada N2L 3G1

Received July 28, 1977

TERRENCE B. FIELD and W. A. E. MCBRYDE. Can. J. Chem. **56**, 1202 (1978).

Data from simulated titrations (p*H*, titer, and p*M*) were generated from literature values of equilibrium constants, and then submitted to various published methods of calculation to regenerate the indicated equilibrium constants. These calculations were done with error-free input data, and the same with imposed random errors. In other experiments data from real titrations were subjected to the same analysis, and additional checks were made on the output of the calculations with an ion-selective electrode as a probe for p*M*. One method of data analysis was prone to cause errors in the finally recovered constants, and causes for this are suggested.

TERRENCE B. FIELD et W. A. E. MCBRYDE. Can. J. Chem. **56**, 1202 (1978).

On a pu déterminer des données de titrations simulées (p*H*, titre et p*M*) à partir de valeurs extraites de la littérature pour des constantes d'équilibre; on a ensuite soumises ces valeurs à diverses méthodes de calcul qui avaient été publiées pour regénérer les constantes d'équilibre indiquées. On a effectué ces calculs en introduisant les données sans erreurs ou avec des erreurs occasionnelles imposées. Dans d'autres expériences, on a soumis des données provenant de titrations réelles à la même analyse et des vérifications additionnelles ont été faites sur le produit de ces calculs avec une électrode sélective vis-à-vis un ion comme sonde pour le p*M*. Une méthode d'analyse des données était susceptible de causer des erreurs dans les constantes récupérer à la fin et on suggère des causes pour cet état de chose.

[Traduit par le journal]

Introduction

For collecting data with which to evaluate acidity constants of weak acids or bases or stability constants of metal complexes titrations are often preferred because of their capability of furnishing a large amount of experimental information from the interaction of a small number of standardized solutions. The subsequent numerical manipulation of the data so collected can take various forms according to the amount and kind of information available. This paper reports a study of one recently described way of conducting titrations and utilizing the results for the calculation of metal complex stability constants, and compares this with some longer established practices.

Sarkar and Kruck (1) recently extended a procedure developed by Osterberg (2) to determine p*L* in the presence of metal ions by p*H* titration, showing that it could also be applied to determine p*M*. This proposal possesses two desirable characteristics; first, that p*M* and p*L* can be measured during the formation of complexes without regard to which species may subsequently be inferred to be present; secondly, that it is not vitiated, as some other procedures are, by the formation of protonated or deprotonated complex species. An independent derivation of the relationships underlying this method (3) appears to confirm the limitation stated by Osterberg that it should be applied only to mononuclear complexes. Certain features of the procedure have come to light during extensive use of it, and these are described here for the benefit of other prospective users.

Data Treatment

At any point in a titration designed to study metal-complex formation there will be three stoichiometric concentrations: C_H, C_M, and C_L. C_H is the net concentration of ionizable hydrogen, i.e., the total ionizable hydrogen put in as ligand, mineral acid, etc., *less* the total of any strong base added as titrant, etc.; C_M is the total concentration of metal in all species; and C_L is the total concentration of ligand in all species. The concentrations of the corresponding unbound species will be represented by square brackets, e.g., [H], or in exponential form, e.g., p*H*. Strictly speaking the latter should be written as p[H], but the simpler notation will be used. Suitable probes such as the glass electrode, suitable metal-ion-sensitive electrodes, and a few electrodes of the second kind, can be calibrated in terms of the concentrations of hydrogen ion (4), metal ions (5), or ligand, respectively, and thus used to determine p*H*, p*M*, or p*L*.

A set of values of C_M, C_L, and C_H defines a point in a titration of the sort being considered, and might be designated the external coordinates of that point. There is also a set of internal coordinates, [M], [L], and [H] which are uniquely defined for that point by the outer coordinates and the relevant equilibrium

Can. J. Chem. Downloaded from www.nrcresearchpress.com by 210.87.254.105 on 09/05/12
For personal use only.

Can. J. Chem. Downloaded from www.nrcresearchpress.com by 210.87.254.105 on 09/05/12
For personal use only.

constants in accordance with eqs. 1 to 3. The complex species formed in solution may be represented by $M_pH_qL_r$, with formation constant β_{pqr}. Where $p = 0$ the species are protonated forms of the ligand; where $r = 0$ the species are products of hydrolysis of the metal ion; metal complexes may form in which q is positive, negative, or zero. In this discussion these are stoichiometric equilibrium constants the justification for whose use is the implicit assumption that they apply to systems of constant, and probably appreciable, ionic strength. Simple mass balances then yield the following relationships:

$$[1] \quad C_H - [H] + [OH] = \sum^{p}\sum^{q}\sum^{r} q\ \beta_{pqr}\,[M]^p[H]^q[L]^r$$

$$[2] \quad C_M - [M] = \sum^{p}\sum^{q}\sum^{r} p\ \beta_{pqr}\,[M]^p[H]^q[L]^r$$

$$[3] \quad C_L - [L] = \sum^{p}\sum^{q}\sum^{r} r\ \beta_{pqr}\,[M]^p[H]^q[L]^r$$

Determination of β_{pqr} by Measurement of [H] Only

In the absence of protonated or deprotonated metal complexes [1] can be used to evaluate [L] from C_H and [H], provided protonation constants of the ligand are known; then [2] can be used to evaluate the auxiliary function $\bar{n}$ for each point in the titration. Since for mononuclear metal complexes $\bar{n}$ is a function of [L] and the metal complex stability constants only, a variety of procedures, numerical and graphical, have been suggested for finding the latter from sets of values $\bar{n}$,[L]. Even for a limited number of polynuclear species such data are capable of yielding satisfactory formation constants (6). It has, however, been observed that for certain systems of stable complexes this treatment of experimental data can lead to erroneous results (7, 8).

The use of computers for handling the determination of stability constants enables more complicated systems to be dealt with. For example, the computer program SCOGS (9) refines trial values of equilibrium constants for postulated species by systematically adjusting these constants in such directions as to minimize the sum of squares of residuals which are the difference between the titer calculated by the provisional constants and the observed titer. Since the titer is a factor determining C_H, the strategy of this program might be described as a search for equilibrium constants that yield a calculated value of this coordinate closest to the observed value. The method can accommodate complex species that are protonated, hydrolyzed, or polynuclear, and has the further capability not utilized in this study of handling two metals and/or two ligands and the formation of mixed complexes. For each point in a titration the output includes indicated values of [M] and [L] and, importantly, the residual. Trends in the values of the latter can often be a guide to inclusion of other species to give a more complete description of the system of complexes. As with the simpler Bjerrum procedure mentioned previously, the formation of very stable complexes can give rise to difficulties owing to the inability of the mass balances to give precisely defined values of [M] or [L] during the calculations.

Determination of β_{pqr} by Solving Linear Equations

If all three inner coordinates were known for each point throughout a titration the values of these and the external coordinates could be inserted into [1], [2], and/or [3] to yield a set of linear equations in the β_{pqr} the solution of which is relatively simple by a linear least-squares matrix inversion procedure (LLSQ). This procedure is, in contrast to SCOGS and similar programs, very economical of computer time. Sarkar and Kruck have shown how pH titrations may be utilized to yield values of the other two inner coordinates. Before commenting on their procedure further, some account is offered of an alternative strategy incorporating the solution of linear equations in β_{pqr}.

If two of the inner coordinates are measured for each point in a titration values of the third can be found, as well as equilibrium constants for postulated species, by a simple iteration based on the same LLSQ routine. In this case provisional values of [L] or [M], whichever are now known, are put into a set of [2] or [3] respectively; these are solved to give first estimates of the β_{pqr} for the assumed complex species. The first provisional values are such as would apply if *no* metal complex formation occurred. With the trial constants new values of [L] or [M] can then be found by treating [3] or [2] in the same way, and the process is repeated until convergence occurs. When suitable probes for [M] or [L] are available this procedure is much to be recommended, especially for systems of very stable metal complexes for which methods based on measurement of [H] alone will sometimes give rise to difficulties. A computer program designated CLLSQ was written to accomplish the treatment of data.

The HOSK Method and Computer Program

Osterberg (2) showed that the differential quotient of two external coordinates of a titration $(\partial C_H/\partial C_L)_{H,C_M}$ could be evaluated experimentally at selected values of pH, and that this function could be used to determine the difference in pL between two points differing in pH (eq. 4).

$$[4] \quad pL - pL_0 = \int_{pH}^{pH_0} (\partial C_H/\partial C_L)_{H,C_M}\, dpH \Big|_{C_L}$$

Can. J. Chem. Downloaded from www.nrcresearchpress.com by 210.87.254.105 on 09/05/12
For personal use only.

If pH_0 is selected such that at it pL_0 is known, e.g., a value low enough that no metal complex formation occurs, then [4] can be used to find pL at any other chosen pH. Sarkar and Kruck (1) showed that the analogous function $(\partial C_H/\partial C_M)_{H,C_L}$ could be determined experimentally and used to determine pM at a selected pH provided that at some reference pH_0 the value of pM_0 was known [5].

$$[5] \quad pM - pM_0 = \int_{pH}^{pH_0} (\partial C_H/\partial C_M)_{H,C_L}\, dpH \Big|_{C_M}$$

In practice, to obtain C_H, C_L, and C_M at constant [H] each is curve-fitted vs. pH and values taken from the curve at the same pH for each titration. Then all C_H and C_L values at the same pH are curve-fitted at constant C_M and $(\partial C_H/\partial C_L)_{H,C_M}$ calculated from the curve. In the same way C_H and C_M values generate $(\partial C_H/\partial C_M)_{H,C_L}$. The values of these differential quotients are then curve-fitted vs. pH, and integrated by Simpson's rule from pH_0 to pH to get either pL or pM from pL_0 or pM_0 and the area under the curve. This is done for each pH for which values of pL and pM are desired. The initial pH, called pH_0, is chosen so that no significant metal complex formation occurs. This is generally one pH unit lower than the initial pH used in SCOGS or CLLSQ. At pH_0, $pM = -\log C_M$, and $pL_0 = -\log C_L(1 + \beta_{011}[H] + \beta_{021}[H]^2 + \cdots)^{-1}$ where β_{011} are protonation constants of the ligand.

All of the foregoing evaluations have been incorporated into a single computer program designated HOSK (Hedström, Osterberg, Sarkar, Kruck), which then continues to evaluate equilibrium constants for selected species by the subroutine LLSQ described previously. The complete program is available from the authors on request. It differs from those developed by Sarkar and Kruck in a number of important respects too detailed to itemize here. In general the HOSK program makes no simplifying assumptions and includes all corrections, as for dilution, etc.

Tests of Data Handling

The initial objective to evaluate the Sarkar–Kruck procedure and the computer program HOSK has been extended to some other data-handling procedures. Evaluation was based on the following: (*i*) the ability of the method to regenerate initial values of equilibrium constants from simulated titration data (pH, titer) which had been calculated for certain model systems with the aid of equilibrium constants from the literature. The simulated titration data were applied both error-free and with varying amounts of superimposed random error. It was possible in this way to check the data handling by HOSK at each stage, e.g., errors in curve fit of C_H, C_L, or C_M, comparison of found vs. theoretical values of $(\partial C_H/\partial C_L)$, etc., recovery of pL or pM values, and effects of changing pH_0, pH_{start}, or pH_{end} on these, and so forth. (*ii*) Comparisons of values of equilibrium constants as found by several methods from data obtained in titrations of real systems. (*iii*) Comparisons of pM values calculated from real titration data with values obtained directly with a metal-ion sensitive electrode.

In addition to the HOSK and SCOGS computer programs, certain simpler procedures were applied to the simulated or real titration data. These included the CLLSQ method mentioned previously and a simple procedure suggested by Romary (10) to solve the Bjerrum relationship for the several β values simultaneously by matrix column elimination. Two other very simple methods were also tested, although their usefulness is somewhat restricted: these are the HALF-$\bar{n}$ values of pL (11), and a DIRECT method in which individual solutions are found for the equation

$$\log K_i = pL_{\bar{n}} + \log(\bar{n} - i + 1) - \log(i - \bar{n})$$

Results

A number of stability constants obtained by the foregoing computational procedures from input data based on real or simulated titrations are shown in Tables 1–7 and 9. In addition to this evidence the authors have over a period of three years accumulated comparable data from many hundreds of titrations in aqueous and mixed solvent systems which support the conclusions drawn in this paper.

Tables 1–4 illustrate the common case of determining metal–complex stability constants. When small errors, comparable to those that might accidentally be incurred in practice, are applied to simulated titration data the starting constants are reasonably well recovered. It is to be stressed that the grouped sets of results in these tables have been calculated from a common set of input data, so that any variation among the constants must be attributed to the method of processing the data. Tables 3 and 4 contain two groups of results according to whether the titrations are conducted from low pH to high, or vice versa.

Tables 5 and 6 illustrate what happens to the stability constants and other parameters derived from these various calculations when the random error on the simulated titration data is progressively increased. The titration volumes onto which the random error is loaded were in all cases less than 1 cm^3. The initial volume was 50.0 cm^3 in all cases.

Tables 7 and 9 show the recovery of equilibrium

TABLE 1. Calculated formation constants for copper(II)–glycine complexes, input values: $\log \beta_{101} = 8.26$, $\log \beta_{102} = 15.16$*

Line	Program	$\log \beta_{101}$ (found)	$\log \beta_{102}$ (found)	S.D. fit	S.D. pM	S.D. pL
1	SCOGS	8.26	15.16	3.6×10^{-5}	0.000	0.000
2	HOSK	8.24	15.16	3.0×10^{-2}	0.013	0.002
3	CLLSQ	8.26	15.14	6.3×10^{-4}	—	0.004
4	HALF-$\bar{n}$	8.33	15.16		0.032	0.000
5	DIRECT	8.32	15.18		0.031	0.000
6	ROMARY	8.26	15.16		0.006	0.000
7	SCOGS(VB)	8.25	15.13	1.3×10^{-3}	0.015	0.003
8	HOSK(VB)	8.24	15.14	3.9×10^{-2}	0.014	0.004
9	CLLSQ(VB)	8.26	15.14	6.3×10^{-4}	—	0.004
10	HALF-$\bar{n}$(VB)	8.33	15.16		0.031	0.005
11	DIRECT(VB)	8.31	15.19		0.027	0.005
12	ROMARY(VB)	8.25	15.16		0.013	0.005
13	SCOGS(pH)	8.26	15.16	9.0×10^{-5}	0.002	0.001
14	HOSK(pH)	8.19	15.16	5.6×10^{-2}	0.033	0.003
15	CLLSQ(pH)	8.26	15.13	1.9×10^{-3}	—	0.005
16	HALF-$\bar{n}$(pH)	8.34	15.17		0.039	0.002
17	DIRECT(pH)	8.31	15.17		0.024	0.002
18	ROMARY(pH)	8.26	15.16		0.005	0.002
19	CLLSQ(E)	8.24	15.20	2.5×10^{-2}	0.009	0.007

*Simulated titration data: lines 1–6 results generated by error-free data; lines 7–12 generated by random error in titer up to ± 0.002 cm^3 in total titer < 1 cm^3; lines 13–18 generated by random error in pH up to ± 0.0025; line 19 generated by random error in electrode potential up to ± 0.5 mV. S.D. = standard deviation: for SCOGS S.D. in titer; for HOSK and CLLSQ S.D. in left side of [2] or [3] scaled to unity; for ROMARY S.D. in $\bar{n}$.

TABLE 2. Determined formation constants for copper(II)–glycine complexes at 25.0°C, $\mu = 0.1$ M ($NaNO_3$)*

Line	Program	$\log \beta_{101}$ (found)	$\log \beta_{102}$ (found)	S.D. fit	S.D. pM
1	SCOGS	8.07	14.88	7.5×10^{-5}	0.089, 0.086
2	HOSK	7.95	15.19	1.25×10^{-1}	0.142, 0.168
3	CLLSQ	8.23	14.89	2.3×10^{-2}	—
4	ROMARY	8.08	14.89	9.0×10^{-3}	0.085, 0.088
5	HALF-$\bar{n}$	8.14	14.89	—	—
6	DIRECT	8.15	14.88	—	—

*Experimentally determined titration data, pH and pM measured. S.D. pM refers to differences between values measured and calculated from derived constants.

constants for systems more complicated than the preceding examples. The copper(II) citrate system (Table 7) has been interpreted by several investigators to include one or more binuclear complexes; since the HOSK procedure has only been shown valid for mononuclear species there was interest in checking how it handled data for a non-conforming case. The iron(III) citrate system has been interpreted in terms of three 1:1 complexes differing in degree of protonation; it is known at first hand to be extremely sensitive to variance in experimental data. Incidentally, to do a HOSK analysis requires data from three titrations at least. However five titrations will allow the curve fitting routine to work on C_H vs. C_L and C_H vs. C_M (i.e. 3 points for 2 coefficients: slope and intercept). In Table 8 we show how data from nine titrations were arranged in sets of five to give enough information for nine independent calculations of stability constants; from these in Table 9 we show the minimum, mean, and maximum values obtained.

Discussion

The results in Tables 1 and 3 show that the assumed values of the metal complex stability constants are fairly successfully regenerated when simulated titration data are treated by the three methods of data analysis, SCOGS, HOSK, or CLLSQ, especially when the input data are applied error-free. When small random errors about equivalent to those associated with real titrations are superimposed the results are still quite good though some small discrepancies are noticeable, viz., line 14, Table 1, or lines 5 and 11, Table 3. In Tables 5 and 6 one can see the onset of more serious errors in the regeneration

Can. J. Chem. Downloaded from www.nrcresearchpress.com by 210.87.254.105 on 09/05/12
For personal use only.

Can. J. Chem. Downloaded from www.nrcresearchpress.com by 210.87.254.105 on 09/05/12
For personal use only.

TABLE 3. Calculated formation constants for copper(II)–ethylenediamine complexes, input values: log β_{101} = 10.44, log β_{102} = 19.60*

Line	Program	log β_{101} (found)	log β_{102} (found)	S.D. fit	S.D. p*M*	S.D. p*L*
Acid titrant						
1	SCOGS	10.44	19.60	2.5×10^{-7}	0.000	0.000
2	HOSK	10.43	19.59	6.7×10^{-2}	0.016	0.005
3	CLLSQ	10.44	19.60	8.2×10^{-4}	—	0.000
4	SCOGS(VA)	10.46	19.65	4.8×10^{-4}	0.030	0.002
5	HOSK(VA)	10.30	19.59	1.5×10^{-1}	0.056	0.003
6	CLLSQ(VA)	10.44	19.60	8.0×10^{-4}	—	0.000
Base titrant (following addition of excess acid)						
7	SCOGS	10.44	19.60	3.2×10^{-7}	0.000	0.000
8	HOSK	10.46	19.63	5.4×10^{-2}	0.018	0.005
9	CLLSQ	10.44	19.60	1.5×10^{-4}	—	0.000
10	SCOGS(VB)	10.45	19.60	1.0×10^{-3}	0.005	0.000
11	HOSK(VB)	10.29	19.69	2.1×10^{-1}	0.022	0.010
12	CLLSQ(VB)	10.44	19.60	1.6×10^{-4}	—	0.000
13	SCOGS(p*H*)	10.44	19.60	1.0×10^{-4}	0.002	0.002
14	HOSK(p*H*)	10.45	19.66	3.8×10^{-2}	0.246	0.177
15	CLLSQ(p*H*)	10.44	19.60	1.0×10^{-4}	—	0.002
16	CLLSQ(E)	10.42	19.61	2.8×10^{-2}	0.008	0.002

*Simulated titration data: lines 1–3 and 7–9 error-free data; lines 4–6 and 10–12 random error in titer as in Table 1; lines 13–15 random error in p*H* as in Table 1; line 16 random error in *E* as in Table 1.

TABLE 4. Determined formation constants for copper(II)–ethylenediamine complexes at 25°C, μ = 0.1 *M* (KNO_3)*

Line	Program	log β_{101} (found)	log β_{102} (found)	S.D. fit	S.D. p*M*
Acid titrant					
1*a*	SCOGS	10.45	19.46	1.9×10^{-3}	0.139
1*b*	SCOGS	10.51	19.61	1.3×10^{-3}	0.077
1*c*	SCOGS	10.55	19.59	1.2×10^{-3}	0.209
	Mean	*10.50*	*19.55*		
2*a*	HOSK	10.43	19.47	2.4×10^{-2}	0.140
2*b*	HOSK	10.43	19.55	3.4×10^{-2}	0.054
2*c*	HOSK	10.32	19.61	1.2×10^{-1}	0.107
	Mean	*10.39*	*19.54*		
3*a*	CLLSQ	10.63	19.00	3.0×10^{-1}	—
3*b*	CLLSQ	10.54	19.39	1.1×10^{-1}	—
3*c*	CLLSQ	10.43	19.09	5.3×10^{-1}	—
	Mean	*10.53*	*19.16*		
Base titrant (following addition of excess acid)					
4*a*	SCOGS	10.00	18.30	6.2×10^{-3}	0.482
4*b*	SCOGS	10.58	19.63	1.0×10^{-3}	0.199
	Mean	*10.29*	*18.99*		
5*a*	HOSK	11.66	21.48	3.6×10^{-1}	1.21
5*b*	HOSK	6.12	Negative	9.0×10^{-1}	1.84
	Mean				
6*a*	CLLSQ	10.49	19.03	9.6×10^{-2}	—
6*b*	CLLSQ	10.63	19.04	1.6×10^{-1}	—
	Mean	*10.56*	*19.04*		

*Experimentally determined titration data, p*H* and p*M* measured. See note on Table 2 for S.D. p*M*.

of stability constants as increasing amounts of random error are applied to the titer or the p*H* in typical titration data. It is clear that none of the methods of data analysis can tolerate input data of poor quality, and it appears that the HOSK treatment is the most susceptible to invalidation from this cause.

Provided that p*M* is accurately measurable by an auxiliary probe CLLSQ gives excellent recovery of

TABLE 5. Effect of random error in input data, calculated values of equilibrium constants, simulated titration data of copper(II)–ethylenediamine complexes*

	Value for random error in volume of base titrant (cm^3) =				
Parameter	Error-free	±0.001	±0.01	±0.02	±0.1
SCOGS					
log β_{101}	10.44	10.43	10.47	10.32	
log β_{102}	19.60	19.60	19.56	19.61	
S.D. fit	2.4×10^{-7}	6.7×10^{-4}	2.8×10^{-3}	8.7×10^{-3}	Failed
S.D. pM	0.000	0.004	0.014	0.057	
S.D. pL	0.000	0.001	0.003	0.006	
HOSK					
log β_{101}	10.47	10.48	10.35	10.72	11.85
log β_{102}	19.51	19.53	19.71	18.93	Negative
S.D. fit	5.5×10^{-2}	5.5×10^{-2}	1.4×10^{-1}	3.9×10^{-1}	8.8×10^{-1}
S.D. pM	0.220	0.216	0.260	0.337	4.08
S.D. pL	0.192	0.191	0.200	0.183	0.640
CLLSQ					
log β_{101}	10.44	10.44	10.44	10.44	10.44
log β_{102}	19.60	19.60	19.60	19.60	19.60
S.D. fit	1.2×10^{-3}	1.1×10^{-3}	1.1×10^{-3}	1.1×10^{-3}	1.3×10^{-3}
S.D. pL	0.000	0.000	0.000	0.000	0.000
ROMARY					
log β_{101}	10.44	10.43	10.48	10.31	
log β_{102}	19.60	19.58	19.52	19.52	
S.D. fit	7.4×10^{-7}	1.7×10^{-3}	2.1×10^{-2}	9.8×10^{-2}	Failed
S.D. pM	0.000	0.015	0.025	0.094	
S.D. pL	0.000	0.001	0.005	0.011	
HALF-$\bar{n}$					
log β_{101}	10.35	10.35	10.35	10.34	8.38
log β_{102}	19.59	19.59	19.22	19.58	17.24
S.D. pM	0.046	0.046	0.175	0.059	1.24
S.D. pL	0.000	0.001	0.005	0.011	0.078
DIRECT					
log β_{101}	10.50	10.48	10.51	10.42	9.05
log β_{102}	19.60	19.58	19.53	19.55	18.57
S.D. pM	0.030	0.016	0.029	0.038	0.762
S.D. pL	0.000	0.001	0.005	0.011	0.078

*Input values log β_{101} = 10.44, log β_{102} = 19.60. For significance of S.D. values see Table 1.

known equilibrium constants; and it is a feature of this procedure that it is insensitive to variance in the titer and relatively insensitive for many complexes to uncertainty in pH values.

Experience with simulated titration data has revealed that the SCOGS program consistently achieves good recovery of the starting equilibrium constants (with the possible exception, as already noted, of values for unusually stable metal complexes) and also the smallest values of standard deviations in pM and pL. In view of this performance the authors have come to place most reliance on this program to indicate 'correct' equilibrium constants derived from real titrations, and hence to provide a basis for comparison of other methods. While limited in its application to systems of simple mononuclear complexes, ML_r, the ROMARY program, insofar as we have tested it, performed almost as well as SCOGS and required only a fraction of the computer time demanded by the latter. The procedures HALF-$\bar{n}$ and LINEAR perform well only on systems where there is no overlap of equilibrium constants; for the copper–glycine complexes ($K_1/K_2 = 23$) these methods consistently returned slightly high values of K_1 which in turn led to values of pM higher than the preceding methods.

Turning to results based on real titrations we note in Tables 2 and 4 two kinds of discrepancies warranting comment. The first is a tendency for the HOSK procedure to generate equilibrium constants significantly at variance with those from SCOGS and the other methods illustrated here. An extreme case is seen in line 5, Table 4, although the base titrations gave some poor results in line 4a as well. Smaller discrepancies are apparent in line 2, Tables 2 or 4. But these tables reveal only a few such problems. We have determined 25 different pK values and 65 different stability constants for glycine and iminodi-

Can. J. Chem. Downloaded from www.nrcresearchpress.com by 210.87.254.105 on 09/05/12
For personal use only.

Can. J. Chem. Downloaded from www.nrcresearchpress.com by 210.87.254.105 on 09/05/12
For personal use only.

TABLE 6. Effect of random error in input data, calculated values of equilibrium constants, simulated titration data of copper(II)–ethylenediamine complexes*

	Value for random error in pH =			
Parameter	Error-free	±0.001	±0.01	±0.1
SCOGS				
log β_{101}	10.44	10.44	10.44	10.51
log β_{102}	19.60	19.60	19.61	19.67
S.D. fit	2.4×10^{-7}	7.3×10^{-5}	8.3×10^{-4}	6.1×10^{-3}
S.D. pM	0.000	0.002	0.017	0.122
S.D. pL	0.000	0.001	0.012	0.082
HOSK				
log β_{101}	10.47	10.47	10.47	10.24
log β_{102}	19.51	19.51	19.46	19.18
S.D. fit	5.5×10^{-2}	5.7×10^{-2}	5.6×10^{-2}	2.9×10^{-1}
S.D. pM	0.220	0.217	0.200	0.097
S.D. pL	0.192	0.192	0.196	0.227
CLLSQ				
log β_{101}	10.44	10.44	10.44	10.48
log β_{102}	19.60	19.60	19.59	19.40
S.D. fit	1.2×10^{-3}	2.9×10^{-3}	2.4×10^{-2}	1.8×10^{-1}
S.D. pL	0.000	0.001	0.009	0.072
ROMARY				
log β_{101}	10.44	10.44	10.44	10.50
log β_{102}	19.60	19.60	19.59	19.72
S.D. fit	7.4×10^{-7}	7.5×10^{-4}	1.4×10^{-2}	3.6×10^{-2}
S.D. pM	0.000	0.003	0.013	0.014
S.D. pL	0.000	0.002	0.013	0.101
HALF-$\bar{n}$				
log β_{101}	10.35	10.35	10.36	10.39
log β_{102}	19.59	19.59	19.62	19.77
S.D. pM	0.046	0.044	0.038	0.103
S.D. pL	0.000	0.002	0.013	0.101
DIRECT				
log β_{101}	10.50	10.50	10.50	10.57
log β_{102}	19.60	19.60	19.60	19.77
S.D. pM	0.030	0.031	0.032	0.186
S.D. pL	0.000	0.002	0.013	0.101

*Input values log β_{101} = 10.44, log β_{102} = 19.60. For significance of S.D. values see Table 1.

TABLE 7. Calculated formation constants for copper(II)–citrate complexes, simulated titration data, input values: log β_{111} = 9.29, log β_{202} = 14.88, log β_{1-11} = 1.63(11)*

Line	Program	log β_{111}	log β_{202}	log β_{1-11}	S.D. fit	S.D. pM	S.D. pL
1	SCOGS	9.29	14.88	1.63	1.7×10^{-7}	0.000	0.000
2	HOSK	9.26	15.15	1.71	2.5×10^{-2}	0.019	0.016
3	CLLSQ	9.29	14.88	1.63	1.5×10^{-4}	—	0.000

*Error-free data used only.

acetic acid and their complexes with three metals in aqueous and in aqueous methanol solutions. The actual results will be published in the near future. The data were so taken as to permit them to be processed in the various ways described in this paper. Good agreement was found among the results based on SCOGS, ROMARY, HALF-$\bar{n}$, and DIRECT calculations. In 6 of the pK's and 38 of the log β values the results from the HOSK calculation differed by more than 0.2 unit from the remainder. Of these 38, twenty-five differed by 0.5 unit or more from the remainder and that number included five negative values.

The second discrepancy to note appears in Table 4 in the form of lower values for log β_{102} generated by the CLLSQ procedure as compared to those found

Can. J. Chem. Downloaded from www.nrcresearchpress.com by 210.87.254.105 on 09/05/12
For personal use only.

TABLE 8. A table showing how the results of nine titrations differing in ratio $C_L:C_M$ can be combined in nine sets of five for analysis by HOSK. The middle titration in each row was used for analysis by SCOGS or CLLSQ

8:1	8:1	6:1	8:2	8:2	6:2	8:3	8:3	6:3
7:1	6:1	7:1	7:2	6:2	7:2	7:3	6:3	7:3
6:1	7:1	8:1	6:2	7:2	8:2	6:3	7:3	8:3
6:2	7:2	8:2	6:1	7:1	8:1	6:2	7:2	8:2
6:3	7:3	8:3	6:3	7:3	8:3	6:1	7:1	8:1

by SCOGS or HOSK. Agreement among these values is much better in Table 2. In view of the excellent recovery of equilibrium constants when CLLSQ was applied to simulated titration data it must be concluded that a systematic error has been introduced into the experimental values of pM through nonlinear response of the probe electrode at low concentrations of copper ion in the ethylenediamine study. This inference is supported by comparison with pM values calculated by SCOGS. No such systematic error appears in the pM data shown in Table 10 where experimental values determined by two electrodes are compared with values calculated from the constants generated by SCOGS and HOSK for the system copper(II)–glycine. The HOSK values showed appreciably larger deviations than those obtained by SCOGS.

The results given in Tables 7 and 9 indicate that even with error-free titration data the HOSK treatment is less successful than the other two methods in regenerating equilibrium constants for the systems selected. It is particularly noteworthy that HOSK returned a poor value for log β_{202} in Table 7 since the method has not yet been shown capable of dealing with polynuclear complex species.

Sources of Error in HOSK Method of Data Treatment

We have sought causes for the occasional appearance of evidently incorrect values among the equilibrium constants generated by HOSK. In general the problem arises from the large amount of data handling required by this method, and in the necessity to set values of pM_0 and pL_0 for evaluating [4] and [5]. Our analysis suggests that the standard deviations in pM and pL derived by this method are often higher than the corresponding quantities found by other methods (see Tables 5 and 6), though errors in these are to some extent compensated in the calculation of stability constants, especially for 1:1 complexes, owing to the fact that $(\partial C_H/\partial C_L)_H$ and $(\partial C_H/\partial C_M)_H$ are in part reciprocally related (3).

Some specific difficulties in this procedure are discussed next.

Evaluation of C_H

Both SCOGS and HOSK depend on accurate evaluation of C_H. The necessity in the latter method to extend titrations to an extreme pH (= pH_0) at which pH or pM can be evaluated from C_L or C_M leads to a situation where C_H may become poorly defined. This problem can be avoided in the other methods by restricting the data to the buffer regions ($0.2 < \bar{n} < 0.8$, etc.). To fix the high pK of an amino acid by the HOSK method requires that the titration be carried to a high pH where [L] $\sim C_L$. In this region $C_H = C_L$ − added base, and is poorly defined; this lack of definition carries over into $(\partial C_H/\partial C_L)_H$

TABLE 9. Calculated formation constants for iron(III)–citrate complexes, simulated titration data (9 sets), input values: log β_{111} = 12.37, log β_{101} = 11.18, log β_{1-11} = 8.49(11)

		Error-free data			Random error in VB = ±0.002 cm³		
Parameter	Program	Minimum	Mean	Maximum	Minimum	Mean	Maximum
log β_{111}	SCOGS	12.37	12.37	12.37	12.23	12.37	12.48
	HOSK	12.56	12.60	12.64	12.53	12.58	12.63
	CLLSQ	12.37	12.37	12.37	12.36	12.37	12.37
log β_{101}	SCOGS	11.18	11.18	11.18	11.16	11.18	11.19
	HOSK	11.23	11.36	11.47	11.24	11.37	11.49
	CLLSQ	11.18	11.18	11.18	11.18	11.18	11.19
log β_{1-11}	SCOGS	8.49	8.49	8.49	8.44	8.49	8.53
	HOSK	8.49	8.58	8.67	8.46	8.56	8.65
	CLLSQ	8.49	8.49	8.49	8.48	8.49	8.49
S.D. fit	SCOGS	2.2×10^{-7}	2.6×10^{-7}	3.4×10^{-7}	7.0×10^{-4}	1.2×10^{-3}	1.5×10^{-3}
	HOSK	1.5×10^{-2}	2.5×10^{-2}	4.1×10^{-2}	1.4×10^{-2}	2.7×10^{-2}	4.5×10^{-2}
	CLLSQ	3.4×10^{-4}	8.5×10^{-4}	3.3×10^{-3}	4.5×10^{-4}	2.1×10^{-3}	1.2×10^{-2}
S.D. pM	SCOGS	0.000	0.000	0.000	0.004	0.012	0.022
	HOSK	0.042	0.081	0.152	0.043	0.081	0.137
S.D. pL	SCOGS	0.000	0.000	0.000	0.000	0.000	0.001
	HOSK	0.073	0.165	0.455	0.075	0.136	0.176
	CLLSQ	0.000	0.000	0.000	0.000	0.000	0.002

Can. J. Chem. Downloaded from www.nrcresearchpress.com by 210.87.254.105 on 09/05/12
For personal use only.

TABLE 10. Comparison of pM values for one titration, system: copper(II)–glycine 25°C, μ = 0.1 M ($NaNO_3$)

	pM observed		pM calculated	
pH	Electrode 1	Electrode 2	HOSK	SCOGS
3.91	3.448	3.442	3.342	3.399
3.98	3.469	3.458	3.358	3.415
4.11	3.513	3.509	3.395	3.452
4.20	3.543	3.539	3.422	3.479
4.35	3.614	3.610	3.481	3.539
4.45	3.648	3.648	3.522	3.581
4.54	3.705	3.695	3.568	3.627
4.65	3.756	3.756	3.624	3.683
4.75	3.824	3.824	3.687	3.746
4.85	3.901	3.891	3.753	3.811
4.96	3.969	3.967	3.826	3.884
5.08	4.07	4.060	3.918	3.974
5.19	4.158	4.158	4.011	4.066
5.31	4.266	4.263	4.118	4.170
5.44	4.391	4.388	4.241	4.291
5.56	4.503	4.503	4.358	4.407
5.68	4.634	4.632	4.488	4.536
5.80	4.770	4.767	4.619	4.666
5.93	4.915	4.912	4.761	4.812
6.06	5.074	5.071	4.918	4.974
6.20	5.260	5.254	5.092	5.154
6.37	5.473	5.473	5.303	5.373
6.55	5.730	5.734	5.563	5.634
S.D. pM(1)	—	0.005	0.160	0.089
S.D. pM(2)	0.005	—	0.142	0.086

and hence pL. When enough base has been added C_H is well defined but negative resulting in a negative $(\partial C_H/\partial C_L)_H$ and a pL smaller than pL_0. Likewise to start a titration involving metal complexes at a pH low enough for [M] = C_M may require the addition of so much acid that C_H (= added acid − added base) is poorly defined over much of the titration. At the start of the titration for small added base C_H is well defined but usually a trend in C_M results in a change of sign for $(\partial C_H/\partial C_M)_H$. (This is the problem in line 5*b*, Table 4.)

Evaluation of $(\partial C_H/\partial C_L)_H$ *or* $(\partial C_H/\partial C_M)_H$

For metal–ligand systems the plots of C_H vs. C_L or C_H vs. C_M may depart from linear, the more so if $\bar{n}C_M$ is not much less than C_L (3). Curve fitting in this event becomes more difficult, and errors in taking derivatives are more apt to be introduced.

The same values of the derivatives are obtained no matter which titration is considered for pM and pL evaluation when C_H vs. C_L and C_H vs. C_M are linear. When these plots are curved, errors in taking the derivatives are greater than differences between selecting separate titrations for pM and pL calculations.

Occasionally the assignment of pH_0 may be too low or too high. For metal–ligand complexes $(\partial C_H/\partial C_M)_H$ should be essentially zero at pH_0, and then steadily increase for a few points. If pH_0 is chosen too high this differential quotient starts with a positive value, or the converse if pH_0 is too low. The consequences are respectively to over or underestimate β_{pqr}.

It should be noted that the simulated titration curves had the same small changes, due to dilution correction, in C_M and C_L as for the experimental data. From Tables 1 and 3 no major problem is caused by this 1 to 2% change in C_M and C_L for simulated data. Since all titrations require similar volumes of titrant C_M is essentially constant at each pH for $(\partial C_H/\partial C_L)_{H,C_M}$ and C_L is essentially constant at each pH for $(\partial C_H/\partial C_M)_{H,C_L}$. When the constants are calculated, dilution-corrected C_M and C_L values are used with the result of cancelling most of this effect upon the constant.

Uncertainty in Data

As a consequence of the two preceding difficulties values of $(\partial C_H/\partial C_M)_H$ are ill-defined in the unbuffered regions of the titrations from which data are required in order to perform the integration of [5]. Close examination shows that in a number of such cases the values of $(\partial C_H/\partial C_M)_H$ fluctuate, sometimes positive, sometimes negative, and the integration leads to poor estimates of pM.

To sum up then, the HOSK method is capable of yielding, without the user's knowledge, results for pM, pL, and the several β_{pqr} that are appreciably in error. Prospective users of the method should acquaint themselves fully with the factors that may cause such erroneous results, and should perform checks on results by an independent computational method.

Experimental

Titrations were carried out in a thermostatted glass vessel maintained at 25.0°C, with solutions containing 0.1 M $NaNO_3$ as background electrolyte. Titrant was added from a 0.5 cm^3 syringe dispenser equipped with micrometer drive. Measurement of pH was made by the response of a Beckman glass electrode (#39301) calibrated with NBS buffers. Measurement of pM was by an Orion solid state copper(II) ion-selective electrode (#94-29) calibrated with solutions of known metal ion concentration. The titration vessel was wrapped in foil owing to the light-sensitive response of the latter electrode. These electrodes with suitable reference electrodes were connected to the input of suitable pH meters (Orion 801 or Radiometer No. 4). Analar-grade glycine was recrystallized before use; ethylenediamine was dried by potassium hydroxide and by sodium metal, and then distilled. All other chemicals were of reagent grade, and solutions were standardized by well established methods. Titrations were carried out and alkali solutions were stored under nitrogen to restrict carbonate formation.

Acknowledgement

The support of this research by the National Research Council of Canada is gratefully acknowledged.

1. B. SARKAR and T. P. A. KRUCK. Can. J. Chem. **51**, 3541 (1973).
2. R. OSTERBERG. Acta Chem. Scand. **14**, 471 (1960).
3. W. A. E. MCBRYDE. Can. J. Chem. **51**, 3572 (1973).
4. W. A. E. MCBRYDE. Analyst, **94**, 337 (1969); **96**, 739 (1971).
5. D. D. PERRIN and B. DEMPSEY. Buffers for p*H* and metal ion control. Chapman and Hall, London. 1974.
6. F. J. C. ROSSOTTI and H. S. ROSSOTTI. The determination of stability constants. McGraw-Hill, New York. 1961.
7. W. A. E. MCBRYDE. Can. J. Chem. **45**, 2093 (1967).
8. G. SCHWARZENBACH and E. FREITAG. Helv. Chim. Acta, **34**, 1492 (1951).
9. I. G. SAYCE. Talanta, **15**, 1397 (1968).
10. J. K. ROMARY, D. L. DONNELLY, and A. C. ANDREWS. J. Inorg. Nucl. Chem. **29**, 1805 (1967).
11. T. B. FIELD, J. L. MCCOURT, and W. A. E. MCBRYDE. Can. J. Chem. **52**, 3119 (1974).

Can. J. Chem. Downloaded from www.nrcresearchpress.com by 210.87.254.105 on 09/05/12
For personal use only.

Synthesis, characterization, and X-ray structural studies of octahedral transition metal complexes incorporating the novel anionic tridentate ligand, dimethyl(ethanolamino)(1-pyrazolyl)-gallate, $[Me_2Ga(OCH_2CH_2NH_2)(N_2C_3H_3)]^-$

KENNETH S. CHONG, STEVEN J. RETTIG, ALAN STORR, AND JAMES TROTTER

Department of Chemistry, University of British Columbia, 2075 Wesbrook Mall, Vancouver, B.C., Canada V6T 1W5

Received October 21, 1977

KENNETH S. CHONG, STEVEN J. RETTIG, ALAN STORR, and JAMES TROTTER. Can. J. Chem. **56**, 1212 (1978).

Details of the synthesis and physical properties of octahedral transition metal complexes of the tridentate tris chelating ligand $[Me_2Ga(OCH_2CH_2NH_2)(N_2C_3H_3)]^-$ are given. Crystals of *sym-fac*-bis[dimethyl(ethanolamino)(1-pyrazolyl)gallato(*N*(2),*O*,*N*)]nickel(II) are monoclinic, $a = 11.7908(6)$, $b = 7.3158(6)$, $c = 12.5797(8)$, $\beta = 97.035(7)°$, $Z = 2$, space group $P2_1/n$ and crystals of the *mer* isomer are monoclinic, $a = 18.6617(7)$, $b = 8.7941(4)$, $c = 13.5670(8)$, $\beta = 91.766(4)°$, $Z = 4$, space group $P2_1/c$. The structures were solved by Patterson and Fourier syntheses and were refined by full-matrix least-squares procedures to final R values of 0.048 and 0.052 for 1881 and 2573 reflections with $I \geq 3\sigma(I)$ for the *fac* and *mer* isomers respectively. The nickel atoms in both structures were found to have distorted octahedral coordination geometry. Bond lengths (corrected for libration) are: Ni—O, 2.090(3); Ni—N, 2.085(3) and 2.112(3); Ga—O, 1.908(3); Ga—N, 2.010(3); and Ga—C, 1.979(5) and 1.981(6) Å for the *fac* isomer, and Ni—O, 2.045(4) and 2.049(4); Ni—N, 2.091(4)–2.156(5); Ga—O, 1.898(4) and 1.899(4); Ga—N, two at 1.991(5); and Ga—C, 1.948(8)–1.971(7) Å for the *mer* isomer.

KENNETH S. CHONG, STEVEN J. RETTIG, ALAN STORR et JAMES TROTTER. Can. J. Chem. **56**, 1212 (1978).

On rapporte les détails de la synthèse et des propriétés physiques de complexes octaédriques de métaux de transition du ligand tris chélatant tridentate $[Me_2Ga(OCH_2CH_2NH_2)(N_2C_3H_3)]^-$. Les cristaux du bis[diméthyle(éthanolamino)(pyrazolyl-1)gallato(*N*(2),*O*,*N*)]*sym-fac* de nickel(II) sont monocliniques $a = 11.7908(6)$, $b = 7.3158(6)$, $c = 12.5797(8)$, $\beta = 97.035(7)°$, $Z = 2$, groupe d'espace $P2_1/n$ et les cristaux de l'isomère *mer* sont monocliniques, $a = 18.6617(7)$, $b = 8.7941(4)$, $c = 13.5670(8)$, $\beta = 91.766(4)°$, $Z = 4$, groupe d'espace $P2_1/c$. On a résolu les structures par les méthodes de Patterson et de Fourier et on les a affinées par la méthode des moindres carrés (matrice complète) jusqu'à des valeurs finales de R qui sont respectivement de 0.048 et 0.052 pour 1881 et 2573 réflexions avec $I \geq 3\sigma(I)$ pour les isomères *fac* et *mer*. On a trouvé que les atomes de nickel dans chacune des structures possèdent une géométrie de coordination octaédrique déformée. Les longueurs de liaison (corrigées pour la libration) sont: Ni—O, 2.090(3); Ni—N, 2.085(3) et 2.112(3); Ga—O, 1.908(3), Ga—N, 2.010(3) et Ga—C, 1.979(5) et 1.981(6) Å pour l'isomère *fac* et Ni—O, 2.045(4) et 2.049(4); Ni—N, 2.091(4)–2.156(5); Ga—O, 1.898(4) et 1.899(4); Ga—N, deux à 1.991(5) et Ga—C, 1.948(8)–1.971(7) Å pour l'isomère *mer*.
[Traduit par le journal]

Introduction

A previous publication (1) described the first of a new class of tridentate ligand systems incorporating the dimethyl gallium and pyrazolyl moieties, **1**. In that study binuclear transition metal complexes were isolated. The present account reports the synthesis of the less sterically demanding anionic tridentate ligand, dimethyl(ethanolamino)(1-pyrazolyl)gallate, $[Me_2Ga(OCH_2CH_2NH_2)(N_2C_3H_3)]^-$, **2**, and its coordinating properties towards selected transition metal ions, M^{2+} (M = Mn, Fe, Co, Ni, Cu, or Zn). Octahedral complexes were isolated in each case and the realization of *fac*/*mer* isomerism has been demonstrated through crystal structure determinations of two nickel isomers.

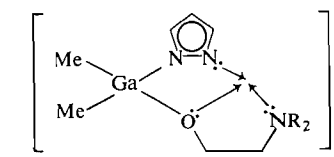

1, R = Me
2, R = H

Experimental

Starting Materials

Air-sensitive materials were handled in oxygen-free dry nitrogen. Tetrahydrofuran (THF) was dried by refluxing over lithium aluminum hydride and was used immediately following distillation. Benzene was dried by refluxing over molten potassium followed by distillation. Pyrazole (K and K Laboratories) and sodium hydride (Alfa Inorganic) were used as supplied.

Can. J. Chem. Downloaded from www.nrcresearchpress.com by 210.87.254.40 on 09/05/12
For personal use only.

TABLE 1. Analytical data for $[Me_2Ga(OCH_2CH_2NH_2)(N_2C_3H_3)]_2M$ complexes

M	Color	Transition metal precursor	Isomer	Analysis: Found (%) C	H	N	Calcd. (%) C	H	N	Comments
Mn	White	$MnCl_2$	*mer*	33.1	6.1	16.3	33.1	5.9	16.5	Air sensitive
Fe	Yellow	$FeCl_2 \cdot 1.5THF$	*mer*	33.9	6.0	16.8	33.0	5.9	16.5	Air sensitive
Co	Magenta	$CoCl_2$	*mer*	32.9	5.9	16.3	32.8	5.9	16.4	Solution air sensitive
Ni	Blue	$NiBr_2$	*mer*	32.9	5.8	16.6	32.8	5.9	16.4	Air stable
Ni	Purple	$NiBr_2$	*fac*	32.9	6.0	16.6	32.8	5.9	16.4	Air stable
Cu	Blue	$CuBr_2$	*fac*	33.9	4.9	18.1	32.5	5.8	16.3	Air sensitive
Zn	White	$ZnCl_2$	*fac*	32.7	5.9	16.7	32.4	5.8	16.2	Air sensitive

Ethanolamine was refluxed over anhydrous $CaSO_4$ and distilled prior to use. Gallium trimethyl (2) and $FeCl_2 \cdot 1.5$ THF (3) were prepared as described previously.

Preparative Details

Sodium Dimethyl(ethanolamino)(1-pyrazolyl)gallate

$$[1]\ NaH + N_2C_3H_4 \xrightarrow{THF,N_2atm.} Na^+N_2C_3H_3^- + H_2$$

$$[2]\ Na^+N_2C_3H_3^- + Me_3Ga \xrightarrow{THF,N_2atm.} Na^+Me_3Ga(N_2C_3H_3)^-$$

$$[3]\ Na^+Me_3Ga(N_2C_3H_3)^- + HOCH_2CH_2NH_2 \xrightarrow[reflux]{THF,N_2atm.} Na^+[Me_2Ga(OCH_2CH_2NH_2)(N_2C_3H_3)]^- + CH_4$$

Trimethyl gallium (3.19 g, 27.8 mmol) in THF was added to sodium pyrazolide (27.8 mmol) (made from sodium hydride (0.667 g, 27.8 mmol) and pyrazole (1.89 g, 27.8 mmol) in THF) in the same solvent. Ethanolamine (1.695 g, 27.8 mmol) in THF was added to the resulting solution and on refluxing a slow evolution of methane occurred. The reaction was complete in approximately 24 h. The resultant solution was cooled and made up to a standard volume in the glove box. Aliquots of this solution were used in the preparation of the transition metal complexes.

Preparation of $[Me_2Ga(OCH_2CH_2NH_2)(N_2C_3H_3)]_2M$ Complexes, where M = Mn, Fe, Co, Ni, Cu, Zn

The procedure was very similar for each experiment and can be illustrated by the preparation of the nickel complexes. The transition metal starting materials for all the preparations are listed in Table 1, along with physical data for the resulting complexes.

An aliquot of the ligand solution prepared as described above and containing $Na^+[Me_2Ga(OCH_2CH_2NH_2)(N_2C_3H_3)]^-$ (1.388 g, 5.56 mmol) was added to a slurry of $NiBr_2$ (0.607 g, 2.78 mmol) in THF. The resulting mixture was stirred overnight and yielded a blue solution and a white precipitate. The solid was allowed to settle and the solvent was then removed from the isolated clear solution. The resulting solid was recrystallized from benzene and yielded predominantly purple crystals together with a small amount of blue crystalline material. The crystals were separated manually and were found to be *fac* and *mer* isomers of the same octahedral compound. The purple crystals were found to be the 'all-*trans*' *fac* isomer, Fig. 1*a*; the blue crystals the *mer* isomer, Fig. 1*b*.

Conversion of one isomer to the other could be effected by correct choice of solvent for recrystallization. The non-polar *fac* isomer (purple crystals) when dissolved in acetone gave the polar *mer* isomer (blue crystals) on recrystallization. Conversely the *mer* isomer dissolved in benzene gave the *fac* isomer on recrystallization. Heating the *fac* isomer causes a color change from purple to blue at ~130°C, suggesting a rearrangement to the *mer* isomer. Continued heating causes decomposition at ~190°C. The blue *mer* isomer itself darkens and decomposes at ~190°C, with no observable color change below this temperature.

No evidence for *fac*/*mer* isomerism in the remaining complexes has been found. The isomer obtained (deduced from ir spectra as discussed later) for each metal is given in Table 1. Numerous attempts were made to obtain a purer copper derivative but recrystallization failed to yield a complex of higher purity.

Spectra

A Varian MAT CH4 was used to record mass spectra at 70 eV with an ion source temperature of 100–180°C. Infrared spectra were recorded on a Perkin–Elmer 457 spectrophotometer as Nujol mulls and electronic absorption solution spectra on a Cary 14 spectrometer.

X-Ray Crystallographic Analyses

sym-fac-*Bis[dimethyl(ethanolamino)(1-pyrazolyl)gallato-(N(2),O,N)]nickel(II)*

The crystal was mounted with (0 1 1) normal to the goniostat axis and had dimensions of ca. 0.49 × 0.49 × 0.54 mm. Unit-cell parameters were refined by least-squares on 2 sin θ/λ values for 16 reflections measured on a diffractomer with Cu K_α radiation (λ = 1.5418 Å). Crystal data (at 22°C) are:

$C_{14}H_{30}Ga_2N_6NiO_2$ fw = 512.58

Monoclinic, a = 11.7908(6), b = 7.3158(6), c = 12.5797(8) Å, β = 97.035(7)°, V = 1076.9(1) Å^3, Z = 2, ρ_c = 1.581 g cm^{-3}, $F(000)$ = 524, μ(Cu K_α) = 42.9 cm^{-1}. Absent reflections: $0k0$, $k \neq 2n$, and $h0l$, $h + l \neq 2n$ defined uniquely the space group $P2_1/n$ (non-standard setting of $P2_1/c$, C_{2h}^5, No. 14).

Intensities were measured with Ni-filtered Cu K_α radiation on a Datex-automated General Electric XRD-6 diffractometer. A θ–2θ scan at 4° min^{-1} over a range of (1.80 + 0.86 tan θ) degrees in 2θ was employed. Background counts of 10 s were measured at each end of the scan. Data were measured to 2θ = 160°. The intensities of the check reflections, measured every 50 reflections throughout the data collection, remained constant to within ±5%. After data reduction, an absorption correction was applied using the Gaussian integration method (4, 5). Transmission factors ranged from 0.102 to 0.338. Of

Can. J. Chem. Downloaded from www.nrcresearchpress.com by 210.87.254.40 on 09/05/12
For personal use only.

Can. J. Chem. Downloaded from www.nrcresearchpress.com by 210.87.254.40 on 09/05/12
For personal use only.

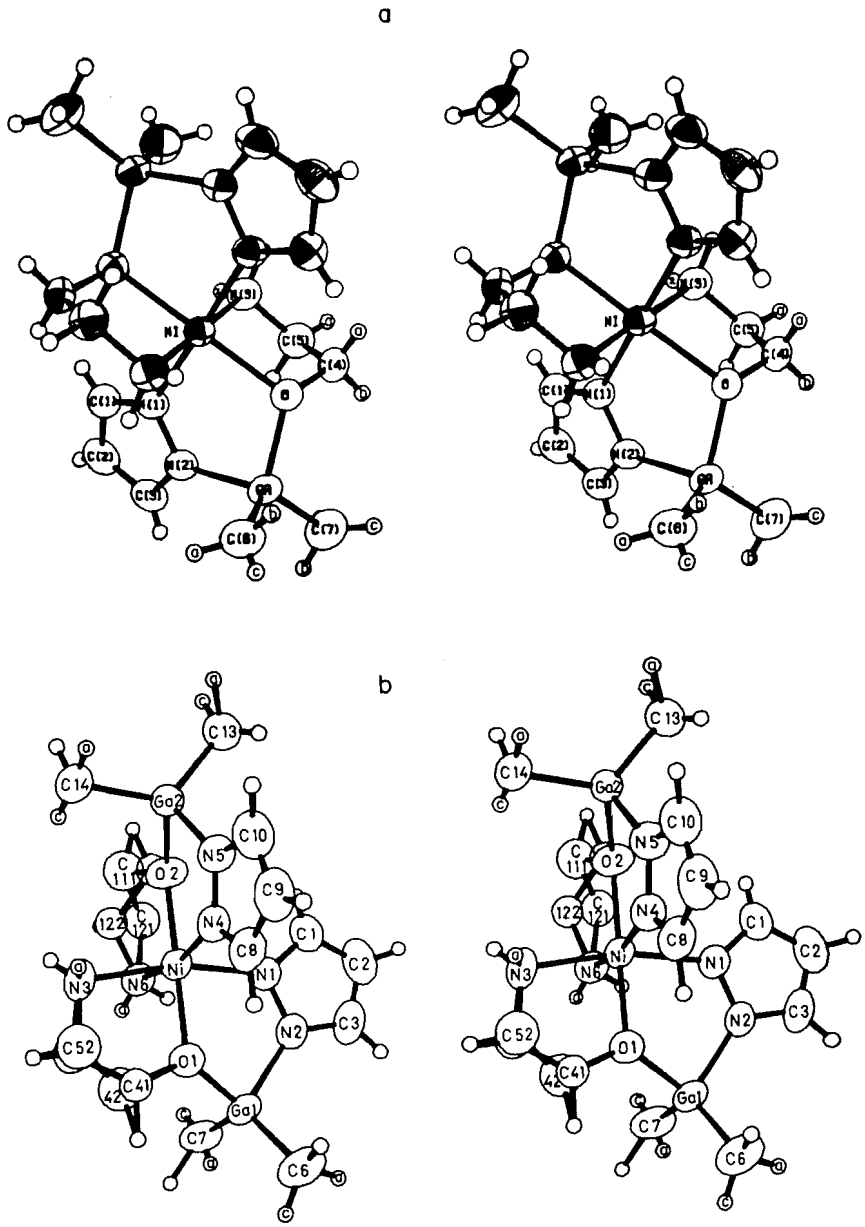

FIG 1. Stereo views of the *sym–fac* (*a*) and *mer* (*b*) isomers of the bis[dimethyl(ethanolamino)(1-pyrazolyl)gallato(*N*(2),-*O*,*N*)]nickel(II) molecule; 50% ellipsoids are shown for the non-hydrogen atoms. Hydrogen atoms have been assigned artificially small thermal parameters for the sake of clarity.

the 2355 independent reflections measured, 1902 (81%) had intensities greater than $3\sigma(I)$ above background where $\sigma^2(I) = S + B + (0.06S)^2$ with S = scan count and B = time-averaged background count.

With Ni at the origin the position of the gallium atom was determined from the Patterson function. After full-matrix refinement with anisotropic thermal parameters to $R = 0.068$, a difference map gave the positions of all 15 hydrogen atoms subsequently included with isotropic thermal parameters. The scattering factors of ref. 6 were used for non-hydrogen atoms and those of ref. 7 for hydrogen atoms. Anomalous scattering factors from ref. 8 were used for the Ga, Ni, O, and N atoms. The weighting scheme, $w = 1/\sigma^2(F)$ where $\sigma^2(F)$ is derived from the previously defined $\sigma^2(I)$, gave uniform average values of $w(|F_o| - |F_c|)^2$ over ranges of $|F_o|$ and was employed in the final stages of refinement. A correction for secondary extinction was approximated by basing the least-squares refinement on the minimization of $\Sigma w[|F_o| - |F_c/(1+gI)|]^2$ where g is the extinction parameter and I the uncorrected intensity. The final value of g was $3.3(6) \times 10^{-8}$. Convergence was reached at $R = 0.048$ and $R_w = 0.057$ for 1881 reflections with $I \geq 3\sigma(I)$ (21 reflections with $||F_o| - |F_c|| > 3\sigma(F)$ were treated as unobserved in the final stages of refinement; instrumental error was suspected, but it seemed unwise to bias the data by

Can. J. Chem. Downloaded from www.nrcresearchpress.com by 210.87.254.40 on 09/05/12
For personal use only.

remeasurement; the discrepancies were not large). For all 2355 reflections $R = 0.061$ and $R_w = 0.078$.

On the final cycle of refinement the mean and maximum parameter shifts were 0.03 and 0.38σ respectively. The mean error in an observation of unit weight was 1.758.

mer-*Bis[dimethyl(ethanolamino)(1-pyrazolyl)gallato*(N(2), O,N)*]nickel(II)*

Experimental details are the same as for the *fac* isomer except where noted. The crystal used, mounted with (0 1 1) normal to the goniostat axis, was ca. 0.4 × 0.4 × 0.35 mm. Thirty-two reflections were used in the refinement of the unit-cell parameters. Crystal data are:

Monoclinic, $a = 18.6617(7)$, $b = 8.7941(4)$, $c = 13.5670(8)$ Å, $\beta = 91.766(4)°$, $V = 2225.5(2)$ Å^3, $Z = 4$, $\rho_c = 1.530$ g cm^{-3}, $F(000) = 1048$, μ(Cu K_α) = 41.5 cm^{-1}. Absent reflections: $0k0$, $k \neq 2n$, and $h0l$, $l \neq 2n$ defined uniquely the space group $P2_1/c$ (C_{2h}^5, No. 14).

The intensity of the check reflection remained constant to within ±3% during data collection. Of 4401 independent reflections measured (to $2\theta = 145°$), 2573 (58.5%) had intensities greater than $3\sigma(I)$ above background. An absorption correction was applied, transmission factors ranging from 0.188 to 0.421.

The coordinates of the nickel and gallium atoms were determined from the three-dimensional Patterson function. All four ethanolamine carbon atoms are positionally two-fold disordered and were refined with site occupancies fixed at 0.5. The positions of most hydrogen atoms (Table 3[1]) were located on subsequent difference maps. Attempts to refine the disordered carbon atoms with anisotropic thermal parameters were unsuccessful. The structure (ordered non-hydrogen atoms having anisotropic thermal parameters) was refined for four cycles giving a final R of 0.052 and R_w of 0.067 for 2573 reflections with $I \geq 3\sigma(I)$ (for all 4401 reflections $R = 0.084$ and $R_w = 0.074$). No correction for secondary extinction was applied. The weighting scheme used was: $w = 1$ for $|F_o| \leq 18$, $w = (18/|F_o|)^2$ for $|F_o| > 18$, and $w = 0.063$ for the unobserved reflections. The mean and maximum parameter shifts on the final cycle of refinement were 0.06 and 0.82σ. The mean error in an observation of unit weight was 0.9415.

The final positional and thermal parameters for both structures are given in Tables 2 and 3[1] respectively. Measured and calculated structure factors have been placed in the Depository of Unpublished Data.[1]

The thermal motions of both molecules have been analysed in terms of rigid-body modes of translation, libration, and screw motion (9) using the computer program MGTLS. For the *fac* isomer (rms $\sigma U_{ij} = 0.0020$ Å^2), analysis of all non-hydrogen atoms (rms $\Delta U_{ij} = 0.0047$ Å^2) gave physically reasonable rigid-body parameters but the Ga coordination group showed significant independent motion and was analysed separately (rms $\Delta U_{ij} = 0.0017$ Å^2). For the *mer* isomer (rms $\sigma U_{ij} = 0.0034$ Å^2), four analyses gave reasonable parameters: the two Ga coordination groups, the Ni coordination group, and a 17 atom group consisting of all ordered non-hydrogen atoms except the methyl carbon atoms (rms σU_{ij} = 39, 28, 23, and 60 × 10^{-4} Å^2 respectively). The appropriate bond distances have been corrected for libration (10, 11), using shape parameters q^2 of 0.08 for all atoms involved. Corrected bond lengths appear in Table 4 along with the uncorrected values. Changes in bond angles were not significant and thus only the uncorrected angles are given in Table 5.

[1]Copies of the structure factor table and Table 3 (thermal parameters) are available, at a nominal charge, from the Depository of Unpublished Data, CISTI, National Research Council of Canada, Ottawa, Ont., Canada K1A 0S2.

Results and Discussion

In a previous study the first of a series of potentially multidentate ligands incorporating the dimethyl gallium and pyrazolyl moieties was described (1). The use of ethanolamine in reaction 3 (see Experimental section) of the ligand synthesis reduces steric crowding around the amino nitrogen and allows the formation of bis(tridentate) octahedral complexes. Predictably, reaction 3 of the ligand synthesis proceeds exclusively at the 'OH' rather than the 'NH_2' group of the ethanolamine. It is known that molecules with amino groups coordinated to gallium trimethyl require elevated temperatures for elimination of methane whereas molecules with hydroxyl groups coordinated to the gallium alkyl eliminate alkane much more readily at lower temperatures (12).

The isolation and characterization of a number of octahedral complexes has demonstrated the versatility of the new chelating legand in that it is capable of both *facial* and *meridional* coordination. Present evidence indicates that when the ligand is *facial*, the non-polar *sym* (all-*trans*) isomer is preferred for octahedral complexes. Thus far there is no evidence for other *fac* isomers but molecular models indicate that these would be polar molecules with much greater steric crowding than occurs in the polar *mer* isomer.

Infrared Spectra

The spectra of the *fac* and *mer* isomers, Fig. 2, illustrate the two types of spectra which have been observed for the complexes listed in Table 1. With use of these spectra as a guide, the complexes isolated for the remaining metals were assigned as *fac* or *mer* isomers on the basis of their ir spectra. Differences in the two spectra are primarily in regions attributable to N—H vibrations. The N—H stretching region at ~3300 cm^{-1} displays two bands in the *sym–fac* isomer but at least three bands in the *mer* isomer. In the N—H deformation region of the spectrum, ~1600 cm^{-1}, the *mer* isomer shows a single band but a three-band envelope is observed for the *fac* isomer. A third fingerprint region of the spectra occurs between 400 and 500 cm^{-1}. In the spectrum of the *mer* isomer two bands occur close together at 460 and 475 cm^{-1} whereas in the spectrum of the *fac* isomer these bands are absent and two new bands occur in this region at 400 and 500 cm^{-1}.

The assignments of *fac* and *mer* isomers on the basis of their infrared spectra are tentative in that *fac* isomers other than the all-*trans sym* isomer might give spectra closely resembling that of the *mer* isomer

Can. J. Chem. Downloaded from www.nrcresearchpress.com by 210.87.254.40 on 09/05/12
For personal use only.

TABLE 2. Final positional parameters (fractional × 10^4, Ga and Ni × 10^5, H × 10^3) with estimated standard deviations in parentheses

Atom	x	y	z
	fac isomer		
(equivalent positions: $\pm(x, y, z; 1/2-x, 1/2+y, 1/2-z)$)			
Ga	23529(4)	48707(6)	56611(4)
Ni	50000	50000	50000
O	3920(2)	5193(3)	6191(2)
N(1)	3765(3)	3381(4)	4129(2)
N(2)	2705(3)	3282(4)	4447(2)
N(3)	5627(3)	2694(5)	5889(3)
C(1)	3808(4)	2150(5)	3356(3)
C(2)	2787(4)	1227(6)	3164(3)
C(3)	2118(4)	1974(6)	3865(4)
C(4)	4382(4)	4071(6)	7053(3)
C(5)	4800(4)	2278(5)	6652(4)
C(6)	1741(6)	7245(9)	5112(5)
C(7)	1538(6)	3330(11)	6605(6)
H(N1)	636(5)	297(7)	628(5)
H(N2)	569(4)	194(7)	554(4)
H(1)	440(5)	215(7)	308(4)
H(2)	269(5)	34(7)	277(5)
H(3)	145(6)	181(8)	395(5)
H(4a)	494(5)	465(6)	748(4)
H(4b)	389(4)	377(7)	748(4)
H(5a)	512(4)	156(6)	725(3)
H(5b)	415(5)	168(6)	622(4)
H(6a)	154(6)	729(9)	437(6)
H(6b)	220(9)	830(16)	554(8)
H(6c)	122(7)	732(11)	524(6)
H(7a)	164(10)	199(18)	663(9)
H(7b)	85(9)	294(12)	616(8)
H(7c)	162(6)	395(11)	732(6)
	mer isomer		
Ga(1)	40047(3)	46733(10)	35614(5)
Ga(2)	7835(3)	77293(8)	41007(5)
Ni	24022(4)	59771(10)	42899(6)
O(1)	3496(2)	5999(5)	4380(3)
O(2)	1311(2)	5900(4)	4194(3)
N(1)	2518(2)	5058(5)	2886(3)
N(2)	3178(3)	4615(6)	2608(3)
N(3)	2549(3)	6765(7)	5777(4)
N(4)	2299(2)	8214(5)	3766(3)
N(5)	1632(2)	8790(5)	3591(3)
N(6)	2232(3)	3712(6)	4835(5)
C(1)	2078(4)	4949(7)	2115(4)
C(2)	2428(4)	4443(7)	1302(5)
C(3)	3114(4)	4244(8)	1637(5)
C(6)	4790(5)	5705(15)	2941(9)
C(7)	4106(5)	2717(13)	4215(7)
C(8)	2753(3)	9198(7)	3429(4)
C(9)	2400(4)	10478(8)	3040(5)
C(10)	1705(4)	10158(8)	3141(5)
C(13)	20(4)	7610(11)	3086(6)
C(14)	608(5)	8444(13)	5441(6)
C(4a)	3772(5)	6818(13)	5213(8)
C(4b)	3723(8)	6046(20)	5437(12)
C(5a)	3311(6)	6371(17)	6071(10)
C(5b)	3303(9)	7046(24)	5946(14)
C(11a)	1028(8)	4726(19)	4818(13)
C(11b)	1011(6)	4449(13)	4354(9)
C(12a)	1455(7)	3358(16)	4603(11)
C(12b)	1490(6)	3649(14)	5122(9)

TABLE 2 (*Concluded*)

Atom	x	y	z
H(N3a)	256(4)	800(9)	577(5)
H(N3b)	227(4)	666(8)	617(6)
H(1)	163(3)	504(6)	217(4)
H(2)	232(5)	437(11)	63(7)
H(3)	349(4)	409(8)	122(5)
H(4)	432(3)	649(7)	531(4)
H(5)	337(5)	711(11)	663(7)
H(6a)	492(6)	511(13)	237(9)
H(6b)	468(8)	720(17)	276(11)
H(6c)	525(6)	526(13)	327(9)
H(7a)	443(5)	254(11)	413(7)
H(7b)	457(7)	204(14)	482(10)
H(7c)	378(8)	223(17)	442(12)
H(N6a)	256(4)	351(9)	517(6)
H(N6b)	244(4)	315(8)	439(5)
H(8)	330(2)	896(5)	345(3)
H(9)	261(3)	1119(7)	277(4)
H(10)	134(4)	1096(10)	311(6)
H(11)	49(2)	453(5)	456(3)
H(12)	133(3)	240(7)	529(5)
H(13a)	−28(5)	903(12)	319(7)
H(13b)	20(5)	815(11)	258(8)
H(13c)	−41(5)	741(9)	328(5)
H(14a)	45(5)	955(11)	521(7)
H(14b)	15(5)	839(9)	562(6)
H(14c)	84(5)	779(11)	574(7)

illustrated for the nickel compound. Noteworthy features in both spectra are the weak bands of low frequency in the C—H stretching region (~2600 cm^{-1}) and the complex region around 550—600 cm^{-1}, a region normally associated with symmetric and asymmetric Ga—C stretching modes.

Mass Spectra

The mass spectra of the octahedral complexes displayed signals due to the parent ions. Table 6 lists the peaks observed in the spectrum of the cobalt derivative as an illustration of the type of fragmentation patterns observed. The isotopic patterns of the individual signals are in good agreement with those predicted from the isotopic distributions of metal atoms (^{69}Ga, 60%; ^{71}Ga, 40%; ^{59}Co, 100%). The appearance of certain peaks in the Co spectrum (see Table 6) indicates a facile loss of amino protons from some ions. The mass spectra of the two nickel isomers were essentially identical which is surprising considering the different bonding in the crystal structures of the two isomers. Perhaps the *fac* isomer is converted to the *mer* isomer at the temperature of the experiment (see Experimental section) before ionization occurs.

Electronic Spectra

The electronic spectra of the complexes were recorded over the range 300–1400 nm and are listed and assigned in Table 7. The spectra of the two nickel isomers are shown in Fig. 3. As expected, three spin-

TABLE 4. Bond lengths (Å) with estimated standard deviations in parentheses
(*a*) Non-hydrogen atoms

Bond	Length		Bond	Length	
	Uncorr.	Corr.		Uncorr.	Corr.
			fac isomer		
Ga —O	1.901(3)	1.908	N(1) —N(2)	1.360(4)	1.362
Ga —N(2)	2.003(3)	2.010	N(1) —C(1)	1.330(5)	1.332
Ga —C(6)	1.973(6)	1.981	N(2) —C(3)	1.344(5)	1.345
Ga —C(7)	1.971(5)	1.979	N(3) —C(5)	1.481(5)	1.484
Ni —O	2.086(3)	2.090	C(1) —C(2)	1.376(6)	1.377
Ni —N(1)	2.083(3)	2.085	C(2) —C(3)	1.367(7)	1.369
Ni —N(3)	2.108(3)	2.112	C(4) —C(5)	1.510(6)	1.512
O —C(4)	1.415(4)	1.417			
			mer isomer		
Ga(1)—O(1)	1.886(4)	1.898	Ga(2) —O(2)	1.888(4)	1.899
Ga(1)—N(1)	1.983(5)	1.991	Ga(2) —N(5)	1.981(5)	1.991
Ga(1)—C(6)	1.938(8)	1.948	Ga(2) —C(13)	1.953(7)	1.964
Ga(1)—C(7)	1.942(11)	1.951	Ga(2) —C(14)	1.961(7)	1.973
Ni —O(1)	2.042(4)	2.049	Ni —O(2)	2.038(3)	2.045
Ni —N(1)	2.086(4)	2.091	Ni —N(4)	2.098(4)	2.102
Ni —N(3)	2.142(5)	2.148	Ni —N(6)	2.152(5)	2.156
N(1) —N(2)	1.358(6)	1.361	N(4) —N(5)	1.358(6)	1.361
O(1) —C(4a)	1.42(1)		O(2) —C(11a)	1.44(2)	
O(1) —C(4b)	1.48(2)		O(2) —C(11b)	1.41(1)	
N(1) —C(1)	1.314(7)	1.316	N(4) —C(8)	1.304(7)	1.307
N(2) —C(3)	1.359(8)	1.359	N(5) —C(10)	1.357(8)	1.359
N(3) —C(5a)	1.51(1)		N(6) —C(12a)	1.51(1)	
N(3) —C(5b)	1.44(2)		N(6) —C(12b)	1.45(1)	
C(1) —C(2)	1.374(10)	1.375	C(8) —C(9)	1.399(10)	1.401
C(2) —C(3)	1.356(11)	1.359	C(9) —C(10)	1.340(11)	1.342
C(4a)—C(5a)	1.52(2)		C(11a)—C(12a)	1.48(2)	
C(4b)—C(5b)	1.38(2)		C(11b)—C(12b)	1.52(2)	

(*b*) Bonds involving hydrogen atoms, both isomers

Bond	Length (Å)
N—H	0.71–1.09(3–8)
C(*pz*)—H	0.81–1.05(5–10)
C(sp^3)—H	0.63–1.38(4–15)

allowed bands are observed for both complexes. In addition, a much weaker band, which has been assigned to the $^3A_{2g} \rightarrow {}^1E_g$ transition, is also observed for both complexes. It is noteworthy that the absorptions due to the *mer* isomer are significantly more intense than those for the *sym–fac* isomer. This may be due to the presence of a centre of symmetry in the immediate ligand environment of the *fac* isomer. (This centre of symmetry is not present in the *mer* isomer.)

The spectrum of the cobalt complex exhibits two main absorption bands, assigned as ν_1 and ν_3, with a shoulder on the more intense of these (ν_3). This shoulder has been tentatively assigned to the 'two electron' transition, $^4A_{2g} \leftarrow {}^4T_{1g}(F)$. The spectrum of the iron complex displays a very weak absorption in the infrared region. Since it occurs as a shoulder on a strong charge transfer band, its position is not definitive.

The nickel and cobalt spectra have been analysed on the basis of the energy levels discussed in ref. 13. *Dq* and *B* values are listed in Table 7. The observed ν_2 and ν_3 bands of the nickel complexes were used in the calculation of these parameters. This leads to calculated ν_1 values of 10.9 and 10.65 kK for the *fac* and *mer* isomers respectively; the expected $\rightarrow {}^1E_g$ transitions are 13.2 and 13.4 kK ($C/B = 4.5$ has been assumed for the calculation of the ^1E_g transition (13)). Similarly, ν_1 and ν_3 have been used to calculate *Dq* and *B* of the cobalt complex. This leads to a calculated value of 19.9 kK for ν_2 which does not agree well with the experimental value of 18.6 kK. The observed shoulder could be due to a spin forbidden band or a splitting of the $^4T_{1g}(P)$ level, rather than

Can. J. Chem. Downloaded from www.nrcresearchpress.com by 210.87.254.40 on 09/05/12
For personal use only.

TABLE 5. Bond angles (deg) with estimated standard deviations in parentheses
Non-hydrogen atoms*

Bonds	Angle (deg)	Bonds	Angle (deg)
	fac isomer		
O(1) —Ga —N(2)	93.2(1)	Ni —O —C(4)	107.4(2)
O(1) —Ga —C(6)	108.2(2)	Ni —N(1) —N(2)	119.0(2)
O(1) —Ga —C(7)	112.6(2)	Ni —N(1) —C(1)	133.1(3)
N(2) —Ga —C(6)	110.2(2)	N(2) —N(1) —C(1)	107.3(3)
N(2) —Ga —C(7)	106.9(3)	Ga —N(2) —N(1)	118.5(2)
C(6) —Ga —C(7)	122.0(3)	Ga —N(2) —C(3)	133.4(3)
O —Ni —N(1)	88.1(1)	N(1) —N(2) —C(3)	108.0(3)
O —Ni —N(3)	83.0(1)	Ni —N(3) —C(5)	107.0(2)
N(1) —Ni —N(3)	90.1(1)	N(1) —C(1) —C(2)	110.5(4)
O —Ni —N(1)′	91.9(1)	C(1) —C(2) —C(3)	104.6(4)
O —Ni —N(3)′	97.0(1)	N(2) —C(3) —C(2)	109.6(4)
N(1) —Ni —N(3)′	89.9(1)	O —C(4) —C(5)	111.0(3)
Ga —O —Ni	113.1(1)	N(3) —C(5) —C(4)	107.8(3)
Ga —O —C(4)	117.6(2)		
	mer isomer		
O(1) —Ga(1)—N(2)	90.3(2)	O(2) —Ga(2) —N(5)	90.3(2)
O(1) —Ga(1)—C(6)	111.5(4)	O(2) —Ga(2) —C(13)	111.6(3)
O(1) —Ga(1)—C(7)	108.8(3)	O(2) —Ga(2) —C(14)	108.2(3)
N(2) —Ga(1)—C(6)	108.2(4)	N(5) —Ga(2) —C(13)	110.7(3)
N(2) —Ga(1)—C(7)	109.7(3)	N(5) —Ga(2) —C(14)	109.3(3)
C(6) —Ga(1)—C(7)	123.3(4)	C(13) —Ga(2) —C(14)	122.1(4)
O(1) —Ni —N(1)	85.8(2)	O(2) —Ni —N(4)	85.9(2)
O(1) —Ni —N(3)	80.9(2)	O(2) —Ni —N(6)	80.4(2)
N(1) —Ni —N(3)	166.2(2)	N(4) —Ni —N(6)	166.2(2)
O(1) —Ni —N(4)	95.3(2)	O(2) —Ni —N(1)	93.4(2)
O(1) —Ni —N(6)	98.4(2)	O(2) —Ni —N(3)	99.7(2)
N(1) —Ni —N(6)	88.6(2)	N(4) —Ni —N(3)	91.3(2)
N(1) —Ni —N(4)	93.7(2)	N(3) —Ni —N(6)	89.5(2)
O(1) —Ni —O(2)	178.6(2)		
Ga(1)—O(1) —Ni	118.6(2)	Ga(2)—O(2) —Ni	119.6(2)
Ga(1)—O(1) —C(4a)	127.2(5)	Ga(2)—O(2) —C(11a)	116.7(7)
Ga(1)—O(1) —C(4b)	116.9(7)	Ga(2)—O(2) —C(11b)	124.9(5)
Ni —O(1) —C(4a)	112.8(5)	Ni —O(2) —C(11a)	111.6(7)
Ni —O(1) —C(4b)	108.2(6)	Ni —O(2) —C(11b)	114.9(5)
Ni —N(1) —N(2)	119.1(3)	Ni —N(4) —N(5)	118.9(3)
Ni —N(1) —C(1)	132.5(4)	Ni —N(4) —C(8)	133.4(4)
N(2) —N(1) —C(1)	107.9(5)	N(5) —N(4) —C(8)	107.0(5)
Ga(1)—N(2) —N(1)	120.4(3)	Ga(2)—N(5) —N(4)	120.1(3)
Ga(1)—N(2) —C(3)	133.0(5)	Ga(2)—N(5) —C(10)	131.8(4)
N(1) —N(2) —C(3)	106.6(5)	N(4) —N(5) —C(10)	107.8(5)
Ni —N(3) —C(5a)	105.5(6)	Ni —N(6) —C(12a)	105.7(6)
Ni —N(3) —C(5b)	107.6(8)	Ni —N(6) —C(12b)	106.2(5)
N(1) —C(1) —C(2)	111.2(6)	N(4) —C(8) —C(9)	111.2(6)
C(1) —C(2) —C(3)	103.9(6)	C(8) —C(9) —C(10)	103.8(6)
N(2) —C(3) —C(2)	110.3(6)	N(5) —C(10) —C(9)	110.0(6)
O(1) —C(4a)—C(5a)	106.2(9)	O(2) —C(11a)—C(12a)	105(1)
O(1) —C(4b)—C(5b)	111(1)	O(2) —C(11b)—C(12b)	107.2(9)
N(3) —C(5a)—C(4a)	107(1)	N(6) —C(12a)—C(11a)	108(1)
N(3) —C(5b)—C(4b)	112(2)	N(6) —C(12b)—C(11b)	110.1(9)

*Primed atoms at $1 - x$, $1 - y$, $1 - z$.

the ${}^4A_{2g} \leftarrow {}^4T_{1g}(F)$ transition which is usually very weak and is often obscured.

Comparison of the above spectral parameters with those of the corresponding hexammine complexes is of interest. The relevant parameters are: $Dq = 1020$ cm^{-1}, $B = 885$ for $Co(NH_3)_6^{2+}$ (13); $Dq = 1080$ cm^{-1}, $B = 900$ for $Ni(NH_3)_6^{2+}$ (13); and $Dq = 1120$ cm^{-1} for $Fe(NH_3)_6^{2+}$ (14). The similarity of the Dq values shows that the tridentate ligand lies in approximately the same position as NH_3 in the spectrochemical series. The B values of the chelate complexes, however, are much lower than those of the hexammine complexes, indicating a greater degree of delocalization or covalency in the former.

Can. J. Chem. Downloaded from www.nrcresearchpress.com by 210.87.254.40 on 09/05/12
For personal use only.

Can. J. Chem. Downloaded from www.nrcresearchpress.com by 210.87.254.40 on 09/05/12
For personal use only.

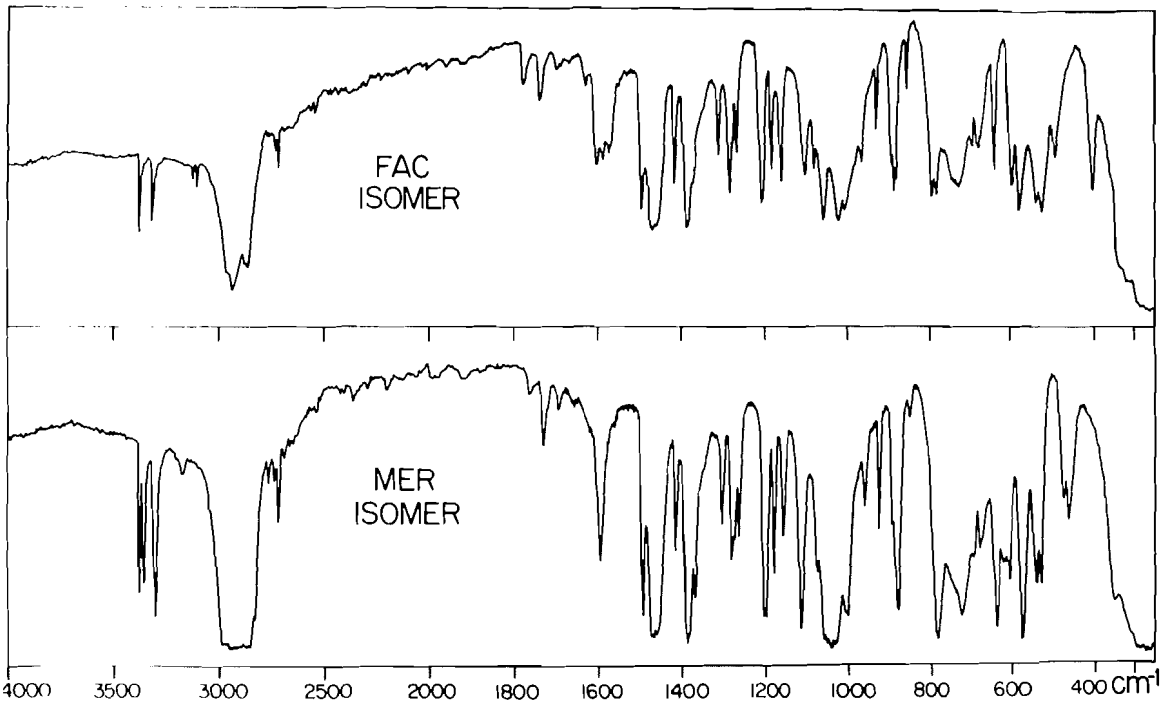

FIG. 2. Infrared spectra of *sym–fac*- and *mer*-bis[dimethyl(ethanolamino)(1-pyrazolyl)gallato(*N*(2),*O*,*N*)]nickel(II).

Crystal Structures

Both crystal structures consist of discrete mononuclear molecular units separated by normal van der Waals distances (see Fig. 4). The nickel atoms of both isomers are bonded to two tridentate $[Me_2Ga(OCH_2CH_2NH_2)(N_2C_3H_3)]^-$ ligands via the amino nitrogen, oxygen, and pyrazolyl nitrogen atoms. While the coordination geometry about the nickel atom is distorted octahedral in both cases, the distortions from 'ideal' geometry are greater for the asymmetric *mer* isomer than for the centrosymmetric *sym–fac* isomer (see Tables 4 and 5).

The geometry of the ligands in the *mer* isomer is very similar to that of the related $[Me_2Ga(OCH_2CH_2NMe_2)(N_2C_3H_3)]^-$ ligand in the binuclear square-pyramidal copper(II) complex $[Me_2Ga(OCH_2CH_2NMe_2)(N_2C_3H_3)_2Cu]_2$ (I). *Facial* coordination by the $[Me_2Ga(OCH_2CH_2NH_2)(N_2C_3H_3)]^-$ ligand is realized by a fold about the Ni—O bond (see Fig. 1). The coordination of the trivalent oxygen atom is pyramidal in the *fac* isomer and more nearly planar in the *mer* isomer (mean bond angles at O are 112.7° in the *fac* isomer and 117.5° in the *mer* isomer). The Ni—N(pyrazolyl) distances (2.085(3) for *fac*, 2.091(4) and 2.102(4) Å for *mer*) are nearly the same in the two isomers while the Ni—N(amino) (2.112(3) for *fac*, 2.148(5) and 2.156(5) Å for *mer*) and Ni—O (2.090(3) for *fac*, 2.049(4) and 2.045(3) Å for *mer*) are significantly different. A combination of steric and electronic effects is probably responsible for these differences. The conformations of the OCCNNi and GaONiNN chelate rings (see torsion angles in Table 8) are very similar in the two isomers. The marked non-planarity of the GaONiNN rings in both isomers is in contrast with the near planarity of the GaOCuNN rings in $[Me_2Ga(OCH_2CH_2NMe_2)(N_2C_3H_3)_2Cu]_2$ (I).

The pyrazolyl ring in the *fac* isomer is planar within experimental error ($\chi^2 = 1.5$) and both metal atoms are significantly displaced from the mean plane of the pyrazolyl ring (Ga by 0.0985(5) and Ni by 0.2701(5) Å). In the *mer* isomer the pyrazolyl ring containing N(1) is planar ($\chi^2 = 0.3$) while the other ring is possibly non-planar ($\chi^2 = 7.8$). The metal

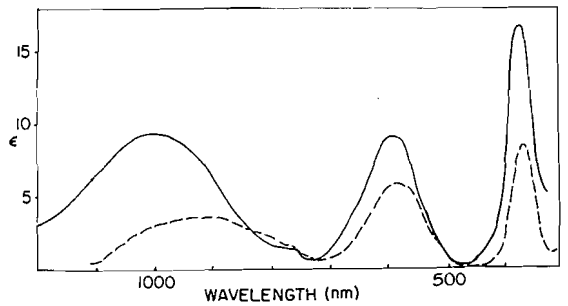

FIG. 3. Electronic spectra of the *fac* (broken line) and *mer* (solid line) isomers of bis[dimethyl(ethanolamino)(1-pyrazolyl)-gallato(*N*(2),*O*,*N*)]nickel(II).

Can. J. Chem. Downloaded from www.nrcresearchpress.com by 210.87.254.40 on 09/05/12
For personal use only.

TABLE 6. Mass spectrum of $[Me_2Ga(OCH_2CH_2NH_2)(N_2C_3H_3)]_2Co$

m/e	Intensity	Assignment
515	10.0	
513	26.2	$Me_4Ga_2(OCH_2CH_2NH_2)_2(N_2C_3H_3)_2Co^+$
511	21.5	
500	4.6	
498	13.1	$Me_3Ga_2(OCH_2CH_2NH_2)_2(N_2C_3H_3)_2Co^+$
496	9.2	
439	4.6	
437	12.3	$Me_3Ga_2(OCH_2CH_2NH)(N_2C_3H_3)_2Co^+$
435	8.5	
432	15.4	$Me_3Ga_2(OCH_2CH_2NH_2)(OCH_2CH_2NH)$-
430	47.8	$(N_2C_3H_3)Co^+$
428	34.6	
388	6.2	
386	14.6	$Me_4Ga_2(OCH_2CH_2NH_2)(N_2C_3H_3)Co^+$
384	12.3	
339	66.9	$MeGa(OCH_2CH_2NH_2)(N_2C_3H_3)_2Co^+$
337	100.0	$MeGa(OCH_2CH_2N)(N_2C_3H_3)_2Co^+$
335	12.0	
		$MeGa(OCH_2CH_2NH_2)_2(N_2C_3H_3)Co^+$
332	10.0	$MeGa(OCH_2CH_2NH_2)(OCH_2CH_2N)$-
330	17.9	$(N_2C_3H_3)Co^+$
328	10.0	$MeGa(OCH_2CH_2NH)_2(N_2C_3H_3)Co^+$
287	5.0	$Me_2Ga(OCH_2CH_2NH_2)(N_2C_3H_3)Co^+$
285	8.0	
146	22.0	$MeGa(OCH_2CH_2NH_2)^+$
144	40.7	$MeGa(OCH_2CH_2N)^+$
142	12.0	
101	8.5	Me_2Ga^+
99	11.5	
71	4.6	Ga^+
69	6.9	
68	53.0	$N_2C_3H_4^+$
67	7.7	$N_2C_3H_3^+$

TABLE 7. Electronic spectra for $[Me_2Ga(OCH_2CH_2NH_2)(N_2C_3H_3)]_2M$ complexes*

M	Energy (kK)	ε	*Dq* (cm^{-1})	*B* (cm^{-1})	Assignment
Ni(*fac*)	10.9	3.6	1090	800	$^3A_{2g} \rightarrow {}^3T_{2g}$
	13.1	0.4			$^3A_{2g} \rightarrow {}^1E_g$
	17.2	5.8			$^3A_{2g} \rightarrow {}^3T_{1g}(F)$
	27.5	8.5			$^3A_{2g} \rightarrow {}^3T_{1g}(P)$
Ni(*mer*)	10.0	9.2	1065	810	$^3A_{2g} \rightarrow {}^3T_{2g}$
	13.1	0.6			$^3A_{2g} \rightarrow {}^1E_g$
	16.9	8.7			$^3A_{2g} \rightarrow {}^3T_{1g}(F)$
	27.2	16.7			$^3A_{2g} \rightarrow {}^3T_{1g}(P)$
Co	9.4	4.3	1055	800	$^4T_{1g}(F) \rightarrow {}^4T_{2g}$
	18.6(sh)	~2			
	20.2	23.2			$^4T_{1g}(F) \rightarrow {}^4T_{1g}(P)$
Fe	12.1	7.5	1210		$^5T_{2g} \rightarrow {}^5E_g$
Cu	16.5	130	1650		$^2E_g \rightarrow {}^2T_{2g}$

*Measured as benzene solutions except for Ni(*mer*) where acetone was used as solvent.

atoms are again significantly displaced from the pyrazolyl mean planes (Ga by 0.0557(8) and 0.1810(6) Å, Ni by 0.2316(8) and −0.2367(8) Å from the N(1) and N(4) pyrazolyl rings respectively).

The gallium atoms in both structures have distorted tetrahedral coordination geometry with O—Ga—N angles of 90.3(2)–93.2(1)° and C—Ga—C angles of 122.0(3)–123.3(4)°. The bond lengths involving gallium are similar to those in related molecules (1, 15–22). Bond lengths and angles in the remainder of the *fac* molecule and the ordered part of the *mer* molecule are as expected; details are given in Tables 4, 5, and 8.

TABLE 8. Intra-annular torsion angles (deg)*

Bond	Obs.	Bond	Obs.
	fac isomer		
Ga —O	28.0(1)	Ni —O	15.6(2)
O —Ni	−25.5(1)	O —C(4)	−42.3(3)
Ni —N(1)	12.0(2)	C(4) —C(5)	55.5(4)
N(1) —N(2)	5.2(2)	C(5) —N(3)	−38.2(3)
N(2) —Ga	−21.0(2)	N(3) —Ni	13.3(2)
	mer isomer		
Ga(1)—O(1)	24.6(2)	Ga(2)—O(2)	22.5(2)
O(1) —Ni	−22.3(2)	O(2) —Ni	−17.2(2)
Ni —N(1)	9.4(3)	Ni —N(4)	1.6(3)
N(1) —N(2)	5.3(3)	N(4) —N(5)	13.7(3)
N(2) —Ga(1)	−17.8(3)	N(5) —Ga(2)	−21.6(3)
Ni —O(1)	−14.0(5) 17.5(7)	Ni —O(2)	19.9(7) −9.6(5)
O(1) —C(4)	42.5(8) −42(1)	O(2) —C(11)	−48(1) 34.3(8)
C(4) —C(5)	−57.8(9) 51(1)	C(11)—C(12)	59(1) −51.2(9)
C(5) —N(3)	44.7(8) −34(1)	C(12)—N(6)	−41.5(9) 42.2(7)
N(3) —Ni	−17.8(6) 7.3(8)	N(6) —Ni	12.0(6) −18.5(5)

*For the disordered ethanolamine chelate rings in the *mer* isomer, the two columns refer to carbon atoms labelled a and b respectively.

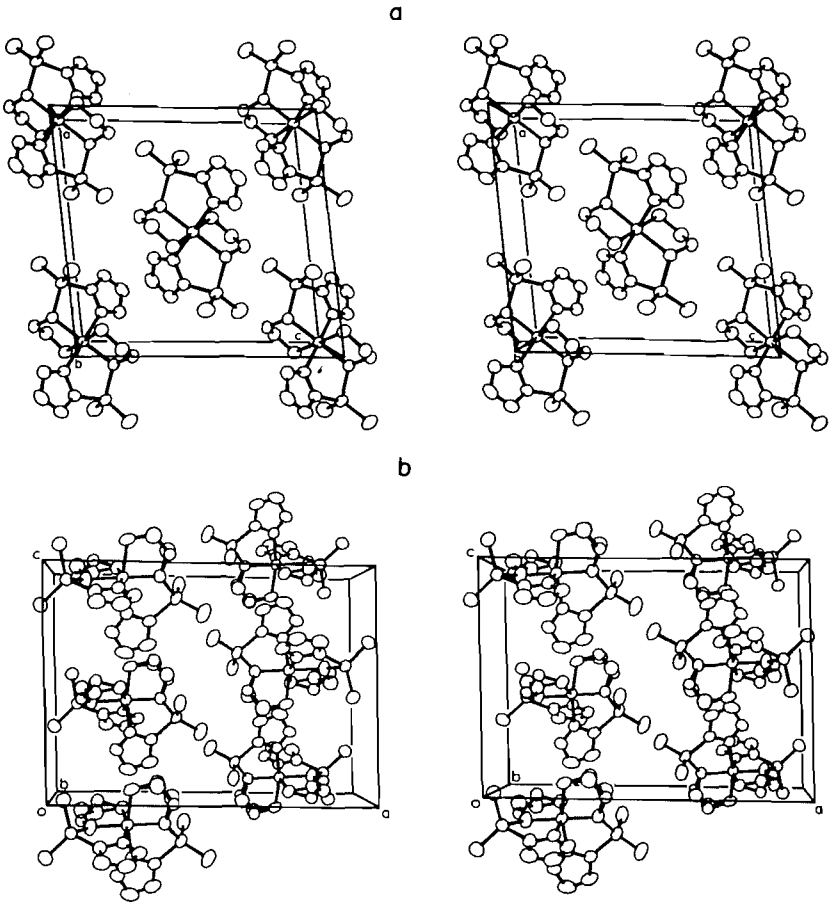

FIG. 4. The crystal structures of the *fac* (*a*) and *mer* (*b*) isomers of bis[dimethyl(ethanolamino)(1-pyrazolyl)gallato(*N*-(*2*),*O*,*N*)]nickel(II) viewed perpendicular to the *ac* plane.

Acknowledgments

We thank the National Research Council of Canada for financial support and the University of British Columbia Computing Centre for assistance. We are grateful to Mr. J. Nip for mass spectra; Mr. P. Borda for C, H, N analyses; and Dr. R. C. Thompson for helpful discussion.

1. K. S. CHONG, S. J. RETTIG, A. STORR, and J. TROTTER. Can. J. Chem. **55**, 4166 (1977).
2. A. STORR and B. S. THOMAS. Can. J. Chem. **48**, 3667 (1970).
3. M. ARESTA, C. F. NOBILE, and D. PETRUZZELLI. Inorg. Chem. **16**, 1817 (1977).
4. P. COPPENS, L. LEISEROWITZ, and D. RABINOVICH. Acta Crystallogr. **18**, 1035 (1965).
5. W. R. BUSING and H. A. LEVY. Acta Crystallogr. **22**, 457 (1967).
6. D. T. CROMER and J. B. MANN. Acta Crystallogr. Sect. A, **24**, 321 (1968).
7. R. F. STEWART, E. R. DAVIDSON, and W. T. SIMPSON. J. Chem. Phys. **42**, 3175 (1965).
8. D. T. CROMER and D. LIBERMAN. J. Chem. Phys. **53**, 1891 (1970).
9. V. SCHOMAKER and K. N. TRUEBLOOD. Acta Crystallogr. Sect. B, **24**, 63 (1969).
10. D. W. J. CRUICKSHANK. Acta Crystallogr. **9**, 747 (1956); **9**, 754 (1956).
11. D. W. J. CRUICKSHANK. Acta Crystallogr. **14**, 896 (1961).
12. G. E. COATES and K. WADE. Organometallic compounds: the main group elements. Vol. 1. 3rd. ed. Methuen, London. 1967.
13. A. P. B. LEVER. Inorganic electronic spectroscopy. Elsevier, New York. 1968.
14. C. FURLANI. Gazz. Chim. Ital. **87**, 371 (1957).
15. D. F. RENDLE, A. STORR, and J. TROTTER. J. Chem. Soc. Dalton Trans. 2252 (1973).
16. D. F. RENDLE, A. STORR, and J. TROTTER. Can. J. Chem. **53**, 2930 (1975).
17. D. F. RENDLE, A. STORR, and J. TROTTER. Can. J. Chem. **53**, 2944 (1975).
18. D. J. PATMORE, D. F. RENDLE, A. STORR, and J. TROTTER. J. Chem. Soc. Dalton Trans. 718 (1975).
19. S. J. RETTIG, A. STORR, and J. TROTTER. Can. J. Chem. **53**, 58 (1975).
20. R. T. BAKER, S. J. RETTIG, A. STORR, and J. TROTTER. Can. J. Chem. **54**, 343 (1976).
21. S. J. RETTIG, A. STORR, and J. TROTTER. Can. J. Chem. **53**, 753 (1975).
22. K. S. CHONG, S. J. RETTIG, A. STORR, and J. TROTTER. Can. J. Chem. **55**, 2540 (1977).

Can. J. Chem. Downloaded from www.nrcresearchpress.com by 210.87.254.40 on 09/05/12
For personal use only.

The chiroptical properties of the strychnine alkaloids: strychnine, β-colubrine, brucine, and their dihydro derivatives

JULIAN W. SNOW[1] AND THOMAS M. HOOKER, JR.[2]

Department of Chemistry, University of California, Santa Barbara, CA 93106, U.S.A.

Received September 6, 1977

JULIAN W. SNOW and THOMAS M. HOOKER, JR. Can. J. Chem. **56**, 1222 (1978).

Ultraviolet absorption and circular dichroism spectra of the strychnine alkaloids strychnine, β-colubrine, brucine, dihydrostrychnine, dihydro-β-colubrine, and dihydrobrucine have been investigated under various experimental conditions. It appears that at least five electronic transitions are required to account for the spectroscopic properties of these molecules in the ultraviolet region above 190 nm. Transitions, which are tentatively assigned as the ^1L_b, ^1L_a, ^1B_b, and ^1B_a in the notation due to Platt, and an $n \rightarrow \pi^*$ transition apparently make significant contributions to the spectra of all of the molecules studied.

JULIAN W. SNOW et THOMAS M. HOOKER, JR. Can. J. Chem. **56**, 1222 (1978).

On a étudié, sous diverses conditions expérimentales, les spectres d'absorption ultraviolet et de dichroïsme circulaire de divers alcaloïdes de la strychnine: la strychnine, la β-colubrine, la brucine, la dihydrostrychnine, la dihydro β-colubrine et la dihydrobrucine. Il semble que l'on doit faire appel à au moins cinq transitions électroniques pour tenir compte des propriétés spectroscopiques de ces molécules dans la région ultraviolette au dessus de 190 nm. On attribue d'une façon temporaire les transitions sous forme ^1L_b, ^1L_a, ^1B_b et ^1B_a, dans la notation qui est due à Platt, et ces transitions autant d'une transition $n \rightarrow \pi^*$ semble apporter une contribution importante aux spectres de toutes les molécules étudiées.

[Traduit par le journal]

Introduction

An experimental investigation of the optical properties of β-colubrine, brucine, and strychnine, and the dihydro-derivatives of these alkaloids, has recently been carried out in this laboratory. The intent of this work has been to investigate the nature of the chromophoric groups of the molecules and the optical properties that arise from their associated electronic transitions. In the spectral region of 190–300 nm, the chromophoric groups of interest are associated with the dihydroindole nucleus and the ethylenic group (Fig. 1). Absorption (uv) and circular dichroism (CD) spectra have been acquired over this wavelength region in organic and aqueous solvent systems.

The molecular framework of these alkaloids is a rigid polycyclic structure that consists of seven fused rings. Thus, the conformational freedom of the molecule is very restricted. This is a very attractive feature when one considers the extreme sensitivity of optical activity to molecular conformation. Solvent effects, for example, are easier to interpret as are the effects of other experimental variables such as p*H*, temperature, and concentration.

The nitrogen atom of the dihydroindole nucleus of strychnine is bonded to a carbonyl group (C_{21}–O_1 of Fig. 1). As a result, the structure of the strychnine aromatic chromophore is similar to an *ortho*-substituted acetanilide, except for the fact that N_1 is tertiary instead of secondary. Strychnine may thus be considered to contain a perturbed acetanilide chromophore. Likewise, brucine and β-colubrine

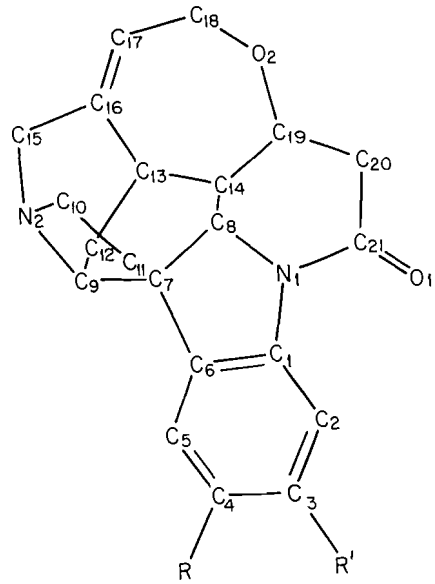

FIG. 1. Diagram of alkaloid framework. Strychnine, R = R′ = H; brucine, R = R′ = OCH_3; β-colubrine, R = OCH_3, R′ = H.

[1]Present address: Department of Chemistry, University of Massachusetts, Amherst, MA 01002, U.S.A.

[2]To whom correspondence should be addressed.

Can. J. Chem. Downloaded from www.nrcresearchpress.com by 210.87.254.105 on 09/05/12
For personal use only.

Can. J. Chem. Downloaded from www.nrcresearchpress.com by 210.87.254.105 on 09/05/12
For personal use only.

contain the analogous 3,4-dimethoxy and *para*-methoxy chromophores, respectively.

The ultraviolet absorption spectrum of acetanilide has been reported several times in the literature (1–4). The spectra of the *ortho*-, *meta*-, and *para*-methoxy derivatives have been measured as well (2). The pertinent features may be summarized as follows. The two lowest energy bands of acetanilide occur at 277 and 243 nm in ethanol (2). The second band is considerably more intense than the first ($\log \varepsilon_{\lambda_{277}} = 2.74$, $\log \varepsilon_{\lambda_{243}} = 4.19$). A third band of greater intensity occurs at 200 nm in iso-octane.

Assignments of the lower energy bands of acetanilide have been made previously. Based on experimental considerations Lutskii *et al.* (2) assigned the lowest energy band to the analog of the B_{2u} transition of benzene. The next transition was assigned to an n_N–π_{CO}* transition, primarily because the wavelength and intensity of this band were not those which would be expected of the analog of the B_{1u} transition of benzene.

The results of a semi-empirical molecular orbital calculation that was carried out by Baba and Suzuki (4) are in agreement with the experimental assignments insofar as the lowest energy band is concerned. The direction of polarization of this transition was calculated to lie along a line perpendicular to the C_1–N_1 axis. The second transition was determined to have considerable charge transfer character as a result of electron transfer from the nitrogen and the aromatic ring to the carbonyl group. The direction of polarization of this transition was determined to make an angle of 20.5° with the C_1–N_1 axis, being inclined toward the carbonyl group. A third transition was calculated to have a direction of polarization identical to that of the lowest energy band.

The polarized absorption studies of acetanilide crystals by Tanaka (5) are in close agreement with the results of Baba and Suzuki. Polarization directions were reported only for the two lower energy bands. The experimental and theoretical polarizations for the lowest energy band were in excellent agreement. The direction of polarization of the second band was found to be 35.6° from the C_1–N_1 axis, which is slightly more inclined to the carbonyl group than that calculated by Baba and Suzuki.

There is one significant dissimilarity insofar as the aromatic chromophores of strychnine and acetanilide are concerned. Whereas the acetamino group of acetanilide and related molecules is usually considered to be coplanar with the aromatic ring, such may not be true in the case of the strychnine alkaloids. The crystalline structure of strychnine hydrobromide has been determined by X-ray diffraction studies (6). These data indicate that the carbon and oxygen atoms of the acetamino group of strychnine lie approximately 0.4 Å below the plane of the aromatic ring. This structural distortion, providing that it exists in solution, may diminish the conjugation of the π-systems of these two groups, with the result that it might be appropriate to consider the phenyl and acetamino groups as independent systems. However, there are marked similarities in the absorption spectra of the strychnine alkaloids and related substituted acetanilides, so the acetanilide interpretation is probably valid. Although the theoretical interpretation of the CD spectra of the strychnine alkaloids will obviously be affected by the nature of the chromophoric groups that are present, the conclusions of the present investigation are not crucially dependent upon this factor.

The notation due to Platt (7) will be utilized in this work to designate the electronic transitions associated with the acetanilide chromophore. In this notation the lowest energy band will be designated as the ^1L_b transition, the second band is the ^1L_a, and the third transition is assigned as the ^1B_b.

The strychnine alkaloids also contain an ethylenic chromophore. The ultraviolet absorption spectrum of ethylene has been reviewed by Merer and Mulliken (8). The broad absorption in the spectrum of liquid ethylene that extends from 265 nm to a maximum near 160 nm was assigned to the N–V system. There appears to be at least one additional transition in the spectrum of solid ethylene (9) and in various substituted olefins (10–12). Calculations of the rotatory strengths of the twisted olefin, *trans*-cyclooctene show that a π_z–π_y* transition is required in addition to the conventional π_z–π_z* transition to explain the observed chiroptical properties near 200 nm (in this notation the ethylenic double bond lies along the *x*-axis and the *z*-axis is perpendicular to the plane of the double bond). The π_z–π_y* transition is electric dipole forbidden in planar ethylene. However the linear dichroism studies of Yogev *et al.* (10) on unsymmetrically substituted olefins confirm the presence of an additional band that could be due to such a transition.

The X-ray diffraction data for crystalline strychnine hydrobromide indicate that the ethylenic double bond is very nearly planar (6). Thus, unless the conformation of the molecule is markedly different in solution, there should be only a minimal amount of skewness associated with this group. It is difficult to estimate the magnitude of the contribution of this small amount of inherent dissymmetry of the ethylenic chromophore to its optical activity, but it is probably minimal. As a result of this planarity, the π_z–π_z* transition, which is polarized along the

Can. J. Chem. Downloaded from www.nrcresearchpress.com by 210.87.254.105 on 09/05/12
For personal use only.

double bond (11), probably makes the dominant contribution to the optical activity of the ethylenic chromophore by means of the dipole coupling mechanism (13). The situation might be expected to be similar to that of gliotoxin, where Nagarajan and Woody (14) found that the spectrum could be adequately reproduced by including only the π_z–π_z^* transition of the ethylenic chromophore in their chiroptical calculations.

Experimental

Strychnine and brucine were obtained from the Sigma Chemical Company. β-Colubrine was obtained from the Pierce Chemical Company. The dihydro derivatives of these compounds were prepared according to the procedure of Oxford and Perkin and Ackmatowicz *et al.* (15, 16), which involves catalytic hydrogenation in 50% aqueous acetic acid. A Parr hydrogenation apparatus was employed for this purpose with the pressure of hydrogen maintained between 20–25 psi. In all cases, hydrogen uptake ceased after 2–5 h with the theoretical amount being consumed. The free base was precipitated from solution by the dropwise addition of 40% sodium hydroxide solution. Dihydrostrychnine was recrystallized from 50% methyl alcohol and dried *in vacuo* over silica gel. The melting point of the resultant needle-like crystals was 222–223°C, compared to the literature value of 220–222°C (15). Dihydrobrucine was recrystallized from hot water and was found to melt at 70°C. Dihydrobrucine tetrahydrate has been reported to melt at 70–72°C (16). Dihydrocolubrine was recrystallized from a mixture of ethanol–water and dried *in vacuo* over silica gel. The resulting crystals were found to melt at 220°C.

The uv absorption spectra were measured on a Cary 118 recording spectrophotometer that is equipped with the Cary far uv modification. All absorption spectra were determined at ambient laboratory temperature.

CD spectra were measured on a Cary 60 recording spectropolarimeter that is equipped with a highly modified prototype 6003 CD accessory. Fused silica cells with path lengths between 0.1 and 1 cm were used. The majority of the CD data were acquired with the aid of a PDP-11 digital computer that was interfaced to the spectropolarimeter, thereby allowing multiple scanning and signal averaging. Details are provided elsewhere (25).

CD data are reported as molar ellipticity, M_θ, which is defined as

$$\theta = \frac{M_\theta c l}{100}$$

where θ is the observed ellipticity in degrees, l is the path length in cm, and c is solute concentration in moles per litre.

When necessary, CD spectra were analyzed by a curvefitting technique based on the method due to Fletcher and Powell (17). The data were fitted to Gaussian band shapes by means of an iterative computer program which minimizes residual mean squares.

All aqueous solutions were prepared with doubly distilled water and were filtered with a millipore apparatus prior to use. Triethylphosphate (TEP) was obtained from Aldrich Chemical Company, and was distilled under vacuum. Solutions prepared with TEP were filtered through sintered glass.

Results

The uv absorption spectrum of dihydro-β-colubrine in water is shown in Fig. 2. The bands at 296 and 262 nm apparently arise from the ^1L_b and ^1L_a transitions, respectively. These bands occur almost 20 nm to the red of the analogous bands in acetanilide. The inductive effect of the methoxy group must be largely responsible for this difference. Similar red-shifts, somewhat smaller in magnitude, were noted for *p*-methoxy acetanilide (2). The absorption maximum at 197 nm is probably due to the ^1B_b transition. The analogous degenerate E_{1u} transitions of benzene would be expected to split into two non-degenerate transitions in this chromophoric group. Thus, an additional transition (^1B_a in Platt's notation) might be expected to absorb in this region as well.

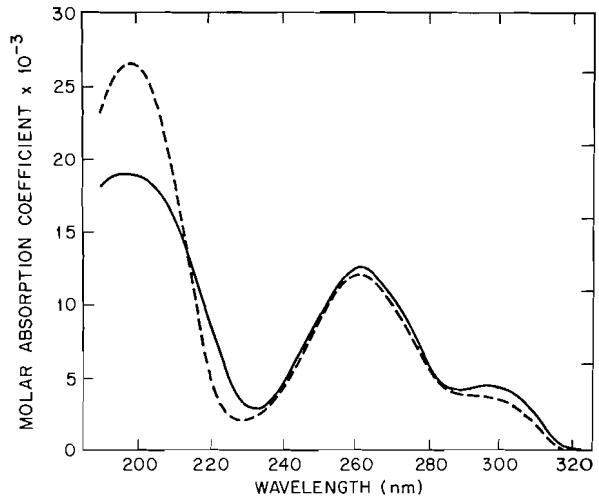

FIG. 2. The uv absorption spectra of dihydro-β-colubrine (—) and β-colubrine (---) in neutral water.

The CD spectra of dihydro-β-colubrine in water as a function of pH, and in triethylphosphate (TEP), are shown in Fig. 3. An interesting feature of these spectra is that at least four, and probably five, Cotton effects are present in each case. Tentative electronic transition assignments are indicated along the bottom of the figure.

A noticeable pH dependence of the molar ellipticity occurs at higher energies (lower wavelengths) in aqueous solution. This dependence is manifested by a decrease in positive ellipticity as the pH is increased. At pH 12.5 there is a small amount of negative ellipticity between 230 and 238 nm which is indeed evidence of a negative Cotton effect in this region. Thus, there must be an additional electronic transition (band III) even though no obvious absorption band appears in the uv spectrum in this wavelength region. The transition giving rise to this Cotton effect is obviously very weakly absorbing and is quite likely electric dipole forbidden.

Removal of a proton from the tertiary nitrogen atom of dihydrocolubrine (N_2 of Fig. 1) appears to be responsible for the change in sign of the Cotton

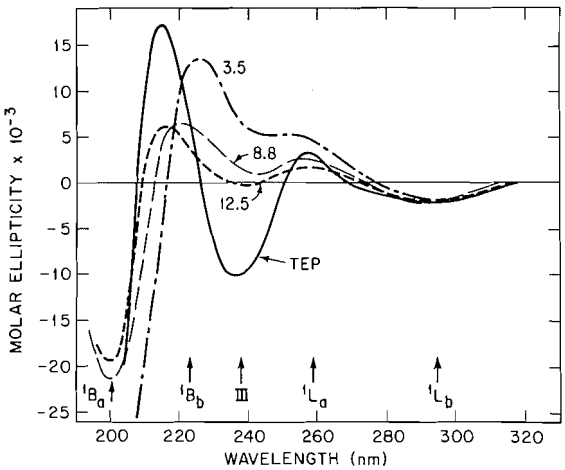

FIG. 3. CD spectra of dihydro-β-colubrine in water and TEP. The numerals in the figure indicate the p*H* of the aqueous solutions. Transition assignments are indicated along the bottom of the figure.

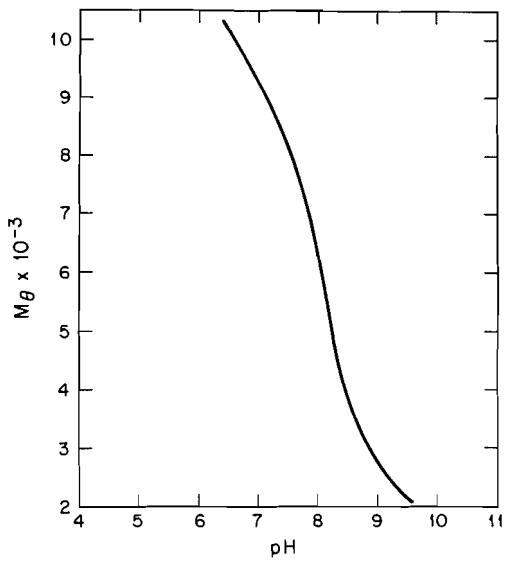

FIG. 4. Plot of M_θ vs. p*H* for dihydro-β-colubrine at 230 nm.

effect due to band III. This can be seen more clearly in Fig. 4 in which molar ellipticity at 230 nm is plotted against p*H*. The plot has the appearance of a sigmoidal curve with the point of inflection at approximately the pK_a of the tertiary nitrogen atom (7.85). The effect of going to a less polar solvent such as TEP is to lower the effective pK_a, hence the negative Cotton effect at 237 nm in this solvent is quite likely due to this effect as well.

The aqueous CD spectra at p*H* 3.5 and 12.5 were subjected to careful analysis by curvefitting. The results are presented in Table 1. In both cases it was found that the spectra required five Cotton effects for best results. The Cotton effect arising from band III clearly undergoes a change in sign from positive to negative and a significant shift to the blue upon going from acidic to basic solution.

The uv absorption spectrum of β-colubrine in water is also shown in Fig. 2. The absorption maximum at 199 nm is presumably due to the ^1B transitions and the π_z–π_z^* transition of the ethylenic chromophore. The increase in intensity of absorption in this region relative to the spectrum of dihydrocolubrine must result from the ethylenic chromophore.

The CD spectra of β-colubrine in aqueous solution, methanol, and TEP are shown in Fig. 5. In view of the results obtained for dihydro-β-colubrine, one would expect to observe five Cotton effects above 200 nm. The ethylenic chromophore of β-colubrine might be expected to give rise to a sixth Cotton effect, but it probably occurs below 200 nm. Although there is some qualitative evidence for five Cotton effects above 200 nm in the spectra of Fig. 5, it is certainly not as compelling as it was in the case of dihydrocolubrine. Thus, assignment of the Cotton effects was made only after conducting careful curvefitting analyses of the data. Attempts were made to fit the spectrum using only four Cotton effects, but it was found that better fits and more reasonable spectral parameters were obtained by using five bands. The results of the curvefitting procedure are presented in Table 2 for the aqueous spectra at acidic and alkaline p*H* values, and in TEP.

The higher energy Cotton effects of β-colubrine exhibit a rather pronounced p*H* and solvent dependence. From the curvefitting results in Table 2 it can be seen that a change in sign of three Cotton effects takes place in going from aqueous acidic solution to basic solution and TEP. Similar sign inversions are also observed in methanol. Cotton effects that arise from the ^1L_a and ^1B_b transitions and band III appear to be affected. The Cotton effect due to band III is red shifted in TEP relative to methanol and base, the minimum being well resolved at 241 nm.

It should be noted that by repetitively scanning the CD spectra a small amount of positive ellipticity was observed to consistently occur in methanol between 255 and 265 nm, and in TEP between 267 and 274 nm. This provides evidence for a positive ^1L_a Cotton effect in these solvents. Although no obvious evidence of positive ellipticity in this wavelength region was observed in the alkaline CD spectrum, the curvefitting analysis indicates that a positive ^1L_a Cotton effect is present.

The uv absorption spectra of brucine and dihydrobrucine are shown in Fig. 6. The ^1L_b absorption maxima for both molecules are considerably more intense and are red shifted approximately 6 nm relative to β-colubrine and dihydro-β-colubrine. The

Can. J. Chem. Downloaded from www.nrcresearchpress.com by 210.87.254.105 on 09/05/12
For personal use only.

Can. J. Chem. Downloaded from www.nrcresearchpress.com by 210.87.254.105 on 09/05/12
For personal use only.

TABLE 1. Curvefitting results for CD spectra of dihydrocolubrine in water

		Rotatory strength[a]		Wavelength[b]		Bandwidth[c]	
Transition	Assignment	$pH = 3.5$	$pH = 12.5$	$pH = 3.5$	$pH = 12.5$	$pH = 3.5$	$pH = 12.5$
I	^1L_b	−0.013	−0.017	293.0	291.9	15.5	17.5
II	^1L_a	0.027	0.011	258.3	259.8	14.7	13.5
III	n–π^*	0.042	−0.113	237.7	223.2	16.3	14.7
IV	^1B_b	0.065	0.120	224.5	217.4	9.4	17.6
V	^1B_a	−0.276	−0.132	201.6	201.4	10.7	9.2

[a]Rotatory strengths given in units of Debye–Bohr magnetons.
[b]Wavelengths are in nm.
[c]Bandwidths are half-widths in nm at $1/e$ of maximum ellipticity.

TABLE 2. Curvefitting results for CD spectra of colubrine in water and TEP

		Rotatory strength[a]			Wavelength[b]			Bandwidth[c]		
Transition	Assignment	$pH = 3.5$	$pH = 12.5$	TEP	$pH = 3.5$	$pH = 12.5$	TEP	$pH = 3.5$	$pH = 12.5$	TEP
I	^1L_b	−0.016	−0.020	−0.024	290.7	290.0	298.2	16.5	17.7	16.4
II	^1L_a	−0.017	0.003	0.003	261.5	261.2	259.7	17.3	14.9	10.0
III	n–π^*	0.036	−0.116	−0.095	238.3	235.9	240.8	16.6	13.3	11.7
IV	^1B_b	0.233	−0.100	−0.107	220.7	220.0	215.0	11.0	9.0	12.5
V	^1B_a	−0.569	−0.130	−0.208	209.6	211.8	205.4	14.2	6.1	8.4

[a]Rotatory strengths given in units of Debye–Bohr magnetons.
[b]Wavelengths are in nm.
[c]Bandwidths are halfwidths in nm at $1/e$ of maximum ellipticity.

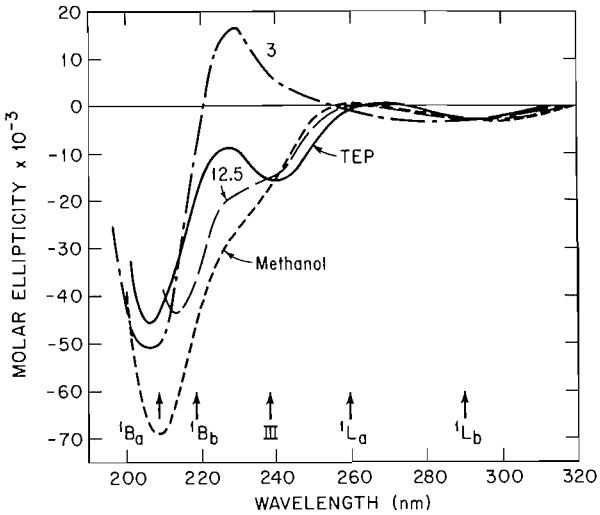

FIG. 5. CD spectra of β-colubrine in water, TEP, and methanol. The numerals in the figure indicate the pH of the aqueous solutions. Transition assignments are indicated along the bottom of the figure.

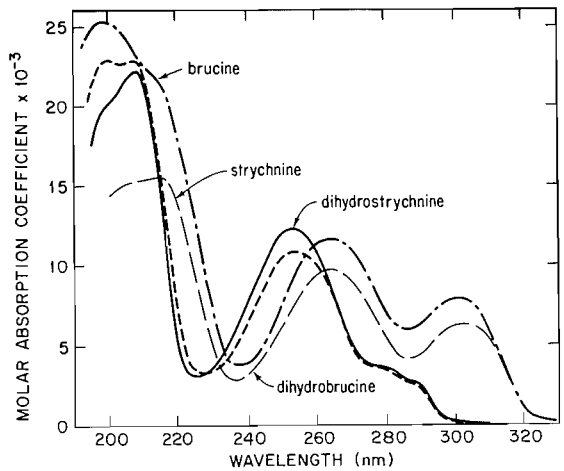

FIG. 6. The uv absorption spectra of brucine, dihydrobrucine, strychnine, and dihydrostrychnine in neutral water.

loss in intensity at 198 nm in dihydrobrucine relative to brucine indicates that the π_z–π_z^* transition of the ethylenic chromophore in the former compound probably occurs slightly to the blue of the ^1B transitions.

The CD spectra of dihydrobrucine in water ($pH = 3.03$) and in TEP are shown in Fig. 7. Again, transition assignments are indicated along the bottom of the figure. Analysis of the CD spectra as a function of pH was not attempted in the case of this compound because of apparent aggregation at alkaline pH values. Both the ^1L_b and ^1L_a Cotton effects were observed to split into positive and negative components at higher pH values, probably as a result of intermolecular exciton coupling. This phenomenon was found to be sensitive to solute

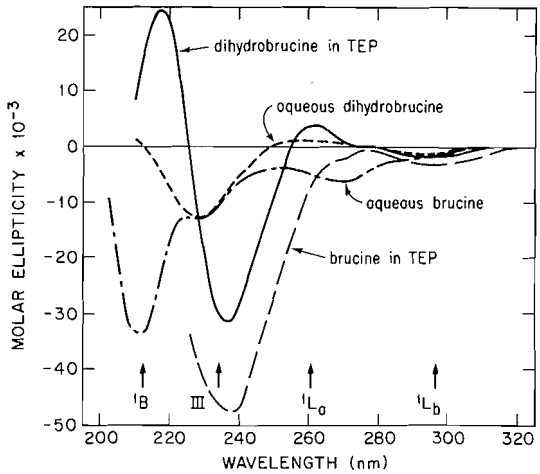

FIG. 7. CD spectra of brucine and dihydrobrucine in aqueous solution at p*H* 3 and TEP. Transition assignments are indicated along the bottom of the figure.

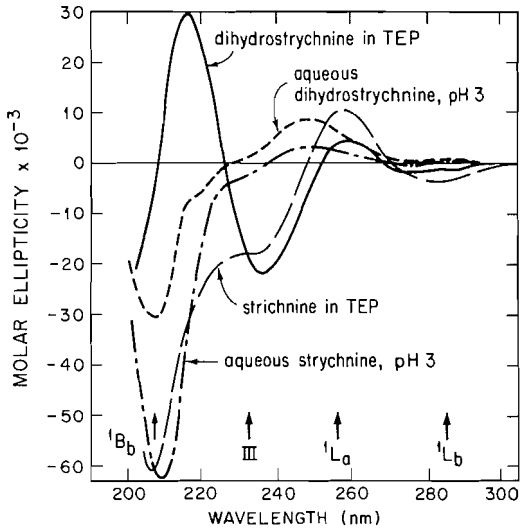

FIG. 8. CD spectra of strychnine and dihydrostrychnine in aqueous solution at p*H* 3 and TEP. Transition assignments are indicated along the bottom of the figure.

concentration, which is evidence that aggregation is occurring.

The 236 nm extrema apparently arise from the same transition that has been designated as band III in the CD spectra reported for β-colubrine and dihydro-β-colubrine. However, unlike the preceding cases, a change in sign of this Cotton effect does not occur as a result of changing the solvent from acidic water to TEP. Nevertheless, this CD band occurs in a region of the spectrum where very little absorbance is observed, as was true of the other molecules that were investigated.

The CD spectra of brucine in acidic aqueous solution and in TEP are also shown in Fig. 7. In aqueous solution an intense negative Cotton effect occurs at 211 nm with a negative shoulder at 228 nm, which probably arises from the ^1B band and band III respectively.

In TEP, the ^1L_a Cotton effect is negative, but is apparently extensively overlapped by a strong negative Cotton effect that arises from band III. As a result, the ^1L_a transition gives rise to a poorly resolved shoulder just below 270 nm. This is probably due to an increase in intensity of the Cotton effect arising from band III, which appears as a negative band with an apparent extremum at 237 nm.

The uv absorption spectra of strychnine and dihydrostrychnine are shown in Fig. 6. The ^1L_b band appears as two distinct shoulders near 287 and 277 nm in both strychnine and dihydrostrychnine. The blue-shift and decrease in intensity of the ^1L_b transitions relative to those observed for the other molecules is a result of the absence of the substituent effect that arises from the methoxy groups. The marked sensitivity of the ^1L_b transition to such substituent effects is typical of a large number of substituted benzene derivatives (18).

CD spectra of strychnine and dihydrostrychnine as determined in acidic aqueous solutions and TEP are shown in Fig. 8. These spectra appear to be rather similar except in the regions of the ^1L_b and ^1B_b transitions. The signs of the ^1L_b and ^1B_b Cotton effects of dihydrostrychnine appear to be solvent dependent, and the ^1L_b band of strychnine appears to give rise to two bands of opposite sign in the aqueous solution spectrum. However, all of the spectra determined in aqueous solution exhibited concentration dependence, which suggests that aggregation may have been taking place. All four curves exhibit evidence for band III Cotton effects, although they appear only as ill-defined negative shoulders near 220 nm in the spectra determined in aqueous solution.

Discussion

Most of the optical activity of the strychnine alkaloids appears to arise from the aromatic acetanilide-like chromophore. In the case of the dihydro derivatives it is the only chromophoric group present that is capable of generating the observed spectral features in the wavelength region that was investigated. Thus, it appears that most of the rotatory strength of these molecules is the result of local mechanisms that are operative in the vicinity of this chromophoric group. In the molecules in which the ethylenic group is present, it is possible for the ethylenic chromophore to contribute to the optical activity. This chromophore might make such con-

Can. J. Chem. Downloaded from www.nrcresearchpress.com by 210.87.254.105 on 09/05/12
For personal use only.

Can. J. Chem. Downloaded from www.nrcresearchpress.com by 210.87.254.105 on 09/05/12
For personal use only.

tributions by virtue of its inherent dissymmetry, or by means of dipole–dipole coupling with some of the aromatic transitions. However, as pointed out earlier, the ethylenic group in strychnine is almost planar, so a large contribution from inherent dissymmetry would not be expected. Furthermore, the plane of the double bond of the ethylenic group is very nearly parallel to the plane of the aromatic ring, and is oriented such that very little dipole coupling would be expected on the basis of Schellman's helical symmetry rule (19).

It appears that five Cotton effects are observed at wavelengths above 200 nm for all of the molecules that were investigated. The two highest wavelength bands must arise from the ^1L_b and the ^1L_a transitions, the latter of which probably includes a significant amount of intramolecular charge transfer character. The two lowest wavelength bands presumably arise from the ^1B_b and ^1B_a bands. If the molecular orbital calculations for acetanilide by Baba and Suzuki can be assumed to be applicable, the higher wavelength band of these two is the ^1B_b transition. Thus, the lowest wavelength transition must be in the ^1B_a, except in the case of the molecules which also include an ethylenic chromophore. All of these assignments should be valid for strychnine, dihydrostrychnine, β-colubrine, and dihydro-β-colubrine, because the pertinent chromophore in each molecule can be considered to approximate C_{2v} symmetry (4). However, the assignments for the two lowest energy transitions may not be valid for brucine and dihydrobrucine, because the chromophore of the molecules clearly does not fulfill these symmetry requirements. Since there is no twofold symmetry axis for this chromophoric group, unambiguous classification of the B states is not possible (18).

There was evidence of an additional transition in most of the molecules that were investigated. In most cases, a Cotton effect (band III) was observed in the wavelength region between the bands that have been assigned to the ^1L_a and ^1B_b transitions. In each case, although there was definite evidence of a circular dichroism band in this region, there was no evidence of a corresponding absorption band. Thus, it seems likely that the Cotton effect that was observed must arise from a transition that is electrically forbidden. Such a transition apparently has not been reported previously insofar as acetanilide or acetanilide derivatives are concerned. However, this band must be associated with the acetanilide group, since it persists even when the only other chromophoric group that could possibly be responsible for it, i.e., the ethylenic group, has been eliminated.

One can think of several possible assignments for this Cotton effect. For example, it could be of vibronic origin, e.g., vibronic components of a nearby band such as the ^1L_a could give rise to such a feature. Another possibility is that this band arises from an as yet unassigned transition. For example, a transition to a state related to the E_{2g} state of benzene or a ^1C transition such as has been reported by Klevens and Platt (20) in certain cata-condensed hydrocarbons might be responsible for it. In fact, Auer (21) has suggested the possibility of a ^1C transition being associated with the optical activity of the indole chromophore of a number of tryptophan derivatives.

Another possibility, which is perhaps more likely, is that the Cotton effect in question arises from an electrically forbidden, magnetically allowed n–π* transition, which is associated with the excitation of a nonbonding electron of the carbonyl oxygen atom. Such transitions are known to occur at widely different wavelengths among various carbonyl compounds. For example, the n–π* transition of ketones occurs near 290 nm (22). On the other hand, it occurs near 212 nm in a number of simple amides (23), but occurs as high as 230 nm in several cyclic dipeptides (24, 25). Such transitions are very sensitive to their environment, and are known to undergo appreciable red-shifts as the polarity of the solvent is decreased. The Cotton effect which was designated as band III certainly exhibited properties that are characteristic of an n–π* transition, i.e., it was sensitive to solvent polarity, pH, etc.

On the basis of the results of this investigation, it is not possible to distinguish between these possibilities as to the origin of the Cotton effect referred to as band III. However, the occurrence of an n–π* transition in the molecules under study could not be regarded as unlikely. On the other hand, definite evidence for other transitions that might fall in the appropriate wavelength region is scant. There is some evidence for ^1C transitions, but this is restricted to only a few molecules, primarily cata-condensed hydrocarbons, which are rather dissimilar to the chromophores under consideration here. In addition, there is no precedent for a vibronically split ^1L_a Cotton effect. Thus, it seems reasonable to assign the Cotton effects that were observed to occur around 220–240 nm in most of the molecules studied to an n–π* transition, although this assignment must be regarded as a tentative one for the present.

Because of their structural similarities there are, as one might expect, a number of correlations that can be observed in the CD spectra of the various strychnine alkaloids and their dihydro derivatives. These correlations are exhibited in tabular form in Table 3, where the signs of the Cotton effects associated with the three lowest energy transitions of each of the

TABLE 3. Signs of CD bands associated with the three lowest energy transitions

	^1L_b		^1L_a		n–π*	
	Water[b]	TEP	Water[b]	TEP	Water[b]	TEP
Strychnine	[a]	–	+	+	–	–
Dihydrostrychnine	+	–	+	+	–	–
β-Colubrine	–	–	–	+	+	–
Dihydro-β-colubrine	–	–	+	+	+	–
Brucine	–	–	–	–	–	–
Dihydrobrucine	–	–	+	+	–	–

[a]The ^1L_b transition of strychnine gives rise to a positive couplet in aqueous solution at low p*H*.
[b]Water refers to aqueous solutions at p*H* 3.

molecules are shown. The two higher energy bands, i.e., those arising from the ^1B transitions, are not included because of uncertainties in their assignments for some of the molecules. Data for solutions in water at p*H* 3 and in TEP are reported. Data for alkaline aqueous solution are not included because such data closely resembled the TEP data in all cases where intermolecular aggregation could be ruled out, except for the fact that the n–π* band was red-shifted in TEP.

The data of Table 3 clearly indicate numerous sign inversions upon going from the free base form of the alkaloids in TEP to acidic aqueous solution. With few exceptions, these changes are the result of titration of the tertiary amino function, i.e., they are not the result of solvent effects. For example, each of the five Cotton effects of β-colubrine and dihydro-β-colubrine have the same relative sign in alkaline aqueous solution and TEP, which seems to rule out solvent dependent mechanisms as the origin of the sign inversions. However, it should be remembered that evidence of intermolecular aggregation was observed in alkaline aqueous solutions of several of the molecules studied, especially strychnine, dihydrostrychnine, and dihydrobrucine.

The sensitivity of the CD spectra of these molecules to the titration of the tertiary amino function appears to arise primarily from the ^1L_a, the n–π*, and the ^1B_b transitions. There is an apparent change in the sign of the ^1L_b transitions of strychnine and dihydrostrychnine, but the data are somewhat questionable because of difficulties with aggregation of these molecules in aqueous solution. In dihydro-β-colubrine removal of the nitrogen proton resulted in a change in sign of the Cotton effect arising from the n–π* transition alone, whereas in β-colubrine three Cotton effects changed sign (^1L_a, n–π*, ^1B_b).

One can think of several possible origins for the p*H* dependence of the CD spectra that was observed with these molecules. For example, a p*H* dependent conformational equilibrium, direct perturbation of the electronic states of the molecules, charge dependence of the chiroptical mechanism, and p*H* dependent solvation are some of the possibilities. However, it is difficult to distinguish between the various mechanisms upon the basis of the present experimental data alone. The resolution of the question of the origins of the p*H* dependence of the CD spectra must await the completion of a thorough theoretical analysis of the mechanisms by which these molecules generate optical rotatory power.

Some interesting similarities between the CD spectra of the various alkaloids and their dihydro-derivatives are also revealed by the data of Table 3. For example, in TEP solution, where aggregation effects are minimized, the CD spectrum of a given alkaloid is very similar to the corresponding dihydro derivative. This is especially true insofar as the three lowest energy transitions are concerned; the ^1L_b and n–π* Cotton effects are consistently negative for all of the molecules. In only one instance, i.e., the ^1L_a bands of brucine and dihydrobrucine, does one of these transitions give rise to Cotton effects that are of opposite sign in the dihydro derivative and the parent alkaloid. This particular case is not surprising, since the polarization direction of the ^1L_a transitions of brucine and dihydrobrucine may well be quite different from that of the corresponding transitions in β-colubrine and strychnine. Thus, this transition may couple more favorably with the ethylenic chromophore in brucine than in the other alkaloids. Reduction of the ethylenic group would obviously eliminate any contribution by this mechanism.

The similarities between the CD spectra of the parent alkaloids and their dihydro derivatives even carry over into aqueous solution, where only the ^1L_a transitions of β-colubrine and dihydro-β-colubrine give rise to Cotton effects of opposite sign. Thus, elimination of the ethylenic chromophore by reduction appears to have only minimal effects on the CD spectra of these alkaloids. This is somewhat surprising, since reduction introduces a new chiral center. However, most of the rotatory strength is apparently being generated locally, i.e., on the

Can. J. Chem. Downloaded from www.nrcresearchpress.com by 210.87.254.105 on 09/05/12
For personal use only.

chromophore that has been designated as an acetanilide chromophore, at least in the case of β-colubrine and strychnine and their dihydro derivatives. The new chiral center is apparently so far removed from this chromophoric group that it exerts no appreciable influence. A similar situation has been reported in the case of other alkaloids. For example, Finch and Taylor (26) found that introduction of chiral centers at similar locations on certain heteroyohimbine alkaloids resulted in no major changes in the optical rotatory dispersion spectra.

In summary, significant differences and similarities were observed in the CD spectra of the closely related molecules which were studied in this investigation. It is not possible to arrive at definite conclusions regarding the origins of these observations at the present time, but the differences which were observed cannot be regarded as surprising from a qualitative point of view. The essential similarity to be noted among the CD spectra of these molecules is the presence of the same number of Cotton effects. It is especially significant that the CD spectra of all of the molecules which were investigated yield evidence for an electronic transition that is not discernable in the uv absorption spectra. This transition, which has been tentatively assigned as an $n-\pi^*$ transition, appears to give rise to Cotton effects between 230 and 240 nm in all of the molecules that were investigated.

Acknowledgements

The support of the National Institute of General Medical Sciences of the National Institutes of Health through Grant GM-18092 is gratefully acknowledged. Equipment purchased with funds from Biomedical Sciences Support Grant S04-RR07099 was utilized in this research.

We would also like to acknowledge the graphic artwork of Dottie McLaren of the Department of Chemistry, University of California, Santa Barbara.

1. H. E. UNGNADE. J. Am. Chem. Soc. **76**, 5133 (1954).
2. A. E. LUTSKII, A. S. GOL'BERKOVA, and A. S. BUGAI. Zh. Obshch. Khim. **33**, 1624 (1963).
3. W. F. FORBES and M. B. SHERATTE. Can. J. Chem. **33**, 1829 (1955).
4. H. BABA and S. SUZUKI. J. Chem. Phys. **32**, 1706 (1960).
5. J. TANAKA. Bull. Chem. Soc. Jpn. **36**, 833 (1963).
6. J. H. ROBERTSON and C. A. BEEVERS. Acta Crystallogr. **4**, 270 (1951).
7. J. R. PLATT. J. Chem. Phys. **17**, 484 (1949).
8. A. J. MERER and R. S. MULLIKEN. Chem. Rev. **69**, 639 (1969).
9. A. LUBEZKY and R. KOPELMAN. J. Chem. Phys. **45**, 2526 (1966).
10. A. YOGEV, J. SAGIV, and Y. MAZUR. J. Am. Chem. Soc. **94**, 5122 (1972).
11. M. YARIS, A. MOSCOWITZ, and R. S. BERRY. J. Chem. Phys. **49**, 3150 (1968).
12. C. C. LEVIN and R. HOFFMAN. J. Am. Chem. Soc. **94**, 3446 (1971).
13. J. G. KIRKWOOD. J. Chem. Phys. **5**, 479 (1937).
14. R. NAGARAJAN and R. W. WOODY. J. Am. Chem. Soc. **95**, 7212 (1973).
15. A. E. OXFORD and W. H. PERKIN, JR. J. Chem. Soc. **130**, 2389 (1927).
16. O. ACKMATOWICZ, R. C. FAWCETT, W. H. PERKIN, JR., and R. ROBINSON. J. Chem. Soc. London, 1769 (1930).
17. R. FLETCHER and M. J. D. POWELL. Comput. J. **6**, 163 (1963).
18. J. N. MURRELL. The theory of the electronic spectra of organic molecules. Wiley, New York, NY. 1963.
19. J. A. SCHELLMAN. Acc. Chem. Res. **1**, 144 (1968).
20. J. R. PLATT. J. Chem. Phys. **17**, 484 (1949); H. B. KLEVENS and S. R. PLATT. J. Chem. Phys. **17**, 470 (1949).
21. H. E. AUER. J. Am. Chem. Soc. **95**, 3003 (1973).
22. H. H. JAFFÉ and M. ORCHIN. Theory and applications of ultraviolet spectroscopy. Wiley, New York, NY. 1962.
23. E. B. NIELSEN and J. A. SCHELLMAN. J. Phys. Chem. **71**, 2297 (1967).
24. T. M. HOOKER, JR., P. M. BAYLEY, W. RADDING, and J. A. SCHELLMAN. Biopolymers, **13**, 549 (1974).
25. J. W. SNOW and T. M. HOOKER, JR. J. Am. Chem. Soc. **97**, 3506 (1975).
26. N. FINCH and W. I. TAYLOR. Tetrahedron, **22**, 1327 (1966).

Can. J. Chem. Downloaded from www.nrcresearchpress.com by 210.87.254.105 on 09/05/12
For personal use only.

Fluidities and conductances of glass-forming melts of cadmium nitrate tetrahydrate and transition metal chlorides

N. ISLAM, S. KUMAR, AND K. P. SINGH

Department of Chemistry, Aligarh Muslim University, Aligarh 202001, India

Received August 17, 1977

N. ISLAM, S. KUMAR, and K. P. SINGH. Can. J. Chem. **56**, 1231 (1978).

The temperature dependences of fluidities and equivalent conductances of $Cd(NO_3)_2 \cdot 4.1H_2O$–$(Ni/Co)Cl_2$ melts have been explained in terms of Vogel–Tammann–Fulcher and Adam–Gibbs equations. The differences in the values of the glass transition temperatures and the preexponential factors corresponding to the Ni^{2+} and Co^{2+} melts were attributed to the differences in the masses of the two systems. The linear decrease and increase observed in the values of the preexponential factor and the glass transition temperature, respectively, with increasing concentration of the solute were discussed. The overall composition dependences of transport properties were analyzed using expressions derived on the basis of both the above equations.

N. ISLAM, S. KUMAR et K. P. SINGH. Can. J. Chem. **56**, 1231 (1978).

On a expliqué le fait que les fluidités et les conductivités équivalentes de masses fondues $Cd(NO_3) \cdot 4.1H_2O$–$(Ni/Co)Cl_2$ dépendent de la température en termes des équations de Vogel–Tamman–Fulcher et Adam–Gibbs. On attribue les différences dans les valeurs des températures de transition vitreuse et les facteurs préexponentiels correspondants aux masses fondues de Ni^{2+} et Co^{2+} aux différences dans les masses de ces deux systèmes. On discute de la diminution et de l'augmentation linéaire observées respectivement dans les valeurs des facteurs préexponentiels et des températures de transition vitreuse avec une augmentation de la concentration du soluté. On a analysé le fait que les propriétés de transport dépendent de la composition globale en utilisant des expressions qui sont dérivées à l'aide des deux équations mentionnées plus haut.

[Traduit par le journal]

Introduction

In the non-Arrhenius region, there are satisfactory analytical expressions (1, 2) for explaining the temperature dependence of transport properties. On the other hand, there is a lack of suitable expressions for the illustration of their composition dependence. However, in recent years such equations are being developed based essentially on the Vogel–Tammann–Fulcher (isothermal) as well as on the Adam–Gibbs equations (3–5). In an earlier paper (3), the better feasibility of the latter equation than the isothermal equation (4, 5) has been discussed. It seems to be worthy to make further investigations on the applicability of these less familiar equations in explaining the composition dependence of transport properties of molten salt mixtures. Binary mixtures of nickel and cobalt chlorides with molten cadmium nitrate tetrahydrate have been chosen here for this purpose and fluidities and electrical conductances have accordingly been measured as functions of temperature and composition. These binary systems were selected mainly due to their readiness to supercool to permit measurements in the ordinary temperature range.

Experimental

Commercial cadmium nitrate tetrahydrate (REACHIM, U.S.S.R.; mp 59.4°C) was used as solvent in the molten state. Anhydrous nickel(II) and cobalt(II) chlorides were prepared (6) from their recrystallized hexahydrate salts and these solutes were found to dissolve up to ~12 mol% in the solvent under consideration. The molten mixtures were prepared in a thermostated water bath at ~70°C. Water of crystallization of the hydrated cadmium nitrate was determined before sample preparation by comparing the measured densities with those reported (7) and was found to be 4.1.

Density, viscosity, and conductance measurements were made in a manner described earlier (8) with the same precision.

Results and Discussion

The measured densities, ρ, at eleven different temperatures of both the systems under investigation were least-squares fitted to a linear equation

$$[1] \qquad \rho = a - bT$$

with T in K. Although the computed values of the two empirical parameters, a and b (Table 1[1]), fluctuate randomly with composition, the overall change in the density with composition has been found to be monotonous (Fig. 1[1]).

The measured fluidities and equivalent conductances decrease with increasing composition (Table 2[1]) and show non-Arrhenius temperature dependence.

[1]Copies of Tables 1 and 2 and Fig. 1 are available at a nominal charge, from the Depository of Unpublished Data, CISTI, National Research Council of Canada, Ottawa, Ont., Canada K1A 0S2.

Can. J. Chem. Downloaded from www.nrcresearchpress.com by 210.87.254.40 on 09/05/12
For personal use only.

TABLE 3. Computed parameters for [2] for equivalent conductance and fluidity* of binary molten mixtures

$[Ni^{2+}]$ (mol%)	A_Y	k_Y	$T_{0,Y}$	Std. dev. in Y	$[Co^{2+}]$ (mol%)	A_Y	k_Y	$T_{0,Y}$	Std. dev. in Y
0.00	3950.0	591.5	193.5	0.018	0.00	3950.0	591.5	193.9	0.018
	(12368.0)	(696.1)	(193.0)	(0.029)		(12368.0)	(696.1)	(193.0)	(0.029)
2.26	3803.7	595.9	197.3	0.012	2.32	3800.0	591.0	196.5	0.014
	(11740.0)	(694.0)	(196.6)	(0.019)		(11610.0)	(692.7)	(195.8)	(0.013)
4.08	3642.3	594.1	200.0	0.010	4.10	3680.0	591.2	199.0	0.023
	(11170.0)	(693.9)	(199.2)	(0.016)		(11170.0)	(692.0)	(198.2)	(0.013)
6.10	3427.7	593.5	202.4	0.013	6.16	3450.0	593.8	201.0	0.023
	(10400.0)	(688.0)	(202.1)	(0.021)		(10773.0)	(693.4)	(200.8)	(0.011)
8.25	3324.5	598.2	205.5	0.017	8.37	3410.0	594.1	203.5	0.013
	(9760.0)	(687.1)	(204.8)	(0.015)		(10229.0)	(688.2)	(203.3)	(0.016)
10.02	3177.3	597.0	208.2	0.019	10.06	3253.0	592.9	206.0	0.022
	(9240.1)	(688.3)	(207.2)	(0.015)		(9671.1)	(688.7)	(205.8)	(0.022)
11.55	3040.2	599.0	210.0	0.011	11.65	3100.0	597.8	208.8	0.023
	(8800.2)	(688.1)	(209.3)	(0.023)		(9200.0)	(690.7)	(208.0)	(0.026)

*Parameters for fluidity are within parentheses.

Therefore, these data were least-squares fitted to the Fulcher or Vogel–Tammann–Fulcher equation

$$[2] \qquad Y(\phi, \Lambda) = A_Y T^{-1/2} \exp\left[-k_Y/(T - T_0)\right]$$

in a manner to obtain approximately constant values for the empirical parameter k_Y. The significance of such a data analysis has been discussed elsewhere (9, 10). The best fit values of the parameters A_Y, k_Y, and T_0 thus obtained are given in Table 3.

The composition dependence of the transport properties is equally important and may indirectly be explained by considering only the variations of the parameters A_Y and T_0 with composition since the third parameter, k_Y, is apparently independent of composition. Therefore, we may consider firstly the variation of glass transition temperature, T_0, with composition. In both the systems, viz., $Cd(NO_3)_2 \cdot 4.1H_2O$–$CoCl_2$ and $Cd(NO_3)_2 \cdot 4.1H_2O$–$NiCl_2$, it has been observed (Fig. 2) that T_0 increases linearly with $[Co^{2+}]$ and $[Ni^{2+}]$. The increase of T_0 with $[Co^{2+}]$ and $[Ni^{2+}]$ in both the systems may be explained by the $m^{-1/2}$ dependence (11) of T_0, m being the average molecular mass. On addition of Co^{2+} and Ni^{2+} to $Cd(NO_3)_2 \cdot 4.1H_2O$, m decreases which may cause an increase in T_0. Moreover, a slightly higher T_0 value observed for the molten mixture of $Cd(NO_3)_2 \cdot 4.1H_2O$–$NiCl_2$ than that of $Cd(NO_3)_2 \cdot 4.1H_2O$–$CoCl_2$ melt at a particular composition may be explained in terms of the cationic potentials (12) or cohesive energies of the systems. The charge:radius ratio for hydrated Ni^{2+} ion (0.578) is higher than that of hydrated Co^{2+} ion (0.575) and, therefore, accounts for the higher T_0 values of the $Cd(NO_3)_2 \cdot 4.1H_2O$–$NiCl_2$ systems.

It is also worthy to note that the T_0 values obtained from the analysis of conductance and viscosity

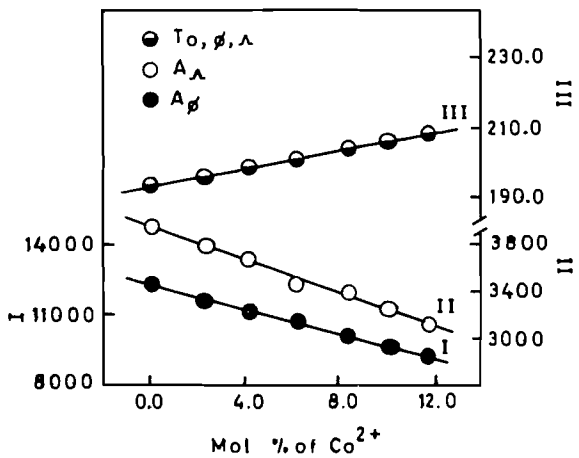

FIG. 2. Variations of A_Y and $T_{0,Y}$ with composition for molten $Cd(NO_3)_2 \cdot 4.1H_2O$–$CoCl_2$ systems (plots are similar for Ni^{2+} systems).

data are very close to each other. This emphasizes the thermodynamic nature of T_0 unlike A_Y and k_Y terms which behave like kinetic parameters.

On the other hand, both A_ϕ and A_Λ appear to decrease linearly (Fig. 2) with increase in $[CO^{2+}]$ and $[Ni^{2+}]$, showing a reverse of their expected $m^{-1/2}$ dependences. There is a difference in the strength of interactions between H_2O–Co^{2+} and H_2O–Ni^{2+} as well as between H_2O–Cd^{2+} which results into the formation of complex species (13) like $Ni(H_2O)_4Cl_2$ and $Co(H_2O)_4Cl_2$. The linear decrease of A_ϕ and A_Λ with increase in mol% of the solute (5, 10) may be attributed to such differences in the strength of interactions. However, the $m^{-1/2}$ dependence relation appears to explain the slightly higher values of A_Y terms observed for the Co^{2+} systems than those for the Ni^{2+} systems. The in-

Can. J. Chem. Downloaded from www.nrcresearchpress.com by 210.87.254.40 on 09/05/12
For personal use only.

Can. J. Chem. Downloaded from www.nrcresearchpress.com by 210.87.254.40 on 09/05/12
For personal use only.

TABLE 4. Parameters for [3] for the fluidity* and equivalent conductance of binary molten mixtures

Melt	T (K)	A_{0Y}	Q_{1Y}	k_Y	Q_{2Y}	X_0	Std. dev. in Y
$Cd(NO_3)_2 \cdot 4.1H_2O$	298.0	3955.0	78.00	590.0	1.288	80.86	0.023
+ $CoCl_2$	303.0	3946.0	76.49	588.2	1.297	84.11	0.023
	308.0	3953.0	76.12	587.0	1.294	88.00	0.028
		(12372.0)	(226.40)	(687.0)	(1.297)	(87.97)	(0.030)
	313.0	3940.0	74.41	588.3	1.287	92.40	0.041
		(12279.0)	(212.70)	(688.0)	(1.294)	(92.02)	(0.033)
	318.0	3956.0	78.85	588.7	1.290	96.37	0.023
		(12370.0)	(211.90)	(687.0)	(1.291)	(95.78)	(0.037)
	323.0	3936.8	76.24	588.4	1.292	99.99	0.031
		(12376.0)	(203.60)	(686.0)	(1.285)	(99.85)	(0.039)
$Cd(NO_3)_2 \cdot 4.1H_2O$	298.0	3991.6	88.46	593.7	1.380	74.88	0.027
+ $NiCl_2$	303.0	4009.6	110.48	594.8	1.389	78.50	0.011
		(12453.0)	(311.50)	(692.6)	(1.397)	(78.48)	(0.018)
	308.0	4042.8	99.11	589.6	1.373	82.08	0.018
		(12442.0)	(311.30)	(689.6)	(1.389)	(82.11)	(0.020)
	313.0	3964.9	88.77	591.4	1.375	85.98	0.012
		(12358.0)	(258.40)	(693.2)	(1.389)	(85.92)	(0.014)
	318.0	3983.5	90.22	593.8	1.378	89.99	0.024
		(12446.0)	(259.80)	(692.6)	(1.384)	(89.68)	(0.017)
	323.0	3999.9	91.29	593.4	1.386	93.06	0.022
		(12444.0)	(279.60)	(697.3)	(1.387)	(93.57)	(0.028)
	328.0	4056.7	90.61	594.0	1.381	96.71	0.027
		(12413.0)	(257.60)	(692.1)	(1.382)	(96.97)	(0.016)
	333.0	3990.3	87.52	594.9	1.392	99.95	0.032
		(12420.0)	(262.90)	(691.8)	(1.390)	(99.99)	(0.026)

*Parameters for fluidity are within parentheses.

crease in the rigidity of the systems with composition may also account for the decrease in the pre-exponential factors as reported earlier (3).

Substitution of the linear composition dependences of T_0 and A_Y into [2] provides the isothermal equation (5).

$$[3] \quad Y = (A_{0Y} - Q_{1Y}X)T^{-1/2} \times \exp\,[-k_Y/Q_{2Y}(X_0 - X)]$$

X refers to the mol% of the solute whereas A_{0Y}, Q_{1Y}, Q_{2Y}, and X_0 have the significances explained earlier (5). In order to explain the applicability of this isothermal equation the conductance and fluidity data were least-squares fitted to eq. 3 at an interval of 5 K over 298 to 333 K and over 308 to 333 K in the molten mixtures of $Cd(NO_3)_2 \cdot 4.1H_2O$–$NiCl_2$ and of $Cd(NO_3)_2 \cdot 4.1H_2O$–$CoCl_2$, respectively. The best fit parameters along with the standard deviation in Λ and ϕ are given in Table 4. Linear plots (Fig. 3) of $\log\,[(A_{0Y} - Q_{1Y}X)/YT^{1/2}]$ vs. $1/(X_0 - X)$ pass through the origin which reinforce the applicability of [3] in describing such behaviour. Moreover, the computer fitted values of the parameters A_{0Y}, Q_{1Y}, Q_{2Y}, and X_0 were found to be in good agreement with their values obtained from the corresponding plots. In molten mixtures of Co^{2+} the values of X_0 ap-

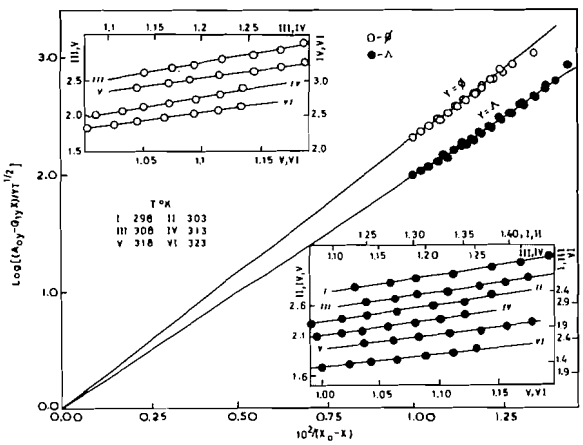

FIG. 3. Plots of $\log\,[(A_{0Y} - Q_{1Y}X)/YT^{1/2}]$ vs. $1/(X_0 - X)$ for molten $Cd(NO_3)_2 \cdot 4.1H_2O$–$CoCl_2$ systems (plots are similar for Ni^{2+} systems).

proach ~100 mol% at 323 K indicating it as the T_0 value for the pure solute, $CoCl_2$. Similarly, T_0 value for $NiCl_2$ has been found to be 333 K. Such a higher value of T_0 for Ni^{2+} than for Co^{2+} was reported previously in melts (5) as well as in aqueous solutions (14) of $NiCl_2$ and $CoCl_2$.

However, it may be observed from Table 4 that the upper temperature limits for the application of

TABLE 5. Computed parameters for [4] for equivalent conductance and fluidity* of binary molten mixtures

$[Ni^{2+}]$ (mol%)	A_Y'	k_Y'	$T_{0,Y}$	Std. dev. in Y	$[Co^{2+}]$ (mol%)	A_Y'	k_Y'	$T_{0,Y}$	Std. dev. in Y
0.00	89.9	598.0	195.4	0.017	0.00	89.9	598.0	195.4	0.017
	(241.9)	(698.2)	(195.5)	(0.048)		(241.9)	(698.2)	(195.5)	(0.048)
2.26	84.6	599.1	198.8	0.017	2.32	85.0	592.3	198.3	0.015
	(226.0)	(695.4)	(198.5)	(0.045)		(227.6)	(693.1)	(198.4)	(0.034)
4.08	81.1	596.8	201.4	0.015	4.10	81.0	591.2	200.5	0.020
	(216.0)	(693.8)	(201.3)	(0.036)		(219.4)	(693.3)	(200.5)	(0.032)
6.10	76.1	593.7	204.0	0.017	6.16	77.0	589.9	202.8	0.014
	(205.0)	(689.8)	(204.0)	(0.024)		(210.8)	(694.1)	(203.0)	(0.028)
8.25	71.0	594.9	206.7	0.038	8.37	73.0	587.2	205.3	0.035
	(196.0)	(692.0)	(206.5)	(0.023)		(202.3)	(690.7)	(205.2)	(0.032)
10.02	67.0	594.3	209.2	0.056	10.06	70.0	586.0	207.8	0.042
	(187.0)	(692.9)	(209.0)	(0.026)		(191.3)	(693.0)	(207.3)	(0.040)
11.55	64.0	594.5	211.2	0.038	11.65	66.0	599.0	209.2	0.027
	(181.5)	(695.5)	(211.5)	(0.024)		(184.0)	(698.8)	(209.2)	(0.034)

*Parameters for fluidity are within parentheses.

TABLE 6. Computed parameters for [5] ($c = 1.5$) for the fluidity* and equivalent conductance of binary molten mixtures

Melt	A_{0Y}'	Q_{1Y}'	k_Y'	$T_{0(0)}$	Q_{2Y}	Std. dev. in Y
$Cd(NO_3)_2 \cdot 4.1H_2O + CoCl_2$	90.1	2.110	597.4	195.4	1.184	0.019
	(241.4)	(4.983)	(698.0)	(195.3)	(1.183)	(0.029)
$Cd(NO_3)_2 \cdot 4.1H_2O + NiCl_2$	90.0	2.250	597.0	195.4	1.370	0.015
	(237.0)	(4.760)	(697.0)	(195.0)	(1.437)	(0.012)

*Parameters for fluidity are within parentheses.

[3] in the two systems under consideration are different. Such limitations in the temperature range for the applicability of the isothermal equation has been discussed in an earlier publication (3).

Therefore, the composition dependence of Λ and ϕ in the present systems has been re-examined by considering T_0 as a basis for the corresponding temperatures, T. For this purpose, the measured equivalent conductance and fluidity data have been fitted to the Adam–Gibbs equation

$$[4] \qquad Y = A_Y' \exp\left[-k_Y'/T \ln (T/T_0)\right]$$
$$= A_Y' \exp\left[-k_Y'/T_0\, c \ln c\right]$$

at $T/T_0 =$ constant $= c$. The variations in A_Y' and T_0 with composition (Table 5) are identical to those in the corresponding parameters of [2]. k_Y' remains independent of composition as k_Y. By accounting for the linear composition dependences of T_0 and A_Y' eq. 4 may be expressed as

$$[5] \quad Y = (A_{0Y}' - Q_{1Y}'X) \times \exp\left[-k_Y'/(T_{0(0)} + Q_{2Y}X)c \ln c\right]$$

The fluidities and conductances data of $Cd(NO_3)_2 \cdot 4.1H_2O$–$CoCl_2$ and $Cd(NO_3)_2 \cdot 4.1H_2O$–$NiCl_2$ systems at constant T/T_0 ($c = 1.5$) values were computed from the Adam–Gibbs equation and they were in turn least-squares fitted to [5]. Reasonably good fits were obtained as it is apparent from Table 6 in the entire experimental range of temperature. The values of parameters A_{0Y}', Q_{1Y}', $T_{0(0)}$, and Q_{2Y} were found to be in good agreement with those obtained from the corresponding linear plots of A_Y and T_0 vs. composition for both the systems under investigation. Furthermore, the plots (Fig. 4) of log $[(A_{0Y}' - Q_{1Y}'X)/Y]$ vs. $1/(T_{0(0)} + Q_{2Y}X)$ were linear and pass through the origin showing the applic-

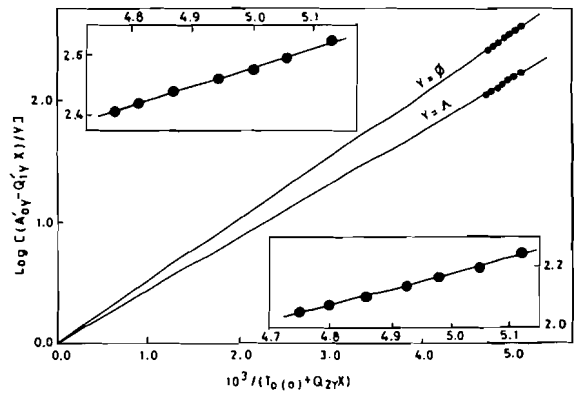

FIG. 4. Plots of log $[(A_{0Y}' - Q_{1Y}'X)/Y]$ vs. $1/(T_{0(0)} + Q_{2Y}X)$ for molten $Cd(NO_3)_2 \cdot 4.1H_2O$–$CoCl_2$ systems (plots are similar for Ni^{2+} systems).

Can. J. Chem. Downloaded from www.nrcresearchpress.com by 210.87.254.40 on 09/05/12
For personal use only.

ability of [5]. These two linear plots corresponding to $Y = \phi$ and $Y = \Lambda$ of $Cd(NO_3)_2 \cdot 4.1H_2O$–$CoCl_2$ melts appear to overlap on those of $Cd(NO_3)_2 \cdot 4.1H_2O$–$NiCl_2$ melts. This may be expected due to the fact that their slopes equal to $k_Y'/c \ln c$ are close to one another in the two binary molten systems owing to the universal constant values of k_Y' terms.

Therefore, eq. 5 appears to have a better applicability than [3] as far as the temperature range is concerned. However, it may be pointed out that before testing the applicability of [5] the conductance and fluidity data have to be fitted independently to [4] for obtaining T_0 values and this puts a restriction on the direct application of [5]. It may, therefore, be concluded that eq. 5 is a better expression for describing the composition dependence of transport properties provided these properties have been measured as functions of both temperature and composition.

Acknowledgements

The authors wish to express their thanks to Professor W. Rahman, Head of the Department of Chemistry, for providing necessary research facilities and to the C.S.I.R. (New Delhi) for the financial assistance to two of them (S.K. and K.P.S.). The authors are specially indebted to Dr. Ismail K. for his suggestions and interest shown during the progress of this work.

1. M. H. COHEN and D. TURNBULL. J. Chem. Phys. **31**, 1164 (1959).
2. G. ADAM and J. H. GIBBS. J. Chem. Phys. **43**, 139 (1965).
3. N. ISLAM, ISMAIL K., K. P. SINGH, and S. KUMAR. To be published.
4. C. A. ANGELL. J. Phys. Chem. **70**, 3988 (1966).
5. N. ISLAM and ISMAIL K. J. Phys. Chem. **80**, 1929 (1976).
6. T. MOELLER. Inorganic synthesis. Vol. V. McGraw-Hill, New York, NY. 1957. p. 153.
7. W. W. EWING and C. H. HERTY. J. Phys. Chem. **57**, 245 (1953).
8. N. ISLAM, M. R. ISLAM, S. AHMAD, and B. WARIS. Appl. Spectrosc. **29**, 68 (1975); J. Am. Chem. Soc. **97**, 3026 (1975).
9. N. ISLAM and ISMAIL K. J. Phys. Chem. **79**, 2180 (1975).
10. C. T. MOYNIHAN, C. R. SMALLEY, C. A. ANGELL, and E. J. SARE. J. Phys. Chem. **73**, 2287 (1969).
11. C. A. ANGELL. J. Am. Ceram. Soc. **51**, 117 (1968).
12. C. A. ANGELL. J. Phys. Chem. **68**, 1917 (1964).
13. C. J. BALLHAUSEN. Introduction to ligand field theory. McGraw-Hill, New York, NY. 1962. p. 256.
14. C. A. ANGELL and E. J. SARE. J. Chem. Phys. **52**, 1085 (1970).

Can. J. Chem. Downloaded from www.nrcresearchpress.com by 210.87.254.40 on 09/05/12
For personal use only.

Aldol-type condensations of $C(\alpha)$-dianions of azines

STEVEN E. DAVIS, NEAL L. SHEALY, KEITH D. SHEALY, LYNN M. SHAFFER, AND CHARLES F. BEAM[1]

Department of Chemistry, Newberry College, Newberry, SC 29108, U.S.A.

Received November 21, 1977

STEVEN E. DAVIS, NEAL L. SHEALY, KEITH D. SHEALY, LYNN M. SHAFFER, and CHARLES F. BEAM. Can. J. Chem. **56**, 1236 (1978).

The $C(\alpha)$-dianions of azines prepared from acetophenone or substituted acetophenones underwent dialdol condensations with ketones to give dihydroxyazines.

STEVEN E. DAVIS, NEAL L. SHEALY, KEITH D. SHEALY, LYNN M. SHAFFER et CHARLES F. BEAM. Can. J. Chem. **56**, 1236 (1978).

Les dianions $C(\alpha)$ des azines préparés à partir de l'acétophénone ou d'acétophénones substitués subissent des condensations di-aldoliques avec les cétones pour conduire aux dihydroxy-azines.

[Traduit par le journal]

Introduction

In comparison with the reports on the preparation and condensation of $C(\alpha)$-anions of oximes and hydrazones with electrophilic reagents (1–3), the synthesis of materials from $C(\alpha)$-dilithioazines has received little attention; in fact, we found the results of the earlier alkylation studies difficult to reproduce (4).

Results and Discussion

The $C(\alpha)$-dianions of acetophenone azines and substituted acetophenone azines (symmetrical and unsymmetrical) were prepared from *n*-butyllithium in tetrahydrofuran (preferable to ether (4)) at 0°C, and they were condensed with ketones, such as benzophenone and cyclohexanone, to give dialdol products. Each dihydroxyazine **1**–**7** (Table 1) contained ^{1}Hmr methylene resonances at δ 3.25 $\pm$ 0.05 ppm and ir absorptions for hydroxyl at approximately 3275 cm^{-1}. As anticipated, hydroxyazines **1** and **5** underwent linear dehydration with concentrated sulfuric acid at 0°C to give azines **8** and **9**, in 49 and 50% yields, respectively (Scheme 1).

TABLE 1. Dihydroxyazines

Compound No.	Empirical formula	R_1	R_2	X	Y	Yield[a] (%)	mp[b] (°C)	Elemental analyses[c,d,e] Calculated C	H	N	Found C	H	N
1	$C_{42}H_{36}N_2O_2$	C_6H_5	C_6H_5	H	H	32	206–207[f]	83.97	6.04	4.66	84.04	6.23	4.45
2	$C_{44}H_{40}N_2O_2$	C_6H_5	C_6H_5	CH_3	CH_3	80	198[g]	84.02	6.41	4.48	83.92	6.50	4.45
3	$C_{43}H_{37}ClN_2O_2$	C_6H_5	C_6H_5	CH_3	Cl	29	198–200[f]	79.55	5.74	4.32	79.32	5.82	4.31
4	$C_{43}H_{38}N_2O_2$	C_6H_5	C_6H_5	CH_3	H	28	193–195[f]	84.01	6.23	4.56	84.30	6.43	4.33
5	$C_{42}H_{34}Cl_2N_2O_2$	C_6H_5	*p*-ClC_6H_4	H	H	24	187–189[f]	75.33	5.12	4.18	75.56	5.35	4.08
6	$C_{28}H_{36}N_2O_2$	CH_2CH_2 / CH_2 / CH_2CH_2	C	H	H	33	176–177[h]	77.74	8.38	6.47	77.78	8.46	6.22
7	$C_{30}H_{40}N_2O_2$	CH_2CH_2 / CH_2 / CH_2CH_2	C	CH_3	CH_3	19	182–183[h]	78.22	8.75	6.08	78.20	8.64	5.92

[a]The percentage yield recorded in the table may not necessarily be the maximum yield possible.
[b]Melting points were obtained in a Thomas-Hoover melting point apparatus in open capillary tubes and are uncorrected.
[c]Combustion analyses were performed by Robertson's Laboratory, 73 West End Ave., Florham Park, NJ 07932.
[d]Infrared spectra were obtained on a Perkin-Elmer 700 infrared spectrometer; Nujol mulls for 1–5 gave spectra that contained broad OH absorption from 3250–3275 cm^{-1}; solution spectra ($CHCl_3$) for **6** and **7** contained broad OH absorption from 3275–3300 cm^{-1}.
[e]Nuclear magnetic resonance spectra were obtained on a Varian Associates EM-300X NMR Spectrometer; 1–5 were slightly soluble in DMSO-d_6 δ:3.25 $\pm$ 0.05 ppm for methylene resonance, 2.25 $\pm$ 0.05 ppm for $ArCH_3$ in **2**–**4**; **6** ($CDCl_3$) δ:1.43 (m, 10 H, cyclohexyl), 3.23 (s, 2H, —CH_2—), 4.8 (s, 1H, OH), and 6.90 ppm (m, 5H, ArH): **7** ($CDCl_3$) δ: 1.42 (m, 10H, cyclohexyl), 2.37 (s, 3H, $ArCH_3$), 3.20 (s, 2H, —CH_2—), 4.97 (b, OH), and 6.77–7.9 (m, 4H, ArH).
[f]Recrystallized from THF–DMF.
[g]Recrystallized from THF.
[h]Recrystallized from 95% ethanol.

[1]Author to whom correspondence should be addressed.

Can. J. Chem. Downloaded from www.nrcresearchpress.com by 210.87.254.5 on 09/05/12
For personal use only.

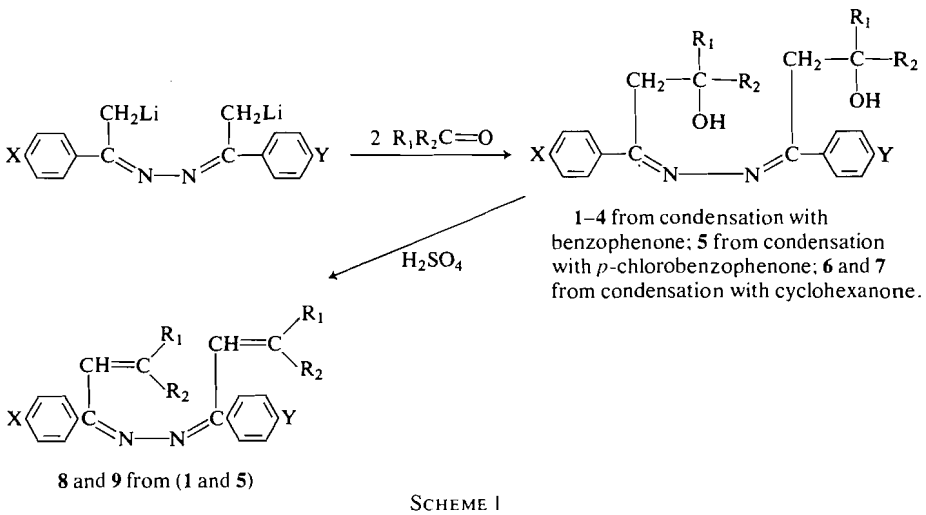

SCHEME I

Experimental

Preparation of Azines

The symmetrical azines were prepared by treating the ketone with hydrazine hydrate (20% molar excess) in 95% ethanol containing a catalytic amount of acetic acid and heating under reflux for ca. 1 h. The unsymmetrical azines were prepared by treating the ketone with a hydrazine in 95% ethanol containing a catalytic amount of acetic acid and heating under reflux for ca. 1 h. All starting materials were recrystallized from 95% ethanol.

General Procedure for Preparation of C(α)-Dilithioazines

A 0.02-mol sample was dissolved in 100–150 ml of dry tetrahydrofuran, cooled to 0°C, blanketed with nitrogen, and stirred; 0.042 mol of *n*-butyllithium (1.6 *M* in hexane) was added dropwise and the resulting red-brown mixture was stirred 30–45 min.

General Procedure for Dialdol Condensation

A solution of 0.042 mol of ketone in 50–75 ml of THF was added to the C(α)-dilithioazine (see procedure above) and stirred for 30–60 min and inversely neutralized by pouring the entire solution into 200–300 ml of ice and water (containing 1 or 2 milliliters of concentrated HCl). The layers were separated and the water layer was extracted with 2 × 75 ml portions of ether. The organic layers were combined, dried ($MgSO_4$), concentrated (Rotovac), and crystallized from ethanol. Recrystallization solvents are listed in the footnotes of Table 1.

General Procedure for Linear Dehydration of Hydroxyazines

A 1 g sample of hydroxyazines **1** or **5** was added to 10 ml of cold concentrated sulfuric acid (0°C) and stirred at this temperature until solution was complete, ca. 1 h. The solution was then poured on to 200–300 g of crushed ice, filtered, washed with water, dried, and recrystallized from ethanol–benzene to give azines **8** (from **1**) mp 214–215°C and 9 (from **5**) mp 190–192°C in 49 and 50% yield, respectively. The infrared (Nujol) spectra of these materials contained no hydroxyl absorption characteristic of hydroxyazines **1**–**7**. *Anal.* calcd. for $C_{42}H_{32}N_2$ (**8**): C 89.33, H 5.71, N 4.96; found: C 89.58, H 5.95, N 4.67. *Anal.* calcd. for $C_{42}H_{30}Cl_2N_2$ (9): C 79.62, H 4.74, N 4.42; found: C 79.36, H 4.93, N 4.40.

Acknowledgements

This project was supported at Newberry College by grants received from the Cottrell Science Grants Program of the Research Corporation, and the South Carolina Heart Association, Inc.

1. C. F. BEAM, M. C. D. DYER, R. A. SCHWARZ, and C. R. HAUSER. J. Org. Chem. **35**, 1806 (1970).
2. R. S. FOOTE, C. F. BEAM, and C. R. HAUSER. J. Heterocycl. Chem. **7**, 589 (1970).
3. C. F. BEAM, R. S. FOOTE, and C. R. HAUSER. J. Chem. Soc. C, 1658 (1971).
4. F. E. HENOCH, K. G. HAMPTON, and C. R. HAUSER. J. Am. Chem. Soc. **91**, 676 (1969).

Can. J. Chem. Downloaded from www.nrcresearchpress.com by 210.87.254.5 on 09/05/12
For personal use only.

Excited state acid–base equilibrium of tyrosine[1]

DAVID MICHAEL RAYNER, DONALD THEODORE KRAJCARSKI, AND ARTHUR GUSTAV SZABO
Division of Biological Sciences, National Research Council of Canada, Ottawa, Ont., Canada K1A 0R6

Received October 20, 1977

DAVID MICHAEL RAYNER, DONALD THEODORE KRAJCARSKI, and ARTHUR GUSTAV SZABO. Can. J. Chem. **56**, 1238 (1978).

Fluorescence attributable to the tyrosinate form of the amino acid tyrosine, previously only observed at $pH > pK(S_0) = 10.3$ where tyrosinate exists in the ground state, has been observed at neutral pH in the presence of high buffer base concentrations. This observation is consistent with the large shift in $pK(S_1)$ predicted from absorption measurements and confirms that proton transfer is indeed a mechanism by which carboxylate ions quench tyrosine fluorescence. The dependence of the fluorescence quantum yields of tyrosine and tyrosinate on pH does not fit a simple excited state acid–base equilibrium model but a more complicated system where carboxylate is also capable of simultaneously quenching tyrosine fluorescence by a mechanism not involving proton transfer. Kinetic analysis of the system allows calculation of $pK(S_1) = 4.2$ for tyrosine. The quantum yield of tyrosinate fluorescence can be appreciably higher than that normally measured at alkaline pH where a separate quenching mechanism must operate. These results have significance in the interpretation of the fluorescence properties of proteins.

DAVID MICHAEL RAYNER, DONALD THEODORE KRAJCARSKI et ARTHUR GUSTAV SZABO. Can. J. Chem. **56**, 1238 (1978).

On a observé de la fluorescence attribuable à la forme tyrosinate de l'acide aminé tyrosine, observé antérieurement uniquement à des $pH > pK(S_0) = 10.3$ auquel le tyrosinate existe dans son état fondamental, à un pH neutre en présence de concentrations élevées de tampons basiques. Cette observation est en accord avec un grand déplacement dans le $pK(S_1)$ qui peut être prédit à partir de mesures d'absorption et confirme que le transfert de proton est de fait un mécanisme par lequel les ions carboxylates piègent la fluorescence de la tyrosine. Le fait que les rendements quantiques de la fluorescence de la tyrosine et du tyrosynate dépendent du pH ne cadre pas avec un modèle acide–base à l'équilibre d'un état excité simple mais avec un système plus compliqué dans lequel le carboxylate est aussi capable de piéger simultanément la fluorescence de la tyrosine par un mécanisme n'impliquant pas un transfert de proton. Une analyse cinétique du système permet de calculer le $pK(S_1) = 4.2$ pour la tyrosine. Le rendement quantique de la fluorescence du tyrosinate peut être beaucoup plus élevé que celui mesuré normalement au pH alcalin quand un mécanisme de piégeage séparé peut être en opération. Ces résultats ont une signification dans l'interprétation des propriétés de fluorescence des protéines.

[Traduit par le journal]

Introduction

In the course of our studies of the fluorescence properties of proteins and amino acids and their structural implications we were struck by the lack of attention paid in recent reviews (1, 2) to the excited state acid–base properties of tyrosine. As a substituted phenol tyrosine would be expected to show similar behaviour to 2-napthol, Weller's (3) classic example of a compound which is far more acidic in the excited state than the ground state ($pK(S_0) = 9.46$, $pK(S_1) = 2.8$). An estimate of ΔpK, ($pK(S_1) - pK(S_0)$), for tyrosine can be obtained from its absorption spectra with the phenol hydroxyl group ionized and unionized using the Förster (4) cycle. By this method Feitleson (5) was able to make the rough estimate $\Delta pK \approx -5$. This predicts $pK(S_1) = 5.3$ for $pK(S_0) = 10.3$ (6). The lack of dependence of the quantum yield of fluorescence of tyrosine in water on pH in the range $pH = 4$ to $pH = 8$ (5, 7) must then be accounted for by the dominance of the rate of deactivation of excited singlet tyrosine to the ground state over the rate of deprotonation to form excited singlet tyrosinate even when the latter pathway is thermodynamically favoured. However, one cannot go on to conclude that the possibility of tyrosinate being formed in the excited state in solutions of $pH < pK(S_0)$ can be ruled out in all cases. Feitleson (5) has shown that weak bases such as acetate quench tyrosine fluorescence under Stern–Volmer kinetics and he reasonably suggests that the mechanism involves transfer of the phenolic proton to the base. Such a mechanism has also been cited by Weber and Rosenheck (8) to explain the quenching of fluorescence in tyrosine copolymers compared to that in their *O*-methylated analogues. Konev (9) lists evidence for such a mechanism being responsible for

[1]NRCC No. 16468.

Can. J. Chem. Downloaded from www.nrcresearchpress.com by 210.87.254.105 on 09/05/12
For personal use only.

Can. J. Chem. Downloaded from www.nrcresearchpress.com by 210.87.254.105 on 09/05/12
For personal use only.

fluorescence quenching in tyrosine proteins containing glutamic and aspartic acid. Weller's (3) quantitative studies of the 2-napthol/acetate system provide a well investigated model system for such quenching.

In a recent review Longworth (2) dismissed proton transfer as the mechanism for the quenching by carboxylate in tyrosine polymers. For the model compound *N*-acetyl-L-tyrosinamide which is expected to show similar excited state acid–base behaviour to tyrosine Longworth and Rahn (10) concluded that the excited state protolytic constant of the phenolic hydroxyl is identical to that of the ground state constant because the inflection point in the fluorimetric titration of this compound is found at the ground state p*K*. This conclusion is not consistent with the large shift found in the absorption spectrum on ionization and these authors have overlooked the implications of excited state acid–base behaviour.

These differences in opinion as to the importance of proton transfer in the quenching of tyrosine fluorescence have led us to conduct this present study of the excited state acid–base properties of tyrosine.

Experimental

Compounds and Materials

L-Tyrosine (Aldrich; 99+%) was recrystallized three times from water. Sodium acetate and acetic acid were analytical reagent grade. Water was purified using an Aqua Media 25 water purification system which we have found as satisfactory as double distillation in reducing background fluorescence.

Methods

Buffered solutions were made up exactly in acetate concentration and their p*H* adjusted by the addition of acetic acid ($pK_a = 4.75$). Hydrogen ion concentration was determined using a Radiometer 26 p*H* meter with a glass electrode. Absorption measurements were made using a Cary 118 spectrophotometer. Corrected fluorescence spectra were measured using a Perkin-Elmer MPF 44A fluorimeter with a Corrected Spectra Unit previously calibrated using quantum counter solutions. Tyrosine fluorescence quantum yields were calculated from fluorescence intensity measurements taken at a fixed wavelength by assuming Chen's (11) value of 0.14 for the quantum yield of tyrosine in water at neutral p*H*. Tyrosinate fluorescence quantum yields were calculated in a similar manner relative to the value of Cornog and Adams for tyrosinate (12) revised to 0.006 to be relative to Chen's value for tyrosine. Where necessary intensity measurements were first corrected for background fluorescence measured from blank solutions identical to the sample solutions in every respect save the presence of tyrosine. The excitation wavelength was 280 nm at which the tyrosine solutions (10^{-4} *M*) in the p*H* range 7.0 to 3.75 had an optical density of 0.124 ± 0.001 unaffected by buffer concentration. The tyrosine concentration in 0.1 *M* NaOH was adjusted to 0.82×10^{-4} *M* to give the same optical density at 280 nm for the purpose of quantum yield measurements. Emission and excitation bandwidths were 4 nm. Fluorescence lifetimes were measured using an NRCC built fluorimeter and correction and deconvolution techniques which have been described previously (13–15). All fluorescence measurements were made in 10 mm × 10 mm quartz cells thermostated at 21°C.

Direct Evidence for Proton Transfer as a Mechanism for Weak Base Quenching

In the absence of buffer the extent to which the excited state equilibrium in the reaction scheme

[1] $$\overset{*}{RH} \underset{k_2[H^+]}{\overset{k_1}{\rightleftharpoons}} \overset{*}{R^-} + H^+$$

with $\overset{*}{RH}$ decaying by k_f and k_0, and $\overset{*}{R^-}$ decaying by k_f' and k_0',

is established on excitation of RH alone depends on the relative magnitude of the rate constant k_1 to $(k_f + k_0)$. As previously stated for tyrosine we must have $(k_f + k_0) \gg k_1$ to account for the lack of inflection in the fluorescence titration near the estimated $pK(S_1) \approx 5$. In the presence of buffer we must also consider the equlibrium

[2] $$\overset{*}{RH} + B^- \underset{k_b'[HB]}{\overset{k_b[B^-]}{\rightleftharpoons}} \overset{*}{R^-} + HB$$

With buffer concentrations high enough for $k_b[B^-]$ to become significant compared with $(k_f + k_0)$ one would expect to observe a drop in $\overset{*}{RH}$ fluorescence and a corresponding rise in $\overset{*}{R}^-$ fluorescence provided the p*H* is appropriate for the equilibrium to be established.

In aqueous tyrosine solutions of p*H* 13 Cornog and Adams (15) have observed weak fluorescence, quantum yield 0.006 ± 0.001 (adjusted to Chen's (11) value for tyrosine), which can be attributed to the tyrosinate species (12). In water – dimethylsulphoxide–ethylene glycol solvent mixture the quantum yield for tyrosinate is given as 0.03 compared with 0.23 for tyrosine (10). The proton transfer quenching mechanism requires at least the partial establishment of the equilibrium 2 and the production of excited tyrosinate ($\overset{*}{R}^-$). If this is the case then it should prove possible, although difficult, to observe emission characteristic of tyrosinate in solutions of high buffer concentration with $pH < 10$.

Figure 1 shows the corrected emission spectra for tyrosine in acetate/acetic acid buffer solutions of varying buffer concentration all with $pH = 6.05$. As the buffer concentration is increased overall quenching is observed but also the relative strength of the emission at 340 nm to that at 302 nm increases until a definite shoulder can be observed in the 2 *M* acetate solution. This is more obvious in Fig. 2 where the spectra in 10^{-2} *M* acetate and 2 *M* acetate are shown normalized to their peak emissions after subtraction of blank solution fluorescence to remove the scatter observable in Fig. 1. The shoulder can be attributed

Can. J. Chem. Downloaded from www.nrcresearchpress.com by 210.87.254.105 on 09/05/12
For personal use only.

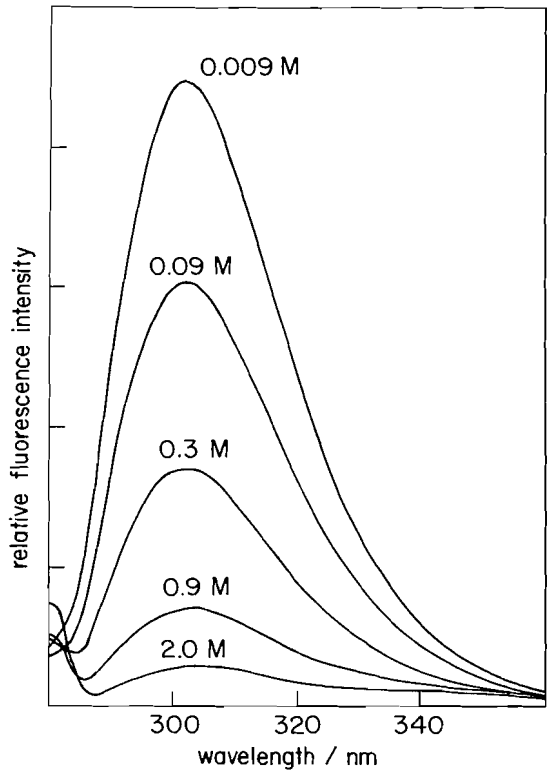

FIG. 1. Corrected fluorescence emission spectra of tyrosine in acetate/acetic acid buffer solutions of differing buffer concentration. pH = 6.05.

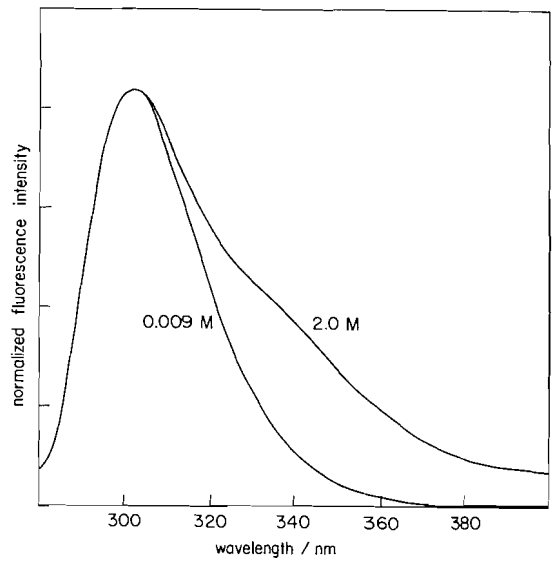

FIG. 2. Corrected fluorescence emission spectra of tyrosine in 0.009 and 2 M acetate solutions at pH = 6.05.

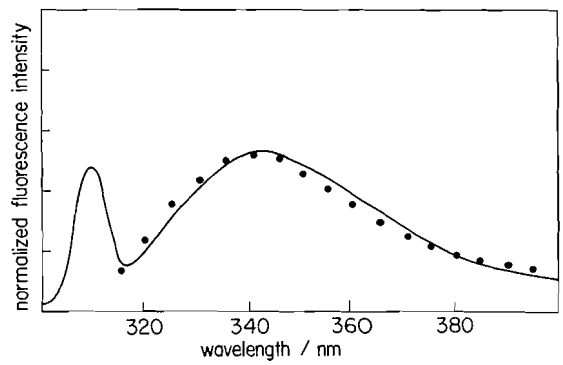

FIG. 3. Corrected fluorescence emission spectrum of tyrosinate in 0.1 M NaOH (solid line) and the spectrum found in 2 M acetate at pH = 6.05 after subtraction of the tyrosine contribution from the overall spectrum (points).

to a second emitting species produced by the addition of acetate. The spectrum of the second species can be generated by assuming that it does not extend down to 302 nm and then subtracting the spectrum in 10^{-2} M acetate from the spectrum in 2 M acetate having previously normalized the two at 302 nm. The spectrum attained in this manner is superimposable with that from a solution of tyrosine in 0.1 M NaOH, i.e. with the tyrosinate fluorescence spectrum (Fig. 3). We therefore assign the observed shoulder to fluorescence from tyrosinate. This is direct evidence for proton transfer as a mechanism for the weak base quenching of tyrosine fluorescence. We have been able to reproduce this behaviour qualitatively using buffer systems other than acetate. Similar results using phosphate, cacodylate, and citrate buffers with high base concentrations show that the mechanism is general and does not apply only for acetate.

pH Dependance of Tyrosine and Tyrosinate Fluorescence at High Buffer Concentration

Table 1 shows the dependance of the quantum yield of the fluorescence assigned in the previous section to tyrosinate and tyrosine as a function of pH in the absence of buffer and in acetate/acetic acid buffers with the acetate concentration held at 0.9 M. Tyrosinate relative intensities, from which the quantum yields were found, were calculated by assuming that tyrosinate does not emit at 302 nm. From the ratio of relative intensities at 302 and 340 nm in very dilute (10^{-3} M) buffer, where we assume only unionized tyrosine fluorescence is observed, and the intensity of the sample in question at 302 nm we can calculate the tyrosine contribution to the fluorescence at 340 nm. Subtraction from the measured value at 340 nm then gives us a measure of the intensity due to tyrosinate. Restrictions of the buffer system prevent measurements below pH = 3.7. The tyrosinate points are a good fit to a theoretical

Can. J. Chem. Downloaded from www.nrcresearchpress.com by 210.87.254.105 on 09/05/12
For personal use only.

TABLE 1. Quantum yields of fluorescence of tyrosine (ϕ) and tyrosinate (ϕ') in aqueous solution

pH	$[AcO^-]/M\ \ell^{-1}$	ϕ	ϕ'
7.0	—	0.14* (ϕ_1)	—
13.0 (0.1 M NaOH)	—	—	0.0060† (ϕ_0'')
3.78	0.9	0.0244	0.0072
3.85	0.9	0.0241	0.0089
3.91	0.9	0.0240	0.0101
3.98	0.9	0.0237	0.0105
4.06	0.9	0.0233	0.0117
4.16	0.9	0.0230	0.0139
4.27	0.9	0.0227	0.0144
4.41	0.9	0.0226	0.0152
4.59	0.9	0.0219	0.0166
4.92	0.9	0.0220	0.0193
5.16	0.9	0.0216	0.0193
5.42	0.9	0.0219	0.0201
5.68	0.9	0.0221	0.0208
5.96	0.9	0.0216	0.0208
6.61	0.9	0.0220	0.0212
7.28	0.9	0.0220	0.0211

*ϕ values are relative to this value of Chen (11) for tyrosine in water.
†ϕ' values are relative to the value of Cornog and Adams (15) adjusted for the revised quantum yield of tyrosine in water of Chen (11).

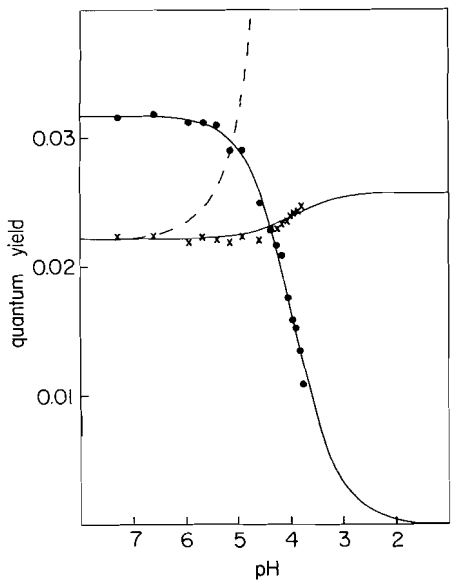

FIG. 4. Quantum yields of fluorescence of tyrosine (×) and tyrosinate (●) as a function of pH in 0.9 M acetate solutions.

sigmoid titration curve with midpoint at pH = 3.95 (solid line in Fig. 4). Over the same pH range the tyrosine fluorescence, as measured at 302 nm, increases. The behaviour of this system is then typical of a partially established excited state acid–base equilibrium.

A qualitative treatment of the results along the lines used by Weller can be attempted. The following straightforward reaction scheme can be proposed,

$$\overset{*}{R}H \underset{k_2[H^+]}{\overset{k_1}{\rightleftharpoons}} \overset{*}{R}^- + H^+$$

$$\overset{*}{R}H + B^- \underset{k_b'[BH]}{\overset{k_b[B^-]}{\rightleftharpoons}} \overset{*}{R}^- + BH$$

$$\overset{*}{R}H \xrightarrow{k_f} RH + h\nu \qquad \overset{*}{R}H \xrightarrow{k_0} RH$$

$$\overset{*}{R}^- \xrightarrow{k_f'} R^- + h\nu \qquad \overset{*}{R}^- \xrightarrow{k_0'} R^-$$

where RH = tyrosine, R^- = tyrosinate, B^- and BH are the two buffer species, and * denotes a species in its first excited singlet state. By setting up the steady state equations for $[\overset{*}{R}H]$ and $[\overset{*}{R}^-]$ and applying the condition that only RH is present in the ground state in the pH range used the following expressions can be obtained.

$$[3] \qquad \frac{\phi}{\phi_0} = \frac{1}{1 + (k_1 + k_b[B^-])\tau/(1 + (k_2[H^+] + k_b'[HB])\tau')}$$

$$[4] \qquad \frac{\phi'}{\phi_0'} = \frac{1}{1 + (1 + (k_2[H^+] + k_b'[HB])\tau')/(k_1 + k_b[B^-])\tau}$$

Can. J. Chem. Downloaded from www.nrcresearchpress.com by 210.87.254.105 on 09/05/12
For personal use only.

where ϕ and ϕ' are the quantum yields of fluorescence from $\overset{*}{R}H$ and $\overset{*}{R}^-$ respectively. $\tau = 1/(k_f + k_0)$, $\tau' = 1/(k_f' + k_0')$, $\phi_0 = k_f\tau$, and $\phi_0' = k_f'\tau'$ are the respective lifetimes and quantum yields where only the one species exists in both ground and excited states. However the tyrosine results are not totally consistent with these expressions. At low pH ϕ/ϕ_0 is predicted by [3] to reach a limiting value of 1 and the tyrosine fluorescence titration curve should follow the dotted curve in Fig. 4. This is clearly not the case, although restrictions of the buffer system and the added complication of the protonation equilibrium of the tyrosine carboxylate group prevent us from measuring a low pH value directly. We therefore propose that acetate is capable of quenching tyrosine fluorescence simultaneously by two mechanisms, one involving proton transfer and the other not. Conflicting statements exist in the literature as to whether carboxylate ions will quench *O*-methylated tyrosine (2, 9, 16) but where quenching has been observed it is clearly not by proton transfer. It has also been stated (5) that carboxylic acids quench tyrosine fluorescence but such conclusions have to be drawn from indirect measurements as the strongly quenching carboxylate ion must also be present in appreciable quantities to maintain a constant pH. We find no evidence for carboxylic acid quenching. Tyrosine fluorescence has a constant yield in 0.9 M acetate in the pH range 7 to 4.9 where the acetic acid concentration ranges from 0.0005 to 0.6 M. When we studied the quenching of tyrosine fluorescence by acetate – acetic acid buffer at two different acidities, pH = 6.05 and pH = 4.75, we obtained the same Stern–Volmer quenching constant (5.7 M^{-1}) despite the greatly increased acetic acid concentrations at the lower pH (Fig. 5).

Our proposal that acetate quenches tyrosine fluorescence by two mechanisms means that another deactivation pathway

$$\overset{*}{R}H + B^- \xrightarrow{k_q[B^-]} RH + B^-$$

must be considered in addition to the straightforward reaction scheme discussed above. If ρ and ρ' are the probabilities that RH and R^-, respectively, are still excited at time t after excitation then

$$[5] \quad \frac{d\rho}{dt} = \rho'(k_b'[HB] + k_2[H^+]) - \rho(k_1 + k_b[B^-] + k_f + k_0 + k_q[B^-])$$

and

$$[6] \quad \frac{d\rho'}{dt} = \rho(k_1 + k_b[B^-]) - \rho'(k_2[H^+] + k_b'[HB] + k_f' + k_0')$$

Applying the condition that only RH is present in the ground state and with

$$\phi = k_f \int_0^\infty \rho \, dt$$

$$\phi' = k_f' \int_0^\infty \rho' \, dt$$

$\phi_0 = k_f\tau$ and $\phi_0' = k_f'\tau'$ where $1/\tau = (k_f + k_0)$, $1/\tau' = (k_f' + k_0')$, and $1/\tau_Q = k_f + k_0 + k_q[B^-]$, it can be shown that

$$[7] \quad \frac{\phi}{\phi_0} = \frac{1}{(\tau/\tau_Q) + (k_1 + k_b[B^-])\tau/\{1 + (k_2[H^+] + k_b'[HB])\tau'\}}$$

and

$$[8] \quad \frac{\phi'}{\phi_0'} = \frac{1}{1 + \{1 + (k_2[H^+] + k_b'[HB])\tau'\}/(k_1 + k_b[B^-])\tau_Q}$$

It can also be shown that

$$[9] \quad (k_2[H^+] + k_b'[HB])\tau' = (k_1 + k_b[B^-])[H^+]\tau'/K^*$$

where $K^* = [\overset{*}{R}^-][H^+]/[\overset{*}{R}H]$, the excited state acid–base dissociation constant. Equations 7 and 8 then become

$$[10] \quad \frac{\phi}{\phi_0} = \frac{1}{(\tau/\tau_Q) + (k_1 + k_b[B^-])\tau/\{1 + (k_1 + k_b[B^-])[H^+]\tau'/K^*\}}$$

and

$$[11] \quad \frac{\phi'}{\phi_0'} = \frac{1}{1 + \{1 + (k_1 + k_b[B^-])[H^+]\tau'/K^*\}/(k_1 + k_b[B^-])\tau_Q}$$

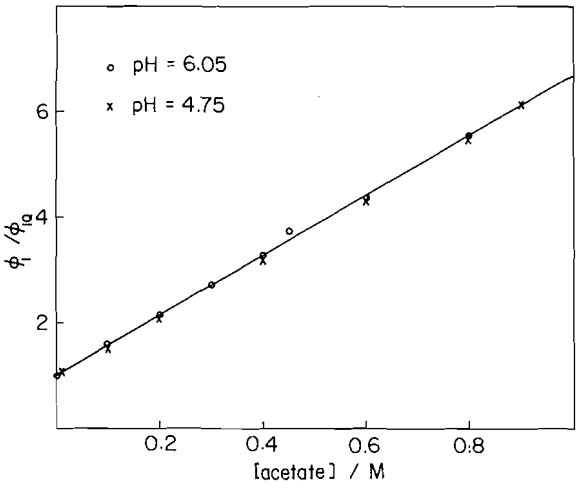

FIG. 5. Stern–Volmer plots at pH = 6.05 and pH = 4.75 for acetate quenching of tyrosine fluorescence.

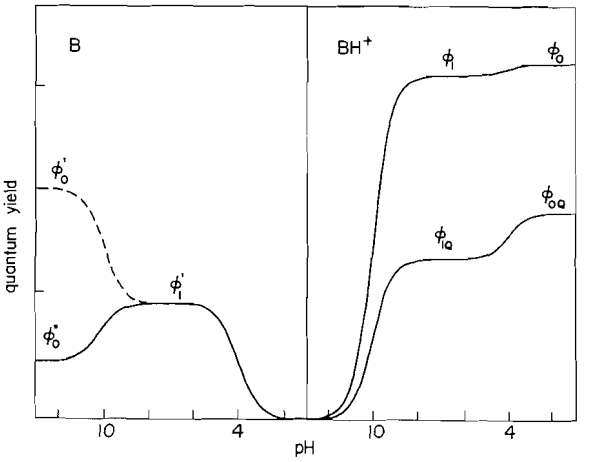

FIG. 6. Dependance of the quantum yields of fluorescence of tyrosine (ϕ) and tyrosinate (ϕ') as predicted when two mechanisms for acetate quenching of tyrosine are considered.

These are the general relationships which describe the dependence of the steady state fluorescence of tyrosine and tyrosinate respectively on buffer and proton concentration. From them it is possible to determine K^* if ϕ_0 or ϕ_0' and τ, τ_Q, and τ' are known.

For the tyrosine–tyrosinate system, however, it is impossible to measure either ϕ_0 or ϕ_0' directly. At low pH where one would measure ϕ_0 the system is further complicated by the drop in fluorescence yield associated with the ground state protonation of the tyrosine carboxylate group (5, 7). At pH = 13 where both ground and excited states are of the tyrosinate form the quantum yield (ϕ' = 0.006) is considerably lower than that found for tyrosinate in the plateau region at p$H \simeq 7$ (ϕ' = 0.021). There is therefore some other quenching mechanism of tyrosinate operating at p$H \simeq$ 13. At pH = 13 the α amino group of ground state tyrosinate is unprotonated (pK = 9.35) and the emitting species will be of form I while at pH = 6 tyrosinate is generated as a

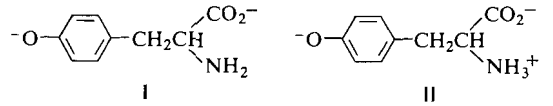

zwitterion in the excited state (II) from the zwitterion form of tyrosine. Perhaps in form I tyrosinate has a lower quantum yield than in form II which exists only in the excited state at lower pH. For the same reason we cannot measure τ' directly.

It is, however, still possible to find K^*. Figure 6 shows the theoretical form of the dependence of ϕ and ϕ' on pH predicted by [10] and [11] in the presence and absence of buffer for a set of quantum yield and pK values chosen for demonstration purposes. This figure helps in the definition of the symbols used in the following treatment where: the subscript 0 refers to yields in the plateau regions attained at the extremes of the acidity range; the subscript Q refers to yields in the presence of a fixed concentration of buffer, its absence indicating no buffer present; the subscript 1 refers to yields attained in the mid-acidity range plateau. The dotted line in Fig. 6 is the line predicted in the absence of the extra quenching mechanism for tyrosinate at pH > p$K(S_0)$ discussed earlier. A single prime superscript is used for yields on this line and a double prime for the experimentally found quenched yield. Equation 11 rearranges to give

$$[12]\quad \frac{1}{\phi'} = \frac{1}{\phi_0'}\left(1 + \frac{1}{(k_1 + k_b[B^-])\tau_Q}\right) + \frac{1}{\phi_0'}\frac{\tau'}{\tau_Q}\frac{[H^+]}{K^*}$$

A graph of $1/\phi'$ vs. $[H^+]$ at constant $[B^-]$, Fig. 7, is linear with

$$\text{Slope} = \left\{\frac{1}{\phi_0'}\frac{\tau'}{\tau_Q}\frac{1}{K^*}\right\}$$

and

$$\text{Intercept} = \frac{1}{\phi_0'}\left\{1 + \frac{1}{(k_1 + k_b[B^-])\tau_Q}\right\}$$

The problem then is to find $(k_1 + k_b[B^-])\tau_Q$, τ', and τ_Q. At negligibly low proton concentration [10] simplifies to give

$$[13]\quad \frac{\phi_{1Q}}{\phi_0} = \frac{1}{(\tau/\tau_Q) + (k_1 + k_b[B^-])\tau}$$

Can. J. Chem. Downloaded from www.nrcresearchpress.com by 210.87.254.105 on 09/05/12
For personal use only.

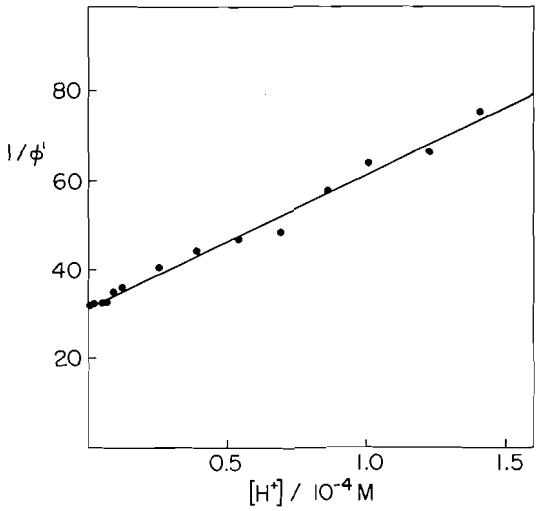

FIG. 7. Reciprocal of the quantum yield of tyrosinate fluorescence as a function of hydrogen ion concentration.

and at high proton concentration

$$[14] \qquad \frac{\phi_{0Q}}{\phi_0} = \frac{\tau_Q}{\tau}$$

where ϕ_{1Q} is the centre plateau value and ϕ_{0Q} the high acidity plateau value attained by ϕ_Q in the presence of a fixed concentration of buffer base (Fig. 6). Eliminating ϕ_0 from [13] and [14] we get

$$\frac{\phi_{0Q}}{\phi_{1Q}} = 1 + (k_1 + k_b[B^-])\tau_Q$$

Although we cannot measure ϕ_{0Q} directly for our system a value can be estimated as our ϕ_Q values should lie on a titration curve with its inflection point at pH = 3.95, the inflection point found for ϕ', the tyrosinate yield. We find $\phi_{1Q} = 0.0222 \pm 0.003$ and ϕ_Q(pH 3.95) = 0.0240, giving $\phi_{0Q} = 0.0257 \pm 0.0003$ for [acetate] = 0.9 $M\ \ell^{-1}$. Therefore $(k_1 + k_b[B^-])\tau_Q = 0.16 \pm 0.02$. From Fig. 7 we find intercept = 46.2 ± 1.1 and hence $\phi_0' = 0.16 \pm 0.02$. Taking slope = $(4.45 \pm 0.11) \times 10^5\ \ell\ M^{-1}$ from Fig. 7 and this value of ϕ_0' we find $\tau'/\tau_Q K^* = (7.01 \pm 1.2) \times 10^4\ M^{-1}$.

The fluorescence lifetime of tyrosine at pH = 7, τ_1, is related to τ (which we cannot measure) by the expression $\tau_1/\tau = \phi_1/\phi_0$ and τ_Q is related to τ by the expression $\tau_Q/\tau = \phi_{0Q}/\phi_0$ hence

$$\tau_Q = \tau_1 \frac{\phi_{0Q}}{\phi_1}$$

We measured τ_1 = 3.52 ns (lit. 3.6 (7)) for tyrosine in aqueous solution (pH = 6.05) at 20.5°C. Using the above value of 0.0257 for ϕ_{0Q} in 0.9 M acetate and 0.14 for ϕ_1 we find τ_Q = 0.64 ns. To obtain a value for τ' we must assume that both of the forms of tyrosinate, I and II, have the same radiative rate of fluorescence (the same k_f), i.e. the differences in quantum yield are due to differences in the non-radiative rates. This is reasonable as the α-amino group is not conjugated to the chromophore. We can then write

$$\tau' = \tau'' \frac{\phi_0'}{\phi_0''}$$

where ϕ_0'' is the measured quantum yield, and τ'' is the measured lifetime of tyrosinate at pH = 13. We found $\phi_0'' = 0.011$ and $\tau'' = 0.10 \pm 0.05$ ns and hence find $\tau' = 2.7 \pm 1.3$ ns.

Using the values estimated for τ_Q and τ' we find $K^* = (0.60 \pm 0.40) \times 10^{-4}\ M$. Therefore, the first excited singlet state acid–base dissociation constant of tyrosine, p$K(S_1)$ is found experimentally to be 4.2 ± 0.4; a shift, ΔpK = 6.1 from the ground state pK = 10.3. This measurement is in agreement with Feitleson's Forster cycle estimate of Δp$K \sim -5$ considering the errors expected in such estimates (17), and the errors and assumptions involved in our measurement. It must be noted that our p$K(S_1)$ value is unavoidably measured at high ionic strength (I = 0.9 M). A correction can be applied for the Brønsted dependence of k_2 and hence K on ionic strength (17). However, the size of the correction proves to be less than the error with which p$K(S_1)$ is calculated.

Discussion and Conclusions

We have shown experimentally that tyrosinate fluorescence can be seen in neutral aqueous solution of tyrosine under the right buffer conditions. These conditions are analogous to those which may be obtained in the local environment of proteins which have tyrosine residues in close proximity to basic groups. Previous theoretical arguments for a large shift in the pK of the tyrosine phenol group on excitation have often been neglected in the interpretation of the fluorescence spectra of peptides and proteins. Our results suggest that this ΔpK effect must be considered when analysing the fluorescence of tyrosine containing proteins. Tyrosinate has its fluorescence maximum at 340 nm which is also the fluorescence maximum shown by tryptophan. From the excitation spectra for emission in the tryptophan band of proteins (i.e. ~340 nm) it has been reasonably proposed that energy transfer takes place from tyrosine to tryptophan (2). Although we have no argument with this mechanism the results can be explained, for proteins containing basic residues, equally well by proton transfer from excited tyrosine giving rise to tyrosinate emission at 340 nm.

Can. J. Chem. Downloaded from www.nrcresearchpress.com by 210.87.254.105 on 09/05/12
For personal use only.

Can. J. Chem. Downloaded from www.nrcresearchpress.com by 210.87.254.105 on 09/05/12
For personal use only.

We have also shown that the quantum yield of fluorescence of tyrosinate ($\phi_0 = 0.16$) predicted by our measurements at neutral pH is actually 26 times greater than that found experimentally at pH = 13. We propose that the yield must be lowered by a separate quenching mechanism possibly involving a change in solute–solvent interactions on deprotonation of the $-NH_3^+$ group. Thus the contribution of tyrosinate to the fluorescence of a protein can be greater than expected from its yield measured directly in alkaline solution.

Although we have shown that carboxylate ions do certainly quench tyrosine fluorescence by a proton transfer mechanism we also find that, on close analysis, our results require them to quench simultaneously by another mechanism which produces no other fluorescent species. This other mechanism may be either a dynamic or ground state effect, although we see no effect by acetate on the tyrosine absorption spectrum. The existence of the second mechanism is consistent with the previously observed quenching of *O*-methyl tyrosine fluorescence by carboxylate and explains the existence of the controversy found in the literature in this area. To rule out other possible explanations of our results than the existence of the second quenching mechanism we had to show that tyrosine fluorescence was not, as previously suggested, quenched by acetic acid.

In conclusion we have demonstrated a large shift in the phenolic pK of tyrosine on excitation to its first excited singlet, finding $pK(S_1) = 4.2 \pm 0.4$ cf. $pK(S_0) = 10.3$, which can have significant implications in the interpretation of the fluorescence properties of polypeptides and proteins.

1. R. W. COWGILL. *In* Biochemical fluorescence: concepts. Vol. II. *Edited by* R. F. Chen and H. Edelhoch. M. Dekker, New York, NY. 1976.
2. J. LONGWORTH. *In* Excited states of proteins and nucleic acids. *Edited by* R. F. Steiner and I. Weinryb. Plenum Press, New York, NY. 1971.
3. A. WELLER. Z. Elektrochem. **58**, 849 (1954).
4. TH. FÖRSTER. Z. Elektrochem. **54**, 42 (1950); **54**, 53 (1950).
5. J. FEITLESON. J. Phys. Chem. **68**, 391 (1964).
6. R. B. MARTIN, J. T. EDSALL, D. B. WETLAUFER, and B. R. HOLLINGWORTH. J. Biol. Chem. **233**, 1429 (1958).
7. M. FAYET and P. WAHL. Biochim. Biophys. Acta, **229**, 102 (1971).
8. G. WEBER and K. ROSENHECK. Biopolymers, Symposia 1, 333 (1964).
9. S. V. KONEV. Fluorescence and phosphorescence of proteins and nucleic acids. Plenum Press, New York, NY. 1967.
10. J. W. LONGWORTH and R. O. RAHN. Biochim. Biophys. Acta, **147**, 526 (1967).
11. R. F. CHEN. Anal. Lett. **1**, 35 (1967).
12. D. M. RAYNER, A. E. MCKINNON, A. G. SZABO, and P. A. HACKETT. Can. J. Chem. **54**, 3246 (1976).
13. D. M. RAYNER, A. E. MCKINNON, and A. G. SZABO. Rev. Sci. I, **48**, 1050 (1977).
14. A. E. MCKINNON, A. G. SZABO, and D. MILLER. J. Phys. Chem. **81**, 1564 (1977).
15. J. L. CORNOG and W. R. ADAMS. Biochim. Biophys. Acta, **66**, 356 (1963).
16. J. FEITLESON. Photochem. Photobiol. **9**, 401 (1969).
17. J. F. IRELAND and P. A. H. WYATT. *In* Advances in physical organic chemistry. Vol. 12. *Edited by* V. Gold. Academic Press, London. 1976.

Constituents of commercial methoxychlor-III.[1] The mechanism of tetraanisylethylene formation. *unsym*-Tetraarylethylenes ($Ar_2C{=}CAr_2'$): synthesis from DT class pesticides, and conversion to phenanthrenes and dibenzo[*g*,*p*]chrysenes

REGINALD H. MITCHELL,[2] LUDVIK MAZUCH, BARRY SHELL, AND PAUL R. WEST[2]

Department of Chemistry, University of Victoria, Victoria, B.C., Canada V8W 2Y2

Received November 28, 1977

REGINALD H. MITCHELL, LUDVIK MAZUCH, BARRY SHELL, and PAUL R. WEST. Can. J. Chem. **56**, 1246 (1978).

Reaction of DT type pesticides with anisole and $AlCl_3$ in CS_2 yielded *unsym*-tetraarylethylenes ($Ar_2C{=}Ar_2'$), which on photocyclisation yielded phenanthrenes. Further oxidative closure to dibenzo[*g*,*p*]chrysenes occurs under conditions that favour cation radical intermediates. Chromatography of commercial methoxychlor (DMDT) yielded tetraanisylethylene together with minor amounts of the corresponding photo products, 3,6-dimethoxy-9,10-dianisylphenanthrene and 3,6,11,14-tetramethoxydibenzo[*g*,*p*]chrysene, as well as other chloroanisylethylenes.

REGINALD H. MITCHELL, LUDVIK MAZUCH, BARRY SHELL et PAUL R. WEST. Can. J. Chem. **56**, 1246 (1978).

La réaction des pesticides du type DT avec l'anisole et le $AlCl_3$ dans CS_2 produit des tétraaryléthylènes non-symétriques ($Ar_2C{=}CAr_2'$) qui par photocyclisation conduisent à des phénanthrènes. Une fermeture oxydante subséquente conduisant à des dibenzo[*g*,*p*]chrysènes se produit dans des conditions qui favorisent les intermédiaires radicaux cationiques. La chromatographie du méthoxychlore commercial (DMDT) conduit à du tétraanisyléthylène avec des quantités plus faibles de photo-produits correspondants, du diméthoxy-3,6 dianisyl-9,10 phénanthrène et tétraméthoxy-3,6,11,14 dibenzo[*g*,*p*]chrysène de même qu'à d'autres chloro-anisyléthylènes.

[Traduit par le journal]

Introduction

Since 1969 methoxychlor (DMDT), **1***b*, has widely replaced the more persistent DDT, **1***c*, in the control of insect populations especially in Canada (3). Whereas the toxicology of methoxychlor itself seems to be reasonably well reported (ref. 3, p. 59), we can find no mention of studies on impurities present in commercial samples of the pesticide. That such studies were desirable became evident when we discovered (1) the presence of the activated olefin tetraanisylethylene (TAE), **3***bb'*, both in technical laboratory grade methoxychlor and in locally available home garden grades and that no report[3] of TAE in methoxychlor nor of its short- or long-term toxicity had appeared. This paper reports a further analysis of impurities that are present in commercial methoxychlor and that are formed on subjecting the DT class pesticides, **1**, to Friedel–Crafts conditions. Further experiments indicate that oxidative photoclosure of TAE, **3***bb'*, can lead to polycyclic aromatic hydrocarbons, one of which has been shown by us (2) to be actively mutagenic and potentially carcinogenic.

[1]For previous papers in this series see refs. 1 and 2.

[2]Authors to whom correspondence should be addressed.

[3]Literature survey by Chemical Data Centre, Columbus, OH, U.S.A.

Results and Discussion

Treatment of commercial methoxychlor (Sigma Chemical Company, U.S.A.) with bromine in acetic acid gave an immediate deep blue colour which suggested a reactive impurity was present. Thin-layer chromatographic examination confirmed the presence of more than six impurities one of which was fluorescent. After an initial recrystallisation, column chromatography of the residue followed by fractional crystallisation separated the fluorescent contaminant as very pale yellow crystals, mp 185–186°C in ca. 0.4% by weight yield (4000 ppm). This was identified as, tetrakis(*p*-methoxyphenyl)ethylene, **3***bb'* (lit. (4) mp 186°C), commonly referred to as tetraanisylethylene (TAE), on the basis of its ^{1}Hmr spectrum which showed only methoxyl protons at δ 3.70 and aromatic protons as an apparent[4] AB quartet at δ 6.93 and 6.51, and its mass spectrum in which the molecular ion was at *m*/*e* 452. As anticipated pure TAE underwent reaction with bromine in glacial acetic acid – methylene chloride solution to give the characteristic blue solution (λ_{max} ca. 540 nm) that had been originally observed with the pesticide. Indeed several previous studies (5) have established that

[4]Although the spin system is AA'BB', it appears like an AB quartet, in all of the following examples.

Can. J. Chem. Downloaded from www.nrcresearchpress.com by 210.87.254.42 on 09/05/12
For personal use only.

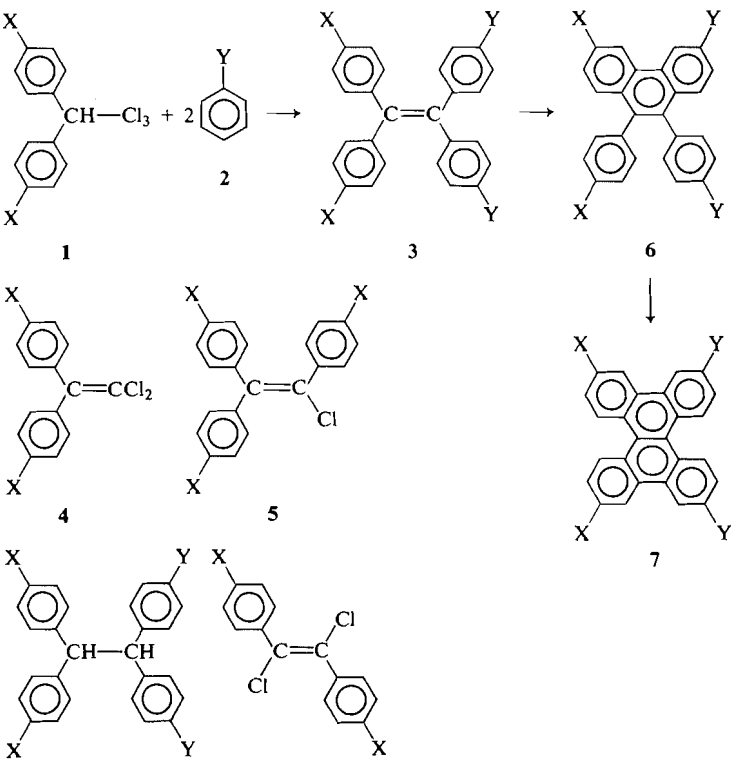

a X = H; *a'* Y = H
b X = OCH_3; *b'* Y = OCH_3
c X = Cl; *c'* Y = Cl

TAE reacts rapidly with a variety of electron acceptors to give the dication, λ_{max} ca. 540 nm. Spectrophotometric analysis (see Experimental) based on this colour reaction indicated that the original technical methoxychlor (Sigma Chemical Co.) contained ca. 0.5% TAE in good agreement with the isolated yield. Several locally available home garden grades (sold at 50% strength) were also tested and these contained ca. 0.2% TAE as might be anticipated. A sample of methoxychlor[5] (labelled 99% pure) obtained through the Department of Health and Welfare, Health Protection Branch, Ottawa, Ont., Canada, also tested for ca. 0.3% TAE.

By further chromatography of the mother liquors left over after crystallisation of TAE two fractions could be obtained. The first contained 1,1-dichloro-2,2-bis(*p*-methoxyphenyl)ethylene (DMDE), **4***b*, and 1-chloro-1,2,2-tris(*p*-methoxyphenyl)ethylene, **5***b* (commonly called chlorotrianisene), identified by ^{1}Hmr and tlc comparison with authentic samples (see below). It is estimated that these are present at 400 and 40 ppm, respectively, in the technical pesticide. The presence of the chlorotrianisene (also called Hormonisene, Merbentul) is interesting since it is known to be a powerful estrogen (6). The second fraction contained the phenanthrene, **6***bb'*, and chrysene, **7***bb'*, identified by comparison with the authentic samples prepared as described below. Although we estimate the final amount of **6***bb'* and **7***bb'* found to be approximately 50 and 5 ppm, respectively, it is quite likely that most of **6***bb'* and nearly all of **7***bb'* forms during the separation procedure, since we subsequently show that exposure of TAE to sunlight forms **6***bb'* which can then be oxidatively closed to **7***bb'* (see below). In fact a major manufacturer (DuPont) has informed us that they have developed a gas chromatographic detection procedure for **7***bb'* (sensitivity < 1 ppm), that indicates the absence of the chrysene **7***bb'* in their technical methoxychlor at the time of manufacture.

[5]Provided by a major Canadian supplier (E. I. DuPont de Nemours Company).

Syntheses

Methoxychlor can be prepared from anisole and chloral at room temperature using $AlCl_3$ (7), H_2SO_4

Can. J. Chem. Downloaded from www.nrcresearchpress.com by 210.87.254.42 on 09/05/12
For personal use only.

Can. J. Chem. Downloaded from www.nrcresearchpress.com by 210.87.254.42 on 09/05/12
For personal use only.

(8), or 15% oleum (9) as catalysts; however in our hands, only use of $AlCl_3$ gave detectable (photometrically) amounts of TAE. This is consistent with the note of Biltz (10) in 1897 that tetraphenylethylene is formed amongst other products from benzene and chloral in CS_2. It is interesting that tetrakis(*p*-chlorophenyl)ethylene, **3***cc'*, has been identified in DDT spray deposits on citrus (10*b*), an observation that is consistent with formation of the analogous impurity during manufacture of DDT.

To maximise the yield of TAE, we substituted methoxychlor (DMDT) for chloral and heated under reflux in CS_2 with 4 molar equiv. of anisole and 5 equiv. of $AlCl_3$. Under these conditions a 50% yield of TAE could be realised.[6] Other products of the reaction were 1.1% of the ethylene (DMDE) **4***b*, identified by comparison with an authentic sample (11), 4% of the half reacted product, chlorotrianisene, **5***b*, identified by its mp 110–112°C (lit. (12) mp 113–114°C), a molecular ion at *m/e* 380 in the mass spectrum, and a ^{1}Hmr spectrum which showed three different $-OCH_3$ signals at δ 3.80, 3.77, and 3.71. Finally, 2% of the tetraphenylethane, **8***bb'*, was formed. The latter was identified by its mp 188–189°C (lit. (13) mp 189–190°C), molecular ion at *m/e* 454, and ^{1}Hmr spectrum which clearly showed the methine and methoxyl protons as singlets at δ 4.56 and 3.64 in a ratio 1:6, respectively. We suspect that this last compound arises through disproportionation of protonated **3***bb'* to give dication and dihydroproduct **8***bb'*. Certainly tetraarylethane formation accompanying or replacing tetraarylethylene formation has been observed previously (10, 14).[6]

The synthesis was extended to other tetraarylethylenes by substitution of the diaryltrichloroethane (DT) component: reaction of DT itself (**1***a*) with anisole and $AlCl_3$ yielded 37% of the dianisyldiphenylethylene, **3***ab'*, whereas reaction of DDT (**1***c*) yielded 1,1-bis(*p*-chlorophenyl)-2,2-bis(*p*-methoxyphenyl)ethylene, **3***cb'* in 42% yield. Ethylene **3***ab'*, mp 153–155°C (lit. (15) mp 154–155°C), gave a strong molecular ion at *m/e* 392. In its ^{1}Hmr spectrum two distinctive types of aromatic protons appeared as a singlet at δ 7.02 and a quartet at δ 6.57 assigned to the phenyl and anisyl protons, respectively, with the methoxyl protons at δ 3.67. The ethylene **3***cb'*, mp 192–193°, molecular ion at *m/e* 460, showed a multiplet for the aryl protons at δ 7.4–6.5 and a singlet for the six methoxyl protons at δ 3.77. A minor amount of the ethane **8***ab'* was also obtained along with **3***ab'*. Variation of the other component was less successful, since reaction of DMDT, **1***b*, with benzene and $AlCl_3$ gave 35% DMDE, **4***b*, and 0.9% 3-methoxy-10-(*p*-methoxyphenyl)-9-phenylphenanthrene, **6***ab'*, mp 248–250°C. The structure of the latter was based on analysis, a molecular ion at *m/e* 390, and its ^{1}Hmr spectrum which showed strongly deshielded aryl protons at δ 8.7–6.7 and two types of methoxyl singlets at δ 3.75 and 3.68. It seems likely, that a small amount of the tetraarylethylene forms, but this is photolytically transformed to phenanthrene during work-up (see below). Change of catalyst to $SnCl_4$, did not improve the reaction. In this case, apart from DMDE and DMDT, a minor amount (0.6%) of 1,2-dichloro-1,2,-bis(*p*-methoxyphenyl)-ethylene, **9***b*, mp 166–168°C (lit. (16, 17) mp 170°C, 166–168°C) was formed. The presence of the latter arises via a 1,2-aryl (Wagner–Meerwein) shift within the catalyst complex, followed by reversion to halide and elimination (Scheme 1).

Stilbene formation from DT compounds has also been observed under other conditions (11, 18*a* and refs. therein). In summary, since a wide variety of different DT compounds, **1**, is known and easily synthesised (18*b*) a straightforward approach to a series of unsymmetrical tetraarylethylenes is at hand.

Conversion to Phenanthrenes and Chrysenes

To confirm the probable origin of the phenanthrene **6***bb'* and chrysene **7***bb'* detected in the fractions obtained after chromatography of technical methoxychlor, we allowed pure TAE, **3***bb'*, to stand both in cyclohexane solution in air and as a solid film in air, while exposed to direct sunlight. We were aware that ready net photoclosure at the *ortho* positions of *cis*-stilbenes in the presence of oxidising agents (eg. I_2, O_2) has been well documented (19). Ready conversion of **3***bb'* to phenanthrene **6***bb'* occurred (44% isolated after 10 days in solution).

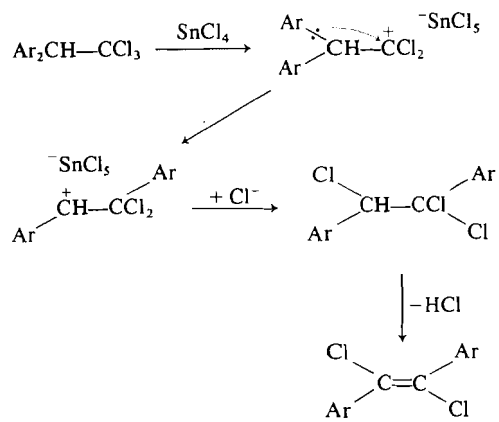

SCHEME 1

[6]A complete list of experiments tried, additional spectral results, and Table 1 are available, at a nominal charge, from the Depository of Unpublished Data, CISTI, National Research Council of Canada, Ottawa, Ont., Canada K1A 0S2.

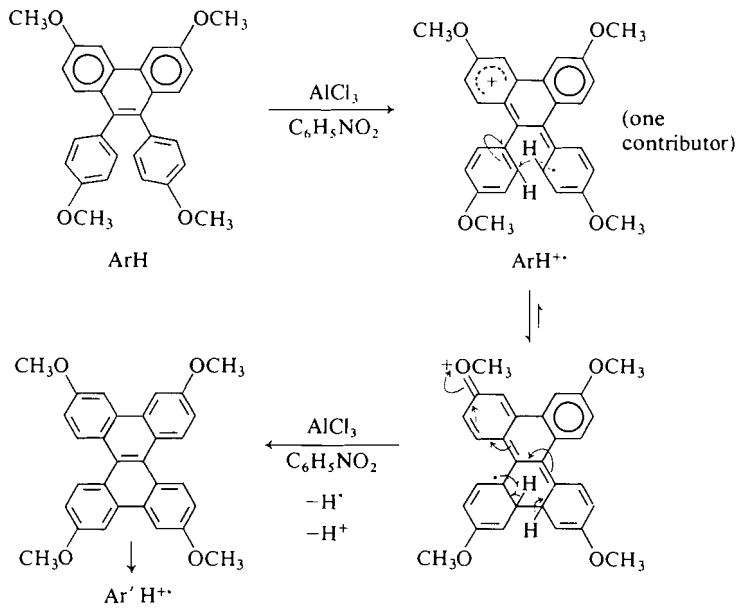

SCHEME 2

Under these conditions we could not detect chrysene **7***bb'* (i.e. the second *ortho* closure). However, when chrysene obtained by an alternative route was exposed to such conditions, oxidative and/or photolytic degradation occurred.

In the laboratory, **6***bb'* could be obtained in 57% yield, using a Hanovia medium pressure lamp with either I_2 or O_2 as oxidant, as rather insoluble crystals, mp 317–319°C, showing a clear molecular ion at *m/e* 450, aryl protons at δ 8.2–6.7, and two methoxyl singlets at δ 4.02 and 3.78 in its ^{1}Hmr spectrum. Correct elemental analysis was obtained. Prolonged photolysis of either **3***bb'* or phenanthrene in the presence of O_2 or I_2 led to further decomposition products, none of which corresponded to the chrysene (tlc) which itself decomposes under these conditions.

In the same way the unsymmetrical phenanthrene **6***bc'*, mp 325–327°C could be obtained from **3***bc'* in 20–40% yield.

To provide an authentic sample of the tetramethoxydibenzo[*g,p*]chrysene **7***bb'* and to demonstrate the feasibility of synthesis of chrysenes from the pesticide impurities, we performed a Scholl reaction (20, 21) on **6***bb'* using $AlCl_3$ in hot nitrobenzene. After chromatography, **7***bb'* could be obtained in 23% yield as crystals which rapidly brown on their surface, mp 210–212°C. The structure was assigned on the basis of a strong molecular ion at *m/e* 448 and its simple ^{1}Hmr spectrum showing three types of aromatic protons at δ 8.55, 8.00, and 7.25 (d, d, and dd respectively) and methoxyl singlet at δ 4.04.

This closure of **6***bb'* does not occur with $AlCl_3$ in CS_2. The apparent necessity of the nitrobenzene suggested that an oxidative mechanism might be operative (Scheme 2). The mechanism is consistent with the observation by Buck *et al.* (22) that cation radical formation occurs very easily on treatment of π-donor aromatics with $AlCl_3$ in either CH_3NO_2 or $C_6H_5NO_2$.

Related esr studies support Scheme 2 for the Scholl reaction. When we treated a dilute solution of **3***bb'* in N_2 purged dry nitrobenzene with a solution of $AlCl_3$ in nitrobenzene, an immediate yellow green colour appeared. Over a 12-h period at 20°C, the colour changed to pale violet. Concurrently the initial complex esr spectrum gradually changed in hyperfine pattern.[7] However the *total* signal intensity remained constant. The final spectrum was identical to that obtained when chrysene **7***bb'* was treated with $AlCl_3$ in nitrobenzene. Moreover the sequence can be duplicated using nitromethane. In this case resolution of the esr spectra at 20°C was not as great as with nitrobenzene.

The lack of rapid reaction in CS_2 where cation radical formation with $AlCl_3$ is less efficient (23), together with the persistence of a constant substantial cation concentration throughout the process is consistent with the proposed mechanism. In fact it has been suggested that conversion to radical cations in CH_3NO_2–$AlCl_3$ may be complete for dialkoxybenzenes (24).

[7]Spectral analysis (including related species) to be published elsewhere.

Can. J. Chem. Downloaded from www.nrcresearchpress.com by 210.87.254.42 on 09/05/12
For personal use only.

Can. J. Chem. Downloaded from www.nrcresearchpress.com by 210.87.254.42 on 09/05/12
For personal use only.

Experiments in concentrated H_2SO_4 demonstrate the well-known complexity of such radical ion systems. On dissolution in thoroughly N_2 purged sulphuric acid, phenanthrene **6***bb'* again yielded a yellowish-green solution that had a weak single broad line esr spectrum. However no colour change corresponding to conversion to chrysene cation was observed over 48 h. A combination of slow phenanthrene cation radical formation coupled with extensive competitive sulphonation (23) may prevent significant net cyclization. In contrast though, when the chrysene **7***bb'* was added to concentrated sulphuric acid, an initial weak unresolved epr spectrum gradually further diminished over 5 min during which time the solution developed an intense blue colour (λ_{max} 620 nm) assigned to the dication of **7***bb'*. Eventual two electron oxidation to the dication is also observed on dissolving tetraanisylethylene **3***bb'* in sulphuric acid (5). As expected nitrobenzene–$AlCl_3$ solutions containing either chrysene **7***bb'*, or phenanthrene **6***bb'* (after standing) provided the same intense blue colour (λ_{max} 620 nm) on quenching with an excess of concentrated sulphuric acid. The apparently instantaneous development of the colour in these cases suggests that a shift in the disproportion equilibrium [1] contributes to dication formation (25).

$$[1] \qquad 2Ar^{+\cdot} \rightleftarrows Ar^{++} + Ar$$

It is useful to consider the photolysis of the phenanthrene **6***bb'* in light of these Scholl reaction results. Firstly, although this phenanthrene does not rapidly degrade when the photolysis ($\lambda > 300$ nm) is carried out in the absence of air or iodine, in their presence, rapid and extensive tar production results. Initially we attributed the lack of chrysene **7***bb'* production to a steric inhibition to the second ring closure. However such inhibition should also be present in the Scholl reaction. Clearly it seems likely in retrospect, that initially formed chrysene is oxidatively degraded in the system (solutions of chrysene **7***bb'* darken rapidly in air).

Finally, from the biological standpoint, one can project from the charge transfer character of the Scholl reaction the distinct possibility that phenanthrene thermal or photo charge transfer closure to the chrysene may occur in the presence of natural electron acceptors (e.g. quinones). Further photochemical study of **6***bb'* phenanthrene charge transfer activity is planned.

Experimental

All melting points were determined on a Kofler hot stage and are uncorrected. The ^{1}Hmr spectra were determined in $CDCl_3$ (unless otherwise stated) on a Perkin-Elmer R12A (60 MHz) or R32 (90 MHz) spectrometer and are reported in ppm downfield from tetramethylsilane as internal standard. Mass spectra were determined on a Hitachi Perkin–Elmer RMU-7 or Finnigan 3300 mass spectrometer at 70 eV. The ir spectra were recorded on a Pye-Unicam SP1000 spectrometer and the uv spectra on a Carey 17 spectrophotometer. Microanalyses were performed by this department. All evaporations were carried out under reduced pressure on a rotary evaporator at ca. 40°C. Extracts were dried with anhydrous sodium sulfate. A table of all additional spectral and experimental results is available in the Depository of Unpublished Data.[6]

*Chromatography of Commercial Methoxychlor (DMDT). Isolation of Tetraanisylethylene, 3*bb'

Crystallisation of technical methoxychlor (90% active DMDT, Sigma Chemical Co., St. Louis, U.S.A.) (100 g) from chloroform (40 ml) – ethanol (100 ml) yielded 76 g of pure DMDT, **1***b*, and 24 g of residue concentrated in impurities. The latter were separated chromatographically on basic Al_2O_3 (1200 g, Woelm, Activity II–III). After elution of the *o*- and *p*-isomers of DMDT with benzene–pentane (1:1), a mixture of ca. six compounds (by tlc) was eluted with benzene. These fluorescent fractions gave a positive blue bromine test (see below) for TAE (500 mg, 0.5 wt.% by uv). Careful recrystallisation from CH_2Cl_2–ethanol yielded ca. 300 mg of pure TAE, mp 185–186°C (lit. (5) mp 186°C).[6]

After removal of TAE, rechromatography of the mother liquors from the above crystallisation yielded a fraction (45 mg) containing 1,1-dichloro-2,2-bis(*p*-methoxyphenyl)ethylene, **4***b*, and chlorotrianisene (1-chloro-1,2,2-tris(*p*-methoxyphenyl)-ethylene), **5***b*, in ca. 10:1 ratio, by comparison (^{1}Hmr and tlc) to authentic samples (described below). A second fraction (< 5 mg) contained the phenanthrene **6***bb'* and chrysene **7***bb'* by tlc comparison to authentic samples (described below). Despite several efforts at multiple chromatography, including preparative tlc, we were unable to isolate pure samples of these latter compounds.

The Colorimetric Analysis of TAE as the Dication

Bromine-blue Colour Test

The sample to be analysed in CH_2Cl_2 solution (ca. 0.3 ml) is added to a uv cell containing 0.1 *M* Br_2 in glacial acetic acid (*Warning*: causes blisters) and its absorbance relative to the same solvent reference is measured immediately by scanning through the maximum at ca. 540 nm. By comparison to the absorbance obtained from a known TAE concentration (e.g. 0.90 for 13 mg/100 ml), the sample concentration can be calculated. Although added DMDT does not interfere, anisole, ethanol, or water must be absent.

Syntheses

Tetrakis(p-*methoxyphenyl)ethylene, TAE, 3*bb'. *Reaction of DMDT with Anisole and AlCl$_3$*

$AlCl_3$ (67 g, 0.5 mol) was added in small portions to a cooled (0–3°C) mechanically stirred mixture of anisole (43 g, 0.4 mol), DMDT **1***b* (35 g, 0.1 mol), and CS_2 (200 ml). The mixture was allowed to warm to room temperature and then heated under reflux for 5 h. After cooling, the mixture was poured onto ice and extracted with CH_2Cl_2. The organic extract was washed with aqueous $NaHCO_3$ and water, dried, and evaporated. The resultant oil was preabsorbed onto alumina and chromatographed using pentane–benzene mixtures as eluant. Eluted first was 1,1-dichloro-2,2,-bis(*p*-methoxyphenyl)ethylene **4***b*, 340 mg (1.1%) as colourless crystals from ethanol, mp 111–112°C (lit. (12) mp 109°C), identical to an authentic sample (11).[6]

Next eluted was chlorotrianisylethylene, **5***b*, 1.5 g (4%) as almost colourless crystals from benzene–cyclohexane, mp 110–112°C (lit. (12) mp 113–114°C).[6]

Can. J. Chem. Downloaded from www.nrcresearchpress.com by 210.87.254.42 on 09/05/12
For personal use only.

Eluted next in the main fraction was TAE, 22.6 g (50%), identical to the sample obtained above. Eluted finally was tetrakis(*p*-methoxyphenyl)ethane **8***bb'*, 900 mg (2%), as white needles from benzene–hexane, mp 188–189°C (lit. (13) mp 189–190°C).[6]

The yield of TAE was also about 50% when CH_2Cl_2 replaced CS_2 as solvent. The results of other experiments are given in Table 1.[6]

*1,1-Bis(*p*-methoxyphenyl)-2,2-diphenylethylene, DADPE, 3*ab'*. Reaction of DT with Anisole and $AlCl_3$*

Using the general method described above for TAE there was obtained from DT, **1***a*, (12 g, 42 mmol), anisole (18.2 g, 168 mmol), $AlCl_3$ (28 g, 210 mmol), and CS_2 (70 ml), product DADPE, **3***ab'*, 6.1 g (37%) as colourless crystals from $CHCl_3$–ethanol, mp 153–155°C (lit. (15) mp 154–155°C).[6]

Eluted after the DADPE was a small amount (~1%) of a substance with mp ca. 155°C identified as 1,1-bis(*p*-methoxyphenyl)-2,2-diphenylethane **8***ab'*, on the basis of ^{1}Hmr and mass spectra data; ^{1}Hmr δ (60 MHz) 7.08 (s, 10H, ϕH), 7.04 and 6.62 (quartet, ^4J = 9 Hz, 8H, MeO-ϕ*H*), 4.61 (s, 2H, —CH—), and 3.62 (s, 6H, —OCH_3); ms, fragment ions at *m/e* 227 ($M^+ - \phi_2CH$), 197 ($M^+ - \phi_2CH$, OCH_2), and 167 ($M^+ - (MeO\text{-}\phi)_2CH$), but no M^+ (cf. **8***bb'*).

Reaction of DMDT with Benzene

Using the same conditions as above, from DMDT **1***b* (14.5 g, 42 mmol), benzene (13.1 g, 168 mmol), $AlCl_3$ (28 g, 210 mmol), and CS_2 (70 ml), there was obtained DMDE **4***b* (35%) identical to previous samples and ca. 0.9% of 3-methoxy-10-(*p*-methoxyphenyl)-9-phenylphenanthrene **6***ab'*, as almost colourless crystals from benzene, mp 248–250°C; ^{1}Hmr (60 MHz) δ: 8.7–6.7 (m, 16H, —ArH), 3.75 and 3.68 (s, 3H each, —OCH_3); ms M^+ at *m/e* 390 (100); uv (ether) λ_{max} (log ε_{max}): 340 nm (2.94), 302 inf (3.96), 279 sh (4.40), and 260 (4.72). *Anal.* calcd. for $C_{28}H_{22}O_2$: C 86.13, H 5.68; found: C 86.07, H 5.80.

When $SnCl_4$ was used as catalyst with benzene as solvent apart from DMDE and unchanged DMDT there was obtained 0.6% of 1,2-dichloro-1,2-bis(*p*-methoxyphenyl)ethylene **9***b*, mp 166–168°C (lit. (16, 17) mp's 170 and 166–168°C).[6]

*1,1-Bis(*p*-chlorophenyl)-2,2-bis(*p*-methoxyphenyl)ethylene, DCDAE, 3*bc'*. Reaction of DDT with Anisole and $AlCl_3$*

Using the general method described above for TAE there was obtained from DDT (10 g, 28 mmol), anisole (12.5 g, 116 mmol), $AlCl_3$ (18.8 g, 141 mmol), and either CS_2 or CH_2Cl_2 (100 ml), product DCDAE, **3***bc'*, 5.41 g (42%) as light yellow crystals from benzene–cyclohexane, mp 192–193°C; ^{1}Hmr (90 MHz) δ: 7.4–6.5 (m, 16H, ArH) and 3.77 (s, 6H, —OCH_3); ms M^+ at *m/e* 460 (100, $^{35}Cl_2$); ir (KBr): 1610 (s), 1515 (s), 1248 (s), 1178 (s), 1090 (s), 1033 (s), 1012 (s), 831 (s), and 808 (s) cm^{-1}; uv ($CHCl_3$) λ_{max} (log ε_{max}): 330 (4.22), 298 (4.18), and 256 nm (4.44). *Anal.* calcd. for $C_{28}H_{22}O_2Cl_2$: C 72.89, H 4.81; found: C 73.01, H 4.66.

*Irradiation of TAE 3*bb'*. 3,6-Dimethoxy-9,10-bis(*p*-methoxyphenyl)phenanthrene, 6*bb'

(*a*) *In the laboratory*—A solution of TAE **3***bb'* (800 mg, 1.77 mmol) and I_2 (7 mg) in benzene (400 ml) was irradiated using a 450 W Hanovia medium pressure lamp with Pyrex filter while bubbling air through the solution for ca. 9 h. The white crystals of product were removed by filtration and dried to yield **6***bb'*, 452 mg (57%), mp 317–319°C; ^{1}Hmr (90 MHz) δ: 8.2–6.7 (m, 14H, ArH), 4.02 and 3.78 (s, 6H each, —OCH_3); ms peaks at *m/e* 450 (M^+, 100), 435 ($M - CH_3$, 14); uv (CH_2Cl_2) λ_{max} (log ε_{max}): 372 (3.41), 355 (3.43), 313.5 (4.13), 305 inf (4.08), 289 (4.39), 283 (4.38), 262 sh (4.72), and 256 nm (4.73). *Anal.* calcd. for $C_{30}H_{26}O_4$: C 79.97, H 5.82; found: C 79.74, H 5.95.

Use of acetonitrile or cyclohexane as solvent reduced the yield of **6***bb'*.

(*b*) *In sunlight*—(*i*) In solution: TAE (50 mg) in cyclohexane (50 ml) was placed in a Pyrex flask and exposed to bright sun (July) for 10 days. Thin-layer chromatography indicated only TAE and phenanthrene **6***bb'* to be present. By crystallisation 22 mg of **6***bb'* (44%) could be isolated, identical to previous samples. (*ii*) In solid state: TAE (50 mg) was coated on a glass Petri dish by means of CH_2Cl_2 solvent. One sample was covered with a Pyrex lid and a second left open to air. Both samples were left in bright sunlight for 10 days. Again tlc and nmr indicated presence of TAE and phenanthrene **6***bb'* in both samples. The dishes were also coated with a light brown insoluble compound.

*Irradiation of DCDAE, 3*bc'*. 3-Chloro-10-(*p*-chlorophenyl)-6-methoxy-9-(*p*-methoxyphenyl)phenanthrene, 6*bc'

Using the same procedure as above there was obtained from **3***bc'* a white precipitate (20–40%) of product, mp 325–327°C; ^{1}Hmr (90 MHz) δ: 8.1–6.5 (m, 14H, ArH), 4.04 and 3.80 (s, 3H each, —OCH_3); ms M^+ at *m/e* 458 (100, $^{35}Cl_2$); uv ($CHCl_3$) λ_{max} (log ε_{max}): 368 (3.28), 350 (3.28), 316 (4.09), 307 inf (4.06), 284 (4.38), 263 inf (4.64), and 255 nm (4.65). *Anal.* calcd. for $C_{28}H_{20}Cl_2O_2$: C 73.21, H 4.39; found: C 73.08, H 4.52.

3,6,11,14-Tetramethoxydibenzo[g,p]*chrysene, 7*bb'

Phenanthrene **6***bb'* (350 mg, 0.78 mmol) was dissolved in warm nitrobenzene (30 ml) and then cooled before the addition of $AlCl_3$ (3 g). After standing overnight at room temperature the mixture was heated on the steam bath for 4 h. After pouring onto ice, nitrobenzene was removed by steam distillation. The residue was extracted with CH_2Cl_2, and the extract washed, dried and evaporated. The dark residue (240 mg) was chromatographed on silica gel using benzene–CH_2Cl_2 (19:1) as eluant to yield product **7***bb'*, 80 mg (23%) as crystals which rapidly turn brown on their surface, mp 210–212°C; ^{1}Hmr (90 MHz) δ: 8.55 (d, J = 9 Hz, 4H, H-1, 8, 10, 16), 8.00 (d, J = 3 Hz, 4H, H-4, 5, 12, 13), 7.25 (dd, J = 9 Hz, 3 Hz, 4H, H-2, 7, 10, 15), and 4.04 (s, 12H, —OCH_3); ms M^+ at *m/e* 448 (100); uv (CH_2Cl_2) λ_{max} (log ε_{max}) 402 (3.83), 363 (4.23), 350 sh (4.21), 304 (4.94), 293 sh (4.73), 276 (4.56), 248 (4.55), and 228 nm (4.43); we were not able to obtain satisfactory analyses for this compound, probably because of its rapid oxidation.

Acknowledgements

We thank the National Research Council of Canada, the Government of British Columbia, and the University of Victoria for support of this investigation.

1. L. Mazuch, R. H. Mitchell, and P. R. West. Chem. Ind. 399 (1975).
2. E. L. Grant, R. H. Mitchell, P. R. West, L. Mazuch, and M. J. Ashwood-Smith. Mutat. Res. **40**, 225 (1976).
3. D. R. Gardner and J. R. Bailey. Methoxychlor: its effects on environmental quality. NRCC Publ. No. 14102. Ottawa, Ont. 1975. p. 15.
4. A. Schönberg, O. Schütz, and S. Nickel. Ber. Dtsch. Chem. Ges. B, **61**, 1384 (1928).
5. R. E. Buckles and W. D. Womer. J. Am. Chem. Soc. **80**, 5055 (1958); R. E. Buckles, R. E. Erikson, J. D. Snyder, and W. B. Person. J. Am. Chem. Soc. **82**, 2444 (1960);

H. M. BUCK, W. BLOEMHOFF, and L. J. OOSTERHOFF. Tetrahedron Lett. 5 (1960); J. A. VALENZUELA and A. J. BARD. J. Phys. Chem. **72**, 286 (1968); N. C. BAENZIGER, R. E. BUCKLES, and T. D. SIMPSON. J. Am. Chem. Soc. **89**, 3405 (1967).
6. M. WINDHOLZ (*Editor*). The Merck Index. 9th Ed. Merck and Company, NJ. 1976.
7. G. SCHNELLER and G. B. L SMITH. J. Am. Chem. Soc. **70**, 4057 (1948).
8. D. A. SHIRLEY (*to DuPont*). U.S. Patent No. 2,477,665. (August 2, 1949); Chem. Abstr. **43**, 9085c (1949).
9. Société Industrielle de Chimie Organique. Fr. Patent No. 1,121,559 (Aug. 21, 1956), Chem. Abstr. **53**, 15010d (1959).
10. (*a*) H. BILTZ. Ann. **296**, 219 (1897); (*b*) F. A. GUNTHER, G. E. CORMAN, and M. I. ELLIOT. J. Econ. Entomol. **41**, 895 (1948).
11. E. E. HARRIS and G. B. FRANKFORTER. J. Am. Chem. Soc. **48**, 3144 (1926).
12. K. SHISHIDO, K. OKANO, T. ISHIDA, and H. NOZAKI. J. Am. Chem. Soc. **77**, 6580 (1955).
13. E. BERGMANN and S. I. FUJISE. Ann. **483**, 65 (1930).
14. R. H. MITCHELL, T. FYLES, and L. M. RALPH. Can. J. Chem. **55**, 1480 (1977).
15. E. BERGMANN and S. I. FUJISE. Ann. **483**, 65 (1970).
16. E. C. DODDS, L. GOLBERG, E. I. GRÜNFIELD, W. LAWSON, C. M. SAFFER, JR., and R. ROBINSON. Proc. R. Soc. B, **132**, 83 (1944).
17. M. OKI. Bull. Chem. Soc. Jpn. **26**, 37 (1953).
18. (*a*) J. FORREST, O. STEPHENSON, and W. A. WATERS. J. Chem. Soc. 333 (1946); (*b*) O. STEPHENSON and W. A. WATERS. J. Chem. Soc. 339 (1946).
19. F. B. MALLORY, C. S. WOOD, and J. T. GORDON. J. Am. Chem. Soc. **86**, 3094 (1964).
20. A. T. BALABAN and C. D. NENITZESCU. *In* Friedel-Crafts and related reactions. Vol. II. *Edited by* G. A. Olah. Interscience Publishers, New York, NY. 1964. p. 979.
21. I. M. DAVIDSON, O. C. MUSGRAVE, and D. L. MANSON. J. Chem. Soc.3040 (1965).
22. H. M. BUCK, W. BLOEMHOFF, and L. J. OOSTERHOFF. Tetrahedron Lett. 5 (1960).
23. A. J. BARD, A. LEDWITH, and H. J. SHINE. Adv. Phys. Org. Chem. **13**, 155 (1976)
24. W. F. FORBES and P. D. SULLIVAN. J. Am. Chem. Soc. **88**, 2862 (1966).
25. U. SVANHOLM, B. SVENSMARK JENSEN, and V. D. PARKER. J. Chem. Soc. Perkin II, 907 (1974).

Can. J. Chem. Downloaded from www.nrcresearchpress.com by 210.87.254.42 on 09/05/12
For personal use only.

The photolysis of chlorinated *p*-terphenyls

BROCK CHITTIM, STEPHEN SAFE, NIGEL J. BUNCE, AND LUIS O. RUZO

Guelph–Waterloo Centre for Graduate Work in Chemistry, Department of Chemistry, University of Guelph, Guelph, Ont., Canada N1G 2W1

AND

KARL OLIE AND OTTO HUTZINGER

Department of Environmental Chemistry, University of Amsterdam, Nieuwe Achtergracht 166, Amsterdam, The Netherlands

Received August 16, 1977

BROCK CHITTIM, STEPHEN SAFE, NIGEL J. BUNCE, LUIS O. RUZO, KARL OLIE, and OTTO HUTZINGER. Can. J. Chem. **56**, 1253 (1978).

A variety of chlorinated *p*-terphenyls was photolyzed in organic media at 300 nm. Replacement of chlorine by hydrogen (dechlorination) was the major reaction. Substitution products were much more prominent than in the corresponding reactions of polychlorinated biphenyls.

Quantum yields of reaction were substantially higher for *ortho*-chlorinated compounds. Xenon-assisted reactions and benzophenone sensitization indicate a triplet reactive state, although energy transfer from benzophenone is very inefficient. Triethylamine promoted an electron transfer pathway but only for those compounds that were least photolabile.

BROCK CHITTIM, STEPHEN SAFE, NIGEL J. BUNCE, LUIS O. RUZO, KARL OLIE et OTTO HUTZINGER. Can. J. Chem. **56**, 1253 (1978).

On a effectué la photolyse, dans des milieux organiques à 300 nm, d'un certain nombre de *p*-terphényles chlorés. La réaction principale correspond au remplacement du chlore par un hydrogène (déchloration). Les produits de substitution sont beaucoup plus importants que dans les réactions correspondantes des biphényles polychlorés.

Les rendements quantiques des réactions sont beaucoup plus élevés pour les composés *ortho*-chlorés. Les réactions assistées par le xénon ou par une sensibilisation par le benzophénone indiquent la présence d'un état réactif triplet quoique le transfert d'énergie de la benzophénone est très inefficace. La triéthylamine aide un chemin de transfert d'électron mais uniquement pour les composés qui sont les moins photolabiles.

[Traduit par le journal]

Introduction

The photochemistry of halogenated aromatic compounds has recently received considerable attention (1–4). Much of this interest stems from the widespread occurrence of aryl chlorides as environmental contaminants (5, 6). Mechanistically, two photolysis pathways have been elucidated (7): direct C—X fission [1], and mechanisms involving excimers or exciplexes [2].

$$[1] \qquad ArX^* \rightarrow Ar^{\cdot} + X^{\cdot}$$

$$[2] \qquad D + ArX^* \rightarrow D^{\cdot +} + Ar^{\cdot} + X^-$$

The recent implication of polychlorinated terphenyls (PCTs) as widespread pollutants has prompted this investigation of their photochemistry, since PCTs absorb light of $\lambda > 300$ nm (8) and hence might be susceptible to solar photodegradation. Preliminary results have suggested that, like the polychlorinated biphenyls (PCBs), the PCTs lose chlorine atoms upon photolysis (9). In this paper we present our results on the mechanism of PCT photodegradation, with emphasis on comparing the results with those of the structurally related PCBs.

Results and Discussion

Identification of Photoproducts

Preliminary product studies involved photolysis of a range of PCTs to ~50% conversion and analysis of the photolysate by gas chromatography – mass spectrometry (gc–ms). These photolyses were carried out in both methanol (Table 1) and cyclohexane (Table 2) solutions using 300 nm radiation and concentrations of ca. 10^{-3} *M*. Air was not excluded.

In Tables 1 and 2, compounds identified only by molecular formulae were not characterised; only the relative molecular mass of the presumed parent ion and the chlorine isotope pattern were available. For compounds assigned structures, the glc retention times of authentic samples were also available, or a sample was isolated by preparative tlc and characterised spectroscopically.

In both methanol and cyclohexane, the most prominent products resulted from dechlorination (replacement of Cl by H). This is in line with results on PCBs (10). Material balances in the early stages of the reactions of 2,5-dichloro- and 2,4,6-trichloro-*p*-terphenyl were >95%, indicating that arylation

Can. J. Chem. Downloaded from www.nrcresearchpress.com by 210.87.254.42 on 09/05/12
For personal use only.

TABLE 1. Photoproducts of chlorinated-*p*-terphenyls in methanol at 300 nm

Substituents	Gas–liquid chromatography retention time (min)[a]	Parent ion; *m/e* ($^{35}Cl_x$ isotope)[a]	Formula or structure[a,b]	% total products formed[c,d]
4	2.6	230	*p*-terphenyl	85
	4.8	264	4-chloro-*p*-terphenyl	sm
	9.0	298	$C_{18}H_{12}Cl_2$	15
2,4	4.8	264	4-chloro-*p*-terphenyl	28
	5.0	298	2,4-dichloro-*p*-terphenyl	sm
	7.3	294	$C_{18}H_{12}Cl(OCH_3)$	72
2,5	4.5	264	$C_{18}H_{13}Cl$	69
	5.1	298	2,5-dichloro-*p*-terphenyl	sm
	7.7	294	5-chloro-2-methoxy-*p*-terphenyl[e]	31
2,6	2.6	230	*p*-terphenyl	22
	3.4	264	$C_{18}H_{13}Cl$	21
	4.2	260	$C_{18}H_{13}(OCH_3)$	t
	4.6	298	2,6-dichloro-*p*-terphenyl	sm
	5.1	297	*	nd
	5.4	262	$C_{18}H_{11}Cl$	8
	5.9	290	$C_{18}H_{12}(OCH_3)_2$	36
	6.2	294	$C_{18}H_{12}Cl(OCH_3)$	11
	6.9	290	$C_{18}H_{12}(OCH_3)_2$	t
	7.8	294	$C_{18}H_{12}Cl(OCH_3)$	t
	9.3	324	$C_{18}H_{11}Cl(OCH_3)_2$	nd
	9.6	358	$C_{18}H_{10}Cl_2(OCH_3)_2$	nd
	12.2	328	$C_{18}H_{11}Cl_2(OCH_3)$	nd
3,5	2.6	230	*p*-terphenyl	5
	4.6	264	$C_{18}H_{13}Cl$	85
	6.4	298	3,5-dichloro-*p*-terpheny	sm
	10.0	294	$C_{18}H_{12}Cl(OCH_3)$	10
	11.8	308	*	nd
2,3,4	4.8	264	4-chloro-*p*-terphenyl	36
	8.7	298	$C_{18}H_{12}Cl_2$	58
	11.2	332	2,3,4-trichloro-*p*-terphenyl	sm
	12.7	328	$C_{18}H_{11}Cl(OCH_3)_2$	3
	13.5	332	$C_{18}H_{11}Cl_3$	3

(formation of hexaphenyls) is not important in the PCT series. This contrasts with the behavior of chlorobenzene (1, 11) and 1-chloronaphthalene (12) but corresponds to the photochemistry of PCBs (10). A phenylated biphenylene was a significant photoproduct of 2,4,6-trichlorobiphenyl; although easy to rationalize, the analogous product has never been reported in the PCB series.

Another difference between PCB and PCT photochemistry is the relatively high yields of methoxy PCTs formed in the photolyses in methanol. These substitution products rarely exceed 2–3% of the product distribution from PCBs (10); from PCTs as much as one third of the product was methoxylated. Especially noteworthy is the fact that only the *o*-chloro-PCTs afforded these high yields of methoxy-compounds; in one case (2,4,6-trichloro-*p*-terphenyl) two of the methoxy products were isolated. Both resulted from replacement of *ortho* chlorines by methoxy.

Although a simple radical mechanism (eq. 1) can account for the dechlorination products, it seems unlikely that methoxy substitution occurs by this route. Attack of methanol as nucleophile upon the aryl radical ($S_{RN}1$) is improbable, both because methanol is a weak nucleophile and also because of the nonbonded interactions which result from the introduction of an *ortho* substituent into a polyphenyl (cf. ref. 13 on biphenyl derivatives). Abstraction of hydrogen would thus seem to be a much more likely fate of an *ortho* aryl radical.

We postulate that substitution more likely occurs by attack of a nucleophile directly upon the excited chloroaromatic; cf. related studies in the benzene series (1, 14). Formation of a σ-bonded intermediate with an sp^3 hybridised *ortho* carbon would relieve nonbonded interactions between the *ortho* chlorine and the hydrogens on the adjacent ring; ejection of chloride ion would then lead to the ground state of the methoxylated product.

Can. J. Chem. Downloaded from www.nrcresearchpress.com by 210.87.254.42 on 09/05/12
For personal use only.

TABLE 1 (*Concluded*)

Substituents	Gas–liquid chromatography retention time (min)[a]	Parent ion; *m/e* ($^{35}Cl_x$ isotope)[a]	Formula or structure[a,b]	% total products formed[c,d]
2,3,6	4.6	264	$C_{18}H_{13}Cl$	44
	5.2	298	2,5-dichloro-*p*-terphenyl	48
	7.0	328	$C_{18}H_{11}Cl_2(OCH_3)$	t
	7.9	332	2,3,6-trichloro-*p*-terphenyl	sm
	8.6	298	$C_{18}H_{12}Cl_2$	2
	9.4	324	$C_{18}H_{11}Cl(OCH_3)_2$	6
2,4,6	4.7	264	4-chloro-*p*-terphenyl	10
	5.1	298	2,4-dichloro-*p*-terphenyl	18
	5.6	332	2,4,6-trichloro-*p*-terphenyl	sm
	6.5	332	$C_{18}H_{11}Cl_3$	22
	7.2	294	$C_{18}H_{12}Cl(OCH_3)$	12
	7.6	296	2,4-dichloro-7-phenylbiphenylene[e]	9
	8.7	328	2,4-dichloro-6-methoxy-*p*-terphenyl[e]	23
	11.1	324	4-chloro-2,6-dimethoxy-*p*-terphenyl[e]	6
3,4,5	4.7	264	4-chloro-*p*-terphenyl	28
	6.4	264	$C_{18}H_{13}Cl$	6
	8.7	298	$C_{18}H_{12}Cl_2$	42
	10.1	332	3,4,5-trichloro-*p*-terphenyl	sm
	12.0	294	$C_{18}H_{12}Cl(OCH_3)$	t
	14.3	332	$C_{18}H_{11}Cl_3$	t
	22.7	328	$C_{18}H_{11}Cl_2(OCH_3)$	23
2,4,4″	4.7	264	4-chloro-*p*-terphenyl	6
	5.4	390	*	nd
	7.4	390	*	nd
	9.4	298	$C_{18}H_{12}Cl_2$	25
	11.2	332	2,4,4″-trichloro-*p*-terphenyl	sm
	12.9	366	$C_{18}H_{10}Cl_4$	5
	14.2	328	$C_{18}H_{11}Cl_2(OCH_3)$	57

[a]Using gc–ms; see Experimental.
[b]By comparative glc retention times using column *A*; see Experimental.
[c]Using column *A* (see Experimental) and assuming (*i*) that the detector response is equivalent for all photoproducts and (*ii*) that the relative retention times using this column are equal to those using the column in the gc–ms system.
[d]t, trace; nd, not detected on glc using column *A*; sm, starting material.
[e]Structure previously determined (ref. 10).

In cyclohexane solution, the *ortho* chloro PCTs furnished (usually) small amounts of cyclohexyl substituted products. Again, these find no precedent in PCB photochemistry. It is tempting to speculate that, once again, the cyclohexyl group has replaced an *ortho* chlorine but we have no information at present upon the genesis of such products.

Minor amounts of chlorination products were obtained with some of the PCTs. Analogous products were previously seen on photolysis of 1-chloronaphthalene (12) but have not been reported in the PCB series.

Quantum Yields of Reaction

Quantum yields for the disappearance of PCT (ϕ_r) were determined for 17 PCTs in methanol and cyclohexane, in both degassed and aerated solutions (Table 3).

In all cases, the ϕ_r values were higher in cyclohexane and, in both solvents, were increased with degassing (in most cases, by a factor of 2). In general, the ϕ_r values were highest for those PCTs containing *ortho* chlorines. In the absence of *ortho* chlorines, *meta*-chlorinated-*p*-terphenyls were the next most photolabile while 4-chloro-*p*-terphenyl was substantially more resistant to photolysis. The most reactive chloroterphenyls were those containing both *ortho* and *para* chlorines, (e.g. 2,4-dichloro-*p*-terphenyl) and the presence of an additional chlorine in the 4″ position usually caused a slight increase in ϕ_r values (e.g. 2,4,4″-trichloro-*p*-terphenyl decomposed more efficiently than 2,4-dichloro-*p*-terphenyl).

The ϕ_r values are very much higher than the corresponding ones reported for the PCBs at 300 nm (10) but are comparable with those recently measured for the PCBs at 254 nm (26). In the PCB series too, compounds having *ortho* chlorines are photolyzed very much more efficiently than those without.

The greater lability of the *ortho* chlorines most probably arises from the higher energy of the excited

Can. J. Chem. Downloaded from www.nrcresearchpress.com by 210.87.254.42 on 09/05/12
For personal use only.

TABLE 2. Photoproducts of chlorinated-*p*-terphenyls in cyclohexane at 300 nm

Substituents	Gas–liquid chromatography retention time (min)[a]	Parent ion; *m/e* ($^{35}Cl_x$ isotope)[a]	Formula or structure[a,b]	% total products formed[c,d]
4	2.5	230	*p*-terphenyl	84
	4.7	264	4-chloro-*p*-terphenyl	sm
	8.6	232	*	16
2,4	4.7	264	4-chloro-*p*-terphenyl	79
	5.0	298	2,4-dichloro-*p*-terphenyl	sm
	9.3	346	$C_{18}H_{12}Cl(C_6H_{11})$	21
2,5	4.4	264	$C_{18}H_{13}Cl$	88
	5.4	298	2,5-dichloro-*p*-terphenyl	sm
	14.4	346	$C_{18}H_{12}Cl(C_6H_{11})$	12
2,6	2.5	230	*p*-terphenyl	54
	3.4	264	$C_{18}H_{13}Cl$	26
	4.6	298	2,6-dichloro-*p*-terphenyl	sm
	5.9	332	$C_{18}H_{11}Cl_3$	2
	6.3	312	$C_{18}H_{13}(C_6H_{11})$	9
	9.6	346	$C_{18}H_{12}Cl(C_6H_{11})$	9
3,5	2.5	252	*	nd
	3.2	264	$C_{18}H_{13}Cl$	t
	4.5	264	$C_{18}H_{13}Cl$	66
	4.6	280	*	nd
	6.4	298	3,5-dichloro-*p*-terphenyl	sm
	11.2	266	*	33
2,3,4	2.5	230	*p*-terphenyl	4
	4.7	264	4-chloro-*p*-terphenyl	16
	8.7	298	$C_{18}H_{12}Cl_2$	72
	11.0	332	2,3,4-trichloro-*p*-terphenyl	sm
	13.4	366	$C_{18}H_{10}Cl_4$	3
	17.0	380	$C_{18}H_{11}Cl_2(C_6H_{11})$	2
	18.9	380	$C_{18}H_{11}Cl_2(C_6H_{11})$	3
2,3,6	4.6	264	$C_{18}H_{13}Cl$	67
	5.4	298	2,5-dichloro-*p*-terphenyl	20
	7.9	332	2,3,6-trichloro-*p*-terphenyl	sm
	8.7	298	$C_{18}H_{12}Cl_2$	2
	9.9	366	$C_{18}H_{10}Cl_4$	2
	11.8	346	$C_{18}H_{12}Cl(C_6H_{11})$	3
	13.4	380	$C_{18}H_{11}Cl_2(C_6H_{11})$	6
2,4,6	4.7	264	4-chloro-*p*-terphenyl	45
	5.0	298	2,4-dichloro-*p*-terphenyl	10
	5.6	332	2,4,6-trichloro-*p*-terphenyl	sm
	6.4	332	$C_{18}H_{11}Cl_3$	20
	7.7	296	2,4-dichloro-7-phenylbiphenylene[e]	3
	11.1	346	$C_{18}H_{12}Cl(C_6H_{11})$	5
	14.0	380	$C_{18}H_{11}Cl_2(C_6H_{11})$	8
3,4,5	4.7	264	4-chloro-*p*-terphenyl	9
	6.3	298	$C_{18}H_{12}Cl_2$	15
	8.5	298	$C_{18}H_{12}Cl_2$	38
	10.1	332	3,4,5-trichloro-*p*-terphenyl	sm
	17.0	332	$C_{18}H_{11}Cl_3$	10
	18.5	366	$C_{18}H_{10}Cl_4$	16
	23.5	400	$C_{18}H_9Cl_5$	22
2,4,4''	9.8	298	$C_{18}H_{12}Cl_2$	79
	11.2	332	2,4,4''-trichloro-*p*-terphenyl	sm
	12.9	366	$C_{18}H_{10}Cl_4$	3
	22.2	380	$C_{18}H_{11}Cl_2(C_6H_{11})$	18

[a]Using gc–ms; see Experimental.
[b]By comparative glc retention times using column *A*; see Experimental.
[c]Using column *A* (see Experimental) and assuming (*i*) that the detector response is equivalent for all photoproducts and (*ii*) that the relative retention time using this column are equal to those using the column in the gc–ms system.
[d]t, trace; nd, not detected by glc using column *A*; sm, starting material.
[e]Structure previously determined (ref. 10).

Can. J. Chem. Downloaded from www.nrcresearchpress.com by 210.87.254.42 on 09/05/12
For personal use only.

TABLE 3. Quantum yields of reaction (ϕ_r) for the chlorinated-*p*-terphenyls in methanol and cyclohexane at 300 nm

	Cyclohexane			Methanol		
	ϕ_r			ϕ_r[a,b]		
Substituents	Degassed	Nondegassed	% dechlorination[b,c,d]	Degassed	Nondegassed	% dechlorination
2,2,4′′	0.70	0.36	79	0.31	0.14	37
2,4	0.66	0.34	80	0.13	0.05	28
2,3,4	0.53	0.36	92	0.12	0.06	94
2,4,6,4′′	0.44	0.09	60	0.17	0.03	25
2,3,4,4′′	0.44	0.38	90	0.12	0.11	96
2,4,6	0.33	0.18	64	0.08	0.05	28
2,5,4′′	0.26	0.01	62	0.12	0.03	40
2,3,6,4′′	0.22	0.20	83	0.20	0.03	94
2,3,6	0.22	0.19	87	0.06	0.01	92
2,6,4′′	0.16	0.06	72	0.11	0.03	32
2,6	0.14	0.08	80	0.10	0.03	43
2,5	0.14	0.07	88	0.10	0.07	69
3,4,5,4′′	0.005	0.003	56	0.004	0.002	74
3,5,4′′	0.005	0.003	85	0.004	0.003	80
3,5	0.003	0.002	66	0.002	0.002	88
3,4,5	0.003	0.002	62	0.002	0.002	76
4	<0.001	<0.001	84	<0.001	<0.001	85

[a]In order of decreasing reactivity in cyclohexane, degassed.
[b]By quantitative glc using column *B*, see Experimental; conversions <20%.
[c]Percentage of total products formed assuming (*i*) all the products were detected by glc with the column and conditions used; (*ii*) products resulting from dechlorination were those with shorter retention times than the starting material, and (*iii*) the detector response (glc) was equivalent for all the products formed.
[d]The products referred to as dechlorination products were those formed by replacement of chlorines on the PCT with hydrogen (e.g. does not include biphenylene type products, methoxy substituted products, etc.).

state when *ortho* substituents are present. The blue shift in the uv absorption spectrum of an *ortho*-substituted compound is well documented for biphenyls (15) and has recently been observed also for the PCTs (8). Analogously, the onset of phosphorescence of *o*-chlorobiphenyls lies at higher energy than that of the parent compound (13, 17) and we assume that this is true also in the terphenyl series.

Thus *ortho* substitution increases the energy of both singlet and triplet excited states. In both biphenyls (18) and terphenyls (19) the first excited state is believed to be planar, the π-bond order of the inter-ring bonds being increased from the ground state. Wagner and Scheve (13, 20) have concluded that when only one *ortho* substituent of the size of methyl or chloro is present, the excited state molecule remains planar and the increase in energy is due to nonbonded interaction. In a 2,2′-disubstituted biphenyl two excited state geometries can be inferred, the *E* being presumed to be planar and the *Z* twisted. In our study, no more than one ring of the PCT ever carried *ortho* chlorines, hence the excited states were most probably planar in all cases.

We thus attribute the greater decomposition efficiency of *o*-chloroterphenyls to the increase in energy of the excited state. Aryl chlorides are thought (21) to have C—Cl bond dissociation energies around 80 kcal/mol; for *p*-terphenyl itself the energies of the singlet and triplet states lie, respectively, ~80 and ~60 kcal/mol above the ground state (22). For *o*-chloroterphenyls these excited state energies will be higher but we do not know by how much.

Assignment of Reactive Excited State

The quantum yields of reaction (ϕ_r) for all the PCTs decreased in the presence of oxygen (Table 3) which quenches long-lived excited states (24). The effect of oxygen varied with the PCT studied but was not sufficiently pronounced to support a triplet excited state unequivocally.

Quantum yields of fluorescence (ϕ_f) were measured in cyclohexane for three of the PCTs studied (Table 4), relative to *p*-terphenyl whose quantum yield of fluorescence was known (22). Among this small group it was found that ϕ_f decreased with increasing chlorine content and with *o*-substitution, as has been observed with PCBs (17). The compounds having the higher values of ϕ_r were the compounds that fluoresced least efficiently. However, this could be compatible with reaction from either a singlet or triplet state. If reaction is from the singlet, then reaction and fluorescence are in direct competition; if a reactive triplet state is involved, fluorescence competes with intersystem crossing. However, intersystem crossing, and hence reaction, would be facilitated by increasing the chlorine content of the

Can. J. Chem. Downloaded from www.nrcresearchpress.com by 210.87.254.42 on 09/05/12
For personal use only.

TABLE 4. Quantum yields of fluorescence (ϕ_f) of *p*-terphenyl and some chlorinated-*p*-terphenyls

Substituents	Excitation wavelength (nm)	Fluorescence maximum emission wavelength (λ_{max}, nm)	Relative intensity[a]	ϕ_f[b]
None	320	342	1.00	0.93
4	325	346	0.90	0.84
2,5	315	343	0.20	0.19
2,4,6	312	345	0.04	0.04

[a]Relative to *p*-terphenyl; 2×10^{-3} *M* solutions in cyclohexane.
[b]Assuming ϕ_f for *p*-terphenyl = 0.93 (22).

molecule and, by analogy with the PCBs (17), by introducing *ortho* substituents.

Two sets of experiments were conducted to try to assign the multiplicity of the excited state: a limited group of PCTs was photolysed in the presence of xenon and of benzophenone (Tables 5 and 6).

The heavy atom effect of xenon (which was present at ca. 1 atm) should tend to enhance intersystem crossing ($S_1 \rightarrow T_1$) (26). For PCTs with low chlorine content and a high fluorescence quantum yield, such as 4-chloro-*p*-terphenyl, ϕ_{isc} is relatively small. The photodegradation efficiency of such a compound should be enhanced in the presence of xenon if the triplet is reactive, but reduced if a reactive singlet is involved. Those PCTs with high ϕ_{isc} should not have ϕ_r greatly affected by xenon.

Experimentally, it was found that ca. 1 atm of xenon decreased ϕ_f for 4-chloro-*p*-terphenyl from 0.84 to 0.72. Thus the combination of ϕ_{isc} and ϕ_{ic} (internal conversion) increased from 0.16 to 0.28. Correspondingly, the efficiency of photodecomposition increased about 70%. Thus this result is entirely compatible with a predominantly triplet state reaction for 4-chloro-*p*-terphenyl.

For 2,5-dichloro- and 2,4,6-trichloro-*p*-terphenyl, xenon had little effect upon the fluorescence and almost no effect upon the ϕ_r value. This suggests, but not conclusively, that ϕ_{isc} is already high, and is compatible with triplet state photoreactivity. This point was examined further by carrying out the reaction of these two compounds in the presence of benzophenone as a triplet sensitiser. Concentrations of benzophenone and PCT were, respectively, 0.1 and 10^{-4} *M*, to ensure that most of the light was absorbed by the sensitiser.

The results support a triplet reactive state (see Table 6). Sensitisation is seen to occur but energy transfer does not take place at each encounter. From the photon flux determined experimentally, the production of $^3Ph_2CO$ (triplet benzophenone) is 4.5×10^{15} s^{-1}. Samples were 2.0 ml and knowing τ_p for Ph_2CO (in isooctane) is 2.5 μs (23) we have $[^3Ph_2CO] = 9.3 \times 10^{-12}$ *M*. Then assuming a rate constant for diffusion of 8×10^9 ℓ mol^{-1} s^{-1} in cyclohexane (24), the rate of encounter is $(8.9 \times 10^9) \times (9.3 \times 10^{-12}) \times (1.0 \times 10^{-4})$ or 8.3×10^{-5} mol ℓ^{-1} s^{-1}. Knowing ϕ_r and the irradiation time we can calculate how much PCT should be degraded if energy transfer took place at every collision. In both cases, fewer than 1% of the collisions resulted in energy transfer. Thus the situation for *ortho*-substituted PCTs is similar to that observed in the PCBs in that energy transfer from benzophenone to the *o*-substituted compounds is inefficient (13).

TABLE 5. Fluorescence and relative reaction rates of some chlorinated-*p*-terphenyls with xenon[a]

Substituents	Relative fluorescence intensity[b]	Relative reaction rate[b,c]
4	0.85	1.72
2,5	1.11	0.98
2,4,6	0.92	0.99

[a]1 atm xenon.
[b]Relative to those degassed samples containing no xenon.
[c]By quantitative glc using column *A*.

TABLE 6. Benzophenone sensitisation of 2,5-dichloro- and 2,4,6-trichloro-*p*-terphenyl photolyses[a]

Parameter	Value	
	2,5-Cl_2	2,4,6-Cl_3
Absorbance of PCT[b]	0.38	0.13
% light absorbed by Ph_2CO	94	98
Irradiation time (s)	120	60
PCT reacted (control) (*M*)	1.6×10^{-5}	1.5×10^{-5}
PCT reacted (sensitised) (*M*)	6.5×10^{-6}	6.5×10^{-6}
Reaction from direct reaction (*M*)	1.0×10^{-6}	3.0×10^{-7}
Reaction due to sensitisation (*M*)	5.5×10^{-6}	6.2×10^{-6}
ϕ_r (from Table 3)	0.14	0.33
Extent of reaction if energy transfer is 100% efficient (*M*)	1.4×10^{-3}	1.6×10^{-3}
% successful collisions	0.4	0.4

[a]In cyclohexane; $[PCT] = 1 \times 10^{-4}$ *M*; $[Ph_2CO] = 0.1$ *M*; duplicate samples.
[b]5-mm pathlength.

Reactions in the Presence of Triethylamine

Tertiary amines are well known to enhance the photolability of many aryl chlorides, through the

Can. J. Chem. Downloaded from www.nrcresearchpress.com by 210.87.254.42 on 09/05/12
For personal use only.

Can. J. Chem. Downloaded from www.nrcresearchpress.com by 210.87.254.42 on 09/05/12
For personal use only.

TABLE 7. Relative reaction rates and fluorescence quenching of *p*-terphenyl and some chlorinated-*p*-terphenyls with triethylamine (TEA)

Substituents	Fluorescence quenching $k_q\tau^a$ (M^{-1})	Relative reaction rates[b]
None	11.1	—
4	10.5	3.14
2,5	6.4	0.40
2,4,6	11.0	1.44

[a]Calculated from Stern Volmer plots.
[b]TEA concentration = 0.1 *M*; by comparing percentage conversions to that of a PCT solution containing no TEA; and by quantitative glc using column *A*.

intervention of an exciplex (eq. 2). For *p*-terphenyls substituted with chlorine at the 4, at the 2,5, and at the 2,4,6 positions, triethylamine quenched the fluorescence and linear Stern Volmer plots of I^0/I vs. [Q] were obtained (Table 7). In contrast to the PCBs no fluorescent exciplexes were observed.

The photodecomposition of these three substances was examined in the presence of triethylamine. Only 4-chloro-*p*-terphenyl had its ϕ_r increased substantially in the presence of amine. This suggests that, just as for the PCBs, an exciplex photodecomposition mechanism only operates for those PCTs that are inherently light stable.

In summary, at the present time it is not possible to assess whether photodegradation of PCTs is important environmentally. It is clear, however, that PCTs absorb light in an environmentally accessible region of the spectrum and that for some of the derivatives photodecomposition can be very efficient, at least in organic solvents. Whereas the related PCBs undergo almost exclusively dechlorination, the PCTs have a more varied photochemistry, with biphenylenes and substitution products appearing prominently in the product mixture. As with the PCBs, those PCTs bearing *ortho* chlorines are very much more photolabile than those without. Mechanistic studies implicate the triplet state as the seat of the photoreaction and suggest that electron transfer routes of decomposition are likely to be important only for the most photostable PCTs.

Experimental

Materials and Methods

Chemicals

Chloro-p-*terphenyls*—These were synthesized as described in a previous publication and were further purified by preparative thin-layer chromatography (tlc) until >99% purity was obtained.

Cyclohexane—This compound (Fisher, spectroanalyzed) was used as received for photolysis product studies and quantum yields of reaction determinations. For the studies involving fluorescence measurements, this solvent was further purified by first washing with concentrated sulfuric acid. It was then washed twice with deionized water and once with a 5% solution of sodium bicarbonate in deionized water. It was finally dried over anhydrous sodium sulfate and glass distilled from P_2O_5.

Potassium ferrioxalate—This compound (Pfaltz and Bauer) was recrystallized twice from water and stored in the dark until needed. All other chemicals were obtained commercially and used without purification.

Gas–Liquid Chromatography

Gas–liquid chromatography was performed on a Hewlett-Packard 5710 gas chromatograph fitted with a flame ionization detector and using a 183 m × 0.64 cm glass column packed with either 3% OV-225 on Gas-Chrom Q, 80–100 mesh (column *A*), or 3% SE-30 on Chromosorb W, 60–80 mesh (column *B*). Both injection port and detector temperatures were 300°C; oven temperature using either column was 250°C.

Gas Chromatography — Mass Spectrometry

Gas chromatography–mass spectrometry analysis was obtained using a Hewlett-Packard 5982-A system operated at 70 eV in the EI mode. The glc column used was column *A*, as described, and it was operated isothermally at 240°C.

Fluorescence Spectroscopy

Fluorescence measurements for the xenon quenching experiments were performed using a Farrand Mark I fluorimeter for which sample chambers were designed and constructed in this department. All other fluorescence measurements were recorded at room temperature in 1 cm × 1 cm square quartz cuvettes using a Hitachi-Perkin-Elmer Fluorescence spectrophotometer MPF-2A.

Photolysis Procedures

All irradiations were carried out in a Rayonet Reactor (The Southern N.E. Ultraviolet Co.) fitted with RUL 3000 lamps which have a peak output energy at 300 ± 10 nm. For quantum yield determinations or relative rate experiments using quenchers, duplicate samples were irradiated in parallel using a rotating 'merry-go-round' apparatus to ensure equal irradiation of all samples. To monitor the light output from the reactor lamps, the modified ferrioxalate actinometer was used (25).

(*i*) *Photoproduct Studies*

The 10 PCTs listed in Tables 1 and 2 were photolyzed in methanol (Fisher, spectroanalyzed) and cyclohexane for gc–ms analysis. Solutions of the PCTs (25 ml, 10^{-3} *M*) were irradiated in Pyrex flasks (Reacti Flasks, Chromatographic Specialties) at 300 nm until approximately 50% of the starting material had reacted as determined by glc. The solvent was then evaporated and the crude mixture analyzed by gc–ms and glc using column *A*.

(*ii*) *Quantum Yields of Reaction* (ϕ_r)

Quantum yields of reaction (ϕ_r) were determined for 17 chlorinated-*p*-terphenyls (listed in Table 3) in cyclohexane and methanol, under both degassed and nondegassed conditions. All determinations (e.g. methanol, degassed) were determined in duplicate using 2-ml samples of 10^{-3} *M* solutions of the PCTs which were irradiated at 300 nm in Pyrex ampoules (8 mm od). Degassed samples were prepared by the freeze–pump–thaw method (usually two cycles at 0.02 mm). Percentage conversions were determined by quantitative glc (column *B*). Owing to possible competitive absorption by the photoproducts, irradiation times were adjusted so that less than 20% conversion of the PCT was obtained. Percentage conversions of 2,5-dichloro- and 2,4,6-trichloro-*p*-terphenyl in degassed cyclohexane and methanol were linear with respect to irradiation times (up to 30%) indicating that the photoproducts did not affect the ϕ_r values when conversions of starting material were kept below 30%.

(iii) Quantum Yields of Fluorescence (ϕ_f)

Quantum yields of fluorescence were determined for three chlorinated terphenyls, 4-chloro, 2,5-dichloro-, and 2,4,6-trichloro-*p*-terphenyl, assuming that the intensity of fluorescence was proportional to ϕ_f. It was also assumed that the fluorimeter response was linear over the wavelengths of interest.

In this method, the intensity of fluorescence of 2×10^{-3} *M* solutions of these three PCTs and *p*-terphenyl, in purified cyclohexane, were determined at their fluorescence maxima. The ϕ_f values for the PCTs were then determined by comparing their fluorescence intensities to that of *p*-terphenyl whose ϕ_f is reported to be 0.93 (22).

(iv) Triethylamine-assisted Photolyses

Fluorescence quenching experiments were performed on *p*-terphenyl and the three chloroterphenyls studied in section *iii*. The fluorescence intensities of 10^{-3} *M* solutions of the terphenyls, containing varying amounts of triethylamine (TEA), were measured at their fluorescence maxima. These intensities were compared with the fluorescent intensity of a terphenyl solution containing no quencher.

To determine the effect of TEA on the PCT reaction rates, 2-ml degassed solutions of the three chloroterphenyls (10^{-3} *M* in purified cyclohexane, Pyrex ampoules) containing TEA (0.1 *M*) or no quencher, were irradiated in duplicate at 300 nm until ~20% of the PCTs reacted in the samples containing no TEA by quantitative glc; relative reaction rates were then calculated taking the reactivity of the PCT solution containing no TEA equal to 1.00.

(v) Xenon-assisted Photolyses

To test the effect of xenon on the fluorescence and the reactivity of the three chloroterphenyls studied above, four samples (2 ml) of the PCTs (10^{-3} *M*) in purified cyclohexane were placed in quartz ampoules (8 mm od) and degassed. Xenon (Matheson; ca. 1 atm) was added to two of these samples using the method described by Bunce *et al.* (26) and all the tubes sealed. After sealing, the fluorescence intensities and photoreactivities of the samples containing xenon were compared with those without xenon.

(vi) Benzophenone-assisted Photolyses

Benzophenone sensitization experiments were performed on 2,5-dichloro- and 2,4,6-trichloro-*p*-terphenyl with and without benzophenone. Degassed 2 ml samples of the chloroterphenyls (10^{-4} *M* in purified cyclohexane, Pyrex ampoules) containing benzophenone or no sensitiser were irradiated in duplicate and the percentage of the PCT reacted (kept below 20%) determined by quantitative glc.

1. J. A. Barltrop, N. J. Bunce, and A. Thomson. J. Chem. Soc. C, 1142 (1967).
2. J. T. Pinhey and R. D. G. Rigby. Tetrahedron Lett. 1267 (1969).
3. R. K. Sharma and N. Kharasch. Angew. Chem. Int. Ed. Engl. **7**, 36 (1968).
4. D. R. Arnold and P. C. Wong. J. Am. Chem. Soc. **99**, 3361 (1977).
5. S. Safe, O. Hutzinger, and V. Zitko. Environ. Health Perspect. **1**, 15 (1972).
6. J. L. Herring, E. J. Hannon, and D. D. Bills. Environ. Contam. Toxicol. **8**, 153 (1972).
7. N. J. Bunce, P. Pilon, L. O. Ruzo, and D. J. Sturch. J. Org. Chem. **41**, 3023 (1976).
8. B. Chittim, S. Safe, L. O. Ruzo, O. Hutzinger, and V. Zitko. J. Agric. Food Chem. **25**, 323 (1977).
9. B. Chittim and S. Safe. Chemosphere, **5**, 269 (1977).
10. L. O. Ruzo, M. J. Zabik, and R. D. Schuetz. J. Am. Chem. Soc. **96**, 3809 (1974).
11. G. E. Robinson and J. M. Vernon. J. Chem. Soc. C, 3363 (1971).
12. L. O. Ruzo, N. J. Bunce, and S. Safe. Can. J. Chem. **53**, 688 (1975).
13. P. J. Wagner and B. J. Scheve. J. Am. Chem. Soc. **99**, 2888 (1977).
14. J. T. Pinhey and R. D. G. Rigby. Tetrahedron Lett. 1271 (1969).
15. H. Suzuki. Electronic absorption spectra and geometry of organic molecules. Academic Press, New York, NY. 1967. Chapt. 12.
16. C. M. O'Donnell, K. E. Harbaugh, R. P. Fisher, and J. D. Winefordner. Anal. Chem. **45**, 609 (1973).
17. H. Dreeskamp, O. Hutzinger, and M. Zander. Z. Naturforsch. A, **27**, 756 (1972).
18. H. H. Jaffe and M. Orchin. Theory and applications of ultraviolet spectroscopy. Wiley, New York, NY. 1964. Chapt. 15.
19. J. Dale. Acta. Chem. Scand. **11**, 640 (1957); **11**, 650 (1957); K. R. Naqvi, J. Donatsch, and U. P. Wild. Chem. Phys. Lett. **34**, 285 (1975).
20. B. J. Scheve and P. J. Wagner. Chem. Phys. Lett. **25**, 324 (1974); P. J. Wagner. J. Am. Chem. Soc. **89**, 2820 (1967).
21. S. W. Benson. The foundations of chemical kinetics. McGraw-Hill Book Co., New York, NY. 1960. p. 760.
22. I. B. Berlman. Handbook of fluorescence spectra of aromatic molecules. Academic Press, New York, NY. 1971. pp. 67–86.
23. L. Giering, M. Berger, and C. Steel. J. Am. Chem. Soc. **96**, 953 (1974).
24. J. G. Calvert and J. N. Pitts, Jr. Photochemistry. Wiley, New York, NY. 1966. p. 599.
25. K. C. Kurien. J. Chem. Soc. B, 2081 (1971).
26. N. J. Bunce, Y. Kumar, L. Ravanal, and S. Safe. J. Chem. Soc. Perkin Trans. II. In press.

Can. J. Chem. Downloaded from www.nrcresearchpress.com by 210.87.254.42 on 09/05/12
For personal use only.

The proton magnetic resonance determination of the hindered rotation in α,α,α′,α′,3,4,6-heptachloro-*o*-xylene

HAROLD M. HUTTON[1] AND WALTER E. HIEBERT
Department of Chemistry, University of Winnipeg, Winnipeg, Man., Canada R3B 2E9
AND
VICTOR MARK
Plastics Department, General Electric Company, Mount Vernon, IN 47620, U.S.A.

Received November 25, 1977

HAROLD M. HUTTON, WALTER E. HIEBERT, and VICTOR MARK. Can. J. Chem. **56**, 1261 (1978).

A high resolution proton magnetic resonance investigation of the hindered rotation of the dichloromethyl groups as a function of temperature in α,α,α′,α′,3,4,6-heptachloro-*o*-xylene (HCOX) has been conducted using dynamic nuclear magnetic resonance line shape analysis, supplemented with a homonuclear double resonance saturation transfer technique. The rate process in HCOX involves a coupled rotation of the two substituted methyl groups and the nonmutual exchange of the three pairs of protons between two equally populated conformers. The Arrhenius and transition state parameters were determined from the rate constants obtained over a temperature range of −5°C to 93°C for a 5 mol% solution of HCOX in methylcyclohexane: $\Delta G^* = 17.22 \pm 0.07$ kcal mol^{-1} at 298 K, $\Delta H^* = 14.6 \pm 0.3$ kcal mol^{-1}, $\Delta S^* = -8.8 \pm 0.8$ cal mol^{-1} deg^{-1}, and $E_a = 15.3 \pm 0.3$ kcal mol^{-1}. The results obtained for HCOX are compared with those for other chloro-substituted xylenes and toluenes.

HAROLD M. HUTTON, WALTER E. HIEBERT et VICTOR MARK. Can. J. Chem. **56**, 1261 (1978).

On a effectué, en faisant appel à une analyse de la forme des raies en résonance magnétique nucléaire dynamique complémentée par une technique de transfert de saturation de double résonance homonucléaire, une étude par résonance magnétique nucléaire du proton à haute résolution de la rotation empêchée des groupes dichlorométhyles en fonction de la température dans des α,α,α′,α′,3,4,6-heptachloro-*o*-xylène (HCOX). Le processus observé dans HCOX implique une rotation couplée des deux groupes méthyles substitués et l'échange non-mutuel des trois paires de protons entre deux conformères qui sont de population égale. On a déterminé les paramètres d'Arrhénius et d'état de transition à partir des constantes de vitesse obtenues à des températures allant de −5°C jusqu'à 93°C pour une solution à 5 mol% de HCOX dans le méthylcyclohexane: $\Delta G^* = 17.22 \pm 0.07$ kcal mol^{-1} à 298 K, $\Delta H^* = 14.6 \pm 0.3$ kcal mol^{-1}, $\Delta S^* = -8.8 \pm 0.8$ cal mol^{-1} deg^{-1} et $E_a = 15.3 \pm 0.3$ kcal mol^{-1}. On compare les résultats obtenus pour HCOX avec ceux obtenus pour d'autres xylènes et toluènes substitués par des atomes de chlore.

[Traduit par le journal]

Introduction

Proton magnetic resonance (^{1}H nmr) studies of the hindered rotation of the dichloromethyl group in a series of substituted toluenes (1–3), substituted xylenes (4, 5), and a substituted mesitylene (6) have been examined by Schaefer *et al.* In this paper we present the results of the study of the hindered rotation in α,α,α′,α′,3,4,6-heptachloro-*o*-xylene (HCOX) as a 5 mol% solution in methylcyclohexane. Mark and Pattison (7) have previously studied the hindered rotation in a series of *o*-bis(dichloromethyl) benzenes, including HCOX in tetradecane, using the variation of the line width of the coalescing resonances as a function of temperature (7). Because the results for HCOX were somewhat ambiguous using this technique the activation parameters were not reported and were left to be determined by a complete line shape analysis.

Steric considerations (8) indicate that the rotation of the two methyl groups in HCOX is synchronized and of opposite direction giving two conformers, **1** and **2**, with roughly equal populations. The stable

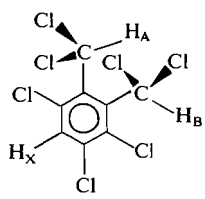

1

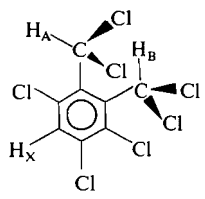

2

conformations are with H_A (**1**), H_B (**1**), H_A (**2**), H_B (**2**) in the plane of the ring (1–6) and are related by a concerted 180° rotation of the two side chain groups

[1]Author to whom correspondence should be addressed.

Can. J. Chem. Downloaded from www.nrcresearchpress.com by 210.87.254.5 on 09/05/12
For personal use only.

Can. J. Chem. Downloaded from www.nrcresearchpress.com by 210.87.254.5 on 09/05/12
For personal use only.

about their respective C—C bonds. Such a rotation effectively changes the magnetic environment of all three protons, giving a ^{1}H nmr spectrum which consists of the time averaged resonances corresponding to the two conformers. The rate constants for the hindered rotation were determined by comparing the experimental spectra with those generated with Binsch's computer program DNMR2 (9). The relatively large errors obtained with this visual matching technique in the slow exchange region were substantially reduced by using the decay and recovery curves of the saturation transfer technique proposed by Forsen and Hoffman (10–12) and developed further by Anet and Bourn (13).

Experimental

Preparation of HCOX

HCOX was prepared by the following steps. (*i*) Ring chlorination of *o*-xylene. A solution of 424 g (4.0 mol) of *o*-xylene in 1500 ml of CCl_4 was chlorinated in the presence of 1 g of aluminum chloride between 30 and 50°C until the theoretical amount of chlorine (851 g) has been added. Stripping of the solvent in a rotary evaporator yielded an oil, which on cooling deposited solids. These, after filtration and trituration with warm hexane, weighed 45 g and were identified as tetrachloro-*o*-xylene, mp 227–228°C (lit. (14) mp 227–228°C). The filtrate of the hexane trituration, for which gc indicated the absence of tetrachloroxylene and the presence of 80% of tri- and 20% of dichloroxylenes, was stripped of solvent and triturated with pentane. Crystals (22 g) separated out overnight and these were shown by gc to contain 95% of *ar*-trichloro-*o*-xylenes. (*ii*) Side-chain chlorination of *ar*-trichloro-*o*-xylenes. The mixture of trichloroxylenes obtained above (20.9 g) was dissolved in 100 ml of CCl_4, the solution heated to reflux and chlorinated exhaustively while irradiating with a bright sunlamp. As shown by gc (11-in. SG column, 225°C), after 4 h of chlorination all of the starting material had disappeared; removal of the solvent in a rotary evaporator left behind 32.8 g of residue (theoretical, 35 g), consisting of two main components with residence times of 10.0 and 12.0 min, in a 20 to 80 ratio. The separation of the two isomeric α,α,α′,α′,-*ar*,*ar*,*ar*-heptachloro-*o*-xylenes was effected by elution chromatography: 10.0 g of the chlorination mixture was chromatographed over 450 g of alumina, using 1350 ml pentane as eluant. The isomer with the 10.0 min gc residence time was eluted first and was obtained in pure form after recrystallization from hexane, mp 114–117°C; ^{1}H nmr indicated the α,α,α′,α′,3,4,5-heptachloro-*o*-xylene structure for this isomer (7). *Anal.* calcd. for $C_8H_3Cl_7$: C 27.7, H 0.87, Cl 71.5; found: C 27.8, H 0.83, Cl 71.6. The other isomer, with the 12.0-min gc residence time, was eluted as the second component and obtained in pure form by recrystallization from hexane, mp 70–72°C; ^{1}H nmr confirmed the α,α,α′,α′,3,4,6-heptachloro-*o*-xylene structure (HCOX). *Anal.* calcd. for $C_8H_3Cl_7$: C 27.7, H 0.87, Cl 71.5; found: C 27.9, H 0.8, Cl 71.5.

^{1}H Nuclear Magnetic Resonance Spectra

A 5 mol% solution of HCOX in methylcyclohexane, containing small amounts of hexamethyldisilane for the internal lock and methylene chloride for the line-width standard, was degassed by the freeze–pump–thaw technique and then sealed.

The ^{1}H nmr spectra were recorded from −60°C to 96°C on a Varian HA-100D spectrometer. Each spectrum was normally recorded three times with some, at temperatures near coalescence, recorded up to eight times using a sweep rate of 0.05 Hz/s with a 1 Hz/cm chart width. Temperatures were measured with an iron–constantan thermocouple placed in a toluene sample in the probe before and after each HCOX spectrum, as previously described by Peeling *et al.* (2) and are estimated to be accurate to ±1°C. The double resonance spin transfer technique was used to assign the proton resonances of the two conformers in HCOX. In the slow exchange region at lower temperatures the chemical shifts of the individual protons and the relative populations of **1** and **2** were determined. Effective spin–spin relaxation times were estimated from the half-height line width of the methylene chloride proton resonance at each temperature. Rate constants of hindered rotation were determined for the temperature range of 27 to 96°C.

Double Resonance Saturation Transfer

A Hewlett-Packard audio oscillator, model 4204A, was used in the double resonance saturation transfer experiment with an external recorder connected to the HA 100 spectrometer to observe the intensity of a resonance as a function of time. The observing frequency was adjusted to the maximum intensity of a selected resonance and the time dependence of the decay curve was measured when the resonance of a second proton with which it exchanged was saturated. The recovery curve was obtained by measuring the change in intensity with time when the saturating frequency was removed. Care was taken not to saturate the resonance with the observing rf field. In addition, the observing and saturating frequencies were adjusted by trial and error to compensate for the shift in peak positions that occurs with the saturating field. This method was used to determine rate constants for HCOX at −5°C and 5°C.

Results and Discussion

Assignment of Peaks Under Conditions of Slow Exchange

The ^{1}H nmr spectrum of HCOX at ambient temperature, where the exchange is relatively slow is given in Fig. 1. Due to the interactions of the two substituted *ortho* groups only two conformers with roughly equal populations are observed. The concerted 180° rotation between **1** and **2** effectively changes the environment of all three protons resulting in a spectrum of six resonances, as in Fig. 1. At ambient temperature the rate of exchange between the two conformers is sufficient to use the saturation transfer technique (11) to assign the protons exchanging between **1** and **2**.

By inspection H_A (**1**) and H_X (**1**) of conformer **1** were assigned by the long range 'zig-zag' coupling (15). The splitting of these two peaks was more evident with lower temperature spectra than in Fig. 1. In keeping with earlier assignments of analogous compounds (1, 16) peak 2 in Fig. 1 was assigned to the methine proton H_A (**1**) and peak 4 to H_X (**1**).

Using the double resonance technique, peak 1 and peak 3 were assigned to the same proton in the two conformers by saturating peak 1 and observing the

TABLE 1. The chemical shifts of HCOX in methylcyclohexane

Temperature (°C)	Chemical shift (Hz)*					
	H_B (2)	H_A (1)	H_B (1)	H_X (1)	H_X (2)	H_A (2)
−60.0	792.8	788.2	755.8	755.8	745.4	742.5
−20.0	795.0	789.7	755.1	754.8	745.6	742.8
0.0	794.22	789.72	755.16	754.9	745.15	742.80
5.0	794.37	789.82	755.26	754.96	745.0	742.7
17.3	794.61	790.11	755.43	754.75	745.18	742.98
20.0	794.64	790.16	755.38	754.70	745.07	742.95
25.7	794.75	790.28	755.44	754.57	745.00	742.96
27.7	794.83	790.31	755.47	754.58	745.04	743.03
32.8	794.70	790.27	755.33	754.44	744.79	742.94
36.5	794.96	790.43	755.35	754.34	744.77	743.00
41.1	795.00	790.54	755.42	754.25	744.79	743.06

*To low field from internal hexamethyldisilane at 100 MHz.

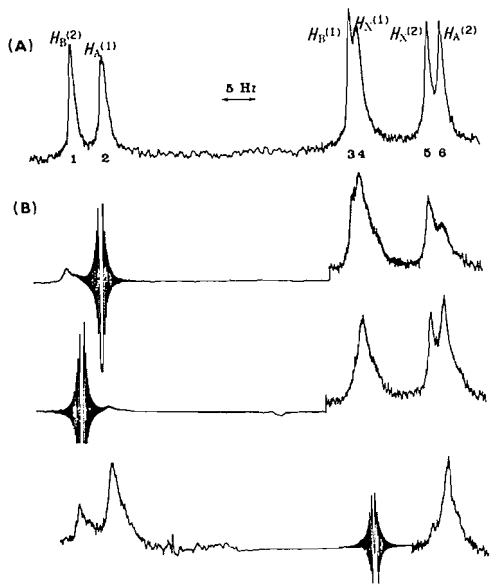

FIG. 1. Comparison of the ^1H nmr spectrum of a 5 mol% solution of HCOX in methylcyclohexane at ambient temperature (A) with spectra obtained by double resonance (B).

decrease in intensity of peak 3, as shown in Fig. 1. Saturation of peak 2 caused a significant reduction in the intensity of peak 6, thus peak 2 and peak 6 are related by an exchange of the conformers; the partial reduction of peak 3 in this experiment is probably due to the partial saturation of peak 1. The third proton in the two conformers is assigned to peaks 4 and 5. This was confirmed by saturating peaks 3 and 4 and observing intensity changes for peaks 1 and 5, as in Fig. 1. Using this information and the previous assignment of H_A (**1**) and H_X (**1**), the peaks may be assigned as indicated in Fig. 1. Peak 1 was assigned to H_B (**2**) as the environment of H_B (**2**) should be similar to that of H_A (**1**).

This assignment was confirmed with the steric crowding method of Peeling *et al.* (6). The magnitude of the crowding was estimated from a scale diagram of the molecule using standard covalent atomic radii and bond angles, and a maximum of 5° bond angle distortion (6). H_A (**1**) and H_B (**2**) are most crowded and thus their resonances are farthest down field; H_X (**2**) and H_A (**2**) are least crowded so are to highest field; while H_B (**1**) and H_X (**1**) occur at intermediate field. Long range coupling permits the unambiguous assignment, as before, for H_A (**1**), H_X (**1**) and thus H_B (**1**) and H_B (**2**) but there appears to be no intuitive way to distinguish H_A (**2**) and H_X (**2**) using this procedure.

^1H Nuclear Magnetic Resonance

At lower temperatures, where the lifetime of each conformer is relatively long, the spectrum consists of a superposition of the resonances of the two conformers. The chemical shifts were measured as a function of temperature and are given in Table 1. Increasing the temperature decreases the lifetime and the conformers interconvert more rapidly causing the peaks to coalesce. In this region the chemical shifts of the resonances were obtained by an extrapolation of the plot of the chemical shifts vs. temperature, using the data from Table 1.

The long range coupling constant between the methine proton H_A (**1**) and H_X (**1**) was measured at lower temperatures to be $^5J_{H_A(1)H_X(1)} = 0.45 \pm 0.04$ Hz with no observable variation with temperature.

At the lower temperatures in the slow exchange region the resonances of the two conformers were sufficiently dispersed to allow a determination of their relative populations. For five temperatures from −60°C to 27°C the ratio of **1**:**2** was 1.00 ± 0.04 indicating that the population difference was not significant.

Representative spectra, together with the spectra calculated with the computer program DNMR2 (9,

Can. J. Chem. Downloaded from www.nrcresearchpress.com by 210.87.254.5 on 09/05/12
For personal use only.

Can. J. Chem. Downloaded from www.nrcresearchpress.com by 210.87.254.5 on 09/05/12
For personal use only.

17) are given in Fig. 2. The effective spin–spin relaxation times were determined at each temperature using internal methylene chloride and were typically 1.4–1.6 s. At slow exchange the line widths of HCOX were comparable to that of the methylene chloride. The rate constants for the hindered rotation with an estimation of the error due to the fitting procedure are given in Table 2.

Double Resonance Saturation Transfer

When the rate process is relatively slow or very fast the determination of reliable rate constants by matching experimental and computer-simulated spectra is difficult because the line shape is relatively insensitive to a change in the preexchange lifetime. An alternative procedure for the slow exchange region, the method of saturation transfer, is complementary and allows data to be acquired over a larger temperature range.

(i) The Decay Process

For two protons H_A, H_B which are interconverted by an exchange process, the instantaneous saturation of the protons at H_B will decrease the intensity of the absorption signal of the H_A protons to a lower nonzero value, as long as the preexchange time between the two sites is approximately the same as the spin–lattice relaxation time (10). Considering a system, such as is found for HCOX, where the average lifetime of proton H_A, τ_A, is equal to the average lifetime of proton H_B, τ_B, the decay of the magnetization $M_Z^A(t)$ with the saturation of H_B is given by

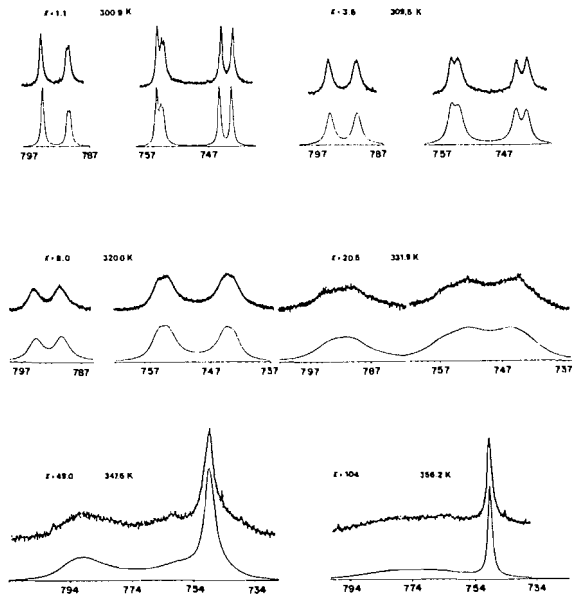

FIG. 2. Experimental and calculated ^1H nmr spectra of HCOX for a few representative temperatures and rate constants.

TABLE 2. Rate constants for HCOX at various temperatures as determined by the line shape analysis

Temperature* (K)	k† (s^{-1})	Temperature (K)	k (s^{-1})
300.7	1.1±0.2	331.9	20.5±0.5
305.8	2.6±0.2	336.4	26.0±1
309.5	3.5±0.2	342.1	36.0±1
314.1	4.2±0.3	347.5	49.0±2
318.1	6.6±0.3	352.5	72.0±2
320.0	8.0±0.3	356.2	104.0±4
323.8	11.0±0.4	363.0	160.0±5
327.1	12.5±0.5	369.0	198.0±6

*Maximum error in temperature ±1 K, except at 369 K where the error is ±2 K.
†Rate constants calculated using the shift data in Table 1 with T_2 from CH_2Cl_2 peak at each temperature; $J_{A(1)\times(1)} = 0.45$ Hz; all other $J = 0$.

eq. 1 (13):

$$[1] \quad M_Z^A(t) - M_Z^A(\infty) = M_Z^A(\infty)\frac{T_{1A}}{\tau_{1A}}\exp\left(\frac{-t}{\tau_{1A}}\right)$$

In [1] $M_Z^A(\infty)$ is the saturation transfer equilibrium magnetization, T_{1A} is the spin–lattice relaxation time, and $1/\tau_{1A} = 1/T_{1A} + 1/\tau_A$. From [1] the initial magnetization of H_A in the absence of any saturating field, M_Z^A, would be given by eq. 2 (13):

$$[2] \quad M_Z^A(\infty)/M_Z^A = \tau_{1A}/T_{1A}$$

Using [1] a plot of $\ln(M_Z^A(t) - M_Z^A(\infty))$ vs. time would give the value of τ_{1A} from the slope; T_{1A} can then be obtained from [2] and thus the lifetime τ_A and rate constant k.

For HCOX at 5°C a representative plot of $\ln(M_Z(t) - M_Z(\infty))$ vs. time is shown in Fig. 3*A* for the decay of H_B (**2**) with the saturation of H_B (**1**). The results for the decay experiments are given in Table 3.

(ii) The Recovery Process

The instantaneous removal of the saturating field at H_B is followed by the increase in the magnetization of H_A to its unsaturated equilibrium value. The magnetization at site A for the recovery process when $t = 0$, $M_Z^A(0)$, will be identical to the value previously designated by $M_Z^A(\infty)$ for the saturation process. The expression for the magnetization as a function of time is given by eq. 3 (13):

$$[3] \quad M_Z^A(t) = M_Z^A + c_1\exp(-\lambda_1 t) + c_2\exp(-\lambda_2 t)$$

M_Z^A is the magnetization in the absence of any saturating field, as before. The values of c_1 and c_2 are determined by the initial saturated state and λ_1 and λ_2 are defined under conditions of slow exchange by (10):

TABLE 3. Rate constants determined for HCOX by double resonance saturation transfer

Temperature (K)	Proton		Decay*				Recovery*	
	Saturated	Observed	$M_Z(\infty)/M_Z$	τ_{1A}	T_1(s)	k (s^{-1})	T_1 (s)	k (s^{-1})
268	H_A (1)	H_A (2)	0.409	4.55	11.1	0.131	9.36	0.108
278	H_A (1)	H_A (2)	0.200	2.94	14.7	0.273	14.0	0.270
	H_A (2)	H_A (1)	0.152	2.77	18.2	0.316	12.7	0.282
	H_B (1)	H_B (2)	0.200	2.87	14.4	0.278	14.2	0.280
					Average†	0.276		0.275

*Average values of a minimum of two trials for each decay and recovery.
†Average value calculated takes into account the number of trials for each decay and recovery.

[4] $$\lambda_1 = 1/\tau_{1A} + 1/\tau_A$$
$$\lambda_2 = 1/\tau_{1A} - 1/\tau_A = 1/T_{1A}$$

This assumes that the lifetimes τ_A and τ_B are equal, as found in HCOX.

From [3] the recovery curve for $M_Z{}^A(t)$ can be reduced to the single exponential term if $\lambda_1 > \lambda_2$:

[5] $$M_Z{}^A(t) - M_Z{}^A = c_2 \exp(-t/T_{1A})$$

In the experiments under consideration the average relaxation time was about 13 s and the lifetime at the slowest rate about 8 s. From [4] this gives a value of $\lambda_1/\lambda_2 = 4.3$ which is larger than the lower limit set by Anet and Bourn (13). Using the single exponential approximation given by [5], a plot of ln $(M_Z{}^A(t) - M_Z{}^A)$ or more appropriately ln $(M_Z{}^A - M_Z{}^A(t))$ vs. time can be used to determine T_{1A}. An example of one of these plots is given in Fig. 3*B* for the recovery of the magnetization of H_B (2) in HCOX at 5°C when the saturation of H_B (1) is removed. To use [5] the first 6 s of data were not included in the analysis of the recovery curves to allow for the approximations made to [3]. The rate constant can be calculated from the value of T_{1A} and the value of τ_{1A} from the saturation experiment. The results are given in Table 3.

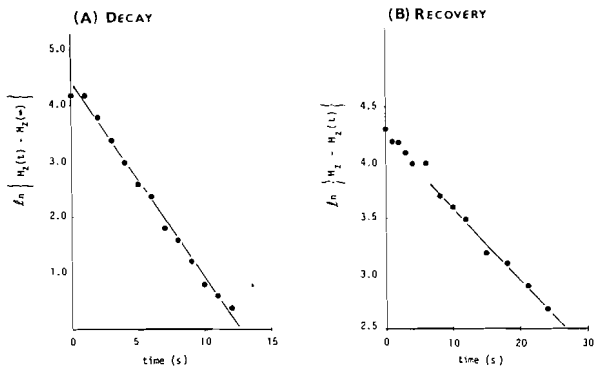

FIG. 3. A plot of ln $(M_Z(t) - M_Z(\infty))$ vs. time (*A*) and of ln $(M_Z - M_Z(t))$ vs. time (*B*) for the decay and recovery respectively of proton H_B (2) with the saturation of H_B (1) at 278 K.

For both the decay and recovery experiments the most reliable data were obtained from the observation of H_A (1) and the saturation of H_A (2). Table 3 includes data from different saturation–recovery sequences to show that similar results are obtained by interchanging the observation-saturation proton and by using different exchanging protons. Since the results are the same for the different methine protons in HCOX both methyl groups must rotate at the same rate.

In Table 3 the values of T_1 and hence the rate constant k are not identical for the decay and recovery techniques. For the decay process τ_{1A} is obtained from the slope; T_1 depends on the measurement of the intensities $M_Z(\infty)$ and M_Z. For the recovery process T_1 is obtained from the slope. Since the measurement of the slopes is usually more reliable, the rate constant calculated with τ_{1A} from the decay and T_1 from the recovery is probably more accurate.

The average value of T_1 of approximately 13 s is about what would be expected for a proton relaxation in a protonated solvent, where the value of T_1 is undoubtedly dominated by the intermolecular spin–lattice relaxation term (18).

Determination of Activation Parameters

The data necessary for both the Arrhenius plot and the Eyring plot are found in Tables 2 and 3. The plot of ln k vs. $1/T$ in Fig. 4 was used to determine E_a, the activation energy; the plot of ln (k/T) vs. $1/T$ in Fig. 5 was used for the transition state parameters $\Delta H^{\ddagger}$, $\Delta S^{\ddagger}$, $\Delta G^{\ddagger}$. For the transition state calculations the transmission coefficient is taken to be unity which is probably more consistent with a concerted process. A summary of the activation and transition state parameters for HCOX and some related compounds is given in Table 4. The standard errors reported in Table 4 for HCOX were obtained from Binsch's program ACTPAR (19) which incorporates errors

Can. J. Chem. Downloaded from www.nrcresearchpress.com by 210.87.254.5 on 09/05/12
For personal use only.

TABLE 4. Summary of activation parameters for HCOX,* and some related chloro-substituted compounds

Compound	Solvent	Temperature (K)	Arrhenius parameters E_a (kcal mol^{-1})	log A	Transition state parameters† $\Delta H^{\ddagger}$	$\Delta S^{\ddagger}$	$\Delta G^{\ddagger}$	Reference
HCOX	Methylcyclohexane	298	15.3 ±0.3	11.3 ±0.2	14.6±0.3	−8.8±0.8	17.22±0.07	(This paper)
OCMX	Toluene-d_8	298	14.93±0.13	12.45±0.09	14.3±0.14	−2.0±0.5	14.9 ±0.5	(4)
OCPX	Toluene-d_8	286	13.6 ±0.4	11.3 ±0.3	13.1±0.4	−7.3±1.3	15.4 ±0.1	(5)
2,3,6-PCT	Toluene-d_8	298	14.0 ±0.3	11.3 ±0.2	13.3±0.3	−7.0±0.7	15.4 ±0.1	(3)
2,4,6-PCT	Toluene-d_8	300	15.2 ±0.2	12.7 ±0.2	14.6±0.2	−1.1±0.7	14.9 ±0.1	(1)
	Methylcyclohexane		14.3 ±0.6	12.0 ±0.5	13.7±0.6	−4.4±2.2	15.0 ±0.2	(1)
OCOX	Tetradecane	356 (T_c)					17.7	(7)
HXCOX	Tetradecane	350 (T_c)					17.4	(7)

*The values for the activation parameters of HCOX are obtained from the program ACTPAR (12) using the data from Tables 2 and 3.
†kcal mol^{-1} for $\Delta H^{\ddagger}$, $\Delta G^{\ddagger}$ and cal mol^{-1} deg^{-1} for $\Delta S^{\ddagger}$.

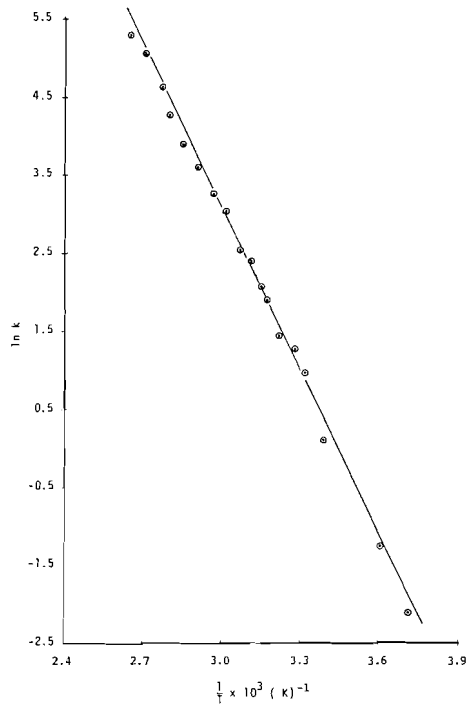

FIG. 4. A plot of ln k vs. the reciprocal of the absolute temperature for HCOX in methycyclohexane. Correlation coefficient 0.9969.

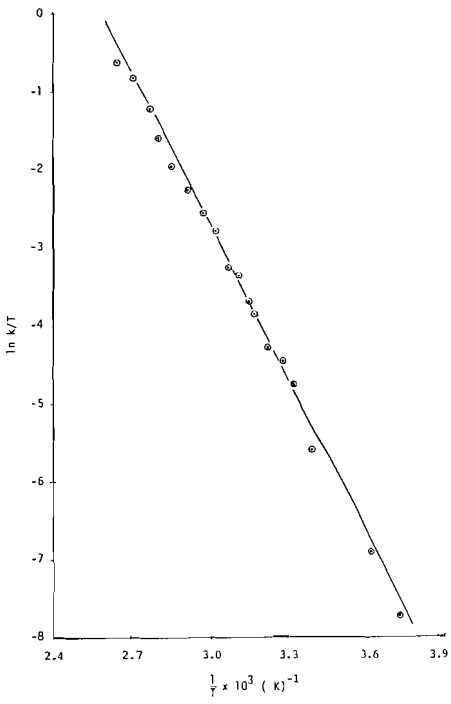

FIG. 5. A plot of ln k/T vs. the reciprocal absolute temperature for HCOX in methylcyclohexane. Correlation coefficient 0.9967.

in k and in T to determine the errors in the activation parameters. The uncertainty in $\Delta G^{\ddagger}$, $\sigma(\Delta G^{\ddagger})$, was determined (ref. 20 and ref. 19 therein)[2] from the equation:

$$[6] \quad \sigma^2(\Delta G^{\ddagger}) = \sigma^2(\Delta H^{\ddagger}) + T^2\sigma^2(\Delta S^{\ddagger}) - 2T\rho\sigma(\Delta H^{\ddagger})\sigma(\Delta S^{\ddagger})$$

The last term in [6] represents the covariance between $\Delta H^{\ddagger}$, $\Delta S^{\ddagger}$ where ρ is the correlation coefficient from the data used to determine $\Delta H^{\ddagger}$, $\Delta S^{\ddagger}$, and $\sigma(\Delta H^{\ddagger})$, $\sigma(\Delta S^{\ddagger})$ are the uncertainties in $\Delta H^{\ddagger}$, $\Delta S^{\ddagger}$. From [6] $\sigma(\Delta G^{\ddagger})$ for the other compounds in Table 4 in kcal/mol would be: OCMX: $\sigma(\Delta G^{\ddagger}) = 0.01$; OCPX: $\sigma(\Delta G^{\ddagger}) = 0.05$; 2,3,6-PCT: $\sigma(\Delta G^{\ddagger}) = 0.10$; 2,4,4-PCT in toluene-$d_8$: $\sigma(\Delta G^{\ddagger}) = 0.01$; 2,4,6-PCT in methylcyclohexane: $\sigma(\Delta G^{\ddagger}) = 0.06$. For both solutions of α,α,2,4,6-pentachlorotoluene the correlation coefficient ρ was assumed to be unity. The inclusion of the covariance term would indicate that the values of $\Delta G^{\ddagger}$ should be more accurate than previously reported.

[2]We are indebted to Dr. Gerhard Binsch for pointing out this procedure.

Coalescence Temperature Calculations

Because of the overlapping line positions it was not possible to determine the coalescence temperatures

Can. J. Chem. Downloaded from www.nrcresearchpress.com by 210.87.254.5 on 09/05/12
For personal use only.

Can. J. Chem. Downloaded from www.nrcresearchpress.com by 210.87.254.5 on 09/05/12
For personal use only.

for the individual protons from the observed spectra. However, the rate constants at coalescence, k_c, for each of the three pairs of exchanging protons in HCOX were determined from the expression (21):

$$[7] \qquad k_c = \pi\Delta\nu/\sqrt{2}$$

where $\Delta\nu$ is the nonexchanging chemical shift difference of the proton in the two conformers. The coalescence temperatures were calculated from k_c and the first order fit of ln k vs. $1/T$ from Fig. 4, ln $k_c = 26.01 - (7653/T_c)$. The values of $\Delta G_c^{\ddagger}$, the transition state free energy at coalescence, were obtained from eq. 8 (22):

$$[8] \qquad \Delta G_c^{\ddagger} = 0.004573\, T_c\,(9.97 + \log T_c/\Delta\nu)$$

The coalescence data are given in Table 5.

Comparison of Activation Parameters for Related Compounds

The activation parameters for HCOX and a number of related compounds are given in Table 4. It is satisfying to note that the values of $\Delta S^{\ddagger}$ are all small and negative for the compounds studied by line shape analysis. This would be expected as the transition states should all be somewhat similar, perhaps with a loss of vibrational contribution to the entropy in the more sterically crowded, and hence more rigid, transition state (16).

The transition state free energy may be the most reliable measure of differences in hindered rotation since it is the least sensitive to error (23). Although the values for $\Delta G^{\ddagger}$ from Table 4 are not all at the same temperature, the values of $\Delta S^{\ddagger}$ are small so that $\Delta G^{\ddagger}$ is insensitive to these small temperature variations.

Earlier studies rationalized the increase in $\Delta G^{\ddagger}$ from α,α,2,4,6-pentachlorotoluene (2,4,6-PCT), $\Delta G^{\ddagger} = 14.9 \pm 0.1$ kcal mol^{-1} in toluene-d_8 (1), to α,α,2,3,6-pentachlorotoluene (2,3,6-PCT), $\Delta G^{\ddagger} = 15.4 \pm 0.1$ kcal mol^{-1} in toluene-d_8 (3), on the basis of the buttressing effect of adjacent chlorine atoms on the ring (3). The barrier for α,α,α′,α′,2,3,5,6-octachloro-*p*-xylene (OCPX), $\Delta G^{\ddagger} = 15.4 \pm 0.1$ kcal mol^{-1} in toluene-d_8 (5) appeared to confirm this explanation. However, such rationale does not account for the free energy being lower for α,α,α′,α′,2,4,5,6-octachloro-*m*-xylene (OCMX), $\Delta G^{\ddagger} = 14.9 \pm 0.5$ kcal mol^{-1} in toluene-d_8 (4) and an explanation has been advanced suggesting that buttressing may increase the ground state energy more than the transition state energy (5). If each of the dichloromethyl groups of α,α,α′,α′,α″,α″,2,4,6-nonachloromesitylene (NCM) were treated as an independent rigid rotor flanked by a single chlorine on each side, the value of $\Delta G^{\ddagger}$ should be comparable to that for 2,4,6-PCT; however, the consideration of the 'effective' size (24) for the dichloromethyl groups suggests that the $\Delta G^{\ddagger}$ value be comparable to OCMX. The experimental value for NCM, $\Delta G^{\ddagger} = 16.1 \pm 0.06$ kcal mol^{-1} in toluene-d_8 (6) indicates that these trends are not reliably predicted using buttressing effects.

Two molecules that are very similar to HCOX have been studied by Mark and Pattison (7), α,α,α′,α′,3,4,5,6-octachloro-*o*-xylene (OCOX, corresponding to compound **1** in ref. 7) and α,α,α′,α′,3,6-hexachloro-*o*-xylene (HXCOX, corresponding to **2** in ref. 7). The free energy of activation of these two molecules should correspond closely to that of HCOX as all three should exhibit similar 'cogwheel' effects and the ring distortion and/or buttressing due to the chlorine atoms on the ring would predict that the value of $\Delta G^{\ddagger}$ for HCOX would be between that for HXCOX and OCOX. With $\Delta G^{\ddagger}$ for OCOX at coalescence equal to 17.7 kcal mol^{-1} and $\Delta G^{\ddagger}$ for HXCOX at coalescence equal to 17.4 kcal mol^{-1} (7), both obtained in tetradecane, the values are comparable for HCOX within experimental error.

TABLE 5. Summary of coalescence temperatures and $\Delta G^{\ddagger}$ values* for the protons of HCOX in methylcyclohexane

Exchanging proton	Δν (Hz)	k_c (s^{-1})	T_c (K)	$\Delta G^{\ddagger}$ (T_c) (kcal mol^{-1})
H_A	47.1	104.6	358.3	17.8
H_B	39.2	87.1	355.3	17.8
H_X	9.6	21.3	333.5	17.6

*Calculated as described in the text.

Acknowledgements

We are indebted to Dr. J. Peeling for the helpful discussions, to Dr. T. Schaefer for his assistance and the use of the spectrometer, and to Dr. V. Pattison for his participation in the HCOX synthesis.

1. B. J. Fuhr, B. W. Goodwin, H. M. Hutton, and T. Schaefer. Can. J. Chem. **48**, 1558 (1970).
2. J. Peeling, T. Schaefer, and C. M. Wong. Can. J. Chem. **48**, 2839 (1970).
3. M. A. H. Stewart, T. Schaefer, H. M. Hutton, and C. M. Wong. Can. J. Chem. **49**, 1085 (1971).
4. J. Peeling, B. W. Goodwin, T. Schaefer, and C. M. Wong. Can. J. Chem. **49**, 1489 (1971).
5. B. H. Barber and T. Schaefer. Can. J. Chem. **49**, 789 (1971).
6. J. Peeling, B. W. Goodwin, T. Schaefer, and J. B. Rowbotham. Can. J. Chem. **51**, 2110 (1973).
7. V. Mark and V. A. Pattison. Chem. Commun. 553 (1971).
8. C. Roussel, M. Chenon, and J. Metzger. Tetrahedron Lett. 1861 (1971).
9. G. Binsch. J. Am. Chem. Soc. **91**, 1304 (1969).
10. S. Forsen and R. A. Hoffman. J. Chem. Phys. **39**, 2892 (1963).
11. S. Forsen and R. A. Hoffman. Acta Chem. Scand. **17**, 1787 (1963).

12. S. FORSEN and R. A. HOFFMAN. J. Chem. Phys. **40**, 1189 (1964).
13. F. A. L. ANET and A. J. R. BOURN. J. Am. Chem. Soc. **89**, 760 (1967).
14. L. E. HINKEL, E. E. AYLING, and L. C. BEVAN. J. Chem. Soc. 1874 (1928).
15. M. BARFIELD and B. CHAKRABARTI. Chem. Rev. **69**, 757 (1969).
16. J. PEELING, L. ERNST, and T. SCHAEFER. Can. J. Chem. **52**, 849 (1974).
17. G. BINSCH and D. A. KLEIER. The computation of complex exchange-broadened NMR spectra. Program 140, Quantum Chemical Program Exchange, Indiana University, 1969.
18. J. H. NOGGLE and R. E. SCHRIMER. The nuclear Overhauser effect. Academic Press, New York, NY. 1971.
19. G. BINSCH. J. Am. Chem. Soc. **94**, 2770 (1972).
20. R. R. KRUG, W. G. HUNTER, and R. A. GRIEGER. J. Phys. Chem. **80**, 2335 (1976); and reference 19 therein.
21. I. O. SUTHERLAND. *In* Annual reports on NMR spectroscopy. Vol. 4. *Edited by* E. F. Mooney. Academic Press, New York, NY. 1971.
22. S. GLASSTONE, K. J. LAIDLER, and H. EYRING. Theory of rate processes. McGraw-Hill Book Co., New York, NY. 1941.
23. G. BINSCH. *In* Dynamic nuclear magnetic resonance spectroscopy. *Edited by* L. M. Jackman and F. A. Cotton. Academic Press, New York, NY. 1975. Chapt. 3.
24. B. NILSSON, P. MARTINSON, K. OLSSON, and R. E. CARTER. J. Am. Chem. Soc. **96**, 3190 (1974).

Can. J. Chem. Downloaded from www.nrcresearchpress.com by 210.87.254.5 on 09/05/12
For personal use only.

Photoinduced chlorination and bromination of haloadamantanes in tetrachloromethane and bromotrichloromethane[1]

ROBERT R. PERKINS[2] AND RICHARD E. PINCOCK

Department of Chemistry, University of British Columbia, Vancouver, B.C., Canada V6T 1W5

Received October 21, 1977

ROBERT R. PERKINS and RICHARD E. PINCOCK. Can. J. Chem. **56**, 1269 (1978).

Irradiation of 1-fluoro-, 1-chloro-, and 1-bromoadamantanes in halogenated solvents leads to free radical halogenation of the adamantane skeleton without exchange of the 1-halo atom. Reactions in tetrachloromethane yield products substituted at both the secondary carbons (i.e., bridge carbons) and at tertiary bridgehead carbons. Bridgehead substituted bromo-products greatly predominate when bromotrichloromethane is used as a solvent. Using this difference in the type of products formed from CCl_4 and $BrCCl_3$ a variety of mixed-halo substituted adamantanes were prepared from 1-monohaloadamantanes. Irradiation of 1-iodoadamantane in either solvent proceeds initially only with halogen exchange rather than halogenation of the ring system.

ROBERT R. PERKINS et RICHARD E. PINCOCK. Can. J. Chem. **56**, 1269 (1978).

L'irradiation des fluoro-1, chloro-1 et bromo-1 adamantanes dans des solvants halogénés conduit à l'halogénation radicalaire du squelette adamantane sans échange de l'atome d'halogène en position 1. Les réactions dans le tétrachlorométhane conduisent à des produits substitués aux deux carbones secondaires (i.e. les atomes de carbone de pont) ainsi qu'à des produits substitués au niveau des carbones tertiaires des têtes de pont. Les produits bromés substitués sur les têtes de pont prédominent grandement quand on utilise le bromotrichlorométhane comme solvant. Faisant appel à cette différence dans les types de produits formés à partir de CCl_4 et $BrCCl_3$, on a pu préparer un grand nombre d'adamantanes substitués par divers halogènes à partir d'adamantanes monohalogénés en position 1. L'irradiation de l'iodo-1 adamantane dans tous les solvants conduit initialement à un échange d'halogène plutôt qu'à l'halogénation du système cyclique.

[Traduit par le journal]

The rapid growth in the field of adamantane chemistry has been a result of the ready availability of the parent compound from Schleyer's rearrangement synthesis (1). From adamantane itself the further production of many interesting and useful derivatives has usually involved an initial substitution reaction at a tertiary bridgehead position (2). Most of these substitution reactions have involved carbonium ion intermediates and, because reactions involving substitution or elimination of hydrogens at secondary (bridge) positions are relatively unfavoured (3) or nearly impossible (4), the ionic reactions at bridgeheads generally proceed in good yields.

The free radical chemistry of adamantanes has received relatively less attention. The free radical substitutions usually occur with less discrimination at both tertiary and secondary positions and give rise to complex mixtures of structural and stereoisomers (5–7). In an early study by Smith and Williams (8) the photochlorination of adamantane with molecular chlorine in various solvents was examined. A mixture of bridge and bridgehead chlorides, the ratio being solvent dependent, was isolated. It was also found that extensive polychlorination occurred when carbon tetrachloride was the solvent.

In previous papers (9, 10) it has been shown that, depending upon the halogen involved, products derived from carbonium ion and/or free radical substitution processes could be isolated from irradiation of adamantyl halides in methanol. We have further examined the photochemical reaction of these halides in halogenated solvents to determine if the chlorination and polychlorination reported by Smith and Williams (8) arises from reactions involving the solvent rather than from added molecular chlorine. Synthetic aspects are also of interest. New mixed halo-substituted adamantanes would be made available by beginning with a 1-monohaloadamantane and then introducing a different halogen at secondary and tertiary positions by a free radical route. These cannot be formed by ionic halogenation conditions (e.g., Br_2 with Lewis acids (11)) which substitute for all halogens present as well as introduce halogen atoms essentially exclusively in bridgehead positions.

Results and Discussion

In initial experiments the products of photolysis of

[1]Presented in part at the 2nd Joint Conference of the Canadian Institute of Chemistry and the American Chemical Society, Montreal, Quebec, May 1977.

[2]Department of Chemistry, Memorial University, Regional College, Corner Brook, Nfld. A2H 6P9.

Can. J. Chem. Downloaded from www.nrcresearchpress.com by 210.87.254.6 on 09/05/12
For personal use only.

Can. J. Chem. Downloaded from www.nrcresearchpress.com by 210.87.254.6 on 09/05/12
For personal use only.

adamantane in methylene chloride, chloroform, and carbon tetrachloride were investigated. Solutions were placed in quartz tubes, carefully degassed, and irradiated with a medium pressure mercury lamp for 48 h. Analysis by glc indicated that no reaction had occurred in methylene chloride, the chloroform solution contained adamantane, 1-chloroadamantane, and 2-chloroadamantane in the relative ratio 68:30:2. The reaction in carbon tetrachloride was faster, contained no unreacted adamantane, and produced seven chlorinated products in addition to hexachloroethane. Liquid chromatography allowed partial separation of the products which were then purified by preparative gas–liquid chromatography (glc). The products (in order of elution on an OV-17 column) were found to be hexachloroethane, 1-chloroadamantane (29%), 2-chloroadamantane (18%), 1,3-dichloroadamantane (16%), unknown minor product (6%), *anti*-1,4-dichloroadamantane and *syn*-1,4-dichloroadamantane (18% combined), and 1,3,5-trichloroadamantane (13%) (approximate yields in parentheses were dependent on irradiation time). These compounds were identified by ir and nmr spectral comparisons with authentic compounds. Authentic samples of the two isomeric 1,4-dichloroadamantanes were prepared by aluminum chloride promoted rearrangement reactions (12). Gas–liquid chromatographic comparisons of retention times with that of authentic 1,2-dichloroadamantane (13) showed that it was absent.

Irradiation of a carbon tetrachloride solution of either 1-fluoro-, 1-chloro-, or 1-bromoadamantane led to introduction of chlorine with a distribution of products similar to that described above for adamantane. The mixed polyhalo products were separated by glc and their structures assigned by glc retention times, nmr spectra, mass spectra, or elemental analysis. The configurations of the *syn*- and *anti*-1-halo-4-halo-adamantane stereoisomers were assigned by analogy to the known (12) and calculated (14) nmr spectra for the *syn*- and *anti*-1,4-dichloroadamantanes; the α-hydrogen on the C4 carbon of the *anti* compound having a larger δ value than that of the *syn* isomer.

For production of the several different compounds in each case of halogenation given above no molecular chlorine was initially present. The trichloromethyl radical or the chlorine atom formed from photolysis of the solvent (9, 10) are the possible hydrogen abstracting agents; the former is usually found to be a more selective agent (5–7). The nearly indiscriminate behaviour of the actual abstracting agent shows up in the variety of products formed by photohalogenation in CCl_4 solutions. The only possible products not produced in sufficient yields

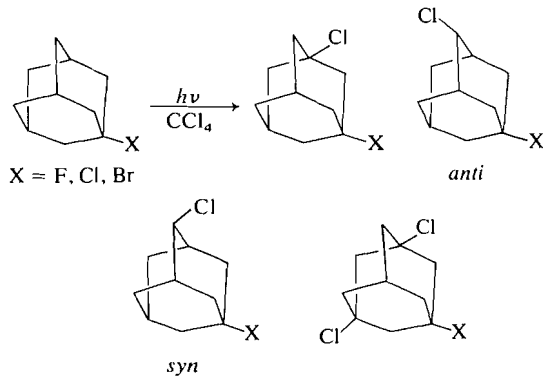

to isolate were the 1-halo-2-chloroadamantanes. The absence of such 1,2-disubstituted products may reflect the steric requirements for abstraction by a large radical as well as an unfavourable polar character of the abstraction reaction when the substrate halogen is close to the reactive site. The lack of selectivity is indicative of chlorine atoms and additional evidence comes with the presence of hydrogen chloride and hexachloroethane formed in copious amounts during the irradiation of carbon tetrachloride solutions containing adamantanes.

When the solvent was changed to bromotrichloromethane the 1-haloadamantanes gave only brominated products. This is consistent with the known (15) greater transferability of the bromine atom over a chlorine atom of $BrCCl_3$. More unusual was the formation of essentially only products for bridgehead substitutions rather than from bridge substitution.

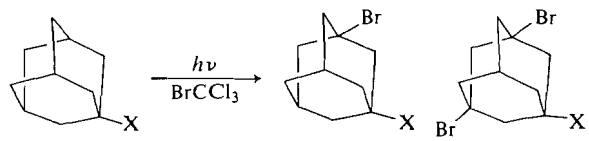

Although secondary products are formed on longer irradiations, the different initial products from CCl_4 and $BrCCl_3$ show that the same radical ($Cl_3C^{\cdot}$) can not be responsible in both systems for the product distributions. Another difference is that hexachloroethane is not formed in the $BrCCl_3$ system. Probably abstraction by the more selective radical $Cl_3C^{\cdot}$ is the major product forming step in $BrCCl_3$ while chlorine atoms are most active in CCl_4.

The transfer of bromine only and the more selective attack at bridgehead positions in $BrCCl_3$ made possible the synthesis of mixed bridgehead substituted halides, e.g., from 1-fluoroadamantane was produced only two major products 1-fluoro-3-bromoadamantane and 1-fluoro-3,5-dibromoadamantane. (The corresponding chlorination reaction

Can. J. Chem. Downloaded from www.nrcresearchpress.com by 210.87.254.6 on 09/05/12
For personal use only.

of 1-fluoroadamantane in CCl_4 distributed the substrate among four products; 1-fluoro-3-chloroadamantane, 1-fluoro-3,5-dichloroadamantane, and the *syn*- and *anti*-1-fluoro-4-chloroadamantanes.) Other substituted haloadamantanes are also made available by photochemical halogenations; 1-fluoro-3,5-dimethyladamantane was chlorinated and brominated at the remaining bridgehead position in CCl_4 and $BrCCl_3$, respectively, and 1-cyanoadamantane was brominated to 1-cyano-3-bromoadamantane.

The above reactions of 1-fluoro-, 1-chloro-, and 1-bromoadamantane involve substitution at new positions on the adamantyl ring without disruption of the 1-halo atom. With 1-iodoadamantane, in either CCl_4 or $BrCCl_3$, the initial reaction is direct photochemical exchange of the 1-iodo atom with solvent halogen. No doubt the propensity of iodo compounds to undergo photoactivation and give ionic intermediates leads to this exchange (9, 10). Unfortunately this activity prevents the preparation by photochemical means of mixed halogenated adamantanes that contain any iodine atoms.

Experimental

Melting points (uncorrected) were obtained with a Thomas Hoover capillary melting point apparatus using sealed tubes. Proton nuclear magnetic resonance spectra are for 10–15% solutions in benzene or carbon tetrachloride and are reported relative to tetramethylsilane at $\delta = 0.0$. High resolution mass spectra were obtained from an Atlas AE1-MS-902 spectrometer. Analytical gas–liquid chromatography was performed with a Perkin Elmer 900 instrument utilizing a flame ionization detector; preparative glc was carried out on a Varian Model 90-P instrument. Microanalyses were by Mr. P. Borda (University of B.C.).

Materials

Adamantane, 1-bromoadamantane, 1-chloroadamantane, and 1-cyanoadamantane were obtained from commercial sources. 1,3-Dimethyladamantane was kindly supplied by Sun Oil Company, Philadelphia, PA. 1-Fluoro- and 1-iodoadamantane were prepared according to literature procedures (11, 16). 1,3-Dichloro- and 1,3-dibromoadamantane as well as 1,3,5-trichloro- and 1,3,5-tribromoadamantane were available by published procedures (11). Samples of authentic *syn*- and *anti*-1,4-dichloroadamantanes and 1,2-dichloroadamantane were prepared by the method of Cuddy *et al.* (12, 13).

General Procedure for Photochemical Reactions

In a quartz vessel equipped with a nitrogen gas inlet and a condenser was placed 0.5–2 g of the haloadamantane and 50–70 ml of CCl_4 or $BrCCl_4$. The reaction vessel was clamped to a stand 10 cm from a GE UA-3 360 watt medium pressure mercury lamp contained in a water cooled quartz immersion well. The entire set-up was surrounded by aluminum foil to minimize loss of light. The degassed solution was irradiated and the reaction followed by glc (182 cm by 0.32 cm OD 8% OV-17 on Chromsorb W AW-DMCS 80/100 mesh), normally for 24 h.

The reaction mixture was poured into a saturated sodium bicarbonate solution and the organic phase washed well with water and dried over magnesium sulfate. Evaporation yielded a sticky yellow solid which was subjected to column chromatography. In the carbon tetrachloride reactions passage down a short silica gel column with pentane allowed separation of the hexachloroethane. The chlorides were washed from the column with chloroform and then eluted down an alumina column using pentane as the eluting solvent. Purified samples were obtained by preparative glc (152 cm by 0.64 cm OD 10% Carbowax 20 m on Chromsorb W 80/100 mesh).

Chlorination of 1-Bromoadamantane

The following monobromo compounds were prepared by irradiation of 1-bromoadamantane in CCl_4.

1-Bromo-3-chloroadamantane: mp 101.5–103°C. (lit. (6) mp 99–100°C); nmr (benzene) δ: 1.05, (unresolved t, 2H δ to both halogens), 1.61 (bs, bridgehead hydrogens γ to both halogens), 1.74 (d, β to Cl), 1.88 (d, β to Br), 2.55 (s, β to both halogens).

syn- *and* anti-*1-Bromo-4-chloroadamantane*: these could not be separated by glc; nmr (CCl_4) δ: 1.80–2.95 (m's), 4.20 (s, for *syn* compound), 4.36 (s, for *anti* compound). *Anal.* calcd. for $C_{10}H_{14}BrCl$: C 48.14, H 5.65; found: C 47.85, H 5.50.

1-Bromo-3,5-dichloroadamantane: colourless solid, mp 104.5–106°C; nmr (CCl_4) δ: 2.02 (unresolved d, 4H β to Cl atoms), 2.16 (unresolved d, 2H β to Br), 2.36 (m, 1H α to each halogen), 2.42 (s, 2H β to both Cl atoms), 2.56 (s, 4H β to Cl and Br); *Anal.* calcd. for $C_{10}H_{13}BrCl_2$: C 42.29, H 4.61; found: C 42.20, H 4.70.

Chlorination of 1-Fluoroadamantane

The following monofluoro compounds were prepared by irradiation of 1-fluoroadamantane in CCl_4.

1-Chloro-3-fluoroadamantane: colourless solid, mp 177–178°C; nmr (CCl_4) δ: 1.55 (unresolved t, 2H δ to both halogens), 1.81 (m, $J = 5.5$ Hz, 4H β to F), 2.01 (unresolved d, 4H β to Cl), 2.23 (d, $J = 5.5$ Hz, 2H β to both F and Cl), 2.35 (broad s, 2H γ to both F and Cl). *Anal.* calcd. for $C_{10}H_{14}FCl$: C 63.66, H 7.48; found: C 63.58, H 7.52.

syn-*4-Chloro-1-fluoroadamantane*: colourless white solid, mp 207–208°C; nmr (CCl_4) δ: 1.45–2.58 (m's), 4.09 (s, 1H); high resolution ms calcd. for $C_{10}H_{14}FCl$: 188.0767; found: 188.0766.

anti-*4-Chloro-1-fluoroadamantane*: colourless white solid, mp 213–215°C; nmr (CCl_4) δ: 1.40–2.45 (m's), 4.18 (s, 1H); high resolution ms calcd. for $C_{10}H_{13}FCl$: 188.0767; found: 188.0765.

1,3-Dichloro-5-fluoroadamantane: colourless solid, mp 135.5–137°C; nmr (CCl_4) δ: 1.80 (t, $J = 3.5$ Hz, 2H β to F), 1.93 (s, 4H β to Cl), 2.20 (d, $J = 5.5$ Hz, 4H, β to both Cl and F), 2.39 (s, 2H, β to both Cl atoms), 2.47 (m, 1H γ to all three halogen atoms); *Anal.* calcd. for $C_{10}H_{13}FCl_2$: C 53.83, H 5.87; found: C 53.50, H 5.99.

Bromination of 1-Fluoroadamantane

The following monofluoro compounds were prepared by irradiation of 1-fluoroadamantane in $BrCCl_3$.

1-Bromo-3-fluoroadamantane: colourless solid, mp 136–137°C; nmr (benzene) δ: 1.05 (unresolved t, 2H δ to both F and Br), 1.58 (m, 4H, β to F), 1.72 (s, 2H γ to both Br and F), 1.91 (s, 4H β to Br), 2.40 (d, $J = 5.5$ Hz, 2H β to both Br and F); *Anal.* calcd. for $C_{10}H_{14}BrF$: C 51.42, H 6.05; found: C 51.44, H 6.17.

1,3-Dibromo-5-fluoroadamantane: colourless solid, mp 160–162°C; nmr (benzene) δ: 1.32 (m, 2H β to F), 1.47 (m, 1H, γ to all three halogen atoms), 1.58 (s, 4H β to Br), 2.13 (d, $J = 5.5$ Hz, 4H β to both Br and to F), 2.44 (s, 2H β to both Br atoms); high resolution ms calcd. for $C_{10}H_{13}Br_2F$: 309.9369; found: 309.9351.

Bromination of 1-Chloroadamantane

In addition to the major product 1-bromo-3-chloroadamantane (see above), 1-chloro-3,5-dibromoadamantane, mp 99–102°C, was formed by irradiation of 1-chloroadamantane in $BrCCl_3$; nmr (benzene) δ: 1.45 (s, 3H, one γ to all three halogen atoms and two β to Cl), 1.59 (unresolved d, 4H β to Br), 2.27 (s, 4H β to both Cl and Br), 2.42 (s, 2H, β to both Br atoms); high resolution ms (no parent) calcd. for $C_{10}H_{13}BrCl$: 248.9869; found: 248.9874.

1-Bromo-3-cyanoadamantane

This compound was isolated from the photolysis of a solution of 1-cyanoadamantane in $BrCCl_3$ (crude yields 48% after irradiation for 24 h). After chromatography through alumina, recrystallization from hexane gave colourless platelets, mp 128.5–130°C; nmr (benzene) δ: 1.00 (s, 2H δ to CN and Br), 1.38 (s, 6H β to CN plus α to both CN and Br), 1.82 (s, 4H β to Br, 2.18 (s, 2H β to both Br and CN); *Anal.* calcd. for $C_{11}H_{14}BrN$: C 55.02, H 5.87, N 5.83; found: C 55.02, H 5.90, N 5.80.

Halogenation of 1-Fluoro-3,5-dimethyladamantane

1-Bromo-3,5-dimethyl-7-fluoroadamantane, mp 31–32°C, was the major product of irradiation of the parent fluoro compound in $BrCCl_3$ for 6 h. Minor products were not isolated; nmr (benzene) δ: 0.58 (s, methyl groups), 0.88 (s, 2H β to both methyl groups), 1.28 (d, J = 5.5 Hz, 4H β to F and methyl), 1.62 (s, 4H β to Br and methyl), 2.27 (d, J = 5.5 Hz, 2H β to both Br and F); high resolution ms calcd. for $C_{12}H_{18}BrF$: 261.1806; found: 261.1803.

Similarly 1-chloro-3,5-dimethyl-7-fluoroadamantane, an oil, mp ca. 20°C, was the major product when the parent compound was irradiated 12 h in CCl_4; nmr (benzene) δ: 0.61 (s, methyl groups), 0.87 (s, 2H β to both methyl groups), 1.27 (d, J = 5.5 Hz, 4H β to F and methyl), 1.45 (s, 4H, β to Cl and methyl), 2.10 (d, J = 5.5 Hz, 2H β to both Cl and F); high resolution ms calcd. for $C_{12}H_{18}FCl$: 216.1080; found: 216.1067.

Acknowledgement

Financial support provided by a grant from the National Research Council of Canada is gratefully acknowledged.

1. P. v. R. Schleyer. J. Am. Chem. Soc. **79**, 3293 (1957).
2. R. C. Fort, Jr. Adamantane, the chemistry of diamond molecules. *In* Studies in organic chemistry. Vol. 5. Marcel Dekker Inc., New York, NY. 1976.
3. R. C. Fort, Jr. and P. v. R. Schleyer. Adv. Alicyclic Chem. **1**, 283 (1966).
4. W. Burns and M. A. McKervey. Chem. Commun. 858 (1974).
5. C. V. Smith and W. E. Billups. J. Am. Chem. Soc. **96**, 4307 (1974).
6. I. Tabushi, Y. Aoyama, S. Kojo, J. Hamuro, and Z. Yoshida. J. Am. Chem. Soc. **94**, 1177 (1972).
7. P. H. Owens, G. J. Gleicher, and L. M. Smith, Jr. J. Am. Chem. Soc. **90**, 4122 (1968).
8. C. V. Smith and H. D. Williams. J. Org. Chem. **26**, 2207 (1961).
9. P. J. Kropp, G. S. Poindexter, N. J. Pienta, and D. C. Hamilton. J. Am. Chem. Soc. **98**, 8135 (1976).
10. R. R. Perkins and R. E. Pincock. Tetrahedron Lett. 943 (1975).
11. J. W. McKinley, R. E. Pincock, and W. Bruce Scott. J. Am. Chem. Soc. **95**, 2030 (1973).
12. B. D. Cuddy, D. Grant, A. Karim, M. A. McKervey, and E. J. F. Rea. J. Chem. Soc. Perkin Trans. 1, 2701 (1972).
13. B. D. Cuddy, D. Grant, and M. A. McKervey. J. Chem. Soc. C, 3173 (1971).
14. H. W. Geluk and J. L. M. A. Schlatmann. Tetrahedron, **24**, 5369 (1968).
15. C. Rüchardt, K. Herwig, and S. Eichler. Tetrahedron Lett. 421 (1969); B. Giese. Angew. Chem. Int. Ed. Engl. **15**, 173 (1976).
16. K. S. Bhandari and R. E. Pincock. Synthesis, 655 (1974).

Can. J. Chem. Downloaded from www.nrcresearchpress.com by 210.87.254.6 on 09/05/12
For personal use only.

Aqueous trifluoroacetic acid as a medium for organic reactions. II. The oxidation of hydrocarbons by manganese(VII)

ROSS STEWART AND UDO A. SPITZER

Department of Chemistry, University of British Columbia, Vancouver, B.C., Canada V6T 1W5

Received November 21, 1977

ROSS STEWART and UDO A. SPITZER. Can. J. Chem. **56**, 1273 (1978).

The oxidation of 11 alkanes, 4 cycloalkanes, and 10 arenes by potassium permanganate in aqueous trifluoroacetic acid has been studied. The reaction rates are approximately first order in h_R, the antilogarithm of the acidity function $-H_R$, and the active oxidant is believed to be MnO_3^+, either free or complexed. The rate of abstraction of primary, secondary, and tertiary hydrogen atoms in the C_5H_{12} isomers is in the ratio 1:60:2100 and the rate per methylene in normal alkanes increases with increasing chain length. Cyclohexane is the least reactive of the cycloalkanes and the isotope effect in the oxidation of cyclo-C_6D_{12} is 4.3 at 25°C. The mechanism of oxidation of the aliphatic hydrocarbons is believed to be hydrogen-atom abstraction by MnO_3^+. The oxidation of arenes C_6H_5Z has a ρ^+ value of -5.29 when appropriate σ^+ values of Z are used, and there is no isotope effect when the reaction rates of $C_6H_5CH_3$, $C_6H_5CD_3$, and $C_6D_5CD_3$ are compared. The mechanism of oxidation of the aromatic compounds is believed to be electrophilic attack of MnO_3^+ at the activated positions of the ring followed by rapid degradation of the ring system.

ROSS STEWART et UDO A. SPITZER. Can. J. Chem. **56**, 1273 (1978).

On a étudié l'oxydation de 11 alcanes, de 4 cycloalcanes et de 10 arènes par le permanganate de potassium dans de l'acide trifluoroacétique aqueux. Les vitesses de réaction sont approximativement du premier ordre en h_R, l'antilogarithme de la fonction d'acidité $-H_R$ et l'on croit que l'oxydant actif est le MnO_3^+ soit à l'état libre ou complexé. Les vitesses d'enlèvement des atomes d'hydrogène primaire, secondaire et tertiaire des isomères du C_5H_{12} sont dans le rapport de 1:60:2100 et la vitesse d'enlèvement par méthylène, dans les alcanes normaux, augmente lorsque l'on augmente la longueur de la chaîne. Le cyclohexane est le moins réactif des cycloalcanes et l'effet isotopique lors de l'oxydation du cyclo-C_6D_{12} est de 4.3 à 25°C. On croit que le mécanisme d'oxydation des hydrocarbures aliphatiques procède par l'enlèvement d'un atome d'hydrogène par MnO_3^+. La valeur de ρ^+ pour l'oxydation des arènes C_6H_5Z est de -5.29 quand les valeurs σ^+ appropriées de Z sont utilisées; il n'y a aucun effet isotopique quand on compare les vitesses de réaction de $C_6H_5CH_3$, $C_6H_5CD_3$ et $C_6D_5CD_3$. On croit que le mécanisme de l'oxydation des composés aromatiques procède par une attaque électrophile du MnO_3^+ sur les positions activées du cycle suivie par une dégradation rapide du système cyclique.

[Traduit par le journal]

Introduction

Permanganate is an extremely versatile oxidizing agent, being able to oxidize many different types of organic compounds under a wide variety of experimental conditions (1). Activation by both acids and bases is commonly found, the latter usually resulting from the organic compound being converted to a more reactive form by base, e.g. alkoxide ions being formed from alcohols, whereas the former is usually the result of a change in the state of the oxidant. Hydrocarbons lack an ionizable functional group and, in any case, are insoluble in aqueous base, and hence alkaline permanganate is generally an ineffective oxidant for such compounds. Aqueous acid activates the manganese(VII) but the problem of water insolubility of hydrocarbons remains. Mixed solvents such as aqueous acetic acid have been used (2) but they present the problem of degradation of the solvent by permanganate. Phase transfer catalysis (3) using a benzene–water pair shows promise but, again, solvent degradation prevents less reactive substrates being studied.

Trifluoroacetic acid (TFA) has been shown to be a useful medium for a number of reactions, including chromium(VI) and other oxidations (4) and electrophilic aromatic substitution (5, 6), and we have investigated its use as a medium for manganese(VII) oxidation. It turns out to have the virtues of being highly resistant to oxidation by permanganate and being sufficiently acidic to convert permanganate ion to a more reactive entity. Furthermore, most organic solvents are quite soluble in TFA solutions, as is potassium permanganate.

The chemical changes that occur as the TFA content of an aqueous TFA solution of potassium permanganate is increased were the subject of a previous paper (7). There we showed that the green species that appears in solutions containing more than 82

Can. J. Chem. Downloaded from www.nrcresearchpress.com by 210.87.254.6 on 09/05/12
For personal use only.

Can. J. Chem. Downloaded from www.nrcresearchpress.com by 210.87.254.6 on 09/05/12
For personal use only.

TABLE 1. Correlation of oxidation rate with acidity function for various hydrocarbons

Compound	log $k_2/-H_0$ correlation, slope	Correlation coefficient	log $k_2/-H_R$ correlation, slope	Correlation coefficient
Pentane	2.86	0.985	1.03	0.987
Hexane	2.59	0.994	1.16	0.991
Cyclohexane	2.95	0.992	1.22	0.989
Cyclohexane-d_{12}	2.95	0.986	1.23	0.990
Cycloheptane	2.78	0.995	0.79	0.986
Benzene	4.89	0.981	0.98	0.997
Toluene	5.81	0.996	0.82	0.9995
Toluene-d_8	5.88	0.993	0.82	0.997

wt.% TFA is the permanganyl cation MnO_3^+, either in the free form or as its trifluoroacetate complex (or ester) $MnO_3 \cdot O_2CCF_3$. The present paper deals with the mangenese(VII) oxidation of 11 alkanes, four cycloalkanes, and 10 arenes and derivatives in aqueous TFA.

Results and Discussion

Permanganate's oxidizing powers rise markedly as the concentration of the TFA component of aqueous TFA is increased. For hydrocarbons, both aliphatic and aromatic, the oxidation rate is roughly proportional to the increase in the h_R value of the solution, where h_R and its negative logarithm, the acidity function H_R (8), represent the ability of an acidic solution to convert aryl alcohols to carbonium ions.

[1] $$ROH + H^+ \rightleftharpoons R^+ + H_2O$$

The increase in rate is very much larger than would be the case if the activation were governed by the acidity function H_0, which measures the ability of an acidic system to protonate a series of amine indicators. Although both H_R and H_0 give linear plots when log k is plotted against acidity function the slopes in the case of H_R are grouped near unity, whereas those for H_0 range from a low of 2.59 for hexane to a high of 5.88 for toluene-d_8. Figure 1 shows a plot of log k_2, where k_2 is the bimolecular rate constant, against $-H_R$ for hexane, cyclohexane, and cyclohexane-d_{12} and Table 1 lists the slopes and correlation coefficients for both the H_0 and H_R correlations.

The kinetics of the oxidation of alkanes and arenes at all acidities have been found to be first order in permanganate and first order in hydrocarbon. Since the slopes of the log $k_2/-H_R$ plots are near unity the general rate expression for the reaction in aqueous TFA is approximated by [2].

[2] $$-d[MnO_4^-]/dt = k[MnO_4^-][RH]h_R$$

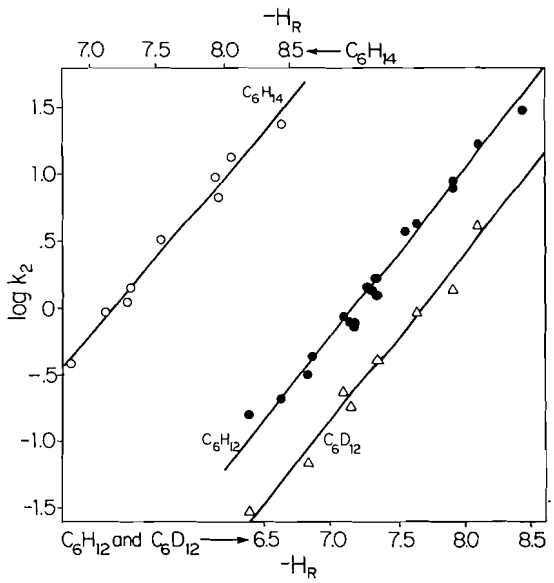

FIG. 1. Correlation of logarithm of oxidation rate with acidity function H_R for hexane, cyclohexane, and cyclohexane-d_{12}.

Furthermore, since the concentration of the green manganese species (MnO_3^+ or $MnO_3 \cdot O_2CCF_3$) in higher concentration of aqueous TFA has been previously shown to be governed by H_R one can infer that it is the active oxidant.[1] The slopes for the two processes, the equilibrium governing the production of MnO_3^+ or $MnO_3 \cdot O_2CCF_3$, and the hydrocarbon oxidation rates are not identical, however, being 0.76 in the former case and between 0.79 and 1.23 in the latter. Most of the oxidations were, of necessity, conducted in solutions where the extent of formation of the green species was much too small to measure and the variability in h_R dependence may reflect this fact.

It is possible to rationalize the approximate unit dependency of rate on h_R by making a number of

[1]An early suggestion that MnO_3^+ might be the active oxidant in acidic permanganate was made by L. S. Levitt (15).

Can. J. Chem. Downloaded from www.nrcresearchpress.com by 210.87.254.6 on 09/05/12
For personal use only.

assumptions regarding activity coefficient behaviour of the various species involved in the equilibrium and the oxidation but we will not burden the reader with what seems to us to be a tenuous line of reasoning. Suffice it to state that to a first approximation H_R governs both the equilibrium production of the active manganese species and the rate of hydrocarbon oxidation. Since MnO_3^+ will almost certainly be more reactive than the complex or ester $MnO_3 \cdot O_2CCF_3$ with which it will be in equilibrium, we believe that it is probably responsible for the bulk of the oxidation in aqueous TFA, even if it is present in smaller concentration. Permanganate ion, MnO_4^-, is, of course, the principal manganese component in all solutions less acidic than 90 wt.% TFA.

Alkanes

The rate of oxidation of alkanes by Mn(VII) in TFA is sensitive to structural differences in the substrate, in particular to chain-branching. Thus the isomeric compounds pentane, isopentane, and neopentane react at the rates shown in Table 2.

It is clear that primary hydrogen atoms are much less subject to attack than those at secondary positions, and that the lone tertiary hydrogen atom in isopentane is responsible for the compound's high reactivity. When appropriate statistical corrections are made for the number of hydrogen atoms of each type, the following reactivity ratio emerges, 1°:2°:3° = 1:60:2100. Such a ratio is not unreasonable for a reaction proceeding by way of hydrogen atom abstraction and producing radicals. Both much larger and much smaller ratios have been found in known radical processes (see for example data tabulated in ref. 9). On the other hand, if hydride ion were the abstracted species and carbonium ions the intermediates thus formed, a very much larger reactivity ratio would be expected (10).

The initial bond-breaking step is followed by further reactions that degrade the molecule, most of these steps being faster than the original reaction. The oxidation of pentane under conditions of excess substrate gives 2-pentanone, 3-pentanone, and a trace of propanoic acid as the reaction products. The corresponding alcohols, 2-pentanol and 3-pentanol, are presumably intermediates in this sequence since we have found them to react with Mn(VII)–TFA at a faster rate than either pentane or the ketones. In fact, 2-pentanol and 3-pentanol react at identical rates. Furthermore, twice as much 2-pentanone as 3-pentanone (66 to 34%) is isolated by glc from the oxidation of pentane (the statistical ratio is 2:1). We can, therefore, calculate all the relevant rate constants for the various steps in the oxidation (Scheme 1).[2]

TABLE 2. Rate constants for the oxidation of the C_5H_{12} isomers by Mn(VII) in 82 wt.% aqueous TFA at 25°C

Isomer	k_2 (M^{-1} s^{-1})	Relative rate
$CH_3(CH_2)_3CH_3$	6.0	30
$(CH_3)_2CHCH_2CH_3$	37[a]	185
$(CH_3)_4C$	0.2	1

[a]Extrapolated from rates at lower acidities, assuming a linear relation between h_R and k; an almost identical ratio for the rates of pentane and isopentane is found at lower acidity.

TABLE 3. Oxidation rates of normal alkanes C_nH_{2n+2} by Mn(VII) in 82 wt.% aqueous TFA at 25°C

n	k_2 (M^{-1} s^{-1})	k_2/n	$k_2/n - 2$
5	6.0	1.2	2.0
6	10.5	1.8	2.6
7	23.0	3.3	4.6
8	30.0	3.8	5.0
9	41.5	4.6	5.9
10	49.6	5.0	6.2
11	61.0	5.5	6.8
12	72.4	6.0	7.2
13	82.5	6.3	7.5

The effect of chain length on rate of reaction of *n*-alkanes by Mn(VII)–TFA is shown in Table 3. The rate constants rise as the chain length increases, as might be expected, since there are more sites of attack. The rate per carbon atom also rises. We have seen that methylene groups are much more reactive than methyl groups and it might be expected that the rate per methylene group would not be significantly affected by chain length but this is not the case. As can be seen from the results in the first column of Table 3 there is a marked increase in rate per methylene ($k_2/n - 2$), which tends to level off somewhat at longer chain length.[3] Presumably there is a cumulative inductive, or other, effect operating to make the methylene groups in the higher alkanes more reactive than those in shorter chains. When electron-withdrawing groups are present the oxidation is slowed drastically. (Nitroethane, propanonitrile, and propanoic acid are highly resistant to oxidation by potassium permanganate in 80 wt.% TFA, con-

[2]Although the product-isolation experiments were conducted in 80 wt.% TFA and the rate measurements in 76 wt.% TFA the identical dependency of rate on acidity for 2- and 3-pentanol suggests that the difference is not of significance.

[3]The larger difference between C_6 and C_7 than between C_5 and C_6 is probably an artifact. The rate constants given for the C_7–C_{13} compounds were obtained by interpolation whereas the values for C_5 and C_6 come from direct measurements.

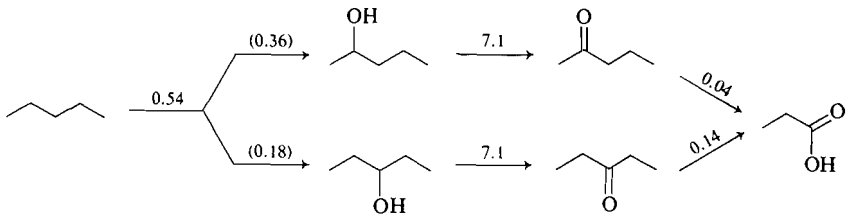

SCHEME 1. Steps in the manganese(VII) oxidation of pentane to propanoic acid in aqueous TFA. The numbers above each arrow represent the rate constant, M^{-1} s^{-1}, for that step in 76 wt.% TFA. The values in parentheses are partial rate constants calculated using the results of product isolation experiments.

ditions under which propane and other alkanes react readily.)

Whether alkyl groups have the same or different inductive effects (as expressed by their σ_I or σ^* values) is a matter of current controversy (11, 12) and the present work may be pertinent in this regard. Our results show that a methylene C—H bond becomes more reactive to Mn(VII)–TFA the greater the number of methylenes in the two attached alkyl groups. Since electron release favours the reaction it is clear that, in our case, higher alkyl groups have larger effective inductive effects than do the lower alkyl groups. (A similar effect is observed for the ionization potential of alkanes (13).)

Cycloalkanes

The effect of ring size on oxidation of the cycloalkanes from C_5–C_8 is shown in Table 4. The preference of six-membered ring systems for tetragonal rather than trigonal bonding is well known and the lower rate of oxidation of cyclohexane is in agreement with such experience. Further, the oxidation of the four cycloalkanes with CrO_3 in glacial acetic acid shows similar behaviour: a ratio of 2.0:1.0:6.6:22.4 is obtained for the rates of oxidation of the C_5–C_8 compounds (10*d*). It is likely that the latter reaction takes place by hydrogen-atom abstraction (10*b*) and this is further evidence supporting the mechanism given earlier in this paper. (Processes involving carbonium ion intermediates show similar orders of reactivity within the C_5–C_8 series but the effects are generally much more pronounced (14).)

It is worth noting that cyclohexane and hexane are oxidized at almost identical rates. All the other cycloalkanes studied here react at least twice as fast as their open-chain analogs. A similar effect has been observed in a number of other hydrogen-atom abstraction processes studied by Bunce.[4]

An isotope effect of 4.3 has been found for the oxidation of cyclohexane-d_{12} at 25°C (Fig. 1). A primary isotope effect of such magnitude shows clearly that the rate-controlling step is carbon–hydrogen bond cleavage, although it is not helpful in distinguishing between hydrogen-atom and hydride-ion abstraction (16).

TABLE 4. Oxidation rates for cycloalkanes by Mn(VII) in 76 wt.% TFA at 25°C

Cycloalkane	k_2 (M^{-1} s^{-1})
C_5	3.1
C_6	1.0
C_7	5.2
C_8	14.0

Arenes

Aromatic compounds containing alkyl side chains are oxidized by Mn(VII)–TFA predominantly at the ring rather than at the side chain in sharp contrast to the behaviour of most transition metal oxidants in particular Mn(III), Ce(IV), and Cr(VI), which attack the side chain preferentially (17). Indeed, Mn(VII) under ordinary conditions does the same (1*a*, 17*a*).[5] That ring attack occurs in our case is clear from evidence based on (*a*) isotope effects, and (*b*) substituent effects. Product analysis was not particularly helpful in locating the position of attack since extensive degradation of the arenes occurred in almost all cases, although small amounts of benzoic acid were isolated from the toluene oxidation, showing that side-chain attack was not completely absent.

It is clear from the results in Table 5, spanning a 600-fold range of reactivity, that the effect of deuterium substitution on the rate of toluene oxidation is negligible. Neither $C_6H_5CD_3$ nor $C_6D_5CD_3$ produces effects that are outside experimental error. The reaction thus appears to proceed by rate-controlling addition of MnO_3^+ to the ring, probably forming a σ complex of the following type, in which the manganese is reduced to manganese(V).

The effect on the reaction of varying the side chain

[4]N. J. Bunce. Personal communication.

[5]Reasonably stable solutions of permanganate ion in benzene can be prepared using tetraalkylammonium counter ions and these can be convenient oxidants for substrates of low polarity (ref. 3 and U. A. Spitzer and R. Stewart, unpublished results).

Can. J. Chem. Downloaded from www.nrcresearchpress.com by 210.87.254.6 on 09/05/12
For personal use only.

Can. J. Chem. Downloaded from www.nrcresearchpress.com by 210.87.254.6 on 09/05/12
For personal use only.

TABLE 5. Kinetic isotope effects in the oxidation of toluene by Mn(VII) in aqueous TFA at 25°C

wt.% TFA	$k_{C_6H_5CH_3}$ (M^{-1} s^{-1})	$k_{C_6H_5CD_3}$ (M^{-1} s^{-1})	$k_{C_6D_5CD_3}$ (M^{-1} s^{-1})	$k_{C_6H_5CH_3}/k_{C_6H_5CD_3}$	$k_{C_6H_5CH_3}/k_{C_6D_5CD_3}$
32.7	0.057	0.060	0.053	0.95	1.07
39.6	0.21		0.19		1.10
42.3	0.36		0.37		0.97
44.3	0.43	0.43	0.46	1.00	0.94
47.8	0.77		0.77		1.00
53.1	1.61	1.55	1.60	1.04	1.00
53.8	2.33		2.55		0.92
57.1	4.27		4.22		1.01
62.5	12.4	11.3	12.0	1.10	1.03
66.7	34.3		37.0		0.93
			Mean	1.03	1.00

in alkylbenzenes also demonstrates clearly that attack takes place at the ring in preference to the alkyl groups. Cumene possesses a tertiary hydrogen atom in the side chain, yet it is oxidized at essentially the same rate as ethylbenzene, with toluene and *tert*-butylbenzene being slightly less reactive (Table 6). If side-chain oxidation were appreciable there should be large variations in the rates of these four compounds. Cumene with one hydrogen atom that is both tertiary and benzylic should be much more reactive than ethylbenzene which has two hydrogen atoms that are secondary and benzylic, followed by toluene with hydrogens that are primary and benzylic, followed by *tert*-butylbenzene which has only primary nonbenzylic hydrogens.

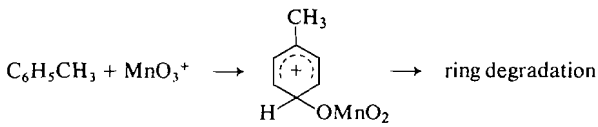

As might be expected electron-donating substituents in the ring increase the rate of reaction of arenes with Mn(VII)–TFA. Figure 2 shows the Hammett plot using σ^+ substituent constants that are appropriate for the most reactive sites. That is, σ_m^+ has been used for *meta* directing groups and σ_p^+ for *ortho-para* directing groups. No statistical corrections have been applied and partitioning between *ortho* and *para* substitution has, of necessity, been neglected. Nonetheless, it is clear that a satisfactory correlation exists. The ρ^+ value of -5.29 is entirely reasonable for a reaction of the type suggested here, i.e. electrophilic attack at ring carbon. Nitration, which of all the common electrophilic substitution reactions perhaps resembles this reaction most closely, has ρ^+ values in this neighbourhood (18).

It is noteworthy that the group that deviates most from the regression line in Fig. 2 is fluoro. Fluorobenzene reacts too slowly by almost an order of magnitude and it appears to be significantly less reactive than benzene, despite the presence of the fluoro group, which has a negative value of σ_p^+. Much of this discrepancy is doubtless statistical in origin. The *meta* and *ortho* positions in fluorobenzene are relatively unreactive towards electrophiles (19) and one is, in effect, comparing six positions of substitution in benzene with one in fluorobenzene.

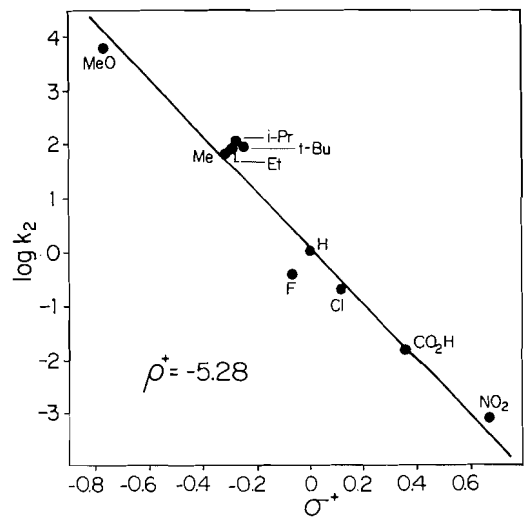

FIG. 2. Hammett plot for oxidation of substituted benzenes.

Electron abstraction from the ring, as occurs in the cobalt(III) oxidation of arenes (20), is a possible alternative mode of reaction. We do not favour this path in the present case since there are a number of points of difference between the cobalt(III) and manganese(VII) reactions. In the cobalt(III) reaction a much lower ρ value is found, there is a substantial isotope effect when $C_6H_5CD_3$ is oxidized, and side-chain oxidation predominates.

Activation Parameters

The reactions studied have activation parameters

TABLE 6. Oxidation rates for alkylbenzenes by Mn(VII) in aqueous TFA at 25°C

wt.% TFA	$k_{C_6H_5CH_3}$ (M^{-1} s^{-1})	$k_{C_6H_5C_2H_5}$ (M^{-1} s^{-1})	$k_{C_6H_5CH(CH_3)_2}$ (M^{-1} s^{-1})	$k_{C_6H_5C(CH_3)_3}$ (M^{-1} s^{-1})
39.6	0.21	0.39	0.38	
41.5	0.43	0.65	0.64	0.46
42.3	0.36	0.61	0.61	
47.8	0.77	1.07	1.13	
50.8	0.98	1.25	1.56	1.43
57.1	4.27	5.32	5.91	
63.5	21.4	32.9	33.4	29.7

TABLE 7. Activation parameters for oxidation of various hydrocarbons by Mn(VII) in aqueous TFA

Compound	wt.% TFA	$\Delta H^{\ddagger}$ (kcal mol^{-1})	$\Delta S^{\ddagger}$ (eu mol^{-1})
Hexane	81	5.8	−35
Cyclohexane	81	5.2	−37
Toluene	34	11.4	−25
Toluene	62	5.6	−36

that are comparable to those found in many other manganese(VII) oxidations (1*b*), $\Delta H^{\ddagger}$ is low and $\Delta S^{\ddagger}$ is large and negative (Table 7). The largest value of $\Delta H^{\ddagger}$ is for toluene at low acidity, 11.4 kcal mol^{-1}. As the acidity is raised the rate of oxidation, of course, rises, and this increase is principally due to a decrease in $\Delta H^{\ddagger}$. The activation parameters for alkanes and arenes are similar when compared under conditions of equal rate but not when compared under conditions of equal acidity since the aromatic hydrocarbons are all considerably more reactive than the alkanes.

Experimental

Materials

Commercial TFA was purified by distillation from a small quantity of potassium permanganate. All hydrocarbons were purified by distillation and the purity checked by vpc. Toluene-α-d_3 (98% D), toluene-d_8 (98% D), and cyclohexane-d_{12} (99% D) were obtained from Merck, Sharpe, and Dohme of Canada.

Kinetic Procedure

The rate of disappearance of permanganate was followed at 526 nm (1*a*) in a thermostatted spectrometer compartment. All rate constants, except where noted, refer to 25°C. A considerable excess of organic substrate was used (20-fold excess or more) and a first-order treatment applied in almost all cases.

Stock solutions in aqueous TFA of hydrocarbons of low or moderate volatility were prepared by straightforward mixing of the components with the TFA concentration being determined by titration. Compounds that are gaseous or highly volatile were prepared by dissolving the hydrocarbon at low temperature (0°C for neopentane) and measuring the increase in weight after the solution was returned to room temperature and opened to the atmosphere for a short time.

Product Analysis

Potassium permanganate (0.5 g) was dissolved in 20–25 ml of the desired TFA–water solution and 4 ml of the substrate added. After 1 h of stirring the reaction was quenched by the addition of 40 ml water; the mixture was saturated with sodium chloride and then extracted three times with 50 ml ether. The ether extracts were combined, dried over anhydrous magnesium sulfate, and flash evaporated and the concentrated ether extracts analyzed by vpc for volatile components. The only nonvolatile compound found in significant amount, benzoic acid, was recovered by evaporating the extracts to dryness and then purifying the crude products by sublimation and recrystallization.

Several problems were encountered in the product analysis, the most severe of which was that large quantities of TFA were extracted along with products. For example, propanoic acid was the only carboxylic acid that could be collected as a product of oxidation of the C_5 alkanes. Although one would expect some acetic acid none of the columns, even Chromosorb 101, which is specifically designed for low-molecular-weight acids, were capable of separating it from the larger amounts of TFA. It was also found that 2-pentanone and 3-pentanone could not be separated from each other. This problem was finally avoided by collecting the small amounts present of this ketone mixture and verifying their identities by nmr. The 2-pentanone to 3-pentanone ratio could be calculated from the peak integrals of the nmr spectrum of the mixture.

Cyclohexane gave trace amounts of cyclohexanol and cyclohexanone and a 75% yield of adipic acid; cyclohexanol gave trace amounts of cyclohexanone and tar and an 86% yield of adipic acid; cyclohexanone gave tar (~9% by weight) and an 81% yield of adipic acid. (Yields are based on reactants consumed.)

The inorganic products of the reaction of Mn(VII)–TFA with a 10-fold molar excess of hydrocarbon are manganese(II) and manganese(IV), the latter usually being observable as a fine brown precipitate. The alkanes yielded approximately equal amounts of manganese(II) and manganese(IV) whereas with the arenes much more of the manganese was found to be in the divalent state, indicating that manganese(IV) in TFA can oxidize aryl rings or the intermediate degradation products.

The initially formed manganese(VI) species that is believed to result from the reaction of alkanes with MnO_3^+ is $HMnO_3^+$, which presumably undergoes disproportionation, and similarly with the manganese(V) intermediate believed formed in the reaction of MnO_3^+ with arenes.

Acknowledgements

The financial support of the National Research Council of Canada is gratefully acknowledged. We thank Dr. N. J. Bunce for providing us with unpublished data.

Can. J. Chem. Downloaded from www.nrcresearchpress.com by 210.87.254.6 on 09/05/12
For personal use only.

1. (*a*) R. STEWART. *In* Oxidation in organic chemistry. Part A. *Edited by* K. B. Wiberg. Academic Press, New York, NY. 1965; (*b*) R. STEWART. Oxidation mechanisms, applications to organic chemistry. W. A. Benjamin, New York, NY. 1964. pp. 58–70.
2. C. F. CULLIS and J. W. LADBURY. J. Chem. Soc. 555 (1955); 1407 (1955); 2850 (1955); H. A. NEIDIG, D. L. FUNK, R. UHRICH, R. BAKER, and W. KREISER. J. Am. Chem. Soc. **72**, 4617 (1950).
3. C. M. STARKS. J. Am. Chem. Soc. **93**, 195 (1971); N. A. GIBSON and J. W. HOSKING. Aust. J. Chem. **18**, 123 (1965).
4. (*a*) D. G. LEE and D. T. JOHNSON. Can. J. Chem. **43**, 1952 (1965); (*b*) N. C. DENO and L. A. MESSER. Chem. Commun. 1051 (1976); (*c*) U. FROMMER and V. ULLRICH. Naturforsch. **266**, 322 (1971).
5. H. C. BROWN and R. A. WIRKKALA. J. Am. Chem. Soc. **88**, 1447 (1966).
6. U. A. SPITZER and R. STEWART. J. Org. Chem. **39**, 3936 (1974).
7. U. A. SPITZER, T. W. TOONE, and R. STEWART. Can. J. Chem. **54**, 440 (1976).
8. (*a*) C. H. ROCHESTER. Acidity functions. Academic Press, London. 1970; (*b*) N. C. DENO, J. J. JARUZELSKI, and A. SCHRIESHEIM. J. Am. Chem. Soc. **77**, 3044 (1955).
9. T. H. LOWRY and K. S. RICHARDSON. Mechanism and theory in organic chemistry. Harper and Row, New York, NY. 1976. p. 502.
10. (*a*) F. MAREŠ and J. ROČEK. Coll. Czech. Chem. Commun. **26**, 2370 (1961); (*b*) K. B. WIBERT. *In* Oxidation in organic chemistry. Part A. *Edited by* K. B. Wiberg. Academic Press, New York, NY. 1965. pp. 119–122; (*c*) F. P. LOSSING and A. MACCOLL. Can. J. Chem. **54**, 990 (1976); (*d*) F. MAREŠ, J. ROČEK, and J. SICHER. Coll. Czech. Chem. Commun. **26**, 2355 (1961).
11. (*a*) R. W. TAFT. *In* Steric effects in organic chemistry. *Edited by* M. S. Newman. John Wiley, New York, NY. Chapt. 13; (*b*) L. S. LEVITT and H. F. WIDING. *In* Progress in physical organic chemistry. Vol. 12. *Edited by* R. W. Taft. Wiley-Interscience, New York, NY. 1976; (*c*) J. A. MACPHEE and J.-E. DUBOIS. Tetrahedron Lett. 2471 (1976).
12. (*a*) M. CHARTON. J. Am. Chem Soc. **99**, 5687 (1977); (*b*) F. G. BORDWELL and H. E. FRIED. Tetrahedron Lett. 1121 (1977).
13. (*a*) H. F. WIDING and L. S. LEVITT. Tetrahedron, **30**, 611 (1974); (*b*) K. WATANABE, T. NAKAYAMA, and J. MOTTL. J. Quant. Spectrosc. Radiat. Transfer, **2**, 369 (1962).
14. H. C. BROWN and G. HAM. J. Am. Chem. Soc. **78**, 2735 (1956).
15. L. S. LEVITT. J. Org. Chem. **20**, 1297, 1955.
16. R. STEWART. *In* Isotopes in organic chemistry. Vol II. *Edited by* E. Buncel and C. C. Lee. Elsevier Press, Amsterdam. 1976.
17. (*a*) D. G. LEE. *In* Oxidation. Vol. 1. *Edited by* R. L. Augustine. Marcel Dekker, New York, NY. 1969; (*b*) D. BENSON. Mechanism of oxidation by metal ions. Elsevier, Amsterdam. 1976.
18. (*a*) J. G. HOGGETT, R. B. MOODIE, J. R. PENTON, and K. SCHOFIELD. Nitration and aromatic reactivity. Cambridge University Press, Cambridge. 1971; (*b*) L. M. STOCK. *In* Progress in physical organic chemistry. Vol. 12. *Edited by* R. W. Taft. Wiley-Interscience, New York, NY. 1976.
19. L. M. STOCK and H. C. BROWN. *In* Advances in physical organic chemistry. Vol. 1. *Edited by* V. Gold. Academic Press, London. 1963.
20. E. I. HEIBA, R. M. DESSAU, and W. J. KOEHL. J. Am. Chem. Soc. **91**, 6830 (1969).

Can. J. Chem. Downloaded from www.nrcresearchpress.com by 210.87.254.6 on 09/05/12
For personal use only.

Rates and activation energies of nitronium ion formation and reaction in the nitration of toluene in ~78% sulphuric acid

GEORGE F. SHEATS

Department of Chemistry, State University College of Arts and Science, Plattsburg, NY 12901, U.S.A.

AND

ALEC N. STRACHAN

Department of Chemistry, Loughborough University of Technology, Loughborough, Leics., LE11 3TU, United Kingdom

Received November 2, 1978

GEORGE F. SHEATS and ALEC N. STRACHAN. Can. J. Chem. **56**, 1280 (1978).

A stopped-flow spectrometer has been used to investigate the mechanism of the nitration of toluene, and to determine kinetic parameters for the formation and reaction of nitronium ion, in 77.3 and 78.45 wt.% sulphuric acid. The protonation of nitric acid to form nitronium ion and water is found to occur at similar rates at both acid concentrations and to have an activation energy of 18.3 ± 4.0 kcal mol^{-1}. The activation energy of the reverse reaction, the heat of the reaction, and the activation energy of encounter complex formation between nitronium ion and toluene are estimated to be respectively 10.5 ± 4.0, 7.8 ± 0.5, and 5.9 ± 0.1 kcal mol^{-1} in 77.3% H_2SO_4 and 12.0 ± 4.0, 6.3 ± 0.5, and 6.0 ± 0.1 kcal mol^{-1} in 78.45% H_2SO_4.

GEORGE F. SHEATS et ALEC N. STRACHAN. Can. J. Chem. **56**, 1280 (1978).

On a utilisé un spectomètre à flux stoppé pour étudier le mécanisme de nitration du toluène et pour déterminer les paramètres cinétiques de la formation et de la réaction de l'ion nitronium dans de l'acide sulfurique à 77.3 et 78.45% en poids. On a trouvé que la protonation de l'acide nitrique pour former l'ion nitronium et de l'eau se produit à des vitesses semblables aux deux concentrations d'acide et qu'elle possède une énergie d'activation de 18.3 ± 4.0 kcal mol^{-1}. On a évalué que l'énergie d'activation de la réaction inverse, que la chaleur de la réaction et que l'énergie d'activation de la formation du complexe de rencontre entre l'ion nitronium et le toluène sont respectivement de 10.5 ± 4.0, 7.8 ± 0.5 et 5.9 ± 0.1 kcal mol^{-1} dans H_2SO_4 à 77.3% et 12.0 ± 4.0, 6.3 ± 0.5 et 6.0 ± 0.1 kcal mol^{-1} dans H_2SO_4 à 78.45%.

[Traduit par le journal]

Introduction

Recently (1) the following mechanism for aromatic nitration has been proposed as the simplest which can accommodate all the known facts.

$$[1] \qquad HNO_3 + H^+ \underset{k_{-1}'}{\overset{k_1'}{\rightleftharpoons}} NO_2^+ + H_2O$$

$$[2] \qquad NO_2^+ + ArH \underset{k_{-2}'}{\overset{k_2'}{\rightleftharpoons}} \text{Encounter complex}$$

$$[3] \qquad \text{Encounter complex} \xrightarrow{k_3'} \text{Benzenonium ion} \longrightarrow \text{Product} + H^+$$

A steady state assumption made with respect to the nitronium ion and the encounter complex leads to the following expression for the rate of nitration.

$$[4] \qquad \frac{-d[ArH]}{dt} = \frac{k_1'k_2'k_3'a_{H^+}[HNO_3][ArH]}{k_{-1}'a_{H_2O}(k_3' + k_{-2}') + k_2'k_3'[ArH]} = \frac{k_1k_2[HNO_3][ArH]}{k_1 + k_2[ArH]}$$

where

$$k_1 = k_1' a_{H^+}$$

and

$$k_2 = \frac{k_1'a_{H^+}k_2'}{k_{-1}'a_{H_2O}} \frac{k_3'}{k_3' + k_{-2}'}$$

When $k_2[ArH] \gg k_1$, [4] simplifies to

$$[5] \qquad -d[ArH]/dt = k_1[HNO_3]$$

which accounts for the rate being zero order with respect to the aromatic substrate under certain conditions such as those that often occur in organic solvents (2–5). On the other hand when $k_1 \gg k_2[ArH]$, [4] simplifies to

$$[6] \qquad -d[ArH]/dt = k_2[HNO_3][ArH]$$

which accounts for the rate being first order with respect to the aromatic substrate under other conditions such as those which normally obtain in aqueous sulphuric acid.

However, when k_1 and $k_2[ArH]$ are of comparable magnitude there should be a transition region in which neither [5] nor [6] is valid but where the nitration rate is still given by [4]. Chapman and Strachan

Can. J. Chem. Downloaded from www.nrcresearchpress.com by 210.87.254.40 on 09/05/12
For personal use only.

Can. J. Chem. Downloaded from www.nrcresearchpress.com by 210.87.254.40 on 09/05/12
For personal use only.

(6) observed a change from first- to zero-order kinetics with respect to the aromatic substrate in the nitration of toluene at concentrations of sulphuric acid between 74.7 and 81.45%. It was with the purpose of testing the proposed mechanism by checking the validity of equation [4] in a transition region such as that which should be found at sulphuric acid concentrations midway between 74.7 and 81.45% that this work was undertaken. In addition it was hoped to determine the temperature dependence of k_1 and k_2, which was not investigated by Chapman and Strachan (6).

Experimental

The materials were all of high purity. The toluene, sulphuric acid, and nitric acid were analytical reagent grade and the hexane spectroscopic grade. The apparatus consisted of a Nortech SF-3A stopped-flow spectrometer connected to an Advance OS 2200 storage oscilloscope. The two reactant solutions were prepared by making up small known amounts of nitric acid and toluene, respectively, to known volumes with aqueous sulphuric acid whose concentration had previously been determined by titration. The nitric acid was assumed to dissolve completely and its concentration calculated accordingly. The concentration of toluene was determined by extracting the toluene from a known weight of solution into 15 cm^3 of hexane and measuring the absorbance of the hexane solution at 262 nm. The two sulphuric acid solutions were driven together under a driving pressure of 103.5 kPa and the reaction monitored at 350 nm. For each run an oscilloscope trace was obtained from which readings were taken of the voltage at different times.

Results and Discussion

Equation [4] can be integrated to yield

$$[7]\quad \frac{[ArH]_0}{[ArH]_0 - [ArH]} \ln \frac{[ArH]_0}{[ArH]} + \frac{k_2[ArH]_0}{k_1} = k_2[HNO_3] \frac{[ArH]_0}{[ArH]_0 - [ArH]} t$$

where $[ArH]_0$ is the initial substrate concentration. In the stopped-flow apparatus the voltage V recorded by the oscilloscope is proportional to the transmitted light intensity. Hence by Beer's Law

$$[8]\quad \frac{[ArH]_0}{[ArH]} = \frac{\log_{10}(V_0/V_\infty)}{\log_{10}(V/V_\infty)}$$

where V_0 and V_∞ are the initial and final voltages respectively.

Substitutions of [8] into [7] leads to

$$[9]\quad \underbrace{\frac{\log_{10}(V_0/V_\infty)}{\log_{10}(V_0/V)} \ln \frac{\log_{10}(V_0/V_\infty)}{\log_{10}(V/V_\infty)}}_{Y} + \frac{k_2[ArH]_0}{k_1} = \underbrace{k_2[HNO_3] \frac{\log_{10}(V_0/V_\infty)}{\log_{10}(V_0/V)} t}_{X}$$

Figures 1 and 2 show plots of

$$Y = \frac{\log_{10}(V_0/V_\infty)}{\log_{10}(V_0/V)} \ln \frac{\log_{10}(V_0/V_\infty)}{\log_{10}(V/V_\infty)}$$

vs.

$$X = \frac{\log_{10}(V_0/V_\infty)}{\log_{10}(V_0/V)} t$$

at two concentrations of sulphuric acid and several temperatures. It can be seen that in all cases good straight lines are obtained. If the limiting case given by [5] applied, the lines would all be vertical, whereas if the other limit and [6] applied the lines would all pass through the origin. The fact that the lines are neither vertical nor pass through the origin is proof of a transition region, and the fact that the plots are linear confirms the validity of [4] in such a region. This in turn is added evidence in favour of aromatic nitration proceeding by the mechanism made up of reactions 1–3. The slopes of the plots shown in Figs. 1 and 2 are equal to $k_2[HNO_3]$ and the intercepts (when $Y = 0$) equal to $[ArH]_0/k_1[HNO_3]$. The slopes and intercepts of the least squares lines through the points and the values of $[HNO_3]$ and $[ArH]_0$ (after mixing) for each run are listed in Table 1, together with the values of k_1 and k_2 derived from them.

Studies of the two phase nitration of toluene (7) lead to an estimate for the value of k_1 at 25°C and 78.45% H_2SO_4 of 0.4 s^{-1}. It can be seen from Table 1 that the value of k_1 directly determined under these conditions is 0.62 s^{-1}. The agreement between the estimated and actual value is thus very satisfactory. Previously Chapman and Strachan (6) reported results which suggest that the value of k_1 under the same conditions should be much higher and between 4.0 and 5.0 s^{-1}. These authors undoubtedly overestimated the value of $[ArH]_0$. They assumed that when small quantities of toluene, insuf-

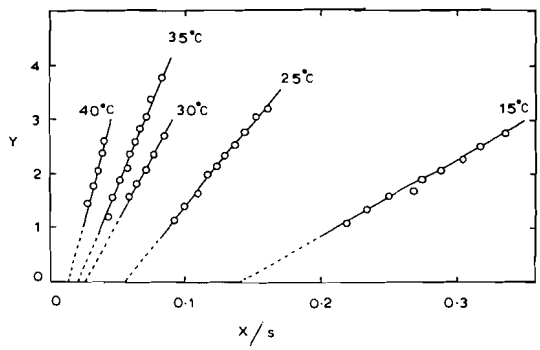

FIG. 1. Nitration of toluene at several temperatures in 77.3% H_2SO_4. Plots of

$$Y = \frac{\log_{10}(V_0/V_\infty)}{\log_{10}(V_0/V)} \ln \frac{\log_{10}(V_0/V_\infty)}{\log_{10}(V/V_\infty)} \text{ vs. } X = \frac{\log_{10}(V_0/V_\infty)}{\log_{10}(V_0/V)} t$$

Can. J. Chem. Downloaded from www.nrcresearchpress.com by 210.87.254.40 on 09/05/12
For personal use only.

TABLE 1. Values of k_1 and k_2 derived from the intercepts and slopes of the plots in Figs. 1 and 2

Temperature (°C)	Wt.% H_2SO_4	Intercept (s)	Slope (s^{-1})	$[HNO_3]$ (mol dm^{-3})	$[ArH]_0$ (mol dm^{-3})	k_1 (s^{-1})	k_2 (dm^3 mol^{-1} s^{-1})
15	77.3	0.141	14.0	2.03×10^{-2}	6.8×10^{-4}	0.24	690
	78.45	0.173	20.6	1.27×10^{-2}	5.0×10^{-4}	0.23	1620
20	78.45	0.122	29.6	1.27×10^{-2}	5.0×10^{-4}	0.32	2330
25	77.3	0.054	30.8	2.02×10^{-2}	6.7×10^{-4}	0.61	1520
	78.45	0.064	42.5	1.26×10^{-2}	5.0×10^{-4}	0.62	3370
30	77.3	0.024	45.4	2.02×10^{-2}	6.7×10^{-4}	1.4	2250
	78.45	0.040	66.0	1.26×10^{-2}	5.0×10^{-4}	1.0	5240
35	77.3	0.019	58.9	2.01×10^{-2}	6.7×10^{-4}	1.8	2930
	78.45	0.019	79.5	1.26×10^{-2}	5.0×10^{-4}	2.1	6310
40	77.3	0.013	101	2.01×10^{-2}	6.7×10^{-4}	2.6	5020

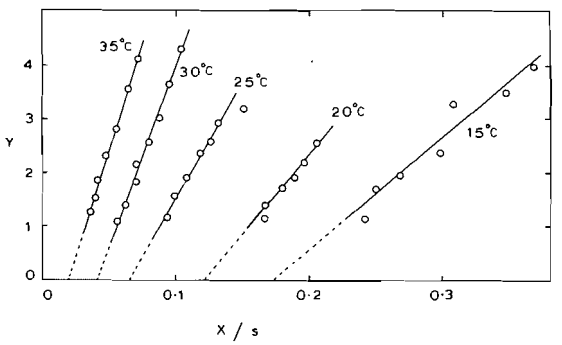

FIG. 2. Nitration of toluene at several temperatures in 78.45% H_2SO_4. Plots of

$$Y = \frac{\log_{10}(V_0/V_\infty)}{\log_{10}(V_0/V)} \ln\frac{\log_{10}(V_0/V_\infty)}{\log_{10}(V/V_\infty)} \text{ vs. } X = \frac{\log_{10}(V_0/V_\infty)}{\log_{10}(V_0/V)}\, t$$

ficient to produce a saturated solution (8), are shaken with aqueous sulphuric acid, all the toluene dissolves, and calculated $[ArH]_0$ on this basis. Later work by Chapman (9) showed this assumption to be invalid and that ~50% or more of the toluene either evaporates or remains undissolved. In the determinations of k_1 the quantity which is measured experimentally is $[ArH]_0/k_1[HNO_3]$. If $[ArH]_0$ is overestimated, so will be the value of k_1. This appears to be the main reason why Chapman and Strachan's k_1 values are out of line with both the estimate from two phase work (7) and the values reported here.

In the present work $[ArH]_0$ was determined spectroscopically after extraction of the toluene from a sample of the acid solution with hexane. While this should lead to values of $[ArH]_0$ which are more reliable, the concentrations of aromatic involved are very low and thus still subject to some uncertainty. In addition because mixing in stopped flow experiments with viscous solutions is not instantaneous (10), there is an uncertainty about the origin of time (the time at which the reaction starts). This affects the intercepts and hence introduces further uncertainties into the k_1 values derived from them. As a result the k_1 values in Table 1 are probably only accurate to within a factor of 2. Table 1 shows that the values of k_1 do not vary significantly between the two acid concentrations. Chapman and Strachan (6) reported an increase of k_1 by a factor of ten as the sulphuric acid concentration was increased from 74.7 to 81.45%. Certainly, since $k_1 = k_1' a_{H^+}$, $\log_{10} k_1$ would be expected to vary approximately as the acidity function, H_0, which does change by a factor of unity between these two concentrations of sulphuric acid (11). However the two acid concentrations employed in this work differ by only 1.15% H_2SO_4, and hence the factor by which the k_1 values would be expected to change is only 1.48. The uncertainties in the k_1 values are larger than this for the reasons discussed above, and this could explain why no significant change of k_1 with acid concentration is apparent. A combined Arrhenius plot of k_1 values at both acid concentrations leads to a value for the activation energy E_1 associated with k_1 of 18.3 ± 4.0 kcal mol^{-1}.

In contrast to the k_1 values, the k_2 values shown in Table 1 are entirely independent of a knowledge of $[ArH]_0$ and largely unaffected by the uncertainty about the origin of time. Hence they should be more accurate, and better agreement with previous work is to be expected. This expectation is realised. The value of k_2/dm^3 mol^{-1} s^{-1} at 25°C of 1520 in 77.3% H_2SO_4 is in good agreement with previously reported values of 1700 in 77.0% (6), 1900 in 77.5% (12) and 1600 in 77.7% H_2SO_4 (12). Likewise the value of 3370 in 78.45% H_2SO_4 accords well with the previous finding of 3400 in 78.15% H_2SO_4 (6). Arrhenius plots of the k_2 values lead to values for the activation energy E_2 associated with k_2 of 13.7 ± 0.5 and 12.3 ± 0.5 kcal mol^{-1} at 77.3 and 78.45% H_2SO_4 respectively. It is highly likely that with toluene at these high acid concentrations $k_3' \gg k_{-2}'$ and formation of the encounter complex (reaction 2) is rate controlling when the nitration rate is first order in toluene (13). If this is so, k_2 =

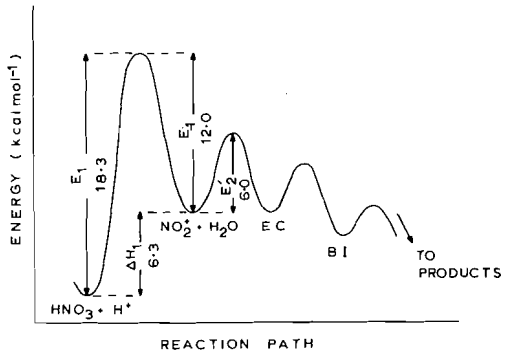

FIG. 3. Activation energy profile for the nitration of toluene in 78.45% H_2SO_4; EC, encounter complex; BI, benzenonium ion.

$(k_1'a_{H^+}/k_{-1}a_{H_2O})k_2'$ and $k_2' = 8RT/3\eta$ where η is the viscosity of the medium. It follows that $E_2 = \Delta H_1 + E_2'$, ΔH_1 being the heat of reaction [1].

From the data on the viscosity of sulphuric acid solutions (14) Arrhenius plots of $\log_{10}(T/\eta)$ vs. $1/T$ can be constructed. They prove to be linear over a limited temperature range and lead to values for E_2' of 5.9 ± 0.1 and 6.0 ± 0.1 kcal mol^{-1} at 77.3 and 78.45% H_2SO_4, respectively. Hence the corresponding ΔH_1 values must be 7.8 ± 0.5 and 6.3 ± 0.5 kcal mol^{-1}. The decrease in ΔH_1 with increasing acid concentration is in line with observations on the E_2 values for aromatics less reactive than toluene (15). With these it is likely that $k_{-2}' \gg k_3'$ and [3] is rate controlling, so that $k_2 = (k_1'a_{H^+}/k_{-1}a_{H_2O})(k_2'/k_{-2}')k_3'$ and $E_2 = \Delta H_1 + \Delta H_2 + E_3'$, ΔH_2 being the heat of reaction 2, the formation of the encounter complex. One expects ΔH_2 to be small and E_3' to be relatively independent of the medium. Hence the decrease of E_2 with increased acid concentration can only be explained if ΔH_1 falls as the $\%H_2SO_4$ rises.

Since $\Delta H_1 = E_1 - E_{-1}$ and E_1 has been found to be 18.3 ± 4.0 kcal mol^{-1}, the value of E_{-1}, the activation energy for the reaction of the nitronium ion with water, must be 10.5 ± 4.0 and 12.0 ± 4.0 kcal mol^{-1} at 77.3 and 78.45% H_2SO_4, respectively. The activation energies and heats of reaction established by this work for the higher acid concentration are summarized in Fig. 3.

1. L. M. STOCK. *In* Industrial and laboratory nitrations. *Edited by* L. F. Albright and C. Hanson. American Chemical Society, Washington, DC. 1976. Chapt. 2.
2. G. BENFORD and C. K. INGOLD. J. Chem. Soc. 929 (1938).
3. E. D. HUGHES, C. K. INGOLD, and R. I. REED. J. Chem. Soc. 2400 (1950).
4. T. G. BONNER, R. A. HANCOCK, and F. R. ROLLE. Tetrahedron Lett. 1665 (1968).
5. R. G. COOMBES. J. Chem. Soc. B, 1256 (1969).
6. J. W. CHAPMAN and A. N. STRACHAN. J. Chem. Soc. Commun. 293 (1974).
7. J. W. CHAPMAN, P. R. COX, and A. N. STRACHAN. Chem. Eng. Sci. **29**, 1247 (1974).
8. H. CERFONTAIN. Recl. Trav. Chim. Pays-Bas, **84**, 491 (1965).
9. J. W. CHAPMAN. Ph.D. Thesis, Loughborough University of Technology, Leics., U.K. 1974.
10. G. F. SHEATS and A. N. STRACHAN. J. Phys. E, **10**, 273 (1977).
11. M. A. PAUL and F. A. LONG. Chem. Rev. **57**, 1 (1957).
12. R. G. COOMBES, R. B. MOODIE, and K. SCHOFIELD. J. Chem. Soc. B, 800 (1968).
13. J. G. HOGGETT, R. B. MOODIE, and K. SCHOFIELD. J. Chem. Soc. B, 1 (1969).
14. O. FASULLO. Sulphuric acid. McGraw-Hill, New York, NY. 1965.
15. J. W. CHAPMAN and A. N. STRACHAN. *In* Industrial and laboratory nitrations. *Edited by* L. F. Albright and C. Hanson. American Chemical Society, Washington, DC. 1976. Chapt. 14.

Can. J. Chem. Downloaded from www.nrcresearchpress.com by 210.87.254.40 on 09/05/12
For personal use only.

Novel aspects of the optical spectra of dichlorotetrakis(thiourea)iron(II)

PAUL JAMES MCCARTHY
Department of Chemistry, Canisius College, Buffalo, NY 14208, U.S.A.
AND
IAN MUNRO WALKER
Department of Chemistry, York University, 4700 Keele St., Downsview, Ont., Canada M3J 1P3

Received October 6, 1977

PAUL JAMES MCCARTHY and IAN MUNRO WALKER. Can. J. Chem. **56**, 1284 (1978).

The low-temperature optical spectra of dichlorotetrakis(thiourea)iron(II) contain strong bands at 16.24 and 24.66 kK. The former gives an intense green color to freshly prepared crystals of this material. Upon long standing at room temperature or when briefly heated to about 150°C the crystals become colorless and both bands disappear. The bands are assigned to allowed metal-to-ligand electron-transfer processes in an $FeCl_2(thiourea)_2(disulfide)$ impurity, which is postulated to be present in minute amounts. Most freshly prepared crystals also show ligand field bands ca. 8 kK which are identical at room temperature and 10 K. Disorder in the crystals is presumed to set up an unsymmetrical ligand field which provides the intensity-gaining mechanism for these forbidden transitions. Well-aged crystals, or fresh crystals that have been heated for 15 min at 150°C, are more ordered and show typical vibronic spectra with the bands decreasing greatly in intensity as the temperature is lowered. The ground state of the complex is shown to be $^5B_{2g}$.

PAUL JAMES MCCARTHY et IAN MUNRO WALKER. Can. J. Chem. **56**, 1284 (1978).

Le spectre optique à basse température du dichlorotétrakis(thiourée)fer(II) contient des bandes fortes à 16.24 et 24.66 kK. La première bande fournit une couleur verte intense aux cristaux de ce composé fraîchement préparés. Après être restés longtemps à la température ambiante ou après avoir été chauffés brièvement à environ 150°C, les cristaux deviennent incolores et les deux bandes disparaissent. On attribue les bandes à des processus permis de transfert d'électrons de métal vers ligand dans une impureté de $FeCl_2(thiourée)_2(disulfure)$, que l'on suppose être présente en très faible quantité. La plupart des cristaux fraîchement préparés présentent aussi des bandes de champ de ligand à environ 8 kK qui sont identiques à la température ambiante et à 10 K. On fait l'hypothèse que les désordres dans les cristaux provoquent la présence d'un champ de ligand asymétrique qui fournit le mécanisme permettant une augmentation d'intensité pour ces transitions non permises. Les cristaux qui ont vieillis, ou des cristaux fraîchement préparés qui ont été chauffés pendant 15 min à 150°C, sont plus ordonnés et présentent des spectres vibroniques typiques alors que l'intensité des bandes diminue grandement à mesure que la température est abaissée. On démontre que l'état fondamental du complexe est $^5B_{2g}$.

[Traduit par le journal]

Introduction

The well-known compound, dichlorotetrakis-(thiourea)iron(II), $Fetu_4Cl_2$, has been the subject of spectrophotometric studies by Bailey and Peterson (1) and Gerloch, Lewis, and Smail (2). The former employed reflectance spectroscopy and the latter made use of low-temperature polarized crystal spectroscopy. We have recently observed several unusual optical properties of fresh crystals of this substance which we felt warranted more extensive investigation. In particular, the crystals, when freshly grown, are emerald-green in color, the color is unevenly distributed in many crystals and fades slowly at room temperature and very rapidly at elevated temperatures, and the spectra of the colorless crystals change upon long standing. In this report we attempt to offer a reasonable explanation for these observations, which are quite unique for a transition metal complex.

Experimental

Preparation of the Compound

Varying amounts of reagents and conditions of preparation were employed. A typical preparation is as follows: about 4.5 g of $FeCl_2 \cdot 4H_2O$ were dissolved in approximately 10 cm^3 of 35% $HClO_4$, and then a small amount of powdered iron was added to reduce any Fe(III) present. When this was accomplished, about 5 g of thiourea were dissolved in the solution, which was then filtered and left standing in a crystal dish until crystals were formed. If the amount of liquid is kept as small as possible, crystals may form overnight; otherwise the process may be very slow. The compound may be similarly prepared in methanol or ethanol with substitution of a few drops of HCl for $HClO_4$, but the crystals which result are generally quite small.

Can. J. Chem. Downloaded from www.nrcresearchpress.com by 210.87.254.105 on 09/05/12
For personal use only.

Spectral Measurements

Polarized absorption spectra of single crystals were measured at room temperature (about 295 K) and 10 K using a Cary-14 spectrophotometer and an Air Products Displex cryogenic refrigerator. The light was polarized by means of a pair of Glan-Thompson prisms, and spectra were recorded with the electric vector of the light parallel to the various extinction axes of the crystal.

Crystals of the compound were examined at 80 K on a Varian E-4 spectrometer operating at 9.1 GHz.

Analyses

Iron was determined as the dipyridyl complex by spectrophotometry.

Results

Crystal Structure and Habit

$Fetu_4Cl_2$ is isomorphous with $Cotu_4Cl_2$ (3). X-ray structural determination of the latter compound has shown that it contains the *trans*-CoS_4Cl_2 chromophore with approximate D_{4h} symmetry (4), and belongs to the tetragonal space group, $P4_2/n$, with four molecules per unit cell.

The lustrous, bright-green crystals of $Fetu_4Cl_2$ appear in two principal habits. The most common (type 1) has an irregular hexagonal face uppermost, and under polarized light these crystals are green in any orientation. The other less numerous crystals (type 2) have a rectangular face uppermost and appear green when light is polarized parallel to the long edge of the rectangle and colorless in the perpendicular direction. Both types of crystals analyze according to the stoichiometry $Fetu_4Cl_2$. *Anal.* calcd. for $Fetu_4Cl_2$: Fe 12.95; found: 12.90 (type 1) and 12.96 (type 2).

The unique orientation is that in which the crystal is colorless under polarized light (i.e., with light polarized perpendicular to the long axis of the rectangular face); this we arbitrarily denote as polarization #1. It can with reasonable certainty be assigned to that in which the electric vector is parallel to C_4(Cl—Fe—Cl axis) (π). The other polarization (#2) on this face is of course perpendicular to $C_4(\sigma)$. The two polarizations recorded on the hexagonal face of the type 1 crystals are, respectively, perpendicular to C_4 (denoted #3), and, perpendicular to that, polarization #4, which is an approximate 50:50 mixture of (#1) and (#2), since the hexagonal face lies at about 43° to the rectangular face. In general, the features in polarization (#3) are all more intense than in polarization (#4).

The Green Color

Examination under a polarizing microscope reveals a most striking property of the freshly prepared crystals, namely, that in most crystals the green color is not evenly distributed throughout, but tends to be found associated with cracks or flaws in the crystal. Crystals of type 2 with light polarized parallel to the long edge of the rectangular face, while appearing generally green, frequently show a colorless band with irregular edges running down the center of the face.

The green color of these crystals is lost on prolonged standing (a few weeks or months) at room temperature, and very rapidly (~5 min) at 150°C. The process is slowed up considerably by storing the crystals below 0°C.

When air is rigorously excluded during the preparation, and all Fe(III) is removed by addition of iron powder, the green color is absent from the product. Similarly, if freshly prepared green crystals are dissolved in oxygen-free methanol or ethanol, and are allowed to redeposit under a nitrogen atmosphere, the green color is greatly reduced or totally absent. On the other hand, active passage of air through the solution during deposition of the crystals results in a product whose green color is markedly enhanced.

It thus appears that the green color of freshly prepared crystals of $Fetu_4Cl_2$ is not due to any *d–d* transition on Fe(II) but to a transient substance which becomes trapped in the lattice during the deposition. It further appears that oxygen or some other oxidizing agent is required for its occurrence. In order to characterize this phenomenon further, we now turn to the crystal spectra.

Crystal Spectra

The visible–near-uv region in freshly prepared crystals contains an intense band at 16.24 kK (1 kK = 1000 cm^{-1}), which is primarily responsible for the green color, and also an intense band at 24.66 kK. Both of these bands are σ polarized (electric vector perpendicular to C_4) and are completely absent from the π polarization (#1). Solution spectra of freshly prepared green crystals were examined in anhydrous deaerated methanol, acetone, dimethylsulfoxide, and dimethylformamide. None of the solutions was green at any time, nor was there any trace of the above bands in any of the solutions.

The visible spectra of a freshly prepared crystal of $Fetu_4Cl_2$ are shown in Fig. 1. The spectra are of polarization (#3) at room temperature and 10 K, both before and after heating the crystal for about 5 min at 150°C. The spectra of the orthogonal polarization (#4) are quite similar but less intense than those recorded in Fig. 1.

Two features of the spectra are noteworthy: first, the two intense bands disappear completely on heating the crystals for 5 min at 150°C. Similar results are obtained for crystals which stand for

Can. J. Chem. Downloaded from www.nrcresearchpress.com by 210.87.254.105 on 09/05/12
For personal use only.

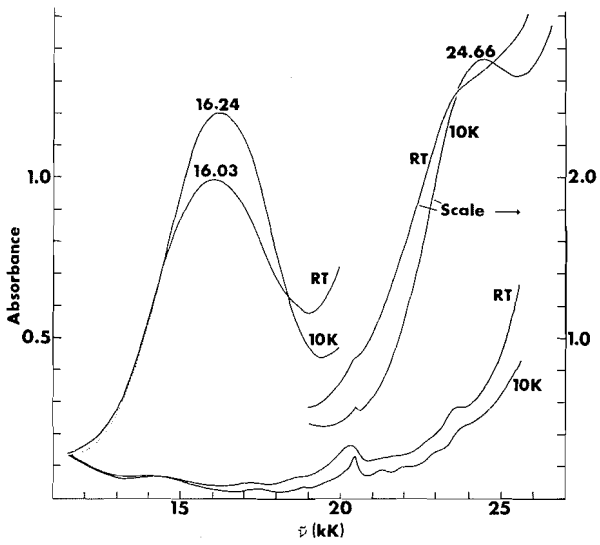

FIG. 1. Crystal spectra of $Fetu_4Cl_2$ (polarization 3) at room temperature (RT) and 10 K before (upper traces) and after (lower traces) heating for 5 min at 150°C. Crystal thickness was 1.75 mm. The weak bands in the lower traces are quintet–triplet transitions.

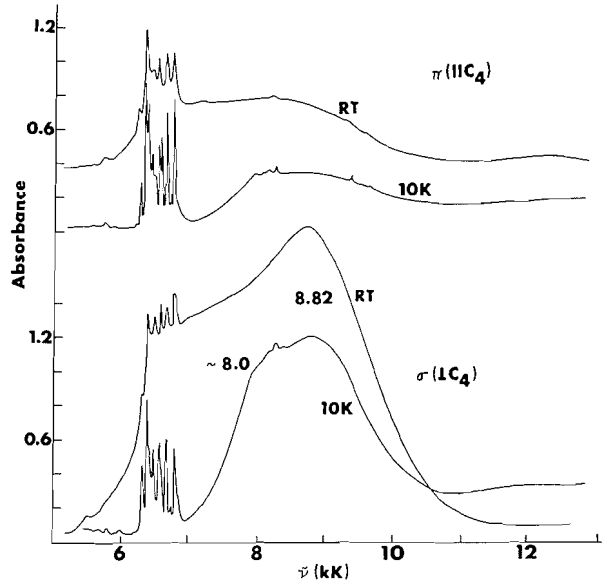

FIG. 2. Polarized crystal spectra of $Fetu_4Cl_2$ at room temperature (RT) and 10 K. The crystal had been heated 15 min at 150°C before the spectra were recorded. Crystal thickness was 1.0 mm.

several months at room temperature. The energies of these bands at 10 K are in a ratio of 2 to 3 (16.24 and 24.66 kK). It is not clear whether it is significant that the energies are almost exact multiples of 8 kK, the approximate value of the low-energy component of the spin-allowed band. Secondly, when the 16 kK bands (room temperature and 10 K) are set at the same absorption value at 11.4 kK (the minima in the curves) as was done in Fig. 1, the band contours on the low-energy side are identical. This indicates that the vibronic mechanism is not responsible for the absorption band. This is confirmed by the fact that the area under the band does not decrease as the temperature is lowered. A small increase in area (~8%) was actually observed, but this may be due to uncertainty in estimating the base line.

Most of the spin-forbidden (quintet–triplet) bands in the visible region are not apparent in the green crystal even at 10 K, but become well-resolved after the green substance has been removed either by heating or long standing. In general, they are 1–2% as intense as the spin-allowed crystal-field transition. The latter occurs in the near-ir region at ca. 8 kK (see Fig. 2). On the low energy side of the band is a set of sharp lines associated with thiourea vibrational overtones. These absorptions are also found in the corresponding cobalt complex, as expected.

The spectra in this region are very sensitive to the manner in which the crystal has been treated. Unlike the 16 kK band, the spin-allowed band in well-aged (9 months) or heat-treated (15 min at 150°C) crystals is vibronic in origin, as expected for a *d–d* transition in a complex of D_{4h} symmetry. Use of the intensity law (5)

$$[1] \qquad I_T = I_{(T=0)} \coth \frac{h\nu}{2kT}$$

with band intensities, I_T, at room temperature and 10 K allows us to establish the frequency (ν) of the allowing vibration as ~150 cm^{-1}.

On the other hand, most crystals which are either freshly prepared or not sufficiently aged (4 months) have spectra which are virtually *identical* at room temperature and 10 K. Thus the spin-allowed band is apparently not of vibronic origin under these circumstances. For these crystals, the intensity-gaining mechanism may best be ascribed to the unsymmetrical field set up by the disorder inherent in the crystal (see below).

It is noteworthy that the two features discussed here, namely, the intense bands at 16 and 24 kK and the vibronic or non-vibronic nature of the 8 kK bands, are independent phenomena. Most crystals that we studied showed non-vibronic bands at 8 kK when the 16 and 24 kK bands were present. Vibronic bands were normally found only after the disappearance of the 16 and 24 kK bands. But one crystal showed both the latter two bands and also vibronic bands at 8 kK.

The treatment of the crystals has little or no effect on the degree of resolution of the quintet–triplet bands in the visible region, once the green band has been removed.

Can. J. Chem. Downloaded from www.nrcresearchpress.com by 210.87.254.105 on 09/05/12
For personal use only.

Can. J. Chem. Downloaded from www.nrcresearchpress.com by 210.87.254.105 on 09/05/12
For personal use only.

Discussion

The spin-allowed bands of the spectrum can be assigned by means of the following energy diagram:

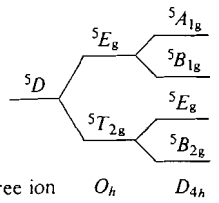

The ordering of the B_{2g} and E_g levels in D_{4h} is not immediately evident. If E_g is the ground state, then on the basis of orbital symmetry alone, the transitions $E_g \rightarrow B_{1g}$ or A_{1g} are allowed in σ, and no transitions are allowed in π. If B_{2g} is the ground state, $B_{2g} \rightarrow B_{1g}$ is allowed in π, and no transitions are allowed in σ. Since the former situation more nearly represents the observed spectra, Gerloch *et al.* (2) assumed an E_g ground state. Since, however, the bands decrease significantly in size on cooling, the vibronic selection rules must be considered before the ground state can be determined unambiguously.

The u vibrations of the *trans*-FeS_4Cl_2 group are $2a_{2u} + b_{2u} + 3e_u$. From an E_g ground state the two excited states (A_{1g} and B_{1g}) become accessible by coupling with e_u vibrations (π spectrum) and a_{2u} or b_{2u} vibrations (σ spectrum). The e_u vibrations of FeS_4Cl_2 are ν(Fe—S), δ(Cl—Fe—Cl), and $\delta(FeS_4)$ (in-plane). None of these has any component along C_4 and so cannot activate a π electronic transition. Likewise, the a_{2u} vibrations are ν(Fe—Cl) and $\delta(FeS_4)$ (out-of-plane), and the b_{2u} vibration is also $\delta(FeS_4)$ (out-of-plane). None of these has any component perpendicular to C_4 and so cannot activate a σ electronic transition.

From a B_{2g} ground state both excited states become accessible in σ by coupling with e_u vibrations, while in π the non-existent a_{1u} and b_{1u} vibrations would be required to render the transition allowed. This approximates what one sees in the spectra, namely, a strong σ and weak π spectrum. The appearance of some intensity in the π spectrum indicates (*a*) that some weak coupling occurs with the vibrations of the *whole* thiourea ligand and that consideration of the skeleton FeS_4Cl_2 is not sufficient, and/or (*b*) that the slight distortions from D_{4h} symmetry which actually occur in the CoS_4Cl_2 chromophore (4) also occur here and lower the symmetry enough to make the D_{4h} selection rules only approximately valid.

The designation of B_{2g} as the ground state agrees with the observation of Birchall and Morris (6) that the magnitude of the quadrupole splitting in the Mössbauer spectrum of $Fetu_4Cl_2$ requires the complex to have the d_{xy} orbital lowest in energy. This would make B_{2g} the ground state. This splitting of the octahedral T_{2g} level implies that the z ligand is stronger than the xy, i.e., $Dq(Cl) > Dq(tu)$. The observations made in this work do not, however, determine the ordering of the A_{1g} and B_{1g} excited states.

The accumulated data, especially the variation in spectral band shapes, point strongly to the occurrence of lattice disorder in most of the freshly prepared crystals, which generally formed rapidly overnight. Heat treatment or long standing appears to repair much of the disorder. The behaviour of the spin-allowed band with temperature can be nicely explained by the hypothesis that a centre of symmetry is absent in the freshly prepared (disordered) case, but on heat treatment or long standing, annealing takes place, resulting in an ordered metal environment with D_{4h} symmetry and vibronic allowedness. It is likely that the crystal which showed the normal vibronic spectrum in the infrared together with the intense green color was a crystal which grew slowly from solution. The slow growth favored ordered arrangement in the crystal.

As for the substance responsible for the 16 and 24 kK bands, the data indicate that we are dealing with a solid-state effect, since these bands are not found in the solution spectra. It is also clear from the rapid disappearance of the bands with heating that they cannot be assigned to quintet–triplet transitions, as was done for the 16 kK band by Gerloch *et al.* (2) and Bailey and Peterson (1).

We offer the following hypothesis which we feel best fits the experimental data: two electron oxidation of adjacent coordinated thioureas by dissolved oxygen near a growing crystal could result in a complex of the composition:

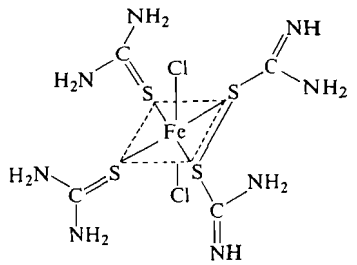

The disulfide ligand is a known oxidation product of thiourea, and would be a singlet, in agreement with the epr results. (Freshly-prepared green crystals showed no epr signal at 80 K.) Since the above complex bears a strong steric resemblance to *trans*-$Fetu_4Cl_2$, it might be expected to be readily incorporated into growing crystals. Heating or long

standing would cause the disulfide, a very weakly bonding ligand, to separate from the complex, thus destroying the color-producing species.

If, as our evidence suggests, the color-producing material is present only in trace amounts, the electronic transitions must be intrinsically intense and so may be allowed transitions. They are too low in energy to be $n \rightarrow \pi^*$ or $\pi \rightarrow \pi^*$ transitions on the ligand. So they are most probably either $L \rightarrow M$ or $M \rightarrow L$ electron transfers. The former can readily be ruled out; if $Fetu_4Cl_2$ itself shows no low-lying $L \rightarrow M$ electron transfer, the complex containing a disulfide ligand (an oxidized species) would be even less likely to show one. $M \rightarrow L$ electron transfer involves a spectroscopic oxidation of the metal, and, in fact, Fe(II) can be rather easily oxidized. This does not occur, however, when the only ligands are Cl^- and thiourea. The Fe(III)–thiourea complex is quite unstable, being quickly reduced to the Fe(II)–thiourea complex with the production of sulfur-containing oxidation products.

The fact that we here postulate an already oxidized disulfide bonded to the Fe(II) means that the Fe(II) $\rightarrow$ disulfide transfer might occur with some ease and therefore be spectroscopically induced by photons of relatively long wavelength. The two bands at 16 and 24 kK may represent such $M \rightarrow L$ electron transfers. Since these are allowed transitions, only a small amount of this complex would have to be present to obtain the intensity observed. With the data presently available, however, it is not possible to specify further the nature of these two bands, nor to show why they are both σ-polarized.

Acknowledgements

P.J.M. is grateful to the Research Corporation for a grant for the purchase of the Displex Cryogenic Refrigerator. I.M.W. is grateful to York University for support of this research.

1. R. A. Bailey and T. R. Peterson. Can. J. Chem. **45**, 1135 (1967).
2. M. Gerloch, J. Lewis, and W. R. Smail. J. Chem. Soc. Dalton, 1559 (1972).
3. J. E. O'Connor and E. L. Amma. Chem. Commun. 892 (1968).
4. J. E. O'Connor and E. L. Amma. Inorg. Chem. **8**, 2367 (1969).
5. C. J. Ballhausen. Introduction to ligand field theory. McGraw-Hill, New York. 1962. p. 187.
6. T. Birchall and M. F. Morris. Can. J. Chem. **50**, 201 (1972).

Can. J. Chem. Downloaded from www.nrcresearchpress.com by 210.87.254.105 on 09/05/12
For personal use only.

A consistent derivation of the Wilson–Decius *s* vectors, including new out-of-plane wag formulae

D. F. McIntosh,[1] K. H. Michaelian,[1] and M. R. Peterson

Department of Chemistry, Lash Miller Chemical Laboratories, University of Toronto, Toronto, Ont., Canada M5S 1A1

Received December 13, 1977

D. F. McIntosh, K. H. Michaelian, and M. R. Peterson. Can. J. Chem. **56**, 1289 (1978).

A consistent derivation of the complete set of *s* vectors needed for vibrational analysis by the Wilson **GF** matrix method is presented. The vectors obtained for the out-of-plane wag are given by new formulae which are considerably simpler than those presently in use. The formulae for the linear bending coordinate are also derived.

D. F. McIntosh, K. H. Michaelian et M. R. Peterson. Can. J. Chem. **56**, 1289 (1978).

On présente une dérivation concordante d'un ensemble complet de vecteurs *s* nécessaire pour l'analyse vibrationnelle par la méthode des matrices **GF** de Wilson. Les vecteurs obtenus pour le balancement hors-plan sont donnés par de nouvelles formules qui sont beaucoup plus simples que celles utilisées présentement. On a aussi dérivé une formule pour la coordonnée de déformation linéaire.

[Traduit par le journal]

Can. J. Chem. Downloaded from www.nrcresearchpress.com by 210.87.254.6 on 09/05/12
For personal use only.

Introduction

Vibrational spectroscopists have long been familiar with the Wilson **GF** matrix method (1). Wilson set up the initial analysis in terms of two internal coordinates, the bond stretch and the valence angle bend. Two additional important internal coordinates, the out-of-plane wag and the torsion, were subsequently defined by Decius, who also showed that the set of four internal modes constitutes a complete set of basis vectors with which a vibrational analysis can be performed (2, 3). This material was later collected in the well known text "Molecular Vibrations" (4). In this book, Decius first explicitly stated the *s* vector expressions for the wag, although he had previously used them implicitly (3).

Several methods for the derivation of the *s* vectors for the four internal coordinates were given in "Molecular Vibrations" and since this publication several other authors have developed new ways of deriving some of the *s* vectors. Perhaps the most notable of these is Steele's vector construction method (5), which was outlined for the valence angle bend and two of the four torsion *s* vectors. However, no consistent method of derivation of all the *s* vectors has been published up to the present time; indeed, the application of any one method usually presents difficulty when all of the *s* vectors are considered.

An even more serious difficulty arises when one attempts to use the valence angle bend formulae for the case of the linear bend. In this case the Wilson–Decius formulae "blow-up" and cannot be used. This problem was recognized quite some time ago and was corrected by Schachtschneider in his well known computer programs for vibrational analysis (6). These formulae have not been published in the literature, but most spectroscopists are aware of this situation and consequently use Schachtschneider's programs or correct for the difficulty themselves.

We have recently derived all of the *s* vectors by means of a consistent and relatively simple method. This procedure results in a new set of formulae for the wag which has the advantage that the formulae are considerably simpler to visualize and to use than are any previous set of formulae.

These new formulae have been incorporated into a new set of programs available from the Quantum Chemistry Program Exchange (7). Altogether there are 3 programs the first of which computes the Wilson **B** matrix. The BMAT program is a modification of the original GMAT program of Schachtschneider and allows for the calculation of five different types of internal coordinates, namely, (*1*) bond stretch, (*2*) valence angle bend, (*3*) out-of-plane wag, (*4*) torsion, and (*5*) linear bend. Two important differences between Schachtschneider's original GMAT program and BMAT are the different set of wag formulae and the inclusion of Hilderbrandt's method of normalization of the torsional coordinate (8). The three programs have the additional feature that a vibrational analysis can be carried out without recourse to the use of symmetry coordinates although, if desired, such a method may be used.

The purpose of this paper then is to introduce a consistent method of derivation of all the *s* vectors, to collect all the *s* vector formulae together in one

[1]Authors to whom correspondence should be addressed.

Can. J. Chem. Downloaded from www.nrcresearchpress.com by 210.87.254.6 on 09/05/12
For personal use only.

source, to note important refinements published recently, and to publish the new formulae of the out-of-plane wag.

The *s* Vectors

Wilson and Decius set out to define a set of internal coordinates that could be expressed exclusively in terms of parameters readily determined from the molecular geometry such as bond lengths, angles, and the like. This can be done for all of the internal coordinates except one. The linear bend cannot be handled in this manner. It is necessary to define a new vector external to the molecule.

All of the s vectors will be expressed in terms of the e vectors (except for the linear bend). The set of e vectors are conveniently expressed in terms of the following formulae:

$$e_{ij} = [(x_j - x_i)\boldsymbol{i} + (y_j - y_i)\boldsymbol{j} + (z_j - z_i)\boldsymbol{k}]/r_{ij}$$

where (x_i, y_i, z_i) and (x_j, y_j, z_j) are the Cartesian coordinates of atoms i and j, respectively, r_{ij} is the distance between the atoms, and $\boldsymbol{i}, \boldsymbol{j}$, and $\boldsymbol{k}$ are unit vectors directed along the positive x, y, and z Cartesian axes, respectively.

Each of the internal coordinates will be considered in turn.

(1) Bond Stretch (Δr_{ij})

This internal coordinate is the simplest to visualize and the s vectors can be written down from inspection.

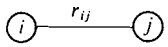

The s vectors for atoms i and j are

$$s_i = -e_{ij} \qquad s_j = e_{ij}$$

(2) Valence Angle Bend ($\Delta\alpha_{ijk}$)

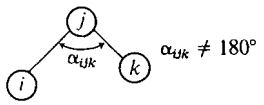

We shall use Steele's vector construction method to obtain the expression for s_i and then derive s_k in terms of s_i. Finally we shall derive s_j in terms of s_i and s_k.

s_i will be perpendicular to the side j,i. Furthermore, the length of s_i is $1/r_{ji}$ since a unit (infinitesimal) displacement of i along s_i will increase α_{ijk} by an amount $1/r_{ji}$.

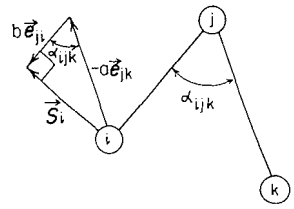

FIG. 1. The vector construction necessary for the definition of s_i in the valence angle bend.

Figure 1 illustrates the vector construction needed to define s_i in terms of e_{jk} and e_{ji}. s_i is a unit vector perpendicular to j,i. Vectors are then constructed parallel to e_{ji} and e_{jk} as illustrated in the figure.

It is clear that the following relationships hold:

$$\sin\alpha_{ijk} = 1/a \quad \text{and} \quad \cos\alpha_{ijk} = b/a$$

Therefore

$$a = 1/\sin\alpha_{ijk}$$

$$b = a\cos\alpha_{ijk} = \cos\alpha_{ijk}/\sin\alpha_{ijk}$$

Therefore

$$s_i = \frac{1}{r_{ji}}[-ae_{jk} + be_{ji}] = \frac{\cos\alpha_{ijk}\, e_{ji} - e_{jk}}{r_{ji}\sin\alpha_{ijk}}$$

We could naturally carry out a similar vector construction to obtain the expression for s_k. For the purpose of unity, however, we will illustrate the method which will be used in the cases of the out-of-plane wag and the torsion.

We will make use of two expressions throughout which express the invariance to rigid translations and rotations (9):

$$\sum_i s_i = \mathbf{0} \quad \text{and} \quad \sum_i R_i \times s_i = \mathbf{0}$$

where R_i is the vector from an arbitrary origin to the equilibrium position of atom i.

In the case of the bend the rotational invariance relation yields:

$$R_i \times s_i + R_j \times s_j + R_k \times s_k = \mathbf{0}$$

Placing the origin at j we have:

$$R_i = r_{ji}e_{ji} \quad R_j = \mathbf{0} \quad R_k = r_{jk}e_{jk}$$

Therefore

$$r_{ji}e_{ji} \times s_i = -r_{jk}e_{jk} \times s_k$$

Multiplying through by e_{jk} we obtain

$$r_{ji}e_{jk} \times (e_{ji} \times s_i) = -r_{jk}e_{jk} \times (e_{jk} \times s_k)$$

We may expand this relationship with the aid of the following vector identity

[1] $$v_1 \times (v_2 \times v_3) = (v_1 \cdot v_3)v_2 - (v_1 \cdot v_2)v_3$$

Can. J. Chem. Downloaded from www.nrcresearchpress.com by 210.87.254.6 on 09/05/12
For personal use only.

Thus we have

$$r_{ji}[(\boldsymbol{e}_{jk}\cdot\boldsymbol{s}_i)\boldsymbol{e}_{ji} - (\boldsymbol{e}_{jk}\cdot\boldsymbol{e}_{ji})\boldsymbol{s}_i] = -r_{jk}[(\boldsymbol{e}_{jk}\cdot\boldsymbol{s}_k)\boldsymbol{e}_{jk} - (\boldsymbol{e}_{jk}\cdot\boldsymbol{e}_{jk})\boldsymbol{s}_k]$$

Evaluating some of the scalar products

$$r_{ji}[(\boldsymbol{e}_{jk}\cdot\boldsymbol{s}_i)\boldsymbol{e}_{ji} - \cos\alpha_{ijk}\,\boldsymbol{s}_i] = -r_{jk}[0\boldsymbol{e}_{jk} - 1\boldsymbol{s}_k]$$

The remaining scalar product can be evaluated by substituting for $\boldsymbol{s}_i$

$$r_{ji}\left[\boldsymbol{e}_{jk}\cdot\left(\frac{\cos\alpha_{ijk}\,\boldsymbol{e}_{ji} - \boldsymbol{e}_{jk}}{r_{ji}\sin\alpha_{ijk}}\right)\right]\boldsymbol{e}_{ji} - r_{ji}\cos\alpha_{ijk}\left[\frac{\cos\alpha_{ijk}\,\boldsymbol{e}_{ji} - \boldsymbol{e}_{jk}}{r_{ji}\sin\alpha_{ijk}}\right] = r_{jk}\boldsymbol{s}_k$$

Expanding the above expression and evaluating the scalar products leads to the following equation

$$\frac{\cos^2\alpha_{ijk}\,\boldsymbol{e}_{ji} - \boldsymbol{e}_{ji} - \cos^2\alpha_{ijk}\,\boldsymbol{e}_{ji} + \cos\alpha_{ijk}\,\boldsymbol{e}_{jk}}{\sin\alpha_{ijk}} = r_{jk}\boldsymbol{s}_k$$

Therefore

$$\boldsymbol{s}_k = \frac{\cos\alpha_{ijk}\,\boldsymbol{e}_{jk} - \boldsymbol{e}_{ji}}{r_{jk}\sin\alpha_{ijk}}$$

We finally employ the translational invariance rule

$$\boldsymbol{s}_j = -(\boldsymbol{s}_i + \boldsymbol{s}_k)$$

For convenience we summarize the $\boldsymbol{s}$ vectors for the valence angle bend

$$\boldsymbol{s}_i = (\cos\alpha_{ijk}\,\boldsymbol{e}_{ji} - \boldsymbol{e}_{jk})/r_{ji}\sin\alpha_{ijk} \qquad \boldsymbol{s}_k = (\cos\alpha_{ijk}\,\boldsymbol{e}_{jk} - \boldsymbol{e}_{ji})/r_{jk}\sin\alpha_{ijk} \qquad \boldsymbol{s}_j = -(\boldsymbol{s}_i + \boldsymbol{s}_k)$$

(3) Out-of-plane Wag (Δθ)

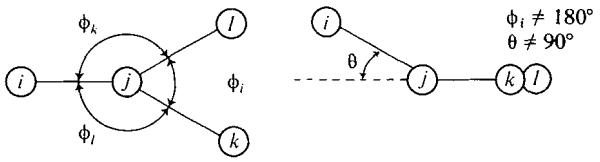

The formulae derived in this section represent new expressions. The numerical results are identical to the results given by the old formulae in "Molecular Vibrations" (p. 60). Our formulae are, however, much easier to visualize and, in fact, require fewer computations.

We will require four $\boldsymbol{s}$ vectors in this case. The direction of $\boldsymbol{s}_i$ is perpendicular to the bond j,i and in a plane perpendicular to the plane k,j,l while the directions of $\boldsymbol{s}_k$ and $\boldsymbol{s}_l$ are each perpendicular to the plane k,j,l.

We might then expect formulae for $\boldsymbol{s}_k$ and $\boldsymbol{s}_l$ to be factors of the unit vector $(\boldsymbol{e}_{jk} \times \boldsymbol{e}_{jl})/\sin\phi_i$. Furthermore, in the case of a planar conformation of the wag (i.e. $\theta = 0$), we would expect $\boldsymbol{s}_i$ also to be merely a factor of this vector. This will turn out to be the case.

We will follow the same lines in our derivation as we did with the bend. $\boldsymbol{s}_k$ and $\boldsymbol{s}_l$ will be expressed in terms of $\boldsymbol{s}_i$. Finally $\boldsymbol{s}_j$ will be expressed in terms of $\boldsymbol{s}_i$, $\boldsymbol{s}_k$, and $\boldsymbol{s}_l$.

Figure 2 illustrates the vector construction needed to define $\boldsymbol{s}_i$. Vectors are constructed parallel to $(\boldsymbol{e}_{jk} \times \boldsymbol{e}_{jl})/\sin\phi_i$ and $\boldsymbol{e}_{ji}$. Referring to the figure it should be clear that the following relationships hold:

$$\cos\theta = 1/a \quad \text{and} \quad \sin\theta = b/a$$

Thus

$$a = 1/\cos\theta \quad \text{and} \quad b = a\sin\theta = \sin\theta/\cos\theta = \tan\theta$$

As in the case of the valence angle bend $\boldsymbol{s}_i$ must be normalized by a factor $1/r_{ji}$. Therefore

$$\boldsymbol{s}_i = \frac{1}{r_{ji}}\left[a\frac{(\boldsymbol{e}_{jk} \times \boldsymbol{e}_{jl})}{\sin\phi_i} - b\boldsymbol{e}_{ji}\right] = \frac{1}{r_{ji}}\left[\frac{(\boldsymbol{e}_{jk} \times \boldsymbol{e}_{jl})}{\cos\theta\sin\phi_i} - \tan\theta\,\boldsymbol{e}_{ji}\right]$$

Again we will use the rotational invariance relation

$$\boldsymbol{R}_i \times \boldsymbol{s}_i + \boldsymbol{R}_j \times \boldsymbol{s}_j + \boldsymbol{R}_k \times \boldsymbol{s}_k + \boldsymbol{R}_l \times \boldsymbol{s}_l = \boldsymbol{0}$$

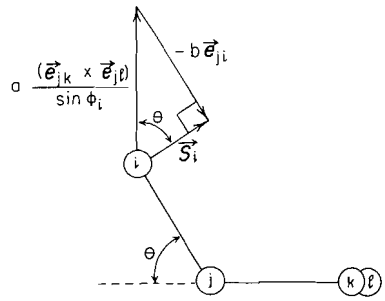

FIG. 2. The vector construction necessary for the definition of s_l in the out-of-plane wag.

Putting the origin at atom j we have

$$R_i = r_{ji}e_{ji} \quad R_j = 0 \quad R_k = r_{jk}e_{jk} \quad R_l = r_{jl}e_{jl}$$

Thus

[2] $$r_{ji}e_{ji} \times s_i = -r_{jk}e_{jk} \times s_k - r_{jl}e_{jl} \times s_l$$

Multiplying [2] by e_{jk} we obtain

$$r_{ji}e_{jk} \times (e_{ji} \times s_i) = -r_{jk}e_{jk} \times (e_{jk} \times s_k) - r_{jl}e_{jk} \times (e_{jl} \times s_l)$$

Utilizing the vector identity of [1] we may expand the above expression

$$r_{ji}[(e_{jk}\cdot s_i)e_{ji} - (e_{jk}\cdot e_{ji})s_i] = -r_{jk}[(e_{jk}\cdot s_k)e_{jk} - (e_{jk}\cdot e_{jk})s_k] - r_{jl}[(e_{jk}\cdot s_l)e_{jl} - (e_{jk}\cdot e_{jl})s_l]$$

Evaluation of some of the scalar products leads to

[3] $$r_{ji}(e_{jk}\cdot s_i)e_{ji} - r_{ji}\cos\phi_l\, s_i = r_{jk}s_k + r_{jl}\cos\phi_i\, s_l$$

Multiplying [2] by e_{jl} and simplifying we obtain an expression analogous to [3]

[4] $$r_{ji}(e_{jl}\cdot s_i)e_{ji} - r_{ji}\cos\phi_k\, s_i = r_{jk}\cos\phi_i\, s_k + r_{jl}s_l$$

We can, at this point, choose to eliminate either s_k or s_l since we have two simultaneous equations in two unknowns. Thus, choosing the elimination of s_l, simplifying and collecting terms we obtain

$$(r_{jk} - r_{jk}\cos^2\phi_i)s_k = (r_{ji}\cos\phi_i\cos\phi_k - r_{ji}\cos\phi_l)s_i + [r_{ji}(e_{jk}\cdot s_i) - r_{ji}\cos\phi_i\,(e_{jl}\cdot s_i)]e_{ji}$$

The left-hand side of this equation simplifies quite easily

$$(r_{jk} - r_{jk}\cos^2\phi_i)s_k = r_{jk}(1 - \cos^2\phi_i)s_k = r_{jk}\sin^2\phi_i\, s_k$$

The evaluation of the scalar products of the right-hand side of the equation can be carried out by substituting in the expression for s_i. Several cancellations will occur. After some algebra one obtains the following expression

$$\frac{\cos\phi_i\cos\phi_k - \cos\phi_l}{\cos\theta\sin\phi_i}(e_{jk} \times e_{jl})$$

Thus the final expression for s_k is

$$s_k = \frac{1}{r_{jk}}\left[\frac{(e_{jk} \times e_{jl})}{\sin\phi_i}\cdot\frac{\cos\phi_i\cos\phi_k - \cos\phi_l}{\cos\theta\sin^2\phi_i}\right]$$

The expression for s_l can be obtained now in a variety of ways. One could eliminate s_k from the expressions [3] and [4] or the values of s_i and s_k could be substituted into either [3] or [4] and rearranged to yield the expression for s_l. Finally s_j is expressed in terms of s_i, s_k, and s_l using the translational invariance relation.

For convenience all the s vectors are summarized below:

$$s_i = \frac{1}{r_{ji}}\left[\frac{(e_{jk} \times e_{jl})}{\cos\theta\sin\phi_i} - \tan\theta\, e_{ji}\right] \qquad s_l = \frac{1}{r_{jl}}\left[\frac{(e_{jk} \times e_{jl})}{\sin\phi_i}\cdot\frac{\cos\phi_i\cos\phi_l - \cos\phi_k}{\cos\theta\sin^2\phi_i}\right]$$

$$s_k = \frac{1}{r_{jk}}\left[\frac{(e_{jk} \times e_{jl})}{\sin\phi_i}\cdot\frac{\cos\phi_i\cos\phi_k - \cos\phi_l}{\cos\theta\sin^2\phi_i}\right] \qquad s_j = -(s_i + s_k + s_l)$$

Can. J. Chem. Downloaded from www.nrcresearchpress.com by 210.87.254.6 on 09/05/12
For personal use only.

This set of formulae is considerably simpler to evaluate with only one vector cross product and three scalar products. The formulae in "Molecular Vibrations" require only one scalar product evaluation but three vector cross product evaluations.

The case of the planar wag ($\theta = 0$) deserves special comment. The formulae given above simplify considerably.

When $\theta = 0$, $\phi_i + \phi_k + \phi_l = 360°$.

Thus

$$\cos \phi_k = \cos [360° - (\phi_i + \phi_l)] = \cos (\phi_i + \phi_l) = \cos \phi_i \cos \phi_l - \sin \phi_i \sin \phi_l$$

Rearranging we have

$$\sin \phi_l = \frac{\cos \phi_i \cos \phi_l - \cos \phi_k}{\sin \phi_i}$$

Similarly

$$\sin \phi_k = \frac{\cos \phi_i \cos \phi_k - \cos \phi_l}{\sin \phi_i}$$

Thus, the expressions simplify to

$$s_i = \frac{1}{r_{ji}}\left[\frac{(e_{jk} \times e_{jl})}{\sin \phi_i}\right] \qquad s_l = \frac{1}{r_{jl}}\left[\frac{(e_{jk} \times e_{jl})}{\sin \phi_i} \cdot \frac{\sin \phi_l}{\sin \phi_i}\right]$$

$$s_k = \frac{1}{r_{jk}}\left[\frac{(e_{jk} \times e_{jl})}{\sin \phi_i} \cdot \frac{\sin \phi_k}{\sin \phi_i}\right] \qquad s_j = -(s_i + s_k + s_l)$$

While the wag formulae have been derived for a general case (i.e. unrestricted θ) the use of the wag as a basis vector should be restricted only to the planar case (i.e. $\theta = 0$) since the non-planar wag corresponds to the symmetric combination of the valence angle bends $\Delta\phi_i$, $\Delta\phi_k$, and $\Delta\phi_l$. It is only in the case of a planar configuration of the atoms that the wag is needed, since out-of-plane deformations cannot be handled by combinations of the valence angle bends $\Delta\phi_i$, $\Delta\phi_k$, and $\Delta\phi_l$. Clearly this is not the case when $\theta \neq 0$ and inclusion of the wag in the basis set along with $\Delta\phi_i$, $\Delta\phi_k$, and $\Delta\phi_l$ in the non-planar configuration would cause serious problems in the determination of a proper force field.

(4) Torsion[2] *($\Delta\tau$)*

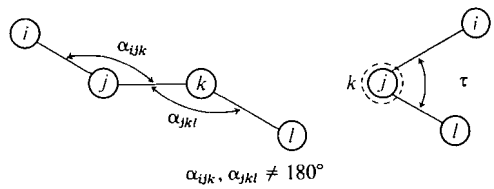

We will initially consider only a 4 atom torsion and will derive the s vectors for that case. The addition of further atoms on either j or k will require the use of the normalization scheme of Hilderbrandt (8).

We will derive the expressions for s_j and s_k after obtaining the expressions for s_i and s_l.

Considering the diagrams above we require atom i to move in a direction perpendicular to bond j,i and j,k. This can be carried out by defining the unit vector $-(e_{ij} \times e_{jk})/\sin \alpha_{ijk}$. The normalization of s_i will be by the length of the projection of bond j,i onto the plane perpendicular to the j,k bond. This length is, in fact, $r_{ij} \sin \alpha_{ijk}$. Thus the s_i vector will be given by the expression

$$s_i = -(e_{ij} \times e_{jk})/r_{ij} \sin^2 \alpha_{ijk}$$

Similar considerations will yield the following expression for s_l

$$s_l = -(e_{lk} \times e_{kj})/r_{lk} \sin^2 \alpha_{jkl}$$

The derivation of the s_j and s_k vectors is now, in fact, simpler than was the case of the wag. We know two vectors explicitly instead of one. Elimination of one is carried out by conveniently choosing it to be the

[2]An in-depth treatment of the torsion has been given recently in ref. 10.

Can. J. Chem. Downloaded from www.nrcresearchpress.com by 210.87.254.6 on 09/05/12
For personal use only.

Can. J. Chem. Downloaded from www.nrcresearchpress.com by 210.87.254.6 on 09/05/12
For personal use only.

origin in the rotational invariance relation. We will then have the last vector expressed as a directly soluble combination of the two known vectors.

$$\boldsymbol{R}_i \times \boldsymbol{s}_i + \boldsymbol{R}_j \times \boldsymbol{s}_j + \boldsymbol{R}_k \times \boldsymbol{s}_k + \boldsymbol{R}_l \times \boldsymbol{s}_l = \boldsymbol{0}$$

Putting k as the origin we have

$$\boldsymbol{R}_i = r_{ki}\boldsymbol{e}_{ki} = r_{kj}\boldsymbol{e}_{kj} + r_{ji}\boldsymbol{e}_{ji} \quad \boldsymbol{R}_j = r_{kj}\boldsymbol{e}_{kj} \quad \boldsymbol{R}_k = \boldsymbol{0} \quad \boldsymbol{R}_l = r_{kl}\,\boldsymbol{e}_{kl}$$

Rearranging the first expression and multiplying through by $\boldsymbol{e}_{kj}$ we obtain

$$r_{kj}\boldsymbol{e}_{kj} \times (\boldsymbol{e}_{kj} \times \boldsymbol{s}_j) = -r_{kj}\boldsymbol{e}_{kj} \times (\boldsymbol{e}_{kj} \times \boldsymbol{s}_i) - r_{ji}\boldsymbol{e}_{kj} \times (\boldsymbol{e}_{ji} \times \boldsymbol{s}_i) - r_{kl}\boldsymbol{e}_{kj} \times (\boldsymbol{e}_{kl} \times \boldsymbol{s}_l)$$

Utilizing the vector identity we may expand this expression

$$r_{kj}[(\boldsymbol{e}_{kj}\cdot\boldsymbol{s}_j)\boldsymbol{e}_{kj} - (\boldsymbol{e}_{kj}\cdot\boldsymbol{e}_{kj})\boldsymbol{s}_j] = -r_{kj}[(\boldsymbol{e}_{kj}\cdot\boldsymbol{s}_i)\boldsymbol{e}_{kj} - (\boldsymbol{e}_{kj}\cdot\boldsymbol{e}_{kj})\boldsymbol{s}_i] - r_{ji}[(\boldsymbol{e}_{kj}\cdot\boldsymbol{s}_i)\boldsymbol{e}_{ji} - (\boldsymbol{e}_{kj}\cdot\boldsymbol{e}_{ji})\boldsymbol{s}_i] - r_{kl}[(\boldsymbol{e}_{kj}\cdot\boldsymbol{s}_l)\boldsymbol{e}_{kl} - (\boldsymbol{e}_{kj}\cdot\boldsymbol{e}_{kl})\boldsymbol{s}_l]$$

Evaluating the scalar products we have

$$-r_{kj}\boldsymbol{s}_j = r_{kj}\boldsymbol{s}_i - r_{ji}\cos\alpha_{ijk}\,\boldsymbol{s}_i + r_{kl}\cos\alpha_{jkl}\,\boldsymbol{s}_l$$

Therefore

$$\boldsymbol{s}_j = \frac{-r_{kj} + r_{ji}\cos\alpha_{ijk}}{r_{kj}}\boldsymbol{s}_i + \frac{-r_{kl}\cos\alpha_{jkl}}{r_{kj}}\boldsymbol{s}_l$$

Substituting in for $\boldsymbol{s}_i$ and $\boldsymbol{s}_l$ we have the final expression for $\boldsymbol{s}_j$

$$\boldsymbol{s}_j = \frac{r_{kj} - r_{ji}\cos\alpha_{ijk}}{r_{kj}r_{ji}\sin\alpha_{ijk}} \cdot \frac{(\boldsymbol{e}_{ij} \times \boldsymbol{e}_{jk})}{\sin\alpha_{ijk}} + \frac{\cos\alpha_{jkl}}{r_{kj}\sin\alpha_{jkl}} \cdot \frac{(\boldsymbol{e}_{lk} \times \boldsymbol{e}_{kj})}{\sin\alpha_{jkl}}$$

The expression for $\boldsymbol{s}_k$ can be obtained in precisely the same manner this time putting j as the origin in the rotational invariance expression and proceeding as above.

A more general case though would be that of a non-4 atom torsion. In that case Hilderbrandt (8) showed that the following expressions are the correct ones for the $\boldsymbol{s}$ vectors of all the atoms involved. It should be pointed out that ni, the number of "i-type" atoms, need not equal nl, the number of "l-type" atoms. That is the two ends of the torsional coordinate need not be symmetrical.

The general expressions for the $\boldsymbol{s}$ vectors then are

$$\boldsymbol{s}_i = -\frac{1}{ni}\frac{(\boldsymbol{e}_{ij} \times \boldsymbol{e}_{jk})}{r_{ij}\sin^2\alpha_{ijk}} \qquad \text{for each } i\text{-type atom}$$

$$\boldsymbol{s}_l = -\frac{1}{nl}\frac{(\boldsymbol{e}_{lk} \times \boldsymbol{e}_{kj})}{r_{lk}\sin^2\alpha_{jkl}} \qquad \text{for each } l\text{-type atom}$$

$$\boldsymbol{s}_j = \frac{1}{ni}\sum_{ni}\frac{r_{jk} - r_{ij}\cos\alpha_{ijk}}{r_{ij}r_{jk}\sin^2\alpha_{ijk}} \cdot (\boldsymbol{e}_{ij} \times \boldsymbol{e}_{jk}) + \frac{1}{nl}\sum_{nl}\frac{\cos\alpha_{jkl}}{r_{jk}\sin^2\alpha_{jkl}} \cdot (\boldsymbol{e}_{lk} \times \boldsymbol{e}_{kj})$$

$$\boldsymbol{s}_k = \frac{1}{nl}\sum_{nl}\frac{r_{jk} - r_{kl}\cos\alpha_{jkl}}{r_{kl}r_{jk}\sin^2\alpha_{jkl}} \cdot (\boldsymbol{e}_{lk} \times \boldsymbol{e}_{kj}) + \frac{1}{ni}\sum_{ni}\frac{\cos\alpha_{ijk}}{r_{jk}\sin^2\alpha_{ijk}} \cdot (\boldsymbol{e}_{ij} \times \boldsymbol{e}_{jk})$$

(5) Linear Valence Angle Bend[3] *(Δϕ)*

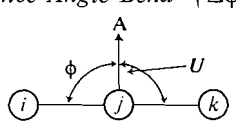

As mentioned previously the valence angle bend formulae "blow-up" in the case of a linear conformation. Schachtschneider (6) recognized this when he published his well known computer programs and allowed for the inclusion of the linear bend as a special type of internal coordinate.

The linear bend is in many respects a very special type of internal coordinate since we cannot use the $\boldsymbol{e}$ vectors as we did in the four preceding types of internal coordinates. We must now define a new type of vector by a point above j at right angles to the linear bend i–j–k as illustrated in the diagram above. Let $\boldsymbol{U}$ be the unit vector along j–A. The $\boldsymbol{s}$ vectors are then defined in terms of the $\boldsymbol{U}$ vector. They must, as

[3]While Schachtschneider (6) treated the linear bend properly with his own vector construction in his computer programs, Ferigle and Meister (11) were the first to correct the deficiency in the Wilson–Decius valence-angle bend formulae following the work of Eliashevich (12).

in all previous cases, be normalized by the respective bond lengths r_{ji} and r_{jk}.

The s vectors for the linear bend then are

$$s_i = -U/r_{ji} \qquad s_k = -U/r_{jk} \qquad s_j = -(s_i + s_k)$$

Schachtschneider made provision in his original GMAT program for the automatic generation of a second linear bend, at right angles to the first. (This is also included in our BMAT program (7).) This situation would arise in an example like carbon dioxide where two degenerate linear bends occur. (In a general case the two linear bends need not necessarily be degenerate.)

To handle this case a second "U" vector may be generated by the following expression

$$UP = e_{jk} \times U$$

The second linear bend is defined by formulae similar to those above

$$s_i = -UP/r_{ji} \qquad s_k = -UP/r_{jk} \qquad s_j = -(s_i + s_k)$$

With this set of five internal coordinates we have completed our set of basis vectors needed for a complete general vibrational analysis.

Acknowledgments

The authors would like to gratefully acknowledge the invaluable assistance of Dr. J. C. Decius without whose help this paper could not have been written.

They would also like to thank the National Research Council of Canada and the University of Toronto for financial assistance.

1. E. B. WILSON, JR. J. Chem. Phys. 7, 1047 (1939); **9**, 76 (1941); **15**, 736 (1947).
2. J. C. DECIUS. J. Chem. Phys. **16**, 1025 (1948).
3. J. C. DECIUS. J. Chem. Phys. **17**, 1315 (1949).
4. E. B. WILSON, JR., J. C. DECIUS, and P. C. CROSS. Molecular vibrations. McGraw-Hill, New York. 1955.
5. D. STEELE. Theory of vibrational spectroscopy. W. B. Saunders, Philadelphia. 1971.
6. J. H. SCHACHTSCHNEIDER. Reports 231/64 and 57/65, Shell Development Co., West Hollow Research Centre, P.O. Box 1380, Houston, Texas 77001, U.S.A.
7. D. F. MCINTOSH and M. R. PETERSON. General vibrational analysis programs utilizing the Wilson **GF** matrix method for a general unsymmetrical molecule. Quantum Chemistry Program Exchange, Room 204, Department of Chemistry, Indiana University, Bloomington, Indiana 47401, U.S.A.
8. R. L. HILDERBRANDT. J. Mol. Spectrosc. **44**, 599 (1972).
9. R. J. MALHIOT and S. M. FERIGLE. J. Chem. Phys. **22**, 717 (1954).
10. I. H. WILLIAMS. J. Mol. Spectrosc. **66**, 288 (1977).
11. S. M. FERIGLE and A. G. MEISTER. J. Chem. Phys. **19**, 982 (1951).
12. M. ELIASHEVICH. C.R. Acad. Sci. URSS, **28**, 604 (1940).

Can. J. Chem. Downloaded from www.nrcresearchpress.com by 210.87.254.6 on 09/05/12
For personal use only.

Kinetics of Z–E isomerization of spiroindolinopyrans

ILONA GRUDA

Département de Chimie-Biologie, Université du Québec à Trois-Rivières (Qué.), Canada G9A 5H7

AND

ROGER M. LEBLANC

Groupe de Recherche en Biophysique, Département de Chimie-Biologie, Université du Québec à Trois-Rivières (Qué.), Canada G9A 5H7

AND

JERZY SOCHANSKI

Département de Physique, Université du Québec à Trois-Rivières (Qué.), Canada G9A 5H7

Received July 4, 1977

ILONA GRUDA, ROGER M. LEBLANC, and JERZY SOCHANSKI. Can. J. Chem. **56**, 1296 (1978).

The kinetics of the Z–E isomerization of a series of 3′-nonsymmetrically substituted spiroindolinopyrans has been studied by nmr in different solvents.

The rate-determining step in nonpolar solvents was found to be the cleavage of the C—O bond whereas in polar solvents it was the C(2)—C(3) bond rotation.

A strong steric hindrance of substituents at carbon 3 was observed. It was found that the rate of the isomerization is more sensitive to the bulkiness of the substituent at C(3′) than at the N(1′). Protic solvents enhance the reaction more than nonprotic polar solvents.

ILONA GRUDA, ROGER M. LEBLANC et JERZY SOCHANSKI. Can. J. Chem. **56**, 1296 (1978).

La cinétique de l'isomérization Z–E d'une série de spiroindolinopyrannes asymétriquement substitués en 3′ a été étudiée par la rmn dans différents solvants.

Dans les solvants apolaires l'étape déterminant la vitesse est la scission de la liaison C—O tandis que dans les solvants polaires c'est la rotation autour de la liaison C(2)—C(3) de l'intermédiaire qui détermine la vitesse.

L'empechement stérique des substituants en C(3) est très fort. La réaction est plus sensible à l'encombrement du substituant en C(3′) qu'en N(1′). Les solvants protiques favorisent plus la réaction que les solvants polaires aprotiques.

Introduction

Spiroindolinopyrans **1** in solution undergo an inversion at the spiro carbon (1, 2). When the compounds are nonsymmetrically substituted at C(3′)[1] the inversion leads to an equilibrium between two isomers **1***a* and **1***b* (Scheme 1).

We have observed previously (3) that nmr spectra of these isomers are different and that this method allows the determination of the concentration of each isomer.

It is well known (1) that spiroindolinopyrans (SP) in solution are in equilibrium with a small amount of an open-ring isomer (OR) which may be detected by uv–visible spectroscopy. This species is identical to the one formed in a photochromic process (4, 5).

Scheme 1 shows the mechanistic possibilities of the transformation of the cyclic isomer **1***a* into its diastereoisomer **1***b*. The open-ring isomer which is a mixture of several species obviously contributes to this transformation.

The cleavage of the C—O bond and the subsequent rehybridization of C(2) yields a nonplanar very unstable intermediate OR-Z'. The *cis–trans* isomerization at the exocyclic double bond leads to an equilibrium between this species and the much more stable OR-E isomer which, in fact, is the only one open-ring isomer that has been observed experimentally.

Two reaction paths, A and B, may lead from **1***a* to **1***b*. Path A: rotation around the single C(2)—C(3) bond converts OR-Z' into OR-Z'' and reclosure of the latter yields **1***b*. Path B: alternatively, **1***b* may be formed in the course of the *cis–trans* isomerization of the exocyclic double bond and the subsequent rotation OR-E' → OR-E → OR-E'', the reverse *trans–cis* isomerization and the final reclosure of OR-Z''.

Toppet *et al.* (2) who investigated spiroindolinopyrans containing up to 95% of the open-ring isomer at equilibrium concluded from dnmr data that in spite of the extreme predominance of the OR-E (*trans*) over the OR-Z (*cis*) isomer, the former is not responsible for the process of inversion.

This is a rather unexpected result since (*i*) the rate of inversion is known to be dependent on the concentration of the OR-E (2); (*ii*) the ratio OR-E/OR-Z is very high; and (*iii*) the steric hindrance to rotation around the C(2)—C(3) bond which is a necessary step in the isomerization, increases drastically in the open-ring isomer OR-Z compared with OR-E. Hence

[1]For numbering see formula **2**.

Can. J. Chem. Downloaded from www.nrcresearchpress.com by 210.87.254.42 on 09/05/12
For personal use only.

Can. J. Chem. Downloaded from www.nrcresearchpress.com by 210.87.254.42 on 09/05/12
For personal use only.

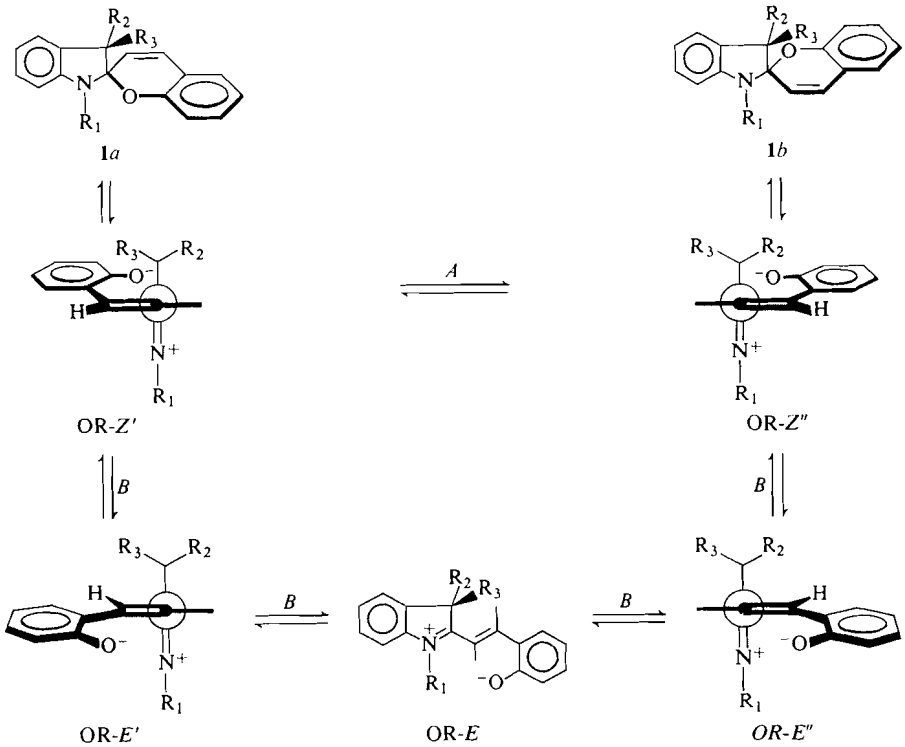

SCHEME 1. OR-*Z'* and OR-*Z''*, nonplanar open-ring isomers with *cis* configuration at the exocyclic double bond. Projection along the C(2)—C(3) single bond. OR-*E'* and OR-*E''*, nonplanar open-ring isomers with *trans* configuration at the double bond.

it could be anticipated that a study of the inversion in a series of spiroindolinopyrans with substituents of varying steric requirements will throw some light on the problem of the steric hindrance of rotation.

Another point of interest was the role of the solvent in the inversion process since the concentration of the intermediate is known to depend on the polarity of the medium.

The results obtained in this investigation enabled us to draw some conclusions with regard to the relative rates of the particular isomerization steps.

Results and Discussion

The following spiroindolinopyrans (**2**) containing a chiral carbon at 3′ have been synthesized.

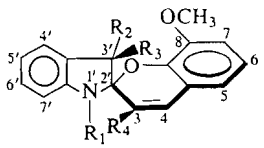

2

a $R_1 = R_2 = CH_3$, $R_3 = C_2H_5$, $R_4 = H$
b $R_1 = R_2 = CH_3$, $R_3 = CH_2C_6H_5$, $R_4 = H$
c $R_1 = CH_2C_6H_5$, $R_2 = CH_3$, $R_3 = C_2H_5$, $R_4 = H$
d $R_1 = R_2 = CH_2C_6H_5$, $R_3 = CH_3$, $R_4 = H$
e $R_1 = R_2 = CH_3$, $R_3 = CH_2C_6H_5$, $R_4 = CH_3$
f[2] $R_1 = R_2 = CH_3$, $R_3 = C_{16}H_{33}$, $R_4 = H$

[2]From ref. 3.

Nuclear magnetic resonance spectra of compounds **2***a*–**2***d* in CCl_4 had two peaks for OCH_3 protons with $\Delta\tau = 0.03$–0.13. Other well-resolved peaks were N—CH_3 in **2***a*, **2***b*, and **2***f* with $\Delta\tau = 0.11$–0.20 and 3′-CH_3 in **2***a* and **2***d* with $\Delta\tau = 0.07$–0.08. Compound **2***e* in CCl_4 had only one resonance peak for each group of protons, two isomers could be seen only in more polar solvents. In 20% CD_3OD–CCl_4 solution $\Delta\tau_{OCH_3} = 0.22$, $\Delta\tau_{N-CH_3} = 0.07$, $\Delta\tau_{3-CH_3} = 0.63$, and $\Delta\tau_{3'-CH_3} = 0.1$.

It can be anticipated that the predominant isomer is the SP-*E* one which is formed by an attack of the anionic oxygen of the open-ring form on the electrophilic carbon from the less crowded side, as shown in Scheme 2, where R_2 is more bulky than

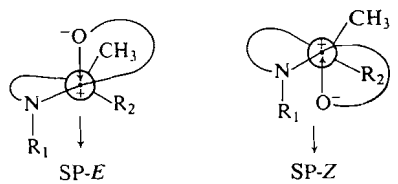

SCHEME 2

the methyl. The above assumption was confirmed by the nuclear Overhauser effect experiments.[3] The

[3]I. Gruda. To be published.

integration of nmr signals shows that in an equilibrated solution the ratio SP-*E*/SP-*Z* is in the range of 1.3–2.2 and is almost independent of the solvent, as shown in Table 1.

Slow crystallisation of synthesized compounds (**2***a*–**2***f*) from ethanol gave solid products containing 80–95% of one isomer, SP-*E* in the case of **2***a*, **2***b*, and **2***d* and SP-*Z* for **2***c* and **2***e*. Nuclear magnetic resonance measurements give the variation of isomers' concentration with time, hence the rate of the isomerization. The kinetics of the above process is represented by two consecutive reversible reactions:

$$X_1 \underset{k_2}{\overset{k_1}{\rightleftharpoons}} X_2 \underset{k_4}{\overset{k_3}{\rightleftharpoons}} X_3$$

where X_1 = SP-*E*, X_2 = OR, X_3 = SP-*Z*. The exact solution of the rate equations for this process is given by a linear combination of two exponential terms (6). In our experiments we have always observed a simple exponential dependence involving a single time constant. The above fact together with the observation that X_2 was always considerably smaller than both X_1 and X_3 has led us to the conclusion that the steady state hypothesis can be applied to the rate equations

$$[1] \quad dx_1/dt = k_2x_2 - k_1x_1$$

$$[2] \quad dx_2/dt = k_1x_1 - k_2x_2 - k_3x_2 + k_4x_3$$

$$[3] \quad dx_3/dt = k_3x_2 - k_4x_3$$

$$[4] \quad x_1 + x_2 + x_3 = 1$$

where x_1, x_2, x_3 are molar fractions of X_1, X_2, X_3, respectively.

Under this hypothesis we have $x_2 \ll x_1, x_3$, together with $dx_2/dt \cong 0$ which enables us to eliminate x_2 thus leading to a system of approximate equations involving two apparent rate constants k_1' and k_{-1}'

$$[5] \quad dx_1/dt = -k_1'x_1 + k_{-1}'x_3$$

$$[6] \quad x_1 + x_3 = 1$$

corresponding to an apparent reaction scheme

$$x_1 \underset{k_{-1}'}{\overset{k_1'}{\rightleftharpoons}} x_3$$

Solving the above system of equations gives

$$[7] \quad x_1 = (x_1^0 - x_1^{eq})e^{-kt} - x_1^{eq}$$

$$[8] \quad x_3 = 1 - x_1$$

whereas the assumption $dx_2/dt = 0$ gives

$$[9] \quad x_2 = p + q\,x_1$$

TABLE 1. The isomer ratio SP-*E*/SP-*Z* in equilibrated solutions

Compound	Solvent	SP-*E*/SP-*Z*
2*a*	CCl_4	2.0
	CD_3COCD_3	1.9
	C_6H_6	2.0
	$CHCl_3$	1.9
2*b*	CCl_4	2.0
	CH_2Cl_2	2.2
	CD_3COCD_3	2.1
	20%CD_3OD–CCl_4	2.2
2*c*	CCl_4	1.5
	CH_2Cl_2	1.3
	CD_3COCD_3	1.5
2*d*	CCl_4	2.2
	CD_3COCD_3	2.5
2*e*	20%CD_3OD–CCl_4	1.4
2*f*	CCl_4	1.8
	C_6H_6	1.8

where x_1^0 = the initial value of x_1,
$x_1^{eq} = k_2k_4/(k_1k_3 + k_2k_4)$ the equilibrium value of x_1,
$k = (k_1k_3 + k_2k_4)/(k_2 + k_3)$ the effective rate constant,
$p = k_4/(k_2 + k_3)$, and
$q = (k_1 - k_4)/(k_2 + k_3)$.

The values of x_1^0, x_1^{eq} and k are easily obtained from the experimental $x_1(t)$ dependence using a computer least-squares curve-fitting procedure. The parameters p and q are similarly obtained from the relationship between x_2 and x_1 provided the $x_2(t)$ data are available. In the absence of any experimental information on x_2, the only parameters which can be obtained from the kinetics experiments are the apparent rate constants given by

$$[10] \quad k_1' = k(1 - x_1^{eq})$$

$$[11] \quad k_{-1}' = kx_1^{eq}$$

The relationships between k_1' and k_{-1}' and the true rate constants k_1, k_2, k_3, and k_4 are

$$[12] \quad k_1' = k_1k_3/(k_2 + k_3)$$

$$[13] \quad k_{-1}' = k_2k_4/(k_2 + k_3)$$

The above relationships lead to

$$[14] \quad \frac{k_{-1}'}{k_1'} = \frac{k_2}{k_3}\frac{k_4}{k_1}$$

which gives us information on the ratio k_2/k_3 provided that we can make some plausible hypothesis about the ratio k_4/k_1. In several cases where it was possible to determine p and q we were able to evaluate all four rate constants

$$[15] \quad k_1 = k[(p + qx^{eq})/p]$$

Can. J. Chem. Downloaded from www.nrcresearchpress.com by 210.87.254.42 on 09/05/12
For personal use only.

TABLE 2. Numerical results for the apparent rate constants

Compound	Solvent	Total concentration (mol ℓ^{-1})	k_1' (min^{-1})	k_{-1}' (min^{-1})
2*a*	CCl_4	0.250	5.25×10^{-3}	10.50×10^{-3}
2*a*	C_6H_6	0.250	4.98×10^{-3}	9.96×10^{-3}
2*a*	CD_3COCD_3	0.125	27.50×10^{-3}	52.00×10^{-3}
2*b*	CCl_4	0.250	3.30×10^{-3}	6.60×10^{-3}
2*b*	CD_3COCD_3	0.078	5.83×10^{-3}	14.20×10^{-3}
2*b*	20% CD_3OD–CCl_4	0.125	38.50×10^{-3}	78.20×10^{-3}
2*c*	CCl_4	0.250	6.00×10^{-3}	9.60×10^{-3}
2*c*	CCl_4	0.125	6.30×10^{-3}	10.10×10^{-3}
2*c*	CD_3COCD_3	0.090	18.30×10^{-3}	28.50×10^{-3}
2*d*	CCl_4	0.250	5.70×10^{-3}	12.50×10^{-3}
2*d*	CD_3COCD_3	0.125	7.40×10^{-3}	19.10×10^{-3}
2*e*	CCl_4	0.250	No isomerization after 24 h	
2*e*	20% CD_3OD–CCl_4	0.125	1.21×10^{-3}	1.69×10^{-3}
2*f*	CCl_4	0.125	8.70×10^{-3}	15.60×10^{-3}

[16] $$k_2 = k\,(x_1^{eq}/p)$$

[17] $$k_3 = k\,((1 - x_1^{eq})/(p + q))$$

[18] $$k_4 = k\,((p + qx^{eq})/(p + q))$$

It is interesting to note that in a particular situation when $x_2 = p$ = constant we obtain

[19] $$k_1 = k_4 = k_1' + k_{-1}'$$

[20] $$k_2/k_3 = k_{-1}'/k_1'$$

It has to be pointed out that all the above relationships can be obtained without the steady state hypothesis following a rigorous mathematical treatment of the time rate equations using the following simplifying assumptions: $k_1, k_4 \ll k_2, k_3$ which results in a small value of x_2 and $t \gg 1/(k_2 + k_3)$ i.e., after the induction period has passed. These inequalities represent a mathematical basis of the steady state hypothesis. The numerical results obtained from the analysis of our experimental data show that the above conditions are very well satisfied in practice.

In our study we were not able to measure the concentration of the open-ring intermediate in nonpolar solvents hence only the apparent rate constants k_1' and k_{-1}' could be calculated [10] and [11]. Table 2 gives calculated apparent rate constants for all investigated compounds. One can see from Table 2 that the rate of isomerization in a nonpolar solvent such as CCl_4 depends only slightly on the bulkiness of the substituents at 1′ and 3′. The most plausible explanation of this result is a hypothesis that in nonpolar solvents the rate-determining step is the bond cleavage in the pyran ring. In a more polar solvent like CD_3COCD_3 both constants are higher for the less crowded compound **2***a* than for **2***b*, **2***c*, and **2***d*. The observed differentiation of isomerization rates can readily be rationalized by the well-known enhancement of heterolytic bond cleavage by polar solvents. It can be assumed for the compounds investigated here that polar solvents enhance considerably the rate of ring opening, the C(2)—C(3) bond rotation thus becoming the rate determining step. The ring closure is always very fast. The role of steric hindrance in the inversion is strongly substantiated by the extremely slow isomerization of the compound **2***e*: in 20% CD_3OD–CCl_4 solution its conversion is 17.5 times slower than for **2***b* which is an analog of **2***e* without a methyl at C3.

For the isomerization in polar solvents we have been able to measure the concentration of the open-ring species by uv-visible spectroscopy and calculate the four true rate constants ([15]–[18]) which are given in Table 3.

The partitioning coefficient of the open-ring form $f = k_2/k_3$, may be considered as a factor representing the steric hindrance of the rotation. Examination of Table 3 shows that when a methyl at nitrogen is replaced by a more bulky benzyl (**2***a* and **2***c*) the steric hindrance is practically unaffected. A more important steric hindrance is provided by introduction of the benzyl group at C(3′) (**2***b* and **2***d*). Comparing the coefficient f for compound **2***b* in two solvents one can see that the solvent has no influence on the rotation hindrance.

The data of Tables 2 and 3 also show that a slightly polar but protic solvent enhances the isomerization much more than a polar nonprotic solvent (compound **2***b*). The open-ring form is strongly stabilized by the hydrogen bond in protic solvents.

The k_1/k_4 ratio is close to 1 in all studied reactions in polar solvents, but we do not feel we can assume a similar ratio in nonpolar solvents. Therefore we do not think the coefficient k_1'/k_{-1}' represents the

Can. J. Chem. Downloaded from www.nrcresearchpress.com by 210.87.254.42 on 09/05/12
For personal use only.

TABLE 3. Numerical results for the true rate constants

Compound	Solvent	Total concentration (mol ℓ^{-1})	k_1 (min^{-1})	k_2 (min^{-1})	k_3 (min^{-1})	k_4 (min^{-1})	x_1^0 (mol ℓ^{-1})	k_2/k_3
2a	CD_3COCD_3	0.125	0.066±0.005	169 ±14	121 ± 7	0.090±0.006	0.111	1.40
2b	CD_3COCD_3	0.078	0.020±0.001	79.4± 5.1	32.7± 2.6	0.020±0.001	0.077	2.47
2c	CD_3COCD_3	0.090	0.048±0.003	289 ±17	178 ±14	0.046±0.002	0.0338	1.62
2d	CD_3COCD_3	0.125	0.028±0.002	98 ± 7.2	35.5± 3.1	0.026±0.001	0.122	2.76
2b	20%CD_3OD–CCl_4	0.125	0.133±0.013	31.2± 3.4	12.7± 1.9	0.110±0.008	0.120	2.46

TABLE 4. Physical and analytical data of spiroindolinopyrans

		Analyses						
		Calculated			Found			
Compound	mp (°C)	C	H	N	C	H	N	Nuclear magnetic resonance (in CCl_4) (τ)
2a	118–119	78.51	7.16	4.36	78.30	7.44	4.52	2.85–3.55 (m, 8H, aromatic and 1 olefinic), 4.35 (d, 1H, olefinic), 6.30[a] and 6.33[b] (s's, 3H, OCH_3), 7.22[b] and 7.33[a] (s's, 3H, N—CH_3), 8.67[b] and 8.74[a] (s's, 3H, 3′-CH_3), 8.30–8.60 (m, 2H, CH_2), 8.85–9.25 (m, 3H, CH_3).
2b	146–147	81.46	6.52	3.65	80.91	6.89	3.77	2.80–4.00 (m, 13H, aromatic and 1 olefinic), 4.25 (d, 1H, olefinic), 6.32[a] and 6.45[b] (s's, 3H, OCH_3), 6.85[a] and 7.32[b] (broad s's, 2H, CH_2), 7.25[b] and 7.45[a] (s's, 3H, N—CH_3), 8.80 (broad s, 3H, 3′-CH_3).
2c	117–118	81.60	6.80	3.50	81.60	6.79	3.58	2.70–3.90 (m, 13H, aromatic and 1 olefinic), 4.30 (d, 1H, olefinic), 5.50–6.15 (m, 2H, N—CH_2—), 6.38[a] and 6.41[b] (s's, 3H, OCH_3), 8.30–8.50 (m, 2H, CH_2), 8.75 (broad s, 3H, 3′-CH_3), 9.00–9.45 (m, 3H, CH_3).
2d	138–139	83.66	6.32	3.05	84.01	6.78	3.26	2.80–3.80 (m, 18H, aromatic and 1 olefinic), 4.15 (d, 1H, olefinic), 5.50–6.05 (m, 2H, N—CH_2—), 6.28[a] and 6.40[b] (s's, 3H, OCH_3), 6.75[a] and 7.15[b] (broad s's, 2H, CH_2), 8.68[a] and 8.75[b] (s's, 3H, 3′-CH_3).
2e	164–165	81.61	6.80	3.53	82.20	7.14	3.22	2.80–4.15 (m, 13H, aromatic and 1 olefinic), 6.20 (s, 3H, OCH_3), 6.60–7.30 (m, 2H, CH_2), 7.20 (s, 3H, N—CH_3), 8.55 (d, 3H, 3-CH_3), 8.86 (s, 3H, 3′-CH_3).

[a]Isomer *Z*.
[b]Isomer *E*.

steric hindrance of rotation which would have been true if $k_1 = k_4$ [14].

In conclusion it should be stressed that in polar solvents where the bond rotation is the rate-determining step the rate of the spiro carbon inversion is strongly affected by steric hindrance of substituents at C(3), less strongly by substituents at C(3′) and almost unaffected by substituents at N(1). Examination of Stuart space-filling molecular models of all OR species shows that the above results fit better into the reaction path *B* than into path *A*. The fact that the equilibrium between the two cyclic isomers and the OR-*E* was established very rapidly and the concentration of the latter remained constant in the course of the reaction SP-$E \rightleftharpoons$ SP-Z ($k_1 = k_4$) shows that the system OR-$Z' \rightleftharpoons$ OR-$E \rightleftharpoons$ OR-Z'' (Scheme 1) was at a dynamic equilibrium during all the time of the reaction. Hence the reaction proceeds along path *B*, at least partly. It is hardly possible to evaluate from the present study how large this fraction is. The choice of the reaction path (*A* or *B*) is likely to depend on the ratio of two activation energies: (*i*) that of the rotation of the OR-*Z*, and (*ii*) the OR-$E \rightarrow$ OR-*Z* isomerization. Usually the activation energy of *cis–trans* isomerization is much higher than the barriers to rotation around single bonds but the situation may be reverse if the formal double bond is strongly polarized (7–9).

Can. J. Chem. Downloaded from www.nrcresearchpress.com by 210.87.254.42 on 09/05/12
For personal use only.

With the spiroindolinopyrans, the contribution of a quinoid form (**3**) may considerably lower the activation energy of the OR-*E* → OR-*Z* isomerization, thus making path *B* accessible.

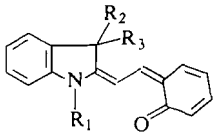

3

It seems probable that paths *A* and *B* are competitive, path *A* being favoured if OR-*E* is very stable (as for the compounds of Ref. 2), whereas a less stable OR-*E* favours path *B*.

Experimental

Melting points are uncorrected. Microanalyses were performed by Schwarzkopf Microanalytical Lab., New York, NY. The nmr spectra were recorded at 60 MHz using a Perkin–Elmer R-12 spectrometer with TMS as standard. The absorption spectra were measured with a Colman 124 spectrometer. The Spectrograde solvents for kinetic experiments were used without further purification. Some control experiments were performed with CCl_4 treated with K_2CO_3. The rate of isomerization remained unchanged.

All compounds were prepared according to the methods described in a previous paper (3). Melting points, analytical data, and nmr data of synthesized compounds are given in Table 4.

The kinetic data were obtained by integration of the nmr peaks of the two isomers (OCH_3 or N—CH_3 protons) in 1-min intervals. The concentration of the newly formed isomer was calculated from the formula:

$$C_1 = C_0 h_1/(h_1 + h_2)$$

where C_0 = the total initial concentration; h_1 = integration data for the newly formed isomer; h_2 = integration data for the other isomer.

The concentration of the OR in acetone was estimated by measuring the absorption at $\lambda = 560$ nm and using the value $3.5 \times 10^4\ \ell\ mol^{-1}\ cm^{-1}$ for the molar extinction coefficient (4).

Acknowledgements

The authors are indebted to the Université du Québec à Trois-Rivières (FIR) and the Ministère de l'Education du Québec (FCAC) for financial assistance.

1. R. C. Bertelson. *In* Photochromism. Vol. III. Techniques of chemistry. Wiley-Interscience, New York, NY. 1971.
2. S. Toppet, W. Quintens, and G. Smets. Tetrahedron, **31**, 1957 (1975).
3. I. Gruda and R. M. Leblanc. Can. J. Chem. **54**, 576 (1976).
4. J. B. Flannery, Jr. J. Am. Chem. Soc. **90**, 5660 (1968).
5. O. Chaudé. Cah. Phys. **50**, 37 (1954).
6. A. A. Frost and R. G. Pearson. Kinetics and mechanism, John Wiley and Sons, New York, NY. 1965.
7. K. I. Dahlqvist. Acta Chem. Scand. **24**, 1941 (1970).
8. Y. Shvo, E. C. Taylor, and J. Bartulin. Tetrahedron Lett. 3259 (1967).
9. J. Sandström and I. Wennerbeck. Chem. Commun. 307 (1969).

Can. J. Chem. Downloaded from www.nrcresearchpress.com by 210.87.254.42 on 09/05/12
For personal use only.

A study of ^{14}N relaxation and nitrogen–proton spin coupling in nucleoside, indole, and ε-caprolactam systems through Fourier transform measurements of NH proton spin–lattice relaxation in the rotating frame

MICHAEL EUGENE MOSELEY AND PETER STILBS

Department of Physical Chemistry, Uppsala University, Box 532, S-751 21 Uppsala, Sweden

Received November 23, 1977

MICHAEL EUGENE MOSELEY and PETER STILBS. Can. J. Chem. **56**, 1302 (1978).

Measurements of nitrogen-14 nuclear spin–lattice relaxation times and direct proton coupling constants are presented for a series of nucleosides and nucleoside bases and indole derivatives in DMSO-d_6 and for a series of ε-caprolactam concentrations in $CDCl_3$. The data were obtained through NH proton $T_{1\rho}$ measurements, a potentially useful alternative to direct ^{14}N and ^{15}N nuclear magnetic resonance for the study of e.g. NH hydrogen bonding.

MICHAEL EUGENE MOSELEY et PETER STILBS. Can. J. Chem. **56**, 1302 (1978).

On a déterminé des temps de relaxation nucléaire spin–réseau pour de l'azote 14 et des constantes de couplage de proton directes pour une série de nucléosides, de bases nucléosides et de dérivés de l'indole dans le DMSO-d_6 et pour une série de concentrations d'ε-caprolactame dans le $CDCl_3$. On a obtenu les données à l'aide de mesures de $T_{1\rho}$ pour le proton NH, une méthode qui pourrait s'avérer une alternative utile à la résonance magnétique nucléaire directe du ^{14}N et du ^{15}N dans des études, par exemple, de lien hydrogène NH

[Traduit par le journal]

Introduction

Nitrogen is a key element in biochemical and biophysical processes. Unfortunately, it is also a difficult nucleus to study by nmr methods. The most abundant isotope (^{14}N, 99.7%) has $I = 1$ and hence a nuclear quadrupole moment, which furthermore happens to be sufficiently large to make resonances very broad (usually >500 Hz). This reduces sensitivity and may result in overlapping resonances in molecules with more than one type of nitrogen. The other nitrogen isotope (^{15}N) has a favourable spin of $\frac{1}{2}$, but a low natural abundance (0.3%). Additional complications are a low, negative gyromagnetic ratio and fairly long spin–lattice relaxation times. Proton broad-band decoupling which may enhance nmr sensitivity due to the nuclear Overhauser effect, is rather a complication in ^{15}N nmr, since this effect will be negative. ^{15}N is therefore a very difficult nucleus to study; sensitivity is more than a magnitude lower than ^{13}C, corresponding to more than two magnitudes in measurement time.

Apart from simple spectra, other nuclear properties are of interest. Nuclear spin relaxation rates are uniquely detailed and quantitative sources of information about molecular mobility, in particular with regard to rotational diffusion and internal motions. Unfortunately their measurement requires roughly 10 times more spectrometer time than running just a single spectrum. One can thus conclude that measurements of ^{15}N relaxation rates will, at best, be difficult. Studies on dilute, natural abundance samples are impossible with presently available spectrometer technology and therefore ^{14}N is usually the only accessible isotope.

Direct measurement of ^{14}N relaxation rates is possible either by pulse methods or through band-shape studies. Since relaxation rates commonly exceed 1000 s^{-1} the latter method is usually the easiest one (although a large number of short nitrogen relaxation times in the literature (see e.g. ref. 1) have been determined by pulse methods). Bands are usually so broad that contributions from instrumental broadening and heteronuclear spin–spin couplings are negligible and the resonance is a Lorentzian curve with a width at half height equal to $1/(\pi \cdot T_2)$. On the other hand, the broad bands may overlap in complex molecules, where one will also face an assignment problem.

Indirect measurement of ^{14}N relaxation rates is, however, possible through band-shape studies of directly bonded spin $\frac{1}{2}$ nuclei, provided that these are subject to slow chemical exchange. Primary and secondary amino protons, in particular, are suited for this approach. Sensitivity is now of proton magnitude, which allows dilute solutions to be used.

The ^{14}N relaxation rate has a profound effect on the amino proton line shapes; resonances are usually more than 10 Hz wide. Matching theoretical and observed band shapes yields the ^{14}N relaxation rate directly, provided that the proton–nitrogen coupling constant and other band shape influencing factors can be determined and accounted for. Unfortunately, this is not normally the case. The direct spin–spin coupling must usually be estimated,

Can. J. Chem. Downloaded from www.nrcresearchpress.com by 210.87.254.42 on 09/05/12
For personal use only.

Can. J. Chem. Downloaded from www.nrcresearchpress.com by 210.87.254.42 on 09/05/12
For personal use only.

although, in favourable cases, it can be measured indirectly in ^{15}N spectra. Significant band shape contributions also arise through proton–proton dipolar relaxation and through proton spin–spin couplings. These can, of course, be accounted for in the simulations, although the band-shape equations rapidly tend to become very complex when additional factors are added. A review of the theory relevant to the above discussion has been given by Lehn and Kintzinger (1).

Measurement of amino proton longitudinal relaxation rates in the rotating frame ($T_{1\rho}$, spin-locking) is a method which eliminates effects on proton relaxation other than proton–nitrogen scalar coupling.[1] It was used as early as 1959 by Salomon (2) to determine proton–nitrogen coupling constants as well as ^{14}N relaxation rates in formamide. A reasonable agreement between theory and experiment was obtained.

To our knowledge, this is the only published application of the technique, as applied to nitrogen relaxation. We have found the method to be a powerful and accurate (although time-consuming) method for determining direct proton–nitrogen coupling constants and ^{14}N relaxation rates, even in very complex systems. With presently available attachments to Fourier transform spectrometers measurement accuracy and convenience is very much improved. Reviews on the spin-locking technique can be found in refs. 3 and 4.

^{14}N relaxation rates are usually completely dominated by the quadrupolar relaxation mechanism (1). Under extreme-narrowing conditions, and the assumption of an exponential correlation function for molecular reorientation, relaxation rates will be given by [1]:

$$[1] \quad \frac{1}{T_{1q}} = \frac{1}{T_1} = \frac{1}{T_2} = \frac{3}{8}\left(\frac{e^2qQ}{\hbar}\right)^2\left(1 + \frac{\eta^2}{3}\right)\tau_c$$

Here eq is the electric field gradient at the nitrogen nucleus, η is the asymmetry parameter of the field gradient, eQ is the electric quadrupole moment of ^{14}N and τ_c is the rotational correlation time. Without additional information the interpretation of ^{14}N relaxation rates is therefore not a completely straightforward task. In addition to rotational diffusion rates the electronic structure around the ^{14}N nuclei also becomes of importance. Nuclear quadrupole resonance methods do provide a way of measuring $e^2qQ/\hbar$ and η in the solid state (1). However, such information is of little value for the interpretation of T_1 changes in solution. Fortunately, τ_c can be obtained in an independent way from either ^2H or ^{13}C T_1 measurements. ^{14}N relaxation times are thus primarily a source of information about the electronic structure in the NH moiety. In systems where it has been established that eq and η are relatively constant however, changes in T_{1N} can be directly related to changes in τ_c.

The present paper concerns measurements made on nucleosides and indoles in DMSO-d_6 and on ε-caprolactam in $CDCl_3$ to illustrate the possibility of employing the technique in a variety of biological and hydrogen bonding systems. ε-Caprolactam was included in the study since it is a simple model of a compound which dimerizes through hydrogen bonding. This effect has previously been studied by measurements of the concentration dependence of its molecular polarization (5). In ^1H nmr the dimerization manifests itself very clearly in concentration-dependent downfield shifts of the NH proton. Since these shift changes reflect changes in the electronic environment of the NH moiety a parallel study of the nitrogen relaxation rate and the proton–nitrogen coupling should be of interest, as both depend on this factor.

Experimental

The nucleosides, parent bases, base derivatives, indole, and indole derivatives were obtained from Sigma Chemical Co. and Pfaltz and Bauer Research Chemicals. ε-Caprolactam was obtained from Merck Chemical Co., and deuterated dimethyl sulphoxide from Ciba–Geigy. All materials were used without further purification except 2-methylindole, which was recrystallized from H_2O.

Samples were prepared in 5 mm thin-wall nmr tubes and were not degassed. Relaxation contributions from dissolved oxygen are anticipated to be negligible since T_1 values were always less than 1.4 s (aniline) and usually in the 0.1–0.3 s range. Furthermore, the electron–nuclear relaxation times are expected to make equally large contributions to the T_1 and $T_{1\rho}$ values (since electron spin relaxation times are very short) and therefore eliminated through the evaluation procedure (cf. [2] below). These expectations are supported by later experiments on carefully degassed samples. Even in nondegassed samples we found $T_1 = T_{1\rho}$ (within experimental error) for signals not subject to chemical exchange or scalar coupling.

All measurements were made by Fourier transform methods on a JEOL FX-100 pulsed nmr spectrometer with double quadrature detection, under control of either the JEOL Autostacking or Auto-T_1 programs. For each sample, T_1 (by the inversion–recovery method) as well as $T_{1\rho}$ was measured for all NH_2 and NH proton signals at an ambient temperature of 25°C. The latter quantity, $T_{1\rho}$, which is sensitive to the proton resonance frequency in the spin-locking field ω_1 (*vide supra*), was measured at five values of ω_1 in the range 1200 to 19 000 rad/s. ω_1 was determined by measurement of the time required to produce a 180° pulse. Great care was taken to insure that all pulse widths and phasings were properly set. These were always checked and, if necessary, adjusted for each sample. Furthermore, the measurements were made with the spectrometer carrier frequency centered on the studied band

[1]An exception is relaxation induced by chemical exchange among nonequivalent sites. We have not found any indications that this mechanism seriously affects the results quoted in the present study (cf. Experimental).

Can. J. Chem. Downloaded from www.nrcresearchpress.com by 210.87.254.42 on 09/05/12
For personal use only.

(within 10 Hz). This is highly essential for spin-locking measurements at low values of ω_1, since the directions of the effective field in the rotating frame (B_{eff}) and the nuclear magnetization after the initial 90° pulse are not exactly parallel off-resonance. Since $B_0 = \omega_0/\gamma$, the z-component of B_{eff} in the rotating frame is $(\omega_0/\gamma)\cdot[1 - \omega_0/(\omega_0 + 2\pi\nu_d)]$, where ω_0 is the carrier frequency in rad/s and γ is the gyromagnetic ratio of the nucleus; ν_d is the deviation from exact resonance. Since $2\pi\nu_d \ll \omega_0$ this expression simplifies to $2\pi\nu_d/\gamma$. During a perfect spin-locking sequence, the nuclear magnetization should point in the y-direction along B_1, which is equal to ω_1/γ or $\pi/(PW(\pi)\cdot\gamma)$ where $PW(\pi)$ is the time required for B_1 to produce a π or 180° pulse. The misalignment angle between B_{eff} and B_1 is thus equal to arctan $(B_{(eff)z}/B_1)$ or arctan $(2\pi\nu_d\cdot PW(\pi))$. One finds that for low ω_1 ($\approx$2000 rad/s) only a range of a few Hz around ω_0 will be properly spin locked.

After the T_1 and $T_{1\rho}$ measurement series, each consisting of 10 spectra, signal amplitudes were fitted to their respective decay functions by a nonlinear least-squares procedure utilizing the general FORTRAN IV minimization subroutine STEPIT (6). T_1 and $T_{1\rho}$ were then fitted to their theoretical ω_1 dependence (3, 4) again by the nonlinear least-squares procedure yielding A ($\equiv {}^1J_{^{14}N-^1H}$) and T_{1N} from the equation

$$[2]\quad \frac{1}{T_{1\rho(sc)}} = \frac{1}{T_{1\rho(obs)}} - \frac{1}{T_1} = \frac{2}{3}A^2\frac{T_{1N}}{1 + \omega_1^2 T_{1N}^2}$$

Here $1/T_{1\rho(sc)}$ is the extracted proton relaxation contribution from proton–nitrogen scalar coupling and T_{1N} and A are the ^{14}N spin–lattice relaxation time and proton coupling constant (in rad/s), respectively.

We wish to emphasize that the procedure commonly suggested in the literature, extracting A and T_{1N} through a linear plot of $T_{1\rho(sc)}$ against ω_1^2 (3, 4) is entirely unsound, since for high values of ω_1, $T_{1\rho(obs)}$ is almost equal to T_1. This approach therefore gives a lower weight to the most accurately known $T_{1\rho(sc)}$ values and a high weight to the least accurately known values.

Error estimation in the present nonlinear least-squares simulations has been done through Monte Carlo methods as suggested by Chandler in the program manual for the STEPIT subroutine (6). The quoted error limits correspond to a 90% confidence interval and include only random errors. The mutual element in the correlation matrix regarding A and T_{1N} was calculated in some cases through the normal STEPIT error estimation features and was typically found to be relatively large and negative (−0.5 to −0.9).

As an initial check on the validity and accuracy of the measurement procedure outlined above $^1J_{^{14}N-^1H}$ and T_{1N} values of neat aniline were measured at 25°C. The results were 57.5 ± 1.0 Hz and 230 ± 20 μs, respectively. The latter value is in excellent agreement with the reported linewidth 1300 Hz (7), which corresponds to T_{2N} (= T_{1N}) = 240 μs. The direct proton–nitrogen coupling in neat aniline has not, however, been reported. Values in various solvents range from 55.6 to 58.7 Hz (recalculated from ^{15}N data (8)).

In samples having two or more exchangeable proton types (e.g. NH, NH_2, COOH, H_2O), chemical exchange may affect the $T_{1\rho}$ values. The effect on the results was found to be a definite overestimation in the value of A although an undetermined change in T_{1N}. There is reason to believe that the trends to an increase of A with concentration in Table I is partially due to this effect. The scatter of A values in Table 3 exceeds the estimated confidence intervals and is believed to be due to traces of water. Systematic over estimations of A do however, seem to be less than 10%.

^{13}C relaxation times were determined by the inversion–recovery method.

Results and Discussion

Pyrimidine and Purine Derivatives

The results are summarized in Table 1. It is seen that the coupling constants are essentially the same throughout the series of compounds and concentrations. The ^{14}N relaxation times vary appreciably, however. Within the same molecule NH_2 nitrogens have a shorter T_1 than NH nitrogens. Concentration effects are small, although a trend towards a decrease in T_{1N} with increasing concentration is found for 9-ethylguanine. This effect is expected, since the solute molecules, subject to increased hydrogen bonding, are less mobile at higher concentrations.

The effect on molecular mobility is quite pronounced going from e.g. 9-ethylguanine to guanosine or from adenine to adenosine. The presence of the ribose ring appears to decrease mobility, since no large differences in *eq* or η are expected within these pairs.

Indoles and Tryptophan

The results in Table 2 show a significantly lower ^{14}N T_1 for the methylindoles than for indole. This is probably due to decreased mobility rather than to

TABLE 1. ^{14}N spin–lattice relaxation times and ^{14}N–proton coupling constants in nucleosides, bases, and derivatives in DMSO-d_6 solution at 25°C

Compound	Concentration (M)	$^1J_{^{14}N-H}$ (Hz)	T_{1N} (μs)
Adenosine-NH_2	0.20	65.8±11.4	37±15
Guanosine-NH_2	0.20	71.7± 3.0	36± 3
Guanosine-NH		64.9± 4.0	42± 5
Adenine-NH_2	0.05	63.2± 1.9	108±11
	0.10	65.5± 1.9	97± 8
9-Ethylguanine-NH_2	0.05	62.4± 6.2	79±25
	0.10	67.2± 1.9	68± 3
	0.20	69.8± 3.4	64± 6
9-Ethylguanine-NH	0.05	66.0± 1.8	131± 9
	0.10	67.5± 4.5	170±31
	0.20	76.5± 4.5	103±16
1-Methylthymine-NH	0.10	65.0± 1.1	226±13
	0.20	65.6± 1.0	244±19
Uracil-N-H1	0.05	61.6± 1.7	246±17
Uracil-N-H3	0.05	65.7± 1.1	247± 8

TABLE 2. ^{14}N spin–lattice relaxation times and ^{14}N–proton coupling constants in indoles and *l*-tryptophan in DMSO-d_6 solution at 25°C

Compound	Concentration (M)	$^1J_{^{14}N-H}$ (Hz)	T_{1N} (μs)
Indole	0.10	69.0±0.1	360± 5
2-Methylindole	0.10	69.2±0.3	227± 4
3-Methylindole	0.10	69.1±0.2	247± 2
1-Tryptophan[a]	0.05	73.4±1.5	435±30

[a]Ring nitrogen.

TABLE 3. ^{14}N spin–lattice relaxation times and ^{14}N–proton coupling constants in ε-caprolactam in $CDCl_3$ at 25°C

ε-Caprolactam concentration (M)	$^1J_{^{14}N-H}$ (Hz)	T_{1N} (μs)
0.05	64.0±0.4	1034±27
0.10	59.0±0.5	787±15
0.25	60.7±0.9	572±29
0.50	64.1±0.6	558±21
1.00	60.8±0.8	477±28

differences in *eq*, since 2- and 3-methylindole both give approximately the same results. The tryptophan results are slightly affected by proton exchange (making A too large). It can be seen, however, that the NH relaxation time is larger than in the indoles. A possible explanation is that the indoles may tend to stack or aggregate in the DMSO solvent, with a subsequent decrease in mobility.

ε-Caprolactam

As shown by Huisgen and Waltz (5) ε-caprolactam forms dimers even at quite low concentrations. The concentration dependence of the ^{14}N T_1 is shown in Table 3. An approximately twofold decrease is found in the region 0.05–1 M. For comparison, the average ^{13}C T_1 decrease is approximately 25% going from a 1 M to a 0.25 M solution (lower concentrations could not be studied). The corresponding ^{14}N T_1 decrease is 17%, suggesting that the electric field gradient of the nitrogen is lower in the dimer than in the monomer.

Conclusions

It is seen that determination of the ^{14}N spin-lattice relaxation time and direct proton–nitrogen coupling constants through proton spin–lattice relaxation in the rotating frame is a feasible and useful technique even in quite complex systems.

It is evident from [1] that the method cannot be applied if $\omega_1 T_{1N}$ is much less than unity. The very short nitrogen relaxation times in the nucleosides (30–50 μs) thus do represent a lower limit for the technique, determined by the maximum available spin-locking field. On our spectrometer set up ω_1(max) is 19 000 rad/s for protons.

An independent (although in practice correlated) restricting factor is the NH proton T_1 value. In larger hydrogen bonded molecules T_1 may become so short that the evaluation of $T_{1\rho(sc)}$ becomes very uncertain.

Since [2] is valid only under conditions of fast nitrogen relaxation an upper limit for the determination of T_{1N} also exists. In this case, however, nitrogen relaxation times can conveniently be determined through NH proton band-shape studies, since instrumental broadening and proton spin–spin couplings will be essentially negligible for these broad signals.

The largest limitation of the method is probably that slow proton exchange is required. This normally precludes its use on aqueous solutions. We have also found that large solvent peaks cause baseline distortions which are extremely troublesome in spin-locking measurements.

Acknowledgements

We wish to thank Professor G. Bergson for putting the spectrometer at our disposal and Dr. U. Obenius for technical assistance.

1. J. M. LEHN and J. P. KINTZINGER. *In* Nitrogen NMR. *Edited by* M. Witanowski and G. A. Webb. Plenum Press, London and New York. 1973.
2. I. SALOMON. C. R. Acad. Sci. Paris, **248**, 92 (1959).
3. N. BODEN. *In* Determination of organic structures by physical methods. Vol. 4. *Edited by* F. C. Nachod and J. J. Zuckerman. Academic Press, New York, NY. 1971.
4. T. C. FARRAR and E. D. BECKER. Pulse and Fourier transform NMR. Academic Press, New York and London. 1971.
5. R. HUISGEN and H. WALTZ. Chem. Ber. **89**, 2616 (1956).
6. J. P. CHANDLER. Subroutine STEPIT. QCPE, Chemistry Dept., Indiana University, Bloomington, IN 47401, U.S.A.
7. M. BOSE, N. DAS, and N. CHATTERJEE. J. Mol. Spectrosc. **18**, 32 (1965).
8. L. PAOLILLO and E. D. BECKER. J. Magn. Reson. **2**, 168 (1970).

Erratum: The chromous chloride promoted addition of *N*-haloamides to olefins. V. The addition of *N*-chloroamides to enol ethers: synthesis of acyloxy and acyl derivatives of α-amino acetals and ketals (aldehydes and ketones) and of 2-amino sugars

HUGUES DRIGUEZ, JEAN-PAUL VERMES, AND JEAN LESSARD

Département de Chimie, Université de Sherbrooke, Sherbrooke (Qué.), Canada J1K 2R1

Received March 3, 1978

(Ref.: Can. J. Chem. **56**, 119 (1978))

In Scheme 6, the yield of **16** is 59% (62% by vpc) and that of **17** is 10% (by vpc).

Can. J. Chem. Downloaded from www.nrcresearchpress.com by 210.87.254.42 on 09/05/12
For personal use only.

Can. J. Chem. Downloaded from www.nrcresearchpress.com by 210.87.254.40 on 09/05/12
For personal use only.

Canadian Journal of Chemistry

Published by
THE NATIONAL RESEARCH COUNCIL OF CANADA

Journal canadien de chimie

Publié par
LE CONSEIL NATIONAL DE RECHERCHES DU CANADA

Volume 56 Number 10 May 15, 1978

Volume 56 numéro 10 15 mai 1978

The reaction of methyl radicals with formaldehyde in dimethyl ether pyrolysis

KIM C. MANTHORNE AND PHILIP D. PACEY

Department of Chemistry, Dalhousie University, Halifax, N.S., Canada B3H 3J5

Received September 13, 1977

KIM C. MANTHORNE and PHILIP D. PACEY. Can. J. Chem. **56**, 1307 (1978).

Dimethyl ether was pyrolyzed in a flow system at 788, 856, and 935 K and 38–401 Torr. Measurement of the yields of CH_4 and C_2H_6 and of either H_2 or CO enabled calculation of high pressure limiting values of the rate constant quotient $k_9k_6^{-1/2}$, where reaction 9 is

$$CH_3 + CH_2O \rightarrow CH_4 + CHO$$

and reaction 6 is the recombination of two methyl radicals. Including literature data from 357–1005 K, the Arrhenius plot for this quotient is a curve.

KIM C. MANTHORNE et PHILIP D. PACEY. Can. J. Chem. **56**, 1307 (1978).

On a effectué la pyrolyse de l'éther diméthylique dans un système à flux à 788, 856 et 935 K et à des pressions allant de 38 à 401 Torr. La mesure des rendements de CH_4 et de C_2H_6 et de soit H_2 ou CO permet de calculer les valeurs limites à hautes pressions du quotient des constantes de vitesse $k_9k_6^{-1/2}$ où la réaction 9 est

$$CH_3 + CH_2O \rightarrow CH_4 + CHO$$

et la réaction 6 est une recombinaison des deux radicaux méthyles. Si l'on inclut des données provenant de la littérature pour des températures allant de 357 à 1005 K, la droite d'Arrhénius pour ce quotient est une courbe.

[Traduit par le journal]

Introduction

The reaction of methyl radicals with formaldehyde has one of the smallest activation energies known for transfer of a hydrogen atom from a carbon atom to a methyl radical (1). Recent experiments, using CH_3 and CH_2O generated in the flow pyrolysis of dimethyl ether at 1063 to 1223 K (2) and 1005 K (3), have indicated that the reaction is faster at these temperatures than predicted from Arrhenius parameters determined at 357–435 K (4, 5). In the present work, this pyrolysis system has been reinvestigated with slower flow rates and smaller conversions at 788 to 935 K.

The rate-determining reactions in the mechanism, numbered consistently with ref. 3, are as follows:

[1] $$CH_3OCH_3 \rightarrow CH_3 + CH_3O$$

[3] $$H + CH_3OCH_3 \rightarrow H_2 + CH_2OCH_3$$

[5] $$CH_3 + CH_3OCH_3 \rightarrow CH_4 + CH_2OCH_3$$

[6] $$2CH_3 \rightarrow C_2H_6$$

[9] $$CH_3 + CH_2O \rightarrow CH_4 + CHO$$

The radicals formed in reactions 1, 3, and 5 decompose rapidly to form CH_2O; the radical formed in reaction 9 decomposes to form CO.

Making the steady-state assumption for each radical, assuming long chains and integrating the rate equations for product formation, the following expressions are obtained:

[20] $$[CH_4] = k_5C[CH_3]t + \ldots$$

[21] $$[CH_2O] = k_5C[CH_3]t + \ldots$$

[22] $$[CO] = \tfrac{1}{2}k_5k_9C[CH_3]^2t^2 + \ldots$$

[23] $$[H_2] - [C_2H_6] = [CO]$$

Here C is the initial concentration of dimethyl ether. Terms in higher powers of t, resulting from stoichiometric expansion, reactant depletion and minor re-

Can. J. Chem. Downloaded from www.nrcresearchpress.com by 210.87.254.40 on 09/05/12
For personal use only.

actions, have been omitted. The assumptions will be reconsidered in the Discussion. Combining the above equations, one obtains, for short t,

$$[24] \quad \frac{2C[CO]}{[CH_4]^2} = \frac{2C([H_2] - [C_2H_6])}{[CH_4]^2} \doteq \frac{k_9}{k_5}$$

Measurement of the yields, at short residence times, of CH_4 and CO or of CH_4, H_2, and C_2H_6, then, enables estimation of the ratio k_9/k_5.

The quotient $k_5k_{6,\infty}^{-1/2}$ can be determined from CH_4 and C_2H_6 yields as described previously (6). Multiplying, one obtains $k_9k_{6,\infty}^{-1/2}$, the quotient determined at lower temperatures in previous work (4, 5).

Experimental

The apparatus and technique have been described previously (6).

The flow rate of dimethyl ether was kept below 0.23 mol/h to prevent the cooler entering gas from distorting the temperature profile. Conversions were kept to less than 15%.

The reagent, passed through the cold reactor into the gas chromatograph, was found to contain about 10 ppm of O_2.

Results

Experiments have been performed at temperatures close to 788, 856, and 935 K.[1]

The dependence of rates of product formation on reactor residence times were as depicted in Figs. 1 and 2 of ref. 6. Figure 1 of the present work shows values of $2CA[CH_4]^{-2}$, where A is [CO] or ($[H_2] - [C_2H_6]$), at various reactor residence times, for experiments at 789 K and 40 Torr and 938 K and 330 Torr.

Extrapolated, initial values of the quotients are listed in Table 1, with values calculated from the raw data of refs. 7 and 8. The extrapolation of the data of ref. 8 may not be reliable, as the conversions reported were from 14 to 70%. The authors of ref. 8 estimated k_9/k_5 was 3, based on dimethyl ether pyrolysis experiments with added formaldehyde. It can be seen that no trend was observed with changing pressure and that there was no significant difference between data obtained using [CO] and those obtained from ($[H_2] - [C_2H_6]$).

In previous work (6) values of $k_5k_{6,\infty}^{-1/2}$ were determined by a Lindemann–Hinshelwood extrapolation of $k_5^2k_6^{-1}$ vs. P^{-1}. Since then the pressure dependence of the reverse of reaction 6 at 778 to 878 K has been investigated experimentally and a Rice–Ramsperger–Kassel–Marcus model has been developed, which, though involving some assump-

[1]Tables of data are available, at a nominal charge, from the Depository of Unpublished Data, CISTI, National Research Council of Canada, Ottawa, Ont., Canada K1A 0S2.

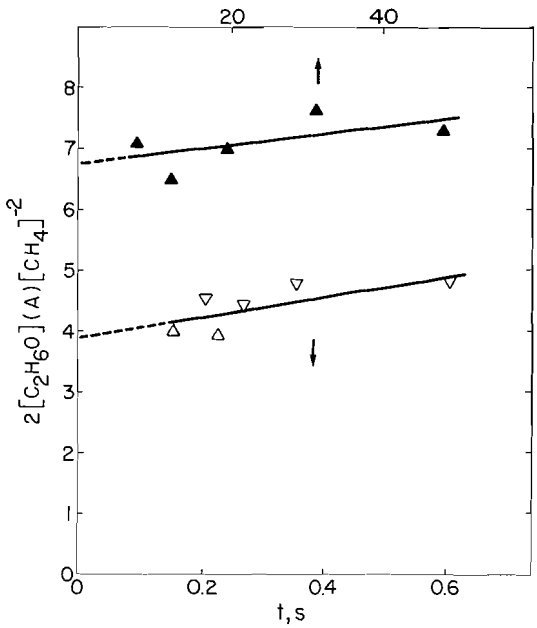

FIG. 1. Values of $2[C_2H_6O]A[CH_4]^{-2}$ as a function of reactor residence time for experiments at 789 K and 40 Torr (filled points) and 938 K and 330 Torr (open points). A is [CO] for the inverted triangles (▽) and ($[H_2] - [C_2H_6]$) for the regular triangles. The lines were determined by the method of least squares.

TABLE 1. Experimental estimates of k_9/k_5

T (K)	P (Torr)	$2[CO][C_2H_6O][CH_4]^{-2}$ (Initial values)
633	95	90[a]
653	95	27[a]
673	95	14[a]
693	55–223	10[a]
713	95	11[a]
780	350	8[b]
859	58	4.7
938	327	4.3
938	400	4.5
T (K)	P (Torr)	$2([H_2] - [C_2H_6])[C_2H_6O][CH_4]^{-2}$ (Initial values)
786	38	6.1
789	40	6.7
788	95	4.7
786	303	6.2
856	50	5.8
856	148	4.8
935	76	4.4
938	122	4.2
937	138	3.5
934	207	4.7
934	241	3.9
935	297	3.9
934	342	4.0

[a, b]Calculated from the analytical data of ref. 7 (*a*) and ref. 8 (*b*). The other data used were from the present work.

Can. J. Chem. Downloaded from www.nrcresearchpress.com by 210.87.254.40 on 09/05/12
For personal use only.

tions, does adequately represent the pressure dependence of the reaction (9). Using this model, values of $k_5k_{6,\infty}^{-1/2}$ have been calculated from the data of ref. 6 and the present work, in a manner analogous to that used in ref. 3 for $k_{6,\infty}$ itself. (See curve *a* of Fig. 4 of ref. 3.) Dimethyl ether was assumed to have the same deactivating efficiency as C_2H_6, on a pressure for pressure basis. Varying the deactivating efficiency to improve the agreement with the pressure dependence observed in this work would have changed the high pressure values of $k_5k_{6,\infty}^{-1/2}$ by less than 5%.

Values of $k_5k_{6,\infty}^{-1/2}$, determined as above, were combined with a value of 2.43×10^{10} ℓ mol^{-1} s^{-1} for $k_{6,\infty}$ (10) to calculate Arrhenius parameters for k_5 of log $A = 10.3 \pm 0.1$ (ℓ mol^{-1} s^{-1}) and $E_A = 60 \pm 2$ kJ mol^{-1}, both within the uncertainty limits reported earlier (6). Here and unless otherwise specified, quoted uncertainties are standard deviations.

Multiplying values of k_9/k_5 from Table 1 by values of $k_5k_{6,\infty}^{-1/2}$ calculated from the above Arrhenius expression allows calculation of $k_9k_{6,\infty}^{-1/2}$. Values are shown in the form of an Arrhenius plot in Fig. 2, with values from earlier work. The value of ref. 3 was calculated from the independent values of k_9 and $k_{6,\infty}$ reported. The experimental Arrhenius parameters for k_9 from this work were calculated to be $\log_{10} A$ (ℓ mol^{-1} s^{-1}) $= 10.1 \pm 0.2$ and $E_A = 45 \pm 3$ kJ mol^{-1}. These are greater than low temperature values of 8.1 ± 0.1 and 26.0 ± 0.7 kJ mol^{-1} from ref. 4 and 8.3 and 28 kJ mol^{-1} from ref. 5.

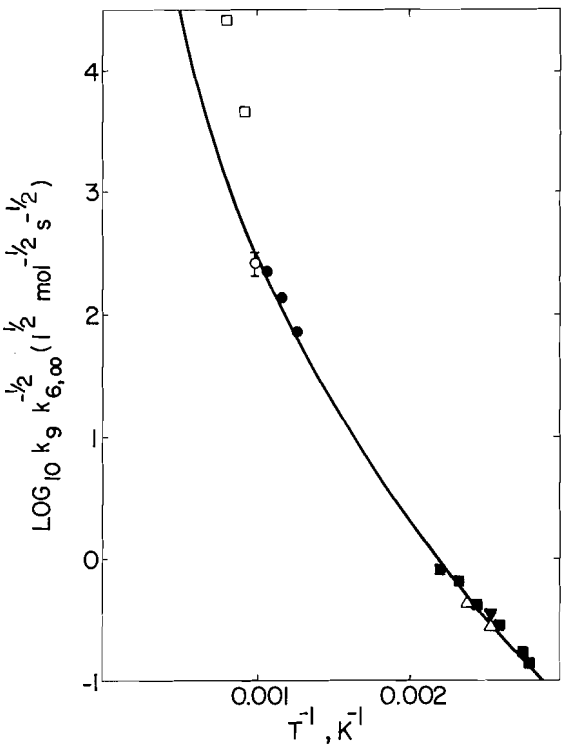

FIG. 2. Arrhenius plot for $k_9k_{6,\infty}^{-1/2}$: ■, ref. 4; △, ref. 5; □, ref. 2; ○, ref. 3; ▼, ref. 11; ●, this work. The solid line, of the form $k = AT^n \exp(-E_A/RT)$, was calculated by the method of least squares for the data from 357 to 1005 K.

Discussion

Formaldehyde was not determined in these experiments. However, Benson and Jain (8) have shown that the initial rate of formation of formaldehyde is equal to the initial rate of removal of dimethyl ether, as required by eqs. 20 and 21.

The assumptions made in deriving eq. 24 were tested using the computer simulation of ref. 3, extended to include the cross-combination of CH_3 and CH_2OCH_3 radicals. The program took into account the initial warming of the reagent on entering the reactor, the build-up of the steady-state radical concentrations, reactant depletion, expansion, the finite chain length, and 11 possible minor reactions. By varying the parameters as described in ref. 3, it was estimated that cumulative errors in the extrapolated initial values of k_9/k_5 from this work should have been 20% or less. Including uncertainty in the extrapolation of $k_5k_6^{-1/2}$ to infinite pressure (taken as 20%) and experimental scatter, the uncertainties in the Arrhenius parameters should be increased to ± 0.9 log units and ± 13 kJ mol^{-1}.

The values of k_9 of Aronowitz and Naegeli (2) were almost an order of magnitude faster than predicted by an Arrhenius line passing through the present results. However, Aronowitz and Naegeli assumed that k_6 had its high pressure limiting value in their system. This could have led to an underestimation of $[CH_3]$ and hence an overestimation of k_9. Furthermore, the low value of $[CH_3]$ could have led to an underestimation of the amount of CH_4 formed by reaction 5 and other reactions, overestimating the remaining amount of CH_4 formed by reaction 9.

All values in Fig. 2, except those from ref. 2, have been fitted by non-linear least-squares to an expression of the form $k_9k_{6,\infty}^{-1/2} = AT^n \exp(-E_A/RT)$. The resulting curve, seen in Fig. 2, is in satisfactory agreement with the data below 1005 K. The parameters of the curve were: log $A = -13.7 \pm 3.7$, $n = 5.6 \pm 1.1$, $E_A = 9.8 \pm 5.5$ kJ mol^{-1}. To fit these points by a straight line, it would be necessary to suppose that the highest and lowest temperature points of ref. 4 are in error by factors of 0.7 and 1.5, respectively, or, if ref. 4 is correct, that the present points are in error by factors of 5 to 8. We conclude that the data are more easily explained on the basis of a curved Arrhenius plot.

Acknowledgements

The authors wish to thank H. P. Reinholdt and Dr. H. Furue for experimental assistance and the National Research Council of Canada for a grant in support of this research.

1. P. Gray, A. A. Herod, and A. Jones. Chem. Rev. **71**, 247 (1971).
2. D. Aronowitz and D. Naegeli. Int. J. Chem. Kinet. **9**, 471 (1977).
3. A. M. Held, K. C. Manthorne, P. D. Pacey, and H. P. Reinholdt. Can. J. Chem. **55**, 4128 (1977).
4. S. Toby and K. O. Kutschke. Can. J. Chem. **37**, 672 (1959).
5. A. R. Blake and K. O. Kutschke. Can. J. Chem. **37**, 1462 (1959).
6. P. D. Pacey. Can. J. Chem. **53**, 2742 (1975).
7. N. Imai and O. Toyama. Bull. Chem. Soc. Jpn. **34**, 328 (1961).
8. S. W. Benson and D. V. S. Jain. J. Chem. Phys. **31**, 1008 (1959).
9. J. A. Clark and C. P. Quinn. J. Chem. Soc. Faraday Trans. I, **72**, 706 (1976).
10. H. E. van den Bergh, A. B. Callear, and R. J. Norstrom. Chem. Phys. Lett. **4**, 101 (1969).
11. D. E. Hoare. Trans. Faraday Soc. **49**, 1292 (1953).

Can. J. Chem. Downloaded from www.nrcresearchpress.com by 210.87.254.40 on 09/05/12
For personal use only.

Nickel(II) and copper(II) complexes of the 'tripod' ligand tris(2-benzimidazylmethyl)amine

LAURENCE K. THOMPSON,[1] BARATHAM S. RAMASWAMY, AND ROBERT D. DAWE

Department of Chemistry, Memorial University of Newfoundland, St. John's, Nfld., Canada A1C 5S7

Received October 27, 1977

LAURENCE K. THOMPSON, BARATHAM S. RAMASWAMY, and ROBERT D. DAWE. Can. J. Chem. **56**, 1311 (1978).

A series of nickel(II) and copper(II) complexes of the title ligand are reported which appear to exhibit predominantly pseudo-octahedral structures in the solid state. Anion bridged dimeric structures are proposed for both nickel and copper; $[Ni_2(NTB)_2X_2]Y_2$ (X = Y = Cl, Br; X = Cl, Br, NCS; Y = BPh_4), $[Cu_2(NTB)_2X_2]X_2 \cdot 2H_2O$ (X = Cl, Br). The other octahedral derivatives appear to be monomeric; $(Ni(NTB)X_2]$ (X = NO_3, NCS), $[Ni(NTB)(H_2O)X]Y$ (X = NCS, Y = BPh_4; X = CH_3CN, Y = $(ClO_4)_2$), $[Ni(NTB)(H_2O)_2]X_2 \cdot 2H_2O$ (X = ClO_4, BF_4), $[Cu(NTB)(NO_3)_2] \cdot H_2O$. Five-coordinate derivatives were uncommon and in the case of three copper complexes trigonalbipyramidal structures are suggested in the solid state; $[Cu(NTB)Cl]BPh_4$, $[Cu(NTB)(H_2O)]X_2 \cdot nH_2O$ (X = BF_4, $n = 0$; X = ClO_4, $n = 1$). In acetone solution all the copper complexes appear to be five-coordinate. Electron spin resonance data confirm trigonalbipyramidal solution structures and indicate $g_{\parallel} < g_{\perp}$ with very small values of $A_{\parallel}$ (60–80 × 10^{-4} cm^{-1}).

LAURENCE K. THOMPSON, BARATHAM S. RAMASWAMY et ROBERT D. DAWE. Can. J. Chem. **56**, 1311 (1978).

On rapporte la préparation d'une série de complexes du nickel(II) et du cuivre(II) avec le ligand mentionné dans le titre qui semblent montrer dans l'état solide des structures qui sont d'une façon prédominante pseudo-octaédriques. On propose des structures dimères possédant un anion ponté tant pour les complexes de nickel que ceux du cuivre; $[Ni_2(NTB)_2X_2]Y_2$ (X = Y = Cl, Br; X = Cl, Br, NCS; Y = BPh_4), $[Cu_2(NTB)_2X_2]X_2 \cdot 2H_2O$ (X = Cl, Br). Les autres dérivés octaédriques semblent être des monomères; $[Ni(NTB)X_2]$ (X = NO_3, NCS), $[Ni(NTB)(H_2O)X]Y$ (X = NCS, Y = BPh_4; X = CH_3CN, Y = $(ClO_4)_2$), $[Ni(NTB)(H_2O)_2]X_2 \cdot 2H_2O$ (X = ClO_4, BF_4), $[Cu(NTB)(NO_3)_2] \cdot H_2O$. Les dérivés pentacoordonnés ne sont pas communs et dans le cas de trois complexes du cuivre on suggère pour l'état solide des structures trigonalbipyramidales; $[Cu(NTB)Cl]BPh_4$, $[Cu(NTB)(H_2O)]X_2 \cdot nH_2O$ (X = BF_4, $n = 0$; X = ClO_4, $n = 1$). En solution dans l'acétone, il semble que tous les complexes du cuivre soient pentacoordonnés. Des données de résonance paramagnétique électronique confirment des structures trigonalbipyramidales en solution et indiquent $g_{\parallel} < g_{\perp}$ avec de petites valeurs de $A_{\parallel}$ (60–80 × 10^{-4} cm^{-1}).

[Traduit par le journal]

Introduction

Recent work has indicated the involvement of imidazole groups in the coordination sphere of copper(II) in copper metalloproteins (1) and the possibility of five-coordinate metal centres in such systems has also been proposed (2, 3). In a previous paper (4) we described the synthesis and characterization of a series of cobalt(II) and zinc(II) complexes of the title ligand (Fig. 1, ligand abbreviated NTB) in which its geometrical constraints appeared responsible for the formation of five-coordinate pseudo-trigonalbipyramidal derivatives. These studies have now been extended to include complexes of nickel and copper. The copper complexes, which exhibit both octahedral and trigonalbipyramidal stereochemistries, provide further examples of copper imidazole systems and add to the paucity of spectral data available for such five-coordinate species.

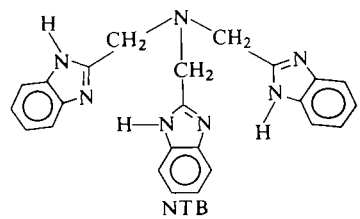

NTB

FIG. 1. Tris(2-benzimidazylmethyl)amine.

Structural assignments are supported by electronic, vibrational, and electron spin resonance spectra and magnetic and conductance data.

Experimental

Electronic spectra were recorded using a Cary 17 spectrometer, infrared spectra were obtained using a Perkin-Elmer model 283 spectrometer and electron spin resonance spectra were recorded at −196°C on a Varian E-3 X-band spectrometer, the magnetic field strength being calibrated with an nmr probe and with Mn(II) in MgO powder. Magnetic susceptibilities were obtained at room temperature by the Faraday

[1]To whom correspondence should be addressed.

Can. J. Chem. Downloaded from www.nrcresearchpress.com by 210.87.254.42 on 09/05/12
For personal use only.

Can. J. Chem. Downloaded from www.nrcresearchpress.com by 210.87.254.42 on 09/05/12
For personal use only.

method using a Cahn model #7600 Faraday Magnetic Susceptibility system, coupled to a Cahn gram electrobalance and conductance data were obtained using a General Radio Company bridge with impedance comparator and a constant temperature bath adjusted to 25°C. Microanalyses were carried out in part in the Chemistry Department at Memorial University using a Perkin-Elmer model #240 Elemental Analyzer and by Altantic Microlab, Inc., Atlanta, Georgia. Metal analyses were determined by Atomic Absorption using a Varian Techtron AA-5, after digestion of the samples in concentrated HNO_3 or aqua-regia.

Metal Complexes of NTB

The ligand, tris(2-benzimidazylmethyl)amine, was prepared as described previously (4). Hydrated or anhydrous metal salts were used.

$[Ni_2(NTB)_2X_2]X_2$ ($X = Cl, Br$), $[Ni(NTB)X_2]$ ($X = NO_3$, NCS)

Solutions of equimolar quantities of the metal salt and NTB were prepared in hot ethanol and mixed. After stirring for a few minutes the solutions were filtered hot (where possible) and volumes reduced to the point of crystallization. Purification was effected by recrystallization from or soxhlet extraction in ethanol and the products dried at 90°C under vacuum.

$[Ni_2(NTB)_2X_2](BPh_4)_2 \cdot nH_2O$ ($X = Cl, Br$; $n = 0$; $X =$ NCS, $n = 3$)

Equimolar quantities of sodium tetraphenylborate and NTB were dissolved together in hot ethanol and added to a hot ethanolic solution of the metal salt. After stirring and cooling pale green products were obtained (X = Cl, Br). In the case of the thiocyanate complex a bright green solution formed from which blue crystals began to form (subsequently shown to be $[Ni(NTB)(NCS)_2]$). Rapid filtration of the hot solution followed by rapid reduction in volume produced bright green crystals. It was found to be difficult to repeat this preparation. Recrystallization of this compound from methanol gave a blue complex $[Ni(NTB)(NCS)(H_2O)](BPh_4)$. The chloro- and bromo-derivatives were purified by soxhlet extraction in ethanol and all compounds were dried at 90°C under vacuum.

$[Ni(NTB)(H_2O)_2]X_2 \cdot 2H_2O$ ($X = ClO_4, BF_4$)

Reaction of equimolar amounts of NTB and the metal salt in hot ethanol produced turquoise–blue solutions from which crystalline products could not be obtained due to the extreme solubility of the complexes. Addition of water to the concentrated ethanolic solutions gave pale blue crystals after stirring for a few minutes. Recrystallization was effected by dissolving the complexes in ethanol and adding water as before. The complexes were dried at 90°C under vacuum.

$[Ni(NTB)(H_2O)(CH_3CN)](ClO_4)_2$

Reaction of equimolar quantities of NTB and nickel perchlorate hexahydrate in acetonitrile gave a mauve solution from which mauve crystals were obtained after prolonged standing in the freezer (−20°C). The mother liquor was decanted and the product washed with cold acetonitrile. Recrystallization was effected from acetonitrile and the compound dried at 90°C under vacuum.

$[Cu_2(NTB)_2X_2]X_2 \cdot 2H_2O$ ($X = Cl, Br$), $[Cu(NTB)(NO_3)_2] \cdot H_2O$, $[Cu(NTB)(H_2O)]X_2 \cdot nH_2O$ ($X = BF_4$, $n = 0$; $X = ClO_4$, $n = 1$)

Equimolar quantities of the metal salt and NTB were dissolved separately in hot methanol and the solutions mixed. In the case of the nitrate complex a green crystalline product was obtained rapidly. The other solutions were filtered hot and their volumes reduced to the point of crystallization. Recrystallization was effected from methanol and the products dried at 90°C under vacuum.

$[Cu(NTB)Cl]BPh_4$

Equimolar quantities of NTB and sodium tetraphenylborate were dissolved together in hot ethanol and added to a hot ethanolic solution of a stoichiometric amount of copper chloride. After reduction in volume to induce crystallization the product was recrystallized from acetone and dried at 90°C under vacuum.

Analytical data for the nickel and copper complexes are given in Table 1.

Results and Discussion

Characterization of the Complexes

Cobalt and zinc complexes of NTB (4) were found to have trigonalbipyramidal structures in which the ligand acts as a tetradentate 'tripod' ligand rather like Me_6tren (5). The stable nickel complexes of NTB all appear to be pseudo-octahedral in structure and can be divided into two groups; a series of blue complexes which are monomeric and a series of green complexes, for which dimeric structures, involving bridging anions, are proposed. Examples of both trigonalbipyramidal and octahedral structures are found among the copper complexes and for some octahedral complexes anion bridged, dimeric structures are also proposed. In all cases NTB appears to behave as a tetradentate ligand coordinating through the apical nitrogen and three benzimidazole nitrogen atoms.

Electronic Spectra

Basically three bands are observed in the electronic spectra of all the NTB nickel complexes, both in the solid state and in solution, in the ranges 8 900 – 10 400 cm^{-1} (ν_1), 15 000 – 17 500 cm^{-1} (ν_2), and 25 000 – 28 000 cm^{-1} (ν_3) (Table 2). Little evidence exists for the splitting of any of these bands in the solid state (mull transmittance) spectra at room temperature or in solution and the band positions are typical of octahedrally coordinated nickel(II) (6, 7). In all cases a very weak absorption is observed around 13 000 cm^{-1}, which is assigned to the spin-forbidden transition $^1E_g \leftarrow {}^3A_{2g}$. The blue perchlorate complex $[Ni(NTB)(H_2O)_2](ClO_4)_2 \cdot 2H_2O$ dehydrates on heating under vacuum to produce a very moisture-sensitive green compound. The mull transmittance spectrum of this compound (Table 2) is very different from those of the other nickel complexes and the band positions and relative intensities bear some resemblance to known trigonalbipyramidal nickel complexes, e.g., $[Ni(Me_6tren)X]X$ (X = Cl, Br, I) (5).

NTB is assumed to behave as a tetradentate ligand occupying four coordination positions around *cis*-pseudo-octahedral metal ions in the case of all the stable nickel complexes. A number of nickel com-

TABLE 1. Analytical and other data

Compound	Colour	Found				Calcd.			
		C	H	N	M	C	H	N	M
$[Ni_2(NTB)_2Cl_2]Cl_2$	Pale green	53.8	4.19	18.2	10.3	53.6	3.91	18.2	10.9
$[Ni_2(NTB)_2Cl_2](BPh_4)_2$	Pale green	70.4	5.36	12.1	6.90	70.2	5.00	11.9	7.16
$[Ni_2(NTB)_2Br_2]Br_2$	Pale green	46.0	3.62	15.2	8.90	46.0	3.25	15.6	9.38
$[Ni_2(NTB)_2Br_2](BPh_4)_2$	Pale green	66.4	5.10	10.9	6.52	66.6	4.74	11.3	6.79
$[Ni_2(NTB)_2(NCS)_2](BPh_4)_2 \cdot 3H_2O$	Green	67.4	5.19	12.7	6.51	67.6	5.06	12.9	6.78
$[Ni(NTB)(NCS)_2]$	Pale blue	53.2	3.85	21.4	9.80	53.6	3.61	21.6	10.1
$[Ni(NTB)(NO_3)_2]$	Pale blue	48.5	3.77	20.8	9.64	48.8	3.56	21.4	9.95
$[Ni(NTB)(H_2O)_2](BF_4)_2 \cdot 2H_2O$	Pale blue	40.9	3.59	14.0	8.20	40.5	4.07	13.8	8.29
$[Ni(NTB)(H_2O)_2](ClO_4)_2 \cdot 2H_2O$	Pale blue	39.1	3.17	13.5	7.63	39.1	3.39	13.3	8.00
$[Ni(NTB)(NCS)(H_2O)]BPh_4$	Pale blue	68.1	5.12	12.9	6.80	68.3	5.00	13.0	6.61
$[Ni(NTB)(H_2O)(CH_3CN)](ClO_4)_2$	Mauve	43.1	3.50	15.5	7.88	43.1	3.59	15.5	8.15
$[Cu_2(NTB)_2Cl_2]Cl_2 \cdot 2H_2O$	Yellow-buff	51.6	4.25	17.5	10.8	51.5	4.11	17.5	11.3
$[Cu(NTB)Cl]BPh_4$	Lime-green	69.5	5.10	11.9	7.31	69.8	4.97	11.9	7.70
$[Cu_2(NTB)_2Br_2]Br_2 \cdot 2H_2O$	Buff	44.4	3.59	15.1	9.38	44.4	3.55	15.1	9.80
$[Cu(NTB)(NO_3)_2] \cdot H_2O$	Green	47.0	3.82	20.4	10.1	47.0	3.76	20.5	10.4
$[Cu(NTB)(H_2O)](BF_4)_2$	Lime-green	43.4	3.33	14.7	9.24	43.5	3.47	14.8	9.58
$[Cu(NTB)(H_2O)](ClO_4)_2 \cdot H_2O$	Lime-green	40.8	3.41	13.8	8.53	40.8	3.54	13.9	9.00

plexes with *cis*-N_4 chromophores have been shown to have dimeric anion bridged structures, e.g., $[Ni_2(en)_4Cl_2]Cl_2$ (8), $[Ni_2(en)_4(NCS)_2]I_2$ (9), $[Ni_2(tren)_2(NCO)_2](BPh_4)_2$ (10), $[Ni_2(trien)_2Cl_2](ClO_4)_2$ (11). These dimeric systems have solid state electronic spectra which are very similar to those of the green NTB complexes and it is suggested that the NTB complexes could have similar structures in the solid state. The blue complexes are assumed to be monomeric with coordinated water, solvent, and/or anion. Support for the dimeric nature of the green complexes and the monomeric nature of the blue complexes is obtained by considering the solution spectra of these complexes in a variety of solvents. Spectral bands for the chloro- and bromo-derivatives remain fairly constant in such solvents as methanol, dimethylsulfoxide, and pyridine implying that the metal is not solvated and that the proposed halogen bridged structures remain intact in solution regardless of solvent. The green thiocyanate complex is much less stable and breaks apart to give a monomeric species in polar solvents. However, it is assumed to have a thiocyanate bridged structure in the solid state. The spectral changes on varying the solvent for some of the blue complexes are much more marked implying solvation of the complex and monomeric structures.

The two coordinated water molecules in the blue perchlorate and tetrafluoroborate complexes appear to be fairly labile. Solution electronic spectra of the perchlorate complex vary according to the solvent used and the band positions follow the energy sequence $CH_3CN > CH_3NO_2 > CH_3OH$. In methanol it is likely that the solution species is $[Ni(NTB)(H_2O)_2]^{2+}$ (Table 2), but in acetonitrile and nitromethane one or both coordinated water molecules are displaced by solvents. The nickel perchlorate complex can be prepared from acetonitrile and is obtained as a mauve crystalline solid. Analysis (Table 1) reveals the presence of one molecule of acetonitrile, which is substantiated by infrared data, and the complex is assumed to have one coordinated water and one coordinated acetonitrile in the solid state. The similarity of the acetonitrile solution spectrum with that of the solid state spectrum suggests the same species exists in solution. Electronic spectral bands of this complex in acetone (blue solution) occur at much lower energy suggesting coordinated acetone. On recrystallization of the mauve complex from acetone a blue compound is obtained which appears to have coordinated acetone according to infrared studies.

All the copper complexes exhibit one major absorption in the solid state, mull transmittance, spectrum in the range 8 000 – 13 000 cm^{-1} (Table 2) but with either a low energy or high energy shoulder. The complexes $[Cu(NTB)(H_2O)](BF_4)_2$, $[Cu(NTB)(H_2O)](ClO_4)_2 \cdot H_2O$, and $[Cu(NTB)Cl]BPh_4$ all exhibit a single absorption with a high energy shoulder. This spectral pattern is typical of five-coordinate trigonalbipyramidal copper(II). Known trigonalbipyramidal systems, e.g., $[Cu(Me_6tren)X]^+$ (5) and $[Cu(tren)L]^{n+}$ (L = OH, py, NH_2Ph, NCS, NH_3) (12), exhibit very similar spectra. The remaining complexes exhibit low energy shoulders, which is typical of pseudo-octahedral copper(II) (Fig. 2). Halogen bridged dimeric structures are proposed for the complexes $[Cu_2(NTB)_2X_2]X_2 \cdot 2H_2O$ (X = Cl, Br) in the solid state. In acetone solution the electronic spectra of all the copper complexes are

Can. J. Chem. Downloaded from www.nrcresearchpress.com by 210.87.254.42 on 09/05/12
For personal use only.

TABLE 2. Electronic spectra (cm^{-1})*

Compound		$^3T_{2g} \leftarrow {}^3A_{2g}(\nu_1)$	$^3T_{1g}(F) \leftarrow {}^3A_{2g}(\nu_2)$	$^3T_{1g}(P) \leftarrow {}^3A_{2g}(\nu_3)$
(*i*) Nickel complexes				
$[Ni_2(NTB)_2Cl_2]Cl_2$	*a*	9350	15600	26400
	b	9250(11)	15700(24)	25300(37)
$[Ni_2(NTB)_2Cl_2](BPh_4)_2$	*a*	9100	15400	26300
	b	9800(12)	16100(26)	25600(37)
$[Ni_2(NTB)_2Br_2]Br_2$	*a*	9100	15300	25600
	b	9500(12)	15800(22)	25600(35)
$[Ni_2(NTB)_2Br_2](BPh_4)_2$	*a*	8900	15200	25300
	b	9600(15)	15800(22)	25600(37)
$[Ni_2(NTB)_2(NCS)_2](BPh_4)_2 \cdot 3H_2O$	*a*	9350	16000	25000
	b	[9900] 10200(16)	16600(25)	26400(36)
$[Ni(NTB)(NCS)_2]$	*a*	10200	16800	27400
	b	10100(20)	16700(28)	26800(43)
$[Ni(NTB)(NO_3)_2]$	*a*	10000	17400	[24400] [28200]
	b	9800(15)	16400(18)	26200(27)
$[Ni(NTB)(H_2O)_2](BF_4)_2 \cdot 2H_2O$	*a*	9800	16400	27000
	b	9850(16)	16400(18)	27000(39)
$[Ni(NTB)(H_2O)_2](ClO_4)_2 \cdot 2H_2O$	*a*	9800	16400	27000
	b	9800(16)	16400(19)	27000(33)
$[Ni(NTB)(NCS)(H_2O)]BPh_4$	*a*	10700	16400	27000
	b	10000(16)	16600(25)	26400(36)
$[Ni(NTB)(H_2O)(CH_3CN)](ClO_4)_2$	*a*	10400	17500	27900
	c	10800	17600	28000
	d	10000	16700	27100
(*ii*) Green dehydrated perchlorate complex	*a*	6700, 9800, [13200], 14800, [23000]		
(*iii*) Copper complexes				
$[Cu_2(NTB)_2Cl_2]Cl_2 \cdot 2H_2O$	*a*	[8000] [11000] 13000		
	d	8600(115) [11600](60)		
$[Cu(NTB)Cl]BPh_4$	*a*	8800 [11800]		
	d	8500(112) [11500](58)		
$[Cu_2(NTB)_2Br_2]Br_2 \cdot 2H_2O$	*a*	[8000] 13700		
	b	8500 [12000] 13500		
	d	8400(117) [11900](80)		
$[Cu(NTB)(NO_3)_2]H_2O$	*a*	[10300] 13800		
	b	10000(85) [13300](76)		
$[Cu(NTB)(H_2O)](BF_4)_2$	*a*	9800 [13000]		
	d	9500(125) [13000](60)		
$[Cu(NTB)(H_2O)](ClO_4)_2 \cdot H_2O$	*a*	9600 [13000]		
	d	9600(124) [13000](55)		

*Labels mean the following: *a*, mull transmittance spectrum (room temperature); *b*, solution in methanol; *c*, solution in acetonitrile; *d*, solution in acetone. [] shoulder, () molar extinction coefficient.

similar, exhibiting a fairly intense major peak with a high energy shoulder, typical of trigonalbipyramidal copper(II) (Fig. 2). The acetone solution spectra of the compounds $[Cu_2(NTB)_2Cl_2]Cl_2 \cdot 2H_2O$ and $[Cu(NTB)Cl]BPh_4$ are identical suggesting the same trigonalbipyramidal solution species. In methanol all the solution species appear to be five-coordinate with the exception of the bromo-complex. In this case five-coordinate spectral bands are observed, but in addition a high energy band appears at 13 300 – 13 500 cm^{-1} (Table 2). This band may well be associated with a solvated, octahedral species in an equilibrium mixture with the five-coordinate cation.

Infrared Data

The region of the infrared spectra in the range 3200 – 3600 cm^{-1} was generally characterized by rather broad absorptions associated with N—H stretch and coordinated and lattice water. There seemed to be little logical pattern associated with the positions of bands attributable to N—H stretch. This could possibly arise from hydrogen bonding associations with oxygen-containing ligands or ions or benzimidazole units in neighbouring molecules. Coordinated water was clearly defined for the bis-aquo nickel complexes $[Ni(NTB)(H_2O)_2]X_2 \cdot 2H_2O$ (X = BF_4, ClO_4) and the aquo copper complexes $[Cu(NTB)(H_2O)]X_2 \cdot nH_2O$ (X = BF_4, $n = 0$; X = ClO_4, $n = 1$) by a broad doublet between 3500 – 3700 cm^{-1}. The green thiocyanate complex $[Ni_2(NTB)_2(NCS)_2](BPh_4)_2 \cdot 3H_2O$ was characterized by a sharp doublet (3290, 3315 cm^{-1}) due to N—H

Can. J. Chem. Downloaded from www.nrcresearchpress.com by 210.87.254.42 on 09/05/12
For personal use only.

Can. J. Chem. Downloaded from www.nrcresearchpress.com by 210.87.254.42 on 09/05/12
For personal use only.

TABLE 3. Infrared data (cm^{-1})

(*a*) Thiocyanato derivatives

Compound	ν CN[NCS]
$[Ni_2(NTB)_2(NCS)_2](BPh_4)_2 \cdot 3H_2O$	2114
$[Ni(NTB)(NCS)_2]$	2060, 2065
$[Ni(NTB)(NCS)(H_2O)]BPh_4$	2118

(*b*) Perchlorato derivatives

Compound	ClO_4^- $\nu_3(T_2)$	Monodentate perchlorate A_1	Monodentate perchlorate E	CH_3CN (co-ordinated)* ν_2	CH_3CN (co-ordinated)* $\nu_3 + \nu_4$
$[Ni(NTB)(H_2O)_2](ClO_4)_2 \cdot 2H_2O$	1100				
Green dehydrated form	1105	1035	1130		
$[Cu(NTB)(H_2O)](ClO_4)_2 \cdot H_2O$	1090				
$[Ni(NTB)(H_2O)(CH_3CN)](ClO_4)_2$	1100			2280	2305

*References 24–26.

(*c*) Nitrato derivatives

Compound	NO_3^- $\nu_2(A_2'')$	NO_3^- $\nu_3(E')$	NO_3^- $\nu_1 + \nu_4$					$\nu_1 + \nu_4$
$[Ni(NTB)(NO_3)_2]$	822	1395	1750	807	1310	1540	1730	1773*
$[Cu(NTB)(NO_3)_2] \cdot H_2O$					1300	1450	1755	1771†

*Bidentate nitrate.
†Monodentate nitrate.

(*d*) Far infrared

Compound	ν (CuCl)
$[Cu(NTB)Cl]BPh_4$	294

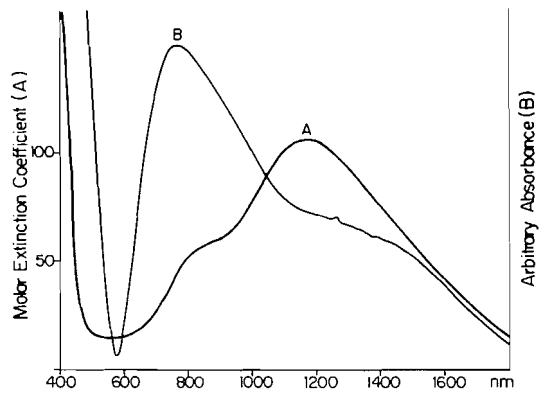

FIG. 2. Electronic spectra of NTB complex $[Cu_2(NTB)_2Cl_2]Cl_2 \cdot 2H_2O$: (*A*) acetone (trigonalbipyramidal), (*B*) mull transmittance (octahedral).

stretch, which was replaced by a sharp singlet ($3310\ cm^{-1}$) in the blue form produced by recrystallization from methanol.

The blue thiocyanate complex $[Ni(NTB)(NCS)_2]$ gave two clearly defined absorptions at 2060 and $2065\ cm^{-1}$ (Table 3) associated with CN stretch in two *cis*-isothiocyanate groups and the green dimeric complex exhibited a sharp singlet at $2114\ cm^{-1}$ associated with CN stretch in a bridging thiocyanate group. In the blue complex $[Ni(NTB)(NCS)(H_2O)]BPh_4$ νCN occurred at $2118\ cm^{-1}$ as a sharp singlet. This represents a very high energy absorption for a terminally bound isothiocyanate and could possibly be due to a sulphur bound thiocyanate. The appearance of a relatively weak band at $719\ cm^{-1}$ for this compound could be associated with CS stretch in a thiocyanate group. Typically N-bonded thiocyanates have νCN less than $2100\ cm^{-1}$ (13) and class '*a*' acceptors usually favour this mode of bonding. Methanol thus appears to cleave the green dimeric thiocyanate bridged complex at the nickel–nitrogen bond, rather than the nickel–sulphur bond.

Both the blue and mauve nickel perchlorate and the copper perchlorate complexes exhibit strong, fairly broad absorptions around $1100\ cm^{-1}$ (Table

TABLE 4. Magnetic moment and conductance data

Compound	Λ_M* (mho mol^{-1} cm^2)	μ (BM) (room temperature)†
$[Ni_2(NTB)_2Cl_2]Cl_2$	220	3.15
$[Ni_2(NTB)_2Cl_2](BPh_4)_2$	187[a]	3.19
$[Ni_2(NTB)_2Br_2]Br_2$	206	3.19
$[Ni_2(NTB)_2Br_2](BPh_4)_2$	222	3.18
$[Ni_2(NTB)_2(NCS)_2](BPh_4)_2 \cdot 3H_2O$	—	3.22
$[Ni(NTB)(NCS)_2]$	79.6	3.11
$[Ni(NTB)(NO_3)_2]$	167	3.16
$[Ni(NTB)(H_2O)_2](BF_4)_2 \cdot 2H_2O$	160	3.25
$[Ni(NTB)(H_2O)_2](ClO_4)_2 \cdot 2H_2O$	156	3.27
$[Ni(NTB)(NCS)(H_2O)]BPh_4$	84.0	3.38
$[Ni(NTB)(H_2O)(CH_3CN)](ClO_4)_2$	—	3.10
$[Cu_2(NTB)_2Cl_2]Cl_2 \cdot 2H_2O$	73.7	1.94
$[Cu(NTB)Cl]BPh_4$	75.1	1.85
$[Cu_2(NTB)_2Br_2]Br_2 \cdot 2H_2O$	80.5	1.87
$[Cu(NTB)(NO_3)_2] \cdot H_2O$	120	1.90
$[Cu(NTB)(H_2O)](BF_4)_2$	155[b]	1.87
$[Cu(NTB)(H_2O)](ClO_4)_2 \cdot H_2O$	184, 159[b]	1.97

*Solvent methanol at approximately 10^{-3} M (25°C); *a*, solvent acetone at approximately 10^{-4} M (25°C); *b*, solvent nitromethane at approximately 10^{-3} M (25°C).
†Magnetic moment per metal measured in solid state by Faraday method.

3) associated with ionic perchlorate while the unstable, moisture sensitive green nickel complex obtained by heating $[Ni(NTB)(H_2O)_2](Cl0_4)_2 \cdot 2H_2O$ exhibited more complex perchlorate absorptions; a strong singlet at 1105 cm^{-1} associated with an ionic perchlorate group and a strong doublet at 1035, 1130 cm^{-1} associated with monodentate perchlorate (14, 15).

Comparison of the copper and nickel nitrate complexes with the corresponding halide derivatives allows certain bands to be identified which can be associated with ionic and bidentate nitrate (nickel) and monodentate nitrate (copper) (Table 3) (14). Nitrate compounds give combinations bands around 1750 cm^{-1} which are often diagnostically useful (16). $[Ni(NTB)(NO_3)_2]$ exhibits three main absorptions in this region, when strong Nujol mulls are employed (Table 3), associated with ionic and bidentate nitrate groups. In the case of the copper nitrate complex two combination bands are observed (Table 3) and are assigned to monodentate nitrate groups.

In the far infrared (600–200 cm^{-1}) there is a close similarity between the spectra of the dimeric halogen bridged nickel species and bands associated with terminal nickel–halogen bonds appear to be absent thus supporting the halogen bridged nature of these species. The general complexity of the spectra in this low energy region prevented any definitive assignments of bridging metal–halogen vibrations. The case of the copper halide compounds was similar. In the chloro-complex $[Cu(NTB)Cl]BPh_4$ a strong band at 294 cm^{-1} is assigned to terminal copper–chlorine stretch.

Magnetism and Conductance

Magnetic moments for the nickel complexes lie in the range 3.1–3.4 BM at room temperature (Table 4) typical of pseudo-octahedral nickel(II) (17), while those of the copper complexes (Table 4) fall in the range 1.85–1.97 BM and appear to be normal for five-coordinate and octahedral copper(II) (5, 12).

Conductance data were obtained for the nickel and copper complexes in solvents appropriate to solubility, at approximately 10^{-3} M (Table 4) and values compared with those of known electrolytes at similar concentrations (18). In the case of the nickel halide complexes the molar conductance values, based on dimeric formula units (Table 4), can be associated with 1:2 electrolytes (18). A concentration dependent study of the molar conductance of $[Ni_2(NTB)_2Br_2]Br_2$ was carried out in methanol in the range $10^{-4} - 2.5 \times 10^{-3}$ M at 25°C. Λ_0 was found to be 170 and the slope of the Kohlrausch plot ($\Lambda_0 - \Lambda_e$ vs. $\sqrt{c}$) was found to be $\sim$1500. Slopes in the range 250–290 have been reported for 1:1 electrolytes in methanol (19) clearly indicating a polymeric or associated solution species. The general similarity between the halide complexes both in the solid state and in solution suggests similar solution species for the other halide complexes. The molecular nature of these solution species may be an aggregate of hydrogen bonded sub-units. Associated solution structures, due to hydrogen bonding, were proposed for some of the cobalt and zinc complexes of NTB (4).

The blue isothiocyanato complex $[Ni(NTB)(NCS)_2]$ appears to behave as a 1:1 electrolyte in methanol, presumably by loss of one coordinated thiocyanate

Can. J. Chem. Downloaded from www.nrcresearchpress.com by 210.87.254.42 on 09/05/12
For personal use only.

TABLE 5. Electron spin resonance data*

Compound	$g_{\parallel}$	$g_{\perp}$	$\lvert A_{\parallel}\rvert$†	$\lvert A_{\perp}\rvert$†
$[Cu_2(NTB)_2Cl_2]Cl_2\cdot 2H_2O$	1.974	2.217	61	89
$[Cu(NTB)Cl]BPh_4$	1.980	2.233	~60	96
‡	—	2.240	—	90
$[Cu_2(NTB)_2Br_2]Br_2\cdot 2H_2O$	1.975	2.214	62	94
$[Cu(NTB)(NO_3)_2]H_2O$	2.014	2.229	75	98
$[Cu(NTB)(H_2O)](BF_4)_2$	2.015	2.225	77	94
$[Cu(NTB)(H_2O)](ClO_4)_2\cdot H_2O$	2.010	2.224	80	97

*Spin-Hamiltonian parameters for frozen methanol solutions (−196°C).
†All hyperfine coupling constants in units 10^{-4} cm^{-1}.
‡Doped solid solution of $[Cu(NTB)Cl]BPh_4$ in $[Zn(NTB)Cl]BPh_4$ (~3%) (−196°C).

to produce a solvated cation. The bis-nitrato complex dissociates to form a 1:2 electrolyte and both the perchlorate and tetrafluoroborate complexes behave as 1:2 electrolytes in methanol. Molar conductance data for the copper complexes indicate the perchlorate and tetrafluoroborate complexes to be 1:2 electrolytes, while the remaining solution species are assumed to be 1:1 electrolytes. The calculated values of Λ_M for the copper halide complexes are based on monomeric five-coordinate species in keeping with the electronic spectral data.

Electron Spin Resonance Data

Electron spin resonance spectra of the copper complexes were run as solids and methanol solutions at −196°C. Figure 3 illustrates a typical spectrum. The frozen glass spectra are characterized by four clearly resolved lines in the perpendicular region and usually two or three in the parallel region and bear a striking resemblance to the few spectra reported for known trigonalbipyramidal systems with tripod ligands (20–22). Copper complexes of tren, Me_6tren, Et_6tren which have trigonalbipyramidal structures have $g_{\parallel} < g_{\perp}$ and $A_{\parallel}$ in the range ~65–100 ($\times 10^{-4}$ cm^{-1}). Spin-Hamiltonian parameters for the copper/NTB systems are reported in Table 5. $A_{\parallel}$ values are typically low, the values for the chloro- and bromo-complexes being the lowest so far reported for trigonalbipyramidal systems with tripod ligands and some $g_{\parallel}$ values are greater than g_e. Systems of this type are interpreted in terms of a d_{z^2} ground state in a trigonalbipyramid but the large values of $g_{\parallel}$ imply the mixing of d_{xy} or $d_{x^2-y^2}$ orbitals into the ground state via vibronic coupling (23). In the solid state the spectra were in general characterized by broad single resonances with some g resolution in the case of the chloro- and nitrato-complexes.

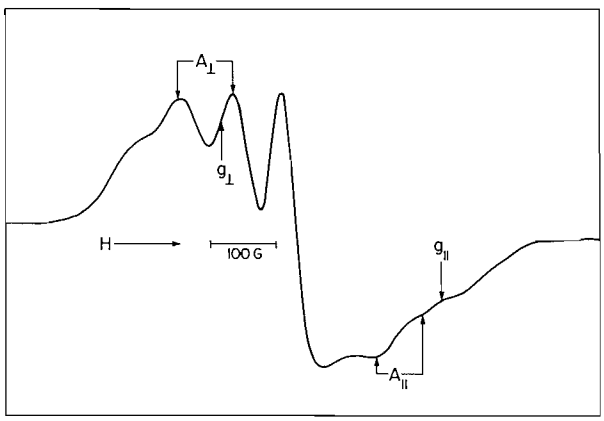

FIG. 3. Electron spin resonance spectrum (X-band) of frozen solution of $[Cu_2(NTB)_2Cl_2]Cl_2\cdot 2H_2O$ in methanol at 77 K.

A doped solid solution of $[Cu(NTB)Cl]BPh_4$ in the trigonalbipyramidal zinc complex $[Zn(NTB)Cl]BPh_4$ (3%) (4) gave a solid spectrum at −196°C which was very similar to its frozen solution spectrum in methanol, except for certain weak features which suggested the presence of a small amount of another species. Poor resolution in the parallel region of the spectrum prevented determination of $g_{\parallel}$ and $A_{\parallel}$ but the perpendicular spin-Hamiltonian parameters are very close to those obtained from the frozen methanol spectrum.

The similarity of the frozen solution spectra of all the halide complexes suggests the presence of similar species in solution in methanol. The spin-Hamiltonian parameters for the complexes $[Cu(Et_6tren)X]X$ (X = Cl, Br) in frozen methanol solution (cation unsolvated) show very small differences indicating the small change in axial crystal field perturbation on replacing chloride by bromide in systems of this type (21). The esr spectra of the nitrate, tetrafluoroborate and perchlorate complexes are almost superimposable, suggesting the presence of similar cations in solution. Values of $g_{\parallel}$, $g_{\perp}$, and $A_{\perp}$ for this set of complexes are close to those observed for the halide complexes. However, $A_{\parallel}$ values increase by 25–30% on replacing an axial halogen by an oxygen donor, e.g., H_2O, NO_3^-.

Acknowledgements

We thank the National Research Council of Canada for financial support for this study and in particular for the purchase of the Cary 17 Spectro-

Can. J. Chem. Downloaded from www.nrcresearchpress.com by 210.87.254.42 on 09/05/12
For personal use only.

meter. Also we express our gratitude to Linda G. Thompson for magnetic susceptibility and conductance measurements and to the Chemistry Department at the University of British Columbia for the use of esr facilities.

1. A. R. AMUNDSEN, J. WHELAN, and B. BOSNICH. J. Am. Chem. Soc. **99**, 6730 (1977) and references therein.
2. V. MISKOWSKI, S. P. W. TANG, T. G. SPIRO, E. SHAPIRO, and T. H. MOSS. Biochemistry, **14**, 1244 (1975).
3. L. MORPURGO, A. FINNAZZI-AGRO, G. ROTILIO, and B. MONDOVI. Eur. J. Biochem. **64**, 453 (1976).
4. L. K. THOMPSON, B. S. RAMASWAMY, and E. A. SEYMOUR. Can. J. Chem. **55**, 878 (1977).
5. M. CIAMPOLINI and N. NARDI. Inorg. Chem. **5**, 41 (1966).
6. A. B. P. LEVER. Inorganic electronic spectroscopy. Elsevier, Amsterdam. 1968.
7. A. B. P. LEVER. Coord. Chem. Rev. **3**, 119 (1968).
8. A. S. ANTSYSHKINA and M. A. PORAI-KOSHITS. Dokl. Akad. Nauk. SSSR, **143**, 105 (1962).
9. A. F. SHVELASHVILI, M. A. PORAI-KOSHITS, and A. S. ANTSYSHKINA. J. Struct. Chem. (USSR), **10**, 552 (1969).
10. D. M. DUGGAN and D. N. HENDRICKSON. Inorg. Chem. **13**, 2056 (1974).
11. N. F. CURTIS and H. K. J. POWELL. J. Chem. Soc. (A), 3070 (1968).
12. G. ALBERTIN, E. BORDIGNON, and A. A. ORIO. Inorg. Chem. **14**, 1411 (1975).
13. E. KONIG and K. MADGEJA. Inorg. Chem. **6**, 48 (1967).
14. K. NAKAMOTO. Infrared spectra of inorganic and coordination compounds. 2nd ed. Wiley-Interscience, New York. 1970.
15. A. E. WICKENDEN and R. A. KRAUSE. Inorg. Chem. **4**, 404 (1965).
16. A. B. P. LEVER, E. MANTOVANI, and B. S. RAMASWAMY. Can. J. Chem. **49**, 1957 (1971).
17. A. B. P. LEVER. Inorg. Chem. **4**, 763 (1965).
18. W. J. GEARY. Coord. Chem. Rev. **7**, 81 (1971).
19. R. D. FELTHAM and R. G. HAYTER. J. Chem. Soc. 4587 (1964).
20. G. A. SENYUKOVA, I. D. MIKHEIKIN, and K. I. ZAMARAEV. J. Struct. Chem. Engl. Transl. **11**, 18 (1970).
21. R. BARBUCCI and M. J. M. CAMPBELL. Inorg. Chim. Acta, **15**, L15 (1975).
22. R. BARBUCCI, A. BENCINI, and D. GATTESCHI. Inorg. Chem. **16**, 2117 (1977).
23. M. C. O'BRIEN. Proc. R. Soc. London, A**281**, 323 (1964).
24. P. VENKATESWARLU. J. Chem. Phys. **19**, 293 (1951).
25. R. J. H. CLARK, J. LEWIS, D. J. MACHIN, and R. S. NYHOLM. J. Chem. Soc. 379 (1963).
26. R. A. WALTON. Spectrochim. Acta, **21**, 1795 (1965).

Can. J. Chem. Downloaded from www.nrcresearchpress.com by 210.87.254.42 on 09/05/12
For personal use only.

SCF molecular orbitals and the photoelectron spectrum of 5,5-dimethyl-Δ^3-1,3,4-oxadiazolin-2-one

ANTHONY JAMES PAINE[1] AND NICK HENRY WERSTIUK

Department of Chemistry, McMaster University, Hamilton, Ont., Canada L8S 4M1

Received November 10, 1977

ANTHONY JAMES PAINE and NICK HENRY WERSTIUK. Can. J. Chem. **56**, 1319 (1978).

CNDO/2 Frontier molecular orbital densities, ionization potentials (IP's), and electronic transition energies were calculated for the title compound (**2***b*) and the 5,5-diprotio (**2***a*), and 5,5-difluoro (**2***d*) analogs. Bond lengths and angles were not optimized but rather taken from a crystal structure of the 2-imino system **3**, with an assumed carbonyl bond length of R_{CO} = 1.19 Å. This value is supported by a high infrared stretching frequency (1835 cm^{-1}), X-ray crystal data of **3**, and the effect of R_{CO} variation on calculated IP's. The first three bands of the photoelectron spectrum of **2***b* were assigned as n_N^- (10.20 eV), π_1 (11.52 eV), and n_{CO} (13.26 eV) (vertical IP's). This unusually large n_{CO} IP is attributed to an inductive effect of the neighbouring strongly electron withdrawing azo group. The IP's obtained by CNDO/2 calculation (12.81, 13.37, and 15.15) are 1.5 to 2.5 eV higher than the experimental values, well within the predictive capability of the method, establishing that this theoretical treatment gives a good representation of the MO's of **2***b*.

ANTHONY JAMES PAINE et NICK HENRY WERSTIUK. Can. J. Chem. **56**, 1319 (1978).

On a calculé, par la méthode CNDO/2 des orbitales moléculaires frontières, les densités, les potentiels d'ionisation (PI) et les énergies de transition électronique du composé mentionné dans le titre (**2***b*) et de ses analogues diprotoné en 5,5 (**2***a*) et difluoro-5,5 (**2***d*). On n'a pas optimisé les longueurs des liens et des angles; on a plutôt utilisé les valeurs provenant d'une structure cristalline du système imino-2 (**3**) en faisant l'hypothèse que la longueur de la liaison carbonyle R_{CO} = 1.19 Å. La validité de cette hypothèse est confirmée par une vibration de fréquence infra-rouge élevée (1835 cm^{-1}), par des données cristallographiques de rayon-X de **3** et par l'effet de la variation de R_{CO} sur les PI calculés. On a attribué les trois premières bandes du spectre photoélectronique de **2***b* aux modes n_N^- (10.20 eV), π_1 (11.52 eV) et n_{CO} (13.26 eV) (PI verticaux). On attribue cette valeur très élevée du PI n_{CO} à un effet inductif du groupe azo qui est fortement électro-affinitaire. Les valeurs de PI obtenues par calculs CNDO/2 (12.81, 13.37 et 15.15) sont de 1.5 à 2.5 eV plus élevées que les valeurs expérimentales, bien à l'intérieur des capacités de prédiction de la méthode, établissant ainsi que ce traitement théorique donne une bonne représentation des orbitales moléculaires de **2***b*.

[Traduit par le journal]

Introduction

Δ^3-1,3,4-Oxadiazolin-2-ones are readily prepared in good yield from the lead tetraacetate oxidative cyclisation of ketone semicarbazones (1). They exhibit competing parallel thermal decomposition modes: one generating nitrogen, carbon monoxide, plus ketone; the other diazoalkane and carbon dioxide (2).

Frontier molecular orbital (FMO) theory has successfully provided insight into the problems of transition state structure, mechanism, stereo-, regio-, and periselectivity as well as into relative reactivity of substrates in a variety of thermal, photochemical, nucleophilic, and electrophilic reactions (3–5). As one of many probes in ongoing mechanistic studies of the thermal, photochemical, and acid- and base-catalysed decomposition of oxadiazolinones we sought to determine the FMO's of the system.

Expensive energy minimization calculations could

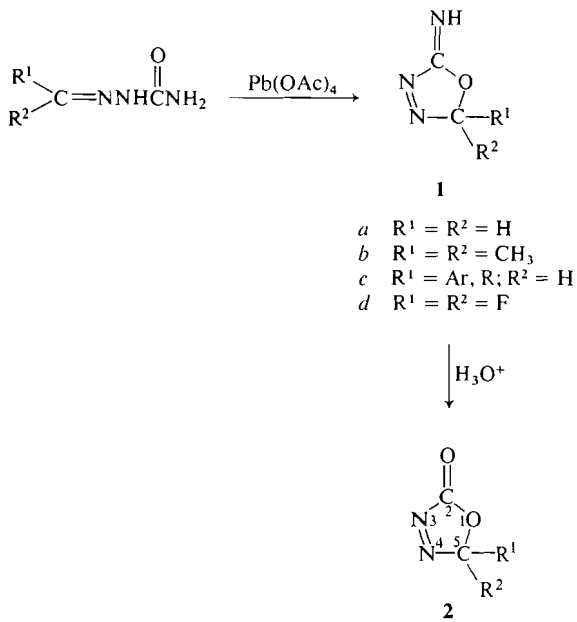

1

a $R^1 = R^2 = H$
b $R^1 = R^2 = CH_3$
c R^1 = Ar, R; R^2 = H
d $R^1 = R^2 = F$

2

[1]Address correspondence to this author.

Can. J. Chem. Downloaded from www.nrcresearchpress.com by 210.87.254.105 on 09/05/12
For personal use only.

Can. J. Chem. Downloaded from www.nrcresearchpress.com by 210.87.254.105 on 09/05/12
For personal use only.

be avoided if accurate values for bond lengths and angles could be inferred from a previous crystal structure of the closely related compound 2-*p*-bromophenylimino-5,5-dimethyl-Δ^3-1,3,4-oxadiazoline (**3**). We now report the results of CNDO/2 orbital calculations on a series of oxadiazolinones. To check the validity of the computed MO's, the photoelectron spectrum of dimethyloxadiazolinone (**2***b*) was obtained, and the assigned IP's compared to the IP's computed by the application of Koopmans' Theorem (6). In later publications we will apply these theoretical results to the mechanistic problems mentioned above.

Methods

Estimation of Bond Lengths and Angles

Oxadiazolinone ring bond lengths and angles were set equal to those reported (7) for the X-ray crystal structure of **3** (Fig. 1). Since the methyl groups in that structure were not perfectly tetrahedral (presumably because of constraints of the crystal phase and/or limitations in the structure solution) these standard parameters were used for the methyl groups: R_{CH} = 1.09 Å, HCH = 109.45° (8). Calculations were also performed on the 5,5-diprotio compound **2***a*[2] and on the 5,5-difluoro compound **2***d* to establish the effect of electron withdrawing groups on the Frontier MO's. For the latter case the CF bond contraction owing to the electron-withdrawing azo function was set equal to the difference between a paraffinic CC bond length (1.541(3) Å) (8) and R_{C-CH_3} = 1.512(9) Å in **3**. When applied to the $R_{CF}(CH_2F_2)$ = 1.360(5) Å (8), this correction yielded the value R_{CF} = 1.331(11) Å for **2***d*. Although some shortening of the N4—C5 bond may also be expected on fluorine substitution, the oxadiazolinone ring parameters were not modified.

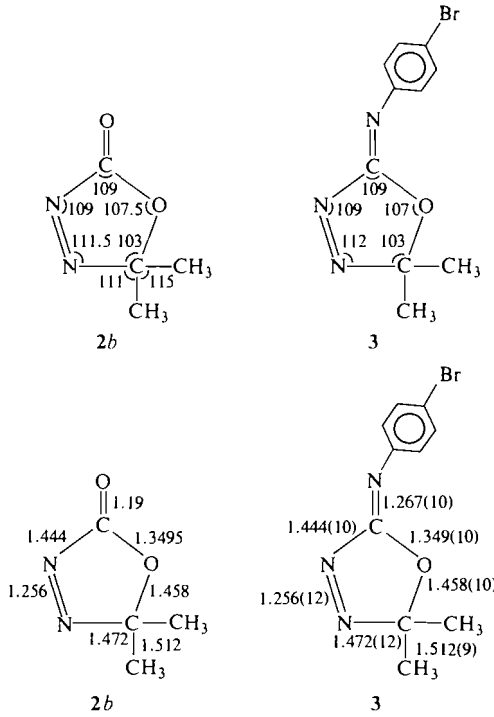

FIG. 1. Bond lengths and angles in dimethyloxadiazolinone (**2***b*) compared to those from the crystal structure of the iminooxadiazoline **3**. Estimated standard deviations for the X-ray crystals are ±1° for angles and ±0.01 Å for bond lengths.

The parameter requiring the greatest attention was the carbonyl bond length. Lack of data on azocarbonyl bond lengths hampers estimation of a reasonable value for oxadiazolinones. For simple carbonyl compounds of the type XCOY (where X, Y = H, CH_3, CF_3, CCl_3, CN, OH, OR, NH_2, NR_2, F, Cl, Br, ..., etc.) there exists a reasonable correlation (10) between the infrared stretching frequency and bond length. As the electron withdrawing power (σ_I) of the attached groups increases (11), an accompanying increase in the CO stretching frequency reflects a shorter bond length (Table 1).

Fixing a carbonyl group in a five-membered ring usually raises the stretching frequency by 35 ± 10 cm^{-1} (12). Correction of the observed CO stretching frequency of **2***b* (1835 cm^{-1} in CCl_4 (1)) for the ring size implies that the azo nitrogens of **2***b* have an effective σ_I between those of the methoxy and chloro substituents, in qualitative agreement with the value of σ_I (0.25) for the phenylazo group (11).

It may also be useful to compare the change in $R_{C=X}$ for X = N—C_6H_4Br-*p* and X = O. Bond lengths in the imino group of **3** (1.267(12) Å) and that in the *p*-bromoanil of benzaldehyde (1.281(10) Å) (13) differ by 0.014(18) Å. Since the benzaldehyde CO bond length is 1.211 Å (14), one might infer an oxadiazolinone CO bond length of 1.196(18) Å by difference.

Since the oxadiazolinone carbonyl is flanked by both an azo nitrogen and an ester oxygen, these criteria combine to suggest a reasonable value of 1.19 Å for this bond length. This value was used in the computations and the effect of the actual choice of R_{CO} on the calculated IP's of the diprotio parent **2***a* is examined in a later section. For a summary of the

[2]No oxadiazolinone with a hydrogen at C5 has yet been isolated due to the rapid tautomerism of the precursor (**1***a* or **1***c*) to the more stable 2-amino-1,3,4-oxadiazole (9):

Can. J. Chem. Downloaded from www.nrcresearchpress.com by 210.87.254.105 on 09/05/12
For personal use only.

TABLE 1. Change in bond length and stretching frequency of the carbonyl group as a function of substituent

	R_{CO} (Å)[a]	ν_{CO} (gas, cm^{-1})[a]	σ_I[b]
CH_3COCH_3	1.22	1737	0.00
CH_3COOCH_3	1.200	1770	0.25
CH_3COCl	1.192	1822	0.47
CH_3COF	1.181	1869	0.52

[a]Reference 10.
[b]Reference 11.

parameters employed in the calculation on **2***b* see Fig. 1.

Calculation

Details of the CNDO/2 method and actual parameters have been fully discussed elsewhere (15–17). Calculations were performed on an HP 3000 computer using a FORTRAN program developed by D. P. Santry of this department. Electronic excitation energies $\Delta E_{i\to j}$ were also calculated using K_{ij} and J_{ij} obtained from the CNDO LCAO expansion coefficients (**C** matrix) and the CNDO atomic electron–electron repulsion integrals γ_{AB} (17).

$$\Delta E_{i\to j} = \varepsilon_j - \varepsilon_i - J_{ij} + 2K_{ij}$$

where:

$$J_{ij} = \int\int \psi_i^*(1)\psi_j^*(2)\frac{1}{r_{12}}\psi_i(1)\psi_j(2)\,d\tau_1 d\tau_2$$

$$K_{ij} = \int\int \psi_i^*(1)\psi_j^*(2)\frac{1}{r_{12}}\psi_j(1)\psi_i(2)\,d\tau_1 d\tau_2$$

which become:

$$J_{ij} = \sum_{A=1}^{NA}\sum_{B=1}^{NA}\sum_{\mu=1}^{NBA}\sum_{\nu=1}^{NBB} C_{\mu i}^2 C_{\nu j}^2 \gamma_{AB}$$

$$K_{ij} = \sum_{A}^{NA}\sum_{B}^{NA}\sum_{\mu}^{NBA}\sum_{\nu}^{NBB} C_{\mu i}C_{\mu j}C_{\nu i}C_{\nu j}\gamma_{AB}$$

where NA = number of atoms

NBA = number of basis functions on atom A

and

$$\gamma_{AB} = \int\int S_A^2(1)\frac{1}{r_{12}}S_B^2(2)\,d\tau_1 d\tau_2,$$

the average coulomb integral between valence S orbitals on atoms A and B.

Results and Discussion

Based on analogy with the ring of oxadiazoline **3**, the oxadiazolinone ring is planar and symmetrical substitution at C5 produces a plane of symmetry. Under C_s symmetry any orbital transforming as a'' is a π orbital and any as a' is a σ orbital. Since the trivial designation as π or σ is meaningful in these cases we adopt it, even when there is no true plane of symmetry (as in **2***b* with staggered methyl groups).

The CNDO/2 LCAO solution gives 26 orbitals for the diprotio compound **2***a* of which 10 are vacant. Of the remaining 16 filled MO's, 6 are 'nonbonding,' containing the so-called lone pairs, and 10 are 'bonding' MO's. In all, 7 of the 26 orbitals have π symmetry. These result from the combinations of five obvious $2p_z$ atomic orbitals on O1, C2, N3, N4, and O6 plus two symmetry orbitals on the CH_2 moiety, designated π_{CH} and π_{CH}^*. These can be viewed as arising from the symmetric and antisymmetric combinations of hydrogen $1S$ orbitals with the $2p_z$ AO of C5. Thus, the π_{CH} is of correct symmetry to interact with the other π orbitals of the molecule and four highly delocalized filled π MO's result. Buried in each of these are contributions from π_{NN}, π_{CO}, π_{n_O} (lone pair on O1), and π_{CH}.

For dimethyloxadiazolinone (**2***b*) a 'staggered' conformation of the methyl groups was assumed for the computation. Although this has the effect of destroying the plane of symmetry present in the diprotio and difluoro analogs, the orbital assignments of symmetry are nonetheless made by comparison to the parent **1***a*.

Computed valence energy levels for **2***a*, **2***b*, and **2***d* are compared to the experimental IP's for **2***b* in Fig. 2. As expected (18), the electron withdrawing fluorines at C5 lower orbital energies and increase the calculated gaps between the first few IP's.

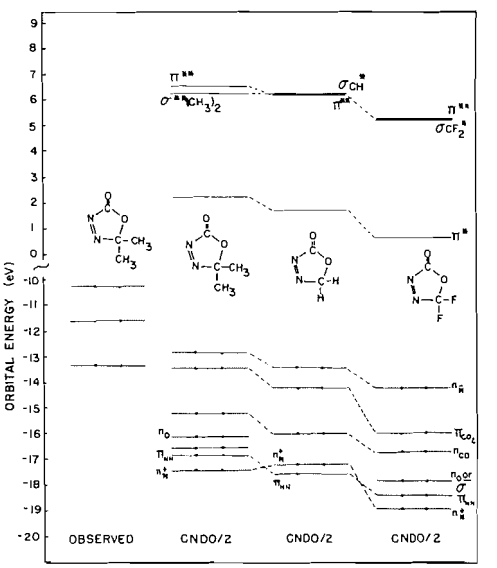

FIG. 2. Calculated and observed energy levels of oxadiazolinones.

TABLE 2. Valence orbital parameters for dimethyloxadiazolin-2-one

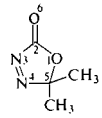

2*b*

Assignment		Sym-metry[a]	Orbital energy (eV)[b] Obs.	Orbital energy (eV)[b] Calcd.	Orbital densities[c] O1	C2	N3	N4	$C(Me)_2$	O6
Unoccupied ABMO	π^{**}	π		6.59	0.038	0.453	0.193	0.066	0.070	0.191
	$\sigma^*_{C(Me)_2}$	σ		6.31	0.182	0.032	0.014	0.043	0.718	0.013
	π^*	π		2.32	0.019	0.129	0.250	0.429	0.049	0.125
Doubly occupied BMO and NBMO	n_N^-	σ	−10.20	−12.81	0.052	0.092	0.312	0.185	0.143	0.215
	π_{CO_2}	π	−11.52	−13.37	0.229	0.014	0.110	0.060	0.318	0.268
	n_{CO}	σ	−13.26	−15.15	0.172	0.039	0.066	0.171	0.207	0.345
	n_O	σ		−16.07	0.436	0.009	0.089	0.108	0.313	0.046
	$C(Me)_2$ symmetry	π		−16.48	0.133	0.043	0.011	0.000	0.668	0.145
	π_{NN}	π		−16.79	0.285	0.005	0.277	0.280	0.145	0.008
	n_N^+	σ		−17.35	0.083	0.075	0.225	0.284	0.144	0.189

[a]Symmetry assignment assumes a mirror plane.
[b]Orbital energies assume Koopmans' Theorem (6).
[c]Orbital density on atom A in orbital $i = \sum_{\mu}^{on\,A} C_{\mu i}^2$.

According to FMO theory (3, 4) nucleophilic and electrophilic attack are favoured at the site of greatest orbital density of the LUMO and HOMO, respectively. Klopman (19), Salem (20), and others, however, recognize the extremes of a continuum from frontier controlled to charge controlled reaction. Although examination of the LUMO of oxadiazolinone (Table 2) suggests possible nucleophilic attack on nitrogen, the fact that both nitrogens are formally negative in overall charge, as indicated in Fig. 3, may mitigate against such attack via the LUMO. On the other hand, attack at C2 via the next lowest unoccupied orbital (NLUMO) is reasonable as this site carries nearly a half-integral total positive charge in addition to a huge frontier density, according to the calculations. Likewise, electrophilic attack (e.g., protonation) on nitrogen via the HOMO (lone pair attack) or on carbonyl oxygen (NHOMO, π attack) is possible. The roles these orbitals play in controlling acid- and base-catalysed reactions of oxadiazolinones is currently under investigation in this laboratory.

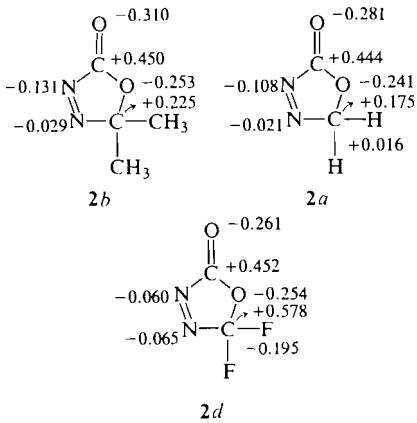

FIG. 3. CNDO/2 net charge densities.

The Photoelectron Spectrum of 2b

Only the three resolved low energy bands of the photoelectron spectrum of **2***b* (Fig. 4) are readily assigned by comparison to suitable models. The ordering of these IP's is verified by reference to the CNDO/2 orbital densities in Table 2. In all cases, the following discussion quotes only vertical IP's.

In *cis*-azoalkanes, the highest energy orbital, at 8–9 eV, is typically the n_N^- or antisymmetric combination of nitrogen lone pair orbitals. Most frequently, the π_{NN} MO is next highest (10.5–11.5 eV),

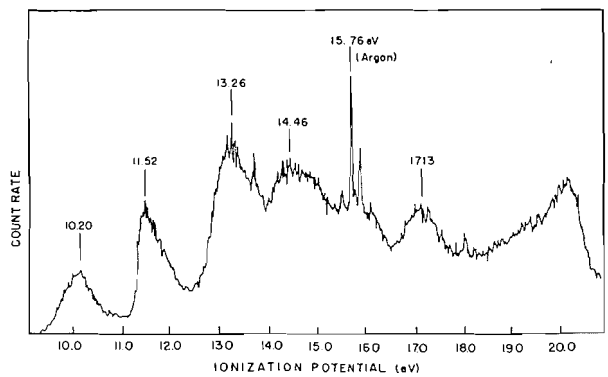

FIG. 4. Photoelectron spectrum of dimethyloxadiazolinone (**2***b*).

Can. J. Chem. Downloaded from www.nrcresearchpress.com by 210.87.254.105 on 09/05/12
For personal use only.

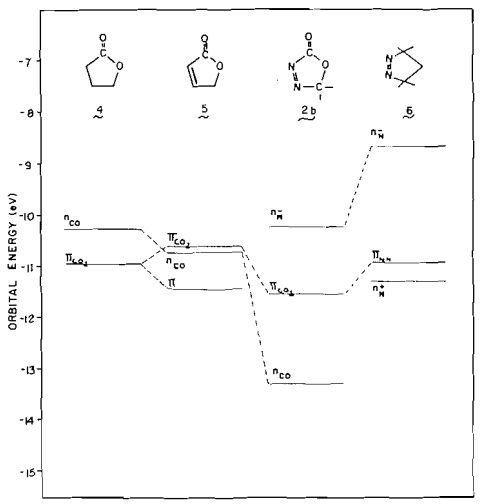

FIG. 5. Correlation diagram using measured valence IP's.

followed by the n_N^+ symmetric combination of nitrogen lone pair orbitals at 11–12 eV (5). Photoelectron spectra of oxadiazolinones are further complicated by the presence of the conjugated ester functional group. Oxygen lone pairs are usually of lower energy than nitrogen lone pairs owing to the increase in effective nuclear charge on going across the first row from C, N, O, to F. For example, n_{CO} and n_O IP's for ketones and esters range between 9.5 and 10.5 eV (21). Based on these and the following considerations, the first three resolved bands for **2***b* have been assigned to n_N^-, π, and n_{CO} (Table 2).

For the purposes of the assignment, the Correlation Diagram for Valence IP's (Fig. 5) features γ-butyrolactone (**4**), γ-crotonolactone (**5**), and 3,3,5,5-tetramethylpyrazoline (**6**) as suitable models. There are not really any more complex heterocyclic models appropriate for **2***b* in the PES literature.[3] CNDO/2 calculations and photoelectron spectra of lactones **4** and **5** have been reported (22).

The highest occupied π-type orbital in each of **4** and **5** contains significant contributions from the formally $2p_z$ lone pair on the ring oxygen and correlates more strongly with HO-π in **2***b* than does the π_{NN} of **6**. In recognition of this fact, the subscript CO_2 has been appended, where appropriate, to describe the electron distribution in this MO. Mixing of π_{NN} and π_{CO_2} in oxadiazolinones ought to raise the HO-π level by resonance but lower it inductively for a net stabilization. At 11.52 eV, the second IP is 0.6 eV lower than the isolated π_{CO_2} orbitals of **4** or **5** or π_{NN} of **6**.

Excluding the π-mixed lone pair orbital on the ring oxygen, four hetero atom lone pair IP's are important. Since they are on adjacent atoms, the nitrogen lone pairs interact the most, with carbonyl oxygen and ring oxygen lone pairs intermediate in energy. One expects the sequence $n_N^- > n_O, n_{CO} > n_N^+$, where n_O refers to the in-plane lone pair orbital on O1 with σ symmetry. The interaction of the azo nitrogen symmetry orbitals with the other lone pair orbitals of σ symmetry results in a widening of the n_N^-/n_N^+ energy gap (a resonance effect) and a lowering of the energy levels (a stabilizing inductive effect). The magnitude of the total effect may be seen by comparing the IP's of dimethyloxadiazolinone (**2***b*) and 3,3,5,5-tetramethylpyrazoline (**6**) (5).

Parameter	6	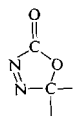 2*b*
n_N^-	8.63 (eV)	10.20 (eV)
n_N^+	11.26 (eV)	>13.3 (eV)
$\Delta(n^-/n^+)$	2.63	>3.1

Because the 13.26 eV ionization has been assigned to the carbonyl oxygen lone pair, the n_N^+ orbital must have an IP higher than 13.3 eV. Thus, the interaction energy $\Delta(n^-/n^+)$ has to be greater than 3.1 eV, which is indeed greater than in the pyrazoline. The CNDO/2 calculations predict $\Delta(n^-/n^+)$ to be 4.54 eV.

The observed carbonyl oxygen lone pair ionization for **2***b*, assigned at 13.26 eV, is much larger than the values of 10.25 eV for γ-butyrolactone (**4**) and 10.70 eV for γ-crotonolactone (**5**) (22), and well outside the normal range for ketones and esters (9.5–10.5 eV (21)). The effect of the double bonds on n_{CO} in **5** and **2***b* can only be inductive and the effect of N=N in this regard is much greater than C=C (compare the carbonyl stretching frequencies (footnote 3), to the 0.5 and 3.0 eV stabilization of n_{CO} in **5** and **2***b* with respect to **4**). Additionally, interaction of lone pair orbitals in **4** and **5** is of the n_{CO}/n_O type and acts to

[3]A referee has suggested that 5,5-dimethyl-2-oxazolidinone (**7**) might also be a useful model but this has been resisted because the lactam nitrogen in **7** is electron donating by virtue of the fact that its lone pair has π symmetry and is strongly mixed with the carbonyl π bond and ring oxygen lone pair of π symmetry. In contrast, lone pairs on the electron withdrawing azo nitrogens of **2***b* are in the plane of the molecule (σ symmetry). Furthermore, the carbonyl stretching frequencies of **4**, **5**, **7**, and **2***b* occur at 1740 (29*a*), 1785 and 1750 (a doublet in the unsaturated lactone (30)), 1750 (29*b*) and 1835 cm^{-1}, respectively, indicating that there is no profit in using the lactam nitrogen to model the effect of the azo group on carbonyl IP's of **2***b*.

7

Can. J. Chem. Downloaded from www.nrcresearchpress.com by 210.87.254.105 on 09/05/12
For personal use only.

Can. J. Chem. Downloaded from www.nrcresearchpress.com by 210.87.254.105 on 09/05/12
For personal use only.

raise the n_{CO} level in these compounds while σ mixing in **2***b* is more complex but will raise n_N^-, lower n_O, and might not affect n_{CO} too much. The n_N^- orbital of **2***b* is stabilized 1.6 eV with respect to that of **6**, with an IP (10.20 eV) well above the usual value of 8–9 eV (5). Without the oppositely acting destabilizing σ interactions anticipated for the n_N^-, the n_{CO} orbital might well be stabilized by more than this amount. CNDO/2 calculated IP's adequately predict a dramatic stabilization: 12.83, 13.74, and 15.15 eV for n_{CO} in **4**, **5**, and **2***b*.

Also salient to this discussion are the effects of substitution at C5, as in **2***a* and **2***d*, on the calculated IP's. Successive substitution of hydrogen then fluorine for methyl reduces the electron density on the carbonyl oxygen by 9 and 16%, respectively (Fig. 3), and this is reflected in 1 to 2 eV stabilizations of all three valence orbitals in **2***d* with respect to **2***b* (Fig. 2). In spite of their physical remoteness, fluorines at C5 are able to transmit their effect to the carbonyl oxygen because the CF_2 moiety contributes π-type symmetry orbitals, strongly withdrawing π electron density to reduce the net charge densities, even at O6. In a qualitative sense, these MO calculations fortify attributing the large stabilization of n_{CO} to a generalized inductive effect of the strongly electron-withdrawing azo function adjacent to the carbonyl.

Consistent then with carbonyl stretching frequency data, the three model compounds and the MO calculations on the three oxadiazolinones, 13.26 eV seems the most reasonable assignment of the n_{CO} band.

As usual, the CNDO/2 calculation has overestimated the ionization potentials, in this case by some 1.5 to 2.5 eV (compared to the usual figure of 4 eV (22–24)), and has correctly reproduced the ordering of the first few highest occupied MO's. Hence, the assigned photoelectron spectrum does seem to validate our initial choice of structural parameters.

Electronic Transition Energies

A further check on our calculation entailed an examination of the electronic transitions of dimethyloxadiazolinone (**2***b*). The uv–visible spectrum in hexane (Fig. 6) exhibits two bands: one at 372 nm ($\varepsilon_{max} = 348\ M^{-1}\ cm^{-1}$) whose structure collapses in more polar solvents, and another at 214 nm ($\varepsilon_{max} = 2880\ M^{-1}\ cm^{-1}$). Even for simple azoalkanes electronic transition assignments of all but $n_N^- \rightarrow \pi^*$ have been frequently disputed (5, 25, 26). Here the CNDO/2 method predicts five possible transitions (Table 3) which might be responsible for the observed higher energy transition, often casually assigned as $\pi \rightarrow \pi^*$. Of these, the single $\pi \rightarrow \pi^*$ candidate ought to be most intense ($\varepsilon_{max} \gtrsim 10\,000$). Any

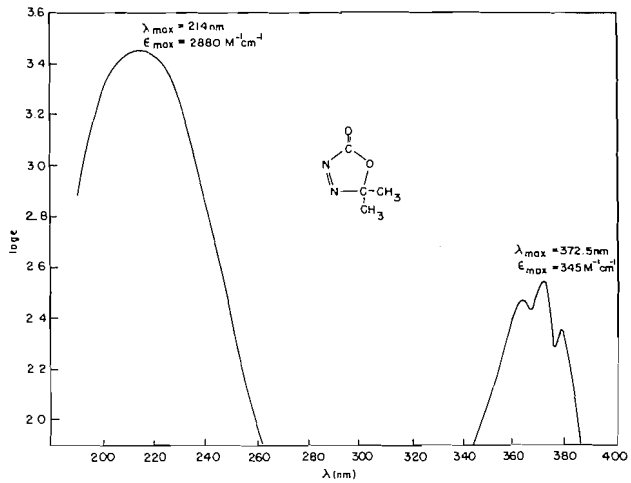

FIG. 6. Absorption spectrum of dimethyloxadiazolinone (hexane).

TABLE 3. Calculated and observed excitation energies for dimethyloxadiazolin-2-one (**2***b*)[a]

Transition	J_{ij}	K_{ij}	$\Delta E_{i\rightarrow j}$	Observed
$n_N^- \rightarrow \pi^*$	9.95	0.00	5.2	3.24
$\pi_{CO_2} \rightarrow \pi^*$	7.83	1.21	10.3	
$n_{CO} \rightarrow \pi^*$	8.52	0.01	9.0	
$n_O \rightarrow \pi^*$	7.85	0.01	10.6	5.80
$n_N^+ \rightarrow \pi^*$	9.80	0.03	9.9	
$n_N^- \rightarrow \pi^{**}$	9.57	0.00	9.8	

[a]All energies in eV.

of the $n \rightarrow \pi^*$ type should have an $\varepsilon_{max} \sim 100$, similar to that for α,β-unsaturated esters (27). However, the observed intensity is intermediate. It is not beyond the realm of possibility that an ε_{max} of 2880 $M^{-1}\ cm^{-1}$ reflects a fortuitous combination of several nearly degenerate $n \rightarrow \pi^*$ transitions, perhaps on the low energy tail of a $\pi \rightarrow \pi^*$ band. Further speculation on this matter would be inappropriate here.

Effects of Variations in R_{CO}

The carbonyl bond length turns out to be one of the key parameters in the entire calculations, and as such deserves some attention. Computations on the oxadiazolinone **2***a* with R_{CO} = 1.16, 1.19, 1.21, 1.24, 1.27, and 1.29 Å found a CNDO/2 total energy minimum at 1.261 Å. Although CNDO bond lengths are known to be unreliable (17) and nothing can be inferred from this particular value, it is significant, however, that the calculated energy gap between first and second IP's is a strong function of the selected bond length: declining from 0.97 eV at 1.16 Å to 0.04 eV at 1.29 Å (Fig. 7). That a gap of 1.32 eV is observed for **2***b* strongly supports our choice of a relatively short carbonyl distance and may well indicate the possibility $R_{CO} < 1.19$ Å.

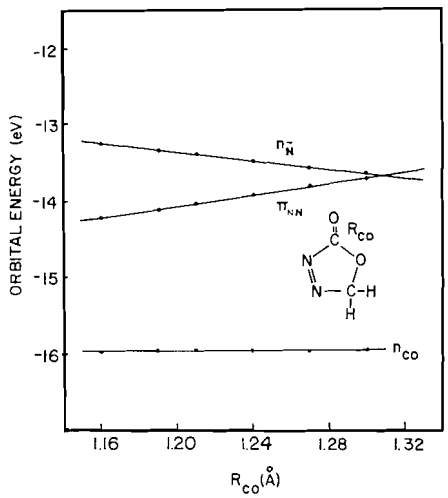

FIG. 7. Valence orbital energy depends on choice of R_{CO} for oxadiazolinone **2***a*.

Smoothly monotonic against decreasing R_{CO}, frontier densities change as expected for increasing electronegativity of the CO moiety but are not significantly altered. Shrinking the CO bond increases the electrophilicity of C3, N4, and N5 in both the charge and frontier controlled senses, thereby rationalizing the high reactivity of oxadiazolinones toward nucleophiles.

As a final note on the bond dimension issue, an apparently minor change in heteroatom; that is replacement of ring oxygen by nitrogen (i.e., in a Δ^1-1,2,4-triazolin-3-one) would result in a substantially longer equilibrium bond length (cf. R_{CO} = 1.26 in azodicarbonamide (8)) and also much different chemistry. In particular, triazolinones are less susceptible to aqueous hydrolysis than oxadiazolinones.[4]

Conclusions

The choice of an alternate theoretical procedure is unlikely to effect a metamorphosis of the electron distributions reported herein. Even though we have shown that the CNDO/2 computational method gives a reasonable picture of Δ^3-1,3,4-oxadiazolin-2-ones, it is obvious from the orbital densities in Table 2 that the classification or assignment of orbitals as n_N, n_{CO}, n_O, π_{CO_2}, π_{NN}, etc., is unrealistic and oversimplified. It is extremely difficult to identify orbital mixing patterns for such a complex molecule, in spite of its low symmetry. For example, π_{NN} contains about a third of the electron density on O1 as well as on each of N3 and N4; because the C—H bonds in **2***a* transform with π symmetry, they are mixed into every π orbital; in the orbitals designated as n_N^- and n_N^+, only half the σ electron density is found on the nitrogens and the third highest occupied molecular orbital, n_{CO} has only a third of the electron density on the oxygen. Under circumstances such as these, the significance of the terms 'lone pair' and two electron 'bond' crumbles.

[4]A. J. Paine and J. Warkentin. Unpublished results.

Experimental

5,5-Dimethyl-Δ^3-1,3,4-oxadiazolin-2-one (**2***b*) was prepared in 80% yield from the ketone semicarbazone as previously described (1). Samples for PES were twice sublimed at 0.01 Torr from 0°C to a Dry Ice – acetone cold finger and maintained at −20°C in the dark prior to use. The photoelectron spectrometric equipment of Professor D. C. Frost (28) was used to obtain the spectrum of **2***b*: a sample pressure of 10^{-5} Torr was employed and no evidence for any decomposition product IP's was observed during spectrum acquisition.

Hexane for the ultraviolet spectrum was purified by overnight treatment with H_2SO_4 and careful fractionation from $CaSO_4$. This material had a uv cutoff at 190 nm on a Cary Model 14 spectrophotometer.

Acknowledgements

We would like to thank Professor D. P. Santry for his program and helpful comments. Professor D. C. Frost and Dr. N. P. C. Westwood of the Department of Chemistry, University of British Columbia, provided assistance during N.H.W.'s sabbatical leave. The National Research Council of Canada supported this work by grants and a postgraduate scholarship to A.J.P.

1. (*a*) S. L. LEE, G. B. GUBELT, A. M. CAMERON, and J. WARKENTIN. Chem. Commun. 1074 (1970); (*b*) P. KNITTEL, S. L. LEE, and J. WARKENTIN. Can. J. Chem. **50**, 3248 (1972).
2. S. L. LEE, A. M. CAMERON, and J. WARKENTIN. Can. J. Chem. **50**, 2326 (1972).
3. K. FUKUI. Top. Curr. Chem. **15**, 1 (1970).
4. (*a*) K. FUKUI, T. YONEZAWA, and C. NAGATA. J. Chem. Phys. **27**, 1247 (1957); (*b*) K. FUKUI, T. YONEZAWA, and C. NAGATA. Bull. Chem. Soc. Jpn. **27**, 423 (1954).
5. K. N. HOUK, Y.-M. CHANG, and P. S. ENGEL. J. Am. Chem. Soc. **97**, 1824 (1975).
6. T. KOOPMANS. Physica, **1**, 104 (1934).
7. A. PRAKASH, C. CALVO, A. M. CAMERON, and J. WARKENTIN. J. Cryst. Mol. Struct. **3**, 71 (1973).
8. Tables of interatomic distances. Chemical Society, London, U.K. 1958.
9. P. KNITTEL. Ph.D. Thesis. Department of Chemistry, McMaster University, Hamilton, Ont. 1976.
10. G. BERTHIER and J. SERRE. *In* The chemistry of the carbonyl group. *Edited by* S. Patai. Interscience, New York, NY. 1970. Chapt. 1.
11. E. M. KOSOWER. An introduction to physical organic chemistry. John Wiley and Sons Inc., New York, NY. 1968. p. 49.
12. N. L. ALPERT, W. E. KEISER, and H. A. SZYMANSKI. IR — theory and practice of infrared spectroscopy. Plenum Press, New York, NY. 1970.
13. J. BERNSTEIN and I. IZAK. J. Chem. Soc. Perkin II, 429 (1976) and refs. cited therein.

Can. J. Chem. Downloaded from www.nrcresearchpress.com by 210.87.254.105 on 09/05/12
For personal use only.

14. R. K. KAKAR, E. A. RINEHART, C. R. QUADE, and T. KOJIMA. J. Chem. Phys. **52**, 3803 (1970).
15. J. A. POPLE, D. P. SANTRY, and G. A. SEGAL. J. Chem. Phys. **43**, 5129, 5135 (1965).
16. J. A. POPLE and G. A. SEGAL. J. Chem. Phys. **44**, 3289 (1966).
17. J. A. POPLE and D. L. BEVERIDGE. Approximate molecular orbital theory. McGraw-Hill, New York, NY. 1970.
18. J. D. ROBERTS. Notes on molecular orbital theory. Benjamin, New York, NY. 1961.
19. G. KLOPMAN. J. Am. Chem. Soc. **90**, 223 (1968).
20. L. SALEM. J. Am. Chem. Soc. **90**, 543, 553 (1968).
21. S. P. MCGLYNN and J. L. MEEKS. J. Electron Spectrosc. Relat. Phenom. **8**, 85 (1976).
22. A. D. BAIN. M.Sc. Thesis. Department of Chemistry, University of British Columbia, Vancouver, BC. 1972.
23. D. W. DAVIES. Chem. Phys. Lett. **2**, 173 (1968).
24. D. C. FROST, F. G. HERRING, C. A. MCDOWELL, and I. A. STENHOUSE. Chem. Phys. Lett. **4**, 533 (1970).
25. E. HASELBACH and A. SCHMELZER. Helv. Chim. Acta, **54**, 1575 (1971) and refs. cited therein.
26. M. B. ROBIN. Higher excited states of polyatomic molecules. Vol. 2. Academic Press, New York, NY. 1975. pp. 68–75.
27. D. H. WILLIAMS and I. FLEMING. Spectroscopic methods in organic chemistry. McGraw-Hill, New York, NY. 1973.
28. D. C. FROST, N. P. C. WESTWOOD, N. H. WERSTIUK, L. M. CABELKOVA-TAGUCHI, and J. WARKENTIN. Can. J. Chem. **55**, 3677 (1977).
29. Sadtler Standard Grating Spectra. Sadtler Research Labs., Philadelphia, PA. 1972. (*a*) No. 25048; (*b*) No. 20236.
30. C. C. PRICE and J. M. JUDGE. Org. Syn. **45**, 22 (1965).

Can. J. Chem. Downloaded from www.nrcresearchpress.com by 210.87.254.105 on 09/05/12
For personal use only.

Horseradish peroxidase. XXVIII. Formation and reactivity of the alkaline form. Evidence for an enzyme–substrate complex in compound 1 formation

DOMINIQUE JOB[1] AND H. BRIAN DUNFORD

Department of Chemistry, University of Alberta, Edmonton, Alta., Canada T6G 2G2

Received August 30, 1977

DOMINIQUE JOB and H. BRIAN DUNFORD. Can. J. Chem. **56**, 1327 (1978).

The rate of formation of **1** from horseradish peroxidase and hydrogen peroxide is investigated as a function of p*H* between p*H* 9.5 and 11.5. For p*H* values smaller than 10, the rate depends linearly on hydrogen peroxide concentration, whereas between p*H* 10 and 11.5, the rate displays saturation kinetics. Evidence is presented for the formation of an intermediate complex before compound **1** formation. Two parameters were measured as a function of p*H*: k_{app}, the apparent rate constant for compound **1** formation, and k_d, the dissociation rate constant of the intermediate complex to **1**. A third parameter, K_{app}, similar to a dissociation constant for the reaction was deduced from the two rate constants. The apparent rate constant k_{app} is p*H* independent for p*H* values <9.5 and is directly affected by ionization of only one group on the native enzyme with a p*K* of 11. The p*H* dependences of k_d and K_{app} require a minimum of two ionizations. One corresponds to a group on the native enzyme which ionizes at a p*H* lower than that of the present study, the second corresponds to the ionizable group with p*K* of 11. For cyanide binding to horseradish peroxidase over the same p*H* interval, saturation kinetics were not observed, yet the p*H* profile for k_{app} exactly parallels that for formation of **1** (when corrected for the effect of the ionization of HCN) and shows an inflection at the same p*H* value.

DOMINIQUE JOB et H. BRIAN DUNFORD. Can. J. Chem. **56**, 1327 (1978).

On a étudié, en fonction du p*H* entre 9.5 et 11.5, la vitesse de formation du composé **1** à partir de la peroxydase du raifort et du peroxyde d'hydrogène. A des valeurs de p*H* plus basses que 10, la vitesse dépend d'une façon linéaire de la concentration de peroxyde d'hydrogène alors qu'à des p*H* allant de 10 à 11.5, la vitesse présente une cinétique de saturation. On présente des données indiquent qu'il y a formation d'un complexe intermédiaire avant la formation du composé **1**. On a mesuré deux paramètres en fonction du p*H*: k_{app}, la constante de vitesse apparente pour la formation du composé **1** et k_d, la constante de vitesse de dissociation du complexe intermédiaire en composé **1**. On a pu déduire un troisième paramètre, K_{app}, semblable à une constante de dissociation, de la réaction à partir des deux constantes de vitesse. La constante de vitesse apparente k_{app} est indépendante du p*H* à des valeurs de p*H* < 9.5 et est directement affectée par l'ionisation d'un seul groupe de l'enzyme à un p*K* de 11. Les relations qui existent entre le p*H* et k_d et K_{app} nécessitent la présence d'au moins deux ionisations. L'une correspond à un groupe sur l'enzyme qui s'ionise à un p*H* plus faible que celui utilisé dans l'étude présente alors que le deuxième correspond à un groupe ionisable avec un p*K* de 11. Pour la fixation de cyanure à la peroxydase de raifort au même intervale de p*H*, on n'a pas observé de cinétique de saturation même si le profil de p*H* pour k_{app} est exactement parallèle à celui de la formation du composé **1** (lorsqu'on l'a corrigé pour l'effet de l'ionisation de HCN) et présente une inflexion à la même valeur de p*H*.

[Traduit par le journal]

Introduction

The presence of a water molecule coordinated to the iron atom of peroxidase has been accepted for many years (1–10). Recent nmr results have been interpreted to indicate both the presence[2] and absence (11) of water in the sixth coordination position of horseradish peroxidase (HRP) although the latter interpretation is suspect since it requires an explanation of why the sixth coordination position of the ferric iron is readily accessible to other ligands (12). Absorbance changes which are induced in an HRP solution by a p*H* jump from neutrality to above 10 have been attributed to the formation of a low-spin hydroxide complex of peroxidase (1, 8–10, 13). From a kinetic study of the alkaline transition of this enzyme the interesting proposal was made that an amino acid residue deprotonates in alkaline solution and becomes the sixth iron ligand as a slow conformational change occurs (14). A recent kinetic study of the alkaline transition of two turnip peroxidases has led to the proposal that these transitions can be explained most simply in terms of deprotonation reactions by hydroxide ions of a heme-linked

[1]Present address: Laboratoire de Biochimie Végétale associé au CNRS (n° 84), centre de Luminy, Université d'Aix-Marseille, 70 route Léon Lachamp, 13288 Marseille Cedex 2, France.

[2]R. J. P. Williams. Personal communication.

Can. J. Chem. Downloaded from www.nrcresearchpress.com by 210.87.254.40 on 09/05/12
For personal use only.

Can. J. Chem. Downloaded from www.nrcresearchpress.com by 210.87.254.40 on 09/05/12
For personal use only.

group for each enzyme (15). Since the alkaline transition of horseradish peroxidase is known to occur at a rate sufficiently slow to be studied with a conventional stopped-flow apparatus (14, 16) we have studied the effect of p*H* jumps on the absorption spectrum of HRP.

We also report the reactivity of alkaline peroxidase towards hydrogen peroxide and evidence for an intermediate in the formation of **1** is presented. Since cyanide binding to peroxidase is a simple ligand reaction (17, 18) this paper also compares it to formation of **1** over the p*H* range 9.5–11.5.

Experimental

Horseradish peroxidase (HRP) was purchased from two sources. One sample was obtained from Boehringer-Mannheim Corp. (lot 716 5528) and the second from Sigma Chemical Co. (lot 25C 9570). They were prepared for use by extensive dialysis against water which had been distilled five times. This water was used to prepare all solutions. The distillation procedure has been described (19) and the quality of the water is such that **1** prepared from stoichiometric amounts of HRP and hydrogen peroxide has a half-life greater than 2 h at 25°C and neutral p*H*. The purity of the enzyme prepared in this manner, as determined by the ratio of absorbances at 403 nm and 280 nm was 3.34 for the Boehringer enzyme and 3.0 for the Sigma enzyme. The concentration of peroxidase was determined spectrophotometrically at 403 nm using a molar absorptivity of 1.02×10^5 M^{-1} cm^{-1} (20). Analytical reagent grade hydrogen peroxide was obtained from Mallinckrodt Chemical works as a 30% aqueous solution. Its concentration was determined spectrophotometrically as described elsewhere (21) using the HRP assay. Potassium cyanide, potassium nitrate, and all buffer components were reagent grade and used without further purification. Carbonate–NaOH buffers were used between p*H* 9.0 and 10.9 and phosphate–NaOH buffers between 10.9 and 11.7. Stopped-flow experiments were performed on a Durrum–Gibson (model D-110) spectrophotometer, equipped with a 2-cm light path cuvette in which solutions of equal volumes were mixed. The temperature was maintained at 25 ± 0.1°C by circulating thermostated water. For p*H*-jump experiments a solution of unbuffered peroxidase, for which the ionic strength, μ, was adjusted to 0.1 with potassium nitrate, was mixed with buffered solutions (ionic strength 0.1 or 0.02 and then adjusted to 0.1 with potassium nitrate) of various p*H* values. Kinetics were recorded at 419 nm where alkaline peroxidase has its maximum absorptivity. For compound **1** formation or cyanide binding to peroxidase, one drive syringe contained peroxidase and buffer and the second drive syringe contained the substrate and buffer. Here too, the ionic strength was adjusted to 0.1 using potassium nitrate. All kinetic curves recorded were found to be first order. The observed rate constants were determined as described (22). Usually, eight individual determinations of the rate constant were performed. These were then averaged for a single best value with known standard deviation. After reaction, the solutions were collected for p*H* measurements with an Orion 801 digital p*H* meter in conjunction with a Fisher combination electrode. Absorbance measurements and optical spectra were obtained with a Cary 14 spectrophotometer.

Results

Alkaline Peroxidase Formation

For all p*H* values first-order kinetic curves have been recorded. The observed rate constant for the alkaline peroxidase formation process, $k_{obs}^{OH^-}$, increases linearly with hydroxide ion concentration as shown in Fig. 1 and leads to the relation

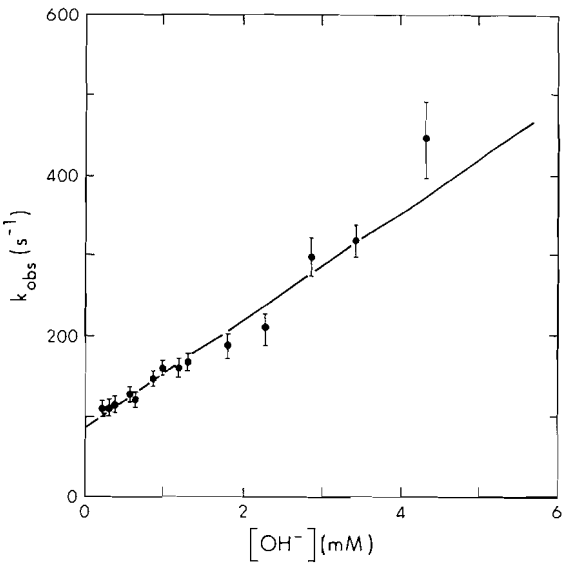

FIG. 1. Alkaline ionization of horseradish peroxidase. An unbuffered solution of HRP (2.45 μ*M*) is mixed with buffered solutions. Absorbance changes were recorded at 419 nm, temperature was 25°C, total ionic strength 0.1. The straight line obtained by a least-squares analysis corresponds to [1] in the text.

$$k_{obs}^{OH^-} = k_b[OH^-] + k_{-b} \quad [1]$$

The values of the slope and the intercept of this straight line determined by linear least-squares analysis[3] are $(7.8 \pm 0.5) \times 10^4$ M^{-1} s^{-1} and 78 ± 9 s^{-1}. These constants differ from those of Epstein and Schejter (14) by about 50 and 20%, respectively. Results similar to ours have been obtained by Yamazaki and Araiso (16). It was also observed that in addition to the process described above, two slow kinetic processes occurred. The spectral changes were small compared to the first fast step and they had half-lives of about 0.5 and 30 s. It is notable that the same behaviour was observed for the alkaline ionization of turnip peroxidase P_1 (15). The p*K* value of the alkaline HRP transition can be measured at equilibrium in a conventional way, by plotting $1/\Delta A_{419\ nm}$ vs. $1/[OH^-]$. One should obtain a straight line for which intercept with the $1/[OH^-]$ axis permits the evaluation of the p*K*. Such a plot constructed from 15 experimental points had a slope of 9.4 ± 0.7 m*M* and a $1/\Delta A_{419\ nm}$ intercept of 9.2 ± 0.5. The p*K* value deduced from

[3]Results are available, at a nominal charge, from the Depository of Unpublished Data, CISTI, National Research Council of Canada, Ottawa, Ont., Canada K1A 0S2.

Can. J. Chem. Downloaded from www.nrcresearchpress.com by 210.87.254.40 on 09/05/12
For personal use only.

this plot was 11.00 ± 0.05, in agreement with the value reported (4) for 25°C and 0.11 μ.

Compound 1 Formation

The formation of **1** from HRP and hydrogen peroxide is described by the stoichiometric eq. 2 (23)

$$[2] \qquad \text{HRP} + H_2O_2 \xrightarrow{k_{app}^{H_2O_2}} \text{HRP-1}$$

For a sufficiently large excess of hydrogen peroxide below p*H* 10, a pseudo-first-order rate constant, $k_{obs}^{H_2O_2}$ can be defined as

$$[3] \qquad k_{obs}^{H_2O_2} = k_{app}^{H_2O_2}[H_2O_2]$$

Plots of $k_{obs}^{H_2O_2}$ vs. hydrogen peroxide concentration are linear at p*H* values of 9.51 and 9.87 (Fig. 2) as was found at more acidic p*H* values (18). For p*H* values >10, nonlinear plots are observed. In this high p*H* region

$$[4] \qquad k_{obs}^{H_2O_2} = \frac{k_d[H_2O_2]}{K_{app} + [H_2O_2]}$$

The significance of the symbols is found in the Discussion.

For $K_{app} > [H_2O_2]$ [4] reduces to the form of [3] so that $k_{app}^{H_2O_2} = k_d/K_{app}$. Equation 4 can be rearranged to

$$[5] \qquad \frac{1}{k_{obs}^{H_2O_2}} = \frac{1}{k_{app}^{H_2O_2}[H_2O_2]} + \frac{1}{k_d}$$

From the linear double-reciprocal plots (Fig. 3) $k_{app}^{H_2O_2}$ and k_d are obtained from the slopes and intercepts, and hence K_{app} can be calculated. To ascertain that the saturation effect obtained in the plot of $k_{obs}^{H_2O_2}$ vs. $[H_2O_2]$ at high H_2O_2 concentrations does indeed correspond only to HRP-**1** formation, absorption spectra were recorded on the Cary 14 spectrophotometer after mixing HRP at p*H* 11.2 with an excess of H_2O_2. One can see from the results of Fig. 4 that the first absorption spectrum that can be recorded after mixing contains a high percentage of HRP-**1**. The spectra presented in Fig. 4 also show that for wavelengths near 430 nm HRP-**1** and the native enzyme are nearly isosbestic at p*H* 11.2. Kinetic curves were recorded at 433 nm and it was observed that during the time of the fast process corresponding to HRP-**1** formation (based on the A_{410} nm measurements) almost no absorbance change occurred at 433 nm. Using a much slower time base, the absorbance at 433 nm does increase perhaps due to the spontaneous decay of HRP-**1** to HRP-**2**. These results indicate that the observed saturation effect in Fig. 2 is not due to some artifact such as the formation of HRP-**2**.

Plots of log (absorbance change) vs. time obtained at 410 nm illustrate that HRP-**1** formation at p*H* 11.55 obeys pseudo-first-order kinetics to a good approximation (Fig. 5). Figure 5 also shows that at p*H* 11.55, increasing the hydrogen peroxide concentration by a factor of 10 only increases the observed rate constant fourfold. The values of k_d, and $k_{app}^{H_2O_2}$ which were deduced at several p*H* values

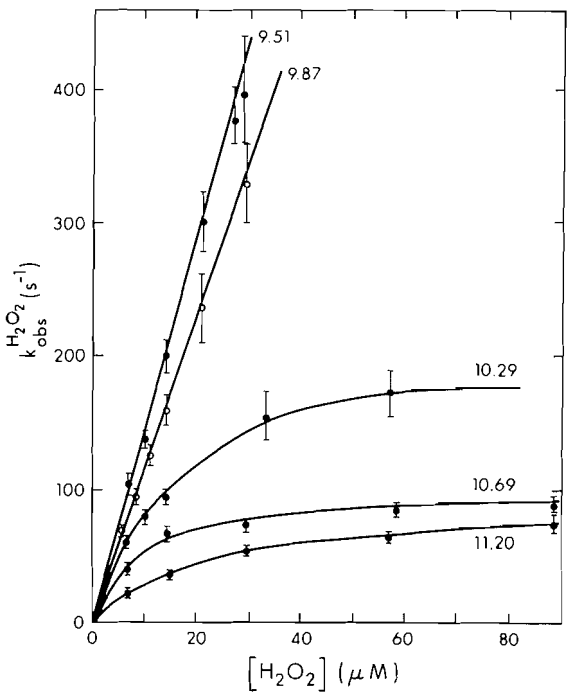

FIG. 2. Plots of k_{obs}, the pseudo-first-order rate constants for compound **1** formation, vs. $[H_2O_2]$. Peroxidase concentration was 0.77 μ*M*, temperature 25°C, total ionic strength 0.1. The p*H* at which each experimental point was determined is indicated on the plots.

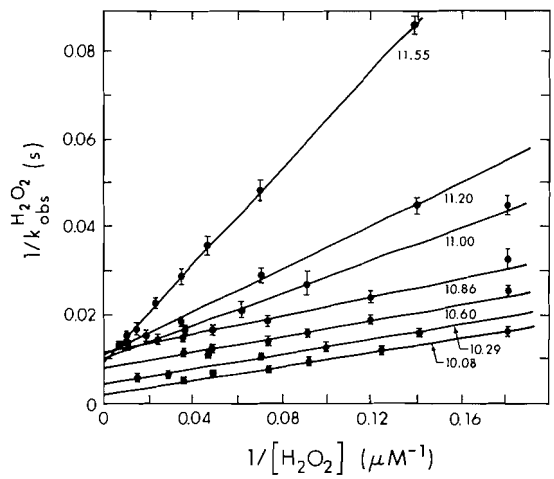

FIG. 3. Linear least-squares analysis of the double reciprocal plots for compound **1** formation. The conditions are those of Fig. 2.

Can. J. Chem. Downloaded from www.nrcresearchpress.com by 210.87.254.40 on 09/05/12
For personal use only.

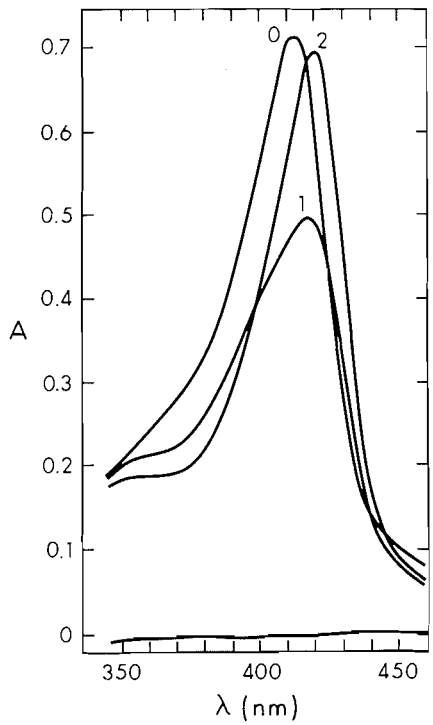

FIG. 4. Absorption spectra recorded after mixing HRP (7.7 μ*M*) with an excess of H_2O_2 (54.5 μ*M*) at p*H* 11.2 (phosphate–NaOH buffer 0.1 μ). Temperature was 25°C. Spectrum 0 was the spectrum of native enzyme, spectrum 1 was recorded just after mixing, and spectrum 2, 1 min after spectrum 1. The H_2O baseline is included.

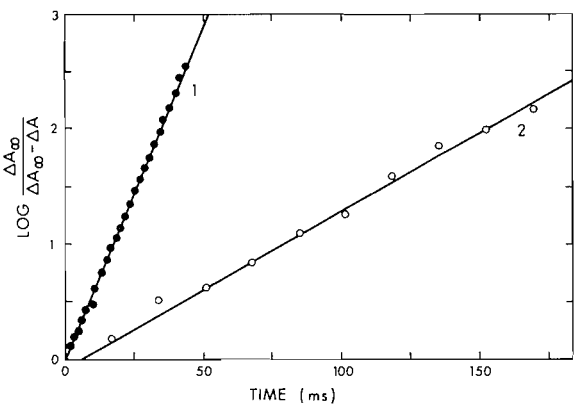

FIG. 5. Semilogarithmic plot of absorbance change at 410 nm vs. time for compound **1** formation, at p*H* 11.55, 0.1 μ, and 25°C The observed rate constants are given by the slopes of the straight lines: (*1*) $[H_2O_2] = 72$ μ*M*, $k_{obs} = 59$ s^{-1}; (*2*) $[H_2O_2] = 7.2$ μ*M*, $k_{obs} = 13$ s^{-1}; for both (*1*) and (*2*) [HRP] = 0.38 μ*M*. An induction period appears to be indicated by the results of (2).

from linear least-squares analysis of the Lineweaver–Burk plots of Fig. 3, are listed.[3] From these the value of K_{app} can be calculated. The values of K_{app} and $k_{app}^{H_2O_2}$ were corrected at the highest p*H* values in order to eliminate the effect of H_2O_2 ionization, since by use of the diffusion control limit rule (18) it has been shown that only the neutral form of hydrogen peroxide is reactive towards HRP to form compound **1**. A pK_a value of 12.0 was used for the dissociation of H_2O_2. Computed best fit curves obtained by nonlinear least-squares analysis to the $k_{app}^{H_2O_2}$ and k_d data as a function of p*H* are shown in Figs. 6 and 7 and the K_{app} data as a function of p*H* are shown in Fig. 8.

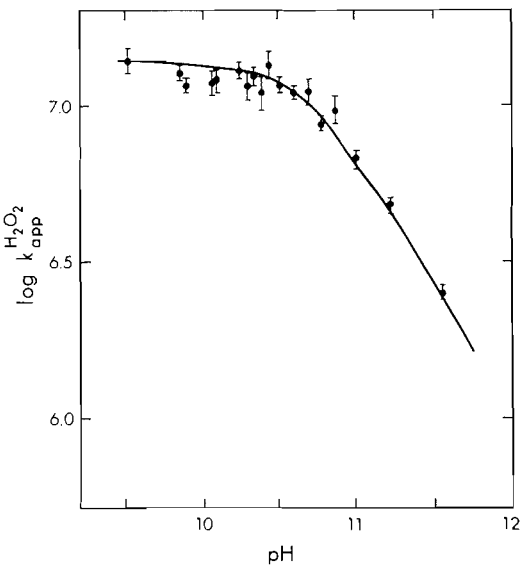

FIG. 6. Best fit curves to the data of k_{app} for compound **1** formation vs. p*H*. The curve was calculated from a nonlinear least-squares fit of the data to [9].

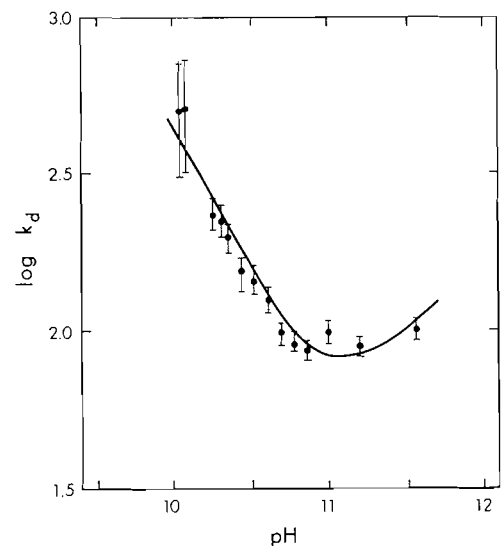

FIG. 7. Best fit curve to the data of k_d for compound **1** formation vs. p*H*. The curve was calculated from a nonlinear least-squares fit of the data to [11].

Can. J. Chem. Downloaded from www.nrcresearchpress.com by 210.87.254.40 on 09/05/12
For personal use only.

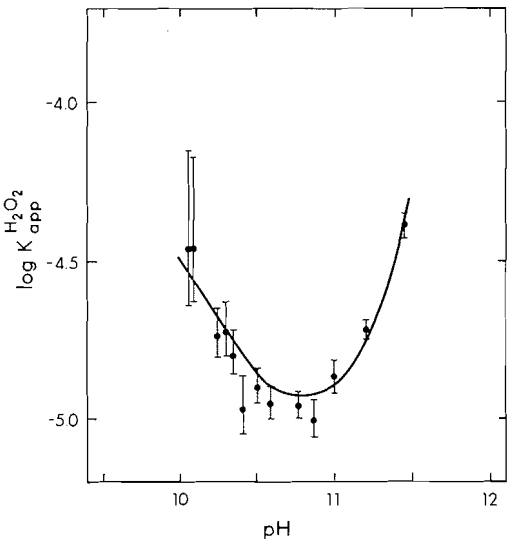

FIG. 8. Best fit curve to the data of log K_{app} for compound **1** formation vs. p*H*. The curve was calculated from the nonlinear correlations shown in Figs. 6 and 7.

Cyanide Binding to HRP

As previously shown for the acidic p*H* range (17, 18), cyanide binding to HRP can be described by [6]

$$\text{HRP} + \text{HCN} \xrightarrow{k_{app}^{CN}} \text{HRP–CN} + \text{H}^+ \qquad [6]$$

where the behaviour of the proton is unknown (17, 18). Using a large excess of cyanide over HRP, the observed pseudo-first-order rate constant for the appearance of the HRP–cyanide complex is given by [7]

$$k_{obs}^{CN} = k_{app}^{CN}[\text{HCN}]_{total} \qquad [7]$$

while at p*H* values >10 plots of $k_{obs}^{H_2O_2}$ for HRP-**1** formation vs. $[H_2O_2]$ show a saturation effect at high H_2O_2 concentrations, the corresponding plots for the HRP–CN complex formation are linear.[3]

*p*H *Dependence of Kinetic Parameters*

Cyanide Binding to Peroxidase

Reaction 8 can account for the k_{app}^{CN} values

$$\begin{array}{ccccc} \text{H–HRP} & + & \text{HCN} & \xrightarrow{k} & \text{HRP–CN} + \text{H}^+ \\ K_{alk}\big\downarrow\big\uparrow \text{H}^+ & & K_L\big\downarrow\big\uparrow \text{H}^+ & & \\ \text{HRP} & & \text{CN}^- & & \end{array} \qquad [8]$$

where K_{alk} is the equilibrium constant for the formation of alkaline HRP and K_L the acid dissociation constant of HCN. The best values obtained from the analysis of the data are $k = (1.2 \pm 0.2)\ 10^5\ M^{-1}\ s^{-1}$, $pK_L = 9.00 \pm 0.08$, and $pK_{alk} = 11.00 \pm 0.15$ in comparison with previous values of $k = (1.1 \pm 0.2)\ 10^5\ M^{-1}\ s^{-1}$ and $pK_{alk} = 10.85 \pm 0.15$ (24).

*p*H *Dependence of the Kinetic and Equilibrium Parameters for HRP-1 Formation*

The data on the saturation effect are not extensive as a function of p*H* because (*i*) the saturation effect can only be detected with the stopped-flow machine above p*H* 10 and (*ii*) denaturation of the enzyme becomes noticeable above p*H* 11.6.

*(i) p*H *Dependence of* $k_{app}^{H_2O_2}$

The simplest empirical equation fitting these data was found to be

$$k_{app}^{H_2O_2} = \frac{(A_1/A_2)[H^+]}{1 + ([H^+]/A_2)} \qquad [9]$$

Use of a nonlinear least-squares program fitting the data to [9] led to the nonlinear correlation shown in Fig. 6 and the best fit parameters listed in Table 1.

The empirical eq. 9 can be interpreted in terms of collision theory using the simple scheme

$$\begin{array}{ccccc} \text{H–HRP} & + & \text{H}_2\text{O}_2 & \xrightarrow{k_1} & \mathbf{1} + \text{H}_2\text{O} \\ K_{alk}\big\downarrow\big\uparrow \text{H}^+ & & & & \\ \text{HRP} & & & & \end{array} \qquad [10]$$

which leads to

$$k_{app}^{H_2O_2} = \frac{(k_1/K_{alk})[H^+]}{1 + ([H^+]/K_{alk})} \qquad [11]$$

Reaction 10 is identical in form to reaction 8 used to account for k_{app}^{CN} values. From the data in Table 3,[3] $k_1 = (1.6 \pm 0.1) \times 10^7\ M^{-1}\ s^{-1}$ and $pK_{alk} = 10.85 \pm 0.07$, the identical value obtained from the cyanide results.

*(ii) p*H *Dependence of* k_d

Two empirical equations were found to fit equally well the data of k_d vs. p*H* for HRP-**1** formation.

$$k_d = A_3[H^+]^2 + A_4 \qquad [12]$$

or

$$k_d = A_5[H^+] + A_6 + (A_7/[H^+]) \qquad [13]$$

A linear least-squares analysis of k_d vs. $[H^+]^2$ is shown in Fig. 9, [12]. In the case of [13], A_6 has a

TABLE 1. Parameters obtained from analysis of k_{app}, K_{app}, and k_d for compound **1** formation

Parameter (Eq. No.)		Numerical values[a]
A_1 (Eq. 9)	k_1 (Eq. 11)	$(1.6\pm0.1)10^7\ (M^{-1}s^{-1})$
A_2 (Eq. 9)	K_{alk} Eq. 11)	$(1.4\pm0.3)10^{-11}\ (M)$
A_3 (Eq. 12)		$(5.4\pm0.3)10^{22}\ (M^{-2}s^{-1})$
A_4 (Eq. 12)		$(88\pm3)\ (s^{-1})$
A_5 (Eq. 13)		$(4.4\pm0.5)10^{12}\ (M^{-1}s^{-1})$
A_6 (Eq. 13)		$(145\pm175)\ (s^{-1})$
A_7 (Eq. 13)		$(2.5\pm0.9)10^{-10}\ (M\,s^{-1})$

[a]Errors estimated from the standard deviations of the nonlinear least-squares fits.

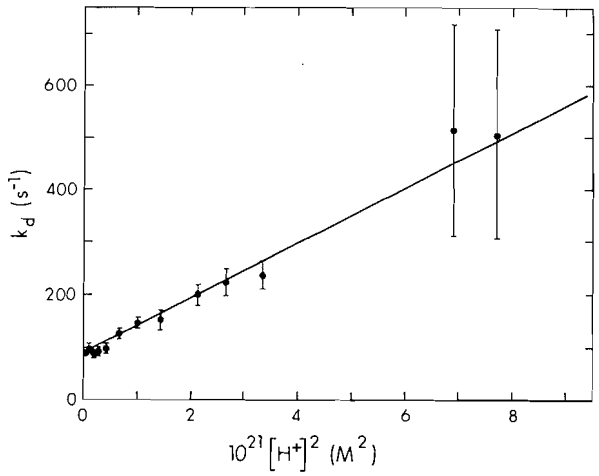

FIG. 9. Linear least-squares analysis of k_d vs. $[H^+]^2$ for compound **1** formation. The straight lines correspond to [12] in the text.

very large standard deviation ($A_6 = 145 \pm 175\ s^{-1}$). Making $A_6 = 0$ led to $A_5 = (4.6 \pm 0.3)10^{12}\ M^{-1}\ s^{-1}$ and $A_7 = (3.3 \pm 0.5)10^{-10}\ M\ s^{-1}$, values compatible with the values of A_5 and A_7 listed in Table 1. The nonlinear correlation using the parameters of Table 1 and [13] is shown in Fig. 7.

(iii) pH Dependence of K_{app}

The K_{app} values were obtained experimentally by the ratio $K_{app} = k_d/k_{app}^{H_2O_2}$. A relatively satisfactory fit for the data of K_{app} vs. p*H* was obtained using the nonlinear correlation fitting the data for $k_{app}^{H_2O_2}$ [9] and for k_d [12] or [13]. From these relations, it was possible to generate empirical curves for K_{app} vs. p*H* going through the experimental points as shown in Fig. 8.

Discussion

The detection of saturation kinetics at alkaline p*H* values indicates that an enzyme–substrate complex exists which is a precursor to **1**. Similar results have been observed for deuterohemin (25, 26) and catalase (27). The two-step mechanism shown in [14],

$$[14]\quad HRP + H_2O_2 \underset{k_{-s}}{\overset{k_s}{\rightleftharpoons}} (HRP\text{-}H_2O_2) \xrightarrow{k_d} HRP\text{-}\mathbf{1}$$

is characterized by [15] (see for instance ref. 28)

$$[15]\quad (k_{1,2})^2 - k_{1,2}(k_d + k_{-s} + k_s[H_2O_2]) + k_s k_d[H_2O_2] = 0$$

where $k_{1,2}$, a parameter yet to be determined, can be defined as

$$[16]\quad k_{1,2} = (k_d + k_{-s} + k_s[H_2O_2] \pm \sqrt{D})/2$$

with

$$\sqrt{D} = (k_d + k_{-s} + k_s[H_2O_2]) \times \left(1 - \frac{4k_d k_s[H_2O_2]}{(k_d + k_{-s} + k_s[H_2O_2])^2}\right)^{1/2}$$

For the particular case that

$$[17]\quad 4k_d k_s[H_2O_2] \ll (k_d + k_{-s} + k_s[H_2O_2])^2$$

$$[18]\quad k_1 = k_d + k_{-s} + k_s[H_2O_2]$$

$$[19]\quad k_2 = \frac{k_d k_s[H_2O_2]}{k_d + k_{-s} + k_s[H_2O_2]}$$

Equation 19 is of the same form as [4] with $k_2 = k_{obs}^{H_2O_2}$ and $(k_d + k_{-s})/k_s = K_{app}$. This is a direct analogy to equations derived under steady-state conditions where K_{app}, the Michaelis–Menten constant equals $(k_d + k_{-s})/k_s$ according to the Briggs–Haldane treatment (29) and can lie between k_{-s}/k_s (Michaelis–Menten assumption (30)) and k_d/k_s (Van Slyke and Cullen assumption (31)). Equation 18 predicts that an induction period $\tau_1 = 1/k_1$ should exist for compound **1** formation (32). Since k_d is the only experimentally determined constant in [18] it can be used to place limits on the other constants of the equation. If $k_d > k_{-s}$ and $k_s[H_2O_2]$, then use of the listed values[3] of k_d indicates that τ_1 should be close to 10 ms for p*H* values between 10.7 and 11.6. There appears to be a finite induction period for plot 2 in Fig. 5, where $[H_2O_2]$ is small.

The similarity of cyanide binding to HRP and compound **1** formation in regard to the p*H* effect on the second-order rate constant has been previously reported for the acidic p*H* range (18). The present results show that this trend is also found for the alkaline p*H* range: cyanide binding to HRP is also inhibited by ionization of a group with p*K* of 11.00 ± 0.15, as is compound **1** formation. Cyanide binding to HRP could perhaps also be described by a two-step mechanism analogous to [14].

$$[20]\quad HRP + HCN \underset{k_{-s}^{CN}}{\overset{k_s^{CN}}{\rightleftharpoons}} (HRP\text{–}HCN) \xrightarrow{k_d^{CN}} HRP\text{–}CN + H^+$$

No saturation effect on k_{obs}^{CN} was obtained at high cyanide concentrations. One possibility might be that in [20], the constant, $K^{CN} = (k_d^{CN} + k_{-s}^{CN})/k_s^{CN}$ is much greater than [HCN]. Then (by comparison with [4])

$$[21]\quad k_{obs}^{CN} = \frac{k_d^{CN} k_s^{CN}}{k_d^{CN} + k_{-s}^{CN}}[HCN] = k_{app}^{CN}[HCN]$$

The p*H* dependence of the k_{app}^{CN} and $k_{app}^{H_2O_2}$ data are simply explained in terms of collision theory by reactions 8 and 11 in which ionization of a single

Can. J. Chem. Downloaded from www.nrcresearchpress.com by 210.87.254.40 on 09/05/12
For personal use only.

Can. J. Chem. Downloaded from www.nrcresearchpress.com by 210.87.254.40 on 09/05/12
For personal use only.

group defined by K_{alk} inhibits the two reactions. However, when the $k_{app}^{H_2O_2}$ results are analyzed in terms of their component parts, k_d and K_{app}, a more complicated picture arises. An explanation of the saturation kinetics requires the formation of an enzyme–substrate complex and the pH dependence of k_d (hence K_{app}) requires a minimum of two ionizations. A full description of the analysis is available.[3] The two-step mechanism in [14] in which preequilibrium formation of a precursor complex occurs before formation of **1** is in agreement with theoretical considerations (12). The rate controlling step in both reactions may represent the displacement of the water molecule, if present in the sixth coordination position of the heme iron. An associative, rather than a dissociative mechanism is indicated, since in the latter case, the loss of the water molecule would be rate limiting, yet the rates of compound **1** formation and cyanide binding differ by a factor of 100. The similarity of the k_{app} data vs. pH for both cyanide binding and compound **1** formation does not extend to lactoperoxidase where there must be mechanistic differences for the two processes (33, 34).

The alkaline ionization of HRP can be discussed in terms of the proton transfer process

$$[22] \qquad BH^+ + OH^- \underset{k_{-b}}{\overset{k_b}{\rightleftharpoons}} B + H_2O$$

for which the rate expression is

$$[23] \qquad k_{obs}^{OH^-} = k_b[OH^-] + k_{-b}$$

This is of identical form to the HRP results fitted to [1] and leads to a value of pK = 11.00 ± 0.08 for the formation of the alkaline form of HRP, in agreement with the value determined from equilibrium measurements. As proposed for the turnip peroxidases (15), the simplest explanation for the observed results presented in Fig. 1 is that BH^+ represents a water molecule in the sixth coordination position of the heme iron and that B represents the hydroxide ion in the sixth coordination position as in methemoglobin and metmyoglobin. The small rate constants corresponding to [1] would indicate that hydroxide ion is displacing the water molecule (in which case the removal of the water molecule might be rate limiting), or if it is abstracting a hydrogen ion from the ligand water molecule, the reaction is slowed by an appropriately placed and negatively charged electrostatic gate (35). The possibility that an amino acid residue deprotonates in alkaline solution and becomes the sixth iron ligand cannot be excluded by our data (14). The latter mechanism (analogous to [15] for instance) predicts that the reaction should display first-order saturation kinetics. This behavior was not observed (Fig. 1) but rather k_{obs} was found to be a linear function of $[OH^-]$, as it was for turnip peroxidases P_1 and P_7 (15). However there is an experimental limitation on the magnitude of $[OH^-]$. In this regard the elegant work of Iizuka *et al.* (36) is of great interest. These workers have combined the quadrature phase detection technique with high resolution nmr, which enables them to detect hyperfine shifts in the immediate environment of a paramagnetic ion. Also conformational changes of the protein during the overall process leading to alkaline peroxidase formation are indicated, since the sedimentation constant value of HRP decreases from $S_{20,w}$ = 3.61 at pH 7.2 to 3.03 S at pH 11.0 (37). The two slow kinetic processes observed during the alkaline transition of HRP might correspond to such conformational changes.

The pK value for the formation of alkaline HRP would appear to be well established by four independent methods: 10.85 ± 0.08 (Fig. 7, log $k_{app}^{H_2O_2}$ vs. pH); 11.00 ± 0.15 (log k_{app}^{CN} vs. pH); 11.00 ± 0.05 (spectrophotometric titration with hydroxide ion); and 11.00 ± 0.08 ([5] results from [1], from the kinetics of the OH^- reaction with HRP). The mean value is 10.96 ± 0.09 at 25°C and μ = 0.1 which can be compared with results of other workers under somewhat different conditions (1, 13, 36, 38, 39).

Acknowledgements

We acknowledge financial support from the National Research Council of Canada which also provided a Postdoctoral Fellowship for one of us (D.J.). Certain aspects of the present problem have been studied independently (T. Araiso and I. Yamazaki, submitted for publication, and H. Kihara, S. Saigo, T. Iizuka, and Y. Ishimura, submitted for publication).

1. D. Keilin and E. F. Hartree. Biochem. J. **49**, 88 (1951).
2. W. D. Ellis and H. B. Dunford. Arch. Biochem. Biophys. **133**, 313 (1969).
3. S. Vuk-Palović and B. Benko. Biochem. Biophys. Res. Commun. **66**, 1154 (1975).
4. J. Ricard, G. Mazza, and R. J. P. Williams. Eur. J. Biochem. **28**, 566 (1972).
5. D. Job and J. Ricard. Arch. Biochem. Biophys. **170**, 427 (1975).
6. R. J. P. Williams, P. E. Wright, G. Mazza, and J. Ricard. Biochim. Biophys. Acta, **412**, 127 (1975).
7. R. K. Gupta and G. R. Schonbaum. Fed. Proc. **36**, 756 (1977).
8. T. Yonetani. *In* The enzymes. Vol. 13. *Edited by* P. D. Boyer. Academic Press, New York, NY. 1976. p. 345.
9. M. Morrison and G. R. Schonbaum. Ann. Rev. Biochem. **45**, 861 (1976).
10. H. B. Dunford and J. S. Stillman. Coord. Chem. Rev. **19**, 187 (1976).

11. A. LANIR and A. SCHEJTER. Biochem. Biophys. Res. Commun. **62**, 199 (1975).
12. P. JONES and H. B. DUNFORD. J. Theor. Biol. **69**, 457 (1977).
13. H. THEORELL. Ark. Kemi Mineral. Geol. **16**A, No. 3 (1943).
14. M. EPSTEIN and A. SCHEJTER. FEBS Lett. **25**, 46 (1972).
15. D. JOB, J. RICARD, and H. B. DUNFORD. Arch. Biochem. Biophys. **179**, 95 (1977).
16. I. YAMAZAKI and T. ARAISO. Jpn. Biophys. Soc. Abstr. 337 (1976).
17. B. CHANCE. J. Cell. Comp. Physiol. **22**, 33 (1943).
18. D. DOLMAN, G. A. NEWELL, M. D. THURLOW, and H. B. DUNFORD. Can. J. Biochem. **53**, 495 (1975).
19. W. D. HEWSON and H. B. DUNFORD. J. Biol. Chem. **251**, 6036 (1976).
20. G. R. SCHONBAUM and S. LO. J. Biol. Chem. **274**, 3360 (1972).
21. M. L. COTTON and H. B. DUNFORD. Can. J. Chem. **51**, 582 (1973).
22. R. ROMAN, H. B. DUNFORD, and M. EVETT. Can. J. Biochem. **49**, 3059 (1971).
23. B. CHANCE. Arch. Biochem. Biophys. **22**, 224 (1949).
24. W. D. ELLIS and H. B. DUNFORD. Biochemistry, **7**, 2054 (1968).
25. D. PORTSMOUTH and E. BEAL. Eur. J. Biochem. **19**, 479 (1971).
26. P. JONES, J. PRUDHOE, T. ROBSON, and K. C. KELLY. Biochemistry, **13**, 4279 (1974).
27. P. JONES and A. SUGGETT. Biochem. J. **110**, 617 (1968).
28. A. A. FROST and R. G. PEARSON. Kinetics and mechanism. 2nd ed. John Wiley and Sons, Inc., New York, NY. 1961. pp. 173–177.
29. G. E. BRIGGS and J. B. S. HALDANE. Biochem. J. **19**, 338 (1925).
30. L. MICHAELIS and M. L. MENTEN. Biochem. Z. **49**, 333 (1913).
31. D. D. VAN SLYKE and G. E. CULLEN. J. Biol. Chem. **19**, 141 (1914).
32. K. J. LAIDLER. The chemical kinetics of enzyme action. Oxford University Press, London. 1958. pp. 113–116.
33. R. J. MAGUIRE, H. B. DUNFORD, and M. MORRISON. Can. J. Biochem. **49**, 1165 (1971).
34. D. DOLMAN, H. B. DUNFORD, D. M. CHOWDHURY, and M. MORRISON. Biochemistry, **7**, 3991 (1968).
35. D. M. DAVIES, P. JONES, and D. MANTLE. Biochem. J. **157**, 247 (1976).
36. T. IIZUKA, S. OGAWA, T. INUBUSHI, T. YONEZAWA, and I. MORISHIMA. FEBS Lett. **64**, 156 (1976).
37. A. J. OSBAHR and G. L. EICHORN. J. Biol. Chem. **237**, 1820 (1962).
38. H. THEORELL and A. EHRENBERG. Acta Chem. Scand. **5**, 823 (1951).
39. H. YAMADA and I. YAMAZAKI. Arch. Biochem. Biophys. **165**, 728 (1974).

Can. J. Chem. Downloaded from www.nrcresearchpress.com by 210.87.254.40 on 09/05/12
For personal use only.

Nuclear analogs of β-lactam antibiotics. VIII. Synthesis of 3-acetoxymethyl-Δ^3-*O*-2-isocephems[1]

TERRY THOMAS CONWAY,[2] GARY LIM, JAMES LESLIE DOUGLAS,[2] MARCEL MENARD, TERRENCE WILLIAM DOYLE,[3] PIERRE RIVEST, DONALD HORNING, LEESON R. MORRIS, AND DENIS CIMON

Bristol Laboratories of Canada, 100 Industrial Boulevard, Candiac, P.Q., Canada J5R 1J1

Received December 12, 1977

TERRY THOMAS CONWAY, GARY LIM, JAMES LESLIE DOUGLAS, MARCEL MENARD, TERRENCE WILLIAM DOYLE, PIERRE RIVEST, DONALD HORNING, LEESON R. MORRIS, and DENIS CIMON. Can. J. Chem. **56**, 1335 (1978).

The synthesis of 7β-(-2′-thienylacetamido)-3-acetoxymethyl-Δ^3-*O*-2-isocephem-4-carboxylic acid (**17**) is described. Thus treatment of enol mesylate **3***a* or triflate **3***b* with triethylamine gave the allene **4** which gave the diiodide upon treatment with iodine. The diiodide gave benzyl 7β-azido-3-acetoxymethyl-Δ^3-*O*-2-isocephem-4-carboxylate (**12**) on treatment with potassium acetate in DMF. Hydrogenolysis of **12** gave the amino acid **16** which was converted to **17** upon treatment with 2-thienylacetyl chloride. Resolution of **17** into its optical antipodes was carried out. The antibiotic activities of racemic **17** and each antipode is compared to that of cephalothin. Antibiotic activity was found to reside in the dextrorotatory isomer.

TERRY THOMAS CONWAY, GARY LIM, JAMES LESLIE DOUGLAS, MARCEL MENARD, TERRENCE WILLIAM DOYLE, PIERRE RIVEST, DONALD HORNING, LEESON R. MORRIS et DENIS CIMON. Can. J. Chem. **56**, 1335 (1978).

On décrit la synthèse de l'acide (thiényl-2′ acétamido-7β) acétoxyméthyl-3 Δ^3-*O*-isocéphem-2 carboxylique-4 (**17**). Ainsi le traitement du mésylate énolique **3***a* ou triflate **3***b* par la triéthylamine conduit à l'allène **4** qui fournit le dérivé diiodé par réaction avec l'iode. Le diiodure conduit à l'azido-7β acétoxyméthyl-3 Δ^3-*O*-isocéphem-2 carboxylate-4 de benzyle (**12**) par réaction avec l'acétate de potassium dans le DMF. L'hydrogénolyse de **12** fournit l'acide aminé **16** qui peut être transformé en **17** par réaction avec le chlorure de thiényl-2 acétyle. La résolution de **17** en antipodes optiques a été réalisée. On compare les activités antibiotiques du **17** racémique et de chacun de ses antipodes avec celles de la céphalothine. On a trouvé que l'isomère dextrorotatoire possède l'activité antibiotique.

[Traduit par le journal]

Recent reports from a number of laboratories attest to the continuing interest in β-lactam antibiotics with modified nuclei, both from natural sources and by total synthesis (2). In the earlier papers of this series we have described the syntheses of a number of nuclear analogs of the cephalosporins **1***a–m* in which the sulfur at the 1 position has been replaced by a carbon atom and the carbon atom at the 2 position by a hetero atom. In each of these cases the substituent at position 3 was hydrogen, methyl, or aralkyl. In view of the pronounced improvement of activity observed when the 3 substituent is acetoxy methyl in the natural series, we desired an entry into these systems as well. In this paper we should like to report the synthesis of the 3-acetoxymethyl-*O*-2-isocephem system **1***n*.[4]

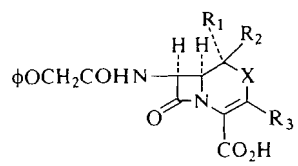

	X	R_1	R_2	R_3
a	O	H	H	H
b	O	H	H	CH_3
c	O	H	H	$CH_2\phi$
d	O	H	H	$(CH_2)_2\phi$
e	O	CH_3	H	CH_3
f	O	H	CH_3	CH_3
g	O	— O	—	CH_3
h	NCH_3	H	H	CH_3
i	NCO_2Et	H	H	CH_3
j	S	H	H	CH_3
k	S	H	H	CH_3
l	SO	H	H	CH_3
m	SO_2	H	H	CH_3
n	O	H	H	CH_2OAc

Our initial attempts to prepare the 3-substituted methyl systems by free radical bromination of the methyl group using either bromine or NBS under a variety of conditions failed completely as did a

[1]For Part VII of this series see ref. 1.

[2]To whom correspondence concerning this paper may be addressed.

[3]Present address: Bristol Laboratories, P.O. Box 657, Syracuse, New York, NY 13201.

[4]For a review of some of the earlier literature on nuclear modifications of β-lactams and an explanation of the trivial nomenclature used throughout this series, see ref. 3.

Can. J. Chem. Downloaded from www.nrcresearchpress.com by 210.87.254.6 on 09/05/12
For personal use only.

TABLE 1. Nuclear magnetic resonance spectra[a]

Compound	Aromatic protons			AR—CH_2	CH_3	Other
3*b*[d]	7.32(s, 5H)	4.91(d) $J = 5$	—	5.24(s)	2.89(s) 2.83(s)[c] 2.47(s) 2.25(s)[e]	4.3(m, 3H)[b]
4	7.30(s, 5H)	4.92(d) $J = 4.5$	—	5.18(s)	2.92(s)[c]	5.65(s, 2H)[f] 4.40(m, 3H)[b]
7 and **8***b*	7.30(s, 5H)	—	—	5.21(s)	2.91(s)[c]	4.0–5.0(m, 6H)[g]
7 and **8***a*	7.20(s, 5H)			5.13(s)	2.91(s)[c]	4.2–5.2(m, 6H)[g]
7 and **8***d*	7.35(s, 5H)	—	—	5.21(s)	2.92(s)[c] 2.49(s)[j] 2.47(s)[j]	4.2–5.3(m, 4H)[h] 2.42(br, 2H)[i]
11	7.42(s, 5H)	—	—	5.37(s)	—	7.02(d, 1H, $J = 3$) 6.80(d, 1H, $J = 3$)
12	7.40(bs, 5H)	5.20(m)	4.60(m)	5.27(s)	2.05(s)[i]	5.09(s, 2H)[k] 3.5–4.1(m, 2H)[m]
13	7.50(s, 5H)	—	—	5.35(s)	2.08(s)[i]	5.15(s, 2H)[k] 1.63(bs, 2H)[n] 4.9–4.6, 4.2–3.7(4H, m)
14	6.8–7.7(m, 10H)	5.62(dd) $J_1 = 7$ $J_2 = 5$	—	5.33(s)	2.05(s)[i]	5.15(s, 2H)[k] 4.56(s, 2H)[o] 3.8–4.6(m, 3H)
15[q]	6.9–7.6(m, 5H)	5.77(m)	—	—	2.07(s)[i]	5.06(s, 2H)[k] 4.65(s, 2H)[o] 3.6–4.6(m, 3H)
16[r]		5.32(d)	—	—	2.17(s)[i]	5.20(s, 2H)[k] 4.0–5.0(m, 3H) 4.90(b, 2–3H)[n]
17[s]	6.9 and 7.3[t] (m, 3H)	5.55(dd) $J_1 = 8$ $J_2 = 4.5$	—	—	2.02(s)[i]	4.96(s, 2H)[k] 3.70(s, 2H)[f] 8.75(d, $J = 8$, 1H)[u] 4.50(d, 1H, $J = 6$)[p] 3.6–4.1(m, 2H)

[a]All spectra were recorded on a Varian A-60A at 60 MHz in $CDCl_3$ unless otherwise noted. Shifts are in δ and couplings are in Hz.
[b]CH—CH_2OMes.
[c]SO_2CH_3.
[d]Two isomers 1:5 ratio.
[e] .
[f] .
[g]H-3, H-4, CH_2—OMes, CH_2Br(or I).
[h]H-3, H-4 + CH_2—OMes.
[i]CH_2Cl.
[j]SCH_3.
[k]CH_2OAc.
[l]CH_3C.
[m]—CH_2—O—.
[n]NH_2.
[o]ϕOCH—.
[p]Either $H_{1\alpha}$ or $H_{1\beta}$.
[q]DMSO-d_6.
[r]D_2O–DMSO-d_6.
[s]$CDCl_3$–DMSO-d_6.
[t] 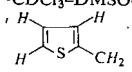
[u]NH.

number of other attempts to oxidize the 3-methyl group. The fortuitous observation that the enol mesylate **3** could be converted in high yields to the allene **4** eventually provided an entry into the desired 3-acetoxymethyl-*O*-2-isocephems (Scheme 1). Thus in the preparation of **3***a* (4) it was noticed that if an excess of triethylamine was used in the reaction of the enol **2** (5) with mesyl chloride and the reaction mixture was allowed to stand at room temperature, the bismesylate disappeared and a new olefinic signal appeared at 5.65 δ in the nmr spectrum which was assigned to the allenic protons in **4** (Table 1). A by-product of this reaction was the *O*-2-isocephem **6** which was formed in variable yields. We speculate

Can. J. Chem. Downloaded from www.nrcresearchpress.com by 210.87.254.6 on 09/05/12
For personal use only.

Can. J. Chem. Downloaded from www.nrcresearchpress.com by 210.87.254.6 on 09/05/12
For personal use only.

that **6** was formed by fragmentation of the initially formed mesylate to give **5** which under the reaction conditions cyclized to yield **6** (Scheme 2). To avoid this side reaction it was decided to prepare **4** via the triflate **3***b* rather than the mesylate **3***a*. Thus treatment of **2** with triflic anhydride (6) in the presence of triethylamine at $-10°C$ gave, after work-up, **3***b* as a mixture of geometric isomers in 71% yield.

Stang and Hargrove (7) have reported the conversion of vinyl triflates to allenes in low to moderate yields by treatment of the triflates at 100°C in quinoline. In the case of **3***b* the conversion to **4** proceeded in high yield (>90%) under mild conditions. Treatment of **3***b* in methylene chloride at 0°C with 1 equiv. of triethylamine and letting the solution come to 23°C over 15 min gave a virtually quantitative yield of allene. Although the allene could be isolated it proved to be relatively unstable and was usually used immediately in the subsequent step. The observation of facile allene formation in our case represents an extension of Stang and Hargrove's original work (7) to vinyl triflates derived from β-keto esters and may well provide access to other members of this elusive class of compounds.

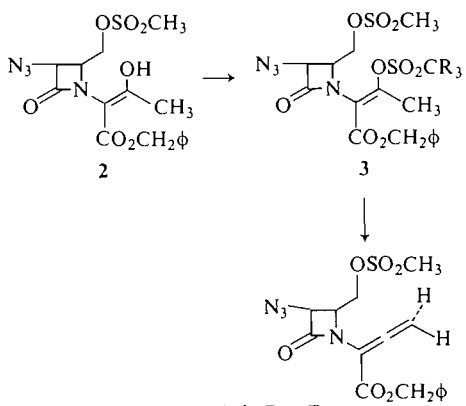

a R = H *b* R = F

SCHEME 1

A priori a number of ways to convert the allene **4** to the desired 3-methyl-substituted-*O*-2-isocephems might be envisioned. Electrophilic addition to the allene might well be expected to give products at the right level of oxidation. Accordingly, the halogenation of **4** was examined. In principle one would expect to obtain as many as four possible products from the reaction (8) arising from the four possible allylic cations which might be generated (Scheme 3).

Treatment of **4** with 1 equiv. of chlorine in methylene chloride gave a mixture of products. The product mixture exhibited olefinic signals in the nmr at 6.23 and 5.83 δ as sets of doublets, and singlets at 4.74 and 4.27 δ. These have been assigned

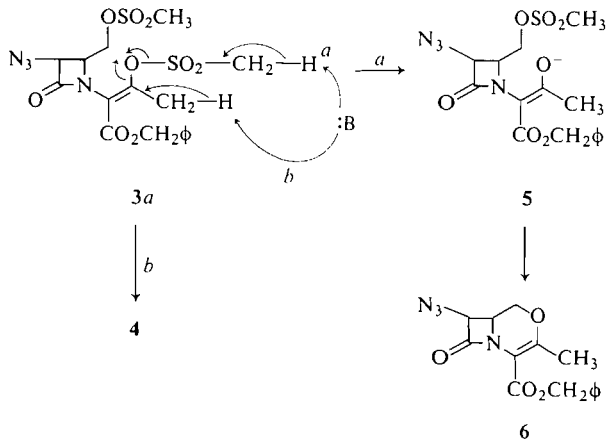

SCHEME 2

to **9***c* and **10***c*, and **7***c* and **8***c*, respectively, and are in an approximate ratio of 1:1:1:1. In view of the complexity of the mixture, further work using chlorination was abandoned. We next turned our attention to bromination of **4**. Treatment of **4** with 1 equiv. of bromine led to a mixture of dibromides. Chromatography of the mixture on silica gel gave a

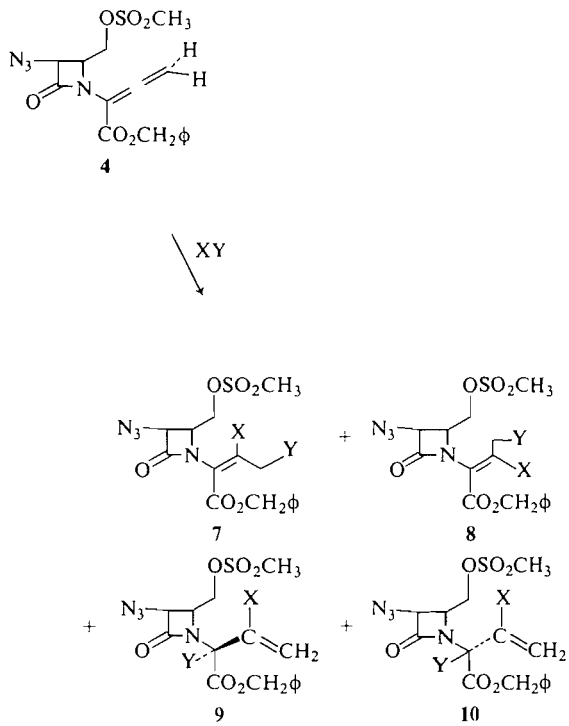

7 ⟶ **10** *a* X = I = Y
b X = Br = Y
c X = Cl = Y
d X = SMe Y = Cl

SCHEME 3

Can. J. Chem. Downloaded from www.nrcresearchpress.com by 210.87.254.6 on 09/05/12
For personal use only.

mixture of the desired dibromides **7***b* and **8***b*[5] in 45% yield.

Treatment of **4** with a solution of iodine in methylene chloride gave the diiodides **7***a* and **8***a* analytically pure in 91% yield. In addition to the above halogenations, attempts were also made to react the allene with a number of other electrophiles such as 2,4-dinitrobenzenesulfenyl chloride, isobutanesulfenyl chloride, methane sulfenyl chloride, *tert*-butyl hypochlorite, sodium hypochlorite, hydrogen peroxide, potassium permanganate, and peracids. For the most part these experiments yielded only polymer. In the case of methanesulfenyl chloride (9) a low yield of an adduct (32%) identified as a mixture of **7***d* and **8***d* by its spectral characteristics was obtained. The uv maximum at 307 nm (ε 7700) was especially diagnostic of the sulfur atom bound at the central atom of the allene (1).[6]

With the dibromides (**7***b* and **8***b*) and diiodides (**7***a* and **8***a*) in hand the conversion of these to the *O*-2-isocephem system was examined next. Thus treatment of either the diiodide or the dibromide with an excess of potassium acetate in dimethylformamide gave the desired intermediate **12** in 35–60% yields (Scheme 4). Although the yield of **12** from the dibromides was higher, the overall yield from the allene was greater using the diiodide. It should also be noted that it was possible to go from the enol **2** to the 3-acetoxymethyl-*O*-2-isocephem **12** without the necessity of isolating the intermediates. Presumably compound **12** arose via displacement of the terminal iodide or bromide by acetate, Michael addition of acetate to the double bond with halide elimination,

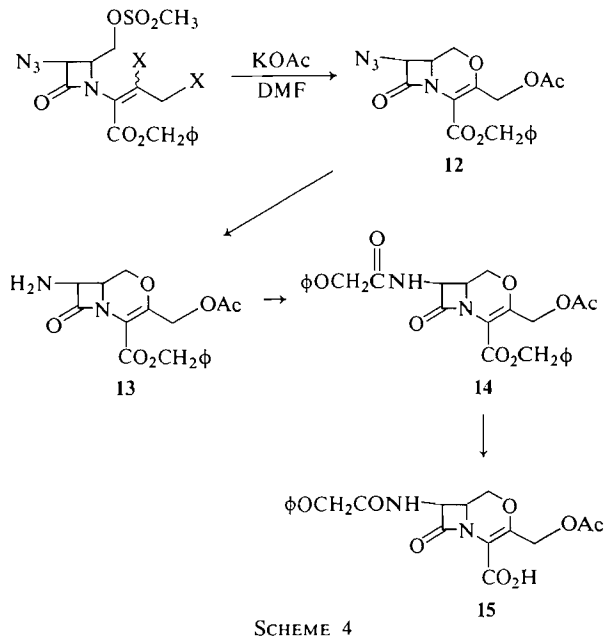

SCHEME 4

hydrolysis of the vinyl acetate to give the enolate, and finally ring closure of enolate. The sequence in which the displacement steps occur is unclear. Attempts to selectively displace the allylic halide failed. The structure of **12** was supported by its elemental analysis, ir and nmr spectra, and by subsequent conversions.

Reduction of **12** using hydrogen sulfide – triethylamine gave the amine **13** in 60% yield. Treatment of **13** with *N*-ethoxycarbonyl-2-ethoxy-1,2-dihydroquinoline (10) (EEDQ) and phenoxyacetic acid gave the amide **14** in 69% yield. Hydrogenolysis of **14** yielded the desired 7β-(phenoxyacetamido)-3-acetoxymethyl-Δ^3-*O*-2-isocephem-4-carboxylic acid (Scheme 4). Compound **15** showed antibiotic activity greater than that observed for the 3-methyl analog.

To provide a comparison of the antibiotic activity of a 2-isocephem with a commercially available cephalosporin, the synthesis of a cephalothin analog was attempted next. Thus hydrogenation of the azido ester **12** over palladium gave a near quantitative yield of the crude amino acid **16** as its hydrochloride salt. Suspension of this salt in aqueous sodium bicarbonate followed by addition of 2-thienylacetyl chloride (11) gave after work-up the racemic 7β-(2′-thienylacetamido)-3-acetoxy methyl-Δ^3-*O*-2-isocephem-4-carboxylic acid (**17**) in 51% overall yield from **12** (Scheme 5). Resolution of the racemic mixture was achieved using (+)-α-methylbenzylamine to give the dextrorotatory enantiomer and (−)-α-methylbenzylamine to give the levorotatory enantiomer. The antibiotic activities of the racemic mixture, both

[5]In addition to **7***b* and **8***b*, a small amount of a third component tentatively identified as **11** on the basis of its spectral characteristics was isolated.

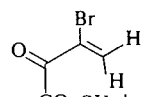

11

[6]Although the products from the addition of Cl_2, Br_2, or I_2 to the allene would not permit one to distinguish between the mechanistic pathways proceeding through the allylic or vinyl cations, those from the addition of methane sulfenyl chloride to **4** do.

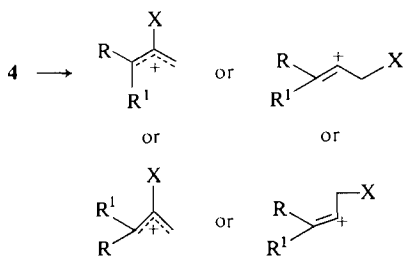

Can. J. Chem. Downloaded from www.nrcresearchpress.com by 210.87.254.6 on 09/05/12
For personal use only.

TABLE 2. Antibiotic activities[a]

Compound	*Streptococcus pneumoniae*	*Staphylococcus aureus* Smith	*Staphylococcus aureus* Meth. Res.	*Escherichia coli*	*Proteus mirabilis*
(±)-**17**	0.03	0.5	2	63	1
(+)-**17**	0.016	0.06	0.25	32	0.13
(−)-**17**	0.5	4	>125	>125	16
Cephalothin	0.08	0.16	1	63	1

[a]Expressed as MIC's (μg/ml) and determined by a two-fold serial dilution assay in Difco nutrient broth by the method of Pursiano *et al.* (12).

enantiomers, and cephalothin against a number of organisms is summarized in Table 2.

As is evident from Table 2 the activity of our cephalothin analog resides primarily in the dextrorotatory isomer (+)-**17** (13). The activity of (+)-**17** compares favorably with that of cephalothin. A more extensive discussion of the bioactivities of compounds in this series will appear elsewhere.

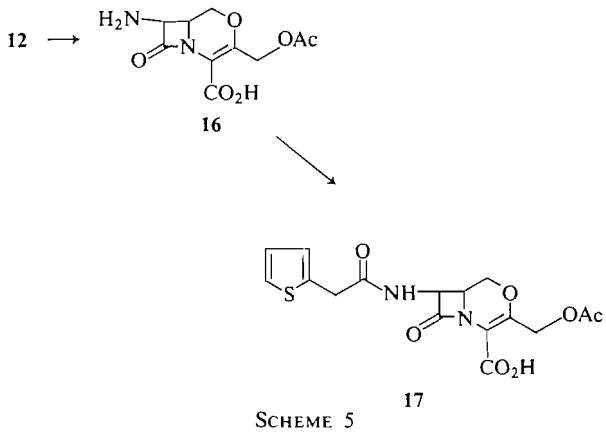

SCHEME 5

Experimental

The ir spectra were recorded on a Unicam Sp-200G grating, ir spectrometer. The nmr spectra were determined on a Varian A60-A spectrometer using tetramethylsilane as an internal standard. Melting points are uncorrected and were determined on a Gallenkamp melting point apparatus. The analyses were performed by Micro-Tech Laboratories, Skokie, Illinois.

Synthesis of **3**b

A solution of the enol **2** (48.0 g, 0.117 mol) in 400 ml of dichloromethane was cooled to −10°C under nitrogen and a solution of triflic anhydride (33.0 g, 0.117 mol) in 100 ml of dichloromethane was added over several minutes. A 10% solution of triethylamine in dichloromethane was added dropwise with stirring until the reaction mixture was weakly basic to p*H* paper (about 0.14 mol of triethylamine was required). The reaction solution was immediately washed with cold 10% hydrochloric acid (500 ml) followed by water (2 × 500 ml). The dichloromethane solution was dried (sodium sulfate) and filtered through 260 g of activity III silica gel. The silica gel was extracted with a further 2 L of dichloromethane. The dichloromethane was evaporated *in vacuo* from the combined extracts to give the triflate **3***b* as a yellow oil 38.3 g (71% yield) (mixture of two isomers). This material was of adequate purity for subsequent reactions. An analytical sample containing one isomer was prepared by recrystallization from ethanol, mp 57–59°C; ir (Nujol mull): 2150, 2120, 1785, 1730 cm^{-1}. *Anal.* calcd. for $C_{17}H_{17}F_3N_4O_4S_2$: C 37.67, H 3.14, N 10.33, S 11.82; found: C 37.40, H 3.12, N 10.43, S 11.73.

Preparation of **7** *and* **8**

A solution of triethylamine (1.01 g, 10 mmol) in 14 ml of dichloromethane was added with stirring to a solution of triflate **3***b* (5.42 g, 10 mmol) in 54 ml of dichloromethane at 0°C. The solution was allowed to warm to 23°C over 15 min.[7] A solution of halogen (10 mmol) in 75 ml of dichloromethane was added dropwise with stirring over 30 min. The resulting solution was washed with water (2 × 150 ml), dried (sodium sulfate), treated with activated charcoal (ca. 1 g), filtered, and the solvent was evaporated *in vacuo* to give **7** and **8** as an oil.

Diiodide 7 and **8***a* was obtained analytically pure, 5.88 g (91% yield). *Anal.* calcd. for $C_{16}H_{16}I_2N_4O_6S$: C 29.74, H 2.50, N 8.67, I 39.28, S 4.96; found: C 29.76, H 2.47, N 8.61, I 39.37, S 5.18.

Dibromide **7** and **8***b* was obtained as a mixture of isomers which could be purified by column chromatography on activity I silica gel (elution with dichloromethane) to give pure **7** and **8***b*, 2.5 g (45% yield). *Anal.* calcd. for $C_{16}H_{16}Br_2N_4O_6S$: C 34.80, H 2.92, N 10.15; found: C 35.25, H 2.97, N 10.02.

Dichloride 7 and **8***c* was obtained as a crude mixture of four isomers plus degradation products.

A by-product isolated by chromatography of the bromination reaction was tentatively identified as compound **11**: ir (mull): 1735, 1705 cm^{-1}.

Preparation of **7** *and* **8**d

The allene was prepared immediately before use in this reaction from 1.08 g (2.00 mmol) of the triflate in the usual manner.

The methanesulfenyl chloride was prepared immediately before use by the method of Douglass (9).

The allene (2.00 mmol) in 20 ml of CH_2Cl_2 was cooled to −5 to −10°C and the freshly prepared solution of MeSCl (2.00 mmol) in 3 ml of CH_2Cl_2 was added with stirring under nitrogen. After 10 min at −5°C, the solution was washed with dilute $Na_2S_2O_3$, then brine, and evaporated *in vacuo* to give a yellow oil. The oil was absorbed from CH_2Cl_2 onto 5 g of silica gel and placed (dry) on a 50 g silica gel column (activity III). The column was eluted with ether; 30 ml fractions were collected and monitored by tlc (silica, ether). Fractions showing one spot at about R_f 0.43 were combined and the solvent was evaporated *in vacuo* to give the product (306 mg, 32%

[7]The allene **4** may be isolated at this point by washing the solution with water, drying (Na_2SO_4), and evaporating the solvent *in vacuo*. The allene decomposes over several days at 0°C.

Can. J. Chem. Downloaded from www.nrcresearchpress.com by 210.87.254.6 on 09/05/12
For personal use only.

yield) as a pale yellow oil; uv λ_{max} 309 mμ (ε 7700); (film): 2120, 1775, 1705 cm^{-1}.

Benzyl 7β-Azido-3-acetoxymethyl-Δ³-O-2-isocephem-4-carboxylate (12)

A mixture of dihalide **7** and **8***a* or *b* (10 mmol), potassium acetate (40 mmol, finely ground), dimethylformamide (50 ml), and water (0.1 ml) was stirred vigorously at 23°C for 20 h. The resulting solution was mixed with ether (250 ml) and washed with water (5 × 250 ml). The ether solution was dried (sodium sulfate) and evaporated *in vacuo* to give a brown residue. The residue was dissolved in dichloromethane and passed through 10 times its weight of activity III silica gel. The solvent was evaporated *in vacuo* and the crude product was recrystallized from benzene–hexane to give pure *O*-2-cephem **12** (35–60% yield),[8] mp 97–98°C; ir (Nujol mull): 2160, 2110, 1775, 1750, 1705, 1600 cm^{-1}. *Anal.* calcd. for $C_{17}H_{16}N_4O_6$: C 54.84, H 4.33, N 15.05; found: C 55.19, H 4.47, N 14.89.

Benzyl 7β-Amino-3-acetoxymethyl-Δ³-O-2-isocephem-4-carboxylate (13)

Hydrogen sulfide was bubbled into a solution of azide **12** (793 mg, 2.1 mmol), triethylamine (210 mg, 2.1 mmol), and dichloromethane (15 ml) for 10 min. Nitrogen was passed through the solution to remove excess hydrogen sulfide and the solvent was evaporated *in vacuo*. The residue was mixed with ether and extracted with 10% hydrochloric acid three times. The acid extract was washed with ether, made basic with sodium bicarbonate, saturated with sodium chloride, and extracted three times with dichloromethane. The dichloromethane extract was washed with saturated sodium chloride, dried (Na_2SO_4), and the solvent was evaporated *in vacuo* to give amine **13** as a colorless oil, 415 mg (60% yield); ir (film): 3400, 1775, 1745, 1715, 1620 cm^{-1}. *Anal.* calcd. for $C_{17}H_{18}N_2O_6$: C 58.95, H 5.24, N 8.09; found: C 58.39, H 5.32, N 7.95.

Benzyl 7β-(Phenoxyacetamido)-3-acetoxymethyl-Δ³-O-2-isocephem-4-carboxylate (14)

A solution of amine **13** (415 mg, 1.2 mmol), phenoxyacetic acid (183 mg, 1.2 mmol), EEDQ (325 mg, 1.3 mmol), and dichloromethane (15 ml) was stirred at 23°C for 1.5 h. The solution was washed with 10% hydrochloric acid, saturated sodium chloride, 10% sodium bicarbonate, and saturated sodium chloride (20 ml each). The resulting solution was dried (Na_2SO_4) and the solvent was evaporated *in vacuo* to give an oil. The oil was chromatographed on activity III silica gel (elution with ether). Amide **14** was obtained as colorless crystals, 400 mg (69% yield), mp 146°C; ir (Nujol mull): 3320, 1775, 1745, 1725, 1690, 1535, 1625 cm^{-1}. *Anal.* calcd. for $C_{25}H_{24}N_2O_8$: C 62.49, H 5.04, N 5.83; found: C 62.58, H 5.07, N 5.83.

7β-(Phenoxyacetamido)-3-acetoxymethyl-Δ³-O-2-isocephem-4-carboxylic Acid (15)

A mixture of ester **14** (100 mg, 0.21 mmol), 10% palladium-on-charcoal (100 mg), and tetrahydrofuran (50 ml) was hydrogenated with agitation at 23°C and 40 psi for 15 min. The catalyst was removed by filtration and the solvent was evaporated *in vacuo*. The crude product was recrystallized from ethanol to give *O*-2-cephem **15**, 50 mg (62% yield), mp 160–170°C (dec.); ir (Nujol mull): 3400–2500, 1785, 1720, 1705, 1645, 1550, 1620 cm^{-1}. *Anal.* calcd. for $C_{18}H_{18}N_2O_8$: C 55.38, H 4.65, N 7.18; found: C 55.32, H 4.88, N 7.13.

[8]Higher yields were obtained if pure dibromide was used rather than pure diiodide; however, since the yield of dibromide from allene was less than diiodide, better overall yields were obtained via the diiodide.

7β-Amino-3-acetoxymethyl-Δ³-O-2-isocephem-4-carboxylic Acid (16)

A mixture of azide **12** (5.0 g, 13.4 mmol), palladium chloride (1.2 g, 7.1 mmol), and anhydrous ethanol (300 ml) was hydrogenated with agitation at 23°C and 50 psi for 1 h. The catalyst was removed by filtration and the solvent was evaporated *in vacuo* to give the hydrochloride salt **16** as an amorphous solid, 4.2 g (100% yield). Because of its instability, the product was not purified further; ir (Nujol mull): 3400–2500, 1770, 1740–1690, 1610 cm^{-1}.

7β-(2′-Thienylacetamido)-3-acetoxymethyl-Δ³-O-2-isocephem-4-carboxylic Acid (17)

Hydrochloride salt **16** (4.2 g, 13.4 mmol) was mixed with 150 ml of water and sodium bicarbonate (7.5 g, 90 mmol) was added at 0°C. A solution of 2-thienylacetic acid chloride[9] (4.5 g, 28 mmol) in 50 ml of acetone was added with stirring to the aqueous solution. The mixture was stirred for 1 h at 0°C, then washed with ether (2 × 100 ml). The aqueous solution was acidified with 10% hydrochloric acid and extracted with dichloromethane (2 × 100 ml). The dichloromethane extract was dried (Na_2SO_4) and the solvent was evaporated *in vacuo*. The residue was crystallized by trituration with ether to give (±)-*O*-2-cephalothin **17**, 2.6 g (51% overall yield from **12**). An analytical sample was prepared by recrystallization from anhydrous ethanol, mp 182°C (dec.); uv_{max} (EtOH): 272 nm, ε 8650; ir (Nujol mull): 3300–2500, 1780, 1750, 1720, 1680, 1535, 1620 cm^{-1}. *Anal.* calcd. for $C_{16}H_{16}N_2O_5S$: C 50.52, H 4.24, N 7.37, S 8.43; found: C 50.34, H 4.41, N 7.47, S 8.45.

The acid **17** (1.0 g, 2.64 mmol) was dissolved in warm isopropyl alcohol (50 ml) and (+)-α-methylbenzylamine (0.32 g, 2.64 mmol) was added. The precipitate was collected by filtration and washed with isopropanol and ether. The precipitate was mixed with 10% hydrochloric acid and extracted with dichloromethane. The dichloromethane extract was dried (Na_2SO_4) and the solvent was evaporated *in vacuo*. The residue was crystallized by trituration with ether. The resolution procedure was repeated twice more (until material of constant rotation was obtained) to give (+)-*O*-2-cephalothin ((+)-**17**) with $[\alpha]_D$ +116° (acetone); (145 mg, 14.5% yield). The mother liquors from the above resolution were similarly treated with (−)-α-methylbenzylamine to give (−)-*O*-2-cephalothin ((−)-**17**) with $[\alpha]_D$ −115° (acetone).

Acknowledgements

Partial financial support of this work by the National Research Council of Canada, through its Industrial Research Assistance Plan, is gratefully acknowledged. We also wish to thank Prof. Bernard Belleau of McGill University for helpful discussions in the course of this work.

1. T. W. Doyle, J. L. Douglas, B. Belleau, J. Meunier, and B.-Y. Luh. Can. J. Chem. **55**, 2873 (1977).
2. (*a*) J. Finkelstein, K. G. Holden, R. Sneed, and C. D. Perchonock. Tetrahedron Lett. 1855 (1977); (*b*) W. F. Huffman, K. G. Holden, T. F. Buckley III, J. G. Gleason, and L. Wu. J. Am. Chem. Soc. **99**, 2352 (1977); (*c*) D. B. Bryan, R. F. Hall, K. G. Holden, W. F. Huffman, and J. G. Gleason. J. Am. Chem. Soc. **99**, 2353 (1977); (*d*) T. T. Howarth, A. G. Brown, and T. J. King.

[9]The acid chloride was obtained from 2-thienyl acetic acid by stirring with oxalyl chloride for 3 h, then evaporating the excess oxalyl chloride *in vacuo* (11).

Chem. Commun. 276 (1976); (*e*) A. G. BROWN, D. F. CORBETT, and T. T. HOWARTH. Chem. Commun. 359 (1977).
3. T. W. DOYLE, B. BELLEAU, B.-Y. LUH, C. F. FERRARI, and M. P. CUNNINGHAM. Can. J. Chem. **55**, 468 (1977).
4. T. W. DOYLE, B.-Y. LUH, D. T. CHU, and B. BELLEAU. Can. J. Chem. **55**, 2719 (1977).
5. T. W. DOYLE, B. BELLEAU, B.-Y. LUH, T. T. CONWAY, M. MENARD, J. L. DOUGLAS, D. T.-W CHU, G. LIM, L. R. MORRIS, P. RIVEST, and M. CASEY. Can. J. Chem. **55**, 484 (1977).
6. T. GRAMSTAD and R. N. HAZELDINE. J. Chem. Soc. 4069 (1957).
7. P. J. STANG and R. J. HARGROVE. J. Org. Chem. **40**, 657 (1975).
8. H. FISCHER. *In* The chemistry of the alkenes. *Edited by* S. Patai. Interscience, London, New York and Sydney. 1964. p. 1025.
9. I. B. DOUGLASS. J. Org. Chem. **24**, 2004 (1959).
10. B. BELLEAU and G. MALEK. J. Am. Chem. Soc. **90**, 1651 (1968).
11. F. F. BLICKE and M. F. ZIENTY. J. Am. Chem. Soc. **63**, 2945 (1941).
12. T. A. PURSIANO, M. MISIEK, F. LEITNER, and K. E. PRICE. Antimicrob. Agents Chemother. **3**, 33 (1973).
13. J. C. SHEEHAN and K. R. HENERY-LOGAN. J. Am. Chem. Soc. **81**, 3089 (1959).

Can. J. Chem. Downloaded from www.nrcresearchpress.com by 210.87.254.6 on 09/05/12
For personal use only.

Nuclear magnetic resonance studies. XXXII.[1] Rearrangement, isomerization, and deuterium exchange via β-enolization in bicyclooctenones. A ^{2}H nuclear magnetic resonance study

A. K. CHENG[2] AND J. B. STOTHERS

Department of Chemistry, University of Western Ontario, London, Ont., Canada N6A 5B7

Received December 2, 1977

A. K. CHENG and J. B. STOTHERS. Can. J. Chem. **56**, 1342 (1978).

The equilibration of the α,α-dimethyl derivatives of bicyclo[2.2.2]octenone, bicyclo[3.2.1]-oct-2-en-6-one, and its Δ^3 isomer has been examined at 155 and 185°C in *tert*-BuO$^-$/*tert*-BuOH. Using ^{2}Hmr spectroscopy the rates and stereoselectivity of hydrogen–deuterium exchange in each of these ketones have been determined for equilibrations with *tert*-BuOD as solvent. The relative reactivities for exchange at the allylic and vinylic sites compared to the analogous results for the corresponding olefins reveal a significant activating effect of the carbonyl group. Comparison of the data with those for the corresponding saturated ketones shows that the double bond enhances the rate of isomerization appreciably and increases the bias of the equilibrium toward the [3.2.1] skeleton.

A. K. CHENG et J. B. STOTHERS. Can. J. Chem. **56**, 1342 (1978).

On a étudié, à 155 et 185°C dans le *tert*-BuO$^-$/*tert*-BuOH, l'équilibration des dérivés α,α-diméthylés de la bicyclo[2.2.2]octénone, de la bicyclo[3.2.1]octène-2 one-6 et de son isomère Δ^3. Utilisant la spectrométrie rmn du ^{2}H, on a déterminé les vitesses et la stéréosélectivité des échanges hydrogène-deutérium dans chacune de ces cétones au cours d'équilibrations faisant appel au *tert*-BuOD comme solvant. Les réactivités relatives pour l'échange aux sites allyliques et vinyliques comparées aux résultats analogues pour les alcènes correspondants mettent en relief un effet activant important du groupement carbonyle. Une comparaison de ces données avec celles obtenues pour les cétones saturées correspondantes montre que la double liaison augmente d'une façon appréciable la vitesse d'isomérisation et augmente la préférence de l'équilibre en faveur du squelette [3.2.1].

[Traduit par le journal]

Our earlier examinations of bicyclooctanones in strongly basic media had shown that the [2.2.2] and [3.2.1] skeletons are interconvertible and that the rate of isomerization is enhanced significantly in the unsaturated derivatives (1). We had found that the α,α-dimethyl derivatives of bicyclo[2.2.2]octenone (**1**), bicyclo[3.2.1]oct-2-en-6-one (**2**), and its Δ^3 isomer **3** are equilibrated at 185°C in *tert*-butoxide – *tert*-butyl alcohol much more readily than their saturated analogs. From experiments in deuterated solvent it was found that hydrogen–deuterium exchange occurred at five carbon sites in **1–3** by examination of their ^{13}Cmr spectra (1*a*). These sites were C-2, -3, -4, -5, and the *exo*-methyl in **2** and **3**. Exchange at C-4 and the methyl site occur by β-enolization whereas that at C-2 (and C-4) involves an allylic carbanion and that at C-3 a vinyl anion presumably. For **1** exchange occurred at C-1, -5, -6, -7, and the *exo*-methyl sites. It was of interest to determine the relative rates of exchange at these sites and to examine the stereoselectivity at the methylene positions. A comparison of these data with the results of our examination of hydrogen–deuterium exchange in bicyclo[2.2.2]octene and bicyclo[3.2.1]oct-2-ene (2) would reveal an activating effect of the carbonyl group on the reactivity of the allylic and vinyl anions in these skeletons. To this end we have followed the progress of deuterium incorporation into ketones **1–3** as a function of time and determined the rates of isomerization using each of the three ketones as starting material. Experiments were carried out at 155 and 185°C. At the higher temperature, the data are directly comparable to the results obtained for a variety of ketonic substrates (3) but for some of the rate processes only lower limits could be estimated. Consequently a series of measurements at 155°C was performed to permit an improved assessment of the relative rates at the different sites in ketones **1–3**. Deuterium incorporation was monitored by examination of the ^{2}Hmr spectra of the deuterated products (4). Analysis of the proton spectra of **1–3** aided by the use of the Eu(fod)$_3$ shift reagent and spin decoupling allowed unambiguous assignments of the signals in the ^{2}H spectra. We wish to present the results of these experiments in this paper.

Experimental

The preparations of **1–3** have been described (1*a*, 5) as has the general procedure for the rearrangement and exchange

[1]For part XXXI see ref. 1*b*.

[2]Present address: Department 367, Beckman Instruments, Fullerton, CA.

Can. J. Chem. Downloaded from www.nrcresearchpress.com by 210.87.254.42 on 09/05/12
For personal use only.

Can. J. Chem. Downloaded from www.nrcresearchpress.com by 210.87.254.42 on 09/05/12
For personal use only.

experiments (4). To a solution of the base, prepared *in situ* by dissolving potassium metal in dry *tert*-butyl alcohol under a nitrogen atmosphere, was added the ketone to give a solution containing ketone–*tert*-BuO$^-$–*tert*-BuOH in a molar ratio of 1:4:40. Aliquots were placed in glass tubes which were sealed after degassing and heated at the appropriate temperatures for various times. For the exchange experiments, *tert*-butyl alcohol-*O*-d_1 (99% deuterated and <0.005 *M* in water) was used. After cooling, the ketonic products were isolated by pentane extraction and the product mixtures analyzed by gas chromatography (gc). Preparative gc using either a 10% FFAP or 15% DEGS column was employed to isolate samples of each ketone. Their ^{2}H spectra, obtained as previously described (4), were recorded to determine the sites and extents of ^{2}H incorporation while the total ^{2}H content was determined by mass spectrometry using a Varian MAT-311A instrument. A Varian XL-100-15 system operating in the Fourier transform mode at 15.4 MHz was used for the ^{2}H spectra while proton spectra were recorded with a Varian HA-100 instrument. The effect of the shift reagent, Eu(fod)$_3$, was utilized to increase the proton shift dispersion to permit unambiguous assignments for specific protons by spin decoupling experiments. This information allowed definitive assignments in the ^{2}H spectra since ^{1}H and ^{2}H shieldings are essentially identical. These spectra were obtained for solutions in carbon tetrachloride containing 20% hexafluorobenzene (v/v) which was required for locking purposes for the ^{2}H spectra.

Results

A series of experiments using each of ketones **1–3** was carried out and the product compositions were determined as a function of time by analytical gc. Representative data from experiments with **1** are listed in Table 1. At 185°C the equilibrium composition was found to be 8:44:48 for **1**:**2**:**3** and equilibrium was established in less than 24 h. The half-life for the experiments with **1** as starting material was approximately 7 h corresponding to a rate constant for the disappearance of **1** of approximately 2.4×10^{-5} s^{-1}, the slow process being the skeletal rearrangement. With either **2** or **3** as starting material, the product is a nearly **1**:**1** mixture of **2** and **3** within several minutes with only trace quantities of **1** detectable by gc. At 155°C, the disappearance of **1** gave a rate constant of ca. 2.4×10^{-6} s^{-1}, i.e. a half-life of ca. 80 h. These rates indicate an activation energy

TABLE 1. Composition of products[a] from **1** at 155 and 185°C

At 185°C				At 155°C			
Time (h)	**1**	**2**	**3**	Time (h)	**1**	**2**	**3**
3	84	8	8	16	90	5	5
6	59	19	22	23	79	10	11
10	40	29	31	43	64	17	19
14	21	38	41	98	40	28	32
24	8	44	48	103	36	27	37
69	8	45	47	148	24	36	40
158	8	44	48	217	15	40	45

[a]Percentage by gc analysis, ±1%.

of approximately 30 kcal/mol for the skeletal isomerization.

A corresponding series of experiments was conducted using *tert*-butyl alcohol-*O*-d_1 as the solvent and the products after isolation were analyzed for total deuterium content by mass spectrometry while the extent of deuterium incorporation at the individual sites was determined from their ^{2}Hmr spectra. In each case the ^{2}H spectra contained six signals for the samples obtained after the longer reaction times. Two of these signals appeared at significantly lower field than the others and were readily assigned to the olefinic centres while the highest field signal could be ascribed to the methyl group. To assign these signals unambiguously, the proton spectra of **1–3** were recorded and the effects of added Eu(fod)$_3$ examined.

For **1**, the proton spectrum contained methyl singlets at 1.05 and 1.10 ppm, a complex multiplet at 1.2–2.2 ppm arising from four protons, as well as four multiplets, each corresponding to the absorption for a single proton centred at 2.56, 3.09, 6.10, and 6.52 ppm. The latter two patterns appeared as triplets of multiplets. Upon the addition of Eu(fod)$_3$, most of the patterns exhibit downfield shifts with the most pronounced effect apparent for the multiplet originally at 3.09 ppm which therefore arose from H-1. In the presence of 0.17 equiv. of Eu(fod)$_3$ the four lower field multiplets shifted to 3.04, 4.57, 6.60, and 6.99 ppm, respectively. Double irradiation centred at 6.60 ppm significantly narrowed the multiplet at 4.57 ppm while the absorption at 3.04 ppm was little affected. The opposite effects were found upon double irradiation at 6.99 ppm. These observations permitted assignment of these four multiplets to H-5, -6, -1, and -4 in order of increasing field. In this spectrum the methyl signals appeared at 1.96 and 1.99 ppm partially obscuring a multiplet which integrated for two protons. A second 2-proton pattern centred at 2.60 ppm was clearly resolved. The ^{2}H spectrum of **1**-d_x isolated from the product mixture after heating **1** at 185°C for 149 h contained six

Can. J. Chem. Downloaded from www.nrcresearchpress.com by 210.87.254.42 on 09/05/12
For personal use only.

signals which were assigned as follows: 6.5(D-5), 6.1(D-6), 3.0(D-1), 1.8, 1.5(D-7), and 1.05 ppm (*exo*-methyl-D). The three higher field assignments are based on the results obtained for **2**-d_x and **3**-d_x but, in any event, these are not crucial for any of the mechanistic conclusions drawn. The major concern is the assignment of the olefinic signals which was straightforward from the proton results.

Six signals also appeared in the ^{2}H spectra of most of the **2**-d_x samples. The positions and assignments are: 6.0(D-2), 5.5(D-3), 2.6(D-5), 2.4(*exo*-D-4), 2.1(*endo*-D-4), and 1.1 ppm (*exo*-methyl-D), based on the following observations. The proton spectrum contained one pattern at 5.96 ppm which was a triplet of multiplets and one at 5.50 ppm, a doublet of multiplets. These were readily assigned to the olefinic protons H-2 and -3, respectively, from their positions and multiplicities since the pattern for H-2 is expected to exhibit comparable spin coupling of 8–10 Hz to the vicinal bridgehead and olefinic protons while the pattern for H-3 would contain one of these interactions with smaller couplings to the allylic protons at C-4. An ill-defined multiplet at 2.55 ppm was ascribed to H-5 and verified upon finding that this pattern was most sensitive to the presence of Eu(fod)$_3$. The methyl protons were equivalent at 1.09 ppm but became nonequivalent in the presence of the shift reagent. A doublet, $J \sim 10$ Hz, at 1.85 ppm was assigned to the *anti*-8-proton and a 4-proton multiplet centred at 2.25 ppm contained the absorptions of the remaining protons. Upon the addition of Eu(fod)$_3$, each of the multiplets exhibited sufficiently different sensitivities such that with 0.3 equiv. of shift reagent each pattern could be unambiguously assigned to a specific proton. The broad multiplet originally at 2.55 ppm showed the largest shift to 9.14 ppm while the H-2 and -3 patterns shifted to 8.09 and 7.31 ppm, respectively. The methyl signals appeared at 5.61 and 4.77 ppm and the *anti*-8-proton absorbed at 4.30 ppm. A doublet at 7.02 ppm ($J \sim$ 18 Hz), each component of which was broad, could be assigned to the *endo*-4 proton, since it was essentially unaffected by double irradiation at H-5. Double irradiation at 7.02 ppm collapsed a pattern near 4.65 ppm thereby revealing the *exo*-4 proton, the lower field component of which coincided with the absorption for H-1 at 4.77 ppm. Finally, the absorption for the *syn*-8 proton appeared at 5.36 ppm. A number of multiple irradiation experiments confirmed these assignments. From similar experiments with solutions containing different amounts of shift reagent, plots of the individual proton shieldings vs. [Eu(fod)$_3$] showed that the *endo*- and *exo*-4-proton patterns crossed over with added reagent; thus, the assignments for each of the deuterium signals could be assigned in the ^{2}H spectrum recorded without added Eu(fod)$_3$. The spectrum of one of the heavily deuterated **2**-d_x samples was examined as a function of added shift reagent to confirm that the induced shifts agreed with those found from the ^{1}H results as a further confirmation of the assignments. As reported previously (1*a*), the methyl signals are readily assigned in the ^{13}C spectrum of **2** and the methyl absorption in the ^{2}H spectrum of **2**-d_x was shown to arise exclusively from the methyl nuclei more sensitive to Eu(fod)$_3$, i.e. exchange occurred only at the *exo*-methyl site in the limits of detection by ^{2}H spectra.

A similar approach was employed to unravel the ^{2}H spectra of the **3**-d_x samples, using initially those from the longer reaction times. In the absence of Eu(fod)$_3$, six signals were evident although the olefinic absorptions at 5.75 and 5.70 ppm were too close for precise integration or for specific assignments. In addition, signals appeared at 2.75, 2.45, 2.25, and 1.10 ppm. That at 2.75 ppm could be assigned to D-5 from its large relative shift upon the addition of Eu(fod)$_3$ while the highest field signal was the methyl absorption. In the proton spectrum of **3** the olefinic pattern is deceptively simple and it was essential to examine the effect of added Eu(fod)$_3$ to distinguish between the two olefinic protons. In the presence of Eu(fod)$_3$ patterns analogous to those described above for **2** emerged to permit unambiguous assignments. Also, as in the case of **2**, the methyl protons became nonequivalent with added shift reagent but, within our limits of detection, deuterium incorporation occurred only at the *exo*-methyl site. In contrast to **2**, it was more difficult to assign the patterns specifically for H-1 and -2, the more remote bridgehead and allylic methylene protons. However, in the ^{2}H spectra of **3**-d_x samples from short reaction times the signal at 2.45 was much more intense than that at 2.25 ppm leading to their assignments as the *exo*- and *endo*-2-deuterons, respectively. With added shift reagent these patterns cross over, behavior which is analogous to that of the 4-protons (deuterons) in **2**. The chemistry observed for the system also requires these assignments for **3**.

With the assignments for **1**–**3**, the ^{2}H spectra of each of the samples isolated after treatment in the deuterated medium were recorded and integrated using line-shape fitting as described previously (4) to determine the relative ^{2}H incorporation at each site. For this purpose the samples of **1**-d_x and **2**-d_x were examined without shift reagent since the individual signals are sufficiently separated. For the **3**-d_x samples, however, the relative amounts of deuterium at C-2, -5, and the methyl site were obtained without added Eu(fod)$_3$ and then the relative amounts at

TABLE 2. Deuterium incorporation[a] in **1–3** at 155°C

Reactant	Time (h)	^{2}H assay of **1** C-5	C-6
1	1	—	0.42
	2.5	—	0.73
	4	—	0.86
	7	0.05	0.97
	12	0.15	1.00
	24	0.17	1.00
	35	0.26	1.00

		^{2}H assay of **2**				^{2}H assay of **3**			
			C-4			C-2			
Reactant		C-2	*exo*	*endo*	C-5	*exo*	*endo*	C-4	C-5
3	2	—	0.82	0.61	0.23	0.15	—	0.14	0.12
	4	—	0.93	0.76	0.51	0.61	—	0.47	0.25
	6	0.13	0.94	0.88	0.74	0.83	0.21	0.83	0.73
	16	0.16	0.92	0.89	0.78	0.83	0.22	0.83	0.76

[a]^{2}H assay by ^{2}Hmr, atoms ^{2}H, ±0.01; total atoms ^{2}H by mass spectrometry, ±0.001.

C-3, -4, and -5 were determined for shifted spectra. In the latter the overlap in the higher field region precluded precise integration. From the two sets of ratios the relative amounts at each site could be derived. For each sample, the total deuterium content was determined by mass spectrometry. With these data the deuterium concentrations at each site were calculated and a summary of these results is tabulated in Tables 2 and 3 for the two temperatures studied.

Discussion

The first feature which is apparent from the present results is the enhanced rate of rearrangment relative to the behavior found for a variety of other bicyclic ketones (3). At 185°C, the temperature at which most of the earlier results were obtained, equilibrium was established in ca. 20 h. The rate of rearrangement for **1** is more than 100 times faster than that found for its saturated analog (*1b*) and deuterium incorporation at most of the sites of exchange in **1–3** was too fast to permit the extraction of even crude rate data. At 155°C approximate rate constants could be generated from the experimental results and it is interesting to compare these with earlier data for closely related systems. The decreased rearrangement rate for **1** corresponds to an activation energy of 30 kcal/mol which seems reasonable for this isomerization. The presence of the double bond in the bicyclo[2.2.2]octane skeleton also appears to bias the equilibrium more toward the [3.2.1] skeleton by comparison with the results for the saturated analogs (*1b*). Since the [3.2.1] system constitutes 92% of the mixture at equilibrium and the rate of **1** → **2**(**3**) is approximately 2.4×10^{-5} s^{-1} at 185°C, the rate of the slower interconversion **2** → **1** is $\sim 2 \times 10^{-6}$ s^{-1}. The corresponding values for 155°C are reduced by a factor of 10.

From the results for the **1**-d_x samples it is evident that exchange at C-6 is much more facile than at C-5; estimated first-order rate constants for ^{2}H incorporation at 155°C are 130×10^{-6} and 2.5×10^{-6} s^{-1}, respectively, i.e. a ratio of ~50. At 185°C, the rate constant for C-5 exchange is 30×10^{-6} s^{-1} while that at C-6 is $>400 \times 10^{-6}$ s^{-1}. These values may be compared to the value of 5.6×10^{-7} s^{-1} found for bicyclo[2.2.2]octene (2). Clearly, the carbonyl group has a pronounced activating effect on the vinyl exchange process in the ketone increasing the rate at C-5 by a factor of 50 and the rate at C-6 by perhaps 10^3. Conceivably, these rate enhancements could signal a change in mechanism but, without further information, it seems sufficient to attribute the enhancement to the polarity of the carbonyl bond either through an inductive or a field effect. At the higher temperature deuterium incorporation was also observed at C-1 and C-7 in the **1**-d_x samples but the rate of appearance was very much slower, $k \sim 2 \times 10^{-6}$ s^{-1}. Since this is comparable to the rate of rearrangement **2** → **1**, the incorporation probably occurred in the [3.2.1] skeleton rather than directly in **1**. This conclusion is supported by the fact that *endo* exchange at C-7 in the 10 h sample is greater than *exo* exchange. This carbon is the bridgehead carbon in **2** and **3** which undergoes rapid exchange at 185°C. Subsequent formation of the β-enolate **4**, followed by opening with inversion to **1** places the deuterium in

Can. J. Chem. Downloaded from www.nrcresearchpress.com by 210.87.254.42 on 09/05/12
For personal use only.

Can. J. Chem. Downloaded from www.nrcresearchpress.com by 210.87.254.42 on 09/05/12
For personal use only.

TABLE 3. Deuterium incorporation in **1**–**3** at 185°C; products (^{2}H assay by ^{2}Hmr)[a]

Reactant	Time (h)	**1** %	**1** C-1	**1** C-5	**1** C-6	**1** C-7 *exo*	**1** C-7 *endo*	**1** Me	**2** %	**2** C-2	**2** C-3	**2** C-4 *exo*	**2** C-4 *endo*	**2** C-5	**2** Me	**3** %	**3** C-2 *exo*	**3** C-2 *endo*	**3** C-3	**3** C-4	**3** C-5	**3** Me
1	2	84	—	0.24	1.00				8	0.59	0.87	1.00	0.98	0.80		8	0.92	0.66	0.82	0.95	0.84	
	5	58	0.04	0.59	0.94				20	0.83	0.90	0.99	0.91	0.80	0.06	22	0.96	0.83	0.89	0.92	0.81	0.06
	10	38	0.06	0.68	0.85	0.03	0.05	Trace	30	0.92	0.99	0.85	0.82	0.86	0.07	32	0.89	0.89	0.82	0.93	0.86	0.09
	149	8	0.74	0.71	0.70	0.74	0.72	0.80	44	0.70	0.74	0.83	0.81	0.61	0.94	48	0.78	0.72	0.74	0.72	0.73	0.86
2	5	2[b]							48	0.54	0.05	0.97	0.96	0.66		50	0.85	0.74	0.10	0.77	0.71	
	10	3[b]							45	0.80	0.12	1.00	0.96	0.71	0.04	52	1.00	0.89	0.09	0.77	0.85	0.03
3	2	2[b]							46	0.73	0.06	0.99	0.91	0.74	0.03	52	0.93	0.88	0.04	0.73	0.83	0.01
	5	3[b]							44	0.82	0.17	1.00	0.93	0.71	0.05	53	1.00	0.85	0.13	0.77	0.88	0.03

[a]Atoms ^{2}H, ± 0.01; product composition by gc analysis ± 1%.
[b]Samples not assayed.

the *endo* orientation at C-7. From the results for other systems (2–4) and the data discussed below, it has been established that β-enolate opening with inversion is the preferred process.[3] Bridgehead exchange (C-1) in **1** also probably arises from exchange at the allylic methylene carbon in **2** which is very rapid at 185°C. Since the allylic site in **2** is essentially completely deuterated in the 2 h sample, conversion of **2** to **1** will account for deuterium at the bridgehead position in **1**. It may be noted that exchange was not observed at C-1 in the saturated analog of **1** under comparable reaction conditions (1*b*). The appearance of deuterium in the *exo*-methyl group of **1** after long reaction times may arise from slow direct exchange or via **2** and **3** but the available data do not permit a distinction. It may be noted that methyl exchange in the bicyclo[2.2.2]octanone case (1*b*) exhibited a rate constant of 5×10^{-8} s^{-1} and the corresponding process in **1** could be expected to be similarly slow.

A series of experiments was performed at 155°C using **3** as the starting material and isolating samples of **2**-d_x and **3**-d_x at various times (Table 2). Deuterium assay of these samples permitted assessment of the relative rates of exchange at C-2, -4, and -5 in each case. From the rate of change of the d_0 peak in the mass spectra of **3**-d_x a deprotonation rate of 8×10^{-5} s^{-1} was found. The fastest process is undoubtedly formation of the allylic anion **5** which can protonate at either C-2 reforming **3** or at C-4 generating **2**. The apparent rate of exchange at the *exo*-4 position in **2** is $\sim 18 \times 10^{-5}$ s^{-1} indicating some stabilization of the negative charge at C-4 by the carbonyl group. As expected the rate of formation of **2** from **3** is 2×10^{-4} s^{-1}, i.e. the same as the deuteration rate at C-4. The *exo*/*endo* ratio at C-4 in **2** is approximately 2 which is essentially the same as that found previously for bicyclo[3.2.1]oct-2-ene at 185°C (2) but the exchange rates in the ketone at the lower temperature are 250 times faster, suggesting a rate enhancement of ca. 10^3 for comparable temperatures. Of course, the anion can exist as **4** the cleavage of which is heavily biased to **5** rather than **1**. In contrast to **2**, the stereoselectivity of allylic exchange at C-2 in **3** is higher; the *exo*/*endo* rate ratio at this site is ca. 6. Conceivably this may arise from a steric effect of the *endo*-methyl at C-7 hindering approach of the deuterium donor. It is interesting that bridgehead exchange (C-5) appears to be approximately twice as fast in **2** as in **3** indicating that somewhat less strain is associated with α-enolization to form a noncon-

[3]A referee suggests that the intermediates from *exo* and *endo* proton abstraction from C-7 in **1** could differ in reactivity such that the intermediate from *exo* abstraction undergoes isomerization preferentially while that from *endo* abstraction is more rapidly reprotonated (deuterated).

Can. J. Chem. Downloaded from www.nrcresearchpress.com by 210.87.254.42 on 09/05/12
For personal use only.

jugated enolate which can be pictured as **6**. It is apparent that methyl exchange and generation of a vinyl anion in **2** and **3** are much higher energy processes since no deuterium was detected at these sites in the experiments at 155°C. At 185°C, however, both processes were observable and the rate of exchange at the *exo*-methyl site is similar to that found for 7,7-dimethylbicyclo[3.2.1]octan-6-one (*1b*), namely 3×10^{-6} s^{-1}. It may be noted that this is a lower limit since the deuterium pool is appreciably diluted by the exchange processes at the other centres. In the saturated system it was possible to detect small amounts of deuterium at the *endo*-methyl position although the rate of *endo*-methyl exchange was 100 times slower than *exo*-methyl exchange. Presumably a similar difference exists for **2** and **3** but is unobservable because of more extensive dilution of the deuterium pool. As in the earlier cases, β-enolate formation of the *exo*-methyl group is implicated although, again, rearrangement to a ring-expanded skeleton was not detected. As noted previously, cyclopropoxides cleave in base to form the product from the more stable anion and the absence of ring expansion is not unexpected. The presence of the double bond in **2** and **3** apparently has no effect on the methyl exchange process. The appearance of deuterium at C-3 presumably via a vinyl anion was noted in our preliminary communication (*1b*) and we investigated deuterium exchange in the corresponding olefins (2). Both vinyl and allylic exchange occur in bicyclo[3.2.1]oct-2-ene and at similar rates. From the results for **2**-d_x and **3**-d_x, however, it is apparent that the rates differ by approximately an order of magnitude. Even so, the rates of vinyl exchange in the ketones, $\sim 8 \times 10^{-6}$ s^{-1}, are significantly faster than that found for the olefins, 2×10^{-7} s^{-1}. The factor of 40 relating the two processes is appreciably smaller than that found for the [2.2.2] system discussed above but it does indicate a significant enhancement by the carbonyl group, presumably through a field effect.

In summary, introduction of the double bond into the [2.2.2] system enhances its reactivity toward β-enolate formation and subsequent rearrangement to the [3.2.1] skeleton. Also, the double bond tends to increase the bias of the equilibrium toward the latter system. The carbonyl group accelerates both allylic and vinylic exchange in both skeletons but does not appear to affect the stereoselectivity of allylic exchange at C-4 in **2** relative to that found for the parent olefin. The effect of the double bond on β-enolization in this system suggests a number of extensions which are worthy of study to gain a better understanding of the utility of the process for synthetic purposes.

Acknowledgements

We are grateful to the National Research Council of Canada for financial support and to Ms. Marlene Brown for technical assistance. We thank Professor D. H. Hunter for valuable discussion.

1. (*a*) D. M. HUDYMA, J. B. STOTHERS, and C. T. TAN. Org. Magn. Reson. **6**, 614 (1974); (*b*) A. K. CHENG, J. B. STOTHERS, and C. T. TAN. Can. J. Chem. **55**, 447 (1977).
2. A. K. CHENG and J. B. STOTHERS. Can. J. Chem. **55**, 50 (1977).
3. A. NICKON, J. L. LAMBERT, J. E. OLIVER, D. F. COVEY, and J. MORGAN. J. Am. Chem. Soc. **98**, 2593 (1976); M. B. RAMPERSAD and J. B. STOTHERS. J. Chem. Soc. Chem. Commun. 709 (1976) and references cited therein.
4. A. L. JOHNSON, J. B. STOTHERS, and C. T. TAN. Can. J. Chem. **53**, 212 (1975).
5. K. R. STEPHENS, J. B. STOTHERS, and C. T. TAN. *In* Mass spectrometry and N.M.R. spectroscopy in pesticide chemistry. *Edited by* R. Haque and J. F. Boros. Plenum Press, New York, NY. 1974. pp. 179–196.

Ipso nitration. XVIII.[1] Nitration of 2-chloro-1,3,5-trimethylbenzene: nitration *ipso* to chlorine

ALFRED FISCHER AND SACHDEV SINGH SEYAN

Department of Chemistry, University of Victoria, Victoria, B.C., Canada V8W 2Y2

Received November 28, 1977

ALFRED FISCHER and SACHDEV SINGH SEYAN. Can. J. Chem. **56**, 1348 (1978).

Nitration of 2-chloro-1,3,5-trimethylbenzene in acetic anhydride gives the *cis* and *trans* isomers of 4-chloro-1,3,5-trimethyl-4-nitrocyclohexa-2,5-dienyl acetate (**1**, 21%), the *cis* and *trans* isomers of 3-chloro-2,4,6-trimethyl-4-nitrocyclohexa-2,5-dienyl acetate (**2**, 6%), and 2-chloro-1,3,5-trimethyl-4-nitrobenzene (73%). Diene **1** reacts with acidified aqueous acetone to form the corresponding dienol, acidified methanol to form the methyl ether, and hydrogen chloride to form the corresponding chloride. In acetic acid a mixture of 4-chloro-3,5-dimethylbenzyl derivatives and 3-chloro-2,4,6-trimethylphenyl acetate are formed. In trifluoroacetic acid – trifluoroacetic anhydride and also in boron trifluoride etherate, 2-chloro-1,3,5-trimethyl-4-nitrobenzene is the predominant product. Diene **2** on reaction with acetic acid, acidified methanol, trifluoroacetic acid – trifluoroacetic anhydride, and boron trifluoride etherate gives 3-chloro-2,4,6-trimethylphenyl acetate. Some 2-chloro-4-nitromesitylene is obtained in trifluoromethanesulfonic acid. Diene **2** also gives the acetate on standing at ambient temperature or at −20°C, and on pyrolysis. Diene **1** gives 4-chloro-3,5-dimethylphenylnitromethane on standing at ambient temperature or at −20°C but a mixture of 2-chloro-1,3,5-trimethyl-4-nitrobenzene, chloromesitylene, and 3-chloro-2,4,6-trimethylphenyl acetate on pyrolysis.

ALFRED FISCHER et SACHDEV SINGH SEYAN. Can. J. Chem. **56**, 1348 (1978).

La nitration du chloro-2 triméthyl-1,3,5 benzène dans l'anhydride acétique conduit aux isomères *cis* et *trans* de l'acétate du chloro-4 triméthyl-1,3,5 nitro-4 cyclohexadiène-2,5 yle (**1**, 21%), aux isomères *cis* et *trans* de l'acétate du chloro-3 triméthyl-2,4,6 nitro-4 cyclohexadiène-2,5 yle (**2**, 6%) et au chloro-2 triméthyl-1,3,5 nitro-4 benzène (73%). Le diène **1** réagit avec de l'acétone en solution aqueuse acidulée pour conduire à la formation du diénol correspondant, avec du méthanol acidulé pour conduire à la formation de l'éther méthylique et avec du chlorure d'hydrogène pour conduire à la formation du chlorure correspondant. Dans l'acide acétique, il y a formation d'un mélange de dérivés du chloro-4 diméthyl-3,5 benzyle et de l'acétate du chloro-3 triméthyl-2,4,6 phényle. Dans un mélange d'acide trifluoroacétique et d'anhydride trifluoroacétique ainsi que dans l'éthérate du trifluorure de bore, le produit prédominant est le chloro-2 triméthyl-1,3,5 nitro-4 benzène. La réaction du diène **2** avec l'acide acétique, le méthanol acidulé, le mélange acide trifluoroacétique – anhydride trifluoroacétique et l'éthérate du trifluorure de bore conduit à l'acétate ou chloro-3 triméthyl-2,4,6 phényle. On obtient du chloro-2 nitro-4 mésithylène dans l'acide trifluorométhanesulfonique. Le diène **2** conduit aussi à l'acétate lorsqu'on le laisse à la température ambiante, à −20°C, ou lorsqu'on le pyrolyse. Le diène **1**, laissé à la température ambiante ou à −20°C, conduit au chloro-4 diméthyl-3,5 phénylnitrométhane; toutefois par pyrolyse on obtient un mélange de chloro-2 triméthyl-1,3,5 nitro-4 benzène, de chloromésithylène et d'acétate du chloro-3 triméthyl-2,4,6 phényle.

[Traduit par le journal]

Introduction

Addition of nitronium ion at an *ipso* position is an important reaction path in the nitration of aromatic derivatives (2–8). In acetic anhydride the *ipso*-nitrocyclohexadienyl cation so formed adds acetate to form the nitronium acetate (acetyl nitrate) adduct. In the benzene series adducts have been isolated in which the nitro group is *ipso* to methyl (9), methylene (10), and ethyl (7), and a cyclohexadienone has been obtained in which nitro is *ipso* to methoxyl (11). Nitration is known to occur *ipso* to other groups, such as isopropyl (12) or bromo (13), but in these cases the *ipso* group is lost and no adduct is obtained. In the naphthalene series an example of nitration *ipso* to bromine and to chlorine has long been known in the formation of 1-bromo-1-nitro-2(1*H*)-naphthalenone and 1-chloro-1-nitro-2(1*H*)-naphthalenone from 1-bromo-2-naphthol and 1-chloro-2-naphthol, respectively (14, 15).

In the present paper we report the isolation of a benzene series adduct with nitro *ipso* to chlorine.

Results and Discussion

Nitration and Formation of Adducts

Nitration of 2-chloro-1,3,5-trimethylbenzene (chloromesitylene) in acetic anhydride gave a mixture of diene adducts (30%) and 2-chloro-4-nitromesitylene (70%). The products were separated by low-tempera-

[1]For part XVII see ref. 1.

Can. J. Chem. Downloaded from www.nrcresearchpress.com by 210.87.254.6 on 09/05/12
For personal use only.

Can. J. Chem. Downloaded from www.nrcresearchpress.com by 210.87.254.6 on 09/05/12
For personal use only.

ture chromatography on alumina and, in addition to the nitro substitution product, the two diastereoisomers of 4-chloro-1,3,5-trimethyl-4-nitrocyclohexa-2,5-dienyl acetate[2] (**1***a* and **1***b*) and one diastereo-

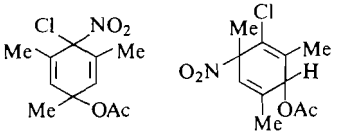

1 **2**

isomer of 3-chloro-2,4,6-trimethyl-4-nitrocyclohexa-2,5-dienyl acetate[3] (**2***b*) were obtained. The second diastereoisomer of 3-chloro-2,4,6-trimethyl-4-nitro-1,4-dihydrophenyl acetate (**2***a*) was not isolated in a pure state but it was present as a major constituent in certain column fractions. Product recovery after chromatography represented a yield, based on the chloromesitylene of ca. 90%. Nuclear magnetic resonance analysis of the column fractions indicated that the ratio 2-chloro-4-nitromesitylene – (**1***a* + **1***b*) – (**2***a* + **2***b*) was 73:21:6. The amount of the adduct **2** varied from run to run but it was always less than the amount of adduct **1**. The variation is probably a reflection of the difficulty of measuring the small proportion of material rather than a variation of the portion of adduct **2** actually formed.

The ir and elemental analytical data confirm the presence of the acetate and nitro groups in the adducts. Adducts **1***a* and **1***b* have a plane of symmetry, as is evident from both the ^1H and ^{13}C nmr spectra. It follows that **1***a* and **1***b* must be 1,4 adducts and not 1,2 adducts which would have six chemically different ring carbon atoms with no chemically identical attached hydrogen atoms or methyl groups. Furthermore the symmetry requires the nitro group to be located at C-2 and the acetate at C-5 of the original 2-chloromesitylene, or vice versa. On addition of the shift reagent tris(1,1,1,2,2,3,3-heptafluoro-7,7-[$^2H_6$]dimethyl-4,6-[$^2H_3$]octanedionato)europium(III) (Eu([$^2H_9$]fod)$_3$) the peak attributed to the single methyl group (at C-5 of the original 2-chloromesitylene) moves downfield more rapidly (Table 1) than that of the two symmetrical methyl groups (at C-1 and C-3). The europium and thus the acetate group at which it is complexed must therefore be closer to C-5 than to C-1 and C-3. Thus the 5-acetoxy-2-nitro structure is correct and the alternative 2-acetoxy-5-nitro structure must be rejected. The latter structure is chemically unlikely since it contains a geminal chlorine and acetate. By analogy with the behaviour of related bromo compounds (16), the elements of acetyl chloride would be expected to be readily eliminated from such a structure to form a cyclohexadienone, i.e. 2,4,6-trimethyl-4-nitrocyclohexa-2,5-dienone is the expected product on addition of the nitronium ion at C-5 of 2-chloromesitylene.

The symmetry present in adducts **1***a* and **1***b* is not present in adduct **2***b*: ^1H nmr reveals the presence of four different methyl groups and two different ring protons and ^{13}C nmr shows that the six ring carbon atoms are chemically distinct. The absence of ultraviolet absorption around 255 nm shows that **2***b* is not a conjugated diene. It cannot be a 1,2 adduct and must therefore be a 1,4 adduct. The shift reagent studies (Table 1) show that one proton (relative slope 1.64) must be attached to the same site as acetate and the other (relative slope 0.22) is at least two carbon atoms away. Two of the methyl groups (relative slopes 0.51 and 0.53) must be equidistant from the acetate and closer than the third (relative slope 0.10). These observations can only be accommodated by the 4-acetoxy-1-nitro structure shown for **2***b* but not by any other structure. Diene **2***a* was identified as a diastereoisomer of **2***b* on the basis of its closely similar nmr spectrum. This is supported by the similar chromatographic behaviour: diene **2***a* was eluted in admixture with **2***b*.

2-Chloromesitylene has four chemically different ring carbon atoms at which the nitronium ion might be added and in so doing four different cyclohexadienyl cations, **3**–**6**, would be generated. There are

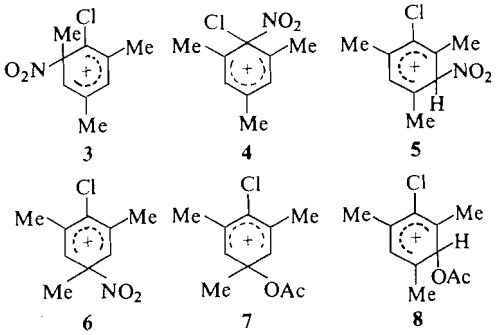

3 **4** **5**

6 **7** **8**

two (chemically identical) atoms at which nitronium ion can be added to form **3** and similarly for **5**. Thus, there is a statistical factor of 2 favouring the formation of these cations. The four cations are the key intermediates whose formation is the rate-determining step in the reaction paths potentially leading to adduct **2**, adduct **1**, 2-chloro-4-nitromesitylene and 2,4,6-trimethyl-4-nitro-cyclohexa-2,5-dienone, respectively. The relative energies of the transition states leading to these ions, and therefore the stabilities of the ions themselves, which are expected to parallel those of the transition states, should determine the relative yields of the products, due allowance being made for the statistical factors already mentioned. In cations

[2]4-Chloro-1,3,5-trimethyl-4-nitro-1,4-dihydrophenyl acetate.
[3]3-Chloro-2,4,6-trimethyl-4-nitro-1,4-dihydrophenyl acetate.

Can. J. Chem. Downloaded from www.nrcresearchpress.com by 210.87.254.6 on 09/05/12
For personal use only.

4 and **5** the methyl groups are similarly (favourably) located with respect to the positive charge: they are *ortho* and *para* with respect to the site of addition and attached to atoms bearing formal positive charges. The resonance (hyperconjugative) as well as the inductive effect of the methyl groups will be operative in stabilization of **4** and **5**. On the other hand the chlorine atoms in **4** and **5** are so located at formally neutral carbon atoms *ipso* and *meta* to the site of addition of nitronium ion that there is little or no opportunity for the stabilizing resonance effect to be called upon and, for this substituent, it is mainly the destabilizing electron-withdrawing inductive effect that is operative. In cations **3** and **6** the reverse situation exists: the chlorine is favourably located at a formally positive carbon (*ortho* or *para*) and its electron-donating resonance effect will be operative and will offset its electron-withdrawing inductive effect, whereas the methyl groups are less favourably located at the formally neutral carbons (*ipso* and *meta*) where the resonance effect of the substituent is reduced. In principle the relative yields of all four potential products are calculable from the appropriate substituent effects for the methyl and chloro groups. In practice, this cannot be done with useful accuracy for all four products, in part because the effect of the methyl groups is so disproportionate in favouring **4** and **5** over **3** and **6** that the relative effect of the methyl groups cannot be estimated reliably and cannot be measured directly from nitration of mesitylene. The relative effect of the methyl groups in directing the nitronium ion to the 1 or 2 position of mesitylene, estimated from the partial rate factors for methyl (17), is a factor of 5000:1 in favour of attack *ortho* and *para* to the three groups. (It is therefore not surprising that mesitylene gives only nitromesitylene on nitration and that the amount of adduct is too small to detect.) This very large factor is partially offset by the effect of the chlorine. From the data of Roberts *et al.* (18) for nitration of chlorobenzene the ratio of the *meta* to *ortho* partial rate factors, $m_f^{Cl}:o_f^{Cl}$, is 1:33 so that, e.g., the ratio of **5**:**3** and thus of chloronitromesitylene to adduct **2** is predicted to be 150:1 (5000:33). This ratio is much larger than the observed ratio of products from these ions, 12:1. In addition to the difficulty of estimating reliably the effects of the methyl groups the substituent effect of the chlorine is known to vary according to the system in which it is measured (2).[4] However, in spite of these difficulties the calculation does lead to the correct qualitative prediction: adduct **2** should be a minor product of the reaction. The relative amounts of adduct **1** and chloronitromesitylene can be calculated with more confidence, since the substituent effect of the methyl groups is the same in the intermediate cations **4** and **5** and thus the relative stability of **4** and **5** is determined only by the effect of the chlorine in the *ipso* and *meta* positions. The ratio[5] $i_f^{Cl}:m_f^{Cl}$ is 1:1.1 (2). Thus, allowing for the statistical factor the ratio of adduct **1** to chloronitromesitylene is predicted to be 1:2.2 whereas the observed ratio is 1:3.5. Likewise, in the comparison of cations **3** and **6** the effect of the methyl groups can be ignored and the amount of adduct **2** to diene should be determined only by the ratio $o_f^{Cl}:p_f^{Cl}$ = 1:4.7 and the statistical factor. The ratio of **2** to dienone is thus predicted to be 1:2.4. No dienone was detected although in one nitration reaction the appropriate absorptions in the ^1H nmr spectra of some column fractions suggested that 2,6-dimethyl-4-nitromethylphenol, the product of rearomatization of the dienone,[6] was present. It is unlikely that the amount of dienone formed, if any, could have exceeded the amount of adduct **2**. However, in spite of the absence of quantitative agreement between calculated and observed product yields both of these lead to the conclusion that the cations **4** and **5** with *ortho* and *para* methyl groups, and *ipso* and *meta* chlorine, respectively are of comparable stability and significantly more stable than cations **3** and **6**, with *meta* and *ipso* methyl groups, and *ortho* and *para* chlorine, respectively.

Reactions of the Adducts

The initial step in the solution reactions of diene adducts (4-nitro-2,5-cyclohexadienyl acetates) involves formation (or reformation) of cyclohexadienyl cations (3, 19). Two competititive pathways exist, one involving loss of nitro group as nitrite and formation of the substituted acetoxycyclohexadienyl cation, the other involving protonation of the acetate group and loss of acetic acid to form the substituted nitrocyclohexadienyl cation. Increased acidity of the reaction medium favours the formation of the nitrocyclohexadienyl cation and products derived from it. The cations that would be generated from adduct **1** by the two competititive paths are **7** and **4**, and from adduct **2**, **8** and **3**. Cations **7** and **8** are the acetoxy

[4]There is also some evidence for a variation in the partial rate factors of the methyl groups. Using partial rate factors more appropriate to polymethylbenzenes (17) the effect of the methyl groups is reduced to a factor of 1500:1 and the factor including the effect of the chlorine is 45:1. The change is in the correct direction but does not account for all of the discrepancy between calculation and observation.

[5]It can be shown that if the reason for the change of partial rate factors with substrate is because of the changes in the Hammett reaction constant for the reaction then partial rate factors of similar magnitude will be similarly affected i.e. a partial rate factor ratio which is close to unity in one system well not be significantly affected by change in the system.

[6]Unpublished work with G. N. Henderson.

Can. J. Chem. Downloaded from www.nrcresearchpress.com by 210.87.254.6 on 09/05/12
For personal use only.

TABLE 1. Relative gradients (gradient 1-$OCOCH_3$ = 1.00) of proton chemical shifts for diene adducts from the addition of Eu($[^2H_9]$fod)$_3$

1*a*		**1***b*		**2***b*	
Assignment	Relative gradient	Assignment	Relative gradient	Assignment	Relative gradient
1-CH_3	0.66	1-CH_3	0.70	1-H	1.64
2-H	0.79	2-H	0.86	2-CH_3	0.51
3-CH_3	0.14	3-CH_3	0.17	4-CH_3	0.10
				5-H	0.22
				6-CH_3	0.53

analogs of cations **6** and **5**, respectively. Cation **7**, like **6**, has the methyl and chlorine substituents less favourably located for net stabilization than does **4**, whereas **8**, like **5**, has the substituents more favourably located for net stabilization than does **3**. It follows that ionization of **1** to give **7** should be less effective in competing with the acid-catalysed loss of acetate to give **4** than is ionization of **2** to give **8** in competition with protonation, and loss of acetate from **2** to give **3**. In fact the formation of cation **8** from adduct **2** is so favoured that 3-chloro-2,4,6-trimethylphenyl acetate, the product of deprotonation of **8**, was not only the sole product obtained in the weak acid, acetic acid, but it was also the only product obtained on treatment of **2** with sulfuric acid in methanol and in the much more strongly acidic conditions of trifluoroacetic acid – trifluoroacetic anhydride and boron trifluoride etherate. Only in the most extreme acidic conditions of neat trifluoromethanesulfonic acid was any product other than the aryl acetate obtained. 2-Chloro-4-nitromesitylene (17%) is clearly a product from cation **3**. From **3** a 1,2 shift of the nitro group would give cation **5**, which is in turn rapidly deprotonated to the chloronitromesitylene. Some 3-chloro-2,4,6-trimethylphenyl acetate (11%) was obtained indicating that even under conditions most conducive to reaction via the nitrocyclohexadienyl cation **3** the reaction via the acetoxycyclohexadienyl cation **8** is still competitive. The major product was 3-chloro-2,4,6-trimethylphenol (44%). This could be formed from the corresponding phenyl acetate by hydrolysis and thus indicative of the predominance of reaction via cation **8**. Alternatively its formation could involve solvolysis via cation **3** to form the nitrocyclohexadienol, which then undergoes ionization of the nitro group to form the hydroxycyclohexadienyl cation followed by deprotonation to the phenol. Although this latter pathway does not involve cation **8** itself it would point to the relative ease of formation of the hydroxy analog of cation **8**.

In contrast to the reactions of adduct **2** adduct **1** gave, almost exclusively, with the exception of the reactions carried out in the presence of silver salts, products derived from the nitrocyclohexadienyl cation, in this case **4**. The simplest reaction of cation **4** is combination with a nucleophile to form a pair of diastereoisomeric nitrocyclohexa-2,5-dienyl derivatives, the overall reaction from **1** being replacement of acetate by the S_N1 mechanism. Examples of this reaction are provided by the reactions of adduct **1** in acidified aqueous acetone (to give 4-chloro-1,3,5-trimethyl-4-nitrocyclohexa-2,5-dienol (**9***x*)), in acidified methanol (to give the corresponding methyl ether **9***y*), and with hydrogen chloride (to give the corresponding chloride **9***z*). In less strongly nucleophilic

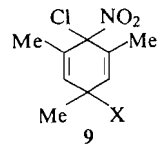

9

x X = OH
y X = OMe
z X = Cl

conditions nitrocyclohexadienyl cations undergo rearomatization reactions. In the particular case, as in **4**, that the nitrocyclohexadienyl cation contains a methyl or primary or secondary alkyl group attached to the position *para* to the quaternary centre, i.e. attached to a formally positively charged carbon, then the methyl group can be deprotonated to form a triene (**10** from **4**) and eventually substituted by the sequence shown for **4** in Scheme 1. More generally, migration of the nitro group to an unsubstituted position followed by rapid deprotonation gives a nitro substitution product of the original aromatic compound. Both 1,2 and 1,3 nitro migrations have been observed (19, 20) and 2-chloro-4-nitromesitylene could conceivably be formed by either two successive 1,2 shifts or, less likely, by a direct 1,3 shift. The deprotonation of the methyl group to form the triene can apparently compete successfully with the nitro migration process when the solvent is of at least modest basicity. Reaction of **1** in acetic acid gave, as the major component of the product, a mixture of four side-chain derivatives. Some 3-chloro-2,4,6-trimethylphenyl acetate was also formed, presumably from the acetoxycyclohexadienyl cation **7**

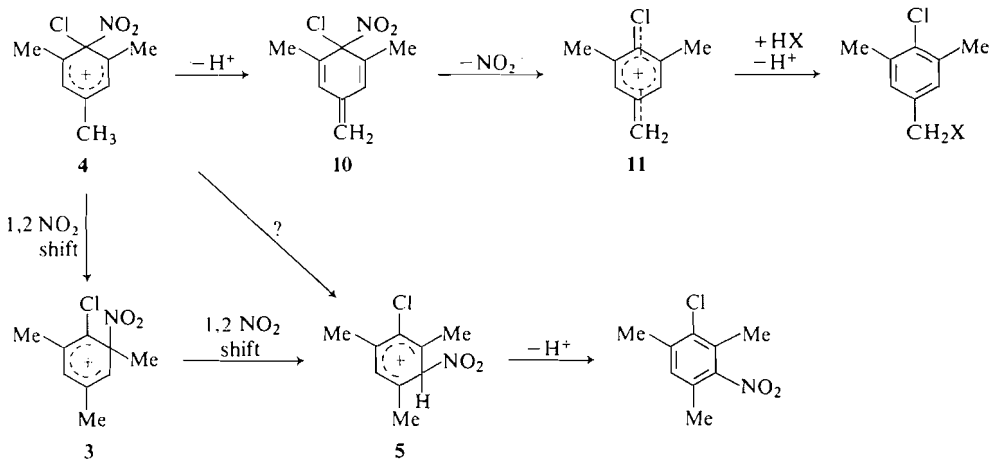

SCHEME 1. Formation of side-chain derivatives and 2-chloro-4-nitromesitylene.

by 1,2 shift of the acetoxy group followed by deprotonation, but only trace amounts of 2-chloro-4-nitromesitylene could be detected. Of the four side-chain products 4-chloro-3,5-dimethylphenylnitromethane and 4-chloro-3,5-dimethylbenzyl acetate were identified by comparison (glc, nmr) with authentic samples. The compound with methylene peak at lowest field (δ 5.58 ppm) and which gave the corresponding benzaldehyde on standing is assigned as 4-chloro-3,5-dimethylbenzyl nitrite since this is an expected product of the reaction, the methylene peak of benzyl nitrite is at the corresponding position and also at lower field than that of phenylnitromethane and benzyl nitrate, and it would be expected to give the corresponding benzaldehyde on standing (21). The compound with methylene peak at highest field (δ 4.56 ppm) was always obtained in smallest amount and was most likely the corresponding alcohol. In the series benzyl nitrite, phenylnitromethane, benzyl acetate, and benzyl alcohol the methylene absorption of the alcohol is at highest field. In reactions carried out under varying conditions, neat acetic acid, acetic acid plus 10% acetic anhydride, acetic acid plus 10% water, the dominant side-chain product was, in turn, the nitromethane, nitrite, and acetate. However in all of these reactions the sum of the side-chain derivatives constituted the major proportion of the product. Formation of the different side-chain products involves combination of the chlorodimethylbenzyl cation with (*i*) nitrous acid, at oxygen, to generate, after deprotonation, the nitrite ester; (*ii*) nitrous acid, at nitrogen, to give the phenylnitromethane; (*iii*) acetic acid to give the benzyl acetate; (*iv*) water to give the benzyl alcohol. The nitrous acid required is from the nitrite released in forming the chlorodimethylbenzyl cation **11** and it is possible that cage recombination from a benzyl cation – nitrite anion ion pair could give rise to the nitrite ester and the nitromethane (22).

In more strongly acidic conditions (boron trifluoride etherate, trifluoroacetic acid – trifluoroacetic anhydride) 2-chloro-4-nitromesitylene was the major reaction product. The basicity of these media is lower than that of acetic acid and deprotonation of the cation **4** to form the triene **10** does not compete so effectively with the nitro shift process which results in the conversion of **4** to **5**. Deprotonation of **5** leads to the observed chloronitromesitylene.

In the rearomatization reactions of **1** discussed so far it is evident that the nitro group migrates or is eliminated in preference to chlorine. Perrin (15) has shown that the Cl^+ group is a poorer leaving group than NO_2^+. It is therefore to be expected (as has been assumed in the foregoing) that cation **4** would undergo preferential migration of the nitro group to give the chloronitromesitylene, although it is not possible to distinguish between this process and the similar migration of the chlorine, since both processes would lead to the same product. The nitro group is also preferentially lost as an anion, as in the reactions of adduct **1** in acetic acid. The unimolecular ionization of the nitro group (as nitrite) to give **7** as an intermediate in the formation of 3-chloro-2,4,6-trimethylphenyl acetate is doubtless a lower energy process than the unimolecular ionization of chloride because the latter leads to cation **12** which is much less stable than **7**. Similarly in the formation of

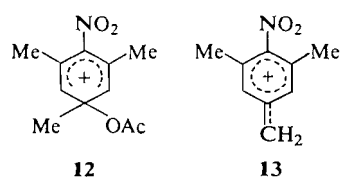

Can. J. Chem. Downloaded from www.nrcresearchpress.com by 210.87.254.6 on 09/05/12
For personal use only.

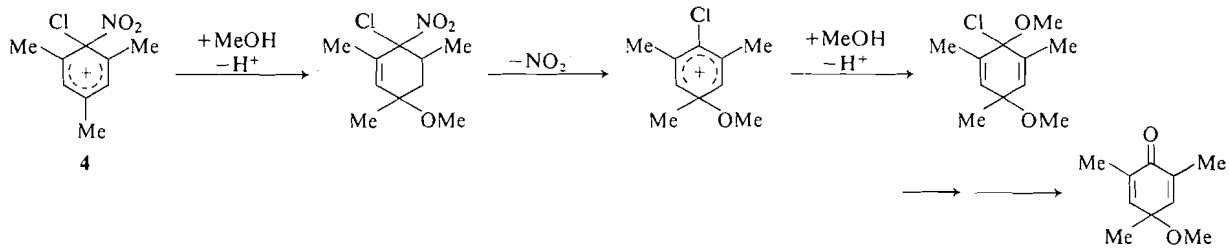

SCHEME 2

the side-chain derivatives (Scheme 1) the chlorodimethylbenzyl cation **11** should be of lower energy than its nitro analog **13** and this accounts for the preferential loss of the nitro group rather than chlorine from triene **10**, as shown by the fact that the side-chain products retain the nuclear chlorine. The energy difference between the benzyl cations **11** and **13** should be smaller than that between the cyclohexadienyl cations **7** and **12** but even this smaller difference is apparently too large to be offset by the anionic leaving group ability of chlorine (presumably) being greater than that of nitro. In an attempt to bring about the loss of chloride some reactions were carried out in the presence of silver salts: silver nitrate in methanol, silver nitrite in methanol, and silver acetate in aqueous acetone. Although a minor amount of 2,4,6-trimethyl-3-nitro-phenyl acetate was obtained, in which the nitro was retained and the chlorine lost, the major component of the product in all of the reactions was 3-chloro-2,4,6-trimethylphenyl acetate. Presumably the formation of 2,4,6-trimethyl-3-nitrophenyl acetate involves silver-ion-catalysed loss of chloride to give cation **12** followed by the 1,2 shift of the acetate group and deprotonation. In the course of the reaction with silver nitrate in methanol a compound was formed with nmr peaks at δ 1.37, 1.92, and 6.47 ppm representing 3, 6, and 2 protons, respectively. It is likely that this compound was 4 - methoxy - 2,4,6 - trimethylcyclohexa - 2,5 - dienone, formed by the sequence shown in Scheme 2. The nmr spectrum of the compound is similar to that[6] of 2,4,6-trimethyl-4-nitrocyclohexa-2,5-dienone with the peaks of the 4-methyl and ring protons moved upfield. Formation of this compound could account for the component of mass 166 (169 from [$^2H_4$]methanol) observed by glc – mass spectrometry and attributed to 3-methoxy-2,4,6-trimethylphenol. A surprising feature of the reactions carried out in the presence of silver salts is the formation of 2-chloro-5-nitromesitylene. It is unlikely that cation **4** would survive long enough to allow the nitro shift process to occur. Even if some **4** was able to leak into a pathway other than recombination with methanol to give the methyl ether it should be deprotonated to form the triene **10**, and thus side-chain product, in preference to undergoing shift of the nitro group. It seems clear that some process other than that shown in the lower portion of Scheme 1 is required to account for the formation of the chloronitromesitylene under these conditions.

Dienes **1***a* and **1***b* decomposed on standing at ambient temperature and even at −20°C to give mainly 4-chloro-3,5-dimethylphenyl nitromethane. Diene **2***b* decomposed to 3-chloro-2,4,6-trimethylphenyl acetate. These reactions neatly illustrate the preference for **1** to react by initial loss of the acetate group and for **2** to undergo loss of the nitro group. On thermolysis **1** gave a mixture of chloromesitylene, 2-chloro-4-nitromesitylene, and 3-chloro-2,4,6-trimethylphenyl acetate and **2** gave 3-chloro-2,4,6-trimethylphenyl acetate.

Experimental

General experimental methods have been described previously (23). Chloromesitylene was obtained by chlorination of mesitylene in chloroform (24). It had bp 67°C/0.55 kPa and was pure by glc; ir (film): 3025 (w), 2975 (m), 2950 (m), 2920 (m), 2850 (w), 1460 (s), 1365 (w), 1173 (m), 1056 (s), 850 (s), 702 (m), 623 (w); ^{1}H nmr δ: 2.07 (s, 3, 5-CH_3) 2.18 (s, 6, 1-CH_3 and 3-CH_3) 6.57 ppm (s, 2, 4-*H* and 6-*H*); ^{13}C nmr ($CDCl_3$) δ_C: 20.5 (1-*C*H$_3$, 3-*C*H$_3$, and 5-*C*H$_3$), 129.2 (*C*-4 and *C*-6), 131.6 (*C*-2), 135.4 (*C*-5), 135.7 ppm (*C*-1 and *C*-3). The assignment of the C-5 and C-1,C-3 absorptions was made on the basis of the intensity difference of the peaks at 135.4 and 135.7 ppm. The 135.4 peak was only half as intense as that at 135.7 ppm.

Nitration of Chloromesitylene in Acetic Anhydride

Preliminary nmr scale experiments established the optimum conditions for the formation of adducts. A cold solution of nitric acid (28.5 g, 0.45 mol) in acetic anhydride (75 cm^3) was added slowly to a vigorously stirred slurry of chloromesitylene (23.3 g, 0.15 mol) in acetic anhydride (150 cm^3) at −78°C. The mixture was allowed to warm to −50°C, maintained at that temperature for 2 h, and cooled again to −78°C. Cold ether (1 dm^3) was added and the reaction mixture was worked up in the usual manner (23) to yield 34 g of pale yellow solid. Integration of the nmr spectrum of the crude product indicated that it was a mixture of diene adducts (30%) and 2-chloro-4-nitromesitylene (70%). Chromatography on alumina[7] at −40°C and elution with pentane and ether–pentane mixtures gave, in the 0–40% ether fractions, 2-chloro-4-nitromesitylene, which was recrystallized from ethanol and had mp 55–57°C (lit. (25) mp 56–57°C); ir (Nujol): 1530 cm^{-1} (NO_2); ^{1}H nmr (CCl_4) δ:

[7]Basic alumia, activity I (Camag) was deactivated with 3% (v/v) of 10% (v/v) aqueous acetic acid.

Can. J. Chem. Downloaded from www.nrcresearchpress.com by 210.87.254.6 on 09/05/12
For personal use only.

Can. J. Chem. Downloaded from www.nrcresearchpress.com by 210.87.254.6 on 09/05/12
For personal use only.

2.19 (s, 3, 5-CH_3), 2.26 (s, 3, 1-CH_3), 2.33 (s, 3, 3-CH_3), 6.98 ppm (s, 1, 6-*H*); ^{13}C nmr ($CDCl_3$) δ_C: 15.7 (3-CH_3), 16.9 (5-CH_3), 20.8 (1-CH_3), 127.0 (*C*-5), 127.8 (*C*-3), 130.4 (*C*-6), 133.0 (*C*-2), 138.5 (*C*-1), 150.9 ppm (*C*-4); ms[8] (70 eV) *m/e* (relative intensity): 199* (87, M), 182* (100, *M* − OH), 154* (48), 127* (54), 115 (56), 91 (65). *Anal.* calcd. for $C_9H_{10}ClNO_2$: C 54.14, H 5.01, N 7.02; found: C 53.99, H 4.92, N 7.19.

The 45 and 50% ether fractions afforded one diastereomer of 4-chloro-1,3,5-trimethyl-4-nitrocyclohexa-2,5-dienyl acetate (**1***a*). Crystallization from ether–pentane gave colourless crystals mp 46–49°C; ir (Nujol): 1740 and 1240 ($OCOCH_3$), 1560 cm^{-1} (NO_2); ^{1}H nmr (CCl_4) δ: 1.56 (s, 3, 1-CH_3), 1.87 (s, 6, 3-CH_3 and 5-CH_3), 1.94 (s, 3, $OCOCH_3$), 6.04 ppm (s, 2, 2-*H* and 6-*H*); ^{13}C nmr ($CDCl_3$) δ_C: 17.5 (3-CH_3 and 5-CH_3), 21.7 ($OCOCH_3$), 26.9 (1-CH_3), 74.0 (*C*-1), 104.7 (*C*-4), 129.8 (*C*-3 and *C*-5), 132.2 (*C*-2 and *C*-6), 170.0 ppm ($OCOCH_3$); ms (chemical ionization, methane) *m/e* (relative intensity): 213* (30, *M* − NO_2), 171* (100), 154* (71), 135 (30), 119 (22). *Anal.* calcd. for $C_{11}H_{14}ClNO_4$: C 50.86, H 5.39, N 5.39; found: C 50.58, H 5.33, N 4.91.

The 55% ether fraction contained as the major constituent the other diastereomer of 4-chloro-1,3,5-trimethyl-4-nitrocyclohexa-2,5-dienyl acetate (**1***b*) together with some **1***a*. Diene **1***b* was crystallized from ether–pentane. The colourless crystals had mp 63.5–64.5°C; ir (Nujol): 1745 and 1235 ($OCOCH_3$), 1570 cm^{-1} (NO_2); ^{1}H nmr ($CDCl_3$) δ: 1.52 (s, 3, 1-CH_3), 1.85 (s, 6, 3-CH_3 and 5-CH_3), 2.00 (s, 3, $OCOCH_3$), 6.17 ppm (s, 2, 2-*H* and 6-*H*); ^{13}C nmr ($CDCl_3$) δ_C: 17.0 (3-CH_3 and 5-CH_3), 21.8 ($OCOCH_3$), 25.3 (1-CH_3), 74.9 (*C*-1), 103.0 (*C*-4), 129.7 (*C*-3 and *C*-5), 133.6 (*C*-2 and *C*-6), 169.8 ppm ($OCOCH_3$); ms (chemical ionization, methane) *m/e* (relative intensity): 224 (13, *M* − Cl), 213* (25, *M* − NO_2), 171* (100), 154* (62), 135 (13), 119 (10). *Anal.* calcd. for $C_{11}H_{14}ClNO_4$: C 50.86, H 5.39, N 5.39; found: C 50.67, H 5.51, N 5.67.

The 60% ether fractions contained two other dienes, **2***a* and **2***b*, as well as **1***b*. Diene **2***a*, one diastereoisomer of 3-chloro-2,4,6-trimethyl-4-nitrocyclohexa-2,5-dienyl acetate was not isolated but its ^{1}H nmr could be determined from the mixture: (CCl_4) δ: 1.74 (s, 3, 6-CH_3), 1.82 (s, 3, 4-CH_3), 1.90 (s, 3, 2-CH_3), 2.10 (s, 3, $OCOCH_3$), 5.73 (s, 1, 5-*H*), 5.96 ppm (s, 1, 1-*H*).

The 65–100% ether fractions afforded the second diastereoisomer of 3-chloro-2,4,6-trimethyl-4-nitrocyclohexa-2,5-dienyl acetate (**2***b*), obtained as colourless crystals from ether–pentane, mp 54–56°C; uv (CH_3OH): 217.5 nm (800 m^2 mol^{-1}); ir (Nujol): 1735 and 1225 ($OCOCH_3$), 1550 cm^{-1} (NO_2); ^{1}H nmr ($CDCl_3$) δ: 1.76 (s, 3, 6-CH_3), 1.86 (s, 3, 4-CH_3), 1.92 (s, 3, 2-CH_3), 2.18 (s, 3, $OCOCH_3$), 5.73 (s, 1, 5-*H*), 5.93 ppm (s, 1, 1-*H*); ^{13}C nmr ($CDCl_3$) δ_C: 16.8 (2-CH_3), 19.1 (6-CH_3), 20.7 ($OCOCH_3$), 24.7 (4-CH_3), 69.8 (*C*-1), 89.3 (*C*-4), 125.0 (*C*-5), 128.5 (*C*-3), 134.0 (*C*-2), 136.4 (*C*-6), 170.1 ppm ($OCOCH_3$); ms (chemical ionization, methane) *m/e* (relative intensity): 213* (100, *M* − NO_2), 171* (25), 154* (35), 123 (82). *Anal.* calcd. for $C_{11}H_{14}ClNO_4$: C 50.86, H 5.39, N 5.39; found: C 50.84, H 5.53, N 5.61.

3-Chloro-2,4,6-trimethylphenol and 3-Chloro-2,4,6-trimethylphenyl Acetate

2-Chloro-4-nitromesitylene was reduced with stannous chloride in hydrochloric acid to 3-chloro-2,4,6-trimethylaniline; ir (film): 3460 and 3395 (m, NH_2), 2925 (m), 1627 (s), 1474 (s), 985 cm^{-1} (m); ^{1}H nmr (CCl_4) δ: 2.00 (s, 3, 6-CH_3), 2.13 (s, 3, 2-CH_3), 2.18 (s, 3, 4-CH_3), 3.25 (s, 2, NH_2), 6.60 ppm (s, 1, 5-*H*); the signal at 3.25 ppm disappeared on treatment with D_2O. Sodium nitrite (1.5 g, 22 mmol) in water (10 cm^3) was added slowly to a solution of the arylamine (3 g, 18 mmol) in sulfuric acid (30 cm^3) at 0°C. After 2 h the solution of the diazonium salt was slowly added to a solution of sulfuric acid (20 cm^3) in water at 50°C. After cooling and neutralization with aqueous sodium bicarbonate the phenol was extracted with ether and purified by chromatography, followed by crystallization from ethanol. 3-Chloro-2,4,6-trimethylphenol had mp 84–85°C; ir (Nujol): 3350 cm^{-1} (OH); ^{1}H nmr (CCl_4) δ: 2.17 (s, 3, 6-CH_3), 2.27 (s, 6, 2-CH_3 and 4-CH_3), 4.46 (s, 1, *OH*), 6.79 ppm (s, 1, 5-*H*); ^{13}C nmr ($CDCl_3$) δ_C: 13.2 (2-CH_3), 15.7 (6-CH_3), 20.0 (4-CH_3), 121.2 (*C*-6), 121.9 (*C*-2), 127.7 (*C*-4), 129.5 (*C*-5), 132.4 (*C*-3), 150.6 ppm (*C*-1); ms (70 eV) *m/e* (relative intensity): 170* (73, M), 155* (24, *M* − CH_3), 135 (100, *M* − Cl), 105 (21), 91 (42), 77 (39). *Anal.* calcd. for $C_9H_{11}ClO$: C 63.53, H 6.47; found: C 63.42, H 6.58.

A solution of the chloromesitol (300 mg) in pyridine (1 cm^3) and acetic anhydride (4 cm^3) was heated under reflux for 30 min. Cooling in ice, dilution with water, and extraction with ether afforded 3-chloro-2,4,6-trimethylphenyl acetate, ir (film): 1770 and 1212 cm^{-1} ($OCOCH_3$); ^{1}H nmr ($CDCl_3$) δ: 2.07 (s, 3, 6-CH_3), 2.17 (s, 3, 2-CH_3), 2.31 (s, 6, 4-CH_3 and $OCOCH_3$), 6.93 ppm (s, 1, 5-*H*); (CCl_4) δ: 2.03 (s, 3, 6-CH_3), 2.13 (s, 3, 2-CH_3), 2.24 (s, 3, $OCOCH_3$), 2.29 (s, 3, 4-CH_3), 6.87 ppm (s, 1, 5-*H*); ^{13}C nmr ($CDCl_3$) δ_C: 14.0 (2-CH_3), 16.0 (6-CH_3), 20.2 ($OCOCH_3$), 20.3 (4-CH_3), 128.2 (C-6), 128.5 (*C*-2), 129.8 (*C*-5), 132.4 (*C*-3), 133.6 (*C*-4), 146.5 (*C*-1), 169.2 ppm ($OCOCH_3$); ms (70 eV) *m/e* (relative intensity): 212* (10, M), 170* (100, *M* − CH_2CO), 135 (75, *M* − C_2H_2ClO), 91 (70).

2-Chloro-3,5-dimethylbenzyl Acetate and 4-Chloro-3,5-dimethylbenzyl Acetate

A solution of chloromesitylene (5 g, 32 mmol) and *N*-bromosuccinimide (6.4 g, 65 mmol) in carbon tetrachloride (100 cm^3) was heated under reflux and irradiated with uv light for 2 h. The succinimide was filtered, the solution washed with water, dried, and evaporated to give a mixture of side-chain bromides (8.3 g). The crude product (6.2 g, 20 mmol) was heated under reflux with potassium acetate (5.5 g, 50 mmol) in 95% ethanol (100 cm^3) for 2.3 h. After dilution with water and extraction with ether a mixture of side-chain acetates (5 g) was obtained. Chromatography on silica gel and elution with ether–pentane mixtures gave, in the 12.5% ether fraction, 4-chloro-3,5-dimethylbenzyl acetate, ir (film): 1735 and 1215 cm^{-1} ($OCOCH_3$); ^{1}H nmr (CCl_4) δ: 1.96 (s, 3, $OCOCH_3$), 2.27 (s, 6, 3-CH_3 and 5-CH_3), 4.83 (s, 2, CH_2), 6.94 ppm (s, 2, 2-*H* and 6-*H*); ^{13}C nmr ($CDCl_3$) δ_C: 20.6 (3-CH_3, 5-CH_3, $OCOCH_3$), 65.6 (CH_2), 128.3 (*C*-2 and *C*-6), 134.0 (*C*-1), 134.4 (*C*-4), 136.3 (*C*-3 and *C*-5), 170.4 ppm ($OCOCH_3$); ms (70 eV) *m/e* (relative intensity): 212* (53, M), 170* (100, *M* − CH_2CO), 153* (56, *M* − CH_3CO_2), 135 (74, *M* − C_2H_2ClO), 117 (47), 91 (22), 77 (20). The 22.5% ether fraction afforded 1,5-bisacetoxymethyl-2-chloro-3-methylbenzene (0.42 g), ir (film): 1740 and 1225 cm^{-1} ($OCOCH_3$); nmr (CCl_4) δ: 2.00 (s, 3, 5-CH_2OCOCH_3), 2.04 (s, 3, 1-CH_2OCOCH_3), 2.34 (s, 3, 3-CH_3), 4.90 (s, 2, 5-CH_2), 5.04 (s, 2, 1-CH_2), 7.12 ppm (s, 2, 4-*H* and 6-*H*).

The 10% ether fraction contained a mixture of monoacetates which were separated on a second column to give 2-chloro-3,5-dimethylbenzyl acetate, ir (film): 1740 and 1230 cm^{-1} ($OCOCH_3$); ^{1}H nmr (CCl_4) δ: 2.00 (s, 3, $OCOCH_3$), 2.23 (s, 3, 5-CH_3), 2.27 (s, 3, 3-CH_3), 5.00 (s, 2, CH_2), 6.92 (broad s, 2, 4-*H* and 6-*H*); ^{13}C nmr ($CDCl_3$) δ_C: 20.2 and 20.7 (3-CH_3

[8]Peaks containing ^{35}Cl are marked with an asterisk. Each such peak was accompanied by a ^{37}Cl peak of approximately one-third the intensity.

Can. J. Chem. Downloaded from www.nrcresearchpress.com by 210.87.254.6 on 09/05/12
For personal use only.

and 5-CH_3), 20.7 ($OCOCH_3$), 64.1 (CH_2), 128.0 (*C*-6), 130.7 (*C*-2), 131.5 (*C*-4), 133.4 (*C*-1), 136.1 (*C*-5), 136.3 (*C*-3), 170.4 ppm ($OCOCH_3$); ms (70 eV) *m/e* (relative intensity): 212* (52, M), 177 (68, $M - Cl$), 170* (63, $M - CH_2CO$), 153* (58, $M - OCOCH_3$), 135 (100, $M - C_2H_2ClO$), 119 (79), 117 (83), 91 (38), 77 (44).

Decomposition of Dienes at Ambient Temperature. Pyrolysis

Rearomatization of the dienes occurred on prolonged storage even at −20°C. Dienes **1***a* and **1***b* gave mainly 4-chloro-3,5-dimethylphenylnitromethane which was recrystallised from ethanol, mp 92–93°C; ir (Nujol): 1545 cm^{-1} (NO_2); ^1H nmr ($CDCl_3$) δ: 2.37 (s, 6, 3-CH_3 and 5-CH_3), 5.29 (s, 2, CH_2), 7.12 ppm (s, 2, 2-*H* and 6-*H*); ^{13}C nmr ($CDCl_3$) δ_C: 20.7 (3-CH_3 and 5-CH_3), 79.4 (CH_2), 127.3 (*C*-4), 128.9 (*C*-1), 129.7 (*C*-2 and *C*-6), 137.2 (*C*-3 and *C*-5); ms (chemical ionization, methane) *m/e* (relative intensity): 199* (2, M), 181* (4, $M - H_2O$), 164 (1, $M - Cl$), 153* (100, $M - NO_2$); *Anal.* calcd. for $C_9H_{10}ClNO_2$: C 54.14, H 5.01, N 7.02; found: C 54.29, H 5.07, N 7.11.

On prolonged standing at room temperature the colourless solid diene **2***b* gave off brown fumes of nitrogen dioxide and formed a green liquid which contained essentially pure 3-chloro-2,4,6-trimethylphenyl acetate of identical ir, ^1H nmr, and ^{13}C nmr to that of the authentic acetate described above.

A sample of diene **1***a* in carbon tetrachloride was injected into the inlet of a gas chromatograph at 200°C. Analysis by glc and glc – mass spectrometry indicated the following product composition: chloromesitylene (22%) *m/e* (relative intensity): 154* (100, M), 119 (45, $M - Cl$); 2-chloro-4-nitromesitylene (27%), *m/e* (relative intensity): 199* (100, M), 182* (25, $M - OH$); 3-chloro-2,4,6-trimethylphenyl acetate (32%), *m/e*: 212* (37, M), 170* (100, $M - CH_2CO$); minor products 19%. A similar experiment with diene **1***b* gave chloromesitylene (56%), 2-chloro-4-nitromesitylene (14%), and 3-chloro-2,4,6-trimethylphenyl acetate (30%). Similar thermolysis of diene **2***b* gave 3-chloro-2,4,6-trimethylphenyl acetate (97%).

*Reaction of Diene **1** with Hydrogen Chloride*

Hydrogen chloride was bubbled through a solution of diene **1***a* (175 mg, 0.8 mmol) in ether (15 cm^3) at −12°C for 30 min. The reaction mixture was aspirated for 30 min and then neutralised with gaseous ammonia at −15°C. Excess NH_4Cl was filtered off and the solution dried and evaporated to give 3,6-dichloro-1,3,5-trimethyl-6-nitro-1,4-cyclohexadiene; ^1H nmr ($CDCl_3$) δ: 1.77 (s, 3, 3-CH_3), 1.86 (s, 3, 1-CH_3 and 5-CH_3), 6.06 ppm (s, 2, 2-*H* and 4-*H*), together with a smaller amount of aromatic compound, predominantly 2-chloro-4-nitromesitylene. A small peak at 1.72 ppm was likely the 3-CH_3 of the minor diastereoisomer.

Reaction of Diene 2b *with Trifluoromethanesulfonic Acid*

Trifluoromethanesulfonic acid (300 mm^3) at −78°C was added to a solution of diene **2***b* (56 mg, 0.2 mmol) in $CDCl_3$ (75 mm^3) also at −78°C. An immediate reaction occurred. After work-up[9] the products were identified by glc and glc – mass spectrometry (relative retention time, *m/e* of molecular ion, % composition) 1,3,5-trimethylbenzene-2,4-diol (3.5, 152, 12%), 3-chloro-2,4,6-trimethylphenol (4.5, 170*, 44%), 2-chloro-4-nitromesitylene (5.6, 199*, 17%), 3-chloro-2,4,6-trimethylphenyl acetate (6.8, 212*, 11%). Components at 2.5, 4%, and 13.7, 12%, were not identified.

[9]Small-scale reactions were worked up by addition of the solution to methylene chloride, neutralization with gaseous ammonia, drying over magnesium sulfate, followed by evaporation of the solvent.

Reaction of Dienes with Boron Trifluoride

$BF_3{\cdot}OEt_2$ (200 mm^3) was added to diene **1***a* (50 mg, 0.2 mmol) at −78°C. The ^1H nmr spectrum showed that 2-chloro-4-nitromesitylene and 4-chloro-3,5-dimethylphenylnitromethane were formed. When $BF_3{\cdot}OEt_2$ was added to a solution of diene **1***b* in $CDCl_3$ at 0°C only the 2-chloro-4-nitromesitylene was obtained on work-up, identified by nmr.

$BF_3{\cdot}OEt_2$ (300 mm^3) was added to a solution of diene **2***b* (57 mg) in $CDCl_3$ (50 mm^3) at −78°C and the solution allowed to warm to ambient temperature. Only 3-chloro-2,4,6-trimethylphenyl acetate was obtained on work-up (nmr).

Reaction of Dienes with Trifluoroacetic Acid – Trifluoroacetic Anhydride

A mixture of trifluoroacetic acid (150 mm^3) and its anhydride (150 mm^3) was added to diene **1***a* (107 mg, 0.4 mmol) in $CDCl_3$ (75 mm^3) at −78°C and the solution allowed to warm to ambient temperature. ^1H nmr showed that the major product was 2-chloro-4-nitromesitylene, confirmed after work-up by glc.

The same reaction carried out on diene **2***b* gave only 3-chloro-2,4,6-trimethylphenyl acetate, identified by ir, nmr, glc, and mass spectrometry, on work-up.

Reaction of Dienes in Acetic Acid

Diene **1***a* (86 mg, 0.3 mmol) was added to [$^2H_4$]acetic acid and the reaction monitored by ^1H nmr at 35°C. The diene slowly rearomatised ($t_{1/2} \sim 1$ h) to four side-chain derivatives with CH_2 peaks (and approximate composition) at δ: 5.58 (13%), 5.36 (30%, 4-chloro-3,5-dimethylphenylnitromethane), 4.98 (13%, 4-chloro-3,5-dimethylbenzyl acetate), 4.56 ppm (5%), and 3-chloro-2,4,6-trimethylphenyl acetate (38%). When the reaction was repeated using diene **1***b* in a solution of [$^2H_4$]acetic acid (180 mm^3) containing acetic anhydride (20 mm^3) the same products were obtained but the compound with δ 5.58 ppm was now the major product (~35%). The nitromethane and benzyl acetate derivatives were identified by addition of authentic samples and observing enhancement of the appropriate peaks in the nmr spectra. The CH_2 peak at δ 5.58 ppm disappeared on standing the reaction mixture for 3 months and new peaks appeared at 7.6, 7.8, and 9.88 ppm. Rearomatization of diene **1***b* was accompanied by partial isomerization to diene **1***a*. When the reaction was repeated using diene **1***a* in a solution of [$^2H_4$]acetic acid (270 mm^3) containing D_2O (30 mm^3) rearomatization occurred rapidly ($t_{1/2} \approx 20$ min) and the side-chain derivatives with CH_2 peaks at 5.58, 5.36, and 4.98 ppm were again formed as well as the phenyl acetate. The benzyl acetate was the major side-chain product. The CH_2 peak at 5.58 ppm again disappeared when the reaction mixture was allowed to stand for two months and new peaks appeared at 7.6, 7.8, and 9.8 ppm. Analysis of the worked-up reaction mixture by glc – mass spectrometry revealed a compound with $M = 168$, assigned as 4-chloro-3,5-dimethylbenzaldehyde, as well as the 3-chloro-2,4,6-trimethylphenyl acetate, 4-chloro-3,5-dimethylbenzyl acetate, and 4-chloro-3,5-dimethylphenylnitromethane. The last three compounds had the appropriate mass spectra and glc retention times were the same as those of authentic samples. The examination of the spectra of the initial reaction carried out in [$^2H_4$]acetic acid revealed that in this case too the compound with $\delta = 5.58$ disappeared on standing and the peaks attributed to the benzyaldehyde appeared. On work-up the compound with mass 168 was detected by glc – mass spectrometry. The characteristic methyl peaks of 3-chloro-2,4,6-trimethylphenyl acetate were recognised in the nmr spectrum of the worked-up product and the presence of this compound, 4-chloro-3,5-dimethylbenzyl acetate and 4-chloro-3,5-dimethylphenylnitromethane were confirmed by comparison

Can. J. Chem. Downloaded from www.nrcresearchpress.com by 210.87.254.6 on 09/05/12
For personal use only.

of glc retention times and glc – mass spectrometry. The benzyaldehyde and phenyl acetate were also detected by glc – mass spectrometry in the worked-up product of the reaction in [$^2H_4$]acetic acid containing acetic anhydride.

Diene **2***b* in [$^2H_4$]acetic acid at 35°C gave very rapidly ($t_{1/2}$ < 5 min) 3-chloro-2,4,6-trimethylphenyl acetate with identical ir, ^{1}H nmr, and glc retention time to an authentic sample.

Reaction with Aqueous Acid in [$^2H_6$]Acetone

A solution of diene **1***a* (53 mg, 0.2 mmol) in aqueous [$^2H_6$]acetone containing 10% (v/v) water and 0.1% sulfuric acid by volume was made up at 0°C and the reaction was observed by nmr at 35°C. After 1 h new absorptions, attributed to the hydroxydiene **9***x*, appeared at δ 1.27 and 1.36 (1-CH_3 of each diastereoisomer), 1.83 (3-CH_3 and 5-CH_3)$_3$, and 6.06 ppm (2-*H*- and 6-*H*). A new acetate peak (CH_3CO$_2$H) appeared at slightly higher field than that of the acetate peak of **1***a*. After 20 h the peak of **1***a* at 1.53 ppm (1-CH_3) had almost completely disappeared. The half-life of the original acetate was ~6 h. The diastereoisomer with 1-CH_3 at 1.27 was present to ca. 50% of that with 1-CH_3 at 1.36 ppm.

Reaction of Dienes with Acidified Methanol

Diene **1***a* (50 mg, 0.2 mmol) was added to a solution of sulfuric acid (6 μmol) in methanol (300 mm^3) at 0°C. Examination by nmr showed that no appreciable reaction occurred at this temperature but exchange was observed when the temperature was raised to 20°C and was more rapid at 30°C. The signal at δ 1.50 ppm associated with the 1-CH_3 of **1***a* decreased and disappeared and was replaced by two signals at 1.22 and 1.31 (1-CH_3 of the isomeric methoxy dienes). Simultaneously the sharp signal at 1.80 (3-CH_3 and 5-CH_3 of **1***a*) broadened (3-CH_3 and 5-CH_3 of isomeric methoxy dienes) the acetate signal at 1.95 was replaced by one at 1.97 (CH_3CO$_2$H) and the latter itself was gradually replaced by a new peak, attributed to methyl acetate formed by esterification of the liberated acetic acid; the signal at 6.07 (2-*H* and 6-*H* of **1***a*) was replaced by signals at 5.83 and 5.87 ppm (2-*H* and 6-*H* of isomeric methoxy dienes). After work-up a 1:1 mixture of the *cis* and *trans* isomers of 4-chloro-1,3,5-trimethyl-4-nitrocyclohexa-2,5-dienyl methyl ether (**9***y*) was obtained, ^{1}H nmr (CDCl$_3$) δ: 1.28 and 1.37 (s, 3 and 3, 1-CH_3), 1.87 (broad s, 6 and 6, 3-CH_3 and 5-CH_3), 3.03 and 3.15 (s, 3 and 3, OCH_3), 5.80 ppm (broad s, 2 and 2, 2-*H* and 6-*H*); ^{13}C nmr (CDCl$_3$) δ_C: 17.1 and 17.4 (3-*C*H$_3$ and 5-*C*H$_3$), 26.6 and 27.4 (1-*C*H$_3$), 52.4 and 52.8 (O*C*H$_3$), 71.9 (*C*-1), 132.3 and 132.6 (*C*-3 and *C*-5), 134.8 and 136.0 (*C*-2 and *C*-6). It was not possible to distinguish with certainty the peaks of *C*-4 (90.4?) from the background. These peaks are expected to be of low intensity.

Reaction of diene **2***b* under the same conditions gave only 3-chloro-2,4,6-trimethylphenyl acetate, identified by ir, nmr, glc, and mass spectrometry.

*Reaction of Diene **1** with Silver Nitrate in Methanol*

Diene **1***a* (79 mg, 0.3 mmol) was added to a solution of silver nitrate (98 mg, 0.6 mmol) in methanol (500 mm^3) at −78°C and the reaction was monitored by ^{1}H nmr at 35°C. Rearomatization occurred rapidly and was accompanied by the exchange of the acetate group for methoxyl as indicated by the development of signals at δ 1.23, 1.33, and 5.8 ppm characteristic of the diastereoisomer mixture of methoxy-nitro adducts. After work-up the nmr spectrum indicated the absence of methylene peaks and therefore of side-chain derivatives. Analysis by glc and glc – mass spectrometry gave major peaks whose structures were assigned from the mass spectra, on the assumption that the basic mesitylene structure was retained, as follows (relative retention time, *m/e* of molecular ion, % composition): 3-methoxy-2,4,6-trimethylphenol (1.5, 166, 15%), 2-chloro-4-nitromesitylene (5.6, 199, 24%), 3-chloro-2,4,6-trimethylphenyl acetate (6.8, 212, 52%), and 2,4,6-trimethyl-3-nitrophenyl acetate (10, 223, 8%). Authentic samples of 2-chloro-4-nitromesitylene and 3-chloro-2,4,6-trimethylphenyl acetate had the same retention time as the respective components assigned these structures.

The experiment was repeated in [$^2H_4$]methanol, which simplified ^{1}H nmr observation of the progress of the reaction. After 50 h aromatic products constituted ca. 80% of the reaction mixture which was worked up and examined by glc and glc – mass spectrometry which indicated the following composition: 3-[$^2H_3$]methoxy-2,4,6-trimethylphenol (1.5, 169, 20%), 2-chloro-4-nitromesitylene (5.3, 199, 21%), 3-chloro-2,4,6-trimethylphenyl acetate (6.5, 212, 45%), 3-nitro-2,4,6-trimethylphenyl acetate (10, 223, 8%), as well as other minor components. Examination of the nmr spectra taken as the reaction proceeded resulted in the following observations: within the first fifteen minutes a substantial amount of rearomatisation occurred, accompanied by the formation of the diastereoisomeric methoxy-nitro dienes (δ 1.23, 1.31, 5.85 ppm) and the disappearance of the acetoxy-nitro diene (δ 1.51, 6.10 ppm); a peak appeared at δ 1.46 ppm and appeared to be associated with a peak at 6.7 ppm since these disappeared again together over a 2 h period; as the peak at 6.7 ppm disappeared a new peak appeared at 6.58 ppm; the methoxy, nitro diene peaks (δ 1.23, 1.31, 5.85 ppm) disappeared over 50 h; the peak at 6.58 ppm is associated with peaks at 1.92 and 1.37 ppm since these peaks appeared together (the 1.92 ppm peak is also present in the acetoxy-nitro diene and the methoxy-nitro dienes and is the absorption of the six protons of the two identical methyl groups attached to the double bonds in these compounds; the peak remained but became sharper as the methoxy-nitro dienes disappeared; similarly, there is an overlap of the 1.31 ppm peak of one methoxy-nitro diene isomer and the 1.37 ppm peak); the last three peaks were also present at 6.47, 1.92, and 1.37 ppm in the worked-up reaction product and integrated for 2, 6, and 3 protons, respectively, appropriate for two ring protons, two methyl groups attached to double bonds, and one methyl group attached to saturated carbon; the diene component constituted 20% of the reaction mixture after work-up. Re-examination of the spectra of the reaction carried out in the nondeuterated methanol supported the foregoing observations.

*Reaction of Diene **1** with Silver Nitrite in Methanol*

Diene **1***a* (94 mg, 0.4 mmol) was added to a solution of silver nitrite (81 mg, 0.5 mmol) in [$^2H_4$]methanol (500 mm^3) at −78°C and the reaction monitored by nmr at 35°C. The changes that ensued parallelled those for the reaction with silver nitrate. After work-up, glc and glc – mass spectrometry gave the following product composition: 3-[$^2H_3$]methoxy-2,4,6-trimethylphenol (1.5, 169, 19%), 2-chloro-4-nitromesitylene (5.3, 199, 22%), 3-chloro-2,4,6-trimethylphenyl acetate (6.5, 212, 51%), 3-nitro-2,4,6-trimethylphenyl acetate (10, 223, 4%).

*Reaction of Diene **1** with Silver Acetate in Acetone*

Silver acetate (38 mg, 0.23 mmol) was added to a solution of diene **1***a* (97 mg, 0.4 mmol) in [$^2H_6$]acetone (500 mm^3) at 0°C and the reaction monitored at 35°C by ^{1}H nmr. The diene was largely rearomatized over 24 h. Work-up and analysis by glc and glc – mass spectrometry gave the following major components: 2-chloro-4-nitromesitylene (5.1, 199, 15%), 3-chloro-2,4,6-trimethylphenyl acetate (6.2, 212, 56%), 3-nitro-2,4,6-trimethylphenyl acetate (10, 223, 23%). The presence of nitro and acetate functions was confirmed by ir. The reaction was repeated with an excess of silver acetate (0.2 mmol of diene,

0.36 mmol of siver acetate) and similar results were obtained: 2-chloro-4-nitromesitylene (5.2, 199, 24%), 3-chloro-2,4,6-trimethylphenyl acetate (6.3, 212, 54%), 3-nitro-2,4,6-trimethylphenyl acetate (10, 223, 15%).

1. A. FISCHER and C. C. GREIG. Can. J. Chem. **56**, 1063 (1978).
2. C. L. PERRIN and G. A. SKINNER. J. Am. Chem. Soc. **93**, 3389 (1971).
3. T. BANWELL, C. S. MORSE, P. C. MYHRE, and A. VOLLMAR. J. Am. Chem. Soc. **99**, 3042 (1977).
4. K. FUJIWARA, J. C. GIFFNEY, and J. H. RIDD. J. Chem. Soc. Chem. Commun. 301 (1977).
5. R. B. MOODIE and K. SCHOFIELD. Acc. Chem. Res. **9**, 287 (1976).
6. H. SUZUKI. Synthesis, 217 (1977).
7. A. H. CLEMENS, M. P. HARTSHORN, K. E. RICHARDS, and G. J. WRIGHT. Aust. J. Chem. **30**, 103 (1977).
8. R. C. HAHN and M. B. GROEN. J. Am. Chem. Soc. **95**, 6128 (1973).
9. D. J. BLACKSTOCK, A. FISCHER, K. E. RICHARDS, J. VAUGHAN, and G. J. WRIGHT. Chem. Commun. 641 (1970).
10. A. FISCHER and D. R. A. LEONARD. Can. J. Chem. **50**, 3367 (1972).
11. B. A. COLLINS, K. E. RICHARDS, and G. J. WRIGHT. J. Chem. Soc. Chem. Commun. 1216 (1972).
12. G. A. OLAH and S. J. KUHN. J. Am. Chem. Soc. **86**, 1067 (1964).
13. D. V. NIGHTINGALE. Chem. Rev. **40**, 117 (1947).
14. K. FRIES. Justus Liebigs Ann. Chem. **389**, 315 (1912).
15. C. L. PERRIN. J. Org. Chem. **36**, 420 (1971).
16. (*a*) D. J. BLACKSTOCK, M. P. HARTSHORN, A. J. LEWIS, K. E. RICHARDS, J. VAUGHAN, and G. J. WRIGHT. J. Chem. Soc. B, 1212 (1971); (*b*) A. H. CLEMENS, M. P. HARTSHORN, K. E. RICHARDS, and G. J. WRIGHT. Aust. J. Chem. **30**, 113 (1977).
17. A. FISCHER and G. J. WRIGHT. Aust. J. Chem. **27**, 217 (1974).
18. J. D. ROBERTS, J. K. SANFORD, F. L. J. SIXMA, H. CERFONTAIN, and R. ZAGT. J. Am. Chem. Soc. **76**, 4525 (1954).
19. P. C. MYHRE. J. Am. Chem. Soc. **94**, 7921 (1972).
20. A. FISCHER and C. C. GREIG. Can. J. Chem. **52**, 1231 (1974).
21. R. G. GILLIS. J. Org. Chem. **21**, 805 (1956).
22. H. SUZUKI, H. YONEDA, and T. HANAFUSA. Bull. Chem. Soc. Jpn. **48**, 2116 (1975).
23. A. FISCHER and K. C. TEO. Can. J. Chem. **56**, 258 (1978).
24. L. I. SMITH and C. L. MOYLE. J. Am. Chem. Soc. **58**, 1 (1936).
25. R. ADAMS and M. J. GORTATOWSKI. J. Am. Chem. Soc. **79**, 5525 (1957).

Can. J. Chem. Downloaded from www.nrcresearchpress.com by 210.87.254.6 on 09/05/12
For personal use only.

Conformational studies on cyclohexa-1,4-diene derivatives. The crystal and molecular structures of 1,2,4,5-tetraphenyl-3,6-dicarbomethoxycyclohexa-1,4-diene and 1,2-dicarbomethoxy-4,5-dimethylcyclohexa-1,4-diene

M. J. BENNETT AND J. T. PURDHAM[1]

Department of Chemistry, University of Alberta, Edmonton, Alta., Canada T6G 2G2

Received July 29, 1977

M. J. BENNETT and J. T. PURDHAM. Can. J. Chem. **56**, 1358 (1978).

1,2,4,5-Tetraphenyl-3,6-dicarbomethoxycyclohexa-1,4-diene crystallizes in the monoclinic space group $I2/a$ (a non-standard setting of $C2/c$) with $a = 20.052(2)$, $b = 5.756(1)$, $c = 22.782(2)$ Å, $\beta = 95.73(1)°$, and $Z = 4$. 1,2-Dicarbomethoxy-4,5-dimethylcyclohexa-1,4-diene crystallizes in the orthorhombic space group *Pbca* with $a = 25.627(2)$, $b = 11.240(1)$, $c = 8.342(1)$ Å, and $Z = 8$. Both structures were solved by direct methods and refined by full matrix least-squares techniques to $R = 0.040$ and $R = 0.036$, respectively. Carbon–carbon double bond lengths are similar in the two compounds (1.326 and 1.333 Å, respectively), but the single bond lengths are significantly longer in 1,2,4,5-tetraphenyl-3,6-dicarbomethoxycyclohexa-1,4-diene (1.518 Å) compared with the 1.493 Å average found in 1,2-dicarbomethoxy-4,5-dimethylcyclohexa-1,4-diene. This and the fact that there are also small deviations from planarity in the former compound are thought to be due to the presence of substituents on the methylenic carbon atoms.

M. J. BENNETT et J. T. PURDHAM. Can. J. Chem. **56**, 1358 (1978).

Le tétraphényl-1,2,4,5 dicarbométhoxy-3,6 cyclohexadiène-1,4 cristallise dans le groupe d'espace $I2/a$ (un arrangement anormal de $C2/c$) avec $a = 20.052(2)$, $b = 5.756(1)$, $c = 22.782(2)$ Å, $\beta = 95.73(1)°$ et $Z = 4$. Le dicarbométhoxy-1,2 diméthyl-4,5 cyclohexadiène-1,4 cristallise dans le groupe d'espace orthorhombique *Pbca* avec $a = 25.627(2)$, $b = 11.240(1)$, $c = 8.342(1)$ Å et $Z = 8$. On a résolu les deux structures par les méthodes directes et on les a affinées par la méthode des moindres carrés (matrice complète) jusqu'à des valeurs finales respectives de $R = 0.040$ et $R = 0.036$. Les longueurs des liaisons doubles carbone–carbone sont semblables dans les deux composés (respectivement 1.326 et 1.333 Å) mais les longueurs des liaisons simples sont passablement plus longues dans le tétraphényl-1,2,4,5 dicarbométhoxy-3,6 cyclohexadiène-1,4 (1.518 Å) que dans le dicarbométhoxy-1,2 diméthyl-4,5 cyclohexadiène-1,4 (1.493 Å). Ce résultat et le fait qu'il y a aussi de petites déviations de planarité dans le premier composé seraient probablement dus à la présence de substituants sur les atomes de carbone méthyléniques.

[Traduit par le journal]

The conformation of cyclohexa-1,4-diene has been investigated by various techniques (1–14), with conflicting conclusions being reached as to the planarity of the six-membered ring.

In two independent and conflicting electron diffraction studies of cyclohexa-1,4-diene itself, Dallinga and Toneman (13) concluded that the molecule was essentially planar, but that small deviations leading to the chair form could not be precluded with certainty. The suggested deviations from the plane were less than 0.05 Å. Oberhammer and Bauer (14), on the other hand, obtained a structure with a boat conformation, with a significant deviation from the diene plane for the methylenic type carbon atoms.

Similar conflicting conclusions involving boat and planar conformations have resulted from nmr studies of cyclohexa-1,4-diene derivatives (9–12).

Three other cyclohexa-1,4-diene derivatives have been studied by single crystal X-ray diffraction. The conformations of 1,4-dicarbomethoxycyclohexa-1,4-diene (15, 16) and cyclohexa-1,4-diene-1-glycine (17) were found to be planar within experimental error, but standard deviations on the atomic parameters were such that small deviations from planarity could not be detected. The conformation of diethyl succinyl succinate (18) was also found to be essentially planar, small deviations from planarity being deemed insignificant.

In view of the contradictory conclusions arrived at, regarding the conformation of cyclohexa-1,4-diene and its derivatives, the molecular structures of 1,2,4,5-tetraphenyl-3,6-dicarbomethoxycyclohexa-1,4-diene (TDCD) and 1,2-dicarbomethoxy-4,5-dimethylcyclohexa-1,4-diene (DDCD) were undertaken in order to provide additional evidence concerning the planarity of the cyclohexa-1,4-diene ring system. The preparation and preliminary structure of TDCD have been reported earlier (19).

[1]Author to whom all correspondence should be sent. Present address: Alberta Labour, Occupational Health and Safety Division, Occupational Hygiene Branch, 9820 – 106th Street, Edmonton, Alta., Canada T5K 2J6.

Can. J. Chem. Downloaded from www.nrcresearchpress.com by 210.87.254.5 on 09/05/12
For personal use only.

Can. J. Chem. Downloaded from www.nrcresearchpress.com by 210.87.254.5 on 09/05/12
For personal use only.

Experimental Section

1,2,4,5-Tetraphenyl-3,6-dicarbomethoxycyclohexa-1,4-diene

Crystal data:

$C_{34}H_{28}O_4$ fw = 500

Monoclinic, $a = 20.052(2)$, $b = 5.756(1)$, $c = 22.782(2)$ Å, $\beta = 95.73(1)°$, $V = 2616.24$ Å^3, $\rho_o = 1.26(1)$ g/ml, $Z = 4$, $\rho_c = 1.269$ g/ml (20°C; CuKα, $\lambda = 1.54182$ Å).

From film data, the space group was identified as either $I2/a$ or Ia with systematic absences occurring for hkl reflections when $h + k + l = 2n + 1$ and for $h0l$ reflections when $h = 2n + 1$. Since there are four molecules per unit cell, this required that each molecule occupied a special position in the space group $I2/a$ while there were no restrictions for the space group Ia. The successful refinement of the structure later confirmed that the space group was in fact $I2/a$. The standard cell C_2/c was not used because of its very obtuse β angle (134.57°). The equivalent positions for the I_2/a cell are: x,y,z; $\bar{x},\bar{y},\bar{z}$; $x,\bar{y},\frac{1}{2}+z$, $\bar{x},y,\frac{1}{2}-z$; $\frac{1}{2}+x,\frac{1}{2}+y,\frac{1}{2}+z$; $\frac{1}{2}-x,\frac{1}{2}-y,\frac{1}{2}+z$; $\frac{1}{2}+x,\frac{1}{2}-y,z$; $\frac{1}{2}-x,\frac{1}{2}+y,\bar{z}$.

Intensity data were collected on a Picker manual diffractometer. 1940 reflections were measured of which 1065 were considered to be significantly above background ($I > 3\sigma(I)$). These data were corrected for Lorentz and polarization effects. No attempt was made to correct for absorption, since this was considered to be negligible ($\mu = 6.67$ cm^{-1}, crystal dimensions 0.15 mm × 0.07 mm × 0.07 mm). However, a correction for the polarization term in the secondary extinction correction was applied (20). Structure factor amplitudes and standard deviations were then calculated.

The structure amplitudes were converted to normalized structure factors and the phases of 162 of the largest of these were determined by the symbolic addition procedure (21). In the E map calculated from these, a six-membered ring occupying a centre of symmetry at the cell origin was easily detected. Further inspection of this map revealed the positions of all 19 carbon and oxygen atoms.

The coordinates of these atoms were used as input to a structure factor calculation, which gave an R_1 value ($\Sigma(||F_o| - |F_c||)/\Sigma|F_o|$) of 0.273 that reduced to 0.097 after three cycles of full matrix least-squares refinement, in which each observation was assigned a weight equal to the reciprocal of its variance. The calculated phases were used to compute an electron density difference map from which the positions of all the hydrogen atoms in the asymmetric unit, other than the three methyl hydrogens, were determined.

These 11 hydrogen atoms were included in the least-squares refinement and R_1 fell to 0.082. The remaining three hydrogen atoms were located in an electron density difference map calculated using only data for which $\sin\theta/\lambda \leq 0.35$. These were included in all the remaining structure factor calculations.

In four more cycles of least-squares refinement, in which the carbon and oxygen atoms were allowed to refine anisotropically, R_1 fell to 0.043. At this point, the correction was made to the data for secondary extinction and the refinement converged in two more cycles to $R_1 = 0.040$ and R_2 ($[\Sigma w(|F_o| - |F_c|)^2/\Sigma w|F_o|^2]^{1/2}$) = 0.042. The largest peak in an electron density difference map computed at the end of the refinement was 0.17 electrons per Å^3.

1,2-Dicarbomethoxy-4,5-dimethylcyclohexa-1,4-diene

Crystal data:

$C_{12}H_{16}O_4$ fw = 224

Orthorhombic, $a = 25.627(2)$, $b = 11.240(1)$, $c = 8.342(1)$ Å, $V = 2405.64$ Å^3, $\rho_o = 1.23(1)$ g/ml, $Z = 8$, $\rho_c = 1.234$ g/ml (20°C; CuKα, $\lambda = 1.54182$ Å).

The compound was prepared by the Diels–Alder reaction betweeen 2,3-dimethyl-1,3-butadiene and dicarbomethoxyacetylene. The impure product was recrystallized from cyclohexane and found to crystallize in the orthorhombic space group $Pbca$, with systematic absences occurring in the $0kl$ data when $k = 2n + 1$, in the $h0l$ data when $l = 2n + 1$, and in the $hk0$ data when $h = 2n + 1$. Intensity data were collected on a Picker FACS I automatic diffractometer. Of the 1501 reflections measured, 1100 were considered to be significantly above background ($I > 2\sigma(I)$). These data were corrected for Lorentz and polarization effects and absorption and extinction were also corrected for ($\mu = 7.73$ cm^{-1}, crystal dimensions 0.35 mm × 0.18 mm × 0.12 mm). The results of these latter calculations indicated that correction for the polarization term in the extinction correction would have sufficed, the absorption term in the extinction correction and the absorption correction itself having little effect.

Structure factor amplitudes and standard deviations were calculated and, from the amplitudes, normalized structure factors were obtained. The phases of 147 of the largest of these were determined by the symbolic addition procedure (21), and in one of the E maps computed the positions of all 16 heavy atoms were located.

A structure factor calculation based upon these coordinates gave a $R_1 = 0.286$ which fell in four cycles of full matrix, least-squares refinement to 0.140. In the refinement, each observation was assigned a weight equal to the reciprocal of its variance. At this point the heavy atoms were allowed to refine anisotropically and two more cycles of refinement reduced R_1 to 0.094.

A difference electron density map was computed, from which the coordinates of all 16 hydrogen atoms were found. These were included in the refinement, but in order to reduce the number of variable parameters the hydrogens of the four methyl groups were included as hindered rotors (22). In four more cycles of refinement, R_1 fell to 0.041.

Absorption and extinction corrections were applied to the data at this stage and in two more cycles, the refinement converged at $R_1 = 0.036$ and $R_2 = 0.036$.[2]

For both compounds the scattering factors for the carbon and oxygen atoms were those of Cromer (23), while for hydrogen those of Mason and Robertson were used (24).

Tables of observed and calculated structure factor amplitudes (Tables 1 and 2) and tables of anisotropic temperature factors (Tables 4 and 6) are available.[3] Tables 3 and 5 give the atomic coordinates of the two compounds. Tables 7–10 give the various bond distances and angles within the two molecules. Table 11 gives the least-squares planes data for the two molecules.[3]

Discussion

The molecular structure of TDCD is shown in Fig. 1. The substance crystallizes with the cyclohexadiene ring occupying a crystallographic inver-

[2]For both structures, apart from certain local programs, the computer programs used were: a locally modified version of SFLS5 by C.T.P. Prewitt; FORDAP, by A. Zalkin, modified by B. Foxman; ORTEP by C. K. Johnson; MGEOM, by J. S. Wood; FAME and MAGIC by R. Dewar and A. Stone.

[3]Copies of the tables of observed and calculated structure factors (Tables 1, 2), anisotropic temperature factors (Tables 4, 6), and least-squares planes (Table 11) are available, at a nominal charge, from the Depository of Unpublished Data, CISTI, National Research Council of Canada, Ottawa, Ont., Canada K1A 0S2.

Can. J. Chem. Downloaded from www.nrcresearchpress.com by 210.87.254.5 on 09/05/12
For personal use only.

TABLE 3. Atomic coordinates and isotropic temperature factors for 1,2,4,5-tetraphenyl-3,6-dicarbomethoxycyclohexa-1,4-diene

Atom	*x*	*y*	*z*	*B*
C1	0.0489(2)	−0.0090(6)	0.0510(1)	2.22*
C2	−0.0143(2)	0.0307(6)	0.0604(1)	2.29*
C3	−0.0706(2)	0.0377(7)	0.0104(1)	2.31*
C4	−0.1180(2)	−0.1633(8)	0.0220(1)	2.78*
C5	−0.2113(3)	−0.2643(13)	0.0726(3)	5.83*
C11	0.1057(2)	−0.0239(6)	0.0990(1)	2.31*
C12	0.1169(2)	0.1543(7)	0.1403(2)	2.89*
C13	0.1707(2)	0.1402(8)	0.1845(2)	3.57*
C14	0.2132(2)	−0.0475(8)	0.1871(2)	3.77*
C15	0.2022(2)	−0.2249(8)	0.1461(2)	3.81*
C16	0.1488(2)	−0.2129(7)	0.1021(2)	3.28*
C21	−0.0383(2)	0.0590(7)	0.1204(1)	2.35*
C22	−0.0731(2)	0.2576(7)	0.1334(2)	3.18*
C23	−0.0985(2)	0.2832(8)	0.1876(2)	3.52*
C24	−0.0900(2)	0.1078(8)	0.2288(2)	3.54*
C25	−0.0558(2)	−0.0923(8)	0.2164(2)	3.50*
C26	−0.0301(2)	−0.1163(7)	0.1624(1)	2.83*
O1	−0.1080(1)	−0.3626(5)	0.0113(1)	4.21*
O2	−0.1704(1)	−0.0852(5)	0.0481(1)	3.96*
H12	0.090(2)	0.290(7)	0.139(2)	4.9(10)
H13	0.179(2)	0.272(7)	0.213(2)	5.0(9)
H14	0.253(2)	−0.053(6)	0.219(1)	4.4(8)
H15	0.232(2)	−0.363(7)	0.146(2)	5.3(10)
H16	0.142(2)	−0.355(7)	0.072(1)	4.8(8)
H22	−0.080(2)	0.376(6)	0.104(1)	4.1(8)
H23	−0.121(2)	0.429(7)	0.194(2)	5.2(10)
H24	−0.106(2)	0.125(6)	0.267(2)	4.7(9)
H25	−0.050(2)	−0.225(8)	0.247(2)	7.1(12)
H26	−0.006(2)	−0.247(7)	0.152(1)	4.0(9)
H51	−0.257(3)	−0.184(9)	0.074(2)	8.0(13)
H52	−0.194(2)	−0.282(10)	0.111(2)	8.9(16)
H53	−0.214(3)	−0.404(10)	0.043(2)	10.8(20)
H3	−0.097(1)	0.182(5)	0.012(1)	1.8(6)

*These are equivalent isotropic temperature factors corresponding to the anisotropic parameters listed in Table 4.[3]

TABLE 5. Atomic coordinates and isotropic temperature factors for 1,2-dicarbomethoxy-4,5-dimethylcyclohexa-1,4-diene

Atom	*x*	*y*	*z*	*B*
C1	0.10689(8)	0.4046(2)	0.4355(3)	3.75*
C2	0.14395(9)	0.3318(2)	0.4897(3)	3.74*
C3	0.1379(1)	0.1995(2)	0.4834(4)	4.87*
C4	0.0879(1)	0.1546(2)	0.4139(3)	4.61*
C5	0.05103(9)	0.2279(2)	0.3600(3)	4.57*
C6	0.0570(1)	0.3601(2)	0.3668(4)	4.63*
C7	0.11068(9)	0.5372(2)	0.4368(3)	4.05*
C8	0.1938(1)	0.3725(2)	0.5604(3)	4.56*
C9	0.0845(1)	0.0210(3)	0.4093(3)	6.14*
C10	−0.0001(1)	0.1887(3)	0.2894(4)	6.37*
C11	0.1514(1)	0.7049(3)	0.3184(4)	6.95*
C12	0.2405(1)	0.5274(3)	0.6852(4)	7.21*
O1	0.08468(7)	0.6004(1)	0.5200(2)	5.82*
O2	0.14422(6)	0.5763(1)	0.3271(2)	5.27*
O3	0.23197(7)	0.3120(2)	0.5685(3)	8.68*
O4	0.19291(6)	0.4826(1)	0.6153(2)	5.71*
H31	0.1680(9)	0.168(2)	0.428(3)	6.13
H32	0.1445(9)	0.168(2)	0.591(3)	6.13
H61	0.0519(9)	0.392(2)	0.259(3)	6.00
H62	0.0276(9)	0.396(2)	0.428(3)	6.04
H91	0.096(3)	−0.014(2)	0.51(1)	5.3†
H92	0.108(3)	−0.012(1)	0.319(3)	
H93	0.047(1)	−0.008(2)	0.385(8)	
H101	−0.032(1)	0.212(3)	0.373(3)	6.8†
H102	−0.009(1)	0.234(3)	0.184(4)	
H103	0.001(1)	0.102(2)	0.278(5)	
H111	0.171(5)	0.733(3)	0.43(1)	6.6†
H112	0.176(4)	0.712(3)	0.22(2)	
H113	0.116(1)	0.744(3)	0.31(1)	
H121	0.271(1)	0.519(5)	0.597(2)	6.7†
H122	0.249(2)	0.477(4)	0.783(6)	
H123	0.233(1)	0.614(2)	0.707(6)	

*These are equivalent isotropic temperature factors corresponding to the anisotropic parameters listed in Table 6.[3]
†These are the isotropic temperature factors used in the hindered rotor group refinement.

TABLE 7. Interatomic distances (Å) in 1,2,4,5-tetraphenyl-3,6-dicarbomethoxycyclohexa-1,4-diene

Atoms	Distance	Atoms	Distance
C1—C2	1.326(4)	C16—C11	1.387(5)
C1—C3′	1.513(4)	C21—C22	1.387(5)
C2—C3	1.523(4)	C22—C23	1.390(5)
C1—C11	1.501(4)	C23—C24	1.378(5)
C2—C21	1.502(4)	C24—C25	1.384(5)
C3—C4	1.537(5)	C25—C26	1.387(5)
C11—C12	1.395(5)	C26—C21	1.390(5)
C12—C13	1.402(5)	C4—O1	1.194(4)
C13—C14	1.374(5)	C4—O2	1.336(4)
C14—C15	1.386(5)	C5—O2	1.462(5)
C15—C16	1.395(5)		

sion centre, with the plane of the ring almost perpendicular to the *b* axis. Because it occupies an inversion centre, the compound is necessarily in the *anti*-configuration and any deviations from planarity lead to a chair, not a boat form.

The structure of DDCD is illustrated in Fig. 2.

The carbon–carbon double bond lengths within the cyclohexadiene ring are similar in both compounds, as are all internal angles. In TDCD the C(sp^2)—C(sp^2) bond length is 1.326 Å, angles of the type C(sp^2)—C(sp^2)—C(sp^3) average 122.3° and the angle at the methylenic carbon is 115.4°. In DDCD these parameters are 1.333 Å, 122.0°, and 116.0° respectively.

The single bond lengths within the rings, however, are significantly different. In TDCD they average 1.518 Å longer than the 1.493 Å average found in DDCD and also longer than the 1.493 Å average of diethyl succinyl succinate (18) and 1.485 Å in cyclohexa-1,4-diene-1-glycine (17), all of which lack substituents attached to the methylenic carbon atoms.

The ester group in TDCD is attached to a sp^3 hybridized carbon atom, but is unable to attain the preferred conformation with the torsion angle Cβ—Cα—C=O equal or close to zero (25), be-

Can. J. Chem. Downloaded from www.nrcresearchpress.com by 210.87.254.5 on 09/05/12
For personal use only.

TABLE 8. Intermolecular angles (deg) in 1,2,4,5-tetraphenyl-3,6-dicarbomethoxycyclohexa-1,4-diene

Atoms	Angle	Atoms	Angle
C3′—C1—C2	122.4(3)	C14—C15—C16	120.5(4)
C3′—C1—C11	113.7(3)	C15—C16—C11	120.3(4)
C11—C1—C2	124.4(3)	C2—C21—C22	119.8(3)
C1—C2—C3	122.1(3)	C2—C21—C26	121.4(3)
C1—C2—C21	124.4(3)	C22—C21—C26	118.6(3)
C21—C2—C3	113.4(3)	C21—C22—C23	120.9(4)
C2—C3—C1′	115.4(3)	C22—C23—C24	119.8(4)
C2—C3—C4	106.1(3)	C23—C24—C25	120.0(4)
C1′—C3—C4	108.4(3)	C24—C25—C26	120.0(4)
C1—C11—C12	120.6(3)	C25—C26—C21	120.7(4)
C1—C11—C16	120.3(3)	C3—C4—O1	124.7(4)
C12—C11—C16	119.0(3)	C3—C4—O2	110.6(3)
C11—C12—C13	120.1(4)	O1—C4—O2	124.7(4)
C12—C13—C14	120.4(4)	C4—O2—C5	115.4(4)
C13—C14—C15	119.6(4)		

TABLE 9. Interatomic distances (Å) in 1,2-dicarbomethoxy-4,5-dimethylcyclohexa-1,4-diene

Atoms	Distance	Atoms	Distance
C1—C2	1.333(3)	C7—O1	1.196(3)
C2—C3	1.496(3)	C7—O2	1.330(3)
C3—C4	1.493(4)	C11—O2	1.459(3)
C4—C5	1.332(3)	C8—O3	1.193(3)
C5—C6	1.494(3)	C8—O4	1.319(3)
C6—C1	1.487(3)	C12—O4	1.443(3)
C1—C7	1.493(3)		
C2—C8	1.479(3)		
C4—C9	1.505(4)		
C5—C10	1.502(4)		

TABLE 10. Intramolecular angles (deg) in 1,2-dicarbomethoxy-4,5-dimethylcyclohexa-1,4-diene

Atoms	Angle	Atoms	Angle
C6—C1—C2	122.4(2)	C1—C7—O1	124.1(2)
C6—C1—C7	113.3(2)	C1—C7—O2	111.5(2)
C2—C1—C7	124.3(2)	O1—C7—O2	124.2(2)
C1—C2—C3	121.6(2)	C7—O2—C11	116.4(2)
C1—C2—C8	124.1(2)	C2—C8—O3	123.7(2)
C3—C2—C8	114.3(2)	C2—C8—O4	114.4(2)
C2—C3—C4	116.1(2)	O3—C8—O4	121.9(2)
C3—C4—C5	122.0(2)	C8—O4—C12	117.0(2)
C3—C4—C9	113.4(2)		
C5—C4—C9	124.6(3)		
C4—C5—C6	122.0(2)		
C4—C5—C10	124.7(2)		
C6—C5—C10	113.4(2)		
C5—C6—C1	116.0(2)		

cause of steric interference by the phenyl rings. This steric interference causes the carbomethoxy group to rotate about the C4—C3 bond, giving a torsion angle of 45.9° for C1′—C3—C4 = O1.

The cyclohexadiene ring of TDCD has small but significant deviations from planarity (Table 11[3]),

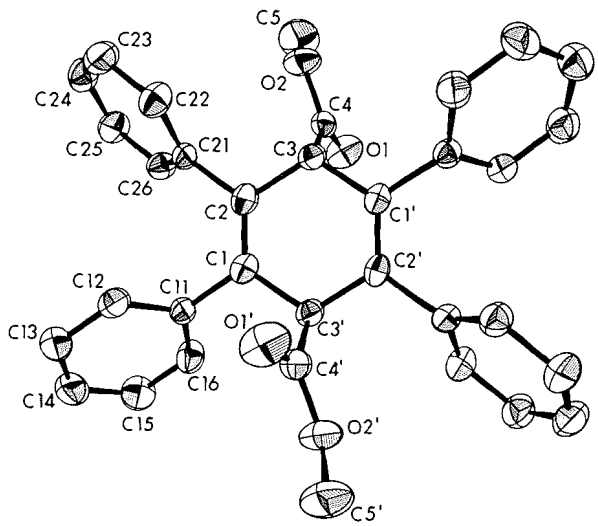

FIG. 1. The molecular structure of 1,2,4,5-tetraphenyl-3,6-dicarbomethoxycyclohexa-1,4-diene.

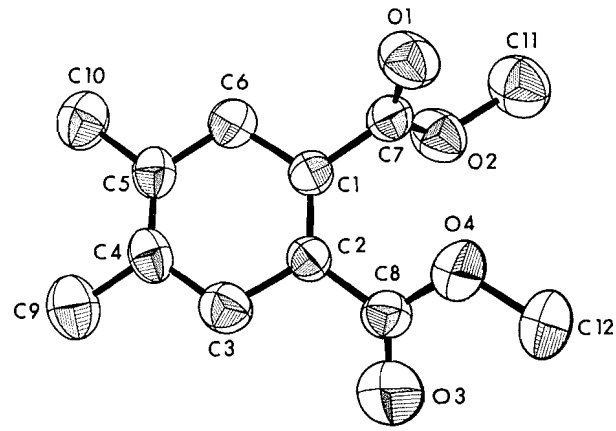

FIG. 2. The molecular structure of 1,2-dicarbomethoxy-4,5-dimethylcyclohexa-1,4-diene.

each of the six atoms lying 0.011 to 0.012 Å out of the least-squares plane. If we define the reference plane as the one containing the four olefinic carbon atoms, then the deviation of the methylenic carbon atom from this plane is 0.037 Å. The dihedral angle between the plane formed by C2C3C1′ and that by C1C2C1′C2′ is 177.4°. This agrees well with the electron diffraction work of Dallinga and Toneman (13), who refined a planar form of cyclohexa-1,4-diene to completion but could not rule out the possibility that other nearly planar conformations, especially the chair form, were present, with a maximum deviation from the plane of 0.05 Å. The results are, however, in disagreement with the electron diffraction study of Oberhammer and Bauer (14), who concluded that the cyclohexa-1,4-diene molecule had a pronounced boat conformation, the dihedral angle

Can. J. Chem. Downloaded from www.nrcresearchpress.com by 210.87.254.5 on 09/05/12
For personal use only.

between the two halves of the molecule being 159.3°, corresponding to deviations from the diene plane of 0.23 Å for the methylenic type carbon atoms.

However, one must always be cautious when extrapolating results obtained from solid state studies to molecules in the liquid or gaseous phase. While the cyclohexa-1,4-diene ring in this structure is not severely constrained, as it would be in a fused ring system, the question remains as to whether the slight chair conformation is a preferred conformation, or whether it is imposed upon the ring as a result of either intermolecular forces in the condensed phase or intramolecular forces due to the bulky substituents.

The intermolecular forces would appear not to be responsible. The closest C---C contacts occur between phenyl rings and are all greater than 3.74 Å. The closest carbon–hydrogen contacts are about 3.0 Å or more, and hydrogen–hydrogen contacts are 2.54 Å or greater. All these distances are greater than the sum of Van der Waals radii of the atoms concerned. The intermolecular interaction between the carbonyl oxygen and the methylenic carbon atom and its hydrogen atom in the molecule one unit cell away in the direction of the short *b* axis also is not important. The O1---H3 distance of 2.63 Å and the O1---C3 distance of 3.533 Å are both greater than the sum of the Van der Waals radii of the atoms involved, 2.6 Å and 3.1 Å respectively.

Intramolecular forces, on the other hand, are very important in this sterically overcrowded molecule. The phenyl–phenyl repulsions are reduced to some extent by the widening of the C_{phen}—C=C angle to 124.4° from the expected 120°. Of course, they would be further reduced by the adoption of a slight chair conformation by the molecule, since, normally, this would lead to a slightly staggered conformation of C11 and C21 with respect to the olefinic bond. It should be noted that this distortion would be expected to lead to a slight reduction in the π-bond overlap. However, an examination of the olefinic plane (Table 11[3]) indicates that this is not the case in this structure. The deviations of C11 and C21 from the least-squares olefinic plane are not what would be expected for the normal chair structure. The situation is shown, much exaggerated, in Fig. 3*a* and *b*. If we again use the plane defined by the four ethylenic carbon atoms as the reference plane, then C3 and C3′ lie 0.037 Å below and above this plane respectively. For the chair structure, one would expect deviations opposite in sign for C21 and C11 and of more or less the same magnitude as for C3 and C3′. Also, C21 should lie on the opposite side of the plane to C3, and C11 should lie on the opposite side of the plane to

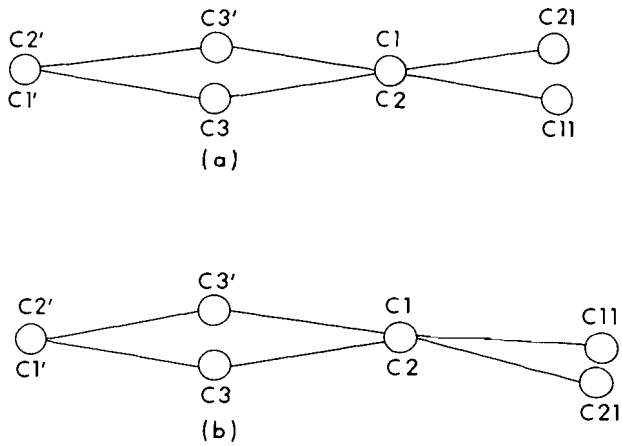

FIG. 3. 1,2,4,5-Tetraphenyl-3,6-dicarbomethoxycyclohexa-1,4-diene: exaggerated Newman projections. (*a*) Theoretical view down C2—C1 bond for chair conformation; (*b*) actual view down C2—C1.

C3′ (Fig. 3*a*). However, the deviations of these atoms from the plane (Table 11[3]) are 0.0015 Å for C11 which is smaller than expected, but in the right direction and 0.044 Å for C21 which is slightly larger than expected, and in the wrong direction (Fig. 3*b*). The atoms C11 and C21, therefore, have assumed positions closer to what one would expect for a completely planar or even boat form of the molecule. This situation lends itself to two possible interpretations; either the inter- and intramolecular forces are attempting to constrain the molecule in a planar or boat conformation and despite this the ring retains a slight chair conformation, or the preferred conformation is that assumed by the substituents and the inter- and intramolecular repulsive interactions are forcing the ring to take up a chair conformation.

Examination of the intramolecular contacts involving the carbomethoxy group greatly favours the latter interpretation. The C4---C21 and C4---C11′ distances are 2.916 and 2.993 Å respectively, while the C4---C2 and C4---C1′ are 2.445 and 2.474 Å, all significantly shorter than the Van der Waals contact of 3.4 Å and are therefore repulsive in nature. Since C4 lies below the plane of the four ethylinic carbon atoms and C11′ and C21, the effect of this repulsive interaction would be to force it even further below the plane, which in turn will cause C3 to move below this plane. The centrosymmetrically related C3′ will be correspondingly raised above the plane, thus leading to a chair conformation.

The lengthening of the single bonds in the cyclohexadiene ring over that found in cyclohexadienes without a methylenic carbon substituent is regarded as further evidence of this repulsive interaction as is

the C3—C4 bond length of 1.537 Å which is 0.02–0.03 Å longer than that commonly observed in the literature for this type of bond.

It is postulated then that for solid state cyclohexadiene derivatives the presence of substituents on the methylenic carbon atoms in the *anti*-configuration leads to a slight chair conformation. Conversely, it would be expected that substituents in the *syn*-configuration would lead to a slight boat conformation and that an absence of methylenic substituents would give a rigorously planar conformation.

It was precisely to test this latter hypothesis that the structure of DDCD was determined. Since this compound bears no methylenic substituents it would be expected to have a planar cyclohexadiene ring. Examination of the least-squares plane (Table 11[3]) shows that this is indeed so, the maximum deviation of any of the six atoms from the plane being 0.004 Å, and C3 and C6 lie 0.004 and 0.008 Å respectively out of the plane defined by the four olefinic carbon atoms.

Acknowledgements

We wish to thank the National Research Council of Canada and the University of Alberta for financial support.

1. H. Gerding and F. A. Haak. Rec. Trav. Chim. **68**, 293 (1949).
2. B. J. Monsotori and A. Weber. J. Mol. Spectrosc. **12**, 129 (1964).
3. H. D. Stidham. Spectrochim. Acta, **21**, 23 (1965).
4. J. Laane and R. C. Lord. J. Mol. Spectrosc. **39**, 340 (1971).
5. I. Miyagawa, Y. Mornio, and R. Riemschneider. Bull. Chem. Soc. Jpn. **27**, 177 (1954).
6. W. D. Kumler, R. Boikess, P. Bruck, and S. Winstein. J. Am. Chem. Soc. **86**, 3126 (1961).
7. F. H. Herbstein. J. Chem. Soc. **2292** (1959).
8. G. Favini, F. Zuccarello, and G. Buemi. J. Mol. Struct. **3**, 385 (1969).
9. L. J. Durham, J. Studebaker, and M. J. Perkins. Chem. Commun. 456 (1965).
10. D. J. Atkinson and M. J. Perkins. Tetrahedron Lett. 2335 (1969).
11. J. L. Marshall, K. C. Erickson, and T. K. Folsom. J. Org. Chem. **35**, 2038 (1970).
12. J. W. Paschal and P. W. Rabideau. J. Am. Chem. Soc. **96**, 272 (1974).
13. G. Dallinga and L. H. Toneman. J. Mol. Struct. **1**, 117 (1967).
14. H. Oberhammer and S. H. Bauer. J. Am. Chem. Soc. **91**, 10 (1969).
15. P. Ganis, C. Pedone, and P. A. Temussi. Atti Accad. Naz. Lincei Cl. Sci. Fis. Mat. Nat. **35**, 68 (1963).
16. P. Ganis, C. Pedone, and P. A. Temussi. Atti Accad. Naz. Lincei Cl. Sci. Fis. Mat. Nat. **35**, 175 (1963).
17. R. J. Jandaceck and S. H. Simonsen. J. Am. Chem. Soc. **91**, 6663 (1969).
18. H.-C. Mez and G. Rihs. Helv. Chim. Acta, **56**, 2766 (1973).
19. M. J. Bennett, J. T. Purdham, S. Takada, and S. Masamune. J. Am. Chem. Soc. **93**, 4063 (1971).
20. W. H. Zachariesen. Acta Crystallogr. **16**, 1139 (1963).
21. J. Karle and I. L. Karle. Acta Crystallogr. **21**, 849 (1966).
22. M. J. Bennett, W. L. Hutcheon, and B. M. Foxman. Acta Crystallogr. Sect. A, **31**, 488 (1975).
23. D. T. Cromer. Acta Crystallogr. Sect. A, **24**, 321 (1968).
24. R. Mason and G. B. Robertson. *In* Advances in structure research by diffraction methods. Vol. 2. *Edited by* R. Brill and R. Mason. Interscience Division, Wiley, New York, NY. 1966.
25. J. D. Dunitz and P. Strickler. *In* Structural chemistry and molecular biology. *Edited by* A. Rich and N. Davidson. W. H. Freeman and Co., San Francisco and London. 1968.

Can. J. Chem. Downloaded from www.nrcresearchpress.com by 210.87.254.5 on 09/05/12
For personal use only.

The crystal and molecular structure of *anti*-1,2,4,5-tetraphenyl-3,6-dicarbomethoxytricyclo[3.1.0.0^{2,4}]hexane

M. J. BENNETT AND J. T. PURDHAM[1]

Department of Chemistry, University of Alberta, Edmonton, Alta., Canada T6G 2G2

Received July 29, 1977

M. J. BENNETT and J. T. PURDHAM. Can. J. Chem. **56**, 1364 (1978).

1,2,4,5-Tetraphenyl-3,6-dicarbomethoxytricyclo[3.1.0.0^{2,4}]hexane crystallizes in the monoclinic space group $P2_1/c$ with $a = 10.044(4)$, $b = 9.500(2)$, $c = 14.172(4)$ Å, $\beta = 104.38(2)°$, and $Z = 2$. Using 1032 unique reflections with $I > 3\sigma(I)$, the structural data were refined by full matrix least-squares techniques to $R = 0.038$. The molecule was found to be in the *anti*-configuration. All bond lengths within the highly strained central tricyclic framework were equal within experimental error and average 1.531 Å.

M. J. BENNETT et J. T. PURDHAM. Can. J. Chem. **56**, 1364 (1978).

Le tétraphényl-1,2,4,5 dicarbométhoxy-3,6 tricyclo[3.1.0.0^{2,4}] hexane cristallise dans le groupe d'espace monoclinique $P2_1/c$ avec $a = 10.044(4)$, $b = 9.500(2)$, $c = 14.172(4)$ Å, $\beta = 104.38(2)°$ et $Z = 2$. Faisant appel à 1032 réflexions uniques avec $I > 3\sigma(I)$, on a affiné les données structurales par la méthode des moindres carrés (matrice complète) jusqu'à une valeur finale de $R = 0.038$. On a trouvé que la molécule existe dans une configuration *anti*. Toutes les longueurs de liaison à l'intérieur du tricycle central hautement tendu sont égales, à l'intérieur des erreurs expérimentales, à 1.531 Å.

[Traduit par le journal]

Can. J. Chem. Downloaded from www.nrcresearchpress.com by 210.87.254.5 on 09/05/12
For personal use only.

The preparation and preliminary structure of 1,2,4,5-tetraphenyl-3,6-dicarbomethoxy [3.1.0.0^{2,4}]-tricyclohexane (TDTC) were described in an earlier report (1). Similar compounds have been prepared by other workers (2), but the stereochemistry of the product was either undetermined or the assignment uncertain. The X-ray crystal structure analysis of this photodimer of 3-carbomethoxy-1,2-diphenylcyclopropene was undertaken in order to unambiguously establish the stereochemistry of the product and to determine the exact geometry of the novel, strained tricyclic system, since it afforded the opportunity to observe the effect of ring fusion upon the geometry of the cyclopropane and cyclobutane rings.

Experimental

Crystal data:

$C_{34}H_{28}O_4$ fw = 500

Monoclinic, $a = 10.044(4)$, $b = 9.500(2)$, $c = 14.172(4)$ Å, $\beta = 104.38(2)°$, $V = 1309.90$ Å^3, $\rho_o = 1.28(1)$ g/ml, $Z = 2$, $\rho_c = 1.272$ g/ml (20°C; CuKα, $\lambda = 1.54182$ Å).

The molecule crystallized in the space group $P2_1/c$ with systematic absences for the $0k0$ reflections when $k = 2n + 1$ and for the $h0l$ reflections when $l = 2n + 1$. Since there were only two molecules in the unit cell, this required that each molecule occupied a crystallographic inversion centre.

Intensity data were collected on a Picker manual diffractometer. Of the 1958 reflections measured, 1032 were considered to be significantly above background ($I > 3\sigma(I)$). These data were corrected for Lorentz and polarization effects. No attempt was made to correct for absorption, since this was considered negligible ($\mu = 6.67$ cm^{-1}). However, a correction for the polarization term in the secondary extinction correction was applied (19). Structure factor amplitudes and standard deviations were then calculated.

The structure amplitudes were converted to normalized structure factors and the phases of 118 of the large E factors were determined by the symbolic addition procedure (3). All but four of the carbon atoms in the asymmetric unit were located in the E map calculated from these phases.

These 15 atom positions were used as input to a structure factor calculation, and the calculated phases were used to compute an electron density map which revealed the locations of the remaining four carbon atoms.

In the initial stages of the refinement, the phenyl rings were refined as rigid bodies with a C—C distance of 1.397 Å and C—C—C angle of 120°. The function being minimized in the refinement was $\Sigma w(|F_o| - |F_c|)^2$. The weight given to each observation was the reciprocal of its variance.

After three cycles of isotropic refinement by full matrix least squares the R_1 value ($\Sigma(||F_o| - |F_c||)/\Sigma|F_o|$) was 0.153, at which point the rigid body restriction was removed from the phenyl rings. One more cycle of refinement reduced R_1 to 0.136 and a difference electron density map calculated at this point showed clearly the positions of all the hydrogen atoms. These were included in the refinement and the heavy atoms allowed to refine anisotropically. The refinement converged at an $R_1 = 0.040$, R_2 ($[\Sigma w(|F_o| - |F_c|)^2/\Sigma w|F_o|^2]^{1/2}$) $= 0.048$. After the data had been corrected for the polarization part of the extinction correction, the refinement reconverged at $R_1 = 0.038$ and $R_2 = 0.038$.[2] The largest peak in

[1]Author to whom all correspondence should be addressed. Present address: Alberta Labour, Occupational Health and Safety Division, Occupational Hygiene Branch, 9820 – 106th Street, Edmonton, Alta., Canada T5K 2J6.

[2]Apart from certain local programs, the computer programs used in the structure determination were: a locally modified version of SFLS 5 by C.T.P. Prewitt; FORDAP, by A. Zalkin, modified by B. Foxman; ORTEP by C.K. Johnson; MGEOM, by J.S. Wood; NRC-4 SAP by S.R. Hall (revised version).

Can. J. Chem. Downloaded from www.nrcresearchpress.com by 210.87.254.5 on 09/05/12
For personal use only.

an electron density difference map computed at the end of the refinement was 0.13 electrons per Å^3.

A table of observed and calculated structure factor amplitudes is available (Table 1).[3]

The scattering factors for the carbon and oxygen atoms were those of Cromer (4), and for hydrogen, the scattering factors of Mason and Robertson were used (5).

Discussion

Table 2 gives the atomic coordinates and isotropic temperature factors while the anisotropic thermal parameters are available (Table 3).[3]

The molecule crystallizes on a crystallographic inversion centre and consequently is in the *anti*-configuration and has a planar cyclobutane ring. The carbomethoxy groups are in the *exo*-position. A diagram of the molecule is shown in Fig. 1 and bond lengths and angles are listed in Tables 4 and 5 respectively.

The most outstanding detailed structural feature of the molecule is that all bond lengths within the tricyclohexane framework are equal within experimental error and average 1.531 Å. The bond distances in the cyclopropane ring average 1.530 Å and the bond angles within the ring average 60.0°. The bond lengths in the cyclobutane ring average 1.534 Å and the ring is planar and square. The cyclopropane and cyclobutane rings meet at an angle of 109°.

The bond distances from the tricyclic system to the substituent phenyl and carbomethoxy groups are all about 0.02 Å shorter than is normally found in unstrained systems. This bond shortening to substituent groups is characteristic of highly strained systems and has been observed in many compounds (6–8). The phenyl ring attached to C2 is perpendicular to the plane of the cyclobutane ring while that attached to C1 is skewed. A similar situation is found in tetraphenyl cyclobutane (14).

The bond distances and angles within the carbomethoxy group are all normal, and the group is planar within experimental error. The torsion angle C2—C3—C4—O1 is 38.3°, which means that the carbomethoxy group has not taken up what has been described as the preferred conformation, with the carbonyl group *syn*-planar with the Cα—Cβ bond (9, 10). This may be entirely due to the intramolecular forces preventing the carbomethoxy group from taking up this preferred conformation, but Hoffman and Davidson (11) have pointed out that, for a carbomethoxy group attached to a cyclopropane ring, the *syn*-planar arrangement may not be the preferred conformation. They showed that the low lying Π* orbital of the carbonyl can interact with a pseudo-Π ring orbital, and that this interaction is greatest if the plane containing the carbomethoxy group is perpendicular to the plane of the cyclopropane ring and the C=O is *anti*-planar with respect to the ring C—H bond, that is, if the torsion angle O=C—C—H is 180°. This they termed the bisected conformation and is precisely the conformation found in this compound, the torsion angle O1—C4—C3—HB being 178°.

Fusion of the cyclopropane and cyclobutane rings affects the geometry of both. The bond lengths in the cyclopropane ring average 1.530(4) Å, longer than the 1.510 Å bond lengths found in cyclopropane itself (12), while the bond lengths in the cyclobutane ring average 1.534(4) Å, shorter than the 1.548 Å bond lengths found in cyclobutane itself (13).

In highly strained fused systems, there does seem to be a tendency towards the shortening of cyclobutane bonds and the lengthening of cyclopropane

TABLE 2. Atomic coordinates and isotropic temperature factors

Atom	*x*	*y*	*z*	*B*
C1	−0.1037(3)	−0.0163(3)	−0.0442(2)	2.95*
C2	0.0235(3)	0.0630(3)	−0.0575(2)	2.80*
C3	0.0600(3)	0.1703(3)	0.0250(2)	3.11*
C4	0.1672(3)	0.2756(4)	0.0210(2)	3.46*
C5	0.2256(6)	0.5160(5)	0.0455(5)	6.33*
O1	0.2699(2)	0.2549(3)	−0.0057(2)	4.90*
O2	0.1317(2)	0.4010(2)	0.0486(2)	4.51*
C11	−0.2453(3)	0.0339(3)	−0.0862(2)	3.15*
C12	−0.2938(4)	0.0369(5)	−0.1865(3)	4.86*
C13	−0.4242(4)	0.0872(5)	−0.2292(3)	5.51*
C14	−0.5063(4)	0.1349(4)	−0.1722(4)	4.96*
C15	−0.4609(4)	0.1337(5)	−0.0744(4)	5.51*
C16	−0.3300(4)	0.0844(4)	−0.0313(3)	5.09*
C21	0.0556(3)	0.0841(4)	−0.1540(2)	3.04*
C22	0.0286(4)	0.2130(4)	−0.2008(3)	4.26*
C23	0.0496(4)	0.2329(5)	−0.2930(3)	5.03*
C24	0.0977(4)	0.1249(4)	−0.3388(3)	4.64*
C25	0.1237(4)	−0.0034(4)	−0.2946(3)	4.56*
C26	−0.0241(4)	−0.0241(4)	−0.2030(3)	3.91*
H51	0.223(5)	0.533(5)	−0.018(3)	8.2(16)
H52	0.319(4)	0.490(5)	0.080(3)	7.4(13)
H53	0.190(5)	0.596(6)	0.074(3)	10.5(17)
HB	−0.012(3)	0.209(3)	0.051(2)	3.6(7)
H12	−0.238(4)	−0.001(4)	−0.228(2)	6.0(9)
H13	−0.454(4)	0.091(4)	−0.299(3)	6.4(10)
H14	−0.596(4)	0.166(4)	−0.203(2)	5.3(8)
H15	−0.518(4)	0.156(4)	−0.030(3)	6.5(10)
H16	−0.303(3)	0.073(3)	0.032(2)	4.0(8)
H22	−0.004(3)	0.289(4)	−0.165(2)	5.4(8)
H23	0.020(4)	0.325(4)	−0.323(3)	7.2(10)
H24	0.114(3)	0.144(4)	−0.399(3)	5.7(10)
H25	0.159(3)	−0.080(4)	−0.323(2)	5.0(8)
H26	0.119(3)	−0.110(3)	−0.176(2)	3.6(7)

*These are equivalent isotropic temperature factors corresponding to the anisotropic parameters given in Table 3.[3]

[3]Copies of the table of observed and calculated structure factor amplitudes (Table 1) and the table of anisotropic thermal parameters (Table 3) are available, at a nominal charge, from the Depository of Unpublished Data, CISTI, National Research Council of Canada, Ottawa, Ont., Canada K1A 0S2.

Can. J. Chem. Downloaded from www.nrcresearchpress.com by 210.87.254.5 on 09/05/12
For personal use only.

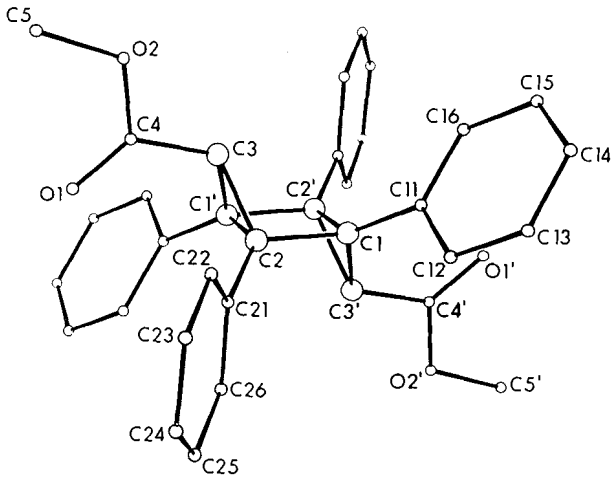

FIG. 1. A perspective view of the molecular structure of 1,2,4,5-tetraphenyl-3,6-dicarbomethoxytricyclo[3.1.0.0^{2,4}]hexane.

TABLE 4. Interatomic distances (Å)

Atoms	Distance	Atoms	Distance
C1—C2	1.535(4)	C12—C13	1.384(5)
C2—C1′	1.532(4)	C13—C14	1.368(5)
C2—C3	1.526(4)	C14—C15	1.347(6)
C3—C1′	1.532(4)	C15—C16	1.386(6)
C3—C4	1.481(4)	C16—C11	1.374(4)
C4—O1	1.199(3)	C21—C22	1.387(4)
C4—O2	1.330(4)	C22—C23	1.386(5)
O2—C5	1.450(5)	C23—C24	1.366(5)
C1—C11	1.478(4)	C24—C25	1.366(5)
C2—C21	1.495(4)	C25—C26	1.385(5)
C11—C12	1.384(4)	C26—C21	1.382(4)

TABLE 5. Intramolecular angles (deg)

Atoms	Angle	Atoms	Angle
C3′—C1—C2′	59.7(2)	C13—C14—C15	120.3(4)
C2′—C1—C2	89.9(2)	C23—C24—C25	120.2(4)
C3′—C1—C11	125.8(3)	C2—C3—C1′	60.1(2)
C2′—C1—C11	134.5(3)	C2—C3—C4	117.4(3)
C11—C1—C2	122.6(3)	C1′—C3—C4	118.2(3)
C3′—C1—C2	106.3(2)	C3—C4—O1	126.3(3)
C1—C2—C1′	90.1(2)	C3—C4—O2	110.1(3)
C1—C2—C21	123.6(3)	O1—C4—O2	123.6(3)
C1—C2—C3	106.4(2)	C14—C15—C16	119.9(4)
C21—C2—C3	123.1(3)	C15—C16—C11	121.3(4)
C21—C2—C1′	135.8(3)	C2—C21—C22	119.6(3)
C3—C2—C1′	60.1(2)	C2—C21—C26	122.3(3)
C1—C11—C12	118.6(3)	C22—C21—C26	117.8(3)
C1—C11—C16	123.7(3)	C21—C22—C23	120.9(4)
C12—C11—C16	117.7(3)	C22—C23—C24	120.0(4)
C11—C12—C13	120.6(3)	C24—C25—C26	120.0(4)
C12—C13—C14	120.0(4)	C25—C26—C21	121.1(4)

bonds. In a tricyclo[2.1.0.0^{2,5}]pentane derivative (15), all the bond lengths except one average 1.53 Å. In bicyclo[2.1.0]pentane (16), the cyclopropane bonds average 1.517 Å and the cyclobutane bonds 1.534 Å, while in a bicyclo[3.2.0]heptene derivative, the cyclobutane ring has an average bond length of 1.532 Å (17).

The microwave structure of bicyclo[2.1.0]pentane is interesting from the point of view of comparison with TDTC, since it simply consists of one less cyclopropane ring in the fused system. Suenram and Harmony argue that since the rings have three and four centre Π-like orbitals, it is possible for them to relocate the total available electron density around the system, as needed to satisfy geometrical strain or other factors. The observed changes in bond length, a slight lengthening of the bonds in the cyclopropane ring and shortening of bonds in the cyclobutane ring, would then correspond to a small shift of electron density from the cyclopropane to the cyclobutane ring. The geometry observed in TDTC would certainly support this delocalization argument, especially if the effect of the substituents is taken into account. Hoffman pointed out that depending upon whether the substituents have electron donating or accepting groups, they can greatly affect the geometry of the cyclopropane ring (18). In a norcardiene derivative (6), the lengthening of two bonds in the cyclopropane ring is rationalized on the basis of a delocalization of electrons from the pseudo-Π orbital on the cyclopropane ring into the Π* orbitals of two geminally substituted cyanide groups. The carbomethoxy group in TDTC is in the correct position to maximize this type of pseudo Π–Π* interaction. This further delocalization would explain the even greater lengthening of the cyclopropane bond length in this compound compared with that found in bicyclo[2.1.0]pentane.

Acknowledgements

We wish to thank the National Research Council of Canada and the University of Alberta for financial support.

1. M. J. BENNETT, J. T. PURDHAM, S. TAKADA, and S MASAMUNE. J. Am. Chem. Soc. **93**, 4063 (1971).
2. (*a*) H. H. STECHL. Chem. Ber. **97**, 2681 (1964); (*b*) N OBUTA and I. MORITANI. Bull. Chem. Soc. Jpn. **39**, 225((1966); (*c*) C. DEBOER and R. BRESLOW. Tetrahedron Lett **11**, 1033 (1967); (*d*) H. DÜRR. Tetrahedron Lett. **17**, 164 (1967); (*e*) E. L. ALLRED and J. C. HINSHAW. J. Am. Chem Soc. **90**, 6885 (1968); (*f*) H. TANIDA and S. TERETAKE Tetrahedron Lett. **57**, 4991 (1970); (*g*) J. SCHIPPERIJN and J LUKAS. Tetrahedron Lett. **3**, 231 (1972).
3. J. KARLE and I. L. KARLE. Acta Crystallogr. **21**, 849 (1966)
4. D. T. CROMER. Acta Crystallogr. Sect. A, **24**, 321 (1968).

5. R. MASON and G. B. ROBERTSON. *In* Advances in structure research by diffraction methods. Vol. 2. *Edited by* R. Brill and R. Mason. Interscience Division, Wiley, New York, NY. 1966.
6. C. J. FRITCHIE. Acta Crystallogr. **20**, 27 (1966).
7. H. A. BENT. Chem. Rev. **61**, 275 (1961).
8. M. J. S. DEWAR. Tetrahedron, 1817 (1965).
9. L. LEISEROWITZ and G. M. J. SCHMIDT. Acta Crystallogr. **18**, 1058 (1965).
10. J. D. DUNITZ and P. STRICKLER. *In* Structural chemistry and molecular biology. *Edited by* A. Rich and N. Davidson. W. H. Freeman & Co., San Francisco and London. 1968.
11. R. H. HOFFMANN and R. B. DAVIDSON. J. Am. Chem. Soc. **93**, 5699 (1971).
12. O. BASTIANSEN, F. N. FRITSCH, and K. HEDBERG. Acta Crystallogr. **17**, 538 (1964).
13. A. ALMENNINGEN, O. BASTIANSEN, and P. N. SKANCKE. Acta Chem. Scand. **15**, 711 (1961).
14. J. DUNITZ. Acta Crystallogr. **2**, 1 (1949).
15. C. S. GIBBONS and J. TROTTER. J. Chem. Soc. A, 2027 (1967).
16. R. D. SUENRAM and M. D. HARMONY. J. Chem. Phys. **56**, 3837 (1972).
17. P. R. BROOK, A. J. DUKE, and J. R. DUKE. J. Chem. Soc. D574 (1970).
18. R. H. HOFFMANN. Tetrahedron Lett. **33**, 2907 (1970).
19. W. H. ZACHARIASEN. Acta Crystallogr. **16**, 1139 (1963).

Can. J. Chem. Downloaded from www.nrcresearchpress.com by 210.87.254.5 on 09/05/12
For personal use only.

Synthesis of *trans*- and *cis*-α-damascone

HSING-JANG LIU, HING-KWOK HUNG,
GEORGE L. MHEHE, AND M. L. DUARTE WEINBERG
Department of Chemistry, University of Alberta, Edmonton, Alta., Canada T6G 2G2

Received July 12, 1977

HSING-JANG LIU, HING-KWOK HUNG, GEORGE L. MHEHE, and M. L. DUARTE WEINBERG. Can. J. Chem. **56**, 1368 (1978).

Selective thioketalization of a mixture of keto esters **5** and **6** resulted in the exclusive formation of thioketal **7** and complete recovery of keto ester **6**. Lithium aluminum hydride reduction of thioketal **7** followed by Moffatt oxidation of the resulting alcohol **8** gave aldehyde **10** which on treatment with a mixture of *cis*- and *trans*-1-propenyl magnesium bromide afforded *trans*-alcohol **11** and its *cis* isomer **12**. Manganese dioxide oxidation of alcohol **11** followed by desulfurization gave *trans*-α-damascone (**3**). Similarly, alcohol **12** was converted to *cis*-α-damascone (**4**).

HSING-JANG LIU, HING-KWOK HUNG, GEORGE L. MHEHE et M. L. DUARTE WEINBERG. Can. J. Chem. **56**, 1368 (1978).

La thiocétalisation sélective d'un mélange des céto esters **5** et **6** conduit à la formation exclusive du thiocétal **7** et une récupération complète du céto ester **6**. La réduction par $LiAlH_4$ du thiocétal **7**, suivie par une oxydation de Moffatt effectuée sur l'alcool **8**, fournit l'aldéhyde **10** qui, par traitement avec un mélange *cis* et *trans* des bromures de propène-1 yle magnésium, donne naissance à l'alcool *trans*-**11** et à son isomère *cis*-**12**. L'oxydation de l'alcool **11** par le dioxyde de manganèse, suivie par une désulfurisation, permet d'obtenir l'α-damascone *trans* (**3**). De la même manière, on peut transformer l'alcool **12** en α-damascone *cis* (**4**).

[Traduit par le journal]

β-Damascenone (**1**) (1-5) and β-damascone (**2**) (2, 6) are highly odoriferous compounds found in nature as trace components in the essential oils of several plant species. Because of their industrial importance and limited availability from natural sources, much attention (1, 7–15) has been drawn to the synthesis of these ketones as well as their structurally related compounds which are of equal industrial interest. Several syntheses of *trans*-α-damascone (**3**) and of *cis*-α-damascone (**4**) have previously been reported involving modifications of α-cyclocitral (1) or α-ionone (7, 11–13). In this paper we describe a full account of an efficient synthesis of **3** and **4** without relay (16).

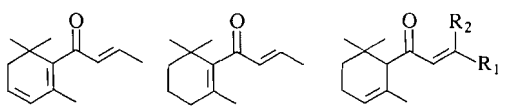

1 **2** **3** $R_1 = CH_3$; $R_2 = H$
4 $R_1 = H$; $R_2 = CH_3$

Keto ester **5** was chosen as the starting compound since it possesses the three methyl groups of the target molecules **3** and **4** as well as suitable functionalities for subsequent transformations. Several methods are available for the preparation of **5** (17–20). The procedure of Rubinstein (17) was adapted for its simplicity. Although it was reported that a single isomer was obtained, the BF_3-catalysed condensation of acetone and ethyl acetoacetate under the described conditions gave, in our hand, a mixture of the desired keto ester **5** and its positional isomer **6** in a ratio of ca. 2:1. Attempts to separate these two isomers by distillation were fruitless. A similar mixture was also obtained previously by Surmatis *et al.* (20), using zinc chloride as a catalyst. They found that **6** could be selectively hydrolyzed by heating the mixture with zinc chloride in ethanol and water to facilitate the separation of **5**. Efforts made toward this end did not result in substantial change of the mixture composition. The desired compound **5** could however be separated from its isomer **6** by extensive column chromatography as noted (20) and its thioketalization gave rise to the thioketal **7** in quantitative yield. A more convenient procedure involves the treatment of the mixture of **5** and **6** with 1,2-ethanedithiol and boron trifluoride etherate at 0°C for 7 h. Under these reaction conditions, keto ester **5** underwent thioketal formation exclusively and quantitatively whereas **6** remained totally unchanged.

The conversion of thioketal **7** into ketones **3** and **4** requires the removal of the thioketal group and the modification of the ester substituent. The required side chain was first installed. Lithium aluminum hydride reduction of thioketal **7** afforded crystalline alcohol **8** in 82% yield. Moffatt oxidation of alcohol **8** using dicyclohexylcarbodiimide, dimethyl sulfoxide, trifluoroacetic acid, and pyridine (21) produced a substantial quantity of the dehydration product **9**.

Can. J. Chem. Downloaded from www.nrcresearchpress.com by 210.87.254.40 on 09/05/12
For personal use only.

Can. J. Chem. Downloaded from www.nrcresearchpress.com by 210.87.254.40 on 09/05/12
For personal use only.

An 80% yield of the desired aldehyde **10** could however be obtained when phosphoric acid (22) was substituted for trifluoroacetic acid and pyridine. Subsequent treatment of aldehyde **10** with propenylmagnesium bromide (1) derived from a mixture of *cis*- and *trans*-1-bromopropene (ca. 1:1) gave a 93% yield of the isomeric alcohols **11** and **12** in approximately equal amounts. It is noted that, in principle, each of these isomers, if so desired, can be specifically prepared by the use of the stereochemically homogeneous reagent. Indeed, when aldehyde **10** was subjected to treatment with *trans*-1-propenyllithium (23), alcohol **11** was formed exclusively. This transformation also facilitated the differentiation of the isomeric pair **11** and **12** at this stage. Oxidation of alcohol **11** with a 30-fold (by weight) excess of manganese dioxide (24) in methylene chloride afforded an 85% yield of enone **13** whose nmr spectrum showed a large coupling constant of 15 Hz for the two vicinal vinylic protons at δ 6.80 and 6.21, confirming the *trans* nature of the conjugated double bond. Upon oxidation under the same conditions, alcohol **12** gave a 45% yield of the expected *cis*-enone **14** and a 31% yield of the *trans* isomer **13**.[1] Interestingly, when the oxidation of **12** was carried out using a lesser amount (12-fold excess) of manganese dioxide, it resulted in the exclusive formation of **14** in 91% yield.

The thioketal groups of **13** and **14** were removed by brief treatment with W-2 Raney nickel (25) which was deactivated in advance in refluxing acetone. Under these conditions, enone **13** gave exclusively

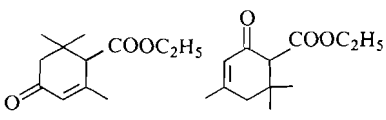

5 **6**

7 R = $COOC_2H_5$
8 R = CH_2OH
10 R = CHO

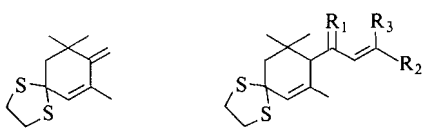

9

11 R_1 = H,OH; R_2 = CH_3; R_3 = H
12 R_1 = H,OH; R_2 = H; R_3 = CH_3
13 R_1 = O; R_2 = CH_3; R_3 = H
14 R_1 = O; R_2 = H; R_3 = CH_3

[1]The required isomerization most likely occurred before the oxidation since further treatment of *cis*-enone **14** with manganese dioxide under the same conditions did not produce any detectable amount of this compound.

trans-α-damascone (**3**) in 56% yield whereas enone **14** afforded equal amounts of *trans*- and *cis*-α-damascone (**3** and **4**)[2] in a total yield of 64%. The ir, nmr, and mass spectra of the two α-damascones thus obtained were in agreement with those reported in the literature (1, 7).

Experimental

General

Mass spectra were recorded on AEI MS-50, MS-9 and MS-2 mass spectrometers. Infrared spectra were obtained using Perkin-Elmer Models 457 and 337 spectrometers. Nuclear magnetic resonance spectra were recorded on Varian A-60 and HR-100 spectrometers, using tetramethylsilane as internal standard. Elemental analyses were performed by the microanalytical laboratory of this department. Melting points were determined on Kofler hot stage apparatus and are uncorrected.

4-Carbethoxy-3,5,5-trimethyl-2-cyclohexen-1-one (5) and 6-Carbethoxy-3,5,5-trimethyl-2-cyclohexen-1-one (6)

The procedure of Rubinstein (17) was used for the boron trifluoride catalysed condensation of ethyl acetoacetate and acetone. The product (55.9 g from 134 g of ethyl acetoacetate) was shown by the nmr spectrum to be a mixture of **5** and **6** in a ratio of ca. 2:1. A sample of the mixture (500 mg) was separated by column chromatography on silica gel. Elution with a solution of 10% ether in Skelly B gave 120 mg of **6** (faster moving) and 230 mg of **5** (20).

8-Carbethoxy-7,9,9-trimethyl-1,4-dithiospiro[4.5]dec-6-ene (7)

From Pure 5

At 0°C, to a solution of **5** (130 mg, 0.62 mmol) in 1,2-ethanedithiol (0.6 ml), was added boron trifluoride etherate (0.1 ml). The resulting solution, after stirring at room temperature for 16 h, was poured into ice-cold 2 *N* aqueous sodium hydroxide (25 ml) and extracted with chloroform. The chloroform solution was washed with water, dried ($MgSO_4$), filtered, and concentrated. Column chromatography of the residue on silica gel, using benzene as eluent, gave **7** (176 mg, 99%): ir (film): 1732 (ester) and 1665 cm^{-1} (double bond); nmr (CCl_4) δ: 5.63 (broad s, 1H, =CH—), 4.09 (q, 2H, J = 7 Hz, —OCH_2—), 3.28 (s, 4H, —SCH_2CH_2S—), 2.63 (d, 1H, J = 14 Hz, —C*H*(H)—), 2.52 (s, 1H, —CHCO—), 1.97 (d, 1H, J = 14 Hz, —C*H*(H)—), 1.66 (broad, s 3H, =CCH_3), 1.24 (t, 3H, J = 7 Hz, —OCH_2CH_3), 1.05 (s, 3H, —CH_3), and 0.95 (s, 3H, —CH_3); ms M^+ calcd. for $C_{14}H_{22}O_2S_2$: 286.10613; found: 286.10606.

From the Mixture of 5 and 6

At 0°C, a mixture of **5** and **6** (5 g, 23.8 mmol) obtained from the condensation reaction (*vide supra*) was dissolved in 1,2-ethanedithiol (20 ml) and boron trifluoride etherate (2 ml) was added. After stirring at the same temperature for 7 h, the reaction mixture was worked up according to the procedure described above to give an oily product which was purified by column chromatography on silica gel. Elution with benzene gave **7** (4.23 g, ~100% based on **5**). Further elution with benzene resulted in the recovery of **6** (1.45 g).

8-Hydroxymethyl-7,9,9-trimethyl-1,4-dithiospiro[4.5]-dec-6-ene (8)

Lithium aluminum hydride (990 mg, 26.05 mmol) was

[2]We have not been able to effect the desulfurization of **14** without partial isomerization of the double bond.

Can. J. Chem. Downloaded from www.nrcresearchpress.com by 210.87.254.40 on 09/05/12
For personal use only.

slowly added to a well stirred solution of **7** (5 g, 17.48 mmol) in ether (60 ml) at −78°C. Stirring was continued under an atmosphere of nitrogen at room temperature overnight. Methanol was added dropwise until the evolution of hydrogen gas ceased. Water and saturated aqueous ammonium chloride (30 ml each) were added. The mixture was acidified with 1 *N* hydrochloric acid to ~p*H* 2 and extracted with chloroform. The extracts were washed with water and combined. Drying ($MgSO_4$), filtration, and concentration gave the crude product. Purification of the crude product by silica gel column chromatography using pentane–benzene (1:1) as eluent gave **8** (3.4 g, 82%): mp 46–47°C (ether); ir ($CHCl_3$): 3430 (alcohol) and 1650 cm^{-1} (double bond); nmr (CCl_4) δ: 5.64 (m, 1H, —CH=), 3.65 (m, 2H, —OCH_2—) 3.26 (s, 4H, —SCH_2CH_2S—), 1.79 (d, 3H, J = 2 Hz, =CCH_3), 1.05, and 1.08 (both s, 3H each, —$C(CH_3)_2$); ms M^+ calcd. for $C_{12}H_{20}OS_2$: 244.0955; found: 244.0952. *Anal.* calcd. for $C_{12}H_{20}OS_2$: C 58.97, H 8.25, S 26.24; found: C 59.15, H 8.16, S 26.07.

Alcohol **8** was found to be unstable, deteriorating when stored in chloroform over magnesium sulfate at room temperature overnight to give diene **9**: ir (film): 1670 and 1598 cm^{-1} (double bonds); nmr (CCl_4) δ: 5.63 (broad s, 1H, =CH—), 4.88 (broad s, 2H, =CH_2), 3.18 (s, 4H, —SCH_2CH_2S—), 2.17 (s, 2H, —CH_2—), 1.73 (d, 3H, J = 1.5 Hz, =CCH_3), 0.90 (s, 6H, —$C(CH_3)_2$); ms M^+ calcd. for $C_{12}H_{18}S_2$: 226.08519; found: 226.08496.

*8-Formyl-7,9,9-trimethyl-1,4-dithiospiro[4.5]dec-6-ene (**10**)*

To a solution of **8** (153 mg, 0.63 mmol) in dimethyl sulfoxide (0.7 ml), were added a solution of dicyclohexylcarbodiimide (400 mg, 1.94 mmol) in benzene (0.35 ml) and a solution of 85% phosphoric acid (4 μl) in dimethyl sulfoxide (0.4 ml). The reaction mixture was stirred at room temperature under a nitrogen atmosphere for 20 h. Ethyl acetate (1.5 ml) and a solution of oxalic acid (153 mg, 1.21 mmol) in methanol (3 ml) were added sequentially and the resulting mixture after stirring at room temperature for 30 min was filtered. The filtrate was added to water and extracted with chloroform. The chloroform solution after washing with saturated aqueous sodium bicarbonate, was dried over magnesium sulfate, filtered, and concentrated. The crude product thus obtained was subjected to preparative thin-layer chromatography using silica gel as adsorbant and a solution of 20% ether in petroleum ether as eluent to give **10** (122 mg, 80%): mp 62–63°C (ether); ir (film): 2730, 1715 (aldehyde), and 1648 cm^{-1} (double bond); nmr (CCl_4) δ: 9.39 (d, 1H, J = 5 Hz, —CHO), 5.79 (m, 1H, =CH), 2.39 (s, 4H, —SCH_2CH_2S—), 2.46, 2.19 (both d, 1H each, J = 15 Hz, —CH_2—), 2.28 (d, 1H, J = 5 Hz, —CHCHO), 1.67 (d, 3H, J = 1.5 Hz, =CCH_3), 1.07 and 1.04 (both s, 3H each, —$C(CH_3)_2$); ms M^+ calcd. for $C_{12}H_{18}OS_2$: 242.0799; found: 242.0799. *Anal.* calcd. for $C_{12}H_{18}OS_2$: C 59.46, H 7.48, S 26.45; found: C 59.52, H 7.50, S 26.09.

trans- *(**11**) and* cis-*1-(2,6,6-Trimethyl-4,4-ethylenedithio-2-cyclohexenyl)-2-buten-1-ol (**12**)*

Using trans- *and* cis-*1-Propenylmagnesium Bromide*

To a suspension of magnesium turnings (60 mg, 2.47 g-atom) in tetrahydrofuran (6 ml), was added a solution of *cis*- and *trans*-1-bromo-1-propene (ca. 1:1; obtained from Aldrich; 0.25 ml) in tetrahydrofuran (1 ml). The mixture was refluxed under a nitrogen atmosphere for 45 min and cooled to −10°C. A solution of **10** (418 mg, 1.73 mmol) in tetrahydrofuran (5 ml) was introduced. After stirring at −5°C for 2 h and at room temperature for an additional 2 h, the reaction mixture was filtered. The filtrate was poured into saturated aqueous ammonium chloride and extracted with chloroform. Work-up of the extracts in the usual manner gave an oil which was purified by silica gel preparative thin-layer chromatography. Elution with ether – petroleum ether (1:1) gave **11** (220 mg, 45%; faster moving) and **12** (234 mg, 48%). Alcohol **12**, mp 93–94°C (ether), showed the following spectral data: ir (CCl_4): 3540 (alcohol) and 1650 cm^{-1} (double bond); nmr (CCl_4) δ: 5.79 (d, 1H, J = 1.5 Hz, —C=CH), 5.38 (m, 2H, —CH=CH—), 4.68 (m, 1H, —CHOH), 3.24 (s, 4H, —SCH_2CH_2S—), 1.79 (d, 3H, J = 1.5 Hz, =CCH_3), 1.67 (d, 3H, J = 5 Hz, =$CHCH_3$), 1.11 and 1.01 (both s, 3H each, —$C(CH_3)_2$); ms M^+ calcd. for $C_{15}H_{24}OS_2$: 284.1269; found: 284.1251. *Anal.* calcd. for $C_{15}H_{24}OS_2$: C 63.33, H 8.50, S 22.54; found: C 63.25, H 8.38, S 22.39.

The following spectral data were obtained for **11**: ir (film): 3470 (alcohol) and 1645 cm^{-1} (double bonds); nmr (CCl_4) δ: 5.71 (broad s, 1H, —C=CH—), 5.52 (m, 2H, —CH=CH—), 4.36 (m, 1H, —CHOH), 3.27 (s, 4H, —SCH_2CH_2S—), 1.75 (d, 3H, J = 2 Hz, =CCH_3), 1.67 (m, 3H, =$CHCH_3$), 1.05 and 0.99 (both s, 3H each, —$C(CH_3)_2$); ms M^+ calcd. for $C_{15}H_{24}OS_2$: 284.1269; found: 284.1255.

Using trans-*1-Propenyllithium*

At −10°C, to a solution of **10** (90 mg; 0.37 mmol) in ether (10 ml), was added a 0.37 *N* solution of *trans*-1-propenyllithium (23) in ether (2 ml, 0.74 mmol). The resulting solution was stirred under an atmosphere of argon for 20 min. Methanol (2 ml) was added and the mixture was poured into saturated aqueous ammonium chloride solution and extracted with ether. The crude product obtained after the usual work-up of the extracts was purified by silica gel preparative thin-layer chromatography with ether – petroleum ether (1:1) elution to give **11** (70 mg, 67%).

*7,9,9-Trimethyl-8-(*trans-*1-oxo-2-butenyl)-1,4-dithiospiro[4.5]dec-6-ene (**13**)*

Alcohol **11** (600 mg, 2.11 mmol) was dissolved in methylene chloride (120 ml) and activated manganese dioxide (18 g) was added. The mixture was stirred at room temperature for 10 h and filtered. Concentration of the filtrate gave an oil. Preparative thin-layer chromatography (silica gel) of the oil eluted with a solution of 20% ether in *n*-pentane afforded **13** (501 mg, 85%): ir (film): 1685 (ketone), 1665 (double bond), and 1625 cm^{-1} (double bond); nmr (CCl_4) δ: 6.80 (qd, 1H, J = 15, J' = 6.5 Hz, =$CHCH_3$), 6.21 (qd, 1H, J = 15, J' = 1.5 Hz, —COCH=), 5.69 (broad s, 1H, —C=CH—), 3.29 (s, 4H, —SCH_2CH_2S—), 1.90 (dd, 3H, J = 6.5, J' = 1.5 Hz, =$CHCH_3$), 1.60 (d, 3H, J = 2 Hz, =CCH_3), 1.07 and 0.86 (both s, 3H each —$C(CH_3)_2$); ms M^+ calcd. for $C_{15}H_{22}OS_2$: 282.1113; found: 282.1113. *Anal.* calcd. for $C_{15}H_{22}OS_2$: C 63.78, H 7.85, S 22.70; found: C 63.83, H 7.72, S 22.51.

*Manganese Dioxide Oxidation of **12***

(*A*) Activated manganese dioxide (3.7 g) was added to a solution of **12** (300 mg, 1.06 mmol) in methylene chloride (80 ml). The reaction mixture was stirred at room temperature for 6 h. Filtration and concentration gave an oil which was purified by preparative thin-layer chromatography on silica gel. Elution with a solution of 20% ether in *n*-pentane afforded

Can. J. Chem. Downloaded from www.nrcresearchpress.com by 210.87.254.40 on 09/05/12
For personal use only.

7,9,9-trimethyl-8-(*cis*-1-oxo-2-butenyl)-1,4-dithiospiro[4.5]-dec-6-ene (**14**) (273 mg, 91%); ir (film): 1680 (ketone), 1655 (double bond), and 1610 cm^{-1} (double bond); nmr (CCl_4) δ: 6.16 (m, 2H, —CH=CH—), 5.67 (broad s, 1H, =CH—), 3.26 (s, 4H, $-SCH_2CH_2S-$), 2.07 (m, 3H, $=CHCH_3$), 1.63 (d, 3H, J = 2 Hz, $=CCH_3$), 1.07 and 0.99 (both s, 3H each, $-C(CH_3)_2$); ms M^+ calcd. for $C_{15}H_{22}OS_2$: 282.1113; found: 282.1112. *Anal.* calcd. for $C_{15}H_{22}OS_2$: C 63.78, H 7.85, S 22.70; found: C 64.15, H 7.74, S 22.62.

(*B*) A mixture of **12** (900 mg, 3.17 mmol) and activated manganese dioxide (27 g) in methylene chloride (150 ml) was stirred at room temperature for 11 h. Work-up of the reaction in the usual manner followed by preparative thin-layer chromatography (silica gel; 20% ether in *n*-pentane elution) of the crude product gave 402 mg (45%) of **14** and 277 mg (31%) of **13**.

trans-α-*Damascone (3)*

A suspension of W-2 Raney Nickel (25) (2 ml) in acetone (5 ml) was refluxed for 8 min. After acetone was removed, a solution of **13** (52 mg, 0.18 mmol) in 98% ethanol (10 ml) was added and the resulting mixture was stirred at room temperature for 10 min. Filtration and concentration followed by preparative thin-layer chromatography of the crude product on silica gel with ether – petroleum ether (1:9) elution gave **3** (20 mg, 56%): ir (film): 1690 (ketone), 1662 (double bond), and 1628 cm^{-1} (double bond); nmr (CCl_4) δ: 6.77 (qd, 1H, J = 15.5, J' = 6.5 Hz, $=CHCH_3$), 6.18 (qd, 1H, J = 15.5, J' = 1.5 Hz, —COCH=), 5.52 (m, 1H, =CH—), 2.75 (broad s, 1H, —CHCO—), 1.88 (dd, 3H, J = 6.5, J' = 1.5 Hz, $=CHCH_3$), 1.55 (t, 3H, J = 1.5 Hz, $=CCH_3$), 0.92, and 0.83 (both s, 3H each), $-C(CH_3)_2$); ms M^+ calcd. for $C_{13}H_{20}O$: 192.1514; found: 192.1514.

cis-α-*Damascone (4)*

A solution of **14** (60 mg, 0.21 mmol) in 98% ethanol (10 ml) was added to the deactivated (by the same procedure described in the previous experiment) W-2 Raney nickel (2 ml) and the resulting mixture was stirred at room temperature for 1.5 h. The mixture was filtered and the filtrate concentrated. Preparative thin-layer chromatography of the oily product on silica gel using a solution of 10% ether in *n*-pentane as eluent gave **3** (faster moving; 13 mg, 32%) and **4** (13 mg, 32%). *cis*-α-Damascone (**4**) thus obtained showed the following spectral data: ir (film): 1685 (ketone), 1673 (double bond), and 1615 cm^{-1} (double bond); nmr (CCl_4) δ: 6.14 (m, 2H, —CH=CH—), 5.50 (m, 1H, =CH—), 2.67 (broad s, 1H, —CHCO—), 2.05 (d, 3H, J = 6 Hz, $=CHCH_3$), 1.55 (t, 3H, J = 1.5 Hz, $=CCH_3$), 0.91 and 0.85 (both s, 3H each $-C(CH_3)_2$); ms M^+ calcd. for $C_{13}H_{20}O$: 192.1514; found: 192.1512.

Acknowledgments

We are grateful to the National Research Council of Canada and the University of Alberta for financial support.

1. E. DEMOLE, P. ENGGIST, U. SÄUBERLI, M. STOLL, and E. SZ. KOVÁTS. Helv. Chim. Acta, **53**, 541 (1970).
2. E. DEMOLE and D. BERTHET. Helv. Chim. Acta, **54**, 681 (1971); **55**, 1866 (1972).
3. M. WINTER and P. ENGGIST. Helv. Chim. Acta, **54**, 1891 (1971).
4. K. KARLSSON, I. WAHLBERG, and C. R. ENZELL. Acta Chem. Scand. **26**, 2837 (1972).
5. J. STRATING and P. VAN EERDE. J. Inst. Brewing, **79**, 414 (1973).
6. B. KIMLAND, A. J. AASEN, and C. R. ENZELL. Acta Chem. Scand. **26**, 2177 (1972).
7. G. OHLOFF and G. UHDE. Helv. Chim. Acta, **53**, 531 (1970).
8. G. BÜCHI and H. WÜEST. Helv. Chim. Acta, **54**, 1767 (1971).
9. K. H. SCHULTE-ELTE, V. RAUTENSTRAUCH, and G. OHLOFF. Helv. Chim. Acta, **54**, 1805 (1971).
10. K. H. SCHULTE-ELTE, B. L. MÜLLER, and G. OHLOFF. Helv. Chim. Acta, **54**, 1899 (1971).
11. G. BÜCHI and J. C. VEDERAS. J. Am. Chem. Soc. **94**, 9128 (1972).
12. K. H. SCHULTE-ELTE, B. L. MÜLLER, and G. OHLOFF. Helv. Chim. Acta, **56**, 310 (1973).
13. V. RAUTENSTRAUCH. Helv. Chim. Acta, **56**, 2492 (1973).
14. K. S. AYYAR, R. C. COOKSON, and D. A. KAGI. Chem. Commun. 161 (1973); J. Chem. Soc. Perkin I, 1727 (1975).
15. W. G. DAUBEN, A. P. KOZIKOWSKI, and W. T. ZIMMERMAN. Tetrahedron Lett. 515 (1975).
16. H. J. LIU, H. K. HUNG, and G. L. MHEHE. Tetrahedron Lett. 4129 (1976).
17. H. RUBINSTEIN. J. Org. Chem. **27**, 3886 (1962).
18. E. KNOEVENAGEL. Ann. **297**, 185 (1897).
19. G. MERLING and R. WELDE. Ann. **366**, 141 (1909).
20. J. D. SURMATIS, A. WALSER, J. GIBAS, and R. THOMMEN. J. Org. Chem. **35**, 1053 (1970).
21. J. G. MOFFATT. Org. Synth. **47**, 25 (1967).
22. K. E. PFITZNER and J. G. MOFFATT. J. Am. Chem. Soc. **87**, 5670 (1965).
23. G. LINSTRUMELLE, J. K. KRIEGER, and G. M. WHITESIDES. Org. Synth. **55**, 103 (1976).
24. J. ATTENBURROW, A. F. B. CAMERON, J. H. CHAPMAN, R. M. EVANS, B. A. HEMS, A. B. A. JANSEN, and T. WALKER. J. Chem. Soc. 1094 (1952).
25. R. L. AUGUSTINE. Catalytic hydrogenation. Marcel Dekker Inc., New York, NY. 1965. p. 147.

Field desorption mass spectrometry of carboxylic acids: characteristic spectra and analysis of mixtures and impure samples[1]

GORDON WALTER WOOD,[2] EMILY JANE OLDENBURG, PUI-YAN LAU, AND DONNA LEE WADE

Department of Chemistry, University of Windsor, Windsor, Ont., Canada N9B 3P4

Received November 28, 1977

GORDON WALTER WOOD, EMILY JANE OLDENBURG, PUI-YAN LAU, and DONNA LEE WADE. Can. J. Chem. **56**, 1372 (1978).

Field desorption mass spectra were obtained for a variety of saturated and unsaturated carboxylic acids containing 12 or more carbons. At best anode temperature molecular ions were dominant and small peaks representing $[M + 1]^+$, $[2M + 1]^+$, $[M - 17]^+$, and $[M - 44]^+$ were present in several compounds. At higher temperatures several novel ions were found, including one corresponding to $[2M + 1 - 18]^+$ which may represent anhydride formation. In a mixture of *cis*-5-eicosenoic and elaidic acids each molecular ion desorbed as expected but at higher temperatures the three possible anhydride ions appeared, with the cross product $[M_1 + M_2 + 1 - H_2O]^+$ as the base peak. Isomeric hydroxystearic acids (2-OH, 12-OH, 17-OH) gave predominantly ions in the molecular ion region with some differences in spectra which may relate to structure. Apparent polyester formation has been observed in 3-hydroxypropanoic acid where ions of the general formula $[xM - (x - 1)H_2O + H]^+$ with $x = 2, 3, \ldots 13$ were found. Several other hydroxyacids show dimer formation and lactic acid has ions up to $x = 5$ in the above formula. Two of four technical grade dicarboxylic acids tested were seriously contaminated by sodium ions and gave useful spectra only after extraction by dibenzo-18-crown-6 ether. After this treatment both adipic and azelaic acid have $[M + 1]^+$ as base peak, although adipic acid decarboxylates readily ($[M - 44]^+ = 74\%$). Other technical grade acids showed the presence of homologues and related structures as impurities.

GORDON WALTER WOOD, EMILY JANE OLDENBURG, PUI-YAN LAU et DONNA LEE WADE. Can. J. Chem. **56**, 1372 (1978).

On a obtenu les spectres de masse par désorption de champ pour un certain nombre d'acides carboxyliques saturés et insaturés contenant au moins 12 atomes de carbone. Dans les meilleures conditions de température d'anode, des ions moléculaires sont prédominants et des petits pics représentant $[M + 1]^+$, $[2M + 1]^+$, $[M - 17]^+$ et $[M - 44]^+$ sont présents dans plusieurs composés. A des températures plus élevées, on a trouvé plusieurs nouveaux ions y compris un ion correspondant à $[2M + 1 - 18]^+$ qui peut représenter la formation de l'anhydride. Dans un mélange d'acides eicosène-5 oïque *cis* et élaidique, il y a, tel que prévu, une désorption de chaque ion moléculaire; toutefois à des températures plus élevées, les ions des trois anhydrides possibles se forment avec le produit croisé $[M_1 + M_2 + 1 - H_2O]^+$ comme pic de base. Les acides hydroxystéariques isomères (OH-2, OH-12, OH-17) conduisent d'une façon prédominante à des ions dans la région de l'ion moléculaire avec quelques différences dans les spectres qui peuvent être dues à leurs structures. Dans le cas de l'acide hydroxy-3 propanoïque, on a observé une formation apparente de polyesters indiqués par la présence d'ions de formule générale $[xM - (x - 1)H_2O + H]^+$ où $x = 2, 3 \ldots 13$. Plusieurs autres hydroxyacides semblent conduire à la formation de dimères; dans le cas de l'acide lactique on a observé la présence d'ions allant jusqu'à $x = 5$ dans la formule mentionnée ci-dessus. Deux des quatres acides dicarboxyliques de pureté commerciale qui ont été examinés étaient sérieusement contaminés par des ions sodium et ne donnaient des spectres utiles qu'après extraction par l'éther dibenzo-18 couronne-6. Après ce traitement, l'acide adipique de même que l'acide azélaïque possèdent un pic de base de $[M + 1]^+$ alors que l'acide adipique se décarboxyle rapidement ($[M - 44]^+ = 74\%$). Dans le cas d'autres acides de pureté commerciale on a observé la présence d'impuretés correspondant aux homologues et à des composés de structures semblables.

[Traduit par le journal]

Introduction

In recent years field desorption mass spectrometry (fdms) has been shown to be a useful technique for characterizing molecules of limited volatility and thermal stability (1, 2). One such class of compound is the higher molecular weight carboxylic acids, materials which are often sold and used as mixtures of moderate complexity. With the ultimate goal of evaluating fdms for analysis of such mixtures, we undertook a study of a range of pure acids containing varying degrees of unsaturation, hydroxyl or additional carboxylic acid groups, and related metal

[1]Taken in part from the M.Sc. Thesis of E.J.O., University of Windsor, Windsor, Ont., 1977.

[2]Author to whom correspondence should be addressed.

Can. J. Chem. Downloaded from www.nrcresearchpress.com by 210.87.254.5 on 09/05/12
For personal use only.

TABLE 1. Field desorption mass spectra of selected carboxylic acids[a]

Acid (n)[b]	x	y	Anode heating current (mA)	Relative intensity (%) 2M + 1	M + 1	M	M − 17	M − 44
$CH_3(CH_2)_{n-2}COOH$								
Lauric (12)[c]			0[d]	1	37	100	3	
Palmitic (16)			0[d]	1	42	100	3	
Stearic (18)			0[d]	4	45	100		3
Behenic (22)			4		56	100		3
$CH_3(CH_2)_xCH{=}CH(CH_2)_yCOOH$								
Myristoleic (14)	3	7	0[d]	6	46	100	1	
Palmitoleic (16)[e]	5	7	5	1	22	100		
Palmitelaidic (t, 16)	5	7	3		21	100		
Oleic (18)	7	7	6		18	100		
Elaidic (t, 18)[f]	7	7	2		23	100		
5-Eicosenoic (20)[g]	13	3	10	5	38	100	2	1
$CH_3(CH_2)_xCH{=}CHCH_2CH{=}CH(CH_2)_yCOOH$								
Linoleic (18)	4	7	4		21	100		
Linolelaidic (t, 18)	4	7	12		28	100		
$CH_3(CH_2)_xCH{=}CHCH_2CH{=}CHCH_2CH{=}CH(CH_2)_yCOOH$								
Linolenic (18)	1	7	0[d]		28	100		

[a]Samples were deposited on the field anode from $CHCl_3$ solutions. For behenic acid, a mixture of $CHCl_3/CH_3OH$ was necessary. Spectra are reported as a set of intensities relative to base peak = 100.
[b]Compounds are identified by common name followed by carbon number (n). All olefinic bonds are *cis* except those marked (t) for *trans*.
[c]Lauric acid, $C_{11}H_{23}COOH$, is the lowest molecular weight carboxylic acid amenable to fdms. Caproic (n = 6), caprylic (n = 8), and capric (n = 10) when admitted to the ion source as gases gave spectra (field ionization) with M+ as base peak. The only other peaks of importance were found in the caproic acid spectrum: $[M + 1]^+ = 76\%$, $[M - 17]^+ = 9\%$.
[d]Spectra recorded at 0 mA are likely to contain a large component of ions produced in gas phase (fims).
[e]Palmitoleic acid showed a peak at $[2M + 1 - 18]^+ = 1\%$.
[f]At 8 mA the base peak for this acid becomes m/e 502 ($[2M + H - H_2O - COOH]^+$); at 15 mA, the base peak is 2M − H.
[g]At higher anode temperatures, the base peak for this acid shifted successively to $[2M - 17]^+$ (ahc = 14 mA), $[2M - 1]^+$ (16mA), and $[3M - 2H]^+$ (18 mA).

salts. The present paper reports the results for free acids, including some deductions about the behavior of these compounds under fd conditions and a comparison with the spectra obtained from representative samples of technical purity.

Experimental

Mass spectra were obtained on a Varian MAT Model CH5 DF instrument equipped with a fi/fd/ei source. Magnet scanning and data acquisition were under the control of an interfaced INCOS model 2000 data system. The field anode was a 10 μm tungsten wire activated by benzonitrile (3) in a modified Varian apparatus. For fd measurements an anode voltage of +3 kV and a cathode voltage of −7 to −8 kV were applied in an unheated source (70–100°C) at ca 10^{-6} Torr. The magnet was scanned quadratically from m/e 900 to 10 in 20 s with a nominal resolution of 1500 and the secondary electron multiplier at 1.75 kV.

A solution (ca. 5 mg/mL) of the sample was deposited on the activated anode by dipping (4). Initial focussing was done on acetone introduced via the batch inlet. During scanning the anode temperature was adjusted manually to achieve optimum desorption rate. After each sample the anode current was increased to its maximum value to clean the wire. Operation in fi mode differed only in that the sample was introduced via the batch inlet. Spectra are not corrected for ^{13}C content.

Myristoleic and 12-hydroxystearic acids were purchased from Sigma; all other monocarboxylic acids were obtained from Applied Science Laboratories. Azelaic, adipic, and isophthalic acids were obtained from Eastman and dibenzo-18-crown-6 ether from Aldrich. All solvents and other reagents were A.C.S. grade and were used without further purification. A series of technical grade fatty acids was kindly donated by Imperial Oil Enterprises Ltd., Sarnia.

The diacids were purified by twofold extraction of a 1% solution in water–methanol with equal volumes of 0.01 M dibenzo-18-crown-6 ether in CH_2Cl_2. The aqueous layer was evaporated *in vacuo* to recover the pure acid.

Results and Discussion

Carboxylic acids of high purity generally give fd mass spectra in which the molecular ion is dominant. As shown by the representative data in Table 1, several acids have significant $[M + 1]^+$ ions (after allowance for ^{13}C isotope) and these latter ions are accompanied by small amounts of complex ions ($[2M + 1]^+$) and/or fragments ($[M - 17]^+$, $[M - 44]^+$). These fragments are most reasonably assigned to loss from $[M + H]^+$ of H_2O and COOH, respectively. General structural correlations for the presence of the $[M + H]^+$ ion and these related species are thus far lacking, as is any explanation for the significant differences in anode temperature necessary for desorption. The most unusual behavior of elaidic and *cis*-5-eicosenoic acids with increasing anode temperature may reveal an increased tendency of these compounds to form dimer and higher complexes but comparisons with other acids must be made with caution. These results could equally well

Can. J. Chem. Downloaded from www.nrcresearchpress.com by 210.87.254.5 on 09/05/12
For personal use only.

TABLE 2. Comparison of isomeric hydroxystearic acids by fdms[a]

Acid	Anode heating current (mA)	Relative intensity (%) 2M + 1	M + 2	M + 1	M	M − 1	M − 17	M − 45	Others(%)
2-Hydroxystearic	12.5	16		49	100			10	2M − 45(6)
12-Hydroxystearic	10.5		14	100		2	21		
17-Hydroxystearic[b]	8		11	100	7		18		

[a]Spectra were obtained from $CHCl_3$ solutions, except for 17-OH where addition of CH_3OH was necessary. Intensities are reported relative to base peak = 100.
[b]Some scans showed ions in the region *m/e* 141–142 corresponding to $[M + H - H_2O]^{2+}$ and $[M - H_2O]^{2+}$.

arise from the higher temperature of desorption which in turn may reflect the physical state of the desorbed sample.

For several of the acids studied, desorption at higher anode temperatures produced peaks corresponding to $[2M + H - H_2O]^+$. In further study of this process which is at least formally equivalent to anhydride formation, we have observed the expected cross product from high temperature fdms of a mixture. For example, a 1:1 mixture of *cis*-5-eicosenoic acid (M_1) and elaidic acid (M_2) behaved normally at low temperatures, with desorption of elaidic acid occurring first as predicted from the behavior of the single compounds. At higher anode temperatures ions of the type $[2M + H - H_2O - COOH]^{\ddagger}$ become more prominent until at 15 mA both 'pure dimer' ions are present and the 'cross-product dimer' $[M_1 + M_2 + H - H_2O - COOH]^{\ddagger}$ is the base peak. At 18 mA the 'mixed anhydride' $[M_1 + M_2 + H - H_2O]^+$ is the base peak and protonated dimer $[M_1 + M_2 + H]^+$ has a relative intensity of 56%. This experiment may be added to earlier work showing that processes resembling known chemical reactions may occur on the field anode (5–8).

The results in Table 2 show that three isomeric hydroxystearic acids are readily field desorbed to give dominant peaks in the molecular ion region. The relative importance of molecular ion and $[2M + 1]^+$ ions for the 2-OH isomer may be related to the ease of formation of intra- and intermolecular hydrogen bonds as illustrated in Scheme 1.

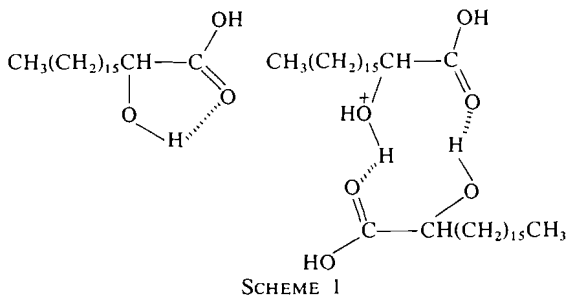

SCHEME 1

Another notable difference between the 2-isomer and the others is the importance of COOH loss (from $M^{\ddagger}$ and $2M^{\ddagger}$) for the former and H_2O loss (from $[M + 1]^+$) for the latter two. At higher anode temperatures the intensity of $[2M + 1]^+$ and an accompanying $[2M + 1 - H_2O]^+$ becomes more important for the 2-isomer until at 15 mA the latter is the base peak.

There is no firm basis for differentiation of the 12- and 17-isomers, although the presence of a weak molecular ion peak for the 17-isomer suggests some tendency for intramolecular hydrogen bonding which may relate to a ring size effect or to differences in orientation in the condensed phase on the field anode.

The most dramatic difference among the dicarboxylic acids presented in Table 3 involves their ease of decarboxylation. The presence of strong $[M + 1]^+$ peaks along with lesser ions corresponding to $[2M + 1]^+$, $[M - 17]^+$, and $[M - 44]^{\ddagger}$ attests to the ease of desorption of these initially protonated species. Whether this behavior is related to ease of protonation or the relative difficulty in ionizing the neutral molecule is not clear (9). In any case, it is tempting to attribute the presence of $M^{\ddagger}$ for azelaic acid to intramolecular H-bonding. The 'self-protonated' species thus formed would involve a ring-size of 12, whereas the other members of the series would be required to form 9- or 15-membered rings to achieve comparable structures.

A number of technical grade carboxylic acids were submitted to fdms with the results summarized in Table 4. These results have been examined with two principal questions in mind. Perhaps most important is the ability of the technique to produce a recognizable mass spectrum of the main component in spite of the presence of contaminants. A secondary question involves the extent to which the major contaminants can be identified.

With the exception of two diacids heavily contaminated with sodium and potassium ions, the compounds tested gave the same base peak ($M^{\ddagger}$ or $[M + 1]^+$) as the pure sample previously discussed.

Can. J. Chem. Downloaded from www.nrcresearchpress.com by 210.87.254.5 on 09/05/12
For personal use only.

TABLE 3. Field desorption mass spectra of selected dicarboxylic acids[a]

Acid (n)[b]	Anode heating current (mA)	Relative intensity (%) 2M + 1	M + 2	M + 1	M	M − 17	M − 44
$HOOC(CH_2)_{n-2}COOH$							
Adipic (6)	7		4	47		7	100
Azelaic (9)	8	1	11	100	2	2	6
Dodecanedioic (12)	10	1	17	100		18	19
$C_6H_4(COOH)_2$							
Isophthalic	12			11	100		

[a]Spectra were obtained from CH_3OH solutions, except for isophthalic acid where C_2H_5OH was used. Intensities are reported relative to base peak = 100.
[b]Compounds are identified by common name. For the aliphatic diacids n refers to the carbon number.

TABLE 4. Analysis of some technical grade carboxylic acids by fdms[a]

Acid	Anode heating current (mA)	Relative intensity (%) 2M + 1	M + 2	M + 1	M	M − 17	Others(%)
Palmitic	7	16	6	55	100	44	3M+1(14), 450(39), 451(22)
Stearic	6	18	8	60	100	3	3M+1(12), 256(2), 312(3), M − 45(1)
Oleic	10		4	20	100		280(6), 254(4)
2-OHstearic	10	9	8	53	100	1	272(5), 284(16), M − 45(6)
12-OHstearic	12		12	100	50		141.7(5),[b] 142.2(3),[b]
Adipic[c]	8	2	9	100		6	360(5),[c] 383(4),[c] M − 44(74)
Azelaic[c]	10		12	100		19	360(16),[c] 383(7),[c] 161(22)
Dodecanedioic	10		19	100		47	M − 44(50)
Isophthalic	13		1	8	100		2M + 23(1)

[a]Solutions were prepared in the same solvents used for the pure acid.
[b]Doubly-charged ions, $141.7 = 283^{2+}$; $142.2 = 284^{2+}$. See text.
[c]Spectra obtained after extraction with dibenzo-18-crown-6 ether, M = 360. Ion m/e 383 is $[M + Na]^+$.

Technical grade palmitic and stearic acids required a higher temperature for optimum desorption, perhaps as a result of the presence of minor impurities. Whatever the cause, a change from 0 to 6–7 mA involves two effects on the resulting spectra: any gas-phase (field ionization) component present at 0 mA will be removed and the higher temperature of desorption would be expected to increase the relative amount of complex ions and fragments. The latter effect is easily seen in the presence of $[3M + 1]^+$ and $[2M + 1]^+$ ions as well as fragments corresponding to loss of H_2O ($[M - 17]^+$) and loss of both H_2O and COOH (m/e 450 for palmitic acid).

Several ions were found which provide evidence for the presence of homologues and related compounds in these spectra. For instance, the ions at m/e 256 and 312 in the stearic acid sample probably represent contamination by saturated C_{16} and C_{20} homologues. Likewise, from peaks at m/e 280 and 254, the oleic acid sample appears to contain both a doubly unsaturated C_{18} (linoleic acid?) and a C_{16} homologue (palmitoleic acid?). Not surprisingly, 2-hydroxystearic acid shows important ions corresponding to stearic acid (m/e 284) and to an homologous hydroxypalmitic acid (m/e 272).

The significance of apparent $[M + 1 - H_2O]^{2+}$ and $[M - H_2O]^{2+}$ ions at m/e 142.7 and 142.2 for technical grade 12-hydroxystearic acid is not known. The authentic sample of this material did not show these ions although its spectrum was otherwise similar (Table 2). Careful examination of the spectrum of the authentic 17-hydroxy isomer revealed small amounts of these same ions.

As already noted, the technical grade samples of adipic and azelaic acids were contaminated with sodium and potassium ions to the point where no useful spectra could be obtained. The spectra reported in Table 4 were obtained after extraction of an aqueous solution of the sample with an organic solution of dibenzo-18-crown-6 ether. These spectra are comparable to those recorded for the standards (Table 3) with the important exception that decar-

Can. J. Chem. Downloaded from www.nrcresearchpress.com by 210.87.254.5 on 09/05/12
For personal use only.

TABLE 5. Apparent polyester ions in fdms of 3-hydroxypropanoic acid[a]

Current (mA)	Relative intensity (%) of $xM - (x-1)H_2O + H$ for x = 1	2	3	4	5	6	7	8	9	10	11	12
0	100	64										
10			24	100								
11			100	44								
12				100								
13				35	100	48	47					
18						100	30	22				
19						40	100	40	27	12	21	
20							70	100	51	18	3	4
21								53	100	63	24	8
22								9	78	100	50	8
23									10	16	100	59

[a]Extension of data presented in ref. 8.

boxylation is considerably less important for the samples purified by extraction. The presence of ions at *m/e* 360 and 383 representing ligand and ligand–sodium complex is not unexpected. From an analytical viewpoint, the most significant part of these results is the demonstration that the simple procedure of alkali metal extraction results in a dramatic improvement in the fd spectrum obtained.

Several hydroxyacids included in this study showed complex behavior. Some results for 3-hydroxypropanoic acid have been communicated (8). Other acids studied included glycolic, $HOCH_2COOH$; malic, $HOOCCHOHCH_2COOH$; lactic, $CH_3CHOHCOOH$; and glucuronic, $HOCH_2(CHOH)_4COOH$. The results obtained are rather complex and comparisons are rendered difficult by the wide differences in best anode temperature for these compounds. The often observed strong dependence of field desorption spectra on anode temperature has now been rationalized by increasing awareness that the desorption process is at least in large part thermal (10) and mechanisms for the desorption processes which take this fact into account have been proposed (9). The fact that three of the acids studied (3-hydroxypropanoic, glycolic, and lactic) desorbed at 0 mA while malic and glucuronic acids required 14 and 19.5 mA, respectively, no doubt has an important bearing on the results. In the discussion which follows, attention will be focussed on ions in the molecular region, complexes and peaks representing loss of water with or without apparent polymer formation.

At 0 mA glycolic acid ($M = 76$) had *m/e* 59 ($[M + 1 - H_2O]^+$) as base peak, major fragments at *m/e* 31 (70%) and 45 (54%), molecular ions (76 = 27%, 77 = 23%) and complex ions at *m/e* 153 (8%, $[2M + 1]^+$), 135 (15%, $[2M + 1 - H_2O]^+$), and 116 (5%, $[2M - 2H_2O]^{+\cdot}$). At 11 mA, *m/e* 59 was much less prominent, *m/e* 45 had become the base peak, and *m/e* 31 and 76 were next in importance.

Lactic acid also desorbed at 0 mA to produce a complex spectrum with ions up to *m/e* 398. This latter ion is assigned to $[5M + 2 - 3H_2O]^{+\cdot}$ and other 5M ions include *m/e* 380 ($[5M + 2 - 4H_2O]^{+\cdot}$), 365 ($[5M + 2 - 4H_2O - CH_3]^+$), 350 ($[5M + 2 - 4H_2O - 2CH_3]^+$), and *m/e* 335. This latter could be $[5M + 2 - 4H_2O - 3CH_3]^+$ or equally $[5M + 2 - 4H_2O - COOH]^+$. It should be noted here and later that all of these assignments have no backing other than their implicit reasonableness which arises largely from the observation that for such a molecule as lactic acid the number of protons associated with a given complex seems to be constant, and all the prominent ions can be 'explained' by loss of such likely fragments as H_2O, COOH, and CH_3.

Ions assigned to 4M species include *m/e* 326 ($[4M + 2 - 2H_2O]^{+\cdot}$), 308 ($[4M + 2 - 3H_2O]^{+\cdot}$), and 245 ($[4M + 2 - 4H_2O - COOH]^+$). With 3M we come for the first time to ions with different degrees of protonation. For example, *m/e* 254 could be $[3M + 2 - H_2O]^{+\cdot}$ whereas *m/e* 217 and 208 may be $[3M + 1 - 3H_2O]^+$ and $[3M + 1 - H_2O - COOH]^{+\cdot}$ and *m/e* 234, 216, and 189 correspond to $[3M - 2H_2O]^{+\cdot}$, $[3M - 3H_2O]^{+\cdot}$, and $[3M - 2H_2O - COOH]^+$, respectively. With 2M and below, the number of possible assignments increases but a major ion at *m/e* 162 appears to be the first member of the 'polyester series' for this molecule i.e. $[2M - H_2O]^{+\cdot}$. Other ions of note may represent loss of H_2O and COOH from dimers (*m/e* 117, 118, 119) and loss of H_2O from $M^{+\cdot}$ and $[M + 1]^+$ (*m/e* 91, 90, 73, 72 are all present). Finally, the base peak in this spectrum is *m/e* 45 which could represent either $[COOH]^+$ or $[M - COOH]^+$ but we favor the latter since $[COOH]^+$ is not ordinarily important.

Malic acid ($M = 134$) produces a relatively uncomplicated spectrum at 14 mA. $[M + 1]^+$ is the

Can. J. Chem. Downloaded from www.nrcresearchpress.com by 210.87.254.5 on 09/05/12
For personal use only.

Can. J. Chem. Downloaded from www.nrcresearchpress.com by 210.87.254.5 on 09/05/12
For personal use only.

base peak and the most important fragments correspond to loss of COOH from that ion and from $M^{\ddagger}$. The only complex ions of significance are *m/e* 269 ($[2M + H]^+$) and 193 whose origin is uncertain.

Since glucuronic acid does not desorb below 16 mA and the best anode temperature is at 19.5 mA it is not surprising that it produces many ions whose structural significance is not obvious. Dimer ion at *m/e* 392 was the highest mass observed. Loss of 2, 3, and 4 H_2O from dimers in various degrees of protonation are seen. A monodehydration ion at *m/e* 179 (base at 16 mA) is the only peak near $M^{\ddagger}$. Among the fragments, *m/e* 31 is base and 61 is second in importance. These two latter ions dominate the spectrum at all values from 17–21 mA.

The apparent polymerization of 3-hydroxypropanoic acid has been shown to continue with increased anode temperature at least to 23 mA. As shown in Table 5, the base peak continues to increase in mass from 451 (degree of polymerization (dp) = 6) to 811 (dp = 11) over this temperature range.

Since the commercial product used in this work is known to contain some dimer and perhaps higher molecular weight oligomers, we have attempted to find out how much of the behavior observed here is related to species already present in the sample. Handling of the sample by fi gave no polymerization peaks. The base peak is *m/e* 72 and molecular ion is weak (3% or less). Attempts to remove all water from the sample before fd gives no spectrum at all. This may reflect the formation of a high polymer on the anode. Proton magnetic resonance spectra of the original sample showed three well separated signals which we assign as follows:

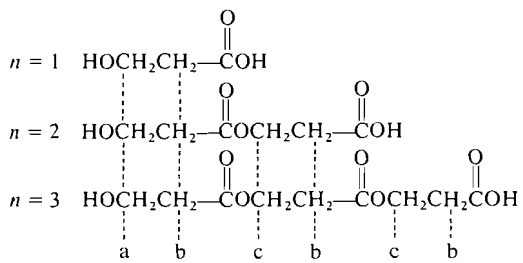

a = 4.8 ppm, 22% of intensity
b = 2.7 ppm, 49% of intensity
c = 4.4 ppm, 29% of intensity

That is, methylenes next to carbonyl are not distinguishable (δ 2.7) but terminal CH_2—O (δ 4.8) is separated from interior CH_2—O (δ 4.4). Integration of these signals and comparison with various compositions shows that an equimolar mixture of n = 1–4 agrees with the nmr intensities. Attempts to allow for higher polymers require the increase of monomer or dimer to maintain balance, e.g. 15% of hexamer with 60% dimer and 25% monomer also fits as does 30% hexamer and 70% monomer. Among the many solutions which can be considered for the nmr data, it appears that all of them must contain at least 50% of total monomer and dimer. Further, the higher polymers change the ratio more and thus less polymer can be mixed in. In summary, although it is not possible to exclude higher oligomers than dimer from the original sample, no combination of molecular species can give rise to the high intensities of high molecular weight ions found in fdms. Further, the fact that total ionization increases above 12 mA means that in general the intensities reported above tetramer represent more material than the ones at lower anode temperatures.

Acknowledgements

Support of this work by an Imperial Oil Limited University Research Grant and by the National Research Council of Canada is gratefully acknowledged. Helpful discussions with Dr. Gordon Alexander, Imperial Oil Enterprises Ltd., Sarnia, Ont., who also provided samples of technical grade acids, are acknowledged with thanks.

1. (*a*) J. M. Wilson. *In* Mass spectrometry. Vol. 4. *Edited by* R. A. W. Johnstone. Specialist Periodical Report, The Chemical Society, London. 1977. Chapt. 5; (*b*) P. J. Derrick. *In* Mass spectrometry. Vol. 4. *Edited by* R. A. W. Johnstone. Specialist Periodical Report, The Chemical Society, London. 1977. Chapt. 6; (*c*) D. E. Games. *In* Mass spectrometry. Vol. 4. *Edited by* R. A. W. Johnstone. Specialist Periodical Report, The Chemical Society, London. 1977. Chapt. 11.
2. A. L. Burlingame, B. J. Kimble, and P. J. Derrick. Anal. Chem. **48**, 368R (1976).
3. H.-R. Schulten and H. D. Beckey. Org. Mass Spectrom. **6**, 885 (1972).
4. H. D. Beckey. Int. J. Mass Spectrom. Ion Phys. **2**, 500 (1969).
5. G. W. Wood and P.-Y. Lau. Org. Mass Spectrom. **10**, 1147 (1975).
6. G. W. Wood, P.-Y. Lau, and G. N. S. Rao. Biomed. Mass Spectrom. **3**, 172 (1976).
7. C. N. Sukenik, J. A. P. Bonapace, N. S. Mandel, P.-Y. Lau, G. Wood, and R. G. Bergman. J. Am. Chem. Soc. **99**, 851 (1977).
8. G. W. Wood and D. L. Wade. Can. J. Chem. **53**, 3500 (1975).
9. J. F. Holland, B. Soltmann, and C. C. Sweeley. Biomed. Mass Spectrom. **3**, 340 (1976).
10. B. Soltmann, C. C. Sweeley, and J. F. Holland. Anal. Chem. **49**, 1164 (1977).

The synthesis of hypecorinine and bicucullinine

BALA C. NALLIAH AND DAVID B. MACLEAN
Department of Chemistry, McMaster University, Hamilton, Ont., Canada L8S 4M1

Received December 20, 1977

BALA C. NALLIAH and DAVID B. MACLEAN. Can. J. Chem. **56**, 1378 (1978).

The total synthesis of two isoquinoline alkaloids of unusual structure, hypecorinine **2** and bicucullinine **3**, from a common intermediate, dehydrobicuculline (**1**), is described.

BALA C. NALLIAH et DAVID B. MACLEAN. Can. J. Chem. **56**, 1378 (1978).

On décrit la synthèse totale de deux alcaloïdes de la série isoquinoléine possédant des structures inhabituelles soit l'hypécorinine **2** et la bicucullinine **3**; ces synthèses font intervenir un intermédiaire commun, la déhydrobicuculline **1**.

[Traduit par le journal]

Can. J. Chem. Downloaded from www.nrcresearchpress.com by 210.87.254.6 on 09/05/12
For personal use only.

The synthesis of dehydrobicuculline (**1**) and its conversion to three spirobenzylisoquinoline and two phthalideisoquinoline alkaloids has been reported recently (1). Here we report the use of **1** in the synthesis of hypecorinine **2** and bicucullinine **3**, two alkaloids which have not been previously synthesised.

The isolation of hypecorinine was reported in 1972 from *Hypecoum erectum* and its structure and that of a companion alkaloid were established at that time (2). The same alkaloid was also found in *Corydalis incisa* Pers. and its structure established by spectral and chemical methods in 1975 (3); the name corydalispirone was given to the alkaloid. The latter work was apparently carried out without knowledge of the previous study. Since the name hypecorinine has precedence we have used this name for the alkaloid.[1]

We reported previously (1) that dehydrobicuculline **1** underwent reduction with diisobutylaluminum hydride to the keto aldehyde **5** which was converted in an aldol ring closure to sibiricine **6** and corydaine **7**. The reduction of intermediate **5** selectively to the keto alcohol **8** followed by oxidation of **8** with mercuric acetate would be expected to yield an immonium salt such as **4** which would then suffer ring closure to hypecorinine **2**. Previous experience with similar compounds led us to use lithium aluminum hydride as the preferred reducing agent (4) for the conversion of **1** into **8**. We found that when a solution of dehydrobicuculline in dry THF was treated with lithium aluminum hydride at 0°C the characteristic yellow colour of **1** disappeared and on work-up a product was obtained which by tlc was a mixture of two components, presumably **8** and **2**. When this product was dissolved in methanol and the solution was allowed to stand overnight, colorless prisms were deposited which were identical with an authentic sample of hypecorinine. We were unable to isolate **8** as a crystalline product presumably because of its ease of oxidation.

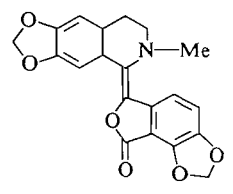

1

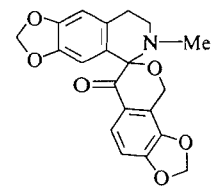

2

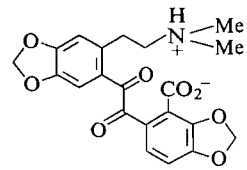

3

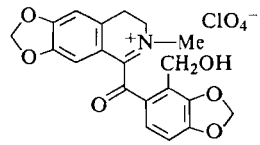

4

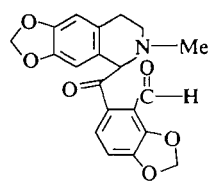

5

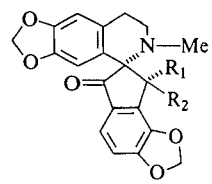

6 $R_1 = H$, $R_2 = OH$ (Sibiricine)
7 $R_1 = OH$, $R_2 = H$ (Corydaine)

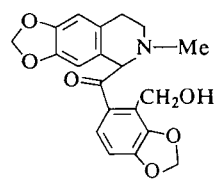

8

We also found that the hydride reduction product was oxidized readily to **2** if it was dissolved in 5% aqueous acetic acid and stirred with mercuric acetate at room temperature for an hour (5). This is the pre-

[1]We thank a referee for drawing the work on hypecorinine to our attention.

Can. J. Chem. Downloaded from www.nrcresearchpress.com by 210.87.254.6 on 09/05/12
For personal use only.

ferred procedure for synthesis of **2**. The perchlorate salt of our synthetic hypecorinine, prepared by the published procedure (3), was also identical with an authentic sample.

Bicucullinine (**3**) (6) is structurally related both to the phthalideisoquinoline alkaloid narceine (**9**) and to the alkaloid cryptopleurospermine (**10**). We anticipated that the quaternary salt **11** which contains all the carbon atoms of bicucullinine, might be converted into **3**, first by opening the lactone ring and then by allowing the ring-opened product to undergo aerial oxidation.

In practice **11** was prepared in good yield by treatment of **1** with methylfluorosulfonate in methylene chloride. When **11** was suspended in ethanol containing Triton B and potassium iodide it slowly dissolved upon stirring, presumably, through opening of the lactone ring, to give the zwitter ion **12**. The solution so obtained was allowed to stand at room temperature for one week and during this period compound **12** apparently reacted with atmospheric oxygen to form the hydroperoxide **13** which was then reduced to the carbinolamine **14** by the iodide ions present in the solution. Before or upon acidification with hydrochloric acid the carbinolamine **14** underwent ring opening and bicucullinine was isolated as its hydrochloride as yellow needles (mp 172–174°C), identical with an authentic sample. Analogous oxidations are reported in the literature (7). The hydrochloride was converted to bicucullinine and this too was identical with an authentic specimen.

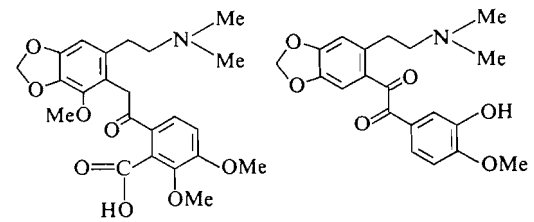

9 **10**

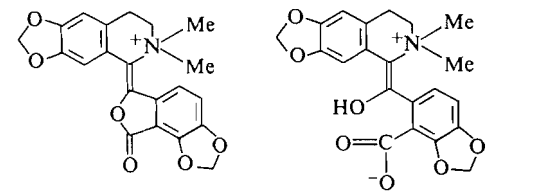

11 **12**

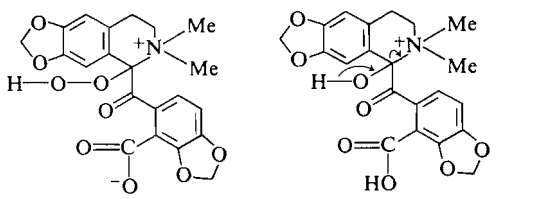

13 **14**

These syntheses illustrate further the use of dehydrophthalides as synthetic intermediates in the synthesis of isoquinoline alkaloids.

Experimental

Preparation of Hypecorinine (2) from Dehydrobicuculline (1)

Lithium aluminum hydride (100 mg) was added to a stirred and ice-cooled solution of dehydrobicuculline (1) (100 mg) in dry THF (50 ml). After 1 h the reaction mixture was decomposed with a saturated solution of sodium sulfate and the precipitate removed by filtration. The filtrate was evaporated to dryness under reduced pressure and dissolved in 5% aqueous acetic acid (25 ml). Mercuric acetate (100 mg) was added and the solution stirred for 1 h at room temperature. The solution was basified (concentrated NH_4OH), extracted with CH_2Cl_2, and the extract evaporated to dryness. The residue was crystallized from methanol yielding colorless prisms, mp 196–198°C (51 mg), identical in mp, mixture mp, and spectroscopic properties (ir, nmr) with an authentic specimen; $\nu_{max}(CHCl_3)$: 1630 and 1692 cm^{-1}; δ ($CDCl_3$): 7.81 and 6.90 (q, 2H, J_{AB} = 8 Hz), 6.62 (s, 1H), 6.56 (s, 1H), 6.10 (s, 2H), 5.88 (s, 2H), 5.17 and 4.84 (q, 2H, J_{AB} = 15.5 Hz), 2.50–3.60 (m, 4H), 2.38 (s, 3H). *Anal.* calcd. for $C_{20}H_{17}O_6N$: C 65.39, H 4.67, N 3.81; found: C 65.53, H 4.80, N 3.64.

N-*Methyldehydrobicuculline (11)*

Freshly distilled methylfluorosulfonate (2 ml) was added to a solution of dehydrobicuculline (1 g) in dry CH_2Cl_2 and the solution stirred for 24 h at room temperature. The orange precipitate which separated was filtered and recrystallized from acetonitrile–MeOH (yield 950 mg). The perchlorate salt was obtained by adding a few drops of 60% perchloric acid to a warm concentrated solution of the salt in acetonitrile. It crystallized in yellow needles, mp 315–316°C (dec.); ν_{max}(Nujol): 1785 cm^{-1}; δ (DMSO): 7.37 (s, 1H), 7.17 (s, 1H), 7.33 and 7.03 (q, 2H, J_{AB} = 8.0 Hz), 6.37 (s, 2H), 6.13 (s, 2H), 3.63 (s, 6H), 3.4–3.7 (m, 2H), 2.9–3.2 (m, 2H). *Anal.* calcd. for $C_{21}H_{18}O_{10}NCl$: C 52.56, H 3.78, N 2.92, Cl 7.39; found: C 52.69, H 3.88, N 2.96, Cl 7.18.

Conversion of N-*Methyldehydrobicuculline (11) to Bicucullinine (3)*

Triton B (40% in MeOH) was added to a stirred suspension of the quaternary salt **11** (200 mg) in absolute ethanol until a clear solution was obtained. Potassium iodide (50 mg) was added, the solution stirred for another hour, and then let stand for a week. The solution was acidified with concentrated hydrochloric acid and left for another day. The residue obtained on evaporation of the solvent was dissolved in the minimum amount of 5% KOH and extracted with CH_2Cl_2 to remove both the iodine formed in the reaction and the excess Triton B. The aqueous solution was acidified with concentrated hydrochloric acid. Yellow needles separated on standing (86 mg), mp 172–174°C. The hydrochloride of the authentic bicucullinine was identical with the synthetic product, ν_{max}(Nujol): 1690, 1658, and 1595 cm^{-1}; δ (DMSO): 7.36 (s, 1H), 7.30 and 7.20 (q, 2H, J_{AB} = 8 Hz), 7.17 (s, 1H), 6.27 (s, 2H), 6.17 (s, 2H), 3.20 (br, s, 4H), 2.77 (s, 6H).

Bicucullinine hydrochloride was converted to bicucullinine in the following way. The hydrochloride was dissolved in aqueous base, this solution treated with freshly prepared silver hydroxide, filtered, and the filtrate acidified with acetic acid. The bicucullinine which crystallized from the aqueous mixture was identical with an authentic specimen.

Acknowledgments

We wish to thank Dr. G. Nonaka, Faculty of Pharmaceutical Sciences, Kyushu University, Fukuoka, Japan for providing us with a sample of corydalispirone (hypecorinine) and the National Research Council of Canada for financial support of this work.

1. B. C. NALLIAH, D. B. MACLEAN, R. G. A. RODRIGO, and R. H. F. MANSKE. Can. J. Chem. **55**, 922 (1977).
2. L. D. YAKHONTOVA, M. N. KOMAROVA, M. E. PEREL'SON, K. F. BLINOVA, and O. N. TOLKACHEV. Khim. Prir. Soedin. 624 (1972); Chem. Abstr. **78**, 108177 (1973).
3. G. NONAKA and I. NISHIOKA. Chem. Pharm. Bull. **23**, 294 (1975).
4. B. NALLIAH, R. H. F. MANSKE, R. RODRIGO, and D. B. MACLEAN. Tetrahedron Lett. 2795 (1973).
5. N. J. LEONARD and W. K. MUSKER. J. Am. Chem. Soc. **82**, 5148 (1960).
6. R. G. A. RODRIGO, R. H. F. MANSKE, H. L. HOLLAND, and D. B. MACLEAN. Can. J. Chem. **54**, 471 (1976).
7. B. NALLIAH, R. H. F. MANSKE, and R. RODRIGO. Tetrahedron Lett. 1765 (1974).

Can. J. Chem. Downloaded from www.nrcresearchpress.com by 210.87.254.6 on 09/05/12
For personal use only.

Electron transport via metalloporphyrins

EUGENE C. JOHNSON, TONY NIEM,[1] AND DAVID DOLPHIN[2]

The Department of Chemistry, The University of British Columbia, Vancouver, B.C., Canada V6T 1W5

Received September 9, 1977

EUGENE C. JOHNSON, TONY NIEM, and DAVID DOLPHIN. Can. J. Chem. **56**, 1381 (1978).

The controlled potential electrolysis of Ni(II) *meso*-tetraphenylporphyrin (Ni(II)TPP) gives at room temperature the corresponding metalloporphyrin π-cation radical $[Ni(II)TPP]^{+\cdot}$. Upon freezing a solution of the π-cation radical to 77 K an internal electron transfer occurs to give $[Ni(III)TPP]^{+}$. A discussion of the routes of electron transport in heme proteins is given, and the roles of metalloporphyrin π-cation radicals in electron transport is evaluated.

EUGENE C. JOHNSON, TONY NIEM et DAVID DOLPHIN. Can. J. Chem. **56**, 1381 (1978).

L'électrolyse à potentiel contrôlé de la *méso*-tétraphénylporphyrine de Ni(II) (Ni(II)TPP) conduit, à température ambiante, au radical π cation métalloporphyrine correspondant $[Ni(II)TPP)^{+\cdot}$. Lorsque l'on congèle une solution du radical π cation à 77 K, un transfert interne d'électron se produit pour conduire au $[Ni(III)TPP]^{+}$. On discute des diverses routes de transport d'électron dans des protéines contenant de l'hème et on évalue le rôle des radicaux π cation métalloporphyrine dans le transport des électrons.

[Traduit par le journal]

Introduction

Redox reactions play critical roles in many biochemical transformations (1), and amongst the coenzymes and cofactors involved the iron porphyrins (hemes) play many varied and crucial functions. Hemes not only transport and store oxygen via hemoglobin and myoglobin, but in the form of cytochromes P-450 activate oxygen which, as monooxygenases bring about numerous biochemical oxidations (2). Other heme enzymes such as catalase and the peroxidases act as two electron reductants of hydrogen peroxide to hydroxide, and are concomitantly oxidized by two electrons to the so-called primary complexes of the enzymes. In the case of catalase the primary complex then acts as a two electron oxidant of hydrogen peroxide to oxygen, and is reduced to the resting ferrihemoprotein. Another group of heme-containing proteins, the cytochromes, function between Fe(II) $\rightleftharpoons$ Fe(III) couples, and by linking centres of different redox potentials couple the free energy change of the electron transport to covalent bond formation (e.g. oxidative phosphorylation (3)).

An insight into the modes of electron transport of metalloporphyrins was gained when it was shown that the initial, photochemically promoted, electron transport in photosynthesis involves the loss of an electron from one of the filled π-molecular orbitals of chlorophyll *a* to generate a chlorophyll (or bacteriochlorophyll) π-cation radical (4–6). Stable π-cation radicals of simpler metalloporphyrins had been reported earlier (7), and shortly after their occurrence in photosynthetic systems was elucidated it was found that similar π-cation radicals were the catalytically active forms of both the catalases and peroxidases (8, 9). Thus when either catalase or peroxidase is oxidized by hydrogen peroxide one electron is removed from the ferric iron and one from the π-cloud to give, in the primary complexes, an Fe(IV) π-cation radical electronic configuration. However, the ground states of these primary complexes differ in that in one the remaining unpaired electron is in an a_{2u}, and in the other in an a_{1u} orbital. The corresponding $^2A_{2u}$ and $^2A_{1u}$ ground states, as a result of their different electronic ground states, exhibit different optical and enzymic properties (8).

A change in the ground state from $^2A_{1u}$ to $^2A_{2u}$ can be demonstrated with the π-cation radical of cobaltic octaethylporphyrin (7). Thus in the presence of bromide ion the cobalt coordinates two ligands to give $[Co(III)OEP]^{2+\cdot}2Br^{-}$ which exhibits a $^2A_{1u}$ ground state. When the bromide ions are removed and replaced by perchlorate the ground state changes to that of $^2A_{2u}$. It is apparent that small changes in the environment about the metal (and at the porphyrin periphery) can bring about a change in the ground state, and this is consistent with calculations which suggest that the two ground states differ in energy by about 1500–2000 cm^{-1} or 4.3–5.7 kcal mol^{-1} (10).

We have been explicit in describing the electronic configuration of an oxidized metalloporphyrin and one might ask if it is possible to describe these configurations as resulting entirely from a metal or a ligand oxidation. Thus a cobaltic π-cation radical which has two electrons less than the Co(II) species

[1]Work carried out by T.N. as a postdoctoral fellow in the Chemistry department, Harvard University.

[2]Author to whom correspondence should be addressed.

Can. J. Chem. Downloaded from www.nrcresearchpress.com by 210.87.254.105 on 09/05/12
For personal use only.

Can. J. Chem. Downloaded from www.nrcresearchpress.com by 210.87.254.105 on 09/05/12
For personal use only.

could formally be described as both a derivative of cobalt(IV) or a π-dication of cobalt(II). One might be inclined to conclude that each of these descriptions are extreme resonance forms of the same molecule and that the molecule should be described as some contribution of all of them. This is not, however, the case since the epr spectrum of $[Co(III)OEP]^{2+\cdot}$ shows that the unpaired electron spends less than 5% of its time on the metal (9). Since the unpaired electron is in a ligand based orbital it can be described as a π-cation radical of cobalt(III). Similarly the oxidation of ferric porphyrins removes electrons from the metal, not the ligand, since the optical spectra (which are dominated by π–π* transitions of the ligand) remain essentially unchanged upon oxidation whereas a dramatic change in the optical spectra would be observed if the ligand were oxidized (11).

The ground state electronic configuration of a metalloporphyrin can, from optical and epr measurements, be accurately determined; and the electronic configuration adopted will depend upon a variety of factors including the metal, the porphyrin and its peripheral substituents, and the axial ligands. Even in the 'simplest' metalloporphyrins small changes will influence the ground state. Thus the electrochemical one-electron oxidation of ruthenium(II) complexes of *meso*-tetraphenylporphyrin (TPP) gave a π-cation of [Ru(II)TPP](CO)(py) (viz. $[Ru(II)TPP]^{+\cdot}$(CO)(py)) but caused oxidation of the metal with $[Ru(II)TPP](py)_2$ to give $[Ru(III)TPP]^{+}(py)_2$ (12). Hence the substitution of the weakly backbonding ligand pyridine for the more strongly backbonding CO destabilized Ru(II) vs. Ru(III) and changed the electronic configuration of the one-electron oxidized species.

Even though the electronic configuration of a metalloporphyrin can now be readily determined, the mechanism, or route, of electron transfer by which such systems undergo redox chemistry is still a subject of much speculation with respect to even simple metalloporphyrins, which may be used as models of heme proteins; while the mechanisms by which heme proteins themselves transport electrons still remain, in general, largely unexplained (1).

As with other coordination complexes metalloporphyrins have been found to effect electron transfer via two well-characterized mechanisms; inner sphere (13), where electron transfer occurs through a bridging species between oxidant and reductant, and outer sphere, where a bridging species is absent and electron transfer must occur through the extended π-systems of the oxidant and reductant (14). While inner sphere mechanisms may operate with some model metalloporphyrins it is apparent, on spatial considerations alone, that for most heme proteins in general an inner sphere mechanism cannot obtain.

Wolberg and Manassen (15) have reported that the electrochemical oxidation of Ni(II)TPP in benzonitrile initially gives a $Ni(III)TPP^{+}$ species which decayed to a $Ni(II)TPP^{+\cdot}$ species. The presence of the two complexes was suggested by epr. In contrast we have recently reported that a similar oxidation in CH_2Cl_2 gives the $[Ni(II)TPP]^{+\cdot}$ species, which is in thermodynamic equilibrium with a $[Ni(III)TPP]^{+}$ species at 77 K, as shown by epr and electronic absorption spectra (16). We describe here a detailed study of these systems and suggest evidence of possible modes for outer sphere mechanisms of electron transfer in metalloenzymes.

Experimental

Materials

Dichloromethane (Fischer, reagent) was refluxed over calcium hydride and distilled and stored over 4 Å molecular sieves. Tetra-*n*-butylammonium hexafluorophosphate (TBAH) was prepared by treating an acetone solution of tetra-*n*-butylammonium iodide and ammonium hexafluorophosphate with water. The precipitated product was twice recrystallized from ethanol–water and dried in vacuum for 10 h at 100°C. Tetra-*n*-butylammonium perchlorate (TBAP) (Eastman) was twice recrystallized from ethanol–water and dried under vacuum for 10 h at 70°C. Tetraphenylporphyrinato nickel(II) was prepared from chlorin-free TPP since Ni(II)TPP is sparingly soluble and difficult to separate from chlorin impurity. ^{61}Ni(II)TPP was prepared similarly except that ^{61}Ni (99% enriched, Oakridge, TN) was initially dissolved in concentrated HCl, evaporated to dryness, and the resultant $^{61}NiCl_2$ used in place of $Ni(OAc)_2$.

Measurements

Ultraviolet–visible absorption spectra were recorded on a Cary 17 recording spectrophotometer. Room temperature spectra were recorded in CH_2Cl_2 using 1.0 cm cells. Spectra at 77 K were measured using a variation of the opal glass method (17). A Pyrex cell was made by flattening a tube (0.5 cm OD) until the pathlength was ~0.1 mm. A quantity of a methylene dichloride solution was transferred to the cell by syringe and the sample frozen, evacuated, and sealed. After warming the cell to room temperature a strip of thin Teflon tape was stretched over the flat face and the cell was then placed in a windowed quartz Dewar filled with liquid nitrogen and placed in the sample beam of the spectrometer. A piece of opal glass was placed in the reference beam and optical spectra were then recorded as usual. The epr measurements, at both room temperature and 77 K, were made on a Varian E-3 EPR spectrometer in degassed methylene dichloride solutions in evacuated quartz epr tubes (4 mm OD).

Electrochemical measurements were made at a Pt electrode in CH_2Cl_2 using 0.1 *M* TBAH or TBAP as supporting electrolyte. A Ag/AgCl couple was used as reference. Standard 3 electrode operational amplifier circuitry was utilized as described previously (6). Due to the sparing solubility of Ni(II)TPP, special care was taken to ensure that no solid material was present during electrochemical or epr measurements. Solutions were either filtered prior to use or, for coulometric measurements, accurately weighted samples of ~3 mg were stirred for 30 min in 30 ml of degassed CH_2Cl_2 prior to use to

Can. J. Chem. Downloaded from www.nrcresearchpress.com by 210.87.254.105 on 09/05/12
For personal use only.

ensure complete solution. Such solutions were then used without further treatment.

Results

Electrochemistry

The shape of the cyclic voltammograms varied significantly according to the supporting electrolyte used. Figure 1 shows cyclic voltammograms of Ni(II)TPP in CH_2Cl_2 using TBAH and TBAP. In the presence of TBAP the cyclic voltammogram, as previously reported (16), is consistent with two overlapping electrochemically reversible couples centered at 1.17 and 1.29 V, while the data for the TBAH system display two well-defined electrochemically reversible couples centred at 1.07 and 1.39 V. Exhaustive electrolysis at 1.24 V in either system produced a green solution which gave a cyclic voltammogram identical to the starting material. Controlled potential coulometry (at 1.24 V) gave *n*-values of 1.01 ± 0.05, consistent with a one-electron oxidation of the Ni(II)TPP. The green solution was stable for several days when protected from the light and the atmosphere, and upon electrolysis at 0.80 V the starting material was quantitatively regenerated ($n = 1$), such that the cycle was completely reversible. Further electrolysis of the green oxidation product at potentials anodic to the second couple gave a brown solution which decomposed over a period of a few hours. Immediate cathodic electrolysis of freshly prepared solutions of the second electrolysis product gave, by coulometry, $n = 0.92 \pm 0.05$, but the appearance of additional cycles indicated decomposition.

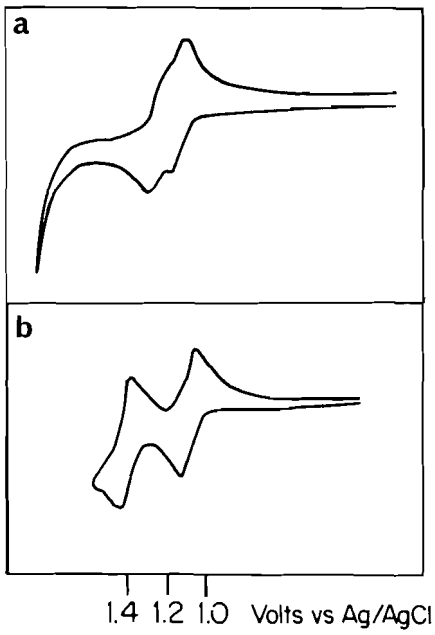

FIG. 1. Cyclic voltammogram of Ni(II)TPP in methylene dichloride using a Ag/AgCl couple as reference; (*a*) tetra-*n*-butylammonium perchlorate and (*b*) tetra-*n*-butylammonium hexafluorophosphate as supporting electrolytes at 0.1 *M*.

Spectra

Figure 2 follows the changes in the absorption spectra of Ni(II)TPP during electrolysis at 1.24 V to give the green one-electron oxidation product. The appearance of isosbestic points in the spectra indicates a clean conversion to the oxidized form. A comparison of the optical spectrum of the green oxidation product to that of the well characterized π-cation radical of Mg(II)OEP (Fig. 3) shows that the product is the π-cation radical $[Ni(II)TPP]^{+\bullet}$ and that further electrolysis generates the corresponding π-dication $[Ni(II)TPP]^{2+}$ (Fig. 3) which has an optical spectrum similar to other metalloporphyrin π-dications. This dication is a powerful electrophile reacting with a variety of nucleophiles such as methanol, or water, to give isoporphyrins (18).

Figure 4 shows the optical spectrum of $[Ni(II)TPP]^{+\bullet}PF_6^-$ at room temperature and after freezing to 77 K. The dramatic spectral changes are accompanied by a change from a green solution to an

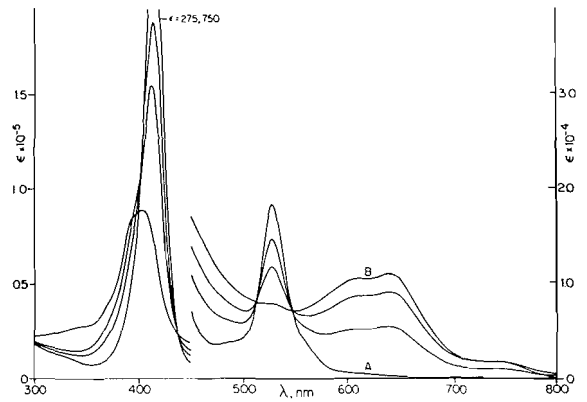

FIG. 2. Optical absorption spectra of Ni(II)TPP (*A*), during its electrochemical oxidation, in CH_2Cl_2, to the π-cation radical $[Ni(II)TPP]^{+\cdot}$ (*B*).

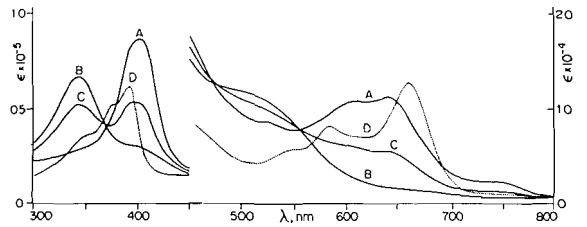

FIG. 3. Optical absorption spectra, in CH_2Cl_2, of the π-cation radical $[Ni(II)TPP]^{+\cdot}$ (*A*), the π-dication $[Ni(II)TPP]^{2+}$ (*B*). *C* is the optical spectrum during oxidation of *A* to *B* showing isosbestic points. *D* is the π-cation radical $[Mg(II)OEP]^{+}$.

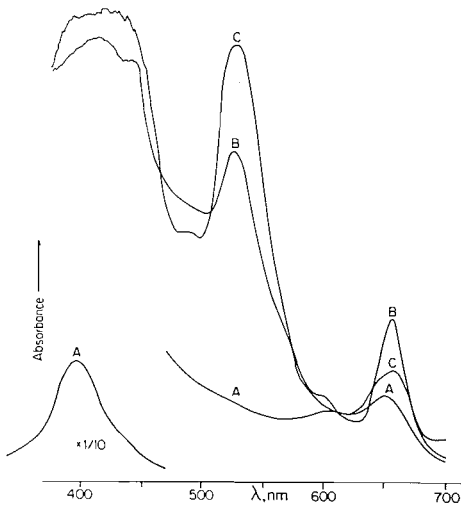

FIG. 4. Optical absorption spectra, in CH_2Cl_2, of [Ni(II)-TPP]$^{+\cdot}PF_6^-$ at room temperature (*A*), the same sample at 77 K showing spectrum of [Ni(III)TPP]$^+PF_6^-$ (*B*), and Ni(II)-TPP at 77 K (*C*).

orange-red frozen solid which has a strong band at 526 nm. The spectra of both Ni(II)TPP and [Ni(II)-TPP]$^{+\cdot}$ when measured in CH_2Cl_2 in the presence of both TBAH and TBAP at 77 K show a band centered at 654 nm (in the absence of TBAP or TBAH Ni(II)TPP does not exhibit this absorption). In addition Ni(II)TPP$^{+\cdot}$ at room temperature exhibits a broad absorption at 668 which moves to 656 at 77 K.

The optical spectra of methylene dichloride solutions of the π-cation radical [Ni(II)TPP]$^{+\cdot}$ [PF_6 or ClO_4]$^-$ showed no major changes upon cooling to 77 K when small amounts of water were present, nor were any changes observed with the bromide salt [Ni(II)TPP]$^{+\cdot}$ Br^-.

Electron Paramagnetic Resonance

The epr of the one-electron oxidation product were recorded at room temperature and at 77 K. At room temperature the green solution in the presence of PF_6^-, ClO_4^-, or Br^- exhibited a single signal, $g = 2.0041$ with a peak-to-peak separation of 47.2 G, indicative of a π-cation radical. At 77 K the orange-red solid showed signals at $g_\perp = 2.286$ and $g_\parallel = 2.086$, consistent with a low spin d^7 (Ni(III)) electronic configuration and in good agreement with spectra reported by Busch and co-workers (19) and by Wolberg and Manassen (15) for Ni(III) complexes. The epr signal of the Ni(III) species slowly decayed with time, being replaced after ~24 h by a weak isotropic signal which also decayed with time.

We have already noted above that upon cooling solutions of the PF_6^- or ClO_4^- salts, in the presence of small amounts of water, or the pure bromide salt no color change is observed. Similarly, these same solutions show no change in their epr spectra when cooled to 77 K, and only the isotropic signal at $g = 2.0041$ is present.

Discussion

From the physical studies described above we can conclude that when Ni(II)TPP is electrolyzed in methylene dichloride (with either TBAH, or TBAP as supporting electrolyte) at 1.24 V it undergoes a clean, reversible, one-electron oxidation to give the corresponding π-cation radical [Ni(II)TPP]$^{+\cdot}$. At room temperature this species shows all of the properties of other similar, and well characterized, metalloporphyrin π-cation radicals with a $^2A_{2u}$ ground state (5). The stability and ease of preparation of this π-cation radical is indicated by the clean electrochemistry and solution stability over long time periods. In addition this π-cation radical behaves like other metalloporphyrin π-cation radicals in that it can quantitatively be reduced back to Ni(II)TPP, and can be made to undergo a further one-electron oxidation to the π-dication [Ni(II)TPP]$^{2+}$.

In all of these respects [Ni(II)TPP]$^{+\cdot}$ is no different from other porphyrin π-cation radicals, which have been reported on in great detail, except for its quite exceptional thermal behavior. All of the above data are consistent with an internal electron transfer occurring as the temperature is lowered, with the hole jumping from the periphery to the metal. These redox reactions can be summarized as follows:

$$\text{Ni(II)TPP} \underset{+e^-}{\overset{-e^-}{\rightleftharpoons}} [\text{Ni(II)TPP}]^{+\cdot} \underset{+e^-}{\overset{-e^-}{\rightleftharpoons}} [\text{Ni(II)TPP}]^{2+}$$
$$\Big\downarrow\Big\uparrow \Delta$$
$$[\text{Ni(III)TPP}]^+$$

The strongest electronic transitions in metalloporphyrins (and their oxidized and reduced derivatives) are $\pi \rightarrow \pi^*$ in nature with molecular extinction coefficients of from 10 000 to 1 000 000 (20, 21). In such systems the weak *d–d* transitions of the metal are hidden. Except when charge transfer between metal and ligand occurs, the oxidation state of a specific metal makes only minor perturbation on the optical transitions of metalloporphyrins. The spectra of Ni(II)TPP and that of the orange frozen samples of the π-cation radical [Ni(II)TPP]$^{+\cdot}$ are quite similar (Fig. 4) which show that all of the bonding π-molecular orbitals are filled. Since the π-cation radical has lost an electron from its highest filled bonding π–MO, then upon cooling an electron must move from the metal to fill the π-system and generate Ni(III). The formation of a nickel(III) complex at low temperatures is confirmed by epr spectroscopy which shows two signals having *g* values comparable to

Can. J. Chem. Downloaded from www.nrcresearchpress.com by 210.87.254.105 on 09/05/12
For personal use only.

Can. J. Chem. Downloaded from www.nrcresearchpress.com by 210.87.254.105 on 09/05/12
For personal use only.

those of previously reported Ni(III) complexes (17, 22). When the same series of epr experiments were carried out using ^{61}Ni ($I = 3/2$) no change in the epr spectra of either the cation radical or the Ni(III) species was observed. However, ^{61}Ni has a small magnetic moment (-0.75) resulting in a small hyperfine interaction which is lost under the relatively broad signal.

Wolberg and Manassen (15) have reported that the initial one-electron oxidation product of Ni(II)-TPP in benzonitrile/TBAP is the metal oxidized $[Ni(III)TPP]^+$, and that upon standing at room temperature solutions of $[Ni(III)TPP]^+$ began to show a weak epr signal which was assigned to $[Ni(II)TPP]^{+\bullet}$. The epr signal which they assigned to $[Ni(III)TPP]^+$ was only observed at 77 K, and it is possible that these authors were observing a similar phenomenon to that reported here. However, the cyclic voltammogram reported for Ni(II)TPP in benzonitrile/TBAP and that reported here using methylene dichloride/TBAP exhibit features which are atypical of most metalloporphyrins (22–25). In the former case the cyclic voltammogram showed two overlapping successive one-electron oxidations which were separated by not more than 100 mV. In the latter case we can resolve the two peaks at 1.17 and 1.29 V which differ by 120 mV. In the numerous cases where it has been shown that the two oxidations occur at the porphyrin periphery (to give π-cation and π-dication) the difference between the two potentials is 290 ± 50 mV (23), and deviations from this value suggest that the metal, rather than the ring, is the redox reactive centre. When Ni(II)TPP is oxidized in CH_2Cl_2/TBAH the two oxidation waves are separated by 320 mV consistant with two ring oxidations, suggesting that the oxidations described above, which were carried out in the presence of perchlorate, involve an initial oxidation of the metal. In benzonitrile the $[Ni(III)TPP]^+$ is sufficiently stable to be observed at room temperature before it converts over to the $[Ni(II)TPP]^{+\bullet}$ whereas we find that at the end of a bulk electrolysis in methylene dichloride any $[Ni(III)TPP]^+$, if formed, has already converted to $[Ni(II)TPP]^{+\bullet}$.

Similar internal electron transfers have been reported previously (19, 26), and Barefield and Mocella (27) showed that a nickel Curtis-type macrocycle exhibited a similar temperature-dependent internal electron transfer, i.e. **1** ⇌ **2**. Although the total charge on these complexes is 3+ instead of the 1+ for the systems reported here, the same general physical behavior was noted. Barefield attributed this phenomenon to the phase change in going from solution to the solid state, and suggested that axial ligation might play an important role in the process. A similar situation obtains here, for when a frozen

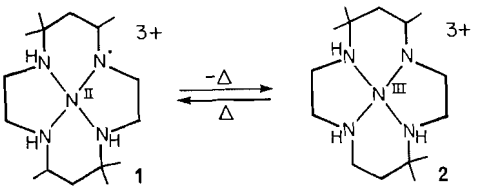

sample is in thermal equilibrium with its solution the solid is orange while the solution is green, and only when the green solution freezes does it change color. It is not yet clear what happens, as the phase changes, to bring about the internal electron transfer and stabilize the hole on the metal rather than the periphery. One might anticipate that the higher oxidation state of the metal would be stabilized by the axial coordination of a donor ligand. The situation is not as clear cut as this, however, since in the presence of bromide or water only the π-cation radical is observed even at 77 K. Moreover, the fact that we have found no other prophyrin π-cation which exhibits this internal electron transfer (including the π-cation radical of Ni(II) octaethylporphyrin) suggests that the phenomenon must depend upon a number of closely balanced factors such that small perturbations can stabilize one or another of the two species undergoing the internal electron transfer. Nonetheless, the degree of axial ligation does play a role here since in addition to the intense band at 525 nm the nickel(III) complex shows a broad weak absorption around 650 nm. While the origin of this charge transfer band is unclear, a similar band also occurs in the Ni(II) complex, but only in the presence of ligands which would axially coordinate, and the appearance of a similar band in the spectrum of the Ni(III) complex suggests that at 77 K even PF_6^- and ClO_4^- are coordinating to the metal.

Other metalloporphyrins show similar internal electron transfers. Ferguson *et al.* (28) while studying octaethylporphyrinato Pb(II) (Pb(II)OEP) found two reversible oxidations on the cyclic voltammetric time scale (s) which they attributed to successive, and reversible, one-electron oxidations of the ring. The resulting π-dication decays, in rigorously purified solvents, with a half-life of ~5 min to a Pb(IV) complex (6), i.e.

$$\text{Pb(II)OEP} \overset{-e^-}{\rightleftharpoons} [\text{Pb(II)OEP}]^{+\bullet} \overset{-e^-}{\rightleftharpoons} [\text{Pb(II)OEP}]^{2+} \downarrow [\text{Pb(IV)OEP}]^{2+}$$

Having shown that a facile and reversible internal electron transfer can occur between a metal and the periphery of a coordinating porphyrin one can ask could such an internal transfer play any role in biochemical systems? Even though many cytochromes function via an Fe(II)–Fe(III) couple, and while it is

Can. J. Chem. Downloaded from www.nrcresearchpress.com by 210.87.254.105 on 09/05/12
For personal use only.

TABLE 1. Electron transfer rates for oxidation/reduction of cytochrome *c*

Reagent	Rate (M^{-1} s^{-1})	Reference
e_{aq}^-	1.3×10^{11}	29
$Fe(dipy)_2(CN)_2^+$	1.9×10^8	35
$Fe(CN)_6^{3-}$	8.0×10^6	35
Azurin	6.25×10^6	37
$Ru(NH_3)_6^{2+}$	3.8×10^4	32
$Fe(CN)_6^{4-}$	2.6×10^4	51
Fe(II) cyt *c*	2×10^4	52
Cr(II)	1.2×10^4	33
$Co(phen)_3^{3+}$	1.5×10^3	32

abundantly clear that the final oxidation states are indeed ferric and ferrous, how is ferrous cytochrome oxidized to its ferric state?

Much kinetic data have been gathered on the redox reactions of cytochromes, particularly the cytochromes *c*, using a variety of redox reagents ranging from hydrated electrons (e_{aq}^-) (29–31) through simple inner- and outer-sphere inorganic reagents (32–36) to those macromolecules which transfer electrons to and from cytochrome *c* in nature (37–41). Table 1 lists some of these redox reagents and observed rates of electron transfer, and while the rates vary they are generally in the range of 10^3–10^6 M^{-1} s^{-1}. Cytochrome *c* contains an axially coordinated methionine (42–43). Sutin has measured the rate of breaking the Fe—S bond, and of opening a heme crevice, which should be rate limiting for an inner sphere pathway (44). The measured value of 60 s^{-1} would appear to rule out an inner sphere process as a major route of electron transfer even with small inorganic redox reagents.

X-ray crystallography has shown that both the reduced and oxidized forms of cytochrome *c* have essentially the same structure (43). One striking feature of the crystal structure is the partially exposed edge of the heme porphyrin ring (a similar structural feature is observed with cytochrome b_5 (45), and we anticipate that other cytochromes in the respiratory chain will show similar exposed hemes). The tertiary structure of the protein will, of course, impose severe steric restraints upon the accessibility of the heme coordinated iron to even the smallest redox reagent, such that it is inconceivable that the iron atoms of two adjacent cytochromes could come close enough to transfer an electron via an inner sphere mechanism. How then do cytochromes transfer electrons amongst themselves? Kinetic studies have suggested three main routes.

(i) A remote transfer through aromatic residues in the protein—which can be seen in the crystal structure of cytochrome *c* to form a channel from the surface of the protein to the heme. Similar remote pathways with an electron tunneling through several Ångstroms of a hydrophobic protein channel have been proposed for some non-heme iron proteins, the ferredoxins (46). Thorough articulations of these arguments can be found elsewhere (47), but it should be noted such a pathway does not appear to be operative in cytochrome *c*.

(ii) A direct electron transfer through space—In addition to the classical inner- and outer-sphere modes of electron transfer the possibilities that direct electron transfer via quantum mechanical electron tunneling, or transfer to and transport through a solvent (as a hydrated electron (e_{aq}^-) in biochemical systems) must be considered. Even in redox reactions with simple inorganic ions the intermediacy, or lack thereof, of e_{aq}^- has yet to be satisfactorily demonstrated (48). The same situation applies to the more complex biochemical systems even though the reduction of ferricytochrome *c* by externally generated e_{aq}^- has been reported (49).

Quantum mechanical electron tunneling is, however, well documented, and tunneling through distances of tens of Ångstroms of inert solvents has been observed with non-biochemical systems (49). While application of the simple one-dimensional theory (49) to complex macromolecules is unwarranted, it does suggest that such mechanisms are possible in nature even though none has yet been documented.

(iii) Oxidation at the porphyrin periphery—A number of both kinetic and product isolation studies suggest that the oxidation of a coordinated metal can proceed through an outer-sphere mechanism, and studies with ferrocytochrome *c* and complexes of tris(1,10-phenantholine)cobalt(III) ions show that an outer sphere mechanism is operative and these studies have led Gray and co-workers (14) to suggest that the point of electron transfer is the partially exposed heme edge. But having concluded that electron transfer occurs via the porphyrin π-cloud how, in fact, is the ferrocytochrome *c* oxidized to the ferric state? We suggest that a process analogous to the oxidation of the Ni(II)TPP to the $Ni(III)TPP^+$ might be operative, that is via the intermediacy of a porphyrin π-cation radical, such that the oxidation of ferro- to ferricytochrome *c* could be described as:

$$\underset{\text{I}}{\text{Fe(II) cyt } c} \underset{+e}{\overset{-e^-}{\rightleftharpoons}} \underset{\text{II}}{[\text{Fe(II) cyt } c]^{+\cdot}} \rightleftharpoons \underset{\text{III}}{[\text{Fe(III) cyt } c]^+}$$

Since ferric and ferrous iron have different covalent

Can. J. Chem. Downloaded from www.nrcresearchpress.com by 210.87.254.105 on 09/05/12
For personal use only.

radii there must be conformational changes around the iron and its ligands between ferro- and ferricytochrome *c* (I and III) and between the postulated ferrocytochrome *c* π-cation radical (II) and ferricytochrome *c* (III). Thus II and III would not be extreme resonance forms of the same species and an activation energy will be required to convert II to III. It has been suggested that the slow interconversion of $[Pb(II)OEP]^{2+}$ to $[Pb(IV)OEP]^{2+}$, discussed above, may be due to a Frank–Condon forbidden transition since the Pb(II) is out of plane and the Pb(IV) in plane (50); and that since there is no overlap between the empty a_{1u} porphyrin orbital and the $a_{2u}(6p_z)$ lead orbital the probability for charge transfer is small. In the case of the nickel complexes described here the system is more finely tuned and the electronic configurations are adjusted to a thermally controlled level. A similar situation might be anticipated in the cytochromes, and the rapid rate of electron transfer for self exchange in cytochromes *c* suggest that an intermediate such as II will be short lived ($<10^{-5}$ s), and as yet none have been detected.

Acknowledgements

This work is a contribution from the Bioinorganic Chemistry Group and was supported by operating and negotiated development grants from the National Research Council of Canada and the United States National Institutes of Health (AM 17989).

1. G. R. Moore and R. J. P. Williams. Coord. Chem. Rev. **18**, 125 (1976).
2. R. Lemberg and J. Barrett. Cytochromes. Academic Press, New York, NY. 1973.
3. J. H. Wang. On the coupling of oxidation to phosphorylation in biological systems. *In* Biological aspects of inorganic chemistry. *Edited by* A. W. Addison, W. R. Cullen, D. Dolphin, and B. R. James. Wiley Interscience, New York, NY. 1977. p. 1.
4. D. H. Kohl. *In* Biological applications of electron spin resonance. *Edited by* H. M. Swartz, J. R. Bolton, and D. C. Borg. Wiley Interscience, New York, NY. 1972. p. 213.
5. J. D. McElroy, G. Feker, and D. Mauzerall. Biochem. Biophys. Acta, **267**, 363 (1972).
6. D. C. Borg, J. Fajer, R. H. Felton, and D. Dolphin. Proc. Natl. Acad. Sci. U.S.A. **67**, 813 (1970).
7. J. Fajer, D. C. Borg, A. Forman, D. Dolphin, and R. H. Felton. J. Am. Chem. Soc. **92**, 3451 (1970).
8. D. Dolphin and R. H. Felton. Acc. Chem. Res. **7**, 26 (1974).
9. D. Dolphin, A. Forman, D. C. Borg, J. Fajer, and R. H. Felton. Proc. Natl. Acad. Sci. U.S.A. **68**, 614 (1971).
10. J. Fajer, D. C. Borg, A. Forman, R. H. Felton, L. Vegh, and D. Dolphin. Ann. N.Y. Acad. Sci. **206**, 349 (1973).
11. R. H. Felton, G. S. Owen, D. Dolphin, and J. Fajer. J. Am. Chem. Soc. **93**, 6332 (1971).
12. G. M. Brown, F. R. Hopf, J. A. Ferguson, T. J. Meyer, and D. G. Whitten. J. Am. Chem. Soc. **95**, 5939 (1973).
13. E. B. Fleischer and S. K. Cheung. J. Am. Chem. Soc. **98**, 8381 (1976).
14. J. V. McArdle, K. Yocom, and H. B. Gray. J. Am. Chem. Soc. **99**, 4141 (1977).
15. A. Wolberg and J. Manassen. Inorg. Chem. **9**, 2365 (1970).
16. D. Dolphin, T. Niem, R. H. Felton, and S. Fujita. J. Am. Chem. Soc. **97**, 5288 (1975).
17. K. Shibata. Methods Biochem. Anal. **7**, 7 (1959).
18. D. Dolphin, R. H. Felton, D. Borg, and J. Fajer. J. Am. Chem. Soc. **92**, 743 (1970).
19. N. E. Tokel, K. Farmery, L. Anderson, F. V. Lovecchio, E. S. Gore, and D. H. Busch. J. Am. Chem. Soc. **96**, 731 (1974).
20. M. Gouterman. Optical spectra and electron structure of porphyrins. *In* The porphyrins. Vol. III. *Edited by* D. Dolphin. Academic Press, New York, NY. In press. Chapt. 1.
21. M. P. Gouterman. J. Mol. Spectrosc. **6**, 138 (1961); C. Weiss, H. Kobayashi, and M. P. Gouterman. J. Mol. Spectrosc. **16**, 415 (1965).
22. J.-H. Fuhrhop and D. Mauzerall. J. Am. Chem. Soc. **91**, 4174 (1969).
23. J.-H. Fuhrhop, K. M. Kadish, and D. G. Davis. J. Am. Chem. Soc. **95**, 5140 (1973).
24. A. Wolberg and J. Manassen. J. Am. Chem. Soc. **92**, 2982 (1970).
25. D. G. Davis. Electrochemistry of porphyrins. *In* The porphyrins. Vol. V. *Edited by* D. Dolphin. Academic Press, New York, NY. In press. Chapt. 4.
26. N. S. Huck and I. S. Woolsey. J. Am. Chem. Soc. **94**, 4107 (1972).
27. E. K. Barefield and M. T. Mocella. J. Am. Chem. Soc. **94**, 4107 (1972).
27. E. K. Barefield and M. T. Mocella. J. Am. Chem. Soc. **97**, 4238 (1975).
28. J. A. Ferguson, T. J. Meyer, and D. G. Whitten. Inorg. Chem. **11**, 2767 (1972).
29. J. Pecht and M. Faraggi. Proc. Natl. Acad. Sci. U.S.A. **69**, 902 (1972).
30. A. Shafferman and G. Stein. Biochim. Biophys. Acta, **416**, 287 (1975).
31. N. N. Lichtin, A. Shafferman, and G. Stein. Biochim. Biophys. Acta, **314**, 117 (1973).
32. S. Wherland and H. B. Gray. Proc. Natl. Acad. Sci. U.S.A. **73**, 2950 (1976).
33. J. W. Dawson, H. B. Gray, R. A. Holwerda, and E. W. Westhead. Proc. Natl. Acad. Sci. U.S.A. **69**, 30 (1972).
34. J. K. Yandell, D. P. Fay, and N. Sutin. J. Am. Chem. Soc. **95**, 1131 (1973).
35. J. C. Cassatt and C. P. Marini. Biochemistry, **13**, 5323 (1974).
36. C. Creutz and N. Sutin. Proc. Natl. Acad. Sci. U.S.A. **70**, 1701 (1973).
37. E. Antonini, A. Finazzi-Agro, L. Avigliano, P. Guerrieri, G. Rotilio, and B. Mondovi. J. Biol. Chem. **245**, 4847 (1970).
38. S. Pecht and P. Rosen. Biochem. Biophys. Res. Commun. **50**, 853 (1973).
39. M. Brunori, C. Greenwood, and M. T. Wilson. Biochem. J. **137**, 113 (1974).
40. M. T. Wilson, C. Greenwood, M. Brunori, and E. Antonini. Biochem. J. **145**, 449 (1975).
41. P. Rosen and S. Pecht. Biochemistry, **15**, 775 (1976).
42. R. E. Dickerson, T. Takano, D. Eisenberg, O. B. Kallai, L. Samson, A. Cooper, and E. Margoliash. J. Biol. Chem. **246**, 1511 (1971).

43. R. E. DICKERSON and R. TIMKOVICH. The enzymes. Vol. XI. *Edited by* P. D. Boyer. Academic Press, New York, NY. 1975. Chapt. 7.
44. N. SUTIN and J. K. YANDELL. J. Biol. Chem. **247**, 6932 (1972).
45. F. S. MATHEWS, M. LEVINS, and P. ARGOS. J. Mol. Biol. **64**, 449 (1972).
46. R. H. HOLM. Identification of active sites in iron–sulfur proteins. *In* Biological aspects of inorganic chemistry. *Edited by* A. W. Addison, W. R. Cullen, D. Dolphin, and B. R. James. Wiley-Interscience, New York, NY. 1977. p. 71.
47. S. FERGUSON-MILLER, D. L. BRAUTIGAN, and E. MARGOLIASH. The electron transfer function of cytochrome c. *In* The porphyrins. Vol. VII. *Edited by* D. Dolphin. Academic Press, New York, NY. In press. Chapt. 4.
48. G. A. KENNEY and D. C. WALKER. *In* Electroanalytical chemistry. Vol. 5. *Edited by* A. J. Bard. Marcel Dekker, Inc., New York, NY. 1971. pp. 1–66.
49. J. R. MILLER. J. Chem. Phys. **56**, 5173 (1972).
50. R. H. FELTON. Primary redox reactions of metalloporphyrins. *In* The porphyrins. Vol. V. *Edited by* D. Dolphin. Academic Press, New York, NY. In press. Chapt. 3.
51. K. G. BRANDT, P. C. PARKS, G. H. CZERLINSKI, and G. P. HESS. J. Biol. Chem. **241**, 4180 (1966).
52. R. K. GUPTA, S. H. KOENIG, and A. G. REDFIELD. J. Magn. Reson. **7**, 66 (1972).

Can. J. Chem. Downloaded from www.nrcresearchpress.com by 210.87.254.105 on 09/05/12
For personal use only.

A reformulation of the theory of unimolecular reactions

ANDREW W. YAU AND HUW O. PRITCHARD

Centre for Research in Experimental Space Science, York University, Downsview, Ont., Canada M3J 1P3

Received September 1, 1977

ANDREW W. YAU and HUW O. PRITCHARD. Can. J. Chem. **56**, 1389 (1978).

The theory of unimolecular reactions is reformulated in a way which makes no reference to the concepts of a transition state, a reaction coordinate, or of an activated complex: the present theory is based, instead, on a simple master-equation approach using the estimated positions and lifetimes of the rotation–vibration energy levels of the molecule. The fundamental basis of this reformulation is that the unimolecular rate is derived from the perturbation of the normal modes of internal relaxation of the reactant molecule by the microscopic reaction processes. The thermal decompositions of cyclobutane, cyclopropane, ethyl isocyanide, ethyl chloride, and methyl isocyanide are examined in detail, and it is shown that not only is the present theory much easier to use than is conventional RRKM theory, but also that it gives better results.

An Appendix provides a set of algorithms required for these calculations.

ANDREW W. YAU et HUW O. PRITCHARD. Can. J. Chem. **56**, 1389 (1978).

On propose une reformulation de la théorie des réactions unimoléculaires d'une façon telle que l'on ne fasse aucune référence aux concepts d'état de transition, de coordonnée de réaction ou de complexe activé: on base plutôt la nouvelle théorie sur une équation maîtresse simple utilisant des positions et des temps de vie évalués des niveaux énergétiques rotation–vibration de la molécule. Le concept fondamental de cette reformulation repose sur la notion que la vitesse unimoléculaire provient d'une perturbation des modes normaux de relaxation interne de la molécule réactive par des processus réactionnels microscopiques. On a examiné en détail les décompositions thermiques du cyclobutane, du cyclopropane, de l'isocyanure d'éthyle, du chlorure d'éthyle et d'isocyanure de méthyle et on a montré que la théorie est plus facile à utiliser que la théorie RRKM conventionnelle et qu'elle donne aussi de meilleurs résultats.

Un appendice fournit l'ensemble d'algorithmes requis pour ces calculs.

[Traduit par le journal]

I. Introduction

This examination of the theory of unimolecular reactions was undertaken principally out of a desire to see the theory cast in modern molecular-dynamic terms. We do not claim that the theory set out below satisfies this desire completely: in a purely formal sense it does, but in practice our estimates of the effective lifetimes of the reactive states with respect to predissociation are not, at present, derived by molecular-dynamic methods.

The most successful current theory of thermal unimolecular reactions is the RRKM theory (1–6), but despite its obvious success in describing reasonably well a very wide range of reaction processes, it suffers from some frustrating deficiencies. Most importantly, although much emphasis is placed upon the selection of a hypothetical reaction coordinate and the corresponding activated complex, it hardly matters what reaction coordinate is chosen (5, 7, 8) because the calculated fall-off behaviour is very insensitive to this choice. Less serious, but nevertheless unsettling, are the problems surrounding the assumed collisional deactivation efficiency: one is that markedly different collision efficiencies are often required to make the calculated and experimental fall-off curves coincide at different temperatures (5), or sometimes these efficiencies do not vary monotonically with temperature (9, 10); another is that collision efficiencies of the order of unity are often found, and yet it is reasonably well established that the vessel walls are more effective in transferring internal energy than are collisions with other molecules (11–13). These difficulties do not arise in the present reformulation: the concepts such as reaction coordinate do not appear, and it becomes evident in the later discussion (section XI*B*) that the puzzle surrounding collision efficiencies is part experimental in origin, and part a matter of theoretical interpretation.

II. List of Symbols

The nomenclature used in this presentation has been chosen to remain, as far as possible, in conformity with existing practices (5) where an identical or nearly identical concept is being represented; for the remainder, we have chosen the simplest nomenclature which appears possible.

- $\mathbf{A}$ internal relaxation matrix (s^{-1}); elements a_{ij}.
- A_∞ Arrhenius frequency factor at infinite pressure (s^{-1}).
- a_i coefficient in the numerator of the generalised Lindemann form, eqs. 46, 47; $\bar{a}_i$ is grouped value in graining procedure, and $\bar{\bar{a}}_i$ is scaled value used in the practical algorithm.

Can. J. Chem. Downloaded from www.nrcresearchpress.com by 210.87.254.42 on 09/05/12
For personal use only.

Can. J. Chem. Downloaded from www.nrcresearchpress.com by 210.87.254.42 on 09/05/12
For personal use only.

B symmetrised relaxation matrix (s^{-1}).
b_i ith coefficient in the denominator of the generalised Lindemann form, eqs. 46, 47; $\bar{b}_i$ and $\tilde{b}_i$ are respectively grouped and scaled quantities.
β inverse temperature (cm; $= 1/kT$).
D predissociation matrix; diagonal elements $d_i = -k_i$ (s^{-1}).
E equilibrium population matrix—non-dissipative system; diagonal elements $\tilde{n}_j$.
ε energy (cm^{-1} or kcal mol^{-1}).
ε_0 critical energy (cm^{-1} or kcal mol^{-1}; $= \varepsilon_\infty$ assuming eq. 34).
ε_∞ activation energy at infinite pressure for strict Arrhenius rate law.
ε_{act} activation energy at arbitrary pressure.
g_i degeneracy of state i.
$G(\varepsilon)$ state-sum up to energy ε.
Γ diagonalised reaction matrix; γ_j is jth eigenvalue.
k Boltzmann constant.
k_{il} predissociation rate constant from reactant in state i to product in state l (s^{-1}).
k_i decay rate constant from state i to all product channels (s^{-1}; $= \sum_l k_{il}$).
$k(\varepsilon)$ average decay rate constant over all states i at energy ε (s^{-1}).
k_{uni} unimolecular rate constant (s^{-1}; $= -\gamma_{n-1}$).
k_∞ infinite pressure rate constant (s^{-1}).
$\mathscr{L}$ Laplace transform.
Λ diagonalised relaxation matrix; λ_j is jth eigenvalue.
λ collisional efficiency in RRKM theory.
$\bar{\lambda}$ collisional efficiency or pressure-shift parameter.
[M] concentration of inert-gas molecules (molecules cm^{-3}).
n number of levels in relaxing system.
$\tilde{n}_i$ equilibrium (fractional) population of the ith state—non-dissipative system; $\sum_i \tilde{n}_i = 1$.
$\bar{n}_r$ total equilibrium (fractional) population within the rth reactive channel grain.
$\eta_i(t)$ population of the ith state at time t—dissipative system; $\sum_i \eta_i(0) = 1$.
p pressure (Torr).
p_{ij} transition probability per collision *from* state i *to* state j.
$P(\varepsilon)$ state-degeneracy at energy ε; $= \sum_i g_i$ over states at ε.
$\rho(\varepsilon)$ density of states at energy ε (cm).
q_{ij} transition rate constant *from* state i *to* state j (cm^3 $molecule^{-1}$ s^{-1}).
R symmetrised reaction matrix (s^{-1}).
S eigenvector matrix of relaxation matrix **B**; S_{ij} is ith element of jth eigenvector.
Ψ eigenvector matrix of reaction matrix **R**; ψ_{ij} is ith element of jth eigenvector.
s Kassel shape parameter for unimolecular fall-off curve.
σ collision diameter.
T temperature.
μ internal relaxation time constant of molecule (s^{-1}).
μ' internal relaxation rate constant (cm^3 $molecule^{-1}$ s^{-1}).
$\bar{\mu}$ internal relaxation rate constant ($Torr^{-1}$ s^{-1}; $= \mu' \times 9.88 \times 10^{18} T^{-1}$).
ν_i vibrational frequency of ith oscillator (cm^{-1}).
x_i anharmonicity factor of vibration, assumed to be a Morse oscillator.
$Z(T)$ collision number at temperature T (cm^3 $molecule^{-1}$ s^{-1}).
$\mathscr{Q}(\beta)$ partition function at inverse temperature β.

III. The Reaction Model

This treatment follows from an extension of the primitive master-equation model we described earlier this year (14). The reactant molecule X is considered to possess a denumerable set of rotation–vibration states X_i, and is diluted in a heat bath of structureless inert gas molecules M; transitions among the various internal states X_i are induced by collisions with M, and should a molecule X find itself in a state with energy greater than a critical amount ε_0, predissociation to products may occur with a set of characteristic time constants, in competition with collisional deactivation. The model then, is no more than a generalised Lindemann scheme (5, 6, 14)

$$X_i + M \underset{q_{ji}(T)}{\overset{q_{ij}(T)}{\rightleftharpoons}} X_j + M$$

$$X_i \xrightarrow{k_{il}} Y_l$$

where Y_l represents the product in the lth internal state; for the time being, we ignore the internal structure of the product molecules.

Implicit in the model are the following assumptions. The temperature of the heat bath remains unchanged during the reaction, and the heat-bath molecules maintain their translational equilibrium. The mutual interactions between the X molecules are neglected in order to preserve the linearity of the master equation. The model is also dissipative in the sense that the reverse reaction is excluded, a simplification justified by the fact that most unimolecular reactions are studied far away from equilibrium (14).

In this treatment, we have readopted the natural ordering of subscripts, so that $q_{ij}(T)$ is the *rate constant* for the transition of X *from* internal state i *to*

Can. J. Chem. Downloaded from www.nrcresearchpress.com by 210.87.254.42 on 09/05/12
For personal use only.

internal state j upon collision with M at temperature T. This rate constant is related to the transition probability per collision $p_{ij}(T)$ *via* the collision number $Z(T)$, assumed to be independent of i, viz.

$$[1] \qquad q_{ij}(T) = Z(T) \cdot p_{ij}(T)$$

where

$$Z(T) = 2\sigma^2(2\pi/\beta m)^{1/2}$$

σ being the collision diameter and $\beta = 1/kT$, the inverse temperature, and m is the reduced mass of X and M. The quantities q_{ij} and q_{ji} are related by the principle of detailed balancing

$$[2] \qquad \tilde{n}_i q_{ij} = \tilde{n}_j q_{ji}$$

where $\tilde{n}_i$ is the equilibrium fractional population of the ith state in the *absence of reaction* (i.e. when $k_{il} = 0$ for all i); the internal-relaxation process is also Markovian, so that

$$[3] \qquad \sum_j p_{ij} = 1$$

The microscopic rate constant k_{il} for the conversion of the reactant in state i to the product in state l is assumed to be independent of both temperature and the concentrations of X and M. Thus, the master equation for the evolution of the population of the ith state of X is readily written as

$$[4] \qquad \frac{d\eta_i(t)}{dt} = \sum_j a_{ij}\eta_j(t) + d_i\eta_i(t)$$

where $\eta_i(t)$ is the fractional population of the ith state at time t, and

$$[5a] \quad a_{ij} = Z[M]\{(1 - \delta_{ij})p_{ji} - \delta_{ij}\sum_k (1 - \delta_{ik})p_{ik}\}$$

$$[5b] \quad d_i = -\sum_l k_{il}$$

Thus, d_i is zero for all unreactive states, and the summation in [5*b*] is understood to be over all accessible product channels; the quantity $-d_i$ will be redesignated as k_i later, in section V.

Since [4] is linear, it may be written in matrix notation

$$[6] \qquad \frac{d\boldsymbol{\eta}(t)}{dt} = (\mathbf{A} + \mathbf{D})\boldsymbol{\eta}(t)$$

where

$$d_{ij} = d_i\delta_{ij}$$

and the matrix sum $(\mathbf{A} + \mathbf{D})$ can be symmetrised in the usual way (15) using the equilibrium population vector, i.e.

$$[7] \qquad \mathbf{R} = \mathbf{E}^{-1/2}(\mathbf{A} + \mathbf{D})\mathbf{E}^{1/2}$$

where

$$e_{ij} = \tilde{n}_i\delta_{ij}$$

and $\mathbf{R}$ is now symmetric; under this transformation [6] becomes

$$[8a] \qquad \frac{d\boldsymbol{\chi}(t)}{dt} = \mathbf{R}\boldsymbol{\chi}(t)$$

with

$$[8b] \qquad \boldsymbol{\chi}(t) = \mathbf{E}^{-1/2}\boldsymbol{\eta}(t)$$

as the 'symmetrised population evolution vector'. Finally, if $\mathbf{R}$ is diagonalised using the matrices $\boldsymbol{\Psi}$ and $\boldsymbol{\Psi}^T$ to give

$$[9] \qquad \boldsymbol{\Gamma} = \boldsymbol{\Psi}^T\mathbf{R}\boldsymbol{\Psi}$$

$\boldsymbol{\Gamma}$ has the property that all the eigenvalues are real and negative, i.e.

$$0 > \gamma_{n-1} \gg \gamma_{n-2} \geq \gamma_{n-3} \geq \cdots \geq \gamma_0$$

since $\mathbf{R}$ is symmetric and negative definite. Because $\mathbf{R}$ and $(\mathbf{A} + \mathbf{D})$ are related by a similarity transformation, their eigenvalues are identical, and hence (14) we identify the experimentally observed unimolecular rate constant with the eigenvalue of largest algebraic magnitude, i.e.

$$[10] \qquad k_{uni} = -\gamma_{n-1}$$

It follows also that the evolution of the populations of the states of the molecule X is given by

$$[11] \quad \eta_i(t) = \tilde{n}_i^{1/2}\sum_j \exp(\gamma_j t)\psi_{ij}\sum_k \psi_{kj}\eta_k(0)\tilde{n}_k^{-1/2}$$

This equation has been used repeatedly in describing non-dissipative systems (16), but it is equally valid for dissipative systems.

The first aim of the master-equation formulation of unimolecular reactions is therefore the determination of the eigenvalue γ_{n-1}; subsequent aims will involve the determination of the eigenvector elements ψ_{ij}. However, whilst the formal solutions may be readily written, the explicit determination of the exact analytic solution for a general system, with a general set of transition probabilities p_{ij} and microscopic rate constants k_{il}, is a formidable task because of a general lack of theorems in this area; hence, our previous approach using numerical experiment (14). Consequently, we will attempt here to establish, as a first step in this direction, explicit relations between k_{uni} and the normal modes of internal relaxation (17), given a set of microscopic rate constants k_{il}. Note here that the term *internal relaxation* refers to changes between rotation–vibration states of X brought about by collision with M; thus, this avenue of attack is simply one way of trying to solve the generalised Lindemann scheme, as presented at the beginning of this section.

Can. J. Chem. Downloaded from www.nrcresearchpress.com by 210.87.254.42 on 09/05/12
For personal use only.

IV. The Relation Between k_{uni} and the Normal Modes of Relaxation

Following our earlier work on molecular relaxation (16, 17) we define, for the internal relaxation system, the symmetrised transition matrix **B** as

$$[12] \qquad \mathbf{B} = \mathbf{E}^{-1/2}\mathbf{A}\mathbf{E}^{1/2}$$

which has eigenvalues λ_j and eigenvectors $\boldsymbol{S}_j$;

$$[13] \qquad \mathbf{B} = \mathbf{S}\Lambda\mathbf{S}^T$$

Recalling briefly the properties of the conservative relaxation system, we have

$$[14] \quad n_i(t) = \tilde{n}_i^{1/2} \sum_j \exp(\gamma_j t) S_{ij} \sum_k S_{kj} n_k(0) \tilde{n}_k^{-1/2}$$

where $n_i(t)$ is the fractional population of state i in the absence of the reaction; notice the similarity with eq. 11. In the conservative case, however, the eigenvalue sequence is

$$0 = \lambda_{n-1} \gg \lambda_{n-2} \geq \lambda_{n-3} \geq \ldots \geq \lambda_0$$

with the zero eigenvalue ensuring conservation of particles, and the particular sequence of eigenvector elements

$$[15] \qquad S_{i,n-1} = \tilde{n}_i^{1/2}$$

ensuring the attainment of the Boltzmann equilibrium distribution as $t \to \infty$. Finally

$$[16] \qquad \lambda_i = \lambda_i'[\mathrm{M}]$$

where the λ_i' are constants, in other words, the relaxation time constants are proportional to [M].

We now rewrite the eigenvalue equation [9], i.e.

$$[17] \qquad \mathbf{R}\boldsymbol{\Psi}_i = \gamma_i \mathbf{I}\boldsymbol{\Psi}_i$$

in the iterative form (18)

$$[17a] \qquad \boldsymbol{\Psi}_i = (\gamma_i \mathbf{I} - \mathbf{B})^{-1}\mathbf{D}\boldsymbol{\Psi}_i$$

Then, using [13], we have

$$[18] \qquad (\gamma_i \mathbf{I} - \mathbf{B})^{-1} = \{\mathbf{S}(\gamma_i \mathbf{I} - \Lambda)\mathbf{S}^T\}^{-1} = \mathbf{S}(\gamma_i \mathbf{I} - \Lambda)^{-1}\mathbf{S}^T$$

whence

$$[19] \qquad \boldsymbol{\Psi}_i = \mathbf{S}(\gamma_i \mathbf{I} - \Lambda)^{-1}\mathbf{S}^T\mathbf{D}\boldsymbol{\Psi}_i$$

The perturbed eigenvector elements are then

$$[20] \qquad \psi_{ki} = \sum_l \left(\sum_m \frac{S_{km}S_{lm}}{\gamma_i - \lambda_m}\right)\left(\sum_j d_{lj}\psi_{ji}\right)$$

and since **D** is diagonal, this reduces to

$$[20a] \qquad \psi_{ki} = \sum_l \sum_m \frac{S_{km}S_{lm}}{\gamma_i - \lambda_m} \cdot d_l\psi_{li}$$

remembering that the summation over l refers to the predissociating states only. For a system with r predissociating states [20] leads to a system of r equations in r unknowns, γ_i and the $(r-1)$ ratios of ψ_{ki}. The utility of [20] follows from the particular spacings of the eigenvalues γ_i and λ_i, where, using a theorem of Courant and Hilbert (19), it may be shown that

$$[21] \quad 0 = \lambda_{n-1} < |\gamma_{n-1}| \ll |\lambda_{n-2}| \leq |\lambda_{n-3}| \leq \ldots \leq |\lambda_0|$$

whence, to an excellent degree of approximation

$$\psi_{k,n-1} = \sum_l \frac{S_{k,n-1}S_{l,n-1}}{\gamma_{n-1}} \cdot d_l\psi_{l,n-1} - \sum_l \sum_{m=0}^{n-2} \frac{S_{km}S_{lm}}{\lambda_m} \cdot d_l\psi_{l,n-1}$$

or, using [15]

$$[22] \quad \psi_{k,n-1} = \tilde{n}_k^{1/2}\gamma_{n-1}^{-1} \sum_l \tilde{n}_l^{1/2} d_l\psi_{l,n-1} - \sum_l \sum_{m=0}^{n-2} \frac{S_{km}S_{lm}}{\lambda_m} \cdot d_l\psi_{l,n-1}$$

Equation 22 lends itself to further development along two distinct lines. First, it provides a framework for the explicit examination of the dependence of k_{uni} on the normal modes of relaxation, at least for model systems, and will be used in this way in subsequent papers to treat other thermal reactions including dielectronic ionisation of hydrogen atoms, and shock wave dissociation of H_2 and D_2. Second, its linearity in γ_{n-1}^{-1} facilitates direct evaluation of k_{uni} for realistic systems of known microscopic rate constants k_{il} and normal modes of relaxation. We will pursue the first point insofar as it pertains to the theory of unimolecular reactions in the remainder of this section, and thereafter devote our attention to the second one.

Suppose there is only one predissociating state r, i.e.

$$d_i = d_r\delta_{ir}$$

Then, for the element $\psi_{r,n-1}$, [22] reduces to

$$[23] \quad \psi_{r,n-1} = \left\{\tilde{n}_r d_r \gamma_{n-1}^{-1} - \sum_{m=0}^{n-2} \frac{S_{rm}^2}{\lambda_m} \cdot d_r\right\}\psi_{r,n-1}$$

which, together with [10] and [16], leads to k_{uni} in the Lindemann form

$$[24] \qquad k_{uni} = -\gamma_{n-1} = \frac{-\tilde{n}_r d_r}{1 - d_r\kappa_{rr}/[\mathrm{M}]}$$

In this equation the term in the denominator

Can. J. Chem. Downloaded from www.nrcresearchpress.com by 210.87.254.42 on 09/05/12
For personal use only.

[25] $$\kappa_{rr} = -\sum_{m=0}^{n-2} \frac{S_{rm}^{\ 2}}{\lambda_m'}$$

represents an average of all the normal modes of relaxation (S_{rm}^2) associated with the state r, *weighted* by their respective characteristic times $\tau_m = -\lambda_m^{-1}$; in fact, the quantity $\kappa_{rr}/[M] \simeq \tau$, the macroscopic relaxation time for the internal energy. Thus, for a system with only one predissociating state, the internal relaxation amongst its various states has the overall effect of grouping all the nonpredissociating states into one, and the fall-off of k_{uni} with pressure is determined principally by the internal energy relaxation rate and, to a lesser extent, by the fine structure of the relaxation, i.e. the detailed nature of the transition probabilities.

It is important to realise that [24] depends on the approximations made in [21], but since

$$|\gamma_{n-1}| \leq \tilde{n}_r|\lambda_{n-2}| \leq \ldots \leq \tilde{n}_r|\lambda_0|$$

and $\tilde{n}_r < 10^{-10}$ for systems of interest, the reason for our earlier numerical finding (14) that such a reaction obeyed Lindemann behaviour to better than one part in 10^6 becomes apparent. On the other hand, for a system with two predissociating states labelled r and s, we have, from [22]

[26] $$k_{uni} = \frac{(\tilde{n}_r\kappa_{rr} + \tilde{n}_s\kappa_{ss} - 2\tilde{n}_r^{1/2}\tilde{n}_s^{1/2}\kappa_{rs})d_rd_s[M]^{-1} - (\tilde{n}_rd_r + \tilde{n}_sd_s)}{1 + \{(\kappa_{rr}\kappa_{ss} - \kappa_{rs}^{\ 2})d_rd_s[M]^{-2} - (\kappa_{rr}d_r + \kappa_{ss}d_s)[M]^{-1}\}}$$

where, as before,

[26a] $$\kappa_{rs} = -\sum_{m=0}^{n-2} \frac{S_{rm}S_{sm}}{\lambda_m'}$$

Thus, with two predissociating channels open, k_{uni} no longer has the Lindemann form, as we found numerically earlier (14); moreover, it can be seen that, in general, k_{uni} cannot be written as a superposition of the Lindemann expressions for the respective channels. This latter observation, then, cuts away at one of the fundamental building blocks of conventional formulations, that k_{uni} can be expressed as the integral over all energy of the differential contribution, dk_{uni}, to the unimolecular rate constant, i.e.

[27] $$k_{uni} = \int_{\varepsilon_0}^{\infty} dk_{uni}$$

where the dk_{uni} are all in Lindemann form (5). The inadequacy of this integral formulation lies in its failure to take account of the perturbation of one predissociating state by all the other predissociating states: this mutual perturbation is of course implicit in the determination of γ_{n-1} through eq. 9. On the other hand, the failure of this integral representation is not catastrophic, for otherwise the development of theories of unimolecular reactions could not have progressed as far as they have done over the last 50 years; nevertheless, the abandonment of [27] is one of the factors contributing to the superiority of the present reformulation over existing theories.

V. The Choice of the k_i

The use of the master-equation formulation to describe chemically reacting systems presents us with a curious paradox. On the one hand, it would appear that, even for quite simple molecules, many millions or billions of state-to-state and state-to-product processes are taking place and therefore their rate constants need to be known. On the other hand, it has been found repeatedly for diatomic dissociation reactions that the rates of observable processes are either only weakly dependent on, or else totally independent of, the assumed state-to-state or state-to-product rate constants (20); we have elaborated on this point elsewhere already (14, 20). In this section, therefore, we will deduce an approximate choice for the numerical values of the k_i, in the following section we will suggest a logical choice for the numerical values of the a_{ij} and, thereafter, we will show that these two choices lead to an excellent representation of all the known unimolecular reaction characteristics for five reactions which have been subjected to extensive experimental scrutiny.

At infinite pressure, the rate constant k_{uni} becomes (14)

[28] $$k_\infty(\beta) = \sum \tilde{n}_i k_i$$

[28a] $$= \sum k_i g_i \exp(-\beta\varepsilon_i)/\mathcal{Q}(\beta)$$

where $\mathcal{Q}(\beta)$ is the molecular partition function of the reactant at the inverse temperature β. Thus, the sum of g_ik_i over all the states i at energy ε is the inverse Laplace transform of $k_\infty(\beta)\mathcal{Q}(\beta)$; i.e.

[29] $$\sum_{\varepsilon} k_i g_i = \mathcal{L}^{-1}\{k_\infty(\beta)\mathcal{Q}(\beta)\}$$

where the summation is over states at energy ε. We now define $k(\varepsilon)$ as the average of k_i over the states at ε, i.e.

[30] $$k(\varepsilon) = \sum_{\varepsilon} k_i g_i / P(\varepsilon); \quad P(\varepsilon) \neq 0$$

Can. J. Chem. Downloaded from www.nrcresearchpress.com by 210.87.254.42 on 09/05/12
For personal use only.

where

$$[31] \qquad P(\varepsilon) = \sum_{\varepsilon} g_i$$

is the state-degeneracy at energy ε. Since $\mathscr{Q}(\beta)$ is just the Laplace transform of $P(\varepsilon)$, the product $k_\infty(\beta)\mathscr{Q}(\beta)$ in [29] is simply the Laplace transform of the convolution of $\mathscr{L}^{-1}\{k_\infty(\beta)\}$ and $P(\varepsilon)$; whence

$$[32] \qquad P(\varepsilon)k(\varepsilon) = \mathscr{L}^{-1}\{k_\infty(\beta)\} * P|_\varepsilon$$

where $f * g|_\varepsilon$ denotes the convolution of functions f and g from zero to ε. Thus, given $k_\infty(\beta)$ one may, at least in principle, obtain $k(\varepsilon)$, as was first done by Slater (21) in 1955. Over the years, considerable misgivings have been voiced about the validity of such procedures (22–26). However, it may be seen that the derivation of [32] from [28] is rigorous.[1] In particular, it may be shown that for a *discrete system* of predissociating levels, the $k(\varepsilon)$ function is given rigorously by

$$[33] \qquad k(\varepsilon) = A_\infty P(\varepsilon - \varepsilon_\infty)/P(\varepsilon); \quad P(\varepsilon) \neq 0$$

if *the rate law is strict Arrhenius in form*, i.e.

$$[34] \qquad k_\infty(T) \equiv k_\infty(\beta) = A_\infty \exp(-\varepsilon_\infty/kT) = A_\infty \exp(-\beta\varepsilon_\infty)$$

Similarly, it follows, again rigorously, that if the rate law is in modified Arrhenius form, viz.

$$[35] \qquad k_\infty(T) \equiv k_\infty(\beta) = B_\infty T \exp(-\varepsilon_\infty^*/kT) = B'\beta^{-1} \exp(-\beta\varepsilon_\infty^*)$$

where $B' = B_\infty/k$, then

$$[36] \qquad k(\varepsilon) = B'G(\varepsilon - \varepsilon_\infty^*)/\rho(\varepsilon)$$

where $G(\varepsilon)$ is the sum of states up to and including ε and $\rho(\varepsilon)$ is the state density at ε.

It is customary to present experimental data for the infinite-pressure rate constant k_∞ in Arrhenius form, eq. 34. Whether or not experimental rate data for thermal unimolecular reactions obey [34] *rigorously* is a matter which we will discuss further below, cf. Appendix 1; deviations from [34], on the other hand, are clearly small, so that we may write a generalised form of the Arrhenius equation, i.e.

$$[37] \qquad k_\infty = \sum_j A_{\infty j} \exp(-\beta\varepsilon_{\infty j}), \quad j = 1, 2, 3, \ldots$$

where obviously $\varepsilon_{\infty j} \simeq \varepsilon_{\infty 1}$ and $0 < A_{\infty j} \ll A_{\infty 1}$ for all $j \geq 2$, and of course, $\varepsilon_{\infty 1} \equiv \varepsilon_\infty$, $A_{\infty 1} \equiv A_\infty$. We then have, using [32],

$$[38] \qquad P(\varepsilon)k(\varepsilon) = \sum_j \mathscr{L}^{-1}\{A_{\infty j} \exp(-\beta\varepsilon_{\infty j})\} * P|_\varepsilon$$

$$[39] \qquad = \sum_j A_{\infty j} P(\varepsilon - \varepsilon_{\infty j})$$

$$[40] \qquad \simeq A_\infty P(\varepsilon - \varepsilon_\infty)$$

Thus, despite existing doubts, [37]–[40] demonstrate conclusively that the inverse transform of the experimental rate law *is* a good *approximation* to $P(\varepsilon)k(\varepsilon)$ in [33]. Equation 33 is not new, in the sense that it was first derived in the continuous form

$$[41] \qquad k(\varepsilon) = A_\infty \rho(\varepsilon - \varepsilon_\infty)/\rho(\varepsilon)$$

by Slater (21). Yet, the obvious conceptual difficulty, that of the density of states at zero energy, is not encountered in the present derivation of [33]. The two $k(\varepsilon)$ functions, [33] and [36], are quite different in form, as is shown for the example of cyclopropane in Fig. 1; however, they give rise to almost imperceptibly different rate laws given the present precision with which most thermal rate constants can be measured. In the present reformulation, we will adopt [33] for $k(\varepsilon)$, based on two arguments presented in Appendix 1: briefly, the use of [33] always gives a better representation of the shape of the fall-off curve than does the use of [36], as is shown, for example, for cyclopropane in Fig. 2, and there is no other overriding reason for preferring [36] over [33].

VI. The Choice of the a_{ij}

The evaluation of the detailed transition probability matrix elements is clearly a formidable task. Yet, it is now well recognised that the macroscopic behaviour of a relaxation system depends predominantly on the overall relaxation rate and much less so on the pattern of the transition probabilities; this is especially so when the internal relaxation rate is many orders of magnitude faster than the reaction rate, as is the case with most thermal unimolecular reactions. Given this degree of freedom, it is desirable that our choice of the a_{ij} shall satisfy two criteria, one, that it leads to an algebraically tractable solution and two, that its physical implications are clear, so that the limits of its usefulness can be well understood. Figure 3*a* shows in schematic form a set of unperturbed eigenvalues for the internal relaxation of a molecule as a function of [M], and Fig. 3*b* shows schematically the result of allowing this eigenvalue spectrum to be perturbed by a set of k_i elements. This is essentially the result obtained earlier in our numerical experiments (14) and foreseen a long

[1]It should be remembered, however, that $k_\infty(\beta)$ may not be defined in the form of eq. 28 if β is too small, but our treatment using the Laplace transform rather than a finite Laplace series implicitly assumes the validity of such definition. The precise effect of this assumption remains to be deduced although, fortunately, because of the inverse relationship between β and ε, any such effect should be most pronounced at infinitely high energy.

Can. J. Chem. Downloaded from www.nrcresearchpress.com by 210.87.254.42 on 09/05/12
For personal use only.

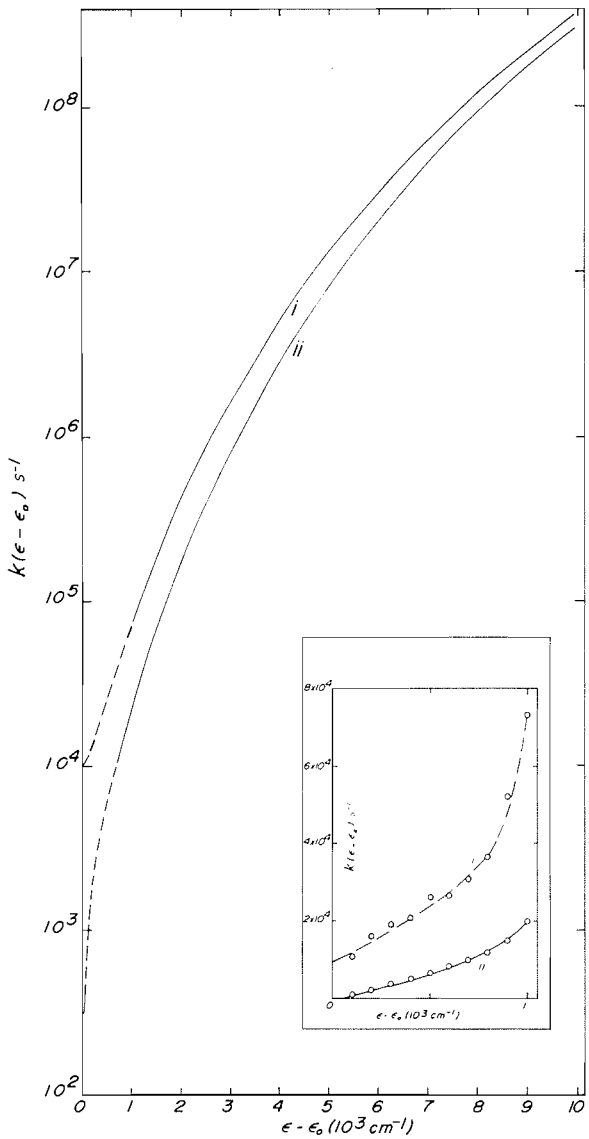

FIG. 1. $k(\varepsilon)$ vs. ε for the isomerisation of cyclopropane above the critical energy. (*i*) Equation 33 with $A_\infty = 1.88 \times 10^{15}\ s^{-1}$, $\varepsilon_\infty = 22\,944\ cm^{-1}$; $\varepsilon_{act} = \varepsilon_\infty$ at all T. (*ii*) Equation 36 with $B' = 1.33 \times 10^{12}\ s^{-1}\ cm^{-1}$, $\varepsilon_\infty{}^* = 22\,414\ cm^{-1}$; $\varepsilon_{act} = \varepsilon_\infty{}^* + kT$ and $\varepsilon_\infty{}^*$ is chosen such that $\varepsilon_{act} = \varepsilon_\infty$ at $T = 763.15$ K. Both functions are step-like (on the scale of the figure) near the critical energy; the dashed segments represent smoothed functions. The inset shows the respective curves near threshold in linear scale.

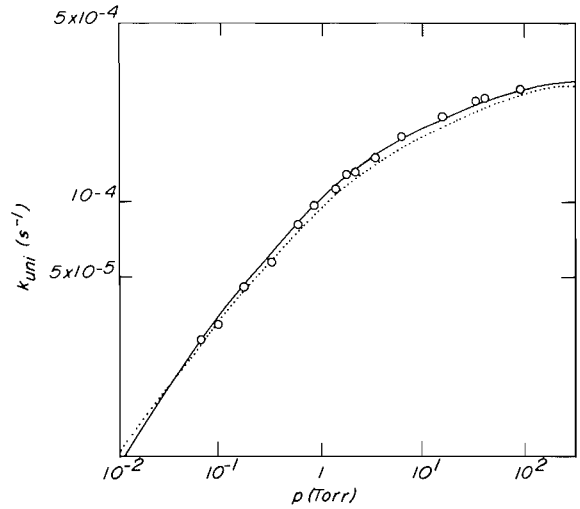

FIG. 2. Fall-off curves for the isomerisation of cyclopropane at 490°C. ○ Experimental data of Pritchard, Sowden, and Trotman-Dickenson (57, 58); — theory using strict Arrhenius rate law, eqs. 33 and 34; ····· theory using modified Arrhenius rate law, eqs. 35 and 36.

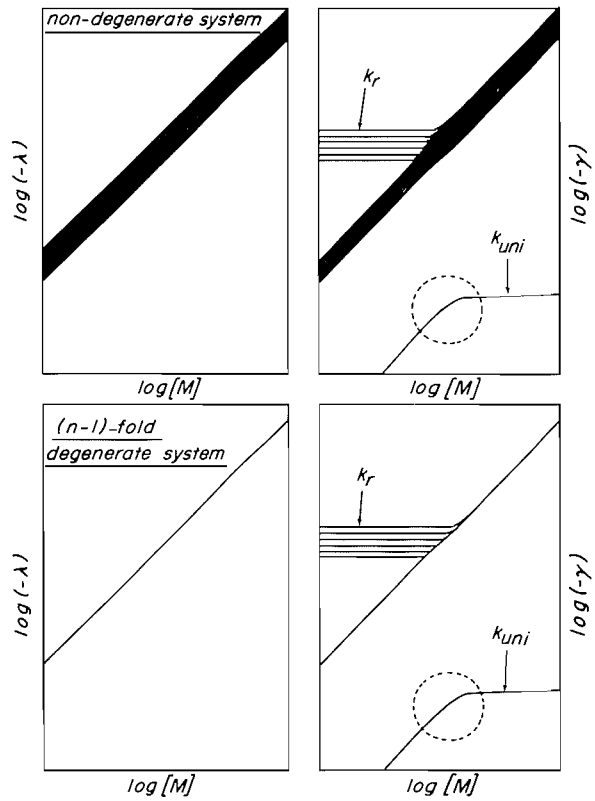

FIG. 3. Schematic representation of the eigenvalue behaviour of (*a*) a general relaxation matrix, (*b*) a general reaction matrix, (*c*) a relaxation matrix with $(n-1)$-fold degeneracy (eq. 42), and (*d*) a reaction matrix with relaxation behaviour of (*c*). Circles indicate pressure region of interest in unimolecular reaction studies.

time ago by Buff and Wilson (40): the important point for our argument is the wide separation between the bundle of eigenvalues representing the internal relaxations and the one representing the reaction rate. We propose, principally on the grounds of algebraic tractability, but also because no great injustice is done to the physical reality (as we shall argue below), to assume that the internal relaxations

Can. J. Chem. Downloaded from www.nrcresearchpress.com by 210.87.254.42 on 09/05/12
For personal use only.

can be treated as being completely degenerate, Fig. 3*c*. The set of transition probabilities corresponding to this $(n-1)$-fold degeneracy of the eigenvalues is (16, 41)

$$[42] \quad a_{ij} = \bar{\lambda}Z[\mathrm{M}]\{(1-\delta_{ij})\tilde{n}_j - \delta_{ij}(1-\tilde{n}_i)\}$$

where $0 < \bar{\lambda} \leq 1$; for such a system, all the non-zero eigenvalues of the symmetrised transition matrix **B** will be degenerate, i.e.

$$\lambda_{n-2} = \lambda_{n-3} = \ldots = \lambda_0 = -\bar{\lambda}Z[\mathrm{M}] = -\mu < \lambda_{n-1} = 0$$

The quantity $\bar{\lambda}$ is therefore a (unknown) collisional efficiency parameter, analogous to the collisional deactivation efficiency (usually denoted by λ) in conventional theory (5, 6): it will be used here in a similar fashion, to effect a lateral shift in the calculated fall-off curve so as to obtain the optimum coincidence with the experimental observations; the quantity μ is of course the time constant for the internal relaxation.

It is important to understand clearly the implications of this approximation. Using [42], the unperturbed system relaxes in a purely exponential manner (16, 41), and it is this property which gives rise to a drastic simplification in the subsequent algebra. When the series of k_i elements is introduced, the behaviour of the perturbed eigenvalues changes to that depicted schematically in Fig. 3*d*, and the contention is that the encircled portion of the curve for k_{uni} in this diagram will be a good approximation to the encircled portion of the curve for k_{uni} in Fig. 3*b*; this is because the bundle of internal-relaxation eigenvalues is so well separated from the reaction-rate eigenvalue, and of course, as far as thermal unimolecular reactions are concerned, we are not interested in the eigenvalue behaviour elsewhere on these diagrams. In physical terms, the set of probabilities given by [42] will lead to a population evolution in which there are no fluctuations during the transient phase (42), but since we are interested only in the steady state in considering thermal unimolecular reactions, this artefact is unlikely to have serious consequences. On the other hand, examination of [42] reveals that the probability of an inelastic transition from state i to state j is proportional to the equilibrium population of the final state: this means that [42] will tend to overestimate the probabilities of transitions to states of high j, and we will return to a discussion of this problem later in the paper.

VII. The Unimolecular Rate Constant, k_{uni}

We are now interested in the way in which the presence of predissociation terms perturbs the solutions of [42]. In the absence of any perturbation, the behaviour of these solutions is very simple (16), namely that both the total energy $\xi(t)$ and each of the individual populations $n_i(t)$ evolve in a pure-exponential way, i.e.

$$[43] \quad \frac{\mathrm{d}\xi(t)}{\mathrm{d}t} = \mu[\xi(t) - \tilde{\xi}]$$

$$[44] \quad n_i(t) = \tilde{n}_i + [n_i(0) - \tilde{n}_i]\mathrm{e}^{-\mu t}$$

Making use of the orthogonality relations between the vectors, together with eq. 15, it then follows that if we have r decay channels present, eq. 22 for the perturbed eigenvector elements simplifies to

$$[45] \quad \psi_{k,n-1} = \tilde{n}_k^{1/2}\gamma_{n-1}^{-1}\sum_l \tilde{n}_l^{1/2} d_l \psi_{l,n-1} + \mu^{-1}\sum_l (\delta_{kl} - \tilde{n}_k^{1/2}\tilde{n}_l^{1/2}) d_l \psi_{l,n-1}$$

where the index l runs over only the predissociating states. Extracting k_{uni} (i.e. $-\gamma_{n-1}$) out of this set of r equations, we have

$$[46] \quad k_{\mathrm{uni}} = \frac{\sum_{i=1}^{r} a_i[\mu\mathrm{M}]^{1-i}}{1 + \sum_{i=1}^{r} b_i[\mu\mathrm{M}]^{-i}}$$

with

$$[47a] \quad a_i = \sum_{\{i\}}^{\{r\}} [(\sum \tilde{n}_j) \cdot (\prod k_j)]$$

$$[47b] \quad b_i = \sum_{\{i\}}^{\{r\}} [(1 - \sum \tilde{n}_j) \cdot (\prod k_j)]$$

where $\sum_{\{i\}}^{\{r\}}$ refers to summation over the $\left\{ {r \atop i} \right\}$ combinatorial terms and the summations and products are over the combinatorial elements.[2] Equation 46 can clearly be regarded as a generalised Lindemann equation, but not the conventional generalised form [27].

In a real system, where there are millions of either discrete or quasi-continuous decay channels, eqs. 46 and 47 would become hopelessly cumbersome. It is therefore necessary to group the decay channels into

[2]The combinatorial terms appearing in eqs. 47*a* and 47*b* are defined as follows, for example

$$a_2 = \sum_{\{2\}}^{\{r\}} \left[\left(\sum_j \tilde{n}_j \right) \cdot \left(\prod_j k_j \right) \right]$$
$$= k_1k_2(\tilde{n}_1 + \tilde{n}_2) + k_1k_3(\tilde{n}_1 + \tilde{n}_3) + \ldots + k_1k_r(\tilde{n}_1 + \tilde{n}_r) + k_2k_3(\tilde{n}_2 + \tilde{n}_3) + \ldots + k_2k_r(\tilde{n}_2 + \tilde{n}_r) + \ldots + k_{r-1}k_r(\tilde{n}_{r-1} + \tilde{n}_r)$$

Can. J. Chem. Downloaded from www.nrcresearchpress.com by 210.87.254.42 on 09/05/12
For personal use only.

pseudo-levels, much in the same way as has been done previously in earlier master-equation formulations (5, 6, 14). However, in previous formulations, the graining procedure has been considered to apply to all states of the molecule, both reactive and unreactive, whereas here, we only need to coarse-grain the reactive levels into pseudo-levels: this is because, *in this approximation*, the information relating to the internal relaxation of the unreactive states has been incorporated into [46] through the use of [45]. This graining procedure is depicted schematically in Fig. 4, which is drawn in such a way as to emphasise the fact that the grain sizes need not correspond to equal energy gaps; the grain widths can be chosen in any way which optimises the calculation with respect to truncation errors and computing costs. In practice, the choice of the number of grains required and the grain widths is straightforward, and is based on the following observations. The first is that for all the reactions considered, 99% of the total rate comes from states within 30 kcal mol^{-1} of the threshold, whatever the pressure, so that the summations in [46] can be terminated at about this energy. The second goes back to our earlier observation that if only one decay channel is present, the calculated fall-off curve is Lindemann in form, but as more decay channels are included in the calculation, the fall-off curve becomes more gradual (corresponding to a higher value of the Kassel shape parameter s) (14). This behaviour is shown in Fig. 5 for cyclopropane at 490°C with

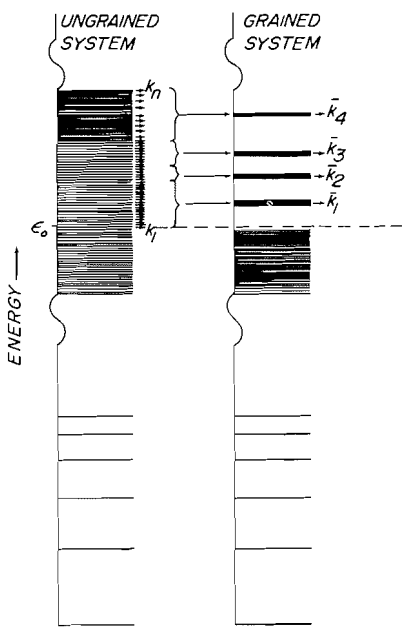

FIG. 4. Schematic representation of the graining procedure. Only the reactive states are grouped. The grain-widths need not be equal in energy.

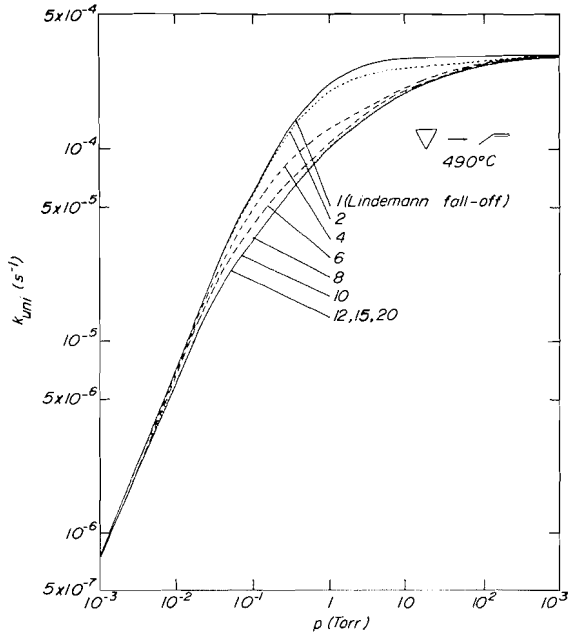

FIG. 5. Calculated fall-off curves for the isomerisation of cyclopropane at 490°C with r = 1, 2, 4, 6, 8, 10, 12, 15, and 20 pseudolevels. The last four curves are graphically indistinguishable. The first (r = 1) curve is exactly Lindemann in form. $A_\infty = 1.88 \times 10^{15}$ s^{-1}, ε_∞ = 65.6 kcal/mol.

r = 1, 2, 4, 6, 8, 10, 12, 15, and 20 decay channels: the calculated fall-off behaviour rapidly 'converges' as r increases, and in no case have we found it necessary to use more than 15 pseudo-levels to represent the spectrum of reactive states.

The use of this grouping procedure necessitates some redefinition of the meanings of terms used in eqs. 46 and 47 where the summations and products are over the individual predissociating states. For the ungrained system, the low-pressure and high-pressure limiting forms of the rate constant are

$$[48] \quad \lim_{[M]\to 0} k_{uni}(M) \equiv k_{bim}[M] = \mu \sum_r \tilde{n}_r/(1 - \sum_r \tilde{n}_r)$$

$$[49] \quad \lim_{[M]\to \infty} k_{uni}(M) \equiv k_\infty = \sum_r \tilde{n}_r k_r$$

If we let $\bar{n}_r$ and $\bar{k}_r$ be the *grouped* equilibrium population and decay constant respectively for the *grained* system, we require that

$$[50] \quad \lim_{[M]\to 0} k_{uni}(M) = \mu \sum_j \bar{n}_j/(1 - \sum_j \bar{n}_j)$$

$$[51] \quad \lim_{[M]\to \infty} k_{uni}(M) = \sum_j \bar{n}_j \bar{k}_j$$

where the summations are now over the *grained* 'pseudo-levels'. Equations 48–51 may be satisfied if

Can. J. Chem. Downloaded from www.nrcresearchpress.com by 210.87.254.42 on 09/05/12
For personal use only.

we have, for each grain

$$[52] \qquad \bar{n}_j = \sum_l \tilde{n}_l$$

$$[53] \qquad \bar{k}_j = \sum_l \tilde{n}_l k_l / \bar{n}_j$$

where the summations l in [52] and [53] are only over the levels within each grain. Explicitly,

$$[54] \qquad \bar{n}_j = [\mathcal{Q}(\beta)]^{-1} \sum_{\varepsilon_l = \varepsilon_j}^{\varepsilon_{j+1}} g_l \exp(-\beta\varepsilon_l)$$

$$[55] \qquad \bar{k}_j = A_\infty [\mathcal{Q}(\beta)\bar{n}_j]^{-1} \exp(-\beta\varepsilon_\infty) \times \sum_{\varepsilon_l = \varepsilon_j - \varepsilon_\infty}^{\varepsilon_{j+1} - \varepsilon_\infty} g_l \exp(-\beta\varepsilon_l)$$

However, as we will discuss further below, the mean width $\Delta\varepsilon$ of the predissociating levels (arising from the uncertainty principle) is several orders of magnitude greater than the mean spacing between the levels for the molecules considered here (i.e. $\rho(\varepsilon) \cdot \Delta\varepsilon \gg 1$), so that [54] may readily be written in integral form, viz.

$$[56] \qquad \bar{n}_j = [\mathcal{Q}(\beta)]^{-1} \int_{\varepsilon_j}^{\varepsilon_{j+1}} \rho(\varepsilon) \exp(-\beta\varepsilon)\, d\varepsilon$$

where we define

$$[57] \qquad \rho(\varepsilon) = \sum_i P(\varepsilon_i)\delta(\varepsilon - \varepsilon_i)$$

$\delta(\varepsilon)$ being the Dirac delta function and the summation goes over all states i. Similarly [55] may be written as

$$[58] \qquad \bar{k}_j = A_\infty [\mathcal{Q}(\beta)\bar{n}_j]^{-1} \exp(-\beta\varepsilon_\infty) \times \int_{\varepsilon_j - \varepsilon_\infty}^{\varepsilon_{j+1} - \varepsilon_\infty} \rho(\varepsilon) \exp(-\beta\varepsilon)\, d\varepsilon$$

Thus, the final expression for k_{uni} remains as eq. 46, but the expressions [56] and [58] for $\bar{n}_j$ and $\bar{k}_j$ are used in [47a] and [47b] instead of $\tilde{n}_j$ and k_j, and the index r is reinterpreted to be the number of pseudo-channels. For the remainder of this paper, for the reasons just mentioned above, the distinction between the discrete form for $k(\varepsilon)$, eq. 33, and the continuous form, eq. 41, will be relaxed, and [33] and [41] will be used interchangeably.

A major advantage of this computational scheme is that once the grain size and the number of grains (usually 15) have been chosen, the unimolecular rate constant k_{uni} at any pressure can be evaluated explicitly, and the calculation needs not be started anew, as is the case with RRKM (and RRK) procedures, for each pressure: this is one of the two reasons why our method is so much more economical in computer time than the pre-existing procedures; the other reason is that our new procedure for calculating densities and sums of states (43) can be up to two orders of magnitude faster than existing methods for complex molecules.

VIII. Which States to Count?

Our reformulation of unimolecular reaction theory is now complete, in a formal sense, the relevant equations being [46], [47a], [47b], [56], and [58]; however, the latter two equations contain the state-degeneracy of the molecule in the non-reactive region, and the density of states of the molecule in the reactive region. Tracing back the origins of this involvement of $P(\varepsilon)$ and $\rho(\varepsilon)$, it arises in our approach as part of a semi-empirical estimate (eq. 33) for the predissociation rate constants of the reactive states of the molecule, and our subsequent approximation using $\rho(\varepsilon)$ for $P(\varepsilon)$ in [57] which reduces [33] to the continuous form [41]. We have yet to consider in this context the problem of counting states, and to decide, for example, whether rotational or vibrational states can be regarded as making equal contributions to $k(\varepsilon)$. Consequently, we have to examine the interrelationship between the state density and the fall-off properties for a molecule.

It has been recognised since the early days of unimolecular reaction theory that both the position and curvature of the fall-off curve are related to the complexity of the molecule. Usually, the number of atoms in the molecule, or the number of vibrational degrees of freedom, is used as an indicator of this complexity, but in fact we are really dealing with a manifestation of the *distribution* of state density in the molecule; a more useful measure of the complexity would be the number of vibrational degrees of freedom weighted by the reciprocals of their respective fundamental frequencies. The more complex a molecule is, the more vibrational degrees of freedom (of lower average frequency) it has, and hence the more drastic its increase in state density with energy. This causes the fall-off in unimolecular reaction rate with decreasing pressure to be more gentle in two ways. First, there are relatively more reactive states accessible by collisional or intramolecular energy transfer, so that at low pressure there will be a relatively higher rate of reaction, and hence a less drastic fall-off. Second, the more complex the molecule, the smaller is the ratio $P(\varepsilon - \varepsilon_\infty)/P(\varepsilon)$ in eq. 33; thus, for fixed values of A_∞ and ε_∞, $k(\varepsilon)$ is smaller and the depletion of population by reaction at any particular pressure is not as severe.

It is of interest to note earlier attempts to characterise the fall-off behaviour of a unimolecular reaction in terms of the complexity of the reactant molecule, along such lines. These include the semi-empirical interpretation of the effective oscillator num-

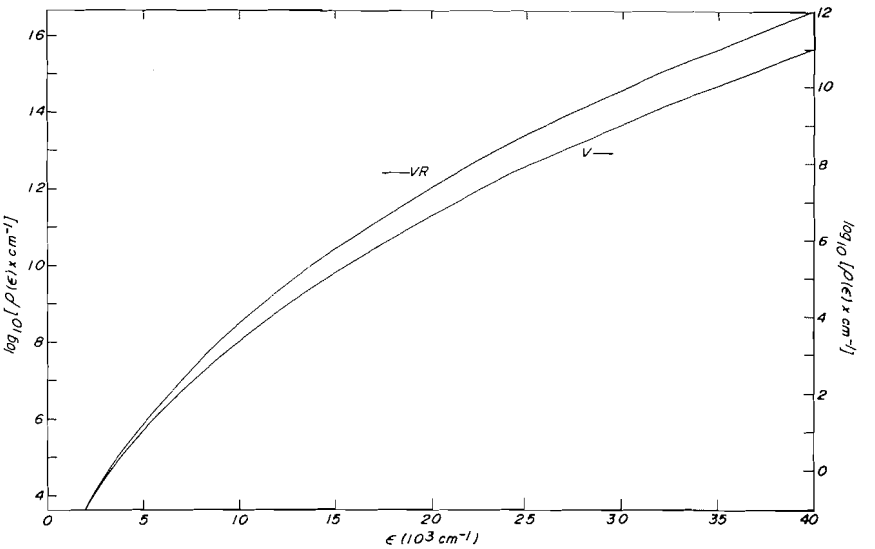

FIG. 6. Vibrational (V) and vibration–rotational (VR) state density of cyclopropane, using spectroscopic data in Appendix 3.

ber s in the Kassel integral in terms of the specific heat of the molecule (44), which is of course related to the distribution of energy levels (and the state density) in the molecule (43). The effective oscillator number s is no more than a fitting parameter (44, 45) whose role is essentially to calibrate the state density (albeit a classical and an inadequate one) of the reactant molecule. Yet the fact that most reactions consistently have a value of s equal to about half of the number of vibrational degrees of freedom tends to confirm the central role of state density in determining the fall-off behaviour, without the need to postulate additional parameters.

In conventional unimolecular rate theories, it has been customary to model a molecule as a collection of independent harmonic oscillators despite two longstanding difficulties. The first one is conceptual: a molecule consisting of pure harmonic oscillators can undergo neither dissociation nor internal energy randomisation. The second one is practical; until recently, fast, reliable methods for calculating state sums and state densities have been restricted to harmonic oscillators (46–48) and the apparent agreement between experiment and theory has certainly led to general acceptance of the harmonic oscillator model over the years, although this agreement has puzzled some authors (49). The actual distribution of states in a molecule is still very much unknown, especially at high energy. However, with the recent development of very efficient computational procedures for the calculation of state densities and state sums, both for harmonic and anharmonic oscillators (43, 50, 51), it is now possible to examine the consequences of assuming such models, with and without rotation, and for a wide range of reactions.

Certainly rotational effects are important in diatomic dissociation (20), and rotational predissociation of polyatomic molecules, although poorly documented, is believed to be a common process (52). Indeed, there are no arbitrary reasons to exclude rotation, in the sense that in the transition probability matrix [42], the a_{ij} elements can equally well be regarded to exclude or include rotational transitions, either alone or simultaneously with vibrational transfer. The density of states for cyclopropane in the interesting energy range is shown in Fig. 6, both with and without rotation. It can be seen that the inclusion of rotational degrees of freedom increases the state density at high energy, and also changes the shape of the state-density curve: this will lead to a shallower fall-off curve, and a shift in the position of the fall-off to lower pressure for a fixed value of $\bar{\lambda}$.[3]

The consequence of inclusion of anharmonicity in the model reactant molecule is less obvious. Yet, it is clear that a minimal description of any unimolecular reaction should treat the molecule, at the very least, as a collection of independent *anharmonic* oscillators. This certainly would be more realistic than the usual harmonic oscillator approximation,

[3]The fall-off behaviour is, however, insensitive to the rotational constants of the molecule: indeed, in the present treatment, using the classical approximation for the rotational partition function and the steepest-descent method (53), the rotational constants only appear as multiplicative factors in $\rho(\varepsilon)$ and $G(\varepsilon)$, and they drop out of the final expression for k_{uni}.

Can. J. Chem. Downloaded from www.nrcresearchpress.com by 210.87.254.42 on 09/05/12
For personal use only.

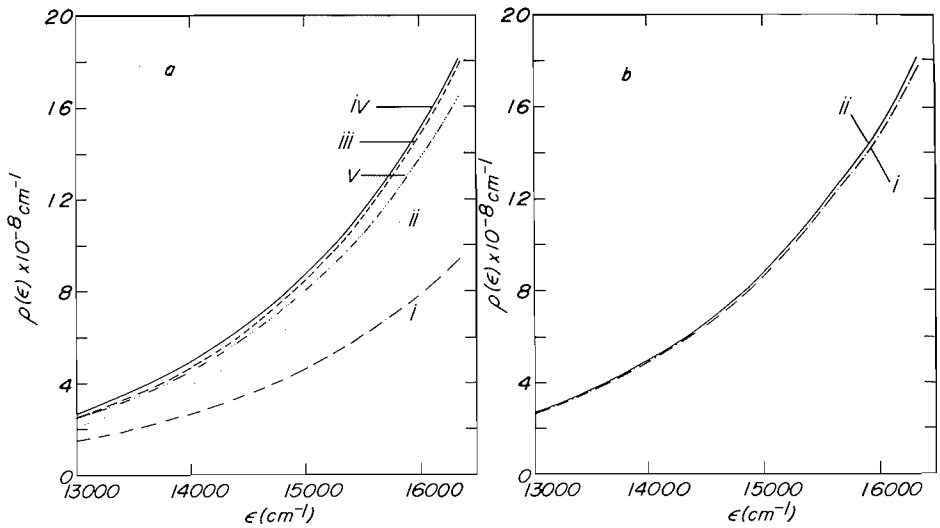

FIG. 7. (*a*) State density of methyl isocyanide in the reactive energy range, with the molecule modelled as (*i*) a set of harmonic oscillators and (*ii*)–(*v*) a set of independent Morse oscillators with $\nu_s = 263$ cm^{-1} and $x_s = 0, 0.01, 0.02$, and 0.03 respectively. All frequencies and anharmonicity factors are given in Appendix 3. All curves are essentially the same shape. (*b*) Variation of state density of methyl isocyanide in the reactive energy range with the anharmonicity factor of high-frequency vibrational mode $\nu_1 = 2966$ cm^{-1}; $x_1 = 0$ (*i*) and 0.08 (*ii*) respectively. All other frequencies and anharmonicity factors are given in Appendix 3. Curves for $0 < x_1 < 0.08$ fall in between (*i*) and (*ii*).

and would remove the conceptual difficulties noted above: on the other hand, the longstanding success of harmonic oscillator models would appear to suggest that the additional complexity might be unnecessary, either because the fall-off behaviour is too insensitive to the anharmonicity, or else because of some fortuitous cancellation of errors. Moreover, anharmonicity data are very limited (54) indeed for the complex molecules of interest here, and so it is necessary to undertake a thorough examination of the effects of anharmonicity before we can have any confidence in the theoretical predictions. The information on anharmonicities that is available comes from first-overtone measurements and/or approximate theoretical calculations (55), and it would appear that with few exceptions, regarding the vibrations as Morse oscillators of frequency ν_i, anharmonicity factors x_i lie in the range of 1–3%, i.e. $0.01 \leq x_i \leq 0.03$ (see Appendix 3 for definitions of ν_i and x_i). Qualitatively, the effect of introducing this anharmonicity is to increase the state density in the intermediate energy range, but to reduce it at high energies, since the set of energy levels now converges to a maximum value of the vibrational quantum number $v_{i,\max}$. Given the typical values of x_i, $v_{i,\max}$ will commonly be between 15 and 50. In order to focus our attention on the nature of the problem, we may subdivide the vibration frequencies of molecules roughly into three classes, those around 300, 1000, and 3000 cm^{-1}. We note that the interesting energy range for thermal unimolecular reactions is between 10 000 and 25 000 cm^{-1}: for example, the Arrhenius activation energy for the isomerisation of methyl isocyanide is about 13 360 cm^{-1}; states in this energy range could either have only very few high-frequency quanta, or at the other extreme, some tens of low-frequency quanta. It follows therefore that the calculated state density $\rho(\varepsilon)$ will not be very sensitive to variations in the anharmonicity factors for the high-frequency modes, but might be so for the low-frequency modes. No systematic study of this point has been reported in the literature, to our knowledge. We have therefore presented in Appendix 2 (and Figs. 7 and 8) such an analysis for methyl isocyanide and cyclopropane.

With the results displayed in Figs. 6–8, we can summarise the conclusions of this section as follows. The complexity of a reactant molecule can be identified with the distribution of energy states of the molecule, particularly at high energy, and this complexity property determines the shape of the fall-off curve, and also, more-or-less, its position. Through the operation of eqs. 46, 47, 56, and 58, the *shape* of the state-density function determines the *shape* of the fall-off curve, and the *magnitude* of the state density in the interesting energy range determines the *position* of the fall-off curve on the pressure axis, to within a factor of $\bar{\lambda}$. Clearly then, the position and shape of the fall-off curve are related, although not explicitly. Also, the calculated form of k_{uni} will depend upon whether $\rho(\varepsilon)$ is determined assuming harmonic or anharmonic oscillators, with or without rotation: as

Can. J. Chem. Downloaded from www.nrcresearchpress.com by 210.87.254.42 on 09/05/12
For personal use only.

Can. J. Chem. Downloaded from www.nrcresearchpress.com by 210.87.254.42 on 09/05/12
For personal use only.

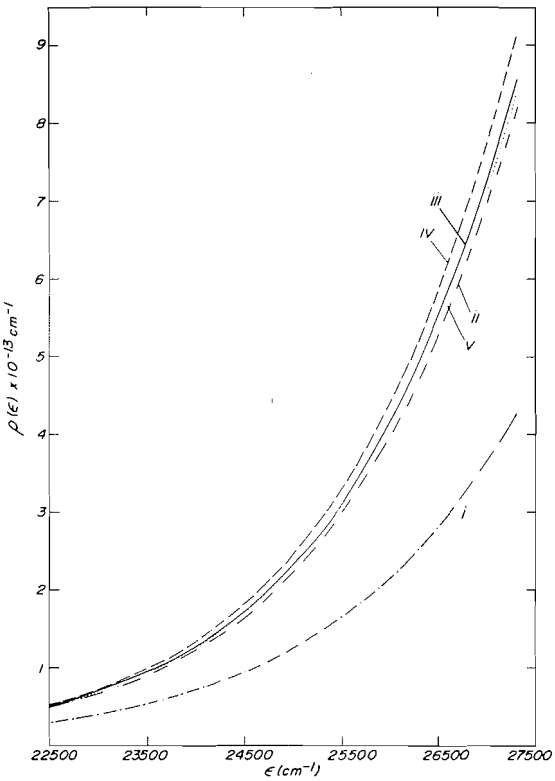

FIG. 8. Variation of state density of cyclopropane in the reactive energy range with the anharmonicity factor of the rocking mode (ν_8 = 854 cm^{-1}). (*i*) Harmonic-oscillator model (all modes); (*ii*)–(*v*) Morse-oscillator model (see Appendix 3), with x_8 = 0, 0.015, 0.03, and 0.09 respectively.

we shall find in the following sections, the best agreement between theory and experiment always results from the anharmonic oscillator model, with rotation. Fortunately, the sensitivity of the results to small imperfections in the assumed model is not great. Consequently, if the anharmonicity factors x_i can be estimated to within ± 0.01, the shape of the $\rho(\varepsilon)$ function will be of acceptable accuracy, and the absolute magnitude of the $\rho(\varepsilon)$ function in the interesting energy range (which determines the pressure shift $\bar{\lambda}$) will be correct to within about 30–50%. Similarly, imperfections in calculating the rotational contribution to $\rho(\varepsilon)$ will also be relatively unimportant: the model system of independent rotors and oscillators is an acceptable approximation.

IX. Comparison with Experiment

In most cases, experimental tests of the theory of unimolecular reactions have been confined to a comparison of the shapes of the experimental and theoretical fall-off curves; however, for some reactions, additional important information is available, namely the variation of the Arrhenius temperature coefficient and/or of the kinetic isotope effect with pressure. In this section we will show that our reformulation gives consistently better agreement with experiment than do any existing theories of unimolecular reactions for five important thermal unimolecular reactions. In fact, a thorough test of the theory is only possible for the isomerisation of cyclopropane, because this is the only molecule for which fairly complete anharmonicity data are available, and it is from the detailed examination of this reaction that we came to the conclusions of the preceding section: that our state count must refer to anharmonic oscillators and include all rotational degrees of freedom. Guided by the anharmonicity data for cyclopropane, we have deduced a set of rules for *estimating* anharmonicity factors for other molecules (see Appendix 3): with these estimated anharmonicity factors, our method gives virtually exact agreement with experiment for the thermal decompositions of cyclobutane and ethyl chloride, and it gives better agreement than exists at present for the isomerisations of methyl isocyanide and ethyl isocyanide (and in these two cases, we believe there may be valid reasons for the remaining discrepancies). The required molecular constants and other parameters are collected together in Appendix 3 and straightforward and efficient computer programs for the calculation of k_{uni} therefrom are described in Appendix 4. In this section, we will confine our attention to the description of the results of these calculations, and the comparison of the computed results with experiment; for the sake of brevity we will take as read earlier extensive comparisons of this nature, particularly those of Wieder and Marcus (3, 4), Lin and Laidler (56), and Robinson and Holbrook (5).

A. The Shape of the Fall-off Curve

Figure 9 shows the experimental results for the thermal isomerisation of cyclopropane at 490°C, obtained by Pritchard, Sowden, and Trotman-Dickenson (57, 58), compared with three model calculations for k_{uni}. The model calculations use the spectroscopic constants of Cyvin (55), the value of ε_∞ found by Falconer, Hunter, and Trotman-Dickenson (59), a value of k_∞ found by extrapolating k vs. $1/p$ (58), and A_∞ consistent with k_∞ and ε_∞ (see Appendix 3 for details). The dotted line shows a conventional RRKM calculation with these parameters (5), using harmonic oscillators and no rotation. The dashed curve shows the results of the present reformulation, again using harmonic oscillators with no rotation; the difference between these two curves stems, in part, from the difference between eq. 27 and eq. 46 and, in part, from the difference in the respective forms of the $k(\varepsilon)$ function (cf. Fig. 2). Thirdly, the

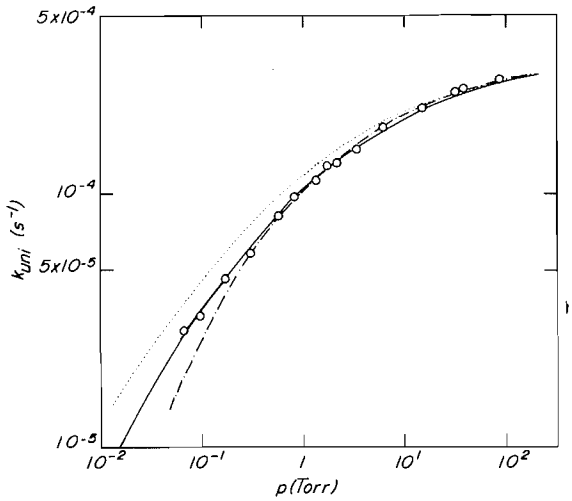

FIG. 9. Thermal isomerisation of cyclopropane at 490°C: ○ Experiment of Pritchard, Sowden, and Trotman-Dickenson (57, 58); ··· RRKM theory, with the antisymmetric CH stretch ($\nu = 3103$ cm^{-1}) mode isolated as reaction coordinate; -·-· this formulation, harmonic oscillator; — this formulation, rotating Morse oscillator.

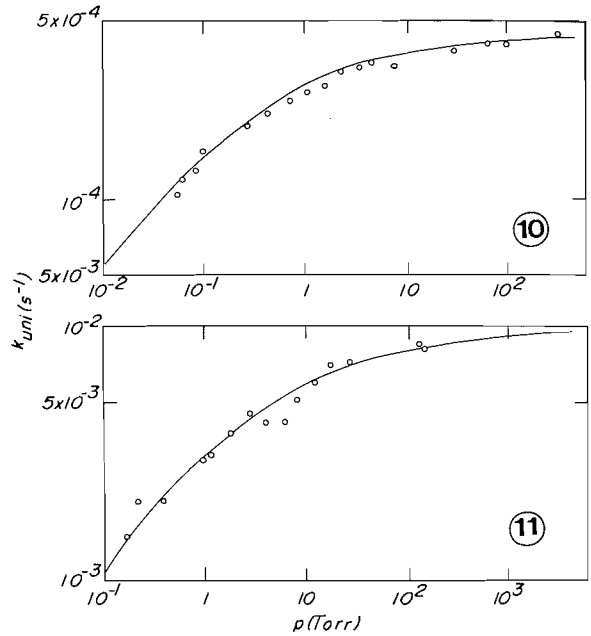

FIG. 10. Thermal decomposition of cyclobutane at 448.3°C: ○ Experiment of Pritchard, Sowden, and Trotman-Dickenson (58, 60); — calculation, eq. 33.

FIG. 11. Thermal decomposition of ethyl chloride at 521°C: ○ Experiment of Holbrook and Marsh (64); — calculation, eq. 33.

solid line shows the results of the present reformulation using Morse oscillators and including rotation: other alternative choices, viz. Morse oscillators without rotation or harmonic oscillators with rotation are not as good, and are omitted for the sake of clarity. We remind the reader at this point that all three theoretical curves in Fig. 9 have been subjected to a lateral (pressure) shift in order to bring them into the best coincidence with the experimental data: the magnitudes of these shifts will be discussed separately below.

Figure 10 shows the experimental results for the thermal decomposition of cyclobutane to two ethylene molecules at 448°C, again obtained by Pritchard, Sowden, and Trotman-Dickenson (58, 60); other experimental data are very closely coincident (5, 61, 62) and are omitted for clarity. The solid line represents the form of k_{uni} calculated from the present reformulation, suitably shifted, and using the molecular constants and reaction-rate parameters given in Appendix 3.

Another reaction which has attracted much attention is the thermal decomposition of ethyl chloride to form ethylene and hydrogen chloride (5); the data are, however, much more scattered than the cyclopropane or cyclobutane data, and not always concordant (5, 63). Figure 11 shows the experimental data of Holbrook and Marsh (64) at 521°C, compared with our calculated form of k_{uni}; the agreement is equally satisfactory at other temperatures also, but unfortunately, because of the scatter inherent in the experimental measurements, does not provide a very stringent test of this reformulation.

The thermal isomerisation of methyl isocyanide to methyl cyanide represents, to date, the most thoroughly studied unimolecular reaction (5, 9, 34). The fall-off behaviour was first studied by Schneider and Rabinovitch (9) at 200, 230, and 260°C; they also derived the infinite-pressure Arrhenius parameters as $A_\infty = 10^{13.6}$ s^{-1} and $\varepsilon_\infty = 38.4$ kcal mol^{-1}. Unfortunately, the isomerisation is an exothermic reaction, and corrections had to be applied to the high-pressure data to allow for self-heating. Collister and Pritchard (34) have recently studied this reaction over the temperature range 120–320°C, in the rigorous absence of self-heating. The highest pressure they used in any of their experiments was 100 Torr and in the region of overlap of the two studies, i.e. $2 \leq p \leq 100$ Torr, $200 \leq T \leq 260$°C the agreement is excellent. Collister and Pritchard extrapolated their rate data (using an iterative RRKM procedure to find the most consistent set of ε_∞ and k_∞) to give $A_\infty = 10^{13.35\pm0.11}$ s^{-1} and $\varepsilon_\infty = 38.2 \pm 0.2$ kcal mol^{-1}, apparently in excellent agreement also with the values given by Schneider and Rabinovitch; however, Schneider and Rabinovitch's values of k_∞ are about 50% greater than those of Collister and Pritchard, which complicates the comparisons somewhat.

Schenider and Rabinovitch (9) examined a whole series of reaction models, but were never able to obtain consistent agreement between the theoretical and

Can. J. Chem. Downloaded from www.nrcresearchpress.com by 210.87.254.42 on 09/05/12
For personal use only.

Can. J. Chem. Downloaded from www.nrcresearchpress.com by 210.87.254.42 on 09/05/12
For personal use only.

experimental fall-off curves (cf. also ref. 5), nor were the pressure shifts monotonic (as they would be expected to be) at the three experimental temperatures. The shape of the fall-off at 230°C has been re-examined by Forst (23, 24) confirming that the experimental and theoretical shapes are not the same. Figure 12 shows the theoretical fall-off curve calculated by our new procedure, including anharmonicity and rotation, together with the experimental points of Schneider and Rabinovitch (9); again, the calculated and experimental curves do not have the same shape, and in the way we have adjusted the pressure shift, there seems to be a sudden rise in the rate constant above 300 Torr. We believe there could be a logical explanation of this observation. Schneider and Rabinovitch estimated the degree of self-heating in their high-pressure reactions on the basis of a ΔH of isomerisation of -15 kcal mol^{-1} and a thermal conductivity of 0.25 mW cm^{-1} deg^{-1}. We have recently remeasured both ΔH as -23.70 ± 0.14 kcal mol^{-1} (65) and the thermal conductivity, about 0.20 mW cm^{-1} deg^{-1} at 230°C (66), which implies that all of the correction factors for self-heating estimated by Schneider and Rabinovitch are *too small by about a factor of two*. It seems likely that if sufficient *raw* experimental data are still available to enable these self-heating corrections to be calculated properly, some of the present discrepancies might be eliminated. As will be shown below, our calculated curve for k_{uni} fits the data of Collister and Pritchard (34)

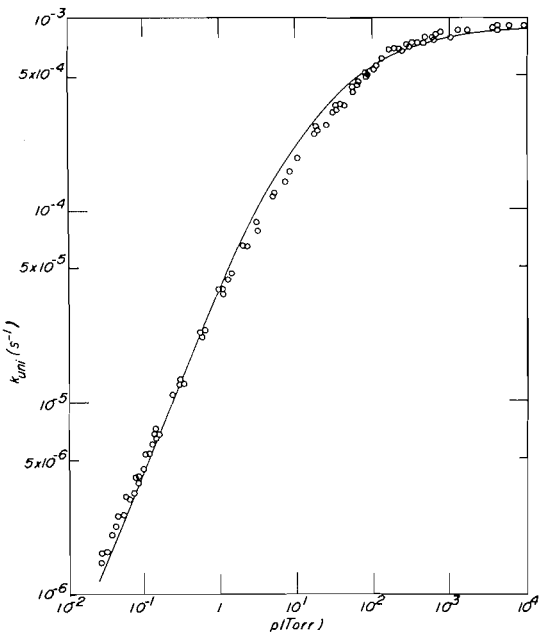

FIG. 12. Thermal isomerisation of methyl isocyanide at 230.4°C: ○ Experiment of Schneider and Rabinovitch (9);— calculation, eq. 33.

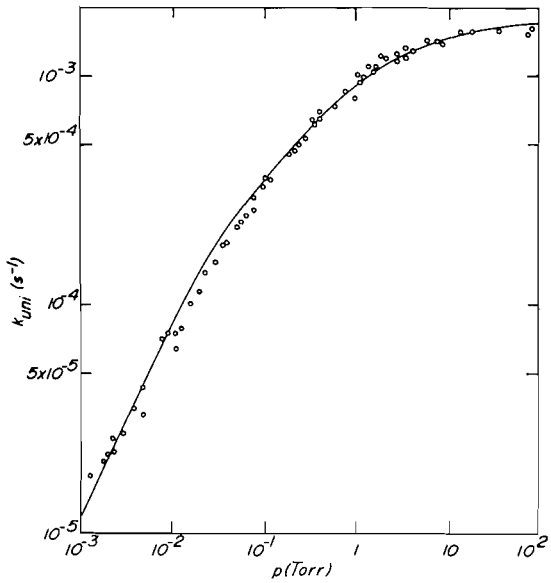

FIG. 13. Thermal isomerisation of ethyl isocyanide at 230.9°C: ○ Experiment of Maloney and Rabinovitch (10);— calculation, eq. 33.

very well, but in view of the short pressure range of this work ($2 \leq p \leq 100$ Torr), this again is not a very stringent test of the new theory.

Figure 13 shows the experimental data of Maloney and Rabinovitch (10) for the thermal isomerisation of ethyl isocyanide at 231°C, plotted together with the theoretical k_{uni} curve calculated from the present reformulation. There is a similar discrepancy to that shown for methyl isocyanide in Fig. 12, which again could be interpreted as an unexpected rise in the experimental rates above 1 Torr. As before, the self-heating corrections are suspect, and should be re-evaluated on the basis of the new value for ΔH (about -22 kcal mol^{-1}) (65) and a new estimate for the thermal conductivity; however, self-heating should not be important at pressures as low as 1 Torr, so there may be other, as yet undiscerned, reasons for this poor agreement.

B. The Position of the Fall-off Curve

As we noted earlier, and in common with other theories of unimolecular reactions, the calculation of k_{uni} does not establish the absolute position of the fall-off curve on the pressure axis. In conventional theory, a collisional deactivation efficiency parameter λ is used to move the calculated fall-off curve along the pressure axis to obtain the best fit with the experimental data. However, this collision efficiency parameter has two disconcerting properties.

The first is that it either varies widely with temperature, or does not vary in a monotonic fashion with temperature, and thus it does not appear to have the kind of properties required of an energy-

transfer probability. For example, for 1,1-dichlorocyclopropane (5), a value of $\lambda = 1.0$ would appear to be satisfactory near 360°C, whereas $\lambda = 0.4$ fits the data better at 425°C: in view of the common occurrence of values of λ of the order of unity, this large variation over such a short temperature range seems surprising. Better documented examples come from experiments on the methyl isocyanide and ethyl isocyanide isomerisations where the pressure correction factors (with the 'E-300' model) (9, 10) at three consecutive temperatures are CH_3NC: 0.91, 1.11, and 0.95; C_2H_5NC: 0.88, 1.37, and 1.25 respectively. It seems unlikely that energy-transfer collision efficiencies would vary in this random fashion, and it is not entirely clear to us whether recalculation of the self-heating corrections (alluded to above) would remove these anomalies altogether. That they are in fact anomalies is shown in Fig. 14 where we plot the data of Collister and Pritchard (34) for three different temperatures: the three lines which pass through the experimental data points all have the same value of the shift parameter $\bar{\lambda}$, and they all fit equally well. The representation of these agreements in this fashion does, however, require some amplification. We do not know how the relaxation time constant μ (cf. eqs. 42–44) for the internal relaxations varies with temperature: in the absence of more definite information, the least biased guess we can make is that $\mu = cT^{1/2}$ (note that $\mu = \bar{\lambda}Z[M]$), and it is this assumption that brings all the experimental data and the theoretical lines into coincidence with a single value of $\bar{\lambda}$. Clearly, if μ were assumed to be constant, the $\bar{\lambda}$ would be monotonic with temperature, unlike the earlier data (9, 10): thus, it seems that this particular difficulty may be mainly experimental in origin.

The second disconcerting property of the collision deactivation efficiency parameter λ is that it often seems to have a value very close to unity. The precise significance of λ is of course unclear because its numerical magnitude must depend upon the choice of the collision rate. It is well recognised that collision rates must be internal-state dependent, and that the 'structureless' collision numbers in common use represent nothing more than macroscopically averaged quantities. Clearly this averaging is very insensitive to the detailed distribution of collision efficiencies, and in the absence of more specific information, we can usually do no more than to use normal gas-kinetic collision diameters in calculating these collision rates (67). Given these difficulties, the occasional occurrence of values of λ slightly in excess of unity, by perhaps 10 or 20% (57, 60) is not alarming, and their observation has actually been interpreted as being supportive of the concept of unit deactivation probability (68). However, in very-low pressure experiments, where activation takes place predominantly at the wall rather than in gaseous collisions, molecule–wall collisions appear to be some 5–10 times as efficient as molecule–molecule collisions (11–13). Some doubts have been voiced about one of these experiments, and it was alleged (69) that the levelling off of the rate constant at low pressure, originally ascribed to wall activation, was really due to water vapour outgassing to a constant pressure from the vessel walls; the critics omitted to observe that a trap at −80°C was permanently in contact with the reaction vessel during each low-pressure run, in order to suppress unwanted pressures of both mercury and water vapours. Let us assume that accommodation coefficients for internal energy of complex molecules at the surface are of the order of 1 in a few collisions: to our knowledge, the only measurements which exist (70) relate to simple molecules at room temperature, but one can easily build an argument based

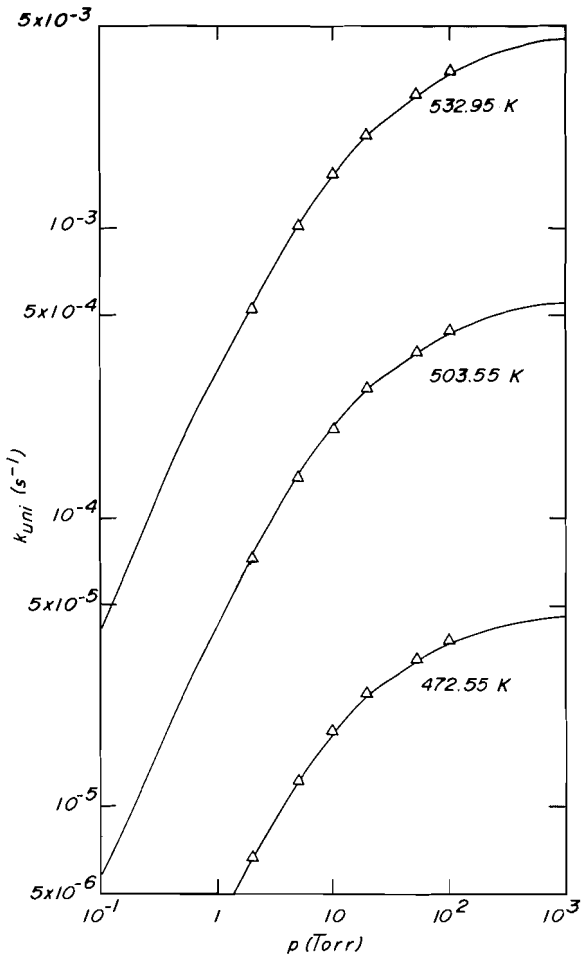

FIG. 14. Thermal isomerisation of methyl isocyanide at 472.55 K, 503.55 K, and 532.95 K. △ Experiment of Collister and Pritchard (34, 35); — eq. 33.

Can. J. Chem. Downloaded from www.nrcresearchpress.com by 210.87.254.42 on 09/05/12
For personal use only.

TABLE 1. Calculated collision efficiency parameters $\bar{\lambda}$

Molecule	T (K)	m (g/mol)	σ (Å)	$10^{10} \times Z$ (cm^3 molecule^{-1} s^{-1})	$10^{11} \times \mu'$ (cm^3 molecule^{-1} s^{-1})	$\bar{\lambda}$
CH_3NC	472.6	41.0	4.5	4.4_4	4.31	0.09_7
	503.6			4.5_9	4.86	0.10_6
	533.0			4.7_2	5.26	0.11_1
C_2H_5NC	504.1	55.1	5.5	5.9_2	6.91	0.11_7
C_3H_6	763.2	42.1	4.0	4.4	4.43	0.10
C_4H_8	721.5	56.1	4.5	4.7	4.22	0.09_9
C_2H_5Cl	794.2	64.5	4.5	4.6	4.77	0.10_4

on the results of these measurements in favour of our assumption. Accepting that the low-pressure kinetic experiments (11–13) demonstrate molecule–wall collisions to be almost an order of magnitude more efficient than molecule–molecule collisions, then we might guess that λ would lie in the range $10^{-1.5}$ to 10^{-1} and that, certainly, λ would not be unity as it generally appears to be in RRKM treatments.

The use of the master-equation formulation enables us to shed some light on this problem, although in a cascading relaxation system the concept of a collision efficiency is not always a well-defined one, since the observed relaxation time depends upon the initial distribution (17). However, it takes on a theoretical meaning when, as in our reformulation, the internal relaxation can be described by a single relaxation time: in our case, cf. eq. 42, the 'sum rule' is obeyed (16) whence, unambiguously

$$[59] \qquad \mu = \bar{\lambda} Z[\mathrm{M}] \quad \text{or} \quad \bar{\lambda} = \mu/Z[\mathrm{M}]$$

where Z, the collision number, is defined as in eq. 1, or since (cf. ref. 5, p. 164) M is usually another molecule of the same kind,

$$[60] \qquad Z = 4\sigma^2(\pi kT/m)^{1/2}$$

where m is the mass of the molecule. It is also convenient to define a relaxation rate constant

$$[61] \qquad \mu' = \mu/[\mathrm{M}] = \bar{\lambda} Z$$

Given the fact that there is excellent coincidence between the experimental and theoretical fall-off curves for the five molecules considered in this paper, the determination of μ' is straightforward, and the results are shown in Table 1. It appears that all the collision efficiency parameters $\bar{\lambda}$ are of the order of 0.1, which is certainly more in line with modern ideas about energy transfer (11–13, 70) than is the unit efficiency of the RRKM theory.

This could, however, be an artefact (but we think not). The a_{ij} in eq. 42 overestimate the importance of large-energy transitions with respect to small-energy transitions, so that all cascading processes coalesce into a single process; however, experiments on these molecules have not yet resolved the cascading processes, so clearly this contraction is reasonably acceptable. The effect of overemphasising large-energy transitions is clearly shown in Fig. 15 which shows the population depletion in the reactive region at low-pressure, i.e. $\tilde{n}_i/\tilde{n}_i$, so that the equilibrium distribution is represented by $\tilde{n}_i/\tilde{n}_i = 1$. It can be seen that the populations of states begin to fall away below the threshold ε_0, and in a real system should continue to fall away to zero at very high energies (5, 14); in our case, however, somewhat above the topmost predissociating state, the values of $\tilde{n}_i/\tilde{n}_i$ return to the equilibrium value, because of the strength of the large-energy transitions implicit in using [42]. This presents no difficulty in our numerical formulation though, since we continue to include predissociating states up to a sufficiently high energy that there is no further contribution to the total rate, as shown in the shaded portion of the diagram. The only point we make here, then, is that the interpretation of the physical meaning of $\bar{\lambda}$ still requires a little circumspection.

C. The Pressure Dependence of the Activation Energy

The pressure dependence of the activation energy provides a sensitive test for unimolecular rate theories. At any pressure p and inverse temperature β, the formal expression for the activation energy

$$[62] \qquad \varepsilon_{\mathrm{act}}(\beta;p) = -\mathrm{d} \ln k_{\mathrm{uni}}(\beta;p)/\mathrm{d}\beta$$

may be obtained directly using the Hellman–Feynmann theorem,

$$[63] \qquad \varepsilon_{\mathrm{act}}(\beta;p) = (k_{\mathrm{uni}})^{-1} \psi_{n-1}{}^T (\partial \mathbf{B}/\partial\beta) \psi_{n-1}$$

The evaluation of [63] for a general system is clearly a formidable task, although some general properties regarding the pressure dependence of $\varepsilon_{\mathrm{act}}$ have been derived by various authors (6, 71, 72). It is simpler, in fact, to compute $\varepsilon_{\mathrm{act}}$ directly from the analytic expression for k_{uni}, if it is available. Indeed, in the present treatment, since $\varepsilon_{\mathrm{act}}$ is only weakly temperature-dependent at all pressures (and independent of temperature at infinite pressure by virtue of the strict

Can. J. Chem. Downloaded from www.nrcresearchpress.com by 210.87.254.42 on 09/05/12
For personal use only.

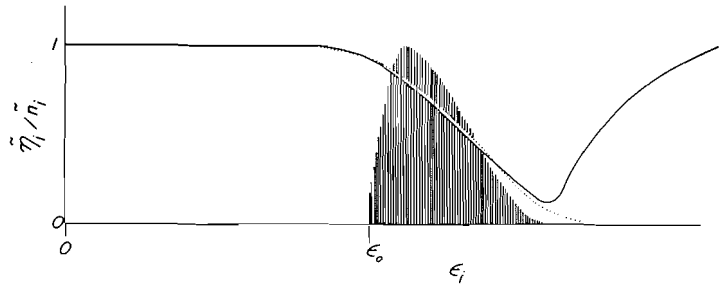

FIG. 15. Schematic representation of population depletion of states $\tilde{n}_i/\tilde{n}_i$ at low pressure as a function of reactant energy ϵ_i, in the $(n-1)$-fold degenerate system (solid line) and in a realistic system (dotted line). ϵ_0 is the critical energy. The shaded area is the distribution profile of reacting molecules.

Arrhenius behaviour), it may be computed from

$$[64] \quad \epsilon_{act}(\beta;p) = \frac{1}{\Delta\beta}\left\{1 - \frac{k_{uni}(\beta + \Delta\beta;p)}{k_{uni}(\beta;p)}\right\}$$

where $\Delta\beta$ is a small change in the inverse temperature β.

The most extensive data available on the pressure dependence of ϵ_{act} are for the thermal isomerisation of methyl isocyanide, from the work of Schneider and Rabinovitch (9) and of Collister and Pritchard (34); in the former work, the activation energy at low pressure was regarded as being temperature-independent, but in the latter work, ϵ_{act} was represented as being both pressure-dependent and temperature-dependent, as required by the present theoretical framework. Figure 16 compares the calculated values of ϵ_{act} from eq. 64 at 230°C with the experimental data of Collister and Pritchard (for that temperature) and of Schneider and Rabinovitch (mean values derived from Arrhenius plots over the range 200–260°C). The agreement between the present theory and experiment is excellent, and is superior to the RRKM description.

Figure 17 shows a similar comparison, using the experimental data of Maloney and Rabinovitch (10), for ethyl isocyanide: the solid line is the present theory, and the two dashed lines are those given by two RRKM models calculated by Maloney and Rabinovitch. The agreement here is not as good as it was for methyl isocyanide, but this is to be expected because the pressure shifts are more irregular for ethyl isocyanide (see preceding subsection). The present theory also gives a very good representation of $\Delta\epsilon_{act} = \epsilon_{act}(\infty) - \epsilon_{act}(0)$: Maloney and Rabinovitch estimated this to be about 4 kcal mol^{-1} compared with our calculated value of 4.5 kcal mol^{-1}.

Figure 18 compares theory and experiment for cyclobutane: the experimental data are deduced from the low-pressure rate constants of Vreeland and Swinehart (62) in the range 410–500°C and the high-pressure rate constants of Carr and Walters (73) between 419 and 460°C. The theoretical curve is calculated for 448°C, and the agreement is again excellent. However, the calculated value of $\Delta\epsilon_{act}$ cannot be compared satisfactorily with experiment because

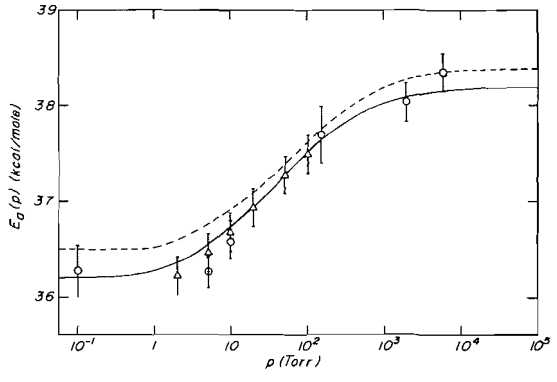

FIG. 16. Variation of activation energy ϵ_{act} with pressure of CH_3NC isomerisation at 230°C: ○ Experiment of Schneider and Rabinovitch (9); △ experiment of Collister and Pritchard (34); --- RRKM calculation (9) with ϵ_∞ = 38.4 kcal/mol; — present formulation, eq. 64 with ϵ_∞ = 38.2 kcal/mol; n.b. activation energy at low pressure is insensitive to the choice of ϵ_∞.

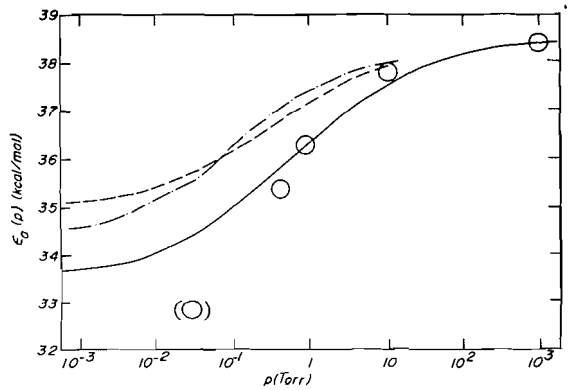

FIG. 17. Variation of activation energy ϵ_{act} with pressure of C_2H_5NC isomerisation at 231°C: ○ Experiment of Maloney and Rabinovitch (10); --- and -·-· RRKM calculations for two models (10); — present formulation, eq. 64.

Can. J. Chem. Downloaded from www.nrcresearchpress.com by 210.87.254.42 on 09/05/12
For personal use only.

Can. J. Chem. Downloaded from www.nrcresearchpress.com by 210.87.254.42 on 09/05/12
For personal use only.

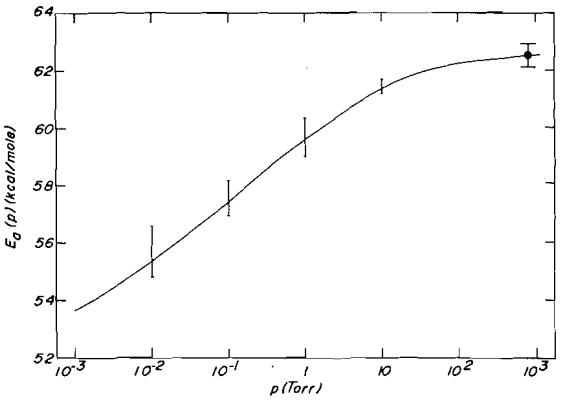

FIG. 18. Variation of activation energy ε_{act} with pressure for the decomposition of cyclobutane at 448.3°C. I value derived from experimental data of Vreeland and Swinehart (62) between 410 and 500°C; ‡ data of Carr and Walters (73); — present formulation, eq. 64.

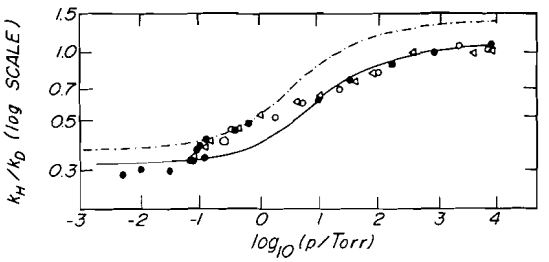

FIG. 19. Kinetic isotope ratio k_H/k_D of CH_3NC, CD_3NC isomerisation vs. pressure p. The three symbols refer to three different groups of experiments of Schneider and Rabinovitch (75). — Present formulation, eq. 65; ····· RRKM calculation using the 'E-300' model of Schneider and Rabinovitch (75).

of the abnormal levelling off of the rate data below 10^{-3} Torr.

Paradoxically, similar experiments have not been performed for cyclopropane: however, an approximation to $\Delta\varepsilon_{act}$ is available from the difference between the high-pressure (59) and low-pressure (11) activation energies, giving 8.4 ± 2 kcal mol^{-1} in the range 477–517°C compared with the theoretical value of $\Delta\varepsilon_{act}$ = 8.2 kcal mol^{-1}, at 490°C.

D. The Pressure Dependence of the Kinetic Isotope Effect

The kinetic isotope effect is an immediate consequence of any statistical rate theory based on molecular densities of states, such as the present formulation. The quantum-statistical effect at low pressure, from the RRKM point of view, has been described by Rabinovitch, Setser, and Schneider (74). Our reformulation, not unexpectedly, leads to a similar limiting form for the isotope ratio $\gamma = k_{uni,a}/k_{uni,b}$ (for isotopes a and b) at low pressure, except that the respective rates $k_{uni,a}(p \to 0)$ and $k_{uni,b}(p \to 0)$ are governed by the relaxation rate constants μ' rather than the collision numbers Z, whence

$$[65] \quad \gamma(p \to 0) = \frac{\mu_a' Z_b}{\mu_b' Z_a} \cdot \frac{\sum \bar{n}_{r,a}(1 - \sum \bar{n}_{r,b})}{\sum \bar{n}_{r,b}(1 - \sum \bar{n}_{r,a})}$$

Although Z_a and Z_b are simply related (via the square roots of the molecular masses), there is no need for μ_a' and μ_b' to be similarly related. However, since isotope-effect experiments are customarily performed by internal comparison, the required value of μ_a' would have to be that appropriate to the relaxation of species a by the mixture of isotopic molecules, and likewise for μ_b'; under these conditions, it seems likely that μ_a'/μ_b' would be close to unity, and with this simplifying assumption, the calculation of γ at all pressures is straightforward if the infinite-pressure Arrhenius parameters are known.

The isomerisation of trideuteriomethyl isocyanide has been studied by Schneider and Rabinovitch (75) at 230°C and over a range from 10^{-2} Torr to greater than 10^4 Torr; the isotope ratio γ varied from 0.28 at the low pressures to 1.07 at the highest pressures. The solid line in Fig. 19 shows the ratio $\gamma(p) = k_H(p)/k_D(p)$ calculated using eq. 65 and using the observed values of $\gamma(\infty)$ = 1.07 and $\varepsilon_{act,D}(\infty) - \varepsilon_{act,H}(\infty)$ = 0.1 kcal mol^{-1}. The dotted line is the 'E-300' RRKM model of Schneider and Rabinovitch (75) based on the same values of $\gamma(\infty)$ and $\Delta\varepsilon_{act}(\infty)$. The agreement with experiment of the reformulation, eq. 65 is again superior to that of the RRKM calculation, and considering the difficulties inherent in the experiments, may be regarded as, at least, satisfactory. Since the thermal conductivities and enthalpies of isomerisation will be very similar for the two isotopic species, the interpretation of these isotope-ratio experiments is probably not seriously jeopardised by possible errors in the self-heating corrections, to which we referred above.

X. Future Developments

This reformulation of the theory of unimolecular reactions removes the need to invoke such troublesome artefacts as the 'activated complex', the 'reaction coordinate', and the 'reaction path degeneracy'. One might ask why it is that RRKM theory, with all these hypothetical constructs, could have been so successful? Its use of the generalised Lindemann form [27] instead of the generalised Lindemann form [46] would obviously not be a major cause of error; likewise the use of a $k(\varepsilon)$ function rather like eq. 36 (based on the sum of states) rather than eq. 41 (based on the density of states) only has a minor effect, cf. Fig. 2. The basic reason why RRKM theory works so well is because, through the use of the entropy of activation to define the 'activated complex', the state

Can. J. Chem. Downloaded from www.nrcresearchpress.com by 210.87.254.42 on 09/05/12
For personal use only.

sum of the latter is increased from the state density of the molecule given by the harmonic oscillator approximation to a form more nearly like that given by the rotating anharmonic oscillator approximation (cf. Fig. 7*a*): this is usually achieved in conventional calculations by reducing the frequencies of some of the oscillators in the molecule (5). The fall-off behaviour of a reaction is predominantly determined by the distribution of $\rho(\varepsilon)k(\varepsilon)$, which varies as $G_v^+(\varepsilon - \varepsilon_0)$, the vibrational state sum of the activated complex in the RRKM formulation. The vibrational state density ρ_v and state sum G_v of a molecule of v vibrations vary roughly as ε^s and ε^{s+1} respectively where s is related to the number of low-frequency modes (see section VIII in text). On the other hand, the vibration–rotational state density ρ_{vr} varies as $\varepsilon^{s+(3/2)}$. The lowering of some (typically a few) of the oscillator frequencies in the activated complex means that s for the complex will be greater than that of the molecule. Hence $(s_{\text{complex}} + 1) \simeq (s_{\text{molecule}} + \frac{3}{2})$ and the functional forms of G_v^+ and ρ_{vr} are comparable.

A major impediment, of course, to the application of this reformulation is the remarkable paucity of anharmonicity data for the vibrational motions of polyatomic molecules. It is obvious, then, that particularly in the consideration of the unimolecular break-up of photochemically excited states, of transient species, or of ionic species, the RRKM approach, which is here in its infancy (76), will not be rapidly superseded: the problem of estimating both vibration frequencies and their anharmonicities for such transient species will not readily be overcome.

In the immediate future, extension of this work can proceed in three well-defined directions. The first is towards the consideration of simpler molecules, where we expect that some of our cavalier assumptions will begin to break down. One can envisage at least four kinds of failure. For very simple molecules, e.g. H_2^+ or H_2, the lifetimes of quasibound states with respect to predissociation appear to be entirely random as a function of $(\varepsilon - \varepsilon_0)$ (77, 78), and so we can expect that for very simple molecules, eq. 33 for $k(\varepsilon)$ will become inadequate. Along with this, the density of states in such small molecules will be reduced, so that the states above threshold do not overlap, and therefore energy cannot be regarded as flowing freely throughout the molecule. For methyl isocyanide and cyclopropane, the predissociation widths of the states above ε_∞ implied by eq. 41 are respectively of the order 10^4 and 10^5 times the mean spacings between the levels, and the only qualm one needs to have about unlimited intramolecular energy exchange is the requirement to conserve angular momentum. Even below threshold, the density of states is such that collision broadening causes them to overlap significantly, dependent of course on the complexity of the molecule, the nature and duration of the collision, and the pressure. All this free intramolecular exchange of energy must die away as the molecule becomes too simple: we will do no more than mention a small selection of a growing literature related to this problem (79–82). Thirdly, there is the assumption, implicit in our use of eq. 33 that rotational and vibrational energy are equally effective in bringing about predissociation; while the actual effect of rotationally-induced predissociation remains to be documented, one may note the possible important implication of rotation in the 'anomalous' Arrhenius factors of some reactions (14). Fourthly, it may become impermissible to lump together, as does eq. 42, with a single relaxation time, the rotational and the vibrational relaxations of these small molecules. Obviously, it is some or all of these effects, in concert, that lie at the cause of the difference in shock-wave dissociation behaviour between very simple molecules and more complex molecules (83).

A second possible extension might be to the problems of multiphoton induced dissociation and of laser separation of isotopic molecules (84, 85). Many of the ideas implicit in this approach, including several outlined in the preceding paragraph, can be carried across to these new problems (85, 86). Unfortunately, until very recently (87), molecules which undergo well-characterised thermal unimolecular decompositions have not been studied by these new methods. It would be interesting to see laser isotope separation experiments undertaken for one of the five molecules discussed in this paper: ethyl chloride is the obvious candidate, despite the fact that the thermal rate constants are the least reproducible of the five sets of data we have analysed.

The third obvious extension is to the discussion of chemical activation. The problem is a little more difficult here, and to follow our present approach would require a set of matrix elements a_{ij} rather like those of eq. 42, but having two non-degenerate eigenvalues. This $(n - 2)$-fold degenerate formulation would also be useful for describing thermal reactions yielding two distinctly different products, and perhaps with distinctly different fall-off characteristics (88, 89).

Finally, there is the problem of completing the achievement of our original objective, that of putting the theory of thermal unimolecular reactions on a sound, modern molecular-dynamic footing. This requires us to understand why it is that the predissociation rate constants for individual states, i.e. the k_i, which almost certainly will have random values over

a small range of ε, can have a coarse-grain average which is reasonably well[4] approximated by eq. 33. A start on this problem was made by Polanyi and Wigner (90) in 1928, but we are still far from a complete understanding of this particular facet. In this year of his death, it seems entirely appropriate to us to dedicate this paper to the memory of Michael Polanyi (1892–1977) who, among his many feats of intellect, was the father of modern molecular dynamics.

Acknowledgement

This work was supported by the National Research Council of Canada, both through the award of an Operating Grant (to H.O.P.) and a Postgraduate Scholarship (to A.W.Y.).

1. R. A. Marcus and O. K. Rice. J. Phys. Chem. **55**, 894 (1951).
2. R. A. Marcus. J. Chem. Phys. **20**, 359 (1952).
3. G. M. Wieder and R. A. Marcus. J. Chem. Phys. **37**, 1835 (1962).
4. G. M. Wieder. Ph.D. Thesis, Polytechnic Institute of Brooklyn, Brooklyn. 1961.
5. P. J. Robinson and K. A. Holbrook. Unimolecular reactions. John Wiley, London. 1972.
6. W. Forst. Theory of unimolecular reactions. Academic Press, New York, NY. 1973.
7. B. Noble, H. Carmichael, and C. L. Bumgardner. J. Phys. Chem. **76**, 1680 (1972).
8. B. D. Neely and H. Carmichael. J. Phys. Chem. **77**, 307 (1973).
9. F. W. Schneider and B. S. Rabinovitch. J. Am. Chem. Soc. **84**, 4215 (1962).
10. K. M. Maloney and B. S. Rabinovitch. J. Phys. Chem. **73**, 1652 (1969).
11. A. D. Kennedy and H. O. Pritchard. J. Phys. Chem. **67**, 161 (1963).
12. P. C. Beadle, D. M. Golden, K. D. King, and S. W. Benson. J. Am. Chem. Soc. **94**, 2943 (1972).
13. D. M. Golden, G. N. Spokes, and S. W. Benson. Agnew. Chem. **12**, 534 (1973).
14. H. O. Pritchard. Can. J. Chem. **55**, 284 (1977).
15. K. E. Shuler. Phys. Fluid, **2**, 442 (1959).
16. A. W. Yau and H. O. Pritchard. Can. J. Chem. **55**, 737 (1977).
17. H. O. Pritchard and N. I. Labib. Can. J. Chem. **54**, 329 (1976); H. O. Pritchard. Can. J. Chem. **54**, 2372 (1976).
18. J. H. Wilkinson. The algebraic eigenvalue problem. O.U.P., London. 1965.
19. R. Courant and D. Hilbert. Methods of mathematical physics. Vol. I. Wiley Interscience, New York, NY. 1962.
20. H. O. Pritchard. Spec. Period. Rep. React. Kinet. **1**, 243 (1975).
21. N. B. Slater. Proc. Leeds Philos. Lit. Soc. Sci. Sect. **6**, 259 (1955).
22. N. B. Slater. Theory of unimolecular reactions. Methuen, London. 1959.
23. W. Forst. *In* Reaction transition states. *Edited by* J. E. Dubois. Gordon and Breach, London. 1972. p. 75.
24. W. Forst. J. Phys. Chem. **76**, 342 (1972).
25. M. Christianson, D. Price, and R. Whitehead. J. Phys. Chem. **78**, 2326 (1974).
26. P. J. Robinson. Spec. Period. Rep. React. Kinet. **1**, 93 (1975).
27. A. Maccoll. *In* Techniques of chemistry. Vol. VI. 3rd ed. *Edited by* E. S. Lewis. Wiley Interscience, New York, NY. 1974. Pt. 1, p. 47.
28. H. M. Frey and R. Walsh. Chem. Rev. **69**, 103 (1969).
29. D. H. Shaw and H. O. Pritchard. Can. J. Chem. **46**, 2721 (1968).
30. M. J. Perona and D. M. Golden. Int. J. Chem. Kinet. **5**, 55 (1973).
31. D. K. Lewis. Can. J. Chem. **54**, 581 (1976).
32. K. N. Klump and J. P. Chesick. J. Am. Chem. Soc. **85**, 130 (1963).
33. S. H. Luu, K. Glänzer, and J. Troe. Ber. Bunsenges. Phys. Chem. **79**, 856 (1975).
34. J. L. Collister and H. O. Pritchard. Can. J. Chem. **54**, 2380 (1976).
35. J. L. Collister. Ph.D. Thesis, York University, Downsview, Ont. 1976.
36. H. Eyring and A.-L. Leu. Proc. Natl. Acad. Sci. U.S.A. **72**, 1717 (1975).
37. J. N. Bradley and M. A. Frend. Trans. Faraday Soc. **67**, 72 (1971).
38. J. A. Barnard, A. T. Cocks, and R. K-Y. Lee. J. Chem. Soc. Faraday Trans. I, **70**, 1782 (1974).
39. D. K. Lewis. J. Phys. Chem. **81**, 1887 (1977).
40. F. P. Buff and D. J. Wilson. J. Chem. Phys. **32**, 677 (1960).
41. I. Procaccia, Y. Shimoni, and R. D. Levine. J. Chem. Phys. **65**, 3302 (1976).
42. A. W. Yau and H. O. Pritchard. Can. J. Chem. **55**, 1588 (1977).
43. A. W. Yau and H. O. Pritchard. Can. J. Chem. **55**, 992 (1977).
44. D. M. Golden, R. K. Solly, and S. W. Benson. J. Phys. Chem. **75**, 1333 (1971).
45. J. Troe. Ber. Bunsenges. Phys. Chem. **78**, 478 (1974).
46. W. Forst. Chem. Rev. **71**, 339 (1971).
47. W. Forst and Z. Prášil. J. Chem. Phys. **51**, 3006 (1969).
48. G. Z. Whitten and B. S. Rabinovitch. J. Chem. Phys. **38**, 2466 (1963); **41**, 1883 (1964).
49. D. W. Setser. *In* MTP international review of science. Vol. 9. *Edited by* J. C. Polanyi. Butterworths, London. 1972. p. 1.
50. T. Beyer and D. F. Swinehart. Comm. ACM, **16**, 379 (1973).
51. S. E. Stein and B. S. Rabinovitch. J. Chem. Phys. **58**, 2438 (1973).
52. G. Herzberg. Electronic spectra and electronic structure of polyatomic molecules. Van Nostrand, New York, NY. 1966.
53. M. R. Hoare and Th. W. Ruijgrok. J. Chem. Phys. **52**, 113 (1970).
54. S. Califano. Vibrational states. John Wiley, London. 1976.
55. S. J. Cyvin. Spectrochim. Acta, **16**, 1022 (1960).
56. M. C. Lin and K. J. Laidler. Trans. Faraday Soc. **64**, 927 (1968).

[4]Very recently, Reddy and Berry (87) have studied the isomerisation of methyl isocyanide induced by intense laser radiation at 7265 Å: this corresponds to a value of $\varepsilon = 39.3$ kcal mol^{-1}, i.e. 1.1 kcal mol^{-1} above threshold (cf. Table 3). From the pressure dependence of the isomerisation rate, one can deduce that $k(\varepsilon)$ at this energy is $\sim 1 \times 10^7$ s^{-1}, whereas eq. 33 (or 41) gives $k(\varepsilon) = 1.0 \times 10^7$ s^{-1} for the same energy.

Can. J. Chem. Downloaded from www.nrcresearchpress.com by 210.87.254.42 on 09/05/12
For personal use only.

Can. J. Chem. Downloaded from www.nrcresearchpress.com by 210.87.254.42 on 09/05/12
For personal use only.

57. H. O. PRITCHARD, R. G. SOWDEN, and A. F. TROTMAN-DICKENSON. Proc. R. Soc. London A, **217**, 563 (1953).
58. R. G. SOWDEN. Ph.D. Thesis, Manchester University, Manchester. 1954.
59. W. E. FALCONER, T. F. HUNTER, and A. F. TROTMAN-DICKENSON. J. Chem. Soc. 609 (1961).
60. H. O. PRITCHARD, R. G. SOWDEN, and A. F. TROTMAN-DICKENSON. Proc. R. Soc. London A, **218**, 416 (1953).
61. C. T. GENAUX, F. KERN, and W. D. WALTERS. J. Am. Chem. Soc. **75**, 6196 (1953).
62. R. W. VREELAND and D. F. SWINEHART. J. Am. Chem. Soc. **85**, 3349 (1963).
63. H. HEYDTMANN, B. DILL, and R. JONAS. Int. J. Chem. Kinet. **7**, 973 (1975).
64. K. A. HOLBROOK and A. R. W. MARSH. Trans. Faraday Soc. **63**, 643 (1967).
65. M. H. BAGHAL-VAYJOOEE, J. L. COLLISTER, and H. O. PRITCHARD. Can. J. Chem. **55**, 2634 (1977).
66. J. L. COLLISTER and H. O. PRITCHARD. Can. J. Chem. **55**, 3815 (1977).
67. J. S. ROWLINSON. Q. Rev. **8**, 168 (1954).
68. A. F. TROTMAN-DICKENSON. Gas kinetics. Butterworths, London. 1955.
69. D. F. SWINEHART. J. Am. Chem. Soc. **91**, 7611 (1969).
70. R. S. LEMON and G. M. ROSENBLATT. Surf. Sci. **48**, 432 (1975); **48**, 449 (1975).
71. D. C. TARDY. Chem. Phys. Lett. **17**, 431 (1972); R. G. GILBERT and I. G. ROSS. J. Chem. Phys. **57**, 2299 (1972).
72. R. C. BHATTACHARJEE and W. FORST. Chem. Phys. Lett. **26**, 395 (1974).
73. R. W. CARR, JR. and W. D. WALTERS. J. Phys. Chem. **67**, 1370 (1963).
74. B. S. RABINOVITCH, D. W. SETSER, and F. W. SCHNEIDER. Can. J. Chem. **39**, 2609 (1961).
75. F. W. SCHNEIDER and B. S. RABINOVITCH. J. Am. Chem. Soc. **85**, 2365 (1963).
76. W. N. OLMSTEAD, M. LEV-ON, D. M. GOLDEN, and J. I. BRAUMAN. J. Am. Chem. Soc. **99**, 992 (1977).
77. G. HUNTER, A. W. YAU, and H. O. PRITCHARD. At. Data Nucl. Data Tables, **14**, 11 (1974).
78. R. J. LEROY. J. Chem. Phys. **54**, 5433 (1971); Eigenvalues and certain expectation values for all bound and quasi-bound levels of ground-state H_2, HD and D_2. Report No. WIS-TCI-387. University of Wisconsin Theoretical Chemistry Institute. January 15th, 1971.
79. N. SAITÔ, H. HIROOKA, and N. OOYAMA. J. Phys. Soc. Jpn. **26**, Suppl. 233 (1969).
80. S. NORDHOLM and S. A. RICE. J. Chem. Phys. **62**, 157 (1975).
81. E. W. SCHLAG and W. E. HOWARD. *In* Molecular energy transfer. *Edited by* R. D. Levine and J. Jortner. John Wiley, New York, NY. 1976. p. 227.
82. P. BRUMER and J. W. DUFF. J. Chem. Phys. **65**, 3566 (1976).
83. D. G. RUSH and H. O. PRITCHARD. Eleventh symposium (international) on combustion. The Combustion Institute, Pittsburgh, PA. 1969. p. 37.
84. D. P. HODGKINSON and J. S. BRIGGS. Chem. Phys. Lett. **43**, 451 (1976).
85. R. V. AMBARTZUMIAN and V. S. LETOKHOV. Acc. Chem. Res. **10**, 61 (1977).
86. N. BLOEMBERGEN. Opt. Commun. **15**, 416 (1975).
87. K. V. REDDY and M. J. BERRY. Chem. Phys. Lett. **52**, 111 (1977).
88. O. K. RICE. Z. Phys. Chem. B, **7**, 226 (1930).
89. M. H. BAGHAL-VAYJOOEE, A. W. YAU, and H. O. PRITCHARD. Can. J. Chem. **55**, 1595 (1977); M. C. FLOWERS. Can. J. Chem. **56**, 29 (1978).
90. M. POLANYI and E. WIGNER. Z. Phys. Chem. **139**, 439 (1928).
91. F. A. MILLER, R. J. CAPWELL, R. C. LORD, and D. G. REA. Spectrochim. Acta, **28A**, 603 (1972).
92. T. SHIMANOUCHI. Tables of molecular vibrational frequencies. Pt. 3. NSRDS-NBS 17. 1968. p. 23.
93. K. BOLTON, N. L. OWEN, and J. SHERIDAN. Spectrochim. Acta, **25A**, 1 (1969).
94. T. SHIMANOUCHI. Tables of molecular vibrational frequencies. Pt. 1. NSRDS-NBS 6. 1967. p. 40.
95. R. C. LORD and B. P. STOICHEFF. Can. J. Phys. **40**, 725 (1962).
96. R. N. DIXON. Spectrochim. Acta, **9**, 59 (1957).
97. Hs. H. GUNTHARD, R. C. LORD, and T. K. MCCUBBIN, JR. J. Chem. Phys. **25**, 768 (1956).
98. R. H. SCHWENDEMAN and G. D. JACOBS. J. Chem. Phys. **36**, 1245 (1962).
99. N. DAVIDSON. Statistical mechanics. McGraw Hill, New York, NY. 1962.
100. N. E. DUNCAN and G. J. JANZ. J. Chem. Phys. **23**, 434 (1955).

Appendix 1

Our choice of [33] for $k(\varepsilon)$ is based on two arguments, one theoretical and one experimental. Firstly, for every molecule considered in this paper, the use of [33] in this reformulation gives a better representation of the shape of the fall-off curve than does the use of [36]: the latter formula always leads to a slightly flatter fall-off curve; an example of this is shown in Fig. 2 for cyclopropane. However, we do not place excessive weight on this coincidence, since it could be an artefact of our particular choice for the a_{ij} elements, eq. 42. Secondly, we conclude from the analysis of experimental data in this appendix that there is no experimental justification for preferring modified Arrhenius [35] over strict Arrhenius [34] rate laws for thermal unimolecular reactions.

A survey of the literature would indicate wide acceptance for the view that experimental rate constants probably have a more complex temperature dependence than is given by eq. 34; common variants are the modified Arrhenius form [35], or more complicated forms in which both the activation energy and pre-exponential factor are temperature-dependent (27, 28). It is, of course, extraordinarily difficult to distinguish among these various forms for any particular set of experimental rate constants because this would require accurate measurements of the rates over very wide ranges of temperature (27), and to our knowledge, only three unimolecular reactions have been so studied. The thermal decomposition of di-*tert*-butylperoxide has been studied over a range of temperature from 363–677 K (29–31): over this range, the rate constant changes by about ten orders of magnitude, from about 10^{-7} s^{-1} to about 10^{3} s^{-1}, and there is no clear evidence that it cannot be represented by the strict Arrhenius form [34]. The

TABLE 2. Spectroscopic constants in cm^{-1}

Molecule	C_3H_6	C_4H_8	CH_3NC	CD_3NC	C_2H_5NC	C_2H_5Cl
Reference	55	91	92	92	93	94
ν_i; $100x_i(g_i)$	739; 1.5 (2)	199; 0.0	263; 2.0 (2)	249; 1.9 (2)	226; 2.5[a]	336; 2.0
	854; 1.5	626; 1.5	945; 2.0	877; 1.9	270; 2.0[a]	676; 3.0
	869; 1.8 (2)	737; 1.5	1129; 1.5 (2)	900; 1.2 (2)	466; 2.0	785; 1.5
	963; 1.8	749; 1.5 (2)	1429; 2.5	1117; 1.2	720; 1.5	972; 1.5
	1029; 2.0 (2)	901; 2.0 (2)	1467; 2.5 (2)	1058; 1.8 (2)	801; 1.5	972; 3.0
	1133; 2.0	926; 0.0	2166; 2.0	2166; 2.0	842; 3.0	1080; 1.5
	1188; 0.0	999; 2.0	2966; 8.0	2251; 6.0	1013; 3.0	1244; 2.0
	1188; 2.0 (2)	1005; 2.0	3014; 4.0 (2)	2263; 3.0 (2)	1108; 1.5	1287; 1.5
	1442; 2.5 (2)	1224; 2.0 (2)			1146; 2.0	1383; 2.0
	1479; 0.0	1225; 2.0			1354; 1.5	1452; 2.0 (3)
	3028; 5.3 (2)	1234; 2.0			1390; 2.5	2890; 8.0
	3038; 8.0	1257; 2.0			1457; 2.5	2946; 8.0
	3082; 4.3 (2)	1260; 2.0 (3)			1461; 2.5 (2)	2983; 4.0 (2)
	3103; 2.9	1452; 2.0 (2)			2155; 2.5	3012; 3.0
		1454; 2.0			2901; 8.0	
		1469; 2.0			2958; 8.0	
		2887; 8.0 (2)			2974; 3.0	
		2905; 8.0			2990; 3.0	
		2945; 8.0			3005; 3.0	
		2965; 3.0 (2)				
		2974; 3.0				
		2987; 3.0				
$B_{\|\|}$	0.670 (97)	0.355 (93)	0.335 (9)	0.30[b]	0.161[c]	0.174[d]
B_z	0.435[b]	0.226 (95)	5.22 (9)	2.61[b]	0.926 (93)	1.05 (96)
$\nu_{torsion}$					203	243
V					1239[f]	1291 (98)
zpe[e]					518	524
B_r[e]					3326	45.74

[a]Frequencies estimated by Maloney and Rabinovitch (10).
[b]Estimated.
[c]Mean of $B_x = 0.170\ cm^{-1}$ and $B_y = 0.152\ cm^{-1}$ (93).
[d]Mean of $B_x = 0.183\ cm^{-1}$ and $B_y = 0.165\ cm^{-1}$ (96).
[e]$zpe = \frac{1}{2}(V - \nu)$ where V is the barrier height and ν is the torsional frequency; the rotational constant is then $B_r = \nu^2/V$ (99).
[f]Estimated from barrier for $C_2H_5CN = 1819\ cm^{-1}$ (100), i.e. $V(C_2H_5NC) \simeq V(C_2H_5CN) \times \nu(C_2H_5NC)/\nu(C_2H_5CN) \simeq 1819 \times 203/298\ cm^{-1}$.

thermal isomerisation of cycloheptatriene has been studied over the temperature range 600–1400 K (32, 33); again, the rate constant, ranging from about $10^{-4}\ s^{-1}$ to about $10^5\ s^{-1}$, is well represented by [34]. Likewise, the thermal isomerisation of methyl isocyanide has been studied over the range 393–593 K, with the rate constant changing by about seven orders of magnitude from about $10^{-8}\ s^{-1}$ to about $10^{-1}\ s^{-1}$ at the high pressures (34): in this case, the (extrapolated) infinite-pressure rate data were fitted by least squares to an equation of the form

$$[66] \qquad \ln k_\infty = A + BT^{-1} + CT^{-2}$$

and then the quadratic term was discarded as not being statistically significant (35). On the other hand, there have been some indications, backed by theoretical arguments (36), that the rates of decomposition of cyclopropane and cyclobutane fall markedly below those predicted by eq. 34 at very high temperatures, i.e. about 1100 K (37, 38); however, recent evidence suggests that these results are incorrect and that the rate constants for these reactions can be represented by eq. 34 at least up to 1500 K (39). On the basis of these observations, taken together with the fact that the observed fall-off behaviour is always more consistent with [33] and [34] than with [35] and [36], we propose, as far as *unimolecular* reactions are concerned, to proceed on the basis that until proved otherwise, infinite-pressure rate constants obey the strict Arrhenius form, eq. 34.

Appendix 2

The purpose of this appendix is to study the sensitivity of the state density of a molecule to variations in anharmonicity factor.

Figure 7 illustrates the sensitivity of the state density of methyl isocyanide for $\varepsilon \geq 13\,000\ cm^{-1}$ to variations in anharmonicity factor: Fig. 7*a* examines variations in the anharmonicity factor for $\nu_8 = 263\ cm^{-1}$ and Fig. 7*b* for $\nu_1 = 2966\ cm^{-1}$. Figure 7*a*, curve (*i*) shows the function $\rho(\varepsilon)$ calculated assuming that all the vibrations in the molecule are harmonic; curves (*ii*)–(*v*) are calculated assuming that all the oscillators are anharmonic (with the x_i as listed in Table 2) except for the bending mode ν_8, for which x_8 values of 0 (harmonic), 0.01, 0.02, and 0.03 respectively are assumed. Three conclusions can be drawn from Fig. 7*a*. One, that all the curves are essentially

Can. J. Chem. Downloaded from www.nrcresearchpress.com by 210.87.254.42 on 09/05/12
For personal use only.

Can. J. Chem. Downloaded from www.nrcresearchpress.com by 210.87.254.42 on 09/05/12
For personal use only.

the same shape: for example $\rho(16\,000)/\rho(13\,000) \simeq 5.5$ for all curves, which implies that the calculated *shape* of the fall-off curve will be essentially the same for all five models; on the other hand, the absolute magnitude of $\rho(\varepsilon)$ for model (*i*) differs from the rest by as much as a factor of 2, which corresponds to a factor of two difference in the absolute pressure shift (i.e. the collisional efficiency factor λ, or $\bar{\lambda}$). Two, that as the anharmonicity factor increases from zero, the state density first increases to a maximum and then decreases, as is to be expected for low-frequency modes in the interesting energy range. Three, that $\rho(\varepsilon)$ only changes by about 10% for a change in x_8 from 0.01 to 0.03 (the estimated range), so that one can expect to derive reasonably meaningful results using estimated x_i values. In Fig. 7*b*, similar results are presented for the symmetric stretching mode $\nu_1 = 2966\ \text{cm}^{-1}$. Curves (*i*) and (*ii*) show the function $\rho(\varepsilon)$ for the anharmonic oscillator model (Table 2) but with $x_1 = 0$, and $x_1 = 0.08$ respectively; curves for $0 < x_1 < 0.08$ fall in between, and are omitted for clarity. Thus, for high-frequency modes, the state density is very insensitive indeed to the chosen values of x_i.

Finally, we examine in Fig. 8 the behaviour of $\rho(\varepsilon)$ as x_i changes from 0 to 0.09 for the rocking mode ($\nu_8 = 854\ \text{cm}^{-1}$) of cyclopropane to ensure that the conclusions just reached are equally valid at much higher energies; the $\rho(\varepsilon)$ curve for the harmonic oscillator model is also shown for comparison. Again, all the curves have essentially the same shape: for example $\rho(27\,400)/\rho(22\,500)$ is about 16 for Morse oscillators and about 14 for harmonic oscillators. Also, the absolute magnitude of $\rho(\varepsilon)$ changes by about 12% for a change in x_8 from 0 to 0.03, compared with a 10% change for methyl isocyanide as x_8 went from 0.01 to 0.03, despite the higher values of ε in this case: indeed, numerical examination shows that the sensitivity of $\rho(\varepsilon)$ to x_i varies roughly as the ratio of ε/ν.

Appendix 3. Molecular Constants and Reaction-rate Parameters

Reliable vibrational assignments, in the harmonic-oscillator approximation, are virtually complete for all the molecules considered in this paper: the only exceptions are for ethyl isocyanide where Maloney and Rabinovitch (10) estimated $\nu_{13} = 226\ \text{cm}^{-1}$ and $\nu_{20} = 270\ \text{cm}^{-1}$, and for the torsional oscillations of both ethyl chloride and ethyl isocyanide which we have treated as free internal rotations with the rotational constants derived from the torsional frequency and barrier height (99), cf. Table 2.

The calculation of anharmonic force constants, on the other hand, has been largely restricted to triatomic molecules, because of the enormous increase in the number of anharmonic terms in the potential function as the number of atoms increases (54). For unimolecular reaction systems, the most complete set of anharmonicity factors is that for cyclopropane, derived from approximate calculations by Cyvin (55). The anharmonicity factors x_i for the various modes are generally between 0.01 and 0.03, except for the stretching mode ($\nu_1 = 3038\ \text{cm}^{-1}$) for which $x_1 \simeq 0.08$; to our knowledge, no complete set of anharmonicity factors exists for any other large molecule of interest in thermal unimolecular reactions. To define our notation, we denote the standard frequency assignments for the molecule by ν_i and the anharmonicity factors x_i ($\equiv$ the x^* of Cyvin) such that

$$[67] \qquad \varepsilon_{v,i} = \frac{v}{1 - x_i}[\nu_i - v\nu_i x_i]$$

Since such data are unlikely to be available in the near future, and in view of the mild insensitivity of $\rho(\varepsilon)$ and the fall-off behaviour to the anharmonicity, we feel that, for the time being, it is a useful procedure to estimate values of x_i as follows, based on a comparison with Cyvin's (55) data for cyclopropane:

CH_3 rocking	$x_i \simeq 0.015$
CH_2 rocking	$x_i \simeq 0.015$
CH_2 twisting	$x_i \simeq 0.02$
CH_2 wagging	$x_i \simeq 0.02$
CH_2 deformation	$x_i \simeq 0.025$
CH antisymmetric stretch	$x_i \simeq 0.03$
CH degenerate stretch	$x_i \simeq 0.04$
CH symmetric stretch	$x_i \simeq 0.08$
C—C stretch	$x_i \simeq 0.02$
C—N stretch	$x_i \simeq 0.02$
Bending modes	$x_i \simeq 0.02$

Since the CH stretching modes have high frequencies, of the order of 3000 cm^{-1}, the state density is not sensitive to their larger values of x_i in the interesting energy range. All the lower-frequency modes, which make the largest contributions to $\rho(\varepsilon)$, appear to have values of x_i near 0.02, and in the absence of very refined calculations, this would appear to be about as close as one can get to the correct values. In the case of the isotopic pair of molecules CH_3NC and CD_3NC, we have assumed that the anharmonicity corrections are related by

$$[68] \qquad \frac{\nu_i x_i(\text{D})}{\nu_i x_i(\text{H})} = \left[\frac{\nu_i(\text{D})}{\nu_i(\text{H})}\right]^2$$

Table 2 lists all pertinent spectroscopic information, observed or estimated, for the six molecular species treated in this paper, i.e. vibration frequencies ν_i, anharmonicity factors, listed as $100x_i$, degen-

Can. J. Chem. Downloaded from www.nrcresearchpress.com by 210.87.254.42 on 09/05/12
For personal use only.

eracies g_i (where they are different from unity), and external rotational constants B_z, $B_{||}$. Table 3 gives a complete self-consistent set of kinetic parameters, with reference to the source of each key entry.

Appendix 4. Algorithm for Calculating k_{uni} and Computer Program

An annotated program of the algorithm for calculating k_{uni}, written in FORTRAN, together with detailed explanations of formulae, sample input data, and specimen output, is lodged with the Depository of Unpublished Data.[5]

The algorithm includes the following key steps:

(*i*) The vibrational state-degeneracy $g_v(\varepsilon)$ is computed from $\varepsilon = 0$ to ε_m by direct count. This procedure is similar to the Stein–Rabinovitch (51) method, but differs from it in some important respects. Counting is performed only at energies where an energy state is present which results in an appreciable saving in time when ε_m is not high (as in the case here where ε_m is a few thousand wave numbers). This is because there are only a few states near $\varepsilon = 0$, and one is therefore performing the counting and convolution only over these states, and not at all the energy grids, as in the Stein–Rabinovitch method. Also, the convolution is performed before round-off of the energy levels: this reduces to a minimum (with little additional programming effort) the propagation of round-off errors in the subsequent convolution with the rotational state-sum.

(*ii*) The rotational state-sum $G_r(\varepsilon)$ is calculated up to ε_m, and convoluted to obtain the vibration–rotation state-sum $G_{vr}(\varepsilon)$. Again, this is a conventional procedure, but the convolution is performed downwards towards $\varepsilon = 0$ (as opposed to the conventional scheme of starting upwards from $\varepsilon = 0$), resulting in a saving of half the required storage space.

(*iii*) If there are any internal rotational degrees of freedom, the state-deneracy $g_i(\varepsilon)$ of the internal rotation is convoluted with $G_{vr}(\varepsilon)$ to obtain the sum of internal states $G(\varepsilon)$ of the molecule. Again, this convolution procedure is performed downward.

(*iv*) The sum of states from $\varepsilon = \varepsilon_m + \Delta\varepsilon$ to $\varepsilon = \varepsilon_{max}$ is calculated at intervals of $\Delta\varepsilon$ using the non-iterative steepest-descent procedure (43).

(*v*) The density of states $\rho(\varepsilon)$ is calculated from ε_∞ to $\varepsilon_\infty + \varepsilon_{max}$ using the same procedure.

(*vi*) The reactive energy range (ε_∞ to $\varepsilon_\infty + \varepsilon_{max}$) is grained into r channels, with states between ε_l and ε_{l+1} being grouped into the lth channel: the channels are not necessarily equally spaced; the values of $\bar{n}_l$

[5]Complete set of material is available upon request, at a nominal charge, from the Depository of Unpublished Data, CISTI, National Research Council of Canada, Ottawa, Ont., Canada K1A 0S2.

TABLE 3. Assumed values of the chemical kinetic rate parameters at infinite pressure: ε_∞ in kcal mol^{-1}, A_∞ and k_∞ in s^{-1}[a]

Molecule	C_3H_6	C_4H_8	CH_3NC[b]	CD_3NC	C_2H_5NC	C_2H_5Cl
Figure	9	10	12	19	13	11
ε_∞ (kcal/mol)	65.6 (59)	62.5 (73)	38.4 (9)	38.5 (75)	38.4 (10)	58.4 (64)
A_∞ (s^{-1})	1.88×10^{15}	3.66×10^{14}	3.98×10^{13} (9)	4.46×10^{13}	7.76×10^{13} (10)	1.07×10^{14} (64)
k_∞ (s^{-1})	3.07×10^{-4} (58)	4.26×10^{-5} (58)	8.57×10^{-4}	8.65×10^{-4} (75)	1.73×10^{-3}	8.88×10^{-3}
At T (K)	763.15	721.45	503.55	503.55	504.05	794.15

[a]Reference numbers in parentheses.
[b]The alternative set of values (34) used to construct Fig. 14 are $\varepsilon_\infty = 38.2$ kcal mol^{-1}; $A_\infty = 2.24\times10^{13}$ s^{-1}; $k_\infty = 4.81\times10^{-5}$ s^{-1} at 472.55 K, 5.89×10^{-4} s^{-1} at 503.55 K, and 4.83×10^{-3} s^{-1} at 532.95 K.

and $\bar{k}_l$ are calculated. The grouped decay rates $\bar{k}_l$ are scaled by the characteristic relaxation rate $\bar{\mu}$ (the relaxation rate at $p = 1$ Torr as defined in eq. 61) to avoid overflow or underflow difficulties in (*vii*) and (*viii*).

(*vii*) The scaled coefficients $\bar{\bar{a}}_i$ and $\bar{\bar{b}}_i$ for use in eq. 46 are computed using $\bar{n}_l$ and $\bar{\bar{k}}_l$; ($\bar{\bar{k}}_l = \bar{k}_l/\bar{\mu}$).

(*viii*) The unimolecular reaction rate constant k_{uni} may then be calculated for any value of the pressure p.

The FORTRAN program consists of the MAIN routine, which handles the flow of the program and the input data, and the following subroutines. (*1*) COUNT which makes a direct count of the vibrational energy level at low energy; (*2*) RINCNT which effects the convolution of any *internal* rotational degrees of freedom with the vibrational states; (*3*) EXTROT which brings about the convolution of the external rotational degrees of freedom; (*4*) DESENT which computes the state sum and state density of the molecule at higher energy by the non-iterative steepest-descent procedure (43); (*5*) GRAIN which divides the reactive energy region into grains and evaluates the quantities $\bar{n}_i$ and $\bar{k}_i$; (*6*) UNIRAT which computes the unimolecular rate constant at the desired values of the pressure p; (*7*) SETPLT (optional), which makes a Calcomp plot of the calculated rate constants as a function of pressure: this subroutine also reads in and plots specimen sets of experimental data, having determined the optimum value of the pressure-shift parameter $\bar{\lambda}$ required to effect the best coincidence between the calculated and experimental fall-off curves; (*8*) PFNCTN: a utility subroutine for calculating the molecular partition function; (*9*) FNPHI1 and FNPHI2: utility subroutines for the evaluation of the average internal energy and its first two derivatives, using exact and approximate (53) Morse partition functions respectively. All the desired options are specified in the input data set, and detailed descriptions of the input parameters and the structures of the respective subroutines are given as comments in the program listings.

The sample calculation evaluates k_{uni} for the methyl isocyanide isomerisation at about 50 values of p and matches the calculated curve with the experimental results of Collister and Pritchard (34) for the temperature $T = 230.4$°C, i.e. the middle curve of Fig. 14; the complete calculation took about 20 s on the York University IBM 370/158 Computer.

Can. J. Chem. Downloaded from www.nrcresearchpress.com by 210.87.254.42 on 09/05/12
For personal use only.

Calorimetric study of an electrochemical reduction

PETER J. TURNER AND HUW O. PRITCHARD
Chemistry Department, York University, Downsview, Ont., Canada M3J 1P3

Received December 13, 1977

PETER J. TURNER and HUW O. PRITCHARD. Can. J. Chem. **56**, 1415 (1978).

The aqueous trichloroacetate ion is reduced irreversibly and with unit current efficiency to the dichloroacetate ion. From the total energy release observed when this process is carried out inside a calorimeter, it is possible to deduce the enthalpy change for the reduction reaction.

PETER J. TURNER et HUW O. PRITCHARD. Can. J. Chem. **56**, 1415 (1978).

L'ion trichloroacétate en solution aqueuse se réduit d'une façon irréversible et avec une efficacité de courant égale à l'unité pour conduire à l'ion dichloroacétate. A partir de l'observation de l'énergie totale qui est dégagée lorsque ce processus est effectuée à l'intérieur d'un calorimètre, il est possible de déduire le changement d'enthalpie pour la réaction de réduction.
[Traduit par le journal]

Can. J. Chem. Downloaded from www.nrcresearchpress.com by 210.87.254.40 on 09/05/12
For personal use only.

Introduction

In recent years, with the enormous growth in our knowledge of electrochemical synthesis, many electrochemical reactions having unit current efficiency have been discovered (1–4). Provided that there are no unwanted side reactions accompanying the reaction of interest, it would seem that the observation of such reactions taking place inside a calorimeter could, in principle at least, lead to valuable thermochemical data. For example, bromobenzene, neopentyl bromide, and 1-bromohexane all appear to be reduced with unit current efficiency in dimethylformamide solution using a mercury cathode: the first two yield the corresponding hydrocarbons in 100% yield, but the latter gives a mixture of hexane, hexene, and dihexylmercury (5); whereas the first two reactions might be suitable for calorimetric study, the latter clearly would not. If it is possible to establish such a calorimetric electrochemical route to enthalpy changes in chemical reactions, then improved enthalpy of formation data would be obtainable for many difficult molecules: these would include bromobenzene and various other aryl or alkyl halides as just mentioned or, for example, carbon tetrachloride, chloroform, etc. (6, 7).

Theory

The investigation of electrochemical reactions by calorimetry has received singularly little attention since Jahn's investigation of heats of cell reactions at the end of the last century (8, 9). For reversible electrochemical reactions, of course, it is both simpler and more accurate to obtain enthalpies of reaction from the temperature dependence of cell emf values (9); however, the electrode reactions to which we have referred above have associated with them, in general, large energy barriers and are irreversible.

The relationship between the electrical power input W_E, the energy release into the calorimeter $(-Q)$, and ΔH for the chemical reaction is simple and straightforward. Under the influence of the passage of an electric current, the contents of the calorimeter change from a defined initial state to a defined final state, at constant pressure and (in our diphenylether calorimeter, see Experimental section below) constant temperature. For the purposes of this argument, we regard the central part of the calorimeter, including the reaction vessel, as the thermodynamic system, and the diphenyl ether as the surroundings. Then

$$[1a] \qquad \Delta E = Q + W$$

$$[2a] \qquad = Q + W_E - P\Delta V$$

Therefore

$$[3] \qquad \Delta H = \Delta E + P\Delta V = W_E + Q$$

i.e., ΔH is the *numerical difference* between the total input power W_E and the energy release Q measured by the calorimeter, and in the limit, if the process could be carried out reversibly, Q would be identified with $T\Delta S$ and W_E with ΔG (9).

This simple thermodynamic argument is unsatisfactory in one respect, that it gives us no indication of the relative magnitudes of the quantities W_E, Q, and ΔH, which is especially important if $\Delta H \simeq 0$ as it turned out to be in the experiment described below. Consequently, we present an alternative derivation, based on electrokinetic considerations, which establishes this connection. For an electrochemical cell operating reversibly, there will be an energy input equal to ΔG from the external circuit, and an absorption of heat from the surroundings (i.e. the calorimeter) equivalent to $T\Delta S$, where ΔG and $T\Delta S$ refer to the total cell process (9). When the

Can. J. Chem. Downloaded from www.nrcresearchpress.com by 210.87.254.40 on 09/05/12
For personal use only.

cell is operating irreversibly, however, we may argue simply that activation energy $E^{\neq}$ is supplied by the external power supply and is returned as heat evolved when the system (i.e. the cell) returns to equilibrium. Thus, the total electrical input is

$$[1b] \qquad W_E = \Delta G + E^{\neq}$$

and upon return to equilibrium, the total heat absorption from the surroundings is now

$$[2b] \qquad Q = T\Delta S - E^{\neq}$$

Thus

$$[3] \qquad W_E + Q = \Delta G + T\Delta S = \Delta H$$

and although $E^{\neq}$ cancels out, it is clear that the larger $E^{\neq}$, the greater will be the numerical magnitudes of W_E and Q compared with that of ΔH. We note in passing that there appears to have been a single exploratory investigation some years ago of this route to the measurement of ΔS, using an equation similar to [2*b*] and adjusting the overpotential to make Q zero (10); this approach, however, is not applicable to the reactions considered here since it is not possible to obtain reliable values for the open-circuit voltage, so that neither ΔG nor the overpotential is an accessible quantity.[1]

Experimental

One of the most thoroughly documented series of electrochemical reductions having unit current efficiency is the reduction of the haloacetic acids, particularly trichloro- and dichloro-acetic acids (11–13). These reactions have certain advantages for our exploratory study over the more exciting ones noted in the Introduction: in particular the simplifications arising from the fact that a completely aqueous system can be used, and that auxiliary thermochemical data are available, especially heats of dilution. Consequently, we chose to study the reduction of the trichloroacetate to the dichloroacetate ion. The reaction is irreversible (11), quantitative (14), and has been used (without 100% recovery of product) as a demonstration experiment in electro-organic chemistry (15); two reduction waves are observed with half-wave potentials of -0.73 and -1.65 V, corresponding to the consecutive removal of two chlorine atoms from the trichloroacetate ion (14).

The calorimetric measurements were made in our large diphenyl-ether isothermal calorimeter (16): this is not an ideal instrument for this investigation because the reaction-vessel space is severely restricted, being 10–15 cm in height but only 4 cm in diameter. Consequently, we decided to omit a third (reference) electrode (17) from the system. The reaction cell consisted of a cylindrical Pyrex vessel, using a pool of mercury on the floor as one electrode, and another pool held on an annular shelf as the other; each electrode consisted of about 10 ml of mercury, and a typical electrolyte volume was 40 ml. Since it is necessary to exclude oxygen from the reaction (14), the solution was deoxygenated using a stream of nitrogen and the reaction vessel was then isolated. Moreover, because of the small space available, and also because we were unable to achieve very high current densities (and therefore obtained rather small heats), we decided we would incur smaller errors by omitting a stirrer from this exploratory system as well.

Electrical input was from a Power Designs 2005 or Hewlett-Packard 2802A DC power supply operating in constant-voltage mode. The voltage across the cell and the current passing through it (the latter measured as the voltage across a Leeds and Northrup standard 1 ohm resistor in series) were displayed simultaneously on a Hewlett-Packard 7100 B two-channel recorder. Using the integrator facility of the recorder, the current was integrated to give the total number of coulombs passing: independent calibration showed this to be accurate to better than $\pm 0.3\%$. The power consumed was determined by graphical integration of the product of the voltage and the current: this integration was greatly simplified by the constancy of the voltage resulting from the characteristics of the power supply and from the approximately isothermal conditions obtaining in the cell; in addition, over the main period of the integration (i.e. after the initial transients had died out), voltage measurements made with a Hewlett-Packard 3465A digital multimeter were substituted for the graphically recorded values, thus improving the accuracy of the power measurement to about $\pm 0.4\%$.

Results

In our early experiments, we hoped to follow closely the work of Meites and Meites (14) using a chloride supporting electrolyte. With two mercury electrodes, the overall cell reaction is

$$[4] \quad 2Hg + Cl_3C{\cdot}CO_2^- + H^+ + Cl^- \rightarrow HCl_2C{\cdot}CO_2^- + Hg_2Cl_2$$

which according to the tabulated data (18) is exothermic to the extent of about $\Delta H = -22.6$ kcal mol^{-1}. However, the anode rapidly became coated with calomel and after about 2 min, the cell current became too small to yield useful calorimetric results. The use of nitric acid as the supporting electrolyte appeared to be more promising: at first, the products are (as expected) dichloroacetate and chloride ions at the cathode and mercurous ions (soluble in the nitrate electrolyte) at the anode. As the products diffuse together, calomel is precipitated, but recovery and subsequent analysis gave only 95% of the expected yield; this is because some of the calomel (inevitably) falls onto the cathode and is reduced. The measured values of ΔH, derived according to eq. 3, were in the region of -15 to -25 kcal mol^{-1} and were very irreproducible.

Our final technique, following Meites (17), was to introduce a membrane into the cell to prevent the mixing of the mercurous and chloride ions. Because of space limitations, we used dialysis tubing (Fisher) and a double layer of this material was found to be sufficient to keep the ions apart long enough for a satisfactory calorimetric determination. In the final

[1] NOTE ADDED IN PROOF: Dr. L. G. Hepler has called to our attention another attempt, about 20 years ago, to measure the heats of some electrochemical reactions in a calorimeter (20).

TABLE 1. Determination of ΔH for reaction 5 using eq. 3*

Power input nW_E (cal)	Energy released $-nQ$ (cal)	Difference $n(W_E + Q)$ (cal)	Extent of reaction† n (μmol)	ΔH (kcal mol^{-1})
29.15±0.12	28.17±0.28	0.98±0.31	322±1	3.04±0.97
27.24±0.11	26.54±0.04	0.70±0.12	303±1	2.31±0.40
34.42±0.14	33.82±0.06	0.60±0.15	382±1	1.58±0.39
35.68±0.14	35.00±0.02	0.68±0.14	395±1	1.73±0.35
31.32±0.12	30.71±0.02	0.62±0.12	347±1	1.77±0.35
30.15±0.12	29.24±0.20	0.91±0.23	333±1	2.74±0.69
32.48±0.13	31.81±0.05	0.67±0.14	360±1	1.85±0.39
			(Mean ± sdm)‡	1.92±0.16

*1 cal = 4.184 J.
†From total coulombs used.
‡Errors are assigned to each individual measurement in columns 1, 2, and 4; errors in columns 3 and 5 follow from the normal rules for combining errors. The final value for ΔH of 1.92 ± 0.16 kcal mol^{-1} is obtained by taking the weighted mean of the entries in column 5.

arrangement, the dialysis tubing was folded in on itself to form a double-walled tube, then folded into a U-shape and supported away from the bottom of the cell: this 'bag' was filled with 10 ml of 1.0 *M* sodium nitrate and 10 ml of mercury. The remainder of the cell was filled with a mixture comprising 0.1 *M* trichloroacetic acid plus 1.0 *M* sodium nitrate, with 10 ml of mercury to act as the cathode. The solutions were deoxygenated with nitrogen and the reaction vessel was then isolated and placed in the calorimeter to establish a satisfactory fore-period.

Electrolysis was carried out for 1000 s using an applied potential of 2 V, giving a current of about 30 mA. Separate bench tests had established that it takes approximately 1 V to drive the anode, and therefore the cathode voltage is also about 1 V, thus falling well below the second wave for trichloroacetic acid. Both waves are rather broad, indicating a high degree of irreversibility: the first, corresponding to the removal of the first chlorine atom lies between −0.4 and −1.1 V and the second, corresponding to the reduction of the resulting dichloroacetate ion to monochloroacetate begins at about −1.3 V; the current density achieved under our conditions was very similar to that obtained by Meites and Meites (14, 17).

After the electrolysis was terminated, it took approximately 1 h for the calorimeter to achieve a linear after-period, which it sustained for about another 2 h, enabling us to estimate the total energy release satisfactorily (in most cases). Thereafter, an accelerated energy release into the calorimeter took place, due to diffusion of the catholyte and anolyte into each other with precipitation of calomel. We may write the overall cell reaction before this mixing occurs as

[5] $2Hg + Cl_3C{\cdot}CO_2^-(300H_2O) + H^+ \rightarrow \{HCl_2C{\cdot}CO_2^- + Cl^- + Hg_2^{2+}\}(9000H_2O)$

and ignoring small heats of mixing inherent in representing the cell reaction as [5], the estimated value of ΔH for this reaction is about +2 kcal mol^{-1} (18). The results listed in Table 1 show that the use of eq. 3 leads to a value of ΔH for reaction 5 of +1.9 ± 0.3 kcal mol^{-1}; this agreement has to be, to some extent, fortuitous since Cox and Pilcher (19) estimate uncertainties as large as ±2 kcal mol^{-1} in the recommended thermochemical data for both these acids.

Conclusions

The exploratory experiment described in this paper represents by no means an ideal thermochemical determination. The use of an isothermal calorimeter (both by Jahn (8) and ourselves) is, it seems, somewhat of an advantage in minimizing current and voltage changes during the experiment. On the other hand, our inability to achieve a homogeneous final solution renders this experiment far from perfect from a thermochemical point of view. Since most reactions of thermochemical interest will be halide reductions, this means that the use of mercury electrodes has to be abandoned in favour of some other metal with a high overpotential but with soluble halides, perhaps zinc. We think that such a change, together with the ability to stir the final solution, would remove most of the variability from the determination of Q found in column 2 of Table 1. Inspection of Table 1 reveals also that an improvement by an order of magnitude in the precision of the power-input measurement would be beneficial. Nevertheless, we believe that this experiment demonstrates that the calorimetric study of electrochemical reductions should be able, given careful experimental design and some ingenuity, to provide accurate enthalpy of formation data in many cases where combustion calorimetry or reaction calorimetry is difficult.

Can. J. Chem. Downloaded from www.nrcresearchpress.com by 210.87.254.40 on 09/05/12
For personal use only.

Acknowledgements

This work was supported by the National Research Council of Canada. We are also grateful to Drs. O. R. Lundell, H. A. Skinner, G. Pilcher, and C. E. Vanderzee for helpful comments.

1. K. KORINEK and T. F. W. MCKILLOP. Ann. Repts. Chem. Soc. London, B**70**, 245 (1973).
2. I. T. HARRISON and S. T. HARRISON. Compendium of organic synthetic methods. Wiley, New York. 1973.
3. N. L. WEINBERG. Technique of electro-organic synthesis. Vol. 5, Part 2. Wiley, New York. 1974.
4. M. R. RITI and F. H. COVITZ. Introduction to organic electrochemistry. Dekker, New York. 1974.
5. J. W. SEASE and R. C. REED. Extended abstracts of Electro-organic Division of Electrochemical Society, **4**, 328 (1969).
6. M. V. STACKELBERG and W. STRACKE. Z. Elektrochem. **53**, 118 (1949).
7. I. M. KOLTHOFF, T. S. LEE, D. STOCESOVA, and E. P. PARRY. Anal. Chem. **22**, 521 (1950).
8. H. JAHN. Z. Phys. Chem. **18**, 399 (1895).
9. D. A. MACINNES. Principles of electrochemistry. Reinhold, New York. 1939.
10. J. C. ERIKSSON and B. SÖDERQVIST. Acta Chem. Scand. **15**, 1701 (1961).
11. P. J. ELVING and C.-S. Tang. J. Am. Chem. Soc. **72**, 3244 (1950); Anal. Chem. **23**, 341 (1951).
12. P. J. ELVING, I. ROSENTHAL, and M. K. KRAMER. J. Am. Chem. Soc. **73**, 1717 (1951).
13. P. HEISEL. German Patent 848,807, September 8th, 1952.
14. T. MEITES and L. MEITES. Anal. Chem. **27**, 1531 (1955).
15. P. E. IVERSON. J. Chem. Ed. **48**, 136 (1971).
16. J. V. DAVIES and H. O. PRITCHARD. J. Chem. Thermodyn. **4**, 9 (1972).
17. L. MEITES. Anal. Chem. **27**, 1116 (1955).
18. Selected values of chemical thermodynamic properties. National Bureau of Standards, Washington. Technical Notes 270-3 and 270-4. 1968 and 1969.
19. J. D. COX and G. PILCHER. Thermochemistry of organic and organometallic compounds. Academic Press, London. 1970.
20. J. M. SHERFEY and A. BRENNER. J. Electrochem. Soc. **105**, 665 (1958).

Can. J. Chem. Downloaded from www.nrcresearchpress.com by 210.87.254.40 on 09/05/12
For personal use only.

Complex fluoroanions in solution. VIII. Mixed anions containing fluoride and trifluoromethanesulfonate or fluorosulfate[1]

S. BROWNSTEIN, J. BORNAIS, AND G. LATREMOUILLE

Division of Chemistry, National Research Council of Canada, Ottawa, Ont., Canada K1A 0R9

Received December 7, 1977

S. BROWNSTEIN, J. BORNAIS, and G. LATREMOUILLE. Can. J. Chem. **56**, 1419 (1978).

Binary fluorides of groups III, IV, V, and VI of the periodic table form fluoroanions with the trifluoromethanesulfonate and fluorosulfate ions. The complexes are weaker and there is less disproportionation than with the trifluoroacetate ion. Fluorine exchange reactions in these anions are generally slow on the nmr time scale at −70°C.

S. BROWNSTEIN, J. BORNAIS et G. LATREMOUILLE. Can. J. Chem. **56**, 1419 (1978).

Les fluorures binaires des groupes III, IV, V et VI du tableau périodique forment des fluoroanions avec les ions trifluorométhanesulfonates et fluorosulfates. Les complexes sont plus faibles que ceux obtenus avec l'ion trifluoroacétate et il y a aussi moins de disproportionation. Les réactions d'échange du fluor dans ces anions sont généralement lentes à l'échelle de la rmn à −70°C.

[Traduit par le journal]

Introduction

The literature on trifluoromethanesulfonic acid and its derivatives has recently been reviewed (1). In addition to salts it forms the anionic species $[I(OSO_2CF_3)_4]^-$ and $[Sn(OSO_2CF_3)_6]^{2-}$ (2, 3). There do not appear to be any reports of mixed anionic species containing both fluoride and trifluoromethanesulfonate radicals. Fluorosulfates and mixed fluorosulfates of the form $M(FSO_3)_n$ (4–6) and $MF_n(FSO_3)_p$ (7, 8) have been reported as well as $M(FSO_3)_n^{p-}$ (9). From conductivity studies in fluorosulfonic acid the existence of the species $MF_n(FSO_3)_p^{q-}$ has been implied where M is Sb, As, and Bi (10). The ion $AsF_5SO_3F^-$ has been prepared and its Raman spectrum reported (11).

Both trifluoromethanesulfonic and fluorosulfonic acids are very strong acids, comparable in strength to the strongest mineral acids. In view of the extensive chemistry recently found with mixed anionic species containing fluoride and trifluoroacetate radicals (12) it is of interest to investigate the existence of similar species with the anions of the very strong acids trifluoromethanesulfonic and fluorosulfonic acid.

Experimental

Techniques for obtaining fluorine resonance spectra, vapor pressure measurements, and sample preparation were identical to those used for the corresponding trifluoroacetates (12). Tetramethylammonium trifluoromethanesulfonate and tetrabutylammonium trifluoromethanesulfonate were prepared by neutralization of an ice cold aqueous solution of the quaternary ammonium hydroxide with trifluoromethanesulfonic acid, and removal of the solvent under vacuum. The corresponding fluorosulfates were prepared in the same manner. Tetramethylammonium fluorosulfate was recrystallized from water; mp 349°C (dec.). *Anal.* calcd.: C 27.75, H 6.94, N 8.09, S 18.50; found: C 27.96, H 7.02, N 7.93, S 18.64.

Tetrabutylammonium fluorosulfate was recrystallized from methylene chloride – diethyl ether; mp 179°C. *Anal.* calcd.: C 56.30, H 10.56, N 4.11, S 9.38; found: C 56.46, H 10.45, N 4.04, S 9.47.

Tetramethylammonium trifluoromethanesulfonate was recrystallized from water; mp > 360°C. *Anal.* calcd.: C 26.91, H 5.38, N 6.28, S 14.35; found: C 26.92, H 5.48, N 6.31, S 14.51.

Tetrabutylammonium trifluoromethanesulfonate was recrystallized from methylene chloride – diethyl ether; mp 110°C. *Anal.* calcd.: C 52.17, H 9.21, N 3.58, S 8.18; found: C 52.28, H 9.11, N 3.63, S 8.29.

The fluorine resonance spectra showed no evidence of fluorine containing impurities. All spectra were of the tetramethylammonium salts in sulfur dioxide solution at −70°C except as specifically noted.

Results and Discussion

$(CH_3)_4NCF_3SO_3$ has a single, sharp fluorine resonance signal at −78.6 and $(CH_3)_4NFSO_3$ at 41.2 ppm. The complexes will be described in the order of their position in the periodic table.

Group III

Boron Trifluoride

Complexes of 1:1 stoichiometry are formed with both $(CH_3)_4NCF_3SO_3$ and $(CH_3)_4NFSO_3$. Their fluorine resonance parameters are listed in Table 1. Vapor pressure measurements give no indication of BF_3 complexing beyond 1:1 but the fluorine resonance spectra show rapid exchange between free and complexed BF_3 when an excess of BF_3 is present.

Group IV

Silicon Tetrafluoride

No complexes are formed with $(CH_3)_4NCF_3SO_3$ or $(CH_3)_4NFSO_3$.

[1]Issued as NRCC No. 16548.

Can. J. Chem. Downloaded from www.nrcresearchpress.com by 210.87.254.6 on 09/05/12
For personal use only.

Can. J. Chem. Downloaded from www.nrcresearchpress.com by 210.87.254.6 on 09/05/12
For personal use only.

TABLE 1. Fluorine resonance parameters of some complex trifluoromethylsulfonate and fluorosulfate anions

Species	δF_1 (ppm)	δF_2 (ppm)	$J_{F_1-F_2}$ (Hz)	J_{M-F_1} (Hz)	J_{M-F_2} (Hz)	δF_4 (ppm)	$J_{F_3-F_4}$ (Hz)
$BF_3CF_3SO_3^-$	−137.5						
$BF_3FSO_3^-$	−140.2						
cis-$SnF_4(CF_3SO_3)_2^{2-}$	−139.1	−129.8	55				
cis-$SnF_4(FSO_3)_2^{2-}$	−142.6	−134.9	54				
trans-$SnF_4(CF_3SO_3)_2^{2-}$	−130.3						
trans-$SnF_4(FSO_3)_2^{2-}$	−134.7						
trans-$TiF_4(CF_3SO_3)_2^{2-}$	276.9						
trans-$TiF_4(FSO_3)_2^{2-}$	277.5						
$PF_5CF_3SO_3^-$	−82.7	−56.4	62.6	762	792		
$PF_5(FSO_3)^-$	−82.6	−60.1	63.0	750	791		
$AsF_5CF_3SO_3^-$	−69.1	−41.4	124				
$AsF_5(FSO_3)^-$	−69.6	−47.5	100				
$V_2F_{10}CF_3SO_3^-$	492	422.2	120			416.8	120
$V_2F_{10}(FSO_3)^-$	489	421	110			416	120
$NbF_5CF_3SO_3^-$	181.7	143.5					
$NbF_5(FSO_3)^-$	184	143.6					
$TaF_5CF_3SO_3^-$	103.5	70.4	25				
$TaF_5(FSO_3)^-$	103.9	70.4	24				
cis-$TaF_4(CF_3SO_3)_2^-$	92.5	127.2	26				
cis-$SF_4(CF_3SO_3)_2^{2-}$	−39.3	13.3	74				
cis-$SF_4(FSO_3)_2^{2-}$	33.1	85.6	75				

Germanium Tetrafluoride

The fluorine resonance spectra indicate that complex formation is occurring but are not amenable to simple interpretation.

Tin Tetrafluoride

A complex of structure **1** is formed with $(CH_3)_4NCF_3SO_3$ and there is also a single line which may arise from *trans*-$SnF_4(CF_3SO_3)_2^{2-}$. Similar results are found with $(CH_3)_4NFSO_3$ and the parameters are listed in Table 1. These results were obtained on freshly prepared samples at −20°C. Over a period of weeks at room temperature the spectra became more complicated. Group IV fluorides normally give *cis* complexes (13) but *trans* complexes have also been reported (14).

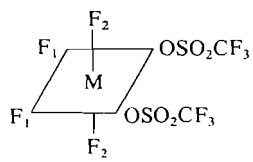

1

Titanium Tetrafluoride

There appear to be two complexes formed with $(CH_3)_4NCF_3SO_3$. One is probably *trans*-$TiF_4(CF_3SO_3)_2^{2-}$ and the other contains bridging and nonbridging fluorines but the spectrum could not be sufficiently resolved for a spectral analysis. The fluorine resonance spectrum of a freshly prepared sulfur dioxide solution with 2 equiv. of $(CH_3)_4NFSO_3$ per TiF_4 has a single line attributed to *trans*-$TiF_4(FSO_3)_2^{2-}$, an unresolved multiplet at 267 ppm, a broad signal from bridging fluorines at −19 ppm, and two other multiplets at low field. After a few weeks at room temperature the multiplet at 267 has disappeared and the spectrum of the other two multiplets is stronger and shown in Fig. 1. Irradiation of the higher field multiplet collapsed the other to a pair of doublets. A simulated spectrum for the case ABCXY is also shown in Fig. 1, where X and Y are bridging fluorines. Structure **2** and the fluorine resonance parameters shown fit these observations. Triple fluorine bridged titanium fluoroanions (15) and multidentate fluorosulfonate groups (6) have been reported. The existence of an ion of structure **2** must, however, be considered hypothetical until more and better evidence is accumulated.

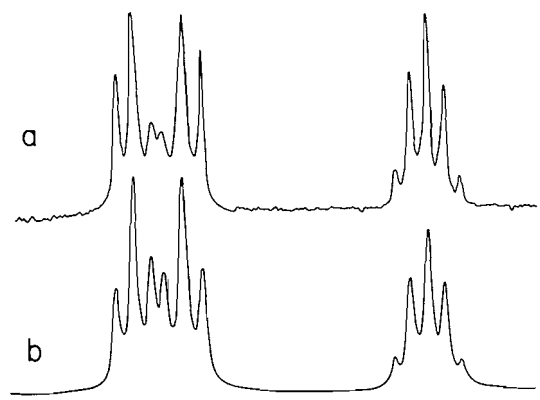

FIG. 1. Terminal fluorine resonance spectrum of $Ti_2F_8(SO_3F)^-$: (*a*) experimental; (*b*) theoretical.

Can. J. Chem. Downloaded from www.nrcresearchpress.com by 210.87.254.6 on 09/05/12
For personal use only.

$\delta_A = 261.9$ $J_{A-B} = 0$ $J_{A-Y} = 0$ $J_{B-Y} = 50$
$\delta_B = 260.4$ $J_{A-C} = 50$ $J_{B-C} = 50$ $J_{C-X} = 50$
$\delta_C = 252.9$ $J_{A-X} = 50$ $J_{B-X} = 0$ $J_{C-Y} = 50$

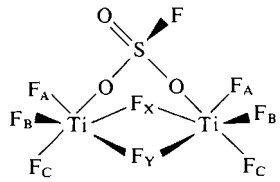

2

Group V

Phosphorus Pentafluoride and Arsenic Pentafluoride

Octahedral 1:1 complexes are completely formed. The parameters are listed in Table 1 with the axial fluorine as F_1. Tetrabutylammonium salts in methylene chloride as solvent at −90°C were employed with PF_5 in order to slow down axial–equatorial fluorine exchange and obtain well resolved spectra.

Vanadium Pentafluoride

The fluorine resonance spectrum of the complex with $CF_3SO_3^-$ is shown in Fig. 2 and interpreted as arising from structure **3**. The tetrabutylammonium

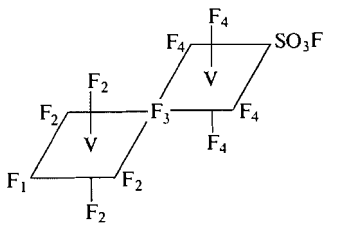

3

salt was employed in SO_2ClF as solvent since VF_5 reacts with SO_2. The single line at 345 arises from VF_6^-. The multiplet at 492 is assigned to F_1, which is spin coupled to F_2 and F_3. The triplet at 422.2 is assigned to F_2, almost equally coupled to F_1 and F_3. The doublet at 416.8 is assigned to F_4, which is spin coupled to F_3. No signal could be found for F_3, presumably because it is so broadened by spin coupling. This assignment cannot be considered as proven, but is consistent with the fact that only a bridged fluoroanion was found with trifluoroacetate as the other anion. Similar results were obtained with FSO_3^- and the fluorine resonance parameters are listed in Table 1.

Niobium Pentafluoride

Signals in the regions to be expected for axial and equatorial fluorines in a complex NbF_5L are found with both $CF_3SO_3^-$ and FSO_3^-. Their intensity ratios are appropriate but fluorine–fluorine spin coupling could not be resolved due to incomplete quadrupolar averaging of niobium–fluorine spin coupling.

Tantalum Pentafluoride

A sulfur dioxide solution with 2 equiv. of $CF_3SO_3^-$ for each TaF_5 has signals from $TaF_5CF_3SO_3^-$ and *cis*-$TaF_4(CF_3SO_3)_2^-$ of structure **1**. The fluorine resonance parameters are listed in Table 1. With a 1:1 solution additional broad lines are observed in the fluorine on tantalum region of the spectrum. They may arise from a condensed species. Only the 1:1 complex and perhaps some condensed species are found with FSO_3^- as the added anion. *Cis*-disubstituted fluoroanions of tantalum have been observed with trifluoroacetate (12) and ethoxide (16) as ligands, while both *cis* and *trans* complexes were observed with chloride and bromide ligands (17).

Group VI

Sulfur Tetrafluoride

Cis complexes of composition $SF_4L_2^{2-}$ are formed with both $CF_3SO_3^-$ and FSO_3^-. These complexes are the only example where there is a large chemical shift difference between the fluorines bonded to the central atom with different complexing anions. From a comparison with the trifluoroacetate complex (12) it would appear that the chemical shifts of $SF_4(CF_3SO_3)_2^{2-}$ are the unusual ones.

Molybdenum and Tungsten Hexafluorides

There is no significant complex formation with $CF_3SO_3^-$ or FSO_3^-. With a twofold excess of the anion a broad weak fluorine resonance peak was observed which might indicate a slight formation of a complex.

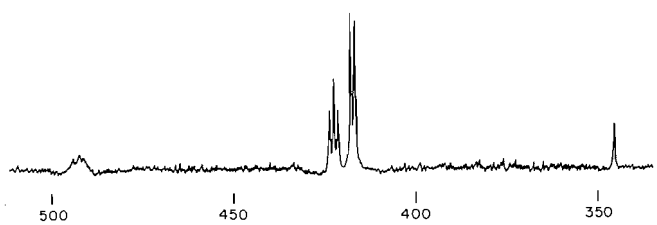

FIG. 2. Fluorine on vanadium region of the fluorine resonance spectrum of an SO_2ClF solution at −90°C with equivalent amounts of VF_5 and TBATFMS.

Group VII

Iodine Pentafluoride

No complex formation is found with $CF_3SO_3^-$ or FSO_3^-.

Conclusions

The two ions $CF_3SO_3^-$ and FSO_3^- behave very similarly in their reactions with binary fluorides. The chemical shifts of the corresponding fluorine atoms bonded to the central element in complexes with $CF_3SO_3^-$ are on average 1.5 ppm to lower field than in the complexes with FSO_3^-, except for the complexes with SF_4. There is no complex formation of these ions with several binary fluorides where trifluoroacetate ion does form complexes (12). There is also less disproportionation to yield more highly substituted fluoroanions with $CF_3SO_3^-$ and FSO_3^- than with trifluoroacetate ion. The weaker complexing can be correlated with the greater strength of the parent sulfonic acids or with the lesser steric requirements of the trifluoroacetate ion at the coordination site. Studies of other anions are needed to distinguish between these possibilities. The chemical shifts of the corresponding fluorine atoms bonded to the central element in complexes with trifluoroacetate ion are on average 14 ppm to lower field than in the complexes with $CF_3SO_3^-$. This is some indication of greater electron donation by $CF_3SO_3^-$ than trifluoroacetate ion, which is contrary to the acid strengths of the parent acids.

1. R. D. Howells and J. D. McCown. Chem. Rev. **77**, 69 (1977).
2. J. R. Dalziel and F. Aubke. Inorg. Chem. **12**, 2707 (1973).
3. R. J. Batchelor, J. N. R. Ruddick, J. R. Sams, and F. Aubke. Inorg. Chem. **16**, 1414 (1977).
4. E. L. Muetterties and D. D. Coffman. J. Am. Chem. Soc. **80**, 5914 (1958).
5. H. C. Clark and H. J. Emeleus. J. Chem. Soc. 4778 (1957).
6. K. C. Lee and F. Aubke. Can. J. Chem. **55**, 2473 (1977).
7. R. J. Gillespie and R. A. Rothenbury. Can. J. Chem. **42**, 416 (1964).
8. L. E. Levchuk, J. R. Sams, and F. Aubke. Inorg. Chem. **11**, 43 (1972).
9. H. A. Carter, S. P. L. Jones, and F. Aubke. Inorg. Chem. **9**, 2485 (1970).
10. R. J. Gillespie, K. Ouchi, and G. P. Pez. Inorg. Chem. **8**, 63 (1969).
11. P. A. Yeats and F. Aubke. J. Fluorine Chem. **4**, 243 (1974).
12. S. Brownstein. Can. J. Chem. **56**, 343 (1978).
13. E. L. Muetterties. J. Am. Chem. Soc. **82**, 1082 (1960).
14. A. D. Adley, D. F. R. Gilson, and M. Onyszchuck. Proc. XIIth. Int. Conf. Coord. Chem. **2**, 169 (1970).
15. P. A. W. Dean. Can. J. Chem. **51**, 4024 (1973).
16. Yu A. Buslayev, Yu V. Kokunov, V. D. Kopanev, and M. P. Gustyakova. J. Inorg. Nuclear Chem. **36**, 1569 (1974).
17. Yu A. Buslayev and E. G. Ilyin. J. Fluorine Chem. **4**, 271 (1974).

Can. J. Chem. Downloaded from www.nrcresearchpress.com by 210.87.254.6 on 09/05/12
For personal use only.

Phosphorus pentasulfide as a mild, selective reagent for the reduction of sulfoxides to sulfides[1]

IAN W. J. STILL,[2] S. KHAQAN HASAN,[3] AND KENNETH TURNBULL
Erindale College, University of Toronto, Mississauga, Ont., Canada L5L 1C6

Received December 28, 1977

IAN W. J. STILL, S. KHAQAN HASAN, and KENNETH TURNBULL. Can. J. Chem. **56**, 1423 (1978).

It has been shown that phosphorus pentasulfide (P_4S_{10}) is a mild, effective reagent for the reduction of sulfoxides to sulfides and that this conversion can be achieved selectively in the presence of other reactive groups such as ketone, ester, amide, nitro, and halogen. Phosphorus pentasulfide also appears to be a promising reagent for reducing selenoxides but is ineffective in reducing sulfones, sulfinates, or sulfites. The mechanistic evidence presented indicates a probable four-centre (Wittig-like) intermediate or transition state for the reduction of sulfoxides by P_4S_{10}.

IAN W. J. STILL, S. KHAQAN HASAN et KENNETH TURNBULL. Can. J. Chem. **56**, 1423 (1978).

On a montré que le pentasulfure de phosphore (P_4S_{10}) est un réactif doux et efficace permettant de transformer les sulfoxydes en sulfures et que cette réduction peut être effectuée d'une façon sélective en présence d'autres groupes réactifs comme des cétones, des esters, des amides, des dérivés nitrés et halogénés. Il semble aussi que le pentasulfure de phosphore soit un réactif qui offre beaucoup de promesses pour réduire les sélénoxydes; il serait toutefois inefficace pour réduire les sulfones, les sulfinates ou les sulfites. Les données mécanistiques présentées indiquent que la réaction de réduction des sulfoxydes par le P_4S_{10} se produit vraisemblablement par un intermédiaire à quatre centres (comme un Wittig).
[Traduit par le journal]

There has been a great deal of current interest in devising new reagents for both the mild, selective oxidation of sulfides to sulfoxides (1, 2) and, to an even greater extent, for the reverse process of reduction of sulfoxides to sulfides (3–6). The reduction of sulfoxides has also been the subject of a recent comprehensive review by Oae and co-workers (7).

It seemed to us that many of the published procedures suffered from one or more of the following disadvantages: expensive or difficultly accessible reagents, relatively severe reaction conditions, or lack of selectivity of the reducing agent. With this in mind we have examined the feasibility of using phosphorus pentasulfide (P_4S_{10}), a reagent which had briefly been reported as being successful for the reduction of sulfoxides in two very specific instances (8), and we would now like to present our findings; (for a preliminary account see ref. 9). As will be discussed later, we have not restricted our study to simple sulfoxides but have also investigated the reaction of P_4S_{10} with structurally related compounds such as sulfinates, sulfites, sulfones, and sulfilimines, as well as briefly examining the reaction of P_4S_{10} with selenoxides.

Results and Discussion

Synthetic Scope of the Reaction

Although the successful use of trivalent phosphorus compounds for the reduction of sulfoxides has been known for several years (10, 11) we believe that this is the first time that the readily available, inexpensive phosphorus pentasulfide has been employed generally for this reduction. As the results in Table 1 clearly illustrate, phosphorus pentasulfide is capable of reducing a wide variety of structural types of sulfoxide, under very mild reaction conditions, in yields ranging from fair to excellent. We are at present unable to satisfactorily explain the relatively poor yields obtained for the cyclic sulfoxides, thiolan 1-oxide and thian 1-oxide. A comparison of the three types of butyl sulfoxide reported in Table 1 was made to establish whether a significant steric hindrance factor exists in this reaction. From the results obtained it appears not, although examination of Dreiding models would suggest that the better conversion achieved in the di-*tert*-butyl sulfoxide case can be rationalized on steric grounds.

The final entry in Table 1 is of interest in that it clearly demonstrates that the reaction between the S=O group and P_4S_{10} is much faster than that between the C=O group and P_4S_{10}. In this case, as in many other examples in the literature, it is possible

[1]Part of this work has been presented at the 2nd Joint Conference of the Chemical Institute of Canada and the American Chemical Society, Montreal, P.Q., May 29–June 2, 1977.

[2]Author to whom correspondence should be addressed.

[3]Postdoctoral fellow, 1976. Present address: Pharmaceutical and Fine Chemicals Research Division, Pakistan Council of Scientific and Industrial Laboratories, Off University Road, Karachi-39, Pakistan.

Can. J. Chem. Downloaded from www.nrcresearchpress.com by 210.87.254.5 on 09/05/12
For personal use only.

Can. J. Chem. Downloaded from www.nrcresearchpress.com by 210.87.254.5 on 09/05/12
For personal use only.

TABLE 1. Reduction of sulfoxides to sulfides

Sulfoxide	Yield[a,b] of sulfide (%)	Melting or boiling (Torr) point[c]
$(CH_3)_2SO$	67	37–39(760)
$(n\text{-}C_4H_9)_2SO$	51	78–80(20)
$(sec\text{-}C_4H_9)_2SO$	42	162–163(760)
$(tert\text{-}C_4H_9)_2SO$	69	148–149 (760)
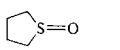	50	118–119(760)
	31	142(760)
$(C_6H_5CH_2)_2SO$	61	48–50
$(C_6H_5)_2SO$	72	160–165(20)
$(p\text{-}CH_3C_6H_4)_2SO$	99	53–55
$(p\text{-}ClC_6H_4)_2SO$[d]	61[d]	92–93
$(p\text{-}CH_3OC_6H_4)_2SO$	100	44–46
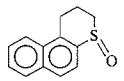	78	91–92
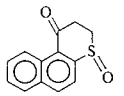	60	67–68

[a]Yield of isolated product, based on starting material actually consumed.
[b]Reaction times of 4–5 h at 25°C in CH_2Cl_2, unless otherwise noted.
[c]These data were consistent with the literature data.
[d]After 16 h.

to convert the carbonyl group to a thiocarbonyl group but only by using much higher-boiling solvents such as toluene or pyridine. Micetich (8) had earlier reported that in the deoxygenation of penicillin and cephalosporin sulfoxides there was no concomitant reaction of P_4S_{10} with ester or amide groups present in the sulfoxides. Further examples of functional groups which are not affected by the P_4S_{10} reagent are provided in Tables 1 and 2: they include aromatic nitro, chloro, and methoxy compounds, as well as a number of other sulfur-containing functional groups; (see below for a discussion of this). On the other hand, it is not likely that the reaction will be applicable to sulfoxides containing any kind of amino or hydroxyl group, or a cyano grouping, because reactions of P_4S_{10} with these functional groups have been well described (12–14).

TABLE 2. Effect of *para*-substituents on reduction of symmetrically substituted phenyl sulfoxides

Para substituent	Extent of conversion to sulfide (%)[a]
NO_2	11
Cl	24
H	39
CH_3	81
OCH_3	100

[a]All reactions were run for 4 h at 25°C in CH_2Cl_2 using the same concentrations of reagents.

Before taking up the discussion of a possible mechanism for the reduction of sulfoxides with phosphorus pentasulfide, its effect on a number of structurally related compounds will be considered. It was obviously of great interest, for example, to observe the behavior of sulfones with P_4S_{10} since there is a paucity of reliable methods for achieving the reduction of sulfones to sulfides, although reagents such as lithium aluminum hydride (15) and diisobutylaluminum hydride (16) have been used successfully in a number of instances. Unfortunately, both di-*n*-butyl sulfone and di-*p*-methoxyphenyl sulfone were recovered unchanged even after prolonged treatment (up to 72 h) with P_4S_{10} in refluxing dichloromethane or benzene. Acid catalysis of the reaction did not produce even a trace of sulfide. It should be noted that the sulfoxides analogous to these sulfones were among the most reactive of those reported in Table 1. Although disappointing from the synthetic standpoint, the lack of reactivity of phosphorus pentasulfide with sulfones can be rationalized in terms of our understanding of the mechanism of the sulfoxide reduction.

We have also examined the reaction of P_4S_{10} with the cyclic sulfinates **1** and **2**.[4] Again, perhaps more surprisingly, a lack of reactivity towards P_4S_{10} was evident. In the case of **1**, a 78% recovery of starting material was observed, while for **2**, starting material was recovered to the extent of only 50% but tlc analysis indicated that at least four products were being formed and accordingly the reaction was not pursued further.

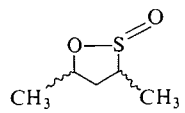

1

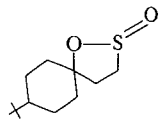

2

A similar situation prevailed when we attempted to extend the reaction with phosphorus pentasulfide to the cyclic sulfite **3**. This compound was readily obtained by the literature procedure (17) but, although only 50% of the starting sulfite survived the reaction with P_4S_{10} and a significant amount of stilbene was formed, we were unable to obtain any conclusive evidence for the formation of either the sulfoxylate ester **4** or a thioxosulfite **5** in this reaction.

One other reaction which was successfully

[4]Samples of these two compounds were generously provided by Professor T. Durst, University of Ottawa, Ottawa, Ont.

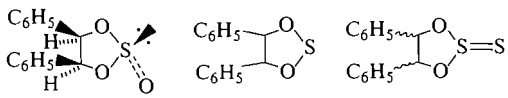

3 4 5

achieved with P_4S_{10} was the reduction of selenoxides to selenides. In fact, perhaps because of the longer Se—O bond, the reduction of diphenyl selenoxide (85% conversion in 3 h) was considerably faster than the diphenyl sulfoxide analogue (39% conversion in 4 h). Although we have not made a detailed study of a series of selenoxides, we also attempted the reduction of dibenzyl selenoxide to illustrate the generality of the procedure. In this case also the reaction proceeded even more smoothly than for the analogous sulfoxide, with an 83% isolated yield of dibenzyl selenide being obtained. Attempts to reduce selenoxides have not been widely reported in the literature to date, although the successful use of various phosphine selenides in halogenated solvents at 25°C for this purpose was very recently reported (18).

$$R_2SeO \xrightarrow[25°C]{P_4S_{10}} R_2Se$$

We were also interested in comparing the effectiveness of phosphorus pentaselenide with phosphorus pentasulfide in the reduction of sulfoxides. Phosphorus pentaselenide (P_4Se_{10}) is readily available and its use for the selenation of uracil derivatives by the reaction of P_4Se_{10} with the appropriate thiocarbonyl analogue has recently been reported (19). However, no reaction between diphenyl sulfoxide and P_4Se_{10} was observed after 6 h in dichloromethane at 40°C. In the light of our discussion of a possible mechanism for the sulfoxide reduction (see below) it is possible that this failure of P_4Se_{10} to react can be explained in terms of unfavorable S—Se bond polarization in the likely intermediate (or transition state) **6**.

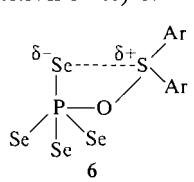

6

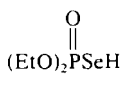

7

It is worth noting at this point that a more complex selenium-containing reagent, *O,O*-diethyl hydrogen phosphoroselenoate (**7**), has been successfully employed very recently for the reduction of sulfoxides to sulfides (20). Mikolajczyk (21, 22) had earlier reported the reduction of dimethyl sulfoxide by a series of related sulfur and selenium derivatives of phosphoric, phosphonic, and phosphinic acid, with concomitant replacement of the P=S (Se) functionality by P=O.

Mechanistic Aspects

There is a considerable difference in the ease with which aliphatic and aromatic sulfoxides react with phosphorus pentasulfide. With DMSO, for example, external cooling was required in the early stages of the reaction and reaction is essentially complete in a few minutes, whereas for diphenyl sulfoxide the conversion to sulfide is barely 40% complete after 4 h (Table 2). This led us to suspect that the electron density at the oxygen atom and hence a rate-determining nucleophilic attack of the oxygen in the $S^+—O^-$ bond at the phosphorus atom in P_4S_{10} are implicated in the reaction mechanism. Strong support for this view is provided by the results in Table 2 which show a clear-cut correlation between the rate of the reduction and increasing electron-donor capability of X in a series of sulfoxides $(p\text{-}XC_6H_4)_2SO$. Given the structure (in the solid state) of P_4S_{10} (23), with its adamantane-like skeleton and four equivalent P=S bonds, this result suggested a Wittig-like intermediate or transition state **8** reacting via the mechanism shown in eq. 1.

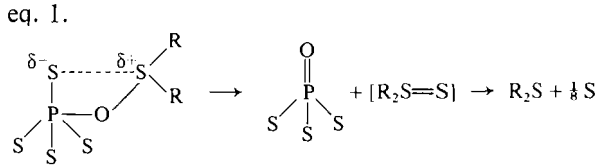

8

This suggestion is somewhat different from a mechanistic proposal by Mikolajczyk and Luczak (24) for the *strong-acid-catalyzed* reduction of dimethyl sulfoxide by a series of substituted phosphine sulfides and selenides. Under the acidic conditions, these authors propose initial protonation of the sulfoxide oxygen atom and the intermediacy of a tetracovalent sulfur species, **9**.

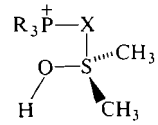

9
(X = S, Se)

A similar intermediate has been proposed by Oae and his co-workers (25) for the reduction of sulfoxides with *O,O*-dialkyl dithiophosphoric acids, $(RO)_2P(S)SH$, where the protonation step is presumably initiated by the phosphorus-containing reagent itself, since there is no strong acid catalyst present in their work.

On the other hand, Sakaki and Oae (18) have

Can. J. Chem. Downloaded from www.nrcresearchpress.com by 210.87.254.5 on 09/05/12
For personal use only.

Can. J. Chem. Downloaded from www.nrcresearchpress.com by 210.87.254.5 on 09/05/12
For personal use only.

proposed an intermediate similar to our Wittig-like structure **8**, or a six-centre analogue involving two selenoxide molecules, for the reduction of selenoxides with phosphine selenides. In their case the argument for such an intermediate was strengthened by the isolation of the corresponding phosphine oxides in high yield, whereas in the reaction which we are investigating, the possibility of isolating the (unknown) by-product $P_4O_4S_6$ was explored without success. Indirect evidence in our case in favor of the four-centre intermediate or transition state was provided by the isolation of triphenylphosphine sulfide (17%) from the reaction between triphenylphosphine oxide and P_4S_{10}. No triphenylphosphine was detected in this reaction, and this should be contrasted with the finding of Oae *et al.* (25) that the reaction between triphenylphosphine oxide and his *O,O*-diethyl dithiophosphoric acid reagent gave, after prolonged reaction times, only a 'minute amount' of triphenylphosphine sulfide.

In terms of the stoichiometry required by [1] we have verified that elemental sulfur is indeed produced in the reaction in an amount almost 100% of that required by theory. We have obtained no direct evidence as yet for the existence of a thiosulfoxide intermediate en route to the sulfide but further experiments are planned with a view to resolving this question. Although a 4:1 molar ratio of sulfoxide to P_4S_{10} should suffice for the conversion to sulfide, we have found that the reaction is much slower under these conditions and that a 2:1 ratio works much better in practice.

Two mechanistic suggestions made by Micetich (8) have also been examined in the present work. Micetich had suggested that because no particular care had been taken to exclude moisture in his experiments the effective reagent might be thiophosphoric acids, rather than P_4S_{10} itself. However, we have run comparison experiments in carefully dried dichloromethane and can find no significant difference in reaction rate between these and experiments run in regular laboratory-grade solvent. We have also demonstrated that the presence of pyridine is not necessary for the success of the reaction, in contrast to Micetich's proposal. In connection with this, it is interesting that Weintraub (13) reports the ready formation of a 4:1 molecular complex between pyridine (but not some pyridine derivatives) and phosphorus pentasulfide.

To add further credence to our proposal for an intermediate such as **8** in the reaction of sulfoxides with phosphorus pentasulfide we carried out a comparison of the rates of reaction, as measured by the extent of reduction in a fixed time period, in solvents of differing polarity (Table 3). It might be

TABLE 3. Effect of solvent polarity on reduction of diphenyl sulfoxide

Solvent	Dielectric constant (ε)[a]	Conversion to sulfide (%)[b]
CS_2	2.64	65
CH_2Cl_2	8.93	41
CH_3COCH_3	20.70	55
CH_3CN[c]	37.50	20[c]
	43.30	0[d]

[a]Reference 35.
[b]All reactions were run for 5 h at 25°C, using identical concentrations of diphenyl sulfoxide.
[c]Control experiments revealed that there is a slow competing reaction of P_4S_{10} with the solvent to produce thioacetamide (see Experimental).
[d]Difficulty in removal of the solvent makes this result slightly suspect. No sulfide was detectable by tlc but the recovery of starting sulfoxide was far from quantitative.

expected, given the polarity of the P=S and S=O bonds, that the reactants would be highly solvated in polar media, in contrast to the four-centre intermediate **8**, and thus that there would be an inverse correlation of rate with the dielectric constant of the medium. Although the data in Table 3 are not conclusive, there is some evidence that this is indeed the case, as was noted by Sakaki and Oae (18) for the selenoxide – phosphine selenide reaction. The reactivity of phosphorus pentasulfide towards hydroxylic solvents already referred to, however, limited the number of the more polar solvents which could be used. Again, although it is not clear from the data in Table 3, which are based on conversions, dichloromethane emerged from this part of our study as the solvent of choice for synthetic purposes, since high yields could be obtained in this solvent even although the reaction times were longer than those in acetone or carbon disulfide.

Direct evidence in favor of the mechanism outlined in [1] is not yet available but it must be pointed out that the proposal of an initial attack of the sulfoxide oxygen at phosphorus in P_4S_{10} does help to explain not only the observed order of reactivity within the sulfoxide series but also the lack of reactivity observed for the sulfones and sulfinate esters. Dipole–dipole repulsion between the S—O bonds in a sulfone has been used to rationalize the much smaller difference in dipole moment between dimethyl sulfone and DMSO (0.35 D) than between the latter and dimethyl sulfide (2.45 D) (26) and would presumably account for a lesser activity of the sulfone oxygen atoms in a nucleophilic sense. The apparent lack of reactivity of the sulfinate derivatives strongly suggests that the inductive electron-withdrawal effect of the σ-bonded oxygen atom plays a greater role in determining the nucleophilic reactivity

of the sulfinyl oxygen than does a resonance contribution of the type shown below.

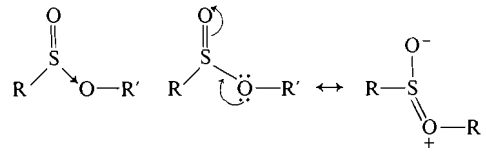

Finally, the greater reactivity of the selenoxides than their sulfoxide counterparts can be rationalized in terms of an intrinsically more polar Se—O bond in the selenoxide, although the greater bond length of this bond is probably also a factor.

The use of the readily available phosphorus pentasulfide affords an effective general method for converting sulfoxides to sulfides under mild conditions, and with a high degree of selectivity. Although the mechanism of this interesting reaction cannot be considered as established, there is a considerable weight of evidence in favor of an initial nucleophilic attack involving the oxygen atom of the sulfoxide at phosphorus, leading to the products via a relatively nonpolar intermediate or transition state. Further work to establish whether a thiosulfoxide intermediate is also formed is currently under way.

Experimental

Infrared spectra were recorded with a Perkin-Elmer 267 grating spectrophotometer, mass spectra with a Bell and Howell 21-490 spectrometer, and ^{1}H nmr spectra with a Varian EM-360 instrument. For the latter, solutions in deuteriochloroform containing tetramethylsilane as internal reference were used. Reactions were monitored by tlc on Merck DC-Alufolien Kieselgel 60F-254, with dichloromethane – hexane as solvent. Melting points were determined using an Electrothermal Mark II melting point apparatus and are corrected.

Sulfoxides

The sulfoxides used in this investigation were either commercially available or were prepared from the corresponding sulfides by one of two general procedures (27, 28). In the former case, the preliminary extraction of the crude reaction mixture with ether is best omitted.

Reduction of Sulfoxides with Phosphorus Pentasulfide

A representative procedure has already been described (9).

Attempted Reaction of Di-(p-methoxyphenyl) Sulfone with Phosphorus Pentasulfide

To a stirred solution of the sulfone (0.50 g, 1.80 mmol) in dichloromethane (10 ml) was added phosphorus pentasulfide (0.80 g, 1.80 mmol). The mixture was heated for 18 h under reflux. After cooling and dilution with water (20 ml) the organic layer was separated, dried ($MgSO_4$), and evaporated under reduced pressure to leave a colorless solid (0.42 g, 84%) identified (mp, mmp, ir) as unreacted starting material (29).

Attempted Reaction of 3,5-Dimethyl-1,2-oxathiolane-2-oxide (1) with Phosphorus Pentasulfide

The sulfinate (**1**) (1.00 mmol) was allowed to react with phosphorus pentasulfide (0.50mmol) in dichloromethane under the standard conditions. After the normal work-up procedure only starting material (78%) was recovered.

Preparation of 1β,2β-Diphenylethylene Sulfite

The title compound was prepared (17) as a 9:1 (*trans–cis*) mixture of isomers by the action of pyridine and thionyl chloride on *meso*-hydrobenzoin (30).

Reaction of 1β,2β-Diphenylethylene Sulfite with Phosphorus Pentasulfide

To a stirred mixture of the sulfite (**3**) (1.30 g, 5.00 mmol) in dichloromethane (15 ml) was added phosphorus pentasulfide (1.10 g, 2.50 mmol). After 12 h at room temperature the mixture was filtered and the solvent was removed under reduced pressure. The resultant yellow oil was chromatographed on silica gel; elution with hexane gave *trans*-stilbene (0.15 g, 17%) as colorless crystals, mp 122–124°C (lit. (31) mp 124°C). Further elution with a methylene chloride – hexane mixture (1:2, v/v) gave only the starting sulfite isomers (0.62 g, 48%),[5] mp 125–126°C (lit. (17) mp 122–126°C).

Reaction of Diphenyl Selenoxide with Phosphorus Pentasulfide

To a stirred solution of diphenyl selenoxide (32) (0.89 g, 3.57 mmol) in dichloromethane (12 ml) at 10°C was added phosphorus pentasulfide (0.79 g, 1.78 mmol). After 3 h, water (20 ml) was added and the organic layer was separated, dried ($MgSO_4$), and evaporated under reduced pressure to yield a pale yellow oil which was chromatographed on silica gel. Elution with a dichloromethane–hexane mixture (1:9, v/v) gave diphenyl selenide (0.71 g, 85%) as a colorless oil, spectroscopically identical (ir, nmr) with an authentic sample.[6]

Reaction of Dibenzyl Selenoxide with Phosphorus Pentasulfide

To a stirred solution of dibenzyl selenoxide (32) (0.12 g, 0.43 mmol) in dichloromethane (10 ml) was added phosphorus pentasulfide (0.098 g, 0.22 mmol). After 4 h at room temperature, water (20 ml) was added and the organic layer was separated, dried ($MgSO_4$), and evaporated under reduced pressure to yield a yellow oil which was chromatographed on silica gel. Elution with a dichloromethane–hexane mixture (1:9, v/v) gave dibenzyl selenide (0.094 g, 83%) as a pale yellow oil, spectroscopically identical (nmr, ms) with an authentic sample (33).

Attempted Reaction of Diphenyl Sulfoxide with Phosphorus Pentaselenide

To a stirred solution of diphenyl sulfoxide (1.01 g, 5.00 mmol) in dry (P_2O_5) dichloromethane (20 ml) was added phosphorus pentaselenide (2.31 g, 2.50 mmol) under an atmosphere of dry nitrogen. The mixture was heated 5 h under reflux, allowed to cool, and then filtered to remove insoluble inorganic material. Water (30 ml) was added and the organic layer was separated, dried ($MgSO_4$), and evaporated under reduced pressure to yield a colorless solid (0.90 g, 90%) spectroscopically identical (nmr, ms) with the starting sulfoxide.

Reaction of Triphenylphosphine Oxide with Phosphorus Pentasulfide

To a stirred solution of triphenylphosphine oxide (2.79 g, 10.00 mmol) in dichloromethane (30 ml) at 10°C was added phosphorus pentasulfide (2.22 g, 5.00 mmol). After 4 h the mixture was diluted with water (40 ml) and the organic layer was separated, dried ($MgSO_4$), and evaporated under reduced

[5]Although nmr evidence had indicated the presence of products other than the starting material in the crude reaction mixture, attempts to isolate these were unsuccessful.

[6]Commercially available from Ventron Corporation (Alfa Products).

Can. J. Chem. Downloaded from www.nrcresearchpress.com by 210.87.254.5 on 09/05/12
For personal use only.

pressure to yield a colorless solid which was chromatographed on silica gel. Elution with dichloromethane gave successively triphenylphosphine sulfide (0.50 g, 17%) as a colorless solid, mp 160–162°C (lit. (34) mp 157.5°C), spectroscopically identical (nmr, ms) with an authentic sample; and triphenylphosphine oxide (0.936 g, 34%), mp 151–153°C (lit. (31) mp 156°C), identical in all respects with authentic starting material.

*Reaction of Di-(*p*-tolyl) Sulfoxide with Phosphorus Pentasulfide (1 Equivalent)*

To a stirred solution of the sulfoxide (2.30 g, 10.00 mmol) in dichloromethane (30 ml) was added phosphorus pentasulfide (1.11 g, 2.50 mmol). After 4 h at room temperature the precipitated solid was removed by filtration. Soxhlet extraction (dichloromethane) for 6 h gave a yellow solid, mp 268–278°C, which could not be further purified. The filtrate was evaporated under reduced pressure and the residual oil was chromatographed on silica gel; elution with toluene gave successively, elemental sulfur (0.14 g, 98% of theory) and di-(*p*-tolyl) sulfide (0.96 g, 45%), mp 54–56°C (lit. (31) mp 57.3°C). Further elution with ethyl acetate gave the starting sulfoxide (0.78 g, 34%), mp 94–96°C (lit. (31) 94–96°C).

Reaction of Acetonitrile with Phosphorus Pentasulfide

A mixture of phosphorus pentasulfide (2.22 g, 5.00 mmol) in acetonitrile (10 ml) was stirred 12 h at room temperature and then diluted with water (100 ml). Evaporation of the dried ($MgSO_4$) dichloromethane extract (50 ml) under reduced pressure afforded a pale yellow oil which was chromatographed on silica gel. Elution with a dichloromethane–hexane mixture (2:1, v/v) gave thioacetamide (0.3 g, 20%), mp 114–116°C (lit. (31) mp 115–116°C), spectroscopically identical (nmr, ms) with an authentic sample.

Acknowledgements

We are grateful to the National Research Council of Canada and to the University of Toronto for financial support.

1. M. Hojo and R. Masuda. Tetrahedron Lett. 613 (1976).
2. Y. Ueno, T. Inoue, and M. Okawara. Tetrahedron Lett. 2413 (1977).
3. H. D. Durst, J. W. Zubrick, and G. R. Kieczykowski. Tetrahedron Lett. 1777 (1974).
4. M. Dreux, Y. Leroux, and P. Savignac. Synthesis, 506 (1974).
5. J. Drabowicz and S. Oae. Chem. Lett. 767 (1977).
6. R. G. Nuzzo, H. J. Simon, and J. San Filippo. J. Org. Chem. **42**, 568 (1977).
7. J. Drabowicz, T. Numata, and S. Oae. Org. Prep. Proced. Int. **9**, 63 (1977).
8. R. G. Micetich. Tetrahedron Lett. 971 (1976).
9. I. W. J. Still, S. K. Hasan, and K. Turnbull. Synthesis, 468 (1977).
10. J. P. A. Castrillon and H. H. Szmant. J. Org. Chem. **30**, 1338 (1965).
11. E. H. Amonoo-Neizer, S. K. Ray, R. A. Shaw, and B. A. Smith. J. Chem. Soc. 4296 (1965).
12. A. H. Cowley. J. Chem. Educ. **41**, 530 (1964).
13. P. M. Weintraub. Int. J. Sulfur Chem. **8**, 321 (1973).
14. B. Tornetta. Ann. Chim. **51**, 930 (1961).
15. W. P. Weber, P. Stromquist, and T. I. Ito. Tetrahedron Lett. 2595 (1974).
16. J. N. Gardner, S. Kaiser, A. Krubiner, and H. Lucas. Can. J. Chem. **51**, 1419 (1973).
17. Q. E. Thompson, M. M. Crutchfield, and M. W. Dietrich. J. Org. Chem. **30**, 2696 (1965).
18. K. Sakaki and S. Oae. Chem. Lett. 1003 (1977).
19. C. D. Mickey and R. A. Zingaro. Int. J. Sulfur Chem. **8**, 557 (1976).
20. D. L. J. Clive, W. A. Kiel, S. M. Menchen, and C. K. Wong. J. Chem. Soc. Chem. Commun. 657 (1977).
21. M. Mikolajczyk. Angew. Chem. Int. Ed. **5**, 419 (1966).
22. M. Mikolajczyk. Chem. Ind. (London), 2059 (1966).
23. A. F. Wells. Structural inorganic chemistry. 4th ed. Clarendon Press, Oxford, England. 1975. p. 695.
24. M. Mikolajczyk and J. Luczak. Chem. Ind. (London), 701 (1974).
25. S. Oae, A. Nakanishi, and N. Tsujimoto. Tetrahedron **28**, 2981 (1972).
26. A. L. McClellan. Tables of experimental dipole moments. W. H. Freeman & Co., San Francisco, CA. 1963. pp. 72–73.
27. M. S. Chauhan and I. W. J. Still. Can. J. Chem. **53**, 2880 (1975).
28. N. J. Leonard and C. R. Johnson. J. Org. Chem. **27**, 282 (1962).
29. F. Loth and A. Michaelis. Ber. **27**, 2540 (1894).
30. L. F. Fieser and K. L. Williamson. Organic experiments. 3rd ed. D. C. Heath and Co., Lexington, MA. 1975. pp. 266–268.
31. R. C. Weast (*Editor*). Handbook of chemistry and physics. 53rd ed. The Chemical Rubber Co., Cleveland, OH. 1972–1973.
32. M. Cinquini, S. Colonna, and R. Giovini. Chem. Ind. 1737 (1969).
33. D. L. Klayman and T. S. Griffin. J. Am. Chem. Soc. **95**, 197 (1973).
34. A. Michaelis and L. Gleichmann. Ber. **15**, 801 (1882).
35. Eastman Org. Chem. Bull. **47**, 1 (1975).

Can. J. Chem. Downloaded from www.nrcresearchpress.com by 210.87.254.5 on 09/05/12
For personal use only.

Recherches en série hétérocyclique. XXIX. Sur des voies d'accès à des thiéno, sélénolo, furo et pyrrolopyrroles[1]

SAMRETH SOTH ET MICHEL FARNIER[2]

Laboratoire de Polarographie Organique associé au C.N.R.S., Chimie des Hétérocycles, Faculté des Sciences Gabriel – 21000 Dijon, France

ET

CLAUDE PAULMIER

Laboratoire de Chimie Organique des Hétérocycles, U.E.R. Sciences – 76130 Mont-Saint-Aignan, France

Reçu le 11 octobre 1977

SAMRETH SOTH, MICHEL FARNIER et CLAUDE PAULMIER. Can. J. Chem. **56**, 1429 (1978).

L'action de l'azidoacétate d'éthyle sur les monoaldéhydes furanniques, thiophéniques et sélénophéniques permet l'accès aux furo-, thiéno- et sélénolo[2,3-*b*]- et -[3,2-*b*]pyrroles. Selon cette voie, seul le pyrrolo[2,3-*b*]pyrrole a pu être synthétisé en utilisant comme substrat le formyl-4 pyrrolecarboxylate-2 d'éthyle. Les thiéno et sélénolo[3,2-*b*]pyrroles peuvent aussi être obtenus par action du bromacétate d'éthyle sur un acétamido-3 thiophène ou sélénophène aldéhyde-2, puis cyclisation des acétamides *N*-substitués formés.

Pour les divers produits décrits, les caractéristiques observées en rmn, uv et spectrométrie de masse sont indiquées.

SAMRETH SOTH, MICHEL FARNIER, and CLAUDE PAULMIER. Can. J. Chem. **56**, 1429 (1978).

The reaction of ethyl azidoacetate with the monoaldehydes of furan, thiophene and selenophene yields furo-, thieno-, and selenolo[2,3-*b*]- and [3,2-*b*]pyrroles. Only pyrrolo[2,3-*b*]pyrrole could be prepared by this route using ethyl 4-formylpyrrole-2-carboxylate as the substrate. The thieno- and selenolo[3,2-*b*]pyrroles also could be obtained by the action of ethyl bromoacetate on 3-acetamidothiophene-2-aldehyde, or the corresponding selenolo compound, followed by cyclization of the *N*-substituted acetamide products.

The nmr, uv, and mass spectra are recorded for the various products described.

[Journal translation]

Introduction

Les systèmes hétérocycliques contenant un cycle pyrrolique orthocondensé à un cycle thiophénique, furannique, sélénophénique ou pyrrolique sont encore assez mal connus. Or de tels composés revêtent, à priori, une importante pharmacologique en tant qu'isostères de l'indole. Dans ce travail, nous proposons des voies d'accès aux systèmes hétérocycliques fondamentaux en séries aréno[2,3-*b*]- et

Série [2,3-*b*]

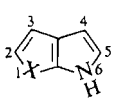

5*b* X = S
5*c* X = Se
10 X = NH

Série [3,2-*b*]

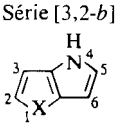

17*a* X = O
17*b* X = S
17*c* X = Se

-[3,2-*b*]pyrroliques. Nous envisagerons successivement les résultats obtenus dans chacune de ces deux séries.

[1]Une partie de ce travail a fait l'objet d'une publication préliminaire (1).

[2]Auteur auquel la correspondance peut être adressée.

Résultats

*Synthèses en série aréno[2,3-*b*]pyrrolique*

Antérieurement à nos travaux, aucun des hétérocycles de ce type n'avait été isolé. A priori, une méthode aisée pour accéder à de tels composés paraîssait être celle qui découle des travaux de Hemetsberger et Knittel (2), méthode utilisant la condensation de l'azidoacétate d'éthyle sur un aldéhyde hétérocyclique. C'est d'ailleurs cette voie qui a été mise en œuvre (3) pour obtenir selon le schéma 1 le thiéno[2,3-*b*]pyrrole **5***b*, le rendement global de la transformation **1***b* → **5***b* étant d'environ 35%.

Nous avons appliqué cette méthode en séries furannique et sélénophénique: les aldéhydes **1***a* et **1***c* se condensent avec l'azidoacétate d'éthyle avec de bons rendements. Par cyclisation, les acrylates substitués **2***a* et **2***c* donnent naissance aux esters **3***a* et **3***c*. Mais seule l'hydrolyse de l'ester **3***c* et la décarboxylation de l'acide **4***c* correspondant ont pu être réalisées, le sélénolo[2,3-*b*]pyrrole **5***c* étant isolé avec un rendement global de 20% par rapport à l'aldéhyde **1***c* de départ. A partir de l'ester **3***a*, il ne nous a pas été possible d'obtenir le système hétérocyclique fondamental correspondant, c'est-à-dire le furo[2,3-

Can. J. Chem. Downloaded from www.nrcresearchpress.com by 210.87.254.5 on 09/05/12
For personal use only.

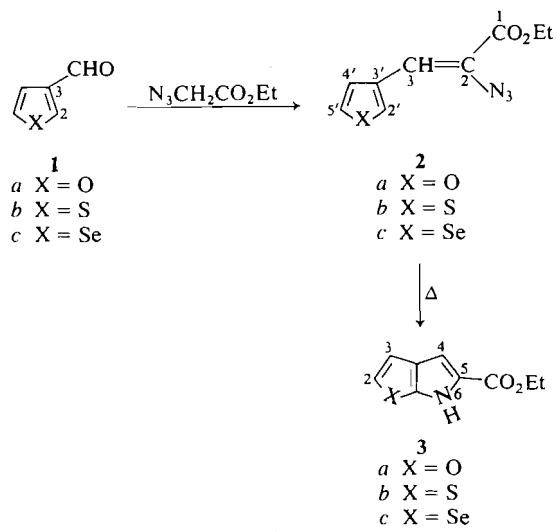

SCHÉMA 1

b]pyrrole. Ce résultat est vraisemblablement dû à l'instabilité de ce dérivé; d'ailleurs le furo[3,2-*b*]pyrrole est également nettement moins stable que ses isostères thiophénique et sélénophénique.

En série pyrrolique, tous nos essais de condensation de l'azidoacétate d'éthyle sur le pyrrolecarbaldéhyde-3 se sont soldés par des échecs. Par contre cette condensation a pu être réalisée sur l'ester aldéhyde-2,4 **6** (voir schéma 2); la réaction doit alors être con-

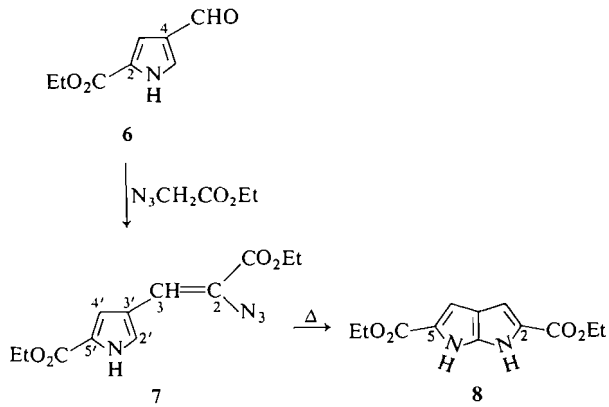

SCHÉMA 2

duite en utilisant l'azidoacétate d'éthyle comme solvant et en présence de pipéridine. Le produit de condensation **7** est isolé avec un rendement de 20%. Sa cyclisation conduit avec un bon rendement (80%) au diester pyrrolique **8** dont l'hydrolyse alcaline fournit le diacide **9**. La décarboxylation de ce dernier permet d'accéder au pyrrolo[2,3-*b*]pyrrole **10** mais seulement avec un rendement de 18%. A noter que ce pyrrolopyrrole est très instable: il doit être conservé à basse température et est très sensible à la moindre trace d'acidité.

*Synthèses en série aréno[3,2-*b*]pyrrolique*

Dans cette série, le thiéno[3,2-*b*]pyrrole est connu depuis les travaux de Snyder et coll. (4, 5). Beaucoup plus récemment Gronowitz *et al.* (6) ont obtenu ce même composé au départ de l'azido-3 thiophènecarbaldéhyde-2. Mais une méthode générale pour l'accès à ce même produit et à ses isostères sélénophénique et furannique paraîssait être celle envisagée en série [2,3-*b*]. Hemetsberger et Knittel (2) ont d'ailleurs condensé l'azidoacétate d'éthyle sur les aldéhydes-2 furannique **11***a* et thiophénique **11***b* et isolé les esters **13***a* et **13***b* (voir schéma 3). Nous avons étendu ces résultats à la série sélénophénique: par condensation de l'aldéhyde-2 **11***c* avec l'azidoacétate d'éthyle, on accède à l'acrylate substitué **12***c* dont la cyclisation fournit l'ester **13***c* (rendement global 45%).

Nous avons également cherché une autre voie d'accès aux esters **13** et nous avons opéré au départ des acétamido aldéhydes **14**. Les dérivés thiophénique **14***b* et sélénophénique **14***c* ont déjà été décrits (7). Quant à l'acétylamino-3 furannecarbaldéhyde-2 **14***a*, nous l'avons préparé comme ses homologues thiophénique et sélénophénique par formylation selon Vilsmeier et Haack du furyl-3 acétamide. Ce dernier composé a déjà été isolé (7) mais avec un faible rendement (20%): nous avons modifié le mode d'obtention préconisé et obtenu le furyl-3 acétamide avec un rendement de 70%. Sa formylation fournit l'aldéhyde **14***a* avec un rendement de 50%. La *N*-substitution des acétamides **14** par le bromacétate d'éthyle s'effectue dans l'acétone en présence de carbonate de potassium anhydre. Après chromatographie sur colonne de silicagel, les composés **15** ont pu être isolés mais avec un faible rendement (environ 30%) et non à l'état de pureté analytique. La cyclisation des composés thiophénique **15***b* et sélénophénique **15***c* s'effectue aisément et avec un excellent rendement (90%) et conduit aux esters **13***b* et **13***c*. Dans les mêmes conditions la réaction conduite à partir du dérivé furannique **15***a* se traduit par la formation de goudrons.

L'hydrolyse alcaline des esters **13** est quantitative et la décarboxylation des acides **16** obtenus conduit aux trois systèmes hétérocycliques fondamentaux **17***a* (rendement 30%), **17***b* (40%) et **17***c* (35%). Ainsi l'obtention des furo, thiéno et sélénolo[3,2-*b*]pyrroles à partir des aldéhydes-2 s'effectue globalement avec un rendement variant de 15 à 20%: la condensation de l'azidoacétate d'éthyle sur un aldéhyde hétérocyclique apparaît donc bien être la méthode de choix pour accéder à des aréno[3,2-*b*]pyrroles. Cependant cette condensation n'a pu être réalisée en série pyrrolique, ni au départ de l'aldéhyde-2, ni à partir de l'ester aldéhyde-2,5.

Can. J. Chem. Downloaded from www.nrcresearchpress.com by 210.87.254.5 on 09/05/12
For personal use only.

Can. J. Chem. Downloaded from www.nrcresearchpress.com by 210.87.254.5 on 09/05/12
For personal use only.

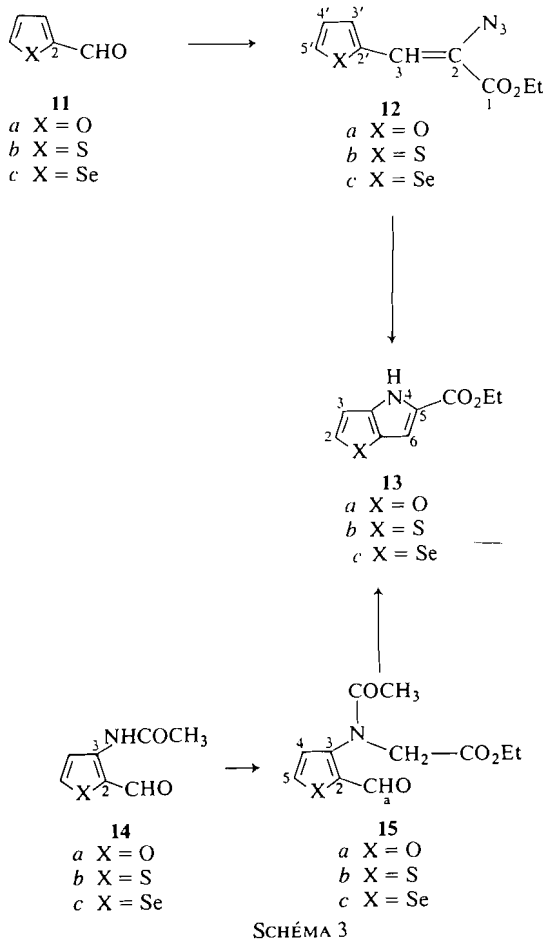

SCHÉMA 3

Spectres de résonance magnétique nucléaire

Les caractéristiques rmn des produits non cyclisés sont indiquées dans la partie expérimentale. Celles des furo, thiéno, sélénolo et pyrrolopyrroles substitués ou non sont groupées dans le tableau 1. Notons que nous avons reporté par ailleurs (3) les données relatives au thiéno[2,3-*b*]pyrrole **5***b*. Les valeurs indiquées au tableau 1 pour le thiéno[3,2-*b*]pyrrole **17***b* sont compatibles avec celles données par Gronowitz *et al.* (6) qui ont relevé ce spectre dans le tétrachlorure de carbone.

En dehors des couplages propres aux protons des cycles thiophénique, furannique, sélénophénique et pyrrolique, on note systématiquement la présence de couplages à longue distance: dans le cas des arénopyrroles de type [3,2-*b*], apparaissent un couplage $^5J_{36}$ de l'ordre de 0.7–0.9 Hz et un couplage $^6J_{25}$ de 1.1–1.2 Hz; pour les isomères de type [2,3-*b*], on relève un couplage $^6J_{25}$ de l'ordre de 0.8–1.0 Hz. Ces résultats sont tout à fait comparables à ceux observés (9) pour les thiénothiophènes.

Signalons enfin que l'ajout de D_2O se traduit normalement par l'élimination des couplages entre le proton lié à l'atome d'azote et ceux liés aux atomes de carbone du cycle pyrrolique. Ainsi, par exemple, le spectre du furo[3,2-*b*]pyrrole **17***a* relevé dans le DMSO-d_6 sans D_2O montre deux couplages supplémentaires: J_{45} = 2.9 et J_{46} = 1.7 Hz.

Spectres dans l'ultraviolet

Le tableau 2 regroupe les caractéristiques uv observées dans l'éthanol pour les arénopyrroles synthétisés. A noter que sur le spectre du furo[3,2-*b*]pyrrole **17***a* apparaît un épaulement vers 220 nm et sur celui du pyrrolo[2,3-*b*]pyrrole **10** une bande vers 190–200 nm difficilement analysable. A titre de comparaison, dans le même solvant, le pyrrole et le thiophène présentent respectivement des bandes à 207 nm (ε_{max} 7100) et 230 nm (ε_{max} 5400). Ainsi par rapport aux hétérocycles initiaux, on observe, et ce classiquement, un déplacement bathochrome. Si une certaine similitude se manifeste pour des systèmes appartenant à une même série [2,3-*b*] ou [3,2-*b*], par contre pour les séries [2,3-*b*] et [3,2-*b*], des différences apparaissent dans les valeurs des ε_{max} des deux bandes: la bande la plus intense se situe entre 210 et 220 nm pour la série [2,3-*b*] et entre 250 et 260 nm pour la série [3,2-*b*]. Enfin, signalons que les calculs théoriques de Klasinc et Trinajstic (10) concernant les spectres uv des thiénopyrroles ne prévoyaient pas cette différence entre les intensités relatives des bandes observées dans les deux séries étudiées.

Spectres de masse

Les spectres des deux sélénolopyrroles **5***c* et **17***c* ne diffèrent que par quelques variations dans les intensités relatives des pics observés. La présence du pic à 91 traduit la perte de l'atome de sélénium, la même fragmentation ayant d'ailleurs déjà été observée pour le sélénolo[3,2-*b*]sélénophène (11). De plus, le pic à 63 correspond à une perte de masse de 28 à partir de 91: c'est cette fois le cycle pyrrolique qui est fragmenté par perte de $CH_2N^{\bullet}$.

Si pour les sélénolopyrroles la perte initiale de l'atome de sélénium ne fait aucun doute, il est plus difficile pour les thiénopyrroles et pour le furopyrrole étudiés de préciser le cycle qui est fragmenté le premier: pour les thiéno[2,3-*b*]- et -[3,2-*b*]pyrroles dont les spectres sont très voisins, le pic moléculaire (*m/e* 123) est faible vis-à-vis du pic $M - H^{\bullet}$ et surtout du pic à 96. Celui-ci peut correspondre soit à la perte de C_2H_2 à partir du pic 122, coupure caractéristique du cycle thiophénique (réf. 12, p. 243), soit à la coupure du cycle pyrrolique (réf. 12, p. 325) par perte de HCN ou de $C_2H_3^{\bullet}$ à partir de 123. Pour le furo[3,2-*b*]pyrrole, le même problème se pose; cependant l'éventualité la plus probable semble être la coupure initiale du cycle furannique donnant le pic à 79

Can. J. Chem. Downloaded from www.nrcresearchpress.com by 210.87.254.5 on 09/05/12
For personal use only.

TABLEAU 1. Caractéristiques rmn de furo, thiéno, sélénolo et pyrrolopyrroles (solvant DMSO-d_6)

	Déplacement chimique des protons (ppm)[a]											
	Cycliques					Exocycliques	Constantes de couplage (Hz)					
Composé	H_2	H_3	H_4	H_5	H_6	$CO_2C_2H_5$	J_{23}	J_{25}	J_{36}	J_{45}	J_{46}	J_{56}
3*a*	7.59(d)	6.67(d)	6.80(s)			4.29(q) 1.29(t)	2.0					
3*c*	7.56(d)	7.17(d)	7.02(s)			4.28(q) 1.31(t)	5.6					
4*c*	7.54(d)	7.17(d)	6.97(s)				5.6					
5*c*[b]	7.41(2d)	7.15(d)	6.34(d)	7.01(2d)			5.5	0.9		2.9		
8		6.79(s)	6.79(s)			4.25(q) 1.30(t)						
9		6.80(s)	6.80(s)									
10[b]	6.52(d)	5.90(d)	5.90(d)	6.52(d)			2.9[d]					
13*a*	7.80(d)	6.64(2d)			6.80(2d)	4.31(q) 1.29(t)	2.1		0.9		1.8	
13*b*[c]	7.52(d)	7.02(2d)			7.12(s*)	4.32(q) 1.30(t)	5.4		0.7			
13*c*	7.98(d)	7.24(2d)			7.11(d)	4.29(q) 1.31(t)	5.6		0.7			
16*a*	7.77(d)	6.62(2d)			6.80(2d)		2.1		0.9		1.8	
16*b*	7.39(d)	6.97(2d)			6.99(s*)		5.2		0.7			
16*c*	7.97(d)	7.23(2d)			7.08(d)		5.5		0.7			
17*a*[b]	7.44(2d)	6.52(2d)		6.78(2d)	6.02(2d)		2.1	1.2	0.9			2.9
17*b*[b]	7.17(2d)	7.02(2d)		7.08(2d)	6.37(2d)		4.9	1.1	0.7			2.8
17*c*[b]	7.66(2d)	7.26(2d)		6.99(2d)	6.38(2d)		5.5	1.2	0.7			2.8

[a]s, singulet; d, doublet; t, triplet; q, quadruplet; s*, singulet élargi.
[b]Ajout de D_2O.
[c]Valeurs en bon accord avec celles de Gale *et al.* (8).
[d]$J_{23} = J_{45}$.

TABLEAU 2. Spectres dans l'ultraviolet (solvant éthanol)

Composé	λ_{max} (nm)	ε_{max}
5*b*	212	18 000
	250	3 600
5*c*	214	19 800
	251	4 100
10	243	8 800
17*a*	248	15 800
17*b*[a]	217	7 100
	258	12 600
17*c*	219	6 400
	266	12 200

[a]Le spectre uv du thiéno[3,2-*b*]pyrrole a déjà été relevé par Matteson et Snyder (5).

correspondant à la perte de CO (réf. 12, p. 108), suivie des fragmentations spécifiques du cycle pyrrolique (réf. 12, p. 325).

Quant au pyrrolo[2,3-*b*]pyrrole, on observe successivement la coupure des deux cycles pyrroliques avec les pertes caractéristiques (réf. 12, p. 325) pour chaque cycle, des fragments C_2H_2, HCN, $C_2H_3^{\bullet}$ et $CH_2N^{\bullet}$.

Partie expérimentale

Les analyses élémentaires out été effectuées par le Laboratoire Central de Microanalyses du C.N.R.S. Les spectres rmn ont été relevés sur un appareil Jeol C 60 HL en utilisant le TMS comme référence interne (m, multiplet; M, massif). Les spectres de masse ont été obtenus à l'aide d'un appareil Finnigan 3300 (température de la source 90°C, tension d'accélération 70 eV) et les spectres uv sur un appareil Beckman DK 2.

Matières premières

Les aldéhydes non commerciaux ont été préparés selon les méthodes décrites dans la littérature: furannecarbaldéhyde-3 (13), sélénophènecarbaldéhyde-2 (14), sélénophènecarbaldéhyde-3 (15), formyl-4 pyrrolecarboxylate-2 d'éthyle (16), acétylamino-3 thiophènecarbaldéhyde-2 et acétylamino-3 sélénophènecarbaldéhyde-2 (7).

*Condensation de l'azidoacétate d'éthyle sur le sélénophènecarbaldéhyde-3 1*c

A une solution d'éthanolate de sodium (0.92 g (0.04 at. g) de Na dans 30 cm^3 d'éthanol absolu), on ajoute goutte à goutte et à 0°C une solution de 1.59 g (0.01 mol) d'aldéhyde **1***c* et 5.16 g (0.04 mol) d'azidoacétate d'éthyle dans 20 cm^3 d'éthanol absolu. L'addition terminée, l'agitation est maintenue 2 h à 0°C; puis on verse sur une solution glacée de chlorure d'ammonium et on extrait à l'éther. La phase éthérée est lavée à l'eau à neutralité, séchée ($MgSO_4$) et évaporée. Le résidu est élué sur colonne d'acide silicique par le mélange benzène–hexane (1:2). Après recristallisation dans le pentane, on isole 1.62 g (60%) d'azido-2 (séléniényl-3′)-3 acrylate d'éthyle (**2***c*), pf 27°C; rmn ($CDCl_3$) δ: 1.37 (t, 3H), 4.34 (q, 2H), 6.88 (s élargi, H_3), 7.72 (2d, $J_{2'4'} = 1.1$ et $J_{4'5'} = 5.1$ Hz, $H_{4'}$), 7.97 (2d, $J_{2'5'} = 2.3$ et $J_{4'5'} = 5.1$ Hz, $H_{5'}$), 8.60 (m, $J_{2'4'} = 1.1$, $J_{2'5'} = 2.3$ et $J_{2'3} = 0.6$ Hz, $H_{2'}$). *Anal.* calc. pour $C_9H_9N_3O_2Se$: C 40.01, N 15.55, Se 29.23; trouvé: C 40.30, N 15.45, Se 29.39.

*Condensation de l'azidoacétate d'éthyle sur le furannecarbaldéhyde-3 1*a

On opère comme décrit ci-dessus mais au départ de l'aldéhyde **1***a* (0.96 g, 0.01 mol). Après recristallisation dans l'éther de pétrole, on obtient 1.43 g (69%) d'azido-2 (furyl-3′)-3 acrylate d'éthyle (**2***a*), pf 24°C; rmn ($CDCl_3$) δ: 1.36 (t, 3H), 4.37 (q, 2H), 6.78 (M, H_4· et H_3), 7.39 (M, $H_{5'}$), 7.82 (M, $H_{2'}$). Ce composé a tendance à se cycliser spontanément et aucun résultat analytique satisfaisant n'a pu être obtenu.

*6H-Sélénolo[2,3-*b*]pyrrolecarboxylate-5 d'éthyle (3*c*)*

On chauffe 45 min à reflux le dérivé **2***c* (1.75 g) dans 100

Can. J. Chem. Downloaded from www.nrcresearchpress.com by 210.87.254.5 on 09/05/12
For personal use only.

cm^3 de xylène. Après évaporation du solvant puis recristallisation dans un mélange benzène–hexane (1:2), on recueille 1.35 g (86%) de l'ester **3***c*, pf 133°C. *Anal.* calc. pour $C_9H_9NO_2Se$: C 44.64, N 5.78, Se 32.61; trouvé: C 44.64, N 5.80, Se 32.56.

*6H-Furo[2,3-*b*]pyrrolecarboxylate-5 d'éthyle (3*a*)*

On porte 1 h à reflux le composé **2***a* (1 g) dans 40 cm^3 de xylène. Le résidu obtenu après élimination du solvant est élué sur acide silicique par le chloroforme. On obtient, après recristallisation dans l'éther de pétrôle, 430 mg (50%) de l'ester **3***a*, pf 94°C. *Anal.* calc. pour $C_9H_9NO_3$: C 60.33, H 5.06, N 7.81, O 26.79; trouvé: C 60.49, H 5.16, N 7.86, O 26.60.

Hydrolyse de l'ester **3**c

On chauffe 2 h à reflux l'ester **3***c* (1.21 g, 0.005 mol) et 0.56 g de potasse dans 10 cm^3 d'eau. On acidifie par une solution glacée d'acide chlorhydrique 5 *N*. Le précipité qui apparaît, essoré, lavé à l'eau glacée à neutralité et séché, fournit quantitativement l'acide 6*H*-sélénolo[2,3-*b*]pyrrolecarboxylique-5 (**4***c*), pf (déc.) 208°C.

*6H-Sélénolo[2,3-*b*]pyrrole (***5***c)*

On chauffe 30 min à 160°C, 1 g d'acide **4***c* et 300 mg de chromite de cuivre (activé par du baryum) dans 30 cm^3 de quinoléine. Puis on refroidit rapidement par un bain d'eau glacée et on verse dans de l'éther. Le sel de cuivre est éliminé par filtration; la phase éthérée est traitée par une solution d'acide chlorhydrique *N*, puis lavée à l'eau à neutralité et séchée; enfin le solvant est évaporé. Après recristallisation dans le pentane, on isole 300 mg (38%) de sélénolo[2,3-*b*]pyrrole **5***c*, pf 54°C; spectre de masse: M^+ 173 (11%), 171 (72), 169 (34), 168 (15), 167 (12), 91 (100), 64 (17), 63 (55). *Anal.* calc. pour C_6H_5NSe: C 42.37, H 2.97, N 8.24, Se 46.42; trouvé: C 42.60, H 2.97, N 7.99, Se 46.03.

Condensation de l'azidoacétate d'éthyle sur le formyl-4 pyrrolecarboxylate-2 d'éthyle **6**

On porte 6 h à 70°C l'ester aldéhyde **6** (16.7 g, 0.1 mol) dans 15 cm^3 de pipéridine et 80 cm^3 d'azidoacétate d'éthyle. Après retour à température ambiante, on verse dans 400 cm^3 d'éther, lave à l'acide chlorhydrique *N*, puis à l'eau jusqu'à neutralité. La phase éthérée est séchée et évaporée. L'excès d'azidoacétate d'éthyle est récupéré par distillation sous 0.05 Torr. L'huile résiduelle ainsi obtenue est éluée sur colonne d'acide silicique par le mélange chloroforme–acétone (10:1). Après recristallisation dans le benzène, on recueille 5.55 g (20%) d'azido-2 (éthoxycarbonyl-5′pyrrolyl-3′)-3 acrylate d'éthyle (7), pf 139°C; rmn ($CDCl_3$) δ: 1.37 (t, 6H), 4.37 (q, 2H), 4.40 (q, 2H), 6.94 (s, H_3), 7.34 (m, $H_{4'}$), 7.57 (m, $H_{2'}$). *Anal.* calc. pour $C_{12}H_{14}N_4O_4$: C 51.79, H 5.07, N 20.14, O 23.00; trouvé: C 51.95, H 5.00, N 20.01, O 22.86.

*1H,6H-Pyrrolo[2,3-*b*]pyrroledicarboxylate-2,5 de diéthyle (***8***)*

A 500 cm^3 de xylène portés à ébullition, on ajoute, par petites portions et en 15 min environ, 5 g du composé **7** fraîchement recristallisé. L'addition terminée, le reflux est maintenu durant 15 min, puis on refroidit rapidement par un bain d'eau glacée. Le précipité formé est essoré. Le filtrat est évaporé et le résidu, repris par de l'éther, abandonne également des cristaux de diester. Après recristallisation dans un mélange éthanol–eau (4:1) de l'ensemble des solides recueillis, on obtient 3.6 g (80%) du diester **8**, pf 216°C. *Anal.* calc. pour $C_{12}H_{14}N_2O_4$: C 57.59, H 5.64, N 11.20, O 25.58; trouvé: C 57.50, H 5.58, N 11.17, O 25.64.

*Acide 1H,6H-pyrrolo[2,3-*b*]pyrroledicarboxylique-2,5 (***9***)*

On chauffe 35 min à 75°C 3.5 g du diester **8** et 3.0 g de potasse dans 60 cm^3 d'eau. Après retour à température ambiante, une partie du diester qui n'a pas réagi est recueillie par filtration. Le filtrat est d'abord extrait au chloroforme pour récupérer le diester à l'état dissous, puis acidifié à 0°C par une solution d'acide chlorhydrique 5 *N*. Le précipité ainsi obtenu est essoré, lavé à l'eau glacée et séché. Au total, on obtient 1.45 g du diester **8** de départ et on isole 1.51 g (rendement 95% par rapport à la quantité de diester qui a réagi) du diacide **9**, pf (déc.) 255°C.

*1H,6H-Pyrrolo[2,3-*b*]pyrrole (***10***)*

A une suspension de 2 g de chromite de cuivre dans 40 cm^3 de quinoléine portés à 140°C, on ajoute, en une fois, le diacide **9** (5.82 g, 0.03 mol) et on maintient à 140°C pendant 45 min. Après avoir été refroidi rapidement, le mélange réactionnel est versé dans de l'éther (préalablement lavé par une solution de potasse). Le sel de cuivre est éliminé par filtration, le solvant évaporé et la quinoléine distillée sous 0.01 Torr. Le résidu est repris par de l'hexane (traité également par une solution de potasse) et le précipité qui apparaît est recristallisé dans le benzène. On obtient ainsi 570 mg (18%) de pyrrolo[2,3-*b*]pyrrole **10**, pf 153°C; spectre de masse: M^+ 106 (100%), 105 (27), 80 (5), 79 (60), 78 (16), 53 (14), 52 (48), 51 (25), 50 (14). *Anal.* calc. pour $C_6H_6N_2$: C 67.92, H 5.66, N 26.41; trouvé: C 67.86, H 5.87, N 26.44.

Condensation de l'azidoacétate d'éthyle sur le sélénophènecarbaldéhyde-2 **11**c

On opère comme décrit précédemment pour l'isomère **1***c*: au départ de l'aldéhyde **11***c* (1.59 g, 0.01 mol), après chromatographie sur acide silicique (éluant benzène–hexane (1:1)) et recristallisation dans l'éther de pétrole, on recueille 1.5 g (55%) d'azido-2 (séléniényl-2′)-3 acrylate d'éthyle **12***c*, pf 50°C; rmn ($CDCl_3$) δ: 1.38 (t, 3H), 4.34 (q, 2H), 7.21 (m, $J_{33'} = 0.7$ et $J_{35'} = 0.9$ Hz, H_3), 7.25 (2d, $J_{3'4'} = 3.9$ et $J_{4'5'} = 5.3$ Hz, $H_{4'}$), 7.44 (m, $J_{3'4'} = 3.9$, $J_{3'5'} = 1.3$ et $J_{33'} = 0.7$ Hz, $H_{3'}$), 8.23 (m, $J_{3'5'} = 1.3$, $J_{4'5'} = 5.3$ et $J_{35'} = 0.9$ Hz, H_5). *Anal.* calc. pour $C_9H_9N_3O_2Se$: C 40.01, H 3.36, N 15.55, Se 29.23; trouvé: C 40.07, H 3.49, N 15.54, Se 29.18.

*4H-Sélénolo[3,2-*b*]pyrrolecarboxylate-5 d'éthyle (***13***c)*

On chauffe 45 min à 110°C 4 g du composé **12***c* dans 200 cm^3 de xylène. Après évaporation du solvant et recristallisation dans un mélange benzène–hexane (1:1), on isole 2.95 g (82%) de l'ester **13***c*, pf 140°C. *Anal.* calc. pour $C_9H_9NO_2Se$: C 44.64, N 5.78, Se 32.61; trouvé: C 44.37, N 5.89, Se 32.40.

*4H-Furo[3,2-*b*]pyrrolecarboxylate-5 d'éthyle (***13***a)*

Cet ester a été préparé avec un rendement de 58% à partir du furfural selon le procédé décrit par Hemetsberger et Knittel (2); pf 121°C (litt. (2) pf 121.5°C).

*4H-Thiéno[3,2-*b*]pyrrolecarboxylate-5 d'éthyle (***13***b)*

Ce composé a été obtenu selon Hemetsberger et Knittel (2); pf 130°C (litt. (2) pf 131°C, litt. (8) pf 132.5–133°C).

N-*Furyl-3 acétamide*

A une solution refroidie à 0°C de 8 g d'acétyl-3 furanne dans 150 cm^3 de chloroforme, on ajoute 8 cm^3 d'acide sulfurique concentré en maintenant la température au dessous de 5°C. Puis on introduit, goutte à goutte et à 0°C, 80 cm^3 d'une solution chloroformique d'acide hydrazoïque préparée à partir de 35 g d'azoture de sodium et 200 cm^3 de chloroforme. L'addition terminée, l'agitation est maintenue 15 min puis on traite par 200 cm^3 d'eau. La phase organique est lavée à la soude, puis à l'eau à neutralité. Les phases aqueuses rassemblées sont rendues basiques puis extraites en continu par l'éther pendant plusieurs heures. Après évaporation de l'ensemble des phases organiques puis recristallisation dans un mélange chloroforme–hexane (1:1), on obtient 6.4 g (70%) de furyl-3 acétamide, pf 112°C (litt. (7) pf 112°C).

Can. J. Chem. Downloaded from www.nrcresearchpress.com by 210.87.254.5 on 09/05/12
For personal use only.

*Acétylamino-3 furannecarbaldéhyde-2 (**14**a)*

A une solution de 2.4 g de furyl-3 acétamide dans 10 cm^3 de diméthylformamide, on ajoute goutte à goutte, à 0°C et sous agitation, 3.5 g d'oxychlorure de phosphore. Le mélange se solidifie et il est laissé 30 min à température ambiante. On verse alors dans 200 cm^3 d'eau contenant 12 g d'acétate de sodium. L'extraction en continu par l'éther fournit l'aldéhyde **14***a* que l'on recristallise (rendement 50%) dans un mélange chloroforme–éther de pétrole (1:9), pf 76°C; rmn ($CDCl_3$) δ: 2.15 (s, 3H), 7.46 (m, H_4 et H_5), 9.77 (s, 1H). *Anal.* calc. pour $C_7H_7NO_3$: C 54.90, H 4.58, N 9.15; trouvé: C 54.82, H 4.90, N 9.04.

*Condensation du bromacétate d'éthyle sur les acétamido aldéhydes **14***

Une solution de 5 mmol d'un acétamido aldéhyde **14** dans 25 cm^3 d'acétone est portée 3 jours à reflux en présence de 1.1 g de bromacétate d'éthyle et de 1.5 g de carbonate de potassium anhydre. Après refroidissement, filtration et concentration, on recueille un résidu qui est repris par l'eau. On extrait trois fois à l'éther. La solution éthérée est lavée à l'eau, séchée et évaporée. L'huile brune obtenue est éluée sur colonne de silicagel d'abord par le benzène pour séparer l'acétamido aldéhyde **14** de départ, puis par un mélange benzène–chloroforme (1:1) pour isoler l'ester **15**. On obtient ainsi les composés de structure **15** sous forme d'huiles avec un rendement voisin de 30%. Ils sont caractérisés par leurs spectres de rmn et n'ont pu être isolés à l'état de pureté analytique. Spectres rmn ($CDCl_3$) δ: **15***a*: 1.27 (t, 3H), 2.05 (s, 3H), 4.17 (q, 2H), 4.24 (s, 2H), 6.66 (d, J_{45} = 1.7 Hz, H_4), 7.65 (d, J_{45} = 1.7 Hz, H_5), 9.81 (s, H_a); **15***b*: 1.20 (t, 3H), 1.95 (s, 3H), 4.15 (q, 2H), 4.35 (s, 2H), 7.18 (d, J_{45} = 5.3 Hz, H_4), 7.79 (d, J_{45} = 5.3 Hz, H_5), 10.08 (s, H_a); **15***c*: 1.20 (t, 3H), 1.92 (s, 3H), 4.13 (q, 2H), 4.32 (s, 2H), 7.43 (d, J_{45} = 5.9 Hz, H_4), 8.47 (d, J_{45} = 5.9 Hz, H_5), 9.98 (s, H_a).

*Cyclisation des composés **15***

*Cyclisation de **15**b*

A une solution d'éthanolate de sodium (100 mg de Na dans 20 cm^3 d'éthanol absolu), on ajoute 1 mmol du composé **15***b* et on porte à reflux pendant 1 h. Après refroidissement on verse dans l'eau et on extrait à l'éther. La phase éthérée est lavée à l'eau, séchée et évaporée. Après recristallisation (solvant éther de pétrole–chloroforme (9:1)), on isole (90%) l'ester **13***b*, pf 130°C.

*Cyclisation de **15**c*

De même au départ de **15***c*, on obtient (90%) l'ester **13***c*, pf 140°C.

*Cyclisation de **15**a*

Par contre, dans les mêmes conditions, la réaction effectuée sur **15***a* ne fournit que des goudrons.

*Hydrolyse des esters **13***

Les acides **16** sont obtenus quantitativement par hydrolyse alcaline des esters **13** selon le mode opératoire décrit pour l'hydrolyse de l'ester **3***c*.

Acide 4*H*-furo[3,2-*b*]pyrrolecarboxylique-5 (**16***a*), pf (déc.) 237°C.

Acide 4*H*-thiéno[3,2-*b*]pyrrolecarboxylique-5 (**16***b*), pf (déc.) 239°C (solvant de recristallisation, eau), (litt. (4) pf 203–204°C).

Acide 4*H*-sélénolo[3,2-*b*]pyrrolecarboxylique-5 (**16***c*), pf (déc.) 220°C.

*Décarboxylation des acides **16***

La décarboxylation des acides **16** est réalisée comme décrit précédemment dans le cas de l'acide **4***c*, mais en ne dépassant pas 120–130°C pour le dérivé furannique **16***a*, en remplaçant le chromite de cuivre par de la poudre de cuivre dans le cas de l'acide thiophénique **16***b* et en acidifiant avec précaution avec de l'acide chlorhydrique 0.2 *N* pour les dérivés furannique et thiophénique.

4*H*-Furo[3,2-*b*]pyrrole (**17***a*), pf 39°C (solvant de recristallisation, pentane); spectre de masse: M^+ 107 (97%), 79 (26), 53 (53), 52 (100), 51 (19), 50 (14). *Anal.* calc. pour C_6H_5NO: C 67.28, H 4.70, N 13.07, O 14.94; trouvé: C 67.28, H 4.90, N 12.96, O 14.77.

4*H*-Thiéno[3,2-*b*]pyrrole (**17***b*), pf 29°C (solvant de recristallisation, hexane) (litt. (5) pf 25–28°C, (6) pf 24–26°C); spectre de masse: M^+ 123 (5%), 122 (25), 96 (100), 95 (15), 70 (25), 69 (19).

4*H*-Sélénolo[3,2-*b*]pyrrole (**17***c*), pf 38°C (solvant de recristallisation éther de pétrole); spectre de masse: M^+ 173 (5%), 171 (53), 169 (24), 168 (8), 167 (8), 91 (100), 64 (14), 63 (39). *Anal.* calc. pour C_6H_5NSe: C 42.37, N 8.24, Se 46.42; trouvé: C 42.14, N 8.26, Se 46.20.

1. K. N. Java, S. Soth, M. Farnier et C. Paulmier. C. R. Acad. Sci. Ser. C, **281**, 793 (1975).
2. H. Hemetsberger et D. Knittel. Monatsh. Chem. **103**, 194 (1972).
3. S. Soth, M. Farnier et P. Fournari. Bull. Soc. Chim. Fr. 2511 (1975).
4. H. R. Snyder, L. A. Carpino, J. F. Zack et J. F. Mills. J. Am. Chem. Soc. **79**, 2556 (1957).
5. D. S. Matteson et H. R. Snyder. J. Org. Chem. **22**, 1500 (1957).
6. S. Gronowitz, C. Westerlund et A.-B. Hörnfeldt. Acta Chem. Scand. B, **30**, 391 (1976).
7. G. Ah-Kow, C. Paulmier et P. Pastour. Bull. Soc. Chim. Fr. 151 (1976).
8. W. W. Gale, A. N. Scott et H. R. Snyder. J. Org. Chem. **29**, 2160 (1964).
9. A. Bugge, B. Gestblom et O. Hartmann. Acta Chem. Scand. **24**, 105 (1970).
10. L. Klasinc et N. Trinajstic. Tetrahedron, **27**, 4045 (1971).
11. S. Gronowitz, T. Frejd et A.-B. Hörnfeldt. Chem. Scr. **5**, 236 (1974).
12. Q. N. Porter et J. Baldas. Mass spectrometry of heterocyclic compounds. Wiley-Interscience, New York, NY. 1971.
13. S. Gronowitz et U. Michael. Ark. Kemi, **32**, 283 (1971).
14. Yu. K. Yur'ev et N. N. Mezentsova. Zh. Obshch. Khim. **27**, 179 (1957).
15. C. Paulmier et P. Pastour. C. R. Acad. Sci. Ser. C, **265**, 926 (1967).
16. P. Fournari, M. Farnier et C. Fournier. Bull. Soc. Chim. Fr. 283 (1972).

Gas phase photolysis of 1-pentene and 1-pentene-d_{10} at 7.1 and 7.6 eV. Kinetic considerations

ANDRZEJ WIĘCKOWSKI[1] AND GUY J. COLLIN

Département des Sciences Pures, Université du Québec à Chicoutimi, Chicoutimi (Qué.), Canada G7H 2B1

Received December 13, 1977

ANDRZEJ WIĘCKOWSKI and GUY J. COLLIN. Can. J. Chem. **56**, 1435 (1978).

The gas phase photolysis of *n*-pentene was carried out in a static system using nitrogen resonance lines at 7.10–7.11 eV (≃ 174 nm) and the bromine line at 7.6 eV (≃ 163 nm). The mechanism for the photolysis was proposed and compared to what was concluded at 8.4 eV (147 nm, the xenon resonance line). The kinetics of the decomposition of the excited C_3H_5* radicals formed in the primary photochemical process and the C_5H_{11}* radicals formed by the addition of hydrogen atoms to the parent molecules were discussed. The investigations were extended to the *n*-C_5D_{10} photolytic system. The observed decomposition rate constants of the excited pentyl radicals as well as the secondary non-equilibrium isotope effects agree with the data published earlier. It is concluded from these experiments that, at least at 7.6 eV, hot hydrogen atoms are produced.

Only a small fraction of the C_3H_5* radicals decompose and yield allene. At the same time the combined primary–secondary non-equilibrium isotope effects are much less than those calculated for the 'pure' primary isotope effects. To account for these observations, it is assumed that the C_3H_5* radicals are formed with a wide spread in the internal energies. Since the threshold of the decomposition of the excited C_3H_5* radical lies above its mean excess energy (calculated on the statistical basis), an analogy in the energy-distribution functions on the radicals activated photochemically and thermally may be suggested. If so, an inverse secondary isotope effect may contribute to the gross effect involved in the C_3H_5* radical decomposition.

ANDRZEJ WIĘCKOWSKI et GUY. J. COLLIN. Can. J. Chem. **56**, 1435 (1978).

Nous avons étudié la photolyse du pentène normal en phase gazeuse en utilisant l'émission d'une lampe basse pression à azote (7.10–7.11 eV, ≃ 174 nm) et à brome (7.6 eV, ≃ 163 nm). La décomposition de la molécule photoexcitée a été observée et comparée à celle observée à 8.4 eV (147 nm) en utilisant une lampe de résonance à xénon. La cinétique de fragmentation des radicaux C_3H_5* formés dans les processus primaires de fragmentation et C_5H_{11}* formés par addition des atomes d'hydrogène sur la molécule parente a été discutée. La photolyse du pentène-d_{10} a aussi été faite à ces longueurs d'onde. Les constantes de vitesse de décomposition ainsi que l'effet isotopique secondaire "non à l'équilibre" observés des radicaux pentyls excités sont en bon accord avec les données publiées dans la littérature. De ces expériences, on conclue qu'au moins à 7.6 eV, des atomes d'hydrogène chauds sont impliqués dans le système.

Une fraction mineure des radicaux C_3H_5* se fragmentent en produisant l'allène. Dans ce cas un effet isotopique "non à l'équilibre" primaire et secondaire combiné est plus petit que celui prévu sur la base d'un seul effet primaire. Le fait que les radicaux C_3H_5* sont formés avec une distribution très large d'énergie, est utilisé pour réconcilier l'effet observé à celui prévu. Puisque le seuil de fragmentation des radicaux C_3H_5* est situé bien au-dessus de l'énergie moyenne contenu par ces radicaux (calculé sur une base statistique), on suggère que le présent système (photochemiquement activé) est analogue à un système thermiquement activé. S'il en est ainsi, un effet isotopique secondaire, inverse, peut contribuer à l'effet isotopique total mesuré pour la fragmentation des radicaux C_3H_5*–C_3D_5*.

Introduction

In recent work in our laboratory, the vacuum uv photolysis (for a review, see ref. 1) of *cis*- and *trans*-2-butene (2, 3) and normal and isobutene (4) at 7.1 eV (a nitrogen resonance lamp) has been studied. All the systems had major primary processes involving the elimination of methyl radicals and hydrogen atoms:

[1] $$C_4H_8^{**} \rightarrow C_3H_5^* + CH_3$$

$$\Delta H = 75.4 \text{ kcal mol}^{-1}$$

[2] $$C_4H_8^{**} \rightarrow C_4H_6 + 2H$$

The resulting C_3H_5* radicals decompose, yielding mainly allene (2), and the mode of the decomposition has been found of particular interest since it reflects the energy partitioning between the radical fragments formed in process [1]. The hydrogen atoms formed predominantly in process [2] added to the parent molecules producing a C_4H_9* species with excess internal energy capable of undergoing decomposition (except for isobutene):

[3] $$s\text{-}C_4H_9^* \rightarrow C_3H_6 + CH_3$$

The yield of propylene formed in this process was reported as a function of butene pressure, with the conclusion that hot hydrogen atoms were formed in

[1]Permanent address: Chemistry Department, Warsaw University, Radiochemistry, Zwirki i Wigury 101, 02-089 Warsaw, Poland.

Can. J. Chem. Downloaded from www.nrcresearchpress.com by 210.87.254.40 on 09/05/12
For personal use only.

Can. J. Chem. Downloaded from www.nrcresearchpress.com by 210.87.254.40 on 09/05/12
For personal use only.

the system studied. The excess kinetic energy carried by the H atoms is probably different in each photolytic butene system (3).

The gas phase photolysis of *n*-pentene represents another possibility where photochemically initiated radicals possessing a certain excess energy are produced (5, 6)

[4] $$C_5H_{10}^{**} \rightarrow C_3H_5^{*} + C_2H_5$$
$$\Delta H = 71.4 \text{ kcal mol}^{-1}$$

and

[5] $$C_5H_{10} + H \rightarrow C_5H_{11}^{*}$$
$$\Delta H = -41.2 \text{ kcal mol}^{-1}$$

[6] $$C_5H_{11}^{*} \rightarrow C_3H_6 + C_2H_5$$
$$\Delta H = 24 \text{ kcal mol}^{-1}$$

Thus, the present report is a logical continuation of our earlier work. In order to investigate the primary photochemical processes of *n*-pentene as a function of photon energy, two resonance lamps have been applied (a nitrogen lamp, 7.1 eV, and a bromine lamp, 7.6 eV). For the purpose of comparison, the earlier data on this system obtained at 8.4 eV (a xenon resonance lamp) are included and discussed. Experiments with perdeuterated *n*-pentene have also been carried out. It is hoped that the presented rate constants of the decomposition of the excited radicals, as well as the observed non-equilibrium isotope effects, will be of some value from the viewpoint of the theory of unimolecular decomposition processes initiated by the absorption of a quantum of light by organic molecules (7).

Experimental

The spectral characteristics of the nitrogen lamp have been reported previously (2). The all-suprasil quartz bromine lamp (8) was filled with bromine (0.5 cm^3) and argon (0.3 Torr) and operated by electrodeless discharge from a Raytheon microwave power unit connected to a U-shaped microwave cavity. In the preparation of this lamp all measures recommended by Loucks and Cvetanović (8) were observed. The vapour pressure of bromine was controlled by placing a 'cold finger' of the lamp in a Dewar flask containing the Dry Ice – methanol bath (ca. −78°C). The emission spectrum was taken with a 0.5 m vacuum monochromator (235 GCA/McPherson instrument) with a 50 μm slit at a scanning speed of 5 nm/min. The spectrum is presented in Fig. 1. Substantial improvement in the performance (spectral purity) of the lamp as compared to the spectra previously reported was achieved (8). The output of the lamp was about 2×10^{14} quanta s^{-1} as determined by ethylene actinometry with $\Phi(C_2H_2) = 0.75$ (9).

The remaining details on the experimental and chromatographical procedure were essentially the same as described in previous studies of this laboratory (2, 6, 10). The results described below were corrected for the presence of small amounts of impurities (propylene, propane, 1,3-butadiene, less than 0.001%) in *n*-C_5H_{10} (NBS standard sample) and *n*-C_5D_{10} (Merck, Sharp and Dohme, Canada Ltd.) starting materials.

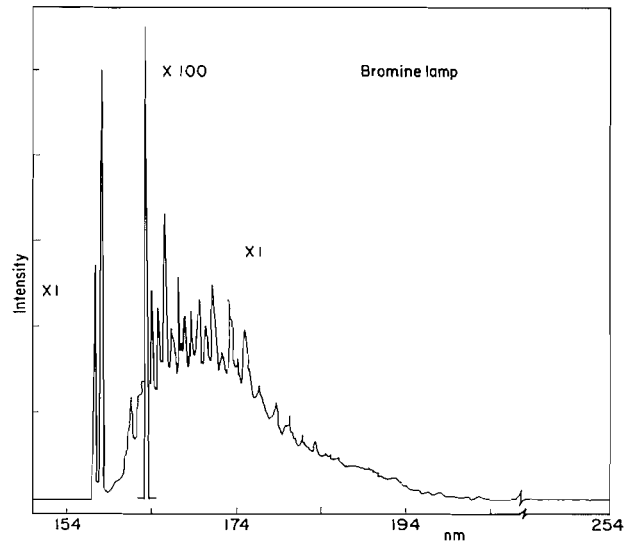

FIG. 1. Emission spectra from the bromine lamp between 150 and 260 nm. Note that the 163 nm (7.6 eV) line has been attenuated by a factor of 100.

Results

With ethylene as an actinometer, the quantum yields of the products at the 7.1 eV as well as the 7.6 eV photolysis of *n*-pentene were determined, and the results are shown in Table 1. The results of unscavenged experiments are given in the first columns of the table and NO and HI scavenged experiments are summarized in the second and the third columns, respectively. If not otherwise indicated it was found that a 10% addition of HI was sufficient to scavenge the radicals present. This observation appears to be of general validity for many organic photochemical systems, although some exceptions have been noted (11). Among the products given in Table 1 only propylene and allene quantum yields were strongly dependent on the *n*-pentene pressure and the pertinent results are summarized in Figs. 2 and 3. The experiments with the perdeuterated compound, C_5D_{10}, are also included in these figures. It should be noted that for each case a constant quantum yield value, no longer dependent on the total pressure, was attained at pressure above 20 Torr (Table 2). Assuming steady-state conditions for allene and propylene precursors, it is thus possible to construct a Stern–Volmer plot for the reciprocal of the product quantum yields, from which these constant values were subtracted, vs. total pressure, and such plots for propylene (H and D) and allene (H and D) for both photon energies are shown in Figs. 2 and 3, respectively.

Discussion

As shown in Table 1, the yields of acetylene, ethy-

TABLE 1. The photolysis of 1-pentene at 7.1–7.6 eV. The experimental product quantum yields in the absence and presence of additives at the total pressure 2.5 Torr (333 N m^{-2})[a]

	No additives		10% NO added		10% HI added	
	7.1 eV	7.6 eV	7.1 eV	7.6 eV	7.1 eV	7.6 eV
Methane	n.d.[b]	0.008	n.d.	n.d.	0.13	0.17
Acetylene	0.004	0.010	0.005	0.010	0.007	0.017
Ethylene	0.26	0.33	0.26	0.33	0.31	0.39
Ethane	0.020	0.030	n.d.	n.d.	0.49	0.54
Propylene	0.061	0.075	0.063	0.078	0.65	0.58
Propane	0.032	0.016	n.d.	n.d.	0.022	0.022
Allene	0.015	0.031	0.016	0.032	0.016	0.032
1,3-Butadiene	0.080	0.090	0.080	0.090	0.080	0.090
1-Butene	0.006	0.006	n.d.	n.d.	0.020	0.020
n-Butane	0.050	0.060	n.d.	n.d.	n.d.	n.d.

[a]C_5 and C_6 products were observed but they are not discussed here.
[b]Not determined is designated by n.d.

TABLE 2. The photolysis of 1-C_5H_{10} at 7.1 and 7.6 eV. The constant quantum yield values of propylene and allene obtained at a pressure higher than 2700 N m^{-2}[a]

	7.1 eV		7.6 eV	
	C_5H_{10}	C_5D_{10}	C_5H_{10}	C_5D_{10}
Φ(propylene)	0.040	0.030	0.040	0.035
Φ(allene)	0.011	0.004	0.024	0.008

[a]20 Torr.

lene, and 1,3-butadiene are virtually the same in unscavenged experiments and experiments scavenged by NO. Moreover, they were only slightly dependent on the total pressure. This suggests that they are formed in the primary processes and that their yields may be calculated directly from the actinometry. Allene and propylene, whose yields are no longer pressure dependent (the constant values determined at high pressure, Table 2), are also probably formed in the primary processes. The yields of radicals formed in the studied systems were obtained by subtracting the yields of the hydrocarbons found in the presence of NO from those obtained in the experiments with HI (Table 1). They represent the major products of the primary photodecomposition of *n*-pentene molecules at both photon energies. As seen in Tables 1 and 4, the C_3H_5, C_2H_5, and CH_3 radicals are formed in the prevalent amounts. The remaining products found in the unscavenged or the HI scavenged experiments are formed in secondary processes which are not discussed in the present report. The exceptions are the decomposition processes of the radicals which are propylene and allene precursors (see below).

Considering the material presented in Tables 1 and 2 and the above remarks, the mechanisms shown in Table 3 for 7.1 eV and 7.6 eV photolysis are proposed. For the purpose of comparison, this table also includes the data obtained at 8.4 eV (5, 6). The particular reactions are not discussed since it has been done for 8.4 eV photolysis in the earlier work in this laboratory (5, 6). The similar criteria of choice have been applied to the present interpretation. One may judge whether or not a good, consistent account has been made by comparing the experimental and mechanistic product quantum yields. For 7.6 eV photolysis, it is done in Table 4. If not otherwise indicated, the same features have been found for the 7.1 eV photolysis.

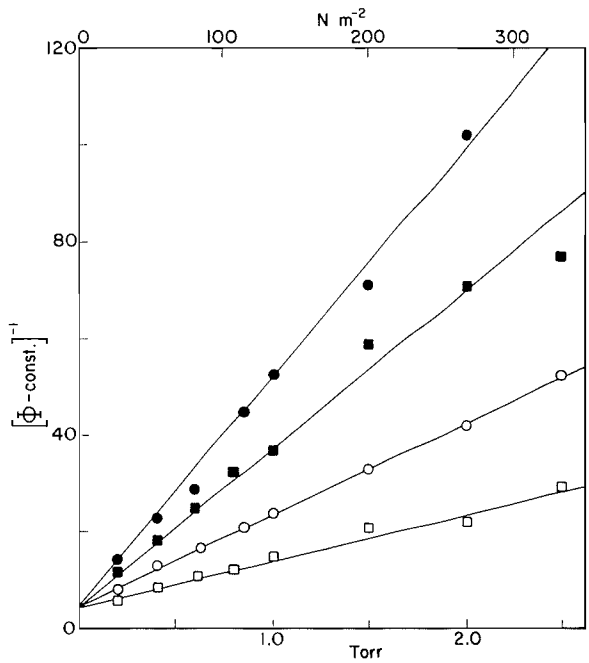

FIG. 2. The photolysis of 1-C_5H_{10} and 1-C_5D_{10}. Stern–Volmer plots of $[\Phi - \text{constant}]^{-1}$ vs. total pressure for the formation of propylene-H (open symbols) and propylene-D (solid symbols) at 7.1 eV (circles) and 7.6 eV (squares) respectively. The constant values are taken from Table 2.

Can. J. Chem. Downloaded from www.nrcresearchpress.com by 210.87.254.40 on 09/05/12
For personal use only.

Can. J. Chem. Downloaded from www.nrcresearchpress.com by 210.87.254.40 on 09/05/12
For personal use only.

TABLE 3. Primary photochemical processes of 1-pentene molecules at different photon energies. Quantum yields: $1\text{-}C_5H_{10} + h\nu \rightarrow (1\text{-}C_5H_{10})^*$

Process No.	$(1\text{-}C_5H_{10})^* \rightarrow$	7.1 eV	7.6 eV	8.4 eV[a]
[4]	$C_3H_5 + C_2H_5$	0.48 ±0.04	0.50 ±0.04	0.10
[7]	$C_3H_5 + C_2H_4 + H$	0.17 ±0.02	0.22 ±0.02	0.24
[8]	$C_4H_6 + CH_3 + H$	0.08 ±0.01	0.09 ±0.01	0.15
[9]	$C_2H_4 + CH_3 + C_2H_3$	0.04 ±0.01	0.05 ±0.01	0.16
[10]	$C_2H_4 + C_3H_6$	0.04 ±0.01	0.04 ±0.01	n.d.
[11]	$C_4H_7 + CH_3$	0.02 ±0.01	0.02 ±0.01	n.d.
[12]	$C_3H_4 + C_2H_5 + H$	0.011±0.005	0.024±0.005	0.14
[13]	$C_3H_7 + C_2H_3$	0.010±0.005	0.010±0.005	n.d.
[14]	$C_3H_7 + C_2H_2 + H$	0.005±0.002	0.010±0.005	0.06
[15]	$C_3H_8 + C_2H + H$	0.002±0.001	0.007±0.002	n.d.
[16]	$C_5H_8 + 2H$	n.d.[b]	n.d.	0.06
[17]	$C_3H_6 + C_2H_3 + H$	n.d.	n.d.	0.04
Total		0.86 ±0.11	0.97 ±0.12	0.95

[a]Reference 6.
[b]Not determined designated by n.d.

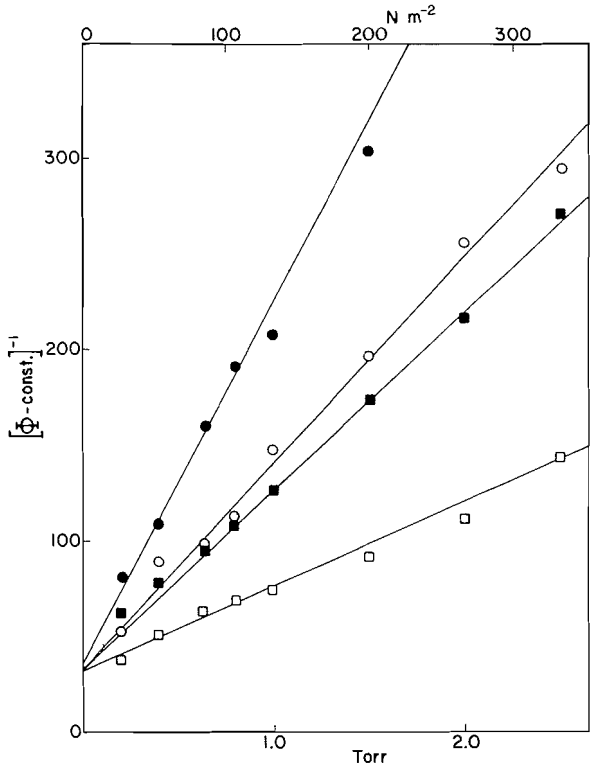

FIG. 3. The photolysis of $1\text{-}C_5H_{10}$ and $1\text{-}C_5D_{10}$. Stern–Volmer plots of $[\Phi - \text{constant}]^{-1}$ vs. total pressure for the formation of allene-H (open symbols) and allene-D (solid symbols) at 7.1 eV (circles) and 7.6 eV (squares), respectively. The constant values are taken from Table 2.

As seen from the data given in Table 4, the general agreement is good, remaining well within the experimental error. The calculated yield of the C_3H_5 radical is higher than that experimentally observed. This difference is outside of the experimental error and means that the experimental yield of this radical

TABLE 4. The photolysis of 1-pentene at 7.6 eV. The experimental and mechanistic primary product quantum yields (see text)

Products	Experimental	Mechanistic
CH_3	0.17	0.17
C_2H	0.007	0.007
C_2H_3	0.06	0.06
C_2H_5	0.54	0.52
C_3H_5	0.54	0.72
C_3H_7	0.018	0.02
C_4H_7	0.02	0.03
C_2H_2	0.01	0.01
C_2H_4	0.33	0.31
C_3H_6	0.04	0.04
C_3H_4	0.024	0.024
1,3-Butadiene	0.09	0.09

is probably underestimated (Table 1). This was also observed at 8.4 eV (6). It should be noted that much better agreement between calculated and measured $\Phi(C_3H_5)$ values (0.65 against 0.62) was obtained at 7.1 eV, suggesting that the difficulties in the quantitative titration of C_3H_5 radicals by HI may be due to their excess energy.

The total product quantum yield at 7.1 eV, less than one (Table 3), implies that some other minor processes are probably not accounted for.

The increase in the photon energy from 7.1 to 7.6 eV causes no substantial changes in the primary photochemical processes of *n*-pentene molecules (Table 3). However, some trends observed in this region are much more pronounced in the 7.6–8.4 eV region. As shown in Table 3 the importance of processes [7]–[9] increases with the photon energy and, at the same time, the yield of process [4] drops five times. Process [12] is also noteworthy since its quantum yield increases more than an order of magnitude

TABLE 5. Summary of the decomposition rate constants (k^{dec}) and the secondary non-equilibrium isotope effects for the decomposition of 2-pentyl and allyl radicals at 7.1 and 7.6 eV, respectively

	$C_5H_{11}^* \rightarrow C_3H_6 + C_2H_5$		$C_3H_5^* \rightarrow C_3H_4 + H$	
	7.1 eV	7.6 eV	7.1 eV	7.6 eV
k_H^{dec} (10^6 s^{-1})	4.4±0.5[a]	11 ±1	5.1±0.3	12.8±0.7
k_D^{dec} (10^6 s^{-1})	1.2±0.2	2.9±0.3	3.4±0.3	7.5±0.5
k_H^{dec}/k_D^{dec}	3.7±1.0	3.8±0.7	1.5±0.3	1.7±0.3

[a]Estimated error.

with the increase in photon energy in the studied region. The quantum yield of the C_2H_3 radical is much higher at 8.4 eV (5, 6) than at 7.1 and 7.6 eV (Table 1), explaining why process [17] (8.4 eV) is replaced by process [10] (this work).

Process [16] was virtually undetected at 7.1 eV as well as at 7.6 eV. The increase in the quantum yield of processes [7] and [12] with the increase in photon energy may not necessarily reflect a change in the primary photochemical processes since it may result from the increased decomposition of the higher energized C_3H_5 and C_2H_5 radicals formed in process [4]. However, on the basis of the Φ values of the remaining processes some substantial changes in the primary fragmentation pattern are concluded to occur along with the increase in photon energy in the 7.6–8.4 eV region.

Secondary Processes. Kinetic Considerations

As mentioned above, only the fate of the propylene and allene precursors will be followed. As to the former process no unambiguity exists (5, 12) regarding its formation process (processes [5] and [6]). On the other hand, allene may result from excited $C_3H_5^*$ radicals,

[18] $$C_3H_5^* \rightarrow C_3H_4 + H$$
$$\Delta H = 56.6 \text{ kcal mol}^{-1}$$

or from $C_4H_7^*$ radicals (11, 13)

[11] $$C_5H_{10}^{**} \rightarrow C_4H_7^* + CH_3$$
$$\Delta H = 85 \text{ kcal mol}^{-1}$$

[19] $$C_4H_7^* \rightarrow C_3H_4 + CH_3$$
$$\Delta H = 32.9 \text{ kcal mol}^{-1}$$

As indicated by HI scavenged experiments both C_3H_5 and C_4H_7 radicals are present in the system studied (Table 1). However, according to the earlier data the $CH_2CH_2CH{=}CH_2$ (1-buten-4-yl) radicals formed in process [11] either decompose to butadiene (14) or isomerize to the 1-buten-3-yl form (14, 15). It has recently been shown by Diaz and Doepker (11) that this 3-yl radical decomposes yielding 1,3-butadiene. The allene formation would demand the isomerization of the 4-yl radical involving 2,4 hydrogen atom shift but this mode of isomerization, which is less probable than the 3,1 shift due to the resonance energy of the 1-buten-3-yl radical, has not yet been reported. Therefore we conclude, as we did in our earlier works (2, 3), that the C_3H_5 (allylic) radical formed in process [4] is the only allene precursor.

The least-squares slopes and intercepts of the lines in Figs. 2 and 3 were used to determine the decomposition rate constants of the $C_5H_{11}^*$ and $C_3H_5^*$ radicals, and they are given in Table 5. The kinetic isotope effects are also included in this table. It is assumed that the deactivation of the excited radicals

[20] $$R^* + M \rightarrow R + M$$

([20]) occurs at each collision and the collision numbers were calculated in the normal way (16). The radical and molecular diameters used for the calculations are:

$$\sigma C_5H_{11} = 0.70 \text{ nm}$$
$$\sigma C_5H_{10} = 0.70 \text{ nm} \quad (12)$$

and

$$\sigma C_3H_5 = 0.467 \text{ nm} \quad (17)$$

Photon Energy Effect

More than a twofold increase in the decomposition rate constants of both radicals with the increase in photon energy is clearly demonstrated in Table 5. According to the theory of unimolecular reactions, this effect results from the increase in the internal energy of the radical species (18). Higher excess energy on the $C_3H_5^*$ radical at 7.6 eV than at 7.1 eV reflects the higher excitation energy gained in the primary photophysical process:

[21] $$C_5H_{10} + h\nu \rightarrow C_5H_{10}^{**}$$
$$\Delta H = 163 \text{ kcal mol}^{-1} \text{ (7.1 eV)}$$
$$\Delta H = 175 \text{ kcal mol}^{-1} \text{ (7.6 eV)}$$

The increase in the decomposition rate of the 2-$C_5H_{11}^*$ radical may result only from the increase in the exothermicity of process [5]. This proves that, at least in the 7.6 eV photolysis of 1-pentene, hot hydrogen atoms are produced.

Can. J. Chem. Downloaded from www.nrcresearchpress.com by 210.87.254.40 on 09/05/12
For personal use only.

Can. J. Chem. Downloaded from www.nrcresearchpress.com by 210.87.254.40 on 09/05/12
For personal use only.

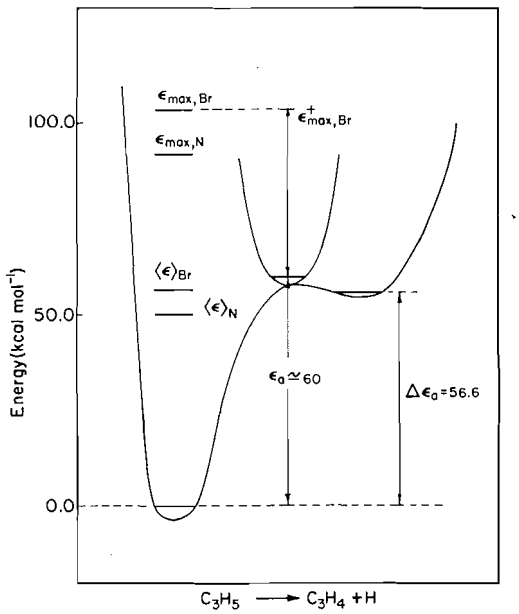

FIG. 4. Schematic potential energy diagram of the C_3H_5* radical decomposition process (see text). Subscripts N and Br refer to experiments done at 7.1 eV (nitrogen lamp) and 7.6 eV (bromine lamp). Activation energy of the process $H + C_3H_4 \rightarrow C_3H_5$ has been estimated from ref. 22.

The decomposition process of the chemically activated 2-pentyl radicals has previously been investigated by Pearson and Rabinovitch (12). Virtually thermal H-atoms were used for the activation. The average value of the rate constant of process [6] obtained by these authors between 0.5 and 2 Torr[2] was equal to 9.0×10^6 s^{-1} and this value is higher than the one found by us for 7.1 eV photolysis (Table 5). This means that a systematic error is probably involved between both studies. No conclusion on the energy of hydrogen atoms produced in the 7.1 eV system can thus be drawn. However, some evidence in favour of the presence of hot hydrogen atoms even at 7.1 eV comes from the isotope effect data (Table 5) which are discussed below.

The assumption has already been made that allene (whose yield is pressure dependent) results only from the C_3H_5* radical decomposition. The Φ(allene) value extrapolated to zero pressure equal to 0.03 ± 0.01 for both photon energies is very small as compared to the C_3H_5 radical quantum yield equal to 0.5 (process [4], Table 3). However, this result is consistent with our earlier observation of the *n*-butene photolysis at 7.1 eV (3), where the complete decomposition of the (C_3H_5)* radicals (formed in process [1]) was not attained either. Considering the thermochemical parameters of processes [1] and [4], and assuming the statistical distribution of energy among the internal degrees of freedom, one may calculate the average excess energies, $\langle\varepsilon\rangle$, on the C_3H_5* radicals formed from the photoexcited C_4H_8** and C_5H_{10}** molecules, respectively. At the photon energy of 7.1 eV these values are 66 kcal mol^{-1} (process [1]) and 50 kcal mol^{-1} (process [4], 56.5 kcal mol^{-1} at 7.6 eV) (19[3]). A schematic potential energy diagram for the decomposition of the allylic C_3H_5* radicals is shown in Fig. 4. It should be noted that the $\langle\varepsilon\rangle$ value (process [4]) estimated on the simple statistical basis lies below the critical energy for the reaction ($\varepsilon_0 = 60$ kcal/mol). Thus, if there is not any spread in the internal energies (2) of the (C_3H_5)* radicals (process [4]), no decomposition of these radicals should be expected. It may also be concluded that even if a single or multipeak energy distribution function is assumed (2), the maximum (maxima) for this function is (are) probably at energies well below the threshold energy for process [18]. As a result, only a minor fraction of the C_3H_5* radicals have sufficient energy to decompose, thus accounting for the small experimental allene quantum yield value.

Isotope Effects

Assuming the radical decomposition mechanisms discussed above, the observed isotope effects for the C_5H_{11}–C_5D_{11} and C_3H_5–C_3D_5 pairs may be classified as secondary and combined primary–secondary non-equilibrium kinetic isotope effects, respectively (7). In the low pressure region where the monoenergetic excitation (the 'δ' energy distribution function) may be assumed, both effects are mainly of the quantum statistical weight origin (due account being taken of the difference in zero point energies on isotope substitution in the case of the primary isotope effects).

For the secondary non-equilibrium isotope effect a large normal effect is predicted by theory and confirmed by experiments (7, 20). The magnitude of this effect depends on the number of isotopic substitutions in the molecules, on the average excess energy above the critical threshold ($\varepsilon^+ = \varepsilon - \varepsilon_0$), and on ε_0, the critical threshold of the reaction (7).

The isotope effects for the C_5H_{11}–C_5D_{11} system summarized in Table 5 may be compared with the secondary non-equilibrium isotope effects for the decomposition of *s*-butyl radicals investigated by Rabinovitch and co-workers (7, 21). The average value of the k_H^{dec}/k_D^{dec} ratio between 0.5 and 2 Torr found by the authors cited (21) were equal to 3.9 ± 0.3 (the external comparison experimental method)

[2]We were unable to detect the dependence of the $k^{dec}(2\text{-}C_5H_{11})$* on *n*-pentene pressure (11).

[3]The thermochemical data used in this work were taken from ref. 19.

Can. J. Chem. Downloaded from www.nrcresearchpress.com by 210.87.254.40 on 09/05/12
For personal use only.

and 3.95 ± 0.19 (the internal method). For the C_5H_{11}–C_5D_{11} system the isotope effects (assuming the same experimental conditions) might be expected to be higher, but it need not be so since the increase in the number of D atoms may be compensated for by the decrease in the critical energy (from 33 kcal mol^{-1} for *s*-C_4H_9 decomposition to 31.2 kcal mol^{-1}, process [6] (12)). The slightly smaller k_H^{dec}/k_D^{dec} ratio than that observed by Rabinovitch and co-workers for the C_4H_9–C_4D_9 system may be due to the higher excess energy on the 2-C_5H_{11}* radicals than on *s*-C_4H_9* obtained by the addition of thermal H atoms to the *cis*-2-butene double bond (21). This may suggest that hot hydrogen atoms are present even in 7.1 eV photolysis. However, the increase in the photon energy is not reflected by the diminishing of the secondary effect (Table 5). This discouraging observation is probably due to experimental error. The magnitude of the 'pure' primary non-equilibrium isotope effects declines with the increase in ε^+ and with the decrease in ε_0 (7). Assuming $\varepsilon_H = \varepsilon_D$ (the active energies of the molecules), which is a common case, the maximum value of this effect ($\varepsilon^+ \to 0$) varies from 6.1 to 6.96 at $\varepsilon_{0D} = 35$ kcal mol^{-1} and $\varepsilon_{0D} = 85$ kcal mol^{-1}, respectively (the results of the model calculations (7)). Since, as indicated above, a substantial excess energy on the (C_3H_5)* radicals cannot be expected, the result $k_H/k_D = 1.6 \pm 0.3$ (Table 5) is somewhat surprising. However, it should be recalled that: (*1*) the experimentally observed kinetic isotope effects for the C_3H_5–C_3D_5 pair should be treated in terms of a combined primary secondary effect, and (*2*) the energy distribution function at the (C_3H_5)* radicals, far from the δ function, should be taken into account.

Considering the above remarks and the preceding discussion, the low experimental isotope effects may be explained if we assume that an inverse secondary kinetic isotope effect contributes to the gross effect. The inverse non-equilibrium secondary effects are predicted by theory and experimentally observed in the low pressure region of thermally activated systems (7, 20). It is of interest to note that a close resemblance may be traced between the photochemically initiated C_3H_5* radicals and thermally activated species. As a result of the wide spread in the internal energies of the C_3H_5* radicals and due to the relationship $\langle\varepsilon\rangle < \varepsilon_0$, the unimolecular decomposition process involving these radicals probably amounts to averaging the energy-dependent unimolecular rate constant over the tail of the energy distribution function rather than over its entire energy range. This is a common feature of the thermally activated systems (18). This analogy indicates that the occurrence of the inverse secondary isotope effects is not, at least, improbable. Further study involving normal and perdeuterated *n*-butene is in preparation and it is hoped that it will throw more light on this interesting behaviour.

Acknowledgments

We would like to express our gratitude to the NRCC for its financial help throughout this work and to the Chemistry Division of the NRCC, Ottawa, who provided us with the quartz lamp (Dr. G. Paraskevopoulos and colleagues).

1. G. J. COLLIN. J. Chim. Phys. **74**, 302 (1977).
2. A. WIĘCKOWSKI and G. J. COLLIN. J. Phys. Chem. **81**, 2592 (1977).
3. A. WIĘCKOWSKI and G. J. COLLIN. Can. J. Chem. **55**, 3636 (1977).
4. G. J. COLLIN and A. WIĘCKOWSKI. J. Photochem. **8**, 103 (1978).
5. P. M. PERRIN and G. J. COLLIN. Can. J. Chem. **51**, 724 (1973).
6. G. J. COLLIN and K. BUKKA. J. Photochem. **6**, 381 (1976/77).
7. B. S. RABINOVITCH and D. W. SETSER. Adv. Photochem. **3**, 1 (1964).
8. L. F. LOUCKS and R. J. CVETANOVIĆ. J. Chem. Phys. **56**, 321 (1972).
9. P. POTZINGER, L. C. GLASGOW, and G. VON BÜNAU. Z. Naturforsch. Sect. A, **27**, 628 (1971); H. HARA and I. TANAKA. Bull. Chem. Soc. Jpn. **46**, 3012 (1973).
10. G. J. COLLIN and P. M. PERRIN. Can. J. Chem. **50**, 2823 (1972).
11. Z. DIAZ and R. D. DOEPKER. J. Phys. Chem. **81**, 1442 (1977).
12. M. J. PEARSON and B. S. RABINOVITCH. J. Chem. Phys. **42**, 1624 (1965).
13. J. HERMAN, K. HERMAN, and P. AUSLOOS. J. Chem. Phys. **52**, 28 (1970).
14. S. W. BENSON and H. E. O'NEIL. Kinetic Data on Gas Phase Unimolecular Reactions. NSRDS-NBS 21, 1970.
15. A. S. GORDON, S. R. SMITH, and C. M. DREW. J. Chem. Phys. **36**, 824 (1962).
16. J. G. CALVERT and J. N. PITTS, JR. Photochemistry. 2nd ed. John Wiley and Sons, Inc. New York. N.Y. 1967. p. 605.
17. T. IBUKI, T. MURATA, and Y. TAKEZAKI. J. Phys. Chem. **78**, 2543 (1974).
18. W. FORST. *In* Theory of unimolecular reactions. Academic Press, Inc. New York. N.Y. 1973.
19. H. M. ROSENSTOCK, K. DRAXL, B. W. STEINER, and J. T. HERRON. J. Phys. Chem. Ref. Data, **6**, Suppl. 1 (1977).
20. B. S. RABINOVITCH, D. W. SETSER, and F. W. SCHNEIDER. Can. J. Chem. **39**, 2609 (1961); B. S. RABINOVITCH and J. H. CURRENT. Can. J. Chem. **40**, 557 (1962).
21. J. W. SIMONS, B. S. RABINOVITCH, and R. F. KUBIN. J. Chem. Phys. **40**, 3343 (1964).
22. J. A. KERR and M. J. PARSONAGE. *In* Evaluated kinetic data on gas phase addition reactions. CRC Press, Cleveland, OH. 1972; P. I. Abel. Compr. Chem. Kinet. **18**, Chapt. III (1976).

The viscosity of concentrated electrolyte solutions. II. Temperature dependence

DOUGLAS E. GOLDSACK AND RAYMOND C. FRANCHETTO

Department of Chemistry, Laurentian University, Sudbury, Ont., Canada P3E 2C6

Received April 4, 1977[1]

DOUGLAS E. GOLDSACK and RAYMOND C. FRANCHETTO. Can. J. Chem. **56**, 1442 (1978).

The temperature dependence of the viscosity of concentrated aqueous electrolyte solutions has been explained in terms of the temperature dependence of the E and V parameters of an equation previously developed for the viscosity of such solutions. Analysis of the V parameters for the alkali halide and ammonium halide salts leads to absolute ionic hydration numbers. The temperature dependence of these hydration numbers reveals two types of ionic behaviour: structure making ions and structure breaking ions. The Gourary–Adrian scale of ionic radii is found to be more consistent with these data and the temperature dependence than the Pauling ionic radii scale.

Analysis of the E parameters leads to the ionic free energy of activation parameters for viscous flow of the ions. The Furth model for hole formation in a liquid is found to correlate these ionic free energy values with the absolute ionic volume parameters obtained from the analysis of the V parameter for all salts. Again the ions are found to break into structure making and structure breaking groups in terms of the surface tension values for the water about the hydrated ions.

DOUGLAS E. GOLDSACK et RAYMOND C. FRANCHETTO. Can. J. Chem. **56**, 1442 (1978).

La relation qui existe entre la température et la viscosité de solutions électrolytiques aqueuses concentrées peut être expliquée en terme de la relation qui existe entre la température et les paramètres E et V d'une équation développée antérieurement pour la viscosité de telles solutions. L'analyse des paramètres V pour des sels d'halogénures alcalins ou d'ammonium conduit à des nombres absolus d'hydratation ionique. La relation qui existe entre la température et ces nombres d'hydratation révèle la présence de deux types de comportement ionique: les ions formant la structure et les ions brisant la structure. On a trouvé que l'échelle Gourary–Adrian des rayons ioniques est plus en accord avec ces données et les relations avec la température que l'échelle des rayons atomiques de Pauling.

L'analyse des paramètres E conduit aux paramètres de l'énergie libre d'activation ionique pour des écoulements visqueux des ions. On a trouvé que le modèle de Furth pour la formation de trous dans un liquide permet d'établir une corrélation entre ces valeurs d'énergie libre ionique et les paramètres absolus de volume ionique obtenus à partir d'une analyse du paramètre V de tous les sels. On a trouvé encore une fois que les ions se divisent en deux groupes les uns formant la structure et les autres brisant la structure de l'eau en terme des valeurs de la tension de surface de l'eau autour des ions hydratés.

[Traduit par le journal]

Introduction

In the first paper of this series (1) it was shown that a simple extension of the absolute rate theory of viscosity to include the contributions from all the particles in a concentrated electrolyte solution led to an equation which quantitatively accounted for the concentration dependence of the viscosity of electrolyte solutions in the 1–10 m range at fixed temperature. For a 1:1 electrolyte this equation is given by

$$[1] \qquad \eta = \frac{\eta_1 \, e^{XE}}{1 + XV}$$

where η is the viscosity of the electrolyte solution at a concentration m and temperature T, η_1 is the viscosity of the solvent at temperature T, X is the mole fraction of the cation or anion in solution, and the parameters E and V are defined as

$$[2] \qquad E = (\Delta G_c^* + \Delta G_a^* - 2\Delta G_1^*)/RT$$

$$[3] \qquad V = \left(\frac{V_c + V_a}{V_1}\right) - 2$$

where V_c = molar volume of the cation particle, V_a = molar volume of the anion particle, V_1 = molar volume of the solvent particle, ΔG_c^* = molar free energy of activation for viscous flow of the cation particle, ΔG_a^* = molar free energy of activation for viscous flow of the anion particle, ΔG_1^* = molar free energy of activation for viscous flow of the solvent particle, and $X = m/(55.5 + 2m)$, where m is the molality of the salt.

The previous paper dealt with a discussion of the concentration dependence of the viscosity of various 1:1 electrolyte solutions at 25°C. It is the purpose of this paper to show that eq. [1] also accounts for the

[1]Revision received January 20, 1978.

Can. J. Chem. Downloaded from www.nrcresearchpress.com by 210.87.254.5 on 09/05/12
For personal use only.

Can. J. Chem. Downloaded from www.nrcresearchpress.com by 210.87.254.5 on 09/05/12
For personal use only.

concentration dependence of the viscosity of 1:1 electrolyte solutions at various temperatures through the temperature dependence of the parameters V and E. The individual ionic components of the V parameter will be shown to be related to ionic solvation numbers, and the individual ionic free energy of activation components of the E parameters will be shown to be related to a surface free energy for formation of a hole in the liquid.

Experimental Results and Treatment of Data

The details of the experimental methods are given in the previous paper of this series (1). Viscosities of aqueous solutions of NaI, KI, NH_4Cl, NaBr, KBr, NH_4Br, NaF, and KF at several concentrations and at six temperatures between 5 and 55°C were determined. These data are presented in Table 1. Viscosities of other salts at several temperatures were obtained from the literature (2, 12, 16–30). All data were analyzed using [1] via a computerized iteration procedure as indicated in the previous paper (1). The $(V_c + V_a)/V_1$ and the E parameters for each salt as a function of temperature obtained by this method are given in Tables 2 and 3 respectively. The viscosity of water as a function of temperature was obtained from the Handbook of Physics and Chemistry (2). Figures 1 and 2 illustrate the reproducibility of the viscosity data for NH_4Br and NaBr as a function of concentration and temperature using the V and E parameters derived from [1].

Discussion

1. The Volume and Free Energy Parameters of the Solvent

The analysis of the concentration dependence of the viscosity of aqueous electrolyte solutions at fixed temperatures yields two parameters for any salt. These parameters, E and V, according to the theory outlined in the previous paper (1) are related to individual ionic parameters as given by [2] and [3]. However, in order to obtain these individual ionic parameters, it is first necessary to determine the molar volume, V_1, for the kinetic species which is involved in the viscous flow process for the solvent. The free energy of activation for viscous flow of the solvent, ΔG_1^*, can be determined from the following relationship for the viscosity of the solvent:

$$[4] \qquad \eta_1 = \frac{hN}{V_1} \exp(\Delta G_1^*/RT)$$

This relationship was one of the assumptions in the theoretical development of [1]. Thus, once V_1 is specified, then this activation free energy can be calculated at any temperature from

$$[5] \qquad \Delta G_1^* = RT \ln(\eta_1 V_1/hN)$$

Analysis of the temperature dependence of the self-diffusion coefficients and the dielectric relaxation times of water (3) has clearly shown that the kinetic species involved in both cases is a single water molecule at all temperatures. These methods allow a calculation of the radius of the kinetic entity involved in the diffusion and relaxation processes, and it was found that the radius so calculated was approximately the same as that of the radius of the water molecule as determined from X-ray analysis, i.e. 1.38 Å (4). For these reasons, V_1 was assumed to be independent of temperature and calculated to be 6.63 cm^3/mol. This implies that ΔG_1^* at any temperature, as given by [5], is solely dependent on the viscosity of water at that temperature. Combining $V_1 = 6.63$ cm^3/mol with [5] and [2], and the E parameters shown in Table 3, the total salt free energies of activation

$$\Delta G_{salt}^* = \Delta G_c^* + \Delta G_a^*$$

were then calculated for all salts at all temperatures studied. These data are displayed in Table 4.

2. Hydration Numbers and the V *Parameters of the Ions*

In the previous paper (1), it was shown that the Jones–Dole B viscosity parameter was related to the two parameters V and E of eq. [1] by the relation

$$B = (E - V)/55.51$$

Furthermore since B has been shown to be an additive parameter with contributions from all ions of a salt, and since E and V are composed of additive ionic parameters, then both the E and V parameters can be analyzed by arbitrarily assuming that the contributions of the potassium and chloride ions are equal at all temperatures, as is done in the analysis of B parameters for salts. Any subsequent conclusions from this arbitrary factoring method must bear this in mind.

Individual ionic V parameters based on V_{K^+} equal to V_{Cl^-} at all temperatures enabled average values of V_{ion} for each ion to be calculated from the total salt V parameters given in Table 2 and the assumed value of V_1 for the solvent. Assuming that these volumes reflect the degree of hydration of each ion, then it is possible to calculate average ionic hydration numbers for each ion as a function of temperature. By subtracting out the volume of the central cation (calculated using the Gourary and Adrian (9) radii scale), and including a dead space correction as given by Conway *et al.* (5), the remaining volume is assumed to be that of the hydration sphere. The hydration number at each temperature can then be obtained by dividing this volume by the volume V_1 =

Can. J. Chem. Downloaded from www.nrcresearchpress.com by 210.87.254.5 on 09/05/12
For personal use only.

TABLE 1. Absolute viscosities of electrolyte solutions (cP)

Molality	5°C	15°C	25°C	35°C	45°C	55°C
			NaF			
0.100	1.546	1.160	0.9082	0.7355	0.6100	0.5167
0.200	1.575	1.183	0.9270	0.7515	0.6239	0.5289
0.300	1.607	1.207	0.9466	0.7687	0.6379	0.5410
0.400	1.643	1.235	0.9690	0.7854	0.6523	0.5534
0.500	1.681	1.264	0.9917	0.8031	0.6668	0.5659
0.600	1.722	1.295	1.015	0.8219	0.6826	0.5786
0.700	1.763	1.325	1.039	0.8416	0.6991	0.5931
0.800	1.801	1.354	1.070	0.8675	0.7210	0.6116
			KF			
0.500	1.560	1.212	0.9518	0.7712	0.6420	0.5444
1.000	1.633	1.289	1.020	0.8245	0.6898	0.5872
2.000	1.843	1.451	1.148	0.9382	0.7840	0.6675
3.000	2.121	1.652	1.303	1.066	0.8886	0.7661
4.000	2.446	1.877	1.479	1.210	1.012	0.8969
5.000	2.795	2.133	1.672	1.366	1.161	1.034
6.000	3.128	2.419	1.900	1.540	1.324	1.191
7.000	3.474	2.738	2.144	1.736	1.507	1.370
			NaBr			
0.500	1.526	1.161	0.9171	0.7470	0.6222	0.5274
1.000	1.544	1.188	0.9445	0.7728	0.6471	0.5523
2.000	1.643	1.284	1.025	0.8433	0.7080	0.6076
3.000	1.811	1.416	1.139	0.9350	0.7809	0.6650
4.000	2.024	1.574	1.273	1.044	0.8781	0.7492
5.000	2.263	1.769	1.421	1.171	0.9866	0.8376
6.000	2.577	2.051	1.646	1.360	1.147	0.9815
7.000	3.084	2.430	1.947	1.607	1.352	1.157
			KBr			
0.500	1.351	1.094	0.8771	0.7153	0.5969	0.5083
1.000	1.325	1.071	0.8641	0.7121	0.5994	0.5140
1.500	1.301	1.055	0.8564	0.7099	0.6014	0.5205
2.000	1.281	1.046	0.8561	0.7126	0.6085	0.5289
2.500	1.267	1.040	0.8549	0.7179	0.6150	0.5375
3.000	1.260	1.039	0.8607	0.7268	0.6252	0.5475
3.500	1.256	1.042	0.8662	0.7342	0.6335	0.5582
4.000	1.256	1.049	0.8745	0.7465	0.6461	0.5694
4.500	1.259	1.057	0.8865	0.7595	0.6589	0.5815
5.000	—	1.067	0.9129	0.7825	0.6823	0.5927
			NH_4Br			
0.500	1.437	1.111	0.8751	0.7139	0.5944	0.5066
1.000	1.392	1.081	0.8618	0.7084	0.5940	0.5095
2.000	1.306	1.038	0.8416	0.7015	0.5952	0.5157
3.000	1.261	1.009	0.8300	0.6994	0.6000	0.5232
4.000	1.235	1.001	0.8325	0.7072	0.6111	0.5358
5.000	1.223	1.000	0.8385	0.7164	0.6250	0.5517
6.000	1.213	1.009	0.8509	0.7306	0.6415	0.5669
7.000	—	1.025	0.8662	0.7497	0.6584	0.5824
			NaI			
0.500	1.382	1.145	0.9042	0.7376	0.6158	
1.000	1.392	1.152	0.9138	0.7506	0.6275	
1.250	1.400	1.157	0.9211	0.7573	0.6355	
1.500	1.413	1.166	0.9327	0.7676	0.6458	
1.750	1.420	1.178	0.9445	0.7755	0.6570	
2.000	1.434	1.194	0.9585	0.7870	0.6675	
2.250	1.450	1.210	0.9729	0.8014	0.6795	
2.500	1.468	1.229	0.9891	0.8169	0.6906	
2.750	1.488	1.250	1.006	0.8379	0.7047	
3.000	1.513	1.277	1.025	0.8519	0.7220	

TABLE 1 (*Concluded*)

Molality	5°C	15°C	25°C	35°C	45°C	55°C
			KI			
0.500	1.412	1.086	0.8615	0.7036	0.5850	
1.000	1.316	1.049	0.8345	0.6918	0.5838	
1.250	1.281	1.028	0.8257	0.6880	0.5838	
1.500	1.254	1.009	0.8194	0.6850	0.5844	
1.750	1.232	0.9977	0.8146	0.6833	0.5864	
2.000	1.214	0.9906	0.8111	0.6829	0.5889	
2.250	1.204	0.9852	0.8093	0.6835	0.5917	
2.500	1.190	0.9820	0.8079	0.6852	0.5948	
2.750	1.182	0.9795	0.8075	0.6872	0.5975	
3.000	1.178	0.9782	0.8078	0.6901	0.6006	
Molality	10°C	20°C	30°C	40°C	50°C	60°C
			NH_4Cl			
0.500	1.280	0.9914	0.7984	0.6573	0.5540	0.4738
1.000	1.258	0.9853	0.8003	0.6620	0.5607	0.4819
2.000	1.228	0.9794	0.8050	0.6742	0.5754	0.4981
3.000	1.208	0.9781	0.8095	0.6865	0.5904	0.5148
4.000	1.198	0.9804	0.8163	0.6896	0.6057	0.5318
5.000	1.199	0.9885	0.8285	0.7139	0.6214	0.5489
6.000	1.214	1.001	0.8438	0.7328	0.6397	0.5665
7.000	—	1.022	0.8649	0.7508	0.6594	0.5843

TABLE 2. $(V_c + V_a)/V_1$ parameters as a function of temperature

Salt	0°C	5°C	10°C	15°C	20°C	25°C	30°C	35°C	40°C	45°C	50°C	55°C	60°C
NaF	—	24.0	—	22.3	—	22.5	—	17.9	—	15.7	—	11.1	—
KF	—	16.0	—	10.8	9.61	9.51	8.78	8.24	—	9.12	—	10.4	—
RbF	—	—	—	12.0	9.53	9.67	9.68	8.96	—	—	—	—	—
CsF	—	—	—	13.7	11.8	11.7	11.3	11.2	—	—	—	—	—
LiCl	10.3	—	8.11	8.94	9.12	8.03	7.83	—	7.96	—	—	—	7.75
NaCl	19.6	—	14.9	—	12.3	13.4	11.7	12.9	11.8	11.1	9.80	9.34	—
KCl	—	—	13.0	11.1	9.57	10.8	7.95	9.95	9.15	8.41	7.94	8.06	8.52
RbCl	—	—	—	13.8	12.9	11.7	11.4	10.9	—	—	—	—	—
CsCl	20.4	—	—	16.3	14.2	12.6	13.6	12.8	—	—	10.3	—	—
NH_4Cl	11.6	—	9.93	—	8.49	8.19	6.91	—	6.21	—	5.62	—	5.38
LiBr	10.7	—	—	—	10.0	—	10.1	—	—	—	10.0	—	—
NaBr	—	20.4	—	18.3	14.3	18.2	—	15.5	—	15.3	—	14.4	—
KBr	18.3	16.1	15.9	15.1	13.3	13.1	12.1	12.1	11.1	11.1	—	9.11	8.31
NH_4Br	—	14.2	—	11.5	—	10.5	—	9.40	—	9.02	—	7.76	—
LiI	11.1	—	—	—	10.9	—	10.9	—	—	—	10.3	—	—
NaI	—	30.5	29.4	15.3	23.9	13.4	16.7	12.0	—	10.5	—	—	—
KI	21.3	22.9	20.4	17.9	16.2	15.1	—	13.7	15.7	13.8	—	—	—
RbI	—	—	—	—	—	15.6	—	—	—	—	—	—	—
CsI	—	—	—	—	—	14.8	—	—	—	—	—	—	—
NH_4I	—	—	20.3	18.8	16.5	16.5	—	—	—	—	—	—	—

6.63 cm^3/mol of a mole of water molecules. These resulting hydration numbers are shown in Table 5. As expected, these hydration numbers decrease with increasing temperature for each ion.

The temperature dependence of these numbers shows that these ions can be broken into two groups. The hydration numbers of Li^+, Na^+, and F^- ions are not as affected by an increase in temperature as are those of the K^+, Rb^+, Cs^+, Cl^-, Br^-, and I^- ions. This grouping of these ions has been previously characterized as "structure making ions" and "structure breaking ions" respectively based on a variety of physical properties of electrolyte solutions (6).

For instance, the ionic B coefficients of the Jones–Dole viscosity equation for electrolytes are negative

Can. J. Chem. Downloaded from www.nrcresearchpress.com by 210.87.254.5 on 09/05/12
For personal use only.

TABLE 3. E^* parameters as a function of temperature

Salt	0°C	5°C	10°C	15°C	20°C	25°C	30°C	35°C	40°C	45°C	50°C	55°C	60°C
NaF	—	31.5	—	30.4	—	31.0	—	27.4	—	25.8	—	22.0	—
KF	—	17.3	—	14.9	14.4	14.2	13.8	13.5	—	14.4	—	15.9	—
RbF	—	—	—	14.5	13.5	13.9	14.1	13.9	—	—	—	—	—
CsF	—	—	—	14.4	13.6	13.9	13.9	14.0	—	—	—	—	—
LiCl	14.7	—	13.4	14.1	14.2	13.5	13.5	—	13.6	—	—	—	13.6
NaCl	18.0	—	15.5	—	14.4	15.2	14.2	14.9	14.5	14.0	13.2	12.9	—
KCl	—	—	7.81	7.06	6.49	7.87	6.40	8.00	7.84	7.61	7.58	7.88	8.43
RbCl	—	—	—	7.59	7.64	7.51	7.74	7.86	—	—		—	—
CsCl	8.04	—	—	8.63	7.97	7.61	8.79	8.80	—	—	8.46	—	—
NH_4Cl	4.88	—	5.10	—	5.14	5.27	4.71	—	4.85	—	4.91	—	5.15
LiBr	12.4	—	—	—	12.8	—	13.2	—	—	—	13.6	—	—
NaBr	—	16.8	—	16.5	14.0	17.0	—	15.8	—	15.8	—	15.5	—
KBr	7.68	7.63	8.05	8.25	7.89	8.16	8.04	8.45	8.20	8.52	—	7.81	7.79
NH_4Br	—	5.76	—	5.51	—	5.80	—	5.86	—	6.26	—	5.95	—
LiI	10.5	—	—	—	11.4	—	11.8	—	—	—	12.2	—	—
NaI	—	18.2	19.2	12.4	17.7	11.8	15.3	11.5	14.7	10.9	—	—	—
KI	7.95	9.16	9.07	8.63	8.37	8.08	—	8.33	10.0	9.58	—	—	—
RbI	—	—	—	—	—	7.61	—	—	—	—	—	—	—
CsI	—	—	—	—	—	6.34	—	—	—	—	—	—	—
NH_4I	—	—	7.91	8.15	7.66	8.48	—	—	—	—	—	—	—

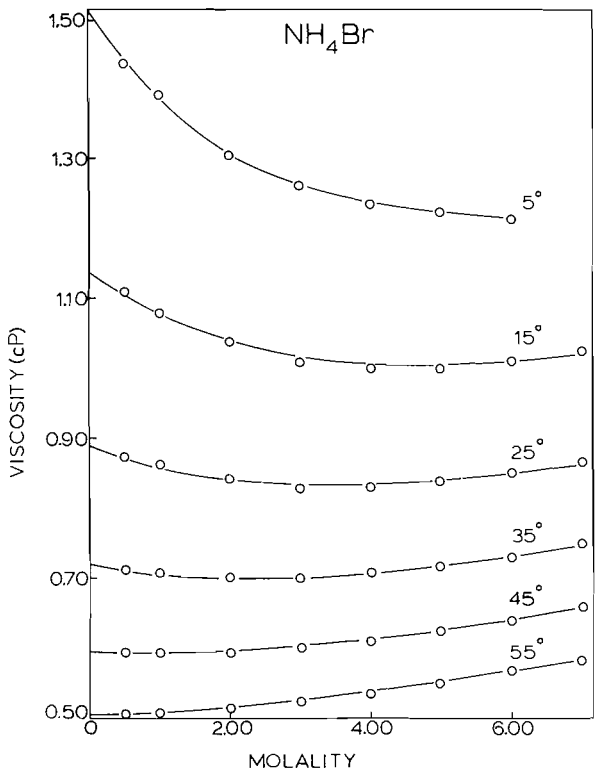

FIG. 1. Absolute viscosities of NH_4Br at several temperatures. The solid lines are calculated with [1] and the parameters given in Tables 2 and 3.

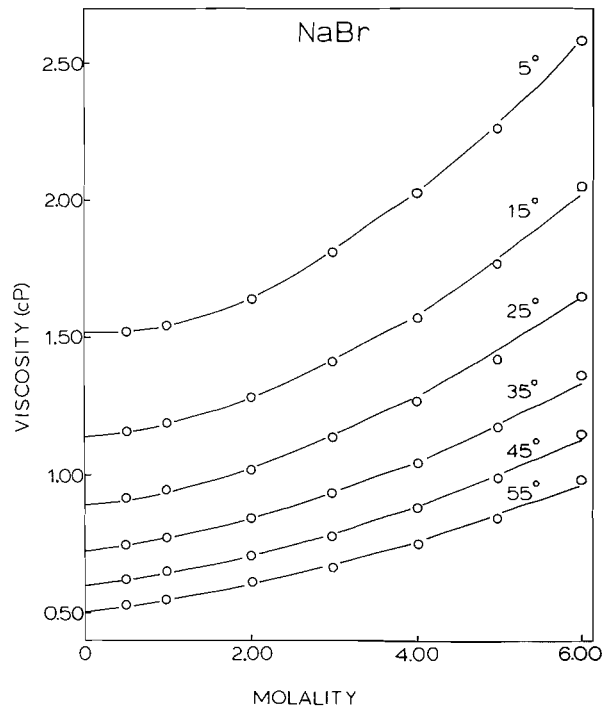

FIG. 2. Absolute viscosities of NaBr at several temperatures. The solid lines are calculated with [1] and the parameters given in Tables 2 and 3.

for structure breaking ions and positive for structure making ions at room temperatures. These differences are reduced at higher temperatures where the "structure" of water is destroyed (7).

One simple explanation of the temperature dependence of these hydration numbers, as well as the grouping of these cations into structure making and structure breaking ions, can be postulated as follows. For an ion to fit into a cavity formerly occupied by a water molecule, its radius must be less than or equal to that of a water molecule (1.38 Å). Thus, if one uses the Pauling ionic radii scale, then the Li^+,

Can. J. Chem. Downloaded from www.nrcresearchpress.com by 210.87.254.5 on 09/05/12
For personal use only.

TABLE 4. Salt free energies, ΔG_{salt}* (kcal/mol), at several temperatures

Salt	0°C	5°C	10°C	15°C	20°C	25°C	30°C	35°C	40°C	45°C	50°C	55°C	60°C
NaF	—	21.0	—	20.8	—	21.5	—	19.8	—	19.2	—	17.1	—
KF	—	13.1	—	11.9	11.6	11.6	11.5	11.3	—	12.0	—	13.2	—
RbF	—	—	—	11.7	11.1	11.4	11.6	11.5	—	—	—	—	—
CsF	—	—	—	11.6	11.2	11.4	11.5	11.6	—	—	—	—	—
LiCl	11.7	—	11.0	11.4	11.5	11.2	11.2	—	11.4	—	—	—	11.7
NaCl	13.4	—	12.2	—	11.7	12.2	11.7	12.2	12.0	11.7	11.3	11.2	—
KCl	—	—	7.86	7.41	7.06	7.85	6.97	7.94	7.85	7.71	7.70	7.91	8.29
RbCl	—	—	—	7.71	7.73	7.64	7.77	7.85	—	—	—	—	—
CsCl	8.04	—	—	8.31	7.92	7.70	8.41	8.43	—	—	8.27	—	—
NH_4Cl	6.33	—	6.33	—	6.27	6.32	5.95	—	5.99	—	5.98	—	6.12
LiBr	10.4	—	—	—	10.8	—	11.1	—	—	—	11.6	—	—
NaBr	—	12.8	—	12.8	11.5	13.3	—	12.7	—	12.9	—	12.9	—
KBr	7.85	7.79	7.99	8.09	7.87	8.03	7.96	8.21	8.07	8.28	—	7.86	7.87
NH_4Br	—	6.75	—	6.52	—	6.63	—	6.62	—	6.86	—	6.65	—
LiI	9.37	—	—	—	9.94	—	10.2	—	—	—	10.6	—	—
NaI	13.6	—	14.3	10.5	13.6	10.2	12.3	10.1	—	9.76	—	—	—
KI	8.00	8.63	8.57	8.31	8.15	7.98	—	8.14	9.21	8.95	—	—	—
RbI	—	—	—	—	—	7.70	—	—	—	—	—	—	—
CsI	—	—	—	—	—	6.95	—	—	—	—	—	—	—
NH_4I	—	—	7.92	8.04	7.74	8.22	—	—	—	—	—	—	—

TABLE 5. Ion hydration numbers as a function of temperature

Ion	0°C	5°C	10°C	15°C	20°C	25°C	30°C	35°C	40°C	45°C	50°C	55°C	60°C
Li^+	2.1	5	0.9	2.6	3.6	1.9	3.1	—	2.7	—	—	—	2.8
Na^+	10.8	—	7.1	—	6.2	6.7	6.4	6.6	5.9	5.6	4.5	4.0	—
K^+	(5.2)[b]	(4.6)[b]	4.2	3.3	2.5	3.1	1.7	2.7	2.3	1.9	1.7	1.7	2.0
Rb^+	—	—	5.3	5.2	3.4	4.5	3.0	—	—	—	—	—	—
Cs^+	8.8	—	—	6.6	5.3	3.1	5.5	3.7	—	—	2.2	—	—
NH_4^+	1.8	—	1.1	—	1.4	0.5	0.6	—	0	—	0	—	0
F^- [a]	—	—	—	4.0	3.6	2.9	3.6	2.0	—	3.7	—	5.2	—
Cl^- [a]	(5.2)[b]	(4.6)[b]	4.2	3.3	2.5	3.1	1.7	2.7	2.3	1.9	1.7	1.7	2.0
Br^- [a]	7.0	5.3	5.6	5.7	4.7	3.9	4.3	3.3	2.7	3.1	—	1.3	0.2
I^- [a]	8.5	—	8.6	7.0	6.1	4.4	—	3.4	5.8	4.3	—	—	—

[a]Obtained from potassium salt values.
[b]Estimate from trend with temperature.

Na^+, and K^+ ions should fit into such a cavity without disruption of the water structure (the primary and secondary hydration layers about this cavity) since their radii are respectively 0.60, 0.95, and 1.33 Å on this scale. On the other hand, the Rb^+, Cs^+, and NH_4^+ ions whose radii are 1.48, 1.69, and 1.44 Å respectively would be expected to disrupt the primary hydration layer, consisting of four water molecules tetrahedrally oriented about the cavity, by pushing these water molecules apart from each other. Furthermore, this would also result in a disruption of the secondary hydration layer consisting of eight water molecules (4). This disruption should lead to a weakening of the bonds holding these water molecules together in these hydration layers. Hence one would expect a similar temperature dependence of the hydration numbers for Li^+, Na^+, and K^+ ions and furthermore one would expect that the temperature dependence of the hydration numbers for Rb^+, Cs^+, and NH_4^+ ions should be larger than this first group because the water molecules in the primary and secondary hydration layers are not held as strongly in the latter group. However, the data of Table 5 show that the temperature dependence of the hydration numbers of the K^+ ion is not the same as that of the Li^+ and Na^+ ions, but in fact resembles that of the Rb^+, Cs^+, and NH_4^+ ions group. This anomaly is removed, however, if the ionic radii of these ions are re-examined.

The ionic radii scale of Pauling has recently been challenged by several groups of investigators (8, 10) as has been discussed by Desnoyers and Jolicoeur (11). In particular, the ionic radii scale of Gourary and Adrian (9) reveals that the Li^+ and Na^+ ions have radii of 0.94 and 1.17 Å respectively, whereas K^+, Rb^+, and Cs^+ are 1.49, 1.63, and 1.86 Å respectively. These new ionic radii are more consistent with the above explanation of the temperature dependence of the hydration numbers given in Table 5 than are the corresponding Pauling ionic radii. Hence, ionic

Can. J. Chem. Downloaded from www.nrcresearchpress.com by 210.87.254.5 on 09/05/12
For personal use only.

TABLE 6. Ionic surface tension (γ) parameters at all temperatures (in erg/cm^2)

Ion	0°C	5°C	10°C	15°C	20°C	25°C	30°C	35°C	40°C	45°C	50°C	55°C	60°C
Li^+	114	—	151	98	83	112	87	—	96	—	—	—	98
Na^+	52	—	58	—	59	60	58	61	63	62	67	70	—
F^-	—	62	—	78	79	87	78	99	—	81	—	78	—
$K^+(Cl^-)$	30	31	33	36	40	37	45	39	41	43	45	45	43
Rb^+	—	—	—	27	27	32	30	36	—	—	—	—	—
Cs^+	22	—	—	26	26	30	29	33	—	—	37	—	—
NH_4^+	27	—	31	—	29	35	30	—	45	—	45	—	60
Br^-	24	26	27	27	28	31	29	34	34	35	—	39	46
I^-	21	22	23	24	23	24	—	29	31	32	—	—	—

volumes were calculated using radii of 1.64 Å for Cl^-, 1.80 Å for Br^-, and 2.05 Å for I^- as given by Gourary and Adrian. The resulting hydration numbers calculated using this ionic radii scale, and including a dead space correction, are shown in Table 5.

Another indication that the Gourary and Adrian ionic radii scale is more consistent with this interpretation of the viscosity of electrolyte solutions is revealed in the behaviour of the fluoride salt solutions. For instance, from Table 1 one can observe that the concentration dependence of the viscosity of KF is that of a typical structure making salt (that is, a salt containing a structure making ion such as Li^+ or Na^+). The other fluoride salts show similar structure making characteristics (12). This implies then that the fluoride ion should be grouped with the Li^+ and Na^+ ions in the structure making group of ions. On the Pauling scale of ionic radii, F^- has a radius of 1.36 Å which is similar to that of the K^+ ion (1.33 Å). However, on the Gourary and Adrian scale the radius of the F^- ion is 1.16 Å, which is almost identical to that of the Na^+ ion (1.17 Å). Therefore the fluoride ion on the Gourary and Adrian ionic radii scale fits the pattern of a structure making ion in aqueous solutions with a radius much smaller than that of the water molecule.

Hence the Gourary and Adrian ionic radii scale allows a simple explanation of the different temperature dependences of the hydration numbers observed for both groups of ions. It also accounts for the individual grouping of these ions into the so-called 'structure making' and 'structure breaking' groups on the basis of ionic size relative to the water molecule. It should also be noted that this explanation does suggest why K^+, Rb^+, and Cs^+ ions can be properly labelled as structure breaking ions since their size alone causes disruption of the normal water structure. Any further calculations requiring the use of ionic radii will be done with the Gourary and Adrian scale.

3. A Model for the Ionic Free Energy of Activation Parameters for Viscous Flow

A simple model for calculating the size, distribution, and free energy of formation of holes in liquids, originally formulated by Furth (13), has been shown to be highly successful in explaining the temperature dependence of the viscosity and diffusion coefficients of molten salts (14). This model assumes that the kinetic species involved in the transport property moves into a cavity or hole of radius r and that the work involved in forming this hole in the liquid medium is given by the work required in forming the hole against the surface tension of the liquid. This work is equated with the free energy of activation for the flow property. In this case then it is assumed that the free energy of activation for viscous flow of an ion will be given by

$$\Delta G^* = 4\pi r^2\gamma \qquad [6]$$

where r is the radius of the hole in the liquid into which the ion moves and γ is the surface tension of the liquid surrounding the ion. Since the free energy of activation parameter for viscous flow of the salt, ΔG_{salt}^*, according to [2], is a linear addition of the contributions from the cation and anion, then combining [2] and [6] gives

$$\Delta G_s^* = \Delta G_{salt}^* = 4\pi r_c^2\gamma_c + 4\pi r_a^2\gamma_a \qquad [7]$$

where r_c is the radius of the cation kinetic species, γ_c is the surface tension of the water surrounding the cation, r_a is the radius of the anion kinetic species, and γ_a is the surface tension of the water surrounding the anion. Now the volume of this cavity into which the ion moves is assumed to be the volume of the kinetic species involved in the transport. This volume is given by the absolute ionic volume parameters V_{ion}. Hence, assuming these kinetic species are spherical in shape and the γ values are given in erg/cm^2, then including the appropriate conversion factor to yield ΔG_s^* values in calories, eq. [7] can be written as

Can. J. Chem. Downloaded from www.nrcresearchpress.com by 210.87.254.5 on 09/05/12
For personal use only.

Can. J. Chem. Downloaded from www.nrcresearchpress.com by 210.87.254.5 on 09/05/12
For personal use only.

[8] $$\Delta G_s^* = 9.76V_c^{2/3}\gamma_c + 9.76V_a^{2/3}\gamma_a$$

As in the case of the analysis of V parameters where V_{K^+} was equated to V_{Cl^-} at all temperatures based on the additivity of the Jones–Dole B parameter, so in like fashion one can assume $\Delta G_{K^+}^*$ is equal to $\Delta G_{Cl^-}^*$ at all temperatures. This enables a calculation of the surface tension for the solvent surrounding each ion as a function of temperature from the relation

[9] $$\gamma_{ion} = \Delta G_{ion}^*/9.76V_{ion}^{2/3}$$

where the ΔG_{ion}^* values for each ion at each temperature were obtained by averaging the ΔG^* values obtained for each ion from the total salt parameters of Table 4 and the assumed $\Delta G_{K^+}^* = \Delta G_{Cl^-}^*$ values. The average V_{ion} values were obtained from the analysis of Section 2 for the hydration numbers of each ion. The resultant ionic surface tension values are displayed in Table 6.

Again as noted for the hydration values of the ions, these ionic surface tension parameters show two major classes. The group of ions Li^+, Na^+, and F^- all show values of γ typical of structured solvents (e.g. water 72 erg/cm^2, glycerol 63 erg/cm^2, hydrazine 92 erg/cm^2), whereas the remaining ions K^+, Rb^+, Cs^+, NH_4^+, Cl^-, Br^-, and I^- show surface tension values characteristic of unstructured solvents (20–30 erg/cm^2). These values of the surface tension for each of these major groups fit in with the concept of structure making and structure breaking ions as discussed earlier since it would be expected that those ions which disrupt the liquid structure about them in solution should have some effect on the properties of the liquid about them. It is assumed that, according to the Frank–Wen model for ionic hydration (15), the property of water beyond the first hydration layer is roughly the same for all structure breaking ions. The parameters of Table 6 seem to agree with this assumption to a first approximation.

The temperature dependence of these ionic surface tension values is anomalous since the surface tension of normal liquids decreases with increase in temperature, whereas these calculated ionic surface tension parameters increase with an increase in temperature.

This anomaly may be due to the arbitrary assumption that the γ values of the potassium and chloride ion are the same at all temperatures. This may not be true in fact and until a method for obtaining absolute ionic viscosity parameters similar to those devised for absolute ionic molal volume parameters is devised only other arbitrary assumptions for obtaining a scale of ionic parameters can be explored. For instance since the ammonium ion seems to be minimally hydrated by this analysis one could assume the ammonium ion is unhydrated at all temperatures and that its energy of activation for viscous flow is the same as that of the solvent at all temperatures. These assumptions would yield another scale of ionic hydration and surface tension parameters.

Conclusions

The two-parameter equation for the viscosity of an electrolyte solution previously derived (eq. [1]) has been shown to account for the temperature dependence of the viscosity of concentrated electrolyte solutions. Analysis of the volume parameters has led to hydration numbers for each ion. The temperature dependence of these hydration numbers has indicated that the Gourary and Adrian ionic radii scale accounts for the grouping of the cations into structure making and structure breaking ions in a more consistent fashion than the Pauling ionic radii scale. Furthermore it gives a simple explanation of the basic differences between these two classes of ions.

A simple model previously used to account for the free energy of activation parameter for the viscosity of molten electrolytes has been shown to correlate the activation free energy parameters for viscous flow of salt ions in concentrated electrolyte solutions with the viscosity volume parameters for these same solutions. Analysis of these free energy of activation data leads to surface tension values for the water about structure making and structure breaking ions which are in agreement with surface tension data of structured and unstructured liquids respectively.

Acknowledgements

We would like to thank the National Research Council of Canada for a scholarship for one of us (R.F.) and the International Business Machine Company (IBM) of Canada for funds in aid of this project.

1. D. E. GOLDSACK and R. C. FRANCHETTO. Can. J. Chem. **55**, 1062 (1977).
2. R. C. WEAST (*Editor*). Handbook of chemistry and physics. 53 ed. Chemical Rubber Co., Cleveland, OH. 1974.
3. R. H. STOKES and R. A. ROBINSON. Electrolyte solutions. 2nd ed. Butterworths, London. 1959.
4. D. EISENBURG and W. KAUZMANN. The structure and properties of water. Oxford, New York. 1969.
5. B. E. CONWAY, R. E. VERRAL, and J. E. DESNOYERS. Z. Phys. Chem. Leipzig, **230**, 157 (1965).
6. H. S. FRANK and M. W. EVANS. J. Chem. Phys. **13**, 507 (1945).
7. R. H. STOKES and R. MILLS. International encyclopedia of physical chemistry and chemical physics. Vol. 16. Pergamon Press, New York. 1969.
8. T. C. WADDINGTON. Trans. Faraday Soc. **62**, 1482 (1966).

9. B. S. GOURARY and F. J. ADRIAN. Solid State Phys. **10**, 127 (1960).
10. M. F. C. LADD. Theor. Chim. Acta Berlin, **12**, 333 (1968).
11. J. E. DESNOYERS and C. JOLICOEUR. Modern aspects of electrochemistry. Vol. 5. *Edited by* J. O'M. Bockris and B. E. Conway. Plenum Press, New York, NY. 1969.
12. S. LENGYEL, J. TAMAS, J. GIBER, and J. H. HOLDERITH. Acta Chim. Acad. Sci. Hung. **40**, 125 (1964).
13. R. FURTH. Proc. Cambridge Phil. Soc. 252 (1941); 276 (1941); 281 (1941).
14. J. O'M. BOCKRIS and A. K. REDDY. Modern electrochemistry. Vol. 1. Plenum Press, New York, NY. 1970.
15. H. S. FRANK and W. Y. WEN. Discuss. Faraday Soc. **24**, 133 (1957).
16. E. W. WASHBURN (*Editor*). International Critical Tables. McGraw-Hill, New York, NY. 1933.
17. C. V. SURYANARAYANA and V. K. VENKATESAN. Acta Chim. Acad. Sci. Hung. **17**, 327 (1958).
18. N. M. BARON and M. U. SCHERBA. Zh. Prikl. Khim. **44**, 2118 (1971).
19. J. E. DESNOYERS and G. PERRON. J. Solution Chem. **1**, 199 (1972).
20. S. K. JALOTA and R. PATTERSON. J. Chem. Soc. **69**, 1510 (1973).
21. V. R. SUHRMANN and I. WEIDERSICH. Z. Anorg. Allg. Chem. **272**, 167 (1953).
22. J. TIMMERMANS. The physico-chemical constants of binary systems in concentrated solutions. Vol. 3. Interscience, New York, NY. 1959.
23. A. G. OSTROFF, B. S. SNOWDEN, and D. E. WOESSNER. J. Phys. Chem. **73**, 2784 (1969).
24. V. P. MASHOVETS, N. M. BARON, and M. U. SCHERBA. Zh. Prikl. Khim. **44**, 1981 (1971).
25. G. JONES and S. M. CHRISTIAN. J. Am. Chem. Soc. **59**, 484 (1937).
26. M. TANAKA. Nippon Kagaku Zasshi, **83**, 639 (1962).
27. M. TANAKA. Nippon Kagaku Zasshi, **82**, 147 (1961).
28. G. JONES and S. K. TALLEY. J. Am. Chem. Soc. **55**, 624 (1933).
29. J. D'ANS *et al.* (*Editors*). Landolt-Bornstein. II Band, 5 Teil. Springer-Verlag, Berlin. 1969.
30. G. JONES and S. K. TALLEY. J. Am. Chem. Soc. **55**, 4124 (1934).

Can. J. Chem. Downloaded from www.nrcresearchpress.com by 210.87.254.5 on 09/05/12
For personal use only.

Can. J. Chem. Downloaded from www.nrcresearchpress.com by 210.87.254.6 on 09/05/12
For personal use only.

A new stereospecific total synthesis of chasmanine and 13-desoxydelphonine

KAREL WIESNER, THOMAS Y. R. TSAI, AND KRISHNAN P. NAMBIAR

Natural Products Research Center, The University of New Brunswick, P.O. Box 4400, Fredericton, N.B., Canada E3B 5A3

Received March 10, 1978

KAREL WIESNER, THOMAS Y. R. TSAI, and KRISHNAN P. NAMBIAR. Can. J. Chem. **56**, 1451 (1978).

A simple synthesis of the title compounds, which is more than 10 steps shorter and an order of magnitude more efficient than our recent photochemical synthesis of chasmanine, is described. The main feature of the new process is a stereo- and regiospecific addition of benzyl vinyl ether to an *o*-quinone intermediate masked by a spirolactone group according to the method of Deslongchamps.

KAREL WIESNER, THOMAS Y. R. TSAI et KRISHNAN P. NAMBIAR. Can. J. Chem. **56**, 1451 (1978).

On décrit une synthèse simple des composés mentionnés dans le titre; cette synthèse est 10 étapes plus courte et au moins 10 fois plus efficace que notre synthèse photochimique que nous avons récemment rapportée pour la chasmanine. La principale caractéristique du nouveau processus est une addition stéréo- et régiospécifique de l'éther vinylbenzylique à un intermédiaire *o*-quinone masqué par un groupe spirolactone faisant appel à la méthode de Deslongchamps.

[Traduit par le journal]

We have described recently (1) the total synthesis of the alkaloid chasmanine (**4**) starting with the 'aromatic intermediate' **1** via the 'nordenudatine intermediate' **2** and the rearrangement product **3**. The construction of compound **2** was accomplished by a modification of our photochemical method.

In spite of the fact that the synthesis was stereospecific in all the steps and that all the substituents emerged in the correct positions simultaneously with the construction of the polycyclic skeleton, it turned out to be capable of considerable improvement. We have now developed a fundamentally different synthesis (see ref. 2 for model experiments) which is more than 10 steps shorter and an order of magnitude more efficient.

This new process represents the final generation of our effort to try out (with the aconite alkaloids) an 'engineering approach' (3) to the systematic development and simplification of synthetic strategy for polycyclic polysubstituted compounds.

In the present communication we wish to disclose the direct synthesis of racemic 13-desoxydelphonine and a formal synthesis of chasmanine by the new method. The starting material was the aromatic intermediate **5** (mp 163–164°C) which was prepared from vanillin by the aziridine rearrangement method (cf. ref. 3). The synthesis is fully stereo- and regiospecific and has been described in detail (4).

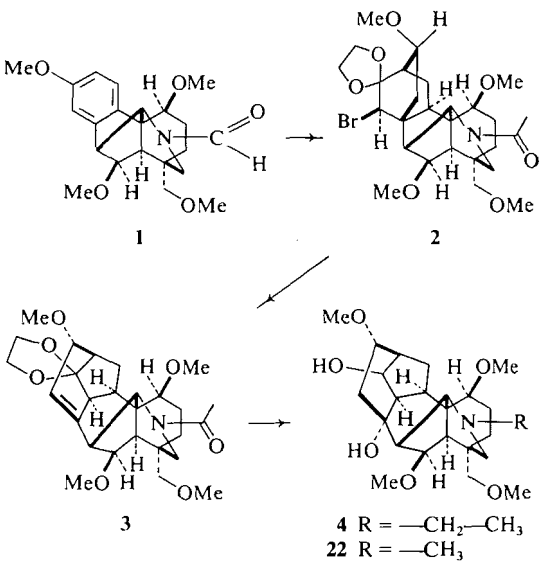

SCHEME 1

A more efficient route to the same compound starting from *o*-cresol has also been developed.[1]

The aromatic methoxyl in compound **5** was selectively cleaved with sodium thioethoxide in dimethylformamide at 120°C for 1.5 h. The phenol **6** (mp

[1]T. Y. R. Tsai, K. P. Nambiar, D. Krikorian, R. Marini-Bettolo, M. Botta, and K. Wiesner. In preparation.

Can. J. Chem. Downloaded from www.nrcresearchpress.com by 210.87.254.6 on 09/05/12
For personal use only.

189–190°C) was obtained in a yield of 95%.[2] Phenol **6** was alkylated with methyl bromoacetate in dry acetone in the presence of potassium carbonate and 18-crown-6 ether at room temperature for 6 h. The oily ester **7** was obtained in a yield of 90%.

The methoxymethyl protecting group and the ester group of compound **7** were hydrolysed with hydrochloric acid in THF at 55°C and the resulting phenolic acid was immediately oxidized to the corresponding masked *o*-quinone according to the method of Berney and Deslongchamps (5). The oxidation was carried out by stirring the solution of the phenolic acid in methylene chloride with an aqueous solution of sodium acetate and *N*-bromosuccinimide for 30 min with ice cooling. The masked *o*-quinone thus obtained was treated with an excess of benzyl vinyl ether for 24 h at room temperature (cf. ref. 2). The adduct **8** was isolated by chromatography on silica gel in an overall yield of 70%. It was separated into the components **8***a* and **8***b* by preparative tlc (ptlc). The ratio of **8***a*:**8***b* was approximately 2:1 and we were unable to suppress the formation of **8***b*. Fortunately, this turned out to be not only unnecessary but to our advantage.

Compound **8***a* was crystalline and melted broadly at 164–176°C since it is a mixture of epimers at the spirolactone carbon. Compound **8***b* was oily and was purified by preparative tlc. It was practically identical in ir and nmr spectroscopy with compound **8***a* except for the nmr peak of the vinylic hydrogen which was in this case a singlet at τ 4.21. In **8***a* the vinylic proton appears as a doublet (J = 6 Hz) at τ 4.35.

The adduct **8***b* was reduced with zinc in glacial acetic acid in the presence of 18-crown-6 ether under reflux for 15 h. The oily product **9** was purified by ptlc and was obtained in a yield of 85%. The same result was also obtained with compound **8***a* and the mixture of **8***a* and **8***b*.[3]

The benzyl protecting group in compound **9** was removed by hydrogenolysis in absolute ethanol over palladium-on-charcoal. The mixture of epimeric alcohols **10** was obtained in a yield of 96% and was immediately acetylated with acetic anhydride in pyridine. The acetates **11** (90%) crystallized from ether–chloroform (mp 166–167°C). The partial epimerization of the hydroxyl in compound **10** was clearly due to a reverse aldol–aldol condensation reaction during the hydrogenolysis or work-up.

Compound **11** is fully analogous in structure to the corresponding intermediate of our photochemical synthesis, which was reached only after many more synthetic operations. The only difference in the two series from this point on is that the photochemical intermediates were *N*-acetyl tertiary amides.

The keto acetate **11** was converted to the saturated compound **12** by hydrogenation with 5% rhodium-on-alumina in methanol at 85 psi for 18 h, followed by oxidation with chromium trioxide – pyridine. The saturated keto acetate **12** was obtained stereospecifically in a yield of **88**% and it was crystallized from ether–chloroform (mp 198–199°C).

Compound **12** was transformed to the keto acetal **13** by the following three operations: (*i*) reflux with *p*-toluenesulfonic acid and ethylene glycol in benzene; (*ii*) hydrolysis with methanolic sodium hydroxide; (*iii*) oxidation with chromium trioxide in pyridine.

The intermediate **13** was obtained in an overall yield of 88% and recrystallized from ether–chloroform to a mp of 206–207°C; ir: 1720, 1620 cm^{-1} (ketone, lactam C=O); ^{1}Hmr τ: 6.05 (s, 4H, O—CH_2—CH_2—O), 6.63, 6.70 (s, 9H, 3 OCH_3), 7.08 (s, 3H, N—CH_3). Reduction of the keto acetal **13** with sodium borohydride in methanol yielded quantitatively the alcohol **14**, mp 271–272°C (ether–chloroform).

Methylation of **14** under our standard conditions (1, 2) with sodium hydride and methyl iodide in dioxane gave 97% of the methoxy derivative **15**, mp 178–179°C (chloroform–ether); ir: 1625 cm^{-1} (lactam C=O); ^{1}Hmr τ: 6.13 (bs, 4H, O—CH_2—CH_2—O), 6.62, 6.63, 6.69, 6.73 (s, 3H each, 4 OCH_3), 7.10 (s, 3H, N—CH_3).

The acetal **15** was heated for 3 h in 80% acetic acid and the corresponding ketone **16** was obtained in a yield of 94% (mp 169–170°C, chloroform–ether); ir: 1720, 1625 cm^{-1} (ketone, lactam C=O).

Bromination of compound **16** with bromine in a mixture of ether and dioxane at room temperature for 4 h gave 90% of the bromo derivative **17** (mp 212–214°C, chloroform–hexane). The configuration of the bromine in formula **17** was assigned on the basis of the subsequent rearrangement, which requires antiplanarity of the leaving group and ring carbon–carbon bond. The bromo ketone **17** was transformed into the dioxolane **18** by reflux with an excess of ethylene glycol and an equimolar amount of *p*-toluenesulfonic acid in benzene for 24 h. Compound **18** (mp 150–152°C) was obtained in 80% yield.

The bromo derivative **18** was heated to 180°C for 6 h with an excess of DBN in a mixture (1:1) of

[2]All compounds gave correct molecular ions in mass spectrometry; all crystalline compounds gave satisfactory results in elemental analysis. The ir and nmr spectra are completely consistent with the assigned structures.

[3]Before this process was discovered the adduct **8***a* was converted to compound **9** via the diketone, dimethylketoacetal, dimethylhydroxyacetal, hydroxyketone, and mesyloxyketone (cf. ref. 2) which was finally reduced with zinc and acetic acid.

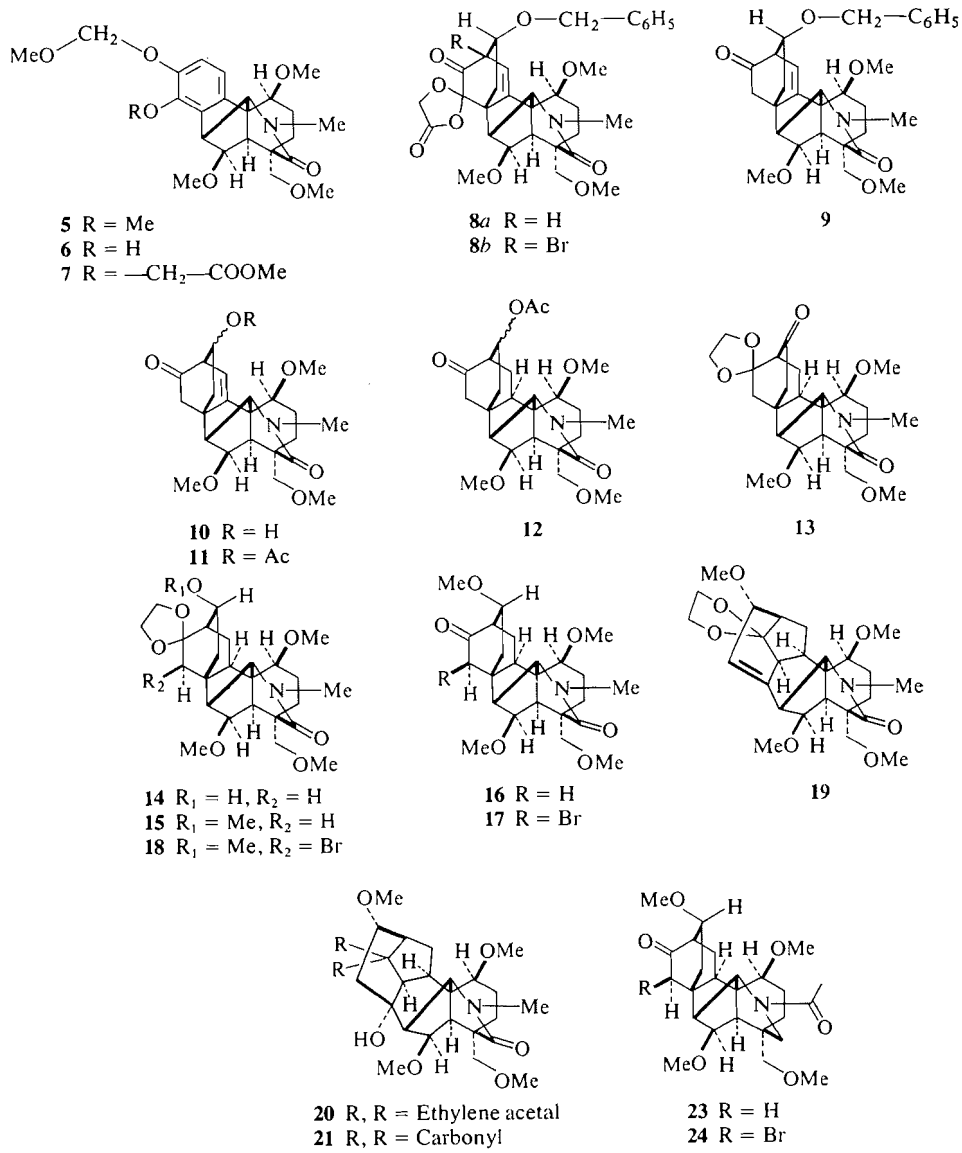

SCHEME 2

DMSO and *o*-xylene (cf. ref. 1). The oily rearranged compound **19** was the only product formed and was isolated by ptlc in a yield of 89%; ir: 1620 cm^{-1} (lactam C=O); ^{1}Hmr τ: 4.43 (d, J = 6 Hz, 1H, vinylic), 6.07 (m, 4H, O—CH_2—CH_2—O), 6.60, 6.67, 6.73, 6.77 (s, 3H each, 4 OCH_3), 7.10 (s, 3H, N—CH_3).

The pyro-oxo derivative **19** was subjected to oxymercuration followed by sodium borohydride reduction in THF (*1*). The oily alcohol **20** was isolated by ptlc in a yield of 65%; ir: 3550, 1622 cm^{-1} (OH, lactam C=O).

Compound **20** was heated in 80% acetic acid for 3 h to 85°C. The oily β-oxo-13-desoxy-14-ketodelphonine (**21**) was isolated by ptlc in quantitative yield; ir: 3560, 3440, 1745, 1622 cm^{-1} (OH, ketone, lactam C=O); ^{1}Hmr τ: 6.63, 6.68, 6.72 (s, 6H, 3H, 3H, 4 OCH_3), 7.04 (s, 3H, N—CH_3).

The keto lactam **21** was refluxed with lithium aluminum hydride in dioxane under nitrogen for 15 h. The *racemic totally synthetic 13-desoxydelphonine* (**22**) was recrystallized from hexane (64% yield). It melted constantly at 124–125.5°C and was identical by ir, nmr, mass spectrometry, and tlc in several systems with the optically active compound of the same structure, mp 92°C, prepared according to Marion and co-workers (6).

We have connected the new synthesis with our

Can. J. Chem. Downloaded from www.nrcresearchpress.com by 210.87.254.6 on 09/05/12
For personal use only.

photochemical synthesis of chasmanine (1) as follows; the intermediate **15** was reduced with lithium aluminum hydride to the corresponding tertiary amine and this was oxidized with $KMnO_4$ in acetone in the presence of acetic acid at room temperature for 15 min. The crude *N*-formyl derivative which was thus obtained was hydrolyzed with 6 *N* HCl at reflux for 3 h and the product was acetylated with acetic anhydride and pyridine. The oily *N*-acetyl derivative **23** was isolated by ptlc in 20% yield. It was identical by ir, nmr, mass spectrometry, and tlc with the corresponding intermediate of our photochemical synthesis (1).

Compound **23** (obtained by the present route) was brominated by the described (1) procedure. The bromo derivative **24** melted after crystallization from ether–chloroform at 244–246°C alone and in mixture with our photochemical intermediate (1) of the same structure (mp 244–246°C). Both materials were indistinguishable by ir, nmr, mass spectrometry, and tlc. The present synthesis represents a completely stereo- and regiospecific construction without the use of a relay of a racemate *containing 13 chiral centres*. All the substituents emerged in the course of the synthesis at the correct positions simultaneously with the construction of the hexacyclic skeleton. This seems to be at the present time the record for chiral control in total synthesis.[4]

Acknowledgements

We wish to thank the National Research Council of Canada, Ottawa, Ontario, Hoffmann – La Roche, Inc., Nutley, New Jersey and Vaudreuil, Quebec, and Merck Sharp and Dohme, Pointe-Clair–Dorval, Quebec for the financial support of this work.

1. T. Y. R. Tsai, C. S. J. Tsai, W. W. Sy, M. N. Shanbhag, W. C. Liu, S. F. Lee, and K. Wiesner. Heterocycles, **7** (Woodward Volume), 217 (1977).
2. K. S. Atwal, R. Marini-Berttolo, I. H. Sanchez, T. Y. R. Tsai, and K. Wiesner. Can. J. Chem. In press.
3. K. Wiesner. Chem. Soc. Rev. **6**, 413 (1977).
4. K. P. Nambiar. Ph.D. Thesis, University of New Brunswick, Fredericton, N.B. 1977. (Microfilm copies are obtainable by writing to the Natural Products Research Center, University of New Brunswick, Fredericton, N.B.)
5. D. Berney and P. Deslongchamps. Can. J. Chem. **47**, 515 (1969).
6. O. Achmatowicz, J. R., Y. Tsuda, and L. Marion. Can. J. Chem. **43**, 2336 (1965).

[4]We thank Professor Gilbert Stork, Columbia University, for pointing this out to one of us.

Can. J. Chem. Downloaded from www.nrcresearchpress.com by 210.87.254.6 on 09/05/12
For personal use only.

Canadian Journal of Chemistry

Published by
THE NATIONAL RESEARCH COUNCIL OF CANADA

Journal canadien de chimie

Publié par
LE CONSEIL NATIONAL DE RECHERCHES DU CANADA

Volume 56 Number 11 June 1, 1978

Volume 56 numéro 11 1 juin 1978

Can. J. Chem. Downloaded from www.nrcresearchpress.com by 210.87.254.42 on 09/05/12
For personal use only.

The chemistry of *N,N'*-dimethylformamidine. I. Formation from potassium methylamide and its thermal stability[1]

JAMES D. HALLIDAY, E. ALLAN SYMONS, AND J. DOUGLAS BONNETT

Physical Chemistry Branch, Chalk River Nuclear Laboratories, Atomic Energy of Canada Limited, Chalk River, Ont., Canada K0J 1J0

Received October 12, 1977

JAMES D. HALLIDAY, E. ALLAN SYMONS, and J. DOUGLAS BONNETT. Can. J. Chem. **56**, 1455 (1978).

The thermal decomposition of methylamine solutions of potassium methylamide (PMA) to form the potassium salt (PDMFA) of *N,N'*-dimethylformamidine (DMFA) has been studied as a function of PMA concentration at 60°C. Although concentrated solutions yield normal pseudo-first-order plots (analysis by ultraviolet–visible spectrophotometry), dilute solutions (<0.05 mol L^{-1} PMA) show an increase to a new rate after about 20 h reaction.

The mechanism for this novel amidine salt synthesis is discussed in terms of rate-limiting β-hydride elimination from the PMA ion pair. The relatively sharp rate increase with time for the low concentration runs may arise from a slow buildup of one or more intermediates. The resulting inverse dependence of k_{obs} on PMA concentration is probably related to ion pair – dimer association phenomena.

Pure DMFA has been produced by this reaction, and its thermal stability examined. DMFA decomposes above 100°C to form bis-*N*-(*N'*-methylmethylenimine)methylamine and methylamine; the series of equilibria involved have been shown to be reversible.

JAMES D. HALLIDAY, E. ALLAN SYMONS et J. DOUGLAS BONNETT. Can. J. Chem. **56**, 1455 (1978).

On a étudié, en fonction de la concentration de la MAP à 60°C, la décomposition thermique de solutions de méthylamidure de potassium (MAP) dans la méthylamine conduisant à la formation du sel de potassium (DMFAP) de la *N,N'*-diméthylformamidine (DMFA). Alors que des solutions concentrées conduisent à des courbes normales de pseudo premier ordre (analyse par spectrophotométrie ultraviolet-visible), des solutions diluées (<0.05 mol L^{-1} MAP), indiquent une augmentation vers une nouvelle vitesse après environ 20 h de réaction.

On discute du mécanism pour cette nouvelle synthèse du sel d'amidine en terme d'une élimination β d'hydrure provenant d'une paire d'ions de MAP et déterminant la vitesse de réaction. L'augmentation relativement rapide de la vitesse en fonction du temps aux concentrations basses peut provenir d'une accumulation lente de l'un ou de plusieurs intermédiaires. La relation résultante inverse de k_{obs} avec la concentration de map est probablement due au phénomène d'association de paires d'ions dimères.

On a pu produire de la DMFA pure par cette réaction et on a évalué sa stabilité thermique. La DMFA se décompose au-dessus de 100°C pour conduire à de la bis-*N*-(*N'*-méthylméthylenimine) méthylamine et à de la méthylamine; on a montré que la série des équilibres impliqués est réversible.

[Traduit par le journal]

Although there are few references in the literature to *N,N'*-dimethylformamidine (DMFA) (1), the general chemistry of the amidine group, 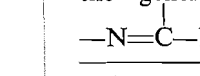 , has been well studied (2–4).

The potassium salt of DMFA had been identified[2] as one of the major products formed when a solution

[1]AECL No. 6117.

[2]Product identification for the thermal decomposition of PMA was done by Raylo Chemicals Ltd., Edmonton, Alta., under research contract to Atomic Energy of Canada Limited, 1969–1972.

Can. J. Chem. Downloaded from www.nrcresearchpress.com by 210.87.254.42 on 09/05/12
For personal use only.

of potassium methylamide (PMA) in methylamine (MA) was heated above ambient temperature (eq. [1]). Reported here are the results of an investigation into this interesting thermal decomposition reaction. Also discussed are DMFA recovery and purification procedures, and a brief study of the thermal stability of liquid DMFA.

[1] $2CH_3NH_2 + CH_3NHK \rightarrow 2H_2 + NH_3 + CH_3N{=}CHNKCH_3$

Experimental

Apparatus

The extremely reactive nature of PMA–MA solutions necessitated vacuum line and dry box techniques for preparation and handling. Details have been reported previously (5).

Ultraviolet–visible (uv–visible) spectra were run on Perkin Elmer 450 and Cary 17 spectrophotometers. Nuclear magnetic resonance spectra were recorded with a Bruker HX90 spectrometer, operating at 90 MHz for protons in a field of 2.114 T. Infrared spectra were obtained with a Perkin Elmer 467 instrument.

PMA Solution Preparation

The stock potassium methylamide solutions were prepared by reacting potassium (5 g ampoules, purity 99.95%, from Alfa Products, Ventron Corp.) with methylamine in 2.3 L stainless steel tanks. The water and ammonia in commercial methylamine (Matheson of Canada, Ltd.) had been removed by multiple treatments of the liquid with lithium metal (platinum black mesh catalyst), followed by vacuum distillation at each stage. In this way the ammonia level could be reduced to less than 8×10^{-3} mol L^{-1}, as determined by gas chromatography.

The stock solutions were stored at $-10°C$ to minimize thermal decomposition. The tanks had been fitted with stainless steel dip tubes for convenience in dispensing samples. The concentrations were determined by adding anhydrous ethanol to vacuum-dried sample residues and analyzing the resulting ethanol solutions of methylamine by gas chromatography. Nitrogen was used as carrier gas and the packing was 28% Pennwalt 223 plus 4% KOH on Gas Chrom R.

PMA Thermolysis Kinetic Runs

The thermal decomposition reaction was studied by monitoring the methylamide ion absorption spectrum by uv–visible spectrophotometry. Because of the elevated temperatures and resultant high methylamine vapour pressures involved, a stainless steel pressure cell assembly with thick quartz windows was used (variable path 0.01–0.1 cm). A sketch of the system is shown in Fig. 1. It was necessary to rinse the unit with dry methylamine at least twice to remove traces of water from the internal surfaces (6). Stock solution was then loaded under vacuum and the desired concentration obtained by dilution or concentration. Final solution volume was generally 40 mL.

Most kinetic runs were carried out at $60.0 \pm 0.1°C$ (oil bath). At appropriate times the reaction was quenched by cooling the tank to ambient temperature and the uv–visible spectrum run. Pseudo-first-order rate constants were obtained from least-squares plots of log absorbance at fixed λ (corrected for solvent baseline) vs. time. Tests had shown that Beer's Law was fairly well obeyed in this region.

The loss of PMA could not be measured *in situ* by nmr, because of rapid amino proton exchange. However, confirmation of the uv–visible analytical approach to measuring the thermolysis rate was obtained by nmr, utilizing the fact that DMFA is stable in aqueous acid solution at ambient temperature (7). For several thermolysis runs, 2 mL samples of PMA reaction solution were removed from the vessel each time a uv–visible spectrum was run. After the solvent and volatiles were distilled off, the residue was reacted with 1–2 mL of 0.7 mol L^{-1} DCl in D_2O to produce a solution about 0.1 mol L^{-1} in dissolved salts. A comparison of the methyl group peak areas for DMFA·DCl and CH_3ND_2·DCl yielded a pseudo-first-order plot which gave rate constants for DMFA formation in agreement with the values for PMA loss from the uv–visible plots (e.g. 2.8×10^{-6} vs. 3.2×10^{-6} s^{-1}, respectively, at 0.15 mol L^{-1}). However, this nmr procedure was used only to confirm the other results, since sample preparation was more involved and the system sensitivity was not as good.

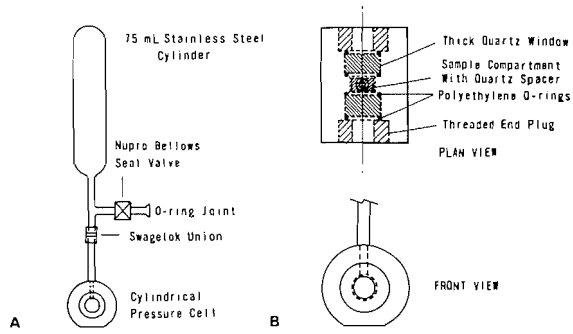

FIG. 1. (*A*) System used to study PMA thermolysis. (*B*) Detail of high pressure (to 6 MPa) uv–visible cell.

DMFA Synthesis

Potassium (13 g) and methylamine (210 g) were heated in a 1 L stainless steel tank at 100°C for 40 h, at which time the thermolysis reaction was complete. The hydrogen gas pressure was then released, the almost colourless solution transferred under vacuum to a Pyrex flask, residual methylamine and other volatiles distilled out, and *n*-dodecanol (300 g, Eastman technical) added to the potassium dimethylformamidide salt. The latter did not dissolve immediately but went into solution slowly as the alcohol was heated to 80°C and the generated DMFA was removed through a distillation column under

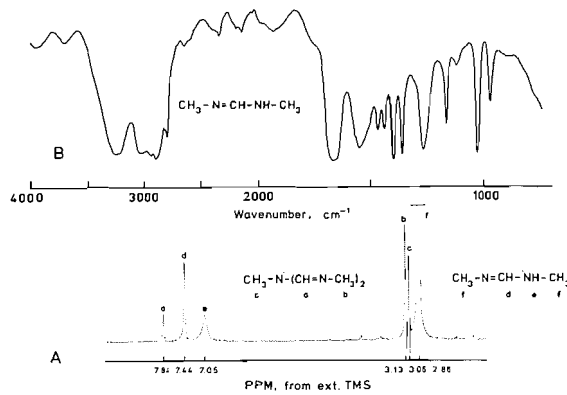

FIG. 2. (*A*) ^1H nuclear magnetic resonance spectrum of neat DMFA and its thermal decomposition product **12** (intentionally thermolyzed). (*B*) Infrared spectrum of neat DMFA, 0.025 mm IRTRAN 2 cell.

Can. J. Chem. Downloaded from www.nrcresearchpress.com by 210.87.254.42 on 09/05/12
For personal use only.

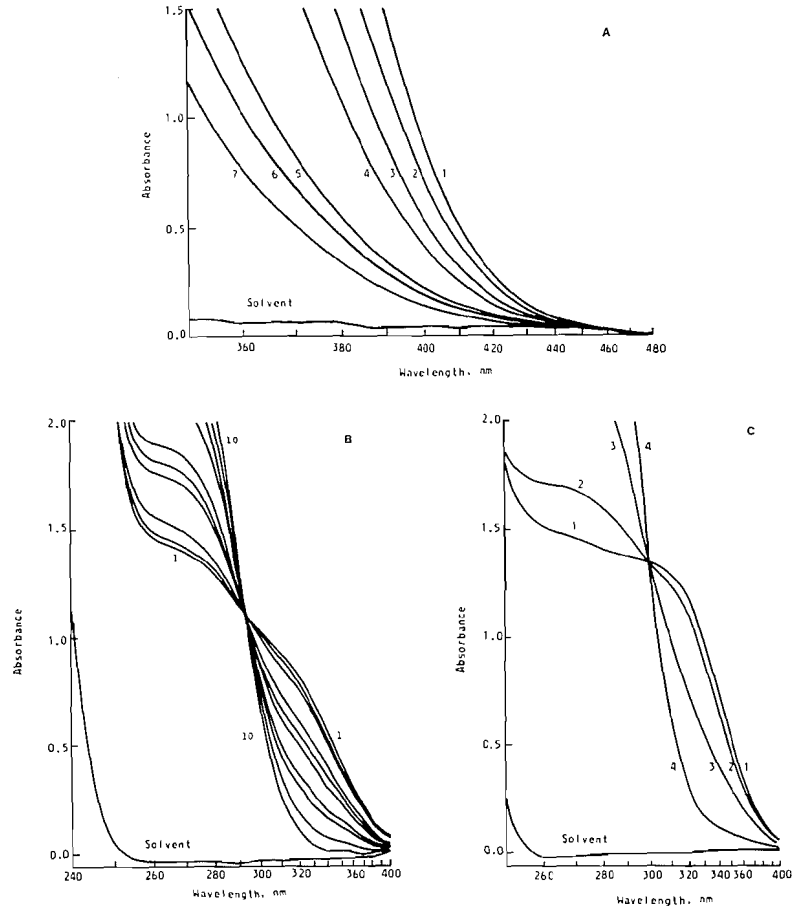

FIG. 3. (*A*) Change in uv–visible spectrum for 0.15 mol L^{-1} PMA at 60.0°C over time period 0–184 h. (*B*) Change for 0.035 mol L^{-1} PMA at 60.0°C, 0–74 h, final scan at 233 h. (*C*) Addition of neat DMFA to 0.085 mol L^{-1} PMA, in concentration ratios 0, 0.054, 0.46, and 1.2, at 23°C, 0.10 mm cell.

reduced pressure. This fraction contained several percent alcohol as determined by nmr. First stage yield was normally about 80%.

Final vacuum distillation through a packed 18 cm column (middle fraction 37.0–38.5°C at 0.5–0.7 kPa, uncorrected (lit. (1*a*) 59°C at 2.7 kPa, (1*c*) 50–53°C at 2.0 kPa) yielded a clear, colourless liquid whose spectral properties (infrared N—C=N stretch absorption at 1660–1680 cm^{-1} (8) (Fig. 2*B*) and ^1H nmr peaks at 7.44, 7.05, and 2.86 ppm (external TMS), ratios 1:1:6) and elemental analysis (*Anal.* calcd. for $C_3H_8N_2$: C 49.97, H 11.18, N 38.85; found: C 49.97, H 11.18, N 38.80) were in agreement with compound **1**. The nmr spectrum is shown in Fig. 2*A*, together with that of its thermal decomposition product (intentionally thermolyzed, see below). The purified DMFA was stored at −1°C to prevent decomposition.

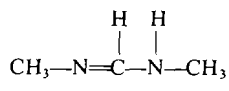

1

The results of an ^1H nmr study of tautomeric exchange in DMFA and its solutions is reported in Part III of this series (9), while its hydrolysis is discussed in Part II (7).

DMFA Thermal Stability

The thermal decomposition of neat DMFA was studied by ^1H nmr spectrometry. Samples in 5 mm nmr tubes capped with Teflon plugs were heated to 143°C in an oven. Periodically they were cooled to ambient temperature and the nmr spectrum run. A capillary of TMS, inserted after the samples were cooled, served both as a lock material and an external reference.

Results and Discussion

Formation of DMFA

PMA Thermal Decomposition

Because the CTTS band (6) of the methylamide ion has a fairly large extinction coefficient (1.54×10^3 L mol^{-1} cm^{-1} at 300 nm), the absorbance decrease with time for the more concentrated solutions had to be measured on the steep shoulder, usually over the range 370–405 nm (Fig. 3*A*). For the dilute solutions more of the absorption band was visible and both growth of the DMFA anion peak and loss of the methylamide ion peak could be seen (Fig. 3*B*). The latter set of spectra compares favourably with that for a synthetic run derived by adding samples of

Can. J. Chem. Downloaded from www.nrcresearchpress.com by 210.87.254.42 on 09/05/12
For personal use only.

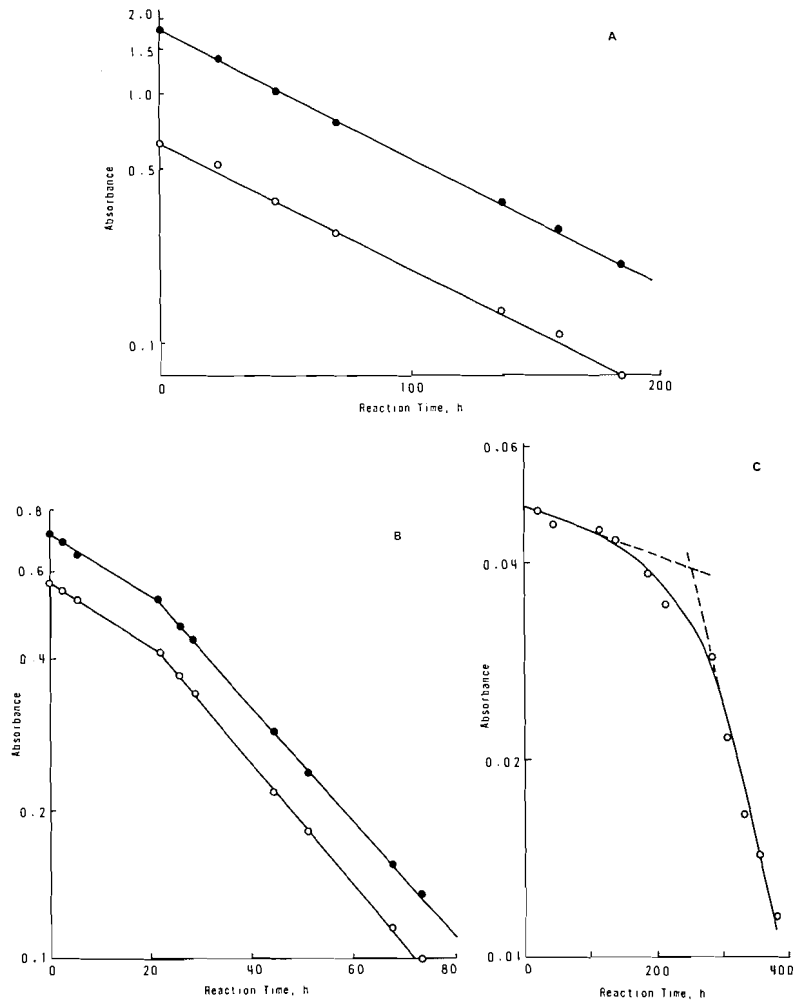

FIG. 4. (*A*) Pseudo-first-order plot of uv–visible data from Fig. 3*A*, half-life 59 h: ●, 386; ○, 405 nm. (*B*) Similar plot for data from Fig. 3*B*, initial half-life 47 h, final 26 h: ●, 330; ○, 340 nm. (*C*) Similar plot for data from run at 23°C with 6×10^{-6} mol L^{-1} PMA, 350 nm.

pure DMFA to a fresh potassium methylamide solution (Fig. 3*C*).

Plots of log absorbance vs. time for concentrated solutions were linear for 1 to 3 half-lives and showed negligible dependence on wavelength within the range 370–405 nm (Fig. 4*A*). On the other hand, for the more dilute solutions studied (below 0.05 mol L^{-1}) there was a distinct induction period of about 20 h before attainment of the final rate (Fig. 4*B*). There was no indication of a precipitate. Because of the lower absorbance for some of these solutions, measurements were occasionally made at somewhat shorter wavelengths (340–360 nm). However, the break in the curve was still evident for data at longer wavelength, although experimental error in the smaller absorbance values contributed to increased scatter. The results of a PMA decomposition run with a solution at very low concentration (6×10^{-6} mol L^{-1}, in all-glass apparatus equipped with a 100 mm optical cell) further support these observations (Fig. 4*C*). This run was carried out at 23°C since the apparatus could not safely withstand any higher internal pressure. Thus it is unlikely that the heating-for-reaction–cooling-for-analysis cycles are responsible for the rate change in the other runs.

Absorption by the potassium salt of DMFA does not interfere significantly with analysis of the decrease in methylamide ion spectrum with time (Fig. 3*C*). However, the contribution from initial product potassium amide (eqs. [8*a*] and [10*b*] below) was of concern. The amide ion is a strong enough base that it can react with solvent to regenerate some methylamide ion via equilibrium [2]. K_2 has not been measured directly but estimates range from 9 to 50

Can. J. Chem. Downloaded from www.nrcresearchpress.com by 210.87.254.42 on 09/05/12
For personal use only.

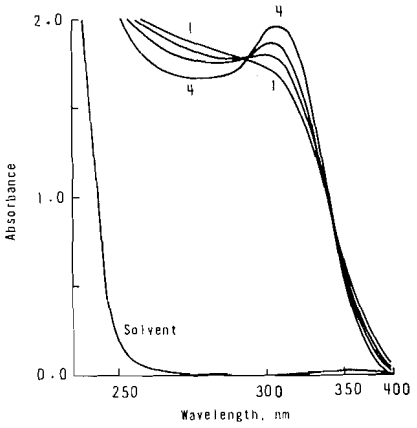

FIG. 5. Change in uv–visible spectrum upon addition of ammonia to 0.085 mol L^{-1} PMA at 23°C, concentration ratios 0, 0.46, 1.0, 2.2.

$$[2]\quad NH_3 + CH_3NH^-K^+ \overset{K_2}{\rightleftharpoons} NH_2^-K^+ + CH_3NH_2$$

(footnote 2 and ref. 10). The corresponding equilibrium for methylamine and the DMFA salt is known to lie well to the right, the dimethylformamidide ion being a much weaker base. Because of the excess CH_3NH_2 as solvent, early in the reaction the NH_2^- formed is all converted to NH_3. However, by the first half-life a small percentage will remain as NH_2^-, as shown for a test solution in Fig. 5. Since the spectra of the methylamide and amide salts are fairly similar, the result will have only a minor effect on the kinetic plots.

The pseudo-first-order rate constant data are presented in Table 1 and Fig. 6. The k_{obs} values calculated for both the initial and final phases of the kinetic plots for the low concentration runs are indicated. One such run, however, at about 0.05 mol L^{-1} PMA, did not exhibit any break in the kinetic plot.

Reaction Mechanism

The individual steps considered to be involved in moving from reactants to products are the following, based *in part* on reactions proposed by staff at Raylo Chemicals Limited,[2] L. G. Walker,[3] and W. J. Holtslander.[4]

Some general points can be made concerning relative stabilities of the various proposed intermediates. Both methylenimine (**2**) and *N*-methylmethylenimine (**5**) are known to be extremely reactive (11), often disappearing via polymerization reactions (3), and hence should be only transient species under the present strongly basic conditions.

[3]L. G. Walker, attached staff, CRNL, AECL, 1970.

[4]W. J. Holtslander, Chemical Engineering Branch, CRNL, AECL.

TABLE 1. Dependence of k_{obs} for PMA thermolysis at 60°C on initial [PMA]

[PMA] (mol L^{-1})	$k_{obs} \times 10^6$ (s^{-1})	[PMA] (mol L^{-1})	$k_{obs} \times 10^6$ (s^{-1})
0.028	2.1,[a] 6.1[b]	0.14	3.2
0.033	4.2[a], 7.6[b]	0.14	3.1
0.038	4.8[a], 6.6[b]	0.15	4.2
0.043	6.5[c]	0.15	4.1
0.047	2.5[a], 6.2[b]	0.15	2.9
0.067	4.9	0.15	3.9
0.086	3.5	0.17	3.3
0.10	3.4	0.18	3.0
0.12	3.2	0.23	3.0

[a]Initial slope value (cf. Fig. 4*B*).
[b]Final slope value (cf. Fig. 4*B*).
[c]No slope change observed.

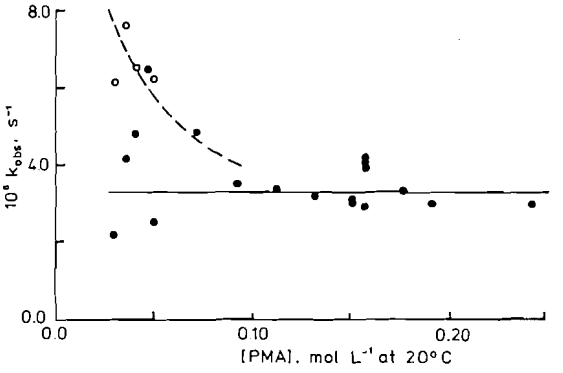

FIG. 6. Dependence of k_{obs} for PMA thermolysis at 60.0°C on PMA concentration. For dilute runs: ●, initial slope; ○, final slope.

A pungent, pyridine-like odour, probably arising from traces of cyclic nitrogen compounds, was often detected at the end of a run. Aminals (*gem*-diamines) are also unstable (3), so that their salts, such as **4**, **6**, and **8**, should have short lifetimes in these solutions, decomposing to amines, imines, and the corresponding salts (3). Evidence for the involvement of the *N*-methylmethylenimine (**5**) comes from the observation that when the thermolysis run is carried out with high hydrogen overpressure (7–30 MPa), dimethylamine is formed as a minor product.[4] This likely occurs through reaction of KH, produced to its solubility limit via equilibrium [13],[4] with **5** according to [14] and [15]. Methylenimine, *N*-methylmethylenimine, and hydrogen cyanide have been proposed as intermediates in the pyrolysis of methylamine (12). Step [13] has been shown to be rapid in the presence of freshly prepared, finely divided KH.[4] Thus, if proton transfer from one nitrogen atom to another is also considered to be rapid, then the main route steps given by eqs. [7], [8*a*], [9*a*], [9*b*], [10*b*], [11], [12], and [13] can all be expected to be fast.

Can. J. Chem. Downloaded from www.nrcresearchpress.com by 210.87.254.42 on 09/05/12
For personal use only.

[3] $CH_3NH^-K^+(\text{ion pair}) \rightarrow KH + \underset{\mathbf{2}}{CH_2{=}NH}$

[4] $\mathbf{2} + CH_3NHK \rightleftharpoons \underset{\mathbf{3}}{CH_2{=}NK} + CH_3NH_2$ ⎫ Cyanide side reaction

[5] $\mathbf{3} \rightarrow KH + HC{\equiv}N$ ⎭

[6] $HCN + CH_3NHK \rightarrow KCN + CH_3NH_2$

[7] $CH_3NHK + \mathbf{2} \rightleftharpoons \underset{\mathbf{4}}{CH_3NKCH_2NH_2}$

[8*a*] $\mathbf{4} \rightleftharpoons \underset{\mathbf{5}}{CH_3N{=}CH_2} + NH_2K$ ⎫

[9*a*] $CH_3NHK + \mathbf{5} \rightleftharpoons \underset{\mathbf{6}}{CH_3NKCH_2NHCH_3}$ ⎬ Route *A*

[10*a*] $\mathbf{6} \rightarrow \underset{\mathbf{1}}{CH_3N{=}CHNHCH_3} + KH$ ⎭

[8*b*] $\mathbf{4} \rightarrow \underset{\mathbf{7}}{CH_3NHCH{=}NH} + KH$ ⎫

[9*b*] $CH_3NHK + \mathbf{7} \rightleftharpoons \underset{\mathbf{8}}{CH_3NK\!\left(CH_3NH\right)\!CHNH_2}$ ⎬ Route *B*

[10*b*] $\mathbf{8} \rightleftharpoons \mathbf{1} + NH_2K$ ⎭

[11] $\mathbf{1} + CH_3NHK \rightarrow \underset{\mathbf{9}}{CH_3N{=}CHNKCH_3} + CH_3NH_2$ ⎫

[12] $NH_2K + CH_3NH_2 \rightleftharpoons NH_3 + CH_3NHK$ ⎬ Products

[13] $KH + CH_3NH_2 \rightleftharpoons H_2 + CH_3NHK$ ⎭

[14] $CH_3N{=}CH_2 + KH \rightleftharpoons CH_3NKCH_3$ ⎫ Dimethylamine side reaction

[15] $CH_3NKCH_3 + CH_3NH_2 \rightleftharpoons CH_3NHCH_3 + CH_3NHK$ ⎭

The rate-limiting steps are therefore believed to be those involving potassium hydride formation, i.e. [3], [8*b*], and/or [10*a*]. Similar metal hydride elimination reactions are known to occur in the decomposition of transition metal alkyl complexes when a β-hydrogen is available (13, 14). The stability of transition metal dialkylamides was ascribed to the absence of suitable β-hydrogen atoms in these compounds (15). Thermal decomposition of alkali metal alkyls leads to the formation of olefins and the alkali metal hydrides (16). Because methylamine has such a low dielectric constant (about 8.0 at 60°C), the dissociation of PMA ion pairs to free ions is slight ($K_d \simeq 10^{-7}$ mol L^{-1} at −25°C (17)). Thus the slow formation of KH probably occurs from the PMA ion pair, [4], via intramolecular elimination (13) either in the α-mode (A) or, more likely, the β-mode (B).

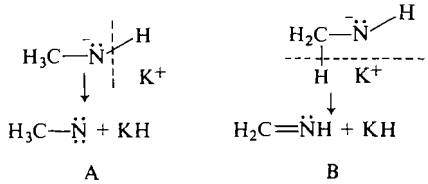

Lithium and sodium methylamides have been reported to yield the cyanides upon heating in methylamine solution or in a vacuum (18). Although this route does not appear to be an important one for the potassium case, there is evidence that the formation of cyanide is the *primary* route in the lithium case (see below). The cyanide must arise through a second hydride elimination step [5], from the methylenimide salt **3**. It is interesting that DMFA is a major product in the reaction between liquid methylamine and anhydrous hydrogen cyanide (1*a*).

The important role of the cation is clear from the more limited results of thermolysis studies with lithium methylamide (LMA). The rate of loss of LMA, as measured by uv–visible spectrophotometry, was roughly a factor of 10 slower than for the potassium salt at the same temperature. Two other runs were carried out in sealed, medium wall nmr tubes at 80°C; the nmr spectra were run at ambient temperature. The formation of lithium *N,N'*-dimethylformamidide was very slow relative to the rate of loss of LMA predicted from the uv–visible measurements but no new peaks appeared in the nmr spectrum. Because lithium cyanide would not be detected under these conditions, alternate tests were

[16]

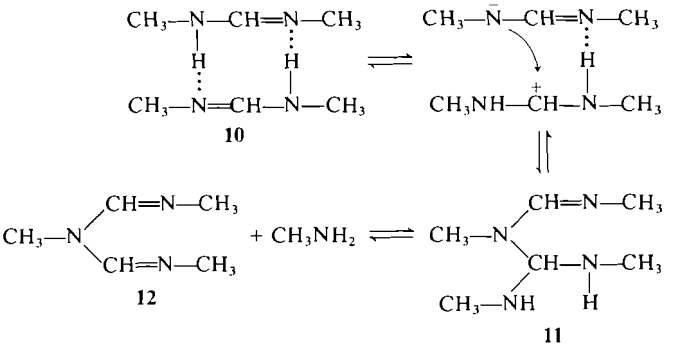

made. The residue from one of these solutions was examined in a Nujol mull by ir and gave good evidence for the presence of cyanide ion, by comparison with the spectrum of potassium cyanide powder in Nujol. The residue from the other solution gave a positive response to a copper sulphide cyanide test (19).

Rate Constant Dependence on PMA Concentration

The high initial PMA concentration runs gave simple first order kinetic plots but for most of the dilute solution runs, below ca. 0.05 mol L^{-1}, an increase in rate was observed after a period of time (e.g. Figs. 4*B* and *C*). The question then arises as to which phase of these runs is comparable to the data for the high concentration runs. The simpler approach is to consider the initial rates as comparable, which yields the horizontal straight line in Fig. 6 (considerable scatter), and the straightforward conclusion that the reaction is indeed first order in PMA concentration. The rate acceleration measured for the dilute PMA runs is then assigned to an unknown side reaction, perhaps triggered by a change in degree of ion pairing, such as the cyanide scheme (eqs. [4] and [5]).

The alternative is to assume that the final rates are comparable, and that the low PMA concentration runs start slowly because of interference from some inhibitor which is gradually consumed. However, one is then left with the problem of explaining a decrease in k_{obs} with increasing PMA concentration, the dashed curve in Fig. 6. In either case, it is difficult to reconcile the fact that the very dilute PMA run behaves the same way (Fig. 4*C*). For this run, ion association will be much less extensive, yet interference from any inhibitor should be much more pronounced.

The effect of a slow buildup of some intermediate(s) must be considered, because of the complicated sequence of steps involved, eqs. [3]–[15]. It was possible, by assigning reasonable values to the various *k*'s (omitting steps 4, 5, 6, 8*b*–10*b*, 14, and 15), to simulate the shape of Fig. 4*B* by computer calculation.[5] Also, the curvature was reduced for higher PMA concentrations. However, as a result, the concentrations of intermediates **2** and **5** rose to levels approaching the initial PMA concentration and then remained constant, a situation which is unlikely in reality. Because of the number of variables involved, it was not feasible to examine all possible combinations of rate constants, but it is clear that a slow buildup of one or more intermediates could cause the behaviour seen in Figs. 4*B* and *C*.

If the last argument above is the correct one, then the problem of explaining the dashed curve in Fig. 6 returns. The phenomenon may arise from an increase in association of reactive ion pair monomers to form unreactive dimers and larger aggregates.

Thermal Stability of DMFA

During the most recent DMFA preparation, an efficient distillation from the *n*-dodecanol left negligible alcohol in the DMFA. However, after subsequent fractional vacuum distillation, a new impurity was discovered in the distillate by nmr; an additional distillation only raised the concentration of this impurity from about one to several percent. A sample of this DMFA, when heated in a sealed nmr tube for a period of 216 h at 143°C, slowly yielded about 15% conversion to the new compound.

The reaction sequence involved is postulated to have been the following (eq. [16]): autoprotolysis of one DMFA molecule by another via a dimeric structure,[6] transfer of the positive charge centre to carbon in the protonated molecule, attack by the anion on the cation of the pair, and finally elimination of methylamine from the unstable aminal **11** (3) to form bis-*N*-(*N'*-methylmethylenimine)methylamine (**12**). The ^{1}H nmr spectrum of **12** in DMFA, Fig. 2*A*, has peaks at 7.84, 3.13, and 3.06 ppm (external TMS) in the ratio 2:6:3.

[5]FORSIM Program, M. Carver, Math and Computation Branch, CRNL, AECL.

[6]There is good infrared and ^{1}H nmr evidence for formation of a cyclic DMFA dimer **10** (9).

Can. J. Chem. Downloaded from www.nrcresearchpress.com by 210.87.254.42 on 09/05/12
For personal use only.

This set of reactions was shown to be reversible. When a sample of DMFA containing a small percentage of **12** was treated with an excess of methylamine, relative to **12**, at ambient temperature for 18 h, the concentration of **12** was reduced to below 0.1%. The remaining methylamine was then quickly removed under vacuum below ambient temperature. It would appear that the forward reaction in [16] is inhibited by the presence of traces of protic species such as the alcohol, which would prevent the formation of DMFA anion initially.

Acknowledgements

The authors are grateful for discussions with Drs. J. H. Rolston and W. J. Holtslander at CRNL, and for the considerable assistance provided by Dr. Rolston in adapting the general computer simulation program[5] to the present problem. They also wish to thank Messrs. P. E. Bindner and J. P. Johnson for some assistance in the laboratory.

1. (*a*) Y. YAMADA, I. KUMASHIRO, and T. TAKENISHI. J. Org. Chem. **33**, 642 (1968); (*b*) M. SEEFELDER and W. JENTZSCH. Chem. Abstr. **60**, 2791a (1964); (*c*) W. JENTZSCH and M. SEEFELDER. Chem. Abstr. **62**, 16240e (1965); (*d*) H. BREDERECK, F. EFFENBERGER, and E. HENSELEIT. Chem. Abstr. **63**, 11353d (1965).
2. R. L. SHRINER and F. W. NEUMANN. Chem. Rev. **35**, 351 (1944).
3. P. A. S. SMITH. Open-chain nitrogen compounds. Vol. 1. W. A. Benjamin, Inc., New York, NY. 1965.
4. I. T. MILLAR and H. C. SPRINGALL. A shorter Sidgwick's organic chemistry of nitrogen. Clarendon Press, Oxford, England. 1969.
5. J. D. HALLIDAY and P. E. BINDNER. Can. J. Chem. **54**, 3775 (1976).
6. R. E. CUTHRELL and J. J. LAGOWSKI. J. Phys. Chem. **71**, 1298 (1967).
7. J. D. HALLIDAY and E. A. SYMONS. Can. J. Chem. **56**, 1463 (1978).
8. D. C. PREVORSEK. J. Phys. Chem. **66**, 769 (1962).
9. J. D. HALLIDAY, E. A. SYMONS, and P. E. BINDNER. Can. J. Chem. **56**, 1470 (1978).
10. K. BAR-ELI and F. S. KLEIN. J. Chem. Soc. 3083 (1962).
11. (*a*) D. E. MILLIGAN. J. Chem. Phys. **35**, 1491 (1961); (*b*) A. G. ABATJOGLOU and E. L. ELIEL. J. Org. Chem. **39**, 3042 (1974); (*c*) J. HINZE and R. F. CURL. J. Am. Chem. Soc. **86**, 5068 (1964).
12. G. W. MEADOWS and J. J. KIRKLAND. J. Phys. Chem. **65**, 2139 (1961).
13. R. R. SCHROCK and G. W. PARSHALL. Chem. Rev. **76**, 243 (1976).
14. P. J. DAVIDSON, M. F. LAPPERT, and R. PEARCE. Acc. Chem. Res. **7**, 209 (1974).
15. D. C. BRADLEY and M. H. CHILHOLM. Acc. Chem. Res. **9**, 273 (1976).
16. (*a*) W. H. GLAZE and G. M. ADAMS. J. Am. Chem. Soc. **88**, 4653 (1966); (*b*) R. L. EPPLEY and J. A. DIXON. J. Organometal. Chem. **11**, 174 (1968); R. A. FINNEGAN and H. W. KUTTA. J. Org. Chem. **30**, 4138 (1965).
17. (*a*) E. ROCHARD and J. RAVOIRE. J. Chim. Phys. **68**, 1183 (1971); (*b*) E. A. SYMONS and J. D. BONNETT. Can. J. Chem. **56**, 1518 (1978).
18. R. JUZA and E. HILLENBRAND. Z. Anorg. Allg. Chem. **273**, 297 (1953).
19. F. FEIGL and V. ANGER. Spot tests in inorganic analysis. *Translated by* R. E. Oesper. 6th English ed. Elsevier, New York, NY. 1972.

Can. J. Chem. Downloaded from www.nrcresearchpress.com by 210.87.254.42 on 09/05/12
For personal use only.

The chemistry of *N,N'*-dimethylformamidine. II. Hydrolysis. Kinetically controlled formation of *cis*-*N*-methylformamide[1]

JAMES D. HALLIDAY AND E. ALLAN SYMONS

Physical Chemistry Branch, Chalk River Nuclear Laboratories, Atomic Energy of Canada Limited, Chalk River, Ont., Canada K0J 1J0

Received October 12, 1977

JAMES D. HALLIDAY and E. ALLAN SYMONS. Can. J. Chem. **56**, 1463 (1978).

The hydrolysis of *N,N'*-dimethylformamidine (DMFA) has been investigated in acid and alkaline aqueous media by ^{1}H nmr; only a narrow basic p*H* range could be extensively studied kinetically. The pseudo-first-order k_{obs} rose steadily from p*H* 11.5 to 13.0 (reaction approximately first order in OH^-), then became independent of p*H* above 13.5 (9.3×10^{-4} s^{-1} at 10°C). In contrast to many amidines, DMFA is quite stable in acid solution (estimated value of the pseudo-first-order hydrolysis rate constant is 1.4×10^{-11} s^{-1} at 10°C, p*H* 0.05, from measurements at 100 and 140°C). This stability is ascribed to the difficulty of eliminating the fairly strong base methylamine from the tetrahedral intermediate in acid solution.

N-Methylformamide (NMF), one of the products, is formed initially as the *cis* isomer. A somewhat slower conversion then occurs to the thermodynamically more stable *trans* isomer. This unusual result is explained in terms of Deslongchamps and co-workers' theory of stereoelectronic control for the orbital-assisted breakdown of tetrahedral intermediates.

JAMES D. HALLIDAY et E. ALLAN SYMONS. Can. J. Chem. **56**, 1463 (1978).

On a étudié l'hydrolyse de la *N,N'*-diméthylformamidine (DMFA) en milieu aqueux acide et alcalin en faisant appel à la rmn du ^{1}H; on n'a pu étudier d'une façon exhaustive la cinétique de cette réaction qu'à l'intérieur d'une région alcaline limitée de p*H*. La valeur k_{obs} pour une réaction du pseudo premier ordre augmente régulièrement lorsque le p*H* passe de 11.5 à 13.0 (la réaction est approximativement du premier ordre en OH^-) et elle devient alors indépendante du p*H* au dessus de 13.5 (9.3×10^{-4} s^{-1} à 10°C). Par opposition à plusieurs amidines, la DMFA est très stable en solution acide (on a évalué que la constante de vitesse hydrolyse du pseudo premier ordre est 1.4×10^{-11} s^{-1} à 10°C, pour un p*H* de 0.05; cette valeur a été évaluée à partir de mesures à 100 et 140°C). On attribue cette stabilité à la difficulté d'éliminer la méthylamine, qui est une base relativement forte, de l'intermédiaire tétraédrique en solution acide.

La *N*-méthylformamide (NMF), l'un des produits, se forme au départ sous la forme de l'isomère *cis*. Une conversion un peu plus lente se produit alors pour conduire à l'isomère *trans* qui est thermodynamiquement plus stable. On explique ce résultat inhabituel en terme de la théorie de Deslongchamps et de ses collaborateurs relative au contrôle stéréoélectronique de la décomposition assistée par les orbitales d'intermédiaires tétraédriques.

[Traduit par le journal]

When methylamine solutions of potassium methylamide are heated they decompose to form hydrogen, ammonia, and the potassium salt (PDMFA) of *N,N'*-dimethylformamidine (DMFA) (**1**) (1).[2] Al-

$$\underset{\mathbf{1}}{CH_3NKCH{=}NCH_3}$$

though a uv–visible spectrophotometric method was successfully applied to the measurement of the rate of this thermolysis reaction (1), an alternate confirmatory method was desirable which could also monitor the formation of products. Proton nmr was used but direct solution analysis was not practical; the technique is unable to distinguish the PMA methyl resonance in the presence of methylamine, because of rapid amino proton exchange. When the salts were isolated from reaction solution samples and dissolved in water to facilitate analysis, the DMFA, under these alkaline conditions, was fairly rapidly hydrolyzed. However, in acid solution, hydrolysis occurred very slowly and for analytical purposes at ambient temperature the rate was negligible. The p*H* dependence of the hydrolysis rate was examined in more detail and the results of this study are reported here.

The temperature dependence of tautomeric exchange in the neat liquid and in several solvents is discussed separately (2).

Experimental

The synthesis, identification, and purification of DMFA have been reported elsewhere in this series (1).

[1]AECL No. 6118.

[2]Product identification was done by Raylo Chemicals Ltd., Edmonton, Alta., under research contract to Atomic Energy of Canada Ltd., CRNL, 1969–1972.

Can. J. Chem. Downloaded from www.nrcresearchpress.com by 210.87.254.6 on 09/05/12
For personal use only.

Can. J. Chem. Downloaded from www.nrcresearchpress.com by 210.87.254.6 on 09/05/12
For personal use only.

Most hydrolysis kinetic runs (0.21 mol L^{-1} DMFA) were carried out at constant ionic strength (0.50 mol L^{-1}), with HCl, KOH, and KCl being employed. The H_2O was triple distilled and the D_2O (99.7 at.% D, AECL) was used as received. Reaction solutions were prepared cold in 2 mL Pyrex tubes; samples were transferred immediately to nmr tubes.

Proton nmr spectra were recorded on a Bruker HX90 spectrometer equipped with a B-ST 100/700 variable temperature controlled probe (±0.5°C). The methyl region was scanned repeatedly as a function of time, using the H_2O signal as internal lock. For the runs with D_2O as solvent, a capillary of TMS was added as an external lock. Depending on the rate of reaction, from 20 to 50 kinetic points could be obtained per run over a period of 1 to 3 half-lives.

The chemical shifts of the species involved in the hydrolysis reaction are shown with the representative spectra in Fig. 1. In general, the DMFA methyl peak fell between the *cis*- and *trans*-*N*-methylformamide (NMF) peaks but their relative positions were dependent on p*H*. The methyl group of the second product of hydrolysis, methylamine (MA), was always to high field of the NMF and DMFA. When overlap of the DMFA and NMF peaks was too great to allow direct measurement of the DMFA integral, it was obtained by subtraction of the MA integral from the combined DMFA and NMF integrals.

Ultraviolet spectra were run on a Cary 17 spectrophotometer, and infrared spectra on a Perkin Elmer model 467 instrument.

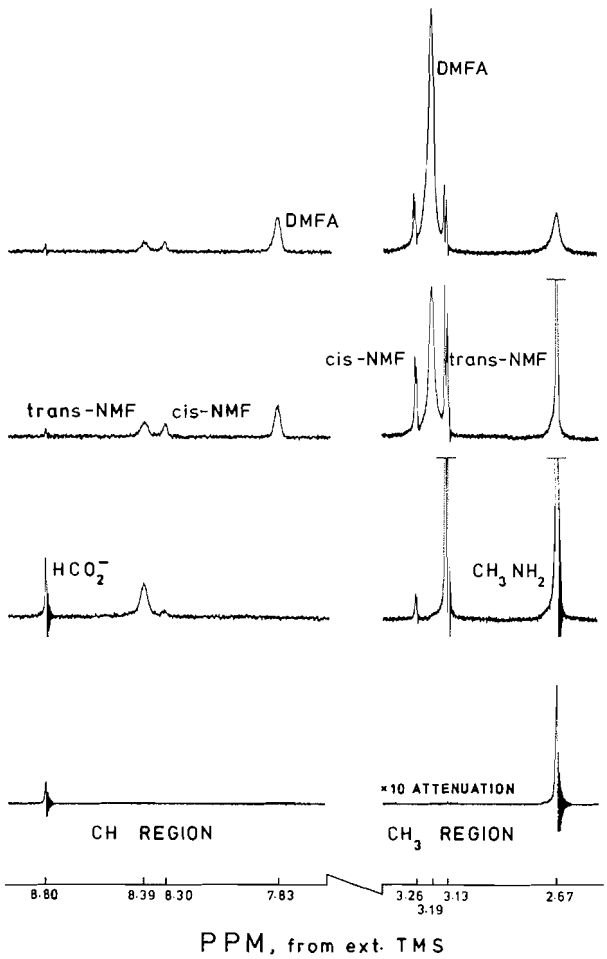

FIG. 1. Changes in the nmr spectrum during 0.21 mol L^{-1} DMFA hydrolysis. Top to bottom: 5 min at 0°C, 15 min at 0°C, 1 h at 23°C, 64 h at 23°C, p*H* 13.0.

Results

Hydrolysis Products

The general hydrolysis sequence, eqs. [1] and [2],

[1] $CH_3N{=}CHNHCH_3 + H_2O \xrightarrow{^-OH} CH_3NHCHO + CH_3NH_2$

[2] $CH_3NHCHO + H_2O \xrightarrow{^-OH} CH_3NH_2 + HCO_2H$

was confirmed by comparing the nmr and infrared spectra of reaction samples with those of aqueous solutions of authentic samples of *N*-methylformamide, methylamine, formic acid, and sodium formate.

Hydrolysis of the NMF, eq. [2], was found to occur at a rate at least a factor of 10 slower than for the DMFA over the p*H* range 11.5–14; however, at p*H* 1 the NMF reacted many orders of magnitude faster than the DMFA.

DMFA pK_a

For one hydrolysis run at 25°C with 0.21 mol L^{-1} DMFA and 0.50 mol L^{-1} KCl, a portion of the reaction sample was monitored with a p*H* meter to determine the extent of p*H* change during a run in the unbuffered system. It was found that the p*H* (glass and solid state electrodes) decreased slowly from 12.9 (extrapolated zero time value), levelling off at 12.2 over a period of 5 DMFA hydrolysis half-lives (as measured by nmr). From the zero time value, the pK_a of the DMFA conjugate acid was estimated to be 12.40 ± 0.10; this compares with the value of 12.40 for acetamidine at 25°C (3). *N,N'*-Diphenylformamidine is a much weaker base, with pK_a 6.15 (4). The p*H* of the various reaction solutions was then calculated via the equations provided by Kolthoff *et al.* (5), using the 12.40 estimate for the DMFA pK_a.

p*H Dependence of* k_{obs}

Least-squares treatment of linear plots of log DMFA integral vs. time yielded the pseudo-first-order rate constants for DMFA hydrolysis. One such plot is shown in Fig. 2. Above p*H* 13 such plots were linear for at least 2 half-lives ($R > 0.995$). Runs were reproducible to better than 10%. Below p*H* 13, the region of linearity for the plots decreased: 1 half-life at 12.5, less than 0.5 half-life at 12.0.

Can. J. Chem. Downloaded from www.nrcresearchpress.com by 210.87.254.6 on 09/05/12
For personal use only.

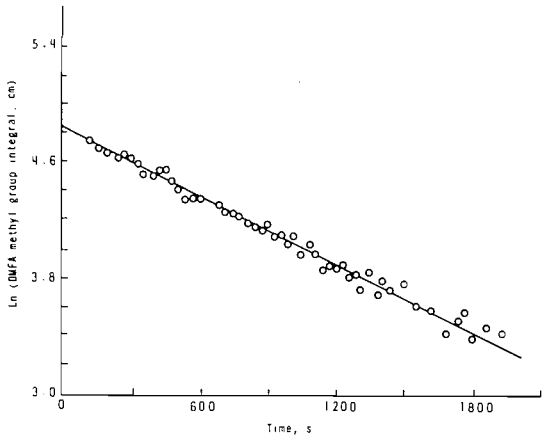

FIG. 2 Pseudo-first-order plot of nmr data for 0.21 mol L^{-1} DMFA hydrolysis at 10.8°C, p*H* 12.97.

The hydrolysis rate at 10.0°C was found to be practically independent of p*H* above 13.5 but it dropped rapidly as the starting p*H* was decreased below this value (Fig. 3). Because buffer solutions could not be used (see below), for the run at starting p*H* 11.5 the initial broad DMFA methyl group singlet changed slowly to a square-topped peak during the first 5% of reaction and then to a resolved doublet by 15% reaction, as the solution p*H* dropped and more extensive protonation of the remaining DMFA occurred. For this run, only the nmr data for the first 5% of reaction were used to calculate k_{obs}.

Accurate k_{obs} measurements could not be made in the p*H* range 2–11; because of sensitivity limitations, the DMFA concentration could not be lowered enough to permit proper buffering action by normal buffer solutions. As an alternate analytical technique the possibility of using uv–visible spectrophotometry was examined, since substrate concentrations in the range 10^{-2}–10^{-4} mol L^{-1} are ideal. Unfortunately, there is no strong chromophoric group in the DMFA molecule and tests showed that no suitable absorption peak was present in the aqueous solution spectrum. There was strong interference from the hydroxide and chloride ion absorption bands below about 240 nm, the region where DMFA begins to absorb.

At very low p*H* the acid hydrolysis of DMFA could be measured without buffers, although elevated temperatures (sealed nmr tubes) were required because of the much slower rates. For a solution at p*H* 0.05, the k_{obs} values at 100 and 140°C were 5.5×10^{-7} and 1.4×10^{-5} s^{-1}, respectively. Extrapolation via the Arrhenius activation energy, E_a, at this p*H* (Table 1) yields an approximate rate constant at 10°C of 1.4×10^{-11} s^{-1}, a value which is nearly 8 orders of magnitude slower than for the base-catalyzed reaction at p*H* 13. A direct extrapolation of the linear portion in Fig. 3 to p*H* 0 gives a value for k_{obs} of 2.4×10^{-17} s^{-1}, which suggests some catalytic effect in the strong acid.

Activation Parameters

Activation parameters were determined from rate constant data at several temperatures in the range −1 to 33°C for the high p*H* region and at 100 and 140°C for p*H* 0.05. The results for H_2O and D_2O are given in Table 1, together with the kinetic solvent isotope effect (KSIE) measured at p*H* 12.9. Figure 4

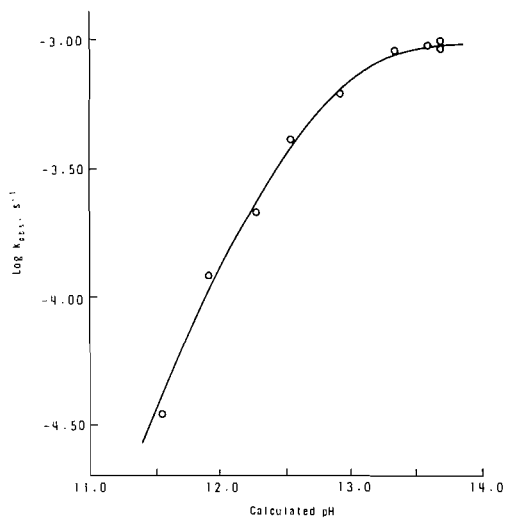

FIG. 3. Dependence of DMFA hydrolysis k_{obs} (0.21 mol L^{-1}) at 10.0°C on initial solution p*H*.

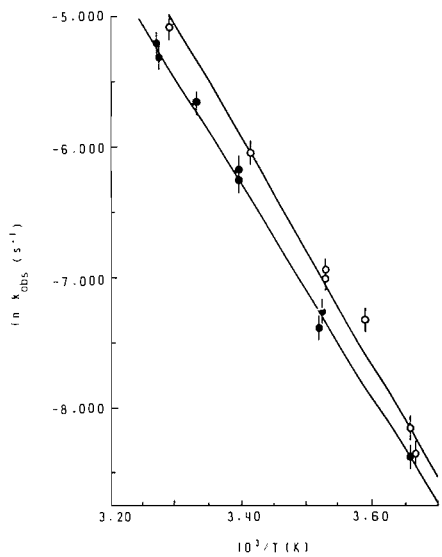

FIG. 4. Arrhenius activation energy plots for DMFA hydrolysis at p*H* 12.9 (●) and 13.7 (○). Bars indicate ±10%.

TABLE 1. Activation parameters and KSIE data for DMFA hydrolysis

Solvent	p*H*	Temperature (°C)	E_a (kJ mol^{-1})	$\Delta S^{\ddagger}$ (J deg^{-1} mol^{-1})	k_{D_2O}/k_{H_2O}
H_2O	12.9	0–33	68.1±1.6		
H_2O	13.7	0–33	70.0±2.9		
D_2O	12.9	0–33	70.2±1.7		
H_2O	0.05	100, 140	103		
H_2O	13.7	20		−65±10 (−15±3 eu)	
	12.9	0			0.85
	12.9	33			0.90

shows the good linearity of the Arrhenius plots over the range studied.

Discussion

DMFA Hydrolysis Mechanism

The following set of equations ([3] to [7]) should represent the overall reaction scheme for DMFA hydrolysis (6). Protonation occurs on the imino nitrogen (7). Jencks (6) states that the cationic imine **2** is likely to be the reactive form of DMFA, with the role of the free imine being insignificant. Nuclear magnetic resonance evidence points to the structure of **2** as more like $[N{=}{=}{=}C{=}{=}{=}N]^+$ than $N{-}{-}C{=}N^+$ (2, 8).

[3] $CH_3NHCH{=}NCH_3 + H_2O$ (DMFA) $\rightleftharpoons$ (K_b) $CH_3\underset{}{N}H\overset{+}{C}H\underset{}{N}HCH_3 + {}^-OH$ **2**

[4] **2** + $^-OH \rightleftharpoons CH_3NHCH(OH)NHCH_3$ **3**

[5] **3** + ^-OH (general base) $\rightleftharpoons CH_3NHCH(O^-)NHCH_3 + H_2O$ **4**

[6] **4** + H_2O (general acid) $\rightleftharpoons CH_3NHCH(O^-)\overset{+}{N}H_2CH_3 + {}^-OH$ **5**

[7] **5** $\longrightarrow CH_3NHCHO + NH_2CH_3$

Direct nucleophilic attack by the hydroxide ion on carbon in **2** is favoured over hyroxide-catalyzed attack of a water molecule (6), to give the tetrahedral intermediate **3**. Breakdown of the intermediate is assisted first by hydroxyl proton removal from **3** and then protonation of one nitrogen in **4** before or during formation of the observed products from **5**, a zwitterionic isomer of **3**.

The DMFA hydrolysis is approximately first order in hydroxide ion from p*H* 11.5 to 13.0 but the rate becomes independent of p*H* above 13.5 (Fig. 3). The same type of limiting behaviour was observed by Robinson (9) for hydrolysis of a cyclic formamidinium compound, 1,3-diphenyl-2-imidazolium chloride; at lower p*H* the hydroxide ion dependence approached second order. The levelling off of k_{obs} at high p*H* was attributed to complete conversion of the tetrahedral intermediate (e.g. **3**) to its conjugate base (e.g. **4**), with an estimated pK_a of 12.75 (9). In his system, Robinson (9) was able to detect the intermediate by ultraviolet spectrophotometry.

The rapid drop in hydrolysis rate with decreasing p*H* into the acid region is assigned to the difficulty of eliminating the relatively strong base, methylamine, from intermediate **3**. It is felt (6) that methylamine expulsion must occur from the conjugate base **4**, with the assistance of general acids, and the concentration of **4** is effectively suppressed at lower p*H*. This is not as severe a requirement for hydrolysis of substituted *N,N'*-diphenylformamidines (DPFA), where weaker amine bases, substituted anilines, are involved (6). DeWolfe found that these formamidines do undergo acid-catalyzed hydrolysis, at a rate only an order of magnitude slower than the base-catalyzed reaction (e.g. for DPFA itself, at 25°C and 1.0 mol L^{-1} HCl, k_{obs} is ca. 1.6×10^{-5} s^{-1} (4) and in 0.64 mol L^{-1} NaOH – 20% dioxane k_{obs} is 6.5×10^{-5} s^{-1} (10)). In contrast, the rate is faster in base but much slower in acid for DMFA relative to DPFA (in 0.50 mol L^{-1} KOH at 25°C k_{obs} is 3.8×10^{-3} s^{-1} but in 1.0 mol L^{-1} acid is calculated via E_a to be only ca. 1.3×10^{-10} s^{-1} at 25°C). For DPFA com-

Can. J. Chem. Downloaded from www.nrcresearchpress.com by 210.87.254.6 on 09/05/12
For personal use only.

Can. J. Chem. Downloaded from www.nrcresearchpress.com by 210.87.254.6 on 09/05/12
For personal use only.

pounds with electron-withdrawing substituents, DeWolfe (10) observed a levelling off of the hydrolysis rate constant at high base concentration, over the range 0.2–0.6 mol L^{-1}. In this range for the other DPFA compounds, the rate constant was already independent of hydroxide concentration.

The results of Cegan *et al.* (11) for hydrolysis of *N'*-aryl-*N*,*N*-dimethylformamidines (ADMFA) are similar to those for the DMFA and substituted DPFA systems. The k_{obs} values for the ADMFA compounds increased with p*H* over the range 4 to 8–10 but were independent of p*H* above this point (buffered solutions); the individual limiting values of k_{obs} were dependent on the phenyl substituents. For the unsubstituted phenyl compound, k_{obs} at 60°C and p*H* 14 was 2.6×10^{-3} s^{-1}, which is about a factor of 10 slower than for DMFA. At p*H* 5 the value was 1.7×10^{-6} s^{-1}. The activation parameters measured at p*H* 13 and 60°C were $E_a = 67.8$ kJ mol^{-1} and $\Delta S^{\ddagger} = -100$ J deg^{-1} mol^{-1}. The corresponding data for DMFA at 20°C (Table 1) are comparable.

The KSIE data obtained in the present study (Table 1) are consistent with the small or inverse effects found for other general acid–base catalyzed reactions, including hydrolysis of formamidinium compounds (12).

cis-N-*Methylformamide Formation via Stereoelectronic Control*

There is an interesting aspect to the NMF formation at breakdown of the tetrahedral intermediate during DMFA hydrolysis. The *trans* isomer of NMF is known to be thermodynamically more stable than

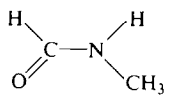

trans-NMF

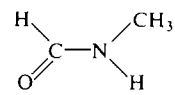

cis-NMF

the *cis* isomer, both neat and in aqueous solution (approximately 90% *trans* at equilibrium) (13). However, during the initial phase of the DMFA hydrolysis runs the *cis*-NMF peak was larger than the *trans* isomer, often by a factor of two or more depending on how soon the first spectral scans were taken. The *cis* peak soon reached a maximum value, then decreased to a fairly low steady state level, while the *trans* peak grew to its final intensity ratio of about 9:1 over the *cis*. The first spectrum in Fig. 1 shows the *cis* and *trans* peaks about equal in size. The NMF was itself hydrolyzed under these reaction conditions but at a considerably slower rate; data are available in the literature (14), so this stage was not studied in detail.

There was a remote possibility that the '*cis*' peak was in fact the tetrahedral intermediate (very few have ever been seen (9)) but the evidence presented below confirms that *cis*-NMF is the correct assignment. The nmr spectral peaks for reaction solutions were compared with those for a standard alkaline aqueous NMF solution. The CH_3 and CH peaks assigned in the reaction solutions to *cis*- and *trans*-NMF corresponded exactly with those in the standard solution, with final *cis*:*trans* peaks ratio of 1:9 as expected at equilibrium. The separation between the *cis*- and *trans*-methyl groups was 12 Hz, with the latter to higher field. The coupling constants, J_{H_3CNH}, were *cis*, 0.5_6 Hz and *trans*, 0.9_7 Hz for the standard solution, and *cis*, 0.5_5 Hz and *trans*, 0.9_5 Hz for one of the kinetic samples where the scans were made slowly enough to permit accurate measurement of the *J* values. Literature values reported for the coupling constants are (13): *trans*, 0.8 Hz (33% in water), 0.9 Hz (neat); *cis*, not measured; chemical shift difference, *cis*- and *trans*-methyl groups, 12 Hz.

The *cis–trans* conversion rate, which appeared to be only slightly slower than the rate of DMFA hydrolysis, could not be reliably obtained in the present study because of overlap of the NMF and DMFA nmr peaks in the methyl region and low sensitivity in the C—H region. However, a computer simulation of the system DMFA → *cis*-NMF ⇌ *trans*-NMF indicated that a *cis–trans* conversion rate constant in the range $5–10 \times 10^{-4}$ s^{-1} at 10°C gives the best fit to our data. This is reasonable, considering that a value of 6×10^{-5} s^{-1} at 10°C can be derived from the data of Neuman *et al.* (15) for C—N rotation in *neat* NMF. The corresponding k_{obs} values for DMFA hydrolysis at 10°C in the present study were in the range 3×10^{-5} to 1×10^{-3} s^{-1}.

It is clear from the experimental evidence that formation of the *cis* isomer of NMF is kinetically favoured during breakdown of the tetrahedral intermediate. Although a small amount of *trans*-NMF may be formed directly, most is produced through *cis*-NMF. The reason for this preferred reaction was not obvious from a preliminary examination of molecular models (Fisher–Hirschfelder–Taylor). However, the orientation of electron lone pairs on the hetero atoms (N and/or O) in hemiorthoesters and hemiorthoamides was considered by Deslongchamps *et al.* (16, 17) to be the governing factor in the base-catalyzed cleavage of these compounds to give the observed thermodynamically unfavoured products. It was required that *both* hetero atoms not involved in the leaving group must have an electron lone pair orbital oriented antiperiplanar to the leaving group for cleavage to occur. This proper orientation was believed to be a key factor in lowering the energy barrier.

Can. J. Chem. Downloaded from www.nrcresearchpress.com by 210.87.254.6 on 09/05/12
For personal use only.

Their stereoelectronic control theory of orbital-assisted cleavage, which is supported by theoretical calculations (18), was applied to the breakdown of the DMFA hydrolysis intermediate, a hemiorthoformamidine. Benkovic and co-workers (19, 20) also had observed in some cases the formation of thermodynamically unfavoured products during hydrolysis or aminolysis of a series of acyclic and cyclic formamidinium compounds, and recently explained the hydrolysis results in terms of stereoelectronic control of the breakdown of the tetrahedral intermediates (20). For DMFA the two potential leaving groups are identical. The appropriate scheme (Scheme 1) is shown below, for attack by hydroxide ion perpendicular to the plane of each of the three possible conformers, **2***a*, **2***b*, and **2***c*, of the protonated DMFA. For this discussion R is substituted for the methyl groups.

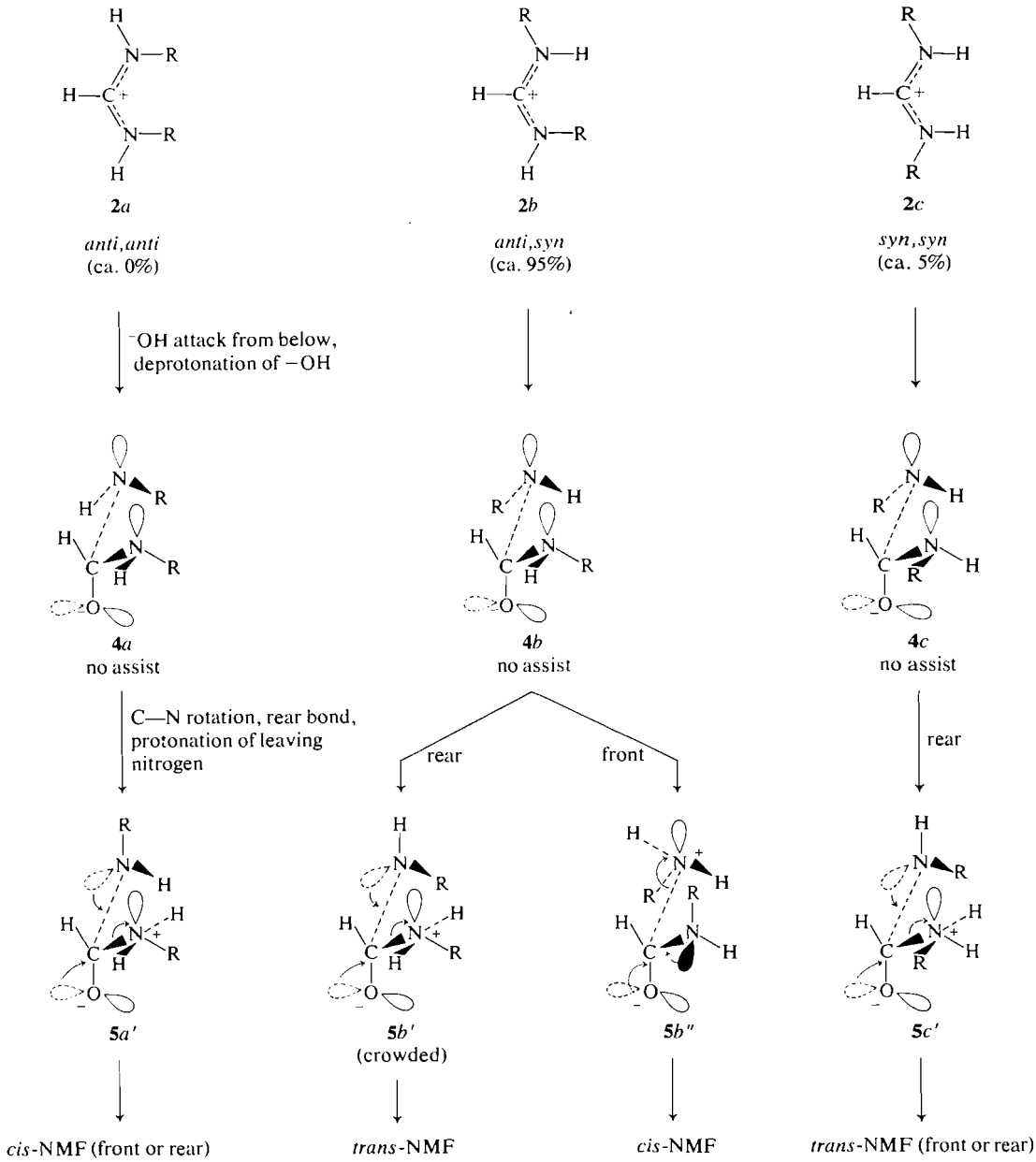

SCHEME 1

When molecular models are examined for each step in this scheme, it becomes clear that steric crowding is a dominant factor in forcing formation of *cis*-NMF.

^{1}H nuclear magnetic resonance spectra of DMFA in dilute acid solution indicate that monoprotonated DMFA is present mostly as conformer **2***b*, with about 5% **2***c* and no detectable **2***a* (2). The last is quite sterically crowded because of the adjacent methyl groups. *cis*-NMF is formed via route *b* and intermediate **5***b*''; the structure required for *trans* formation (**5***b*') is so crowded that **5***b* should proceed predominantly to **5***b*''. Deslongchamps *et al.* (16) argue that *under conditions of proper orbital orientation* the energy barrier for elimination from the tetrahedral intermediate becomes lower than for conformational change. Thus **5***b*' does not occur in significant concentration, since it would immediately lead to *trans*-NMF, and the observed *initial* low concentration of *trans*-NMF must be formed via route *c* (which yields *only* the *trans* isomer, regardless of front or rear C—N bond rotation). It is concluded from the above discussion that the easiest route to *orbital-assisted* breakdown of the hydrolysis intermediate leads preferentially to the *cis* isomer of NMF, which then changes to the more stable *trans* isomer.

Acknowledgements

The authors wish to thank Messrs. P. E. Bindner and J. P. Johnson for some laboratory assistance.

1. J. D. Halliday, E. A. Symons, and J. D. Bonnett. Can. J. Chem. **56**, 1455 (1978).
2. J. D. Halliday, E. A. Symons, and P. E. Bindner. Can. J. Chem. **56**, 1470 (1978).
3. A. Albert and E. P. Serjeant. The determination of ionization constants. 2nd ed. Chapman and Hall Ltd., London, England. 1971.
4. R. H. DeWolfe. J. Am. Chem. Soc. **82**, 1585 (1960).
5. I. M. Kolthoff, S. Bruckenstein, and R. G. Bates. Acid-bases in analytical chemistry. Wiley-Interscience, New York, NY. 1964.
6. W. P. Jencks. Catalysis in chemistry and enzymology. McGraw-Hill, New York, NY. 1969. Chapt. 10.
7. K. M. Wellman and D. L. Harris. Chem. Commun. 256 (1967).
8. G. S. Hammond and R. C. Neuman, Jr. J. Phys. Chem. **67**, 1655 (1963).
9. D. R. Robinson. J. Am. Chem. Soc. **92**, 3138 (1970).
10. R. H. DeWolfe. J. Am. Chem. Soc. **86**, 864 (1964).
11. A. Cegan, G. Stehlik, and M. Vecera. Report SGAE Ber No. 2574, Österreichischen Studiengesellschaft für Atomenergie G.M.B.H., Vienna, Austria. 1975; Chem. Abstr. **85**, 108066v (1976).
12. D. R. Robinson and W. P. Jencks. J. Am. Chem. Soc. **89**, 7088 (1967).
13. L. A. LaPlanche and M. T. Rogers. J. Am. Chem. Soc. **86**, 337 (1964).
14. A. Saika. J. Am. Chem. Soc. **82**, 3540 (1960).
15. R. C. Neuman, Jr., V. Jonas, K. Anderson, and R. Barry. Biochem. Biophys. Res. Commun. **44**, 1156 (1971).
16. P. Deslongchamps, C. Lebreux, and R. Taillefer. Can. J. Chem. **51**, 1665 (1973).
17. P. Deslongchamps, S. Dubé, C. Lebreux, D. R. Patterson, and R. J. Taillefer. Can. J. Chem. **53**, 2791 (1975).
18. J. M. Lehn and G. Wipff. J. Am. Chem. Soc. **96**, 4048 (1974).
19. S. J. Benkovic, T. H. Barrows, and P. R. Farina. J. Am. Chem. Soc. **95**, 8414 (1973).
20. B. A. Burdick, P. A. Benkovic, and S. J. Benkovic. J. Am. Chem. Soc. **99**, 5716 (1977).

Can. J. Chem. Downloaded from www.nrcresearchpress.com by 210.87.254.6 on 09/05/12
For personal use only.

The chemistry of *N,N'*-dimethylformamidine. III. Tautomerism and hindered rotation[1]

JAMES D. HALLIDAY, E. ALLAN SYMONS, AND PATRICK E. BINDNER

Physical Chemistry Branch, Chalk River Nuclear Laboratories, Atomic Energy of Canada Limited, Chalk River, Ont., Canada K0J 1J0

Received October 12, 1977

JAMES D. HALLIDAY, E. ALLAN SYMONS, and PATRICK E. BINDNER. Can. J. Chem. **56**, 1470 (1978).

Proton nmr and infrared studies of neat *N,N'*-dimethylformamidine (DMFA) have shown that the *cis* isomer **1** is present exclusively and that it undergoes tautomerism. At 25°C, $k_{taut} = 8.2 \times 10^2\ s^{-1}$, $E_a = 41.5 \pm 1.5\ kJ\ mol^{-1}$, $\Delta H^* = 39.1 \pm 1.5\ kJ\ mol^{-1}$, and $\Delta S^* = -57.5 \pm 5.0\ J\ mol^{-1}\ K^{-1}$. The tautomerism is proposed to occur through a hydrogen-bonded cyclic dimer. The effects of solvent on the tautomeric rate in DMFA have also been investigated for CD_3NH_2 and $CDCl_3$ solutions.

Potassium *N,N'*-dimethylformamidide (PDMFA) in CD_3NH_2 does not exhibit hindered rotation about the single C—N bond on the nmr time scale over the temperature range −56 to 25°C. However, protonated DMFA undergoes hindered rotation about this bond in highly acidic media (97 wt.% H_2SO_4 at 25°C, $k_{rot} = 0.16 \times 10^2\ s^{-1}$, $E_a = 35.4 \pm 0.8\ kJ\ mol^{-1}$). The acid catalysis is interpreted as occurring through formation of the diprotonated species. The two nitrogens in protonated DMFA have different base strengths.

JAMES D. HALLIDAY, E. ALLAN SYMONS et PATRICK E. BINDNER. Can. J. Chem. **56**, 1470 (1978).

Des études par rmn du proton et par infrarouge de la *N,N'*-diméthylformamidine (DMFA) à l'état pur ont montré que l'isomère *cis* **1** est le seul isomère présent et qu'il subit une réaction de tautomérie. A 25°C, $k_{taut} = 8.2 \times 10^2\ s^{-1}$, $E_a = 41.5 \pm 1.5\ kJ\ mol^{-1}$, $\Delta H^* = 39.1 \pm 1.5\ kJ\ mol^{-1}$ et $\Delta S^* = -57.5 \pm 5.0\ J\ mol^{-1}\ K^{-1}$. On suggère que la réaction de tautomérie se produit par l'intermédiaire d'un dimère cyclique comportant un pont hydrogène. On a aussi étudié les effets de solvant sur les vitesses de tautomérisation de la DMFA en solution dans CD_3NH_2 et $CDCl_3$.

La *N,N'*-diméthylformamididure de potassium (DMFAP) dans le CD_3NH_2 ne présente pas de rotation empêchée autour du lien simple C—N à l'échelle de temps de la rmn, à des températures allant de −56 à 25°C. Toutefois dans le cas de la DMFA protonée il existe une rotation empêchée autour de ce lien en milieu fortement acide (H_2SO_4 à 97% en poids à 25°C $k_{rot} = 0.16 \times 10^2\ s^{-1}$, $E_a = 35.4 \pm 0.8\ kJ\ mol^{-1}$). La catalyse acide suggèrerait la formation d'espèces diprotonées. Les deux azotes de la TMFA protonée ont des basicités différentes.

[Traduit par le journal]

In this series Part I (1) dealt with the thermal decomposition of both potassium methylamide in methylamine solutions (which yielded potassium *N,N'*-dimethylformamidide (PDMFA)) and the neat free base, *N,N'*-dimethylformamidine (DMFA). Part II (2) discussed the hydrolysis of the DMFA as a function of p*H*. In the course of these studies several unusual features associated with isomerism (geometrical, rotational) and tautomerism (3) in the structure of DMFA have been elucidated.

This paper describes an nmr study of tautomerism and hindered rotation in the title compound and its cationic and anionic forms as functions of solvent and temperature.

Experimental

All nmr samples were handled using dry box (He atmosphere) and vacuum line techniques to minimize moisture contamination. All nmr tubes were flame sealed.

PDMFA and DMFA were synthesized as described previously (1). DMFA·HCl was prepared by reacting DMFA with gaseous HCl at reduced temperature in the nmr tube. DMFA·H_2SO_4 was prepared by addition of DMFA directly to the precooled H_2SO_4 solution in the nmr tube. The acids used were (*a*) anhydrous HCl (Matheson), (*b*) aqueous HCl (Anachemia), and (*c*) H_2SO_4 (Baker). DCl (>99 at.% D) (Merck, Sharp, and Dohme), 38 wt.% in D_2O, was used to remove NH proton coupling in one sample of DMFA·H^+.

The solvents CD_3NH_2 (>98 at.% D) and $CDCl_3$ (>99.8 at.% D) (Merck, Sharp, and Dohme), the former dried over lithium metal, were distilled under vacuum before use. $CHCl_3$ (Fisher Spectranalyzed) was used for the infrared measurements.

Although there is a reaction between DMFA and CD_3NH_2, eq. [1] (4*a*), that produces the isotopically labeled mono- and di-CD_3 DMFA species, it is sufficiently slow that measurements of the tautomerism in DMFA can be made without appreciable deuterium isotope effects interfering.

Proton nmr spectra were recorded on a Bruker HX90 nmr spectrometer operating at 90 MHz in a field of 2.114 T. Variable temperature studies were performed using a Bruker variable temperature controller, B-ST 100/700 (±0.5°C). Probe temperatures were checked with a small calibrated Pt

[1]AECL No. 6119.

Can. J. Chem. Downloaded from www.nrcresearchpress.com by 210.87.254.5 on 09/05/12
For personal use only.

Can. J. Chem. Downloaded from www.nrcresearchpress.com by 210.87.254.5 on 09/05/12
For personal use only.

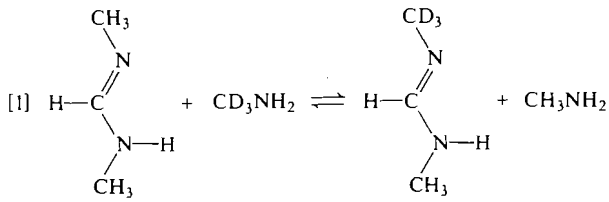

resistance thermometer (Rosemount, model #146MA100F element, 1.5 mm diameter × 15 mm long). Infrared spectra of DMFA were run on a Perkin Elmer 467 spectrophotometer.

Results

DMFA

Temperature effects on the nmr spectra were studied for the neat material (ca. 14 *m*) and for solutions in CD_3NH_2 (1.4 *m*) and $CDCl_3$ (0.5–2.9 *m*). Rates for tautomeric exchange were obtained by complete lineshape analysis using the computer program DNMR3 (5). Coupling constants were corrected for peak overlap effects where necessary. Figure 1 shows the effect of solvent and Fig. 2 the variation with temperature of the measured exchange rate for tautomerism, τ^{-1} (s^{-1}), for DMFA. Representative nmr spectra for the system are illustrated in Fig. 3. No coupling owing to the NH protons could be observed in these solutions.

The infrared spectrum of DMFA as a function of concentration in $CHCl_3$ is shown in Fig. 4.

PDMFA

The salt PDMFA, a very strong base, has been studied in liquid CD_3NH_2 in which it is both soluble and stable. No significant change was observed in the methyl group nmr spectra for a 0.45 *m* sample over the temperature range −56 to 25°C. The spectra resembled those of DMFA in its high temperature limit, where the two methyl groups are equivalent. However J_{HCNCH} is smaller than in DMFA, 0.5_0 Hz instead of 0.7_8 Hz.

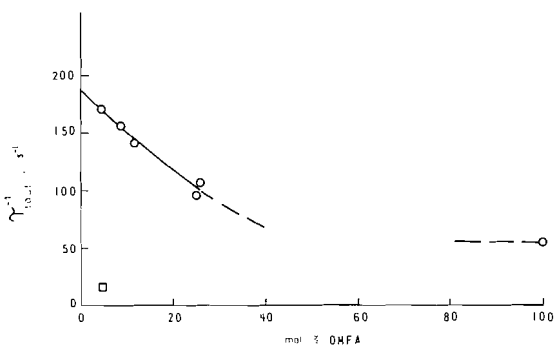

FIG. 1. Concentration effect on the rate (τ^{-1}) for DMFA tautomerism in $CDCl_3$ and CH_3ND_2 solutions at −16.2°C: ○, $CDCl_3$ solution; □, CD_3NH_2 solution.

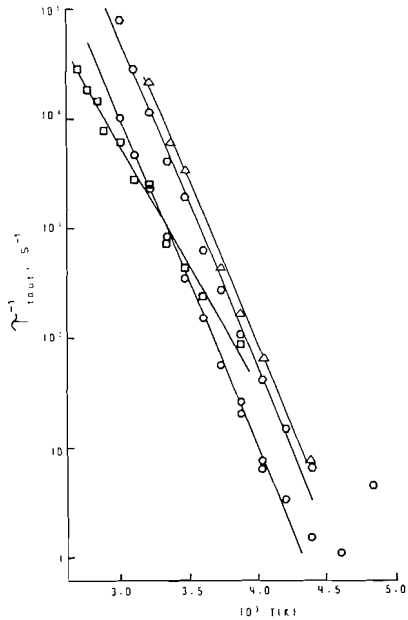

FIG. 2. Temperature dependence of the DMFA tautomerism rate (τ^{-1}): □, neat; ○, 1.4 *m* in CD_3NH_2; ⬡, 2.9 *m* in $CDCl_3$; △, 0.5 *m* in $CDCl_3$.

DMFA·H$^+$

It has been shown that aqueous acid solutions of DMFA·H^+ are very stable to hydrolysis (2).

DMFA·H^+ nmr spectra were run for a number of aqueous solutions with varying acid concentrations (0–97 wt.% H_2SO_4). Representative spectra are shown in Fig. 5.

Temperature dependence studies were done on the 6 mol L^{-1} HCl and 97 wt.% H_2SO_4 (0.2–1.0 *m* DMFA) solutions. In the former, except for effects associated with the change with temperature (−15 to 110°C) in quadrupolar relaxation owing to the ^{14}N, no exchange effects were observable. However, in the latter, two time-dependent processes could be seen occurring over this temperature range: first, increasing rates of exchange of NH protons, leading to collapse of the methyl doublets, and second, increasing rates of hindered rotation about the C—N bonds, leading to equivalent methyl groups. The rate constant and the Arrhenius activation energy measured for the latter process for both 0.2 and 1.0 *m* solutions at 40°C are 0.31×10^2 s^{-1} (0.16×10^2 s^{-1}, extrapolated to 25°C) and 35.4 ± 0.8 kJ mol^{-1}, respectively. Calculation of accurate exchange rates for the coalescence of the methyl groups is complicated by the NH proton – solvent exchange since it broadens the methyl lines during coalescence. The activation energy was taken from the higher temperature data where the effects of this latter exchange were minimal.

Can. J. Chem. Downloaded from www.nrcresearchpress.com by 210.87.254.5 on 09/05/12
For personal use only.

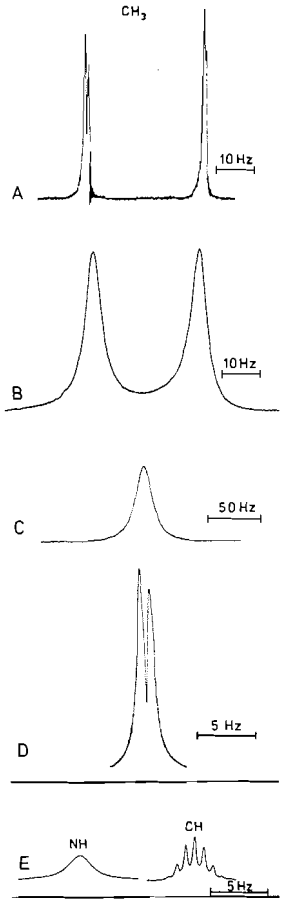

FIG. 3. Representative nmr spectra of DMFA as a function of temperature: (*A*) −56.5°C in CD_3NH_2; (*B*) −35.6°C in $CDCl_3$; (*C*) −15.0°C in $CDCl_3$; (*D* and *E*) +80.1°C in $CDCl_3$. The CH and NH peaks for *A*, *B*, and *C* are featureless, broad singlets.

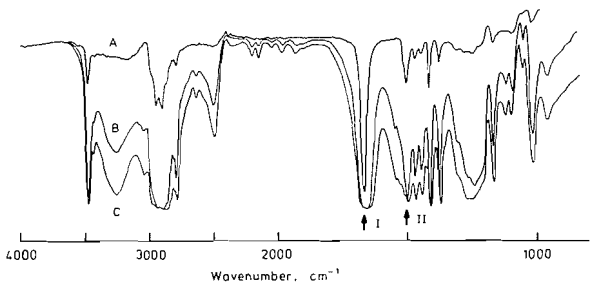

FIG. 4. Effect of concentration on the ir spectrum of DMFA in $CHCl_3$ at 25°C, 0.20 mm CaF_2 cells, $CHCl_3$ reference: (*A*) 0.04 *m*, (*B*) 0.4 *m*, (*C*) 0.8 *m*. The amidine I and II bands of DMFA are indicated.

Discussion

DMFA

DMFA has four possible configurations, based on a planar N—C=N structure:

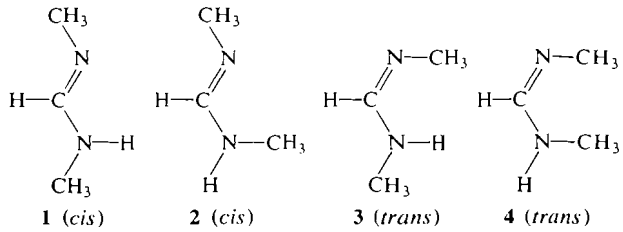

As with amides (6, 7), there is partial double bond character in the single C—N bond. The charge delocalization through the —N=C—N< structure will be indicated throughout this paper where it is appropriate to the discussion. The above isomers may interchange through (*i*) rotational isomerism (**1** and **2**, **3** and **4**), (*ii*) geometrical isomerism (**1** and **3**, **2** and **4**), and (*iii*) tautomerism. Tautomerism in **1** or **4** produces no effective change but in **2** yields **3** and vice versa. Owing to pronounced steric interactions (molecular models) the fraction of DMFA likely to be present as **4** is very small. To further complicate the analysis, a combination of geometric and rotational isomerism in **2** will also give **3**.

Based solely on the nmr spectral data, the

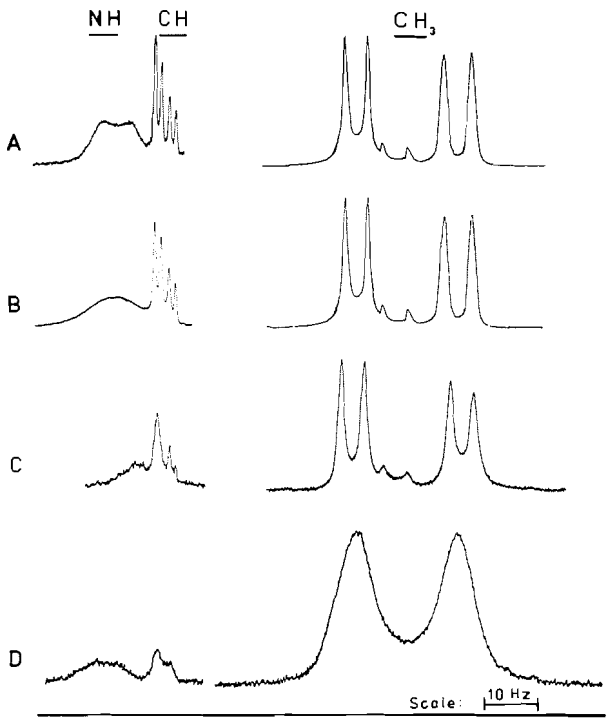

FIG. 5. Effect of acid concentration and temperature on the nmr spectrum of protonated DMFA: (*A*) −15°C, 6 mol L^{-1} HCl; (*B*) 25°C, 6 mol L^{-1} HCl; (*C*) 25°C, 66 wt.% H_2SO_4; (*D*) 25°C, 97 wt.% H_2SO_4.

Can. J. Chem. Downloaded from www.nrcresearchpress.com by 210.87.254.5 on 09/05/12
For personal use only.

mechanism for the exchange occurring in this symmetrically *N,N'*-disubstituted amidine cannot be unambiguously assigned. However, with the addition of our infrared results and those of Prevorsek (3) we can show that the mechanism must be tautomerism in structure **1**.

Prevorsek (3) has studied a number of *N,N'*-ring substituted aryl amidines by infrared spectroscopy and concluded that they exhibit a tautomerism in solution, which leads at the same time to a geometrical isomerism with respect to both single and double CN bonds, i.e. corresponding to **2** ⇌ **3**. Evidence for his conclusion came from the observation of two ν(N—H) bands and two ν(C=N) bands for unsymmetrical *N,N'*-aryl-substituted acetamidines and even for the symmetrical *N,N'*-diphenylacetamidine. These duplicate bands indicated two isomers for each compound. In addition, the presence of a strong amidine II band at ca. 1500 cm^{-1} showed that there must be a *trans* isomer (3) in the acetamidines since this can only arise from that configuration (corresponding to **3** and/or **4**).

The ir spectra of DMFA in $CHCl_3$ solution (Fig. 4) show a major band (3480 cm^{-1}) and a very weak one (3435 cm^{-1}) in the ν(N—H) region and a single strong band (1670 cm^{-1}) in the ν(C=N) region. This suggests there is only one principal isomer in solution. Because the amidine II band (1505 cm^{-1}) is present at much reduced intensity, it appears there is very little *trans* configuration, i.e., **3** and/or **4** (3). Therefore DMFA in $CHCl_3$ solution must be present principally as **1** or **2**. Prevorsek (3) assigns the high frequency NH stretch to the *trans* configuration and the low frequency to the *cis* in the *N,N'*-diarylacetamidines. However, from our results for DMFA, it would appear that the high frequency band must be due to the *cis* configuration, since very little of the *trans*, **3** and/or **4**, is present.

From the nmr data obtained at reduced temperature for DMFA in CD_3NH_2, only one isomeric form predominates (Fig. 3*A*). At elevated temperature in this sample the methyl groups become equivalent. Rotational isomerism alone about the C—N bond, **1** to **2**, cannot produce equivalent methyl groups. Therefore the only mechanism that can be operative in the DMFA system is *tautomerism in 1*, since tautomerism in **2** would give **3**.

The ir data for DMFA in $CHCl_3$ (Fig. 4) and neat (1) illustrate the extent of molecular association via hydrogen bonding in these solutions. Dilution of DMFA from 0.8 to 0.04 *m* in $CHCl_3$ significantly reduces the broad band centred at 3260 cm^{-1} which arises from the hydrogen-bonded N—H stretch in the associated species in the neat and concentrated solutions. Effectively 100% association is shown for neat DMFA since the monomer band, which should be at 3480 cm^{-1}, is not present (1). The structure of these species can be determined from changes in the bands in the region 1900–2200 cm^{-1}, which are characteristic of imine salts (8). The most probable associated form is the cyclic dimer **5***a–c* (4). As White and Kilpatrick (4*b*) showed for *N,N'*-diphenylformamidine (K_{dimer} = 69), this should be a particularly stable dimer since it has an eight-membered ring structure, in which the two hydrogens (with presumably 180° valence bonds) reduce it in effect to a six-membered ring. The charge-separated structure (**5***b*) has been proposed as playing a role in

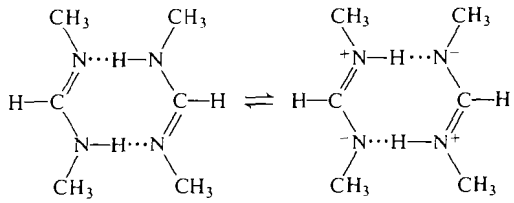

5*a* **5***b*

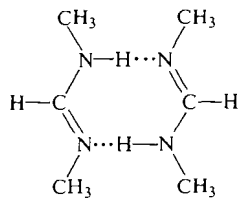

5*c*

the thermal breakdown of neat DMFA to produce bis-*N*-(*N'*-methylmethylenimine)methylamine (1). The dimer structures **5***a–c* are an example of Hunter's mesohydric tautomerism (9). The necessary transfer of a proton from one nitrogen to the other within the molecule to effect the tautomerism results directly from the H-bond association.

Activation Parameters for DMFA Tautomerism

The Arrhenius plot of the neat DMFA kinetic data is shown in Fig. 2 and the activation parameters calculated from it in Table 1. The error ranges

TABLE 1. Kinetic and thermodynamic parameters calculated from nmr data for DMFA tautomerism at 25°C

Solvent	k_{taut} (s^{-1})	$\Delta H^{\ddagger}$ (kJ mol^{-1})	$\Delta S^{\ddagger}$ (J mol^{-1} K^{-1})
Neat	8.2×10^{2}	39.1±1.5	−57.5±5.0
CD_3NH_2 (1.4 *m*)	7.4×10^{2}	55.7±0.4	1.2±2.7
$CDCl_3$ (0.5 *m*)	6.3×10^{3}	54.1±1.3	10.3±5.2
(2.9 *m*)	4.2×10^{3}	55.7±1.8	12.3±4.4

Can. J. Chem. Downloaded from www.nrcresearchpress.com by 210.87.254.5 on 09/05/12
For personal use only.

reported were determined by a least-squares analysis of the data.

The activation energies for hindered rotation about the C—N bond in amides and amidinium ions were studied by Neuman and Jonas (10*a*) and found to be in the range 84–100 kJ mol^{-1}, much higher than the 41 kJ mol^{-1} measured for tautomerism in DMFA. Since these amidinium compounds had no N—H protons and could not exhibit tautomerism, this is additional evidence that tautomerism, and not hindered rotation, is operating in DMFA.

Solvent Effects

Dilution of DMFA in $CDCl_3$ and CD_3NH_2 produces interesting changes in the observed rate of tautomerism (Fig. 1) and in the activation parameters calculated from the temperature dependence of τ^{-1} as a function of concentration (Table 1). The changes in τ^{-1} may be caused by changes in the monomer – hydrogen bonded dimer equilibrium with dilution (see ir spectra, Fig. 4) and/or solvent effects on the dimer structure itself. Changes in hydrogen-bond association between substrate and solvent can play an important role in determining the magnitude of the rate constant and activation energy in solution; e.g. for hindered rotation in neat *N,N*-dimethylformamide, $k_{rot} = 1.2 \times 10^{-2}$ s^{-1} with $E_a = 78$ kJ mol^{-1}, whereas for a 12 mol% solution in formamide $k_{rot} = 1.6 \times 10^{-4}$ s^{-1} with $E_a = 109$ kJ mol^{-1} (11).

Our results for the hydrogen-bonding solvent CD_3NH_2 follow the same trend, a decrease in τ^{-1} with an increase in E_a relative to neat DMFA (Fig. 1). However, for the $CDCl_3$ solutions the τ^{-1} values show a marked increase. Defining the principal component responsible for these changes is difficult. If a constant for monomer–dimer equilibrium in the range 10–100 is used ($K = 69$ for *N,N'*-diphenylformamidine in benzene (4*b*)) then the percentage monomer can rise to ~10–15% (consistent with the ir spectra for DMFA–$CDCl_3$ solutions) for the most dilute solutions studied. This is probably not sufficient to have a pronounced effect on the results. We believe that it is small changes in the dimer structure with different solvents that produces the observed effects, since tautomerism in the dimer inherently should be easier than in the monomer. However, without further data on the extent of monomer and solvent participation in solutions of DMFA, our solution activation parameters must be considered qualitative, because the τ^{-1} cannot be related directly to a specific rate constant for tautomerism.

Nuclear Magnetic Resonance Spectral Assignments

Spectral assignments in the nmr results can be made on the basis of the chemical shifts and the coupling constants J_{HCNCH}. At 25°C the chemical shifts with respect to TMS for the CH_3, NH, and CH in neat DMFA are 2.85, 7.11, and 7.39 ppm, respectively. At low temperatures (Fig. 3*A*) the splitting of the high field methyl group ($J_{HCNCH} = 0.5_2$ Hz) originates from the amine nitrogen side and that for the low-field methyl group ($J_{HCNCH} = 0.9_8$ Hz) from the imino nitrogen side. The chemical shift difference between the methyl groups is 0.338 ppm. No coupling owing to the amino proton is observed. At elevated temperatures (Fig. 3*D*) magnetic equivalence of the methyl groups is shown by the doublet ($J_{HCNCH} = 0.7_8$ Hz) and septet ($J_{HCNCH} = 0.7_8$ Hz) in the CH_3 and CH positions, respectively. These lines exhibit some distortion due not to non-first-order effects but apparently to the presence of small quantities of isomers **2** and **3** which are formed at higher temperatures.

PDMFA

Removal of the DMFA amino proton forms the anion, PDMFA, whose structure can be **6** and/or **7**.

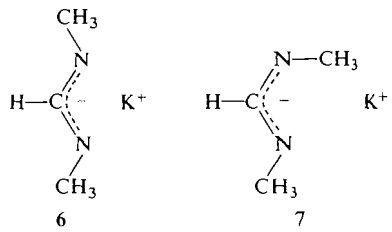

6 **7**

The third possible isomer, with both methyl groups *trans* to the CH, is ruled out on grounds of steric hindrance.

The nmr spectrum of PDMFA in CD_3NH_2 showed no significant change with temperature. Even at −56°C the methyl region resembled that of DMFA at high temperature with equivalent methyl groups. Although the only evidence for assigning a structure to PDMFA is the average coupling constant $J_{HCNCH} = 0.5_0$ Hz, which can be influenced by bond angles and charges in the molecule, it suggests that **6** is the only isomer in solution. The *trans* structure (**7**) would be expected to have a larger J value (see DMFA results) and hence an average J value greater than 0.5 Hz.

DMFA·H$^+$

In contrast, addition of a proton to the DMFA yields a much more interesting system. Structures **8**, **9**, and **10** are possible. Hammond and Neuman (12) studied *N,N'*-dimethylacetamidinium chloride (DMAA·HCl) in aqueous acid solutions and observed only one isomer, which was identified as that corresponding to **9**. Our spectrum of DMFA·HCl (Fig. 5) shows a predominance of **9** (methyl doublets at 3.70 and 3.49 ppm) and suggests a small quantity (ca. 5%) of the symmetrical isomer **8**

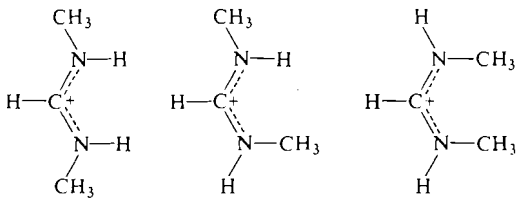

8 **9** **10**

(methyl doublet at 3.62 ppm). No evidence was seen for the third isomer (**10**). Since DMFA·HCl is less sterically hindered than DMAA·HCl the presence of a small amount of **8** is not surprising.

Spectral assignments can be made based on the lineshapes observed in protiated and deuterated solvents, and on a comparison with the assignments for DMAA·HCl (12). The high field methyl group doublet in Fig. 5 (3.49 ppm) is broadened by unresolved coupling to the CH proton and the lines deviate from Lorentzian shape accordingly. Since $J_{trans} > J_{cis}$ in amides (13) and other similar compounds (14), the high field broadened doublet can be attributed to the methyl group *trans* to the CH proton; the low field methyl doublet at 3.70 ppm then arises from the methyl group *cis* to the CH proton. These methyl doublets arise from coupling to the adjacent nitrogen protons, since they collapse to singlets in deuterated acid solution. The coupling constants observed for H—N—CH_3 in the different isomers are: **9**, high field 5.2 Hz, low field 4.4 Hz; **8**, 4.1 Hz.

The significantly distorted doublets at low field (Fig. 5, 8.50, 8.34 ppm) become one singlet in deuterated acid solution and belong to the CH proton coupled to the two nonequivalent nitrogen protons. The NH and CH protons comprise an ABC system, with the nitrogen proton portion of the spectrum (8.94 ppm) significantly broadened by quadrupolar relaxation. At lower temperatures (−15°C) the effect of this relaxation on the amino proton lines is reduced and they narrow sufficiently to show the broad outline of the BC component of the spectrum. Coupling constants extracted from simulation of this system using DNMR3 (5) gave J_{HNCH} of ca. 6 and 14 Hz.

This ABC subspectrum is further evidence for the nonequivalence of the two N—H protons and confirmation of structure **9** as the predominant species present.

Other than the above effects associated with the change in ^{14}N quadrupolar relaxation, no significant changes were observed in the spectrum of this sample over the temperature range −15 to 100°C. Partial coalescence of the methyl group signals through hindered rotation about the C—N bond had been expected, since this was observed for *N,N*-dimethylacetamidium chloride in DMSO-d_6 (10*a*).

The observed spectra are markedly affected by changes in the acid concentration. For an aqueous solution of DMFA·H^+ the spectrum is similar to that shown in Fig. 5*a*. However, as the acid concentration is raised (to achieve high acid concentrations, H_2SO_4 was used) the methyl doublets begin to collapse, as seen in the 66% H_2SO_4 spectrum, Fig. 5*c*. The high-field doublet shows the greater effect, indicating a difference in the basicity of the two nitrogens. At 97% H_2SO_4 the two methyl lines are beginning to coalesce. Thus two acid catalyzed exchange mechanisms would appear to be operating. First, there is exchange between the amino protons in the mono protonated cation and protons in the solvent, catalyzed through formation of the diprotonated species DMFA·H_2^{2+}. This exchange rate increases with added acid, and ultimately in media of high acidity becomes sufficiently fast to show loss of coupling to the N—CH_3 groups and collapse of the doublets. Second, the lifetimes of these diprotonated species become long enough to allow magnetic equivalence of the N—CH_3 groups by rotation about C—$\overset{+}{N}H_2CH_3$ bonds.

These results are in qualitative agreement with the more extensively studied DMAA·HCl system (12). However, there are differences in the relative rates of these reactions. In weakly acid solution DMAA·HCl shows only two singlets for the methyl groups when there is no added acid, and it is not until 14% H_2SO_4 is reached that the NH coupling is seen (12). For DMFA·HCl this inverse dependence of N—H proton exchange on acid concentration is not seen and the NH coupling is present even in very weakly acidic solutions, i.e., the residence time of the protons is long on the nmr time scale. At the other extreme, in strongly acid solution DMAA·HCl shows coalescence of the two methyl groups in 90.7% H_2SO_4 (12) but even at 97% H_2SO_4, the DMFA salt still has two broad but resolved singlets.

The pK_a of DMAA is estimated at ca. 13 (12) and that of DMFA was found to be 12.4 (2). DMAA, being slightly more basic, would be expected to diprotonate faster in acid and therefore show the effects of this second protonation sooner than DMFA·H^+, i.e., a lower acid concentration is required to coalesce the methyl group signals in DMAA·H^+. The behaviour at low acid concentrations, where the DMFA·H^+ does not show the inverse dependence of the NH proton exchange rate while DMAA·H^+ does, may result from dimer formation in the DMFA·H^+, forcing an initial longer residence time for the protons.

The mechanism for these exchange reactions with DMAA·HCl at higher acid concentrations, proposed by Neuman and Hammond (12), applies equally well to DMFA·H^+ (Scheme 1).

Can. J. Chem. Downloaded from www.nrcresearchpress.com by 210.87.254.5 on 09/05/12
For personal use only.

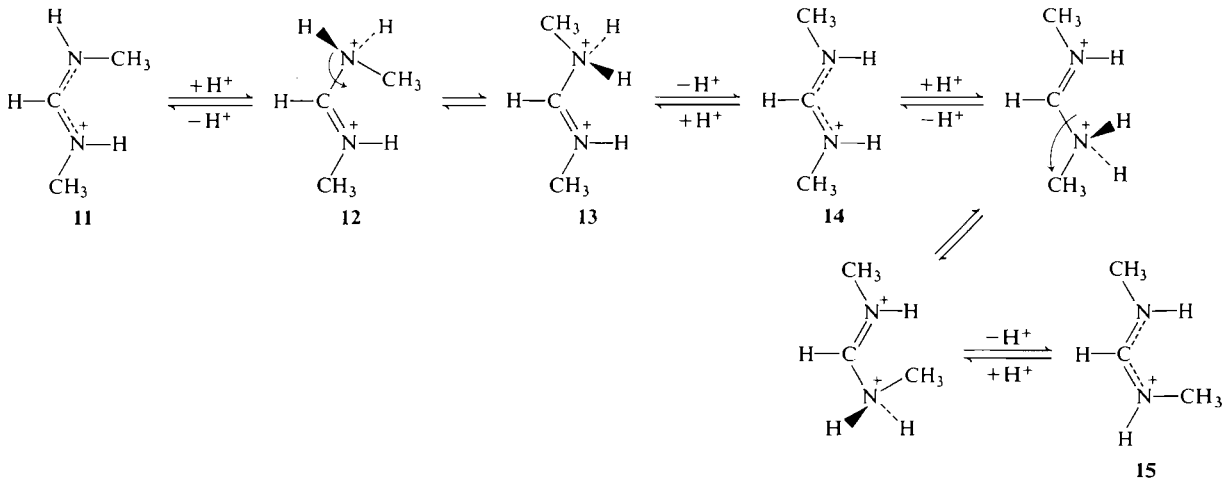

SCHEME 1

The exchange reactions with the solvent occur via protonation of **11** to form **12**. Equivalence of the two methyl groups of **11** requires that each CN bond must undergo hindered rotation, and that the higher energy symmetrical formamidinium ions **8** and **10** must be intermediates. This would be consistent with the observation that methyl equivalence is slower than NH exchange with the solvent.

The activation energy of 35 kJ mol^{-1} is very much less than that measured for hindered rotation about the C—N bond in *N*,*N*-dimethylacetamidinium cations in DMSO-d_6 (10*a*) or *N*,*N*,*N*′,*N*′-tetramethylformamidinium perchlorate in $CDCl_3$ (10*b*). This can be explained by assuming that the double bond character of the C—N single bond in the diprotonated species is significantly reduced from that in the monoprotonated amidinium ion, since the C=N double bond is more effectively frozen in these strongly acid solutions.

Acknowledgements

The authors would like to thank Drs. R. D. McAlpine and J. H. Rolston for helpful discussions and Mr. J. P. Johnson for assistance with the initial portion of this work.

1. J. D. HALLIDAY, E. A. SYMONS, and J. D. BONNETT. Can. J. Chem. **56**, 1455 (1978).
2. J. D. HALLIDAY and E. A. SYMONS. Can. J. Chem. **56**, 1463 (1978).
3. D. C. PREVORSEK. J. Phys. Chem. **66**, 769 (1962).
4. (*a*) R. L. SHRINER and F. W. NEUMANN. Chem. Rev. **35**, 351 (1944); (*b*) N. E. WHITE and M. KILPATRICK. J. Phys. Chem. **59**, 1044 (1955).
5. D. A. KLEIER and G. BINSCH. Quantum chemistry program exchange, Chemistry Department, Indiana University, Bloomington, IN. Program #165 DNMR3, modified to run on a CDC6600/Cyber 175 computer.
6. L. PAULING. The nature of the chemical bond. 3rd ed. Cornell University Press, Ithaca, NY. 1960. p. 281.
7. W. E. STEWART and T. H. SIDDALL III. Chem. Rev. **70**, 517 (1970).
8. R. T. CONLEY. Infrared spectroscopy. 2nd ed. Allyn and Bacon Inc., Boston, MA. 1972.
9. (*a*) H. O. CHAPLIN and L. HUNTER. J. Chem. Soc. 1114 (1937); (*b*) L. HUNTER and H. T. HAYES. J. Chem. Soc. 1 (1941).
10. (*a*) R. C. NEUMAN, JR. and V. JONAS. J. Phys. Chem. **75**, 3532 (1971); (*b*) J. RANFT and S. DÄHNE. Helv. Chim. Acta, **47**, 1160 (1964).
11. R. C. NEUMAN, JR. and L. B. YOUNG. J. Phys. Chem. **69**, 2570 (1965).
12. (*a*) G. S. HAMMOND and R. C. NEUMAN, JR. J. Phys. Chem. **67**, 1655 (1963); (*b*) R. C. NEUMAN, JR. and G. S. HAMMOND. J. Phys. Chem. **67**, 1659 (1963).
13. V. J. KOWALEWSKI and D. G. DE KOWALEWSKI. J. Chem. Phys. **32**, 1272 (1960).
14. (*a*) R. R. FRASER. Can. J. Chem. **38**, 549 (1960); (*b*) J. H. RICHARDS and W. F. BEACH. J. Org. Chem. **26**, 623 (1961).

Can. J. Chem. Downloaded from www.nrcresearchpress.com by 210.87.254.5 on 09/05/12
For personal use only.

Arene–chromium complexes: Photochemical substitution of phosphine and phosphite ligands by olefin

G. Paul Donnini and Alan Shaver[1]

Department of Chemistry, McGill University, 801 Sherbrooke St. West, Montreal, P.Q., Canada H3A 2K6

Received October 26, 1977

G. Paul Donnini and Alan Shaver. Can. J. Chem. **56**, 1477 (1978).

Complexes of the type (η^6-$C_6H_5XCH_2CH{=}CH_2$)$Cr(CO)_2L$, where X = O, CH_2 and L = $P(C_6H_5)_3$, $P(OC_6H_5)_3$, $P(OC_2H_5)_3$, and $P(CH_3)_2(C_6H_5)$ are photochemically labile. Ultraviolet irradiation leads to rapid displacement of L and coordination of the pendent olefin. [1,3,5-$(CH_3)_3C_6H_3$]$Cr(CO)_2P(C_6H_5)_3$ undergoes the same reaction in the presence of *cis*-cyclooctene. These observations are related to the general inability to substitute a second carbonyl ligand in (arene)$Cr(CO)_2Y$ by photochemical methods. Two new complexes (η^6-$C_6H_5XCH_2CH{=}CH_2$)$Cr(CO)_2CS$ are reported but these decompose under ultraviolet irradiation.

G. Paul Donnini et Alan Shaver. Can. J. Chem. **56**, 1477 (1978).

Les complexes du type (η^6-$C_6H_5XCH_2CH{=}CH_2$)$Cr(CO)_2L$, où X = O, CH_2 et L = $P(C_6H_5)_3$, $P(OC_6H_5)_3$, $P(OC_2H_5)_3$ et $P(CH_3)_2(C_6H_5)$ sont photochimiquement labiles. Par irradiation ultraviolette, on obtient un déplacement rapide du groupe L et une coordination de l'oléfine pendante. Le [1,3,5-$(CH_3)_3C_6H_3$]$Cr(CO)_2P(C_6H_5)_3$ subit la même réaction en présence de cyclooctène-*cis*. Ces observations sont reliées au fait qu'il est généralement impossible de substituer un second ligand carbonyle dans l'arène$Cr(CO)_2Y$ par des méthodes photochimiques. On rapporte la préparation de deux nouveaux complexes (η^6-$C_6H_5XCH_2CH{=}CH_2$)$Cr(CO)_2CS$ mais ceux-ci se décomposent sous l'influence d'une irradiation ultraviolette.

[Traduit par le journal]

Introduction

The stereochemistry of chiral organometallic complexes has been receiving increased attention (1). In particular arene–chromium carbonyl complexes have been the subject of a number of studies. The first examples of resolved enantiomeric complexes of this type have already been reported (2). The chromium tricarbonyl unit can also be used to 'label' one side of organic molecules containing an arene ring. With the plane of symmetry so removed, intricate asymmetric reactions may be carried out on the organic moiety (3).

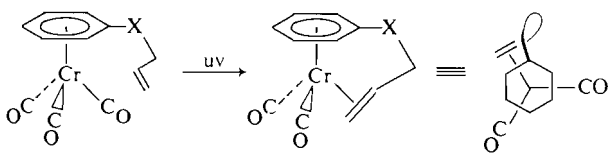

1
a X = O
b X = CH_2

2
a X = O
b X = CH_2

Complexes of type **1** are interesting since stable olefin complexes **2** are obtained upon irradiation (4). Complexes of type **2** are chiral owing to the link between the olefin and the arene (i.e. the olefin is prochiral (5)). Racemization can only occur by dissociation of the olefin and recoordination of its other 'face'. Diastereoisomerism in **2** has been generated by the use of an asymmetrically substituted arene ring (6). However, the same thing may be achieved if one of the remaining carbonyls could be effectively replaced by a different ligand, thus creating a second chiral center. During our studies on these complexes, we have discovered that uv irradiation of arenechromiumdicarbonylphosphine or -phosphite complexes in the presence of an olefin (free or attached to the arene) causes facile replacement of the phosphine or phosphite by the olefin.

[1]Author to whom correspondence should be addressed.

Experimental

All operations were carried out in a nitrogen atmosphere; all evaporations were performed *in vacuo*. All solvents were distilled in a nitrogen atmosphere before use. Hexane was distilled from sodium wire. Benzene and tetrahydrofuran (THF) were distilled from sodium–benzophenone. The ultraviolet irradiation source was a 100 W Hanovia high-pressure quartz mercury vapor immersion lamp in a water-cooled Pyrex photochemical immersion cell (Ace Glass Inc., catalogue numbers 6515-30 and 6517, respectively). The major ultraviolet band is at 366 nm (1.4 W); other lines in the visible and their radiated energy (W) are 4045(0.75), 4350(1.08), 5461(1.35), and 5780(1.55) as quoted by Ace Glass Inc., Vineland, NJ. (Pyrex glass seriously absorbs at wavelengths shorter than 330 nm (7).) The sample chamber had a capacity of 70 ml. Agitation of the reaction solution was achieved by continuously bubbling nitrogen from an inlet at the bottom of the chamber. Nuclear magnetic resonance (^{1}H nmr) spectra were obtained on a Varian T-60 instrument, using tetramethylsilane (TMS) as internal standard, unless otherwise noted. Infrared (ir) spectra were taken on a Perkin-Elmer 257 grating spectrophotometer. Mass spectra were obtained at 70 eV using a direct inser-

Can. J. Chem. Downloaded from www.nrcresearchpress.com by 210.87.254.40 on 09/05/12
For personal use only.

Can. J. Chem. Downloaded from www.nrcresearchpress.com by 210.87.254.40 on 09/05/12
For personal use only.

tion probe at the Mass Spectroscopy Unit, McGill University, and at the Department of Chemistry, University of Alberta. Melting points were determined in open capillaries in a Thomas Hoover Uni-Melt apparatus and are uncorrected. Chromatographic separations were carried out with neutral activated alumina. Compounds **1***a* and *b* and **2***a* and *b* were prepared via published techniques [4, 8].

*Preparation of Phosphine and Phosphite Complexes (***3***a–e)*

These yellow-orange adducts were prepared by irradiation of tricarbonyl **1** (2–3 mmol) in benzene (THF for **3***a*) until it was converted to olefin adduct **2**. The progress of the reaction was followed by monitoring the carbonyl stretching bands in the infrared and generally took 1.5 h. The red solution was transferred by means of a syringe to a 100 ml, three-neck flask equipped with a N_2 inlet. A slight excess of the appropriate ligand was added, and the solution was heated (50–55°C) with stirring overnight (15 h). Evaporation to dryness and chromatographic purification on alumina, eluting with CH_2Cl_2–hexane (1:2), afforded fairly pure adducts. Purer products, but lower overall yields (based on **1***b*), could be obtained by reacting recrystallized (hexane) **2***b* with the appropriate ligand in benzene.

The preparation of **3***a* was slightly different from the above procedure and is described in greater detail below. Infrared data are given in Table 1.

*(η⁶-Allyl phenyl ether)(triphenylphosphine)dicarbonylchromium (***3***a)*

A solution of 575 mg (2.2 mmol) of tricarbonyl **1***a* in 70 ml THF was irradiated for 1.5 h. The solution was transferred to a 100-ml three-neck flask and evaporated to dryness. The residue was extracted with 3 × 15 ml hexane and the combined extracts were filtered. Then 600 mg (2.3 mmol) of triphenylphosphine was added and the solution was heated to 45°C overnight. Evaporation to dryness and chromatography afforded a 50% overall yield of crude orange solid, which was recrystallized from CH_2Cl_2–hexane, mp 112–113°C; nmr (acetone-d_6, external TMS) δ: 4.27–4.67 (m's, 5H, 3ArH and CH_2O), 4.75–5.58 (m's, 4H, 2ArH and CH_2=CH), 5.65–6.38 (m, 1H, CH=CH_2), 7.2–7.80 ppm (m, 15H, $P(C_6H_5)_3$); ms *m/e*: 504 (M^+), 448 ($M^+ - 2CO$), 407 ($M^+ - 2CO - C_3H_5$), 314 ($CrP(C_6H_5)_3$), 262, 183, 108. *Anal.* calcd. for $C_{29}H_{25}CrO_3P$: C 69.04, H 5.00; found: C 68.96, H 5.09.

*(η⁶-4-Phenyl-1-butene)(triphenyl phosphite)dicarbonylchromium (***3***b)*

Compound **3***b* was obtained in 75% yield, mp (hexane) 100–101°C; nmr ($CDCl_3$) δ: 2.12 (d, 4H, CH_2—CH_2), 4.00 (m, 1H, *p*-ArH), 4.25–4.50 (m, 2H, ArH), 4.6–4.95 (m, 3H), 5.05 (bs, 1H), 5.3–6.0 (bm, 1H, CH=CH_2), 7.0–7.4 ppm (m, 15H, $P(OC_6H_5)_3$); ms *m/e*: 550 (M^+), 494 ($M^+ - 2CO$), 362 ($CrP(OC_6H_5)_3$). *Anal.* calcd. for $C_{30}H_{27}CrO_5P$: C 65.45, H 4.94; found: C 65.48, H 4.76.

*(η⁶-4-Phenyl-1-butene)(triethyl phosphite)dicarbonylchromium (***3***c)*

Compound **3***c* was obtained in 65% yield (oil); nmr ($CDCl_3$) δ: 1.27 (t, 9H, 3 × CH_3), 2.43 (m, 4H, CH_2—CH_2), 3.91 (quintet, 6H, 3 × CH_2OP), 4.7–5.3 (m, 7H, 5ArH and CH_2=CH), 5.3–6.2 ppm (bm, 1H, CH=CH_2); ms *m/e*: 406 (M^+), 361 (M^+ – OEt), 350 ($M^+ - 2CO$), 218 ($CrP(OEt)_3$), 184 ($CrC_6H_5CH_2CH_2CH$=CH_2). *Anal.* calcd. for $C_{18}H_{27}CrO_5P$: C 53.20, H 6.70; found (average of two analyses): C 53.64, H 6.72.

*(η⁶-4-Phenyl-1-butene)(triphenylphosphine)dicarbonylchromium (***3***d)*

Compound **3***d* was obtained in 60% yield, mp (hexane) 101–102°C; nmr ($CDCl_3$) δ: 2.37 (m, 4H, CH_2—CH_2), 4.4–5.2 (m's, 7H, 5ArH and CH_2=CH), 5.45–6.1 (bm, 1H, CH=CH_2), 7.15–7.70 ppm (m, 15H, $P(C_6H_5)_3$); ms *m/e*: 502 (M^+), 446 ($M^+ - 2CO$), 314 ($CrP(C_6H_5)_3$), 262 ($P(C_6H_5)_3$). *Anal.* calcd. for $C_{30}H_{27}CrO_2P$: C 71.71, H 5.42; found: C 71.38, H 5.69.

*(η⁶-4-Phenyl-1-butene)(dimethylphenylphosphine)dicarbonylchromium (***3***e)*

Compound **3***e* was obtained in 60% yield (oil); nmr ($CDCl_3$) δ: 1.57 (d, 6H, $P(CH_3)_2$, J_{PCH} = 8 Hz), 2.25 (m, 4H, CH_2—CH_2), 4.3–5.15 (m's, 7H, 5ArH and CH_2=CH), 5.4–6.15 (bm, 1H, CH=CH_2), 7.15–7.75 ppm (bm, 5H, C_6H_5—P); ms *m/e*: 378 (M^+), 322 ($M^+ - 2CO$), 190 ($CrP(C_6H_5)Me_2$), 184 ($CrC_6H_5CH_2CH_2CH$=CH_2). *Anal.* calcd. for $C_{20}H_{23}CrO_2P$: C 63.49, H 6.13; found: C 62.52, H 6.24.

Irradiation of Phosphine and Phosphite Complexes

The concentration, solvent, and reaction time are given in Table 2. The progress of the reaction was followed by monitoring the carbonyl stretching bands. Once the production of **2***a* or *b* was complete, a 30-ml portion of the reaction mixture was transferred to a 100-ml three-neck flask and evaporated to dryness. Nuclear magnetic resonance analysis of the residue confirmed the presence of **2** and the disappearance of **3**. The remaining portion of the reaction mixture was heated to 50°C; a clean regeneration of **3** was noted in all cases.

*(η⁶-Allyl phenyl ether)dicarbonylthiocarbonylchromium (***7***a)*

A solution of 300 mg (1.1 mmol) of tricarbonyl **1***a* in 70 ml benzene was irradiated for 1.5 h, then filtered. The filtrate was evaporated to 30 ml and 5 ml dry CS_2 was added. The solution was heated to 40–45°C in the dark for several hours and the reaction was monitored by ir spectroscopy. The resulting dark mixture was cooled, filtered, and the filtrate was evaporated to dryness. The residue was chromatographed on alumina, eluting with hexane–CH_2Cl_2 (3:2). A 20% yield of yellow oily product was recovered. This was crystallized from hexane, mp 61–62°C (dec.); ir (hexane): 1970, 1927 cm^{-1}; nmr (benzene-d_6, external TMS) δ: 3.90 (m, 2H, CH_2O), 4.20 (m, 1H, *p*-ArH), 4.36–5.35 (m's, 6H, 4ArH and CH_2=CH), 5.40–6.20 ppm (m, 1H, CH=CH_2); ms *m/e*: 286 (M^+), 230 ($M^+ - 2CO$), 186 ($M^+ - 2CO - CS$), 145 ($M^+ - 2CO - CS - C_3H_5$). *Anal.* calcd. for $C_{12}H_{10}CrO_3S$: C 50.35, H 3.52; found: C 50.91, H 4.70.

*(η⁶-4-Phenyl-1-butene)dicarbonylthiocarbonylchromium (***7***b)*

One millimole (240 mg) of olefin adduct **2***b* was dissolved in 30 ml benzene and a solution of 265 mg (1 mmol) of triphenylphosphine in 5 ml dry CS_2 was added. The mixture was heated to 50°C in the dark and the reaction was monitored by ir spectroscopy. After 4 h, the mixture was allowed to cool to room temperature. One hour later, the solvents were stripped off and the dark residue was chromatographed on alumina, eluting with CH_2Cl_2–hexane (1:2). Careful elution afforded 153 mg (60% yield) of a yellow oil. This could be further purified by crystallization from hexane at low temperature but the yellow solid melted below room temperature; ir (hexane): 1973, 1931 cm^{-1}; nmr ($CDCl_3$) δ: 2.45 (m, 4H, CH_2—CH_2), 4.95 (m, 1H, CHH=CH), 5.15 (m, 1H, CHH=CH), 5.3–6.2 ppm (m's, 6H, 5ArH and CH=CH_2); ms *m/e*: 284 (M^+), 228 ($M^+ - 2CO$), 184 ($M^+ - 2CO - CS$), 91, 52.

Irradiation of Thiocarbonyl Adducts **7***a and* b

When either adduct **7***a* or *b* (0.2–0.7 mmol) was irradiated in either benzene or hexane, a brownish precipitate formed almost immediately. Continued irradiation (20–30 min) caused the gradual disappearance of the ir carbonyl absorptions of **7***a* and *b* and other, much weaker bands appeared.

TABLE 1. Infrared absorption frequencies[a]

Complex					
No.	X	L	THF	Benzene	Hexane
2*a*	O		1920, 1864	1925, 1867	1940, 1888
2*b*	CH_2			1913, 1857	1932, 1882
3*a*	O	$P(C_6H_5)_3$	1889, 1833	1892, 1840	1905, 1854
3*b*	CH_2	$P(OC_6H_5)_3$		1913, 1860	1927, 1877
3*c*	CH_2	$P(OEt)_3$		1897, 1843	1907, 1857
3*d*	CH_2	$P(C_6H_5)_3$		1891, 1838	1905, 1856
3*e*	CH_2	$P(C_6H_5)Me_2$		1883, 1827	1898, 1848

[a]Spectra taken in 0.1 mm or 1 mm NaCl solution cells; all values are in cm^{-1}.

Results and Discussion

The yellow complexes **3** were prepared by reacting **2** with the appropriate ligand in warm benzene or hexane. These reactions proceed very smoothly and in good yield. The general preparation of (arene)Cr-$(CO)_2$L complexes often consists of irradiation of (arene)$Cr(CO)_3$ in a donor solvent such as THF, whereby (arene)$Cr(CO)_2$THF is presumably produced. The THF is replaced by the desired ligand after the irradiation. In **2** the coordinated pendent olefin plays the same role as THF, stabilizing the dicarbonyl. The chelate nature of the arene–olefin ligand is undoubtedly the reason (4) for the greatly increased stability of **2** over unchelated (arene)Cr-$(CO)_2$olefin complexes, which are seldom isolated. The progress of the reactions can be followed by monitoring the infrared spectrum in the carbonyl stretching region. The two bands due to **2** are gradually replaced by two others which are lower in energy (Table 1). The reaction is accompanied by a red to yellow colour change.

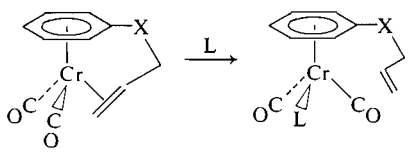

2 *a* and *b* 3

a X = O, L = $P\phi_3$
b X = CH_2, L = $P(O\phi)_3$
c X = CH_2, L = $P(OEt)_3$
d X = CH_2, L = $P\phi_3$
e X = CH_2, L = $PMe_2\phi$

The preparation of **3***a* is of note because of the recent report of the production of **4** by stirring **2***a* in benzene with or without $P(C_6H_5)_3$ for 93 h (9).

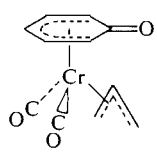

4

In contrast, we observed that the same reaction in warm hexane gave **3***a* in over 50% yield. Some minor bands in the infrared spectrum of the reaction mixture might be due to **4** but only **3***a* was isolated after chromatography. We found that refluxing the reaction in benzene resulted in extensive decomposition. Stirring in benzene at room temperature gave **4** as reported (9). This reaction provides a striking example of solvent effects on the path of organometallic reactions.

The complexes **3***a–e* were irradiated in an attempt to generate **5**, which would have two centers of optical activity and thus be diastereotopic. Although substitution of the second carbonyl is rare (10), it was hoped that the presence of the pendent olefin might trap out any monocarbonyl produced. However,

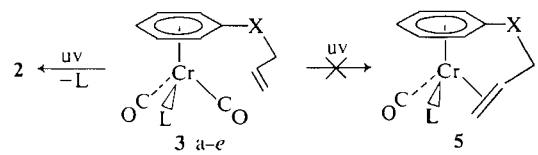

irradiation of **3***a–e* in benzene or hexane rapidly regenerated **2**. The irradiations were accompanied by a colour change from yellow to the characteristic red of **2**. The reactions are quite rapid, being up to three times faster than the photosubstitution of a carbonyl in **1** to produce **2** (Table 2). If the uv lamp is shut off and the reaction solution is stirred, **3** is gradually regenerated. This process can be speeded by warming. The reactions are quite clean and irradiation–heating cycles can be repeated several times. After work-up, the presence of **2** was confirmed by nmr spectroscopy. Within the limits of our detection (ca. 7%), no monocarbonyl **5** was produced, although continued irradiation of **2***a* causes a gradual decrease in intensity of its carbonyl stretching bands. Eventually no **2***a* remains and a pale yellow solid (mp 147–148°C dec.) having a band in the infrared at 1888 cm^{-1} (benzene or THF) is isolated in low yield. This is not **5**, since it does not have any arene ligand but

Can. J. Chem. Downloaded from www.nrcresearchpress.com by 210.87.254.40 on 09/05/12
For personal use only.

TABLE 2. Irradiation of phosphine and phosphite complexes *3a–e*

Complex irradiated					Reaction period to completion (min)
No.	X	L	mmol	Solvent[a]	
3a	O	$P(C_6H_5)_3$	0.55	THF[b]	15–20
			0.55	Benzene[b]	20
3b	CH_2	$P(OC_6H_5)_3$	0.35	Benzene[c]	15–20
			0.34	Hexane[c]	15–20
3c	CH_2	$P(OEt)_3$	0.75	Benzene	30–35
			0.75	Hexane	30–35
3d	CH_2	$P(C_6H_5)_3$	1.0	Benzene	35
3e	CH_2	$P(C_6H_5)Me_2$	0.80	Hexane	30–35

[a]Sixty-five millilitres, N_2 purge.
[b]Further irradiation causes decomposition and appearance of a new peak at 1888 cm^{-1}.
[c]Difficult to follow because absorptions overlap.

does contain triphenylphosphine. We have been unable to characterize it further.

Similar photosubstitutions of ligands by an olefin have been reported for complexes containing η^6-benzonorbornadiene (11). This may be regarded as a special case, since the olefin is held close to the metal by the rigid, multicyclic nature of the ligand. The substitution of another ligand by the olefin might be

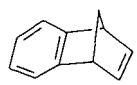

Benzonorbornadiene

accelerated in this case, in order to reduce steric crowding at the chromium. The olefins used in our study are attached to the arene ring by only one connection. The olefin is free to swing away from the metal. Therefore, we assume that the olefin does not promote phosphine loss; rather, that the Cr—P bond is particularly photosensitive under the reaction conditions. To test this idea, $[1,3,5\text{-}(CH_3)_3C_6H_3]Cr(CO)_2P(C_6H_5)_3$, **6**, a complex with no pendent olefin, was prepared (12) and irradiated in the presence of excess *cis*-cyclooctene. The irradiation in benzene was accompanied by a yellow to red colour change, characteristic of the generation of the olefin complex. As the reaction progressed, the two infrared bands at 1896 and 1848 cm^{-1} (hexane) due to **6** were replaced by two bands at 1904 and 1855 cm^{-1}. The latter bands were assigned to $[1,3,5\text{-}(CH_3)_3C_6H_3]Cr(CO)_2[cis\text{-}C_8H_{14}]$, since they appeared when $[1,3,5\text{-}(CH_3)_3C_6H_3]Cr(CO)_3$ was irradiated in the presence of *cis*-cyclooctene during our preparation of **6**. Lack of a pendent olefin requires use of excess free olefin and also results in reduced yields of the olefin complex.

These observations are relevant to an understanding of the reactivity of (arene)$Cr(CO)_2L$ complexes. The lack of monocarbonyl derivatives has been attributed to the stabilizing effect (10) which the initial loss of CO from (arene)$Cr(CO)_3$ has on the remaining carbonyls. We propose an alternative explanation. Irradiation of the tricarbonyl with uv light leads to the loss of the only two electron donor that can be displaced, namely CO. However, in **3** there is a choice of two such ligands. Apparently the Cr—P bond is very labile when the molecule is photoexcited, as has been predicted (13). This seems to be general for all (arene)$Cr(CO)_2L$ studied so far (11, 13). Loss of L is due to the photolability of the Cr—L bond and not necessarily due to any increased stability of the Cr—CO bond in the dicarbonyl complex.

The one reported example (14*a*) of substitution of a carbonyl ligand is the irradiation (290–370 nm) of $(C_6H_5CO_2Me)Cr(CO)_2P(OEt)_3$ in the presence of $P(OMe)_3$. The complexes isolated are $(C_6H_5CO_2Me)Cr(CO)L_1L_2$ where $L_1 = CO$, $L_2 = P(OMe)_3$ (20%); $L_1 = L_2 = P(OMe)_3$ (10%); and $L_1 = P(OEt)_3$, $L_2 = P(OMe)_3$ (15%). Disubstitution occurs but ligand exchange, $P(OMe)_3$ for $P(OEt)_3$, is very evident. The disubstitution was attributed to the π acidity of the $P(OEt)_3$ and CO_2Me groups, which weakened the Cr—CO bond as reflected in infrared and pK_a studies. This may be so, but the exchange of phosphite ligands is probably due to the photolability of the Cr—P bond. Moreover, irradiation of $(C_6H_5CO_2Me)Cr(CO)_2L$, where L = $P(OMe)_3$, $P(OEt)_3$, and $P(C_6H_5)_3$, in the presence of $P(C_6H_5)_3$ and $P(OEt)_3$, results in the displacement of L by the new ligand (14*a*).

The factors that affect the photoreactivity of (arene)$Cr(CO)_2L$ complexes are not understood. Although correlations of photoreactivity with metal carbonyl stretching frequencies are attractive, they are not necessarily relevant to the molecules in excited states. The photoreactivity of these complexes is likely to be very dependent on the wavelength of irradiation, as has already been observed when L = *trans*-4-styrylpyridine (13). This may be the explanation of why, under our reaction conditions, the Cr–olefin bond is less photolabile than the Cr—P

Can. J. Chem. Downloaded from www.nrcresearchpress.com by 210.87.254.40 on 09/05/12
For personal use only.

bond. Wavelength dependence studies on the photochemistry of (arene)$Cr(CO)_2L$ complexes are needed.

In contrast to the cases where L = phosphine and other ligands, CO is displaced when L = CS, as in (arene)$Cr(CO)_2CS$ [2, 14*b*]. Accordingly, we prepared the new complexes **7** according to slightly modified published techniques [14]. They were characterized by their infrared, nmr, and mass spectra. Both complexes decomposed when exposed to fluorescent lighting. When they were irradiated in an attempt to synthesize **8**, they rapidly decomposed

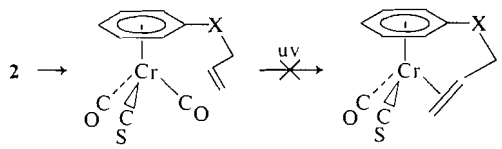

7 **8**

a X = O
b X = CH_2

under a variety of reaction conditions, including the presence of $P(C_6H_5)_3$. A dark, high-melting precipitate formed in all cases.

Conclusions

The failure to photosynthesize monocarbonyl **5** is due to the photolability of the Cr—P bond and not due to increased stability of the dicarbonyl precursor. The prediction (13) of the general photolability of the Cr—L bond in (arene)$Cr(CO)_2L$ is thus substantiated for L = phosphines and phosphites. Under our reaction conditions, the Cr–olefin bond is less photolabile than the Cr—P bond.

Acknowledgments

This work was supported by a grant from the National Research Council of Canada. G.P.D. acknowledges the Department of Chemistry, McGill University, for a Teaching Postdoctorate Fellowship (1976–1978). The authors are grateful to Professor J. Takats, Department of Chemistry, University of Alberta for providing some of the mass spectra.

1. (*a*) H. Brunner. Topics Curr. Chem. **56**, 67 (1975); (*b*) A. Davison and N. Martinez. J. Organometal. Chem. **74**, C17 (1974) and references therein.
2. G. Simonneaux, A. Meyer, and G. Jaouen. J. Chem. Soc. Chem. Commun. 69 (1975).
3. G. Jaouen and A. Meyer. J. Am. Chem. Soc. **97**, 4667 (1975).
4. W. S. Trahanovsky and R. A. Hall. J. Organometal. Chem. **96**, 71 (1975).
5. G. Paiaro. Organometal. Chem. Rev. Sect. A, **6**, 319 (1970).
6. Yu. T. Struchkov, V. G. Andrianov, A. N. Nesmeyanov, V. V. Krivykh, V. S. Kaganovich, and M. I. Rybinskaya. J. Organometal. Chem. **117**, C81 (1976).
7. J. G. Calvert and J. N. Pitts. Photochemistry. John Wiley & Sons, New York, NY. 1966 as quoted by A. J. Gordon and R. A. Ford. The chemists companion. John Wiley & Sons, New York, NY. 1972.
8. A. N. Nesmeyanov, M. I. Rybinskaya, V. V. Krivykh, and V. S. Kaganovich. J. Organometal. Chem. **93**, C8 (1975).
9. W. S. Trahanovsky and R. A. Hall. J. Am. Chem. Soc. **99**, 4850 (1977).
10. W. E. Silverthorn. Adv. Organometal. Chem. **13**, 47 (1975).
11. B. A. Howell and W. S. Trahanovsky. J. Am. Chem. Soc. **97**, 2136 (1975).
12. B. V. Lokshin, V. I. Zdanovich, N. K. Baranetskaya, V. N. Setkina, and D. N. Kursanov. J. Organometal. Chem. **37**, 331 (1972); W. Strohmeier and H. Hellmann. Chem. Ber. **96**, 2859 (1963).
13. M. Wrighton. Chem. Rev. **74**, 401 (1974).
14. (*a*) G. Jaouen and R. Dabard. J. Organometal. Chem. **72**, 377 (1974); (*b*) I. S. Butler, N. J. Coville, and D. Cozak. J. Organometal. Chem. **133**, 59 (1977).

Can. J. Chem. Downloaded from www.nrcresearchpress.com by 210.87.254.40 on 09/05/12
For personal use only.

Aminoglycoside antibiotics: Chemical conversion of neomycin B, paromomycin, and lividomycin B into bioactive pseudosaccharides[1,2]

STEPHEN HANESSIAN, TETSUYOSHI TAKAMOTO,[3] ROBERT MASSÉ, AND GHANSHYAM PATIL

Department of Chemistry, University of Montreal, Montreal, P.Q., Canada H3C 3V1

Received October 28, 1977

STEPHEN HANESSIAN, TETSUYOSHI TAKAMOTO, ROBERT MASSÉ, and GHANSHYAM PATIL. Can. J. Chem. **56**, 1482 (1978).

Pseudosaccharides containing various natural combinations of rings present in aminoglycoside antibiotics were prepared from the parent antibiotics, neomycin B, paromomycin, and lividomycin B, by oxidation of available vicinal diols and β-elimination. Pseudotrisaccharides comprising rings A, B, and C of paromomycin and lividomycin B, a pseudotrisaccharide comprising rings B, C, and D of the three antibiotics, and a 'core' pseudotrisaccharide containing rings B and C were thus prepared. These are valuable biological probes and intermediates for semisynthetic work in this series.

STEPHEN HANESSIAN, TETSUYOSHI TAKAMOTO, ROBERT MASSÉ et GHANSHYAM PATIL. Can. J. Chem. **56**, 1482 (1978).

Des pseudosaccharides qui contiennent des combinaisons naturelles de noyaux présents chez les antibiotiques aminoglycosidiques, néomycine B, paromomycine et lividomycine B, ont été préparés par une séquence impliquant l'oxydation des diols vicinaux chez les substances parentes, suivie d'une β-élimination. Ainsi les pseudotrisaccharides contenant les noyeaux A, B et C des antibiotiques néomycine et paromomycine, ceux qui portent les noyeaux B, C et D des trois antibiotiques, et un pseudodisaccharide 'core' contenant les noyeaux B et C ont été préparés. Ces substances peuvent être utilisées en tant qu'intermédiaires en synthèse dans cette série et aussi comme outils biologiques.

The aminoglycoside (aminocyclitol) antibiotics are a group of naturally occurring substances that exhibit powerful antibacterial effects on a wide variety of bacteria, by interfering with their normal process of protein biosynthesis at the ribosomal level (for recent reviews see refs. 2 and 3). A better understanding of their modes of action, as well as of other physiological properties necessitates a knowledge of structural, functional, conformational, and related parameters associated with these molecules. Correlations between structure and biological functions have been somewhat hampered by the unavailability of suitable model substrates that bear structural resemblance to the parent antibiotics. Only recently has it been possible to compile data (4) relating structural and functional features within a given series of aminoglycoside antibiotics to their biological activities, their susceptibilities to bacterial inactivating enzymes (see ref. 5 for recent reviews) and to their potential toxicity (6).

Despite the commercial availability of a number of aminoglycoside antibiotics and their extensive use in the treatment of pathogenic infections there is, at the present time, an ever-increasing interest in discovering novel types or analogs that have broader antibacterial spectra, with much lower degrees of toxicity and susceptibility to inactivating enzymes. Extensive research programs are currently in progress, particularly in the industrial sector, involving chemical modification and semisynthetic analogs (2) starting from the readily available, bioactive antibiotics and, whenever possible, from suitable fragments derived from these substances.

In the 4,6-*O*-glycosylated 2-deoxystreptamine group of antibiotics, such as neomycin B (**1**) and paromomycin (**2**) (Scheme 1), it has been known, since their discovery, that the corresponding pseudodisaccharides neamine and paromamine, isolated by methanolysis of the parent antibiotics, were only weakly antibacterial when tested in vitro. With the discovery of ribostamycin (**6**), a 5-*O*-β-D-ribofuranosylneamine (7), it became evident that the presence of the 2,6-diamino-2,6-dideoxyhexosyl unit attached to the ribofuranosyl portion in neomycin and paromomycin was not mandatory for biological activity as ribostamycin is more active than neamine but still less active than neomycin.[4]

At the inception of this study, there remained at least two other natural combinations of glycosidically-linked pseudosaccharides in molecules such as neomycin B and paromomycin that were unavailable either chemically or from other sources. It was there-

[1]For a previous publication in this series, see ref. 1.

[2]Portions of this work were reported at the 58th Meeting of the Chemical Institute of Canada, Symposium on Aminoglycoside Antibiotics, Toronto, Ontario, May 25–28, 1975.

[3]Postdoctoral associate, 1973–1975.

[4]It should be noted, however, that ribostamycin LD_{50} 260 mg/kg (mouse) is less toxic than neomycin, LD_{50} 24–44 mg/kg (mouse) (6).

Can. J. Chem. Downloaded from www.nrcresearchpress.com by 210.87.254.6 on 09/05/12
For personal use only.

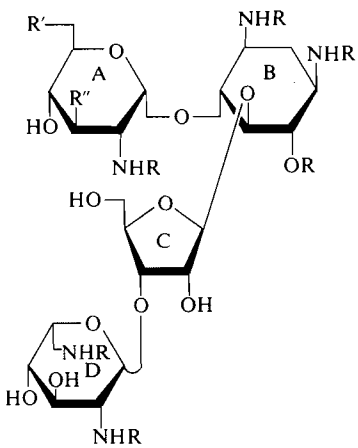

1 R = H; R′ = NH_2; R″ = OH
2 R = H; R′, R″ = OH
3 R, R″ = H; R′ = OH
4 R = Cbz; R′ = NHCbz; R″ = OH
5 R = Cbz; R′, R″ = OH

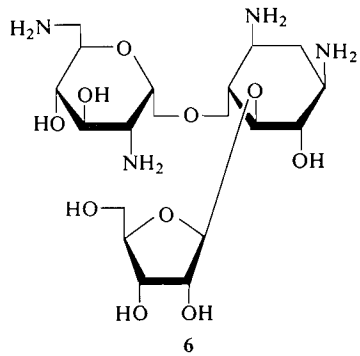

6

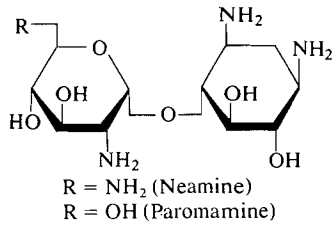

R = NH_2 (Neamine)
R = OH (Paromamine)

SCHEME 1

fore of paramount importance to devise practical and efficient means of obtaining such pseudosaccharides and to assess their utility in a general program concerned with the chemistry and biochemistry of aminoglycoside antibiotics. An examination of the structure of paromomycin reveals that there are three such pseudosaccharides in its skeletal framework. These constitute the two pseudotrisaccharides having rings A, B, C and rings B, C, D, and the 'core' pseudodisaccharide containing rings B, C. The latter two subunits are also common to the neomycins, lividomycin B (**3**) (8), ribostamycin, and related antibiotics.

In previous communications (1, 9), we have reported on the oxidative degradations of derivatives of neomycin B and paromomycin. In this paper, we report details of these conversions, as well as other pertinent transformations in this series.

Access to the pseudotrisaccharide comprising rings A, B, and C was considered first because of the inherent biological properties of such aminoglycosides. The basic strategy involved the use of the readily available neomycin B and paromomycin as starting materials and to effect, through suitably protected derivatives, periodate oxidation of the vicinally situated diol at C-3‴—C-4‴ of the diamino sugar unit D, followed by a base-catalyzed elimination of the resulting dialdehyde to release the aglycone, as illustrated in Scheme 2.

Paromomycin was chosen as the starting substrate because it should lend itself to preferential functionalization in ring A via the formation of a 4′,6′-*O*-benzylidene acetal. In such a derivative, the only vicinal diol is situated in ring D and the oxidative degradation discussed above should prove feasible. The classical procedure for the preparation of *O*-benzylidene acetals in the carbohydrate series involves the use of benzaldehyde in the presence of anhydrous zinc chloride (10). Under these conditions, and particularly in the presence of excess zinc chloride and benzaldehyde, penta-*N*-benzyloxycarbonylparomomycin (**5**) led to the corresponding 4′,6′-*O*;4‴,6‴-*O*,*N*-dibenzylidene derivative (11). However, treatment of **5** with benzaldehyde in the presence of 98% formic acid, as described in the case of methyl α-D-mannopyranoside (12), gave the desired 4′,6′-*O*-acetal **7** in high yield (Scheme 3). Periodate oxidation of **7** was found to proceed efficiently with a moderate excess of periodic acid in tetrahydrofuran in the presence of 4-Å molecular sieves. The resulting dialdehyde derivative[5] was isolated as an amorphous solid that exhibited the expected color tests for aldehydes (see Experimental). Treatment of the dialdehyde in methanol solution with triethylamine effected the desired β-elimination to give a crystalline product

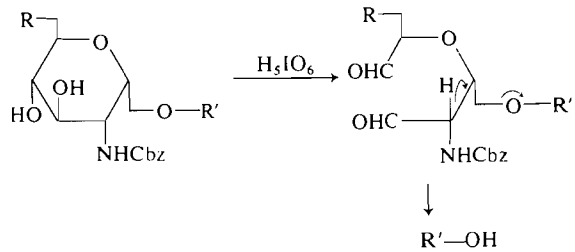

SCHEME 2

[5]For convenience the dialdehyde derivatives are represented in their acyclic forms rather than as internal acetals.

Can. J. Chem. Downloaded from www.nrcresearchpress.com by 210.87.254.6 on 09/05/12
For personal use only.

Can. J. Chem. Downloaded from www.nrcresearchpress.com by 210.87.254.6 on 09/05/12
For personal use only.

TABLE 1. ^{13}C magnetic resonance data of neomycin B and pseudotrisaccharide **13** (ppm from TMS)[a]

Compound	Ring	Carbon atoms[b] 1	2	3	4	5	6
Neomycin B	A	100.3	56.4	74.1	72.2	74.1	42.6
$pD \geq 11$	B	51.2	36.5	51.2	83.2	82.4	78.4
	C	109.2	74.1	77.0	85.1	62.3	—
	D	99.8	53.7	71.6	69.4	77.0	42.1
13	A	99.8	55.7	73.1	70.8	73.7	60.9
$pD \geq 11$	B	50.3	35.6	49.8	84.3	84.8	77.7
	C	109.5	75.8	70.5	84.3	62.4	—
13[c]	A	96.1	53.7	68.8	69.1	73.7	60.2
$pD \cong 1$	B	49.5	27.9	49.5	77.2	82.4	72.0
	C	109.9	74.0	69.1	83.9	60.7	—

[a]Chemical shifts corrected to TMS scale taking δ dioxane as 67.4 ppm.
[b]For simplicity and space conservation, the carbon atoms are not primed; ring A atom should be singly primed, ring C doubly primed, and ring D triply primed as in the text.
[c]Using methanol as internal reference at δ 49.8 ppm.

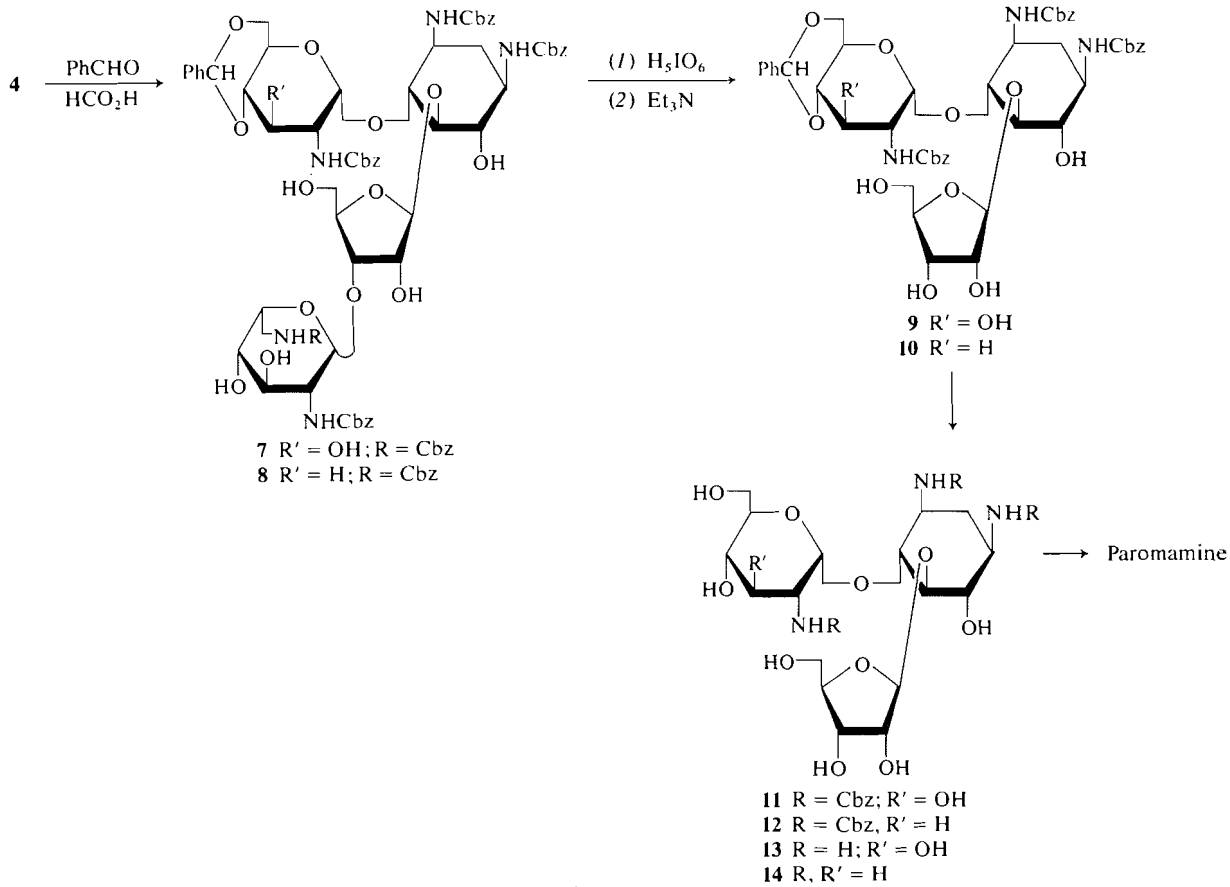

SCHEME 3

that was assigned the expected pseudotrisaccharide structure **9**, based on chemical and spectroscopic data. This product gave an amorphous tetraacetate derivative. Cleavage of the acetal function in the presence of dilute acetic acid in the usual manner led to the crystalline product **11** in high yield. Finally, removal of the benzyloxycarbonyl groups by hydrogenolysis gave the desired pseudotrisaccharide **13**, isolated as the amorphous free base. The structure of the pseudotrisaccharide was substantiated by

Can. J. Chem. Downloaded from www.nrcresearchpress.com by 210.87.254.6 on 09/05/12
For personal use only.

high resolution mass spectral data (9), by ^{13}Cmr data (Table 1), as well as by chemical means. Thus, by virtue of the presence of the vicinal, *cis*-diol group in the ribose moiety of **9**, it was possible to effect periodate oxidation of **9** to the corresponding dialdehyde. Reduction of the latter with sodium borohydride led to the corresponding diol, which upon acid hydrolysis, hydrogenolysis, and cleavage of the labile glycosidic linkage comprising the ring-C-opened ribose unit, led to paromamine as the sole product.

Pseudotrisaccharide **13** is structurally closely related to ribostamycin **6**, the only difference being a peripheral, functional replacement of an amino group at C-6′ in the latter by an alcohol group in the former. It was, therefore, of interest that the antibacterial spectrum of **13** was comparable to that of ribostamycin (7) but weaker than that of neomycin B or paromomycin. It was also not altogether unexpected that the pseudotrisaccharide **13**, like its parent antibiotic and related analogs, was an effective substrate for phosphotransferases I and II,[6] which are known to inactivate the neomycin–kanamycin group of antibiotics by phosphorylation at the C-3′ hydroxyl group (5).

The pseudotrisaccharide related to **13** has been recently obtained from an alkaline hydrolysis of an aminoglycoside antibiotic, isolated from *Bacillus circulans* and designated Bu-1709E$_2$ (13). This substance differs from **13** in that it contains an *N*-1 (*S*)-(−)-4-amino-2-hydroxybutyryl unit, as in the butirosin group of aminoglycosides (14). ^{13}C magnetic resonance data on **13** at p$D \geq 11$ and p$D \simeq 1$ are listed in Table 1 and are in accord with the structure and in good agreement with data published for the closely related ribostamycin (15).

Since ribostamycin was the only naturally occurring pseudotrisaccharide related to the neomycins at the inception of this study, it was of interest to extend the oxidative degradation described for paromomycin, to its 3′-deoxy analog, lividomycin B (**3**).

Application of the sequential periodic acid oxidation and β-elimination reaction to the lividomycin B (**3**) series was possible with the 4′,6′-benzylidene derivative **8** (16),[7] which was prepared from the corresponding *N*-benzyloxycarbonyl derivative **4**. The pseudotrisaccharide derivative **10** was obtained in good yield and was subsequently treated with dilute acid to give the crystalline derivative **12**. Removal of the benzyloxycarbonyl groups by hydrogenolysis led to the pseudotrisaccharide **14** (desneosaminyllividomycin B), isolated as the amorphous sulfate salt. As lividomycin B lacks the C-3′ hydroxyl group, its antibacterial activity is somewhat broader than that of paromomycin, particularly against strains capable of producing phosphotransferases. The antibacterial activity of **14** was found to be disappointingly weak against strains of *E. coli* that were known to be resistant to kanamycin and was generally marginal against a limited number of other susceptible strains. It appears therefore that the diaminosugar (neosamine B) portion of lividomycin B plays an integral part in dictating its overall biological activity, unlike the case of paromomycin and neomycin whose corresponding A, B, C pseudotrisaccharides maintain substantial intrinsic activities. The 6′-amino derivative of **14** (3′-deoxyribostamycin) possesses superior antibacterial activity compared to ribostamycin itself (17). These findings demonstrate the profound influence of subtle functional changes in seemingly identical molecules on their biological properties and provide valuable information concerning functional requirements. The readily obtained pseudotrisaccharides **13** and **14**, and their respective derivatized precursors, can be regarded as useful intermediates to bioactive analogs in the ribostamycin and butirosin series, since methods of selective functionalization at C-6′ are now available (18). It should also be mentioned that our originally published procedure (9) for the conversion of paromomycin into **13** has been recently adapted to the oxidative degradation of penta-*N*-acetyllividomycin B (19) and should prove useful in other cases also.

In their elegant studies on the neomycins, Rinehart *et al.* (20) had observed that *N*-acylated derivatives of neosamine B (2,6-diamino-2,6-dideoxy-L-idose, corresponding to ring D in **1**–**2**) were resistant to periodate oxidation and they had invoked conformational arguments to explain this behavior, particularly that the C-5 epimeric neosamine C derivatives were susceptible to oxidation. On the basis of these observations and related studies in our laboratory, it was anticipated that a preferential cleavage of ring A might be possible in derivatives of neomycin B and paromomycin, leading eventually to a pseudotrisaccharide comprising rings B, C, and D. Indeed, treatment of hexa-*N*-benzyloxycarbonylneomycin B (**15**) (1) (Scheme 4) with a slight excess of periodic acid in tetrahydrofuran led to a dialdehyde **19** (Scheme 5), which when treated with triethylamine in methanol underwent β-elimination to give the crystalline pseudotrisaccharide derivative **16** in 63% yield. Hydrogenolysis in the presence of 20% palladium-hydroxide-on-charcoal (21) gave the pseudotrisaccharide **17** as an amorphous solid, whose structure was confirmed by mass spectral analysis of the

[6]We thank Prof. J. Davies, University of Wisconsin, for these tests, June 24, 1974.

[7]We thank Prof. H. Umezawa for a generous gift of this compound.

Can. J. Chem. Downloaded from www.nrcresearchpress.com by 210.87.254.6 on 09/05/12
For personal use only.

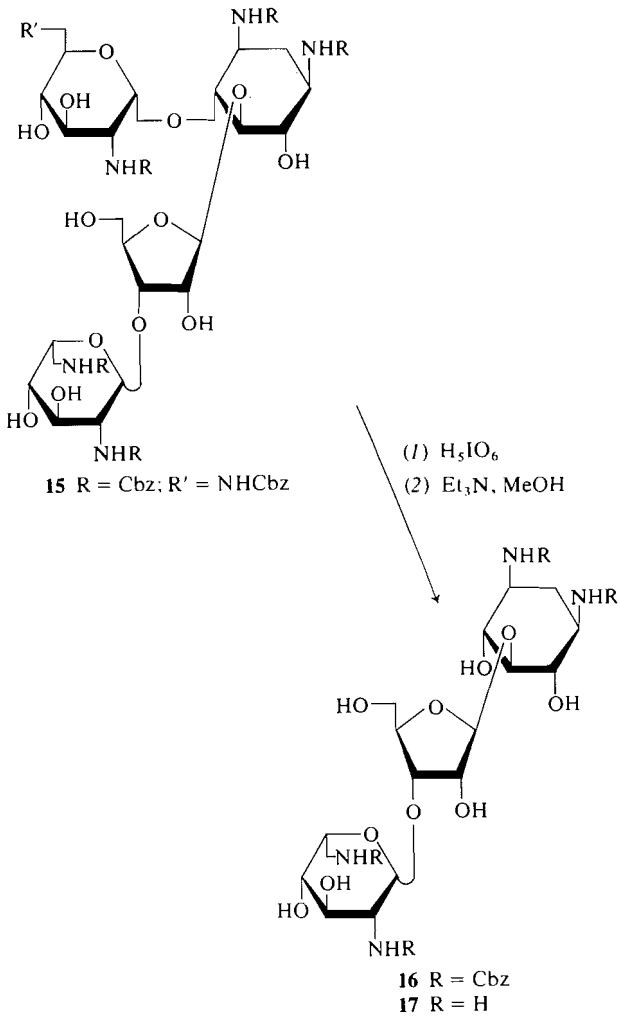

15 R = Cbz; R′ = NHCbz

16 R = Cbz
17 R = H

SCHEME 4

corresponding *N*-acetylated, *O*-trimethylsilyl derivative in accord with previous studies (22). The same product **17** could also be obtained from penta-*N*-benzyloxycarbonylparomomycin (**5**). It should be noted that a pseudotrisaccharide found as a minor component in commercial samples of neomycin (23) had been assigned a gross structure as in **17**. This had led to the suggestion (23) that it may be a biosynthetic precursor to the antibiotic (24). It appears that the neobiosamine portion (rings C, D) is formed at a relatively early stage in the biosynthesis of the neomycins (24) but it is as yet uncertain whether the remaining steps of the biosynthetic process involve the stepwise assembly of the 2-deoxystreptamine (ring B) and ultimately the neosamine C (ring A) portion, or a direct glycosylation of a preformed neamine. In a recent study, Pearce *et al.* (25) have shown that neamine is converted into neomycin (30%) by *Streptomyces rimosus* which was deoxystreptamine-negative. It still remains to be seen, however, if the pseudotrisaccharide **17**, which is found in commercial samples of neomycin, contributes to the biosynthetic pathway and, if so, to what extent. With the availability of the pseudotrisaccharide **17**, it will now be possible to provide conclusive evidence for the existence of an alternate biosynthetic pathway.[8] Surprisingly, the pseudotrisaccharide **17** was found to have some antibacterial activity, being 4–10 times less active than neamine.

In connection with these oxidative degradations of the neomycins and related antibiotics, it might be of interest to comment on ^{13}Cmr data which corroborate the difference in ground state conformations of rings A and D in these compounds. The ^{13}Cmr spectrum of neomycin B was recorded at $pD \geq 11$ in order to eliminate effects associated with the protonated or partially protonated amino groups. The assignments are in accord with data published on related aminoglycosides (26). Although the ground state conformation of the 2,6-diamino-2,6-dideoxy-α-D-glucopyranosyl portion (ring A, neosamine C) in neomycin B is most likely one that approximates a *C*1(D) form, that of the 5-epimeric 2,6-diamino-2,6-dideoxy-β-L-idopyranosyl portion (ring D, neosamine B) cannot be defined with certainty. Extensive ^{13}Cmr studies have shown that the conformations of the idopyranosides can vary considerably between the extreme *C*1 and 1*C* forms, depending on the configuration of the anomeric carbon, the oxidation state at C-6, the solvent, and the temperature (27). Examination of the ^{13}Cmr data in Table 1 reveals that the chemical shifts of the anomeric carbon atoms C-1′ and C-1‴ of rings A and D, respectively, are essentially identical. There is, however, a notable upfield shift of the signals associated with C-2‴, C-3‴, and C-4‴, compared to their counterparts in the ring A portion. As in the case of paromomycin and its analogs (11), this is most likely due to a distortion of the *C*1(L) conformation in the plane of at least three carbon atoms. A 1*C* conformation, as is known for idopyranosides, would place the aglycone in an equatorial orientation. The coincidence of chemical shifts of C-1′ and C-1‴ could, in this case, be due to the presence of different aglycones in rings A and D. Proton magnetic resonance data (20) in connection with the coupling constants of the anomeric hydrogen atoms in the neomycins reveal a much smaller dihedral angle (J_{12} = 1.6 Hz) in the β-L-*ido* portion (ring D), compared to the α-D-*gluco* portion (J_{12} = 2.7 Hz) indicating a departure from the idealized equatorial, axial (*C*1 form) or axial, equatorial (1*C* form) orientations of hydrogen atoms

[8]In collaboration with Prof. K. L. Rinehart, Jr.

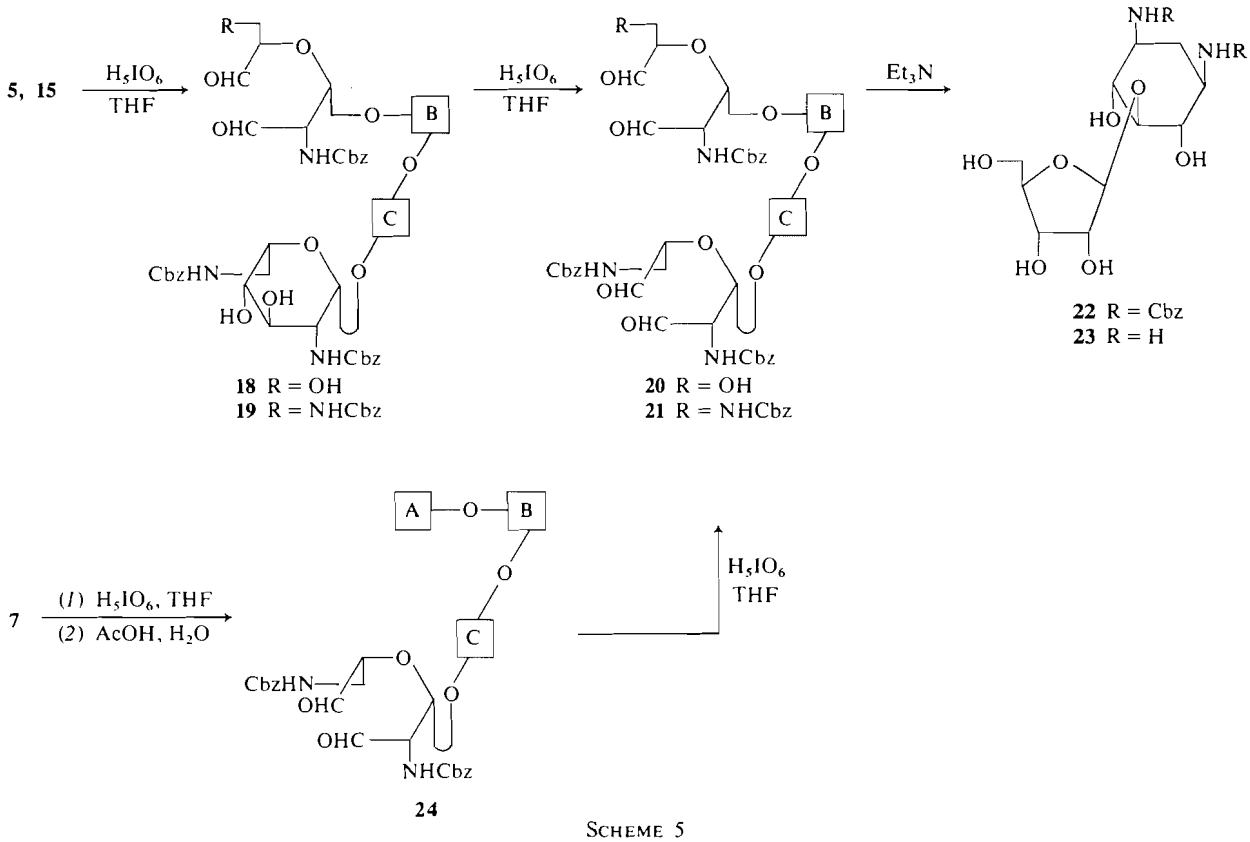

SCHEME 5

in the former case. Unfortunately the ^{1}Hmr spectra of the neomycins are not amenable to analysis in the region of other ring protons which would shed light on the solution conformations of the respective rings. In this regard, a study of proton-coupled ^{13}Cmr spectra might be informative, particularly in conjunction with appropriate model compounds.

^{13}C magnetic resonance data on hexa-*N*-acetylneomycin B (28) show that the signals associated with C-3′′′—C-4′′′ (ring D) are also at higher field compared to those of C-3′—C-4′ (ring A), with a maximum shift of +2.9 Hz for C-4′′′. While H-bonding effects might indeed contribute to the preponderance of certain conformations in solution, it appears that *N*-acylation does not change the solution conformation drastically. In a derivative such as **15**, the angles subtended by the C-3′′′—C-4′′′ hydroxyl groups in ring D will depart considerably from that in the D-gluco counterpart ($\simeq$60°) (20), hence a preferential periodate oxidation of the latter under controlled conditions would be a reasonable expectation.

To obtain the core pseudodisaccharide comprising rings B and C, advantage was taken of the presence of the vicinal diol function in ring D of **7**. Thus, treatment of **7** with a moderate excess periodic acid ($\cong$3 equiv.) gave the dialdehyde derivative which was subjected to mild acid hydrolysis to cleave the acetal function. The resulting dialdehyde derivative **24** was isolated as an amorphous solid in good yield (Scheme 5). A second periodic acid oxidation with only 1.5 equiv. of oxidant led to the tetraaldehyde **20** which, after β-elimination as previously described, gave the crystalline pseudodisaccharide derivative **22** in 18.8% overall yield. The latter could also be obtained in fewer steps from the oxidative degradation of **5** or **15** using a large excess of periodic acid. Hydrogenolysis then gave the pseudodisaccharide **23** as an amorphous solid which was found to be inactive in the standard antibacterial test. It is of interest that a recent synthesis of ribostamycin **6** utilizes the pseudodisaccharide derivative **22** obtained by glycosylation procedures, followed by chromatographic separation of positional isomers (29).

In addition to their potential antibacterial activities, the pseudodisaccharides described in this work could be of interest in other contexts as well. As already discussed above, they can be regarded as versatile, readily available intermediates for semisynthetic work, particularly that their modes of formation lead to *N*-acylated, preferentially *O*-substituted derivatives suitable for various transformations in-

Can. J. Chem. Downloaded from www.nrcresearchpress.com by 210.87.254.6 on 09/05/12
For personal use only.

cluding the all important glycosylation reactions. In addition, some of these pseudosaccharides can be regarded as ideal biochemical probes to study a variety of functions at the molecular level, since they encompass some of the structural and functional units present in the parent antibiotics. They could therefore be useful in bridging the last gap in relating structure–activity relationship in this series. Finally, they constitute potentially useful biosynthetic building blocks for the biotransformation of aminoglycosides (see, for example, ref. 30) and they could provide the 'missing link' in the biosynthetic pathway of the neomycin–paromomycin group of antibiotics.

Experimental

Melting points are uncorrected. Optical rotations were measured on a Perkin-Elmer automatic spectropolarimeter, model 141. Proton magnetic resonance spectra were recorded on a JEOL instrument at 60 MHz unless otherwise stated, with tetramethylsilane as internal standard, in deuteriochloroform as solvent. ^{13}C magnetic resonance spectra were recorded on a Bruker WH-90 instrument at 22.6 MHz. Mass spectra were recorded on an AEI-902 mass spectrometer at low and high resolution. Column chromatography was done using silica gel G254, with application of moderate suction.

Penta-N-*benzyloxycarbonylparomomycin (5)*

Benzyloxycarbonyl chloride (4.8 ml) was added dropwise and with vigorous stirring to a mixture of paromomycin **2** (4.8 g), sodium carbonate (8.64 g) in water (4.8 ml), and methanol (120 ml). After stirring at 5°C for 2 h, the mixture was stirred at room temperature for 17 h. Methanol (150 ml) was added, the inorganic precipitate was removed by filtration, and the filtrate was evaporated to dryness. Trituration of the residue with water (300 ml, total), filtration, and washing the solid with petroleum ether, gave the title compound; yield 7.37 g (92%). The colorless amorphous solid was suitable for further manipulations, although tlc indicated the presence of a trace amount of a second product (EtOAc–$CHCl_3$–MeOH, 25:40:9); a portion was purified by chromatography over silica gel; mp 139–141°C; $[\alpha]_D^{20}$ +22.6° (*c* 0.4, MeOH). *Anal.* calcd. for $C_{63}H_{75}N_5O_{24}\cdot 1.5H_2O$: C 57.62, H 5.95, N 5.34; found: C 57.25, H 5.87, N 5.40.

4′,6′-O-*Benzylidenepenta*-N-*benzyloxycarbonylparomomycin (7)*

Formic acid (1 ml) was added at 0°C to a mixture of **5** (0.73 g) in 7 ml of freshly distilled benzaldehyde and the clear solution was allowed to stand at 0°C for 25 h. The solution was added dropwise to a stirred solution of aqueous sodium bicarbonate with occasional addition of petroleum ether. The resulting amorphous solid was filtered, washed with water and petroleum ether, the solid was dissolved in methanol, and refiltered to remove a trace of insoluble material. Evaporation of the filtrate gave a syrup that solidified when triturated with petroleum ether to give the title compound as an essentially chromatographically homogeneous, amorphous solid; yield 0.775 g (95%); this material was suitable for utilization in the next step. Purification of a small quantity by preparative tlc ($CHCl_3$–EtOAc–MeOH, 10:2:1) gave material having mp 142–144°C (sinters ~135°C); $[\alpha]_D^{20}$ +17.8° (*c* 0.6, MeOH). This material gave a green colored spot when sprayed with acidic ammonium molybdate spray (31). *Anal.* calcd. for $C_{70}H_{79}N_5O_{24}\cdot 1.5H_2O$: C 60.00, H 5.86, N 5.00; found: C 59.71, H 5.82, N 5.12.

Acetylation of a portion (103 mg) in pyridine containing acetic anhydride (0.5 ml) during 5 days at 25°C, followed by evaporation of the solution gave the corresponding hexaacetyl derivative as a chromatographically homogeneous syrup; 75 mg (62%). An nmr spectrum of the product showed the correct ratio of protons in the integrated areas corresponding to acetyl methyl groups.

Periodic Acid Oxidation of 7

A mixture containing **7** (2.27 g, 1.59 mmol), periodic acid (545 mg, 2.39 mmol), and 4-Å molecular sieves (1.5 g) in 60 ml of redistilled tetrahydrofuran was allowed to stand at 0°C for 24 h. It was then poured into aqueous sodium bicarbonate with stirring and the solution was extracted with chloroform (4 × 50 ml). The organic phase was washed with water, dried over anhydrous sodium sulfate, and processed as usual to give a colorless syrup. Trituration with ether gave the dialdehyde derivative resulting from **7**, as an amorphous solid, which was suitable for use in the next step; yield 2.12 g (93%). The product showed one major spot on tlc (R_f 0.6, $CHCl_3$–EtOAc–MeOH, 20:4:3) and gave an orange color with the aniline hydrogen phthalate spray and a blue color with the ammonium molybdate spray; this is characteristic of aldehydes and hemiacetals (compare with green color in case of **7**, **9**, etc.).

4-O-*(4,6*-O-*Benzylidene-2-benzyloxycarbonylamino-2-deoxy*-α-D-*glucopyranosyl)-5*-O-*(*β-D-*ribofuranosyl)-1,3-di*-N-*benzyloxycarbonyl-2-deoxystreptamine (9)*

A solution containing the above-described dialdehyde derivative (2.13 g) and triethylamine (1 ml) in 70 ml of methanol was stirred at room temperature for 4 h. Evaporation of the solution gave a solid residue which was triturated with ether and filtered. Crystallization from ethanol gave the title compound (0.89 g, 63%) which was essentially pure by tlc ($CHCl_3$–EtOAc–MeOH, 20:5:3) and gave a characteristic greenish color when sprayed with acidified ammonium molybdate. Recrystallization from ethanol, or purification by preparative thick-layer chromatography gave an analytical sample; mp 221–222°C; $[\alpha]_D^{20}$ +35.4° (*c* 0.7, acetone). *Anal.* calcd. for $C_{48}H_{57}N_3O_{18}\cdot H_2O$: C 59.81, H 5.92, N 4.36; found: C 59.61, H 5.80, N 4.27.

Acetylation of a portion (50 mg) as described for **7** gave the peracetate as a chromatographically homogeneous foam (96%); $[\alpha]_D^{20}$ +12° (*c* 1, acetone).

4-O-*(2-Benzyloxycarbonylamino-2-deoxy*-α-D-*glucopyranosyl)-5*-O-*(*β-D-*ribofuranosyl)-1,3-di*-N-*benzyloxycarbonyl-2-deoxystreptamine (11)*

A suspension of **9** (450 mg) in 80% acetic acid was stirred at room temperature. After 30 h the clear solution was evaporated to dryness and the residue was washed with ether by decantation to give the crystalline title compound; yield 410 mg (quantitative). Purification by a sample (50 mg) preparative tlc ($CHCl_3$–EtOAc–MeOH, 4:1:1), followed by recrystallization from methanol gave an analytical sample (41 mg); mp 213–215°C; $[\alpha]_D^{20}$ +31.7° (*c* 0.88, dioxane). *Anal.* calcd. for $C_{41}H_{51}N_3O_{17}\cdot H_2O$: C 54.55, H 6.21, N 4.66; found: C 54.87, H 5.95, N 4.72.

The corresponding peracetate was obtained as a foam which exhibited the expected ^1Hmr spectral characteristics.

4-O-*(2-Amino-2-deoxy*-α-D-*glucopyranosyl)-5*-O-*(*β-D-*ribofuranosyl)-2-deoxystreptamine (13)*

A solution containing **11** (150 mg) in a mixture of methanol (20 ml) and dioxane (10 ml) was hydrogenated in the presence of 20% palladium-hydroxide-on-charcoal (21) (100 mg) and 0.64 ml of *N* hydrochloric acid. After 2.5 h, 10 ml of water was added and the hydrogenation was continued for 1.5 h. The suspension was filtered, the neutral filtrate was treated with

Can. J. Chem. Downloaded from www.nrcresearchpress.com by 210.87.254.6 on 09/05/12
For personal use only.

Can. J. Chem. Downloaded from www.nrcresearchpress.com by 210.87.254.6 on 09/05/12
For personal use only.

Rexyn (OH^-), and the filtered solution was evaporated to dryness below 40°C to give a cream-colored solid; yield 75 mg (94%). The product was dissolved in the minimum volume of water and reprecipitated by addition of ethanol to give 31 mg of the chromatographically homogenous pseudotrisaccharide. Processing of the mother liquors gave an additional 35 mg of material; mp 160–175°C with decomposition at ~200°C; $[\alpha]_D^{20}$ +21° (*c* 1, H_2O); tlc (MeOH – $CHCl_3$ – 28% NH_4OH, 3:1:2) R_f 0.42, $R_{paromamine}$ 0.85; paper chromatography (1-PrOH–pyridine–H_2O–AcOH, 15:10:12:3) $R_{paromamine}$ 1.25 (pseudotrisaccharide **13** lit. (13) mp 168–170°C (for the carbonate salt); $[\alpha]_D$ +42° (H_2O)).

Mass spectral data on the *N*-acetyl *O*-trimethylsilyl derivative (22): *m/e* calcd. for $C_{31}H_{64}N_3O_{11}Si_4$ fragment: 766.3617; found: 766.3612; *m/e* calcd. for a $C_{28}H_{59}N_2O_{10}Si_4$ fragment: 695.3246; found: 695.3249. The ^{1}Hmr spectrum (D_2O, 100 MHz) of the pseudotrisaccharide **10** showed the two anomeric protons at −0.52 and −0.54 ppm relative to the HOD signal. ^{13}C magnetic resonance data are listed in Table 1.

Oxidative Degradation of ***9****: Isolation of Paromamine*

A solution containing **9** (300 mg) in 50 ml of methanol was treated with an aqueous solution of sodium metaperiodate (150 mg, 6 ml). After standing at room temperature overnight the solution was treated with 0.5 ml of ethylene glycol and the solvent was evaporated. The residue consisting essentially of the corresponding dialdehyde derivative was dissolved in methanol (15 ml) and 0.5 *N* HCl (5 ml) was added. After stirring for 24 h, the solution was evaporated partially and the resulting insoluble solid was filtered, washed with water, and dried; yield 250 mg. This product was dissolved in a 1:1 mixture of methanol and tetrahydrofuran, and 45 mg (4 equiv.) of sodium borohydride in 1 ml of water was added. After stirring the solution for 5 h, tlc ($CHCl_3$–EtOAc–MeOH, 20:5:4) indicated the complete conversion of the dialdehyde into the corresponding triol derivative, R_f 0.26. Evaporation of the solution and chromatographic separation, gave 140 mg of the triol. This material was dissolved in 30 ml of methanol and subjected to hydrogenolysis in the presence of 20% palladium-on-charcoal (50 mg) and 25 ml of *N* HCl. After 1 h, 10 ml of water was added to the mixture and the hydrogenation was continued for another 2 h. The mixture was filtered, the filtrate was neutralized with Rexyn 203 (OH^-) and processed as usual to give the triol derivative as a colorless solid (72 mg, quantitative); mp ~180°C (dec.); $[\alpha]_D$ +18.5° (*c* 0.34, H_2O); $R_{paromamine}$ 1.18 (MeOH – $CHCl_3$ – 28% NH_4OH, 3:1:2).

Treatment of the above product in 6 *N* HCl (18 h, 25°C) gave paromamine hydrochloride (53 mg) identical in all respects to an authentic sample (32).

*4-O-(4,6-O-Benzylidene-2-benzyloxycarbonylamino-2,3-dideoxy-α-D-ribo-hexopyranosyl)-5-O-(β-D-ribofuranosyl)-1,3-di-N-benzyloxycarbonyl-2-deoxystreptamine (****10****)*

To a solution containing 4′,6′-*O*-benzylidenepenta-*N*-benzyloxycarbonyllividomycin B (**8**) (16) (200 mg) in 10 ml of tetrahydrofuran was added 187 mg (5.5 equiv.) of periodic acid and 1 g of 4-Å molecular sieves at 0°C. The mixture was stirred gently at 0–5°C for 20 h after which time tlc ($CHCl_3$–EtOAc–MeOH, 20:5:3) indicated the complete consumption of **8** and the formation of a new, less polar product. The mixture was poured into aqueous sodium bicarbonate, the solution was extracted with chloroform, and the latter was processed as usual to give the dialdehyde resulting from **8** as a syrup (180 mg). This material gave the characteristic blue color for aldehydes with the ammonium molybdate spray. The syrup was dissolved in methanol (30 ml), traces of insoluble salts were filtered, and the filtrate was treated with 0.5 ml of triethylamine. After stirring overnight, the mixture was evaporated to dryness, the residue was triturated with ether and filtered to give the title compound as an amorphous, chromatographically homogenous solid; yield 125 mg. This material gave a green color when sprayed with acidified ammonium molybdate. It was used as such in the following step.

*4-O-(5-Benzyloxycarbonylamino-2,3-dideoxy-α-D-ribo-hexopyranosyl)-5-O-(β-D-ribofuranosyl)-1,3-di-N-benzyloxycarbonyl-2-deoxystreptamine (****12****)*

The above obtained product (125 mg) was dissolved in 8 ml 80% aqueous acetic acid and the solution was stirred at room temperature overnight. The solution was evaporated to dryness, the residue was triturated with water, and the resulting solid was filtered, washed with petroleum ether, and dried. The crude product, consisting of one major component (tlc, $CHCl_3$–EtOAc–MeOH, 4:1:1) was purified by preparative thick-layer chromatography to give the title compound as a crystalline solid (76 mg, 61% overall from **8**). Recrystallization of a portion of ethanol, gave fine colorless crystals; mp 228–229°C; $[\alpha]_D^{25}$ +27.7° (*c* 1, dioxane). *Anal.* calcd. for $C_{41}H_{51}N_3O_{16}$: C 58.50, H 6.06, N 5.00; found: C 58.92, H 6.18, N 4.87.

*4-O-(2-Amino-2,3-dideoxy-α-D-ribo-hexopyranosyl)-5-O-(β-D-ribofuranosyl)-2-deoxystreptamine (Deneosaminyllividomycin B) (****14****)*

The preceding compound (60 mg) was dissolved in 20 ml containing 0.34 ml of *N* hydrochloric acid, 60 mg of 20% palladium-hydroxide-on-charcoal and the mixture was hydrogenated for 3 h. Filtration, treatment of the filtrate with Rexyn (OH^-), and usual manipulation gave a syrup that was chromatographed on Amberlite CG-50 (NH_4^+) using *N* ammonia as developer the fractions containing the product were combined to give 15 mg (~45%) of a syrup that solidified upon trituration with ethanol. The corresponding sulfate salt was obtained as an amorphous solid by adding the required volume of aqueous sulfuric acid and evaporation in the presence of ethanol; mp 170–175°C (dec.); $[\alpha]_D^{25}$ +28° (*c* 0.8, H_2O) (lit. (19) mp 170–174°C (dec.); $[\alpha]_D^{25}$ +30° (H_2O)).

Treatment of **14** (10 mg) with 2,4-dinitrofluorobenzene (15 mg) in aqueous sodium bicarbonate – ethanol, followed by diluting with water and stirring overnight, gave a yellow precipitate that was purified by preparative thick-layer chromatography ($CHCl_3$–EtOAc–MeOH, 3:2:1), to give the corresponding tri-*N*-dinitrophenyl derivative as an amorphous, yellow powder (10 mg, 43%); mp 215–220°C (gradual dec.).

*Hexa-N-benzyloxycarbonylneomycin B (****15****)*

A solution containing neomycin sulfate (11.44 g) in 150 ml of water containing 25 g of sodium carbonate was diluted with 200 ml of methanol. The solution was cooled to 0°C and treated dropwise and with stirring, with 25 ml of benzyloxycarbonyl chloride. After 4 h, the mixture was diluted with 500 ml of cold water, and the whole was poured into 1 ℓ of ice-water with vigorous stirring. The resulting oily residue was separated from the supernatant by decantation and it was repeated by trituration with petroleum ether, then with water. The resulting paste was dissolved in a mixture of chloroform and methanol (1:1), the solution was filtered to separate traces of insoluble material, and the filtrate was evaporated to a colorless foam. Trituration with water gave a solid that was filtered and air dried. It was then suspended in petroleum ether and the mixture was vigorously stirred to give a fine colorless powder; yield 16.06 g (89%). Thin-layer chromatography ($CHCl_3$–EtOAc–MeOH, 20:5:3) indicated the presence of a major component and two minor components corresponding to the title product, the neomycin C analog, and a partially *O*-esterified derivative, respectively. The latter could be trans-

Can. J. Chem. Downloaded from www.nrcresearchpress.com by 210.87.254.6 on 09/05/12
For personal use only.

formed into the neomycin derivative by treatment with sodium methoxide.

A portion of the above product (4.76 g) was dissolved in refluxing chloroform (50 ml), the solution was cooled and added to a column containing 250 mg of silica gel. Elution with chloroform (100 ml), then with the solvent mixture $CHCl_3$–EtOAc–MeOH, 20:5:2, gave successively, the *O*-benzyloxycarbonyl derivative (0.26 g), the title compound (3.67 g), and hexa-*N*-benzyloxycarbonylneomycin C (0.5 g). A second chromatographic treatment of the title compound (which contained traces of the C isomer) gave 3.03 of chromatographically homogenous material; mp 116–120°C; $[\alpha]_D^{25}$ +32.9° (*c* 0.54, $CHCl_3$).

5-O-[3-O-(2,6-Dibenzyloxycarbonylamino-2,6-dideoxy-α-L-idopyranosyl)-β-D-ribofuranosyl]-1,3-di-N-benzyloxycarbonyl-2-deoxystreptamine (16)

The preceding product **15** (1 g, 0.78 mmol) was dissolved in 60 ml of anhydrous tetrahydrofuran, the solution was cooled to 0°C, and treated with 10 g of 4-Å molecular sieves and 210 mg (0.92 mmol) of periodic acid. The mixture was left at 0–2 C for 20 h after which tlc indicated the disappearance of **15** and the formation of a less polar product (the dialdehyde **19**) which gave a positive test when chromatoplates were sprayed with aniline hydrogen phthalate. The mixture was treated with Rexyn 203 (OH^-), and the neutral supernatant was separated and combined with washings. The solution was evaporated to dryness, the syrupy residue (0.942 g) was dissolved in methanol (30 ml) containing triethylamine (1 ml), and the solution was heated at 55°C for 2 days. Evaporation of the solution gave a solid residue that was triturated with ether. The residue was chromatographed on silica gel ($CHCl_3$–EtOAc–MeOH, 20:5:2) to give the crystalline title compound (370 mg, 46%) and starting material (160 mg). Based on recovered **15**, the yield of **16** was 56%. Recrystallization from hot 2-propanol gave an analytical sample; mp 228–230°C; $[\alpha]_D^{25}$ +22.9° (*c* 0.9, dioxane). *Anal.* calcd. for $C_{49}H_{58}N_4O_{18}$: C 59.38, H 5.89, N 5.15; found: C 59.29, H 5.80, N 5.61.

5-O-[3-O-(2,6-Diamino-2,6-dideoxy-α-L-idopyranosyl)-β-D-ribofuranosyl]-2-deoxystreptamine (17)

A solution containing **16** (470 mg, 0.47 mmol) in 60 ml of methanol and 2.9 ml of *N* hydrochloric acid was treated with 20% palladium-hydroxide-on-charcoal (250 mg) and the mixture was hydrogenated. After 3 h, the mixture was processed in the usual manner to give a syrup which was redissolved in water (5 ml) and the solution was treated with Rexyn 203 (OH^-) until the p*H* became neutral. Filtration and evaporation of the filtrate gave a residue which solidified by trituration with ethanol, to give the title compound as an amorphous colorless solid (179 mg, 83%); mp 210–212°C (dec.); $[\alpha]_D^{25}$ +22.5° (*c* 0.25, H_2O); R_f 0.38 ($CHCl_3$ – MeOH – 28% NH_4OH, 1:3:2); paromamine had R_f 0.48; neomycin, R_f 0.21 in the same solvent system; mass spectral data for the *N*-acetylated, *O*-trimethylsilyl derivative: *m/e* calcd. for a fragment $C_{16}H_{33}N_2O_4Si_2$: 373.1977; found: 373.1987; *m/e* calcd. for $C_{16}H_{33}N_2O_5Si_2$: 388.1928; found: 389.1947.

This product could also be prepared from penta-*N*-benzyloxycarbonylparomomycin (**5**), essentially by the same procedure as described in the sequence **15** → **16** → **17**.

5-O-(β-D-Ribofuranosyl)-1,3-di-N-benzyloxycarbonyl-2-deoxystreptamine (22)

From 7

A sample of **7** (820 mg, previously dehydrated by dissolving in pyridine and distillation of the solvent) was oxidized with periodic acid (430 mg, 3.16 equiv.) in tetrahydrofuran (30 ml) in the presence of 4-Å molecular sieves. After 24 h at 0–5°C the mixture was poured in aqueous sodium bicarbonate solution and was processed as previously described to give the corresponding dialdehyde as a syrup (720 mg). The latter was dissolved in 80% aqueous acetic acid and, after 2 days, the solution was evaporated to dryness. The residue was triturated with water and then dried to give the dialdehyde derivative **24** as an amorphous solid (670 mg).

A second periodic acid oxidation (178 mg, 1.5 equiv.) in 30 ml of tetrahydrofuran as described above gave the tetraaldehyde derivative **20** (614 mg), which was dissolved in 20 ml of methanol containing 0.5 ml of triethylamine and the solution was stirred at 50°C for 2 days. Evaporation to dryness and trituration of the residue with ether gave a solid which was purified by preparative thick-layer chromatography ($CHCl_3$–EtOAc–MeOH, 4:1:1) to give the title compound in the form of colorless needles (63 mg, 18.8% overall). Recrystallization from ethanol gave an analytical sample; mp 235–237°C (sintering); $[\alpha]_D^{25}$ −44° (*c* 1, MeOH); mass spectral data for the *O*-TMS derivative: *m/e* 675 for a fragment containing the 2-deoxystreptamine portion and a $O—CH=\overset{+}{O}TMS$ substituent (arising from C-1 of the ribose unit with $\overset{+}{O}TMS$ migration). *Anal.* calcd. for $C_{27}H_{34}N_2O_{11}$: C 57.65, H 6.05, N 4.98; found: C 57.42, H 5.92, N 4.91.

From 5

Penta-*N*-benzyloxycarbonylparomomycin **5** (1 g) was oxidized with periodic acid (1.42 g, 8 equiv.) in 70 ml of tetrahydrofuran containing 4-Å molecular sieves. After standing at 0°C for 20 h, the mixture was poured into aqueous sodium bicarbonate and processed as usual to give 890 mg of the tetraaldehyde intermediate **20**. Treatment of the latter in methanol (70 ml) containing triethylamine (1 ml) for 15 h at room temperature and processing as described above gave the crude, chromatographically homogenous title compound (170 mg, 39–40% overall). Recrystallization from ethanol gave the crystalline product (70 mg, 16%) identical to that obtained above.

The same results were obtained starting from the neomycin derivative **15** and proceeding via the corresponding tetraaldehyde derivative **21**.

5-O-(β-D-Ribofuranosyl)-2-deoxystreptamine (23)

A solution containing 210 mg of the preceding compound in 50 ml of methanol containing 1.3 ml of *N* hydrochloric acid was hydrogenated in the presence of 20% palladium-hydroxide-on-charcoal (100 mg). After 4 h, the catalyst was filtered and the filtrate was processed in the usual manner to give a syrup (104 mg, 98%) which solidified from ethanol. The chromatographically homogenous product showed R_f 0.56 in $CHCl_3$ – MeOH – 28% NH_4OH, 1:3:2, $R_{paromamine}$ 1.12, and $R_{deoxystreptamine}$ 1.36; mp ~135°C (with foaming); $[\alpha]_D^{25}$ −24.6°C (*c* 0.22, H_2O).

Acknowledgements

We thank the National Research Council of Canada for financial support (PRAI Grant). We also thank R. Mayer for the ^{13}Cmr spectra and Dr. M. S. B. Nayar for recording the mass spectra.

1. S. HANESSIAN, T. TAKAMOTO, and R. MASSÉ. J. Antibiot. **28**, 835 (1975).
2. S. UMEZAWA. Adv. Carbohydr. Chem. Biochem. **30**, 111 (1974); *In* Drug action and drug resistance in bacteria. 2. Aminoglycoside antiobiotics. *Edited by* S. Mitsuhashi. University Park Press, Baltimore, MD. 1975. pp. 3–35.

Can. J. Chem. Downloaded from www.nrcresearchpress.com by 210.87.254.6 on 09/05/12
For personal use only.

3. N. TANAKA. *In* Drug action and drug resistance in bacteria. 2. Aminoglycoside antibiotics. *Edited by* S. Mitsuhashi. University Park Press, Baltimore, MD. 1975. pp. 125–139, and references cited therein.
4. K. E. PRICE, J. C. GODFREY, and H. KAWAGUCHI. Adv. Appl. Microbiol. **18**, 191 (1974).
5. H. UMEZAWA. Adv. Carbohydr. Chem. Biochem. **30**, 183 (1974); R. BENEVISTE and J. DAVIES. Annu. Rev. Biochem. **42**, 471 (1973).
6. K. FUJISAWA, T. HOSHIYA, and H. KAWAGUCHI. J. Antibiot. **28**, 677 (1974).
7. E. AKITA, T. TSURUOKA, N. EZAKI, and T. NIIDA. J. Antibiot. **23**, 173 (1970).
8. T. MORI, T. ICHIVANAGI, H. KONDO, K. TOKUNAGA, T. ODA, and K. MUNAKATA. J. Antibiot. **24**, 339 (1971); see also T. MORI, Y. KYOTANI, I. WATANABE, and T. ODA. J. Antibiot. **25**, 149 (1972).
9. T. TAKAMOTO and S. HANESSIAN. Tetrahedron Lett. 4009 (1974).
10. N. K. RICHTMYER. Methods Carbohydr. Chem. **1**, 107 (1962); O. T. H. SCHMIDT. Methods Carbohydr. Chem. **1**, 349 (1962).
11. S. HANESSIAN, R. MASSÉ, and G. EKBORG. Can. J. Chem. This issue.
12. J. G. BUCHANAN and J.-C. P. SCHWARZ. J. Chem. Soc. 4770 (1962).
13. T. TSUKIURA, K. SAITO, S. KOBARU, M. KONOSHI, and H. KAWAGUCHI. J. Antibiot. **26**, 386 (1973).
14. P. W. K. WOO, H. W. DION, and Q. R. BARTZ. Tetrahedron Lett. 2625 (1971).
15. S. OMOTO, S. INOUYE, M. KOJIMA, and T. NIIDA. J. Antibiot. **26**, 717 (1973).
16. S. UMEZAWA, I. WATANABE, T. TSUCHIYA, H. UMEZAWA, and M. HAMADA. J. Antibiot. **25**, 617 (1972).
17. D. IKEDA, T. TSUCHIYA, S. UMEZAWA, and H. UMEZAWA. J. Antibiot. **26**, 799 (1973).
18. S. HANESSIAN, R. MASSÉ, and T. NAKAGAWA. Can. J. Chem. This issue; see also S. HANESSIAN and P. LAVALLEE. Methods Carbohydr. Chem. **7**, 49 (1976).
19. T. YAMAGUCHI, K. KAMIYA, T. MORI, and T. ODA. J. Antibiot. **30**, 332 (1977).
20. K. L. RINEHART, JR., M. HICHENS, A. D. ARGOUDELIS, W. S. CHILTON, H. E. CARTER, M. P. GEORGIADIS, C. P. SCHAFFNER, and R. T. SCHILLINGS. J. Am. Chem. Soc. **84**, 3218 (1962); see also K. L. RINEHART, JR. The neomycins and related antibiotics. John Wiley & Sons, Inc., New York. 1964. pp. 29–31.
21. W. PEARLMAN. Tetrahedron Lett. 1663 (1967).
22. D. C. DE JONGH, E. B. HILLS, J. D. HRIBAR, S. HANESSIAN, and T. CHANG. Tetrahedron, **29**, 2707 (1973) and references cited therein.
23. P. J. CLAES, F. COMPERNOLLE, and H. VANDERHAEGE. J. Antibiot. **27**, 931 (1974).
24. K. L. RINEHART, JR. and R. F. SCHIMBOR. *In* Antibiotics biosynthesis. *Edited by* D. Gottlieb and P. D. Shaw. Springer Verlag, Inc., New York. 1967. pp. 359–372, and references cited therein; see also K. L. RINEHART, JR., J. M. MALIK, R. S. NYSTROM, R. M. STROSHANE, S. T. TRUITT, M. TANIGUCHI, J. P. ROLLS, W. J. HAAK, and B. A. RUFF. J. Am. Chem. Soc. **96**, 2263 (1974).
25. C. J. PEARCE, J. E. G. BARNETT, C. ANTHONY, M. AKHTAR, and S. D. GERO. Biochem. J. **159**, 601 (1976).
26. S. N. ROSENTHAL and J. H. FENDLER. Adv. Phys. Org. Chem. **13**, 279 (1976) and references cited therein.
27. A. S. PERLIN, B. CASU, G. R. SANDERSON, and J. TSE. Carbohydr. Res. **21**, 123 (1972).
28. K. L. RINEHART, JR., J. M. MALIK, R. S. NYSTROM, R. M. STROSHANE, S. T. TRUITT, M. TANAGUCHI, J. P. ROLLS, W. J. HAAK, and B. A. RUFF. J. Am. Chem. Soc. **96**, 2263 (1974).
29. H. FUKAMI, K. KITAHARA, and M. NAKAJIMA. Tetrahedron Lett. 545 (1976).
30. R. T. TESTA and B. C. TILLEY. J. Antibiot. **28**, 573 (1975); S. J. DAUM, D. ROSI, and W. A. GOSS. J. Antibiot. **30**, 98 (1977) and references cited therein.
31. W. MEYER ZU RECKENDORF. Chem. Ber. **96**, 2019 (1963).
32. T. H. HASKELL, J. C. FRENCH, and Q. R. BARTZ. J. Am. Chem. Soc. **81**, 3840 (1959).

Aminoglycoside antibiotics: The formation and characterization of dihydrooxazine derivatives in the paromomycin series[1]

STEPHEN HANESSIAN, ROBERT MASSÉ, AND (IN PART) GORAN EKBORG[2]

Department of Chemistry, University of Montreal, Montreal, P.Q., Canada H3C 3V1

Received October 28 1977

STEPHEN HANESSIAN, ROBERT MASSÉ, and GORAN EKBORG. Can. J. Chem. **56**, 1492 (1978).

Treatment of penta-*N*-benzyloxycarbonylparomomycin with benzaldehyde and excess zinc chloride gives a dibenzylidene derivative in high yield. This consists of the 4′,6′-*O*-benzylidene 4‴,6‴-*N*,*O*-benzylidene (dihydrooxazine) derivative of penta-*N*-benzyloxycarbonylparomomycin. Chemical evidence is presented to support this structure and model studies are reported for the formation of dihydrooxazine and oxazolidine derivatives of benzyloxycarbonylamino sugars containing suitably situated hydroxyl groups. The easily obtained dihydrooxazine derivative of paromomycin constitutes an interesting, preferentially blocked derivative, that is useful for the chemical modification of the parent antibiotic.

STEPHEN HANESSIAN, ROBERT MASSÉ et GORAN EKBORG. Can. J. Chem. **56**, 1492 (1978).

Le traitement de la penta-*N*-benzyloxycarbonylparomomycine par la benzaldehyde et un excès de chlorure de zinc donne un dérivé dibenzylidenique avec des hauts rendements. Ce dérivé implique les cycles 4′,6′-*O*-benzylidenique et 4‴,6‴-*N*,*O*-benzylidenique (dihydrooxazinique) de la penta-*N*-benzyloxycarbonylparomomycine. La structure de ce produit a été élucidée par des méthodes chimiques. Des transformations sur des subtrats modèles sont effectuées en vue d'obtenir des dérivés dihydrooxaziniques et oxazolidiniques. Les dérivés ainsi obtenue dans la série de la paromomycine sont des intermédiaires utiles, amenable à des transformations chimiques.

The knowledge that certain enzymes elaborated by bacterial strains carrying resistance transfer factors are capable of inactivating a group of aminoglycoside antibiotics (1) has been an important stimulus for intensive research work directed at the synthesis (2) and chemical modification of these substances (1*c*, 3). The planning of a synthetic sequence aimed at the selective chemical modification at a specific site in these molecules is sometimes hampered by their multifunctional character. There exists, therefore, a crucial need for the development of methods leading to preferentially blocked derivatives within a given series, by which critical portions of a given molecule are temporarily masked by appropriate functionalities, thus exposing other regions for various manipulations. The problem becomes all the more difficult if one considers that, in a large number of aminoglycosides that contain one or more sugars anchored around a 2-deoxystreptamine unit for example, the orientations and relative dispositions of amino and hydroxyl groups are, for the most part, very similar. One may be faced, for example, with the need to effect selective reactions at one vicinal *trans*-diol group in a hexopyranose unit, but not at another, located on a different sugar unit in a given aminoglycoside.

We were interested in probing the chemical reactivities of pairs of amide and alcohol functions having a 1,2- or a 1,3 disposition, in an aminoglycoside antibiotic such as paromomycin (**1**) (4) (Scheme 1) toward aldehydes and ketones, with the object of preparing oxazolidine and dihydrooxazine derivatives. Such derivatives would constitute interesting synthetic intermediates for further chemical modification work. Paromomycin (**1**) contains four sets of amine alcohol functions, two of which are situated on different rings, whereas the other two are in the 2,6-diamino sugar unit (paromose) (5). Previous work (6) has shown that it is possible to prepare a 4′,6′-*O*-benzylidene derivative in high yield by the treatment of *N*-benzyloxycarbonylparomomycin (**2**)

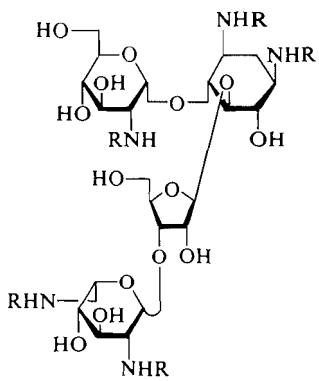

1 R = H, Paromomycin I
2 R = Cbz

SCHEME 1

[1]Taken, in part, from the Ph.D. Thesis submitted by R. Massé, Université de Montréal, Montréal, P.Q., 1975.

[2]Postdoctoral Associate, 1975–1976.

Can. J. Chem. Downloaded from www.nrcresearchpress.com by 210.87.254.5 on 09/05/12
For personal use only.

Can. J. Chem. Downloaded from www.nrcresearchpress.com by 210.87.254.5 on 09/05/12
For personal use only.

with benzaldehyde in the presence of formic acid. Using excess zinc chloride as catalyst, **2** was transformed into a product that contained two benzylidene groups. This compound isolated in over 80% yield was not oxidized by periodic acid in tetrahydrofuran. An acetal spanning a *trans*-diol group in the diamino sugar portion was excluded because of the relative acid stability of the new compound (see below). The possibility of the formation of an oxazolidine of dihydrooxazine ring, spanning favorably situated amide and hydroxyl functions, was therefore contemplated. In view of the existence of several possibilities involving such rings, we deemed it necessary to study the reaction with some model compounds which encompass some of the structural and functional features present in the various units of paromomycin.

Treatment of methyl 4,6-*O*-benzylidene-2-benzyloxycarbonylamino-2-deoxy-α-D-glucopyranoside (7) with benzaldehyde and excess zinc chloride gave back unchanged starting material, indicating the reluctance of the *trans* amide–alcohol system to form an oxazolidine derivative. It was apparent, therefore, that the newly introduced 'acetal' function in **2** did not involve any of the three sets of vicinal *trans*-oriented amide hydroxyl units. On the other hand, treatment of methyl 4,6-*O*-benzylidene-2-benzyloxycarbonylamino-2-deoxy-α-D-allopyranoside (**3**) (8) (Scheme 2) with benzaldehyde and excess zinc chloride gave the corresponding crystalline oxazolidine derivative **4**. It was of interest to study the relative stabilities of the acetal and oxazolidine rings in **4**, as it would be expected that the acetal group would be preferentially cleaved under controlled conditions. Indeed, treatment of **4** with 80% aqueous acetic acid at room temperature effected complete cleavage of the acetal function to give the oxazolidine derivative **5** in high yield. When treated with 50% aqueous formic acid, the latter compound was transformed into methyl 2-benzyloxycarbonylamino-2-deoxy-α-D-allopyranoside (**6**) (8).

Attention was next turned to the formation of *N,O*-benzylidene derivatives of the dihydrooxazine type, spanning three carbon atoms. Methyl 2,6-dibenzyloxycarbonylamino-2,6-dideoxy-α-D-glucopyranoside (**7**), which contains an unreactive *trans*-vicinal amide hydroxyl unit and a potentially reactive unit having a 1,3-disposition at C-4 and C-6, was treated with benzaldehyde and excess zinc chloride (Scheme 2). As anticipated, the corresponding *N,O*-benzylidene derivative **8** was indeed formed, although there remained some unchanged starting material. Treatment of the product with 50% aqueous formic acid gave, as in the previous case, starting compound **7** in good yield.

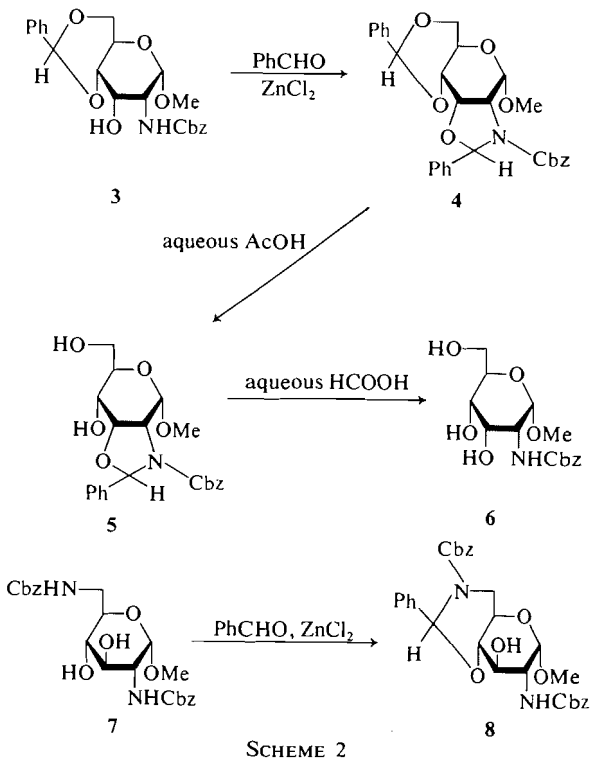

SCHEME 2

Finally, in an effort to simulate the structural and configurational requirements of the diamino sugar unit in paromomycin toward an *N,O*-benzylidenation reaction, a suitable degradation product of the antibiotic was sought as a model. Methanolysis of paromomycin gives, in addition to paromamine (9), the disaccharide glycoside, methyl paromobiosaminide **9** (10) (Scheme 3) in which the D-ribose portion has undergone ring expansion. Aside from this structural variation, however, the diamino sugar unit remains unchanged and should be an excellent model to simulate, as closely as possible, the dihydrooxazine ring forming reaction in the parent antibiotic derivative. Treatment of the *N*-benzyloxycarbonyl derivative of methyl paromobiosaminide (**10**) with benzaldehyde and zinc chloride gave a high yield of a new product to which the structure **11** can be assigned. This product was not oxidized with sodium metaperiodate and upon treatment with aqueous formic acid gave **10** in 70% yield.

Based on the results obtained with the model compounds, it was reasonable to assume that the new product formed in the reaction of **2** or **12** with benzaldehyde and excess zinc chloride was actually the dibenzylidene derivative **14** (Scheme 4). We then proceeded to seek direct chemical proof of this structure and to study some of its properties.

The dihydrooxazine ring formation was dependent on the concentration of zinc chloride, as a minimum

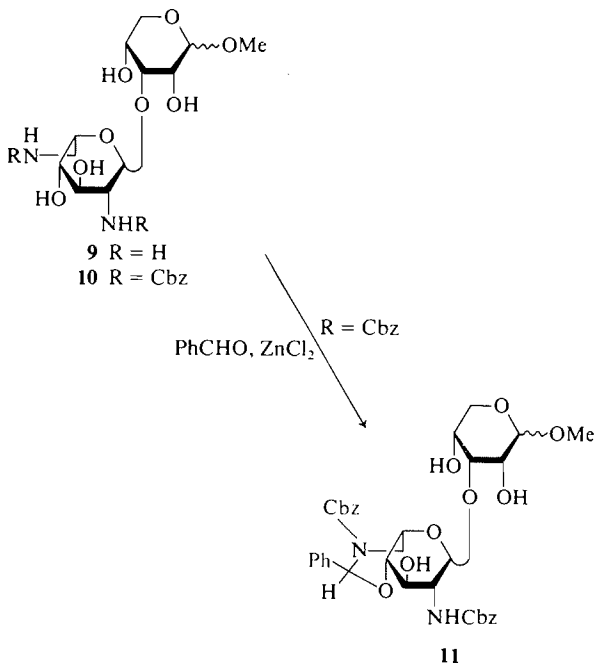

SCHEME 3

of 4 equiv. of the Lewis' acid was needed for complete reaction. With 1 or 2 equiv., the major product was the acetal derivative **12**. Treatment of **12** with benzaldehyde and zinc chloride gave the product **14** which was identical to that obtained from the direct treatment of **2**. *N,O*-Benzylidenation also took place with 4′,6′-*O*-cyclohexylidene-*N*-benzyloxycarbonylparomomycin (**13**) to give **15**. Treatment of **14** and **15** individually with aqueous acetic acid effected selective cleavage of the 4′,6′-acetal group to give the preferentially blocked paromomycin derivative **16**. Treatment with aqueous formic acid at 50°C resulted in the formation of the parent **2** but the reaction was accompanied by extensive degradation, no doubt owing to the presence of the relatively acid-labile *O*-β-D-ribofuranosyl residue. The regeneration of the parent antibiotic, paromomycin, was possible however, under conditions of hydrogenolysis, where the only detectable side product was paromamine.

Unlike their respective precursors, compounds **14** and **15** were not susceptible to periodate oxidation owing to the lack of vicinal diol groups. In previous papers (6, 11), we described a method for the controlled degradation of amino glycoside antibiotics, based on the cleavage, with periodate, of vicinal diol groups situated on C-3,C-4 on amino sugar units, followed by treatment with mild base. This sequence provides not only useful, selectively blocked predisposed amino glycoside fragments for semisynthetic work but with the proper choice of substrates it can lead to pseudodisaccharide and pseudotrisaccharide fragments that can be used as biological probes. Treatment of **16** with 1 equiv. of periodic acid in dry tetrahydrofuran gave a dialdehyde derivative **17**, which was subjected to β-elimination in the presence of triethylamine. Based on its physical characteristics and mode of formation, the product, formed in high yield from the sequence shown in Scheme 5, was assigned structure **18**. Acid hydrolysis with 50% aqueous formic acid gave several products, among which *N*-benzyloxycarbonyl-2-deoxystreptamine and D-ribose were identified by chromatography. Hydrogenolysis in the presence of palladium-hydroxide-on-charcoal (12) gave the known (11) pseudotrisaccharide **19**.

The formation of oxazolidine derivatives in the aminoglycoside series has been demonstrated in the gentamicin group (13), and has been used as supporting evidence for the *cis* disposition of the vicinal methylamino and tertiary hydroxyl groups in the garosamine moiety (14). Thus, on gentle warming in the presence of various aromatic aldehydes in ethanol, gentamicin C_2 is converted into the corresponding oxazolidine Schiff base derivative. The benzylidene analog has been used as an intermediate in the preparation of *N*-benzyl (13) and deoxygenated derivatives (15).

An oxazolidine derivative has also been reported to arise as a by-product in the treatment of penta-*N*-ethoxycarbonylribostamycin with 2,2-dimethoxypropane and *p*-toluenesulfonic acid in DMF at 70°C (16). It is of interest that in this case the oxazolidine ring encompasses the vicinally situated C-1 ethoxycarbonylamino and C-6 hydroxyl groups in the central 2-deoxystreptamine ring, and that these groups bear a *trans* relationship to each other. The instability of such a strained ring is evident from its hydrolytic behavior in the presence of an *O*-isopropylidene group.

Finally, an oxazolidine derivative of *N*-acetylepiinosamine-1 has been prepared in the course of ketal forming reactions, also under forcing conditions (2,2-dimethoxypropane, DMF, TsOH, at 80°C) (17). Because of the *cis* arrangement of the vicinal acetamido and hydroxyl groups, it was possible to selectively hydrolyze an *O*-isopropylidene group in the *O,O*:*N,O*-diisopropylidene derivative of *N*-acetylepiinosamine-1.

To the best of our knowledge, we are not aware of the formation of stable dihydrooxazine derivatives in the aminoglycoside series. Preliminary results have shown that the mild treatment of other aminoglycosides containing benzyloxycarbonylamino and alcohol functions in a 1,3 orientation with benzaldehyde and zinc chloride leads to the formation of the corresponding dihydrooxazine (*N,O*-benzylidene)

Can. J. Chem. Downloaded from www.nrcresearchpress.com by 210.87.254.5 on 09/05/12
For personal use only.

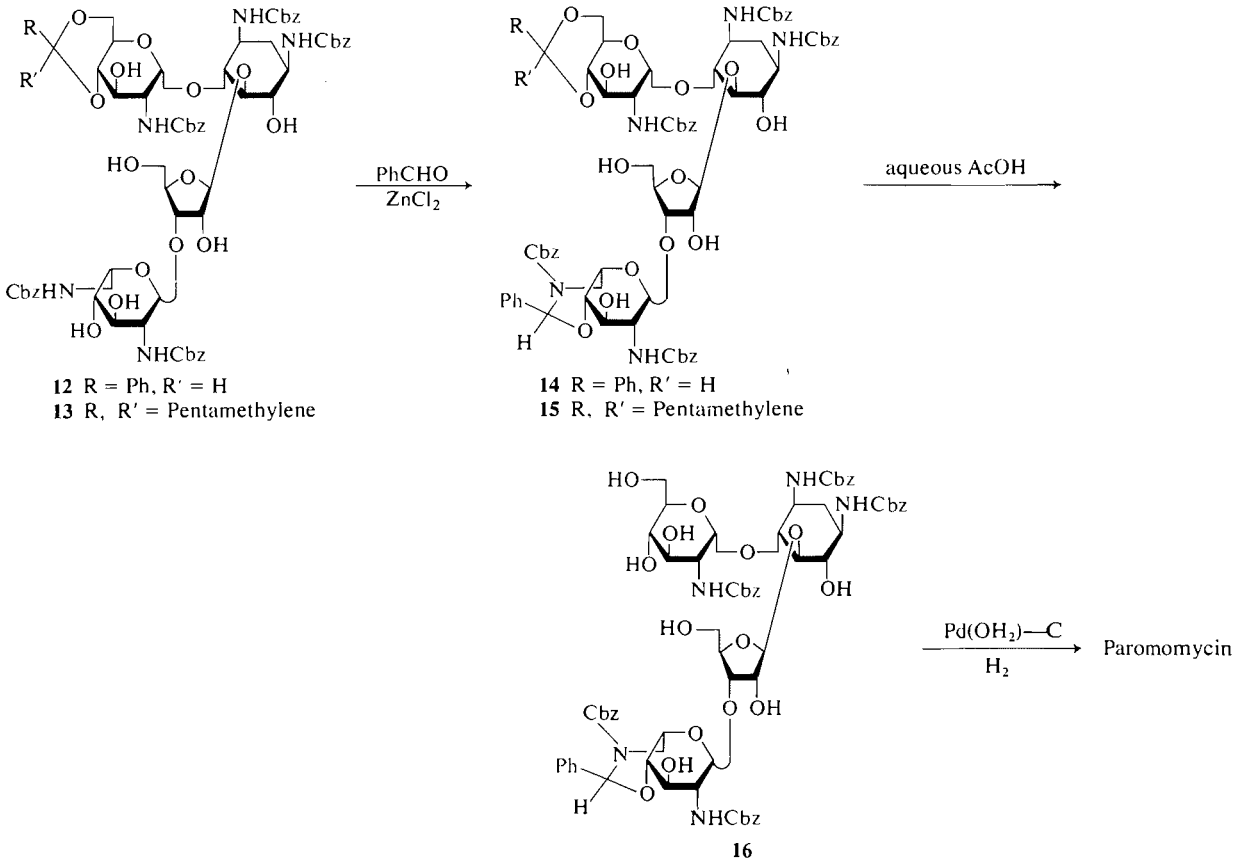

12 R = Ph, R′ = H
13 R, R′ = Pentamethylene

14 R = Ph, R′ = H
15 R, R′ = Pentamethylene

16

SCHEME 4

derivatives. In the paromomycin series, the reaction leads in high yield to a derivative in which the 2,6-diamino-2,6-dideoxy-L-idopyranosyl (paromose) moiety is effectively protected as the O^4,N^6-benzylidene derivative, thus paving the way for modifications at the other rings, particularly the 2-amino-2-deoxy-α-D-glucopyranosyl moiety, which is the site of enzymatic inactivation (1). By treatment with benzaldehyde and excess zinc chloride, it is thus possible to preferentially protect sets of amino alcohol groups in the multifunctional aminoglycosides, depending on their relative dispositions (1,2 or 1,3) and spatial orientations.

Finally, it may be of interest to recall the relative tendencies for the formation of oxazolidine and dihydrooxazine rings from the respective benzyloxy-

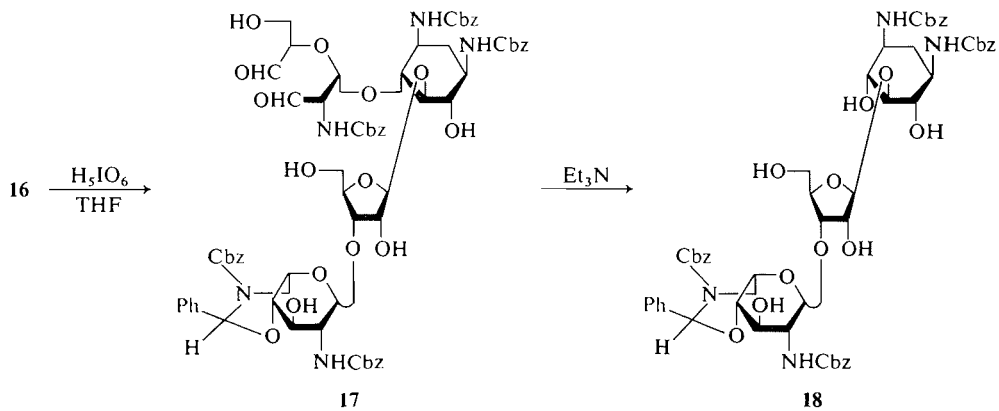

17

18

SCHEME 5

Can. J. Chem. Downloaded from www.nrcresearchpress.com by 210.87.254.5 on 09/05/12
For personal use only.

Can. J. Chem. Downloaded from www.nrcresearchpress.com by 210.87.254.5 on 09/05/12
For personal use only.

TABLE 1. ^{13}C magnetic resonance spectra of paromomycin (**1**), neamine, and methyl nebiosaminide (**9**) (ppm from TMS)[a]

Compound	Ring	Carbon atoms[b] 1	2	3	4	5	6
Paromomycin[c]	A	100.2	56.3	74.4	70.8	73.8	61.6
$pD \geq 11$	B	50.1	36.5	50.1	84.4	82.5	78.3
	C	109.1	74.4	77.0	84.9	62.3	—
	D	100.3	53.6	71.5	69.3	77.0	42.0
Neamine	A	101.9	56.4	74.7	72.5	74.3	42.9
$pD \geq 11$	B	51.5	36.8	50.5	88.5	77.1	78.6
Methyl	C	102.0	69.5	75.3	68.6	64.2	—
neobiosaminide[d]	D	99.5	53.9	71.7	69.5	76.9	42.0
$pD \geq 11$							

[a]Chemical shifts corrected to TMS scale taking δ dioxane as 67.4 ppm.
[b]For simplicity and space conservation, the carbon atoms are not primed; ring A atoms should be singly primed; ring C, doubly primed; and ring D, triply primed, as in the text.
[c]Assignments corroborated by appropriate β-shifts at acid p*D*, and by correlation with model compounds (E. Wenkert and E. W. Hagaman. Private communcation).
[d]The anomeric methoxyl group showed a signal at 56.6 ppm, corresponding to the carbon nucleus of the major α-anomer in the sample.

carbonyl amino and alcohol functions (e.g. **3** → **4**, **7** → **8**, and **10** → **11**).

The moderate yield (34%) and the recovery of unreacted starting material in the conversion of **3** → **4** can be attributed to the high energy of the conformationally biased pyranose ring, as the attachment of a five-membered oxazolidine ring is expected to introduce considerable ring strain. Molecular models show that the hexopyranose ring in **4** is forced into a half-chair conformation as a result of the presence of the oxazolidine ring. The

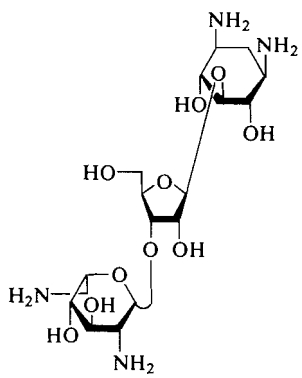

19

exceptionally facile formation of the dihydrooxazine ring in the disaccharide derivative **11** (89%) and in the paromomycin derivatives **14** and **15** (84%) compared to the model compound **8** (54%) is somewhat unexpected. Recent ^{13}Cmr spectroscopic studies (18) have shown that the conformations of methyl D-idopyranosides can depart significantly from the ground state *C*1(D) or 1*C*(D) forms. If the reasonable assumption is made that the 2-amino-2-deoxy-α-D-glucopyranosyl moiety in paromomycin adopts the *C*1(D) conformation, the conclusions derived from ^{13}Cmr data on paromomycin (Table 1) are that the 2,6-diamino-2,6-dideoxy-β-L-idopyranosyl portion adopts a time-averaged conformation that is substantially different than *C*1(L), particularly in the environment of C-2‴—C-4‴. Thus, we find that the chemical shifts of C-1′ and C-1‴ corresponding to the anomeric carbon atoms of the α-D-*gluco* and β-L-*ido* units, respectively, are coincident at $pD \geq 11$, while the signals due to C-2‴, C-3‴, and C-4‴ are at higher field (Δ 2.7, 2.9, and 1.5 Hz, respectively), compared to their C-2′—C-4′ counterparts, indicating quasi-axial orientations approaching a 1*C* form. Comparison of the ^{13}Cmr assignments of the carbon atoms of the diamino sugar portion in methyl neobiosaminide **9** and in neamine (19), respectively, reveal a similar upfield shift for signals associated with C-3—C-4 in the former case, indicating a different conformation (Table 1). It is of interest to recall the ^{1}Hmr studies on penta-*N*-acetylparomomycin by Rinehart *et al.* (20) who found a smaller H-1‴—H-2‴ coupling constant ($J_{1,2}$ = 1.8 Hz) in the 2,6-diamino-2,6-diamino-β-L-idopyranosyl moiety compared to that in the 2-amino-2-deoxy-α-D-glucopyranosyl moiety ($J_{1,2}$ = 3.5 Hz), reflecting a smaller dihedral angle for the vicinally disposed hydrogen atoms in the former sugar. A departure from a *C*1(L) conformation is also evident from periodate oxidation studies (refs. 11, 21, and 10*c*, pp. 29–31), as was originally proposed by Rinehart *et al.* (refs. 21 and 10*c*, pp. 29–31). Assuming that the conformation of the 2,6-diamino sugar moiety in paromomycin and methyl neobiosaminide does not change significantly in the derivatives **2** and **10**, it is not clear why the formation of the corresponding *N*,*O*-benzylidene derivatives is

Can. J. Chem. Downloaded from www.nrcresearchpress.com by 210.87.254.5 on 09/05/12
For personal use only.

more favored compared to a D-*gluco* structure (as in **9**). It is possible that in such a conformation the nucleophilicity of the C-4‴ hydroxyl group toward the benzaldehyde–$ZnCl_2$ complex is enhanced through H-bonding with the carbonyl group of the 2-benzyloxycarbonylamino group. Such an enhancement cannot be envisaged for **7** in its ground state.

Experimental

Melting points are uncorrected. Optical rotations were measured on a Perkin-Elmer automatic spectropolarimeter, model 141. ^1H magnetic resonance spectra were recorded on a JEOL instrument at 60 MHz unless otherwise stated, with tetramethylsilane as internal standard, in deuteriochloroform as solvent. Spectra were not well resolved except in certain regions but were consistent with the structures. ^{13}C magnetic resonance spectra were recorded on a Bruker WH-90 instrument at 22.6 MHz. Mass spectra were recorded on an AEI-902 mass spectrometer at low resolution. Column chromatography was done using silica gel G254, with application of moderate suction.

*Methyl 4,6-*O*-Benzylidene-2,3-*N,O*-benzylidene-2-benzyloxycarbonylamino-2-deoxy-α-*D*-allopyranoside (**4**)*

A mixture containing **3** (340 mg, 0.9 mmol) and anhydrous zinc chloride (408 mg, 3 mmol) in 3 ml of benzaldehyde was stirred at room temperature overnight. The solution was poured into aqueous 10% sodium bicarbonate (200 ml) and extracted with chloroform (2 × 50 ml). The organic phase was processed in the usual manner to give an oily residue, from which excess benzaldehyde was removed by distillation at 50°C under vacuum. The viscous residue solidified after trituration with petroleum ether to give a product that contained the title compound (tlc $CHCl_3$–EtOAc, 10:1), in addition to an appreciable amount of starting material. Separation by thick-layer chromatography gave **3** (115 mg) and the title compound (120 mg). Recrystallization of the latter from 2-propanol – petroleum ether gave 110 mg (34%) of an analytical sample; mp 180–181°C; $[\alpha]_D^{21}$ +117.5° (*c* 0.3, $CHCl_3$); ν_{max} (KBr): 1725 cm^{-1} (C=O). *Anal.* calcd. for $C_{29}H_{29}O_7N$: C 69.17, H 5.80, N 2.78; found: C 69.43, H 6.07, N 2.95.

*Methyl 2,3-*N,O*-Benzylidene-2-benzyloxycarbonylamino-2-deoxy-α-*D*-allopyranoside (**5**)*

The preceding compound (40 mg) was dissolved in 5 ml of 80% aqueous acetic acid and the solution was stirred 12 h at room temperature. Evaporation of the solvent gave a syrupy residue that was triturated with aqueous sodium bicarbonate then with water and finally with petroleum ether. The residual syrup was dissolved in 2-propanol and the solution was diluted with petroleum ether to give the title compound as a colorless amorphous solid that was homogeneous by tlc ($CHCl_3$–EtOAc–MeOH, 25:15:3); yield 28 mg (82%); mp 110–115°C; $[\alpha]_D^{25}$ +189.3° (*c* 0.14, $CHCl_3$); ν_{max} (film): 3450 cm^{-1} (C=O).

Heating a solution of the product (10 mg) in 1.5 ml of 50% formic acid at 50°C for 20 h followed by conventional work-up gave 5.5 mg of methyl 2-benzyloxycarbonylamino-2-deoxy-α-D-allopyranoside (8); mp 79–81°C; $[\alpha]_D^{25}$ +70° (*c* 0.1, MeOH), identical with an authentic sample.

*Methyl 2,6-Dibenzyloxycarbonylamino-2,6-dideoxy-α-*D*-glucopyranoside (**7**)*

A solution containing methyl 6-azido-2-benzyloxycarbonylamino-2,6-dideoxy-α-D-glucopyranoside (**22**) (235 mg, 0.67 mmol) in 40 ml of methanol and 5 ml of water was hydrogenated in the presence of 200 mg of 20% palladium-hydroxide-on-charcoal (12). After 2 h, the catalyst was filtered, the filtrate was evaporated to dryness, and the residue was dissolved in 15 ml of 3:1 aqueous methanol. The solution was treated with 1 ml of benzyloxycarbonyl chloride, 0.5 g of sodium bicarbonate, and the suspension was stirred at 0°C for 10 h. Dilution with a mixture of chloroform and petroleum ether resulted in the precipation of the product, which was filtered and dried; yield 171 mg of an amorphous colorless solid; mp 158–160°C; $[\alpha]_D^{25}$ +37.5° (*c* 0.12, $CHCl_3$).

*Methyl 4,6-*N,O*-Benzylidene-2,6-dibenzyloxycarbonylamino-2,6-dideoxy-α-*D*-glucopyranoside (**8**)*

Anhydrous zinc chloride (150 mg, 1.1 mmol) was added to a solution containing **7** (130 mg, 0.28 mmol) in 2 ml of freshly distilled benzaldehyde and the mixture was stirred at room temperature for 24 h. The solution was poured into 10% aqueous sodium bicarbonate with vigorous stirring and the resulting precipitate was collected by filtration. The filtrate was diluted with petroleum ether to give a sticky solid that was washed with the same solvent by decantation. The remaining solid consisted of a major product, contaminated with a small amount of unreacted starting material (tlc $CHCl_3$–EtOAc, 10:1). Separation by preparative thick-layer chromatography gave the title compound (61 mg, 52% based on recovered starting material). Recrystallization from 2-propanol gave an analytical product; mp 111–112°C; $[\alpha]_D^{27}$ +33° (*c* 0.10, $CHCl_3$). *Anal.* calcd. for $C_{30}H_{32}N_2O_8$: C 65.68, H 5.81, N 5.10; found: C 65.55, H 5.97, N 4.92.

Treatment of the above obtained derivative (15 mg) with 50% aqueous formic acid (50%, 20 h), followed by neutralization with Rexyn 203 (OH^-) and processing as usual, gave methyl 2,6-dibenzyloxycarbonylamino-2,6-dideoxy-α-D-glucopyranoside (7) (10 mg); mp 157–160°C; $[\alpha]_D^{27}$ +36.8° (*c* 0.1, $CHCl_3$).

*Methyl Di-*N*-benzyloxycarbonylparomobiosaminide (**10**)*

Methyl paramobiosaminide dihydrochloride (**9**) (1.2 g), obtained by methanolysis of paromomycin **1** (10), was dissolved in a mixture of water (25 ml) and methanol 10 ml, containing 2.3 g of sodium carbonate. The solution was cooled to 0°C and treated dropwise and with vigorous stirring with 1.41 g of benzyloxycarbonyl chloride. After 30 min, the mixture was left at 0°C for 10 h. Addition of cold water (200 ml) gave a sticky solid that was washed with cold water by decantation. Trituration with petroleum ether gave an amorphous solid that was dissolved in 50 ml of chloroform and the solution was filtered to eliminate a small amount of insoluble material. Evaporation of the solvent and purification by chromatography ($CHCl_3$–EtOAc–MeOH, 20:5:3) gave the title compound as a colorless solid. It was dissolved in chloroform and reprecipitated with petroleum ether; yield 490 mg; mp 230–235°C (foams with dec.); $[\alpha]_D^{27}$ +29.2° (*c* 0.51, $CHCl_3$); this chromatographically homogeneous product was used as such in the next step.

*Methyl 3-*O*-(4,6-*N,O*-Benzylidene-2,6-dibenzyloxycarbonylamino-2,6-dideoxy-β-*L*-idopyranosyl)α,β-*D*-ribopyranoside (**11**)*

A solution containing 200 mg (0.33 mmol) of the preceding compound in 5 ml of freshly distilled benzaldehyde was treated with 328 mg (2.41 mmol) of zinc chloride. After vigorous stirring for 4 h, the solution was added dropwise into 10% aqueous sodium bicarbonate and the resulting colorless precipitate was washed with water, dried, and dissolved in chloroform. The solution was dried with sodium sulfate, filtered, and the filtrate was evaporated to give a syrup that solidified from a mixture of chloroform and petroleum ether;

Can. J. Chem. Downloaded from www.nrcresearchpress.com by 210.87.254.5 on 09/05/12
For personal use only.

yield 205 mg (89%). This product was chromatographically homogeneous (benzene–EtOAc, 1:1). An analytical sample was obtained by preparative thick-layer chromatography; the colorless amorphous product softened at 95–98°C and melted at 105–110°C; $[\alpha]_D^{27}$ +29.7° (*c* 0.16, $CHCl_3$); ^{1}Hmr: 3.36 (s, OCH_3), 6.78 ppm (b, PhCH<N,O>), etc. The product was unaffected by periodic acid in tetrahydrofuran (0°C, 24 h). *Anal.* calcd. for $C_{35}H_{40}O_{12}N_2$: C 61.76, H 5.92, N 4.11; found: C 61.88, H 6.10, N 3.88.

Acetylation of the dihydrooxazine derivative **11** (94 mg) in pyridine and acetic anhydride gave 97 mg (87%) of an amorphous triacetate derivative; mp ~ 112–115°C; $[\alpha]_D^{27}$ +30.9° (*c* 0.41, $CHCl_3$). Nuclear magnetic resonance data indicated the incorporation of three *O*-acetyl groups, as judged from the relative integration of appropriate areas in the spectrum.

Acid Stability of the Dihydrooxazine Derivative ***11***

Acetic Acid

The dihydrooxazine derivative **11** (10 mg) was dissolved in 80% aqueous acetic acid and the solution was left overnight at room temperature. Thin-layer chromatographic examination indicated no change. Heating the solution at 50°C for 24 h also showed unchanged starting material.

Formic Acid

An amount of the dihydrooxazine derivative **11** (35 mg) in 5 ml of 50% aqueous formic acid was heated at 50°C for 19 h, the solution was then treated with Rexyn 203 (OH^-), and processed in the usual manner to give methyl di-*N*-benzyloxycarbonylparomobiosaminide (**10**) 21 mg (70%); $[\alpha]_D^{27}$ +30° (*c* 0.29, $CHCl_3$).

*4′,6′-*O*-Benzylidene-4‴,6‴-*N,O*-benzylidenepenta-*N*-benzyloxycarbonylparomomycin (**14**)*

To a suspension containing 420 mg (0.32 mmol) of penta-*N*-benzyloxycarbonylparomomycin (**2**) (6) in 10 ml of freshly distilled benzaldehyde, was added anhydrous zinc chloride (620 mg, 4.52 mmol) and the mixture was stirred overnight. The mixture was then poured into 100 ml of cold 2% aqueous sodium bicarbonate and the resulting precipitate containing zinc salts was filtered and thoroughly washed with petroleum ether (200 ml), then with methanol. The filtrate, now containing an amorphous precipitate,[3] was diluted with a further 100 ml of petroleum ether. Filtration and washing with the same solvent gave a solid that was dissolved in 100 ml of chloroform containing 3 drops of triethylamine; the solution was concentrated to about 5 ml, then it was diluted with petroleum ether. The resulting colorless precipitate was transformed into a fine powder by vigorous stirring of the mixture. The crude product 370–445 mg (87–98%) consisted of a major component when analysed by tlc ($CHCl_3$–EtOAc–MeOH, 20:5:3). Purification by chromatography on a silica gel (80 g; developed with chloroform, 100 ml, then the above stated tlc solvent) gave 385 mg (84%) of a chromatographically homogeneous solid. The product could be reprecipitated several times from chloroform – petroleum ether, with minimal loss in weight; mp 139–142°C; $[\alpha]_D^{27}$ +31.3° (*c* 4.78, $CHCl_3$). *Anal.* calcd. for $C_{77}H_{83}N_5O_{23}\cdot 1.5H_2O$: C 62.51, H 5.68, N 4.84; found: C 62.76, H 5.68, N 4.75.

The product could also be obtained from 4′,6′-*O*-benzylidenepenta-*N*-benzyloxycarbonylparomomycin (**12**) (6), using essentially the same conditions but only half the volume of benzaldehyde; yield 76%; mp 141–143°C; $[\alpha]_D^{27}$ +30.9° (*c* 3.74, $CHCl_3$).

The product **14** was unaffected when treated with periodic acid in tetrahydrofuran (0°C, 48 h) and it was recovered unchanged (98%).

Treatment with 50% aqueous formic acid (55%, 48 h), followed by neutralization with Rexyn 203 (OH^-) and tlc examination revealed the presence of **2** as the major product. Also present were traces of more polar components resulting from further degradation of the molecule. The parent penta-*N*-benzyloxycarbonylparomomycin (**2**) was subsequently recovered by preparative thick-layer chromatography; $[\alpha]_D^{27}$ +21° (*c* 0.1, $CHCl_3$) (lit. (11) $[\alpha]_D^{27}$ +22.6° ($CHCl_3$)).

*Penta-*N*-benzyloxycarbonyl-4′,6′-*O*-cyclohexylideneparomomycin (**13**)*

A solution containing 616 mg (0.48 mmol) of penta-*N*-benzyloxycarbonylparomomycin (**2**), 21 mg of *p*-toluenesulfonic acid, and 2 ml of 1,1-dimethoxycyclohexane in 20 ml of anhydrous DMF was heated at 45°C under reduced pressure (~20 Torr) for 1 h. The cooled solution was neutralized with Rexyn 253 (OH^-) and the solvent was removed by co-distillation with 1-butanol. The residue was triturated with petroleum ether to give 650 mg (~quantitative) of an amorphous solid, that consisted of a major component (tlc, $CHCl_3$–EtOAc–MeOH, 20:5:3). Purification by chromatography on silica gel, as described in the previous preparation, gave the title compound as a colorless amorphous solid. It was dissolved in chloroform and reprecipitated with hexane; yield 450 mg (68%); mp 124°C (softens), ~145°C (foams); $[\alpha]_D^{27}$ +38.1° (*c* 0.32, $CHCl_3$). *Anal.* calcd. for $C_{69}H_{83}N_5O_{24}$: C 60.65, H 6.12, N 5.12; found: C 60.18, H 6.24, N 5.48.

*4‴,6‴-N,O-Benzylidenepenta-N-benzyloxycarbonyl-4′,6′-O-cyclohexylideneparomomycin (**15**)*

A solution containing 120 mg (0.088 mmol) of **13** in 50 ml of freshly distilled benzaldehyde was treated with anhydrous zinc chloride (435 mg, 3.20 mmol) and the resulting suspension was stirred and processed as described in the preparation of **14**. Chromatography of the crude product (110 mg) gave 95 mg (80%) of the title dihydrooxazine derivative **15**; mp 142–145°C; $[\alpha]_D^{27}$ +30.6° (*c* 3.94, $CHCl_3$). *Anal.* calcd. for $C_{76}H_{87}N_5O_{24}\cdot 0.5H_2O$: C 62.37, H 5.99, N 4.78; found: C 62.44, H 5.54, N 4.58.

The product was not affected by treatment with periodic acid in tetrahydrofuran (0°C, 48 h), whereas the parent **13** was transformed to the corresponding dialdehyde derivative under the same conditions.

Treatment of the product (10 mg) with 50% aqueous formic acid (50°C, 48 h) resulted in the formation of the parent **13** in addition to several degradation products (tlc).

*4‴,6‴-N,O-Benzylidenepenta-N-benzyloxycarbonylparomomycin (**16**)*

*From **14***

A solution containing 198 mg of the dihydrooxazine derivative **14** in 10 ml of 80% acetic acid was stirred at room temperature for 30 h. Evaporation of the solvent gave a colorless syrup that solidified when triturated with cold 1% aqueous sodium bicarbonate. The solid was filtered, washed with water, dried, and redissolved in 20 ml of chloroform. Drying over sodium sulfate, filtration, and evaporation of the solvent gave an amorphous solid that showed a major spot on tlc ($CHCl_3$–EtOAc–MeOH, 20:5:3), yield 165 mg (94%). Purification by thick-layer chromatography gave the title compound as an amorphous colorless solid (from chloroform – petroleum ether); yield 138 mg (79%); mp 143–146°C; $[\alpha]_D^{27}$ +24.7° (*c* 1.04, $CHCl_3$). *Anal.* calcd. for $C_{70}H_{79}N_5O_{24}\cdot 2H_2O$: C 59.60, H 5.64, N 4.96; found: C 59.81, H 5.54, N 5.00.

[3]If a syrup is formed, it is stirred under petroleum ether until it solidifies. Decantation and trituration with cold water will also cause solidification.

From 15

The dihydrooxazine derivative **15** (77 mg) was dissolved in 4 ml of 80% acetic acid, and the solution was stirred at room temperature for 30 h. The product was isolated as described in the preceding section; yield 60 mg (81%); mp 142–146°C; $[\alpha]_D^{27}$ +25° (*c* 0.71, MeOH).

Acid hydrolysis of the product (50 mg) in 50% formic acid (50°C, 24 h), followed by neutralization with Rexyn 203 (OH^-) and chromatography gave penta-*N*-benzyloxycarbonylparomomycin (**2**) (15 mg, 32%); $[\alpha]_D^{27}$ +21° (*c* 0.15, $CHCl_3$), in addition to several degradation products (tlc).

5-O-[3-O-(4,6-N,O-Benzylidene-2,6-dibenzyloxycarbonylamino-2,6-dideoxy-α-L-idopyranosyl)-β-D-ribofuranosyl]-1,3-di-N-benzyloxycarbonyl-2-deoxystreptamine (18)

Periodic acid (5 mg, 2.9 mmol) was added to a solution of the dihydrooxazine derivative **16** (63 mg) in 5 ml of dry tetrahydrofuran. After 24 h at 0°C and 6 h at room temperature, tlc examination indicated the absence of starting material (benzene–EtOAc, 1:1) and the conversion into the dialdehyde derivative **17**; this could be detected as a major component and gave a positive test with the aniline hydrogen phthalate test for aldehydes. The solution was then neutralized with Rexyn 203 (OH^-) and was processed in the usual manner to give a syrup. The latter was dissolved in 2 ml of methanol, 1 ml of triethylamine was added, and the solution was heated at 60°C overnight. Evaporation of the solvent gave a syrup that was purified by chromatography on silica gel ($CHCl_3$, 50 ml, then $CHCl_3$–EtOAc–MeOH, 20:5:3), to give the title compound as an amorphous solid the latter was dissolved in chloroform and reprecipitated with petroleum ether; yield 42 mg (80%); mp 114–116°C; $[\alpha]_D^{27}$ +20.1° (*c* 0.42, $CHCl_3$). *Anal.* calcd. for $C_{56}H_{62}N_4O_{18}$: C 62.32, H 5.79, N 5.19; found: C 62.07, H 5.91, N 5.21.

A portion of the above product (11 mg) was subjected to acid hydrolysis in 50% formic acid (50°C, 24 h); tlc examination revealed the presence of 1,3-di-*N*-benzyloxycarbonyl-2-deoxystreptamine, ribose, and two other unidentified components.

Hydrogenolysis in the presence of 20% palladium-hydroxide-on-charcoal (13) in 1:1 aqueous methanol gave the known (12) pseudotrisaccharide **19**, in addition to a small amount (5–10%, estimated from tlc) of paromamine.

Acknowledgements

We thank the National Research Council of Canada (PRAI Grant) for financial support. We also thank R. Mayer and G. Patil for ^{13}C spectra.

1. (*a*) H. UMEZAWA. Adv. Carbohydr. Chem. Biochem. **30**, 183 (1974); (*b*) R. BENVENISTE and J. JAVIES. Annu. Rev. Biochem. **42**, 471 (1973); (*c*) H. UMEZAWA. *In* Aminoglycoside antibiotics. *Edited by* S. Mitsuhashi. University Park Press, Baltimore, MD. 1974.
2. S. UMEZAWA. Adv. Carbohydr. Chem. Biochem. **30**, 111 (1974).
3. K. E. PRICE, J. C. GODFREY, and H. KAWAGUCHI. Adv. Appl. Microbiol. **18**, 191 (1974).
4. T. H. HASKELL, J. C. FRENCH, and Q. R. BARTZ. J. Am. Chem. Soc. **81**, 3482 (1959).
5. S. HANESSIAN and T. H. HASKELL. J. Org. Chem. **28**, 2598 (1963).
6. T. TAKAMOTO and S. HANESSIAN. Tetrahedron Lett. 4009 (1974).
7. A. B. FOSTER, M. STACEY, and S. V. VARDHEIM. Acta Chem. Scand. **13**, 281 (1959).
8. S. HANESSIAN, R. MASSÉ, and T. NAKAGAWA. Can. J. Chem. This issue.
9. T. H. HASKELL, J. C. FRENCH, and Q. R. BARTZ. J. Am. Chem. Soc. **81**, 3480 (1959).
10. (*a*) T. H. HASKELL, J. C. FRENCH, and Q. R. BARTZ. J. Am. Chem. Soc. **81**, 3481 (1959); (*b*) K. L. RINEHART, JR. and P. W. K. WOO. J. Am. Chem. Soc. **80**, 6463 (1958); (*c*) K. L. RINEHART, JR. The neomycins and related antibiotics. John Wiley & Sons, Inc., New York, NY. 1964.
11. S. HANESSIAN, T. TAKAMOTO, and R. MASSÉ, J. Antibiot. **28**, 835 (1975).
12. W. PEARLMAN. Tetrahedron Lett. 1663 (1967).
13. D. J. COOPER, J. WEINSTEIN, and J. A. WAITZ. J. Med. Chem. **14**, 1118 (1971).
14. D. J. COOPER, M. D. YUDIS, R. D. GUTHRIE, and A. M. PRIOR. J. Chem. Soc. C, 960 (1971).
15. P. J. L. DANIELS, J. WEINSTEIN, R. W. TKACH, and J. MORTON. J. Antibiot. **27**, 150 (1974).
16. S. INOUE, T. TSURUOKA, Y. OGAWA, S. OMOTO, and T. NIIDA. Sci. Rep. Meiji Seika Kaisha, No. 13, 1 (1973).
17. A. HASEGAWA and M. NAKAJIMA. Carbohydr. Res. **29**, 239 (1973).
18. A. S. PERLIN, B. CASU, G. R. SANDERSON, and J. TSE. Carbohydr. Res. **21**, 123 (1972); A. S. PERLIN, B. CASU, and H. J. KOCH. Can. J. Chem. **48**, 2596 (1970); see also A. S. PERLIN. *In* MTP international review of science, organic chemistry series 2. Vol. 7. Carbohydrates. *Edited by* G. O. Aspinall. Butterworths, London, England. 1976. pp. 1–34.
19. P. W. K. WOO and R. D. WESTLAND. Carbohydr. Res. **26**, 522 (1973).
20. K. L. RINEHART, JR., W. S. CHILTON, and M. HICHENS. J. Am. Chem. Soc. **84**, 3216 (1962).
21. K. L. RINEHART, JR., M. HICHENS, A. D. ARGOUDELIS, W. S. CHILTON, H. E. CARTER, M. P. GEORGIADIS, C. P. SCHAFFNER, and R. T. SCHILLINGS. J. Am. Chem. Soc. **84**, 3218 (1962).
22. S. HANESSIAN, D. DUCHARME, R. MASSÉ, and M. L. CAPMAU. Carbohydr. Res. In press.

Can. J. Chem. Downloaded from www.nrcresearchpress.com by 210.87.254.5 on 09/05/12
For personal use only.

Aminoglycoside antibiotics: Synthesis of pseudotrisaccharides derived from neamine and paromamine

STEPHEN HANESSIAN, TOMOYA OGAWA,[1] AND TETSUYOSHI TAKAMOTO[1]

Department of Chemistry, University of Montreal, Montreal, P.Q., Canada H3C 3V1

Received October 28, 1977

STEPHEN HANESSIAN, TOMOYA OGAWA, and TETSUYOSHI TAKAMOTO. Can. J. Chem. **56**, 1500 (1978).

Pseudotrisaccharides of paromamine having a 6-*O*-(β-D-ribofuranosyl) and 6-*O*-(α-D-arabinofuranosyl) moieties were prepared from appropriately *N,O*-substituted derivatives of paromamine by glycosylation reactions. Selective functionalization at C-6′ in 6-*O*-(β-D-ribofuranosyl)paromamine led to the corresponding neamine-containing pseudotrisaccharide. None of these semisynthetic aminoglycosides possessed antibacterial activity, although at least one of them has been shown to be a substrate for the phosphotransferases I and II. The unnatural attachment of a pentofuranosyl moiety at C-6 of the 2-deoxystreptamine unit in these pseudotrisaccharides is, therefore, detrimental to their antibacterial action, unlike amino sugar containing analogs at the same position.

STEPHEN HANESSIAN, TOMOYA OGAWA et TETSUYOSHI TAKAMOTO. Can. J. Chem. **56**, 1500 (1978).

Des pseudotrisaccharides de la paromamine contenant les unités 6-*O*-(β-D-ribofuranosyl) et 6-*O*-(α-D-arabinofuranosyl) ont été préparés à partir des dérivés de la paromamine, par des réactions de glycosylation. Des transformations sélectives ont été effectuées sur la position C-6′ dans la 6-*O*-(β-D-ribofuranosyl)paromamine, menant à un analogue contenant un résidu néamine. Aucun de ses dérivés semisynthétiques s'est avéré avoir des propriétés antibactériennes, quoique au moins un pseudotrisaccharide s'est montré comme substrat à l'action des phosphotransférases I et II. L'attachement nonnaturel d'une unité pentofuranosyl sur C-6 de la 2-deoxystreptamine est au détriment de l'action antibactérienne, contrairement aux analogues qui contiennent un sucre aminé à la même position.

In spite of the large variation in the nature of the sugar units in aminoglycoside antibiotics of the 2-deoxystreptamine type, a unique feature exists in this group of potent antibacterial agents in that the pattern of substitution of the sugar residues is invariably at positions 4,5 and 4,6 of the central cyclitol ring; (see ref. 1 for recent reviews). In the former case, all the known, microbially-derived pseudotrisaccharides have been found to contain a β-D-pentofuranosyl moiety attached at C-5 of the 2-deoxystreptamine ring, the other sugar being, without exception, of the aminodeoxy type. To date, the β-D-*ribo* and β-D-*xylo* configurations have been found, as in the case of ribostamycin (**1**) (2), butirosin B (**3**) (3), antibiotic Bu-1709E$_1$ (**5**) (4), and butirosin A (**2**) (3), and xylostatin (**4**) (5), respectively (Scheme 1). It should be noted that with the exception of the butirosin types, in which the *N*-1 group is acylated with (*S*)-(−)-4-amino-2-hydroxybutyric acid, all these compounds have a common three-ring pseudotrisaccharide structure with only minor variations in the configuration of an isolated hydroxyl group, e.g. C-3 in the β-D-pentofuranosyl unit. It is also important to note that other peripheral modifications involving the exchange of an amino group for hydroxyl or the deoxygenation at a specific site, such as in Bu-1975C$_1$ and C$_2$ (6), may have important consequences at the molecular level. For example, it is known that neamine is more active than paromamine, while ribostamycin **1**, its 6′-hydroxy analog, **6** (7) and xylostatin **4**, its C-3′′ epimer, are of comparable biological activity in an in vitro test, which emphasizes the role of the β-D-pentofuranosyl moiety in these pseudotrisaccharides (8).

In a general program directed toward the synthesis

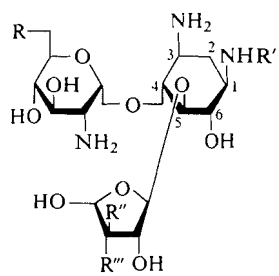

1 (Ribostamycin) R = NH$_2$; R′, R″ = H; R‴ = OH
2 (Butirosin A) R = NH$_2$; R″ = OH; R‴ = H; R′ = L-HABA
3 (Butirosin B) R = NH$_2$; R″ = H; R‴ = OH; R′ = L-HABA
4 (Xylostatin) R = NH$_2$; R′, R‴ = H; R″ = OH
5 (Bu-1709E$_2$) R, R‴ = OH; R″ = H; R′ = L-HABA
6 R,R‴ = OH; R′, R″ = H

SCHEME I

[1]Postdoctoral Associate, 1973–1974.

Can. J. Chem. Downloaded from www.nrcresearchpress.com by 210.87.254.105 on 09/05/12
For personal use only.

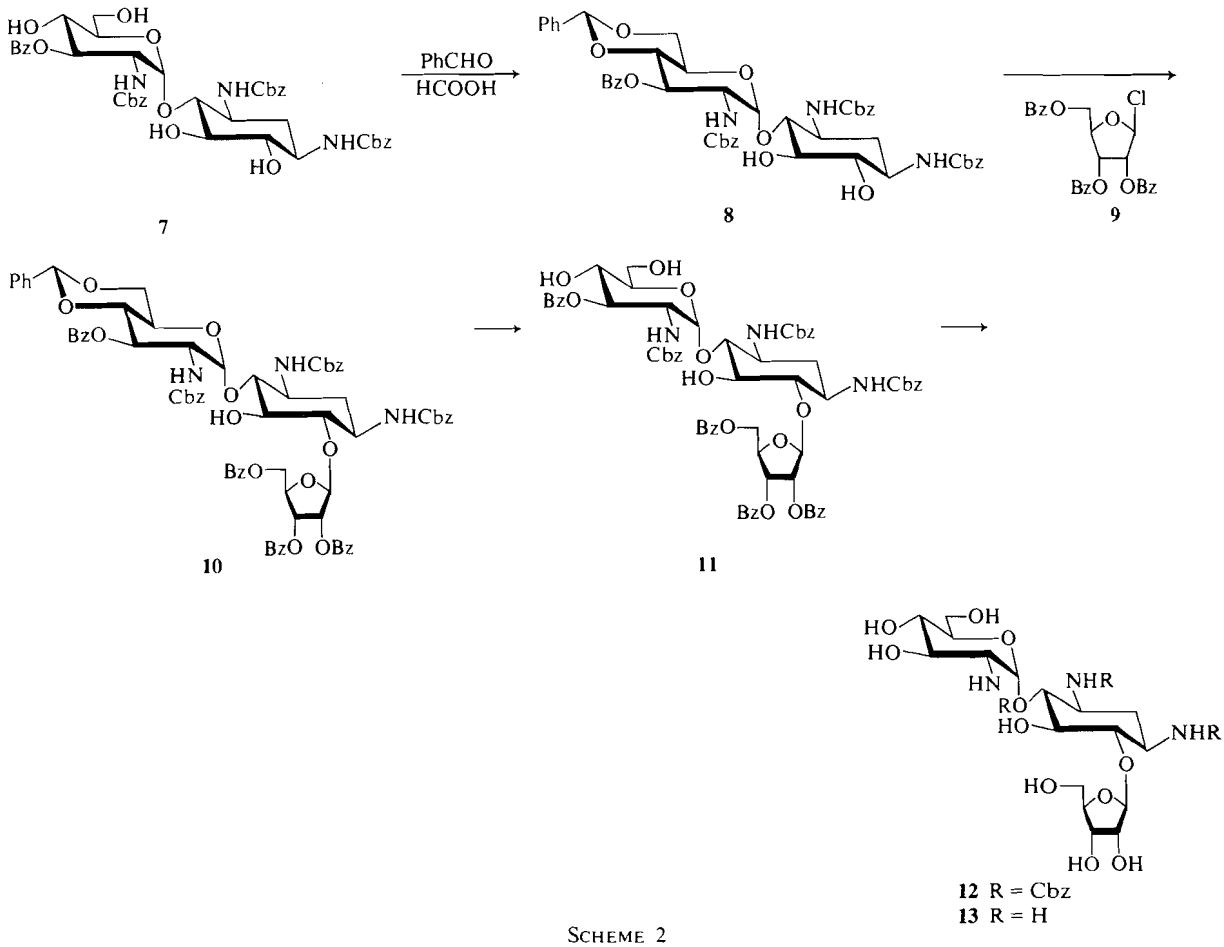

SCHEME 2

and chemical modification of aminoglycoside antibiotics, it was of interest to prepare pseudotrisaccharides derived from paromamine and neamine containing a β-D-ribofuranosyl unit glycosidically attached to the 'unnatural' C-6 position of the 2-deoxystreptamine ring. In this respect, the target compounds would be positional isomers of the naturally occurring ribostamycin and of its bioactive 6-hydroxy analog (7). In a preliminary communication (9), we described the preparation of 6-*O*-(β-D-ribofuranosyl)paromamine, which was also reported by the Farmitalia group (10). We now disclose details of this and related syntheses in this series.

The pseudosaccharides neamine and paromamine, which are readily available from the methanolysis of the respective antibiotics (11, 12), constitute ideal starting materials for semisynthetic work. In this work, paromamine was chosen as the substrate for glycosylation reactions because it lends itself to preferential functionalization in the 2-amino-2-deoxy-D-glucopyranosyl moiety, thus allowing transformations in the 2-deoxystreptamine portion. Furthermore, it was anticipated that pseudotrisaccharides derived from paromamine, could be easily converted into their neamine counterparts by selective transformations at the C-6′ position (13).

The readily available di-*O*-isopropylidene derivative of tri-*N*-benzyloxycarbonylparomamine (14) was benzoylated in the usual manner and the acetal groups were preferentially hydrolyzed to give crystalline 3′-*O*-benzoyl-tri-*N*-benzyloxycarbonylparomamine (**7**) in high yield (Scheme 2). The latter was then transformed into the corresponding 4′,6′-*O*-benzylidene derivative **8** by an adaptation of a procedure used for methyl α-D-mannopyranoside (15). The crystalline derivative **8**, was ideally suited for glycosylation reactions at C-5 and/or C-6 of the 2-deoxystreptamine unit. The readily available 2,3,5-tri-*O*-benzoyl-β-D-ribofuranosyl chloride (**9**) (16) was an obvious derivative for such a reaction as it encompasses the configurational as well as structural features to be found in the target compound. Furthermore, there were ample precedents in the literature for the formation of 1,2-*trans* glycosidic

Can. J. Chem. Downloaded from www.nrcresearchpress.com by 210.87.254.105 on 09/05/12
For personal use only.

Can. J. Chem. Downloaded from www.nrcresearchpress.com by 210.87.254.105 on 09/05/12
For personal use only.

linkages using this glycosyl halide derivative; (see for example, ref. 17). Although the site of *O*-glycosylation was not as predictable, it was anticipated that reaction might occur preponderantly at the C-6 hydroxyl group of the 2-deoxystreptamine moiety of **8**, based mainly on steric considerations. Previous glycosylation reactions of 2-deoxystreptamine had shown that the newly introduced sugar units were attached to the hydroxyl groups situated at C-4 and C-6 (18). Treatment of **8** with the glycosyl halide derivative **9** in the presence of mercuric cyanide as catalyst led to a major product in high yield, which, after chromatographic separation gave the pseudotrisaccharide derivative **10** as an amorphous colorless solid. Proof of homogeneity was secured by further transformations and by comparative reactions with the isomeric pseudotrisaccharide derivative in which the β-D-ribofuranosyl unit was at C-5 of the 2-deoxystreptamine (7).

Preferential hydrolysis of the acetal function of **10** gave the pseudotrisaccharide derivative **11** which had distinctly different chromatographic properties compared to its positional isomer, prepared by oxidative degradation of paromomycin (7). Furthermore, when **10** was subjected to debenzoylation and the resulting product was acetylated, only a derivative corresponding to **10** could be obtained, in which the C-5 hydroxyl group remained free. On the other hand, parallel reactions of the positional isomer corresponding to structure **6**, resulted in complete *O*-acetylation. This behavior can be rationalized on steric grounds as models show that the C-5 hydroxyl group is severely hindered and not readily accessible in derivatives of type **11**. In fact, total di-*O*-acetylation and benzoylation of derivatives such as **8** required unusually severe conditions, compared to analogous acylations of other polyhydroxy compounds (Scheme 3). Monoacetylation of **8**, occurred under very mild conditions to give the corresponding 6-acetate **15**, whereas acetylation under the same conditions of 4′,6′-*O*-benzylidenetri-*N*-benzyloxycarbonylparomamine (**14**) led to the corresponding 3′,6-diacetate derivative **18**. Acylation of **14**, **15**, or **18** under forcing conditions gave the fully *O*-acylated crystalline derivatives **16**, **17**, and **19**. The partially acylated derivatives **15** and **18** could be considered as preferentially protected synthetic intermediates for further reactions at the C-5 hydroxyl group (e.g. glycosylation) although as seen, this position is not too readily accessible.

Preferential hydrolysis of the benzoyl groups in **11** led to the pseudotrisaccharide derivative **12** in good yield. Subsequent removal of the benzyloxycarbonyl groups by hydrogenolysis gave the free pseudotrisaccharide **13** which was isolated as the free base and was found to be different from its positional isomer **6** by chromatography and identical to the product obtained by the Farmitalia group (10). The gross structural features of **13** were established by high resolution mass spectrometry on the corresponding *N*-acetylated *O*-trimethylsilyl derivative (19). The fragmentation patterns of this derivative and those derived from its positional isomer **6** were too similar to allow a differentiation between them. The same observation was made with the corresponding *N*-acetylated *N*,*O*-permethylated derivatives; however the peak at *m/e* 530 corresponding to the loss of a 2,3,5-tri-*O*-methyl-D-ribofuranosyloxy unit from the pseudotrisaccharide derivative was much more prominent in the spectrum of the product derived from **6** compared to that from **13**. Recent studies along these lines on kanamycin analogs allow a distinction to be made regarding the pattern of substitution on the 2-deoxystreptamine ring (20). Unlike its positional isomer **6**, pseudotrisaccharide **13** was found to be inactive against a variety of gram-positive and gram-negative strains in a standard antibacterial assay.[2] Interestingly it was also found to be a good substrate for phosphotransferases I and II, enzymes which are known to inactivate aminoglycoside antibiotics by phosphorylation at the C-3′-hydroxyl group (21).[3]

As previously mentioned, seemingly minor peripheral modifications in the basic molecular architecture of the aminoglycoside molecule may have profound effects on their biological properties. Since neamine was known to be a more effective inhibitor of the in vitro growth of bacteria than its 6′-hydroxy

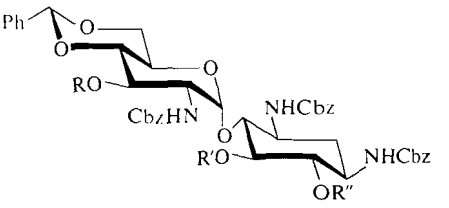

14 R, R′, R″ = H
15 R = Bz; R′ = H; R″ = Ac
16 R = Bz; R′, R″ = Ac
17 R, R′, R″ = Bz
18 R, R″ = Ac; R′ = H
19 R, R′, R″ = Ac

SCHEME 3

[2]The MIC values were 25–100 μg/ml. We thank Dr. H. Baker, Ayerst Laboratories, Montreal, P.Q., for these tests.

[3]We are grateful to Professor J. Davies, University of Wisconsin, for these tests, June 24, 1974.

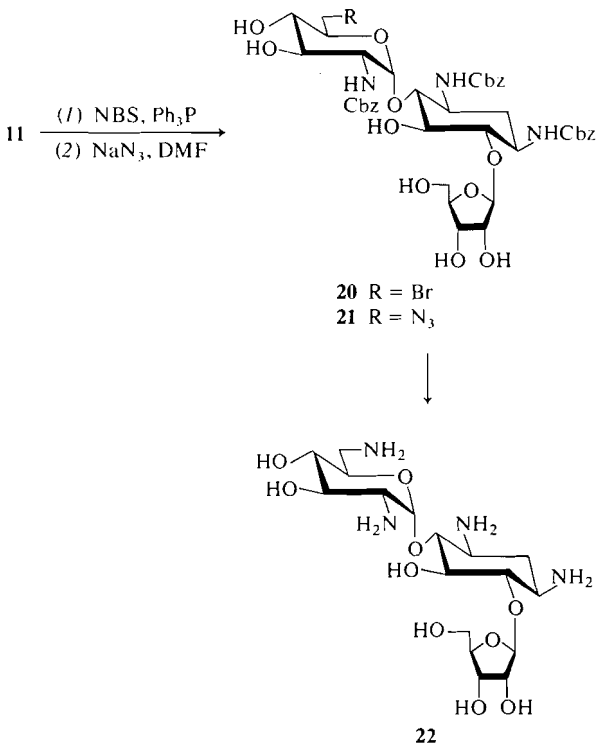

SCHEME 4

analog paromamine, it was of interest to convert the pseudotrisaccharide **13** into its neamine counterpart, i.e. 6-*O*-(β-D-ribofuranosyl)neamine. The *N*,*O*-protected intermediate **11** appeared to be ideally suited as a precursor for such a transformation, which necessitated a selective functionalization of one of two primary hydroxyl groups in the molecules, namely at C-6′. Thus, treatment of **11** with the reagent pair *N*-bromosuccinimide and triphenylphosphine in DMF gave, as previously shown for other polyfunctional molecules (13), including aminoglycosides (22), the selectively brominated derivative **20** in 85% yield (Scheme 4). The potential amino group at C-6′ was introduced via a displacement reaction with sodium azide in DMF in the usual way (83%) and hydrogenolysis of the resulting 6′-azido derivative **21** gave the pseudotrisaccharide **22** as an amorphous solid. The latter had distinctly different chromatographic mobilities compared to its positional isomer, ribostamycin (**1**). Unfortunately, like its precursor **13**, pseudotrisaccharide **22** was devoid of antibacterial activity when tested in the standard in vitro assay. At the time of the completion of this part of our program, the same compound was reported by the Farmitalia group (10), based essentially on the same sequence, namely, preferential glycosylation of a suitable *N*,*O*-protected paromamine derivative at C-6, followed by chemical conversion to the neamine analog via selective sulfonylation and amination. More recently, Suami *et al.* (23), based on our initial observation (9) that 6-*O*-(β-D-ribofuranosyl)paromamine (**13**) was much less active than its isomer **6** (14), have also prepared the neamine containing pseudotrisaccharide **22** by a sequence involving indirect acetylation of *N*,*O*-substituted neamine derivatives at the C-5 and C-6 hydroxyl groups, via several steps from tetra-*N*-ethoxycarbonylneamine and glycosylation of the derived isomer, essentially as previously described for **10**. At this point, it should be mentioned that Ito *et al.* (25) have effected a similar glycosylation reaction between the halide **9** and 3′,4′-di-*O*-benzyl-tri-*N*-benzyloxycarbonylneamine, and have reported the isolation of a major product in moderate yield in which the D-ribofuranosyl moiety was attached to the 5-position of the 2-deoxystreptamine unit. In our studies and those of the Farmitalia group (10), the major products in similar glycosylations were, as already discussed, the 6-*O*-substituted glycosides, with only trace amounts of the isomeric glycosides being found in the crude reaction mixtures. Except for the presence of a 4′,6′-acetal in the 2-amino-2-deoxy-α-D-glucopyranosyl portion of our substrates (e.g. **8**), the remaining structural and functional features are very similar to the neamine derived substrate (25) and it is difficult to rationalize the divergence in the sites of glycosylation. An assessment of these results, particularly in the light of the antibacterial assays, revealed to us that there exists a critical positional requirement with regard to the site of attachment of the pentofuranosyl ring in these pseudosaccharides. It was also evident that the role of functional parameters, such as the presence of a neamine rather than a paromamine containing unit in these compounds was not critical enough at the molecular level to compensate for the adverse effects associated with unnatural attachment of the third ring.

In contrast to cases such as **1**–**6**, where the pentofuranosyl moiety is at position-5 of the pseudodisaccharide, the sugar residue which occurs at position-6 in antibiotics such as kanamycin, are all *cis*-1,2 linked pyranosides. Therefore, it was of interest to find out if the adverse effect of the attachment of a 6-*O*-β-D-pentofuranosyl unit was due to its intrinsic structure or to the presence of the 'unnatural' anomeric configuration. To separate these effects, the synthesis of an 6-*O*-(α-D-pentofuranosyl)paromamine was planned. The D-*arabino* configuration was chosen because of the ready availability of *O*-esterified glycosyl halides in this series which, by virtue of

Can. J. Chem. Downloaded from www.nrcresearchpress.com by 210.87.254.105 on 09/05/12
For personal use only.

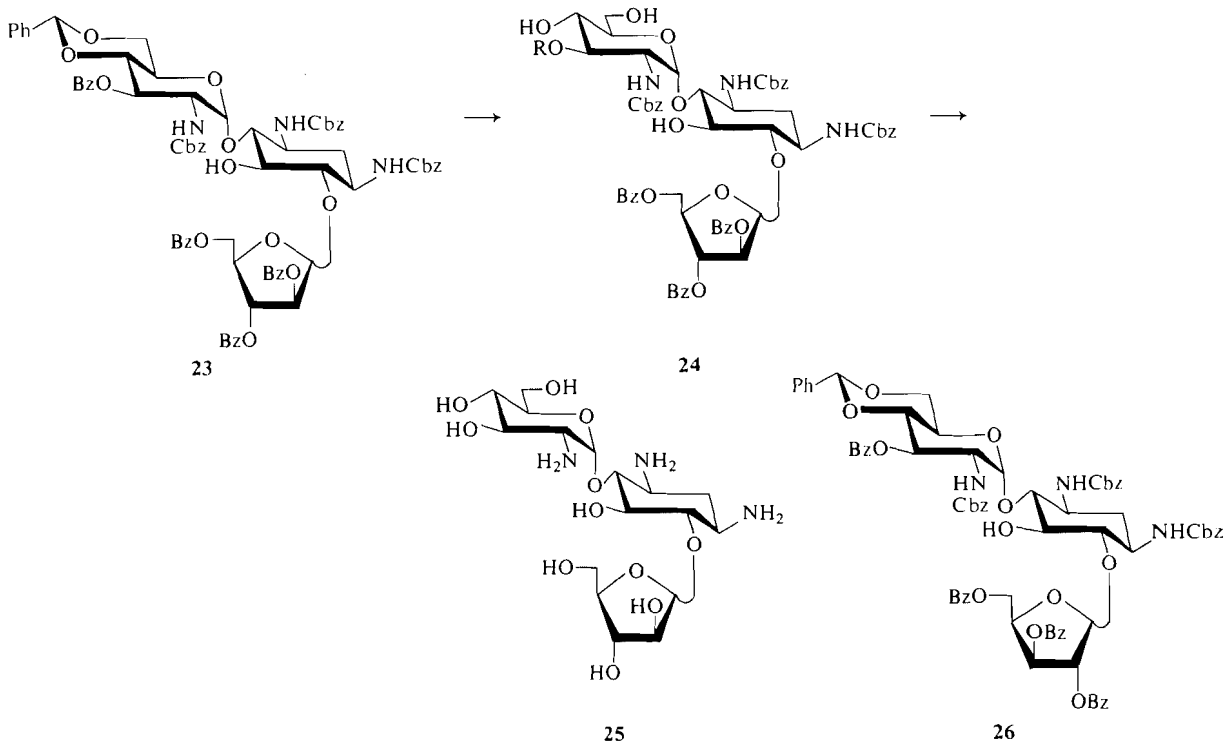

SCHEME 5

neighboring group participation during the glycosylation reaction, would be expected to lead to the desired α-D linkage. Thus, treatment of **8** with 2,3,5-tri-*O*-benzoyl-α-D-arabinofuranosyl bromide in the presence of mercuric cyanide as catalyst, gave the corresponding glycoside **23** in 50% yield (Scheme 5). Once again acylation reactions were found to be extremely slow, as in the D-*ribo* analog **10**. Removal of the 4′,6′-acetal group led to the derivative **24**, isolated as a chromatographically homogeneous solid. Debenzoylation followed by hydrogenolysis gave the desired 6-*O*-(α-D-arabinofuranosyl)paromamine (**25**) as an amorphous solid. Its gross structural features were estabilshed by mass spectral analysis of the corresponding *N*-acetylated *O*-trimethysilyl derivative. The pseudosaccharide **25** was found to be devoid of antibacterial activity. In this context, it is of interest that Suami *et al.* (23) have extended their glycosylations to include 6-*O*-α- and -β-D-glucopyranosyl and galactopyranosyl derivatives of neamine. As expected, only the α-D series showed activity, which emphasizes the role of *ring size and anomeric configuration* in conjunction with sites of attachment of sugars to 2-deoxystreptamine. Finally, the synthesis of a pseudotrisaccharide derivative **26**, containing the β-D-xylofuranosyl moiety at C-6 was also accomplished. However, in view of the results of biological testing on the analogs **13**, **22**, and **27**, it was not converted into the free pseudotrisaccharide, which would be a positional isomer of xylostatin (5).

In conclusion, it is evident, that the presence of at least one amino group in the sugar moiety at C-6 in neamine–paromamine type aminoglycosides is an important functional prerequisite for attaining acceptable thresholds of antibacterial activity as is the case with the naturally occurring kanamycins, gentamicins, and related aminoglycosides.

Experimental

Melting points are uncorrected. Optical rotations were measured on a Perkin-Elmer automatic spectropolarimeter, model 141. ^{1}H magnetic resonance spectra were recorded on a Jeol instrument at 60 MHz, unless otherwise mentioned, with tetramethylsilane as internal standard in deuteriochloroform as solvent. Mass spectra were recorded on an AEI-902 mass spectrometer, at low and high resolution. Reference material in peak matching experiments was tris(pentadecafluoroheptyl)-*s*-triazine, the exact mass of the $C_{13}F_{23}N_2$ ion being taken as *m/e* 620.9693. Column chromatography was done using silica gel G254, with application of moderate suction.

*4′,6′-O-Benzylidenetri-N-benzyloxycarbonylparomamine (**14**)*

To a suspension containing tri-*N*-benzyloxycarbonylparomamine (**7**) (9) (0.5 g) in 4.2 ml of freshly distilled benzaldehyde, was added 98% formic acid (1.7 ml). After 30 min the mixture was transformed into a gelatinous mass which was kept at room temperature for 24 h, after which time it was poured into aqueous sodium bicarbonate. Addition of petroleum ether with vigorous stirring resulted in the precipitation of the product, which was filtered and washed successively with aqueous bicarbonate, water, and finally with

Can. J. Chem. Downloaded from www.nrcresearchpress.com by 210.87.254.105 on 09/05/12
For personal use only.

Can. J. Chem. Downloaded from www.nrcresearchpress.com by 210.87.254.105 on 09/05/12
For personal use only.

petroleum ether. Recrystallization from a mixture of tetrahydrofuran and methanol gave the title compound, 427 mg (76%); mp 299–300°C (dec.); $[\alpha]_D^{20}$ +52.8° (*c* 0.1, dioxane); R_f 0.29 (tlc, $CHCl_3$–EtOAc–MeOH, 20:50:1). *Anal.* calcd. for $C_{43}H_{47}N_3O_{13}$: C 63.46, H 5.82, N 5.16; found: C 63.22, H 5.68, N 5.02.

3′,5,6-Tri-O-*acetyl-4′,6′*-O-*benzylidenetri*-N-*benzyloxycarbonylparomamine* (**19**)

A mixture containing **14** (100 mg) in pyridine (2 ml) and acetic anhydride (0.1 ml) was heated at 100–105°C for 4 h, and the solution was concentrated under reduced pressure. The residue was recrystallized from a mixture of chloroform, ethanol, and petroleum ether, to give the title compound (99 mg, 86%); mp 270–272°C; $[\alpha]_D^{25}$ +36.1° (*c* 1.0, dioxane); R_f 0.71 (tlc, $CHCl_3$–EtOAc–MeOH, 20:5:1). *Anal.* calcd. for $C_{49}H_{53}N_3O_{16}$: C 62.62, H 5.64, N 4.50; found: C 62.46, H 5.69, N 4.34.

3′,5,6-Tri-O-*benzoyl-4′,6′*-O-*benzylidenetri*-N-*benzyloxycarbonylparomamine* (**17**)

A solution containing 1 g of **7** in 20 ml of dry pyridine was treated with benzoyl chloride (3 ml) at 0°C. The solution was stirred at room temperature for 2 h, and then at 45–50°C for 3 days, when tlc examination indicated that esterification was complete. Water (0.5 ml) was added and after standing for 1 h, the solution was poured into ice-water. Extraction with dichloromethane and processing of the organic phase as usual, gave a syrup (1.6 g) which crystallized from a mixture of toluene and pyridine. Recrystallization from chloroform and ether gave the title compound (1.2 g, 87%); mp 227–230°C; $[\alpha]_D^{20}$ +22.4° (*c* 0.5, $CHCl_3$). *Anal.* calcd. for $C_{64}H_{59}N_3O_{16}$: C 68.28, H 5.28, N 3.73; found: C 68.12, H 5.14, N 3.50.

Selective hydrolysis of the acetal function was affected in a 4:1 acetic acid–water solution, at 80–85°C for 5.5 h. Chromatographic separation (toluene – ethyl acetate, 4:1) gave 3′,5,6-tri-*O*-benzoyltri-*N*-benzyloxycarbonylparomamine as a syrup, ~90%.

3′,6-Di-O-*acetyl-4′,6′*-O-*benzylidenetri*-N-*benzyloxycarbonylparomamine* (**18**)

A mixture of **14** (80 mg), acetic anhydride (0.1 ml), and pyridine (2 ml) was left at 5°C overnight; the solvent was co-distilled with toluene and the residue was triturated with a mixture of tetrahydrofuran and acetone to give the title compound as an amorphous, chromatographically homogenous solid (75 mg, 85%); mp 269–275°C (dec.); $[\alpha]_D^{25}$ +36.0° (*c* 1, dioxane); R_f 0.51 (tlc, $CHCl_3$–EtOAc–MeOH, 20:5:1). Acetylation of this product under forcing conditions (100°C, 4 h) gave the crystalline triacetate **19** (quantitative).

3′-O-*Benzoyltri*-N-*benzyloxycarbonylparomamine* (**7**)

To a solution containing tribenzyloxycarbonyl-4′,6′:5,6-di-*O*-isopropylideneparomamine (**14**) (2.65 g) in 14 ml of dry pyridine was added benzoyl chloride (1.1 ml) with cooling and stirring. The reaction mixture was diluted with chloroform after standing at room temperature overnight and the solution was washed with aqueous bicarbonate, then with water. Drying the organic phase and evaporation gave a syrup that solidified when triturated with petroleum ether. The benzoylated intermediate was dissolved in 75 ml of 80% acetic acid and after stirring at room temperature for 27 h, water was added to give the title compound; yield 2.4 g. Recrystallization from ethanol gave an analytical sample (2.3 g, 95%); mp 247–248°C; $[\alpha]_D^{20}$ +91.6° (*c* 1, DMF). *Anal.* calcd. for $C_{37}H_{43}N_3O_{13}$: C 60.23, H 5.87, N 5.7; found: C 60.05, H 5.87, N 5.62.

6-O-*Acetyl-3′*-O-*benzoyl-4′,6′*-O-*benzylidenetri*-N-*benzyloxycarbonylparomamine* (**15**)

Acetylation of **8** (50 mg) as described above gave the title compound as a chromatographically homogenous solid; mp 257–264°C; $[\alpha]_D^{25}$ +34.6° (*c* 1, dioxane); R_f 0.53 (tlc, $CHCl_3$–EtOAc–MeOH, 20:5:1). Acetylation of this product under forcing conditions gave the crystalline diacetate derivative **16** (quantitative).

5,6-Di-O-*acetyl-3′*-O-*benzoyl-4′,6′*-O-*benzylidenetri*-N-*benzyloxycarbonylparomamine* (**16**)

A mixture containing **8** (28 mg), acetic anhydride (0.05 ml), and pyridine (1 ml) was heated at 100–110°C for 5 h with stirring. Co-distillation of the solvent with toluene gave a residue which was triturated with ethanol and the solution evaporated to give a solid. Recrystallization from a mixture of chloroform and ethanol, gave the title compound (21 mg, 64%) as needles; mp 289–291°C (dec.); $[\alpha]_D^{20}$ +21.6° (*c* 1, dioxane); R_f 0.33 (tlc, benzene–2-butanone, 3:1); R_f 0.81 ($CHCl_3$–EtOAc–MeOH, 20:5:1). *Anal.* calcd. for $C_{54}H_{55}N_3O_{16}$: C 67.74, H 5.49, N 4.20; found: C 64.84, H 5.56, N 4.00.

3′-O-*Benzoyl-4′,6′*-O-*benzylidenetri*-N-*benzyloxycarbonylparomamine* (**8**)

A suspension of **7** (2.5 g) in freshly distilled benzaldehyde (20 ml), was treated with 4 ml of 98% formic acid, after which the solution became clear and homogenous. After stirring for 1 h, a gelatinous mass was obtained and was left at room temperature for 27 h. Pouring into aqueous bicarbonate and dilution with petroleum ether gave the title compound as a solid (2.36 g), which was filtered and washed as previously described. Dissolution of the product in tetrahydrofuran followed by addition of acetone gave the title compound as a chromatographically homogenous colorless solid; yield 2.2 g (81%); $[\alpha]_D^{2}$ +44.3° (*c* 1, dioxane); R_f 0.4 (tlc, $CHCl_3$–EtOAc–MeOH, 15:5:1). This material was suitable for use in subsequent transformations.

6-O-*(2,3,4-Tri*-O-*benzoyl*-β-D-*ribofuranosyl)-3′*-O-*benzoyl-4′,6*-O-*benzylidenetri*-N-*benzyloxycarbonylparomamine* (**10**)

Mercuric cyanide (2 g) and calcium sulfate (5 g) were added to a solution of **8** (1 g, previously dried by azeotropic removal of traces of water with DMF) in a mixture of DMF (10 ml) and 1,2-dichloroethane (30 ml). To the stirred suspension was added a solution of 2,3,5-tri-*O*-benzoyl-β-D-ribofuranosyl chloride (**9**), prepared from 2 g of the corresponding 1-acetate derivative (**26**), in 5 ml of 1,2-dichloroethane. After stirring the mixture at 50°C for 18 h, it was filtered through a bed of Celite (this latter having been well washed with dichloromethane) and the pooled filtrates and washings were extracted with aqueous bicarbonate, then with water. Processing of the organic phase as usual gave a syrup which solidified upon trituration with di-2-propyl ether. Filtration of the solid and washing with the same solvent gave the title compound; yield 1.35 g (91%). The product exhibited one major spot on tlc (toluene – ethyl acetate, 3:2, R_f ~0.65). A portion of the product was dissolved in a 4:1 mixture of carbon tetrachloride and acetone, and the solution was poured through a short column of silica gel. Elution with a 3:1 mixture of the same solvents, followed by isolation and reprecipitation from a mixture of dichloromethane and di-2-propyl ether gave an analytical sample; mp 278–279°C; $[\alpha]_D^{20}$ +26.8° (*c* 1, dioxane). *Anal.* calcd. for $C_{76}H_{71}N_3O_{21}$: C 67.00, H 5.25, N 3.09; found: C 66.77, H 5.02, N 3.15.

Attempts to acylate the above product were not successful, and starting material was recovered without loss; e.g. acetic anhydride in pyridine, 25°C, 5 days; benzoyl chloride in pyridine, 25°C, 65 h. A portion of the product (100 mg) was treated with sodium methoxide in a mixture of methanol and

Can. J. Chem. Downloaded from www.nrcresearchpress.com by 210.87.254.105 on 09/05/12
For personal use only.

dichloromethane. After standing overnight, acetic acid was added to p*H* ~ 5 and the solution was evaporated to dryness to give a chromatographically homogenous product, mp > 250°C, corresponding to the debenzoylated analog of **10**. This product had the same chromatographic mobility as its positional isomer derived from **6** (24); tlc, $CHCl_3$–EtOAc–MeOH, 15:5:4. Acetylation of the two products, individually (acetic anhydride, pyridine, 25°C, 5 days) gave distinctly different acetylated products owing to a total *O*-acetylation in the case of the 5-*O*-(β-D-ribofuranosyl) derivative and only partial acetylation in the case of the positional isomer because of the sterically hindered C-5 hydroxyl group in the latter. Benzoylation (25°C, 65 h) led to the same results.

*6-O-(2,3,5-Tri-*O*-benzoyl-*β*-D-ribofuranosyl)-3′-O-benzoyltri-*N*-benzyloxycarbonylparomamine (**11**)*

Compound **10** (1.34 g) was dissolved in a mixture of acetic acid (40 ml), dioxane (20 ml), and water (10 ml), and the solution was stirred at 50–55°C for 4 days. Evaporation gave a syrup, that was chromatographed on short silica gel column ($CHCl_3$). The fractions containing the major component were combined and evaporated to a syrup. Trituration with dichloromethane – di-2-propyl ether gave the title compounds as a chromatographically homogenous solid; yield 760 mg (64%); mp 242–243°C; $[\alpha]_D^{20}$ +52.8° (*c* 0.75, dioxane); tlc (toluene–EtOAc–MeOH, 15:10:3), R_f ~ 0.55. The product was suitable for transformations without further purification. A portion was subsequently purified by preparative thick-layer chromatography. *Anal.* calcd. for $C_{69}H_{67}N_3O_{21}$: C 65.03, H 5.30, N 3.30; found: C 64.68, H 5.23, N 3.13.

*6-O-(β-D-ribofuranosyl)tri-*N*-benzyloxycarbonylparomamine (**12**)*

A solution containing 300 mg of the preceding compound in 5 ml of dichloromethane was treated with a 0.1 solution of sodium methoxide in methanol (12 ml). After standing at room temperature overnight, the solution was treated with aqueous acetic acid to p*H* 5 and the solvents were removed under reduced pressure. Trituration of the residue with aqueous methanol gave the title compound as a chromatographically homogenous solid; yield 200 mg (98%); mp 260–265°C (dec.); $[\alpha]_D^{20}$ +41.4° (*c* 0.5, DMF). *Anal.* calcd. for $C_{41}H_{51}N_3O_{17}$: C 57.40, H 5.99, N 4.90; found: C 57.44, H 5.95, N 4.77.

*6-O-(β-ribofuranosyl)paromamine (**13**)*

A mixture containing 135 mg of **12** and 100 mg of 20% palladium-hydroxide-on-charcoal (27) in 30 ml of methanol–dioxane (2:1) was hydrogenated in the presence of 0.48 ml of *N* HCl. After 1 h, mixture was diluted with 10 ml of water and hydrogenation was continued for an additional 2 h. The suspension was filtered, the filtrate was treated with Rexyn 203 (OH^-), and the neutralized solution was processed as usual to give a colorless solid; yield 55 mg (77%). The product was chromatographically homogenous in several solvent systems; R_f 0.47; tlc, ($CHCl_3$ – MeOH – 28% NH_4OH, 1:3:2); $R_{paromamine}$ 1.00; paper chromatography (1-PrOH–pyridine–H_2O–AcOH, 15:10:12:3) $R_{paromamine}$ 1.24. The product could be precipitated from aqueous solution (minimum volume) by the addition of methanol or ethanol; mp 174–175°C (sintering at 145°C); $[\alpha]_D^{20}$ +34.2° (*c* 1, H_2O). As the free base, the product had a tendency to absorb variable amounts of carbonic acid depending on the periods of exposure to air. Its chromatographic properties were not altered however. For further characterization, a sample (2 mg) of the free base was acetylated (acetic anhydride in pyridine, 25%, 6 days), the product was treated with sodium methoxide, and the resulting *N*-acetyl derivative was *O*-silylated according to a previously described standard procedure (19), to give the *N*-acetyl *O*-trimethylsilyl derivative which was analyzed by high resolution mass spectrometry; *m/e* calcd. for a $C_{30}H_{63}N_3O_{10}Si_4$ fragment (containing the deoxystreptamine and D-glucosamine portions): 737.3590; found: 737.3586; *m/e* calcd. for a $C_{27}H_{57}N_2O_8Si_4$ fragment (deoxystreptamine, ribose): 649.3192; found: 649.3198, corresponding to the following fragments.

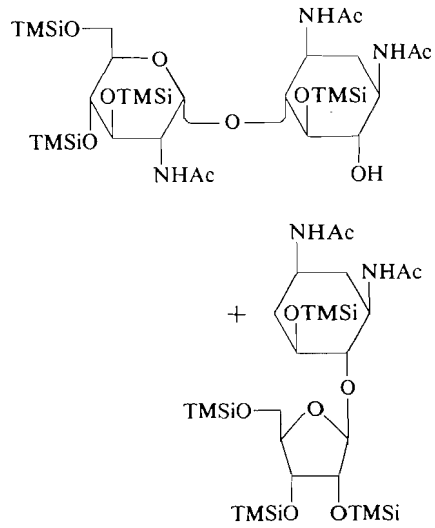

The mass spectral data of the corresponding tri-*N*-acetyl-*N*,*O*-permethyl derivative was also in accord with the gross structure, *m/e* 260 (D-glucosaminyl portion); *m/e* 175 (D-ribofuranosyl portion); *m/e* 530 (paromamine portion with loss of D-ribofuranosyloxy moiety), etc.

*6-O-(2,3,5-Tri-*O*-benzoyl-*β*-D-ribofuranosyl)-3′-O-benzoyl-6′-bromo-6′-deoxytri-*N*-benzyloxycarbonylparomamine (**20**)*

A solution containing 500 mg (0.4 mmol) of **20** (previously dried by azeotropic removal of traces of moisture with DMF at 110°C) and 330 mg (1.25 mmol) of triphenylphosphine in 15 ml of dry DMF was treated at 0°C and with stirring, with 125 mg (1.2 mmol) of *N*-bromosuccinimide. The solution was heated at 50°C for 3 days. After cooling, methanol (2 ml) was added to destroy excess halogenating reagent and the solution was evaporated under reduced pressure by co-distillation with 1-butanol. The residue was triturated with ether several times, until the remaining solid contained no more triphenylphosphine oxide. This solid (460 mg) was dissolved in 30 ml of chloroform and the solution was added to a short column (1.5 × 2.5 cm) containing silica gel. Elution with chloroform gave the title compound as a chromatographically homogenous colorless solid; yield 427 mg (85%); mp 215–218°C; $[\alpha]_D^{20}$ +64.0° (*c* 0.5, DMF). *Anal.* calcd. for $C_{69}H_{60}N_3O_{20}Br$: C 61.98, H 4.98, N 3.14; found: C 61.77, H 5.45, N 2.96.

*6-O-(β-D-Ribofuranosyl)-6′-azido-6′-deoxytri-*N*-benzyloxycarbonylparomamine (**21**)*

The preceding compound (370 mg) was dissolved in dry DMF (10 ml), sodium azide (200 mg) was added, and the mixture was heated at 100°C overnight. Evaporation of the solvent to a small volume, followed by a pouring in the water, gave a solid (300 mg, 83%); mp 213–215°C; this corresponded to the 6′-azido analog of **21**, which was suitable for use in the next step. Debenzoylation of this product in the presence of 0.5 *N* sodium methoxide in methanol (20 ml), followed by neutralization with aqueous acetic acid, evaporation, and

Can. J. Chem. Downloaded from www.nrcresearchpress.com by 210.87.254.105 on 09/05/12
For personal use only.

trituration of the residue with water, gave a colorless solid; yield 170 mg (83%). The product was chromatographically homogenous; tlc ($CHCl_3$–EtOAc–MeOH, 15:5:3) R_f 0.5; mp 233–237°C (dec.); $[\alpha]_D^{20}$ +48.4° (*c* 0.62, DMF); ν_{max} (KBr): 2100 cm^{-1}, N_3. *Anal.* calcd. for $C_{41}H_{50}N_6O_{16}$: C 39.41, H 4.03, N 6.72; found: C 39.22, H 4.15, N 6.42.

6-O-(β-D-Ribofuranosyl)neamine (22)

The preceding compound (128 mg) was hydrogenated in a 1:2 dioxane–methanol (30 ml) containing 0.7 ml of *N* HCl in the presence of 20% palladium-hydroxide-on-charcoal (100 mg). After 1 h, water (10 ml) was added and the hydrogenation was continued for 2.5 h. After filtration and processing of the filtrate as described for **13**, there was obtained a chromatographically homogeneous colorless solid (68 mg). The product was dissolved in a small volume of methanol and precipitated with ethanol to give the amorphous title compound; mp ~ 140°C (dec.); $[\alpha]_D^{20}$ +27.0° (*c* 0.5, H_2O); R_f 0.41 (tlc, $CHCl_3$–MeOH–NH_4OH, 1:3:2); R_f of ribostamycin, 0.35; R_f of **13**, 0.47 (lit. (23) mp 140°C (dec.); $[\alpha]_D^{20}$ +33.0° (H_2O); lit. (10) mp 175°C; $[\alpha]_D^{20}$ +33.0° (H_2O)). The corresponding *N*-dinitrophenyl derivative was obtained as follows. The product (50 mg) in 2.5 ml of water was treated with 50 mg of sodium bicarbonate followed by 20 mg of 2,4-dinitrofluorobenzene dissolved in 1.5 ml of ethanol. After stirring for 22 h, water (10 ml) was added and the resulting yellow solid was collected by filtration. The product was dissolved in dioxane and reprecipitated by the addition of ethanol and water; yield 65 mg; mp 195–198°C (dec.); $[\alpha]_D^{20}$ +186.6° (*c* 0.5, DMF); R_f 0.63 (tlc, $CHCl_3$–EtOAc–MeOH, 3:2:1).

6-O-(2,3,5-Tri-O-benzoyl-α-D-arabinofuranosyl)-3′-O-benzoyl-4′,6′-O-benzylidenetri-N-benzyloxycarbonylparomamine (23)

To a suspension containing **8** (1 g), mercuric cyanide (2 g) calcium sulfate (5 g) in 10 ml of DMF, and 30 ml of 1,2-dichloroethane was added a solution of 2,3,5-tri-*O*-benzoyl-α-D-arabinofuranosyl bromide (prepared from 2 g of the corresponding methyl glycoside by treatment with 10:1 acetic acid – acetic anhydride saturated with hydrogen bromide) in 10 ml of 1,2-dichloroethane. The mixture was stirred at 55°C for 18 h; it was then diluted with dichloromethane and the suspension was filtered through a layer of Celite. The filtrate was washed with aqueous bicarbonate, then with water. Processing of the organic phase in the usual manner gave a solid (1.15 g) which showed a major spot on tlc (toluene–EtOAc, 3:2). Further purification was achieved by chromatography on silica gel with chloroform as eluent. The title compound was thus obtained as a colorless amorphous solid. It was dissolved in dichloromethane and precipitated with di-2-propyl ether; yield 740 mg (50%); mp 238–241°C; $[\alpha]_D^{20}$ +28.3° (*c* 1, dioxane). *Anal.* calcd. for $C_{76}H_{71}N_3O_{21}$: C 67.00, H 5.25, N 3.09; found: C 66.96, H 5.25, N 3.22.

6-O-(α-D-Arabinofuranosyl)paromamine (25)

A solution containing **23** (130 mg) was dissolved in a mixture of acetic acid (4 ml), dioxane (2 ml), and water (1 ml), and the solution was stirred at 50°C for 4 days. Processing as described for **11** gave an amorphous solid that was homogenous by tlc, except for the presence of trace amounts of **7** (yield, 80 mg); purification by preparative tlc and debenzoylation as described for **12**, gave a product which was subjected to hydrogenation as in the case of **12**, to give the title pseudotrisaccharide (25 mg), as a colorless amorphous solid; mp foams ~120°C, decomposes ~140°; $[\alpha]_D$ +77.3° (*c* 1.01, H_2O); R_f 0.47 (tlc $CHCl_3$ – MeOH – 28% NH_4OH, 1:3:2); ms data on the corresponding *N*-acetyl-*O*-trimethylsilyl derivative *m/e*: 737 (4%), 649 (2%), see data under the preparation of **13**.

6-O-(2,3,5-Tri-O-benzoyl-β-D-xylofuranosyl)-3′-O-benzoyl-4′,6′-O-benzylidenetri-N-benzyloxycarbonylparomamine (26)

A suspension containing **8** (200 mg), mercuric cyanide (400 mg), and calcium sulfate (1 g) in a mixture of DMF (2 ml) and 1,2-dichloroethane (6 ml) was treated with 2,3,5-tri-*O*-benzoyl-D-xylofuranosyl bromide (2 ml; obtained from 0.7 g of the corresponding methyl glycoside derivative by treatment with a mixture of acetic acid saturated with hydrogen bromide and acetic anhydride (0.25 ml in 2 ml of 1,2-dichloroethane)). The mixture was stirred at 50°C for 3 days and processed as described for **10** to give a solid residue (from chloroform – di-2-propyl ether; yield 188 mg; 70%) which showed essentially one major spot on tlc. A portion was purified by preparative tlc (toluene–EtOAc, 3:2, R_f ~ 0.65) to give the title compound as a colorless amorphous solid; mp 251–256°C; $[\alpha]_D^{25}$ +11.0 (*c* 0.5, dioxane). *Anal.* calcd. for $C_{76}H_{71}N_3O_{21}$: C 67.00, H 5.25, N 3.09; found: C 66.47, H 5.30, N 3.09.

Acknowledgements

We thank the National Research Council of Canada for financial support (PRAI Grant).

1. S. UMEZAWA. Adv. Carbohydr. Chem. Biochem. **30**, 111 (1974); S. UMEZAWA. *In* Drug action and drug resistance in bacteria. 2. Aminoglycoside antibiotics. *Edited by* S. Mitsuhashi. University Park Press, Baltimore, MD. 1975. pp. 3–35.
2. T. SHOMURA, N. EZAKI, T. TSURUOKA, T. NIWA, E. AKITA, and T. NIIDA. J. Antibiot. **23**, 155 (1970).
3. P. W. K. WOO, H. W. DION, and Q. R. BARTZ. Tetrahedron Lett. 2617 (1971); 2621 (1971); 2625 (1971).
4. H. TSUKIURA, K. SAITO, S. KUBARU, M. KONISHI, and H. KAWAGUCHI. J. Antibiot. **26**, 386 (1973).
5. S. HORII, I. NOGAMI, N. MIZOKAMI, Y. ARAI, and M. YONEDA. Antimicrob. Agents Chemother. **5**, 578 (1974).
6. M. KONISHI, K. NUMATA, K. SHIMUDA, H. TSUKIURA, and H. KAWAGUCHI. J. Antibiot. **27**, 471 (1974).
7. S. HANESSIAN, T. TAKAMOTO, R. MASSÉ, and G. PATIL. Can. J. Chem. This issue.
8. K. E. PRICE, J. C. GODFREY, and H. KAWAGUCHI. Adv. Appl. Microbiol. **18**, 191 (1974).
9. T. OGAWA, T. TAKAMOTO, and S. HANESSIAN. Tetrahedron Lett. 4013 (1974).
10. F. ARCAMONE, G. CASSINELLI, P. B. CUCCIA, and G. DI COLO. Ann. Chim. **64**, 485 (1974).
11. J. D. DUTCHER, N. HOSANSKY, M. N. DONIN, and O. WINTERSTEINER. J. Am. Chem. Soc. **73**, 1384 (1951); R. L. PECK, C. E. HOFFHINE, JR., P. GALE, and K. FOLKERS. J. Am. Chem. Soc. **71**, 2590 (1949); **75**, 1018 (1953).
12. T. H. HASKELL, J. C. FRENCH, and Q. R. BARTZ. J. Am. Chem. Soc. **81**, 3480 (1959).
13. S. HANESSIAN, R. MASSÉ, and T. NAKAGAWA, Can. J. Chem. This issue; see also S. HANESSIAN and P. LAVALLEE. Methods Carbohydr. Chem. **7**, 49 (1976) and references cited therein.
14. S. UMEZAWA, S. KUTO, K. TATSUTA, and T. TSUMURA. Bull. Chem. Soc. Jpn. **42**, 529 (1969).
15. J. G. BUCHANAN and J. C. P.-SCHWARZ. J. Chem. Soc. 4770 (1962).
16. N. YUNG and J. J. FOX. Methods Carbohydr. Chem. **2**, 108 (1963); see also S. HANESSIAN and A. G. PERNET. Can. J. Chem. **52**, 1280 (1974).

17. G. WULFF and R. ROHLE. Angew. Chem. Int. Ed. Engl. **13**, 157 (1974); S. HANESSIAN and J. BANOUB. *In* Synthetic methods for carbohydrates. *Edited by* H. ElKhadem. ACS Symposium Series, No. 39. 1976. pp. 36–63.
18. S. UMEZAWA and Y. ITO. Bull. Chem. Soc. Jpn. **34**, 1540 (1961); S. KOTO, Y. ITO, and S. UMEZAWA. Bull. Chem. Soc. Jpn. **38**, 1447 (1965).
19. D. C. DE JONGH, J. D. HRIBAR, S. HANESSIAN, and P. W. K. WOO. J. Am. Chem. Soc. **89**, 3364 (1976); see also D. C. DE JONGH, E. B. HILLS, J. D. HRIBAR, and S. HANESSIAN. Tetrahedron, **29**, 2707 (1973).
20. D. C. DE JONGH, M. S. B. NAYAR, G. PATIL, and S. HANESSIAN. Tetrahedron. In press.
21. H. UMEZAWA. Adv. Carbohydr. Chem. Biochem. **30**, 183 (1974); R. BENEVISTE and J. DAVIES. Annu. Rev. Biochem. **42**, 471 (1973); Antimicrob. Agents Chemother. **4**, 402 (1973).
22. S. HANESSIAN and P. LAVALLEE. J. Antibiot. **25**, 683 (1972).
23. T. SUAMI, S. NISHIYAMA, Y. ISHIKAWA, and S. KATSURA. Carbohydr. Res. **52**, 187 (1976).
24. T. TAKAMOTO and S. HANESSIAN. Tetrahedron Lett. 4009 (1974).
25. Y. ITO, E. AKITA, T. TSURUOKA, and T. NIIDA. Antimicrob. Agents Chemother. **1**, 33 (1970).
26. E. F. RECONDO and H. RINDERKNECHT. Helv. Chim. Acta, **42**, 1171 (1959); R. K. NESS, W. DIEHL, and H. G. FLETCHER, JR. J. Am. Chem. Soc. **76**, 763 (1954).
27. W. PEARLMAN. Tetrahedron Lett. 1663 (1967).

Can. J. Chem. Downloaded from www.nrcresearchpress.com by 210.87.254.105 on 09/05/12
For personal use only.

Aminoglycoside antibiotics: Studies directed toward the selective modification of hydroxyl groups: Synthesis of 3′-epiparomamine and 3′-epineamine[1,2]

STEPHEN HANESSIAN, ROBERT MASSÉ, AND TOSHIO NAKAGAWA[3]
Department of Chemistry, University of Montreal, Montreal, P.Q., Canada H3C 3V1

Received October 28, 1977

STEPHEN HANESSIAN, ROBERT MASSÉ, and TOSHIO NAKAGAWA. Can. J. Chem. **56**, 1509 (1978).

Based on the knowledge that certain bacterial strains can produce enzymes that are capable of phosphorylating the 3′-hydroxyl group of a series of aminoglycoside antibiotics, the pseudodisaccharide 3′-epiparomamine was prepared through a series of high yielding steps, starting from paromamine. Application of selective halogenation and subsequent amination reactions allowed the efficient transformation of 3′-epiparomamine to 3′-epineamine. The two compounds were not substrates for the inactivating enzymes, however, they are also much weaker antibiotics compared to the parent compounds paromamine and neamine. Model synthetic studies in the 2-amino-2-deoxy-D-glucose series are also reported.

STEPHEN HANESSIAN, ROBERT MASSÉ et TOSHIO NAKAGAWA. Can. J. Chem. **56**, 1509 (1978).

La synthèse de la 3′-epiparomamine et la 3′-epineamine fut réalisée à partir de la paromamine par des transformations chimiques, basée sur la connaissance que des enzymes dans certaines souches bactériennes sont capables d'inactiver une série d'antibiotiques aminoglycosidiques par phosphorylation sur la fonction 3′-hydroxyle. Les nouveaux pseudodisaccharides ne sont pas des substrats pour ces enzymes, pourtant leur pouvoir antibactérien est beaucoup plus faible comparé aux molécules parentes. Des réactions modèles dans la série D-glucosamine furent aussi réalisées.

Because of their therapeutic importance in the control of certain infections caused by gram-negative bacteria, the aminoglycoside antibiotics have recently been the target of extensive research work on several fronts (1–4). Experience has shown that even minor structural variations, induced chemically or enzymatically, can result in dramatic changes in the biological profile of a given aminoglycoside antibiotic (5–7). A delicate balance exists, therefore, between functional, structural, configurational, and conformational factors that is reflected in the biological roles of these substances at the molecular level. In view of the highly multifunctional, polar nature of these molecules, progress in the selective chemical modification at strategic positions has been relatively slow. For these and other reasons, we have been interested in exploring chemical methods for selective transformations involving hydroxyl groups, with the objective of ultimately applying them to the aminoglycosides.

One of the principal modes of enzymatic inactivation (3–5) of this group of antibiotics of the 2-deoxystreptamine type, that bear a C-3′ hydroxyl group, is via phosphorylation, mediated by a phosphotransferase, such as NPT_I.[4] The resulting 3′-phosphate esters of these aminoglycosides are devoid of biological activity. The presence of the entire molecule is not necessary for such enzymatic reactions, since pseudodisaccharides and pseudotrisaccharides in the same series are also substrates for these enzymes. The need for functional modifications specifically at C-3′ (and C-4′), based on the preceding biochemical rationales is, therefore, evident in a continuing quest for aminoglycosides that are less susceptible to the action of the phosphotransferases yet maintain, if not improve, their biological potency. Since enzyme–substrate interactions are particularly sensitive to configurational and conformational changes, chemical modifications of the paromamine and neamine pseudodisaccharides were envisaged, that should, in principle, result in an aberrant recognition by the phosphorylating enzymes. Epimerization, chain branching, and deoxygenation reactions at C-3′ were thus explored with model compounds, the premise being that promising results would encourage extension of these modifications to the parent antibiotics containing the above mentioned pseudodisaccharide units.

Peripheral transformations, as in the passage from a primary hydroxyl group to an amino group, were also studied in this context.

Model Substrates

A suitable, readily available model substrate for three of the above mentioned modifications was methyl 4,6-*O*-benzylidene-2-benzyloxycarbonylamino-2-deoxy-α-D-glucopyranoside (**1**) (8), in which the desired C-3 hydroxyl group is unsubstituted and can

[1]For the previous paper in this series, see ref. 1.

[2]Taken in part from the Ph.D. thesis submitted by R.M., University of Montreal, Montreal, P.Q., 1975.

[3]Postdoctoral Associate, 1972.

[4]Neomycin phosphotransferase I; also known as neomycin–kanamycin phosphotransferase, see refs. 3–6.

Can. J. Chem. Downloaded from www.nrcresearchpress.com by 210.87.254.105 on 09/05/12
For personal use only.

Can. J. Chem. Downloaded from www.nrcresearchpress.com by 210.87.254.105 on 09/05/12
For personal use only.

TABLE 1. ^{13}C magnetic resonance data of compounds **8** and **9** (in ppm from TMS)

	Carbon atom						
Compound	1	2	3	4	5	6	OMe
8	100.3	55.7	74.4	69.8	72.8	61.5	56.1
9	97.4	50.9	68.5	66.7	67.8	61.5	56.5
Δδ	+2.9	+4.8	+5.9	+3.1	+5.0	—	+0.4

be effectively modified. Moreover, the parent sugar, its analogs, and its positional isomers, constitute one of the amino sugar units in several aminoglycosides that are susceptible to the action of the phosphotransferases. The choice of the *N*-protecting benzyloxycarbonyl group was important, since, in addition to its anticipated compatibility with various conditions of reactions that were planned, it could be cleaved under mild hydrogenolytic conditions.

Oxidation of **1** with acetic anhydride in dimethyl sulfoxide (9) gave a 76% yield of the crystalline 3-uloside **4** and a small amount of the methylthiomethyl ether derivative **2**. Formation of the latter was avoided when the oxidation was done using dimethyl sulfoxide – *N*,*N*-dicyclohexylcarbodiimide (10) and the yield of crystalline material remained essentially unchanged. Based on a literature precedent involving the corresponding 2-benzamido derivative (11), it was anticipated that reduction of **4** with sodium borohydride would lead preponderantly to the D-*allo* analog **5**. Indeed, reduction of **4** gave a quantitative yield of **5**, which had discernibly different chromatographic properties compared to the epimeric **1**. Further confirmation of the structure of **5** was obtained from comparison of the nmr spectral characteristics of the acetate derivatives **3** and **6**, and the ^{13}C magnetic resonance spectra of the *N*,*O*-deblocked methyl glycosides **8** and **9**. Thus, selective cleavage of the acetal function in **5** gave methyl 2-benzyloxycarbonylamino-2-deoxy-α-D-allopyranoside (**7**), which was subjected to hydrogenolysis to give methyl 2-amino-2-deoxy-α-D-allopyranoside (**8**), isolated as the amorphous hydrochloride salt. Similar treatment of **1** gave the epimeric methyl 2-amino-2-deoxy-α-D-glucopyranoside (**9**), isolated as the hydrochloride. These reactions are summarized in Scheme 1.

The ^{13}C spectral characteristics for the epimeric compounds **8** and **9** are recorded in Table 1. Except for the resonances of the hydroxymethyl and methoxyl carbon atoms, all other resonances undergo an upfield shift in the D-*allo* isomer. The most significant shift is observed for C-3 and agrees with data in the monosaccharide series (12) for upfield shifts associated with ^{13}C nuclei bearing axial hydroxyl groups. The large shielding effect observed for C-5 in compound **8** can be explained in the terms expressed by Perlin *et al.* (12), as there could exist a strong H_5–O_3 *syn*-diaxial interaction. Since the exact conformation of **8** relative to that of **9** is not known, some of the shielding effects could also presumably result from subtle conformational changes, thus enhancing the initial effect experienced by the ^{13}C nuclei adjacent to the one bearing the axial hydroxyl group.

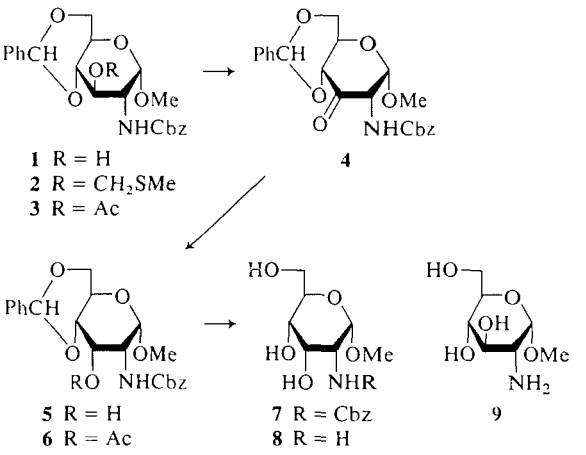

SCHEME 1

It was next decided to explore the feasibility of a chain branching reaction at C-3 with the uloside derivative **4** as a model. Treatment of the latter with methylmagnesium iodide in tetrahydrofuran gave a high yield of the 3-*C*-methyl derivative **10** (Scheme 2). Mechanistic arguments and literature precedents (13) strongly favored the D-*allo* configuration for this product. A second objective in this series was to attempt a ring opening of the benzylidene acetal function in **10**, with *N*-bromosuccinimide (NBS) (14), as a means of functionalizing the terminal primary carbon atom. Treatment of **10** with NBS gave a 57% yield of the expected product **11**, thus encouraging

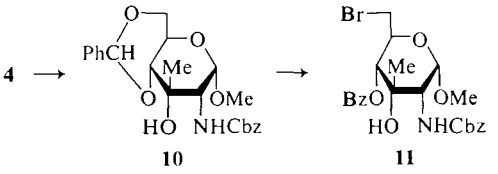

SCHEME 2

Can. J. Chem. Downloaded from www.nrcresearchpress.com by 210.87.254.105 on 09/05/12
For personal use only.

applications of the same sequence in the aminoglycoside series. Unfortunately, when the Grignard reaction was extended to a suitably protected paromamine derivative, no reaction occurred, presumably owing to the formation of an insoluble complex. Further work on chain branching reactions in this series was therefore abandoned.

It was of interest next to study newer methods for the introduction of deoxy functions at C-3 and/or C-4 using a D-glucosamine derivative as a model. In previous work, we had shown that the reaction of methyl 2-azido-3,4-*O*-benzylidene-6-bromo-2,6-dideoxy-α-D-altropyranoside with NBS was highly stereoselective, since the preponderant product was the corresponding 3,6-dibromo derivative (15). The presence of a *cis*-diol group in **7** prompted us to prepare the corresponding *O*-benzylidene acetal and to study its reaction with NBS (Scheme 3). To avoid multiple blocking and deblocking steps, it was decided to first convert **5** into the corresponding 6-bromo derivative **12** via an NBS reaction. Sequential debenzoylation to **13** and acetal formation gave the 3,4-*O*-benzylidene derivative **14**. Treatment of the latter with NBS gave a mixture of two products **15** and **16** in a ratio of 1:1. The isomeric relationship between the two products was indicated by mass spectral data of the individual compounds. ^{1}H magnetic resonance spectral data allowed a tentative assignment of the D-*gulo* structure to the crystalline isomer **15**. In view of the moderate yield of the NBS reaction (42%) and the nonregiospecific distribution of products in the model studies, this approach to deoxygenation of aminoglycosides was not pursued further.

Finally, a practical method was sought to replace a primary hydroxyl group by an amino group, that could be adapted to the aminoglycoside series. Such a transformation is the basis of a well known and now classical procedure that consists in the nucleophilic displacement of primary sulfonic acid esters by a nitrogen nucleophile such as ammonia or azide ion; (see for example ref. 16).

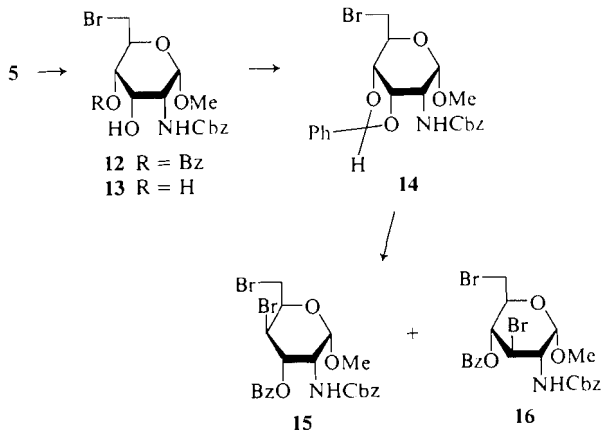

SCHEME 3

Although this procedure has been extensively used in monosaccharide chemistry, its applications in the area of aminoglycosides have been few and the yields have been moderate or low in most cases (17–19), except where selectivity was of little concern because of prior protection of many of the existing hydroxyl groups (20). In previous papers (21) we reported on the selective halogenation of primary hydroxyl groups in polyhydroxy compounds, containing a variety of substituents, with triphenylphosphine and the appropriate *N*-halosuccinimide. The reaction has been found to be remarkably suitable in the case of the polyfunctional *N*-substituted aminoglycosides as exemplified by the transformation of tri-*N*-benzyloxycarbonylparomamine (**18**) into neamine **21** in high overall yield via the corresponding 6′-bromo **19** and 6′-azido **20** derivatives (Scheme 4).

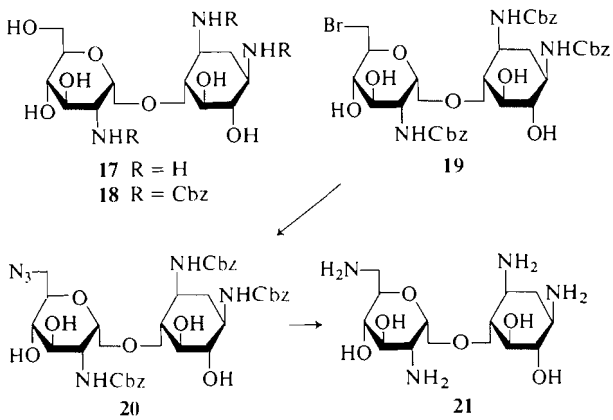

SCHEME 4

3′-Epiparomamine (28) and 3′-Epineamine (31)

The virtually stereospecific reduction of the 3-uloside derivative **4** paved the way to a similar reaction sequence in the paromamine series (**17**) with the objective of preparing 3′-epiparomamine (**28**) (22). The disposition of the hydroxyl groups in tri-*N*-benzyloxycarbonylparomamine (**18**) is such that acetal formation can take place, under somewhat forcing conditions, to the corresponding diisopropylidene derivative **22** (23) (Scheme 5). Oxidation of the latter with dimethyl sulfoxide and acetic anhydride gave the desired 3′-uloside derivative **24** in over 80% yield, after chromatographic purification. Reduction of **24** with sodium borohydride in a mixture of methanol and DMF, or with tri-*tert*-butylaluminium hydride in tetrahydrofuran, gave in each case the corresponding 3′-epiparomamine derivative **25** in high yield. This product has a significantly different chromatographic mobility compared to its

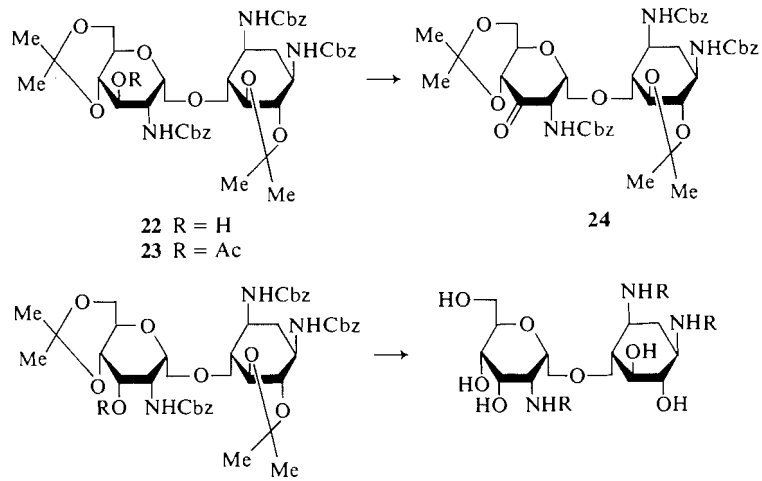

SCHEME 5

epimer **22**. Confirmation of the D-*allo* stereochemistry of the amino sugar portion was secured by chemical and spectroscopic means. Thus, acetylation of **22** and **25** individually, gave the respective 3′-acetates **23** and **26**, in which the signals for the acetyl methyl resonances were distinctly different, as would be expected from the presence of equatorial and axial acetate groups, respectively (24). This was further confirmed in the ^{1}Hmr spectrum of a sample of **26**, to which progressively increasing amounts of **23** were added. Treatment of **25** with 80% aqueous acetic acid effected cleavage of the acetal groups to give crystalline tri-*N*-benzyloxycarbonyl-3′-epiparomamine (**27**), which had discernibly different chromatographic properties compared to **17**. Finally, reductive cleavage of the *N*-protecting groups gave 3′-epiparomamine, isolated as the amorphous trihydrochloride salt **28**. Acid hydrolysis of **27** and chromatographic examination of the mixture revealed the presence of 2-deoxystreptamine and 2-amino-2-deoxy-D-allose. Ninhydrin degradation of this amino sugar gave rise to a neutral sugar that was identified as ribose by chromatography in several solvent systems. An identical degradation of 2-amino-2-deoxy-D-glucose gave arabinose as expected. The gross structural features of 3′-epiparomamine were also confirmed by high resolution mass spectral data, obtained on the corresponding *N*-benzyloxycarbonyl and *N*-acetyl *O*-trimethylsilyl derivatives (25). It is of interest that such *N*-benzyloxycarbonyl derivatives are amenable to mass spectral analysis, and give fragmentation patterns similar to those already known (25) in the *N*-acetyl series, with the exception that the fragments containing the amino sugar and 2-deoxystreptamine components give rise to peaks that have much lower relative intensities compared to the *N*-acetyl series.

Extension of the bromination reaction with the reagent pair Ph_3P–NBS to **27** was also successful and led to the formation of tri-*N*-benzyloxycarbonyl-6′-bromo-6′-deoxy-3′-epiparomamine (**29**) in high yield. In this case, the selective bromination was done at room temperature in HMPT as solvent, which illustrates the preparative utility of this reaction in this series (Scheme 6). Displacement of the bromine atom in **29** with azide ion in the usual manner led to the corresponding 6′-azido derivative **30** in high yield. Previous studies in this laboratory have in fact shown that it is possible to effect a sequential bromination and azide displacement reaction in one flask, which simplifies the manipulative part of these reactions, while maintaining the elements of practicality and efficacy. Finally, catalytic reduction of **30** caused a simultaneous hydrogenolysis of the benzyloxycarbonyl groups to give 3′-epineamine (**31**) isolated as the amorphous tetrahydrochloride salt. Its structural and functional features were confirmed by high resolution mass spectrometry and by ^{13}C spectral data. Like in the monosaccharide series, the effect of an inversion of configuration at C-3 in 3′-epiparomamine and 3′-epineamine, compared to the naturally occurring pseudodisaccharides (26, 27), is manifested by an upfield shift in the absorption of the ^{13}C nuclei corresponding to C-2′,C-5′ of the amino sugar moiety. Shielding of C-5′, however, was much less pronounced compared to **8**, possibly owing to orientational (rotamer) effects (28, 29) associated with the presence of a larger aglycone in the pseudodisaccharides. Upon acidification to $pH \simeq 1$, the expected β-shifts were observed in both

Can. J. Chem. Downloaded from www.nrcresearchpress.com by 210.87.254.105 on 09/05/12
For personal use only.

TABLE 2. ^{13}C magnetic resonance data of paromamine, 3′-epiparomamine, neamine, and 3′-epineamine (ppm from TMS)

Carbon[a,b]	Paromamine (17)	3′-Epiparomamine (28)		Neamine (21)	3′-Epineamine (31)	
	p*H* ≃ 11	p*H* ≃ 11	p*H* ≃ 1	p*H* ≃ 11	p*H* ≃ 11	p*H* ≃ 1
1	51.3	51.0	51.2	51.2	51.2	50.7
2	33.8	33.6	28.7*	35.8	33.1	28.4*
3	50.1	49.7	49.8	50.1	49.5	49.8
4	86.6	86.8	78.4*	86.7	83.9	76.2*
5	75.6	76.0	75.7	76.7	75.2	75.2
6	76.3	76.3	73.2*	77.6	76.3	73.4*
1′	100.9	101.2	95.4*	101.0	99.2	95.0*
2′	55.9	51.4	50.2	55.9	51.4	50.9
3′	73.9	68.6	66.4*	74.1	68.7	65.8*
4′	70.7	67.4	67.0	72.3	64.8	67.1
5′	73.6	71.1	70.6	72.3	70.4	68.0*
6′	61.8	61.4	61.2	42.1	41.5	41.2

[a]Primed numbers refer to the carbon atoms of the amino sugar portion.
[b]Numbers with asterisks denote carbon atoms susceptible to β-shifts at acid p*H* values.

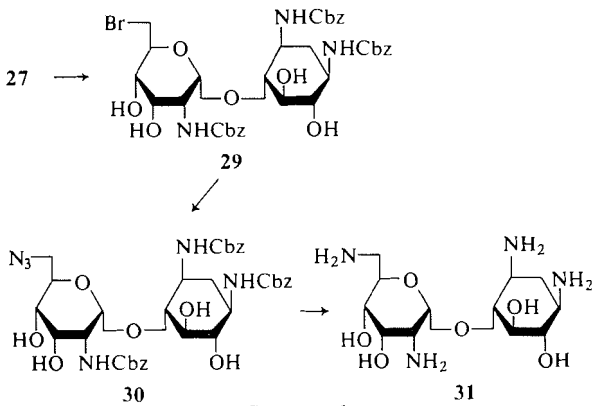

SCHEME 6

series, as can be seen in Table 2. An interesting feature in the spectrum of 3′-epineamine is the apparent large upfield shift of the C-4′ signal compared to that found in 3′-epiparomamine. This could be due to increasing 1,3-*syn* interactions with H-4–O-5, or more likely, to the presence of different rotamer populations (28, 29) associated with the $—CH_2NH_2$ group in 3′-epineamine. Such a γ effect (30) would be reflected in the spectrum of 3′-epineamine, upon changing the p*H*, but not as much in the case of the 3′-epimeric pseudodisaccharide **28**.

As anticipated at the outset of this study, 3′-epiparomamine was not a substrate[5] for the phosphotransferases that normally attack neomycin, paromomycin, and kanamycin among other related aminoglycosides (3, 4). Unfortunately, the antibacterial spectra of 3′-epiparomamine and 3′-epineamine were disappointing, compared to their respective parent pseudodisaccharides, although as expected, 3′-epineamine showed a better relative activity. Thus, while the effects of inactivating enzymes could be curtailed by inversion at C-3′ in paromamine and neamine, the subtle prerequisites for effective penetration into bacterial cells, and for binding to the ribosomes appear not to be fulfilled in the modified analogs.

[5]We are grateful to Professor J. Davies, University of Wisconsin, for these studies.

Experimental

Melting points are uncorrected. Optical rotations were measured on a Perkin-Elmer automatic spectropolarimeter, model 141. ^1H magnetic resonance spectra were recorded on a JEOL instrument at 60 MHz unless otherwise mentioned, with tetramethylsilane as internal standard and deuteriochloroform as solvent. ^{13}C spectra were recorded on a Bruker WH-90 instrument at 22.6 MHz, utilizing a frequency decoupler at 90 MHz. Samples (50–200 mg) were dissolved in deuterium oxide (0.8–1.2 ml) which was previously degassed. Dioxane or methanol were used as internal standards and showed signals at 67.4 and 49.8 ppm, respectively, downfield from tetramethylsilane (TMS). Spectra were measured at neutral p*H*, at p*H* ≃ 11, and p*H* ≃ 1, with appropriate p*H* adjustment with an anion exchange resin (Rexyn 203 OH^- form) and sulfuric acid, respectively. Sweeping frequencies varied from 10 000–90 000 scans depending on the concentration of the sample. Mass spectra were recorded on an AEI-902 mass spectrometer, at low and high resolutions. Column chromatography was done using silica gel G254, with application of moderate suction.

Methyl 4,6-O-Benzylidene-2-benzyloxycarbonylamino-2-deoxy-α-D-ribo-hexopyranosid-3-ulose (4)

Oxidation with DMSO–Ac_2O

A solution containing 846 mg (2.05 mmol) of methyl 4,6-*O*-benzylidene-2-benzyloxycarbonyl-amino-2-deoxy-α-D-glucopyranoside (**1**) (8) in 16 ml of a 1:1 mixture of dimethyl sulfoxide and acetic anhydride was left at room temperature overnight. The solution was poured into 200 ml of ice-water with vigorous stirring, and the resulting precipitate was recovered by filtration and washing with cold water. The colorless solid (710 mg) consisted of the desired product, contaminated by a small amount of the corresponding methylthiomethyl ether derivative **2**. Recrystallization from 2-propanol gave 480 mg

Can. J. Chem. Downloaded from www.nrcresearchpress.com by 210.87.254.105 on 09/05/12
For personal use only.

Can. J. Chem. Downloaded from www.nrcresearchpress.com by 210.87.254.105 on 09/05/12
For personal use only.

(58%) of the ketone **4**. Additional material was obtained from the mother liquors by preparative thick-layer chromatography (benzene–EtOAc, 1:1); total yield, 640 mg (76%); mp 201–202°C; $[\alpha]_D^{27}$ +89.3° (*c* 2.45, $CHCl_3$); ν_{max} (KBr): 3295 (NH), 1745, 1685 cm^{-1} (C=O). *Anal.* calcd. for $C_{22}H_{23}NO_7$: C 63.91, H 5.60, N 3.38; found: C 64.19, H 5.45, N 3.40.

The methylthiomethyl ether derivative **2** was isolated from the above preparative thick-layer chromatographic separations; mp 188–189°C (2-propanol); $[\alpha]_D^{27}$ +154.5° (*c* 2.48, $CHCl_3$); nmr: 1.97 (s, CH_3S—), 3.35 (s, CH_3O—), 4.80 ppm (s, O—CH_2—S), etc. *Anal.* calcd. for $C_{24}H_{29}O_7NS$: C 60.61, H 6.14, N 2.94; found: C 60.69, H 6.09, N 2.88.

Oxidation with DMSO–DCC

A solution containing 1.49 g (3.91 mmol) of **1** in 25 ml of dimethyl sulfoxide was treated with 2.92 g (14.15 mmol) of dicyclohexylcarbodiimide and 1 g of phosphoric acid at 0°C. After 50 h at room temperature, the suspension was filtered and the filtrate was partitioned between chloroform (400 ml) and aqueous sodium bicarbonate (75 ml). Processing of the organic phase, evaporation to a small volume (~40 ml), and pouring into ice-water (500 ml) gave a colorless precipitate which was isolated by filtration. Drying under vacuum and recrystallization from 2-propanol gave the title compound (1.15 g, 77%); mp 201–202°C.

*Methyl 4,6-O-Benzylidene-2-benzyloxycarbonylamino-2-deoxy-α-D-allopyranoside (**5**)*

To a solution containing 477 mg (1.15 mmol) of **4** in 5 ml of DMF and 15 ml of methanol was added 411 mg of sodium borohydride, in small portions and with external cooling. After 1 h at room temperature, the solution was evaporated to a small volume, diluted with chloroform (100 ml), and the solution was washed with water. Processing of the organic phase in the usual manner gave 480 mg of colorless chromatographically homogeneous solid. Recrystallization from a mixture of ethyl acetate and hexane gave the title compound (465 mg, 97%); mp 103–104°C; $[\alpha]_D^{27}$ +56.2° (*c* 3.15, $CHCl_3$); ν_{max} (KBr): 3420 (OH), 3330 (NH), 1685 cm^{-1} (NHCO). Compounds **1** and **5** had discernibly different chromatographic mobilities (tlc, $CHCl_3$–EtOAc, 5:1) showing R_f 0.42 and 0.55, respectively. *Anal.* calcd. for $C_{22}H_{25}NO_7$: C 63.60, H 6.06, N 3.37; found: C 63.42, H 6.12, N 3.49.

The 3-*O*-acetyl derivative **6**, prepared by acetylation of **5** with pyridine and acetic anhydride, was obtained as a colorless foam; $[\alpha]_D^{27}$ +28° (*c* 0.21, $CHCl_3$); ^{1}Hmr: 2.08 ppm (OAc). The epimeric acetate **3**, prepared from **1**, showed mp 188–189°C; $[\alpha]_D^{27}$ +154.4° (*c* 2.48, $CHCl_3$); ^{1}Hmr: 1.82 ppm (OAc).

*Methyl 2-Benzyloxycarbonylamino-2-deoxy-α-D-allopyranoside (**7**)*

A solution containing 211 mg of **5** in 80% aqueous acetic acid was left at room temperature for 12 h. Evaporation of the solvent gave a syrup that solidified from a mixture of 2-propanol and petroleum ether (bp 30–60°C); yield, 145 mg (87%); mp 82–83°C; $[\alpha]_D^{27}$ +69.4° (*c* 0.37, MeOH); ν_{max} (KBr): 1700 cm^{-1} (NHCO); R_f 0.24 (tlc, $CHCl_3$–EtOAc–MeOH, 25:15:3).

*Methyl 2-Amino-2-deoxy-α-D-allopyranoside Hydrochloride (**8**)*

A solution containing 250 mg of the preceding compound **7**, in 25 ml of methanol, was hydrogenated, in the presence of 100 mg of 20% palladium-hydroxide-on-charcoal (31). After 2 h, the suspension was filtered, the filtrate was evaporated to a syrup that was dissolved in 20 ml of methanol containing 1 ml of *N* hydrochloric acid. The yellow solution was decolorized with charcoal and processed in the usual way to give a colorless syrup that solidified under vacuum; yield 140 mg (90%); mp 80–85°C (softening); 112–115°C (foaming and decomposition); $[\alpha]_D^{27}$ +82.4° (*c* 0.21, MeOH). The product was chromatographically homogeneous, R_f 0.59 (tlc, $CHCl_3$ – MeOH – 28% NH_4OH, 1:3:1). The ^{13}C spectral parameters are listed in Table 1.

*Methyl 2-Amino-2-deoxy-α-D-glycopyranoside Hydrochloride (**9**)*

Catalytic hydrogenation of **1** (310 mg) in 20 ml of methanol as described above gave a syrup that solidified from aqueous ethanol to give 161 mg (88.5%) of the title compound; mp 118–120°C; $[\alpha]_D^{27}$ +126.5° (*c* 0.39, H_2O) (lit. (32) mp 119°C; $[\alpha]_D^{27}$ +129° (H_2O)); R_f 0.73 (tlc, $CHCl_3$ – MeOH – 28% NH_4OH, 1:3:1). The ^{13}C spectral parameters are listed in Table 1.

*Methyl 4,6-O-Benzylidene-2-benzyloxycarbonylamino-2-deoxy-3-C-methyl-α-D-allopyranoside (**10**)*

To a cooled solution of methylmagnesium iodide (prepared from 1.5 g (61.7 mmol) of magnesium turnings and 4 ml of methyl iodide in 30 ml of ether) was added the ketone **4** (811 mg, 1.96 mmol) in 40 ml of tetrahydrofuran, dropwise and with stirring. The mixture was heated at reflux for 5 h, excess reagent was destroyed with a 20% solution of ammonium chloride (50 ml), and the solution was extracted with chloroform. Processing of this solution in the usual manner gave a crystalline product that showed a major component on tlc ($CHCl_3$–EtOAc, 5:1). Recrystallization from ethanol gave the title compound; yield 673 mg, 80%; mp 138.5–140°C. A second recrystallization gave an analytical sample; mp 142–143°C; $[\alpha]_D^{27}$ +50.5° (*c* 4.69, $CHCl_3$); ^{1}Hmr: 1.30 (s, C—CH_3), 3.02 (bs, OH), 3.34 (s, OCH_3), 4.70 (d, H-1, $J_{1,2}$ = 3.7 Hz), 5.12 (s, $PhCH_2O$—), 5.52 (s, PhCH<O>O), 7.35 ppm (m, Ph), etc. *Anal.* calcd. for $C_{23}H_{27}NO_9$: C 64.32, H 6.33, N 3.26; found: 64.51, H 6.36, N 3.36.

*Methyl 4-O-Benzoyl-2-benzyloxycarbonylamino-6-bromo-2,6-dideoxy-3-C-methyl-α-D-allopyranoside (**15**)*

To a solution containing 468 mg (1.08 mmol) of **14** and 207 mg (1.16 mmol) of *N*-bromosuccinimide in 50 ml of carbon tetrachloride was added 2 g of barium carbonate and the mixture was heated at reflux for 20 min. Processing the mixture in the usual manner gave a pale yellow syrup that was purified by chromatography ($CHCl_3$–EtOAc, 25:2). The title compound was thus obtained as colorless crystals (316 mg, 57%); recrystallization was effected from a mixture of 2-propanol and petroleum ether; mp 89.5–90.5°C; $[\alpha]_D^{27}$ +58° (*c* 1.52, $CHCl_3$); ^{1}Hmr: 1.18 (s, C—CH_3), 3.48 (s, OCH_3), 4.83 ppm (d, H-1, $J_{1,2}$ = 3.7 Hz), etc. *Anal.* calcd. for $C_{23}H_{26}NO_7Br$: C 54.34, H 5.16, N 2.75; found: C 53.94, H 5.95, N 2.38.

*Methyl 4-O-Benzoyl-2-benzyloxycarbonylamino-6-bromo-2,6-dideoxy-α-D-allopyranoside (**12**)*

To a solution of **5** (323 mg, 0.87 mmol) in 50 ml of carbon tetrachloride was added 196 mg (1.1 mmol) of *N*-bromosuccinimide, followed by 1.3 g of barium carbonate. The suspension was heated at reflux for 30 min, the inorganic solids were filtered, and the filtrate was washed with water (20 ml) and dried. Evaporation gave a colorless syrup that crystallized from a mixture of 2-propanol and petroleum ether at 0°C; yield 231 mg, 60%; mp 151–151.5°C; $[\alpha]_D^{27}$ +74° (*c* 2.56, $CHCl_3$). *Anal.* calcd. for $C_{22}H_{24}NO_7Br$: C 53.44, H 4.85, N 2.8, Br 16.17; found: C 53.18, H 4.59, N 2.88, Br 16.05.

*Methyl 2-Benzyloxycarbonylamino-6-bromo-2,6-dideoxy-α-D-allopyranoside (**13**)*

Debenzoylation of compound **12** (312 mg) in the usual manner (sodium methoxide, methanol, 25°C, 30 min) followed by

Can. J. Chem. Downloaded from www.nrcresearchpress.com by 210.87.254.105 on 09/05/12
For personal use only.

treatment of the solution with a small amount of Dowex-50 (H^+) and processing the solution gave the title compound as a syrup. Crystallization was effected from a mixture of 2-propanol and petroleum ether; yield, 240 mg, 93%; mp 114–115.5°C; $[\alpha]_D^{27}$ +66.8° (*c* 0.15, $CHCl_3$). *Anal.* calcd. for $C_{15}H_{20}NO_6Br$: C 46.16, H 4.16, N 3.51; found: C 46.22, H 4.45, N 3.32.

*Methyl 3,4-O-Benzylidene-2-benzyloxycarbonylamino-6-bromo-2,6-dideoxy-α-D-allopyranoside (**14**)*

Zinc chloride (1.5 g) was added to a solution containing **13** (250 mg, 0.64 mmol) in 5 ml of benzaldehyde and the resulting suspension was stirred at room temperature for 36 h. The mixture was poured into ice-water containing 10 g of sodium bicarbonate, the solids were filtered, and the filtrate was extracted with chloroform. Processing as usual gave a syrup that was purified by chromatography (benzene–EtOAc, 5:1) to give the title compound as a homogeneous syrup, yield 182 mg, 60%; $[\alpha]_D^{27}$ +15.8° (*c* 2.21, $CHCl_3$). ^1H magnetic resonance spectral analysis indicated the presence of a 4:1 mixture of diastereoisomers: 3.49 (bs, 2H, $PhCH_2O$—), 5.95 and 6.27 ppm (s, PhCH<O/O>), etc. This compound was used as such for subsequent transformations.

*Reaction of Acetal **14** with* N-*Bromosuccinimide*

A suspension containing **14** (170 mg, 0.35 mmol), *N*-bromosuccinimide (71 mg, 0.39 mmol), and 800 mg of barium carbonate in 25 ml of carbon tetrachloride was heated at reflux for 2 h. Filtration and evaporation of the filtrate gave a colorless syrup (107 mg) which showed the presence of two major products by tlc (benzene–EtOAc, 5:1). Separation by preparative thick-layer chromatography gave 41 mg of a product having R_f 0.71, and 42 mg of a product having R_f 0.84 (total yield, 42%).

The former product is tentatively assumed to be *methyl 4-O-benzoyl-2-benzyloxycarbonylamino-3,6-dibromo-2,3,6-trideoxy-α-D-glycopyranoside* (**16**); $[\alpha]_D^{27}$ +40.6° (*c* 1.04, $CHCl_3$). The product having R_f 0.84 crystallized from 2-propanol and was assigned the isomeric structure *methyl 3-O-benzoyl-2-benzyloxycarbonylamino-4,6-dibromo-2,4,6-trideoxy-α-D-glucopyranoside* (**15**); mp 101–102°C; $[\alpha]_D^{27}$ +41.7° (*c* 0.12, $CHCl_3$); nmr: 3.60 (s, 3H, OCH_3), 4.22 (dd, H-4, $J_{4,3}$ = 1.5 Hz, $J_{4,5}$ = 6.7 Hz), 4.48 (dd, H-2, $J_{2,1}$ = 3.7 Hz, $J_{2,3}$ = 3.3 Hz), 5.16 (s, $PhCH_2O$—), 5.60 (t, H-3, $J_{3,2}$ = 3.3 Hz, $J_{3,4}$ = 1.5 Hz), 7.60, 7.80 ppm (m, Ph), etc. *Anal.* calcd. for $C_{22}H_{23}NO_6Br_2$: C 47.42, H 4.16, N 2.51; found: C 47.97, H 4.59, N 2.24.

*Selective Bromination of Tri-*N*-benzyloxycarbonylparomamine. Synthesis of Tri-*N*-benzyloxycarbonyl-6′-bromo-6′-deoxyparomamine (**19**)*

A 349 mg (0.48 mmol) sample of tri-*N*-benzyloxycarbonylparomamine (**18**) (23), previously freed from traces of moisture by azeotropic removal of water with pyridine, was added to 258 mg (0.98 mmol) of triphenylphosphine in 15 ml of dry hexamethylphosphoramide (HMPT). To the stirred and cooled solution was added 158 mg (0.89 mmol) of NBS, in portions, over a period of 5 min. The pale yellow solution was stirred at 55°C for 10 h, excess reagent was destroyed by addition of methanol (5 ml), and the solvents were removed *in vacuo* at 70°C. The syrupy dark yellow residue solidified when triturated with cold water. A major portion of triphenylphosphine oxide was removed by successive trituration with hot petroleum ether. The residual solid was recrystallized from ethanol to give 341 mg (82%) of the title compound; mp 241–243°C; $[\alpha]_D^{27}$ +49.3° (*c* 0.80, DMF). *Anal.* calcd. for $C_{36}N_{42}N_3O_{12}Br$: C 54.82, H 5.36, N 5.32; found: C 54.60, H 5.40, N 5.21.

A slightly lower yield (76%) was obtained in DMF but longer times were required to effect complete reaction (72 h) and there was considerable discoloration of the mixture.

Acetylation of **19** gave the crystalline tetraacetate derivative; mp 211.5–212.5°C; $[\alpha]_D^{27}$ +79.5° (*c* 0.22, $CHCl_3$).

*6′-Azidotri-*N*-benzyloxycarbonyl-6′-deoxyparomamine (**20**)*

A mixture containing 210 mg (0.36 mmol) of the preceding bromo derivative and 215 mg of sodium azide in 6 ml of dry HMPT was heated at 55°C for 5 h. The solution was poured dropwise and with vigorous stirring into ice-water (200 ml) and the resulting precipitate was filtered, washed well with water, and dried. The desired product was reprecipitated from hot ethanol; yield 163 mg (81.5%); mp 240–242°C; $[\alpha]_D^{27}$ +68° (*c* 0.75, DMF); ν_{max} (KBr): 3400–3350 (OH, NH), 2100 (N_3), 1665 cm^{-1} (C=O). The product was chromatographically homogeneous and was used as such in the following step.

The yield was essentially the same when the reaction was done in DMF (90°C, 20 h).

The amorphous tetraacetate derivative of **20** (mp 123–125°C; $[\alpha]_D^{27}$ +66° (*c* 0.29, $CHCl_3$)) was obtained in the usual manner.

*Neamine (**21**)*

The preceding compound (139 mg, 0.18 mmol) was hydrogenated in the presence of 20% palladium-hydroxide-on-charcoal (31) in a mixture of methanol (2 ml) and dioxane (12 ml) containing 5 ml of 0.1 *N* hydrochloric acid. After 2.5 h, the catalyst was filtered and washed with water. Processing the filtrate gave a colorless syrup that was dissolved in a few drops of water; addition of ethanol gave the title compound as the hydrochloride salt; yield 71.5 mg (83%); mp 220–225°C (dec.); $[\alpha]_D^{27}$ +82.9° (*c* 0.66, H_2O) (lit. (18) mp 233°C (dec); $[\alpha]_D^{27}$ +86.8° (H_2O)).

The product was identical to authentic neamine in two solvent systems. ^{13}C spectral data are provided in Table 2.

*4-O-(3-O-Acetyl-2-benzyloxycarbonylamino-2-deoxy-4,6-O-isopropylidene-α-D-glycopyranosyl)-1,3-di-*N*-benzyloxycarbonyl-5,6-O-isopropylidene-2-deoxystreptamine (**23**)*

A solution containing 400 mg (0.49 mmol) of tri-*N*-benzyloxycarbonyl-di-*O*-isopropylideneparomamine (**22**) (23) in 2 ml of dry pyridine as treated with acetic anhydride (0.4 ml). After 18 h, the solvent was co-distilled with toluene at 30–35°C and the residual syrup was triturated from a mixture of dioxane and cyclohexane. The resulting colorless solid was filtered and dried; yield 358 mg (85%). That product was chromatographically homogeneous; mp 123–135°C; $[\alpha]_D^{27}$ +46.1° (*c* 1.0, $CHCl_3$); ^1Hmr: 1.93 ppm (s, CH_3COO), etc. *Anal.* calcd. for $C_{44}H_{53}N_3O_{14}\cdot H_2O$: C 61.03, H 6.40, N 4.96; found: C 61.30, H 6.25, N 4.88.

*4-O-(2-Benzyloxycarbonylamino-2-deoxy-4,6-O-isopropylidene-α-D-ribohexopyranose-3-ulosyl)-1,3-di-*N*-benzyloxycarbonyl-5,6-O-isopropylidene-2-deoxystreptamine (**24**)*

A solution containing **22** (1.83 g, 2.27 mmol) in a mixture of dimethyl sulfoxide (20 ml) and acetic anhydride (20 ml) was kept in the dark at room temperature for 3 days. Evaporation of the solvent gave a residue that was dissolved in dichloromethane (60 ml) and the solution was washed with aqueous sodium bicarbonate and then with water. Processing of the organic phase gave a solid residue that was purified by chromatography (CH_2Cl_2–ether, 1:1). The product was isolated as an amorphous solid and reprecipitated from dioxane – cyclohexane (containing a drop of triethylamine); yield 1.51 g (82.5%); mp 152–154°C; $[\alpha]_D^{27}$ +39° (*c* 0.40, $CHCl_3$). *Anal.* calcd. for $C_{42}H_{49}N_3O_{19}$: C 62.75, H 6.14, N 5.25; found: C 62.43, H 6.12, N 5.28.

Can. J. Chem. Downloaded from www.nrcresearchpress.com by 210.87.254.105 on 09/05/12
For personal use only.

4-O-(2-Benzyloxycarbonylamino-2-deoxy-4,6-O-isopropylidene-α-D-allopyranosyl)-1,3-di-N-benzyloxycarbonyl-5,6-O-isopropylidene-2-deoxystreptamine (25)

To a cooled solution of the ketone **24** (713 mg, 0.89 mmol) in 1.5 ml of DMF and 30 ml of methanol was added, in portions and with stirring, 299 mg (7.94 mmol) of sodium borohydride. After 18 h at room temperature, the solution was diluted with cold water (50 ml) and the resulting precipitate was collected by filtration, washed, and dried. Recrystallization from a mixture of ethanol and petroleum ether in the presence of a drop of triethylamine gave 565 mg (80%) of the title compound; mp 174–176°C; $[\alpha]_D^{27}$ +26° (*c* 0.50, $CHCl_3$). The product was discernibly different on tlc (benzene–EtOAc, 1:1) showing R_f 0.55, compared to the epimeric **22**, which showed R_f 0.32. *Anal.* calcd. for $C_{42}H_{51}N_3O_{13}$: C 62.60, H 6.38, N 5.21; found: C 62.00, H 6.43, N 5.38.

Reduction in the presence of lithium tri-*tert*-butylaluminium hydride (0°C, then 12 h at 25°C, in THF) gave the same product, in essentially the same yield as above. The mother liquors did not contain detectable amounts of the epimeric alcohol **22**, as evidenced by tlc, but consisted of more of the same product.

4-O-(3-O-Acetyl-2-benzyloxycarbonylamino-2-deoxy-4,6-O-isopropylidene-α-D-allopyranosyl)-1,3-di-N-benzyloxycarbonyl-5,6-O-isopropylidene-2-deoxystreptamine (26)

The preceding compound (100 mg) was acetylated in a mixture of pyridine (1 ml) and acetic anhydride (0.5 ml). After 24 h, the solvent was removed by co-distillation with toluene and the syrupy residue was heated with a mixture of dioxane and cyclohexane to give a colorless solid (95 mg, 90%) that was chromatographically homogeneous; mp 106–108°C; $[\alpha]_D^{27}$ +35° (*c* 0.54, $CHCl_3$); ^{1}Hmr: 2.13 ppm (s, CH_3COO), etc.; compare with 1.93 ppm for the equatorial acetate group in the epimeric **21**. *Anal.* calcd. for $C_{44}H_{53}N_3O_{14}\cdot H_2O$: C 61.03, H 6.40, N 4.96; found: C 61.30, H 6.25, N 4.88.

4-O-(2-Benzyloxycarbonylamino-2-deoxy-α-D-allopyranosyl)-1,3-di-N-benzyloxycarbonyl-2-deoxystreptamine (Tri-N-benzyloxycarbonyl-3′-epiparomamine) (27)

A solution of **25** (300 mg) in 10 ml of 80% acetic acid was heated at 65–70°C for 1 h. The solvent was evaporated under reduced pressure and the residual crystalline solid was triturated with 50 ml of cold water. Filtration, washing with water, and drying gave the title compound which was recrystallized from methanol; yield 227 mg (84%); mp 243–245°C; $[\alpha]_D^{27}$ +42.8° (*c* 2.12, DMF); $[\alpha]_D^{27}$ +40° (*c* 2.10, dioxane); R_f 0.47 (tlc, $CHCl_3$–EtOAc–MeOH, 20:5:3). The C-3′ epimeric paromamine analog **18** showed R_f 0.40. *Anal.* calcd. for $C_{36}H_{43}N_3O_{13}$: C 59.58, H 5.97, N 5.79; found: C 59.15, H 6.26, N 5.59.

4-O-(2-Amino-2-deoxy-α-D-allopyranosyl)-2-deoxystreptamine (3′-Epiparomamine Trihydrochloride) (28) (23)

A mixture containing 467 mg of the preceding compound and 311 mg of palladium-hydroxide-on-charcoal (31) in 20 ml of methanol and 25 ml of dioxane containing 10 ml of 0.1 *N* hydrochloric acid was hydrogenated for 5 h. The catalyst was filtered on a layer of Celite, washed with 10 ml of water, and the filtrate was evaporated to dryness. The resulting yellow syrup was dissolved in water, the solution was decolorized with charcoal and processed as usual to give a colorless syrup that solidified from a mixture of water and ethanol. The colorless amorphous solid was dried at 50°C for 24 h; yield 254 mg (91%) of 3′-epiparomamine trihydrochloride (**28**); mp > 240°C (dec.); $[\alpha]_D^{27}$ +72.5° (*c* 0.60, H_2O); R_f 0.44 (tlc, $CHCl_3$–MeOH–28% NH_4OH, 1:3:2). On paper chromatograms (1-propanol – pyridine – acetic acid – water, 15:10:3:12) the product showed $R_{glucosamine}$ 0.19 and $R_{paromamine}$ 0.23 (21 h elution); high resolution mass spectral data for the tri-*N*-acetylper-*O*-trimethylsilyl derivative: *m/e* calcd. for fragment $C_{17}H_{38}NO_5Si_3$: 420.2058; found: 420.2072; calcd. for fragment $C_{16}H_{33}N_2O_4Si_2$: 373.1979; found: 373.1984; ^{13}C spectral data for 3′-epiparomamine are shown in Table 2.

Chemical characterization of 3′-epiparomamine was effected by hydrolytic studies. Acid hydrolysis (acetic acid – water – hydrochloric acid – 2-methoxymethanol, 10:3:2:5) (23) of tri-*N*-benzyloxycarbonyl-3′-epiparomamine at 100–110°C for 15 h, followed by paper chromatographic examination of the mixture, revealed the presence of two components, corresponding to 2-amino-2-deoxyallose (R_f 0.46) and 2-deoxystreptamine (R_f 0.20 (1-butanol – pyridine – water – acetic acid, 5:5:3:1) (33). In the same system, 2-amino-2-deoxy-D-glucose showed R_f 0.49 and the two amino sugars were easily separated, when analyzed individually or as a mixture.

4-O-(2-Benzyloxycarbonylamino-6-bromo-2,6-dideoxy-α-D-allopyranosyl)-1,3-di-N-benzyloxycarbonyl-2-deoxystreptamine (29)

Tri-*N*-benzyloxycarbonyl-3′-epiparomamine (**27**) (303 mg, 0.41 mmol) was dissolved in 20 ml of HMPT and the solution was reduced to half its volume by distillation under reduced pressure at 90°C to remove traces of moisture. The solution was diluted with 10 ml of dry HMPT, 227 mg (0.86 mmol) of triphenylphosphine was added, the solution was cooled to 0°C then treated with *N*-bromosuccinimide (146 mg, 0.82 mmol) as previously described. After stirring at room temperature for 10 h, tlc analysis revealed that the starting material had been transformed to a less polar product. Excess reagent was destroyed with methanol and the solvents were removed at 70°C *in vacuo*. The resulting syrup was dissolved in 3 ml of chloroform and the solution was diluted with ether to give a solid. This treatment eliminated a major portion of the triphenylphosphine oxide which remained in solution. The residual solid was isolated by decantation of the supernatant solution. It was then triturated with water, filtered, and air dried. Thin-layer chromatographic examination of the solid revealed the presence of a major product and traces of triphenylphosphine oxide and polar impurities. These were removed by trituration with chloroform, to leave a chromatographically homogeneous solid (200 mg). The filtrate was concentrated and applied to thick-layer plates ($CHCl_3$–EtOAc–MeOH, 20:5:2) to give 60 mg of the expected bromo derivative; total yield 260 mg (79%). Recrystallization was effected from ethanol; mp 209–211°C; $[\alpha]_D^{27}$ +25.9° (*c* 0.7, EtOH); *m/e*: 502 (corresponding to the glycosyl cation), 412, 315, etc; *m/e* 557 (corresponding to the 2-deoxystreptamine cation, with loss of a glycosyloxy portion from M^+), etc.

4-O-(6-Azido-2-benzyloxycarbonylamino-2,6-dideoxy-α-D-allopyranosyl)-1,3-di-N-benzyloxycarbonyl-2-deoxystreptamine (30)

A solution containing 217 mg (0.27 mmol) of the preceding compound and 225 mg of sodium azide in 7 ml of HMPT was heated at 55°C with stirring for 4 h. The solution was then cooled and added dropwise to 100 ml of ice-water, and the resulting precipitate was collected by filtration. The solid was dissolved in methanol, traces of insoluble material were removed by filtration, the filtrate was evaporated to dryness, and the residue was recrystallized from ethanol to give the title compound; yield 115 mg (56%); mp 195–197°C; $[\alpha]_D^{27}$ +36° (*c* 0.80, MeOH); ν_{max} (KBr): 2100 cm^{-1} (N_3). *Anal.* calcd. for $C_{36}H_{42}N_6O_{12}\cdot H_2O$: C 56.24, H 5.50, N 10.93; found: C 56.27, H 5.17, N 10.76.

4-O-(2,6-Diamino-2,6-dideoxy-α-D-allopyranosyl)-2-deoxystreptamine Tetrahydrochloride (3′-Epineamine Tetrahydrochloride) (31)

A suspension containing the preceding compound (104 mg,

0.13 mmol), 105 mg of palladium-hydroxide-on-charcoal catalyst in a 1:1 mixture of dioxane (10 ml), and 0.5 *N* hydrochloric acid (10 ml) was hydrogenated for 5 h. After filtration and evaporation of the filtrate, a pale yellow syrup was obtained. Treatment of an aqueous solution with decolorizing carbon and processing in the usual manner gave a colorless solid that was dissolved in the minimum volume of water containing 0.5 ml of methanol and was reprecipitated by addition of ethanol. The title compound was thus obtained as a chromatographically homogeneous solid; yield 60 mg (93%); mp 200–205°C (dec.); $[\alpha]_D^{27}$ +62.1° (*c* 0.66, H_2O); R_f 0.37 in $CHCl_3$ – MeOH – 28% NH_4OH, 1:3:2. Neamine showed R_f 0.45 in the same solvent system; high resolution mass spectral data for the tetra-*N*-acetylper-*O*-trimethylsilyl derivative: *m/e* calcd. for fragment $C_{16}H_{33}N_2O_5Si_2$: 389.1928; found: 389.1949; calcd. for fragment $C_{16}H_{33}N_2O_4Si_2$: 373.1979; found: 373.1990; ^{13}C spectral data for 3′-epineamine are shown in Table 2.

Acknowledgements

We thank the National Research Council of Canada (PRAI Grant) for financial support. We also thank R. Mayer for recording ^{13}C spectra and P. Coulombe for mass spectral measurements.

1. S. HANESSIAN, T. TAKAMOTO, and R. MASSÉ. J. Antibiot. **28**, 835 (1975).
2. S. UMEZAWA. Adv. Carbohydr. Chem. Biochem. **30**, 111 (1974)
3. H. UMEZAWA. Adv. Carbohydr. Chem. Biochem. **30**, 183 (1974).
4. R. BENVENISTE and J. DAVIES. Annu. Rev. Biochem. **42**, 471 (1973); Antimicrob. Agents Chemother. **4**, 402 (1973).
5. K. E. PRICE, J. C. GODFREY, and H. KAWAGUCHI. Adv. Appl. Microbiol. **18**, 191 (1974).
6. S. MITSUHASHI (*Editor*). Aminoglycoside antibiotics. University Park Press, Baltimore, MD. 1975.
7. K. FUJISAWA, T. HOSHIYA, and H. KAWAGUCHI. J. Antibiot. **28**, 677 (1974).
8. A. B. FOSTER, M. STACEY, and S. V. VARDHEIM. Acta Chem. Scand. **13**, 281 (1959).
9. J. D. ALBRIGHT and L. GOLDMAN. J. Org. Chem. **30**, 1107 (1965); see also S. HANESSIAN and R. F. BUTTERWORTH. Synthesis, 70 (1971) and references cited therein.
10. K. E. PFITZNER and J. G. MOFFATT. J. Am. Chem. Soc. **85**, 3027 (1963).
11. B. R. BAKER and D. H. BUSS. J. Org. Chem. **30**, 2308 (1965).
12. A. S. PERLIN, B. CASU, and H. J. KOCH. Can. J. Chem. **48**, 2596 (1970); see also G. KOTOWYCZ and R. U. LEMIEUX. Chem. Rev. **73**, 669 (1973).
13. B. R. BAKER and D. H. BUSS. J. Org. Chem. **31**, 217 (1966).
14. S. HANESSIAN. Carbohydr. Res. **1**, 86 (1966); S. HANESSIAN. Methods Carbohydr. Chem. **6**, 183 (1972) and references cited therein.
15. S. HANESSIAN and R. MASSÉ. Carbohydr. Res. **35**, 175 (1974).
16. D. HORTON. *In* The amino sugars. Vol. 1A. *Edited by* R. W. Jeanloz. Academic Press, New York, NY. 1969. pp. 3–190; L. HOUGH and A. C. RICHARDSON. *In* Rodd's chemistry of carbon compounds. Vol. 1F. *Edited by* S. Coffey. Elsevier, Amsterdam. 1967. pp. 449–500.
17. S. UMEZAWA, K. TATSUTA, T. TSUCHIYA, and E. KITAZAWA. J. Antibiot. **20**, 53 (1962).
18. T. TSUCHIYA and S. UMEZAWA. J. Antibiot. **18**, 1181 (1965).
19. T. P. CULBERTSON, D. R. WATSON, and T. H. HASKELL. J. Antibiot. **26**, 790 (1973).
20. I. WATANABE, T. TSUCHIYA, S. UMEZAWA, and H. UMEZAWA. J. Antibiot. **26**, 802 (1973).
21. M. M. PONPIPOM and S. HANESSIAN. Carbohydr. Res. **18**, 342 (1971); S. HANESSIAN and P. LAVALLEE. Methods Carbohydr. Chem. **7**, 49 (1976) and references cited therein.
22. S. HANESSIAN, R. F. BUTTERWORTH, and T. NAKAGAWA. Carbohydr. Res. **26**, 261 (1973).
23. S. UMEZAWA, S. KOTO, K. TATSUTA, and T. TSUMURA. Bull. Chem. Soc. Jpn. **42**, 529 (1969).
24. F. W. LICHTENTHALER. Chem. Ber. **96**, 845 (1963); see also F. W. LICHTENTHALER and P. EMIG. Carbohydr. Res. **7**, 121 (1967).
25. D. C. DE JONGH, J. D. HIRBAR, S. HANESSIAN, and P. W. K. WOO. J. Am. Chem. Soc. **89**, 3364 (1967); see also D. C. DE JONGH, E. B. HILLS, J. D. HRIBAR, and S. HANESSIAN. Tetrahedron, **29**, 2707 (1973).
26. P. W. K. WOO and R. D. WESTLAND. Carbohydr. Res. **26**, 522 (1973).
27. S. OMOTO, S. INOUYE, M. KOJIMA, and T. NIIDA. J. Antibiot. **26**, 717 (1973).
28. T. L. NAGABUSHAN and P. J. L. DANIELS. Tetrahedron Lett. 747 (1975).
29. K. F. KOCH, J. A. RHOADES, E. W. HAGAMAN, and E. WENKERT. J. Am. Chem. Soc. **96**, 3300 (1974).
30. H. EGGERT and C. DJERASSI. J. Am. Chem. Soc. **95**, 3710 (1973).
31. W. PEARLMAN. Tetrahedron Lett. 1663 (1967).
32. A. NEUBERGER and R. PITT-RIVERS. J. Chem. Soc. 122 (1939).
33. F. G. FISCHER and H. J. NEBEL. Z. Physiol. Chem. 302 (1955).

Can. J. Chem. Downloaded from www.nrcresearchpress.com by 210.87.254.105 on 09/05/12
For personal use only.

The dissociation constant for potassium methylamide ion pairs in methylamine[1]

E. ALLAN SYMONS AND J. DOUGLAS BONNETT

Physical Chemistry Branch, Chalk River Nuclear Laboratories, Atomic Energy of Canada Limited, Chalk River, Ont., Canada K0J 1J0

Received November 24, 1977

E. ALLAN SYMONS and J. DOUGLAS BONNETT. Can. J. Chem. **56**, 1518 (1978).

The limiting equivalent conductance (Λ_0) and ion pair dissociation constant (K_d) have been obtained for potassium methylamide in methylamine from conductance data measured over the temperature range -55 to $+25$°C. The value of K_d increases from 6.3×10^{-8} mol L^{-1} at the highest temperature to 9.4×10^{-7} mol L^{-1} at the lower limit. The results show good agreement with literature data for potassium amide in ammonia after corrections for differences in solvent viscosity and dielectric constant. The heat of dissociation is -26 kJ mol^{-1} above -15°C, but decreases gradually at progressively lower temperatures as a shift occurs from tight to loose ion pair structures.

E. ALLAN SYMONS et J. DOUGLAS BONNETT. Can. J. Chem. **56**, 1518 (1978).

On a déterminé la conductivité équivalente limite (Λ_0) et la constante de dissociation des paires d'ions (K_d) pour le méthylamidure de potassium dans la méthylamine à partir de données de conductivité mesurées à des température allant de -55 à $+25$°C. La valeur de K_d augmente de 6.3×10^{-8} mol L^{-1} jusqu'à 9.4×10^{-7} mol L^{-1} lorsque l'on passe de la température la plus élevée à la limite inférieure. Les résultats montrent une bonne concordance avec les données de la littérature pour l'amidure de potassium dans l'ammoniac après corrections pour les différences de viscosité de solvant et de constante diélectrique. La chaleur de dissociation est de -26 kJ mol^{-1} au dessus de -15°C mais cette valeur diminue graduellement à mesure que la température diminue; ce résultat est le reflet d'un déplacement qui se produit dans les structures des paires d'ions qui passent d'une nature intime vers une structure plus lâche.

[Traduit par le journal]

Introduction

A chemical process based on isotopic exchange between molecular hydrogen and methylamine has been considered (1) as an alternative to the hydrogen sulphide – water exchange process currently used in Canada for the production of heavy water. Unlike the latter process, the methylamine system requires an added catalyst (eq. [1]) to accelerate the deuterium isotope exchange rate to a useful level. The compounds examined as potential catalysts have been the alkali metal salts of methylamine, with potassium methylamide (PMA) receiving the most study.

$$[1] \qquad HD + CH_3NH_2 \xrightarrow{PMA} H_2 + CH_3NHD$$

In spite of the extensive body of kinetic data now available from Holtslander,[2] Kalra and Otto (2), and Rochard and Ravoire (3) for isotope exchange in concentrated solution, the mechanism of reaction [1] has yet to be clarified. A major problem has been the lack of information concerning the degree of dissociation of the catalyst PMA into free ions, eq. [2]. Since methylamine has a fairly low dielectric constant (about 9.4 at 25°C), concentrated PMA solutions should consist of a mixture of free ions, ion pairs, triple ions, and larger ion aggregates. Rochard has reported the values 3×10^{-7} mol L^{-1} at -90°C and 4×10^{-7} mol L^{-1} at -62°C for the ion pair dissociation constant, K_d, in dilute solution (3, 4).

$$[2] \qquad CH_3NH^-K^+ \overset{K_d}{\rightleftharpoons} CH_3NH^- + K^+$$

The results of an electrical conductivity study of K_d for PMA as a function of temperature over the range -55 to $+25$°C are now presented.

Experimental

Reagents

Water and most of the ammonia were removed from commercial methylamine (Matheson) by at least one treatment of the liquid with lithium metal. The precipitated mixture of lithium hydroxide and amide was left behind during subsequent fractional vacuum distillation onto fresh lithium. Ammonia analysis was by gas chromatography: TC detector, He at 30 mL min^{-1}, 2 m × 6 mm column packed with 28% Pennwalt 223 – 4% KOH on 80–100 mesh Gas Chrom R. Liquid amine samples were diluted 1:3 with absolute ethanol, 100 μL of the resultant solutions being injected at 65°C isothermal. Purified methylamine was found to contain between 3×10^{-3} and 2×10^{-2} mol L^{-1} NH_3.

Stock PMA solutions were prepared as described previously (5). Standard KCl solutions were made up with J. T. Baker Ultrex grade KCl and quadruple-distilled water (acidic dichromate and alkaline permanganate treatments).

[1] AECL No. 6196.

[2] W. J. Holtslander and co-workers at Chalk River Nuclear Laboratories (CRNL), Atomic Energy of Canada Limited (AECL).

Can. J. Chem. Downloaded from www.nrcresearchpress.com by 210.87.254.6 on 09/05/12
For personal use only.

Can. J. Chem. Downloaded from www.nrcresearchpress.com by 210.87.254.6 on 09/05/12
For personal use only.

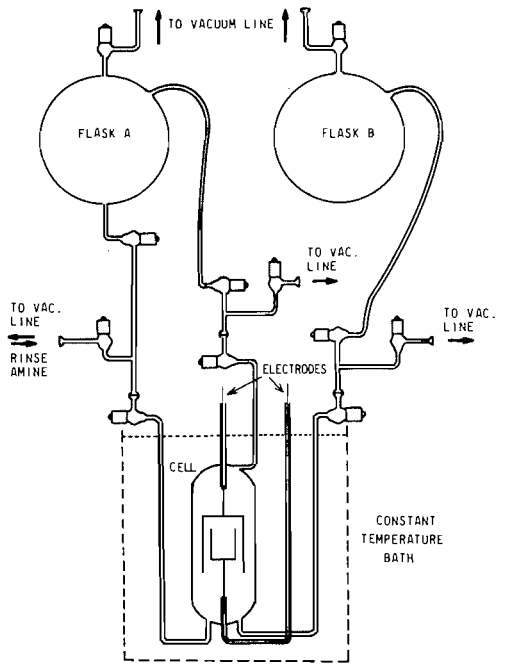

FIG. 1. Apparatus used to study electrical conductivity of methylamine solutions.

Apparatus

The constant temperature bath was a Neslab model LTV 40 low temperature type with a side window. Absolute ethanol was used as bath fluid over the range −60 to +25°C; control was better than ±0.02°C. Temperatures were measured with a Stolab 911 PL electronic thermometer that had been calibrated against a standard platinum resistance thermometer; accuracy was ±0.02°C.

Conductivity cell resistance was measured with a Beckman RC-18A bridge, with a specified accuracy of ±0.05% over the range 500 to 50 000 Ω. The design of the electrode system was based on the recommendations of Nichol and Fuoss (6). The pair of concentric platinum cylinders (1 cm diameter × 2 cm long and 2 cm diameter × 3 cm long) was mounted vertically in the conductivity cell (see Fig. 1). The cell was calibrated at 25.0°C with KCl solutions. The cell constant, an average of 0.0351 ± 0.0012 cm^{-1} for three determinations, was obtained by using the equation of Fuoss and co-workers (7).

Conductivity Measurements

The solution handling and conductivity cell systems are illustrated in Fig. 1. The vessels were constructed of Pyrex glass, with liquid feedthrough tubes ring-sealed at the vertical O-ring joint connection points to prevent solution contact with the ethylene–propylene rubber O-rings. The latter had been pretreated with concentrated PMA solution. The standard Teflon–glass stems in the J. Young Co. greaseless valves were replaced with chemically more resistant low density polyethylene stems.

To remove water still on the vessel walls after normal vacuum drying (8), the system was rinsed with concentrated PMA solution and then dry methylamine. The temperature of the bath was lowered or raised from ambient to facilitate liquid transfer into the cell from flask A or out of the cell to waste storage flask B, respectively.

The conductance solutions were prepared in flask A by successive dilution with dry methylamine (vacuum transfer), starting from a stock concentrated PMA solution of known concentration. The first portion of each such solution was used to rinse the cell again. The concentrations of the diluted solutions were calculated from the measured weight of added methylamine at each stage.

A series of resistance readings was made at 1000 and 3000 Hz as a function of temperature for each concentration. The readings normally stabilized within 15 to 20 min after a change in temperature. For values above about 90 kΩ, a 10 kΩ precision resistor (0.01%) was placed in parallel with the cell (9). A correction (usually less than 0.1%) was made for the effects of electrode polarization, using the procedure of Robinson and Stokes (10).

Equivalent conductance values (Λ) were calculated from the resistance data in the normal manner. The correction for the specific conductance of the solvent ranged from two percent for the concentrated solutions to ten percent for the most dilute ones. The Λ data are believed to be accurate within ±10% for these highly reactive solutions, based on likely errors in resistance and concentration values.

Results

Plots of Λ at constant temperature versus the square root of the stoichiometric concentration produced the curves normally expected for an ion-paired electrolyte in a solvent of moderately low dielectric constant (11) (see Fig. 2). However, when some data obtained by Holtslander[2] at higher concentrations up to 0.4 mol L^{-1} were included, there was no indication of the shallow minimum usually seen at the onset of formation of triple ions (10).

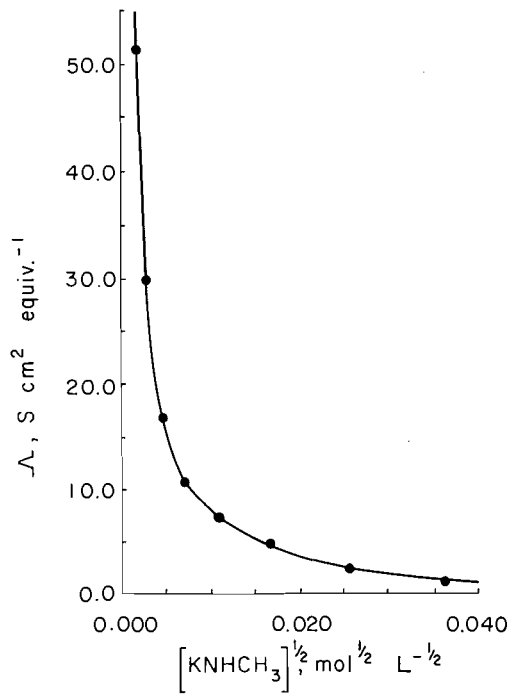

FIG. 2. Dependence of potassium methylamide solution equivalent conductance on concentration at 25.0°C.

Can. J. Chem. Downloaded from www.nrcresearchpress.com by 210.87.254.6 on 09/05/12
For personal use only.

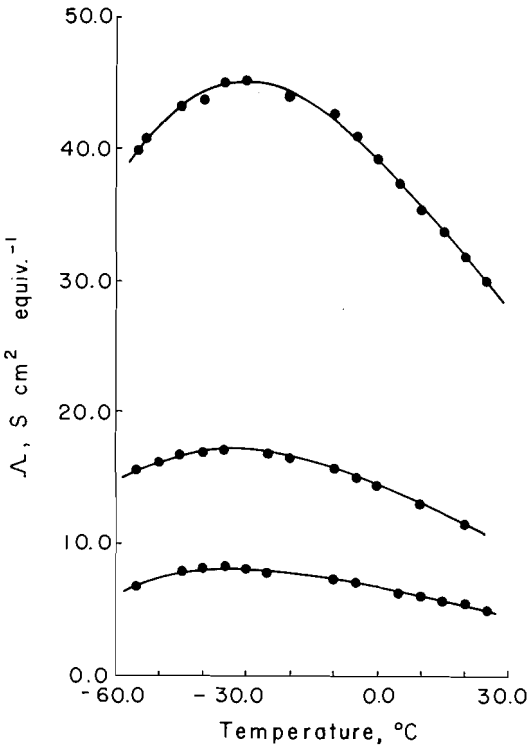

FIG. 3. Dependence of potassium methylamide solution equivalent conductance on temperature at (top to bottom) 9.04×10^{-6}, 5.01×10^{-5}, and 2.84×10^{-4} mol L^{-1} (25°C).

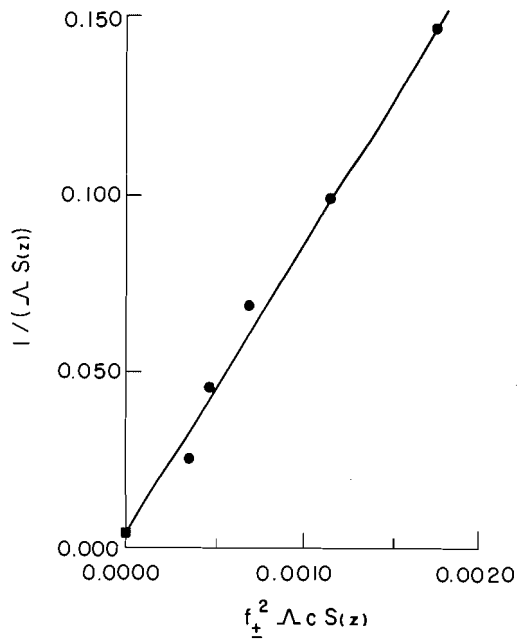

FIG. 4. Fuoss plot (11–13) for potassium methylamide in methylamine at 0.0°C (a = 3 Å, $\Lambda_0\eta$ = 66 mPa s S cm² equiv.$^{-1}$).

The dependence of Λ on temperature for three representative concentrations is shown in Fig. 3. An explanation for the distinct maximum seen in each case at about −30°C is considered in the Discussion section.

The limiting equivalent conductance, Λ_o, and the ion pair dissociation constant, K_d, were determined by the procedure of Fuoss and co-workers (12–14), as outlined below. Only conductivity data measured at stoichiometric concentrations (c) below 5×10^{-4} mol L^{-1} were used; above this concentration, calculated from the equation $c = 1.19 \times 10^{-14} D^3T^3$ (14) (where D is solvent dielectric constant and T the absolute temperature), triple ion formation becomes important.

There are two similar equations which may be employed to obtain Λ_o and K_d, both of which give identical results when K_d is less than 10^{-3} mol L^{-1} (12, 14). The one chosen for the present study was:

$$[3] \qquad 1/(\Lambda S(z)) = 1/\Lambda_0 + c\Lambda f_{\pm}^2 S(z)/(K_d\Lambda_0^2)$$

The function $S(z)$ is defined in ref. 14. The equation used to calculate $\log f_{\pm}^2$ (mean activity coefficient $f_{\pm}$) was that given by Robinson and Stokes (ref. 10, p. 229).

A computer program was used to evaluate and plot the terms in eq. [3], starting with an estimate for Λ_0 (based on an extrapolation of the Λ data to zero concentration at each temperature) and assigning the value 3 Å to the ion pair size parameter "a" in the log $f_{\pm}^2$ equation.[3] A Fuoss plot of $1/(\Lambda S(z))$ vs. $c\Lambda f_{\pm}^2 S(z)$ for each set of data gave a line of slope $1/(K_d\Lambda_0^2)$ and intercept $1/\Lambda_0$, from which K_d and Λ_0 could be determined. This value of Λ_0 was fed back into eq. [3] on an iterative basis until new and old values agreed within 1.0 S cm² equiv.$^{-1}$.

A typical Fuoss plot is shown in Fig. 4. Included is a refinement brought about by the observation of a random scatter in the final computer Λ_0 data as a function of temperature (see Table 1). To smooth out the data Walden's Rule (15) was applied, the product of the computer Λ_0 and the solvent viscosity, η, being averaged for the temperature range −45 to +15°C. A refined value of the limiting equivalent conductance, Λ_0', was then calculated from this average $\eta\Lambda_0$ (66 mPa S cm² equiv.$^{-1}$) and the η at each temperature. Finally, the Λ_0' values were run through the computer program to obtain the set of X, Y coordinates for the final Fuoss plot (no optimization). A least-squares line was drawn through these coordinates, including the $X = 0$, $Y = 1/\Lambda_0'$ point (shown as a square point in Fig. 4), to permit a calculation of K_d.

[3]A change from 3 to 4 to 5 Å for "a" had no significant effect on the values of Λ_0 and K_d obtained.

Can. J. Chem. Downloaded from www.nrcresearchpress.com by 210.87.254.6 on 09/05/12
For personal use only.

TABLE 1. Measured and refined limiting equivalent conductance for $KNHCH_3$ in methylamine as a function of temperature

Temperature (°C)	Viscosity, η (mPa s)*	Computer Λ_0† (S cm² equiv.$^{-1}$)	$\eta\Lambda_0$ (mPa s S cm² equiv.$^{-1}$)	Λ_0'‡ (S cm² equiv.$^{-1}$)
25.0	0.205	221	45	322
20.0	0.212	253	54	311
15.0	0.219	290	64	301
10.0	0.228	284	65	289
5.0	0.237	304	72	278
0.0	0.250	301	75	264
−5.0	0.264	251	66	250
−10.0	0.280	242	68	236
−15.0	0.298	226	67	221
−20.0	0.318	207	66	208
−25.0	0.340	179	61	194
−30.0	0.366	254	56	180
−35.0	0.393	141	55	168
−40.0	0.425	149	63	155
−45.0	0.460	175	81	143
−50.0	0.500	274	137	132
−55.0	0.545	§	—	121

*From unpublished data compiled by W. E. Lockerby *et al.*, CRNL.
†Parameter a = 3 Å.
‡Based on average $\eta\Lambda_0$ = 66 mPa s S cm² equiv.$^{-1}$.
§Fuoss plot intercept was negative.

TABLE 2. Experimental K_d for $KNHCH_3$ in methylamine as a function of temperature

Temperature (°C)	$10^7 K_d$* (mol L^{-1})	Temperature (°C)	$10^7 K_d$ (mol L^{-1})
25.0	0.63	−20.0	3.9
20.0	0.77	−25.0	4.7
15.0	0.94	−30.0	5.8
10.0	1.2	−35.0	6.8
5.0	1.4	−40.0	7.8
0.0	1.8	−45.0	8.7
−5.0	2.2	−50.0	9.2
−10.0	2.6	−55.0	9.4
−15.0	3.3		

*Based on a = 3 Å and $\eta\Lambda_0$ = 66 mPa s S cm² equiv.$^{-1}$.

The resultant K_d data as a function of temperature are given in Table 2, while Fig. 5 shows a Van't Hoff plot of the results (16). Because of the procedure used to obtain Λ_0 and K_d, the uncertainty in their values may be as high as 20% for Λ_0 and 30% for K_d, although relative agreement appears to be better than this.

Discussion

Potassium Methylamide or Amide?

Some ammonia is always present in methylamine solutions of methylamide salts, either from the solvent itself or from slow thermal decomposition of the salts (5). Ammonia can react with potassium methylamide to form potassium amide, eq. [4]. K_{eq}

$$[4] \qquad KNHCH_3 + NH_3 \overset{K_{eq}}{\rightleftharpoons} CH_3NH_2 + KNH_2$$

has not been measured directly but estimates reported are 9 and 50 (footnote 4 and ref. 17, respectively). The question therefore arose as to whether the conductivity data, obtained at low PMA concentrations, were in fact applicable to PMA or to KNH_2.

Although $K_{eq} > 1$, the high concentration of the methylamine as solvent (ca. 21 mol L^{-1}) will suppress the formation of KNH_2 at least for reasonably low concentrations of NH_3. In the present work, the NH_3 concentration was generally in the range 3×10^{-3} to 1×10^{-2} mol L^{-1}, which would convert no more than 0.4% of the PMA, assuming a value of $K_{eq} = 10$. For Rochard's work with methylamine containing up to 0.1 mol L^{-1} NH_3 (3, 4), the conversion would have been closer to 5%.

Some success was later achieved in substantially lowering the concentration of ammonia in the methylamine by using a low-temperature fractional distillation technique.[5] A 1 m long vacuum-jacketed column, based on a design in the literature (18), was operated under reflux with cooling fluid pumped through the central condenser tube at about −21°C (bp NH_3 −33.4°C, CH_3NH_2 −6.5°C). By removing up to eight 2 ml condensed vapour samples from the top of the column over a period of 48 h, it was possible to decrease the NH_3 content of the methyl-

[4]Raylo Chemicals Limited, Edmonton, Alta., under research contract to AECL, 1969–1972.

[5]The procedure was developed in cooperation with Dr. J. D. Halliday and P. E. Bindner at CRNL.

Can. J. Chem. Downloaded from www.nrcresearchpress.com by 210.87.254.6 on 09/05/12
For personal use only.

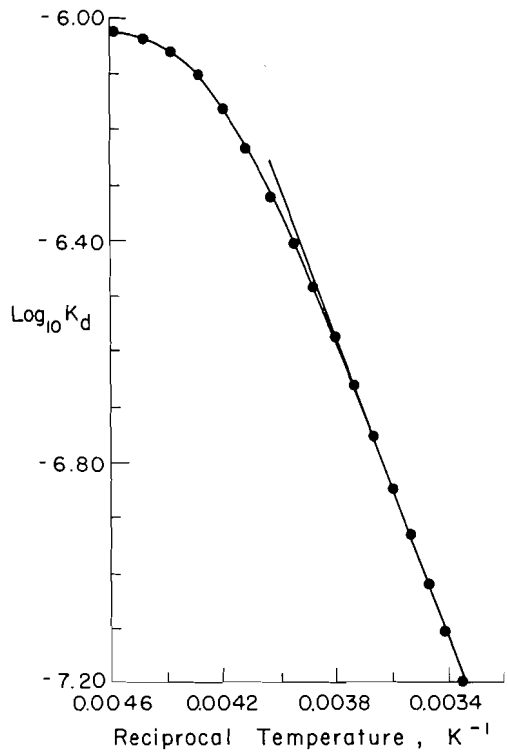

FIG. 5. Van't Hoff plot for potassium methylamide ion pair dissociation in methylamine. ΔH_d from linear portion is -26 kJ mol^{-1}.

amine in the 2 L pot (initially 4×10^{-3} mol L^{-1} NH_3) to below 1×10^{-5} mol L^{-1}.

In spite of this ability to obtain methylamine *initially* very low in NH_3, it was found impossible to maintain a low level for any useful period of time. The thermal decomposition of methylamide salts in methylamine solutions that occurs at higher temperatures and concentrations to produce ammonia (5) still proceeds at a significant rate under the conditions of conductivity measurement. In addition, the reaction of potassium with low-NH_3 methylamine to make moderately dilute $KNHCH_3$ solutions for study tended to generate NH_3 at concentrations up to 5×10^{-4} mol L^{-1}.

Theoretical Value of K_d *for* $KNHCH_3$

Fuoss has derived a relation between the ion *association* constant, K_a, and the solvent dielectric constant (D) for 1:1 electrolytes (19). In eq. [5], e is the electronic charge and k the Boltzmann constant. No allowance is made for specific ions or solute–solvent interactions.

$$[5] \quad K_a = 1/K_d = 2.524 \times 10^{-3}\, a^3 e(e^2/akDT)$$

The values calculated at several temperatures for a 1:1 electrolyte in methylamine are compared in Table 3 with the data measured for $KNHCH_3$. The agreement between theoretical and experimental K_d is best for a value of "a" (in eq. [5]) just greater than 3 Å. Delmas (20) chose 3 Å for KNH_2 in ammonia, based on the sum of the ionic radii for this salt. The K_d derived from Rochard's conductivity data at -90°C is smaller than expected by at least a factor of 10 (Table 3) but the reason is not known.

TABLE 3. Dependence of theoretical K_d for $KNHCH_3$ in methylamine on value of "a" and comparison with experimental results

Temperature (°C)	Theoretical K_d* (mol L^{-1}) $a = 3$ Å	$a = 4$ Å	$a = 5$ Å	Measured K_d† (mol L^{-1})
25.0	3.8×10^{-8}	2.3×10^{-6}	—	6.3×10^{-8}
0.0	8.5×10^{-8}	4.1×10^{-6}	3.6×10^{-5}	1.8×10^{-7}
-50.0	4.9×10^{-7}	1.5×10^{-5}	1.0×10^{-4}	9.2×10^{-7}
-90.0	8.2×10^{-7}	2.2×10^{-5}	—	9.2×10^{-8}‡

*Via eq. 5.
†Based on $\eta\Lambda_0 = 66$ mPa s S cm^2 equiv.$^{-1}$; practically insensitive to value chosen for "a", $a = 3$ Å.
‡Calculated from Rochard's data (4) via Fuoss plot.

Temperature Dependence of K_d *for* $KNHCH_3$

A Van't Hoff plot of log K_d vs. $1/T$ provides the heat of dissociation, ΔH_d, for the ion pairs (16). The plot for $KNHCH_3$ in methylamine, Fig. 5, yields a value of -26 kJ mol^{-1} for the linear region above about -15°C. This result is comparable to those found for other ion pairing equilibria (16).

The marked curvature seen in this plot below -15°C has also been observed in other systems (21, 22). It has been explained on the basis of an equilibrium between two types of ion pairs, 'tight' and 'loose', with the latter containing one or more solvent molecules sandwiched between the anion and cation (21). The tight ion pair, with a larger heat of dissociation, is favoured at higher temperature, while the other, with a smaller ΔH_d, is favoured at low temperature (21).

The above results help to explain the shape of the Λ–temperature plots in Fig. 3. The distinct maximum, seen also by Holtslander[2] at much higher PMA concentrations up to the solubility limit of 0.4 mol L^{-1}, can arise from a combination of two factors (23). The solution conductance is dependent on both the number of ions and their mobilities. When the temperature is raised, from e.g. -60°C, the ion mobilities will increase because the solvent viscosity decreases, but at the same time K_d decreases (Fig. 5), thereby lowering the total number of ions. Thus the viscosity effect dominates at temperatures below the conductance maximum, while the

decrease in K_d becomes dominant at higher temperatures.

A Comparison of $KNHCH_3$ in CH_3NH_2 with KNH_2 in NH_3

The present results for $KNHCH_3$ in methylamine can be compared with the data of Delmas *et al.* (20, 24) for KNH_2 in ammonia. First, the Λ_0 of a salt at a given temperature should only differ, to a first approximation, by the ratio of the solvent viscosities (Walden's Rule (15)). At $-33.4°C$ $\eta_{NH_3} = 0.255$ and $\eta_{CH_3NH_2} = 0.384$ mPa s. Delmas gives $\Lambda_{0(KNH_2-NH_3)} = 308$ S cm^2 equiv.$^{-1}$ at this temperature, so that $\Lambda_{0(KNH_2-CH_3NH_2)}$ is predicted to be 205 S cm^2 equiv.$^{-1}$. The experimental value for $\Lambda_{0(KNHCH_3-CH_3NH_2)}$, based on the assumption of constant $\Lambda_0\eta$ in methylamine (as discussed earlier), is somewhat lower at about 172 S cm^2 equiv.$^{-1}$, which is consistent with $^-NHCH_3$ being a slightly larger ion than $^-NH_2$.

The K_d values for the salts in the two solvents should be related by the respective dielectric constants through eq. [5]. The conversion factor $\exp [(e^2/akT)(1/D_{CH_3NH_2} - 1/D_{NH_3})]$ was used. At $-33.4°C$, $D_{NH_3} = 22.4$, $D_{CH_3NH_2} = 13.1$, and $K_{d(KNH_2-NH_3)} = 1.0 \times 10^{-4}$ mol L^{-1} (20). The value thus predicted for $K_{d(KNH_2-CH_3NH_2)}$ is 1.2×10^{-6} mol L^{-1} for $a = 3$ Å and 3.9×10^{-7} mol L^{-1} for $a = 4$ Å. These compare favourably with the experimental $K_{d(KNHCH_3-CH_3NH_2)}$ at this temperature, 6.5×10^{-7} mol L^{-1}, and suggest again that "a" for $KNHCH_3$ lies between 3 and 4 Å.

Acknowledgements

The authors are grateful for discussions with Drs. J. H. Rolston, J. D. Halliday, and W. J. Holtslander at CRNL, and for the assistance provided by J. G. Wesanko in the construction of the conductivity cell. The provision of some data by Dr. Holtslander prior to publication is appreciated.

1. A. R. Bancroft and H. K. Rae. Atomic Energy of Canada Limited, Report AECL-3684. 1970.
2. H. Kalra and F. D. Otto. Can. J. Chem. Eng. **52**, 258 (1974).
3. E. Rochard and J. Ravoire. J. Chim. Phys. **68**, 1183 (1971); E. Rochard. Centre d'Études Nucléaires de Saclay, France. Report CEA-R-3835. June 1969.
4. E. Rochard. Centre d'Études Nucléaires de Saclay, France. Report DPC.SIS.SCI./70. 133/ER/NG. May 1970.
5. J. D. Halliday, E. A. Symons, and J. D. Bonnett. Can. J. Chem. **56**, 1455 (1978).
6. J. C. Nichol and R. M. Fuoss. J. Phys. Chem. **58**, 696 (1954).
7. J. E. Lind, Jr., J. J. Zwolenik, and R. M. Fuoss. J. Am. Chem. Soc. **81**, 1557 (1959).
8. R. E. Cuthrell and J. J. Lagowski. J. Phys. Chem. **71**, 1298 (1967).
9. H. Wang and P. Hemmes. J. Am. Chem. Soc. **95**, 5119 (1973).
10. R. A. Robinson and R. H. Stokes. Electrolyte solutions. 2nd ed., revised. Butterworths, London, England. 1970.
11. R. M. Fuoss. J. Chem. Educ. **32**, 527 (1955).
12. R. M. Fuoss and T. Shedlovsky. J. Am. Chem. Soc. **71**, 1496 (1949).
13. R. M. Fuoss. J. Am. Chem. Soc. **79**, 3301 (1957).
14. R. M. Fuoss and F. Accascina. Electrolytic conductance. Interscience, New York, NY. 1959. Chapt. 17.
15. H. S. Harned and B. B. Owen. The physical chemistry of electrolytic solutions. Reinhold Publishing Corp., New York, NY. 1958. pp. 283–286.
16. C. W. Davies. Ion association. Butterworths, London, England. 1962. Chapt. 12.
17. K. Bar-Eli and F. S. Klein. J. Chem. Soc. 3083 (1962).
18. D. F. Shriver. The manipulation of air-sensitive compounds. McGraw-Hill, New York, NY. 1969.
19. R. M. Fuoss. J. Am. Chem. Soc. **80**, 5059 (1958).
20. R. Delmas. Centres d'Études Nucléaires de Saclay, France. Report CEA-R-3377. 1968.
21. M. Szwarc. Ions and ion pairs in organic reactions. Vol. 1. Wiley-Interscience, New York, NY. 1972.
22. M. Szwarc. Carbanions, living polymers and electron transfer processes. Interscience, New York, NY. 1968.
23. C. A. Kraus. J. Phys. Chem. **60**, 129 (1956).
24. R. Delmas, R. Courvoisier, and J. Ravoire. Adv. Chem. Ser. **89**, 25 (1969).

Can. J. Chem. Downloaded from www.nrcresearchpress.com by 210.87.254.6 on 09/05/12
For personal use only.

Reduction of cyclic anhydrides. II. Factors affecting regioselectivity of attack on the carbonyl group by metal hydrides

MARGARET M. KAYSER AND PETER MORAND

Department of Chemistry, University of Ottawa, Ottawa, Ont., Canada K1N 6N5

Received November 21, 1977

MARGARET M. KAYSER and PETER MORAND. Can. J. Chem. **56**, 1524 (1978).

The reduction of unsymmetrically substituted cyclic anhydrides with metal hydrides often leads to the preferential formation of one of the two possible lactones. In the light of recent experimental findings and theories concerning metal hydride addition to the carbonyl function, the electronic and steric factors influencing regioselectivity of cyclic anhydride reductions are discussed and an explanation for the observed patterns is proffered. Similar considerations may be extended to predict the major lactonic products in the reductions of various other unsymmetrical cyclic anhydrides.

MARGARET M. KAYSER et PETER MORAND. Can. J. Chem. **56**, 1524 (1978).

La réduction par les hydrures métalliques d'anhydrides cycliques substitués d'une façon non-symétrique conduit souvent à la formation préférentielle d'une des deux lactones possibles. A la lumière de résultats expérimentaux récents et des théories concernant l'addition des hydrures métalliques sur les fonctions carbonyles, on discute des facteurs électroniques et stériques influençant la régiosélectivité des réductions d'anhydrides cycliques et on présente une explication pour les tendances observées. On peut étendre des considérations similaires pour prédire la nature des produits lactoniques principaux formés lors de la réduction de divers autres anhydrides cycliques non-symétriques.

[Traduit par le journal]

The direct conversion of a cyclic anhydride into the corresponding lactone is of general interest to chemists, as it is well established that lactones are important intermediates in the synthesis of a variety of compounds, particularly natural products; see, for example, ref. 1*a*. Several methods have been used to accomplish this conversion (1*b* and *c*) but the simplest and most effective are reductions with metal hydrides. Unsymmetrically substituted anhydrides can potentially yield two lactones. Catalytic hydrogenations generally produce lactones resulting from the reduction of the less hindered carbonyl function (1*b*). Reductions with metal hydrides, often but not always, take place selectively at the more hindered carbonyl group (2, 3). In this paper, an attempt is made to identify the factors which appear to govern regioselectivity in metal hydride reductions.

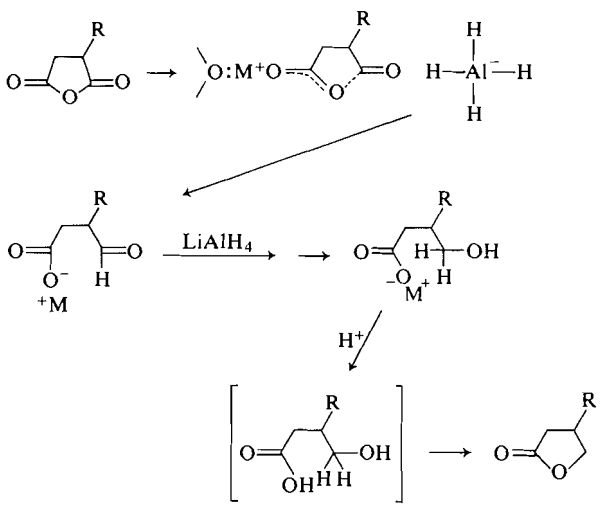

FIG. 1. Mechanism for anhydride reductions with metal hydrides proposed by Bloomfield and Lee (2*b*).

Selective reduction of the more sterically encumbered carbonyl group with metal hydrides has been explained by a mechanism involving initial attack of a metal cation on the less hindered carbonyl function, followed by the transfer of a hydride ion to the more hindered carbonyl group (2*a* and *b*).[1] The intermediate aldehyde is then rapidly reduced to yield an alcohol function and cyclization occurs upon acidification (Fig. 1). Although never challenged, the mechanism of Bloomfield and Lee (2*b*) fails to explain known cases of preferential reduction of the less hindered carbonyl group (3*c* and *d*).

In the course of our work on reductions of cyclic anhydrides, we have encountered other cases of

[1]Such selectivity has been reported in the reactions of steroidal cyclic anhydrides (3*a* and *b*) with lithium aluminum hydride and lithium tri-*tert*-butoxyaluminum hydride. With the latter reagent, lactols (hemiacylals) are formed by closure of the intermediate carboxyaldehyde. The authors explained the regioselectivity observed in terms of inter- or intramolecular complex formation similar to that invoked by Bloomfield and Lee (2*b*). We have examined the Dreiding model of **19** and concluded that it is the slightly more accessible carbonyl group which undergoes reduction. However, in view of the very similar steric environment around the carbonyl groups the perception of which one is more hindered remains disputable.

Can. J. Chem. Downloaded from www.nrcresearchpress.com by 210.87.254.5 on 09/05/12
For personal use only.

Can. J. Chem. Downloaded from www.nrcresearchpress.com by 210.87.254.5 on 09/05/12
For personal use only.

selective nucleophilic additions to the less hindered carbonyl group (**10** and **11**), as well as examples of reduction of the more sterically congested carbonyl function (**1**, **3**, **5**, **16**). Reductions of two anhydrides (**12** and **15**) lead to a mixture of lactones, a result of diminished preference for the more hindered carbonyl group.

To explain the observed patterns of regioselectivity in these reactions, we would like to propose an alternative approach, based on the following assumptions: (*i*) the mechanism of cyclic anhydride reductions bears a fundamental resemblance to the mechanism of hydride ion addition to the carbonyl group of cyclic ketones; (*ii*) the attack of the cation and hydride ion occurs on the *same* carbonyl function; (*iii*) the site of the attack is controlled by electronic factors, when the two carbonyl functions are electronically different.

Metal Hydride Reductions of the Carbonyl Function

Reductions of ketones with simple metal hydrides have been studied and used extensively for over three decades (4). Although the mechanism of the reaction and the factors determining its stereochemistry remain an area of speculation and controversy, the results of recent investigations and quantum mechanical calculations provide guidelines for a working mechanistic model.

Molecular Orbital Picture of Electrophilic and Nucleophilic Addition to the Carbonyl Group

The most favourable mechanism in terms of MO theory for electrophilic and nucleophilic additions to the carbonyl function is generally accepted to occur in the following manner: the electrophile attacks the frontier HOMO orbital, the so-called nonbonding orbital of the carbonyl oxygen. The product has a plane of symmetry, i.e., the five atoms involved remain in one plane, whereas the π bond of the carbonyl group is orthogonal to this plane. The association of a cation with the oxygen atom of the carbonyl function enhances the addition of a nucleophile to the LUMO π orbital and specifically, to the carbon atom of the carbonyl group (5). The maximum overlap (in the transition state) would suggest an initial approach perpendicular to the molecular plane but the polarity of the molecule favours a greater separation between nucleophile and the oxygen atom. The above conclusion is derived from the work of Bürgi *et al.* (6), who calculated the minimum energy path for addition of hydride ion to formaldehyde. At a distance of 2 Å the line of approach of the nucleophile is not perpendicular, but forms an angle of about 110° with the C=O bond (Fig. 2).

Baldwin (7) extended these results into a simple method of assessing the stereochemical restraints in hydride reductions of other carbonyl functions. Using Baldwin's approximation, the approach vector of H^- (representing the most favourable reaction coordinate) on an ester or anhydride function is shifted (angle β) from the symmetric position, as in a ketone (Fig. 3*a*), to a position in space away from the oxygen atom (Fig. 3*b*) and directed at the molecular plane at an angle (α) of approximately 110° (Fig. 3*c*).

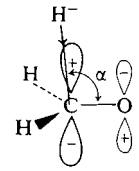

FIG. 2. The attack of hydride ion on the molecular plane of formaldehyde.

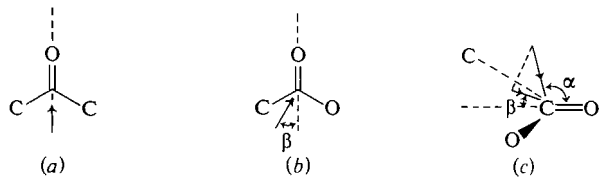

FIG. 3. The projections of H^- attack on the molecular plane.

The term 'steric hindrance' needs to be revised in view of the above considerations (8). The steric congestion in the vicinity of the carbonyl function with respect to the perpendicular approach of a nucleophile is not the same as when the angle of approach is wider (8, 9). However, for reasons of simplicity, theoretical calculations generally assume a perpendicular approach (10).

Kinetics of Metal Hydride Reductions and Catalytic Activity of Li^+ Cation

Kinetic studies (11) have shown that the reaction of mesityl phenyl ketone with $LiAlH_4$ in THF is first order in both ketone and metal hydride.[2]

The reaction of metal hydrides with ketones depends on the nature of the cation (11). The effects of the cation on the reactivity of the ketone is not entirely clear. However, it has been demonstrated (15) that upon removal of the Li^+ cation with the appropriate crown ether, no reaction (within a reasonable reaction time)[3] took place before hydroly-

[2]The same kinetics apparently apply to reductions with sodium borohydride (12). Wiegers and Smith (13) studied the reduction of 2,4,6-trimethoxy benzophenone in diethylether solution and found the reaction first order in ketone, but 0.5–0.6 order in $LiAlH_4$. This, according to the authors, indicates participation of both monomeric and dimeric lithium aluminum hydride. Ashby (14) suggests that the difference between $LiAlH_4$ in THF and $LiAlH_4$ in diethyl ether is due to the difference in solvation of $Li^+AlH_4^-$ in those two solvents.

[3]It is possible that the role of cation, especially Li^+ cation, is catalytic and in its absence, reactions are very slow. Apparently, Li^+ cation is not necessary for reductions with aluminum hydrides, since $NaAlH_4$ and NR_4AlH_4 reduce ketones, although at a considerably slower rate (14).

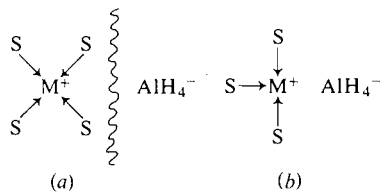

(*a*) (*b*)

FIG. 4. Solvent separated (*a*) and contact (*b*) ion pairs.

sis. Concurrent or prior association of the carbonyl oxygen with Li^+ cation, followed by hydride transfer has been suggested by Ashby *et al.* (16). Pierre and Handel (17) have proposed that a cation intervenes in a catalytic fashion and that stereoselection is fixed from the first step in the mechanism, namely the association of the cation with the carbonyl oxygen atom.

Solvent Effects

Conductance experiments indicate that $LiAlH_4$ in THF exists predominantly as solvent-separated ion pairs (Fig. 4*a*) whereas $NaAlH_4$ appears to be a mixture of solvent-separated (Fig. 4*a*) and contact ion pairs (Fig. 4*b*) (11). Thus, solvation offers a partial explanation for superior reactivity (11) and selectivity (3*b*, 16) of Li^+ cation with respect to Na^+ cation.

Mechanism of $LiAlH_4$ Reduction of the Carbonyl Group

In summary, the mechanism of this reaction is generally accepted to involve the following steps: (*i*) association of the cation with the oxygen atom of the carbonyl group (a fast process in which the solvent separated ion pair falls apart); (*ii*) approach of the AlH_4^- nucleophile[4] from above or below the molecular plane to the carbon end of the carbonyl group,[5] at an angle wider than 90 and as close as possible to 110°; (*iii*) passage through the transition state; (*iv*) formation of the products.

Metal Hydride Reductions of Cyclic Anhydrides

We assume as a working hypothesis that the same principal steps apply to the reduction of anhydrides. However, in the case of unsymmetrically substituted cyclic anhydrides, there are two different carbonyl groups which may undergo reduction. In the majority of cases studied (Table 1), there is a definite preference for reduction to occur at the more electron rich carbonyl function. The preferential association of the Li^+ cation with the carbonyl group bearing the most basic, most isolated, nonbonding electrons on its oxygen atom, is followed by the addition of the hydride ion to the carbon end of the *activated* carbonyl function. The stereochemistry of nucleophilic approach is illustrated in Fig. 3*b* and *c*.

Several anhydrides (**1**, **6**, **8**, **10**, **11**, and **16**) were reduced with both $LiAlH_4$ and $NaBH_4$. The site of reduction was consistently the same and the yields of lactones comparable.[6]

A survey of the data presented in Table 1 reveals that the course of reaction must be governed by electronic effects which induce differences in electron availability on the two carbonyl groups: (*i*) conjugation with aromatic systems; (*ii*) presence of a tertiary carbon atom α to one of the carbonyl functions; (*iii*) presence of electron-withdrawing (phenyl or nitro) or electron-releasing (alkyl) groups on the carbon atom α to the carbonyl function.

Conjugation with aromatic systems results in delocalization of electrons which weakens the carbonyl dipole. This effect is illustrated by the reduction of homophthalic anhydride **13**. The only product isolated, lactone **13***b*, results from reduction of the carbonyl function *not* conjugated with the benzene ring.

The attack of Li^+ cation occurs preferentially on the oxygen atom having the most basic, nonbonding electrons. Not surprisingly, greater reactivity is exhibited by the carbonyl group adjacent to a tertiary carbon atom.[7] Inasmuch as the addition of nucleophile to the carbonyl group is enhanced by the interaction of the cation with the oxygen atom, the transfer of hydride ion to the activated carbonyl group follows. Such a sequence of events adequately describes the results obtained in the reduction of anhydrides **1**, **3**, **5**, **16**, and **17**, as well as compounds **6**, **7**, **8**, and **9**, reported in the literature. The steric hindrance about the carbonyl group in these compounds does not deter hydride transfer where simple metal hydrides (AlH_4^- and BH_4^-) are used. It

[4]In the case of $LiBH_4$ reductions (18) hydride addition was found to be the rate-determining step.

[5]The variety of steric and/or electronic effects will determine the direction of hydride approach. Obvious steric congestion, and in cases of nonhindered carbonyls, the torsional interactions (19) and unequal distortion of electron density about the carbonyl group (20, 21) are examples of such effects.

[6]Since the Na^+ cation is a poor catalyst, the mechanism of $NaBH_4$ reduction differs from $LiAlH_4$ reduction in the first step, i.e., association with the cation. It is generally believed (ref. 2*a* pp. 51, 52) that $NaBH_4$ reductions are catalyzed by protic solvent or, in cases of reductions carried out in anhydrous alcohol free solvents, the reaction may actually occur only during the isolation procedure when water, acid or alcohol is added. From the practical point of view, it is simpler to reduce an anhydride to a lactone, using $NaBH_4$, rather than $LiAlH_4$. The products obtained in the majority of cases studied are the same. The only example, to our knowledge, where the reductions with $NaBH_4$ and $LiAlH_4$ yielded significantly different ratios of lactones has been reported for the Inhoffen adduct (**19**, ref. 3*b*).

[7]The greater reactivity of the carbonyl function next to the most highly substituted carbon atom has also been manifested in esterification reactions of cyclic anhydrides to half-acid esters (22).

Can. J. Chem. Downloaded from www.nrcresearchpress.com by 210.87.254.5 on 09/05/12
For personal use only.

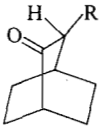

FIG. 5. Example of ketone having Cram's model conformation built in.

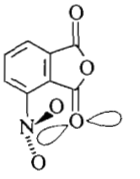

FIG. 6. Nitro group is twisted from the plane of the molecule.

should be pointed out that under conditions of overpowering steric crowding, the course of the reaction might be reversed, but at present, there are no known examples in the cyclic anhydride series. A somewhat analogous situation, encountered in the reduction of ketones, has been recently discussed by Chérest *et al.* (21). A number of 3-alkyl bicyclo[2.2.2]octan-2-ones (example, Fig. 5) undergo reduction with $LiAlH_4$ from the more hindered side leading to *trans* alcohols,[8] when R is methyl, ethyl or isopropyl. However, when R is *tert*-butyl, the *cis* alcohol is obtained as the major product. The authors attribute these results to the anisotropic inductive effects of the alkyl groups which lead to differences in electron density on the two faces of the plane containing the trigonal carbon atom.[9] When the R group becomes large enough to block completely the path of nucleophilic attack, the reaction becomes subject to steric control.

The subtle differences engendered by the presence of electron-releasing and electron-withdrawing groups are illustrated by the following examples from Table 1. 2-Methylsuccinic anhydride (**2**) is preferentially reduced on the more sterically crowded side of the molecule. According to the mechanism proposed by Bloomfield and Lee (2*b*) (Fig. 1), 2-phenylsuccinic anhydride (**4**) should lead to a higher ratio in favour of the lactone formed by reduction on the more hindered side, since a phenyl group is more important sterically than a methyl group (24). However, the experimental results show that **4** is reduced to a lesser extent at the more hindered carbonyl function. It is obvious that the electron-withdrawing phenyl group weakens the neighbouring carbonyl function, thus slightly promoting reduction of the less hindered carbonyl group, (40% reduction on the less hindered side in **4**, *vs.* 30% in **2**).

Electronic factors operating in these reactions may be complicated by other effects not obvious at first glance. The case which illustrates well the danger of hasty predictions, is exemplified in the reduction of 3-nitrophthalic anhydride **15**. Considering the electron-withdrawing effects of the nitro group, we might have expected 7-nitrophthalide (**15***a*) as the major product but, in fact, the isomeric 4-nitrophthalide (**15***b*) is produced preferentially. In this case, the nitro group, twisted from the molecular plane, owing to the proximity of the neighbouring carbonyl group, cannot undergo electron delocalization and therefore does not deactivate the carbonyl group in the *ortho* position. On the other hand, the cation will be attracted to this highly oxygenated end of the molecule (Fig. 6) and consequently, will preferentially activate the *ortho* carbonyl function.

The ring system to which the anhydride is attached greatly influences the site of metal hydride reduction. A case in point is the complete reversal in regioselectivity observed in the reduction of the anhydrides **10** and **11**, compared to anhydride **6**. The former two compounds differ from **6** only by having a methylene or ethylene bridge respectively. Since it is known that the formation of enolate anion greatly inhibits the reduction of carbonyl groups (25, 26), one is tempted to explain the above results[10] by evoking the relative ease of enolization of the carbonyl group in **6**, as opposed to resistance to enolization in the bridgehead compounds **10** and **11**. The enolate anion of succinic anhydride has been generated (27) but it appears that under the reduction conditions employed, enolization does not occur to any significant extent.[11]

The difference in reactivity between the two carbonyl functions of cyclic anhydrides may be ascribed to hyperconjugative effects (28, 29). The carbonyl group for which one or more no-bond resonance canonical forms can be written should be a weaker dipole due to electron delocalization. The two bridged anhydrides **10** and **11** have folded structures and are not able to flatten out. Consequently, neither enolization nor hyperconjugation can contribute to the delocalization of electrons and the two carbonyl groups are essentially equivalent. An approach (by nucleophile) from the concave side is

[8]With $LiAl(tOBu)_3H$ more sensitive to steric hindrance, reduction always occurs selectively from the less hindered side of the molecule (21).

[9]Klein (23) evokes this effect to explain and predict addition to trigonal carbon, sulfur and pyramidal nitrogen atoms.

[10]It is equally tempting to use enolization to justify the results of reductions for all the anhydrides possessing one carbonyl group α to the tertiary carbon atom, while the other one is α to the primary or secondary carbon atom.

[11]No incorporation of deuterium is observed when the reaction is quenched with DCl–D_2O. Also, no significant amount of H_2 gas is evolved during the reductions of cyclic anhydrides.

Can. J. Chem. Downloaded from www.nrcresearchpress.com by 210.87.254.5 on 09/05/12
For personal use only.

Can. J. Chem. Downloaded from www.nrcresearchpress.com by 210.87.254.5 on 09/05/12
For personal use only.

TABLE 1. Lactones produced from the metal hydride reductions of cyclic anhydrides

Starting anhydride	Products *a*	Products *b*	% yield of lactonic products	Ratio *a*:*b*	Reference no.
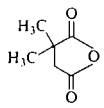 **1**	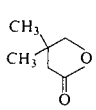	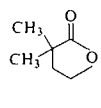	70[a,c] 74[b,c,f]	19:1	31 2*c*
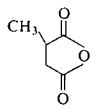 **2**	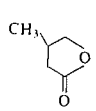	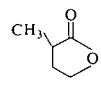	69[a,c]	2.2:1	2*b*
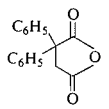 **3**	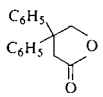	—	67[b,c,e,f]		
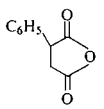 **4**	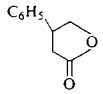	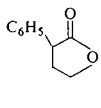	72[a,c]	1.5:1	2*b*
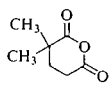 **5**	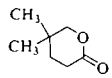		72[a,c,e]	8:1	
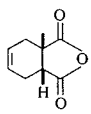 **6**		—	80[a,b,d,f]		2*d*, 41
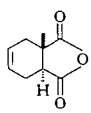 **7**		—	75[a,d,f]		2*b*
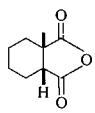 **8**		—	80[a,b,d,f]		2*b*, 41
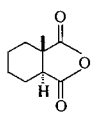 **9**		—	85[a,d,f]		2*b*
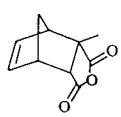 **10**	Trace	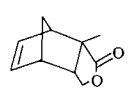	84[a–c,e,f]		

TABLE I (*Concluded*)

Starting anhydride	Products *a*	Products *b*	% yield of lactonic products	Ratio *a*:*b*	Reference no.
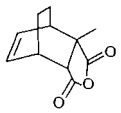 11	—	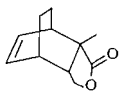	86[a-c,e,f]		
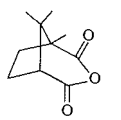 12	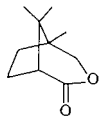	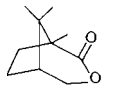	76[a,c,e]	3:2	
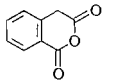 13	—	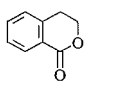	55[b,c,f]		2*c*
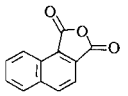 14	—	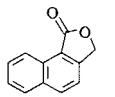	67[a,f]		3*d*
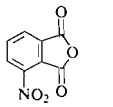 15	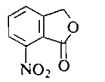	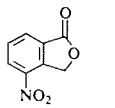	80[a,d,e]	1:2	
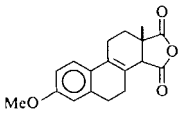 16	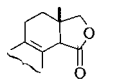	—	80–90[a,b,e,f]		41
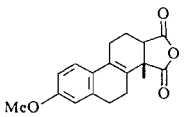 17	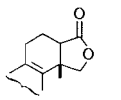	—	80–90[b,e,f]		41
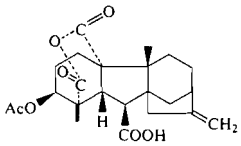 18	—	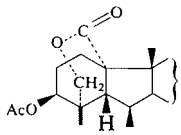	50[a,f]		3*c*
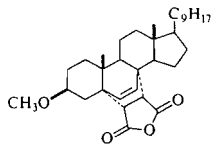 19	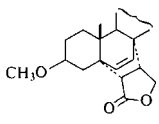	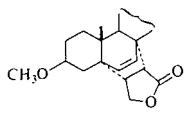	47[a,d] 30[b,d]	13:1 1:1	3*a*

[a] $LiAlH_4$ reduction.
[b] $NaBH_4$ reduction.
[c] Gas-liquid chromatography analyzed.
[d] Column chromatography.
[e] Reported in this paper.
[f] Only one product isolated.

Can. J. Chem. Downloaded from www.nrcresearchpress.com by 210.87.254.5 on 09/05/12
For personal use only.

Can. J. Chem. Downloaded from www.nrcresearchpress.com by 210.87.254.5 on 09/05/12
For personal use only.

prevented by the electrons of the π bond. The hydride ion therefore must approach from the convex face. Here, the cation may associate itself with one or the other carbonyl group but this step is fast and reversible and the nucleophile will be transferred to the less crowded group.

Camphoric anhydride **12** presents another case where subtle electronic effects influence the selectivity of the reaction. By analogy to the stereoselectivity observed in the reduction of camphor (10), the nucleophile should add from the *endo*, more 'overt' side. There is little difference in steric environment between the two carbonyl groups when the approach is from the *endo* side. We would have expected a mixture of two lactones in a 1:1 ratio. The slight preference shown for the 'more' hindered carbonyl may be due to the inductive effect of the angular methyl group.

The results of the metal hydride reductions of 19 cyclic anhydrides presented in Table 1 clearly show that these reactions cannot be governed by steric factors alone. The observed pattern may be rationalized by evoking a different electronic character for the two carbonyl groups,[12] when applicable. Obviously, in the absence of electronic differences, the reduction is subject to steric factors. It is yet to be established at what point steric factors begin to dominate the course of the reaction when electronic differences exist. It should be emphasized that the above considerations may not be valid for reduction of cyclic anhydrides with bulky metal hydrides (e.g. $LiAl(tOBu)_3H$) which are more sensitive to steric hindrance.

Experimental

Melting points were determined on a Thomas–Hoover capillary melting point apparatus and are uncorrected. Infrared spectra were obtained on a Beckman IR-20 spectrophotometer and proton nmr spectra in $CDCl_3$, with TMS as internal standard, on a Varian T-60 or HA-100 instrument. Tetrahydrofuran was distilled under argon from lithium aluminum hydride into oven-dried and argon-flushed flasks containing the lithium aluminum hydride. The transfer of tetrahydrofuran, when necessary, was accomplished with an argon-swept syringe. Gas–liquid chromatographic analyses were carried out with an Autoprep Model A-700 gas chromatograph.

The general procedure for the reductions was as follows. Lithium aluminum hydride (0.005–0.01 mol) was placed in an oven-dried, argon-swept, three-neck flask into which 25–50 ml of tetrahydrofuran was subsequently distilled. The flask was fitted with an inlet port for syringes, a magnetic stirrer, a thermometer, and a gas outlet tube. The flask, swept with a slow stream of nitrogen, was cooled in a Dry Ice – acetone bath. The gas tube was then connected to the gas measuring system and anhydride (0.01 mol) dissolved in a small quantity of distilled tetrahydrofuran (20–30 ml) was injected into the flask. The hydrogen evolved was noted. The temperature of the reaction mixture was maintained below −55°C, throughout the addition process. The stirred solution was slowly warmed to 0°C over a period of 2 h. The flask was then cooled again to −20°C and 5 ml of 6 *N* HCl was added slowly. The reaction mixture was left overnight. The layers were separated and the acidic aqueous layer was extracted with ether. The combined organic layers were dried, concentrated, and analyzed by glc. Reductions with sodium borohydride were carried out according to the procedure of Belleau and Puranen (1*a*).

2,2-Dimethylsuccinic anhydride (**1**) was prepared from 2,2-dimethylsuccinic acid by dehydration with acetyl chloride and was reduced according to the procedure described above (31). Yields of lactones ranged from 50–75% and 10–15% of diacid was recovered. Gas–liquid chromatographic analysis (6 ft, 10% carbowax, 120°C), showed the ratio of the two lactones to be 19:1. The major product *β,β-dimethyl-γ-butyrolactone* (**1***a*) was purified by distillation under reduced pressure (*2c*,32); ν_{max}: 1720 cm^{-1} (lactone C=O); δ:1.20 (s, 6H, 2 × CH_3), 2.34 (s, 2H, CH—C=O), 3.98 (s, 2H, CH_2—O). This lactone was compared with α,α-dimethyl-γ-butyrolactone (1*b*) prepared by $RuCl_2(Ph_3P)_3$ catalyzed hydrogenation of the anhydride **1** (31); δ:1.28 (s, 6H, 2 × CH_3), 2.12 (t, 2H, CH_2—C=O), 4.26 (t, 2H, CH_2—O).

2,2-Dimethylglutaric anhydride (**5**), upon reduction with $LiAlH_4$, yielded lactone **5***a* as a major product. Gas–liquid chromatographic analysis (6 ft, 10% carbowax, 135°C) indicated the ratio **5***a*:**5***b* to be 9:1. γ,γ-Dimethyl-δ-valerolactone (**5***a*): ν_{max}: 1730 cm^{-1} (lactone C=O) (lit.(33)); δ:0.98 (s, 6H, 2 × CH_3), 1.62 (t, 2H), 3.90 (s, 2H, CH_2—O). This lactone was compared with α,α-dimethyl-δ-valerolactone (**5***b*) which was obtained as a major product of catalytic hydrogenation ($RuCl_2(Ph_3P)_3$) of the anhydride **5**: δ:4.22 (t, 2H, CH_2—O).

2,2-Diphenylsuccinic acid was prepared according to the method of Makosza (34*a*) by condensing, under phase transfer conditions, diphenylacetonitrile with methyl bromoacetate. The product *3,3-diphenyl-3-cyanopropionic acid* was obtained in 76% yield; mp 178–181°C; *m/e* (70 eV): 251 (M^+); ν_{max}: 2220 cm^{-1} (C≡N; δ:3.5 (s, 2H), 7.3 (s, 10H). 3,3-Diphenyl-3-cyanopropionic acid was hydrolyzed by refluxing for 12 h in a mixture of concentrated H_2SO_4 and glacial acetic acid (1:1). 2,2-Diphenylsuccinic acid was obtained in 60% yield; mp 179–180°C (lit. (34*a*) mp 175°C); *m/e*: 252 ($M - H_2O$); ν_{max}: 1710 cm^{-1}; δ: 3.6 (s, 2H), 7.33 (s, 10H). 2,2-Diphenylsuccinic acid was heated to melting and it solidified to give needle-like crystals of *2,2-diphenylsuccinic anhydride* (**3**); mp 89–91°C (lit. (34*b*) mp 90.5–90°C); ν_{max}: 1700 and 1770 cm^{-1} (C=O anhydride); δ:3.66 (s, 2H), 7.36 (s, 10H).

Reduction of 2,2-Diphenylsuccinic Anhydride

The anhydride **3**, 1.26 g (0.005 mol) was dissolved in isopropyl alcohol (350 ml). The stirred solution was cooled to 0°C and $NaBH_4$ 0.185 g (0.005 mol) added in small portions over a period of 2 h. The solution was then allowed to warm to room temperature and was stirred for an additional 2 h. The isopropyl alcohol was distilled under reduced pressure and excess 3 *N* HCl was added, followed by 150 ml of chloroform. The reaction mixture was stirred for a few hours and the layers separated. The aqueous layer was extracted twice with chloroform and the combined organic layers were dried and evaporated. The residue was chromatographed on silica gel. Lactone **3***a* was eluted first with benzene, yield 67%; mp 109–110°C (lit. (35) mp 109–110°C); ν_{max}: 1780 cm^{-1} (C=O); δ:3.19 (s, 2H), 4.73 (s, 2H), 7.40 (10H). The anhydrides **10** and

[12]It is quite likely that the same mechanism could explain the results of the reductions of unsymmetrical succinimides (30*b*).

Can. J. Chem. Downloaded from www.nrcresearchpress.com by 210.87.254.5 on 09/05/12
For personal use only.

11 were prepared by Diels–Alder addition (36) of citraconic anhydride to cyclopentadiene and 1,3-cyclohexadiene, respectively. exo-*2-Methylnorborn-5-ene*-endo-*2,3-dicarboxylic acid anhydride* (**10**); mp 139–141°C; ν_{max}: 1770 and 1850 cm^{-1} (anhydride C=O); δ: 1.6 (s, 3H, Me), 1.86 (m, 2H), 3.08 (m, 1H). *Anal.* calcd. for $C_{10}H_{10}O_3$: C 67.42, H 5.62; found: C 67.71, H 5.76. exo-*2-Methylbicyclo[2.2.2]oct-5-ene-2,3*-endo-*dicarboxylic acid anhydride* (**11**); mp 182–184°C; ν_{max}: 1775 and 1850 cm^{-1} (anhydride C=O); δ: 1.41. *Anal.* calcd. for $C_{11}H_{12}O_3$: C 68.73, H 6.17; found: C 68.92, H 6.29.

Reduction of the anhydride **10** with $LiAlH_4$ according to the general procedure as well as with $NaBH_4$ in dimethylformamide gave the crystalline lactone, *exo*-2-methylnorborn-5-ene-*endo*-(3-methyl-2-carbo-3a)-lactone (**10***b*; yield 84%; mp 137–139°C; ν_{max}: 1745 cm^{-1} (lactone C=O); δ: 1.52 (s, 3H, CH_3), 4.02 (m, 2H, CH_2—O), 6.33 (m, 2H); δ (0.5 *N* NaOD): 3.60 (d, 2H, CH_2—O). *Anal.* calcd. for $C_{10}H_{12}O_2$: C 73.17, H 7.31; found: C 73.01, H 7.54). A trace of the lactone resulting from the reduction on the more hindered side could be detected by glc.

Reduction of the anhydride **11** with $LiAlH_4$ or with $NaBH_4$ gave the crystalline lactone **11***b*; yield 86%; mp 184–185°C; ν_{max}: 1755 cm^{-1} (lactone C=O); δ: 1.37 (s, 3H, Me), 4.05 (m, 2H, CH_2—O), 6.30 (m, 2H). *Anal.* calcd. for $C_{11}H_{14}O_2$: C 74.15, H 7.86; found: C 74.75, H 7.91.

Reduction of *camphoric anhydride* (**12**) with $LiAlH_4$ produced 70–78% yields of the mixture of **12***a* and **12***b* in the ratio 3:2 determined by glc analysis. The unreacted anhydride 20–25% was recovered. The two lactones were separated on base-washed alumina, crystallized from low boiling petroleum ether, and sublimed. β-*Campholide* (**12***a*) mp 214–216°C (lit. (37, 38) mp 213–216°C); ν_{max}: 1735 cm^{-1} (lactone C=O); δ: 0.90 (d, 6H, CH_3), 1.08 (s, 3H, CH_3), 4.05 (m, 2H, CH_2—O). α-*Campholide* (**12***b*) mp 210–211°C (lit. (41) mp 210–211°C); ν_{max}: 1730 cm^{-1} (lactone C=O); δ: 0.95 (s, 3H, CH_3), 1.10 (s, 3H, CH_3), 1.20 (s, 3H, CH_3), 4.35 (m, 2H, CH_2—O). Unequivocal proof of structure for the two lactones was obtained by direct comparison of the lactone **12***b* with α-campholide obtained by the Baeyer–Villiger oxidation of camphor (39).

Reduction of *3-nitrophthalic anhydride* (**15**) was carried out according to the general procedure. The reduction product, a yellow crystalline substance was isolated in 80% yield. The proton nmr analysis showed the presence of two lactones in the ratio 2:1, where *4-nitrophthalide* (**15***b*) is a major product. Chromatography on silica gel yielded pure **15***b*; mp 135–136°C (lit. (40) mp 136°C); ν_{max}: 1780 (lactone C=O), 1550, and 1370 cm^{-1} (NO_2); δ: 5.75 (s, 2H, CH_2—O). *7-Nitrophthalide* (**15***a*) showed proton resonance δ 5.40 (s, CH_2—O).

The anhydride **16** (41), upon reduction with sodium borohydride in DMF, gave lactone **16***a*. Yields ranged from 80–90%; mp 175–176°C; analysis, ir, and proton nmr spectra were consistent with assigned structure.

Reduction with ½ mol of $NaBH_4$ to 1 mol of the anhydride (16) yielded corresponding hemiacylal which was further reduced with $NaBH_4$ to give the lactone **16***a*. The anhydride **17** reduced under similar conditions yielded a mixture of the lactone **17***a* and hemiacylal. The hemiacylal could be reduced with excess $NaBH_4$ to give **17***a*. Lactone **17***a*, mp 159–160°C; hemiacylal, mp 178–179°C; analysis, ir, and proton nmr spectra were consistent with assigned structures.

Acknowledgements

The Diels–Alder adducts were prepared by Mr. P. Crosby. We are grateful to Dr. P. Wolkoff for helpful discussions and would like to thank the National Research Council of Canada for financial support.

1. (*a*) B. Belleau and J. Puranen. Can. J. Chem. **43**, 2551 (1965); P. M. Wege, R. D. Clark, and C. H. Heathcock. J. Org. Chem. **41**, 3144 (1976); E. J. Corey and B. B. Snider. Tetrahedron Lett. 3091 (1973); R. H. Cornforth, J. W. Cornforth, and G. Popjak. Tetrahedron, **18**, 1351 (1962); A. R. Pinder. Chem. Rev. **64**, 551 (1964); M. Kato, M. Kageyama, and A. Yoshikoshi. J. Chem. Soc. Perkin I, 1305 (1977); E. J. Corey, H. E. Ensley, and J. W. Suggs. J. Org. Chem. **41**, 380 (1976); (*b*) R. McCrindle, K. H. Overton, and R. A. Raphael. J. Chem. Soc. 313 (1961); (*c*) F. Fichter and A. Beisserenger. Ber. **36**, 1200 (1903); O. Salomon. Ber. **20**, 883 (1887).
2. (*a*) H. O. House. Modern synthetic reactions. 2nd ed. W. A. Benjamin, Inc., Reading, MA. 1972. pp. 88 and 89; (*b*) J. J. Bloomfield and S. L. Lee. J. Org. Chem. **32**, 3919 (1967); (*c*) D. M. Bailey and R. E. Johnson. J. Org. Chem. **35**, 3575 (1970); (*d*) R. Granger and H. Techer. C. R. Acad. Sci. Ser. C, **250**, 142 (1960).
3. (*a*) M. E. Birckelbaw, P. W. LeQuesne, and C. K. Wocholski. J. Org. Chem. **35**, 558 (1970); (*b*) D. E. Burke and P. H. LeQuesne. J. Org. Chem. **36**, 2397 (1971); (*c*) B. E. Cross and J. C. Stewart. Tetrahedron Lett. 3589 (1968); (*d*) F. Weygand, K. G. Kinkel, and D. Tietjen. Chem. Ber. **83**, 394 (1950).
4. N. G. Gaylord. Reductions with complex metal hydrides. Interscience Publishers, New York, NY. 1956; R. L. Augustine. Reductions; techniques and applications in organic synthesis. Decker, New York, NY. 1968; M. P. Doyle and C. T. West. Stereoselective reductions. Dowden, Hutchingon and Ross Inc., Stroudsburg, PA. 1976.
5. R. G. Pearson. Symmetry rules for chemical reactions. Wiley-Interscience Publications, New York, NY. 1976. p. 341 and the references therein.
6. H. B. Bürgi, J. D. Dunitz, J. M. Lehn, and G. Wipff. Tetrahedron, **30**, 1563 (1974); H. B. Bürgi, J. D. Dunitz, and E. Shefter. J. Am. Chem. Soc. **95**, 5065 (1973); H. B. Bürgi, J. M. Lehn, and G. Wipff. J. Am. Chem. Soc. **96**, 1956 (1974).
7. J. E. Baldwin. J. Chem. Soc. Chem. Commun. 738 (1976).
8. R. Süess. Helv. Chim. Acta, **60**, 1650 (1977).
9. D. C. Wigfield and F. W. Gowland. J. Org. Chem. **42**, 1108 (1977).
10. W. T. Wipke and P. Gund. J. Am. Chem. Soc. **98**, 8107 (1976); J.-C. Perlberger and P. Müller. J. Am. Chem. Soc. **99**, 6316 (1977).
11. E. C. Ashby and J. R. Boone. J. Am. Chem. Soc. **98**, 5524 (1976).
12. H. C. Brown, O. H. Wheeler, and K. Ichikawa. Tetrahedron, **1**, 214 (1957).
13. K. E. Wiegers and S. G. Smith. J. Am. Chem. Soc. **99**, 1480 (1977).
14. E. C. Ashby and J. R. Boone. J. Org. Chem. **41**, 2890 (1976).
15. J.-L. Pierre and H. Handel. Tetrahedron Lett. 2317 (1974).
16. E. C. Ashby, J. R. Boone, and J. P. Oliver. J. Am. Chem. Soc. **95**, 5427 (1973).
17. H. Handel and J.-L. Pierre. Tetrahedron, **31**, 997 (1975).
18. H. Uelzmann. J. Org. Chem. **25**, 671 (1960).
19. M. Chérest and H. Felkin. Tetrahedron Lett. 2205 (1968).
20. J. Klein. Tetrahedron Lett. 4307 (1973).
21. M. Chérest, H. Felkin, and P. Tacheau. J. Chem. Soc. Chem. Commun. 372 (1977).
22. H. S. Bajaj, P. D. Desai, R. K. Gautam, and G. S. Saharia. J. Indian Chem. Soc. **52**, 1076 (1975).
23. J. Klein. Tetrahedron, **30**, 3349 (1974).

24. E. L. ELIEL, N. ALLINGER, S. ANGYAL, and G. MORRISON. Conformational analysis. Interscience Publishers, New York, NY. 1965. p. 44.
25. H. O. HOUSE. Modern synthetic reactions. 2nd ed. W. A. Benjamin, Inc., Reading, MA. 1972. p. 54.
26. D. H. R. BARTON, R. H. HESSE, C. WILSHIRE, and M. PECHET. J. Chem. Soc. Perkin I, 1075 (1977).
27. N. MINAMI and I. KUWAJIMA. Tetrahedron Lett. 1423 (1977).
28. M. J. S. DEWAR. Hyperconjugation. The Ronald Press Company, New York, NY. 1962.
29. M. J. S. DEWAR and H. N. SCHMEISING. Tetrahedron, **5**, 166 (1959); R. S. MULLIKEN. Tetrahedron, **17**, 247 (1962).
30. J. C. HUBERT, J. B. WYNBERG, and W. N. SPECKAMP. Tetrahedron, **31**, 137 (1975); J. B. WYNBERG, W. N. SPECKAMP, and H. E. SCHOEMAKER. Tetrahedron Lett. 4073 (1974).
31. P. MORAND and M. KAYSER. J. Chem. Soc. Chem. Commun. 314 (1976).
32. A. WINDAUS and F. KLANHART. Chem. Ber. **54**B, 58 (1921).
33. J. FALBE, H. J. SCHULZE-STEINEN, and F. KORTE. Chem. Ber. **98**, 886 (1965).
34. (*a*) M. MAKOSZA. Rocz. Chem. **43**, 79 (1969); (*b*) E. J. CRAGOE, C. M. ROBB, and J. M. SPRAGUE. J. Org. Chem. **15**, 381 (1950).
35. F. SALMON-LEGAGNEUR. C. R. Acad. Sci. Ser. C, **227**, 437 (1948).
36. O. DIELS and K. ALDER. Ann. **460**, 98 (1928).
37. A. HALLER and G. BLANC. C.R. Acad. Sci. Ser. C, **141**, 697 (1905).
38. R. R. SAUER. J. Am. Chem. Soc. **81**, 925 (1951); **83**, 2759 (1961).
39. A. BAEYER and V. VILLIGER. Chem. Ber. **32**, 3625 (1899).
40. F. K. BEILSTEIN and V. KURBATOV. Ann. **202**, 219 (1880); W. BORSCHE, K. DIACONT, and H. ANAU. Ber. **67**, 676 (1934).
41. P. MORAND, A. HANCOCK, and P. CROSBY. Unpublished work from this laboratory.

Can. J. Chem. Downloaded from www.nrcresearchpress.com by 210.87.254.5 on 09/05/12
For personal use only.

Mechanism of L-ascorbic acid oxidation on a mercury electrode. II. Basic medium

JUAN JOSÉ RUIZ,[1] ANTONIO ALDAZ,[2] AND MANUEL DOMINGUEZ

Departamento de Química Física, Facultad de Ciencias, Universidad de Sevilla, Spain

Received June 16, 1977

JUAN JOSÉ RUIZ, ANTONIO ALDAZ, and MANUEL DOMINGUEZ. Can. J. Chem. **56**, 1533 (1978).

A polarographic study of the oxidation mechanism of L-ascorbic acid is carried out in a basic medium and two oxidation waves are observed.

An analysis of these waves shows that the limiting current is governed by diffusion and that in each reaction a two electron transfer takes place. On the rising portion of the waves, the oxidation process consists of two consecutive one electron transfers. In the first wave, the second transfer is the rate determining step, whilst in the second wave, a chemical stage subsequent to the second electron transfer is the rate determining step. The reaction orders, together with the Tafel slopes, are calculated.

The oxidation mechanism of this acid in basic media is different from that in acid media.

JUAN JOSÉ RUIZ, ANTONIO ALDAZ et MANUEL DOMINGUEZ. Can. J. Chem. **56**, 1533 (1978).

On a effectué une étude polarographique du mécanisme d'oxydation de l'acide L-ascorbique en milieu acide et on a observé deux vagues d'oxydation.

Une analyse de ces vagues montre que le courant limite est gouverné par la diffusion et que dans chacune d'elle il se produit un transfert de deux électrons. Sur la portion montante des vagues, le processus d'oxydation comporte deux transferts consécutifs d'un électron. Dans la première vague, le deuxième transfert détermine la vitesse alors que dans la deuxième vague l'étape déterminante se trouve dans une étape chimique subséquente au deuxième transfert d'électron. On a calculé les ordres des réactions de même que les pentes de Tafel.

Le mécanisme d'oxydation de cet acide en milieu basique diffère de celui obtenu en milieu acide.

[Traduit par le journal]

Introduction

In a previous paper (1), we studied the polarographic behaviour of L-ascorbic acid and dehydro-L-ascorbic acid in an acid medium. A study was also made of the *i–E* curves in the rising portion of the polarographic wave. These data, together with those obtained from the microcoulometric study from electron spin resonance and from electrolysis with the identification of products by paper chromatography, led us to propose a reaction mechanism that fully agrees with the experimental results.

The polarographic behaviour of L-ascorbic acid differs with acid and basic media. This paper describes a study of the oxidation mechanism of this acid in a basic medium.

Experimental

All apparatus, cells, electrodes, solutions, and measurements are identical to those described in our previous paper (1).

Results

General Behaviour

The L-ascorbic acid, in a basic medium, oxidizes over the drop mercury electrode (DME), producing two polarographic waves. The second wave is only completely defined from p*H* 8 onwards (Fig. 1).

Microcoulometric Measurements

It is not possible to determine the number of electrons taking part in the oxidation waves of L-ascorbic acid in a basic medium from the decrease of the limiting current with the time of electrolysis.

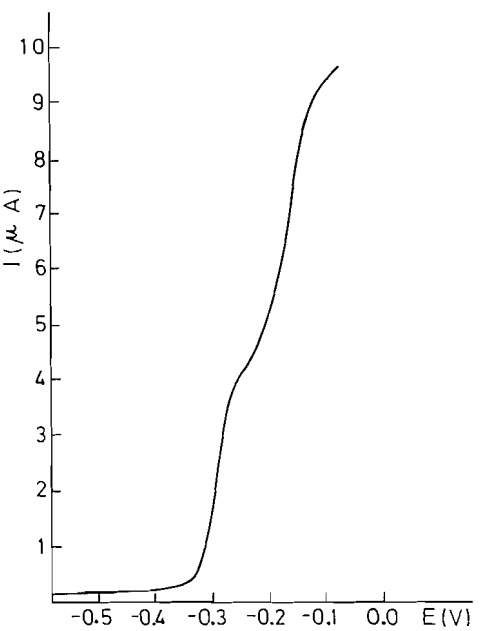

FIG. 1. Oxidation waves of L-ascorbic acid; p*H* = 8.20, $c = 5 \times 10^{-4}$ *M*.

[1]To whom all correspondence should be addressed.

[2]Present address: Departamento de Investigaciones Químicas, Centro Coordinado del C.S.I.C., Universidad Autónoma, Canto Blanco, Madrid 34, Spain.

Can. J. Chem. Downloaded from www.nrcresearchpress.com by 210.87.254.5 on 09/05/12
For personal use only.

Can. J. Chem. Downloaded from www.nrcresearchpress.com by 210.87.254.5 on 09/05/12
For personal use only.

This is due to the fact that L-ascorbic acid is unstable in this medium and therefore the decrease of the current is not only caused by the electrochemical oxidation of the acid but also by its homogeneous decomposition in solution.

If we consider, however, that the limiting current of the first wave is the same for both acid and basic media, that the second wave has practically the same height as the first, and that the compounds originating these waves must have, as will be seen later, similar diffusion coefficients, it can be concluded that the number of electrons transferred in both waves is equal to that of the first wave in an acid medium, i.e. two.

Polarographic Behaviour

For the first oxidation wave, the limiting current is independent of the p*H* whilst $E_{1/2}$ varies linearly with the p*H*. The value of the slope of the plot $E_{1/2}$ vs. p*H* is -68 mV/p*H* unit. This variation corresponds to the ultimate linear portion of Fig. 2. The two previous linear portions demonstrate the behaviour of $E_{1/2}$ vs. p*H* in acid and neutral media (1) (p*H* between 2.5–8).

$E_{1/2}$ is independent of the concentration of L-ascorbic acid. The logarithmic analysis of the wave gave a straight line with a slope of 30 mV per decade that is practically independent of the p*H*.

The limiting current is governed by diffusion as $\log i_{lim}$ vs. $\log h$ (corrected for the back pressure) is linear with a slope of 0.50. The limiting current has a temperature coefficient of 1.1% per °C and is proportional to the L-ascorbic acid concentration in the bulk of the solution.

The second oxidation wave appears at p*H* 7, although it is not completely defined until p*H* 8. The limiting current is independent of the p*H* whilst $E_{1/2}$ varies linearly with the p*H*. The slope of the plot of $E_{1/2}$ vs. p*H* is -79 mV/p*H* unit (Fig. 3).

With a decrease in the L-ascorbic acid concentration, $E_{1/2}$ shifts to more anodic values, whilst i_{lim} varies linearly. The limiting current is governed by diffusion the plot $\log i_{lim}$ vs. $\log h$ being linear with a slope of 0.51.

Tafel Curves and Reaction Orders

(a) Influence of pH

In the case of the first oxidation wave, the Tafel curves are independent of the p*H* and their slopes have an average value of 42 mV per decade (Fig. 4).

The reaction orders with respect to the H^+ con-

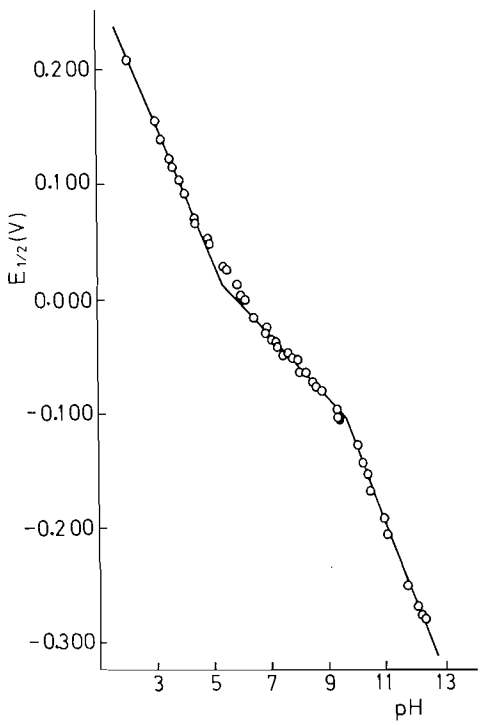

FIG. 2. First wave: variation of $E_{1/2}$ with p*H*.

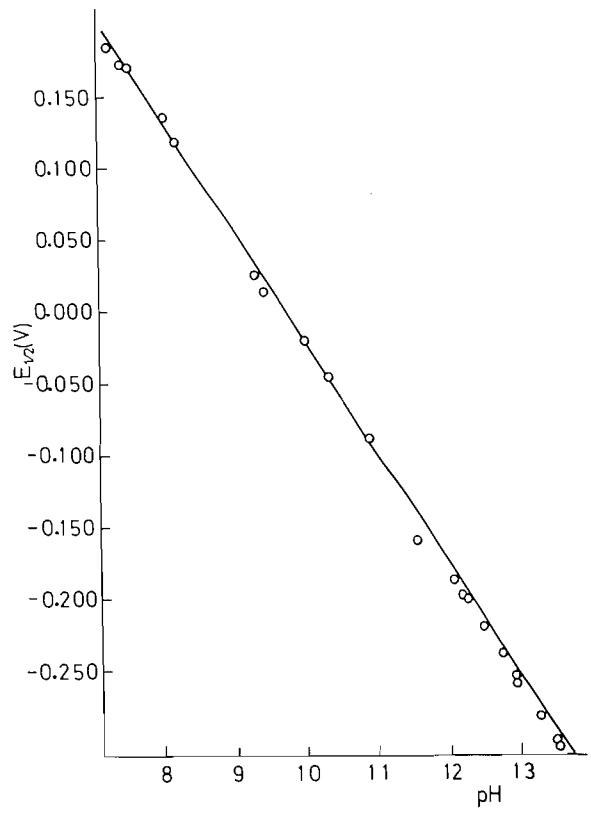

FIG. 3. Second wave: variation of $E_{1/2}$ with p*H*.

Can. J. Chem. Downloaded from www.nrcresearchpress.com by 210.87.254.5 on 09/05/12
For personal use only.

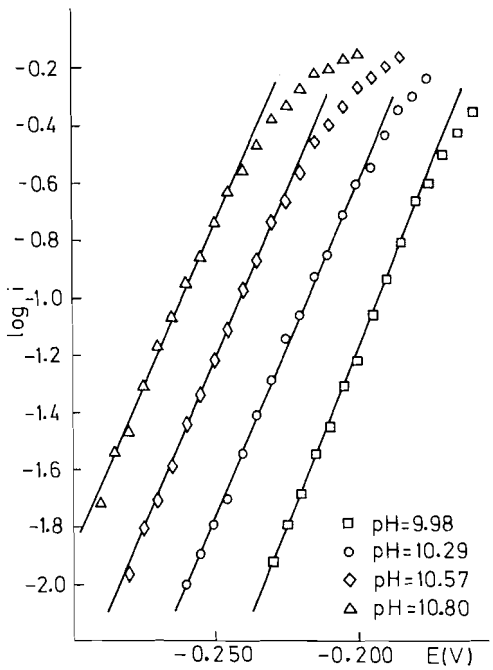

Fig. 4. Representation of Tafel curves, first wave.

centration are:

$$\left[\frac{\partial \log i}{\partial \log \mathrm{H}^+}\right]_{E,T,c_{i\neq j}} = -2.0 \quad \text{at } pH = 10\text{–}11$$
$$= -1.1 \quad \text{at } pH = 12\text{–}13$$

The order is independent of the potential in the zone where Tafel's law is obeyed (Fig. 5).

In the case of the second oxidation wave, the Tafel slopes are equally independent of the H^+ concentration, and the slopes have an average value of 30 mV per decade. The reaction order with respect to the H^+ concentration in the pH range 7–9 is -2.0.

(b) Influence of L-*Ascorbic Acid Concentration*

For both oxidation waves, the order with respect to the concentration was 1 in all cases and was independent of the potential in the zone where Tafel's law is obeyed.

Identification of Intermediate Products

It has already been established (1) that the first product from the L-ascorbic acid oxidation is dehydro-L-ascorbic acid. This acid or any of its derivatives could therefore be responsible for the electron transfer that originates the second oxidation wave.

Using the Mapson and Partridge technique (2) the first product of oxidation in an acid medium was identified as dehydro-L-ascorbic acid from its R_F characteristics (0.07 weak and 0.49 strong). As the position of the weak spot (0.07) corresponds approximately with that assigned to 2,3-diketogulonic acid, it can be assumed that there is a rupture of the lactone ring of dehydro-L-ascorbic acid. This fact was confirmed when the chromatography was carried out in a basic medium (pH 10) and the spot was accentuated. It can therefore be supposed that, in a basic medium, L-ascorbic acid, or its first oxidation product, undergoes hydrolysis with rupture of the lactone ring.

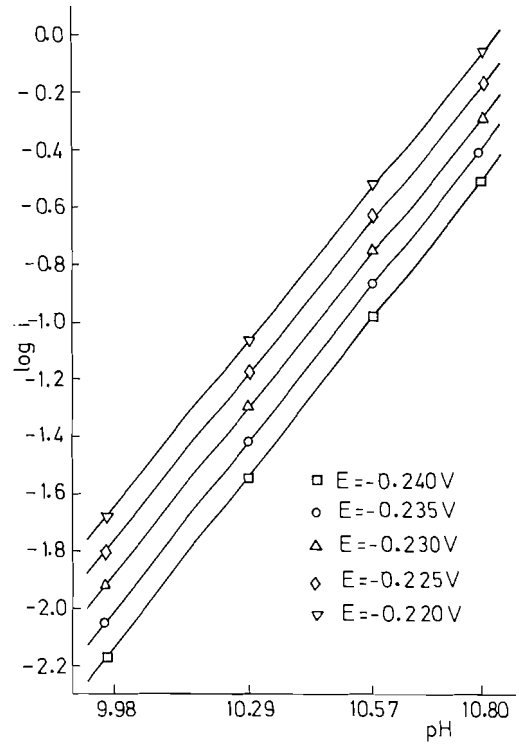

FIG. 5. Reaction orders.

On the other hand, Euler and Hasselquist (3) detected the formation of an enediol type compound during the decomposition of dehydro-L-ascorbic acid in a basic medium. In the present study, we have obtained the corresponding disodium salt by using the technique described by Kenyon and Munro (4). The structure of this salt was confirmed by infrared spectroscopy where it was observed that the C—O band (1160 cm^{-1}), characteristic of γ-lactones, had disappeared and that a band of double bonding existed (1640 cm^{-1}).

Therefore, from these results, one can assume that dehydro-L-ascorbic acid undergoes, in a basic medium, the **1**, **2**, **3** sequence.

The final products of the reaction form an extremely complex mixture in which L-treonic and oxalic acids are found, together with fructose and

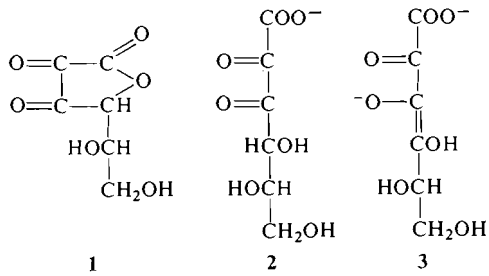

1 2 3

other sugars. These products are identified by paper chromatography on a concentrated solution which has undergone electrolysis.

Discussion and Conclusions

(a) First Oxidation Wave

In a previous paper (1) the oxidation mechanism of L-ascorbic acid in an acid medium was established. The reaction orders with respect to the H^+ concentration were -2 and -1 depending on whether the acid was nondissociated or in its monodissociated form. The potentials varied as predicted with the pH, i.e. the plot of $E_{1/2}$ vs. pH gave two linear segments with slopes of -59 and -27 mV/pH unit which correspond to a process in which a two proton and a one proton transfer takes place respectively.

If this oxidation mechanism were also true for basic media, the reaction orders would be -1 and 0 depending on whether the acid was in its monodissociated form or was completely dissociated. The plot of $E_{1/2}$ vs. pH should give two linear segments with slopes of -27 and 0 mV/pH unit, respectively.

However, the reaction orders were found to be -2.0 for pH 10–11 and -1.1 for pH 12–13, whilst the plot of $E_{1/2}$ vs. pH is linear with a slope of -68 mV/pH unit.

The fact that, with respect to the H^+ concentration, the reaction order increases from -1 (in neutral medium) to -2 and that the slope of the plot $E_{1/2}$ vs. pH increases from -27 mV/pH unit (neutral medium) to -68 mV/pH unit indicates the existence of a chemical step, with the participation of an H^+ ion, before the rate determining step (r.d.s.).

On the other hand, from data obtained from the identification of products, 2,3-diketogulonic acid in solution is converted to the enolate shown in structures **1**, **2**, **3**.

From the above conclusions, the oxidation mechanism in a basic medium can be represented by Scheme 1, where reaction 1 represents hydrolysis with rupture of the lactone ring, reactions 2 and 3 represent the one electron transfers, and reaction 4 represents dissociation (enolate formation) of 2,3-diketogulonic acid.

Assuming reaction 3 to be the r.d.s. and applying the approximation of equilibrium state, the value of the intensity in the rising portion of the wave could be expressed as

$$[1] \qquad i = 2FK_1K_2k_3 \frac{c_T}{K_1c_H + c_H^2} \exp(2-\beta)FE/RT$$

where c_T is the total concentration of L-ascorbic acid in the bulk of the solution, c_H the concentration of H^+ ions, K_1 and K_2 the equilibrium constants of reactions 1 and 2, and k_1 the rate constant of the rate determining step.

Table 1 gives a comparison of the theoretical results from the aforementioned mechanism and the experimental results.

As is logical, when pK_2 is less than the pH of the medium, reaction 1 of Scheme 1 should be ignored.

The close agreement between the experimental and theoretical results indicates that the oxidation process probably takes place as shown in Scheme 1.

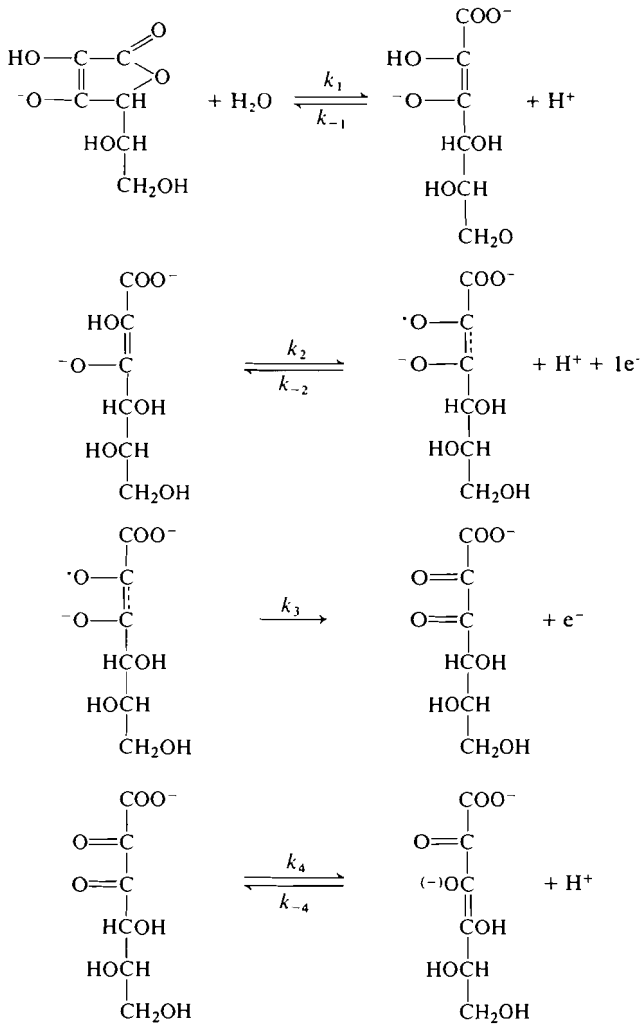

SCHEME 1. Reaction kinetic pathways of L-ascorbic acid (first wave).

Can. J. Chem. Downloaded from www.nrcresearchpress.com by 210.87.254.5 on 09/05/12
For personal use only.

Can. J. Chem. Downloaded from www.nrcresearchpress.com by 210.87.254.5 on 09/05/12
For personal use only.

TABLE 1. Comparison between theoretical and experimental results for first wave

Parameter	Value: Theoretical ($\beta = 0.5$)	Value: Experimental
Tafel slope	39 mV	42 mV
Order with respect to L-ascorbic acid concentration	1	1
Order with respect to H^+ ion	-2 for $K_1 \ll c_H$ -1 for $K_1 \gg c_H$	-2.0 (pH 10–11) -1.1 (pH 12–13)

(b) Second Oxidation Wave

The fact that this wave has practically the same intensity as the first seems to indicate that the wave is caused by the product of the first oxidation of L-ascorbic acid in a basic medium, i.e. 2,3-diketo-

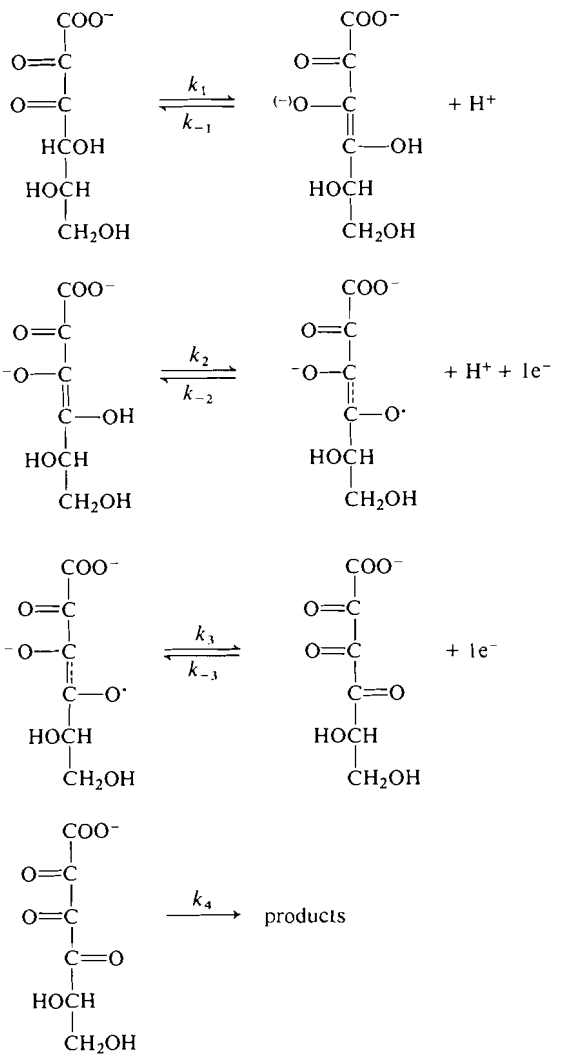

SCHEME 2. Reaction kinetic pathways of L-ascorbic acid (second wave).

TABLE 2. Comparison between theoretical and experimental results for second wave

Parameter	Value: Theoretical	Value: Experimental
Tafel slope	29.5 mV	29.7 mV
Order with respect to L-ascorbic acid concentration	1	1
Order with respect to H^+ ion	-2 for $(1 + K_1)c_H \gg K_1K_2$ -1 for $K_1K_2 \gg (1 + K_1)c_H$	-2 —

gulonic acid. As this compound undergoes, in a basic solution, a series of consecutive chemical reactions, these can perhaps be considered as being the primary stages of oxidation, that is, enolization and dissociation (reaction 1 of Scheme 2).

Following the formation of the enolate, oxidation can take place by means of two one electron transfers forming 2,3,4-triketogulonic acid (reactions 2 and 3 of Scheme 2). This acid is believed to be highly unstable owing to the presence of four adjoining carbonyl groups and decomposition follows giving substances with a shorter carbon chain (reaction 4 of Scheme 2), as observed in the results from the chromatography.

Considering reaction 4 to be the r.d.s. and applying the approximation of equilibrium state, the value of the current in the rising portion of the wave can be expressed by

$$[2]\quad i = 2FK_1K_2K_3k_4 \frac{c_T}{K_1K_2c_H + (1 + K_1)c_H^2} \times \exp(2FE/RT)$$

where c_T is the total concentration of L-ascorbic acid in the bulk of the solution, K_1, K_2, and K_3 are the equilibrium constants of the reactions 1, 2, and 3, and k_4 is the rate constant of the rate determining step.

Table 2 gives a comparison between theoretical values deduced from the above mechanism and the experimental results.

The close agreement between the theoretical and experimental results clearly indicates that the oxidation process probably takes place as shown in Scheme 2.

Acknowledgment

This study was supported by the Comisión Asesora de Investigación Científica y Técnica, Madrid.

1. J. J. RUIZ, A. ALDAZ, and M. DOMINGUEZ. Can. J. Chem. **55**, 2799 (1977).
2. L. V. MAPSON and S. M. PARTRIDGE. Nature, **164**, 479 (1949).
3. H. V. EULER and H. HASSELQUIST. Ark. Kemi, **8**, 67 (1955).
4. J. KENYON and M. J. MUNRO. J. Chem. Soc. 158 (1948).

Synthesis and nuclear magnetic resonance study of the compounds (2-X-1,3-dithiane) (X = H, Me, $SiMe_3$, $GeMe_3$, $SnMe_3$, $PbMe_3$) and their tetracarbonyliron complexes

DAVID J. CANE, WILLIAM A. G. GRAHAM, AND LIVIU VANCEA

Department of Chemistry, University of Alberta, Edmonton, Alta., Canada T6G 2G2

Received August 3, 1977

DAVID J. CANE, WILLIAM A. G. GRAHAM, and LIVIU VANCEA. Can. J. Chem. **56**, 1538 (1978).

A series of (1,3-dithiane)$Fe(CO)_4$ complexes, (2-X-1,3-dithiane)$Fe(CO)_4$, X = H, Me, $SiMe_3$, $GeMe_3$, $SnMe_3$, $PbMe_3$, has been prepared and characterized, and both the complexes and the free ligands studied by ^1H and ^{13}C nmr spectroscopy. The energy barrier to ring inversion in (1,3-dithiane)$Fe(CO)_4$, ΔG_{298}†, is 14.7 ± 0.2 kcal mol^{-1}, some 4.4 kcal mol^{-1} higher than in free 1,3-dithiane. ^{13}C nmr spectra showed that within the $Fe(CO)_4$ moiety, rapid averaging of carbonyl groups occurs down to at least −80°C.

DAVID J. CANE, WILLIAM A. G. GRAHAM et LIVIU VANCEA. Can. J. Chem. **56**, 1538 (1978).

On a préparé et caractérisé une série de complexes (dithiane-1,3)$Fe(CO)_4$, (2-X-1,3-dithiane)$Fe(CO)_4$, X = H, Me, $SiMe_3$, $GeMe_3$, $SnMe_3$ et $PbMe_3$ et on a étudié aussi bien les complexes que les ligands libres par spectroscopie rmn ^1H et ^{13}C. La barrière d'énergie à l'inversion du cycle dans le (dithiane-1,3)$Fe(CO)_4$, ΔG_{298}†, est 14.7 ± 0.2 kcal mol^{-1}, soit une valeur qui est 4.4 kcal mol^{-1} plus élevée que dans le dithiane-1,3 libre. Les spectres rmn du ^{13}C montrent qu'à l'intérieur de la fraction $Fe(CO)_4$ il se produit des transpositions rapides des groupes carbonyles jusqu'à une température d'au moins −80°C.

[Traduit par le journal]

Introduction

Over the past few years, the six-membered heterocycle 1,3-dithiane and its derivatives have been the subject of many investigations. Initially, the interest arose because of their structural similarity to cyclohexane and 1,3-dioxane. Most efforts were directed at understanding the conformational preferences in these heterocycles, and this was tackled using the equilibrium method (1, 2), ^1H (3–7) and ^{13}C (3, 8) nmr spectroscopy, dipole moment measurements (6), and X-ray structural determinations (9). Recently, 1,3-dithianes have become increasingly important reagents in organic (10) and organometallic synthesis (11, 12).

Transition metal complexes of 1,3-dithianes have been comparatively little studied. In 1975, the synthesis and crystal structure of the first metal carbonyl complex of this type, (1,3-dithiane)$Fe(CO)_4$, was reported (13). In the solid state structure of this compound the dithiane ring adopts a chair conformation in which one of the sulphur atoms occupies an axial site in the trigonal bipyramidal arrangement around iron. Some mercury (14), niobium (15), tantalum (15), and copper (16) complexes of 1,3-dithiane have also been described.

In the course of a study of transition metal derivatives of 1,3-dithiane, we have prepared a series of 2-substituted dithianes, together with the corresponding iron tetracarbonyl complexes, (2-X-1,3-dithiane)$Fe(CO)_4$, X = Me, $SiMe_3$, $GeMe_3$, $SnMe_3$, $PbMe_3$. We report here full characterization of the previously unknown members of this series, together with the results of ^1H and ^{13}C nmr studies on all the compounds, and on (1,3-dithiane)$Fe(CO)_4$.

Results and Discussion

Reaction of diiron nonacarbonyl with 1,3-dithiane (13) or its derivatives proceeds smoothly in THF (17) at room temperature according to reaction 1:

[1] 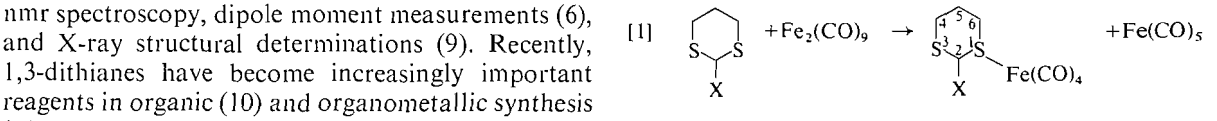

X = H, Me, $SiMe_3$, $GeMe_3$, $SnMe_3$, $PbMe_3$

The (dithiane)$Fe(CO)_4$ complexes are yellow or red–brown crystalline solids, which are reasonably stable in air. For example, infrared spectroscopy of (2-Me_3Si-1,3-dithiane)$Fe(CO)_4$ showed no appreciable decomposition after the crystals were exposed to the atmosphere for 4 days. However, solutions of the complexes are sensitive to air and light.

The (dithiane)$Fe(CO)_4$ complexes were fully characterized by analysis, mass spectrometry (low and high resolution), infrared, ^1H and ^{13}C nmr spectroscopy.

Infrared Spectra

Assuming that the solid-state structure (13) of (1,3-dithiane)$Fe(CO)_4$ is preserved in solution, idealized C_{3v} symmetry at iron would predict three infrared-active carbonyl stretching bands ($2A_1 + E$).

Can. J. Chem. Downloaded from www.nrcresearchpress.com by 210.87.254.6 on 09/05/12
For personal use only.

TABLE 1. Infrared spectra of (1,3-dithiane)$Fe(CO)_4$ complexes

(2-X-1,3-dithiane)$Fe(CO)_4$ X =	Carbonyl stretching bands[a]			
H	2056 (7.7)	1981 (7.1)	1954 (10)	1943 (9.7)
Me	2054 (8.1)	1978 (7.7)	1954 (10)	1939 (9.6)
Me_3Si	2054 (7.2)	1975 (7.0)	1952 (10)	1937 (9.4)
Me_3Ge	2053 (7.8)	1976 (7.6)	1952 (10)	1937 (9.9)
Me_3Sn	2052 (7.0)	1975 (7.2)	1951 (9.5)	1937 (10)
Me_3Pb	2051 (6.8)	1974 (6.9)	1948 (9.0)	1936 (10)

[a]In *n*-hexane solution. Band positions in cm^{-1}, with intensities in parentheses relative to the strongest band as 10, using a percent transmission scale.

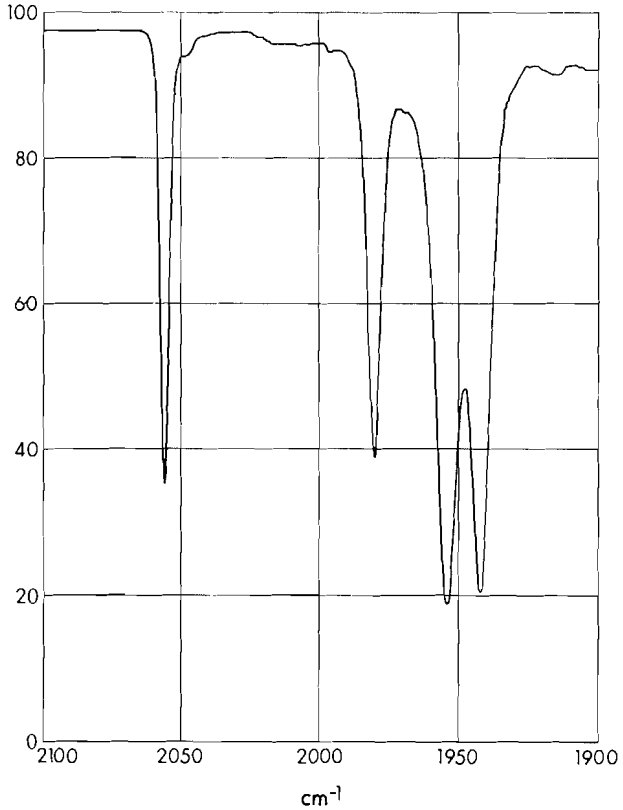

FIG. 1. Carbonyl stretching region of the infrared spectrum of (1,3-dithiane)$Fe(CO)_4$ in *n*-hexane solution.

The infrared spectrum of this compound in fact showed four terminal carbonyl bands[1] (Fig. 1), which may be understood in terms of the asymmetry introduced by the dithiane ligand (C_s symmetry, $3A' + A''$ modes (19)).

The carbonyl stretching frequencies observed for the series of complexes prepared here differ very little (Table 1), although there is a general trend to lower frequencies upon substitution.

[1]The previously reported (13) infrared spectrum of (1,3-dithiane)$Fe(CO)_4$ is now agreed to be in error (18).

^1H *Nuclear Magnetic Resonance Spectra*

In the absence of ring inversion, the ^1H nmr spectrum of 1,3-dithiane can be roughly described (see below) as consisting of both AB and AA'BB'CD spin systems. Coordination of one of the sulfur atoms to iron reduces the symmetry of the molecule, and AB and ABCDEF spin systems are obtained. The following discussion will deal mainly with the H-2 resonances. The numbering scheme adopted is shown in reaction 1.

At $-30°C$, the ^1H nmr spectrum of (1,3-dithiane)-$Fe(CO)_4$ in toluene-d_8 showed an AB pattern with calculated chemical shifts at 3.12 and 2.58 ppm, and three sets of multiplets with estimated positions at 1.9, 1.7, and 1.1 ppm (Fig. 2). The upfield part of the AB pattern was considerably broader (width at half-height 4 Hz) than the lower field part (width 1.5 Hz). Selective decoupling confirmed that this differential broadening is due to coupling to the multiplets centered at 1.7 and 1.9 ppm. The resonance at 2.58 ppm is assigned to H-2_{eq} and the one at 3.12 ppm to H-2_{ax}. H-2_{eq} can couple via a planar W-pathway to H-4_{eq} and H-6_{eq} and this broadens its signal relative to that of H-2_{ax} for which no such couplings exist. Analysis of the AB system (20) afforded $^2J(\text{H-}2_{ax} - \text{H-}2_{eq}) = 13.5$ Hz and $\delta(\text{H-}2_{ax}) - \delta(\text{H-}2_{eq}) = 54.2$ Hz.

The three multiplets at higher field in the spectrum are tentatively assigned to H-4, H-6, and H-5, on the basis of their upfield shifts on complex formation.

On warming, the AB pattern broadens, coalesces, and at 35°C becomes a single resonance (Fig. 2). At this temperature, ring inversion occurs rapidly on the nmr time scale. The coalescence temperature is 25°C and this gives a value for the free energy of activation for ring inversion ($\Delta G_{298}\dagger$) of 14.7 ± 0.2 kcal mol^{-1}. It therefore appears that coordination of a ring sulfur atom to iron results in a considerable increase in the free energy barrier for ring inversion over that in free 1,3-dithiane ($\Delta G_{213}\dagger = 10.3$ kcal mol^{-1}) (21).

^1H nmr data for the other (dithiane)$Fe(CO)_4$ com-

Can. J. Chem. Downloaded from www.nrcresearchpress.com by 210.87.254.6 on 09/05/12
For personal use only.

Can. J. Chem. Downloaded from www.nrcresearchpress.com by 210.87.254.6 on 09/05/12
For personal use only.

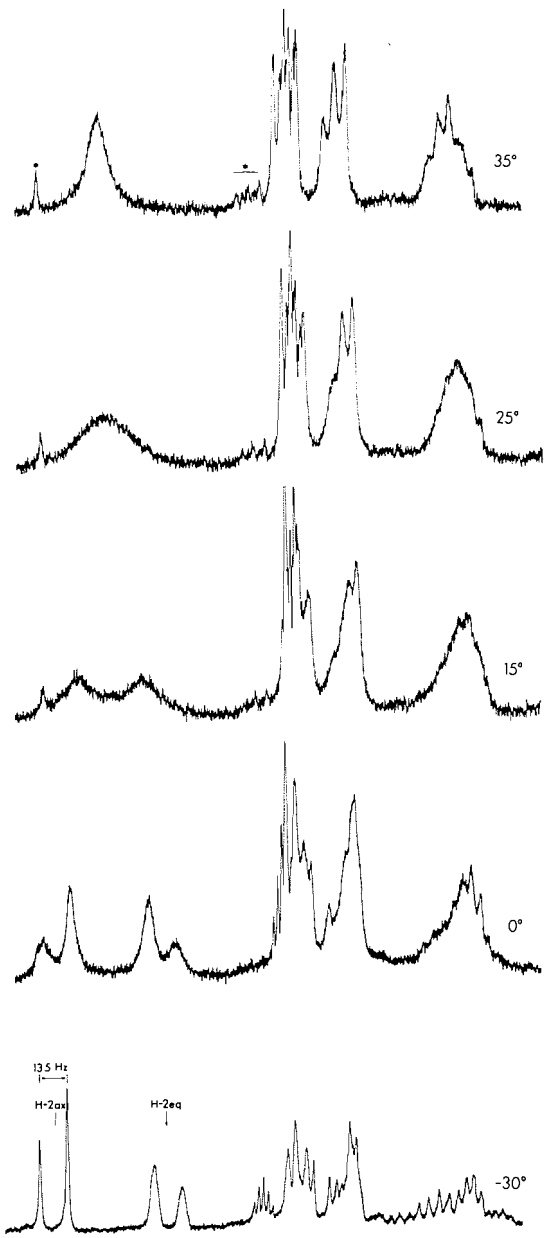

FIG. 2. Proton nmr spectra of (1,3-dithiane)$Fe(CO)_4$ in toluene-d_8 at a series of temperatures. Peaks marked with asterisks are due to free 1,3-dithiane. Quintet visible at centre of −30°C spectrum is due to residual toluene-d_7.

plexes are given in Table 2. The corresponding parameters for the free ligands are listed in Table 3. The ^1H nmr of 1,3-dithiane and 2-Me-1,3-dithiane in CS_2 have been previously reported, but not analyzed (22). The analysis of such AA'BB'CD systems has been described (23), and the 220 MHz spectrum of 2-Ph-1,3-dithiane has been interpreted using iterative methods (23, 24).

Generally speaking, the H-2 resonance in the free ligands is deshielded on going from silicon to lead derivatives. Complexation to iron results in a general upfield shift of the ring proton resonances, H-2 being most affected. The methyl protons attached to the group IV substituent atom, on the other hand, frequently shift to lower field.

Considerable difficulty was encountered in obtaining the ^1H nmr spectra of (dithiane)$Fe(CO)_4$ complexes. Although samples were prepared in the dark using dry, oxygen-free solvents, rapid decomposition of the lower members of the series frustrated many attempts at spectral determination. However, it was found that spectra of high quality could be obtained by sealing the samples in cyclohexane-d_{12} or toluene-d_8 under 1 atm of carbon monoxide.[2]

^{13}C *Nuclear Magnetic Resonance Spectra*

The ^{13}C nmr spectrum of 1,3-dithiane is expected to show three resonances, due to C-2, C-4,6, and C-5. The presence of a substituent in the 2-position makes the assignment unambiguous: C-2 can be differentiated from C-5 by off-resonance decoupling, and C-4,6 has twice the intensity of C-2 or C-5. Coordination of 1,3-dithiane to iron removes the plane of symmetry and four signals of equal intensity are expected for the ring carbons of (1,3-dithiane)$Fe(CO)_4$. Unambiguous assignment is possible using model compounds such as (2-Me_3E-1,3-dithiane)-$Fe(CO)_4$ where E has an isotope with spin of 1/2 in sufficient abundance, for example $^{117,119}Sn$ or ^{207}Pb.

^{13}C nmr data for the (dithiane)$Fe(CO)_4$ complexes and for the free ligands are given in Tables 4 and 5, respectively. The ^{13}C nmr spectra of 1,3-dithiane and 2-Me-1,3-dithiane in $CDCl_3$ have been reported previously (8).

Complexation of dithianes to iron results in a downfield shift for C-2, C-5, C-6, and for the methyl carbons. As expected, C-2 and C-6 are the most affected; the downfield shift for C-2 is between 9.9 and 12.5 ppm, and the corresponding shift for C-6 between 13.6 and 15.9 ppm. The downfield shift of the methyl carbons is only 1.6–4.0 ppm and C-5 is even less affected: downfield shift 0.5–2.4 ppm. In contrast, C-4, the ring carbon most distant from iron, is shifted upfield by 0.3 to 1.3 ppm.

The carbonyl chemical shifts differ little on changing the group IV substituent on the dithiane ligand.

The ^{13}C–$^{117,119}Sn$ or ^{13}C–^{207}Pb coupling constants for the ring carbons decrease on complexation, the most affected being the one-bond coupling to C-2.

[2]On one occasion, an nmr tube containing (1,3-dithiane)-$Fe(CO)_4$ in toluene-d_8 under carbon monoxide shattered as the spectrum was being run, damaging the probe.

TABLE 2. ^{1}H nmr data for (1,3-dithiane)Fe(CO)$_4$ complexes

(2-X-1,3-dithiane)Fe(CO)$_4$ X =	Chemical shift[a] H-2	H-4,6	H-5	Me
H	3.67 (s, broad)	2.7 (m)	2.2 (m)[b]	
H	3.04 (s, broad)	2.1 (m), 1.9 (m)	1.3 (m)	
Me	3.74 (q)[c]	2.8 (m)	2.1 (m)	1.57 (d)[b,c]
Me_3Si	3.59 (s)	2.8 (m), 2.6 (m)	2.1 (m)	0.03 (s)[b]
Me_3Ge	3.48 (s)	2.3 (m)	1.9 (m)	0.40 (s)
Me_3Sn	3.62 (s)	2.3 (m)	1.9 (m)	0.31 (s) [54, 57]
Me_3Pb	3.93 (s) [11]	2.1 (m)		1.06 (s) [65]

[a]In ppm from TMS; multiplicities in parentheses; ambient temperature. Values in square brackets are ^{1}H–^{117,119}Sn or ^{1}H–^{207}Pb coupling constants in Hz. Toluene-d_8 solvent, unless otherwise stated.
[b]Cyclohexane-d_{12} solvent.
[c]^3J(H—CH$_3$) = 7 Hz.

TABLE 3. ^{1}H nmr data for 1,3-dithianes

(2-X-1,3-dithiane) X =	Chemical shift[a] H-2	H-4,6	H-5	Me
H	3.67 (s)	2.7 (m)	2.0 (m)	
	3.41 (s)	2.4 (m)	1.6 (m)	
Me	4.03 (q)[b]	2.8 (m)	1.9 (m)	1.38 (d)[b]
	3.85 (q)[b]	2.4 (m)	1.6 (m)	1.34 (d)[b]
Me_3Si	3.65 (s)	2.7 (m)	2.0 (m)	0.13 (s)
	3.56 (s)	2.4 (m)	1.7 (m)	0.16 (s)
Me_3Ge	3.77 (s)	2.7 (m)	2.0 (m)	0.27 (s)
	3.73 (s)	2.5 (m)	1.8 (m)	0.28 (s)
Me_3Sn	3.92 (s) [46]	2.6 (m)	2.1 (m)	0.21 (s) [54, 56]
	3.84 (s) [46]	2.4 (m)	1.8 (m)	0.23 (s) [54, 56]
Me_3Pb	4.26 (s) [31]	2.6 (m)	2.1 (m)	0.92 (s) [64]
	4.22 (s) [31]	2.4 (m)	1.8 (m)	0.91 (s) [64]

[a]In ppm from TMS; multiplicities in parentheses; ambient temperature. Values in square brackets are ^{1}H–^{117,119}Sn or ^{1}H–^{207}Pb coupling constants in Hz. Solvent: cyclohexane-d_{12} (top entry) or toluene-d_8 (bottom entry).
[b]^3J(H—CH$_3$) = 7 Hz.

The similar coupling to the methyl carbons increases on complexation. No coupling was observed to the carbonyl carbons.

Although the solid state structure of (1,3-dithiane)-Fe(CO)$_4$ indicates nonequivalent carbonyl groups, in solution at room temperature the carbonyl carbon resonances of this and of all the other (dithiane)Fe-(CO)$_4$ complexes appear as a sharp singlet. This indicates a rapid carbonyl rearrangement on the nmr time scale.

Spectra at lower temperatures were recorded in the hope of slowing down the carbonyl scrambling process. However, the carbonyl signals of all complexes investigated here remained sharp to the lowest accessible temperatures (−80°C for (1,3-dithiane)Fe(CO)$_4$, (2-Me-1,3-dithiane)Fe(CO)$_4$, and (2-Me$_3$Ge-1,3-dithiane)Fe(CO)$_4$ and −90°C for the others). This perhaps is not too surprising in view of the extremely low barrier for carbonyl scrambling in Fe(CO)$_5$ (25, 26) and its derivatives, such as Fe(CO)$_4$L (L = C_5H_5N (27), PF_3 (28)) and Fe(CO)$_3$(L—L) (L—L = $Me_2PCH_2CH_2PMe_2$ (29), $Ph_2PCH_2PPh_2$ (30), to mention but a few).

The ring carbons of the (dithiane)Fe(CO)$_4$ complexes showed fairly sharp resonances in the room temperature spectra. As the temperature was decreased, these resonances broadened and at −80 or −90°C, the ring signals had in many cases disappeared into the baseline. The methyl carbons exhibited sharp resonances throughout this temperature range.

The temperature dependence of the ^{13}C nmr spectra described above is presumably due to nonrigidity in the dithiane ring. For (1,3-dithiane)Fe-

Can. J. Chem. Downloaded from www.nrcresearchpress.com by 210.87.254.6 on 09/05/12
For personal use only.

TABLE 4. ^{13}C chemical shifts and coupling constants for (1,3-dithiane)$Fe(CO)_4$ complexes[a]

(2-X-1,3-dithiane)$Fe(CO)_4$ X =	CO	C-2	C-4	C-5	C-6	Me
H	214.2	43.7	28.6	28.5	43.4	—
Me	214.6	52.6	30.3	27.8	44.8	19.6
Me_3Si	215.7	44.1	30.0	26.9	46.5	−1.5
Me_3Ge	215.6	43.9	30.2	27.9	47.2	−1.3
Me_3Sn	215.5	39.6	30.8	28.8	47.4	−7.8
		[210, 219]	[27]	[—]	[17]	[342, 359]
Me_3Pb	215.5	39.2	32.1	29.0	48.1	2.9
		[27]	[32]	[6]	[15]	[274]

[a]In ppm downfield from TMS. Values in square brackets are ^{13}C–$^{117,119}Sn$ or ^{13}C–^{207}Pb coupling constants in Hz. Toluene-d_8 solvent. Temperature 303 K.

TABLE 5. ^{13}C chemical shifts and coupling constants for 1,3-dithianes[a]

(2-X-1,3-dithiane) X =	C-2	C-4,6	C-5	Me
H	31.9	29.8	26.8	—
Me	42.1	30.6	25.4	21.3
Me_3Si	34.2	30.9	26.4	−3.1
Me_3Ge	33.6	31.3	26.5	−3.5
Me_3Sn	27.1	32.0	26.8	−10.4
	[b]	[32]	[d]	[334, 350]
	27.3	32.3	26.9	−10.2[c]
	[252, 264]	[31]	[d]	[337, 353]
Me_3Pb	28.8	33.4	26.9	−1.1
	[102]	[43]	[7]	[258]

[a]In ppm downfield from TMS. Values in square brackets are ^{13}C–$^{117,119}Sn$ or ^{13}C–^{207}Pb coupling constants in Hz. Toluene-d_8 as solvent unless otherwise stated. Temperature 303 K.
[b]Tin coupling satellites obscured by other resonances.
[c]CD_2Cl_2 solvent.
[d]Coupling constant too small to observe.

$(CO)_4$ it is likely that we are observing the same ring inversion process in both ^1H and ^{13}C spectra. Ring inversion has also been observed in the compounds cyclohexyltrimethyltin and cyclohexyltrimethyllead (31). The exact nature of the processes involved in the 2-substituted dithiane complexes is open to speculation.

Experimental Section

All experiments were carried out under an atmosphere of dry, oxygen-free argon or nitrogen. Solvents were distilled from lithium aluminum hydride or calcium hydride and saturated with argon or nitrogen before use. Nuclear magnetic resonance solvents were dried over type 4A Molecular Sieves. In general, starting materials were commercially available and were used as received. Me_3PbBr was prepared by a literature method (32).

^1H nmr spectra were recorded on Varian A-56/60A or HA-100 instruments. Spectra were referenced vs. internal tetramethylsilane (TMS) or the residual proton from deuterated solvents (cyclohexane-d_{12} 1.38 ppm, toluene-d_8 6.98 ppm (33). Our own measurements confirm these values). Nuclear magnetic resonance tubes containing (dithiane)$Fe(CO)_4$ complexes in toluene-d_8 or cyclohexane-d_{12} (previously degassed by several freeze–thaw cycles) were sealed off under 1 atm of carbon monoxide,[2] and were stored at liquid nitrogen temperature in the dark. The free energy of activation for ring inversion in (1,3-dithiane)$Fe(CO)_4$ was calculated from the chemical shift separation at slow exchange and the coalescence temperature (34, 35). The chemical shift difference between the axial and equatorial H-2 resonances below the region of coalescence (243–273 K) was temperature dependent. A least-squares analysis of the chemical shift difference ($\Delta\delta$) in toluene-d_8 against temperature (T, K) suggested the following relationship:

$$\Delta\delta = -0.1445T + 89.35$$

From this relationship, $\Delta\delta$ at coalescence could be calculated.

^{13}C nmr spectra were recorded in the pulse Fourier transform mode of operation on a Bruker HFX-90-Nicolet 1085 spectrometer operating at 22.6 MHz. Spectra were obtained using proton broad-band decoupling conditions and with quadrature detection. Assignment of resonances was carried out using the off-resonance decoupling technique, as well as $^{117,119}Sn$ or ^{207}Pb satellites. The number of data points (channels) was usually 8000 and the sweep width 6000 Hz (for the (dithiane)$Fe(CO)_4$ complexes) or 5000 Hz (for the free ligands). This afforded a digital resolution of approximately 0.03 ppm. Other operating conditions were as given elsewhere (36). Toluene-d_8 served as nmr solvent and lock and TMS was employed as internal standard. For most spectra, tris(acetylacetonato)chromium(III) was used as a relaxation agent (37). Most sample tubes, especially for the lower members of the (dithiane)$Fe(CO)_4$ series, were sealed off under vacuum. Chemical shifts downfield from TMS are taken as positive.

Infrared spectra were recorded using a Perkin-Elmer 337 grating spectrometer with scale expansion, operating at a speed of 39 cm^{-1} min^{-1} and calibrated with carbon monoxide gas. Reported infrared stretching frequencies are considered accurate to ± 1 cm^{-1}.

Can. J. Chem. Downloaded from www.nrcresearchpress.com by 210.87.254.6 on 09/05/12
For personal use only.

Can. J. Chem. Downloaded from www.nrcresearchpress.com by 210.87.254.6 on 09/05/12
For personal use only.

TABLE 6. Yields, analytical data, and physical properties

Compound	Yield[a] (%)	Appearance	bp (°C/mm Hg) or mp (°C)	Calculated				Found			
				Mol. wt.	% C	% H	% S	Mol. wt.[b]	% C	% H	% S
2-Me_3Ge-1,3-dithiane	76	Colorless	89/1.4	238	35.49	6.81	27.07	238	35.58	6.86	27.09
2-Me_3Sn-1,3-dithiane	54	Colorless	98/1.5	284	29.71	5.70	22.66	284	29.88	5.78	22.53
2-Me_3Pb-1,3-dithiane	23	Colorless	112/0.4	372	22.63	4.34	—	372	22.64	4.34	—
(1,3-Dithiane)$Fe(CO)_4$	43	Red–brown	43–44 (decomp.)	287.92133	33.35	2.80	22.26	287.92118	33.42	2.75	22.09
(2-Me-1,3-dithiane)$Fe(CO)_4$	30	Lt.-brown	49–50 (decomp.)	302	35.78	3.34	21.22	302	35.19	3.27	20.61
(2-Me_3Si-1,3-dithiane)$Fe(CO)_4$	20	Lt.-brown	53–54 (decomp.)	360	36.67	4.48	17.80	360	36.86	4.49	17.34
(2-Me_3Ge-1,3-dithiane)$Fe(CO)_4$	50	Lt.-brown	55–57 (decomp.)	405.9052	32.64	3.98	—	405.9057	32.55	4.21	—
(2-Me_3Sn-1,3-dithiane)$Fe(CO)_4$	48	Orange–yellow	80–81 (decomp.)	451.8861	29.30	3.58	14.22	451.8848	29.15	3.51	13.95
(2-Me_3Pb-1,3-dithiane)$Fe(CO)_4$	56	Red–orange	80–81 (decomp.)	540	24.49	2.99	—	540	24.75	3.04	—

[a]Yields quoted are of pure material.
[b]Determined by mass spectrometer. Values quoted refer to the most intense peak of the isotopic multiplet due to the parent ion.

Routine mass spectra were obtained using AEI MS-12 or modified MS-2 instruments. Exact mass measurements were performed on MS-9 and MS-50 spectrometers. Samples were introduced by direct evaporation or sublimation, with the inlet systems of the mass spectrometers at room temperature. Computer-calculated isotope combination patterns were in excellent agreement with those observed for the parent ions of the new compounds.

Microanalyses were carried out by the Microanalytical Laboratory of this Department. Melting points were determined in sealed tubes on a Gallenkamp apparatus, and are uncorrected.

Preparation of 2-Substituted 1,3-Dithianes

Preparations of 2-Me-1,3-dithiane (38), 2-*tert*-Bu-1,3-dithiane (39), and 2-Me_3Si-1,3-dithiane (12) were carried out according to published procedures. Compounds 2-Me_3E-1,3-dithiane (E = Ge, Sn, Pb) were prepared from Me_3GeBr, Me_3SnCl, and Me_3PbBr using the method quoted above for 2-Me_3Si-1,3-dithiane. Yields, analytical data, and physical properties of new compounds are given in Table 6.

Preparation of (Dithiane)$Fe(CO)_4$ Complexes

The synthesis of (1,3-dithiane)$Fe(CO)_4$ (in 28% yield) has been described (13). We prepared the compounds (2-Me-1,3-dithiane)$Fe(CO)_4$ and (2-Me_3E-1,3-dithiane)$Fe(CO)_4$ (E = Si, Ge, Sn, Pb) using a similar procedure, although we found that purification by low-temperature crystallization gave improved yields over chromatographic work up. Yields, analytical data, and physical properties are given in Table 6. In attempted preparations of (2-*tert*-Bu-1,3-dithiane)$Fe(CO)_4$, infrared spectra suggested that the compound was formed, but the crystals obtained decomposed on reaching room temperature.

Synthesis of (1,3-Dithiane)$Fe(CO)_4$

All operations were carried out with precautions to exclude light. To $Fe_2(CO)_9$ (3.8 g, 10.5 mmol) was added a solution of 1,3-dithiane (1.26 g, 10.5 mmol) in 75 ml THF. The mixture was stirred under a static argon atmosphere for 4 h, and then solvent and $Fe(CO)_5$ were removed at room temperature under vacuum. The dark brown, oily residue was extracted with petroleum-ether (bp 50–80°C, 50 ml) and after filtration the yellow–brown solution was cooled to −20°C overnight to give (1,3-dithiane)$Fe(CO)_4$ as long, red–brown crystals (1.3 g, 43%). Further cooling of the mother liquor to −78°C gave a secondary yield of 0.9 g of slightly less-pure material.

Acknowledgements

We thank Professor Ernest L. Eliel for helpful discussions, Mrs. L. C. Kong, Miss K. Thompson, and Mr. T. W. Brisbane for their courage in determining the ^1H nmr spectra, and the National Research Council of Canada for financial support.

1. E. L. ELIEL and R. O. HUTCHINS. J. Am. Chem. Soc. **91**, 2703 (1969).
2. K. PIHLAJA. J. Chem. Soc. Perkin Trans. II, 890 (1974).
3. E. L. ELIEL, V. S. RAO, F. W. VIERHAPPER, and G. Z. JUARISTI. Tetrahedron Lett. 4339 (1975); F. A. CAREY, O. D. DAILEY, JR., and W. C. HUTTON. J. Org. Chem. **43**, 96 (1978).
4. K. BERGESEN, B. M. CARDEN, and M. J. COOK. Tetrahedron Lett. 4479 (1975).
5. I. STAHL and J. GOSSELCK. Tetrahedron, **30**, 3519 (1974).
6. M. J. COOK and A. P. TONGE. J. Chem. Soc. Perkin Trans. II, 767 (1974).
7. K. PIHLAJA, D. M. JORDAN, A. NIKKILÄ, and H. NIKANDER. Adv. Mol. Rel. Proc. **5**, 227 (1973).

8. E. L. ELIEL, V. S. RAO, and F. G. RIDDELL. J. Am. Chem. Soc. **98**, 3583 (1976).
9. F. A. CAREY, P. M. SMITH, R. J. MAHER, and R. F. BRYAN. J. Org. Chem. **42**, 961 (1977); R. F. BRYAN, F. A. CAREY, O. HERNANDEZ, and I. F. TAYLOR, JR. J. Org. Chem. **43**, 85 (1978).
10. E. L. ELIEL. Tetrahedron, **30**, 1503 (1974).
11. A. G. BROOK, J. M. DUFF, P. F. JONES, and N. R. DAVIS. J. Am. Chem. Soc. **89**, 431 (1967).
12. E. J. COREY, D. SEEBACH, and R. FREEDMAN. J. Am. Chem. Soc. **89**, 434 (1967).
13. F. A. COTTON, J. R. KOLB, and B. R. STULTS. Inorg. Chim. Acta, **15**, 239 (1975).
14. K. BRODERSEN, G. LIEHR, and W. RÖLZ. Chem. Ber. **108**, 3243 (1975).
15. A. MERBACH and J.-C. BÜNZLI. Chimia, **25**, 222 (1971).
16. F. CHASTRETTE, M. HASSAMBAY, and M. CHASTRETTE. Bull. Soc. Chim. Fr. 607 (1976).
17. D. J. CANE. Ph.D. Thesis. University of Birmingham. 1976; D. J. CANE and E. J. FORBES. To be published.
18. F. A. COTTON. Private communication.
19. D. J. PATMORE and W. A. G. GRAHAM. Inorg. Chem. **6**, 981 (1967).
20. E. W. GARBISCH, JR. J. Chem. Ed. **45**, 311 (1968).
21. H. FRIEBOLIN, H. G. SCHMID, S. KABUSS, and W. FAISST. Org. Magn. Res. **1**, 67 (1969).
22. H. T. KALFF and E. HAVINGA. Recl. Trav. Chim. **85**, 467 (1966).
23. H. R. BUYS. Recl. Trav. Chim. **89**, 1244 (1970).
24. J. MARTIN and J. B. ROBERT. Org. Magn. Res. **7**, 76 (1975).
25. J. P. JESSON and P. MEAKIN. J. Am. Chem. Soc. **95**, 1344 (1973).
26. H. W. SPIESS, R. GROSESCU, and U. HAEBERLEN. Chem. Phys. **6**, 226 (1974).
27. F. A. COTTON and J. M. TROUP. J. Am. Chem. Soc. **96**, 3438 (1974).
28. H. MAHNKE, R. J. CLARK, R. ROSANSKE, and R. K. SHELINE. J. Chem. Phys. **60**, 2997 (1974).
29. M. AKHTAR, P. D. ELLIS, A. G. MACDIARMID, and J. D. ODOM. Inorg. Chem. **11**, 2917 (1972).
30. F. A. COTTON, K. I. HARDCASTLE, and G. A. RUSHOLME. J. Coord. Chem. **2**, 217 (1973).
31. W. KITCHING, D. DODDRELL, and J. B. GRUTZNER. J. Organometal. Chem. **107**, C5 (1976).
32. L. C. WILLEMSENS and G. J. M. VAN DER KERK. Investigations in the field of organolead chemistry. International Lead–Zinc Research Organization, Inc., New York. 1965.
33. Merck, Sharp & Dohme Canada. Deuterated nmr solvents, handy reference data. Undated.
34. R. K. POMEROY, L. VANCEA, H. P. CALHOUN, and W. A. G. GRAHAM. Inorg. Chem. **16**, 1508 (1977).
35. G. BINSCH. *In* Dynamic nuclear magnetic resonance spectroscopy. *Edited by* L. M. Jackman and F. A. Cotton. Academic Press, NY. 1975. p. 45.
36. L. VANCEA, R. K. POMEROY, and W. A. G. GRAHAM. J. Am. Chem. Soc. **98**, 1407 (1976).
37. O. A. GANSOW, A. R. BURKE, and G. N. LAMAR. J. Chem. Soc. Chem. Commun. 456 (1972).
38. E. J. COREY and D. SEEBACH. Angew. Chem. Int. Ed. **4**, 1075 (1965).
39. D. SEEBACH. Synthesis, 17 (1969).

Can. J. Chem. Downloaded from www.nrcresearchpress.com by 210.87.254.6 on 09/05/12
For personal use only.

A study of the ion $[Ta_2OF_{10}]^{2-}$ [1]

J. SALA-PALA, J. Y. CALVES, AND J. E. GUERCHAIS

Laboratoire de chimie inorganique moléculaire, U.E.R. Sciences, 6, Avenue Le Gorgeu, 29283 Brest-Cedex, France

AND

S. BROWNSTEIN

Division of Chemistry, National Research Council of Canada, Ottawa, Ont., Canada K1A 0R9

AND

J. C. DEWAN AND A. J. EDWARDS

Chemistry Department, University of Birmingham, P.O. Box 363, Birmingham, B15-2TT England

Received October 24, 1977

J. SALA-PALA, J. Y. CALVES, J. E. GUERCHAIS, S. BROWNSTEIN, J. C. DEWAN, and A. J. EDWARDS. Can. J. Chem. **56**, 1545 (1978).

Hydrolysis of $(Et_4N)[TaF_6]$ with Et_4NOH in organic medium gives $(Et_4N)_2[Ta_2OF_{10}]$. The Ta—O—Ta infrared and Raman frequencies reflect the linearity of the bridge, in agreement with a previous X-ray study. The ^{19}F nmr spectrum is of the type $AA'E_4E_4'$. Chemical shifts are compared with other pseudo-octahedral species of tantalum with formula $[TaF_5L]$.

J. SALA-PALA, J. Y. CALVES, J. E. GUERCHAIS, S. BROWNSTEIN, J. C. DEWAN et A. J. EDWARDS. Can. J. Chem. **56**, 1545 (1978).

Le composé $(Et_4N)_2[Ta_2OF_{10}]$ a été obtenu lors de l'hydrolyse d'une solution organique de $(Et_4N)[TaF_6]$ par de l'hydroxyde de tétraéthylammonium. Les fréquences caractéristiques du groupement Ta—O—Ta (ν_{as} = 880 cm^{-1}, ν_s = 270 cm^{-1}) sont en accord avec la linéarité du pont décelée lors d'une étude antérieure par diffraction de rayons-X. Le spectre rmn (^{19}F) est de type $AA'E_4E_4'$ avec δ_A = 13.0 et δ_E = 32.0 ppm ($CFCl_3$); $J_{A-A'}$ = 9.2, J_{A-E} = 33.4, $J_{A-E'}$ = 0.6 et $J_{E-E'}$ = 0 Hz. Les valeurs des déplacements chimiques des fluors sont comparées à celles d'autres espèces pseudo-octaédriques du tantale de type $[TaF_5L]$.

Introduction

Several tantalum fluoride species, $[TaF_6]^-$, $[TaF_7]^{2-}$, $[TaF_8]^{3-}$, and $[TaF_9]^{4-}$, have been reported in hydrofluoric acid solution (1, 2). The first three species have been well characterized by X-ray crystallography (3), while the last has been inferred by a study in solution (1). The hydrolysis of these species has excited little interest except for two articles. The solid $K_4[Ta_2OF_{12}]$ was obtained by the reaction of $K_2[TaF_7]$ with KOH (4). The hydrolysis of $[TaF_6]^-$ in aqueous solution was studied by fluorine magnetic resonance (5). There are some ambiguities in the latter article, e.g. a fluorine resonance doublet attributed to the equatorial fluorines of a pseudo-octahedral species $[TaF_5L]^{n-}$ could be due to $[TaF_5(OH_2)]$, $[TaF_5OH]^-$, $[TaOF_5]^{2-}$, or a polymeric species.

An attempt to isolate, as solids, the various species produced in the hydrolysis of $[TaF_6]^-$ was made to fill the gaps in the previous studies. Such a procedure, although slower and more difficult than solution studies alone, is probably the only certain means of identifying the species produced and their degree of polymerization.

[1]NRCC No. 16542.

Experimental

$Et_4N[TaF_6]$ was prepared by the addition of Et_4NF to a hydrofluoric acid solution of $TaCl_5$(Et_4N/Ta = 1). Upon concentrating the solution the product precipitated. It was filtered, dried under vacuum (60°C and 15 Torr) for several days, and recrystallized from anhydrous CH_3CN.

$(Et_4N)_2[Ta_2OF_{10}]$

To an anhydrous methanol solution of $Et_4N[TaF_6]$ was added an aqueous methanolic solution of 20% Et_4NOH (Et_4N/Ta = 1.05). After shaking for several minutes the solution was slowly evaporated under vacuum until a precipitate was formed. This was filtered, washed with ether, and stored over P_4O_{10}. Its infrared spectrum and X-ray powder pattern were identical with those obtained for single crystal material of formula $(Et_4N)_2[Ta_2OF_{10}]$ used for the X-ray structure determination of that compound (6). *Anal.* calcd. for $C_{16}H_{40}F_{10}N_2OTa_2$: C 23.20, H 4.87, F 22.93, N 3.38; found: C 23.45, 23.60, H 4.89, 4.95, F 22.51, 22.51, N 3.25, 3.35.

Infrared and Raman Spectroscopy

Infrared spectra were obtained on a 1% KBr pellet with a 'Perkin-Elmer 225' apparatus. The infrared spectrum is shown in Fig. 1, with principal bands (cm^{-1}):

Can. J. Chem. Downloaded from www.nrcresearchpress.com by 210.87.254.5 on 09/05/12
For personal use only.

Can. J. Chem. Downloaded from www.nrcresearchpress.com by 210.87.254.5 on 09/05/12
For personal use only.

1405 m (a)	880 vs (b)
1310 m (a)	795 s (a)
1185 s (a)	575 vs (c)
1080 m (a)	530 vs (c)
1030 m (a)	350 m
1006 m (a)	250 vs
	225 vs

(a) arises from the cation Et_4N^+
(b) ν(Ta—O—Ta)
(c) ν(Ta—F)

Raman spectra were obtained by excitation with a 300 mW argon laser (514.5 nm excitating radiation) using a CODERG PHE spectrometer with a slit width of 550 nm.

The Raman spectrum is presented in Fig. 2 with principal bands (cm^{-1}):

270 s 392 m 470 w 669 s 897 w 1074 m

Fluorine Resonance Spectroscopy

Spectra were obtained at 94.1 MHz on a 'Varian Associates XL-100A-12' (at −70°C in liquid SO_2), at 250 MHz on a 'CAMECA' (from −30 to +20°C in CH_2ClCN), and at 56.4 MHz on a 'JEOL C-60HL' (from −30 to +60°C in CH_2ClCN). Chemical shifts are relative to internal $CFCl_3$ with positive shifts to low field.

Results and Discussion

Preparation

The slow evaporation of a solution of $Et_4N[TaF_6]$ in hydrogen peroxide gives a mixture of $Et_4N[TaF_6]$, $(Et_4N)_2[Ta(O–O)F_5]$, $Et_4N[Ta(O–O)F_4(H_2O)]$, and a fourth compound (7). The presence of an infrared band at 880 cm^{-1} in the latter compound was tentatively assigned to ν(O–O). However an X-ray diffraction study has shown that in fact it is an oxo compound of formula $(Et_4N)_2[Ta_2OF_{10}]$ in which the dimerisation is effected by a linear Ta—O—Ta bridge as in Fig. 3 (6). The origin of the 880 cm^{-1} band is described below.

In order to confirm, by a chemical path, the absence of a peroxo group we attempted a synthesis in a medium containing no peroxide. The precipitate obtained by addition of an Et_4NOH solution to an alcoholic solution of $Et_4N[TaF_6]$ had identical infrared spectra and Debye–Scherrer powder patterns with the previously obtained crystals of $(Et_4N)_2[Ta_2OF_{10}]$ (6). The formation of this anion, the first of the type $[M_2OF_{10}]^{2-}$ with a transition metal, might arise via an intermediate hydroxy compound (eq. [1]) followed by a condensation (eqs. [2] or [2′]).

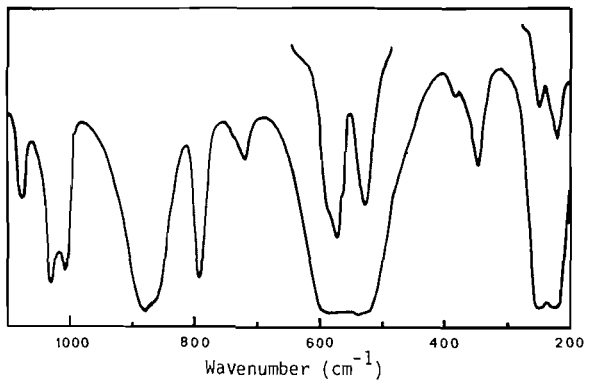

FIG. 1. The infrared spectrum of $(Et_4N)_2[Ta_2OF_{10}]$.

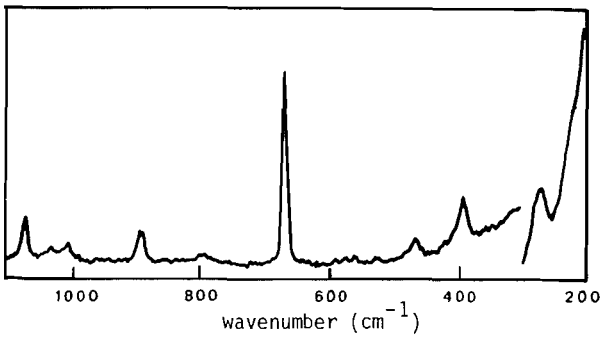

FIG. 2. The Raman spectrum of $(Et_4N)_2[Ta_2OF_{10}]$.

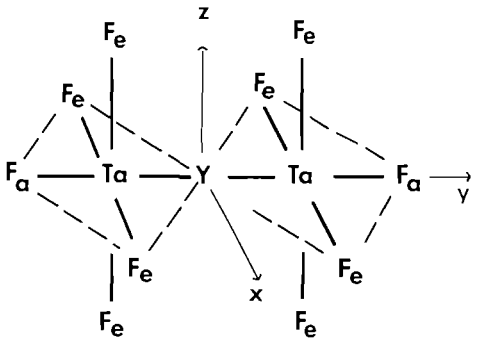

FIG. 3. The geometry of the anions F_5Ta—Y—TaF, where Y = O or F.

[1] $TaF_6^- + OH^- \rightleftharpoons TaF_5OH^- + F^-$

[2] $2TaF_5OH^- \rightleftharpoons Ta_2OF_{10}^{2-} + H_2O$

[2′] $[TaF_6]^- + [TaF_5(OH)]^- \leftrightarrows [Ta_2OF_{10}]^{2-} + HF$

Infrared and Raman Studies

For an anion $[M_2OX_{10}]^{n-}$ of symmetry D_{4h}, group theory predicts 33 normal modes ($4a_{1g}$, a_{1u}, $4a_{2u}$, $2b_{1g}$, b_{1u}, b_{2g}, $2b_{2u}$, $4e_g$, $5e_u$) of which 14 are infrared active (a_{2u} and e_u modes) and 15 are Raman active (g modes) (8).

In the present case the assignment of all these modes is not possible because of the intense bands arising from the organic cation. Nevertheless by comparison with studies of the anions $[M_2OX_{10}]^{n-}$ where M = Ru, Os, W; X = Cl and n = 4 (8–10) the following assignments are made. A very strong and wide infrared absorption at 880 cm^{-1} is attributed to the valence vibration ν_{as}(Ta—O—Ta).

Two strong infrared bands at 530 and 575 cm^{-1}

Can. J. Chem. Downloaded from www.nrcresearchpress.com by 210.87.254.5 on 09/05/12
For personal use only.

are assigned to the valence vibrations ν_{as}(Ta—F_{axial}) and ν_{as}(Ta—$F_{equatorial}$).

In the Raman spectrum the most intense bands at 270 and 669 cm^{-1} are assigned to ν_s(Ta—O—Ta) and ν_s(Ta—F) respectively. The frequencies of ν_{as} and ν_s(Ta—O—Ta) (at 880 and 270 cm^{-1} respectively) are close to those of the bridge in the ion $[Os_2OCl_{10}]^{4-}$ (ν_{as} = 852 cm^{-1}, ν_s = 225 cm^{-1}; ∠Os—O—Os = 180°) (11) and quite different from those of the ion $[\{WO(O_2)_2(H_2O)\}_2O]^{2-}$ (ν_{as} = 790 cm^{-1}, ν_s = 556 cm^{-1}; ∠W—O—W = 139°) (12). This difference in the frequency separation of ν_{as} and ν_s is attributable to the difference in the angle ∠M—O—M in the anion. The high value of ν_{as} and the low value of ν_s found for the anions of tantalum and osmium arise from the linearity of the M—O—M bridge, a linearity which implies the existence of multiple-oxygen bonding because of overlap of the empty d_{xy} and d_{yz} orbitals of Ta(V) with the filled orbitals p_x and p_z of oxygen (see Fig. 3 for notations).

Fluorine Magnetic Resonance Studies

The fluorine resonance spectrum of $[Ta_2OF_{10}]^{2-}$, a doublet at 32 ppm and a quintuplet at 13 ppm with relative intensities of 4/1, is consistent with the structure found in the solid state. Fine structure in the quintuplet is particularly marked at −70°C in liquid sulfur dioxide (Fig. 4*b*). The origin of this fine structure was shown to be magnetic, rather than chemical, non-equivalence by a double irradiation experiment. When the doublet (equatorial fluorines) is irradiated only a single collapsed line is observed for the axial fluorines (Fig. 4*c*). A theoretical spectrum for the system $AA'E_4E_4'$ with $J_{A-A'}$ = 9.2, J_{A-E} = 33.4, $J_{A-E'}$ = 0.6, and $J_{E-E'}$ = 0 Hz is shown in Fig. 4*d*. It was calculated by the program NUMARIT[2].

Spectra in CH_2ClCN solution at −30°C and 250 MHz are very similar to those shown in Fig. 4 except for somewhat poorer resolution of the fine structure of the quintuplet. This fine structure disappears with increasing temperature such that at room temperature only a simple moderately resolved quintuplet is found.

In Table 1 are listed the fluorine resonance parameters for several species (TaF_5L) with a pseudo-octahedral structure about tantalum. They can be divided into two groups. One group has an axial–equatorial fluorine coupling constant of about 25 Hz, has the axial fluorine resonance at lower field than the equatorial fluorine resonance, and has both of them at lower field than the signal of $[TaF_6]^-$. The second group has a coupling constant of about 35 Hz, the axial fluorine at higher field than the equatorial fluorine, and both often at higher field than the signal of $[TaF_6]^-$. The species $[Ta_2OF_{10}]^{2-}$ clearly belongs to the second group.

[2]J. S. Martin. Private communication.

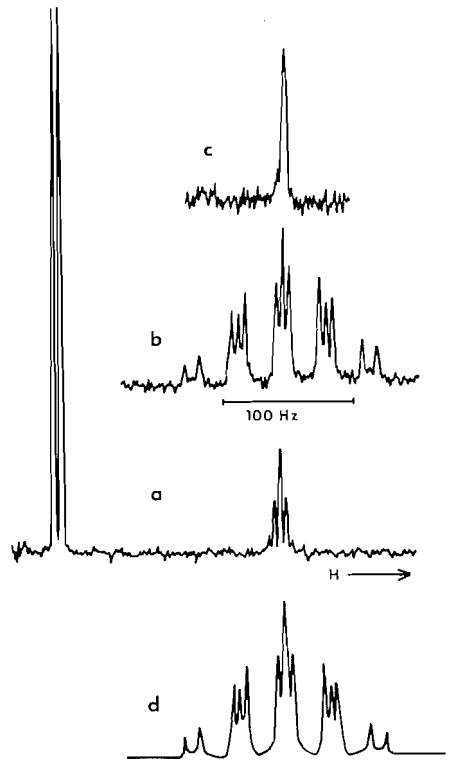

FIG. 4. Fluorine resonance spectra of $(Et_4N)_2[Ta_2OF_{10}]$. (*a*) Entire spectral region (at −20°C in CH_2ClCN; 56.4 MHz). (*b*) Fine structure of quintuplet (at −70°C in SO_2; 94.18 MHz). (*c*) Irradiation of doublet, same spectral region and conditions as (*b*). (*d*) Simulated spectrum with same scale as (*b*) (see text).

TABLE 1. Fluorine resonance parameters for $[TaF_5L]$ species

L	δ_A	δ_E	J_{A-E}	Reference
$OTaF_5^{2-}$ [a]	13.0	32.0	See text	This work
$FTaF_5^-$ [b]	115.1	72.0	23.0	14
F^- [c]	40.4	40.4		14
$O(CH_3)_2$	112.8	73.6	23.1	15
O—CO—CF_3^-	73.7	56.6	27.5	16
O—SO_2—CF_3^-	103.5	70.4	25	17
O—SO_2—F^-	103.9	70.4	25.2	17
O—$P(OCH_3)_3$	96.7	62.4	25	18
Cl^-	54.2	64.4	33 [d]	19
Br^-	57.9	71.4		19
$OCH_2CH_3^-$	−5.0	18.5	38	20
H_2O	12.4	34.7	35	13
O—$S(CH_3)_2$	0.6	19.7	35	13
H—CO—$N(CH_3)_2$	−3.2	18.0	37	13
HO—CH_2—CH_3	−29.9	16.7	39	13

[a]Species $[F_5Ta—Y—TaF_5]^{2-}$ with Y = O (see Fig. 3).
[b]Species $[F_5Ta—Y—TaF_5]^-$ with Y = F (see Fig. 3). δ_Y = 80.8, J_{A-Y} = 165, J_{E-Y} = 48.
[c]Species $[TaF_6]^-$ with all fluorines equivalent.
[d]Measured by the present authors.

The main group V elements, where there are no free *d* electrons, have the chemical shifts of axial fluorines at higher field than equatorial fluorines in their complexes while the reverse is found for the transition group V elements in those complexes where bonding via the *d* electrons is not possible (14). Therefore those complexes of TaF_5 which have the axial fluorine resonance at higher field than the equatorial may have multiple bonding between the tantalum and the ligand, employing the *d* orbitals of tantalum.

Conclusions

The hydrolysis of $[TaF_6]^-$ with Et_4NOH yields initially the dinuclear species $[Ta_2OF_{10}]^{2-}$. Further hydrolysis of $[TaF_6]^-$ or $[Ta_2OF_{10}]^{2-}$ yields compounds less rich in fluorine which are presently being studied by the same experimental techniques used in this work. The contribution of infrared, Raman, fluorine magnetic resonance, and X-ray structure determination on the same material provides a solid base for the study of further compounds in this series.

Acknowledgements

The authors thank Prof. J. Dehand and Dr. P. Braunstein (Strasbourg, France) for the Raman spectra and CAMECA (Courbevoie, France) for the very high field fluorine resonance spectra.

1. L. P. VARGA and M. FREUND. J. Phys. Chem. **66**, 21 (1962); **66**, 187 (1962).
2. O. L. KELLER and A. CHETHAM-STRODE. Inorg. Chem. **5**, 367 (1966).
3. (*a*) J. H. CANTERFORD and R. COLTON. Halides of the second and third row transition metals. Wiley-Interscience, London. 1968; (*b*) J. H. HOARD, W. J. MARTIN, M. E. SMITH, and J. F. WHITNEY. J. Am. Chem. Soc. **76**, 3820 (1954).
4. R. RITCHIE and G. MITRA. J. Fluorine Chem. **6**, 291 (1975).
5. YU. A. BUSLAEV and E. G. ILYIN. Koord. Khim. **1**, 451 (1975).
6. J. C. DEWAN, A. J. EDWARDS, J. Y. CALVES, and J. E. GUERCHAIS. J. Chem. Soc. Dalton, 978 (1977).
7. J. Y. CALVES. Thesis, Brest, France. 1975.
8. R. J. H. CLARK, M. L. FRANKS, and P. C. TURTLE. J. Am. Chem. Soc. **99**, 2473 (1977).
9. J. S. FILIPPO, R. L. GRAYSON, and H. J. SNIADOCH. Inorg. Chem. **15**, 269 (1976).
10. J. S. FILIPPO, P. J. FAGAN, and F. J. DI SALVO. Inorg. Chem. **16**, 1016 (1977).
11. K. F. TEBB and H. G. VON SCHNERING. Z. Anorg. Allg. Chem. **396**, 66 (1973).
12. R. M. WING and K. P. CALLAHAN. Inorg. Chem. **8**, 871 (1969).
13. YU. A. BUSLAEV and E. G. ILYIN. Dokl. Akad. Nauk SSSR, **190**, 1351 (1970).
14. S. BROWNSTEIN and G. LATREMOUILLE. Can. J. Chem. **52**, 2236 (1974).
15. S. BROWNSTEIN and M. J. FARRAL. Can. J. Chem. **52**, 1958 (1974).
16. S. BROWNSTEIN. Can. J. Chem. **56**, 343 (1978).
17. S. BROWNSTEIN, J. BORNAIS, and G. LATREMOUILLE. Can. J. Chem. In press.
18. C. M. P. FAVEZ and A. E. MERBACH. J. Fluorine Chem. **8**, 409 (1976).
19. YU. A. BUSLAEV and E. G. ILYIN. J. Fluorine Chem. **4**, 271 (1974).
20. YU. A. BUSLAEV, YU. V. KOKUNOV, V. D. KOPANEV, and M. P. GUSTYAKOVA. J. Inorg. Nucl. Chem. **36**, 1569 (1974).

Can. J. Chem. Downloaded from www.nrcresearchpress.com by 210.87.254.5 on 09/05/12
For personal use only.

Equilibrium decomposition pressures of the compounds K_2ZrCl_6 and K_2HfCl_6

G. J. KIPOUROS AND S. N. FLENGAS

Department of Metallurgy and Materials Science, University of Toronto, Toronto, Ont., Canada M5S 1A4

Received October 3, 1977

G. J. KIPOUROS and S. N. FLENGAS. Can. J. Chem. **56**, 1549 (1978).

The chemical equilibria representing the reactions

$$K_2ZrCl_{6(S\text{ or }L)} \geq 2KCl_{(S\text{ or }L)} + ZrCl_{4(vap,P,T)}$$

and

$$K_2HfCl_{6(S\text{ or }L)} \geq 2KCl_{(S\text{ or }L)} + HfCl_{4(vap,P,T)}$$

were investigated by direct vapour pressure measurements. The thermodynamic data for these reactions, such as free energies and enthalpies of reaction, have been calculated. With reference to the separation of Hf from Zr by a recently developed process based on the selective reactivity of $ZrCl_4$ and $HfCl_4$ vapours with alkali chlorides, it is shown that KCl is a better separating agent than LiCl.

G. J. KIPOUROS et S. N. FLENGAS. Can. J. Chem. **56**, 1549 (1978)

On a étudié, par des mesures directes de pression de vapeur, l'équilibre chimique représentant les réactions

$$K_2ZrCl_{6(S\text{ ou }L)} \geq 2KCl_{(S\text{ ou }L)} + ZrCl_{4(vap,P,T)}$$

et

$$K_2HfCl_{6(S\text{ ou }L)} \geq 2KCl_{(S\text{ ou }L)} + HfCl_{4(vap,P,T)}$$

Pour ces réactions on a calculé les données thermodynamiques telles que les énergies libres et les enthalpies de la réaction. Dans l'optique d'une séparation du Hf du Zr à l'aide d'un processus développé récemment, basé sur une réactivité sélective des vapeurs de $ZrCl_4$ et $HfCl_4$ avec des chlorures alcalins, on a montré que le KCl est un meilleur agent pour la séparation que le LiCl.

[Traduit par le journal]

Introduction

In previous publications from this laboratory (1–4) the vapour pressures of $ZrCl_4$ in equilibrium with its solutions containing alkali chlorides such as LiCl, NaCl, KCl, and CsCl, and of $HfCl_4$ in equilibrium with its solutions containing alkali chlorides such as LiCl and CsCl, have been determined by direct experimental techniques involving the use of a spoon type Bourdon gauge (1, 2) or a molten tin isoteniscope (3, 4).

In the present investigation, a quartz spiral type Bourdon gauge has been applied to the determination of the vapour pressures of $ZrCl_4$ and of $HfCl_4$ in equilibrium with the two pure compounds K_2ZrCl_6 and K_2HfCl_6 respectively, over a temperature range extending below and above their melting points.

In addition, part of the phase diagram of the system K_2ZrCl_6–K_2HfCl_6 has been determined by cryoscopy.

From the results of this study, the equilibrium dissociation constants, free energies, and enthalpies for the reactions

$$[1] \qquad K_2MCl_{6(S)} \rightleftarrows 2KCl_{(S)} + MCl_{4(vap)}$$

where M represents Zr or Hf, have been calculated.

The equilibrium constant for the exchange reaction

$$[2] \qquad K_2ZrCl_6\ (\text{in solid solution}) + HfCl_4\ (\text{vapour}) \geq K_2HfCl_6\ (\text{in solid solution}) + ZrCl_4\ (\text{vapour})$$

was also calculated

From the above data, the theoretical efficiency for the separation of hafnium from zirconium by a previously developed process based on the selective reactivity of $ZrCl_4$ and $HfCl_4$ vapours with alkali halides (5, 6) has been calculated. The results indicate that KCl should be more efficient for separating those two elements than LiCl.

Experimental

At specific partial pressure and temperature, pure $ZrCl_4$ and $HfCl_4$ vapours react with solid KCl to form the stoichiometric solid complex compounds K_2ZrCl_6 and K_2HfCl_6 respectively. The corresponding reactions may be written as:

$$[3] \qquad 2KCl\ (\text{solid}) + ZrCl_4\ (\text{vapour})\ \text{at } P,T \rightarrow K_2ZrCl_6\ (\text{solid})\ P,T$$

and

$$[4] \qquad 2KCl\ (\text{solid}) + HfCl_4\ (\text{vapour})\ \text{at } P,T \rightarrow K_2HfCl_6\ (\text{solid})\ P,T$$

The KCl–K_2ZrCl_6 (1) and KCl–K_2HfCl_6 (7) binary systems are related by simple eutectic type phase diagrams which clearly indicate the stability of these congruently melting complex compounds.

Can. J. Chem. Downloaded from www.nrcresearchpress.com by 210.87.254.6 on 09/05/12
For personal use only.

Can. J. Chem. Downloaded from www.nrcresearchpress.com by 210.87.254.6 on 09/05/12
For personal use only.

The general method applied for the preparation of the pure stoichiometric compounds was developed in this laboratory earlier (1, 2) and involves the reaction of finely ground KCl, having a particle size of less than 325 mesh, with $ZrCl_4$ or $HfCl_4$ vapours at 1 atm pressure.

The optimum reaction temperature for both K_2ZrCl_6 and K_2HfCl_6 has been found to be 485°C. Reaction time was of the order of 80 to 100 h.

When the formation of the complex compounds has been completed, the weight gain of KCl, which is converted to either K_2ZrCl_6 or K_2HfCl_6, remains constant with time and it indicates mole ratios of KCl/ZCl_4 or $KCl/HfCl_4$ respectively equal to 2.

The $ZrCl_4$ and $HfCl_4$ salts were purchased from the Wah Chang Corporation of America, Albany, New York. As they were always received in a partially hydrolyzed condition, they were purified by repeated sublimations in vacuum through a molten tin plug, as reported earlier (3).

The KCl used in the present investigation was reagent grade containing less than 0.01% total impurities, and supplied by Fisher Scientific. It was dehydrated under vacuum, at 500°C.

Handling of materials, preparation of samples, and transfer to the reaction cells were conducted in a dry box filled with argon gas.

The apparatus for measuring the equilibrium vapour pressures of $ZrCl_4$ and $HfCl_4$ over the pure complex compounds K_2ZrCl_6 and K_2HfCl_6 respectively is shown in Fig. 1. It consisted of a hollow fused quartz spiral Bourdon type gauge, made by Worden Quartz Products, Houston, Texas. The gauge was connected to the quartz reaction cell as shown in Fig. 1.

The gauge serves only as a null point detector, while the pressure is read directly on the attached closed end mercury manometer. After connecting the gauge to the apparatus, the gauge was checked for distortion using two closed end mercury manometers and comparing the two readings. The null point of the quartz spiral was determined with the aid of a telescope to the nearest 0.2 mm, while the mercury levels in the manometers were measured by a cathetometer.

Heat was supplied by a nichrome resistance furnace containing independent heating zones. The lower zone heated the sample to the desired reaction temperature, while the upper zone was controlled at a constant temperature, higher than the sublimation point of the corresponding tetrachloride. By inserting part of the two furnace windings into each other, the temperature profile within the entire system was such that condensation of the volatile vapours was prevented in all regions. The temperature was measured by means of a 22-gauge chromel–alumel thermocouple contained in a glass tube immersed in the salt sample. The thermocouple had been calibrated against a certified platinum 13% rhodium vs. platinum standard. The temperature variation within the zone occupied by the sample was ±0.4 K.

The quartz spiral type gauge was used recently in this laboratory (8) and was found to be superior to both the spoon type Bourdon gauges (1, 2) and the molten tin isoteniscopes (3, 4) used previously, because of its ability to sustain large and sudden pressure changes of an order of 1 atm without shattering. This eliminated the need for close supervision of the apparatus. In addition, because the gauge is connected directly to the sample container, and because of its small volume, the initial composition of the sample is not altered during an experiment. Furthermore, the salt sample and its vapour are contained in a closed system, thus preventing material losses and creating truly equilibrium conditions.

In a typical experiment, the sample container was loaded with the appropriate amount of salt through the tube A (Fig. 1), quickly sealed, heated to about 200°C, and periodically evacuated through the tube B to remove any gaseous hydrolysis products which might have been formed during the glass blowing operations, as well as any gas which may have been absorbed by the finely ground salt. The cell was then sealed under vacuum at the constriction C, placed in the furnace, and subjected to repeated heating and cooling cycles over the entire temperature range of interest. Experiments lasted usually a period of 30 days, and during this period the quartz cells were not visibly attacked by any of the salts. Pressure measurements during heating were in excellent agreement with those obtained during cooling.

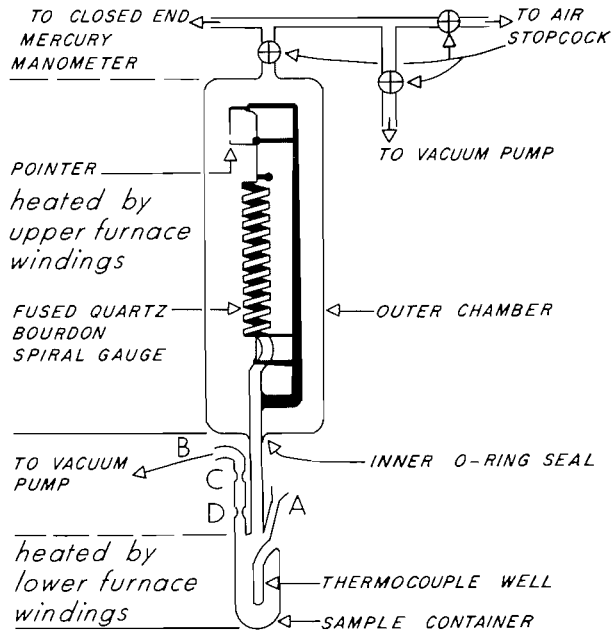

FIG. 1. Apparatus for measurement of the vapour pressures.

The apparatus for determining the phase diagram for the system K_2ZrCl_6–K_2HfCl_6 has been described elsewhere (1, 3). The containers for the mixtures to be measured were heart-shaped quartz cells having the thermocouple well at the centre of the charge, and were sealed under vacuum. Applied cooling rates were ¼°C to 1°C per min. The measurements are obtained under the pressure of $ZrCl_4$ or $HfCl_4$, respectively, in equilibrium with the two compounds or their solutions.

Experimental Results

Determination of the K_2ZrCl_6–K_2HfCl_6 Phase Diagram

The characteristic data for this diagram are given in Table 1. The liquidus tie line, when drawn, is continuous and linear and indicates a continuous series of ideal solid–liquid solutions between the two compounds. This type of behaviour, which is typical of zirconium–hafnium compounds, was also found in the systems Li_2ZrCl_6–Li_2HfCl_6 (3) and $ZrCl_4$–$HfCl_4$ (9).

The melting point for pure K_2ZrCl_6, given in Table 1, is in good agreement with that reported by Lister and Flengas (1). The melting point for pure K_2HfCl_6 determined in this work is higher than that reported by Morozov and Sun-In-Chzhu (7) by about

TABLE 1. Characteristics of the phase diagram of the binary system K_2ZrCl_6–K_2HfCl_6

Mol% of K_2HfCl_6	T (°C) of liquid line
0	799
15.0	800
34.5	802
52.5	804
67.0	805
100.0	808

6°C. The disagreement may be attributed to the presence of impurities in the K_2HfCl_6, probably in the form of hydrated zirconium oxychlorides, used by those workers. Their method of preparing K_2HfCl_6 consisted of intimately mixing the stoichiometric amounts of $HfCl_4$ and KCl, and the hydrated oxychlorides which are always present in 'pure' zirconium tetrachloride would be expected to remain in the mixture.

Vapour Pressure Measurements

The vapour pressures of $ZrCl_4$ and $HfCl_4$, in equilibrium with the pure compounds K_2ZrCl_6 and K_2HfCl_6 respectively, have been determined. Pressures were measured in mm Hg, and corrections were made for mercury expansion and for gravity effects (10, 11) to convert to standard conditions, i.e., at 273.15 K and an acceleration of free fall of 9.80665 m/s^2. These corrected pressures are given in Table 2. Temperatures reported herein are based on the IPTS-68 (12). In Fig. 2 these data are plotted as $\ln P_{MCl_4}$ vs. $1/T$, and the lines shown on the graphs are calculated by the least-squares method, while the points are experimental.

Some experimental points for the equilibrium decomposition pressures of K_2ZrCl_6 obtained previously in the laboratory (1) using the fragile quartz spoon type gauges are also shown in Fig. 2 and are in good agreement with the present work. These previous data were obtained only at higher temperatures near the melting temperature of K_2ZrCl_6, as at lower temperatures the measurements became irreversible due to gases absorbed by the sample.

It should be noted that in the present work, due to the ability of the spiral type gauge to withstand large pressure gradients, the samples could be degassed extensively prior to measurement, thus making possible accurate low pressure readings.

The corresponding equations for the temperature dependence at the equilibrium pressures within the characteristic temperature ranges were calculated and are given in Table 3. Reaction 1 in Table 3 defines the equilibrium pressure of $ZrCl_4$ over pure solid K_2ZrCl_6 and solid KCl at temperatures lower than the eutectic temperature shown in Fig. 2.

TABLE 2. Measured vapour pressure of $ZrCl_4$ and $HfCl_4$ over the pure compounds K_2ZrCl_6 and K_2HfCl_6 respectively

$ZrCl_4$		$HfCl_4$	
T (°C)	P (mm Hg)	T (°C)	P (mm Hg)
421	15.9	427	10.9
505	22.8	452	11.4
524	23.8	470	11.9
560	27.8	525	12.9
594	30.8	545	13.9
625	33.8	589	14.4
653	37.8	636	15.9
686	41.7	660	17.9
723	55.7	685	19.9
743	81.5	709	24.8
772	173.0	732	34.8
792	355.1	758	55.7
800	484.3	771	80.5
808	551.9	791	130.2
838	751.8	802	184.0
866	865.2	812	385.0
847	815.5	816	474.6
826	854.4	853	686.5
803	514.2	863	760.2
777	231.8	872	840.8
753	111.3	860	708.3
726	61.6	844	621.8
676	40.7	827	524.3
579	29.8	821	489.3
530	25.8	805	245.6
465	19.9	798	178.9
		782	107.3
		751	53.7
		665	18.8
		548	13.9
		524	12.9
		456	11.9

Reaction 2 in Table 3 represents the equilibrium pressure of $ZrCl_4$ over pure solid K_2ZrCl_6 at temperatures higher than the eutectic temperature and in the presence of a solution of KCl and K_2ZrCl_6 of liquidus composition, as predicted by the phase diagram (1). Due to the temperature and composition dependence of the activity of KCl in this region, the $\ln P_{ZrCl_4}$ vs. $1/T$ plot exhibits a curvature (nonlinear part in Fig. 2).

Reaction 3 in Table 3 represents the equilibrium pressure of $ZrCl_4$ over pure molten K_2ZrCl_6 at temperatures higher than its melting point.

Similar considerations apply to reactions 4, 5, and 6 for K_2HfCl_6 given in Table 3. It should be noted that the nonlinear and upper linear portions of the pressure curves for K_2ZrCl_6 and K_2HfCl_6 in Fig. 2 intercept at temperatures which are in agreement with the melting points of the compounds K_2ZrCl_6 and K_2HfCl_6 respectively.

Discussion

Below the corresponding eutectic temperatures of

Can. J. Chem. Downloaded from www.nrcresearchpress.com by 210.87.254.6 on 09/05/12
For personal use only.

Can. J. Chem. Downloaded from www.nrcresearchpress.com by 210.87.254.6 on 09/05/12
For personal use only.

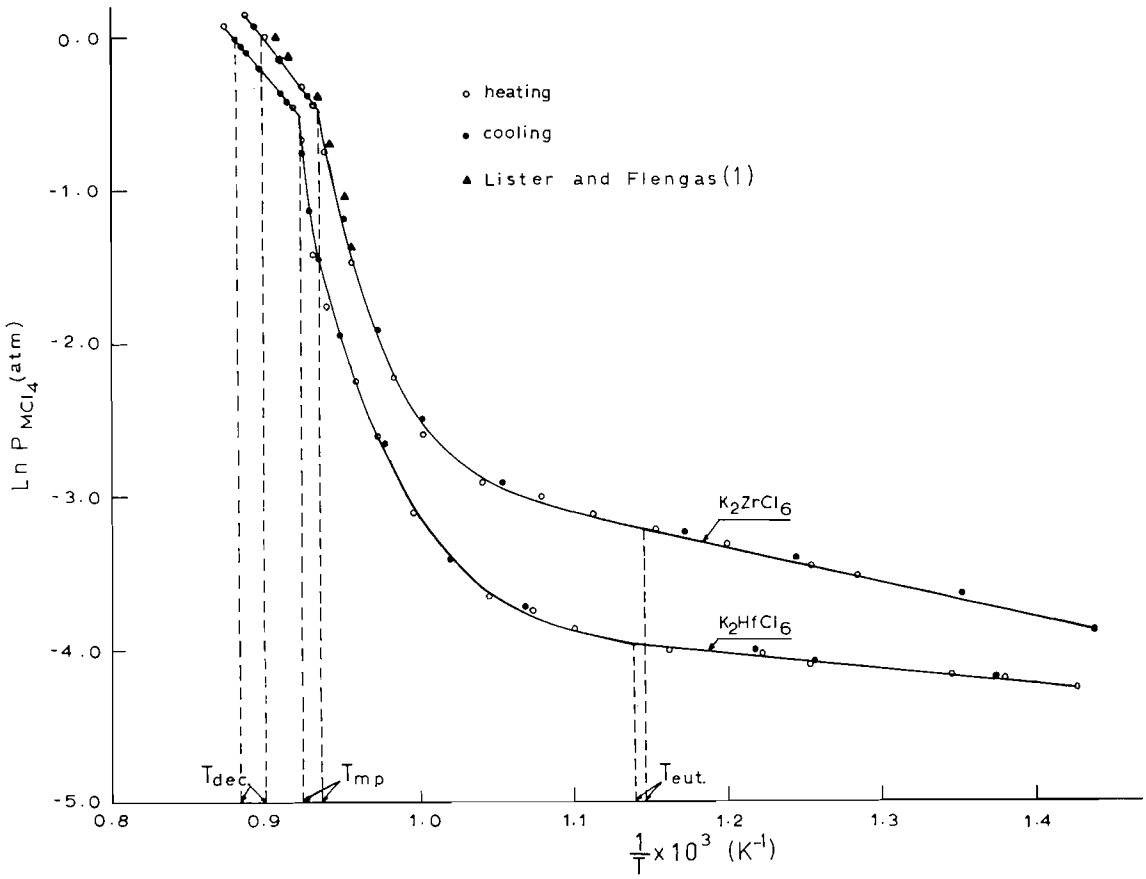

FIG. 2. Diagram of ln P_{MCl_4} vs. $1/T$ for the pure complex compounds K_2ZrCl_6 and K_2HfCl_6.

the pseudo-binary systems KCl–K_2ZrCl_6 and KCl–K_2HfCl_6 respectively, the thermal decomposition of the chlorozirconate and chlorohafnate complex compounds are described by the reactions:

[5] $$K_2ZrCl_{6(s)} \rightleftarrows 2KCl_{(s)} + ZrCl_{4(vap)}$$

[6] $$K_2HfCl_{6(s)} \rightleftarrows 2KCl_{(s)} + HfCl_{4(vap)}$$

If the standard states for the condensed phases are chosen as the pure solids at all temperatures and for the vapour phases, the pure vapours at 1 atm, the thermodynamic equilibrium constants for the decomposition reactions [5] and [6] can be written as:

[7] $$K_5 = P_{ZrCl_4(vap)}$$

[8] $$K_6 = P_{HfCl_4(vap)}$$

In these equations, actual pressures have been used instead of fugacities, as the zirconium tetrachloride vapour has been shown to be unimolecular and ideal (13, 14), and hafnium tetrachloride vapour should be expected to be quite similar.

The standard heat for the decomposition reactions ΔH_R^0 may be obtained from the van't Hoff equation, written as:

[9] $$\frac{d \ln k}{dT} = -\frac{\Delta H_R^0}{RT^2}$$

while the standard free energy and the average standard entropy can be determined from the well-known equations:

[10] $$\Delta G^0 = -RT \ln k$$

[11] $$\Delta G_R^0 = \Delta H_R^0 - T\Delta S_R^0$$

The results of these calculations for pure K_2ZrCl_6 and K_2HfCl_6 are given in Table 4. From these data, the equilibrium constant of the exchange reaction:

[12] $HfCl_4$ (vapour) + K_2ZrCl_6 (as a solid solution of K_2ZrCl_6 in K_2HfCl_6) = $ZrCl_4$ (vapour) + K_2HfCl_6 (as a solid solution of K_2HfCl_6 in K_2ZrCl_6)

is calculated as:

[13] $$K_{ex} = (P_{ZrCl_4}/P_{HfCl_4})_{vapour} \times (X_{K_2HfCl_6}/X_{K_2ZrCl_6})_{in\ solid\ solution}$$

In this equation, mole fractions (X's) have been

TABLE 3. Equilibrium vapour pressures of $ZrCl_4$ and $HfCl_4$ over the pure compounds K_2ZrCl_6 and K_2HfCl_6 respectively

Equilibrium reactions	K_2MCl_6 (mol%)	Temperature range (K)	$\ln P_{MCl_4}$ (atm) $= A + (B/T)$ A	B	Standard error of
1. K_2ZrCl_6 (solid) = 2KCl (solid) + $ZrCl_4$ (vapour)	100	694–867	−0.5447	−2 298	±0.0252
2. K_2ZrCl_6 (solid) = 2KCl (in solution) + $ZrCl_4$ (vapour)	100	867–1072	Nonlinear		
3. K_2ZrCl_6 (liquid) = 2KCl (in solution) + $ZrCl_4$ (vapour)	100	1072–1139	10.0861	−11 263	±0.0468
4. K_2HfCl_6 (solid) = 2KCl (solid) + $HfCl_4$ (vapour)	100	700–877	−2.3446	−1 347	±0.0454
5. K_2HfCl_6 (solid) = 2KCl (in solution) + $HfCl_4$ (vapour)	100	877–1081	Nonlinear		
6. K_2HfCl_6 (liquid) = 2KCl (in solution) + $HfCl_4$ (vapour)	100	1081–1145	13.2736	−15 073	±0.0676

TABLE 4. Thermodynamic values for the decomposition of the pure compounds K_2ZrCl_6 and K_2HfCl_6

Compound	Temperature range (K)	ΔH_R^0 (dec.) (cal/mol)	ΔS_R^0 (dec.) (eu)
K_2ZrCl_6	694–867	4570	−1.08
K_2HfCl_6	700–877	2678	−4.66

substituted for activities, because of the suggested ideal behaviour of the solid solutions.

Since [12] was derived by subtracting [5] from [6], given in Table 3, the temperature dependence on the equilibrium constant given by [13] may be calculated by combining [7] and [8] as:

$$[14] \quad \ln K_{ex} = 1.799 - (951/T) \qquad \text{st. dev.} = 0.1097$$

A plot of K_{ex} vs. T (in °C) is shown in Fig. 3.

It has been shown in a previous publication (6) that impure $ZrCl_4$ containing $HfCl_4$ may be purified in a closed two-compartment reaction cell in which the impure $Zr(Hf)Cl_4$ mixture is placed in the first compartment, which is kept at a temperature T_1, while an alkali chloride ACl is placed in the second compartment, which is kept at a temperature T_2.

The separation is based on the formation of the complex compounds A_2ZrCl_6 and A_2HfCl_6, which appear in the second compartment as a solid solution. The efficiency of the separation process depends upon the magnitude of the equilibrium constant for the exchange reaction [12].

The efficiency of separation η is defined as:

$$[15] \quad \eta = \frac{(\text{wt.\% } HfCl_4)_{\text{initial}} - (\text{wt.\% } HfCl_4)_{\text{final}}}{(\text{wt.\% } HfCl_4)_{\text{initial}}} \times 100$$

and may be calculated from the previously derived relationship

$$[16] \quad K_{ex} = \frac{2(X^1_{ZrCl_4})a - b + 2Z}{2(X^1_{HfCl_4})a - 2Z} \times \left(\frac{P^0_{ZrCl_4}}{P^0_{HfCl_4}}\right)_{T_1} \frac{2Z}{b - 2Z}$$

where $X^1_{ZrCl_4}$ and $X^1_{HfCl_4}$ are the mole fractions of $ZrCl_4$ and $HfCl_4$ respectively in the $Zr(Hf)Cl_4$ mixture initially present in the first compartment of the separation cell prior to reaction; a represents the

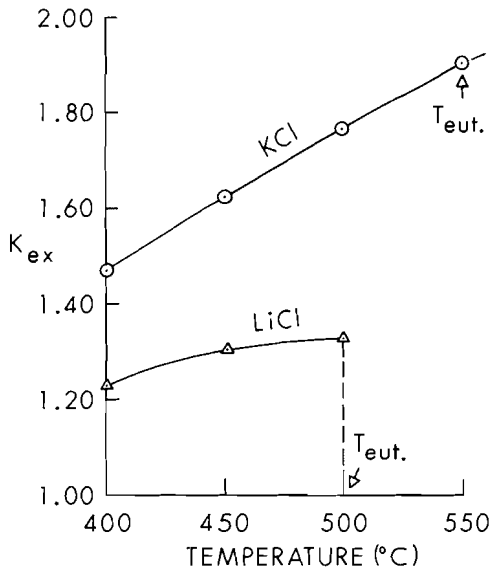

FIG. 3. Temperature dependence of the equilibrium constants K_{ex} for the exchange reactions:

$$HfCl_4 \text{ (vapour)} + K_2ZrCl_6 \text{ (solid solution)} \rightleftharpoons K_2HfCl_6 \text{ (solid solution)} + ZrCl_4 \text{ (vapour)}$$

and

$$HfCl_4 \text{ (vapour)} + Li_2ZrCl_6 \text{ (solid solution)} \rightleftharpoons Li_2HfCl_6 \text{ (solid solution)} + ZrCl_4 \text{ (vapour)}$$

Can. J. Chem. Downloaded from www.nrcresearchpress.com by 210.87.254.6 on 09/05/12
For personal use only.

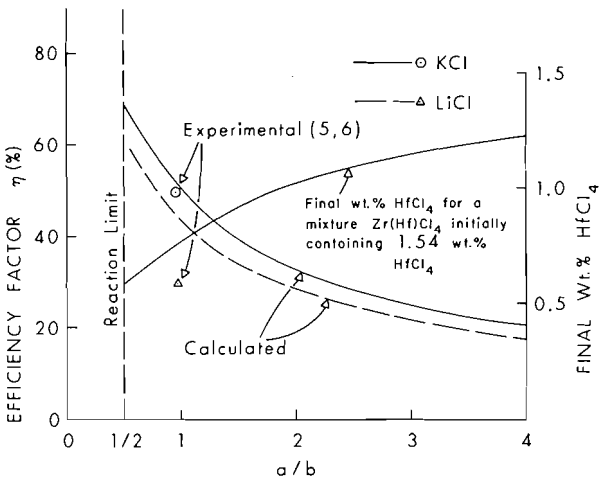

FIG. 4. Variation of the separation efficiency factor η with the molar ratio a/b of $Zr(Hf)Cl_4$ to LiCl or KCl respectively. Calculations are based on $Zr(Hf)Cl_4$ initially containing 1.54 wt.% $HfCl_4$. T_1 and T_2 temperatures are respectively 330 and 450°C.

total number of moles of $Zr(Hf)Cl_4$ present in the first compartment of this reactor, prior to separation; b represents the number of moles of ACl present in the second compartment of the reactor; Z is the number of moles of $HfCl_4$ which have reacted with ACl and are retained in the second compartment of the reactor after equilibrium has been reached; $P^0_{ZrCl_4}$ and $P^0_{HfCl_4}$ are the sublimation pressures (15) of pure $ZrCl_4$ and $HfCl_4$ respectively, at the temperature T_1.

Considering a reactor containing KCl and T_1 and T_2 temperatures of 330 and 450°C respectively, the separation efficiency factor η may be calculated from the determined values of K_{ex} and for various ratios of a/b.

Figure 4 illustrates the variation of η with the a/b ratio for LiCl and KCl. As is seen, η increases as the a/b ratio decreases. Hence the separation becomes more efficient when the amount of the $Zr(Hf)Cl_4$ mixture placed in compartment I is close to that required by the stoichiometry for the formation of K_2ZrCl_6 and K_2HfCl_6. The reaction limit is reached at $a/b = 0.5$, at which point all the added tetrachloride vapours react with the KCl. On the other hand, as the a/b ratio approaches the value of 0.5, most of the $Zr(Hf)Cl_4$ ends up as a K_2ZrCl_6–K_2HfCl_6 solid solution in compartment II. Hence for practical purposes, the a/b ratio must be larger than 0.5, and a value of about 0.8 to 1.0 appears optimum. At $a/b = 0.8$ the calculated separation efficiency is about 56%.

By comparing LiCl and KCl as separating agents for Hf, it is also evident that at 450°C KCl is more efficient than LiCl. In addition, potassium chloride is a more readily available chemical, and does not require the very elaborate dehydration procedure which is necessary for producing anhydrous lithium chloride.

In Fig. 3, it is seen that the K_{ex} for the reaction with KCl increases significantly with temperature and the separation process may be conducted at temperatures as high as 594°C, which is the eutectic temperature for the binary system K_2ZrCl_6–KCl. At this temperature the complexes K_2ZrCl_6 and K_2HfCl_6 would not decompose, since their decomposition temperatures have been found to be 840 and 863°C, respectively.

On the contrary, in the LiCl system the temperature range for a gas–solid reaction extends only up to 496°C, which is the corresponding eutectic temperature for the system Li_2ZrCl_6–LiCl, and at this temperature the pure Li_2ZrCl_6 and Li_2HfCl_6 compounds also decompose thermally (3).

Considering the reaction with KCl at a temperature of 550°C, for which $K_{ex} = 1.92$, and for $a/b = 1$, the separation efficiency factor is calculated to be 56.49%. This should be compared with η = 43% for the LiCl reaction at 450°C.

Therefore, it should be possible to reduce the $HfCl_4$ content from an initial level of 1500 ppm to less than 50 ppm in only four successive separation steps.

1. R. L. LISTER and S. N. FLENGAS. Can. J. Chem. **43**, 2947 (1965).
2. R. L. LISTER and S. N. FLENGAS. J. Electrochem. Soc. **111**, 343 (1964).
3. J. E. DUTRIZAC and S. N. FLENGAS. Advances in extractive metallurgy symposium. Paper 24. April 17–20. The Institution of Mining and Metallurgy, London, England. 1967.
4. D. A. ASVESTAS, P. PINT, and S. N. FLENGAS. Can. J. Chem. **55**, 1154 (1977).
5. J. E. DUTRIZAC and S. N. FLENGAS. Can. Patent No. 863 258 (February 9, 1971).
6. S. N. FLENGAS and J. E. DUTRIZAC. Metall. Trans. B, **8B**, 377 (1977).
7. I. S. MOROZOV and SUN-IN-CHZHU. Russ. J. Inorg. Chem. **4**, 307 (1959).
8. D. R. SADOWAY and S. N. FLENGAS. Can. J. Chem. **54**, 1692 (1976).
9. L. A. NISELSON. Zh. Neorg. Khim. **7**, 693 (1962); Russ. J. Inorg. Chem. 354 (1962).
10. D. AMBROSE. Vapour pressures. *In* Chemical thermodynamics. Vol. I. *Edited by* M. L. McGlashan. The Chemical Society, London. 1973. Chapt. 7.
11. W. G. BROMBACHER, D. R. JOHNSON, and J. L. CROSS. Mercury barometers and manometers. National Bureau of Standards, Washington, DC. Monograph 8. 1960.
12. R. L. POWELL *et al.* Thermocouple reference tables based on the IPTS-68. National Bureau of Standards, Washington, DC. Monograph 125. 1974.
13. O. RAHLFS and W. FISCHER. Z. Anorg. Allg. Chem. **211**, 349 (1933).
14. J. A. N. FRIEND, A. T. W. COLLEY, and R. S. HAYES. J. Chem. Soc. 494 (1930).
15. A. A. PALKO, A. D. RYON, and D. W. KUHN. J. Phys. Chem. **62**, 319 (1958).

Can. J. Chem. Downloaded from www.nrcresearchpress.com by 210.87.254.6 on 09/05/12
For personal use only.

ESCA spectra and molecular charge distributions for some pyrimidine and purine bases

JAMES PEELING[1] AND FRANK E. HRUSKA
Department of Chemistry, University of Manitoba, Winnipeg, Man., Canada R3T 2N2
AND
N. STEWART MCINTYRE
Analytical Science Branch, Whiteshell Nuclear Research Establishment, Pinawa, Man., Canada R0E 1L0

Received November 29, 1977

JAMES PEELING, FRANK E. HRUSKA, and N. STEWART MCINTYRE. Can. J. Chem. **56**, 1555 (1978).

A series of pyrimidine and purine bases has been studied experimentally by electron spectroscopy for chemical analysis. Individual component peaks in the spectra were assigned on the basis of known substituent effects on core electron binding energies. Binding energies for all the core levels in the molecules provide sufficient data to determine the molecular charge distributions. The results compare favourably with atomic charges determined theoretically in the CNDO/2 molecular orbital formalism.

JAMES PEELING, FRANK E. HRUSKA et N. STEWART MCINTYRE. Can. J. Chem. **56**, 1555 (1978).

On a étudié expérimentalement, en faisant appel à la spectroscopie d'émission photoélectronique induite par rayons-X (ESCA), une série de bases purine et pyrimidine. On a attribué les composantes individuelles des spectres en se basant sur des effets connus des substituants sur les énergies de liaison des électrons des couches internes. Les énergies de liaison pour tous les niveaux internes des molécules fournissent des données suffisantes pour déterminer les distributions des charges moléculaires. Les résultats se comparent favorablement avec les charges atomiques déterminées d'une façon théorique par un formalisme d'orbitale moléculaire du type CNDO/2.

[Traduit par le journal]

Introduction

Electron spectroscopy for chemical analysis (ESCA) or X-ray photoelectron spectroscopy (XPS) has proven to be a valuable tool in studies of structure and chemical bonding. The binding energies and relative intensities of core photoelectron peaks provide a direct elemental analysis of a sample. At a finer level of observation, chemical shifts in core electron binding energies relate directly to the charge distributions in molecular solids, in cases where lattice effects on the binding energies are of secondary importance. In the realm of biologically important molecules, although a number of studies of amino acids (1–4) and proteins (3, 5–8) have been reported, relatively few investigations have been directed towards the area of nucleic acids and their components. The ESCA spectra of tRNA and a few of its components were described briefly (9), and studies on metal complexes of DNA (10), AMP (11), and some thiouracils (12) have appeared. Detailed studies of the ESCA spectra of the purine and pyrimidine bases themselves appear to be limited to the early investigations of Barber and Clark on adenine (13), cytosine and thymine (14), in spite of the interest which this work created (15–18). Clark has also recently published the spectra of 5- and 6-azauracil (19).

In this paper we describe the core electron spectra of common purine and pyrimidine bases, some of their aza analogs, and one fluorinated analog (Fig. 1). These analogs have chemotherapeutic value (20), which ultimately must be due to the electronic perturbations elicited by the chemical modifications to the base. The measured binding energies are used to derive experimental charge distributions in the molecules. These are compared with the results of

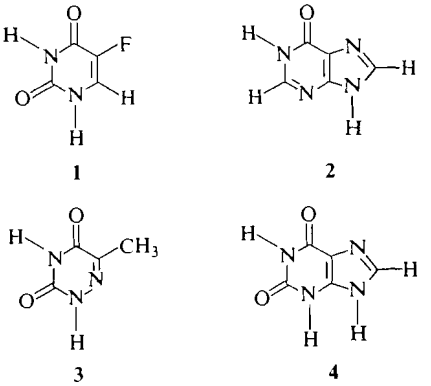

FIG. 1. Chemical formulae for several of the purine and pyrimidine bases studied here: 5-fluorouracil (**1**), 6-azathymine (**2**), hypoxanthine (**3**), and xanthine (**4**).

[1]Post-doctoral fellow: present address: University of Petroleum and Minerals, Dhahran, Saudi Arabia.

Can. J. Chem. Downloaded from www.nrcresearchpress.com by 210.87.254.6 on 09/05/12
For personal use only.

Can. J. Chem. Downloaded from www.nrcresearchpress.com by 210.87.254.6 on 09/05/12
For personal use only.

CNDO (21) molecular orbital theory calculations. Although extensive theoretical studies have been directed towards the elucidation of charge distributions in nucleic acid bases (22–25), a limited quantity of independent experimental data are available.

Experimental

The bases were all commercial samples (Sigma Chemical Company) and were examined, without further purification, as powders mounted on the spectrometer probe either using double-sided tape or by pressing into finely grooved copper flats fixed to the probe. Spectra of the C_{1s}, N_{1s}, O_{1s}, and F_{1s} core levels were obtained on a McPherson ESCA-36, calibrated as described previously (26), using $MgK_{\alpha_{1,2}}$ radiation (1253.6 eV). Several of the samples were run over extended periods of time, and all were examined visually, to check for radiation damage. The constancy of the ratios of the core level peak intensities and their positions were taken as evidence that no substantial radiation damage occurred.

Peak positions in incompletely resolved bands were determined by computer deconvolution using the peak fitting routine described by Bancroft *et al.* (27). The bands used in fitting a peak envelope are defined according to their centroid position, half-width, shape (an equal combination of Gaussian and Lorentzian distributions), and intensity. These parameters are then varied to obtain a minimum in the error sum of squares between the values for the experimental curve and the trial combination of bands. An important feature of this program is its ability to constrain certain parameters of selected bands within set limits, while allowing the others to vary freely. Peak parameters for the intensity of a given core line were constrained to give peak areas proportional to those required by the molecular formula. C_{1s} peak widths were constrained to half-widths (FWHM) between 1.4 and 1.6 eV, since preliminary studies showed that peak widths for all carbon sites investigated fell in this range. N_{1s} half-widths were constrained between 1.3 and 1.4 eV. Figure 2 shows some examples of envelopes deconvoluted in this manner. Binding energies were determined relative to the C_{1s} peak ascribed to hydrocarbon contamination, which was assigned a value of 285.0 eV (28). This peak gradually increased in intensity with time as residual hydrocarbons deposited on the sample surface.

Results and Discussion

ESCA Spectra

Table 1 gives the experimental binding energies for the bases examined, with corresponding sites in the purines and pyrimidines listed in the same column. In Fig. 2 are some representative examples of deconvoluted C_{1s} bands. The reproducibility of the deconvolution procedure, and of the spectra themselves, was checked for several of the compounds by processing spectra obtained in repeated measurements on a number of different samples. For the pyrimidines the absolute binding energies determined in this fashion generally agreed to better than ± 0.15 eV (2σ), while the relative binding energies for peaks under any one envelope were reproducible to better than ± 0.10 eV. In the case of the purine bases, the generally greater number of peaks under a given spectral envelope, combined with a smaller spread in binding energies, resulted in increased uncertainties

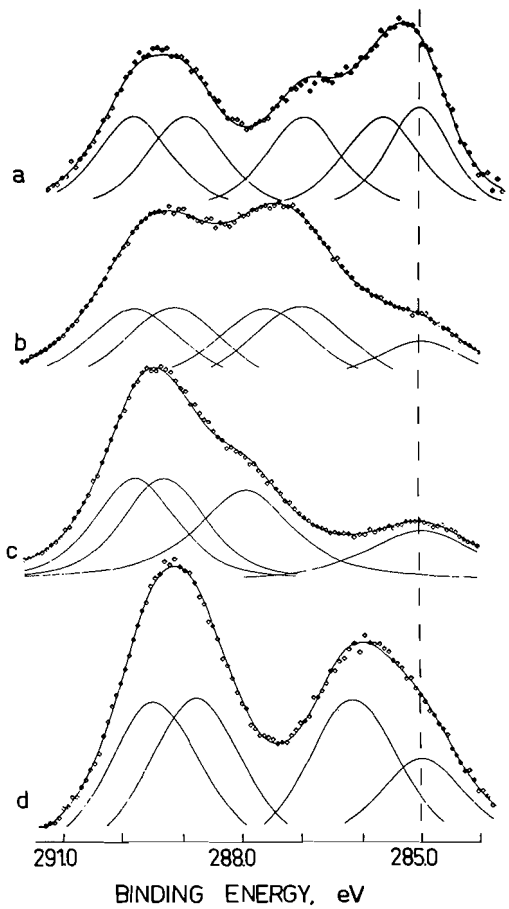

FIG. 2. Computer deconvoluted C_{1s} bonds for (*a*) uracil, (*b*) 5-fluorouracil, (*c*) 5-azauracil, and (*d*) 6-azauracil. The hydrocarbon contamination peak used for reference is the peak at the lowest binding energy. For clarity, the full extent of each Gaussian–Lorentzian band has been truncated in the fitted spectra.

in peak positions, the standard deviations being about ± 0.2 eV for the C_{1s} bands. The poorly resolved N_{1s} bands of the purines presented some difficulties. For xanthine, visual inspection of the N_{1s} spectral region showed that it consisted of two poorly resolved peaks of relative intensities 3:1. Computer deconvolution based on this assumption gave a good fit to the experimental spectrum, the peaks being of equal width. The linewidth was about the same as that for N_{1s} peaks in the pyrimidines, so the reported binding energies are probably accurate to better than ± 0.3 eV. A similar approach to the hypoxanthine N_{1s} band showed that it could be fitted well by two peaks of equal intensity. However, for 8-azaxanthine, guanine, and 8-azaguanine, the N_{1s} envelopes consisted of featureless bands, and the deconvolution procedure consisted of a random fitting under the broad spectral envelopes of the number of peaks of equal intensity required by the molecular formulae.

Can. J. Chem. Downloaded from www.nrcresearchpress.com by 210.87.254.6 on 09/05/12
For personal use only.

The N_{1s} binding energies listed in Table 1 for these latter compounds give a satisfactory but not necessarily unique fit to the experimental spectra. It is difficult to assess quantitatively the accuracy of these data but a reasonable uncertainty in the binding energy of any one component peak is ± 0.4 eV.

The N_{1s} peaks for uracil, 5-fluorouracil, and thymine consisted of single peaks with linewidths indistinguishable from those found for chemically unique N_{1s} peaks. The same is true in the case of the O_{1s} bands; the peaks observed for the single oxygen in hypoxanthine, guanine, and 8-azaguanine were not sharper than those of the other bases which contain two chemically distinct oxygen species.

The lack of resolution in the ESCA technique which becomes apparent in the above discussion is likely to be the limiting factor in carrying out detailed structural studies of the type reported here. The number of incompletely resolved peaks under a given core level band that can be determined uniquely is generally quite small, so even moderately complex molecules like the purine bases are often not amenable to a thorough analysis. Although improved resolution, for instance using monochromatic X-ray sources (29), undoubtedly helps to some extent, the limited resolution is inherent in the method and the complexity of the molecules that can be studied is thus restricted.

Assignment of C_{1s} Spectra

The assignments of the deconvoluted C_{1s} spectral peaks can be carried out using known substituent effects on core electron binding energies (29). The factors giving rise to ESCA chemical shifts in molecular solids are generally short range in nature. Although in the case of the nucleic acid bases, intermolecular effects, such as hydrogen bonding, may not be insignificant, they are likely to be of secondary importance in comparing similar molecular sites. That they are of secondary importance becomes clear on considering the binding energy data in Table 1. Where the immediate environment of the C(2) carbon is unchanged through the series of compounds, the binding energy remains fairly constant. Replacing the 2-keto oxygen of xanthine and 8-azaxanthine with the less electronegative $-NH_2$ group results in a decrease in the binding energy of this carbon. A further decrease in binding energy occurs on removing the $-NH_2$ group to form hypoxanthine. Similarly C(4) shows a significant change in binding energy only for 5-azauracil and 5-fluorouracil, where the substitution of the nearby electronegative group induces an increase in binding energy at this site. As expected, the fluorine substitution also gives rise to an increase in the binding energy of C(6), and to a much more substantial

TABLE 1. Core electron binding energies (eV) for the pyrimidine and purine bases

Compound	C(2)	C(4)	C(5)	C(6)	CH_3	C(8)	N(1)	N(3)	N(5)	N(6)	N(7)	N(8)	N(9)	NH_2	O	F
Uracil	289.7$_5$	288.9$_5$	285.6$_5$	286.8$_5$	—	—	400.8$_0$	400.8$_0$							531.8$_5$	
5-Fluorouracil	289.9$_5$	289.3$_0$	287.1$_0$	287.7$_0$	—	—	401.2$_0$	401.2$_0$							532.2$_5$	687.9$_0$
5-Azauracil	289.9$_0$	289.4$_0$	—	288.0$_0$	—	—	401.2$_0$	400.7$_0$	399.6$_0$						532.0$_5$	
6-Azauracil	289.6$_0$	288.9$_0$	286.1$_5$	—	—	—	401.2$_5$	401.0$_5$		400.4$_5$					531.9$_0$	
Thymine	289.8$_0$	288.7$_5$	285.8$_5$	286.6$_5$	285.4$_5$	—	400.9$_5$	400.9$_5$							532.0$_0$	
6-Azathymine	289.6$_0$	288.7$_5$	286.5$_0$	—	285.7$_0$	—	401.2$_0$	400.9$_0$		400.3$_0$					531.9$_5$	
	C(2)	C(6)	C(5)	C(4)		C(8)	N(3)	N(1)			N(7)	N(8)	N(9)	NH_2	O	
Xanthine	289.7	288.8	285.8	287.2	—	286.7	400.8	400.8			399.5	—	400.8	—	531.8	
Hypoxanthine	287.5	288.8	285.7	287.1	—	286.0	399.8	401.0			399.8	—	401.0	—	531.9	
8-Azaxanthine	289.7	288.8	286.0	287.3	—	—	400.9	400.9			400.3	401.8	400.3	—	531.8	
Guanine	288.5	288.7	285.8	287.2	—	286.5	399.5	400.8			399.5	—	400.8	399.5	531.8	
8-Azaguanine	288.7	288.9	285.8	287.4	—	—	399.6	401.0			400.2	401.0	401.0	399.6	531.7	

TABLE 2. Experimental and theoretical

Compound	C(2)	C(4)	C(5)	C(6)	CH_3		N(1)	N(3)
Uracil	0.44(0.45)* [0.33]†	0.34(0.37) [0.27]	−0.05(−0.16) [0.01]	0.11(0.18) [0.26]	—		−0.21(−0.18) [−0.20]	−0.24(−0.2 [−0.22]
5-Fluorouracil	0.40(0.44)	0.32(0.33)	0.10(0.08)	0.13(0.10)	—		−0.18(−0.18)	−0.19(−0.2
5-Azauracil	0.46(0.46)	0.45(0.42)	—	0.21(0.26)	—		−0.18(−0.19)	−0.27(−0.2
6-Azauracil	0.39(0.44)	0.32(0.35)	0.01(−0.03)	—	—		−0.14(−0.15)	−0.19(−0.2
Thymine	0.42(0.45)	0.32(0.37)	−0.04(−0.09)	0.08(0.15)	0.02(−0.00)		−0.20(−0.18)	−0.22(−0.2
6-Azathymine	0.40(0.45)	0.32(0.33)	0.03(0.05)	—	0.03(−0.02)		−0.15(−0.17)	−0.20(−0.2
	C(2)	C(6)	C(5)	C(4)		C(8)	N(3)	N(1)
Xanthine	0.42(0.45)	0.33(0.35)	−0.02(−0.08)	0.14(0.21)		0.12(0.15)	−0.26(−0.21)	−0.24(−0.2
Hypoxanthine	0.17(0.24)	0.33(0.35)	−0.04(−0.08)	0.14(0.20)		0.07(0.14)	−0.17(−0.24)	−0.22(−0.1
8-Azaxanthine	0.42(0.44)	0.33(0.36)	−0.03(−0.06)	0.14(0.19)		—	−0.22(−0.23)	−0.25(−0.2
Guanine	0.35(0.39)	0.34(0.36)	−0.02(−0.11)	0.16(0.22)		0.11(0.13)	−0.23(−0.33)	−0.24(−0.2
8-Azaguanine	0.37(0.39)	0.36(0.36)	−0.05(−0.12)	0.17(0.23)		—	−0.26(−0.34)	−0.26(−0.2

*Values in parentheses represent theoretical charges calculated by CNDO/2 molecular orbital method.
† Square brackets contain experimental charges for uracil obtained from *L*-shell STO scattering factors (ref. 36).

increase in that of C(5). Similarly, C(5) and C(6) in the 6- and 5-azapyrimidines, respectively, show higher binding energies, a consequence of replacing a ring carbon with a more electronegative nitrogen. However, in the purine bases, the influence of the imidazole nitrogens on the binding energies of the analogous carbons (C(5) and C(4)) is considerably smaller.

Assignment of N_{1s} Spectra

In spite of the difficulties discussed above in determining the N_{1s} binding energies, a qualitative analysis of substituent effects can be used in assigning the peaks. The data in Table 1 show that the binding energies of N(3) in the pyrimidine bases and N(1) of the purines, being isolated from major structural changes, are constant to within ±0.15 eV. An increase to 401.20 eV for 5-fluorouracil is the largest change. For the 6-azapyrimidines, N(1) is closer to the structural change and an increase in binding energy is apparent here as well as for 5-fluorouracil. In the purines hypoxanthine, guanine, and 8-azaguanine, the binding energy of N(3) decreases by ~1.2 eV relative to xanthine. The lower binding energy for the $\diagdown\!\!=\!\!\diagup$N compared to the $\diagdown\!\!-\!\!\diagup$NH structural feature has been noted before (1) and is also evident in the case of N(5) and N(6) in the azapyrimidines. Similarly, N(7) in xanthine, hypoxanthine, and guanine has a binding energy of ~399.6 eV, while N(9), whose immediate environment is similar to that of N(1), is assigned to a component at ~400.9 eV. (An X-ray crystallographic study of guanine (30) has shown that only the tautomeric form having N(9) protonated is formed in the crystals; we assume that this is also the case for xanthine and hypoxanthine.) In 8-azaxanthine N(8) is protonated and N(9) is unprotonated (31). The immediate environments of N(7) and N(9) are thus similar and they are assigned identical binding energies, which, because of the influence of N(8), are greater than those of other $\diagdown\!\!=\!\!\diagup$N structural features. The N(8) nitrogen, being adjacent to two other nitrogen atoms, is assigned to the N_{1s} peak at highest binding energy. The structure of 8-azaguanine (32) on the other hand shows that N(9) is protonated instead of N(8), so N(7) remains lower in binding energy than N(9). The limited resolution does not permit a distinction in the binding energies of N(8) and N(9). The —NH_2 nitrogen in guanine and 8-azaguanine is assigned to the peaks at 399.5 and 399.6 eV, respectively. Barber and Clark (13) previously have assigned a peak at 399.5 eV to an —NH_2 group in the structurally similar adenine molecule.

In 5-azauracil the assignment of the N_{1s} peaks at 401.20 and 400.60 eV to N(1) and N(3), respectively, is not obvious from substituent effects. Therefore, CNDO/2 calculations were carried out for this molecule, and the calculated atomic charges were used to determine the relative binding energies through application of the charge potential model (see below). The order of the N_{1s} binding energies in Table 1 was confirmed. Further support for this ordering is found in the results of detailed *ab initio* molecular orbital theory studies (25, 33), which also show the 1s binding energy of N(1) to be greater than that of N(3).

Tautomeric Forms

The binding energy data in Table 1 also provide information on the tautomeric forms of the bases. In general, the diketo forms of uracil and its derivatives predominate in the crystal (as well as solution) state (24, 34), and the N_{1s} binding energies and the C_{1s} binding energies for C(2) and C(4) are in accord with this structure for each of our pyrimidines. Thus, experimental and theoretical studies on model com-

Can. J. Chem. Downloaded from www.nrcresearchpress.com by 210.87.254.6 on 09/05/12
For personal use only.

atomic charges in the pyrimidine and purine bases

N(5)	N(6)					O(2)	O(4)	F
—	—					−0.35(−0.37)	−0.29(−0.36)	
						[−0.30]	[−0.28]	
—	—					−0.32(−0.36)	−0.26(−0.31)	−0.25(−0.18)
−0.23(−0.28)	—					−0.40(−0.37)	−0.30(−0.36)	
—	0.00 (0.00)					−0.35(−0.37)	−0.31(−0.33)	
—	—					−0.34(−0.39)	−0.30(−0.33)	
—	−0.02(−0.04)					−0.35(−0.39)	−0.30(−0.33)	

	N(7)	N(8)	N(9)	NH_2	O(2)	O(6)
	−0.10(−0.16)	—	−0.15(−0.13)	—	−0.36(−0.38)	−0.30(−0.36)
	−0.06(−0.16)	—	−0.15(−0.11)	—	—	−0.33(−0.38)
	−0.01(−0.04)	0.04(0.07)	−0.14(−0.16)	—	−0.37(−0.39)	−0.32(−0.33)
	−0.10(−0.16)	—	−0.15(−0.12)	−0.37(−0.24)	—	−0.32(−0.39)
	−0.04(−0.05)	0.08(−0.07)	−0.14(−0.17)	−0.40(−0.23)	—	−0.35(−0.38)

pounds have shown that the C_{1s} binding energy of an alcoholic carbon is about 1 eV lower than that of a ketonic carbon (35). Furthermore, in the enol form either N(1) or N(3) (or both) assumes the $\diagdown\!\!=\!\!\text{N}$ structure, the N_{1s} binding energy of which is substantially lower ($\sim$1.5 eV) than in the $\diagdown\!\text{NH}$ unit. No crystal structure of 5-azauracil has appeared as yet. Our C_{1s} and N_{1s} binding energies show no evidence of the enol form, the only significant change compared to uracil being an increase in the binding energy of C(4) owing to the influence of N(5). Therefore, it is apparent that this base also exists in the diketo form. Similar arguments utilizing the binding energy data for the purine bases indicate that xanthine and 8-azaxanthine exist in the diketo structure, while in hypoxanthine, guanine, and 8-azaguanine the keto form is assumed at C(6). This is consistent with crystallographic studies on 8-azaxanthine (31), guanine (30), and 8-azaguanine (32). A study of selectively-methylated bases is planned in order to examine more thoroughly the influence of tautomeric forms on the ESCA spectra.

Charge Distributions

In the electrostatic potential model (36) core electron binding energies E_i for a molecular solid are related to the molecular charge distribution by

$$[1] \qquad E_i = E_i^0 + k_i q_i + \sum_{j \neq i} \frac{q_j}{r_{ij}}$$

where E_i^0 is a reference level, q_i is the charge on atom i, q_j is the charge on atom j situated at a distance r_{ij} from i, and k_i is a constant. The determination of molecular charge distributions from experimental binding energies using eq. [1] requires knowledge of the parameters k_i and E_i^0 for the different core levels. Clark and Thomas (36) used the CNDO/2 molecular orbital formalism to determine charge distributions in a number of model carbon and oxygen compounds. These charges were used with the experimental binding energies and molecular geometries to yield values of k_i and E_i^0 for the C_{1s} and O_{1s} levels via eq. [1]. We used a similar approach with published N_{1s} binding energies for a number of simple compounds examined in the solid phase and values of $k_N = 18.5 \pm 2.5$ and $E_N^0 = 399.7 \pm 0.5$ eV were found.

In a system composed of C, N, and O, for which the geometry and all the core level binding energies are known, the potential model eq. [1] are sufficient to determine all the atomic charges q_i, and the neutrality requirement gives one additional equation. However, the nucleic acid bases all contain several hydrogen atoms in addition to C, N, and O, so it is necessary to make some approximations. Experience with CNDO/2 calculations on a variety of molecular systems has shown that in neutral molecules the charge on a hydrogen atom bonded to a carbon is small, whereas hydrogen in an N—H bond has a deficiency of about 0.10 to 0.15 electrons. For all the bases reported here we have therefore set $q_H = 0.0$ for C—H and $q_H = 0.13$ for N—H hydrogens. With these approximations there are enough equations for 5-fluorouracil to determine the charges on the C, N, O, and F atoms, while for the other bases there is one equation more than required to find the charge distributions.

The internuclear distances, r_{ij}, required in eq. [1], were determined from geometries obtained in X-ray crystallographic studies of uracil (37), 5-fluorouracil (38), 6-azauracil (39), thymine (40), 6-azathymine (39), guanine (31), 8-azaguanine (32), and 8-azaxanthine (31). The geometries of 5-azauracil, xanthine, and hypoxanthine were estimated by comparison with the experimental geometries of the other bases.

Can. J. Chem. Downloaded from www.nrcresearchpress.com by 210.87.254.6 on 09/05/12
For personal use only.

Can. J. Chem. Downloaded from www.nrcresearchpress.com by 210.87.254.6 on 09/05/12
For personal use only.

The experimentally determined charges are given in Table 2. Uncertainties in the values originate to some extent from uncertainties in the binding energies but mainly from uncertainties in the values for k_i and E_i^0. The experimental N_{1s} and O_{1s} binding energies used to determine the constants appropriate to these core levels spanned rather limited ranges, so these constants are less certain than those for the C_{1s} levels. Based on the precision of the experimental binding energies and the constants, uncertainties in the experimental charges are estimated to be: N_{1s}, 0.08; O_{1s}, 0.06; and C_{1s}, 0.03 electrons.

The values of k_i in eq. [1] depend on the definition of atomic charge and, when determined using a molecular orbital theory treatment, on the basis set used. The values used in this work were derived from CNDO/2 molecular orbital calculations, so it is appropriate to compare our experimental charges to charges calculated within this theoretical framework. Using the molecular geometries described above, atomic charges were calculated by the CNDO/2 molecular orbital method, and the results are included in Table 2 (in parentheses), Using X-ray scattering factors, Stewart (41) has also obtained an experimental estimate of the charge distribution in uracil, and his data, obtained from *L* shell Slater type orbitals (STO's) are included in Table 2.

The CNDO/2 charges refer to free molecules while the ESCA data refer to the solid phase, where such effects as intermolecular hydrogen bonding may be expected to affect the molecular charge distributions. However, the agreement evident in Table 2 between the experimental and theoretical charges is very good and lends support to the original ESCA peak assignments. For some of the bases, different assignments were assumed and the charges recalculated. In all instances this yielded charges further removed from the theoretical results and in most cases the calculated changes were strongly changed by the alternative assignment.

For uracil, and the pyrimidines in general, some consistent trends in the experimental and theoretical results for the relative atomic charges are evident. The larger uncertainties in the experimental data for the purines possibly mask some of the more subtle differences but the major trends in variations in the charge distributions are reproduced.

The chemical and biochemical implications of differences in the electron distributions in the nucleic acid bases have been discussed extensively (22–25) and comments here are restricted to a brief mention of inconsistencies between the experimental and theoretical numbers. In the pyrimidines the most notable difference is at the 5 and 6 positions of uracil, 5-azauracil, and thymine. The theoretically calculated electron excess at the 5 position is greater than that indicated by the ESCA results, and the corresponding electron deficiency at C(6) is also greater. It has been noted that use of [1] with CNDO/2 charges predicts the wrong ordering of the C_{1s} levels in 5-azauracil (25, 33), a consequence of the apparent over-polarization of the 5—6 bond suggested by the CNDO/2 calculations. In the purines the magnitudes of the calculated charges at C(5) and C(4) also exceed those determined by the ESCA procedure. At N(7) the molecular orbital theory calculations show the negative charge to be greater than the ESCA-derived value. Finally, major disagreement is apparent between the theoretical and experimental charge at the $-NH_2$ nitrogen of guanine and 8-azaguanine.

Some of these discrepancies could result from effects such as hydrogen bonding or from the hydrogen charge approximations made in the CNDO/2 calculations. However, a more likely reason for the discrepancies resides in the CNDO/2 method itself which, using Koopmans' theorem, does not take account of core hole relaxation energy differences in differing sites in the molecule. Clark and co-workers (25) have made *ab initio* calculations of the neutral and core hole states in 5-azauracil and have shown that the C_{1s} and N_{1s} relaxation energies in this molecule differ with the chemical environment. They have suggested that specific group relaxation energy shifts can be used to refine charge calculations which are based on the charge potential model. We intend to apply such procedures to determine if the discrepancies observed in this work can be completely accounted for by relaxation effects.

Conclusions

This study has shown that in favourable cases application of the charge potential model (eq. [1]) with experimental core electron binding energies can yield atomic charges in the pyrimidine and purine bases. The accuracy of the results for small molecules is sufficient to study differences in electron distributions originating in structural modifications. Difficulties in assigning the ESCA spectra, and in the subsequent derivation of charges, arise from the somewhat low resolution of the technique, and apparently limit the complexity of the systems amenable to this sort of analysis. The pyrimidine bases are readily analyzed, while the purines appear to be close to the limit of complexity for thorough analysis.

Acknowledgements

This research was supported by operating grants from the National Research Council of Canada and

the Rh Institute of Manitoba. Thanks are due to D. G. Zetaruk, Atomic Energy of Canada Limited, and K. Marat, University of Manitoba, for computing assistance.

1. D. T. CLARK, J. PEELING, and L. COLLING. Biochim. Biophys. Acta, **453**, 533 (1976).
2. H. RUPP and U. WESER. Biochim. Biophys. Acta, **446**, 151 (1976).
3. M. M. MILLARD. Adv. Exp. Med. Biol. **48**, 589 (1974).
4. H. RUPP and U. WESER. Bioinorg. Chem. **5**, 21 (1975).
5. J. PEELING, D. T. CLARK, I. M. EVANS, and D. BOULTER. J. Sci. Food Agric. **27**, 331 (1976).
6. J. PEELING, B. G. HASLETT, I. M. EVANS, D. T. CLARK, and D. BOULTER. J. Am. Chem. Soc. **99**, 1025 (1977).
7. M. M. MILLARD and M. S. MASRI. Anal. Chem. **46**, 1820 (1974).
8. P. T. ANDREWS, C. E. JOHNSON, B. WALLBANK, R. CAMMACK, D. O. HALL, and K. K. RAO. Biochem. J. **149**, 471 (1975).
9. L. D. HULETT and T. A. CARLSON. Clin. Chem.677 (1970).
10. M. M. MILLARD, J. P. MACQUET, and T. THEOPHANIDES. Biochim. Biophys. Acta, **402**, 166 (1975).
11. U. WESER, G. J. STROBEL, and W. VOELTER. FEBS Lett. **41**, 243 (1974).
12. W. H. THOMAS and U. WESER. Hoppe-Seyler's Z. Physiol. Chem. **358**, 47 (1977).
13. M. BARBER and D. T. CLARK. Chem. Commun. 23 (1970).
14. M. BARBER and D. T. CLARK. Chem. Commun. 24 (1970).
15. A. VAN DER AVOIRD. Chem. Commun. 727 (1970).
16. R. REIN, A. HARTMAN, and S. NIR. Israel J. Chem. **10**, 93 (1972).
17. A. ISHIDA, H. KATO, H. NAKATSUJI, and T. YONEZAWA. Bull. Chem. Soc. Jpn. **45**, 1574 (1972).
18. A. IMAMURA, H. FUJITA, and C. NAGATA. J. Am. Chem. Soc. **94**, 6287 (1970).
19. D. T. CLARK. ESCA applied to organic and polymeric systems. *In* Handbook of X-ray and ultraviolet photoelectron spectroscopy. *Edited by* D. Briggs. Heyden and Son Ltd., London. 1977.
20. J. SKODA. Prog. Nucleic Acid Res. **2**, 197 (1963).
21. J. A. POPLE and G. A. SEGAL. J. Chem. Phys. **43**, S 136 (1965).
22. B. PULLMAN and A. PULLMAN. Prog. Nucleic Acid Res. Mol. Biol. **9**, 327 (1969).
23. B. PULLMAN and A. PULLMAN. Adv. Heterocycl. Chem. **13**, 77 (1971).
24. J. S. KWIATKOWSKI and B. PULLMAN. Adv. Heterocycl. Chem. **18**, 199 (1975).
25. D. T. CLARK, I. W. SCANLAN, and J. MULLER. Theor. Chim. Acta, **35**, 341 (1974).
26. N. S. MCINTYRE and M. G. COOK. Anal. Chem. **47**, 2208 (1975).
27. G. M. BANCROFT, I. ADAMS, L. L. COATSWORTH, C. D. BENNEWITZ, J. D. BROWN, and W. D. WESTWOOD. Anal. Chem. **47**, 586 (1975).
28. U. GELIUS, E. BASILIER, S. SVENSSON, T. BERGMARK, and K. SIEGBAHN. J. Electron Spectrosc. Relat. Phenom. **2**, 405 (1973).
29. U. GELIUS, P. F. HEDEN, J. HEDMAN, B. J. LINDBERG, R. MANNE, R. NORDBERG, C. NORDLING, and K. SIEGBAHN. Phys. Scr. **2**, 70 (1970).
30. U. THEWALT, C. E. BUGG, and R. E. MARSH. Acta Crystallogr. B, **27**, 2358 (1971).
31. H. C. MEZ and J. DONOHUE. Z. Krist. **130**, 376 (1969).
32. J. SLETTEN, E. SLETTEN, and L. H. JENSEN. Acta Crystallogr. B, **24**, 1692 (1968).
33. D. T. CLARK, I. SCANLAN, J. MULLER, and D. B. ADAMS. *In* Proc. SRC Atlas Symp. No. 4, Oxford, April 1974. *Edited by* V. R. Saunders and J. Brown. 1974. p. 235.
34. D. VOET and A. RICH. Prog. Nucleic Acid Res. Mol. Biol. **10**, 83 (1970).
35. D. T. CLARK. *In* Electron emission spectroscopy. *Edited by* W. Dekeyser. D. Reidel Publ. Co., Dordrecht, Holland. 1973. p. 373.
36. D. T. CLARK and T. R. THOMAS. J. Polym. Sci. Polym. Chem. Ed. **14**, 1671 (1976).
37. R. F. STEWART and L. H. JENSEN. Acta Crystallogr. **23**, 1102 (1967).
38. L. FALLON. Acta Crystallogr. B, **29**, 2549 (1973).
39. P. SINGH and D. J. HODGSON. J. Chem. Soc. Chem. Commun. 439 (1973).
40. T. SAKURAI and M. OKUNUKI. Acta Crystallogr. B, **27**, 1445 (1971).
41. R. F. STEWART. J. Chem. Phys. **53**, 205 (1970).

Can. J. Chem. Downloaded from www.nrcresearchpress.com by 210.87.254.6 on 09/05/12
For personal use only.

The solid phase synthesis of monoester monoamides and monoester monoalcohols from symmetrical diacid chlorides[1,2,3]

JUDAH M. GOLDWASSER AND CLIFFORD C. LEZNOFF

Department of Chemistry, York University, Downsview, Ont., Canada M3J 1P3

Received January 18, 1978

JUDAH M. GOLDWASSER and CLIFFORD C. LEZNOFF. Can. J. Chem. **56**, 1562 (1978).

A 2% crosslinked divinylbenzene–styrene copolymer, incorporating benzyl alcohol groups, was used to monoprotect the symmetrical diacid chlorides, $ClOC(CH_2)_nCOCl$ (where $n = 2, 3, 4$, and 8), terephthaloyl chloride and isophthaloyl chloride. Subsequent reaction of the resulting polymer-bound monoester monoacid chloride with aniline, benzylamine, dimethylamine, *tert*-butylamine, or ammonia yielded polymer-bound monoester monoamides, which on base cleavage and esterification gave monoester monoamides in high yield. Borohydride reduction of polymer-bound sebacoyl chloride, terephthaloyl chloride, and isophthaloyl chloride gave their respective polymer-bound monoester monoalcohols, which on base cleavage from the polymer and esterification yielded the monoester monoalcohols in good yield along with some recovered dimethyl esters of the respective starting diacid chlorides.

JUDAH M. GOLDWASSER et CLIFFORD C. LEZNOFF. Can. J. Chem. **56**, 1562 (1978).

On a utilisé un copolymère divinylbenzène–styrène reticulé à 2% et incorporant de l'alcool benzylique pour effectuer la monoprotection des chlorures de diacides symétriques $ClOC(CH_2)_nCOCl$ (où $n = 2, 3, 4$ et 8) de téréphtaloyle et d'isophtaloyle. Une réaction ultérieure, du chlorure de monoacide monoester lié au polymère qui en résulte, avec de l'aniline, de la benzylamine de la diméthylamine, de la *tert*-butylamine ou de l'ammoniac fournit des monoamides monoesters liés au polymère qui, par clivage basique et estérification, conduisent à des monoamides monoesters avec de bons rendements. Une réduction au borohydrure des chlorures de sébacoyle, de téréphtaloyle et d'isophtaloyle liés au polymère conduit aux monoalcools monoesters correspondants liés au polymère qui, par clivage basique du polymère et estérification, fournissent des monoesters monoalcools avec de bons rendements aux côtés des esters diméthyliques récupérés de leurs chlorures de diacides de départs respectifs.

[Traduit par le journal]

Introduction

Monoester monoamides have invariably been prepared by treatment of a monoester monoacid chloride with an amine. This method was used by Wohl (1) in 1910 in the preparation of methyl *N*-methylisophthalamate and more recently by Johnson (2) to prepare a number of ethyl adipamates in low yield. Furthermore, the monoester monoacid precursors are prepared from the symmetrical diesters or diacids in less than 50% yield as base hydrolysis of symmetrical diesters (3, 4) or esterification of symmetrical diacids (4, 5) leads to a 1:2:1 ratio of diester, desired monoester monoacid, and diacid. Only in the preparation of monoamides of diacids such as succinic acid, where the anhydride can be used as the precursor, are the yields as high as 70% and even for this example (6) the solid phase synthesis gives higher yields (see below).

ω-Hydroxyaliphatic acids and hydroxymethylbenzoic acids have been prepared by several different routes but *rarely* from the readily available symmetrical diacids or diesters (7). Ruzicka and Stoll (8) prepared long chain ω-hydroxyacids in low yield by the Baeyer–Villiger oxidation on poorly accessible macrocyclic ketones. Ozonolysis of naturally occurring olefinic acids followed by reduction with $NaBH_4$ gives ω-hydroxyaliphatic acids in high yield as shown by Diaper and Mitchell (9) and Lyncan and Adams (10) provided an inexpensive long chain olefinic acid is available. Hydroxymethylbenzoic acids have been usually made from unsymmetrical precursors such as *p*-toluic acid chloride (11), bromobenzyl bromide (12), or *p*-cyanotoluene (13).

We have previously shown how insoluble polymer supports can be used as monoblocking agents of symmetrical diols (14, 15), dihydric phenols (16), dials (17, 18), and diamines (19) and that the free functional group is available for elaboration to insect sex attractants (20, 21) and unsymmetrical carotenoids (22). In a preliminary report of this article (23) we showed how solid phases can be used to monoblock symmetrical aliphatic diacid chlorides, which can be elaborated to aliphatic monoester monoamides in high yield. In this paper we present the details of the solid phase preparation of a variety

[1]The use of polymer supports in organic synthesis. Part XVI. For part XV, see ref. 21.

[2]Taken in part from the M.Sc. Thesis of J. M. Goldwasser.

[3]Presented in part, at the 2nd Joint CIC–ACS Conference, Montreal, Quebec, May 29 – June 2, 1977.

Can. J. Chem. Downloaded from www.nrcresearchpress.com by 210.87.254.42 on 09/05/12
For personal use only.

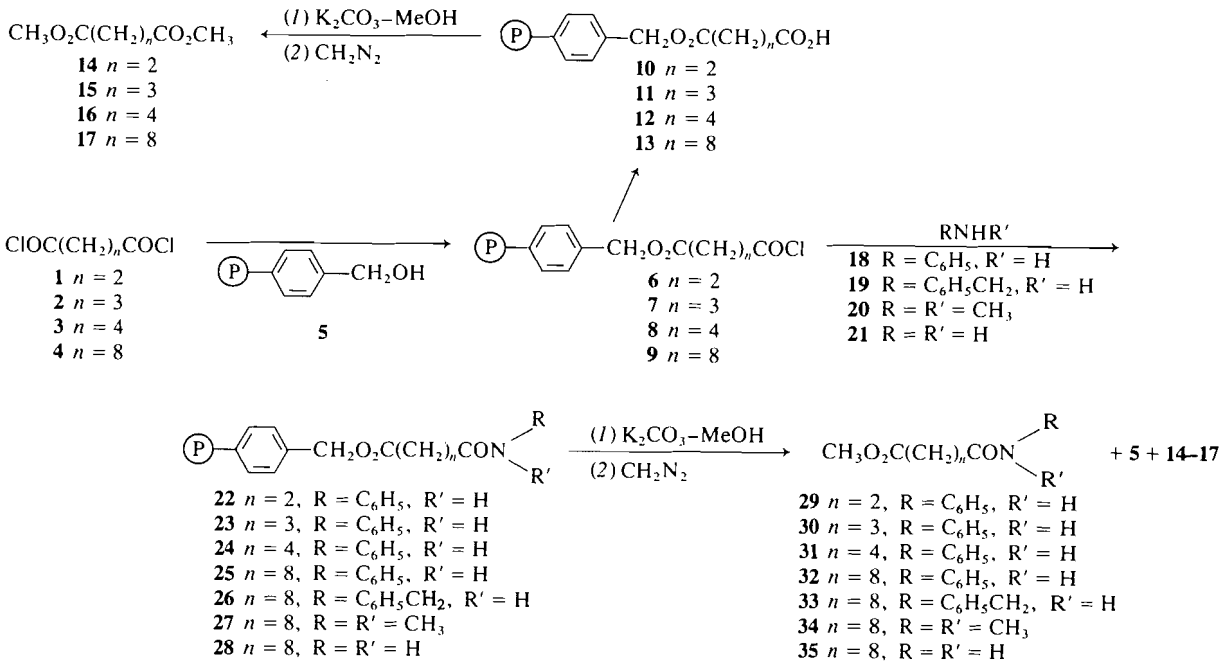

SCHEME I

of aliphatic and aromatic monoester monoamides and monoester monoalcohols.

Results and Discussion

Monoester Monoamides

A large excess of succinyl (**1**), glutaryl (**2**), adipoyl (**3**), or sebacoyl chloride (**4**) was added to a suspension of a 2% crosslinked divinylbenzene–styrene copolymer, containing benzyl alcohol groups, (**5**) (24), in tetrahydrofuran (THF) and the mixture stirred overnight under argon. Filtration of the polymers under anhydrous conditions (15) gave their respective polymer-bound monoester monoacid chlorides (**6–9**) as shown in Scheme 1. The infrared (ir) spectra of **6–9**, exhibited strong absorptions at 1740 cm^{-1} indicative of the monoester group, a shoulder at 1760 cm^{-1} and an enhancement of an absorption peak at 1812 cm^{-1}, normally associated with the polystyrene resin but also indicative of an acid chloride. The loading capacities of polymer **5** for their respective acid chlorides were determined by hydrolysis of **6–9** in aqueous dioxane to give polymer-bound monoester monoacids **10–13**, respectively. The ir spectra of **10–13** exhibited strong absorptions at 1740 and 1710 cm^{-1} indicative of the ester and acid groups, respectively. The absorption peak at 1710 cm^{-1} was absent in **6–9**, indicating that the free acid chloride groups in **6–9** had not hydrolysed in the work-up or in the preparation of the KBr pellets, used to take the ir of **6–9**. Cleavage of **10–13** with either tetra-*n*-butylammonium hydroxide in THF at room temperature for 48 h or with potassium carbonate (K_2CO_3) in methanol at the reflux temperature for 12 h, gave the diacids derived from **1–4**. The diacids liberated from **10–13** were treated with diazomethane in ether to give dimethyl succinate (**14**), dimethyl glutarate (**15**), dimethyl adipate (**16**), and dimethyl sebacate (**17**), respectively. In some instances sebacic acid was isolated directly from cleavage of **13** and not esterified. Thus, the loading capacities of polymer **5** for **1–4** were determined by isolation of their respective diesters **14–17** and are recorded in Table 1. Treatment of the polymer-bound acid chlorides (**6–9**) with aniline (**18**) and **9** with benzylamine (**19**), dimethylamine (**20**), and ammonia (**21**), respectively, gave the polymer-bound monoester monoamides **22–28**, respectively. The ir spectra of **22–28** all exhibited intense absorptions at 1740 cm^{-1} and between 1650–1700 cm^{-1} indicative of the ester and amide functional groups, respectively. In addition, the secondary amides **22–26** exhibited peaks at 1510–1550 cm^{-1} indicative of amide II absorptions of secondary amides. Cleavage of **22–28** with K_2CO_3 in methanol followed by esterification with diazomethane yielded methyl *N*-phenylsuccinamate (**29**) (6), methyl *N*-phenylglutaramate (**30**), methyl *N*-phenyladipamate (**31**), methyl *N*-phenylsebacamate (**32**) (3), methyl *N*-benzylsebacamate (**33**), methyl *N*,*N*-dimethylsebacamate (**34**), and methyl sebacamate (**35**) (4) in high yield (Table 1). In some preparations a small amount of the symmetrical diesters **14–17** were recovered (Table 1)

Can. J. Chem. Downloaded from www.nrcresearchpress.com by 210.87.254.42 on 09/05/12
For personal use only.

Can. J. Chem. Downloaded from www.nrcresearchpress.com by 210.87.254.42 on 09/05/12
For personal use only.

TABLE 1. Yields of monoester monoamides **29–35**, **44**, **45**, recovered from cleavage of polymers **22–28**, **42**, **43** with K_2CO_3

Monoester monoamide	Loading capacity of **5**, quantity of **14–17**, **41** per gram of **5**		Recovered product, quantity of **29–35**, **44**, **45** per gram of **5**		Recovered diester, quantity of **14–17**, **41** per gram of **5**		% yield
	mg/g	(mmol/g)	mg/g	(mmol/g)	mg/g	(mmol/g)	
29	50	(0.34)[a]	66	(0.32)	—	—	94
30	72	(0.45)[a]	96	(0.43)	—	—	97
31	92	(0.53)[a]	97	(0.41)	19	(0.11)	77
32	113	(0.56)[b,c]	161	(0.55)	—	—	98
	104	(0.45)[a]	85	(0.29)	34	(0.15)	65
35	113	(0.56)[b,c]	108	(0.50)	—	—	90
34	113	(0.56)[b,c]	117	(0.48)	—	—	86
	104	(0.45)[a,c]	71	(0.29)	27	(0.12)	71
33	104	(0.45)[a,c]	101	(0.33)	30	(0.10)	77
44	59	(0.30)[a]	56	(0.24)	10	(0.05)	80
45	[d]	[d]	49	(0.21)	—	—	—

[a]Reactions carried out with recycled polymer.
[b]Reactions carried out with new polymer.
[c]Isolated as sebacic acid.
[d]Cleavage took place when **39** was converted to monoester monoacid derivative.

along with **29–35** and were separated from **29–35** by preparative thin-layer chromatography (tlc). The spectral and physical data for **29–35** are consistent with the assigned structures (see Experimental). *It should be emphasized that in almost all cases the crystalline monoester monoamides can be cleanly separated from the oily symmetrical dimethyl esters by crystallization* and that preparative tlc was done simply to obtain the accurate yield data recorded in Table 1.

Similarly, treatment of the symmetrical aromatic diacid chlorides, terephthaloyl chloride (**36**), and isophthaloyl chloride (**37**) yielded the polymer-bound monoester monoacid chlorides **38** and **39**, respectively, as shown in Scheme 2. The ir spectra of **38** and **39** showed absorption peaks at 1730 and 1770–1785 cm^{-1} indicative of aromatic esters and aromatic acid chlorides respectively. Hydrolysis of **38** with aqueous dioxane gave the polymer-bound monoester monoacid (**40**), which exhibited absorptions in its ir spectrum at 1730 and 1700 cm^{-1} typical of aromatic esters and aromatic acids, respectively, but similar hydrolysis of **39** resulted in substantial cleavage from the polymer to liberate isophthalic acid. Polymer **40** could be cleaved as before but this time the resulting terephthalic acid was esterified with HCl in methanol to give dimethyl terephthalate (**41**) as the intermediate acid is insoluble in ether making esterification with diazomethane inefficient. Treatment of **38** and **39** with *tert*-butylamine led to the polymer-bound monoester monoamides **42** and **43**, respectively, which exhibited absorption peaks at 1730, 1650–1680, and 1520–1560 cm^{-1}, in their ir spectra, indicative of ester, amide I, and amide II absorptions,

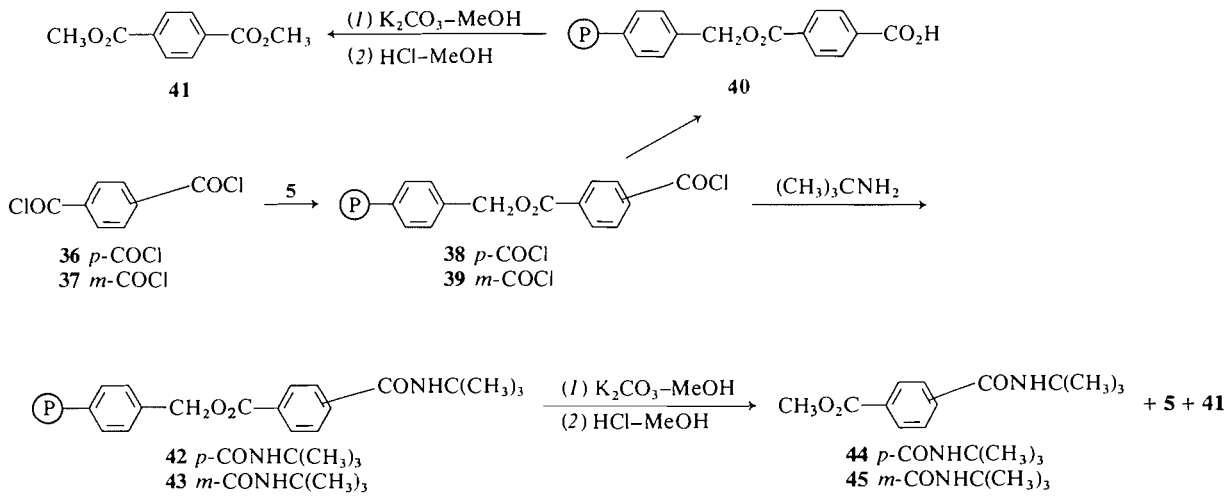

SCHEME 2

TABLE 2. Yields of monoester monoalcohols recovered from cleavage of **46**, **48**, and **49**

Monoester monoalcohol	Loading capacity of **5**, quantity of **17**, **41** per gram of **5**		Recovered product, quantity of **47**, **50**, **51** per gram of **5**		Recovered diester, quantity of **17**, **41** per gram of **5**		% yield
	mg/g	(mmol/g)	mg/g	(mmol/g)	mg/g	(mmol/g)	
47[a,b,c]	113	(0.49)[d]	59	(0.29)	41	(0.18)	59
47[a,c,e]	113	(0.49)[d]	59	(0.29)	46	(0.20)	59
47[b,c,f]	127	(0.55)[d]	75	(0.37)	39	(0.17)	67
47[b,f,g]	117	(0.51)[d]	67	(0.33)	41	(0.18)	65
47[b,f,h]	129	(0.56)[d]	34	(0.17)	30	(0.13)	30
50[b,c,f]	59	(0.30)	38	(0.23)	14	(0.07)	77
51[b,c,f]	—	—	38	(0.23)	—	—	—

[a]Reaction time of 5 h.
[b]Reaction carried out at room temperature.
[c]Reaction carried out using $NaBH_4$.
[d]Isolated as sebacic acid.
[e]Reaction carried out at reflux in dioxan.
[f]Reaction time of 12 h.
[g]Reaction carried out using $NaBH_3CN$.
[h]Reaction carried out using $Zn(BH_4)_2$.

respectively. Cleavage of **42** and **43** and esterification of the product with HCl in methanol gave methyl *N-tert*-butylterephthalamate (**44**) and methyl *N-tert*-butylisophthalamate (**45**), respectively (Table 1). A small amount of **41** was recovered in the preparation of **44**. No dimethyl isophthalate was found in the preparation of **45** but this was expected as any unreacted **39** would probably have been cleaved in the work-up of **43**. The spectral and physical data for **44** and **45** are consistent with the assigned structures (Experimental). It may be noted in Table 1 that the use of freshly prepared **5** yielded the monoester monoamides exclusively while recycled **5** yielded the monoester monoamides in high yield but this time accompanied by some diester. Whether the formation of the diester results from some initial double-binding of **1**–**4** and **36**–**37** with recycled **5** or is due to subsequent incomplete reaction of the polymer-bound monoester monoacid chlorides with the appropriate amine is still conjecture.

Monoester Monoalcohols

The successful monoprotection of symmetrical diacid chlorides as represented by the polymer-bound monoester monoacid chloride **9** allows for the possibility of reducing **9** to the polymer-bound ω-hydroxymonoester **46** shown below. Sodium borohydride ($NaBH_4$) is known to reduce acid chlorides but not esters (25). Hence reduction of **9** with $NaBH_4$ in THF under argon for 12 h gave **46**, which on cleavage with K_2CO_3 in methanol and esterification with diazomethane yielded methyl 10-hydroxydecanoate (**47**) (10) in 67% yield (Table 2), the

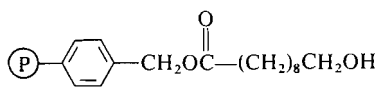

46

remaining material being **17**, derived from unreacted **9**. As some **17** was recovered from the reduction of **9** some attempts were made to optimize the yield of **47** by changing the reaction conditions. These variations and their results are recorded in Table 2. Similar results were obtained with new or recycled polymer **5**. Since $NaBH_4$ is not very soluble in THF or dioxane, other reducing agents selective for reducing acid chlorides or acids but not esters were sought. Borane in THF, known to selectively reduce acids in the presence of esters (26), when added to polymer-bound monoester monoacid **13** caused cleavage of the ester linkage to the polymer and hence was unsuitable. Zinc borohydride [$Zn(BH_4)_2$] (27) caused partial cleavage of the ester linkage of polymer **9** and still did not result in complete reduction of **9** to **47** (Table 2). We also perceived that incomplete reduction of **9** might be due to increased crosslinking of the intermediate borate esters due to the fact that the borane reagents have multiple hydrides. Thus, as the reduction of **9** proceeds, crosslinking increases and the reaction eventually stops as further reducing agent cannot penetrate to the interior of the polymer beads. We did attempt to reduce **9** with the *monohydride* sodium monohydridotris(2-methoxyethoxo)-borate, $NaBH(OCH_2CH_2OCH_3)_3$ (28) but this reagent is more reactive than $NaBH_4$ causing partial reduction of **9** to 1,10-decanediol.[4] Sodium cyanoborohydride, $NaBH_3CN$ (29), is less reactive than $NaBH_4$ and is soluble in THF. Reduction of **9** with $NaBH_3CN$ gave **46** and hence **47** in a yield comparable but no better than that using $NaBH_4$ (Table 2).

Similarly, reduction of the polymer-bound aromatic monoester monoacid chlorides **38** and **39** with

[4]Experiment done by V. Yedidia.

Can. J. Chem. Downloaded from www.nrcresearchpress.com by 210.87.254.42 on 09/05/12
For personal use only.

Can. J. Chem. Downloaded from www.nrcresearchpress.com by 210.87.254.42 on 09/05/12
For personal use only.

$NaBH_4$ gave the polymer-bound monoester monoalcohols **48** and **49** shown below. Cleavage of **48** and **49** as before and esterification with HCl in methanol yielded methyl *p*-hydroxymethylbenzoate (**50**) (11) and methyl *m*-hydroxymethylbenzoate (**51**), respectively (Table 2). Some dimethylterephthalate (**41**) was recovered from the cleavage of **48**.

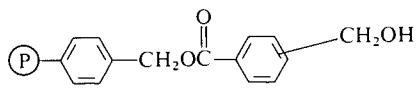

48 *p*-CH_2OH
49 *m*-CH_2OH

Conclusions

It has been shown that monoester monoamides can be prepared, often in quantitative yield, from a variety of inexpensive symmetrical aliphatic and aromatic diacid chlorides using a readily available functionalized solid phase. Polymer-bound symmetrical aliphatic and aromatic diacid chlorides can also be selectively reduced to monoester monoalcohols in good yield.

Experimental

A chloromethylated 2% divinylbenzene (DVB) – styrene copolymer, containing 1.16 mequiv. Cl/g of resin,[5] obtained from Sigma Chemical Company was used as the starting resin in all resin transformations. Filtration was done under vacuum using sintered glass Büchner funnels. Suspensions and solutions were stirred using magnetic stirrers. Matheson high purity argon was used to maintain inert atmosphere conditions. Filtration under an inert atmosphere was accomplished under positive pressure in a modified fritted Schlenk tube apparatus (15). Infrared (ir) spectra were recorded on a Pye Unicam SP1000 infrared spectrophotometer using KBr discs for solids or as neat films between NaCl discs. Nuclear magnetic resonance (nmr) spectra were recorded on a Varian EM 360 spectrometer using deuterochloroform as solvent and tetramethylsilane as the internal standard. The positions of the signals are reported in δ units. The splittings of the signals are described as singlets (s), doublets (d), triplets (t), quartets (q), or multiplets (m). Mass spectra (ms) were recorded at 70 eV on a Hitachi Perkin Elmer RMU 6E mass spectrometer. The number in parentheses after the indicated ion shows the percentage of the base peak represented by that ion. Melting points (mp) were determined using a Kofler hot stage melting point apparatus and are uncorrected. Thin-layer chromatography (tlc) was performed using silica gel G as the adsorbent and benzene–ether (7:3) as eluant unless otherwise stated. Microanalyses were done by G. Gygli of Toronto and Dr. C. Daesslé of Montreal. Spectral and analytical data are given for all new compounds and for known compounds where data are unreported.

Preparation of Polymer-bound Acid Chlorides ***6–9, 38, and 39***

Thirteen millimoles of the symmetrical diacid chloride (**1–4**, **36**, or **37**) was added to 3 g (containing a maximum of 3.48 mequiv. of benzyl alcohol groups) of **5** suspended in 50 ml of dry THF in a modified Schlenk tube apparatus (15) and stirred under an inert atmosphere for 12 h at room temperature. The suspensions were filtered under argon and washed with dry THF in a modified Schlenk tube apparatus and stirred under argon for 12 h at room temperature to give the polymer-bound monoester monoacid chlorides (**6–9**, **38**, and **39**); ir (KBr): 1812–1760 (COCl), 1740–1730 (CO_2R), and 1180–1150 cm^{-1} (C—O).

Preparation of Polymer-bound Monoester Monoacids ***10–13 and 40***

Polymer **6–9** or **38** (1 g) was suspended in 50 ml of aqueous THF and stirred at the reflux temperature for 5 h. The resultant polymer was then filtered, washed once with THF, three times with methanol, and twice with ether to give the polymer-bound monoacid **10–13** or **40**; ir (KBr): 1740–1730 (CO_2R), 1710–1700 (CO_2H), and 1180–1150 cm^{-1} (C—O).

Cleavage of the Polymer-bound Monoester Monoacids ***10–13 and 40 with*** K_2CO_3

A polymer-bound acid **10–13** or **40** (1.1 g) and 0.75 g of K_2CO_3 were suspended in 50 ml of methanol and stirred at the reflux temperature for 12 h. Regenerated polymer **5** was filtered, washed four times with methanol, once with benzene, three times with methanol, and twice with ether. An ir spectra of **5** exhibited no absorption peaks at 1740–1730 and 1710–1700 cm^{-1} due to uncleaved acid. The filtrate was evaporated almost to dryness, acidified with HCl, and esterified with diazomethane in ether. The product was then extracted with ether three times. The ether layer was then washed once with dilute H_2SO_4, once with dilute NaOH, and once with water. The ether layer was dried over $MgSO_4$ and evaporated to dryness to give pure dimethyl succinate (**14**), dimethyl glutarate (**15**), dimethyl adipate (**16**), dimethyl sebacate (**17**), and dimethyl terephthalate (**41**), identical to the commercially available diesters. The cleavage product from **13** was sometimes acidified with HCl and isolated directly as sebacic acid by extraction with ether. The cleavage product from **40** was esterified with HCl in methanol to give **41**. The amount of recovered **5** was determined. The loading capacities of the diesters **14–17** and **41** for polymer **5** are recorded in Tables 1 and 2. Thus, approximately one-half to one-third of the benzyl alcohol groups of **5** are available for reaction with the symmetrical acid chloride.

Preparation of the Polymer-bound Monoester Monoamides ***22–28, 42, and 43***

A suspension of 1.1 g of polymer **6–9** in dry THF was treated with 5 mmol of aniline (**18**) and the mixture stirred under argon for 5 h at room temperature. The polymer was subsequently filtered and washed once with THF, three times with methanol, once with benzene, three times with methanol and twice with ether to give the polymer-bound monoester monoamide **22**, **23**, **24**, or **25**; ir (KBr): 3450–3300 (broad) (N—H), 1740 (CO_2R), 1700–1670 (amide I), and 1550–1510 cm^{-1} (amide II).

Similarly, **9** reacted with benzylamine (**19**) to give polymer-bound monoester monoamide **26**; ir (KBr): 3450–3300 (broad) (NH), 1740 (CO_2R), 1690–1660 (amide I), and 1550–1510 cm^{-1} (weak) (amide II).

Similarly, **9** reacted with dimethyl amine (**20**) to give the polymer-bound monoester monoamide **27**; ir (KBr): 1740 (CO_2R) and 1660–1650 cm^{-1} (amide I).

Similarly, **9** reacted with ammonia to give the polymer-bound monoester monoamide **28**; ir (KBr): 3500–3350 (broad) and 3200 (weak, NH), 1740 (CO_2R), and 1690–1670 cm^{-1} (amide I).

Similarly, **38** or **39** reacted with *tert*-butylamine to give the

[5]Thus, it can be calculated (30) that approximately one in eight of the benzene rings is chloromethylated.

Can. J. Chem. Downloaded from www.nrcresearchpress.com by 210.87.254.42 on 09/05/12
For personal use only.

polymer-bound monoester monoamide **42** or **43**; in (KBr): 3600–3350 (broad) (NH), 1730 (CO_2R), 1680–1660 (amide I), and 1540–1510 cm^{-1} (amide II).

*Preparation of the Monoester Monoamides **29–35**, **44**, and **45***

A suspension of 1.1 g of **22** was cleaved with K_2CO_3 in methanol, esterified, and extracted with ether as described above for the cleavage of **10**. The amount of recovered **5** was determined. The product was purified by preparative tlc to give as the sole product (Table 1) 66 mg of methyl *N*-phenylsuccinamate (**29**); mp 94–94.5°C (lit. (6), mp 97–99°C); ir (KBr): 3320 (NH), 1742 (CO_2R), 1670 (amide I), 1550 (amide II), 1600 (phenyl), and 1165 cm^{-1} (C—O); nmr δ: 8.1 (s, 1, N*H*), 7.7–7.2 (m, 5, aromatic *H*), 3.8 (s, 3, CH_3O), and 2.8 (s, 4, $CH_2C{=}O$); ms: 207 (53) (M^+), 176 (36), 93 (100).

Similarly, **23** yielded methyl *N*-phenylglutaramate (**30**); mp 72–72.5°C; ir (KBr): 3370 (NH), 1730 (CO_2R), 1690 (amide I), 1605 (phenyl), 1540 (amide II), and 1165 cm^{-1} (C—O); nmr δ: 8.1 (s, 1, N*H*), 7.7–7.1 (m, 5, aromatic *H*), 3.7 (s, 3, CH_3O), 2.5 (m, 4, $CH_2C{=}O$), and 2.1 (m, 2, CH_2); ms: 221 (82) (M^+), 129 (65), 93 (100). *Anal.* calcd. for $C_{12}H_{15}NO_3$: C 65.14, H 6.83, N 6.33; found: C 65.43, H 6.88, N 6.37.

Similarly, **24** gave methyl *N*-phenyladipamate (**31**); mp 43°C; ir (KBr): 3430 (NH), 1740 (CO_2R), 1670 (amide I), 1605 (phenyl), 1550 (amide II), and 1180 cm^{-1} (C—O); nmr δ: 7.9 (s, 1, N*H*), 7.7–7.1 (m, 5, aromatic *H*), 3.8 (s, 3, CH_3O), 2.5 (m, 4, $CH_2C{=}O$), and 1.8 (m, 4, CH_2); ms: 235 (8) (M^+), 93 (100). *Anal.* calcd. for $C_{13}H_{17}NO_3$: C 66.36, H 7.28, N 5.95; found: C 66.28, H 7.37, N 6.02.

Similarly, **25** gave methyl *N*-phenylsebacamate (**32**); mp 68°C (lit. (3) mp 68°C); ir (KBr): 3370 (NH), 1720 (CO_2R), 1690 (amide I), 1605 (phenyl), 1550 (amide II), and 1170 cm^{-1} (C—O); nmr δ: 8.3 (s, 1, N*H*), 7.7–7.1 (m, 5, aromatic *H*), 3.8 (s, 3, CH_3O), 2.4 (m, 4, $CH_2C{=}O$), and 1.9–1.1 (m, 12, CH_2).

Similarly, **26** yielded methyl *N*-benzylsebacamate (**33**); mp 70–71°C; ir (KBr): 3390 (NH), 1742 (CO_2R), 1635 (amide I), 1555 (amide II), and 1175 cm^{-1} (C—O); nmr δ: 7.4 (s, 5, aromatic *H*), 6.3 (s, 1, N*H*), 5.6 (d, 2, J = 6 Hz, NCH_2Ph), 3.7 (s, 3, CH_3O), 2.4 (m, 4, $CH_2C{=}O$), and 1.9–1.1 (m, 12, CH_2). *Anal.* calcd. for $C_{18}H_{27}NO_3$: C 70.79, H 8.91, N 4.59; found: C 70.63, H 8.54, N 4.59.

Similarly, **27** yielded methyl *N*,*N*-dimethylsebacamate (**34**) as an oil; ir (neat): 1742 (CO_2R), 1645 (amide I), and 1165 cm^{-1} (C—O); nmr δ: 3.8 (s, 3, CH_3O), 3.1, 3.05 (d, 6, CH_3N), 2.4 (m, 4, $CH_2C{=}O$), and 1.9–1.2 (m, 12, CH_2). *Anal.* calcd. for $C_{13}H_{26}NO_3$: C 64.16, H 10.36, N 5.76; found: C 63.99, H 10.26, N 5.64.

Similarly, **28** gave methyl sebacamate (**35**); mp 74–76°C (lit. (4) mp 74–76°C); ir (KBr): 3400, 3200 (NH_2), 1738 (CO_2R), 1650 (amide I), and 1175 cm^{-1} (C—O); nmr δ: 5.7 (s, 2, NH_2), 3.7 (s, 3, CH_3O), 2.2 (m, 4, $CH_2C{=}O$), and 1.9–1.2 (m, 12, CH_2).

Similarly, **42** gave methyl *N-tert*-butylterephthalamate (**44**); mp 124.5–125°C; ir (KBr): 3310 (NH), 1725 (CO_2R), 1640 (amide I), 1550 (amide II), and 1290, 1110 cm^{-1} (C—O); nmr δ: 8.3–7.7 (m, 4, aromatic *H*), 6.2 (s, 1, N*H*), 4.1 (s, 3, CH_3O), and 1.6 (s, 9, CH_3C); ms: (235) (88) (M^+), 220 (77) ($M^+ - CH_3$), 180 (90), 163 (100) ($M^+ - NHC(CH_3)_3$). *Anal.* calcd. for $C_{13}H_{17}NO_3$: C 66.36, H 7.28, N 5.95; found: C 66.73, H 7.74, N 5.52.

Similarly, **43** yielded methyl N-*tert*-butylisophthalamate (**45**); mp 77.5°C; ir (KBr) 3350 (NH), 1730 (CO_2R), 1640 (amide I), 1550 (amide II), and 1270, 1150 cm^{-1} (C—O); nmr δ: 8.4–7.4 (m, 4, aromatic *H*), 6.2 (s, 1, N*H*), 4.0 (s, 3, CH_3O), and 1.5 (s, 9, CH_3C); ms: (235) (25) (M^+), 220 (23) ($M^+ - CH_3$), 182 (38), 163 (100) ($M^+ - NHC(CH_3)_3$). *Anal.* calcd. for $C_{13}H_{17}NO_3$: C 66.36, H 7.28, N 5.95; found: C 66.33, H 7.29, N 5.84.

In the isolation of **31–34** and **44**, some of the corresponding dimethyl esters **16**, **17**, and **41** were detected and separated from the monoamide monoesters by preparative tlc (see Table 1).

*Preparation of Polymer-bound Monoester Monoalcohols **46**, **48**, and **49***

To a suspension of 1.0 g of **9**, was added 4 mmol of $NaBH_4$, $NaBH_3CN$ or $Zn(BH_4)_2$ in 40 ml of dry THF. The mixture was stirred under argon at room temperature for 12 h. The excess borohydride was decomposed with water and dilute HCl. The resultant polymer was filtered and washed four times with methanol, once with benzene, three times with methanol, and twice with ether to give the polymer-bound monoester monoalcohol (**46**); ir (KBr): 3600–3400 (O—H), 1740 (CO_2R), 1600 (phenyl), and 1160 cm^{-1} (C—O).

Similarly, reduction of **38** yielded the polymer-bound monoester monoalcohol (**48**); ir (KBr): 3600–3400 (O—H), 1730 (CO_2R), 1602 (phenyl), and 1170 cm^{-1} (C—O).

Similarly, reduction of **39** gave the polymer-bound monoester monoalcohol (**49**): ir (KBr): 3600–3400 (OH), 1730 (CO_2R), 1602 (phenyl), and 1180 cm^{-1} (C—O).

*Preparation of the Monoester Monoalcohols **47**, **50**, and **51***

A suspension of 1.1 g of **46** was cleaved with K_2CO_3 in methanol, esterified, and extracted with ether as described above for the cleavage of **10**. The amount of recovered **5** was determined. The product was purified by preparative tlc to yield (Table 2) some recovered **9** and methyl 10-hydroxydecanoate (**47**) as an oil (10); ir (neat): 3500–3300 (OH), 1743 (CO_2R), and 1175 cm^{-1} (C—O); nmr δ: 3.72 (s, 3, CH_3O), 3.65 (t, 2, J = 6 Hz, CH_2O), 2.0 (s, 1, O*H*), 2.35 (t, 2, J = 7 Hz, $CH_2C{=}O$), and 1.8–1.2 (m, 14, CH_2).

Similarly, **48** yielded (Table 2) some recovered **41** and methyl 4-hydroxymethylbenzoate (**50**); mp 49.5–50°C (lit. (11) bp 155–157°C/4–5 Torr); ir (KBr): 3340–3200 (OH), 1730 (CO_2R), 1620 (phenyl), and 1290, 1175 cm^{-1} (C—O); nmr δ: 8.2–7.3 (m, 4, aromatic *H*), 4.7 (s, 2, CH_2O), 4.0 (s, 3, CH_3O), and 2.5 (s, 1, O*H*); ms: 166 (88) (M^+), 135 (97) ($M^+ - OCH_3$ or CH_2OH), 107 (100) ($M^+ - CO_2CH_3$). *Anal.* calcd. for $C_9H_{10}O_3$: C 65.07, H 6.07; found: C 65.64, H 6.25.

Similarly, **49** gave methyl 3-hydroxymethylbenzoate (**51**) as an oil; ir (neat): 3550–3300 (OH), 1730 (CO_2R), 1600 (phenyl), and 1290, 1200 cm^{-1} (C—O); nmr δ: 8.2–7.3 (m, 4, aromatic *H*), 4.7 (s, 2, CH_2O), 4.0 (s, 3, CH_3O), and 2.8 (s, 1, O*H*); ms: 166 (84) (M^+), 135 (98) ($M^+ - OCH_3$ or CH_2OH), 107 (100) ($M^+ - CO_2CH_3$). *Anal.* calcd. for $C_9H_{10}O_3$: C 65.07, H 6.07; found: C 64.94, H 6.20.

*Attempted Preparation of **46** by the Borane Reduction of **13***

To a suspension of 1.0 g of **13** in 30 ml of dry THF cooled in ice, was added borane (two mmol) in THF. The mixture was allowed to warm to room temperature and was stirred under argon for 12 h. Excess hydride was decomposed with water and dilute HCl. The resultant polymer was filtered and washed once with THF, four times with methanol, twice with benzene, three times with methanol, and twice with ether. The ir spectrum of the resultant polymer showed complete loss of absorption at 1740 cm^{-1}, indicating that total cleavage of the ester linkage had taken place.

Acknowledgements

We are grateful for the financial assistance of the National Research Council of Canada.

1. A. Wohl. Chem. Ber. **43**, 4374 (1910).
2. D. H. Johnson. J. Chem. Soc. 1624 (1958).
3. G. T. Morgan and E. Walton. J. Chem. Soc. 902 (1936).

4. M. D. SOFFER, N. S. STRAUSS, M. D. TRAIL, and K. W. SHERK. J. Am. Chem. Soc. **69**, 1684 (1947).
5. G. B. BROWN, M. D. ARMSTRONG, A. W. MOYER, W. P. ANSLOW, JR., B. R. BAKER, M. V. QUERRY, S. BERNSTEIN, and S. R. SAFIR. J. Org. Chem. **12**, 160 (1947).
6. G. M. ROBINSON and R. ROBINSON. J. Chem. Soc. 175 (1925).
7. P. CHUIT and J. HAUSSER. Helv. Chim. Acta, **12**, 463 (1929).
8. L. RUZICKA and M. STOLL. Helv. Chim. Acta, **11**, 1159 (1928).
9. D. G. DIAPER and D. L. MITCHELL. Can. J. Chem. **38**, 1976 (1960).
10. W. H. LYNCAN and R. ADAMS. J. Am. Chem. Soc. **51**, 625 (1929).
11. A. SINGH, L. J. ANDREWS, and R. M. KEEFER. J. Am. Chem. Soc. **84**, 1179 (1962).
12. H. GITMAN and D. G. MELSTROM. J. Am. Chem. Soc. **70**, 4179 (1948).
13. F. H. CASE. J. Am. Chem. Soc. **47**, 1143 (1925).
14. J. Y. WONG and C. C. LEZNOFF. Can. J. Chem. **51**, 2452 (1973); J. M. J. FRÉCHET and L. J. NUYENS. Can. J. Chem. **54**, 926 (1976).
15. T. M. FYLES and C. C. LEZNOFF. Can. J. Chem. **54**, 935 (1976).
16. C. C. LEZNOFF and D. M. DIXIT. Can. J. Chem. **55**, 3351 (1977).
17. C. C. LEZNOFF and J. Y. WONG. Can. J. Chem. **51**, 3756 (1973).
18. C. C. LEZNOFF and S. GREENBERG. Can. J. Chem. **54**, 3824 (1976).
19. D. M. DIXIT and C. C. LEZNOFF. J. Chem. Soc. Chem. Commun. 798 (1977).
20. C. C. LEZNOFF and T. M. FYLES. J. Chem. Soc. Chem. Commun. 251 (1976); C. C. LEZNOFF, T. M. FYLES, and J. WEATHERSTON. Can. J. Chem. **55**, 1143 (1977); T. M. FYLES, C. C. LEZNOFF, and J. WEATHERSTON. J. Chem. Ecol. **4**, 109 (1978). T. M. FYLES, C. C. LEZNOFF, and J. WEATHERSTON. Can. J. Chem. **55**, 4135 (1977).
21. T. M. FYLES, C. C. LEZNOFF, and J. WEATHERSTON. Can. J. Chem. **55**, 4135 (1978).
22. C. C. LEZNOFF and W. SYWANYK. J. Org. Chem. **42**, 3203 (1977).
23. C. C. LEZNOFF and J. M. GOLDWASSER. Tetrahedron Lett. 1875 (1977).
24. J. M. STEWART and J. D. YOUNG. Solid phase peptide synthesis. W.H. Freeman Ltd., San Francisco, CA. 1969. pp. 27–28.
25. S. W. CHAIKEN and W. G. BROWN. J. Am. Chem. Soc. **71**, 122 (1949).
26. N. M. YOON, C. S. PAK, H. C. BROWN, S. KRISHNAMURTHY, and T. P. STOCKY. J. Org. Chem. **38**, 2786 (1973).
27. N. M. YOON, H. J. LEE, H. K. KIM, and J. YANG. J. Kor. Chem. Soc. **20**, 59 (1976).
28. O. KRIZ, J. STUCHLIK, P. SOCHOR, and O. STROUF. Coll. Czech. Chem. Commun. **42**, 421 (1977).
29. H. C. BROWN. Boranes in organic chemistry. Cornell University Press, Ithaca, NY. 1972. Chapts. 12 and 13.
30. TH. J. NIEUWSTAD, A. P. G. KIEBOOM, A. J. BREIJER, J. VAN DER LINDEN, and H. VAN BEKKUM. Recl. Trav. Chim. Pays-Bas, **95**, 225 (1976).

Can. J. Chem. Downloaded from www.nrcresearchpress.com by 210.87.254.42 on 09/05/12
For personal use only.

Propriétés hydrodynamiques des conformations ordonnées et desordonnées du poly(γ-L-glutamate de benzyle): dimensions et flexibilité de la chaîne

NGA HO-DUC

Département de Chimie, Université de Montréal, C.P. 6210, Succ. A Montréal (Qué.), Canada H3C 3V1

Reçu le 13 octobre 1977

NGA HO-DUC. Can. J. Chem. **56**, 1569 (1978).

Théoriquement, on peut déterminer la structure désordonnée ou ordonnée des polypeptides en solution, ainsi que leurs dimensions à partir des propriétés hydrodynamiques. Nous avons un certain nombre suffisant de théories pour interpréter les résultats expérimentaux. En ce qui concerne la conformation ordonnée hélicoidale, ces théories se basent sur des modèles physiques d'un ellipsoide de révolution allongé, d'une chaîne vermiforme plus ou moins flexible, d'une chaîne cylindrique rigide ou semi-flexible.

Les données expérimentales de viscosité des sept échantillons de poly(γ-L-glutamate de benzyle) dans le dichloro-1,2 éthane à 25°C ont été étudiées. La longueur d'un résidu h a été calculée selon le modèle ellipsoidal. Le degré de flexibilité est caractérisée par le nombre de monomères par segment rigide (N_S). La valeur de N_S a été déterminée selon l'équation de Yamakawa et Fujii réarrangée par Vitovskaya et Tsvetkov. Nous obtenons pour h, en supposant que la chaîne est rigide, des valeurs se situant entre 1.3 et 2 Å. Nous constatons pour les échantillons de poids moléculaires suivants: 1.8×10^5, 1.7×10^5, 1.5×10^5, que la valeur de h est voisine de 1.5 Å. Ce sont, précisément, des échantillons dont la longueur de chaîne est du même ordre de grandeur que celle d'un segment rigide.

L'analyse des données de la viscosité du poly(γ-L-glutamate de benzyle) dans l'acide dichloroacétique indique qu'à part de la formation de liaisons hydrogène entre le polypeptide et le solvant, d'autres interactions sont présentes.

Bref, nous constatons que, si l'étude de la transition conformationnelle est jugée satisfaisante à partir des données hydrodynamiques, la détermination des dimensions caractéristiques permettant de décrire la conformation reste ambigue. Un des problèmes est la flexibilité de la chaîne. Pour contourner cette difficulté, nous proposons une méthode qui consiste à déterminer le nombre de monomères par segment rigide à partir des différentes valeurs obtenues pour h pour les différents poids moléculaires et ensuite les dimensions à partir des échantillons dont la longueur des chaînes est en bon accord avec celle du segment rigide ainsi déterminée.

NGA HO-DUC. Can. J. Chem. **56**, 1569 (1978).

Theoretically we can determine the disordered or ordered structure of polypeptides and their dimensions in dilute solutions from hydrodynamic properties. We have presently a wealth of theories for random coil chains and a limited but sufficient number of theories for ordered chains for interpreting experimental results.

Viscosity data for seven poly(γ-benzyl-L-glutamate) samples in 1,2-dichloroethane at 25 C are analyzed and the length per monomeric residue (h) is calculated according to the equivalent ellipsoid approach. The degree of flexibility or rigidity is characterized by calculating N_S, the number of monomer units in a rigid segment or a Kuhn statistical segment; the determination of N_S is made by applying Yamakawa and Fujii's equation modified by Vitovskaya and Tsvetkov.

Values obtained for h assuming the solute molecule to be a rigid, stiff chain, range between 1.3 to 2 Å. One notices that the h value close to 1.5 Å is found for the three following molecular weights: 1.8×10^5, 1.7×10^5, and 1.5×10^5. They are, in fact, the samples having a length in good quantitative agreement with that of the rigid segment determined by the method of Vitovskaya and Tsvetkov. This rigid segment corresponds to a sample of 700 ± 100 monomer units.

The analysis of the experimental data of poly(γ-benzyl-L-glutamate) in dichloroacetic acid indicates that, in addition to the formation of hydrogen bonds, other interactions between the polypeptide and the solvent are present.

In summary, we may conclude that the study of the helix–coil transition using hydrodynamic measurements is judged satisfactory but the determination of characteristic dimensions used to describe exactly the conformation of the macromolecule is somewhat ambiguous. One major problem is the degree of flexibility encountered with high molecular weight chains. However, to get around this difficulty, we propose, according to our results, a method which consists in determining the number of monomer units within a rigid segment from the different values found for h and then the dimensions from the samples for which the chain length is in good agreement with that of a rigid segment thus determined.

Can. J. Chem. Downloaded from www.nrcresearchpress.com by 210.87.254.6 on 09/05/12
For personal use only.

Can. J. Chem. Downloaded from www.nrcresearchpress.com by 210.87.254.6 on 09/05/12
For personal use only.

Introduction

L'étude des conformations ordonnée et désordonnée des polypeptides synthétiques a donné naissance ces 15 dernières années à un certain nombre de théories thermodynamiques. Au point de vue hydrodynamique, nous constatons que l'effort se développe d'une façon remarquable depuis 1970. Il existe actuellement quelques théories raffinées (1–6) dont les différences fondamentales proviennent des simplifications apportées aux modèles physiques décrivant le phénomène concerné. Cependant, il faut noter que l'information correspondant à la conformation ordonnée est limitée théoriquement par plusieurs facteurs.

Comme ces propriétés hydrodynamiques se déduisent du coefficient de frottement de la macromolécule en solution et que ce coefficient dépend de la forme et de la grandeur du soluté, nous essayons de calculer ces quantités à partir de la viscosité intrinsèque et plus tard du coefficient de sédimentation en se basant sur les théories ayant pour modèles physiques un ellipsoide de révolution allongé, un batonnet rigide ou semi-flexible ou la chaîne vermiforme.

A partir des données expérimentales de la viscosité intrinsèque des échantillons de poly(γ-L-glutamate de benzyle) dans le dichloro-1,2 éthane et dans l'acide dichloroacétique nous calculons les dimensions de la chaîne et la longueur statistique de Kuhn. Nous étudions ensuite l'effet de la flexibilité de la chaîne sur les dimensions et proposons un moyen permettant de faire un choix convenable parmi les différentes valeurs obtenues.

Considérations théoriques

L'interprétation des données hydrodynamiques d'une macromolécule en solution peut se faire à l'aide des relations théoriques entre la viscosité intrinsèque $[\eta]$ et les dimensions de la chaîne ainsi que son poids moléculaire et certains paramètres d'interaction. Les relations théoriques exactes sont bien connues pour les particules sphériques ou d'équivalence hydrodynamique sphérique (7) et pour les particules d'ellipsoïde de révolution (8); les expressions de $[\eta]$ pour la structure hélicoïdale assimilé à un ellipsoïde de révolution allongé, à une chaîne cylindrique ou semi-flexible ou une chaîne vermiforme sont encore discutables. Nous résumons sommairement ces approximations couramment utilisées pour élucider ce problème.

L'approximation qui consiste à assimiler l'hélice à un ellipsoïde de révolution discutée par plusieurs auteurs (9, 10) a pour base les équations de Simha (11) avec l'hypothèse que le grand axe a de l'ellipsoïde est proportionnel au poids moléculaire du soluté, a étant égal à la longueur de contour de la chaîne (L).

Le petit axe b est relié au diamètre d de l'hélice par la relation suivante:

$$b = (3/2)^{0.5} d$$

Dans le cas où $(L/d) \gg 1$, la viscosité intrinsèque d'une particule d'ellipsoïde allongé peut s'écrire:

$$[1] \quad [\eta] = \frac{\pi N_A M^2}{4 M_L^3} \left\{ \frac{14}{15} \left(\frac{d}{L}\right)^2 + \frac{2}{45[\ln (2L/d) - 1.70]} + \frac{2}{15[\ln (2L/d) - 0.7]} \right\}$$

où $M_L = M/L$ ou sous la forme qui la relie directement à h, la longueur d'un résidu ou d'un motif de base

$$[2] \qquad hM = 6.86 M_0 ([\eta]/M)^{1/3} [p/\Lambda(p)]^{1/3}$$

où M_0 le poids moléculaire du motif de base et p le rapport axial. Notons que pour une chaîne rigide $h = M_0/M_L$ et

$$\Lambda(p) = \frac{14}{15} + \frac{p^2}{15(\ln 2p - 1.5)} + \frac{p^2}{5(\ln 2p - 0.5)}$$

Notons que dans l'éq. [2] h est exprimé en Å et $[\eta]$ en dl/g.

Hearst et Tagami (13) ont dérivé une équation pour la viscosité d'une chaîne vermiforme en appliquant la théorie générale de Kirkwood en tenant compte de la distribution à symétrie cylindrique du modèle. Quelques années plus tard Hearst *et al.* (14) ont repris ce modèle continu en ajoutant une force de flexion permettant de calculer la viscosité d'une chaîne vermiforme à un certain degré de flexibilité. Le résultat théorique de Hearst peut s'écrire selon la relation linéaire suivante entre $M/[\eta]$ et $M^{1/2}$

$$[3] \quad \frac{M}{[\eta]} = \frac{(\lambda M_L)^{3/2}}{\phi} \left[K \left(\frac{M_L}{\lambda}\right)^{1/2} + M^{1/2} \right]$$

où ϕ est une constante, λ^{-1} la longueur statistique de Kuhn, le paramètre K, une constante pour un polypeptide donné, est donné par la relation suivante: $K = -K_2 [K_3 + \ln(\lambda d)]$; K_2, K_3 sont des constantes numériques. Il faut noter que l'éq. [3] et celle donnée par Noda (15) en tenant compte du volume exclu ne sont valides que pour des chaînes ayant une flexibilité relativement grande. Nous verrons plus tard, dans la partie des résultats, que ce modèle ne peut s'appliquer à la chaîne de poly(γ-benzyl-L-glutamate), cette dernière étant "trop"

Can. J. Chem. Downloaded from www.nrcresearchpress.com by 210.87.254.6 on 09/05/12
For personal use only.

rigide. Plus récemment Yamakawa et Fujii (6) ont évalué la viscosité intrinsèque des chaînes rigides ou faiblement flexibles en appliquant les procédés de calculs hydrodynamiques d'Oseen Burgers au modèle de chaîne vermiforme cylindrique. L'approche de Yamakawa et Fujii (6) conduit à l'expression analytique semi-empirique suivante pour $[\eta]$

$$[4]\quad [\eta] = \frac{\pi N_A L^3}{24M \ln\left(\frac{L}{d}\right)} \frac{f(L)}{1 + \sum_{i=1}^{4} A_i \left[\ln\left(\frac{d}{L}\right)\right]^{-1}}$$

où A_i sont des grandeurs numériques indépendantes de L et d

$$f(L) = \frac{3}{2L^4}(e^{-2L} - 1 + 2L - 2L^2 + -\tfrac{3}{4}L^3)$$

Toutefois il faut noter que cette équation n'est qu'approximative pour $L/d < 100$. Selon les calculs des auteurs si $L = 10$, $d = 0.1$ l'erreur est de l'ordre de 0.5%, si $L = 10$ et $d = 0.25$ l'erreur passe à 3%.

Récemment Vitovskaya et Tsvetkov (16) ont réarrangé l'équation de Yamakawa et Fujii sous une forme plus pratique permettant de mesurer la rigidité ou la flexibilité de la chaîne. Ils substituent $f(L)$ par $f(x)$

$$f(x) = \frac{24}{x^4}\left(e^{-x} - 1 + x - \frac{x^2}{2} + \frac{x^3}{6}\right)$$

où $x = 2\,L\lambda$. A partir de l'éq. [4] ils obtiennent facilement avec ce changement de variable l'expression suivante:

$$[5]\quad y = h^3 f(x) = \frac{[\eta]}{M^2}\frac{24}{\pi N_A} M_0{}^3 \left[\ln\frac{L}{d} - 1.839 + \frac{8.24}{\ln\frac{L}{d}} - \frac{32.85}{\ln^2\frac{L}{d}} + \frac{41.10}{\ln^3\frac{L}{d}}\right]$$

ou

$$[6]\quad y = h^3\left(1 - \frac{2}{5}\frac{1}{M_0 N_S} M + \frac{2}{15}\frac{1}{M_0{}^2 N_S{}^2} M^2 - \ldots\right)$$

où N_S = nombre de monomères ou de résidus par segment rigide. Nous calculons à partir de N_S le poids correspondant M_{NS}. Cette quantité sera utilisée comme l'intermédiaire valable pour faire un choix judicieux parmi les différentes valeurs obtenues pour les dimensions de la chaîne déterminées à l'aide des données viscosimétriques.

Partie expérimentale

Les échantillons de poly(γ-benzyl-L-glutamate) ont été fournis par la compagnie Sigma. Les poids moléculaires ont été déterminés par viscosimétrie selon les calibrations de Doty *et al.* (17) et de Fujita *et al.* (18). Les solvants utilisés, l'acide dichloroacétique et dichloro-1,2 ethane, ont été purifiés par distillation sous vide. Toutes les mesures de viscosité ont été effectuées à l'aide d'un viscosimètre semi-micro Cannon Ubbelhode en utilisant le montage automatique de Hewlett Packard modèle 5901 B. Pour éviter la dégradation du polypeptide dans l'acide dichloroacétique, la mise en solution et les mesures ont été faites dans le minimum de temps possible. La température est maintenue à 25.00 ± 0.02°C; la concentration varie entre 1 à 0.2% p/v.

Résultats et discussions

Les résultats viscosimétriques des systèmes étudiés $[Glu(OBzl)]_n$-Cl_2AcOH et $[Glu(OBzl)]_n$-Cl_2Et et $[Glu(OBzl)]_n$-Cl_2AcOH/Cl_2Et sont groupés dans le tableau 1.

Mentionnons, en passant, qu'à partir de ces données nous traçons les graphiques de $[\eta]$ en fonction de M (fig. 1) et nous avons trouvé les relations suivantes respectivement pour Cl_2AcOH et Cl_2Et.

$$[7]\quad [\eta]\ \mathrm{dl/g} = 1.12 \times 10^{-4} M^{0.75}$$

$$[8]\quad [\eta]\ \mathrm{dl/g} = 1.2 \times 10^{-7} M^{1.40}$$

L'exposant pour le système $[Glu(OBzl)]_n$-Cl_2AcOH est inférieur à celui de Doty *et al.* (17).

Notons également le point d'isoviscosité intrinsèque (i.e. le point où la viscosité intrinsèque est indépendante du changement de conformation) est aux environs de 0.35 ce qui correspond à un poids moléculaire approximativement de 5×10^4. Le volume hydrodynamique moyen d'un tel poids moléculaire ne change pas lors de la transition hélice–pelote.

Dimensions et flexibilité de la chaîne dans Cl_2Et: conformation hélicoïdale

Nous avons déterminé h à partir de l'éq. [2] en posant pour le $[Glu(OBzl)]_n$, $p = 3.8 \times 10^{-4}$ M. La constante de proportionnalité 3.8×10^{-4} correspond à une hélice α rigide de 15 Å de diamètre. L'erreur sur p affecte peu la détermination de h à cause du

TABLEAU 1. Viscosité intrinsèque des systèmes étudiés (dl/g)

	[η]			
$M \times 10^5$	Cl_2Et	60% Cl_2Et + 40% Cl_2AcOH	40% Cl_2Et + 60% Cl_2AcOH	Cl_2AcOH
3.0	4.95	3.90	3.19	1.55
1.8	2.34	2.23	1.70	0.92
1.7	1.90	1.69	1.50	0.91
1.5	1.70	1.50	1.40	0.86
0.65	0.61	0.57	0.59	0.42
0.52	0.41	0.41	0.41	0.38
0.24	~0.16	~0.21	~0.2	~0.22

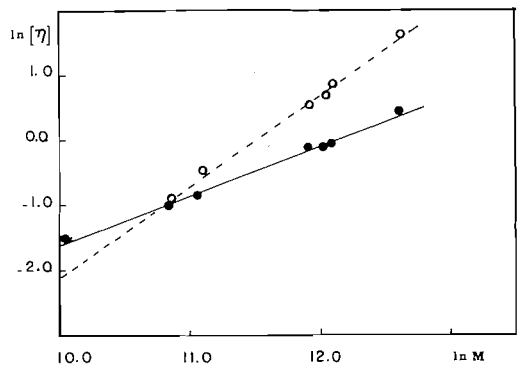

FIG. 1. Viscosité intrinsèque du poly(γ-benzyl-L-glutamate) dans le dichloroethane (●) et dans l'acide dichloroacétique (○) en fonction du poids moléculaire.

TABLEAU 2. Résultats expérimentaux de la longueur d'un résidu de $[Glu(OBzl)]_n$

	h (Å)	
$M \times 10^5$	éq. [2]	éq. [1*a*]
3	1.40	
1.8	1.49	
1.7	1.53	Valeur
1.5	1.56	moyenne
0.65	1.7	$\simeq 1.3$
0.52	1.7	
0.24	2.0	

terme $[p^2/\Lambda(p)]^{1/3}$. Nous trouvons les valeurs de h ainsi calculées dans le tableau 2.

Notons en passant que la valeur de h peut être évaluée graphiquement à partir de l'éq. [1]. En effet lorsque $\ln L/d > 1.5$, i.e. dans le cas d'une hélice α, une chaîne d'au moins cinquante motifs de base, l'éq. [1] peut être remplacée approximativement par la relation [1*a*]

$$[1a] \qquad \frac{N_A M^2}{[\eta]} = \frac{45}{2\pi}\left[\ln\frac{L}{d} - \text{cte}\right] M_L{}^3$$

Le graphique $N_A M^2/[\eta]$ en fonction de ln M (fig. 2) nous permet de calculer M_L et ensuite h. La valeur de h calculée de cette façon est de 1.3 Å qui est plutôt une valeur caractéristique de l'hélice π que de l'hélice α, i.e. 1.5 Å. Cette faible valeur est due à la flexibilité de la chaîne et à l'approximation apportée à l'équation. Examinons plutôt les valeurs de h obtenues par l'éq. [2] pour chaque échantillon; les points à noter dans ces résultats sont les valeurs de h trop élevées pour des échantillons de faible masse, légèrement faibles pour le poids moléculaire 3×10^5 et égales, aux erreurs expérimentales près, à celle attendue pour les échantillons de poids moléculaire s'étalant de 1 à 2×10^5.

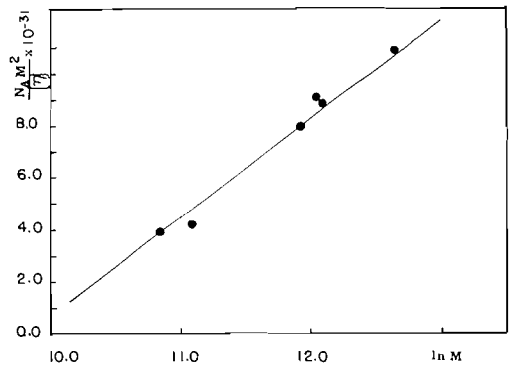

FIG. 2. Courbe permettant le calcul de h pour l'équivalence hydrodynamique ellipsoïdale allongée (système cgs).

Passons maintenant au degré de flexibilité de la chaîne. Ce degré peut être caractérisé par la longueur de persistance ou par la longueur du segment de Kuhn ou par N_S le nombre de monomère par segment rigide. Ce dernier peut être déterminé à partir de l'éq. [6] qui est représentée graphiquement, à partir de résultats expérimentaux, sur la fig. 3. En effet l'ordonnée à l'origine nous donne la valeur numérique de h, elle est égale à 1.6 Å et la pente initiale de la courbe nous permet de calculer N_S. La valeur de N_S ainsi déterminée est égale à 700 ± 100 ce qui correspond à un poids moléculaire M_{NS} d'environ 1.5×10^5 pour le $[Glu(OBzl)]_n$, autrement dit hélice α dont la longueur dépasse 1200 Å n'est plus rigide, elle devient plus ou moins flexible. Cet ordre de grandeur de poids moléculaire se compare favorablement avec celui des échantillons dont h est égal à 1.5 Å, i.e. les trois échantillons suivants: 1.8×10^5, 1.7×10^5 et 1.5×10^5. La valeur un peu faible 1.4 Å s'explique facilement par une légère flexibilité de la chaîne. Les valeurs 1.7 et 2 Å pour des chaînes courtes pourraient être expliquées par l'approximation de l'équivalence hydrodynamique d'un ellipsoïde de révolution pour la chaîne héli-

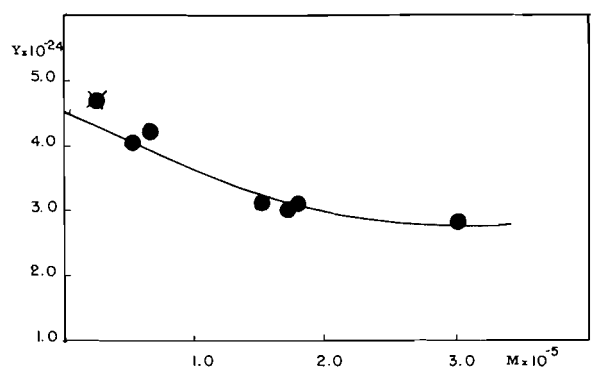

FIG. 3. Détermination de la longueur de persistance selon l'équation de Yamakawa et Fujii (6) (système cgs).

Can. J. Chem. Downloaded from www.nrcresearchpress.com by 210.87.254.6 on 09/05/12
For personal use only.

Can. J. Chem. Downloaded from www.nrcresearchpress.com by 210.87.254.6 on 09/05/12
For personal use only.

coïdale. Elle donne des valeurs élevées à cause probablement des effets des bouts effilés de l'ellipsoïde. D'après nos résultats expérimentaux, au moins pour le $[Glu(OBzl)]_n$ le modèle d'équivalence hydrodynamique ellipsoïdale est valable pour des chaînes ayant une longueur supérieure à 650 Å; par contre lorsque la chaîne devient très longue le facteur de flexibilité intervient.

Enfin nous essayons d'étudier la flexibilité de la chaîne avec l'éq. [3] de Hearst *et al.* La fig. 4 dont la pente du graphique $M/[\eta]$ en fonction de $M^{1/2}$ est négative, nous indique que le $[Glu(OBzl)]_n$ est "trop" rigide, il n'a pas la conformation vermiforme statistique, i.e. un long batonnet cylindrique très peu rigide. Notons que la pente reste encore négative pour un solvant mixte de Cl_2Et et de Cl_2AcOH à 60% d'acide, sûrement nous constatons que la rigidité diminue. C'est une façon d'illustrer qualitativement la variation de la rigidité de la chaîne.

Dimensions de la chaîne dans Cl_2AcOH:conformation pelote statistique

La viscosité intrinsèque d'une chaîne de conformation pelote statistique est reliée à la masse et au rayon quadratique moyen $\langle\overline{R^2}\rangle^{1/2}$ par la relation simple et bien connue

$$[9] \qquad [\eta] = \phi_0 \frac{\langle\overline{R^2}\rangle^{3/2}}{M}$$

ou ϕ_0 est la constante de Flory, elle est égale à 1.9×10^{21} pour le $[Glu(OBzl)]_n$ à 100% désordonnée (19).

Les valeurs de $\langle\overline{R^2}\rangle^{1/2}$ calculées à partir de l'expression [9] sont groupées dans le tableau 3. Les valeurs de $\langle\overline{R_0^2}\rangle^{1/2}$ données dans le même tableau, sont calculées à partir du graphique $[\eta]/M^{0.5}$ en fonction de $M^{0.5}$ selon la méthode de Stockmayer–Fixman. Elles sont du même ordre de grandeur que celles calculées à partir des données de Brant et

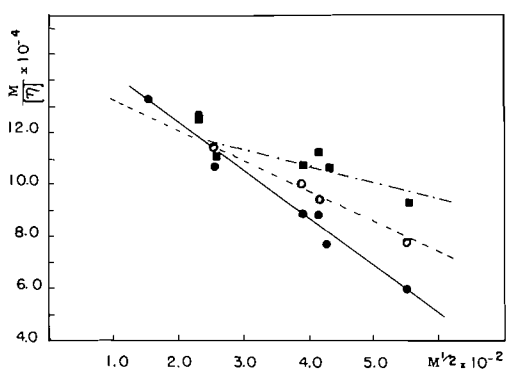

FIG. 4. Flexibilité de la chaîne en fonction de la composition des solvants (système cgs): (●) 100% Cl_2Et; (○) 60% Cl_2Et + 40% Cl_2AcOH; (■) 40% Cl_2Et + 60% Cl_2AcOH.

TABLEAU 3. Valeurs numériques de $\langle\overline{R_0^2}\rangle^{1/2}$ et $\langle\overline{R^2}\rangle^{1/2}$ du système $[Glu(OBzl)]_n$–Cl_2AcOH

		$\langle\overline{R_0^2}\rangle^{1/2}$(Å)		
M	$\langle\overline{R^2}\rangle^{1/2}$(Å)	Réference 20	Ce travail	α
300 000	625	417	418	1.50
180 000	444	323	324	1.38
170 000	433	314	315	1.38
150 000	408	295	296	1.38
65 000	243	194	195	1.25
52 000	214	174	174	1.23
24 000	140	118	118	1.19

Flory (20). Notons que Norisuye (19) a trouvé la même valeur pour le rapport $\overline{R_0^2}/nl_p^2$ où l_p est la difference entre deux α-C successifs.

Le volume exclu est calculé à partir de l'équation suivante:

$$[10] \qquad u = 2(\alpha^5 - \alpha^3)\frac{4\pi}{3}(\overline{R_G^2})_0^{3/2}F(x)$$

ou

$$\langle R_G^2\rangle = \frac{1}{6}\langle\overline{R^2}\rangle$$

et

$$F(x) = 1 - \frac{x}{2^{3/2}2!} + \frac{x^2}{3^{3/2}3!} - \cdots$$

$$x = 2(\alpha^2 - 1)$$

Nous avons calculé les volumes V_{SF} et V_{BL} théoriquement d'une façon très approximative selon la méthode de Kopp, d'une chaîne solvatée selon le mécanisme proposé par Sayama *et al.* (21) et selon celui de Bixon et Lifson (22). Nous avons discuté ces mécanismes dans une publication antérieure (23).

La fig. 5 représente seulement l'allure de variation de u et des V_{YF}, V_{BL} en fonction du poids molécu-

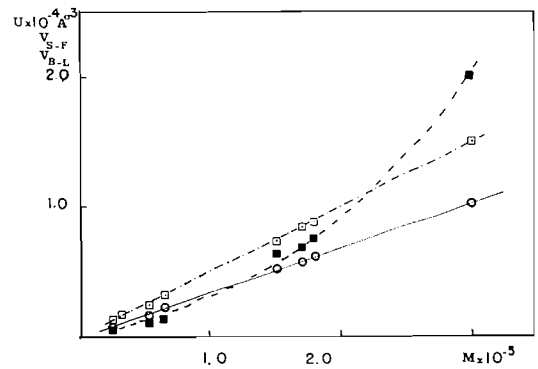

FIG. 5. Relation entre le volume exclu ou le volume occupé par une chaîne solvatée et le poids moléculaire: (■) volume exclu (u) calculé à partir des données viscosimétrique; (○) V_{SF} volume occupé par une chaîne solvatée selon le mécanisme de Sayama *et al.* (21); (□) V_{BF} volume occupé par une chaîne solvatée selon le mécanisme de Bixon et Lifson (22).

Can. J. Chem. Downloaded from www.nrcresearchpress.com by 210.87.254.6 on 09/05/12
For personal use only.

laire. Il faut noter que les valeurs absolues de V_{SF} et de V_{BL} n'ont aucun sens, ce qui nous intéresse c'est l'allure de la variation. En comparant la variation de u avec celle de V_{YF} et de V_{BL} nous devrions conclure, à titre d'indication, qu'à part de la formation des liaisons hydrogène entre le polypeptide et le solvant, l'interaction polymère–solvant, d'ordre différent du cas précédent, est loin d'être négligeable.

Conclusions

Théoriquement on peut déterminer la conformation, les dimensions des polypeptides en solution à partir des propriétés hydrodynamiques. En effet, nous avons un certain nombre limité mais suffisante de théories pour interpréter les résultats expérimentaux, mais nous constatons que, si l'étude de la transition conformationnelle est jugée satisfaisante, la détermination des dimensions caractéristiques permettant de définir d'une façon précise la conformation de la chaîne en hélice est fortement influencée par plusieurs facteurs. Un des problèmes majeurs qui se pose est le degré de flexibilité de la chaîne. Cependant nous pensons, d'après nos résultats, qu'on peut contourner ce problème, dans une certaine mesure, en déterminant le nombre de monomères par segment rigide selon l'équation de Yamakawa–Fujii réarrangée par Vitovskaya et Tsvetkov, à partir des différentes valeurs de h trouvées pour différents échantillons, puis ensuite les dimensions à partir des échantillons dont la longueur des chaînes est en bon accord avec celle du "segment rigide" ainsi déterminée. En effet pour un polypeptide donné on pourrait classer les valeurs de h calculées à partir de l'équation de Simha en trois catégories selon le schéma suivant:

$$M_x \text{ (chaîne courte)} \ll M_{NS} \qquad h_x > h_{réel}$$

$$M_x \leq M_{NS} \qquad h_x \approx h_{réel}$$

$$M_x \gg M_{NS} \qquad h_x < h_{réel}$$

En utilisant une valeur de h trouvée à partir d'un échantillon de poids moléculaire M_h pour déterminer N_S ou M_{NS} trois cas pourraient se présenter: (*i*) $M_{NS} \gg M_h$; (*ii*) $M_{NS} \approx M_h$; (*iii*) $M_{NS} \ll M_h$. La valeur la plus proche de la valeur réelle de h devrait être celle qui satisfait le cas (*ii*). Nous remarquons également que l'effet des bouts effilés de l'équivalence hydrodynamique ellipsoïdale ne semble négligeable que pour des chaînes moyennement longues. Le modèle n'est valable, pour le cas de poly(γ-L-glutamate de benzyle), que pour des chaînes ayant plus de 200 motifs de base. Nous pensons qu'on pourrait vérifier l'existence de cet effet en comparant les résultats viscosimétriques avec ceux de la sédimentation. En effet les théories traitant la viscosité et la sédimentation des polymères sont basées sur le même modèle physique, mais il y a une différence fondamentale entre ces deux phénomènes. Pour la viscosité, la molécule de soluté se déplace en même temps que le solvant et la force de frottement est due au mouvement de rotation de la molécule tandis que dans la sédimentation, la molécule de soluté se déplace toute seule et la force de frottement est due surtout au mouvement de translation de la molécule, les bouts effilés ont un effet plus accentué dans ce dernier cas. Nous effectuons actuellement des mesures de sédimentation sur ces mêmes échantillons dans les mêmes conditions.

Remerciement

Nous remercions le Ministère de l'Education du Québec pour l'aide financière accordée.

1. J. E. Hearst and W. H. Stockmayer. J. Chem. Phys. **37**, 1425 (1962).
2. J. E. Hearst. J. Chem. Phys. **40**, 1506 (1964).
3. R. Ullman. J. Chem. Phys. **53**, 1734 (1970).
4. P. Sharp and U. A. Blomfield. J. Chem. Phys. **48**, 2149 (1968).
5. H. Yamakawa and M. Fujii. Macromolecules, **6**, 407 (1973).
6. H. Yamakawa and M. Fujii. Macromolecules, **7**, 128 (1974).
7. P. J. Flory. Principles of polymer chemistry. Cornell University Press, Ithaca, NY. 1953.
8. C. Tanford. Physical chemistry of macromolecules. John Wiley and Sons, New York, London. 1961.
9. J. T. Yang. Adv. Protein Chem. **16**, 331 (1961).
10. H. Benoit, L. Freud, and G. Spach. Poly and amino acids. Marcel Dekker Inc., New York, NY. 1967. Chapt. 3.
11. R. Simha. J. Phys. Chem. **44**, 25 (1940).
12. H. A. Scheraga and L. Mandelkern. J. Am. Chem. Soc. **75**, 179 (1953).
13. J. E. Hearst and Y. Tagami. J. Chem. Phys. **42**, 4149 (1965).
14. J. E. Hearst, E. Beals, and R. A. Harris. J. Chem. Phys. **48**, 5371 (1968).
15. I. Noda. Biopolymers, **13**, 591 (1974).
16. M. G. Vitovskaya and V. N. Tsvetkov. Eur. Polymer J. **12**, 251 (1976).
17. P. Doty, J. H. Bradbury, and A. M. Holtzer. J. Am. Chem. Soc. **78**, 947 (1956).
18. H. Fujita, A. Teramoto, T. Yamashita, K. Okita, and S. Ikeda. Biopolymers, **4**, 781 (1966).
19. T. Norisuye. Ph.D. Thesis. Osaka University, Osaka, Japan. 1973.
20. D. A. Brant and P. J. Flory. J. Am. Chem. Soc. **87**, 2788 (1966).
21. N. Sayama, K. Kida, T. Norisuye, A. Teramato, and H. Fujita. Polymer J. **3**, 538 (1972).
22. M. Bixon and S. Lifson. Biopolymers, **4**, 815 (1966).
23. H. Daoust, M. Choquette, and N. Ho-Duc. Biopolymers, **15**, 2059 (1976).

The near-ultraviolet absorption spectrum of diimide: a re-examination[1]

R. A. BACK AND C. WILLIS

Division of Chemistry, National Research Council of Canada, Ottawa, Ont., Canada K1A 0R6

AND

D. A. RAMSAY

Herzberg Institute of Astrophysics, National Research Council of Canada, Ottawa, Ont., Canada K1A 0R6

Received December 21, 1977

R. A. BACK, C. WILLIS, and D. A. RAMSAY. Can. J. Chem. **56**, 1575 (1978).

The absorption spectra of N_2H_2 and N_2D_2 in the region 3000–4300 Å have been re-examined with somewhat higher resolution than was used in earlier work. The vibrational assignments of the principal progressions are unchanged except for the revision of the vibrational numbering suggested by the calculations of Perić, Buenker, and Peyerimhoff in 1977. The transition is electronically forbidden ($^1B_g - {}^1A_g$) but is made vibronically allowed by excitation of one quantum of the antisymmetric stretching vibration $\nu_5'(b_u)$. Weaker progressions are induced by the torsional vibration $\nu_4'(a_u)$ and the antisymmetric H—N—N bending vibration $\nu_6'(b_u)$. Agreement between experiment and theory is generally satisfactory though some significant discrepancies in Franck–Condon factors have been noted.

R. A. BACK, C. WILLIS et D. A. RAMSAY. Can. J. Chem. **56**, 1575 (1978).

On a redéterminé les spectres d'absorption du N_2H_2 et du N_2D_2 dans la région de 3000–4300 Å avec une résolution meilleure que celle utilisée dans un travail antérieur. Les attributions vibrationnelles des principales progressions sont inchangées excepté pour la revision de la numérotation vibrationnelle suggérée par les calculs de Perić, Buenker et Peyerimhoff en 1977. La transition est électroniquement défendue ($^1B_g - {}^1A_g$) mais est rendue vibroniquement permise par excitation d'un quantum de la vibration de valence antisymétrique $\nu_5'(b_u)$. Des progressions plus faibles sont induites par la vibration de pivotement $\nu_4'(a_u)$ et la vibration de déformation angulaire H—N—N antisymétrique $\nu_6'(b_u)$. L'accord entre l'expérience et la théorie est généralement satisfaisante quoique quelques disparités importantes ont pu être notées dans les facteurs Franck–Condon.

[Traduit par le journal]

Introduction

The near-ultraviolet spectra of N_2H_2 and N_2D_2 in the region 3000–4300 Å have been studied recently by the present authors (1). Vibrational analyses of the weak diffuse bands indicated that there are three long progressions in ν_2', the symmetric H—N—N bending frequency, corresponding to the excitation of 0, 1, and 2 quanta of ν_3', the N—N stretching frequency. The system was assigned to the symmetry-forbidden $^1B_g - {}^1A_g(\pi^* \leftarrow n_+)$ transition, probably made allowed by vibronic interaction. The long progressions in ν_2' indicated a large change in the H—N—N angle between the ground and excited states, estimated by simple Franck–Condon calculations to be 25 ± 2°. Since the inducing mode was not known, the vibrational numberings could not be determined unambiguously and there was some uncertainty in this estimate.

In 1975, Vasudevan *et al.* (2) reported *ab initio* calculations for the ground and first excited state of *trans*-diimide which predicted a difference of only 15° in the H—N—N angle. They suggested a reinterpretation of the near-ultraviolet absorption spectrum, assigning the long progressions to excitation of the antisymmetric bending frequency, $\nu_6'(b_u)$, which is clearly contrary to the Herzberg–Teller selection rules. More recently, Perić, Buenker, and Peyerimhoff (3) have published detailed calculations of Franck–Condon factors and of the relative activities of the three possible inducing modes, ν_4', ν_5', and ν_6'. Their results indicate that the antisymmetric N—H stretching frequency $\nu_5'(b_u)$ is the most active in making the transition vibronically allowed and that the original identification of the progressions is correct but the values for v_2' were incorrect and should be reduced by 3. A few bands at the long wavelength end of the spectrum were reassigned to similar though weaker progressions made allowed by the excitation of one quantum of the torsional frequency, $\nu_4'(a_u)$.

In view of these interesting results, we have undertaken a re-examination of the spectra of N_2H_2 and N_2D_2 using somewhat higher resolution than in the earlier work, especially at the longer wavelengths.

Experimental

Most of the experimental conditions were the same as described previously (1). However, spectra were obtained using

[1]NRCC No. 16582.

Can. J. Chem. Downloaded from www.nrcresearchpress.com by 210.87.254.40 on 09/05/12
For personal use only.

Can. J. Chem. Downloaded from www.nrcresearchpress.com by 210.87.254.40 on 09/05/12
For personal use only.

TABLE 1. Wavenumbers of bands and vibrational assignments for the 3000–4300 Å band system of N_2H_2[a]

	Inducing mode												
	$\nu_5'(b_u)$ N—H stretching					$\nu_4'(a_u)$ torsion					$\nu_6'(b_u)$ H—N=N bending		
v_2'/v_3'	0		1		2	0		1		2	0		1
0	23 896	(1579)	25 475	(1510)	26 985								
	(1 184)		(1 172)		(1 172)								
1	25 080	(1567)	26 647	(1510)	28 157								24 601
	(1 185)		(1 159)		(1 179)								(1 178)
2	26 265	(1541)	27 806	(1530)	29 336	23 251	(1535)	24 786	(1550)	26 336[b]	24 235	(1544)	25 779
	(1 185)		(1 185)		(1 169)	(1 185)		(1 186)		(1 175)	(1 161)		(1 120)
3	27 450	(1541)	28 991	(1514)	30 505	24 436	(1536)	25 972	(1539)	27 511[b]	25 396	(1503)	26 899[b]
	(1 190)		(1 152)		(1 120)	(1 181)		(1 165)			(1 161)		
4	28 640	(1503)	30 143	(1482)	31 625	25 617	(1520)	27 137			26 557[b]		
	(1 155)		(1 138)		(1 097)	(1 172)					(1 152)		
5	29 795	(1486)	31 281	(1441)	32 722	26 789					27 709		
	(1 128)		(1 098)										
6	30 923	(1456)	32 379										
	(1 104)												
7	32 027												

[a]All wavenumbers in cm^{-1} *in vacuo*. Wavenumber differences are given in parentheses.
[b]Frequencies less certain owing to overlap with neighbouring band(s).

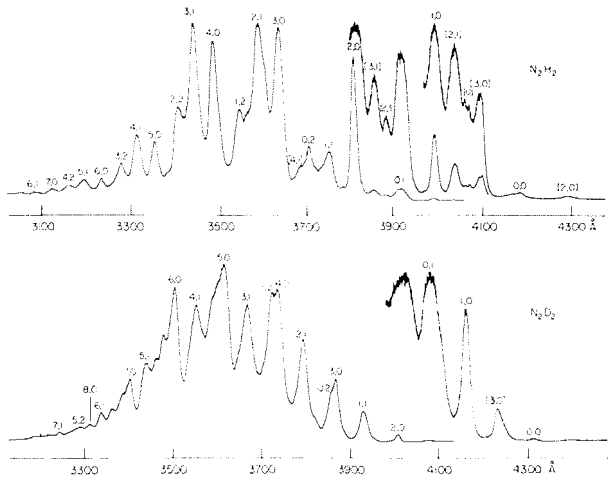

FIG. 1. Microphotometer curves of the absorption spectra of N_2H_2 and N_2D_2. Assignments refer to the values of $v_2'v_3'$. Assignments without brackets refer to ν_5'-induced progressions; [ ] denotes ν_4'-induced progressions and { } indicates ν_6'-induced bands.

a 7.3 m vacuum Ebert spectrograph in the first order with a reciprocal dispersion of 4.5 Å/mm. This spectrograph has from 4 to 10 times the dispersion of the medium Hilger spectrograph used in the earlier work and is adequate in view of the diffuse nature of most of the bands. Some of the bands at longer wavelengths ($\lambda > 3800$ Å)[2] show coarse rotational structure; for example, the band of N_2H_2 near 4184 Å shows at least six head-like features which are presumably caused by *K*-structure. Microphotometer curves of the complete spectra of N_2H_2 and N_2D_2 are shown in Fig. 1. New measurements of the frequencies of the bands of both isotopic species were made and usually agreed with the earlier measurements to within 10 or 20 cm^{-1} except for weak bands which are heavily overlapped. Several new bands were found for N_2H_2 and the frequencies and assignments for all the bands are given in Table 1. For N_2D_2, fewer new bands were found and these are discussed in the text.

Discussion

The three vibrational modes which can make the $^1B_g - {}^1A_g$ transition vibronically allowed are $\nu_4(a_u)$, $\nu_5(b_u)$, and $\nu_6(b_u)$. The torsional vibration ν_4 gives rise to bands with vibronic species $^1B_u - {}^1A_g$ for which the transition moment lies in the molecular plane.[3] The bands therefore consist of sub-bands with $\Delta K_a = 0$ (*a*-type) and $\Delta K_a = \pm 1$ (*b*-type), the relative intensities depending on the direction of the transition moment with respect to the inertial axes. Bands which are induced by ν_5 or ν_6 have vibronic species $^1A_u - {}^1A_g$ and give rise to *c*-type structures with only $\Delta K_a = \pm 1$. The rotational constants for the ground state of N_2H_2 are well known from the infrared studies of Carlotti, Johns, and Trombetti (5) ($A'' = 10.000$, $B'' = 1.304$, and $C'' = 1.150$ cm^{-1}) and constants for the excited state can be estimated from the calculated structures of Perić *et al.* (3) ($A' = 13.0$, $B' = 1.12$, $C' = 1.07$ cm^{-1}). The *K*-structures of the bands are therefore expected to be violet-degraded and the *J*-structures red-degraded. For *a*-type bands the origin is expected to

[2]The diffuseness of the spectrum has been attributed to rapid intersystem crossing to the ground state at large torsional displacements (4). The rather abrupt loss of rotational structure below 3800 Å suggests the onset of a more efficient intersystem crossing at this energy, about 75 kcal/mol.

[3]Throughout this discussion we treat the excited state as though it were planar. The calculations of Perić *et al.* (3) indicate a twisted structure but the essential arguments are unchanged.

Can. J. Chem. Downloaded from www.nrcresearchpress.com by 210.87.254.40 on 09/05/12
For personal use only.

lie close to the low frequency edge; for *b*-type and *c*-type bands the *K*-structure forms a 'head of heads' estimated to lie about 30 cm^{-1} below the band origin. The measurements in Table 1 reflect these considerations. As noted above, a few bands at the long wavelength end of the spectrum show evidence of *K*-structure although it is not sufficiently well developed to permit an unambiguous assignment of the *K*-numbering.

The calculations of Perić *et al.* (3) indicate that the relative activities of the three inducing modes for N_2H_2 are $\nu_4:\nu_5:\nu_6::\frac{1}{3}:1:\frac{1}{40}$. The strongest progressions should therefore be ν_5'-induced. The revision of the vibrational numberings of the principal progressions for N_2H_2 and N_2D_2 appears reasonable in view of the Franck–Condon calculations and also the irregularities of the vibrational intervals for low v_2' (<3) in the original assignments. For N_2H_2, the strongest bands are the (3,1), (2,1), (3,0), (4,0), and (2,0) bands with respect to (v_2', v_3') (Fig. 1). The unassigned bands are readily accommodated into ν_4'-induced progressions and weaker ν_6'-induced progressions with similar values of (v_2', v_3'). The validity of the assignments is supported by the consistency of the values which are obtained for the vibrational differences ($\nu_5' - \nu_4'$) and ($\nu_5' - \nu_6'$) (Table 2). Apart from a weak feature[4] at 26 444 cm^{-1} all the N_2H_2 bands are now assigned, including some weak bands unassigned in the earlier work and some weak additional bands found in the present work.

For N_2D_2 the strongest bands in the ν_5'-induced progressions are the (5,0), (6,0), (4,0), (3,1), and (4,1) bands (Fig. 1). The band at 23 601 cm^{-1}, originally assigned as the (2,1) band, is reasonably reassigned as the (3,0) band of the ν_4'-induced progression, giving ($\nu_5' - \nu_4'$) = 2278 cm^{-1} (Table 2). Unfortunately, all the higher members of this progression and of the progression with $v_3' = 1$ are overlapped by stronger ν_5'-induced bands so that it is not possible to obtain a satisfactory confirmation of this vibrational interval. Five new weak bands were found at 24 413 (overlapped), 25 292, 26 199, 25 762, and 26 626 cm^{-1}.[5] It is tempting to assign these bands as the (3,0), (4,0), (5,0), (3,1), and (4,1) bands induced by ν_6'. However, the first three bands give values for ($\nu_5' - \nu_6'$) ranging from 1437–1444 cm^{-1} and the latter two give values of 1500 and 1538 cm^{-1}. These discrepancies are larger than the experimental errors and it is possible that the latter two bands are the (5,0) and (6,0) bands induced by $3\nu_4'$. One of the problems in the earlier work was an apparent doubling of the higher members of the third principal progression with $v_3' = 2$, which was tentatively ascribed to Fermi resonance. The bands appear with the same relative intensities in the present work (see Fig. 1) and hence are presumably not caused by an impurity, e.g., N_2HD. The frequencies of the bands are too high for ν_4'- or ν_6'-induced bands and the Fermi resonance interpretation involving levels (1, v_2', 0) and (0, $v_2' + 1$, 1) still seems the most reasonable.

TABLE 2. Excited state frequency differences for N_2H_2 and N_2D_2 (in cm^{-1})

		N_2H_2		N_2D_2	
v_2'	v_3'	($\nu_5' - \nu_4'$)	($\nu_5' - \nu_6'$)	($\nu_5' - \nu_4'$)	($\nu_5' - \nu_6'$)
2	0	3014	2030		
3	0	3014	2054	2278	
4	0	3023	(2083)		
5	0	3006	2086		
1	1		2046		
2	1	3020	2027		
3	1	3019	(2092)		
4	1	3006			
2	2	(3000)[b]			
3	2	(2994)			
Mean		3015	2049	2278	1440[c]
Calcd.[a]		3080	2235	2203	1580

[a]Perić *et al.* (3).
[b]Numbers in parentheses are less certain.
[c]See Discussion.

The calculations of Perić *et al.* account for the relative activities of the inducing modes in a very satisfactory manner. However, the calculations of Franck–Condon factors are less satisfactory. The strongest bands in the observed progressions occur at slightly higher values of v_2' than in the calculated. The observed intensity distributions are noticeably different in some of the progressions indicating a breakdown of the zero-order Born–Oppenheimer approximation; for example, the (3,0) and (4,0) bands of N_2H_2 are comparable in intensity, whereas the (3,1) band is much stronger than the (4,1) band (Fig. 1). A more dramatic difference between the observed and calculated intensities occurs for the lowest values of v_2', where the band intensities decrease much more rapidly with increasing wavelength than predicted. For example, the calculated value for the ratio of the intensities of the (0,0) and (2,0) bands of N_2H_2 is 0.64 but the experimental value is certainly less than 0.1; similar differences exist for N_2D_2. The reason for these differences is not clear but may be associated with the low barrier for the torsional vibration

[4]This feature may be the (3,1) or possibly the (4,0) band induced by $3\nu_4'$; the calculations of Perić *et al.* (3) predict that these bands should have $\frac{1}{23}$ of the intensities of the corresponding ν_5'-induced bands.

[5]Weak unassigned shoulders have also been seen near 27 435 and 28 622 cm^{-1}.

in the excited state and the sensitivity of this barrier to the excitation of other vibrations. Finally, the agreement between the observed and calculated frequency differences ($\nu_5' - \nu_4'$) and ($\nu_5' - \nu_6'$) for the excited state lies within 10% (Table 2); however, the calculated anharmonicities for the N—N stretching frequency ν_3' (81 cm^{-1} for N_2H_2, 75 cm^{-1} for N_2D_2) are much larger than the experimental and seem unreasonably high. The overall agreement between theory and experiment is most encouraging though some differences need to be resolved.

Acknowledgements

We wish to thank W. Goetz and M. Barnett for assistance with the experimental work.

1. R. A. Back, C. Willis, and D. A. Ramsay. Can. J. Chem. **52**, 1006 (1974).
2. K. Vasudevan, S. D. Peyerimhoff, R. J. Buenker, W. E. Kammer, and H.-L. Hsu. Chem. Phys. **7**, 187 (1975).
3. M. Perić, R. J. Buenker, and S. D. Peyerimhoff. Can. J. Chem. **55**, 1533 (1977).
4. C. Willis, R. A. Back, and J. M. Parsons. J. Photochem. **6**, 253 (1976/77).
5. M. Carlotti, J. W. C. Johns, and A. Trombetti. Can. J. Phys. **52**, 340 (1974).

Can. J. Chem. Downloaded from www.nrcresearchpress.com by 210.87.254.40 on 09/05/12
For personal use only.

Quelques aspects du spectre d'absorption infrarouge de complexes par liaison hydrogène

WILLIE A. BUENO[1] ET NEUSA M. MAZZARO[2]

Depto Química da F.F.C.L.R.P.-U.S.P. 14100, Ribeirão Prêto, SP, Brésil

Reçu le 21 septembre 1977

WILLIE A. BUENO et NEUSA M. MAZZARO. Can. J. Chem. **56**, 1579 (1978).

Les spectres infrarouges, dans la région de 4000 à 1600 cm^{-1}, de 24 complexes par liaison hydrogène des oxydes d'amines aliphatiques avec certains dérivés du phénol sont discutés.

WILLIE A. BUENO and NEUSA M. MAZZARO. Can. J. Chem. **56**, 1579 (1978).

A discussion is given of the infrared spectra in the region 4000 to 1600 cm^{-1} of 24 hydrogen-bonded complexes between aliphatic amine oxides and a number of phenol derivatives.

[Traduit par le journal]

Introduction

Le caractère semipolaire de la liaison N—O dans les oxydes d'amines aliphatiques en fait d'excellents accepteurs de proton pour la formation de liaisons hydrogène (1, 2). Toutefois, la liaison hydrogène entre des dérivés du phénol et des oxydes d'amines aliphatiques est peu connue, que ce soit du point de vue de sa nature, de la structure des bandes d'absorption infrarouge ou de l'influence des substituants à l'état liquide pur. Ce travail étudie la formation de tels complexes et discute les caractéristiques des bandes d'absorption du spectre infrarouge, dans la région de 4000 à 1600 cm^{-1}.

Conditions expérimentales

Les oxydes d'amine ont été préparés à partir de l'amine et d'eau oxygénée. On obtient un liquide visqueux qui cristallise en aiguilles aprés quelques jours sous vide en présence de P_2O_5 (3).[3] Les phénols commerciaux ont été purifiés suivant les méthodes usuelles de recristallisation ou de sublimation et déséchage. Les complexes sont obtenus par mélange du donneur et de l'accepteur de proton dans la proportion 1:1, malaxage en atmosphère sèche et chauffage jusqu'à la température de fusion. Ils sont ensuite sèchés sous vide. Aucun des complexes obtenus n'a cristallisé. Les spectres infrarouges ont été obtenus avec un spectromètre Perkin-Elmer, modèle 457, en film entre des faces de NaCl, à la température moyenne de 30°C. Les intensités des bandes ont été mesurées relativement à celle de la bande qui apparait aux environs de 1585 cm^{-1} vu qu'elle est pratiquement constante dans tous les cas étudiés.

Résultats et discussion

L'observation des spectres infrarouges montre que la vibration de valence de la liaison N—O (ν(NO)) se situe autour de 945 cm^{-1} pour l'oxyde de triméthylamine (TMAO) et pour l'oxyde de triéthylamine (TENO) et autour de 965 cm^{-1} pour l'oxyde de tripropylamine (TPNO). La vibration δ(ONC) n'a pas été analisée vu qu'elle ne se presente pas comme une bande d'absorption "pure" (4). La formation des complexes ne déplace pas la ν(NO), mais diminue son intensité. Cette diminution peut être expliquée, qualitativement, par le modèle de Orville-Thomas (5), étant donné que la formation de la liaison hydrogène B—O···H—OR induit une polarization de la paire d'electrons de la base provocant ainsi une augmentation de l'intensité de la ν(OH···). Les spectres montrent aussi qu'il y a déplacement de la fréquence d'absorption ν(OH) vers des valeurs plus basses. Cette absorption se présente sous la forme de bandes larges et relativement intenses. Ces faits sont causés par la liaison hydrogène qui se forme entre l'hydrogène du groupe O—H phénolique et l'oxygène d'amines.

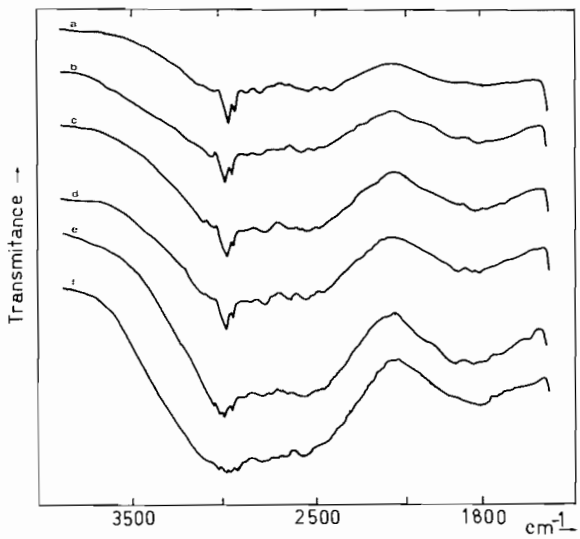

FIG. 1. Spectre infrarouges de complexes entre le TENO et (*a*) *p*-nitrophénol, (*b*) *m*-nitrophénol, (*c*) *m*-chlorophénol, (*d*) *p*-chlorophénol, (*e*) *p*-phenilphénol et (*f*) phénol.

[1]Prof. Ass. Dr. de la Faculdade de Filosofia Ciências e Letras de Ribeirão Prêto, Depto Química, Univ. S. Paulo.

[2]Boursiére de la Fundação de Amparo à Pesquisa do Estado de São Paulo, SP, Brésil.

[3]Le nombre de molécules d'eau associées aux oxydes d'amines a été déterminé par un titrage Karl Fisher (14).

Can. J. Chem. Downloaded from www.nrcresearchpress.com by 210.87.254.105 on 09/05/12
For personal use only.

Can. J. Chem. Downloaded from www.nrcresearchpress.com by 210.87.254.105 on 09/05/12
For personal use only.

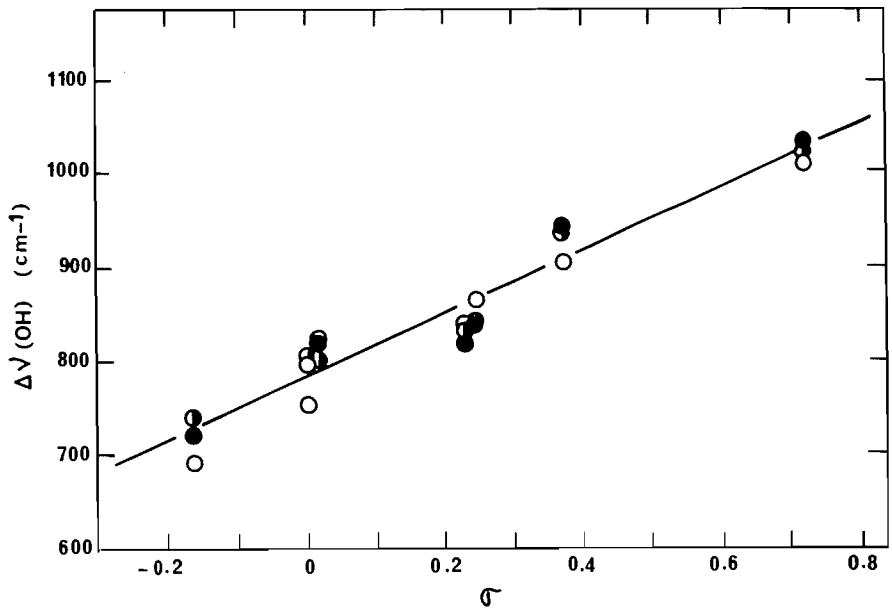

FIG. 2. Déplacement de la fréquence de valence de la liaison O—H vs. le sigma de Hammett. ○ = TMAO, ● = TENO et ◑ = TPNO.

L'analyse des spectres, dans la région de 4000 à 1600 cm^{-1}, montre qu'il existe une large bande dont l'intensité croit du *p*-nitrophénol au *p*-méthylphénol et qui présente plusieurs épaulements (Fig. 1) dont on a essayé d'expliquer la nature de diversès manières (6). On a tenté de trouver des modes de combinaisons ou harmoniques faisant intervenir les frequences fondamentales se situant entre 1650 à 1150 cm^{-1}. Il apparait que la large bande vers 3000 cm^{-1} contient plusieurs bandes dues à des résonances de Fermi qui s'ajoutent à l'absorption ν(OH) qui, à cause de la liaison hydrogène, se déplace vers des fréquences plus basses. Aprés élimination des absorptions dues aux bandes de combinaison (de la même manière que Hall et Wood (10)) et aux vibrations ν(CH) il est possible de préciser la fréquence de la vibration ν(OH) des complexes, en utilisant le méthode de Nelson et coll. (1), et donc Δν(OH) (tableau 1). Cette valeur est aussi fondée sur l'obtention d'une relation entre Δν(OH) et σ (discutée dans la littérature (7, 8), pour les dimères d'acides organiques), avec un coefficient de corrélation satisfaisant[4] ($r = 0.961$, sauf pour le *p*-nitrophénol). La relation obtenue entre la constante du substituant donné par Hammett (11) (σ) et les Δν(OH), fig. 2, est donnée par

$$\Delta\nu(OH)\ (\text{en cm}^{-1}) = 334\sigma + 785$$

[4]Les valeurs statistiques de la correlation entre Δν(OH) et les constants du substituant ont été calculées à partir de Jaffè (9) ($r = 0.961$; $s = 27.02$; $s_\rho = 21.95$; $n = 21$).

La valeur positive de la pente de la droite obtenue (désignée par Hammett comme ρ) indique que la constante d'equilibre de formation du complexe augmente avec l'affinité du substituant des noyaux phénoliques pour les electrons. Toutefois, cela n'explique pas les intensités des bandes d'absorption dans la région vers 3000 cm^{-1}.

Dans les spectres du type *i*, décrits par Hadzi (12), comme cela a déjà été indiqué, on distingue trois larges bandes d'absorption: la bande *A* (ν(OH) > 2800 cm^{-1}), la bande *B* (~2550 cm^{-1}) et la bande *C* (~1900 cm^{-1}). Le tableau 2 donne les fréquences des trois types de bandes observées. Les bandes dues aux ν(CH) et aux vibrations harmoniques du noyau aromatique se superposent aux bandes *A*.

TABLEAU 1. Déplacement de la fréquence des vibrations de valence O—H de divers phénols dans les complexes avec oxyde d'amines aliphatiques*

Substituant du phénol	σ (11)	ν(OH) (8)	Δν(OH)† TMAO	TENO	TPNO
m-NO_2	0.710	3604	1014	1034	1024
m-Cl	0.373	3607	907	947	947
p-Br	0.232	3609	859	839	839
p-Cl	0.227	3610	830	820	830
p-ϕ	0.009	3610	820	820	820
H	0	3612	752	802	802
p-CH_3	−0.170	3614	694	724	744

*L'erreur sur les fréquences déterminée est de l'ordre de ± 10 cm^{-1}.
†Le Δν(OH) est déterminé à partir de Δν(OH) = ν(OH) − ν(OH···) où ν(OH) et ν(OH···) sont les vibrations de valence de la liaison O—H libre et associée, respectivement.

TABLEAU 2. Fréquences approximatives (en cm^{-1}) des trois types de bandes dans la région 3000 à 1600 cm^{-1}

Substituant du phénol	TMAO			TENO			TPNO		
	A	*B*	*C*	*A*	*B*	*C*	*A*	*B*	*C*
p-NO_2	—	2500	1900	—	2560	1800	2730	2550	1770
m-NO_2	—	2550	1860	—	2570	1800	2780	2580	1810
m-Cl	2700	2550	1880	2780	2570	1820	2780	2560	1800
p-Br	2750	2570	1870	2775	2560	1815	2775	2570	1830
p-Cl	2780	2560	1870	2790	2560	1820	2780	2570	1820
p-ϕ	2790	2570	1875	2790	2570	1820	2790	2570	1815
H	2860	2580	1870	2810	2590	1825	2810	2560	1810
p-CH_3	2920	2500	1875	2780	2550	—	2810	2560	—

En accord avec les observations de Hadzi et coll. (12, 13) l'intensité des bandes *A* et *B* diminue quand la force de l'acide augmente (fig. 1). Quand le pK_a de l'acide décroit (c'est-à-dire, quand la forçe de l'acide augmente) l'intensité des bandes *A*, *B* et *C* diminue mais l'intensité de la bande *C* ne diminue pas dans la même proportion. Ceci est contraire aux observations de Hadzi (12) qui, en utilisant différents dérivés de l'acide acétique, a observé que *C* augmente avec la forçe de l'acide. On observe aussi que, dans les complexes les plus faibles, la bande *A* est du type ν(OH) alors que c'est la bande *B* qui possède ce caractère dans les complexes les plus forts. Cependant, la deutération déplace les bandes *A* et *B* vers des fréquences plus basses et toutes les bandes de cette region sont dues aux interactions entre ν(OH) avec des bandes de combinaisons (10). Dans les cas du *m*-chlorophénol et du *m*-nitrophénol, le maximum d'absorption, qui probablement n'est pas une bande de résonance de Fermi, apparaît déjà à des fréquences inférieures à celles de la bande *A*, ce qui semble indiquer que la force de ces complexes se situe entre celle des autres. Quand l'acide est le *p*-nitrophénol, la bande *A* a la plus faible intensité, et il y a une forte et large bande d'absorption au – dessous de 1600 cm^{-1} (13). Cette large bande au – dessous de 1600 cm^{-1} est peut-être due à l'apparition d'autres bandes d'absorption dues aux formes $AH^+\cdots B$ et $BH^+\cdots B$ (2). De cette manière, il pourrait être faux que les spectres des complexes entre le *p*-nitrophénol et les récepteurs de protons suivent la tendance observée dans les spectres des complexes avec les phénols moins acides (fig. 1) étant donné qu'il est difficile de situer le bande d'absorption de la vibration ν(OH) parce que ces composés absorbent fortement entre 2000 et 300 cm^{-1} (2).

Remerciements

Les auteurs remercient la F.A.P.E.S.P. (Brésil), le C.R.Q.-IV dont les subsides ont permis la réalisation de ce travail et le Depto de Física e Química da F.F.O.R.P.-U.S.P. pour l'enregistrement de quelques spectres infrarouges.

1. J. H. NELSON, L. C. NATHAN et R. O. RADSGALE. J. Am. Chem. Soc. **90**, 5754 (1968).
2. W. SAFFIOTI et W. A. BUENO. J. Chim. Phys. **78**, 731 (1976).
3. W. R. DUNSTAN et G. E. GOULDING. J. Chem. Soc. **75**, 1005 (1899).
4. Y. KURODA et M. KIMURA. Spectrochim. Acta, **22**, 47 (1966).
5. G. J. BOOBYER et W. J. ORVILLE-THOMAS. Spectrochim. Acta, **22**, 147 (1966).
6. A. NOVAK. J. Chim. Phys. **77**, 981 (1975).
7. C. LAURENCE et B. WOJTKOWIAK. Bull. Soc. Chim. Fr. 2780 (1968); 3124 (1971); 3833 (1971); 3870 (1971); 662 (1973).
8. M. D. JOESTEN et L. J. SHAAD. Hydrogen bonding. Marcel Dekker Publ., Amsterdam. 1976. p. 230.
9. H. H. JAFFÈ. Chem. Rev. **53**, 191 (1953).
10. Q. HALL et J. L. WOOD. Spectrochim. Acta, **23A**, 1257 (1967).
11. L. P. HAMMETT. J. Am. Chem. Soc. **59**, 96 (1937).
12. D. HADZI. Pure Appl. Chem. **11**, 435 (1965).
13. D. HADZI, C. KLOFUTAR et S. OBLAK. J. Chem. Soc. A, 905 (1968).
14. A. I. VOGEL. Quantitative inorganic analysis. 3º ed. Longmans Co., London. 1961. p. 944.

Can. J. Chem. Downloaded from www.nrcresearchpress.com by 210.87.254.105 on 09/05/12
For personal use only.

Les fonctions de Hartree–Fock–Slater comme base pour des calculs de perturbation à un électron pour molécules. III. Le calcul de la première hyperpolarisabilité

M. TRSIC ET W. G. LAIDLAW

Department of Chemistry, University of Calgary, Calgary, Alta., Canada T2N 1N4

Reçu le 19 octobre 1977

M. TRSIC et W. G. LAIDLAW. Can. J. Chem. **56**, 1582 (1978).

On a calculé les premières hyperpolarisabilités des molécules CO, CH_4, HCHO et CN^- par une méthode Hartree–Fock–Slater non couplé. Différentes fonctions de base ont été essayées.

M. TRSIC and W. G. LAIDLAW. Can. J. Chem. **56**, 1582 (1978).

Uncoupled Hartree–Fock–Slater first hyperpolarizabilities have been calculated for CO, CH_4, HCHO, and CN^-. Different basis sets have been tested for CH_4 and CO.

Can. J. Chem. Downloaded from www.nrcresearchpress.com by 210.87.254.105 on 09/05/12
For personal use only.

Introduction

Etant donné qu'une méthode Hartree–Fock–Slater (HFS) non couplée a produit des résultats satisfaisants pour des polarisabilités moléculaires (1), on a entrepris le calcul des premières hyperpolarisabilités β par la même technique. On rapporte ici les valeurs obtenues pour les cas de CO, CN^-, CH_4 et HCHO quand on maintien les orbitaux 1*s* de C, N et O "congelés". Dans les cas de CO et HCHO on peut comparer avec des autres méthodes et dans le cas de CH_4 on a des résultats de calcul et aussi un résultat expérimental approché pour comparaison.

La méthode de perturbation

Pour une molécule dans un champ électrique uniforme F, la théorie des perturbations donne l'expression suivante pour le tenseur β (2, 3):

$$[1]\quad -\tfrac{1}{6}\sum_{\nu,\mu,\omega}\beta_{\nu\mu\omega}F_\nu F_\mu F_\omega = \sum_{m,n\neq 0}\frac{\langle 0|H^{(1)}|m\rangle\langle m|H^{(1)}|n\rangle\langle n|H^{(1)}|0\rangle}{(W_0-W_m)(W_0-W_n)} - \sum_{m\neq 0}\frac{\langle 0|H^{(1)}|m\rangle\langle 0|H^{(1)}|0\rangle\langle m|H^{(1)}|0\rangle}{(W_0-W_m)^2}$$

avec

$$[2]\qquad H^{(1)} = -\sum_\nu\sum_i q_i r_\nu^{(i)}F_\nu$$

$H^{(1)}$ étant la perturbation produite par le champ. W_m est l'énergie de l'état non perturbé $|m\rangle$ et q_i est la charge de la particule *i*.

Si l'on exprime la formule 1 à l'aide des orbitaux moléculaires (OM), on obtient pour l'élément tensoriel $\beta_{\nu\mu\omega}$

$$[3]\quad \beta_{\nu\mu\omega} = S\left\{2\sum_{k,a,b}\frac{\langle k|er_\nu|a\rangle\langle a|er_\mu|b\rangle\langle b|er_\omega|k\rangle}{(\varepsilon_a-\varepsilon_k)(\varepsilon_b-\varepsilon_k)} + 2\sum_{k,l,a}\frac{\langle k|er_\nu|a\rangle\langle k|er_\mu|l\rangle\langle a|er_\omega|l\rangle}{(\varepsilon_a-\varepsilon_k)(\varepsilon_a-\varepsilon_l)} - 4\sum_{k,a}\frac{\langle k|er_\nu|a\rangle\langle k|er_\mu|k\rangle\langle a|er_\omega|k\rangle}{(\varepsilon_a-\varepsilon_k)^2}\right\}$$

Les integrals $\langle k|er_\nu|a\rangle$, $\langle a|er_\mu|b\rangle$, etc. sont mono-électroniques et construites sur les OM–HFS, k, l sont des orbitaux occupés dans l'état fondamental et a, b sont des orbitaux virtuels, e est le charge électronique et r_ν, r_μ et r_ω sont des coordonnés des électrons. La lettre S indique une somme sur toutes les permutations des coordonnés r_ν, r_μ et r_ω et ε_a et ε_k sont des énergies HFS mono-électroniques.

L'expression 3 est le résultat de l'interaction de l'état fondamental non perturbé avec des états mono-excités et les interactions entre les différents états mono-excités, la dernière somme étant originé par "l'auto-interaction" de l'état fondamental. Les éléments matricielles avec des états doublement et poli-excités sont tous zéro. Dans le cas des molécules avec un moment dipolaire on peut s'attendre que les termes diagonaux en [3] auront beaucoup d'importance dans la somme totale.

La partie nucléaire de l'éq. 1, originé par l'opérateur [2], est annulé quand on utilise l'approximation de Born et Oppenheimer et, par conséquence, n'apparaît pas dans l'éq. 3.

La qualité des fonctions d'onde de HFS

La qualité des fonctions de base employés pour constuire les OM–HFS est un des facteurs qui détermine la qualité des résultats obtenus par la méthode de perturbation. Pour illustrer cet effet, on rapporte les résultats obtenus pour CO et CH_4 quand on utilise les bases optimisées pour les atomes (4), une fonction pour chaque orbitale atomique (BS) et deux fonctions pour chaque orbitale atomique (BD) et aussi, les bases étendues et optimisées pour la molécule (BM) de CH_4 par Baerends et Ros (5) et pour la molécule de CO par McLean et Yoshimine (6). Les aspects plus spécifiques de la méthode utilisé pour obtenir les fonctions de HFS (7), c'est à dire, l'effet de l'intégration numérique et la façon de rapprocher la densité électronique (ressemblable aux techniques LEDO (8) et PDDO (9)) ne seront pas rapportés en détail. Il suffit de dire (on utilise CO comme example) que le nombre de points pour l'intégration numérique

TABLEAU 1. Premières hyperpolarisabilités[a]

	β_{zzz}			β_{zyy}		
	Résultats HFS	Littérature[k]		Résultats HFS	Littérature[k]	
CO $\xrightarrow{z}$	10.37(BS)	24.98[b]		3.32(BS)	2.14[b]	
	14.24(BD)	−10.13[b]	10.13[b]	3.70(BD)	−1.88[b]	1.88[b]
	13.84(BM)	−9.83[b]	9.83[b]	2.77(BM)	−1.52[b]	1.52[b]
		1.86[c]	12.13[f]		−1.71[d]	1.25[f]
		1.12[c]			−1.25[i]	
		0.84[c]				
		1.97[d]				
		−12.13[f]				

	β_{xyz}			
	Résultats HFS	Littérature[k]		Expérience
CH_4	−8.27(BS)	0.40[e]	−1.89[i]	±0.1[g]
	−10.34(BD)	0.19[e]		
	−5.33(BM)	0.98[h]		
		1.38[h]		
		1.62[h]		
		0[j]		
		1.89[i]		
		−0.21[d]		
		−2.1[f]		

	β_{zzz}			β_{zyy}		
	Résultat HFS	Littérature[k]		Résultat HFS	Littérature[k]	
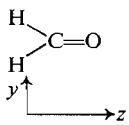	30.61(BD)	−16.76[i]	16.76[i]	19.33(BD)	−1.38[i]	1.38[i]

	β_{zxx}		
	Résultat HFS	Littérature[k]	
	1.40(BD)	−0.60[i]	0.60[i]

	β_{zzz} Résultat HFS	β_{zyy} Résultat HFS
$CN^- \xrightarrow{z}$	10.85(BD)	6.06(BD)

[a] β en 10^{-31} esu.
[b] Référence 10, différentes bases atomiques.
[c] Référence 13.
[d] Référence 12.
[e] Référence 15.
[f] Référence 3.
[g] P. D. Maker, valeur cité dans la réf. 2.
[h] Résultats BS, BD et base étendue de la réf. 14.
[i] Référence 11.
[j] Référence 17.
[k] La deuxième colonne répète la valeur de β avec le signe changé dans les cas où on a pu établir que les auteurs ont utilisé une convention opposée à la notre.

est tel que, si on le double, le changement dans la valeur de $\beta_{\mu\nu\omega}$ est moins de 3% et que la densité électronique est représenté d'une façon telle que, si on introduit d'autres fonctions de base pour la densité, la valeur de $\beta_{\mu\nu\omega}$ change, au plus 10%, généralement moins de 1%.

Résultats et discussion

Les résultats obtenus sont résumés dans le tableau 1, dans la première colonne dessous chaque élément tensoriel. Les résultats de la littérature se trouvent dans la deuxième colonne dessous chaque élément tensoriel. On trouve que la convention utilisé pour

Can. J. Chem. Downloaded from www.nrcresearchpress.com by 210.87.254.105 on 09/05/12
For personal use only.

Can. J. Chem. Downloaded from www.nrcresearchpress.com by 210.87.254.105 on 09/05/12
For personal use only.

choisir le signe de β n'est pas uniforme dans la littérature et on a choisi celle décrite par Buckingham et Orr (2) pour les résultats de ce calcul. Dans les cas où on a pu clairement établir l'emploi d'une convention pour le signe opposé à celle de Buckingham et Orr, on montre aussi, dans la deuxième colonne dessous chaque élément de β, le valeur prise en utilisant cette dernière convention. C'est le cas pour deux des résultats pour CO de O'Hare et Hurst (la convention utilisé est décrite en bas du tableau VII de la réf. 10). Aussi, Liebmann et Moskowitz comparent leurs résultats avec ceux de O'Hare et Hurst au même temps qu'ils rapportent le résultat de Buckingham et Stephen (3) avec le signe changé (voir le tableau VIII de la réf. 11). En conséquence, on montre les résultats de Liebmann et Moskowitz (11) avec le signe changé. La convention utilisé par McLean et Yoshimine (13) semble être la même que la notre. La convention utilisé par les autres auteurs n'est pas aussi simple pour nous de retrouver. On peut seulement dire qu'on trouve le même signe que Hush et Williams (12) avec un calcul semi-empirique à "champ fini" pour CH_4 et CO et le signe contraire que Lazzeretti et Zanasi (14) et Arrighini *et al.* (15) pour CH_4. Aussi pour CH_4, on a le même signe que le calcul semi-empirique de type Unsold de Buckingham et Stephen (3).

On voit que nos résultats pour β montrent l'effet de la base utilisée pour obtenir les fonctions HFS; néanmoins, cette influence n'est pas très prononcée (on trouve des effets plutôt drastiques, comme dans le travail d'O'Hare et Hurst où même un changement de signe est produit par un changement de base). Pour le CO, le changement de β (BS) à β (BD) est plus prononcé que le changement de β (BD) à β (BM); cependant, le calcul BD ne paraît pas capable d'apporter une relative stabilité dans le cas du CH_4. Ceci paraît raisonable si on s'aperçoit que la base BD n'améliore pas l'espace variationel dans la région des atomes de H du CH_4 tandis qu'elle représente une amélioration pour les deux atomes du CO. Il faut la base BM pour introduire une flexibilité suffisante dans la région des H du CH_4.

Les variations des valeurs de β pour CH_4 et CO publiées sont d'un ordre de grandeur, les valeurs pouvant être positives ou negatives (la convention pour le signe n'est pas, malheureusement, à l'origine de toutes les différences de signe). Pour CH_4, en principe, on devrait donner préférence aux résultats de Lazzeretti et Zanasi et d'Arrighini *et al.* obtenus par une méthode HF *ab initio* couplée; de façon similaire, pour CO on choisirait les résultats de McLean et Yoshimine obtenus à l'aide d'une technique de "champ fini" (méthode qui est essentiellement de caractère couplée). On est, toutefois, mal à l'aise pour choisir la valeur HF couplée correcte du CH_4 etant donné que les valeurs proposées par Lazzeretti et Zanasi et Arrighini *et al.* diffèrent par un ordre de grandeur et, même, révèlent une tendance divergente avec l'amélioration de la base atomique. La valeur expérimentale $\beta = |0.1|$ proposée par Maker (2) ne paraît pas suffisamment concluante pour résoudre cette différence. Si l'on considère que les résultats d'Arrighini *et al.* (16) pour la polarisabilité sont toujours bas par rapport à l'expérience, on peut s'attendre à une situation pareille pour β.

Ce que la comparaison des différents résultats semble révéler c'est que les valeurs HFS non couplées de ce travail pour CO sont ressemblables aux celles d'O'Hare et Hurst obtenues par une méthode HF non couplée et double perturbation et des ensembles de base comparables ($\beta_{zzz} = 13.8$ avec 10.1 et 9.8). La comparaison avec le calcul HF non couplé avec double perturbation de Liebmann et Moskowitz qui utilisent une base de qualité à peu près BD permet la même conclusion ($\beta_{zzz} = 14.2$ avec 12.1). Tous ces résultats non couplés montrent le même signe et un ordre de grandeur en dessus des résultats HF "à champ fini" de McLean et Yoshimine ($\beta \simeq 1$).

Dans le cas du CH_4 on obtient le même ordre de grandeur et le même signe que Liebmann et Moskowitz ($\beta_{xyz} = -5.3$ avec -1.9). Comme on a remarqué en haut, la comparaison avec le résultat HF couplé correct n'est pas facile, il est seulement évident que les valeurs non couplées se trouvent en dessus des valeurs couplées.

On peut conclure que la méthode HFS non couplée rends des résultats ressemblables aux calculs HF du type non couplé quand on utilise des bases de qualité comparable. Aussi, une base BD paraît suffisante pour se rapprocher à la limits HFS non couplée, l'atome de H faisant exemption. On peut alors considérer la valeur obtenue pour l'ion CN^- comme suffisamment proche de la limite HFS non couplée, tandis qu'on est moins rassuré sur la signification du résultat pour la molécule de HCHO. Finalement, il faudra attendre des nouveaux résultats expérimentaux pour décider le degré de crédit dû aux résultats non couplés par rapport des résultats couplés.

Remerciements

On remercie le soutien du Conseil national de recherches du Canada. On remercie messieurs E. Baerends et T. Ziegler pour l'emploi de quelques fonctions d'onde. Aussi, on a profité des commentaires de M. le Professeur A. D. Buckingham.

1. M. TRSIC, T. ZIEGLER et W. G. LAIDLAW. Chem. Phys. **15**, 383 (1976).
2. A. D. BUCKINGHAM et B. J. ORR. Q. Rev. **21**, 195 (1967).
3. A. D. BUCKINGHAM et M. J. STEPHEN. Trans. Faraday Soc. **53**, 884 (1957).
4. E. CLEMENTI et C. ROETTI. At. Data Nucl. Data Tables, **14**, 177 (1974).
5. E. J. BAERENDS et P. ROS. Chem. Phys. **8**, 412 (1975).
6. A. D. MCLEAN et M. YOSHIMINE. Tables of linear molecule wave functions. IBM, San Jose, CA. 1976.
7. E. J. BAERENDS, D. E. ELLIS et P. ROS. Chem. Phys. **2**, 41 (1973).
8. F. P. BILLINGSLEY II et J. E. BLOOR. J. Chem. Phys. **55**, 5178 (1971).
9. M. D. NEWTON. J. Chem. Phys. **51**, 3917 (1969).
10. J. M. O'HARE et R. P. HURST. J. Chem. Phys. **46**, 2356 (1967).
11. S. P. LIEBMANN et J. W. MOSKOWITZ. J. Chem. Phys. **54**, 3622 (1971).
12. N. S. HUSH et M. L. WILLIAMS. Theor. Chim. Acta, **25**, 346 (1972).
13. A. D. MCLEAN et M. YOSHIMINE. J. Chem. Phys. **46**, 3682 (1967).
14. P. LAZZERETTI et R. ZANASI. Chem. Phys. Lett. **39**, 323 (1976).
15. G. P. ARRIGHINI, M. MAESTRO et R. MOCCIA. Symp. Faraday Soc. No. 2, 48 (1968).
16. G. P. ARRIGHINI, C. GUIDOTTI, M. MAESTRO, R. MOCCIA et O. SALVETTI. J. Chem. Phys. **49**, 2224 (1968).
17. R. S. RINN et J. WEID. J. Chem. Phys. **60**, 454 (1974).

Can. J. Chem. Downloaded from www.nrcresearchpress.com by 210.87.254.105 on 09/05/12
For personal use only.

Enthalpies of formation of crystalline selenium(IV) chloride and bromide

ALAN D. WESTLAND AND RAMESH MAKHIJA

Department of Chemistry, University of Ottawa, Ottawa, Ont., Canada K1N 9B4

Received January 16, 1978

ALAN D. WESTLAND and RAMESH MAKHIJA. Can. J. Chem. **56**, 1586 (1978).

Standard enthalpies of formation of crystalline selenium(IV) halides were determined by solution calorimetry relative to that of selenium(IV) oxide. The values obtained were: $\Delta H^{\ominus}_{f,298}$ $SeCl_4$(c), -42.7 ± 0.4 and $\Delta H^{\ominus}_{f,298}$ $SeBr_4$(c), -17.9 ± 0.5 kcal mol^{-1}.

ALAN D. WESTLAND et RAMESH MAKHIJA. Can. J. Chem. **56**, 1586 (1978).

On a déterminé les enthalpies standard de formation des halogénures cristallins du selenium(IV) en faisant appel à la calorimétrie en solution relative aux propriétés de l'oxyde de selenium(IV). On a obtenu les valeurs suivantes: $\Delta H^{\ominus}_{f,298}$ $SeCl_4$(c), -42.7 ± 0.4 et $\Delta H^{\ominus}_{f,298}$ $SeBr_4$(c), -17.9 ± 0.5 kcal mol^{-1}.

[Traduit par le journal]

In a study of the enthalpies of reaction of selenium(IV) halides with the corresponding alkali halides, it was useful to know the standard enthalpies of formation of $SeCl_4$(c) and $SeBr_4$(c). The value -43.8 kcal mol^{-1} is given for the chloride in the most recent tabulation published by the National Bureau of Standards, Washington (1). This value appears to derive from the measurements made by Thompsen (2) in the last century. His original value has undergone revision because it is now realized that the hexagonal form of selenium is the most stable state (3), whereas Thompsen chose glassy selenium as the standard state. It appeared desirable to repeat the determination by means of an alternative method. There is no reported value of the enthalpy of formation of $SeBr_4$.

We have measured both of these enthalpies by solution calorimetry. Thus, a determination of the enthalpy of the process

[1] $$SeO_2(c) + 4HCl(g) = SeCl_4(c) + 2H_2O(l)$$

enables us to obtain $\Delta H_f^{\ominus}$ for $SeCl_4$ from the tabulated enthalpies of formation for the other compounds in the equation. The partial processes, the enthalpies for which were either measured or evaluated from published data, are as follows:

[2] $$SeCl_4(c) + \{316HCl + 4029H_2O\} = \{SeCl_4 + 316HCl + 4029H_2O\}$$

[3] $$SeO_2(c) + \{320HCl + 4027H_2O\} = \{SeCl_4 + 316HCl + 4029H_2O\}$$

[4] $$4HCl(g) + \{316HCl + 4029H_2O\} = \{320HCl + 4029H_2O\}$$

[5] $$2H_2O(l) + \{320HCl + 4027H_2O\} = \{320HCl + 4029H_2O\}$$

The braces indicate solutions. It is seen that $\Delta H_1 = -\Delta H_2 + \Delta H_3 + \Delta H_4 - \Delta H_5$ where the subscripts correspond to the numbers of the equations.

The foregoing represents the typical case in which 1 g of SeO_2 is dissolved in 200 cm^3 of 4.0 *M* hydrochloric acid. The enthalpies of reactions [2] and [3] were measured and ΔH_4 and ΔH_5 were evaluated from published data (1).

In order for the method to give a correct result, it is necessary that the selenium species in solution be labile. We were unable to discover from the literature what period of time is required for the oxyhalo species to reach equilibrium but the shape of our temperature–time plots for the dissolution of selenium(IV) halides suggested that all enthalpic processes were complete within 2–6 min. Raman spectra indicate that identical solutions result from dissolving either $SeCl_4$ or SeO_2 in hydrochloric acid.[1]

The relevant equations for the study of $SeBr_4$ are as follows:

[6] $$SeO_2(c) + 4HBr(g) = SeBr_4(c) + 2H_2O(l)$$

[7] $$SeBr_4(c) + \{320HCl + 4029H_2O\} = \{SeBr_4 + 320HCl + 4029H_2O\}$$

[8] $$SeO_2(c) + \{4HBr + 320HCl + 4027H_2O\} = \{SeBr_4 + 320HCl + 4029H_2O\}$$

[9] $$4HBr(g) + 18.7H_2O = \{4HBr + 18.7H_2O\}$$

[10] $$\{4HBr + 18.7H_2O\} + \{320HCl + 4008.3H_2O\} = \{4HBr + 320HCl + 4027H_2O\}$$

[11] $$20.7H_2O + \{320HCl + 4008.3H_2O\} = \{320HCl + 4029H_2O\}$$

We see that $\Delta H_6 = -\Delta H_7 + \Delta H_8 + \Delta H_9 + \Delta H_{10} - \Delta H_{11}$. Equation [9] represents the formation of

[1] J. B. Milne. Private communication.

Can. J. Chem. Downloaded from www.nrcresearchpress.com by 210.87.254.42 on 09/05/12
For personal use only.

TABLE 1. Enthalpies of solution of $SeCl_4$, $SeBr_4$, SeO_2, and HBr*

Compound	Range of sample weight (g)	No. of determinations	Mean molar enthalpy of solution (kcal mol^{-1})	Reaction enthalpy
$SeCl_4$	0.249–0.487	6	-24.22 ± 0.13	ΔH_2
$SeBr_4$	0.517–0.998	7	-7.18 ± 0.11	ΔH_7
SeO_2	0.399–0.988	4	$+1.69 \pm 0.03$	ΔH_3
SeO_2*	0.510–1.258	7	$+1.04 \pm 0.05$	ΔH_8
HBr (48.97% solution)	1.901–3.062	4	-1.10 ± 0.02	$\Delta H_{10}/4$

*The solvent was 4.02 *M* hydrochloric acid for all cases except for ΔH_8. In this case, the solvent was 4.02 *M* hydrochloric acid containing the stoichiometric amount of HBr.

49% w/w hydrobromic acid from HBr gas. The enthalpy for this process was interpolated from literature data (1). The enthalpy of mixing the two acids was measured calorimetrically. The enthalpies of the other partial processes were obtained as in the $SeCl_4$ case.

Experimental

Preparation of $SeCl_4$

Selenium pearls (99.999%) were treated with chlorine in a Pyrex tube according to the procedure given by Brauer (5). The product was sublimed in chlorine and stored in sealed ampoules under nitrogen. *Anal.* calcd. for $SeCl_4$: Se 35.8, Cl 64.2; found: preparation 1: Se 35.7, Cl 63.6; preparation 2: Se 35.7, Cl 64.5.

Preparation of $SeBr_4$

Selenium pearls were placed in a Pyrex tube which was evacuated and sealed. A supply of excess purified bromine was attached to this tube via a break-seal. After breaking the seal, bromine entered the reaction space and combination of the elements proceeded spontaneously. The excess bromine was removed by condensing it in the original bromine reservoir and the product was removed in the inert atmosphere box and stored in N_2-filled ampoules. *Anal.* calcd. for $SeBr_4$: Se 19.8, Br 80.2; found: preparation 1: Se 20.1, Br 79.7; preparation 2: Se 19.6, Br 80.2.

Selenium(IV) Oxide

Two commercial samples of SeO_2 (Ventron, 99.9%) were used. One of these was used as received, the other was sublimed in a slow stream of oxygen. The samples were kept in a closed system during handling operations in order to avoid contamination by hydrolysis.

Hydrochloric and hydrobromic acids were reagent grade and were analyzed by titration with 1.0 *N* sodium hydroxide solution.

Analyses

Selenium was determined iodometrically according to a procedure described by Vogel (method *C*) (6). Halogen was determined by potentiometric or Volhard titration.

Calorimetric Measurements

The calorimeter has been described previously (7). The data were treated by the method of Kubaschewski to correct for heat loss or gain (8). The accuracy of the calorimeter was checked by measuring the heat of neutralization of tris(hydroxymethyl)aminomethane with excess 0.1 *N* HCl at 298 K (found: 29.6, 29.7; lit. (9) 29.72 kJ mol^{-1}).

Results

Table 1 contains the results of our calorimetric measurements of enthalpies of solution. Two preparations of each of the tetrahalides were used to obtain the results shown. The mean values for the independent preparations differed in both cases by much less than the overall standard deviations given in the table. The enthalpy of solution of SeO_2 was slightly less endothermic when the calorimeter liquid contained 4 mol of HBr per mole of SeO_2.

Commercial hydrobromic acid was titrated with 1.0 *M* NaOH and found to have a concentration of 48.97% w/w. The glassware used in this analysis was carefully standardized by weighing deliveries of distilled water. Samples of the acid were mixed in the calorimeter with 4.02 *M* hydrochloric acid. The entry in the table refers to the enthalpy of mixing expressed per mole of HBr. The enthalpy of equation [10] is thus four times this quantity.

ΔH_f° of $SeCl_4$

We obtained -24.22 ± 0.13 and 1.69 ± 0.03 kcal mol^{-1} respectively for ΔH_2 and ΔH_3. The enthalpy of reaction [4] was taken to be -63.3 ± 0.3 kcal. This was obtained by graphical interpolation of literature data (1) and is the difference in the integral heats of solution of HCl(g) to form the solutions $\{316HCl + 4029H_2O\}$ and $\{320HCl + 4029H_2O\}$. The data are very precise: the uncertainty limits here reflect chiefly the assumed error in the interpolation procedure while assuming that the literature data provide correct first order differences. The heat of dilution ΔH_5 was found in a similar way to be -0.16 kcal when 2 mol of water dissolve in the solution $\{320HCl + 4027H_2O\}$. These data give -37.2 ± 0.6 kcal as the enthalpy of reaction [1]. For the literature values (1) of standard enthalpies of formation we have: SeO_2(c), -53.86, HCl(g), -22.062, and H_2O(l), -68.315 kcal mol^{-1}. The value for SeO_2(c) is that recorded by Gattow (3) for the hexagonal modification. Previously reported values for

Can. J. Chem. Downloaded from www.nrcresearchpress.com by 210.87.254.42 on 09/05/12
For personal use only.

Can. J. Chem. Downloaded from www.nrcresearchpress.com by 210.87.254.42 on 09/05/12
For personal use only.

SeO_2 were obtained in most cases with glassy or poorly defined selenium. The data lead to $\Delta H^{\ominus}_{f,298}$ $SeCl_4(c) = -42.7 \pm 0.4$ kcal mol^{-1}. The standard deviation given here is the root mean square value of those for the partial processes.

The value obtained is 1.1 kcal mol^{-1} less negative than that cited in ref. 1. However, the uncertainty on Thompsen's value has been estimated to be ± 1.5 kcal mol^{-1} (4) which overlaps with our value. In order to decide upon the best value, the following points should be considered. The present method of determination is indirect while Thompsen measured the enthalpy of the process $Se_2Cl_2(l) + 3Cl_2(g) = 2SeCl_4(c)$. This was combined with the result for the process $2Se(glass) + Cl_2(g) = Se_2Cl_2(l)$. However, Thompsen failed to give experimental details so that a proper assessment of his work is not possible.

The indirectness of our method does not appear to introduce an appreciable cumulative error as the precision of the quantities used in the calculations is very good. The literature data for HCl and H_2O are especially precise. One must consider the purity of the SeO_2 and the $SeCl_4$. Sublimation of the former had no effect on its enthalpy of solution. The chloride is subject to hydrolysis and possible contamination with Se_2Cl_2. We measured the enthalpies of solution of H_2SeO_3 and Se_2Cl_2 in 4.02 *M* hydrochloric acid and obtained +4.5 and −5.1 kcal mol^{-1} respectively. It follows that an error of 0.1 kcal mol^{-1} in the heat of solution of $SeCl_4$ would be caused by 0.5 mol% of either one of these impurities. Such a mixture of $SeCl_4$ and Se_2Cl_2 was prepared and it was found to have a distinct yellow colour. As the $SeCl_4$ used was almost pure white it was evident that there was no appreciable contamination with Se_2Cl_2. As Se—O bands in the infrared spectrum are normally weak, we were unable to devise a method to specifically detect hydrolysis. The chlorine analyses lead us to believe that no more than 1 mol% hydrolysis had occurred.

$\Delta H_f^{\ominus}$ of $SeBr_4$

We obtained -7.18 ± 0.11, $1.04 + \pm 0.05$, and -4.40 ± 0.08 kcal for ΔH_7, ΔH_8, and ΔH_{10} respectively. ΔH_9 and ΔH_{11} were interpolated graphically from literature data (1) and were taken to be -71.24 ± 0.2 and -1.58 ± 0.05 kcal respectively. The literature data appear to be highly reliable: the uncertainty in ΔH_9, the integral heat of solution of 4 mol of HBr, reflects the uncertainties in the published data combined with that of our analysis of the concentrated acid. The data yielded -65.8 ± 0.3 kcal for the enthalpy of reaction [6].

In order to calculate the standard enthalpy of formation of $SeBr_4$, ΔH_6, $\Delta H_f^{\ominus} SeO_2$, $\Delta H_f^{\ominus} H_2O$ and $\Delta H_f^{\ominus} HBr$ were used. This last was taken to be -8.70 kcal mol^{-1} (1). These data give $\Delta H^{\ominus}_{f,298}$ $SeBr_4(c) = -17.9 \pm 0.3$ kcal mol^{-1}.

As before with $SeCl_4$, the limiting factor in the accuracy of the determination was held to be the purity of the $SeBr_4$ in respect of both the initial stoichiometry and possible subsequent hydrolysis during handling. Because of its colour, it was not possible to assess the purity of the $SeBr_4$ by its appearance alone; however, the analytical purity was very good. Separate preparations of $SeBr_4$ gave good agreement in heats of solution.

Acknowledgment

This work was supported by a grant from the National Research Council of Canada.

1. D. D. WAGMAN, W. H. EVANS, V. B. PARKER, I. HALOW, S. M. BAILEY, and R. H. SCHUMM. Selected values of chemical thermodynamic properties. Technical note 270-3. National Bureau of Standards, Washington, DC. 1968.
2. J. THOMPSEN. Ber. **15**, 3024 (1882).
3. G. GATTOW. Z. Anorg. Allg. Chem. **317**, 245 (1962).
4. F. D. ROSSINI. Selected values of chemical thermodynamic properties. Circular 500. National Bureau of Standards, Washington, DC. 1952.
5. G. BRAUER (*Editor*). Handbook of preparative inorganic chemistry. Vol. 1. 2nd ed. Academic Press, New York. 1965.
6. A. I. VOGEL. A textbook of quantitative inorganic analysis. 3rd ed. Longman, New York. 1962. p. 303.
7. P. GELBMAN and A. D. WESTLAND. J. Chem. Soc. Dalton Trans. 1598 (1975).
8. O. KUBASCHEWSKI, E. LL. EVANS, and C. B. ALCOCK. Metallurgical thermochemistry. 4th ed. Pergamon, Oxford. 1967. p. 90.
9. R. J. IRVING and I. WADSÖ. Acta Chem. Scand. **18**, 195 (1964).

Pyrolysis of bromobenzene by the toluene carrier technique and determination of $D(C_6H_5—Br)$

R. JOHN KOMINAR AND MICHAEL J. KRECH
Chemistry Department, Wilfrid Laurier University, Waterloo, Ont., Canada N2L 3C5
AND
STANLEY JAMES W. PRICE
Chemistry Department, University of Windsor, Windsor, Ont., Canada N9B 3P4

Received December 20, 1977

R. JOHN KOMINAR, MICHAEL J. KRECH, and STANLEY JAMES W. PRICE. Can. J. Chem. **56**, 1589 (1978).

The pyrolysis of C_6H_5Br has been studied by the toluene carrier technique over the temperature range 1018 to 1126 K using contact times of 1.18 to 2.85 s and total pressures of 3.8 to 4.4 kPa. Percent decomposition based on analyses of residual C_6H_5Br ranged from 4 to 89%. When HBr was trapped out and quantitatively determined it accounted for more than 95% of the bromine expected. Within the limits of the experimental method the decomposition was found to be homogeneous and first order.

[1] $$C_6H_5Br \rightarrow C_6H_5 + Br$$

The Arrhenius equation for reaction [1] is

$$\log k_1 (s^{-1}) = (14.6 \pm 0.26) - \frac{317\ 000 \pm 5400}{19.15T}$$

Making an approximate correction of the activation energy to 298 K then gives $D(C_6H_5—Br) = 313 \pm 5.4$ kJ mol^{-1}.

R. JOHN KOMINAR, MICHAEL J. KRECH et STANLEY JAMES W. PRICE. Can. J. Chem. **56**, 1589 (1978).

On a étudié la pyrolyse du C_6H_5Br à l'aide de la technique de l'entraînement par le toluène à des températures allant de 1018 à 1126 K, utilisant des temps de contact de 1.18 à 2.85 s et des pressions totales allant de 3.8 à 4.4 kPa. Les pourcentages de décomposition, basés sur l'analyse du C_6H_5Br résiduel, vont de 4 à 89%. Lorsque l'on piège le HBr et qu'on le détermine quantitativement, on récupère ainsi plus de 95% du brome attendu. A l'intérieur des limites de la méthode expérimentale, on a trouvé que la décomposition est homogène et du premier ordre.

[1] $$C_6H_5Br \rightarrow C_6H_5 + Br$$

L'équation d'Arrhénius pour la réaction [1] est

$$\log k_1 (s^{-1}) = (14.6 \pm 0.26) - \frac{317\ 000 \pm 5400}{19.15T}$$

Si l'on fait une correction approximative de l'énergie d'activation à 298 K, on obtient alors $D(C_6H_5—Br) = 313 \pm 5.4$ kJ mol^{-1}.

[Traduit par le journal]

Introduction

In an earlier toluene carrier study of C_6H_5Br a value of the order of 297 kJ mol^{-1} was reported for $D(C_6H_5—Br)$ (1). This is considerably lower than the value suggested by Benson and O'Neal (2) of 339 kJ mol^{-1} based on thermochemical kinetic evidence. In a recent paper by two of the present authors (3) comparing values of $D(C_6H_5—X)$ and $D(C_6F_5—X)$ the bromo analogs were not included. A recent thermochemical study gives a value of 436 kJ mol^{-1} for $D(C_6F_5—Br)$ (4). The present study was undertaken in an attempt to resolve the discrepancy between the earlier toluene carrier study and the more recent thermochemical suggestion of $D(C_6H_5—Br)$, and to extend the $D(C_6H_5—X)$, $D(C_6F_5—X)$ comparison to include the bromo analogs.

Experimental

Materials

(a) Bromobenzene

The bromobenzene used was obtained from Eastman Organic Chemicals #43. Prior to use, the bromobenzene was distilled and head and tail fractions were discarded. Analysis by gas chromatography (6 ft × 0.125 in. 15% Apiezon L on chromosorb W, N_2 carrier, 30 cm^3/min, isothermal for 4 min at 100°C and temperature programmed from 100–160°C at 32°C/min) showed only minor impurities estimated at a maximum of 0.01% of the sample.

(b) Benzene

Analar grade benzene from British Drug House was simi-

larly tested by gas chromatography and the minor impurities were estimated at a maximum of 0.01% of the sample.

(c) Toluene

Toluene from sulfonic acid (Eastman Organic X325) was prepared for use by refluxing over sodium under vacuum and then degassing by bulb-to-bulb distillation.

(d) n-*Undecane*

n-Undecane was obtained from Polyscience Corporation and used as received.

(e) Diethyl Mercury

Diethyl mercury was obtained from Alpha Inorganics and used as received.

Apparatus and Procedure

The basic toluene carrier system has been previously described (5). The quantity of C_6H_5Br required for a run was injected via a gas-tight syringe through a silicone rubber septum. It was then subjected to controlled evaporation into the toluene carrier stream. Total pressures were taken by a differential manometer after the C_6H_5Br had been removed from the system while only toluene was flowing. The reaction vessel was treated with hot fuming nitric acid prior to use. Residual acid was baked out under vacuum after the vessel was installed in the system.

Toluene, unreacted C_6H_5Br, HBr, and other condensibles were trapped at −80°C. After the run, in experiments where the amount of HBr produced was quantitatively determined, the liquid products were isolated, the cold bath removed, and 25 ml of standardized NaOH introduced into the flask. The entire contents were stirred for 10–15 min with a magnetic stirrer, while still under vacuum. The contents of the trap were quantitatively transferred to a separatory funnel, the aqueous layer separated, and titrated with standard HCl. The organic layer was transferred to an amber sample bottle with a Teflon lined top, weighed, and a weighed amount of internal standard *n*-undecane added. In experiments where HBr analyses were not carried out the collected liquid products were transferred directly to the amber bottles, weighed, and a weighed amount of internal standard introduced. The samples were analyzed on a P.E. Model 3600 Gas Chromatograph for residual C_6H_5Br, toluene, and benzene by an internal standard technique. The areas were determined using a Columbia Scientific Industries Model CSI38 digital electronic integrator. The integrator was acquired half-way through the course of this work and the quantitative gc analysis showed a marked increase in precision when the integrator was put into use.

Results and Discussion

Selected experimental results are given in Table 1 and the Arrhenius plot for the decomposition of C_6H_5Br is shown in Fig. 1. The results may be discussed in terms of the following mechanism.

[1] $C_6H_5Br \rightarrow C_6H_5 + Br$

[2] $Br + C_6H_5CH_3 \rightarrow C_6H_5CH_2 + HBr$

[3] $C_6H_5 + C_6H_5CH_3 \rightarrow C_6H_6 + C_6H_5CH_2$

[4] $C_6H_5 + C_6H_5CH_2 \rightarrow C_6H_5CH_2C_6H_5$

[5] $2C_6H_5CH_2 \rightarrow (C_6H_5CH_2)_2$

[6] $2C_6H_5 \rightarrow (C_6H_5)_2$

The products of reactions [3] through [6] were identified qualitatively by gas chromatography.

TABLE 1. Selected experimental results for the toluene carrier flow decomposition of bromobenzene

T^* (K)	P (kPa)	t_c (s)	Decomposition (%)	Toluene / C_6H_5Br molar ratio	k_1 (s^{-1})
1126	4.18	2.44	89.1	99	0.9108
1119	4.18	2.17	76.7	92	0.6716
1112P	4.16	1.27	48.1	102	0.5184
1104	4.35	2.85	69.2	90	0.4129
1094	4.07	2.26	49.6	68	0.3031
1087	3.99	2.24	43.1	91	0.2515
1079	4.03	2.34	32.4	88	0.1771
1070	4.02	2.32	26.7	82	0.1342
1070P	4.12	1.18	16.1	110	0.1496
1059P	3.84	1.31	11.8	82	0.0964
1057	4.16	2.26	18.5	103	0.0906
1049	4.18	2.16	14.3	80	0.0714
1048P	4.10	1.20	7.9	126	0.0682
1045	4.10	2.19	11.7	104	0.0565
1019	4.19	2.21	4.2	125	0.0193
1018	4.04	2.26	5.8	103	0.0263

* P denotes runs in packed reaction vessel, surface-to-volume ratio 17 times that in unpacked vessel.

Over the temperature range 1018 to 1126 K the C_6H_5Br decomposition ranged from 4 to 89%. Over this same temperature range it is estimated (6) that 0.08 to 4.4% of the toluene carrier decomposed. Since the toluene to phenyl bromide ratio was usually about 100:1 it is therefore also necessary to consider the following additional reactions.

[7] $C_6H_5CH_3 \rightarrow C_6H_5CH_2 + H$

[8] $H + C_6H_5CH_3 \rightarrow H_2 + C_6H_5CH_2$

[9] $H + C_6H_5CH_3 \rightarrow CH_3 + C_6H_6$

[10] $H + C_6H_5Br \rightarrow C_6H_5 + HBr$

The major concern here is the possible occurrence of reaction [10] to a significant extent. Reaction [8] should be approximately 40 kJ more exothermic than reaction [10] and should have an added statistical advantage (three H on CH_3 available for abstraction versus one Br). It, therefore, seems likely that k_8 should be somewhat larger than k_{10}. Given this, and the fact that the toluene–C_6H_5Br ratio was generally in the range 80:1 to 120:1, it seems unlikely that reaction [10] would be significant.

As an experimental check on this conclusion three experiments were carried out using approximately equimolar amounts of C_6H_5Br and $Hg(C_2H_5)_2$. At the temperatures used reactions [11] and [12] occurred extremely rapidly producing an effective increase in the rate of H atom production of at least a

[11] $Hg(C_2H_5)_2 \rightarrow 2C_2H_5 + Hg$

[12] $C_2H_5 \rightarrow C_2H_4 + H$

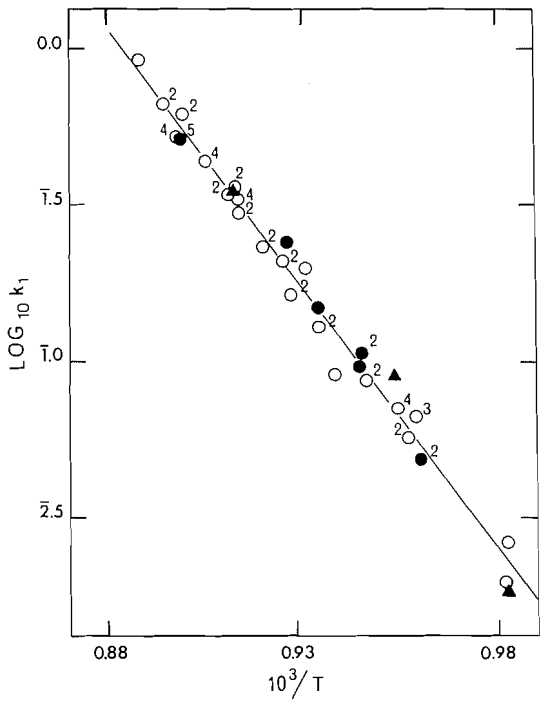

FIG. 1. Arrhenius plot for the decomposition of bromobenzene. Open circles, ○, represent unpacked vessel runs. Full circles, ●, represent packed vessel runs. Full triangles, ▲, represent addition of $Hg(C_2H_5)_2$ in selected runs. Numbers beside points indicate the number of experiments averaged to obtain the plotted point.

factor of 10 at the lowest temperature and a factor of 2 at the highest temperature used. The results of these runs are shown in Table 2. No significant increase in the decomposition of C_6H_5—Br was observed. It therefore seems unlikely that reaction [10] plays any significant role in the proposed mechanism.

The rate constants given in Table 1 have been calculated from the amount of undecomposed C_6H_5Br. As a check, the quantity of HBr produced was measured in a number of runs and was found to be 94–99% of the expected value.

TABLE 2. Effect of $Hg(C_2H_5)_2$ on C_6H_5—Br decomposition

T (K)	Decomposition (%)	k_1 (s^{-1})
1018*	3.8	0.0179
1018	4.2	0.0193
1049*	16.7	0.0862
1049	14.3	0.0714
1075*	52.4	0.3499
1075	51.2	0.3355

*Denotes the addition of $Hg(C_2H_5)_2$ to C_6H_5Br.

It is also possible that small quantities of CH_3Br were formed; however, no CH_3Br was observed when analyzed for by gas chromatography.

Benzene analyses were carried out on the liquid samples but the amount of benzene cannot be quantitatively related to the primary reaction because of the benzene coming from the toluene carrier decomposition.

Approximately one quarter of the experiments were carried out using a packed reaction vessel, with surface to volume ratio 17 times that in the unpacked vessel. No detectable surface effects were observed (Fig. 1).

Values of k_1 have been calculated from the usual first-order expression. The data in Table 3 indicate that values of k_1 determined in this way show no significant variation when the C_6H_5Br concentration is varied over a range of up to a factor of 7.4. Within experimental limits the decomposition is first order in C_6H_5Br.

The linear regression line for all the data points in Fig. 1 may be represented by (stated error limits are $\pm\sigma$)

$$\log k_1\,(s^{-1}) = (14.63 \pm 0.26) - \frac{317\ 000 \pm 5400}{19.15T}$$

Approximate correction of the activation energy to 298 K then gives $D(C_6H_5—Br) = 313.0 \pm 5.4$ kJ mol^{-1}. Using $\Delta H^0_{f298}(C_6H_5, g) = 325.1$ kJ mol^{-1} (7) to revise Benson and O'Neal's (2) value for the C_6H_5Br decomposition gives

$$\log k = 14.8 - 328/19.15T$$

in reasonable agreement with the present results.

In Fig. 2 a comparison is made of $D(C_6F_5—X)$ and $D(C_6H_5—X)$ bond dissociation energies (3, 4). In general the enhanced electron density on the carbon attached to X in C_6F_5X leads to stronger C—X bonds. In C_6F_6 all of the carbon atoms are positive but the p-orbital overlap is optimum.

TABLE 3. Test of the effect of C_6H_5Br concentration on k_1

T (K)	Bromobenzene concentration (mol cm^{-3} × 10^9)	k_1 (s^{-1})
1095	28.9	0.3377
	21.3	0.2941
	14.1	0.3092
	12.2	0.3522
	10.1	0.3506
	9.0	0.3465
	8.6	0.3207
	3.9	0.3280

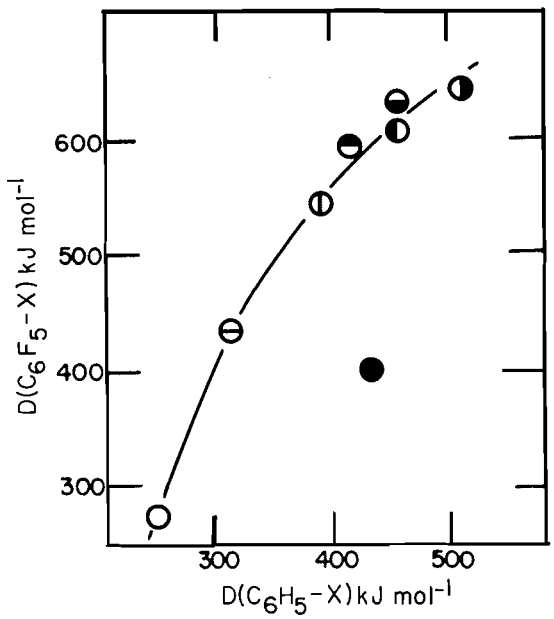

FIG. 2. Comparison of $D(C_6F_5—X)$ and $D(C_6H_5—X)$ bond dissociation energies for X = I (○), Br (⊖), Cl (◑), CH_3 (◓), H (◒), OH (◐), F (◑), and CF_3 (●).

The marked exception to the correlation shown is for X = CF_3. In this and in similar groups where the carbon in X is bonded to highly electronegative atoms the sp^3 hybrid orbitals on this carbon will be distorted to such an extent that overlap with the ring carbon orbitals is drastically reduced. The low value for $D(C_6F_5—CF_3)$ is therefore not unexpected.

Acknowledgements

This work has been supported in part by the National Research Council of Canada. Two of the authors (R.J.K. and M.J.K.) are also indebted to Wilfrid Laurier University for summer research support. The authors wish to thank Mr. C. Langford for his assistance in computer processing of the experimental data.

1. M. SZWARC and D. W. WILLIAMS. J. Chem. Phys. **20**, 1171 (1952).
2. S. W. BENSON and H. E. O'NEAL. Kinetic data on gas phase unimolecular reactions. Natl. Stand. Ref. Data Ser. Natl. Bur. Stand. **21**, 503 (1970).
3. M. J. KRECH, S. J. W. PRICE, and W. F. YARED. Can. J. Chem. **52**, 2673 (1974).
4. M. J. KRECH, S. J. W. PRICE, and H. J. SAPIANO. Can. J. Chem. **55**, 4222 (1977).
5. M. J. KRECH and S. J. W. PRICE. Can. J. Chem. **41**, 224 (1963).
6. S. J. W. PRICE. Can. J. Chem. **40**, 1310 (1962).
7. G. A. CHAMBERLAIN and E. WHITTLE. Trans. Faraday Soc. **67**, 2077 (1971).

Can. J. Chem. Downloaded from www.nrcresearchpress.com by 210.87.254.6 on 09/05/12
For personal use only.

Diastereoisomeric 4a,10a-dihydrofusarubins: True metabolites of *Fusarium solani*[1]

ITSUO KUROBANE AND LEO C. VINING
Department of Biology, Dalhousie University, Halifax, N.S., Canada B3H 4J1
AND
A. GAVIN MCINNES AND DONALD G. SMITH
Atlantic Regional Laboratory, National Research Council of Canada, Halifax, N.S., Canada B3H 3Z1

Received March 6, 1978

ITSUO KUROBANE, LEO C. VINING, A. GAVIN MCINNES, and DONALD G. SMITH. Can. J. Chem. **56**, 1593 (1978).

In alkaline cultures of *Fusarium solani* fusarubin is formed by nonenzymic oxidation of two previously unknown dihydrofusarubins, *rel*-(3*R*,4a*R*,10a*R*)- and *rel*-(3*R*,4a*R*,10a*S*)-5,10-dioxo-3,4,4a,5,10,10a-hexahydro-7-methoxy-3-methyl-3,6,9-trihydroxy-1*H*-naphtho[2,3-*c*]pyran.

ITSUO KUROBANE, LEO C. VINING, A. GAVIN MCINNES et DONALD G. SMITH. Can. J. Chem. **56**, 1593 (1978).

Dans des cultures alcalines de *Fusarium solani*, il y a formation de fusarubine par l'oxydation non-enzymatique de deux dihydrofusarubines inconnues jusqu'à maintenant soit les *rel*-(3*R*,4a*R*,10a*R*) et *rel*-(3*R*,4a*R*,10a*S*) dioxo-5,10 hexahydro-3,4,4a,5,10,10a méthoxy-7 méthyl-3 trihydroxy-3,6,9 1*H* naphto[2,3-*c*] pyrannes.

[Traduit par le journal]

Fusarubin (oxyjavanicin (1)), which has structure **1** (2–5), has been regarded as a metabolite of *F. solani* and *F. javanicum* for over 30 years. Fusarubinogen, an ammonium sulfate ester of a reduced form of **1**, has been reported as a possible progenitor metabolite in one strain of *F. solani* (3) but more probably is an artifact produced by the isolation procedure. We now report the isolation of two diastereoisomeric dihydrofusarubins (**2** and **3**) from *F. solani* cultures, and present evidence that air oxidizes them under alkaline conditions to yield **1**.

Cultures of *F. solani* grown on a maltose (2%) – ammonium tartrate (0.46%) – salts medium were harvested at 2 days when the p*H* had dropped to 3 from an initial value of 5. An ethyl acetate extract of the filtrate was taken to dryness and the residue chromatographed on silicic acid. Elution with a 5:1 benzene – ethyl acetate mixture gave **2**, $[\alpha]_D^{20}$ +145.4° (*c* 0.31, acetone); mp 153–154°C (reddish-orange needles from CH_2Cl_2); $M^{\ddagger}$ at *m/e* 308.0905 (calcd. for $C_{15}H_{16}O_7$: 308.08961); λ_{max} (95% EtOH): 213, 243, 273, 300, and 391 nm (log ε: 4.17, 4.30, 3.87, 3.71, and 3.94). Decreasing the benzene – ethyl acetate ratio to 3:1 gave **3**, $[\alpha]_D^{20}$ +23.3° (*c* 0.31, acetone); mp 117–118°C (pale-yellow needles from methanol); $M^{\ddagger}$ peak too small for mass measurement, $M - 18$ (also observed in the mass spectrum of **2**) at *m/e* 290.0784 (calcd. for $C_{15}H_{14}O_6$: 290.07904; λ_{max} (95% EtOH): 213, 243, 273, 300, and 391 nm (log ε: 4.15, 4.31, 3.89, 3.70, and 3.96).

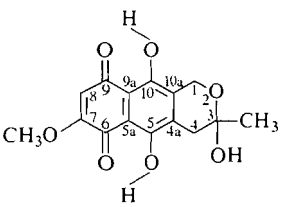

1

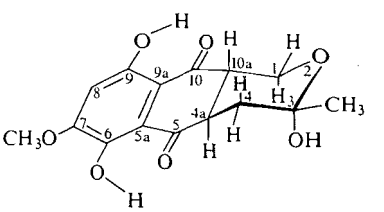

2

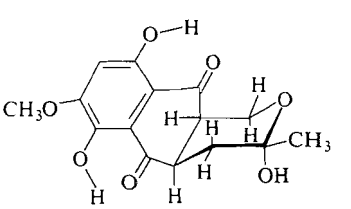

3

[1]Issued as NRCC No. 16690.

TABLE 1. ^{1}H nmr data (100 MHz) for dihydrofusarubins*

Compound	CH_3	OCH_3	H-8	3-OH	6,9-OH	
2	1.75(s)	3.87(s)	6.98(s)	7.96(bs)	12.58,12.83(bs)	
3	1.38(s)	3.94(s)	6.72(s)	2.50(s)	12.34,12.69(s)	
	H-1ax	H-1eq	H-10a	H-4a	H-4eq	H-4ax
2	4.46 $J_{1ax,1eq}$ −11.4 $J_{1ax,10a}$ 10.8	4.45 $J_{1eq,10a}$ 5.0	3.37 $J_{10a,4a}$ 13.2	3.97 $J_{4a,4ax}$ 11.6 $J_{4a,4eq}$ 3.5	2.72 $J_{4eq,4ax}$ −13.2	1.92
3	4.51 $J_{1ax,1eq}$ −11.6 $J_{1ax,10a}$ 3.2	4.00 $J_{1eq,10a}$ 1.4	3.00 $J_{10a,4a}$ 5.4	3.55 $J_{4a,4ax}$ 13.6 $J_{4a,4eq}$ 4.2	1.97 $J_{4eq,4ax}$ −13.2 $J_{4eq,10a}$ 1.2	1.59

*Compound 2 in $C_5{}^2H_5N$ at 0°C and compound 3 in $C^2H_2Cl_2$ at 28°C. Chemical shifts in ppm relative to TMS. Coupling constants $J_{p,q}$ in Hz. The protons H-1ax through H-4ax form a coupled six-spin system which was analyzed with the Varian spin simulation program on a 620L data system.

Conversion of **2** and **3** to **1** occurs rapidly at room temperature in 0.1 *N* NaOH solution and when *F. solani* cultures are basified at 2 days with NaOH. The conversions also take place in pyridine although **2** is stable at solution temperatures <0°C. The uv data are consistent with **2** and **3** containing a 5,8-dihydroxy-1,4-dioxo-1,2,3,4-tetrahydronaphthalene ring system (6) whereas the chemical evidence requires that they be isomeric dihydrofusarubins.

The signals for the methyl and methoxy groups in the ^{1}H nmr spectra of **2** and **3** (see Table 1) were readily assigned. Resonances for the ketal and intramolecularly hydrogen-bonded phenolic hydroxyl groups were temperature dependent and removed by exchange with ^2H_2O. H-8 was deshielded relative to its counterpart (δ 6.36) in **1** (5) and was, therefore, present in a phenolic rather than a quinone ring (5, 7). From the chemical shifts and spin–spin coupling constants (e.g., ref. 8) the ketal ring systems giving rise to the coupled six-spin systems had the conformations shown, with H-4a and H-10a antiperiplanar in **2** and synclinal in **3**. Conformational free energy calculations (9) indicate that the hydroxyl group at C-3 in both **2** and **3** is axially orientated, assuming a methyl group has a stronger 1,3-diaxial interaction with hydrogen (0.9 kcal mol^{-1}) than a hydroxyl group and the 'anomeric effect' favours the epimer with an axial hyroxyl group (0.55 kcal mol^{-1}). Thus the combined evidence establishes **2** and **3** as *rel*-(3*R*,4a*R*,10a*R*)- and *rel*-(3*R*,4a*R*,10a*S*)-5,10-dioxo-3,4,4a,5,10,10a-hexahydro-7-methoxy-3-methyl-3,6,9-trihyroxy-1*H*-naphtho[2,3-*c*]pyran.

The total weight of crude extract (347 mg ℓ^{-1}) from *F. solani* cultures changed little after 2 days but the amount of **2** and **3** rapidly decreased after 3 days. This loss was accompanied by a rapid increase in the p*H* of the medium from 3 to 8, and an increasing proportion of **1** in the product. Maintaining the p*H* of the culture at about 3 by adding acetic acid prevented this conversion. We presume that enolization involving H-4a, H-10a, and the carbonyl groups of **2** and **3** is promoted by alkaline conditions, and the hydroquinones thus obtained are oxidized by air to quinones. The tautomeric form of fusarubin initially formed subsequently rearranges to **1**.

Acknowledgements

We thank Mr. J. Van Ingen for valuable technical assistance.

1. G. P. ARSENAULT. Can. J. Chem. **43**, 2423 (1965).
2. H. R. V. ARNSTEIN and A. H. COOK. J. Chem. Soc. 1021 (1947); H. R. V. ARNSTEIN, A. H. COOK, and M. S. LACEY. Nature, **157**, 333 (1946).
3. H. W. RUELIUS and A. GAUHE. Ann. **569**, 38 (1950); **570**, 121 (1951).
4. E. HARDEGGER, K. STEINER, E. WIDMER, and A. PFIFFNER. Helv. Chim. Acta, **47**, 2027 (1964).
5. W. S. CHILTON. J. Org. Chem. **33**, 4299 (1968).
6. D. B. BRUCE and R. H. THOMSON. J. Chem. Soc. 1089 (1955).
7. R. E. MOORE and P. J. SCHEUER. J. Org. Chem. **31**, 3272 (1966).
8. L. CANUEL and M. ST.-JACQUES. J. Org. Chem. **41**, 1380 (1976); C. B. ANDERSON and M. P. GEIS. Tetrahedron, **31**, 1149 (1975).
9. E. L. ELIEL, N. L. ALLINGER, S. J. ANGYAL, and G. A. MORRISON. Conformational analysis. Wiley (Interscience), New York, NY. 1965. pp. 351–432.

Can. J. Chem. Downloaded from www.nrcresearchpress.com by 210.87.254.6 on 09/05/12
For personal use only.

Canadian Journal of Chemistry

Published by
THE NATIONAL RESEARCH COUNCIL OF CANADA

Volume 56 Number 12 June 15, 1978

Journal canadien de chimie

Publié par
LE CONSEIL NATIONAL DE RECHERCHES DU CANADA

Volume 56 numéro 12 15 juin 1978

Can. J. Chem. Downloaded from www.nrcresearchpress.com by 210.87.254.6 on 09/05/12
For personal use only.

Deactivation of singlet oxygen and triplet pentacene by transition metal complexes

HIROSHI FURUE AND KENNETH E. RUSSELL

Department of Chemistry, Queen's University, Kingston, Ont., Canada K7L 3N6

Received October 4, 1977

HIROSHI FURUE and KENNETH E. RUSSELL. Can. J. Chem. **56**, 1595 (1978).

Rate constants, k_Q, have been determined for the deactivation of singlet oxygen in carbon tetrachloride by a range of transition metal complexes. The singlet oxygen was produced by flash photolysis of air-saturated carbon tetrachloride solutions with methylene blue as sensitizer, and the decay followed by observing the concentration of the acceptor 1,3-diphenylisobenzofuran at 435 nm. The high rate constants of certain diamagnetic nickel complexes are accounted for by a spin-allowed transfer of electronic energy from singlet oxygen to the complex. Rate constants have also been determined for the deactivation of triplet pentacene by a number of these metal complexes. The triplet pentacene was produced by flash photolysis of dilute solutions of pentacene in benzene and the decay monitored at 492 nm. The rate constants for quenching of triplet pentacene are generally lower than those for quenching of singlet oxygen but there is a good correlation between the two sets of results. Both processes appear to proceed by way of electronic energy transfer without the intervention of complex formation between donor and acceptor.

HIROSHI FURUE et KENNETH E. RUSSELL. Can. J. Chem. **56**, 1595 (1978).

On a déterminé les constantes de vitesse, k_Q, des réactions de désactivation de l'oxygène singulet dans le tétrachlorure de carbone par un certain nombre de complexes de métaux de transition. On a produit l'oxygène à l'état singulet par la photolyse éclair de solutions d'air saturées de tétrachlorure de carbone en utilisant le bleu de méthylène comme sensibilisateur et on a suivie la décroissance en observant la concentration de l'accepteur diphényl-1,3 isobenzofuranne à 435 nm. On explique les constantes de vitesse élevées, observées avec certains complexes diamagnétiques du nickel, par un transfert d'énergie électronique permise par le spin de l'état singulet de l'oxygène vers le complexe. On a aussi déterminé les constantes de vitesse de la réaction de désactivation de l'état triplet du pentacène par un certain nombre de ces complexes métalliques. On a produit l'état triplet du pentacène par photolyse éclair de solutions diluées de pentacène dans le benzène et on a contrôlé la décroissance à 492 nm. Les constantes de vitesse de la réaction de piégeage de l'état triplet du pentacène sont généralement plus faibles que celles observées pour le piégeage de l'état singulet de l'oxygène mais il existe une bonne corrélation entre les deux séries de données. Les deux processus semblent se produire par l'intermédiaire d'un transfert d'énergie électronique sans l'intervention de la formation d'un complexe entre le donneur et l'accepteur.

[Traduit par le journal]

Introduction

Deactivation of singlet oxygen ($^1\Delta_g$) by transition metal complexes has attracted attention because of its possible involvement in the stabilization of polyolefins against photodegradation (1). The effectiveness of such complexes in deactivating singlet oxygen in solution has been studied by various groups, usually by determining the rate of consumption of rubrene in the presence of a steady state concentration of $^1\Delta$ O_2 (2–4). Adams and Wilkinson (5) and Merkel and Kearns (6) demonstrated some years ago that laser photolysis can be used to study directly the decay of singlet oxygen in solution. We have shown that the decay in carbon disulfide can equally well be studied by flash photolysis (7) and that quenching rate constants, k_Q, of transition metal complexes can be obtained from rates of decay of $^1\Delta$ O_2 in the presence and absence of the quencher. In our earlier study, the $^1\Delta$ O_2 was produced by flash photolysis of oxygen-saturated carbon disulfide solu-

Can. J. Chem. Downloaded from www.nrcresearchpress.com by 210.87.254.6 on 09/05/12
For personal use only.

tions containing methylene blue as sensitizer; the decay was observed by monitoring the disappearance of the acceptor 1,3-diphenylisobenzofuran (DPBF) at 435 nm. $^1\Delta$ O_2 has an even longer lifetime in the solvent carbon tetrachloride (6) and the original study has now been extended to yield k_Q values for a wide range of metal complexes in carbon tetrachloride solution.

The quenching of $^1\Delta$ O_2 may occur by a number of different routes. Water and alcohols appear to deactivate by an electronic–vibrational energy transfer mechanism (6). The intermediate quenching ability of amines is associated with the formation of charge transfer complexes between the amines and the $^1\Delta$ O_2, with its high electron affinity; the required 'spin-flip' may be assisted by spin–orbit interactions in the complex (8). β-Carotene is an extremely efficient quencher of $^1\Delta$ O_2 and the quenching proceeds by spin-allowed energy transfer with the formation of triplet β-carotene (9).

$$^1\Delta\ O_2 + {}^1C \rightarrow {}^3\Sigma\ O_2 + {}^3C$$

The rapid transfer of electronic energy is possible because the triplet energy of β-carotene is less than that of singlet oxygen. The very high quenching constants of some transition metal complexes may also be associated with their possessing low energy excited states (cf. ref. 10). Since it was not possible to obtain direct information on these energies, e.g. by phosphorescence studies, a study of the quenching of triplet pentacene by transition metal complexes was made. Triplet pentacene has an excitation energy of the order of 7000 cm^{-1} (11, 12), compared with 7882 cm^{-1} for $^1\Delta$ O_2, and it was anticipated that the ease of quenching of triplet pentacene by a metal complex would parallel its ability to deactivate singlet oxygen if a spin-allowed energy transfer mechanism were operative.

Experimental

Materials

Carbon tetrachloride, methanol, benzene, and pyridine were of certified A.C.S. grade. Methylene blue, 1,3-diphenylisobenzofuran, and pentacene were used as supplied (Aldrich Chemical Corp.). 2-Hydroxy-4-dodecyloxybenzophenone, octadecyl 3-(3′,5′-di-*tert*-butyl-4′-hydroxyphenyl)-propionate, bis(di-*n*-butyldithiocarbamato)nickel(II), Ni(di-*n*-butyl-dtc)$_3$, and bis(di-*n*-butyldithiocarbamato)zinc(II), recrystallized from a chloroform–acetone mixture, were gifts from Drs. D. J. Carlsson and D. M. Wiles. Bis(di-*i*-propyldithiophosphato)nickel(II), Ni(di-*i*-propyl-dtp)$_2$, bis(2,4-pentanedionato)diaquonickel(II), Ni(acac)$_2$aq$_2$, were used as supplied and 2,2′-thiobis-4-(*tert*-octyl)phenolato[*n*-butylamine]nickel(II) was recrystallized from a chloroform–ethanol mixture. Bis(di-*n*-butyldithiocarbamato)copper(II), bis(diethyldithiocarbamato)nickel(II), and tris(di-*n*-butyldithiocarbamato)cobalt(III) were prepared in water from copper(II) sulfate, nickel(II) chloride, and cobalt(II) nitrate respectively and the appropriate potassium dialkyldithiocarbamate (13, 14). Bis(di-*i*-propyldithiophosphato)bis[pyridine]nickel(II) was prepared by adding pyridine dropwise to a benzene solution of bis(di-*i*-propyldithiophosphato)nickel(II). Bis(diethyldithiophosphato)palladium(II) was prepared from potassium tetrachloropalladate(II) and ammonium diethyldithiophosphate (14). Bis(dithiobenzil)nickel(II) was prepared from benzoin, phosphorus pentasulfide, and nickel(II) chloride (15). Tris(2,2′-bipyridine)ruthenium(II) chloride pentahydrate, Ru(bipy)$_3$Cl$_2$, was a gift from Dr. M. C. Baird.

Apparatus

The flash photolysis apparatus was similar to that used in an earlier investigation (7). For the singlet oxygen study, the monitoring light source (435 nm) consisted of a 200 W high pressure mercury lamp and a grating monochromator. Filters of red photographic film (Diazochrome Red KRD Tecnifax) were installed between the flash tubes and the reaction cell to cut off radiation below 600 nm, in order to prevent bleaching of DPBF by light from the flash. In the pentacene study, the monitoring light source (492 nm) was a 55 W, 12 V quartz–iodine tungsten lamp. Plates of window glass (4 mm) were installed between the flash tubes and the reaction cell to reduce decomposition of the pentacene by ultraviolet radiation from the flash.

Procedure

For the singlet oxygen investigation, the sensitizer methylene blue was dissolved in methanol, and the DPBF and the quencher in carbon tetrachloride. The solvent normally consisted of carbon tetrachloride containing 2 vol% methanol, although 1 vol% methanol was adequate to solubilize the methylene blue. The solvent was saturated with air and the oxygen concentration was about 2.5×10^{-3} *M* (16). Some results were obtained using the solvent mixture saturated with oxygen at 1 atm in order to determine the effect of oxygen concentration on the decay. A typical reaction mixture contained methylene blue (5×10^{-6} *M*), DPBF (2.94×10^{-6} *M*), oxygen (2.5×10^{-3} *M*), and quencher, e.g. bis(di-*i*-propyl-dithiophosphato)nickel(II) (1.0×10^{-6} *M*). DPBF fades slowly even in the monitoring light and the initial settings of the apparatus were made with a reaction mixture containing no DPBF. The cell was then filled with a normal reaction mixture containing DPBF and the final adjustments made. Finally a fresh reaction mixture was placed in the cell and flashed (2×20 μF, 4 kV) and the decay curve on the oscilloscope screen photographed by means of a Polaroid camera.

The cell for the triplet pentacene study had a path length of 42.6 cm. A weighed amount (ca. 0.5 mg) of pentacene was placed in the degassing ampoule attached to the cell and benzene (70 ml), or a benzene solution of the quencher, added. The mixture was carefully degassed three times on the vacuum line and left overnight to allow complete solution of the pentacene. The reaction mixture was then transferred to the cell compartment, the condenser banks (10 μF) charged to 6 kV, and the decay curve recorded in the usual manner.

Results and Discussion

Decay of Singlet Oxygen in Carbon Tetrachloride – Methanol Mixtures

The decay of singlet oxygen was first studied in the absence of added quencher. The rate of decay was determined by monitoring the bleaching of the acceptor DPBF photometrically. The $^1\Delta$ O_2 is formed by energy transfer from triplet methylene blue, ^{3}MB,

[I] $$^3\text{MB} + {}^3\Sigma\ O_2 \rightarrow {}^1\text{MB} + {}^1\Delta\ O_2$$

Can. J. Chem. Downloaded from www.nrcresearchpress.com by 210.87.254.6 on 09/05/12
For personal use only.

and it decays to ground state oxygen either by physical deactivation

[2] $$^1\Delta\, O_2 \rightarrow {}^3\Sigma\, O_2$$

with rate constant $1/\tau$, or by reaction with DPBF (A) to give the peroxide AO_2

[3] $$^1\Delta\, O_2 + A \rightarrow AO_2$$

with rate constant k_A. The decay is observable over a period of about 1 ms with carbon tetrachloride + 2% methanol as solvent. If $[AO_2]$ and $[AO_2]_\infty$ are the concentrations respectively of AO_2 at time t and after the decay of $^1\Delta\, O_2$ is complete, and $[^1\Delta]_0$ is the concentration of $^1\Delta\, O_2$ at the start of the decay, it can be shown (10) that

[4] $$[AO_2]_\infty - [AO_2] = \frac{k_A[A][^1\Delta]_0}{1/\tau + k_A[A]} \times \exp -(1/\tau + k_A[A])t$$

[5] $$2.30 \log ([A] - [A]_\infty) = -(1/\tau + k_A[A])t + \text{constant}$$

If OD, OD_∞ represent optical densities of DPBF at time t and after complete decay of $^1\Delta\, O_2$,

[6] $$2.30 \log (OD - OD_\infty) = -(1/\tau + k_A[A])t + \text{constant}$$

Plots of log $(OD - OD_\infty)$ vs. t yield lines of slope $-(1/\tau + k_A[A])/2.30$. Typical first order decay plots for initial DPBF concentrations of 1.47×10^{-6} and 6.12×10^{-6} M are shown in Fig. 1. The plots show slight curvature due to the change in [A], and hence of $k_A[A]$, during the course of an experiment. A summary of the experimental conditions used and the derived $1/\tau + k_A[A]$ values is given in Table 1. Following the suggestion of Young *et al.* (17), the results have been analyzed using the average acceptor concentration $[A]_{AV}$. A plot of $1/\tau + k_A[A]$ vs. $[A]_{AV}$ is linear and values of $\tau = 310 \pm 50$ μs and $k_A = (5.3 \pm 1.7) \times 10^8\ M^{-1}\ s^{-1}$ were derived for the solvent carbon tetrachloride + 2 vol% methanol.

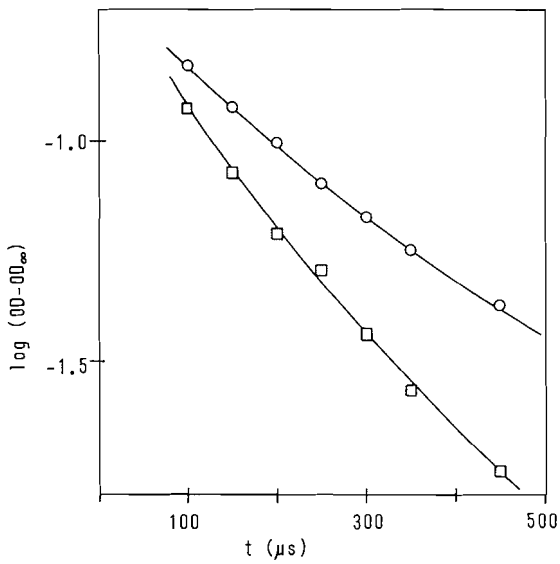

FIG. 1. First order decay plots for singlet oxygen. □, $[A]_0 = 6.12 \times 10^{-6}$ M, 5 cm cell; ○, $[A]_0 = 1.47 \times 10^{-6}$ M, 20 cm cell.

The effect of changing the methanol content from 1 to 5 vol% was examined. The first order decay constants, $1/\tau$, are plotted against methanol content of the solvent in Fig. 2. Linear extrapolation yields a value of $1/\tau = (1.42 \pm 0.40) \times 10^3\ s^{-1}$ for pure carbon tetrachloride, corresponding to a lifetime of 700^{+280}_{-150} μs in this solvent (cf. Merkel and Kearns (6), 700 ± 200 μs). It was not expected that quenching by methylene blue and oxygen would contribute significantly to $1/\tau$, and, in agreement with this, changing the concentration of methylene blue and of oxygen by factors of 2 and 5 respectively did not affect the decay rates of $^1\Delta\, O_2$ in carbon tetrachloride containing 2 vol% methanol.

The rate constants, k_A, for the reaction of singlet oxygen with DPBF are respectively 7.3, 4.8, 5.4, 5.2, and $6.0 \times 10^8\ M^{-1}\ s^{-1}$ at 25°C for methanol contents of 1, 2, 3, 4, and 5 vol%. There may be some change with methanol content but the results are all in the range $4.8–7.3 \times 10^8\ M^{-1}\ s^{-1}$ and they are the same within the margin of experimental error. These values compare with k_A values of $3 \times 10^8\ M^{-1}\ s^{-1}$ for carbon disulfide containing 2 vol% methanol as solvent (7) and $2 \times 10^9\ M^{-1}\ s^{-1}$ for pyridine (17).

TABLE 1. Effect of acceptor DPBF concentration [A] on decay of singlet oxygen ($^1\Delta$) in carbon tetrachloride containing 2 vol% methanol

Cell length	$[A]_0$[a] ($\times 10^6\ M$)	$[A]_\infty$[b] ($\times 10^6\ M$)	$[A]_{AV}$[c] ($\times 10^6\ M$)	$1/\tau + k_A[A]$ ($\times 10^{-3}\ s^{-1}$)
20	1.46	0.97	1.22	3.93
15	1.45	0.92	1.19	4.05
		0.73	1.09	4.12
10	2.94	1.82	2.38	4.38
		1.77	2.36	4.40
		1.83	2.39	4.38
		1.82	2.38	4.37
		1.71	2.33	4.29
		1.98	2.46	4.67
7	4.99	2.98	3.99	5.62
		2.92	3.97	5.67
	5.02	3.10	4.06	5.84
		3.42	4.22	5.40
5	6.12	4.35	5.24	5.87
		4.39	5.26	5.95

[a] $[A]_0$ is the initial acceptor DPBF concentration.
[b] $[A]_\infty$ is the acceptor concentration at $t = \infty$ after all singlet oxygen ($^1\Delta$) has decayed.
[c] $[A]_{AV}$ is the average of $[A]_0$ and $[A]_\infty$.

Can. J. Chem. Downloaded from www.nrcresearchpress.com by 210.87.254.6 on 09/05/12
For personal use only.

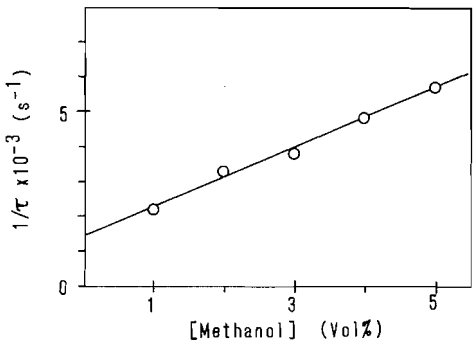

FIG. 2. Effect of methanol on $1/\tau$ for singlet oxygen ($^1\Delta$) in carbon tetrachloride.

Quenching of Singlet Oxygen by Polyolefin Stabilizers

Addition of a polyolefin stabilizer, Q, such as bis(di-*i*-propyldithiophosphato)nickel(II) to the solution provides an additional mode of decay of $^1\Delta\ O_2$

$$[7] \qquad {}^1\Delta\ O_2 + Q \rightarrow {}^3\Sigma\ O_2 + Q$$

If k_Q is the rate constant for deactivation via reaction [7] the dependence of $[AO_2]$ on time is given by

$$[8] \quad 2.3 \log \{[AO_2]_\infty - [AO_2]\} = -(1/\tau + k_A[A] + k_Q[Q])t + \text{constant}$$

so that

$$[9] \quad 2.3 \log (OD - OD_\infty) = -(1/\tau + k_A[A] + k_Q[Q])t + \text{constant}$$

Thus values of k_Q may be obtained from plots of log $(OD - OD_\infty)$ vs. t in the absence and in the presence of quencher. A relatively high quencher concentration results in only slight bleaching of the DPBF so that the useful range of quencher concentrations is generally only two- or threefold. It was confirmed, however, that over this range the slopes of log $(OD - OD_\infty)$ vs. t plots increase linearly with [Q] for all nickel and cobalt chelates investigated. For example, the magnitudes of these slopes for concentrations of $Ni(acac)_2aq_2$ of 0, 4.4×10^{-5}, and 8.8×10^{-5} M were found to be 10.1×10^3, 16.8×10^3, and 23.7×10^3 s^{-1}; the slopes are reproducible to better than $\pm 4\%$.

The rate constants, k_Q, for the quenching of $^1\Delta\ O_2$ by a range of polyolefin stabilizers and related compounds are given in Table 2. In some instances the k_Q values quoted are upper limits. At concentrations of 2-hydroxy-4-dodecycloxybenzophenone up to 10^{-2} M, no increase in slope of the decay plot was observed. The highest concentrations of Cu(di-*n*-butyl-dtc)$_2$ and $Ru(bipy)_3Cl_2$ which could be used were 5×10^{-6} and 1×10^{-6} M respectively because these complexes absorb significantly at the wavelength of the monitoring light. At these concentrations, the copper and ruthenium complexes had no effect on the decay of singlet oxygen.

TABLE 2. Rate constants for quenching of singlet oxygen ($^1\Delta$) and triplet pentacene by polyolefin stabilizers and related transition metal complexes

Quencher	Singlet oxygen ($^1\Delta$)[a] k_Q ($\times 10^{-8}$ M^{-1} s^{-1})	Triplet pentacene[b] k_Q ($\times 10^{-8}$ M^{-1} s^{-1})
2-Hydroxy-4-dodecycloxybenzophenone	<0.002	—
Octadecyl 3-(3′,5′-di-*tert*-butyl-hydroxyphenyl)propionate	0.0046 ± 0.0006	—
Bis[2,2′-thiobis-4-(*tert*-octyl)phenolato]nickel(II)	6.0 ± 3.2[c]	—
Zn(di-*n*-butyl-dtc)$_2$	0.2 ± 0.1[c]	0.0018 ± 0.0015
$Ni(acac)_2aq_2$	0.66 ± 0.06	0.54 ± 0.06
2,2′-Thiobis-4-(*tert*-octyl)phenolato[*n*-butylamine]nickel(II)	6.0 ± 3.2[c,d]	0.23 ± 0.15
Co(di-*n*-butyl-dtc)$_3$	12 ± 2	3.3 ± 0.7
Ni(diethyl-dtc)$_3$	66 ± 6	7.0 ± 0.8
Ni(di-*i*-propyl-dtp)$_3$	76 ± 10	7.8 ± 3.4
Bis(dithiobenzil)nickel(II)	147[e]	47 ± 7
Ni(di-*n*-butyl-dtc)$_3$	$41 \pm 6 (40 \pm 15)$[c]	—
Cu(di-*n*-butyl-dtc)$_3$	<5	—
$Ru(bipy)_3Cl_2$	<10	—
Ni(di-*i*-propyl-dtp)$_3$py$_2$	—	3.6 ± 0.6
Pd(diethyl-dtp)$_2$	—	<0.2
Pt(diethyl-dtp)$_2$	—	<0.02

[a]Values obtained in carbon tetrachloride containing 2 vol% methanol.
[b]Values obtained in benzene at room temperature.
[c]Values obtained by Flood *et al.* (7) in carbon disulfide containing 2 vol% methanol.
[d]Value revised as a tetramer (3).
[e]Value estimated from reported datum (4) assuming that the quenching rate constant for β-carotene is 2×10^{10} M^{-1} s^{-1} in toluene.

As has been noted in earlier studies (2–4), nickel complexes containing sulfur ligands are efficient quenchers of singlet oxygen. A change in the metal in the complex may result in a considerable reduction in k_Q. For example Ni(di-*n*-butyl-dtc)$_2$ has a k_Q of 4.1×10^9 M^{-1} s^{-1} whereas Zn(di-*n*-butyl-dtc)$_2$ has a k_Q of only 2×10^7 M^{-1} s^{-1}. This wide variation indicates that enhancement of intersystem crossing by heavy atoms is not a major factor with these quenchers. There is also no correlation between k_Q and the paramagnetism of the complexes. The rate constants for the diamagnetic complexes investigated range from 2×10^7 M^{-1} s^{-1} (Zn(di-*n*-butyl-dtc)$_2$) to 7.6×10^9 M^{-1} s^{-1} (Ni(di-*i*-propyl-dtp)$_2$). Paramagnetic complexes include $Ni(acac)_2aq_2$ for which $k_Q = 6.6 \times 10^7$ M^{-1} s^{-1}, Cu(di-*n*-butyl-dtc)$_2$ ($k_Q < 5 \times 10^8$ M^{-1} s^{-1}), and probably 2,2′-thiobis-4-(*tert*-octyl)phenolato[*n*-butylamine]nickel(II) (18) for which $k_Q = 6.0 \times 10^8$ M^{-1} s^{-1}.

The high rate constants for the diamagnetic nickel

Can. J. Chem. Downloaded from www.nrcresearchpress.com by 210.87.254.6 on 09/05/12
For personal use only.

complexes can be accounted for by a spin-allowed transfer of electronic energy from singlet oxygen to the metal complex

[10] $$^1\Delta O_2 + {}^1Q \rightarrow {}^3\Sigma O_2 + {}^3Q$$

For efficient transfer, the energy of the lowest triplet state of the complex must be lower than or near to the excitation energy of $^1\Delta O_2$ (9). Experimental data on triplet energies of the diamagnetic d^8 nickel dialkyldithiocarbamates and dialkyldithiophosphates are not available since these substances do not phosphoresce. However, their lowest singlet–singlet absorptions, which are due to metal *d–d* transitions, are observed and they can be used to make rough estimates of the required triplet energies. It is found that the energy differences between singlet–singlet absorption maxima and estimated triplet (0–0) energies for complexes of first and second transition metals (e.g. ruthenocene)[1] are of the order of 8000 cm^{-1}. If the same difference applies to Ni(diethyl-dtc)$_2$ and Ni(diethyl-dtp)$_2$, their respective triplet energies are close to 8000 and 7000 cm^{-1}. These estimates are only approximate but they indicate that low lying triplet levels are available to permit deactivation of singlet oxygen via reaction [10]. A low triplet energy of ~8000 cm^{-1} is also estimated for diamagnetic d^6 Co(di-*n*-butyl-dtc)$_3$ for which a k_Q of 1.2×10^9 M^{-1} s^{-1} is observed. On the other hand Ru(bipy)$_3$Cl$_2$ phosphoresces with a maximum at 15 700 cm^{-1} (20) and the lowest singlet–singlet absorption in d^{10} Zn(di-*n*-butyl-dtc)$_2$, an internal ligand transition, is about 36 000 cm^{-1} (14). These complexes do not possess triplet energies close to the excitation energy of $^1\Delta O_2$ and their k_Q values are correspondingly low ($<1 \times 10^9$ M^{-1} s^{-1} for the ruthenium complex and 2×10^7 M^{-1} s^{-1} for the zinc complex).

Decay of Triplet Pentacene in Benzene

The decay of triplet pentacene in benzene solution was first studied in the absence of added quenchers. In these experiments, the concentration of pentacene is very low ($<3 \times 10^{-5}$ *M*) so that quenching by ground state pentacene is small (11). Triplet–triplet quenching may be observable with flash times of 4 μs (11), but it is not important under the conditions used in this work. The decay can therefore be analysed assuming a simple first order process,

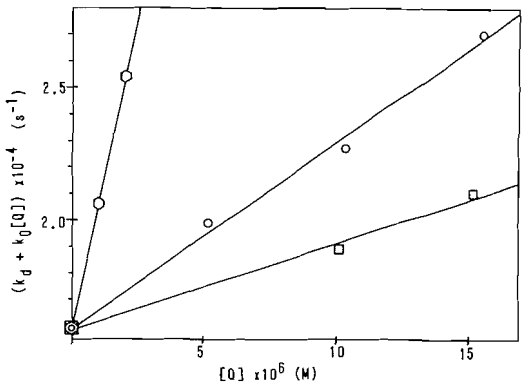

FIG. 3. Effect of quenchers on the decay of triplet pentacene. ⬡, Bis(dithiobenzil)nickel(II); ○, nickel(diethyl-dtc)$_2$; □, Co(di-*n*-butyl-dtc)$_3$.

[11] $$2.3 \log OD = -k_d t + \text{constant}$$

where OD represents the optical density of triplet pentacene at time *t* and k_d is the first order decay constant. Plots of log OD vs. *t* are linear;[2] the value of k_d obtained from results with a number of initial solutions was $(1.59 \pm 0.06) \times 10^4$ s^{-1}. This compares with a value of $(1.43 \pm 0.07) \times 10^4$ s^{-1} recorded by Hellner *et al.* (11). The result was unaffected when the pentacene concentration was lowered by a factor of three. The same k_d was obtained when a given solution was flashed a dozen times suggesting that the residual concentration of oxygen is sufficiently low to have no measurable effect on the rate of decay (cf. ref. 24). The effect of adding 1 vol% pyridine was determined because it was necessary to have pyridine present in the quenching study of Ni(di-*i*-propyl-dtp)$_2$py$_2$. The k_d value for benzene containing 1 vol% pyridine was $1.45 \pm 0.05 \times 10^4$ s^{-1}.

Quenching of Triplet Pentacene by Transition Metal Complexes

Addition of a quencher, Q, provides a further route for the decay of triplet pentacene,

[12] $$^3P + Q \rightarrow {}^1P + Q$$

If the rate constant for this process is k_Q, the dependence of log OD on time in the presence of quencher is given by [13]

[13] $$2.3 \log OD = -(k_d + k_Q[Q])t + \text{constant}$$

k_Q values can thus be derived from the slopes of plots

[1]Ruthenocene has its lowest singlet–singlet and singlet–triplet absorptions (19) and phosphorescence maximum (20, 21) at 29 500, 26 000, and 17 000 cm^{-1} respectively. The triplet (0–0) energy was assumed to be midway between the absorption and phosphorescence maxima, i.e. 21 500 cm^{-1}, yielding an energy difference between the singlet–singlet absorption maximum and triplet (0–0) energy of ruthenocene of 8000 cm^{-1}. Similar treatment of Rh(dimethyl-dtc)$_3$ (22) and ferrocene (19, 23) gives differences of 7700 and 7800 cm^{-1} respectively.

[2]Copies of a typical decay curve and a plot of log OD vs. *t* are available, at a nominal charge, from the Depository of Unpublished Data, CISTI, National Research Council of Canada, Ottawa, Ont., Canada K1A 0S2.

Can. J. Chem. Downloaded from www.nrcresearchpress.com by 210.87.254.6 on 09/05/12
For personal use only.

of log OD vs. time. For the quenchers bis(dithiobenzil)nickel(II), Ni(diethyl-dtc)$_2$, and Co(di-*n*-butyl-dtc)$_3$, the concentration of quencher was varied; the decay rate constants, $k_d + k_Q[Q]$, are plotted against [Q] in Fig. 3. The results for all the quenchers investigated are summarized in Table 2. The k_Q values for Pd(diethyl-dtp)$_2$ and Pt(diethyl-dtp)$_2$ are merely upper limits; no quenching was observed at the highest quencher concentrations (respectively 1×10^{-4} and 9×10^{-4} M) which could be used without serious absorption by the quencher at the monitoring wavelength (492 nm). Quenching by Zn(di-*n*-butyl-dtc)$_2$ was small even at a concentration of 10^{-2} M.

The measured k_Q's range from 1.8×10^5 M^{-1} s^{-1} for Zn(di-*n*-butyl-dtc)$_2$ to a maximum of 4.7×10^9 M^{-1} s^{-1} for bis(dithiobenzil)nickel(II). As with the deactivation of singlet oxygen, there is no correlation between k_Q and the paramagnetism of the metal complex. The quenching rate constants for the paramagnetic complexes investigated range from 2.3×10^7 to 3.4×10^8 M^{-1} s^{-1} whereas those for diamagnetic complexes range from 1.8×10^5 to 4.7×10^9 M^{-1} s^{-1}. Square planar complexes appear to be slightly more efficient than the roughly corresponding octahedral complexes. For example, the k_Q for square planar Ni(diethyl-dtc)$_2$ is 7×10^8 M^{-1} s^{-1} whereas that for octahedral Co(di-*n*-butyl-dtc)$_3$ is 3.3×10^8 M^{-1} s^{-1}. Addition of two molecules of pyridine to square planar Ni(di-*i*-propyl-dtp)$_2$ to form the octahedral bis[pyridine] complex reduces k_Q from 7.8×10^8 to 3.6×10^8 M^{-1} s^{-1}.

The quenching of triplet pentacene by transition metal complexes can best be interpreted in terms of an electronic energy transfer mechanism (25–27). Farmilo and Wilkinson determined rate constants for quenching of the triplet states of 16 organic compounds by tris(acetylacetonato)iron(III), -ruthenium(III), and -aluminum(III). They established energy transfer as the mechanism of quenching by relating quenching ability to the energies of the triplet states being quenched and the spectroscopically determined energy levels of the complexes. In the present study the highest k_Q value, 4.7×10^9 M^{-1} s^{-1}, was observed for quenching by diamagnetic bis(dithiobenzil)nickel(II). This is close to the maximum value of about 6×10^9 M^{-1} s^{-1} associated with quenching of triplet states in benzene at room temperature (23, 28). The lowest singlet–singlet electronic transition observed for the dithiobenzil complex has an energy of 11 500 cm^{-1} (15), and a rough estimate of the lowest triplet energy is 5500 cm^{-1}. Since this is almost certainly lower than the triplet energy of pentacene, it is not surprising that the quenching ability of the complex is high. The electronic transition involved is a ligand π–π^* transition so that steric factors are likely to be unimportant.

Ni(diethyl-dtc)$_2$ possesses a *d–d* transition whose triplet energy is estimated to be approximately 8000 cm^{-1}; this is perhaps slightly higher than the triplet energy of pentacene. Its quenching ability would be expected to be lower than that of the benzil complex and in fact its k_Q value is 7.0×10^8 M^{-1} s^{-1}. On the other hand, Ni(diethyl-dtc)$_2$ is approximately 4000 times more efficient than Zn(di-*n*-butyl-dtc)$_2$ in quenching triplet pentacene. The zinc complex has a d^{10} structure and does not possess any low energy triplet levels; it is therefore impossible for it to quench triplet pentacene by an efficient energy transfer process. Furthermore, the replacement of Ni(II) in dialkyldithiophosphato complexes by Pd(II) or Pt(II) increases significantly the energy of the *d–d* transition (rough estimates of the triplet energies are respectively 14 000 and 15 000 cm^{-1}). The k_Q values of these complexes are low because their triplet energies are too large to allow significant energy transfer.

Comparison of Results for Singlet Oxygen and Triplet Pentacene

The rate constants, k_Q, for the quenching of singlet oxygen and triplet pentacene by a number of metal complexes are given in Table 2. There is a good correlation between the two sets of results, although in many cases the k_Q for singlet oxygen is an order of magnitude greater than the k_Q for triplet pentacene. These results add support to the conclusion that the quenching of singlet oxygen and of triplet pentacene both proceed by way of electronic energy transfer. The involvement of similar chemical factors, in e.g. complex formation, is unlikely in view of the dissimilar natures of singlet oxygen and triplet pentacene.

The diffusion controlled rate constants for the quenching of singlet oxygen (6, 29) and triplet pentacene (28) in benzene are about 2×10^{10} and 6×10^9 M^{-1} s^{-1} respectively. The rate constants for bis(dithiobenzil)nickel(II) are about 3/4 of these values; the difference between the rate constants for this highly efficient quencher may have its origin in differing diffusion rates of singlet oxygen and triplet pentacene in solution. The rate constants also depend on the relative magnitudes of the excitation energies of singlet oxygen and triplet pentacene. The value for singlet oxygen is known to be 7882 cm^{-1} but the calculated values for triplet pentacene vary from 6400 to 8500 cm^{-1}, and an experimental value, obtained from phosphorescence studies of pentacene in tetracene (12), is as low as 6500 cm^{-1}. The triplet energy of pentacene is thus probably slightly lower

Can. J. Chem. Downloaded from www.nrcresearchpress.com by 210.87.254.6 on 09/05/12
For personal use only.

than the excitation energy of $^1\Delta$ O_2, and this could lead to a more rapid fall-off of k_Q with triplet pentacene as donor, as opposed to singlet oxygen, as the lowest triplet energy of the acceptor is increased. A steric factor may also affect rate constants in solution, particularly if k_Q is considerably less than that expected for the diffusion controlled reaction (26). Large triplet pentacene molecules are likely to be subject to greater steric hindrance in the process of exchanging energy than small singlet oxygen molecules. This may be of particular significance when the acceptor is a square planar complex with the appropriate orbitals localized on the central metal atom.

Acknowledgements

This work was supported by an operating grant from the National Research Council of Canada. We thank Dr. J. K. S. Wan for the use of flash photolysis equipment and Drs. D. Carlsson and D. M. Wiles for discussion and the gift of additives.

1. D. J. Carlsson and D. M. Wiles. J. Macromol. Sci. Rev. Macromol. Chem. **14**, 65 (1976), and references therein.
2. D. J. Carlsson, G. D. Mendenhall, T. Suprunchuk, and D. M. Wiles. J. Am. Chem. Soc. **94**, 8960 (1972).
3. J. P. Guillory and C. F. Cook. J. Polym. Sci. Polym. Chem. Ed. **11**, 1927 (1973).
4. A. Zweig and W. A. Henderson, Jr. J. Polym. Sci. Polym. Chem. Ed. **13**, 717 (1975).
5. D. R. Adams and F. Wilkinson. J. Chem. Soc. Faraday Trans. II, **68**, 586 (1972).
6. P. B. Merkel and D. R. Kearns. J. Am. Chem. Soc. **94**, 7244 (1972).
7. J. Flood, K. E. Russell, and J. K. S. Wan. Macromolecules, **6**, 669 (1973).
8. E. A. Ogryzlo and C. W. Tang. J. Am. Chem. Soc. **92**, 5034 (1970).
9. C. S. Foote and R. W. Denny. J. Am. Chem. Soc. **90**, 6233 (1968).
10. A. Adamczyk and F. Wilkinson. J. Appl. Polym. Sci. **18**, 1225 (1974); A. Farmilo and F. Wilkinson. Photochem. Photobiol. **18**, 447 (1973).
11. C. Hellner, L. Lindquist, and P. C. Roberge. J. Chem. Soc. Faraday Trans. II, **68**, 1928 (1972).
12. N. E. Geacintov, J. Burgos, M. Pope, and C. Strom. Chem. Phys. Lett. **11**, 504 (1971).
13. H. J. Cavell and S. Sugden. J. Chem. Soc. 621 (1935).
14. C. K. Jørgensen. J. Inorg. Nucl. Chem. **24**, 1571 (1962).
15. G. N. Schrauzer and V. P. Mayweg. J. Am. Chem. Soc. **87**, 1483 (1965).
16. E. Wilhelm and R. Battino. Chem. Rev. **73**, 1 (1973).
17. R. H. Young, D. Brewer, and R. A. Keller. J. Am. Chem. Soc. **95**, 375 (1973).
18. F. A. Cotton and G. Wilkinson. Advanced inorganic chemistry. 3rd ed. Interscience, New York, NY. 1972. p. 892.
19. Y. S. Sohn, D. N. Hendrickson, and H. B. Gray. J. Am. Chem. Soc. **93**, 360 (1971).
20. M. S. Wrighton, L. Pdungsap, and D. L. Morse. J. Phys. Chem. **79**, 66 (1975).
21. G. A. Crosby, G. D. Hager, K. W. Hipps, and M. L. Stone. Chem. Phys. Lett. **28**, 497 (1974).
22. M. K. DeArmond. Acc. Chem. Res. **7**, 309 (1974).
23. A. Farmilo and F. Wilkinson. Chem. Phys. Lett. **34**, 575 (1975).
24. G. Porter and M. W. Windsor. Proc. R. Soc. London Ser. A, **245**, 238 (1958).
25. F. Wilkinson. Pure Appl. Chem. **41**, 661 (1975).
26. F. Wilkinson and A. Farmilo. J. Chem. Soc. Faraday Trans. II, **72**, 604 (1976).
27. W. G. Herkstroeter. J. Am. Chem. Soc. **97**, 4161 (1975).
28. P. J. Wagner and I. Kochevar. J. Am. Chem. Soc. **90**, 2232 (1968).
29. W. R. Ware. J. Phys. Chem. **66**, 455 (1962).

The crystal and molecular structure of *trans*-chloro(3-hydroxypropyl-*N*,*N*-dimethylaminocarbene)-bis(dimethylphenylphosphine)platinum(II) hexafluorophosphate

ROBERT F. STEPANIAK AND NICHOLAS C. PAYNE[1]

Department of Chemistry, University of Western Ontario, London, Ont., Canada N6A 5B7

Received July 4, 1977

ROBERT F. STEPANIAK and NICHOLAS C. PAYNE. Can. J. Chem. **56**, 1602 (1978).

The crystal and molecular structure of *trans*-chloro(3-hydroxypropyl-*N*,*N*-dimethylaminocarbene)bis(dimethylphenylphosphine)platinum(II) hexafluorophosphate has been determined from three-dimensional X-ray data collected on an automated four circle diffractometer using CuKα radiation. The compound crystallizes in the orthorhombic space group $Pna2_1$, with $Z = 4$, and cell dimensions $a = 14.403(2)$, $b = 12.631(2)$, and $c = 16.151(2)$ Å. Full matrix least-squares refinement on F gave a final conventional R factor of 0.047 for 3442 observations with $I > 3\sigma(I)$. The cation coordination geometry is square planar, with the carbene ligand lying approximately perpendicular to the plane. The Pt—Cl bond length is 2.356(4) Å and the Pt—C(carbene) distance is 1.978(12) Å. The C(carbene)—N bond length is 1.293(16) Å. These dimensions are discussed in terms of the *trans* influences of the carbene and chloride ligands and the bonding in the carbene species.

ROBERT F. STEPANIAK et NICHOLAS C. PAYNE. Can. J. Chem. **56**, 1602 (1978).

On a déterminé la structure cristalline et moléculaire de l'hexafluorophosphate du chloro-(hydroxy-3-propyl-*N*,*N*-diméthylaminocarbène)bis(diméthylphénylphosphine) platine(II) *trans* à partir de données de rayon-X tridimensionnelles recueillies sur un diffractomètre automatique à quatre cercles utilisant la radiation CuKα. Le composé cristallise dans le groupe d'espace orthorhombique $Pna2_1$, avec $Z = 4$, et des dimensions de mailles $a = 14.403(2)$, $b = 12.631(2)$ et $c = 16.151(2)$ Å. On a affiné la structure par la méthode des moindres carrés (matrice complète) jusqu'à une valeur finale de R de 0.047 pour 3442 observations avec $I > 3\sigma(I)$. La géométrie de coordination du cation est plan carrée alors que le ligand carbène se trouve approximativement perpendiculaire au plan. La longueur de la liaison Pt—Cl est 2.356(4) Å et la distance Pt—C(carbène) est 1.978(12) Å. La longueur de la liaison C(carbène)—N est 1.293(16) Å. On discute de ces dimensions en terme des influences *trans* des ligands carbène et chlorure et de la nature des liaisons dans les espèces carbène.

[Traduit par le journal]

Introduction

The investigation of the structure, bonding, and geometry of carbene ligands has been the focus of much research. Square planar complexes of Pt(II) containing tertiary carbene ligands have been studied using X-ray crystallographic techniques (1–6). The carbene ligands in these compounds can conveniently be divided into two categories:

A *B*

X, Y = OR, NR′R″, SR
R = alkyl, aryl
R′R″ = H, alkyl, aryl

Several structures of complexes containing ligands of type *A* have been reported (4–6). In general it has been concluded that virtually all the stabilization of the C(carbene) atom is by electron donation from the nucleophilic substituents X and Y. Metal–ligand $d\pi$–$p\pi$ interaction has been shown to be at best very weak by both structural (4, 5)[2] and spectroscopic (8) studies. Pt—Cl bond lengths in complexes where the Cl^- is *trans* to type *A* carbene ligands show that these carbenes exert a very strong *trans* influence (5, 6).

We have determined the structures of several square planar cationic complexes of Pt(II) containing carbene ligands of type *B* (1–3) in order to study the bonding and *trans* influence of these entities. All complexes studied contain a methyl ligand in the coordination site *trans* to the carbene. The Pt—C(methyl) bond lengths observed have proved to be poor indicators of the *trans* influence of the carbene ligands.

Recent successes in estimating the *trans* influence of carbon donor ligands from Pt—Cl bond lengths (9) prompted us to determine the structure of a complex where a chloride ion replaced the methyl ligand opposite a carbene ligand of type *B*. The complex selected was the product of ring cleavage of

[1]Author to whom correspondence should be addressed.

[2]R. F. Stepaniak and N. C. Payne, unpublished results.

Can. J. Chem. Downloaded from www.nrcresearchpress.com by 210.87.254.42 on 09/05/12
For personal use only.

Can. J. Chem. Downloaded from www.nrcresearchpress.com by 210.87.254.42 on 09/05/12
For personal use only.

a cyclic alkoxycarbene ligand (10), which was prepared by the method of Chisholm and Clark (11). Treatment with dimethylamine opened the ring, and the *trans* methyl ligand was subsequently replaced by Cl^- by reaction with HCl. Detailed preparative, spectral, and physical data for the salt are presented elsewhere (12).

In addition to examining the *trans* influence of the carbene, we are also interested in the effect of ligands of varying *trans* influence on the Pt—C(carbene) bond, and in the structure and geometry of the type *B* carbene ligand as compared to carbenes of type *A*.

Experimental

Irregular octahedral blocks of **1**, *trans*-[PtCl{HO$(CH_2)_3$-C=NMe_2}$(PMe_2Ph)_2$]PF_6, were obtained by recrystallization from a mixture of dichloromethane and ether. Preliminary Weissenberg and precession photographs indicated the orthorhombic system. The observed systematic absences, $0kl$; $k + l$ odd, and $h0l$; h odd, are consistent with the centrosymmetric space group *Pnam*, an alternate setting of *Pnma* (D_{16}^{2h} No. 32) and the acentric space group $Pna2_1$ (C_{2v}^9 No. 33) (13).

The density of the crystals, determined by flotation in CH_2BrCH_2Br and CCl_4, and the cell volume indicate a Z value of 4. For *Pnam* the ions must occupy special positions of site symmetry m, while no symmetry restrictions are imposed upon the ions in space group $Pna2_1$. The presence of the long alcoholic group bonded to C(carbene) minimizes the possibility of the presence of a mirror plane through Cl, Pt, and the carbene ligand, so m site symmetry was considered unlikely. The structure solution was therefore initiated in $Pna2_1$, and successfully completed.

A crystal with well developed faces and of dimensions $0.22 \times 0.17 \times 0.18$ mm[3] was selected. Optical goniometry was used to identify the 15 crystal faces, the forms {111}, {11$\bar{1}$}, and {01$\bar{1}$}, and the faces (001), (0$\bar{1}$1), ($\bar{1}\bar{1}$0), (110), and (1$\bar{1}$0). The crystal was mounted on a Picker FACS-1 computer controlled diffractometer taking care that symmetry axes were not coincident with the spindle axis to avoid multiple reflections (14). Twenty-five reflections in the range $34° < 2\theta < 72°$ (CuKα, $\lambda = 1.54056$ Å) were centered. Least-squares refinement of the setting angles[3] was carried out to obtain an orientation matrix, the unit cell constants, and their estimated standard deviations (esd). These and other crystal data are given in Table 1. The ω scans of several intense, low angle reflections were recorded to check crystal mosaicity. The mean width at half height was 0.06°. The conditions for data collection are also given in Table 1. 5296 hkl and $hk\bar{l}$ intensities were recorded out to a 2θ maximum of 125°. The five standard reflections showed a mean increase of 10(1)% over the period of the experiment, and a slight deterioration in peak quality was observed. No correction was applied to the data for this increase in intensity, which is attributed to an increase in crystal mosaicity. All data were corrected for background, Lorentz, and polarization effects, and a standard deviation σ assigned to each value as previously described (15). p was taken as 0.03. 3442 observations were found to have $I > 3\sigma$. The structure solution was based on these reflections only. All data with $I > 0$ were corrected for absorption[3]. The maximum and minimum transmission coefficients are 0.407 and 0.261 respectively.

[3]The computer programs used include local modifications of the following: cell refinement and orientation matrix, PICKTT, from W. C. Hamilton's MODE1; full matrix least-squares, J. A. Ibers' NUCLS; Patterson and Fourier syntheses, A. Zalkin's FORDAP; function and errors, W. R. Busing, K. O. Martin, and H. A. Levy's ORFFE; crystal structure illustrations, C. K. Johnson's ORTEP; absorption correction by the analytical method of de Meulenaer and Tompa in the program AGNOST as modified by Cahen and Ibers (7).

Structure Solution and Refinement

From a three-dimensional Patterson function the positional parameters of the Pt atom were obtained. These values, together with an overall scale factor, were varied in the cycles of least-squares refinement. Agreement factors were obtained of

$$R_1 = \frac{\sum(||F_o| - |F_c||)}{\sum |F_o|} = 0.232$$

and

$$R_2 = \left[\frac{\sum w(|F_o| - |F_c|)^2}{\sum w(F_o)^2}\right]^{1/2} = 0.293$$

where F_o and F_c are the observed and calculated structure factor amplitudes. w is the weighting factor given by $4F_o^2/\sigma^2$. The function minimized in all least-squares calculations was $\sum w(|F_o| - |F_c|)^2$. The scattering factors for Pt, P, Cl, F, O, N, and C were those of Cromer and Waber (16) and those for the H atom were taken from Stewart, Davidson, and Simpson (17). Corrections for the anomalous dispersion of Pt, P, and Cl atoms were those calculated by Cromer and Liberman (18).

Remaining non-hydrogen atom positions were determined from successive least-squares refinements and difference Fourier syntheses. The orientation of the cations in the unit cell was found to be such as to preclude m symmetry as required by space group *Pnam*, so the choice of $Pna2_1$ as the correct space group was confirmed. As a further test for the presence of a centre of symmetry, the distribution of E values was compared to theoretical calculations for centric and acentric crystals. However, the results were inconclusive.

The phosphine phenyl rings were refined as rigid groups (19) with D_{6h} symmetry, and a rigid group of O_h symmetry described the six F atoms of the anion. During refinement with isotropic non-group atom temperature factors and overall group thermal parameters being varied, together with positional parameters and an overall scale factor, the temperature factor of the F6 rigid group increased to about 26 Å^2. An examination of a difference Fourier synthesis suggested either excessive thermal motion of the anion, or the presence of disorder. Two models were proposed to account for this. Refinement of F atoms with anisotropic thermal parameters resulted in unacceptable anion geometry, and large amplitudes of vibration. A better description was obtained by re-

Can. J. Chem. Downloaded from www.nrcresearchpress.com by 210.87.254.42 on 09/05/12
For personal use only.

TABLE 1. Crystal data and experimental conditions for data collection

$C_{22}H_{35}ClF_6NOP_3Pt$	fw = 767.0
Analysis	
Found	C 34.64, H 4.53, N 1.74
Calculated	C 34.45, H 4.60, N 1.83
Cell constants at 23°C	$a = 14.403(2)$ Å
($\lambda = 1.54056$ Å)	$b = 12.631(2)$ Å
	$c = 16.151(2)$ Å
Cell volume	2938 Å^3
Space group	$Pna2_1$
Density	
Observed	1.75(1) g cm^{-3}
Calculated	1.73 g cm^{-3}
μ(CuKα)	113.0 cm^{-1}
Filter	Ni foil prefilter, 0.018 mm
Scan range	−0.70 to +0.70 of K$\bar{\alpha}$ peak
Scan rate	2.0° min^{-1} (θ–2θ scan)
Stationary background count time	10 s
% Bragg intensity obtained	80
Take-off angle	1.8°
Crystal–counter distance	32 cm
Crystal–aperture distance	30 cm
Aperture dimensions	5 × 5 mm
2θ range	$2.5° < 2\theta \leq 125°$
Index limits	$0 \leq h \leq 16, 0 \leq k \leq 14, -18 \leq l \leq 18$

TABLE 2. Atomic positional and thermal parameters

Atom	x	y	z	U_{11}[a]	U_{22}	U_{33}	U_{12}	U_{13}	U_{23}
Pt	0.10441(4)[b]	0.05172(4)	0.2500	548(3)	535(3)	330(2)	24(3)	−124(5)	−101(5)
P(1)	0.2249(2)	−0.0689(3)	0.2431(5)	586(19)	713(23)	374(22)	95(18)	−142(28)	−38(29)
P(2)	−0.0071(3)	0.1818(3)	0.2661(2)	678(24)	535(20)	370(29)	49(19)	25(19)	−97(18)
Cl	0.1881(4)	0.1350(4)	0.3571(3)	1287(47)	1080(40)	966(36)	190(37)	−660(35)	−537(32)
P(3)	0.4534(4)	0.0642(5)	−0.0674(4)	0.093(2)[c]					
C(11)	0.2436(14)	−0.1388(14)	0.3419(9)	1189(163)	750(122)	380(84)	154(125)	−346(97)	139(80)
C(12)	0.3338(11)	−0.005(2)	0.2228(11)	467(96)	1483(157)	811(152)	−104(107)	−88(85)	63(112)
C(21)	0.0408(11)	0.3101(11)	0.2365(13)	876(108)	713(97)	535(136)	−24(84)	−40(106)	−56(97)
C(22)	−0.0473(14)	0.1963(15)	0.3706(10)	1031(153)	987(148)	463(94)	47(122)	293(99)	−247(92)
C(1)	0.0351(9)	−0.0175(11)	0.1592(7)	346(78)	518(91)	302(64)	163(68)	−25(57)	−83(58)
N	−0.0248(8)	−0.0924(9)	0.1702(7)	392(70)	652(82)	425(69)	−210(66)	53(56)	−131(58)
C(2)	−0.0486(10)	−0.1307(11)	0.255(2)	787(99)	692(95)	843(111)	−239(81)	23(175)	316(159)
C(3)	−0.0766(10)	−0.1394(14)	0.1028(11)	422(101)	795(122)	823(118)	−265(86)	−64(84)	−210(99)
C(4)	0.0533(9)	0.0164(11)	0.0702(8)	338(80)	499(88)	444(77)	8(67)	58(62)	33(63)
C(5)	0.1205(11)	0.1058(13)	0.0556(9)	598(111)	777(108)	461(81)	25(92)	−53(80)	19(78)
C(6)	0.1334(13)	0.1319(15)	−0.0354(10)	850(140)	770(120)	517(93)	−18(103)	29(90)	−62(86)
O	0.1704(8)	0.0464(11)	−0.0807(7)	724(80)	1412(117)	554(65)	−193(92)	90(59)	−163(76)

[a]Thermal parameters are given as $U_{ij} \times 10^4$ (Å^2). The form of the ellipsoid is given by $\exp[-2\pi^2(U_{11}h^2a^{*2} + U_{22}k^2b^{*2} + U_{33}l^2c^{*2} + 2U_{12}hka^*b^* \cos\gamma^* + 2U_{13}hla^*c^* \cos\beta^* + 2U_{23}klb^*c^* \cos\alpha^*)]$.
[b]Numbers in parentheses given here and in other tables are estimated standard deviations in the least significant digits.
[c]Isotropic thermal parameters are given as U (Å^2).

taining the group constraints upon the F6 entities, and introducing a second rigid group. A multiplicity parameter was refined, and the appropriate constraints were applied to the derivatives (2). The P atom of the anion, P(3), was assigned an isotropic thermal parameter, and refined as an individual atom.

$Pna2_1$ is a polar space group, so the presence of polar dispersion error must be entertained (20). Each enantiomorphic structure was refined, varying the same parameters in each case. All non-group atoms of the cation were allowed to vibrate anisotropically. Individual isotropic thermal parameters were varied for phenyl ring rigid groups and overall group temperature factors were calculated for the F6 rigid groups. Values of R_1 and R_2 for the original structure were 0.051 and 0.060 respectively. The second model converged at $R_1 = 0.060$ and $R_2 = 0.074$. Application of Hamilton's R factor significance test to the R_2 values showed that the second could be rejected at the 0.005 significance level.

TABLE 3. Rigid group parameters

Group	x_g[a]	y_g	z_g	δ	ε	η	Multiplicity
Ph-1	0.1908(5)	−0.2448(6)	0.1031(5)	2.372(9)	−2.460(7)	1.248(10)	
Ph-2	−0.1851(5)	0.1394(6)	0.1535(5)	−0.581(9)	2.329(6)	1.012(9)	
1-F6	0.4537(10)	0.0582(12)	−0.0628(10)	−0.201(14)	−3.331(13)	−0.449(14)	0.51(2)
2-F6	0.4507(10)	0.0706(13)	−0.0698(10)	−2.477(15)	3.185(13)	2.647(14)	0.49(2)

[a] x_g, y_g, and z_g are the fractional coordinates of the group origin, and δ, ε, and η (rad) are the group orientation angles. See ref. 19.

TABLE 4. Derived group atom parameters

	Atom	x	y	z	B (Å^2)
Ph-1	1C(1)[a]	0.2089(8)	−0.1732(9)	0.1665(6)	4.6(4)
	1C(2)	0.2451(8)	−0.1558(8)	0.0877(8)	5.6(4)
	1C(3)	0.2269(9)	−0.2274(10)	0.0243(5)	7.2(5)
	1C(4)	0.1726(9)	−0.3165(9)	0.0396(7)	7.3(5)
	1C(5)	0.1365(8)	−0.3339(8)	0.1184(8)	6.7(5)
	1C(6)	0.1546(8)	−0.2623(10)	0.1819(6)	5.9(4)
Ph-2	2C(1)	−0.1096(6)	0.1640(8)	0.2038(6)	4.1(3)
	2C(2)	−0.1790(8)	0.0968(8)	0.2329(5)	5.9(4)
	2C(3)	−0.2544(7)	0.0721(8)	0.1826(7)	6.6(4)
	2C(4)	−0.2606(7)	0.1147(9)	0.1033(7)	5.9(4)
	2C(5)	−0.1913(8)	0.1820(9)	0.0742(5)	5.9(4)
	2C(6)	−0.1158(7)	0.2066(8)	0.1245(6)	5.6(4)
1-F6	1F(1)	0.5488(12)	0.026(2)	−0.105(2)	13.8(8)[b]
	1F(2)	0.3587(12)	0.091(2)	−0.0211(15)	
	1F(3)	0.432(2)	−0.0622(13)	−0.044(2)	
	1F(4)	0.475(2)	0.1786(13)	−0.0812(15)	
	1F(5)	0.403(2)	0.048(2)	−0.1494(11)	
	1F(6)	0.504(2)	0.068(2)	0.0237(11)	
2-F6	2F(1)	0.5253(14)	0.141(2)	−0.023(2)	13.8(8)
	2F(2)	0.3761(15)	0.001(2)	−0.116(2)	
	2F(3)	0.383(2)	0.169(2)	−0.074(2)	
	2F(4)	0.518(2)	−0.028(2)	−0.066(2)	
	2F(5)	0.407(2)	0.038(2)	0.0162(12)	
	2F(6)	0.494(2)	0.103(2)	−0.1559(12)	

[a] Ring C atoms are numbered sequentially. 1C(1) is bonded to P(1).
[b] Overall isotropic thermal parameters were applied to each atom in the F6 groups.

The contributions to F_c of 34 H atoms were included in the final least-squares cycles. Ten phenyl H atom positions were obtained using a C—H distance of 0.95 Å. Positional parameters for the 6 methylene H atoms and the 18 methyl H atoms were calculated from an ideal tetrahedral geometry. A C—H distance of 1.00 Å was assumed. The H atom thermal parameters were 1.0 Å^2 greater than those of the atoms to which they are bonded. Definite evidence for the H atom bonded to O was not observed in the electron density maps, so structure factors were not calculated for this atom. However, all others were present in a difference Fourier synthesis.

The final two cycles of full matrix least-squares refinement employed 3421 observations with $I > 3\sigma$. 187 parameters were varied. Final agreement parameters of $R_1 = 0.047$ and $R_2 = 0.054$ were obtained. The largest parameter shift was associated with the disorder model for the anion, 1.81σ, in the final cycle. Other shifts were all less than 0.2 esd. The error on an observation of unit weight is 1.75 electrons. The largest peak in a total difference Fourier synthesis is associated with the disordered PF_6 at (0.269, 0.229, −0.0358), and has an electron density of 1.38(13) e Å^{-3}. The disorder multiplicity parameter was 0.51(2). A statistical examination of the structure factors in terms of Miller indices, magnitudes of F_o, λ^{-1} sin θ, and diffractometer setting angles showed no unusual trends. Examination of F_o and F_c for intense reflections showed no evidence for secondary extinction.

Final positional and thermal parameters of the non-group atoms are presented in Table 2. Rigid group positional and orientation parameters are

Can. J. Chem. Downloaded from www.nrcresearchpress.com by 210.87.254.42 on 09/05/12
For personal use only.

Can. J. Chem. Downloaded from www.nrcresearchpress.com by 210.87.254.42 on 09/05/12
For personal use only.

TABLE 7. Selected intramolecular bond distances and angles

Distances (Å)		Angles (deg)	
	Metal atom inner coordination sphere		
Pt—P(1)	2.312(3)	P(1)—Pt—P(2)	174.3(2)
Pt—P(2)	2.312(4)	Cl—Pt—C(1)	179.4(4)
Pt—Cl	2.356(4)	Cl—Pt—P(1)	86.9(2)
Pt—C(1)	1.978(12)	Cl—Pt—P(2)	87.5(2)
		C(1)—Pt—P(1)	93.0(4)
		C(1)—Pt—P(2)	92.7(4)
	Phosphine ligands		
P(1)—C(11)	1.842(15)	Pt—P(1)—C(11)	112.6(7)
P(1)—C(12)	1.792(17)	Pt—P(1)—C(12)	111.8(7)
P(1)—1C(1)	1.822(12)	Pt—P(1)—1C(1)	114.5(4)
P(2)—C(21)	1.825(15)	Pt—P(2)—C(21)	109.8(5)
P(2)—C(22)	1.795(15)	Pt—P(2)—C(22)	113.7(7)
P(2)—2C(1)	1.801(10)	Pt—P(2)—2C(1)	114.7(4)
		C(11)—P(1)—C(12)	104.1(9)
		C(11)—P(1)—1C(1)	105.1(7)
		C(12)—P(1)—1C(1)	108.0(7)
		C(21)—P(2)—C(22)	106.1(9)
		C(21)—P(2)—2C(1)	108.4(6)
		C(22)—P(2)—2C(1)	107.6(6)
	Carbene ligand		
C(1)—N	1.293(16)	Pt—C(1)—N	123.9(9)
C(1)—C(4)	1.522(17)	Pt—C(1)—C(4)	119(1)
N—C(2)	1.484(29)	N—C(1)—C(4)	117(1)
N—C(3)	1.447(17)	C(1)—N—C(2)	121(1)
C(4)—C(5)	1.505(20)	C(1)—N—C(3)	123(1)
C(5)—C(6)	1.518(20)	C(2)—N—C(3)	116(1)
C(6)—O	1.409(19)	C(1)—C(4)—C(5)	118(1)
		C(4)—C(5)—C(6)	113(1)
		C(5)—C(6)—O	112(1)

given in Table 3, and derived positional and thermal parameters of rigid group atoms are given in Table 4. Calculated H atom positional and thermal parameters are shown in Table 5, and a list of $10|F_o|$ and $10|F_c|$ in electrons, together with the weight $w \times 10^4$, is presented in Table 6.[4]

Description of the Structure

Crystals of the salt result from the packing of discrete ions. The nearest anion-cation approach is 2.93 Å, between O and 1F(2). Disorder of the anion is observed with each possible orientation being equally populated. The cation with the atom labelling scheme is presented in Fig. 1, and an overall stereoview of the cation is shown in Fig. 2. Intraionic bond distances and angles together with their estimated standard deviations are listed in Table 7.

The square plane of the metal atom is slightly distorted, since the P(1)—Pt—P(2) angle is 174.3(2)°.

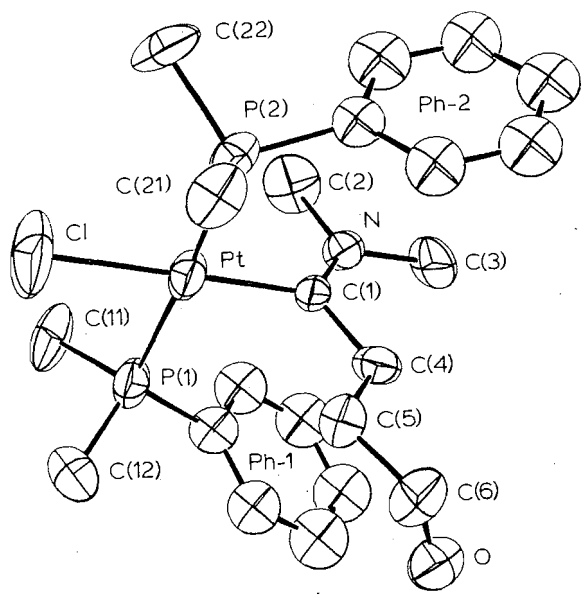

FIG. 1. A view of the cation, showing the atom numbering scheme. Thermal ellipsoids are drawn at the 50% probability level.

[4]Tables 5 and 6 are available, at a nominal charge, from the Depository of Unpublished Data, CISTI, National Research Council of Canada, Ottawa, Ont., Canada K1A 0S2.

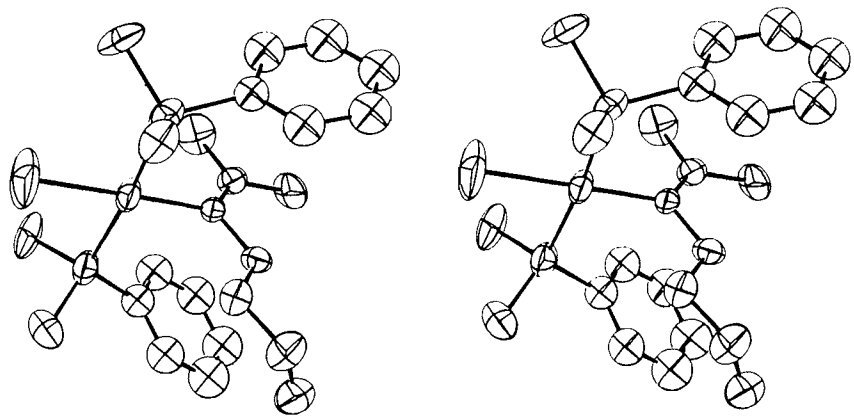

FIG. 2. A stereoview of the cation. Atoms are drawn at the 50% probability level.

The phosphine ligands are bent back away from the carbene ligand. The mean C(1)—Pt—P angle is 92.9(2)° and the average Cl—Pt—P angle is 87.2(3)°. A weighted least-squares plane calculated through Pt, Cl, P(1), P(2), and C(1) is given in Table 8. P(1) lies 0.020(6) Å above this plane and is farthest from it. None of the other atoms deviate significantly from the plane. The Cl—Pt—C(1) angle is 179.4(4)°.

The dimethylphenylphosphine ligand orientations and geometries are similar to those observed in other structures (2, 3). Thus the phenyl rings lie on the carbene side of the square plane and virtually perpendicular to it. The angles between the normals to the planes are 94° and 92° for Ph-1 and Ph-2 respectively. The phosphine P atoms are equidistant from the metal atom at 2.312(4) Å.

The weighted least-squares plane of the carbene ligand (Table 8), defined by C(sp^2), N, and the atoms C(4), C(2), and C(3) to which they are bonded, lies at an angle of 90.2° to the coordination plane of the metal atom. The N atom is farthest from the plane and lies 0.016(12) Å above it. The carbene ligand can be written as $RCH_2C{=}NMe_2$, where R is an ethanolic substituent. Of the atoms making up this group, C(5) and C(6) lie only slightly below the carbene plane, and O is 1.15 Å above it.

TABLE 8. Weighted least-squares planes

Atom	Deviation from plane (Å)
Atoms included: Pt, Cl, P(1), P(2), C(1)	
Equation of plane: $6.763x + 7.207y - 10.88z = -1.641$	
Pt	−0.0002(4)
Cl	0.000(7)
P(1)	0.020(6)
P(2)	0.008(4)
C(1)	0.020(14)
Atoms included: C(1), N, C(2), C(3), C(4)	
Equation of plane: $10.31x - 8.759y - 1.355z = 0.3068$	
C(1)	−0.008(12)
N	0.016(12)
C(2)	−0.008(16)
C(3)	−0.014(18)
C(4)	0.003(13)
C(5)	−0.067
C(6)	−0.039
O	1.15

The Pt—C(sp^2) bond distance is 1.978(12) Å and is shorter by 5.6σ than that of 2.079(13) Å observed for complex **2**, $[Pt(MeC{=}NMe_2)Me(PMe_2Ph)_2]PF_6$ (2). Within the carbene ligand, the C(sp^2)—N bond length is 1.293(16) Å. This is not significantly longer than that of 1.266(15) Å observed in **2**, for the bond lengths differ by 1.2σ. The mean N—C(methyl) distance is 1.465(15) Å and the C(sp^2)—C(4) bond length is 1.505(20) Å. These values too are equivalent to those obtained for **2**. The angles about the C(carbene) atom have a mean value of 120(2)°. The mean C(1)—N—C(methyl) angle is 122(1)° and the C(2)—N—C(3) angle is 116(1)°. Coplanarity of C(1), N, C(2), C(3), and C(4), as well as the magnitude of the angles about C(1) and N, are indicative of sp^2 hybridization. The C(sp^3)—N—C(sp^3) angle for the dimethylamino substituent in **2** is 113(1)°. The mean C(sp^3)—C(sp^3) bond length in the alcoholic substituent is 1.511(7) Å, and the mean angle at the C(sp^3) atoms of this group is 114(3)°.

The Cl ligand is located *trans* to the carbene and a Pt—Cl bond of 2.356(4) Å is observed. This value is of comparable magnitude to those of 2.362(3) and 2.361(5) Å obtained for **3**, *cis*-$PtCl_2\{C(NPhCH_2)_2\}PEt_3$ (5) and **4**, *cis*-$PtCl_2\{C(OEt)NHPh\}PEt_3$ (6) respectively. In these complexes carbene ligands also lie opposite a Cl ligand.

The disorder model for the anion is satisfactory, in that the mean P—F bond length is 1.58(2) Å, and the mean F—P—F angles are 89.9(6) and 174.2(7)° for *cis* and *trans* F atoms, respectively.

Can. J. Chem. Downloaded from www.nrcresearchpress.com by 210.87.254.42 on 09/05/12
For personal use only.

TABLE 9. Bonding in carbene ligands

Complex	*trans* Ligand	Pt—C(sp^2) (Å)	C—N (Å)	Carbene ligand	Reference
cis-Pt{C(OEt)NHPh}Cl_2PEt_3 **4**	Cl	1.962(18)	1.33(3)	*A*	6
trans-[Pt{$HO(CH_2)_3C$—NMe_2}Cl$(PMe_2Ph)_2$]PF_6 **1**	Cl	1.978(12)	1.293(16)	*B*	This work
trans-Pt{$C(NPhCH_2)_2$}Cl_2PEt_3	PEt_3	2.020(16)	1.37(2) 1.33(2)	*A*	5
cis-Pt{$C(NPhCH_2)_2$}Cl_2PEt_3 **3**	Cl	2.009(13)	1.327(11) 1.327(11)	*A*	5
[Pt{$C(NHMe)_2$}$_4$]$(PF_6)_2$	—$C(NHMe)_2$	2.047(1)	1.310(3)	*A*	22
trans-[Pt{C(NHMe)SEt}$_2$(C≡$NMe)_2$]$(PF_6)_2$	—C(NHMe)SEt	2.058(7)	1.300(10)	*A*	4
trans-[Pt(MeC—NMe_2)Me$(PMe_2Ph)_2$]PF_6 **2**	Me	2.079(13)	1.266(15)	*B*	2
trans-[Pt(CH_2C—OCH_2CH_2)Me$(PMe_2Ph)_2$]PF_6	Me	2.00(2)		*B*	3
RuI_2{HC—N(Me)-*p*-C_6H_4Me}CO(C≡N-*p*-C_6H_4Me)PPh_3			1.28	[a]	23
$RhCl_3(HC$—$NMe_2)(PEt_3)_2$			1.289(14)	[a]	24

[a]Secondary carbene ligand.

Discussion

Pt—Cl bond lengths are useful for determining the *trans* influence of the ligand in the opposite coordination site (9). For example, the Pt—Cl bond length of 2.276(1) Å in *cis*-$PtCl_2(CO)PPh_3$ (20) is shorter than that of 2.371(3) in *trans*-$PtMeCl(PPh_2Me)_2$ (21) by 31.7σ. In the former complex the Cl ligand lies opposite CO, a ligand of very weak *trans* influence, whereas in the latter Cl is opposite methyl, a strong *trans* influence ligand. In this study, the Pt—Cl bond length is 2.356(4) Å. This is 3.0σ shorter than that where Cl is *trans* to a methyl ligand and 20.0σ longer than that where Cl is *trans* to CO. The type *B* carbene ligand displays a *trans* influence approximately as large as that of the methyl ligand. Comparable Pt—Cl bond lengths of 2.362(3) and 2.361(5) Å have been obtained for the complexes **3** and **4** respectively, where type *A* tertiary carbene ligands lie opposite Cl. Thus the *trans* influences of the different types of tertiary carbene ligands are similar, suggesting that the nature of the Pt—C(sp^2) bonds is also similar.

In Table 9 are presented some Pt—C(carbene) bond length data for square-planar platinum(II) systems. The Pt—C(sp^2) bond lengths in the three complexes where Cl lies opposite carbene ligands are not significantly different. The mean bond length is 1.983(14) Å, shorter by 4.7σ than the bond distance where a carbene lies *trans* to another carbene, and 6.0σ shorter than that where a methyl ligand lies opposite a carbene. The above bond length differences can be attributed to the weak *trans* influence of Cl and to the strong *trans* influences of the methyl and carbene ligands. However, in the complex *trans*-[Pt(CH_2C—OCH_2CH_2)Me$(PMe_2Ph)_2$]PF_6 (3) the Pt—C(carbene) bond of 2.00(2) Å is shorter than expected when methyl is present in the *trans* coordination site, but in this alkoxycarbene compound the high electronegativity of the oxygen atom may result in a greater metal–ligand π interaction (25).

Also shown in Table 9 is a summary of C—N distances for carbene ligands of types *A* and *B*. Values are included for the secondary carbene ligands in RuI_2{HC—N(Me)-*p*-C_6H_4Me}CO(C≡N-*p*-C_6H_4Me)(PPh_3) (23) and $RhCl_3(HC$—$NMe_2)$-$(PEt_3)_2$ (24), where the C—N bonding is expected to be similar to that in the type *B* ligands. The single nucleophilic substituent in type *B* and secondary carbene ligands must contribute more electron density to stabilize the C(sp^2) atom than either of the two substituents in a type *A* ligand. This is apparently reflected in the C—N bond lengths. The majority of type *A* ligands have values around 1.33 Å, whereas the type *B* ligands all have distances less than 1.30 Å.

Acknowledgments

We thank the National Research Council of Canada for financial support of this work. R.F.S. is grateful for the award of an NRCC Scholarship.

1. R. F. STEPANIAK and N. C. PAYNE. J. Organometal. Chem. **57**, 213 (1973).
2. R. F. STEPANIAK and N. C. PAYNE. Inorg. Chem. **13**, 797 (1974).
3. R. F. STEPANIAK and N. C. PAYNE. J. Organometal. Chem. **72**, 453 (1974).
4. W. M. BUTLER and J. H. ENEMARK. Inorg. Chem. **12**, 540 (1973).
5. K. W. MUIR and LJ. MANOJLOVICIC-MUIR. J. Chem. Soc. Dalton, 2427 (1974).
6. E. M. BADLEY, J. CHATT, R. L. RICHARDS, and G. A. SIM. J. Chem. Soc. Dalton, 1930 (1976).
7. D. CAHEN and J. A. IBERS. J. Appl. Crystallogr. **5**, 298 (1972).
8. P. BRANT, J. H. ENEMARK, and A. L. BALCH. J. Organometal. Chem. **114**, 99 (1976).
9. LJ. MANOJLOVICIC-MUIR and K. W. MUIR. Inorg. Chim. Acta, **10**, 47 (1974).

Can. J. Chem. Downloaded from www.nrcresearchpress.com by 210.87.254.42 on 09/05/12
For personal use only.

10. M. H. CHISHOLM, H. C. CLARK, W. S. JOHNS, J. E. H. WARD, and K. YASUFUKU. Inorg. Chem. **14**, 900 (1975).
11. M. H. CHISHOLM and H. C. CLARK. Inorg. Chem. **10**, 1711 (1971).
12. R. F. STEPANIAK and N. C. PAYNE. Data to be published.
13. International Tables for X-ray Crystallography. 3rd ed. Kynoch Press, Birmingham, England. 1969.
14. W. A. ZACHARIESEN. Acta Crystallogr. **18**, 705 (1965).
15. P. W. R. CORFIELD, R. J. DOEDENS, and J. A. IBERS. Inorg. Chem. **6**, 197 (1967).
16. D. T. CROMER and J. T. WABER. Acta Crystallogr. **18**, 104 (1965).
17. R. F. STEWART, E. R. DAVIDSON, and W. T. SIMPSON. J. Chem. Phys. **42**, 3175 (1965).
18. D. T. CROMER and D. LIBERMAN. J. Chem. Phys. **53**, 1891 (1970).
19. R. EISENBERG and J. A. IBERS. Inorg. Chem. **4**, 773 (1965).
20. R. WALKER, LJ. MANOJLOVICIC-MUIR, and K. W. MUIR. J. Chem. Soc. Dalton, 1279 (1976).
21. M. A. BENNETT, P. W. CLARK, G. B. ROBERTSON, and P. O. WHIMP. J. Organometal. Chem. **63**, C15 (1973), and references therein.
22. S. Z. GOLDBERG, R. EISENBERG, and J. S. MILLER. Inorg. Chem. **16**, 1502 (1977).
23. D. F. CHRISTIAN, G. R. CLARK, and W. R. ROPER. J. Organometal. Chem. **81**, C7 (1974).
24. B. CETINKAYA, M. F. LAPPERT, G. M. MCLAUGHLIN, and K. TURNER. J. Chem. Soc. Dalton, 1591 (1974).
25. E. O. FISCHER. Pure Appl. Chem. **30**, 353 (1972).

Can. J. Chem. Downloaded from www.nrcresearchpress.com by 210.87.254.42 on 09/05/12
For personal use only.

Interaction fluorure d'hydrogène – acide perchlorique: Reactivité du nitromethane dans le milieu

CLAUDE BELIN ET JACQUELINE POTIER

Laboratoire des Acides Minéraux (associé au C.N.R.S. N° 79), Université des Sciences et Techniques du Languedoc, Place Eugène Bataillon, 34060 Montpellier Cédex, France

Reçu le 20 septembre 1977

CLAUDE BELIN et JACQUELINE POTIER. Can. J. Chem. **56**, 1610 (1978).

Le fluorure d'hydrogène donne, avec l'acide perchlorique, un composé à fusion non congruente (−117°C); par spectroscopie infrarouge, on montre que $HClO_4$ est fixé sur un polymère $(HF)_n$ par liaison faible. Le liquide de même composition contient encore une faible proportion de ce complexe; HF est bien une base vis-à-vis de $HClO_4$. La réactivité du nitrométhane a été étudiée dans ce milieu liquide acide, on montre que $MeNO_2$ y est une base légèrement plus forte que HF.

CLAUDE BELIN and JACQUELINE POTIER. Can. J. Chem. **56**, 1610 (1978).

Hydrogen fluoride reacts with perchloric acid yielding an incongruently melting compound (−117°C); by ir spectroscopy, we demonstrate that $HClO_4$ is linked to a $(HF)_n$ polymer through a weak hydrogen bond. The liquid of the same composition still contains a small amount of the complex; HF is really a base for $HClO_4$. The reactivity of $MeNO_2$ was studied in this liquid acidic medium and the nitromethane is found to be somewhat stronger than HF.

Introduction

Les solutions anhydres des acides HF et $HClO_4$ doivent être des milieux extrèmement acides; logiquement, leur acidité de Hammett doit varier de −10.8 pour HF (1) à la valeur estimée, −16, pour $HClO_4$ (2). En fait, on ne sait pratiquement rien sur ces solutions à l'exception des conclusions contradictoires de Hantzsch (3) (composé cristallisé $H_2F^+ClO_4^-F$ 57°C) et de Brauer et Distler (4) (inexistence de ce composé).

Dans ce mémoire, on étudie successivement: (*i*) le diagramme des équilibres liquide–solide entre HF et $HClO_4$ où est mis en évidence le composé cristallisé HF–$HClO_4$ en fait très différent de celui envisagé par Hantzsch; (*ii*) la nature des interactions entre les deux acides dans ce composé cristallisé (par spectroscopie de vibration infrarouge); (*iii*) la nature des composés présents dans le liquide de même composition et (*iiii*) la compétition, vis-à-vis de l'acide $HClO_4$, des bases très faibles HF et CH_3NO_2.

Méthodes expérimentales

Le fluorure d'hydrogène est un produit Matheson (pureté 99.9%) bidistillé. Le fluorure de deutérium est obtenu par action, à haute température, de l'acide deutérosulfurique anhydre sur du fluorure de calcium (Merck, 99.95%). D_2SO_4 est préparé par hydratation à l'eau lourde (99.9% en deutérium), de SO_3 synthétisé suivant la méthode de Bernard (5) (pureté 99.98%). Les mélanges sont réalisés à l'abri de toute trace d'humidité et analysés thermiquement dans un tube laboratoire en polytrifluorochloroéthylène (Kel-F). Le nitrométhane CD_3NO_2 est un produit Merck Uvasol titrant au moins 99% en deutérium. L'acide perchlorique anhydre est préparé au laboratoire selon la méthode mise au point par Mascherpa (15) et titre au minimum 99.96 mol%.

Equilibres liquide–solide dans le binaire $HClO_4$–HF

Le diagramme des équilibres liquide–solide a été établi par atd à l'échauffement. La fig. 1 reproduit les résultats obtenus. On relève essentiellement deux paliers d'invariance. Le premier à −117°C entre 0 et 55 mol% de $HClO_4$. Le diagramme des effets thermiques est, dans ce cas, maximum à 50%, ce qui permet de conclure à l'existence dans l'état solide du composé 1·1 HF–$HClO_4$.

Le second palier d'invariance à −118.8°C s'étend sur toutes les concentrations et son diagramme de Tamman[1] présente deux maxima à 50 et 67%; ce palier d'invariance est donc lié à deux phénomènes physiques différents.

La forme du liquidus entre 55 et 67 mol% de $HClO_4$ amène à attribuer ce palier à l'eutectique entre le composé 1·1 et $HClO_4$ cristallisé, ceci rend compte du maximum à 67%. On peut penser que le second maximum est lié à l'existence d'une deuxième forme du composé 1·1 dont la température de transformation serait très voisine de celle de l'eutectique.

Le tableau suivant rend compte des principales

[1]Diagramme de Tamman: il donne en unité arbitraire l'évolution de l'effet thermique corrigé en fonction de la concentration relative des constituants, mais non corrigé en fonction des chaleurs spécifiques:

$$T = sm/(M_1X_1 + M_2X_2);$$

s, surface de l'effet thermique sur la courbe d'enregistrement; *m*, masse de l'échantillon; M_1 et M_2, masses molaires des constituants; X_1 et X_2, fractions molaires des constituants.

Can. J. Chem. Downloaded from www.nrcresearchpress.com by 210.87.254.42 on 09/05/12
For personal use only.

Can. J. Chem. Downloaded from www.nrcresearchpress.com by 210.87.254.42 on 09/05/12
For personal use only.

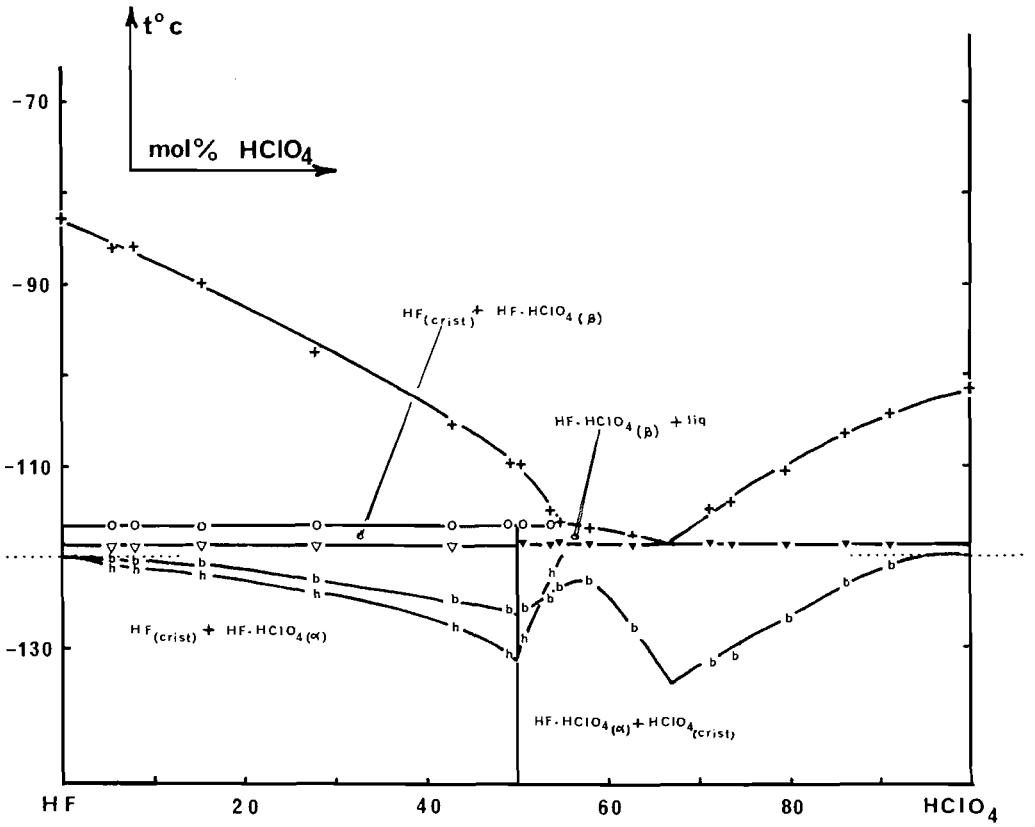

FIG. 1. Diagramme des équilibres liquide–solide du système $HClO_4$–HF; +, fin de fusion; O, invariant de transition; ▼, invariant d'eutexie; ▽, invariant de transformation dans l'état solide; h, effet thermique de l'invariant de transition; b, effet thermique global des invariants d'eutexie et de transformation dans l'état solide.

caractéristiques de ce binaire; α et β représentent les

$$HF_{(crist)} \leftrightarrow HF_{(liq)} \qquad F = -83.6°C$$

$$(HClO_4{\cdot}HF)_{(\beta)} \leftrightarrow HF_{(crist)} + \text{liquide eutectique} \quad \begin{cases} T = -117°C, \\ \text{mol\% } HClO_4 = 55 \end{cases}$$

$$(HClO_4{\cdot}HF)_{(\alpha)} \leftrightarrow (HClO_4{\cdot}HF)_{(\beta)} \quad \begin{cases} T = -118.8°C, \\ \text{mol\% } HClO_4 = 50 \end{cases}$$

$$(HClO_4{\cdot}HF)_{(\beta)} + HClO_{4(crist)} \leftrightarrow \text{liquide eutectique} \quad \begin{cases} T = -118.8°C, \\ \text{mol\% } HClO_4 = 67 \end{cases}$$

deux formes allotropiques cristallisées du composé.

Le composé $HF{\cdot}HClO_4$ se forme bien, mais avec des caractéristiques très différentes de celles indiquées par Hantzsch. Le bas point de fusion observé (fusion non congruente) conduit à penser à une association faible plutôt qu'à une réaction $HClO_4 + HF \leftrightarrow H_2F^+ClO_4^-$. Par ailleurs, le système est totalement miscible au-dessus de −60°C.

Spectroscopie de vibration du composé 1·1 cristallisé

Les spectres ir du composé 1·1 hydrogéné et partiellement deutérié (dans la suite de ce travail, par raison de simplicité on adopte la notation "deutérié"), ont été enregistrés à −150°C, ils sont reproduits sur la fig. 2. On y relève essentiellement deux domaines: entre 4000 et 2000 cm^{-1}, celui des vibrations de valence ν_{XH} et ν_{XD} (X = F ou O) et entre 1400 et 400 cm^{-1}, celui des vibrations de valence de ClO_3, Cl—OH, des déformations δ ClO et évidemment des déformations δ_{XH} et δ_{XD}. L'absence de bandes entre 1000 et 1100 cm^{-1} dues à l'ion perchlorate permet de rejeter définitivement la structure ionique de Hantzsch.

Domaine 4000–2000 cm^{-1}

Trois bandes apparaissent à 3415, 3230 et 3060 cm^{-1}, elles glissent par deutériation (50% en deutérium) respectivement à 2510, 2403 et 2300 cm^{-1} (rapports isotopiques 1.36, 1.34 et 1.33). Ces trois bandes sont retrouvées par dilution isotopique à 3415, 3250 et 3080 cm^{-1}, elles sont donc attribuables à des vibrations fondamentales et correspondent aux vibrations de valence ν_{FH} et ν_{OH}. Cependant pour un échantillon ne contenant que 14% de deutérium,

Can. J. Chem. Downloaded from www.nrcresearchpress.com by 210.87.254.42 on 09/05/12
For personal use only.

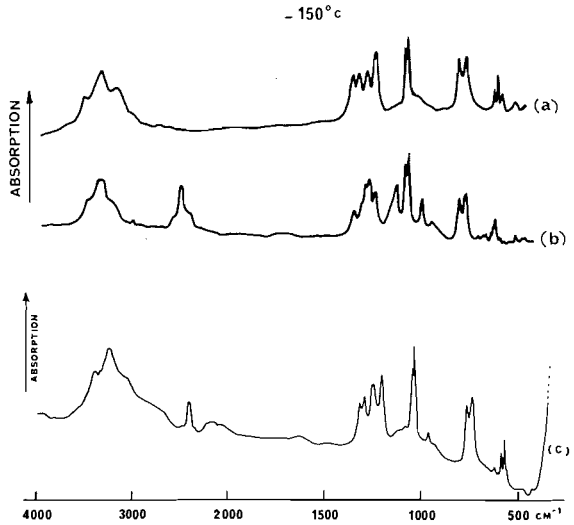

FIG. 2. Spectres infrarouges à $-150°C$ du composé cristallisé $HF{\cdot}HClO_4$: (*a*) hydrogéné; (*b*) partiellement deutérié (50%); (*c*) partiellement deutérié (14%).

on observe dans le domaine ν_{XD} une bande fine à 2410 cm^{-1} et une bande plus large centrée à 2160 cm^{-1}.

Dans ce domaine le spectre de HF cristallisé présente deux bandes à 3401 et 3056 cm^{-1}, l'intensité de la deuxième étant nettement plus importante que celle de la première; ces observations sont en accord avec celles de Kittelberger et Hornig (6), Sastri et Hornig (7), Giguère et Zengin (8). Par ailleurs, Pavia au laboratoire (9) ainsi que Karelin et Grigorovich (10) ont montré que pour $HClO_4$ cristallisé, ν_{OH} apparaît, pour l'un à 3350 cm^{-1}, pour les autres à 3355 cm^{-1}. Manifestement, le spectre obtenu, ici, n'est pas la somme des spectres des composés de départ; il y a donc interaction, probablement par liaison hydrogène.

La formation d'un complexe moléculaire simple par liaison hydrogène de type $HF\cdots HOClO_3$ ou de type $HO—ClO_2—O\cdots HF$ entraînerait l'existence de deux vibrations de valence XH seulement. La présence des trois bandes à 3415, 3230 et 3060 cm^{-1} ne peut s'expliquer que par l'existence d'un polymère pour l'une des molécules d'acide. Or, on sait (9), que $HClO_4$ est toujours monomère, tandis que Atoji et Lipscomb (11) ont montré, par radiocristallographie, que HF est un polymère en chaîne. Dans ces conditions, il semble logique de penser que l'interaction des deux acides est en réalité celle de $HClO_4$ monomère sur HF polymère.

On attend alors, dans ce domaine, au moins trois bandes: deux pour les mouvements en phase et en opposition de phase du polymère $(HF)_x$ et une pour le monomère $HClO_4$ fixé sur le polymère $(HF)_x$ en F comme sur le schéma 1 suivant. Dans ce cas, on admet que les couplages entre les différentes molécules de $HClO_4$ ne peuvent être détectés mais sont responsables de la largeur du massif.

Le spectre du composé à grande dilution isotopique (14%) doit être le plus simple à analyser; en effet on élimine ainsi certains modes de couplage et on doit attendre dans le domaine des ν_{XD} seulement deux bandes correspondant à ν_{FD} et ν_{OD}. La bande fine à 2410 cm^{-1} est à associer à la bande intense à 3230 cm^{-1} sur le spectre du composé totalement hydrogéné ($\rho = 1.34$) et à la bande également intense observée à 2403 cm^{-1} sur le spectre du composé partiellement deutérié (50%); signalons à ce sujet que dans un mélange DF,HF à 99% en HF (7), la bande unique ν_{FD} est observée à 2403 cm^{-1}. Il apparaît donc très logique d'attribuer cette bande à ν_{FD} de l'acide fluorhydrique et par conséquent la bande large de plus basse fréquence (2160 cm^{-1}) à ν_{OD} de l'acide perchlorique; quant à l'épaulement à 2080 cm^{-1}, on pourrait y voir, avec plus de réserves, la trace d'une harmonique (2×1085) vraisemblablement exaltée par résonance de Fermi; l'attribution de la bande à 1085 cm^{-1} est donnée ultérieurement.

Sur le spectre du composé totalement hydrogéné, l'attribution spécifique du triplet à 3415, 3230 et 3060 cm^{-1} est plus difficile. Les deux plus hautes fréquences doivent probablement être reliées aux deux modes ν_{FH} en phase et en opposition de phase du polymère HF_x; la bande à 3060 cm^{-1} est trop haute pour être attribuée purement à ν_{OH} de $HClO_4$ ($\rho = 1.41$ avec ν_{OD}) et on doit penser à un couplage avec ν_{FH}.

Domaine 1400–400 cm^{-1}

A priori, les vibrations de valence du groupe ClO_3 doivent être peu affectées par cette association. La comparaison des spectres de $HClO_4$ anhydre et du composé $HClO_4{\cdot}FH$ cristallisé le confirme (fig. 3).

Les principales différences sont: l'existence d'une nouvelle bande relativement intense à 1315 cm^{-1} et d'un doublet au niveau de 750 cm^{-1}, le déplacement

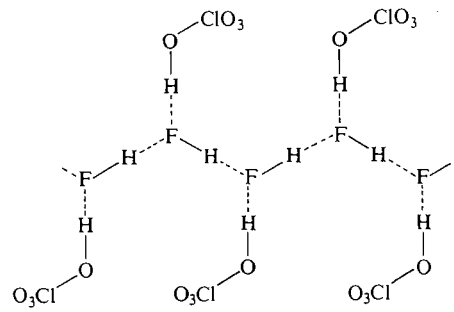

SCHÉMA 1

Can. J. Chem. Downloaded from www.nrcresearchpress.com by 210.87.254.42 on 09/05/12
For personal use only.

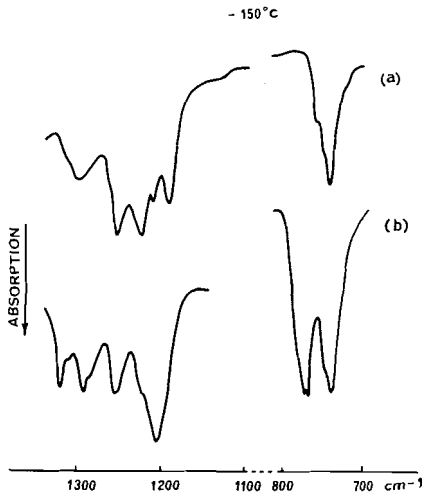

FIG. 3. Spectres ir à −150°C entre 1350 et 700 cm^{-1}; (*a*) $HClO_4$ anhydre cristallisé; (*b*) $HClO_4$·HF cristallisé.

de +15 cm^{-1} de la bande à 1185 cm^{-1} et l'augmentation de son intensité.

Sur le spectre du composé "deutérié" apparaissent (fig. 2), trois nouvelles bandes à 1085, 960 et 595 cm^{-1}. Simultanément, les bandes à 1315, 765 et 565 cm^{-1} diminuent d'intensité tandis que la bande à 1200 cm^{-1} se déplace de +5 cm^{-1} et diminue aussi d'intensité. Les trois nouvelles bandes sont, sans problème, attribuées à des déformations δ_{XD}. Quatre déformations sont attendues, les déformations dans le plan δ_{FH} et δ_{OH} et les déformations hors du plan correspondantes.

Pour $HClO_4$ cristallisé, on observe δ_{OH} à 1190 cm^{-1} et γ_{OH} à 480 cm^{-1}, tandis que, dans CH_3NO_2·$HClO_4$, δ_{OH} est pointé à 1230 cm^{-1} et γ_{OH} à 755 cm^{-1}. Pour $(HF)_x$ cristallisé, selon les auteurs, δ_{FH} est observé à 1200 cm^{-1} (8) ou à 1025 cm^{-1} (6). Il semble que la faiblesse de la liaison hydrogène F···$HOClO_3$ qui se traduit par un abaissement de fréquence ν_{OH} trois fois plus faible que dans CH_3NO_2·$HClO_4$ ne permette pas d'attribuer la bande à 1315 cm^{-1} à δ_{OH}. Le couple 1200 ↔ 960 cm^{-1} pour $\delta_{OH} \leftrightarrow \delta_{OD}$ est beaucoup plus compatible avec la force de la liaison hydrogène observée ici. Le déplacement de δ_{OH} (+10 cm^{-1}), par rapport à δ_{OH} de $HClO_4$, est tout à fait logique, il est cinq fois plus faible que celui observé pour CH_3NO_2·$HClO_4$.

La bande à 1315 cm^{-1} (1085 cm^{-1} dans le composé "deutérié") doit être attribuée à la déformation dans le plan du polymère $(HF)_x$. Le déplacement de fréquence est important, il traduit sans aucun doute la rigidisation du polymère $(HF)_x$ par addition des molécules d'acide perchlorique et aussi le fait que le fluor est tricoordiné dans le composé.

Les déformations hors du plan γ_{XH}, sont toujours attendues à des fréquences inférieures; un raisonnement analogue à celui suivi pour les déformations dans le plan conduit à attribuer à γ_{OH} la bande à 565 cm^{-1} qui diminue d'intensité lors de la deutériation partielle. Le couple 765 ↔ 595 cm^{-1} est dû à $\gamma_{FH} \leftrightarrow \gamma_{FD}$. Il convient de rappeler qu'on relève ces vibrations à des fréquences particulièrement élevées dans les ions H_2F^+, *n*HF (12). En conclusion, le composé HF·$HClO_4$ est dans l'état solide un composé moléculaire dans lequel subsiste le polymère $(HF)_x$ sur lequel des molécules de $HClO_4$ sont liées par de faibles liaisons hydrogènes aux atomes de fluor.

Présence du composé 1·1 dans l'état liquide

Le spectre d'un mélange de composition 1·1 est reproduit sur la fig. 4. Il est différent de celui du composé cristallisé, particulièrement dans le domaine des ν_{XH}. Le massif avec trois maxima est centré autour de 3600, 3360 et 2600 cm^{-1}. Dans une solution partiellement deutériée de stoechiométrie identique, ces maximums ont glissé à 2650, 2500 et 1950 cm^{-1}; les rapports ρ = 1.36, 1.37 et 1.33 sont corrects pour des maxima aussi mal résolus. Il faut noter sa largeur qui passe de 600 cm^{-1} dans le solide à 1700 cm^{-1} dans le liquide.

Pour HF liquide, ν_{FH} se présente sous forme d'une bande unique centrée à 3450 cm^{-1} alors que pour $HClO_4$ liquide, ν_{OH} ne donne qu'une bande à 3340 cm^{-1}. On est obligé d'admettre que dans l'état liquide, il n'y a pas que coexistence des deux bandes mais, interaction entre HF et $HClO_4$; cette déduction est confirmée par la présence de la bande à 1314 cm^{-1} caractéristique de la libration du polymère $(HF)_x$-$(HClO_4)_x$. Puisque pour le composé 1·1 dans l'état solide, les interactions sont faibles, elles le seront *a priori* plus encore dans l'état liquide.

L'évolution du massif ν_{XH} en fonction de la température entre 0, −100 et −150°C où le complexe est cristallisé peut être suivie sur la fig. 5. Il semble que très progressivement, la bande à 3600 glisse à 3400 cm^{-1} tandis que corrélativement celle à 3360 glisse à 3230 cm^{-1}. Cette évolution de fréquence en fonction de la température est normale, elle conduit à proposer d'attribuer la bande à 3600 cm^{-1} à ν_{FH} et celle à 3360 cm^{-1} à ν_{OH}. Sur cette dernière figure, on

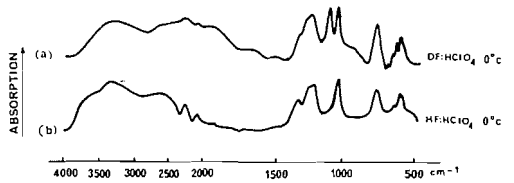

FIG. 4. Spectres ir à 0°C des composés 1·1 dans l'état liquide; (*a*) DF·$HClO_4$; (*b*) HF·$HClO_4$.

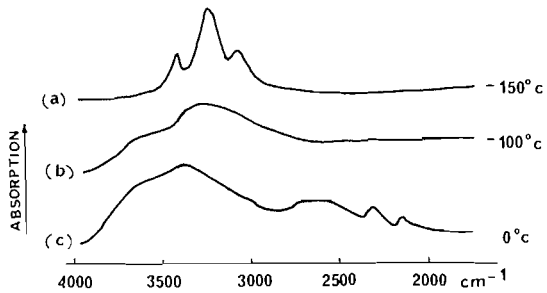

FIG. 5. Evolution du massif XH pour le composé $HF{\cdot}HClO_4$ en fonction de la température; (*a*) −150°C; (*b*) −100°C; (*c*) 0°C.

remarquera la disparition de la bande à 2600 cm^{-1} en fonction de la diminution de la température qui conduit à penser que cette bande est de type A, B, C dans la nomenclature de Hadzi (13). On peut penser qu'elle est liée à l'harmonique de la libration $(FH)_x$ en résonance de Fermi avec la bande large $\nu_{OH} + \nu_{FH}$, comme on l'observe toujours en pareil cas (14). Pour le composé partiellement deutérié, on retrouve cette même forme A, B, C mais avec une intensité moindre; à la bande à 2600 cm^{-1}, on doit associer la bande diffuse autour de 1680 cm^{-1} (fig. 4), qui diminue d'intensité quand la température décroit, pour disparaître presque totalement à −100°C.

La présence de la bande à 1315 cm^{-1} (1050 dans le complexe deutérié) caractéristique du complexe $HF{\cdot}HClO_4$ et l'évolution du massif ν_{XH}, prouve que l'association subsiste dans l'état liquide. Cependant, la largeur du massif entre 4000 et 2000 cm^{-1} ne peut s'expliquer que par la coexistence, à côté du composé 1·1, des molecules $(HF)_x$ et $HClO_4$ libres. Cette conclusion est logique puisque le composé 1·1 ne peut s'autodissocier dans l'état liquide que selon l'équilibre:

$$(HF{\cdot}HClO_4)_x \rightleftarrows (HF)_x + xHClO_4$$

Il est bien évident que dans HF et dans le complexe, les polymères $(HF)_x$ sont d'ordres différents et que, certainement, dans le liquide à la composition du complexe, des polymères de degrés d'association différents peuvent coexister. En conclusion, il y a, dans l'état liquide, interaction entre $(HF)_x$ et $HClO_4$ par liaison hydrogène entre l'atome de fluor et le groupe OH de l'acide perchlorique, mais coexistent simultanément des molécules d'acide perchlorique et de fluorure d'hydrogène.

Etude du mélange liquide CD_3NO_2–HF–$HClO_4$. Basicité relative de HF

Après avoir mis en évidence les propriétés basiques de $(HF)_x$ vis-à-vis de $HClO_4$, il était intéressant d'étudier la compétition vis-à-vis de $HClO_4$ entre cette base et une autre base faible. La base choisie est

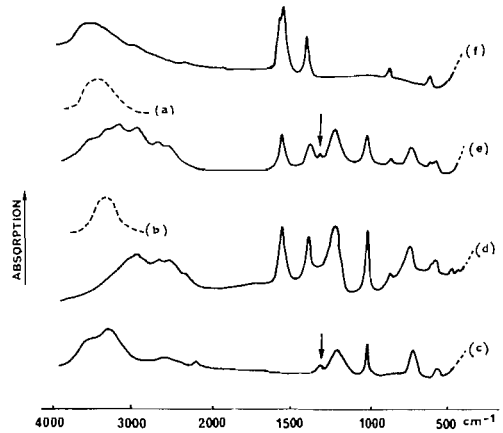

FIG. 6. Spectres ir à +25°C dans l'état liquide; (*a*) HF; (*b*) $HClO_4$; (*c*) $HF{\cdot}HClO_4$; (*d*) $CD_3NO_2{\cdot}HClO_4$; (*e*) CD_3NO_2, $HF,HClO_4$; (*f*) CD_3NO_2,HF; ↓ 1315 cm^{-1}.

le nitrométhane. On a enregistré un spectre d'un mélange de composition molaire: 1 HF, 1 $HClO_4$, 1 CD_3NO_2 (on a utilisé le nitrométhane deutérié pour éviter toute interférence, tant dans le domaine des ν_{XH} que des ν_{ClO_3}). Sur la fig. 6, au spectre obtenu, on a joint, à titre de comparaison, les spectres des différents mélanges binaires correspondants à des composés susceptibles de se former, c'est-à-dire, $HClO_4{\cdot}CD_3NO_2$, $(HF{\cdot}HClO_4)_x$ cristallisé et dans l'état liquide HF,CD_3NO_2, dans le rapport moléculaire 1·1.

On note, tout d'abord, sur le spectre du mélange ternaire HF–$HClO_4$–CD_3NO_2, la présence d'une bande faible à 1315 cm^{-1}: dans ce mélange, existe donc le composé $(HF{\cdot}HClO_4)_x$.

A côté de cette bande, on retrouve un très large massif qui s'étend de 4000 à 2000 cm^{-1}, caractérisé par un maximum vers 3200 cm^{-1} associé à des sous-maxima à 3500 et 2750 cm^{-1}. La comparaison du spectre de $(HF{\cdot}HClO_4)_x$ dans l'état liquide (spectre fig. 7*c*) de $CD_3NO_2{\cdot}HClO_4$ (fig. 7*d*) et de celui du mélange ternaire (fig. 7*e*) montre que ce massif est la somme des différents constituants $(HF{\cdot}HClO_4)_x$, $CD_3NO_2{\cdot}HClO_4$; en particulier, c'est à ce dernier composé que sont associés les sous-maxima à 3200 et 2750 cm^{-1}.

Par ailleurs, il semble que, dans ce milieu, le polymère $(HF)_x$ est moins polymérisé qu'il ne l'est dans le fluorure d'hydrogène liquide, on note en effet, un glissement de +150 cm^{-1} vers les hautes fréquences, déplacement analogue à celui observé aussi bien dans le composé $(HF{\cdot}HClO_4)_x$ que dans le mélange binaire $HF{\cdot}CD_3NO_2$.

En conclusion, dans ce mélange ternaire, existe $(HF{\cdot}HClO_4)_x$, $CD_3NO_2{\cdot}HClO_4$ et $(HF)_x$ largement dépolymérisé. Le nitrométhane n'a donc pas rompu totalement la liaison $HF\cdots HOClO_3$; en conséquence

Can. J. Chem. Downloaded from www.nrcresearchpress.com by 210.87.254.42 on 09/05/12
For personal use only.

vis-à-vis de l'acide perchlorique, les basicités de HF et de CD_3NO_2 doivent être du même ordre de grandeur quoique le nitrométhane soit certainement moins faible, comme le révèlent les glissements de fréquences ν_{OH} et δ_{OH} de $HClO_4$ respectivement $\Delta\nu_{OH}$ de -130 et $-600\ cm^{-1}$ et $\Delta\delta_{OH}$ $+10$ et $+50\ cm^{-1}$.

Conclusion generale

Au cours de ce travail, on a pu montrer que contrairement aux conclusions de Brauer et Distler (4), $HClO_4$ réagit sur la base HF pour former un autre composé $1\cdot1$ dans l'état solide. La force de l'acide $HClO_4$ n'est cependant pas suffisante pour former un complexe moléculaire simple $HF\cdots HO—ClO_3$ même dans l'état solide et, a fortiori, pour protoner HF et donner le composé $H_2F^+ClO_4^-$ annoncé par Hantzsch (3). Le composé formé est dans l'état solide, un polymère $(HF)_x$ fixé à $HClO_4$ par une liaison hydrogène sur l'atome de fluor, beaucoup plus faible que celle existant dans $CD_3NO_2\cdot HClO_4$. Dans le liquide de stoechiométrie $HF:HClO_4$, ce complexe $(HF\cdot HClO_4)_x$ subsiste en équilibre avec $(HF)_x$ et $HClO_4$ libre. Enfin, on a montré que dans une solution ternaire $HF:HClO_4:CD_3NO_2$ coexistent les composés $(HF\cdot HClO_4)_x$ et $HClO_4\cdot CD_3NO_2$ (en grande proportion), et bien entendu $(HF)_x$ et $HClO_4$. L'ensemble de ces faits permet de parler de la basicité de HF dans ces milieux, basicité plus faible que celle de CD_3NO_2.

1. H. H. Hyman, M. Kilpatrick et J. Katz. J. Am. Chem. Soc. **79**, 3668 (1957).
2. K. Yates et H. Wai. J. Am. Chem. Soc. **86**, 5408 (1964).
3. A. Hantzsch. Ber. Deutch. Ges. **63**, 1789 (1930).
4. G. Brauer et H. Distler. Anorg. Allgem. Chem. **275**, 157 (1954).
5. J. Bernard. Thèse. Paris, France. 1957.
6. J. H. Kittelberger et D. F. Hornig. J. Chem. Phys. **46**, 3099 (1967).
7. M. C. M. Sastri et D. F. Hornig. J. Chem. Phys. **39**, 12, 3497 (1963).
8. P. A. Giguere et N. Zengin. Can. J. Chem. **36**, 1013 (1958).
9. A. C. Pavia. Rev. Chim. Min. **7**, 471 (1970).
10. A. J. Karelin et Z. I. Grigorovich. Spectrochim. Acta, **32A**, 851 (1976).
11. M. Atoji et W. M. Lipscomb. Acta Cryst. **7**, 173 (1954).
12. C. Belin et J. Potier. J. Chim. Phys. **78**, 1222 (1972).
13. D. Hadzi. Pure. Appl. Chem. **11**, 435 (1965).
14. D. Hadzi. *Dans* The hydrogen bond. II. Structure and spectroscopy. *Edité par* P. Schuster, G. Zundel et C. Sandorfy. North Holland. 1976. p. 565.
15. G. Mascherpa. Thèse. Montpellier, France. 1965.

Can. J. Chem. Downloaded from www.nrcresearchpress.com by 210.87.254.42 on 09/05/12
For personal use only.

Anthraniloylanthranilamide (*o*-amino-*N*-(*o*-carbamoylphenyl)benzamide): Preparation and use as a synthetic precursor for quinazolino[1,2,3]benzotriazinones

FITZROY D. EDDY AND KEITH VAUGHAN

Department of Chemistry, Saint Mary's University, Halifax, N.S., Canada B3H 3C3

AND

MALCOLM F. G. STEVENS

Department of Pharmacy, University of Aston in Birmingham, Gosta Green, Birmingham, England B4 7ET

Received October 6, 1977

FITZROY D. EDDY, KEITH VAUGHAN, and MALCOLM F. G. STEVENS. Can. J. Chem. **56**, 1616 (1978).

Several synthetic routes to anthraniloylanthranilamide (**6**) are described; the problems involved in *o*-aminobenzoylation reactions are explored. Reduction of *N*-(*o*-nitrobenzoyl)-anthranilamide by stannous chloride gave a low yield of **6**, which was also obtained in low yield by reaction of isatoic anhydride with *o*-aminobenzamide. The possible use of *O*-(*o*-amino-benzoyl)hydroxylamines for *o*-aminobenzoylation was investigated but proved impractical. Diazotisation of **6** affords 3-(*o*-carbamoylphenyl)-1,2,3-benzotriazin-4(3*H*)-one (**2**), which undergoes base-catalysed cyclisation to the quinazolino[3,2-*c*]benzotriazine (**4**). The conversion **2** → **4** probably involves the isomeric quinazolino[1,2-*c*]benzotriazine (**3**), which could not be isolated.

FITZROY D. EDDY, KEITH VAUGHAN et MALCOLM F. G. STEVENS. Can. J. Chem. **56**, 1616 (1978).

On décrit plusieurs chemins de synthèse conduisant à l'anthraniloylanthranilamide (**6**); on explore les problèmes impliqués dans les réactions d'*o*-aminobenzoylation. La réduction de la *N*-(*o*-nitrobenzoyl)anthranilamide par le chlorure stanneux conduit à **6** avec un mauvais rendement; on peut aussi obtenir **6** avec un mauvais rendement par la réaction de l'anhydride isatoïque avec l'*o*-aminobenzamide. On a étudié la possibilité d'utiliser de l'*O*-(*o*-aminobenzoyl) hydroxylamine pour effectuer l'*o*-aminobenzoylation; cette réaction ne s'avère toutefois pas pratique. La diazotisation de **6** conduit à la *o*-carbamoylphényl-3 benzotriazine-1,2,3 (3*H*) one-4 (**2**) qui subit une cyclisation catalysée par les bases pour conduire à la quinazolino-[3,2-*c*]benzotriazine (**4**). La transformation de **2** → **4** implique probablement la quinazolino-[1,2-*c*]benzotriazine (**3**) isomère qui n'a pu être isolé.

[Traduit par le journal]

In a previous report (1), the reactions of the diaryltriazene (**1**) were investigated as a possible synthetic entry to the quinazolinobenzotriazine ring system, i.e. **3** or **4**. Compound **1** was observed to undergo conversion to the triazenophenylquinazolone (**5**) by reaction with piperidine in ethanol at moderate temperatures. The initial step in the conversion **1** → **5** must be cyclisation to the triazinone (**2**), followed by further ring closure to afford the quinazolino[1,2-*c*]benzotriazine (**3**). Interaction of piperidine with the triazine ring of **3** leads to the observed product **5** directly, although the possibility of rearrangement of **3** to the isomer **4**, before interaction with piperidine, could not be ruled out. Indeed, the conversion of **4** (a known compound) to **5** was shown to occur under the same conditions as **1** → **5**. However the intermediate species **2**, **3**, and **4** could not be isolated during the reaction of **1** with piperidine.

Although the triazinone (**2**) does not appear to be stable during cyclisation involving formation of the N3—C4 bond, synthesis via formation of the N2—N3 bond offers more hope for isolation and study of **2**. Diazotization of *o*-aminobenzamides (2) affords triazinones by N2—N3 bond formation; the necessary precursor for this approach to **2** would be anthraniloylanthranilamide (**6**), which surprisingly has been reported in the literature only once (3). The published synthesis involves reduction of the nitro group in *N*-(*o*-nitrobenzoyl)anthranilamide in very low yield (11%). This method has been repeated by us and, although on some occasions the yield improved slightly, lower yields were recorded just as frequently.

An improved method of synthesis of **6** would obviously be useful; a feasible alternative could be direct *o*-aminobenzoylation of anthranilamide. However, methods for the direct introduction of the *o*-aminobenzoyl group are scarce and, whenever possible, the preferred method is *o*-nitrobenzoylation, followed by reduction, as used by Butler and Partridge (3). Perhaps the most frequently used reagent for *o*-aminobenzoylation is isatoic anhydride (**7**), which reacts readily with amines and several

Can. J. Chem. Downloaded from www.nrcresearchpress.com by 210.87.254.5 on 09/05/12
For personal use only.

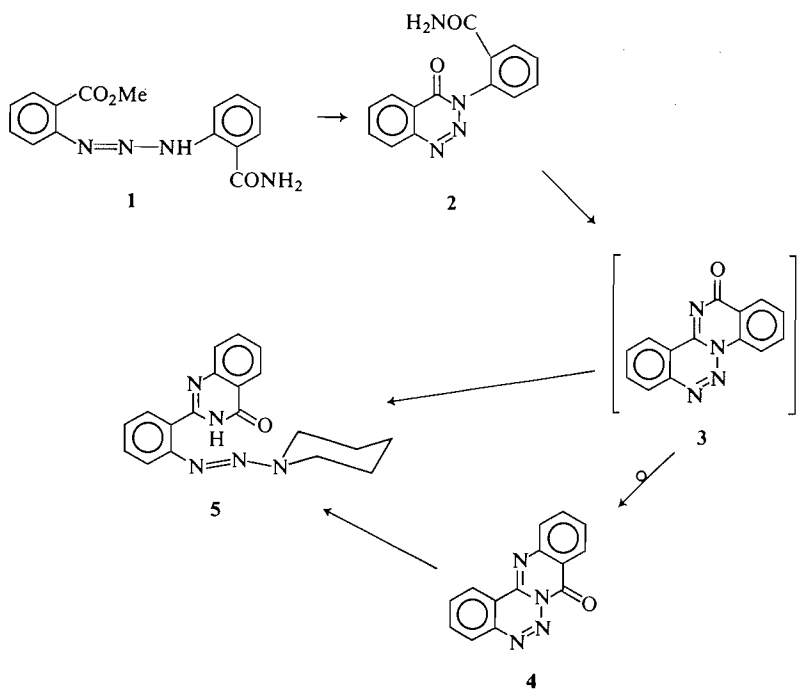

other nucleophiles to afford anthranilamides and other anthraniloyl derivatives (4). A disadvantage of **7** for this application is the competing reactivities of the C2 and C4 carbonyl groups, and reaction with amines often gives rise to ureides, as a result of steric interaction at C4 (5). Nevertheless isatoic anhydride reacts with anthranilic acid in basic solution to afford anthraniloyl anthranilic acid (the parent acid of **6**) (6); however the analogous reaction of **7** with anthranilamide was unsuccessful. Reaction did occur (as evidenced by CO_2 evolution) when **7** and anthranilamide were heated in dimethylformamide at 124°C but the yield of **6** obtained in this way was only 6%.

3-(*o*-Aminobenzoyloxy)-1,2,3-benzotriazin-4(3*H*)-one (**8**) has recently been shown to be a potentially useful reagent for *o*-aminobenzoylation (7). Although the versatility of this reaction has not been thoroughly demonstrated, **8** does react with primary alkylamines to afford anthranilamides (7). When a mixture of **8** and excess anthranilamide was refluxed in nitromethane, formation of anthraniloylanthranilamide (**6**) was quickly evident as adduced by tlc analysis, which also showed the presence of both the starting materials and the expected by-product, *N*-hydroxybenzotriazinone (**9***a*). Because of the tendency of **9***a* to undergo thermolytic conversion to **8** (7), a twofold excess of anthranilamide was used to effect a stoichiometric conversion of **8** → **6**. However, after prolonged refluxing, it was evident (from tlc) that the amount of the required product (**6**) in the reaction mixture was not increasing significantly and that other reactions, e.g. polymerisation (7) of **8**, were interfering. The resulting reaction mixture was somewhat intractable and it was not possible to separate the anthraniloylanthranilamide from the

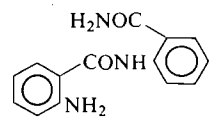

6

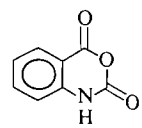

7

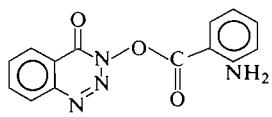

8

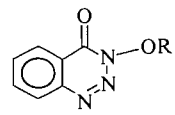

9

a R = H
b R = CH_2Ph

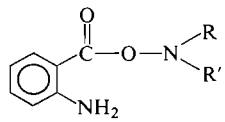

10

a R = R′ = H
b R = R′ = Et
c R = H, R′ = Me

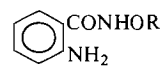

11

a R = H
b R = CH_2Ph

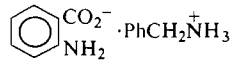

12

Can. J. Chem. Downloaded from www.nrcresearchpress.com by 210.87.254.5 on 09/05/12
For personal use only.

Can. J. Chem. Downloaded from www.nrcresearchpress.com by 210.87.254.5 on 09/05/12
For personal use only.

other products and unreacted anthranilamide. Nevertheless, the fact that **6** is formed from **8** in this reaction is further evidence of the synthetic use of this novel triazine, and suggests that further studies of the reactions of *N*-(*o*-aminobenzoyloxy) derivatives with nucleophiles (reaction [1]) are worthwhile.

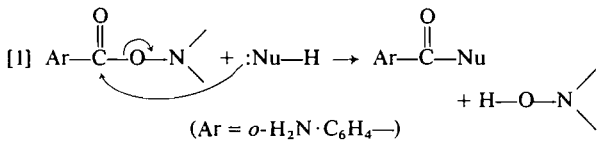

[1] $Ar{-}C(=O){-}O{-}N< + :Nu{-}H \rightarrow Ar{-}C(=O){-}Nu + H{-}O{-}N<$

(Ar = *o*-$H_2N{\cdot}C_6H_4$—)

Indeed, the reaction of isatoic anhydride (**7**) with hydroxylamine in basic solution is reported to afford the *O*-(*o*-aminobenzoyl)hydroxylamine (**10***a*) (8). The structure of **10***a* appears to be unequivocal, especially since it is clearly a different compound from the *N*-(*o*-aminobenzoyl) isomer (**11***a*), which can be obtained by reaction of methyl *o*-aminobenzoate with hydroxylamine (8). This *O*-aroylation of hydroxylamine by isatoic anhydride evidently involves nucleophilic attack by the hydroxyl group, although formation and rearrangement of an *N*-oxide, via nucleophilic attack by the amino group, is feasible (9). However if the latter mechanism was operative during the reaction of **7** with hydroxylamine, the stable *N*-aroyl derivative (**11***a*) would arise and not the observed product **10***a*.

Further evidence for *O*-aroylation is provided by the reaction of isatoic anhydride with *N*-blocked hydroxylamines. Thus, reaction of **7** with *N*,*N*-diethylhydroxylamine affords a single product, which has analytical and spectroscopic data fully consistent with the expected *O*-aroyl structure (**10***b*). Likewise, **7** reacted with *N*-methylhydroxylamine, but gave a lower yield of the *N*-methyl derivative (**10***c*). The *O*-aroylhydroxylamines (**10***a–c*) display carbonyl absorption at 1680–1700 cm^{-1} in the ir spectra and the mass spectra all show an abundant molecular ion, together with a pronounced fragment at *m/e* 137, evidently arising from O—N bond cleavage. The diethyl derivative (**10***b*) is light-sensitive but appears to be stable in the dark unlike the *O*-amino derivative (**10***a*), which often decomposes within a day of preparation.

As previously reported by Kohl and Wolf (10), the reaction of **7** with *O*-benzylhydroxylamine affords the *N*-(*o*-aminobenzoyl)hydroxylamine (**11***b*). Evidently the *O*-blocked hydroxylamine can react as a nucleophile via the N atom with equal reactivity to the *N*-substituted hydroxylamines. The reaction of **7** with *O*-alkylhydroxylamines is a useful step in the synthesis of 3-alkyloxybenzotriazinones; diazotization of **11***b* affords the 3-benzyloxytriazinone (**9***b*), which was also synthesised by direct benzylation of the 3-hydroxytriazinone (**9***a*) (7).

The reaction of the *O*-aroylhydroxylamine (**10***a*) with benzylamine does not follow the predicted pathway (reaction [1]). When **10***a* is treated with neat benzylamine, a vigorous exothermic reaction occurs, after a short induction period, and copious effervescence is observed. The solid product obtained from this reaction was not *N*-benzylanthranilamide but, surprisingly, was found to be the benzylammonium salt of anthranilic acid (**12**). The same salt was obtained when **10***a* and benzylamine reacted in acetonitrile solution. A possible mechanism to explain the formation of this salt involves a base-induced α-elimination from the hydroxylamine (reaction [2]); an analogous intramolecular process

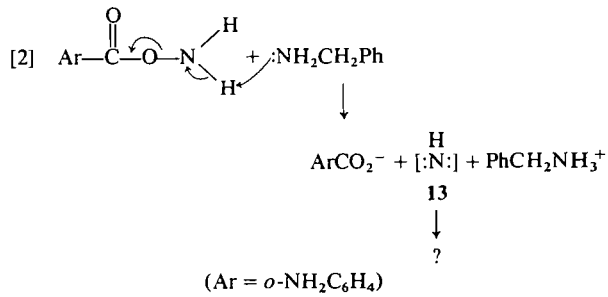

[2] $Ar{-}C(=O){-}O{-}N(H){-}H + :NH_2CH_2Ph \rightarrow ArCO_2^- + [:\overset{H}{N}:] + PhCH_2NH_3^+$

13 → ?

(Ar = *o*-$NH_2C_6H_4$)

could be responsible for the spontaneous slow decomposition of **10***a* previously discussed.

The eventual fate of the nitrogen fragment (**13**) is uncertain but it is quite likely the source of the unidentified gas evolved during the reaction. Also the mass spectrum of **10***a* exhibits a strong peak at *m/e* 137, corresponding to loss of the fragment NH. Further evidence for the proposed mechanism (reaction [2]) is the fact that the diethyl derivative **10***b* does not react in this way, nor does it appear to react by the nucleophilic displacement mechanism (reaction [1]). Reaction of **10***b* with benzylamine did not produce effervescence and gave only an intractable, ether-soluble red oil. Although **10***a* showed the same vigorous reaction with alkylamines, e.g. methyl- and propylamines, no such reaction was seen with other nucleophilic reagents, e.g. ethanol and aniline.

Thus, although the *O*-aroylhydroxylamine (**10***a*) is a reactive species, it clearly behaves differently from the *N*-(*o*-aminobenzoyloxy)triazinone (**8**) in reaction with nucleophiles and, consequently, is not a potential precursor of anthraniloylanthranilamide. The reactivity of **8** towards nucleophilic attack at the aroyl group may be due to the presence of the electron-withdrawing carbonyl group bonded to the N atom of the N—O-aroyl system; this structural feature is not present in **10***a*. In further studies, it is hoped that the structural requirement for a more useful *o*-aminobenzoylating agent will be elaborated.

Diazotization of anthraniloylanthranilamide (**6**) proceeded without complication and afforded a good

Can. J. Chem. Downloaded from www.nrcresearchpress.com by 210.87.254.5 on 09/05/12
For personal use only.

yield of 3-(*o*-carbamoylphenyl)-1,2,3-benzotriazin-4(3*H*)-one (**2**), which is a stable, colourless, crystalline solid. **2** reacted with piperidine in ethanol at 60°C to afford the same triazene (**5**) which had previously been obtained from the amide ester (**1**) under identical conditions (1). This observation confirms the previous hypothesis that **2** is an intermediate in the conversion **1** → **5**. Whereas no intermediate species in the conversion **1** → **5** could be isolated, the reaction of **2** with piperidine in ethanol at room temperature afforded a good yield of the quinazolinobenzotriazinone (**4**), in addition to the triazene (**5**) as a minor product. Compound **2** is evidently much more reactive than the precursor **1**, which required elevated temperatures to react with piperidine, and it is therefore likely that the rate-determining step in the conversion **1** → **5** is the initial reaction **1** → **2**.

Several modifications to these reaction conditions have been attempted in order to isolate the unknown isomeric quinazolinobenzotriazinone (**3**), the presumed intermediate in the conversion **2** → **4**. Compound **2** was recovered quantitatively unchanged after prolonged reflux in ethanol; evidently piperidine, or a similar catalyst, is essential for cyclisation of **2** to occur. Reaction of **2** with DABCO (1,4-diaza[2,2,2]bicyclooctane), which is a base catalyst more sterically hindered as a nucleophile than piperidine, in acetonitrile was much slower than reaction with piperidine; however the only product observed, both at room temperature and under reflux, was the same quinazolinobenzotriazinone (**4**). Compound **2** was found to be stable to solution thermolysis at 160°C and no evidence of cyclisation under these conditions could be found. Attempts to dehydrate the triazinone (**2**) using dicyclohexylcarbodiimide were unsuccessful.

In conclusion, it is evident that the quinazolino-[1,2-*c*]benzotriazinone (**3**) is a very elusive species. Certainly **3** does not appear to be stable under the reaction conditions necessary for the cyclisation of **2** and the rearrangement **3** → **4** must be a very facile process. This rearrangement of **3**, which is a fused 1,4-dihydroquinazoline, is analogous to the well known tautomerisation of 1,4-dihydroquinazolines to 3,4-dihydroquinazolines (11).

Experimental

Anthraniloylanthranilamide (**6**)

(*a*) A solution of *o*-nitrobenzoyl chloride (50 g) in anhydrous benzene (200 ml) was added to a vigorously stirred solution of anthranilamide (33 g) and pyridine (50 ml) in anhydrous benzene (120 ml). After stirring 1 h at room temperature, the benzene was removed under vacuum and the residue treated with water (1 ℓ) to afford *o*-(*o'*-nitrobenzamido)benzamide (80 g), mp 194–196°C (ethanol) (lit. (3) mp 195–196°C).

The nitro amide (20 g) was reduced with stannous chloride (60 g) in glacial acetic acid (150 g) and concentrated HCl (60 ml) at room temperature for 2 h. The product was isolated as the oxalate and tin compounds were precipitated by bubbling H_2S through a suspension of the crude product in 0.5 *N* H_2SO_4. Filtration of the hot suspension and cooling the filtrate afforded pure anthraniloylanthranilamide (yield 7–18%), mp 206–208°C (lit. (3) mp 207.5–208°C); ν_{max}: 3450, 3340, 3200 (broad), and 1650 (broad) cm^{-1}.

(*b*) Isatoic anhydride (1.63 g) and anthranilamide (1.39 g) were heated in dimethylformamide (10 ml) at 124°C for 2.2 h, when effervescence had ceased. After cooling, the reaction mixture was treated with water (42 ml) and the p*H* adjusted to 9.4. After standing for 24 h, the resulting precipitate was filtered to afford the aminoamide (**6**) (0.16 g, 6%), which had identical ir spectrum to that obtained in (*a*).

(*c*) 3-(*o*-Aminobenzoyloxy)-1,2,3-benzotriazin-4(3*H*)-one (**8**) (0.5 g) and anthranilamide (0.5 g) were refluxed in nitromethane (20 ml) for 125 h. The progress of the reaction was followed by tlc analysis on Kieselgel 60 F254 (Merck) using chloroform as solvent. Thin-layer chromatography indicated the presence of the expected reaction products, **6** and **9***a*, in addition to both starting materials, in the reaction mixture after only 1 h reflux. The same four components were still present after 50 h reflux. After 125 h, tlc analysis indicated the presence of the required product (**6**), and only trace amount of **9***a*; in addition, the mixture contained considerable amounts of unreacted anthranilamide and unidentified products. Fractional crystallisation of the reaction mixture eventually afforded a solid (12 mg), but tlc analysis showed that it was a mixture of **6**, anthranilamide, and one other component.

O-*(o-Aminobenzoyl)hydroxylamine* (**10**a)

Hydroxylamine hydrochloride (13.8 g) was dissolved in water (250 ml) and added to a solution of sodium carbonate (21.2 g) in water (250 ml). The mixture was stirred while isatoic anhydride (16.3 g) was added over 10 min with vigorous effervescence. After stirring for 1 h, the solid was filtered and dried in air to afford *O*-(*o*-aminobenzoyl)hydroxylamine (9.8 g), mp 79–81°C; ν_{max}: 3420, 3300, 3200, and 1700 cm^{-1}; M^+ 152 (17%), *m/e*: 137 (23%) (*M* − NH), 120 (100%) ($H_2N{\cdot}C_6H_4CO$), and 92 (58%).

Reaction of isatoic anhydride with *O*- and *N*-substituted hydroxylamines by the above procedure afforded the following compounds.

N-*Methyl*-O-*(o-aminobenzoyl)hydroxylamine* (**10**c)

Yield 45%, mp 48–50°C; ν_{max}: 3430, 3300, 3230, 3160, and 1680 cm^{-1}; M^+ 166 (40%), *m/e*: 137 (91%) (*M* − CH_3N), 120 (100%)($H_2NC_6H_4CO$), and 92 (100%). *Anal.* calcd. for $C_8H_{10}N_2O_2$: C 57.83, H 6.02, N 16.87; found: C 57.28, H 6.08, N 16.62.

N,N-*Diethyl*-O-*(o-aminobenzoyl)hydroxylamine* (**10**b)

Yield 84%, mp 70–72°C, ν_{max}: 3450, 3340, and 1695 cm^{-1}; M^+ 208 (7%), *m/e*: 174 (2%), 161 (3%), 146 (6%), 137 (25%) (*M* − C_4H_9N), 120 (100%); δ ($CDCl_3$): 1.15 (t, *J* = 7 Hz, 6H, Me), 3.03 (q, *J* = 7 Hz, 4H, CH_2), 5.8 (broad s, 2H, NH_2), and 6.5–7.9 ppm (m, 4H, aromatic). *Anal.* calcd. for $C_{11}H_{16}N_2O_2$: C 63.46, H 7.69, N 13.46; found: C 63.23, H 7.58, N 13.90.

O-*Benzyl*-N-*(o-aminobenzoyl)hydroxylamine* (**11**b)

Yield 48%, mp 101–102°C (lit. (10) mp 104–106°C), ν_{max}: 3420, 3350, 3150, 1740(w), 1655, and 1640 cm^{-1}; δ ($CDCl_3$): 4.93 (s, 2H, CH_2), 5.3 (br s, 2H, NH_2), and 6.5–7.4 (m, 9H, aromatic). *Anal.* calcd. for $C_{14}H_{14}N_2O_2$: C 69.42, H 5.79, N 11.57; found: C 69.09, H 6.05, N 11.79.

*3-Benzyloxy-1,2,3-benzotriazin-4(3*H*)-one* (**9**b)

(*a*) *O*-Benzyl-*N*-(*o*-aminobenzoyl)hydroxylamine (486 mg) was dissolved in 2 *M* HCl (5 ml), diluted with water (40 ml), and diazotised at 0°C with sodium nitrite (140 mg) in water.

Can. J. Chem. Downloaded from www.nrcresearchpress.com by 210.87.254.5 on 09/05/12
For personal use only.

After stirring for 3 h at 0°C, the precipitate was filtered and recrystallised from ethanol to afford the triazinone (**9***b*) (400 mg, 78%), mp 151–153°C (ethanol); ν_{max}: 1720 cm^{-1}. *Anal.* calcd. for $C_{14}H_{11}N_3O_2$: C 66.40, H 4.35, N 17.87; found: C 66.52, H 4.56, N 17.68.

(*b*) 3-Hydroxy-1,2,3-benzotriazin-4(3*H*)-one (420 mg) was dissolved in 10% aqueous NaOH (1 ml) and the yellow solution diluted with water (5 ml) and ethanol (2 ml). Benzyl bromide (425 mg) was added and the mixture stirred for 12 h at room temperature. The suspended oil slowly dissolved and was replaced by a white precipitate. The solid was filtered, washed with cold aqueous ethanol and dried to afford the benzyloxybenzotriazinone (**9***b*) (400 mg, 62%), which was identical (ir spectrum, mp and mixture mp 151–153°C) with a sample from above.

Benzylammonium o-*Aminobenzoate* (**12**)

(*a*) *O*-(*o*-Aminobenzoyl)hydroxylamine (**10***a*) (1 g) was treated with benzylamine (1 ml). No immediate reaction took place but within approximately 1 min, a vigorous reaction set in with copious effervescence. The resulting oil solidified on cooling and was triturated with ether, filtered and recrystallised from benzene to afford the anthranilate salt (**12**) (1.25 g), mp 114°C (benzene); ν_{max}: 3450, 3350, 2700 (br), and 1610 cm^{-1}. *Anal.* calcd. for $C_{14}H_{16}N_2O_2$: C 68.85, H 6.56, N 11.48; found: C 67.95, H 6.52, N 11.27. This salt was identical (ir and mixture mp) with a sample prepared from benzylamine and anthranilic acid.

(*b*) *O*-(*o*-Aminobenzoyl)hydroxylamine (0.5 g) was dissolved in acetonitrile (5 ml) and benzylamine (0.5 ml) was added. The mixture was warmed on a steam bath under reflux for 0.5 h, during which slight effervescence was evident. The acetonitrile was removed under vacuum and the residue was dissolved in hot benzene and left to crystallise. Filtration afforded the same benzylammonium salt (**12**) (0.64 g, 67%) as in (*a*).

*3-(*o*-Carbamoylphenyl)-1,2,3-benzotriazin-4(3*H*)-one* (**2**)

Anthraniloylanthranilamide (**6**) (0.5 g) was dissolved in 2 *M* HCl (3 ml), diluted with water (15 ml), and diazotised at 0°C with sodium nitrite (0.14 g) in water. The solution went clear briefly before a white precipitate formed. The reaction mixture was allowed to warm slowly to room temperature and then filtered to afford the triazinone (0.44 g, 85%), mp 201–204°C (dec.) (ethanol); ν_{max}: 3400, 3250, 3150, 1680, and 1650 cm^{-1}. *Anal.* calcd. for $C_{14}H_{10}N_4O_2$: C 63.15, H 3.76, N 21.05; found: C 63.11, H 3.90, N 21.07.

Reactions of the Amide (**2**)

(*a*) Compound **2** (0.1 g) was refluxed in ethanol (5 ml) for 24 h. The cooled solution afforded a crystalline precipitate; both the precipitate and the residue in the filtrate, were identical with the starting material (quantitative recovery).

(*b*) Compound **2** (0.1 g) was suspended in cold ethanol (10 ml) and piperidine (0.03 g) was added. The suspension was stirred at room temperature for 13 days and the residual precipitate was filtered to afford quinazolino[3,2-*c*][1,2,3]-benzotriazin-8-one (**4**) (50 mg, 54%), mp 216–218°C, which was identical (mixture mp 216–218°C and ir spectrum) with an authentic sample (12). The ethanolic filtrate was evaporated and the residue recrystallised from aqueous ethanol to afford the triazene (**5**) (20 mg, 16%), which was identical with the sample prepared as follows (*c*).

(*c*) Compound **2** (0.1 g) was dissolved in ethanol (10 ml) containing piperidine (0.03 g) at 60°C. The clear solution was maintained at 60–70°C for 5 h. The ethanol was removed under vacuum and the oily residue was triturated with 60–80°C petroleum ether – benzene. The insoluble solid was filtered to afford unchanged starting material (0.04 g). Evaporation of the filtrate gave an oil, which solidified on standing and recrystallised from aqueous ethanol to afford 2-[2-(piperidin-1-ylazo)phenyl]quinazolin-4(3*H*)-one (**5**) (0.05 g) (40%), mp 143–145°C, which was identical (ir spectrum and mixture mp 143–145°C) with an authentic sample (1).

(*d*) Compound **2** (0.1 g) was refluxed in anhydrous diglyme (2 ml) for 5 h. Dilution with petroleum ether (60–80°) caused precipitation; filtration afforded unchanged starting material (66 mg).

(*e*) *with DABCO*

(*i*) Compound **2** (0.1 g) was suspended in a solution of DABCO (50 mg) in acetonitrile (10 ml) and the mixture was refluxed for 24 h. Thin-layer chromatographic analysis of the solution showed a mixture of two components, the principle one being the starting material (**2**); the second component, which had the greater R_f value, was the quinazolinobenzotriazinone (**4**). Evaporation of the reaction mixture, trituration with benzene and filtration gave a solid mixture of the two components **2** and **4**. Recrystallisation of this solid from ethanol–acetonitrile afforded the pure quinazolinobenzotriazinone (**4**) (10 mg), which was identical with an authentic sample (12).

(*ii*) The above procedure was repeated at room temperature for 7 days. Thin-layer chromatographic analysis of the solution showed only the presence of the same two components, **2** and **4**.

(*f*) Compound **2** (0.1 g) and dicyclohexylcarbodiimide (0.2 g) were dissolved in acetonitrile (10 ml) with slight warming and the mixture stirred at room temperature for 140 h. (Occasional warming was necessary to maintain a clear solution.) Thin-layer chromatographic analysis showed that no reaction had occurred.

Acknowledgements

The financial assistance of the Saint Mary's University Senate Research Committee (in part) is gratefully acknowledged. We are also indebted to the Department of Pharmacy at the University of Aston in Birmingham for providing facilities, equipment, chemicals, moral encouragement and criticism to one of us (K.V.) during a period of sabbatical leave, 1976–1977, when this work was completed.

1. T. P. AHERN, H. FONG, and K. VAUGHAN. Can. J. Chem. **54**, 290 (1976).
2. M. DAVIS and F. G. MANN. J. Chem. Soc. 945 (1962); G. HELLER and L. HESSEL. J. Prakt. Chem. **120**, 64 (1929); A. WEDDIGE and H. FINGER. J. Prakt. Chem. **35**, 262 (1887).
3. K. BUTLER and M. W. PARTRIDGE. J. Chem. Soc. 2396 (1959).
4. R. P. STAIGER and E. C. WAGNER. J. Org. Chem. **18**, 1427 (1953).
5. R. P. STAIGER and E. B. MILLER. J. Org. Chem. **24**, 1214 (1959).
6. E. MOHR, F. KOHER, and H. ULRICH. J. Prakt. Chem. **79**, 320 (1909).
7. T. P. AHERN, T. NAVRATIL, and K. VAUGHAN. Can. J. Chem. **55**, 630 (1977).
8. A. W. SCOTT and B. L. WOOD. J. Org. Chem. **7**, 508 (1942).
9. V. E. GUNN and J.-P. ANSELME. J. Org. Chem. **42**, 754 (1977).
10. H. KOHL and E. WOLF. Justus Liebigs' Ann. Chem. **766**, 106 (1972).
11. W. L. F. ARMAREGO. *In* The chemistry of heterocyclic compounds: Fused pyrimidines. Part I. *Edited by* D. J. Brown. Interscience, New York, NY. 1967. pp. 74 and 99.
12. A. W. MURRAY and K. VAUGHAN. J. Chem. Soc. C, 2070 (1970).

Indole *N*-alkylation of tryptamines via dianion and phthalimido intermediates. New potential indolealkylamine haptens

S. OSMUND DE SILVA AND VICTOR SNIECKUS

Guelph–Waterloo Centre for Graduate Work in Chemistry, University of Waterloo Campus, Waterloo, Ont., Canada N2L 3G1

Received December 22, 1978

S. OSMUND DE SILVA and VICTOR SNIECKUS. Can. J. Chem. **56**, 1621 (1978).

Tryptamine derivatives **3***a–c* and **4***a*, **4***b*, **4***d* have been converted into the indole *N-p*-carbomethoxybenzyl derivatives **1***a*, **1***b*, **1***g*, and **2***a*, **2***b*, **2***c*, respectively, using dianion and phase-transfer catalytic methodologies. Treatment of these compounds with lithium iodide and sodium cyanide in refluxing dimethylformamide gave the corresponding carboxylic acids **1***d*, **1***e*, **1***h*, and **2***d*, **2***e*, **2***f*. The serotonin analogue **1***f* was obtained by catalytic debenzylation of **1***h*. These products may be useful haptens for eliciting specific antibodies to indolealkylamines.

S. OSMUND DE SILVA et VICTOR SNIECKUS. Can. J. Chem. **56**, 1621 (1978).

Faisant appel à des méthodes impliquant des dianions et une catalyse par transfert de phase, on a pu transformer les dérivés de la tryptamine **3***a–c*, **4***a*, **4***b* et **4***d* en leurs dérivés respectifs *N-p*-carbométhoxybenzyle indoles (**1***a*, **1***b*, **1***g* et **2***a*, **2***b*, **2***c*). La réaction de ces composés avec l'iodure de lithium et le cyanure de sodium dans la diméthylformamide à reflux conduit aux acides carboxyliques correspondants **1***d*, **1***e*, **1***h* et **2***d*, **2***e* et **2***f*. On a obtenu l'analogue de la sérotonine **1***f* par une débenzylation catalytique de **1***h*. Ces composés peuvent être des haptènes utiles pour découvrir des anticorps spécifiques aux indolealkylamines.

[Traduit par le journal]

Introduction

In connection with a problem concerning production of antibodies to tryptamines (1), it was of interest to prepare a series of indole *N*-substituted compounds of the types **1** and **2**. These compounds would possess a free carboxylic acid function (R^2 = H) which would serve as a handle for coupling to protein to afford potential antigens which in turn would be used directly (**1**) or after suitable demasking of the side-chain amino group (**2**) in attempts to elicit specific antibodies (2).

It may be envisaged that compounds **1** and **2** would be most conveniently available by N_a-*p*-carboalkoxybenzylation of either commercially or synthetically (3) available tryptamine derivatives. Although a number of excellent methods have been developed (4), particularly in recent years (5), for *N*-alkylation of simple indole derivatives, this reaction appears not to have been extensively explored (4) for tryptamines. This situation may be explained in part by the observation that relatively few complex indole alkaloids possess N_a-substitution (6) and, since tryptamines are common building blocks for these natural products, a general synthetic need for N_a-alkylated tryptamines has not arisen.

Herein we report on (*i*) the regioselective N_a-*p*-carbomethoxybenzylation of dianions from N_b-acyl tryptamines **3** generated using sodium hydride in DMF (7) or phase-transfer conditions (8) to give **1**, R^2 = Me; (*ii*) similar N_a-benzylation of monoanions of N_b-phthaloyl tryptamines **4**, available using

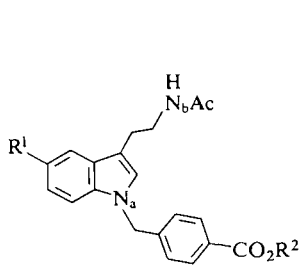

1

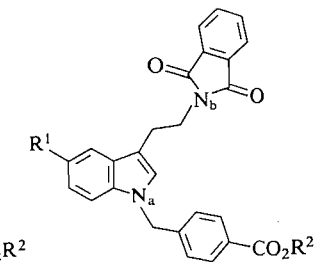

2

a R^1 = H, R^2 = Me
b R^1 = OMe, R^2 = Me
c R^1 = OAc, R^2 = Me
d R^1 = R^2 = H
e R^1 = OMe, R^2 = H
f R^1 = OH, R^2 = H
g R^1 = OCH_2Ph, R^2 = Me
h R^1 = OCH_2Ph, R^2 = H

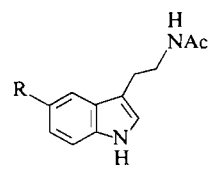

3

a R = H
b R = OMe
c R = OCH_2Ph

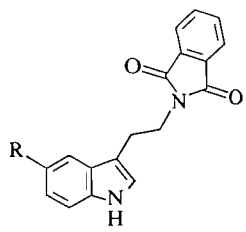

4

a R = H
b R = OMe
c R = OH
d R = OAc

Can. J. Chem. Downloaded from www.nrcresearchpress.com by 210.87.254.40 on 09/05/12
For personal use only.

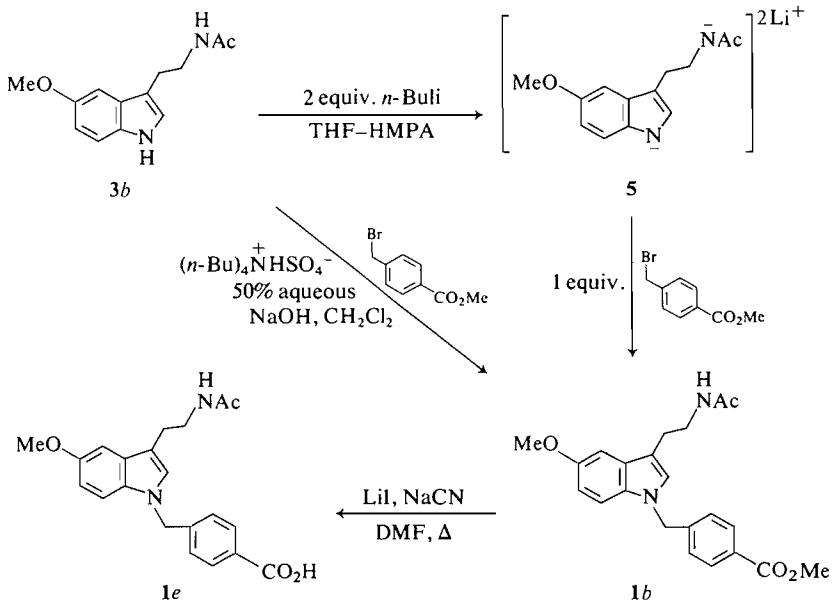

SCHEME 1

Nefkens' reagent **6** (9), to give **2**, R^2 = Me; and (*iii*) selective ester hydrolysis of **1** and **2** (R^2 = Me) to the carboxylic acids, **1** and **2** (R^2 = H) by the nonaqueous procedure of McMurry and Wong (10).

Results and Discussion

It was anticipated that treatment of melatonin (**3***b*) with 2 equiv. of base would generate the dianion **5** which upon reaction with 1 equiv. of *p*-carbomethoxybenzyl bromide would undergo alkylation at the more reactive N_a-anion to provide, after work-up, compound **1***b*.[1] In the event, when this reaction was conducted in a THF–HMPA mixture using *n*-butyllithium as base, the desired product (**1***b*) was formed in 60% yield (Scheme 1). When the N_a-alkylation was carried out in a two-phase system (8) consisting of methylene chloride and concentrated aqueous sodium hydroxide with a phase-transfer catalyst (tetra-*n*-butylammonium hydrogen sulfate), a significant improvement in efficiency and yield was noticed with the added advantage of avoiding the anhydrous conditions that are essential for the procedure using *n*-butyllithium. That the alkylation had occurred in the indole rather than the side-chain nitrogen was ascertained from examination of the ir and nmr spectra which showed absence of characteristic indole NH absorption and presence of a two-proton singlet at τ 4.83 typical of benzylic protons of 1-benzylindole (*vide infra*). For the final stage of the synthesis, **1***b* → **1***e*, it was necessary to use conditions which would selectively hydrolyze the ester without affecting the amide function. The nonaqueous procedure of McMurry and Wong (10) proved suitable for this purpose and provided **1***e* in 50% yield.

Following the route delineated in Scheme 1, compounds **1***d*, **1***f*, and **1***h* were also synthesized (see Tables 1 and 2). In the case of the serotonin analogue **1***f*, the protected *O*-benzylacetylserotonin **3***c* was alkylated with *p*-carbomethoxybenzyl bromide. The resulting product **1***c* underwent deesterification when subjected to reaction with lithium iodide and sodium cyanide in refluxing DMF to give **1***h*. Debenzylation of the blocked phenol to obtain **1***f* was achieved by catalytic hydrogenation.

The N_b-phthaloyl derivatives **2***d–f* were prepared by adaptation of N_a-alkylation conditions extensively used previously in our laboratories (7). The general route is shown in Scheme 2 for the preparation of **2***e* and the results are summarized in Tables 1 and 2. The starting phthaloyl derivatives **4***a–c* were readily prepared from commercially available tryptamines by treatment with phthalic anhydride or, preferably, by application of Nefkens' excellent *N*-carbethoxyphthalimide (**6**) reagent (9) which enjoys moderate use in peptide synthesis (13) but which appears not to be widely employed by organic chemists, e.g., in the Gabriel synthesis. Alkylations were carried out at room temperature using sodium hydride in DMF; as in the case of **3***c*, the protected *O*-acetyl phthaloylserotonin (**4***d*) was used for the base-catalyzed alkylation reaction. The phase transfer method applied to **4***a* gave only low yields of **2***a* and was

[1]For indole *N*-alkylation of tryptophan dianion, see ref. 11; for other synthetic work with indole compounds using dianion intermediates, see ref. 12.

Can. J. Chem. Downloaded from www.nrcresearchpress.com by 210.87.254.40 on 09/05/12
For personal use only.

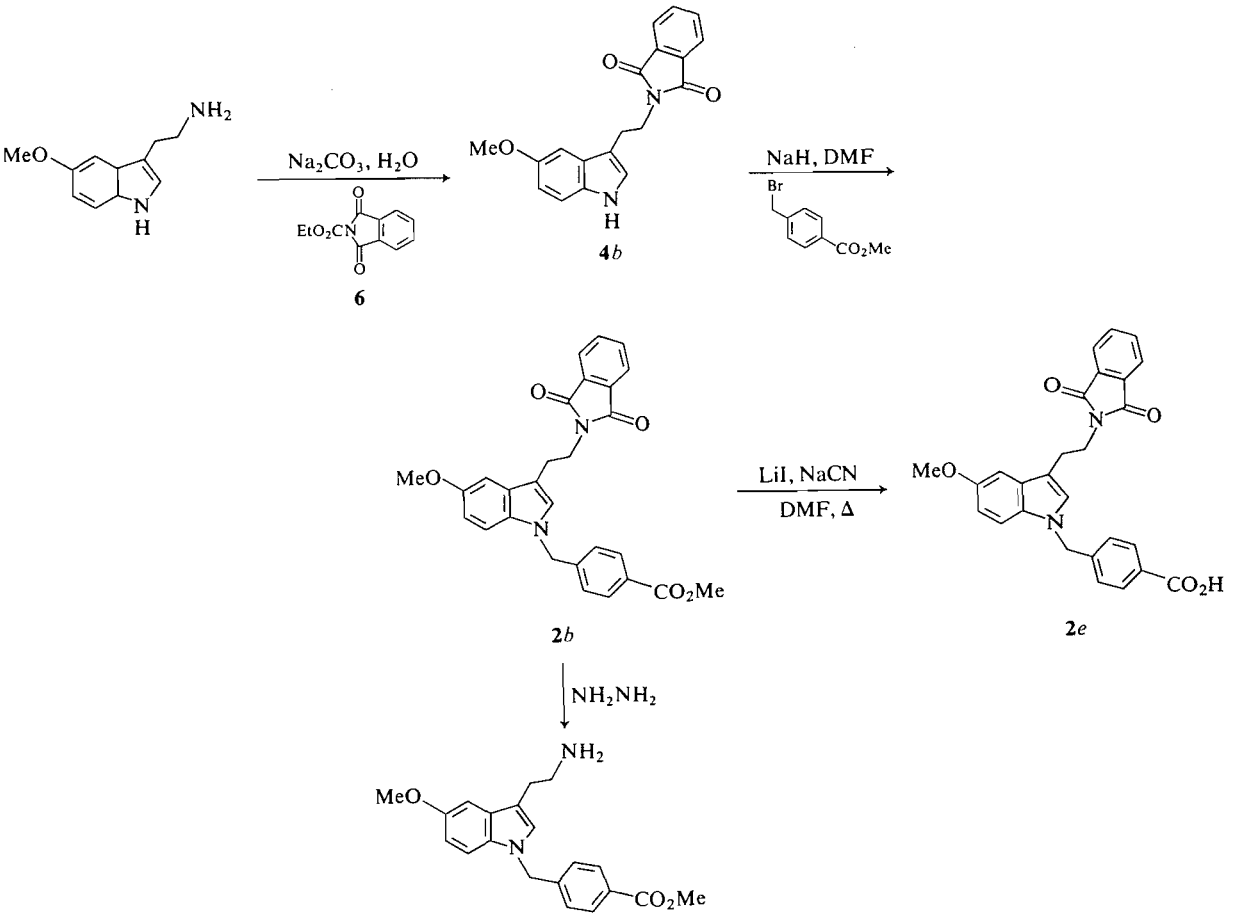

SCHEME 2

therefore not pursued. The nmr spectra of the alkylated products **2***a–c* all showed a two-proton singlet at $\tau \sim 4.8$ which can be unambiguously assigned to the N_a-benzylic hydrogens by analogy with the data obtained in the N_b-acetyl series (**1***a–c*). Finally, deesterifications of **2***a–c* were effected using the LiI–NaCN reagent to give compounds **2***d–f*. The LiI–NaCN reaction on **2***c* gave directly the deesterified-deacetylated product **2***f*. Deacetylation occurs owing to the basic conditions that prevail during aqueous work-up of the reaction mixture.

To test the dephthaloylation step[2] required for antibody generation studies after coupling to protein (1), compound **2***b* was subjected to the standard conditions of hydrazinolysis at room temperature (13). The expected product, **7**, was obtained in good yield.

In conclusion, this work provides ready access to N_a-*p*-carboxybenzyl tryptamine derivatives **1***d–f* and **2***d–f*. These may be useful in radioimmunoassay, immunohistochemical and related studies which are in progress elsewhere.[3]

Experimental

Melting points were measured on a Mel-Temp apparatus and are uncorrected. Microanalyses were performed by A. B. Gygli, Toronto. Infrared spectra were determined with a Beckman IR-5A instrument. Nuclear magnetic resonance spectra were obtained on Varian T-60 and Perkin-Elmer R-12 spectrometers. Thin-layer chromatography was carried out with Merck silica gel GF 254 and column chromatography with Merck silica gel (0.05–0.2 mm) obtained from Brinkmann (Canada) Ltd. THF was dried by refluxing over sodium and benzophenone until a deep blue color persisted in solution. Dry DMF was prepared by refluxing over calcium hydride followed by distillation. HMPA was dried by allowing it to stand over Linde molecular sieves (Type 4A) followed by distillation.

n-Butyllithium was purchased as a solution in *n*-hexane from Alfa Ventron Crop. Tryptamine hydrochloride, 5-methoxytryptamine hydrochloride, and 5-benzyloxytryptamine

[2]For an example of its application in penicillin synthesis see the recent work of Kukolja and Lammert (13).

[3]G. M. Brown and co-workers, Department of Neurosciences, McMaster University, Hamilton, Ont.

Can. J. Chem. Downloaded from www.nrcresearchpress.com by 210.87.254.40 on 09/05/12
For personal use only.

Can. J. Chem. Downloaded from www.nrcresearchpress.com by 210.87.254.40 on 09/05/12
For personal use only.

TABLE 1. N_a-*p*-Carboxybenzyl derivatives of tryptamines and N_b-phthaloyltryptamines (**1** and **2**)

Compound	Starting material	Method[a]	Yield[b] (%)	Melting point[c] (°C)
1*a*	**3***a*	*B*	>95	136 (PhH – 2% EtOH)
1*b*	**3***b*	*A*	60	116 (PhH–*n*-hexane)
		B	98	
1*d*	**1***a*	*C*	69[d]	155 (EtOH)
1*e*	**1***b*	*C*	66	173 ($CHCl_3$ – 2% EtOH)
1*f*	**1***h*	*D*	96	204 (EtOH)
1*g*	**3***c*	*B*	97	Oil[e]
1*h*	**1***g*	*C*	60	141 (EtOH – 10% H_2O)
4*a*	Tryptamine·HCl	*E*	94	165 (EtOH)
		F	90	
4*b*	5-MeO-Tryptamine·HCl	*E*	91	158 (EtOH)
4*c*	Serotonin–creatinine sulfate	*E*	84[f]	210 (EtOH)
		G	69	
4*d*	**4***c*	*H*	99	Foam
2*a*	**4***a*	*A*	48[g]	139 (MeOH – 20% PhH)
2*b*	**4***b*	*A*	54[g]	143 (EtOH)
2*c*	**4***d*	*A*	79	209 (EtOH – 10% CH_2Cl_2)
2*d*	**2***a*	*C*	60[d]	192–193 (EtOH – 10% H_2O)
2*e*	**2***b*	*C*	48[g]	227 (EtOH – 5% $CHCl_3$)
2*f*	**2***c*	*C*	35	193 (EtOH – 20% H_2O)

[a]See Experimental.
[b]Yield of homogeneous product after chromatography (if necessary).
[c]Recrystallization solvent given in parentheses.
[d]Starting material (25–30%) was recovered.
[e]After chromatography (silica gel PhH–Me_2CO–MeOH 8:1:1) homogeneous by tlc.
[f]Yield improved to 96% if **6** is added portionwise to an aqueous mixture of serotonin salt and Na_2CO_3.
[g]Starting material (30–50%) was recovered.

hydrochloride were purchased from Aldrich Chemical Co. Melatonin and serotonin–creatinine sulfate were procured from Sigma Chemical Co. All of these compounds were used without further purification.

*1-(*p*-Carbomethoxy)benzylmelatonin (**1**b)*

Method A

To a solution of melatonin (**3***b*) (0.116 g, 0.5 mmol) in a mixture of dry THF (30 ml) – HMPA[4] (0.5 ml) maintained under an atmosphere of dry nitrogen and cooled in an ice-bath was added via a syringe through a septum cap a solution of *n*-butyllithium (2.4 *M*, 0.42 ml (1 mmol)) in *n*-hexane. Over a period of 4 h stirring at room temperature there accumulated a colorless, gelatinous precipitate. A solution of methyl α-bromo-*p*-toluate (ref. 14 and footnote 5) (0.114 g, 0.5 mmol) in dry THF (5 ml) was introduced dropwise and stirring was continued for a further 4 h. The clear yellow solution was treated with 0.1 *N* hydrochloric acid solution (5 ml) and the resulting mixture was evaporated to dryness *in vacuo*. The residue was suspended in water (50 ml) and extracted with methylene chloride (2 × 50 ml). The organic extract was dried (sodium sulfate) and evaporated to dryness. The residue on chromatography (silica gel, benzene–acetone–methanol eluent, 8:1:1) gave a yellow gum (0.115 g, 60%) which was crystallized from a 1:3 mixture of benzene – petroleum ether (60–80°C) to give **1***b* as a colorless solid.

Method B

A solution of melatonin (**3***b*) (0.232 g, 1 mmol) in methylene chloride (30 ml) was mixed with an aqueous solution (20 ml 50% w/v) of sodium hydroxide. Solid methyl α-bromo-*p*-toluate (0.250 g, 1.09 mmol) and a solution of tetra-*n*-butylammonium hydroxide (a few drops of 40% aqueous solution) were successively introduced and the mixture was stirred at 30–33°C for 3 h. Heating was discontinued and the mixture was stirred at room temperature overnight (~14 h). The reaction mixture was cooled in ice and carefully acidified (litmus paper) with a dilute solution of hydrochloric acid. The organic layer was separated, washed with a saturated solution of sodium carbonate and then with water. Drying (sodium sulfate) of the organic extract followed by evaporation to dryness *in vacuo* gave a gummy material which was purified by column chromatography as in method *A*. Crystallization of the purified product (0.37 g, 98%) from a mixture of benzene–*n*-hexane (1:1) gave a colorless solid. This compound was found to be identical with a sample of **1***b* prepared by method *A*.

*1-(*p*-Carboxy)benzylmelatonin (**1**e)*

Method C

A mixture of 1-(*p*-carbomethoxy)benzylmelatonin (**1***b*) (0.223 g, 0.587 mmol), anhydrous lithium iodide (0.804 g, 6 mmol), and sodium cyanide (0.050 g, 1 mmol) in dry DMF (50 ml) under a blanket of dry nitrogen was heated in an oil bath at 140–145°C (external temperature) for 50 h. Most of the solvent was removed *in vacuo* and the residual gum was suspended in water (25 ml) and extracted with chloroform (2 × 20 ml). The organic extract was dried (Na_2SO_4) and evaporated to dryness to give 0.062 g (28%) of recovered starting material (**1***b*). The aqueous layer was acidified with concentrated hydrochloric acid. Cooling in ice resulted in formation of a gum. The water layer was decanted, ethanol was added and the whole was evaporated to dryness. There was obtained 0.142 g (66%) of **1***e* as a yellow solid.

[4]Dictated by solubility problems. In all other cases of method *A*, DMF was used as the sole solvent.

[5]This compound was prepared by the method of Julia and Chastrette (14).

TABLE 2. Spectral and analytical data of compounds **1**, **2**, and **4**

Compound	ν_{max} (KBr) (cm^{-1})	τ ($CDCl_3$) (*J* in Hz)	Molecular formula	Elemental analysis (%) C Calcd.	C Obs.	H Calcd.	H Obs.	N Calcd.	N Obs.
1*a*	1720 1645	2.0 (d, 2H, *J* = 10), 2.2–3.1 (m, 7H), 3.86 (br s, 1H), 4.72 (s, 2H), 6.13 (s, 3H), 6.47 (q, 2H, *J* = 8), 7.04 (t, 2H, *J* = 8), 8.10 (s, 3H)	$C_{21}H_{22}N_2O_3$	71.98	71.90	6.33	6.29	7.99	7.96
1*b*	1720 1645	2.0 (d, 2H, *J* = 10), 2.5–3.3 (m, 6H), 4.0 (br s, 1H), 4.83 (br s, 2H), 6.23 (s, 3H), 6.27 (s, 3H), 6.47 (q, 2H, *J* = 8), 7.06 (t, 2H, *J* = 8), 8.1 (s, 3H)	$C_{22}H_{24}N_2O_4$	69.46	69.50	6.36	6.38	7.36	7.34
1*d*[a]	3400 1700 1645 1600	2.0 (d, 2H, *J* = 10), 2.35–3.0 (m, 9H), 4.63 (br s, 2H), 6.53 (q, 2H, *J* = 7), 7.03 (t, 2H, *J* = 7), 8.07 (s, 3H)	$C_{20}H_{20}N_2O_3$	71.41	71.46	5.99	5.97	8.33	8.28
1*e*	3400 (br) 1700 1645 1600	2.04 (d, 2H, *J* = 10), 2.7–3.4 (m, 6H), 4.8 (br s, 2H), 6.1 (s, 3H), 6.38 (q, 2H, *J* = 7), 7.08 (t, 2H, *J* = 7), 8.05 (s, 3H)	$C_{21}H_{22}N_2O_4$	68.84	68.81	6.05	6.07	7.65	7.69
1*f*[b]	3500 (v br) 1700 1645 1600	2.02 (d, 2H, *J* = 10), 2.4–3.6 (m, 6H), 4.60 (br s, 2H), 5.30 (m, 3H), 6.46 (2 × t, 2H, *J* = 7), 7.21 (t, 2H, *J* = 7), 8.15 (s, 3H)	$C_{20}H_{20}N_2O_4$	68.17	68.08	5.72	5.77	7.95	7.99
1*g*[c]	1720 1645	2.05 (d, 2H, *J* = 10), 2.3–3.2 (m, 11H), 4.03 (br s, 1H), 4.85 (s, 2H), 4.95 (s, 2H), 6.15 (s, 3H), 6.53 (q, 2H, *J* = 8), 7.13 (t, 2H, *J* = 8), 8.15 (s, 3H)	$C_{28}H_{28}N_2O_4$	Not determined					
1*h*[a]	3400 (br) 1700 1645 1600	2.0 (d, 2H, *J* = 10), 2.4–3.23 (m, 13H), 4.62 (s, 2H), 4.87 (s, 2H), 6.55 (q, 2H, *J* = 8), 7.08 (t, 2H, *J* = 8), 8.10 (s, 3H)	$C_{27}H_{26}N_2O_4$	73.29	73.31	5.92	5.90	6.33	6.29
4*a*[c]	1775 1712	1.7–3.0 (m, 9H), 5.08 (2 × t, 2H, *J* = 8), 6.75 (t, 2H, *J* = 8)	$C_{18}H_{14}N_2O_2$	74.47	74.49	4.86	4.90	9.65	9.63
4*b*[c]	1775 1715	1.7–3.2 (m, 8H), 5.08 (2 × t, 2H, *J* = 8), 6.75 (t, 2H, *J* = 8)	$C_{19}H_{16}N_2O_3$	71.24	71.26	5.03	5.07	8.74	8.79
4*c*[b]	3400 1770 1705	1.95–3.3 (m, 8H), 6.1 (2 × t, 2H, *J* = 8), 7.07 (t, 2H, *J* = 8)	$C_{18}H_{14}N_2O_3$	70.58	70.60	4.61	4.63	9.15	9.17
4*d*[c]	3500 1775 1768 1715	1.4 (br s, 1H), 2.0–3.3 (m, 8H), 6.1 (t, 2H, *J* = 8), 6.97 (t, 2H, *J* = 8), 7.7 (s, 3H)	$C_{20}H_{16}N_2O_4$	Not determined					
2*a*[c]	1775 1715	1.9–3.2 (m, 13H), 4.8 (br s, 2H), 6.0 (2 × t, 2H, *J* = 8), 6.23 (s, 3H), 6.85 (t, 2H, *J* = 8)	$C_{27}H_{22}N_2O_4$	73.96	73.98	5.06	5.03	6.39	6.37
2*b*[c]	1775 1715 (br)	1.82–3.22 (m, 12H), 4.72 (br s, 2H), 5.82 (2 × t, 2H, *J* = 8), 6.08 (s, 3H), 6.12 (s, 3H), 6.88 (t, 2H, *J* = 8)	$C_{28}H_{24}N_2O_5$	71.78	71.80	5.16	5.14	5.98	5.94

Can. J. Chem. Downloaded from www.nrcresearchpress.com by 210.87.254.40 on 09/05/12
For personal use only.

TABLE 2 (*Concluded*)

Compound	ν_{max} (KBr) (cm^{-1})	τ ($CDCl_3$) (*J* in Hz)	Molecular formula	Elemental analysis (%) C Calcd.	C Obs.	H Calcd.	H Obs.	N Calcd.	N Obs.
2*c*	1775 1715 (br)	1.56–3.1 (m, 12H), 4.8 (s, 2H), 5.96 (t, 2H, J = 8), 6.08 (s, 3H), 6.94 (t, 2H, J = 8), 7.04 (s, 3H)	$C_{29}H_{24}N_2O_6$	70.15	70.16	4.87	4.90	5.64	5.68
2*d*	3500 (br) 1780 1720 1715	1.92 (d, 2H, J = 10), 2.0–3.0 (m, 11H), 4.0 (br s, 1H), 4.65 (s, 2H), 5.9 (t, 2H), J = 8), 6.8 (t, 2H, J = 8)	$C_{26}H_{20}N_2O_4$	73.57	73.61	4.75	4.97	6.60	6.62
2*e*[b]	3600 (br) 1780 1715 1700	2.0–3.32 (m, 12H), 4.8 (br s, 2H), 6.05 (t, 2H, J = 8), 6.25 (s, 3H), 6.99 (t, 2H, J = 8)	$C_{27}H_{22}N_2O_5$	71.36	71.39	4.88	4.87	6.16	6.19
2*f*[b]	3600 (v br) 1780 1715 1700	1.70 (br s, 1H), 2.0 (d, 2H, J = 10), 2.20–3.80 (m, 11H), 4.90 (br s, 2H), 6.50 (t, 2H, J = 8), 7.0 (t, 2H, J = 8)	$C_{26}H_{20}N_2O_5$	70.90	70.87	4.54	4.50	6.36	6.40

[a]Nuclear magnetic resonance recorded in DMSO-d_6–$CDCl_3$.
[b]Nuclear magnetic resonance recorded in DMSO-d_6.
[c]Infrared determined in $CHCl_3$.

*1-(*p*-Carboxy)benzyl-*N*-acetylserotonin (**1***f*)*

Method D

A solution of **1***h* (0.161 g, 0.36 mmol) in absolute ethanol (150 ml) containing a suspension of 10% palladium-on-charcoal (0.175 g) was hydrogenated in a Parr apparatus at 45 psi for 18 h. Filtration of the reaction mixture followed by evaporation to dryness and recrystallization gave **1***f* as an off-white crystalline solid (0.123 g, 96%).

*Phthaloyltryptamine (**4**a)*

Method E

Nefkens' method (9) was adapted. Tryptamine hydrochloride (1.967 g, 1 mmol) and *N*-carbethoxyphthalimide (2.41 g, 1.1 mmol) were suspended in water (50 ml) and sodium carbonate decahydrate (5.72 g, 2 mmol) was added with stirring. After 0.5 h at room temperature, an additional amount of *N*-carbethoxyphthalimide (0.48 g, 0.2 mmol) was added and stirring was continued for another 0.5 h. The yellowish-white solid was collected by filtration and recrystallized to give yellow crystals of **4***a* in three crops, 2.74 g (94%).

Method F

A mixture of tryptamine hydrochloride (0.393 g, 2 mmol), phthalic anhydride (0.312 g, 2.02 mmol), anhydrous sodium carbonate (0.110 g, 1.02 mmol) and dry benzene (50 ml) was refluxed under a Dean–Stark water separator. After 20 h, the solvent was removed *in vacuo* and then the residue was pyrolyzed for 15 min in an oil bath preheated to 210°C. The brownish solid residue was allowed to cool to about 80°C and hot water (200 ml) was added with vigorous trituration. The mixture was extracted with methylene chloride (200 ml) and the organic extract was successively washed with a 5% aqueous solution of sodium hydroxide (100 ml) and water (200 ml). The organic layer was treated with decolorizing carbon, filtered, dried (sodium sulfate), and evaporated to dryness. The residual solid was recrystallized from ethanol to give **4***a* (0.523 g, 90%), identical with a sample obtained by method *E*.

*Phthaloyl-5-hydroxytryptamine (**4**c)*

Method G

A mixture of serotonin–creatinine sulfate (0.388 g, 1 mmol), phthalic anhydride (0.5 g, 3.37 mmol), and anhydrous pyridine (20 ml) was heated in an oil bath at 100°C for 20 h. Evaporation to dryness followed by azeotropic distillation with absolute ethanol gave a residual solid which was pyrolyzed in a preheated oil bath at 200°C. The melt was allowed to cool and was then triturated with hot ethanol (30 ml). The mixture was cooled to 0°C. The resulting solid was collected by filtration and was washed successively with water (40 ml), a saturated aqueous solution of sodium carbonate (50 ml), and water (40 ml). The solid was air dried and recrystallized to give a yellow crystalline material (0.210 g, 69%), shown to be identical with a sample of **4***c* prepared by method *E*.

O-*Acetylphthaloylserotonin (**4**d)*

Method H

A stirred solution of **4***c* (0.306 g, 1 mmol) in dry THF (75 ml) maintained at room temperature under an atmosphere of dry nitrogen was treated with sodium hydride (0.060 g, 1.2 mmol, 50% dispersion in mineral oil). Over a period of 0.5 h, a reddish-brown color developed. Acetic anhydride (0.3 ml, 3 mmol) was added to the mixture and stirring was continued for 12 h. The mixture was treated with aqueous hydrochloric acid (0.1 *N*, 5 ml) and most of the THF was removed *in vacuo*. The aqueous solution was diluted with water (200 ml) and the resulting brownish gum was retained by decanting the supernatant aqueous layer. The gummy material was suspended in absolute ethanol and the whole was taken to dryness *in vacuo*. This process was repeated several times. The gum was washed with hot petroleum ether (60–80°C, 50 ml) and dried *in vacuo* to give **4***d* as a cream-colored foam, 0.342 g (99%) which was used without further purification for the preparation of **2***c*.

Can. J. Chem. Downloaded from www.nrcresearchpress.com by 210.87.254.40 on 09/05/12
For personal use only.

N-*Acetyltryptamine (3a)*

Tryptamine hydrochloride (0.200 g, 1.02 mmol) suspended in a mixture of dry pyridine (10 ml), benzene (20 ml), and acetic anhydride (3 ml) was stirred at room temperature for 6 h. The mixture was evaporated to dryness *in vacuo* and the residue was suspended in water (200 ml) and extracted with methylene chloride (2 × 100 ml). Successive washing of the organic extract with 10% aqueous sodium carbonate solution, water, 10% hydrochloric acid, and water followed by drying (sodium sulfate) and removal of solvent *in vacuo* gave a colorless gummy material. This compound was crystallized from a mixture of ether – benzene – petroleum ether (60–80°C) (10:10:1) to give **3***a* as a white crystalline solid (0.192 g, 93%), mp 75°C (lit. (15) mp 75–76°C).

5-Benzyloxy-N-*acetyltryptamine (3c)*

The procedure described for the preparation of **3***a* was employed. From 0.950 g (3.14 mmol) of 5-benzyloxytryptamine hydrochloride and 10 ml of acetic anhydride in a mixture of dry pyridine (40 ml) and benzene (5 ml) there was obtained a gummy product which was crystallized from a mixture of benzene–*n*-hexane (10:1) to give **3***c* as a cream-colored solid (0.943 g, 97%), mp 123°C (lit. (16) mp not recorded); ir ν_{max} (KBr): 1645 cm^{-1}; nmr ($CDCl_3$) τ: 1.30 (br s, 1H, indole NH), 2.3–3.2 (m, 9H, aromatic H), 4.10 (br s, 1H, amide NH), 4.86 (s, 2H, $PhCH_2$), 6.45 (two overlapping triplets, J = 7 Hz, 2H, $N—CH_2$), 7.12 (t, 2H, J = 7 Hz, $—CH_2$), 7.85 (s, 3H, $COCH_3$). *Anal.* calcd for $C_{19}H_{20}N_2O_2$: C 74.00, H 6.54, N 9.08; found: C 73.78, H 6.31, N 8.89.

N-*Carbethoxyphthalimide (6)*

Nefkens' method (9) for the preparation of this compound was modified. A solution of phthalimide (14.7 g, 100 mmol) in dry DMF (100 ml) was added dropwise into a stirred suspension of sodium hydride (5.0 g, 105 mmol, a 50% dispersion in mineral oil, oil removed by washing with dry petroleum ether) kept at room temperature. After 3 h, the evolution of hydrogen had ceased. The mixture was cooled to 5°C and freshly distilled ethyl chloroformate (10 ml, 130 mmol) was added dropwise keeping the temperature below 40°C. The mixture was stirred at 35°C for 3 h and then poured into ice-cold water (1 L) with vigorous stirring. The resulting white solid was collected by filtration and recrystallized from ethanol to give 20 g (91%) of product, mp 80°C (lit. (9) mp 80°C).

Acknowledgements

This work was generously supported by grants from the Medical Research Council of Canada (Grant No. 5372) to V. Snieckus and to G. M. Brown, Department of Neurosciences, McMaster University, Hamilton, Ontario. We are grateful to Ms. L. Leung for the preparation of starting materials and to Professor Jan Bergman for a gift of tetra-*n*-butylammonium hydrogen sulfate.

1. L. J. GROTA and G. M. BROWN. Can. J. Biochem. **52**, 196 (1974).
2. B. F. ERLANGER. Pharmacol. Rev. **25**, 271 (1973); R. S. YALOW. Pharmacol. Rev. **25**, 161 (1973).
3. F. TROXLER. *In* Indoles. Part II. *Edited by* W. J. Houlihan. Wiley, New York, NY. 1972. p. 181.
4. R. J. SUNDBERG. The chemistry of indoles. Academic Press, Inc., New York, NY. 1970. p. 19ff; W. A. REMERS. *In* Indoles. Part I. *Edited by* W. J. Houlihan. Wiley, New York, NY. 1972. pp. 90ff and 128ff; L. R. SMITH. *In* Indoles. Part II. *Edited by* W. A. Houlihan. Wiley, New York, NY. 1972. p. 72.
5. N. NARASIMHACHARI and K. LEINER. J. Chromatogr. Sci. **15**, 181 (1977); A. BANERJI and J. BANERJI. Indian J. Chem. **13**, 945 (1975); H. PLIENINGER, H. P. KRAEMER, and C. ROTH. Chem. Ber. **108**, 1776 (1975); M. A. GARNER, P. J. ALBISSER, M. A. RENSWICK, and M. J. WHITEHEAD. Chem. Ind. 110 (1974); G. M. RUBOTTOM. Org. Synth. **54**, 60 (1974); R. J. SUNDBERG and H. F. RUSSELL. J. Org. Chem. **38**, 3324 (1973) and refs. therein; P. BRAVO, G. GAUDINO, and A. UMANI-RONCHI. Gazz. Chim. Ital. **100**, 652 (1970).
6. M. HESSE. Indolalkaloide in tabellen. Springer-Verlag, Berlin, Germany. 1964.
7. S. O. DE SILVA and V. SNIECKUS. Can. J. Chem. **52**, 1294 (1974).
8. A. BARCO, S. BENETTI, G. P. POLLINI, and P. G. BARALDI. Synthesis, 124 (1976); N. N. SUVOROV, Y. I. SMUSHKEVICH, V. S. VELEZHEVA, V. S. ROSHOV, and S. V. SIMAKOV. Khim. Geterotsikl. Soedin. 191 (1976); Chem. Abstr. **84**, 179957b (1976); E. V. DEHMLOW. Angew. Chem. Int. Ed. Engl. **16**, 493 (1977).
9. G. H. L. NEFKENS, G. I. TESSER, and R. J. F. NIVARD. Recl. Trav. Chim. Pays-Bas, **79**, 688 (1960).
10. J. E. MCMURRY and G. B. WONG. Syn. Commun. **2**, 389 (1972); J. E. MCMURRY. Org. React. **24**, 187 (1976).
11. S. YAMADA, T. SHIOIRI, T. ITAYA, T. HARA, and R. MATSUEDA. Chem. Pharm. Bull. Jpn. **13**, 88 (1965).
12. E. M. KAISER and P. L. A. KNUTSON. Tetrahedron Lett. 3583 (1975); J. L. HERRMANN, R. J. CREGGE, J. E. RICHMAN, C. L. SEMMELHACK, and R. H. SCHLESSINGER. J. Am. Chem. Soc. **96**, 3702 (1974).
13. E. WUNSCH. *In* Methoden der Organischen Chemie (Houben-Weyl). Vol. 15, part 1. *Edited by* E. Muller. Georg Thieme Verlag, Stuttgart, Germany. 1974. pp. 250–261; S. KUKOLJA and S. R. LAMMERT. J. Am. Chem. Soc. **97**, 5582 (1975).
14. S. T. D. GOUGH and R. P. NAPIER. U.S. Patent No. 3, 497, 346; Chem. Abstr. **72**, 131371f (1972); E. S. HUYSER. J. Am. Chem. Soc. **82**, 381 (1962); M. JULIA and F. CHASTRETTE. Bull. Soc. Chim. Fr. 2255 (1962).
15. H. T. HUANG and G. NIEMANN. J. Am. Chem. Soc. **74**, 101 (1952).
16. W. M. MCISAAC and I. H. PAGE. J. Biol. Chem. **234**, 858 (1959).

Can. J. Chem. Downloaded from www.nrcresearchpress.com by 210.87.254.40 on 09/05/12
For personal use only.

Synthesis of the spirosesquiterpene (−)-acorenone and related cyclopentanoid monoterpenes[1]

GORDON L. LANGE, ELI E. NEIDERT, WILL J. ORROM, AND DAVID J. WALLACE

Guelph–Waterloo Centre for Graduate Work in Chemistry, Department of Chemistry, University of Guelph, Guelph, Ont., Canada N1G 2W1

Received January 30, 1978

GORDON L. LANGE, ELI E. NEIDERT, WILL J. ORROM, and DAVID J. WALLACE. Can. J. Chem. **56**, 1628 (1978).

The first total synthesis of the spirosesquiterpene (−)-acorenone (**1**) is described. The critical step involves a spiroannelation of the enamine of aldehyde **11** with 1-methoxy-3-buten-2-one (**16**) in the presence of acetic acid to give ketone **17**. Reaction of **17** with methylmagnesium iodide followed by treatment of the resultant alcohol **18** with *p*-toluenesulfonic acid in refluxing benzene leads directly to **1** in good overall yield. As the starting material for the preparation of the cyclopentanoid aldehyde **11** was (+)-limonene the final product is optically active and thus the absolute configuration of naturally occurring (−)-acorenone (**1**) is established. The preparation of a number of other optically active cyclopentanoid monoterpenes (**4** and **13**) is also described.

GORDON L. LANGE, ELI E. NEIDERT, WILL J. ORROM et DAVID J. WALLACE. Can. J. Chem. **56**, 1628 (1978).

On décrit la première synthèse totale du spirosesquiterpène (−)-acorénone (**1**). L'étape critique implique une spiroannélation de l'énamine de l'aldéhyde **11** avec la méthoxy-1 butène-3 one-2 (**16**) en présence d'acide acétique pour donner la cétone **17**. La réaction de **17** avec l'iodure de méthylmagnésium, suivie par un traitement de l'alcool **18** qui en résulte avec de l'acide *p*-toluènesulfonique dans le benzène au reflux, conduit directement à **1** avec un rendement global qui est bon. Comme le produit de départ pour la préparation de l'aldéhyde cyclopentanique **11** est le (+)-limonène, le produit final est optiquement actif et on a donc établi ainsi la configuration absolue de la (−)-acorénone (**1**) que l'on retrouve dans la nature. On décrit aussi la préparation d'un certain nombre d'autres monoterpènes cyclopentaniques optiquement actifs (**4** et **13**).

[Traduit par le journal]

The spirosesquiterpene (−)-acorenone (**1**) was isolated from sweet flag oil (*Acorus calamus* L.) by Sorm and co-workers (2) and its structure determined by degradation (3) and by comparison with acorenone-B (**2**) (4), which differs only in its configuration at the spiro carbon. Syntheses of **2** were reported by several groups (5) and the conversion of (±)-**2** to (±)-**1** was recently effected (6). In this report we outline the first synthesis of (−)-**1** and also describe the preparation of a number of optically active cyclopentanoid monoterpenes which were synthons in our proposed routes to **1**.

Our initial approach to the synthesis of **1** (Scheme 1) involved as the first and critical step a photocycloaddition of **3** to **4**. Previous investigation of a model system employing methylenecyclopentane as the alkene component had given the desired adduct, which in two additional steps was converted to the spiro[4.5]decan-7-one system in moderate overall yield (7). It was first necessary to prepare a sample of **4** and as we chose (+)-limonene (**7**) as our starting material all subsequent products were optically active. Catalytic hydrogenation of **7** yielded (+)-*p*-menth-1-ene, which was converted by performic acid to a mixture of *trans*-*p*-menthane-1,2-diols (**8**) (8). Cleavage of **8** with periodic acid in aqueous pyridine gave (−)-3-isopropyl-6-oxoheptanal (**9**) (9) which was cyclized using acetic acid and piperidine[2] to the

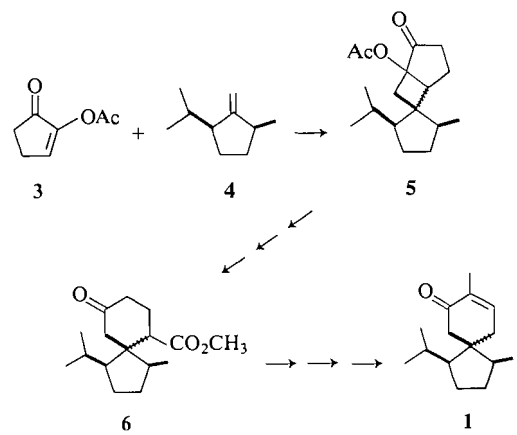

SCHEME 1

[1]A preliminary communication on a portion of this work has appeared (1).

[2]This procedure was used previously for the cyclization of 3-isopropenyl-6-oxoheptanal (10).

Can. J. Chem. Downloaded from www.nrcresearchpress.com by 210.87.254.6 on 09/05/12
For personal use only.

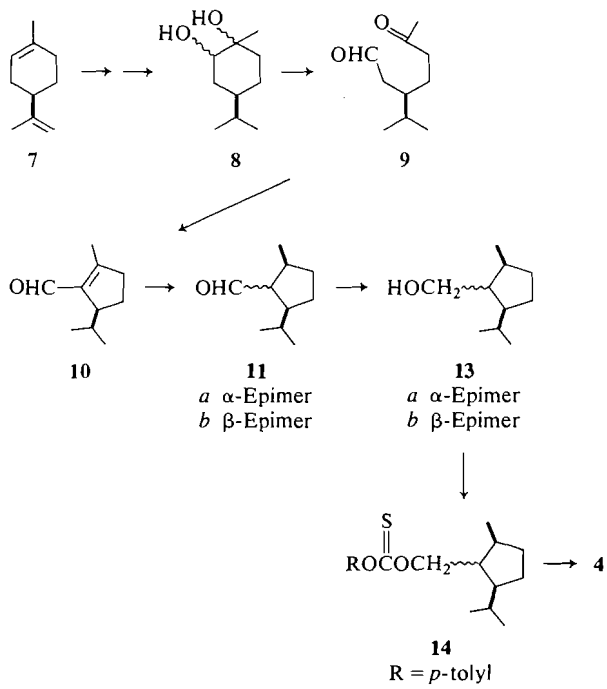

SCHEME 2

(−)-aldehyde **10**. **10** was reported previously (11) but herein we give experimental details for its preparation and complete spectral data.

Reduction of the carbon–carbon double bond in the unsaturated aldehyde **10** was the critical step in establishing the *cis*-orientation of the substituents at the 1 and 3 positions. It was anticipated that the large isopropyl group would block the approach of the reagent to the β-face of **10** and thus attack on the α-face would give the desired *cis* geometry. In the fact, catalytic hydrogenation of **10** with 5% palladium-on-charcoal in absolute ethanol gave an epimeric mixture of the desired aldehydes (**11**) in which the all *cis* product (**11***b*) predominated.[3] To prove the *cis* geometry of the 1 and 3 substituents, pure samples of the two epimers were collected by gc and each was treated with methanolic sodium methoxide to effect epimerization. Gas chromatographic analysis of the products showed a mixture of 90% of **11***a* and 10% of **11***b* in both instances. In a previous investigation, Buchi and Wuest (12) prepared similar aldehydes in which the 1 and 3 substituents were *trans* (**12**) and found that the equilibrium mixture consisted of 75% of **12***a* and 25% of **12***b*. In the case of aldehydes **11**, an even greater preference for one of the aldehydes, namely **11***a*, would be expected as the considerable steric strain in the all *cis* isomer, **11***b*, would be relieved. The physical data for both epimers are recorded in the Experimental section but in subsequent preparative reactions the mixture was used.

Lithium aluminum hydride reduction of aldehyde **11** gave a mixture of alcohols (**13**) with the ratio depending on the ratio of epimeric aldehydes present in the starting material. Gas chromatographic samples of pure **11***a* and **11***b* were reduced separately to confirm the conversions to **13***a* and **13***b*, respectively. Physical data for both alcohols are reported but normally the mixture was used in subsequent steps.

The last step in the preparation of **4** was the dehydration of **13**. Pyrolysis of the xanthate of **13** gave consistently low yields of **4** (<10%) as the favoured pathway appeared to be conversion to the dithiolcarbonate. This side reaction has been noted previously in the case of xanthates of primary alcohols (13). A recently reported pyrolysis method (14), which is particularly effective in the case of hindered alcohols, was attempted next. The thiocarbonate *O*-ester **14** was prepared by reaction of **13** with *O*-4-methylphenyl chlorothioformate (15) in pyridine. Pyrolysis of crude **14** at 230°C with distillation of the product as formed, yielded (−)-*cis*-1-methyl-2-methylene-3-isopropylcyclopentane (**4**)[4] in 68% yield from alcohol **13**. Gas chromatographic analysis on

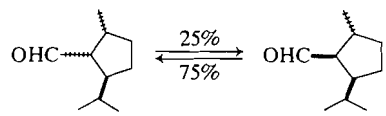

12*a* **12***b*

two columns indicated **4** to be >95% pure and ir, nmr, mass spectral, and elemental analyses were all consistent with the structure proposed. Pyrolysis of **14** prepared from an alcohol mixture which was predominantly either **13***a*[5] or **13***b* gave similar yields of **4** showing that both alcohols were effective precursors of the alkene.

The above sequence describes the synthesis of a variety of derivatives with the 1,2-dimethyl-3-isopropylcyclopentane carbon skeleton which is present in several classes of natural products: the iridoids (17*a*), the insect monoterpenoids (17*b*), and the monoterpene alkaloids (17*c*). In almost all these compounds the methyl and isopropyl moieties at the 1 and 3 positions bear a *trans* relationship to each other and consequently most synthetic investigations have been directed towards the preparation of compounds with this particular stereochemistry (18). This study provides entry not only into optically active cyclopentanoid derivatives with less common

[3]The ratio of the two epimers varied from run to run and longer exposure to the catalyst resulted in epimerization of **11***b* to **11***a*.

[4]Racemic **4**, **13***a* and **13***b* were previously obtained as minor components of a complex reaction mixture but none was isolated or characterized (16).

[5]Prepared by epimerization of **11** before reduction.

Can. J. Chem. Downloaded from www.nrcresearchpress.com by 210.87.254.6 on 09/05/12
For personal use only.

Can. J. Chem. Downloaded from www.nrcresearchpress.com by 210.87.254.6 on 09/05/12
For personal use only.

cis orientation of the 1 and 3 substituents but also yields compounds which are potential synthons for the preparation of more complex natural products.

Now that the desired alkene **4** was available, we were able to investigate the approach to **1** as outlined in Scheme 1. Irradiation of **3** and **4** in benzene using conditions previously described for the model system (7) gave a complex mixture of adducts from which **5** was isolated in low yield. Conversion of **5** to **6** was effected using the procedures previously reported (7) but the overall yield was low and the separation of the products was difficult. Therefore, this approach was abandoned in favour of a shorter and more efficient route to **1** in which it was still possible to use aldehyde **11** (Scheme 2).

In our second approach, the spiro system was formed by an annelation reaction of an enamine with a vinyl ketone. Reaction of **11** with pyrrolidine gave enamine **15** (Scheme 3) as a 4:1 mixture of double bond isomers. When **15** was stirred at room temperature with an excess of 1-methoxy-3-buten-2-one (**16**) (19) and 1 equiv. of acetic acid (in the absence of solvent) a 35% yield of (+)-**17** was isolated. Compound **17** was the spiroannelation product expected from an initial Michael reaction of **16** with the less hindered α-face of **15** followed by cycloaldolization. If acetic acid was not present in the initial stages of the reaction of **15** and **16** a different C_{15} product of undetermined structure, which could not be converted to either **1** or **2**, was formed. The use of less than an equivalent of acetic acid resulted in mixtures of **17** and the unknown compound. Presumably the acetic acid effectively catalyzes the cycloaldolization step without destroying the reactivity of the enamine by protonation. Enone **16** has been used by Wenkert and others (19) in annelation reactions but this is the first report of its use in the preparation of spiro systems. Spiroannelation reactions employing methyl vinyl ketone and enamines of cyclic aldehydes have been reported (20), but the use of solvents resulted in long reaction times. When these procedures were employed with reactants **15** and **16** none of the desired product was isolated. The use of this enamine – enone – acetic acid system in other annelation reactions is presently under investigation.

The successful preparation of **17** gave an ideal synthon for introduction of a methyl group at C(8), a double bond between C(8) and C(9), and a carbonyl group at C(7) as required to complete the synthesis of **1**. Treatment of **17** with methylmagnesium iodide gave alcohol **18** and introduced the desired methyl group. Hydrolysis of the enol ether moiety in **18** with a two-phase ether – aqueous sulfuric acid mixture proceeded much more slowly and in lower yield than

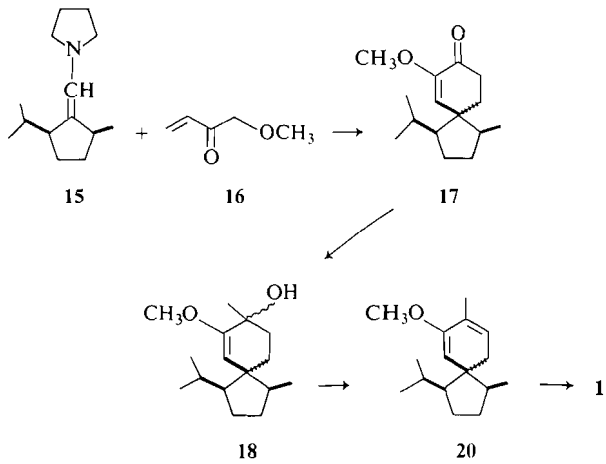

SCHEME 3

was the case with the model system **19**[6] because of steric hindrance in the region of the C(6)—C(7) double bond of **18**. This result provided additional support for the configuration assigned to the spiro carbon in **17**. Finally it was discovered that merely

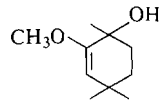

19

by refluxing a solution of **18** in benzene containing a catalytic amount of *p*-toluenesulfonic acid both the dehydration and the hydrolysis steps could be accomplished in one operation to yield (−)-acorenone (**1**) in 74% yield.[7] If the reflux period was halved, diene **20** could be isolated in significant yield. This result indicated that the dehydration step took place first and the water formed then effected hydrolysis of the enol ether. Conversion of **17** → **1** constitutes a new alkylative carbonyl transposition[8] and its utility in the synthesis of other natural products will be reported in a separate publication.

The synthetic sample of (−)-**1** was compared with

[6]Prepared by reaction of methylmagnesium iodide with 2-methoxy-4,4-dimethyl-2-cyclohexenone (19).

[7]Similar treatment of model compound **19** gave a 40:60 mixture of enone and ketol, respectively, indicating that the dehydration and hydrolysis reactions proceeded at about the same rate in this unhindered system. It was not possible to dehydrate the ketol using these conditions and thus our clean conversion of **18** → **1** was dependent on steric hindrance enabling the dehydration to be effected before the hydrolysis step.

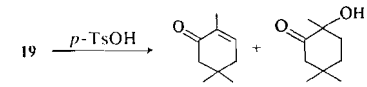

[8]For an extensive list of other carbonyl transposition reactions see ref. 1 in a recent paper by Trost *et al.* (21).

Can. J. Chem. Downloaded from www.nrcresearchpress.com by 210.87.254.6 on 09/05/12
For personal use only.

a natural sample which was isolated as previously described (2) from European calamus oil.[9] The two samples were identical in every respect including the magnitude and sign of the optical rotation (see Experimental).[10] This synthesis of (−)-**1** from a compound of known absolute configuration, (+)-limonene (**7**), establishes for the first time the absolute configuration of the natural product and also represents the first total synthesis of (−)-acorenone.

Experimental

Infrared spectra were recorded on a Beckman Model IR 12 spectrophotometer, nmr spectra on a Varian A-60A spectrometer using TMS (τ 10.0) as internal standard, uv spectra on a Cary 118 spectrophotometer and optical rotations were determined on a Bendix NPL Automatic Polarimeter, Type 143 at 25°C using a 1-cm cell and carbon tetrachloride as solvent. Mass spectra were obtained on a Varian MAT CH7 spectrometer operating at 70 eV while accurate mass determinations were obtained on a VG Micromass 7070F unit. Gas chromatoraphic analyses and collections were performed on an Aerograph Autoprep Model A-700 with either of the following: column *A*, 20% Carbowax 20 M on Chromosorb W, 6 ft × 0.25 in; column *B*, 15% benzyl cyanide – $AgNO_3$ on Chromosorb W, 9 ft × 0.19 in; column *C*, 20% Carbowax 20 M on Chromosorb W, 9 ft × 0.25 in. Thin-layer chromatographic separations and analyses were accomplished on silica gel GF 254 with thickness of 0.50 and 0.25 mm, respectively. Elemental analyses were performed by H. S. McKinnon, University of Guelph or A. B. Gygli, Microanalysis Lab, Toronto.

*(−)-3-Isopropyl-6-oxoheptanal (**9**)*

Freshly distilled limonene (**7**), $[\alpha]_D$ +125°, was hydrogenated using 5% platinum-on-charcoal without solvent (8). The resultant *p*-menth-1-ene was oxidized to the *trans-p*-menthane-1,2-diols (**8**) using performic acid followed by ethanolic potassium hydroxide (8). The viscous mixture of distilled diols was oxidized with periodic acid in pyridine to give **9** after distillation in 78% yield (9).

*(−)-1-Methyl-2-formyl-3-isopropylcyclopentene (**10**)*

A solution of 42.4 g (0.25 mol) of **9**, 3 ml of glacial acetic acid, 3 ml of piperidine in 300 ml of dry benzene was heated to reflux for 2.5 h during which time the water produced (4.5 ml) was removed by use of a Dean–Stark trap. The benzene solution was cooled and extracted with dilute hydrochloric acid, with saturated sodium bicarbonate solution and finally with saturated brine solution. The organic phase was dried ($MgSO_4$), the solvent was removed under vacuum and the residue distilled to give 29.0 g (76%) of **10**, which exhibited only one peak on gc analysis using column *A* at 200°C: bp 68–74°C/1.4 Torr; $[\alpha]_D$ −7.9°; ir (neat): 2970, 2870, 2820, 2710, 1670, 1635 cm^{-1}; uv_{max} (EtOH): 250 nm (ε 12 000); nmr ($CDCl_3$) τ: 0.01 (1H, s), 7.84 (3H, t, J = 1.4 Hz), 7.4–8.5 (6H, m), 9.12 (3H, d, J = 6.8 Hz), 9.35 (3H, d, J = 6.8 Hz).

*1-Methyl-2-formyl-3-isopropylcyclopentane (**11**)*

A sample of 15.6 g (0.103 mol) of freshly distilled **10** in 190 ml of absolute ethanol was placed in a 500 ml hydrogenation flask and 1.0 g of 5% Pd-on-charcoal was added. The suspension was hydrogenated for 45 min at room temperature in a Parr Series 3910 low pressure apparatus (initial pressure 14 psi, final pressure 6 psi). The catalyst was filtered and the solvent was carefully removed at reduced pressure. Fractional distillation of the residue at 80–88°C/4.5 Torr gave 10.3 g (65%) of product which on gc analysis on column *A* at 132°C indicated two major peaks in a ratio of 1:2 in order of elution from the column. The two peaks, **11***a* and **11***b* respectively, were collected as oils by preparative gc and the following physical properties were determined. Aldehyde **11***a*: $[\alpha]_D$ −17.8°; ir (CCl_4): 2968, 2880, 2820, 2714, 1728, 1473, 1390, 1373, 1115 cm^{-1}; nmr (CCl_4) τ: 0.45 (1H, d, J = 3.0 Hz), 7.8–9.0 (8H, m), 9.00 (3H, d, J = 6.5 Hz), 9.11 (3H, d, J = 6.0 Hz), 9.14 (3H, d, J = 6.0 Hz); ms *m/e* (relative intensity): 154 (M^+, 1), 152 (16), 127 (100), 110 (42), 109 (40), 87 (52), 81 (87), 69 (75). *Anal.* calcd. for $C_{10}H_{18}O$: C 77.87, H 11.76; found: C 77.72, H 11.56. Aldehyde **11***b*: $[\alpha]_D$ +16.4°; ir (CCl_4): 2968 2890, 2836, 2728, 1727, 1474, 1390, 1372, 1120 cm^{-1}; nmr (CCl_4) τ: 0.23 (1H, d, J = 5.5 Hz), 7.7–8.6 (8H, m), 8.8–9.2 (9H, three d); ms *m/e* (relative intensity): 154 (M^+, 1), 152 (17), 127 (34), 115 (39), 110 (46), 109 (34), 87 (76), 81 (60), 69 (75). *Anal.* calcd. for $C_{10}H_{18}O$: C 77.87, H 11.76; found: C 77.58, H 11.76.

*Epimerization of **11***

A solution of 75 mg of **11***a* and 75 mg sodium methoxide in one ml of methanol was left under nitrogen at room temperature for 18 h. Water (5 ml) was added to the reaction solution and the product was extracted with ether to yield 67 mg of a colorless residue. Gas chromatographic analysis (column *A*, 132°C) indicated an equilibrium mixture of 90% of **11***a* and 10% of **11***b*. Similarly, treatment of 23 mg of **11***b* as described above gave a mixture of 90% of **11***a* and 10% of **11***b*.

*1-Methyl-2-hydroxymethyl-3-isopropylcyclopentane (**13**)*

A solution of 20 g (0.13 mol) of crude **11** in 20 ml of anhydrous ether was added dropwise over 1 h to a stirred suspension of 5.0 g (0.13 mol) of lithium aluminum hydride in 200 ml of anhydrous ether. The reaction mixture was then heated to reflux for an additional 0.5 h, cooled, and the excess hydride reagent destroyed by successive additions of 5 ml of ether, 5 ml of 4 *M* sodium hydroxide solution, and 15 ml of water. The resultant granular precipitate was removed by filtration and the ether solution was dried with anhydrous $MgSO_4$. The solvent was removed and the residue distilled to give 14 g (70%) of alcohol **13**, bp 65–70°C/1.2 Torr. Gas chromatographic analysis (column *A*, 172°C) of **13** showed the two major peaks at 11 min and 13.5 min were present in a ratio of 1:4, respectively.[11] Pure samples of aldehydes **11***a* and **11***b* were reduced separately and it was shown that **11***a* was converted to the earlier gc peak, alcohol **13***a* and **11***b* was converted to the second gc peak, alcohol **13***b*. Pure samples of alcohols **13***a* and **13***b* were collected by preparative gc and their spectral properties determined. Alcohol **13***a*: $[\alpha]_D$ −15.6°; ir (CCl_4): 3640, 2975, 2895, 1045 cm^{-1}; nmr (CCl_4) τ: 5.90 (1H, s, disappeared on addition of D_2O), 6.48 (2H, m), 7.9–9.1 (8H, m), 8.98 (3H, d, J = 6.5 Hz), 9.08 (3H, d, J = 5.5 Hz), 9.13 (3H, d, J = 5.5 Hz); ms *m/e* (relative intensity): 156 (M^+, 2), 138 (14), 123 (36), 95 (100), 81 (39), 69 (43), 55 (36). *Anal.* calcd. for $C_{10}H_{20}O$: C 76.86, H 12.90; found: C 76.86, H 12.97. Alcohol **13***b*: $[\alpha]_D$ +0.28°; ir (CCl_4): 3640, 2970, 2890, 1473, 1389,

[9]We wish to thank Fritzsche Ltd., Toronto, for a generous sample of this oil.

[10]We thank Professor V. Herout, Czechoslovak Academy of Science, for an ir spectrum of **1** and Professor J. D. White, Oregon State University, for a sample of (−)-**2**.

[11]The ratio in **13** is different than in **11** as the aldehyde undergoes partial epimerization upon distillation.

Can. J. Chem. Downloaded from www.nrcresearchpress.com by 210.87.254.6 on 09/05/12
For personal use only.

1371, 1039 cm^{-1}; nmr (CCl_4) τ: 6.47 (2H, d, J = 4.5 Hz), 7.8–9.0 (8H, m), 8.15 (1H, s, disappeared on addition of D_2O), 8.93 (3H, d, J = 6.5 Hz), 9.10 (6H, m); ms *m/e* (relative intensity): 156 (M^+, 2), 141 (10), 138 (7), 123 (41), 95 (100), 81 (59), 69 (81). *Anal.* calcd. for $C_{10}H_{20}O$: C 76.86, H 12.90; found: C 77.11, H 12.75.

O-4-Methylphenyl Thiocarbonate **14**

To a solution of 6.5 g (42 mmol) of distilled alcohol **13** in 175 ml of pyridine at room temperature was added with stirring 8.2 g (44 mmol) of *O*-4-methylphenyl chlorothioformate (15). The viscous precipitate which formed initially dissolved after one h and stirring was continued an additional 4 h. The reaction solution was poured into water (500 ml) and extracted with chloroform (4 × 100 ml). The combined organic layers were washed with cold 6 *N* HCl (2 × 100 ml), with a saturated solution of sodium bicarbonate, with a saturated brine solution and dried with anhydrous $MgSO_4$. The solvent was removed completely using a rotary evaporator and then a vacuum pump to leave 13.5 g of crude thiocarbonate **14** as a dark amber oil: ir (neat): 2910, 2830, 1540, 1495, 1450, 1270, 1210, 1190 cm^{-1}. Complete removal of the solvent at this stage facilitated the isolation in the next step of alkene product which was not contaminated with chloroform.

*(−)-*cis*-1-Methyl-2-methylene-3-isopropylcyclopentane (4)*

A micro distillation apparatus was assembled with a dropping funnel placed in one neck of the distillation flask. Four millilitres of triethylene glycol in the flask were heated to 230°C and then the 13.5 g of crude thiocarbonate **14** were added dropwise at a rate (addition time about one h) which maintained slow distillation of the alkene product. The pot temperature was then slowly raised to 250°C over an additional hour. The resultant 8.8 g of crude yellow distillate, which contained *p*-cresol as the major impurity, was chromatographed on 75 g of silica gel (60–200 mesh) and the product was eluted with pentane to give 3.9 g (68% from alcohol **13**) of alkene **4** as a colorless liquid with a pinene-type odor. Gas chromatographic analysis on columns *A* (72°C) and *B* (60°C) showed the alkene to be >95% pure: $[\alpha]_D$ −28.5°; ir (neat): 3030, 2940, 2850, 1645, 1470, 1390, 1370, 880 cm^{-1}; nmr (neat) τ: 5.16 (2H, m), 7.4–9.0 (7H, m), 9.00 (3H, d, J = 6.5 Hz), 9.07 (3H, d, J = 6.5 Hz), 9.23 (3H, d, J = 6.5 Hz); ms *m/e* (relative intensity) 138 (M^+, 9), 123 (17), 95 (100), 81 (61), 67 (50). *Anal.* calcd. for $C_{10}H_{18}$: C 86.88, H 13.12; found: C 86.58, H 13.42.

Pyrrolidine Enamine **15**

A solution of 20.4 g (0.132 mol) of **11** and 19.4 g (0.273 mol) pyrrolidine in 50 ml of benzene was refluxed under nitrogen for 6 h. During the reflux period 2.4 ml water was formed and collected in a Dean–Stark water separator. The solvent was removed at reduced pressure and the residue distilled to yield 22.0 g (80%) of **15**. Gas chromatographic analysis on column *C* at 179°C showed the distillate to be a 1:4 mixture of isomers. Compound **15** had bp 80–90°C 0.25 Torr; $[\alpha]_D$ +34.2°; ir (neat): 2950, 1655, 1465, 1455 cm^{-1}; nmr (CCl_4) τ: 4.39 (1H, m), 7.07 (4H, m), 8.1–8.6 (11H, m), 8.9–9.3 (9H, m); ms *m/e* (relative intensity): 207 (M^+, 18), 192 (6), 165 (33), 164 (100), 148 (7), 120 (7), 95 (10), 93 (11), 70 (18). *Mol. wt.* calcd. for $C_{14}H_{25}N$: 207.1987; found: 207.1967.

(+)-1-Isopropyl-7-methoxy-4-methylspiro[4.5]dec-6-en-8-one (17)

To 3.0 g (14 mmol) of **15** was added with stirring under nitrogen through a serum cap 1.7 g (17 mmol) of 1-methoxy-3-buten-2-one (**16**). The yellow solution was cooled in an ice bath and 0.84 g (14 mmol) acetic acid was added dropwise with stirring. After 10 min the ice bath was removed and the stirring was continued for 6 h at which time the reaction mixture was a dark brown viscous liquid. The mixture was dissolved in 100 ml chloroform and extracted three times with water, once with 5% HCl, once with saturated $NaHCO_3$ solution, once with brine and dried with anhydrous $MgSO_4$. Removal of the solvent and short path distillation (bath 80–100°C) gave 1.18 g (35%) of **17**. Analysis by gc (column *C* at 225°C) or tlc ($CHCl_3$) indicated the distillate was >90% pure. An analytical sample was prepared by preparative tlc: $[\alpha]_D$ +34.5°; ir (neat): 2960, 1695, 1625, 1210, 1140 cm^{-1}; uv_{max} (EtOH): 266 nm (ε 8000); nmr (CCl_4) τ: 4.5 (1H, s), 6.44 (3H, s), 7.56 (2H, d, J = 6.5 Hz), 7.8–8.5 (9H, m), 8.9–9.2 (9H, m); ms *m/e* (relative intensity): 236 (M^+, 33), 193 (32), 180 (22), 165 (86), 152 (100), 137 (42), 123 (47). *Mol. wt.* calcd. for $C_{15}H_{24}O_2$: 236.1776; found: 236.1779.

(+)-1-Isopropyl-7-methoxy-4,8-dimethylspiro[4.5]dec-6-en-8-ol (18)

A solution of 0.86 g (3.6 mmol) of **17** in 15 ml anhydrous ether was added dropwise over 15 min to 8.4 ml of a 0.5 *M* (4.2 mmol) solution of methylmagnesium iodide in ether under an atmosphere of nitrogen. The reaction was heated to reflux for 1 h, cooled, and poured into an NH_4Cl solution. The aqueous phase was extracted twice with ether and the combined organic phases were extracted with saturated $NaHCO_3$ solution, with brine, and dried ($MgSO_4$). Removal of the solvent gave 0.89 g (98%) of crude **18** which tlc (50% ether–petrol) showed to be a 40:60 mixture of isomers at R_f's 0.55 and 0.50, respectively. An analytical sample of the mixture of **18** was separated by preparative tlc: $[\alpha]_D$ +33°; ir (neat): 3470, 2970, 1665, 1215, 1140 cm^{-1}; nmr (CCl_4) τ: 5.75 (1H, s), 6.47 (3H, s), 7.83 (1H, s, disappears on addition of D_2O), 8.0–8.6 (11H, m), 8.73 (3H, s), 8.9–9.2 (9H, m); ms *m/e* (relative intensity): 252 (M^+, 36), 237 (11), 196 (32), 168 (100), 149 (91), 136 (67), 109 (86). *Mol. wt.* calcd. for $C_{16}H_{28}O_2$: 252.2089; found: 252.2087.

(−)-Acorenone (1)

A solution of 0.11 g (0.44 mmol) of tlc purified **18** and 0.02 g of *p*-toluenesulfonic acid in 10 ml benzene was heated to reflux under nitrogen for 4 h. The solution was cooled, 30 ml benzene was added, and the solution was extracted with saturated $NaHCO_3$ solution, with brine, and dried ($MgSO_4$). Removal of the solvent gave 94 mg of crude product which was purified by preparative tlc (20% ether–petrol) to yield 71 mg (74%) of pure (−)-acorenone (**1**): $[\alpha]_D$ −28°; ir (CCl_4): 2965, 1677, 1380, 1365, 1190 cm^{-1}; uv_{max} (EtOH): 238 nm (ε 8200); nmr was identical to that previously reported (6). A sample of natural **1** isolated from European calamus oil as previously described (2) and purified by preparative gc had spectral properties identical to the synthetic **1** and $[\alpha]_D$ −27°. The gc retention times of the two samples were also coincident.

Acknowledgements

The authors acknowledge the financial assistance of the National Research Council of Canada and the capable technical assistance of Mr. Richard Shum and Mr. James Herzstock for a portion of this work.

1. G. L. Lange, W. J. Orrom, and D. J. Wallace. Tetrahedron Lett. 4479 (1977).
2. J. Vrkoc, V. Herout, and F. Sorm. Collect. Czech. Chem. Commun. **26**, 1021 (1961).
3. J. Vrkoc, V. Herout, and F. Sorm. Collect. Czech. Chem. Commun. **26**, 3183 (1961).
4. R. J. McClure, K. S. Schorno, J. A. Bertrand, and L. H. Zalkow. Chem. Commun. 1135 (1968).

5. J. F. RUPPERT, M. A. AVERY, and J. D. WHITE. Chem. Commun. 978 (1976); H. WOLF and M. KOLLECK. Tetrahedron Lett. 451 (1975); W. OPPOLZER and K. K. MAHALANABIS. Tetrahedron Lett. 3411 (1975); B. M. TROST, K. HIROI, and N. HOLY. J. Am. Chem. Soc. **97**, 5873 (1975).
6. W. RASCHER and H. WOLF. Tetrahedron, **33**, 575 (1977).
7. G. L. LANGE, H. M. CAMPBELL, and E. NEIDERT. J. Org. Chem. **38**, 2117 (1973).
8. W. F. NEWHALL. J. Org. Chem. **23**, 1274 (1958).
9. Y. KISHIDA. Chem. Pharm. Bull. (Tokyo), **8**, 357 (1960).
10. J. WOLINSKY, M. R. SLABAUGH, and T. GIBSON. J. Org. Chem. **29**, 3740 (1964).
11. R. LALANDE, J. MOULINES, and J. DUBOUDIN. C. R. Acad. Sci. **254**, 1087 (1962); E. E. VAN TAMELEN, G. M. MILNE, M. I. SUFFNESS, M. C. RUDLER CHAUVIN, R. J. ANDERSON, and R. S. ACHINI. J. Am. Chem. Soc. **92**, 7202 (1970).
12. G. BUCHI and H. WUEST. J. Am. Chem. Soc. **87**, 1589 (1965).
13. H. R. NACE. Org. React. **12**, 57 (1962).
14. H. GERLACH, T. T. HUONG, and W. MULLER. Chem. Commun. 1215 (1972).
15. G. HILGETAG and R. PHILIPPSON. Monatsber. Dtsch. Akad. Wiss. Berlin, **6**, 585 (1964); Chem. Abstr. **62**, 5165h (1965).
16. K. SISIDO, S. KUROZUMI, K. UTIMOTO, and T. ISIDA. J. Org. Chem. **31**, 2795 (1966).
17. (*a*) J. M. BOBBITT and K.-P. SEGEBARTH. *In* Cyclopentanoid terpene derivatives. *Edited by* W. I. Taylor and A. R. Battersby. Marcel Dekker, New York, NY. 1969. p. 1. (*b*) G. W. K. CAVILL. *In* Cyclopentanoid terpene derivatives. *Edited by* W. I. Taylor and A. R. Battersby. Marcel Dekker, New York, NY. 1969. p. 203. (*c*) W. C. WILDMAN, J. LE MEN, and K. WIESNER. *In* Cyclopentanoid terpene derivatives. *Edited by* W. I. Taylor and A. R. Battersby. Marcel Dekker, New York, NY. 1969. p. 239.
18. A. F. THOMAS. *In* The total synthesis of natural products. Vol. 2. *Edited by* J. ApSimon. Wiley-Interscience, New York, NY. 1973. p. 59.
19. E. WENKERT, N. F. GOLOB, S. S. SATHE, and R. A. J. SMITH. Syn. Commun. **3**, 205 (1973).
20. V. V. KANE. Syn. Commun. **6**, 237 (1976); S. F. MARTIN. J. Org. Chem. **41**, 3337 (1976).
21. B. M. TROST, K. HIROI, and S. KUROZUMI. J. Am. Chem. Soc. **97**, 438 (1975).

Can. J. Chem. Downloaded from www.nrcresearchpress.com by 210.87.254.6 on 09/05/12
For personal use only.

Etude structurale du fluorure de chloryle en phase solide

GEORGES TANTOT, PHILIPPE JOUBERT ET ROLAND BOUGON[1]

Division de chimie, Département de Génie Isotopique, Centre d'Etudes Nucléaires de Saclay, Boîte Postale No 2, 91190 Gif/Yvette, France

Reçu le 26 juillet 1977

GEORGES TANTOT, PHILIPPE JOUBERT et ROLAND BOUGON. Can. J. Chem. **56**, 1634 (1978).

Le fluorure de chloryle ClO_2F est étudié en phase solide par diffraction des rayons X et des neutrons ainsi que par la spectroscopie vibrationnelle.

Les diagrammes de diffraction ont été indexés en corrélation avec la structure connue de ClF_3. A 77 K, la maille élémentaire de ClO_2F a les paramètres suivants: $a = 8.85 \pm 0.02$ Å, $b = 6.17 \pm 0.02$ Å, $c = 4.62 \pm 0.01$ Å; $\beta = 95.0 \pm 0.1°$; $Z = 4$. Cette maille, qui peut être considérée comme résultant d'une légère déformation monoclinique de la maille orthorhombique de ClF_3, est compatible avec les mesures de densité réalisées sur ClO_2F et ClF_3.

Le groupe d'espace C_{2h}^1 ($P2/m$) permet le mieux de rendre compte des résultats de la spectroscopie vibrationnelle et des raies observées dans les diagrammes de diffraction de ClO_2F poly-cristallin.

GEORGES TANTOT, PHILIPPE JOUBERT, and ROLAND BOUGON. Can. J. Chem. **56**, 1634 (1978).

Chloryl fluoride, ClO_2F was studied in its solid phase by X-ray and neutron diffraction techniques and by vibrational spectroscopy.

The powder diffraction patterns of ClO_2F were indexed by comparison with ClF_3. At 77 K, the parameters of the monoclinic cell of ClO_2F are as follows: $a = 8.85 \pm 0.02$ Å, $b = 6.17 \pm 0.02$ Å, $c = 4.62 \pm 0.01$ Å, $\beta = 95.0 \pm 0.1°$, $Z = 4$. This cell, which can be thought as arising from a slight monoclinic deformation of the orthorhombic cell of ClF_3, is consistent with the density measurements also performed on ClO_2F and ClF_3.

The space group C_{2h}^1 ($P2/m$) was found to be the best compatible with both the vibrational data and the lines observed in the powder diffraction patterns for ClO_2F in the polycrystalline state.

Introduction

Peu de résultats structuraux sont disponibles sur le fluorure de chloryle ClO_2F, composé particulièrement réactif (1). La spectroscopie vibrationnelle infrarouge et Raman (2, 3), puis la spectroscopie de micro ondes (4, 5) ont permis de déterminer la forme de la molécule. Celle-ci a une structure pyramidale de symétrie ponctuelle C_s avec l'atome de chlore au sommet, en accord avec la théorie de la répulsion des paires électroniques de valence (6). La molécule possède six modes fondamentaux de vibration, pour lesquels nous adoptons la dénomination usuelle (3). Quatre sont de type a' parfaitement symétrique et deux de type a'', tous sont actifs en absorption infrarouge et en diffusion Raman.

Il nous a paru intéressant de poursuivre ces études dans la phase solide, pour laquelle aucun résultat n'est connu. En effet, le fluorure de chloryle possède des propriétés relativement voisines du trifluorure de chlore ClF_3, dont la structure cristalline à basse température a été déterminée (7) et qui fait l'objet d'une étude spectroscopique (8). Nous avons employé à la fois la cristallographie et la spectroscopie vibrationnelle, méthodes dont les résultats se complètent souvent (9). Nous avons étudié en phase solide les spectres de diffusion Raman en fonction de la température, et le spectre infrarouge du composé pur et dilué par le chlore. Les résultats structuraux acquis sont complétés par les données déduites du diagramme de poudre et permettent de proposer un groupe d'espace pour ClO_2F.

Partie expérimentale

Le fluorure de chloryle (98%) est fourni par la Société Comurhex (Pierrelatte, France). Il est traité par le fluorure de sodium anhydre, distillé entre −78°C et 0°C. La pureté est vérifiée par spectroscopie infrarouge et par microsublimation (10).

Les spectres infrarouges sont enregistrés de 4000 à 400 cm^{-1} sur un spectromètre Beckman IR 9. Les appareils sont étalonnés en fréquence à l'aide d'un film de polystyrène et de composés gazeux. Pour les spectres de contrôle en phase gazeuse, nous avons utilisé une cellule de dix centimètres en monel, préalablement passivée par ClO_2F, à fenêtres de chlorure d'argent. Le spectre Raman de ClO_2F gazeux a été étudié, sous une pression de 1200 Torr dans une cuve à fenêtres de corindon orientées et des mesures de polarisation ont été faites. A basse température, nous avons employé un cryostat à azote liquide mis au point au laboratoire, à fenêtres de chlorure d'argent. Nous obtenons par conduction une température fixe de 90 K, ce qui explique le choix du chlore comme diluant dans l'étude en matrice au lieu des habituels gaz nobles. Les spectres de diffusion Raman sont enregistrés sur un spectromètre Coderg T 800. La source d'excitation est un laser Spectra-physics modèle 164 à argon ionisé (raies bleue à 488.0 nm et verte à 514.5 nm) dont les raies de plasma sont éliminées par des filtres interférentiels. L'étalonnage est réalisé avec une

[1]A qui toute demande concernant ce travail peut être demandée

lampe au néon (11). Nous avons utilisé principalement un cryostat à hélium liquide de la Société l'Air Liquide, employant un bain de gaz refroidi. Nous avons réalisé les diagrammes de diffraction de poudre à 77 K à l'aide de neutrons thermiques ($\lambda = 1.140$ Å) et de rayons X (raie CuK_α). Une chambre Debye-Scherrer a été spécialement modifiée pour enregistrer ce dernier (12). Les deux spectres sont semblables et, dans les deux cas, les cristallites sont trop gros pour pouvoir considérer les intensités comme fiables. Les échantillons sont contenus dans des tubes de KelF ou de quartz de 6 à 14 mm de diamètre, ou des capillaires de 0.4 mm de diamètre (RX).

La densité de la phase liquide a été mesurée à 24.7°C par pesée d'un même volume de ClF_3, de densité connue (13), et de ClO_2F, soit 1.581 ± 0.006. Nous avons observé la variation de la densité avec la température dans un tube calibré. Nous avons vérifié le bon calibrage du tube et sa dilatation thermique à l'aide d'un composé de référence, l'oxyde d'éthyle (14). Entre 150 et 300 K, la densité de ClO_2F liquide obéit à l'équation

$$d = 1.649 - 2.631.10^{-3}t\,(°C)$$

avec un intervalle de confiance à 95% égal à 0.007.

La densité apparente du solide au point de fusion (150 K) est égale à 2.18. Nous avons corrélé dans les phases liquides et solide la variation de la densité avec la température et le déplacement des raies de diffusion Raman. Ce calcul donne par extrapolation la densité apparente à 77 K (température d'obtention des spectres de diffraction), soit 2.21 ± 0.03.

Le composé ClF_3 servira de comparaison en cristallographie et nous avons obtenu de la même façon à 77 K une densité apparente de 2.47 pour une valeur calculée de 2.53 (7).

Resultats et discussion

Etude spectroscopique

Nous avons enregistré les spectres vibrationnels du fluorure de chloryle (donnés à 90 K en fig. 1). On remarque dans ces spectres la séparation de certaines raies en plusieurs composantes. L'origine de ces éclatements qui peut a priori provenir de couplage intermoléculaires, d'effets isotopiques ou d'effets de site sera considérée plus loin.

Si l'on considère les intensités relatives des raies Raman des modes internes: les bandes ν_3 et ν_4 ont des intensités voisines, et supérieures d'un ordre de grandeur à celles des bandes ν_5 et ν_6. De même en corrigeant l'intensité de ν_1 de la perte de sensibilité du détecteur dans ce domaine on obtiendrait pour cette bande une intensité comparable à celle de ν_3 et ν_4. Les mêmes résultats ont été obtenus en phase gazeuse, où de plus la mesure des taux de polarisation a montré que seules les raies ν_5 et ν_6 étaient dépolarisées (15).

Ceci indique le caractère symétrique du mode ν_4, qui est le mode critique (si la molécule devient plane, il perd le caractère de parfaite symétrie), et résultat important pour cette étude, que la molécule reste probablement, pyramidale en phase solide.

Des mesures calorimétriques[2] ont montré l'existence d'une phase solide unique entre 78 et 150 K.

[2]P. Barberi. Communication personelle.

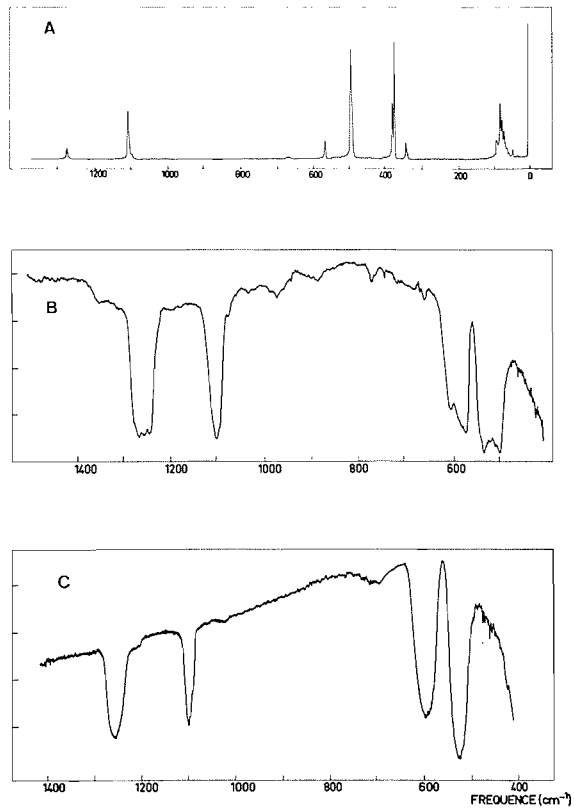

FIG. 1. Spectres vibrationnels de ClO_2F solide (90 K): (A) spectre Raman du solide; (B) spectre infrarouge du solide; (C) spectre infrarouge du composé dilué dans le chlore solide (4.3%).

Par l'étude des spectres Raman en fonction de la température, nous concluons à l'absence de transition jusqu'à 10 K pour les raisons suivantes: (*i*) la conservation de l'allure du spectre (et des intensités relatives), (*ii*) une même analogie dans la zone des modes externes, (*iii*) un déplacement continu et monotone des bandes de diffusion. Le rapport des intensités entre les composantes du mode ν_4 ne varie pas, alors qu'il serait vraisemblablement sensible à une modification du réseau cristallin. L'apparent changement d'allure de certains modes externes entre 140 et 10 K tient à une meilleure résolution à basse température (la largeur moyenne de ces modes passe de 3.4 à 1.6 cm^{-1}), les modes supplémentaires étant masqués par les ailes des modes intenses.

Si l'on considère à présent le spectre infrarouge (fig. 1) du composé à l'état pur ou dilué. Les bandes sont larges et mal résolues, ce phénomènes est fréquent parmi les composés interhalogènes. Dans le solide pur, les bandes comportent de une à quatre composantes. Dans le spectre réalisé en matrice de chlore (4.3% molaire en ClO_2F); les composantes supplémentaires ou toutes disparues et les raies se

sont affinées. Les raies infrarouges supplémentaires du solide pur ne sont donc pas attribuables à l'effet isotopique du chlore, et ceci est en accord avec les observations et calculs de Begun *et al.* (3). Les éclatements de raies sont donc dûs uniquement à des couplages intermoléculaires et/ou des effets de site.

On peut faire aussi une remarque d'incidence importante concernant les intensités relatives: on constate que même si les raies a' et a'' sont actives en infrarouge et en Raman, il existe cependant une certaine exclusion en intensité entre les deux phénomènes. Ainsi par exemple la branche du mode ν_4 à 378 cm^{-1} doit posséder un caractère antisymétrique.

Les attributions des vibrations internes présentées dans le tableau 1 ont été faites en tenant compte de ces remarques. L'examen de ce tableau montre d'importants écarts de fréquence entre les contreparties infrarouge et Raman d'un même mode, tel ν_2. Pour ν_3 cela est moins apparent à cause de la variation d'absorption des fenêtres en AgCl dans ce domaine. En l'absence d'un centre de symétrie, la coïncidence infrarouge Raman doit être observée pour toutes les bandes. Les exclusions observées indiquent donc la présence d'un centre d'inversion dans le motif observé en spectroscopie (9), et ce centre est propre au motif puisque la molécule isolée est de symétrie C_s.

Les modes externes, qu'on observe au nombre de douze à 10 K (15) permettent de préciser le nombre de molécules du motif optique, puisque ce nombre correspond à un couplage, entre au moins trois molécules (16). Par ailleurs la présence du centre d'inversion indique un nombre pair de molécules, la motif optique doit donc comporter quatre éléments.

Etude structurale

Nous avons complété le travail précédent par une étude cristallographique. Le motif optique comporte quatre molécules d'après nos conclusions, et nous avons recherché une maille cristallographique compatible. Des tentatives d'indexation automatique, fondées sur la minimisation du volume de la maille (17), montrent l'absence de solution dans les systèmes autres que monoclinique ou triclinique. Nous avons envisagé la possibilité d'une maille orthorhombique à huit molécules. Le nombre de réflexions absentes, déjà important dans une maille moitié, devient alors prohibitif. De plus, la meilleure solution obtenue dans ce cas est une maille contenant 7.1 molécules, qui n'apparaît pas physiquement acceptable. Les molécules ClF_3 et ClO_2F présentent des propriétés assez voisines (7, 8), dont l'encombrement: la densité obtenue en plaçant quatre molécules de ClO_2F dans la maille de ClF_3 (−120°C) est 2.36. Leurs diagrammes de diffraction sont représentés en fig. 2. Il apparaît des analogies structurelles, en particulier en ce qui concerne les positions de certaines raies. Cette similitude pourrait cependant n'être que fortuite puisque aussi bien en phase gazeuse que condensée, les molécules sont, du moins en ce qui concerne l'arrangement spatial des atomes, de symétries différentes. Nous avons cependant examiné la possibilité, pour la maille de ClO_2F, de dériver de celle de ClF_3 par déformation monoclinique. Remarquons que les raies de ClF_3 d'indexation $hk0$ ou $0kl$ ne se déplacent que très peu, ce qui implique l'absence de permutation d'axes. Un spectre de ClO_2F à 77 K s'indexe en totalité avec les paramètres suivants: $a = 8.85 \pm 0.02$ Å; $b = 6.17 \pm 0.02$ Å; $c = 4.62 \pm 0.01$ Å; $\beta = 95.0 \pm 0.1°$. Les résultats de l'indexation figurent dans le tableau 2. La densité calculée est de 2.29 et 2.23 si l'on adopte un défaut de remplissage analogue à celui de ClF_3, soit un excellent accord avec la valeur expérimentale.

TABLEAU 1. Fréquences fondamentales de ClO_2F en phase solide (fréquences en cm^{-1})

	Infrarouge		
Vibration	Matrice	Solide	Raman
ν_5 (a'')		1269	
	1258	1258	1272
		1247	
ν_1 (a')			1104
	1098	1101	1096
		1094	
ν_2 (a')	598	606	566
		572	
ν_3 (a')	528	533	
		498	495
			492
ν_4 (a')			378
			371
ν_6 (a'')			341
			338

Discussion

En nous aidant de la spectroscopie vibrationnelle, nous avons cherché à préciser le groupe d'espace. Compte tenu des raies observées et des règles d'ex-

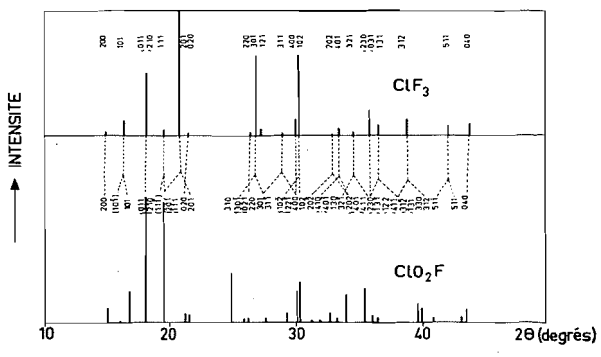

FIG. 2. Diagrammes de diffraction de ClO_2F et ClF_3 solides.

TABLEAU 2. Indexation du diagramme de diffraction de ClO_2F

d(Å)					
Obs.	Cal.	h	h	l	I/I_0
4.38	4.40	2	0	0	13
3.93	3.94	1	0	1	25
3.64	3.38	0	1	1	100
	3.59	2	1	0	
3.375	3.330	2	0	$\bar{1}$	97
3.084	3.084	0	2	0	7
3.049	3.053	2	0	1	6
2.665	2.652	3	1	0	40
2.572	2.579	3	0	$\bar{1}$	
2.558	2.561	0	2	1	8
2.529	2.526	2	2	0	
2.398	2.385	3	0	1	1
2.261	2.263	2	2	$\bar{1}$	8
2.199	2.203	4	0	0	54
2.181	2.180	1	0	2	
2.113	2.116	2	0	$\bar{2}$	2
2.069	2.074	4	1	0	1
	2.057	4	0	$\bar{1}$	
2.021	2.002	1	3	0	6
1.989	1.979	3	2	$\bar{1}$	2
1.947	1.952	4	1	$\bar{1}$	23
1.927	1.923	4	0	1	
1.864	1.863	2	3	0	25
1.829	1.836	4	1	1	6
	1.830	1	2	$\bar{2}$	

tinction qu'elles impliquent (18), nous avons retenu les groupes d'espace suivant (avec les notations de la réf. 9): C_2^1, C_2^2, C_s^1, C_s^2, C_{2h}^1, C_{2h}^2. Seuls les groupes d'espace $C_{2h}^1(P2/m)$ et $C_{2h}^2(P2_1/m)$ sont compatibles avec le centre d'inversion mis en evidence par spectroscopie vibrationnelle.

L'analyse du groupe facteur (16) correspondant à ces groupes montre que les spectres obtenus sont en accord avec cette analyse. En particulier, le nombre de modes externes observés en diffusion Raman correspond à ceux de ces modes qui doivent être actifs ($6a_g + 6b_g$). Le diagramme de corrélation indique que le groupe de site est C_1 ou C_s. Mais par ailleurs si l'on reprend les données cristallographiques des deux groupes retenus, on constate qu'en site C_1, deux molécules se trouvent superposées à une distance $b/2a$, ce qui n'est pas possible d'un point de vue stérique. Le groupe de site des molécules est donc C_s. Des deux groupes $C_{2h}^1(P2/m)$ et $C_{2h}(P2_1/m)$ sélectionnés, seul (18) le premier permet de placer 4 molécules sur des sites C_s, et ceci par une occupation des deux ensembles de sites C_s à 2 équiv. par ensemble. Cette dernière conclusion permet aussi de dire que les séparation de raies observées peuvent avoir pour origine les effets de site aussi bien que les couplages intermoléculaires.

Pour résumer l'ensemble de l'étude, une similitude des diagrammes de diffraction de ClF_3 et de ClO_2F a facilité l'indexation de celui de ClO_2F. La spectroscopie vibrationnelle a permis de compléter les données de diffraction et de proposer le groupe $C_{2h}^1(P2/m)$ pour ClO_2F en phase solide. Cette proposition serait bien entendu à valider par une étude cristallographique plus approfondie.

Remerciements

Nous tenons à remercier M. Meriel de son aide précieuse pour l'obtention des spectres de diffraction de neutrons et Mme Charpin de ses avis expérimentés et de son constant intérêt pour ce travail.

1. K. O. CHRISTE. Inorg. Chem. **11**, 1220 (1972).
2. A. ARVIA et P. AYMONINO. Spectrochim. Acta, **19**, 1449 (1963).
3. G. M. BEGUN, W. H. FLETCHER et D. F. SMITH. Spectrochim. Acta, **20**, 1763 (1964).
4. M. C. I. GERRY et C. R. PARENT. J. Chem. Soc. Chem. Commun. 285 (1972).
5. M. C. L. GERRY et C. R. PARENT. J. Mol. Spectrosc. **49**, 343 (1974).
6. R. J. GILLESPIE. Can. J. Chem. **39**, 318 (1961).
7. F. N. BENSEY et R. D. BURBANK. J. Chem. Phys. **21**, 602 (1953).
8. M. DRIFFORD et R. ROUSSON. J. Chem. Phys. **62**, 1806 (1975).
9. G. TURRELL. Infrared and Raman spectra of crystals. Academic Press, London, England. 1972.
10. P. DELVALLE. Bull. Soc. Chim. Fr. 1611 (1963).
11. J. L. LOADER. Basic laser Raman spectroscopy. Heyden and Sons, London, England. 1970.
12. C. NAULIN et R. BOUGON. J. Chem. Phys. **64**, 4155 (1976).
13. A. A. BANKS et A. J. RUDGE. J. Chem. Soc. 91 (1950).
14. G. J. JANZ et R. P. T. TOMKINS. Non-aqueous electrolytes handbook. Vol. 1. Academic Press, New York, NY. 1972. p. 29.
15. G. TANTOT. Thèse de Doctorat d'Etat, Université Pierre et Marie Curie, Paris. 1976.
16. S. BHAGAVANTAM et T. VENTAKARAYUDU. Theory of groups and its application to physical problems. Academic Press, New York, NY. 1969.
17. D. LOUER et M. LOUER. J. Appl. Cryst. **5**, 271 (1972).
18. International Tables for X-ray Crystallography. Vol. 1. Kynoch Press, Birmingham, England. 1965.

Observation de transitions de phase dans les dérivés dihalogénés du benzène par spectroscopie infrarouge lointain et diffusion Raman

B. WYNCKE, F. BREHAT ET A. HADNI

Equipe de Recherche Associée au CNRS No 14, Université de Nancy I, Laboratoire Infrarouge Lointain, C.O. no 140, 54037 Nancy, Cédex, France

ET

J. SERRIER ET M. BAVEREZ

ENSIC, Laboratoire de Physico-Chimie Industrielle, 1, rue Grandville, 54042 Nancy, Cédex, France

Reçu le 15 juillet 1977

B. WYNCKE, F. BREHAT, A. HADNI, J. SERRIER et M. BAVEREZ. Can. J. Chem. **56**, 1638 (1978).

Spectres d'absorption dans l'infrarouge lointain et spectres de diffusion Raman (15–250 cm^{-1}) des dérivés *ortho* et *méta* disubstitués du benzène ClC_6H_4Cl, ClC_6H_4Br et BrC_6H_4Br ont été enregistrés pour des températures comprises entre 80 et 300 K. Ils permettent de découvrir que les *o*- et *m*-dichlorobenzène présentent une transition de phase à 200 et 220 K respectivement, et que l'*o*-chlorobromobenzène présente deux transitions de phase à 185 et 222 K.

B. WYNCKE, F. BREHAT, A. HADNI, J. SERRIER, and M. BAVEREZ. Can. J. Chem. **56**, 1638 (1978).

Far infrared absorption and Raman spectra were recorded for *ortho*- and *meta*-disubstituted benzene ClC_6H_4Cl, ClC_6H_4Br, and BrC_6H_4Br from 15 to 250 cm^{-1} at different temperatures (80–300 K). From spectroscopic evidence, one phase transition is found for both the *o*- (200 K) and the *m*-dichlorobenzene (220 K), and two for the *o*-chlorobromobenzene (185 and 222 K).

Introduction

Lors d'une étude précédente (1, 2) nous avons enregistré le spectre dans l'infrarouge lointain de composés dihalogénés du benzène substitués en position para. Afin de compléter cette étude, nous examinons les composés ClC_6H_4Cl, ClC_6H_4Br et BrC_6H_4Br substitués en position ortho et méta. Contrairement aux dérivés *para* disubstitués les dérivés *ortho* et *méta* disubstitués sont liquides à température ambiante. Les spectres d'absorption infrarouge et de diffusion Raman à basse température permettent d'étudier l'évolution des modes de réseau de ces dérivés dihalogénés du benzène en fonction de la température. Des changements de phase sont mis en évidence pour la première fois.

Partie expérimentale

Les liquides que nous avons utilisés sont de qualité Purum fournis par les établissement Fluka. Nous ne les avons pas purifiés davantage. Les spectres d'absorption infrarouge sont enregistrés sur un spectromètre Cameca SI 36. Les liquides sont introduits dans une cuve cylindrique d'épaisseur variable, à fenêtres de quartz ou de TPX. Le diamètre du faisceau lumineux est de 18 mm; il existe donc une différence de température entre les bords de la cuve porte-échantillon et le centre de l'échantillon. Dans certains cas le centre, n'atteint qu'une température de 110 K alors que les bords de la cuve sont beaucoup plus froids (78 K). La température de la carotte de cuivre qui supporte la cuve porte-échantillon est régulée et peut être maintenue à toute valeur comprise entre 78 et 320 K. Un étalonnage a été nécessaire pour connaître la température au centre de l'échantillon; c'est cette dernière qui est indiquée sur les courbes et diagrammes.

Les spectres de diffusion Raman ont été enregistrés sur un spectromètre Coderg T 800. La raie excitatrice a une longueur d'onde de 4880 Å, correspondant à la lumière bleue émise par un laser Spectra Physics à argon.

Les liquides sont introduits dans un capillaire de 1 mm de diamètre et sont refroidis dans un cryostat à circulation d'air liquide dont le débit permet de réguler la température entre 85 et 300 K. Le rayonnement diffusé est observé à 90° du rayonnement incident.

Spectres infrarouge et Raman

Les dihalogénobenzènes que nous avons étudiés sont liquides à température ambiante. Les fréquences des maximums d'absorption observés sont rassemblées dans le tableau 1. Le refroidissement de ces liquides donne des solides polycristallins pour lesquels il n'est pas possible de connaître la polarisation des modes infrarouge et Raman.

Sur la fig. 1 nous présentons les spectres d'absorption infrarouge (ir) et de diffusion Raman (R) des dérivés disubstitués du benzène à l'état solide pour quelques températures.

La résolution obtenue avec le spectromètre infrarouge est de 1 cm^{-1} pour les fréquences spatiales $\dot{\nu}$ inférieures à 100 cm^{-1} et de 2 cm^{-1} pour les fréquences supérieures. Le spectrophotomètre Raman utilisé a une résolution de 1 cm^{-1} pour les fréquences spatiales comprises entre 5 et 250 cm^{-1}. L'absorption dans l'infrarouge lointain (15–100 cm^{-1}) est représentée par la variation de l'indice d'absorption $k = K/4\pi\dot{\nu}$ calculé à partir des spectres de transmission. L'intensité I des raies de diffusion Raman est exprimée en unités arbitraires.

Can. J. Chem. Downloaded from www.nrcresearchpress.com by 210.87.254.40 on 09/05/12
For personal use only.

TABLEAU 1. Fréquences spatiales des dihalogénobenzènes liquides à 300 K

$\dot{\nu}$ (cm^{-1})							
o-$C_6H_4Cl_2$				m-$C_6H_4Cl_2$			
Ce travail	Réf. 3	Réf. 4	Réf. 7	Ce travail	Réf. 3	Réf. 4	Réf. 7
45	52	45					
			152 (ν_{16})	60	60	60	
153							175 (ν_{20})
				177			198 (ν_{11})
			202 (ν_{11})	200			
206			239 (ν_{20})				

$\dot{\nu}$ (cm^{-1})			
o-C_6H_4ClBr		m-C_6H_4ClBr	
Ce travail	Réf. 7	Ce travail	Réf. 7
45		50	
	140 (ν_{30})		
143	164 (ν_{21})		163 (ν_{30})
166		166	202 (ν_{21})(ν_{29})
	230 (ν_{29})	204	

$\dot{\nu}$ (cm^{-1})						
o-$C_6H_4Br_2$				m-$C_6H_4Br_2$		
Ce travail	Réf. 3	Réf. 4	Réf. 7	Ce travail	Réf. 3	Réf. 7
40	42					
		44		45		
					48	
			129 (ν_{11})			
131						132 (ν_{20})
				133		
149						
				157		159 (ν_{11})
				196		
218			(?)(ν_{20})			
			251 (ν_{30})			

Nous avons constaté expérimentalement que le spectre infrarouge lointain de l'orthobromochlorobenzène est différent suivant que le liquide est refroidi lentement ou rapidement. Ce composé doit donc présenter des modifications structurales lors du refroidissement. L'analyse thermique différentielle nous a permis de déceler deux transitions de phase à 185 et 222 K. Dans le cas de l'*o*- et du *m*-dichlorobenzène une transition de phase se produit à 200 et 220 K respectivement. Les autres composés ne présentent pas de transition de phase dans le domaine de température étudié.

L'évolution des fréquences des modes de réseau en fonction de la température est représentée sur les figs 2–7. Les fréquences observées vers 240 K sont désignées par ν_i ($i = 1, 2 \ldots n$) dans l'ordre des fréquences croissantes. Sur les figs 2–7 nous avons également représenté la variation de la fréquence

Can. J. Chem. Downloaded from www.nrcresearchpress.com by 210.87.254.40 on 09/05/12
For personal use only.

Can. J. Chem. Downloaded from www.nrcresearchpress.com by 210.87.254.40 on 09/05/12
For personal use only.

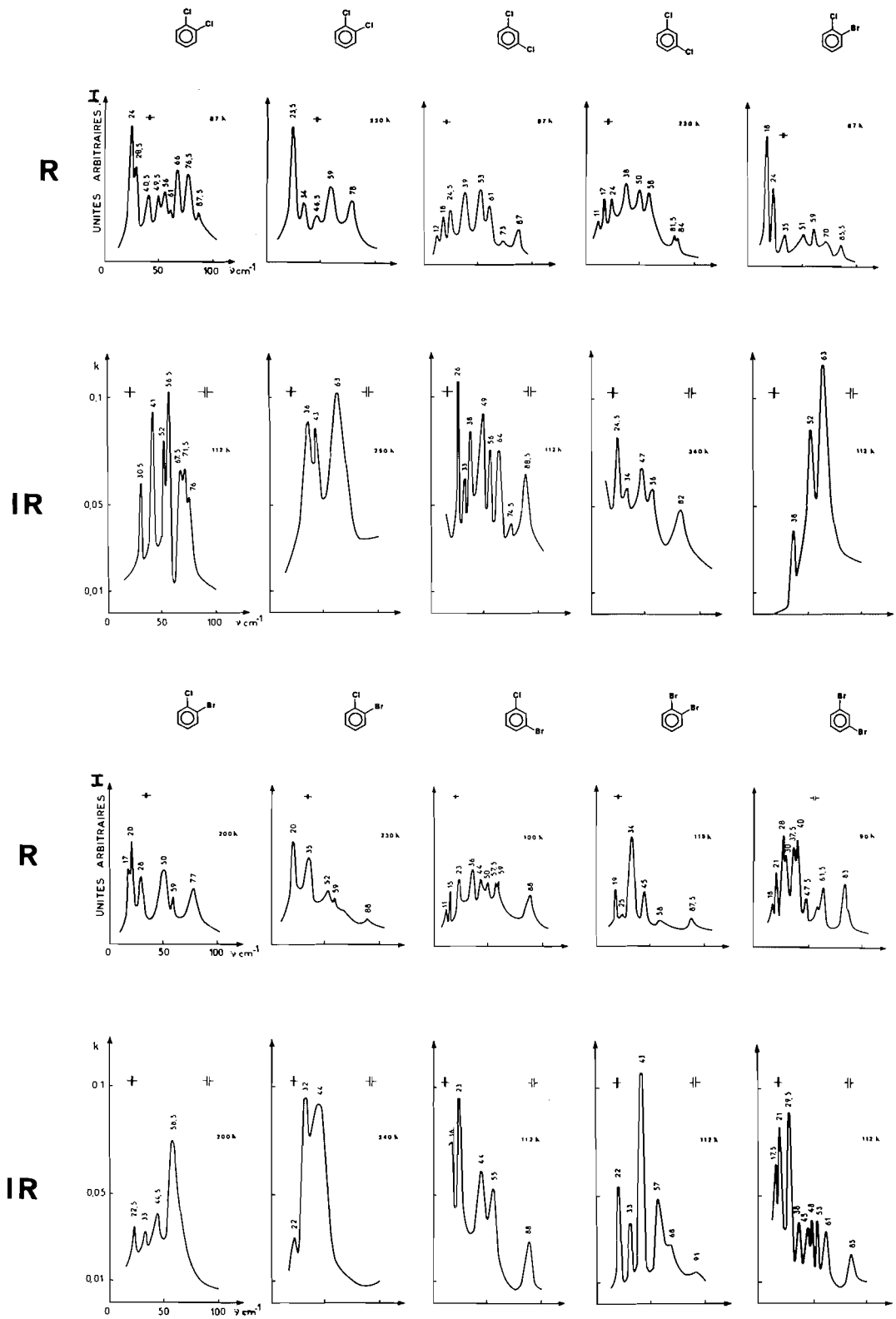

FIG. 1. Indice d'absorption (k) et intensité (I) de six dérivés disubstitués du benzène (*ortho* et *méta*) en fonction de la fréquence spatiale ($\bar{\nu}$) pour quelques températures.

Can. J. Chem. Downloaded from www.nrcresearchpress.com by 210.87.254.40 on 09/05/12
For personal use only.

d'absorption infrarouge du liquide entre la température du point de fusion et 300 K. Dans les liquides polaires la bande d'absorption de basse fréquence est très large et nous avons représenté sur les figures la largeur de la raie à mi-hauteur par une zone hachurée. L'ensemble des résultats obtenus est rassemblé dans le tableau 2.

Discussion

Liquides

Les raies dont les fréquences sont inférieures à 100 cm^{-1} sont dues à l'absorption des liquides polaires. Nos résultats sont en bon accord avec ceux de Mansingh (3). La fréquence du maximum d'absorption et l'intensité de la bande peuvent s'expliquer à l'aide des modèles choisis par Benson *et al.* (4) et Larkin (5). La valeur moyenne du maximum de l'indice d'absorption k est de l'ordre de 4.77×10^{-2} pour les dérivés disubstitués que nous avons étudiés alors qu'il est égal à 0.53×10^{-2} dans le cas du benzène à 300 K (6). Ceci montre le caractère fortement dipolaire de ces liquides.

Les fréquences que nous avons observées au dessus de 100 cm^{-1} sont dues à des mouvements de déformation des molécules. Nos résultats sont en général identiques à ceux que Green (7) a publiés pour les dérivés benzèniques dichlorés et chlorobromés en position *ortho* et *méta*. Nous rappelons dans la colonne 7 du tableau 1 l'attribution proposée par cet auteur. Pour les *o*- et *m*-dibromobenzène seules les fréquences 131, 133 et 157 cm^{-1} sont comparables à celles que Green a observées et attribuées à ν_{11}, ν_{20} et ν_{11} respectivement. Dans l'*o*-dibromobenzène l'absorption observée à 149 cm^{-1} est d'intensité faible et peut être due à un mode de combinaison. La raie intense à 218 cm^{-1} pourrait être attribuée à ν_{20} bien que Green (7) ne l'ait pas observée. Shurvell *et al.* (8) situent un mode b_1 à 220 cm^{-1} qui correspond à l'absorption que nous avons observée à 218 cm^{-1} et confirme l'attribution à ν_{20}. L'absorption observée à 196 cm^{-1} dans le spectre du *m*-dibromobenzène correspond d'après Shurvell à un mode de type a_2 inactif en absorption infrarouge, ce qui pourrait expliquer sa faible intensité comparée à celle des modes situés à 133 et 157 cm^{-1} de type b_1 et a_1 respectivement.

Solides

Dérivés dihalogénés présentant des transitions de phase

L'*o*-dichlorobenzène (fig. 2*a* et *b*) présente une transition de phase à 200 K confirmée par analyse thermique différentielle. C'est au voisinage de 200 K que se produisent les modifications des spectres. Au dessus de 200 K nous observons huit modes de réseau, trois sont actifs en absorption infrarouge et

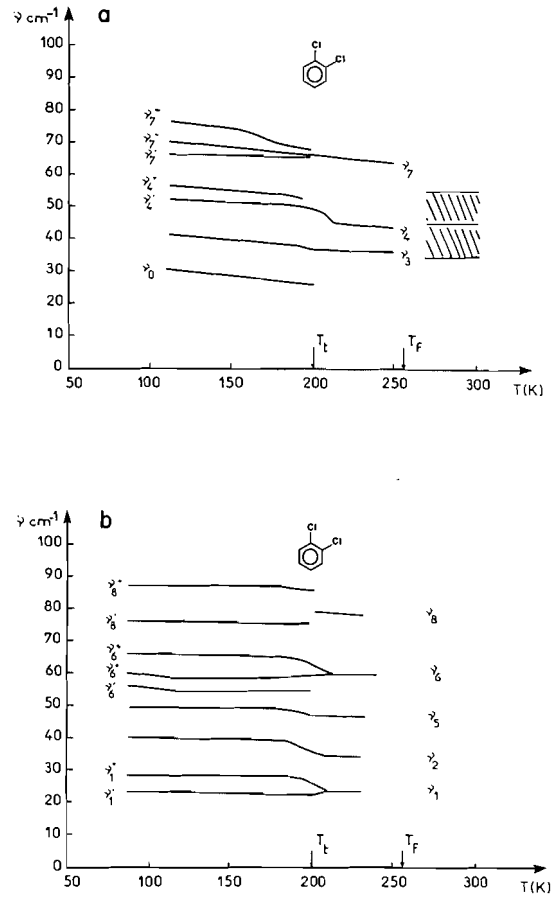

FIG. 2. Variation en fonction de la température des fréquences spatiales ($\tilde{\nu}$) des modes de vibration du réseau: (*a*) actifs en infrarouge et (*b*) actifs en diffusion Raman de l'*o*-dichlorobenzène.

les cinq autres en diffusion Raman. Lorsqu'on abaisse la température et que le changement de phase s'est produit on constate que seul le mode ν_3 conserve une variation linéaire de fréquence en fonction de la température contrairement à ν_2 et ν_5. Les autres modes ν_1, ν_4, ν_6 et ν_7 donnent plusieurs composantes et il apparait dans le spectre infrarouge un mode nouveau ν_0. Au voisinage de la température de transition ν_8 disparaît par affaiblissement d'intensité alors qu'apparaissent deux composantes ν_8' et ν_8'' dont l'intensité se renforce avec l'abaissement de la température.

Le *m*-dichlorobenzène (fig. 3*a* et *b*) présente une transition de phase à 220 K qui produit peu de modifications des spectres. L'*o*-chlorobromobenzène (fig. 4*a* et *b*) présente deux transitions de phase à 185 et 222 K. Ces températures de transition sont confirmées par analyse thermique différentielle, l'aire du pic de la seconde transition est 2.6 fois supérieure à celle de la première, cette différence est attribuée à la disparition brutale du mode ν_7' à 210 K.

Can. J. Chem. Downloaded from www.nrcresearchpress.com by 210.87.254.40 on 09/05/12
For personal use only.

TABLEAU 2. Fréquences des modes de réseau des dérivés *ortho*- et *méta*-dihalogénés du benzène

$\dot{\nu}$ (cm^{-1})							
o-$C_6H_4Cl_2$ (T_t = 200 K, T_f = 256 K)				m-$C_6H_4Cl_2$ (T_t = 220 K, T_f = 252 K)			
Infrarouge		Raman		Infrarouge		Raman	
112 K	250 K	87 K	230 K	112 K	240 K	87 K	230 K
						12	11 (ν_1)
						18	17 (ν_2)
		24	23.5(ν_1)	26	24.5(ν_3)	24.5	24 (ν_4)
30.5		28.5					
				33			
			34 (ν_2)		34 (ν_5)		
	36(ν_3)						
				38		39	38 (ν_6)
41		40.5					
	43(ν_4)						
		49.5	46.5(ν_5)	49	47 (ν_7)		
52						53	50 (ν_8)
56.5		56		56	56 (ν_9)		
			59 (ν_6)				
		61				61	58 (ν_{10})
67.5	63(ν_7)			64			
		66					
71.5							
				74.5		73	
76		76.5	78 (ν_8)				
							81.5(ν_{11})
					82 (ν_{12})		
		87.5		88.5		87	84 (ν_{13})

$\dot{\nu}$ (cm^{-1})							
o-C_6H_4ClBr (T_t = 185 et 222 K, T_f = 260 K)				m-C_6H_4ClBr (T_f = 251.5 K)			
Infrarouge		Raman		Infrarouge		Raman	
112 K	240 K	87 K	230 K	112 K	210 K	100 K	230 K
						11	10 (ν_1)
		18	20(ν_1)	16.5	15.5(ν_3)	15	14.5(ν_2)
	22(ν_2)	24		23	22 (ν_5)	23	22 (ν_4)
	32(ν_3)						
						36	34 (ν_6)
		35	35(ν_4)				
38				44	42 (ν_8)	44	39 (ν_7)
	44(ν_5)						
52		51	52(ν_6)			50	46 (ν_9)
				55	52 (ν_{11})		
		59	59(ν_7)			57.5	53 (ν_{10})
						59	58 (ν_{12})
63			64(ν_8)				
		70					
		85.5	88(ν_9)	88	83 (ν_{14})	88	84 (ν_{13})

D'une manière générale les fréquences observées en diffusion Raman et en absorption infrarouge ne coïncident pas et ne sont pas dues au même mode de vibration. Dans le cas où les fréquences observées en absorption et en diffusion sont voisines comme par exemple les fréquences 34–36 cm^{-1} et 43–46.5 cm^{-1} de l'*o*-dichlorobenzène à 240 K on constate (fig. 1*a*) que la différence de fréquence des modes infrarouges est de 43–36 = 7 cm^{-1} et celle des modes Ramans de 46.5–34 = 12.5 cm^{-1}. Cette différence n'est pas due à une erreur expérimentale et montre bien que les fréquences 34 et 36 cm^{-1} n'ont pas pour origine le même mode normal de vibration. Il en est de même pour les fréquences 43–46.5 cm^{-1}. Le mode 63 cm^{-1} observé à 250 K a une largeur de bande à mi-hauteur qui est de l'ordre de 25 cm^{-1} et s'étend

TABLE 1 (*Concluded*)

$\dot{\nu}$ (cm^{-1})							
o-$C_6H_4Br_2$ (T_f = 280 K)				m-$C_6H_4Br_2$ (T_f = 266 K)			
Infrarouge		Raman		Infrarouge		Raman	
112 K	230 K	115 K	230 K	112 K	230 K	90 K	230 K
		19	18.5(ν_1)	17.5	15 (ν_1)	18	15.5(ν_2)
				21	19 (ν_3)	21	19 (ν_4)
22	21(ν_2)	25	23.5(ν_3)				
						28	26 (ν_5)
				29.5	27 (ν_6)	30	29 (ν_7)
33	30(ν_4)	34	32 (ν_5)				
				38	34 (ν_9)	37.5	34.5(ν_8)
43	41(ν_6)	45	43 (ν_7)	45	40.5(ν_{11})	40	35.5(ν_{10})
				48	43 (ν_{13})	47.5	44 (ν_{12})
57	52(ν_8)			53	48 (ν_{14})	57	54 (ν_{15})
		58	53 (ν_9)				
				61	58 (ν_{16})	61.5	58.5(ν_{17})
68	—(ν_{10})						
				85	80 (ν_{19})	83	79 (ν_{18})
		87.5	85 (ν_{11})				
91	—(ν_{12})						

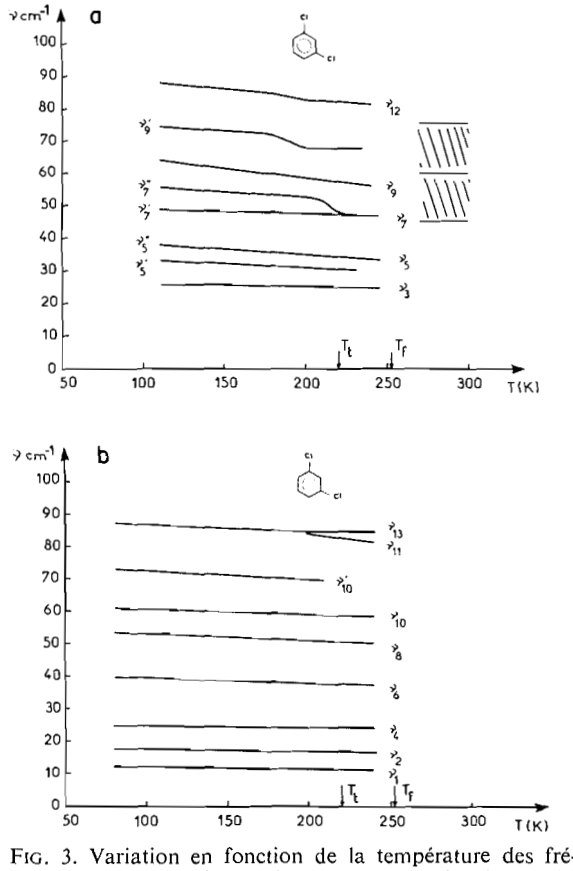

FIG. 3. Variation en fonction de la température des fréquences spatiales ($\dot{\nu}$) des modes de vibration du réseau: (*a*) actifs en infrarouge et (*b*) actifs en diffusion Raman du *m*-dichlorobenzène.

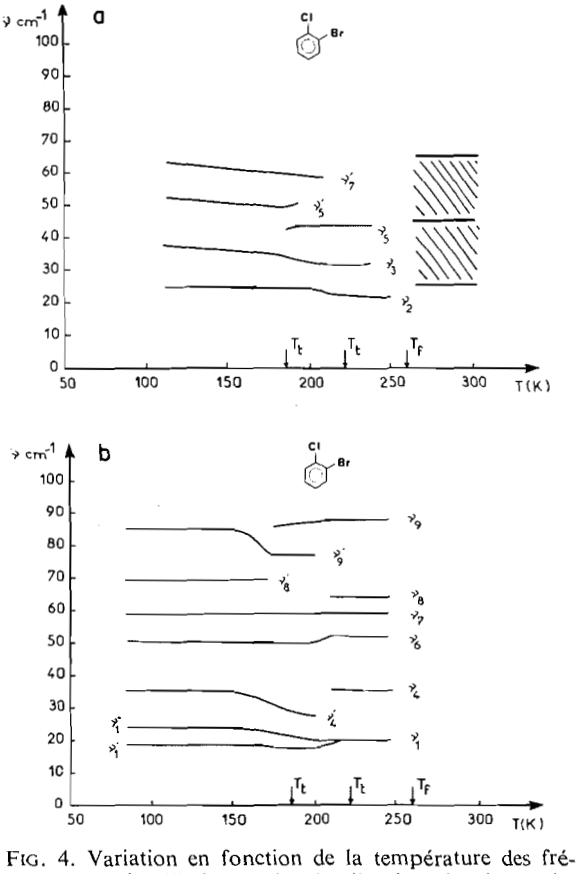

FIG. 4. Variation en fonction de la température des fréquences spatiales ($\dot{\nu}$) des modes de vibration du réseau: (*a*) actifs en infrarouge et (*b*) actifs en diffusion Raman de l'*o*-chlorobromobenzène.

Can. J. Chem. Downloaded from www.nrcresearchpress.com by 210.87.254.40 on 09/05/12
For personal use only.

Can. J. Chem. Downloaded from www.nrcresearchpress.com by 210.87.254.40 on 09/05/12
For personal use only.

de 50 à 75 cm^{-1}. Il recouvre entièrement les modes observés en diffusion à 59 et 78 cm^{-1}. La largeur de bande et l'intensité de ce mode permet de penser qu'il comporte plusieurs composantes dont celles situées à 59 et 78 cm^{-1}. Le changement de phase et l'abaissement de la température nous montrent que ce mode donne naissance à trois composantes en absorption (67.5–71.5 et 76 cm^{-1}) et à deux en diffusion (66 et 76.5 cm^{-1}). La coïncidence des fréquences ne peut alors être admise que pour 67.5–66 cm^{-1} et 76–76.5 cm^{-1}. L'aspect complémentaire des spectres d'absorption et de diffusion nous permet de penser que le groupe facteur du cristal pourrait être C_{2h} ou D_{2h} en supposant que ces composés cristallisent dans le système monoclinique ou orthorhombique. La distinction entre ces deux groupes ne peut se faire que par l'étude de monocristaux en lumière polarisée.

A 240 K les spectres d'absorption des *o*-dichloro- et *o*-chlorobromobenzène présentent trois maximums d'absorption ce qui permet de penser que la cellule de Bravais ne comporte pas plus de deux molécules. Les molécules des composés étudiés ici sont dépourvues de centre de symétrie et le site occupé par celles-ci ne peut être un centre d'inversion de telle sorte que les vibrations de pivotement et de translation ont même type de symétrie. La vibration fondamentale réelle observée est la superposition de ces mouvements de telle sorte qu'il est difficile d'attribuer les fréquences que nous avons observées. Nous pouvons dire seulement que la vibration faisant intervenir le pivotement de la molécule autour de l'axe porteur du moment dipolaire permanent sera peu intense en absorption.

Dérivés dihalogénés ne présentant pas de transition de phase

Les variations en fonction de la température des fréquences des modes de réseau du *m*-chlorobromo-

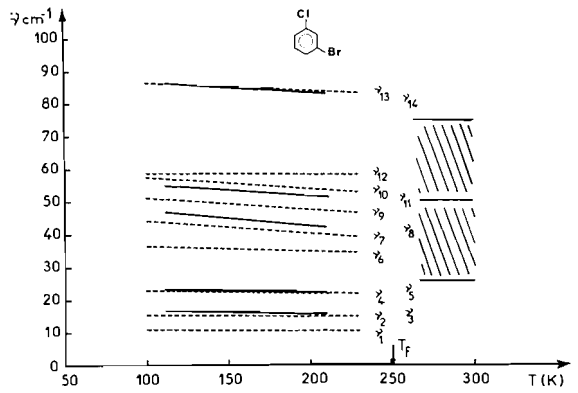

FIG. 5. Variation en fonction de la température des fréquences spatiales ($\dot{\nu}$) des modes de vibration du réseau: — actifs en infrarouge et ---- en diffusion Raman du *m*-chlorobromobenzène.

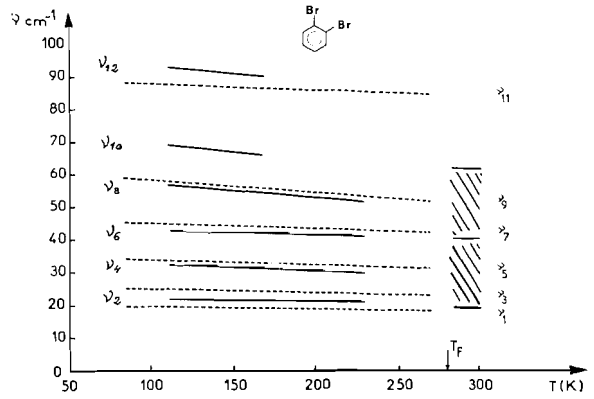

FIG. 6. Variation en fonction de la température des fréquences spatiales ($\dot{\nu}$) des modes de vibration du réseau: — actifs en infrarouge et ---- en diffusion Raman de l'*o*-dibromobenzène.

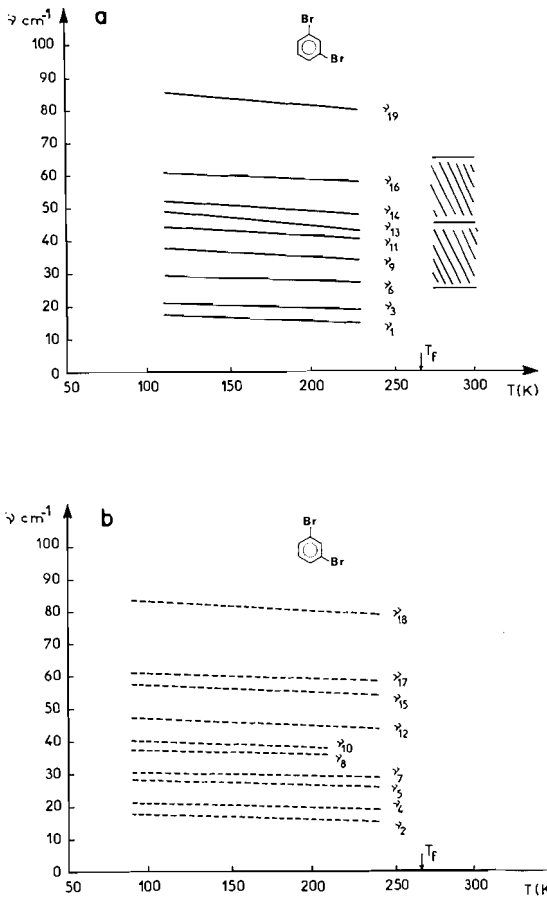

FIG. 7. Variation en fonction de la température des fréquences spatiales ($\dot{\nu}$) des modes de vibration du réseau: (*a*) actifs en infrarouge et (*b*) actifs en diffusion Raman du *m*-dibromobenzène.

benzène et des *o*- et *m*-dibromobenzène sont représentées sur les figs 5, 6 et 7. Ces variations sont linéaires et ces dérivés dihalogénés ne présentent pas de transition de phase dans le domaine de température étudié.

Contrairement aux dérivés présentant des transitions de phase les fréquences de vibration observées en absorption et en diffusion coïncident, à la précision des mesures près, pour ces trois composés. A 112 K les fréquences de vibration du *m*-dibromobenzène peuvent s'associer de la manière suivante: $17.5(\nu_1)$–$18(\nu_2)$, $21(\nu_3)$–$21(\nu_4)$, $38(\nu_9)$–$37.5(\nu_8)$, $48(\nu_{13})$–$47.5(\nu_{12})$, $61(\nu_{16})$–$61.5(\nu_{17})$ et $85(\nu_{19})$–$83(\nu_{18})$ cm^{-1}. Le maximum d'absorption observé à 27 cm^{-1} (ν_6) apparait résolu en deux composantes $26(\nu_5)$ et $29(\nu_7)$ cm^{-1} en diffusion alors que ν_{10}, ν_{11}, ν_{14}, ν_{15} situés respectivement à 40, 45, 53 et 57 cm^{-1} n'apparaissent que dans un seul des deux spectres.

Ces remarques vérifiées dans le cas de l'*o*-dibromobenzène et du *m*-chlorobromobenzène permettent de proposer comme groupe facteur un des groupes C_s, C_2, D_2 ou C_{2v} dans le cas où ces cristaux appartiennent au système monoclinique ou orthorhombique. La cellule de Bravais peut comporter quatre molécules.

Conclusion

Les spectres d'absorption dans l'infrarouge lointain de six dérivés dihalogénés du benzène, étudiés à l'état liquide à 300 K, présentent tous un maximum d'absorption au voisinage de 45 cm^{-1}.

La solidification de ces liquides par refroidissement permet d'observer les modes de réseau par absorption dans l'infrarouge lointain et par diffusion Raman. L'étude de la variation des fréquences en fonction de la température nous a permis de déceler des transitions de phase dans les *o*- et *m*-dichlorobenzène, ainsi que dans l'*o*-chlorobromobenzène. L'attribution définitive des modes de réseau ne pourra être faite que lorsque les structures seront connues.

1. B. WYNCKE, A. HADNI et X. GERBAUX. J. Phys. **31**, 893 (1970).
2. J. BEUCHOT. Thèse. Nancy, France. 1974.
3. A. MANSINGH. J. Chem. Phys. **52**, 5896 (1970).
4. M. BENSON, G. D. MARTIN, S. WALKER, J. WARREN et R. WILSON. Can. J. Chem. **50**, 2610 (1972).
5. I. W. LARKIN. J. Chem. Soc. Faraday Trans. II, **69**, 1278 (1973); **70**, 1457 (1974).
6. B. WYNCKE et A. HADNI. C.R. Acad. Sci. Ser. B, **275**, 825 (1972).
7. J. H. S. GREEN. Spectrochim. Acta A, **26**, 1913 (1970); **26**, 1523 (1970).
8. H. F. SHURVELL, B. DULAURENS et P. PESTEIL. Spectrochim. Acta, **22**, 333 (1966).

Can. J. Chem. Downloaded from www.nrcresearchpress.com by 210.87.254.40 on 09/05/12
For personal use only.

Approaches to the synthesis of triterpenoids. III. Some *cis*-decalins corresponding to rings D and E of some pentacyclic triterpenes[1]

JOHN W. APSIMON,[2] SATYANAND BADRIPERSAUD, TUNG T. T. NGUYEN, AND RICHARD PIKE

Department of Chemistry, Carleton University, Ottawa, Ont., Canada K1S 5B6

Received August 3, 1977

JOHN W. APSIMON, SATYANAND BADRIPERSAUD, TUNG T. T. NGUYEN, and RICHARD PIKE. Can. J. Chem. **56**, 1646 (1978).

The synthesis of 10-methoxycarbonyl-1,7,7-trimethyl-*cis*-2-decalone (**6***c*) is described as well as that of the corresponding *trans* isomer. The stereochemistry of catalytic hydrogenation of the carbon–carbon double bond of $\Delta^{1,9}$-2-octalones is shown to be controlled by the angular substituent at position 10.

The *cis*-decalin system is considered as a synthon for the DE ring system of certain pentacyclic triterpenes.

JOHN W. APSIMON, SATYANAND BADRIPERSAUD, TUNG T. T. NGUYEN et RICHARD PIKE. Can. J. Chem. **56**, 1646 (1978).

On décrit la synthèse de la méthoxycarbonyl-10 triméthyl-1,7,7 décalone-2 *cis* (**6***c*) de même que celle de l'isomère *trans* correspondant. On a montré que la stéréochimie de l'hydrogénation catalytique de la double liaison carbone–carbone des $\Delta^{1,9}$ octalones-2 est contrôlée par le substituant angulaire en position 10.

On considère le système de la décaline *cis* comme un synthon pour le système des cycles DE de certains triterpènes pentacycliques.

[Traduit par le journal]

Can. J. Chem. Downloaded from www.nrcresearchpress.com by 210.87.254.6 on 09/05/12
For personal use only.

For some years our laboratory has been occupied with research directed towards the total synthesis of triterpenes, particularly the biogenetically related pentacyclic species represented by friedelin (**1**), alnusenol (**2**), multiflorenol (**3**), taraxerol (**4**), and β-amyrin (**5**) (2). The pentacyclic triterpenes display a great number of structural variations and complexities, yet in contrast to reports concerning the synthesis of lower terpenes and steroids (3), relatively little attention has been directed towards the laboratory construction of this class of compound (4) until recently when the outstanding researches of a number of groups have provided syntheses of lupeol (5), alnusenone (6), shionone (7), friedelin (8), germanicol (9) serratenediol (10), tetrahymanol (11), δ-amyrin, β-amyrin, and germanicol (12). Heathcock and coworkers (13, 14) have reported the synthesis of several synthons suitable for incorporation in a triterpene synthetic sequence.

In a series of closely related triterpenoids two or more rings present possess the same structural and stereochemical features. For example compounds **1**–**5** all possess a *cis*-fused decalin system as the DE rings (see **1** for ring designations) and only in β-amyrin (**5**) is the C-13 α-methyl group absent. In one of the synthetic routes being investigated in our laboratory we considered a unit represented by **6** as an obvious synthon[3] for triterpenoids of types **1**–**4** and this paper describes some of our experiments directed towards the synthesis of such a species.

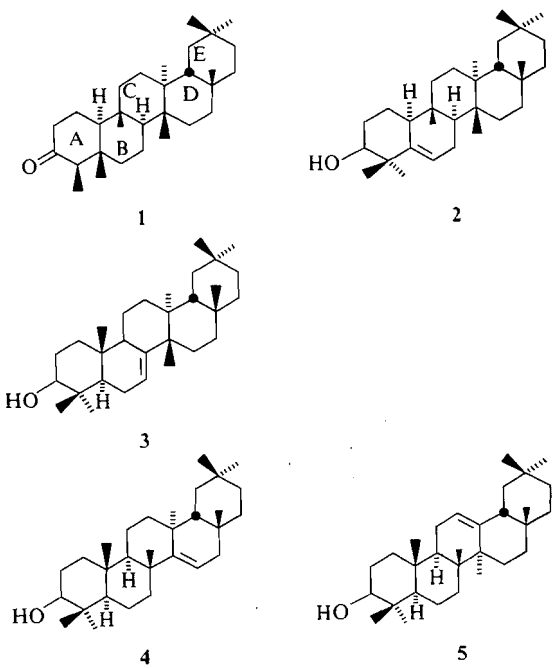

[1]This work is described in the M.Sc. Thesis of T.T.T.N. (Carleton University, Ottawa, Ont., 1971) and the Ph.D. Thesis of S.B. (Carleton University, Ottawa, Ont., 1976). For Part II see ref. 1.

[2]To whom inquiries should be directed.

[3]Except for structures **1**–**5** which represent natural products, all structures used in this paper represent racemates. Only that enantiomer bearing a direct relationship to the natural series is shown for convenience.

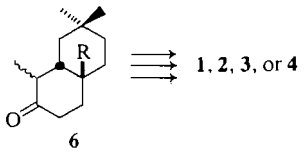

6

a R = CH_3
b R = COOMe
c R = CH_2OH

Similar work has been described by Halsall and Thomas (15) and recently by Heathcock and co-workers (14).

For two reasons, our work was centred on the use of a substrate in which the future C-28 methyl group of the triterpenoids is functionalised. Firstly, we anticipated the activating effect of the methyl ester to be of use in the synthesis of **8** and secondly the synthons **6***b* or **6***c* could conceivably be used for the elaboration of pentacyclic triterpenes in which one or more methyl groups have been oxidised (2).

As a precursor for our studies we chose 10-carbomethoxy-1,7,7-trimethyl-$\Delta^{1,9}$-2-octalone (**8**) the synthesis of which is outlined in Scheme 1. Thus,

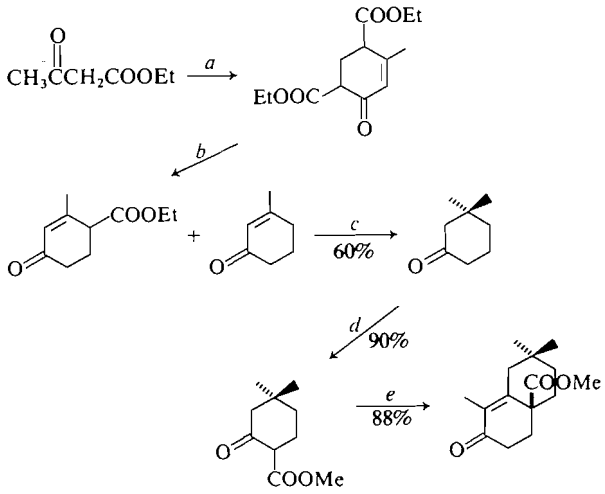

SCHEME 1. Reagents: (*a*) HCHO, piperidine; (*b*) H_2SO_4; (*c*) MeMgI, CuI; (*d*) $CO(OMe)_2$, NaH; (*e*) $CH_3CH_2COCH{=}CH_2$, NaOMe.

carboxymethylation of 3,3-dimethylcyclohexanone (16) by refluxing in dimethylcarbonate containing sodium hydride provided 6-carbomethoxy-3,3-dimethylcyclohexanone (**7**) in excellent yield. A Robinson annelation of this keto ester with ethyl vinyl ketone furnished the octalone **8** in an overall yield of 35% from ethyl acetoacetate.

Next, our work turned to a study of the catalytic hydrogenation of **8**. Literature precedent would suggest either of two routes for this reduction. Thus, the reports of Heathcock and co-workers (14) and Halsall and Thomas (15) suggest reduction should proceed to yield a *cis*-fused decalone, whereas Dauben and Rogan (17) have noted that ester **9** is catalytically hydrogenated to a mixture of the *trans*-decalone **10**, lactone **11**, and hydrogenolysis product **12**. Other reports confirm that the angular substituent has a major role in directing the course of reduction (14, 15, 18) as does the p*H* of the reaction medium (19, 20) and substituents at other positions in the

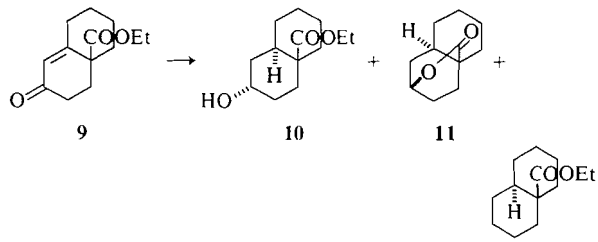

9 **10** **11** **12**

molecule (17, 18*b*). Based on the arguments of Augustine (19) concerning the 1,4 addition of hydrogen to α,β-unsaturated ketones in acidic medium we considered the intermediate **13** leading to a *cis*-decalone more likely than **14** in which the axial C-7 methyl group would incur a severe steric interaction with the metal surface and which would lead to a *trans*-decalone.

In the event, catalytic hydrogenation of **8** provided a variety of products[4] depending on the conditions used. These are summarised in Scheme 2. Thus, hydrogenation in acetic acid at room temperature using platinum provided a 2:1 ratio of alcohol **15** and lactone **16** whilst reduction of the amount of catalyst increased reduction time but reduced the amount of lactone formed.[5] Hydroxy ester **15** on

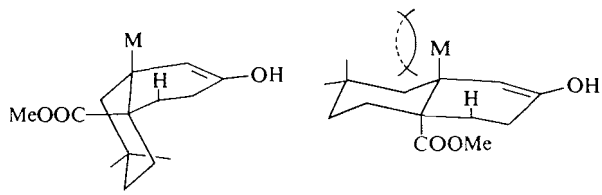

13 **14**

M = Metal

[4]In the majority of cases described in this paper, the spectral and analytical properties of the compounds prepared are unexceptional and lead unequivocally to the structures proposed. In the interests of brevity no extended discussion has been included on the structural elucidation for these materials but all relevant data is reported in the experimental section. The correlation of the various compounds discussed with keto ester **17** whose structure has been demonstrated by a single crystal X-ray analysis leaves no doubt as to the structures proposed.

[5]Unpublished observation of G. Simcoe, B.Sc. Honours Research Report, Carleton University, Ottawa, Ont., 1974.

Can. J. Chem. Downloaded from www.nrcresearchpress.com by 210.87.254.6 on 09/05/12
For personal use only.

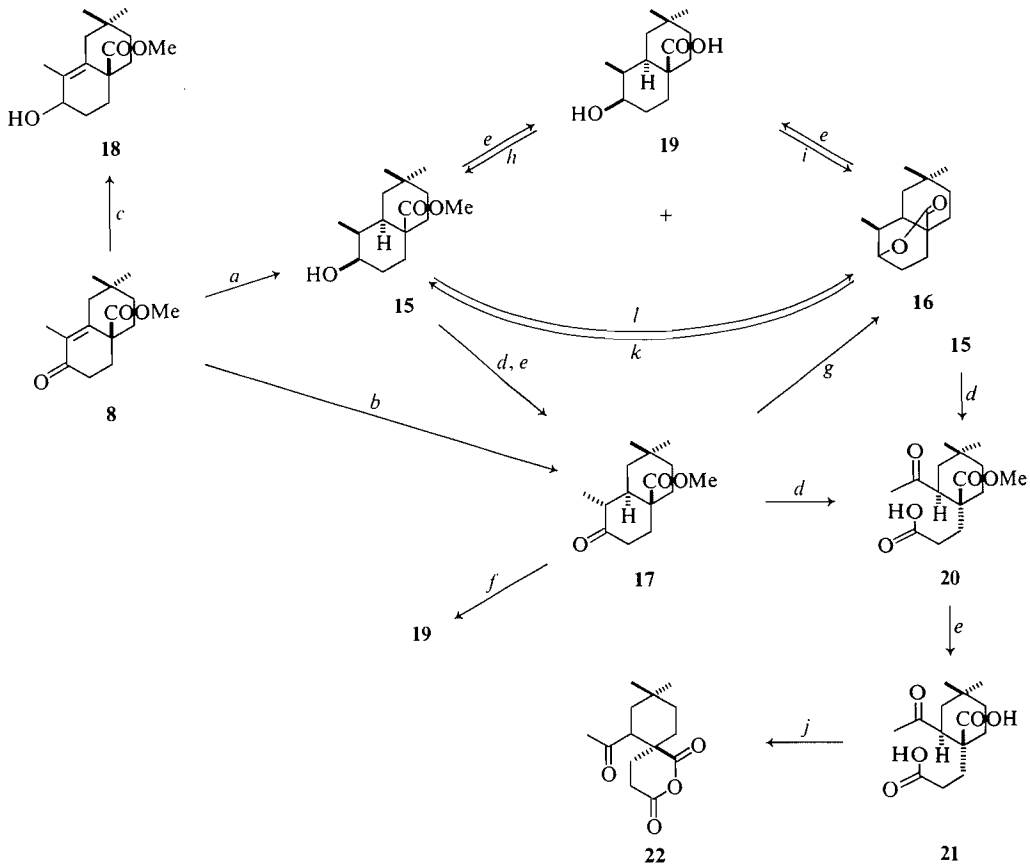

SCHEME 2. Reagents: (*a*) Pt, H_2, CH_3COOH; (*b*) EtOH, 3% 3*N* HCl, 10% Pd–C, H_2; (*c*) Pt, H_2, EtOH, CH_3COOH; (*d*) CrO_3, Me_2CO; (*e*) NaOH; (*f*) Na, isopropanol; (*g*) $NaBH_4$; (*h*) CH_2N_2, Et_2O; (*i*) *p*-toluene sulphonic acid; (*j*) distil; (*k*) NaOMe; (*l*) CH_3COOH.

hydrolysis provided the acid **19** which in turn, on acid treatment yielded lactone **16**, also available directly from **15**. Cleavage of **16** by methoxide furnished **15** and by sodium hydroxide followed by neutralisation gave **19**. Oxidation of **15** by Jones' reagent provided a liquid ketone that yielded crystalline **17** on base treatment. Assuming that this transformation involves equilibration at the C-1 methyl group together with the observation of lactone formation and the X-ray structure data for **17** (22), then stereostructures **15**, **16**, and **19** emerge. Presumably **15** arises by the net *cis*-addition of hydrogen to all four positions of the enone system of **8**. From the Jones' oxidation of **15** we also detected substantial amounts of the ring-cleaved keto acid ester **20** (33), the structure of which was confirmed by hydrolysis to the diacid **21** followed by pyrolytic distillation to the substituted glutaric anhydride **22**.

Reduction of **8** in ethanol with a trace of acetic acid over prereduced platinum oxide furnished allylic alcohol **18**, oxidation of which yielded **8**. The use of 10% palladium-on-charcoal as a catalyst in ethanol acidified with hydrochloric acid yielded the saturated ketone **17** (22) in 60% yield. Although at this stage of our studies we were unsure of the *trans* stereochemistry depicted for **17**, the formation of **15** and **16** were reminiscent of Daubens' report (17, 18*b*). Attempts to prepare **17** by a Birch reduction (12) of **8** were unsuccessful. A single crystal X-ray analysis of **17** was carried out by Huber and Gabe (22) revealing the stereochemistry shown and indicating that in this case the angular carbomethoxyl group possesses a directing effect (18*a*) over any steric effects (19).

Our next tactic was to reverse the stereochemistry of the double bond hydrogenation in **8** by catalytic reduction of 10-hydroxymethyl-1,7,7-trimethyl-$\Delta^{1,9}$-2-octalone (**23**) (17, 18*b*, 23) utilising the haptophilic properties of the hydroxymethyl group. Octalone **23** was obtained from octalone **8** by two routes (Scheme 3). Thus, reduction of **8** with lithium aluminum hydride provided **24** (60%) and **25** (15%), both as mixtures of C-2 epimers. Allylic oxidation of **24** with activated manganese dioxide provided the required keto alcohol **23** in 71% yield. However, the

Can. J. Chem. Downloaded from www.nrcresearchpress.com by 210.87.254.6 on 09/05/12
For personal use only.

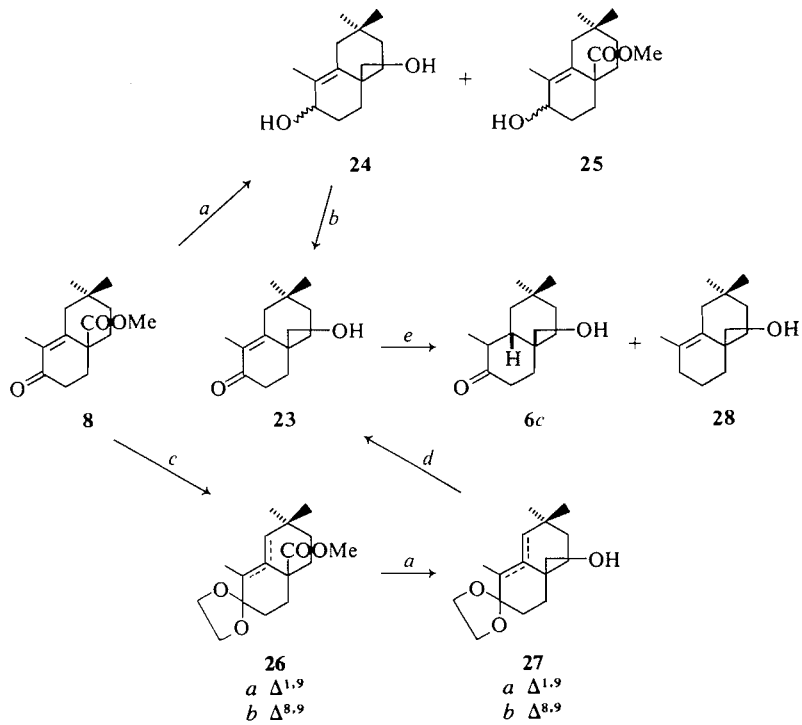

SCHEME 3. Reagents: (*a*) $LiAlH_4$; (*b*) MnO_2; (*c*) $HOCH_2CH_2OH$, *p*-toluene sulphonic acid, benzene azeotrope; (*d*) 10% HCl; (*e*) 10% Pd–C, H_2.

use of large amounts of manganese dioxide (10-fold) required for the oxidation step was not amenable to larger scale preparations; thus **23** was prepared by the alternate route involving ketalisation of **8** to the mixture of double bond isomers **26** reduction to **27** and deketalisation.

Hydrogenation of **23** proceeded over 10% palladium-on-charcoal to yield decalone **6***c* (68%) and hydrogenolysis product **28** (10%). The *cis*-ring junction stereochemistry was assigned on the basis of a comparison of its physical properties with those of 10-hydroxymethyl-1,7,7-trimethyl-*trans*-2-decalone (**29**) obtained by lithium aluminum hydride reduction of the ester group of *trans*-decalone **17** after protection of the keto group as its ethylene ketal, followed by deprotection. Table 1 outlines the major differences in these properties including the gas chromatographic characteristics of their trimethylsilyl derivatives. A similar comparison of the physical properties of esters **6***b* and **17** (see Table 2) emphasises these differences.

Of particular use in the assignment of stereochemistry was the observation that the signals corresponding to the C-10 hydroxymethyl protons (C(10)-CH_2OH) in the *trans*-decalone **29** appearing at δ 3.72 and 4.08 as a pair of doublets have a half-height width of 3 Hz as opposed to the same signals for the *cis*-decalone **6***c* where the pair of doublets at δ 3.77 and 3.95 have a half-height width of only 1 Hz. This observation can be attributed to long range W coupling (**24**) of the hydroxymethyl group protons **29** with three axial protons whereas in **6***c* only one proton is capable of attaining a suitable W arrangement with the angular hydroxymethyl group protons as shown (25).

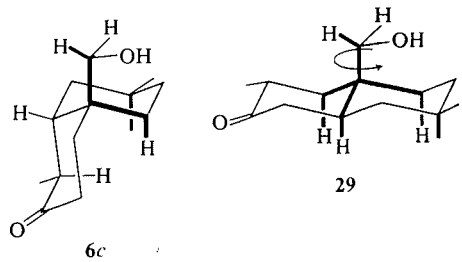

The mass spectra of the pairs of *cis* and *trans* isomers **6***c* and **29**, their corresponding ethylene ketals, and **6***b* and **17**, displayed some striking differences especially in the case of the ketals.[6] Thus the ethylene ketal **30** (C,9H-β) had the molecular ion (M^+ 268) as its parent ion with the expected ketal directed fragmentation (26) to **31** being observed with a relative abundance of 50%, on the other hand

[6]We have, as yet, been unable to observe any regularities in the fragmentation of these parallel series of stereoisomers but hopefully, continuing work in these laboratories will provide more data (27).

Can. J. Chem. Downloaded from www.nrcresearchpress.com by 210.87.254.6 on 09/05/12
For personal use only.

Can. J. Chem. Downloaded from www.nrcresearchpress.com by 210.87.254.6 on 09/05/12
For personal use only.

TABLE 1. Some physical properties of decalones **6***c* and **29**

Compound	Melting point (°C)	^{1}H nmr CH_2*OH (ppm)	$W_{h/2}(CH_2{*}OH) - W_{h/2}(TMS)$ (Hz)	$J_{C(1)H-C(9)H}$	^{13}C nmr CH_2OH (ppm)	Retention times[a] (min)
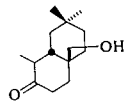 **6***c*	95–97	3.77 and 3.95 (2d, J = 10 Hz)	1	5	68.60	30.8
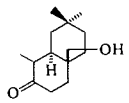 **29**	105–108	3.72 and 4.08 (2d, J = 10 Hz)	3		70.16	27.4

[a]Gas chromatography (column OV-225 at 160°C); retention times of silyl ether derivatives.

TABLE 2. Some differences in the physical properties of decalones **17** and **6***b*

Compound	Melting point (°C)	^{1}H nmr (ppm) $C(=O)-OCH_3$	^{1}H nmr (ppm) $C(1)CH_3$	Retention times[a] (min)
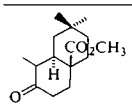 **17**	71–73	3.73	1.01	43
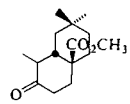 **6***b*	Oil	3.82	0.97	38.4

[a]Gas chromatography (column OV-225 at 160°C).

in the case of the ketal **30** (C,9H-α) the molecular ion showed only a relative abundance of 10% with the fragment *m/e* 99 (i.e. **31**) being the parent ion.

With compound **6***c* in our hands, we next turned our attention to alkylation at C-1, arguing for β-face

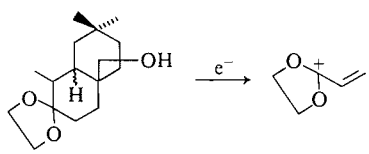

30 **31** (*m/e* 99)

alkylation from the open face of the hinge-like *cis*-fused decalin. Such an event would then lead to the stereochemistry desired for friedelin (**1**). These studies were disappointing although in one experiment we observed that alkylation of the enol acetate **32** with allyl bromide provided a low yield of a product tentatively assigned structure **33**. It is interesting to note that enol acetylation of **6***c* with acetic anhydride, perchloric acid in carbon tetrachloride (28) yielded the expected regioisomer **32** (29). At this stage of our studies we postponed further work on this problem in favour of other more promising synthetic routes to the triterpenoids.

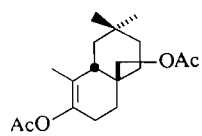

32

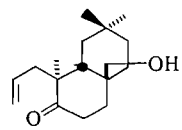

33

Experimental

All melting points were obtained on a Kofler hot stage and are uncorrected. Boiling points are uncorrected. Thin-layer chromatography was carried out on precoated silica gel plates obtained from E.M. reagents (silica gel F-254, 0.25 mm or 2.0 mm); the plates were developed either by exposure to iodine vapour or by spraying with a solution of ceric sulphate and heating. The nuclear magnetic resonance spectra were obtained on a Varian Model T-60 or Varian H-A 100 spectro-

Can. J. Chem. Downloaded from www.nrcresearchpress.com by 210.87.254.6 on 09/05/12
For personal use only.

meter with tetramethylsilane as internal standard. Chemical shifts are expressed in the δ scale and the following abbreviations apply: s, singlet; d, doublet; t, triplet; m, multiplet. Infrared spectra were determined on a Perkin-Elmer Model 237B Grating Infrared spectrometer and Beckman AccuLab 2 infrared spectrometer. The ultraviolet spectra were run on a Cary recording spectrometer Model 14 or Perkin-Elmer 202 ultraviolet–visible spectrophotometer. Gas chromatographic analyses were carried out on a Hewlett-Packard F & M Scientific 402 high efficiency gas chromatograph. Mass spectra were obtained on an AEI MS12 instrument at Trent University, Peterborough. Combustion analyses were performed by Spang Microanalytical Laboratory, Ann Arbor, Michigan. The term 'dry benzene' refers to benzene which has been distilled and stored over sodium wire. The term 'dry tetrahydrofuran' refers to tetrahydrofuran which has been distilled from lithium aluminum hydride under anhydrous conditions. Petroleum ether refers to the fraction boiling at 30–60°C. Boron trifluoride etherate was obtained from Eastman Kodak Company and was purified by distillation from calcium hydride.

3-Methyl-2-cyclohexenone

This compound was prepared by a modification of the method of Smith and Rouault (30). Piperidine (20 ml) was added to a mixture of ethyl acetoacetate (500 g, 3.85 mol) and paraformaldehyde (57.6 g, 1.92 mol). The mixture was warmed to 50°C to initiate the reaction. The solution became yellow and the temperature rose quickly to 70°C. The reaction flask was cooled in an ice bath and the temperature maintained at about 50°C for 15 min and the reaction mixture was left stirring overnight at room temperature. The yellow viscous oil was poured into 1.ℓ of 20% sulphuric acid and refluxed for 24 h. After cooling, the organic material was extracted with methylene chloride (250 ml × 4) and dried over anhydrous sodium sulphate. Removal of the solvent under reduced pressure gave an oil which was vacuum distilled to afford 3-methyl-2-cyclohexenone (124 g; 58%); bp 85–90°C/15 Torr (lit. (30) bp 75–77°C/10 Torr); ir (neat): 1660 (C=O) and 1625 cm^{-1} (C=C); nmr ($CDCl_3$) δ: 1.97 (s, 3, C-3 CH_3) and 5.83 (s, 1, C-2 H).

3,3-Dimethylcyclohexanone

Magnesium turnings (33.6 g, 1.38 mol) were placed in a three-necked round-bottomed flask fitted with a condenser, equilibrating dropping funnel and a nitrogen inlet. The magnesium turnings were covered with anhydrous ether and 1 ml of methyl iodide was added through the dropping funnel. The mixture was stirred until the reaction started and then 200 g (1.4 mol) of methyl iodide diluted with anhydrous ether (300 ml) was added dropwise such that reflux was maintained. After addition was completed the mixture was cooled (ice-bath) and copper iodide (10.8 g, 0.057 mol) was added and stirred. Still at 0°C, 3-methyl-2-cyclohexenone (124 g, 1.12 mol) in an equal volume of anhydrous ether was added slowly and stirring was continued for an additional 15 min. The mixture was poured into 1 ℓ of cold 3 *N* H_2SO_4 and mechanically stirred. The ether layer was separated and washed with sodium thiosulphate solution and dried over anhydrous sodium sulphate. After removal of solvent, the residue was distilled *in vacuo* to yield 86 g (66%) of 3,3-dimethylcyclohexanone as an oil; bp 50–60°C/10 Torr (lit. (16) bp 62–65°C/13 Torr, 71–71.5°C/19 Torr); ir (neat): 1700 cm^{-1} (C=O); nmr ($CDCl_3$) δ: 0.98 (s, 6, *gem*-dimethyl).

6-Methoxycarbonyl-3,3-dimethylcyclohexanone (7)

Sodium hydride (53.5 g, 2.23 mol) and dimethyl carbonate (250.5 g 2.78 mol) were placed in a three-necked round-bottomed flask under a nitrogen sweep and the mixture was stirred vigorously and heated to reflux. While refluxing, 3,3-dimethylcyclohexanone (71.1 g, 0.56 mol) was added dropwise. After addition was completed, the mixture was stirred and refluxed for another 30 min, then cooled and acidified with acetic acid. The organic material was extracted with ether, washed with saturated sodium bicarbonate solution followed by saturated sodium chloride solution and was dried over anhydrous sodium sulphate. After filtration, solvent was evaporated to yield an oil which on distillation furnished 69 g (70%) of the keto ester **7**; bp 60–65°C/10.5 Torr; ir (neat): 1710 (C=O) and 1745 cm^{-1} (ester); nmr ($CDCl_3$) δ: 0.97 (s, 6, *gem*-dimethyl), and 3.77 (s, 3, OCH_3). *Anal.* calcd. for $C_{10}H_{16}O_3$: C 65.19, H 8.75; found: C 64.97, H 8.53.

10-Methoxycarbonyl-1,7,7-trimethyl-$\Delta^{1,9}$-2-octalone (8)

To dry, distilled methanol (200 ml) was added 0.6 g (0.026 mol) of sodium. After all of the sodium had reacted, the solution was cooled to 0°C and 6-methoxycarbonyl-3,3-dimethylcyclohexanone (**7**) (50 g, 0.27 mol) was added dropwise to the stirred solution at 0°C. The solution was stirred for an additional 15 min then ethyl vinyl ketone (22.2 g, 0.26 mol) in 30 ml of methanol was added dropwise, the solution still being at 0°C. An excess of base (2 g (0.087 mol) of Na in 30 ml of MeOH) was added and the mixture was stirred at room temperature overnight. Water was added and the mixture was acidified with 3 *N* H_2SO_4. The organic material was extracted with ether, washed twice with water, saturated sodium chloride solution, and dried over anhydrous magnesium sulphate. After removal of the solvent, the oil obtained was distilled to give 69 g (88%) of the octalone **8**, bp 99–104°C/0.1 Torr. This material solidified on refrigeration but melted after a few hours at room temperature; ir (neat) 1675 (C=O), and 1715 cm^{-1} (ester); nmr ($CDCl_3$) δ: 0.87 (s, 3, C-7 CH_3), 1.03 (s, 3, C-7 CH_3), 1.83 (s, 3, C-1 CH_3), and 3.75 (s, 3, $COOCH_3$). *Anal.* calcd. for $C_{15}H_{22}O_3$: C 71.97, H 8.86; found: C 71.68, H 8.62. M^+ (ms) 250.

10-Methoxycarbonyl-1,7,7-trimethyl-trans-*2-decalone (17)*

A mixture of 10% palladium-on-charcoal (1 g), ethanol (100 ml), and 5 ml 3 *N* HCl was hydrogenated at 1 atm pressure of hydrogen at room temperature for 4 h. 10-Methoxycarbonyl-1,7,7-trimethyl-$\Delta^{1,9}$-2-octalone (10 g) was added and the resulting mixture was hydrogenated for 4 h (uptake of 950 ml H_2). The mixture was filtered, the filtrate was diluted with water and extracted with chloroform (3 × 30 ml). The chloroform layer was washed with saturated sodium bicarbonate solution, saturated sodium chloride solution, and dried over anhydrous magnesium sulphate. Removal of the solvent at reduced pressure gave an oil which crystallized from hexane to give 6.0 g (60%) of the decalone **17**. Recrystallization from hexane produced colorless needles; mp 103–106°C; ir (Nujol): 1715 (ketone), 1730 (ester), and 1360, 1380 cm^{-1} (*gem*-dimethyl); nmr ($CDCl_3$) δ: 0.91, 0.95 (two s, 3 each, *gem*-dimethyl), 1.01 (d, 3, J = 6 Hz, C-1 CH_3), and 3.74 (s, 3, $COOCH_3$); ms *m/e* (relative intensity): 252 (100), 237 (5), 220 (15), 192 (31), 175 (58). *Anal.* calcd. for $C_{15}H_{24}O_3$: C 71.39, H 9.59; found: C 71.47, H 9.77.

Hydrogenation of 10-Methoxycarbonyl-1,7,7-trimethyl-$\Delta^{1,9}$-2-octalone (8)

(*a*) A mixture of 2.00 g. of platinum oxide and 100 ml of acetic acid was hydrogenated at 1 atm pressure for 4 h. The α,β-unsaturated ketone **8** (5.01 g) was added and the resulting mixture was hydrogenated at atmospheric pressure and at room temperature overnight. After filtration, the solution was diluted with water and extracted with chloroform. The chloro-

Can. J. Chem. Downloaded from www.nrcresearchpress.com by 210.87.254.6 on 09/05/12
For personal use only.

form solution was washed with saturated sodium bicarbonate solution, dried over anhydrous sodium sulphate and evaporated to give 4.77 g. of a colorless oil. Thin-layer chromatography showed the presence of two compounds. The crude product was chromatographed on 141 g of Woelm neutral alumina (grade 1). Elution with chloroform gave 2.19 g (66%) of **15** as a colorless oil; ir 3400 (OH), 1725 cm^{-1} ($COOCH_3$); nmr ($CDCl_3$) δ:0.85, 0.98 (s, 3H each, *gem*-dimethyl), 0.93 (d, 3H, CH_3—CH—), 3.68 (s, 3H, $COOCH_3$). Further elution with 25% ether in chloroform gave 1.49 g (34%) of **16** as colorless crystals. Recrystallization from hexane gave an analytical sample; colorless long needles, mp 68–69°C; ir ($CHCl_3$):1736 cm^{-1} (CO of a six-membered ring lactone); nmr ($CDCl_3$) δ: 0.88, 1.06 (s, 3H each, *gem*-dimethyl), 0.93 (d, 3H, CH_3—CH—), 4.33 (m, 1H, —*CH*—O—); ms *m/e*:222 (molecular ion). *Anal.* calcd. for $C_{14}H_{22}O_2$: C 75.67, H 9.91; found: C 75.70, H 9.84.

(*b*) A mixture of 200 mg of platinum oxide, absolute ethanol (20 ml) and acetic acid (1 ml) was hydrogenated at 1 atm for 2 h. The α,β-unsaturated ketone **8** (100 mg) was added and the resulting mixture was hydrogenated at ambient temperature and at atmospheric pressure for 30 min. After filtration, the solution was diluted with water and extracted with chloroform. After washing with sodium bicarbonate solution, and water, the solution was dried and evaporated to provide a colorless oil (0.98 g) that crystallized on standing. Recrystallization twice from aqueous methanol provided an analytical sample of **18**; mp 102–103°C; ir 3200 (OH), 1725 cm^{-1} ($COOCH_3$); nmr ($CDCl_3$) δ: 0.8, 0.9 (s, 3H each, *gem*-dimethyl), 1.8 (s, 3H, *CH*—C=C), 3.64 (s, 3H, $COOCH_3$) and 4.0 (m, 1H, C*H*—OH). *Anal.* calcd. for $C_{15}H_{24}O_3$ (M^+ 252): C 71.39, H 9.59; found (M^+ 252): C 71.53, H 9.84.

Preparation of Lactone ***16***

(a) Stepwise Approach

To a solution of 0.906 g of the crude hydroxy ester **15** in 15 ml methanol was added 12 ml of 2 *N* sodium hydroxide and 10 ml of benzene. The resulting mixture was heated at reflux for 5 h then cooled to room temperature. The reaction mixture was diluted with water and extracted with chloroform. After washing the organic layer with saturated sodium bicarbonate solution and drying over anhydrous sodium sulphate, evaporation gave a yellow oil (0.426 g) which was shown to be the starting material **15** by nmr. The aqueous layer was acidified with hydrochloric acid and extracted thoroughly with chloroform. The chloroform solution was washed with saturated sodium chloride solution, dried over anhydrous sodium sulphate, and evaporated giving a colorless amorphous powder **19** (0.336 g, 94% yield based on recovered starting material); mp 102–105°C; tlc (30:70 ethyl acetate – benzene, iodine development) showed one spot R_f 0.22; nmr ($CDCl_3$) δ: 0.76, 0.93 (s, 3H each, *gem*-dimethyl), 1.00 (d, 3H, CH_3—CH), 3.80 (m, 1H, —*CH*—OH), 6.50 (s, 2H, *OH* and CC*OH*).

A solution of 0.336 g of the hydroxy acid **19** and 0.121 g of *p*-toluenesulfonic acid monohydrate in 25 ml of benzene was heated at reflux overnight using a Dean–Stark trap to collect water. The reaction mixture was cooled and extracted with benzene. The organic layer was washed with saturated sodium bicarbonate solution, dried over anhydrous sodium sulphate, and evaporated to give a yellowish oil (0.236 g, 76% yield) which crystallized from hexane and was shown to be identical in all respects (ir, nmr, tlc) with lactone **16**.

(b) Direct Approach

A solution of 0.103 g of the hydroxy ester **15** in 10 ml of acetic acid was stirred at room temperature overnight. The mixture was poured into water and extracted with chloroform. The organic layer was washed with saturated sodium bicarbonate solution and dried over anhydrous sodium sulphate. Evaporation afforded a yellowish oil (0.077 g, 85% yield) which after crystallization from hexane was shown to be identical with the lactone **16** by tlc, ir, and nmr.

Preparation of Hydroxy Acid ***19*** *from Lactone* ***16***

A mixture of 0.124 g of the lactone **16**, 2 ml of 2 *N* sodium hydroxide, and 10 ml of benzene was refluxed overnight. The resulting solution was cooled and extracted with chloroform. The organic layer was washed with 5% hydrochloric acid solution, dried over anhydrous sodium sulphate, and evaporated to give a colorless amorphous powder (0.098 g, 73% yield) which was shown to be identical in all respects (ir, nmr, and tlc) with the hydroxy acid **19**.

*Collins' Oxidation of 10-Methoxycarbonyl-1α,7,7-trimethyl-*trans*-2β-decalol (**15**)*

Chromium trioxide 0.472 g (0.0047 mol) was added to a solution of 0.770 g (0.0094 mol) of pyridine in 15 ml of methylene chloride under nitrogen. The deep burgundy solution was stirred for 15 min then 0.209 g (0.0008 mol) of the crude hydroxy ester **15** in 5 ml of methylene chloride was added in one portion. A black precipitate appeared and the mixture was stirred for half an hour. Methylene chloride was decanted from the residue which was washed three times with ether. Solvent was removed under vacuum, ether was added, and the solution filtered, washed with saturated sodium bicarbonate solution, saturated sodium chloride solution, and dried over anhydrous magnesium sulphate. Removal of the solvent left a yellowish oil (0.180 g) which showed no trace of starting material. The crude product was chromatographed on 104 g of Woelm neutral alumina (grade 1). Elution with 75% chloroform in benzene gave colorless crystals (0.120 g, 58%). Recrystallization from hexane gave the pure saturated ketone **17** as colorless prismatic needles; mp 84–85°C; ir: 1725 ($COOCH_3$), 1710 cm^{-1} (CO); nmr ($CDCl_3$) δ: 0.88, 1.03 (s, 3H each, *gem*-dimethyl), 0.92 (d, 3H, CH_3—CH—), 3.74 (s, 3H, $COOCH_3$); nmr (C_6D_6) δ: 1.17 (d, 3H, CH_3—CH—). *Anal.* calcd. for $C_{15}H_{24}O_3$: C 71.39, H 9.59; found: C 71.07, H 9.47.

*Sodium Borohydride Reduction of 10-Methoxycarbonyl-1α,7,7-trimethyl-*trans*-2-decalone (**17**)*

To a solution of 0.104 g (0.0004 mol) of the ketone **17** in 5 ml of methanol was added 0.313 g (0.0008 mol) of sodium borohydride in 1 ml of water. The resulting mixture was refluxed overnight. The solution was cooled, acidified with hydrochloric acid, and extracted with chloroform. After washing the organic layer with saturated sodium bicarbonate solution and drying over anhydrous sodium sulphate, evaporation gave colorless crystals in a yellowish oil (0.107 g). Thin-layer chromatography showed two spots, one of which was the starting material. The crude product was chromatographed on 3 g of Woelm neutral alumina (grade 1).

Elution with benzene afforded colorless needles mp 68–70°C after evaporation of solvent (0.041 g, 88% yield based on recovered starting material), shown to be identical with the lactone **16** by infrared and nmr.

*Jones' Oxidation of 10-Methoxycarbonyl-1α,7,7-trimethyl-*trans*-2β-decalol (**15**)*

Jones' reagent was added dropwise to a solution of 0.190 g of the crude hydroxy ester **15** in 5 ml of acetone until the orange color of the reagent persisted while stirring vigorously. The reaction mixture was allowed to stir at room temperature for an additional 15 min and acetone was then evaporated. Water was added, the mixture was shaken vigorously, and additional aliquots of water were added until the green chro-

Can. J. Chem. Downloaded from www.nrcresearchpress.com by 210.87.254.6 on 09/05/12
For personal use only.

mium salts dissolved. The aqueous layer was extracted thoroughly with ether. The combined extracts were washed with saturated sodium bicarbonate solution, water, and dried over anhydrous sodium sulphate. Removal of the solvent left a yellowish oil (0.097 g, 53%), which could not be induced to crystallize; however, after treatment of an alcoholic solution with 2 *N* NaOH solution and reisolation, pure **17** was obtained.

The combined washing layer was acidified with hydrochloric acid and extracted with chloroform. After washing the organic layer with saturated sodium chloride solution, it was dried over anhydrous sodium sulphate, before evaporation to give colorless crystals (0.089 g, 47%). Recrystallization from carbon tetrachloride afforded the pure acid ester **20** as a colorless amorphous powder; mp 112–113°C; ir ($CHCl_3$): 3600–2500 (COOH), 1710 cm^{-1} (CO); nmr ($CDCl_3$) δ: 0.87, 0.94 (s, 3H each, *gem*-dimethyl), 2.18 (s, 3H, CH_3—CO—), 3.70 (s, 3H, $COOCH_3$), 5.77 (m, 1H, *OH*); nmr (C_6D_6) δ: 1.80 (s, 3H, CH_3—CO—); ms *m/e*: 284 (molecular ion), base peak at *m/e* 43 (CH_3CO^+). *Anal.* calcd. for $C_{15}H_{24}O_5$: C 63.36, H 8.51; found: C 63.09, H 8.28.

*Jones' Oxidation of 10-Methoxycarbonyl-1α,7,7-trimethyl-*trans*-2-decalone (17)*

To a solution of 0.300 g of the ketone **17** in 5 ml of acetone, sufficient Jones' reagent was added to maintain an orange coloration. The reaction mixture was stirred at room temperature for 15 min then acetone was removed under reduced pressure. Water was added and the mixture was extracted with chloroform. The organic layer was washed with saturated sodium bicarbonate solution and water, then dried over anhydrous sodium sulphate. Evaporation after filtration gave yellow needle-like crystals (0.053 g) which were shown to be the starting material **17**. The aqueous layer was acidified with hydrochloric acid and extracted with chloroform. The chloroform solution was washed with saturated sodium chloride solution, dried over anhydrous sodium sulphate, and evaporated to give yellowish crystals (0.205 g, 77% yield based on recovered starting material). Sublimation at 180°C under vacuum afforded the diacid **21** as colorless prismatic needles; mp 193–194°C; ir: 3500–2300 (COOH), 1720 (CO of COOH), 1700 cm^{-1} (CO); nmr ($CDCl_3$) δ: 0.95, 0.99 (s, 3H each, *gem*-dimethyl), 2.18 (s, 3H CH_3—CO—). *Anal.* calcd. for $C_{14}H_{22}O_5$: C 62.20, H 8.20; found (M^+ (ms) 270): C 62.37, H 8.41.

*Sodium Reduction of 10-Methoxycarbonyl-1α,7,7-trimethyl-*trans*-2-decalone (17)*

To a solution of 0.44 g (0.0002 mol) of the ketone **17** in 5 ml of isopropanol was added 0.080 g (0.0035 mol) of sodium. The resulting mixture was refluxed under nitrogen overnight. The solution was cooled, acidified with hydrochloric acid, and extracted with chloroform. After washing the organic layer with saturated sodium chloride solution and drying over anhydrous sodium sulphate, evaporation gave a yellowish amorphous powder (0.026 g, 61% yield) which was shown to be identical with the hydroxy acid **19** (tlc, ir, nmr).

Preparation of Anhydride 22 from Acid Ester 20

A solution of 0.200 g of acid ester **20** in 20 ml of methanol was added to 15 ml of 2 *N* sodium hydroxide. The resulting solution was refluxed overnight. The reaction mixture was cooled, acidified with hydrochloric acid, and extracted with chloroform. The organic layer was washed with saturated sodium chloride solution, dried over anhydrous sodium sulphate and evaporated giving colorless needle-shaped crystals (0.148 g, 78% yield). This product was identical in all respects (ir, nmr, tlc) with diacid **21**. This was sublimed at 180°C under vacuum to give a yellowish oil (0.110 g) which showed carbonyl absorptions in its ir spectrum at 1770 and 1720 cm^{-1} for the anhydride **22**. M^+ calcd. for $C_{14}H_{20}O_4$: 252; found (ms): 252.

10-Hydroxymethyl-1,7,7-trimethyl-$\Delta^{1,9}$-2-octalol (24)

A solution of octalone **8** (2.5 g, 0.01 mol) in anhydrous ether (100 ml) was stirred with 0.38 g (0.01 mol) of lithium aluminum hydride at reflux temperature for 2 h. The mixture was cooled in an ice bath and excess of lithium aluminum hydride was decomposed by adding dropwise a saturated solution of Rochelle salt. The ether layer was separated and the aqueous layer extracted with ether (3 × 20 ml). After drying the combined ether extracts over anhydrous magnesium sulphate, the solvent was removed to give an oil. Column chromatography on silica gel eluting with petroleum ether containing increasing amounts of benzene gave two fractions.

Fraction 1

10-Methoxycarbonyl-1,7,7-trimethyl-$\Delta^{1,9}$-2-octalol (**25**) (12%); mp 102–103°C; ir (Nujol): 3400 (OH) and 1730 cm^{-1} (ester); nmr ($CDCl_3$) δ: 0.83, 0.95 (2 s, 3 each, *gem*-dimethyl), 1.80 (s, 3, C-1 CH_3), 3.70 (s, 3, $COOCH_3$), and 4.00 (broad, 1, $W_{h/2}$ = 8 Hz, C-2 H); ms *m/e* (relative intensity): 252 (trace), 238 (26), 191 (45), 175 (100). *Anal.* calcd. for $C_{15}H_{24}O_3$: C 71.39, H 9.59; found: C 71.41, H 9.52.

Fraction 2

10-Hydroxymethyl-1,7,7-trimethyl-$\Delta^{1,9}$-2-octalol (**24**) (60%); ir (neat): 3350 (OH) and 1360, 1380, cm^{-1} (*gem*-dimethyl), nmr ($CDCl_3$) δ: 0.93, 0.97 (2 s, 3 each, *gem*-dimethyl), 1.77 (s, 3, C-1 CH_3), 3.47 (m, 2, CH_2OH), and 4.10 (broad, 1, C-2 H); ms *m/e* (relative intensity): 224 (trace), 206 (8), 176 (100). *Anal.* calcd. for $C_{14}H_{24}O_2$: C 74.95, H 10.78; found (M^+ (ms) 272): C 74.77, H 10.48.

10-Hydroxymethyl-1,7,7-trimethyl-$\Delta^{1,9}$-2-octalone (23)

10-Hydroxymethyl-1,7,7-trimethyl-$\Delta^{1,9}$-2-octalol (**24**) (2.7 g, 12 mmol) and manganese dioxide (31) (7 g, 80 mmol) in 50 ml chloroform were vigorously stirred for 72 h at room temperature. The mixture was filtered under suction and the residue washed with chloroform. The combined chloroform solutions were washed with saturated brine and dried ($MgSO_4$). Evaporation of the solvent gave an oil which was chromatographed on 90 g alumina. Elution with benzene and then benzene containing increasing amounts of ethyl acetate furnished 1.91 g (71%) octalone **23** and further elution gave 0.2 g of starting octalol **24**. Bulb-to-bulb distillation of the octalone **23** at 140°C/0.2 Torr furnished an analytical sample; uv_{max} (95% C_2H_5OH): 251 nm (ε 17 500); ir (neat): 3400 (OH), 1650 (C=O), and 1600 cm^{-1} (C=C); nmr ($CDCl_3$) δ: 0.87, 1.07 (2 s, 3 each, *gem*-dimethyl), 1.78 (s, 3, C-1 CH_3), and 3.75 (s, 2, CH_2OH); ms *m/e* (relative intensity): 222 (50), 193(100), 192 (100), 149 (50). *Anal.* calcd. for $C_{14}H_{22}O_2$: C 75.63, H 9.97; found: C 75.70, H 10.03.

Hydrogenation of 10-Hydroxymethyl-1,7,7-trimethyl-$\Delta^{1,9}$-2-octalone (23)

Run 1

The octalone **23** (525 mg, 2.1 mmol) in ethanol (5 ml) was added to 100 mg prehydrogenated 10% palladium-on-charcoal in 40 ml ethanol. Hydrogenation was carried out for 48 h during which time 60 ml hydrogen was absorbed. The mixture was filtered and the filtrate was diluted with water and extracted with ether (30 ml × 3). The ether extract was washed with water, saturated brine and dried (Na_2SO_4). Removal of the ether gave an oil which was chromatographed on a silica gel plate (2 mm). Development of the plate twice with benzene – ethyl acetate (1 : 1) gave two main products.

Fraction 1—(R_f 0.59, 19%) was identified as 10-hydroxymethyl-1,7,7-trimethyl-$\Delta^{1,9}$-octalin (**28**): ir (neat): 3300 and 1030 cm^{-1} (primary alcohol), no carbonyl absorption; nmr ($CDCl_3$) δ: 0.82, 0.97 (2 s, 3 each, *gem*-dimethyl), 1.65 (s, 3, C-1 CH_3), and 3.42, 3.65 (2 d, 2, J = 4 Hz, AB quartet,

Can. J. Chem. Downloaded from www.nrcresearchpress.com by 210.87.254.6 on 09/05/12
For personal use only.

—CH_2—OH); ms *m/e*: 208 (M^+). *Anal.* calcd. for $C_{14}H_{24}O$: C 80.66, H 11.57; found: C 80.71, H 11.61.

Fraction 2—(R_f 0.43, 19%) was the decalone **6***c*. Two recrystallizations from methanol–water gave an analytical sample: ir (Nujol): 3200 (OH) and 1700 cm^{-1} (C=O); nmr ($CDCl_3$) δ: 0.86, 0.90 (2 s, 3 each, *gem*-dimethyl), 0.93 (d, 3, J = 6 Hz, C-1 CH_3), 3.77, 3.95 (2 d, 2, J = 10 Hz, AB quartet $W_{h/2} - W_{h/2}$ (TMS) = 1.5 Hz, CH_2—OH), and 2.85 (m, 1, C-1 H). Decoupling of the C-1 CH_3 (0.93 caused the signal at 2.85 to collapse to a doublet J = 5 Hz; ms *m/e* (relative intensity): 224 (10), 193 (20), 175 (10). *Anal.* calcd. for $C_{14}H_{24}O_2$: C 74.95, H 10.78; found: C 74.88, H 10.76.

Run 2

The octalone **23** (2.2 g) in 15 ml ethanol was added to 1.1 g of prehydrogenated 10% Pd–C in 75 ml ethanol and 3 ml 3 *N* HCl. Hydrogenation was carried out and in 4 h 305 ml of hydrogen was absorbed. Work-up as above gave an oil which was crystallized directly from hexane to give the decalone **6***c* in 68% yield. Thin-layer chromatography on silica gel plates (0.25 mm) of the mother liquor showed the presence of starting material and hydrogenolysis product **28**.

2-Ethylenedioxy-10-methoxycarbonyl-1,7,7-trimethyl-$\Delta^{1,9}$*-octalin (***26***a) and 3-Ethylenedioxy-10-methoxycarbonyl-1,7,7-trimethyl-*$\Delta^{8,9}$*-octalin (***26***b)*

A mixture of octalone **8** (5 g), *p*-toluenesulfonic acid (375 mg), and excess ethylene glycol (10 ml) in 300 ml benzene was stirred and refluxed for 24 h using a Dean–Stark water separator. The mixture was cooled, washed with 5% sodium bicarbonate solution, water, saturated sodium chloride solution, and dried over anhydrous magnesium sulphate. Distillation of the solvent *in vacuo* yielded a clear oil (5.8 g, 98%) which was indicated by nmr to be a mixture of $\Delta^{1,9}$-ethylene ketal **26***a* (60%) and $\Delta^{8,9}$-ethylene ketal **26***b* (40%). Column chromatography of a sample over alumina (grade III) eluted with petroleum ether and petroleum ether containing increasing amounts of benzene gave pure samples of the two isomers. Evaporative distillation of each isomer at 130–140°C/0.1 Torr afforded analytical samples.

2-Ethylenedioxy-10-methoxycarbonyl-1,7,7-trimethyl-$\Delta^{1,9}$*-octalin (***26***a)*: ir (neat): 1720 (ester), and 1030, 1060, 1130, 1150, 1190 cm^{-1} (ketal); nmr ($CDCl_3$) δ: 0.83, 0.97 (2 s, 3 each, *gem*-dimethyl), 1.67 (s, 3, C-1 CH_3), 3.70 (s, 3, $COOCH_3$), and 4.02 (broad s, 4, —O—CH_2—CH_2—O—); ms *m/e* (relative intensity): 294 (32), 279 (37), 235 (40), 99 (100). *Anal.* calcd. for $C_{17}H_{26}O_4$: C 69.36, H 8.90; found: C 69.28, H 8.92.

3-Ethylenedioxy-10-methoxycarbonyl-1,7,7-trimethyl-$\Delta^{8,9}$*-octalin (***26***b)*: ir (neat): 1720 (ester), and 1020, 1060, 1110, 1130, 1150 cm^{-1} (ketal); nmr ($CDCl_3$) δ: 1.00, 1.03 (2 s, 3 each, *gem*-dimethyl), 1.01 (d, 3, J = 6 Hz, C-1 CH_3), 3.70 (s, 3, $COOCH_3$), 3.93 (broad s, 4, —O—CH_2—CH_2—O—), and 5.37 (d, 1, J = 2 Hz, C-8 H); ms *m/e* (relative intensity): 294 (4), 297 (3), 235 (7), 99 (100). *Anal.* calcd. for $C_{17}H_{26}O_4$: C 69.36, H 8.90; found: C 69.36, H 8.78.

2-Ethylenedioxy-10-hydroxymethyl-1,7,7-trimethyl-$\Delta^{1,9}$*-octalin (***27***a) and 2-Ethylenedioxy-10-hydroxymethyl-1,7,7-trimethyl-*$\Delta^{8,9}$*-octalin (***27***b)*

To a stirred suspension of lithium aluminum hydride (700 mg, 0.018 mol) was added through a dropping funnel 5 g (0.017 mol) of a mixture of $\Delta^{1,9}$- and $\Delta^{8,9}$-ketal esters **26***a* and **26***b*. On completion of addition the mixture was refluxed for 2 h, the reaction mixture was then cooled in an ice bath and the excess lithium aluminum hydride decomposed by careful addition of a saturated solution of Rochelle salt. The ether layer was separated, washed with water, saturated aqueous sodium chloride solution and dried over anhydrous magnesium sulphate. Evaporation of the solvent gave 3.98 g (88%) of the hydroxy ketals as an oil. The two ketal esters **26***a* and **26***b* were reduced separately by above procedure to give samples of the hydroxy ketals **27***a* and **27***b*. Recrystallization twice from methanol afforded analytical samples of each isomer.

Hydroxy ketal ***27***a: mp 81–83°C; ir (Nujol): 3475 (OH), 1040, 1050, 1060, 1145 cm^{-1} (ketal); nmr ($CDCl_3$) δ: 0.83, 0.98 (2 s, 3 each *gem*-dimethyl), 1.62 (s, 3, C-1 CH_3), 3.57 (broad s, 2, CH_2—OH); and 3.98 (s, 4, —O—CH_2—CH_2—O—); ms *m/e* (relative intensity): 266 (5), 222 (35), 193 (80), 192 (75), 99 (100). *Anal.* calcd. for $C_{16}H_{26}O_3$: C 72.14, H 9.84; found: C 72.32, H 9.92.

Hydroxy ketal ***27***b: mp 87–90°C; ir (neat): 3450 (OH), and 1020, 1060, 1110, 1165, 1190 cm^{-1} (ketal); nmr ($CDCl_3$) δ: 1.00 (s, 6, *gem*-dimethyl), 1.00 (d, 3, J = 6 Hz, C-1 CH_3), 3.58 (s, 2, CH_2OH), 3.92 (s, 4, —O—CH_2—CH_2—O—), and 5.28 (broad s, 1, C-8 H); ms *m/e* (relative intensity): 266 (3), 236 (1), 99 (100). *Anal.* calcd. for $C_{16}H_{26}O_3$: C 72.14, H 9.84; found: C 72.23, H 9.83.

10-Hydroxymethyl-1,7,7-trimethyl-$\Delta^{1,9}$*-2-octalone (***23***) from the Ketals* ***27***a *and* ***27***b

A mixture of $\Delta^{1,9}$- and $\Delta^{8,9}$-hydroxymethyl ketal **27***a* and **27***b* (1 g) was dissolved in acetone (15 ml). Aqueous oxalic acid solution (5%) was added until the solution became cloudy and the mixture was refluxed for 1 h. The acetone was evaporated under reduced pressure and the organic material extracted with ether, washed with saturated sodium bicarbonate solution, saturated sodium chloride solution and dried over magnesium sulphate. Rotary evaporation of the solvent gave an oil which was chromatographed on grade III alumina (elution with benzene – ethyl acetate 70:30) to give octalone **23** (484 mg). A short column distillation provided an analytical sample: bp 140–145°C/0.2 Torr; ir (neat): 3400 (OH), 1650 (C=O), and 1600 cm^{-1} (C=C); nmr ($CDCl_3$) δ: 0.87, 1.07 (2 s, 3 each, *gem*-dimethyl), 1.78 (s, 3, C-1 CH_3), and 3.75 (s, 2, CH_2OH); ms *m/e* (relative intensity): 222 (50), 192 (100), 191 (100), 149 (50). *Anal.* calcd. for $C_{14}H_{22}O_2$: C 75.63, H 9.97; found: C 75.42, H 9.84.

*10-Trimethylsilyloxymethyl-1,7,7-trimethyl-*cis*-2-decalone*

This derivative was prepared according to the procedure of Zinkel (32). To a small pear-shaped flask containing a solution of (5 mg) alcohol **6***c* in 5 ml petroleum ether was added 1 ml of hexamethyldisilazine followed by 1 ml trimethylchlorosilane. The flask was gently heated over a steam bath for 1 h. The solvent was removed by rotary evaporation and the trimethylsilyl ether was extracted with petroleum ether, filtered and concentrated. A 1-μL sample of this concentrated solution was injected into a 6 ft × 0.25 in. column of OV-225 (stationary phase: 5% cyanopropylmethyl phenylmethylsilicone fluid on Chromosorb G, 100–80 mesh) at 160°C. A single peak was observed: retention time 30.8 min.

*2-Ethylenedioxy-10-methoxycarbonyl-1,7,7-trimethyl-*trans*-decalin*

A mixture of 500 mg (1.98 mmol) of *trans*-decalone **17**, *p*-toluenesulfonic acid (37 mg), and ethylene glycol 2 ml in 100 ml benzene was stirred and refluxed overnight, water being removed by azeotropic distillation with benzene. The mixture was cooled and saturated aqueous sodium bicarbonate solution was added. The resulting neutral solution was washed twice with water, then with saturated sodium chloride solution and dried over anhydrous magnesium sulphate. Evaporation of the solvent gave a solid in quantitative yield. Recrystallization thrice from methanol/water furnished an analytical sample: mp 85–87°C; ir (Nujol): 1700 cm^{-1} (ester); nmr δ: 0.80 (d, 3, J = 6Hz, C-1 CH_3), 0.97 (s, 6, *gem*-dimethyl), 3.63 (s, 3, $COOCH_3$), and 3.91 (s, 4, —O—CH_2—CH_2—O—); ms *m/e* (relative intensity): 296 (60), 237 (24), 167 (34), 100 (85),

Can. J. Chem. Downloaded from www.nrcresearchpress.com by 210.87.254.6 on 09/05/12
For personal use only.

86 (100). *Anal.* calcd for $C_{17}H_{28}O_4$: C 68.89, H 9.52; found: C 68.85, H 9.43.

2-Ethylenedioxy-10-hydroxymethyl-1,7,7-trimethyl-trans-*decalin*

A solution of ketal ester 1.025 g (3.5 mmol) in dry ether 25 ml was added dropwise to a stirred suspension of lithium aluminum hydride (10 mmol) in dry ether 75 ml. The mixture was stirred for 5 h at room temperature, then cooled in an ice bath, and excess lithium aluminum hydride was destroyed by the careful addition of a saturated solution of Rochelle salt. The ether layer was separated and the aqueous layer extracted two more times with 20 ml each of ether. The combined ether extracts were washed with water, a saturated solution of sodium chloride and dried over anhydrous magnesium sulphate. Evaporation of the solvent gave an oil (99%) which solidified on standing. Recrystallization from methanol yielded 770 mg (83%). Two recrystallizations from methanol afforded an analytical sample: mp 133–135°C; ir (Nujol): 3480 cm^{-1} (OH), no carbonyl absorption; nmr ($CDCl_3$) δ: 0.73 (d, 3, J = 6 Hz, C-1 CH_3), 0.97 (s, 6, *gem*-dimethyl), 3.70 (s, 2, CH_2—OH), and 3.92 (s, 4, —O—CH_2—CH_2—O—); ms *m/e* (relative intensity): 268 (10), 99 (100), 86 (10). *Anal.* calcd. for $C_{16}H_{28}O_3$: C 71.60, H 10.52; found: C 71.63, H 10.62.

10-Hydroxymethyl-1,7,7-trimethyl-trans-*2-decalone (29)*

The hydroxy ketal (770 mg) was dissolved in 50 ml acetone containing 2 ml of 6 *N* HCl and refluxed for 2 h. Water was added to the mixture and the acetone evaporated. The aqueous residue was extracted with ether (3 × 20 ml). The ether extract was washed with water, saturated sodium chloride solution and dried over magnesium sulphate (anhydrous). Evaporation of the ether at reduced pressure gave a solid which was recrystallized from hexane 555 mg (86%) to yield decalone **29** (555 mg, 86%) as colorless needles. Another recrystallization gave an analytical sample: mp 103–104°C; ir (Nujol): 3450 (OH) and 1715 cm^{-1} (C=O); nmr ($CDCl_3$) δ: 0.90, 0.97 (2 s, 3 each, *gem*-dimethyl), 1.00 (d, 3, J = 4 Hz, C-1 CH_3), and 3.72, 4.08 (2 d, 1 each, J = 10 Hz, $W_{h/2} - W_{h/2}$(TMS) = 4 Hz, AB quartet CH_2—OH); ms *m/e* (relative intensity): 224 (22), 193 (16), 176 (35), 165 (34). *Anal.* calcd. for $C_{14}H_{24}O_2$: C 74.94, H 10.78; found: C 74.88, H 10.66.

10-Trimethylsilyloxymethyl-1,7,7-trimethyl-trans-*2-decalone.*

Prepared by the procedure of Zinkel (32) as described above using the alcohol **31** (10 mg). Injection of 1 μL of a concentrated petroleum ether solution of this silyl ether into a 6 ft × 0.25 in. OV-225 column at 160°C (see above) gave a single peak, retention time 27.4 min. Coinjection of a mixture of the *cis* and *trans* silyl ethers indicated two compounds of retention times 27.4 and 30.8 min, respectively.

10-Carboxyl-1,7,7-trimethyl-cis-*2-decalone*

The hydroxy ketone **6***c* (200 mg) was dissolved in 15 ml acetone and cooled in an ice bath. To the stirred solution, Jones' reagent was added dropwise until a permanent orange colour remained. Stirring was continued for a further 30 min at 0°C. The mixture was poured into a separatory funnel, water was added and the organic material was extracted with ether. The ether layer was washed with saturated $NaHCO_3$ solution, then water until clear and then dried over anhydrous magnesium sulphate. Evaporation of the ether under reduced pressure gave a solid, mp 187–192°C; ir (Nujol): 1685 (COOH) and 1710 cm^{-1} (C=O); nmr ($CDCl_3$) δ: 10.87 (COO*H*); no CH_2--OH absorption. This material was esterified without further purification.

10-Methoxycarbonyl-1,7,7-trimethyl-cis-*2-decalone (6*b*)*

To a stirred solution of the acid obtained from 200 mg alcohol **6***c* in 20 ml ether was added an ether solution of diazomethane until there was a permanent yellow colour. The reaction was allowed to stand for 3 h at room temperature when evaporation of the ether and excess diazomethane gave an oil (257 mg). Gas chromatographic analysis on a 6 ft × 0.25 in. OV-225 column at 160°C showed a single peak (43 min retention time). Several attempts to induce crystallization failed. Bulb-to-bulb distillation at 120°C/0.5 Torr provided an analytical sample of ester **6***b*; ir (neat): 1712 (ketone) and 1725 cm^{-1} (ester); nmr ($CDCl_3$) δ: 0.95 (s, 6, *gem*-dimethyl), 0.97 (d, 3, J = 6 Hz, C-1 CH_3), and 3.80 (s, 3, COOCH_3); ms *m/e* (relative intensity): 252 (16), 137 (2), 220 (4), 192 (100), 177 (13), 175 (11). *Anal.* calcd. for $C_{25}H_{24}O_3$: C 71.41, H 9.58; found: C 71.34, H 9.62.

2-Acetoxy-10-acetoxymethyl-1,7,7-trimethyl-$\Delta^{1,9}$-cis-*octalin (32)*

A mixture of 200 mg of ketol **6***c*, acetic anhydride (1 ml) and 1 drop of perchloric acid in carbon tetrachloride (10 ml) was stirred at room temperature for 1 h. The reaction mixture was diluted with water and the carbon tetrachloride layer was separated. The aqueous layer was extracted with (10 ml × 2) chloroform and the combined chloroform and carbon tetrachloride extracts were washed with saturated sodium bicarbonate solution, water and saturated sodium chloride solution and dried over magnesium sulphate (anhydrous). Evaporation of the solvents gave an oil which on bulb to bulb distillation at oil pump pressure furnished a colorless oil which was homogeneous by tlc; ir (neat): 1745 cm^{-1} (acetate); nmr ($CDCl_3$) δ: 0.92 (s, 6, *gem*-dimethyl), 1.50 (s, 3, C-1 CH_3), 2.05, 2.10 (2 s, 3 each, C-CH_3), and 3.90, 4.13 (2 d, 1 each, J = 11 Hz, CH_2—OAc); ms: M^+ 276. *Anal.* calcd. for $C_{18}H_{28}O_2$: C 78.21, H 10.21; found: C 79.88, H 9.95.

Acknowledgements

We thank the National Research Council of Canada for generous financial assistance. We are grateful to Ms. Sue Macauley who provided expert technical assistance.

1. J. W. APSIMON, P. BAKER, J. BUCCINI, J. W. HOOPER, and S. MACAULAY. Can. J. Chem. **50**, 1944 (1972).
2. T. K. DEVON and A. I. SCOTT. Handbook of naturally-occurring compounds. Vol. II. Academic Press, New York, NY. 1972.
3. (*a*) A. F. THOMAS, C. H. HEATHCOCK, and D. TAUB. *In* The total synthesis of natural products. Vol. II. *Edited by* J. W. ApSimon. John Wiley and Co., New York, NY. 1973; (*b*) A. A. AHKREM and YU. A. TITOV. Total steroid synthesis. Plenum Press, New York, NY. 1970.
4. J. W. APSIMON and J. W. HOOPER. *In* The total synthesis of natural products. Vol. II. *Edited* by J. W. ApSimon. John Wiley and Co., New York, NY. 1973.
5. G. STORK, S. UYEO, T. WAKAMATSU, P. GRIECO, and J. LABOVITZ. J. Am. Chem. Soc. **93**, 4945 (1971).
6. (*a*) R. E. IRELAND, D. A. EVANS, D. GLOVER, R. M. RUBOTTOM, and H. YOUNG. J. Org. Chem. **34**, 3717 (1969); (*b*) R. E. IRELAND, M. I. DAWSON, S. C. WELCH, A. HAGENBACH, J. BORDNER, and B. TRUS. J. Am. Chem. Soc. **95**, 7829 (1973); (*c*) R. E. IRELAND, P. BEY, K.-F. CHENG, R. J. CZAMY, J.-F. MOSER, and R. I. TRUST. J. Org. Chem. **40**, 1000 (1975).
7. R. E. IRELAND, C. J. KOWALSKI, J. W. TILLEY, and D. M. WALBA. J. Org. Chem. **40**, 990 (1975).
8. R. E. IRELAND and D. M. WALBA. Tetrahedron Lett. 1071 (1976).

Can. J. Chem. Downloaded from www.nrcresearchpress.com by 210.87.254.6 on 09/05/12
For personal use only.

9. R. E. IRELAND, S. W. BALDWIN, D. J. DAWSON, M. I. DAWSON, J. E. DOLFINI, J. NEWBOULD, W. S. JOHNSON, M. BROWN, R. J. CRAWFORD, P. F. HUDRLIK, G. H. RASMUSSEN, and K. K. SCHMIEGEL. J. Am. Chem. Soc. **92**, 5743 (1970).
10. G. D. PRESTWICK and J. N. LABOVITZ. J. Am. Chem. Soc. **96**, 7103 (1974).
11. E. E. VAN TAMELEN, M. P. SEILER, and W. WIERENGA. J. Am. Chem. Soc. **94**, 8228 (1972).
12. E. E. VAN TAMELEN, M. P. SEILER, and W. WIERENGA. J. Am. Chem. Soc. **94**, 8229 (1972).
13. J. S. DUTCHER, J. C. MACMILLAN, and C. H. HEATHCOCK. J. Org. Chem. **41**, 2663 (1976).
14. J. E. ELLIS, J. S. DUTCHER, and C. H. HEATHCOCK. J. Org. Chem. **41**, 2670 (1976).
15. T. G. HALSALL and D. B. THOMAS. J. Chem. Soc. 2431 (1956).
16. G. BUCHI, O. JEGER, and L. RUZICKA. Helv. Chim. Acta, **31**, 241 (1948); H. O. HOUSE and W. F. FISCHER. J. Org. Chem. **33**, 949 (1968).
17. W. G. DAUBEN and J. B. ROGAN. J. Am. Chem. Soc. **79**, 5002 (1957).
18. (*a*) L. S. MINCKLER, A. S. HUSSEY, and R. H. BAKER. J. Am. Chem. Soc. **78**, 1009 (1956); (*b*) W. G. DAUBEN, J. W. MCFARLAND, and J. B. ROGAN. J. Org. Chem. **26**, 297 (1961); (*c*) R. B. WOODWARD, F. SONDHEIMER, D. TAUB, K. HEUSLER, and W. M. MCLAMORE. J. Am. Chem. Soc. **74**, 4223 (1952).
19. R. L. AUGUSTINE. J. Org. Chem. **23**, 1853 (1958); R. L. AUGUSTINE and A. D. BROOM. J. Org. Chem. **25**, 802 (1960); R. L. AUGUSTINE. Catalytic hydrogenation. Marcel Dekker Inc., New York, NY. 1965.
20. A. MARCHANT and A. A. PINDAR. J. Chem. Soc. 327 (1956); S. MCELVAIN and P. H. PARKER, JR. J. Am. Chem. Soc. **78**, 5312 (1956).
21. D. H. R. BARTON and C. H. ROBINSON. J. Chem. Soc. 3045 (1954); G. STORK and S. D. DARLING. J. Am. Chem. Soc. **82**, 1516 (1960); **87**, 275 (1965).
22. C. S. HUBER and E. J. GABE. Acta Crystallogr. B, **30**, 2519 (1974).
23. H. W. THOMPSON and R. NAIPAWER. J. Am. Chem. Soc. **95**, 6379 (1973); H. W. THOMPSON. Ann. N.Y. Acad. Sci. **214**, 195 (1973); H. W. THOMPSON and E. MCPHERSON. J. Am. Chem. Soc. **96**, 6232 (1974); H. W. THOMPSON, E. MCPHERSON, and B. L. LENCES. J. Org. Chem. **41**, 2903 (1976).
24. L. M. JACKMAN and S. STERNHALL. Applications of nuclear magnetic resonance spectroscopy in organic chemistry. 2nd ed. Pergamon Press, Oxford. 1969. p. 337 and refs. therein.
25. M. BARFIELD. J. Chem. Phys. **41**, 3825 (1964); K. L. WILLIAMSON, T. HOWELL, and T. A. SPENCER. J. Am. Chem. Soc. **88**, 325 (1966); P. MARSHAN, D. A. WIDDOWSON, and J. K. SUTHERLAND. J. Chem. Soc. Perkin I, 238 (1974).
26. H. BUDZIKIEWICZ, C. DJERASSI, and D. H. WILLIAMS. Structural elucidation of natural products by mass spectrometry. Vol. 2. Holden-Day Inc., San Francisco, CA. 1964. Chapt. 18; H. E. AUDIER, M. FETIZON, and J. C. TABET. Org. Mass Spectrom. **10**, 639 (1975) and refs. therein.
27. E. LUND, H. BUDZIKIEWICZ, J. M. WILSON, and C. DJERASSI. J. Am. Chem. Soc. **85**, 441 (1963); J. Am. Chem. Soc. **85**, 1528 (1963); M. M. GREEN. Top. Stereochem. **9**, 35 (1976).
28. H. O. HOUSE and V. KRAMER. J. Org. Chem. **28**, 3362 (1963); H. O. HOUSE, L. J. CZUBA, M. GALL, and H. D. OMSTEAD. J. Org. Chem. **34**, 2324 (1969).
29. H. FAVRE and A. J. LISTON. Can. J. Chem. **47**, 3233 (1969); R. BUCOURT. Top. Stereochem. **8**, 159 (1974).
30. L. E. SMITH and G. F. ROUALT. J. Am. Chem. Soc. **65**, 631 (1943).
31. J. A. ATTENBURROW, A. F. B. CAMERON, J. H. CHAPMAN, R. M. EVANS, B. A. HEMS, A. B. A. JANSEN, and T. WALKER. J. Am. Chem. Soc. **74**, 1094 (1952).
32. D. F. ZINKEL. J. Chromatogr. **29**, 382 (1967).
33. J. R. SCHAEFFER and A. O. SNODDY. Org. Syn. Coll. Vol. IV. J. Wiley, New York, NY. 1963. p. 19.

Decomposition of tetramethyl-2-tetrazene under acidic conditions

LEON J. MADGZINSKI, K. SOMASEKHAREN PILLAY, HERVÉ RICHARD, AND YUAN L. CHOW
Department of Chemistry, Simon Fraser University, Burnaby, B.C., Canada V5A 1S6

Received December 12, 1977

LEON J. MADGZINSKI, K. SOMASEKHAREN PILLAY, HERVÉ RICHARD, and YUAN L. CHOW. Can. J. Chem. **56**, 1657 (1978).

Decompositions of tetramethyl-2-tetrazene (TMT) under acidic conditions were investigated by product analysis and by nmr and esr spectroscopic monitors. Photolysis in acetonitrile containing trifluoroacetic acid generated the dimethylaminium radical which added efficiently to an olefinic double bond. Some adducts contained a $(CH_3)_2NCH_2$— moiety, the immediate precursor of which could be $CH_2{=}N(CH_3)_2^+$ species. Photolytic addition of TMT to norbornenes generated 2-norbornyl radicals that underwent coupling through the *exo* or *endo* side to give the dimers. Thermal decomposition in sulfuric acid in the presence of toluene gave *N*,*N*-dimethyltoluidines, *N*-methylphenethylamine, benzyltoluenes, and a plethora of other minor products in addition to a large amount of formylidene methylamine. The last compound was the major product when thermal decomposition of TMT was carried out in trifluoroacetic acid in the presence of toluene or anisol; amination products of aromatic substrates were low and contained only *ortho* and *para* isomers. TMT dissolved in these solvents exhibited the esr signal of the stable $TMT^{\ddagger}$ (the tetrazene cation radical) which did not react with cyclohexene. In concentrated sulfuric acid, TMT was decomposed in less than 15 min giving formylidene methylamine and dimethylamine as shown by nmr. In trifluoroacetic acid, the esr signal of tetramethylhydrazine cation radical ($TMH^{\ddagger}$) emerged after the TMT solution was irradiated; no dimethylaminium radical signal could be detected. The relationship of $TMT^{\ddagger}$ and $TMH^{\ddagger}$ with formation of the observed products remains unclear.

LEON J. MADGZINSKI, K. SOMASEKHAREN PILLAY, HERVÉ RICHARD et YUAN L. CHOW. Can. J. Chem. **56**, 1657 (1978).

On a étudié, à l'aide de l'analyse des produits et par études spectroscopiques rmn et rpe la décomposition de la tétraméthyltétrazène-2 (TMT) dans des conditions acides. La photolyse dans l'acétonitrile contenant de l'acide trifluoroacétique conduit à la formation de radical diméthylaminium qui s'additionne d'une façon efficace à la double liaison oléfinique. Quelques produits contenaient une portion $(CH_3)_2NCH_2$— dont le précurseur immédiat serait l'espèce $CH_2N(CH_3)_2^+$. L'addition photolytique du TMT aux norbornènes conduit à des radicaux norbornyl-2 qui subissent des couplages par les faces *exo* ou *endo* pour conduire à des dimères. La décomposition thermique dans l'acide sulfurique en présence de toluène conduit aux *N*,*N*-diméthyltoluidines, à la *N*-méthylphénéthylamine, aux benzyltoluènes et à toute une série d'autres produits mineurs en plus d'une grande quantité de formylidène méthylamine. Ce dernier composé est le produit majeur lorsque la décomposition thermique du TMT est effectuée dans l'acide trifluoroacétique en présence du toluène ou d'anisol; les produits d'amination des substrats aromatiques sont faibles et contiennent uniquement les isomères *ortho* et *para*. Lorsque le TMT est dissous dans ces solvants, il présente un signal rpe correspondant à l'entité $TMT^{\ddagger}$ (le radical cation tétrazène) qui ne réagit pas avec le cyclohexène. Dans l'acide sulfurique concentré, le TMT se décompose en moins de 15 minutes pour conduire à la formylidène méthylamine et à la diméthylamine tel que montré par le spectre rmn. Dans l'acide trifluoroacétique, le signal rpe du radical cation tétraméthylhydrazine ($TMH^{\ddagger}$) peut être observé lorsque l'on irradie la solution de TMT; on n'a pu détecter aucun signal correspondant au radical diméthylaminium. La relation qui existe entre la nature des produits observés et la formation de $TMT^{\ddagger}$ et le $TMH^{\ddagger}$ demeure confuse.

[Traduit par le journal]

Introduction

The presence of the thermally (1, 2) and photolytically (2–4) labile azo linkage has attracted many workers to investigate decomposition of tetraalkyl-2-tetrazene in expectation to observe reactive intermediates centered at the amine nitrogen. Most of the investigations were carried out with tetramethyl-2-tetrazene (TMT) from which formylidene methylamine ($CH_2{=}NCH_3$) or its derivatives (e.g., the trimer **1**, *N*,*N*′,*N*″-trimethylhexahydrotriazine, or the hydrolysis products, methylamines and formaldehyde) are invariably the major products isolated (5–8). A number of mechanisms proposed so far may be summarized as shown in eqs. [1–3] (6, 8–10).

Thermolysis or photolysis of TMT to generate the dimethylamine radical (eq. [1]) has been proven by the recording of the esr signal of the radical (3, 4). TMT decomposition in dilute acidic solution produces equimolar yields of nitrogen, formaldehyde, and methylamine from which $TMT{-}H^+$ is proposed

Can. J. Chem. Downloaded from www.nrcresearchpress.com by 210.87.254.42 on 09/05/12
For personal use only.

Can. J. Chem. Downloaded from www.nrcresearchpress.com by 210.87.254.42 on 09/05/12
For personal use only.

to decompose by an ionic process giving the nitrenium ion as in eq. [2] (or its ion pairs with the existing anions) (8, 9). However, other investigators also suggest an intramolecular cyclic proton transfer to account for the decomposition (10). In concentrated sulfuric acid the diprotonated tetraphenyl-2-tetrazene is suggested to homolytically decompose to yield diphenylaminum radicals (11). This leads to speculation that TMT might be homolytically decomposed to the two aminium radicals in concentrated sulfuric acid as shown in eq. [3]. As the observed products could be rationalized equally satisfactorily with aminium radical or nitrenium ion, mechanisms of TMT decomposition remain an open question.

Investigations utilizing esr spectroscopy show that treatments of TMT with alkylating or acylating agent in acidic conditions give the fairly persistent radical cations $TMT^{\ddagger}$ and $TMH^{\ddagger}$ (tetramethylhydrazine), the formations of which have been suggested to involve an electron transfer (oxidation) to aminium radicals (6, 7). Whether these two radicals participate in the subsequent reactions is obscure. The complex reaction patterns of TMT decomposition are further shown by isolation or detection (by esr) of various by-products that are not readily explained by the straightforward mechanisms of eqs. [1–3] (1,

$$[1]\quad (CH_3)_2NN{=}NN(CH_3)_2 \xrightarrow[\Delta]{h\nu \text{ or}} 2(CH_3)_2N\cdot + N_2$$

$$[2]\quad \underset{(TMT\text{–}H^+)}{(CH_3)_2NN{=}\overset{+}{N}NH(CH_3)_2} \xrightarrow{\text{dil. } H^+} (CH_3)_2N^+ + (CH_3)_2NH_2{}^+ + N_2$$

$$[3]\quad TMT\text{–}2H^+ \xrightarrow{\text{conc. } H_2SO_4} 2(CH_3)_2NH^{\ddagger} + N_2$$

6). It appears that heterolysis or homolysis are not the only possible TMT reactions but electron transfer reactions might also occur either as a part of or independently from the reaction.

Provided conditions can be found, acidic decomposition of TMT may be regarded as a clean way to generate two entities of the dimethylaminium radical (eq. 3). Reactivities of aminium radicals have been established to undergo highly specific inter- and intramolecular (the Hofmann–Löeffler type) H-abstraction, addition to olefinic bonds, electrophilic substitution on activated aromatic rings, and α-hydrogen elimination (12–15). It is envisaged that such reactions might give us a clue to the nature of the reactive intermediates in TMT decompositions. We wish to report here the photochemical and thermal decompositions of TMT under acidic conditions.

Photolysis of TMT in Trifluoroacetic Acid – Acetonitrile Solution

Decompositions of TMT in dilute acidic solutions, e.g., 1 *M* hydrochloric acid or trifluoroacetic acid in methanol or acetonitrile, at 0°C was very slow but became faster at room temperatures and higher. In these thermal decompositions, high yields of the trimer of formylidene methylamine **1** were obtained either in the absence or presence of an olefin; basic products incorporating the olefinic molecule were not detected.

When an acetonitrile solution of TMT containing trifluoroacetic acid and cyclohexene was photolysed under an inert atmosphere, a complex mixture was obtained from the basic extract. By direct matching of the vpc peaks with authentic samples, dimethylaminocyclohexane (**4**, 17%),[1] dimethylaminocyclo-

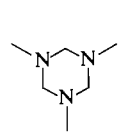

1

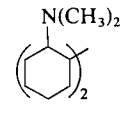

2

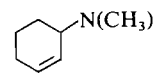

3

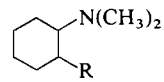

4 R = H
5 R = $CH_2N(CH_3)_2$
6 R = $N(CH_3)_2$
7 R = Cl

hexene (**3**, 8.5%), *trans*-1,2-bisdimethylaminocyclohexane (**6**, 1.2%), bis-2-dimethylaminobicyclohexyl (**2**, 1.4%), and *trans*-2-dimethylaminomethyl-1-dimethylaminocyclohexane (**5**, 16%) and the corresponding *cis*-isomer of **5** (4.1%) were identified. In the presence of hydrochloric acid, instead of trifluoroacetic acid, the TMT photolysis afforded, in addition to the above products, unstable *cis*- and *trans*-1-dimethylamino-2-chlorocyclohexanes **7**. In this case, **2** and **7** were isolated by column chromatography and *trans*-**5** by preparative vpc. In both experiments, trimer **1** was also isolated as the major product.

The reasonably good yields of dimethylaminocyclohexyl derivatives indicate that the dimethylaminium radical is generated as the reactive intermediate and attacks cyclohexene fairly efficiently in agreement with the photoadditions of *N*-nitrosamines (12), *N*-chloramines (13, 15), and *N*-nitroamines (16) to olefins. In the present case, the photolabile species presumably is the monoprotonate TMT ($TMT\text{–}H^+$,

[1]All the percentage yields were calculated on the basis of 1 mol of TMT to yield 1 mol equiv. of the products.

Can. J. Chem. Downloaded from www.nrcresearchpress.com by 210.87.254.42 on 09/05/12
For personal use only.

pK_a 3.9) which has λ_{max} 239 nm (6, 8) and is dissociated to give two dimethylaminium radicals and nitrogen. In contrast, thermolysis of TMT under similar conditions does not yield the addition products indicating that the aminium radical is not generated.

The complexity of the product patterns might arise from the lack of a good counter radical donor or from low concentrations of radicals to react with the dimethylaminocyclohexyl radical intermediate which may undergo dimerization or disproportionation to yield **2**, **3**, and **4**. TMT and other nitrogen containing bases are protonated under the experimental conditions, and are expected to be poor hydrogen atom donors owing to electrostatic repulsion of cationic charges. The $CH_2N(CH_3)_2$ moiety of **5** and chlorine of **7** could be derived from $CH_2{=}N(CH_3)_2$ or $(CH_3)_2NCH_2\overset{+}{N}H(CH_3)_2$ (1) and hydrogen chloride, respectively, but their incorporations by radical mechanisms find no precedence. It is suspected that electron transfer reactions also intervene in the radical processes leading to incorporation of these ionic species into the overall reaction (*vide infra*). In view of the formation of both *cis* and *trans* isomers for **5** and **7**, a purely ionic route, e.g., a nitrenium ion attack to give the aziridinium intermediate, can hardly be a rational alternative. It follows that the observed complexity of products might be avoided if the cyclohexyl radical intermediate is captured with a good radical donor; indeed under oxygen the cyclohexyl radical is efficiently scavenged to give good yields of the 1-dimethylamino-2-hydroperoxycyclohexane (17). Although TMT photoaddition to cyclohexene under nitrogen is not a synthetically useful reaction, those to other olefins, such as norbornene and 1,5-cyclooctadiene, give more amenable results.

In the presence of norbornene, similar TMT photolysis in acetonitrile–TFA gave monomer and dimeric adducts in a ratio of 1:10; the former was assigned as *exo*-2-dimethylaminobicyclo[2.2.1]heptane **9** by comparisons of the ir and nmr data with those published (18). The four dimers were adducts of 1 molecule of TMT to 2 molecules of norbornene less N_2 as shown by gc–ms analysis.[2] Two major components were isolated in the pure state and were shown to be 2-*endo*-(3′-*exo*-dimethylaminobicyclo[2.2.1]hept-2′-*endo*-yl)-3-*exo*-dimethylaminobicyclo[2.2.1]heptane (**10**, 16%) and 2-*endo*-(3′-*exo*-dimethylaminobicyclo-

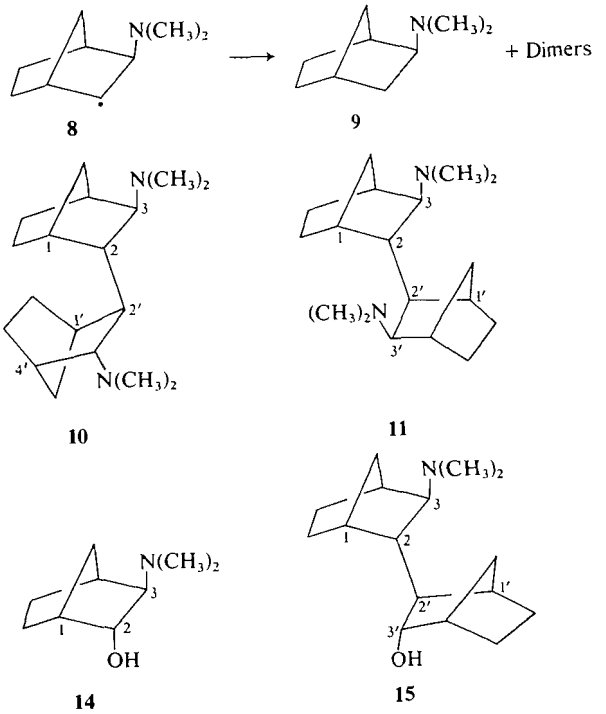

[2.2.1]hept-2′-*exo*-yl)-3-*exo*-dimethylaminobicyclo-[2.2.1]heptane (**11**, 22%). The former is readily proven by the eight ^{13}C nmr signals[2] owing to the presence of the plane of symmetry; the alternative all *exo*-configuration was unlikely since aminium radical initiated addition to norbornene generally gave *trans* configuration as the major product (19). The highly symmetrical structure of **10**, and therefore a low dipole moment, was suggested by its insolubility in methanol and solubility in hexane in contrast to the solubility behavior of **11**. The ^{13}C nmr data obtained by the off-center decouplings were particularly useful in assignments of the stereochemistry. Some assignments of the proton and ^{13}C nmr were ascertained by comparisons with the reported chemical shifts of substituted norbornanes (20) and by single frequency irradiation of proton signals in relation to the ^{13}C spectral changes;[2] for comparisons, two norbornyl derivatives **14** and **15** (17) are also included in Table 1. The relatively low field of the C-7 at 37.3 ppm and the high field of the C-6 at 23.2 ppm indicated an *endo* and *exo* substitution at the C-2 and C-3 in **10** (20). If the $(CH_3)_2N$— groups were *endo*, the shift at C-5 would be in the order of 20 ppm instead of the observed 28.5 ppm. Dimer **11** exhibited a one-proton double doublet at τ 7.56 with the coupling constants of 8.5 and 1.5 Hz assignable to the C-3 *endo*-proton geminal to the $N(CH_3)_2$ group. The coupling pattern clearly indicated a 2,3-*cis* configura-

[2]These and other spectra and decoupling techniques are given in the Thesis by L. J. Madgzinski (ref. 17). The conditions and operation of vpc analyses are also described in the same reference.

Can. J. Chem. Downloaded from www.nrcresearchpress.com by 210.87.254.42 on 09/05/12
For personal use only.

TABLE 1. ^{13}C nuclear magnetic resonance chemical shifts (in ppm from TMS) of the dimer **10** and **11** and related compounds

Carbon position	10	11	14	15
1 + 1′	35.3	25.0 34.2	42.5	33.4 33.4
2 + 2′	40.0	40.0 39.0	78.2	39.9 37.4
3 + 3′	74.9	76.6 71.9	76.6	77.1 82.7
4 + 4′	46.9	45.5 53.2	39.0	47.6 53.0
5 + 5′	28.5	28.4 30.3	28.4	29.2 20.5
6 + 6′	23.2	23.0 29.2	19.4	22.7 27.1
7 + 7′	37.3	37.2 35.0	34.3	34.3 34.3
$N(CH_3)_2$	42.4	43.0 44.8	43.6	44.0

tion of the substitutions on the norbornene system. The other C-3 proton appeared at τ 7.43 as a multiplet. Since the ^{13}C nmr spectrum showed all 16 signals indicating the molecular dissymmetry, structure **11** was assigned. Comparisons of ^{13}C nmr chemical shifts as shown in Table 1 also supported the assignments of structure **10** and **11**. It was noteworthy that for **11** the C-5′ and C-6′ resonated at relatively low fields in comparison to the C-5 and C-6 chemical shifts in agreement with the assignment of the *cis-exo* configuration to one-half of the molecule (20). Two other dimers resisted various efforts of purification methods. In this photolysis, trimer **1** was also obtained in a 40% yield.

In the presence of 1,5-cyclooctadiene (COD), TMT photolysis under similar conditions yielded two compounds which were identified as 5-dimethylaminocyclooctene (**12**, 32%) and 2-*exo*-dimethylamino-6-*exo*-dimethylaminomethyl-*cis*-bicyclo[3.3.0]octane (**13**, 12%). No material was extracted from the acidified photolysate. The structural assignments of **12** and **13** followed readily from their spectral properties and the elemental analyses. The *exo* configuration of the 2-dimethylamino group in **13** was indicated by the double triplet signal at τ 6.40 in the nmr spectrum of the dimethiodide of **13**; this proton must have one *cis*-vicinal interaction (J = 8.5 Hz) and two *trans*-vicinal interactions (J = 6 Hz) in a cyclopentane ring (21). The *cis*-ring fusion as well as the *exo* configuration of the $(CH_3)_2NCH_2$— group were derived from the favored stereochemical course of a radical addition to a COD ring (22).

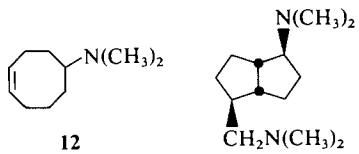

12 13

The relatively simple product pattern in the photoaddition to COD may indicate that COD is a better hydrogen donor than cyclohexene as shown by the higher yield of **12**. The transannular ring closure immediately after the aminium radical attack on COD has ample analogies (22–24) in radical addition reactions but the precursor of the $CH_2N(CH_3)_2$ moiety in **13** poses the same question as mentioned above.

The extensive formation of dimeric compounds (>75%) in contrast to the low yield of **9** in the TMT photoaddition to norbornene under nitrogen is surprising. The stereochemistry of the major dimers **10** and **11** suggests that the dimers are formed by coupling of the norbornyl radicals **8** rather than by a stepwise addition of **8** to norbornene followed by a combination with a dimethylaminium radical. For if the latter occurs, an *endo-endo* connection and an *exo-exo*-dimethylamino orientation to norbornene rings, such as in **10**, would not constitute the major products (19). This has led us to conclude that the norbornyl radical **8** has reasonable concentration, and therefore a reasonable life-time in the reaction system presumably owing to the fact that there is no good H-atom donor in the system. It is known that 2-norbornyl radicals do not have a resonance stabilization similar to that of 2-norbornyl cation (25). In theory, the *endo-endo* coupling of **8** would give a *dl* pair and *meso* isomers and the *endo-exo* coupling two *dl* pairs. From the ^{13}C nmr spectrum, dimer **10** is the *endo-endo meso* isomer. The dimer **11** and two unidentified dimers might be the *dl* pairs.

TMT photoaddition to dicyclopentadiene **16** and 5-vinylnorbornene **17** were also investigated. In methanol solution containing TFA, the photoaddition to **16** gave two monomeric adducts **18** (35%) and a mixture of dimeric adducts **19** (40%) in addition to five minor components. These two groups of closely related isomers showed overlapped peaks in attempted vpc separation and were isolated and identi-

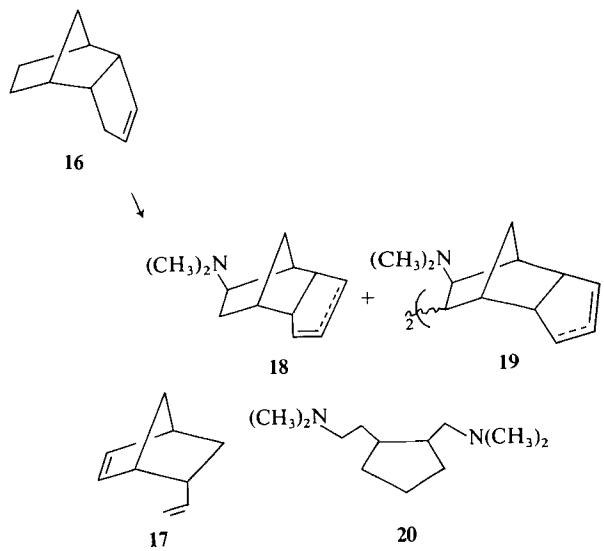

Can. J. Chem. Downloaded from www.nrcresearchpress.com by 210.87.254.42 on 09/05/12
For personal use only.

fied as mixtures. The relatively high yields of monomeric adducts **18** obviously arises from the better hydrogen atom donating solvent, methanol, to intercept the C-radical intermediate. Despite careful analysis of the products, compounds derived from cyclization were not detected in the basic products. TMT photoaddition to **17** in acetonitrile gave at least four dimeric adducts similar to **19** as the major product in 70% yield in addition to many monomeric adducts as shown by gc–ms analysis. The initial attack of the dimethylaminium radical occurred nearly exclusively at the norbornyl double bond as indicated by the strong vinyl proton signal in the nmr spectrum of the crude products. The nmr analysis of the same chromatographic fractions containing the minor products show that tricyclic adducts resulting from cyclization might be formed in small quantities; attempts to isolate these minor products were unsuccessful.

Photoaddition of TMT to 1,6-heptadiene yielded cyclized diamine **20** as the major product which could not be easily extracted due to the solubility in water. The cyclization to a five-membered ring system was inferred in analogy to the radical addition of C_3F_7I to the olefin (26) and the structure was supported by ^{13}C nmr and mass spectra; in both cases the incorporation of an extra methylene group was clearly indicated. In view of the clean ^{13}C nmr spectrum, this sample must contain only one geometric isomer of **20** though the *cis* or *trans* stereochemistry could not be determined.

Spectroscopic Studies of TMT Decomposition

To gain insight on the TMT decomposition under acidic conditions, the decomposition processes were monitored with nmr and esr spectroscopy. While some of these results supported the published reports, there were other observations that could not be conclusively related to the proposed mechanism.

Controlled dissolution of TMT in concentrated sulfuric acid at 0°C caused immediate evolution of nitrogen giving rise to $(CH_3)_2NH_2^+$ (at τ 7.10) and $CH_3NH{=}CH_2^+$ (at τ 6.27 and 1.93) in an equimolar ratio with a small signal of TMH–$2H^+$ at τ 6.40. The nmr signals for TMH–$2H^+$ decayed slowly at 20°C but rapidly at 100°C to be replaced by the signals of the former two species. Although no nmr signal of TMT–H^+ could be detected, this solution exhibited a weak esr signal for $TMT^{\ddagger}$ (6, 7, 27) which decayed slowly over several days giving no new signal.

Solutions of TMT in TFA or in 1 *M* TFA-acetonitrile-d_3 showed the nmr singlets for TMT–H^+ at τ 6.62, 6.82, and 6.92 with the ratio of 1:1:2 at −15°C in analogy to those of the hydrochloride salt of TMT (27). The signals were broadened at 10°C and at 30°C coalesced to the singlet at τ 6.78 which decayed to be replaced by the signals of $(CH_3)_2NH_2^+$ and $CH_3NH{=}CH_2^+$ in an equimolar amount. Irradiation of the TMT–H^+ solution in TFA at 0°C gave the nmr signals of these two species in addition to a weak TMH–H^+ signal at τ 7.14 and other unidentified signals. However irradiation in the TFA–acetonitrile solution gave a complex nmr spectrum.

A TMT solution in TFA–acetonitrile exhibited a strong esr signal for the $TMT^{\ddagger}$ (6, 7) at room temperature or lower with *g*-factor 2.0040 ± 0.0005, a_N = 1.15 (2N), a_N = 10.85 (2N), a_H = 10.40 (6H) and a_H = 10.60 G (6H). This signal persisted for days at −45°C but decayed rapidly in 2 h at room temperature with no appearance of new signals. This solution was irradiated at 25°C without a filter; on interruption of irradiation an esr signal for $TMH^{\ddagger}$ (a_N = 13.2, a_H = 12.7 G and *g*-factor = 2.0039 ± 0.0006) (6) built up rapidly in 5 min and decayed slowly in 1 h. The interruption of irradiation at −45°C generated the persistent esr signals of $TMH^{\ddagger}$ superimposed with a weaker signal of $TMT^{\ddagger}$. Addition of cyclohexene to this solution at −45°C caused immediate disappearance of the $TMH^{\ddagger}$ signal but the $TMT^{\ddagger}$ remained unchanged.

Ubiquitous presence of the persistent $TMT^{\ddagger}$ signal in these experiments indicates that this radical is unreactive even to an olefin. TMH has been proposed to be formed by dimerization of the dimethylamino radicals in the treatment of TMT with acylation or alkylation agents (6, 7). The corresponding $TMT^{\ddagger}$ and $TMH^{\ddagger}$ radicals are suggested to be formed by oxidation using the aminium radicals as the electron acceptor (7). Under the present photolytic conditions, the $TMH^{\ddagger}$ might be formed as shown in eqs. [4–7]. However, neither in the reported (6, 7) nor in the present experiments, the esr signals of the aminium radicals could be detected presumably due to fast reactions of eqs. [5–7]. The lack of

$$\text{TMT–H}^+ \xrightarrow[\text{H}^+]{h\nu} 2(\text{CH}_3)_2\text{NH}^{\ddagger} + \text{N}_2 \quad [4]$$

$$2(\text{CH}_3)_2\text{NH}^{\ddagger} \rightarrow \text{TMH–H}^+ + \text{H}^+ \quad [5]$$

$$\text{TMH–H}^+ + (\text{CH}_3)_2\text{NH}^{\ddagger} \rightarrow \text{TMH}^{\ddagger} + (\text{CH}_3)_2\text{NH}_2^+ \quad [6]$$

$$\text{TMT–H}^+ + (\text{CH}_3)_2\text{NH}^{\ddagger} \rightarrow \text{TMT}^{\ddagger} + (\text{CH}_3)_2\text{NH}_2^+ \quad [7]$$

the $TMH^{\ddagger}$ esr signal during irradiation might arise from photolability of this radical which is consumed as it is formed. The appearance of $TMH^{\ddagger}$ esr signal after interruption of photolysis suggests that a precursor decomposes thermally to generate the dimethylaminium radicals which undergo reactions [5] and [6]. Such a precursor could be the *cis* form of the TMT–H^+ in analogy to the thermally unstable *cis*-

Can. J. Chem. Downloaded from www.nrcresearchpress.com by 210.87.254.42 on 09/05/12
For personal use only.

tetraisopropyl-2-tetrazene reported previously (4). If so, the photoexcitation serves to isomerize the *trans* form to the *cis* form of TMT–H^+. The formation of TMH in the decomposition in sulfuric acid might also indicate the intermediacy of the dimethylaminium radical under the conditions.

While the $TMH^{\ddagger}$ was demonstrably reactive toward cyclohexene, its role in the observed photoaddition could not be ascertained since photolysis of TMH under the same conditions as those used in the TMT photoaddition to cyclohexene did not give addition products. The quantity of $TMT^{\ddagger}$ and $TMH^{\ddagger}$ generated in the decomposition is reported (6) to be very low; the reaction of eqs. [4–7] are probably not the major reaction pathway.

When TMT was added to a 1:1 mixture of cyclohexene–acetonitrile containing TFA, two layers developed: the top cyclohexene layer exhibited a poorly resolved $TMT^{\ddagger}$ esr signal which decayed in 45 min to be replaced by a signal at $g = 2.0024 \pm 0.0004$ with 17 major bands. This signal is tentatively assigned to *N,N,N'*-trimethyldiaminomethyl radical, $(CH_3)_2\dot{N}CHNHCH_3$, on the basis of a computer simulated spectrum using the coupling constants of known α-aminoalkyl radicals (28, 29). The sequence of the spectral formation suggests that $TMT^{\ddagger}$ decomposition is related to the formation of the radical. However, the mechanism remains to be clarified.

Thermal Decomposition of TMT in Concentrated H_2SO_4

N-Chlorodimethylamine has been decomposed in concentrated sulfuric acid thermally, photolytically or catalysed with ferrous, cuprous, or titanous ion in the presence of toluene (15, 30). *N,N*-Dimethyltoluidines are obtained in these reactions in which unusually high yields (5 ~ 54%) of the *meta* isomers are interpreted by a radical mechanism involving dimethylaminium radical as the reactive species (15). Since the aminium radicals generated from *N*-nitrosamine photolysis in 0.1 *M* HCl in methanol fail to give toluidine derivatives (12), high acidity media, such as concentrated H_2SO_4 or mixtures with AcOH, appear to be necessary to stabilize the dimethylaminium radical so that it has a sufficiently long lifetime to successfully attack toluene. As shown above, TMT decomposition in H_2SO_4 also suggests dimethylaminium radical intermediacy; the decomposition in the presence of toluene was therefore investigated.

At the beginning, the reaction of *N*-chlorodimethylamine with toluene in sulfuric acid was repeated according to the procedure of Bock and Kompa (30) from which 35% of toluidines **21** with an *ortho*:*meta*:*para* ratio of 9:61:30 was obtained; previously unisolated *o*- and *p*-benzyltoluenes (**22**) were also isolated in 8% yield from the neutral fraction. These samples were used to establish an efficient analytical procedure by vpc and gc–ms methods as described in the Experimental section. A heterogeneous mixture of TMT, toluene, and concentrated sulfuric acid was allowed to react at room temperature or lower with vigorous stirring from which large amounts of polymeric material containing aromatic rings and dimethylamino groups were obtained. The yields of toluidines **21** ranged 5 ~ 23% with a typical *ortho*:*meta*:*para* ratio of 15:10:75; the ratio however fluctuated considerably and could not be reproduced. The yields were ca. 5% for several hours reaction but increased significantly after 20 h. From the neutral fractions, about 10% of *o*- and *p*-benzyltoluenes (**22**) with a ratio of 4:6 and a trace amount of bibenzyl were also identified.

In the basic fractions, in addition to toluidines **21** and the trimer **1**, minor amounts of *N*-methylphenethylamine (**23**), *N,N*-dimethylbenzylamine (**24**), *N*-methylindoline (**27**), *N,N*-dimethylphenethylamine (**25**), and *p-N*-methyltoluidine (**26**) were also detected by the peak matching method with authentic samples (31). The identity of these compounds were further supported by gc–ms analyses. However, when the reaction was carried out at 80°C for 15 min, the yields of toluidines **21** decreased to 1–2% and those of phenethylamines **23** and **25** increased to 30 and 8%; *o*- and *p*-benzyltoluenes **22** were also formed in 10% in this reaction.

Since the above nmr results indicate that TMT on dissolution in concentrated sulfuric acid decomposes within several minutes, the phenethylamines **23** and **25** and benzyltoluenes **22**, but not toluidine **21**, appear to be formed within this time scale. In a prolonged decomposition, phenethylamines **23** and **25** are presumably decomposed to the polymers and toluidines **21** are formed from a slow reaction of an aminating species attacking on toluene. Assumption that TMH—$2H^+$ in sulfuric acid reversibly generates the dimethylaminium radical in a slow dissociation could not be substantiated since TMH under the same conditions does not react with toluene: the identity of the aminating species remains obscure.

At the present stage, mechanistic interpretations of other basic product formation involve many uncertainties and not warranted. However, lack of *m*-benzyltoluene in the TMT as well as *N*-chlorodimethylamine reaction products implies that the *ortho* and *para* isomers are formed by an electrophilic attack of the benzyl cation on toluene. As the benzyl radical intermediacy is also suggested by the small amounts of bibenzyl in the products, both radical and ionic processes are suspected to operate in

Can. J. Chem. Downloaded from www.nrcresearchpress.com by 210.87.254.42 on 09/05/12
For personal use only.

the decomposition. Both phenethylamine **23** and **25** are expected to be formed from a benzyl moiety reacting with $CH_2{=}NHCH_3^+$ and $CH_2{=}N(CH_3)_2^+$. An analogy to such a reaction is the reverse pathway of the fragmentation of the N-methylphenethylaminium radical (31) which also serves as the precursor to indoline **27** (15).

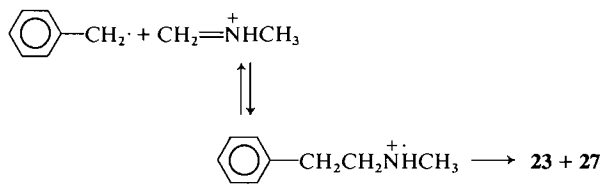

Decompositions of TMT in toluene–TFA (ratio of 0.7:7:4) were also carried out under similar conditions as above to give the trimer **1** as the major product; toluidine **21** was obtained in only *ca.* 2% yields with the *ortho*:*para* ratio of 60:40 but the *m*-toluidine **21** was not obtained. Neither the basic products **23**–**27** nor benzyltoluenes **22** were obtained. The decomposition pattern in TFA is thus much simpler and probably does not involve a dimethylaminium radical. In view of the high ratio of the *o*- to *p*-toluidine and lack of the *m*-toluidine, it is tempting to suggest an electrophilic attack of the nitrenium ion on toluene: similar products patterns have been reported in the nitronium and isopropyl carbonium ion attacks on toluene (32, 33). Decomposition of TMT in a mixture of anisole and TFA gave ca. 10% of *N*,*N*-dimethylanisidine with an *ortho* and *para* isomeric ratio of 2:1. The low yield of the amination product might arise from a rapid proton migration of nitrenium ion to $CH_2{=}NHCH_3$ which could account for the clean formation of the trimer **1** in the TFA decomposition. Such a reaction finds analogies in the rapid rearrangement of methylnitrene (34) and deprotonation of isopropylcarbonium ion (35). However, attempts to intercept the dimethylnitrenium ion with cyclohexene did not give the expected addition products.

The decompositions of TMT discussed above display complex patterns probably owing to concurrence of many side reactions. With the exception of photolysis of TMT—H^+ to generate the dimethylaminium radical, no clear mechanistic conclusion can be made on the thermolysis of TMT in acidic conditions.

Experimental

Unless otherwise specified, the following conditions were used. The ir spectra were recorded with a Perkin-Elmer 457 spectrophotometer as liquid films or Nujol mulls, uv spectra with a Unicam SP 8000 spectrophotometer, mass spectra with a Hitachi-Perkin-Elmer RMU-6E instrument at 80 eV (peak intensity was given as a percentage of the most intense peak), esr spectra with a Varian E-4 EPR spectrometer using a flat quartz Varian E-248 aqueous solution sample cell and diphenylpicrylhydrazyl radical as the external standard, and the nmr spectra with either a Varian A 56/60 or a Varian XL-100 instrument equipped with a Nicolet 1080 computer in CCl_4 or $CDCl_3$ using TMS as internal standard or in H_2SO_4 or CF_3COOH using the dimethylammonium ion signal (τ 7.10) as the internal standard. The gas chromatographic (vpc) analyses were obtained on an F & M Model 810-19 dual flame analytical instrument using a Varian Aerograph Model 20 strip chart recorder equipped with a Model 224 disc chart integrator with a 10% Carbowax 20M on Chromosorb W 100/120 (10 ft × $\frac{1}{16}$ in.) stainless steel column. Preparative vpc separations were performed on a Varian Aerograph Series 1700 thermal conductivity instrument with a 25% Carbowax 20M on Chromosorb W 60/80 (10 ft × $\frac{1}{4}$ in.) stainless steel column and the gc–ms were done on a 5% Carbowax 20M on Chromosorb W 100/120 (6 ft × $\frac{1}{8}$ in.) glass column in a Varian 1400 instrument which was directly coupled to the mass spectrometer.

Preparation of Tetramethyl-2-tetrazene (TMT) and Tetramethylhydrazine (TMH)

The procedure of Watson (1) was slightly modified to give better yields. HgO (158 g, 0.74 mol) was added slowly over 2 h to a stirred solution of dimethylhydrazine (50 ml, 0.66 mol) in ether (400 ml) at −5°C. Solid K_2CO_3 (10 g) was then added and the mixture stirred for 2 h more at −5°C, then 2 h at room temperature. The mixture was filtered, the ether was removed, and the resulting yellow liquid (34.2 g) was distilled to give TMT as a pale yellow liquid (29.5 g, 78%); bp 42°C/28 Torr; uv λ_{max} (ethanol): 277 nm (ε, 8 × 10^3); nmr τ:7.19 (s). The mercury was collected, washed with water, and dried (107 g, 82%).

TMH was prepared as described by Watson (1): nmr τ:7.14 (s) for TMH—H^+ in CF_3CO_2H and 6.40 for TMH—$2H^+$ in H_2SO_4.

Photolysis of TMT under Nitrogen

In the Presence of Cyclohexene

A solution of TMT (4.8 g), cyclohexene (17 g), trifluoroacetic acid (32 g), and acetonitrile (320 ml) was made up in a photocell under a nitrogen atmosphere and was irradiated with a low pressure mercury lamp (Ultraviolet Products Inc.)[3] for 6 h. The residue from the photolysate was acidified with aqueous HCl and extracted to afford a small amount of the neutral fraction. The aqueous phase was basified with Na_2CO_3 and heated over a steam bath for 2 h. Ether extraction afforded the basic fraction (2.87 g).

The major products of the basic fraction were identified by gc analysis (20% Dowfax 9N9 – 10% TEP on Chromosorb) as dimethylaminocyclohexane (**4**, 13 min, 17%), 3-dimethylaminocyclohexene (**3**, 14.5 min, 8.5%), *trans*-diamine **6** (26 min, 1.2%), *trans*-**5** (29 min, 16%), *cis*-**5** (32 min, 4.1%), and **2** (40 min, 1.4%, *vide infra*).

In a separate experiment, the basified aqueous solution was not heated but was extracted to give the basic fraction from which imine trimer **1** was obtained in a 60% yield in addition to the above compounds. In this experiment, a portion of the zero hour sample was kept in the dark at 0 ~ 5°C for 3 days after which time the TMT uv absorption had disappeared. The usual work-up afforded a basic oil which was shown to contain

[3]In all other photolyses, except this case, a Hanovia lamp was used. In all experiments, the zero hour samples kept in the dark at 0°C were examined by uv spectroscopy at the end of the reaction showing no decrease of the intensity at 239 nm.

Can. J. Chem. Downloaded from www.nrcresearchpress.com by 210.87.254.42 on 09/05/12
For personal use only.

only the trimer **1** and showed no nmr signals due to a cyclohexane ring.

In the Presence of Norbornene

A solution containing TMT (3 g), norbornene (6.85 g), trifluoroacetic acid (23 g), and acetonitrile (200 ml) was prepared at 0°C and was photolysed under nitrogen for 2 h at 0°C. The solution turned to deep yellow within 15 min of irradiation but the color faded by the end of the photolysis. The basified aqueous solution was extracted to give the first basic fraction (2.68 g) and further continuously extracted to give the second basic fraction (300 mg). The latter contained only the imine trimer **1** as shown by the nmr signal at τ 6.78 and 7.79.

A part of the first basic fraction was chromatographed on basic alumina. Methylene chloride eluted 2-*endo*-(3′-*exo*-dimethylaminobicyclo[2.2.1]hept-2′-*endo*-yl)-3-*exo*-dimethylaminobicyclo[2.2.1]heptane (**10**) which was recrystallized, as white prisms; mp 165–171°C (sealed tube); ir: 2870, 2775, 1290, 1268, 1179, 1169, 1060, 1042, 1013, 850, and 714 cm^{-1}; ^1H nmr τ: 7.75 (s, 12H), 7.7–7.9 (m, 2H), 8.06 (m, $W_{\frac{1}{2}}$ = 4 Hz, 2H), 8.2–9.2 (m, 16H); ^{13}C nmr: 74.9(d), 46.9(d), 42.4(q), 40.0(d), 37.3(t), 35.3(d), 28.5(t), and 23.2(t); ms (80°C): 276.2561 (M^+, 10, calcd. for $C_{18}H_{32}N_2$: 276.2565), 261(100), 232(10), 218(10), 192.1749 (51, calcd. for $C_{10}H_{22}N$: 192.1753), 150(9), 138.1279 (9, calcd. for $C_9H_{16}N$: 138.1282). *Anal.* calcd. for $C_{18}H_{32}N_2$: C 78.20, H 11.67, N 10.13; found: C 78.25, H 11.58, N 10.13.

Elution with 1% MeOH in CH_2Cl_2 gave a mixture. Elution with 2% MeOH in CH_2Cl_2 gave a solid which was sublimed to give 2-*endo*-(3′-*exo*-dimethylaminobicyclo[2.2.1]hept-2′-*exo*-yl)-3-*exo*-dimethylaminobicyclo[2.2.1]heptane (**11**) as white needles; mp 67–72°C (sealed tube); ir: 2878, 2777, 1680, 1292, 1270, 1260, 1174, 1091, 1056, 1025, 1012, 942, 888, 848, and 760 cm^{-1}; ^1H nmr τ: 7.42 (m, $W_{\frac{1}{2}}$ = 10 Hz, 1H), 7.56 (d, J = 8 Hz, 1H), 7.65–7.85 (m, 2H), 7.76 (s, 12H), 8.16–8.22 (m, 16H); ^{13}C nmr: 76.6(d), 71.9(d), 53.2(d), 45.5(d), 44.8(q), 43.0(q), 40.0(d), 39.0(d), 37.2(t), 35.0(d and t), 34.2(d), 30.3(t), 29.2(t), 28.4(t), 23.0(t); ms: (80°C) 276 (M^+, 8), 261(100), 232(17), 218(17), 192(53), 152(26), 98(22), 84(53), and 58(43). Addition of 20% Europium(III) 2,2,6,6-tetramethylheptanedioate (Ventron Corp., Montreal) separated the low field protons showing at τ 7.43 (m) and 7.55 (dd, J = 8.5 and 1.4 Hz) and also two N—CH_3 singlets with 3 Hz spacing. *Anal.* calcd. for $C_{18}H_{32}N_2$: C 78.20, H 11.67, N 10.13; found: C 78.54, H 11.72, N 10.65.

The crude basic fraction showed five major vpc peaks with retention times (20% Dowfax 9N9 – 19% TEP on chromosorb P 60/80) of 25, 134, 143, 150, and 158 min in a ratio of 8:43:11:31:16. The first peak was isolated from the vpc analysis as oily dimethylaminobicyclo[2.2.1]heptane (**9**); *m/e*(%): 139 (M^+, 38), 124(8), 110(46), 98(38), 84(29), 71(33), and 58(100); ir: 2862(s), 2759(s), 1454(s), 1159, 1147(b), 1072(s), 1040(s), 1021(s), 930, 897, and 819 cm^{-1} (18). The other four peaks were due to the dimeric compounds and the 150 and 134 min peaks were shown to correspond to compounds **10** and **11**.

In a separate experiment under the similar conditions, 2.5 g of the basic fraction was obtained. Analysis by vpc showed the monomer to dimers ratio was 1:10 and the four dimers had a ratio of 40:10; 28:15 in the order of the retention times.

In the Presence of 1,5-Cyclooctadiene

A solution of TMT (4 g), 1.5-cyclooctadiene (4 g), trifluoroacetic acid (25 g), and acetonitrile (100 ml) was prepared in a photovessel at 0°C and was photolysed for 2 hs. Half of the photolysate was worked up to give a basic fraction (1.64 g) but no acidic fraction. The basic fraction gave two vpc peaks at 6.8 and 14.3 min in the ratio of 1.9:1. The mixture (1.48 g) was chromatographed on neutral alumina (75 g); elution with a 1:1 mixture of petroleum ether and ether gave a colorless oil (565 mg) which was distilled to 5-dimethylaminocyclooctene (**12**); ir: 3020, 2828, 2779, 1688(w), 1458, and 727 cm^{-1}; ms: 153 (M^+, 25), 138(5), 136(5), 125(18), 124(18), 110(25), 84(66), 71(100); nmr τ: 4.48 (m, 2H), 7.92 (s, 6H), 7.8–8.1 (m, 11H), 8.15–9.05 (bm, 6H). *Anal.* calcd. for $C_{10}H_{19}N$: C 78.37, H 12.50, N 9.14; found: C 78.15, H 12.36, N 9.49.

The picrate was recrystallized from ethanol: mp 153–167°C (dec.). *Anal.* calcd. for $C_{16}H_{22}N_4O_7$: C 50.26, H 5.80, N 14.65; found: C 50.76, H 5.97, N 14.70.

Further elution gave a mixture (122 mg). Elution with ether gave a colorless oil (266 mg) which was distilled (20°C/0.05 Torr) to give 2-*exo*-dimethylamino-6-*exo*-dimethylaminomethyl-*cis*-bicyclo[3.3.0]octane (**13**); ir: 2818, 2770(s), 1458(s), and 1040(s) cm^{-1}; ms: 210 (M^+, 30), 195(2), 166(22), 165(15) 152(10), 150(6), 137(7), 136(6), 126(23), 124(18), 110(11), 84(49), 71(32), and 58(100); nmr τ 7.74(s), 7.78(s). *Anal.* calcd. for $C_{13}H_{26}N_2$: C 74.23, H 12.46, N 13.36; found: C 74.18, H 12.43, N 13.42.

The dipicrate was recrystallized from ethanol; mp 217–221°C (dec.). *Anal.* calcd. for $C_{25}H_{32}N_8O_{14}$: C 44.91, H 4.82, N 16.76; found: C 44.78, H 4.84, N 16.60.

The dimethiodide was recrystallized from ethanol; mp 155 190°C (dec.): ms: (70°C) 210(4), 142(59), 127(18), 84(17), and 58(100); nmr τ 6.40 (dt, J = 8.5, 6.5, and 6 Hz, 1H), 6.64 and 6.75 (the AB part of a ABX, J_{AB} = 13.5, J_{AX} = 8.9, J_{BX} = 3.9 Hz), 6.99 (s, 9H), 7.04 (s, 9H), 7.32 (bm, 7H), 7.75–8.25 (bm, 7H), 8.30–8.83 (m, 3H). Irradiation at τ 7.93 collapsed the signals at 6.64 and 6.75 to an AB quartet ($\Delta\delta$ = 19 Hz, J = 13.5 Hz). Irradiation at τ 7.32 collapsed the dt at τ 6.40 signal to a double doublet (J = 8.5 and 6 Hz) and at 8.05 the same signal to a double doublet (J = 6.5 and 6 Hz). *Anal.* calcd. for $C_{15}H_{32}N_2I_2$: C 36.45, H 6.53, N 5.67; found: C 36.48, H 6.64, N 5.58.

In the Presence of Cyclohexene

A solution of TMT (3 g), cyclohexene (16 g), concentrated hydrochloric acid (15 ml), and acetonitrile (200 ml) was photolysed as above under nitrogen. The photolysate was worked up as usual to give neutral (22 mg) and basic (2.52 g) fractions. The crude basic fraction was analysed by vpc peak matching method on a 10% Carbowax 20M column to give the peaks of the imine trimer **1** (1.1 min) as the major component and minor peaks of 3-dimethylaminocyclohexene (**3**, 2.2 min), dimethylaminocyclohexane (**4**, 6.1 min), *trans*-chloroamine **7** (8.0 min), and *cis*-chloroamine **7** (9.0 min) (*vide infra*).

The basic fraction (2.5 g) was chromatographed on a silica gel column. With ether as the eluent, it gave what appeared to be a *bis*-dimethylaminodicyclohexane (**2**, 10 mg); ir: 2930(s), 2860, 2780, 1450, 1261, 1185, 1042(s), 805 cm^{-1}; ms: 252.2541 (M^+, 8, calcd. for $C_{16}H_{32}N_2$: 252.2565), 237.2307 (12, calcd. for $C_{15}H_{29}N_2$: 237.2330), 207.1966 (22, calcd. for $C_{14}N_{25}N$; 207.1987), 192.1724 (12, calcd. for $C_{13}H_{22}N$: 192.1752), 167(20), 149(24), 140(24), 125.1201 (36, calcd. for $C_8H_{15}N$: 125.1206), 84(100), and 71(46).

Continued elution with ether gave unstable *trans*-2-chlorodimethylaminocyclohexane (**7**, 285 mg, 7.1%) which was distilled to a pale yellow oil; nmr τ: 6.11 (dt, J = 4 and 10 Hz, 1H), 7.67 (s, 6H), and 7.65 (m, 1H); ms: 163.1011 (calcd. for $C_8H_{16}NCl$: 163.0942), 161.0944 (calcd. for $C_8H_{16}NCl$: 161.0972), 126.1280 (calcd. for $C_8H_{16}N$: 126.1282).

Elution with 10% CH_2Cl_2 in ether gave the *cis*-chloroamine 7 (59 mg, 1.5%); nmr τ: 5.43 (m, $W_{\frac{1}{2}}$ = 7 Hz, 1H), 7.67 (s, 6H), 7.75 (m, 1H); the mass spectrum was very similar to that of the *trans* isomer. With 20% CH_2Cl_2 in ether the imine trimer **1** was obtained.

The column was washed with 1 *N* HCl in methanol and the basic material (725 mg) was recovered. This material was ana-

Can. J. Chem. Downloaded from www.nrcresearchpress.com by 210.87.254.42 on 09/05/12
For personal use only.

lysed by vpc on a 20% Dowfax 9N9/10% TEP column by the peak matching method to give the following peaks: *trans*-diamine **6** (26 min, 2.4%), *trans*-**5** (28 min, 12%), and *cis*-**5** (33 min, 1%).

In the Presence of Dicyclopentadiene

A solution of TMT (3.48 g), *endo*-dicyclopentadiene (3.96 g, bp 38–39°C), and TFA (17.1 g) in methanol (170 ml) was photolysed through a Corex filter under nitrogen for 1 h. The photolysate was worked up to give neutral (217 mg, dicyclopentadiene) and basic fractions (5.18 g); the latter showed an nmr signal at τ 3.80 for a norbornene olefinic proton and τ 4.42 for a cyclopentene olefinic proton in a ratio of 1:14 and the major singlets at τ 7.75 and 7.85 for dimethylamino groups. The ratio of the olefinic and dimethylamino protons is 4:13 indicating no major cyclization products.

The vpc analysis of the basic fraction showed two major clusters of peaks at 8.2 min (**18**, two peaks, 35%) and 21.5 min (**19**, four peaks, 40%), and five sharp minor peaks at 7.7, 9.1, 11.7, 12.5, and 12.8 min. A portion of the basic fraction (1 g) treated with methanol gave a white solid (185 mg) which was recrystallized to give a dimer **19** as colorless needles; mp 181–183°C; ir: 3040, 2820(s), 2760(s), 1610(w), 1278, 1024(s), 942, 740, and 692(s) cm^{-1}; ^1H nmr τ 4.39 (m, 2H), 4.51 (m, 2H), 7.75 (s, 6H), 7.76 (s, 6H), and 8.32–8.36 (AB quartet with further splitting) and other multiplets; ^{13}C nmr 23 peaks; ms (%): at 110°C: 352.2883 (M^+, 50, calcd. for $C_{24}H_{36}N_2$: 352.2878), 337.2636 (70, calcd. for $C_{23}H_{33}N_2$: 337.2644), 308.2383 (15, calcd. for $C_{22}H_{30}N$: 308.2378), 189(30), 149(60), 110(45), 84.0813 (100, calcd. for $C_5H_{10}N$: 84.0813) and 58(85). *Anal.* calcd. for $C_{24}H_{36}N_2$: C 81.76, H 10.29, N 7.95; found: C 81.61, H 10.17, N 7.77.

The basic fraction (1.5 g) was chromatographed on neutral alumina using ether and petroleum ether as eluent. Elution with 30 ~ 40% ether in petroleum ether gave mixtures of monomeric and dimeric compounds. Elution with 45% ether in petroleum ether gave an oil (320 mg) which was distilled at 20°/0.5 Torr to give colorless oil of **18**; ir: 3045, 2950(s), 2860(s), 2820(s), 2770(s), 1610(w), 1050(s), 1040(s), and 700(s) cm^{-1}; nmr τ 4.42 (m, 2H), 6.95 (m, 1H), 7.85 (s, 6H), and other multiplets; ms (%) at 80°C: 177 (M^+, 46), 162(6), 148(5), 136(17), 122(19), 109(100), 84(60), 71(57), and 58(48). *Anal.* calcd. for $C_{12}H_{19}N$: C 81.30, H 10.80, N 7.90; found: C 81.47, H 10.81, N 7.98.

In the Presence of 5-Vinyl-2-norbornene

An acetonitrile (170 ml) solution containing TMT (4.64 g), *endo*-5-vinyl-2-norbornene (4.2 g), and TFA (28.5 g) was photolysed under nitrogen at 0°C until the 235 nm absorption disappeared. The photolysate was worked up in the usual manner to afford a neutral (275 mg) and basic fraction (3.9 g). The basic fraction exhibited nmr signals at τ 4.4 and 5.0 for the vinyl olefinic protons and a weak one at τ 4.0 for the norbornene olefinic protons.

The vpc of the basic fraction showed peaks at 4.5 min (two peaks, 7%), 8.3 min (three peaks, 1%), 10 min (three peaks, 13%), and a cluster of four peaks at 16.4, 17.0, 17.2, and 18.1 min (40%). The gc–ms analysis showed that the first fraction exhibited *m/e* (%) at 165 (M^+, 51), 150(20), 136(22), 110(42), 98(39), 84(52), 71(84), and 58(100) and the peaks of the last fraction showed strong *m/e* at 328 (M^+), 313, 284, 244, 110, 84, 71, and 58. The first fraction was isolated by preparative vpc to give a colorless oil; ir: 3070, 29.40(s), 2860(s), 2810(s), 2760(s), 1635(m), 1035, and 902(s) cm^{-1}; nmr τ 4.34 (m, 1H), 5.14 (m, 2HO, 7.93(s), 7.97(s), and other multiplets.

In the Presence of 1,6-Heptadiene

A solution of TMT (3.3 g, 0.0287 mol), 1,6-heptadiene (2.1 g, 0.0221 mol), and TFA (25 g) in acetonitrile (200 ml) was photolysed under nitrogen in the usual manner. The photolysate was worked up in the usual manner to give only a small amount of neutral and basic fractions. The basic aqueous solution was continuously extracted with ether to afford an oil (450 mg) which showed one major spot on tlc. The basic fraction was chromatographed on alumina using 1% methanol in methylene chloride to give 1-(2′-dimethylaminoethyl)-2-dimethylaminomethylcyclopentane (**20**) as a volatile oil (163 mg); ir: 2820(s), 2760(s), 1265(m), 1040(m), 1030(m), and 845(w) cm^{-1}; ^1H nmr τ 7.75(s), 7.78(s), and other multiplets; ^{13}C nmr (ppm from TMS): 59.8 (t, CH_2N), 58.7 (t, CH_2N), 45.5 (q, CH_3N), 45.2 (q, CH_3N), 39.6 (d, —CH—), 30.1(t), 28.8(t), 27.0(t), and 22.1(t); *m/e* (%): 198(4), 154(22), 153(19), 138(17), 110(19), 84(44), 71(22), 59(27), and 58(100). *Anal.* calcd. for $C_{12}H_{26}N_2$: C 72.66, H 13.12, N 14.12; found: C 72.84, H 13.17, N 14.17.

Synthesis of Authentic Samples

trans-*1,2-Bisdimethylaminocyclohexane (6)*

The procedure of Swift (36) was used to prepare *trans*-1,2-diaminocyclohexane and the methylation was carried out according to Winterwitz *et al.* (37). The crude product was purified by preparative vpc on a 20% Dowfax 9N9/10% TEP column to give **1** as an oil; ir: 2928(s), 2862(s), 2830(s), 2781(s), 1452, 1172, 1047, 1026; nmr τ: 7.71(s); ms: 170 (M^+, 100), 155(6), 125(27), 124(29), 110(25), 97(53), 84(100), 71(84) and 58(65). The picrate (ethanol) was yellow plates; mp 209–211°C (lit. mp (37) 204°C. *Anal.* calcd. for $C_{22}H_{28}N_8O_{14}$: C 42.04, H 4.49, N 17.83; found: C 42.16, H 4.47, N 17.97.

cis- *and* trans-*2-Dimethylaminomethyl-1-dimethylaminocyclohexane (5)*

The oxime of 2-dimethylaminomethylcyclohexanone was prepared according to the known method as white needles; mp 113–116°C (lit. (38) mp 110–120°C). This oxime was reduced with $LiAlH_4$ in ether and was methylated with a mixture of formic acid – formaldehyde to give a mixture of *cis*- and *trans*-**5**. The mixture was separated by preparative vpc on a 20% Dowfax – 10% TEP column in which the *trans* isomer had retention time of 41 min (59%) and the *cis* isomer 57 min (41%). The *trans* isomer had properties as follows: ir: 2925, 2855, 2818, 2763, 1451, 1036 cm^{-1}; ^1H nmr τ 7.81 (s, 6H), 7.87 (s, 6H), 7.58 (dt, J = 3 and 12 Hz, 1H), 7.9–9.2 (m, 9H); ^{13}C nmr in ppm: 17.3, 21.3, 21.7, 30.6 (for C(3), C(4), C(5), and C(6)), 37.9 (C(2)), 39.9 (N—CH_3), 46.0 (N—CH_3), 62.8 (CH_2—N), and 66.2 (C(1)); ms *m/e* (%): 184 (M^+, 27), 140(34), 139(66), 138(21), 126(14), 124(34), 111(36), 110(57), 84(59), 71(48), and 58(100). *Anal.* calcd. for $C_{11}H_{24}N_2$: C 71.68, H 13.12, N 15.20; found: C 71.34, H 13.22, N 15.35.

The dipicrate was recrystallized from ethanol; mp 176–179°C (dec.). *Anal.* calcd. for $C_{23}H_{30}N_8O_{14}$: C 42.99, H 4.71, N 17.44; found: C 42.80, H 4.71, N 17.34.

The *cis*-isomer was isolated as an oil; ir: 2930, 2860, 2818, 2764, 1465, 1452, 1035 cm^{-1}; the ms is identical to that of the *trans* isomer.

Thermal Decomposition of TMT in the Presence of Olefins Under Acidic Conditions

In the Presence of Cyclohexene

A solution of TMT (3 g), concentrated hydrochloric acid (15 ml), cyclohexene (16 g), and methanol (200 ml) kept at 4°C under nitrogen in the dark showed ca. ⅓ of TMT disappearance after 120 h. The remaining TMT decomposed completely at room temperature after 20 h. The solution was worked up in the usual manner to give no neutral fraction but a basic fraction by CH_2Cl_2 extraction (1.13 g) which was almost pure imine trimer **1**; nmr (in H_2SO_4) ppm from H_2SO_4: −7.57 (dt, J = 6 and 1.5 Hz, 3H), −3.38 (m, 1H), −3.15 (m, 1H), and −3.70 (bs, 1H); ir: 2945(s), 2780(s), 2638, 1675(w), 1470, 1445, 1388, 1263(s), 1236(s), 1160, 1115(s), 1004, 915(s), 860 cm^{-1}; ms: 43(62) and 42(100). The yield is quantitative.

Can. J. Chem. Downloaded from www.nrcresearchpress.com by 210.87.254.42 on 09/05/12
For personal use only.

In a separate experiment, a solution of TMT (1 g) and cyclohexene (7.25 g) was added dropwise to trifluoroacetic acid (8 g) under continuous purging of carbon monoxide at room temperature with vigorous stirring. A purple color developed in the lower phase and vigorous evolution of nitrogen was observed. After 30 min, the lower phase turned to pale yellow and nitrogen evolution stopped. In another 90 min, the solution was worked up to give no neutral fraction. The basic fraction was obtained by continuous extraction and gave imine trimer **1** (180 mg, 47%) as the only product.

In the Presence of Norbornene

A solution of TMT (1 g) and norbornene (8.3 g) in acetonitrile (10 ml) was added dropwise to trifluoroacetic acid (8 g) in 2 min under nitrogen with stirring. After 5 h the solution was worked up to give a basic fraction (250 mg) which showed nmr singlets at τ 6.78 and 7.70 (in the 2:3 ratio for **1**) and weak signals at τ 6.15 and 8.0–9.1 regions. The yield of the imine trimer **1** was 30% as determined by vpc.

Nuclear Magnetic Resonance Studies of TMT Decomposition

TMT in H_2SO_4

TMT (0.5 ml) was added dropwise to a 25 ml flask containing H_2SO_4 (5 ml) cooled to -10°C with vigorous stirring. The solution turned to bright yellow and expelled gases. The solution was transferred to a precooled nmr tube and the spectra were recorded at -20°C in 15 min after mixing and at 20°C in 30 min. TMH (100 mg) was dissolved in H_2SO_4 (3 ml) as above and the nmr spectrum was recorded at 20°C. The signal at τ 6.40 for TMH–$2H^+$ persisted for 2 weeks at 20°C but was replaced by the signals at τ 1.93, 6.27 and 7.10 on warming in a water bath.

TMT in TFA

TMT (100 mg) was added to TFA (0.5 ml) at -10°C with stirring. The solution kept at -15°C showed singlets at τ 6.62, 6.82, and 6.92 in a ratio of 1:1:2. The signals showed no change at -15°C for 1 h but broadened at 10°C and coalesced to a singlet at τ 6.78 at 30°C. At 30°C, the singlet decayed with a half-life of ca. 20 min to give the new set of signals at 1.90 (m), 6.25 (m, 2H), and 7.10 (t, 3H).

A solution prepared from TMT (50 mg), CD_3CN (0.5 ml), and TFA (100 mg) at -10°C showed singlets at τ 6.58, 6.88, and 6.96 in a ratio of 1:2:1. Both this and the above solutions were irradiated through a Corex filter. The resulting solution exhibited signals at τ 6.25, 7.10, and 7.14 in addition to other unidentified signals.

Electron Spin Resonance Studies of TMT Decompositions

A solution of TMT in desired solvent was prepared by slow addition and stirring at 0°C or lower. The solution was transferred to an aqueous esr cell and purged with nitrogen for 2 min. The acetonitrile–TFA solution showed the esr spectrum at room temperature of $TMT^{\ddagger}$: a_N (2N) = 1.15, a_N(2N) = 10.85, a_H(6H) = 10.40, a_H(6H) = 11.60 G, and g = 2.0040 ± 0.0005 (lit. (6) a_N = 1.20, a_N = 10.96, a_H = 10.40, a_H = 11.52 G, and g = 2.0036). This solution was irradiated with an Osram 200 W lamp in the esr cavity at room temperature for 5 min. Five minutes after switching off the lamp a strong esr signal of $TMH^{\ddagger}$ was observed: a_N(2N) = 13.5, a_H(12H) = 12.7 G, and g = 2.0034 ± 0.0004) (lit. (39) a_N = 13.5, a_H = 12.7 G, and g = 2.0035). Although $TMT^{\ddagger}$ esr signal persisted for several hours, the $TMH^{\ddagger}$ signal decayed within 1 h at room temperature.

An acetonitrile solution containing TMT (0.17 *M*) and TFA (1.1 *M*) showed a strong $TMT^{\ddagger}$ signal at -45°C. Photolysis of the solution in the cavity caused no change in the esr signal. When the light was shut off, the $TMH^{\ddagger}$ signal started to build up reaching a maximum after 10 min. The $TMH^{\ddagger}$ signal remained unchanged for several hours at -45°C but decayed in 30 min at 30°C. To a solution showing $TMH^{\ddagger}$ and weak $TMT^{\ddagger}$ signals, a drop of cyclohexene was added at -45°C. On rescanning, the $TMH^{\ddagger}$ signal decreased rapidly leaving behind the $TMT^{\ddagger}$ signal. The $TMT^{\ddagger}$ signal persisted even when this solution was warmed to room temperature.

A solution of TMT in cyclohexene (0.5 *M*, 2 ml) was added to TFA in acetonitrile (1.3 *M*, 2 ml) at 20°C to give a binary phase system. The upper phase exhibited a $TMT^{\ddagger}$ signal which disappeared in 45 min to be replaced by a 17 band signal at g = 2.0024 ± 0.004. This signal is very similar to the simulated (EPRCAL) spectrum of the $(CH_3)_2\dot{N}CHNHCH_3$ using a_N = 8, a_N = 6, a_H(N—H) = 8, a_H(α-H) = 15.5, and $a_H(CH_3)$ = 4 G (28).

Decomposition of TMT in H_2SO_4 in the Presence of Toluene

Generally, a solution of TMT in toluene was added to a mixture of toluene and H_2SO_4 at a particular temperature ranging from -10 to 80°C. The reaction was terminated by the addition of ice and extracted with ether. The ether and toluene were removed by distillation at 110°C to provide the 'neutral' fraction. At this point the polymeric material which had separated was collected by scraping it off the sides of the flask. It was washed with 10% aqueous KOH followed by water and then ether. The washings were combined with the major aqueous portion. This was basified with aqueous KOH and extracted with ether. After the ether was removed, the residual oil was analyzed for products. A typical experiment is described below.

A solution of TMT (0.9 g) in toluene (4.1 ml) was added dropwise to a vigorously stirred mixture of toluene (4.0 ml) and concentrated sulfuric acid (2.5 ml) at -5°C; the addition speed was adjusted so that the temperature did not rise above 0°C. Gases were evolved and the mixture turned a deep purple color. The reaction was continued at -5°C for 20 h to give a dark brown mixture.

The neutral oil (142 mg) could not be separated by preparative vpc and exhibited *m/e* peaks at 182 (M^+, 92), 167(100), 165(38), 152(15), 141(4), 128(6), 104(36), 91(19), and 77(10) and ir peaks at 3028, 1604, 1516, 1031, 791(w), 769(w), 746, 729(s), 698(s), and 600 cm^{-1}. The nmr spectrum showed two sets of singlets at τ 6.05 and 7.79 for *o*-benzyltoluene **22** and at τ 6.10 and 7.71 for *p*-benzyltoluene in a ratio of 37:63. A weak singlet at τ 7.15 was tentatively assigned to bibenzyl (40).

The basic fraction (238 mg) was taken up in 5 ml of carbon tetrachloride containing 0.197 *M* chlorobenzene as the internal standard. The solution was analysed on a 10% Carbowax 20 *M* chromosorb W 100/200 column (10 ft × $\frac{1}{16}$ in. stainless steel column, N_2 gas at 30 psi, temperature programmed at 2°/min. from 100 to 200°C) to give the following retention times: 4.6, 6.0, 9.2, 10.2, 15.0, 18.6, 19.4, 20.2, 23.0, and 26.0 for **1**, chlorobenzene, **24**, *o*-**21**, **25**, **23**, *p*-**21**, *m*-**21**, **27**, and **26**, respectively. The percentage yields were calculated based on the technique described in the literature (2). The major peaks were identified by the peak matching with the authentic samples and were further supported by gc–ms patterns.

Decomposition of *N*-chlorodimethylamine in toluene–sulfuric acid mixture was carried out according to Bock and Kampa (30) to give neutral and basic fractions. The latter, in 35% yield, served as reference sample for analysis and was shown to contain *N,N*-dimethyltoluidine with a *o*:*m*:*p* ratio of 9:61:30 by the same analysis. The neutral fraction was shown to contain *o*- and *p*-benzyltoluene in an 8% yield.

TMT Decomposition in TFA in the Presence of Toluene

A solution of TMT (0.9 g) in toluene (4 ml) was added dropwise at a controlled temperature with rapid stirring to a solution of TFA (5.25 g) in toluene (4 ml). During the addition

gases were evolved and two phases were formed. The reaction was terminated by addition of ice and worked up as above. No purple color was observed, nor polymeric material obtained.

In one experiment, *o-N,N*-dimethyltoluidine (**21**) was isolated by preparative vpc as an oil; ir: 2940(s), 2870, 2835(s), 2780, 1600(s), 1494(s), 945(s), 805, 762(s), and 725(s) cm^{-1}.

Acknowledgement

The authors are grateful to the National Research Council of Canada for financial support.

1. J. S. WATSON. J. Chem. Soc. 3677 (1956).
2. C. J. MICHEJDA and W. P. HOSS. J. Am. Chem. Soc. **92**, 6298 (1970).
3. W. C. DANEN and T. T. KENSLER. J. Am. Chem. Soc. **92**, 5235 (1970).
4. J. R. ROBERTS and K. U. INGOLD. J. Am. Chem. Soc. **95**, 3228 (1973).
5. W. E. BULL, J. A. SEATON, and L. F. AUDRIETH. J. Am. Chem. Soc. **80**, 2516 (1958).
6. S. F. NELSEN, R. B. METZLER, and M. IWAMURA. J. Am. Chem. Soc. **91**, 5103 (1969).
7. C. J. MICHEJDA and D. ROMANS. Tetrahedron Lett. 4213 (1969).
8. W. R. MCBRIDE and W. E. THUN. Inorg. Chem. **5**, 1846 (1966).
9. C. G. OVERBERGER and B. S. MARKS. J. Am. Chem. Soc. 77, 4097 (1955).
10. F. EFFENBERGER and P. FISCHER. Tetrahedron, **26**, 3029 (1970).
11. G. S. HAMMOND, B. SEIDEL, and R. E. PINCOCK. J. Org. Chem. **28**, 3275 (1963).
12. Y. L. CHOW. Acc. Chem. Res. **6**, 354 (1973).
13. R. S. NEALE. Synthesis, 1 (1971).
14. M. E. WOLFF. Chem. Rev. **63**, 55 (1963).
15. (*a*) F. MINISCI. Synthesis, 1 (1973); (*b*) A. CLERICI, F. MINISCI, M. PERCHINUNNO, and O. PORTA. J. Chem. Soc. Perkin II, 416 (1974).
16. R. W. LOCKHART, R. W. SNYDER, and Y. L. CHOW. J. Chem. Soc. Chem. Commun. 52 (1976).
17. L. J. MADGZINSKI. M.Sc. Thesis, Simon Fraser University, Burnaby, BC. 1977.
18. A. C. COPE, E. CIGANEK, and N. A. LEBEL. J. Am. Chem. Soc. **81**, 2799 (1959).
19. K. S. PILLAY, S. C. CHEN, T. MOJELSKI, and Y. L. CHOW. Can. J. Chem. **53**, 3014 (1975); K. S. PILLAY, K. HANAYA, and Y. L. CHOW. Can. J. Chem. **53**, 3022 (1975).
20. G. C. LEVY and G. L. NELSON. Carbon-13 nuclear magnetic resonance for organic chemists. Wiley-Interscience, New York, NY. 1972. Chapt. 3.
21. J. B. LAMBERT, J. J. PAPAY, S. A. KHAN, K. A. KAPAUF, and E. R. MAGYAR. J. Am. Chem. Soc. **96**, 6112 (1974).
22. L. FRIEDMAN. J. Am. Chem. Soc. **86**, 1885 (1964).
23. R. DOWBENKO. J. Am. Chem. Soc. **86**, 946 (1964); Tetrahedron, **20**, 1843 (1964).
24. G. PREGALIA and G. GREGARIO. Chim. Ind. (Milan), **45**, 1065 (1963).
25. D. I. DAVIES and S. J. CRISTOL. Adv. Free Radical Chem. **1**, 155 (1965).
26. N. O. BRACE. J. Am. Chem. Soc. **86**, 523 (1964); J. Org. Chem. **31**, 2879 (1966).
27. W. M. TOLLES, D. W. MOORE, and W. E. THUN. J. Am. Chem. Soc. **88**, 3476 (1966).
28. S. F. NELSEN. Nitrogen centred radicals. *In* Free radicals. Vol. II. *Edited by* J. K. Kochi. John Wiley and Sons, New York, NY. 1973. Chapt. 21.
29. R. W. FESSENDEN and P. NETA. J. Phys. Chem. **76**, 2857 (1972).
30. (*a*) H. BOCK and K. L. KOMPA. Chem. Ber. **99**, 1347 (1966); (*b*) H. BOCK and K. L. KOMPA. Chem. Ber. **99**, 1357 (1966); (*c*) H. BOCK and K. L. KOMPA. Chem. Ber. **99**, 1361 (1966).
31. R. A. PERRY. Ph.D. Thesis, Simon Fraser University, Burnaby, BC. 1973.
32. G. A. OLAH. Acc. Chem. Res. **4**, 240 (1971).
33. L. M. STOCK and H. C. BROWN. Adv. Phys. Org. Chem. **1**, 35 (1963).
34. F. D. LEWIS and W. H. SAUNDERS, JR. Alkylnitrenes. *In* Nitrenes. *Edited by* W. Lwowski. Interscience Publishers, New York, NY. 1970. Chapt. 3.
35. G. A. OLAH and P. VON R. SHLEYER. *In* Carbonium ions. Vol. II. Wiley-Interscience, New York, NY. 1970. p. 774.
36. G. SWIFT. J. Org. Chem. **32**, 511 (1967).
37. F. WINTERITZ, M. MOUSSERON, and R. DENNILAULER. Bull. Soc. Chim. Fr. 382 (1956).
38. I. N. NARAZOV and K. V. KUZNETZOV. Dokl. Akad. Nauk SSSR, **111**, 358 (1956).
39. S. F. NELSEN. J. Am. Chem. Soc. **88**, 5666 (1966).
40. Sadtler Research Laboratories, Inc., Standard I.R. and N.M.R. Spectra. Sammuel P. Sadtler and Sons, Inc., Philadelphia, PA. 1977.

Can. J. Chem. Downloaded from www.nrcresearchpress.com by 210.87.254.42 on 09/05/12
For personal use only.

A theoretical study of the energies of solution, association, and migration for univalent substitutional anion impurities in alkali metal chloride crystals

JOHN CORISH AND BRENDA M. C. PARKER
Department of Chemistry, University College, Dublin 4, Ireland
AND
PATRICK W. M. JACOBS
Department of Chemistry, University of Western Ontario, London, Ont., Canada N6A 5B7

Received October 31, 1977

JOHN CORISH, BRENDA M. C. PARKER, and PATRICK W. M. JACOBS. Can. J. Chem. **56**, 1668 (1978).

Theoretical calculations have been made of the energy change accompanying the substitution of a univalent anion, F^-, Br^-, or I^-, into crystals of the alkali metal chlorides LiCl, NaCl, KCl, and RbCl. Association energies for the formation of nearest neighbour (nn) or next nn complexes with a vacancy in the anion sub-lattice and the activation energies for the four basic kinds of single vacancy jumps have also been calculated. The results of these calculations are discussed with respect to ion size and polarization effects and their relation to the activation energy (E') for the diffusion of a univalent impurity in the host crystals. The availability of experimental values of E' for some systems permits an assessment of the contribution to E' from the temperature dependence of the correlation factor and from vacancy pair diffusion.

JOHN CORISH, BRENDA M. C. PARKER et PATRICK W. M. JACOBS. Can. J. Chem. **56**, 1668 (1978).

On a effectué des calculs théoriques sur les changements d'énergie qui accompagnent la substitution par un anion univalent F^-, Br^- ou I^-, dans des cristaux des chlorures de métaux alcalins LiCl, NaCl, KCl et RbCl. On a calculé les énergies d'association correspondant à la formation de complexes entre une lacune du sous-réseau des anions et ses premiers ou deuxièmes voisins; on a aussi calculé les énergies d'activation qui accompagnent les quatre types fondamentaux de sauts d'une monolacune. On discute de ces résultats en termes de la grosseur des ions et d'effets de polarisation et de leur relation avec l'énergie d'activation (E') pour la diffusion d'une impureté monovalente dans les cristaux hôtes. La disponibilité de valeurs expérimentales de E' pour quelques systèmes permet d'évaluer la contribution à E' à partir de la relation température-facteur de corrélation et de la diffusion de bilacunes.
[Traduit par le journal]

Introduction

In a recent paper (1) Catlow, Diller, and Norgett (CDN) derived two alternative self-consistent sets of two-body potentials for the alkali halides with the rock salt structure. The availability of these new potentials makes it possible to perform new calculations on the properties of defects in these crystals. Results communicated hitherto include calculations on vacancy and interstitial defects in NaCl, KCl, and KBr (2), a systematic study of vacancy defects in the 16 alkali halides with the rock salt structure (3), calculations of the equilibrium location and energy of the univalent substitutional impurities Li^+ and F^- in several host crystals (19), and calculations on association and migration energies for seven cation and six anion univalent impurity-host systems (4). In these last calculations we employed the earlier Set I CDN potentials (1) and we also utilized the geometric mean approximation to evaluate the three unknown parameters A_{ij}, ρ_{ij}, C_{ij}, in the short-range Buckingham potential

$$[1] \qquad \phi_{ij} = A_{ij} \exp(-R_{ij}/\rho_{ij}) - C_{ij}/R_{ij}^6$$

for the impurity-host second neighbour interaction. In eq. [1], ϕ_{ij} is the potential energy due to the interaction of ions of types i and j, A_{ij} and ρ_{ij} are the repulsive and hardness parameters in the repulsive interaction, and C_{ij} is the van der Waals coefficient in the attractive dipole–dipole interaction; R_{ij} is the distance between ions i and j.

In this paper we investigate the 12 univalent anion impurity systems obtained by incorporating F^-, Br^-, I^- in the alkali metal chlorides LiCl, NaCl, KCl, RbCl. Two of these systems namely KCl:F^- and KCl:Br^- were investigated previously (19) but are included here for completeness and because we have now, whenever possible, used the CDN Set II (spline) potentials.

Calculations

The calculations were performed using the HADES computer program (5, 6). The ions in the crystal are divided into two sets. One set called

Can. J. Chem. Downloaded from www.nrcresearchpress.com by 210.87.254.42 on 09/05/12
For personal use only.

Can. J. Chem. Downloaded from www.nrcresearchpress.com by 210.87.254.42 on 09/05/12
For personal use only.

region I comprises the defect (that is the impurity plus, in some instances, a vacancy) together with the immediately surrounding ions. The relaxations of the ions in region I are calculated explicitly as the crystal adopts its configuration of minimum energy. Full advantage is taken of symmetry but nevertheless the size of region I is limited by the capacity of the available computers to handle the large numbers of variables required to specify the ion positions. Of the six defect energies evaluated four were calculated with 81 ions in region I; for the remaining two defects the maximum size of region I obtainable was 48 ions because of their lower symmetry. Consequently for one system, namely $LiCl:Br^-$, calculations were performed with a smaller region I as well as for the 81-ion region I to check for any variations due to the size of the explicitly relaxed region. The remainder of the crystal is treated as a dielectric continuum matched to region I at the boundary.

Both the Set I and Set II potentials (1) of CDN are based on the shell model with ion shell charges and spring constants chosen to reproduce the anion polarizabilities and the static and high-frequency permittivities and the frequencies of the transverse optic mode of the crystals. The second neighbour interaction in Set I was of the Buckingham form (eq. [1]) with repulsive parameter A_{ii} and hardness parameter ρ_{ii} determined from calculations based on the electron gas approximation (7). The total attractive component of the second neighbour potential was arbitrarily partitioned equally between anion and cation interactions ($C_{ii} = C_{jj}$). The nearest neighbour (nn) repulsive parameters were fitted to bulk properties. In order to reduce the number of potential constants to be fitted the repulsive parameters were assumed to have the form

$$[2] \qquad A_{ij} = b \exp [(a_i + a_j)/\rho_{ij}]$$

with $a_i + a_j = a$, the nn anion–cation distance, and b a constant for all the 16 halides. The van der Waals interaction between nearest neighbours was assumed to be completely quenched ($C_{ij} = 0, i \neq j$). Potential parameters b, a_i, a_j, ρ_{ij}, and C_{ii} were adjusted to fit the stability condition, cohesive energy, and elastic constants of all the 16 alkali halides. In this procedure a separate C_{ii} is required for each substance.

The potentials of Set II differ from Set I in having separate values of the second neighbour van der Waals coefficients C_{ii}, C_{jj} specific to each interaction. The second neighbour potential is of a more complex form, the repulsive wall and attractive tail being joined to the potential minimum by fifth-order and third-order polynomials respectively, at adjustable spline knots. Both sets give excellent representations of the equilibrium, elastic, and dielectric properties of the crystals.

For the calculations involving an impurity ion (k) the potential describing the nn (ik) interaction should clearly be taken to be the same as for the corresponding pure crystal (ik). However, new second neighbour (kj) potentials are needed. For the calculations based on Set II, the repulsive parameters A_{kj}, ρ_{kj} were calculated using the electron gas approximation, C_{kj} was obtained from the geometric mean $(C_{kk}C_{jj})^{1/2}$, and the spline knots were arithmetic means of the knots for the corresponding kk, jj interactions. The calculations are not in fact sensitive to the precise location of the spline knots.

There are some difficulties concerning calculations for LiCl. There is no splined potential for the Li–I interaction because of insufficient elastic data for LiI (1). It was therefore necessary to use Set I for $LiCl:I^-$. For $LiCl:Br^-$ calculations were also performed with Set I so that the sensitivity of the results to details of the potential could be evaluated.

Defect Energies

The energy change accompanying the process

$$[3] \qquad M^+X^- + X'^- = M^+X'^- + X^-$$

is given by

$$[4] \qquad \Delta u(X') = u(X') - u_c(MX') + u_c(MX)$$

where $u(X')$ is the defect energy calculated for a crystal containing a single X'^- ion at its normal substitutional position in the crystal and u_c denotes the cohesive energy. The energy change accompanying the formation of a complex, with the vacancy on the nn anion site, from an isolated X'^- ion and an anion vacancy $\boxminus$,

$$[5] \qquad X'^- + \boxminus = X'^-\boxminus$$

is

$$[6] \qquad \Delta u_{a1} = u_{a1} - u_-^{\infty} - u(X')$$

where u_{a1} is the energy of the crystal containing one complex and u_-^{∞} is the energy required to remove an anion X^- from a normal lattice site to a point well outside the crystal. Δu_{a2}, the energy to form a complex with the vacancy in the next nn site in the anion sub-lattice, is given by an analogous expression to [6]. Thus in addition to the energies of the various defect configurations u_c and u_-^{∞} had to be calculated in order to obtain $u(X')$ and Δu_{a1}. This information is given in Table 1. The symbols u_1, u_2, $u_{3,4}$ denote the saddle point energies for anion vacancies executing jumps of types w_1, w_2, w_3, or w_4 (Fig. 1); Δu_1, Δu_2, Δu_3, Δu_4 are the corresponding activation energies for these jumps. The defect energies $u(X')$,

Can. J. Chem. Downloaded from www.nrcresearchpress.com by 210.87.254.42 on 09/05/12
For personal use only.

TABLE 1. Calculated values of the cohesive energy (u_c) and of the energy to remove an anion (u_-^∞) to a point well outside the crystal. These results were obtained with the CDN Set II potentials except for LiI for which the Set I potential had to be used (see text)

Substance	u_c/eV	u_-^∞/eV
LiF	−11.051	7.114
LiCl	−8.862	6.026
LiBr	−8.311	5.780
LiI	−7.456	4.684
NaF	−9.747	6.554
NaCl	−8.042	5.714
NaBr	−7.608	5.504
NaI	−7.122	5.272
KF	−8.537	5.406
KCl	−7.370	5.116
KBr	−7.048	4.986
KI	−6.635	4.869
RbF	−8.055	4.773
RbCl	−7.050	4.716
RbBr	−6.782	4.692
RbI	−6.406	4.583

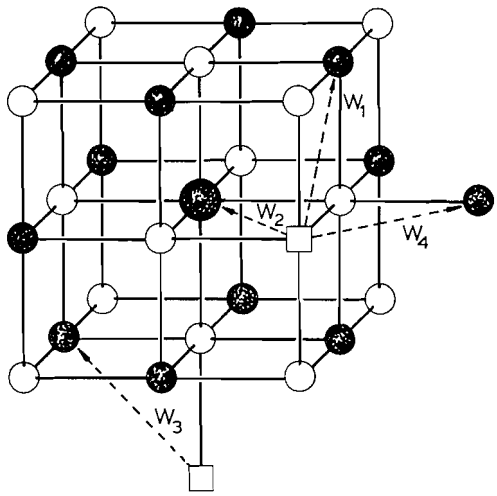

FIG. 1. Definition of the anion vacancy jumps w_1, w_2, w_3, w_4 associated with an anion impurity. The large filled circle denotes the impurity, smaller filled circles denote anions of the host crystal, open circles denote cations, and squares denote anion vacancies. The symbol w_n is used to denote both the type of jump and the corresponding jump frequency.

u_{a1}, u_{a2}, u_1, u_2, and $u_{3,4}$ are given in Table 2, and the substitutional energies, association energies, and activation energies appear in Table 3.

In calculating $u(X')$ the origin was fixed at the lattice site for which the impurity ion is the basis atom, but the impurity was allowed to move off this site to its most stable position. This motion was constrained by symmetry to ⟨110⟩ directions, since experimental work has shown that the F^- ion occupies an off-centre position along ⟨110⟩ in NaBr:F^-, KI:F^-, and RbI:F^- (8, 9). In every system investigated here, with the exception of LiCl:F^-, the impurity relaxed to the lattice site. The choices of origin for the calculation of u_{a1}, u_{a2}, u_1, u_2, $u_{3,4}$ are shown in Figs. 2*a–e*. All the calculations were performed with 81 ions in region I except those of u_1 and $u_{3,4}$ for which 48 ions were used. To test whether this would introduce any untoward effects, the defect energies for LiCl:Br^- were recalculated with a smaller region I. In each case this was chosen to be as close as possible to 48 ions provided that if one ion in a particular symmetry-related set was included, then so were all the ions in that set. The results of these test calculations are shown in Table 4. They show that although minor quantitative differences arise from the choice of a smaller region I, defect energies are little affected and reasonably satisfactory convergence with respect to the size of region I has been achieved. However, the substitutional, association, and activation energies involve taking differences of these defect energies and so uncertainties of a 2–3 hundreths of an eV in those energies that involve $u_{3,4}$ and u_1 can be expected. Table 4*b* compares the above energies calculated from the consistently smaller region I (~48 ions) with those values obtained previously using the 81-ion region I whenever possible. Even though only minor differences arise these could be important if the energy parameter is close to zero. For example Δu_{a1} is +0.011 eV for the small region I but −0.017 eV for the 81-ion region, implying that, although association energies are small for univalent impurity ions, the nn position for the vacancy is marginally favoured for Br^- in LiCl.

The effect of the choice of potential may be judged from Table 5 where we compare Set I and Set II results for LiCl:Br^- and KCl:Br^-. The results clearly show the same trends although some quantitative differences are apparent. For LiCl:Br^- the jump activation energies are lower by about 0.1 eV when calculated from Set I instead of from Set II. For KCl:Br^- the results are very comparable throughout except for the small association energy for the nn vacancy which was expected from ion size considerations. In general, Set II potentials are preferable because of the greater flexibility of the potential function and the specific van der Waals coefficient for each interaction.

Ion Displacements

The calculations for substitutional impurities were done by giving the impurity ion an initial ⟨110⟩ displacement. During the calculation the crystal adopts its minimum energy configuration and in every

TABLE 2. Calculated defect energies for alkali chloride crystals containing a univalent anion impurity. All energies are in eV and the symbols describing the defect are defined in the text

System	$u(X')$	u_{a1}	u_{a2}	u_1	u_2	$u_{3,4}$
LiCl:F^-	−1.218	4.925	4.722	5.547	4.958	5.695
LiCl:Br^-	0.606	6.615	6.702	7.579	7.498	7.590
LiCl:I^-	1.690	6.791	7.063	7.643	7.555	7.837
NaCl:F^-	−0.991	4.691	4.587	5.405	5.027	5.390
NaCl:Br^-	0.482	6.180	6.253	6.959	6.912	7.071
NaCl:I^-	1.267	6.924	7.096	7.774	7.601	7.925
KCl:F^-	−0.696	4.422	4.297	5.115	4.779	5.126
KCl:Br^-	0.353	5.457	5.513	6.197	6.134	6.382
KCl:I^-	0.993	6.063	6.196	6.839	6.717	7.119
RbCl:F^-	−0.624	4.107	3.983	4.726	4.479	4.757
RbCl:Br^-	0.297	5.002	5.054	5.677	5.630	5.864
RbCl:I^-	0.862	5.534	5.650	6.236	6.103	6.904

TABLE 3. The energy change which occurs on substituting an X'^- anion for a chloride ion, the association energies for nn and nnn complexes, and the activation energies for types w_1, w_2, w_3, and w_4 anion jumps. All energies are in eV

System	$\Delta u(X')$	Δu_{a1}	Δu_{a2}	Δu_1	Δu_2	Δu_3	Δu_4
LiCl:F^-	0.971	0.117	−0.086	0.622	0.033	0.973	0.770
LiCl:Br^-	0.055	−0.017	0.070	0.964	0.883	0.888	0.975
LiCl:I^-	0.348	−0.071	0.201	0.852	0.764	0.774	1.046
NaCl:F^-	0.714	−0.032	0.158	0.714	0.336	0.803	0.699
NaCl:Br^-	0.048	−0.016	0.057	0.779	0.732	0.818	0.891
NaCl:I^-	0.346	−0.057	0.115	0.850	0.677	0.829	1.001
KCl:F^-	0.471	0.002	−0.123	0.693	0.357	0.829	0.704
KCl:Br^-	0.031	−0.012	0.044	0.740	0.677	0.869	0.925
KCl:I^-	0.258	−0.046	0.087	0.776	0.654	0.923	1.056
RbCl:F^-	0.381	0.015	−0.109	0.619	0.372	0.774	0.650
RbCl:Br^-	0.019	−0.011	0.041	0.675	0.628	0.810	0.862
RbCl:I^-	0.218	−0.044	0.072	0.702	0.569	1.254	1.370

system, except for LiCl:F^-, this resulted in the impurity ion going back onto the lattice site. The maximum displacement, that for RbCl:I^-, was 0.00026, 0.00026, 0. Such small displacements are considered insignificant. The locations of near neighbour ions up to the fourth neighbours (initially at 2,0,0) are given in Table 6 for the 11 systems which have full cubic symmetry. We notice the importance of ion-size effects. If the substitutional impurity is smaller than the host anion then the first, second, and fourth neighbours move in towards the impurity but if the impurity is larger than the host-crystal anion then these neighbouring ions are displaced outwards. The displacement of the third neighbours from their sites with coordinates $\pm 1, \pm 1, \pm 1$ are very small ($\leq 0.002a$). The displacements of the fourth neighbour ions are significant and are the most important after the nn ions, a fact which seems to be generally true and for which there is experimental evidence from Raman scattering measurements, for example.

In LiCl:F^- the F^- ion does not go on-centre; the displacement is constrained by symmetry to the ⟨110⟩ direction which is known to be the preferred direction for F^- impurity ions. The coordinates of the F^- impurity ion and its near neighbours, up to the fourth neighbours, are given in Table 7 for LiCl:F^-. The coordinates of the ions not given in the table can be worked out by using the fact that the final configuration has a ⟨110⟩ axis of symmetry. Since polarization effects must be important when small impurity ions adopt an off-centre configuration simple ion-size effects alone are unlikely to account for the calculated displacements. However, the fourth neighbours are again seen to undergo significant outward displacements when the adjacent nn ion suffers a large outward displacement (cf. the displacements at the 2,0,0 and 1,0,0 lattice sites).

Discussion

There have been no previous calculations of the energy parameters presented in this paper except the substitutional energies which can be extracted from Fancher and Barsch's (10) results of calculations of the energy of formation of several alkali halide solid

Can. J. Chem. Downloaded from www.nrcresearchpress.com by 210.87.254.42 on 09/05/12
For personal use only.

Can. J. Chem. Downloaded from www.nrcresearchpress.com by 210.87.254.42 on 09/05/12
For personal use only.

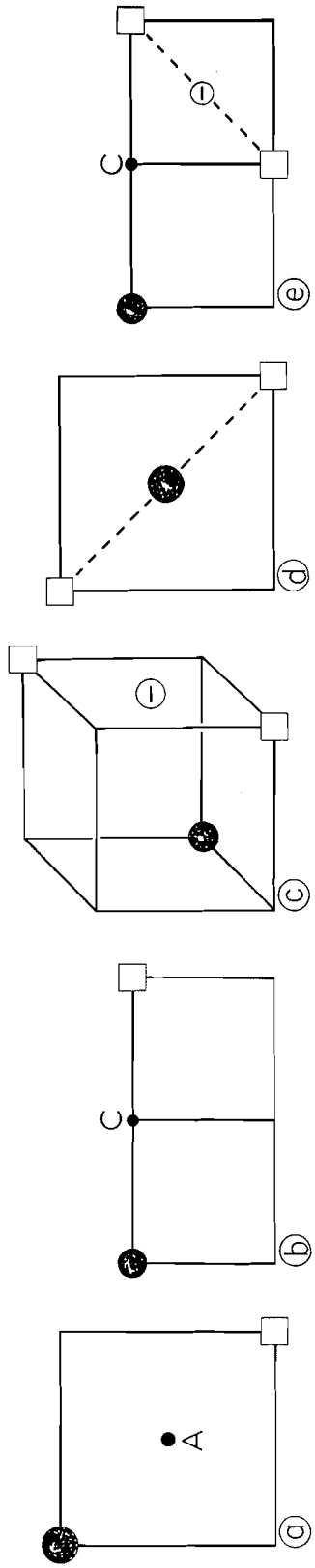

FIG. 2. The large filled circle denotes the anion impurity, the small filled circle the origin of the coordinate system, a square denotes an anion vacancy, and a circle containing a hyphen (⊖) denotes the jumping anion. (*a*) The face-centred (fc) position A denotes the choice of origin used for the nn vacancy complex. (*b*) The cation site C was used as the origin for the nn vacancy complex. (*c*) Saddle point configuration for a w_1-type jump. The origin coincides with the jumping anion at the fc position. (*d*) Symmmetrical saddle point configuration for the w_2-type jump. The origin coincides with the impurity anion at the fc position. (*e*) Saddle point configuration for w_3- and w_4-type jumps. The origin is at the cation site C.

TABLE 4. Test of the effect of a smaller region I on the defect energies of LiCl:Br^- and substitutional, association, and activation energies for LiCl:Br^-

(*a*) Test of the effect of a smaller region I on the defect energies of LiCl:Br^- (all energies are in eV)

Defect	No. of ions	Energy	Energy with larger region I
$u(X')$	50	0.608	0.606
u_{a1}	49	6.639	6.615
u_{a2}	54	6.716	6.702
u_1	48	7.579	—
u_2	49	7.552	7.498
$u_{3,4}$	48	7.590	—
u_-^∞ LiCl	57	6.020	6.026
u_-^∞ LiBr	57	5.774	5.780

(*b*) Substitutional, association, and activation energies for LiCl:Br^- using the smaller region I of Table 4*a*, compared with the values obtained by using the 81-ion region I (except for u_1 and $u_{3,4}$)

Parameter	Small region I	As given previously
$\Delta u(X^{-\prime})$	0.057	0.055
Δu_{a1}	0.011	−0.017
Δu_{a2}	0.088	0.070
Δu_1	0.940	0.964
Δu_2	0.913	0.883
Δu_3	0.874	0.888
Δu_4	0.951	0.975

solutions as functions of composition. Our calculated values should be compared with the limiting slope at infinite dilution of $U(x)$ for X′ in MX, where $U(x)$ is the energy of mixing at mole fraction x, and this was done by estimating this slope as $U(x = 0.01)/0.01$. Fancher and Barsch used the model of Dick and Das (14, 15) which takes account of repulsive interactions for nn only and neglects van der Waals forces entirely. Despite the simpler potential employed by these authors the two sets of results parallel one another quite closely and the same conclusions may be drawn from either set. The first factor is ion size. I^- and Br^- are larger than Cl^- and so the replacement energies are positive with the I^- values being larger than the Br^- energies. Also for a given impurity ion the replacement energy decreases as the cation radius, and therefore deformability increases. The F^- results show that ion size is not the only consideration and the large replacement energies obtained for F^- point to the importance of ion polarization effects. $U(x)$ has been measured experimentally for only two of the systems examined here and these results, which are in reasonable agreement with both calculated values, are also given in Table 8. Again the quoted values are the limiting

Can. J. Chem. Downloaded from www.nrcresearchpress.com by 210.87.254.42 on 09/05/12
For personal use only.

TABLE 5. Comparison of calculated defect energies for LiCl:Br^- and KCl:Br^- using the Set I and Set II (splined) potentials for CDN (1)

System	$\Delta u(X')$	Δu_{a1}	Δu_{a2}	Δu_1	Δu_2	Δu_3	Δu_4
LiCl:Br^-(I)	0.039	−0.018	0.082	0.788	0.740	0.771	0.871
(II)	0.055	−0.017	0.070	0.964	0.883	0.888	0.975
KCl:Br^-(I)	0.026	0.012	0.046	0.748	0.625	0.880	0.913
(II)	0.031	−0.012	0.044	0.740	0.677	0.869	0.925

TABLE 6. The calculated equilibrium locations of the cores of the neighbouring ions up to fourth neighbours for the systems in which the impurity ions effectively occupy lattice sites. All coordinates are given in units of the relevant anion–cation interionic distances, the impurity ions are placed at the origin, and the coordinates of only one ion of each symmetry type are given

System	Locations of the cores of the 6 ions of the type originally at 1,0,0			Locations of the cores of the 12 ions of the type originally at 1,1,0			Locations of the cores of the 8 ions of the type originally at 1,1,1			Locations of the cores of the 6 ions of the type originally at 2,0,0		
LiCl:Br^-	1.032	0.000	0.000	1.006	1.006	0.000	1.000	1.000	1.000	2.005	0.000	0.000
LiCl:I^-	1.089	0.000	0.000	1.013	1.013	0.000	0.999	0.999	0.999	2.022	2.000	0.000
NaCl:F^-	0.919	0.000	0.000	0.990	0.990	0.000	1.002	1.002	1.002	1.985	0.000	0.000
NaCl:Br^-	1.028	0.000	0.000	1.004	1.004	0.000	0.999	0.999	0.999	2.008	2.000	2.000
NaCl:I^-	1.065	0.000	0.000	1.010	1.010	0.000	0.998	0.998	0.998	2.022	0.000	0.000
KCl:F^-	0.932	0.000	0.000	0.992	0.992	0.000	1.002	1.002	1.002	1.979	0.000	0.000
KCl:Br^-	1.023	0.000	0.000	1.002	1.002	0.000	0.999	0.999	0.999	2.009	0.000	0.000
KCl:I^-	1.059	0.000	0.000	1.005	1.005	0.000	0.998	0.998	0.998	2.026	0.000	0.000
RbCl:F^-	0.934	0.000	0.000	0.993	0.993	0.000	1.002	1.002	1.002	1.979	0.000	0.000
RbCl:Br^-	1.023	0.000	0.000	1.002	1.002	0.000	0.999	0.999	0.999	2.010	0.000	0.000
RbCl:I^-	1.058	0.000	0.000	1.005	1.005	0.000	0.998	0.998	0.998	2.025	0.000	0.000

TABLE 7. Calculated equilibrium locations of the core of the impurity ion and those of its neighbouring ions, up to its fourth neighbours, in LiCl:F^-. The coordinates are given in units of the nn anion–cation separation a and the on-centre position of the fluoride ion would be at the origin

Lattice coordinates			Calculated coordinates for ion core		
0.0	0.0	0.0	−0.117	−0.117	0.000
1.0	0.0	0.0	1.070	−0.005	0.000
−1.0	0.0	0.0	−0.894	−0.024	0.000
0.0	0.0	1.0	−0.015	−0.015	0.813
1.0	1.0	0.0	0.987	0.987	0.000
1.0	−1.0	0.0	0.989	−0.984	0.000
−1.0	−1.0	0.0	−1.009	−1.009	0.000
0.0	1.0	1.0	−0.001	0.983	0.974
0.0	−1.0	1.0	−0.003	−0.992	0.988
1.0	1.0	1.0	0.995	0.995	1.003
1.0	−1.0	1.0	0.992	−1.004	1.000
−1.0	−1.0	1.0	−1.006	−1.006	1.002
2.0	0.0	0.0	2.018	0.002	0.000
−2.0	0.0	0.0	−1.998	0.000	0.000
0.0	0.0	2.0	0.001	0.001	1.997

TABLE 8. Comparison of the calculated substitutional energies $\Delta u(X')$ in eV, with the results of Fancher and Barsch (10) (FB) and with experimental data

System	$\Delta u(X')$	FB	Expt.
LiCl:F^-	0.971	0.889	
LiCl:Br^-	0.055	0.063	
LiCl:I^-	0.362	0.417	
NaCl:F^-	0.714	0.503	
NaCl:Br^-	0.048	0.055	0.062[a]
			0.047[b]
NaCl:I^-	0.346	0.359	
KCl:F^-	0.471	0.363	
KCl:Br^-	0.031	0.046	0.037[c]
KCl:I^-	0.258	0.294	
RbCl:F^-	0.381	0.300	
RbCl:Br^-	0.019	0.038	
RbCl:I^-	0.218	0.274	

[a]Fineman and Wallace (11).
[b]Fontell *et al.* (12).
[c]Hovi (13).

partial molar energies for $x \to 0$, obtained from $U(x = 0.01)$.

There are no experimental data yet for association energies or for the activation energies for type w_1, w_2, w_3, or w_4 jumps. The major factor causing association between vacancies and aliovalent impurity ions is electrostatic interaction (16) but ion size also plays a part particularly in determining whether nn or next nn sites (in the same sub-lattice) are favoured. These calculations are for univalent impurities and therefore enable one to assess ion-size factors. Br^- and I^- impurity ions are larger than Cl^- and we should therefore expect the nn sites for the vacancy to be favoured. Table 3 shows that this is so; Δu_{a1} is negative in every case, and more so for I^- than Br^-. An anion vacancy in the next nn anion site, however, does not relieve the local strain and so this site is not favoured, $\Delta u_{a2} > 0$. On size arguments alone one should not expect $\Delta u_{a1} < 0$ for

Can. J. Chem. Downloaded from www.nrcresearchpress.com by 210.87.254.42 on 09/05/12
For personal use only.

substitutional F^- ions. For RbCl it is slightly positive, for KCl it is approximately zero, for NaCl it is slightly negative, and for LiCl it is definitely positive. In all these cases the sign of Δu_{a2} is opposite to that of Δu_{a1}, that is, if the nn position is unstable the next nn position is stable. These more complicated results with F^- are due to polarization effects.

The calculated values (3) of the activation energy (Δu_0) for the motion of a single isolated vacancy in the four host crystals are 0.69 eV for LiCl, 0.72 eV for NaCl, 0.69 eV for KCl, and 0.63 eV for RbCl. We should expect Δu_2, the activation energy for the impurity–vacancy interchange, to be roughly the same as Δu_0 if the anion impurity is not very different in size to the host anion. This is certainly true for Br^- in NaCl, KCl, RbCl for which Δu_2 differs from Δu_0 by $\sim$0.01 eV. For the larger I^- ion larger repulsive interactions will be offset by a greater polarization contribution and it is not possible to predict in advance which will be the more important effect. The results for I^- in NaCl, KCl, RbCl show that Δu_2 is less than Δu_0 by 0.04 to 0.06 eV, so that polarization effects slightly outweigh the increased repulsive energy. For F^- the interchange energy Δu_2 is much less than Δu_0 and this is due not only to its smaller size but also to polarization effects.

The results presented here for the w_2, w_3, w_4 jumps are of some help in predicting activation energies for impurity diffusion by a single vacancy mechanism. The ratio of the impurity diffusion coefficient D' to the self-diffusion coefficient D for the pure crystal is (17)

$$[7] \qquad D'/D = w_2 f_i'/w_0 f_0$$

where w_0 is the jump frequency for the motion of a single vacancy in the pure crystal,

$$[8] \qquad f_i' = f_i w_3/w_4$$

and the correlation factor for the impurity is

$$[9] \qquad f_i = \frac{w_1 + Fw_4}{w_2 + w_1 - Fw_4}$$

with F a slowly varying function of w_3/w_0 in the range 1 to $\frac{7}{2}$. f_0 is the correlation factor for self-diffusion in the pure crystal. From eqs. [7]–[9] we have

$$[10] \quad -k[\mathrm{d}\ln(D'/D)/\mathrm{d}T^{-1}] = E_v' - E_v = \Delta u_2 - \Delta u_0 + \Delta u_3 - \Delta u_4 - k[\mathrm{d}\ln f_i/\mathrm{d}T^{-1}]$$

where E_v, E_v' are the activation energies for the diffusion of host ions and impurity ions, respectively, by single vacancy jumps. We have calculated the first four terms on the right side of [10] but an accurate prediction of $E_v' - E_v$ would require a knowledge of the dependence of the correlation factor f_i on temperature, and hence of the entropies of activation and effective vibrational frequencies as well as of the energies of activation. We may obtain a first approximation to E_v', called $\tilde{E}_v'$, by simply omitting the correlation term in [10] so that

$$[11] \qquad \tilde{E}_v' = \tfrac{1}{2}u_S + \Delta u_2 + \Delta u_3 - \Delta u_4$$

where u_S is the energy to form a Schottky defect. Values of $\tilde{E}_v'$ calculated from [11], using u_S values from ref. 3, are given in Table 9, together with the only currently available values (18) for E', the experimental activation energy for vacancy diffusion. Apart from the neglect of the correlation term in $\tilde{E}_v'$, experimentally measured diffusion coefficients include contributions from both vacancy pair diffusion and the diffusion of single vacancies. Thus a comparison of E' with $\tilde{E}_v'$ gives a measure of the contribution to E' of the combined effects of the temperature dependence of the correlation factor and that from the vacancy pair contribution to D'. Table 9 suggests that these two effects provide a net correction to $\tilde{E}_v'$ which is positive and of the order of a few tenths of an eV.

TABLE 9. Calculated values of the activation energy for diffusion by single vacancies of a univalent anion impurity ($\tilde{E}_v'$) in alkali metal chloride crystals, neglecting the temperature dependence of the correlation factor, compared with experimental values of the activation energy E' for impurity diffusion. All numerical values are in eV

Host crystal	$\tilde{E}_v'$ for: F^-	Br^-	I^-
LiCl	1.57	2.13	1.98
NaCl	1.50	2.08	1.78
KCl	1.76	1.90	1.80
RbCl	1.72	1.80	1.67
Host crystal	**E' for: F^-**	**Br^-**	**I^-**
NaCl	1.83	2.18	2.08

Acknowledgements

P.W.M.J. thanks the North Atlantic Treaty Organization for a Research Grant. B.M.C.P. acknowledges the receipt of a post-graduate research grant from the Irish Department of Education and the cooperation of the Computer Centre at University College, Dublin.

1. C. R. A. CATLOW, K. M. DILLER, and M. J. NORGETT. J. Phys. C, **10**, 1395 (1977).
2. C. R. A. CATLOW, J. CORISH, K. M. DILLER, P. W. M. JACOBS, and M. J. NORGETT. J. Phys. Paris, **37**, C7-253 (1976).
3. C. R. A. CATLOW, J. CORISH, K. M. DILLER, P. W. M. JACOBS, and M. J. NORGETT. Report TP713, A.E.R.E. Harwell, U.K. 1977.
4. J. CORISH, B. M. C. PARKER, and P. W. M. JACOBS. Proc. R. Ir. Acad. **77**, 371 (1977).
5. A. B. LIDIARD and M. J. NORGETT. *In* Computational solid state physics. *Edited by* F. Herman, N. W. Dalton, and T. R. Koehler. Plenum Press, New York, NY. 1972.
6. M. J. NORGETT. Report R7650, A.E.R.E. Harwell, U.K. 1974.
7. P. T. WEDEPOHL. Proc. Phys. Soc. **92**, 79 (1967).
8. A. GONGORA and F. LÜTY. Bull. Am. Phys. Soc. **20**, 469 (1975).
9. J. WAHL and F. LÜTY. Bull. Am. Phys. Soc. **20**, 469 (1975).
10. D. L. FANCHER and G. R. BARSCH. J. Phys. Chem. Solids, **30**, 2517 (1969).
11. M. FINEMAN and W. E. WALLACE. J. Am. Chem. Soc. **70**, 4165 (1948).
12. N. FONTELL, V. HOVI, and L. HYVONEN. Ann. Acad. Sci. Fenn. Ser. A, **I**, No. 65, 1 (1949).
13. V. HOVI. Ann. Acad. Sci. Fenn. Ser. A, **I**, No. 55, 1 (1948).
14. B. G. DICK and T. P. DAS. Phys. Rev. **127**, 1053 (1962).
15. B. G. DICK and T. P. DAS. J. Appl. Phys. **33**, 2815 (1962).
16. C. R. A. CATLOW. Chem. Phys. Lett. **39**, 497 (1976).
17. J. R. MANNING. Diffusion kinetics for atoms in crystals. Van Nostrand Co., Princeton, NJ. 1968.
18. M. BÉNIÈRE, F. BÉNIÈRE, C. R. A. CATLOW, A. K. SHUKLA, and C. N. R. RAO. J. Phys. Chem. Solids, **38**, 521 (1977).
19. C. R. A. CATLOW, J. CORISH, K. M. DILLER, P. W. M. JACOBS, M. J. NORGETT, and B. M. C. PARKER. To be published.

Can. J. Chem. Downloaded from www.nrcresearchpress.com by 210.87.254.42 on 09/05/12
For personal use only.

Crystal and molecular structure of diphenylboron *N*-methylacethydroxamate (4,5-dimethyl-2,2-diphenyl-1,3-dioxa-4-azonia-2-boratacyclopent-4-ene)

STEVEN J. RETTIG AND JAMES TROTTER

Department of Chemistry, University of British Columbia, 2075 Wesbrook Mall, Vancouver, B.C., Canada V6T 1W5

AND

W. KLIEGEL AND D. NANNINGA

Institut für Pharmazeutische Chemie der Technischen Universität, 33 Braunschweig, Bundesrepublik Deutschland

Received December 12, 1977

STEVEN J. RETTIG, JAMES TROTTER, W. KLIEGEL, and D. NANNINGA. Can. J. Chem. **56**, 1676 (1978).

Crystals of diphenylboron *N*-methylacethydroxamate are orthorhombic, $a = 12.5478(8)$, $b = 7.8735(3)$, $c = 13.6809(5)$ Å, $Z = 4$, space group *Pnam*. The structure was solved by direct methods and was refined by full-matrix least-squares procedures to $R = 0.037$ and $R_w = 0.054$ for 1265 reflections with $I \geq 3\sigma(I)$. The molecule features a five-membered BO_2CN ring which lies in the crystallographic mirror plane. The carbon and nitrogen atoms of the heterocyclic ring are positionally disordered. Mean bond lengths (corrected for libration) are: O—B, 1.550(2), B—C, 1.609(2), O—C/N, 1.340(3), C—N, 1.300(2), C/N—CH, 1.470(2), and C—C(phenyl), 1.394(8) Å.

STEVEN J. RETTIG, JAMES TROTTER, W. KLIEGEL et D. NANNINGA. Can. J. Chem. **56**, 1676 (1978).

Les cristaux du *N*-méthylacéthydroxamate de diphénylbore sont orthorhombiques, $a = 12.5478(8)$, $b = 7.8735(3)$, $c = 13.6809(5)$ Å, $Z = 4$, groupe d'espace *Pnam*. On a résolu la structure par des méthodes directes et on l'a affinée par la méthode des moindres carrés (matrice complète) jusqu'à des valeurs de $R = 0.037$ et $R_w = 0.054$ pour 1265 réflexions avec $I \geq 3\sigma(I)$. La molécule comporte un cycle BO_2CN à cinq chaînons qui se trouve dans un plan mirroir cristallographique. Les atomes de carbone et d'azote de l'hétérocycle sont disposés d'une façon désordonnée. Les longueurs moyennes des liaisons (corrigées pour la libration) sont: O—B, 1.550(2), B—C, 1.609(2), O—C/N, 1.340(3), C—N, 1.300(2), C/N—CH, 1.470(2) et C—C(phényle), 1.394(8) Å.

[Traduit par le journal]

Introduction

The search for the best formal description of the boron chelates of *N*-substituted hydroxamic acids led us to the investigation of the difluoroboron derivative of *N*-methylacethydroxamic acid (**1**, R = R^1 = Me, X = F). An X-ray crystallographic analysis of this compound (1) gave evidence for a predominant contribution of the zwitterionic form **1***a* to the resonance structure of the compound. In addition to establishing the boron–nitrogen betaine formulation (**1***a*), a remarkable molecular symmetry was observed. In spite of the chemically different functions (C=O and N—O) in the ligand, the O—B distances in the difluoroboron chelate are equal within experimental error and a comparatively short amide C—N bond indicates **1***a* or **1***c*. In view of these findings it is of great interest to examine the molecular dimensions of an analogous chelate compound in which the extremely electron-deficient difluoroborenium ion (in **1***c*, X = F) is replaced by a less electrophilic diphenylborenium ion (X = Ph).

Other diphenylboron chelates with bidentate oxygen ligands having chemically different oxygen

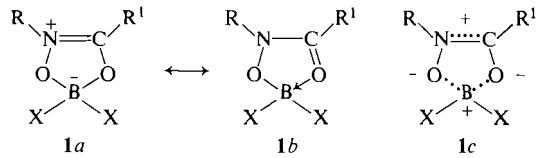

1*a* **1***b* **1***c*

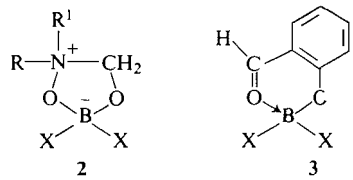

2 **3**

atoms, such as **2** (X = Ph) (2), which can be regarded as a formal reduction product of **1**, and the salicylaldehyde derivative **3** (X = Ph) (3), have significantly different O—B distances. In a B,N-betaine structure **1***a* or **1***c*, two nearly identical O—B bond lengths could also be expected in the case of X = Ph. The main structural difference between the difluoro and diphenyl derivatives should be in the intra-annular bond lengths to boron, expected to be longer for X = Ph.

Can. J. Chem. Downloaded from www.nrcresearchpress.com by 210.87.254.40 on 09/05/12
For personal use only.

Can. J. Chem. Downloaded from www.nrcresearchpress.com by 210.87.254.40 on 09/05/12
For personal use only.

Experimental

4,5-Dimethyl-2,2-diphenyl-1,3-dioxa-4-azonia-2-boratacyclopent-4-ene[1]

N-Methylacethydroxamic acid (2 mmol) (4) and oxybisdiphenylborane (1 mmol) (diphenylborinic acid anhydride) were dissolved in 15 ml of absolute ethanol. Crystals began precipitating after a few minutes at room temperature. The mixture was heated to boiling to complete the reaction. After cooling, 0.44 g (1.74 mmol, 87%) of colorless crystals were isolated and were recrystallized from acetone–chloroform, mp 214°C. *Anal.* calcd. for $C_{15}H_{16}BNO_2$: C 71.18, H 6.37, N 5.53, B 4.27; found: C 71.16, H 6.44, N 5.42, B 4.27; ir (1/300 KBr): 1650 cm^{-1} (C=N/O); ^1H nmr (60 MHz, DMSO-d_6/TMS) δ (ppm): 2.37 (s, 3, C—CH_3), 3.57 (s, 3, N—CH_3), 7.1–7.8 (m, 10, Ph).

X-ray Crystallographic Analysis

The crystal chosen for study was mounted with *b* parallel to the goniostat axis and had dimensions of ca. 0.2 × 0.6 × 0.8 mm. Unit-cell and space group data were obtained from film and diffractometer measurements. The unit-cell parameters were refined by least squares on 2 sin θ/λ values for 27 reflections measured on a diffractometer with Cu K_α radiation (λ = 1.540562 and 1.544390 Å for α_1 and α_2). Crystal data (at 22°C) are:

$C_{15}H_{16}BNO_2$ fw = 253.11

Orthorhombic, a = 12.5478(8), b = 7.8735(3), c = 13.6809(5) Å, V = 1351.6(1) $Å^3$, ρ_m = 1.22 (flotation in aqueous KI), Z = 4, ρ_c = 1.244 g cm^{-3}, $F(000)$ = 536, μ(Cu K_α) = 6.6 cm^{-1}. Absent reflections: $0kl$, $k + l \neq 2n$, and $h0l$, $h \neq 2n$. Space group *Pnam* (non-standard setting of *Pnma*, D_{2h}^{16}, No. 62) from structure analysis.

Intensities were measured with nickel-filtered Cu K_α radiation on a Datex-automated General Electric XRD-6 diffractometer. A θ–2θ scan at 4° min^{-1} over a range of (1.80 + 0.86 tan θ) degrees in 2θ was employed. Background counts of 10 s were measured at each end of the scan. Data were measured to 2θ = 160°. The intensities of the check reflections, measured every 50 reflections throughout the data collection, remained constant to within ±1.7%. After data reduction, an absorption correction was applied using the Gaussian integration method (5, 6). Transmission factors ranged from 0.722 to 0.905. Of the 1534 independent reflections measured, 1271 (83%) had intensities greater than $3\sigma(I)$ above background where $\sigma^2(I) = S + B + (0.06S)^2$ with S = scan count and B = time-averaged background count.

The systematic absences allow space groups $Pna2_1$ or *Pnam*, the latter being indicated by the *E*-statistics. The structure was solved in the centrosymmetric space group by direct methods (7). The positions of the 13 non-hydrogen atoms were given by the 13 highest peaks on an *E*-map calculated from the best set of signs. Full-matrix least-squares refinement of the non-hydrogen atoms with isotropic, then with anisotropic thermal parameters, gave R = 0.088. A difference map revealed the positions of the phenyl hydrogen atoms and indicated a twofold disorder of both sets of methyl hydrogen atoms. In order to determine the location of the nitrogen atom in the heterocyclic ring, parallel refinements were carried out with the nitrogen atom in positions X(1) and X(2). Both refinements gave R = 0.066 with inconsistent anisotropic thermal parameters, indicating probable disordering. The positions X(1) and X(2) were then refined as 50% nitrogen and 50% carbon, giving an R value of 0.060 and reasonable thermal parameters. The occupancies of the disordered hydrogen atoms were set at 0.5 and were not refined.

The scattering factors of ref. 8 were used for non-hydrogen atoms and those of ref. 9 for hydrogen atoms. Anomalous scattering factors from ref. 10 were used for the non-hydrogen atoms. The weighting scheme, $w = 1.0$ if $|F_o| < 8.0$, $w = (8.0/|F_o|)^2$ if $|F_o| \geq 8.0$, and $w = 0.137$ for the unobserved planes, gave uniform average values of $w(|F_o| - |F_c|)^2$ over ranges of $|F_o|$ and was employed in the final stages of refinement. A correction for secondary extinction was approximated by basing the least-squares refinement on the minimization of $\Sigma w[|F_o| - |F_c/(1 + gI)|]^2$ where g is the extinction parameter and I the uncorrected intensity. The final value of g was 8.3×10^{-8}. Convergence was reached at R = 0.037 and R_w = 0.054 for 1265 reflections with $I \geq 3\sigma(I)$ (6 reflections with $||F_o| - |F_c|| > 3\sigma(F)$ were treated as unobserved in the final stages of refinement; instrumental error was suspected, but it seemed unwise to bias the data by remeasurement; the discrepancies were not large). For all 1534 reflections R = 0.048 and R_w = 0.059.

On the final cycle of refinement the mean and maximum parameter shifts corresponded to 0.03 and 0.30σ respectively. The mean error in an observation of unit weight was 0.3406. A final difference map showed maximum fluctuations of ±0.25 e $Å^{-3}$. Final thermal parameters of the disordered hydrogen atoms indicate that for the C(2) methyl group occupancies of 0.5 are correct but for the C(3) group the unprimed positions

TABLE 1. Final positional parameters (fractional × 10^4, H × 10^3) with estimated standard deviations in parentheses; equivalent positions: ±[x, y, z; ½ − x, ½ + y, ½ + z; x, ½ − y, z; ½ + x, ½ − y, z]

Atom	x	y	z
O(1)	2367(1)	5876(2)	2500
O(2)	4230(1)	6255(1)	2500
X(1)	2671(1)	7505(2)	2500
X(2)	3690(1)	7712(2)	2500
C(2)	4287(2)	9313(3)	2500
C(3)	1840(2)	8807(3)	2500
C(4)	3489(1)	3694(1)	1524(1)
C(5)	2619(1)	2779(2)	1169(1)
C(6)	2704(1)	1719(2)	363(1)
C(7)	3671(1)	1547(2)	−112(1)
C(8)	4542(1)	2437(2)	218(1)
C(9)	4451(1)	3497(2)	1025(1)
B	3400(1)	4815(2)	2500
H(2a)*	504(4)	910(6)	250
H(2b)*	411(3)	993(5)	193(3)
H(2a′)*	390(4)	1016(6)	250
H(2b′)*	478(4)	921(6)	190(3)
H(3a)*	222(3)	1000(5)	250
H(3b)*	141(3)	860(4)	186(3)
H(3a′)*	115(9)	841(12)	250
H(3b′)*	194(5)	961(7)	203(4)
H(5)	191(1)	290(2)	150(1)
H(6)	210(2)	98(3)	17(2)
H(7)	375(2)	78(3)	−68(2)
H(8)	525(2)	233(3)	−11(2)
H(9)	507(1)	415(2)	125(1)

*Occupancy fixed at 0.5.

[1]The practice of Chemical Abstracts and tentative IUPAC rules suggest the use of the term 'borata' rather than 'boranata' which we used before to denote tetrahedral boron.

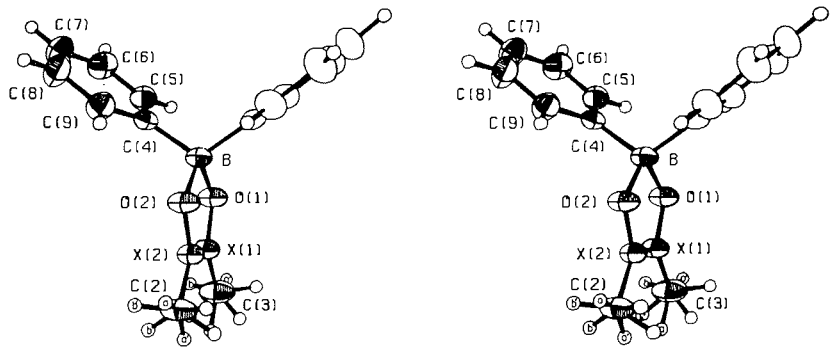

FIG. 1. Stereo view of the diphenylboron *N*-methylacethydroxamate molecule; 50% ellipsoids are shown for the non-hydrogen atoms. Hydrogen atoms have been assigned artificially small thermal parameters for the sake of clarity.

TABLE 3. Bond lengths (Å) with estimated standard deviations in parentheses

(*a*) Non-hydrogen atoms

Bond	Uncorr.	Corr.	Bond	Uncorr.	Corr.
O(1)—B	1.542(2)	1.552	C(4)—B	1.604(2)	1.609
O(2)—B	1.540(2)	1.548	C(4)—C(5)	1.396(2)	1.404
O(1)—X(1)	1.338(2)	1.342	C(4)—C(9)	1.395(2)	1.404
O(2)—X(2)	1.333(2)	1.337	C(5)—C(6)	1.387(2)	1.391
X(1)—X(2)	1.289(2)	1.300	C(6)—C(7)	1.383(2)	1.392
X(1)—C(3)	1.462(3)	1.468	C(7)—C(8)	1.374(2)	1.382
X(2)—C(2)	1.466(2)	1.471	C(8)—C(9)	1.388(2)	1.393

(*b*) Bonds involving hydrogen atoms

Me—H,	0.82–1.05(4–11), mean 0.96(8) Å
C(ar)—H,	0.98–1.00(2), mean 0.99(1) Å

appear to be favored by a factor of about 3:1 over the primed positions. The final positional and thermal parameters appear in Tables 1 and 2[2] respectively. Measured and calculated structure factors have been placed in the Depository of Unpublished Data.[2]

The ellipsoids of thermal motion for the non-hydrogen atoms are shown in Fig. 1. The thermal motion has been analysed in terms of the rigid-body modes of translation, libration, and screw motion (11) using the computer program MGTLS. The rms standard error in the temperature factors σU_{ij} (derived from the least-squares analysis) is 0.0008 Å^2. Analyses of the phenyl ring plus the boron atom and the seven atom group consisting of the non-hydrogen atoms lying in the mirror plane (rms ΔU_{ij} = 0.0015 and 0.0006 Å^2, respectively) gave physically reasonable rigid-body parameters. The appropriate bond distances have been corrected for libration (12) using shape parameters q^2 of 0.08 for all atoms involved. Corrected bond lengths appear in Table 3 along with the uncorrected values. Bond angles are not significantly different from the uncorrected values listed in Table 4.

Results and Discussion

Figure 1 shows a general view of the molecule with the crystallographic numbering scheme and the disordered methyl hydrogen atoms. The packing arrangement viewed along *b* is shown in Fig. 2.

The crystal structure consists of discrete molecules of diphenylboron *N*-methylacethydroxamate. All intermolecular distances correspond to normal van der Waals interactions with the exception of a possible weak hydrogen bond involving a disordered methyl hydrogen atom (C(3)—H(3a')...O(2)[$x - \frac{1}{2}$, $\frac{3}{2} - y$, $\frac{1}{2} - z$]: C...O = 3.275(3), H...O = 2.42(11) Å, and ∠C—H...O = 154(8)°).

The **1***a* molecule with X = F was found to have an essentially planar BO_2CN ring and geometrical symmetry remarkably close to C_{2v} (2/*m*). The diphenyl derivative has crystallographic *m* symmetry, the five-membered ring lying on the mirror plane and therefore exactly planar. The geometrical C_{2v} symmetry of the molecule is again present as expected but in this case the C and N atoms are indistinguishable. The geometry of the *N*-methylacethydroxamate moiety is the same as that found in the difluoro derivative within the limits of experimental error. The symmetrical disposition of the two phenyl rings is unique among diphenylboron chelates (2, 3, 13–16).

[2]Copies of the structure factor table and Table 2 (thermal parameters) are available, at a nominal charge, from the Depository of Unpublished Data, CISTI, National Research Council of Canada, Ottawa, Ont., Canada K1A 0S2.

Can. J. Chem. Downloaded from www.nrcresearchpress.com by 210.87.254.40 on 09/05/12
For personal use only.

TABLE 4. Bond angles (deg) with estimated standard deviations in parentheses

(*a*) Non-hydrogen atoms*

Bonds	Angle (deg)	Bonds	Angle (deg)
B —O(1)—X(1)	106.2(1)	C(9)—C(4)—C(5)	116.6(1)
B —O(2)—X(2)	106.8(1)	C(4)—C(5)—C(6)	121.8(1)
O(1)—X(1)—C(3)	117.9(2)	C(5)—C(6)—C(7)	120.0(1)
O(1)—X(1)—X(2)	113.9(1)	C(6)—C(7)—C(8)	119.5(1)
C(3)—X(1)—X(2)	128.2(2)	C(7)—C(8)—C(9)	120.1(1)
O(2)—X(2)—C(2)	118.7(2)	C(8)—C(9)—C(4)	121.9(1)
O(2)—X(2)—X(1)	113.3(1)	O(1)—B —O(2)	99.8(1)
C(2)—X(2)—X(1)	128.0(2)	O(1)—B —C(4)	110.9(1)
B —C(4)—C(5)	121.3(1)	O(2)—B —C(4)	110.9(1)
B —C(4)—C(9)	122.0(1)	C(4)—B —C(4)′	112.6(1)

(*b*) Angles involving hydrogen atoms

C/N—C(Me)—H,	104–116(2–6),	mean 110(4)
H—C(Me)—H,	90–115(2–7),	mean 109(5)
C—C(ar)—H,	118–122(1),	mean 120(1)

*Primed atom at $x, y, \frac{1}{2} - z$.

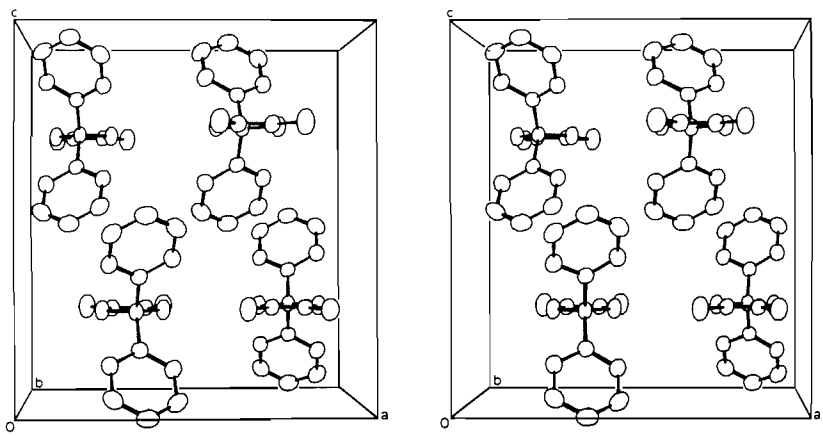

FIG. 2. Stereo view of the packing arrangement of diphenylboron *N*-methylacethydroxamate viewed along *b*.

The O—B distances (1.548(2) and 1.552(2) Å) are, as expected, significantly longer than those in the difluoro analogue (1.496(3) and 1.497(3) Å); they are close to the (N)O—B distance of 1.556(8) Å in **2** (2) but are considerably longer than the true O—B single bonds in the ethanolamine esters of diarylborinic acids (13–15) (mean[3] 1.477(5) Å) and the weakened single bonds in L-prolinatodiphenylboron (16) (1.529(3) Å), **3** (1.500(4) Å), and **2** (1.506(7) Å). The dative O—B bond in **3**, 1.574(4) Å, is significantly longer than the O—B bonds in the present structure. This evidence further supports the earlier contention (1) that the overall structure of **1** is best described as a 3:1 hybrid of resonance forms **1***a* and **1***b*.

The B—C distance of 1.609(2) Å lies near the short end of the range of B—C distances observed in diphenylboron chelates (2, 3, 13–16), 1.603(4) in **3** to 1.639(8) Å in **2** with a mean value of 1.617(8) Å. The mean C—C(phenyl) distance of 1.394(8) Å is normal, but individual bond lengths and angles in the ring differ significantly. This substituent-induced distortion of the phenyl ring is essentially identical to that found in related compounds (15, 16).

[3]Here and elsewhere in this report mean values refer to weighted means with rms deviations from the mean in parentheses.

Acknowledgments

We thank the National Research Council of Canada for financial support and the University of British Columbia Computing Centre for assistance.

Can. J. Chem. Downloaded from www.nrcresearchpress.com by 210.87.254.40 on 09/05/12
For personal use only.

1. S. J. RETTIG, J. TROTTER, W. KLIEGEL, and D. NANNINGA. Can. J. Chem. **55**, 1 (1977).
2. S. J. RETTIG, J. TROTTER, and W. KLIEGEL. Can. J. Chem. **52**, 2531 (1974).
3. S. J. RETTIG and J. TROTTER. Can. J. Chem. **54**, 1168 (1976).
4. O. EXNER. Collect. Czech. Chem. Commun. **16**, 266 (1951).
5. P. COPPENS, L. LEISEROWITZ, and D. RABINOVICH. Acta Crystallogr. **18**, 1035 (1965).
6. W. R. BUSING and H. A. LEVY. Acta Crystallogr. **22**, 457 (1967).
7. R. E. LONG. Ph.D. Thesis, University of California at Los Angeles, Los Angeles, CA. 1965.
8. D. T. CROMER and J. B. MANN. Acta Crystallogr. Sect. A, **24**, 321 (1968).
9. R. F. STEWART, E. R. DAVIDSON, and W. T. SIMPSON. J. Chem. Phys. **42**, 3175 (1965).
10. D. T. CROMER and D. LIBERMAN. J. Chem. Phys. **53**, 1891 (1970).
11. V. SCHOMAKER and K. N. TRUEBLOOD. Acta Crystallogr. Sect. B, **24**, 63 (1969).
12. D. W. J. CRUICKSHANK. Acta Crystallogr. **9**, 747 (1956); **9**, 754 (1956); **14**, 896 (1961).
13. S. J. RETTIG and J. TROTTER. Can. J. Chem. **51**, 1288 (1973).
14. S. J. RETTIG and J. TROTTER. Acta Crystallogr. Sect. B, **30**, 2139 (1974).
15. S. J. RETTIG and J. TROTTER. Can. J. Chem. **54**, 3130 (1976).
16. S. J. RETTIG and J. TROTTER. Can. J. Chem. **55**, 958 (1977).

Can. J. Chem. Downloaded from www.nrcresearchpress.com by 210.87.254.40 on 09/05/12
For personal use only.

Anesthesia and hydrogen bonding. A semi-quantitative infrared study at room temperature

GINETTE TRUDEAU, K. C. COLE, RACHEL MASSUDA, AND C. SANDORFY
Département de Chimie, Université de Montréal, Montréal (Qué.), Canada H3C 3V1

Received December 22, 1977

GINETTE TRUDEAU, K. C. COLE, RACHEL MASSUDA, and C. SANDORFY. Can. J. Chem. **56**, 1681 (1978).

It has been shown previously that certain anesthetics hinder the formation of hydrogen bonds of the O—H---O, N—H---N, N—H---O=C$\diagdown$ types. An attempt has now been made to correlate this hydrogen bond 'breaking' property with anesthetic potency. As a measure of the former, relative intensities of infrared bands related to 'free' and hydrogen bonded species were used. The band which was chosen for this purpose is the OH or NH stretching + in-plane bending combination band. This made it possible to carry out the measurements at room temperature. A semi-quantitative relationship has been found. Its significance for the theories of anesthesia is discussed.

GINETTE TRUDEAU, K. C. COLE, RACHEL MASSUDA et C. SANDORFY. Can. J. Chem. **56**, 1681 (1978).

Il a été démontré dans notre laboratoire que les anesthésiques halogénés entravent la formation des liaisons hydrogène de types O—H---O, N—H---N et N—H---O=C$\diagdown$. Nous avons effectué une étude par spectroscopie infrarouge afin de voir s'il existe une relation entre cette propriété et le pouvoir anesthésique de ces composés. A cette fin nous nous sommes servis des intensités relatives des bandes infrarouges libres et associées (par liaison hydrogène) de systèmes-modèle mesurées en présence et en absence d'anesthésiques. La bande qui nous a permis d'exécuter ce travail est une combinaison de la vibration de valence et de la vibration de déformation du groupement OH ou NH. Cette bande possède, en effet, un rapport libre–associé favorable à des mesures à la température ambiante. Une relation semi-quantitative a été trouvée. On discute son importance pour les théories de l'anesthésie.

Introduction

It has been observed in our laboratory that fluorocarbon type anesthetics containing higher halogens hinder the formation of hydrogen bonds (HB). The HB's were of the O—H---O, N—H---N, N—H---O=C$\diagdown$, or S—H---S types (1–5). When compounds like $CF_3CHClBr$ (halothane), CF_3-$CHCl_2$, or C_3F_7Br, for example, are added to solutions containing alcohols, phenols, amines, amides, thiols engaged in such HB's, the intensity ratio of the free and associated infrared X—H (X = O or N or S) stretching bands is modified in favor of the free (or less associated) species. This effect often takes spectacular proportions at low temperatures. Instead of the expected increase of the intensity of the associated band on lowering the temperature we observe its decrease and the accompanying reappearance of the free band. Therefore, in order to magnify the effect much (but not all) of our previous work was carried out at low temperatures (down to −190°C).

Subsequently we (6) were able to show that similar observations can be made on HB's involving water (for example, water bonded to an ether). Another series of infrared measurements (7) yielded the result that anesthetics like chloroform, halothane, methoxyflurane, enflurane, which contain an acidic hydrogen atom, can form HB's as proton donors whereby hindering the formation of N—H---N, O—H---O, and N—H---O=C$\diagdown$ HB's. Brown and Chaloner (8), Koehler *et al.* (9), and Davies *et al.* (10, 11) using different methods also arrived at the conclusion that HB formation by this acidic hydrogen might play a role in the mechanism of anesthesia.

The mechanism whereby anesthetics perturb or dissociate HB's might involve hydrophobic or polar interactions or the formation of another HB. As to the latter possibility, since available proton acceptor sites in the organism are quite certainly already engaged in HB's, it is clear that competitive HB cannot occur without perturbing or dissociating existing ones.

Present time theories of anesthesia are based on the 'unitary hypothesis' and the 'hydrophobic site theory' which state that the mechanism of action of all inhalation anesthetics is essentially the same and it implies only interactions at hydrophobic sites of the membrane (cf. refs. 12–15). The above-mentioned observations seem to indicate the need for a more

Can. J. Chem. Downloaded from www.nrcresearchpress.com by 210.87.254.6 on 09/05/12
For personal use only.

Can. J. Chem. Downloaded from www.nrcresearchpress.com by 210.87.254.6 on 09/05/12
For personal use only.

balanced theory of anesthesia taking into account, in addition to hydrophobic interactions, the possibility of polar ones including hydrogen bonding.

Most of our previous infrared spectroscopic studies were carried out at low temperatures. This had two drawbacks: the difficulty of making measurements quantitative due to problems inherent with the low temperature solution technique and the remoteness from in vivo conditions. In order to transpose our work to room temperature and to make it at least semi-quantitative we had to use an infrared band other than the X—H stretching fundamental (X = O, N, or S). To understand this we have to remark that at room temperature and at concentrations which have to be used the free band is often too weak and too highly overlapped by the associated band to be amenable to quantitative measurements. Fortunately, the free–associated ratio is different for overtones and combination tones. It generally favors the free band (16–19). The region of the first X—H overtone in the spectrum is usually complicated, however. No freestanding bands are found and, in some cases, we encounter the opposite difficulty: it is the associated band which is too weak (1). Thus we have to look for combination bands. Alcohols and phenols possess bands in the near infrared centered at about 5200–5300 cm^{-1} (or 1.92–1.88 μm) for which the free and associated bands overlap relatively little and the free–associated intensity ratio is moderate. This band is the combination of the O—H stretching and the O—H in-plane bending mode. Luck and Ditter (20) and Bonner and Choi (21) have applied these bands to hydrogen bond studies several years ago. Secondary amides have a band near 5000–4900 cm^{-1} (or 2.00–2.04 μm), also a combination of the N—H stretching mode and the N—H in-plane bending mode. These bands make it possible to carry out quantitative studies at room temperature. The assignment of the bands to the free and associated species respectively has been verified by varying the concentrations and comparison with the related NH or OH fundamentals.

Three model systems were chosen: water and dioxane (O—H---O<), self-associated *N*-methyl and *N*-ethylacetamide (the two gave practically the same results) (N—H---O=C<), and self-associated tertiary butanol. The intensities of the free and associated bands have been determined for a series of anesthetics: $CFCl_3$, CF_2BrCF_2Br, CH_2Cl_2, CF_3CHCl_2, $CHCl_3$, $CF_3CHClBr$ (halothane), and CH_3OCF_2-$CHCl_2$ (methoxyflurane). The concentrations of the solutions were the same in all cases.

The spectra were subjected to a curve analysis described in the Experimental section. Then correlations were sought between the band areas representing the intensities of the vibrational transitions and the anesthetic potencies.

Experimental

A. Purification of Samples and Solvents

Dioxane (from Anachemia) was refluxed on sodium wires for 4 h, then distilled under nitrogen atmosphere. It was kept on molecular sieves (4X) in a dry box and protected from light. We used deionized water obtained by passage through an ion-exchanger resin. *N*-Ethylacetamide (from Eastman Organic Chemicals) was dried on molecular sieves and distilled under vacuum. It was kept in a dry box and protected from light. *Tert*-butanol (Fisher Scientific, spectro grade) was dried on $MgSO_4$ and purified by fractional distillation. Methylcyclohexane (Matheson, Coleman and Bell) was passed through a silica gel column which had been dried at 350°C for 10 h, then dried over P_2O_5 and distilled under nitrogen atmosphere. Chloroform (Fisher Scientific, spectranalyzed) was washed several times with water, dried on $CaCl_2$, and distilled. It was stored in a dry box under nitrogen atmosphere and protected from light. Methylenechloride (Fisher Scientific, spectranalyzed) was dried on P_2O_5 and distilled. $CFCl_3$ (Freon 11), CF_3CHCl_2 (Freon 123), and CF_2BrCF_2Br (Freon 114-B-2), all from the E. I. DuPont de Nemours Company, were treated in the same way. Halothane, from Hoechst Pharmaceuticals of Canada, and methoxyflurane, from Abbott Laboratories of Canada, were used without further purification. The absence of any significant impurity was checked by gas chromatography. The samples were kept over molecular sieves in a refrigerator. The solutions were prepared in a dry box and the spectra recorded forthwith.

B. Preparation of Solutions

For the water–dioxane system first a 5 g/ℓ solution of water in dioxane was prepared (0.277 *M*). Then 0.05 mol of the (liquid) anesthetic was added to 5 ml of the water–dioxane solution and methylcyclohexane was added to the mixture to make the total volume of the solution 13 ml. For example, when $CFCl_3$ was the 'anesthetic', the solution contained 5 ml of the (5 g/ℓ) water–dioxane solution + 5.6 ml (0.05 mol) of $CFCl_3$ + 2.4 ml of methylcyclohexane. In this way the molar concentration of both water (0.107 *M*) and the anesthetic was the same for all anesthetics. In the case of *N*-ethylacetamide we first prepared a 0.594 *M* solution in carbon tetrachloride since the amide was not sufficiently soluble in methylcyclohexane. To 5 ml of this solution we added 0.04 mol of the anesthetic. Then we completed the volume with CCl_4 to 11 ml so that the amide had the same concentration in all solutions (0.270 *M*) as did the anesthetics. For *tert*-butanol we added 0.05 mol of the anesthetic to 5 ml of an initial solution of 2.98 *M* in CCl_4. Then CCl_4 was added to the solution to make the concentration of *tert*-butanol 1.24 *M* in every case. Carbon tetrachloride is, of course, not entirely 'inert' but this does not seriously affect the additional effects exerted by the other compounds.

C. Instrumental

The near-infrared spectra were measured with a Cary-17 spectrometer using silica cells. Both normal and differential spectroscopic methods were used. For the latter the reference cell contained the same amount of dioxane, anesthetic, and methylcyclohexane as the sample cell plus CCl_4 to compensate for water contained in the latter in the case of the water–dioxane system and similarly for the other systems.

Can. J. Chem. Downloaded from www.nrcresearchpress.com by 210.87.254.6 on 09/05/12
For personal use only.

D. Curve Analysis

The computer programs we used have been developed by Jones and co-workers (22–26). They consist of four parts.

CONVERT (Canadian NRC Program II)

This converts the experimental spectra obtained in units of absorbance vs. wavelength to units of transmittance vs. wavenumbers.

CURFIT (CNRC Program X)

This is the basic band fitting program. The experimental band envelope is approximated by Cauchy–Gauss product functions while the 'baseline constant' is also allowed to vary. The program varies and refines the (four) input parameters characteristic of the Cauchy–Gauss functions.

CURCOM (CNRC Program XIV)

With the parameters obtained from CURFIT this program calculates the composite curve and compares it with the experimental curve.

LWIDTH

A program written by one of us (K.C.C.) then computes the half-width, integrated intensity, and the Cauchy–Gauss ratio for each band obtained through the preceding programs.

The computations were carried out using the CYBER-173 (CDC) computer of the Université de Montréal.

A typical example of band decomposition is shown in Fig. 1. The numerical results are given in Table 1. In Figs. 3, 5, and 6, the band areas are given on a relative scale. This scale is different for the different systems since the actual concentrations of the free and associated species are not known and no molar extinction coefficients can be computed. Thus the numerical values should not be compared among different figures.

Results

A. The Water–Dioxane System

The maximum of the free ($\nu_2 + \nu_3$) band of water is at 5288 $\pm$ 6 cm^{-1} in the series of anesthetics which were studied. Two broader, associated bands are found centered at 5223 $\pm$ 9 and 5120 cm^{-1} (shoulder) respectively. Since dioxane is present in great excess the self-association of water can be disregarded as well as complexes which would be formed by one dioxane and more than one water molecule. Thus the most probable associated species are those in which one water molecule connects two dioxane molecules (>O---H—O—H---O<) or the one to one complex with one bonded and one 'free' OH group. The former probably correlates to the band at 5223 cm^{-1}. This is, however, not essential from the point of view of our problem. A qualitative picture of what occurs is given in Fig. 2. As we add to the water–dioxane system equal amounts of CF_2BrCF_2Br, CF_3CHCl_2, $CHCl_3$, or $CH_3OCF_2CHCl_2$, the free band's intensity obviously increases to the detriment of those of the associated bands. The computed band areas of the free band in the presence of different anesthetics appear in Table 1. We did not seek correlations with the associated bands in this case since we do not know the relative intrinsic intensities of the two bands and thus could not make a weighted sum of them.

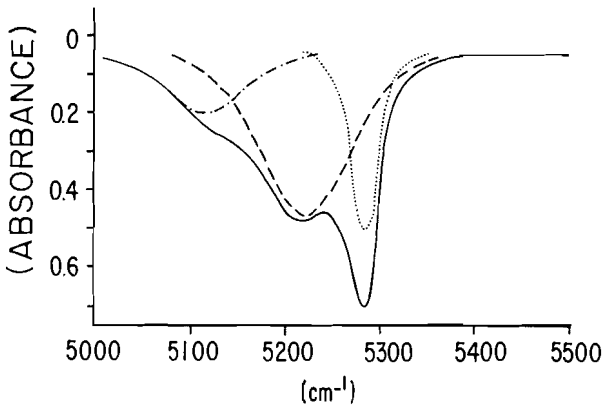

FIG. 1. Curve analysis (band fitting) of the OH stretching + OH in-plane bending region of the near infrared spectrum of the water–dioxane system (see Experimental section).

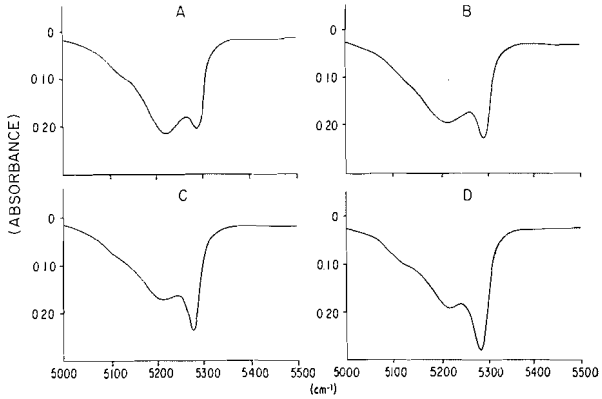

FIG. 2. Changes in the relative intensities of the free and associated ($\nu_2 + \nu_3$) combination band in the water–dioxane system for solutions containing equimolar amounts of one of the following anesthetics: *A*, CF_2BrCF_2Br; *B*, CF_3CHCl_2; *C*, $CHCl_3$; *D*, $CH_3OCF_2CHCl_2$.

In Table 1 and Fig. 3 the band area under the free band is compared to the anesthetic potency represented by log $1/p$ where p is the effective anesthetic pressure in atmospheres (ATA) required to suppress the righting reflex of mice in half of the experimental animals. The p values are those used by Miller and Smith (12), Hansch *et al.* (27), and Di Paolo *et al.* (28) in their critical investigation of the Meyer–Overton relationship. As can be seen a reasonably good correlation is obtained except that CH_2Cl_2 lies off the line by an amount which seems to exceed experimental error. For CF_2BrCF_2Br we found no p value in the literature but a MAC[1] value was given by Suckling (29). From this MAC value we estimated a p value lying between 0.9 and 1.3. The location of this point

[1]Minimum alveolar concentration needed to cause anesthesia.

TABLE 1. Computed relative band areas for the OH or NH stretching + in-plane bending combination. The band areas are on different relative scales for each system and should only be compared within a given column

Anesthetic	Log 1/*p*	Band area water–dioxane free OH	Band area self-associated *N*-ethylacetamide free NH	Band area self-associated *N*-ethylacetamide associated NH	Band area self-associated *tert*-butanol free OH
C_7H_{14}	~0	3.01	37.78	46.68	3.50
$CFCl_3$	0.82	3.88	37.89	45.42	6.11
CF_2BrCF_2Br	0.90–1.30 (estimated)	3.73	—	—	7.30
CH_2Cl_2	1.52	5.35	39.19	42.15	13.10
CF_3CHCl_2	1.57	4.80	40.90	—	—
$CHCl_3$	2.08	5.27	41.73	33.60	14.41
$CF_3CHClBr$	2.11	5.40	42.95	30.75	14.30
$CH_3OCF_2CHCl_2$	2.66	6.49	44.70	29.20	14.81

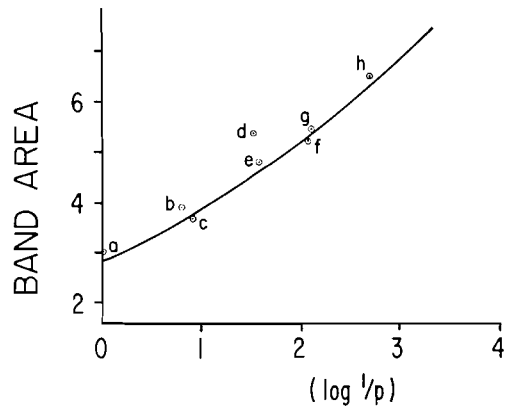

FIG. 3. The relationship between the logarithm of the inverse of the effective anesthetic pressure and the computed relative band area of the free ($\nu_2 + \nu_3$) band of the water–dioxane system in the presence of different anesthetics: *a*, C_7H_{14}; *b*, $CFCl_3$; *c*, CF_2BrCF_2Br; *d*, CH_2Cl_2; *e*, CF_3CHCl_2; *f*, $CHCl_3$; *g*, $CF_3CHClBr$; *h*, $CH_3OCF_2CHCl_2$.

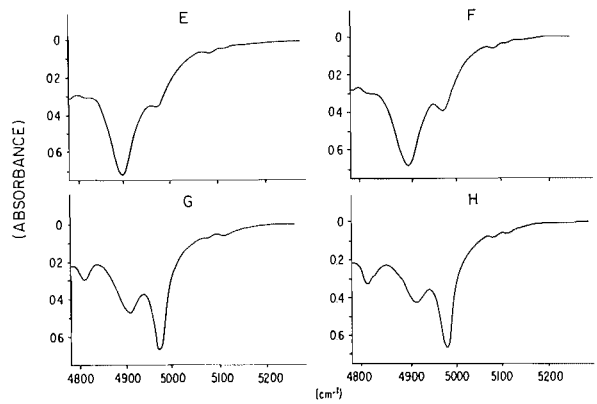

FIG. 4. Changes in the relative intensities of the free and associated NH stretching + NH in-plane bending combination band of self-associated *N*-ethylacetamide. The solutions contained equimolar amounts of one of the following anesthetics: *E*, C_7H_{14}; *F*, $CFCl_3$; *G*, CH_2Cl_2; *H*, $CHCl_3$.

is uncertain but it is clearly located near the point related to $CFCl_3$ and much lower than those related to anesthetics containing an acidic hydrogen.

The case of CH_2Cl_2 presents a special problem which is discussed to some extent below.

B. Self-associated N-*Ethylacetamide*

The free band we used has its maximum at 4978 ± 5 cm^{-1} and the associated band at 4905 ± 10 cm^{-1} in all cases. On the basis of the previous work by Fillaux and DeLozé (30) we can consider these as the NH stretching + NH in-plane bending combinations. *N*-Ethylacetamide might have *cis* and *trans* forms but we cannot distinguish separate bands due to these. They must be contained in the fairly broad bands which we observed.

Figure 4 shows the qualitative aspect; again we see that when anesthetics are added to the amide solution the free band increases and the associated band decreases in intensity in a way parallelling anesthetic potency. Figure 5 and Table 1 give the relation between the integrated intensities of the free band and log 1/*p* as defined above. This time we obtain a smooth relationship which is about equally good for all the anesthetics we used. With the associated band we obtain a relationship which is roughly the inverse of what was found with the free band (Fig. 6).

Similar correlations were obtained when we used absorbances instead of the band areas. This is in keeping with the fact that, in this case, the band widths do not vary widely.

C. Self-associated tert-*Butanol*

Only the free band could be used for reasons similar to those which we encountered in the case of the water–dioxane system. It is located at 4938 ± 5 cm^{-1} (see Asselin and Sandorfy (31)). The results are similar to those for the two other systems and are included in Table 1. $CFCl_3$ and CF_2BrCF_2Br clearly behave differently from the others. CH_2Cl_2 seems to be less irregular in this case.

Can. J. Chem. Downloaded from www.nrcresearchpress.com by 210.87.254.6 on 09/05/12
For personal use only.

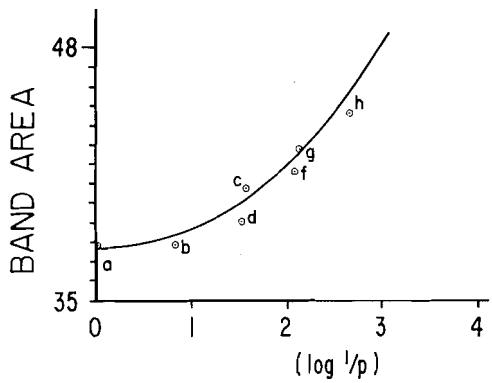

FIG. 5. The relationship between the logarithm of the inverse of the effective anesthetic pressure and the computed relative band area of the free NH stretching + NH in-plane bending combination band for self-associated *N*-ethylacetamide in the presence of different anesthetics: *a*, C_7H_{14}; *b*, $CFCl_3$; *c*, CF_3CHCl_2; *d*, CH_2Cl_2; *f*, $CHCl_3$; *g*, $CF_3CHClBr$; *h*, $CH_3OCF_2CHCl_2$.

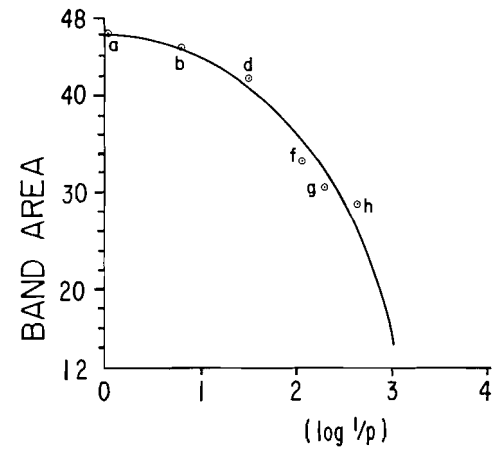

FIG. 6. The relationship between the logarithm of the inverse of the effective anesthetic pressure and the computed relative band area of the associated NH stretching + NH in-plane bending combination band for self-associated *N*-ethylacetamide in the presence of different anesthetics: *a*, C_7H_{14}; *b*, $CFCl_3$; *d*, CH_2Cl_2; *f*, $CHCl_3$; *g*, $CF_3CHClBr$; *h*, $CH_3OCF_2CHCl_2$.

Discussion and Conclusions

The following observations can be made.

(*1*) In all three systems we have studied, the most potent anesthetics are also the most efficient hydrogen bond breakers. These are chloroform, halothane, and methoxyflurane, the latter being the most potent everywhere. The general trend is that halogenated anesthetics containing no acidic hydrogen are less potent and those which contain one are more potent.

(*2*) While this applies to all three of our model systems there are significant differences among the correlations obtained. This shows that the pattern of associations of the different anesthetics with the O—H---O<, O—H---O—H---, and N—H---O=C< systems is to some extent different.

(*3*) A few detailed comments are needed on those anesthetics which do not contain the acidic hydrogen. $CFCl_3$ which we considered as an inert solvent in some of our previous work does have a moderate anesthetic potency. As to its HB breaking ability, in the case of the amide system, it seems to be just slightly greater than that of methylcyclohexane. We have found no data on the anesthetic potency of the latter but it is likely to be somewhat less than that of $CFCl_3$. The same applies to the *tert*-butanol system. In the case of the water–dioxane system, $CFCl_3$ is found to be a more efficient HB breaker. On the whole these are all weak effects, however.

CF_2BrCF_2Br seems to be a somewhat stronger HB breaker for the amide and *tert*-butanol but weaker for the water–dioxane system. As has been shown earlier (1–5) this molecule can be made a powerful HB breaker at low temperatures. Possibly $CFCl_3$ acts mainly by its permanent dipole moment (0.45 D) while CF_2BrCF_2Br through its higher polarisability.

CH_2Cl_2 is a rather intriguing case. While it falls in line for the amide and for *tert*-butanol it is anomalous for water–dioxane. It breaks many more HB's than would be expected from its known log $1/p$ value. According to Oi and Coetzee (32) and Green (33), this molecule can form HB's as a proton donor. Curiously, however, this does not seem to affect its C—H stretching frequencies. It does affect the C—Cl stretching modes. Clearly, this is a complicated case and requires a detailed study. We are examining the problem through low temperature measurements in order to magnify the effect of association. The results will be reported later.

Chloroform, halothane, CF_3CHCl_2, and methoxyflurane behave similarly for all three systems. There is no doubt about the importance of the acidic hydrogen. There are, however, other associative sites in these molecules. These are the chlorine atoms in all of them, the bromine in halothane, and the ether linkage in methoxyflurane. They probably help, to a variable extent.

The correlations we have obtained are far from being perfect. They could not be expected to be so. It is clear, however, that there is a definite parallelism between hydrogen bond breaking power and anesthetic potency. This has been indicated already in our previous, low temperature work. It has now been obtained through a room temperature study, closer to biological conditions and in a semi-quantitative fashion. Observations *1* and *2* lend weight to the

Can. J. Chem. Downloaded from www.nrcresearchpress.com by 210.87.254.6 on 09/05/12
For personal use only.

supposition that the perturbation of hydrogen bonds plays a role in the mechanism of inhalation anesthesia and that this perturbation varies in strength and nature according to the HB system which is perturbed. What we observe under in vivo conditions is probably an integral of many such effects. It is believed that these perturbations are additional to other hydrophobic and polar interactions. On the molecular level, the mechanism of anesthesia is likely to be pluralistic involving a number of different interactions.

Acknowledgments

We are indebted to Dr. R. N. Jones for letting us have the benefit of his programs and his experience on infrared curve analysis. Our thanks are due to Dr. R. Denis and Dr. D. D. Denson for supplying us with samples and for stimulating conversations and correspondence and to Mr. Paul Sauvageau for helping us with the experimental aspects of our work. Financial support from the National Research Council of Canada and le Ministère de l'Education du Québec is gratefully acknowledged.

1. M. C. Bernard-Houplain and C. Sandorfy. J. Chem. Phys. **56**, 3412 (1972).
2. M. C. Bernard-Houplain, C. Bourderon, J. J. Peron, and C. Sandorfy. Chem. Phys. Lett. **11**, 149 (1971).
3. T. Di Paolo and C. Sandorfy. J. Med. Chem. **17**, 809 (1974).
4. T. Di Paolo and C. Sandorfy. Can. J. Chem. **52**, 3612 (1974).
5. R. Bicca de Alencastro and C. Sandorfy. Can. J. Chem. **50**, 3594 (1972).
6. A. Nagyrevi and C. Sandorfy. Can. J. Chem. **55**, 1592 (1977).
7. R. Massuda and C. Sandorfy. Can. J. Chem. **55**, 3211 (1977).
8. J. M. Brown and P. A. Chaloner. Can. J. Chem. **55**, 3380 (1977).
9. L. S. Koehler, W. Curley, and K. A. Koehler. Mol. Pharmacol. **13**, 113 (1977).
10. R. H. Davies, R. D. Bagnall, and W. G. M. Jones. Int. J. Quantum Chem., Quantum Biol. Symp. **1**, 201 (1974).
11. R. H. Davies, R.D. Bagnall, W. Bell, and W. G. M. Jones. Int. J. Quantum Chem., Quantum Biol. Symp. **3**, 171 (1976).
12. K. W. Miller and E. B. Smith. *In* A guide to molecular pharmacology-toxicology. *Edited by* R. M. Featherstone. M. Dekker, New York, NY. 1973. Chapt. 11, Part 2, pp. 427–475.
13. M. J. Halsey. *In* Anesthetic uptake and action. *Edited by* E. I. Eger. Williams and Wilkins, Baltimore, MD. 1974. pp. 45–76.
14. R. D. Kaufman. Anesthesiology, **46**, 49 (1977).
15. D. D. Denson. Chemtech, **7**, 446 (1977).
16. W. A. P. Luck and W. Ditter. J. Mol. Struct. **1**, 261 (1967/1968).
17. A. Burneau and J. Corset. J. Chim. Phys. **69**, 171 (1972).
18. T. Di Paolo, C. Bourderon, and C. Sandorfy. Can. J. Chem. **50**, 3161 (1972).
19. M. C. Bernard-Houplain and C. Sandorfy. Chem. Phys. Lett. **27**, 154 (1974).
20. W. A. P. Luck and W. Ditter. J. Mol. Struct. **1**, 339 (1967/1968).
21. O. D. Bonner and Y. S. Choi. J. Phys. Chem. **78**, 1723 (1974).
22. R. N. Jones, T. E. Bach, H. Fuhrer, V. B. Kartha, J. Pitha, K. S. Seshadri, R. Venkataraghavan, and R. P. Young. Computer programs for absorption spectrometry. NRCC Bulletin No. 11. National Research Council of Canada, Ottawa. 1968.
23. J. Pitha and R. N. Jones. Optimization methods for fitting curves to infrared band envelopes. Computer Programs. NRCC Bulletin No. 12. National Research Council of Canada, Ottawa. 1968.
24. J. Pitha and R. N. Jones. Can. J. Chem. **44**, 3031 (1966).
25. J. Pitha and R. N. Jones. Can. J. Chem. **45**, 2347 (1967).
26. R. N. Jones, R. Venkataraghavan, and J. W. Hopkins. Spectrochim. Acta, **23A**, 925 (1967).
27. C. Hansch, A. Vittoria, C. Silipo, and P. Y. C. Jow. J. Med. Chem. **18**, 546 (1975).
28. T. Di Paolo, L. B. Kier, and L. H. Hall. Mol. Pharmacol. **13**, 31 (1977).
29. C. W. Suckling. Br. J. Anaesth. **29**, 466 (1957).
30. F. Fillaux and C. DeLozé. J. Chim. Phys. **69**, 36 (1972).
31. M. Asselin and C. Sandorfy. Can. J. Chem. **49**, 1539 (1971).
32. N. Oi and J. F. Coetzee. J. Am. Chem. Soc. **91**, 2473 (1969).
33. R. D. Green. Hydrogen bonding by C—H groups. Wiley, New York, NY. 1974. p. 49.

Can. J. Chem. Downloaded from www.nrcresearchpress.com by 210.87.254.6 on 09/05/12
For personal use only.

Synthesis of triquinacene and some of its derivatives

PIERRE DESLONGCHAMPS, UKKEN OUSEPH CHERIYAN, YVON LAMBERT, JEAN-CLAUDE MERCIER, LUC RUEST, ROBERT RUSSO, AND PIERRE SOUCY

Laboratoire de synthèse organique, Département de chimie, Université de Sherbrooke, Sherbrooke (Qué.), Canada J1K 2R1

Received December 13, 1977

PIERRE DESLONGCHAMPS, UKKEN OUSEPH CHERIYAN, YVON LAMBERT, JEAN-CLAUDE MERCIER, LUC RUEST, ROBERT RUSSO, and PIERRE SOUCY. Can. J. Chem. **56**, 1687 (1978).

Several routes for the synthesis of triquinacene (**1**) and 2,3-dihydrotriquinacen-2-one (**3**) are described using Thiele's acid as starting material.

PIERRE DESLONGCHAMPS, UKKEN OUSEPH CHERIYAN, YVON LAMBERT, JEAN-CLAUDE MERCIER, LUC RUEST, ROBERT RUSSO et PIERRE SOUCY. Can. J. Chem. **56**, 1687 (1978).

Les synthèses du triquinacène (**1**) et du dihydro-2,3-triquinacénone-2 (**3**) sont décrites à partir de l'acide de Thiele en utilisant plusieurs voies différentes.

Can. J. Chem. Downloaded from www.nrcresearchpress.com by 210.87.254.40 on 09/05/12
For personal use only.

Tricyclo[5.2.1.$0^{4,10}$]decatriene-2,5,8 (**1**) usually called triquinacene (Scheme 1) was first synthesized by Woodward and his collaborators (1). Since then, several syntheses of triquinacene and some derivatives thereof have appeared in the literature (2–11). Some of these compounds can be considered potential starting materials for the synthesis of dodecahedrane (**2**) (12–16) which is the equivalent of dimeric triquinacene (**1**).

We have reported in preliminary communications (7, 8) syntheses of triquinacene (**1**) and 2,3-dihydrotriquinacen-2-one (**3**). We wish now to report these syntheses in detail as well as the preparation of several other related derivatives.

Strategy

In our preliminary planning, it appeared to us that a good synthetic strategy would be to use a tetrahydrodicyclopentadiene derivative containing two functional groups such as **4** and to convert it into triquinacene via the intermediates **5** and **6**.

Our plan was therefore based on the recognition that (*a*) the tetrahydrodicyclopentadiene skeleton is a tricyclic isomer of hexahydrotriquinacene with which it has two identical five-membered rings (rings A and B); (*b*) the desired starting material **4** should be easily available because dicyclopentadiene chemistry is well known; (*c*) the specific carbon–carbon cleavage on **4** where the functional group W is converted into two new functional groups Y and Z in intermediate **5** should be possible; (*d*) the bicyclic intermediate **5** contains three functional groups, two of which (X and Z) can be used to make a new carbon–carbon bond to generate the hexahydrotriquinacene skeleton **6** having three functional groups conveniently disposed in specific positions, so that triquinacene can be obtained by further appropriate transformations, (*e*) the intermediate **5** also possesses the correct configuration at three asymmetric carbons, so that the right configuration for the four asymmetric carbons of the skeleton of **6** is assured; (*f*) the three external tertiary hydrogen atoms of the skeleton of **6** should behave like bridgehead hydrogens. In such a case, the regiospecific transformation of X, Y, and Z into the desired disubstituted double bonds which are present in triquinacene should be easy.

It is also interesting to point out that the functional groups in intermediate **5** are in such a position that they cannot alter the configuration of the three asymmetric carbons of the skeleton by epimerization. There was also almost no possibility that two of these three functional groups could interact together to generate either new unwanted functional groups or undesired skeleton fragmentations. Such possibilities existed in intermediates of type **6** only. The functional groups X and Z are in a 1,3 relationship in **6** and they could prefer to always react together so that they could not easily be converted into two of the three isolated double bonds of triquinacene. We felt however that this difficulty could be overcome by appropriate protection of one of the functional groups if the tertiary hydrogen between these two functional groups would not behave like a bridgehead hydrogen as previously suggested.

Starting Material

The tricyclic diketone **10** (Scheme 1) was chosen as our first key intermediate since we were convinced that the two carbonyl groups could be easily differentiated. The readily available Thiele's acid (**7**) (17), the structure of which is well established (ref. 18 and references cited therein), was selected as our starting material. The tricyclic diketone **10** was first obtained (7) from **7** in three steps via the diacid chloride **8** (19) and the diazide **9**. We subsequently succeeded in a direct conversion of Thiele's acid (**7**) into the diketone **10** in 35–40% yield using sodium azide in a mixture of sulfuric and trifluoroacetic acid (8). This one-step

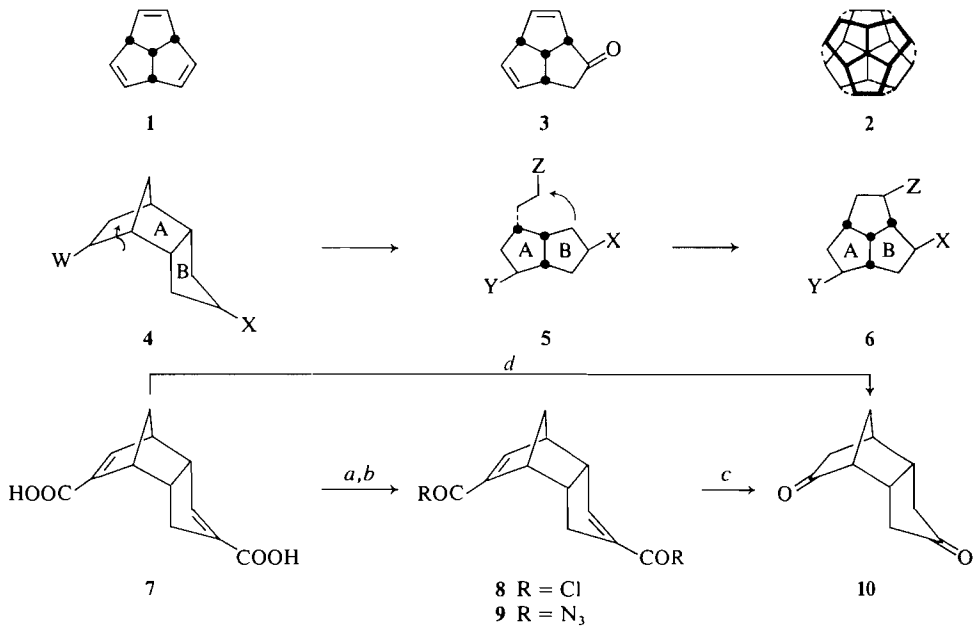

SCHEME 1. (*a*) Oxalyl chloride, CH_2Cl_2; (*b*) NaN_3; (*c*) heat, DME, H_2O; (*d*) NaN_3, CF_3COOH, H_2SO_4.

procedure was preferred because of its simplicity of operation.

The Baeyer–Villiger Route

In our first route to triquinacene derivatives which is described in Scheme 2, we have selected the Baeyer–Villiger reaction to effectuate the desired cleavage **4** → **5**. The diketone **10** was first converted into the monoketal **11**. 3,3-Dimethylpropane-1,3-diol was chosen because the monoketal **11** is highly crystalline and is therefore easily obtained pure by crystallization. Treatment of the monoketal **11** with *m*-chloroperbenzoic acid gave a high yield of a mixture of the lactones **12** (73%) and **13** (27%). The desired lactone **12** was obtained pure by specific basic hydrolysis of the other lactone **13**.[1] The ketal lactone **12** was characterized further by its transformation into the bicyclic methyl ester benzoate **14**.

The conversion of the ketal lactone **12** into the ketal aldehyde acetate **18**, which has the appropriate functional groups to build the hexahydrotriquinacene skeleton (**5** → **6**), was carried out in four steps. The ketal lactone **12** was reduced to the diol **15** which was converted into the diacetate **16**. Basic hydrolysis under mild conditions gave the acetate alcohol **17** as the major product which was oxidized to the ketal aldehyde acetate **18**. Treatment of **18** under acidic conditions gave directly an ≃1:1 mixture of the aldol condensation products, the *cis* and the *trans* tricyclic ketone alcohol acetates **19** and **20** which were separated by chromatography. Oxidation of **19** and **20** gave the same β-diketone acetate **21**. This result shows that **19** and **20** are epimeric alcohols having the same skeleton. The assignment of the *cis* and the *trans* configuration to **19** and **20**, respectively, will be confirmed below. The epimeric alcohols **19** and **20** were further characterized by acetylation which gave the *cis* and *trans* ketone diacetates **22** and **23**, respectively.

The *trans* tricyclic ketone alcohol acetate **20** was then transformed into the ketal alcohol acetate **24** which was hydrolysed under basic conditions to give the ketal diol **25**. The ketal diol **25** was converted into the ketal dimesylate **26** which on treatment with potassium *tert*-butoxide gave a mixture of ketal dienes **27** (10%) and **28** (90%). Mild acid hydrolysis of the mixture of **27** and **28** gave a mixture of dienones **29** (10%) and **3** (90%) which were separated by vapor phase chromatography. The dienone **29** was found to be extremely unstable and it was characterized by its infrared spectrum only. The dienone **3** (2,3-dihydrotriquinacen-2-one) had the expected spectroscopic properties and was characterized by the preparation of a crystalline dinitrophenyl hydrazone derivative. The dienone **3** was shown to be identical with an authentic sample of 2,3-dihydrotriquinacen-2-one which was prepared by the oxidation of 2-*exo*-2,3-dihydrotriquinacenol (**30**) (16).[2]

[1]For a discussion concerning the large difference in the rates of the basic hydrolysis of this type of lactone, see page 2476 of ref. 20.

[2]We are grateful to Professor R. B. Woodward for his generous gift of 2-*exo*-2,3-dihydrotriquinacenol (**30**).

Can. J. Chem. Downloaded from www.nrcresearchpress.com by 210.87.254.40 on 09/05/12
For personal use only.

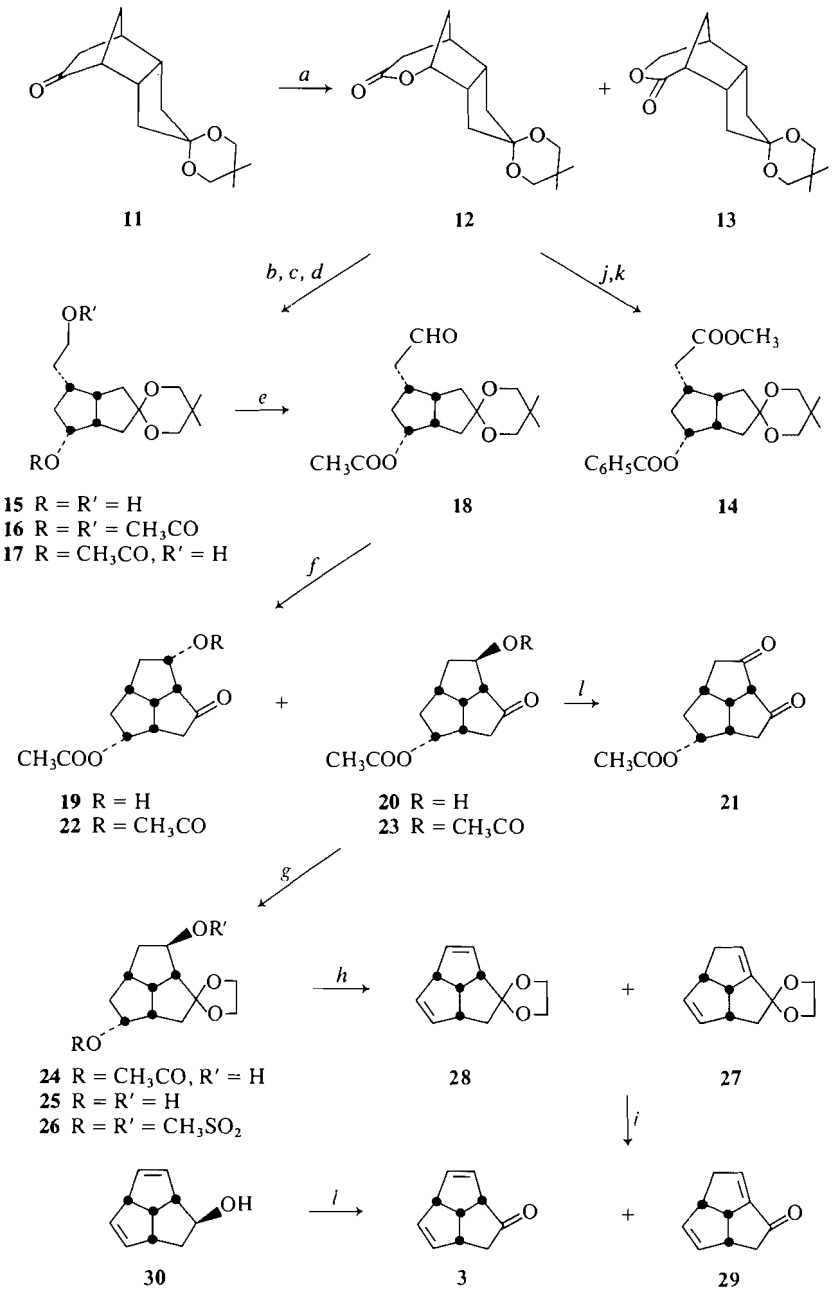

SCHEME 2. (*a*) *m*-$ClC_6H_4CO_3H$, Na_2CO_3, CCl_4; (*b*) $LiAlH_4$, ether; (*c*) $(CH_3CO)_2O$, pyridine; (*d*) Na_2CO_3, H_2O, CH_3OH; (*e*) $CrO_3 \cdot 2C_5H_5N$; (*f*) HCl 3 *N*, acetone; (*g*) ethylene glycol, benzene, *p*-toluenesulfonic acid; (*h*) *t*BuOK, DMSO; (*i*) HCl 2 *N*, THF; (*j*) CH_3ONa, CH_3OH; (*k*) C_6H_5COCl, pyridine, CH_2Cl_2; (*l*) Jones' oxydation.

The preceding results show that we had developed a valuable approach for the synthesis of triquinacene derivatives. It involved however many operations (13 steps, **7** → **10** → **11** → **12** → **15** → **16** → **17** → **18** → **20** → **24** → **25** → **26** → **28** → **3**) and a mixture of **19** and **20** which could not be easily separated. The next task was to develop a shorter route within that scheme.

Reduction of the ketal lactone **12** with diisobutyl aluminium hydride (Scheme 3) gave directly the ketal aldehyde alcohol **31** in excellent yield. Molecular distillation of **31** gave the crystalline tricyclic ketal

Can. J. Chem. Downloaded from www.nrcresearchpress.com by 210.87.254.40 on 09/05/12
For personal use only.

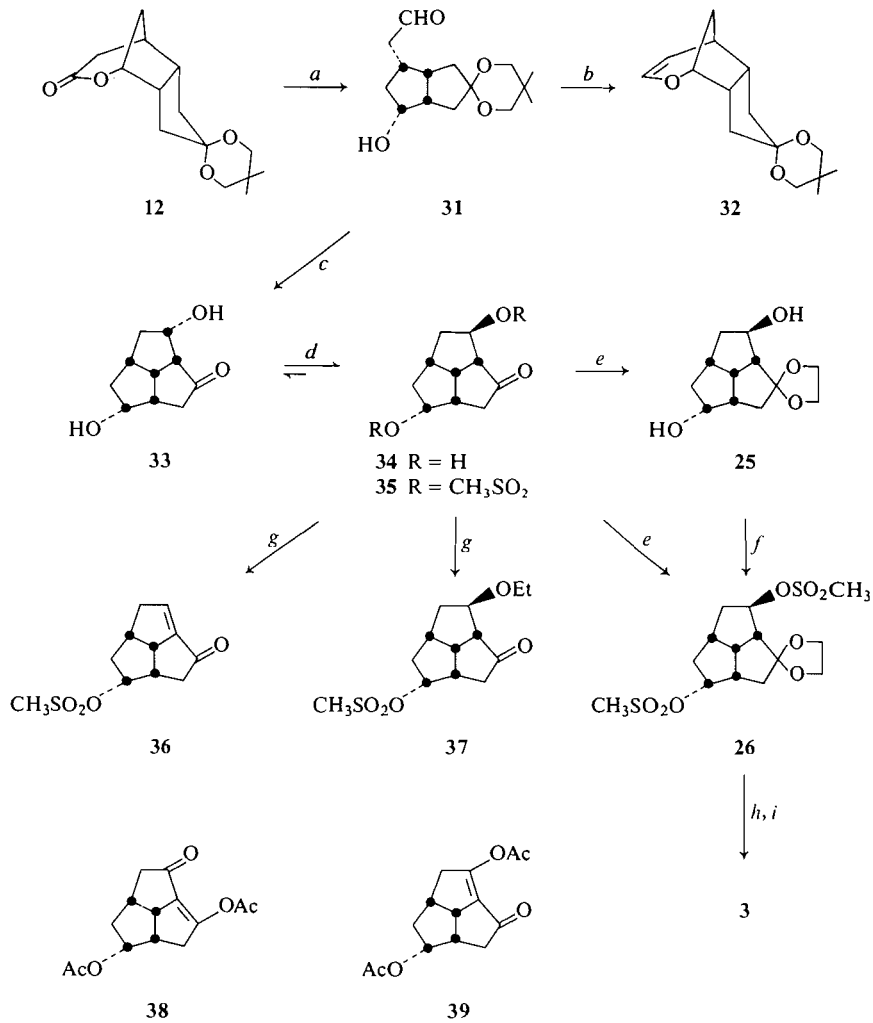

SCHEME 3. (*a*) Diisobutyl aluminium hydride; (*b*) heat; (*c*) HCl 2*N*, acetone; (*d*) EtONa, EtOH; (*e*) ethylene glycol, benzene, *p*-toluenesulfonic acid; (*f*) CH_3SO_2Cl, pyridine, CH_2Cl_2; (*g*) NaOH, EtOH, CH_2Cl_2; (*h*) *t*BuOK, DMSO; (*i*) HCl 2*N*, THF.

enol ether **32** and, upon acetylation, **31** gave the ketal aldehyde acetate **18** which we have previously obtained by a longer procedure described in Scheme 2. Treatment of the ketal aldehyde alcohol **31** under acidic conditions gave an $\simeq 1:1$ mixture (thin-layer chromatography) of the epimeric aldol products, the *cis* and the *trans* ketone diols **33** and **34** which were not separated. Upon treatment with a catalytic amount of sodium ethoxide in ethanol, equilibration occurred to give mainly one product, which was isolated directly by crystallization in $\simeq 63\%$ yield. We have assigned the *trans* diol structure **34** to this product. This assignment is based on the fact that structure **34** has one secondary hydroxyl group in the *exo* configuration. It must therefore be more stable than the *cis* diol structure **33** which has that same hydroxyl group oriented in the less sterically favored *endo* orientation. This can be clearly seen on examination of a molecular model.

Acetylation of the *trans* ketone diol **34** gave the *trans* ketone diacetate **23** which we have described in Scheme 2. The assignment of configuration for the *trans* tricyclic ketone alcohol acetate **20** is thus established. Since, compounds **19** and **20** have been shown to be epimers by their respective transformation into the β-diketone acetate **21**, the configuration of the *cis* tricyclic ketone alcohol acetate **19** is also established.

Ketalization of *trans* ketone diacetate **22** with ethylene glycol followed by basic hydrolysis gave the *trans* ketal diol **25**. We have already described the conversion of compound **25** into the *trans* ketal dimesylate **26**. The same *trans* ketal dimesylate **26** can also be obtained by a simple two-step procedure

Can. J. Chem. Downloaded from www.nrcresearchpress.com by 210.87.254.40 on 09/05/12
For personal use only.

Can. J. Chem. Downloaded from www.nrcresearchpress.com by 210.87.254.40 on 09/05/12
For personal use only.

from the *trans* ketone diol **34**. The *trans* ketone diol **34** upon mesylation gave the ketone dimesylate **35** which could also be converted under carefully controlled conditions into the same *trans* ketal dimesylate **26** in an excellent yield. Since compound **26** gives 2,3-dihydrotriquinacenone (**3**) in two steps, this new route represents a nine-step synthesis of compound **3** (**7** → **10** → **11** → **12** → **31** → **34** → **35** → **26** → **28** → **3**).

It is interesting to note that the ketone dimesylate **35** is a stable compound which can even be transformed into the *trans* ketal dimesylate **26**. This result suggests that the tertiary hydrogen in α-position to the carbonyl group behaves like a bridgehead hydrogen or at least is not easily removed under mild basic (during the mesylation reaction) or acidic (during the ketalization reaction) conditions.

We have found however that in the presence of sodium hydroxide, this tertiary hydrogen α to the carbonyl group can be removed. When the *trans* ketone dimesylate **35** was treated with slightly less than 1 equiv. of sodium hydroxide in ethanol at 0°C, it gave the crystalline conjugated enone mesylate **36** which was well characterized. When the same reaction was carried out at room temperature with an excess of sodium hydroxide, a new compound was isolated to which we have assigned the structure **37** with an ethoxy group in the *exo* position.

These results show that the tertiary hydrogen is not in a completely bridgehead position but the high reactivity of enone mesylate **36** suggests that the trisubstituted double bond must be strained. The preparation of compound **36** and the comparison of its infrared spectrum with that of compound **29** confirmed the structure assignment previously made for **29**.

The infrared spectrum of the β-diketone acetate **21** shows that this compound exists in the β-diketone form only (21). However, on treatment with acetic anhydride and pyridine, compound **21** gave, in high yield, a crystalline ketone enol diacetate which can have structure **38** or **39**. Although, we have not established the exact structure for that compound, it is interesting to note that only one of the two possible enol acetates was observed. This result shows also that it is possible to have triquinacene derivatives with a double bond at one of the bridgehead positions.

The above nine-step sequence represents a convenient method for the preparation of 2,3-dihydrotriquinacen-2-one (**3**). It is still however a lengthy procedure because there are some steps which can be considered unnecessary. In principle, these extra steps are the following: (*a*) the diketone **10** needs to be protected in the form of the ketal ketone **11** before the Baeyer–Villiger reaction; (*b*) the ketal lactone **12** obtained from the Baeyer–Villiger reaction needs a readjustment of its functionality to the ketal aldehyde **31** so that the aldol condensation can take place; (*c*) the carbonyl group in the *trans* ketone diol **34** needs to be protected in the form of a ketal group (→**26**) before the elimination reaction can proceed; (*d*) the alcohol groups need to be activated as mesylates to facilitate the formation of the double bonds; and (*e*) the ketal group must then be removed. Clearly, an ideal synthesis should avoid all these steps! In the following approaches, we have tried to eliminate a good majority of these 'unnecessary' steps.

The Photochemical Route

In our second approach to triquinacene and its derivatives, we have chosen the well-known photochemical fragmentation of ketones (22) to effectuate the cleavage **4** → **5**. Upon ultraviolet irradiation, the ketal ketone **11** (Scheme 4) is transformed into the bicyclic ketal olefin aldehyde **40** in good yield. Upon acidic treatment, compound **40** gave mainly the aldol condensation product, the tricyclic *exo* ketone alcohol **41**. Acetylation of this crude product gave after chromatography the pure *exo* ketone acetate **42** in 75% yield. The *exo* ketone acetate **42** was shown to be identical with an authentic sample obtained from the acid hydrolysis of the *exo* ketal acetate **47** (*vide infra*).

This method represents a four-step synthesis (**7** → **10** → **11**, **40** → **41**) of the triquinacene derivative **41** in which only one step (**10** → **11**) can be considered extra. We have therefore tried to eliminate this unnecessary step and we have found that it is indeed possible to photolyse the diketone **10** directly to give the ketone aldehyde **43** in good yield. The successful specific cleavage of the diketone **10** is presumably due to the fact that the norbornanone carbonyl group is more strained.

The ketone aldehyde **43** was then treated under acidic conditions to effectuate the aldol condensation reaction. This crude product was acetylated and it was shown by vapor phase chromatography to contain ≃80% of the *exo* ketone acetate **42**, ≃15% of the *endo* ketone acetate **51**, and ≃5% of an unidentified product. The *endo* ketone acetate **51** was shown to be identical with an authentic sample obtained from the acid hydrolysis of the *endo* ketal acetate **48** (*vide infra*).

Treatment of the crude aldol condensation product with sodium ethoxide in ethanol followed by acetylation gave a mixture of *exo* ketone acetate **42** (94.5%), *endo* ketone acetate **51** (1.5%), and an unidentified product (4%). Equilibration of **41** and **50** had thus occurred since the crude product obtained from this

Can. J. Chem. Downloaded from www.nrcresearchpress.com by 210.87.254.40 on 09/05/12
For personal use only.

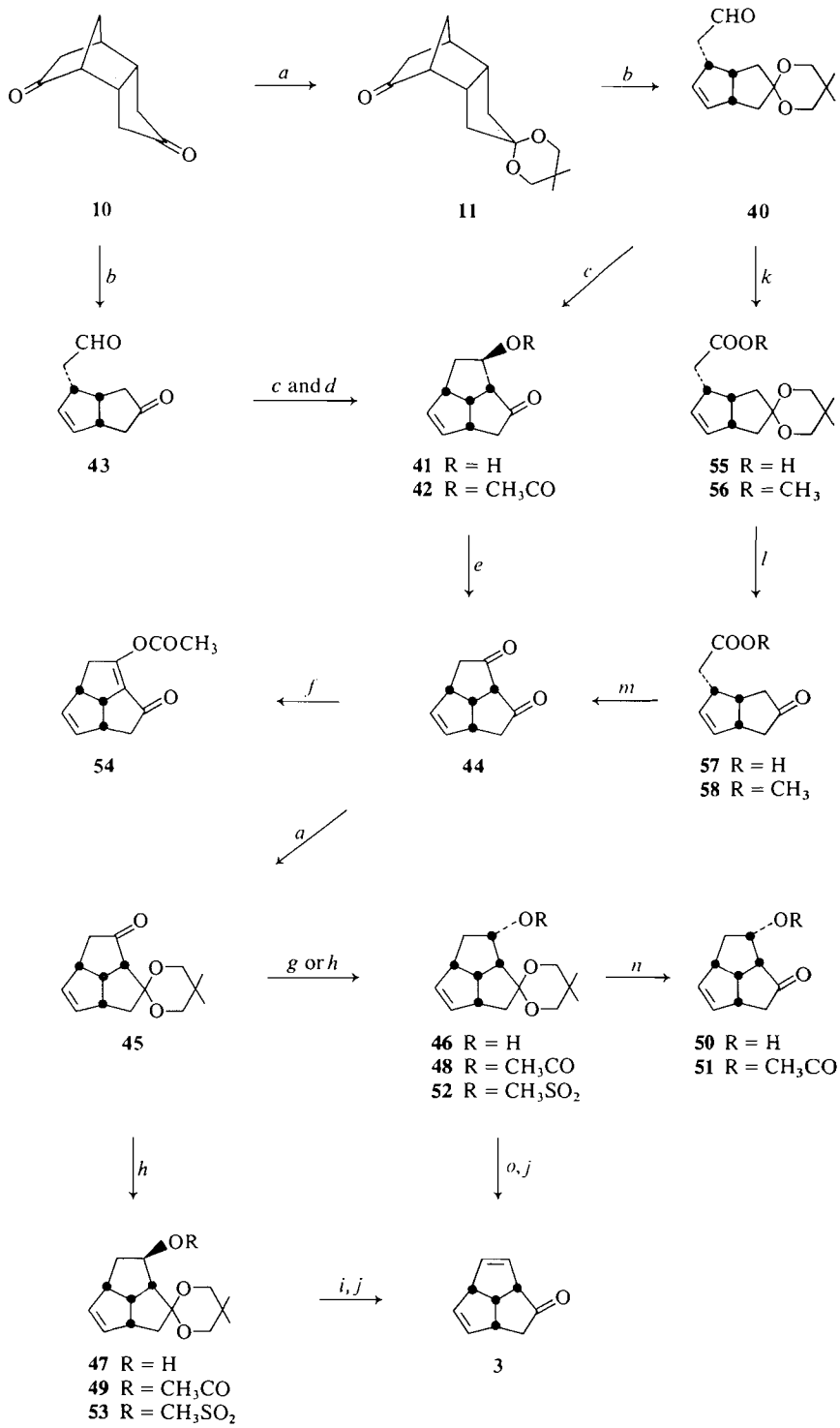

SCHEME 4. (*a*) 2,2-Dimethylpropane-1,3-diol, benzene, *p*-toluenesulfonic acid; (*b*) ultraviolet irradiation; (*c*) HCl 3 *N*, acetone; (*d*) C_2H_5ONa, C_2H_5OH; (*e*) Jones' oxydation; (*f*) $(CH_3CO)_2O$, pyridine; (*g*) $LiAl(tBuO)_3H$, THF; (*h*) sodium, EtOH; (*i*) *t*BuOK, DMSO; (*j*) HCl 2 *N*, THF; (*k*) $AgNO_3$, NaOH, H_2O; (*l*) CH_3COOH–H_2O; (*m*) *p*-toluenesulfonic acid, benzene; (*n*) *p*-toluenesulfonic acid, acetone, H_2O; (*o*) DBN, benzene.

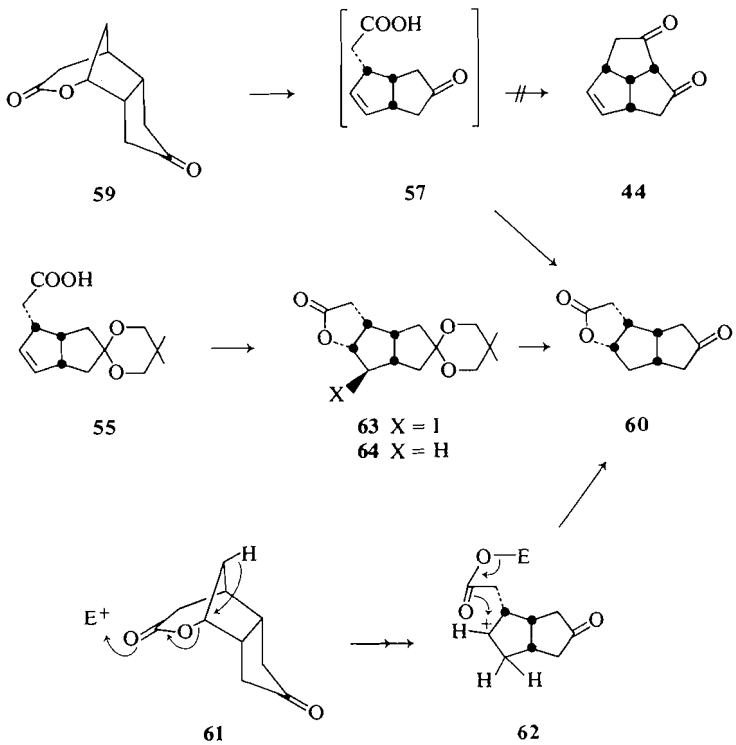

SCHEME 5

basic treatment contains mainly the *exo* ketone alcohol **41**. This crude product was used directly without further purification.

The assignment of the *exo* and *endo* configuration for the hydroxyl group in **41** and **50** comes from the basic equilibration studies. This assignment was also confirmed by the following experiments. The unpurified *exo* ketone alcohol **41** was oxidized to give the highly crystalline β-diketone **44**. Selective ketalization of **44** to give the crystalline ketal ketone **45** was achieved with 3,3-dimethylpropane-1,3-diol. Reduction of the ketal ketone **45** with lithium tri-*tert*-butoxyaluminium hydride gave the *endo* ketal alcohol **46**. The *endo* configuration was assigned because the alcohol product must be the result of an attack by hydride ion on the least hindered *exo* face of the ketal ketone **45**. This conclusion was further confirmed by a chemical reduction of **45**. Treatment of **45** with sodium in ethanol gave a mixture of the epimeric ketal alcohols **46** (13%) and **47** (87%). The *exo* ketal alcohol **47** was obtained pure by crystallization. The *endo* and the *exo* ketal alcohols **46** and **47** were transformed into their corresponding ketal acetates, **48** and **49**, respectively. The ketal acetates **48** and **49** were then hydrolysed under acid conditions to give, respectively, the *endo* and the *exo* tricyclic ketone acetates **51** and **42**. The *exo* configuration of the tricyclic alcohol **41** is thus established.

The *endo* tricyclic ketal alcohol **46** was converted into the *endo* mesylate **52** which on treatment with potassium *tert*-butoxide followed by acid hydrolysis gave the 2,3-dihydrotriquinacen-2-one (**3**) in nine steps (**7** → **10** → **43** → **41** → **44** → **45** → **46** → **52** ⇉ **3**) from Thiele's acid.

A shorter synthesis of **3** was devised by using the *exo* ketone alcohol **41**. Compound **41** was converted into the ketal **47** which, after mesylation (→**53**) followed by dehydromesylation and acid hydrolysis, gave 2,3-dihydrotriquinacen-2-one (**3**) in seven steps (**7** → **10** → **43** → **41** → **47** → **53** ⇉ **3**) from Thiele's acid. This is the shortest and most convenient method for the preparation of the dienone **3**.

The tricyclic β-diketone **44** could also be prepared by an internal acylation reaction. The ketal aldehyde **40** was oxidized to the ketal carboxylic acid **55** which was analysed as its corresponding methyl ester **56**. Acid hydrolysis of the ketal methyl ester **56** gave the ketone methyl ester **58** which was converted into the ketone carboxylic acid **57** by hydrolysis under basic conditions. Upon heating in benzene in the presence of *p*-toluenesulfonic acid, compound **57** gave a good yield of the β-diketone **44**. Upon treatment with acetic anhydride and pyridine, the β-diketone **44** was converted into the ketone enol acetate **54**.

The very facile acylation reaction (**57** → **44**) suggests that there is a possibility to transform directly

Can. J. Chem. Downloaded from www.nrcresearchpress.com by 210.87.254.40 on 09/05/12
For personal use only.

Can. J. Chem. Downloaded from www.nrcresearchpress.com by 210.87.254.40 on 09/05/12
For personal use only.

the ketone lactone **59** (Scheme 5) into the β-diketone **44** by using anhydrous acidic conditions. Under such conditions, it is reasonable to envisage that the lactone **59** would dehydrate to give the olefin ketone carboxylic acid **57** or its equivalent as an intermediate which would then give the β-diketone **44**. The ketone lactone **59** was obtained by acid hydrolysis of the ketal lactone **12**. On treatment with polyphosphoric acid, the ketone lactone **59** did not yield the anticipated β-diketone **44**; instead, the γ-lactone **60** was produced in good yield. This result suggests that, in strong acidic conditions, the lactonization is faster than the acylation reaction or that **59** gives **60** via a process which is expressed in formulas **61** and **62**.

The structure of the γ-lactone **60** was proven chemically: iodolactonization of ketal carboxylic acid **55** gave the ketal iodolactone **63** which was hydrogenolysed to the ketal γ-lactone **64**. Acid hydrolysis of the ketal γ-lactone **64** gave a γ-lactone which was found identical with the tricyclic γ-lactone ketone **60** obtained from the polyphosphoric acid treatment of **59**.

Synthesis of Triquinacene

The tricyclic *exo* ketone alcohol **41** and the highly crystalline β-diketone **44** (Scheme 6), which can be obtained in three and four steps, respectively, from Thiele's acid, appeared as ideal intermediates for a convenient synthesis of triquinacene (**1**).

Reduction of the β-diketone **44** with lithium aluminium hydride gave a 5:1 mixture of the *cis* and the *trans* diols **65** and **66** which were separated by chromatography. Both diols were converted into their corresponding diacetates **67** and **68**.

We have assigned the *endo-cis* structure **65** for the major diol because (*a*) the simplicity of nmr spectra of **65** and its diacetate **67** shows that these products must have a plane of symmetry; (*b*) the major diol can be converted into a cyclic carbonate derivative **69** by reaction with phosgene. Examination of molecular models show clearly that the *cis-endo* diol structure **65** can easily form a cyclic carbonate whereas the *cis-exo* diol structure **70** cannot. In structure **70**, the direction in space of the two *exo* alcohol groups is such that they cannot form a cyclic six-membered ring carbonate. This assignment was further strengthened by the fact that on reduction with a bulkier hydride such as lithium tri-*tert*-butoxy aluminium hydride, the β-diketone **44** gave almost exclusively the diol assigned as structure **65**.

The assignment of the *trans* (*endo-exo*) configuration to the minor diol follows from the examination of the nmr spectra of **66** and its diacetate **68** which indicates a complete lack of symmetry in these compounds. This assignment is further confirmed by the

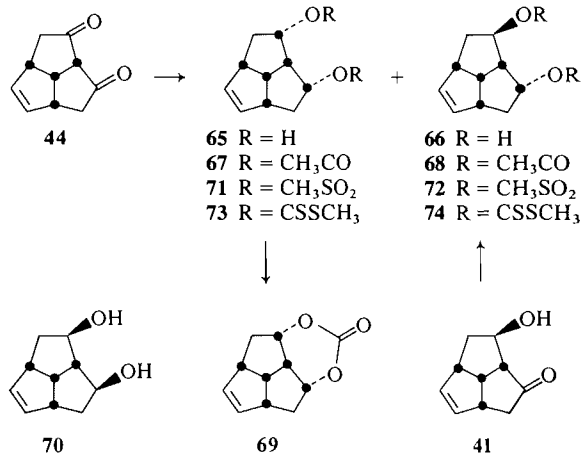

SCHEME 6

fact that the reduction of the *exo* ketone alcohol **41** with lithium tri-*tert*-butoxy aluminium hydride gave almost exclusively the diol **66**.

The *cis* and the *trans* diols **65** and **66** can be transformed into their respective *cis* and *trans* dimesylates **71** and **72** and into their respective *cis* and *trans* dixanthates **73** and **74**. Triquinacene can be prepared in approximately 50% yield from each of these four intermediates. No attempt was made to improve this yield or to develop an alternative higher yielding procedure. Both dimesylates **71** and **72** on treatment with basic alumina (23) give triquinacene **1**. Similarly, pyrolysis of the *cis* and the *trans* dixanthates **73** and **74** give also triquinacene (**1**). A synthesis of triquinacene can therefore be realized in six steps (**7** → **10** → **43** → **41** → **66** → **72** (or **74**) → **1**) or in seven steps (**7** → **10** → **43** → **41** → **44** → **65** → **71** (or **73**) → **1**). The six-step sequence via the *trans* dimesylate **72** appears to be the method of choice.

Experimental

The ir spectra were taken on a Perkin-Elmer 257 spectrophotometer. The ultraviolet (uv) spectra were registered on a Varian Techtron 635 spectrophotometer. Vapor phase chromatographic (vpc) analysis were carried out on a Varian aerograph instrument model 90-P. Proton nmr spectra were recorded on a Varian A-60 instrument. Chemical shifts are reported in δ values relative to tetramethylsilane as internal standard. The mass spectra were taken on a Hitachi-Perkin-Elmer RMU-6 mass spectrometer by Mr. J. R. Martin, Université de Sherbrooke. Microanalyses were carried out by Mr. J. Tamas, Laboratoire de Microanalyse, Université de Sherbrooke, and by Dr. C. Daesslé, Organic Microanalyses, Montreal. Thiele's acid (**1**) was prepared by the method described in reference 24. Anhydrous magnesium sulfate was used as the drying agent in working up reactions. Low boiling petroleum ether (bp 30–60°C) was used.

Diacid Chloride **8**

Oxalyl chloride (63.5 g, 42.6 ml, 0.5 mol) was added with stirring to a suspension of powdered Thiele's acid **7** (50 g, 0.23 mol) in anhydrous methylene chloride (800 ml) under an

Can. J. Chem. Downloaded from www.nrcresearchpress.com by 210.87.254.40 on 09/05/12
For personal use only.

atmosphere of nitrogen. After the addition was complete, the stirring was continued at room temperature for 5 days. The unreacted acid was then filtered off and the filtrate was evaporated to dryness under vacuum. The brown oil obtained was triturated with petroleum ether (10 × 125 ml) and the solution was cooled to yield white crystals (40 g, 73%); mp 61–62°C (lit. (19) mp 62°C); ir (CH_2Cl_2): 1750, 1617, and 1587 cm^{-1}; nmr ($CDCl_3$) δ: 6.93 (1H, quadruplet, J = 2 Hz) and 7.18 (1H, quadruplet, J = 1 and 2 Hz) (two olefinic hydrogens).

*Diazide **9** (2)*

A solution of the diacid chloride **8** (32.3 g, 0.126 mol) in acetone (100 ml) was added dropwise with stirring to a solution of sodium azide (17.9 g, 0.275 mol) in water (100 ml) at 0°C. After the addition was complete the reaction mixture was stirred for 10 min at 0°C. The white precipitate of the diazide obtained was collected by filtration. Owing to the explosive nature of the product, it was immediately converted into the diketone **10** without further purification. An analytical sample was prepared from an aliquot by recrystallization from petroleum ether (white crystals); mp 75–77°C; ir (CH_2Cl_2): 2150, 1683, 1674, 1618, and 1586 cm^{-1}; nmr ($CDCl_3$) δ: 6.60 (1H, quadruplet, J = 2 and 4 Hz) and 6.93 (1H, doublet, J = 3 Hz) (two olefinic hydrogens); ms *m/e*: 149, 107, 79, and 52. *Anal.* calcd. for $C_{12}H_{10}O_2N_6$: C 53.31, H 3.73; found: C 53.95, H 3.86.

*Diketone **10***

*(a) From Diazide **9***

The moist diazide obtained as above was heated in a mixture of dimethoxyethane (170 ml) and water (60 ml) with stirring at 80°C for 2 h under an atmosphere of nitrogen. The reaction mixture was then cooled to 10°C and treated with dilute hydrochloric acid (3 *N*, 50 ml) and stirring continued at room temperature for 1 h. It was then continuously extracted with ether (1 ℓ) for 20 h. Evaporation of the ether extract yielded a white syrup (16 g, 77%). An analytical sample of the diketone **10** was prepared by the hydrolysis of the monoketal **11** as follows. The monoketal **11** (84 mg, 0.34 mmol) was stirred in a mixture of tetrahydrofuran (2 ml) and hydrochloric acid (1 *N*, 1 ml) for 5 h at room temperature. Dichloromethane (50 ml) was then added to the reaction mixture, the organic layer was separated, washed with saturated sodium bicarbonate and sodium chloride solution, and dried. The white syrup (56 mg, 100%) obtained on distilling off the solvent was sublimed under vacuum (80°C/0.1 Torr); mp 113–115°C; ir (CH_2Cl_2): 1750 cm^{-1}; nmr ($CDCl_3$) δ: 6.80–8.50 (12 H, multiplets); ms *m/e*: 164 (M^+). *Anal.* calcd. for $C_{10}H_{12}O_2$: C 73.14, H 7.37; found: C 73.02, H 7.24.

(b) From Thiele's Acid

Thiele's acid (50 g, 0.225 mol) was dissolved in a mixture of sulfuric acid (concentrated, 250 ml) and trifluoroacetic acid (150 ml). Sodium azide (30.5 g, 0.47 mol) was then added in small portions. After the addition was completed, the mixture was heated at 45–50°C (oil bath temperature) for 5 h. After cooling to 0°C, water (1.5 ℓ) was slowly added and the mixture was extracted with dichloromethane (continuous extraction for 4 days). The organic extract was washed with saturated bicarbonate solution, dried with sodium sulfate, and evaporated to dryness. The crude diketone was then purified by column chromatography on Florisil using successively pentane, benzene, and ether. The diketone **10** (≃13.0 g, ≃35%) was obtained in the ether solution as a waxy product which can be used directly for the next operation.

*Monoketal **11***

The crude diketone **10** (23.4 g, 0.142 mol) was dissolved in anhydrous benzene (600 ml) and mixed with 2,2-dimethyl-1,3-propanediol (15.6 g, 0.15 mol) and *p*-toluenesulfonic acid (50 mg). The mixture was refluxed for 20 h using a Dean–Stark water separator. The resulting brown solution was washed successively with saturated sodium carbonate and sodium chloride solution, dried, and concentrated under vacuum to yield a pale yellow solid. The above solid was recrystallized from benzene–ether to give white crystals (24.5 g, 69%); mp 125–126°C; ir ($CHCl_3$): 1740, 1360, 1350, and 1110 cm^{-1}; nmr ($CDCl_3$) δ: 0.87 (3H, singlet, CH_3), 0.98 (3H, singlet, CH_3), 7.00–9.00 (12 H, multiplet), 3.42 (2H, singlet, CH_2O), and 3.48 (2H, singlet, CH_2O); ms *m/e*: 250 (M^+). *Anal.* calcd. for $C_{15}H_{12}O_3$: C 71.97, H 8.86; found: C 71.99, H 9.03.

*Lactone **12***

Anhydrous sodium bicarbonate (33.6 g, 0.4 mol) and *m*-chloroperbenzoic acid (85%, 19.5 g, 96.4 mmol) were added to a solution of the monoketal **11** (20.0 g, 80.0 mmol) in dry carbon tetrachloride and stirred for 45 h. The reaction mixture was then diluted with dichloromethane (1500 ml) and washed thoroughly with a solution of sodium thiosulfate (10%, 2 × 100 ml), water (200 ml), a solution of sodium hydroxide (1 *N*, 2 × 200 ml), and again water (4 × 100 ml). The organic phase was then dried and evaporated to dryness under vacuum to give a white solid (21.1 g) containing the two lactones **12** and **13** in the ratio 73:27; ir (CH_2Cl_2): 1735, 1215, and 1100 cm^{-1}; nmr ($CDCl_3$) δ: 0.90 (singlet), 1.02 (singlet), 1.50–3.00 (multiplets), 3.47 and 3.50 (4H, OCH_2 of the acetal), 4.32 (27% of 2H, CH_2OCO, broad multiplet), and 4.70 (73% of 1H, CHOCO, broad multiplet).

The purification of the lactone **12** was carried out by selective basic hydrolysis of the isomeric lactone **13**. The crude mixture of the isomeric lactones **12** and **13** (21.19 g, 80 mmol) in the ratio 73:27 was dissolved in dimethoxyethane (700 ml) and cooled (5°C). This was treated with a solution of sodium hydroxide (1 *N*, 22 ml, 22 mmol) diluted with water (230 ml) and the reaction mixture was kept at room temperature for 17 h. A further amount of sodium hydroxide solution was then added (1 *N*, 17 ml, 17 mmol) and the disappearance of the lactone was followed by analyzing aliquots of the reaction mixture by nmr (disappearance of the signal at δ 4.32). The hydrolysis was complete in 9 h 30 min. The dimethoxyethane was then distilled off under vacuum and the residue was taken up in dichloromethane (600 ml). The organic phase was separated and washed with sodium hydroxide solution (1 *N*, 100 ml). The aqueous phase was reextracted with dichloromethane (150 ml) and the combined extracts were washed with water (2 × 150 ml), dried, and the solvent evaporated off under vacuum to yield only the lactone **12** as a white solid (13.8 g, 90%). The analytical sample was prepared by recrystallization from dichloromethane–ether; mp 158–159°C; ir (CH_2Cl_2): 1735, 1215, 1120, and 1110 cm^{-1}; nmr ($CDCl_3$) δ: 0.88 (3H, singlet, CH_3), 1.00 (3H, singlet, CH_3), 1.30–3.00 (11 H, multiplet), 3.42 (2H, singlet, CH_2O), 3.47 (2H, singlet, CH_2O), and 4.63 (1H, multiplet, CHOCO); ms *m/e*: 266 (M^+). *Anal.* calcd. for $C_{15}H_{22}O_4$: C 67.64, H 8.33; found: C 67.80, H 8.58.

*Methyl Ester Benzoate **14***

A solution of sodium methoxide in methanol was prepared by adding sodium (430 mg, 18.7 mmol) to anhydrous methanol (10 ml) with the exclusion of moisture. The lactone **12** (1.00 g, 3.76 mmol) dissolved in dry methanol was added to the above solution and stirred at room temperature for 12 h. The methanol was then evaporated off under reduced pressure and the residue dissolved in dichloromethane (250 ml). The organic phase was washed with water (1 × 100 ml and 2 × 50 ml),

Can. J. Chem. Downloaded from www.nrcresearchpress.com by 210.87.254.40 on 09/05/12
For personal use only.

dried, and the solvent distilled off under vacuum to give the corresponding hydroxy methyl ester as an oil (1.07 g, 95%); ir (CH_2Cl_2): 3600, 3460, 1735, 1080, 1062, and 1025 cm^{-1}; nmr ($CDCl_3$) δ: 0.95 (6H, singlet, $(CH_3)_2C$), 7.20–8.80 (11 H, multiplet), 3.42 (4H, singlet, two OCH_2), 3.62 (3H, singlet, OCH_3), and 4.2 (1H, multiplet, CHOH).

The above crude hydroxy methyl ester (690 mg, 2.31 mmol) was dissolved in dichloromethane (10 ml) and pyridine (2 ml). Benzoyl chloride (358 mg, 2.56 mmol) was added to the above solution and stirred at room temperature for 11 h. The reaction mixture was then diluted with water (200 ml) and extracted with dichloromethane (200 ml). The extract was stirred with very dilute hydrochloric acid (100 ml, p*H* 3). The organic phase was separated, washed with sodium bicarbonate solution (5%, 50 ml), and water (50 ml). It was then dried and the solvent was removed by distillation under vacuum to give an oil (896 mg) which was purified by thick-layer chromatography on silica gel using benzene–ether (3:2). This resulted in a white crystalline product (624 mg, 67%). An analytical sample was prepared by recrystallization from ether; mp 86–87°C; ir (CCl_4): 3070, 1741, 1720, 1601, 1580, 1110, and 1000 cm^{-1}; nmr (CCl_4) δ: 0.88 (3H, singlet, CH_3), 0.94 (3H, singlet, CH_3), 1.00–3.10 (11 H, multiplet), 3.39 (4H, multiplet, two OCH_2), 3.65 (3H, singlet, OCH_3), 5.20 (1H, multiplet, CHOCO), 7.45 (3H, multiplet, aromatic hydrogens), and 8.04 (2H, multiplet, aromatic hydrogens); ms *m/e*: 402 (M^+). *Anal.* calcd. for $C_{23}H_{30}O_6$: C 68.63, H 7.51; found: C 68.30, H 7.79.

Diol ***15***

A solution of the lactone **12** (15.4 g, 0.058 mol) in anhydrous tetrahydrofuran (200 ml) was added dropwise with stirring during a period of 60 min to a suspension of lithium aluminium hydride (4.5 g, 0.12 mol) in dry ether (350 ml) at 0°C. The reaction mixture was then stirred at room temperature for 2 h and refluxed for 60 min. It was then cooled and diluted with dichloromethane (500 ml). The complex formed was decomposed by the slow addition of saturated Rochelle salt solution (35 ml). The excess of water was removed by stirring with anhydrous magnesium sulfate. The inorganic salts were filtered off and the filtrate was evaporated to give a colorless oil (14.6 g, 94%) which could not be distilled; ir (CH_2Cl_2): 3610, 3460, 1360, 1350, and 1115 cm^{-1}; nmr ($CDCl_3$) δ: 0.96 (6H, singlet, $(CH_3)_2C$), 3.32 (2H, singlet, CHO*H* and CH_2OH), 3.52 (4H, singlet, two OCH_2), 3.60 (2H, triplet, J = 7 Hz, CH_2OH), and 4.20 (1H, multiplet, CHOH); ms *m/e*: 270 (M^+).

Diacetate ***16***

The ketal diol **15** (14.4 g, 0.053 mol) was dissolved in a mixture of pyridine (100 ml) and acetic anhydride (50 ml) and kept at room temperature in the dark for 13 h. It was then evaporated to dryness under vacuum. The last traces of the solvent were removed by repeated codistillation with benzene to give an oil (18.9 g, 100%). An analytical sample was prepared by molecular distillation; bp 155°C/0.05 Torr; ir (CH_2Cl_2): 1730, 1243, and 1115 cm^{-1}; nmr ($CDCl_3$) δ: 0.97 (3H, singlet, CH_3), 0.94 (3H, singlet, CH_3), 2.00 (6H, singlet, two CH_3CO), 3.46 (4H, singlet, two OCH_2), 4.05 (2H, triplet, J = 7 Hz, CH_2OCO), and 4.95 (1H, multiplet, CHOCO); ms *m/e*: 354 (M^+). *Anal.* calcd. for $C_{19}H_{30}O_6$: C 64.38, H 8.53; found: C 64.45, H 8.54.

Acetate Alcohol ***17***

A solution of potassium carbonate (7.3 g, 0.053 mol) in water (150 ml) was added dropwise with stirring during a period of 50 min to a solution of the ketal diacetate **16** (18.6 g, 0.052 mol) in methanol (850 ml) at 0°C. After the addition was complete the stirring was continued for 30 min. It was then treated with saturated sodium chloride solution (400 ml) and the reaction mixture was extracted several times with dichloromethane. The residue obtained upon distilling off the solvent was again dissolved in dichloromethane (500 ml), dried, and evaporated under vacuum to give a colorless oil (15 g) which was a mixture of the diol **15**, the acetate alcohol **17**, and the starting material **16**. The monoacetate **17** was obtained pure by column chromatography on Florisil (elutions with petroleum ether – benzene) as a colorless oil (8.8 g, 53.7%) which could not be distilled: ir (CH_2Cl_2): 3600, 3500, 1726, 1240, and 1112 cm^{-1}; nmr ($CDCl_3$) δ: 0.93 (3H, singlet, CH_3), 0.98 (3H, singlet, CH_3), 2.02 (3H, singlet, CH_3CO), 2.37 (1H, singlet, CH_2OH), 3.50 (4H, singlet, two OCH_2), 3.64 (2H, triplet, J = 7 Hz, CH_2OH), and 4.95 (1H, multiplet, CHOCO); ms *m/e*: 252 ($M^+ - CH_3COOH$).

Ketal Acetate Aldehyde ***18***

(*a*) *From Acetate Alcohol* ***17***

The acetate alcohol **17** (2.5 g, 8 mmol) dissolved in dichloromethane (100 ml) was added to a solution of chromium trioxide pyridine complex (25) (12.4 g, 48 mmol) in the same solvent (300 ml) at 0°C. The reaction mixture was then stirred at room temperature for 20 min and poured into water (500 ml). The organic layer was separated and the aqueous layer was extracted three times with dichloromethane. The extracts were combined and washed with saturated copper sulfate solution followed by saturated sodium chloride solution. It was then dried and the solvent was distilled off under vacuum to give crude ketal acetate aldehyde **18** as a yellow oil (2.4 g, 97%); ir (CH_2Cl_2): 2730, 1735, 1245, 1060, and 1030 cm^{-1}; nmr ($CDCl_3$) δ: 0.95 (6H, singlet, $(CH_3)_2C$), 3.43 (4H, singlet, two OCH_2), 4.93 (1H, multiplet, CHOCO), and 9.70 (1H, multiplet, CHO).

(*b*) *From Ketal Aldehyde Alcohol* ***31***

The ketal aldehyde alcohol **31** (649 mg, 2.42 mmol) was dissolved in a mixture of pyridine (5 ml) and acetic anhydride (2.5 ml) and kept in the dark at room temperature for 10 h. The residue obtained on removing the solvent under vacuum was dissolved in dichloromethane (200 ml) and washed with water (2 × 30 ml). The organic phase was dried, filtered, and the solvent evaporated off under reduced pressure to yield an oil (608 mg). It was purified by treatment with active charcoal and chromatography on Florisil. Elution with ether–benzene gave the pure ketal acetate aldehyde **18** (209 mg, 28%) identical with the product obtained in the above procedure.

Cis *and* Trans *Ketone Alcohol Acetates* ***19*** *and* ***20*** *(26)*

The ketal aldehyde alcohol **31** (1.994 g, 7.45 mmol) was acetylated by the method described above to yield the crude ketal acetate aldehyde **18** (2.109 g) which was dissolved in a mixture of acetone (800 ml) and hydrochloric acid solution (3 *N*, 16 ml). After 2 h at room temperature, excess solid sodium bicarbonate was added. After filtration, the solvent was evaporated and dichloromethane was added. The resulting solution was dried with sodium sulfate, filtered, and evaporated to dryness. Thick-layer chromatography with silica gel in two successive elutions with ether gave the *cis* and the *trans* ketone alcohol acetates **19** and **20**. The *cis* ketone alcohol acetate **19** was obtained pure by crystallization with ether – petroleum ether (R_f 0.45, 516 mg, 31%); mp 73–74°C; ir (CH_2Cl_2): 3600, 3500, 1730, and 1245 cm^{-1}; nmr ($CDCl_3$) δ: 2.05 (3H, singlet, CH_3CO), 3.64 (1H, broad singlet, OH), 4.58 (1H, quadruplet, J = 7 Hz, CHOH), and 5.30 (1H, multiplet, CHOCO); ms *m/e*: 224 (M^+). *Anal.* calcd. for $C_{12}H_{16}O_4$: C 64.27, H 7.19; found: C 64.17, H 7.37.

The *trans* ketone alcohol acetate **20** was obtained pure as an oil (R_f 0.3, 434 mg, 25%); ir (CH_2Cl_2): 3600, 3450, 1735, and 1245 cm^{-1}; nmr ($CDCl_3$) δ: 2.02 (3H, singlet, CH_3CO), 4.58

Can. J. Chem. Downloaded from www.nrcresearchpress.com by 210.87.254.40 on 09/05/12
For personal use only.

(1H, multiplet, C*H*OH), and 5.31 (1H, multiplet, CHOCO); ms *m/e*: 224 (M^+).

β-*Diketone Acetate* ***21***

(*a*) *From* Cis *Ketone Alcohol Acetate* ***19***

The *cis* alcohol acetate **19** (64 mg, 0.28 mmol) was dissolved in acetone (50 ml) and cooled to 0°C. A slight excess of a solution of chromium trioxide in sulfuric acid (27), was added from a burette to this solution with vigorous stirring. After 10 min the excess oxidizing agent was destroyed by the addition of isopropanol and the reaction mixture was neutralized with solid sodium bicarbonate. It was then filtered and the residue was washed with acetone. The filtrate was evaporated to dryness under reduced pressure to give a solid which was dissolved in dichloromethane. The above solution was dried over sodium sulfate, filtered, and the solvent was distilled off under vacuum to yield a solid (62 mg, quantitative). An analytical sample was prepared by recrystallization from ether – petroleum ether; mp 124–126°C; ir (CH_2Cl_2): 1768, 1741, 1721, and 1230 cm^{-1}; nmr ($CDCl_3$) δ: 1.90 (3H, singlet, CH_3CO), 1.70–4.00 (10 H, multiplet), and 5.47 (1H, multiplet, CHOCO); ms *m/e*: 222 (M^+). *Anal.* calcd. for $C_{12}H_{14}O_4$: C 64.85, H 6.35; found: C 64.87, H 6.30.

(*b*) *From* Trans *Ketone Alcohol Acetate* ***20***

Using the experimental procedure described above, the *trans* alcohol acetate **20** was also converted into the same β-diketone acetate **21** in essentially quantitative yield.

Cis *Ketone Diacetate* ***22***

A solution of the *cis* alcohol acetate **19** (205 mg, 0.83 mmol) in a mixture of pyridine (3 ml) and acetic anhydride (1.5 ml) was kept in the dark at room temperature for 24 h. It was then cooled (5°C) and methanol (2 ml) was added with stirring. The reaction mixture was then shaken with dichloromethane (200 ml) and the organic phase was washed with hydrochloric acid (1 *N*, 100 ml) followed by water (100 ml). The solution was then dried and the solvent was evaporated off under reduced pressure to give an oil (249 mg) which was purified by preparative thick-layer chromatography on silica gel with benzene–ether (70 mg, quantitative); bp 140°C/5 × 10^{-6} Torr, dec.; ir (CH_2Cl_2): 1740 and 1240 cm^{-1}; nmr ($CDCl_3$) δ: 2.08 (6H, singlet, two CH_3CO) and 5.35 (2H, multiplet, two OCHCO); ms *m/e*: 266 (M^+).

Trans *Ketone Diacetate* ***23***

(*a*) *From* Trans *Ketone Alcohol Acetate* ***20***

The *trans* acetate alcohol **20** (86 mg, 0.38 mmol) was dissolved in a mixture of pyridine (1.5 ml) and acetic anhydride (0.8 ml) and kept in the dark for 24 h. The reaction mixture was then cooled (5°C), mixed with methanol (1.5 ml) and stirred at room temperature for 30 min. It was then diluted with ether (200 ml), washed successively with dilute hydrochloric acid (1 *N*, 2 × 50 ml), saturated sodium bicarbonate solution (50 ml), and water (2 × 50 ml). Removal of the dried solvent under vacuum gave an oil (93 mg, 92%) which crystallized from ether – petroleum ether; mp 78–79°C; ir ($CHCl_3$): 1740, 1245, and 1210 cm^{-1}; nmr ($CDCl_3$) δ: 2.02 (6H, singlet, two CH_3COO) and 5.37 (2H, multiplet, two OCHCO); ms *m/e*: 266 (M^+). *Anal.* calcd. for $C_{14}H_{18}O_5$: C 63.15, H 6.81; found: C 63.14, H 6.91.

(*b*) *From* Trans *Ketone Diol* ***34***

The *trans* ketone diol **34** (511 mg, 2.8 mmol) was dissolved in pyridine (15 ml) and acetic anhydride (7.5 ml) and stirred. The above solution was kept at room temperature in the dark for 75 h. It was then evaporated to dryness under reduced pressure. The resulting oil (830 mg) was purified by column chromatography on Florisil. Elution with benzene–ether gave the pure ketone diacetate **23** (628 mg, 84%). Recrystallization from ether – petroleum ether gave white crystals whose physical and spectral properties were identical to the product **23** obtained above.

Ketal Alcohol Acetate ***24***

The ketone alcohol acetate **20** (277 mg, 1.2 mmol) was dissolved in benzene (50 ml) and mixed with ethylene glycol (0.3 ml, 5 mmol) and *p*-toluenesulfonic acid (15 mg). The reaction mixture was refluxed for 8 h using a Dean–Stark water separator. The cooled reaction mixture was diluted with dichloromethane (100 ml) and washed with saturated sodium carbonate and saturated sodium chloride. The dried solution was evaporated to give a yellow oil. Thick-layer chromatography on silica gel using ether as the solvent gave the pure ketal alcohol acetate **24** (205 mg, 64%). It was recrystallized from ether – petroleum ether; mp 73–74°C; ir (CH_2Cl_2): 3600, 3500, 1740, 1245, and 1115 cm^{-1}; nmr ($CDCl_3$) δ: 1.97 (3H, singlet, CH_3CO), 2.32 (1H, singlet, OH), 3.90 (4H, singlet, two OCH_2), 4.27 (1H, multiplet, C*H*OH), and 4.93 (1H, multiplet, CHOCO); ms *m/e*: 268 (M^+). *Anal.* calcd. for $C_{14}H_{20}O_5$: C 62.67, H 7.51; found: C 62.52, H 7.56.

Trans *Ketal Diol* ***25***

(*a*) *From Ketal Alcohol Acetate* ***24***

A solution of ketal alcohol acetate **24** (135 mg, 0.5 mmol) in methanol was mixed with potassium carbonate (345 mg, 2.5 mmol) in water (5 ml). The mixture was left at room temperature for 4 h. Most of the methanol was removed by evaporation and the resulting aqueous mixture was continuously extracted with dichloromethane during 24 h. Drying and evaporation of the solvent gave a yellow crystalline residue (102 mg, 90%) which was recrystallized from ethyl acetate; mp 150–151°C; ir (CH_2Cl_2): 3600 and 3470 cm^{-1}; nmr ($CDCl_3$) δ: 3.50 (2H, broad singlet, two OH), 3.98 (4H, singlet, two OCH_2), and 4.27 (2H, multiplet, two C*H*OH); ms *m/e*: 266 (M^+). *Anal.* calcd. for $C_{12}H_{18}O_4$: C 63.70, H 8.02; found: C 63.80, H 7.92.

(*b*) *From* Trans *Ketone Diacetate* ***23***

A solution of *trans* ketone diacetate **23** (127 mg, 0.48 mmol) in benzene (55 ml) was mixed with ethylene glycol (574 mg, 9.25 mmol) and *p*-toluenesulfonic acid (15 mg). The mixture was heated to reflux during 11 h using a Dean–Stark water separator. Ether (200 ml) was then added and the organic phase washed with saturated sodium bicarbonate (100 ml) and water (100 ml). The dried solution was evaporated to dryness to give the corresponding *trans* ketal diacetate which crystallized from petroleum ether (118 mg, 80%); mp 57–59°C; ir (CH_2Cl_2): 1730 cm^{-1}; nmr ($CDCl_3$) δ: 2.01 and 2.03 (6H, two singlets, two CH_3CO), 3.96 (4H, broad singlet, two CH_2O), and 5.17 (2H, multiplet, two CHOCO); ms *m/e*: 310 (M^+). *Anal.* calcd. for $C_{16}H_{22}O_6$: C 61.92, H 7.15; found: C 62.01, H 7.24.

The above *trans* ketal diacetate (628 mg, 2.03 mmol) was dissolved in methanol (50 ml) and mixed with water (23 ml) and triethylamine (6 ml). This mixture was heated at 70°C for 16 h. The solvent was then removed *in vacuo* and the residue was dissolved in methanol (15 ml) and dichloromethane (500 ml). The solution was dried and the solvent was evaporated. The residual oil was purified by column chromatography on Florisil. The ketal diol **25** (347 mg, 76%) was obtained pure by elution with methanol–ether (1:19). Recrystallization from ethyl acetate gave a product which was found identical with the *trans* ketal diol **25** obtained by the above procedure.

Trans *Ketal Dimesylate* ***26***

(*a*) *From* Trans *Ketal Diol* ***25***

The ketal diol **25** (328 mg, 1.43 mmol) was dissolved in a

Can. J. Chem. Downloaded from www.nrcresearchpress.com by 210.87.254.40 on 09/05/12
For personal use only.

mixture of dichloromethane (60 ml) and pyridine (3.4 ml) at 0°C. Methane sulfonyl chloride (822 mg, 7.7 mmol) was added to the above solution and the reaction mixture was kept in the cold (5°C) for 4½ days. It was then diluted with dichloromethane (500 ml) and washed with hydrochloric acid (1 *N*, 100 ml), sodium carbonate solution (10%, 100 ml), and water (2 × 75 ml). The organic phase was dried and the solvent was distilled off under reduced pressure. The residue was recrystallized from dichloromethane–ether to give the pure dimesylate **26** (384 mg, 70%); mp 122.5–123.5°C; ir (CH_2Cl_2): 1360, 1340, 1180, 1100, and 1000 cm^{-1}; nmr ($CDCl_3$) δ: 3.03 (3H, singlet, CH_3SO_2), 3.10 (3H, singlet, CH_3SO_2), 4.00 (4H, singlet, two OCH_2), and 5.00 (2H, multiplet, two $CHOSO_2$); ms *m/e*: 286 ($M^+ - CH_3SO_2OH$). *Anal.* calcd. for $C_{14}H_{22}O_8S_2$: C 43.96, H 5.80; found: C 43.99, H 5.78.

(b) From Ketone Dimesylate 35

A solution of *p*-toluenesulfonic acid (8 mg) and ethylene glycol (284 mg, 4.6 mmol) in benzene (50 ml) was refluxed for 1 h with a water separator. The ketone dimesylate **35** (142 mg, 0.41 mmol) was then added to the above solution and the reaction mixture was refluxed for 2 h. The solution was cooled and treated with ice cold water (100 ml). The organic phase was separated and the aqueous phase was extracted with dichloromethane (300 ml). The combined extracts were washed with ice cold water (100 ml), dried and the solvent evaporated off under reduced pressure to give the ketal dimesylate **26** (157 mg, quantitative) as an oil. It was crystallized from dichloromethane:ether. The product obtained was found identical with the *trans* ketal dimesylate **26** obtained by the procedure above.

*Dienone **29** and 2,3-Dihydrotriquinacen-2-one (3)*

Potassium *tert*-butoxide purified by sublimation (224 mg, 2 mmol) was added to a solution of the dimesylate **26** (204 mg, 0.53 mmol) in anhydrous dimethyl sulfoxide (20 ml) under an atmosphere of nitrogen and stirred at 30°C for 6 h. The yellow reaction mixture was poured into ice cold water (150 ml) containing sodium chloride and the mixture was extracted with ether. The ether extract was washed with water, dried, and evaporated to give an oil (95 mg, 94%). The oil was distilled (60–70°C/0.5 Torr; 69 mg, 68%) and analyzed by vapor phase chromatography (5 ft × ¼ in., 15% OS-138 on Chromosorb W, 200°C). It was found to contain three products with retention times 10, 11, and 14 min, respectively, in the ratio 71:25:4. The above mixture was separated into two fractions by preparative thick-layer chromatography on silica gel. One of the fractions (20 mg, R_f 0.50) contained the three products and the other (45 mg, R_f 0.39) showed the presence of only two products with retention times 10 and 11 min in the ratio 76:24. It could be shown by hydrolysis that they were the ketals **27** and **28**; ir (CH_2Cl_2): 3040, 1120, and 1102 cm^{-1}; nmr ($CDCl_3$) δ: 1.20–3.9 (multiplets), 3.92 (singlet), and 5.35–5.85 (multiplet).

Hydrochloric acid (2 *N*, 1 ml) was added to a mixture of the ketal dienes **27** and **28** (42 mg, 0.22 mmol) in the ratio 87:13 in tetrahydrofuran (2 ml) and stirred at room temperature for 7 h. The mixture was diluted with saturated sodium chloride solution and extracted with ether. The organic phase was washed with saturated sodium bicarbonate solution, water, and dried. Evaporation of the solvent gave a yellow oil (33 mg), the vapor phase chromatographic analysis of which revealed the presence of two compounds (5 ft × ¼ in., 15% OS-138 on Chromosorb W, 200°C) with retention times 6 and 9 min in the ratio 86:14. They were separated by preparative thick-layer chromatography on silica gel with benzene. The conjugated ketone **29** was obtained as a colorless oil (6 mg, 19%, R_f 0.40). The above compound showed only one peak with retention time 9 min by vapor phase chromatography. It was found to be unstable at room temperature; ir (CH_2Cl_2): 1707 and 1615 cm^{-1}.

The ketone **3** (15 mg, 47%, R_f 0.20) isolated as a yellow oil was pure by vapor phase chromatography with retention time 6 min. It was further purified by molecular distillation (45°C/0.9 Torr); ir (CH_2Cl_2): 3040, 1740, 1614, and 1604 cm^{-1}; nmr ($CDCl_3$) δ: 1.00–4.00 (6H, multiplet) and 5.78 (4H, multiplet, four olefinic hydrogens); ms *m/e*: 146 (M^+).

The 2,4-dinitrophenylhydrazone derivative was prepared by reacting the ketone with a solution of the 2,4-dinitrophenylhydrazine in ethanol containing traces of sulfuric acid. The product was recrystallized from ethyl acetate; mp 155°C. *Anal.* calcd. for $C_{16}H_{14}O_4N_4$: C 58.89, H 4.32; found: C 58.79, H 4.47.

2,3-Dihydrotriquinacen-2-one (3)

*(a) From 2-*exo*-2,3-Dihydrotriquinacenol (30)*

A solution of 2-*exo*-2,3-dihydrotriquinacenol (**30**) (27.2 mg, 0.18 mmol) in dry dichloromethane (3 ml) was added to a solution of Collins' reagent (25) (284 mg, 1.1 mmol) in the same solvent (10 ml) and stirred for 30 min. The reaction mixture was then poured into water (30 ml) and extracted with dichloromethane (3 × 35 ml). The organic phase was washed with dilute hydrochloric acid (1 *N*, 15 ml) saturated sodium bicarbonate solution (25 ml), and saturated sodium chloride solution (25 ml). It was dried and the solvent was distilled off under reduced pressure to give an oil (21 mg) which was purified by filtration through a column of silica gel (3 g). 2,3-Dihydrotriquinacen-2-one (**3**) was obtained pure (15 mg, 54%) as a colorless oil with ether – petroleum ether (1:1).

(b) From Exo *Ketal Mesylate 53*

The *exo* ketal mesylate **53** (100 mg, 0.30 mmol) was dissolved in dry benzene (25 ml) in a flask equipped with a water separator under an atmosphere of nitrogen. Benzene was distilled off (20 ml) and a large excess of 1,5-diazabicyclo[3.4.0]nonene-5 (DBN) (1.00 g, 8 mmol) was added. The temperature of the bath was raised to 160–165°C and the reaction was completed in 3 h (tlc). The reaction mixture was then cooled to room temperature and diluted with benzene (60 ml). The solution was washed with ice cold dilute hydrochloric acid (0.1 *N*), sodium bicarbonate solution (10%), and brine. It was dried over sodium sulfate and the solvent was distilled off to give the crude ketal diene (64 mg, 90%); nmr ($CDCl_3$) δ: 0.95 (3H, singlet, CH_3), 0.97 (3H, singlet, CH_3), 1.36 (1H, quartet), 2.30 (1H, multiplet), 2.91 (1H, multiplet), 3.50 (7H, multiplets, two CH_2O and three allylic hydrogens), and 5.58 (4H, multiplets, four olefinic hydrogens). A solution of the ketal diene (58 mg, 0.25 mmol) in tetrahydrofuran (2 ml) and dilute hydrochloric acid (1 *N*, 1 ml) was stirred for 6 h under nitrogen. Excess solid sodium bicarbonate was added and the reaction mixture was diluted with dichloromethane (50 ml). The organic phase was washed with brine, dried over sodium sulfate, and filtered through a column of silica gel (20 g). The filtrate was concentrated under vacuum to give a product (25 mg, 70%) which was found identical with 2,3-dihydrotriquinacen-2-one (**3**).

(c) From Endo *Ketal Mesylate 52*

A solution of the ketal mesylate **52** (215 mg, 0.65 mmol) in anhydrous dimethyl sulfoxide (12 ml) was heated to 65°C under an atmosphere of nitrogen. Freshly sublimed potassium *tert*-butoxide (145 mg, 1.3 mmol) was added to the above reaction mixture in two equal portions with an interval of 3 h. At the end of 6 h the reaction mixture was poured into water (50 ml) containing sodium chloride and the solution was worked up as already described to give the corresponding ketal diene (140 mg).

The above ketal diene was converted into 2,3-dihydro-

Can. J. Chem. Downloaded from www.nrcresearchpress.com by 210.87.254.40 on 09/05/12
For personal use only.

triquinacen-2-one (**3**) by treatment with dilute hydrochloric acid as described in the above procedure *b*.

*Ketal Aldehyde Alcohol **31** (28)*

A solution of the lactone **12** (1.34 g, 5.04 mmol) in dry benzene (45 ml) was mixed with anhydrous ether (25 ml) and cooled (−5°C) in an atmosphere of nitrogen. Diisobutylaluminium hydride solution (10.3 ml, 5.52 mmol, 11.4% in hexane) was added to the above solution rapidly by means of a syringe. After 35 min it was decomposed by the careful addition of water (2.7 ml) and was allowed to warm up slowly to room temperature. The reaction mixture was then diluted with dichloromethane (500 ml), dried over sodium sulfate, and the solvent was evaporated off under reduced pressure to give an oil (1.45 g, quantitative). This product was directly used for subsequent reactions. A small amount of the product was purified by chromatography on Florisil using ether–benzene and ether; ir (CH_2Cl_2): 3600, 3480, 2730, 1730, 1065, and 1030 cm^{-1}; nmr ($CDCl_3$) δ: 0.97 (6H, singlet, $(CH_3)_2C$), 3.55 (4H, singlet, two OCH_2), 4.27 (1H, multiplet, C*H*OH), and 9.88 (1H, multiplet, CHO); ms *m/e*: 268 (M^+).

*Ketal Enol Ether **32***

The aldehyde alcohol **31** (294 mg, 1.10 mmol) was subjected to microdistillation. Formation of a white solid was observed in the distillate. The distillate was purified by preparative thick layer chromatography with benzene. Two products were isolated: the aldehyde alcohol **31** (183 mg) and the enol ether **32** as a solid (73 mg). An analytical sample of the ketal enol ether **32** was prepared by recrystallization from petroleum ether; mp 94–96°C; ir (CH_2Cl_2): 3080, 1640, 1100, and 1000 cm^{-1}; nmr ($CDCl_3$) δ: 0.95 (3H, singlet, CH_3), 0.98 (3H, singlet, CH_3), 3.50 (4H, singlet, two OCH_2), 4.45 (1H, multiplet, CHO), 4.82 (1H, triplet, J = 6.5 Hz, C*H*=CHO), and 6.20 (1H, doublet, J = 5.5 Hz, C=C*H*O); ms *m/e*: 250 (M^+). *Anal.* calcd. for $C_{15}H_{22}O_3$: C 71.97, H 8.86; found: C 71.61, H 9.06.

Cis *and* Trans *Ketone Diols **33** and **34** (26)*

The aldehyde alcohol **31** (5.49 g, 20.4 mmol) was dissolved in acetone (2.2 ℓ) and treated with dilute hydrochloric acid (2 *N*, 50 ml, 100 mmol). The reaction mixture was stirred at room temperature for 2 h and 15 min. Afterwards, it was neutralized with solid sodium bicarbonate and the stirring was continued for another 45 min. It was filtered and the solvent was evaporated under reduced pressure. The residue obtained was taken up in dichloromethane (1.5 ℓ) and dried over anhydrous sodium sulfate for 30 min. Removal of solvent under vacuum yielded an oil which was purified by chromatography on a column of Florisil (225 g) using ether–methanol. An oil (3.67 g, 98.5%) containing the two isomers in the ratio 1:1 was recovered. Thin-layer chromatography of the mixture on silica gel by double elution with methanol–ether showed two spots of equal intensity corresponding to the *cis* diol **33** (R_f 0.25) and the *trans* diol **34** (R_f 0.20).

The epimerisation of *cis* **33** and *trans* **34** ketone diols was carried out in the following way: the above mixture of the ketone diols **33** and **34** (2.18 g, 11.9 mmol) was dissolved in anhydrous ethanol (220 ml). Nitrogen was bubbled through the solution for 15 min and a solution of sodium ethoxide in ethanol (0.174 *M*, 3.42 ml, 0.56 mmol) was added and the mixture was stirred at room temperature for 21 h. Hydrochloric acid was then added (1 *N*, 0.58 ml) and stirred again for 15 min. The solvent was distilled off under reduced pressure and the residue was taken up in dichloromethane (800 ml). The above solution was dried over anhydrous sodium sulfate and evaporated under reduced pressure to give an oil (2.20 g) containing mainly the *trans* diol **34** with a small quantity of the *cis* diol **33**. The *trans* **34** isomer was isolated in the pure state (866 mg) by crystallization from ethyl acetate. The residue was subjected to dry column chromatography on silica gel. Elution with methanol–ether (3:97 and 1:24) yielded another crop of the *trans* diol **34** (498 mg) (total yield 62.5%); mp 97–99°C; ir (KBr): 3300 and 1720 cm^{-1}; nmr (acetone-d_6) δ: 1.10–4.20 (10H, multiplets) and 4.5 (2H, multiplet, two C*H*OH); ms *m/e*: 182 (M^+). *Anal.* calcd. for $C_{10}H_{14}O_3$: C 65.92, C 7.74; found: C 65.62, H 7.77.

*Ketone Dimesylate **35***

The *trans* ketone diol **34** (626 mg, 3.43 mmol) was dissolved in a warm mixture of dichloromethane (70 ml) and pyridine. The solution was then cooled (−5°C) and methane sulfonyl chloride (1.97 g, 17.2 mmol) was added and the reaction mixture was kept in the cold (5°C) for 4½ days. It was afterwards diluted with ice cold dichloromethane (700 ml). The organic phase was washed with ice cold water (100 ml), cold dilute hydrochloric acid (1 *N*, 200 ml), ice cold saturated sodium bicarbonate solution (100 ml), and again ice cold water (100 ml). The solution was then dried and evaporated under reduced pressure to give an oil which was recrystallized from dichloromethane – ether – petroleum ether (1.10 g, 95%); mp 114–116°C; ir (CH_2Cl_2): 1741, 1360, 1335, and 1170 cm^{-1}; nmr ($CDCl_3$) δ: 1.70–3.70 (10H, multiplet, 3.08 (3H, singlet, CH_3SO_2), 3.10 (3H, singlet, CH_3SO_2), and 5.37 (2H, multiplet, two $CHOSO_2$); ms *m/e*: 338 (M^+). *Anal.* calcd. for $C_{12}H_{18}O_7S_2$: C 42.59, H 5.36; found: C 42.38, H 5.37.

*Enone Mesylate **36***

A solution of sodium hydroxide in ethanol (0.105 *N*, 5.56 ml, 0.58 mmol) was added during a period of 25 min to a solution of the ketone dimesylate **35** (198 mg, 0.58 mmol) in dichloromethane (15 ml) at 0°C. After the addition was complete the reaction mixture was stirred for 10 min, diluted with ice cold water (150 ml), and extracted with dichloromethane (300 ml). The extract was washed with water (50 ml), dried, and the solvent was distilled off under vacuum to yield the enone mesylate **36** (140 mg, quantitative). An analytical sample was prepared by recrystallization from dichloromethane–ether; mp 83–84.5°C; ir (CH_2Cl_2): 3050, 1717, 1626, 1355, 1330, and 1170 cm^{-1}; uv ($CHCl_3$) λ_{max}: 243 nm (ε 9400); nmr ($CDCl_3$) δ: 2.00–3.50 (8H, multiplet), 2.93 (3H, singlet, CH_3SO_2), 3.78 (1H, multiplet), 5.18 (1H, multiplet, $CHOSO_2$), and 6.38 (1H, multiplet, olefinic hydrogen); ms *m/e*: 242 (M^+). *Anal.* calcd. for $C_{11}H_{14}O_4S$: C 54.53, H 5.82; found: C 54.45, H 5.84.

*Ethoxy Ketone Mesylate **37***

The ketone dimesylate **35** (200 mg, 0.59 mmol) was dissolved in a mixture of dichloromethane (10 ml) and ethanol (10 ml). A solution of sodium hydroxide in ethanol (0.1 *N*, 6.2 ml, 0.65 mmol) was added to the above solution with stirring during a period of 20 min at room temperature. After the addition was complete, the stirring was continued for another 40 min. The reaction mixture was then diluted with water (100 ml), the organic phase was separated, and the aqueous phase was extracted with dichloromethane (300 ml). The extracts were combined, washed with water (100 ml), and dried. The removal of solvent under vacuum yielded a yellow oil which was purified by chromatography on Florisil (10 g) with dichloromethane–ether to give the ethoxy ketone mesylate **37** (134 mg, 79%) as an oil; ir (CH_2Cl_2): 1735, 1360, 1340, and 1180 cm^{-1}; nmr ($CDCl_3$) δ: 1.18 (3H, triplet, J = 7 Hz, CH_3CH_2), 3.02 (3H, singlet, CH_3SO_2), 3.50 (2H, quadruplet, J = 7 Hz, CH_3CH_2), 4.13 (1H, multiplet, $CHOCH_2CH_3$), and 5.18 (1H, multiplet, $CHOSO_2$); ms *m/e*: 288 (M^+).

*Ketone Enol Diacetate **38** or **39***

The β-diketone acetate **21** (50 mg, 0.22 mmol) was dissolved

Can. J. Chem. Downloaded from www.nrcresearchpress.com by 210.87.254.40 on 09/05/12
For personal use only.

in a mixture of pyridine (2 ml) and acetic anhydride (1 ml) and kept in the dark at room temperature for 22 h. The reaction mixture was then evaporated to dryness under reduced pressure to give a solid residue (61 mg, quantitative). An analytical sample was prepared by recrystallization from a mixture of dichloromethane – ether – petroleum ether; mp 146–147.5°C; ir (CH_2Cl_2): 1769, 1744, 1722, 1702, 1236, and 1225 cm^{-1}; uv ($CHCl_3$) λ_{max}: 284 (ε 590) and 241 nm (ε 870); nmr ($CDCl_3$) δ: 1.90 (3H, singlet, CH_3COOCH), 2.47 (3H, singlet, CH_3 of enol acetate), 4.37 (1H, multiplet), and 5.43 (1H, multiplet, CHOCO); ms *m/e*: 264 (M^+). *Anal.* calcd. for $C_{14}H_{16}O_5$: C 63.03, H 6.10; found: C 63.55, H 6.07.

Ketal Olefin Aldehyde ***40***

The mono ketal **11** (4 g, 16 mmol) was dissolved in anhydrous tertiary butanol (1 ℓ) and irradiated with a mercury lamp (450 W) equipped with a quartz filter in an atmosphere of nitrogen (22). The entire system was cooled by circulating cold water during the irradiation. The reaction was complete in 90 min. The solvent was distilled off under vacuum to give an oil which was purified by column chromatography on Florisil by eluting successively with pentane, benzene, and ether. About 2.4 g (60–65%) of the aldehyde **40** and 200 mg (5%) of the starting material were recovered. The product was found unstable and therefore should be kept in the cold or used up immediately for the subsequent reaction; ir (CH_2Cl_2): 2720 and 1730 cm^{-1}; nmr ($CDCl_3$) δ: 0.94 (6H, singlet, $(CH_3)_2C$), 3.42 (2H, singlet, CH_2O), 3.48 (2H, singlet, CH_2O), 5.50 (2H, multiplet, two olefinic hydrogens), and 9.55 (1H, triplet, J = 1 Hz, CHO); ms *m/e*: 250 (M^+).

Exo *and* Endo *Ketone Alcohols* ***41*** *and* ***50*** *(26)*

(a) From Ketal Olefin Aldehyde ***40***

A solution of the ketal olefin aldehyde **40** (4.0 g, 16 mmol) in acetone (500 ml) was stirred with hydrochloric acid (3 *N*, 35 ml) at room temperature for 2 h. Sodium bicarbonate (25 g) was then added and stirred for another 15 min. The reaction mixture was filtered and the filtrate was concentrated to remove the acetone. The aqueous solution was then thoroughly extracted with dichloromethane. The extract was dried and the solvent was distilled off under vacuum to give crude *exo* ketone alcohol **41**; ir (CH_2Cl_2): 3585, 3410, and 1730 cm^{-1}; nmr ($CDCl_3$) δ: 4.32 (1H, multiplet, CHOH) and 5.56 (2H, quadruplet, J = 6 Hz, two olefinic hydrogens); ms *m/e*: 164 (M^+). A portion of this crude product (700 mg) was acetylated with pyridine and acetic anhydride. Preparative thin-layer chromatography on Florisil with ether as solvent gave pure *exo* ketone acetate **42** (660 mg, 75%).

(b) From Ketone Olefin Aldehyde ***43***

A solution of the ketone olefin aldehyde **43** (600 mg, 3.66 mmol) in acetone (80 ml) was stirred with hydrochloric acid (3 *N*, 6.4 ml) at room temperature for 1 h. Sodium bicarbonate (2 g) was added, the mixture was filtered, and concentrated. The resulting solution was extracted with dichloromethane. The organic extract was dried, filtered, and evaporated to give a crude product (600 mg). An aliquot (18 mg) of this crude product was acetylated with pyridine and acetic anhydride. Vapor phase chromatography showed that the product obtained was a mixture of *exo* ketone acetate **42** (≃80%), *endo* ketone acetate **51** (≃15%), and an unidentified product (≃5%). The remaining crude aldol condensation product was mixed with ethanol (50 ml) containing a small quantity of sodium ethoxide (4 mg) and the mixture was left at room temperature for 1.5 h under nitrogen. Most of the ethanol was evaporated, dilute hydrochloric acid was added, and the aqueous phase was extracted with dichloromethane (3 × 20 ml). The dried organic phase was evaporated to dryness to give an oil which consisted mainly of *exo* ketone alcohol **41** (580 mg). Acetylation of an aliquot gave *exo* ketone acetate **42** (94.5%), *endo* ketone acetate **51** (1.5%), and an unidentified product (4%).

Exo *Ketone Acetate* ***42***

The *exo* ketal acetate **49** (80 mg, 0.3 mmol) was dissolved in acetone containing a few drops of water and *p*-toluenesulfonic acid (12 mg). After 18 h at room temperature, the solvent was evaporated and dichloromethane (30 ml) was added. The organic solution was washed with water (2 × 5 ml), dried with sodium sulfate, and evaporated to dryness. The resulting oil was purified by preparative thin-layer chromatography on silica gel with ether to give pure *exo* ketone acetate **42** (50 mg, 80%) as a liquid; ir (CH_2Cl_2): 1740 cm^{-1}; nmr ($CDCl_3$) δ: 2.04 (3H, singlet, CH_3CO), 5.24 (1H, quadruplet, J = 6 Hz, CHOCO), and 5.64 (2H, quadruplet (unsymmetric), olefinic hydrogens); ms *m/e*: 206 (M^+); vpc: one peak at 8.24 min (5 ft × ¼ in.; 5% SE-30 on Chromosorb W, 140°C). *Anal.* calcd. for $C_{12}H_{14}O_3$: C 69.89, H 6.84; found: C 69.63, H 7.04.

Ketone Aldehyde ***43***

The diketone **10** (4 g, 24.4 mmol) was dissolved in anhydrous methanol (1 ℓ). The solution was irradiated with a mercury lamp (450 W) in quartz with cooling under an atmosphere of nitrogen (22). After 30 min, analysis by gas chromatography (5 ft × ¼ in., 5% SE-30 on Chromosorb W, 135°C) indicated the presence of a major peak corresponding to the ketone aldehyde (retention time: 3 min) and a minor peak, the starting material (5%, retention time: 5 min). The solvent was then evaporated off under reduced pressure to give an oil (4 g) which was used without purification; ir (CH_2Cl_2): 2710 and 1720 cm^{-1}; nmr ($CDCl_3$) δ: 5.68 (2H, quartet, J = 6 Hz, olefinic hydrogens) and 9.49 (1H, triplet, J = 1 Hz, CHO); ms *m/e*: 164 (M^+).

β-*Diketone* ***44***

(a) From Exo *Ketone Alcohol* ***41***

To a solution of the crude alcohol **41** (2 g, 12.2 mmol) in acetone (100 ml) cooled to 0°C, Jones' reagent (26) was added dropwise until an orange color persisted. After 60 min the solvent was removed and the residue was diluted with water and extracted with dichloromethane. The organic phase was washed with water, dried, filtered through Celite, and evaporated under vacuum. The solid product obtained was recrystallized from ethyl acetate to give colorless needles (600 mg, 30%) of the β-diketone **44**; mp 115°C; ir (CH_2Cl_2): 1760 and 1710 cm^{-1}; nmr ($CDCl_3$) δ: 5.6 (2H, singlet, olefinic hydrogens); ms *m/e*: 162 (M^+); vpc: one peak at 8 min (5 ft × ¼ in., 5% SE-30 on Chromosorb, 140°C). *Anal.* calcd. for $C_{10}H_{10}O_2$: C 74.06, H 6.21; found: C 73.80, H 6.19.

(b) From Ketone Carboxylic Acid ***57***

The crude ketone carboxylic acid **57** (135 mg, 0.75 mmol) was dissolved in anhydrous benzene, *p*-toluenesulfonic acid was added (≃20 mg) and the mixture was refluxed for 17 h in a flask equipped with a Dean–Stark water separator. The solvent was then evaporated off and the residue was dissolved in dichloromethane. It was washed twice with water, dried, and the solvent was distilled off under vacuum to give a yellow solid which was recrystallized from ethyl acetate to give a product (98 mg, 83%) identical with the β-diketone **44** obtained by the above procedure.

Ketal Ketone ***45***

A solution of the β-diketone **44** (1 g, 6.2 mmol) in benzene (150 ml) was mixed with 2,2-dimethyl-1,3-propanediol (744 mg, 7 mmol) and *p*-toluenesulfonic acid (20 mg). The reaction mixture was refluxed for 24 h in a flask equipped with a Dean–Stark water separator. It was then washed with sodium

Can. J. Chem. Downloaded from www.nrcresearchpress.com by 210.87.254.40 on 09/05/12
For personal use only.

bicarbonate solution (5%, 20 ml) and saturated sodium chloride solution (2 × 20 ml). The organic phase was dried and the solvent was distilled off under vacuum to give a mixture containing mainly the ketone ketal **45**. The product was purified by column chromatography on Florisil with benzene–methanol (99:1), followed by crystallization from petroleum ether (850 mg, 55%), mp 64–65°C; ir (CH_2Cl_2): 1730, 1200, and 1000 cm^{-1}; nmr ($CDCl_3$) δ: 0.90 (3H, singlet, CH_3), 0.98 (3H, singlet, CH_3), 3.48 (4H, multiplet, two CH_2O), and 5.70 (2H, singlet, two olefinic hydrogens); ms *m/e*: 248 (M^+). *Anal.* calcd. for $C_{15}H_{20}O_3$: C 72.55, H 8.12; found: C 72.34, H 7.84.

Endo *Ketal Alcohol* ***46***

The ketone ketal **45** (1.2 g, 4.8 mmol) dissolved in dry tetrahydrofuran (20 ml) was added to a suspension of lithium tri-*tert*-butoxyaluminium hydride (2.4 g, 9.6 mmol) in the same solvent (150 ml). The reaction mixture was then refluxed for 40 h and treated with aqueous sodium bicarbonate solution (5%, 1 ml), just enough to destroy the excess hydride. The organic phase was then dried over anhydrous sodium sulfate, filtered, and evaporated. The crude product obtained was purified by crystallization from ether (1 g, 80%); mp 94–95°C; ir (CH_2Cl_2): 3500 cm^{-1}; nmr ($CDCl_3$) δ: 0.95 (3H, singlet, CH_3), 0.98 (3H, singlet, CH_3), 3.51 (2H, singlet, CH_2O), 3.55 (2H, singlet, CH_2O), 4.4 (1H, multiplet, C*H*OH), and 5.60 (2H, quadruplet, J = 6 Hz, two olefinic hydrogens); ms *m/e*: 250 (M^+).

Exo *and* Endo *Ketal Alcohols* ***46*** *and* ***47***

The ketal ketone **45** (154 mg, 0.62 mmol) was dissolved in absolute ethanol (15 ml) and refluxed. Small pieces of sodium were added until a faint precipitate began to appear in the reaction medium. The stirring was continued for another 2 h. The reaction mixture was then cooled in an ice bath and poured into a saturated sodium chloride solution (20 ml). It was extracted with ether (5 × 50 ml), dried, and the solvent was evaporated to give an epimeric mixture of *exo* (87%) and *endo* (13%) ketal alcohols **47** and **46** as an oil. The relative proportion of the two isomers was determined by nmr spectroscopy. Crystallization with ether gave the pure *exo* ketal alcohol **47** (120 mg, 80%). An analytical sample was prepared by recrystallization from ether–pentane; mp 109–110°C; ir (CH_2Cl_2): 3500 cm^{-1}; nmr ($CDCl_3$) δ: 0.83 (3H, singlet, CH_3), 1.06 (3H, singlet, CH_3), 3.48 (4H, multiplet, two CH_2O), 3.95 (1H, multiplet, C*H*OH), and 5.55 (2H, quadruplet, J = 6 Hz, two olefinic hydrogens); ms *m/e*: 250 (M^+). *Anal.* calcd. for $C_{15}H_{22}O_3$: C 71.97, H 8.86; found: C 72.00, H 8.95.

Exo *Ketal Alcohol* ***47***

A solution of the crude *exo* ketone alcohol **41** (587.7 mg, 3.58 mmol) in benzene (70 ml) containing 2,2-dimethyl-1,3-propanediol (0.374 g, 3.58 mmol) and *p*-toluenesulfonic acid was refluxed for 3.3 h with a system equipped with a Dean–Stark water separator. Most of the solvent was removed by evaporation and dichloromethane was added. The organic phase was washed with solutions of saturated sodium carbonate and sodium chloride. The organic phase was dried with sodium sulfate, filtered, and evaporated to dryness. The resulting product can be crystallized with a mixture of ether–pentane. It can also be purified by column chromatography on Florisil using benzene–ether (25:2) as eluent. A yield of approximately 50–55% is obtained. This yield is based on the starting diketone **10**; mp 109–110°C. This product was found identical with the *exo* ketal alcohol **47** obtained from the chemical reduction of the ketal ketone **45**.

Endo *Ketal Acetate* ***48***

The ketal alcohol **46** (350 mg, 1.4 mmol) was dissolved in acetic anhydride (15 ml) containing sodium acetate (250 mg, 2.8 mmol). The reaction mixture was heated at 70°C for 72 h with stirring. The solution was then filtered and the filtrate was concentrated under reduced pressure to give a crystalline residue which was recrystallized from ether (390 mg, 95%). An analytical sample was prepared by recrystallization from ether – petroleum ether; mp 134°C; ir (CH_2Cl_2): 1730 and 1255 cm^{-1}; nmr ($CDCl_3$) δ: 0.84 (3H, singlet, CH_3), 1.05 (3H, singlet, CH_3), 1.94 (3H, singlet, C*H*$_3$CO), 3.40 (2H, singlet, CH_2O), 3.55 (2H, singlet, CH_2O), 5.50 (1H, multiplet, CHOCO), and 5.55 (2H, singlet, two olefinic hydrogens); ms *m/e*: 292 (M^+). *Anal.* calcd. for $C_{17}H_{24}O_4$: C 69.84, H 8.27; found: C 69.91, H 8.82.

Exo *Ketal Acetate* ***49***

The *exo* ketal alcohol **47** (74 mg, 0.3 mmol) was dissolved in a mixture of pyridine (2 ml) and acetic anhydride (1 ml) and left in the dark for 48 h at room temperature. The solvent was distilled off under reduced pressure and the last traces were removed by repeated evaporation with benzene. The product obtained was purified by preparative thick-layer chromatography on silica gel using ether as the eluent to give the *exo* ketal acetate **49** as a solid; mp 131–132°C; ir (CH_2Cl_2): 1730 cm^{-1}; nmr ($CDCl_3$) δ: 0.86 (3H, singlet, CH_3), 1.05 (3H, singlet, CH_3), 2.03 (3H, singlet, CH_3CO), 3.52 (4H, multiplet, two CH_2O), 5.00 (1H, multiplet, CHOCO), and 5.60 (2H, quadruplet, olefinic hydrogens); ms *m/e*: 292 (M^+). *Anal.* calcd. for $C_{17}H_{24}O_4$: C 69.84, H 8.27; found: C 69.94, H 8.22.

Endo *Ketone Acetate* ***51***

A solution of the ketal acetate **48** (390 mg, 1.3 mmol) in wet acetone (50 ml) was treated with *p*-toluenesulfonic acid (40 mg, 10% by weight) and stirred at room temperature for 18 h. The solvent was then evaporated off and the residue was dissolved in dichloromethane (100 ml), washed with water (2 × 15 ml), and dried. The oil obtained on removing the solvent was purified by column chromatography on silica gel using benzene–ether (25:1) as the eluent to give the *endo* ketone acetate **51** as an oil (220 mg, 80%). An analytical sample was prepared by preparative thick-layer chromatography on silica gel with ether; ir (CH_2Cl_2): 1735 cm^{-1}; nmr ($CDCl_3$) δ: 1.93 (3H, singlet, CH_3CO), 5.42 (1H, multiplet, CHOCO), and 5.65 (2H, quadruplet, J = 6 Hz, olefinic hydrogens); ms *m/e*: 206 (M^+); vpc: one peak at 7.48 min (5 ft × $\frac{1}{4}$ in., 5% SE-30 on Chromosorb W, 140°C). *Anal.* calcd. for $C_{12}H_{14}O_3$: C 69.89, H 6.84; found: C 70.20, H 6.97.

Endo *Ketal Mesylate* ***52***

Methane sulfonyl chloride (0.42 ml, 5.4 mmol) was added to a solution of the ketone alcohol **46** (238 mg, 0.95 mmol) in dichloromethane (35 ml) and pyridine (4 ml) and kept in the dark for 5 days at room temperature. The reaction mixture was then diluted with dichloromethane (100 ml), washed with water (2 × 25 ml), and dried. The solvent was evaporated off under reduced pressure and the last traces of pyridine were removed with the aid of benzene. The yellow oil obtained was purified by chromatography on a column of Florisil by eluting successively with petroleum ether (30–60°C), benzene, and ether to give white crystals. An analytical sample was prepared by recrystallization from ether; mp 90°C; ir (CH_2Cl_2): 1360, 1340, 1180, 1100, and 1000 cm^{-1}; nmr ($CDCl_3$) δ: 0.95 (6H, singlet, $(CH_3)_2C$), 2.92 (3H, singlet, CH_3SO_2), 3.44 (2H, singlet, CH_2O), 3.54 (2H, singlet, CH_2O), 5.12 (1H, multiplet, $CHOSO_2$), and 5.58 (2H, singlet, two olefinic hydrogens); ms *m/e*: 328 (M^+). *Anal.* calcd. for $C_{16}H_{24}O_5S$: C 58.51, H 7.37; found: C 58.68, C 7.46.

Can. J. Chem. Downloaded from www.nrcresearchpress.com by 210.87.254.40 on 09/05/12
For personal use only.

Exo *Ketal Mesylate* ***53***

Methane sulfonyl chloride was added (0.62 ml, 7.94 mmol) to a solution of the ketal alcohol **41** (350 mg, 1.4 mmol) in dichloromethane (50 ml) and pyridine (5.9 ml) and the reaction mixture was kept at room temperature for 16 h with the exclusion of light. It was then diluted with dichloromethane (100 ml) and washed with water (2 × 25 ml). The organic phase was dried and concentrated. The last traces of pyridine were removed by codistillation with benzene. The product obtained was recrystallized from ether–pentane (368 mg, 80%); mp 103–104°C; ir ($CHCl_3$): 1345, 1325, 1155, 1100, and 1000 cm^{-1}; nmr ($CDCl_3$) δ: 0.98 (3H, singlet, CH_3), 0.93 (3H, singlet, CH_3), 2.96 (3H, singlet, CH_3SO_2), 3.48 (4H, multiplet, $(CH_2O)_2$), 3.30 (2H, multiplet), 4.67 (1H, quartet, $CHOSO_2$), and 5.51 (2H, quartet, J = 5.5 Hz, two olefinic hydrogens); ms *m/e*: 328 (M^+). *Anal.* calcd. for $C_{16}H_{24}O_5S$: C 58.51, H 7.37; found: C 58.72, H 7.53.

Ketone Enol Acetate ***54***

The β-diketone **44** (175 mg, 1.08 mmol) was dissolved in a mixture of acetic anhydride (1 ml) and pyridine (2 ml) and kept in the dark for 12 h at room temperature. The solvent was then distilled off under reduced pressure. The last traces of pyridine were removed by codistillation with benzene. The yellow solid obtained was recrystallized from benzene–ether (175 mg, 80%); mp 123.5–124°C; ir (CH_2Cl_2): 1765 and 1705 cm^{-1}; uv ($CHCl_3$) λ_{max}: 292 (ε 278) and 244 nm (ε 516); uv (EtOH) λ_{max}: 293 (ε 250) and 212 nm (ε 2750); nmr ($CDCl_3$) δ: 2.38 (3H, singlet, CH_3CO), 3.58 (2H, multiplet, $CH_2C{=}C$), 4.44 (1H, triplet, J = 9 Hz, H_{10}), and 5.68 (2H, singlet, two olefinic hydrogens); ms *m/e*: 204 (M^+). *Anal.* calcd. for $C_{12}H_{12}O_3$: C 70.58, H 5.92; found: C 70.36, H 5.81.

Ketal Carboxylic Acid ***55*** *and its Methyl Ester* ***56***

A solution of silver nitrate (5.77 g, 0.34 mol) in water (32 ml) was added to a solution of the ketal olefin aldehyde **40** (4 g, 0.016 mol) in ethanol (42 ml). A solution of sodium hydroxide (2.62 g, 0.065 mol) in water (90 ml) was added during a period of 15 min. It was then stirred at room temperature for 3 h. The reaction mixture was filtered through Celite, concentrated, diluted with water, and extracted several times with ether. The aqueous phase was then acidified with dilute hydrochloric acid to p*H* 6 and extracted exhaustively with ether. It was dried and the solvent evaporated off to give the crude ketal carboxylic acid **55** as an oil (3.3 g, 75%) which was not further purified.

An excess of diazomethane in ether was added to a solution of the crude acid **55** (3.3 g, 0.012 mol) in ether (20 ml) at room temperature and stirred for 30 min. The evaporation of the solvent at reduced pressure yielded the ketal carboxylic acid methyl ester **56** as an oil which was purified by microdistillation (3.36 g, 100%, 120–130°C/5 Torr); ir ($CHCl_3$): 1730 and 1105 cm^{-1}; nmr ($CDCl_3$) δ: 0.96 (3H, singlet, CH_3), 0.92 (3H, singlet, CH_3), 3.43 (2H, singlet, CH_2O), 3.48 (2H, singlet, CH_2O), 3.67 (3H, singlet, CH_3O), and 5.54 (2H, multiplet, two olefinic hydrogens); ms *m/e*: 280 (M^+). *Anal.* calcd. for $C_{16}H_{24}O_4$: C 68.55, H 8.63; found: C 68.60, H 8.69.

Ketone Carboxylic Acid ***57*** *and its Methyl Ester* ***58***

The ketal ester **56** (1.1 g, 3 mmol) was dissolved in a solution of aqueous acetic acid (70%, 20 ml) and heated at 70°C for 12 h. The reaction mixture was concentrated under reduced pressure and extracted with dichloromethane. The organic phase was washed with water, dried, and the solvent distilled off under vacuum. The remaining acetic acid was removed by distillation with benzene. The oil obtained was dissolved in ether (20 ml) and treated with an excess solution of diazomethane in ether. The above solution was stirred at room temperature for 30 min and the solvent was evaporated off to give the ketone carboxylic acid methyl ester **58** as an oil which was purified by preparative thick-layer chromatography on Florisil to give 20% of the starting ketal carboxylic acid methyl ester **56** and **58** (490 mg, 72%); ir ($CHCl_3$): 1735 cm^{-1}; nmr ($CDCl_3$) δ: 2.00–3.65 (9H, multiplet), 3.70 (3H, singlet, CH_3O), and 5.68 (2H, singlet, two olefinic hydrogens); ms *m/e*: 194 (M^+). *Anal.* calcd. for $C_{11}H_{14}O_3$: C 68.02, H 7.27; found: C 68.23, H 7.28.

A solution of the ketone ester **58** (222 mg, 1.2 mmol) in water (15 ml) was mixed with aqueous sodium hydroxide (1 *N*, 1.8 ml) and allowed to react for 2 h at room temperature. The neutral material was then removed by extraction with ether. The aqueous solution was acidified with dilute hydrochloric acid and was extracted several times with dichloromethane. The extracts were combined, dried, and evaporated under reduced pressure to give the ketone carboxylic acid **57** as an oil (180 mg, 90%) which was not purified further. This crude acid was then used directly for the preparation of the β-diketone **44**.

Ketone δ-Lactone ***59***

The ketal lactone **12** (3.0 g, 0.0113 mol) was dissolved in acetone (300 ml) and treated with dilute hydrochloric acid (3 *N*, 24 ml, 0.072 mol). The reaction mixture was stirred at room temperature for 5 h and then was concentrated and extracted several times with dichloromethane. The organic phase was washed with saturated sodium bicarbonate solution and water. It was dried and the solvent was evaporated off under vacuum to yield white crystals of ketone δ-lactone **59** that were purified by recrystallization from dichloromethane–ether (1.58 g, 80%); mp 148–150°C; ir ($CHCl_3$): 1745 cm^{-1}; nmr ($CDCl_3$) δ: 1.78–3.50 (11H, multiplet) and 4.83 (1H, multiplet, CHOC); ms *m/e*: 180 (M^+). *Anal.* calcd. for $C_{10}H_{12}O_3$: C 66.65, H 6.71; found: C 66.46, H 6.54.

Ketone γ-Lactone ***60***

(a) From Ketone Lactone ***59***

The ketone lactone **59** (2 g, 11 mmol) was added in small portions to polyphosphoric acid (30 g, 92 mmol). The reaction mixture was homogenized and heated on a water bath at 80–90°C for 15 min. The above solution was then poured over crushed ice and extracted several times with dichloromethane. The organic phase was washed several times with saturated sodium carbonate solution and with water. It was then dried and the solvent was removed to give a yellow solid which was recrystallized from dichloromethane–ether (1.67 g, 84%); mp 105–106.5°C; ir ($CHCl_3$): 1780 and 1740 cm^{-1}; nmr ($CDCl_3$) δ: 1.42–3.57 (11H, multiplet) and 5.10 (1H, multiplet, CHOCO); ms *m/e*: 180 (M^+). *Anal.* calcd. for $C_{10}H_{12}O_3$: C 66.65, H 6.71; found: C 66.61, H 6.60.

(b) From Ketal γ-Lactone ***64***

A solution of ketal γ-lactone **64** (119 mg, 0.44 mmol) in acetone (15 ml) containing dilute hydrochloric acid (3 *N*, 2 ml was left at room temperature for 7 h. Most of the acetone was then removed by evaporation, water was added, and the aqueous phase was extracted with dichloromethane. The organic extract was washed with a solution of saturated sodium bicarbonate and water. The dried solution was evaporated to yield the ketone γ-lactone **60** which was recrystallized from dichloromethane–ether (63 mg, 80%). The product obtained was found identical with the ketone γ-lactone **60** obtained in the above procedure.

Ketal Iodolactone ***63*** *(29)*

The crude ketal acid **55** (1.00 g, 3.7 mmol) was stirred in a solution of sodium hydroxide (1 *N*, 3.7 ml, 3.7 mmol) for 20 min and was then saturated with sodium bicarbonate. To the above mixture, an aqueous solution of iodine (1.52 g, 5.9

Can. J. Chem. Downloaded from www.nrcresearchpress.com by 210.87.254.40 on 09/05/12
For personal use only.

mmol) and potassium iodide (1.41 g, 8.5 mmol) was added and stirred at room temperature for 4 h. The excess of iodine was then destroyed by the addition of sodium thiosulfate solution. The reaction mixture was extracted several times with dichloromethane. The extracts were combined, dried and the solvent was distilled off to give crude ketal iodolactone **63** as an oil (1.25 g, 84%) which was not purified further; ir ($CHCl_3$): 1775 cm^{-1}; nmr δ ($CDCl_3$): 0.92 (3H, singlet, CH_3), 0.99 (3H, singlet, CH_3), 3.45 (4H, singlet, two CH_2O), 4.09 (1H, triplet, CHI), and 5.16 (1H, triplet, CHOCO); ms *m/e*: 392 (M^+).

Ketone γ-Lactone ***64***

A solution of the crude iodolactone **63** (62 mg, 1.5 mmol) in anhydrous ethanol (420 ml) was treated with Raney nickel (1.8 g) in the presence of pyridine (0.36 ml). The reaction mixture was stirred under hydrogen at atmospheric pressure and room temperature for 7 h. The solution was filtered through Celite and evaporated to dryness to give the ketal γ-lactone **64** as a crystalline product which was recrystallized from dichloromethane–pentane (360 mg, 86%); mp 85–87°C; ir ($CHCl_3$): 1765 cm^{-1}; nmr ($CDCl_3$) δ: 0.95 (6H, singlet, $(CH_3)_2C$), 1.37–3.27 (11H, multiplet), 3.46 (4H, singlet, two CH_2O), and 4.97 (1H, multiplet, CHOCO); ms *m/e*: 266 (M^+). *Anal.* calcd. for $C_{15}H_{22}O_4$: C 67.65, H 8.33; found: C 67.29, H 8.20.

Cis *and* Trans *Diols* ***65*** *and* ***66***

A solution of the β-diketone **44** (200 mg, 1.2 mmol) in dry tetrahydrofuran (10 ml) was added slowly to a suspension of lithium aluminium hydride (280 mg, 7.0 mmol) in the same solvent (10 ml). The reaction mixture was refluxed for 5 h, cooled, and hydrolysed slowly with water. It was then extracted with dichloromethane. The organic phase was dried and evaporated to give an oil containing the two diols which were separated by preparative thick-layer chromatography on silica gel. The *cis* diol **65** (R_f 0.54, 134 mg) and the *trans* diol **66** (R_f 0.19, 25 mg) were found to be identical with their respective authentic samples obtained as described below.

Cis *Diol* ***65***

A solution of the β-diketone **44** (100 mg, 0.6 mmol) in tetrahydrofuran (10 ml) was added slowly to a suspension of lithium tri-*tert*-butoxy aluminium hydride (1.08 g, 4.2 mmol) in the same solvent (10 ml). The reaction mixture was then refluxed for 40 h. It was cooled, hydrolysed slowly with water, and extracted with dichloromethane. The organic phase was dried and the solvent was distilled off to yield an oil which was purified by thick-layer chromatography on silica gel to give pure *cis* diol **65** (70 mg, 70%) which was recrystallized from ether – petroleum ether; mp 129–130°C; ir ($CHCl_3$): 3520 and 3400 cm^{-1}; nmr ($CDCl_3$) δ: 1.47–3.58 (10H), 4.49 (2H, quadruplet, J = 6.0 Hz, two C*H*OH), and 5.70 (2H, singlet, two olefinic hydrogens); ms *m/e*: 166 (M^+). *Anal.* calcd. for $C_{10}H_{14}O_2$: C 72.26, H 8.49; found: C 71.99, H 8.30.

Trans *Diol* ***66***

A solution of the crude *exo* ketone alcohol **41** (1.5 g, 9 mmol) in ether (30 ml) was added to a suspension of lithium aluminium hydride (1.71 g, 45 mmol) in the same solvent (20 ml) and refluxed for 3 h. The reaction mixture was then cooled, decomposed slowly with water, and extracted with ether. The extract was dried and evaporated. The crystalline *trans* diol **66** obtained was recrystallized from dichloromethane–ether (825 mg, 55%); mp 97.5–98°C; ir ($CHCl_3$): 3580 (weak) and 3390 cm^{-1} (strong); nmr ($CDCl_3$) δ: 1.00–3.47 (8H, multiplet), 4.30 (2H, multiplet, two CHOH), and 5.53 (2H, quadruplet, two olefinic hydrogens); ms *m/e*: 166 (M^+). *Anal.* calcd. for $C_{10}H_{14}O_2$: C 72.26, H 8.49; found: C 72.15, H 8.31.

Cis *Diacetate* ***67***

The *cis* diol **67** (70 mg, 0.4 mmol) was dissolved in a mixture of pyridine (2 ml) and acetic anhydride (2 ml) and stirred at room temperature for 12 h with the exclusion of light. The pyridine and acetic anhydride were distilled off under reduced pressure and the last traces were removed by codistillation with benzene. The product obtained was purified by preparative thick-layer chromatography on silica gel to give the *cis* diacetate **66** as a liquid (70 mg, 70%); ir ($CHCl_3$): 1730 cm^{-1}; nmr ($CDCl_3$) δ: 1.97 (6H, singlet, two CH_3CO), 4.66 (2H, quadruplet, two CHOCO), and 5.57 (2H, singlet, two olefinic hydrogens); ms *m/e*: 250 (M^+); vpc one peak at 4.12 min (5 ft × ¼ in.; 5% SE-30 on Chromosorb W, 165°C).

Trans *Diacetate* ***68***

A solution of the *trans* diol **66** (70 mg, 0.4 mmol) in pyridine (2 ml) and acetic anhydride (2 ml) was stirred at room temperature for 12 h with exclusion of light. The reaction mixture was then worked up and purified as described for the *cis* acetate **67** (80 mg, 80%); mp 53.5–55°C; ir ($CHCl_3$): 1725 cm^{-1}; nmr ($CDCl_3$) δ: 1.96 (3H, singlet, CH_3CO), 2.00 (3H, singlet, CH_3CO), 5.13 (1H, quadruplet, CHOCO), 5.29 (1H, quadruplet, CHOCO), and 5.62 (2H, quadruplet, two olefinic hydrogens); ms *m/e*: 250 (M^+); vpc: one peak at 7.62 min (5 ft × ¼ in., 5% SE-30 on Chromosorb W, 165°C).

Cyclic Carbonate ***69***

A solution of phosgene in dry benzene (1.6 ml, 2.36 g/30 ml, 1.28 mmol) was added to a solution of the *cis* diol **65** (53 mg, 0.32 mmol) in the same solvent (10 ml) containing pyridine (0.1 ml, 1.28 mmol) during a period of 5 min. The reaction mixture was then stirred for 30 min at room temperature. The excess phosgene was destroyed by the slow addition of water and the mixture was extracted several times with dichlorome thane. The extracts were combined, washed with dilute hydrochloric acid (6%), water, and dried. The product obtained on removal of the solvent was recrystallized from dichloromethane–ether (54 mg, 90%); mp 143–153°C; ir ($CHCl_3$): 1730 cm^{-1}; nmr ($CDCl_3$) δ: 1.82–3.80 (8H, multiplet), 4.96 (2H, multiplet, two CHOCO), and 5.60 (2H, singlet, two olefinic hydrogens); ms *m/e*: 192 (M^+). *Anal.* calcd. for $C_{11}H_{12}O_3$: C 68.74, H 6.29; found: C 68.43, H 6.46.

Cis *Dimesylate* ***71***

Methane sulfonyl chloride (0.07 ml, 0.9 mmol) was added to a solution of the *cis* diol **65** (45 mg, 0.3 mmol) in dichloromethane (2 ml) and pyridine (1 ml) in the cold (−20 to −30°C). The reaction mixture was then left in the refrigerator at 0°C for 24 h in the dark. The reaction mixture was then poured into water and extracted several times with dichloromethane. The organic phase was washed with dilute hydrochloric acid (6%), saturated sodium chloride solution, and water. It was dried and the solvent was distilled off under vacuum to yield a crystalline product which was recrystallized from dichloromethane – petroleum ether (80 mg, 92%); mp 151–152°C; ir ($CHCl_3$): 1350, 1335, and 1170 cm^{-1}; nmr ($CDCl_3$) δ: 2.07–3.52 (8H, multiplet), 3.03 (6H, singlet, two CH_3SO_2), 5.26 (2H, quadruplet, two CHO), and 5.65 (2H, singlet, two olefinic hydrogens); ms *m/e*: 322 (M^+). *Anal.* calcd. for $C_{12}H_{18}O_6S_2$: C 44.70, H 5.48; found: C 45.02, H 5.57.

Trans *Dimesylate* ***72***

Methane sulfonyl chloride (3 ml, 38.7 mmol) was added to a cold (−20 to −30°C) solution of the *trans* diol **66** (2.15 g 12.9 mmol) in dichloromethane (126 ml) and pyridine (42 ml) and kept at 0°C in the dark for 60 h. It was then left at room temperature for 24 h. The reaction mixture was worked up as described for the *cis* dimesylate **71**. The product obtained was recrystallized from dichloromethane–ether–pentane (4.52 g,

Can. J. Chem. Downloaded from www.nrcresearchpress.com by 210.87.254.40 on 09/05/12
For personal use only.

84%); mp 111.5–112°C; ir ($CHCl_3$): 1360, 1340, and 1175 cm^{-1}; nmr ($CDCl_3$) δ: 1.50–3.50 (8H, multiplet), 3.04 (6H, singlet, two CH_3SO_2), 5.06 (2H, multiplet, two CHO), and 5.60 (2H, quadruplet, two olefinic hydrogens); ms *m/e*: 226 ($M^+ - CH_3—SO_2OH$). *Anal.* calcd. for $C_{12}H_{18}O_6S_2$: C 44.70, H 5.48; found: C 43.68, H 5.66.

Cis *and* Trans *Dixanthates* ***73*** *and* ***74*** *(30)*

Sodium hydride (192 mg, 8.0 mmol) was added to an equimolar mixture of the *cis* and *trans* diols **65** and **66** (250 mg, 1.5 mmol) dissolved in tetrahydrofuran (20 ml). The reaction mixture was refluxed for 1 h, cooled to room temperature, treated with carbon disulfide (5.0 ml, 12.0 mol), and refluxed again for 1½ h. The reaction mixture was cooled to room temperature, methyl iodide was added (5 ml, 12.4 mmol), and it was refluxed for another 1 h. It was then cooled, concentrated under reduced pressure, and poured into benzene. The organic phase was washed with water, dried, and the solvent was evaporated off. The oil obtained was purified by chromatography on Florisil to give the pure *cis* xanthate **73** (208 mg) and the *trans* xanthate **74** (203 mg) (total yield: 80%).

Cis *xanthate* ***73***: ir ($CHCl_3$): 1240, 1222, 1218, and 1157 cm^{-1}; nmr ($CDCl_3$) δ: 3.49 (6H, singlet, two CH_3S), 6.06 (2H, quadruplet, two CHOC), and 5.60 (2H, singlet, two olefinic hydrogens); ms *m/e*: 346 (M^+). *Anal.* calcd. for $C_{14}H_{18}O_2S_4$: C 48.58, H 5.20; found: C 49.22, H 5.55.

Trans *xanthate* ***74***: mp 69.5–70.5°C; ir ($CHCl_3$): 1225, 1190, 1070, and 1050 cm^{-1}; nmr ($CDCl_3$) δ: 3.47 (3H, singlet, CH_3S), 3.49 (3H, singlet, CH_3S), 5.94 (2H, multiplet, two CHOC), and 5.63 (2H, multiplet, two olefinic hydrogens); ms *m/e*: 346 (M^+). *Anal.* calcd. for $C_{14}H_{18}O_2S_4$: C 48.58, H 5.20; found: C 49.02, H 5.66.

In another experiment, the pure *trans* diol **66** (336 mg, 2.0 mmol) was converted into the *trans* dixanthate **74** as described above (680 mg, 96%).

*Triquinacene (****1****)*

(a) From Cis *Dimesylate* ***71*** *(22)*

Neutral alumina (Woelm, activity I, 5 g) was added to a solution of the *cis* dimesylate **71** (240 mg, 0.12 mmol) in dichloromethane (8 ml). The mixture was magnetically stirred at room temperature during 23 h. The mixture was then filtered and the dichloromethane was removed by distillation at atmospheric pressure to yield crude triquinacene which was distilled at 80–85°C (30–35 min) (40 mg, 42%); ir (CH_2Cl_2): 3040, 2460, 2380, 1605, and 1348 cm^{-1}; nmr ($CDCl_3$) δ: 3.70 (4H, singlet) and 5.63 (6H, singlet, six olefinic hydrogens); ms *m/e*: 130 (M^+), 129 ($M^+ - 1$), 115 ($M^+ - 15$), 78 ($M^+ - 52$), and 77 ($M^+ - 53$); vpc one peak at 2.87 min (5 ft × ¼ in., 5% SE-30 Chromosorb W, 152°C). *Anal.* calcd. for $C_{10}H_{10}$: C 92.26, H 7.74; found: C 91.92, H 7.91.

(b) From Trans *Dimesylate* ***72*** *(22)*

Using an experimental procedure similar to the one described above, the *trans* dimesylate **72** (2 g, 3.1 mmol) gave pure triquinacene (460 mg, 57%).

(c) From Cis *Dixanthate* ***73***

The *cis* dixanthate **73** (90 mg, 0.26 mmol) was heated at 210°C in a sealed tube (under vacuum) during a period of 6 h. The resulting product was dissolved in pentane and purified by chromatography on Florisil. The pentane solution was removed and distillation gave pure triquinacene (17 mg, 50%).

(d) From Trans *Dixanthate* ***74***

Using an experimental procedure similar to one described above, the *trans* dixanthate **74** (470 mg, 1.35 mmol) gave pure triquinacene (**1**) (89 mg, 50%). No special effort was made to improve the yield of triquinacene in these four different experimental procedures.

1. R. B. Woodward, T. Fukunaga, and R. C. Kelly. J. Am. Chem. Soc. **86**, 3162 (1964).
2. I. T. Jacobson. Acta Chem. Scand. **21**, 2235 (1967).
3. J. W. Baum and C. D. Gutsche. J. Org. Chem. **33**, 4312 (1968).
4. L. A. Paquette, G. V. Meehan, and S. S. Marshall. J. Am. Chem. Soc. **91**, 6779 (1969).
5. R. Srinivasan. J. Am. Chem. Soc. **92**, 7542 (1970).
6. A. de Meijere, D. Kaufmann, and O. Schallner. Angew. Chem. Int. Ed. Engl. **10**, 417 (1971).
7. R. Russo, Y. Lambert, and P. Deslongchamps. Can. J. Chem. **49**, 531 (1971).
8. C. Mercier, P. Soucy, W. Rosen, and P. Deslongchamps. Synth. Commun. **3**, 161 (1973).
9. L. A. Paquette, S. V. Ley, and W. B. Farnham. J. Am. Chem. Soc. **96**, 312 (1974).
10. L. A. Paquette and M. J. Wyvratt. J. Am. Chem. Soc. **96**, 4671 (1974).
11. L. A. Paquette, W. B. Farnham, and S. V. Ley. J. Am. Chem. Soc. **97**, 7273 (1975).
12. P. E. Eaton and R. H. Mueller. J. Am. Chem. Soc. **94**, 1014 (1972); P. E. Eaton, R. H. Mueller, G. R. Carlson, D. A. Cullison, G. F. Cooper, T. C. Chou, and E.-P. Krebs. J. Am. Chem. Soc. **99**, 2751 (1977).
13. L. A. Paquette, I. Itoh, and W. B. Farnham. J. Am. Chem. Soc. **97**, 7280 (1975).
14. L. A. Paquette, M. J. Wyvratt, O. Schallner, D. F. Schneider, W. J. Begley, and R. M. Blankenship. J. Am. Chem. Soc. **98**, 6774 (1976).
15. O. Repič. Ph.D. Thesis, Harvard University, Cambridge, MA. 1976.
16. R. C. Kelly. Ph.D. Thesis. Harvard University, Cambridge, MA. 1965.
17. J. Thiele. Chem. Ber. **34**, 68 (1901).
18. G. L. Dunn and J. K. Donahue. Tetrahedron Lett. 3485 (1968).
19. D. Peters. J. Chem. Soc. 1761 (1959).
20. P. Deslongchamps. Tetrahedron, **31**, 2463 (1976).
21. H. Stetter, L. Kruger-Hansen, and M. Rizk. Chem. Ber. **94**, 2702 (1961).
22. T. Matsui. Tetrahedron Lett. 3761 (1967) and references quoted therein.
23. G. H. Posner, R. J. Johnson, and M. J. Whalen. Chem. Commun. 281 (1972).
24. K. Ziegler, H. E. Kuhlhorn, and K. Hofner. Chem. Ber. **89**, 434 (1956).
25. J. C. Collins. Tetrahedron Lett. 3363 (1968).
26. R. A. Bell, R. E. Ireland, and R. A. Partyka. J. Org. Chem. **31**, 2530 (1966); R. A. Bell, R. E. Ireland, and L. N. Mander. J. Org. Chem. **31**, 2536 (1966).
27. K. Bowden, I. M. Heilbron, E. R. H. Jones, and B. C. L. Weedon. J. Chem. Soc. 39 (1946).
28. J. Schmidlin and A. Wettstein. Helv. Chim. Acta, **46**, 2799 (1963).
29. C. S. Rondesvedt and C. V. Dernooy. J. Am. Chem. Soc. **77**, 4878 (1955).
30. K. Wiesner, L. Poon, T. Jirkovsky, and M. Fishman. Can. J. Chem. **47**, 433 (1969).

Crystal structures of medium ring compounds. Part II. The crystal and molecular structure of *cis-anti-cis*-4,5:9,10-biscyclohexano-1,3,6,8-tetraoxecane

ARIS TERZIS, J. BRIAN FAUGHT,[1] AND T. BRUCE GRINDLEY

Department of Chemistry, Dalhousie University, Halifax, N.S., Canada B3H 4J3

Received December 13, 1977

ARIS TERZIS, J. BRIAN FAUGHT, and T. BRUCE GRINDLEY. Can. J. Chem. **56**, 1705 (1978).

The crystal structure of *cis-anti-cis*-4,5:9,10-biscyclohexano-1,3,6,8-tetraoxecane (**2**) has been determined by X-ray diffraction. The crystals are monoclinic, $a = 11.120(1)$, $b = 8.127(1)$, $c = 7.990(1)$ Å, $\beta = 110.01(1)°$, $P2_1/c$, with $Z = 2$. The structure was solved by the application of symbolic addition procedures and refined to a final R value of 0.031 (R_w 0.040) for 989 reflections with $I > 2.0\sigma(I)$.

This structural determination confirms a previous tentative assignment of the relative configuration of **2**. In the crystal, the two *cis*-substituted cyclohexane rings adopt chair conformations in which the equatorial oxygens on different rings are linked through methylene groups to axial oxygens on the other rings. The central 10-membered tetraoxecane ring adopts the boat–chair–boat conformation, the most stable conformation for cyclodecane.

ARIS TERZIS, J. BRIAN FAUGHT et T. BRUCE GRINDLEY. Can. J. Chem. **56**, 1705 (1978).

On a déterminé, par diffraction des rayons-X, la structure cristalline du biscyclohexano-4,5:9,10 tétraoxécanne-1,3,6,8 *cis-anti-cis* (**2**). Les cristaux sont monocliniques $a = 11.120(1)$, $b = 8.127(1)$, $c = 7.990(1)$ Å, $\beta = 110.01(1)°$, $P2_1/c$ avec $Z = 2$. On a résolu la structure par l'application du processus d'addition symbolique et on l'a affinée jusqu'à une valeur finale de R de 0.031 (R_w 0.040) pour 989 réflexions avec $I > 2.0\sigma(I)$.

Cette détermination de structure confirme une attribution antérieure non définitive de la configuration relative de **2**. Dans le cristal, les deux cycles cyclohexaniques substitués *cis* adoptent des conformations chaises dans lesquelles les oxygènes équatoriaux sur les différents cycles sont liés par l'intermédiaire de groupes méthylènes à des oxygènes axiaux sur les autres cycles. Le cycle tétraoxécanne à dix chaînons que l'on retrouve au centre de la molécule adopte une conformation bateau–chaise–bateau; cette conformation est la plus stable pour le cyclodécane.

[Traduit par le journal]

Introduction

Medium rings are one of the few systems where nonbonded interactions are very important in the determination of molecular geometry and therefore there is considerable interest in the properties of these systems (1). The crystal structures of only few medium rings containing hetero atoms have been determined and, in particular, only two crystals containing 10-membered rings with more than one oxygen atom in the ring have been examined. The most stable cyclodecane conformation (1, 2) in the solid state appears to be the boat–chair–boat (BCB) (1,2) and this conformation was observed for the 10-membered ring in *trans-syn-trans*-4,5:9,10-biscyclohexano-1,3,6,8-tetraoxecane (**1**) (3). In this publication, we report the structure of a 4,5:9,10-biscyclohexano-1,3,6,8-tetraoxecane (**2**) obtained as a minor product from the base catalysed reaction of *cis*-1,2-cyclohexanediol and methylene chloride.

This product (**2**) had previously been tentatively assigned the *cis-anti-cis* configuration on symmetry arguments based on its nmr spectra (4). At low temperatures in solution, inversion of the two *cis*-disubstituted cyclohexane rings slows and two conformational possibilities arise, a C_i symmetric form (**2***a*) with equatorial bonds linked to axial and a C_2 symmetric form (**2***b*) with axial bonds linked to axial and equatorial to equatorial (see Fig. 1). Preliminary low temperature nmr results strongly suggest that the latter C_2 symmetric form (**2***b*) is favoured in solution (ref. 5 and footnote 2).

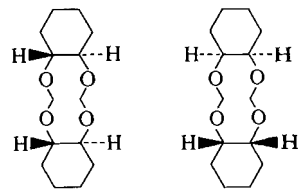

1 **2**

Experimental

Compound **2** was prepared according to the procedure of Brimacombe *et al.* (6). Crystals suitable for study were obtained by recrystallization from ethanol and had mp 143–144°C

[1]Present address: Environmental Protection Service, Environment Canada, Halifax, N.S.

[2]M. St. Jaques and T. B. Grindley. Unpublished results.

Can. J. Chem. Downloaded from www.nrcresearchpress.com by 210.87.254.105 on 09/05/12
For personal use only.

Can. J. Chem. Downloaded from www.nrcresearchpress.com by 210.87.254.105 on 09/05/12
For personal use only.

TABLE 1. Positional and thermal parameters* (esd's) for *cis-anti-cis*-4,5:9,10-biscyclohexano-1,3,6,8-tetraoxecane

Atom	x	y	z	U_{11} or U_{iso}	U_{22}	U_{33}	U_{12}	U_{13}	U_{23}
				Nonhydrogen atoms ($\times 10^4$)					
O(1)	4051(1)	1647(1)	3064(1)	357(4)	431(5)	355(4)	−19(4)	94(4)	77(4)
O(2)	4020(1)	−1479(1)	4486(1)	361(4)	327(4)	320(4)	17(3)	89(3)	4(3)
C(1)	3073(1)	1166(2)	3761(2)	345(6)	340(6)	367(6)	20(5)	123(5)	28(5)
C(2)	3508(1)	−145(1)	5214(1)	351(6)	334(6)	291(5)	−9(5)	96(5)	−19(5)
C(3)	2392(1)	−699(2)	5770(2)	430(7)	453(7)	398(6)	−15(5)	189(6)	15(6)
C(4)	1272(1)	−1315(2)	4190(2)	378(7)	523(8)	534(8)	−74(6)	194(6)	−20(7)
C(5)	843(1)	−2(2)	2751(2)	338(7)	650(9)	532(8)	−9(6)	82(6)	36(7)
C(6)	1950(1)	578(2)	2181(2)	364(7)	490(7)	394(6)	12(6)	68(5)	65(6)
C(7)	5107(1)	2492(2)	4232(2)	376(7)	335(6)	442(7)	−10(5)	97(6)	69(6)
				Hydrogen atoms ($\times 10^3$)					
H(1)	282(1)	214(2)	432(2)	40(3)					
H(2)	420(1)	27(1)	623(1)	36(3)					
H(3A)	271(1)	−156(1)	670(2)	54(4)					
H(3B)	212(1)	26(2)	633(2)	54(4)					
H(4A)	152(1)	−233(2)	369(2)	51(4)					
H(4B)	54(1)	−163(2)	455(2)	52(4)					
H(5A)	12(1)	−40(2)	166(2)	68(4)					
H(5B)	51(1)	94(2)	322(2)	65(4)					
H(6A)	226(1)	−31(1)	163(2)	45(3)					
H(6B)	167(1)	153(2)	129(2)	65(4)					
H(7A)	553(1)	301(2)	345(2)	42(3)					
H(7B)	481(1)	326(2)	492(2)	44(3)					

*The form of the anisotropic vibration is $\exp[-2\pi^2(a^{*2}h^2U_{11} + \ldots 2a^*b^*hkU_{12} + \ldots)]$.

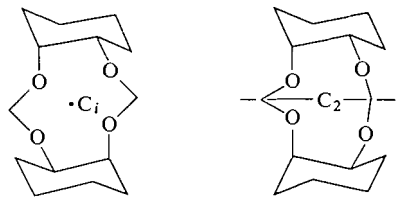

2*a* 2*b*

FIG. 1. The two possible relative orientations of the cyclohexane rings in *cis-anti-cis*-4,5:9,10-biscyclohexano-1,3,6,8-tetraoxecane (**2**).

(lit (6) mp 142–143°C). Crystal data:

$C_{14}H_{24}O_4$ fw = 256.34
Monoclinic, a = 11.120(1), b = 8.127(1), c = 7.990(1) Å, β = 110.01°(1), V = 678.49 Å^3, ρ_{obs} = 1.26 g cm^{-3}, Z = 2, ρ_{calcd} = 1.255 g cm^{-3} (18°C, CuK$_\alpha$, λ = 1.54051 Å).

Preliminary precession and Weissenberg photographs showed the following systematic absences: $h0l$, $l = 2n + 1$; $0k0$, $k = 2n + 1$. These absences uniquely identify the space group as $P2_{1/c}$. The unit cell dimensions were obtained from a least-squares refinement of the diffractometer angular settings of 12 independent reflections.

A crystal (0.21 × 0.21 × 0.18 mm) was mounted with the a axis nearly parallel to the ϕ axis of a Picker FACS-1 automated diffractometer with a graphite monochromator. Data were collected by the $\theta - 2\theta$ scan technique from a point 0.95° below the calculated 2σ position for CuK$_{\alpha 1}$ to 0.95° above the calculated position for CuK$_{\alpha 2}$, at a rate of 1° min^{-1}. Stationary background counts were taken for 20 s at either end of the scan range. During the course of the data collection, three standard reflections were measured at a period of 30 reflections. Their variations were less than 4.5% of their respective mean values.

A total of 1452 intensity measurements, including standards, were made for h, k, $\pm l$ in the region of $2\theta < 127°$ and reduced to a set of 1096 independent reflections after averaging equivalent reflections whose intensities were within 2σ of each other. The integrated intensity was calculated as

$$I(\text{net}) = I(\text{scan}) - 0.5t_T/t_B(B_1 + B_2)$$

where I(scan) is the number of counts over the scan range, t_T is the scan time, and t_B is the time for each background count B_1 and B_2. The standard deviations were calculated according to the expression

$$\sigma(I) = [N_T + 0.25(t_T/t_B)^2(B_1 + B_2) + cI^2 + 0.04^2(I - I_c)^2]^{\frac{1}{2}}$$

where N_T is the total integrated scan count obtained in time t_T, c is the factor to account for instrument instability during data collection (for this structure, c was 0.035), I is the net intensity, and I_c is I corrected for absorption. The last term in brackets is a factor accounting for errors in the absorption correction. Only data for which $I > 2.0\sigma(I)$ were used which left 989 reflections to be entered in the least-squares refinement.

An absorption correction was applied[3] to the data and calculated transmission coefficients based on a linear absorption coefficient of 7.44 cm^{-1} for CuK$_\alpha$ radiation ranged from 0.850 to 0.887. Finally, Lorentz and polarization corrections were applied.

The structure was determined by the application of symbolic addition procedures (10). All the nonhydrogen atoms were found in the first E-map. A structure factor calculation based

[3]The computer programs used were locally modified versions of the following: F. R. Ahmed, NRC-2A (data processing); F. R. Ahmed and C. P. Huber, NRC-2(7) (data reduction); F. R. Ahmed and P. Singh, NRC-3(7) (absorption correction); S. R. Hall, NRC-4, (symbolic addition procedure); F. R. Ahmed, NRC-8(7) (Fourier maps); R. J. Doedens and J. A. Ibers, NUCLS (least-squares refinement), with block-diagonal option introduced by J. Sygusch *et al.* (8); and C. K. Johnson (9) ORTEP (drawings).

Can. J. Chem. Downloaded from www.nrcresearchpress.com by 210.87.254.105 on 09/05/12
For personal use only.

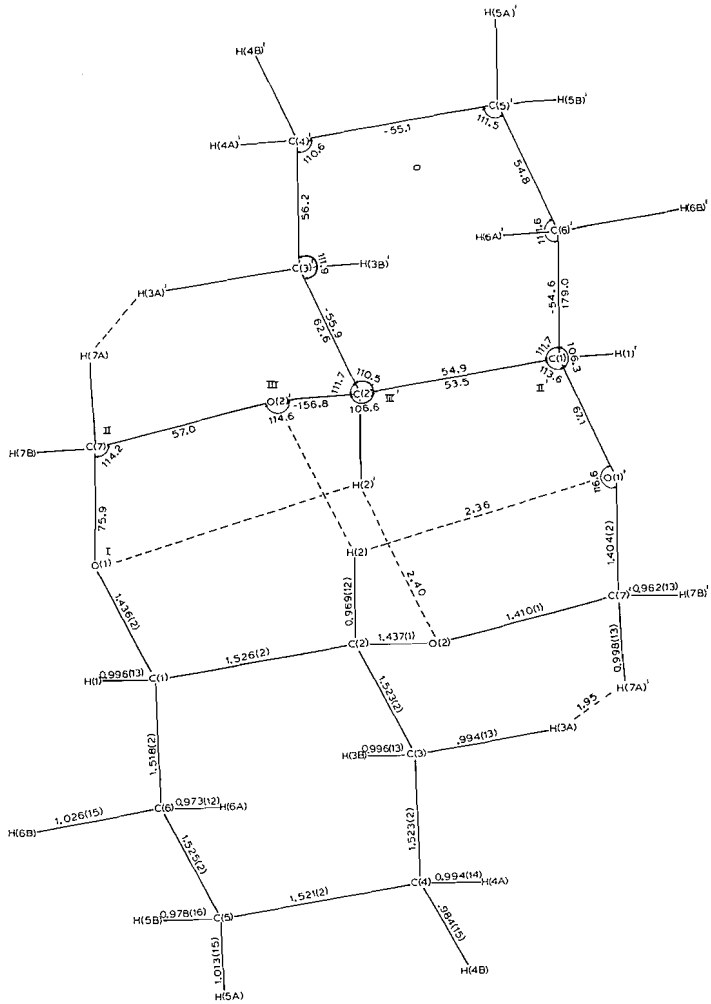

FIG. 2. Numbering and structural parameters for *cis-anti-cis*-4,5:9,10-biscyclohexano-1,3,6,8-tetraoxecane. Bond lengths (Å) with their errors in parentheses (10^3Å), and the more significant calculated short intramolecular distances (---) are shown on the bottom half of the diagram. Bond angles (deg) and torsional angles (deg) between heavy atoms are shown on the top half. All errors in angles were 0.1°. Roman numerals indicate the positions of the three different types of BCB positions on the structure.

on these atoms led to a conventional R factor of 0.287 where $R = \Sigma||F_o| - |F_c||/\Sigma F_o$. Temperature and scale factors were taken from the Wilson plot. Four cycles of block diagonal least-squares refinement (with unit weights) varying atomic positional and isotropic thermal parameters gave $R = 0.117$. All the hydrogen positions were determined from a difference Fourier map calculated at this point. Refinement continued, varying atomic positional and anisotropic thermal parameters for the nonhydrogen atoms, and positional and isotropic thermal parameters for the hydrogen atoms. Inclusion of a secondary extinction correction (11) as well as a weighting scheme ($w = 1/(\sigma F_o)^2$) led to a final $R = 0.031$ (observed data) and $R_w = (\Sigma w(|F_o| - |F_c|)^2/\Sigma w|F_o|^2)^{\frac{1}{2}}$ of 0.040 after seven cycles of refinement. Maximum shifts in the final least-squares refinement were 0.3σ. The 'goodness of fit,' defined as $[\Sigma w(|F_o| - |F_c|)^2/(m - n)]^{\frac{1}{2}}$ was 1.70, where m = number of observations and n = number of refined parameters. The final difference map was featureless and there were no trends in the quantity $\Sigma w(|F_o| - |F_c|)^2$ as a function of $|F_o|$, sin 2θ, or $|h|$ (slowest varying index during data collection). The scattering factors for all atoms were taken from Cromer and Mann (12) and the anomalous dispersion components for carbon and oxygen were taken from Cromer and Lieberman (13).

Results and Discussion

Atomic positions and thermal parameters for **2** are given in Table 1. The structure factor table and Table 2, which contains the bond angles involving hydrogen, were put on deposit.[4] Numbering, bond lengths, bond angles, torsional angles, and short intramolecular distances of interest are shown in Fig. 2. To facilitate comparison with the results from

[4]A complete set of tabular data is available, at a nominal charge, from the Depository of Unpublished Data, CISTI, National Research Council of Canada, Ottawa Ont., Canada K1A 0S2.

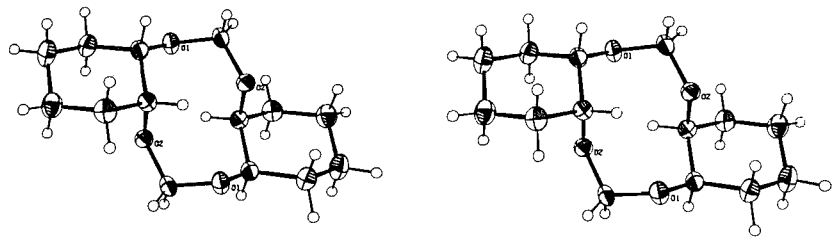

FIG. 3. Stereoscopic view of the solid state structure of *cis-anti-cis*-4,5:9,10-biscyclohexano-1,3,6,8-tetraoxecane.

molecular mechanics calculations, the short intramolecular distances were recalculated using a C—H bond length of 1.1 Å. Figure 3 is an ORTEP diagram of the crystal structure of **2**.

This crystal structure determination confirmed the previous (4) tentative assignment of the *cis-anti-cis* configuration to **2**. In the solid state, **2** adopted the C_i symmetric form **2***a*, in contrast to its preference at low temperature in solution (ref. 5 and footnote 2) and the 10-membered ring was in a BCB conformation. Only **2***a* can adopt a BCB conformation; the particular combination of torsional angles required by the relative orientations of the two cyclohexane rings in **2***b* cannot be accommodated in this type of conformation. Since only the BCB conformation has been observed for unhindered cyclodecane derivatives in the solid state (2) it is not surprising that the crystal structure of **2** contains **2***a*.

The BCB conformation observed for the 10-membered ring of **2** is very similar to that of **1** (see Fig. 4 and Table 3). In particular, this BCB conformation is narrower than those in cyclodecane derivatives because of relief of transannular nonbonded interactions. In cyclodecane the BCB conformation has C_{2h} symmetry which results in three different types of carbon positions termed I, II, and III and the locations of these positions for **1** and **2** are shown in Fig. 4 and Fig. 2, respectively. For **2**, the cyclohexane ring is fused in equatorial orientations at BCB positions type II and III whereas for **1**, the ring fusion differs only in that the orientation at the type II position is axial. Since substituents at either axial or equatorial type II BCB positions have similar steric interactions, this similarity of geometry is expected although it does support the contention (3) that the conformation of **1** was not much affected by intermolecular interactions.

The few differences in geometry between the tetraoxecane rings in **1** and **2** arise from the change in nonbonded interactions when the cyclohexane carbon at the type II positions changes from being an axial carbon on C(1). Removal of this interaction in **2** allowed the bond angle C(1)—O(1)—C(7) to decrease from 118.2 to 116.6° and by reducing the torque on the $C(7)H_2$ group considerably reduced the rocking and particularly twisting distortion of this group from local C_{2v} symmetry (see Tables 3 and 4 and ref. 3).

One extraannular bond angle, C(6)—C(1)—O(1), is markedly smaller in **2** (106.3°) than in **1** (112.8° for the comparable angle). This angle is smaller in **2** because the ethyl methyl ether fragment C(6)—C(1)—O(1)—C(7) is now *anti* rather than *gauche* as in **1**. This decrease in bond angles on changing from *gauche* to *anti* in similar CCOC fragments has been observed in macrocyclic polyethers (14) and has been attributed to relief of the *gauche* interactions. In **2**, additional effects cause the angle under discussion to be particularly small; decreasing this angle decreases the distance between the $C(3)'H_2$ group and the $C(7)H_2$ group and particularly between H(7A) and H(3A)'.

TABLE 3. Comparison of bond angles and torsional angles in **1** and **2**

BCB position type	Atoms involved	Angle (deg) Compound **1**	Compound **2**	Difference
Bond angles				
I	COC	118.2	116.6	−1.6
II	OCO	113.7	114.2	+0.5
III	COC	115.3	114.6	−0.7
III′	OCC	106.9	106.6	−0.3
II′	CCO	114.3	113.6	−0.7
Torsional angles				
I and II	COCO	73.0	75.9	+2.9
II and III	OCOC	60.9	57.0	−3.9
III and III′	COCC	−158.2	−156.8	+1.4
III′ and II′	OCCO	52.6	53.5	+0.9
II′ and I′	CCOC	65.4	67.1	+1.7

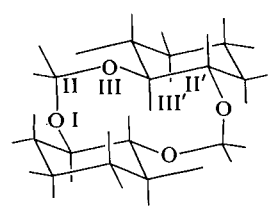

FIG. 4. Approximate representation of the structure of *trans-syn-trans*-4,5:9,10-biscyclohexano-1,3,6,8-tetraoxecane with BCB positions indicated by roman numerals.

Can. J. Chem. Downloaded from www.nrcresearchpress.com by 210.87.254.105 on 09/05/12
For personal use only.

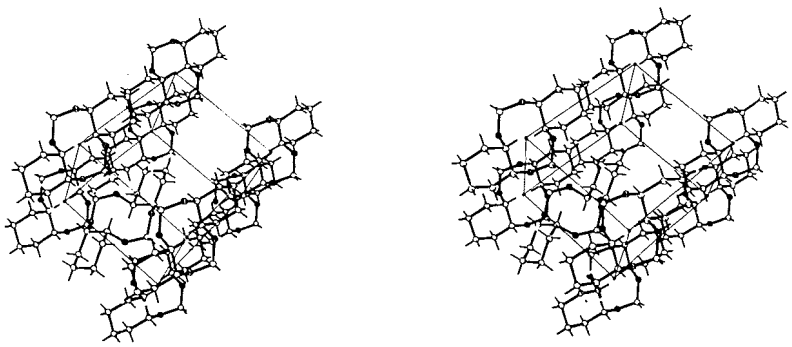

FIG. 5. Stereoscopic view of the molecular packing.

TABLE 4. Comparison of the distortion of the OCH_2O group from local C_{2v} symmetry

Compound	Mean angle size*	Distortion		
		Wag*	Rock*	Twist*
1	108.4	2.0	−3.4	−8.6
2	107.5	−1.7	−1.6	−4.9

*These terms are defined as in ref. 3 and were calculated using bond angles in Tables 2 and 3.

The packing diagram is shown in Fig. 5. There is one H–H intermolecular nonbonded interaction at a distance closer than 2.5 Å, between H(2) and an H(7A) of 2.341 Å. This distance is sufficiently large so as not to significantly influence the conformation of the 10-membered ring.

Acknowledgements

Support of this work by grants from the National Research Council of Canada is gratefully acknowledged.

1. E. M. ENGLER, J. D. ANDOSE, and P. V. R. SCHLEYER. J. Am. Chem. Soc. **95**, 8005 (1973); O. ERMER. Struct. Bonding (Berlin), **27**, 161 (1976); C. ALTONA and D. H. FABER. Fortschr. Chem. Forsch. **45**, 1 (1974).
2. J. D. DUNITZ. *In* Perspectives in structural chemistry. Vol. 2. *Edited by* J. D. Dunitz and J. A. Ibers. John Wiley and Sons, Inc., New York, NY. 1968. p. 1; O. ERMER, J. D. DUNITZ, and I. BERNAL. Acta Crystallogr. Sect. B, **29**, 2778 (1973).
3. A. TERZIS, T. B. GRINDLEY, and J. B. FAUGHT. Can. J. Chem. **55**, 2692 (1977).
4. T. B. GRINDLEY, J. F. STODDART, and W. A. SZAREK. J. Am. Chem. Soc. **91**, 4722 (1969).
5. T. B. GRINDLEY. Ph.D. Thesis. Queens University, Kingston, Ont. 1970.
6. J. S. BRIMACOMBE, A. B. FOSTER, B. D. JONES, and J. J. WILLARD. J. Chem. Soc. C, 2404 (1967).
7. F. R. AHMED, S. R. HALL, M. E. PIPPY, and C. P. HUBER. NRC-Crystallographic programs for the IBM/360 System. National Research Council of Canada, Ottawa, Ont. 1970.
8. J. SYGUSCH, F. R. BRISSE, and S. HANESSIAN. Acta Crystallogr. Sect. B, **30**, 40 (1974).
9. C. K. JOHNSON. ORTEP, Report ORNL-3794. Oak Ridge National Laboratory Oak Ridge, TN. 1965.
10. J. KARLE and I. L. KARLE. Acta Crystallogr. **21**, 849 (1966).
11. P. COPPENS and W. C. HAMILTON. Acta Crystallogr. Sect. A, **26**, 71 (1970).
12. O. T. CROMER and A. MANN. Acta Crystallogr. Sect. A, **24**, 321 (1968).
13. O. T. CROMER and D. LIEBERMAN. J. Chem. Phys. **53**, 1891 (1970).
14. I. GOLDBERG. Acta Crystallogr. Sect. B, **32**, 41 (1976); J. D. DUNITZ and P. SEILER. Acta Crystallogr. Sect. B, **30**, 2741 (1974).

Can. J. Chem. Downloaded from www.nrcresearchpress.com by 210.87.254.105 on 09/05/12
For personal use only.

Can. J. Chem. Downloaded from www.nrcresearchpress.com by 210.87.254.105 on 09/05/12
For personal use only.

Synthesis of covalently-linked dimeric porphyrins

JOHN B. PAINE III AND DAVID DOLPHIN

Department of Chemistry, University of British Columbia, Vancouver, B.C., Canada V6T 1W5

Received March 28, 1978

JOHN B. PAINE III and DAVID DOLPHIN. Can. J. Chem. **56**, 1710 (1978).

Dimeric porphyrins covalently linked directly at their periphery (β,β′-biporphyrins) or via a hydrocarbon chain $(CH_2)_n$, where n = 1–8, have been synthesized from the corresponding β,β′-linked bispyrroles.

JOHN B. PAINE III et DAVID DOLPHIN. Can. J. Chem. **56**, 1710 (1978).

Utilisant les bispyrroles correspondants liés en β,β′ comme produits de départ, on a synthétisé les porphyrines dimères liées d'une façon covalente directement à leur périphérie (β,β′ biporphyrines) ou par l'intermédiaire d'une chaîne hydrocarbonée $(CH_2)_n$ où n = 1–8.

[Traduit par le journal]

Since our first report (1) of covalently-linked dimeric porphyrins, joined by amide linkages, a number of similar dimeric porphyrins with amide, ester, or ether linkages have been reported (2–10). That all of these systems employed the coupling of porphyrins, through these functional groups, results from the 'ready' availability of the porphyrin precursors and the ease of formation of amide, ester, and ether linkages. However, once formed, such linkages have numerous disadvantages in that they generally lower the solubility (of systems which naturally have low solubilities), and increase the reactivity, and thereby decrease the stability. In addition the presence of extraneous functional groups complicates mechanistic and spectral studies on such systems.

Whereas all previous syntheses of dimeric porphyrins consist of joining two preformed porphyrin entities in the final steps, our approach consists of constructing the covalent link *first*, and then building a porphyrin onto either end. To avoid the disadvantages of the linkages discussed above a synthesis has been developed where hydrocarbon chain-linked bispyrroles **1** are converted into the corresponding dimer porphyrins **7** where the hydrocarbon chain plays a passive role both chemically and electronically.

Experimentally, the sequence depicted in Scheme 1 is facile to perform. The preparation of the bispyrroles **1** depends upon the length of the linking chain. When n = 0 the β,β′-bipyrrole was prepared by Ullmann coupling (11) of the corresponding β-iodopyrrole **8** (R = I). For n = 1 the β,β′-dipyrromethane was prepared from **9** (R = H) and acidified methanolic formaldehyde. For $n > 5$ acylation of **8** (R = H) or **9** (R = H) with a diacid chloride (in methylene chloride – nitromethane at 0°C with excess stannic chloride) gave the diketo bispyrroles **13** which were reduced to **1** with an excess of diborane. The diacid chlorides of succinic and glutaric acids could only be mono substituted, presumably owing to the propensity of the intermediate pyrrolyl keto acid chlorides **10***c* to cyclise to the five- and six-membered enol lactones, which upon work up gave the pyrrolyl keto acids **10***a*. These after esterification to the ethyl esters **10***b* were reduced by diborane in ethyl acetate – tetrahydrofuran to **11***a*, which were selectively saponified (carboxylalkyl side-chain esters saponify much faster than nuclear carboxylate esters which are vinylogous carbamates) to **11***b*. These two carboxylic acids along with the pyrrolylpropionic acid **11***b* (n = 3) prepared similarly from the readily available ester (Knorr synthesis with methyl 4-acetyl-5-oxohexanoate and ethyl oximinoacetoacetate) were treated with oxalyl chloride, followed by **8** (R = H) and reduction of the keto bispyrrole with diborane gave **1** (n = 3, 4, and 5) in high yields.

So far the ethane-linked bispyrrole **1** (n = 2) has not been prepared by the above routes owing to the insolubility of the acid **11***b* (n = 2) prepared by reductive alkylation of **8** (R = H) with glyoxylic acid, and the instability of its acid chloride **11***c* (n = 2) under the reaction conditions.

Most of the above pyrrolic intermediates were prepared as the ethyl esters and then transesterified to their benzyl esters, ready for hydrogenolysis to the diacid **2**. Condensation of **2** with the formyl-

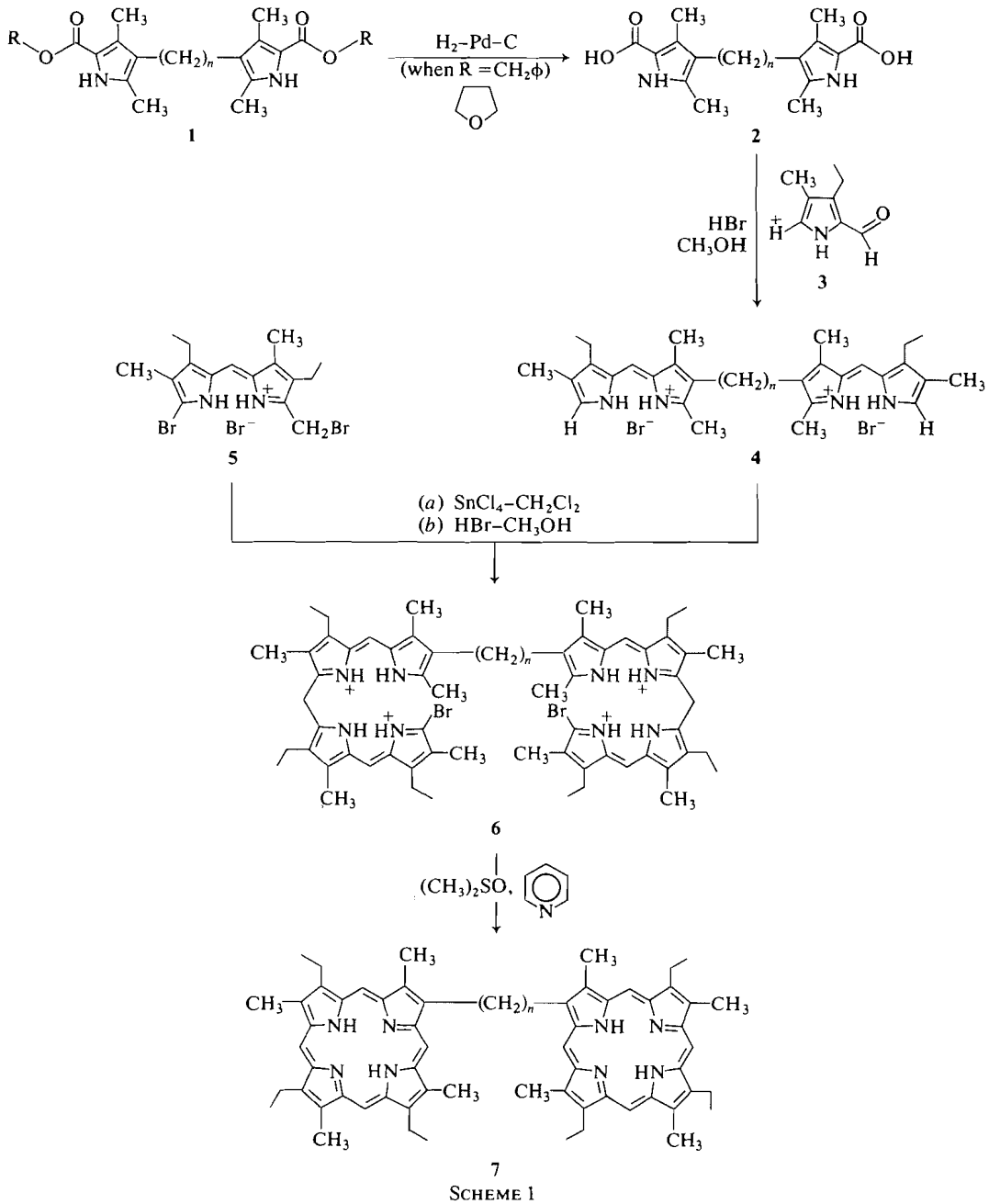

SCHEME 1

pyrrole **3** gave ~90% yields of the bisdipyrromethenes **4** for the cases studied (n = 0–8). Condensation of **4** with an excess of the bromomethyldipyrromethene **5** gave the bisbiladienes-*a*,*c* which were converted, under conditions of the Johnson porphyrin synthesis (12), into the covalently linked dimeric porphyrins[1] **7** in yields of 55–70% for n = 3–8 and in the sterically hindered systems ca. 30% yields based upon **4**.

These systems, and doubly linked cyclophane porphyrins which are available by modifications of

[1]All of the porphyrins and their precursors give elemental analyses, electronic, ^{1}H and ^{13}C nmr, and mass spectra consistent with their proposed structures. All of the sequences leading up to the porphyrins are notable for their excellent yields. The Friedel–Crafts acylations and diborane reductions proceeded in 80–90% yields; the dimeric dipyrromethenes were all isolated in 85–95% yields based upon the preceding dibenzyl esters, and the transbenzylations, where employed, gave 90–95%. The selective saponifications give 95% recovery of the desired product.

Can. J. Chem. Downloaded from www.nrcresearchpress.com by 210.87.254.105 on 09/05/12
For personal use only.

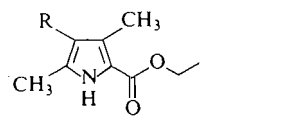

8

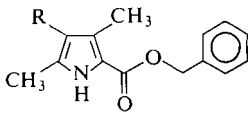

9

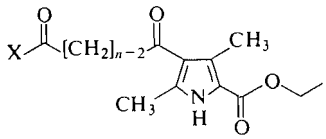

10
a X = OH
b X = OEt
c X = Cl

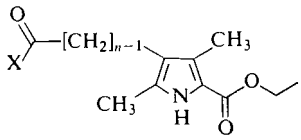

11
a X = OEt
b X = OH
c X = Cl
d X = OMe(n = 3)

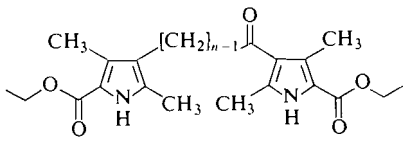

12

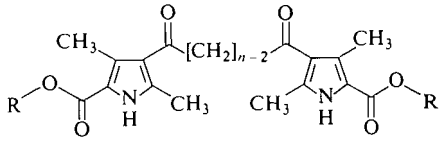

13
R = Et or Bz

the above procedures, have been prepared as models to study electron and photon transfer between porphyrins, and our initial studies on exciton interaction are presented in the following paper.

Acknowledgements

This work was supported by the United States National Institutes of Health (AM 14343) and the National Research Council of Canada.

1. F. P. Schwarz, M. Gouterman, Z. Muljiani, and D. H. Dolphin. Bioinorg. Chem. **2**, 1 (1972).
2. J. A. Anton and P. A. Loach. J. Heterocycl. Chem. **12**, 573 (1975).
3. J. A. Anton, K. Kwong, and P. A. Loach. J. Heterocycl. Chem. **13**, 717 (1976).
4. C. K. Chang, M.-S. Kuo, and C.-B. Wang. J. Heterocycl. Chem. In press.
5. H. Ogoshi, H. Sugimoto, and Z. Yoshida. Tetrahedron Lett. 169 (1977).
6. J. P. Collman, C. M. Elliott, T. R. Halbert, and B. S. Tovrog. Proc. Natl. Acad. Sci. U.S.A. **74**, 18 (1977).
7. N. E. Kagan, D. Mauzerall, and R. B. Merrifield. J. Am. Chem. Soc. **99**, 5484 (1977).
8. S. B. Boxer and G. L. Closs. J. Am. Chem. Soc. **98**, 5406 (1976).
9. L. L. Shipman, T. M. Cotton, J. R. Norris, and J. J. Katz. Proc. Natl. Acad. Sci. U.S.A. **73**, 1791 (1976).
10. M. R. Wasielewski, M. H. Studier, and J. J. Katz. J. Phys. Chem. **81**, 577 (1977).
11. R. Grigg and A. W. Johnson. J. Chem. Soc. 3315 (1964).
12. A. W. Johnson. *In* The porphyrins. Vol. 1. *Edited by* D. Dolphin. Academic Press, New York, NY. 1978. Chapt. 5.

Can. J. Chem. Downloaded from www.nrcresearchpress.com by 210.87.254.105 on 09/05/12
For personal use only.

Exciton and electron interaction in covalently-linked dimeric porphyrins

JOHN B. PAINE III AND DAVID DOLPHIN

Department of Chemistry, University of British Columbia, Vancouver, B.C., Canada V6T 1W5

AND

MARTIN GOUTERMAN

Department of Chemistry, University of Washington, Seattle, WA 93195, U.S.A.

Received February 7, 1978

JOHN B. PAINE III, DAVID DOLPHIN, and MARTIN GOUTERMAN. Can. J. Chem. **56**, 1712 (1978).

The interactions between dimeric porphyrins, covalently linked at their peripheries, have been measured from their electronic absorption spectra and ^{13}C nmr spectra.

8

9

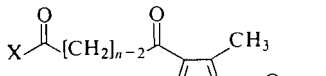

10
a X = OH
b X = OEt
c X = Cl

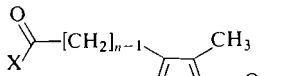

11
a X = OEt
b X = OH
c X = Cl
d X = OMe(n = 3)

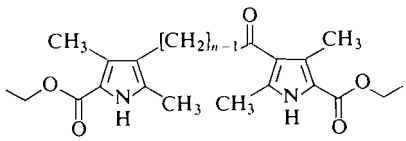

12

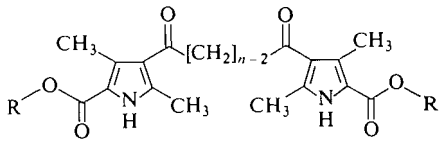

13
R = Et or Bz

the above procedures, have been prepared as models to study electron and photon transfer between porphyrins, and our initial studies on exciton interaction are presented in the following paper.

Acknowledgements

This work was supported by the United States National Institutes of Health (AM 14343) and the National Research Council of Canada.

1. F. P. Schwarz, M. Gouterman, Z. Muljiani, and D. H. Dolphin. Bioinorg. Chem. **2**, 1 (1972).
2. J. A. Anton and P. A. Loach. J. Heterocycl. Chem. **12**, 573 (1975).
3. J. A. Anton, K. Kwong, and P. A. Loach. J. Heterocycl. Chem. **13**, 717 (1976).
4. C. K. Chang, M.-S. Kuo, and C.-B. Wang. J. Heterocycl. Chem. In press.
5. H. Ogoshi, H. Sugimoto, and Z. Yoshida. Tetrahedron Lett. 169 (1977).
6. J. P. Collman, C. M. Elliott, T. R. Halbert, and B. S. Tovrog. Proc. Natl. Acad. Sci. U.S.A. **74**, 18 (1977).
7. N. E. Kagan, D. Mauzerall, and R. B. Merrifield. J. Am. Chem. Soc. **99**, 5484 (1977).
8. S. B. Boxer and G. L. Closs. J. Am. Chem. Soc. **98**, 5406 (1976).
9. L. L. Shipman, T. M. Cotton, J. R. Norris, and J. J. Katz. Proc. Natl. Acad. Sci. U.S.A. **73**, 1791 (1976).
10. M. R. Wasielewski, M. H. Studier, and J. J. Katz. J. Phys. Chem. **81**, 577 (1977).
11. R. Grigg and A. W. Johnson. J. Chem. Soc. 3315 (1964).
12. A. W. Johnson. *In* The porphyrins. Vol. 1. *Edited by* D. Dolphin. Academic Press, New York, NY. 1978. Chapt. 5.

Exciton and electron interaction in covalently-linked dimeric porphyrins

John B. Paine III and David Dolphin

Department of Chemistry, University of British Columbia, Vancouver, B.C., Canada V6T 1W5

and

Martin Gouterman

Department of Chemistry, University of Washington, Seattle, WA 93195, U.S.A.

Received February 7, 1978

John B. Paine III, David Dolphin, and Martin Gouterman. Can. J. Chem. **56**, 1712 (1978).

The interactions between dimeric porphyrins, covalently linked at their peripheries, have been measured from their electronic absorption spectra and ^{13}C nmr spectra.

JOHN B. PAINE III, DAVID DOLPHIN et MARTIN GOUTERMAN. Can. J. Chem. **56**, 1712 (1978).

Faisant appel à la spectroscopie d'absorption électronique et de rmn du ^{13}C, on a mesuré les interactions entre des porphyrines dimères liées d'une façon covalente à leur périphérie.
[Traduit par le journal]

A number of dimeric porphyrins has recently been reported (1–9) covalently joined via amide or ester linkages in a manner similar to the systems which we initially prepared (10). The electronic absorption spectra of these various dimers show a variety of changes in their electronic transitions, compared to the corresponding monomeric species, which are related to small changes in their conformations.

Thus a blue shift in the Soret band of cofacial porphyrin dimers has been observed by Chang *et al.* (1) and Collman *et al.* (2) whereas Kagan *et al.* (7) saw no change in the Soret region but a considerable red shift in the visible region.

We (11) have recently prepared dimeric porphyrins covalently linked directly at their periphery (β,β′-bisporphins), or via a hydrocarbon chain, i.e., **1**

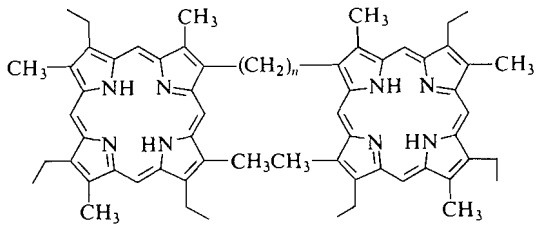

1

where n = 1–8. Figure 1 shows the electronic spectra for the free bases n = 0, 1, and 8, and for monomeric etioporphyrin I.[1] Figure 2 shows the spectra of the same four species in their protonated forms (each porphyrin ring is an *N,N*-diprotonated dication). Recently an extensive discussion of exciton coupling in the μ-oxo dimer of Sc porphyrins has been given (12). The considerations there can be applied with some extension to the present case. In general the exciton coupling parameter between identical units for a dimer electronic band depends on

$$V = (\mu^2/R^3)f$$

Here μ^2 is the transition dipole strength of the monomer and depends on the molar extinction coefficients of the band; R is the distance between centers; and f is a factor depending on the vector relations among the transition dipoles on each unit and the vector direction between centers, with $-2 \leq f \leq 1$. For the visible bands where μ^2 is small, V is comparable to the solution line-width, so the only effect of dimer formation is a slight broadening of the lines and a very small bathochromic shift. For the Soret band, V is substantially larger and more apparent effects are expected.

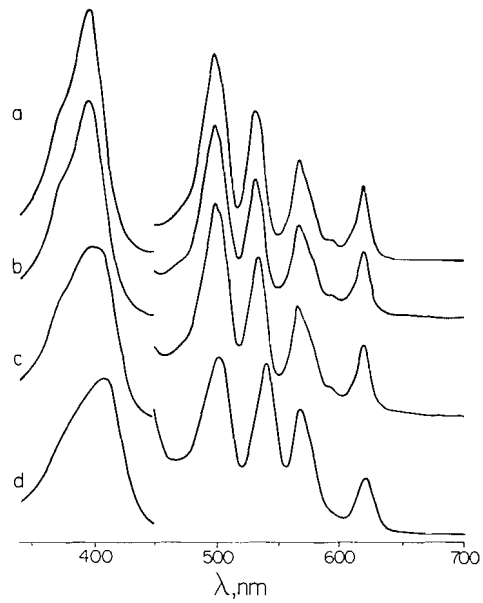

FIG. 1. Electronic spectra of free base porphyrins in CH_2Cl_2: *a* = etioporphyrin I, *b* = **1**, n = 8; *c* = **1**, n = 1, *d* = **1**, n = 0.

For the dimer **1** (n = 8) no changes are observed between its spectra, of both the free base and protonated cations, and those of etioporphyrin I, suggesting that the two porphyrin rings in this dimer (whose centres could be greater than 15 Å apart) do not interact. But in the n = 1 and n = 0 dimers, a significant effect on the Soret band is observed, including the appearance of two resolved bands in the dication case. To understand this it should be recalled that the Soret band of each dication monomer arises from doubly degenerate excited states X_1, Y_1 on one unit and X_2, Y_2 on the other. The

[1]Etioporphyrin I is 2,7,12,17-tetraethyl-3,8,13,18-tetramethylporphyrin and has the same substitution pattern as the dimers **7**, except that the bridging group in the dimer is replaced by an ethyl group.

TABLE 1. ^{13}C nmr shifts (in $CDCl_3$–TFA) relative to internal TMS

δ (ppm)									
$n = 0$	$n = 1$	$n = 3$	$n = 4$	$n = 5$	$n = 6$	$n = 7$	$n = 8$	Etioporphyrin I	Assignment
146.31	145.78	145.09	143.92	145.09	144.53	143.93	144.14	143.43	α and β
145.91	145.40								
145.51	145.09								
143.76[4]	142.92*	142.61		143.04	143.23				
143.44	142.14	142.44	142.34	142.37	142.84	142.54	142.94	142.34	
143.16[6]	141.96	142.01		142.15	142.25	142.25	142.24		
142.66	141.46*	141.81	141.96		142.08				
141.87	141.17	141.54	141.44	141.57	141.66	141.67	141.75	141.56	
141.48	140.67				141.37	141.38	141.37		
141.08									
139.62	139.19	138.98	137.92	138.72	138.31	137.63	137.91	136.74	
	138.91		137.33	138.41	137.91	137.24	137.53		
139.11	138.52								
132.33	138.21	138.41	137.15						
100.83	99.12	98.79	98.25	98.65	98.44	98.25	98.34	98.14	*Meso*
100.23	98.94								
99.35	98.53								
99.04	98.24								
		34.14†	32.08	32.20	32.00	32.27	32.17		Linking chain
				30.41†	29.84	29.44†	29.34		
						29.73	29.85		
	24.99†	26.95	26.56	26.78	26.78	26.70	26.77		
20.37	20.17	20.17	20.07	20.19	02.09	20.09	20.08	20.16	Ethyl
16.36	16.24	16.29	16.26	16.32	16.26	16.42	16.33	16.43	
16.08	15.93								
12.81	12.40								Methyl
11.90	11.79	11.77	11.71	11.81	11.72	11.82	11.71	11.80	
11.01	11.63				11.53				
	11.12								

*Degenerate peaks; superscript indicates probable number of carbons in coincidence. For $n \geq 3$, the amount of degeneracy of a given peak is not always ascertainable.
†Unique carbons for odd numbered carbon linkage.

exact interaction among the four excited states depends on the detailed geometry, which is not as yet known. But for a variety of geometries, to a first approximation the four states interact pairwise. Thus the four resulting dimer excited states are roughly of form $(X_1 \pm X_2)(2)^{-1/2}$ and $Y_1 \pm Y_2)(2)^{-1/2}$. The expected geometry for $n = 0$ would have the transition dipoles of one pair of states, call these X_1 and X_2, parallel to the vector $\boldsymbol{R}$ between centers; the allowed exciton state then is the one at lower energy. The transition dipoles for the other pair, call these Y_1 and Y_2, would be perpendicular to $\boldsymbol{R}$; here the allowed exciton state may be unshifted or blue shifted depending on the detailed orientation. This may account for the well-resolved doublet observed in the Soret band for the dication with $n = 0$. However, in the free base, the Soret states X_1, Y_1 are nondegenerate in the monomer, and the interaction with X_2, Y_2 will be far more complicated. Thus, only an unresolved, highly broadened Soret band is observed. Similar, though less well resolved transitions are observed for the dimer $n = 1$.

The electronic interaction between the two porphyrin rings in the dimers is also evident when examining their ^{13}C magnetic resonance spectra. The spectra were obtained from deuteriochloroform solutions containing an excess of trifluoracetic acid, to increase the solubility and allow the observation of α carbons by eliminating NH tautomerization (13).

For chain length ≥ 3, the porphyrin nucleii are largely pseudosymmetrical, as the charge-repulsion entailed by diprotonation of each macrocycle should tend to minimize the interaction. The 16 α and β carbons (of each porphyrin) which are in fact entirely nonequivalent, give 7 signals of varying degeneracy for $n = 4$, 5, 7, and 8, 9 signals for $n = 6$, 8 for $n = 3$ but 13 each for $n = 0$ or 1 (Table 1).

The *meso* carbons give only a single broad peak for all *n greater* than 2, but resolve into four well-defined peaks for *n less* than 2.

The substituent ethyl groups give single peaks at δ 16 and 20, and the methyls produce a singlet near 11.7 δ, when *n* greater than 2, with the anomalous exception of $n = 6$, which gives an additional methyl

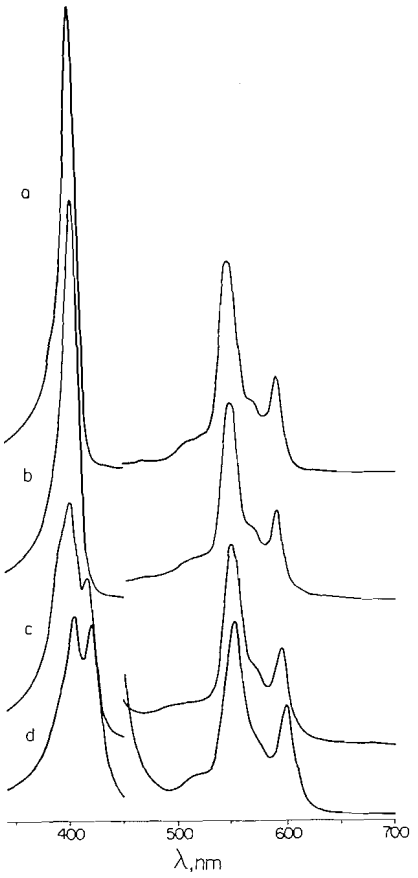

FIG. 2. Electronic spectra of *N,N*-diprotonated porphyrins in CH_2Cl_2–TFA: *a* = etioporphyrin I; *b* = **1**, *n* = 8; *c* = **1**, *n* = 1; *d* = **1**, *n* = 0.

peak at δ = 11.53. The cases *n* = 0 and 1 show an extra ethyl peak near 16, and three (*n* = 0) or four (*n* = 1) methyl peaks.

Thus only when the porphyrins are constrained to be proximate, are the interactions sufficiently strong to reduce the pseudodegeneracy. The *n* = 2 example is clearly of interest as the boundary point of these interactions but is as yet unavailable.

The linking chain itself is of interest: the termini, linked to the porphyrin, are shielded relative to the other carbons, and occur in the range 26.5–27 ppm, except for the *n* = 1 case, which appears even further upfield, at 25. The penultimate carbon is the farthest downfield, typically at 32–32.2 δ, except for the *n* = 3 case, where this carbon has a doubled relationship and is down to 34.1. Interior carbons occur in the 29.3–30.4 range. We anticipate that a more detailed analysis of these and other data on metallo-derivatives of the dimers reported here will give a greater insight into the conformation that these species can adopt, and upon the relationship between the distance and orientation of porphyrin chromophores, and the effect upon energy transfer between porphyrins as a function of the orientation and distance between the chromophores.

Acknowledgements

This work was supported by the United States National Institutes of Health (AM 14343, 16508) and the National Research Council of Canada.

1. C. K. CHANG, M.-S. KUO, and C.-V. WANG. J. Heterocycl. Chem. **14**, 943 (1977). In press.
2. J. P. COLLMAN, C. M. ELLIOTT, T. R. HALBERT, and B. S. TOVROG. Proc. Natl. Acad. Sci. U.S.A. **74**, 18 (1977).
3. J. A. ANTON and P. A. LOACH. J. Heterocycl. Chem. **12**, 573 (1975).
4. J. A. ANTON, K. KWONG, and P. A. LOACH. J. Heterocycl. Chem. **13**, 717 (1976).
5. H. OGOSHI, H. SUGIMOTO, and Z. YOSHIDA. Tetrahedron Lett. 169 (1977).
6. M. R. WASIELEWSKI, M. H. STUDIER, and J. J. KATZ. J. Phys. Chem. **81**, 577 (1977).
7. N. E. KAGAN, D. MAUZERALL, and R. B. MERRIFIELD. J. Am. Chem. Soc. **99**, 5484 (1977).
8. S. G. BOXER and G. L. CLOSS. J. Am. Chem. Soc. **98**, 5406 (1976).
9. L. L. SHIPMAN, T. M. COTTON, J. R. NORRIS, and J. J. KATZ. Proc. Natl. Acad. Sci. U.S.A. **73**, 1791 (1976).
10. F. P. SCHWARZ, M. GOUTERMAN, Z. MULJIANI, and D. H. DOLPHIN. Bioinorg. Chem. **2**, 1 (1972).
11. J. B. PAINE III and D. DOLPHIN. Can. J. Chem. This issue.
12. M. GOUTERMAN, D. HOLTEN, and E. LIEBERMAN. Chem. Phys. In press.
13. (*a*) R. J. ABRAHAM, G. E. HAWKES, and K. M. SMITH. J. Chem. Soc. Perkin Trans. II, **6**, 627 (1974); (*b*) R. J. ABRAHAM, G. E. HAWKES, M. F. HUDSON, and K. M. SMITH. J. Chem. Soc. Perkin Trans. II, **3**, 204 (1975).

Canadian Journal of Chemistry

Published by
THE NATIONAL RESEARCH COUNCIL OF CANADA

Volume 56 Number 13 July 1, 1978

Journal canadien de chimie

Publié par
LE CONSEIL NATIONAL DE RECHERCHES DU CANADA

Volume 56 numéro 13 1 juillet 1978

Can. J. Chem. Downloaded from www.nrcresearchpress.com by 210.87.254.6 on 09/05/12
For personal use only.

Long-range ^1H, ^{19}F spin–spin coupling constants in benzenesulfonyl fluoride and some of its derivatives. Insensitivity of ^{19}F shifts to *ortho* substituents

TED SCHAEFER AND WILLIAM J. E. PARR[1]

Department of Chemistry, University of Manitoba, Winnipeg, Man., Canada R3T 2N2

Received January 6, 1978

TED SCHAEFER and WILLIAM J. E. PARR. Can. J. Chem. **56**, 1717 (1978).

The proton and ^{19}F high resolution nuclear magnetic resonance spectra of benzenesulfonyl fluoride and of some derivatives are analyzed to yield spin–spin coupling constants between ^{19}F and the ring protons. These parameters display a marked dependence on the ring substituents and it is not clear how their conformational behaviour can be distinguished from intrinsic substituent perturbations. The large magnitudes of the couplings over six bonds to the *para* protons, relative to those in benzoyl fluoride, strongly indicate the importance of conformations in which the S—F bond does not lie in the benzene plane. The methyl group replacement technique suggests that the six-bond coupling contains contributions in addition to that from a σ–π mechanism. The chemical shift of the *para* proton yields a π electron density at the contiguous carbon atom which is considerably smaller than in nitrobenzene, for example. The ^{19}F shifts are much less sensitive to *ortho* substituents than are the ^{19}F shifts in benzoyl fluoride derivatives, implying much smaller intramolecular van der Waals interactions in the sulfonyl compounds.

TED SCHAEFER et WILLIAM J. E. PARR. Can. J. Chem. **56**, 1717 (1978).

On a analysé les spectres de résonance magnétique nucléaire à haute résolution du proton et du ^{19}F du fluorure de benzènesulfonyle et de quelques-uns de ses dérivés pour obtenir les constantes de couplage spin–spin entre le ^{19}F et les protons du cycle. Ces paramètres présentent une dépendance marquée sur les substituants du cycle et il n'est pas clair comment leur comportement conformationnel peut être distingué des perturbations intrinsèques dues aux substituants. Les très grandes valeurs des constantes de couplage à travers six liens avec les protons en *para*, relatives à celles obtenues dans le fluorure de benzoyle, indiquent d'une façon bien marquée l'importance des conformations dans lesquelles le lien S—F ne se trouve pas dans le plan du benzène. La technique du remplacement du groupe méthyle suggère que le couplage à travers six liaisons contient des contributions supplémentaires par rapport à celles du mécanisme σ–π. Le déplacement chimique du proton *para* indique la présence d'une densité électronique π au niveau de l'atome de carbone contigu qui est beaucoup plus faible que celle présente, par exemple, dans le nitrobenzène. Les déplacements chimiques du ^{19}F sont beaucoup moins sensibles aux substituants *ortho* que les déplacements chimiques du ^{19}F dans les dérivés du fluorure de benzoyle; ce résultat implique que des interactions de van der Waals intramoléculaires sont beaucoup plus faibles dans le cas des dérivés sulfonyles.

[Traduit par le journal]

Introduction

The long-range couplings between protons or ^{19}F nuclei on the side chain and protons or ^{19}F nuclei on the benzene ring are of interest in the elucidation of spin–spin coupling mechanisms (1), can often be used in the deduction of conformational preferences (ref. 2 and references therein) and even of small barriers to internal rotation (0–3 kcal/mol) about the bonds connecting the side chains to the benzene ring (3). Detailed measurements, frequently accompanied by semiempirical calculations, of the long-range couplings have been made for CH_3 (ref. 4 and references therein), CH_2X, where X = OH, F, Cl, Br, I, CH_3, etc.; cyclo-C_3H_5, CHX_2, SiH_3, SiH_2X,

[1]Postdoctoral fellow, 1974–1976.

Can. J. Chem. Downloaded from www.nrcresearchpress.com by 210.87.254.6 on 09/05/12
For personal use only.

TABLE 1. Spectral data for 3-nitrobenzenesulfonyl fluoride **3** as a 5 mol% solution in $CDCl_3$ and chemical shift data for benzenesulfonyl fluoride, **1**

Parameter	Value		Parameter	Value
ν_F	—	3686.02†	$^4J_{25}$	1.822(2)
ν_2*	885.887(4)‡	800.91	$^4J_{46}$	1.067(5)
ν_3	—	762.53	$^5J_{25}$	0.471(6)
ν_4	865.110(4)	776.96	$^4J_o^{H_2,SF}$	−0.314(8)
ν_5	792.986(4)	762.53	$^4J_o^{H_6,SF}$	−0.454(7)
ν_6	836.310(4)	800.91	$^5J_m^{H,SF}$	1.054(7)
$^3J_{45}$	8.294(5)§	—	$^6J_p^{H,SF}$	−0.568(7)
$^3J_{56}$	7.925(5)	—	Root mean	
$^4J_{24}$	2.223(5)	—	square deviation	0.012_5

*Proton chemical shifts in Hz at 100.001 MHz to low field of internal TMS at 305 K.
†This column refers to a 10 mol% solution of 1 in $CDCl_3$ and the shift of ^{19}F, ν_F is in Hz at 56.443 MHz to low field of internal $CFCl_3$.
‡The numbers in parentheses give the standard deviation in the last place.
§Coupling constants in Hz.

$SiHX_2$; CF_3, SiF_3; CHO, COF; OH, SH, SeH; and other side chains (2–11).

The couplings involving ^{19}F in the SO_2F moiety are available for three benzenesulfonyl fluoride derivatives, $C_6F_5SO_2F$ (12), 2,4,6-tri$(CH_3)C_6H_2$-SO_2F and 2,5-di$(F)C_6H_3SO_2F$ (13). In this paper we report full analyses of the proton and ^{19}F magnetic resonance spectra for benzenesulfonyl fluoride, **1**, and five of its derivatives, **2–6**.

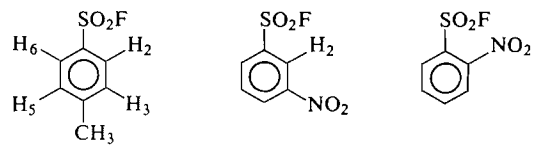

2 **3** **4**

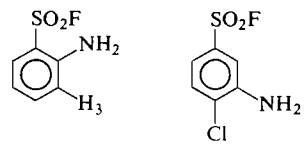

5 **6**

Experimental

Compound **1** was prepared from the sulfonyl chloride by treatment with aqueous KF, as was the *m*-nitro derivative. The other compounds were of commercial origin.

The ^{1}Hmr spectra of 5–10 mol% degassed solutions in $CDCl_3$ (but see Table 2) were recorded in the frequency sweep mode at 100.001 MHz on an HA100 spectrometer at 305 K. Repeated calibrations involved the reading of sweep and of lock oscillator frequencies at approximately 5 Hz intervals. The ^{19}F magnetic resonance spectra were similarly calibrated at 56.443 MHz on a DA60I spectrometer at 302 K. The samples contained tetramethylsilane and $CFCl_3$ as internal lock sources.

The relative signs of the $^1H,^{19}F$ coupling constants were determined by double resonance experiments (14) and have been related to $^1H,^{19}F$ couplings within the ring of the 2,5-difluoro compound (13), so that their absolute signs are fairly certain.

Results and Discussion

Spectral Analyses

These proceeded in a straightforward manner according to the computer program LAME (15, 16). In Table 1, the spectral parameters for 3-nitrobenzenesulfonyl fluoride are tabulated, giving an idea of the precision of the analyses. Rather than tabulate all parameters for the other compounds (the ring proton shifts for **1** being available in Table 1), the coupling constants to ^{19}F and its shift relative to internal $CFCl_3$ are presented in Table 2. These data are most pertinent to the following discussion.

Ring Proton Parameters

The shift of the *para* proton, δ_4, of 8.01 ppm downfield of TMS for **1**, is considerably larger than that for nitrobenzene, 7.65 ppm (17), or benzoyl fluoride, 7.64 ppm (18) in CCl_4. These data suggest that the SO_2F group withdraws π electron density from C4 to a significantly greater degree than do the NO_2 or COF groups. The shift of C_6H_6 can be taken as 7.25 ppm, so that SO_2F is a somewhat stronger π electron withdrawer than NH_2 is a donor, δ_4 being 6.62 ppm is aniline (17). A proton chemical shift of about 11 ppm/π electron at the contiguous carbon (19) indicates an increase in electron density of about 0.13 electrons in going from **1** to aniline. Recent *ab initio* calculations yield a difference of 0.087 electron at C4 in aniline and nitrobenzene (20), in decent agreement with the above considerations (a proportionality factor of 12 ppm/π electron gives almost exact agreement with the observed shift difference of 1.03 ppm but may be fortuitous). In any event, it appears that the SO_2F group reduces the π electron density at the *para* position by 0.06–0.07 electrons when allowance is made for slight differential solvent shifts between CCl_4 and $CDCl_3$ (21).

The plethora of ring proton shifts and coupling

TABLE 2. $^1H,^{19}F$ spin–spin coupling constants and ^{19}F chemical shifts in **1–6** and in 2,5-difluorobenzenesulfonyl fluoride, 7

Parameter	Value*						
	1	**2**	**3**	**4**	**5**	**6**	**7**
ν_F†	3686.0	3707.9	—	3640.2	3571.6	3674.7	3594.4
$^4J_o^{H_2,SF}$	−0.56‡	−0.59	−0.31	—	—	−0.37	—
$^4J_o^{H_6,SF}$	−0.56	−0.59	−0.45	−0.82(0.82)§	−0.46	−0.67	−0.23
$^5J_m^{H_3,SF}$	1.04	0.99	—	0.38(0.38)	0.80	—	0.78
$^5J_m^{H_5,SF}$	1.04	0.99	1.05	0.37(0.34)	1.07	1.07	—
$^6J_p^{H_4,SF}$	−0.67	1.01‖	−0.57	−1.09(−1.13)	−0.66	—	−0.58

*In 5–10 mol% solutions in $CDCl_3$ unless otherwise stated.
†In Hz at 56.443 MHz to low field of internal $CFCl_3$ at 302 K.
‡Coupling constants in Hz, accuracy 0.02 Hz.
§Values in parentheses for a C_6D_6 solution.
‖$^7J_p^{CH_3,SF}$.

constants within the ring will not be further discussed. The data will be forwarded on request.

Substituent and Conformational Dependence of Coupling Constants to ^{19}F

The couplings to *ortho* and *meta* protons in **1**, of −0.56 and 1.04 Hz, respectively, are similar to those in benzoyl fluoride, viz., −0.60 and 1.33 Hz (5). Both couplings are strongly dependent on the presence of ring substituents, e.g., $^5J_m^{H,SF}$ sinks to 0.38 Hz in the presence of an *ortho*-nitro group (Table 2) in both C_6D_6 and $CDCl_3$ solutions. Apparently it would be difficult to separate the substituent from the conformational dependence of these coupling constants.

Part of the complexity arises from our ignorance of the conformational preferences of the SO_2F group. An STO-3G calculation (22), using a regular geometry for the benzene ring and the SO_2F geometry previously described (13), gave **8** as 3.2 kcal/mol higher in energy than **9**; **10** was of intermediate

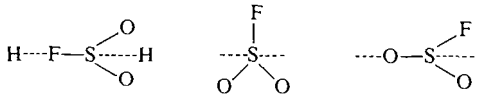

8 **9** **10**

energy. These calculations suggest that $^6J_p^{H,SF}$ should be finite and negative if it arises via a σ–π mechanism (4, 23); just as $^6J_p^{H,CF}$ should vanish in benzoyl fluoride, as it does (5), because the C—F bond prefers the benzene plane by some 4 kcal/mol (24). The σ–π coupling increases in magnitude as $\sin^2\theta$, where θ is the angle by which the S—F bond twists out of the benzene plane.

The observed $^6J_p^{H,SF}$ in **1** is −0.67 Hz (Table 2). However, the σ–π mechanism also implies that replacement of the *para* proton by a methyl group should entail (25–27) $-^6J_p^{H,SF} \simeq {}^7J_p^{CH_3,SF}$. Yet the latter is +1.01 Hz in **2**, of the correct sign but much too large (assuming a *para*-methyl group does not alter the SO_2F conformational preferences). As ^7J does presumably measure the σ–π contribution to ^6J (11, 25–27), it follows that ^6J contains a positive σ electron contribution[2] of about 0.34 Hz. Its angle dependence is not known. Consequently, any hope of using ^6J in the determination of barriers to internal rotation (3, 28) in **1** or its derivatives is probably a forlorn one.

Furthermore, $^6J_p^{H,SF}$ becomes −1.1 Hz in the presence of an *ortho*-nitro group, whereas it remains unchanged in the presence of an *ortho*-amino substituent and changes only slightly on introduction of an *ortho*-fluorine atom (Table 2). Because of the σ electron contribution, it is not possible to decide whether the nitro group exerts an intrinsic substituent effect on this component of ^6J or on the σ–π component, or if it indeed forces the S—F bond farther towards a plane perpendicular to the benzene ring. These complexities stand in sharp contrast to the behaviour of $^6J_p^{H,CH}$ in toluene derivatives (3, 4, 7), which displays only a $\sin^2\theta$ dependence and a minimal dependence on the electronic properties of the ring substituent.

It does appear that the S—F bond spends considerable time away from the benzene plane but the present coupling data cannot confirm the STO-3G predictions of relatively strong conformational preferences. The coupling data are also consistent with weak conformational preferences of the SO_2F group.

The ^{19}F Chemical Shifts

These occur some 40 ppm to low field of the shifts in benzoyl fluoride derivatives (29). The range of

[2]If couplings over six bonds between ^{19}F on a side chain and a ring proton contain σ electron contributions, then previous assumptions about such couplings in benzyl fluoride (28) are incorrect. These problems are under investigation.

Can. J. Chem. Downloaded from www.nrcresearchpress.com by 210.87.254.6 on 09/05/12
For personal use only.

2.3 ppm in the shifts (Table 2) contrasts sharply with the lowfield shift of up to 35 ppm experienced by ^{19}F in *ortho*-substituted benzoyl fluoride derivatives (30). The latter are very likely caused by strong intramolecular van der Waals interactions between the fluorine atom in the COF group and the *ortho* substituents. Such interactions are highly sensitive to interatomic distances. The preferred planar conformation of benzoyl fluoride (24) favors small distances between the fluorine atom and the *ortho* substituents.

Accordingly, the relative insensitivity to *ortho* substituents of the ^{19}F shifts in the sulfonyl fluorides suggests that the S—F bond can easily avoid the *ortho* groups; although, as indicated by $^{6}J_{p}^{H,SF}$, the S—F bond is not forced into conformations analogous to **8**.

Acknowledgments

We are grateful to the National Research Council of Canada for financial assistance.

1. M. Barfield and B. Chakrabarti. Chem. Rev. **69**, 757 (1969).
2. W. Danchura, T. Schaefer, J. B. Rowbotham, and D. J. Wood. Can. J. Chem. **52**, 3986 (1974).
3. W. J. E. Parr and T. Schaefer. J. Am. Chem. Soc. **99**, 1033 (1971).
4. R. Wasylishen and T. Schaefer. Can. J. Chem. **50**, 1852 (1972).
5. R. J. Kostelnik, M. P. Williamson, D. E. Wisnosky, and S. M. Castellano. Can. J. Chem. **47**, 3313 (1969).
6. M. Barfield, C. J. Macdonald, I. R. Peat, and W. E. Reynolds. J. Am. Chem. Soc. **93**, 4195 (1971).
7. W. J. E. Parr and T. Schaefer. J. Magn. Reson. **25**, 167, 171 (1977).
8. W. J. E. Parr and T. Schaefer. Can. J. Chem. **55**, 557 (1977).
9. T. Schaefer and W. J. E. Parr. J. Chem. Phys. **65**, 1197 (1976).
10. T. Schaefer, J. B. Rowbotham, and K. Chum. Can. J. Chem. **54**, 3666 (1976).
11. T. Schaefer, L. J. Kruczynski, and W. J. E. Parr. Can. J. Chem. **54**, 3210 (1976).
12. P. Meakin, D. W. Ovenall, W. A. Sheppard, and J. P. Jesson. J. Am. Chem. Soc. **97**, 522 (1975).
13. W. J. E. Parr and T. Schaefer. Can. J. Chem. **54**, 3564 (1976).
14. R. Freeman and W. A. Anderson. J. Chem. Phys. **37**, 2053 (1962).
15. S. Castellano and A. A. Bothner-By. J. Chem. Phys. **41**, 3863 (1964).
16. C. W. Haigh and J. M. Williams. J. Mol. Spectrosc. **32**, 398 (1969).
17. C. Castellano, C. Sun, and R. Kostelnik. Tetrahedron Lett. **51**, 5205 (1967).
18. C. Castellano *in* W. Brügel. Nuclear magnetic resonance spectroscopy and chemical structure. Academic Press, New York, NY. 1967.
19. T. Schaefer and W. G. Schneider. Can. J. Chem. **41**, 966 (1963).
20. W. J. Hehre, L. Radom, and J. A. Pople. J. Am. Chem. Soc. **94**, 1496 (1972).
21. A. D. Buckingham, T. Schaefer, and W. G. Schneider. J. Chem. Phys. **32**, 1227 (1960).
22. W. J. Hehre, R. F. Stewart, and J. A. Pople. J. Chem. Phys. **51**, 2657 (1969).
23. C. Heller and H. M. McConnell. J. Chem. Phys. **32**, 1535 (1960).
24. R. K. Kakar. J. Chem. Phys. **56**, 1189 (1972).
25. R. A. Hoffman. Mol. Phys. **1**, 326 (1958).
26. C. J. Macdonald and W. F. Reynolds. Can. J. Chem. **48**, 1002 (1970).
27. J. B. Rowbotham and T. Schaefer. Can. J. Chem. **52**, 489 (1974).
28. T. Schaefer, J. B. Rowbotham, W. J. E. Parr, K. Marat, and A. F. Janzen. Can. J. Chem. **54**, 1322 (1976).
29. H. Bildsøe and K. Schaumburg. J. Magn. Reson. **14**, 223 (1974).
30. T. Schaefer, K. Marat, K. Chum, and A. F. Janzen. Can. J. Chem. **55**, 3936 (1977).

Can. J. Chem. Downloaded from www.nrcresearchpress.com by 210.87.254.6 on 09/05/12
For personal use only.

The internal barriers to rotation about the carbon–carbon bond in 3,5-dichlorobenzyl alcohol and selenol by the *J* method

TED SCHAEFER, WERNER DANCHURA, WALTER NIEMCZURA, AND WILLIAM J. E. PARR

Department of Chemistry, University of Manitoba, Winnipeg, Man., Canada R3T 2N2

Received January 17, 1978

TED SCHAEFER, WERNER DANCHURA, WALTER NIEMCZURA, and WILLIAM J. E. PARR. Can. J. Chem. **56**, 1721 (1978).

The *J* method, depending on a comparison between observed spin–spin coupling constants over six bonds between protons on a side chain and *para* ring protons and those calculated by a hindered rotor treatment, is applied to the determination of the twofold barrier to internal rotation about the carbon–carbon bonds in 3,5-dichlorobenzyl alcohol and selenol. In the alcohol, the C—O bond prefers the benzene plane by 0.3 ± 0.2 kcal/mol whereas, in the selenol, the C—Se bond prefers a plane perpendicular to the benzene ring by 3.8 ± 0.7 kcal/mol. Comparison with the thiol suggests that a major component of the barrier arises from repulsive interactions, increasing as the size of the XH (X = O, S, Se) group increases.

TED SCHAEFER, WERNER DANCHURA, WALTER NIEMCZURA et WILLIAM J. E. PARR. Can. J. Chem. **56**, 1721 (1978).

On a appliqué la méthode *J*, qui dépend d'une comparaison entre les constantes de couplage spin–spin observées à travers six liaisons entre des protons d'une chaîne latérale et les protons du cycle en position *para* et les constantes calculées par un traitement de rotor empêché, à la détermination de la barrière binaire à la rotation interne autour des liens carbone–carbone des alcool et sélénol du dichloro-3,5 benzyle. Dans l'alcool, le lien C—O préfère la conformation dans le plan du benzène par 0.3 ± 0.2 kcal/mol alors que dans le sélénol le lien C—Se préfère une conformation perpendiculaire au plan du cycle benzénique par 3.8 ± 0.7 kcal/mol. Une comparaison de ces données avec celles obtenues avec les thiols suggère qu'une composante importante à la barrière à la rotation provient d'interactions de répulsion dont l'importance croît à mesure que la grosseur du groupe XH (X = O, S, Se) augmente.

[Traduit par le journal]

Introduction

In a recent application of the *J* method, a value of 1.8 ± 0.2 kcal/mol was estimated for the twofold barrier to internal rotation about the carbon–carbon bond in 3,5-dichlorobenzyl mercaptan (1). Conformation **1** was demonstrated to be the reasonable low-energy form, with **2** as the conformation of high energy.

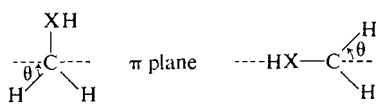

θ = 30° **1** θ = 60° **2**

The *J* method for the determination of small twofold barriers depends on the experimental (2, 3) and theoretical (4) knowledge that $^6J_p^{H,CH}$, the spin–spin coupling constant over six formal bonds between the side-chain proton and the *para* ring proton, is proportional to $\langle \sin^2\theta \rangle$, the average or expectation value of $\sin^2\theta$. The angle θ measures the out-of-plane twist of the C—H bond containing the coupled proton. Application of a hindered rotor formalism (5) leads (6) to a value of $\langle \sin^2\theta \rangle$ as a function of internal barrier, temperature, and the reduced moment of inertia about the bond around which rotation occurs; being quite insensitive to the last parameter. A knowledge of $^6J_{90}$, the six-bond coupling for a conformation in which the side-chain C—H bond lies in a plane perpendicular to the benzene plane, is also required.

The presence of the chlorine atoms at the *meta* positions does not perturb $^6J_p^{H,CH}$ (7, 8) and allows a more accurate determination of this quantity; benzyl systems normally giving rise to very tightly coupled phenyl ring ^{1}H nmr spectra at 100 MHz.

If the barrier in 3,5-dichlorobenzyl mercaptan is determined mainly by steric interactions in **2**, it follows that in the benzyl alcohol the barrier should be considerably reduced and that in the benzyl selenol a higher barrier should exist. Indeed, *ab initio* molecular orbital calculations at the STO3G level (9) suggest that the C—O bond in benzyl alcohol prefers the benzene plane to the extent of 0.22 kcal/mol, perhaps because C—O hyperconjugation is less effective in lowering the energy than is C—H hyperconjugation.

In this paper, the *J* method is applied to the determination of the internal barrier in the alcohol and the selenol. It turns out that the barriers lie at the low and high extremes at which the *J* method becomes insensitive to the actual barrier. Nevertheless, useful

Can. J. Chem. Downloaded from www.nrcresearchpress.com by 210.87.254.5 on 09/05/12
For personal use only.

Can. J. Chem. Downloaded from www.nrcresearchpress.com by 210.87.254.5 on 09/05/12
For personal use only.

conclusions about conformational energetics can be made.

Experimental

The 3,5-dichlorobenzyl alcohol was prepared from the commercial benzoic acid by reduction with $LiAlH_4$. The bromide followed by treatment with PBr_3. The 3,5-dichlorobenzyl selenol was synthesized from the bromide via the Grignard reagent, exactly following the procedure given for the preparation of phenyl selenol (10). The ^1H nmr spectra left no doubt about the identity of the alcohol and selenol.

^1H nmr spectra of the benzyl alcohol were recorded for a 5 mol% solution in C_6D_6 and for a 1 mol% solution in CS_2, whereas, for reasons of spectral dispersion, the selenol had its spectrum recorded as a 10 mol% solution in C_6D_6. All solutions were degassed by the freeze–pump–thaw technique and contained a small amount of internal TMS. Spectra were repeatedly calibrated by interpolation between markers placed at 5 Hz intervals in the frequency sweep mode of an HA100 spectrometer at a probe temperature of 305 K. At sweep rates of 0.02 and 0.01 Hz/s and a dispersion of 1 Hz/cm, this procedure yielded peak positions with a standard deviation comparable to that between calculated and observed spectra in the spectral analyses.

Results and Discussion

Spectral Analyses

Performed by means of the computer program LAME (11, 12), the analyses gave the spectral parameters in Table 1. The standard deviations of well below 0.01 Hz suggest an accuracy of at least 0.02 Hz in the parameters of greatest interest, viz. $^6J_p^{H,CH}$. It may be noted that $^6J_p^{H,CH_2}$ was -0.59 Hz for the alcohol in both CS_2 and C_6D_6 solutions. Because the OH and SeH protons do not couple to the ring protons the spectra are easily assigned as AB_2X_2R spin systems.

The Barriers and Conformations

3,5-Dichlorobenzyl Alcohol

The value of $^6J_p^{H,CH}$ is -0.59 Hz in both CS_2 and C_6D_6 solutions, at concentrations differing by a factor of 5, suggesting that intermolecular association is ineffective at altering this coupling constant. This is not to say that the barrier in the liquid state must be the same as in the gaseous state.

In previous work it was argued that the substituent in the methyl group reduces the magnitude of $^6J_{90}^{H,CH}$ if it is much more electronegative than hydrogen (8). The reduction can occur because the localization of the π type molecular orbitals of the CH_2OH group is greater than in the CH_3 group (13). A value of -1.14 Hz for CH_2Cl led to a reasonable barrier in benzyl chloride, and was estimated on the basis of a monotonic relationship between $^6J_{90}^{H,CH}$ and electronegativity. A linear extrapolation (E_H = 2.1, E_{Cl} = 3.0, E_{OH} = 3.5) yields $^6J_{90}^{H,CH}$ as -1.08_5 Hz for CH_2OH. In that situation, $\langle \sin^2 \theta \rangle$ becomes 0.54 ($0.59/1.08_5$) and the internal barrier is 0.4 ± 0.2 kcal, where an error of 0.02 is assumed in $\langle \sin^2 \theta \rangle$.

An alternative approach to $^6J_{90}^{H,CH}$ for CH_2OH takes the value of -1.09 Hz for CH_2F calculated (6) by INDO–MO–FPT (14). These calculations are successful in finding reasonable values for the β-proton hyperfine coupling constants in the β-fluoroethyl radical; such couplings are also transmitted via a σ-π mechanism (15). Furthermore, the calculations exactly reproduce the magnitude and $\langle \sin^2 \theta \rangle$ dependence of $^6J_p^{H,CH_3}$ in toluene (4). In this situation, $^6J_{90}^{H,CH}$ is -1.13 Hz, $\langle \sin^2 \theta \rangle$ becomes 0.52 and the internal barrier is 0.1 ± 0.2 kcal/mol.

In both instances, the stable form is **2**. If the stable form were **1**, $\langle \sin^2 \theta \rangle$ would be <0.5. Such a situation could be achieved if $^6J_{90}^{H,CH}$ for CH_2OH had a magnitude of greater than 1.18 Hz, i.e., $>0.59/0.5$ Hz. If, in fact, $^6J_{90}^{H,CH}$ were unchanged from its value of -1.24 Hz in toluene,[1] then $\langle \sin^2 \theta \rangle$ would be 0.47_6 and the internal barrier would be 0.2 ± 0.2 kcal/mol, with **1** most stable.

Abraham and Bakke (16, 17) show that the hydroxyl proton chemical shift and the geminal proton coupling constant in benzyl alcohol itself are consistent either with free rotation about the C—C bond or with a conformation in which the C—O bond is rotated by 60° out of the benzene plane. Such a conformation implies that $\langle \sin^2 \theta \rangle$ varies between 0.37_5 for a very large barrier (>3 kcal/mol) and 0.50 for a vanishing barrier. If $^6J_{90}$ is in fact equal to -1.24 Hz, then this conformation as the ground state, but with a barrier to rotation of about 0.5 kcal/mol, is compatible with our coupling data.

In our opinion, the coupling data are best fitted by 0.3 ± 0.2 kcal/mol for the twofold barrier to internal rotation in 3,5-dichlorobenzyl alcohol, **2** being the most stable conformation, in perhaps accidental agreement with STO-3G calculations on benzyl alcohol.

3,5-Dichlorobenzyl Selenol

The value of $^6J_p^{H,CH}$ is -0.37 Hz, yielding $\langle \sin^2 \theta \rangle$ as 0.29_7 if $^6J_{90}^{H,CH}$ is -1.24 Hz; or, if the electronegativity of the SeH· group is taken as 2.4, then $^6J_{90}^{H,CH}$ is -1.21 Hz according to the discussion given for CH_2OH and $\langle \sin^2 \theta \rangle$ is 0.30_4. For a very large barrier, $\langle \sin^2 \theta \rangle$ would be 0.25 for **1** as the ground state conformation. In other words, the barrier is substantial and in a region where the J method is rather insensitive to the barrier. The plot of $\langle \sin^2 \theta \rangle$ vs. barrier yields 3.8 ± 0.7 kcal/mol for

[1]Coupling constant data for compounds of known conformation indicate that the estimated $^6J_{90}$ values are reasonably good (S. Sternhell and C. Fallick. Private communication).

TABLE 1. Proton chemical shifts[a] and coupling constants for 3,5-dichlorobenzyl alcohol and selenol at 305 K

Parameter	Value OH[b]	Value SeH[c]	Parameter	Value OH	Value SeH
ν_{XH}	195.020(5)[d]	−40.299(3)[e]	$^4J_{24}{}^{H,H}$	1.917(5)	1.894(3)
ν_{CH_2}	456.130(6)	298.829(4)	$^4J_o{}^{H,CH_2}$	−0.775(6)	−0.487(4)
ν_2	712.593(5)	674.949(3)	$^6J_p{}^{H,CH_2}$	−0.588(7)[f]	−0.368(3)
ν_4	714.956(5)	694.668(2)	Root mean square		
$^3J^{XH,CH_2}$	5.951(6)	6.804(3)	deviation	0.019	0.012

[a]In Hz at 100 MHz to low field of internal TMS and 305 K.
[b]For a 1 mol% solution in CS_2.
[c]For a 10 mol% solution in C_6D_6.
[d]The numbers in parentheses give the standard deviations in the last place.
[e]To high field of internal TMS.
[f]$^6J_p{}^{H,CH_2}$ for a 5 mol% solution in C_6D_6 was −0.585(7) Hz.

an error of 0.02 in $\langle \sin^2 \theta \rangle$. It seems certain that the barrier is larger than 3 kcal/mol.

An alternative ground state conformation might have been **3**, for which $\langle \sin^2 \theta \rangle$ would have varied

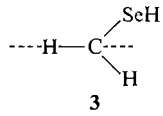

3

between 0.5 for zero barrier and 0.375 for a very large barrier, i.e., the observed $^6J_p{}^{H,CH}$ would have fallen between −0.62 and -0.46_5 Hz. Therefore **3** need not be considered because the observed $^6J_p{}^{H,CH}$ is −0.37 Hz.

The derived barriers for the series OH, SH, and SeH are 0.3 ± 0.2, 1.8 ± 0.2, and 3.8 ± 0.7 kcal/mol, respectively, the value for SH having the lowest percentage error because the J method is most accurate for barriers between about 0.8 and 2.2 kcal/mol when **1** is the low energy conformation. It appears that the sizes of the substituent and, therefore, repulsive forces, play a major role in these barriers. Furthermore, the barriers for the corresponding CH_2F (6), CH_2Cl, and CH_2Br (8) compounds display a similar gradation.

Acknowledgments

We are grateful to Dr. R. J. Abraham and to Dr. S. Sternhell for the communication of data prior to publication. The National Research Council of Canada provided financial support.

1. T. SCHAEFER and W. J. E. PARR. J. Chem. Soc. Faraday Trans. II, **73**, 1501 (1977).
2. C. J. MACDONALD and W. F. REYNOLDS. Can. J. Chem. **48**, 1002 (1970).
3. J. B. ROWBOTHAM and T. SCHAEFER. Can. J. Chem. **52**, 489 (1974).
4. R. WASYLISHEN and T. SCHAEFER. Can. J. Chem. **50**, 1852 (1972).
5. P. B. AYSCOUGH, M. C. PRICE, and R. E. D. MCCLUNG. Mol. Phys. **20**, 41 (1971).
6. T. SCHAEFER, J. B. ROWBOTHAM, W. J. E. PARR, K. MARAT, and A. F. JANZEN. Can. J. Chem. **54**, 1322 (1976).
7. H. ROTTENDORF and S. STERNHELL. Aust. J. Chem. **17**, 1315 (1964).
8. T. SCHAEFER, L. J. KRUCZYNSKI, and W. J. E. PARR. Can. J. Chem. **54**, 3210 (1976).
9. W. J. HEHRE, L. RADOM, and J. A. POPLE. J. Am. Chem. Soc. **94**, 1496 (1972).
10. D. G. FOSTER. Org. Syn. **24**, 89 (1944).
11. S. CASTELLANO and A. A. BOTHNER-BY. J. Chem. Phys. **41**, 3863 (1964).
12. C. W. HAIGH and J. M. WILLIAMS. J. Mol. Spectrosc. **32**, 398 (1969).
13. R. HOFFMAN, L. RADOM, J. A. POPLE, P.v.R. SCHLEYER, W. J. HEHRE, and L. SALEM. J. Am. Chem. Soc. **94**, 6221 (1972).
14. J. A. POPLE and D. L. BEVERIDGE. Approximate molecular orbital theory. McGraw-Hill Book Company, New York, NY. 1970.
15. K. S. CHEN, P. J. KRUSIC, P. MEAKIN, and J. K. KOCHI. J. Phys. Chem. **78**, 2014 (1974).
16. R. J. ABRAHAM and J. M. BAKKE. Org. Magn. Reson. In press.
17. R. J. ABRAHAM and J. M. BAKKE. To be published.

Can. J. Chem. Downloaded from www.nrcresearchpress.com by 210.87.254.5 on 09/05/12
For personal use only.

A novel acid-catalyzed isomerization of the adducts of 1,4-dimethyl-2,3-diphenylcyclopentadiene and dialkyl azodicarboxylates

LÊ H. DAO[1] AND DONALD MACKAY

The Guelph–Waterloo Centre for Graduate Work in Chemistry, Waterloo Campus, Department of Chemistry, University of Waterloo, Waterloo, Ont., Canada N2L 3G1

Received October 7, 1977

LÊ H. DAO and DONALD MACKAY. Can. J. Chem. **56**, 1724 (1978).

The adduct (**4***a*) of 1,4-dimethyl-2,3-diphenylcyclopentadiene with dimethyl azodicarboxylate is isomerized by one or more equivalents of trifluoroacetic acid to the exocyclic alkene **5***a*. The di-*tert*-butyl analogue **4***b* is isomerized by limited amounts of trifluoroacetic acid to a mixture of **5***b* and the oxadiazine **10**, the latter being the only product with 1 equiv. of acid; **5***b* can be made more efficiently from **4***b* by the action of pyridine or triethylamine. Excess acid converts **4***b*, **5***b*, or **10** to the oxadiazinone **7**. A protonated intermediate derived from **4***b* is postulated as the precursor to both **5***b* and **7** in acid, a view supported by deuterium labelling studies.

LÊ H. DAO et DONALD MACKAY. Can. J. Chem. **56**, 1724 (1978).

L'adduit (**4***a*) du diméthyl-1,4 diphényl-2,3 cyclopentadiène avec l'azodicarboxylate de diméthyle peut être isomérisé par un ou plusieurs équivalents d'acide trifluoroacétique pour conduire à l'alcène exocyclique **5***a*. L'analogue di-*tert*-butyle **4***b* peut être isomérisé par des quantités faibles d'acide trifluoroacétique pour conduire à un mélange de **5***b* et d'oxadiazine **10**; ce dernier composé est le seul produit lorsque l'on traite **4***b* par un équivalent acide. On peut obtenir **5***b* d'une façon plus efficace à partir de **4***b* par l'action de la pyridine ou de la triéthyl amine. Le traitement de **4***b*, **5***b* ou **10** par de l'acide en excès conduit à l'oxadiazinone **7**. On fait l'hypothèse qu'un intermédiaire protoné dérivé de **4***b* serait le précurseur aussi bien de **5***b* que de **7** en milieu acide; cette hypothèse est supportée par des études de marquages au deutérium.

[Traduit par le journal]

The role of the substituents X, R_1, R_2, and R_3 in the thermal and acid-catalyzed isomerizations of **1** has been discussed in some detail (1). In particular the rate enhancement trends X = CO > X = CH_2 and R_1 = alkyl or aryl > R_1 = alkoxy or aryloxy have been clearly established (1*e*). Thus *N*-acyloxy groups, unlike their *N*-acyl counterparts, were thermally unreactive in the adducts of cyclopentadiene (**1**, X = CH_2, R_2 = R_3 = H) but participated readily in the thermal or acid-catalyzed isomerization of the adducts of 2,5-dimethyl-3,4-diphenylcyclopentadienone (**1**, X = CO, R_2 = Me, R_3 = Ph) to give both the oxadiazines **2** and the diazetidines **3** (1*c*).

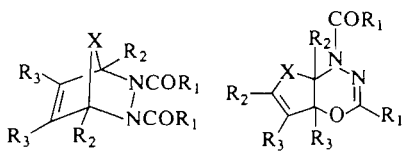

1

2

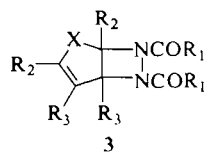

3

We now wish to describe briefly the intermediate case, with the methyl and phenyl substituents but with CH_2 rather than CO in the bridge (**1**, X = CH_2, R_2 = Me, R_3 = Ph). Specifically we have studied the dimethyl and di-*tert*-butyl esters **4***a* and *b* which show that yet another isomerization pathway is available to bridged pyridazine systems like **1**.

The expected Diels–Alder reaction between 1,4-dimethyl-2,3-diphenylcyclopentadiene and dimethyl or di-*tert*-butyl azodicarboxylate occurred readily (the former reaction is extremely fast) in benzene, or in carefully purified chloroform or carbon tetrachloride.[2] The spectroscopic properties of the adducts **4***a* (mp 162–163°C) and **4***b* (mp 157.5–159°C), fully supported the assigned structures, in particular the *C*- and *O*-methyl singlets in the ^{1}Hmr spectra.

In the absence of traces of acid or base, the adducts **4** were thermally much more stable than their carbonyl bridged counterparts. Thus when heated in hydrocarbon solvents at reflux they showed little reaction in toluene but were decomposed slowly in xylene and rapidly in decalin.

Heating **4***a* in benzene containing 1 equiv. or more of trifluoroacetic acid (TFA) resulted in the formation of a glassy isomer (90% yield by ^{1}Hmr analysis).

[1]Present address: Department of Chemistry, York University, Downsview, Ont.

[2]Stock reagents caused isomerization of the adducts, very rapidly in the case of **4***a*, perhaps owing to traces of acid in the solvents.

Can. J. Chem. Downloaded from www.nrcresearchpress.com by 210.87.254.5 on 09/05/12
For personal use only.

Can. J. Chem. Downloaded from www.nrcresearchpress.com by 210.87.254.5 on 09/05/12
For personal use only.

Its ir spectrum (CCl_4) had NH absorptions at 3420 and two ester carbonyl absorptions at 1768 and 1732 cm^{-1}. Of note in its ^{1}Hmr spectrum ($CDCl_3$) were two methoxy singlets at 6.32 and 6.26, a *tert*-methyl singlet at 8.45, a widely separated methylene AB pair, the low field proton obscured by the ester groups, the high field one at 7.18, and two broad absorptions for one proton each at 5.05 and 5.15 τ. The latter absorptions were strongly indicative of a double bond exocyclic to methylene. The most reasonable structure for this isomer is **5***a*, supported by its ready hydrogenation (Pd–C) to a dihydro derivative **6***a*, whose ^{1}Hmr spectrum showed a distorted methyl doublet (second order), a complex tertiary proton absorption, and the absence of vinylic absorptions.

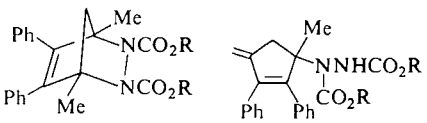

4 **5**

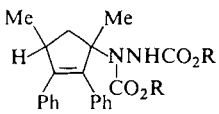

6

a R = Me
b R = CMe_3

The reaction of **4***b* in the presence of TFA was more complex. A solution at room temperature in neat TFA, or in carbon tetrachloride containing more than 1 equiv. of TFA, gave rapidly and quantitatively a compound $C_{25}H_{28}N_2O_4$ of mp 153.5–154.5°C, corresponding to the loss of C_4H_8. Structure **7** could be confidently assigned to this product, both by analogy with the product (**9**) of acid dealkylation of the three isomeric adducts from 2,5-dimethyl-3,4-diphenylcyclopentadienone and dimethyl azodicarboxylate (1*d*), and by its spectra. The ^{1}Hmr pattern derived from the carbocyclic ring resembled that observed in earlier work (1*d*, and *e*) with this ring system. The ir spectrum had, as well as NH absorption, two carbonyl bands at 1784 and 1763 cm^{-1}, attributable to the exo- and endocyclic ester groups, respectively; the value for the latter is more consistent with the six- than with a five-membered ring alternative (2), as in isomer **8**.

The formation of **7** from **4***b* parallels exactly that of **9** from **1** (R_1 = OMe, R_2 = Me, R_3 = Ph, X = CO) with excess TFA; in that case, if limited amounts of TFA were used, isomerization to the 1,3,4-oxadiazine and 1,2-diazetidine was observed to compete with solvolysis (1*d*). Examination by ^{1}Hmr spectroscopy of the reaction of **4***b* in scrupulously

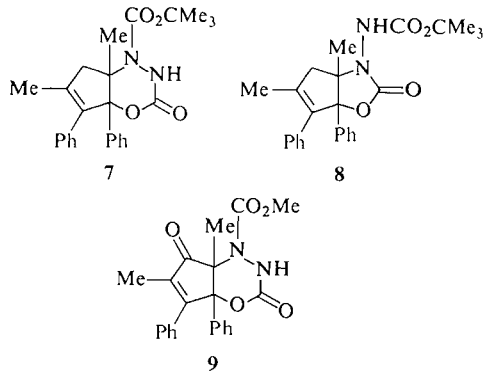

7 **8**

9

dry benzene-d_6 with limited amounts (0.05–1 equiv.) of TFA showed the formation of two isomers. One of these, in amounts never exceeding 25% of product, was readily recognized as the diene **5***b* by the exo- and endocyclic methylene ^{1}Hmr pattern characteristic of **5***a*; as more acid was added these peaks disappeared. The major isomer, whose formation was quantitative after 1 equiv. of acid had been added,[3] had two *tert*-butoxy singlets and otherwise absorptions very similar to those of **7**. Precipitation of the TFA as its pyridinium salt gave a benzene solution of the isomer, obtained on evaporation as an oil to which the structure **10** was assigned on the basis of its ir and ^{1}Hmr spectra.

Efforts to crystallize **10** failed. It proved to be extraordinarily labile to solvolysis, water, alcohols, or acids giving immediately the dealkylated product **7**.

The isomerization reaction of **4***b*, described above, clearly shows that **5***b*, unlike **5***a*, is unstable towards high concentrations of TFA. Compound **5***b* could, however, be obtained as a solid (mp 155–155.5°C), in nearly quantitative yield, by heating **4***b* in carbon tetrachloride containing an excess of pyridine or triethylamine. It had spectra completely in line with

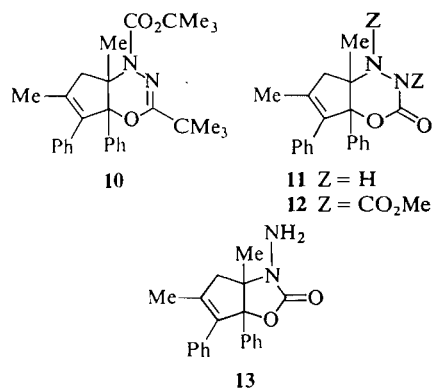

10 **11** Z = H
12 Z = CO_2Me

13

[3]If the equivalent of acid was added all at once the formation of **5***b* was not observed.

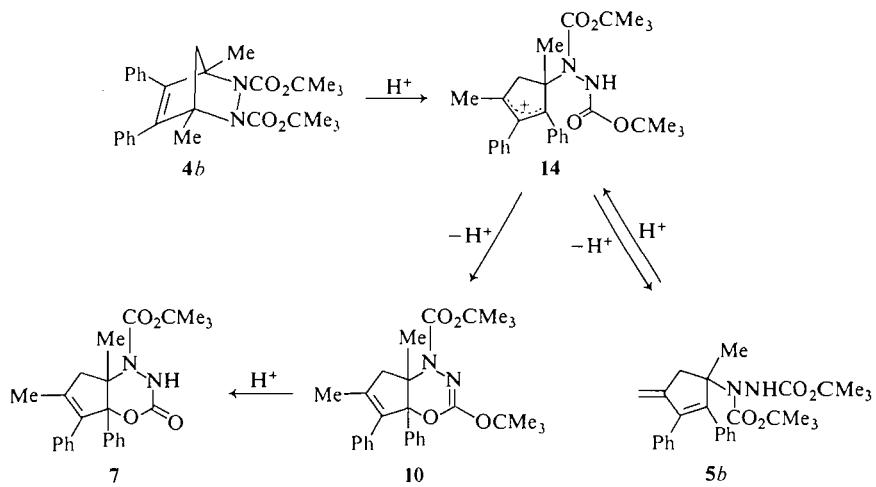

SCHEME 1

those of **5***a* and it too gave a dihydro derivative **6***b*, involving reduction of the exocyclic double bond. Treatment of **5***b* with excess of TFA resulted, as expected, in the quantitative formation of **7**.

Solvolysis of both *tert*-butyl groups could be achieved readily when either **4***b* or **5***b* was refluxed with dilute hydrochloric or sulfuric acid in methanol, or heated neat in TFA; (presumably **10** is an intermediate). The product **11** (M^+ 320) was an oil which resisted crystallization. It was recognized by the methyl and methylene patterns of its ^{1}Hmr spectrum and a weak NH and intense lactone absorption in its ir spectrum. An oily dicarbomethoxy derivative **12** (M^+ 436) was obtained by treatment with 2 equiv. of sodium hydride and methyl chloroformate in pyridine. The nonequivalence of the methoxy singlets in the ^{1}Hmr spectrum (benzene-d_6) of this product permitted rejection of **13** as an alternative isomer of the acid hydrolysis.

The isomerization and solvolysis reactions in acid and base described above are outlined in Scheme 1 for the *tert*-butyl case. The mechanistic relationship suggested between them involves as the key intermediate in acidic conditions the allylic cation **14**, which can be neutralized either by loss of a methyl H to give the diene **5***b* or by loss of amide H in cyclization to **10**. No ready explanation is apparent for the stability of **4***a* to excess of TFA.

The conversion of **14** to **5***b* as a major pathway is in contrast with the behaviour of the analogous protonated intermediates derived from the adducts of cyclones and azo esters, in which only cyclization to the oxadiazine is observed. The intermediate in the latter case is in fact an α-keto allylic cation, **15**. Its degree of positive character at the methyl substituted carbon is expected to be small (contrast the resonance contributions expected of **15***b* and **16***b*) and loss of a methyl H is correspondingly inhibited.

Some support for Scheme 1 is provided by deuterium studies using trifluoroacetic acid-*d*. When **4***b* was treated with excess of the labelled acid in benzene-d_6 the formation of **7** with an unlabelled vinylic methyl peak was observed in the ^{1}Hmr spectrum. Under identical conditions **5***b* gave **7** in which deuterium incorporation in the vinylic methyl group was almost complete. These results are consistent with the intermediacy of **14** to both **5***b* and **7**. They also show that in excess of acid the formation of **5***b* from **4***b* is negligible (a result already implied in footnote 3) and that **5***b* is not an intermediate to **7**.

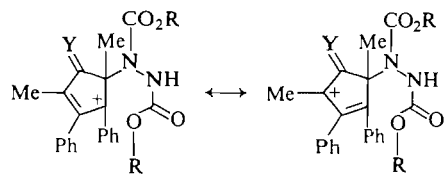

a *b*

15 Y = O
16 Y = H,H

The possibility that acid could catalyze the synthesis of **4**, as well as its isomerization, was examined. Thus in the Diels–Alder reaction protonation of either the 1,4-dimethyl-2,3-diphenylcyclopentadiene or the azo ester could lead to a $4^+ + 2$ (3) or a $4 + 2^+$ reaction (4, 5). It was found (^{1}Hmr analysis) that an equimolar solution of diene and di-*tert*-butyl azodicarboxylate reacted in the presence of 0.5 mol equiv. of TFA in benzene-d_6 faster than without the catalyst but no **4***b* could be detected. The products were a mixture of **5***b* and (mainly) **7**. When **4***b* itself was treated with TFA under identical conditions it formed **5***b* and **7**[4] seven times faster than the previous reaction. This rate factor does not allow

[4]The failure to observe **10** in these reactions is probably because the solvent was not rigorously dried.

Can. J. Chem. Downloaded from www.nrcresearchpress.com by 210.87.254.5 on 09/05/12
For personal use only.

Can. J. Chem. Downloaded from www.nrcresearchpress.com by 210.87.254.5 on 09/05/12
For personal use only.

a decision to be made about the occurrence or otherwise of the acid-catalyzed Diels–Alder reaction.

Experimental

The following spectrometers were used: for ir a Beckman IR10; for uv a Coleman EPS-3T Hitachi; for ms an AEI MS-30; for ^{1}Hmr a Varian T-60.

*2,3-Dialkoxycarbonyl-1,4-dimethyl-5,6-diphenyl-2,3-diazabicyclo[2.2.1]hept-5-enes (**4**)*

The Dimethoxycarbonyl Compound (4a)

The reaction of 1,4-dimethyl-2,3-diphenylcyclopentadiene (246 mg, 1 mmol) and dimethyl azodicarboxylate (146 mg, 1 mmol) in benzene solution (2 ml) at room temperature was rapid and exothermic; nmr analysis of a portion of the solution showed only the formation of the adduct **4***a*, which was complete within a few minutes. Evaporation of the solution and addition of pentane caused crystallization of the product (370 mg, 95%). Recrystallisation from benzene–hexane gave prisms, mp 162–163°C; ν (CCl_4): 1745, 1715 cm^{-1} (C=O); τ (CCl_4): 2.6–3.3 (10H, phenyl), 6.53 (s, 6H, OMe), 7.99 (s, 2H, methylene), 8.17 ppm (s, 6H, *tert*-Me); τ (C_6H_6): 8.29, 8.35 ppm (ABq, 2H, methylene, J = 9 Hz). *Anal.* calcd. for $C_{23}H_{24}N_2O_4$: C 70.39, H 6.16, N 7.14; found: C 70.31, H 6.09, N 6.85.

*The Di-*tert*-butoxycarbonyl Compound (**4**b)*

Under the same conditions the diene and the di-*tert*-butyl azodicarboxylate reacted in about 12 h to give **4***b* quantitatively (^{1}Hmr control experiment). Evaporation and crystallization of the residue by addition of pentane gave the adduct (80%) which was twice crystallized from hexane–cyclohexane as large prisms, mp 157.5–159°C; ν (CCl_4): 1730, 1702 cm^{-1}; τ (CCl_4–$CDCl_3$): 2.86 (broad s, 10H, phenyl), 7.97 (s, 2H, methylene), 8.13 (s, 6H, *tert*-Me), 8.65 ppm (s, 18H, *tert*-BuO); in C_6H_6 the methylene hydrogens are separated, $\Delta\tau$ = 0.23 ppm (J = 9.5 Hz). *Anal.* calcd. for $C_{29}H_{36}N_2O_4$: C 73.08, H 7.61, N 5.88; found: C 73.35, H 7.53, N 6.16.

*Thermal Stability of **4**a and* b

Solutions of the adducts (ca. 05 *M*) were refluxed in appropriate solvents and monitored at intervals by evaporating samples and subjecting the residues to ^{1}Hmr analysis. The results were: **4***a* and *b*, 4 h in toluene, <10%, <5% decomposition; **4***a* and *b*, 3 h in xylene, 30%, 50% decomposition; **4***a*, 3 h in decalin, complete decomposition.

*1,2-Dialkoxycarbonyl-1-(1-methyl-2,3-diphenyl-4-methylidene-2-cyclopentenyl)hydrazines (**5**)*

The Dimethoxycarbonyl Compound (5a)

A solution of **4***a* (100 mg, 0.26 mmol) in benzene (10 ml) containing TFA (29 mg, 0.26 mmol) was kept at room temperature for 1 h. Pyridine (21 mg, 0.27 mmol) was added, followed by *n*-hexane (20 ml) to precipitate the pyridinium salt. The filtered solution was evaporated to a glassy residue which resisted crystallization. Purification by column chromatography (silica gel – methylene chloride) gave **5***a* (70 mg, 70%) as a hard glass which softened between 175–178°C; ν (CCl_4): 3420 (NH), 1768, 1732 cm^{-1} (C=O); τ ($CDCl_3$): 2.8–3.1 (10H, phenyl), 3.36 (s, 1 NH), 5.05 (b, 1H, vinyl), 5.15 (b, 1H, vinyl), 6.32 (s, 3H, OMe), 6.36 (s, 3H, OMe), ~6.4 (1H, methylene, concealed by OMe), 7.18 (d, 1H, methylene, J = 16 Hz), 8.45 ppm (broad s, 3H, *tert*-Me, sharpens >100°C); *m/e* 364 (M^+ – CO, 15%), 246 ($C_{19}H_{18}^+$, 100%).

*The Di-*tert*-butoxycarbonyl Compound (**5**b)*

A solution of **4***b* (100 mg, 0.21 mmol) was refluxed in a mixture of carbon tetrachloride (1 ml) and either pyridine or triethylamine (0.5 ml) for 16 h. Evaporation, followed by crystallization of the residue twice from hexane–cyclohexane gave **5***b* as prisms (80 mg, 80%), mp 155–155.5°C; ν (CCl_4): 3415 (NH), 1752, 1715 cm^{-1} (C=O); τ (CCl_4–$CDCl_3$): 2.6–3.0 (10H, phenyl), 3.80 (1NH), 5.00 (b, 1H, vinyl), 5.10 (b, 1H, vinyl), 6.31 (d, 1H, methylene, J = 17 Hz), 7.13 (d, 1H, methylene), ca. 8.5 (3H, *tert*-Me, concealed by *tert*-BuO), 8.51 (s, 9H, *tert*-BuO), 8.60 ppm (s, 9H, *tert*-BuO). *Anal.* calcd. for $C_{29}H_{36}N_2O_4$: C 73.08, H 7.61, N 5.88; found: C 73.24, H 7.69, N 5.81.

*Alternative Synthesis of **5**b*

A solution of **4***b* (208 mg, 0.44 mmol) in dry benzene (3 ml) containing TFA (29 mg, 0.25 mmol) was kept at room temperature for 30 min. The solvent was evaporated and the residue taken up in chloroform and the product then purified by chromatography on silica gel. This reaction was monitored by ^{1}Hmr analysis using a solution of **4***b* and TFA in benzene-d_6 (dried over molecular sieves) at the same concentration as in the preparative scale experiment. The formation of both **5***b* (52 mg, 25%) and **10** (156 mg, 75%) was observed. Addition of further TFA up to 1 equiv. caused complete formation of **10**.

*1,2-Dialkoxycarbonyl-1-(1,4-dimethyl-2,3-diphenyl-2-cyclopentenyl)hydrazines (**6**)*

The Dimethoxycarbonyl Compound (6a)

Compound **5***a* (79 mg, 0.20 mmol) in dioxane (10 ml) took up hydrogen (0.20 mmol) in 10 h on shaking over palladium–charcoal. Filtration, evaporation, and treatment with hexane gave **6***a* (40%) as a glassy solid, softening between 70–75°C; ν (CCl_4): 3432 (NH), 1765, 1730 cm^{-1} (C=O); τ ($CDCl_3$): 2.6–3.0 (10H, phenyl), 3.60 (1NH), 6.20 (s, 3H, OMe), 6.30 (s, 3H, OMe), 7.50 (m, 2H, methylene), 7.95 (m, 1H, *tert*-H) 8.70 (s, 3H, *tert*-Me), 8.80 ppm (distorted d, 3H, *sec*-Me); *m/e* 394 (M^+, 0.3%), 247 ($C_{19}H_{19}^+$, 100%).

*The Di-*tert*-butoxycarbonyl Compound (**6**b)*

Hydrogenation of **5***b* was carried out under identical conditions on the same scale but the reaction was complete after 2 h. Filtration and evaporation gave **6***b* (94%), which was crystallized from benzene–hexane, mp 129–130°C; ν (CCl_4): 3428 (NH), 1760, 1722 cm^{-1} (C=O); τ ($CDCl_3$): 2.7–3.0 (10H, phenyl), 3.90 (1NH), 7.60 (m, 2H, methylene), 8.46 (s, 9H, *O-tert*-Bu), 8.66 (s, 9H, *O-tert*-Bu), 8.72 (s, 3H, *tert*-Me), 8.90 ppm (distorted d, 3H, *sec*-Me); *m/e* 247 ($C_{19}H_{19}^+$, 100%). *Anal.* calcd. for $C_{29}H_{38}N_2O_4$: C 72.77, H 8.00, N 5.86; found: C 72.50, H 7.82, N 5.76.

Cis-*4*-tert-*Butoxycarbonyl-4a,6-dimethyl-7,7a-diphenyl-2,3,4,4a,5,7a-hexahydrocyclopenta-1,3,4-oxadiazin-2-one (**7**)*

*From **4**b*

The adduct **4***b* (202 mg, 0.4 mmol) was dissolved in carbon tetrachloride (5 ml) containing TFA (0.2 ml). After 4 h at room temperature the solution was evaporated and the residue was dissolved in ether and washed with aqueous sodium hydrogen carbonate. The ether layer afforded an almost quantitative yield of 7 which crystallized as prisms, mp 153.5–154.5°C from carbon tetrachloride – hexane; ν (CCl_4): 3385, 3260 (free and H-bonded NH), 1784, 1763 cm^{-1} (C=O); τ (CCl_4): 2.53 (1NH), 2.75, 2.85 (s, s, 10H, phenyl), 7.06 (d, 1H, methylene, J = 16.5 Hz), 7.57 (d, 1H, methylene), 8.07 (s, 3H, vinyl-Me), 8.53 (s, 9H, *tert*-BuO), 9.12 ppm (s, 3H, *tert*-Me). *Anal.* calcd. for $C_{25}H_{28}N_2O_4$: C 71.41, H 6.71, N 6.66; found: C 71.12, H 6.75, N 6.70.

In a variant on this experiment **4***b* (0.2 mmol) was dissolved in neat TFA (0.3 ml) in an ^{1}Hmr tube. An intense blue-green color developed immediately. The spectrum obtained in less than 1 min was that of the final product (no further change

Can. J. Chem. Downloaded from www.nrcresearchpress.com by 210.87.254.5 on 09/05/12
For personal use only.

with time) and had the absorptions described above in addition to the *tert*-BuO signal of *tert*-butyl alcohol. Evaporation and work-up as before gave a nearly quantitative yield of 7.

From **5**b

The blue-green colour was again observed when **5***b* (0.2 mmol) was dissolved in TFA (1 ml); ^{1}Hmr analysis at this point showed that the formation of 7 was quantitative. The work-up was carried out as before.

cis-*2*-tert-*Butoxy-4*-tert-*butoxycarbonyl-4a,6-dimethyl-7,7a-diphenyl-4,4a,5,7a-tetrahydrocyclopenta-1,3,4-oxadiazine (**10**)*

A solution of **4***b* (238 mg, 0.50 mmol) in benzene (5 ml, dried over molecular sieves) was kept with TFA (57 mg, 0.50 mmol) at room temperature for 30 min. Dry pyridine (41 mg, 0.52 mmol) was added and, after stirring for 5 min, pyridinium trifluoroacetate was precipitated by the addition of excess of *n*-hexane (Na dried) and removed by filtration. The filtrate was finally evaporated in a stream of dry nitrogen to the viscous **10**, which resisted crystallization and decomposed immediately and quantitatively to **7** on contact with hydroxylic solvents. It had ν (CCl_4): 1785, 1760 (C=O), 1670 cm^{-1} (C=N); τ (CCl_4): 2.5–3.2 (10H, phenyl), 7.12 (d, 1H, methylene, J = 17 Hz), 7.76 (d, 1H, methylene), 8.22 (s, 3H, vinyl Me), 8.55 (s, 9H, *tert*-BuO), 8.80 (s, 9H, *tert*-BuO), 9.12 ppm (s, 3H, *tert*-Me); *m/e* 448, 421, 364, 320, 275, 246 ($C_{19}H_{18}^+$).

cis-*4a,6-Dimethyl-7,7a-diphenyl-2,3,4,4a,5,7a-hexahydrocyclopenta-1,3,4-oxadiazin-2-one (**11**)*

A solution of either **4***b* or **5***b* (100 mg, 0.26 mmol) in methanol (15 ml) was stirred for 12 h with 2 *N* HCl or H_2SO_4 (5 ml); alternatively a solution of **4***b* (100 mg) was refluxed for 2 h in TFA (2 ml). The solvent was evaporated and the residue, dissolved in chloroform, was washed with aqueous sodium hydrogen carbonate. The chloroform solution gave **11** (57 mg, 70%) as a glassy product resisting crystallization: ν (CCl_4): 3355 (NH), 1765 cm^{-1} (C=O); τ (CCl_4): 2.74 (s, 5H, phenyl), 2.87 (s, 5H, phenyl), 6.23 (b, 2NH), 7.10 (d, 1H, methylene, J = 18 Hz), 7.52 (d, 1H, methylene), 8.08 (s, 3H, vinyl Me), 9.12 ppm (s, 3H, *tert*-Me); *m/e* 320 (M^+, 30%), 305 (30%), 275 (90%), 246 ($C_{19}H_{18}^+$, 100%).

cis-*3,4-Dimethoxycarbonyl-4a,6-dimethyl-7,7a-diphenyl-2,3,4,4a,5,7a-hexahydrocyclopenta-1,3,4-oxadiazin-2-one (**12**)*

Addition of **11** (80 mg, 0.25 mmol) in tetrahydrofuran (2 ml) to a suspension of 50% sodium hydride – mineral oil (33 mg, 0.69 mmol NaH) in tetrahydrofuran (5 ml) caused vigorous effervescence of hydrogen. Methyl chloroformate (78.5 μl, 1 mmol) was then introduced. After 5 h at room temperature ether and water were added, and the ether layer was shaken out several times with water, dried, and evaporated. The residue was purified by column chromatography on silica gel with elution by benzene. The bisurethane **11** was obtained as a glassy solid: ν (CCl_4): 1760, 1740 cm^{-1} (C=O); τ (CCl_4): 2.64 (m, 5H, phenyl), 2.80 (s, 5H, phenyl), 6.06 (s, 6H, OMe), 7.70 (m, 2H, methylene), 8.04 (s, 3H, vinyl Me), 9.01 ppm (s, 3H, *tert*-Me); τ (C_6D_6): 6.00 (s, 3H, OMe), 6.10 ppm (s, 3H, OMe); *m/e* 436 (M^+, 5%), 392 ($M^+ - CO_2$, 20%), 334 (43%), 319 (7%), 260 (34%), 244 ($C_{19}H_{16}^+$, 100%).

Deuterium Incorporation Studies on **4**b *and* **5**b

A solution of **4***b* (24 mg, 0.05 mmol) in chloroform-*d* (0.3 ml) saturated with D_2O was treated with 1 drop of trifluoroacetic anhydride and the ensuing reaction monitored by ^{1}Hmr analysis. When the conversion to 7 was complete the vinylic methyl peak was found by integration to be lacking in deuterium.

The experiment was repeated under identical conditions with **5***b*. Integration of the peaks for the product **7** showed the vinylic methyl to be exactly two thirds the intensity of the *tert*-methyl peak.

Kinetics Procedures

(a) Acid Catalysis of Diels–Alder Reaction

A solution of 1,5-dimethyl-2,3-diphenylcyclopentadiene and di-*tert*-butyl azodicarboxylate (13 mg each, 0.05 mmol) in benzene-d_6 (0.3 ml, undried stock solvent) was treated with TFA (2 μl, 0.025 mmol) and monitored by ^{1}Hmr analysis. The rate of formation of **7** (major product) and **5***b* (minor) was determined from the concentrations measured by integration of the methyl peaks. The adduct **4***b* was not detected.

(b) Acid Catalysis of Reaction of **4**b

A solution of **4***b* and TFA in benzene-d_6 at exactly the concentrations used in *a* was similarly analyzed. The formation of **7** and **5***b* occurred at a rate seven times greater than that observed in *a*.

Acknowledgment

We thank the National Research Council of Canada for financial assistance.

1. (*a*) J. A. CAMPBELL, D. MACKAY, and T. D. SAUER. Can. J. Chem. **50**, 371 (1972); (*b*) C. Y-J. CHUNG, D. MACKAY, and T. D. SAUER. Can. J. Chem. **50**, 1568 (1972); (*c*) D. MACKAY, C. W. PILGER, and L. WONG. J. Org. Chem. **38**, 2043 (1973); (*d*) D. MACKAY and C. W. PILGER. Can. J. Chem. **52**, 1114 (1974); (*e*) J. A. CAMPBELL, I. HARRIS, D. MACKAY, and T. D. SAUER. Can. J. Chem. **53**, 535 (1975).
2. A. R. KATRITZKY and A. P. AMBLER. *In* Physical methods in heterocyclic chemistry. Vol. II. *Edited by* A. R. Katritzky. Academic Press, New York, NY. 1963. p. 161.
3. R. R. SCHMIDT. Angew. Chem. Int. Ed. Engl. **12**, 212 (1973).
4. W. H. URRY, P. SZECSI, C. IKOKU, and D. W. MOORE. J. Am. Chem. Soc. **86**, 2224 (1964).
5. S. HÜNIG. Helv. Chim. Acta, **54**, 1721 (1971).

A new extraction–spectrophotometric method for the determination of phosphate

KUNNATH S. SUBRAMANIAN AND ALFIO CORSINI

Department of Chemistry, McMaster University, Hamilton, Ont., Canada L8S 4M1

Received December 2, 1977

KUNNATH S. SUBRAMANIAN and ALFIO CORSINI. Can. J. Chem. **56**, 1729 (1978).

A new extraction–spectrophotometric method has been developed for the determination of trace amounts of phosphorus as orthophosphate. The method is based on the chemistry of 12-tungstophosphoric acid, $H_3PW_{12}O_{40}$ (TPA). In the procedure, orthophosphate is converted quantitatively to TPA in aqueous solution at a tungstate–phosphate molar ratio ≥ 24, in the p*H* range 1.2 to 1.9 and in the temperature range 60 to 100°C. The TPA is subsequently extracted into *n*-amyl alcohol and its absorbance measured at 267 nm. Beer's law is followed up to at least 25 μg/ml P. The method is less prone to solution conditions and species interference (especially As(V) and Si(IV)) than the widely used molybdenum-blue methods and is competitive in terms of sensitivity, precision, and accuracy. The TPA method was applied successfully to the determination of phosphate in a variety of phosphorus-containing specimens including natural waters, ores, and alloys.

Based on potentiometric and spectrophotometric studies, a scheme which accounts for the observed heptaproticity of TPA is proposed.

KUNNATH S. SUBRAMANIAN et ALFIO CORSINI. Can. J. Chem. **56**, 1729 (1978).

On a développé une nouvelle méthode d'extraction liée à la spectrophotométrie pour la détermination de phosphore à l'état de trace sous forme d'orthophosphate. La méthode est basée sur la chimie de l'acide tungstophosphorique-12 $H_3PW_{12}O_{40}$ (TPA). Dans cette méthode, on transforme quantitativement l'orthophosphate en TPA en solution aqueuse à un rapport molaire de tungstate–phosphate ≥ 24, à des p*H* allant de 1.2 à 1.9 et à des températures allant de 60 à 100°C. On extrait par la suite le TPA par l'alcool amylique et on mesure son absorption à 267 nm. La loi de Beer peut être appliquée jusqu'à au moins 25 μg/ml P. Cette méthode est moins susceptible aux conditions de solution et d'interférence par diverses substances (spécialement As(V) et Si(IV)) que la méthode plus utilisée du bleu de molybdène; de plus elle est compétitive en terme de sensibilité, de précision et d'exactitude. On a appliqué avec succès la méthode TPA pour la détermination du phosphate dans un grand nombre de spécimens contenant du phosphore comme des eaux naturelles, des minerais et des alliages.

En se basant sur des études potentiométrique et spectrophotométrique, on propose un schéma qui permet de tenir compte de l'heptaproticité observée dans le TPA.

[Traduit par le journal]

Introduction

Phosphorus is usually determined in such matrices as natural waters, minerals, steels, agricultural products, and foodstuffs by spectrophotometric procedures based on the formation of 12-molybdophosphoric acid (MPA) and its reduction to molybdenum-blue (1). The molybdenum-blue method and its various modifications have been thoroughly reviewed (1–3). In spite of its popularity, the molybdenum-blue method has a number of drawbacks, the most important of which are: (*i*) the method is based on empirical grounds (4) and the fundamental steps involved in the chemistry are not fully understood (4, 5); for example, the chemical nature of the 'blue' species is still uncertain and 'blues' have been proposed in which Mo is in some combination of either +4 and +5 or +5 and +6 oxidation states (e.g., ref. 6); (*ii*) serious interferences result from As(V), Cr(VI), Cu(II), Ge(IV), Hg(II), NO_2^-, Si(IV), and V(V) (7–9); and (*iii*) the intensity and stability of the colour, the position of peak maxima, and the extent of interference are all sensitive to the choice and concentration of the reductant, the concentration of molybdate and acid, standing time, and temperature (2, 8). Thus, with each reductant used (e.g., stannous chloride, ascorbic acid, 1-amino-2-naphthol-4-sulphonic acid) conditions must be found in which maximum sensitivity in the presence of phosphate is combined with minimum sensitivity in its absence (10). These difficulties clearly show the need for an alternative method which allows wider flexibility of experimental conditions and greater freedom from interferences and for which the chemistry is understood.

In regard to the above considerations, the analytical potential of 12-tungstophosphoric acid, $H_3PW_{12}O_{40}$ (TPA), for the determination of phosphorus has received scant attention (11) even though TPA is reported to be more stable than MPA to both acid and reducing agents (12) and has a higher molar absorptivity ($\varepsilon_{267} = 4.7 \times 10^4\ \ell\ mol^{-1}\ cm^{-1}$ (13) vs. $\varepsilon_{825} = 2.7 \times 10^4\ \ell\ mol^{-1}\ cm^{-1}$ (14)). Pre-

Can. J. Chem. Downloaded from www.nrcresearchpress.com by 210.87.254.6 on 09/05/12
For personal use only.

Can. J. Chem. Downloaded from www.nrcresearchpress.com by 210.87.254.6 on 09/05/12
For personal use only.

sumably, the complicated aqueous solution chemistry of TPA and tungstate ion (WO_4^{2-}) has discouraged serious analytical study of TPA. For example, the p*H* region in which TPA exists as the undissociated (or ion-associated) acid is still uncertain (15). Furthermore, TPA is reported to be both triprotic and heptaprotic in aqueous solution (e.g., refs. 12, 15). With regard to tungstate ion, its solution chemistry is very complex, involving the formation of isopolytungstate species through condensation reactions (12).

The present paper describes an extraction–spectrophotometric method for the determination of trace amounts of phosphorus, based on the quantitative formation of TPA from tungstate, phosphate, and acid under appropriate conditions. The method has been tested on a number of standard reference materials and applied to natural water samples. In addition, the hydrolytic stability of TPA has been studied and although it was found that TPA is intrinsically triprotic, a scheme that accounts for its observed heptaproticity in water is advanced.

Experimental

Apparatus

Spectra in the uv region were recorded with a Bausch and Lomb Spectronic 600 double-beam spectrophotometer, equipped with a Sargent Model SRL strip-chart recorder. Quartz cells (Hellma) with path lengths ranging from 50 to 0.1 mm were used, depending on sample concentration.

Potentiometric titrations of TPA in aqueous and nonaqueous media were done with a Radiometer Model p*H* M4 meter equipped with a fibre-type saturated calomel electrode and a low sodium-ion error glass electrode.

A Gilmont ultra-precision digital micrometer syringe burette was used for dispensing volumes of phosphate and arsenate solutions.

Reagents and Solutions

Stock solutions of tungstate (0.1 *M*), phosphate (155.5 μg P/ml), and TPA (1.0×10^{-3} *M*) were prepared respectively, from $Na_2WO_4 \cdot 2H_2O$ ('Baker Analyzed' reagent), KH_2PO_4 (primary standard, Analar, B.D.H.), and anhydrous $H_3PW_{12}O_{40}$ (obtained by heating to 280–300°C for 10 h hydrated TPA (Alfa) after purification by extraction into ether). The solutions were stored in polyethylene bottles. Suitable aliquots of the tungstate and phosphate solutions were taken to obtain solutions of lower concentration. Standard solutions (1.0 and 0.1 *M*) of perchloric acid and sodium hydroxide were stored in polyethylene bottles. *n*-Amyl alcohol and 2-butanone were dried over K_2CO_3, distilled at atmospheric pressure, and stored over type 4A Linde molecular sieves (16). (The *n*-amyl alcohol was collected at 138.0–138.2°C and 2-butanone at 79.6–80.2°C.) All other reagents were of suitable purity for the purpose intended.

Procedure

(a) Hydrolytic Stability of TPA

The stability of TPA in aqueous solutions of varying p*H* was studied both spectrophotometrically and potentiometrically. Solutions of TPA (3.21×10^{-5} *M*) with acidities ranging from 4 *M* $HClO_4$ to p*H* 12 were prepared. For solutions of p*H* > 0, the ionic strength was adjusted to unity with $NaClO_4$. Spectra were recorded in the range 200–400 nm (5 cm cells, corresponding reference solutions without TPA) at zero time (i.e., immediately after preparation of each solution) and at 1, 5, 10, 24, and 120 h intervals. Titrations in aqueous medium (50 ml of 10^{-3} *M* TPA) were made with 2.01×10^{-2} and 9.90×10^{-2} *M* solutions of NaOH in the p*H* range 2–7 and 7–12, respectively. The ionic strength was maintained at ~1 by addition of $NaClO_4$. For titrations in nonaqueous media, 0.153 and 0.144 g of anhydrous TPA were dissolved in 50 ml of *n*-amyl alcohol and 2-butanone, respectively, and the solutions titrated with a 0.101 *M* tetra-*n*-butylammonium hydroxide which was standardized as described by Fritz and Gainer (17).

(b) Formation of TPA from Phosphate, Tungstate, and Acid

Experiments to establish conditions for the quantitative conversion of phosphate to TPA in aqueous solution and for the subsequent quantitative extraction of the TPA into *n*-amyl alcohol were carried out. Several solutions were prepared in the p*H* range 0 to 5.4, each solution having final phosphate and tungstate concentrations of 4.0×10^{-5} and 4.8×10^{-4} *M*, respectively (W/P molar ratio = 12). Spectra were recorded at zero time, 0.5, 1, and 5 h and at 1, 5, 10, and 15 days, with cells of appropriate path length and corresponding reference solutions without phosphate. The extent of formation of TPA and of interference from isopolytungstate species was obtained by reference to spectra of standard solutions of TPA and of appropriate isopolytungstate species. In a further experiment, a series of solutions was prepared in the p*H* region 0–3, each solution (10 ml) having final phosphate and tungstate concentrations of 5.0×10^{-5} and 6.0×10^{-4} *M* (W/P ratio = 12, phosphate concentration equivalent to 1.55 μg P/ml). The solutions were then extracted for 2 min with *n*-amyl alcohol (25 ml) under the following conditions; after standing for 0, 0.5, and 24 h at 25°C; and after newly prepared solutions were heated momentarily to 45, 60, or 100°C and cooled to 25°C. The spectrum of the alcohol phase was recorded in the range 200–400 nm. The *n*-amyl alcohol extract of the corresponding blank was used as a reference solution. These experiments were repeated at W/P molar ratios of 24, 48, 96, 144, and 240. For each ratio, the phosphate concentration was kept constant at 1.55 μg/ml P. Similar experiments were performed at 15.5 μg P/ml at the above W/P molar ratios and also at 0.155 μg P/ml at W/P ratios of 24, 48, 144, 240, 480, 960, 1440, and 2400. The extent of formation–extraction of TPA was estimated by comparison to spectra of standard solutions of TPA in *n*-amyl alcohol.

Conformity to Beer's law of the TPA formed in aqueous solution and extracted into the alcohol phase was tested by taking suitable aliquots of phosphate ranging from 0 to 25 μg P/ml. The solution conditions were: W/P molar ratio ≥ 24; p*H* 1.2–1.9; the solution brought momentarily to a boil and cooled to 25°C and extracted as before. The absorbance of the alcohol phase was measured at 267 nm.

(c) Effect of Foreign Ions

The solution conditions for the study of foreign-ion effects were: phosphate concentration, 1.55 μg P/ml; W/P molar ratio, 96; p*H* range, 0–2; initial concentration of foreign ion, $(1.0–5.0) \times 10^3$ μg/ml, depending on the ion, and progressively lowered until the response corresponded to 100% phosphate recovery. The solutions containing tungstate, phosphate, acid, and the foreign ion were boiled, cooled, extracted, and the absorbance of the alcohol phase measured at 267 nm. The foreign ions tested are listed later. Since arsenic, silicon, and germanium form corresponding heteropolytungstates (15) and tungstate ion condenses to isopolytungstates, some of which

Can. J. Chem. Downloaded from www.nrcresearchpress.com by 210.87.254.6 on 09/05/12
For personal use only.

absorb in the region of 270 nm (18), the effect of these species was studied in detail as described below.

(i) Effect of arsenic—The formation and extraction of 12-tungstoarsenic acid (TAA) was studied under the same conditions as described for TPA in section (*b*). The concentrations of arsenate (Na_2HAsO_4) corresponded to 0.75, 1.50, 2.30, and 3.80 and 15.00 μg As/ml. The W/As ratio was ~96. Studies on the recovery of phosphate in the presence of arsenate were done at phosphate concentrations of 0.0155, 0.155, 1.55, and 15.5 μg P/ml. For each P concentration, arsenate concentrations of 0.75, 1.50, 3.80, and 15.0 μg As/ml were used. In each case, the tungstate concentration was 0.01 *M* and the p*H* was 1.5–1.9.

(ii) Effect of silicon and germanium—Solutions (2.0×10^{-5} *M*) of 12-tungstosilicic and -germanic acids ranging in acidity from 4 *M* $HClO_4$ to p*H* 12 were extracted with *n*-amyl alcohol (25°C). Spectra of the aqueous phase before extraction and of the alcohol phase after extraction were taken over the range 200–350 nm.

(iii) Effect of isopolytungstates—Tungstate solutions (10^{-1}–10^{-3} *M*) were adjusted to p*H* 0–2, heated to 60 and 100°C, cooled to 25°C, and extracted with *n*-amyl alcohol. Spectra of the aqueous and final organic phases were recorded over the range 220–400 nm. Similar tests were made on solutions of metatungstate, $H_2W_{12}O_{40}^{6-}$ (2.0×10^{-5} *M*), and paratungstate, $H_2W_{12}O_{42}^{10-}$ ($3.2 \times 10^{-5} - 1.28 \times 10^{-4}$ *M*).

(d) Analytical Application to Phosphorus-containing Materials

(i) Determination of total soluble phosphate in water samples—The following procedure was used for natural water and sewage water samples and is suitable in general for the determination of total soluble phosphate. Pipet an aliquot (25 ml for concentrations < 0.1 μg P/ml; ≤ 10 ml for concentrations ≥ 0.1 μg P/ml) into a 125 ml conical flask, add 1 ml of 5 *M* H_2SO_4, 0.4 g of $(NH_4)_2S_2O_8$, dilute to 50 ml with deionized water, and digest until the volume is reduced to 10–15 ml (~1 h). Allow the solution to cool, transfer to a 50 ml beaker (use 5–10 ml of deionized water to rinse the flask), and adjust the p*H* to >7 with 5 *M* NaOH (dropwise). Add a volume of tungstate solution so that the final analytical concentration $\geq 10^{-3}$ *M*. (For samples containing ≤ 10 μg P/ml, 1–3 ml of 0.1 *M* tungstate is adequate.) Re-adjust the p*H* (potentiometrically) to 1.2–1.9 (1.5–1.9 if As(V) is present) with 1 *M* $HClO_4$. Bring the solution to a boil (heating to 60°C for 2–3 min is also adequate), cool to 25°C in a water bath, and transfer to a separatory funnel, using a few ml of 0.03 *M* $HClO_4$ to rinse the beaker. Then add exactly 10 ml of *n*-amyl alcohol, extract for 2 min, and measure the absorbance of the alcohol phase at 267 nm against the corresponding *n*-amyl alcohol extract of the reagent blank, using cells of suitable path length (e.g., 2 or 5 cm cells for 0 to 0.1 μg P/ml). Between measurements, the cell should be rinsed with the next sample and not with solvents (e.g., acetone) that absorb in the 200–300 nm range. Also, excessive water in the alcohol phase causes cloudiness; in such cases, a period of ~40 min is required for the water to settle. Obtain the concentration of P by reference to a calibration curve prepared from standard phosphate solutions.

Filter sewage-water samples through a 0.45 μ Millipore filter to remove suspended and particulate matter, prior to the determination.

(ii) Application to an organophosphorus compound (triphenyl phosphate, NBS standard, 1071 a)—Between 2–3 mg of the sample (dried over P_2O_5 for 2 h) was quickly weighed and treated with distilled water (50 ml), 6 *M* H_2SO_4 (1.5 ml), and $(NH_4)_2S_2O_8$ (1 g). After digestion as above, the volume was adjusted to 100 ml and a 5 ml aliquot taken for analysis. The aliquot was diluted to 10–15 ml and then processed exactly as in section (*i*).

(iii) Application to alloys. Steel samples (NBS)—To weighed amounts (0.05–0.1 g) in 100 ml beakers were added 5 ml of 1:1 HNO_3 and after the oxides of nitrogen were expelled by gentle boiling, 10 ml of 2% $(NH_4)_2S_2O_8$. The solution was reboiled for 5 min, 4 ml of concentrated HCl added, and the solution evaporated to dryness. The residue was dissolved in 40 ml of 0.01 *M* HCl and the solution passed through an ion-exchange column (Amberlite, CG-120, type $RSO_3^-Na^+$) to remove Fe(III). The phosphate was eluted with 60–80 ml of a 0.2 *M* HCl (3 ml/min flow rate) and collected in a 250 ml beaker. The solution was evaporated to 10–15 ml, cooled, and diluted exactly to 100 ml. A suitable aliquot was taken and processed exactly as in section (*i*) above.

(a) Phosphor-bronze samples (Canada Centre for Mineral and Energy Technology)—To weighed samples (0.05–0.08 g) were added 0.5 ml of concentrated HNO_3 and 1 ml of concentrated HCl. After the vigorous reaction had subsided, 10 ml of distilled water was added and the mixture heated until dissolution was complete. The solution was diluted exactly to 50 ml and a suitable aliquot taken for processing as above.

(iv) Application to ores and a mineral. Nickel–copper–cobalt ore, SU-1 (standard reference material, Canada Centre for Mineral and Energy Technology)—A sample (0.05–0.06 g) of the dried ore (2 h at 110°C) was treated with 5 ml of concentrated HNO_3 and after evaporation, 2 ml of concentrated HCl. After re-evaporation and addition of 10 ml of water, the silica was removed by filtration and the filtrate passed through an ion-exchange column as described for steel samples. The eluate (~100 ml) was evaporated to 25–30 ml, diluted to 50 ml, and a 10-ml aliquot processed in the usual way.

(a) Manganese ore (NBS, 25c)—Ten millilitres of 0.05 *M* HNO_3 was added to a dried sample (~0.07 g), followed by 30–32% (w/w) H_2O_2 (dropwise) until all vigorous action ceased. After heating and dilution to ~25 ml, the solution was filtered to remove silica and the filtrate diluted to 50 ml. A suitable aliquot was processed.

(b) Feldspar (NBS, 99a)—A dried sample (0.1–0.2 g) was fused with $K_2S_2O_7$ (0.8–1.6 g) for 90 min, the crucible was transferred to a 150 ml beaker containing 40–50 ml distilled water, and the mixture boiled until only the silica remained undissolved. After the silica was removed, the filtrate was diluted to 100 ml and a 10 ml aliquot taken for analysis.

Results and Discussion

(a) Hydrolytic Stability of TPA

The isolation of the Ag(I) and guanidine hepta salts led early workers to formulate TPA as $H_7PW_{12}O_{42}$. An element of uncertainty with regard to the proposed heptaproticity in water was introduced after Keggin, on the basis of X-ray studies, formulated the heteropoly anion as $PW_{12}O_{40}^{3-}$, although there followed several physicochemical measurements the results of which again suggested TPA to be heptaprotic (19). Finally, in a heat of neutralization study, Spitsyn and Kosmodemyanskaya (20) concluded that in aqueous solution TPA is triprotic and that its apparent high proticity is due to degradation to a species of higher charge, such as $PW_{11}O_{39}^{7-}$.

In the present study, the intrinsic triprotic nature of TPA was confirmed by titration in *n*-amyl alcohol and in 2-butanone. Each titration curve showed a

Can. J. Chem. Downloaded from www.nrcresearchpress.com by 210.87.254.6 on 09/05/12
For personal use only.

single sharp potentiometric step, with the end-point corresponding to the consumption of precisely 3 mol of base per mole of TPA, based on the formula $H_3PW_{12}O_{40}$. In aqueous solution, however, and as found by others, the titration curve revealed two steps, the first corresponding to 7 mol of NaOH per mole of TPA and the second to an additional 19 mol. The buffer regions occurred in the pH ranges 2–4 and 6–9, respectively.

Based on TPA as $H_3PW_{12}O_{40}$, the overall titration reaction is:

$$[1]\quad H_3PW_{12}O_{40} + 26OH^- \rightleftharpoons 12WO_4^{2-} + HPO_4^{2-} + 14H_2O$$

An empirical scheme that reasonably accounts for the overall stoichiometry is:

$$[2]\quad H_3PW_{12}O_{40} + 3OH^- \rightleftharpoons PW_{12}O_{40}^{3-} + 3H_2O$$

$$[3]\quad PW_{12}O_{40}^{3-} + 4OH^- \rightleftharpoons PW_{11}O_{39}^{7-} + WO_3{\cdot}H_2O + H_2O$$

$$[4]\quad WO_3{\cdot}H_2O + 2OH^- \rightleftharpoons WO_4^{2-} + 2H_2O$$

$$[5]\quad PW_{11}O_{39}^{7-} + 17OH^- \rightleftharpoons 11WO_4^{2-} + HPO_4^{2-} + 8H_2O$$

The reaction scheme is consistent with the titration curve. Reactions [2] and [3] are postulated to occur over the pH range 2–4 without step-wise differentiation. These reactions together could have led earlier workers to conclude that TPA is heptaprotic. Similarly, reactions [4] and [5] are postulated to occur mainly over the pH range 6–9. The unit $PW_{11}O_{39}^{7-}$ has been previously proposed (21) and the degradation of heteropolytungstates to WO_4^{2-} in alkaline solution is well-known (12, 15).

The absorption spectra of solutions of TPA in the range 4 M $HClO_4$ to pH 12 further support the scheme (Fig. 1). The constant absorbance at 267 nm ($\varepsilon_{267} = 5.1 \times 10^4\ \ell\ mol^{-1}\ cm^{-1}$) in the range p$H$ 0.3–1.9 (curve *2*) suggests that TPA exists either as the undissociated acid or as an ion-associated species (e.g., $3H_3O^+$, $PW_{12}O_{40}^{3-}$) below pH 2. (The greater absorbance in 4 M $HClO_4$ (curve *1*) is attributable to strong secondary medium effects in concentrated electrolyte solutions (22).) The progressive decrease in absorbance and shift of peak maximum from 267 to 248 nm (curves *3–6*) and the ultimate disappearance of the 248 nm maximum (curves *7–9*) are indicative of the decomposition of TPA with increasing pH. Curve *9* is identical to the spectrum of simple tungstate ion. The absence of an isosbestic point in the pH range 0.3–5.0 (curves *2–6*) is suggestive of complex behaviour, i.e., a simple acid–base protonic dissociation is not the sole process taking place. Indeed, the time dependence of the absorbance at 248 nm (curves *4–6*) attests to complicated processes. Since each mole of TPA consumed 7 mol of NaOH up to ~pH 4 (3 mol for neutralization, 4 mol for a first-stage decomposition to a species postulated to be $PW_{11}O_{39}^{7-}$), the assignment of the 248 nm band to the $PW_{11}O_{39}^{7-}$ species seems reasonable.

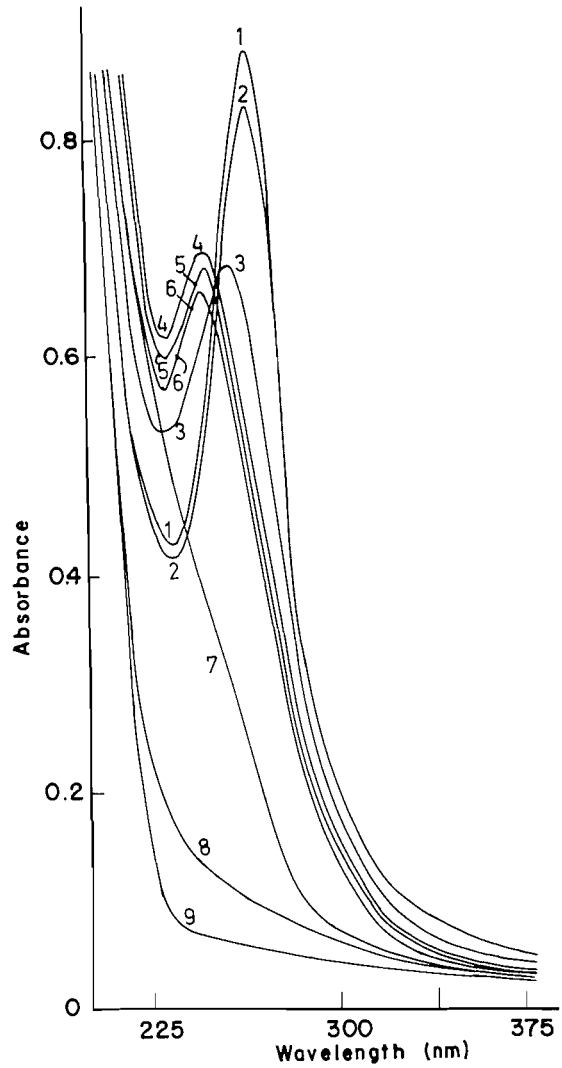

FIG. 1. Absorption spectra of TPA in aqueous solution as a function of pH ($C_{TPA} = 3.21 \times 10^{-5}$ M, $\mu = 1$, 25°C, 5 mm cells, corresponding solution without TPA as reference). (*1*) 4 M $HClO_4$; (*2*) pH 0.3–1.9; (*3*) pH 2.4; (*4*) pH 3.7; (*5*) pH 4.1; (*6*) pH 5.0; (*7*) pH 7.7; (*8*) pH 8.4; (*9*) pH 11.9.

The hydrolytic instability of TPA above pH 2 was further confirmed when the extraction of an aqueous solution of TPA (2.00×10^{-5} M) into *n*-amyl alcohol was found to be quantitative only at p$H \leq 2$; also, Beer's law was valid for aqueous solutions of TPA and the *n*-amyl alcohol extracts of the aqueous solutions only below pH 2.

Can. J. Chem. Downloaded from www.nrcresearchpress.com by 210.87.254.6 on 09/05/12
For personal use only.

The above studies clearly show that any development of a quantitative method for phosphate based on the formation of TPA from phosphate, tungstate, and acid would have to be done at $pH \leq 2$.

(b) Formation of TPA in Solution from Phosphate, Tungstate, and Acid

Preliminary studies in aqueous solution at a W/P ratio of 12 and at 25°C showed that the formation of TPA was not quantitative even after 15 days at $pH < 2$, and that serious interference occurred from the simultaneous formation of isopolytungstates. Therefore, the development of a useful analytical method would require not only optimization of experimental parameters (e.g., temperature, tungstate concentration) for quantitative formation of TPA in solution, but also reduction of interference from the isopolytungstates. Since detailed studies with tungstate ion, paratungstate ($H_2W_{12}O_{42}^{10-}$), and metatungstate ($H_2W_{12}O_{40}^{6-}$) in acid medium showed that isopolytungstates are not extracted into *n*-amyl alcohol at $pH > 1$, and since TPA is quantitatively extracted up to pH 2, subsequent measurements of the formation of TPA were carried out after alcohol extraction of the aqueous phase set at pH 0–3, with particular interest in the pH range 1–2.

These measurements showed that the formation of TPA at 25°C was indeed quantitative (in the pH range 1.2–1.9) at a W/P ratio ≥ 24; however, under these conditions, the aqueous phase reaction required 24 h to be quantitative, even at W/P = 240, and as such is unsuitable for analytical use. Figure 2 (for W/P = 48) is typical of the data obtained. Figure 3 shows that quantitative formation of TPA was instant (in the pH range 1.2–1.9) when the aqueous phase (W/P $\geq$ 24) was brought to a boil. Instant quantitative formation was also achieved at 60°C, but only 90% formation occurred at 45°C. In Fig. 3, the decrease in absorbance above pH 2 is due to the decomposition of TPA; the decrease below pH 1 is due to precipitation of tungstic oxide and to the formation and extraction of isopoly compounds. These processes reduce the effective analytical concentration of tungstate available for reaction with phosphate. Also, the extraction of isopoly species occurs to a greater extent in the reference than in the test solution, resulting in a decrease in absorbance.

For the above studies, the phosphate concentration was 1.55 μg P/ml in the aqueous phase. Similar results were obtained at 15.5 μg P/ml. At 0.155 μg P/ml, however, instant quantitative formation of TPA was achieved only at W/P ratios $\geq$240. At a W/P ratio of 24, for example, the extent of TPA formation was only 33%. The higher W/P ratio required for low concentrations of phosphorus is accommodated in the analytical procedure for water samples by the directive to add 1–3 ml of 0.1 *M* tungstate solution.

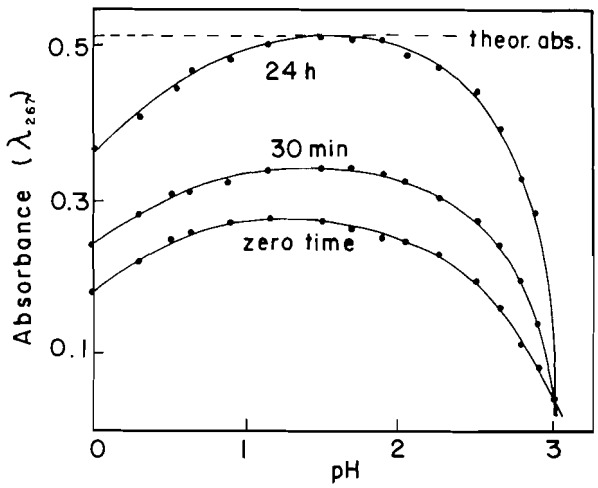

FIG. 2. Formation–extraction of TPA as a function of pH ($C_{WO_4^{2-}} = 2.4 \times 10^{-3}$ *M*, $C_{H_2PO_4^-} = 5.0 \times 10^{-5}$ *M*, W/P = 48, 25°C, 5 mm cells, corresponding *n*-amyl alcohol extract of blank as reference).

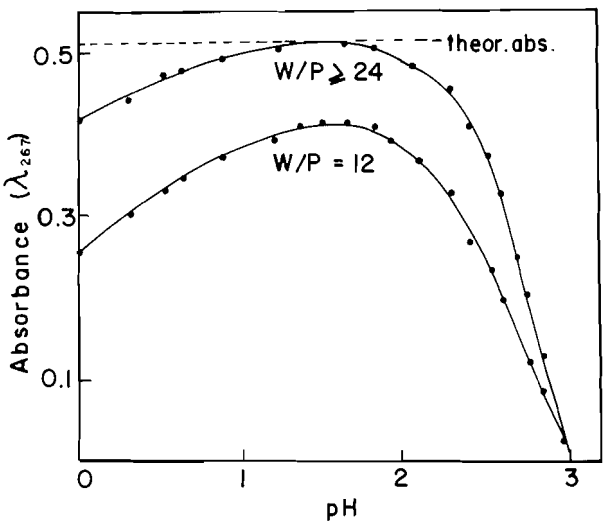

FIG. 3. Instant (zero time) formation–extraction of TPA as a function of pH ($C_{H_2PO_4^-} = 5.0 \times 10^{-5}$ *M*, 100°C, 5 mm cells, corresponding *n*-amyl alcohol extract of blank as reference).

A test of the conditions under which phosphate is converted quantitatively to TPA showed that Beer's law is obeyed for phosphate concentrations at least up to 25 μg P/ml. Furthermore, the absorbance values of TPA in the alcohol phase remained constant for at least 48 h. This stability is a decided advantage over both the popular molybdenum-blue and the molybdovanadophosphate methods (23).

To ensure that the species formed and extracted

Can. J. Chem. Downloaded from www.nrcresearchpress.com by 210.87.254.6 on 09/05/12
For personal use only.

into the alcohol phase under the conditions described above was indeed TPA, the extracted compound was isolated, dried at 275–300°C for 1 h, and an X-ray powder pattern taken. The excellent agreement in *d*-spacings between the isolated compound and a sample of anhydrous TPA obtained by drying commercially available TPA, together with the exact coincidence of spectra in *n*-amyl alcohol, confirmed the matter.

In the course of this work, some observations were made that are of interest with regard to the mechanism of formation of $H_3PW_{12}O_{40}$ in aqueous solution. (*i*) When a small amount of freshly precipitated white tungstic oxide is heated in the presence of phosphate at ca. p*H* 1, the oxide dissolves and TPA is formed and extracted into *n*-amyl alcohol. TPA is not formed from aged oxide. (*ii*) TPA is not formed from metatungstate ($H_2W_{12}O_{40}^{6-}$) and phosphate in the range p*H* 2 to 4 *M* $HClO_4$. In this range, metatungstate is stable. In 7 *M* $HClO_4$, however, decomposition to tungstic oxide is instant. On addition of phosphate to this solution and heating, TPA is formed. (*iii*) An acid solution of paratungstate (p*H* < 2) in the absence of phosphate precipitates the white oxide. In the presence of phosphate, the oxide is not precipitated but, rather, TPA is formed. From these observations, it is almost certain that TPA is not formed by direct reaction of phosphate with a dodecameric species but from smaller isopoly species formed in the degradation of the dodecameric species.

(*c*) *Effect of Foreign Ions*

Studies at 1.55 μg P/ml showed no interference from: K^+, Na^+, Cl^-, NO_3^-, and SO_4^{2-} up to 5000 μg/ml; Mg(II), Ca(II), Mn(II), Co(II), Ni(II), Cr(VI), Mo(VI), and F^- up to 1000 μg/ml; Hg(II), Al(III), Si(IV), Br^-, I^-, CN^-, NO_2^-, S^{2-}, SO_3^{2-}, Si(IV), and SeO_3^{2-} in the range 400–700 μg/ml; Ag(I), Ba(II), Cd(II), As(III), and U(VI) in the range 150–300 μg/ml; Be(II), Cu(II), Zn(II), Pb(II), Sn(IV), and Ge(IV) in the range 50–100 μg/ml; and Ti(IV) and Zn(IV) in the range 20–50 μg/ml.

Serious interference occurred from As(V), Fe(III) (≥3 μg/ml), Sn(II) (≥2 μg/ml), Th(IV) (≥2 μg/ml), and V(V) (≥2 μg/ml). Respectively, these interferences may be due to the formation of $AsW_{12}O_{40}^{3-}$, $FePO_4$ ($K_{sp} = 10^{-21.9}$ at 25°C (24)), tungsten-blue from reduction of TPA by Sn(II), $Th_3(PO_4)_4$ ($K_{sp} = 10^{-78.6}$ at 25°C (24)), and $PVW_{11}O_{40}^{4-}$ (15). Since the effects of Fe(III), Sn(II), Th(IV), and V(V) have not been fully examined in the molybdenum-blue method, valid comparisons with the TPA method could not be made.

Since As(V) interferes seriously in the molybdenum-blue procedure with $SnCl_2$ as the reductant (As is returned as its equivalent of P (8, 25)) and with ascorbic acid – Sb(III) as the reductant (only 0.01 μg As/ml can be tolerated for 1.0 μg P/ml (26)), a

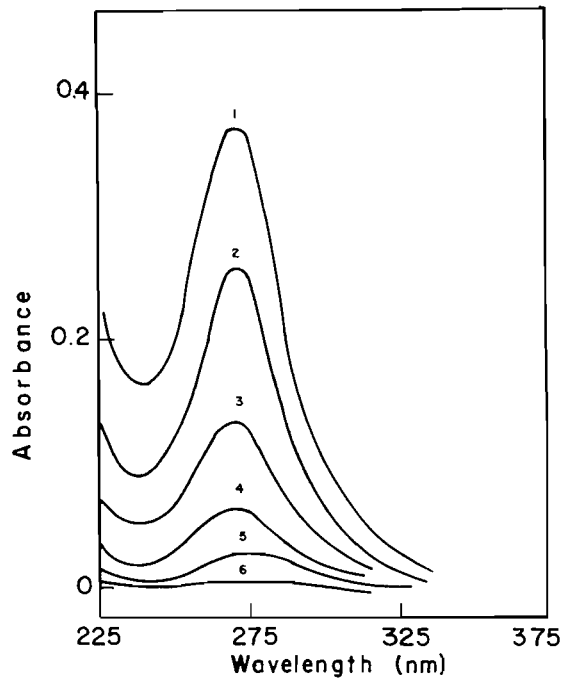

FIG. 4. Absorption spectra for the formation-extraction of $H_3AsW_{12}O_{40}$ ($C_{WO_4^{2-}} = 4.8 \times 10^{-3}$ *M*, $C_{HAsO_4^{2-}} = 5.0 \times 10^{-5}$ *M* (3.75 μg/ml As), 100°C, 5 mm cells, corresponding *n*-amyl alcohol extract of blank as reference). (*1*) p*H* 0.0; (*2*) p*H* 0.7; (*3*) p*H* 1.2; (*4*) p*H* 1.4; (*5*) p*H* 1.7; (*6*) p*H* 1.8.

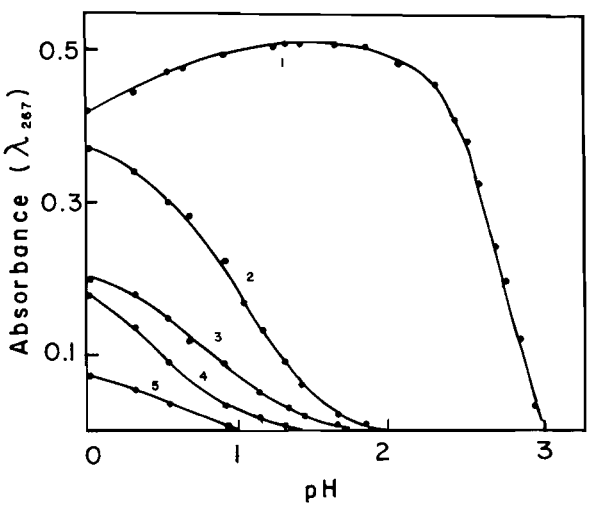

FIG. 5. Formation–extraction of $H_3AsW_{12}O_{40}$ and comparison to TPA (W/As ≥ 24, W/P ≥ 24, 100°C, 5 mm cells, corresponding *n*-amyl alcohol extract of blank as reference). (*1*) 1.55 μg P/ml; curves (*2*)–(*5*), 15.0, 3.75, 1.50, and 0.75 μg As/ml.

Can. J. Chem. Downloaded from www.nrcresearchpress.com by 210.87.254.6 on 09/05/12
For personal use only.

detailed study of the effect of As(V) was made in the present work. The formation of $H_3AsW_{12}O_{40}$ (TAA) in acid solution has been reported recently (27). Figure 4 shows typical absorption spectra in *n*-amyl alcohol of TAA extracted from aqueous solution in the p*H* range 0–2. It is evident that the interference from As(V) arises from the intense absorption at 267 nm. In Fig. 5, the formation–extraction of TAA at concentrations ranging from 0.75 to 15 μg As/ml is shown. Superimposed is the curve for the formation–extraction of TPA (equivalent to 1.55 μg P/ml). Obviously, if the p*H* is set between 1.5–1.9, interference from As is minimized. The data of Table 1 clearly show that even for rather high As/P ratios, the recovery of P is satisfactory in the p*H* range 1.5–1.9. This relative freedom from interference of As(V) represents a significant advantage over the phosphate methods now in routine use.

The high tolerance of the TPA procedure to Si(IV) and Ge(IV) (at 1.55 μg P/ml) arises from the fact that extraction of 12-tungstosilicic and -germanic acids into *n*-amyl alcohol is negligible at acidities lower than 0.3 *M* $HClO_4$. In the molybdenum-blue method, no more than 3.0 μg Si/ml ($SnCl_2$ reduction (2)) and 10 μg/ml (ascorbic acid – Sb(III) reduction (8)) can be tolerated at 10 μg P/ml. No quantitative information is available on the extent of Ge(IV) interference.

As already discussed, the isopoly species do not interfere under the conditions of the TPA method.

(d) Analytical Applications

(i) Water Samples

The water samples, which had been preserved by addition of H_2SO_4 to a p*H* ~ 1, were obtained from the Upper Lakes Pollution Group (Windsor, Ontario) (ULPG) and the Canada Centre for Inland Waters (Burlington, Ontario). A concentrated nutrient reference sample was provided by the Environmental Protection Agency (Cincinnati, Ohio). The analytical results are presented in Table 2. The values by the molybdenum-blue method were obtained by other laboratories. The ULPG values (samples 42, 44, 46) for total soluble phosphate represent the average result of several laboratories which participated in a round-robin analysis. These laboratories used the molybdenum-blue method but a variety of reductants such as $SnCl_2$, 1-amino-2-naphthol-4-sulphonic acid, ascorbic acid, or a combination of ascorbic acid and Sb(III). On the whole, the agreement between the TPA and molybdenum-blue values is good. A comparison of the precision values is not valid since some data represent several different analysts and other data represent only a single determination. The molybdenum-blue method, however, requires much stricter control over the experimental conditions. This disadvantage is somewhat offset by the more tedious TPA procedure.

The literature contains several methods for the determination of phosphorus in natural waters but few for its determination in wastewater (8, 28). According to Heinke (28), many analysts are using methods developed for natural waters for the determination of phosphorus in wastewaters without proof that materials in sewage do not interfere. In this regard, the TPA method was tested by application to raw-sewage influent and effluent from a municipal sewage-treatment plant. The standard-addition technique was used to ascertain the effect of possible interferences. Excellent agreement was obtained between the found and added values for the spike (Table 3).

TABLE 1. Recovery of phosphorus (as phosphate) in the presence of arsenic (as arsenate)[a]

Taken (μg/ml)		
P	As[b]	P found (μg/ml)[c]
0.0155	3.75	0.023 ±0.002
	1.50	0.017 ±0.002
	0.75	0.0153±0.0002
0.155	15.0	0.212 ±0.003
	3.75	0.180 ±0.001
	1.50,0.75	0.156 ±0.002
1.55	15.0	1.75 ±0.02
	3.75,1.50,0.75	1.54 ±0.002
15.50	15.0	16.10 ±0.02
	3.75,1.50,0.75	15.53 ±0.02

[a]T = 100°C, p*H* 1.5–1.9.
[b]For the range 0.01–0.02 μg P/ml, an As/P ratio (μg/ml) of at least 50 is tolerable. For the ranges 0.1–0.2 and 1–2 μg P/ml, ratios of at least 10 and 2, respectively, are tolerable.
[c]Average of two determinations. Precision measure is the average deviation.

(ii) Alloys, Ores, a Mineral, and an Organophosphorus Compound

The results for %P in steel samples (NBS) and phosphor–bronze samples (Canada Centre for Mineral and Energy Technology) and in an organophosphorus compound (NBS) are presented in Table 4. Also reported are the results (as $\%P_2O_5$) for ores and a mineral.

A separation was not required in the analysis of the phosphor–bronze samples since Fe was present at <3 μg/ml and the other metals present (Cu, Sn, Pb, Zn, Ni, and Al) did not interfere. Separation of Fe was, however, necessary in the analysis of the steel samples.

(e) Reliability of the TPA Method

The reliability of a method is characterized by its accuracy, precision, and sensitivity. These properties are discussed in turn with respect to the TPA method.

Can. J. Chem. Downloaded from www.nrcresearchpress.com by 210.87.254.6 on 09/05/12
For personal use only.

TABLE 2. Determination of total soluble phosphate as P in water samples

Sample No.	Source	Total soluble phosphate (mg P/ℓ) Molybdenum-blue[a]	TPA[b]
42	Lake Michigan	0.009±0.004 (17)	0.008±0.001
		0.007±0.003 (11)	
44	S & S Canal	1.83 ±0.15 (16)	1.85 ±0.01
		1.85 ±0.12 (15)	
46	STP-effluent	0.174±0.024 (17)	0.170±0.001
		0.179±0.015 (16)	
1806	St. Mary's River	0.001 (F)[c]	0.002
		0.002 (UF)[c]	0.002
4907	Welland Canal	0.005 (F)[c]	0.003
2412	Well-site	0.038 (UF)[c]	0.042±0.001
1	EPA nutrient reference	0.021[d]	0.019±0.002

[a]The precision measure is the standard deviation. The numbers in parentheses represent the number of laboratories whose results are included in the average. The averages based on less than 17 results were recalculated by ULPG after deletion of suspected data.
[b]Each result (except for those for samples 1806 and 4907) represents the average of three determinations. The precision measure is the standard deviation.
[c]F = filtered; UF = unfiltered.
[d]Calculated value from primary standard P ingredient.

TABLE 3. Determination of total soluble phosphate as P in sewage water

Total phosphorus (ppm)					
		Spike			
Sample + Spike[a]		Found		Added	
Influent	Effluent	Influent	Effluent	Influent	Effluent
3.84±0.03	0.614±0.005	1.22±0.01	0.245±0.005	1.24	0.248
5.07±0.02	0.737±0.002	2.45±0.02	0.368±0.004	2.48	0.372
5.62±0.04	0.983±0.005	3.00±0.01	0.614±0.005	3.10	0.620
6.31±0.02		3.69±0.01		3.72	

[a]The unspiked influent and effluent contained 2.62 ± 0.04 and 0.369 ± 0.006 ppm P, respectively. The spike was added as a volume of standard phosphate solution. Measurements at both 60 and 100°C yielded essentially the same results. Values represent the average of six determinations. The precision measure is the standard deviation.

TABLE 4. Determination of phosphorus in alloys, ores, a mineral, and an organophosphorus compound

Sample No.	%P Certified value[d]	%P TPA[e]
170A[a]	0.005 (0.004 –0.007)	0.0053±0.0001
15f[a]	0.006 (0.004 –0.007)	0.0065±0.0005
14e[a]	0.008 (0.007 –0.010)	0.008 ±0.001
8j[a]	0.095 (0.094 –0.098)	0.093 ±0.002
304[b]	0.007 (0.0045–0.011)	0.0063±0.0002
293[b]	0.030 (0.028 –0.032)	0.029 ±0.002
477[b]	0.43 (0.40 –0.45)	0.422 ±0.002
SU-1 (Ni–Co–Cu)	0.10[f]	0.099 ±0.002
25c (Mn ore)	0.22[f]	0.204 ±0.003
99a (Feldspar)	0.02[f]	0.019 ±0.001
1071a[c]	9.5	9.43 ±0.02

[a]Steel standards.
[b]Phosphor–bronze spectrographic standards.
[c]Triphenyl phosphate standard.
[d]The numbers in parentheses given the range of values from which the certified value was obtained as an average.
[e]The results are the average of three determinations. Precision measure is the standard deviation.
[f]Provisional values, as $\%P_2O_5$. TPA value as $\%P_2O_5$.

TABLE 5. Accuracy of the TPA method for the determination of phosphate in some materials

Sample No.	η	P (ppm) or %P or P_2O_5		Confidence interval[a]	
		$\bar{x}$	s	95%	99%
42	3	0.008	0.001	0.008 ±0.003	0.008 ±0.006
44	3	1.85	0.01	1.85 ±0.025	1.85 ±0.057
46	3	0.170	0.001	0.170 ±0.003	0.170 ±0.006
1	5	0.019	0.002	0.019 ±0.003	0.019 ±0.004
1071a	4	9.43	0.02	9.43 ±0.032	9.43 ±0.058
25c	3	0.204	0.003	0.204 ±0.008	0.204 ±0.017
99a	3	0.019	0.001	0.019 ±0.003	0.019 ±0.006
170A	3	0.0053	0.0001	0.0053±0.0003	0.0053±0.0006
14e	3	0.008	0.001	0.008 ±0.003	0.008 ±0.006

[a]The confidence interval is based on the equation: $\mu = \bar{x} \pm ts/\sqrt{\eta}$.

(i) Accuracy

Both the 95% and 99% confidence intervals (Table 5) are satisfactory for the small number of replicate determinations done. Although the testing is by no means exhaustive, the data show that the TPA method is capable of yielding acceptably accurate results.

(ii) Precision

Based on the 95% confidence limit, the percentage coefficient of variation was found to be 4.8% for 0.0062 ppm P; 2.3% for 0.062 ppm; 1.6% for 0.62 ppm; and 0.65% for 6.2 ppm. The percentage coefficient of variation values reported for the molybdenum-blue methods (8) are: 19% at 0.16 ppm P and 8.5% at 3.2 ppm with stannous chloride as the reductant; 4% at 0.05–0.10 ppm P, 11% at 0.027 ppm, and 100% at 0.81 ppm with ascorbic acid as the reductant. The superior precision of the TPA method is primarily the result of the greater range in experimental conditions which the TPA method allows. A detailed discussion of this topic is given elsewhere (29).

(iii) Sensitivity

If, following Sandell (30), the minimum detectable value of absorbance is taken as 0.001, the use of a 1 cm cell would give for TPA ($\varepsilon_{267} = 5.1 \times 10^4$) a limit of detection corresponding to 0.62 ppb P. This sensitivity, however, is not attainable in practice since it is limited by the accuracy of the apparatus and the magnitude of the blank value. The blank value in the present work corresponded to 0.005 ± 0.002 absorbance units on a total of 20 measurements. If a signal could be considered to be different from the blank value when it is at least as great as the mean blank value plus three standard deviations of the blank value (31), the practical limit of absorbance would be ~0.011, and consequently the practical limit of sensitivity of the TPA method would be ~6 to 7 ppb P for a 1 cm cell. Comparisons are not possible with the molybdenum-blue methods since standard deviations of the blank values do not appear to have been reported.

Conclusions

The TPA method is at least competitive with the molybdenum-blue methods in terms of accuracy, precision, and sensitivity. In addition, it is less prone to interferences, especially from As(V), and it allows greater freedom in the adjustment of experimental conditions. Because of the number and nature of steps required by the TPA procedure, however, it is difficult to automate and, at the present time, is best suited to the analysis of non-routine samples and as a reference method.

TPA is intrinsically triprotic; its apparent heptaproticity in aqueous solution is due to its instability in aqueous solution above p*H* 2.

Acknowledgements

The authors are grateful to the National Research Council of Canada for financial support of this research, and to the Upper Lakes Pollution Group, the Canada Centre for Inland Waters, the Environmental Protection Agency, and the Regional Laboratory of Hamilton–Wentworth for the generous provision of samples.

1. D. F. BOLTZ. *In* Analytical chemistry of phosphorus compounds. Vol. 37. *In* Chemical analysis. *Edited by* M. Halmann. John Wiley and Sons, New York, NY. 1972. Chapt. 1.
2. F. A. J. ARMSTRONG. *In* Analytical chemistry of phosphorus compounds. Vol. 37. *In* Chemical analysis. *Edited by* M. Halmann. John Wiley and Sons, New York, NY. 1972. Chapt. 20.
3. K. S. SUBRAMANIAN. Ph.D. Thesis, McMaster University, Hamilton, Ont., Canada. 1976.
4. S. R. CROUCH and H. B. MALMSTADT. Anal. Chem. **39**, 1084 (1967).
5. P. M. BECKWITH, A. SCHEELINE, and S. R. CROUCH. Anal. Chem. **47**, 1930 (1975).
6. V. F. BASKOVSKII, N. A. ALIKINA, and V. S. SHVRER. J. Anal. Chem. USSR, **25**, 288 (1970).

Can. J. Chem. Downloaded from www.nrcresearchpress.com by 210.87.254.6 on 09/05/12
For personal use only.

7. D. L. JOHNSON and M. E. Q. PILSON. Anal. Chim. Acta, **58**, 289 (1972).
8. J. D. BURTON. Water Res. 7, 291 (1973).
9. R. W. TILLMAN and J. K. SYERS. Analyst London, **100**, 322 (1975).
10. L. DUVAL. Chim. Anal. **45**, 237 (1963).
11. M. JEAN. Anal. Chim. Acta, **42**, 545 (1968).
12. G. A. TSIGDINOS. Bulletin Cdb-12a. Climax Molybdenum Company, New York, NY. 1969.
13. G. M. VARGA, E. PAPACONSTANTINOU, and M. T. POPE. Inorg. Chem. **9**, 662 (1970).
14. H. M. THEASTON and W. R. BANDI. Anal. Chem. **38**, 1764 (1966).
15. T. J. R. WEAKLEY. *In* Structure and bonding. Vol. 18. *Edited by* J. D. Dunitz *et al.* Springer-Verlag, Berlin. 1974. pp. 131–176.
16. D. D. PERRIN, W. L. F. ARMAREGO, and D. R. PERRIN. Purification of laboratory chemicals. Pergamon Press, London. 1966. pp. 38, 70–72.
17. J. S. FRITZ and F. E. GAINER. Talanta, **13**, 939 (1966).
18. D. L. KEPERT. *In* Comprehensive inorganic chemistry. *Edited by* J. C. Bailer. Pergamon Press, London. 1973. pp. 607–672.
19. K. S. SUBRAMANIAN. Ph.D. Thesis, McMaster University, Hamilton, Ont., Canada. 1976. pp. 95–97.
20. V. I. SPITSYN and G. V. KOSMODEMYANSKAYA. J. Inorg. Chem. USSR, **10**, 353 (1965).
21. P. SOUCHAY. Ann. Chim. Paris, **20**, 73 (1945).
22. G. D. CHRISTIAN. *In* CRC critical reviews in analytical chemistry. Vol. 5. *Edited by* B. H. Campbell. CRC Press, Cleveland, Ohio. 1975. pp. 1–84.
23. K. P. QUINLAN and M. A. DESESA. Anal. Chem. **27**, 1626 (1955).
24. I. M. KOLTHOFF, E. B. SANDELL, E. J. MEEHAN, and S. BRUCKENSTEIN. Quantitative chemical analysis. The Macmillan Company, Toronto, Ont. 1969. pp. 1153, 1155.
25. H. LEVINE, J. J. ROWE, and F. S. GRIMALDI. Anal. Chem. **27**, 258 (1955).
26. J. MURPHY and J. P. RILEY. Anal. Chim. Acta, **27**, 31 (1962).
27. B. E. REZNIK, L. P. TSYGANOK, and V. P. STATSENKO. J. Anal. Chem. USSR, **26**, 1409 (1971).
28. G. W. HEINKE. Ph.D. Thesis, McMaster University, Hamilton, Ont., Canada. 1969.
29. K. S. SUBRAMANIAN. Ph.D. Thesis, McMaster University, Hamilton, Ont., Canada. 1976. pp. 175–179.
30. E. B. SANDELL. Colorimetric determination of trace metals. Interscience, New York, NY. 1959.
31. H. KAISER. Z. Anal. Chem. **216**, 80 (1966).

Can. J. Chem. Downloaded from www.nrcresearchpress.com by 210.87.254.6 on 09/05/12
For personal use only.

The volume of activation for benzyl chloride hydrolysis and its pressure dependence

R. LOHMÜLLER, D. D. MACDONALD, M. MACKINNON, AND J. B. HYNE[1]

Department of Chemistry, University of Calgary, Calgary, Alta., Canada T2N 1N4

Received September 15, 1977

R. LOHMÜLLER, D. D. MACDONALD, M. MACKINNON, and J. B. HYNE. Can. J. Chem. **56**, 1739 (1978).

Various equations which have been proposed to provide the 'best' functional form for the dependence of rate upon pressure for reactions in solution have been tested for the extraction of ΔV^* and $d\Delta V^*/dp$ for the hydrolysis of benzyl chloride at 30°C and at pressures over the range 1 to 6895 bar. One hundred individual rate constants were determined for this reaction at pressure increments of 345 bar and provide a sufficiently large body of data to permit application of statistical methods for testing the various rate–pressure functions with little risk of bias.

R. LOHMÜLLER, D. D. MACDONALD, M. MACKINNON et J. B. HYNE. Can. J. Chem. **56**, 1739 (1978).

On a vérifié diverses équations qui ont été proposées pour fournir la "meilleure" forme fonctionnelle exprimant la relation entre la vitesse de réaction et la pression afin d'en tirer le ΔV^* et le $d\Delta V^*/dp$ de réactions d'hydrolyse en solution du chlorure de benzyle à 30°C et à des pressions allant de 1 à 6895 bar. On a déterminé 100 constantes de vitesse individuelle pour cette réaction avec des augmentations de pression de 345 bar et ces données fournissent un ensemble suffisamment étendu pour permettre l'application de méthodes statistiques pour vérifier les diverses fonctions vitesse–pression en impliquant un minimum de risque de polarisation.

[Traduit par le journal]

Introduction

In recent years there has been considerable discussion and controversy as to the best method for determining the activation volume, ΔV^*, and its pressure dependence $(\partial\Delta V^*/\partial p)_T$ from rate vs. pressure data for reactions in solution (1–11). Various methods have been suggested, including the use of polynomial $\ln k$ vs. p functions (6), incremental extrapolation (7), and by assuming that the volume of activation has a functional dependence upon pressure approximated by the empirical Tait equation (8, 9), which has been found to represent satisfactorily the PVT properties of many real substances.

The first two methods rely upon the differentiation of an empirical expression for the pressure dependence of $\ln k$ to evaluate ΔV^* according to [1].

$$[1] \qquad \Delta V^* = -RT\left(\frac{\partial \ln k}{\partial p}\right)_T$$

However, the Tait equation method is, in principle, one of integration, in that ΔV^* is assumed to have some a priori pressure dependence. The function form of the pressure dependence of $\ln k$ is then

$$[2] \qquad \ln (k_p/k_0) = -\frac{1}{RT}\int_{p_0}^{p} \Delta V^*(p)\, dp$$

A previous statistical analysis by Golinkin *et al.* (4) using relatively sparse experimental $\ln k$ vs. pressure data for benzyl chloride solvolysis in aqueous alcohol systems indicated that the second order polynomial function provided the best method for extracting ΔV^* and $(\partial\Delta V^*/\partial p)$ from rate–pressure data. This finding has been questioned frequently (see review by Eckert (10)) and the problem of selecting the best method for evaluating these pseudo-thermodynamic parameters of activation remains. This is of particular importance in the extraction of higher derivative activation parameters such as $d\Delta V^*/dp$. Part of the problem lies in the paucity of good experimental $\ln k$ vs. pressure data for most reactions studied. Furthermore, the data available have seldom been treated by rigorous statistical methods, and the choice of the $\ln k$ vs. pressure function has frequently been subject to bias.

In this paper we re-examine the problem of selecting the best functional dependence of $\ln k$ upon pressure for obtaining ΔV^* and $d\Delta V^*/dp$ values. The reaction chosen as the test case is the hydrolysis of benzyl chloride at 30°C over a pressure range of 1 to nearly 7000 bar. This reaction has been studied previously (11–14) and is particularly suitable in that no reactions (e.g. elimination) have been shown to occur other than the simple hydrolysis, i.e.

$$C_6H_5CH_2Cl + H_2O \rightarrow C_6H_5CH_2OH + HCl$$

In the present study we have made some 100 individual rate determinations at pressure increments of 345 bar. This number of independent data points is larger than has hitherto been available for any single

[1]To whom correspondence should be addressed.

Can. J. Chem. Downloaded from www.nrcresearchpress.com by 210.87.254.5 on 09/05/12
For personal use only.

Can. J. Chem. Downloaded from www.nrcresearchpress.com by 210.87.254.5 on 09/05/12
For personal use only.

reaction in solution at a given temperature under hydrostatic pressure and, for the first time, permits a statistical analysis to be performed with little risk of bias.

Experimental

Materials

House distilled water was passed through a deionizing resin and exhibited a specific conductance of less than 8×10^{-7} S cm^{-1} at 25°C. Benzyl chloride was distilled twice under reduced pressure and the middle fraction collected. Analysis by gas–liquid chromatography showed less than 0.02% impurity.

Rate Measurements

Rate measurements at atmospheric pressure and at pressure increments of 345 bar up to 6895 bar were carried out as previously described (11, 15). The pressure vessel was submerged in a 40 gal thermostat which was controlled to better than ±0.01°C. An automatic pressure control device permitted pressures to be held constant to within ±14 bar over the entire pressure range employed. Approximately 1 h was allowed for temperature and pressure equilibration before rate data were collected.

The rate of production of HCl resulting from the hydrolysis of the benzyl chloride was followed by an *in situ* conductimetric method thereby avoiding uncertainties introduced by aliquot sampling techniques. The type of cells used has been described previously (15). The conductance measurement was carried out with an automatic conductance bridge General Radio Type 1680-A (1 kHz) which printed the results in 4 to 5 digit integers with an average change of 1000 integer units per half-life measured. The reproducibility of the conductance bridge is quoted to better than ±1 in the last digit. The time required for a conductivity reading was less than 1.1 s, according to the manufacturer's specifications. Therefore, a standard deviation of ±2 s in the independent variable (time) in the conductance–time relationship was assumed.

Systematic errors in the rate determinations could occur by contamination of the sample (especially with compression oil through uneven pressurization) and through aquisition of data before thermal equilibrium was achieved. Special procedures were adopted, as described below, in the reaction rate analysis to eliminate experimental results containing systematic errors.

Results and Discussion

The Rate Constant and its Errors

It has been established in earlier work (11) that the hydrolysis of benzyl chloride in dilute aqueous solution follows a strictly pseudo-first order rate expression. The Guggenheim (16) rate analysis technique (eq. [3]) is therefore a convenient way of extracting the rate constant, k, from conductance–time data.

$$[3] \quad \ln(\lambda_{t+\Delta t} - \lambda_t) = kt + \ln(\lambda_\infty - \lambda_0)(1 - e^{k\Delta t})$$

Other methods (17, 18) have been tried and yield identical results, but do not have the advantage of being amenable to linear regression analysis. Furthermore, they are not as sensitive to deviations of the experimental data from a first order rate relationship.

The regression analysis, i.e. the evaluation of the slope k and the intercept of a linear regression, was carried out by computer to reduce the possibility of bias. This statistical treatment also provides several criteria for the final selection of acceptable conductance–time data, i.e. for the exclusion of sets of conductance–time data which carry systematic errors or features that can be ascribed to experimental artifact. No sets of conductance–time data were employed in the final analysis if the correlation coefficient was smaller than 0.99990. Further, if the 95% confidence limit of the slope indicated an error limit in the rate (k) in excess of 1% the data were rejected. This test is sensitive to the number of conductance–time data points taken in each run and used in the regression analysis. This number normally exceeded 20.

Finally a graphical representation of the deviation of the experimental data points from the least-squares regression line was constructed, together with a double-sided test of significance, to detect any systematic deviation of the data from a straight line. In this double-sided test the slope obtained by regression on the first two-thirds of the conductance–time data was compared with the slope calculated from the last two-thirds of data. The 95% confidence limit of the Student's t function was used as the criterion for acceptance. The selected rate constants, k, are presented in Table 1.

Determination of the Error in k

Since the rate constant, k, is not a directly measured quantity, the determination of its error requires elaboration. Excluding systematic errors, the *major* reasons for the deviation of the computed value, k, from κ (the true value of the rate constant) are uncertainties in p, T, λ (conductance), and t, and their mutual dependency (i.e. correlations).

The error in k due to temperature variation can be predicted using the Arrhenius relationship between the reaction rate and temperature.

$$[4] \quad k = A \exp(-E_a/RT)$$

where E_a is the energy of activation and A is a constant. The standard error (SE) of a function $y = f(x)$ is defined as

$$[5] \quad \mathrm{SE}(X) = |\partial y/\partial x|\sigma$$

in which σ is the standard deviation of the parent population. The standard error in k at a given temperature, δk_T, therefore can be evaluated using [6].

$$[6] \quad \delta k_T = \left[\frac{AE_a}{RT^2}\exp(-E_a/RT)\right]\delta T$$

Substitution of values for A and E_a from the work of Dickson and Hyne (15) on benzyl chloride hydrolysis at atmospheric pressure yields $\delta k_T = 2.6 \times 10^{-8}\ s^{-1}$ at 30°C for an assumed error in temperature of

TABLE 1. Hydrolysis of benzyl chloride at 30.00°C

Pressure (p/bar)	Experimental rate ($k/10^5$ s^{-1})	Mean rate ($\bar{k}/10^5$ s^{-1})	Standard deviation (SD/10^5 s^{-1})	Confidence limit (95% CL/10^5 s^{-1})
1	2.438, 2.424, 2.486, 2.474			
	2.473, 2.505, 2.471, 2.526			
	2.510, 2.480, 2.472	2.478	0.030	0.020
345	2.830, 2.763, 2.792, 2.772	2.789	0.030	0.048
689	3.158, 3.152, 3.106, 3.250	3.167	0.060	0.095
1034	3.469, 3.493, 3.537, 3.533			
	3.409, 3.482, 3.491, 3.607			
	3.316, 3.160	3.495	0.088	0.063
1379	3.673, 3.940, 3.835, 3.875			
	3.837, 3.857, 3.846, 3.933	3.850	0.082	0.068
1724	4.274, 4.270, 4.293, 4.290			
	4.263, 4.283	4.279	0.012	0.013
2068	4.659, 4.727, 4.770, 4.767			
	4.633, 4.752	4.718	0.058	0.061
2413	5.251, 5.231, 5.190, 5.162	5.209	0.040	0.064
2758	5.590, 5.634, 5.646	5.623	0.030	0.075
3103	6.033, 6.016, 6.071	6.040	0.028	0.070
3447	6.672, 6.621, 6.625, 6.572			
	6.649, 6.610, 6.584, 6.686	6.627	0.040	0.033
3792	7.144, 7.076	7.110	0.048	0.431
4137	7.528, 7.548, 7.622, 7.483			
	7.764, 7.677, 7.558	7.597	0.097	0.090
4482	8.259, 8.287, 8.133	8.226	0.082	0.204
4826	8.844, 8.899, 8.842, 8.568	8.788	0.149	0.237
5171	9.377, 9.264, 9.509	9.383	0.123	0.305
5516	10.21, 9.881, 10.26, 9.615	9.992	0.302	0.480
5861	10.44, 10.58, 10.48	10.51	0.070	0.174
6205	11.06, 10.86, 11.31, 11.34	11.10	0.218	0.271
6895	12.43, 11.86	12.15	0.403	3.619

Can. J. Chem. Downloaded from www.nrcresearchpress.com by 210.87.254.5 on 09/05/12
For personal use only.

±0.01°C. This represents an uncertainty of ~0.1% of the mean value of k (2.478×10^{-5} s^{-1}) at this temperature.

The relationship between the rate constant, k, and pressure is given by [1], in which terms due to the pressure dependencies of the activity coefficients have been neglected. Since the pressure dependence of $\Delta V^{\neq}$ is generally unknown, the differential has to be solved by approximation. Without further justification at this point we assume that a quadratic relationship between ln k and p is sufficient for the purpose of evaluating the error in k due to uncertainty in pressure. Accordingly, differentiation of [7],

$$[7] \qquad \ln k = A_0 + A_1 p + A_2 p^2$$

yields the error function as

$$[8] \qquad \delta k_p = [k(A_1 + 2A_2 p)]\delta p$$

where the empirical constants A_1 and A_2 were obtained from the quadratic fit (see later discussion). For $\delta p = 14$ bar (i.e. the uncertainty in pressure control), the error in k for $T = 30$°C amounts to 2.12×10^{-7} s^{-1} at 3447 bar ($k = 6.627 \times 10^{-5}$ s^{-1}) and 2.10×10^{-7} s^{-1} at 6895 bar ($k = 1.215 \times 10^{-4}$ s^{-1}). These errors represent uncertainties of 0.32% and 0.17% in the mean values for k at 3447 and 6895 bar, respectively. It appears, therefore, that the error due to uncertainty in pressure is significantly greater than that due to uncertainty in temperature, at least for the data used here.

The rate constant, k, is related to the conductance, λ, by [3] which was used for the Guggenheim rate analysis. After rearranging, and substituting D for the constant term and $\Delta\lambda$ for the conductance difference ($\lambda_{t+\Delta t} - \lambda_t$), eq. [3] reduced to the following expression.

$$[9] \qquad k = \frac{\ln \Delta\lambda}{t} - \frac{D}{t}$$

Since t and λ are both subject to error, and are strongly correlated, the estimation of the δk has to be made (19) using [10].

$$[10] \quad \delta k_{\lambda,t} = \left[\left(\frac{\partial k}{\partial t}\right)^2 \delta^2(t) + \left(\frac{\partial k}{\partial \Delta\lambda}\right)^2 \delta^2(\Delta\lambda) + 2\left(\frac{\partial k}{\partial t}\frac{\partial k}{\partial \Delta\lambda}\right)\delta(t)\delta(\Delta\lambda)\rho(t, \Delta\lambda) \right]^{1/2}$$

Can. J. Chem. Downloaded from www.nrcresearchpress.com by 210.87.254.5 on 09/05/12
For personal use only.

where $\rho(t,\Delta\lambda)$ is the correlation coefficient for t and $\Delta\lambda$.

As an illustration of the numerical evaluation of $\delta k_{\lambda,t}$ we consider a run at 3447 bar and 30°C with a rate constant of 6.625×10^{-5} s^{-1}. The error was calculated using the experimental values of λ_t = 10 101 S and $\lambda_{t+\Delta t}$ = 13 253 S at t = 17 100 s. The actual correlation coefficient of 0.999813 for this run was substituted by the minimal correlation coefficient of 0.9999. An error δt = 2.0 s (i.e. the uncertainty in the time of reading) and a relative error of $\delta\lambda$ = 2 S in the combined conductance readings (i.e. ±1 in each conductance reading) yielded an error in k of $\pm 5.1 \times 10^{-8}$ s^{-1}. This represents an uncertainty of 0.08% in the mean value for the rate constant.

Although temperature, pressure, and conductance are not independent, the errors in these reaction parameters can be considered independent for the present purpose since, in the error range considered, a change in one parameter would not significantly affect the other parameters. The total error δk, therefore, can be calculated from [11].

$$\delta k = \delta k_T + \delta k_p + \delta k_\lambda \qquad [11]$$

This analysis yields values for δk of 1.0×10^{-7} s^{-1} and 3.0×10^{-7} s^{-1} for pressures of 1 and 3447 bar, respectively. The percentage errors in k corresponding to these pressures are ±0.4% (1 bar) and ±0.5% (3447 bar), which we consider to be entirely realistic for the error sources considered.

Error propagation provides a reasonable means for the evaluation of the lower error limit, of the quality of the experiments, and of the magnitude and importance of error parameters when an improvement in the experimental method is planned. For instance, the calculations carried out in the previous section indicate that the greatest source of error in k arises from the uncertainty in pressure. Thus, the total error in k could be markedly reduced by an improvement in the method of pressure control. However, for the evaluation of an *experimental* error the experiments have to be carried out, and whenever experimental findings disagree with computed results the former must take priority. The reason for this, of course, is that a host of possible statistical error sources exist which are not covered by [6], [8], and [10]. Furthermore, the confidence limit for the *mean value* of k (i.e. $\bar{k}$) is sensitive to the number of values from which it was calculated. Therefore, in order to obtain statistically meaningful estimates of $\bar{k}$, and the associated errors, the rate data listed in Table 1 were subjected to detailed statistical analysis. In addition to the previously discussed experimental k values, the mean $\bar{k}$ values for each pressure, their standard deviations, and 95% confidence limits are listed in Table 1. The distribution to the values was found to be close enough to normality, even in their logarithmic form, to justify this statistical treatment.

The observation that the error remains small with rising pressure seems to hold if a sufficient number of experiments are carried out. However, the difficulty of carrying out a successful experiment increases with pressure. Therefore, the number of experiments performed, and hence the precision in determining the mean value of k, usually also decreases with p. The relative sensitivity of the standard deviation and the confidence limit to the number of individual rate determinations at a given pressure is well illustrated by the values at 3447 and 3792 bar (Table 1). Both the standard deviations are quite low (0.040 and 0.048) and it might be concluded that the $\bar{k}$ values are equally precise. However, the 95% confidence limit for the 3792 value (0.431) with only two rate determinations available is an order of magnitude different from that at 3447 (0.033) where eight rate values were used in the determination of the mean. Accordingly, it seems important to cite *both* the overall standard deviation and the overall error limit for 95% confidence when reporting rate constants at elevated pressures.

The Rate–Pressure Functions

In the previous section considerable effort was expended in establishing the reliability of rate constants for the hydrolysis of benzyl chloride as a function of pressure. These data are now used to evaluate various empirical methods for extracting the volume of activation, $\Delta V^{\ddagger}$, and its pressure dependence, $(\partial\Delta V^{\ddagger}/\partial p)_T$ for this reaction. No a priori assumptions are made regarding the quality of any given empirical function in representing the pressure dependence of the rate constant k. The various empirical functions chosen for analysis are described below.

Polynomial Function

The simplest functional dependence of ln k upon pressure is given by the polynomial equation [12*a*]

$$\ln k = \sum_{i=0}^{n} A_i p^i \qquad [12a]$$

where n is the degree of the polynomial with coefficients (A_0, A_1, ..., A_n). Differentiation of [12*a*] with respect to pressure yields the following expressions for $\Delta V^{\ddagger}$ and $(\partial\Delta V^{\ddagger}/\partial p)$ at zero pressure

$$\Delta V_0^{\ddagger} = -RTA_1 \qquad [12b]$$

$$(\partial\Delta V^{\ddagger}/\partial p)_{p=0} = -2RTA_2 \qquad [12c]$$

It should be noted that when n = 1 the resulting linear rate–pressure relationship is the classical van't Hoff equation.

Can. J. Chem. Downloaded from www.nrcresearchpress.com by 210.87.254.5 on 09/05/12
For personal use only.

Incremental Function

Whalley and co-worker (2, 7) proposed that reliable values for the activation volume can be derived graphically using the incremental expression eq. [13]

$$[13a] \quad \ln [k(p_{i+1})/k(p_i)]/(p_{i+1} - p_i) = A_1 + A_2\left[\frac{p_{i+1} + p_i}{2}\right]$$

where

$$[13b] \quad \Delta V_0^{\ddagger} = -RTA_1$$

$$[13c] \quad (\partial \Delta V^{\ddagger}/\partial p)_{p=0} = -2RTA_2$$

It should be noted that the incremental method represents, in mathematical terms, a reduced quadratic equation. Although the incremental method is basically a graphical technique for analysing rate–pressure data, it is treated in this study by computer to obtain statistical data for comparison with the other functions chosen for study.

Benson–Berson Function

Benson and Berson (8) expressed the pressure dependence of $\Delta V^{\ddagger}$ in terms of the empirical Tait equation and, upon integration (eq. [2]), derived the following expression for the dependence of rate upon pressure

$$[14a] \quad [\ln (k_i/k_o)]/p_i = A_1 + A_2 p^{0.523}$$

where

$$[14b] \quad \Delta V_0^{\ddagger} = -RTA_1$$

$$[14c] \quad (\partial \Delta V^{\ddagger}/\partial p)_{p=1} = -0.797RTA_2$$

The exponent 0.523 is strictly valid only for organic solvents, although it has been used for aqueous systems. The Benson–Berson function as written above is included here for reasons of comparison only.

Reduced Quadratic Function

The incremental and Benson–Berson functions described above can be treated as linear regressions after transformation of the variables. This transformation clearly involves a rather drastic change in scale of the dependent variable. In order to assess the effect of transforming an inherently nonlinear function to a linear one, we have carried out a similar transformation on the quadratic function, thereby deriving the following expressions for the pressure dependence of ln k and the corresponding parameters of activation.

$$[15a] \quad [\ln (k_i/k_0)]/p_i = A_1 + A_2 p_i$$

$$[15b] \quad \Delta V_0^{\ddagger} = -RTA_1$$

$$[15c] \quad (\partial \Delta V^{\ddagger}/\partial p)_{p=0} = -2RTA_2$$

Note that in [15] the regression is forced through the initial point (k_0) and the function, therefore, contains one less regression coefficient than the corresponding polynomial of degree 2.

The Regression Analysis

Regression analyses (19–23) were performed with each of the functions discussed above using the rate data unweighted and weighted. In the weighted data cases standard deviation (SD) or the 95% confidence limits (CL) as listed in Table 1 were used separately to calculate statistical weights (21) for each rate–pressure point.

Because of the variety of types of weighted and unweighted data treatment more than 80 regression coefficients and their associated variances were yielded by this analysis. Only the coefficients for the unweighted data treatment are presented here (Table 2). Other values are available on request.

In order to determine the point at which higher order terms in the polynomial expression no longer represents a statistically significant improvement of fit, Student's t-test has been applied. Table 3 lists various t values calculated from the three types of weighted and unweighted regression analyses; t_u unweighted, t_{SD} standard deviation weighted, and t_{CL} confidence limit weighted. Values in each of these categories are shown for various orders of the polynomial. These values can then be compared with t values taken from statistical tables for various levels of confidence. When t_u, t_{SD}, or t_{CL} values for a given polynomial become smaller than the corresponding t value for a given confidence level the highest order term in the polynomial is no longer statistically significant.

Accordingly for a 99% confidence limit the unweighted regression (t_u) indicates that third and higher order terms are not significant, hence the quadratic expression should be used. When the data are weighted by either method (t_{SD}, t_{CL}), however, the third order term is significant, indicating a cubic polynomial is appropriate. Reducing the confidence limit to 95% does not change the cut-off for the weighted data cases.

In extracting the $\Delta V^{\ddagger}$ and $d\Delta V^{\ddagger}/dp$ parameters, therefore, no polynomials above third order have been employed. The nontriviality of the third power pressure term implies the existence of pressure dependence of $d\Delta V^{\ddagger}/dp$. This should be compared with the pressure dependence of the compressibility of real substances and with the temperature dependence of the enthalpy of activation (i.e. $\Delta C_p^{\ddagger}$).

The Pseudo-thermodynamic Parameters

The essential purpose of this detailed and statistically rigorous analysis is to extract the pseudo-

TABLE 2. Regression coefficients

Function	A_0	A_1	A_2
Linear (van't Hoff)	-0.1049×10^{2}	0.2321×10^{-3}	—
Quadratic	-0.1059×10^{2}	0.3349×10^{-3}	-0.1538×10^{-7}
Cubic	-0.1060×10^{2}	0.3472×10^{-3}	-0.1999×10^{-7}*
Reduced quadratic	—	0.3501×10^{-3}	-0.1802×10^{-7}
Benson–Berson	—	0.3608×10^{-3}	-0.1013×10^{-6}
Incremental	—	0.3409×10^{-3}	-0.3198×10^{-7}

*A_3 for cubic 0.4512×10^{-12}.

TABLE 3. Significance of various polynomial terms

Degree of polynomial	Degree of freedom	t values for confidence 95%	t values for confidence 99%	Calculated t values t_u	Calculated t values t_{SD}	Calculated t values t_{CL}
1	18	1.734	2.552	34.04	32.27	33.86
2	17	1.740	2.567	35.87	29.08	38.45
3	16	1.746	2.583	2.19	3.45	4.14
4	15	1.753	2.602	2.30	1.31	0.48
5	14	1.771	2.624	0.62	0.46	0.39

TABLE 4. Summary of $\Delta V^{\ddagger}$ and $d\Delta V^{\ddagger}/dp$ and errors

	$\Delta V^{\ddagger}$ (ml mol^{-1})			$d\Delta V^{\ddagger}/dp\times10^{3}$ (ml mol^{-1} bar^{-1})		
	Unwtd.	SD wtd.	CL wtd.	Unwtd.	SD wtd.	CL wtd.
Linear (van't Hoff)	−5.77(0.17)	−5.99(0.19)	−6.61(0.19)	—	—	—
Quadratic	−8.33(0.07)	−8.38(0.09)	−8.54(0.06)	0.765(0.021)	0.785(0.027)	0.840(0.022)
Cubic	−8.64(0.16)	−8.81(0.14)	−8.81(0.08)	0.995(0.107)	1.162(0.111)	1.130(0.072)
Reduced quadratic	−8.71(0.07)	−8.49(0.05)	−8.53(0.05)	0.897(0.033)	0.806(0.019)	0.822(0.020)
Benson–Berson	−8.98(0.06)	−8.87(0.04)	−8.88(0.04)	2.01 (0.061)	1.92 (0.035)	1.93 (0.037)
Incremental	−8.48(0.28)	−8.33(0.37)	−8.51(0.29)	1.59 (0.145)	1.58 (0.204)	1.56 (0.196)

thermodynamic activation parameters $\Delta V^{\ddagger}$ and $d\Delta V^{\ddagger}/dp$ and to obtain estimates of their reliability depending upon the function used to express the pressure dependence of the rate. The values calculated from the regression coefficients of the various functions are shown together with their standard errors (square root of variance) in Table 4. Three values of each parameter are shown for each function corresponding to the method of data treatment, i.e. weighted by standard deviation, by confidence limit, or unweighted. It will be recalled that the confidence limit weighting is more sensitive to the number of rate determinations made than is the standard deviation weighting.

The values in Table 4 clearly illustrate the inadequacy of the linear or van't Hoff type function. This has been demonstrated previously by several workers but it is important to note that it is not only the standard error that is unacceptably large but the $\Delta V^{\ddagger}$ value itself is significantly different from those obtained using higher power expressions. Such differences could be of considerable significance in mechanistic arguments based on the value of meaured volumes of activation.

There appears to be relatively little difference in $\Delta V^{\ddagger}$ values extracted by the various higher degree functions, whether the data are weighted or unweighted. An overall average value of 8.6 ± 0.4 ml/mol includes all values irrespective of the method of calculation. Bearing in mind the very extensive data base and the rigour with which the analysis was performed it is clear that few, if any, $\Delta V^{\ddagger}$ values currently available on any system can be considered to be more precise than ± 0.5 ml/mol. This is of special significance when considering *differences* between $\Delta V^{\ddagger}$ values as a criterion of reaction mechanism changes.

The Table 4 data also permit some comment to be made on the relative merits of the various nonlinear functional forms. All are clearly adequate in that they all provide a consistent value for $\Delta V^{\ddagger}$. Considering the size of the data base that each expression

Can. J. Chem. Downloaded from www.nrcresearchpress.com by 210.87.254.5 on 09/05/12
For personal use only.

Can. J. Chem. Downloaded from www.nrcresearchpress.com by 210.87.254.5 on 09/05/12
For personal use only.

was fitted to, however, the standard error associated with each value is informative. The quadratic, reduced quadratic, and Benson–Berson equations yield very small $\Delta V^{\ddagger}$ standard errors under all circumstances (<0.1 ml/mol). The cubic function has a somewhat higher value when applied to unweighted or standard deviation weighted data but it will be recalled that the Student *t*-test examination of the polynomial forms (Table 3) indicated that the cubic term was not significant with unweighted data. The large standard error in the $\Delta V^{\ddagger}$ value extracted by the incremental method suggests that when applied to a much more limited rate data set this functional form could yield $\Delta V^{\ddagger}$ values that were somewhat imprecise.

The mere fact that nonlinear functional forms provide a better fit of the rate–pressure data establishes the fact that the pressure dependence of $\Delta V^{\ddagger}$ is nontrivial. The feasibility of quantitative measurement of this important pseudo-thermodynamic activation parameter has, however, been questioned. As in the case of other second order derivatives there is no doubt that good data are essential for meaningful $d\Delta V^{\ddagger}/dp$ values to be obtained. The data in Table 4 illustrate the kind of precision that can be obtained using extensive and high quality rate–pressure data.

Again for the large data set used here there appears to be little difference between values obtained by weighting or not weighting the input data. The Benson–Berson and incremental functions, however, yield values that are significantly higher than the various nonlinear polynomials. The standard error associated with the incremental value is also larger, but that for the Benson–Berson is similar to that for the much lower $\Delta V^{\ddagger}$ values of the polynomials. It may be that the high value of the Benson–Berson $d\Delta V^{\ddagger}/dp$ is a reflection of forcing the data to a 0.523 power term which, as noted previously, is strictly valid only for organic solvents. Such a restriction would be expected to have a more noticeable effect on the second order derivative than on the $\Delta V^{\ddagger}$ term, as is the case.

The $d\Delta V^{\ddagger}/dp$ data would suggest that with extensive high quality rate–pressure data values of this activation parameter can be measured with a precision of $\pm 10\%$. Since even the sign of $d\Delta V^{\ddagger}/dp$ can be a useful piece of information in attempting to unravel the details of reaction mechanism, this level of precision is more than adequate for useful $d\Delta V^{\ddagger}/dp$ parameters.

Acknowledgment

The authors wish to thank the National Research Council of Canada for financial support of this work.

1. C. T. Burris and K. J. Laidler. Trans. Faraday Soc. **51**, 1497 (1955).
2. E. Whalley. Advances in physical chemistry. Vol. 2. Academic Press Inc., New York, NY. 1964.
3. B. T. Baliga and E. Whalley. Can. J. Chem. **43**, 2453 (1963).
4. H. S. Golinkin, W. G. Laidlaw, and J. B. Hyne. Can. J. Chem. **44**, 293 (1966).
5. D. D. Macdonald and A. F. M. Barton. *In* Techniques in chemistry. *Edited by* A. Wiessberger. John Wiley and Sons, Inc. 1976. pp. 317–362.
6. C. Walling and D. D. Tanner. J. Am. Chem. Soc. **85**, 612 (1963).
7. B. T. Baliga and E. Whalley. Can. J. Chem. **48**, 528 (1970).
8. S. W. Benson and J. A. Berson. J. Am. Chem. Soc. **84**, 152 (1962).
9. S. W. Benson and J. A. Berson. J. Am. Chem. Soc. **86**, 259 (1964).
10. C. A. Eckert. Annu. Rev. Phys. Chem. **23**, 239 (1972).
11. J. B. Hyne, H. S. Golinkin, and W. G. Laidlaw. J. Am. Chem. Soc. **88**, 2104 (1966).
12. E. Tommila, E. Paakkala, U. K. Virtauen, A. Evva, and S. Varila. Ann. Acad. Sci. Fenn. Ser. AII, 91 (1959).
13. B. Bensley and G. Kohnstam. J. Am. Chem. Soc. 4747 (1951).
14. K. J. Laidler and R. Martin. Int. J. Chem. Kinet. **1**, 113 (1969).
15. S. J. Dickson and J. B. Hyne. Can. J. Chem. **49**, 2394 (1971).
16. E. A. Guggenheim. Philos. Mag. **2**, 538 (1926).
17. E. J. King. Acid base equilibria. Pergamon Press Inc., London. 1965. pp. 27–36.
18. M. R. Smith and H. A. Buckmaster. J. Magn. Reson. **17**, 29 (1975).
19. A. A. Clifford. Multivariate error analysis. John Wiley & Sons, New York, Toronto. 1973. pp. 32, 34.
20. N. R. Draper and H. Smith. Applied regression analysis. John Wiley & Sons, New York, London, Sidney. 1966. p. 134.
21. O. L. Davies and P. L. Goldsmith (*Editors*). Statistical methods in research and production. 4th ed. Oliver and Boyd, Edinburgh. 1972. p. 203.
22. M. S. Bartlett. Biometrics, **5**, 207 (1949).
23. M. A. Creasy. J. Statist. Soc. B, **18**, 65 (1956).

A Mössbauer study of organotellurium compounds. Part III. Tellurium heterocycles and related compounds

NIGEL S. DANCE AND COLIN H. W. JONES

Department of Chemistry, Simon Fraser University, Burnaby, B.C., Canada V5A 1S6

Received October 20, 1977

NIGEL S. DANCE and COLIN H. W. JONES. Can. J. Chem. **56**, 1746 (1978).

Mössbauer data are reported for a number of heterocyclic compounds containing tellurium. The influence on the Mössbauer parameters of the constraints imposed by accommodating tellurium in these ring systems are discussed. The influence of the bulky aryl ligand 2-biphenylyl, $C_{12}H_9$—, on the Mössbauer parameters of diaryltellurium dihalides and aryltellurium trihalides has also been investigated.

NIGEL S. DANCE et COLIN H. W. JONES. Can. J. Chem. **56**, 1746 (1978).

On rapporte des données de Mössbauer pour un certain nombre de composés hétérocycliques contenant du tellure. On discute de l'influence, sur les paramètres de Mössbauer, des contraintes imposées par l'accommodation d'un tellure dans ces systèmes cycliques. On a aussi étudié l'influence du ligand aryle volumineux biphénylyl-2, $C_{12}H_9$—, sur les paramètres de Mössbauer des dihalogénures de diaryltellure et des trihalogénures d'aryltellure.

[Traduit par le journal]

Can. J. Chem. Downloaded from www.nrcresearchpress.com by 210.87.254.105 on 09/05/12
For personal use only.

Introduction

In previous papers (1–4) we have reported the ^{125}Te Mössbauer spectra of a wide range of organotellurium compounds and in the present paper the study is extended to include a number of tellurium heterocycles and related derivatives. Thus, in addition to forming diaryl and dialkyl tellurides, tellurium is also found in five- and six-membered heterocycles (5). In such compounds the bond lengths and bond angles are largely determined by the constraint of accommodating the tellurium atom in the ring and it was of interest to determine what effects this might have on the ^{125}Te Mössbauer parameters. Similarly, the effect of steric hindrance due to bulky aryl groups was also of interest, particularly for the trihalide derivatives.

It is relevant to briefly review here the important general features of the interpretation of ^{125}Te Mössbauer parameters. The ^{125}Te quadrupole splittings are determined predominantly by the imbalance in the 5*p* orbital populations, while the isomer shifts are influenced by the population of both the 5*s* and 5*p* orbitals. Removal of 5*s* electron density from the tellurium decreases the nuclear *s*-electron density $|\Psi_s(0)|^2$ and results in a more negative isomer shift, while removal of 5*p* electrons increases $|\Psi_s(0)|^2$ through deshielding and leads to a more positive isomer shift. It has been found that an additivity model satisfactorily explains the main features of the quadrupole splitting data for Te II and Te IV organotellurium derivatives (1, 2), this despite the fact that Te II possesses two lone pairs of electrons and Te IV one lone pair. The ^{125}Te isomer shifts span only a small range from -1.2 to $+1.8$ mm s^{-1} and as such are not a particularly useful probe to changes in chemical environment.

Results and Discussion

The computed Mössbauer parameters are reported in Table 1 and structural formulae for some of the compounds studied are presented in Table 2.

The Cyclic Tellurides

Of immediate interest in Table 1 are the Mössbauer parameters for dibenzotellurophene, $C_{12}H_8Te$ (**3**), phenoxtellurine, $C_{12}H_8OTe$ (**5**), and tellurium acetylacetonate, $C_5H_6O_2Te$ (**6**). The crystal structure data for these compounds are compared with that for $(p\text{-}MeC_6H_4)_2Te$ in Table 3. In these relatively simple molecules the C—Te—C bond angles vary from 101 to 81.7° and some variation is also observed in the bond lengths. The quadrupole splittings, and possibly the isomer shifts, show small differences from one compound to another. In the Townes and Dailey theory the quadrupole coupling constants for the compounds R_2Te can be related to the unit coupling constant, e^2q_0Q, the C—Te—C bond angle, θ, and the C—Te bond orbital population, *a*, through the expressions (10)

$$\frac{e^2qQ}{e^2q_0Q}\left(1+\frac{\eta}{3}\right) = 2 - a; \quad \eta = -3\cos\theta$$

for $90° < \theta < 109°$.

These expressions relate e^2qQ to the relative *s* and *p* character of the bonding orbitals and the two lone pairs. When $\theta = 90°$ the bonding would be pure *p* in character. It can be seen that changes in *a* and θ will influence the observed quadrupole splitting, $\frac{1}{2}e^2qQ(1 + \eta^2/3)^{1/2}$. Since the C—Te bond lengths,

TABLE 1. ^{125}Te Mössbauer parameters measured at 4.2 K

	Compound	δ* mm s^{-1} (±0.08)	Δ mm s^{-1} (±0.2)	Γ mm s^{-1}	χ^2/N	Ref.†
1	Me_2Te	0.06	10.5	6.2		2
2	Ph_2Te	0.18	10.5	5.9		2
3	$C_{12}H_8Te$	0.14	9.3	5.8	0.93	
4	$C_{12}H_8Te{\cdot}C_6H_3N_3O_7$	0.05	9.1	5.6	0.95	
5	$C_{12}H_8OTe$	0.24	11.2	4.7	1.01	
6	$C_5H_6O_2Te$	0.39	11.7	5.2	0.97	
7	$(C_{12}H_9)_2Te$	0.22	10.8	5.4	0.97	
8	Ph_2Te_2	0.37	10.7	6.1		2
9	$(C_{12}H_9Te)_2$	0.39	10.3	6.6	1.06	
10	$[Te(CH_2CO_2H)]_2$	0.40	11.1	6.2	1.18	
11	$(p\text{-}MeOC_6H_4)_2TeMe^+I^-$	0.15	5.8	5.9	1.13	
12	$(p\text{-}MeOC_6H_4)_2TeMe^+I^-$ in $CDCl_3$	0.32	5.6	4.8	1.09	
13	$Ph_3Te^+Cl^-$	0.35	5.8	6.0	1.05	
14	$Ph_3Te^+Cl^-$ in DMSO	0.29	5.7	4.7	1.02	
15	$C_{12}H_8OTeMe^+I^-$	0.29	6.2	7.5	1.00	
16	$(p\text{-}MeOC_6H_4)_2TeCl_2$	0.68	9.1	5.9		2
17	$C_{12}H_8TeCl_2$	0.75	8.1	6.9	1.06	
18	$C_{12}H_8OTeCl_2$	0.70	8.0	6.6	1.03	
19	$C_5H_6O_2TeCl_2$	0.71	8.2	5.9	0.90	
20	$C_{12}H_8OTe(NO_3)_2$	0.56	9.3	6.8	1.06	
21	$Ph_2Te(NO_3)_2$	0.07	8.9	6.4	1.16	
22	$(C_{12}H_8OTeNO_3)_2O$	0.41	7.6	6.4	0.93	
23	Ph_2TeO	0.47	6.0	6.5	1.08	
24	$(C_{12}H_9)_2TeCl_2$	0.73	8.2	5.9	1.10	
25	$(C_{12}H_9)_2TeBr_2$	0.50	7.6	4.8	1.01	
26	$(C_{12}H_9)_2TeI_2$	0.55	6.3	7.1	1.03	
27	$p\text{-}MeOC_6H_4TeCl_3$	0.91	9.4	5.9	0.97	
28	$C_{12}H_9TeCl_3$	0.80	8.0	6.1	1.05	
29	$C_{12}H_9TeBr_3$	0.86	7.1	5.5	0.89	
30	$C_{12}H_9TeI_3$	0.90	7.5	6.4	1.02	

* δ with respect to I/Cu, source, and absorbers at 4.2 K.
†With the exception of those compounds noted, all measurements were made in this work.

and hence the tellurium bond orbital populations, vary, a simple dependence of Δ on θ is not to be expected. Moreover the C—Te—C bond angles may not accurately reflect the directed valencies on the tellurium. However, both $C_{12}H_8OTe$ and $C_5H_6O_2Te$, for which $\theta \simeq 90°$, exhibit relatively larger Δ and δ values in comparison with Ph_2Te, for example, and this is consistent with a greater *p* character in the Te—C bonds and hence a greater lone-pair character for the tellurium 5*s* electrons.

The inductive effect of the oxygen atom in $C_{12}H_8OTe$ and of the carbonyl group in $C_5H_6O_2Te$ may be a factor in influencing Δ for these compounds, although the ditelluride $(TeCH_2CO_2H)_2$ (**10**) has very similar parameters to those of Ph_2Te_2 (Table 1).

In $C_{12}H_8Te$ the C—Te—C bond angle (9) is 81.7° and a simple combination of *s* and *p* orbitals cannot be used to rationalise the bonding about the tellurium. The quadrupole splitting for $C_{12}H_8Te$ is significantly smaller than that of the other cyclic tellurides. A contributing factor may be π-delocalisation around the five-membered ring, which is essentially planar.

An adduct of $C_{12}H_8Te$ with picric acid, $C_{12}H_8Te{\cdot}C_6H_3N_3O_7$ (**4**) can be isolated by recrystallizing dibenzotellurophene from ethanol in the presence of picric acid (11). The Mössbauer parameters for this adduct are identical to those obtained for the parent molecule and there is no evidence for any coordination of the molecule of picric acid to the tellurium. The adduct presumably involves a charge-transfer interaction between the two aromatic molecules.

The Cyclic Telluronium Cation, $C_{12}H_8OTeMe^+$

The compound $C_{12}H_8OTeMe^+I^-$ (**15**) contains the telluronium cation $C_{12}H_8OTeMe^+$ in which the tellurium is accommodated in a heterocyclic ring. We have previously reported Mössbauer data for two telluronium salts, Ph_2CH_3TeI and $Ph(CH_3)_2TeI$ (3), and for completeness we report here measurements on $(p\text{-}MeOC_6H_4)_2TeMe^+I$ (**11**) and $Ph_3Te^+Cl^-$ (**13**). The Mössbauer parameters for all the telluronium salts, regardless of anion and the precise nature of the organic groups attached to the tellurium, are very similar (Δ = 5.4 to 6.2 mm s^{-1}). This is consistent

Can. J. Chem. Downloaded from www.nrcresearchpress.com by 210.87.254.105 on 09/05/12
For personal use only.

Can. J. Chem. Downloaded from www.nrcresearchpress.com by 210.87.254.105 on 09/05/12
For personal use only.

TABLE 2. Structural formulae for some of the compounds studied

Ph_2Te **2**	Ph_2Te_2 **8**	$Ph_3Te^+Cl^-$ **13**	$(p\text{-}MeOC_6H_4)_2TeCl_2$ **16**	$p\text{-}MeOC_6H_4TeCl_3$ **30**
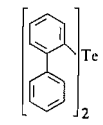 **7**	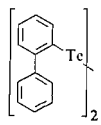 **9**		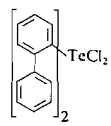 **24**	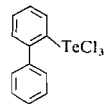 **28**
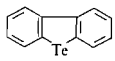 **3**			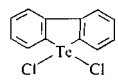 **17**	
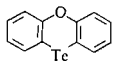 **5**		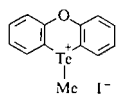 **15**	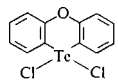 **18**	
			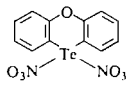 **20**	
			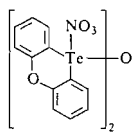 **22**	
6			**19**	

with the presence of an essentially pyramidal telluronium cation in which the electric field gradient at the tellurium arises predominantly from some small stereochemical activity of the lone pair and is not influenced by secondary contacts to the tellurium (12). The fact that $C_{12}H_8OTeMeI$ has a Δ which is similar to the other telluronium salts suggests that even in this complex cation the tellurium finds itself in an essentially pyramidal environment very similar to that of the other telluronium salts, with C—Te—C bond angles approaching 90°.

Another aspect of the chemistry of telluronium salts is the evidence from ir data for ion pairing in solutions of DMSO.[1] Mössbauer spectra of frozen solutions of $(p\text{-}MeOC_6H_4)_2TeMe^+I^-$ in $CDCl_3$ and $Ph_3Te^+Cl^-$ in DMSO gave parameters (Table 1) very similar to those of solid samples, again suggesting that the immediate environment at the tellurium site determines the Mössbauer parameters.

The Cyclic Dichlorides

The dichlorides $C_{12}H_8TeCl_2$ (**17**), $C_{12}H_8OTeCl_2$ (**18**), and $C_5H_6O_2TeCl_2$ (**19**) were studied to allow a comparison with simple diaryltellurium dichlorides. The dichlorides were chosen for investigation, rather than the bromides or iodides, because they exhibit the largest quadrupole splittings. The crystal structures of $C_{12}H_8OTeI_2$ (14) and $C_5H_6O_2TeCl_2$ (8) show the tellurium to be in a Ψ-trigonal bipyramidal geometry with the halogen ligands in *trans*-axial positions. The dihalides exhibit more positive isomer shifts than the parent tellurides, the halogen ligands removing predominantly *p*-electron density from the tellurium. Compounds **17**, **18**, and **19** exhibit isomer shifts comparable with those of $(p\text{-}MeOC_6H_4)_2TeCl_2$. However, the quadrupole splittings of the cyclic dichlorides are all significantly smaller (ca 8.1 mm s^{-1}) than that of $(p\text{-}MeOC_6H_4)_2TeCl_2$ (9.1 mm s^{-1}).

TABLE 3. Crystallographic data for the tellurides

Compound	C—Te—C bond angle (deg)	C—Te bond length (Å)	Ref.
$(p\text{-}MeC_6H_4)_2Te$	101	2.05(5)	6
$C_{12}H_8OTe$	89.4(3)	2.10(9)	7
$C_5H_6O_2Te$	89.5(4)	2.17(1)	8
$C_{12}H_8Te$	81.7(2)	2.087(5)	9

[1]W. R. McWhinnie and N. S. Dance. Unpublished work.

Can. J. Chem. Downloaded from www.nrcresearchpress.com by 210.87.254.105 on 09/05/12
For personal use only.

These differences in Δ may arise in part from differences in asymmetry parameter, η, in the two cases.

Alternatively, the smaller quadrupole splittings for the cyclic dichlorides may be understood in terms of the additivity model. Given the larger splittings of the parent cyclic tellurides, the cyclic dihalides would be expected to have a smaller splitting. This follows from the interpretation of the splittings in tellurides and organotellurium dihalides presented in earlier papers (1–3). It should be noted that the $C_{12}H_8OTe$ moiety in $C_{12}H_8OTeI_2$ is essentially identical (14) with that in the parent telluride (7) and this also holds for $C_5H_6O_2TeCl_2$ and $C_5H_6O_2Te$ (8).

For $C_{12}H_8TeCl_2$ (**17**) the splitting is again relatively small in comparison with $(p\text{-}MeOC_6H_4)_2TeCl_2$. However, the splitting of $C_{12}H_8Te$ was itself relatively small. The crystal structures of $C_{12}H_8Te$ (9) and $C_{12}H_8TeI_2$ (15) show that while the C—Te—C bond angles are the same (ca. 81°), the Te—C bond length is shorter in the former case than the latter. This would be consistent with delocalization around the five-membered ring in $C_{12}H_8Te$, such delocalization being eliminated in the diiodide. The Mössbauer parameters for $C_{12}H_8TeCl_2$ are comparable with those of $C_{12}H_8OTeCl_2$ and $C_5H_6O_2TeCl_2$.

The Cyclic Dinitrate, $C_{12}H_8OTe(NO_3)_2$, and Related Compounds

In addition to the dichlorides discussed above we have recorded the spectra of the dinitrates $C_{12}H_8OTe(NO_3)_2$ (**20**) and $Ph_2Te(NO_3)_2$ (**21**). These compounds exhibit large quadrupole splittings (9.3 and 8.9 mm s^{-1} respectively) comparable with those of dichlorides. This is consistent with the crystal structure of $C_{12}H_8OTe(NO_3)_2$ (16), which shows the tellurium to be in a Ψ-trigonal bipyramidal environment with the nitrate groups in *trans*-axial positions, and with interpretations of the ir data for $Ph_2Te(NO_3)_2$, which suggest a similar structure (17).

While $C_{12}H_8OTeCl_2$ has a smaller splitting than Ph_2TeCl_2, $C_{12}H_8OTe(NO_3)_2$ has a very similar splitting to $Ph_2Te(NO_3)_2$. It is interesting that the crystal structure data for $C_{12}H_8OTe$ (7) and $C_{12}H_8OTe(NO_3)_2$ (16) show that there is a very significant difference in the angle of fold in the heterocyclic ring containing the O and Te atoms in these two molecules. The Mössbauer data suggest that the tellurium environments in $C_{12}H_8OTe(NO_3)_2$ and $Ph_2Te(NO_3)_2$ are very similar.

The compound $(C_{12}H_8OTeNO_3)_2O$ (**22**) has the structure shown in Table 2, the $C_{12}H_8OTeNO_3$ units being linked through an oxygen bridge (18). The isomer shift and quadrupole splitting of this compound are significantly smaller than those of $C_{12}H_8OTe(NO_3)_2$ or $Ph_2Te(NO_3)_2$. The compound Ph_2TeO (**23**) exhibits an even smaller quadrupole splitting (Table 1). The structure of Ph_2TeO has not been determined. It is reasonable to assume that the tellurium finds itself in an essentially trigonal pyramidal environment, possibly with distant contacts *trans* to the oxygen and phenyl groups.

In $(C_{12}H_8OTeNO_3)_2O$ the tellurium may be viewed as being in a distorted trigonal bipyramidal environment with the C—Te—C bonds and the assumed lone pair in the equatorial plane and the Te—O and Te—ONO_2 bonds in *trans*-axial positions, the O—Te—ONO_2 angle being 172°. The heterocyclic ring in $(C_{12}H_8OTeNO_3)_2O$ is intermediate in terms of planarity between that found in $C_{12}H_8OTe$ (7) and $C_{12}H_8OTe(NO_3)_2$ (16). The quadrupole splitting for $(C_{12}H_8OTeNO_3)_2O$, 7.6 mm s^{-1}, lies between that of Ph_2TeO, 5.0 mm s^{-1}, and $C_{12}H_8OTe(NO_3)_2$, 9.3 mm s^{-1}, again suggesting a simple additivity of the components to the electric field gradient.

Aryltellurium Trihalides and Diaryltellurium Dihalides with Bulky Organic Ligands

While full crystal structures on several diaryltellurium dihalides were reported some years ago, similar data have only recently become available for the aryltellurium trihalides. Kobelt and Paulus found that in $ClCH_2CH_2TeCl_3$ the tellurium is present in a square-based pyramidal geometry with the organic ligand in the axial position and four chlorines, two bridging, in the plane (19). Infrared and Raman data have suggested a similar structure for the phenyltellurium trihalides (20, 21). However, recent crystal structures (22, 23) of the α and β forms of 2-biphenylyltellurium triiodide, which are very similar, and of the bromide (24), $C_{12}H_9TeBr_3$, have revealed a Ψ-trigonal bipyramidal geometry about the tellurium with the $C_{12}H_9$ ligand, one halogen and the assumed lone pair in the equatorial plane, and two halogens in *trans*-axial positions.

In previous Mössbauer studies we have measured the spectra of a number of aryltellurium dihalides and trihalides (1–3). Given the recent structural work on the 2-biphenylyl derivatives, and the very bulky nature of this ligand, it was of interest to measure the Mössbauer spectra of the compounds $(C_{12}H_9)_2TeX_2$ and $C_{12}H_9TeX_3$ (X = Cl, Br, I), and to compare their parameters with those of the previously studied halide derivatives. It may also be noted that it was relevant to investigate these compounds in the present study in as much as the trihalides may be used as intermediates in the preparation of $C_{12}H_8Te$.

Whereas aryltellurium trichlorides, tribromides, and triiodides have previously been found to yield Δ values of 9.3, 7.9, and 5.2 mm s^{-1} respectively, the

Can. J. Chem. Downloaded from www.nrcresearchpress.com by 210.87.254.105 on 09/05/12
For personal use only.

2-biphenylyl derivatives gave values of $C_{12}H_9TeCl_3$, 8.0; $C_{12}H_9TeBr_3$, 7.1; and $C_{12}H_9TeI_3$, 7.8 mm s^{-1}. These two sets of values are significantly different and raise some question as to whether the $C_{12}H_9TeX_3$ compounds may be viewed as 'typical' organotellurium trihalides or whether, as a result of steric hindrance arising from the bulkiness of the 2-biphenyl group, the structures of the $C_{12}H_9$ derivatives are significantly different from those of other aryl derivatives. It will be of interest to determine the crystal structure of a phenyltellurium trihalide to see whether it has a distorted trigonal bipryamidal structure or a square-based pyramidal structure as previously proposed. It should be noted that $(C_{12}H_9)_2Te$ (**7**) and $(C_{12}H_9Te)_2$ (**9**) have Mössbauer parameters very similar to those of other tellurides and ditellurides and that the 2-biphenylyl ligand is similar to other aryl ligands in those compounds. It is interesting that $C_{12}H_9TeI_3$ has an unusually large quadrupole splitting for a triiodide, while $C_{12}H_9TeCl_3$ and $C_{12}H_9TeBr_3$ are both smaller than would have been expected. In both the α and β forms of $C_{12}H_9TeI_3$ the three iodine atoms are inequivalent (22, 23), while in $C_{12}H_9TeBr_3$ the *trans*-axial bromine atoms are equivalent (24). In the triiodide the larger Δ value may be explained by the presence of an appreciable asymmetry parameter, η.

In the light of the apparently anomalous quadrupole splittings of the 2-biphenylyltellurium trihalides, it was of interest to measure the Mössbauer spectra of the bis(2-biphenylyl)tellurium dihalides. The data of Table 1 clearly show that, while these dihalides had isomer shifts comparable with other dihalides, the quadrupole splittings were again relatively smaller. Thus, diaryltellurium dichlorides generally exhibit Δ values of ca. 9.2 mm s^{-1}, whereas the bis(2-biphenylyl) derivative had a splitting of only 8.2 mm s^{-1}. The difference in the splittings for the diaryltellurium (8.0 mm s^{-1}) and bis(2-biphenylyl)tellurium dibromide (7.6 mm s^{-1}), however, was much smaller, while the bis(2-biphenylyl)tellurium diiodide appeared similar to other diaryltellurium diiodides (Δ = 6.3 mm s^{-1}). For the chlorides, and possibly the bromides, there is again evidence that the 2-biphenylyl derivatives may have structures which are significantly different from those of the phenyltellurium dihalides.

Experimental

Mössbauer spectra were recorded on compounds naturally abundant in tellurium. The source used was a 20 mCi ^{125}Sb/Cu source provided by New England Nuclear. The absorbers, containing 5–10 mg cm^{-2} of ^{125}Te, and the source were immersed in liquid helium in a Harwell Instruments Dewar. The constant acceleration drive, operating on a ramp which generates single spectra, was a Harwell Instruments MV 200 transducer driven by a MWG 200 wave-form generator and an MSA 200 attenuator. The spectra were accumulated in 256 channels in a Nuclear Data 2200 series multichannel analyser. During the experiments a Xe/CO_2 (Reuter Stokes) proportional counter and a thin NaI/Tl scintillation counter were used, the two giving comparable spectra. The detectors were gated on the Xe or I escape peak and a copper absorber was used to reduce the background under the escape peak. The compounds studied gave percent resonance absorptions in the peak minima of 6–10%. Spectra were routinely accumulated to 1 to 2 × 10^5 counts per channel. The spectra were computer fitted to independent Lorentzians using a program first described in ref. 25. The spectrometer was routinely calibrated using a ^{57}Co/Pd source and an iron foil absorber at room temperature.

Most of the compounds described were prepared following literature procedures (13, 26–28), and were identified by elemental analyses, melting points, mass spectroscopy, infrared, and ^1H nmr spectroscopy. Elemental analyses were not obtained where compounds were shown to be identical to previously prepared samples.

The following new compounds were prepared.

Bis(2-biphenylyl)telluride. 2-Biphenylylmercury chloride (7.75 g, 20 mmol) and tellurium tetrachloride (2.70 g, 10 mmol) were dissolved in 20 ml of dioxane and refluxed for 4 h. The solution was cooled, and the precipitated mercuric chloride – dioxane complex filtered under vacuum. The filtrate was evaporated to an oil, and diethyl ether added to precipitate crude bis(2-biphenylyl)tellurium dichloride. This was dissolved in hot ethanol, and hydrazine added dropwise until evolution of nitrogen ceased. The resulting turbid solution was evaporated to dryness and extracted with light petroleum ether, which on evaporation yielded 3.2 g of red oil. This was added to 2 g of freshly prepared copper powder in 25 ml of dry dioxane and refluxed for 6 h. After this time the initially red solution had become light green, and a heavy black precipitate formed. The solution was filtered and evaporated to dryness. Recrystallization from ethanol produced 0.85 g (19% of theoretical yield) of bis(2-biphenylyl)telluride.

Bis(2-biphenylyl)tellurium dichloride. Chlorine gas was passed into a solution of bis(2-biphenylyl)telluride (0.3 g) in 20 ml of carbon tetrachloride. After a few minutes a small amount of precipitate formed. Evaporation produced a quantitative yield of bis(2-biphenylyl)tellurium dichloride.

Bis(2-biphenylyl)tellurium dibromide and *bis(2-biphenylyl)-tellurium diiodide.* These compounds were similarly prepared in quantitative yields by mixing carbon tetrachloride solutions of equimolar amounts of bis(2-biphenylyl)telluride and the appropriate halogen.

Acknowledgements

The authors wish to thank the National Research Council of Canada for a grant supporting this research and Professor W. R. McWhinnie (University of Aston in Birmingham, England) for helpful discussions.

1. C. H. W. Jones, W. R. McWhinnie, and F. J. Berry. Mössbauer Effect Methodology, **10**, 227 (1976).
2. C. H. W. Jones, R. Shultz, W. R. McWhinnie, and N. S. Dance. Can. J. Chem. **54**, 3234 (1976).
3. F. J. Berry and C. H. W. Jones. Can. J. Chem. **54**, 3737 (1976).
4. W. R. McWhinnie, N. S. Dance, and C. H. W. Jones. J. Organomet. Chem. **125**, 291 (1977).
5. W. V. Farrar and J. M. Gulland. J. Chem. Soc. 11 (1945).

6. W. R. BLACKMORE and S. C. ABRAHAMS. Acta Crystallogr. **8**, 317 (1955).
7. M. R. SMITH, M. M. MANGION, R. A. ZINGARO, and E. A. MENGERS. J. Heterocycl. Chem. **10**, 527 (1973).
8. C. L. RASTON, R. J. SECOMB, and A. H. WHITE. J. Chem. Soc. Dalton Trans. 2307 (1976).
9. J. D. MCCULLOUGH. Inorg. Chem. **14**, 2639 (1975).
10. E. A. C. LUCKEN. *In* Nuclear quadrupole coupling constants. Academic Press, London. 1967. p. 265.
11. D. HELLWINKEL and G. FAHRBACH. Chem. Ber. **101**, 574 (1968).
12. D. D. TITUS and J. LEE and R. F. ZIOLO J. Organomet. Chem. **120**, 381 (1976).
13. G. WITTIG and H. FRITZ. Ann. Chem. **577**, 39 (1952).
14. J. D. MCCULLOUGH. Inorg. Chem. **12**, 2669 (1973).
15. J. D. MCCULLOUGH. Inorg. Chem. **14**, 1142 (1974).
16. M. M. MANGION, M. R. SMITH, and E. A. MEYERS. J. Heterocycl. Chem. **10**, 533 (1973).
17. W. R. MCWHINNIE, B. C. PANT, and N. S. DANCE. J. Organomet. Chem. **63**, 305 (1973).
18. M. M. MANGION, M. R. SMITH, and E. A. MEYERS. J. Heterocycl. Chem. **10**, 543 (1973).
19. D. KOBELT and E. F. PAULUS. Angew. Chem. Int. Ed. Engl. **10**, 73 (1971).
20. W. R. MCWHINNIE and P. THAVORNYUTIKARN. J. Chem. Soc. Dalton Trans. 551 (1972).
21. P. THAVORNYUTIKARN and W. R. MCWHINNIE. J. Organomet. Chem. **50**, 135 (1973).
22. C. KNOBLER and J. D. MCCULLOUGH. Inorg. Chem. **16**, 612 (1977).
23. J. D. MCCULLOUGH. Inorg. Chem. **16**, 2318 (1977).
24. J. D. MCCULLOUGH and C. KNOBLER. Inorg. Chem. **15**, 2728 (1976).
25. G. M. BANCROFT, W. K. ONG, A. G. MADDOCK, R. H. PRINCE, and A. J. STONE. J. Chem. Soc. A, 1966 (1967).
26. D. SCHULZ and G. KLAR. Z. Naturforsch. Teil B, **30**, 43 (1975).
27. J. D. MCCULLOUGH. Inorg. Chem. **14**, 2285 (1974).
28. K. S. IRGOLIC. Organic chemistry of tellurium. Gordon and Breach Ltd., New York. 1974.

Can. J. Chem. Downloaded from www.nrcresearchpress.com by 210.87.254.105 on 09/05/12
For personal use only.

Oxidation of methyl glycopyranosides by *Acetobacter suboxydans*

G. Wayne Schnarr and Walter A. Szarek

Department of Chemistry, Queen's University, Kingston, Ont., Canada K7L 3N6

Received December 19, 1977

G. Wayne Schnarr and Walter A. Szarek. Can. J. Chem. **56**, 1752 (1978).

A synthesis of methyl pentopyranosid-4-uloses has been achieved by microbiological oxidation by *Acetobacter suboxydans* of some methyl pentopyranosides. The oxidation products were isolated as their *O*-methyloxime derivatives, and the assignment of the configuration of the oximes was made on the basis of the carbon-13 magnetic resonance spectra. An analysis of the oxidative specificity of *A. suboxydans* towards methyl glycopyranosides is presented.

G. Wayne Schnarr et Walter A. Szarek. Can. J. Chem. **56**, 1752 (1978).

On a effectué une synthèse des pentopyrannosiduloses-4 de méthyle par une oxydation microbiologique à l'aide d'*Acétobacter suboxydans* de quelques pentopyrannosides de méthyle. On a isolé les produits d'oxydation sous forme de dérivés *O*-méthyloximes et l'attribution de la configuration des oximes a été effectuée en se basant sur les spectres de résonance magnétique nucléaire du carbone 13. On présente une analyse de la spécificité de l'oxydation des glycopyrannosides de méthyle par l'*Acétobacter suboxydans*.

[Traduit par le journal]

Introduction

In a preliminary communication (1), we reported the successful oxidation of methyl α- and β-D-xylopyranosides (**1**, **2**) by the acetic acid bacterium (2) *Acetobacter suboxydans* to give the corresponding glycosid-4-uloses (**3**, **4**) as the major products, with

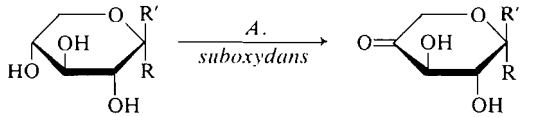

1 R = OMe, R′ = H
2 R = H, R′ = OMe
3 R = OMe, R′ = H
4 R = H, R′ = OMe

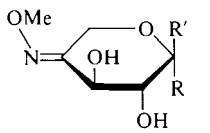

5 R = OMe, R′ = H
6 R = H, R′ = OMe

traces of the glycosid-3-uloses also being present. Chemical procedures were used to determine the site of the oxidation, and the oxidation products were further characterized as their *O*-methyloxime derivatives (**5**, **6**). We now report the results with a series of methyl pento- and hexopyranosides and also present an analysis of the oxidative specificity of *A. suboxydans* towards methyl glycopyranosides in terms of the specificity of the previously known dehydrogenase systems.

Acetobacter suboxydans apparently contains two enzyme systems which are responsible for the oxidation of the alditols. The predominant system oxidizes a polyhydric alcohol containing the structural unit **7**

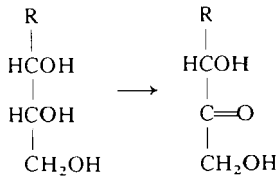

7 **8**

R = H,—(CHOH)$_n$—CH$_2$OH (n = 0–5)

to the ketose **8**, and this oxidative specificity has been formulated as the Bertrand–Hudson rule (3). A more recently recognized system (4), designated as a D-*galacto* dehydrogenase, is responsible for the oxidation of D-galactose diethyl dithioacetal (**9**), to give the corresponding 5-keto compound (**10**), and also for the oxidation of other compounds possessing the D-*galacto* configuration (5).

Acetobacter suboxydans was also found to oxidize the cyclitols and some of their derivatives in a stereospecific manner. Magasanik *et al.* (6) proposed that the oxidative specificity could be defined by two

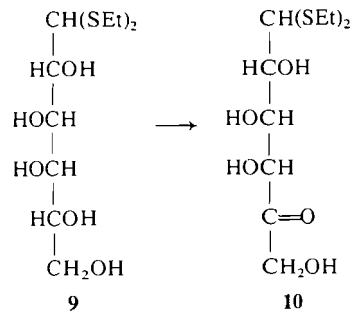

9 **10**

Can. J. Chem. Downloaded from www.nrcresearchpress.com by 210.87.254.5 on 09/05/12
For personal use only.

Can. J. Chem. Downloaded from www.nrcresearchpress.com by 210.87.254.5 on 09/05/12
For personal use only.

rules, with the possibility of a third rule also being applicable. Anderson *et al.* (7) proposed a modification of rule 3 to give the following set of rules: (*1*) only axial hydroxyl groups will be oxidized; (*2*) if an axial hydroxyl group is to be oxidized, there must be an equatorial hydroxyl group in the *meta* position, in a clockwise direction if the molecule is oriented so that the axial hydroxyl group projects downwards; (*3*) if there is an equatorial hydroxyl group in the *para* position, the oxidation will proceed at a faster rate and, if there is a choice, the axial hydroxyl group satisfying this rule will be preferentially oxidized. These rules can be represented by C-2, C-6, and C-5, respectively, in the oxidation of 1,2,3,5/4,6-cyclohexanhexol (**11**, *myo*-inositol) to 2,4,6/3,5-pentahydroxycyclohexanone (**12**).

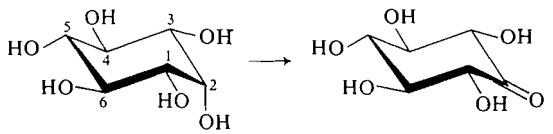

11 **12**

Results and Discussion

Since *A. suboxydans* probably does not contain a glycoside-specific dehydrogenase, the procedure normally used for the oxidation of polyhydric alcohols (8) was modified. Instead of using a proliferating culture in which the glycoside would replace the polyhydric alcohol, cells isolated from cultures grown on D-sorbitol broths were used. Paper chromatography, in which several spray reagents could be used to detect the products, and uv spectroscopy, in which λ_{max} (H_2O) ~ 265 nm changed to λ_{max} ~ 310 nm in 1 *N* sodium hydroxide, were used to determine whether oxidation was occurring. When a sample was treated, successively, with sodium borohydride and sulfuric acid, and the products were examined by paper chromatography, two aldoses, epimeric at the site of microbial oxidation, were revealed.

Since it was also necessary to determine the extent of the oxidation, the *O*-methyloxime derivatives of the oxidation products were prepared and isolated by column chromatography. In some cases, treatment of the oxidation mixture with methoxylamine hydrochloride also resulted in the formation of the bis(*O*-methyloxime) derivative; however, attempts to prepare the bis(*O*-methyloxime) from the *O*-methyloxime **6** by treatment with an excess of methoxylamine hydrochloride were unsuccessful.

The presence of only one geometrical isomer of each oxime (**5**, **6**, and **13**) was indicated by both the ^{1}Hmr and ^{13}Cmr spectra. When some simple, *N*-substituted ketimines were examined by ^{13}Cmr spectroscopy (9), it was found that the shielding of the *syn*-carbon was greater than that of the *anti*-carbon, a phenomenon attributable mainly to differences in steric compression. It was on this basis that the signals for compounds **5**, **6**, and **13** were assigned (see Table 1); the *E*-configuration can also be assigned to the *O*-methyloximes on the basis of the ^{13}Cmr chemical-shift data. The bis(*O*-methyloxime) was shown by hplc to be a mixture of two isomers; the major isomer was assigned the 3*E*,4*E*-configuration on the basis of the ^{13}Cmr chemical-shift data.

The results of the attempted oxidations in a series of methyl glycopyranosides are summarized in Table 2. The yields are based on the combined, isolated yields of the *O*-methyloxime and bis(*O*-methyloxime) derivatives, except for methyl α-D-xylopyranoside (**1**) in which case the quantitative oxidation is based on the absence of starting material after the reaction with methoxylamine hydrochloride. Although there are insufficient examples to allow complete analysis of the oxidative specificity of *A. suboxydans* towards methyl glycopyranosides, there are certain patterns which can be recognized.

The quantitative oxidation of methyl α-D-xylopyranoside (**1**) within 4 days, a time comparable to that required for oxidation of the alditols and cyclitols, makes this an ideal model for comparison with previously known dehydrogenase systems. The likelihood that *A. suboxydans* possesses an enzyme system specific for glycopyranosides is remote and is not considered here. Based strictly on the cyclic nature of the glycopyranosides, the enzyme or enzymes responsible for the oxidation of the cyclitols would have to be considered. However, none of the three requirements for oxidation (see Introduction) are satisfied by methyl α-D-xylopyranoside. There are also the enzymes responsible for oxidation of the cyclic diols and triols (10) but insufficient information is known about these systems to allow a comparison.

The configurational requirements for the two systems responsible for oxidation of the alditols, shown

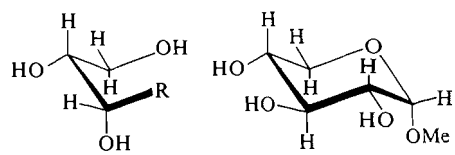

26 **1**

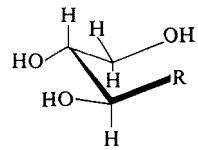

27

Can. J. Chem. Downloaded from www.nrcresearchpress.com by 210.87.254.5 on 09/05/12
For personal use only.

TABLE 1. Carbon-13 chemical-shift data[a] for the *O*-methyloxime derivatives of some methyl pentopyranosid-4-uloses

Compound	Solvent[b]	C-1	C-2	C-3	C-4	C-5	O—CH_3	N—O—CH_3
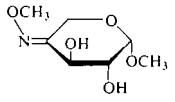 5	A	99.7	72.2	69.1	155.1	55.9	55.5	61.4
	B	99.7	73.8	69.4	154.2	54.4	55.8	62.1
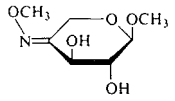 6	A	104.4	74.7	70.1	156.2	56.6	55.1	61.4
	B	104.0	75.7	70.3	155.3	57.5	55.8	62.3
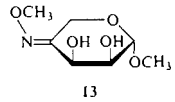 13	A	101.6	71.4	67.6	155.3	55.3	55.3	61.3
	B	100.9	71.1	67.2	155.8	55.1	55.8	62.1
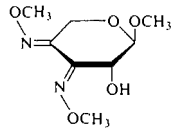 14	B	101.0	64.7	149.6[c]	147.8[c]	58.6	56.0	63.2

[a]In ppm from tetramethylsilane.
[b]A refers to methyl sulfoxide-d_6 solutions and B refers to chloroform-*d* solutions.
[c]Assignments for these peak positions may be reversed.

TABLE 2. Results of the oxidation of methyl glycopyranosides by *Acetobacter suboxydans*

Methyl glycopyranoside		Site of oxidation	Yield (%)	Time (days)
α-D-Arabinopyranoside	(**15**)	C-4	34	30
β-D-Arabinopyranoside	(**16**)	—	—	30
α-L-Arabinopyranoside	(**17**)	C-4	16	30
β-L-Arabinopyranoside	(**18**)	C-2	—[b]	30
α-D-Lyxopyranoside	(**19**)	C-4	43	30
α-L-Lyxopyranoside	(**20**)	—	—	30
β-D-Ribopyranoside[a]	(**21**)	C-2	—[b]	5
α-D-Xylopyranoside	(**1**)	C-4	100	4
β-D-Xylopyranoside	(**2**)	C-4	41	30
α-D-Glucopyranoside	(**22**)	—	—	30
β-D-Glucopyranoside	(**23**)	—	—	30
α-D-Mannopyranoside	(**24**)	—	—	30
β-D-Galactopyranoside	(**25**)	—	—	30

[a]The major component of the Fischer glycosidation mixture.
[b]Products decomposed, or were subjected to further metabolism, and no derivatives could be isolated.

by **26**, representing the Bertrand-Hudson system, and **27**, representing the more recently recognized D-*galacto* system, can be compared to the configurational state in methyl α-D-xylopyranoside (**1**). Assuming the three hydroxyl groups to be the necessary contact points for binding to the enzymes and considering the topographic similarity of **1** and **27**, it is not surprising that oxidation of **1** occurred at C-4. When the model compound is altered, the extent of the oxidation is diminished in a predictable manner. Thus, when the glycopyranosides which are epimeric at C-1 (**2**) and C-2 (**19**) are oxidized, the yields are reduced to 41 and 43%, respectively; also, when an equatorial hydroxymethyl group is introduced at C-5 in any of the three pentopyranosides mentioned above (that is, **22**, **23**, and **24**), there is no oxidation observed. Although this pattern indicates that the D-*galacto*-specific enzyme is responsible for these three oxidations, this suggestion cannot be proven until the oxidations are attempted with the purified enzyme.

A complex pattern is presented by the other four positive oxidations. The enzyme responsible for oxidizing the alditols according to the Bertrand-Hudson rule could be assumed to be responsible for the oxidation of methyl α-D-arabinopyranoside (**15**) when the topographic similarities of **15** and **28** are considered. Structures **26** and **28** possess the same configura-

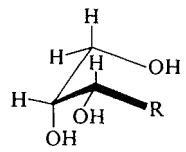
28

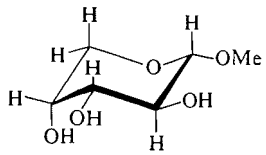
15

tional but different conformational requirements. The oxidation of methyl α-L-arabinopyranoside (**17**) by either of these enzymes cannot be rationalized; however, comparison of **11** and **17** shows that both rule *1* and rule *2* for oxidation of the cyclitols (see Introduction) are satisfied by **17**. Therefore, the

Can. J. Chem. Downloaded from www.nrcresearchpress.com by 210.87.254.5 on 09/05/12
For personal use only.

enzyme, or one of the enzymes, responsible for oxidation of the cyclitols is apparently responsible for the oxidation of methyl α-L-arabinopyranoside. The oxidations which occurred at C-2, for which the products could not be isolated or characterized, may have been caused by the enzyme or enzymes which oxidized some aldonic acids to the corresponding 2-keto compounds (11).

It is apparent from these results that the oxidation of methyl glycopyranosides by *A. suboxydans* is complicated by the presence of at least four active enzymes. The resolution of this problem will not be forthcoming until the enzymes have been purified. Nevertheless, the microbiological synthesis of some methyl pentopyranosid-4-uloses has been achieved, and a large number of cyclic, carbohydrate derivatives are now potential substrates for oxidation by this microorganism.

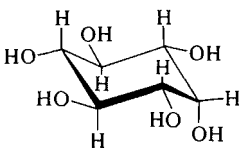

11

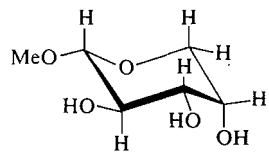

17

Experimental

Melting points were determined with a Fisher–Johns melting point apparatus and are uncorrected. The infrared (ir) spectra were recorded on a Perkin–Elmer 180 spectrophotometer. Ultraviolet (uv) spectra were recorded on a Unicam SP800 B spectrophotometer. Proton magnetic resonance (^{1}Hmr) spectra were recorded at 60 MHz on a Varian EM-360 spectrometer in chloroform-*d* with tetramethylsilane (TMS, δ = 0.00) as the internal standard, unless otherwise indicated. Carbon-13 magnetic resonance (^{13}Cmr) spectra were recorded in chloroform-*d* or methyl sulfoxide-d_6 solutions on a Bruker HX-60 spectrometer equipped with a FT60M Fourier transform accessory at 15.09 MHz; chemical shifts are given in ppm downfield from TMS. Thin-layer chromatography (tlc) was performed with Silica Gel G as the adsorbent in the following solvent systems (v/v): (*A*) ethyl acetate – ethanol, 5:1; (*B*) ethyl acetate; (*C*) petroleum ether (bp 60–80°C) – ethyl acetate, 1:3. The developed plates were air-dried and exposed to uv light and/or sprayed with a solution of cerium sulfate (1.0%) and molybdic acid (1.5%) in 10% aqueous sulfuric acid, and heated at ~150°C. Column chromatography was performed on Brinkmann silica gel (70-325 mesh). Paper chromatography (pc) was performed on Whatman No. 1 chromatography paper using the descending technique. The following solvent systems were used (v/v): (*I*) *n*- propanol – ethyl acetate – water, 7:1:2; (*II*) 0.55% benzeneboronic acid in ethyl acetate – acetic acid – water, 9:2:2 (12); (*III*) *n*-butanol–ethanol–water, 3:1:1. The following spray reagents were used to detect the carbohydrates on the paper chromatograms: (*i*) 2,5-diphenyl-3-(*p*-styrylphenyl)tetrazolium chloride (TSTZ) (13); (*ii*) aniline hydrogen phthalate (14); (*iii*) *p*-anisidine hydrochloride (15); (*iv*) triphenyltetrazolium chloride (TTC) (16); (*v*) *o*-phenylenediamine (17). High performance liquid chromatography (hplc) was performed using a Waters Model ALC-GPC-244 liquid chromatograph with Model 440 Absorbance Detector (254 nm). A μPorasil column was used with hexane – ethyl acetate (1:1, v/v) as the solvent. Solvents were evaporated under reduced pressure below 50°C.

Acetobacter suboxydans (ATCC 621H) was grown as previously described (18). All of the microbiological oxidations were performed in the following manner. *Acetobacter suboxydans* cells were isolated from D-sorbitol broths by centrifugation (~10 000 rpm, ~12 000 g) using an International Refrigerated Centrifuge Model B-20. The substrate was dissolved in distilled water (1–2%, w/v), the isolated cells were added, and the suspension was swirled mechanically. For the oxidation of 2 g of substrate, the cells isolated from 150 ml of standard sorbitol broth were used.

Oxidation of Methyl α-D-Xylopyranoside (1)

(*a*) An aqueous solution of **1** was oxidized by *A. suboxydans* cells. The oxidation was shown to be complete after 4 days, at which time tlc (solvent *A*) showed that no starting material remained when a sample was treated with methoxylamine hydrochloride (see part *b*). Examination of the oxidation mixture by pc (solvent *III*) revealed a streak ($R_{SORBOSE}$ 2.4–3.3) using both spray *i* (purple) and spray *ii* (yellow, faded quickly). When an oxidation sample was examined using uv spectroscopy, the sample showed λ_{max} 262 nm and a sample in ~1 *N* sodium hydroxide showed λ_{max} 308 nm. After 4 days, the cells were removed by centrifugation. When a sample was treated, successively, with sodium borohydride and ~1 *N* sulfuric acid (~70°C, 3 h), and the products were examined by pc (solvents *II* and *III*, spray *iii*), the presence of xylose, arabinose, and a trace of ribose was revealed.

(*b*) Methoxylamine hydrochloride (5.0 g) was added to an oxidation sample containing 4.0 g of oxidized **1**. The solution was adjusted to p*H* 4 and heated at ~70°C for 3 h. Thin-layer chromatography (solvent *A*) revealed the presence of only one major product (R_F 0.71) and traces of two minor components (R_F 0.79, 0.90). The solution was neutralized and concentrated to a syrup which was extracted with hot dichloromethane. The organic solution was dried (magnesium sulfate), concentrated to a syrup, and the major product was isolated by column chromatography (solvent *B*). The major product was identified as methyl β-L-*threo*-pentopyranosid-4-ulose (*E*)-*O*-methyloxime (**5**) and was isolated as a syrup (3.90 g, 84%); $[\alpha]_D$ +133° (*c* 1.50, water) and +174° (*c* 1.37, chloroform); ν_{max} (neat): 1640 (weak, C=N), 3430 cm^{-1} (strong, OH); ^{1}Hmr data δ: 3.46 (s, 3H, OMe), 3.89 (s, 3H, NOMe), 3.5–5.0 (m, 7H, H-1, H-2, H-3, 2H-5's, OH-2, OH-3); ^{13}Cmr data: see Table 1. *Anal.* calcd. for $C_7H_{13}O_5N$: C 44.0, H 6.8, N 7.3; found: C 43.8, H 6.8, N 7.3.

(*c*) A solution of **5** (3.90 g) in distilled water (125 ml) was shaken with Rexyn 101 resin (H^+) until tlc (solvent *A*) indicated that no starting material remained and that a single product (R_F 0.47) had been formed. Paper chromatography (solvent *I*) showed that this product migrated at the same rate as the product formed in the original oxidation. The resin was removed by filtration and the aqueous solution was concentrated to give methyl β-L-*threo*-pentopyranosid-4-ulose (**3**) as a syrup (2.65 g, 81%); $[\alpha]_D$ + 170° (*c* 1.60, water); ν_{max} (neat): 1730 cm^{-1}(strong, C=O), 3350 cm^{-1}(strong, OH); λ_{max}(H_2O) 260 nm (ε 931); λ_{max} (0.1 *N* NaOH): 317 nm (ε 1750), and λ_{sh} 341 nm; ^{1}Hmr data (in deuterium oxide relative to DSS) δ: 3.38 (s, 3H, OMe), 3.4–4.8 (m, 5H, H-1, H-2, H-3, 2H-5's); ^{13}Cmr data: see ref. 1. *Anal.* calcd. for $C_6H_{10}O_5$: C 44.4, H 6.2; found: C 43.9, H 6.1.

Oxidation of Methyl β-D-Xylopyranoside (2)

(*a*) An aqueous solution of **2** was oxidized for a period of 30 days. Paper chromatography (solvent *III*) revealed a streak ($R_{SORBOSE}$ 2.3–3.6) using both spray *i* (purple) and spray *ii*

Can. J. Chem. Downloaded from www.nrcresearchpress.com by 210.87.254.5 on 09/05/12
For personal use only.

(yellow). When a broth sample was examined using uv spectroscopy, the sample showed λ_{max} 268 nm and a sample in ~1 *N* sodium hydroxide showed λ_{max} 313 nm and λ_{sh} 337 nm. After 30 days, the cells were removed by centrifugation. When a sample was treated, successively, with sodium borohydride and ~1 *N* sulfuric acid (~70°C, 3 h) and the products were examined by paper chromatography (solvent *III*, spray *iii*), the presence of xylose, arabinose, and a trace of ribose was revealed.

(*b*) An oxidation sample containing 2.0 g of **2**, both oxidized and unoxidized, was treated with methoxylamine hydrochloride. Thin-layer chromatography (solvent *B*) revealed the presence of one major product (R_F 0.54), one minor product (R_F 0.68) which was visible under uv light, and the unoxidized starting material (R_F 0.09). The reaction mixture was processed as before and the two products were separated using column chromatography (solvent *B*). The slower-moving component was identified as methyl α-L-*threo*-pentopyranosid-4-ulose (*E*)-*O*-methyloxime (**6**) and was obtained as white flakes (700 mg, 30%) having mp 69–70°C (recrystallized from dichloromethane – petroleum ether (30–60°C)); $[\alpha]_D$ −135° (*c* 1.03, water); ν_{max} (KBr): 1645 (weak, C=N), 3380 cm^{-1} (strong, OH); ^{1}Hmr data δ: 3.61 (s, 3H, OMe), 4.06 (s, 3H, NOMe), 3.5–5.0 (m, 7H, H-1, H-2, H-3, 2H-5's, OH-2, OH-3); ^{13}Cmr data: see Table 1. *Anal.* calcd. for $C_7H_{13}O_5N$: C 44.0, H 6.8, N 7.3; found: C 43.9, H 7.0, N 7.3.

The faster-moving component was isolated as a syrup (294 mg), $[\alpha]_D$ −4° (*c* 2.10, chloroform); ν_{max} (neat): 1620, 1725 (conjugated C=N's), 3450 cm^{-1} (OH); λ_{max} (CH_2Cl_2): 265 nm. High performance liquid chromatography revealed that the syrup was a mixture of two isomers in a ratio of ~20:1. The major component was identified as methyl β-D-*glycero*-pentopyranosid-3,4-diulose (3*E*,4*E*)-bis(*O*-methyloxime) (**14**); ^{1}Hmr data δ: 3.20 (s, 1H, OH-2), 3.47 (s, 3H, OMe), 4.02 and 4.07 (s, 3H each, 2 NOMe's), 4.5–4.8 (m, 4H, H-1, H-2, 2H-5's); ^{13}Cmr data: see Table 1. *Anal.* calcd. for $C_8H_{14}N_2O_5$: C 44.0, H 6.5, N 12.8; found: C 44.2, H 6.5, N 12.8.

(*c*) A solution of **6** (650 mg) in distilled water (50 ml) was shaken with Rexyn 101 resin (H^+) until tlc (solvent *B*) indicated that no starting material remained and that a single product (R_F 0.09) had been formed. The hydrolysis mixture was processed to give methyl α-L-*threo*-pentopyranosid-4-ulose (**2**) as a syrup (470 mg, 85%); $[\alpha]_D$ −38° (*c* 1.56, water); ν_{max} (neat): 1730 (C=O), 3390 cm^{-1} (OH); λ_{max} (H_2O): 269 nm (ε 120); λ_{max} (1.0 *N* NaOH): 311 nm (ε 365); ^{1}Hmr data (in deuterium oxide relative to DSS) δ: 3.58 (s, 3H, OMe), 3.2–4.7 (m, 5H, H-1, H-2, H-3, 2H-5's); ^{13}Cmr data: see ref. 1. This product was shown by paper chromatography (solvent *I*) to be identical to that formed in the original oxidation. An accurate elemental analysis could not be obtained as the compound started to decompose as soon as it was concentrated to a syrup.

Oxidation of Methyl α-D-Lyxopyranoside (19)

(*a*) An aqueous solution of **19** was oxidized for a period of 30 days. Paper chromatographic analysis (solvent *I*) revealed a product ($R_{SORBOSE}$ 2.17) when both spray *i* (purple) and spray *iv* (red) were used. When an oxidation sample was examined using uv spectroscopy, the sample showed λ_{max} 294 nm and a sample in 1 *N* sodium hydroxide showed λ_{max} 311 nm and λ_{sh} 347 nm. When a sample was treated, successively, with sodium borohydride and 2 *N* sulfuric acid (~80°C, 3h), paper chromatography (solvent *III*, spray *iii*) revealed the presence of lyxose and a small amount of ribose.

(*b*) An oxidation sample containing 1.5 g of **19**, both oxidized and unoxidized, was treated with methoxylamine hydrochloride and tlc (solvent *A*) showed the presence of a major product (R_F 0.81), a minor product (R_F 0.87) which could be seen under uv light, and unreacted starting material (R_F 0.56). The reaction mixture was processed as before and the two products were separated by column chromatography (solvent *C*). The slower-moving component was isolated as a syrup (455 mg, 26%) and identified as methyl β-L-*erythro*-pentopyranosid-4-ulose (*E*)-*O*-methyloxime (**13**); $[\alpha]_D$ +109° (*c* 2.10, dichloromethane); ν_{max} (neat): 1650 (weak, C=N), 3430 cm^{-1} (strong, OH); ^{1}Hmr data δ: 3.46 (s, 3H, OMe), 3.89 (s, 3H, NOMe), 3.8–4.9 (m, 7H, H-1, H-2, H-3, 2H-5's, OH-2, OH-3); ^{13}Cmr data: see Table 1. *Anal.* calcd. for $C_7H_{13}O_5N$: C 44.0, H 6.8, N 7.3; found: C 44.0, H 6.8, N 7.2.

The faster-moving component was isolated as a syrup (295 mg), $[\alpha]_D$ +5° (*c* 2.10, chloroform); ν_{max} (neat): 1620, 1725 (conjugated C=N's), 3450 cm^{-1} (OH); λ_{max} (CH_2Cl_2): 265 nm. High performance liquid chromatography revealed the syrup to be a mixture of two isomers in an approximate ratio of 20:1. Based on the ^{1}Hmr and ^{13}Cmr data, which were identical to those of **14** from the oxidation of methyl β-D-xylopyranoside, the major isomer was identified as methyl β-L-*glycero*-pentopyranosid-3,4-diulose (3*E*,4*E*)-bis(*O*-methyloxime).

(*c*) When **13** was hydrolyzed with Rexyn 101 resin (H^+) and the reaction mixture was processed as in the previous two cases, the product decomposed before it could be characterized.

Oxidation of Methyl α-D-Arabinopyranoside (15)

(*a*) An aqueous solution of **15** was oxidized for a period of 30 days. Paper chromatography (solvent *I*) revealed a product ($R_{SORBOSE}$ 1.92) when both spray *iv* (red) and spray *i* (purple) were used. When a broth sample was examined using uv spectroscopy, the sample showed λ_{max} 260 nm and a sample in ~1 *N* sodium hydroxide showed λ_{max} 310 nm and λ_{sh} 343 nm. A sample was treated, successively, with sodium borohydride and ~2 *N* sulfuric acid (~85°C, 6 h), and paper chromatography (solvents *II* and *III*, spray *iii*) revealed the presence of arabinose and xylose.

(*b*) An oxidation sample containing 4.0 g of **15**, both oxidized and unoxidized, was treated with methoxylamine hydrochloride and tlc (solvent *B*) revealed the presence of one major product (R_F 0.67), one minor product (R_F 0.83) which could be seen under uv light, and unreacted starting material (R_F 0.06). The reaction mixture was processed as before and the two components were isolated by column chromatography (solvent *B*). The major component was identified as methyl α-D-*threo*-pentopyranosid-4-ulose (*E*)-*O*-methyloxime and was isolated as white flakes (1.30 g, 28%) having mp 64–65°C; $[\alpha]_D$ +132° (*c* 1.21, water). The ir, ^{1}Hmr, and ^{13}Cmr spectra were identical to those of **6** isolated from the oxidation of methyl β-D-xylopyranoside. The faster-moving component was isolated as a syrup (294 mg), $[\alpha]_D$ +5° (*c* 1.33, chloroform); ν_{max} (neat): 1620, 1735 (conjugated C=N's), 3430 cm^{-1} (OH); λ_{max} (CH_2Cl_2): 264 nm. High performance liquid chromatography revealed that the syrup was a mixture of two isomers in an approximate ratio of 11:1. On the basis of hplc retention times, and ^{1}Hmr and ^{13}Cmr spectral data, the major isomer was identified as methyl β-L-*glycero*-pentopyranosid-3,4-diulose (3*E*,4*E*)-bis(*O*-methyloxime).

Oxidation of Methyl α-L-Arabinopyranoside (17)

(*a*) An aqueous solution of **17** was oxidized for 30 days. Paper chromatography (solvent *I*) revealed a product ($R_{SORBOSE}$ 1.95) when both spray *iv* (red) and spray *i* (purple) were used. When an oxidation sample was examined using uv spectroscopy, the sample showed λ_{max} 260 nm and a sample in ~1 *N* sodium hydroxide showed λ_{max} 314 nm and λ_{sh} 341 nm. When a sample was treated, successively, with sodium borohydride

Can. J. Chem. Downloaded from www.nrcresearchpress.com by 210.87.254.5 on 09/05/12
For personal use only.

and 2 *N* sulfuric acid (~85°C, 7 h), paper chromatography (solvents *II* and *III*, spray *iii*) revealed the presence of arabinose and xylose.

(*b*) An oxidation sample containing 4.0 g of **17**, both oxidized and unoxidized, was treated with methoxylamine hydrochloride and tlc (solvent *B*) showed the presence of two products (R_F 0.53, 0.72) and a large amount of unreacted starting material (R_F 0.04). The reaction mixture was processed as before and the two products were isolated by column chromatography. The products were identical in all respects to those obtained from the oxidation of methyl β-D-xylopyranoside; the *O*-methyloxime **6** was isolated in 11% yield (509 mg), and 253 mg of a syrupy mixture of the isomeric bis(*O*-methyloximes) were also isolated.

Oxidation of a Mixture of Methyl D-*Ribosides*

An aqueous solution of a mixture of methyl D-ribosides, prepared by a Fischer glycosidation, was oxidized by a suspension of *A. suboxydans* cells. Examination of the oxidation mixture after 5 days by paper chromatography (solvent *I*) showed the presence of one major product ($R_{SORBOSE}$ 2.2–2.3) and one minor product ($R_{SORBOSE}$ 1.4). With sprays *i* (purple), *ii* (yellow), and *v* (visible using uv light), both products gave in each case the same color reaction, whereas with spray *iii* the major and minor products gave a yellow and a red color, respectively. When an oxidation sample was examined using uv spectroscopy, the sample showed λ_{max} 267 nm, whereas a sample in ~1 *N* sodium hydroxide showed λ_{max} 320 nm and λ_{sh} ~345 nm. An oxidation sample was treated successively, with sodium borohydride and ~2 *N* sulfuric acid (~80°C, 4 h), and paper chromatography (solvents *I* and *III*, spray *iii*) showed the presence of ribose and a trace of arabinose. Attempts to prepare oxime, *O*-methyloxime, and phenylhydrazone derivatives of the oxidation products were unsuccessful.

Oxidation of Methyl β-L-*Arabinopyranoside (18)*

An aqueous solution of **18** was oxidized for 30 days. Examination of an oxidation sample by paper chromatography (solvent *I*) revealed the presence of one product ($R_{SORBOSE}$ 2.03) using spray *iii* (purple). When an oxidation sample was treated, successively, with sodium borohydride and ~2 *N* sulfuric acid (~85°C, 6 h), paper chromatography (solvent *III*, spray *iii*) revealed the presence of arabinose and a small amount of ribose. Attempts to prepare an *O*-methyloxime derivative were unsuccessful.

Oxidation of Methyl β-D-*Glucopyranoside (23)*

An aqueous solution of **23** was oxidized for 30 days. Paper chromatographic analysis of the oxidation mixture revealed a product, having $R_{SORBOSE}$ 1.53 (solvent *I*), which gave a positive reaction with spray *i* (purple) and spray *v* (gray-brown). Paper chromatographic examination (solvent *III*, spray *iii*) of a sample treated, successively, with sodium borohydride and ~2 *N* sulfuric acid (~80°C, 4 h) revealed only the presence of glucose. Attempts to prepare an *O*-methyloxime derivative were unsuccessful.

Oxidation of Methyl α-D-*Mannopyranoside (24)*

An aqueous solution of **24** was oxidized for 30 days. Paper chromatographic analysis of the oxidation mixture revealed a product, having $R_{SORBOSE}$ 1.77 (solvent *I*), which gave positive reactions with both spray *i* (purple) and spray *v* (gray-brown). Paper chromatographic examination of a sample treated, successively, with sodium borohydride and ~2 *N* sulfuric acid (~85°C, 6 h) gave inconclusive results. Attempts to prepare an *O*-methyloxime resulted in the formation of a trace of a product which could not be isolated.

Other Attempted Oxidations

Aqueous solutions of the following methyl aldopyranosides were oxidized for 30 days, and paper chromatographic analysis showed that no oxidation had occurred in each case: methyl α-L-lyxopyranoside (**20**), methyl β-D-arabinopyranoside (**16**), methyl α-D-glucopyranoside (**22**), and methyl β-D-galactopyranoside (**25**).

Acknowledgements

The authors are grateful to the National Research Council of Canada for financial support in the form of a scholarship (to G.W.S.) and a grant (to W.A.S.).

1. W. A. SZAREK and G. W. SCHNARR. Carbohydr. Res. **55**, C5 (1977).
2. T. ASAI. Acetic acid bacteria. University of Tokyo Press, Tokyo, Japan. 1968.
3. R. M. HANN, E. B. TILDEN, and C. S. HUDSON. J. Am. Chem. Soc. **60**, 1201 (1938).
4. D. T. WILLIAMS and J. K. N. JONES. Can. J. Chem. **45**, 741 (1967).
5. D. T. WILLIAMS. Ph.D. Thesis, Queen's University, Kingston, Ont. 1966.
6. B. MAGASANIK, R. E. FRANZL, and E. CHARGAFF. J. Am. Chem. Soc. **74**, 2618 (1952).
7. L. ANDERSON, R. TAKEDA, S. J. ANGYAL, and D. J. MCHUGH. Arch. Biochem. Biophys. **78**, 518 (1958).
8. W. A. SZAREK, G. W. SCHNARR, H. C. JARRELL, and J. K. N. JONES. Carbohydr. Res. **53**, 101 (1977).
9. (*a*) G. C. LEVY and G. L. NELSON. J. Am. Chem. Soc. **94**, 4897 (1972); (*b*) N. NAULET, M. L. FILLEUX, G. J. MARTIN, and J. PORNET. Org. Magn. Reson. **7**, 326 (1975); (*c*) J. CASANOVA and J.-P. ZAHRA. Tetrahedron Lett. 1773 (1977); (*d*) C. A. BUNNELL and P. L. FUCHS. J. Org. Chem. **42**, 2614 (1977).
10. A. RAPIN, A. L. HAENNI, and T. POSTERNAK. Helv. Chim. Acta, **50**, 1801 (1967).
11. (*a*) V. ETTEL, J. LIEBSTER, and M. TADRA. Chem. Listy, **46**, 45 (1952); (*b*) J. LIEBSTER, M. KULHANEK, and M. TADRA. Chem. Listy, **47**, 1075 (1953).
12. E. J. BOURNE, E. M. LEES, and H. WEIGEL. J. Chromatogr. **11**, 253 (1963).
13. J. S. D. BACON. Biochem. J. **73**, 507 (1959).
14. S. M. PARTRIDGE. Nature, **164**, 443 (1949).
15. L. HOUGH, J. K. N. JONES, and M. H. WADMAN. J. Chem. Soc. 1702 (1950).
16. W. E. TREVELYAN, D. P. PROCTER, and J. S. HARRISON. Nature, **166**, 444 (1950).
17. S. S. COHEN and M. C. LANNING. Fed. Proc. **9**, 161 (1950).
18. G. W. SCHNARR, W. A. SZAREK, and J. K. N. JONES. App. Env. Microbiol. **33**, 732 (1977).

Ipso nitration. XX.[1] Nitration of 5-*tert*-butyl-1,2,3-trimethylbenzene in acetic anhydride. Formation and rearomatization of adducts

ALFRED FISCHER AND KHAY CHUAN TEO

Department of Chemistry, University of Victoria, Victoria, B.C., Canada V8W 2Y2

Received January 5, 1978

ALFRED FISCHER and KHAY CHUAN TEO. Can. J. Chem. **56**, 1758 (1978).

Nitration of 5-*tert*-butyl-1,2,3-trimethylbenzene in acetic anhydride gives both diastereomers of the adduct 1-*tert*-butyl-3,4,5-trimethyl-4-nitrocyclohexa-2,5-dienyl acetate and one diastereomer of 1-*tert*-butyl-3,4,5-trimethyl-4-nitrocyclohexa-2,5-dienol, in 91% yield, together with 5-*tert*-butyl-1,2,3-trimethyl-4-nitrobenzene. Solvolysis of the dienyl acetate in acidified aqueous acetone and acidified methanol affords the diastereomers of the dienols and the dienyl methyl ethers, respectively. The dienyl methyl ethers are also formed from the dienyl acetate in neutral methanol and again on reaction with methanolic sodium methoxide. The dienols isomerize (epimerize) in acidified aqueous acetone. Reaction of the dienyl methyl ethers in aqueous methanol, or prolonged reaction in methanol, results in the formation of methyl-1,2,3-trimethylphenyl ether. Similar cleavage of the *tert*-butyl group is the main reaction on solvolysis of the dienyl acetate in aqueous acetic acid. Under more acidic conditions the dienyl acetate gives 5-*tert*-butyl-2,3-dimethylbenzyl nitrite and lesser amounts of 5-*tert*-butyl-2,3-dimethylphenylnitromethane and 5-*tert*-butyl-2,3-dimethylbenzyl acetate. In trifluoromethanesulfonic and fluorosulfonic acids 5-*tert*-butyl-1,2,3-trimethyl-4-nitrobenzene is the major product.

ALFRED FISCHER et KHAY CHUAN TEO. Can. J. Chem. **56**, 1758 (1978).

La nitration du *tert*-butyl-5 triméthyl-1,2,3 benzène dans l'anhydride acétique conduit aux deux diastéréoisomères de l'adduit, acétate de *tert*-butyl-1 triméthyl-3,4,5 nitro-4 cyclohexadiène-2,5 yle, et à un diastéréoisomère du *tert*-butyl-1 triméthyl-3,4,5 nitro-4 cyclohexadiène-2,5 ol avec un rendement de 91% aux côtés du *tert*-butyl-5 triméthyl-1,2,3 nitro-4 benzène. La solvolyse de l'acétate de diényle dans de l'acétone aqueuse acidulée et dans du méthanol acidulé conduit respectivement aux diastéréoisomères des diénols et des éthers méthyliques de diényle. Les éthers méthyliques de diényle se forment aussi à partir de l'acétate de diényle dans le méthanol neutre et aussi par réaction du méthylate de sodium en milieu méthanolique. Les diénols s'isomérisent (épimérisent) en solution dans l'acétone aqueuse acidulée. La réaction des éthers méthyliques de diényle avec le méthanol aqueux ou par action prolongée du méthanol conduit à la formation de l'éther méthylique du triméthyl-1,2,3 phényle. Un clivage semblable du groupe *tert*-butyle correspond à la réaction principale observée lors de la solvolyse de l'acétate de diényle dans l'acide acétique aqueux. Utilisant des conditions plus acides, l'acétate de diényle conduit au nitrite du *tert*-butyl-5 diméthyl-2,3 benzyle et à des quantités plus faibles de *tert*-butyl-5 diméthyl-2,3 phénylnitrométhane et d'acétate du *tert*-butyl-5 diméthyl-2,3 benzyle. Dans les acides trifluorométhanesulfonique et fluorosulfonique, le *tert*-butyl-5 triméthyl-1,2,3 nitro-4 benzène est le produit principal.

[Traduit par le journal]

Nitration of *p*-*tert*-butyltoluene in acetic anhydride results in predominant *ipso* (1) attack by the nitronium ion at the methyl-substituted position and the formation of 1,2 and, to a lesser extent, 1,4 nitronium acetate adducts (2). Nitration of 4-*tert*-butyl-*o*-xylene gives 1,4 adduct (3) although a small amount of 1,2 adduct is also formed. The present investigation of 5-*tert*-butyl-1,2,3-trimethylbenzene (**1**) continues our study of the nitration of the series of *tert*-butylmethylbenzenes. The unusual formation of 1,2 adducts is of specific interest in this series. A related study is the nitration of 1,2,3,5-tetramethylbenzene (4).

[1]For Part XIX see ref. 10.

Results and Discussion

Nitration and Formation of Adducts

Nitration of 5-*tert*-butyl-1,2,3-trimethylbenzene (**1**) in a mixture of acetic anhydride and methylene chloride at −55°C gave a product mixture containing ca. 91% of diene adducts. One diastereoisomer[2] of 1-*tert*-butyl-3,4,5-trimethyl-4-nitrocyclohexa-2,5-dienyl acetate[3] (**2***a*) was crystallized from the product mixture. Low temperature chromatography of the residue after concentration of the mother liquor gave 5-*tert*-butyl-2,3-dimethylbenzyl nitrite (**5**)

[2]Individual members of a pair of diastereoisomeric adducts are designated as *a* and *b*.

[3]1-*tert*-Butyl-3,4,5-trimethyl-4-nitro-1,4-dihydrophenyl acetate.

Can. J. Chem. Downloaded from www.nrcresearchpress.com by 210.87.254.6 on 09/05/12
For personal use only.

Can. J. Chem. Downloaded from www.nrcresearchpress.com by 210.87.254.6 on 09/05/12
For personal use only.

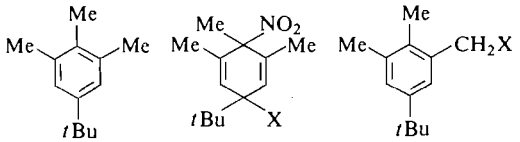

1

2 X = OAc
3 X = OH
4 X = OMe

5 X = ONO
6 X = NO_2
7 X = OAc
8 X = OH

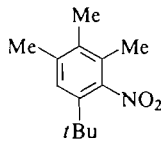

9

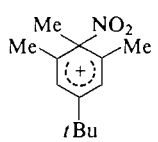

10

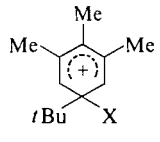

11 X = OAc
12 X = OMe
13 X = OH

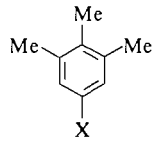

14 X = OMe
15 X = OAc
16 X = OH

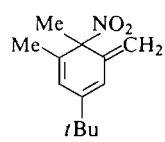

17

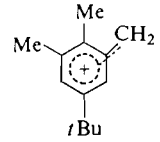

18

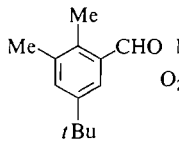

19

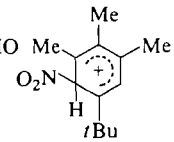

20

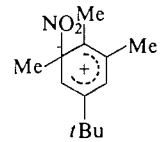

21

5-*tert*-butyl-1,2,3-trimethyl-4-nitrobenzene (**9**), a second diastereoisomer of 1-*tert*-butyl-3,4,5-trimethyl-4-nitrocyclohexa-2,5-dienyl acetate (**2***b*), and 1-*tert*-butyl-3,4,5-trimethyl-4-nitrocyclohexa-2,5-dienol (**3***a*), with stereochemistry corresponding to that of the acetate **2***a*. The correspondence of the stereochemistry was demonstrated by the reduction with aluminum hydride of acetate **2***a* to an alcohol identical to **3***a*. The nitrite **5** was eluted in the early column fractions and was followed by the nitroarene **9**. More nitrite **5** together with acetic acid was obtained in the fractions immediately following **9**. It is clear that these fractions must have contained a diene which decomposed to **5** and acetic acid (and a small amount of other benzylic derivatives, **6** and **7**) subsequent to elution from the column. Probably this diene was **2***a* since it was the major component of the immediately following fraction (0.11 g) which contained a mixture of dienes and it is highly unlikely that all of the **2***a* initially formed could have cleanly crystallized from the reaction mixture before chromatography, without leaving a significant fraction remaining in solution. Diene **2***a* was shown to decompose to **5** and acetic acid, together with variable amounts of the nitromethane **6** and acetate **7**, on standing in solution at ambient temperature and the solid diene decomposed similarly. It is clear that diene **2** is very labile. This was confirmed by allowing a nitration reaction mixture to warm to 0°C before work-up. Under these conditions the nitromethane **6** and nitrite **5** were the predominant reaction products and no dienes were obtained.

The symmetry evident from the ^1H and ^{13}C nmr spectra of **2***a*, **2***b*, and **3***a* shows that these are 2,5 or 5,2 adducts of the original 5-*tert*-butyl-1,2,3-trimethylbenzene. The nitro group must be attached to the C-2 position since the position *ipso* to *tert*-butyl is very hindered and, moreover, addition of the nitronium ion at this position (C-5) would lead to de-*tert*-butylation (5). Addition of nitronium ion *ipso* to *tert*-butyl does not occur to either *p-tert*-butyltoluene (2) or 4-*tert*-butyl-*o*-xylene (3) and is even less likely in 5-*tert*-butyl-1,2,3-trimethylbenzene (*vide infra*). A very small amount of another diene(s) (δ 6.02, 6.08, 6.21 ppm) appeared in one column fraction. It is possible that this was a conjugated diene, such as a 1-acetoxy-2-nitro adduct of the original arene, or a 1-nitro-4-acetoxy adduct. Since the amount was ~0.2% of the total product it was not further investigated. No significant amount of dienes other than those isolated was apparent in the reaction mixture prior to chromatography. Thus it appears that the predominant formation of 1,2 adducts in the case of *p-tert*-butyltoluene is unique.

From the relative extents of attack by the nitronium ion at the nuclear positions of 1,2,3-trimethylbenzene (6, 7) and *tert*-butylbenzene (8) the relative amounts of attack at the nuclear positions of **1** may be calculated on the assumption of additivity (7). Attack at the 2 *ipso* position is predicted to occur to the extent of 95%, with only 1% at the 1 *ipso* position and 5% at the 4 position. Little or no attack is expected at the highly hindered 5 position, *ipso* to *tert*-butyl (2, 5). Although the results of such calculations should be treated with some caution (6, 9) it is clear that, in the case of **1**, calculation is in accord with experiment. The 91% of dienes formed (by nmr), or 91% of diene and benzylic (diene derived) products isolated, reflects that extent of attack at the 2 position. No 5-nitro-1,2,3-trimethylbenzene, the expected product of attack at the 5 position, was detected.

The dienol **3***a* is not a primary reaction product and must have been formed by solvolysis of the dienyl acetate **2**, or other adduct, during work-up.

Reactions of the Adducts

Reactions of diene adducts proceed via cyclohexa-

Can. J. Chem. Downloaded from www.nrcresearchpress.com by 210.87.254.6 on 09/05/12
For personal use only.

dienyl cations. Ionization of the nitro group as nitrite anion gives an acetoxycyclohexadienyl cation. Loss of acetate as acetic acid (acid-catalysed) gives a nitrocyclohexadienyl cation. The competition between the two pathways is controlled by: (*i*) the acidity of the solution, more acid solutions favouring the catalysed loss of acetate to form the nitrocyclohexadienyl cation; (*ii*) the ionizing power of the solvent, increased ionizing power favouring the formation of acetoxycyclohexadienyl cation and nitrite anion; and (*iii*) the other substituents present in the diene. In the case of **2** the nitrocyclohexadienyl cation **10** has two methyl and one *tert*-butyl groups attached to centres bearing a formal positive charge, whereas the acetoxy-cyclohexadienyl cation **11** has only one methyl group attached to such a centre. Thus formation of the nitrocyclohexadienyl cation **10** is greatly favoured by the substituents. The ease of formation of **10** is shown by the facility in which the acetate group of **2** is replaced by other nucleophiles in substitution reactions.

Substitution and Isomerization Reactions of Dienes ('Exchange Reactions')

Reactions in which the acetate group of **2** is exchanged for other nucleophiles occur readily, apparently by the S_N1 mechanism.[4] Similarly the diastereoisomeric dienols **3***a* and **3***b* and ethers **4***a* and **4***b* readily undergo isomerization (epimerization) reactions, again by the S_N1 mechanism. All of these reactions presumably involve the intermediate formation of cation **10**. Thus reaction of acetate **2***a* with [$^2H_4$]acetic acid containing 10% acetic anhydride and sulfuric acid led to rapid exchange of the [$^2H_3$]acetate for acetate. Similarly reaction of both **2***a* and **2***b* with aqueous sulfuric acid in acetone gave the dienols **3***a* and **3***b* (Table 1) and with acidified methanol the ethers **4***a* and **4***b*. The facts that both diastereomers of the product were produced from a single diastereomer of the reactant, that both diastereomers of the reactant gave the same initial ratio of products and that the diastereomers of the product subsequently equilibrated provide strong support for the suggested formation of an intermediate nitrocyclohexadienyl cation in which one of the two original chiral centres has become achiral. The substitution and isomerization reactions were conveniently followed by the changes in the *tert*-butyl region of the ^1H nmr spectra. The reactions provide a potentially excellent route to the preparation of both diastereoisomers of **3** and **4**. Dienol **3***b*, which, unlike **3***a*, was not obtained from the nitration reaction mixture, was isolated from the mixture of diastereomers prepared in this manner. The mixture of the ethers **4***a* and **4***b* was prepared similarly and **4***b* isolated by chromatography. An interesting feature of the exchange reactions is that the isomer formed more rapidly, **3***a* and **4***a*, with the *tert*-butyl peak at lower field, is not the most stable isomer. Prolonged reaction led to the predominant formation of **3***b* and **4***b*, with the higher field *tert*-butyl group. The acid-catalysed methanolysis of **2** was carried out under conditions such that the replacement of acetate by methoxyl and the subsequent equilibration was very fast. Both **2***a* and **2***b* gave the same ratio of **4***a*:**4***b*, 29:71. However, formation of the nitrocyclohexadienyl cation is so facile that it was possible to observe methanolysis in the absence of added acid (Tables 2 and 3). It was then possible to observe the disappearance of **2***a* and the initial formation of an approximately 1:1 mixture of **4***a* and **4***b*, which subsequently equilibrated to a mixture containing ca. 70% of **4***b*, and then slowly rearomatized forming, as the major product, methyl 3,4,5-trimethylphenyl ether (**14**). Epimerization of the dienols **3***a* and **3***b* in acetone containing aqueous sulfuric acid was readily followed (Table 4).

TABLE 1. Acid-catalysed hydrolysis of acetate **2***a*[a]

Time (min)	Amount (mol%)			
	2*a*	**3***a*	**3***b*	ArH
25	64	26	9	1
30	59	31	10	1
45	41	44	12	2
60	30	53	14	3
75	24	57	15	4
90	21	58	16	6
4000[b]		46	46	8[c]

[a]Amounts in mol% from integrals of *tert*-butyl peaks at δ 1.02 (2*a*), 0.99 (3*a*), 0.92 (3*b*), and 1.22 ppm (aromatic product and/or *tert*-butyl alcohol equivalent to aromatic cleavage product).
[b]Reaction mixture allowed to stand at lower temperature for 2 days and then worked-up.
[c]From *tert*-butyl peak at δ 1.30 and also from the aromatic peak at 7.12 ppm.

Acetate **2***a* and dienol **3***a* have the same stereochemistry and hence **2***b* and **3***b* must have the same stereochemistry. The *tert*-butyl and 4-methyl ^1H nmr peaks of **2***b* are at higher field than **2***a* and similarly for **3***b* with respect to **3***a*. In the case of the dienyl methyl ethers the ^1H nmr peaks of *tert*-butyl and 4-methyl protons are at higher field in **4***b* than in **4***a*. On the basis of these parallels it seems reasonable to propose that **4***a* has the same stereochemistry as **2***a* and **3***a* and that **4***b* has the same stereochemistry as **2***b* and **3***b*.

Solvolysis of acetate **2***a* in aqueous methanol gave both the dienols **3***a* and **3***b* and the dienyl methyl

[4]In the acid-catalysed reactions it is the conjugate acid of the diene which undergoes the S_N1 reaction.

Can. J. Chem. Downloaded from www.nrcresearchpress.com by 210.87.254.6 on 09/05/12
For personal use only.

TABLE 2. Methanolysis of diene **2***a* followed by ^{1}H nmr[a]

Time (min)	Amount (mol %) 2*a*	4*a*	4*b*	X	Y
30	47	24	25	5	
45	18	36	39	5	
60	6	41	45	6	
75	1	39	49	7	1
90		35	52	8	2
105		32	52	8	4
120[b]		30	54	9	4
275		22	62	8	5
425[c]		17	51	16	12
1450[d]		6	18	36	36
1700[e]		5	16	37	37
2900[f]		2	5	44	44

[a]Values in mol% from integrals of *tert*-butyl peaks at δ 0.89 (4*b*), 0.96 (4*a*), 1.02 (2*a*), 1.15 (Y, unidentified), 1.18 ppm (X, probably *tert*-butyl methyl ether). A small peak also developed at 1.29 ppm, which increased from 0.5% (at 30 min) to 4% (90 min), and a minor peak at 1.22 ppm.
[b]Aromatic peaks at 7.12 and 6.49 ppm just visible.
[c]Aromatic peak at 7.12 and 6.49, the latter associated with peaks at 3.68, 2.22, and 2.08 ppm (methyl 3,4,5-trimethylphenyl ether (**14**)).
[d]Peak at 5.95 apparent.
[e]From integral of 5.5–7.2 ppm region: 5.73 (4, 16%), 5.93 and 5.97 (25%), 6.50 (36%), 7.15 ppm (24%).
[f]From integral of 5.5–7.2 ppm region of worked-up product: 5.68 (4, 7%), 5.82 and 5.87 (16%), 6.52 (**14**, 50%), 6.95 (19%), 7.10 (7%).

TABLE 3. Methanolysis of diene **2***a* followed by ^{13}C nmr[a]

Time (min)	Amount (mol %) 2*a*[b]	4*a*[c]	4*b*[c]
80	68	17	14
153	21	44	35
1307		39	62
1384		37	63
4300[d]		29	71

[a]Amounts of dienes are in mol% with no account taken of rearomatization products estimated to be ~25% at 4300 min (see text).
[b]From peak height ratios of 174.7 (CH_3CO_2H) and 170.7 ($OCOCH_3$ of 2*a*), and 129.5 plus 129.8 (vinylic C of 4*a* and 4*b*) and 126.6 ppm (vinylic C of 2*a*) peaks.
[c]From peak height ratios of 39.1/38.8, 51.6/52.1, 129.5/129.8, 137.0/136.4 ppm peaks (4*a* peaks cited first).
[d]The mixture was worked-up and the ratio of the ^{1}H peaks at 2.88 (OCH_3 of 4*a*) and 3.14 (OCH_3 of 4*b*) was 32:68.

ethers **4***a* and **4***b*, the products arising from reaction of cation **10** with both solvent species. Since the ratio of **4***b* to **4***a* was close to the equilibrium value (~70% **4***b*) whereas **3***a* appeared to be present in greater amount than **3***b* it would seem that the dienyl ethers epimerize more rapidly than the dienols. This reaction clearly illustrates the preference for formation of cation **10**, from **2**, over cation **11**. Solvolysis in aqueous alcohols normally leads to loss of the nitro group as nitrite (6, 10) and the preferred loss of

TABLE 4. Acid-catalysed interconversion of dienols **3***a* and **3***b*[a]

Time (min)	Amount (mol %) from 3*a* 3*a*	3*b*	*S*[b]	Amount (mol %) from 3*b* 3*a*	3*b*	*S*[b]
0	100				100	
25	78	22	—	6	94	5
50	62	38	—	10	90	9
75	53	47	7	14	86	13
100	49	51	—	16	84	—
125	—	—	8	18	82	21
6000[c]	39	61	15	—	—	—

[a]Amounts of 3*a* and 3*b* in mol% of (3*a* + 3*b*) with no account taken of formation of other dienes or of rearomatization. Values listed interpolated from plots of mol% vs. time.
[b]*S*: substance with absorption at δ 6.47 ppm (probably **16**), values are percentage of the sum of the integrals of the δ 7.12, 6.47, and 5.95 ppm peaks. The integral of the 7.12 peak was ~2% of the sum of the integrals after 125 min.
[c]Solution held in the freezer for 4 days.

acetate in the present instance is a reflection of the degree to which the alkyl substituents preferentially stabilize cation **10** compared with **11**.

Reaction of acetate **2***a* with sodium methoxide in methanol gave as the major product the ethers **4***a* and **4***b* and a small amount of dienol **3**. Reaction of the adducts of *p*-xylene (**11**), *p*-cymene (**12**), and the 1,4 adduct of *p*-*tert*-butyltoluene (**2**) with sodium methoxide leads to the initial formation of the corresponding dienols, by cleavage of the acetate at the acetyl group ($B_{AC}2$ transesterification), followed by rearrangement to the 3,4-dialkylphenol, in the cases of the adducts of *p*-xylene[5] and *p*-cymene, and cleavage of the *tert*-butyl group, in the case of the adduct of *p*-*tert*-butyltoluene. For **2** only a small amount of the reaction, at most, proceeds along this pathway. The main reaction is ionization of the acetate group to form cation **10** which combines with methoxide to form the ether **4**. Two factors presumably contribute to the dominance of the $B_{AL}1$ over the normal $B_{AC}2$ pathway for reaction of the acetate ester. The ease of formation of cation **10** is one. The other is that the bulky *tert*-butyl group shields, to at least some degree, the neighbouring acetyl group from attack by methoxide. It is striking that ionization of acetate dominates ionization of the nitro group as nitrite, even under conditions such that no acid is available for catalysis, not even the acid normally released in the solvolysis.

In the substitution and epimerization reactions which were followed over extended periods of time, and in the rearomatization reactions discussed below, dienes other than those already mentioned appeared to be formed, as shown by the appearance of other peaks in the δ 5.7–6.3 ppm (vinyl hydrogen) and/or 1.5–2.0 ppm (allylic methyl and methyl

[5]Unpublished work with R. J. Thompson.

Can. J. Chem. Downloaded from www.nrcresearchpress.com by 210.87.254.6 on 09/05/12
For personal use only.

bonded to saturated carbon) and/or ~1.1 ppm ('saturated' *tert*-butyl) regions. It is possible that these absorptions arose from the presence of conjugated dienes. However, such absorptions never represented more than a minor amount of the product and the conclusion (*vide supra*) that the special factors which result in the preferential formation of 1,2 adduct (conjugated diene) from *tert*-butyltoluene do not exist in the 5-*tert*-butyl-1,2,3-trimethylbenzene system is reinforced.

Rearomatization Reactions

Rearomatization products of diene adducts are formed via the nitrocyclohexadienyl cation (13) or the acetoxycyclohexadienyl cation (6). Acetate **2** gives the nitrocyclohexadienyl cation **10** much more rapidly than the acetoxycyclohexadienyl cation **11** under all conditions investigated. However this does not result in all of the rearomatization reactions proceeding via **10**, as the transition state barrier between **10** and its aromatic product may be, and in the relevant instances presumably is, higher than that between **2**, **11** and its aromatic product (cf. 14).

As discussed above methanolysis of acetate **2***a* gave the dienyl ethers **4***a* and **4***b*, which subsequently equilibrated (Tables 2 and 3). On prolonged reaction the dienyl ethers rearomatized and the major aromatic product was methyl 3,4,5-trimethylphenyl ether (**14**). Formation of **14** occurs via the methoxycyclohexadienyl cation **12**, which undergoes loss of the *tert*-butyl cation. The ether **14** was formed in close to quantitative yield when the dienyl ethers **4***a* and **4***b* were first prepared and then solvolysed in aqueous methanol, conditions most favourable to the ionization of the nitro group (6). The methoxyl group is a poorer leaving group than acetoxyl and a possible explanation for the formation of the rearomatization product via the methoxycyclohexadienyl cation **12** might be that ionization of the nitro group as nitrite from **4** is faster than loss of methoxide (although slower than loss of acetate from **2**). However, since **4** epimerizes before rearomatization (Tables 2 and 3) formation of **10** would seem to be *faster* than formation of **12**. Thus the barrier for loss of the *tert*-butyl cation from **12** is lower than that (those) for rearomatization of **10**.

Solvolysis of acetate **2***a* in moist [$^2H_4$]acetic acid resulted in rapid exchange of the acetate group prior to rearomatization and epimerization accompanying rearomatization (Table 5). Formation of the nitrocyclohexadienyl cation **10** is evidently faster than formation of the acetoxycyclohexadienyl cation **11**. However the predominant rearomatization products, the [$^2H_3$]acetate **15** and the phenol **16**, are not derived from cation **10** but from **11** (or the hydroxy analog **13**), which ejects the *tert*-butyl cation. Conceivably, the phenol **16** could have been formed by hydrolysis of the aryl acetate **15**. It seems more likely that some dienol **3** was formed from **2***a* by partial exchange of acetate with solvent water, via **10**, and that the phenol was in turn formed from the dienol via ionization to cation **13** followed by loss of the *tert*-butyl cation. A compound of relative molecular mass 192 was also a significant product from the solvolysis of acetate **2***a*. No significant amounts of benzylic derivatives were detectable by nmr hence this product is probably a phenol. Reaction pathways which would lead to both unrearranged phenol, i.e. 6-*tert*-butyl-2,3,4-trimethylphenol, and to rearranged phenol, i.e. 2-*tert*-butyl-3,4,5-trimethylphenol, have been observed in other systems (3, 12), and may apply here. Loss of the *tert*-butyl group also occurred in the solvolysis of the 1,4 adducts of *p*-*tert*-butyltoluene and 4-*tert*-butyl-*o*-xylene, although in the latter case this was a minor reaction, the major reaction being the normal 1,2 acetate shift leading to the aryl acetate.

It is evident that in the solvolytic rearomatization reactions in aqueous acetic acid, aqueous methanol and methanol one mole of *tert*-butyl derivative, viz. *tert*-butyl acetate, alcohol, or methyl ether, as appropriate, must have been formed per mole of aromatic de-*tert*-butylation product. Although the *tert*-butyl cleavage products were not identified as such ^1H nmr peaks were observed at the appropriate positions in the spectra of the reaction mixtures, e.g. at δ 1.30 (*tert*-butyl alcohol (15)) and 1.43 ppm (*tert*-butyl acetate (15)) in the products of solvolysis of **2***a* in moist acetic acid. The formation of these peaks provides a measure of the extent of rearomatization even

TABLE 5. Solvolysis of acetate **2***a* in moist acetic acid[a]

Time (min)	Amount (mol %)		
	2*a*	**2***b*	ArH
0	100		
10	44	26	12
15	35	24	20
20	26	20	30
25	21	16	39
30	16	13	44
35	12	11	48

[a]Reaction carried out in [$^2H_4$]acetic acid containing 2% water. Amounts determined from integrals of *tert*-butyl peaks at δ 0.92 ('2*b*'), 0.99 ('2*a*'), and 1.25 plus 1.29 ('ArH') expressed as a fraction of the total integral from 0.85 to 1.35 ppm. Other (smaller) peaks appeared at 1.07 and 1.14 ppm. '2*a*' may include a contribution from dienol 3*a* and likewise for '2*b*' and 3*b*. 'ArH' may include a contribution from *tert*-butyl alcohol and *tert*-butyl acetate, the expected cleavage products.

though the compounds exhibiting the absorption peaks are not themselves aromatic.

As the acidity of the reaction medium is increased the rate of formation of the nitrocyclohexadienyl cation **10** and its steady-state concentration will increase relative to the acetoxycyclohexadienyl cation **11**, because the loss of acetate group from **2** is acid catalysed but the loss of the nitro group is not. The rate of rearomatization from **10** will also increase and will eventually become faster than the rate of rearomatization via **11**. Addition of 0.05% sulfuric acid and 10% acetic anhydride to acetic acid brings about this transition and the aromatic products formed are derived from the nitrocyclohexadienyl cation **10** (Table 6).[6] Deprotonation of **10** at either of the symmetrical methyl groups leads to the triene **17** which in turn undergoes ionization of the nitro group to form the benzyl carbonium ion **18** and nitrite anion. Combination of **18** and nitrite anion, at oxygen, would give the benzyl nitrite **5** and, at nitrogen, would give the aryl nitromethane **6**. Combination of the benzyl cation with acetate would give the benzyl acetate **7**.[7] Inspection of Table 6 reveals that the aldehyde **19** is not a primary reaction product but is formed from the nitrite **5** in the more strongly acidic solutions and also during work-up. In fact it was possible to follow the conversion of **5** into **19** in the reaction mixtures to which the 5% and 50% sulfuric acid solutions were added. Thus it is clear that the nitrite **5** is the major primary aromatic product over the complete acidity range investigated. Benzyl nitrite itself is known to undergo autodecomposition to benzaldehyde (16) and benzaldehydes often accompany benzylic products obtained from rearomatization of diene adducts (3, 4, 11, 17). The benzyl alcohol **8** which was obtained on work-up of the reaction to which 0.05% sulfuric acid had been added also appears to have been formed from **5**. A small amount of the nitroarene **9** also appeared to have been formed in the reaction to which 50% sulfuric acid was added.

Reaction of acetate **2***a* in deuteriochloroform with 2% aqueous sulfuric acid led to initial partial conversion into dienol **3**. However, rapid rearomatization ensued and the final product was the nitrite **5** and acetic acid. Reaction of acetate **2***a* in ether with hydrogen chloride (in an unsuccessful attempt to prepare the nitrocyclohexadienyl chloride) also gave nitrite **5** as the major product and some nitromethane **6**. The conversion of **5** to benzaldehyde **19**, on standing in the acid solution was again demonstrated. Reaction of **2***a* with boron trifluoride in ether also gave a mixture of the side-chain products **5**, **6**, **7**, and **8** and, on one occasion, the benzaldehyde **19**.

TABLE 6. Yields of products of rearomatization of diene **2***a* with sulfuric acid and 10% acetic anhydride in [$^2H_4$]acetic acid[a]

	Yield immediately before work-up					Yield after work-up				
%H_2SO_4[c]	**19**	**5**	**6**	**7**	X[b]	**19**	**5**	**6**	**7**	X[b]
0.05[d]		47	13	12	14	12	18	33	16	5
0.5	8	43	18	25	6	56		16	22	6
5.0	50	2	13	31	4	48		11	37	4
50[e]	—	—	—	—	—	48		16	19	

[a]Yields in mol% determined by integration of the methylene, vinyl, and aromatic regions of the ^1H nmr spectrum.
[b]Unidentified compound δ 7.00 ppm in both reaction mixture and $CDCl_3$, possibly **1**.
[c]Amount of sulfuric acid by weight in the acetic anhydride – [$^2H_4$]acetic acid solution before addition of 250 mm^3 to a solution of **2***a* (120 mg) in $CDCl_3$ (200 mm^3).
[d]Before work-up peaks between δ 6.0 and 6.5 ppm integrated for ~14% of the products. After work-up 16% of **8** was obtained in addition to the products listed.
[e]Because of phase separation the product distribution prior to work-up could not be measured quantitatively. Qualitatively, **19** increased relatively during the reaction to become the major product, **5** was present initially but disappeared prior to work-up as **19** was formed and **6** and **7** were minor products. Peaks attributed to a minor amount of nitroarene **9** were also present in the ^1H nmr spectrum of the worked-up product.

At very high levels of acidity the opportunity for cation **10** to be deprotonated to the triene **17** is reduced. The life-time of **10** is therefore increased and the opportunity for migration of the nitro group to occur is enhanced. Migration of the nitro group to the unsubstituted position gives cation **20**, the precursor to the nitroarene **9**. When acetate **2***a* was reacted with fluorosulfonic acid and with trifluoromethane sulfonic acid the nitroarene **9** was the major reaction product, although benzylic derivatives, mainly the aldehyde **19**, itself presumably formed from the nitrite **5**, and some nitromethane **6** were also formed. A small amount of **9** was also detected in the reaction with 50% sulfuric acid in acetic acid – acetic anhydride, as mentioned above.

Adduct **2** has a marked preference for the formation of benzylic derivatives. On reaction with sulfuric acid in acetic acid – acetic anhydride the adduct of 4-*tert*-butyl-*o*-xylene gave only modest amounts of benzylic product. The nitroarene was formed at the lowest acidities and became the major product at higher acidities. In trifluoroacetic acid and/or boron trifluoride etherate the adducts of *p*-xylene, *tert*-butyltoluene, and 4-*tert*-butyl-*o*-xylene all gave the nitroarene. Under these conditions, as mentioned, **2** gave benzylic derivatives and only gave the nitro-

[6]These reactions were carried out in a medium which contained 44% deuteriochloroform. The presence of the chloroform and the absence of water would make for a poorly ionizing solution and this factor would contribute to a decreased ease of formation of **11** and hence a reduced extent of rearomatization by this pathway.

[7]These reactions can also be formulated as occurring between the benzyl cation and nitrous and acetic acids, followed by deprotonation.

Can. J. Chem. Downloaded from www.nrcresearchpress.com by 210.87.254.6 on 09/05/12
For personal use only.

Can. J. Chem. Downloaded from www.nrcresearchpress.com by 210.87.254.6 on 09/05/12
For personal use only.

arene under more highly acidic conditions and even then appreciable amounts of benzylic derivatives were still formed. This preference may be attributed to the stability of cation **10** and the fact that the nitro group has to migrate across an interposed *ipso* position to form cation **20** the precursor to nitroarene. If the migration involves successive 1,2 shifts then cation **21** is formed as an intermediate. Cation **21** is much less stable than **10** and it will preferentially reform **10** rather than **20**. Thus the existence of **21** in the sequence **10** → **21** → **20** effectively increases the lifetime of **10** and allows more opportunity for deprotonation to the triene **17** to occur. In addition, there is, of course, a statistical factor of 2 favouring deprotonation of **10** as compared with the 4-*tert*-butyl-1,2-dimethylbenzene case.

Thermolysis of acetates **2***a* and **2***b* gave the parent hydrocarbon **1** and benzylic derivatives as the major products. Thermolysis of the dienol **3***a* gave the phenol **16**, formally the product of the elimination of the elements of *tert*-butyl nitrite, and the benzyl alcohol **8** as the major products.

Experimental

General experimental methods have been described previously (3).

*5-*tert*-Butyl-1,2,3-trimethylbenzene (**1**)*

Alkylation of *m*-xylene (2.5 mol) with *tert*-butyl alcohol and aluminum chloride catalyst (18) gave 5-*tert*-butyl-1,3-dimethylbenzene (73% after distillation at 41°C/55 Pa); ir (film): 1600, 1475, 1360, 845, 701 cm^{-1}; ^1H nmr ($CDCl_3$) δ: 1.26 (s, 9, $C(CH_3)_3$), 2.24 (s, 6, 1-CH_3 and 3-CH_3), 6.75 (s, 1, 2-*H*), 6.95 ppm (s, 2, 4-*H* and 6-*H*); ^{13}C nmr ($CDCl_3$) δ_C: 21.5 (1-CH_3 and 3-CH_3), 31.4 ($C(CH_3)_3$), 34.4 ($C(CH_3)_3$), 123.1 (*C*-4 and *C*-6), 127.1 (*C*-2), 137.3 (*C*-1 and *C*-3), 151.0 ppm (*C*-5); ms (70 eV) *m/e* (relative intensity): 162 (30, M), 148 (18), 147 (100, $M - CH_3$), 119 (30, $M - C_3H_7$), 107 (33), 91 (18).

Chloromethylation of the 5-*tert*-butyl-1,3-dimethylbenzene (1 mol) gave 5-*tert*-butyl-2-chloromethyl-1,3-dimethylbenzene (83% after two recrystallizations from pentane); mp 26–27°C (lit. (19) 25.6–25.9°C); ir (melt): 1610, 1480, 1450, 1360, 1270, 1243, 933, 870, 726, 675 cm^{-1}; ^1H nmr ($CDCl_3$) δ: 1.24 (s, 9, $C(CH_3)_3$), 2.34 (s, 6, 1-CH_3 and 3-CH_3), 4.53 (s, 2, CH_2), 7.01 ppm (s, 2, 4-*H* and 6-*H*); ^{13}C nmr ($CDCl_3$) δ_C: 19.4 (1-CH_3 and 3-CH_3), 31.2 ($C(CH_3)_3$), 34.3 ($C(CH_3)_3$), 41.0 (CH_2Cl), 125.4 (*C*-4 and *C*-6), 131.0 (*C*-2), 136.9 (*C*-1 and *C*-3), 151.3 ppm (*C*-5); ms (70 eV) *m/e* (relative intensity): 212 (8) and 210 (24, M), 197 (33) and 195 (100, $M - CH_3$), 175 ($M - Cl$).

Reduction of the 5-*tert*-butyl-2-chloromethyl-1,3-dimethylbenzene (0.72 mol) with lithium aluminum hydride gave 5-*tert*-butyl-1,2,3-trimethylbenzene (**1**, 99%); mp (sealed tube) 34–35°C (lit. (19) 30–32°C); ir (Nujol): 1470, 1350, 1309, 1240, 1205, 998, 929, 865, 711 cm^{-1}; ^1H nmr ($CDCl_3$) δ: 1.27 (s, 9, $C(CH_3)_3$), 2.10 (s, 3, 2-CH_3), 2.24 (s, 6, 1-CH_3 and 3-CH_3), 7.00 ppm (s, 2, 4-*H* and 6-*H*); ^{13}C nmr ($CDCl_3$) δ_C: 14.9 (2-CH_3), 20.8 (1-CH_3 and 3-CH_3), 31.4 ($C(CH_3)_3$), 34.1 ($C(CH_3)_3$), 124.6 (*C*-4 and *C*-6), 131.9 (*C*-2), 135.8 (*C*-1 and *C*-3), 147.9 ppm (C-5); ms (70 eV) *m/e* (relative intensity): 176 (29, M), 161 (100, $M - CH_3$), 145 (9), 133 (30), 121 (46), 119 (15), 105 (20), 91 (20).

*5-*tert*-Butyl-2,3-dimethylbenzyl Acetate (**7**) and 5-*tert*-Butyl-2,3-dimethylbenzyl Alcohol (**8**)*

Chloromethylation (19) of 4-*tert*-butyl-1,2-dimethylbenzene gave 5-*tert*-butyl-1-chloromethyl-2,3-dimethylbenzene; ir (Nujol) 1470, 1350, 1278, 1262, 1242, 1208, 879, 737, 688, 625 cm^{-1}; ^1H nmr ($CDCl_3$) δ: 1.26 (s, 9, $C(CH_3)_3$), 2.21 (s, 6, 2-CH_3 and 3-CH_3), 4.51 (s, 2, CH_2), 7.12 ppm (s, 2, 4-*H* and 6-*H*); ^{13}C nmr ($CDCl_3$) δ_C: 14.4 (2-CH_3), 20.6 (3-CH_3), 31.3 ($C(CH_3)_3$), 34.1 ($C(CH_3)_3$), 45.9 (CH_2Cl), 124.6 (*C*-6), 127.6 (*C*-4), 132.6 (*C*-2), 135.0 (*C*-1), 136.9 (*C*-3), 148.3 ppm (*C*-5); ms (70 eV) *m/e* (relative intensity): 212 (9) and 210.124 (27, M_r calcd. for $^{12}C_{13}{}^1H_{19}{}^{35}Cl$): 210.118), 197 (40) and 195 (100, $M - 15$), 175 (13, $M - Cl$), 169 (5) and 167 (13, $M - C_3H_7$), 161 (18), 159 (36), 119 (33), 91 (13).

The chloride (1.5 g, 7 mmol) was heated under reflux with silver acetate (1.4 g, 8 mmol) in acetic acid (20 cm^3) for 1 h. After work-up 5-*tert*-butyl-2,3-dimethylbenzyl acetate (**7**, 1.7 g, 7 mmol was obtained); ir (film) 1730 and 1238 ($OCOCH_3$), 1470, 1370, 1350, 1021, 870 cm^{-1}; ^1H nmr ($CDCl_3$) δ: 1.30 (s, 9, $C(CH_3)_3$), 2.00 (s, 3, $OCOCH_3$), 2.16 (s, 3, 2-CH_3), 2.25 (s, 3, 3-CH_3), 5.07 (s, 2, CH_2), 7.15 ppm (s, 2, 4-*H* and 6-H); ms *m/e* 234.161 (M_r($^{12}C_{15}{}^1H_{22}{}^{16}O_2$): 234.162).

Reduction of the acetate 7 with lithium aluminum hydride gave 5-*tert*-butyl-2,3-dimethylbenzyl alcohol (**8**); ir (CCl_4) 3630, 3500–3250 (broad) 1470, 1350, 1240, 1018, 1000, 874 cm^{-1}; ^1H nmr: 1.30 (s, $C(CH_3)_3$), 1.22 (s, 2-CH_3), 1.29 (s, 3-CH_3), 4.70 (s, CH_2), 7.20 ppm (m, 4-*H* and 6-*H*); ms (70 eV) *m/e* (relative intensity): 192.153 (41, M_r calcd. for $^{13}C_{13}{}^1H_{20}{}^{16}O$: 192.151), 175 (100, $M - OH$), 159 (81), 119 (34).

*Nitration of 5-*tert*-Butyl-1,2,3-trimethylbenzene (**1**)*

A solution of freshly distilled nitric acid (18.9 g, 0.30 mol) in acetic anhydride (60 cm^3) was added to **1** (17.6 g, 0.10 mol) in a mixture of acetic anhydride (40 cm^3) and dry methylene chloride (30 cm^3) at a rate such that the temperature of the mixture (cooled in solid carbon dioxide – acetone) did not rise above −55°C. The pale yellow mixture was allowed to stand at −75°C for 1 h and after work-up in the usual manner (3) yielded a yellow crystalline solid (30.7 g) consisting of (by ^1H nmr) ca. 91% of dienes. Recrystallization at low temperature from ether–pentane gave white prismatic crystals of 1-*tert*-butyl-3,4,5-trimethyl-4-nitrocyclohexa-2,5-dienyl acetate (**2***a*, 17.0 g, 61 mmol); mp 80.5–81.5°C (dec.); uv (CH_3OH): 225 nm (ε 160 m^2 mol^{-1});[8] ir (CCl_4): 1735, 1250 and 1222 ($OCOCH_3$), 1540 and 1355 (NO_2), 1154, 1085, 995, 950, 897 cm^{-1}; ^1H nmr ($CDCl_3$) δ: 1.01 (s, 9, $C(CH_3)_3$), 1.75 (d, 6, $J \simeq 0.8$ Hz, 3-CH_3 and 5-CH_3), 1.79 (s, 3, 4-CH_3), 1.93 (s, 3, $OCOCH_3$), 5.75 ppm (d, 2, $J \simeq 0.8$ Hz, 2-*H* and 6-*H*); ^{13}C nmr ($CDCl_3$) δ_C: 18.0 (3-CH_3 and 5-CH_3), 19.0 (4-CH_3), 22.0 ($OCOCH_3$), 25.3 ($C(CH_3)_3$), 39.1 ($C(CH_3)_3$), 80.5 (*C*-1), 92.5 (*C*-4), 125.8 (*C*-2 and *C*-6), 135.1 (*C*-3 and *C*-5), 169.5 ppm ($OCOCH_3$). *Anal.* calcd. for $C_{15}H_{23}NO_4$: C 64.04, H 8.24, N 4.98; found: C 64.27, H 8.29, N 5.00.

The residue (11.9 g) after evaporation of the solvent was subjected to chromatography on alumina (700 g) at −40°C. Elution with pentane and ether–pentane mixtures (250 cm^3 per fraction) gave, in the pentane and 5% ether fractions, 5-*tert*-butyl-2,3-dimethylbenzyl nitrite (**5**, 0.5 g, 2 mmol); ir ($CDCl_3$): 1660 and 1610 cm^{-1} (ONO); nmr ($CDCl_3$) δ: 1.29 (s, $C(CH_3)_3$), 2.17 (s, 3, 2-CH_3), 2.27 (s, 3, 3-CH_3), 5.65 (s, 2, CH_2) 7.15 ppm (broad s, 2, 4-*H* and 6-*H*); ^{13}C nmr ($CDCl_3$) δ_C: 14.5 (2-CH_3), 20.6 (3-CH_3), 31.3 ($C(CH_3)_3$), 34.2 ($C(CH_3)_3$), 69.4 (CH_2), 124.5 (*C*-6), 127.6 (*C*-4), 132.7 (*C*-1 and *C*-2), 136.8 (*C*-3), 148.5 ppm (*C*-5).

[8]The limit of measurement under the conditions used was 225 nm, where only end absorption was observed.

Can. J. Chem. Downloaded from www.nrcresearchpress.com by 210.87.254.6 on 09/05/12
For personal use only.

5-*tert*-Butyl-1,2,3-trimethyl-4-nitrobenzene (**9**, 1.9 g, 9 mmol) was eluted in the second 5% and first 10% ether fractions. After recrystallization from pentane it had mp 89–91°C; ir (CCl_4): 1520 and 1365 cm^{-1} (NO_2); ^1H nmr ($CDCl_3$) δ: 1.34 (s, 9, $C(CH_3)_3$), 2.08 (s, 3, 2-CH_3), 2.16 (s, 3, 1-CH_3), 2.28 (s, 3, 3-CH_3), 7.13 ppm (s, 1, 6-*H*); ^{13}C nmr ($CDCl_3$) δ_C: 14.8 (2-CH_3), 15.7 (3-CH_3), 21.0 (1-CH_3), 30.9 ($C(CH_3)_3$), 35.2 ($C(CH_3)_3$), 126.8 (*C*-6), 127.5 (*C*-3), 134.4 (*C*-2), 136.5 (*C*-1), 137.6 (*C*-5), 149.8 ppm (*C*-4); ms (70 eV) *m/e* (relative intensity): 221.143 (39, M_r calcd. for $^{12}C_{13}{}^1H_{19}{}^{14}N^{16}O_2$: 221.142), 207 (17), 206 (100, $M - CH_3$), 175 (22, $M - NO_2$).

The second 10% and the 20% ether fractions probably contained more diene **2***a* (4.3 g, 15 mmol), however the nmr spectra showed only the rearomatization product, the nitrite **5**, and an equivalent amount of acetic acid. Minor amounts of the nitromethane derivative **6** and the acetate **7** were also present. The second diastereoisomer of 1-*tert*-butyl-3,4,5-trimethyl-4-nitrocyclohexa-2,5-dienyl acetate (**2***b*, 2.2 g, 8 mmol) was obtained in the 30–60% ether fractions. After low temperature recrystallization from ether–pentane **2***b* had mp 82.0–83.0°C (dec.); uv (CH_3OH): 225 nm (ε 130 m^2 mol^{-1});[8] ir (Nujol): 1740, 1247 and 1220 ($OCOCH_3$), 1540 (NO_2), 1155, 1075, 1002, 963, 890, 848, 792 cm^{-1}; ^1H nmr ($CDCl_3$) δ: 0.93 (s, 9, $C(CH_3)_3$), 1.72 (s, 3, 4-CH_3), 1.77 (d, 6, $J \simeq 1$ Hz, 3- and 5-CH_3), 1.99 (s, 3, $OCOCH_3$), 5.80 ppm (d, 2, $J \simeq 1$ Hz, 2- and 6-H); ^{13}C nmr ($CDCl_3$) δ_C: 17.8 (3-CH_3 and 5-CH_3), 21.3 (4-CH_3), 21.6 ($OCOCH_3$), 25.0 ($C(CH_3)_3$), 39.6 ($C(CH_3)_3$), 80.7 (*C*-1), 90.9 (*C*-4), 127.1 (*C*-2 and *C*-6), 133.3 (*C*-3 and *C*-5), 169.2 ppm ($OCOCH_3$). *Anal.* calcd. for $C_{15}H_{23}NO_4$: C 64.04, H 8.24, N 4.98; found: C 64.37, H 8.19, N 4.28.

1-*tert*-Butyl-3,4,5-trimethyl-4-nitrocyclohexa-2,5-dienol (**3***a*, 1.33 g, 5.6 mmol) was obtained in the 90–100% ether fractions. It was recrystallized at low temperature from ether–pentane and had mp 78.5–79.0°C (dec.); uv (CH_3OH): 225 nm (ε 140 m^2 mol^{-1});[8] ir (CCl_4): 3620 (OH), 1530 and 1340 (NO_2), 1218, 1152, 1075, 1059, 1029, 980, 652 cm^{-1}; ^1H nmr ($CDCl_3$) δ: 0.99 (s, 9, $C(CH_3)_3$), 1.39 (s, 1, OH), 1.74 (s, 3, 4-CH_3), 1.77 (d, 6, $J \simeq 0.8$ Hz, 3-CH_3 and 5-CH_3), 5.95 ppm (d, 2, $J \simeq 0.8$ Hz, 2- and 6-*H*); ^{13}C nmr ($CDCl_3$) δ_C: 18.3 (3-CH_3 and 5-CH_3), 22.1 (4-CH_3), 25.3 ($C(CH_3)_3$), 38.1 ($C(CH_3)_3$), 72.0 (*C*-1), 90.7 (*C*-4), 130.5 (*C*-2 and *C*-6), 132.9 ppm (*C*-3 and *C*-5).

When the above reaction was repeated at a temperature of 0°C no diene adduct was obtained and the major products apparent (nmr) in the reaction mixture after work-up were the nitromethane **6** and the nitrite **5**. Crystallization of the crude product from pentane gave 5-*tert*-butyl-2,3-dimethylphenylnitromethane (**6**); mp 77–78°C: ir (CCl_4) 1545 and 1355 (NO_2), 1256, 1210, 1000, 975 cm^{-1}; ^1H nmr ($CDCl_3$) δ: 1.28 (s, 9, $C(CH_3)_3$), 2.20 (s, 3, 2-CH_3), 2.28 (s, 3, 3-CH_3), 5.45 (s, 2, CH_2), 7.12 and 7.26 ppm (q, 2, $J \simeq 2$ Hz, 4-*H* and 6-*H*); ^{13}C nmr ($CDCl_3$) δ_C: 14.8 (2-CH_3), 20.7 (3-CH_3), 31.2 ($C(CH_3)_3$), 34.2 ($C(CH_3)_3$), 78.5 (CH_2), 126.3 (*C*-6), 128.1 (*C*-1), 128.9 (*C*-4), 133.6 (*C*-2), 137.2 (*C*-3), 148.8 ppm (*C*-5); ms (70 eV) *m/e* (relative intensity): 221 (5, M), 176 (22), 175 (100, $M - NO_2$), 160 (25), 145 (23), 133 (13). *Anal.* calcd. for $C_{13}H_{19}NO_2$: C 70.56, H 8.65, N 6.33; found: C 70.81, H 8.74, N 6.33.

Diene **2***a* rearomatized rapidly in $CDCl_3$ solution at ambient temperature to form the nitrite **5** (76%; ^1H nmr δ: 1.28, 2.15, 2.26, 5.65, 7.16 ppm), the nitromethane **6** (16%; δ 5.45 ppm), the acetate **7** (4%; δ 5.12 ppm) and acetic acid (δ 2.03 ppm). On another occasion the nitrite **5** was formed in 90% yield. At 0°C rearomatization occurred within 24 h and the benzylic products were formed in the amounts: **5** (58%), **6** (36%), **7** (6%), together with acetic acid. A sample of **2***a* which had rearomatized at ambient temperature and was then worked-up gave (^1H nmr) the aldehyde **19** (8%; δ: 7.39, 7.66, 10.28 ppm), **5** (25%), **6** (34%), **7** (11%), and **8** (16%). Formation of **19**, **6**, **7**, and **8** was confirmed by glc–mass spectrometry. Dienol **3***a* also rearomatized rapidly in $CDCl_3$ solution at ambient temperature to give the nitrite **5**, identified by ^1H and ^{13}C nmr, and small amounts of **6** (14%; δ 5.45 ppm) and **8** (14%; δ 4.68 ppm).

Aluminum Hydride Reduction of Diene Acetate **2**a

Diene **2***a* (120 mg, 0.40 mmol) in dry tetrahydrofuran (THF) (1 cm^3) was stirred with a solution of excess AlH_3 (2.7 mmol) in THF (15 cm^3) at 0°C for 15 min. After work-up a pale yellow oil (95 mg) was obtained, and the major component (ca. 80%) was identified as the dienol **3***a*; (ir (CCl_4): 3620, 1530, 1340, 1252, 1155, 1075, 1058, 1029, 980, 652 cm^{-1}; ^1H nmr ($CDCl_3$) δ: 0.99, 1.40, 1.73, 1.76, 5.93 ppm).

Hydrolysis of Acetate **2** *in Acidified Aqueous Acetone. 1-tert-Butyl-3,4,5-trimethyl-4-nitrocyclohexa-2,5-dienol (3b)*

The dienyl acetate **2***a* (100 mg) was dissolved in aqueous [$^2H_6$]acetone (400 mm^3; 10:90, v/v) containing sulfuric acid (0.02% w/v) and the disappearance of **2***a* and formation of the diastereoisomeric dienols **3***a* and **3***b*, at 35°C, was followed by integration of the *tert*-butyl peaks at δ 0.92 (**3***b*), 0.99 (**3***a*), and 1.02 (**2***a*). Data are shown in Table 1. A small amount of aromatic compound was also formed as indicated by the appearance of peaks at δ 1.2 ppm ($C(CH_3)_3$) and at 7.2 ppm (Ar*H*). The reaction was worked-up after standing two days at lower temperature.[9] At this time equal amounts of **3***a* and **3***b* were present. Peaks characteristic of both **3***a* and **3***b* were clearly distinct in the nmr spectrum of the worked-up product; **3***a*: ^1H nmr ($CDCl_3$) δ: 0.99, 1.76, 1.78, 5.96 ppm; **3***b*: ^1H nmr ($CDCl_3$) δ: 0.93, 1.69, 1.73, 5.92 ppm. A similar experiment starting with acetate **2***b* likewise gave an initial mixture of dienols in which **3***a* predominated and in which **3***b* increased with time to become eventually larger than **3***a* in the ratio of 1.4:1.

On a preparative scale acetate **2***a* (700 mg) was dissolved in acidified aqueous acetone (3 cm^3) at 31°C. After 95 min, at which time ^1H nmr indicated that 40% yield of dienol **3***b* had been obtained, the mixture was worked-up to yield a yellow oil (660 mg) containing dienols (92%) and aromatic compound(s) (8%). Chromatography on alumina at −30°C and elution with pentane–ether gave dienol **3***a*. Elution with ether gave dienol **3***b* (180 mg); mp 91–95°C (dec.); ^1H nmr ($CDCl_3$) δ: 0.93 (s, 9, $C(CH_3)_3$), 1.69 (s, 3, 4-CH_3) 1.73 (d, 6, $J = 0.7$ Hz, 3-CH_3 and 5-CH_3) 2.20 (s, 1, *OH*), 5.91 ppm (broad s, 2, 2-*H* and 6-*H*); ^{13}C nmr ($CDCl_3$) δ_C: 17.7 (3-CH_3 and 5-CH_3), 21.2 (4-CH_3), 25.0 ($C(CH_3)_3$), 37.8 ($C(CH_3)_3$), 72.5 (*C*-1), 91.2 (*C*-4), 130.5 (*C*-2 and *C*-6), 132.1 ppm (*C*-3 and *C*-5).

Reaction of Acetate **2** *with Acidified Methanol*

Diene **2***a* (100 mg, 0.36 mmol) was added to methanol (400 mm^3) containing sulfuric acid (0.2% w/v). Although acetate **2***a* is not very soluble in methanol it dissolved readily in the acidified methanol, indicative of reaction on solution and, indeed, before the ^1H nmr spectrum of the mixture could be examined (< 4 min) diene **2***a* had been completely converted into a mixture of the ethers **4***a* and **4***b* and the two diastereoisomers had been equilibrated. The ratio of **4***a*:**4***b* as determined by the ratio of the integrals of the *tert*-butyl peaks at 0.96 and 0.89 ppm was 29:71. In a similar experiment with diene **2***b* the exchange and equilibration was complete in less than 2 min and the same ratio of **4***a*:**4***b* was found. In both

[9]Small-scale reactions were worked-up by adding the solution to methylene chloride (5 cm^3) followed by neutralization with gaseous ammonia (for reactions in acid) or ammonium chloride (for reactions in base), drying over magnesium sulfate, and removal of the solvent under reduced pressure.

Can. J. Chem. Downloaded from www.nrcresearchpress.com by 210.87.254.6 on 09/05/12
For personal use only.

cases rearomatization was negligible, less than 2% occurring in 16 min.

On preparation scale acetate **2***a* (0.5 g) was reacted with methanol (3 cm^3) containing sulfuric acid (0.2% w/v) at 0°C for 15 min. After work-up a clean mixture of the ethers **4***a* (36%) and **4***b* (64%) was obtained.

Methanolysis of Acetate **2**a

A suspension of diene **2***a* (100 mg) in methanol (400 mm^3) was prepared in an nmr tube. After treatment in an ultrasonic bath at 21°C for 22 min the solution became homogeneous and the reaction was then followed by ^1H nmr at a probe temperature of 35°C. The relative amounts of reactant and products were determined by integration of the *tert*-butyl peaks and results are summarized in Table 2. Initially a mixture of the dienyl ethers **4***a* and **4***b* was formed and after some time the amount of **4***b* became significantly greater than **4***a*. Eventually rearomatization occurred giving as the main product methyl 3,4,5-trimethylphenyl ether (**14**). Similar results were obtained for a reaction carried out in [$^2H_4$]methanol and followed by ^1H nmr.

The reaction was repeated using a solution of acetate **2***a* (550 mg) in methanol (800 mm^3) and $CDCl_3$ (300 mm^3). After treatment in the ultrasonic bath at 25°C for 25 min, the reaction was followed by ^{13}C nmr at a probe temperature of 27°C. Decoupled spectra (2000 scans) were accumulated at the indicated time intervals (Table 3). The disappearance of the peaks characteristic of acetate **2***a* and the appearance of peaks characteristic of acetic acid (20.9 and 175 ppm) and of the cyclohexadienyl methyl ethers **4***a* and **4***b* were readily observed. No rearomatization was detected by ^{13}C nmr. However, when the reaction mixture was examined by ^1H nmr after 2700 min it was evident that aromatic products, δ 7.1 (12%) and 6.52 ppm (11%, methyl 3,4,5-trimethylphenyl ether (**14**)) had been formed. The 2.08, 2.22, and 3.68 ppm peaks of **14** were also evident. A component with δ 5.9 ppm (10%) was also present. *tert*-Butyl peaks at δ 1.14, 1.16 and 1.18 were also apparent and each was ca. 13% of the total *tert*-butyl peak intensity. The aryl ether (11%) could be clearly discerned in the worked-up product, the *tert*-butyl intensity at 1.15 and 1.18 ppm was reduced to half the amount before work-up and there were aromatic peaks at 7.10 (5%) and 6.95 ppm (7%).

Chromatography of the product on alumina at −50°C and elution with pentane and ether–pentane mixtures gave, in the 5% ether fraction, methyl 3,4,5-trimethyl-4-nitrocyclohexa-2,5-dienyl ether (**4***b*); ^1H nmr ($CDCl_3$) δ: 0.89 (s, $C(CH_3)_3$), 1.70 (s, 4-CH_3), 1.76 (broad s, 3-CH_3 and 5-CH_3) 3.12 (s, OCH_3), 5.72 ppm (s, 2-*H* and 6-*H*); ^{13}C nmr ($CDCl_3$) δ_C: 17.6 (3-CH_3 and 5-CH_3), 21.3 (4-CH_3), 25.3 ($C(CH_3)_3$) 38.4 ($C(CH_3)_3$), 52.0 (OCH_3), 78.3 (*C*-1), 91.2 (*C*-4), 129.4 (*C*-2 and *C*-6), 135.5 ppm (*C*-3 and *C*-5). Methyl 3,4,5-trimethylphenyl ether (**14**) was present as a contaminant. Its isolation and characterisation is described below. The dienyl ether **4***a* was not separately isolated. It was eluted with its diastereoisomer **4***b* (60%) in the 10% ether fraction and had ^1H nmr ($CDCl_3$) δ: 0.97 (s, $C(CH_3)_3$), 1.71 (s, 4-CH_3), 1.80 (broad s, 3-CH_3 and 5-CH_3), 2.90 (s, OCH_3), 5.72 ppm (s, 2-*H* and 6-*H*); ^{13}C nmr δ_C 18.0 (3-CH_3 and 5-CH_3), 22.2 (4-CH_3), 25.6 ($C(CH_3)_3$), 38.6 ($C(CH_3)_3$), 51.4 (OCH_3), 78.3 (*C*-1), 91.2 (*C*-4), 129.1 (*C*-2 and *C*-6), 136.2 ppm (*C*-3 and *C*-5).

Isomerization (Epimerization) of the Dienols **3**a *and* **3**b

The dienol **3***a* was dissolved in aqueous acetone (400 mm^3; 10:90, v/v) containing sulfuric acid (0.05% w/v) and isomerization at 35°C was followed by integration of the *tert*-butyl peaks of the ^1H nmr spectrum at δ 0.98 (**3***a*) and 0.92 ppm (**3***b*). A similar experiment was carried out starting from **3***b*. Peaks characteristic of the isomers were distinct in the aqueous acetone solution; **3***a*: 0.98, 1.75 (s, 3-CH_3, 4-CH_3 and 5-CH_3), 5.99; **3***b*: 0.92, 1.70 (s), 5.99 ppm and the formation of the mixture of isomers from each single isomer was readily discerned. In the course of both reactions small peaks also developed at δ 1.05, 1.12, 1.14, 1.20, 1.28, 6.47, and 7.12 ppm. Results are shown in Table 4.

Solvolysis of Diene **2** *in Aqueous Methanol*

A suspension of acetate **2***a* (100 mg) in CD_3OD–D_2O (80% w/v, 300 mm^3) was agitated in an ultrasonic bath at ca. 20°C for 25 min. After work-up ^1H nmr indicated that a mixture of the ether **4** (δ 5.72, 59%) dienol **3** (δ 5.92, 25%) and aromatic compounds (δ 6.5, 6%; δ 7.1 ppm, 10%) had been formed. The ratio of **4***b* to **4***c* was ~3:1 but **3***a* appeared to be present in greater amount than **3***b*.

Reaction of Diene **2** *with Sodium Methoxide*

A solution of sodium methoxide (2 mmol) in methanol (2 cm^3) was added to a solution of **2***a* (160 mg, 0.6 mmol) in methanol (1 cm^3) at −78°C. The mixture was stirred at 0°C for 60 min. After work-up ^1H nmr showed that the product consisted of 10% aromatic compounds (δ ~ 7.1 and ~7.3 ppm), 7% dienols **3***a* and **3***b* (δ ~ 5.9 ppm), and 83% dienyl ethers **4***a* and **4***b* (δ ~ 5.7 ppm). The ratio of **4***a* to **4***b* was ~1:4, determined from the relative heights of the methoxy peaks at δ 2.90 and 3.12 and qualitatively supported by the relative heights of the *tert*-butyl peaks at 0.97 and 0.89 ppm. It was not possible to establish the ratio of dienol **3***b* to **3***a* because of the overlap of the dienol *tert*-butyl peaks (δ 0.93 and 0.99 ppm) with those of the ether.

Solvolysis of Diene **2**a *in Moist* [$^2H_4$]*Acetic Acid*

A solution of diene **2***a* (160 mg, 0.64 mmol) in a mixture of water (8 mm^3) and [$^2H_4$]acetic acid (400 mm^3) was observed by nmr at 35°C. The diene exchanged acetate rapidly with the solvent since in the first observed spectrum, after 2 min, the only acetate peak was that of acetic acid at 2.03 ppm. Furthermore, in the course of the reaction a higher field *tert*-butyl (δ 0.92 ppm) appeared and disappeared more slowly than the original *tert*-butyl peak as the diene(s) rearomatized over a period of 40 min (Table 5). The formation of brown fumes of NO_2 indicated that the dominant rearomatization reaction involved loss of the nitro group. Aromatic peaks appeared at δ 6.50, 6.64, and 6.69 and a (diene?) peak at 6.28 ppm. The mixture stood at 40°C for a further 30 min. After work-up the δ 5.5–7 ppm region exhibited peaks at δ 5.87 (7%), 6.16 (15%), 6.43 (37%), 6.58 (24%), and 6.70 ppm (15%). Major *tert*-butyl peaks appeared at δ 1.30 (*tert*-butyl alcohol) and 1.43 ppm (*tert*-butyl acetate). Gas–liquid chromatography and glc–mass spectrometry established the products to be a phenol (17%, M^+ 192), the phenol **16** (22%, M^+ 136), the deuterated acetate **15** (32%, M^+ 181), two unidentified components (4% and 3%), the aldehyde **17** (8%), alcohol **8** (5%), acetate **7** (4%), and nitroarene **9** (M^+ 221, 8%). The mass spectra of the peaks identified as **17**, **8**, and **7** were not determined and the identification is based solely on retention time.

Solvolysis of the Dienyl Methyl Ethers **4** *in Aqueous Methanol*

A mixture of the dienyl ethers **4***a* and **4***b* (0.2 g) was reacted with a solution of water (2 cm^3) and methanol (8 cm^3) at 50–55°C for 90 min. After work-up essentially pure (96% by glc) methyl 3,4,5-trimethylphenyl ether (**14**) was obtained; ^1H nmr ($CDCl_3$) δ: 2.01 (s, 3, 4-CH_3), 2.16 (s, 6, 3-CH_3 and 5-CH_3), 3.60 (s, 3, OCH_3), 6.47 ppm (s, 2, 2-*H* and 6-*H*); ^{13}C nmr ($CDCl_3$) δ_C: 14.5 (4-CH_3), 20.8 (3-CH_3 and 5-CH_3), 55.0 (OCH_3), 113.1 (*C*-2 and *C*-6), 127.0 (*C*-4), 137.5 (*C*-3 and *C*-5), 157.0 (*C*-1); ms *m/e* 150 (M). When the reaction was repeated at 25°C 12% of the dienyl ethers **4** was converted into the aryl ether **14** in 90 min.

Can. J. Chem. Downloaded from www.nrcresearchpress.com by 210.87.254.6 on 09/05/12
For personal use only.

Reaction of Diene **2** *with Sulfuric Acid in Acetic Anhydride – [$^2H_4$]Acetic Acid*

In separate experiments solutions of 0.05, 0.5, 5, and 50% H_2SO_4 (by weight) in 10% acetic anhydride – [$^2H_4$]acetic acid (250 mm^3) were added to a solution of diene **2***a* (120 mg, 0.4 mmol) in $CDCl_3$ (200 mm^3) and the ensuing reactions followed by ^{1}H nmr as the temperature was raised from −20°C. In the most dilute sulfuric acid solution exchange of the [$^2H_3$]acetate for the unlabelled acetate in the diene could be followed at −20°C and was substantially complete after 6 min. When, after 16 min, the temperature was raised to −5°C development of rearomatization product, nitrite **5** (δ 1.28, 2.15, 2.26, 5.65, and 7.15 ppm) could be observed. After 42 min and at +15°C 50% of the diene had rearomatized and the minor products, the nitromethane **6** (δ 5.49) and acetate **7** (δ 5.10), were clearly evident. At +15°C/48 min new diene peaks (whose initial formation was just apparent at +5°C/32 min) at 6.13 (major) and 6.08 (minor) integrated for ca. 20% of the mixture, approximately equal to the amount of diene **2**, and a significant amount of diene **2***b* (δ 0.95) was present as well as the original **2***a*. The *tert*-butyl peak of the new diene(s) overlapped with that of the original diene at δ 1.03. However, the diene methyl region, which had initially exhibited only a singlet at δ 1.74 ppm, now had peaks at δ 1.69, 1.75, 1.78, and 1.81 ppm. As the temperature was raised to +35°C (85 min) diene **2** disappeared more rapidly than the new diene and some new peaks appeared at δ 1.06, 6.43 ppm. Before work-up (after 90 min) all of the original diene had disappeared and the new diene(s) constituted ~10% of the mixture. The distribution of the benzylic products was 67% **5**, 18% **6**, 18% **7**. After work-up no diene was present and the product composition was 5-*tert*-butyl-2,3-dimethylbenzaldehyde (**19**); nmr ($CDCl_3$) δ: 1.31 (s, C(CH_3)$_3$), 2.30 (s, CH_3), 2.50 (s, CH_3), 7.39 (d, J = 2 Hz, 1, 4-*H*), 7.66, (d, J = 2 Hz, 1, 6-*H*), 10.28 ppm (s, 1, C*H*O), 12%; **5**, 18%; **6**, 33%; **7**, 16%; **8**, 16%. An unidentified component (δ 7.00 ppm) whose formation had been observed in the course of the variable temperature study, was present to the extent of ~5%. The presence of **19**, **6**, **7**, and **8** in the reaction product was confirmed by glc and glc – mass spectrometry.

In the reaction to which 0.5% sulfuric acid had been added rearomatization occurred at a lower temperature (+5°C) and in the reactions with 5 and 50% acid rearomatization was complete before nmr observation. Aldehyde **19** appeared in the reactions before work-up and in the cases of the reaction with 5 and 50% sulfuric acid the (complete) conversion of **5** to **19** before work-up could be followed. Results are shown in Table 6.

Reaction with added 0.05% sulfuric acid at +7°C and with added 0.5% sulfuric acid at +12°C were also followed by ^{13}C nmr. In the more dilute acid solution, the exchange of the [$^2H_3$]acetate in **2***a* could be followed by the reduction in the intensity of the peak at 171.0 ppm ($OCOCH_3$). In the more concentrated acid solution rearomatization was essentially complete when the spectrum was initially observed and the methylene carbons of **5** (69.7), **6** (78.7), and **7** (66.5) were apparent in the spectrum.

Reaction of Diene **2** *in Acidified Aqueous Chloroform*

Aqueous sulfuric acid (2% w/v, 20 mm^3) was added to a solution of diene **2***a* (100 mg) in [^{2}H]chloroform (400 mm^3) and the ensuing reaction followed by ^{1}H nmr at 35°C. Within 4 min, the peak of the dienol **3***a* at δ 5.92 had appeared and was 25% of the height of the diene **2***a* peak at 5.72 ppm. However the nitrite **5** then formed very rapidly and was detected by a sharp signal at 5.64 ppm which, after 12 min, was the largest peak in this region of the spectrum. Peaks also appeared at 5.83 and 6.07 ppm but all except the 5.65 ppm peak disappeared after 40 min and the spectrum was that of nitrite **5** (1.30, 2.18, 2.28, 5.65, and 7.15 ppm) and acetic acid (2.06 ppm).

TABLE 7. Yields of products from the thermolysis at 260°C of diene adducts[a]

	% yield of product								
Diene	A	**1**	**15**	**16**	**19**	**8**	**7**	**6**	B
2*a*	3	28	5		5	21	26	14	
2*b*	4	38	4	4		14	19	11	
3*a*	7			35		51			7

[a]Yields determined from the gas chromatogram. Compounds are listed from left to right in order of increasing retention time on a 3% SE 30 column at 160°C. A and B are unidentified compounds. The appropriate *m/e* value for the molecular ion was observed in the chemical ionization (methane) mass spectrum of each of the identified compounds.

Reaction of Diene **2** *with Hydrogen Chloride*

Reactions of **2***a* (500 mg) in ether (25 cm^3) at −70 and −78°C with hydrogen chloride, added as the gas and, in other experiments, in ether solution, were carried out in an attempt to prepare the nitrocyclohexadienyl chloride. All of these reactions were unsuccessful, only benzylic products being obtained. The major product was nitrite **5** with a lesser amount (15–25%) of the nitromethane **6**. A reaction which was allowed to stand at room temperature before work-up gave mainly aldehyde **19** and no **5**.

Reaction of Diene **2**a *with Boron Trifluoride*

Boron trifluoride etherate (200 mm^3) was added to a solution of diene **2***a* (120 mg) in dry ether (1 cm^3). After 5 min the reaction was worked-up and the product examined by nmr and glc – mass spectrometry. Reactions were carried out at both −78 and 0°C and essentially similar results were obtained. The side-chain derivatives **5** (22%), **6** (26%), **7** (31%), and **8** (20%) were formed in the typical yields indicated and were identified by the characteristic methylene region absorption of each compound. On glc – mass spectral analysis major peaks with appropriate retention times and *m/e* values for the molecular ions of **6**, **7**, and **8** were obtained and, in addition, a peak with molecular ion *m/e* 190, attributed to 5-*tert*-butyl-2,3-dimethylbenzaldehyde (**19**). A small amount (2%) of **1** (M$^+$ 176) was also observed. On one occasion peaks typical of the aldehyde were apparent in the nmr spectrum of a mixture of side-chain products containing some of the nitrite **5**. Presumably the aldehyde is also formed from the nitrite under the glc conditions.

Reaction of Diene **2** *with Fluorosulfonic Acid and with Trifluoromethanesulfonic Acid*

Fluorosulfonic acid (250 mm^3) was added to a solution of **2***a* (130 mg) in $CDCl_3$ (200 mm^3) at −78°C. The mixture, which separated into two phases, was warmed to ambient temperature and worked-up. ^{1}H nmr showed that the product contained nitroarene **9** (50%), the nitromethane **6** (16%), and the aldehyde **19** (34%).

A solution of diene **2***a* (200 mg) in methylene chloride (1 cm^3) was added to a solution of trifluoromethanesulfonic acid (0.5 cm^3) in methylene chloride (5 cm^3) at −78°C. After warming to ambient temperature and work-up the product was shown to be the nitroarene **9** (81%) and the aldehyde **19** (12%) by ^{1}H nmr and glc – mass spectrometry. Two other unidentified components were detected by glc and ^{1}H nmr also showed the presence of a small amount of the nitromethane **6** (δ 5.46 ppm).

Thermolysis of the Dienyl Acetates 2a *and* 2b *and the Dienol* 3a

Ethereal solutions of the diene acetates 2*a* and 2*b* and of the alcohol 3*a* were injected into the inlet of the gas chromatograph set at 260°C. Thermolysis took place smoothly and well-resolved peaks were observed. Product identification was carried out by comparison of retention times with those of authentic samples, and by glc – mass spectrometry. The results are shown in Table 7.

Acknowledgements

We thank the National Research Council of Canada and the University of Victoria for financial support.

1. C. L. PERRIN and G. A. SKINNER. J. Am. Chem. Soc. **93**, 3389 (1971).
2. A. FISCHER and R. RÖDERER. Can. J. Chem. **54**, 3978 (1976).
3. A. FISCHER and K. C. TEO. Can. J. Chem. **56**, 258 (1978).
4. A. FISCHER and D. R. A. LEONARD. Can. J. Chem. **54**, 1795 (1976).
5. G. A. OLAH and S. J. KUHN. J. Am. Chem. Soc. **86**, 1067 (1964).
6. T. BANWELL, C. S. MORSE, P. C. MYHRE, and A. VOLLMAR. J. Am. Chem. Soc. **99**, 3042 (1977).
7. A. FISCHER and G. J. WRIGHT. Aust. J. Chem. **27**, 217 (1974).
8. J. R. KNOWLES, R. O. C. NORMAN, and G. K. RADDA. J. Chem. Soc. 4485 (1960).
9. J. W. BARNETT, R. B. MOODIE, K. SCHOFIELD, and J. B. WESTON. J. Chem. Soc. Perkin Trans. II, 648 (1975).
10. A. FISCHER, G. N. HENDERSON, and R. J. THOMPSON. Aust. J. Chem. In press.
11. A. FISCHER and J. N. RAMSAY. Can. J. Chem. **52**, 3960 (1974).
12. A. FISCHER and R. RÖDERER. Can. J. Chem. **54**, 423 (1976).
13. P. C. MYHRE. J. Am. Chem. Soc. **94**, 7921 (1972).
14. A. FISCHER and C. C. GREIG. Can. J. Chem. **56**, 1063 (1978).
15. The Aldrich Library of NMR Spectra. Aldrich Chemical Co. Inc., Milwaukee, WI. 1974.
16. R. G. GILLIS. J. Org. Chem. **21**, 805 (1956).
17. D. J. BLACKSTOCK, A. FISCHER, K. E. RICHARDS, and G. J. WRIGHT. Aust. J. Chem. **26**, 775 (1973).
18. J. F. NORRIS and B. M. STURGIS. J. Am. Chem. Soc. **61**, 1413 (1939).
19. M. J. SCHLATTER. J. Am. Chem. Soc. **76**, 4952 (1954).

Can. J. Chem. Downloaded from www.nrcresearchpress.com by 210.87.254.6 on 09/05/12
For personal use only.

Electron spin resonance studies of the surface chemistry of molybdenum–alumina catalysts

K. C. KHULBE, R. S. MANN, AND M. TERNAN[1]

Department of Chemical Engineering, University of Ottawa, Ottawa, Ont., Canada K1N 6N5

Received December 22, 1977

K. C. KHULBE, R. S. MANN, and M. TERNAN. Can. J. Chem. **56**, 1769 (1978).

When alumina was doped with molybdenum oxide, the concentration of the electron accepting sites increased linearly up to 18 wt.% MoO_3, and then decreased. The colour of the Mo–alumina changed from whitish yellow to grayish black when degassed at 320°C for 2 h. This depended on the concentration of Mo. A strong signal for Mo^{5+} was observed. Oxygen species were formed when the degassed sample was treated with oxygen or air. A reversible behaviour of oxygen on these species was observed. A possible mechanism has been discussed for the formation of O_2^- species and the reversible behaviour of oxygen. The concentration of electron accepting centers has been correlated with the activity for the hydrodenitrogenation of heavy oils over MoO_3–alumina catalysts.

K. C. KHULBE, R. S. MANN et M. TERNAN. Can. J. Chem. **56**, 1769 (1978).

Lorsque l'on additionne de l'oxyde de molybdène à de l'alumine, la concentration des sites acceptant des électrons augmente d'une façon linéaire jusqu'à 18% en poids de MoO_3; par la suite cette valeur diminue. La couleur du mélange alumine–molybdène change d'une jaune blanchâtre à un noir grisatre lorsque l'on enlève les gaz à 320°C pendant deux heures. Cette couleur dépend de la concentration de molybdène. On a observé un signal puissant correspondant à du Mo^{5+}. Il se forme des espèces oxygénées lorsque l'on traite un échantillon dans lequel on a enlevé les gaz avec de l'oxygène ou avec de l'air. Le comportement réversible de l'oxygène sur ces espèces a pu être observé. On discute d'un mécanisme possible pour la formation d'espèces de O_2^- et pour le comportement réversible de l'oxygène. On a établi une corrélation entre la concentration des centres accepteurs d'électrons et l'activité lors de l'hydrogènation accompagnée de l'enlèvement d'azote présent dans des huiles lourdes sous l'influence de catalyseurs de MoO_3–alumine.

[Traduit par le journal]

Introduction

Catalysts based on molybdenum oxide – alumina have found ever increasing uses in oxidation (1), hydrodesulphurization (2), hydrodenitrogenation (2), and other hydrocarbon reactions. It was observed that electron accepting centers of alumina increase when doped with metals (3) and of Mo–alumina when doped with promotor ions (4) like Co and Ni. In the present paper we report the effect of the variation in the concentration of electron accepting centers (Lewis acid sites) with the variation of molybdenum concentration and an attempt is made to correlate these centers with the denitrogenation and desulphurization activity. The effect of heating *in vacuo* at 320°C and the reversible behaviour of oxygen on the heated and evacuated catalyst is also reported.

Experimental

The technique for X-ray diffraction studies, infrared absorption spectra, and esr measurements, and the measurement of esr signal intensity are described elsewhere (5, 6). A solution of 0.05 *M* phenothiazine (TDPA) in benzene was used for phenothiazine cation radical formation on the surface of the catalyst. The catalysts used in this work were the same as used earlier by Parson and Ternan (2). The calcined pellets were ground and only 40–60 mesh size grains were used for the present study.

Results

The γ-alumina and pure MoO_3 powder did not give an esr signal under the experimental conditions. The esr spectra of the oxidised catalyst containing 30% MoO_3 on alumina is shown in Fig. 1, I (weak signal). The observed signal was due to Mo^{5+} (7). Catalysts containing less than 20% MoO_3 on alumina did not give an esr signal.

When alumina was treated with phenothiazine (TDPA) solution in benzene a very weak signal of TDPA cation radical was observed suggesting that γ-alumina has electron accepting centers (8, 9). The MoO_3 powder also gave a weak signal of TDPA cation when it was treated in a manner similar to that of alumina.

When 30% MoO_3–alumina was treated with a solution of TDPA, a new esr signal (strong) at $g = 2.003$ was observed in addition to the Mo^{5+} signal at $g = 1.923$ (Fig. 1, II). The new peak was due to the TDPA cation radical (10). The colour of the catalyst changed immediately (from white or yellow to red) on adding TDPA solution in benzene. Whereas in the case of pure alumina, the colour changed

[1]Present address: Canmet, Ottawa, Canada.

Can. J. Chem. Downloaded from www.nrcresearchpress.com by 210.87.254.40 on 09/05/12
For personal use only.

Can. J. Chem. Downloaded from www.nrcresearchpress.com by 210.87.254.40 on 09/05/12
For personal use only.

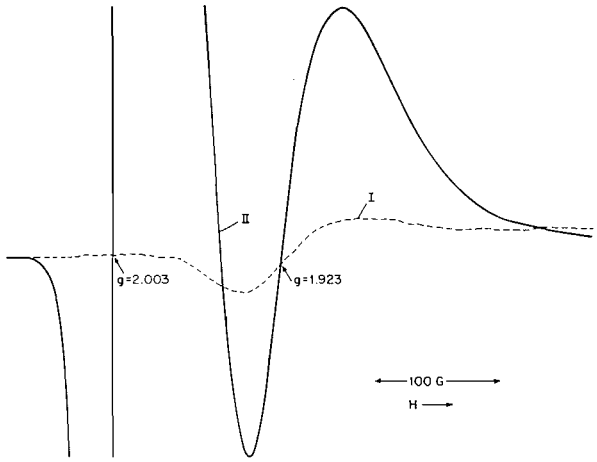

FIG. 1. I, esr spectra of 30 wt.% MoO_3–alumina; II, esr spectra of 30 wt.% MoO_3–alumina + TDPA.

from white to gray, the colour of Mo-doped alumina changed from white or yellow to red or dark red, depending on the concentration of Mo.

The electron acceptor site (Lewis site) is responsible for the oxidation of aromatic hydrocarbons to the corresponding cations (8, 9). The intensity of the esr signal of TDPA cation radicals increased linearly up to 18 wt.% MoO_3 on alumina and then decreased on further increases in Mo concentration (Fig. 2). It is suggested that the electron accepting property of the doped alumina increased with the increase in Mo concentration up to a certain limit and then decreased on further addition of Mo. It was observed (11) that the Mo^{5+} concentration increased linearly with the increase of MoO_3 concentration (up to ~30%).

When 18% MoO_3–alumina was degassed at room temperature for 72 h, a very weak signal of Mo^{5+} ion was obtained. However, when the sample was outgassed at 320°C for 2 h, its colour at room temperature became gray or black and a strong esr

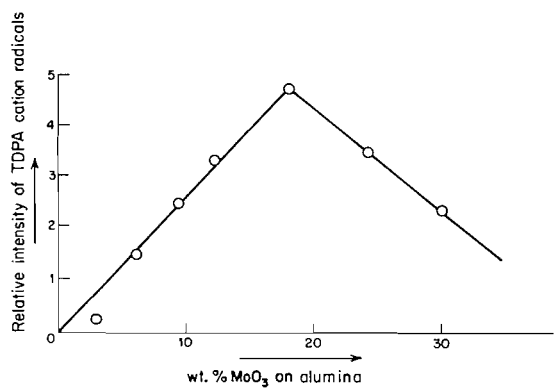

FIG. 2. Relative intensity of esr signals of TDPA cation radical vs. wt.% MoO_3–alumina.

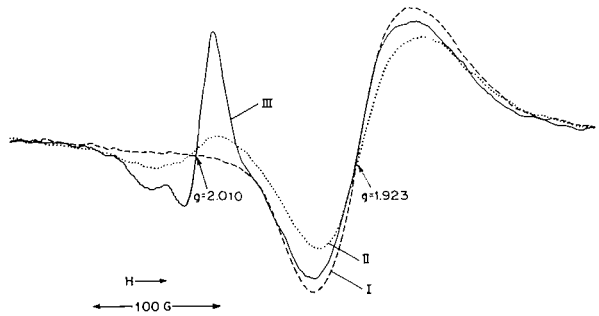

FIG. 3. I (---), esr spectra of 18 wt.% MoO_3–alumina degassed at 320°C for 2 h; II (...), esr spectra of degassed sample + O_2 (100 Torr); III (—), esr spectra of evacuated oxygen treated sample.

signal of Mo^{5+} was observed (Fig. 3, I). The intensity of the signal increased with the increase of Mo concentration. Similar results were obtained by Sheshadri *et al.* (12) on reduced catalysts.

When this black sample (degassed at 320°C, MoO_3–alumina catalyst) was treated with oxygen or air (100 Torr) at room temperature, the esr signal of Mo^{5+} slightly decreased (Fig. 3, II). However, when the adsorbed oxygen was evacuated at room temperature a new signal at g ~2.010 was observed, including the Mo^{5+} signal of almost original intensity as observed before admitting oxygen (Fig. 3, III). The intensity of this new signal depended on the concentration of Mo and the oxygen pressure. This new signal was assigned to the O_2^- species. This signal disappeared when the sample was treated with oxygen or heated. Thus, a reversible effect of oxygen was observed on this new signal. A similar effect was observed by Iyengar *et al.* (13) on TiO_2. Carbon monoxide and hydrogen did not affect this signal at room temperature indicating a negative test for the O^- ion species. The reversible behaviour of O_2 indicates that the signal at g = ~2.010 is associated with the surface oxygen and is subject to dipolar magnetic broadening by molecular O_2.

On heating the black sample at 400°C in the presence of air, the colour of the catalyst changed to white or yellow (original colour), which suggested a deficiency of O_2 in the degassed (at 320°C) MoO_3–alumina catalyst. X-ray and ir analyses did not reveal the existence of a detectable amount of free molybdenum or molybdenum oxide in the alumina supported molybdenum oxide samples (original and the black sample). It could be possible that either free MoO_3 or molybdenum was monodispersed. The blackness of the evacuated and heated alumina supported molybdenum oxides may be due to the presence of different valencies of molybdenum or

Can. J. Chem. Downloaded from www.nrcresearchpress.com by 210.87.254.40 on 09/05/12
For personal use only.

lower oxides of molybdenum. However, other possibilities are not discarded.

Discussion

The Brønsted and Lewis acid sites (electron accepting centers) have always been looked upon as the active catalytic centers of alumina or alumina supported metal catalysts. Upon dehydration at increasing temperatures, the Brønsted acid sites, numerous at high water content, are gradually converted into Lewis acid sites. At high temperatures, the electron deficient character of alumina dominates.

X-ray analysis confirmed that the alumina was of the γ-type. The structure of γ-alumina is very complex. No detectable amount of free molybdenum or its oxides was found in alumina supported molybdenum (before and after evacuation and heating). Surface OH groups of alumina are not completely eliminated. Some of the OH groups of alumina are basic and are capable of forming a salt with the molybdic acid. Thus, with alumina as a carrier, practically all the metal is combined to form Mo—O—Al groups which are active centres for the generation of radicals. However, the possibility of other active centres could not be eliminated. The formation of aluminum molybdate has been discussed by several authors. Sonnemans and Mars (14) suggested that the catalyst prepared according to the normal impregnation method contains molybdenum in two forms, i.e. MoO_3 and aluminium molybdate. The molybdenum trioxide is present on the surface (aluminium molybdate) as a monolayer and has a heterogeneous character. A study by X-ray and ir analyses did not indicate the existence of free molybdenum or molybdenum oxides in the catalysts. It is our view that molybdenum exists in a 'combined form' in alumina. It is also reported that Mo^{6+} on a carrier of γ-alumina is present in tetrahedral coordination at low concentration and in octahedral coordination at high concentration of molybdenum (15). Molybdenum formed a compound with the carrier $Al_2(MoO_4)_3$. It seems that γ-alumina supported molybdenum oxides have a very complicated structure.

Molybdenum is an element with outermost structure $4d^5 4s^1$. It has oxidation states 2− to 6+; the lowest oxidation states (2−, 1−, 0, 1+) are exhibited only by organometallic compounds and compounds of π acceptor ligands. The higher oxidation states (4+, 5+, 6+) are the most stable. The true stability ranges of the various oxides will be very difficult to establish because of the slow reaction and the transformation rates, especially those occurring below about 600°C. There is a pronounced tendency for some of the phases to form and remain for long periods in a metastable state. It is possible that, depending on the method of preparation of the catalyst, molybdenum with different valencies can be present in alumina.

In the present investigation, it was observed that the concentration of electron accepting centers increased with increased Mo concentration up to a certain limit (18% MoO_3) and then decreased with further increase of Mo concentration (Fig. 2).

Parson and Ternan (2) studied hydrocracking, hydrodesulphurization, and hydrodenitrogenation of heavy oils over these catalysts. The activities in hydrocracking and hydrodesulphurization with MoO_3 concentration were quite high, up to 9 and 3% respectively, but the increases were more gradual at higher concentrations. On the other hand, the activity pattern for hydrodenitrogenation and the surface area of the catalyst were similar to that of Fig. 2. Thus, the number of electron accepting sites are directly related to the surface area of the catalysts and to the activity for hydrodenitrogenation. Parson and Ternan (2) also observed that the surface acidity of these catalysts increased linearly with increased concentration of Mo. The pattern for the electron accepting sites with Mo concentration was found to be different in the present study (Fig. 2). It was confirmed from our investigations that different types of acid centres are present on the surface as only the electron accepting centers could give the cation radical on the surface (8).

A comparison of Fig. 1, I with Fig. 1, II for Mo^{5+} concentrations would indicate that Mo^{5+} does not take part in the formation of cation radicals. The increase in Mo^{5+} concentration on the addition of TDPA could be understood by the reduction of Mo^{6+}.

$$Mo^{6+} + e^- \rightarrow Mo^{5+}$$

On evacuation at higher temperatures MoO_3 loses oxygen from the surface and produces the dissociation of Mo^{6+}.

$$Mo^{6+} \rightarrow Mo^{5+} + \text{hole}$$

Mo can exist in any of four valencies, 6+, 5+, 4+, and 3+, corresponding to d^0, d^1, d^2, and d^3 configurations. Hexavalent molybdenum is diamagnetic and therefore will not give an esr signal. Mo^{4+}, even if it were paramagnetic, would not give a spectrum except at a very low temperature. It would be expected that any observed resonance due to d^2 would have a large zero field splitting and would give a broad signal. The value of g for Mo^{3+} is 2.000 (7). It is thus concluded from the esr spectra obtained for Mo^{5+} that Mo^{5+} existed together with Mo^{6+}. How-

Can. J. Chem. Downloaded from www.nrcresearchpress.com by 210.87.254.40 on 09/05/12
For personal use only.

ever, from the colour of the catalyst, it can be presumed that some other species of molybdenum might also be present.

The new peak observed after degassing the adsorbed O_2 from the evacuated and heated Mo–alumina (Fig. 3, III) was due to the O_2^- species. A similar effect of O_2 was observed on rutile (13). The reversible behaviour of O_2 on the evacuated and heated Mo–alumina surface can be understood from the following mechanism:

Mo^{6+} dissociates to Mo^{5+}, and Mo^{5+} to Mo^{4+}

$$Mo^{6+} \rightarrow Mo^{5+} + \square_+$$

$$Mo^{5+} \rightarrow Mo^{4+} + \square_+$$

where $\square_+$ describes a hole with a positive charge and $\square_e$ the hole acting as electron.

It is also possible that an equilibrium exists between Mo^{5+} and Mo^{4+} ions as suggested by Ishii and Matsuura (16)

$$\square_+ + Mo^{4+} \leftrightarrows \square_e + Mo^{5+}$$

A weak signal of Mo^{5+} was observed when Mo–alumina catalyst was degassed at room temperature. It is possible that these Mo^{5+} ions could be different from Mo^{5+} ions formed after dissociation of Mo^{6+} as explained above. On treating with O_2, the original Mo^{5+} was converted into Mo^{6+} and thus reduced the concentration of Mo^{5+} slightly as follows:

[A] $$Mo^{5+} + O_2 \leftrightarrows Mo^{6+} + O_2^-$$

also

[B] $$Mo^{4+} + O_2 \leftrightarrows Mo^{5+} + O_2^-$$

The formation of Mo^{5+} in [B] could be less than Mo^{5+} consumed in [A] and [C]

[C] $$\square_e + O_2 \rightarrow O_2^-$$

On evacuating the adsorbed O_2, O_2^- ions remained behind and gave the esr spectra at $g = 2.010$. The disappearance of the O_2^- signal in the presence of O_2 may be due to dipolar magnetic broadening by molecular O_2.

When TDPA solution was added to the unheated and evacuated catalyst, the concentration of Mo^{5+} increased and TDPA cation radical formed. This suggests that Mo^{6+} ions behaved as electron accepting centers ($Mo^{6+} + e^- \rightarrow Mo^{5+}$). On heating and evacuating the catalyst, Mo^{6+} dissociates into Mo^{5+} as discussed above. On adding TDPA to the heated and evacuated catalyst, the intensity of the observed esr signal of the TDPA cation radical was less than the intensity of the TDPA radical when TDPA was added to the unheated catalyst. However, no appreciable change was observed in the Mo^{5+} signal. It seems from the foregoing observations that there are different types of electron accepting sites on the surface of the molybdenum–alumina catalyst.

Acknowledgements

The authors are indebted to the National Research Council of Canada for financial aid (A-1125), to the Energy Centre, Department of Energy, Mines & Resources for providing the samples, and to Dr. A. Manoogian for valuable discussions.

1. O. Sadao, T. Shigeyuki, F. Akira, and N. Yasuo. Kogyo Kagaku Zasshi, **72**, 2244 (1969).
2. B. I. Parson and M. Ternan. Proc. 6th Int. Congr. Catal. Vol. 2. 1976. p. 965.
3. I. Badrikov, K. C. Khulbe, and R. S. Mann. J. Catal. **43**, 339 (1976).
4. R. Mone. Scientific bases of the preparation of heterogeneous catalysis. Société Chimique de Belgique, Brussels, Belgium, Oct. 14, 1975. p. D3-1.
5. R. S. Mann and K. C. Khulbe. J. Catal. **42**, 115 (1976).
6. K. C. Khulbe, R. S. Mann, and A. Manoogian. J. Chem. Phys. **60**, 4810 (1974).
7. R. S. Mann and K. C. Khulbe. Bull. Chem. Soc. Jpn. **48**, 1021 (1975).
8. J. J. Rooney and R. C. Pink. Trans. Faraday Soc. **58**, 1632 (1962).
9. K. W. Hall. J. Catal. **1**, 53 (1962).
10. K. C. Khulbe, R. S. Mann, and M. K. Sarkar. React. Kinet. Catal. Lett. **7**, 35 (1977).
11. A. S. Sultanov, G. Sh. Talipov, N. Sh. Inoyatov, V. P. Tatarskii, and K. A. Samigov. Kinet. Katal. **12**, 1259 (1971); Engl. Transl. p. 1117.
12. K. S. Seshadri and L. Petrakis. J. Phys. Chem. **74**, 4102 (1970).
13. R. D. Iyengar, M. Codell, J. S. Karra, and J. Turkevich. J. Am. Chem. Soc. **88**, 5055 (1966).
14. J. Sonnemans and P. Mars. J. Catal. **31**, 209 (1973).
15. Y. Ishii and I. Matsuura. Technol. Rep. Kansai Univ. **61**, 41 (1966).
16. Y. Ishii and I. Matsuura. Nippon Kagaku Zasshi, **92**, 320 (1971).

The crystal structure of a dinuclear platinum(II) complex with a bent dihydroxy bridge, di-(μ-hydroxy)tetrakis(triethylphosphine)diplatinum(II).tetrafluoroborate

G. W. BUSHNELL

Chemistry Department, University of Victoria, Victoria, B.C., Canada V8W 2Y2

Received October 4, 1977

G. W. BUSHNELL. Can. J. Chem. **56**, 1773 (1978).

The crystal structure of di-(μ-hydroxo)tetrakis(triethylphosphine)diplatinum(II) fluoroborate has been determined and refined to an R value of 0.032. The space group is $P2_1/c$ and the cell dimensions are a = 1.604(1), b = 1.847(1), c = 1.336(1) nm, β = 101.6°, with 4 molecules per unit cell. The dimeric cation consists of two square planar Pt(II) centres bridged by a pair of hydroxo ligands. The angle between the mean plane normals is 36.4°. One of the BF_4^- groups, situated close to the dihydroxo bridge on the more open side, and having lower thermal parameters than the second fluoroborate anion, is hydrogen bonded to the oxygen atoms. The hydrogen atoms were not located. The interatomic distances (pm) are Pt—P = 223.5 (mean), Pt—O = 213.3 (mean), Pt(1)—Pt(2) = 312.1(1), O(1)—O(2) = 272(2), O(1)—F(1) = 288(2), O(2)—F(2) = 282(3). The mean bond angles (deg) are O—Pt—O = 79.4, P—Pt—P = 97.7, P—Pt—O = 91.5, and Pt—O—Pt = 94. One of the triethylphosphine groups is disordered or in thermal motion and was refined by constrained least squares using two superimposed partial structures. The results are discussed in relation to other known hydroxo bridged platinum species relevant to the field of platinum containing, cancer chemotherapeutic drugs.

G. W. BUSHNELL. Can. J. Chem. **56**, 1773 (1978).

On a déterminé la structure cristalline du fluoroborate du di-(μ-hydroxo)tétrakis(triéthylphosphine)diplatine(II) et on l'a affinée jusqu'à une valeur de R de 0.032. Le groupe d'espace est $P2_1/c$ et les dimensions de la maille sont a = 1.604(1), b = 1.847(1), c = 1.336(1) nm, β = 101.6° avec quatre molécules par maille. Le cation dimère comprend deux Pt(II) plan carré pontés par une paire de ligand hydroxo. L'angle entre les normales aux plans moyens est de 36.4°. Un des groupes BF_4^- situé près du pont dihydroxo du côté le plus dégagé et possédant des paramètres thermiques plus bas que ceux du second anion fluoroborate est lié par un pont hydrogène aux atomes d'oxygène. On n'a pas déterminé la position des atomes d'hydrogène. Les distances interatomiques (pm) sont Pt—P = 223.5 (moyen), Pt—O = 213.3 (moyen), Pt(1)—Pt(2) = 312.1(1), O(1)—O(2) = 272(2), O(1)—F(1) = 288(2), O(2)—F(2) = 282(3). Les angles de liaison moyens (degré) sont O—Pt—O = 79.4, P—Pt—P = 97.7, P—Pt—O = 91.5 et Pt—O—Pt = 94. Un des groupes triéthylphosphine est désordonné ou en mouvement thermique et on l'a affiné par la méthode des moindres carrés contraints utilisant deux structures partielles superposées. On discute des résultats en relation avec d'autres espèces connues de platine, pontées par des groupes hydroxo et reliées aux drogues contenant du platine utilisées dans la chémothérapie du cancer.

[Traduit par le journal]

Introduction

Previous work (1) on the hydroxy complexes of platinum(II) and palladium(II) established a preparative method and dimeric structure for compounds of the type $[M_2(OH)_2L_4](BF_4)_2$ where M = Pt and L = triethylphosphine, triphenylphosphine, or pyridine or where M = Pd and L = triphenylphosphine. These compounds are non-hygroscopic, air-stable solids, with nonlabile hydroxy protons. The hydroxy bridge resists cleavage by tertiary phosphines.

The cancer chemotherapeutic properties of *cis*-dichlorodiammineplatinum(II) and related compounds have excited a great deal of interest recently, and clinical trials on man have been undertaken (2). This compound is known (3) to undergo aquation at hydrogen ion concentrations similar to those found in living organisms, giving the ions $[Pt(NH_3)_2Cl(H_2O)]^+$ and $[Pt(NH_3)_2(H_2O)_2]^{2+}$. The acid dissociation constants of the diaquodiammineplatinum(II) cation are known, and neutralization of a solution of the complex with sodium hydroxide and the application of heat gives a solution containing the dimer $[(NH_3)_2Pt(OH)_2Pt(NH_3)_2]^{2+}$. Two groups of workers have determined the crystal structure of di-μ-hydroxotetramminediplatinum(II) nitrate (4, 5). Different triclinic unit cells have been assigned but the results agree on an approximately planar structure for the $Pt_2O_2N_4$ set of atoms in the cation. The important interatomic distances and bond angles are similar. Hydrogen bonding between the nitrate ions and the dimeric cations is important in this crystal structure.

A yellow hydroxy bridged trimer $[Pt_3(NH_3)_6(OH)_3](NO_3)_3$ was also obtained during the preparation of the above dimer (5). The crystal structure of

Can. J. Chem. Downloaded from www.nrcresearchpress.com by 210.87.254.5 on 09/05/12
For personal use only.

Can. J. Chem. Downloaded from www.nrcresearchpress.com by 210.87.254.5 on 09/05/12
For personal use only.

this compound (6) shows that each platinum atom has an approximately planar coordination, but that the cation as a whole has a three dimensional structure with a pseudo-twofold axis through a Pt atom and the O atom opposite to it in the nonplanar six-membered ring. Hydrogen bonding is prominent in this crystal structure just as it is in the dimer crystal.

The only other bridged hydroxy complexes of platinum(II) well characterized are a binuclear hydroxy bridged species prepared from the ethylenediamine diaquoplatinum(II) cation by Lim and Martin (7). Their work reports titrations of standard base into $[enPt(OH_2)_2]^{2+}$ and $[enPd(OH_2)_2]^{2+}$, and provides excellent evidence for rapid dimer formation in the palladium system, and good evidence of a slower dimerisation of $[enPt(OH_2)(OH)]^{+}$, with $K = 10^6\ M^{-1}$ estimated.

The crystal structure of the tetrameric hydroxytrimethylplatinum(IV) published by Spiro, Templeton, and Zalkin (8) contains $Pt_4O_4(Me)_{12}$ molecules, approximately described as a Pt_4O_4 cube consisting of interpenetrating Pt_4 and O_4 tetrahedra, with three methyl groups joined to each platinum atom, which thus attains octahedral coordination.

Hydroxo bridged species of platinum are currently of interest in connection with the formation of deep blue or purple compounds formed when *cis*-$[Pt(NH_3)_2(H_2O)_2]^{2+}$ is neutralized and reacted with pyrimidines and purines. These compounds, commonly called 'platinum-blues', are water soluble, amorphous compounds which show promise as effective anti-tumour agents of comparatively low toxicity. Their structures are not yet known, but there are indications that mixed valence Pt(II)/Pt(IV) hydroxo bridged species may be involved and that the Pt—Pt distance may be important (5).

Our results show a type of di-μ-hydroxo bridge structure which is new in Pt chemistry and indicate that the anion may influence this bridge structure through hydrogen bonding.

Experimental

The preparation of the material has already been described (1). The colourless transparent crystals grew to 1 mm^3 in size. Photography using CuK_α radiation gave the space group and approximate unit cell dimensions. The crystal data are:

$C_{24}H_{62}B_2F_8O_2P_4Pt_2$ fw = 1070.4
Monoclinic, space group $P2_1/c$ (No. 14), unit cell a = 1.604(1), b = 1.847(1), c = 1.336(1) nm, β = 101.6(1)°; working cell a' = 1.869(1) nm, β′ = 122.8(1)°; cell volume 3.877 nm^3; crystal shape 0,1,1; 0,−1,−1; 0.129 mm; 0,1,−1; 0,−1,1; 0.097 mm; 6,3,−2; −6,3,2; 0.48 mm; density 1.821(5) (meas.), 1.834 (calcd.) g cm^{-3}; molecules per cell 4; absorption coefficient (MoK_α) 78.1 cm^{-1}.

A working unit cell, conveniently related to the morphology, was refined by least squares from diffractometer centering results for 24 pairs of reflections, used for data collection, and transformed to the conventional unit cell by the matrix 1,0,1;0,1,0;0,0,−1. The shape of the crystal used is specified by giving the indices in terms of the working cell and the perpendicular distance to the origin for each of the six crystal faces. The mounting direction was along a'. The intensity measurements were made with a Hilger four circle diffractometer using θ/2θ scans of 50 steps of 0.04° in 2θ, counting for 1 s at each step. Measurements were complete up to 2θ = 50° in one hemisphere using MoK_α radiation and a monochromator. Three standards were measured after every batch of 50 reflections. Absorption corrections were applied by numerical integration using an 8 × 8 × 8 Gaussian grid. To economize on computing time, reflections were rejected if $I < 5\sigma(I)$. Multiple measurements were averaged, the Lorentz and polarization corrections applied, and the indices transformed to match the conventional unit cell. A total of 17 133 measurements gave 5365 reflections in the final data set.

Structure Determination

The structure was solved from the three-dimensional Patterson function. The set of programs employed was that of the Chemical Crystallography Laboratory, Oxford (9). In the structure factor calculations the atomic scattering curves for Pt and P were those of Cromer and Waber (10), and the curves for F, C, and B were from the International Tables (11). All atoms were assumed to be uncharged and a correction was made for the anomalous dispersion of Pt (12). The model containing two Pt and four P atoms gave R = 0.22 initially. The model was refined by minimization of $\sum w(|F_o| - |F_c|)^2$ using the method of least squares. Light atoms were located and added to the model by means of Fourier maps. With further refinement, the R value decreased to 0.042 but at this stage it was clear that the triethylphosphine group containing P(1) was not appearing as clearly as the other three, and that the fluorine atoms F(5) to F(8) had large temperature factors. A structure factor calculation was done with the troublesome atoms removed, and the difference map based on this showed the fluorine atoms as before, but no resolution of the PEt_3 difficulty, since the map clearly showed more than six peaks near to the P(1) atom. The A and B parts of the partial structure factors corresponding to the reliably determined atoms were calculated for use while dealing with the first PEt_3 group and written on a peripheral device. The terminal methyl groups of the first PEt_3 group were temporarily neglected and the three carbon atoms bonded to P(1) were treated as six half atoms in two sets of three. The nomenclature C(51)–C(56) was used for the six extra labels required. Two least-square cycles were calculated using strict constraints (13) within each set to maintain reasonable bond lengths and angles, but allowing unhindered rotation about the Pt—P bond. This was followed by a difference map which showed three nonspherical

Can. J. Chem. Downloaded from www.nrcresearchpress.com by 210.87.254.5 on 09/05/12
For personal use only.

TABLE 1. Constraints applied to the least-squares refinement

(a) Bond length constraints (pm)	
P(1)—C	183.5±2.0
C—C (1st PEt_3)	154 ±0.4
B(2)—F	(Mean B(2)—F length) ± 2
(b) Bond angle constraints (deg)	
Pt(1)—P(1)—C	113.8±1.0
C—P(1)—C	104.8±1.0
P(1)—C—C	112.4±1.0
F—B(2)—F	109.5±2
(c) Vibrational constraints (pm^2)	
P(1)—C	0±100
C—C (1st PEt_3)	0±100

peaks attributable to three pairs of methyl carbon half atoms, which were added to the model and refined by two cycles of constrained least squares with the site occupation factors fixed at 0.5. The occupation factor was then refined giving 0.56 for C(11) to C(16) and 0.44 for C(51) to C(56). Finally the fixed atom file was dispensed with, and the whole structure refined by four cycles of least squares in which the constraints were loosened as far as possible. The final set of constraints is given in Table 1. A vibrational constraint limits the difference between two bonded atoms in the components of their mean square displacements along the bond direction. The full matrix was approximated using various blocking schemes throughout the refinement, but finally by blocks for (*i*) each PEt_3 group, (*ii*) the Pt and O atoms and the first BF_4 group, (*iii*) the second BF_4 group, and (*iv*) the scale and a dummy U (isotropic). A weighting scheme, devised to minimize systematic variations of $w\Delta^2$, took the form $w = 1/(1 + [|F_o| - A)/B]^2)$, with $A = 80$ and $B = 91$. The final R value was 0.032 and $R_w = 0.042$, where R_w is defined as $(\sum w\Delta^2/\sum w|F_o|^2)^{1/2}$. The final difference map gave no indication of any misplaced atom. The hydrogen atoms were not located. The structure factor table and tables containing some of the less interesting structural details are in the Depository for Unpublished Data.[1]

Results

Figure 1 shows the structure of the binuclear cation, consisting of two square-planar Pt(II) halves, joined by the bridging hydroxy groups at a substantial dihedral angle. Figure 1 also shows the juxtaposition of the cation and the first BF_4^- ion, the thermal vibration ellipsoids, and the atom labelling scheme. The atomic parameters are given in Tables 2 and 3. The complete unit cell is shown

[1]Copies may be obtained, at a nominal charge, from the Depository of Unpublished Data, CISTI, National Research Council of Canada, Ottawa, Ont., Canada K1A 0S2.

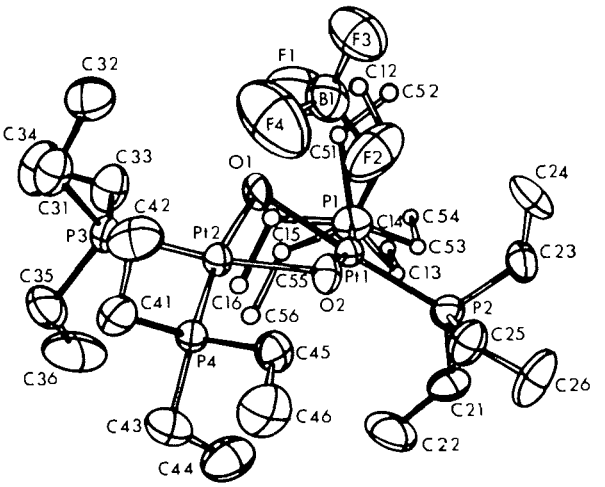

FIG. 1. The molecular structure of the $[(PEt_3)_2Pt(OH)_2Pt(PEt_3)_2]^{2+}$ cation with the first BF_4^- ion in juxtaposition.

in Fig. 2 which has its origin at the front lower right, with axes *a* right to left, *b* vertical, and *c* into the page. The second BF_4^- ion is situated near the right- and left-hand sides of the drawing in all its symmetry positions and is not close to the dihydroxy bridge.

Bond lengths are given in Table 4. The Pt—P lengths are all close to the mean value of 223.5 pm. The bond distances Pt—O(1) seem to differ slightly from the Pt—O(2) distances. It is not known whether this is a consequence of small errors in the structure determination or a real effect caused by differences in the hydrogen atom positions in the bridge. The Pt—O distances are slightly larger than the values 203(1) and 202(2) pm found in $[(NH_3)_2Pt(OH)_2Pt(NH_3)_2](NO_3)_2$ and $[Pt_3(NH_3)_6(OH)_3](NO_3)_3$ respectively, which is reasonable in view of the *trans*-influence of the phosphine ligand. The Pt(IV)—O distance in $(Me_3PtOH)_4$ is 222(1) pm. The Pt—O lengths and the bent nature of the bridge lead to a Pt—Pt distance of 312.1(1) in Table 4 compared to 308.5(1) in the above ammine dimer. In platinum metal, Pt—Pt = 277 pm. With the geometry of our complex and the d^8 electronic structure of Pt(II) it is difficult to imagine any bonding between the platinum atoms. The absence of Pt—Pt interaction is therefore assumed. The P—C lengths, mean = 183 pm, and the C—C lengths, mean = 154 pm, are normal. The mean B—F lengths are 135 and 127 pm in the first and second BF_4^- ions respectively. The shorter distance in the second ion is attributed to its greater thermal motion (14).

Selected bond angles are given in Table 5. The O—Pt—O and Pt—O—Pt angles are slightly smaller than the values of 81.3(4)° and 98.7(4)° found in

Can. J. Chem. Downloaded from www.nrcresearchpress.com by 210.87.254.5 on 09/05/12
For personal use only.

TABLE 2. Fractional atomic coordinates*

Atom	*x*	*y*	*z*
Pt(1)	285.10(4)	−36.28(4)	269.23(5)
Pt(2)	270.84(5)	84.12(4)	103.41(5)
O(1)	358.2(9)	−3.2(7)	157(1)
O(2)	253.0(9)	73.5(7)	254(1)
P(1)	329.0(4)	−150.0(3)	256.7(5)
C(11)	434(1)	−166(2)	338(3)
C(12)	501(3)	−110(3)	322(5)
C(13)	267(2)	−224(1)	296(3)
C(14)	304(4)	−299(2)	276(6)
C(15)	337(3)	−171(2)	125(1)
C(16)	249(3)	−169(4)	55(3)
C(51)	444(1)	−152(2)	264(3)
C(52)	493(3)	−118(4)	364(4)
C(53)	303(4)	−222(2)	340(4)
C(54)	347(6)	−294(2)	323(7)
C(55)	294(3)	−185(3)	126(2)
C(56)	208(4)	−156(4)	68(4)
P(2)	211.3(3)	−53.6(3)	391.7(4)
C(21)	119(1)	−113(1)	361(2)
C(22)	59(2)	−88(2)	264(3)
C(23)	275(2)	−86(1)	512(2)
C(24)	350(2)	−33(2)	551(2)
C(25)	171(2)	33(1)	426(2)
C(26)	126(2)	32(2)	517(2)
P(3)	302.9(3)	80.1(3)	−51.4(4)
C(31)	370(2)	155(1)	−82(2)
C(32)	455(2)	161(2)	−5(2)
C(33)	365(2)	−2(1)	−62(2)
C(34)	391(2)	−10(2)	−165(2)
C(35)	213(2)	74(2)	−161(2)
C(36)	160(2)	7(2)	−159(3)
P(4)	175.2(3)	173.8(3)	72.2(4)
C(41)	200(1)	253(1)	0(2)
C(42)	282(2)	293(1)	60(2)
C(43)	70(1)	146(1)	4(2)
C(44)	31(2)	89(2)	62(3)
C(45)	158(1)	210(1)	193(2)
C(46)	92(2)	272(1)	183(2)
B(1)	454(2)	162(2)	326(2)
F(1)	469(1)	102(1)	274(2)
F(2)	390(2)	150(2)	373(2)
F(3)	524(1)	186(1)	391(1)
F(4)	423(2)	213(1)	259(2)
B(2)	−60(2)	168(1)	338(2)
F(5)	−21(3)	196(3)	419(4)
F(6)	−123(2)	134(2)	358(3)
F(7)	−86(2)	214(2)	267(4)
F(8)	−7(2)	123(2)	312(3)

*x, y, and z values should be multiplied by 10^{-3} to obtain fractional crystal coordinates. Standard deviations are given in parentheses in units of the least significant decimal place.

$[(NH_3)_2Pt(OH)_2Pt(NH_3)_2](NO_3)_2$. The P—Pt—P angles agree closely with the values found in other *cis*-$[(PEt_3)_2PtXY]$ ions, such as X = Cl, Y = phenanthroline, 1,8-naphthyridine, phthalazine, wherein P—Pt—P = 99.5, 99.3, 98.9°, respectively (15). Excluding the first PEt_3 group, the mean values of angles are: Pt—P—C = 114°, C—P—C = 105°, P—C—C = 112°. The applied constraints (Table 1) which were derived from the crystal structure of

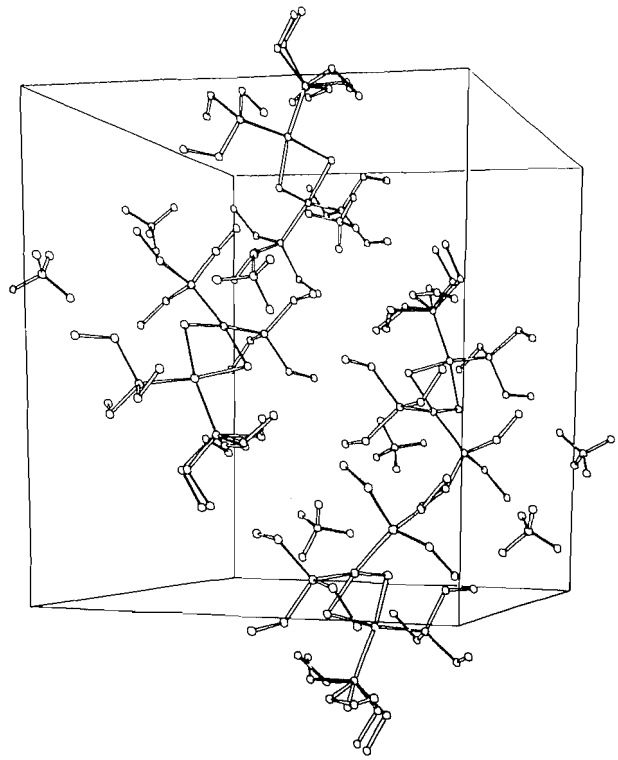

FIG. 2. The packing diagram for μ-dihydroxytetrakis(triethylphosphine)diplatinum(II) tetrafluoroborate.

$[(PEt_3)_2PtCl_2Pt(PEt_3)_2](BF_4)_2$ (16) are consistent with the lengths and angles subsequently found in the normal PEt_3 groups and the first BF_4^- ion.

The use of constraints was necessary to complete this structure determination with a chemically reasonable model. The constraints could not be removed at the end of the refinement, leaving a structure stable in a least-squares cycle based on the X-ray intensities alone. Therefore, the structure of the first PEt_3 group and the second BF_4^- ion has been partly imposed, partly determined. Fortunately the bent bridge structure and the position of the first BF_4^- ion can hardly be dependent on these details.

The conformation of the three normal PEt_3 groups is such that on each ligand the carbon atoms of two ethyl groups and the P atom form a W shape which runs perpendicular to the Pt coordination plane. The P atom and the two carbon atoms of the other ethyl lie approximately in the coordination plane and the direction of the P—C—C sequence is away from the other PEt_3 ligand of the *cis* pair. The P(1),C(51)–C(56) set of sites is similar except that the direction of the approximately in-plane P—C—C sequence is away from O(1). The P(1),C(11)–C(16) set is different in that it lacks the W shape: its conformation

Can. J. Chem. Downloaded from www.nrcresearchpress.com by 210.87.254.5 on 09/05/12
For personal use only.

TABLE 3. Anisotropic temperature parameters*

Atom	$U(11)$	$U(22)$	$U(33)$	$U(23)$	$U(13)$	$U(12)$
Pt(1)	3.64(3)	3.74(4)	3.57(3)	0.35(3)	0.57(3)	−0.01(3)
Pt(2)	4.02(4)	3.54(3)	3.57(3)	0.39(3)	0.77(3)	0.13(3)
O(1)	6.1(9)	4.5(8)	3.6(7)	2.0(6)	0.1(6)	−1.0(7)
O(2)	6.1(9)	3.9(7)	4.0(7)	0.8(6)	1.6(6)	−0.5(6)
P(1)	5.1(3)	4.3(3)	7.7(4)	−0.4(3)	1.6(3)	0.7(2)
P(2)	4.1(3)	4.0(3)	4.1(3)	0.4(2)	1.0(2)	−0.1(2)
P(3)	4.9(3)	4.5(3)	4.1(3)	0.3(2)	1.4(2)	0.4(2)
P(4)	4.2(3)	3.9(3)	4.2(3)	0.1(2)	0.9(2)	0.4(2)
B(1)	7(2)	7(2)	6(2)	−1(1)	1(1)	0(1)
F(1)	8(1)	14(2)	13(2)	−7(1)	0(1)	1(1)
F(2)	14(2)	22(3)	13(2)	−9(2)	8(2)	−9(2)
F(3)	10(1)	9(1)	10(1)	−2(1)	−1(1)	−2(1)
F(4)	20(3)	13(2)	15(2)	4(2)	−3(2)	0(2)
B(2)	7(2)	7(2)	12(3)	2(2)	3(2)	0(2)
F(5)	36(6)	32(5)	42(8)	−24(6)	−1(6)	−12(5)
F(6)	20(3)	28(4)	22(3)	6(3)	8(3)	−8(3)
F(7)	18(3)	40(6)	43(7)	32(6)	17(4)	15(4)
F(8)	27(4)	36(5)	23(4)	10(4)	12(3)	22(4)

*Values should be multiplied by 10^2 to obtain mean square amplitudes in pm^2. The standard deviation is given in parentheses in units of the least significant decimal place.

TABLE 4. Interatomic distances. The platinum coordination and bridge structure

Atoms	Length	Atoms	Length
Pt(1)—P(1)	223.8(6)	Pt(2)—P(3)	223.1(5)
Pt(1)—P(2)	222.7(5)	Pt(2)—P(4)	224.3(5)
Pt(1)—O(1)	216.6(13)	Pt(2)—O(1)	216.7(14)
Pt(1)—O(2)	209.7(13)	Pt(2)—O(2)	210.1(13)
Pt(1)—Pt(2)	312.1(1)	O(1)—O(2)	272(2)
O(1)—F(1)	288(2)	O(2)—F(2)	282(3)

TABLE 5. Bond angles (deg). The platinum coordination and bridge structure

Angle		Angle	
O(1)—Pt(1)—O(2)	79.4(6)	O(1)—Pt(2)—O(2)	79.3(6)
O(1)—Pt(1)—P(1)	89.6(5)	O(1)—Pt(2)—P(3)	91.7(7)
P(1)—Pt(1)—P(2)	98.1(5)	P(3)—Pt(2)—P(4)	97.3(5)
P(2)—Pt(1)—O(2)	93.1(6)	P(4)—Pt(2)—O(2)	91.7(7)
O(1)—Pt(1)—P(2)	171.6(5)	O(1)—Pt(2)—P(4)	170.9(4)
O(2)—Pt(1)—P(1)	168.6(4)	O(2)—Pt(2)—P(3)	171.0(4)
Pt(1)—O(1)—Pt(2)	92(2)	Pt(1)—O(2)—Pt(2)	96(2)
Pt(1)—O(1)—F(1)	100(2)	Pt(1)—O(2)—F(2)	106(2)
Pt(2)—O(1)—F(1)	88.1(7)	Pt(2)—O(2)—F(2)	105(2)
B(1)—F(1)—O(1)	132(2)	B(1)—F(2)—O(2)	114(3)

TABLE 6. Least-squares planes $Ax + By + Cz = D$* and the deviations of atoms from the planes (pm)

Plane	A	B	C	D
1	1081	370.8	752.3	498.1
2	1098	1234	205.6	421.7
		Plane 1		
Pt(1)	P(1)	P(2)	O(1)	O(2)
−0.7	−4.8	5.2	6.4	−6.0
		Plane 2		
Pt(2)	P(3)	P(4)	O(1)	O(2)
0.9	−0.6	0.2	0.3	−0.7

NOTE: The angle between the normals to planes 1 and 2 is 36.4°.
*x, y, and z are fractional crystal coordinates. D = the perpendicular distance to the origin in pm.

resembles one of the PEt_3 ligands in the chloro bridged complex $[(PEt_3)_2PtCl_2Pt(PEt_3)_2](BF_4)_2$ (16).

A least-squares plane has been calculated for the coordination of each Pt atom and the results are given in Table 6. Each half of the binuclear complex is close to planarity. The angle of 36.4° between the plane normals is an interesting feature of the structure. An explanation in terms of the bond angles at the oxygen atoms does not work. Since the O—Pt—O angle is 79.4°, the angle Pt—O—Pt would be 100.6° if the complex were planar. The mean Pt—O—Pt angle is 94°. It can hardly be argued that the cation bends in order to reduce the Pt—O—Pt angle from 100.6° to 94° when the usual bond angle at oxygen is 104.5, as in water, or larger. The dihedral angle is most directly explained as a consequence of hydrogen bonding between the first BF_4^- ion and the bridging hydroxy groups. Evidence for the hydrogen bonding is as follows: (*i*) the temperature factors of the fluorine atoms are lower in the first than in the second fluoroborate ion (Table 3); (*ii*) the short interatomic distances O(1)—F(1) and O(2)—F(2) (Table 4); (*iii*) the suitable bond angles Pt—O(1)—F(1), Pt—O(2)—F(2), B(1)—F(1)—O(1), and B(1)—F(2)—O(2) (Table 5). A search of the literature for structural results giving evidence of hydrogen atom positions in the μ-dihydroxy bridges of binuclear complexes was not very rewarding, since the hydrogen atoms were usually undetected. Often

the M_2O_2 ring is planar, with a central inversion point. The most suggestive structure otherwise was that of *cis*-$[(PPr_3)ClPt(EtS)_2Pt(PPr_3)Cl]$ (17) which has a bent bridge with 50° between the normals. One ethyl group is axial, the S—C bond being approximately perpendicular to the mean plane through the entire heavy atom skeleton, whereas the other ethyl group is equatorial. On the basis of the above it seems that the hydrogen atoms of the μ-dihydroxy bridge are both axial, and equally involved in hydrogen bonding since distance O(1)—F(1) = O(2)—F(2) approximately.

The more clinically successful cancer chemotherapeutic drugs have amine instead of triethylphosphine groups. The inability of the triethylphosphine ligands to engage in hydrogen bonding is partly responsible for the difference in the structures of the μ-dihydroxy bridges of $[(NH_3)_2Pt(OH)_2Pt(NH_3)_2](NO_3)_2$ and $[(PEt_3)_2Pt(OH)_2Pt(PEt_3)_2](BF_4)_2$ in the crystalline state. In the former compound two nitrate ions on opposite sides of the complex are each involved in hydrogen bonding to a bridging hydroxy and a terminal ammine group. The hydrogen atoms were not located (4). In solutions of pyrimidine and purine bases a bending of the ammine complex due to hydrogen bonding from one side cannot be precluded.

The mainstream of chemical thought on the mechanism of action of *cis*-$[PtCl_2(NH_3)_2]$ has been that after passage through cell membranes in the nonionic form, the compound undergoes aquation in two stages and two steps of substitution with pyrimidine or purine bases, which produce cross linking of the DNA strands. The production of binuclear complexes which has now been clearly recognized (4, 5, 7) was initially neglected. Hydrogen bonding of the type discovered in this paper may be important in the mechanism. For example the N—C—O grouping of cytosine might hydrogen bond to a μ-dihydroxy bridge, thus holding the platinum complex in position until the more permanent formation of a Pt—N bond by guanine had been achieved. This would be followed by bridge cleavage and cross linking.

Acknowledgements

This work was carried out at the Chemical Crystallography Laboratory, Oxford, while the author was there on study leave in 1973–1974. Thanks are due to Professor H. M. Powell for generously making available the full facilities of the laboratory and to Drs. C. K. Prout, D. J. Watkin, and R. A. Forder. The versatile, fast, and elegant computer programming by Drs. J. R. Carruthers, J. S. Rollett, and E. White is gratefully acknowledged. Thanks are due to Dr. K. R. Dixon who provided the crystals, and to Mrs. K. Beveridge for Fig. 2. The study leave was supported by the University of Victoria and the National Research Council of Canada provided an operating grant.

1. G. W. Bushnell, K. R. Dixon, R. G. Hunter, and J. J. McFarland. Can. J. Chem. **50**, 3694 (1972).
2. S. K. Carter and M. Slavik. Annu. Rev. Pharmacol. **14**, 157 (1974).
3. J. W. Reishus and D. S. Martin. J. Am. Chem. Soc. **83**, 2457 (1961).
4. R. Faggiani, B. Lippert, C. J. L. Lock, and B. Rosenberg. J. Am. Chem. Soc. **99**, 777 (1977).
5. J. A. Stanko, L. S. Hollis, J. A. Schreifels, and J. D. Hoeschele. Wadley Med. Bull. **7**, 138 (1977).
6. R. Faggiani, B. Lippert, C. J. L. Lock, and B. Rosenberg. Inorg. Chem. **16**, 1192 (1977).
7. M. C. Lim and R. B. Martin. J. Inorg. Nucl. Chem. **38**, 1911 (1976).
8. T. G. Spiro, D. H. Templeton, and A. Zalkin. Inorg. Chem. **7**, 2165 (1968).
9. J. R. Carruthers, J. S. Rollett, and E. White. Crystallographic program manual. Chemical Crystallography Laboratory, Parks Rd, Oxford.
10. D. T. Cromer and J. T. Waber. Acta Crystallogr. **18**, 104 (1965).
11. J. A. Ibers. International tables for X-ray crystallography. Vol. III. Kynoch Press, Birmingham. 1962. p. 201, Table 3.3.1.A.
12. D. T. Cromer. Acta Crystallogr. **18**, 17 (1965).
13. J. S. Rollett. Crystallographic computing. *Edited by* F. R. Ahmed. Munksgaard, Copenhagen. 1970. p. 167.
14. W. R. Busing and H. A. Levy. Acta Crystallogr. **17**, 142 (1964).
15. G. W. Bushnell and K. R. Dixon. Can. J. Chem. **56**, 878 (1978).
16. G. W. Bushnell. Can. J. Chem. To be submitted.
17. M. C. Hall, J. A. J. Jarvis, B. T. Kilbourn, and P. G. Owston. J. Chem. Soc. Dalton, 1544 (1972).

Can. J. Chem. Downloaded from www.nrcresearchpress.com by 210.87.254.5 on 09/05/12
For personal use only.

Rupture du lien C—S lors de la réduction de sulfones par $LiAlH_4$

NORMAND DUFORT ET BERNARD JODOIN

Département de chimie, Université de Montréal, Montréal (Qué.), Canada H3C 3J7

Reçu le 30 décembre 1977

NORMAND DUFORT et BERNARD JODOIN. Can. J. Chem. **56**, 1779 (1978).

Différentes sulfones α,β-insaturées et saturées sont réduites par $LiAlH_4$. Il se produit une rupture du lien C—S dépendant de la nature de la sulfone.

NORMAND DUFORT and BERNARD JODOIN. Can. J. Chem. **56**, 1779 (1978).

Different α,β-unsaturated and saturated sulfones are reduced by $LiAlH_4$. A cleavage of the C—S bond occurs according to the kind of sulfones.

Dans le cadre de nos travaux, nous avons été appelés à étudier la réduction par $LiAlH_4$ de la cyclohexène-1 yl *p*-tolyl sulfone (**1**), de la cyclopentène-1 yl *p*-tolyl sulfone (**2**), de la norbornène-2 yl-2 *p*-tolyl sulfone (**3**) et des sulfones saturées correspondantes **4**, **5** et **6** et nous en rapportons les résultats.

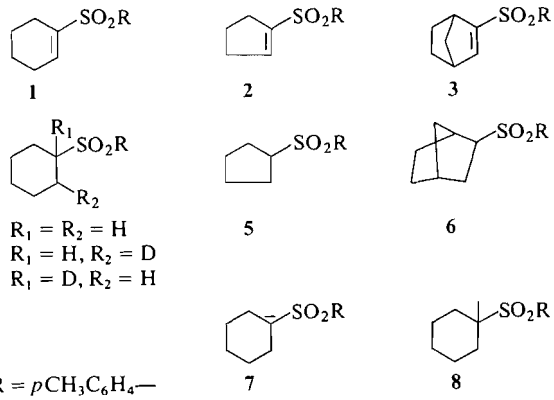

1 **2** **3**

4 $R_1 = R_2 = H$
4*a* $R_1 = H, R_2 = D$
4*b* $R_1 = D, R_2 = H$

5 **6**

$R = pCH_3C_6H_4—$

7 **8**

Les sulfones insaturées **1**, **2** et **3** traitées par $LiAlH_4$ dans l'éther pendant 1 h, donnent les sulfones saturées correspondantes avec d'excellents rendements. Cette réduction chimique s'avère d'ailleurs plus efficace et plus rapide pour réduire la double liaison que la réduction catalytique. Un mécanisme plausible pour cette réduction serait le suivant: il y aurait tout d'abord attaque de l'hydrure sur le carbone en position β du groupe SO_2 pour conduire au carbanion **7** dont la charge négative est localisée sur le carbone en α du groupe sulfonyle (1–6). Le carbanion **7** conduirait ensuite à la sulfone saturée **4** lors de l'hydrolyse. Afin de vérifier ce mécanisme, le composé **1** a été réduit par $LiAlD_4$. Le spectre rmn du produit obtenu indique la disparition du proton oléfinique et la présence d'un hydrogène en α du groupe SO_2 et de neuf autres hydrogènes pour le groupe cyclohexyle confirmant ainsi la formation du composé **4***a* et le mécanisme proposé. Le spectre de masse indique que la deutération est complète puisque le produit monodeutéré **4***a* est pur à 98%. De plus, lorsque le composé **1** est réduit par $LiAlH_4$ suivi d'une hydrolyse par D_2O, on obtient le composé **4***b*.

Si le temps de réduction est prolongé, le produit obtenu n'est pas le sulfure comme on pourrait s'y attendre (7); mais il se produit une rupture du lien C—S pour donner l'acide *p*-toluènesulfinique qui est alors isolé sous forme de méthyl *p*-tolyl sulfone et l'hydrocarbure saturé correspondant (voir tableau 1). Cette réaction impliquerait d'abord la formation d'un carbanion en α du groupe SO_2. Ce dernier pourrait donner par rupture du lien C—S, l'anion *p*-tolyl sulfinate et un carbène par analogie avec la réduction des tosylhydrazones par $LiAlH_4$ (8). Le carbène par migration d'un hydrogène formerait une oléfine (9). Comme il s'est avéré impossible de détecter la présence d'oléfines par chromatographie en phase gazeuse et par résonance magnétique nucléaire, un tel mécanisme ne peut pas être retenu. La formation d'acide *p*-toluènesulfinique et d'hydrocarbure saturé s'expliquerait plutôt par le fait que le carbanion **7** pourrait être protoné par suite de la décomposition de l'éther en alcène (10), pour donner la sulfone saturée qui conduirait à la rupture du lien C—S.

En effet, lorsque les sulfones saturées **4**, **5** et **6** sont traitées par $LiAlH_4$ dans des conditions analogues aux sulfones insaturées, il se produit également une rupture du lien C—S pour donner de l'acide *p*-toluènesulfinique isolé sous forme de méthyl *p*-tolyl sulfone et les hydrocarbures saturés correspondants (voir tableau 1). Afin de s'assurer que la rupture des sulfones saturées n'impliquait pas un carbanion comme intermédiaire comme dans le cas des sulfones insaturées, il suffisait de choisir une sulfone n'ayant pas d'hydrogène en α du groupe SO_2. A cette fin, la méthyl-1 cyclohexyl *p*-tolyl sulfone **8** a été préparée en traitant la cyclohexyl *p*-tolyl sulfone **4** par le méthyl lithium, suivi d'une addition d'iodure de méthyle. Cette sulfone, traitée par $LiAlH_4$ dans les

Can. J. Chem. Downloaded from www.nrcresearchpress.com by 210.87.254.40 on 09/05/12
For personal use only.

Can. J. Chem. Downloaded from www.nrcresearchpress.com by 210.87.254.40 on 09/05/12
For personal use only.

TABLEAU 1. Résultats obtenus en réduisant les sulfones par $LiAlH_4$

Sulfones réduites	Conditions[a]	Produits obtenus (%)[b] Sulfone saturée	Méthyl *p*-tolyl sulfone
Cyclohexène-1 yl *p*-tolyl sulfone (**1**)	A	27	38
	B	24	42
Cyclopentène-1 yl *p*-tolyl sulfone (**2**)	A	35	36
	B	24	23
Norbornène-2 yl-2 *p*-tolyl sulfone (**3**)	A	22	22
	B	16	23
Cyclohexyl *p*-tolyl sulfone (**4**)	A	6[c]	42
	B	31[c]	24
Cyclopentyl *p*-tolyl sulfone (**5**)	A	—	97
	B	28[c]	42
exo-Norbornyl *p*-tolyl sulfone (**6**)	A	24[c]	42
	B	38[c]	27
Hexyl *p*-tolyl sulfone	A	—	42
Benzyl phényl sulfone	A	93[c]	—
Diphényl sulfone	A	100[c]	—
Dibutyl sulfone	A	88[c]	—
Dicyclohexyl sulfone	A	80[c]	—

[a]Conditions: (A) $LiAlH_4$ dans l'éther pendant 144 hs; (B) $LiAlH_4$ dans le tétrahydrofuranne pendant 40 h.
[b]Après purification par cristallisation ou chromatographie pour les sulfones. L'hydrocarbure formé est identifié par chromatographie en phase gazeuse à l'aide d'un échantillon authentique.
[c]Sulfone de départ récupérée.

mêmes conditions, donne également par rupture du lien C—S de l'acide *p*-toluènesulfinique et du méthyl cyclohexane avec un rendement de 33%.

Ce travail permet donc de déduire que la réduction de sulfones α,β-insaturées ou saturées et constituées d'une partie aromatique et non aromatique conduit à la rupture du lien C—S au lieu de donner le sulfure correspondant, tandis que les dialkyl ou les diaryl sulfones dans les mêmes conditions ne réagissent pas (voir tableau 1) à moins qu'il ne s'agisse d'hydroxybenzyl phényl sulfones (11).

Partie expérimentale

Préparation de la méthyl-1 cyclohexyl p-*tolyl sulfone (**8**)*

A 2.6 g de cyclohexyl *p*-tolyl sulfone **4** dissous dans 200 ml d'éther anhydre sous atmosphère d'azote et dans un bain de glace sèche et d'acétone, on ajoute 7.2 ml d'une solution de méthyl lithium 2.2 *M* dans l'éther. La solution se colore rapidement en jaune et on ajoute 10 ml d'iodure de méthyle. Le mélange agité durant une heure est ensuite hydrolysé par l'addition de quelques ml d'eau. Après extraction et évaporation du solvant, le résidu est cristallisé dans un mélange d'éther – éther de pétrole. Par cristallisation fractionnée, on sépare le produit qui n'a pas réagi (0.8 g) du produit méthylé **8** (1.4 g) qui fond à 78–79°C; spectre rmn: 7.60 (m, 4H, hydrogènes du noyau aromatique), 2.41 (s, 3H, méthyle du groupe tolyle), 1.28 ppm (s, 3H, méthyle en α de la sulfone). *Anal.* calc. pour $C_{14}H_{20}SO_2$: C 66.65, H 7.99; trouvé: C 66.92, H 7.78.

Méthode générale de réduction des sulfones α,β-insaturées en sulfones saturées

Une portion (0.002 mol) de sulfone insaturée est ajoutée à une suspension de 0.006 mol de $LiAlH_4$ dans 10 ml d'éther anhydre. Le mélange est porté à reflux durant 1 h. Après extraction et évaporation du solvant, le résidu recristallisé dans un mélange d'éther – éther de pétrole donne la sulfone saturée.

Méthode générale de réduction des sulfones α,β-insaturées avec récupération des produits de rupture

Une portion (0.002 mol) de sulfone est traitée par 0.012 mol de $LiAlH_4$ comme ci-dessus sauf que le temps de réaction est prolongé jusqu'à 144 h. Après extraction, l'éther est évaporé à travers une colonne de Widmer. Le résidu est alors chromatographié en phase gazeuse sur deux colonnes différentes afin d'identifier l'hydrocarbure formé (colonne de 12 pieds × ⅛ po. de diamètre, température 65°C et contenant 3% de JXR sur Chromosorb G AW DMCS et colonne de 20 pieds × ⅛ po. de diamètre, température 100°C et contenant 5% de QF-1 sur Chromosorb G AW DMCS). Par injections mixtes avec le produit authentique, on identifie l'hydrocarbure formé. De la phase organique, on récupère également de la sulfone saturée formée par réduction de la double liaison. A la phase aqueuse, on ajoute un large excès (5 ml) d'iodure de méthyle et quelques ml d'une solution de NaOH à 10%. Après un reflux de 24 h, le mélange est acidifié par une solution de HCl à 10%. Après extraction et évaporation du solvant, on recueille l'acide *p*-toluènesulfinique sous forme de méthyl *p*-tolyl sulfone.

Méthode générale de réduction des sulfones saturées avec récupération des produits de rupture

La même méthode de réduction est utilisée pour les sulfones saturées que pour les sulfones insaturées sauf que les quantités de sulfone et d'hydrure sont dans le rapport de 1 à 3 alors qu'il est de 1 à 6 pour les sulfones insaturées.

Remerciement

Les auteurs remercient le Conseil national de recherches du Canada pour l'aide financière accordée sous forme d'octroi de recherches (A 2030).

1. D. J. CRAM et A. S. WINGROVE. J. Am. Chem. Soc. **85**, 1100 (1963).
2. D. J. CRAM. Fundamentals of carbanion chemistry. Academic Press, New York, NY. 1965. pp. 71–84.
3. J. N. ROITMAN et D. J. CRAM. J. Am. Chem. Soc. **93**, 2225 (1971).
4. A. RAUK, S. WOLFE et I. G. CSIZMADIA. Can. J. Chem. **47**, 113 (1969).
5. S. WOLFE, A. RAUK et I. G. CSIZMADIA. J. Am. Chem. Soc. **91**, 1567 (1969).
6. S. WOLFE, A. RAUK, L. M. TEL et I. G. CSIZMADIA. Chem. Commun. 96 (1970).
7. F. G. BORDWELL et W. H. MCKELLIN. J. Am. Chem. Soc. **73**, 2251 (1951).
8. M. FISHER, Z. PELAH, D. H. WILLIAMS et C. DJERASSI. Ber. **98**, 3236 (1965).
9. L. FRIEDMAN et H. SHECHTER. J. Am. Chem. Soc. **83**, 3159 (1961).
10. R. L. LETSINGER et D. F. POLLART. J. Am. Chem. Soc. **78**, 6079 (1956).
11. B. KOUTEK, L. PAVLICKOVA, J. VELEK et M. SOUCEK. Coll. Czech. Chem. Commun. **41**, 2250 (1976).

Can. J. Chem. Downloaded from www.nrcresearchpress.com by 210.87.254.40 on 09/05/12
For personal use only.

Ligand exchange reactions between ferrocene and 9,10-dimethylanthracene

RONALD G. SUTHERLAND, W. JACK PANNEKOEK, AND CHOI CHUCK LEE

Department of Chemistry and Chemical Engineering, University of Saskatchewan, Saskatoon, Sask., Canada S7N 0W0

Received December 12, 1977

RONALD G. SUTHERLAND, W. JACK PANNEKOEK, and CHOI CHUCK LEE. Can. J. Chem. **56**, 1782 (1978).

The reaction of 9,10-dimethylanthracene (**8**) with ferrocene (FcH) in the presence of $AlCl_3$–Al in decalin gave the stereospecifically hydrogenated product, η^6-*cis*-(*endo*-9,10-dihydro)-9,10-dimethylanthracene-η^5-cyclopentadienyliron cation (**10***a*), the hydrogenation at C-9,10 being *cis* and *endo* or on the same side as the cyclopentadienyliron (CpFe) moiety. When *cis*-9,10-dihydro-9,10-dimethylanthracene, generated from **10***a* by photolysis or pyrolytic sublimation, was used as the arene in the ligand exchange reaction, complexing with the CpFe group could occur from either side of the ring system, giving rise to a mixture of **10***a* and the η^6-*cis*-(*exo*-9,10-dihydro)-9,10-dimethylanthracene-η^5-cyclopentadienyliron cation (**10***b*). The η^6-*cis*-9,10-dihydro-9,10-dimethylanthracene-*trans*-bis-η^5-cyclopentadienyliron dication, with the two CpFe groups *trans*, was also prepared either from a stepwise ligand exchange using **10***a* or directly from reaction of **8** using an excess of FcH. A mechanism is proposed for the hydrogenation that has been found to accompany ligand exchange reactions between polycyclic arenes and FcH and possible applications are pointed out for the synthesis of partially hydrogenated polycyclic aromatic hydrocarbons.

RONALD G. SUTHERLAND, W. JACK PANNEKOEK et CHOI CHUCK LEE. Can. J. Chem. **56**, 1782 (1978).

La réaction du diméthyl-9,10 anthracène (**8**) avec le ferrocène (FcH) en présence de $AlCl_3$–Al dans la décaline conduit à un produit hydrogéné stéréospécifiquement soit le cation η^6 (dihydro-9,10 *endo*) diméthyl-9,10 anthracène η^5 cyclopentadiénylfer *cis* (**10***a*), l'hydrogénation au niveau des atomes de carbone 9,10 se faisant *cis* et *endo*, soit sur le même côté que la portion cyclopentadiénylfer (CpFe). Lorsque l'on utilise du dihydro-9,10 diméthyl-9,10 anthracène *cis*, produit à partir de **10***a* par photolyse ou sublimation pyrolytique, comme arène dans la réaction d'échange de ligand, la complexation avec le groupe CpFe pourrait se produire de chaque côté du système cyclique et pourrait conduire à un mélange de **10***a* et du cation η^6 (dihydro-9,10 *exo*) diméthyl-9,10 anthracène η^5 cyclopentadiénylfer *cis* (**10***b*). On a aussi préparé le dication η^6 dihydro-9,10 diméthyl-9,10 anthracène *cis* bis-η^5 cyclopentadiénylfer *trans* avec les deux groupes CpFe *trans*; on a préparé ce composé soit par un échange par étape du ligand faisant appel à **10***a* soit directement par réaction de **8** avec un excès de FcH. On propose un mécanisme pour l'hydrogénation qui accompagne les réactions d'échange de ligand entre les arènes polycycliques et FcH et on indique des applications possibles pour la synthèse d'hydrocarbures aromatiques polycycliques partiellement hydrogénés.

[Traduit par le journal]

Introduction

In 1963, Nesmeyanov *et al.* (1, 2) first reported that η^6-arene-η^5-cyclopentadienyliron cations could be prepared by the reaction of benzene or substituted benzenes with ferrocene and $AlCl_3$, with Al powder also present in the reaction mixture to minimize the formation of ferricenium ions from ferrocene. Among the more intriguing early observations was the finding that the reaction with chloro- or bromobenzene was complicated by the loss of halogen to give the benzene complex and, in some instances, the biphenyl complex (3, 4). Apart from the synthesis of complexes from naphthalene and fluorene (3), early studies tended to neglect the reactions of polynuclear hydrocarbons with ferrocene. Our work in this area began with a successful attempt to prepare cations by an intramolecular ligand exchange process, whereby bisindenyliron (**1**) was converted to the corresponding η^6-arene-η^5-cyclopentadienyliron cation **2** by treatment with BF_3-etherate (5), a transformation which has since been confirmed by other workers (6).

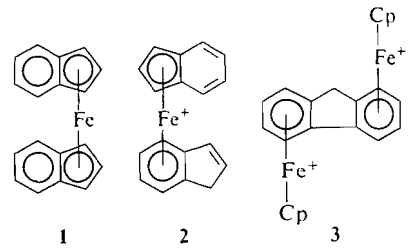

1 2 3

The first successful synthesis of η^6-arene-*bis*-η^5-cyclopentadienyliron dications was reported from this laboratory in 1972 (7), using arenes such as biphenyl, diphenylmethane, and fluorene, and in the latter case, the two cyclopentadienyliron (CpFe)

Can. J. Chem. Downloaded from www.nrcresearchpress.com by 210.87.254.6 on 09/05/12
For personal use only.

Can. J. Chem. Downloaded from www.nrcresearchpress.com by 210.87.254.6 on 09/05/12
For personal use only.

moieties were shown to be *trans* to each other (**3**). Subsequently, Hendrickson and co-workers (8) reported the synthesis of a number of such dications from a variety of aromatic polynuclear hydrocarbons. However, we have found that such reactions with aromatic polynuclear hydrocarbons resulted in a novel hydrogenation process. For example, reaction of naphthalene with ferrocene (FcH)–$AlCl_3$–Al gave rise to both the η^6-naphthalene-η^5-cyclopentadienyliron cation (**4**) and the η^6-tetralin-η^5-cyclopentadienyliron cation (**5**), whereas anthracene gave only the hydrogenated η^6-9,10-dihydroanthracene-η^5-cyclopentadienyliron cation (**6**) and the corresponding dication (**7**) (9). These observations as well as the early work in the field have recently been reviewed (10).

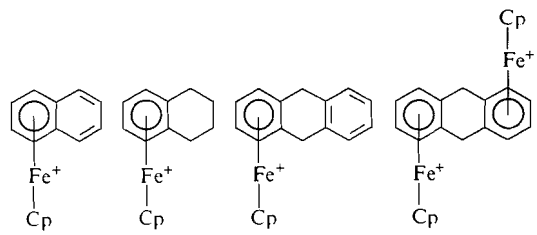

The ligand exchange reaction between FcH and a number of substituted naphthalenes has also been studied (11). It is of interest to note that with 1-bromonaphthalene, the reaction gave a mixture of the expected η^6-1-bromonaphthalene-η^5-cyclopentadienyliron cation, the debrominated cation **4**, and the debrominated-hydrogenated cation **5**. With added radical scavengers such as I_2 or diphenylpicrylhydrazyl (DPPH), the formation of **5** was suppressed, thus implicating radical ions in the hydrogenation process (11). In the present work, ligand exchange reactions between FcH and 9,10-dimethylanthracene, in the presence of $AlCl_3$–Al, were studied with the view of elucidating the stereochemical nature and hence the probable mechanism for the hydrogenation process observed in such reactions.

Results

9,10-Dimethylanthracene (**8**) can be readily prepared in a one-step reaction from vinyl acetate, $AlCl_3$, and benzene (12). By analogy with the ready formation of the 9,10-dihydroanthracene complex **6** from anthracene, it may be anticipated that if hydrogenation occurs in the ligand exchange reaction between FcH and **8**, the hydrogenation could be specifically *trans* to give ion **9**, specifically *cis* and *endo* to the CpFe group to give ion **10***a*, and specifically *cis* and *exo* to the CpFe group to give ion **10***b*,[1] or hydrogenation might take place randomly to give a mixture of these isomers.

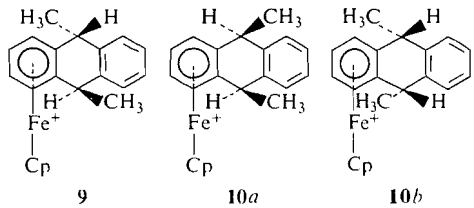

Reaction of **8** with FcH in the presence of $AlCl_3$–Al (molar ratio of 1:1:2:1 for arene–FcH–$AlCl_3$–Al) required a minimum temperature of 130–140°C in decalin to give a single monocationic product, which upon photolysis (9) or pyrolytic sublimation gave the hydrogenated ligand, *cis*-9,10-dihydro-9,10-dimethylanthracene (**11**). The product, therefore, cannot be ion **9** but may be ion **10***a* or **10***b*. Subsequent observations (*vide infra*) showed that this product is **10***a*, the η^6-*cis*-(*endo*-9,10-dihydro)-9,10-dimethylanthracene-η^5-cyclopentadienyliron cation. The dication, **12**, can be prepared in a stepwise manner (7) from treatment of ion **10***a* with FcH, $AlCl_3$, and Al, or in a one-step process (8) from **8** with an excess of FcH (molar ratio of 1:5:10:1 for arene–FcH–$AlCl_3$–Al). When *cis*-9,10-dihydro-9,10-dimethylanthracene (**11**), derived from the photolysis or pyrolytic sublimation of **10***a*, was used as the arene, the ligand exchange reaction with FcH in the presence of $AlCl_3$–Al now gave a mixture of the *cis-endo*-dihydro cation **10***a* and the *cis-exo*-dihydro cation **10***b*, in a ratio of approximately 60:40. The ^1H and ^{13}C nmr spectral data and their assignments for hydrocarbon **11** and ions **10***a*, **10***b*, and **12** are summarized in Table 1 and, as illustrations, the ^{13}C nmr spectra of ions **10***a* and **12** are shown in Fig. 1.

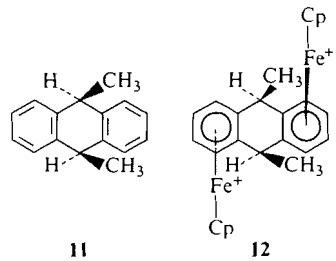

Discussion

From Table 1, it is seen that in agreement with earlier observations (8, 9, 11), the aromatic ring, after complexing with the CpFe group, shows an upfield shift as was first reported by Hendrickson

[1]The *endo* and *exo* designations are used to indicate that the H atoms at C-9,10 and the CpFe group are on the same side and on opposite sides, respectively, of the ring system (13).

TABLE 1. ^1H and ^{13}C nmr data from *cis*-9,10-dihydro-9,10-dimethylanthracene (**11**), η^6-*cis*-(*endo*-9,10-dihydro)-9,10-dimethylanthracene-η^5-cyclopentadienyliron monocation (**10***a*), η^6-*cis*-(*exo*-9,10-dihydro)-9,10-dimethylanthracene-η^5-cyclopentadienyliron monocation (**10***b*), and η^6-*cis*-9,10-dihydro-9,10-dimethylanthracene-*trans*-bis-η^5-cyclopentadienyliron dication (**12**)

	δ (ppm from TMS)*									
	CH_3		C-9,10		Cp		Complexed aromatic		Uncomplexed aromatic	
	^1H	^{13}C	^1H	^{13}C	^1H	^{13}C	^1H	^{13}C	^1H	^{13}C
11	1.51(d) J = 7.4 Hz	28.3	4.12(q) J = 7.4 Hz	39.8					7.3(m)	126.1 127.7 140.3†
10*a*	1.59(d) J = 7.4 Hz	27.2	4.03(q) J = 7.4 Hz	39.2	4.59(s)	76.4	6.27(s)	86.2 86.4 105.8†	7.42(s)	127.2 127.8 137.4†
10*b*	2.00(d) J = 6.8 Hz	11.9	3.69(q) J = 6.8 Hz	34.4	4.24(s)	75.0	6.40(m)	83.4 84.4 108.9†	7.55(s)	123.2 126.7 140.5†
12	1.96(d) J = 7.3 Hz	19.9	4.17(q) J = 7.3 Hz	35.4	4.74(s) 4.79(s)	75.9 77.0	6.42(m)	84.7 85.0 85.6 86.6 103.6† 106.4†		

*The spectra were obtained in CD_3CN solution except that the ^1H spectra of **10***a* and **10***b* were obtained in CD_2Cl_2.
†Quaternary carbons.

and co-workers (8). With regard to the stereochemistry of the hydrogenation, it is of interest to note that for ion **10***a*, in which the H atoms at C-9,10 are *endo* or on the same side of the ring system as the CpFe group, the CH_3 and C-9,10 absorptions are quite similar for **10***a* and the hydrogenated ligand **11**. On the other hand, for ion **10***b* in which the CH_3 groups at C-9,10 are *endo*, there is a steric downfield shift (14) for the CH_3 proton absorption at 2.00 ppm relative to that of **10***a* at 1.59 ppm. Similarly, the same steric effect that caused a loss of electron density for the CH_3 hydrogens gave rise to more shielding for the CH_3 carbons, resulting in an upfield shift (15, 16) for the CH_3 carbon absorption of **10***b* at 11.9 ppm relative to that of **10***a* at 27.2 ppm. Slightly more shielding for the C-9,10 carbons of **10***b* than **10***a* is also observed. Such results, therefore, establish the *cis*-(*endo*-9,10-dihydro) and *cis*-(*exo*-9,10-dihydro) structures for ions **10***a* and **10***b*, respectively.

The ^{13}C spectrum of dication **12** (Table 1, Fig. 1) shows two Cp resonances at 75.9 and 77.0 ppm and only one set of aliphatic peaks at 19.9 (CH_3) and at 35.4 ppm (C-9,10). These findings are consistent only with structure **12** in which the two CpFe groups are *trans*. If the two CpFe groups were *cis*, there would be only one equivalent Cp absorption, and if the two nonequivalent Cp peaks were due to a mixture in which the two CpFe groups were *cis* in one case and *trans* in the other, there would be two sets of resonances at the aliphatic region. Since in **12** the CH_3 groups are *endo* to one of the CpFe groups, the steric effect gave, relative to **10***a*, a downfield shift for the CH_3 proton absorption and an upfield shift for the CH_3 carbon absorption, quite similar to those observed for **10***b* relative to **10***a*, and, therefore, providing a further confirmation for structures **10***a* and **10***b*.

The present results thus indicate that the ligand exchange reaction between 9,10-dimethylanthracene (**8**) and FcH in the presence of $AlCl_3$–Al, as in the analogous reaction with anthracene (9), occurs with hydrogenation at the C-9,10 positions. However, a minimum temperature of 130–140°C is required in the reaction with **8**, in contrast with the reaction with anthracene which took place at about 80°C (9). The addition of the H atoms is stereospecifically *cis* and *endo* or on the same side as the CpFe group to give ion **10***a*. When *cis*-9,10-dihydro-9,10-dimethylanthracene (**11**) is used as the arene, there is no hydrogenation and the CpFe group can complex from either side of the ring system to give a mixture of ions **10***a* and **10***b*.

In our earlier work, it was shown that deuterium was not incorporated from D_2O during work up and that hydrogenation did occur during the ligand exchange reaction (9). The source of the hydrogen is probably the solvent since control experiments have shown that, instead of decalin, the use of hydrocarbons such as nonane, a poorer hydrogen donor, as solvent gave lesser extents of hydrogenation (17). With the naphthalene system, it was also found that

Can. J. Chem. Downloaded from www.nrcresearchpress.com by 210.87.254.6 on 09/05/12
For personal use only.

Can. J. Chem. Downloaded from www.nrcresearchpress.com by 210.87.254.6 on 09/05/12
For personal use only.

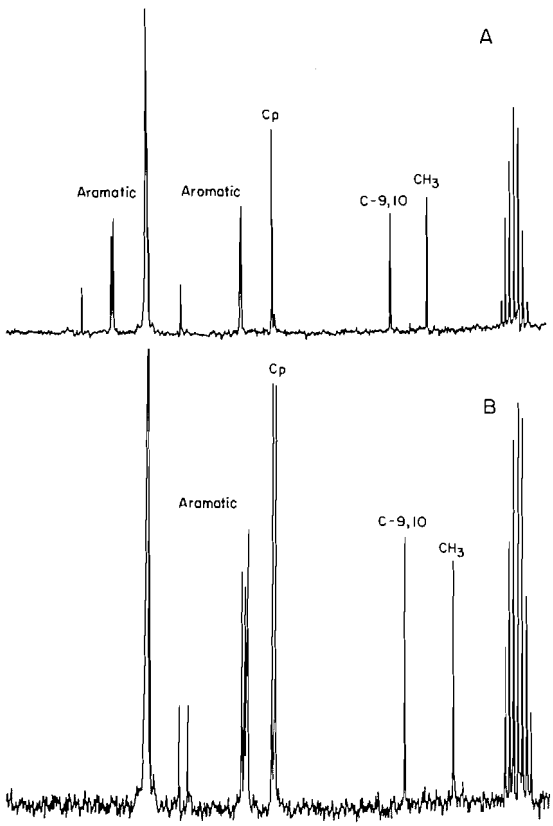

FIG. 1. ^{1}H-decoupled ^{13}C nmr spectra in CD_3CN of the η^6-*cis*-(*endo*-9,10-dihydro)-9,10-dimethylanthracene-η^5-cyclopentadienyliron cation **10***a* (*A*) and the η^6-*cis*-9,10-dihydro-9,10-dimethylanthracene-*trans*-bis-η^5-cyclopentadienyliron dication **12** (*B*).

the extent of hydrogenation was dependent on the concentration of $AlCl_3$ and that extensive scramblings occurred when perdeuteronaphthalene was used in the reaction (11). These observations strongly suggested that hydride abstraction by $AlCl_3$ likely played an important role. In the work with 1-halonaphthalenes (11), the relative ease of dehalogenation (Br > Cl ≫ F) again suggested the removal of halide by $AlCl_3$ as $AlCl_3X^-$ (X = Br, Cl). With 1-bromonaphthalene, the effect of radical scavengers in suppressing the hydrogenation, but not the dehalogenation, indicated that at least two steps were involved in the hydrogenation process, namely, the loss of $AlCl_3X^-$ followed by a radical reduction involving H atoms (11).

The present findings with **8** provided much additional information pertinent to the mechanism of the hydrogenation. The higher reaction temperature required by **8** in contrast to anthracene is consistent with hydride abstraction by $AlCl_3$, since a primary hydrogen has to be removed from **8** to initiate the hydrogenation. The stereospecificity observed in the addition of hydrogen to C-9,10, namely, *cis* and *endo* to the complexed iron, is of mechanistic significance. It suggests that the iron must have been complexed to the arene ligand before hydrogenation and that iron hydride intermediates are likely involved. Such stereospecific transfers of hydrogen via iron hydrides have been observed, for example, in the fragmentation of the complex, cyclohexadienylcyclopentadienyliron (18).

Considering all the information discussed above, a mechanism for the hydrogenation process is outlined in Scheme 1. This is a modification of the previously suggested radical-ion mechanism which was proposed as a working hypothesis (11). The mechanism in Scheme 1 can, of course, be readily adapted to account for the hydrogenation with other arenes such as the formation of **5** from naphthalene. Among the key steps in the mechanism is the intramolecular oxidation–reduction (11) in which an electron is

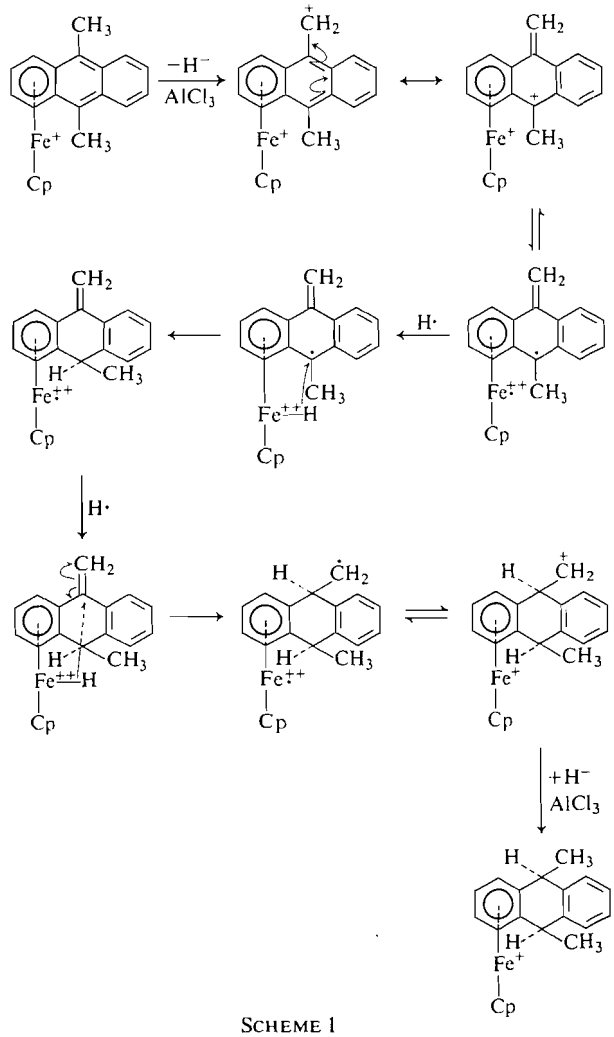

SCHEME 1

Can. J. Chem. Downloaded from www.nrcresearchpress.com by 210.87.254.6 on 09/05/12
For personal use only.

transferred from Fe(II) to give Fe(III) while a carbonium ion center is reduced to a free radical. This has a recent analogy in the work of Cais *et al.* (19) who found that a tertiary amine could transfer an electron to an α-ferrocenyl carbonium ion to give a radical, which subsequently could abstract H to form product.

Aside from the mechanistic aspects of the hydrogenation, the present and related work also indicate that there are synthetic applications. The reaction of **8** to give **10***a*, followed by pyrolytic sublimation to give **11** is the best synthetic route to this hydrocarbon. A number of reductive methods to give 9,10-dihydro-9,10-dimethylanthracene generally resulted in a mixture of the *cis* and *trans* isomers (20–22) while the synthesis of the pure *cis* isomer (**11**) required a sequence of stereospecific reactions (23, 24). Other related work (to be published) with polycyclic aromatics, such as acenaphthene, phenanthrene, chrysene and pyrene, show that hydrogenation occurs readily to give partially reduced polycyclics, which can then be obtained in a pure form by chromatographic separation of the complexes followed by either photolysis or pyrolytic sublimation to give the free ligand; for example, both 4,5-dihydropyrene and 4,5,9,10-tetrahydropyrene can be obtained in this manner from pyrene.

Experimental

η⁶-cis-(endo-*9,10-Dihydro*)-*9,10-dimethylanthracene*-η⁵-*cyclopentadienyliron cation (**10**a)*

A mixture of 5.15 g (25 mmol) of 9,10-dimethylanthracene (**8**) (12), 4.7 g (25 mmol) of ferrocene, 6.7 g (50 mmol) of $AlCl_3$, and 0.65 g (25 mmol) of Al powder in 50 ml of decalin were heated under reflux and under N_2 at 135°C for 12 h. The resulting material was cooled to room temperature and 50 ml of H_2O was added. The mixture was thoroughly shaken, the aqueous layer separated and washed with Skelly B (3 × 100 ml) and then filtered into a concentrated solution of ammonium hexafluorophosphate. The yellow hexafluorophosphate salt of **10***a* that precipitated (3.1 g, 25%) was dried under vacuum for 24 h. Recrystallization could be carried out in CH_3CN–tetrahydrofuran; however, on successive recrystallization, the melting point varied and the nmr spectra showed broadening of the peaks presumably owing to decomposition giving rise to paramagnetic impurities. It was noted that for the complex salts prepared in the present work, the best ^1H and ^{13}C nmr spectra were obtained with a minimum handling of the reaction products. The identification of ions such as **10***a* was, therefore, based on nmr spectroscopic data as summarized in Table 1 and exemplified in Fig. 1.

cis-*9,10-Dihydro-9,10-dimethylanthracene (**11**) from **10**a*

Photolysis

A solution of the hexafluorophosphate salt of **10***a* (2.5 g, 5.3 mmol) in tetrahydrofuran (50 ml) was irradiated under N_2 and with stirring for 16 h in a Rayonet reactor using 253.7 nm radiation. The resulting solution was poured into 200 ml of H_2O, extracted with CH_2Cl_2 (3 × 50 ml), and dried over $MgSO_4$. After removal of the solvent, the residue was subjected to column chromatography over neutral alumina with hexane as eluant. The eluate was concentrated to an oily residue and crystallized from CH_3OH giving 350 mg (30%) of **11**, mp 130-131°C (lit. (23) mp 130–131°C).

Pyrolytic Sublimation

The hexafluorophosphate salt of **10***a* was dissolved in a minimum of acetone or CH_2Cl_2 in a sublimator. The solvent was allowed to evaporate, leaving a thin coating of the material on the glass wall of the apparatus. After evacuation to about 0.1 Torr, heating was applied with a bunsen burner for 0.5 h or in an oil bath at about 180°C for 4 h. The solid sublimate that collected on the cold finger was dissolved in $CHCl_3$ and purified by passage through an alumina column using $CHCl_3$ as eluant. Recrystallization from CH_3OH gave **11** in yields of about 80%.

*Mixture of **10**a and **10**b from Reaction with **11***

A mixture of 940 mg (4.5 mmol) of **11**, 840 mg (4.5 mmol) of ferrocene, 1200 mg (9.0 mmol) of $AlCl_3$, and 120 mg (4.5 mmol) of Al powder in 18 ml of decalin was heated under reflux and under N_2 at 100°C for 16 h. The resulting material was worked up as described in the preparation of **10***a* from **8**. The product (400 mg, 20%) was a mixture of **10***a* and **10***b*, the nmr data for which are given in Table 1. From the ^1H nmr, the relative proportion of **10***a*:**10***b* was estimated to be 60:40.

η⁶-cis-*9,10-Dihydro-9,10-dimethylanthracene*-trans-*bis*-η⁵-*cyclopentadienyliron Dication (**12**)*

*From 9,10-Dimethylanthracene (**8**)*

A mixture of 1.25 g (6.0 mmol) of **8**, 5.58 g (30 mmol) of ferrocene, 8.0 g (60 mmol) of $AlCl_3$, and 0.16 g (6.0 mmol) of Al powder in 50 ml of decalin was heated under reflux and under N_2 at 140°C for 16 h. Work-up of the reaction mixture as described in the preparation of **10***a* from **8** gave 4.0 g (90%) of the hexafluorophosphate salt of **12**. The ^1H and ^{13}C nmr data are given in Table 1 and the ^{13}C nmr spectrum is shown in Fig. 1.

*From Ion **10**a*

A mixture of 1.0 g (0.21 mmol) of the hexafluorophosphate salt of **10***a*, 3.9 g (2.1 mmol) of ferrocene, 5.6 g (4.2 mmol) of $AlCl_3$, and 0.56 g (2.1 mmol) of Al powder in 50 ml of cyclohexane was refluxed (about 80°C) under N_2 for 16 h. Work-up as described above gave 300 mg (20%) of the hexafluorophosphate salt of **12**.

Acknowledgement

Financial support in the form of grants given by the National Research Council of Canada to R.G.S. and to C.C.L. are gratefully acknowledged.

1. A. N. NESMEYANOV, N. A. VOL'KENAU, and I. N. BOLESOVA. Dokl. Acad. Nauk SSSR, **149**, 615 (1963).
2. A. N. NESMEYANOV, N. A. VOL'KENAU, and I. N. BOLESOVA. Tetrahedron Lett. 1725 (1963).
3. A. N. NESMEYANOV, N. A. VOL'KENAU, and I. N. BOLESOVA. Dokl. Acad. Nauk SSSR, **166**, 607 (1966).
4. I. U. KHAND, P. L. PAUSON, and W. E. WATTS. J. Chem. Soc. C, 2261 (1968).
5. C. C. LEE, R. G. SUTHERLAND, and B. J. THOMSON. J. Chem. Soc. Chem. Commun. 1071 (1971).
6. P. M. TREICHEL and J. W. JOHNSON. J. Organomet. Chem. **88**, 207 (1975).
7. C. C. LEE, R. G. SUTHERLAND, and B. J. THOMSON. J. Chem. Soc. Chem. Commun. 907 (1972).
8. W. H. MORRISON, E. Y. HO, and D. N. HENDRICKSON. J. Am. Chem. Soc. **96**, 3603 (1974).
9. R. G. SUTHERLAND, S. C. CHEN, J. PANNEKOEK, and C. C. LEE. J. Organomet. Chem. **101**, 221 (1975).

10. R. G. SUTHERLAND. J. Organomet. Chem. Library, **3**, 311 (1977).
11. R. G. SUTHERLAND, S. C. CHEN, W. J. PANNEKOEK, and C. C. LEE. J. Organomet. Chem. **117**, 61 (1976).
12. J. M. PEPPER, B. P. ROBINSON, and S. W. SCHWANBECK. Can. J. Chem. **40**, 122 (1962).
13. E. A. HILL and J. H. RICHARDS. J. Am. Chem.Soc. **83**, 4216 (1961).
14. L. M. JACKMAN and S. STERNHELL. Applications of nuclear magnetic resonance spectroscopy in organic chemistry. 2nd ed. Pergamon Press, New York, NY. 1969. p. 71.
15. G. C. LEVY and G. L. NELSON. Carbon-13 nuclear magnetic resonance for organic chemists. Wiley-Interscience, New York, NY. 1972. pp. 24 and 84.
16. A. S. PERLIN. *In* Isotopes in organic chemistry. Vol. 3. Carbon-13 in organic chemistry. *Edited by* E. Buncel and C. C. Lee. Elsevier, Amsterdam. 1977. Chapt. 4.
17. R. G. SUTHERLAND, W. J. PANNEKOEK, and C. C. LEE. Ann. N.Y. Acad. Sci. **295**, 192 (1977).
18. C. C. LEE, R. G. SUTHERLAND, and B. J. THOMSON. Tetrahedron Lett. 2625 (1972).
19. M. CAIS, P. ASHKENAZI, S. DANI, and J. GOTTLIEF. J. Organomet. Chem. **122**, 403 (1976).
20. R. G. HARVEY, L. ARZADON, J. GRANT, and K. URBERG. J. Am. Chem. Soc. **91**, 4535 (1969).
21. R. G. HARVEY and L. ARZADON. Tetrahedron, **25**, 4887 (1969).
22. R. G. HARVEY and C. C. DAVIS. J. Org. Chem. **34**, 3607 (1969).
23. A. H. BECKETT and R. G. LINGARD. J. Chem. Soc. 2409 (1959).
24. L. M. JACKMAN and J. W. LOWN. J. Chem. Soc. 2776 (1962).

Can. J. Chem. Downloaded from www.nrcresearchpress.com by 210.87.254.6 on 09/05/12
For personal use only.

On the existence of *cis* and *trans* conformational isomers in 2-methylphenol and 4-chloro-2-methylphenol

TED SCHAEFER AND KALVIN CHUM

Department of Chemistry, University of Manitoba, Winnipeg, Man., Canada R3T 2N2

Received February 2, 1978

TED SCHAEFER and KALVIN CHUM. Can. J. Chem. **56**, 1788 (1978).

The analysis of the proton magnetic resonance spectra of 2-methylphenol and of 4-chloro-2-methylphenol in benzene-d_6 and CCl_4 solutions yields spin–spin coupling constants over five bonds between the hydroxyl proton and the *meta* ring protons. These coupling constants are related to the intramolecular equilibrium between conformers in which the hydroxyl group is oriented *cis* or *trans* to the methyl group. The free energy difference between the conformers is 0.4 ± 0.1 kcal/mol, with the *trans* form being the more stable. The concentration dependence of the hydroxyl proton chemical shift of the chloro compound in CCl_4 suggests that dimerization is relatively unimportant and yields rough values for the extent of self-association. It is argued that the derived free energy values refer to the intramolecular equilibrium for the monomers.

TED SCHAEFER et KALVIN CHUM. Can. J. Chem. **56**, 1788 (1978).

L'analyse des spectres de résonance magnétique nucléaire du proton du méthyl-2 phénol et du chloro-4 méthyl-2 phénol dans des solutions de benzène-d_6 et de CCl_4 conduisent aux constantes de couplage spin–spin à travers cinq liaisons entre le proton de l'hydroxyle et les protons du cycle en position *méta*. On a établi une relation entre ces constantes de couplage et l'équilibre intramoléculaire entre les conformères dans lesquels le groupe hydroxyle est orienté soit *cis* ou *trans* par rapport au groupe méthyle. La différence d'énergie libre entre les conformères est de 0.4 ± 0.1 kcal/mol, la forme *trans* étant la plus stable. La relation qui existe entre la concentration et le déplacement chimique du proton hydroxyle du composé chloré dans CCl_4 suggère que l'importance d'une dimérisation est faible et fournit des valeurs approximatives concernant le taux d'autoassociation. On présente des arguments à l'effet que les valeurs des énergies libres qui en sont dérivées se réfèrent à l'équilibre intramoléculaire des monomères.

[Traduit par le journal]

Introduction

A direct measurement of the *cis–trans* equilibrium for 2-methylphenol in solution is not available. The stretching frequency of the hydroxyl group in 2-methylphenol in CCl_4 solution at 300 K is not resolvable into two components, so that the free energy difference, ΔG, between the *cis* (**1***a*) and *trans* (**1***b*)

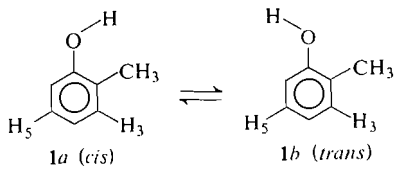

1*a* (*cis*) **1***b* (*trans*)

forms cannot be derived (1). An indirect estimate (1), based on the stretching band intensities in 2-*tert*-butylphenol and in 2-*tert*-butyl-5,6-dimethylphenol, yields $\Delta G = -0.5$ kcal/mol for the above equilibrium (**1***b* more stable) at 300 K in CCl_4.

The far infrared and low frequency Raman spectra in C_6H_{12} solution contain many bands, leading to ambiguous assignments of the torsional modes of the hydroxyl group (2, 3). A molecular mechanics calculation (4) suggests that **1***b* is more stable than **1***a* by 0.86 kcal/mol, the methyl group lying in a staggered conformation relative to the C—O bond.

When intermolecular proton exchange can be retarded sufficiently, it has been shown in this laboratory (5, 6) that ΔG can be deduced from the stereospecific long-range spin–spin coupling constants over five bonds between the hydroxyl proton and the protons or fluorine nuclei in positions *meta* to the hydroxyl site. In particular, it is very likely that ${}^5J_m^{OH,H_3} \equiv {}^5J_c$ is negligibly small in **1***a* and that ${}^5J_m^{OH,H_3} \equiv {}^5J_t$ can be as large as 0.7 Hz in molecules with conformations analogous to **1***b*. Corresponding remarks apply to ${}^5J_m^{OH,H_5}$ in **1***b* and in **1***a*, respectively.

In this paper a full analysis of the proton magnetic resonance spectra of 2-methylphenol (**1**) and of 4-chloro-2-methylphenol (**2**) in CCl_4 and C_6D_6 solutions yields information about the equilibrium between **1***a* and **1***b* and about the coplanarity of the O—H group with the benzene ring. The concentration dependence of the spectral parameters of **2** are also investigated.

Experimental

Solutions of 2-methylphenol, of 4-chloro-2-methylphenol, and of 4,6-dichloro-2-methylphenol at various concentrations (see below) in appropriate solvents, were degassed by the freeze–pump–thaw technique. They contained small amounts

Can. J. Chem. Downloaded from www.nrcresearchpress.com by 210.87.254.40 on 09/05/12
For personal use only.

TABLE 1. Proton chemical shifts[a] and spin–spin coupling constants for 2-methylphenol

Parameter	Value[b] C_6D_6[c]	Value[b] CCl_4[d]	Parameter	Value C_6D_6	Value CCl_4
ν_{OH}	420.421(2)	445.175(2)	$^5J_m^{H_6,CH_3}$	0.408(2)	0.411(2)
ν_{CH_3}	204.681(2)	219.811(1)	$^6J_p^{H,CH_3}$	−0.591(2)	−0.595(2)
ν_3	693.470(2)	699.700(2)	$^3J_{34}$	7.462(3)	7.476(2)
ν_4	673.495(2)	671.955(2)	$^3J_{45}$	7.458(3)	7.439(3)
ν_5	691.410(2)	694.511(2)	$^3J_{56}$	7.921(3)	7.987(3)
ν_6	637.725(2)	660.521(2)	$^4J_{35}$	1.697(3)	1.698(2)
$^4J_o^{H,OH}$	−0.111(3)	−0.116(2)	$^4J_{46}$	1.181(3)	1.197(2)
$^5J_m^{H_5,OH}$	0.484(3)	0.453(3)	$^5J_{36}$	0.376(3)	0.333(3)
$^5J_m^{H_5,OH}$	0.215(3)	0.242(2)	rms deviation	0.018	0.015
$^6J_p^{H_4,OH}$	0.0[e]	0.0[e]	Transitions calculated	671	665
$^4J_o^{H,CH_3}$	−0.771(2)	−0.777(2)	Peaks observed	152	117
$^5J_m^{H_4,CH_3}$	0.354(2)	0.361(2)	Transitions assigned	573	504

[a]In Hz at 100 MHz and 305 K to low field of internal tetramethylsilane.
[b]Numbers in parentheses give the standard deviation in the last place.
[c]5 mol%.
[d]2.5 mol%.
[e]Peaks displayed no change in linewidth on decoupling the OH proton.

TABLE 2. Hydroxyl proton chemical shift[a] and hydroxyl proton spin–spin coupling constants for 4-chloro-2-methylphenol

Parameter	Value[b] C_6D_6 5 mol%	Value[b] CCl_4[c] 2.5 mol%	3.4 mol%	5.0 mol%	8.0 mol%
ν_{OH}	389.700(1)	443.55(1)	452.446(2)	470.11(1)	488.57(1)
$^4J_a^{H,OH}$	−0.141(2)	−0.15	−0.146(2)	−0.145(5)	-0.1_5
$^5J_m^{H_3,OH}$	0.467(2)	0.44	0.436(2)	0.457(5)	0.44
$^5J_m^{H_5,OH}$	0.242(2)	0.26	0.265(2)	0.216(5)	0.24
rms deviation	0.010	—	0.010	0.014	—

[a]In Hz at 100 MHz and 305 K to low field of internal tetramethylsilane.
[b]In Hz; numbers in parentheses are standard deviations.
[c]Hydroxyl proton shifts at other concentrations and 305 K are 0.15 mol%, 428.19 ± 0.02 Hz; 0.3, 428.20 ± 0.03; 0.6, 429.52 ± 0.04; 1.2, 433.81 ± 0.02; 1.9, 438.27 ± 0.02; 3.6, 454.63 ± 0.03.

of tetramethylsilane as an internal reference. Intermolecular hydroxyl proton exchange was retarded as previously described (7).

Proton magnetic resonance spectra were repeatedly calibrated at 5-Hz intervals in the frequency sweep mode at sweep rates of 0.01 and 0.02 Hz/s on an HA100 spectrometer. The probe temperature was 305 ± 1 K. Spectra were also calibrated while decoupling the hydroxyl proton. Consequently, the spectral parameters could be derived and compared for fully coupled (seven or eight spins) and partially decoupled (six and seven spins) conditions.

Results and Discussion

Spectral Analyses

These were performed by the computer program LAME (8, 9). In Table 1 the spectral parameters are entered for 2-methylphenol. Similar analyses yielded data for 4-chloro-2-methylphenol, the immediately relevant numbers being presented in Table 2. Figure 1 displays calculated and observed hydroxyl proton spectra for a 3.4 mol% solution of 4-chloro-2-methylphenol in CCl_4 solution. It illustrates the quality of spectra attainable for **2**.

The Cis–Trans Equilibrium in 1 and 2 2-Methylphenol

If ^5J_c in **1***a* and **1***b* is negligibly small,[1] then the free energy difference between **1***a* and **1***b* is $-RT \times \ln K = -RT \ln {}^5J_t/{}^5J_c = -RT \ln 0.484/0.215 = -490 \pm 50$ cal/mol for **1** in C_6D_6 solution and is -380 ± 40 cal/mol in CCl_4 solution (see Table 1). The estimated errors assume that the standard deviations in Table 1 are to be multiplied by 4.

It is tempting to suggest that the apparently greater stability of the *trans* form in C_6D_6 solution can be rationalized by invoking intermolecular hydrogen bonding to the π system of the solvent molecules, which might well be stronger for the *trans* form. Note that the OH and the H_6 protons of **1** display substantial

[1]A 10 mol% solution of 4,6-dichloro-2-methylphenol in C_6D_6 yielded no observable $^5J_m^{H_5,OH}$, nor was any line-narrowing observed for H_5 peaks when the hydroxyl proton was decoupled, strongly suggesting that ^5J_c is less than 0.03 Hz and that this compound exists predominantly as one conformer.

Can. J. Chem. Downloaded from www.nrcresearchpress.com by 210.87.254.40 on 09/05/12
For personal use only.

Can. J. Chem. Downloaded from www.nrcresearchpress.com by 210.87.254.40 on 09/05/12
For personal use only.

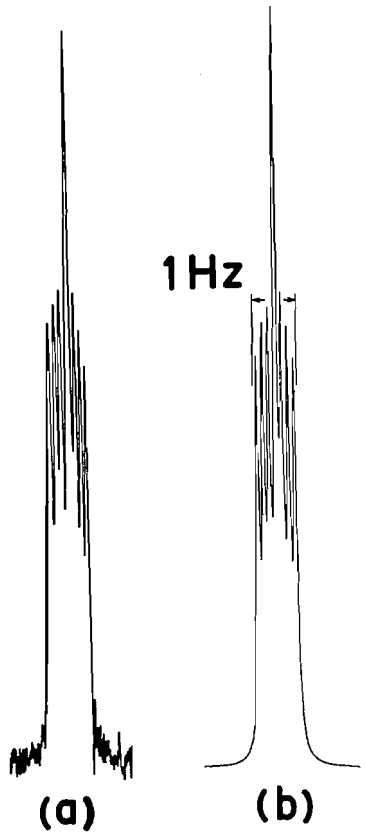

FIG. 1. The observed (*a*) and calculated (*b*) hydroxyl proton magnetic resonance spectra at 100 MHz of a 3.4 mol% solution of 4-chloro-2-methylphenol in CCl_4 at 305 K.

upfield shifts, relative to the CCl_4 solution (Table 1), compared to the other protons in **1**; this is expected if the magnetically anisotropic benzene solvent molecules pack preferentially about that region of the solute molecule. Yet this solvent effect on the *cis–trans* equilibrium must be small, if present at all.

The value of $^6J_p^{H_4,OH}$ is unobservably small in both solutions, as expected (10) if the barrier to rotation about the C—O bond is about 3.5 kcal/mol (11, 12). It is therefore reasonable to ignore any complications arising from an appreciable population of conformers in which the O—H bond lies out of the benzene plane.

Intermolecular hydrogen bonding between solute molecules must be present to some degree at these concentrations (5 mol%), but probably does not alter substantially the observed ^5J values (see discussion of **2** below). Hydrogen bonding to CCl_4 solvent molecules is apparently rather slight, having an *enthalpy* of only about 0.2 kcal/mol for phenol itself (13). Proton magnetic resonance measurements give no evidence for a specific phenol–CCl_4 complex (14).

4-Chloro-2-methylphenyl (2)

From the coupling data in Table 2, it follows that the average free energy difference between the *cis* and *trans* forms of **2** is -380 ± 60 cal/mol (*trans* more stable) in the various solutions. The values of $^5J_m^{H_3,OH}$ and $^5J_m^{H_5,OH}$ do not vary significantly between 2.5 and 8 mol% in CCl_4 and are apparently unchanged in C_6D_6 solution. Intermolecular hydroxyl proton exchange could not be stopped for a 10 mol% solution in CCl_4.

Intramolecular Hydrogen Bonding in 2

The purpose of the concentration studies was to ascertain whether increased intermolecular association could alter the intramolecular equilibrium. The *cis* and *trans* forms are present in appreciable amounts and the present approach should be sensitive to a change of 30% in the apparent intramolecular equilibrium constant, K (for $K \sim 2$). An estimate of the degree of association is necessary. One may argue as follows.

In general, the accurate determination of the type and concentration of the associated species of alcohols or phenols in solution from the hydroxyl proton chemical shift alone is probably impossible (15). For example, if at least two associated species are present; the two observables, total concentration and chemical shift, must be matched to two equilibrium constants and to the two chemical shifts for the associated species. Except in special cases (16), there may well exist more than two associated species. Indeed, infrared (17) and activity (18) data for phenol in CCl_4 can be most satisfactorily interpreted with a monomer – trimer sequential polymer model.

A plot vs. concentration in CCl_4 of the hydroxyl proton chemical shift of **2** implies a zero limiting slope at low concentrations, i.e., below 0.6 mol% or ca. 0.06 M (for **2** in CCl_4, $M \sim 0.1 \times$ mol%). As shown by Tucker *et al.* (15, 19), such is the behaviour expected for an association process in which the dimerization constant is very small and the first important association involves trimerization or a higher polymerization.

Dimerization is probably small; nevertheless, the degree of association of **2** can be only roughly approximated in the following manner. The chemical shift data (20) for phenol in CCl_4 clearly show that it is more highly associated than **2** in CCl_4. A fit of such data to a monomer–timer model (21, 22) overestimates the concentration of phenol monomer (18). A similar model for **2** will yield a small absolute error in the degree of association and will give a lower limit to the degree of association.

Between 0.15 and 8 mol% (ca. 0.15 and 0.8 M), the hydroxyl proton shift of **2** can be roughly fitted by a monomer–trimer model with $K_3 \sim 0.7$ molarity units, implying that about 10% of **2** is associated at 2.5 mol% and that 35% is associated at 8 mol%. The observed coupling constants are number averages for all extant species. It follows directly that, at 8 mol%, K for the intramolecular equilibrium could be as large as 5 in the trimer (compared to, say, 1.5 for the monomer) before an appreciable change ($\sim$0.02 Hz) occurs in the observed ^5J values. Consequently, a reasonable interpretation of the coupling data in Table 2 is that they are a measure of the intramolecular equilibrium in the monomer. Substantial changes in this equilibrium, caused by self-association, could only be measured reliably by this method if the extent of association were varied over a much larger range than is practical for **2**.

Conclusions

2-Methylphenol and 4-chloro-2-methylphenol exist in C_6D_6 and CCl_4 solutions as two conformers in which that conformer containing the O—H bond *trans* to the methyl group is 0.4 $\pm$ 0.1 kcal/mol lower in free energy than the *cis* conformer at 305 K. This result can be compared to 4-bromo-2-trifluoromethylphenol, 3.3 mol% in CCl_4 at 305 K, for which the *cis* conformer has a lower free energy of 0.5 kcal/mol (6). A concentration study of 4-chloro-2-methylphenol suggests that the calculated free energy differences refer to the intramolecular equilibrium for the monomers.

Acknowledgment

We are grateful to the National Research Council of Canada for financial support.

1. K. U. Ingold and D. R. Taylor. Can. J. Chem. **39**, 471 (1961).
2. A. S. Manocha, G. L. Carlson, and W. G. Fateley. J. Phys. Chem. **77**, 2094 (1973).
3. G. L. Carlson and W. G. Fateley. J. Phys. Chem. **77**, 1157 (1975).
4. N. L. Allinger, J. J. Maul, and M. J. Hickey. J. Org. Chem. **36**, 2747 (1971).
5. J. B. Rowbotham, M. Smith, and T. Schaefer. Can. J. Chem. **53**, 986 (1975).
6. T. Schaefer and J. B. Rowbotham. Can. J. Chem. **54**, 2243 (1976).
7. J. B. Rowbotham and T. Schaefer. Can. J. Chem. **52**, 3037 (1974).
8. S. Castellano and A. A. Bothner-By. J. Chem. Phys. **41**, 3863 (1964).
9. C. W. Haigh and J. M. Williams. J. Mol. Spectrosc. **32**, 398 (1969).
10. T. Schaefer, J. B. Rowbotham, and K. Chum. Can. J. Chem. **54**, 3666 (1976).
11. H. D. Bist, J. C. D. Brand, and D. R. Williams. J. Mol. Spectrosc. **24**, 402 (1967).
12. E. Mathier, D. Welti, A. Bauder, and Hs. H. Gunthard. J. Mol. Spectrosc. **37**, 63 (1971).
13. R. S. Drago, L. B. Parr, and C. S. Chamberlain. J. Am. Chem. Soc. **99**, 3207 (1977).
14. T. Gramstad and E. D. Becker. J. Mol. Struct. **5**, 253 (1970).
15. E. E. Tucker and E. Lippert. *In* Recent advances in hydrogen bonding. *Edited by* P. Schuster, G. Zundel, and C. Sandorfy. North-Holland Publishing Co., Amsterdam. 1976. Chapt. 17.
16. E. D. Becker, E. E. Tucker, and C. N. R. Rao. J. Chem. Soc. Faraday Trans. II, **73**, 438 (1977).
17. K. B. Whetsel and J. H. Lady. Spectrometry of fuels. Plenum Press, New York, NY. 1970.
18. E. E. Tucker, S. D. Christian, and Lung-Nan Lin. J. Phys. Chem. **78**, 1443 (1974).
19. E. E. Tucker and E. D. Becker. J. Phys. Chem. **77**, 1483 (1973).
20. F. Kohler, E. Liebermann, R. Schano, H. E. Affsprung, J. K. Morrow, K. Sosnkowska-Kehiaian, and H. Kehiaian. J. Chem. Thermodyn. **7**, 241 (1975).
21. A. J. Dale and T. Gramstad. Spectrochim. Acta A, **28**, 639 (1972).
22. Y. S. Bogachev, L. K. Vasianian, N. N. Shapetko, and T. L. Alexeeva. Org. Magn. Reson. **4**, 453 (1972).

Can. J. Chem. Downloaded from www.nrcresearchpress.com by 210.87.254.40 on 09/05/12
For personal use only.

Kinetics and mechanism of the reaction of dimethyl acetylphosphonate with water. Expulsion of a phosphonate ester from a carbonyl hydrate

RONALD KLUGER, DAVID C. PIKE, AND JIK CHIN

Department of Chemistry, University of Toronto, Toronto, Ont., Canada M5S 1A1

Received January 2, 1978

RONALD KLUGER, DAVID C. PIKE, and JIK CHIN. Can. J. Chem. **56**, 1792 (1978).

Dimethyl acetylphosphonate (DAP) is rapidly cleaved in water to acetate and dimethylphosphonic acid. The half time for reaction at p*H* 7, 25°C is estimated to be 3 s. The reaction is first order in hydroxide ion concentration and first order in DAP concentration. Rates of reaction were measured over the p*H* range 3.8 to 6.5 at 25°C, 6.5 and 7.0 at 5°C, 4.5 to 6.5 at 35°C, and 4.5 to 6.0 at 45°C. The average observed second-order rate constant at 25°C is $2.4 \times 10^6\ M^{-1}\ s^{-1}$. DAP is converted rapidly to a hydrated carbonyl adduct. The mechanism for the formation of the observed products is proposed to be analogous to cleavage reactions of other carbonyl hydrates, proceeding from a monoanion conjugate in this case. The estimated rate constant for the unimolecular cleavage of the carbonyl hydrate anion is $2 \times 10^3\ s^{-1}$. The rapid hydrolysis of DAP results from energetically favourable formation of a hydrate due to the electronic effect of the phosphonate diester. This effect also promotes ionization of the hydrate. The ionized hydrate readily expels the phosphonate diester to achieve the overall rapid hydrolysis.

RONALD KLUGER, DAVID C. PIKE et JIK CHIN. Can. J. Chem. **56**, 1792 (1978).

L'acétylphosphonate de diméthyle (APD) se coupe rapidement dans l'eau pour conduire à l'acétate et à l'acide diméthylphosphonique. Le demi-temps de la réaction à un p*H* = 7, à 25°C, est d'environ 3 s. La réaction est du premier ordre en hydroxyde est du premier ordre en APD. On a mesuré les vitesse de réaction à des p*H* allant de 3.8 à 6.5 à 25°C et 6.5 et 7.0 à 5°C, de 4.5 à 6.5 à 35°C et de 4.5 à 6.0 à 45°C. La valeur moyenne de la constante de vitesse du deuxième ordre à 25°C est de $2.4 \times 10^6\ M^{-1}\ s^{-1}$. Il y a une transformation rapide de APD en un adduit hydraté au niveau du carbonyle. Le mécanisme de formation des produits observés est proposé par analogie avec les réactions de clivage d'autres hydrates de groupements carbonylés qui procèdent, dans le cas actuel, à partir d'un monoanion conjugué. La constante de vitesse évaluée pour le clivage unimoléculaire de l'anion de l'hydrate du carbonyle est de $2 \times 10^3\ s^{-1}$. L'hydrolyse rapide de l'APD provient d'une formation d'un hydrate favorisé du point de vue énergétique à cause de l'effet électronique du diester de phosphonate. Cet effet accélère l'ionisation de l'hydrate. L'hydrate ionisé expulse facilement le diester de phosphonate pour conduire à une hydrolyse globale rapide.

[Traduit par le journal]

Esters of 1-keto phosphonates, such as dimethyl acetylphosphonate (DAP), **1**, were first reported

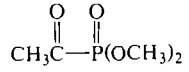

1

more than 30 years ago (1). These compounds are products of the Arbusov reaction between acyl chlorides and trialkyl phosphites. The original report by Kabachnik and Rossiiskaya (1) mentioned that dimethyl benzoylphosphonate reacted with alkali to give products resulting from cleavage of the bond between the carbonyl and phosphonyl groups. This tendency for internal bond cleavage to occur in preference to esterolytic cleavage made preparation of unesterified derivatives a problem (2). Monoesters and free acid derivatives have been prepared recently (3) by the methods first proposed by Zervas and Dilaris (4) for conversion of phosphate triesters to diesters and which were generalized to phosphonates by Kluger and Wasserstein (5).

We have prepared DAP and studied its rapid reaction in neutral aqueous solution. The reaction results in cleavage of the carbonyl-to-phosphonyl bond with attack of water occurring at the carbonyl carbon atom. The reaction is first order in hydroxide ion concentration and has an estimated half time at p*H* 7, 25°C, of 3 s. Nuclear magnetic resonance spectroscopy reveals that DAP reacts with water initially to form a hydrated carbonyl derivative **2**

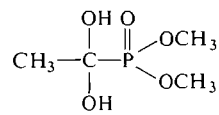

2

which accounts for 90% of the total concentration of DAP added when a slightly acidic solution is utilized (to slow down the cleavage reaction).

The cleavage of hydrated carbonyl group compounds has been studied for a number of cases in which the leaving group is a carbanion (6). This type of intermediate is also invoked in the hydrolysis

Can. J. Chem. Downloaded from www.nrcresearchpress.com by 210.87.254.5 on 09/05/12
For personal use only.

Can. J. Chem. Downloaded from www.nrcresearchpress.com by 210.87.254.5 on 09/05/12
For personal use only.

reactions of esters (7) and amides (8) where the leaving group is an alkoxide ion or amine respectively. However, to our knowledge no previous study has dealt with the quantitative reactivity of a phosphorus anion leaving group departing from a carbonyl hydrate. The phosphorus anion that is expected to be generated is comparable in basicity to an alkoxide ion (9) and thus should decompose at a rate which may be comparable to hydrates derived from esters (7).

Experimental

Materials

All chemicals used for which preparations are not given were purchased from commercial suppliers. Liquids used for synthesis were distilled before use.

Dimethyl Acetylphosphonate (DAP)

This was prepared by the procedure of Kabachnik and Rossiiskaya (1). Trimethyl phosphite (110.1 g, 0.89 mol) was added dropwise with stirring to 67 g (0.89 mol) acetyl chloride under a nitrogenous atmosphere. The reaction mixture was occasionally cooled to maintain a temperature of less than 30°C. After the addition was complete, the mixture was distilled (product bp 42–45°C/0.01 Torr), yielding 101.7 g DAP (0.67 mol, 75%), a clear colourless mobile liquid. Spectroscopic data: ir(cm^{-1}): 3125, 1709, 1492, 1437, 1403, 1335, 1188, 1164, 1057, 1036; proton nmr spectrum 60 MHz, CCl_4 relative to internal TMS) δ: 2.41 (3H, d, $^3J_{PH}$ = 5.0 Hz, $CH_3C(O)$), 3.80 (6H, d, $^3J_{PH}$ = 10.1 Hz, P—O—CH_3), uv ($CHCl_3$) ε_{334}: 65. Proton nmr spectrum of DAP hydrate **2** (60 MHz, D_2O, p*D* 3 relative to internal DSS) δ: 1.32 (3H, d, $^3J_{PH}$ = 12.6 Hz, $CH_3C(OD)_2$), 3.86 (6H, d, $^3J_{PH}$ = 10.5 Hz, P—O—CH_3).

Methods

Product Analysis

The products of hydrolysis of DAP were analyzed by conducting the hydrolysis reaction in deuterium oxide and analyzing the resultant solution by proton nmr spectroscopy (Varian T60). The initial spectrum is due to DAP, **1**, and the deuterium-exchanged hydrate **2**; the latter accounts for approximately 90% of the total DAP concentration. This spectrum is rapidly converted to that of deuteriodimethyl phosphonate ($DP(O)(OCH_3)_2$), which is the predominant tautomer of dimethyl phosphite (9), and acetic acid. The product assignment was confirmed by addition of genuine samples of the two species and observation of appropriate peak enhancements. Furthermore, the hydrolysis of DAP produced a species which hydrolyzed further and at a rate identical to that of dimethyl phosphite. By integration of the original and product nmr spectra this analysis accounts for a quantitative yield of products from DAP.

Kinetics

The rate of conversion of DAP to acetic acid and dimethyl phosphonate was followed by two independent procedures. Since acetic acid dissociates to a significant extent under our reaction conditions, the rate of production of these materials could be followed by automatic p*H*-stat recording (using sodium hydroxide solution to maintain a constant reading on a p*H* meter). A Radiometer p*H* meter PHM 28 controlled by a Radiometer TTT1 automatic titrator was used with a Radiometer ABU12 burette (5). Recording of volume of added base was done with a Heath recorder connected to the ABU12 driveshaft with a 50-to-1 gear reduction potentiometer using a 1.5 V reference cell. The reaction vessel was jacketed and contained water circulated from a constant temperature bath maintained within ±0.1°C.

DAP (2 μl) was injected into 3 ml of a 0.1 *M* potassium chloride solution at a pre-set p*H* value. All DAP dissolved since observed rate *constants* were identical when 5 μl of DAP was used. The p*H*-stat method usually gave recorded plots that could be analyzed by first-order methods since the reactions were conducted under conditions which were pseudo first order in substrate ($[H^+]$, $[OH^-]$, and $[H_2O]$ remained constant and thus the reaction was pseudo-zero-order in those species at all times). However, the further hydrolysis reaction of dimethyl phosphite complicated observations and methods of separation of consecutive reactions had to be utilized (10). For reactions at p*H* 4.0 and 4.5 which were very slow, initial rate methods were used (11). Above p*H* 6.5, the reaction was too fast to measure.

The disappearance of DAP could also be followed spectrophotometrically. The carbonyl moiety of DAP has a local absorbance maximum in water at 320 nm (ε ~ 3). Since from proton nmr spectra it appears that ~90% of DAP is present as carbonyl hydrate, the actual ε_{320} (H_2O) for the carbonyl absorbance of DAP is probably 3 × 10 ≈ 30. The rate of formation of hydrate is too fast to measure by recording spectrophotometry with conventional mixing. However, the disappearance of DAP in equilibrium with hydrate could be followed. A Unicam SP1800A recording spectrophotometer was used to follow the disappearance of absorbance due to the carbonyl group of DAP. Unlike the p*H*-stat method, this disappearance is not complicated by further hydrolysis of dimethyl phosphite. Rate constants were obtained by plotting, by conventional first-order methods, absorbance at a particular time compared to final absorbance as a function of time. Acetic acid – sodium acetate buffer was used to maintain acidity at p*H* 3.80 and the observed rate constant coincided with that observed by p*H* stat in the absence of buffer. Therefore, the methods give comparable results and confirm the validity of the kinetic assumptions we have used.

Results

The observed rate constants for the hydrolysis of DAP to produce acetate and dimethyl phosphite are summarized in Table 1. The reaction appears to be first order in hydroxide ion concentration. A common rate constant was obtained with variation in p*H* when the observed rate constants were divided by hydroxide ion concentration. The rate constants obtained at each p*H* value by first-order plots of p*H*-stat results were averaged, divided by hydroxide concentration and these resultant second-order rate constants were averaged to obtain a mean second-order rate constant for a particular temperature. The data at 5, 25, 35, and 45°C were plotted according to the Arrhenius equation (correlation coefficient = 0.997) with E_a = 17.6 kcal/mol. Analysis by transition state theory (12) gives an activation enthalpy of 17.0 kcal/mol, an activation entropy of 10.3 entropy units and a free energy of activation of 14.0 kcal/mol (at 300 K). These values can be applied to a mechanistic analysis if appropriate equilibrium parameters for ionizations prior to the rate-determining step are incorporated.

Can. J. Chem. Downloaded from www.nrcresearchpress.com by 210.87.254.5 on 09/05/12
For personal use only.

TABLE 1. Observed rate constants and derived values. Hydrolysis of 2 μl DAP in 3 ml 0.1 *M* potassium chloride

Temperature (°C)	p*H* (±0.01)	$k_{obs} \times 10^4$ (s^{-1})	$k_{app} \times 10^{-6}$ ($M^{-1}\ s^{-1}$)[a]
5.0	6.50	110	0.348
	7.00	342	0.342
25.0	3.80	1.25[b]	2.00
		1.16[b]	1.83
		1.31[b]	2.08
		1.31[b]	2.08
	4.00	2.72[c]	2.72
	4.50	6.24[c]	1.97
	5.00	24.2	2.42
	6.00	211	2.11
	6.50	851	2.69
35.0	4.50	18.6	5.88
	5.00	83.2	6.32
	5.50	184	5.82
	6.00	719	7.19
	6.50	1690	5.34
45.0	4.50	64.6	20.4
	5.00	199	19.9
	5.50	700	22.1
	6.00	2240	22.4

[a] $k_{app} = k_{obs}/[OH^-]$.
[b] Spectroscopic method: 10 μl DAP added to 3 ml sodium acetate – acetic acid buffer (0.1, 0.2, 0.3, and 0.4 *M* respectively).
[c] Initial rate method.

Discussion

The hydrolysis of DAP between p*H* 4 and 6.5 occurs by a mechanism involving specific base catalysis. The reaction is first order in hydroxide ion concentration and first order in DAP concentration. The hydrate of DAP forms rapidly and exists in equilibrium with the keto form. A mechanism consistent with other hydrolytic expulsions from carbonyl compounds and accommodating our data is given below.

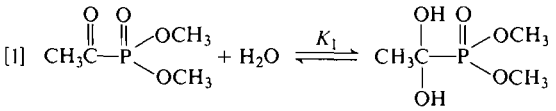

1 **2**

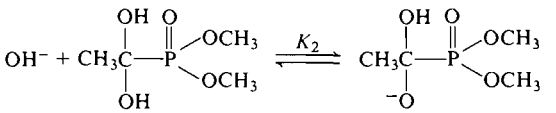

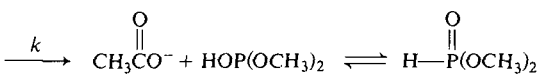

This mechanism leads to the rate expression

[2] $v = kK_1K_2[\mathbf{1}]\,[OH^-] = k_{app}[DAP]\,[OH^-]$;

$$[DAP] = [\mathbf{1}] + [\mathbf{2}]$$

$$v = k_{app}(1 + K_1)\,[\mathbf{1}]\,[OH^-]$$

[3] $$k_{app} = kK_1K_2/(1 + K_1)$$

$$k = k_{app}(1 + K_1)/(K_1K_2)$$

We observe that K_1, the equilibrium constant for the hydration of **1** to give **2**, is approximately 9. The ionization constant, K_2, is the remaining parameter necessary to connect our observed rate constant to the rate constant k in the proposed mechanism [1]. This assumes that a carbonyl hydrate monoanion is the reactive species in the cleavage reaction.

Hine and Koser (6) have summarized mechanisms that have been observed for cleavage of a carbonyl hydrate when the leaving group is a carbanion. The intermediate hydrate ionizes to a monoanionic conjugate which cleaves only if the carbanion is a particularly good leaving group. For most leaving groups, reaction in alkaline solutions proceeds from the dianion of the hydrate; reaction via the monoanion is slow.

Hine and Koser (6) observed that the ionization of carbonyl hydrates conforms to a linear free energy relationship governed by substituent constants of the two substituents on the hydrated carbon atom. The pK_a of a hydroxyl group of a carbonyl hydrate is given by eq. [4].

[4] $$pK_a = 14.19 - 1.32(\sigma_{R_1}^* + \sigma_{R_2}^*)$$

For the hydrate **2**, $R_1 = CH_3$ and $R_2 = P(O)(OCH_3)_2$. The value of σ^* for a phosphonate diester group has been determined by Martin and Griffin (13) to be +2.18. That for a methyl group is zero, by definition (14). Therefore substituting into eq. [4], we estimate the pK_a of a hydroxyl group of **2** to be approximately 11. The equilibrium constant K_2 defined in [1] can be derived from the acid dissociation constant of **2** by dividing the latter by the autoionization constant of water. Therefore K_2 will have an approximate value given by [5].

[5] $$K_2 = (10^{-11}/10^{-14})\,M^{-1} = 10^3\,M^{-1}$$

Substituting K_2 into [3] and the approximate value of k_{app} at 25°C of $2 \times 10^6\ M^{-1}\ s^{-1}$;

[6] $$k \cong (2 \times 10^6)(10)(10^3)^{-1}(9)^{-1} \cong 2 \times 10^3\ s^{-1}$$

The factors controlling the hydrolytic reactivity of DAP are: the extent of hydration (measured by equilibrium constant K_1), the ease of ionization of hydrate **2** (measured by equilibrium constant K_2), and the facility with which the ionized hydrate is cleaved (measured by rate constant k). The hydration equilibrium is enhanced by the strongly electron withdrawing nature of the phosphonate diester sub-

stituent (13) and by the lack of resonance interactions between the phosphonate and carbonly groups. Similarly, the ionization equilibrium is assisted by the electronic nature of the phosphonate as a substituent (6). The magnitude of k is such that along with relatively favourable equilbria preceding the cleavage step, an overall large observed second-order rate constant (k_{app}) results.

Quantitative comparisons of the rate and equilibrium constants in the proposed mechanism to those in other carbonyl cleavage reactions involves assumptions about parallels in mechanism which probably require further study. Jencks (15) has summarized some of the problems which still remain in our understanding of these reactions. For example, the pK_a of the conjugate acid of the leaving group might be an adequate basis for a linear free energy analysis of the rate constant for expulsion of the leaving group. However, although carbanions and oxygen anions of comparable basicities can be expelled, catalysis by Brønsted acids only is observed for the oxygen anions. In this respect the phosphonate behaves like a carbanion.

If a comparison of the rate constant for expulsion of the phosphonate anion (k) is made with the rate constant for expulsion of a thiazolium conjugate base (16), we find that although thiazolium has a considerably higher pK_a than dimethyl phosphonic acid (9, 17), the rate constants are comparable. This suggests that the hydrate anion containing a phosphonate substituent may be relatively more stable than a similar compound with a carbon-based substituent. A complete analysis will therefore require a systematic study within the phosphonate series, including determinations of overall energetics. Such a study is in progress in our laboratory.

Acknowledgment

We thank the National Research Council of Canada for an operating grant that has supported our research.

1. M. I. KABACHNIK and P. A. ROSSIISKAYA. Izv. Akad. Nauk SSSR, Otd. Khim. Nauk, 365 (1945); Chem. Abstr. **40**, 4688 (1946).
2. V. F. COOKE, W. GERRARD, and W. J. GREEN. Chem. Ind. (London), 351 (1953).
3. R. KLUGER and D. C. PIKE. J. Am. Chem. Soc. **99**, 4504 (1977).
4. L. ZERVAS and I. DILARIS. J. Am. Chem. Soc. 77, 5354 (1955).
5. R. KLUGER and P. WASSERSTEIN. J. Am. Chem. Soc. **95**, 1071 (1973).
6. J. HINE and G. F. KOSER. J. Org. Chem. **36**, 1348 (1971).
7. J. P. GUTHRIE. J. Am. Chem. Soc. **95**, 6999 (1973).
8. J. P. GUTHRIE. J. Am. Chem. Soc. **96**, 3608 (1974).
9. P. R. HAMMOND. J. Chem. Soc. 1365 (1962).
10. A. A. FROST and R. G. PEARSON. Kinetics and mechanism. 2nd ed. J. Wiley and Sons, Inc., New York, NY. 1961. pp. 166–169.
11. G. FLECK. Chemical reaction mechanisms. Holt, Rinehart and Winston, Inc., New York, NY. 1971. Chapt. 3.
12. J. E. LEFFLER and E. GRUNWALD. Rates and equilibria of organic reactions. J. Wiley and Sons, Inc., New York, NY. 1963. pp. 163–171.
13. D. J. MARTIN and C. E. GRIFFIN. J. Org. Chem. **30**, 4034 (1965).
14. R. W. TAFT, JR. *In* Steric effects in organic chemistry. *Edited by* M. S. Newman. J. Wiley and Sons, Inc., New York, NY. 1956. Chapt. 13.
15. W. P. JENCKS. Catalysis in chemistry and enzymology. McGraw-Hill Book Company, New York, NY. 1969. pp. 490–517.
16. G. E. LIENHARD. J. Am. Chem. Soc. **88**, 5642 (1966).
17. J. CROSBY and G. E. LIENHARD. J. Am. Chem. Soc. **92**, 5707 (1970).

Can. J. Chem. Downloaded from www.nrcresearchpress.com by 210.87.254.5 on 09/05/12
For personal use only.

Pyrones. III. The alkylation of pyronones. Preferential formation of 2-alkoxy-4-pyrones[1]

TERRY DONALD CYR AND GERALD ARTHUR POULTON
Department of Chemistry, University of Victoria, Victoria, B.C., Canada V8W 2Y2

Received December 5, 1977

TERRY DONALD CYR and GERALD ARTHUR POULTON. Can. J. Chem. **56**, 1796 (1978).

2-Alkoxy-4-pyrones and 2-alkoxychromones were prepared in high yield from 4-hydroxy-2-pyrones (2,4-pyronones) and 4-hydroxycoumarin, respectively. The products of diazomethane methylation of dehydroacetic acid (3-acetyl-4-hydroxy-6-methyl-2-pyrone) were identified.

TERRY DONALD CYR et GERALD ARTHUR POULTON. Can. J. Chem. **56**, 1796 (1978).

Faisant respectivement appel aux hydroxy-4 pyrones-2 (pyronones-2,4) et à l'hydroxy-4 coumarine comme produits de départ, on a préparé, avec de bons rendements, des alkoxy-2 pyrones-4 et des alkoxy-2 chromones. On a identifié les produits obtenus en effectuant la méthylation de l'acide déhydroacétique (acétyl-3 hydroxy-4 méthyl-6 pyrone-2) avec le diazométhane.

[Traduit par le journal]

Introduction

Many investigations have been reported concerning the methylation of pyronones (2,4-pyrandiones) by various reagents; because of the tautomeric equilibrium which can exist between the diketo form **1***a* and enolic forms **1***b* and **1***c*, isomeric alkylated

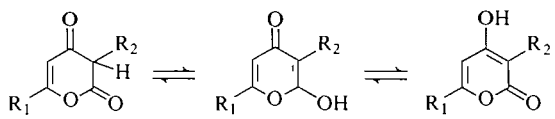

1*a* **1***b* **1***c*

products may be formed. In methylations reported with diazomethane, triacetic acid lactone (6-methyl-2,4-pyrandione) (2, 3), 6-phenyl-2,4-pyrandione (2), 3,5-dialkylpyronones (4, 5), and the precursors to the natural products yangonin (6) and aureothin (7) afford separable mixtures of the 2-alkoxy-4-pyrone **2** and the 4-alkoxy-2-pyrone **3**. The 4-alkoxy-2-pyrone

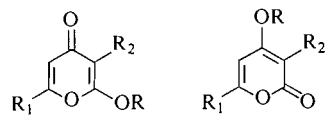

2 **3**

is the major isomer in most of these alkylations; only in alkylations of 6-alkoxy- or 6-hydroxy-2,4-pyrandiones (5, 8) does the 2-alkoxy-4-pyrone sometimes predominate. Methylation of the silver salt of the pyrandione with methyl iodide has also been reported (9) to yield similar results. Methylation using base and dimethyl sulfate produces 4-alkoxy-2-pyrones quantitatively from 6-methyl- (10) and 6-phenyl-2,4-pyrandiones (9), as does the use of 10% methanolic HCl (9). Beak and Lee have recently reported (11) 2-alkylation of triacetic acid lactone with methyl fluorosulfonate. As we have been interested in an efficient route to 3-acyl-2-alkoxy-4-pyrones, we have investigated the alkylation of triacetic acid lactone (**1**, $R_1 = CH_3$, $R_2 = H$), dehydroacetic acid (**1**, $R_1 = CH_3$, $R_2 = CH_3CO$), and several related compounds.

Results and Discussion

Alkylation of dehydroacetic acid has been reported to yield only the 4-alkoxy-2-pyrone when carried out with either diazomethane (12, 13) or methyl or ethyl iodide and the silver salt (ref. 14 and references cited therein). Since recent experience has shown that both 2- and 4-pyrones are generally formed in the diazomethane methylations, we repeated the reaction with the intention of isolating the minor products of the reaction, in the hope of finding the desired 3-acetyl-2-methoxy-6-methyl-4-pyrone. Even using conditions designed (3) to produce increased 2-alkoxy-4-pyrone yields, no trace of the desired compound was detected. 3-Acetyl-4-methoxy-6-methyl-2-pyrone (**4**, Scheme 1) was indeed the major product under all conditions. Three minor products, 3-acetonyl-6-methyl-2,4-pyrandione (**5**), 3-acetonyl-4-methoxy-6-methyl-2-pyrone (**6**), and 3-acetonyl-2-methoxy-6-methyl-4-pyrone (**7**), arise from the initial addition of diazomethane to the acetyl group, followed by rearrangement (15): methylation of the tautomeric enols occurs yielding both possible isomers. We believe that both products can result when hydrogen bonding between the 4-hydroxyl and the 3-acyl substituent is removed. 4-Oxo-3,6-dimethyl-4*H*-furo[3,2-*c*]pyran (**8**) is a previously reported (12) product of this reaction, whereas 2,6-dimethyl-4-pyrone (**9**) is produced from dehydroacetic acid by hydrolysis and rearrangement (16).

[1]For Part II see ref. 1.

Can. J. Chem. Downloaded from www.nrcresearchpress.com by 210.87.254.40 on 09/05/12
For personal use only.

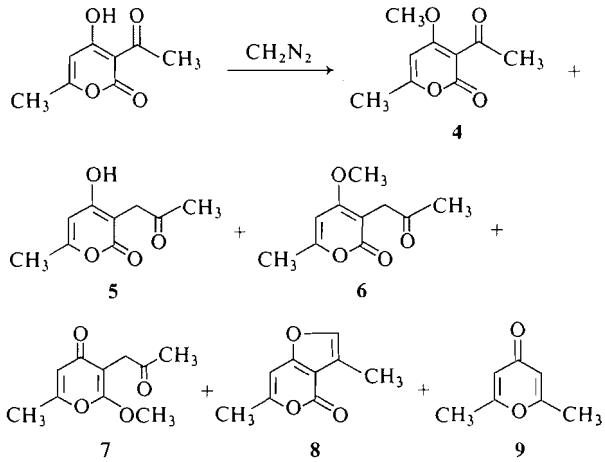

SCHEME 1

In a further attempt to produce the desired 2-alkylated products, the reaction of dehydroacetic acid and its sodium salt with Meerwein-type alkylating agents was investigated. Treatment of dehydroacetic acid with dimethoxycarbonium tetrafluoroborate gave a quantitative yield of 3-acetyl-6-methyl-2*H*-pyran-2-on-4-oxyboron difluoride (**10**). All attempts to force alkylation of this species by prolonged treatment with excess quantities of trimethyloxonium tetrafluoroborate, triethyloxonium tetrafluoroborate, or methyl fluorosulfonate failed. Similar treatment of sodium dehydroacetate (17) again yielded only **10**.

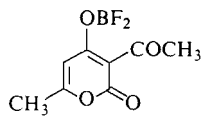

Our inability to produce an alkylated 4-pyrone in the dehydroacetic acid series led us then to triacetic acid lactone and its derivatives. We were successful in achieving virtually quantitative production of 2-ethoxy- or 2-methoxy-6-methyl-4-pyrone from triacetic acid lactone by the following simple procedure: careful base-catalyzed *O*-acylation with acetic anhydride (the absence of acid is essential to prevent the ready O → C Fries-type rearrangement which produces dehydroacetic acid (18)) yields 4-acetoxy-6-methyl-2-pyrone (**11**). Alkylation of this ester with triethyloxonium tetrafluoroborate yields, after mild acid hydrolysis, the desired 2-ethoxy-6-methyl-4-pyrone (**12**, R = Et) in 86% overall yield (Scheme 2). The reaction can also be carried out using trimethyloxonium tetrafluoroborate or dimethoxycarbonium tetrafluoroborate.

To test the applicability of the reaction, some other systems were alkylated. 4-Hydroxycoumarin (**13**) was readily acylated and subsequent alkylation as described above yielded 2-methoxy- or 2-ethoxychromone (**16**). 7-Hydroxycoumarin (**14**) acylated readily but alkylation produced only recovered hydroxy compound and did not give an alkylated product (i.e. **17**). 3-Acetyl-3-bromo-6-methyl-2,4-pyrandione (**15**) (19) was readily alkylated using Meerwein's reagent to yield 3-bromo-2-ethoxy-6-methyl-4-pyrone (**18**, R = Et, 80%).

The production of 2-alkoxy-4-pyrones from 2,4-pyrandiones and of 2-alkoxychromones from 4-hydroxycoumarins in high yields which we have described offers an excellent synthetic alternative to the previous procedures using diazomethane which involve a laborious separation of the two isomer pro-

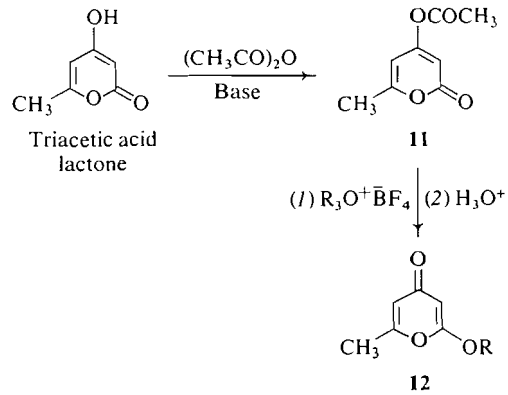

SCHEME 2

ducts or to Beak's recently reported alkylation for which no experimental details have as yet been reported.

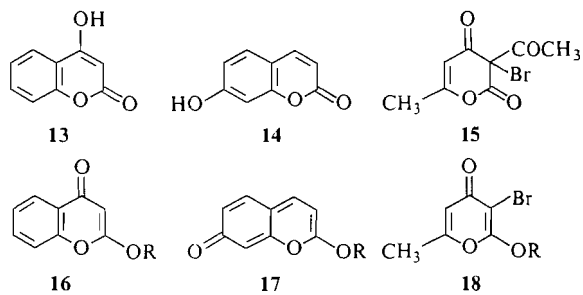

Experimental

Melting points were determined on a Bock Monoscop VS and are uncorrected. Mass spectra were obtained on an Hitachi-Perkin-Elmer RMU-7S double-focussing instrument. Nuclear magnetic resonance spectra were recorded in $CDCl_3$ solution with internal TMS reference on a Perkin-Elmer R12-A spectrometer at 60 MHz. Ultraviolet spectra were obtained using an Unicam SP-800 spectrophotometer.

Thin-layer chromatography was carried out using Merck silica gel GF254 precoated plates, column chromatography with 60–200 mesh silica gel (Davison Chemical) and preparative thin-layer with MN-Kieselgel G/UV 254 (Macherey, Nagel & Co.).

Can. J. Chem. Downloaded from www.nrcresearchpress.com by 210.87.254.40 on 09/05/12
For personal use only.

Can. J. Chem. Downloaded from www.nrcresearchpress.com by 210.87.254.40 on 09/05/12
For personal use only.

Compounds

Dehydroacetic acid was purchased from Aldrich Chemical Co. and recrystallized before use. Triacetic acid lactone (20) and 3-acetyl-3-bromo-6-methyl-2,4-pyrandione (19) were prepared by literature procedures. 4-Hydroxy- and 7-hydroxycoumarin were from Aldrich Chemicals.

Reaction of Dehydroacetic Acid with Diazomethane

(*A*) Dehydroacetic acid (1.00 g, 5.9 mmol) in dry ether (100 ml) was treated at 0°C with ethereal diazomethane (prepared (21) from *N,N'*-dimethyl-*N,N'*-dinitrosoterephthalamide, ca. 36 mmol). The reaction mixture was allowed to warm up to room temperature overnight, filtered, and evaporated to yield the crude product (1.014 g). Chromatography produced, as the major product, 3-acetyl-4-methoxy-6-methyl-2-pyrone (**4**, 705 mg, 65%), mp 90–91°C (lit. (13) mp 93–95°C); nmr δ: 6.11 (1H, s), 3.91 (3H, s), 2.47 (3H, s), and 2.31 ppm (3H, s). Minor products isolated by repeated column and thin-layer chromatography were identified as (*i*) 3-acetonyl-6-methyl-2,4-pyrandione (**5**, 145 mg, 13%), mp 179–180°C; nmr (in D_2O with external TMS reference) δ: 6.04 (1H, s), 3.48 (2H, s), 2.22 (3H, s), and 2.18 ppm (3H, s); *m/e* calcd. for $C_9H_{10}O_4$: 182.058; found: 182.053. (*ii*) 3-Acetonyl-4-methoxy-6-methyl-2-pyrone (**6**, 144 mg, 12%), mp 108.5–109.5°C; nmr δ: 6.04 (1H, s), 3.81 (3H, s), 3.48 (2H, s), 2.28 (3H, s), and 2.18 ppm (3H, s); *Anal.* calcd. for $C_{10}H_{12}O_4$: C 61.22, H 6.16; found: C 60.97, H 6.32. (*iii*) 3-Acetonyl-2-methoxy-6-methyl-4-pyrone (7, trace), nmr δ: 6.00 (1H, s), 3.91 (3H, s), 3.42 (2H, s), 2.26 (3H, s), and 2.18 ppm (3H, s); *m/e* (relative intensity): 196 (92), 168 (12), 154 (99), 153 (82), 139 (91), 113 (100), 85 (19), 69 (10), 59 (45), 43 (58), 39 (14); ir λ_{max}: 1733, 1686 cm^{-1}; (*iv*) 2,6-dimethyl-4-pyrone (**9**, 50 mg, 7%), mp 132°C (lit. (22) mp 132°C); nmr δ: 6.03 (2H, s) and 2.23 ppm (6H, s).

(*B*) From a similar experiment carried out in chloroform solution was isolated 3-acetyl-4-methoxy-6-methyl-2-pyrone (300 mg, 28%) and a second component, identified as 4-oxo-3,6-dimethyl-4*H*-furo[3,2-*c*]pyran (**8**, 120 mg, 12.5%), mp 129–130°C (lit. (12) mp 128–130°C); nmr δ: 7.24 (1H, s), 6.37 (1H, s), and 2.32 ppm (6H, s).

Reaction of Dehydroacetic Acid with Dimethoxycarbonium Tetrafluoroborate

Dehydroacetic acid (1.00 g, 5.9 mmol) in ethyl acetate (25 ml) was treated at room temperature with dimethoxycarbonium tetrafluoroborate (23) (1.70 g, 10.5 mmol) and stirred overnight. The ethyl acetate was evaporated *in vacuo*, the residues added to water (25 ml), and the product extracted with dichloromethane. Drying and evaporation of the solvent yielded 3-acetyl-6-methyl-2*H*-pyran-2-on-4-oxyboron difluoride (**10**, 1.285 g, 96%), mp 86–87°C; nmr δ: 6.14 (1H, s), 2.84 (3H, s), and 2.40 ppm (3H, s); ir λ_{max}: 1185 (B—O) and 1070 cm^{-1} (B—F); *m/e* (relative intensity): 216 (57, $M^{\ddagger}$), 201 (40, $M^{\ddagger} - CH_3$), 197 (17, $M^{\ddagger} - F$), 173 (29, $M^{\ddagger} - COCH_3$), 154 (34, *m/e* 173 − F), 69 (20), 43 (100); δ_{19_F} (relative to $CFCl_3$) 143 ppm; λ_{max} (MeOH) (log ε): 224 (3.98), 316 (4.09). *Anal.* calcd. for $C_8H_7BF_2O_4$: C 44.50, H 3.27; found: C 44.72, H 3.53.

Reaction of Sodium Dehydroacetate with Dimethoxycarbonium Tetrafluoroborate

Sodium dehydroacetate (17) (1.00 g, 5.26 mmol) suspended in ethyl acetate (25 ml) was treated with dimethoxycarbonium tetrafluoroborate (23) (1.51 g, 9.32 mmol) as described above. The same product was isolated in similar yield.

Alkylation of Triacetic Acid Lactone

Acylation

To triacetic acid lactone (4.0 g, 31.7 mmol) dissolved in 10% NaOH (15 ml) and ice (10 g) was added acetic anhydride (10 ml). The mixture was shaken for 10 min, then extracted with dichloromethane (3 × 100 ml), and the extracts dried (Na_2SO_4) and evaporated to yield pure 4-acetoxy-6-methyl-2-pyrone (4.87 g, 92%) (18). As this compound is prone to rearrangement, it was used immediately for the subsequent reaction.

Alkylation

To the above acetoxy compound (4.6 g, 27.4 mmol) was added triethyloxonium tetrafluoroborate (12 g, 63 mmol) and the mixture heated for 20 h under a nitrogen atmosphere. HCl (5%, 100 ml) was added and the product extracted with dichloromethane (3 × 100 ml). Drying and evaporating the extracts gave the crude product as a red oil (4.41 g) which was purified by chromatography to give 2-ethoxy-6-methyl-4-pyrone (**12**, R = Et, 3.77 g, 89%), mp 46–47°C (lit. (24) mp 44–46°C); nmr δ: 5.86 (1H, dd, J = 1.76, 0.84 Hz), 5.39 (1H, d, J = 1.76 Hz), 4.08 (2H, q, J = 7.22 Hz), 2.24 (3H, d, J = 0.88 Hz), 1.44 ppm (3H, t, J = 7.22 Hz); λ_{max} (EtOH): 240 (4.06); *m/e* (relative intensity): 154 (100), 126 (25), 98 (76), 97 (25), 69 (75), 58 (22), 54 (10).

Using similar procedures, the following products were prepared.

*2-Methoxy-6-methyl-4-pyrone (**12**, R = Me)*—from triacetic acid lactone (46%), mp 92–94°C (lit. (2) mp 94–94.5°C); nmr δ: 6.08 (1H, dd, J = 1.8 Hz, 0.8 Hz), 5.54 (1H, d, J = 1.8 Hz), 3.92 (3H, s), 2.28 ppm (3H, d, J = 0.8 Hz); λ_{max} (EtOH): 240 (4.10).

*2-Methoxychromone (**16**, R = Me)*—from 4-hydroxycoumarin (69%), mp 103–106°C (lit. (9) mp 106–107°C); nmr δ: 8.39 (1H, m), 7.9–7.4 (3H, m), 5.74 (1H, s), and 4.05 ppm (3H, s); λ_{max} (EtOH): 220 (4.26), 265 (3.98), 284 (3.90).

*2-Ethoxychromone (**16**, R = Et)*—from 4-hydroxycoumarin (91%), mp 99–102°C; nmr δ: 8.35 (1H, m), 7.9–7.4 (3H, m), 5.73 (1H, s), 4.35 (2H, q, J = 7.2 Hz), 1.52 (3H, t, J = 7.2 Hz); λ_{max} (EtOH): 220 (4.27), 267 (4.03), 285 (3.91); *m/e* 190 (48), 134 (11), 133 (10), 120 (24), 105 (13), 94 (100), 92 (29), 69 (33), 51 (16), 50 (16), 39 (17). *Anal.* calcd. for $C_{11}H_{10}O_3$: C 69.46, H 5.30; found: C 69.41, H 5.33.

Reaction of 3-Acetyl-3-bromo-6-methyl-2,4-pyrandione with Triethyloxonium Tetrafluoroborate

3-Acetyl-3-bromo-6-methyl-2,4-pyrandione (19) (**15**, 16.0 g, 65 mmol) in dichloromethane (150 ml) was treated with triethyloxonium tetrafluoroborate (13.3 g, 70 mmol), and the solution refluxed for 14 h. Most of the solvent was removed *in vacuo*, and HCl (5%, 150 ml) and ether (50 ml) added. The ether layer was removed and the aqueous layer extracted with dichloromethane (5 × 100 ml). From the dichloromethane layer was isolated 3-bromo-2-ethoxy-6-methyl-4-pyrone (**18**, R = Et, 12.1 g, 80%), mp 132–134°C (lit. (24) mp 131–132°C); nmr δ: 6.03 (1H, s), 4.42 (2H, q, J = 6.5 Hz), 2.27 (3H, s), 1.47 ppm (3H, t, J = 6.5 Hz); λ_{max} (EtOH): 200 (4.25), 264 (3.90); *m/e* (relative intensity): 234 (65), 232 (65), 206 (73), 204 (78), 166 (67), 164 (71), 151 (22), 124 (35), 66 (34), 45 (100), and 43 (40).

In a similar manner 2-methoxy-3-bromo-6-methyl-4-pyrone (**18**, R = Me) could be prepared; nmr δ: 6.09 (1H, s), 4.04 (3H, s), and 2.28 ppm (3H, s); λ_{max} (EtOH): 209.5 (4.27), 264 (3.91).

Acknowledgements

Financial support by the National Research Council of Canada and the University of Victoria is gratefully acknowledged.

1. D. L. McGILLIVRAY and G. A. POULTON. Org. Magn. Spectrom. In press.
2. D. HERBST, W. B. MORS, O. R. GOTTLIEB, and C. DJERASSI. J. Am. Chem. Soc. **81**, 2427 (1959).
3. H. NAKATA. Bull. Chem. Soc. Jpn. **33**, 1688 (1960).
4. E. NICCOLI, U. VAGLINI, and G. CECCARELLI. Ann. Chim. (Rome), **58**, 664 (1968).
5. A. CORBELLA, P. GARIBOLDI, G. JOMMI, and G. RUSSO. Gazz. Chim. Ital. **98**, 1096 (1968).
6. I. CHMIELEWSKA, J. CIEŚLAK, K. GORCZYŃSKA, B. KONTNIK, and K. PITAKOWSKA. Tetrahedron, **4**, 36 (1958).
7. Y. HIRATA, H. NAKATA, K. YAMADA, K. OKUHARA, and T. NAITO. Tetrahedron, **14**, 252 (1961).
8. J. LITYŃSKI and R. MALACHOWSKI. Rocz. Chem. **7**, 579 (1927); Chem. Abstr. **22**, 4124 (1928).
9. S. JANISZEWSKA-DRABAREK. Rocz. Chem. **27**, 456 (1953); Chem. Abstr. **49**, 3176c (1955).
10. J. D. BU'LOCK and H. G. SMITH. J. Chem. Soc. 502 (1960).
11. P. BEAK and J. LEE. J. Org. Chem. **40**, 147 (1975).
12. A. A. AKHREM, A. M. MOISEENKOV, F. A. LAKHVICH, and A. I. POSELENOV. Izv. Akad. Nauk SSSR, Ser. Khim. 143 (1972).
13. K. MIYAKI, K. YAMAGISHI, and A. TAKAHASHI. J. Pharm. Soc. Jpn. **76**, 433 (1956).
14. E. E. ROYALS and J. C. LEFFINGWELL. J. Org. Chem. **30**, 1255 (1965).
15. J. MARCH. Advanced organic chemistry: Reactions, mechanisms, and structure. 2nd ed. McGraw Hill Book Co., New York, NY. 1977. p. 997.
16. J. N. COLLIE and T. P. HILDITCH. J. Chem. Soc. **91**, 787 (1907).
17. J. N. COLLIE and H. R. LESUEUR. J. Chem. Soc. **65**, 254 (1894).
18. E. MARCUS, J. F. STEPHEN, and J. K. CHAN. J. Heterocycl. Chem. **6**, 13 (1969).
19. T. M. HARRIS, C. M. HARRIS, and C. K. BRUSH. J. Org. Chem. **35**, 1329 (1970).
20. N. C. BROWN and G. S. PALL. South Africa. Patent No. 67 006 159 (April, 1968); Chem. Abstr. **70**, 87585m (1969).
21. L. F. FIESER and M. FIESER. Reagents for organic synthesis. Vol. I. John Wiley and Sons Inc., New York, NY. 1967. p. 191.
22. I. HEILBRON, A. H. COOK, H. M. BUNBURY, and D. H. HEY (*Editors*). Dictionary of organic compounds. Vol. 2. Eyre and Spottiswoode, London, England. 1965. p. 1218.
23. R. F. BORCH. J. Org. Chem. **34**, 627 (1969).
24. T. KATO, Y. YAMAMOTO, and S. TAKEDA. Chem. Pharm. Bull. **21**, 1047 (1973).

Can. J. Chem. Downloaded from www.nrcresearchpress.com by 210.87.254.40 on 09/05/12
For personal use only.

Activation energy for methoxy group relaxation

M. A. MAZID, J. P. SHUKLA, AND S. WALKER

Department of Chemistry, Lakehead University, Thunder Bay, Ont., Canada P7B-5E1

Received January 12, 1978

M. A. MAZID, J. P. SHUKLA, and S. WALKER. Can. J. Chem. **56**, 1800 (1978).

Dielectric absorption studies have been made on seven compounds which have methoxy groups attached to an aromatic ring and on some related rigid molecules. The solutes have been dispersed in a polystyrene matrix. In some cases, the absorptions due to the group and the molecular process have been separated completely, and this has permitted the estimation of more accurate Eyring enthalpies of activation for methoxy group relaxation. These values have been compared with those in the literature and, on the whole, it would seem likely that the energy barrier to group relaxation is small and of the order of 10 kJ mol^{-1} for cases where there is no mutual conjugation or steric effects.

M. A. MAZID, J. P. SHUKLA et S. WALKER. Can. J. Chem. **56**, 1800 (1978).

On a effectué des études d'absorption diélectrique sur sept composés possédant des groupes méthoxy attachés à un cycle aromatique et sur quelques molécules rigides qui leur sont apparentées. On a dispersé les solutés dans une matrice de polystyrène. Dans quelques cas, on a pu séparer complètement l'absorption due au groupe de celle du processus moléculaire et ceci a permis d'évaluer d'une façon plus précise les enthalpies d'activation de Eyring pour la relaxation du groupe méthoxy. On a comparé ces valeurs avec celles trouvées dans la littérature et, d'une façon générale, il semblerait que la barrière d'énergie à la relaxation du groupe est petite et de l'ordre de 10 kJ mol^{-1} pour les cas ou il n'y a pas de conjugaison mutuelle ou d'effet stérique.
[Traduit par le journal]

Introduction

Molecules which have a methoxy group attached to an aromatic ring have been widely studied by dielectric techniques (1–4). The molecules have been examined either as a pure liquid or as a solute in a dilute solution of a nonpolar solvent and the absorption has been observed in the microwave region. In all cases the molecular and group absorptions have overlapped and the relaxation time for the group had to be deduced from a Budó analysis (5). Such an analysis can sometimes be subject to appreciable errors which possibility in turn leads to serious errors in the enthalpy of activation for group relaxation.

In the dielectric study of flexible molecules it has been found possible in a number of cases studied by Davies *et al.* (6, 7) and Walker and co-workers (8–10) to separate completely the absorption due to the intramolecular and molecular processes by dispersing the solute in a polystyrene matrix. The enthalpies of activation for the intramolecular process have, on the whole, compared quite well with those from the other direct methods of nmr and ultrasonics (7, 10.).

It seemed appropriate to carry out such a dielectric study on a number of methoxy compounds in order to determine the energy barrier for group relaxation more accurately from dielectric data. Moreover, the study seems even more pertinent when it is borne in mind that there is no generally accepted value for methoxy group rotation when the group is attached to an aromatic ring. In fact, there are very serious deviations in the magnitude of the value as estimated theoretically and from vibrational spectra (see later).

Experimental Results

The dielectric measurements have been made on a General Radio 1615A capacitance bridge in the frequency range 50 to 10^5 Hz. The measuring cell was a three-terminal circular parallel plate capacitor mounted in a temperature-controlled chamber flushed with dry nitrogen gas. The cell may be operated from liquid nitrogen temperature to about 400 K. For one of the polystyrene matrix samples, additional measurements have been made using a Hewlett–Packard 4342A Q-meter with a temperature-controlled, two-terminal cell in the range 2.5×10^4 to 1.5×10^7 Hz. The apparatus and measurement techniques have been described previously by Walker and co-workers (8–10).

The polystyrene matrix was prepared in the way described by Davies and Swain (7) and we have adopted their procedures both experimentally and also in the evaluation of the relaxation time and distribution parameter, by means of the Fuoss–Kirkwood equation and the enthalpy of activation from the Eyring equation. The polystyrene used here had a weight average molecular weight, $\bar{M}_w$, of 230 000. The relaxation data and the results of Eyring equation analyses of these data are given in Table 1.

In the fitting of the data of relaxation time as a function of temperature to the Eyring equation,

Can. J. Chem. Downloaded from www.nrcresearchpress.com by 210.87.254.6 on 09/05/12
For personal use only.

Can. J. Chem. Downloaded from www.nrcresearchpress.com by 210.87.254.6 on 09/05/12
For personal use only.

standard statistical techniques have been employed to obtain the slope and intercept of the line and the variances of these two parameters. These data yielded values of the enthalpy (ΔH_E) and entropy (ΔS_E) of activation for the relaxation process along with confidence intervals for each of these two. The 95% confidence intervals on ΔH_E were typically $\pm 10\%$ of the nominal values, or less, in agreement with the work of Davies *et al.* (6, 7). For the ΔS_E term, these confidence intervals were of the order of $\pm 50\%$ of the nominal values in some cases, since this term is often a small part of the intercept, $(\ln (h/k_B) - \Delta S_E/R)$, of the $\ln (T\tau)$ vs. $(1/T)$ plot.

Discussion

2,6-Dimethoxynaphthalene

This is the simplest case of the molecules reported here since in this molecule the $C_{\overline{aromatic}}O$ bonds are collinear across the 2,6 positions of the naphthalene molecule. Since the energy barrier for the rotation of the methoxy group is low (see later), then stable *cis* and *trans* isomers are improbable and thence, a component of the dipole moment fixed with respect to the molecular skeleton (necessary to detect molecular relaxation) is improbable. In fact, only the dipole moments perpendicular to the long axis need to be considered and are the ones which relate to the rotation of the methoxy groups.

The relaxation data from 2,6-dimethoxynaphthalene are obtained from one set of absorption peaks in the temperature range, 91–108 K, characterized by an enthalpy of activation of 11 kJ mol^{-1}. This may be ascribed to the barrier opposing methoxy group relaxation.

1,7-Dimethoxynaphthalene

The dielectric absorption in this case was marked by two separate sets of absorption peaks in the temperature ranges 86–97 K and 275–301 K, respectively. The enthalpy of activation in the lower temperature range is found to be 14 kJ mol^{-1}, whereas the higher temperature process has a $\Delta H_E = 84$ kJ mol^{-1}.

The ΔH_E value observed for the lower temperature process is of the same order as that for the methoxy group relaxation in 2,6-dimethoxynaphthalene and its ΔG_{E150} of 14 kJ mol^{-1} and τ_{150} of 9.5×10^{-6} s also show good agreement with those of 14 kJ mol^{-1} and 1.5×10^{-5} s for 2,6-dimethoxynaphthalene.

For the other relaxation process for 1,7-dimethoxynaphthalene the ΔH_E of 84 kJ mol^{-1} is to be compared with that of 90 kJ mol^{-1} for the fairly similar sized, rigid molecule, 4-bromobiphenyl.[1] This is to be contrasted with the lower temperature process value

[1]K. A. Kwaja (this laboratory). Private communication.

TABLE 1. Relaxation data and Eyring activation parameters for some solutes dispersed in a polystyrene matrix*

Solute	Temperature range (K)	Relaxation time (s)			ΔG_E (kJ mol^{-1})			ΔH_E (kJ mol^{-1})	ΔS_E (J K^{-1} mol^{-1})
		150 K	200 K	300 K	150 K	200 K	300 K		
3,3′-Dimethoxybiphenyl	89–105	9.6×10^{-6}	9.7×10^{-8}	9.0×10^{-9}	14	16	18	10±1	−35±13
2,6-Dimethoxynaphthalene	91–108	1.5×10^{-5}	1.0×10^{-7}	7.8×10^{-9}	14	16	17	11±1	−30±10
1,3-Dimethoxybenzene	86–119	6.0×10^{-5}	5.2×10^{-7}	4.4×10^{-8}	16	18	20	11±2	−46±18
1,7-Dimethoxynaphthalene	86–97	9.5×10^{-6}	2.6×10^{-8}	1.3×10^{-9}	14	14	14	14±3	−3±27
1,7-Dimethoxynaphthalene	275–301	8.7×10^{8}	3.1	1.0×10^{-6}	62	54	39	84	150
3,5-Dimethylanisole	81–109	8.3×10^{-6}	1.2×10^{-7}	1.3×10^{-8}	14	16	18	9.6±2	−42±17
3,5-Dimethylanisole	170–199	1.5×10^{-2}	6.4×10^{-6}	2.4×10^{-9}	31	28	24	37±2	44±9
2,4,6-Tribromoanisole	115–150	4.2×10^{-3}	4.2×10^{-6}	1.2×10^{-7}	19	21	22	16±1	−28±11
2,4,6-Tribromoanisole	178–217	1.7×10^{-2}	1.9×10^{-5}	1.8×10^{-8}	31	30	29	33±3	12±17
3,5-Dichlorobenzonitrile	207–250	1.3	5.3×10^{-4}	1.8×10^{-7}	37	36	35	38±2	11±10
1,3-Diiodobenzene	166–223	9.0×10^{-3}	2.0×10^{-5}	3.7×10^{-7}	30	30	31	29±1	−6±6

*The τ and ΔG_E values are quoted mainly for comparative purposes and only those within or close to a measured temperature range are considered accurate values.

Can. J. Chem. Downloaded from www.nrcresearchpress.com by 210.87.254.6 on 09/05/12
For personal use only.

of 14 kJ mol^{-1} for 1,7-dimethoxynaphthalene. Thus, for this molecule the high temperature process may be ascribed to molecular relaxation and the lower temperature one to group relaxation. Support for this assignment may be gained from the entropy of activation data where for the high temperature process the value of $\Delta S_E \sim 150$ J K^{-1} mol^{-1} is appropriate for molecular relaxation of such a large molecule, whereas the ΔS_E values for methoxy group relaxation are much smaller and have negative values and for 1,7-dimethoxynaphthalene is -3 J K^{-1} mol^{-1}.

3,3'-Dimethoxybiphenyl

This solute has been found to give a set of absorption peaks in the temperature range 89–105 K in the frequency range of the GR bridge. From these data an enthalpy of activation (ΔH_E) of 10 kJ mol^{-1} was deduced. This value is much too small to be attributed to any form of molecular motion nor can it be ascribed to rotation about the C—C bond between the two rings since the barrier for such relaxation is appreciably higher than this (11). Thus, the most likely candidate for such a low barrier is the rotation of the methoxy group.

1,3-Dimethoxybenzene

This molecule yields a $\Delta H_E = 11$ kJ mol^{-1} and absorbs in the 86–119 K range. A rigid molecule of similar size and shape, 1,3-diiodobenzene, has a $\Delta H_E = 29$ kJ mol^{-1} (Table 1). Thus, the 1,3-dimethoxybenzene value cannot be ascribed to molecular relaxation, and its similarity to that obtained for methoxy group relaxation in 2,6-dimethoxynaphthalene would suggest that the relaxation process is, at least, predominantly methoxy group relaxation.

3,5-Dimethylanisole

3,5-Dimethylanisole exhibits two sets of absorption peaks in the temperature ranges 81–109 and 170–199 K, respectively. The enthalpies of activation corresponding to the above two processes are found to be 9.6 and 37 kJ mol^{-1}, respectively. The first process in the lower temperature region may be assigned to the group relaxation whereas the second process would correspond to the molecular reorientation. The ΔH_E of 9.6 kJ mol^{-1} is in good agreement with the ΔH_E of 10, 11, and 14 kJ mol^{-1} values for 3,3'-dimethoxybiphenyl, 1,3-dimethoxybenzene, and 1,7-dimethoxynaphthalene, respectively, and the differences are scarcely greater than the experimental errors involved in the measurements of such low ΔH_E values.

A comparison of the ΔG_{E150} (14 kJ mol^{-1}) with these systems (ΔG_E 14, 16, 14 kJ mol^{-1}) also shows a close agreement in the data, suggesting that the process is that of methoxy group relaxation and this is supported by the τ_{150} value of 8.3×10^{-6} s which is of the same order as the values for methoxy group relaxation values of 9.6×10^{-6} s, 6.0×10^{-5}, and 9.5×10^{-6} s for 3,3'-dimethoxybiphenyl, 1,3-dimethoxybenzene, and 1,7-dimethoxynaphthalene, respectively.

The higher temperature process yields a $\Delta H_E = 37$ kJ mol^{-1} and this may be assigned to molecular reorientation since it has a similar ΔH_E to that for 3,5-dichlorobenzonitrile, a slightly larger molecule, which has a value of 38 kJ mol^{-1} for the molecular relaxation process (see Table 1).

2,4,6-Tribromoanisole

This exhibits two sets of absorption peaks in the temperature ranges 115–150 and 178–217 K, giving rise to ΔH_E values of 16 and 33 kJ mol^{-1}, respectively.

The higher temperature process having a $\Delta H_E = 33$ kJ mol^{-1} would be expected to be attributed to molecular relaxation. It has also $\Delta G_{E150} = 31$ kJ mol^{-1}. These values are to be compared with the corresponding values for a slightly larger molecule, 3,5-dichlorobenzonitrile, which has $\Delta H_E = 38$ kJ mol^{-1}, $\Delta G_{E150} = 37$ kJ mol^{-1}, and also those for the molecular process of 3,5-dimethyanisole with $\Delta H_E = 37$ kJ mol^{-1} and $\Delta G_{E150} = 31$ kJ mol^{-1}. Thus, the higher temperature process for 2,4,6-tribromoanisole may be ascribed to molecular relaxation. The $\Delta H_E = 16$ kJ mol^{-1} for the low temperature process is to be allotted to methoxy relaxation and the increment in value of ~ 5 kJ mol^{-1} could be related to the presence of bromo atoms in the ring which may result in steric and additional conjugative effects.

Conclusions

As Grindley *et al.* (12) have pointed out, there is no generally accepted barrier for methoxy group relaxation in anisole. Dielectric relaxation studies (4) of anisole in a nonpolar solvent yield a value of ~ 6 kJ mol^{-1}. Theoretical calculations (13–15) yield values ranging between 0 and 7.5 kJ mol^{-1}. However, the vibrational spectrum (16) yields a much higher value of 25.1 kJ mol^{-1}. Grindley *et al.* (12) from a somewhat empirical approach, obtained a value of 11 kJ mol^{-1}. The values we have obtained for methoxy relaxation in 1,3-dimethoxybenzene and 3,5-dimethylanisole are 11 and 9.6 kJ mol^{-1}, respectively. These are the two molecules of those we have examined which should be closest to anisole in conjugative effects of the conjugated ring with the methoxy group. It is striking how near this value is to that estimated by Grindley *et al.* (12). In fact, even for 3,3'-dimethoxybiphenyl and 2,6-dimethoxynaphthalene the ΔH_E value is very similar. Only in

the case of 2,4,6-tribromoanisole, where there are appreciable steric effects and possibly increased conjugation involved, is the ΔH_E increased slightly to 16 kJ mol^{-1} for methoxy group relaxation.

It would seem reasonable to conclude that in the absence of appreciable steric or mutual conjugative effects the barrier to methoxy group relaxation, when attached to a conjugated system, is low and of the order of 10 kJ mol^{-1}.

1. D. B. FARMER and S. WALKER. Can. J. Chem. **47**, 4645 (1969).
2. D. M. ROBERTI and C. P. SMYTH. J. Am. Chem. Soc. **82**, 2106 (1960).
3. E. FOREST and C. P. SMYTH. J. Am. Chem. Soc. **86**, 3474 (1964).
4. S. K. GARG and C. P. SMYTH. J. Chem. Phys. **46**, 373 (1967).
5. J. CROSSLEY, S. P. TAY, and S. WALKER. Adv. Mol. Relaxation Processes, **6**, 79 (1974).
6. M. DAVIES and E. EDWARDS. Trans. Faraday Soc. **63**, 2163 (1967).
7. M. DAVIES and J. SWAIN. Trans. Faraday Soc. **67**, 1637 (1971).
8. C. K. MCLELLAN and S. WALKER. Can. J. Chem. **55**, 583 (1977).
9. S. P. TAY and S. WALKER. J. Chem. Phys. **63**, 1634 (1975).
10. S. P. TAY, S. WALKER, and E. WYN-JONES. Adv. Mol. Relaxation Processes. In press.
11. E. MARIT FARBROT and P. N. SKANCKE. Acta Chem. Scand. **24**, 3645 (1970).
12. T. B. GRINDLEY, A. R. KATRITZKY, and R. D. TOPSOM. J. Chem. Soc. Perkin Trans. II, 289 (1974).
13. E. HELGSTRAND. Acta Chem. Scand. **24**, 3687 (1970).
14. N. L. ALLINGER, J. J. MANL, and M. J. HICKEY. J. Org. Chem. **36**, 2747 (1971).
15. K. W. J. HEHRE, L. RADOM, and J. A. POPLE. J. Am. Chem. Soc. **94**, 1496 (1972).
16. N. L. OWEN and R. E. HESTER. Spectrochim. Acta, **25A**, 343 (1969).

Can. J. Chem. Downloaded from www.nrcresearchpress.com by 210.87.254.6 on 09/05/12
For personal use only.

Electrochemical reduction of pyridopyrazines

JOSEPH ARMAND, KHALED CHEKIR, AND JEAN PINSON

Laboratoire de Physicochimie des Solutions, Université Pierre et Marie Curie, Bâtiment F, 8 rue Cuvier, 75230 Paris, Cédex 05 France

Received October 13, 1977

JOSEPH ARMAND, KHALED CHEKIR, and JEAN PINSON. Can. J. Chem. **56**, 1804 (1978).

The electrochemical reduction of several pyrido[2,3-*b*]pyrazines in hydroorganic or aprotic media leads to 1,4-dihydro derivatives which can be isolated in some cases. Most of these derivatives isomerize into 1,2-, 3,4-, or 5,8-dihydro compounds. A molecule of alcohol is added to these last compounds in alkaline medium. The electrochemical reduction of 1,2- or 3,4-dihydro derivatives gives 1,2,3,4-tetrahydropyridopyrazines. In hydroorganic media, the 7-bromopyrido [2,3-*b*]pyrazines give a 1,4-dihydro compound which can either isomerize or debromhydrate. In an aprotic medium, the parent heterocycle is obtained. By electrochemical reduction of pyrido[3,4-*b*]pyrazines, 1,4-dihydro derivatives can be formed which isomerize. The 1,2- or 3,4-dihydro compounds thus obtained can be reduced at the electrode into 1,2,3,4-tetrahydro derivatives.

JOSEPH ARMAND, KHALED CHEKIR et JEAN PINSON. Can. J. Chem. **56**, 1804 (1978).

La reduction électrochimique de diverses pyrido[2,3-*b*]pyrazines en milieu hydroorganique et aprotique fournit des dérivés dihydro-1,4 isolés dans certains cas. Ces dérivés peuvent s'isomériser en solution en dérivés dihydro-1,2 ou -3,4 ou -5,8. Ces derniers additionnent une molécule d'alcool en milieu alcalin. La réduction des dérivés dihydro-1,2 ou -3,4 fournit des tétrahydro-1,2,3,4. Les dérivés 7-bromés conduisent en milieu hydroorganique à une dihydro-1,4 qui peut soit s'isomériser soit se débromhydrater, alors qu'en milieu aprotique il y a coupure de la liaison C—Br pour conduire à la pyrido[2,3-*b*]pyrazinè. La réduction électrochimique des pyrido[3,4-*b*]pyrazines fournit des dérivés dihydro-1,4 qui s'isomérisent uniquement en dérivés dihydro-1,2 ou -3,4 eux mêmes électroréductibles en tétrahydro-1,2,3,4.

Can. J. Chem. Downloaded from www.nrcresearchpress.com by 210.87.254.6 on 09/05/12
For personal use only.

It has been shown in previous papers that by electrochemical reduction of compounds with the —N=C—C=N— group (1, 2), semihydrogenated derivatives can be prepared. We now present the results obtained in the case of pyridopyrazines, whose electrochemistry had never before been investigated in spite of their interesting pharmacological properties.

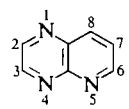

Pyrido[2,3-*b*]pyrazines

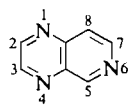

Pyrido[3,4-*b*]pyrazines

*Alkyl- and Arylpyrido[2,3-*b*]pyrazines*

Hydroorganic Media

In a water–methanol mixture (50:50 by volume) 2,3-diphenylpyrido[2,3-*b*]pyrazine (**1**) presents a single two-electron wave, with an $E_{1/2}$ which is pH dependent between pH 1 and 14: $E_{1/2} = -0.09 - 0.07$ pH. It is more easily reduced than the 2,3-diphenylpyrazine (2) for which $E_{1/2} = -0.38 - 0.079$ pH, owing to an increased conjugation with the pyridine ring. Electrolysis of a dilute solution of **1** in neutral or acidic media (Fig. 1) leads to a compound with an anodic wave whose $E_{1/2}$ value is near that of the cathodic wave of **1**. This reduced compound (**2**) precipitates during the electrolysis and is very easily oxidized. When dissolved in a non-deoxygenated solution, this compound is quickly and quantitatively reoxidized to **1**. In alkaline media (Fig. 2), the same primary reduction product is obtained but its anodic wave decreases with time and two cathodic waves appear; a preparative electrolysis

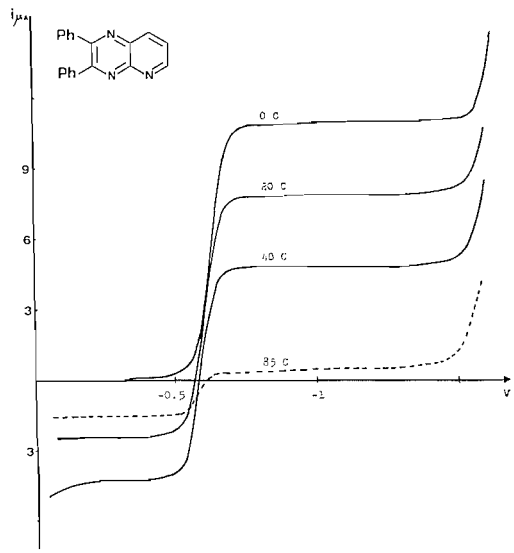

FIG. 1. Electrolysis of **1** in dilute solution: pH 7; $c = 2 \times 10^{-3}$ M, 50% CH_3OH, $E = -0.7$ V/sce, $V = 200$ ml. Polarograms recorded before (0 C), during (20 C, 40 C) and at the end of the electrolysis (85 C).

Can. J. Chem. Downloaded from www.nrcresearchpress.com by 210.87.254.6 on 09/05/12
For personal use only.

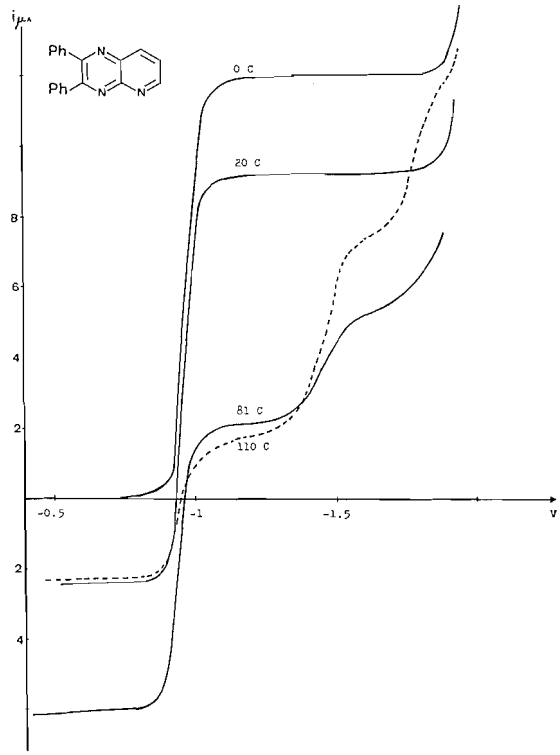

FIG. 2. Electrolysis of **1** in dilute solution: 0.1 *N* NaOH, $c = 2.10^{-3}$ *M*, 80% CH_3OH, $E = -1.1$ V/sce, $V = 200$ ml. Polarograms recorded before (0 C) and during the electrolysis (20 C, 81 C, 110 C).

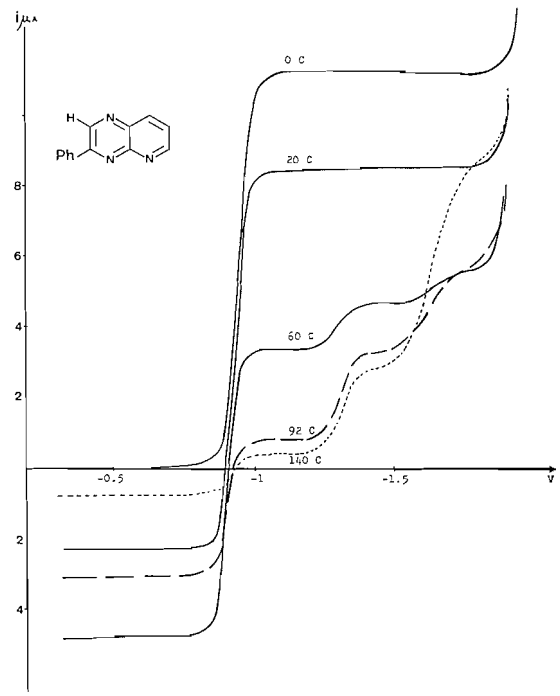

FIG. 3. Electrolysis of **5** in dilute solution: 0.1 *N* NaOH, $c = 2.10^{-3}$ *M*, 50% CH_3OH, $E = -1.05$ V/sce, $V = 200$ ml. Polarograms recorded before (0 C), during (20 C, 60 C, 92 C) and at the end of the electrolysis (140 C).

of **1** gives a mixture of two compounds which can be separated: 3,4-dihydro-2,3-diphenylpyrido[2,3-*b*]-pyrazine (**3**) and 5,6,7,8-tetrahydro-6-methoxy-2,3-diphenylpyrido[2,3-*b*]pyrazine (**4**). These two compounds give the same cathodic waves as those observed in Fig. 2.

*3-Phenylpyrido[2,3-*b*]pyrazine (**5**)*—The polarographic behaviour of **5** is similar to that of **1**; in a 50:50 water–methanol mixture, $E_{1/2}$ varies with p*H* according to the same equation. Electrolysis of dilute solutions also gives a highly oxidizable compound (**6**) which does not precipitate in the medium but is transformed slowly in an acidic or a neutral medium and more rapidly in an alkaline medium. This is shown on the polarograms recorded during the electrolysis (Fig. 3). In an alkaline water–methanol medium, a preparative electrolysis of **5** gives 5,6,7,8-tetrahydro-6-methoxy-3-phenylpyrido[2,3-*b*]pyrazine (**7**); by using C_2H_5OH instead of CH_3OH, one obtains 5,6,7,8-tetrahydro-6-ethoxy-3-phenylpyrido-[2,3-*b*]pyrazine (**8**).

*2,3-Dimethylpyrido[2,3-*b*]pyrazine (**9**)*—The polarograms are similar to those of **1**; $E_{1/2} = -0.15 - 0.07$ p*H* (50:50 water–methanol). During electrolysis in dilute solution, the polarograms show that the primary reduction product **10** is transformed at every p*H* (Fig. 4). A preparative electrolysis of **9** in an alkaline medium gives a 15:85 mixture (nmr titration) of 5,6,7,8-tetrahydro-6-methoxy-2,3-dimethylpyrido[2,3-*b*]pyrazine (**11**) and 1,2- (or 3,4-) dihydro-2,3-dimethylpyrido[2,3-*b*]pyrazine (**12**). This last compound can be purified by recrystallization.

The data in Scheme 1 account for our results. First of all, some of the dihydro and tetrahydro derivatives obtained by preparative electrolysis can be reduced at the dropping mercury electrode and produce a cathodic wave which is identical to that observed during the electrolyses of dilute solutions: the results of these electrolyses are thus in agreement with those of the preparative electrolyses. The primary reduction product shows an anodic wave with an $E_{1/2}$ value near that of the cathodic wave of the starting pyrido[2,3-*b*]pyrazine and it partially isomerizes into a 1,2- or 3,4-dihydro derivative; this behaviour is identical to that of pyrazines (2). Thus, the 1,4-dihydro structure can be assigned to compounds **2**, **6**, and **10** according to route *A*. In the case of **5**, 1,2- (or 3,4-) dihydro-3-phenylpyrido[2,3-*b*]pyrazine could not be isolated; this is indeed what is observed in Fig. 2 where a cathodic wave appears with an $E_{1/2}$ little different from that of **3**. This indicates that the 1,4-dihydro derivative **6** partially isomerizes into a

Can. J. Chem. Downloaded from www.nrcresearchpress.com by 210.87.254.6 on 09/05/12
For personal use only.

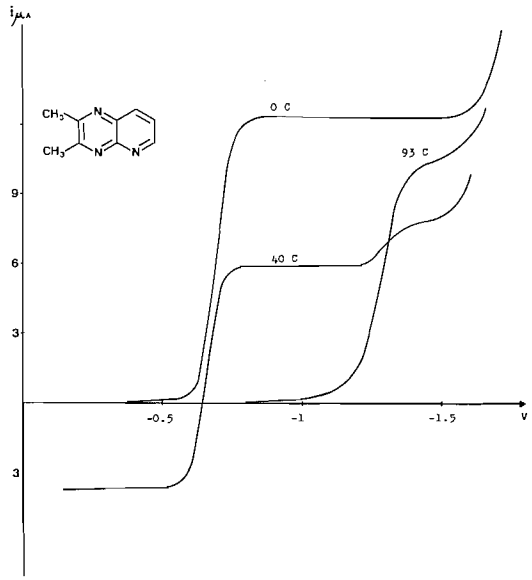

FIG. 4. Electrolysis of **9** in dilute solution: pH = 7.2, $c = 2.10^{-3}$ M; 50% CH_3OH, $E = -0.8$ V/sce, $V = 200$ ml. Polarograms recorded before (0 C), during (40 C) and at the end of the electrolysis (93 C).

1,2- or 3,4-dihydro derivative which could not be isolated because of its low yield and high solubility.

To the best of our knowledge, route B is entirely new. The formation of the tetrahydro derivatives **4**, **7**, **8**, and **11** can be explained by covalent addition of alcohol to a dihydrogenated derivative. This type of addition, which is often observed with nitrogen heterocycles (3), generally takes place on a >C=N— bond. Thus, the most logical hypothesis is that the addition takes place on the 7,8-dihydro derivative. In a nonaqueous medium in the presence of phenol (see below), the electrolysis of the pyrido[2,3-*b*]pyrazines leads to the 5,8-dihydro derivative; this compound is rapidly and quantitatively transformed into the 5,6,7,8-tetrahydro derivative in an alkaline water–methanol mixture. These results indicate that the 1,4-dihydropyrido[2,3-*b*]pyrazine leads to the 5,8-dihydro compound which isomerizes in alkaline medium into the 7,8-dihydro derivative, with addition of a molecule of methanol (Scheme 1). The formation of a 5,8-dihydro compound can be explained either by an intramolecular rearrangement of the 1,4-dihydro compound or by the reduction on the 5,8 position of a molecule of pyrido[2,3-*b*]-pyrazine by a molecule of the 1,4-dihydro compound. The first hypothesis implies that the reaction is of first kinetic order in 1,4-dihydro derivative, whereas in the second hypothesis the reaction would be first order in 1,4-dihydro and first order in pyrido[2,3-*b*]-pyrazine. The isomerization reaction 1,4-dihydro → 1,2- or 3,4-dihydro is also first order in 1,4-dihydro. Thus, a fourfold increase of the initial concentration of **1** should not change the ratio of the number of moles of **4** to the number of moles of **3** if the first hypothesis is the right one, while this ratio should undergo a large increase in the second case. By changing the amount of **1** which is electrolyzed from

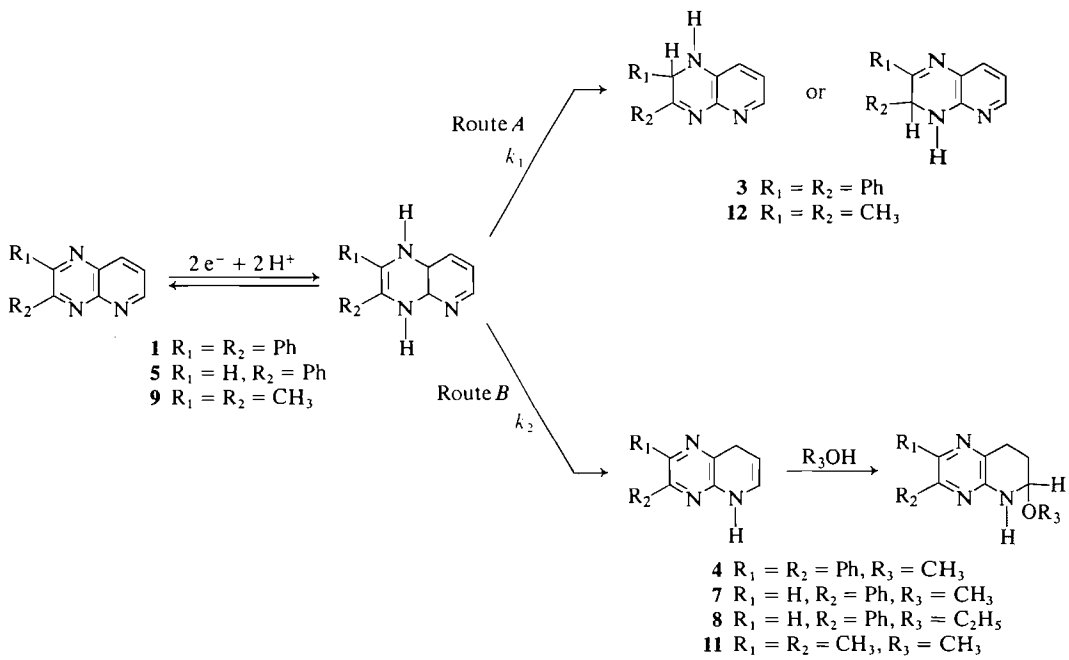

SCHEME 1. Reduction of pyrido[2,3-*b*]pyrazines in hydroorganic media: $1 <$ pH < 14.

Can. J. Chem. Downloaded from www.nrcresearchpress.com by 210.87.254.6 on 09/05/12
For personal use only.

250 mg to 1 g (in the same volume), the above ratio remains constant; therefore, we can conclude that the 5,8-dihydro is obtained by intramolecular rearrangement of the 1,4-dihydro derivative.

Other cosolvents have been used: acetonitrile, dimethylformamide, and diglyme. In each case, the transformation rate of the 1,4-dihydro derivative is too slow to permit the isolation of isomerization products. The relative amounts of 1,2- or 3,4-dihydro and 5,6,7,8-tetrahydro derivatives obtained by routes *A* and *B* depend on the relative values of the rate constants k_1 and k_2. These depend not only on the nature of R_1 and R_2, as shown by the preparative electrolyses, but also on the reduction medium: the reduction of **1** leads to a 40% yield of **3** in an alkaline water – methanol mixture; this yield increases to 63% in dimethylformamide in the presence of phenol and decreases to 0% in acetonitrile in the presence of phenol.

In short, the primary reduction product of pyrido[2,3-*b*]pyrazines is the 1,4-dihydro derivative which isomerizes either to a 1,2- or 3,4-dihydro or to a 5,8-dihydro compound. The ratio of the different compounds depends on k_1, k_2, and the medium.

Nonaqueous Media

Electrochemical reductions in nonaqueous media were used to prepare 1,4-diacetyl-1,4-dihydro derivatives by operating in dimethylformamide (DMF) or acetonitrile (ACN) in the presence of acetic anhydride as shown by Lund and Simonet (4). In addition, nonaqueous media with phenol added as a proton donor were used to prevent the addition of alcohol. In DMF, the potentials are referred to the Ag,AgI/I^- 0.1 *M* electrode and in ACN to the Ag/Ag^+ 0.01 *M* electrode.

In DMF, **1** presents two one-electron waves (Fig. 5). By adding an excess of acetic anhydride, these two waves merge into a single two-electron wave with an $E_{1/2}$ which is slightly more positive than that of the first wave of **1**. A preparative electrolysis gives the 5,8-dihydro-5-acetyl-2,3-diphenylpyrido[2,3-*b*]-pyrazine (**13**). Similar polarographic behaviour is observed for **5**; however, preparative electrolyses led only to gummy products.

In ACN, the polarographic results are similar to that obtained in DMF for **1** and **5**. The electrolysis of **1** also gives **13** whereas with **5**, one obtains the 1,4-dihydro-1,4-diacetyl-3-phenylpyrido[2,3-*b*]pyrazine (**14**).

Upon addition of phenol, the second wave of the polarogram of **1** disappears progressively as the first one increases and becomes a two-electron wave, with an $E_{1/2}$ which is shifted to more positive potentials, both in ACN and DMF. In DMF, electrolysis of **1** gives **3** whereas in ACN, it leads to the 5,8-dihydro-

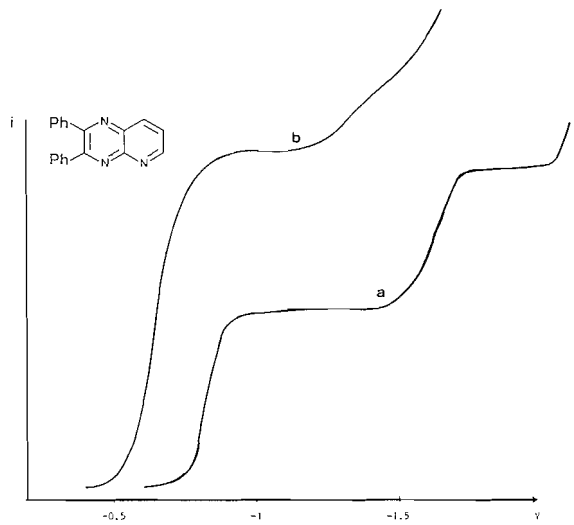

FIG. 5. Polarogram of (*a*) **1** in DMF: $c = 10^{-3}$ *M*, 0.15 *M* TBAI, $V = 50$ ml; and (*b*) after addition of 2 ml acetic anhydride (2.1×10^{-2} mol; mol ratio 10^3). Reference electrode Ag/AgI I^- 0.1 *M*.

2,3-diphenylpyrido[2,3-*b*]pyrazine (**15**). It should be noted that **15** does not acetylate in DMF in the presence of acetic anhydride.

In the case of **5**, polarograms are modified in the same way; electrolysis in DMF gives a mixture containing mostly the 1,4-dihydro-3-phenylpyrido-[2,3-*b*]pyrazine (**6**); in ACN, the 5,8-dihydro-3-phenylpyrido[2,3-*b*]pyrazine (**16**) is obtained.

In the absence of an electrophilic reagent or of a proton donor, the two monoelectronic waves can be assigned to the formation of an anion radical and of a dianion. The unusual stability of the dianion of **1** (Fig. 6) can be explained by its low basicity owing to a high degree of conjugation. It is recalled that the dianion of 2,3-diphenylpyrazine is unstable under the same conditions (Fig. 7).

In the presence of acetic anhydride, the reduction starting from **1** proceeds differently than that starting from **5** (Scheme 2). It should first be recalled that, as stated above, **13** can not be obtained through the acetylation of **15**. In the presence of an electrophile, the acetylation of nitrogen heterocycles can take place before or after the first electronic transfer (4). In the case of a preceding acetylation, which can be sketched as in Scheme 3, the most basic nitrogen in the molecule should be acetylated. In the case of pyridopyrazines, the most basic nitrogen is that of the pyridine ring (5). Thus a preceding acylation would seem to occur in the formation of **13**, whereas in the case of **14** the acetylation would take place after the first electronic transfer according to an ECEC mechanism.

In the presence of phenol, the solutions become

Can. J. Chem. Downloaded from www.nrcresearchpress.com by 210.87.254.6 on 09/05/12
For personal use only.

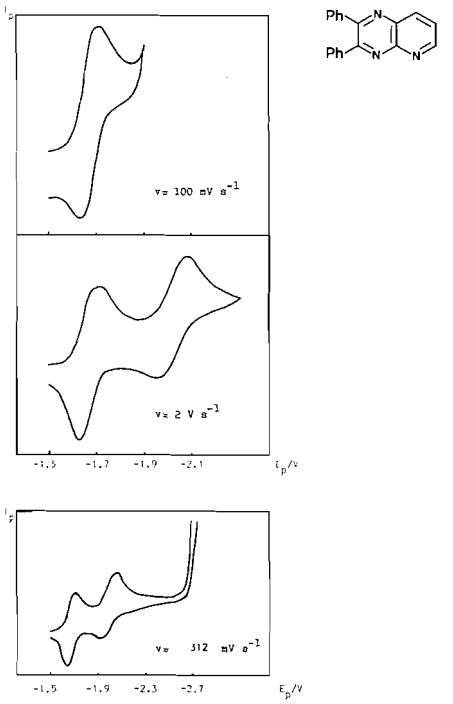

FIG. 6. Voltammograms of **1**: $c = 10^{-3}$ *M*; solvent, ACN; supporting electrolyte, tetraethylammonium perchlorate 0.1 *M*; reference electrode Ag/Ag$^+$ 0.01 *M*.

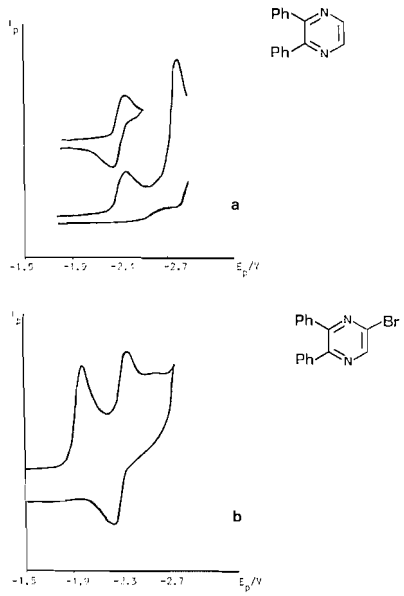

FIG. 7. Voltammogram of (*a*) 2,3-diphenylpyrazine: $c = 10^{-3}$ *M*, $v = 20$ V s^{-1}; and of (*b*) 5-bromo-2,3-diphenylpyrazine: $c = 10^{-3}$ *M*, $v = 1200$ V s^{-1}. Solvent ACN; supporting electrolyte, 0.1 *M* TEAP; reference electrode Ag/Ag$^+$ 0.01 *M*.

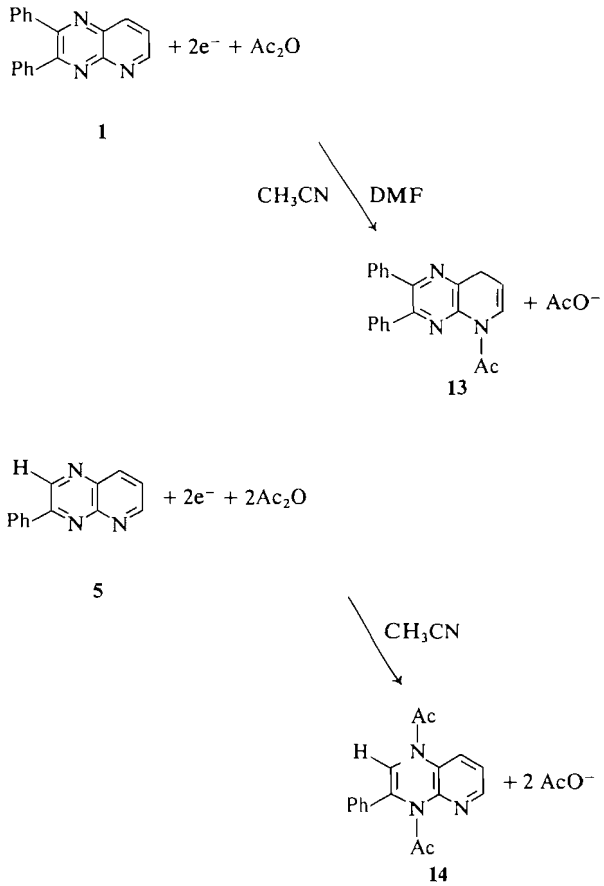

SCHEME 2. Reduction of pyrido[2,3-*b*]pyrazines in nonaqueous media.

deep red during the electrolysis; this colour is stable in the case of **5** in DMF and is due to the 1,4-dihydro derivative as the primary reduction product which is stable in one case and which isomerizes in the three other cases. The rate and the orientation of this isomerization depend on R_1, R_2, and the medium as shown in Scheme 4.

*7-Bromopyrido[2,3-*b*]pyrazines*

These compounds were investigated to find out if their behaviour is similar to that of other aromatics (6, 7) where bromine is cleaved upon reduction, this cleavage being interesting for the synthesis of pyridopyrazines.

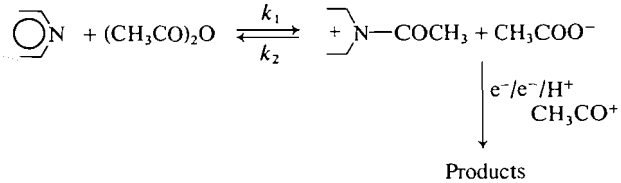

SCHEME 3. Mechanism of a preceding acetylation.

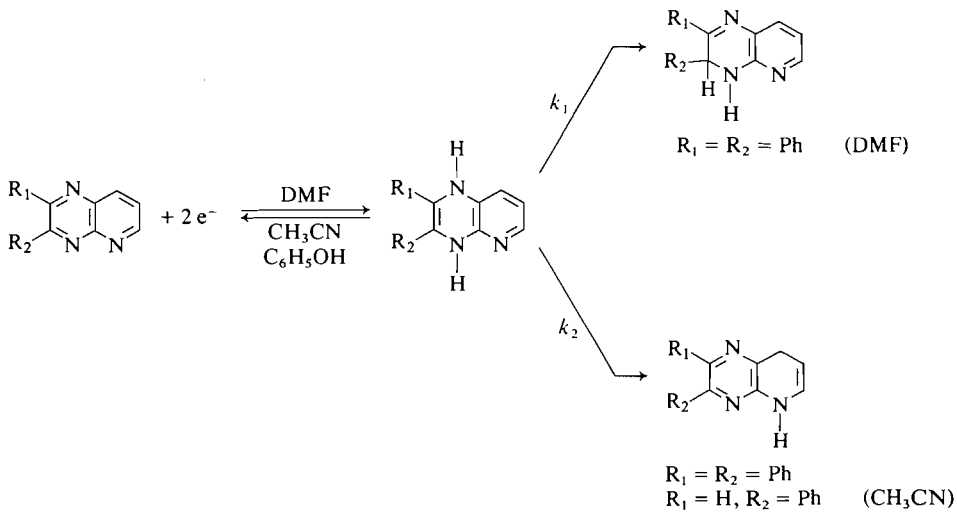

SCHEME 4. Reduction of pyrido[2,3-*b*]pyrazines in DMF and ACN with addition of phenol.

Hydroorganic Medium

In this medium, compounds **17**, **18**, and **19** present a single 2 F wave. The $E_{1/2}$ varies linearly with the pH: $E_{1/2} = -0.08 - 0.055$ pH for **17**, $E_{1/2} = -0.09 - 0.07$ pH for **18**, and $E_{1/2} = -0.15 - 0.068$ pH for **19**. The reductibility of pyrido[2,3-*b*]pyrazines is only slightly modified by the bromine atom as can be seen by comparing the above $E_{1/2}$ with those of the nonbrominated compounds.

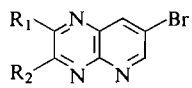

17 $R_1 = R_2 = Ph$
18 $R_1 = H$, $R_2 = Ph$
19 $R_1 = R_2 = CH_3$

Electrolysis of dilute solutions of **17** and **18** in acidic or neutral media leads to a compound with an anodic wave, whose $E_{1/2}$ is near from that of the starting compound (Fig. 8). This compound can be reoxidized by air to give quantitatively the starting compound (nmr and polarograms). Thus, the primary reduction product is a 1,4-dihydro derivative which isomerizes very slowly. In alkaline media, the polarograms recorded during the electrolyses are similar to those obtained with the nonbrominated compounds. When **17** and **18** are electrolyzed under the conditions used for **1** and **5**, the same products are obtained (i.e. **3**, **7**, and **8**) with the same yields.

In alkaline media, the behaviour of **19** is similar to that of **17** and **18** but in acidic or neutral media, the 1,4-dihydro derivative is mainly transformed into a 1,2- (or 3,4-) dihydro derivative as shown by preparative electrolysis of **19** in a neutral medium

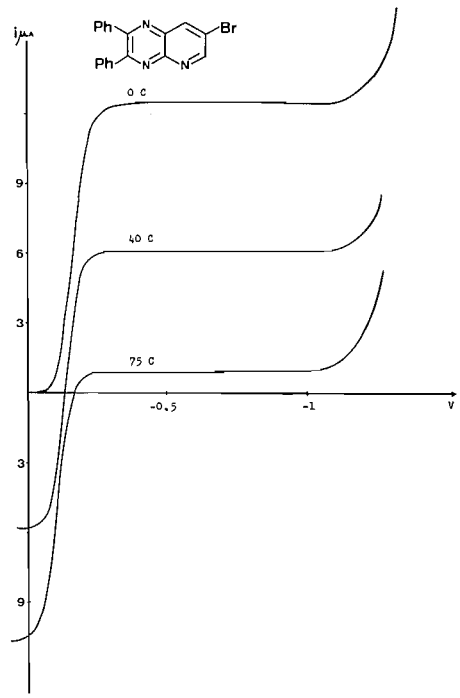

FIG. 8. Electrolysis of **17** in dilute solution: 0.1 N H_2SO_4, $c = 2 \times 10^{-3}$ M, 80% CH_3OH, $E = -0.25$ V/sce, $V = 200$ ml. Polarograms recorded before and during the electrolysis (40 C, 75 C).

where the 1,2- or 3,4-dihydro-2,3-dimethyl-7-bromopyrido[2,3-*b*]pyrazine (**20**) is formed.

These results indicate that in alkaline medium the cleavage of bromine from the 7-bromo compounds takes place at the level of the 1,4-dihydro derivative: the results are summarized in Scheme 5.

Can. J. Chem. Downloaded from www.nrcresearchpress.com by 210.87.254.6 on 09/05/12
For personal use only.

Can. J. Chem. Downloaded from www.nrcresearchpress.com by 210.87.254.6 on 09/05/12
For personal use only.

SCHEME I

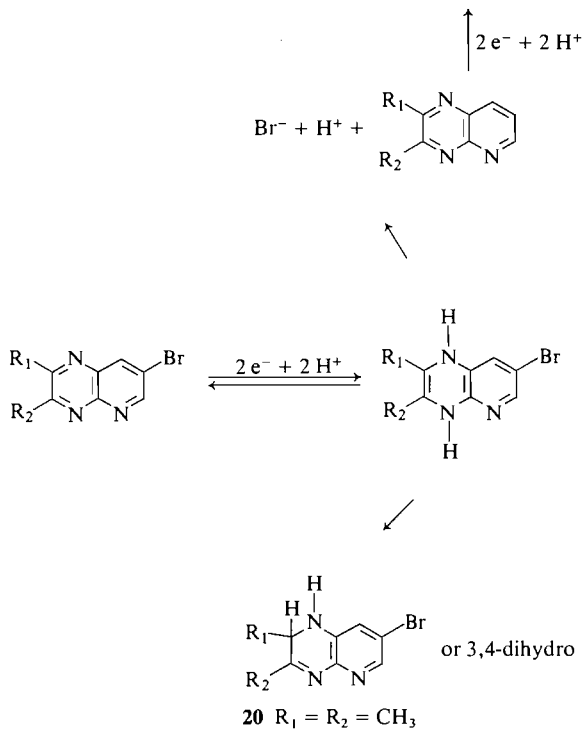

20 $R_1 = R_2 = CH_3$

SCHEME 5. Reduction of 7-bromopyrido[2,3-*b*]pyrazines in hydroorganic media.

Nonaqueous Medium

In acetonitrile and DMF, the three bromo derivatives present a 1 F wave followed by the two waves of the parent heterocycle. The half wave potentials of these three compounds are not too different.

	17	18	19	Reference electrode
DMF	−0.63 V	−0.63 V	−0.80 V	Ag,AgI/I⁻ 0.1 *M*
ACN	−1.51 V	−1.51 V	−1.66 V	Ag/Ag⁺ 0.01 *M*

Voltammograms were recorded at different scan rates in the case of **17** in ACN (Fig. 9). At low scan rates, the first irreversible peak of **17** is followed by the two reversible peaks of **1** (Fig. 9*a*). At higher scan rates (Fig. 9*c*), the voltammogram shows two reversible peaks corresponding to the formation of the radical anion and the dianion of **17** and a small anodic peak of **1** ($\mathbf{1}^{\cdot-} \rightarrow \mathbf{1}$). This anodic peak is higher in Fig. 9*b* recorded at an intermediate sweep rate; therefore, the extent of bromine cleavage is greater than in Fig. 9*c* but is not complete as in Fig. 9*a*. Figure 9*d* is recorded at the same sweep rate as Fig. 9*b* but the cathodic scan is stopped before the second peak of **17**; it shows a single reversible peak which corresponds to the $\mathbf{17}/\mathbf{17}^{\cdot-}$ couple. In the case of **19** (in ACN) at a low scan rate (0.2 V s^{-1}), a single irreversible peak ($E_p = -1.76$ V) is observed, followed by the two peaks of **9** ($E_p = -1.96$ V reversible and $E_p = -2.32$ V irreversible). At a higher scan rate (200 V s^{-1}), the first peak becomes reversible and a new peak appears which corresponds to the formation of the dianion of **19**.

Coulometric experiments were also carried out: in the case of **17**, the electrolysis of a 10^{-3} *M* or 10^{-2} *M* solution consumes 1.5 F/mol and the main product is **1** in 53 and 70% yield, respectively; some by-products are evinced by thin-layer chromatography. The reduction of a 10^{-2} *M* solution of **19** consumes 1.5 F/mol and the yield of **9** is 50%.

The rate of decomposition of the radical anion obtained after the first electronic transfer can be measured by plotting E_p as a function of log v (v = sweep rate in V s^{-1}) (6). We found $k_1 = 18 \pm 6$ s^{-1} for **17** and 385 ± 100 s^{-1} for **19**. These rate constants are very small when compared to the rate constant for the decomposition of the radical anion of the 2,3-diphenyl-5-bromopyrazine (**21**). In the latter case, the first wave of the voltammogram remains irreversible up to 1200 V s^{-1}, indicating that k_1 is higher than 50 000 s^{-1} (Fig. 7).

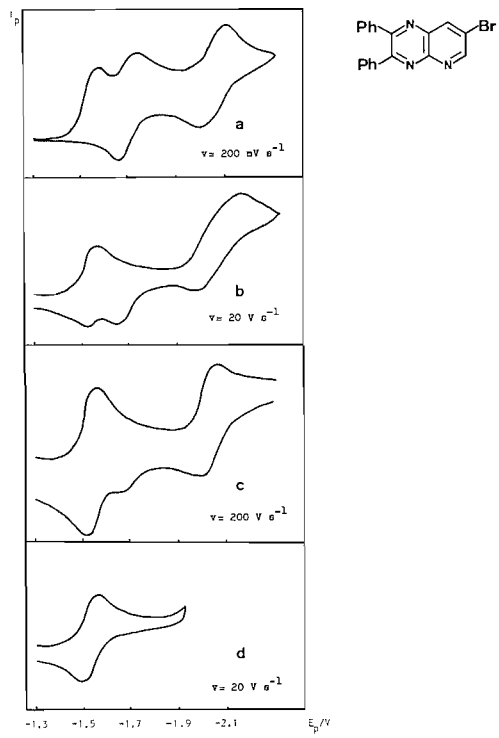

FIG. 9. Voltamograms of 7-bromo-2,3-diphenylpyrido[2,3-*b*]-pyrazine **17**. Solvent ACN; supporting electrolyte, tetraethylammonium perchlorate 0.1 *M*; reference electrode Ag/Ag⁺ 0.01 *M*.

Can. J. Chem. Downloaded from www.nrcresearchpress.com by 210.87.254.6 on 09/05/12
For personal use only.

If RBr represents the bromo heterocycle and RH the parent compound, the cleavage of bromine can take place at the level of the radical anion $RBr^{\cdot -}$ to give a neutral radical R· and a bromine anion. This neutral radical R· can enter into three competitive reactions: (*i*) hydrogen atom abstraction from the solvent; (*ii*) further reduction to R^- at the electrode; or (*iii*) electron exchange in solution. It has been shown (8) that when the rate constant k_1 is low, further electrode reduction is unlikely: the radical anion has enough time to diffuse from the electrode to the solution before it decomposes. Thus R· is obtained in the bulk of the solution and cannot be reduced at the electrode. Between the two last possibilities, the most probable reaction is a hydrogen atom abstraction from the solvent. Not only is it favoured by concentration effect but also the by-products evidenced by tlc can be explained by an attack of the solvent on R· (8)

$$R\cdot + SH \rightarrow RH + S\cdot \quad (SH = \text{solvent})$$

$$S\cdot + e \rightarrow S^-$$

$$R\cdot + S^- \rightarrow RS^{\cdot -}$$

$$RS^{\cdot -} \rightarrow \text{By-products}$$

The reduction of S· to S^- would thus account for more than 1 electron being observed during the coulometric experiments.

An interesting and unusual feature of these compounds is the high stability of the dianion RBr^{2-}: a reversible peak corresponding to the $RBr^{\cdot -}RBr^{2-}$ couple is observed on the voltammogram of **17** even at relatively low scan rates (Fig. 9*b*). This dianion decomposes relatively slowly into R^- and a bromine anion; R^- is most likely protonated to RH by the residual water. At the potential where this reaction takes place, RH is reduced to $RH^{\cdot -}$ and the re-oxidation of this radical anion is seen on the anodic scan of the voltammogram (Fig. 9*b* and *c*).

It should be noted that the cleavage of Br^- from the 7-bromopyrido[2,3-*b*]pyrazines is useful for the synthesis of these series. To prepare pyrido[2,3-*b*]-pyrazines, one follows a synthetic route (9) where the

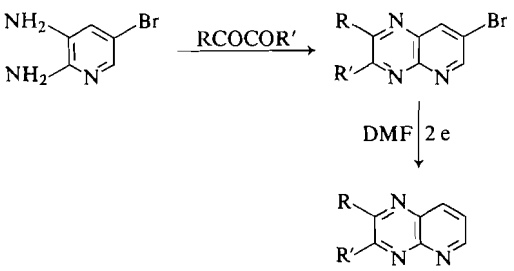

SCHEME 6. Electrochemical preparation of pyrido[2,3-*b*]-pyrazines.

most difficult step in the series of reactions is the chemical debromation of 2,3-diamino-5-bromo-pyridine. Through the sequence of reactions shown in Scheme 6, this chemical debromination step can be avoided. The debromation is carried out electrochemically on the pyrido[2,3-*b*]pyrazines which are easily prepared from 2,3-diamino-5-bromopyridine. For example, a preparative electrolysis of **17** carried out in DMF gives easily 51% of **1**.

*Chemical Preparation of the Reduced Derivatives of Pyrido[2,3-*b*]pyrazines*

Dihydro derivatives have been prepared by reaction of organomagnesium compounds with pyrido-[2,3-*b*]pyrazines (12); no 1,2- or 3,4-dihydropyrido-[2,3-*b*]pyrazines had been described before our preliminary communication (13). We have prepared the 1,4-dihydro derivative of **5** by reduction with sodium dithionite. Unlike compound **2** it cannot be prepared by electrolysis.

1,2,3,4-Tetrahydro derivatives have been obtained by reaction of organomagnesium compounds (12) or by reduction with $AlLiH_4$ (5, 10, 11). This last reagent does not give any result in the case of **5**; the tetrahydro derivative is prepared by hydrogenation with Pd–C. The 1,2,3,4-tetrahydro derivatives can also be obtained by electrolysis of 1,2- or 3,4-dihydro compounds: **3** leads to the *cis*-tetrahydro derivative whereas **2** gives a mixture of *cis* and *trans* isomers. 5,6,7,8-Tetrahydropyrido[2,3-*b*]pyrazines have been prepared by hydrogenation of 5,6-dihydro derivatives (11).

*Pyrido[3,4-*b*]pyrazines*

The electrochemical reduction of 2,3-diphenyl-pyrido[3,4-*b*]pyrazine (**22**) was investigated to assess the influence of the position of the pyridine nitrogen in comparison with the reduction pattern of **1**. This influence is indeed strong since the electrochemical reduction of **22** does not involve the pyridine ring.

Between p*H* 1 and 13 the polarogram of **22** presents a 2 F cathodic wave with an $E_{1/2}$ which varies with the p*H* as $E_{1/2} = 0.07 - 0.08\,pH$ between p*H* 1 and 7 and as $E_{1/2} = -0.07 - 0.069\,pH$ between p*H* 7 and 13 (CH_3OH, 50%). The reducibility of **22** is thus similar to that of **1**. An electrolysis of a dilute solution in a basic medium shows an anodic wave with an $E_{1/2}$ near that of the cathodic wave of **22**. This anodic wave decreases with time and a new cathodic wave appears (Fig. 10) whose half-wave potential is more negative than that of **22**. A preparative electrolysis in a basic medium gives the 1,2- or 3,4-dihydro-2,3-diphenylpyrido[3,4-*b*]pyrazine (**23**). In solution, this compound shows the same cathodic wave as that observed in Fig. 10. The reduction is outlined in Scheme 7.

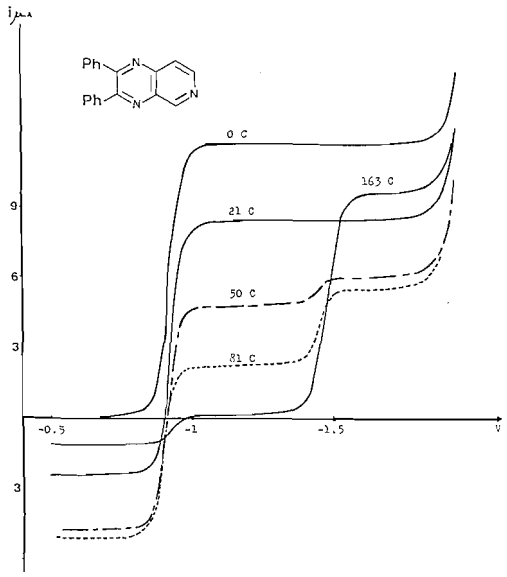

FIG. 10. Electrolysis of 2,3-diphenylpyrido[3,4-*b*]pyrazine **25** in dilute solution: 0.1 *N* NaOH, $c = 2.10^{-3}$ *M*; 75% CH_3OH, $V = 200$ ml. Polarograms recorded before (0 C), during (21 C, 50 C, 81 C), and at the end of the electrolysis (163 C).

The 1,2- (or 3,4-) dihydro-2,3-diphenylpyrido[3,4-*b*]pyrazine (**23**) presents a 2 F cathodic wave $E_{1/2} = -1.47$ V in alkaline media (CH_3OH 75%; NaOH 0.1 *N*). An electrolysis at -1.6 V consumes 2 F/mol and the resulting solution does not present any polarographic wave. Preparative electrolysis yields 1,2,3,4-tetrahydro-2,3-diphenylpyrido[3,4-*b*]pyrazine.

Thus the polarographic behaviour of 2,3-diphenylpyrido[2,3-*b*]pyrazine (**1**) is analogous to that of

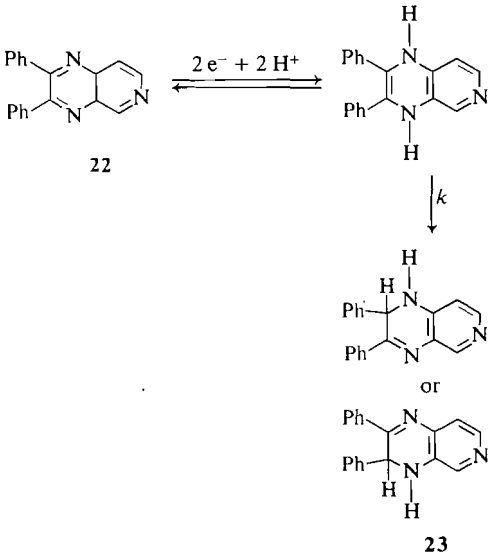

SCHEME 7. Reduction of pyrido[3,4-*b*]pyrazines in hydroorganic medium.

2,3-diphenylpyrido[3,4-*b*]pyrazine (**22**) but the rearrangement of the primary reduction product the 1,4-dihydro derivative does not involve the pyridine ring in the case of **22**. The relative position of the pyridine nitrogen is thus critical in the preparation of compounds containing hydrogenated pyridine rings.

In conclusion, the electrochemical reduction of pyridopyrazines in an aqueous or nonaqueous medium always yields a 1,4-dihydro derivative as the primary reduction product. This compound could be isolated as such or as its diacetyl derivative. This 1,4-dihydro compound usually rearranges rapidly: 1,2- or 3,4-dihydro as well as 5,8-dihydro and 5,6,7,8-tetrahydro derivatives can thus be obtained. The 1,2- or 3,4-dihydro compounds can be reduced into 1,2,3,4-tetrahydro derivatives. The correct choice of the reduction medium and of the potential permits a selective formation of one or the other of these compounds.

Experimental

Techniques

The apparatus and techniques used in hydroorganic medium have been described previously (1, 2). The reference electrode was a saturated calomel electrode. The p*H* values are measured with a Radiometer model 4 p*H* meter equipped with a combined glass–calomel electrode model GK2302B standardized in aqueous buffer. In nonaqueous media a three electrode polarograph Tacussel PRG3 was used to record the polarograms. The high scan rate voltammograms were recorded with the help of an apparatus composed of a Tacussel GSTP3 signal generator, a fast response wide bandpass potentiostat provided with an ohmic drop compensation device (14) and a memory oscilloscope Tektronix 7313. The stationary electrode was a mercury drop suspended on a gold disc 0.8 mm in diameter. The electrolyses were carried out either in the cell described previously or in a classical H cell with a 10 cm^2 mercury pool as a cathode; the potentiostat was a Tacussel ASA 100-1 and the integrator a Tacussel IG5-N. The supporting electrolyte was either 0.1 *M* tetrabutylammonium iodide or 0.1 *M* tetraethylammonium perchlorate. The reference electrodes were Ag/AgI/I^- 0.1 *M* in DMF (−0.51 V vs. sce) and Ag/Ag^+ 0.01 *M* in ACN (+0.29 V vs. sce). The microanalyses were performed by M. E. Dorme (University Pierre and Marie Curie). All the compounds described gave correct elemental analysis. The following abbreviations are used in reporting nmr results: s = singlet, d = doublet, t = triplet, q = quadruplet and m = multiplet.

Preparation of Pyrido[2,3-b]pyrazines

2,3-Diphenylpyrido[2,3-b]pyrazine (1) was prepared according to ref. 15 by reaction of 2,3-diaminopyridine with benzil in a 75:25 alcohol – acetic acid mixture; mp 144°C (alcohol); nmr ($CDCl_3$): 2-Ph + 3-Ph + 7-H, m centered at 7.5 ppm (11H); 8-H, q centered at 8.51 ppm (1H); 6-H, q centered at 9.16 ppm (1H); $J_{6-8} = 2$ Hz, $J_{7-8} = 8$ Hz, and $J_{6-7} = 5$ Hz.

3-Phenylpyrido[2,3-b]pyrazine (5) was prepared by condensation of 2,3-diaminopyridine with phenylglyoxal hydrate (11) in cold alcohol; mp 140°C; nmr ($CDCl_3$): Ph + 7-H + 8-H m centered at 7.6 and 8.3 ppm (7H); 6-H, q centered at 9.1 ppm (1H); 2-H, 9.36 ppm (1H).

Can. J. Chem. Downloaded from www.nrcresearchpress.com by 210.87.254.6 on 09/05/12
For personal use only.

Can. J. Chem. Downloaded from www.nrcresearchpress.com by 210.87.254.6 on 09/05/12
For personal use only.

2,3-Dimethylpyrido[2,3-b]pyrazine (9) was obtained by reaction of 2,3-diaminopyridine with diacetyl (15) in cold alcohol; mp 150°C (dec.) (benzene); nmr ($CDCl_3$): 2-CH_3, s, 2.7 ppm (3H); 3-CH_3, s, 2.81 ppm (3H); 7-H, q centered at 7.65 ppm (1H); 8-H, q centered at 8.38 ppm (1H); 6-H, q centered at 9.13 ppm (1H); and $J_{6-8} = 2$ Hz, $J_{7-8} = 8$ Hz, $J_{6-7} = 5$ Hz.

Electrochemical Reductions of Pyrido[2,3-b]pyrazines in Hydroorganic Media

The electrolyses in dilute solutions were carried out with 100 or 200 ml of solvent and the pyridopyrazine concentration was 2×10^{-3} *M*. The cosolvent was generally 50% methanol but the amount of methanol was increased to 75 or 80% in some cases to prevent the 1,4-dihydro derivative from precipitating.

Electrolysis of 2,3-Diphenylpyrido[2,3-b]pyrazine (1)

Preparation of 3 and 4—One gram of **1** was dissolved in 200 ml of 0.1 *N* NaOH solution (80% MeOH; $E = -1.1$ V). At the beginning of the electrolysis the solution was clear and the current 200 mA; after 720 C (682 C for 2 F/mol) the intensity fell to 5 mA. The solution with a solid in suspension was poured into 800 ml of water; the precipitate was filtered, washed with water, and dried (970 mg). An nmr spectrum showed that this solid was a 60:40 mixture of **3** and **4**. This solid was stirred in a 20:80 water–methanol mixture to give **4**; the filtrate was evaporated and yielded **3**. The analysis and the nmr spectrum of **3** showed that it was either a 1,2- or a 3,4-dihydro compound. As the nmr spectrum of the 1,2-dihydro-2,3-diphenylpyrido[2,3-*b*]pyrazine prepared by the method of ref. 12 was different from that of **3**, this compound must be the 3,4-dihydro-2,3-diphenylpyrido[2,3-*b*]pyrazine; mp 208°C (methanol); nmr ($CDCl_3 + D_2O$): 3-H, s, 5.9 ppm (1H); 7-H, q centered at 6.66 ppm (1H); 3-Ph + 2-Ph + 6-H, m centered at 7.35 and 7.9 ppm (11H); 8-H, q centered at 7.61 ppm (1H).

The analysis and the nmr spectrum showed that **4** was the 5,6,7,8-tetrahydro-6-methoxy-2,3-diphenylpyrido[2,3-*b*]pyrazine; mp 200°C (dec.) (methanol); nmr ($CDCl_3$): —CH_2—CH_2—, m centered at 2.15 and 3.15 ppm (4H); —O—CH_3, s, 3.28 ppm (3H); 6-H, m centered at 4.41 ppm (1H); $\rangle$N—*H*, s, 6.6 ppm disappears upon addition of D_2O (1H); 2-Ph + 3-Ph, m centered at 7.3 ppm (10H).

Acetyl derivative of 3—The product was dissolved in acetic anhydride (16) to give 4-acetyl-3,4-dihydro-2,3-diphenylpyrido[2,3-*b*]pyrazine (50% yield); mp 150°C (methanol); nmr ($CDCl_3$): —COCH_3, s, 2.48 ppm (3H); 2-Ph + 3-Ph + 3-H + 6-H + 7-H + 8-H, m between 7 and 8.3 ppm (14H).

Electrolysis of 3-Phenylpyrido[2,3-b]pyrazine (5)

Preparation of 7—The electrolysis of 1 g of **5** (70% CH_3OH, 0.1 *N* NaOH; $E = -1.1$ V) gave 600 mg of 5,6,7,8-tetrahydro-6-methoxy-3-phenylpyrido[2,3-*b*]pyrazine (**7**) (51% yield) after consumption of 2.06 F/mol; mp 183°C (methanol); nmr ($CDCl_3 + D_2O$): —CH_2—CH_2—, m centered at 2.15 and 3 ppm (4H); —O—CH_3, s, 3.3 ppm (3H); 6-H, m centered at 4.53 ppm (1H); Ph, m centered at 7.45 and 7.9 ppm (5H); 2-H, s, 8.3 ppm (1H).

Preparation of 8—Conditions were the same as above but ethanol instead of methanol was used; 1 g of **5** gave 730 mg of 5,6,7,8-tetrahydro-6-ethoxy-3-phenylpyrido[2,3-*b*]pyrazine (**8**) (59% yield); mp 165°C (ethanol); nmr ($CDCl_3$): —CH_2—CH_2— and —O—CH_2—, m centered at 2.15 and 3.3 ppm (6H); CH_3, t, 1.16 ppm (3H); 6-H, m centered at 7.45 and 7.9 ppm (5H); 2-H, s, 8.3 ppm (1H).

Electrolysis of 2,3-Dimethylpyrido[2,3-b]pyrazine (9)

Preparation of 12—One gram of **9** was electrolyzed (CH_3OH 80%; NaOH 0.2 *N*; $E = -1.2$ V; 2.16 F/mol) and the solution was extracted with five portions of 25 ml $CHCl_3$; the organic layer was dried and evaporated to give 350 mg of a solid containing **11** and **12** in 15:85 ratio as shown by nmr. This solid was dissolved in 2 ml of benzene and, upon addition of cyclohexane, 250 mg of a precipitate identified as 1,2- or 3,4-dihydro-2,3-dimethylpyrido[2,3-*b*]pyrazine (**12**) was obtained (25% yield); mp 106°C; nmr ($CDCl_3 + D_2O$): CH_3—$\underset{|}{C}$—H, d, 1.33 ppm (3H); CH_3—$\underset{|}{C}$=, s, 2.13 ppm (3H); CH_3—$\underset{|}{C}$—*H*, q, 4.3 ppm (1H); 7-H, 8-H, and 6-H, q centered at 6.6, 7.36, and 7.8 ppm (3H); $J_{CH_3-C-H} = 6$ Hz. The nmr of 5,6,7,8-tetrahydro-6-methoxy-2,3-dimethylpyrido[2,3-*b*]pyrazine (**11**) in $CDCl_3 + D_2O$: —O—CH_3, s, 3.3 ppm (3H); 2-CH_3 and 3-CH_3, s, 2.35 and 2.31 ppm (3H each); CH_3—O—$\underset{|}{C}$—*H*, m centered at 4.68 ppm (1H).

Electrochemical Reduction of Pyrido[2,3-b]pyrazines in Non-aqueous Media

The cathodic solution contained 60 ml of solvent, 1 g of substrate, and 8 ml of acetic anhydride or a quantity of phenol corresponding to about 10 times that of the substrate.

Electrolysis of (1) in DMF in the Presence of Acetic Anhydride

Electrolysis was carried out at $E = -1.1$ V; 2.06 F/mol; the electrolyzed solution was poured into 500 ml of water, the precipitate was filtered, washed with water, and dried. This product was dissolved in ether, hexane was added, and the brown precipitate was filtered. The filtrate was evaporated to dryness to give 300 mg of 5,8-dihydro-5-acetyl-2,3-diphenylpyrido[2,3-*b*]pyrazine (**13**) which was recrystallized from methanol (26% yield); mp 128°C; nmr ($CDCl_3$): CH_3—CO—, s, 2.77 ppm (3H); —CH_2—, q centered at 3.78 ppm (2H); 7-H, m centered at 7.41 ppm (1H); 2-Ph + 3-Ph + 6-H, m centered at 7.35 ppm (11H). When 100 mg of **13** was dissolved in 25 ml of alkaline solution (CH_3OH 80%; NaOH 0.1 *N*) a precipitate appeared after 10 min at room temperature. The solution was concentrated, the precipitate filtered, washed with water, and dried to give a quantitative yield of **4**.

Electrolysis of 5 in DMF in the Presence of Acetic Anhydride

Electrolysis was carried out at $E = -1.0$ V, 1.80 F/mol. The solution was treated in the usual way and gave a gummy mixture whose nmr spectrum indicated the presence of the starting pyridopyrazine among other unidentified products. Tentative purifications were unsuccessful.

Electrolysis of 1 in ACN in the Presence of Acetic Anhydride

Electrolysis was carried out at $E = -1.75$ V, 2.00 F/mol. The solution remained yellow during electrolysis; (the characteristic red colour of the 1,4-dihydro derivative did not appear). At the end of electrolysis, the solution was poured into 800 ml of water and a gummy compound precipitated which crystallized after 1 h. The precipitate was filtered, washed with water, and dried to give 1.05 g of **13** (91% yield).

Electrolysis of 5 in ACN in the Presence of Acetic Anhydride

Electrolysis was carried out at $E = -1.8$ V, 2.16 F/mol. During electrolysis the solution became red; at the end, the solution was poured into 1 ℓ of water. After 24 h the red-orange precipitate which formed was filtered, washed with water, and dried; thus, 270 mg of 1,4-dihydro-1,4-diacetyl-3-phenylpyrido[2,3-*b*]pyrazine (**14**) was obtained (19% yield); mp 206°C (methanol); nmr ($CDCl_3$): —CO—CH_3, s at 2.21 and 2.28 ppm (6H); 2-H, s, 6.66 ppm (2H); Ph + 6-H + 7-H + 8-H, m centered at 7.3 and 8.2 ppm (8H). In alkaline solution (CH_3OH 50%, NaOH 0.1 *N*) **14** desacetylated to give **5**.

Can. J. Chem. Downloaded from www.nrcresearchpress.com by 210.87.254.6 on 09/05/12
For personal use only.

*Electrolysis of **1** in DMF in the Presence of Phenol*

Electrolysis was carried out with 1 g of **1**, 1.66 g of phenol at $E = -1.0$ V, 1.80 F/mol. The solution became red during the electrolysis and at the end it was diluted with 500 ml of water; the precipitate was filtered, washed with water, and dried to give 900 mg of a product which, after recrystallization in MeOH, led to 640 mg of 3,4-dihydro-2,3-diphenylpyrido-[2,3-*b*]pyrazine (**3**) (63% yield).

*Electrolysis of **5** in DMF in the Presence of Phenol*

Electrolysis was carried out with 1 g of **5**, 2.3 g of phenol at $E = -1.0$ V, 1.82 F/mol. The solution became red and at the end of the electrolysis, it became yellow when exposed to air; (oxidation of the 1,4-dihydro derivative). An nmr spectrum in $CDCl_3$ showed that the compound which precipitated after dilution in deoxygenated water was a mixture containing mostly the starting pyridopyrazine. A polarogram of this product (MeOH 50%; NaOH 0.1 *N*) showed the anodic wave of **6**. A purification was attempted without results.

*Electrolysis of **1** in DMF in the Presence of Phenol*

Electrolysis was carried out with 1 g of **1**, 2 g of phenol at $E = -1.75$ V, 2.24 F/mol. The solution became red during the electrolysis and a precipitate appeared; it was filtered, washed with ACN, and dried to give 450 mg of 5,8-dihydro-2,3-diphenylpyrido[2,3-*b*]pyrazine (**15**) (45% yield). The filtrate was diluted with 800 ml of water to give a gummy product which was shown by nmr to be a mixture of **1**, **3**, and **15**. For **15**, mp 245°C (CH_3CN); nmr (DMSO-d_6): $-CH_2-$, q, 3.73 ppm (2H); 7-H, m centered at 4.66 ppm (1H); 6-H, m centered at 6.16 ppm (becoming a doublet upon addition of MeOD) (1H); 2-Ph + 3-Ph, m centered at 7.3 ppm (10H); $\rangle$N—H, d, 8.2 ppm (disappears on addition of MeOD) (1H); an irradiation of the $\rangle$NH signal transforms the 6-H signal into a doublet and irradiation of 6-H transforms the 7-H and $-CH_2-$ signals into a triplet and a doublet, respectively.

When 35 mg of **15** was dissolved in 30 ml of CH_3OH the reactant was recovered unchanged after 24 h at room temperature (nmr). Thus, methanol does not add to **15** under these conditions.

When 100 mg of **15** was dissolved in a DMF – acetic anhydride mixture, starting material was also recovered unchanged after 24 h at room temperature; thus **15** does not acetylate into **13** under these conditions.

When 100 mg of **15** was stirred for 24 h in an alkaline solution (80% CH_3OH; 0.1 *N* NaOH (i.e. conditions which allow the formation of **4** by electrolysis), filtered, washed with water, and dried 85 mg of **4** was obtained.

*Electrolysis of **5** in ACN in the Presence of Phenol*

Electrolysis was carried out with 1 g of **5**, 2.3 g of phenol at $E = -1.75$ V, 2.16 F/mol. As in the case of **1**, the solution became red during the electrolysis and a precipitate appeared which was filtered and washed with ACN to give 450 mg of 5,8-dihydro-3-phenylpyrido[2,3-*b*]pyrazine (**16**); by diluting the filtrate with water 150 mg of **16** was obtained (59% yield); mp 225°C (ACN); nmr (DMSO-d_6): $-CH_2-$, q, 3.71 ppm (2H); 7-H, m, 4.6 ppm (1H); 6-H, m centered at 6.2 ppm (becomes a doublet upon addition of MeOD) (1H); 3-Ph, m centered at 7.5 and 8.05 ppm (5H); 2-H + $\rangle$N—H, s, 8.5 ppm and a broad signal which disappears on addition of MeOD.

Preparation of 7-Bromopyrido[2,3-b]pyrazines

*7-Bromo-2,3-diphenylpyrido[2,3-b]pyrazine (**17**)* was obtained by condensation of 5-bromo-2,3-diaminopyridine (**9**) with benzil as (15) in a 25:75 acetic acid – alcohol mixture; mp 155°C (dec.) (alcohol); nmr ($CDCl_3$): 2-Ph + 3-Ph, m centered at 7.4 ppm (10H); 8-H, d, 8.6 ppm (1H); 6-H, d, 9.1 ppm (1H); $J_{6-8} = 2$ Hz.

*7-Bromo-3-phenylpyrido[2,3-b]pyrazine (**18**)* was obtained according to ref. 11 by condensation of 5-bromo-2,3-diaminopyridine with phenyl glyoxal hydrate in alcohol at room temperature; mp 168°C (alcohol); nmr ($CDCl_3$): 3-Ph, m centered at 7.6 and 8.3 ppm (10H); 8-H, d, 8.6 ppm (1H); 6-H, d, 9.16 ppm (1H); $J_{6-8} = 2$ Hz; 2-H, s, 9.43 ppm (1H).

*7-Bromo-2,3-dimethylpyrido[2,3-b]pyrazine (**19**)* was obtained by reaction of 5-bromo-2,3-diaminopyridine with diacetyl at room temperature (15); mp 150°C (dec.) (benzene); nmr ($CDCl_3$): 2-CH_3 and 3-CH_3, s, 2.78 and 2.80 ppm (6H); 8-H, d, 8.43 ppm (1H); 6-H, d, 9.03 ppm (1H); $J_{6-8} = 2$ Hz.

Reduction of 7-Bromopyrido[2,3-b]pyrazines in Hydroorganic Media

The electrolyses in dilute solutions were carried out in 100 or 200 ml of solution at a concentration of 2×10^{-3} *M* but owing to the insolubility of the bromopyridopyrazines, the amount of methanol was always 75–80%. In alkaline medium, the compounds obtained by reduction of **17**, **18**, and **19** are the same and in the same amounts as those obtained from their homologues **1**, **5**, and **9**: reduction of 1 g of **17**: CH_3OH 80%, NaOH 0.1 *N*, $E = -1.1$ V, 4.30 F/mol; reduction of 1 g of **18**: CH_3OH 70%, NaOH 0.1 *N*, $E = -1.1$ V, 4.30 F/mol; reduction of 1 g of **19**: CH_3OH 80%, NaOH 0.1 *N*, $E = -1.2$ V, 4.32 F/mol.

*Electrolysis of 7-Bromo-2,3-dimethylpyrido[2,3-b]pyrazine (**19**) in Neutral Medium*

As the ionic strength of a NaH_2PO_4–Na_2HPO_4 buffer is not high enough in an 80% methanol solution (the solubility of sodium phosphate is low in this medium) an acetic acid – ethylene diamine buffer was used. A solution was prepared from 10 g of acetic acid and 6 g of ethylenediamine in 190 ml CH_3OH; 160 ml of this solution was used to dissolve 2 g of **19** and water was added to 250 ml (p*H* 7.29; $E = -0.8$ V; 2.32 F/mol). At the end of the electrolysis, the solution was poured into 300 ml of water, filtered, and the filtrate extracted with six portions of 50 ml $CHCl_3$. The organic layer was dried and evaporated to give a gum which crystallized in cyclohexane to give 600 mg of **20** (30% yield); mp 160°C (dec.); nmr ($CDCl_3$ + D_2O): $CH_3-\underset{|}{\overset{|}{C}}-H$, d, 1.2 ppm (3H); $CH_3-\overset{|}{C}=$, s, 2.15 ppm (3H); $CH_3-\underset{|}{\overset{|}{C}}-H$, q centered at 4.32 ppm (1H); $J_{CH_3-C-H} = 6$ Hz; 6-H and 8-H, d at 7.48 (1H) and 7.83 ppm (1H), $J_{6-8} = 2$ Hz.

Reduction of 7-Bromopyrido[2,3-b]pyrazine in Aprotic Medium

The coulometric measurements were carried out in 50 ml of ACN at a concentration of 10^{-2} or 10^{-3} *M*. The final products were identified and titrated by polarography and glc (3% OV17 on Varaport 100–120, 1.5 m). An electrolysis of 7-bromo-2,3-diphenylpyrido[2,3-*b*]pyrazine (**17**) was carried out to prepare **1**: 1 g of **17** in DMF; $E = -0.7$ V. After completion of the electrolysis, the solution was poured into 500 ml of water and the precipitate was filtered, washed with methanol (in which **1** only is soluble) to obtain 400 mg of **1** (51% yield).

*Preparation of the 1,4-Dihydro-2,3-diphenylpyrido[2,3-b] pyrazine (**2**) by Electrochemical Reduction of **1***

Electrolysis of a 2×10^{-3} *M* solution of **1** (CH_3OH 50%, p*H* 7, $E = -0.7$ V) gave a red orange precipitate of **2** which was filtered under nitrogen, washed with deoxygenated water, and dried under nitrogen. In a deoxygenated alkaline solution (80% CH_3OH, 0.1 *N* NaOH) **2** presented an anodic wave the

Can. J. Chem. Downloaded from www.nrcresearchpress.com by 210.87.254.6 on 09/05/12
For personal use only.

$E_{1/2}$ of which was identical to that of the anodic wave observed during the electrolysis of **1**. When a solution of **2** was put in contact with air, the red colour disappeared and the polarogram showed only the cathodic wave of **1**.

Reduction of **5** *by Sodium Dithionite. Preparation of 1,4-Dihydro-3-phenylpyrido[2,3-*b*]pyrazine (6)*

The procedure of ref. 16 was used with some modifications: 4 g of sodium dithionite and 130 ml of alcohol were added to a solution of 4 g of sodium carbonate in 130 ml of water vigorously stirred and maintained under nitrogen. The solution was heated to 40°C and 867 mg of **5** in 10 ml of chloroform was added dropwise. The mixture is maintained 4 h at 40°C under nitrogen with continuous stirring: a brown solid appeared in the solution. After cooling, the precipitate was filtered under nitrogen, washed with deoxygenated water, and dried under nitrogen; 750 mg of 1,4-dihydro-3-phenylpyrido[2,3-*b*]pyrazine (**6**) was thus obtained. Compound **6** burned spontaneously in contact with air. In a deoxygenated basic solution (CH_3OH 50%, NaOH 0.1 *N*) **6** presented the same anodic wave as that shown in Fig. 3. In this solution **6** was instantaneously and quantitatively reoxidized to **5** when in contact with air. Tentative acetylations by the method of ref. 16 did not give any positive result.

*Preparation of Tetrahydropyrido[2,3-*b*]pyrazines. Catalytic Hydrogenation of* **5** *on 5% Pd/C*

A catalytic hydrogenation was carried out at room temperature with 300 mg of **5** in 100 ml ethanol in the presence of 75 mg of 5% Pd/C. After 12 h of stirring and consumption of 75 ml of hydrogen (theoretical: 65 ml of H_2 if 2 mol of H_2 are consumed per mole of **5**) the solution was filtered and evaporated to dryness to give a solid which was shown by nmr to be a mixture of 1,2,3,4-tetrahydro- and 5,6,7,8-tetrahydro-3-phenylpyrido[2,3-*b*]pyrazine in an 80:20 ratio. Recrystallization from alcohol afforded 100 mg of 1,2,3,4-tetrahydro derivative (33% yield); mp 181°C; nmr ($CDCl_3$ + D_2O): $-CH_2-$, m centered at 3.40 ppm (2H); Ph—$\underset{|}{C}$—*H*, q centered at 4.62 ppm (1H); 3-Ph + 6-H + 7-H + 8-H, m, 6.4–7.6 ppm (8H).

*Electrolysis of 3,4-dihydro-2,3-diphenylpyrido[2,3-*b*]pyrazine (***3***). Preparation of* cis*-1,2,3,4-Tetrahydro-2,3-diphenylpyrido[2,3-*b*]pyrazine*

Electrolysis was carried out using 100 mg of **3** in 100 ml of solution (60% CH_3OH, 0.1 *N* NaOH) at $E = -1.6$ V, 2.0 F/mol. At the end of electrolysis the methanol was evaporated, water added, and the precipitate was filtered. By recrystallization from alcohol, 85 mg of *cis*-1,2,3,4-tetrahydropyrido-[2,3-*b*]pyrazine was obtained; mp 206°C; nmr ($CDCl_3$): 2-H and 3-H, d, 4.70 and 4.80 ppm (after addition of D_2O) (2H); 2-Ph + 3-Ph + 6-H + 7-H + 8-H, m between 6.5 and 7.7 ppm (13H); $\rangle$N—H broad signals at 4.10 and 5.50 ppm (disappeared on addition of D_2O) (2H).

*Electrolysis of 1,2- (or 3,4-) Dihydro-2,3-dimethylpyrido-[2,3-*b*]pyrazine (***12***)*

Compound **12** was not electroreducible in alkaline medium; this compound was obtained by electrochemical reduction of **9** in a low yield. For this reason, electrolysis was carried out on 1 g of **9** (200 ml of solution; 50% CH_3OH, 0.1 *N* H_2SO_4) at a potential corresponding to the cathodic wave of **12** ($E = -1.1$ V, 3.84 F/mol). After completion of electrolysis, the solution was neutralized with 20 ml of 0.1 *N* NaOH and extracted six times with 25 ml of chloroform. The organic layer was dried and evaporated to give 733 mg (yield 71%) of a solid which was shown by nmr to be a mixture of *cis*- and *trans*-1,2,3,4-tetrahydro-2,3-dimethylpyrido[2,3-*b*]pyrazine; nmr ($CDCl_3$ + D_2O): $CH_3-\underset{|}{\overset{|}{C}}-\underset{|}{\overset{|}{C}}-CH_3$, m centered at 1.1 ppm (6H); $CH_3-\underset{|}{\overset{|}{C}}H-\underset{|}{\overset{|}{C}}H-CH_3$, m centered at 3.3 ppm (2H); 6-H, 7-H, and 8-H, m centered at 6.5 and 7.4 ppm (3H).

*Pyrido[3,4-*b*]pyrazine*

*Preparation of 2,3-Diphenylpyrido[3,4-*b*]pyrazine (***22***)*

This was obtained according to ref. 17 by condensation of the 3,4-diaminopyridine with benzil in alcohol; mp 177°C (alcohol); nmr ($CDCl_3$): 2-Ph + 3-Ph, m centered at 7.5 ppm (10H); 7-H and 8-H, d, 8.06 (1H) and 8.91 ppm (1H) (J_{7-8} = 6 Hz); 5-H, s, 9.71 ppm (1H).

Electrolysis of **22**

One gram of **22** was partially dissolved in 200 ml of 0.1 *N* NaOH solution containing 75% methanol. During the electrolysis (initial current, 150 mA), the solution became red (indicating the formation of the 1,4-dihydro derivative). After consumption of 2.06 F/mol the current falls to 5 mA and all the solid is dissolved. Electrolysis was continued for 2 h after which the red colour had disappeared and a new solid precipitated. This precipitate was filtered, washed with water, and dried (560 mg); more of this compound (360 mg) could be obtained by diluting the filtrate with water (total yield 91%). This product was shown to be 1,2- (or 3,4-) dihydro-2,3-diphenylpyrido[3,4-*b*]pyrazine (**23**); mp 247°C (alcohol); nmr (DMSO-d_6 + D_2O): Ph—$\underset{|}{C}$—*H*, s, 6.13 ppm (1H); 7-H or 8-H, d, 6.61 ppm (J_{7-8} = 6 Hz) (1H); 7-H or 8-H + 2-Ph + 3-Ph, m centered at 7.4 and 8.1 ppm (11H); 5-H, s, 8.36 ppm (1H).

Acetyl Derivative of **23**

Compound **23** was easily acetylated according to the method of ref. 16 to give 1,2- (or 3,4-) dihydro-1- (or 4-) acetyl-2,3-diphenylpyrido[3,4-*b*]pyrazine; mp 150°C (dec.; methanol); nmr ($CDCl_3$): $-CO-CH_3$, s, 2.41 ppm (3H); 2-Ph + 3-Ph, m, 6.9–7.6 ppm (10H); 7-H + 8-H + Ph—$\underset{|}{C}$—*H*, m centered at 8.1 ppm and d at 8.35 ppm (3H); 5-H, s, 8.96 ppm (1H).

Electrolysis of **23**

One gram of **22** was dissolved in 200 ml of solution (70% CH_3OH, 0.1 *N* NaOH) and the potential is set at the level of the cathodic wave of **23**: $E = -1.6$ V, 5.04 F/mol. At the end of the electrolysis, the methanol was evaporated and the solution diluted with 500 ml of water. The precipitate was filtered, washed with water, and dried to give 1 g (98% yield) of *cis*- or *trans*-1,2,3,4-tetrahydro-2,3-diphenylpyrido[3,4,*b*]-pyrazine; mp 110°C (dec.); nmr ($CDCl_3$ + D_2O): Ph—$\underset{|}{C}$*H*—$\underset{|}{C}$*H*—Ph, s, 4.66 ppm (2H); 7-H and 8-H, d, 6.40 and 7.73 ppm (J_{7-8} = 6 Hz) (2H); 2-Ph + 3-Ph, m, 6.6–7.23 ppm (10H); 5-H, s, 7.73 ppm (1H).

1. J. Pinson, J. P. M'Packo, N. Vinot, J. Armand, and P. Bassinet. Can. J. Chem. **50**, 1581 (1972).
2. J. Armand, K. Chekir, and J. Pinson. Can. J. Chem. **52**, 3971 (1974).
3. A. Albert. Adv. Heterocycl. Chem. **20**, 117 (1976).
4. H. Lund and J. Simonet. C.R. Acad. Sci. Ser. C, **277**, 1387 (1973).
5. D. Boutte, G. Queguiner, and P. Pastour. C.R. Acad. Sci. Ser. C, **273**, 1529 (1971).

6. L. NADJO and J. M. SAVEANT. J. Electroanal. Chem. **30**, 41 (1971).
7. K. ALWAIR and J. GRIMSHAW. J. Chem. Soc. Perkin II, 1811 (1973).
8. F. M'HALLA, J. PINSON, and J. M. SAVEANT. J. Electroanal. Chem. In press.
9. M. TISHLER, G. A. STEIN, G. LINDBERG, and M. RYDER. Org. Synth. **44**, 34 (1964).
10. R. C. DE SELMS and H. S. MOSHER. J. Org. Chem. **82**, 3762 (1960).
11. N. VINOT and P. MAITTE. Bull. Soc. Chim. Fr. 3100 (1973).
12. N. VINOT and P. MAITTE. Bull. Soc. Chim. Fr. 251 (1976).
13. J. ARMAND, K. CHEKIR, J. PINSON, and N. VINOT. C.R. Acad. Sci. Ser. C, **281**, 547 (1975).
14. D. GARREAU and J. M. SAVEANT. J. Electroanal. Chem. **35**, 309 (1972).
15. N. VINOT and P. MAITTE. C.R. Acad. Sci. Ser. C, **275**, 681 (1972).
16. H. I. X. MAGER and W. BERENDS. Recl. Trav. Chim. Pays-Bas, **79**, 282 (1960).
17. J. W. CLARK-LEWIS and R. P. SINGH. J. Chem. Soc. 3162 (1962).

Can. J. Chem. Downloaded from www.nrcresearchpress.com by 210.87.254.6 on 09/05/12
For personal use only.

Theoretical and experimental behaviour of a thermal conductivity detector for the determination of the *ortho/para* hydrogen composition of gas mixtures in the temperature-jump region[1]

DAVID N. MITCHELL[2] AND DONALD J. LE ROY

Division of Chemistry, National Research Council of Canada, Ottawa, Ont., Canada K1A 0R6

Received December 13, 1977

DAVID N. MITCHELL and DONALD J. LE ROY. Can. J. Chem. **56**, 1817 (1978).

The theoretical characteristics of a thermistor type thermal conductivity detector were determined for gases in the range 1 to 30 Torr, and were tested experimentally for mixtures of *ortho*- and *para*-hydrogen in pure hydrogen and in dilute mixtures of hydrogen in helium. It was found that the detector could be treated as being spherically symmetric. For temperature-jumps of up to 100 K, the total heat transfer could be adequately explained by a simplified form of the Kennard temperature-jump theory, only two parameters being required, the radius of the thermistor and its accommodation coefficient. The differential behaviour, the sensitivity to changes in *ortho/para* composition, required an additional parameter, the apparent gas phase relaxation rate for rotational energy.

DAVID N. MITCHELL et DONALD J. LE ROY. Can. J. Chem. **56**, 1817 (1978).

On a déterminé les caractéristiques théoriques d'un détecteur de conductivité thermique de type thermistance pour les gaz à des pressions allant de 1 à 30 Torr et on les a vérifiées expérimentalement pour des mélanges d'hydrogène *ortho* et *para* dans de l'hydrogène pur et dans des mélanges dilués d'hydrogène dans l'hélium. On a trouvé que le détecteur peut être traité comme étant sphériquement symétrique. Pour des sauts de température allant jusqu'à 100 K, on peut expliquer adéquatement le transfert total de chaleur par une forme simplifiée de la théorie de Kennard concernant les sauts de température dans lesquels il ne faut que deux paramètres soit le rayon de la thermistance et son coefficient d'accommodation. Le comportement différentiel, la sensibilité à des changements dans des compositions *ortho/para*, nécessite un paramètre additionnel, le taux apparent de relaxation en phase gazeuse pour l'énergie rotationnelle.

[Traduit par le journal]

Introduction

The differing thermal conductivities of *ortho*-hydrogen (*o*-H_2) and *para*-hydrogen (*p*-H_2) have been used for many years for measuring the *ortho/para* composition of hydrogen (1–11). Following the development of gas chromatography, thermal conductivity cells were used in conjunction with chromatographic columns for separating and measuring *o*-H_2 and *p*-H_2, even in the presence of other gases (2, 3, 6–10). However, in gas phase reaction kinetic studies in flow systems at pressures less than 1 atm, the chromatographic method requires *off-line* collection, compression, and processing of the sample, generally at pressures of 1 atm or more. Recently the original, direct, thermal conductivity method was adapted to studies of the kinetics of hydrogen atom exchange in a flow system, by locating the thermal conductivity cells *on-line*, immediately following the reaction vessel, and operating them at the reactor pressure (4, 5, 11). This avoided the considerable time required for *off-line* processing using gas chromatography, as well as the possibility of *ortho/para* equilibration on the chromatographic column (6). A drawback of the *on-line* technique is that heat conduction is pressure dependent at the pressures (1 to 30 Torr) used in these experiments. This effect, attributed to the phenomenon of the "temperature-jump", has been recognized for many years (12–25). It can be avoided by internal calibration (11) or by using relative concentration measurements at fixed pressure (4, 5).

We have recently used the *on-line* method to measure the fraction of *p*-H_2 in hydrogen formed by gas phase three-body recombination in the presence of a large excess of helium (11). Because a wider range of pressures was needed to study the kinetics than had been used previously (4, 5), the pressure dependence of the signal was significant, and so it was decided to investigate the behaviour of the thermal conductivity detector in greater detail. In the paper we develop a theoretical model for the sensitivity of the detector and its pressure dependence, and show experimentally that the model is reasonable.

Experimental

Apparatus

The thermal conductivity detector used in these experiments

[1]NRCC No. 16545.

[2]Present address: Aluminium du Canada, Ltée, Centre de Recherche d'Arvida, C.P. 250, Arvida, Jonquière, Québec, Canada.

Can. J. Chem. Downloaded from www.nrcresearchpress.com by 210.87.254.40 on 09/05/12
For personal use only.

Can. J. Chem. Downloaded from www.nrcresearchpress.com by 210.87.254.40 on 09/05/12
For personal use only.

was similar to that described previously (4, 5), but incorporated several important modifications. The two thermal conductivity cells, *sample* and *reference*, were inserted via T joints in the flow line between the reaction vessel and the pressure control valve immediately before the pump; the former was upstream from the latter. Tungsten filaments, called equilibrators, were inserted between the thermal conductivity cells and the T joints. When heated to incandescence, these converted the hydrogen in the gas diffusing from the flow line to the thermal conductivity cells into *normal* hydrogen (n-H_2), containing a mole fraction of p-H_2 equal to 0.2500. The reference equilibrator was left *on* continuously to produce an n-H_2 reference, and the sample equilibrator was turned *on* in order to zero the bridge, and *off* to observe the difference in the fraction of p-H_2 in the sample gas.

The actual apparatus is shown in Fig. 1. The cylindrical thermal conductivity chambers (A), 3.3 cm deep by 1.9 cm in diameter, were drilled in a single, massive (3 kg) block of stainless steel, machined to fit into a 5 ℓ Dewar flask. Gases diffused from the reactant gas stream, through the equilibrators, to the thermal conductivity chambers via thin-walled stainless steel tubes (B), 4.8 cm in diameter and 18 cm long. The Dewar flask served as a temperature controlling bath and the thin-walled tubing reduced heat conduction from the room. Thus the walls of the thermal conductivity chambers could be maintained at a constant temperature.

The *hot* element of each thermal conductivity cell was a glass-coated bead thermistor (C) (Veco, Type 32A7, nominal resistance 2000 Ω at 25°C), soldered to electrical leads mounted in a long glass tube (D). These tubes were held rigidly in place by spring steel clips (E) at the bottom and O-ring seals (F) at the top of the stainless steel tubes. This arrangement allowed easy removal of the thermistor assembly for inspection or replacement.

The equilibrators (G) consisted of standard 500 W tungsten lamp filaments, stretched between supports to give a total length of 40 cm, and mounted in Pyrex tubes. The Pyrex tubes were jacketed and water was circulated from a thermostatted bath to keep the walls at a constant temperature of 25°C.

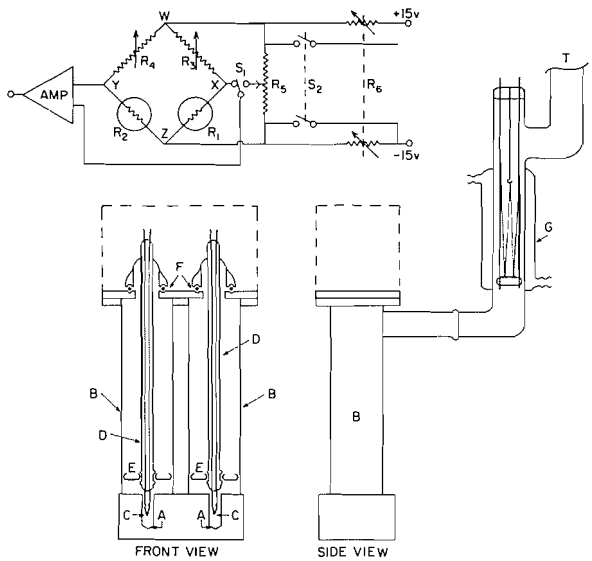

FIG. 1. Thermal conductivity detector. A, thermistor well; B, thin-walled stainless steel tube; C, bead thermistor; D, glass tube; E, spring steel clip; F, O-ring seal; G, equilibrator; T, T-joint connection. Bridge circuit is discussed in the text.

The thermistors comprised two arms of a conventional DC bridge circuit, also shown in Fig. 1. The thermistors R_1 and R_2 are designated as *sample* and *reference* thermistors respectively. The remaining arms of the bridge (R_3 and R_4) consisted of precision decade resistance boxes. The bridge output voltage V, between points X and Y was applied to a Burr Brown Instrumentation Amplifier, Type 3061/25, generally operated at unit gain; the amplifier output was read using a DC digital voltmeter with 10 μV sensitivity. The bridge voltage (E) between points W and Z was fixed at 30 V by applying the full output of a ±15 V stabilized DC power supply (Semiconductor Circuits Incorporated, Type LCD2.15.100A, ±0.001% stability). Consequently, the potential at points X and Y was near ground and saturation of the amplifier was avoided. Adjusting R_3 and R_4 allowed for slight differences in R_1 and R_2 (less than 0.5% at 25°C) and allowed both the temperature of the thermistors and the output voltage (V) to be adjusted simultaneously. The additional resistors (R_5 and R_6) and switches (S_1 and S_2) allowed E to be gradually increased to the final value of 30 V as the thermal conductivity chamber walls were cooled. This prevented the thermistors from either overheating or 'freezing'.

In operation, a change in the p-H_2 composition of the gas in the sample cell (by turning its equilibrator *off*) resulted in a change in thermal conductivity. This in turn caused the heat dissipated by R_1, and hence its resistance, to change, thereby causing a change in the voltage drop across R_1 which was detected as a change in the voltage V between X and Y.

Theory

The objective was to derive an expression for the sensitivity of the detector, defined as dV/dX_p, where X_p is the mole fraction of hydrogen in p-H_2 form in the hydrogen in a mixture of hydrogen and another gas, He in this case. Since n-H_2 is the reference, dV/dX_p is to be evaluated for $X_p = 0.25$. Accordingly, a model was developed for W_1, the power dissipated by the thermistor R_1. The general equation governing steady-state heat conduction from a thermistor through a gas at any pressure to a cylindrical wall, when the thermal conductivity of the gas, K, is dependent on temperature, is not readily solved. We therefore made a number of simplifying assumptions. Firstly, it was assumed that the thermistor bead is spherical. Secondly, it was assumed that the working pressures are sufficiently high that the conventional heat conduction equation (26), with temperature-jump boundary conditions (16), is valid. Finally, it was assumed that the wall radius is sufficiently large compared to the thermistor radius r_1, that the heat flow problem can be treated as that of a spherical heat source in an infinite medium, with the asymptotic gas temperature, as the radial distance tends to infinity, equal to the wall temperature, T_W. These assumptions were later tested experimentally.

For this model, the differential equation governing heat conduction is

$$[1] \qquad r^{-2}\, d[r^{-2}K(T)\, dT/dr]/dr = 0$$

After one integration we obtain

Can. J. Chem. Downloaded from www.nrcresearchpress.com by 210.87.254.40 on 09/05/12
For personal use only.

[2] $$K(T)\,dT/dr = -W_1/4\pi r^2$$

where the form of the integration constant, $-W_1/4\pi$, follows from the observation that the power transmitted through any closed spherical surface of radius $r > r_1$ is equal to W_1, the power dissipated by the thermistor. On integrating [2] between the limits $r_1 < r < \infty$, we obtain the relation

[3] $$W_1 = 4\pi r_1 \int_{T_w}^{T_1'} K\,dT$$

where T_1' is, in general, less than the temperature of the thermistor, T_1, because of the temperature-jump phenomenon. The lower limit of the integration is taken to be the temperature of the wall T_w, i.e. the limit of $T(r)$ as $r \to \infty$.

It is found experimentally that the temperature-jump vanishes at sufficiently high pressures. Thus, for spherical symmetry,

[4] $$\lim_{p\to\infty} W_1 = W_1^{\infty} = 4\pi r_1 \int_{T_w}^{T_1} K\,dT$$

Hence [3] may be written

[5] $$W_1 = W_1^{\infty} - 4\pi r_1 \int_{T_1'}^{T_1} K\,dT$$

The term W_1^{∞} is normally evaluated empirically as the intercept of a plot of $1/W_1$ vs. $1/P$. Values of T_1' may also be evaluated empirically, most easily by using the explicit form[3] $K(T) = AT^B$ in the range $T_1' \leq T \leq T_1$. Thus

[6] $$T_1' = \left[T_1^{B+1} - \frac{(W_1^{\infty} - W_1)}{4\pi r_1}\frac{(B+1)}{A}\right]^{1/(B+1)}$$

where, in the present instance, r_1 is obtained from [4].

In theoretical considerations the temperature-jump is usually expressed (16) in the form

[7] $$T_1' = T_1 + g_1(dT/dr)_{r_1}$$

Thus, from [2] and [7],

[8] $$T_1' = T_1 - g_1 W_1/[4\pi r_1^2 K(T_1')]$$

According to the theory of Kennard (16), the temperature-jump distance, g_1, is given by

[9] $$g_1 = \left(\frac{2-a}{a}\right)(2\pi MRT)^{1/2}\frac{K}{C_P + C_V}\frac{1}{P}$$

where a is the accommodation coefficient, P is the pressure, and the other quantities have their usual significance. It has been pointed out (25) that the various quantities in [9] are to be taken at T_1'. If we use a kinetic theory expression for $K(T_1')$ developed to the same level of sophistication used in developing the temperature-jump theory, then [9] takes the form

[10] $$g_1 = \left(\frac{2-a}{a}\right)\frac{2}{3}\lambda(T_1')$$

in which $\lambda(T_1')$ is the appropriate mean free path. This is the same as the expression developed by Present (29). Thus from [3], [8], and [10],

[11] $$T_1' = T_1 - \left(\frac{2-a}{a}\right)\frac{2}{3}\frac{\lambda(T_1')}{r_1} \times \int_{T_w}^{T_1'} K\,dT/K(T_1')$$

Finally, since simple kinetic theory predicts that $\lambda(T_1')$ should be proportional to T_1' and inversely proportional to P, we may write

[12] $$T_1' = T_1 - \left(\frac{2}{3}\right)\frac{760}{273}\left(\frac{2-a}{a}\right)\frac{\lambda_0}{r_1}\frac{T_1'}{P} \times \int_{T_w}^{T_1'} K\,dT/K(T_1')$$

where λ_0 is the mean free path at 273 K and 760 Torr pressure.

In obtaining an expression for dV/dX_p we use the relation

[13] $$dV = -[R_3(R_1 + R_3)/E(R_1 - R_3)]\,dW_1$$

derived from the electrical properties of the circuit shown in Fig. 1. Also, dW_1 is related to dT_1 by the equation

[14] $$dW_1 = -\frac{(R_1 - R_3)}{(R_1 + R_3)^3}E^2\alpha_1 R_1\,dT_1$$

where the temperature coefficient of the thermistor at T_1 is defined as $\alpha_1 = d\ln R_1/dT_1$.

[3]The particular form $K(T) = AT^B$ is a useful functional form since the first order theory for monatomic gases obeys a similar law, and polyatomic gases follow this law approximately. Over the relatively narrow range of temperatures required in the present work (approximately 150 to 400 K) this function fits the data in refs. 27 and 28 with a precision of 1 to 2%. Using these data we obtain, for He, $K = 3.958 \times 10^{-5}T^{0.6369}$ and, for n-H_2, $K = 1.962 \times 10^{-5}T^{0.7915}$ (in units of W cm^{-1} K^{-1}).

Can. J. Chem. Downloaded from www.nrcresearchpress.com by 210.87.254.40 on 09/05/12
For personal use only.

Now it is evident that for a given mole fraction of total hydrogen, N_{H_2}, at constant pressure and T_W, W_1 will be a function of only two independent variables, T_1 and X_p. Thus, the total differential of W_1 is given by

$$[15] \qquad dW_1 = (\partial W_1/\partial T_1)_{X_p}\, dT_1 + (\partial W_1/\partial X_p)_{T_1}\, dX_p$$

By eliminating dT_1 between [14] and [15] and substituting for dW_1 using [13] we obtain the following equation for the sensitivity function:

$$[16] \qquad \frac{dV}{dX_p} = -\frac{[ER_1R_3/(R_1 + R_3)^2](\partial W_1/\partial X_p)_{T_1}}{E^2R_1(R_1 - R_3)/(R_1 + R_3)^3 + (\partial W_1/\partial T_1)_{X_p}/\alpha_1}$$

Expressions for the partial derivatives in [16] are obtained directly from [3]:

$$[17] \qquad (\partial W_1/\partial T_1)_{X_p} = 4\pi r_1 K(T_1')(\partial T_1'/\partial T_1)_{X_p}$$

$$[18] \qquad (\partial W_1/\partial X_p)_{T_1} = 4\pi r_1 \left\{ \int_{T_W}^{T_1'} (\partial K/\partial X_p)_T\, dT + K(T_1')(\partial T_1'/\partial X_p)_{T_1} \right\}$$

Substituting these expressions in [16] and noting that

$$[19] \qquad W_1 = E^2R_1/(R_1 + R_3)^2 = 4\pi r_1 \int_{T_W}^{T_1'} K\, dT$$

the expression for the sensitivity function becomes

$$[20] \qquad dV/dX_p = -\frac{[ER_1R_3/(R_1 + R_3)^2]\left\{ \int_{T_W}^{T_1'} (\partial K/\partial X_p)_T\, dT + K(T_1')(\partial T_1'/\partial X_p)_{T_1} \right\}}{[(R_1 - R_3)/(R_1 + R_3)] \int_{T_W}^{T_1'} K\, dT + K(T_1')(\partial T_1'/\partial T_1)_{X_p}/\alpha_1}$$

Although [20] is the ultimate form of the sensitivity function used, it is evident that the various quantities in it must be obtained either as observable parameters or by computation. Of these, the electrical quantities R_1, R_3, and E are known, as are T_1 and T_W, and α_1 is determined by separate calibration.

The quantities $K(T_1')$ and $\int_{T_W}^{T_1'} K\, dT$ can be evaluated from available data once the values of T_1' are known. These, in turn, can be evaluated in two ways: (*a*) purely empirically, using [6], or (*b*) by solving the theoretical expression of the modified Kennard theory eq. [12] by an iterative procedure; the possibility of using the latter method will be discussed below.

The partial derivative $(\partial T_1'/\partial T_1)_{X_p}$ in [20] can be evaluated by re-arranging [12] and differentiating logarithmically assuming that a is a weak function of T_1 and T_1'. Thus

$$[21] \qquad (\partial T_1'/\partial T_1)_{X_p} = \left\{ 1 + (T_1 - T_1') \left[1/T_1' + K(T_1') \Big/ \int_{T_W}^{T_1'} K\, dT - (\partial K/\partial T)_{X_p} \Big/ K(T_1') \right] \right\}^{-1}$$

where $(\partial K/\partial T)_{X_p}$ is to be evaluated for T_1' as well as $X_p = 0.25$. The partial derivative $(\partial T_1'/\partial X_p)_{T_1}$ can be evaluated in a similar way, and is most simply expressed as

$$[22] \qquad (\partial T_1'/\partial X_p)_{T_1} = (T_1 - T_1') \times \left[(\partial K/\partial X_p)_{T_1'} \Big/ K(T_1') - \int_{T_W}^{T_1'} (\partial K/\partial X_p)_T\, dT \Big/ \int_{T_W}^{T_1'} K\, dT \right] (\partial T_1'/\partial T_1)_{X_p}$$

To obtain an expression for the derivative $(\partial K/\partial X_p)_T$ appearing in [20] and [22] it was necessary to utilize a theoretical and semi-empirical approach since few relevant experimental data are available (30, 31). Using Hirschfelder's expression for non-polar gases (32), we write the following equation for a H_2–He mixture:

$$[23] \qquad K_{mix} = [K_{mix}]_{mono} + (K_{H_2} - [K_{H_2}]_{mono}) \left(1 - \frac{(1 - N_{H_2})D_{H_2H_2}}{N_{H_2}D_{H_2He}} \right)^{-1}$$

where $[K_{mix}]_{mono}$ and $[K_{H_2}]_{mono}$ are calculated by assuming no contribution from internal energy, and the diffusion coefficients $D_{H_2H_2}$ and D_{HeH_2} are assumed to be independent of the rotational state distribution of H_2.

Thus, for a fixed mole fraction of H_2,

$$[24] \qquad (\partial K/\partial X_p)_T = \frac{N_{H_2} D_{HeH_2}/D_{H_2H_2}}{1 - N_{H_2}(1 - D_{HeH_2}/D_{H_2H_2})} (\partial K_{H_2}/\partial X_p)_T$$

The theoretical value of K for a pure polyatomic gas is normally arrived at by multiplying K_{mono} by the Eucken factor. The latter has been generalized by Hirschfelder (32) in terms of a dimensionless parameter δ_f. In the present instance the theoretical value of K_{H_2} is given by

$$[25] \qquad K_{H_2} = [K_{H_2}]_{mono}\{1 + \delta_f[(2/5)(C_P/R) - 1]\}$$

where

$$[26] \qquad \delta_f = (5/2)P^0 D^0{}_{H_2H_2}/[K_{H_2}]_{mono}T$$

in which the superscript refers to a standard pressure. Since δ_f is independent of the rotational distribution we may write

$$[27] \qquad (\partial K_{H_2}/\partial X_p)_T = 0.1013(D^0{}_{H_2H_2}/T)[\partial(C_P/R)/\partial X_p]_T$$

where K_{H_2} has the units of W cm^{-1} K^{-1} and $D^0{}_{H_2H_2}$ is the self-diffusion coefficient of H_2 in cm^2 s^{-1} at 1 atm. Also, since the molar heat capacity of H_2 is a linear function of X_p,

$$[28] \qquad (\partial C_P/\partial X_p)_T = C_P(p) - C_P(o)$$

Thus from [24], [27], and [28],

$$[29] \qquad (\partial K/\partial X_p)_T = 0.1013 \frac{N_{H_2} D^0{}_{HeH_2}[C_P(p)/R - C_P(o)/R]/T}{1 - N_{H_2}(1 - D^0{}_{HeH_2}/D^0{}_{H_2H_2})}$$

Expressions for all of the quantities appearing in [20] have now been obtained.

Experimental Test of the Model

The assumption of spherical symmetry and the validity of the modified Kennard theory (eq. [12]) were tested experimentally using pure n-H_2 and pure He. Values of W_1 were measured electrically for T_W equal to 77, 195, and 273 K, for T_1 ranging from 277 to 373 K, and for P ranging from 1 to 30 Torr. These were corrected for heat losses through the thermistor leads and by radiation by measuring the power dissipated *in vacuo*.

The assumption of spherical symmetry implies that the 'cell constant' should be equal to $4\pi r_1$ as shown in [4]. To test this, values of $W_1{}^\infty$ were first obtained from plots to $1/W_1$ vs. $1/P$, as shown in Fig. 2. Although the curves for a given gas at fixed T_1 and T_W are not strictly linear, there is little error in extrapolating them to obtain $W_1{}^\infty$.

The values of the integral in [4] were evaluated numerically using the data tabulated by Liley (27, 28) for temperatures below 150 K and by using the form[3] $K(T) = AT^B$ for higher temperatures. Corresponding values of $W_1{}^\infty$ and $\int_{T_W}^{T_1} K\,dT$ are plotted in Fig. 3. It is evident that the data for He and n-H_2 lie on a common straight line through the origin. The value of r_1 derived from the slope is 0.0162 ± 0.0001 cm. The thermistor was actually somewhat ellipsoidal rather than spherical; its minor radius was 0.015 cm. Thus the assumption of spherical symmetry appears to be valid to a good approximation.

To test the validity of the modified Kennard theory we note that if, in [12], we set $K(T_1') = A(T_1')^B$ and if a does not vary appreciably over the range of temperature used, then a plot of $T_1 - T_1'$ vs. $(T_1')^{(1-B)} \int_{T_W}^{T_1'} K\,dT/P$ should give a single straight line for each gas, going through the origin, and having a slope of $(2 - a)/a \times 2/3 \times \lambda_0/r_1 \times 760/273 \times 1/A$. However, as shown in Fig. 4, the data for a given gas are best interpreted as lying on three separate lines, characterized by T_W but independent of T_1. Also, deviations from linearity occur at larger values of the abscissa. Examination of the latter phenomenon showed that in all cases the curves are linear through the origin for $P \geq$ ca. 4 Torr. We suggest that the deviations at lower pressures may arise either from the inadequacy of the Kennard expression for the temperature-jump, eq. [12], when $T_1 - T_1'$ is large or because of a temperature variation in the value of a.

By using published data on λ_0 for each gas the accommodation coefficients derived from the straight-line portions of the curves in Fig. 4 were calculated to be 0.25, 0.21, 0.20, and 0.22, 0.20, 0.17 for He and n-H_2 and T_W equal to 77, 195, and 273 K, respectively. Although the calculated values of a should not depend on T_W their magnitudes are not unreasonable.

Can. J. Chem. Downloaded from www.nrcresearchpress.com by 210.87.254.40 on 09/05/12
For personal use only.

Can. J. Chem. Downloaded from www.nrcresearchpress.com by 210.87.254.40 on 09/05/12
For personal use only.

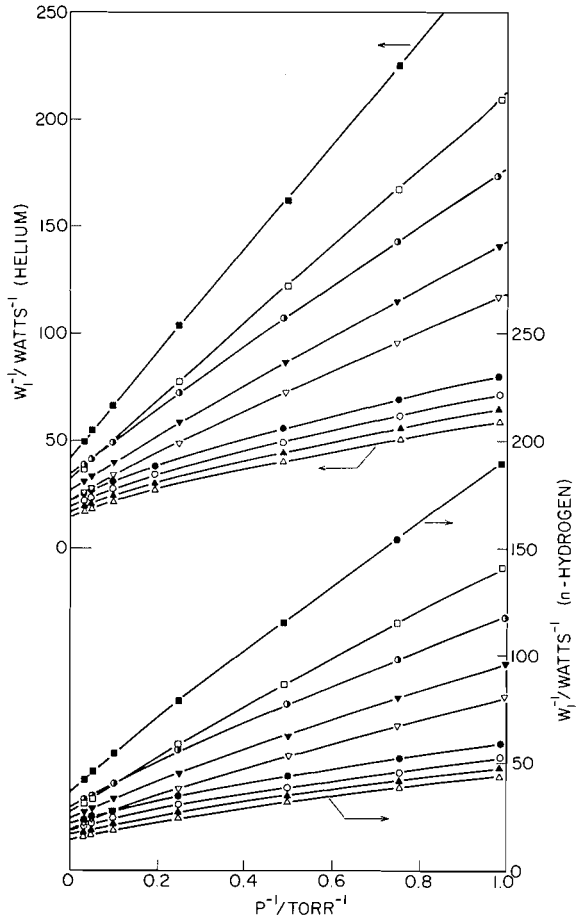

FIG. 2. Pressure dependence of thermistor power dissipation for He and n-H_2. T_W = 77 K: ●, T_1 = 277 K, ○, T_1 = 302 K, ▲, T_1 = 327 K, △, T_1 = 352 K. T_W = 195 K: ◑, T_1 = 302 K, ▼, T_1 = 327 K, ▽, T_1 = 352 K. T_W = 273 K: ■, T_1 = 348 K, □, T_1 = 373 K.

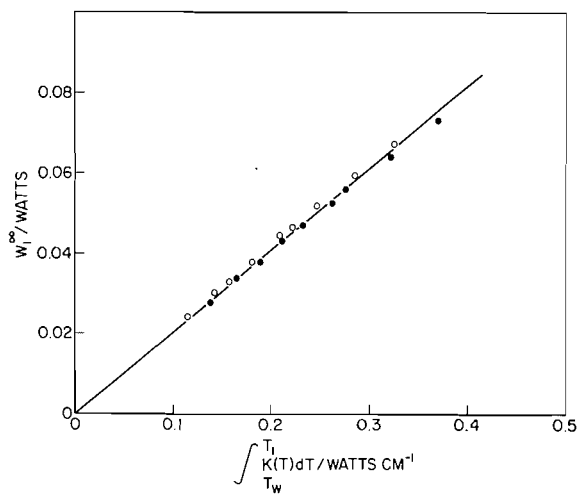

FIG. 3. Test of spherical symmetry at infinite pressure limit (eq. [4]). ●, n-H_2, ○, He.

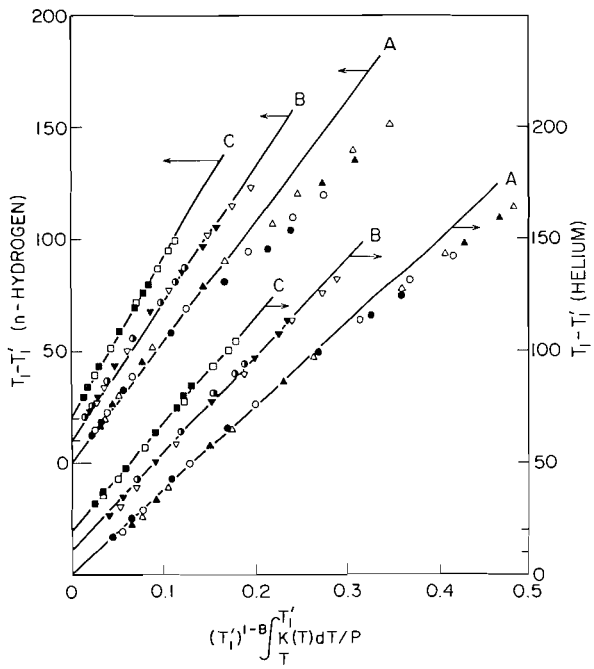

FIG. 4. Test of Kennard temperature-jump theory for He and n-H_2 and determination of accommodation coefficients (eq. [12]). (A) T_W = 77 K: ●, T_1 = 227 K, ○, T_1 = 302 K, ▲, T_1 = 327 K, △, T_1 = 352 K. (B) T_W = 195 K: ◑, T_1 = 302 K, ▼, T_1 = 327 K, ▽, T_1 = 352 K. (C) T_W = 273 K: ■, T_1 = 348 K, □, T_1 = 373 K.

The theoretical expression derived for the sensitivity dV/dX_p, given in [20], was tested experimentally for T_W = 77 K, for a number of different total pressures and values of T_1. This was done for pure H_2 and for dilute mixtures with $0.014 \leq N_{H_2} \leq 0.020$ in He. Various *ortho/para* compositions were obtained by subjecting known fractions of the gas mixture to passage through traps maintained at 77 K and containing a paramagnetic catalyst (Cr_2O_3 on alumina; Harshaw Chemical Company). It was found that H_2 in such portions was converted to the equilibrium composition, that is X_p = 0.5041.

In using pure H_2 the sensitivity was obtained by plotting ΔV, the change in V on equilibrating the sample, against ΔX_p, the corresponding change in X_p. For a fixed pressure these plots were linear through the origin except for $\Delta V > 0.5$ V. Deviations from linearity for larger values of ΔV were found to be due to appreciable changes in R_1, although the corresponding changes in T_1 were negligible. When the experimental values of ΔV were corrected for this purely electrical effect, the curves became linear throughout for all values of P from 1 to 30 Torr.

In the case of the dilute mixtures of H_2 in He the values of ΔV (and dV/dX_p) were, of course, much smaller, and to obtain a precision comparable to that

Can. J. Chem. Downloaded from www.nrcresearchpress.com by 210.87.254.40 on 09/05/12
For personal use only.

with pure hydrogen it was necessary to use samples with $X_p = 0.5041$.

In order to compare the values of the sensitivity for the various mole fractions, N_{H_2}, of hydrogen in the H_2–He mixtures, these were normalized by dividing by N_{H_2}. The validity of this procedure can be investigated by examination of [20]. The values of $K(T_1')$, $\int_{T_w}^{T_1'} K\,dT$, and $(\partial T_1'/\partial T_1)_{X_p}$ are very weak functions of N_{H_2} in the range used; in fact, using the values for pure He introduces very little error. On the other hand, the integrand $(\partial K/\partial X_p)_T$ and the term $(\partial T_1'/\partial X_p)_{T_1}$ in [20] are approximately proportional to N_{H_2}. This can be seen from [22] and [29] and noting that the ratio $D^0_{HeH_2}/D^0_{H_2H_2}$ ranged from 1.06 at 300 K to 1.11 at 77 K.

Experimental values of the sensitivity are shown as functions of pressure and for various values of T_1 in Figs. 5 and 6. The smooth curves labelled A are the theoretical ones given by [20], where the quantities in it are based on the modified Kennard theory of [12]. When $T_1 - T_1'$ was greater than 100 K a correction of up to 10% was used to compensate for the nonlinearity mentioned in connection with Fig. 4.

It can be seen from [12] that if we know λ_0 and

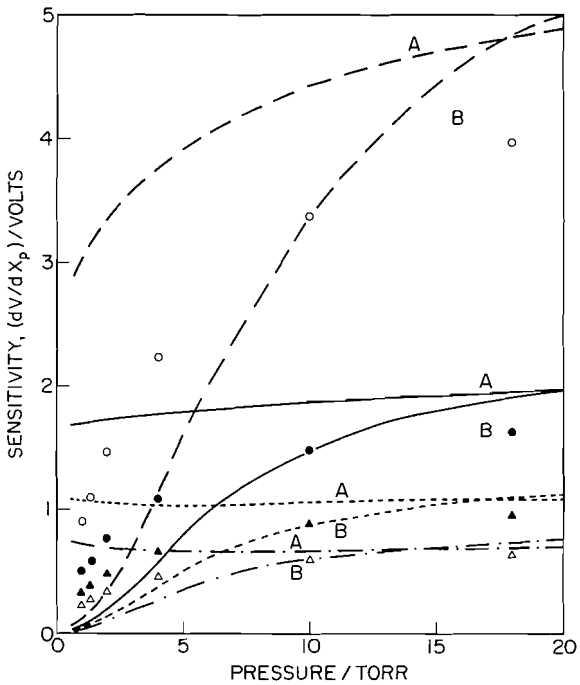

FIG. 5. Sensitivities for pure H_2 with $T_w = 77$ K. — — —, ○, $T_1 = 227$ K; ——, ●, $T_1 = 302$ K; ---, ▲, $T_1 = 327$ K; — · —, △, $T_1 = 352$ K. Points are measured values; smooth curves are theoretically constructed sensitivity functions. Curves A, eq. [20]; curves B, corrected for inefficient rotational accommodation, eq. [33].

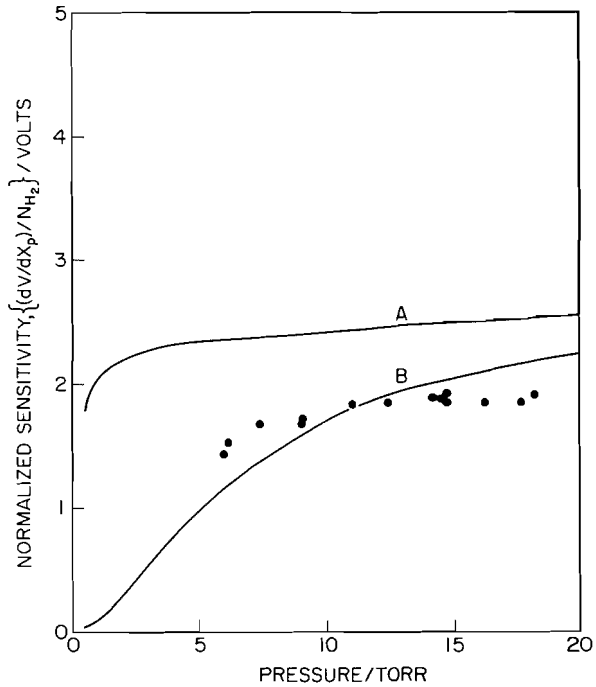

FIG. 6. Normalized sensitivity for He–H_2 mixtures (N_{H_2} = 0.014 to 0.020) with $T_w = 77$ K, $T_1 = 296.1$ K. Points are measured values; smooth curves are theoretically constructed sensitivity functions. Curve A, eq. [20]; curve B, corrected for inefficient rotational accommodation, eq. [33].

$K(T)$ then, once T_1, T_w, and P are chosen, the value of T_1' will be defined provided we know the values of a and r_1. These latter two can be considered to be semi-empirical quantities known from other measurements. In the present instance we set $r_1 = 0.0162$ cm and a at the values given for $T_w = 77$ K, viz. 0.22 for pure H_2 and 0.25 for the dilute mixtures in He. The values of T_1' were then determined by an iterative procedure. From these, all of the nonelectrical quantities in [20] were evaluated using [21], [22], and [29]. Values of C_P for H_2 were calculated directly from spectroscopic data (33) and diffusion coefficients were obtained from a recent literature survey (34). The integral $\int_{T_w}^{T_1'} (\partial K/\partial X_p)_T\,dT$ was evaluated numerically.

By choosing $E = 30.00$ V and obtaining $R_1(T_1)$ and $\alpha_1(T_1)$ from the calibration curve of the thermistor, the iteratively obtained values of T_1' also make it possible to calculate R_3. This follows by equating the electrical expression for W_1, $R_1E^2/(R_1 + R_3)^2$, to [3] after allowing for the heat losses by radiation and conduction through the leads, as described previously.

Discussion

The limiting high pressure behaviour of the de-

Can. J. Chem. Downloaded from www.nrcresearchpress.com by 210.87.254.40 on 09/05/12
For personal use only.

tector (W_1^{∞}) is entirely in accord with the simple spherical model chosen. This agreement would be unlikely if significant convective heat transfer were present (12, 14), leading us to believe that convection is minimal under the experimental conditions used.

In the pressure range 1 to 30 Torr, the total heat transfer is in remarkably good agreement with the simplified form of the Kennard theory for temperature-jumps up to 100 K. The deviation found for larger values may arise from failure of the linear temperature gradient assumption in the Kennard theory. It could also result from the variation of a with T_1 and T_1'. Such variation has been found to occur (35), but in the present case it is not clear which interpretation of the deviation is correct. The other deviation from the theory, the apparent dependence of the accommodation coefficient on the wall temperature, is relatively minor, considering the wide range of wall temperatures used. This may be due to the assumption, in the Kennard theory, that the two surfaces act independently. The Knudsen theory (16, 23), which is valid at much lower pressures, considers the effects at both surfaces simultaneously. While our experimental conditions would be expected to lie outside the Knudsen range it is possible that the results could be better interpreted in terms of a theory covering the intermediate range.

On the basis of the modified Kennard theory it should be possible to predict the sensitivity of the detector to changes in *ortho/para* composition in pure H_2 and in dilute mixtures. Only two parameters should be required (in addition to physical data from other sources), the radius of the thermistor and its accommodation coefficient.

When the sensitivity is calculated in this way, agreement with experimental measurements is poor. Although this might be expected at low pressures (<4 Torr), the fact that the high pressure agreement is also poor leads us to question the way we applied the Eucken–Hirschfelder theory. If values of δ_f in [26] are calculated using the expression $[K_{H_2}]_{mono} = (15/4)(R/M)\eta$ (36), where the viscosity is obtained from a recent survey (37), we find they range from 0.86 at 100 K to 0.89 at 300 K. Thermal conductivity measurements (31), however, yield smaller values of δ_f. The effect of these differences in δ_f is to produce slight reductions (of from 1 to 5%) in the apparent thermal conductivity, which in the nondifferential measurements in this work would be virtually undetectable (although a reduction of K_{H_2} by the amount indicated would improve the already close agreement between the He and n-H_2 results in Fig. 2). The effect on the differential measurements (dV/dX_p), which depend on the internal energy contribution to thermal conductivity, would be very much larger. Various reasons for this effect have been proposed, including poor accommodation of internal energy at a surface, and rapid resonant energy exchange in the gas (31). The second reason is perhaps unlikely in the dilute H_2 in He case and we will therefore consider the first explanation only in this work.

Using a model outlined by Harris (31), we assume that from the thermistor surface out to a distance l, the gas behaves as a monatomic gas which only has translational energy, which it receives from the thermistor surface. The distance l represents the random walk distance through which the molecules go within the rotational relaxation time of H_2. Thus, on the average, the H_2 will convert its excess translational energy to rotational energy at a distance l from the thermistor surface and, from then on, will behave as a polyatomic gas.

A consequence of this is that the gas temperature at r_1, T_1', which was originally obtained from [3] using measured values of W_1, is incorrect, and should be replaced by a corrected temperature, T_1^c. The two are related by the integral equation

$$[30] \qquad \int_{T_1''}^{T_1^c} [K]_{mono}\, dT = \int_{T_1''}^{T_1'} K\, dT$$

obtained on integrating [2] and defining T_1'' as the gas temperature at $r_1 + l$, and $[K]_{mono}$ as the thermal conductivity in the absence of internal energy contributions.

For dilute mixtures of H_2 in He, we assumed that K is equal to K_{He}, so that the above definition means that $[K]_{mono} = K$, for the dilute H_2 in He and $T_1^c = T_1'$. In the case of pure H_2, however, $T_1^c \neq T_1'$. Within the temperature range $T_1'' \leq T \leq T_1^c$, K is independent of X_p, so that

$$[31] \qquad (\partial K/\partial X_p)_T = 0$$

and

$$[32] \qquad \int_{T_W}^{T_1^c} (\partial K/\partial X_p)_T\, dT = \int_{T_W}^{T_1''} (\partial K/\partial X_p)_T\, dT$$

Using these results, together with the relationship between $(\partial T_1^c/\partial X_p)_{T_1}$ and $(\partial T_1^c/\partial T_1)_{X_p}$ (cf. eq. [22]), we may write a corrected sensitivity analogous to [20],

$$[33] \quad (dV/dX_p)_c = -\frac{[ER_1R_3/(R_1+R_3)^2]\displaystyle\int_{T_W}^{T_1''} (\partial K/\partial X_p)_T\, dT \left\{1 - \frac{(T_1 - T_1^c)[K]_{mono}(\partial T_1^c/\partial T_1)_{X_p}}{W_1/4\pi r_1}\right\}}{[(R_1 - R_3)/(R_1 + R_3)]W_1/4\pi r_1 + [K]_{mono}(\partial T_1^c/\partial T_1)_{X_p}/\alpha_1}$$

Can. J. Chem. Downloaded from www.nrcresearchpress.com by 210.87.254.40 on 09/05/12
For personal use only.

where we use $W_1/4\pi r_1$ in place of $\int_{T_w}^{T_1'} K\,dT$.

By equating $(dV/dX_p)_c$ to the measured sensitivity at one mid-range pressure, it is possible to solve numerically the simultaneous nonlinear eqs. [30] and [33] for T_1^c and T_1''. The value of l is then obtained by integrating [2] between the limits $T_W \leq T \leq T_1''$ $(\infty \geq r \geq r_1 + l)$. For the dilute H_2 in He results, a pressure of 12 Torr was chosen and gave a distance $l = 0.006261$ cm, corresponding to a relaxation time of 2.5×10^{-9} atm s. For pure H_2, and a pressure of 10 Torr, the distance l was remarkably constant for the four values of T_1 used, with an average value of 0.01279 ± 0.00010 cm. This gave relaxation times ranging from 8.4×10^{-9} atm s, for $T_1 = 277$ K, to 6.0×10^{-9} atm s, for $T_1 = 352$ K. These results are comparable to those obtained by more direct measurement (38).

By assuming, further, that l depends only on pressure for a given gas, and setting $l = 0.07513/P$ cm for the dilute H_2 in He mixtures and $l = 0.1279/P$ cm for pure H_2 (where P is the pressure in Torr), we may calculate T_1'', T_1^c, and hence $(dV/dX_p)_c$ as a function of pressure. These corrected sensitivity functions are compared to experimental results in Figs. 5 and 6 (curves labelled B). The pressure dependence of the scaled curves is more realistic, although they appear to overestimate the effect of inefficient rotational accommodation. This is not surprising since it was assumed that the accommodation coefficient for internal energy is equal to zero (i.e. monatomic behaviour out to a distance of l), whereas it is likely that it is non-zero, although less than the observed values (39). In principle, the model could be further refined, but it is doubtful whether it would produce any useful additional information.

Conclusions

The thermal conductivity detector, based on a small bead thermistor, has been shown to be adequately described by simple heat transfer theory over a wide range of conditions, when the effects of surface accommodation are considered. Differential measurements (dV/dX_p), which depend on the effect of the small differences in rotational energy of o-H_2 and p-H_2 on the thermal conductivity, are not well described by the simple theory and it was necessary to take into account the efficiency of rotational relaxation, both on the thermistor surfaces and in the gas phase. By assuming negligible rotational relaxation on the thermistor surface, introduction of a single additional parameter, the apparent gas phase relaxation rate for rotational energy, produces theoretical sensitivity curves which are in closer agreement with experiment, and which may be useful in a predictive sense as well.

Acknowledgement

The authors would like to thank Dr. Simon Wauchop for his considerable contributions to the redesigning of the thermal conductivity detector used in this study and his initial work on explaining its operation.

1. A. Farkas. Orthohydrogen parahydrogen and heavy hydrogen. Cambridge University Press, Cambridge. 1935.
2. W. R. Schulz and D. J. Le Roy. Can. J. Chem. **42**, 2480 (1964).
3. W. R. Schulz and D. J. Le Roy. J. Chem. Phys. **42**, 3869 (1965).
4. B. A. Ridley, W. R. Schulz, and D. J. Le Roy. J. Chem. Phys. **44**, 3344 (1966).
5. D. J. Le Roy, B. A. Ridley, and K. A. Quickert. Discuss. Faraday Soc. **44**, 92 (1967).
6. K. A. Quickert and D. J. Le Roy. Can. J. Chem. **48**, 2532 (1970).
7. W. J. Haubach, C. M. Knobler, A. Katirski, and D. White. J. Phys. Chem. **71**, 1398 (1967).
8. W. Moore and H. Ward. J. Am. Chem. Soc. **80**, 2909 (1958).
9. M. Mohnke and W. Saffert. 4th International Gas Chromatography Symposium, Hamburg, 1962. *Edited by* M. Van Swaay. Butterworth Inc., Washington, DC. 1962. p. 216.
10. E. H. Carter and H. A. Smith. J. Phys. Chem. **67**, 1512 (1963).
11. D. N. Mitchell and D. J. Le Roy. J. Chem. Phys. **67**, 1042 (1977).
12. B. G. Dickins. Proc. R. Soc. London Ser. A, **143**, 517 (1934).
13. S. A. Maev. Teplofiz. Vys. Temp. **5**, 114 (1967).
14. N. Kh. Zimina. Russ. J. Phys. Chem. **46**, 929 (1972); **47**, 1573 (1973); **47**, 1674 (1973).
15. G. P. Gupta and S. C. Saxena. Can. J. Phys. **45**, 1418 (1967).
16. E. H. Kennard. Kinetic theory of gases. McGraw-Hill, 1938. p. 311.
17. M. Smoluchowski. Ann. Phys. **64**, 101 (1898); Akad. Wiss. Wien. Abt. 2A, **107**, 304 (1898); **108**, 5 (1899).
18. R. E. Harris. J. Chem. Phys. **46**, 3217 (1967).
19. H. S. Gregory. Proc. R. Soc. London Ser. A, **149**, 35 (1935); Philos. Mag. **22**, 257 (1936).
20. H. Y. Wachman. J. Chem. Phys. **42**, 1850 (1965).
21. K. Schäfer, W. Rating, and A. Eucken. Ann. Phys. **42**, 176 (1942).
22. L. Lees and C-Y. Liu. Phys. Fluids, **5**, 1137 (1962).
23. M. Knudsen. Ann. Phys. **34**, 593 (1911).
24. C. Y. Cha and B. J. McCoy. J. Chem. Phys. **56**, 3265 (1972).
25. L. B. Thomas and R. C. Golike. J. Chem. Phys. **22**, 300 (1954).
26. R. V. Churchill. Fourier series and boundary value problems. McGraw-Hill, New York. 1963. p. 10.
27. P. E. Liley. Proc. 4th Symp. on Thermophysical Properties. Am. Soc. Mech. Eng. 1968. p. 323.
28. C. Y. Ho, R. W. Powell, and P. E. Liley. J. Phys. Chem. Ref. Data, **1**, 279 (1972).
29. R. D. Present. Kinetic theory of gases. McGraw-Hill, New York. 1958. p. 190.

30. W. UEBELHACK, W. EICHENAUER, K. HEINZINGER, and A. KLEMM. Z. Naturforsch. **22a**, 1528 (1967); K. H. MÜLLER, W. EICHENAUER, K. HEINZINGER, and A. KLEMM. Z. Naturforsch. **25a**, 247 (1970); W. UEBELHACH, W. EICHENAUER, K. HEINZINGER, and A. KLEMM. Z. Naturforsch. **26a**, 1303 (1971).
31. L. B. HARRIS. J. Chem. Phys. **49**, 206 (1968).
32. J. O. HIRSCHFELDER. 6th Combustion Symp. Yale University, The Combustion Institute. 1957, p. 351.
33. H. W. WOOLEY, R. B. SCOTT, and F. G. BRICKWEDDE. J. Res. Natl. Bur. Stand. **41**, 379 (1948).
34. T. R. MARRERO and E. A. MASON. J. Phys. Chem. Ref. Data, **1**, 3 (1972).
35. L. B. THOMAS and E. B. SCHOFIELD. J. Chem. Phys. **23**, 861 (1955); L. B. THOMAS. Rarified Gas Dynamics, 5th Symposium, Oxford University. 1966; Academic Press. 1967. p. 155; D. V. ROACH and L. B. THOMAS. Rarified Gas Dynamics, 5th Symposium, Oxford University. 1966; Academic Press. 1967. p. 163; J. KOUPTSIDIS and D. MENZEL. Bunsen Gesell. **74**, 512 (1970).
36. J. O. HIRSHFELDER, C. F. CURTISS, and R. B. BIRD. Molecular theory of gases and liquids. John Wiley and Sons Inc., New York. 1954. p. 534.
37. G. C. MAITLAND and E. B. SMITH. J. Chem. Eng. Data, **17**, 150 (1972).
38. R. M. JONKMAN, G. J. PRANGSMA, I. ERTAS, H. F. P. KNAAP, and J. J. M. BEENAKKER. Physica, **38**, 441 (1968).
39. K. SCHAFER and S. STOTZ. Z. Elektrochem. **65**, 623 (1961).

Can. J. Chem. Downloaded from www.nrcresearchpress.com by 210.87.254.40 on 09/05/12
For personal use only.

Apparent molal heat capacities and volumes of amino acids in aqueous polyol solutions

GIUSEPPA DIPAOLA[1] AND BERNARD BELLEAU[2]

Department of Chemistry, McGill University, Montreal, P.Q., Canada H2A 2K6

Received November 17, 1977

GIUSEPPA DIPAOLA and BERNARD BELLEAU. Can. J. Chem. **56**, 1827 (1978).

Densities (24°C) and volumetric specific heats (25°C) were measured for amino acids (0.05–0.5 *m*) containing apolar side chains in water, and in aqueous solutions of glycerol, mannitol, sorbitol, NaCl, urea, and Gu·HCl, with a flow densimeter and flow microcalorimeter respectively.

The derived apparent molal quantities and transfer functions of the amino acids in aqueous polyol solutions reveal no specificities which might explain the origin of the unique behavior of polyols in protein systems. However, the study did reveal a regular increase in the structure-making ability of the amino acid as the hydrophobicity of the side chains increased. This structure-making tendency was reduced significantly in dilute solutions of the higher polyols.

GIUSEPPA DIPAOLA et BERNARD BELLEAU. Can. J. Chem. **56**, 1827 (1978).

On a mesuré les densités (24°C) et les chaleurs spécifiques volumétriques (25°C) d'acides aminés (0.05–0.5 *m*) contenant des chaînes latérales non-polaires dans l'eau et dans des solutions aqueuses de glycérol, de mannitol, de sorbitol, de NaCl, d'urée et de Gu·HCl en faisant appel respectivement à un densimètre à écoulement et à un microcalorimètre à écoulement.

Les quantités molales apparentes que l'on peut en tirer et les fonctions de transfert des acides aminés dans les solutions de polyol aqueux ne révèlent aucune spécificité qui pourrait expliquer l'origine du comportement unique de polyols dans des systèmes de protéine. Toutefois, les études mettent en évidence qu'il existe une relation entre l'augmentation réguliére de l'habilité à produire des structures par des acides aminés et l'augmentation de l'hydrophobicité de la chaîne latérale. Il y a une réduction importante de cette tendance à former des structures lorsque l'on travaille dans des solutions diluées de polyols de poids moléculaires élevés.

[Traduit par le journal]

Introduction

Amino acids have been useful models for understanding the thermodynamic behavior of proteins, especially in determining apolar group contributions to the biopolymer's conformational stability. This is important because of the unique role played by hydrophobic hydration in the denaturation of proteins (1).

Standard free energies have been determined from solubility measurements of several amino acids in various solvents (2). Data on heats of transfer (3) and standard free energies of transfer from water to mixed aqueous solvents are also available (4). Until recently (3, 5–7), however, no reliable determination of partial molal heat capacities of amino acids in water existed.

The present work, which describes calorimetric and volumetric data on several α-amino acids (with apolar side chains) in a number of polyol–water systems, was undertaken in order to help elucidate possible correlations between structural interactions of amino acids in aqueous polyol solutions and the stabilizing effects of polyols on proteins. In previous publications we reported results of a similar study on other aqueous polyol systems (8, 9).

Experimental

Heat capacities were measured with a flow microcalorimeter capable of detecting differences between the volumetric specific heat of a solution and that of a reference solvent to $\pm 3 \times 10^{-5}$ J K^{-1} cm^{-3}. Densities were determined with a flow digital densimeter sensitive to $\pm 3 \times 10^{-6}$ g cm^{-3}. Details of the experimental procedure have been published previously (8). Apparent molal quantities (ϕ_c, ϕ_v) were calculated in the usual way (8).

Reagent grade polyhydric alcohols were used without further purification: glycerol (Fisher Certified Spectroanalyzed); ethylene glycol and 1,2-propanediol (Matheson, Coleman and Bell, Chromatoquality); 1,3-propanediol (Eastman Kodak Reagents); D-arabitol, D-xylitol, ribitol (Nutritional Biochemicals); D-mannitol, D-sorbitol, *myo*-inositol, sucrose (Fisher certified reagents), and *meso*-erythritol (Aldrich).

Reagent grade amino acids D-alanine, D- and L-valine, and

[1]Holder of a Centennial Predoctoral Scholarship of the National Research Council of Canada. Present address: Department of Chemistry, University of Toronto, Toronto, Ont., Canada M5S 1A1.

[2]Author to whom correspondence should be addressed.

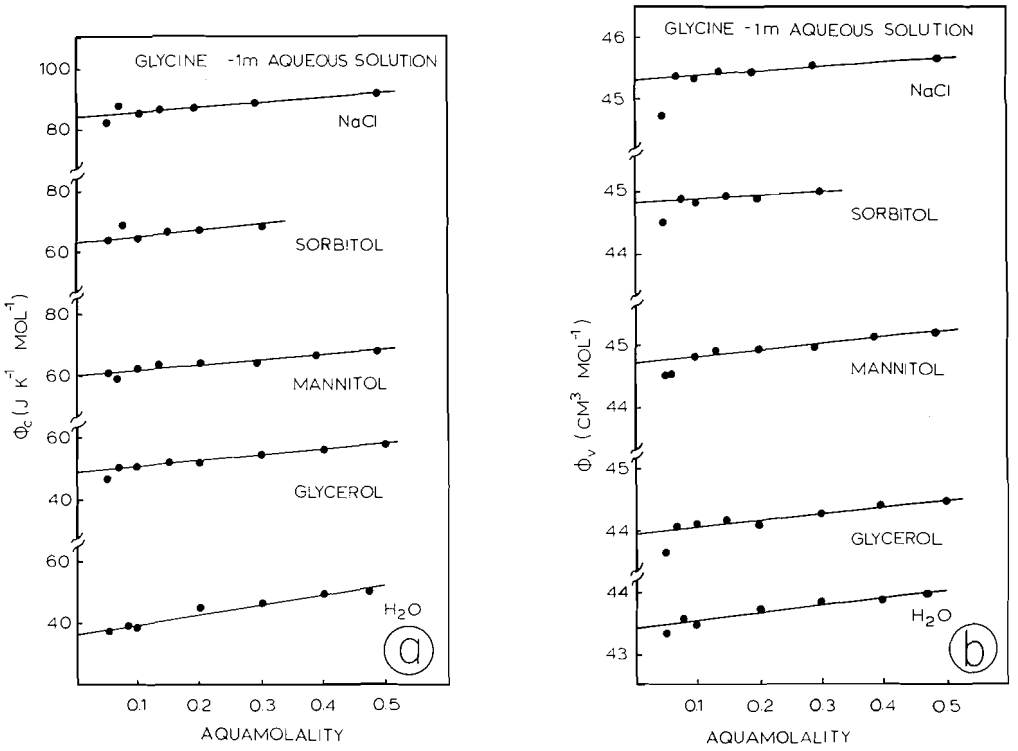

FIG. 1. Apparent molal quantities of glycine in 1 *m* aqueous solution. (*a*) ϕ_c at 25°C; (*b*) ϕ_v at 24°C.

L-leucine were obtained from Nutritional Biochemicals, L-alanine from Aldrich, DL-α-aminobutyric acid from Sigma, DL-norleucine and L-isoleucine from Eastman Kodak, glycine from Fisher Scientific, and DL-norvaline from BDH Chemicals Limited.

Urea (Schwarz-Mann, Ultra-Pure), guanidine·HCl (Sigma), and NaCl (Fisher certified reagents) were used without further purification.

Results

Apparent molal heat capacities (25°C) and volumes (24°C) were derived for several amino acids containing apolar side chains (glycine, D- and L-alanine, DL-α-aminobutyric acid, D- and L-valine, L-leucine, DL-norleucine, and DL-norvaline) in water, 1 *m* and 2 *m* glycerol, and 1 *m* mannitol, sorbitol, NaCl, urea, and Gu·HCl.[3]

The amino acids exhibit a linear dependence of ϕ_c and ϕ_v on concentration in the range of 0.05 to 0.5 *m*. Typical results (for glycine) are illustrated graphically in Fig. 1.[3] Results of a linear regression analysis of the data[4] for all the amino acids are summarized in Table 1; the standard apparent molal quantities and excess coefficients (B_v and B_c) are included.[5] The estimated uncertainties (based on duplicate measurements of 4–7 points) on the infinite dilution properties ϕ_c^0 and ϕ_v^0 are ± 1 J K^{-1} mol^{-1} and $\pm(0.05$–$0.1)$ cm^3 mol^{-1} respectively.

Table 2 compares the present results with data from the recent literature. The heat capacity data were taken from the work of Spink and Wadso (3) and Ahluwalia *et al.* (7); the volumetric data were taken from the papers of Gopal *et al.* (4), Ahluwalia *et al.* (7), and Ellerton *et al.* (10). References to other work in this area can be found in ref. 7. The present standard apparent molal quantities are in reasonable agreement with the previously determined values. Because of their low solubility in water, only a few experimental points at high dilution were obtained for leucine and norleucine. For this reason, the estimated uncertainty for these compounds is much higher than for the rest.

Results for heat capacities and volumes of the

[3]Complete sets of tabular data for d_0/d, σ/σ_0, ϕ_v, and ϕ_c are available, at a nominal charge, from the Depository of Unpublished Data, CISTI, National Research Council of Canada, Ottawa, Ont., Canada K1A 0S2.

[4]Data points outside experimental uncertainty were not considered in the analysis.

[5]Results were fitted by linear regression analysis to equations of the form:

$$[1] \qquad \phi_x = \phi_x^0 + B_x m$$

where m represents the aquamolal concentration of the amino acid and ϕ_x represents the appropriate apparent molal quantity. For most of the excess coefficients, B_x, only the magnitude is significant.

TABLE 1. Concentration dependence of amino acids in 1.0 *m* aqueous polyols

Amino acid	Solvent	ϕ_c^0 (J K^{-1} mol^{-1}) (25°C)	B_c	ϕ_v^0 (cm^3 mol^{-1}) (24°C)	B_v
Gly	H_2O	36.7	31.0	43.39	1.27
	Glycerol	49.4	17.7	43.98	0.98
	Mannitol	60.2	17.2	44.64	1.25
	Sorbitol	63.5	17.9	44.80	0.54
	NaCl	84.3	15.6	45.30	0.77
L-Ala	H_2O	145.6	12.6	60.62	0.79
	Glycerol	144.4	15.6	60.85	1.04
	Mannitol	155.5	8.8	61.78	0.59
	Sorbitol	159.0	5.3	61.83	0.42
D-Ala	H_2O	144.7	14.8	60.68	0.91
	Mannitol	154.3	10.4	61.83	0.47
	Sorbitol	158.2	7.0	61.93	0.22
DL-Aba	H_2O	234.1	5.6	75.92	0.30
	Glycerol	229.9	8.0	76.11	0.33
	Mannitol	235.9	5.8	76.78	0.41
	Sorbitol	238.5	3.6	76.73	0.37
L-Val	H_2O	307.5	19.2	90.98	0.53
	Glycerol	302.6	12.5	91.20	—
	Mannitol	310.9	6.0	91.92	0.37
	Sorbitol	311.8	12.1	92.10	—
D-Val	H_2O	307.8	18.8	90.87	0.97
	Mannitol	309.6	9.6	91.91	0.40
	Sorbitol	310.9	13.5	91.90	—
DL-Norval	H_2O	320.2	10.6	92.05	0.40
	Glycerol	315.0	7.7	92.11	0.53

TABLE 2. Comparison of standard apparent molal quantities in water with literature values

Amino acid	ϕ_c^0 Present (J K^{-1} mol^{-1}) (25°C)	ϕ_c^0 Lit. (J K^{-1} mol^{-1}) (25°C)	ϕ_v^0 Present (cm^3 mol^{-1}) (24°C)	ϕ_v^0 Lit. (ml mol^{-1}) (25°C)
Gly	36.7(±1)[a]	44[b]	43.39±(0.05–0.1)	43.21[c]; 43.22[e]
L-Ala	145.6(±1)	(DL)146[b]; 142.5[d]	60.62±(0.05–0.1)	60.60[c]; 60.47[d]
D-Ala	144.7(±1)		60.68±(0.05–0.1)	
DL-Aba	234.1(±1)	226[b]; 227.2[d]	75.92±(0.05–0.1)	75.54[d]
L-Val	307.5(±1)	(DL)307[b]	90.98±(0.05–0.1)	(DL)90.77[c]
D-Val	307.8(±1)		90.87±(0.05–1)	(DL)90.78[e]
DL-Norval	320.2(±1)		92.05±(0.05–0.1)	
L-LEU	402.4±(2–4)	(DL)382[b]; 399.0[d]	107.96(±0.1)	107.75[d]
DL-Norleu	404.5±(2–4)	400.0[d]	107.95(±0.1)	107.72[d]

[a]Estimated uncertainties are in parentheses.
[b]Reference 3.
[c]Reference 4.
[d]Reference 7.
[e]Reference 8.

amino acids in the mixed solvents could not be compared with literature values, since no such data exist. Any work that has been reported was carried out either at high concentrations (11) or is of dubious reliability (11, 12) because of the magnification of experimental error at low concentrations.

No significant differences are observed in the limiting thermodynamic behavior (ϕ_c^0, ϕ_v^0) of L- and D-configurations of amino acids in solution, e.g. compare D- and L-alanine, and D- and L-valine (Table 1).[6]

Apparent molal heat capacities and volumes of transfer of 0.1 *m* amino acids from water to the various aqueous solvents are summarized in Table 3.

[6]No difference is expected for mirror images; only for racemic, if solute–solute interactions exist, or if the asymmetric polyol interacts directly with the D- or L-form.

TABLE 3. Thermodynamic transfer functions of 0.1 *m* amino acids to 1 *m* aqueous solvent

Amino acid	Solvent	$\Delta\phi_{c\ tr}$[a] (J K^{-1} mol^{-1}) (25°C)	$\Delta\phi_{v\ tr}$[a] (cm^3 mol^{-1}) (24°C)
Gly	H_2O	—	—
	Glycerol	12.7	0.62
	Glycerol (2 *m*)	19.6	1.12
	Mannitol	24.2	1.33
	Sorbitol	26.3	1.33
	Urea	23.5	0.66
	Gu·HCl	40.7	1.65
	NaCl	46.7	1.85
L-Ala	H_2O	—	—
	Glycerol	−0.9	0.33
	Glycerol (2 *m*)	3.3	0.74
	Mannitol	11.0	1.19
	Sorbitol	14.4	1.25
D-Ala	H_2O	—	—
	Mannitol	8.7	1.18
	Sorbitol	12.0	1.13
DL-Aba	H_2O	—	—
	Glycerol	−3.4	0.14
	Glycerol (2 *m*)	−8.4	0.12
	Mannitol	2.8	0.81
	Sorbitol	4.3	0.74
L-Val	H_2O	—	—
	Glycerol	−5.8	0.18
	Glycerol (2 *m*)	−10.0	0.22
	Mannitol	1.8	0.93
	Sorbitol	3.3	1.08
D-Val	H_2O	—	—
	Mannitol	0.6	0.97
	Sorbitol	2.6	0.96
DL-Norval	H_2O	—	—
	Glycerol	−4.9	0.09
	Urea	4.9	0.42
	Gu·HCl	6.7	1.16
	NaCl	22.8	1.29
L-Leu[b]	H_2O	—	—
	Glycerol	−10.9	0.15
	Glycerol (2 *m*)	−15.5	0.38
	Mannitol	−6.1	0.53
	Sorbitol	−1.2	0.84
DL-Norleu[b]	H_2O	—	—
	Glycerol	−12.2	0.06
	Gu·HCl	−1.0	1.73
	NaCl	20.7	1.80

[a]The estimated uncertainties on $\Delta\phi_{c\ tr}$ and $\Delta\phi_{v\ tr}$ are approximately ±2 J K^{-1} mol^{-1} and ±(0.1–0.2) cm^3 mol^{-1} respectively. These uncertainties become respectively ±(4–8) J K^{-1} mol^{-1} and ±0.2 cm^3 mol^{-1} for leucine and norleucine.
[b]Transfer functions of 0.07 *m* amino acid.

Positive volumes of transfer are observed in all cases. The heat capacities of transfer are less systematic, however. Whereas negative values of $\Delta\phi_{c\ tr}$ values are observed for all amino acid transfers (except glycine) to glycerol solutions, the $\Delta\phi_{c\ tr}$ values are positive for all the amino acid transfers (except leucine and norleucine)[7] to the other solvent systems investigated.

[7]It must be noted that the uncertainties for leucine and norleucine are approximately double those for the other amino acids.

Discussion

Standard Apparent Molal Quantities

A consideration of the infinite dilution properties, ϕ_c^0 and ϕ_v^0, for the α-amino acids (Ala, Aba Norval, and Norleu) shows that the CH_2 contribution is similar to that found for aliphatic hydrocarbons (13), 86 J K^{-1} mol^{-1} and 15.8 cm^3 mol^{-1} respectively. The same conclusion was reached recently by Ahluwalia *et al.* (7). These results suggest that the electrostrictive effects of the zwitterion portion of the molecule do not seriously hinder the 'structure-enhancing' characteristics of the neighboring apolar groups. However, care must be exercised in predicting additivity relationships from group contribution data alone. The extrapolated values for ϕ_c^0 and ϕ_v^0 for glycine are significantly higher than the experimentally measured values.

The CH_2 group incremental contribution in mixed solvents (1 *m* glycerol and 1 *m* mannitol) is slightly lower than in water (85 and 80 J K^{-1} mol^{-1} respectively), suggesting a decrease in structural interactions in polyol–water as compared to pure water.

Data on amides, carboxylic acids, amines, and alcohols seem to indicate a negligible effect of branching from primary to secondary carbons (14). The data for leucine and norleucine show no effect within experimental error. However, the valine–norvaline data (Table 2) show an obvious branching effect (lower ϕ_c^0 and ϕ_v^0 for the branched isomer). One must keep in mind that a 1% impurity in the amino acid can probably cause an uncertainty of 5–10 J K^{-1} mol^{-1} in ϕ_c^0 (7).

Concentration Dependence

The concentration dependence (0.05–0.5 *m*) of ϕ_c ϕ_v for the amino acids in the various solvent systems is linear and small, and decreases slightly with increasing size of the aliphatic side chain. One would intuitively expect a greater concentration dependence as the hydrophobicity of the molecule increases, and also a nonlinear dependence, since the structure-making ability of the alkyl side chains should decrease with increasing amino acid concentration. However, this is not observed. Gucker and Allen (15) have also found that the partial molal heat capacity ($C_{p,2}$) for glycine and alanine is relatively insensitive to changes in concentration up to several molalities. A compensation mechanism between opposing electrostrictive and hydrophobic forces might provide a partial explanation.

Transfer Functions

There is an excellent correlation between the increase in hydrophobicity of the amino acid alkyl side chain and the trends in the apparent molal heat capacity of transfer to aqueous glycerol solutions

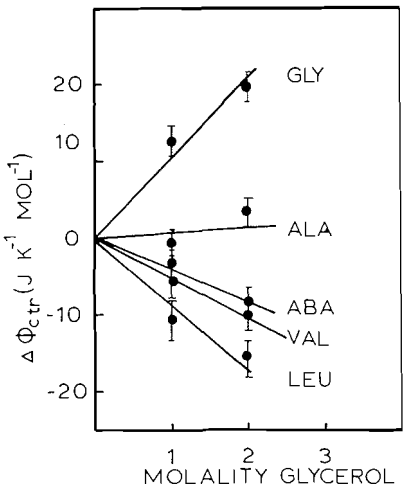

FIG. 2. Apparent molal heat capacities of transfer (25°C) of 0.1 *m* amino acids from water to aqueous glycerol solutions.

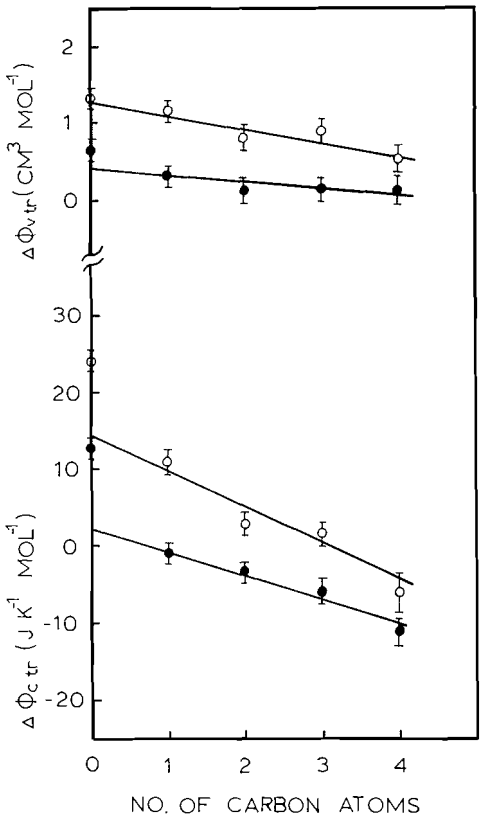

FIG. 3. Apparent molal volumes (24°C) and heat capacities of transfer of 0.1 *m* amino acids* to 1 *m* glycerol (●) and 1 *m* mannitol (○) solutions: *n = 0 ≡ Gly; 1 ≡ Ala; 2 ≡ Aba; 3 ≡ Val/Norval; 4 ≡ Leu/Norleu.

(Fig. 2), which suggests that the transfer functions are reflecting changes in structural interactions. The results can be explained in the manner already proposed for the transfer of the electrostrictive structure breaker, NaCl, and the hydrophobic probe, *n*-Bu_4NBr, to aqueous glycerol (8). Whereas glycine behaves as a typical structure breaker in glycerol–water (i.e. the solution behavior is dominated by the zwitterion portion), α-aminobutyric acid, valine, and leucine behave as typical hydrophobic structure makers (i.e. the solution behavior is dominated by the apolar portion). The structure-altering characteristics of alanine in aqueous glycerol are borderline.

Not only are the structure-altering characteristics of the amino acids differentiated by the transfer functions (Fig. 2), but the degree of structural order in different solvents is also differentiated (Fig. 3). Any differences that might occur in the transfer functions because of chain-branching effects, or differences between stereoisomers, are hidden within the experimental uncertainty. In general, the transfer parameters become increasingly more positive in the following order: glycerol–mannitol–sorbitol–urea–Gu·HCl–NaCl (Table 3). These results reflect the greater structure-breaking tendencies as one proceeds from glycerol to NaCl solutions, and the lowered structure-making ability of the apolar side chains as the degree of structural order in solution decreases. However, no definitive conclusions about changes in structural interactions in such solutions can be reached until more specific models for mixed aqueous solutions become available.

Acknowledgement

This work was generously supported by the National Research Council of Canada.

1. W. KAUZMANN. Adv. Protein Chem. **14**, 1 (1959).
2. Y. NOZAKI and C. TANFORD. J. Biol. Chem. **246**, 2211 (1971).
3. C. H. SPINK and I. WADSO. J. Chem. Thermodyn. **7**, 561 (1975), and references therein.
4. R. GOPAL, D. K. AGARWAL, and R. KUMAR. Indian J. Chem. **11**, 1061 (1973).
5. K. P. PRASAD and J. C. AHLUWALIA. J. Solution Chem. **5**, 491 (1976).
6. S. CABANI, G. CONTI, E. MATTEOLI, and A. TANI. J. Chem. Soc. Faraday Trans. I, **73**, 476 (1977).
7. J. C. AHLUWALIA, C. OSTINGUY, G. PERRON, and J. E. DESNOYERS. Can. J. Chem. **55**, 3364 (1977).
8. G. DiPAOLA and B. BELLEAU. Can. J. Chem. **53**, 3452 (1975).
9. G. DiPAOLA and B. BELLEAU. Can. J. Chem. **55**, 3825 (1977).
10. H. D. ELLERTON, G. REINFELDS, D. E. MULCAHY, and P. J. DUNLAP. J. Phys. Chem. **68**, 398 (1964).
11. J. T. EDSALL. J. Am. Chem. Soc. **57**, 1506 (1935).
12. G. C. KRESHECK. J. Chem. Phys. **52**, 5966 (1970).
13. C. JOLICOEUR and G. LACROIX. Can. J. Chem. **54**, 624 (1976).
14. N. NICHOLS, R. SKOLD, C. SPINK, J. SUURKUUSK, and I. WADSO. J. Chem. Thermodyn. **8**, 1081 (1976).
15. F. T. GUCKER and T. W. ALLEN. J. Am. Chem.Soc. **64**, 191 (1942).

The density, electrical conductivity, freezing point, and viscosity of mixtures of trifluoromethanesulfonic acid and water

RONALD CORKUM AND JOHN MILNE

Department of Chemistry, University of Ottawa, Ottawa, Ont., Canada K1N 6N5

Received January 16, 1978

RONALD CORKUM and JOHN MILNE. Can. J. Chem. **56**, 1832 (1978).

Density, viscosity, specific conductivity, and freezing point measurements over the whole composition range of water – trifluoromethanesulfonic acid mixtures are reported. A maximum in viscosity and minimum in specific conductivity are observed at the composition corresponding to the monohydrate, $H_3O^+SO_3CF_3^-$, and a maximum deviation from the ideal density is found at the composition corresponding to $H_5O_2^+SO_3CF_3^-$. The freezing point curve gives evidence for four hydrates with 1:1, 2:1, 4:1, and 6:1 water/trifluoromethanesulfonic acid mole ratios. An incongruent melting hydrate, probably 2:1 acid to water mole ratio is also indicated.

RONALD CORKUM et JOHN MILNE. Can. J. Chem. **56**, 1832 (1978).

On rapporte des mesures de densité, de viscosité, de conductivité spécifique et de point de fusion à plusieurs compositions de mélanges d'eau et d'acide trifluorométhanesulfonique. On observe une viscosité maximum et une conductivité spécifique minimum à une composition correspondant au monohydrate, $H_3O^+SO_3CF_3^-$, et une déviation maximale de la densité idéale à une composition correspondant à $H_5O_2^+SO_3CF_3^-$. Les courbes de point de fusion donnent des indications à l'effet que quatre hydrates avec des rapports molaires de 1:1, 2:1, 4:1 et 6:1 eau/acide trifluorométhanesulfonique peuvent exister. Il y a aussi des indications à l'effet qu'un hydrate de point de fusion incongruent et de composition 2:1 d'acide par rapport à l'eau existe aussi.

[Traduit par le journal]

Introduction

Physical measurements on trifluoromethanesulfonic acid (HTFMS) and its mixtures with some other solvents have been the subject of several studies. Haszeldine and co-workers (1, 2) have shown that the acid is completely dissociated in water and they have isolated the monohydrate, which may be formulated as $H_3O^+SO_3CF_3^-$, on the basis of its ir spectrum. Gramstad (3) has shown that HTFMS is stronger than perchloric acid in acetic acid medium and Russell and Senior (4) established that the acid is comparable in acid strength to chlorosulfuric acid but weaker than fluorosulfuric acid in 100% sulfuric acid as solvent. Fialkov and Ligus (5) have made density, viscosity, and electrical conductivity measurements on sulfuric acid – HTFMS mixtures and found evidence for a 1:1 compound which they formulate as $H_3SO_4^+SO_3CF_3^-$.

The kinetics of decomposition of HTFMS in aqueous solutions have been studied and the acid has been shown to be remarkably stable (6). No systematic studies have been made of the physical properties of aqueous HTFMS solutions over the complete composition range. This paper concerns the density, viscosity, electrical conductivity, and freezing point diagram of water–HTFMS mixtures.

Experimental

HTFMS (3M Company) was purified by double distillation with HTFMS anhydride added in the initial step. The fraction boiling at 162°C was collected. The anhydride was prepared by distillation of the acid from P_2O_5 (2). Distilled and deionized water were used throughout. For solutions at the acid rich end of the composition diagram, all transfers were made in a dry box.

Density Measurements

The density measurements were made at 25.0 ± 0.1°C in 25 ml volumetric flasks, which were recalibrated at the same temperature with distilled water. The average deviation in these density measurements is ±0.002 g/ml.

Viscosity Measurements

The viscosities were measured at 25.0 ± 0.1°C using an Ostwald viscometer. The viscometer was thoroughly cleaned before use and was calibrated with distilled water. The same volume of liquid was used in all runs. The viscosity was calculated from the average of from 2 to 5 runs. The average deviation of the measurements was ±0.0002 centipoise (cP). It should however be born in mind that a ±0.1°C change in temperature can cause a ±0.2% change in the viscosity of water.

Electrical Conductivity Measurements

Electrical conductivity was measured using an RC18 conductivity bridge from Industrial Instruments. The cell used has been described earlier (7). The measurements were made at 25.00 ± 0.01°C.

Freezing Point Measurements

Freezing points were measured in a vacuum jacketed cryoscope as described earlier (8). Temperature was measured with a chromel–alumel thermocouple with reference junction at 0°C. A Hewlett-Packard multimeter (Model 3465A) was used to measure potential. The thermocouple was calibrated at ice temperature and at the sublimation temperature of carbon dioxide. Freezing points were measured with temperature descending and in most instances, particularly where the

Can. J. Chem. Downloaded from www.nrcresearchpress.com by 210.87.254.42 on 09/05/12
For personal use only.

Can. J. Chem. Downloaded from www.nrcresearchpress.com by 210.87.254.42 on 09/05/12
For personal use only.

cooling curve of the solid–liquid mixture was steep, the freezing temperature was confirmed by remelting the mixture. The cryoscope was cooled with liquid air for all measurements except those above 5°C where ice was used. The initial cooling rate was set at 0.5°C/min, by adjusting the vacuum in the jacket of the cryoscope.

Results and Discussion

The experimental measurements of density, viscosity, electrical conductivity, and freezing points are all available as supplementary material.[1] Interpolated electrical conductivity values over the complete composition range are given in Table 1. Freezing point inflections are given in Table 2.

The results of the density measurements are shown in Fig. 1. Measurements could be made over the range of acid mole fraction 0.44 to 0.575 although solid monohydrate is the stable in this region. The densities in this range are, therefore, those of a supercooled mixture. The density found for the pure acid, 1.696 g/ml, is in excellent agreement with values reported earlier (5, 9). The mixtures show pronounced positive deviation from ideality and, thus, there is a strong interaction between water and HTFMS as expected. Maximum deviation from ideality occurs at 1:2 HSO_3CF_3/H_2O mole ratio.

The measurements of viscosity are plotted in Fig. 2. The viscosity of the pure acid was found to be 2.97 cP. This value is higher than that found by Fialkov and Ligus (5) (2.87 cP). It was not possible to measure the viscosity of the mixtures between acid mole fractions 0.44 and 0.58 at 25°C due to the formation of solid $H_3O^+SO_3CF_3^-$. The very large positive deviations from ideality indicate that the interaction is strong.

The electrical conductivity of dilute solutions of both HTFMS in water (1) and water in the acid (10) has been investigated. In both instances strong electrolyte behaviour has been observed as a result of the protonation reaction:

$$H_2O + HSO_3CF_3 \rightarrow H_3O^+ + SO_3CF_3^-$$

The trifluoromethanesulfonate anion ($TFMS^-$) in HTFMS conducts electricity by a proton transfer mechanism (10)[2] as does the hydronium cation in water. The specific conductivities of water – HTFMS acid mixtures at 25°C are given in Fig. 3. The monohydrate did not crystallize from the solutions with N_{HTFMS} between 0.44 and 0.575, unlike in the case of the viscosity measurements, and specific conductivities in this range are those of supercooled mixtures. The specific conductivity composition diagram exhibits 2 maxima at 0.063 and 0.855 and a minimum at 0.5 mole fraction of acid. As acid is added to water the conductivity increases to its maximum as the concentration of conducting species which conduct by proton transfer increases. In as much as trifluoromethanesulfonic acid is a sufficiently strong acid to protonate even the isolated water molecule (as opposed to bulk water), the ion concentration will in-

TABLE 1. Interpolated electrical conductivity values of water – trifluoromethanesulfonic acid mixtures

Mole fraction N_{HTFMA}	Specific conductivity $10^2\kappa_{sp}$ (Ω^{-1} cm^{-1})
0.00	0.0007
0.05	43.15
0.10	40.58
0.15	29.50
0.20	19.60
0.25	12.18
0.30	6.68
0.35	3.75
0.40	2.10
0.45	1.23
0.50	0.64
0.55	0.72
0.60	0.96
0.65	1.22
0.70	1.48
0.75	1.70
0.80	1.85
0.85	1.97
0.90	1.76
0.95	1.25
1.00	0.006

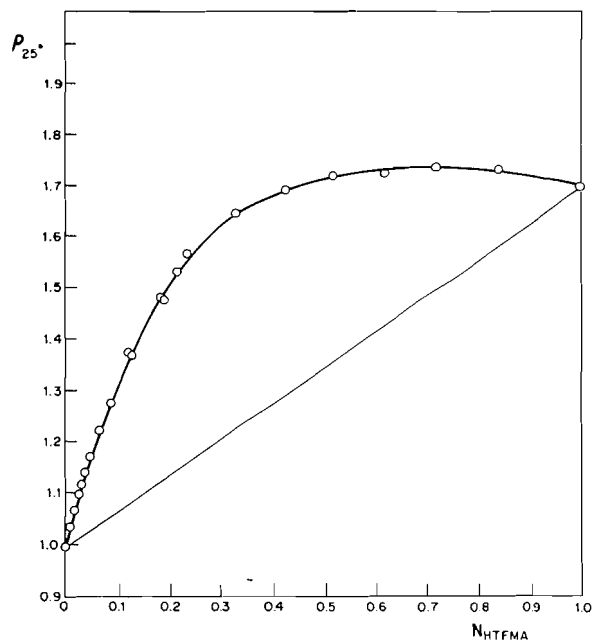

FIG. 1. The density of H_2O–HTFMA mixtures at 25°C.

[1]Copies of material on deposit may be obtained, at a nominal charge, from the Depository of Unpublished Data, CISTI, National Research Council of Canada, Ottawa, Ont., Canada K1A 0S2.

[2]J. B. Milne. Unpublished results.

TABLE 2. Freezing points of eutectic and peritectic mixtures and compounds formed from HTFMS–H_2O mixtures[a]

Mole fraction N_{HTFMS}	Nature of solid	Freezing point (°C)
0.133	Eutectic H_2O–$6H_2O$·HTFMS	−84
0.145	Compound $6H_2O$·HTFMS	−47.5
0.165	Eutectic $6H_2O$·HTFMS–$4H_2O$·HTFMS	−76.5
0.200	Compound $4H_2O$·HTFMS	−49.5
0.227	Eutectic $4H_2O$·HTFMS–$2H_2O$·HTFMS	−60.0
0.333	Compound $2H_2O$·HTFMS	−6.5
0.370	Eutectic $2H_2O$·HTFMS–H_2O·HTFMS	−12.0
0.500	Compound H_2O·HTFMS	+36.0
0.685	Peritectic	−17.5
1.000	Compound HTFMS	−43.53

[a]A peritectic and eutectic are indicated also near 0.85 mole fraction of acid.

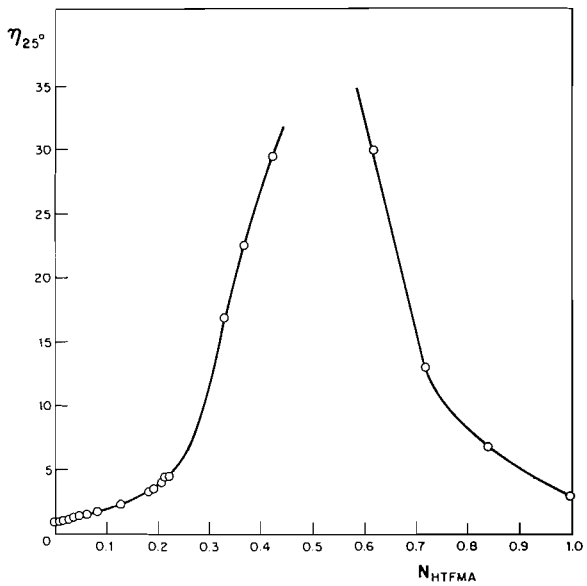

FIG. 2. The viscosity of H_2O–HTFMA mixtures at 25°C.

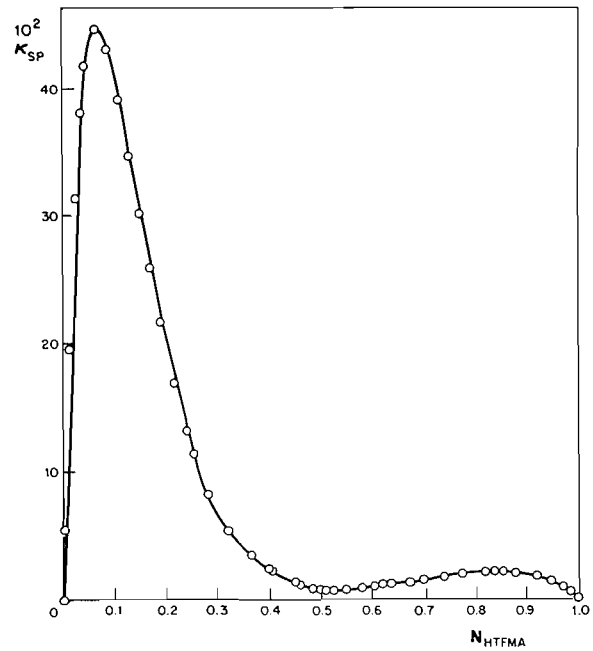

FIG. 3. The specific conductivity of H_2O–HTFMA mixtures at 25°C.

crease with increasing mole fraction of acid. Therefore, the decrease in specific conductivity after 0.063 mole fraction acid is not due to a decrease in the concentration of ions but is a result of increasing viscosity, electrophoretic and relaxation effects, if these are not offset by a change in dielectric constant, and, no doubt most importantly, the decreased efficiency of the proton transfer mechanism as the coordination of the hydronium ion changes from that of only water molecules, which are able to propagate the chain, to coordination with neighbouring $TFMS^-$ anions. The conductivity falls to a minimum at 1:1 HTFMS/water then, as the hydronium ions in the coordination shell of the $TFMS^-$ anion are replaced by HTFMS molecules with increasing acid mole fraction, the proton transfer mechanism, which can occur in bulk HTFMS via the solvent anion, becomes

Can. J. Chem. Downloaded from www.nrcresearchpress.com by 210.87.254.42 on 09/05/12
For personal use only.

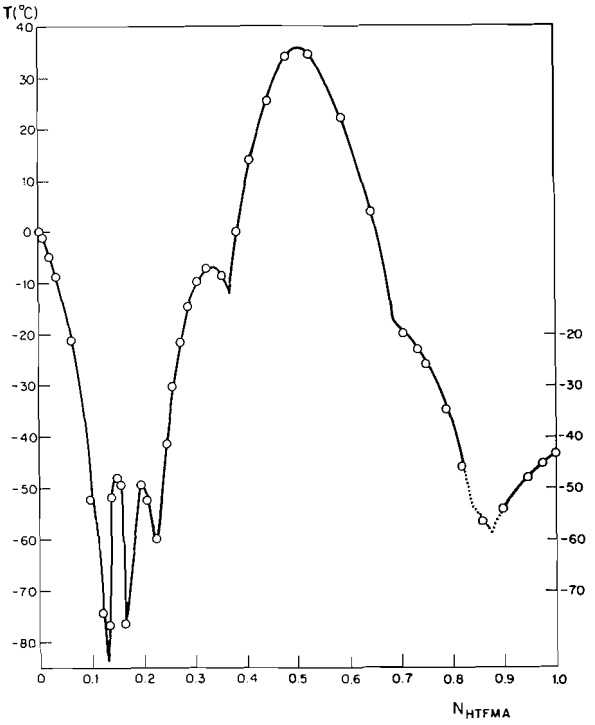

FIG. 4. The freezing point diagram for H_2O–HTFMA mixtures.

more important and the conductivity rises to a maximum. Decreasing viscosity, electrophoretic and relaxation effects will also play a role here. Finally, the conductivity begins to decrease again after 0.855 mole fraction of acid due to a decrease in ion concentration until the conductivity for pure acid is reached. Similar behaviour is observed for sulfuric acid – water mixtures (11).

The freezing point diagram for HTFMS–H_2O mixtures is shown in Fig. 4 and the freezing points of the eutectics, peritectics, and compounds formed are given in Table 2. The diagram gives evidence for trifluoromethanesulfonates of H_3O^+, $H_5O_2^+$, $H_9O_4^+$, and $H_{13}O_6^+$. These hydrates parallel those found in the H_2O–H_2SO_4 system (13) except that no evidence for a trihydrate is found in the H_2O–HTFMA system. The monohydrate is well established (2, 12) and its freezing point was reported by Gramstad and Haszeldine (2) at +34°C. The ir spectrum of the monohydrate confirms that the correct formulation is $H_3O^+SO_3CF_3^-$ (2, 12).

Evidence for a fifth hydrate is the peritectic point at 0.685 mole fraction of acid which indicates the existence of an incongruent melting compound, perhaps $H_2O{\cdot}2$HTFMA. Because of insufficient detail in the diagram near 0.85 mole fraction of acid, no definite conclusions can be drawn as to the exact location of the inflection points. Perchloric acid is known to form a hydrate of composition $H_2O{\cdot}4HClO_4$ (14) and a similar compound may be formed in the H_2O–HTFMA system.

Acknowledgements

Peter Gelbman is thanked for making the density and viscosity measurements and Clement Lau for determining the freezing point of the pure acid. The Defense Research Board of Canada is thanked for financial support.

1. R. N. HASZELDINE and J. M. KIDD. J. Chem. Soc. 4228 (1954).
2. T. GRAMSTAD and R. N. HASZELDINE. J. Chem. Soc. 4069 (1957).
3. T. GRAMSTAD. Tidsskr. Kjemi Bergves. Metall. **19**, 62 (1959).
4. D. G. RUSSELL and J. B. SENIOR. Can. J. Chem. **52**, 2975 (1974).
5. YU. YA. FIALKOV and V. I. LIGUS. Zh. Obshch. Khim. **42**, 267 (1972).
6. L. FABES and T. W. SWADDLE. Can. J. Chem. **53**, 3053 (1975).
7. J. BARR, R. J. GILLESPIE, and R. C. THOMPSON. Inorg. Chem. **3**, 1149 (1964).
8. R. J. GILLESPIE, J. B. MILNE, and R. C. THOMPSON. Inorg. Chem. **5**, 468 (1966).
9. Technical Information FC-24, 3M Company, October 1970.
10. D. G. RUSSELL. M.Sc. Thesis, University of Saskatchewan, Saskatoon, Saskatchewan. 1972.
11. International Critical Tables. Vol. VI. McGraw-Hill, New York, NY. 1929. p. 241.
12. T. G. BALICHEVA, V. I. LIGUS, and YU. YA. FIALKOV. Zh. Neorg. Khim. **18**, 3195 (1973).
13. C. M. GABLE, H. F. BETZ, and S. H. MARRON. J. Am. Chem. Soc. **72**, 1445 (1950).
14. G. S. PEARSON. *In* Inorganic chemistry and radiochemistry. Vol. 8. *Edited by* H. J. Emeleus and A. G. Sharpe. Academic Press, New York, NY. 1966. p. 182.

Can. J. Chem. Downloaded from www.nrcresearchpress.com by 210.87.254.42 on 09/05/12
For personal use only.

Caerulomycin D, a novel glycosidic derivative of 3,4-dihydroxy-2,2′-dipyridyl 6-aldoxime from *Streptomyces caeruleus*[1]

A. GAVIN MCINNES, DONALD G. SMITH, AND JOHN A. WALTER
Atlantic Regional Laboratory, National Research Council of Canada, Halifax, N.S., Canada B3H 3Z1
AND
JEFFREY L. C. WRIGHT AND LEO C. VINING
Biology Department, Dalhousie University, Halifax, N.S., Canada B3H 4J1
AND
GUY P. ARSENAULT
Department of Chemistry, Massachusetts Institute of Technology, Cambridge, MA, U.S.A.

Received December 19, 1977

A. GAVIN MCINNES, DONALD G. SMITH, JOHN A. WALTER, JEFFREY L. C. WRIGHT, LEO C. VINING, and GUY P. ARSENAULT. Can. J. Chem. **56**, 1836 (1978).

Analysis by ^1H and ^{13}C nmr spectrometry showed that caerulomycin D, a new metabolite isolated from *S. caeruleus*, possessed a novel ring system and had the structure (2*S*,3*R*,4*R*,4a*S*,10a*S*)-3,4,4a,10a-tetrahydro-4-hydroxy-3,4a-dimethoxy-2-methyl-9-(2-pyridyl)-2*H*-pyrano[3′,2′:5,6]-*p*-dioxino[2,3-*c*]pyridine-7-carboxaldehyde (*E*)-oxime.

A. GAVIN MCINNES, DONALD G. SMITH, JOHN A. WALTER, JEFFREY L. C. WRIGHT, LEO C. VINING et GUY P. ARSENAULT. Can. J. Chem. **56**, 1836 (1978).

L'analyse des spectres rmn du ^1H et du ^{13}C montre que la caerulomycine D, un nouveau métabolite isolé du *S. caeruleus*, possède un nouveau système cyclique et que sa structure correspond à l'oxime (*E*) du tétrahydro-3,4,4a,10a hydroxy-4 diméthoxy-3,4a méthyl-2 (pyridyl-2)-9 2*H*-pyrano[3′,2′:5,6]*p*-dioxino[2,3-*c*]pyridinecarboxaldéhyde-7 (2*S*, 3*R*, 4*R*, 4a*S*, 10a*S*).

[Traduit par le journal]

A previous paper (1) describes the isolation from cultures of *Streptomyces caeruleus* of several metabolites related to the antibiotic caerulomycin A for which the structure **1***a* has been established (2). Two

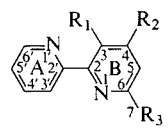

1*a* $R_1 = H, R_2 = OCH_3, R_3 = CH{=}NOH$
1*b* $R_1 = H, R_2 = OCH_3, R_3 = C{\equiv}N$
1*c* $R_1 = H, R_2 = OCH_3, R_3 = CH{=}NOAc$
2 $R_1 = OH, R_2 = OCH_3, R_3 = CH{\equiv}NOH$
3*a* $R_1 = OCH_3, R_2 = OCH_3, R_3 = CH{=}NOH$
3*b* $R_1 = OCH_3, R_2 = OCH_3, R_3 = C{\equiv}N$
3*c* $R_1 = OCH_3, R_2 = OCH_3, R_3 = CH{=}NOAc$

of the new compounds, caerulomycins B and C, were concluded from spectroscopic evidence to have structures **2** and **3***a*. The rationale for assigning resonances in the ^1H and ^{13}C nmr spectra of 2,2′-dipyridyl and the metabolites was explained and forms the basis for much of the additional work on the structure of the fourth metabolite, caerulomycin D, which is reported here.

Caerulomycin D, $C_{19}H_{21}N_3O_7$, displayed a characteristic red color with ferrous ions, and showed absorption maxima in the ultraviolet and infrared regions consistent with a 2,2′-dipyridyl structure (1). An increment of 2 mass units in the molecular ion after gas phase deuterium exchange indicated two active hydrogens in the molecule. Mild acetylation yielded a monoacetate which showed a carbonyl stretching absorption at 1785 cm^{-1} but retained a hydroxyl stretching absorption maximum at 3525 cm^{-1}; more vigorous conditions gave a nitrile (ν_{max} 2230 cm^{-1}) lacking these absorption maxima but showing a carbonyl stretching absorption at 1760 cm^{-1}. This behavior is accounted for if caerulomycin D possesses an aldoxime group and a less acidic hydroxyl function which is acetylated under vigorous conditions.

The structures of caerulomycin D (**4***a*), caerulomycinonitrile D monoacetate (**4***b*), and caerulomycin D monoacetate (**4***c*) have been elucidated mainly by ^1H and ^{13}C nmr studies. Earlier observations (1) on 2,2′-dipyridyl, caerulomycin C (**3***a*), its nitrile (**3***b*) and monoacetate (**3***c*), as well as comparisons with the model compounds 4-*tert*-butylcyclohexanone dimethylketal (**5**), 2,3-dimethoxyisopropylbenzene (**6**), and 1,4-benzodioxan (**7**) were particularly valuable. Proton assignments were confirmed by spin-decoupling experiments (3) and nuclear Overhauser enhancement (nOe) studies (4), while spectral simula-

[1]NRCC No. 16645.

Can. J. Chem. Downloaded from www.nrcresearchpress.com by 210.87.254.42 on 09/05/12
For personal use only.

Can. J. Chem. Downloaded from www.nrcresearchpress.com by 210.87.254.42 on 09/05/12
For personal use only.

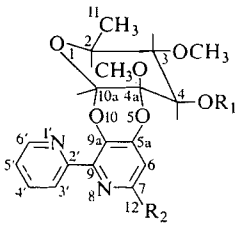

4

a R_1 = H, R_2 = CH=NOH
b R_1 = Ac, R_2 = C≡N
c R_1 = H, R_2 = CH=NOAc

tion techniques (footnote to Table 1) were used to obtain relevant parameters from complex spectral sub-groups. The ^{13}C nmr data were obtained from proton-noise decoupled (pnd) and high resolution (hr) spectra, and assignments were aided by off-resonance (ord) and single ^1H frequency (sfd) decoupling experiments (5).

The ^1H nmr spectra of **4***a* (Table 1) and **3***a* (1) were virtually identical in the region δ 7.0–12.0, and nitrile formation caused similar spectral changes. Signals for the two methoxyl groups in **3***a* and **3***b* were replaced in the spectra of **4***a* and **4***b* by resonances for a methylated hexose residue, and it appeared that caerulomycins C and D differed only in this respect; a 3,4-dioxygenated 2,2′-dipyridyl-6-aldoxime structure being common to both compounds.

The ^{13}C nmr data (Tables 2 and 3) in **4***a* and **4***b* supported this conclusion. Resonances for the ring A, oxime, and nitrile carbons were readily identified (1). Five additional resonances in the spectra of both compounds were assigned to ring B carbons for reasons already given previously for **3***a* and **3***b* (1). Thus on going from **4***a* to **4***b*, C-7 was shielded and its coupling to H-12 removed, C-6 was deshielded and the coupling to H-6 increased, and the chemical shift of C-9 was only slightly affected. ^1H sfd experiments also showed that H-6 was coupled to C-9a of **4***a* and C-9a and C-5a of **4***b* in addition to the oxime and nitrile carbons. A similar change in the multiplicity of the C-5a, but not the C-9a, signal also accompanied the conversion of **3***a* to **3***b* (1).

The high-field portions of the ^1H nmr spectra of **4***a* and **4***b* (Table 1) each contained resonances for one methyl, two methoxyl, and four methine hydrogens; the spectrum of **4***a* also possessed a hydroxyl signal (δ 5.57; proton exchangeable with deuterium) which was replaced by one for an acetoxyl methyl group (δ 1.89) in the spectrum of **4***b*. In each compound one of the methine hydrogens gave a singlet resonance with a chemical shift (**4***a*, δ 5.68; **4***b*, δ 5.83) similar to that of the anomeric hydrogen of aryl glucopyranosides (6). From the absence of spin–spin coupling the adjacent carbon was not bonded to hydrogen. The chemical shifts of the three remaining methine hydro-

TABLE 1. ^1H nuclear magnetic resonance data (100 MHz) for caerulomycin D (**4***a*) and caerulomycinonitrile D monoacetate (**4***b*) in DMSO-d_6*

Compound	H-2	H-3	H-4	H-6	H-10a	H-11	H-12	═NOH	═NO(CO)CH_3
4*a*	3.90(dq)	3.12(t)	3.74(dd)	7.41(s)	5.68(s)	1.30(d)	8.08(s)	11.55(s)	
4*b*	3.92(dq)	3.30(t)	5.00(d)	7.94(s)	5.89(s)	1.33(d)			
4*c*	3.90(dq)	3.12(t)	3.74(dd)	7.55(s)	5.68(s)	1.31(d)	8.53(s)		2.23(s)
	H-3′	H-4′	H-5′	H-6′	3-OCH_3	4-OH	4a-OCH_3	4-O(CO)CH_3	
4*a*	7.94	7.94	7.46	8.71	3.44(s)	5.57(d)	3.44(s)		
4*b*	7.69	7.96	7.48	8.70	3.36(s)		3.46(s)	1.89(s)	
4*c*	7.94	7.94	7.47	8.70	3.44(s)	5.55(d)	3.44(s)		

*H-3′, H-4′, H-5′, and H-6′ form an AMXY sub-spectrum which was analyzed with the Varian spin simulation program on the 620L data system associated with the XL-100 spectrometer. The coupling constants for this system are not listed since they were the same for all compounds, within experimental error (± 0.1 Hz), as those reported previously for 2,2′-bipyridyl, **1***a*, **1***b*, 2, **3***a*, **3***b*, and **3***c* (1). Values for the sugar moiety in **4***a* were $J_{2,3}$ = 8.5 $J_{2,11}$ = 6.4, $J_{3,4}$ = 7.5, $J_{4,OH}$ = 6.2 Hz; in **4***b* they were $J_{2,3}$ = 8.9, $J_{2,11}$ = 6.3, $J_{3,4}$ = 9.1 Hz. The following nuclear Overhauser enhancements were observed (irradiated protons in parentheses). Note that the use of 'and' in these expressions signifies simultaneous irradiation or observation of more than one signal due to their proximity or equivalence; 'or' signifies the separate irradiation or observation of each signal listed. **4***a*: H-10a (3 and 4a-OCH_3) 15%; H-6′ (H-6 and 5′) 0%; H-10a (H-6 and 5′) 14%; H-6, 12, 3′, 4′, 5′, or 6′ (3 and 4a-OCH_3, or H-10a) 0%; H-2, 3, 4, 9, or 11 and 5a-OCH_3 (H-10a) 0%; H-12 (H-6) 0%; **4***b*: H-10a (4a-OCH_3) 23%; H-10a (H-2, 6, O(CO)CH_3, or 3-OCH_3) 0%; H-4 (H-2) 13%; H-4 (H-6, 10a, or 4a-OCH_3) 0%; H-6, 3′, 4′, 5′, 6′, or 3,or 4a-OCH_3 (O(CO)CH_3) 0%.

Can. J. Chem. Downloaded from www.nrcresearchpress.com by 210.87.254.42 on 09/05/12
For personal use only.

TABLE 2. ^{13}C nuclear magnetic resonance (25.16 MHz) chemical shift data (δ_C TMS) for caerulomycin D (**4***a*), caerulomycinonitrile D monoacetate (**4***b*), and model compounds (**5**, **6**, and **7**) in DMSO-d_6*

Compound	C-2	C-3	C-4	C-4a	C-5a	C-6	C-7	C-9	C-9a	C-10a	C-11
4*a*	70.2	83.3	69.0	95.9	142.8	107.5	145.9	148.6	136.6	91.0	17.6
4*b*	70.1	80.5	69.4	95.4	148.3	118.1	125.3	148.8	139.3	91.0	17.1
	C-12	C-2′	C-3′	C-4′	C-5′	C-6′	3-OCH_3	4a-OCH_3	CH_3CO_2	CH_3CO_2	
4*a*	148.1	154.0	124.6	136.4	123.5	149.0	59.4	50.3			
4*b*	117.0	153.2	124.6	136.5	123.9	149.0	59.9	51.0	169.3	20.1	
	C-1	C-2,6	C-3,5	C-4	$C(CH_3)_3$	$C(CH_3)_3$	1-OCH_3				
5	99.1	32.3	23.2	46.9	32.0	27.4	46.7, 46.9				
	C-1	C-2	C-3	C-4	C-5	C-6	$CH(CH_3)_2$	$CH(CH_3)_2$	2-OCH_3	3-OCH_3	
6	141.8	146.4	152.7	110.4	124.1	118.1	26.7	23.5	60.3	55.5	
	C-2,3	C-4a,8a	C-5,8	C-6,7							
7	64.3	143.8	117.3	121.3							

*Pulse Fourier transform 8K, sweep width 5120 Hz, data accuracy ± 0.6 Hz.

TABLE 3. ^{13}C–H coupling constants ($^nJ_{CH}$) for caerulomycin D (**4***a*) and caerulomycinonitrile D monoacetate (**4***b*) in DMSO-d_6

Compound	C-2	C-3	C-4	C-4a	C-5a	C-6	C-7	C-9
4*a*	dbm; $^1J = 146.8$	dbm; $^1J = 147.0$	dbs; $^1J = 142.3$	bs	bs	dd; $^1J = 165.8$, $^3J_{6,12} = 3.5$	d; $^2J_{7,12} = 5.4$	s
4*b*	dbm; $^1J = 149.0$	dbm; $^1J = 146.8$	dbs; $^1J = 147.4$	bs	d; $^2J_{5a,6} = 3.9$		s	s
	C-9a	C-10a	C-11	C-12	3-OCH_3	4a-OCH_3		
4*a*	dd; $^3J_{9a,6} = 5.5$	d; $^1J = 178.1$	bq; $^1J = 126.1$	dd; $^1J = 167.0$, $^3J_{12,6} = 8.7$	dq; $^1J = 141.7$, $^3J_{3,OCH_3} = 5.9$	q; $^1J = 145.3$		
4*b*	d; $^3J_{9a,6} = 5.3$	d; $^1J = 180.9$	bq; $^1J = 126.5$	d; $^3J_{12,6} = 3.6$	dq; $^1J = 142.6$, $^3J_{3,OCH} = 6.0$	q; $^1J = 145.4$		
	C-2′	C-3′	C-4′	C-5′	C-6′			
4*a*	bm	dd; $^1J = 166.3$, $^3J_{3',5'} = 6.6$	dd; $^1J = 165.0$, $^3J_{4',6'} = 6.3$	dbm	dbdd; $^1J = 178.7$			
4*b*	bm	dd; $^1J = 165.9$, $^3J_{3',5'} = 6.9$	dd; $^1J = 165.7$, $^3J_{4',6'} = 5.9$	dt; $^1J = 165.3$, $^2J_{5',6'} \approx {}^3J_{5',3'} \approx 7.5$	ddd; $^1J = 179.9$, $^2J_{6',5'} = 3.8$; $^3J_{6',4'} = 7.3$			

Can. J. Chem. Downloaded from www.nrcresearchpress.com by 210.87.254.42 on 09/05/12
For personal use only.

gens required that they were attached to carbons bearing oxygen (7), and the magnitudes of vicinal couplings (Table 1) indicated that they were axially orientated on adjacent sites of a six-membered ring (8). In addition, one (**4***a*, δ 3.90; **4***b*, δ 3.92) was vicinally coupled to hydrogens of the methyl group. These observations established that H-2, H-3, H-4, and the methyl group must be positioned as in structures **4***a* and **4***b*. In **4***a* H-4 was also coupled to a hydroxyl hydrogen. Acetylation to produce **4***b* removed the coupling and deshielded the signal from δ 3.74 to δ 5.00 as predicted (9) if the hydroxyl and acetoxyl substituents were bonded to C-4. The fragment $C_2H_6O_4$ still unaccounted for must include the two methoxyl groups evident in the ^1H nmr spectra. The methoxyl groups had chemical shifts characteristic of those in carbohydrate derivatives (10) and are plausibly located only at the 2 and 4 positions of a pyranose ring. On this evidence C-10a and C-4a must be linked to the 3 and 4 positions of the 2,2′-dipyridyl ring through oxygen atoms as shown in structures **4***a* and **4***b*.

The ^1H nmr nOe data in Table 1 support the above conclusions. Irradiating H-2 of **4***b* produced a significant nOe for H-4 but not H-10a, whereas irradiation of the low field (δ 3.46) methoxyl hydrogens showed a nOe for H-10a but no intensity change in the signal for H-4. No nOe was obtained for H-10a when the high field (δ 3.36) methoxyl hydrogens were irradiated. These observations confirm the 1,3-diaxial relationship of H-4 and H-2. They also establish that one methoxyl group (δ 3.46) is vicinal and *gauche* to H-10a as well as *trans* to H-4. As H-4 is axial, C-4a bears an axial methoxyl group and H-10a is equatorial. The second C—O bond at C-4a must be equatorially orientated, whereas the corresponding bond at C-10a must be axial. Because the nOe evidence excludes any possibility of the second methoxyl group (δ 3.36) being on C-4a, it has to be on C-3 since C-4 already bears a hydroxyl group. Nuclear Overhauser enhancement studies on **4***a* and **4***b* excluded the possibility of an aromatic hydrogen and a methoxyl group being on contiguous carbons (Table 1). The steric relationships of H-3 to the two methoxyl groups were inaccessible by nOe studies because of the proximity of all three resonances in the spectra of **4***a* and **4***b*.

^{13}C resonances were observed in the region δ_C 17.0–100.0 for all carbons associated with the sugar residue (Table 2). As expected (11) the anomeric carbon C-10a resonated at low field (**4***a* and **4***b*; δ_C 91.0), with a spin–spin coupling to H-10a (**4***a*, $^1J_{CH}$ = 178.1 Hz; **4***b*, $^1J_{CH}$ = 180.9 Hz) indicative of an equatorial orientation for this proton (12). The chemical shifts of the ketal carbon C-4a of **4***a* (δ_C 95.9) and **4***b* (δ_C 95.4) were similar to the value of δ_C 99.1 observed for C-1 of 4-*tert*-butylcyclohexanone dimethylketal (**5**). These carbons gave rise to singlet resonances broadened by long-range coupling to methoxyl and possibly other neighbouring hydrogens in the hr ^{13}C spectra. The chemical shifts of C-4 and C-2 are in the region expected for C-2 through C-5 of aldohexopyranosides which fall within a narrow range centered at about δ_C 70 and are not appreciably altered by acetylation (9). Replacement of a hydroxyl by a methoxyl group is known to deshield such carbons by ≈10 ppm (11) and the chemical shift of C-3 (**4***a*, δ_C 83.3; **4***b*, δ_C 80.5) is consistent with its bearing a methoxyl substituent. Moreover, one of the methoxyl carbons (**4***a*, δ_C 59.4; **4***b*, δ_C 59.9) was coupled ($^3J_{CH}$ ≈ 6.0 Hz) to the C-3 methine hydrogen. No long-range coupling of methoxyl carbons to aromatic hydrogens was observed in **1***a*, **1***b*, **3***a*, **3***b*, and **3***c* (1). Signals arising from the methoxyl group on C-4a (**4***a*, δ_C 50.3; **4***b*, δ_C 51.0) were assigned from proton ord studies. The methyl carbons had chemical shifts similar to the value of δ_C 17.9 observed for the methyl carbon of rhamnose (11). Two remaining resonances in the spectrum of **4***b* were due to the acetoxyl group (CH_3, δ_C 20.1; C=O, δ_C 169.2) attached to C-4.

In the ^{13}C spectrum of 4-*tert*-butylcyclohexanone dimethylketal (**5**) (Table 2) the axial and equatorial methoxyl carbons were almost chemically equivalent (δ_C 46.9 and 46.7), and were abnormally shielded (≈10 ppm) relative to the methoxyl carbons of *O*-methyl derivatives of inositols, monosaccharides, and methyl glycosides (11). Similar shielding was exhibited by the ketal methoxyl at C-4a of **4***a* (δ_C 50.3) and **4***b* (δ_C 51.0) when compared to the methoxyl at C-3 (**4***a*, δ_C 59.4; **4***b*, δ_C 59.9). The ring B carbon of **4***a* and **4***b* which is bonded via oxygen to C-4a should also be shielded by about 10 ppm whereas the one linked through oxygen to C-10a should be normally shielded. Deshielding contributions to C-9a and C-5a of **4***a* and C-3 and C-4 of **3***a* were estimated by comparing their chemical shifts with those of corresponding carbons in 2,2′-dipyridyl (1). Shielding effects of other substituents on ring B were ignored as they would be small compared to those of the directly bonded substituents. The results show that C-3 and C-4 of **3***a* are about equally deshielded (22.7 ± 0.5 ppm) by the directly bonded methoxyl groups (1), whereas C-9a and C-5a of **4***a* (Table 2) are deshielded by 16.1 and 5.6 ppm. The most reasonable explanation for the extra shielding of C-5a in **4***a* is that it is bonded through oxygen to C-4a, C-9a being similarly attached to C-10a. Examination of the data for **3***b* and **4***b* led to the same conclusion.

The chemical shifts of C-6, C-7, and C-9 in **4***a* or

Can. J. Chem. Downloaded from www.nrcresearchpress.com by 210.87.254.42 on 09/05/12
For personal use only.

4*b* are quite similar to those for the corresponding carbons in **3***a* or **3***b* (1) but values for C-5a and C-9a are very different. Examination of the ^{13}C nmr spectrum of 2,3-dimethoxyisopropylbenzene (**6**) in DMSO-d_6 (Table 2) established that the methoxyl groups deshielded C-2 by ≈ 20 ppm and C-3 by ≈ 24 ppm relative to carbons at the same positions in cumene (13). The latter was examined in $CDCl_3$ but solvent effects should be small. The deshielding contributions were almost the same as those experienced by C-3 and C-4 in **3***a* or **3***b* (1). However, the aromatic carbons bonded to oxygen in benzo-1,4-dioxane (**7**) were deshielded by ≈ 15 ppm relative to the carbons of benzene suggesting that the methylene groups partially shield (≥ 5 ppm) these carbons. The same effect in **4***a* would be expected to result in C-5a and C-9a being deshielded by ≈ 15 ppm. The aromatic carbons bonded to oxygen in phenyl-α-D-glucopyranoside (δ_C 157.2), phenyl-β-D-glucopyranoside (δ_C 157.7), and anisole (δ_C 159.3) had almost the same chemical shifts so differences in the substitution at C-10a in **4***a* should not affect the deshielding contribution at C-9a. However, for C-5a the 'ketal' shielding contribution of ≈ 10 ppm must be taken into account and the net deshielding will be only about 5 ppm. From the ^{13}C data for 2,2′-dipyridyl (1) the chemical shifts of C-9a and C-5a in **4***a* are thus calculated to be ≈ 135 ppm (120 + 15 ppm) and 142 ppm (137 + 5 ppm), respectively, which is in reasonable agreement with the experimental values (Table 2).

Chemical shifts of the ring B carbons show consistent trends on going from **1***a* to **1***b*, **3***a* to **3***b*, and **4***a* to **4***b*, except that values for C-5a in the latter pair differ by 5.5 ppm, whereas those for the corresponding carbon (C-4) in **1***a* and **1***b*, or **3***a* and **3***b*, are almost identical (1). Since deshielding of C-5a in **4***b* cannot be attributed to the oxime to nitrile conversion, replacement of the C-4 hydroxyl by an acetoxyl must be responsible. A space-filling molecular model revealed that methoxyl groups at C-3 and C-4a restrict the orientation of an acetoxyl group at C-4. In the most likely conformation of **4***b* the carbonyl group was positioned so that C-5a lay within its deshielding region, thus accounting for the downfield shift on going from **4***a* to **4***b*. Alternatively, but less likely, the chemical shift change might be due to differences of solvation.

No differences were observed between **3***a* and **4***a* in ^1Hmr and ^{13}C nmr data for the oxime group or in the chemical shifts of the ring B hydrogens, hence the oxime substituent in **4***a* must have the *E* configuration and orientation previously deduced for **3***a* (1). Also it was the oxime hydroxyl function of **4***a* which was acetylated under mild conditions to yield the monoacetate **4***c* because the ^1H nmr spectra of the two compounds were essentially indistinguishable except for the replacement of the oxime hydroxyl resonance (δ 11.55 ppm) of **4***a* by an acetyl methyl signal (δ 2.23 ppm) in the spectrum of **4***c*.

The mass spectrum of caerulomycin D showed a series of peaks corresponding to loss of 15 (CH_3), 18 (H_2O), and 30 (CH_2O) mass units, as observed for caerulomycins A and C (1). A strong peak corresponding to *m/e* 332 represented a loss of 71 mass units which did not occur in other dipyridyl compounds and can be accounted for by elimination of a C_4H_7O fragment from the sugar moiety. This initiated two major fragmentation pathways (Scheme 1), neither of which generated the ion at *m/e* 156 corresponding to unsubstituted dipyridyl that was observed in the spectra of caerulomycins B and C.

Information on the absolute configuration at C-2 of the sugar residue of **4***a* was provided by optical rotation measurements. α-D-Aldohexopyranoses and pyranosides, which exist solely in a *C*1 conformation, have positive molecular rotations (14, 15), and when the aglycone is phenyl the rotation increases. Thus phenyl-α-D-glucopyranoside has $[M]_D$ +463 (16). In the compound **8**, which possesses a 2,3-dihydro-1,4-dioxin ring system analogous to that in **4***a* and has $[M]_D$ +602 (17), attachment of the phenanthrene residue has made an even greater positive contribution. Converting the glucose residue of **8** to 6-deoxyglucose would decrease $[M]_D$ by only about 25 (15) and methylation of the C-4 hydroxyl would have little influence on the magnitude and no effect on the sign of rotation (18). Since an axial methoxyl at C-2 of **8** would have to make an improbable contribution of > -500 to the molecular rotation to change its sign the phenanthrene analogue of **4***a* would be expected to have a positive rotation if the sugar had a *C*1 conformation and belonged to the D-series and a negative one if it had a 1*C* conformation and belonged to the L-series. Thus the value of $[M]_D$ −216 found for **4***a* indicates that the sugar moiety has an L-configuration at C-2 and therefore an α-L-configuration at the anomeric center.

The combined evidence establishes caerulomycin D as (2*S*,3*R*,4*R*,4a*S*,10a*S*)-3,4,4a,10a-tetrahydro-4-hydroxy-3,4a-dimethoxy-2-methyl-9-(2-pyridyl)-2*H*-pyrano[3′,2′:5,6]-*p*-dioxino[2,3-*c*] pyridine-7-carboxaldehyde(*E*)-oxime. This structure is unique; the fundamental ring system 2*H*-pyran[3′,2′:5,6]-*p*-dioxino[2,3-*c*]pyridine has not been reported previously and the sugar portion is a derivative of 6-deoxy-L-*arabino*-hexos-2-ulose, a rare monosaccharide only recently synthesized from L-rhamnose (19). L sugars are widely distributed in natural products (20) and some which are constituents of anti-

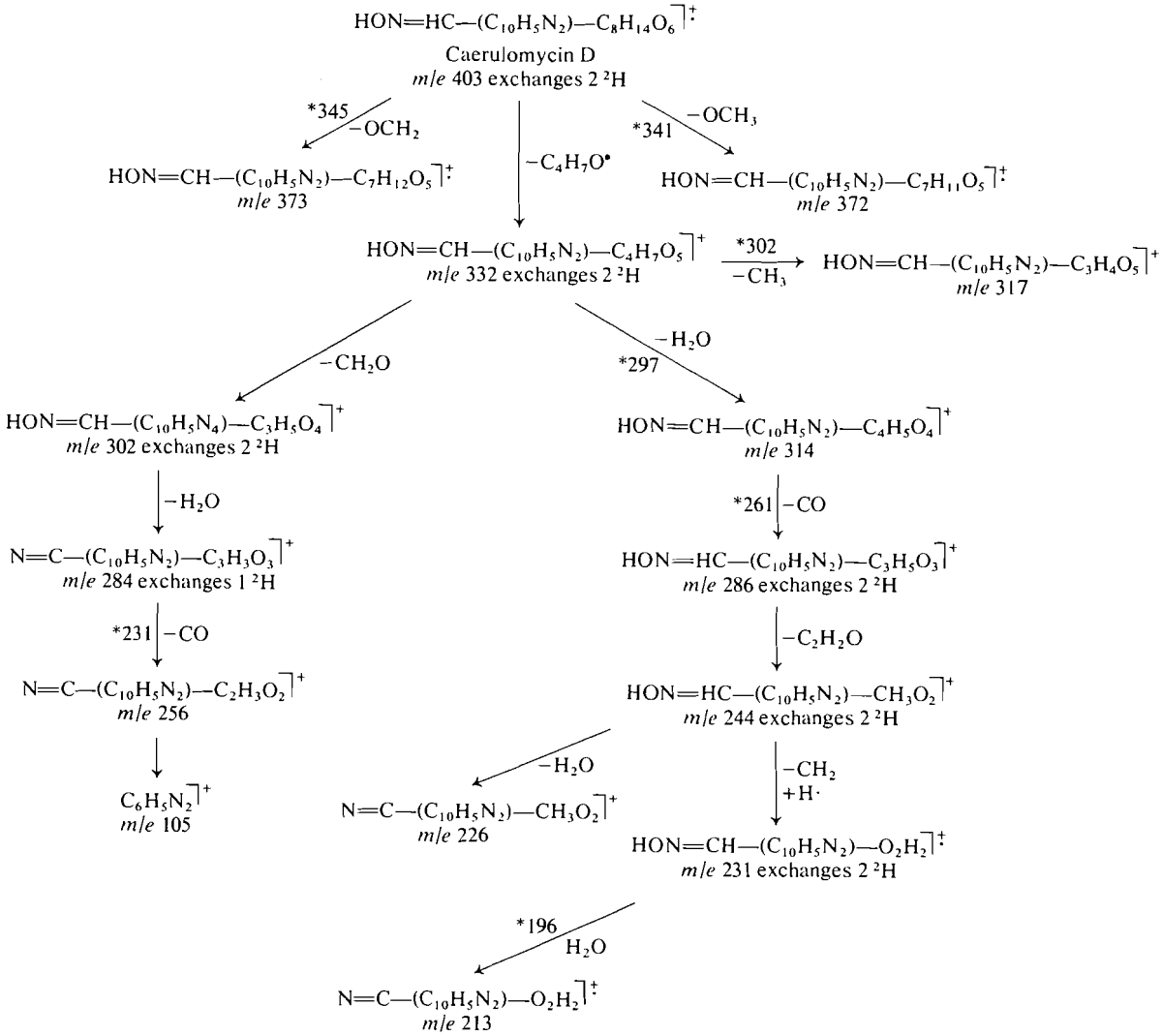

SCHEME I

biotics possess unusual amino, deoxy, and branched-chain structures (21). However, we know of only one other example where a similar ring system was generated by glycosidic type linkages involving vicinal hydroxyl groups of an aglycone and the anomeric center and carbonyl group of a keto sugar. In actinospectacin, an antibiotic produced by *Streptomyces spectabilis*, a decahydro-2*H*-pyrano[2,3-*b*][1,4] benzodioxin ring system was formed from 1,3-dideoxy-1,3-bis(methylamino)-*myo*-inositol and a 4,6-dideoxy-2,3-diulose (22).

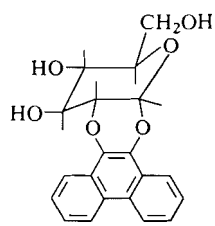

8

Experimental

^{1}H nmr spectra were taken on either a Varian Associates model HA-100D or XL-100-15 spectrometer operating in the continuous wave mode. ^{13}C nmr spectra were recorded at 25.16 MHz on the latter instrument in the pulse Fourier transform mode. Mass spectra were obtained with a Consolidated Electrodynamics Corporation model 110-B double-focusing spectrometer operated in the electrical mode.

Caerulomycin D (4a)

Procedures for the isolation of this compound are given in the previous paper (1). Repeated recrystallization from ethanol yielded fine colorless needles, mp 241–242°C; λ_{max} (MeOH) (log ε): 231 (4.14), 267 (4.00), and 305 nm (inflex.) (3.52);

Can. J. Chem. Downloaded from www.nrcresearchpress.com by 210.87.254.42 on 09/05/12
For personal use only.

ν_{max} (KBr): 3450–3150 (br), 1580, 1570, 1560, 1250, 1125, 1060, 1040, 970, and 790 cm^{-1}; *m/e* (%): 403 (14), 388 (8), 332 (10), 314 (19), 302 (62), 286 (29), 284 (33), 231 (24), 213 (17), 105 (14), 78 (25), 72 (100). Deuterium exchange with D_2O from the heated inlet system of the mass spectrometer caused a shift in $M^{\ddagger}$ from *m/e* 403 to 405. Accurate mass measurement of selected ions (against a perfluorokerosene reference) gave *m/e* 403.1384 (calcd. for $C_{19}H_{21}O_7N_3$: 403.1379), 314.0776 (calcd. for $C_{15}H_{12}O_5N_3$: 314.0797), 302.0781 (calcd. for $C_{14}H_{12}O_5N_3$: 302.0777), 286.0826 (calcd. for $C_{14}H_{12}O_4N_3$: 286.0828) 284.0679 (calcd. for $C_{14}H_{10}O_4N_3$: 284.0671), 231.0656 (calcd. for $C_{11}H_9O_3N_3$: 231.0644), 213.0542 (calcd. for $C_{11}H_7O_2N_3$: 213.0538), and 105.0456 (calcd. for $C_6H_5N_2$: 105.0453). *Anal.* calcd. for $C_{19}H_{21}N_3O_7$: C 56.57, H 5.25, N 10.42; found: C 56.41, H 5.13, N 10.89. Caerulomycin D is relatively stable in acid and was recovered unchanged after 4 h heating under reflux in 2 *N* hydrochloric acid. Partial hydrolysis occurred with 6 *N* acid.

*Caerulomycin D Monoacetate (**4**c)*

Caerulomycin D (25 mg) suspended in acetic anhydride (4 ml) at room temperature dissolved slowly. After 24 h ice was added and the solution was evaporated at 45°C *in vacuo* to an almost colorless product (25 mg) which crystallized from ethanol as needles, mp 143–145°C; λ_{max} (MeOH) (log ε): 231 (4.15), 266 (3.97), and 305 nm (inflex.) (3.37); ν_{max} (CCl_4): 3525 and 1785 cm^{-1}; ν_{max} (KBr): 3600–3100 and 1780 cm^{-1}; $M^{\ddagger}$ at *m/e* 445 (<0.1%) and fragment ions at *m/e* (%): 427 (0.4), 385 (10), 370 (8), 314 (10), 298 (9), 284 (100), 270 (7), 254 (9), 226 (28), 213 (63), 197 (15), and 184 (11). Accurate mass measurement of *M* − 18: 427.1380 (calcd. for $C_{21}H_{21}N_3O_7$: 427.13795).

*Caerulomycinonitrile D Monoacetate (**4**b)*

Caerulomycin D (140 mg) was heated under reflux with acetic anhydride (15 ml) for 3 h. Addition of ice and evaporation of the solution *in vacuo* yielded a pale brown gum. This was purified by preparative thin-layer chromatography (silica gel HF_{254}; eluant 20% acetone–benzene: R_f 0.4) to give a gum which was rechromatographed (silica gel HF_{254}; 3% propanol–ether R_f 0.45) to yield leaflets, mp 63–65°C, λ_{max} (MeOH) (log ε): 229 (4.17), 257 (3.84), and 292 nm (3.50); ν_{max} (CCl_4): 2240 and 1760 cm^{-1}; ν_{max} (KBr): 2235 and 1756 cm^{-1}; $M^{\ddagger}$ at *m/e* 427 (17%) and fragment ions at *m/e* (%): 397 (44), 367 (11), 337 (22), 304 (10), 284 (14), 267 (17), 264 (18), 213 (100), 142 (55), and 127 (50). Accurate mass measurement of $M^{\ddagger}$: 427.1388 (calcd. for $C_{21}H_{21}N_3O_7$: 427.13795).

1. A. G. McInnes, D. G. Smith, J. L. C. Wright, and L. C. Vining. Can. J. Chem. **55**, 4159 (1977).
2. P. V. Divekar, G. Read, and L. C. Vining. Can. J. Chem. **45**, 1215 (1967).
3. R. A. Hoffman and S. Forsen. Prog. Nucl. Magn. Reson. Spectrosc. **1**, 15 (1966).
4. J. H. Noggle and R. E. Schirmer. The nuclear Overhauser effect, chemical applications. Academic Press, New York, NY. 1971.
5. G. C. Levy and G. L. Nelson. Carbon-13 nuclear magnetic resonance for organic chemists. Wiley-Interscience, New York, NY. 1972.
6. T. D. Audichya, T. R. Ingle, and J. L. Bose. Indian J. Chem. **9**, 282 (1971).
7. R. U. Lemieux and J. D. Stevens. Can. J. Chem. **44**, 249 (1966).
8. G. Kotowycz and R. U. Lemieux. Chem. Rev. **73**, 669 (1973).
9. R. U. Lemieux and J. D. Stevens. Can. J. Chem. **43**, 2059 (1965).
10. T. D. Inch. Annu. Rep. NMR Spectrosc. **5A**, 320 (1972).
11. E. Breitmaier and W. Voelter. ^{13}C NMR spectroscopy. Verlag Chemie GmbH, Weinheim/Bergstr. 1974. Chapt. 5.
12. K. Bock, L. Iundt, and C. Pedersen. Tetrahedron Lett. 1037 (1973).
13. L. F. Johnson and W. C. Jankowski. Carbon-13 NMR spectra. Wiley-Interscience, New York, NY. 1972. p. 352.
14. D. H. Whiffen. Chem. Ind. 964 (1956).
15. J. H. Brewster. J. Am. Chem. Soc. **81**, 5483 (1959).
16. W. J. Hickinbottom. J. Chem. Soc. 3140 (1928).
17. B. Helferich, E. N. Mulcahy, and H. Ziegler. Chem. Ber. **87**, 233 (1954).
18. J. Stanek, M. Cerny, J. Kocourek, and J. Pacak. The monosaccharides. Publishing House of the Czechoslovak Academy of Sciences. Prague. (Distributors, Academic Press, New York, NY.) 1963. p. 310.
19. F. H. H. Carlsson, A. J. Charlson, and E. C. Watton. Carbohyd. Res. **36**, 359 (1974).
20. R. Schaffer. *In* The carbohydrates. Vol. IA. *Edited by* W. Pigman and D. Horton. Academic Press, New York, NY. 1972. Chapt. 2.
21. S. Hanessian and T. H. Haskell. *In* The carbohydrates. Vol. IIA. *Edited by* W. Pigman and D. Horton. Academic Press, New York, NY. 1970. Chapt. 31.
22. P. F. Wiley. J. Am. Chem. Soc. **84**, 1514 (1962); H. Hoeksema, A. D. Argoudelis, and P. F. Wiley. J. Am. Chem. Soc. **84**, 3212 (1962); G. Slomp and F. A. MacKellar. Tetrahedron Lett. 521 (1962); L. D. Colebrook and R. H. Gourlay. Proc. Natl. Acad. Sci. U.S. **48**, 1693 (1962); A. L. Johnson, R. H. Gourlay, D. S. Tarbell, and R. L. Autrey. J. Org. Chem. **28**, 300 (1963).

Can. J. Chem. Downloaded from www.nrcresearchpress.com by 210.87.254.42 on 09/05/12
For personal use only.

Can. J. Chem. Downloaded from www.nrcresearchpress.com by 210.87.254.6 on 09/05/12
For personal use only.

Assembly of the carbon skeletal framework of erythronolide A

STEPHEN HANESSIAN, GEORGES RANCOURT,[1] AND YVAN GUINDON[1]

Department of Chemistry, University of Montreal, Montreal, P.Q., Canada H3C 3V1

Received March 17, 1978

STEPHEN HANESSIAN, GEORGES RANCOURT, and YVAN GUINDON. Can. J. Chem. **56**, 1843 (1978).

The construction of the 15-carbon chiral framework of erythronolide A is described, based on a synthetic strategy that uses carbohydrate-derived 'chiral templates' as prefabricated segments of the target molecule.

STEPHEN HANESSIAN, GEORGES RANCOURT et YVAN GUINDON. Can. J. Chem. **56**, 1843 (1978).

La construction du squelette carboné chiral de l'érythronolide A est décrite, basée sur une stratégie synthétique qui utilise des carbohydrates comme 'charpentes chirales.'

The construction of the chiral, polyfunctional carbon framework of macrolide aglycones (1–3) presently constitutes one of the more challenging synthetic endeavors in the chemistry of natural products. We have already described the synthesis of two functionalized chiral precursors I and II to erythronolide A, **1**, comprising 8 out of the 10 chiral centers of this formidable synthetic objective, and representing its C-1—C-6 and C-9—C-15 portions (4, 5).[2] We now describe the completion of a critical phase in the total synthesis of **1**,[3] namely, the bridging of appropriately modified precursors I and II, thus giving access to the entire functionalized carbon skeleton as a suitably protected derivative.

The synthetic plan for the construction of this derivative called for (*a*) the one-carbon homologation of precursors I (R = OMe) and II through C-6 and C-1, respectively, and their transformation, individually, into nucleophilic and electrophilic counterparts; (*b*) the efficient utilization of a C—C bond forming reaction for the union of two such segments; (*c*) introduction of a *C*-methyl group at C-8; and (*d*) elaboration of the tertiary center at C-6.

The nucleophilic component corresponding to C-1—C-6 of the erythronolides was prepared from

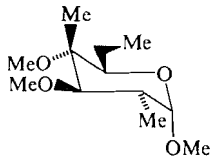

Precursor II

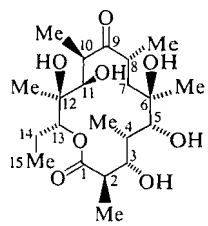

1

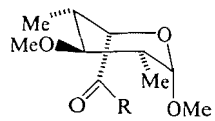

Precursor I R = OMe; Me

the α,β-unsaturated ester **2** (4, 5) (Scheme 1). Treatment of **2** with lithium dimethylphosphonoacetate (ether, 25°C) gave the corresponding ketophosphonate derivative **3** as a syrup (80% after chromatography); $[\alpha]_D$ +142.8°;[4] M^+ 322. Catalytic hydrogenation (5% Pd/C, H_2, MeOH), then gave the desired synthon **4** as a syrup (95%); $[\alpha]_D$ +130.1°; M^+ 324; δ (ppm): 2.93 (t, $J_{3,4}$ = 14 Hz, H-3), 4.38 (d, $J_{5,4}$ = 4 Hz, H-5), 4.73 (d, $J_{1,2}$ = 3.5 Hz, H-1), etc. The electrophilic component corresponding to C-9—C-15 of **1** was obtained from precursor II in the following manner. Acid hydrolysis (70% AcOH, 80°C) gave the free sugar **5** (Scheme 1) as a mixture of anomers (syrup, 74%), which was converted into a mixture of epimeric allylic alcohols **6** by reaction with vinylmagnesium bromide (7) in THF

[1]NRCC Predoctoral Fellow.

[2]Precursor I also represents the C-1—C-6 portion of erythronolide B.

[3]Expression **1** corresponds to one of several planar projections for the erythronolides, where the relative orientation of functional groups may vary according to the arbitrary choice of conformation (4, 5). The spatial disposition of each group in expression **1** is the same as that found in the solution conformation of erythronolide B (6). We therefore prefer the adoption of such an expression whenever the structures of these compounds are represented as plane projections; see also ref. 2.

[4]New compounds had spectroscopic (^{1}H nmr; ir) and mass spectral characteristics that were in accord with their structures. Optical rotations were measured at 25°C in chloroform at concentrations of 0.5–1%.

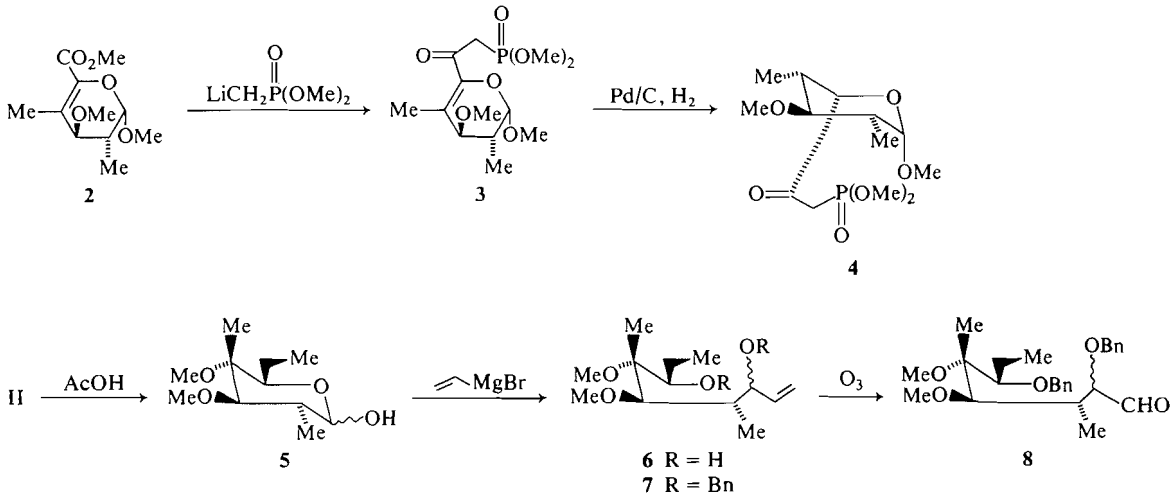

SCHEME 1

(25°C, 18 h, ~98%). Benzylation (BnBr, NaH, DME) then gave a mixture of epimeric compounds **7** as a syrup (73% overall from **6**) which was subjected to ozonolysis to give the desired aldehydo derivative **8** as a syrup (77%); ν_{max} 1725 cm^{-1} (C=O).

Coupling between intermediates **4** (slight excess) and **8** was accomplished in the presence of sodium hydride in THF (18 h, 25°C) to give **9** as a syrupy mixture of C-9 epimers which could be separated by chromatography (59%); $M^{\ddagger}$ 626.3809 ($C_{37}H_{54}O_8$) (Scheme 2). That the L-*ido* stereochemistry had remained intact during the coupling, as required for the C-1—C-6 portion in **1**, was ascertained chemically, by treatment of **9** with NaOMe (pH ~ 9) which led to virtually complete epimerization at C-5 within a few hours.[5]

Conjugate addition of lithium dimethylcuprate to **9** (ether, −5°C) gave the C-8 methyl derivative **10** as a mixture of syrupy diastereoisomers (approximately quantitative) without any detectable epimerization at C-5; δ (ppm): 4.25 ($J_{5,4}$ = 3 Hz, H-5). The tertiary center at C-6 was introduced by reaction of **10** with methyllithium in ether to give **11**, presumably as a mixture of diastereoisomers (syrup, 51%), $[\alpha]_D$ +35.2°. *Since C-9 is the site of the carbonyl group in* **1**, *and C-8* epi *derivatives can be epimerized* (*8*, *9*) *to give the desired configuration, the stereochemical purity at these centers in the mixture of diastereoisomers corresponding to* **11** *is unimportant at this stage of the synthesis.* The yet unknown stereochemistry at C-6 also offers some flexibility, since this center is introduced in the last step of the sequence (**10** → **11**) and the stereochemical control of the reaction could be further studied under a variety of conditions with no loss of chiral efficiency at other centers. In this context, we describe another approach for joining appropriately modified precursors I(R = Me) and II, in which I is used as a source of an electrophilic component, as exemplified in the following model study (Scheme 3). Treatment of precursor I (R = Me) with vinylmagnesium bromide gave a ~6:1 mixture of epimers (syrup > 90%) in which the preponderant product was assigned structure **12** based on literature precedents (10–12). Methylation (MeI, NaH, DMF) followed by oxidative cleavage (OsO_4–IO_4^-) gave the aldehydo derivative **13** (syrup, 65% from **12**) which was transformed via a Wittig or Horner–Emmons reaction into **14** (syrup, ~80% after chromatography); $[\alpha]_D$ +33°; *m/e* 325 ($M^{\ddagger}$ − MeO). Using this approach, the correct stereochemistry at C-6 would be secured early in the synthetic sequence, and subsequent introduction of the C-8 methyl group in the enone derived from **13** and the appropriate ketophosphonate derivative prepared from II, would involve a reductive alkylation process.

The synthetic conquest of only one macrolide aglycone has been achieved so far, in the landmark total synthesis of the 12-membered macrolide antibiotic methymycin (13). Other work in this area has involved lactonization of seco acids derived from 14- and 16-membered natural 'polyoxo' macrolide aglycones (9, 14). Two recent reports (15, 16) have dealt with the generation of aldol-type systems in the search for stereoselective methods that are potentially applicable to the stepwise construction of highly chiral and functional compounds such as **1**. In the Woodward route to **1** (17), a dithiadecalin ring system is ingeneously used as a framework for the systematic introduction of functionality corresponding to segments of the seco acid. Our approach for

[5]The D-*gluco* stereochemistry (C-1—C-6) of the resulting syrupy mixture of epimers at C-9 was clearly evident from nmr studies, $J_{4,5}$ = 11 Hz; *m/e* 594.3513 ($M^{\ddagger}$ − MeOH).

Can. J. Chem. Downloaded from www.nrcresearchpress.com by 210.87.254.6 on 09/05/12
For personal use only.

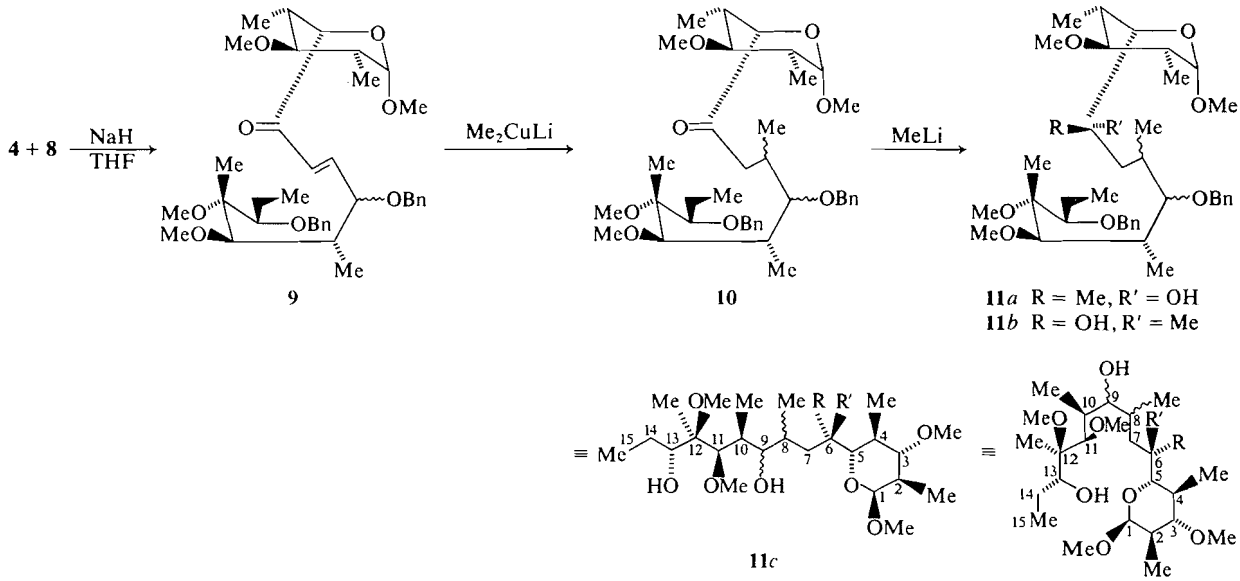

SCHEME 2

the assembly of the carbon skeletal framework of **1** and its 9-dihydro derivative (18), as exemplified by the 1,5-hemiacetal derivative **11***c*, has been based on the efficient utilization of prefabricated 'chiral templates' derived from carbohydrates (5, 7, 19, and references cited therein).[6] As a consequence, all the hydroxyl and methyl groups in **11** have been introduced regiospecifically and the correct absolute stereochemistry of at least eight chiral centers present in **1** has been secured.

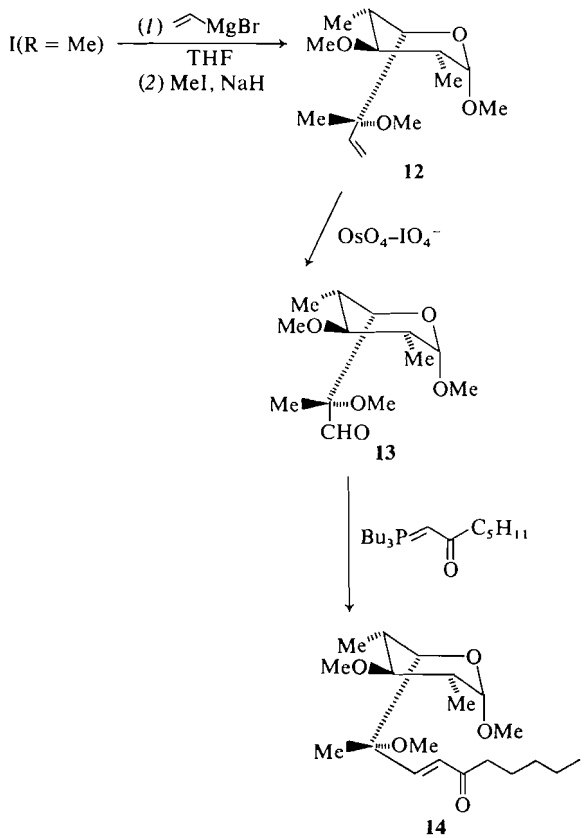

SCHEME 3

Acknowledgments

We thank the National Research Council of Canada and le Ministère de l'Education du Québec for financial support and for fellowships to G.R. and Y.G. We also acknowledge the assistance of R. Mayer and P. Coulombe with spectroscopic measurements.

1. W. D. CELMER. Pure Appl. Chem. **28**, 413 (1971).
2. S. MASAMUNE, G. S. BATES, and (in part) J. W. CORCORAN. Angew. Chem. Int. Ed. Engl. **16**, 585 (1977).
3. K. C. NICOLAOU. Tetrahedron, **33**, 683 (1977).
4. S. HANESSIAN and G. RANCOURT. Can. J. Chem. **55**, 1111 (1977).
5. S. HANESSIAN and G. RANCOURT. Pure Appl. Chem. **49**, 1201 (1977).
6. T. J. PERUN and R. S. EGAN. Tetrahedron Lett. 387 (1969).
7. G. STORK and S. RAUCHER. J. Am. Chem. Soc. **98**, 1583 (1976).
8. J. TADANIER, R. J. MARTIN, R. S. EGAN, A. W. GOLDSTEIN, E. HIRNER, and F. FISHER. J. Am. Chem. Soc. **95**, 592 (1973); J. TADANIER, R. J. MARTIN, R. S. EGAN, A. W. GOLDSTEIN, R. S. STANASZEK, E. HIRNER, and F. FISHER. J. Org. Chem. **39**, 2495 (1974).
9. E. J. COREY, K. C. NICOLAOU, and L. S. MELVIN, JR. J. Am. Chem. Soc. **97**, 654 (1975).

[6]The common intermediate leading to precursors I and II (4) has now been prepared in its *O*-demethylated form, hence the possibility exists for preferential *O*-protection at individual hydroxyl groups for further elaboration into **1**.

Can. J. Chem. Downloaded from www.nrcresearchpress.com by 210.87.254.6 on 09/05/12
For personal use only.

10. D. J. CRAM and F. A. A. ELHAFEZ. J. Am. Chem. Soc. **74**, 5828 (1952); D. J. CRAM and K. R. KOPECKY. J. Am. Chem. Soc. **81**, 2748 (1959).
11. M. L. WOLFROM and S. HANESSIAN. J. Org. Chem. **27**, 1800 (1962).
12. T. D. INCH. Adv. Carbohyd. Chem. Biochem. **27**, 191 (1972).
13. S. MASAMUNE, H. YAMAMOTO, S. KAMATA, and A. FUKUGAWA. J. Am. Chem. Soc. **97**, 3513 (1975).
14. S. MASAMUNE, Y. MAYASE, W. K. CHAN, and R. L. SOBCZAK. J. Am. Chem. Soc. **98**, 7874 (1976).
15. R. E. IRELAND and C. S. WILCOX. Tetrahedron Lett. 2839 (1977).
16. C. T. BUSE and C. H. HEATHCOCK. J. Am. Chem. Soc. **99**, 8109 (1977).
17. R. B. WOODWARD. 25th National Organic Chemistry Symposium, Morgantown, WV, June 19–23, 1977.
18. M. V. SIGAL, JR., P. F. WILEY, K. GERZON, E. H. FLYNN, U. C. QUARCK, and O. WEAVER. J. Am. Chem. Soc. **78**, 388 (1956).
19. See for example, D. SEEBACH and H.-O. KALINOWSKI. Nachr. Chem. Techn. **24**, 415 (1976) and references cited therein.

Can. J. Chem. Downloaded from www.nrcresearchpress.com by 210.87.254.6 on 09/05/12
For personal use only.

Canadian Journal of Chemistry

Published by
THE NATIONAL RESEARCH COUNCIL OF CANADA

Volume 56 Number 14 July 15, 1978

Journal canadien de chimie

Publié par
LE CONSEIL NATIONAL DE RECHERCHES DU CANADA

Volume 56 numéro 14 15 juillet 1978

Can. J. Chem. Downloaded from www.nrcresearchpress.com by 210.87.254.5 on 09/05/12
For personal use only.

The thermal desorption of surface species from sulfur dioxide adsorption on natural chrysotile asbestos and calorimetric sorption heats at 298, 323, 373, and 423 K

WILLIAM JOHN MURPHY AND ROBERT ANDERSON ROSS

Department of Chemistry, Lakehead University, Thunder Bay, Ont., Canada P7B 5E1

Received January 4, 1978

WILLIAM JOHN MURPHY and ROBERT ANDERSON ROSS. Can. J. Chem. **56**, 1847 (1978).

Calorimetric heats of adsorption have been determined for sulfur dioxide adsorbed at 298, 323, 373, and 423 K on both Californian and Quebec chrysotiles. Adsorption isotherms have been measured and some differential molar entropies calculated. Thermal desorption of surface species resulting from the adsorption of sulfur dioxide on Californian chrysotile at 298 K have been studied from 25 to 450°C. Sulfurous and carbonic acids, in addition to sulfites and other trace species, have been shown to result from the adsorbent–adsorbate interactions. A mechanism for sulfur dioxide adsorption on chrysotile has been prepared which accounts for the observed high heats of adsorption measured at low surface coverages.

WILLIAM JOHN MURPHY et ROBERT ANDERSON ROSS. Can. J. Chem. **56**, 1847 (1978).

On a déterminé les chaleurs d'absorption calorimétriques de l'anhydride sulfureux adsorbé à 298, 323, 373 et 423 K sur des chrysotiles de la Californie et du Québec. On a mesuré les isothermes d'adsorption et on a calculé quelques entropies molaires différentielles. On a étudié, de 25 à 450°C, la désorption thermique d'entités de surface provenant d'une adsorption de l'anhydride sulfureux sur une chrysotile de la Californie à 298 K. On a démontré qu'il y a formation d'acides sulfureux et carbonique en plus de sulfites et de traces d'autres entités à partir d'interactions adsorbant–adsorbé. On a préparé un mécanisme pour expliquer l'adsorption de l'anhydride sulfureux sur la chrysotile qui tient compte des chaleurs d'adsorption élevées qui ont été observées et qui ont été mesurées à des valeurs faibles de recouvrement des surfaces.

[Traduit par le journal]

Introduction

Asbestos in its various forms is perhaps the most documented solid pollutant (1) of industrial societies and sulfur dioxide is recognized as one of the major gaseous pollutants (2, 3). Inhalation of the various asbestos types and its possible relationship to the initiation of respiratory disease has long been the subject of intensive research (4–6). It has been reported (7), however, "that neither pulmonary fibrosis (asbestosis) nor bronchogenic carcinoma (lung cancer), the two most common asbestos-related diseases, are peculiarly related to or caused solely by the inhalation of asbestos fibres". In this respect the reported synergetic relationship (8, 9) between cigarette smoke and asbestos with respect to lung cancer incidence is of major interest.

Through recent publications we have described thermodynamic studies of sulfur dioxide adsorption on a wide range of materials including γ-Al_2O_3 (10), charcoal (11), and chrysotile asbestos which had been subjected to various degrees of heat treatment (12). In an endeavour to typify the nature of the specific gas–solid interactions this work has now been extended to an examination of the adsorption of sulfur dioxide on chrysotile asbestos from 298 to 423 K using both thermodynamic and thermodesorption – mass spectrometric techniques. At the same time, these data could be of some value in health-related studies in determining whether synergism, with respect to respiratory diseases, is likely or possible with co-inhalation of the pollutants.

Experimental

Materials

Chrysotile ($Mg_3SiO_5(OH)_4$) samples were supplied by (*a*) Lake Asbestos, Black Lake, Quebec (sample 7T/5, Quebec chrysotile) and (*b*) Union Carbide Corporation (Calidria

Can. J. Chem. Downloaded from www.nrcresearchpress.com by 210.87.254.5 on 09/05/12
For personal use only.

asbestos sample HPO, Californian chrysotile). The major impurities were brucite ($Mg(OH)_2$), 10% in sample (*a*) and magnetite (Fe_3O_4), 3.75% in (*a*) and 0.75% in sample (*b*).

Sulfur dioxide (Matheson of Canada, anhydrous grade, >99.98% pure) was drawn directly from the cylinder, after line flushing, to a trap attached to the apparatus. It was then outgassed at 10^{-4} Torr and vacuum distilled over trays of phosphorus pentoxide. This purification procedure was repeated at least six times. Middle portions only were used and glc analyses showed these to be greater than 99.999% pure.

Surface areas of all samples were determined from nitrogen adsorption–desorption isotherms at 77 K (13) giving 60 and 40 $m^2 g^{-1}$ for Californian and Quebec chrysotiles, respectively.

The samples were pretreated at 423 K and 10^{-4} Torr for 24 h which results in a 0.5% weight decrease due to loss of physically adsorbed water from the surface (13, 19). The samples used in the thermal desorption experiments were initially pretreated as above and then exposed to sulfur dioxide at 600 Torr for 6 h at 298 K. The sulfur dioxide was then pumped off and the samples outgassed by pumping at 298 K for 24 h.

Apparatus and Procedure

Calorimetry

Calorimetric heats of adsorption were determined in a vessel similar to that described by Robinson and Ross (14). The calorimeter was operated in the adiabatic mode and the heat measurement conditions were adapted from those used by Smith and Ford (15) as recently reported (11). Entropies of adsorption were calculated from classical thermodynamic equations (16, 17).

Qualitative chemical tests for sulfite, sulfide, sulfate, and carbonate were performed on all samples from the calorimetric experiments, after desorption of sulfur dioxide and pumping overnight at 10^{-4} Torr.

Thermal Desorption

Thermal desorption of adsorbed species was carried out from 25 to 450°C at a heating rate of 3°C/min. Krypton (Matheson of Canada, Research Purity grade, >99.995% pure), at 1 Torr, was used as the carrier gas and as the internal pressure standard in an all-glass 'static' circulation apparatus similar to that of Boreskov and Popovskii (20), incorporating a differential reactor. The gas analyser was a Vacuum Generator Micromass Q7 mass spectrometer attached to the circulation loop via a capillary leak and operated at $\sim 3 \times 10^{-6}$ Torr.

Results

Adsorption and Calorimetry

Figures 1 and 3 show the adsorption isotherms for sulfur dioxide adsorption on Californian and Quebec chrysotiles, respectively, at substrate temperatures of 298, 323, 373, and 423 K. Californian chrysotile exhibited larger adsorption capacities than the Quebec material at corresponding substrate temperatures. Further, its capacity was more temperature dependent than that for Quebec chrysotile at a corresponding pressure of sulfur dioxide. For example, the adsorption capacity at 600 Torr for Californian chrysotile fell from 4.00 μmol m^{-2} at 298 K to 1.65 μmol m^{-2} at 423 K compared with 2.92 μmol m^{-2} at 298 K and 1.42 μmol m^{-2} at 423 K for the Quebec sample.

Figure 1 (inset) shows the results obtained in pretreatment experiments when Californian chrysotile was exposed to sulfur dioxide at 373 K for 6 h at 600 Torr. The gas was then pumped off and the chrysotile outgassed at 373 K by pumping at 10^{-4} Torr for a further 24 h. A reduction in adsorption capacity of between 25 and 30% over the entire equilibrium pressure range was observed when an isotherm was determined on this surface.

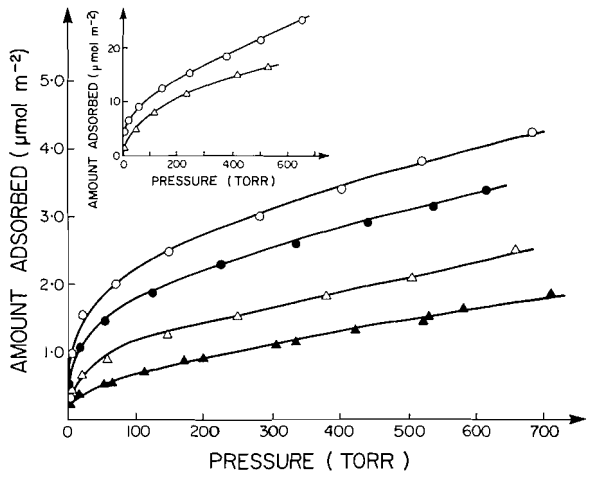

FIG. 1. Adsorption isotherms for sulfur dioxide on Californian chrysotile (HPO) at 298 K (○), 323 K (●), 373 K (△), and 423 K (▲). Inset: adsorption isotherms for sulfur dioxide at 373 K, after pretreatment with sulfur dioxide (○), and after standard pretreatment conditions (△).

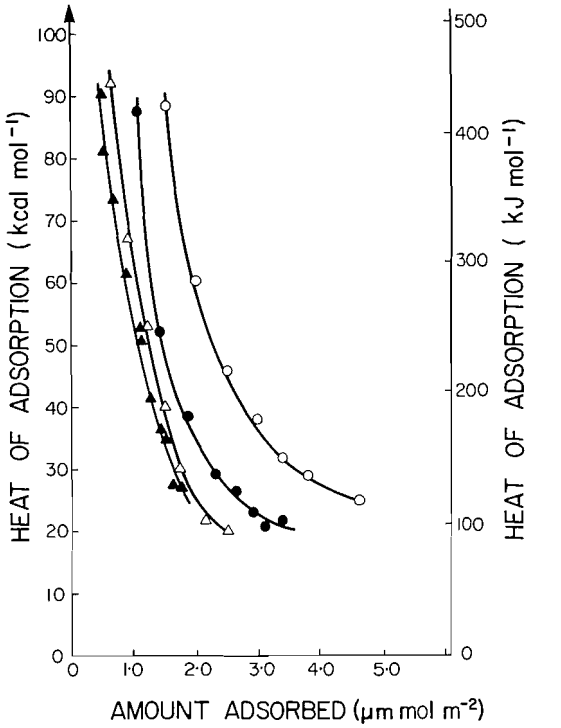

FIG. 2. Heat curves for the adsorption of sulfur dioxide on Californian chrysotile (HPO) at 298 K (○), 323 K (●), 373 K (△), and 423 K (▲).

Can. J. Chem. Downloaded from www.nrcresearchpress.com by 210.87.254.5 on 09/05/12
For personal use only.

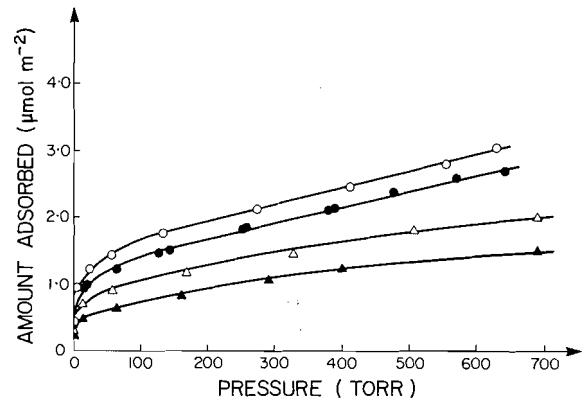

FIG. 3. Adsorption isotherms for sulfur dioxide on Quebec chrysotile (7T/5) at 298 K (○), 323 K (●), 373 K (△), and 423 K (▲).

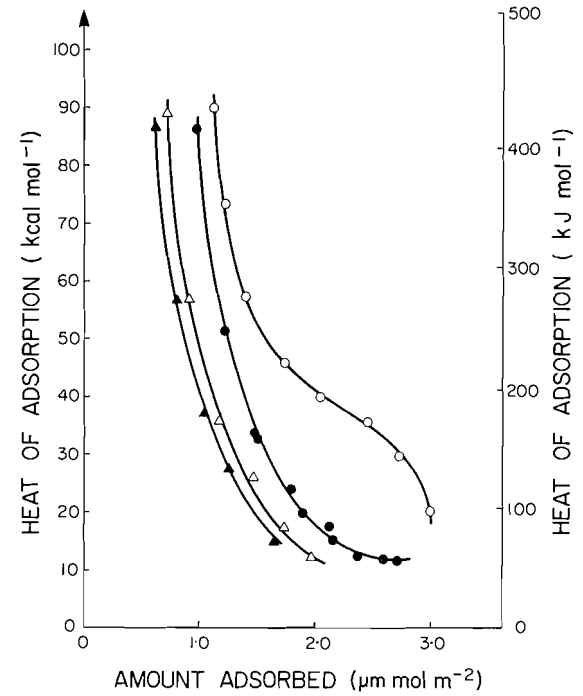

FIG. 4. Heat curves for the adsorption of sulfur dioxide on Quebec chrysotile (7T/5) at 298 K (○), 323 K (●), 373 K (△), and 423 K (▲).

Figures 2 and 4 show the heats of adsorption of sulfur dioxide on Californian and Quebec chrysotiles, respectively, at 298, 323, 373, and 423 K. Both adsorbents exhibited very high heats of adsorption at low coverages which fell sharply with increased coverage. The profile for Quebec chrysotile at 298 K was exceptional in that an inflexion point, which was reproducible, was observed, ~35 kcal mol^{-1} at 2.5 μmol m^{-2} coverage.

Thermal Desorption

Figure 5*a* shows the relative amounts of species

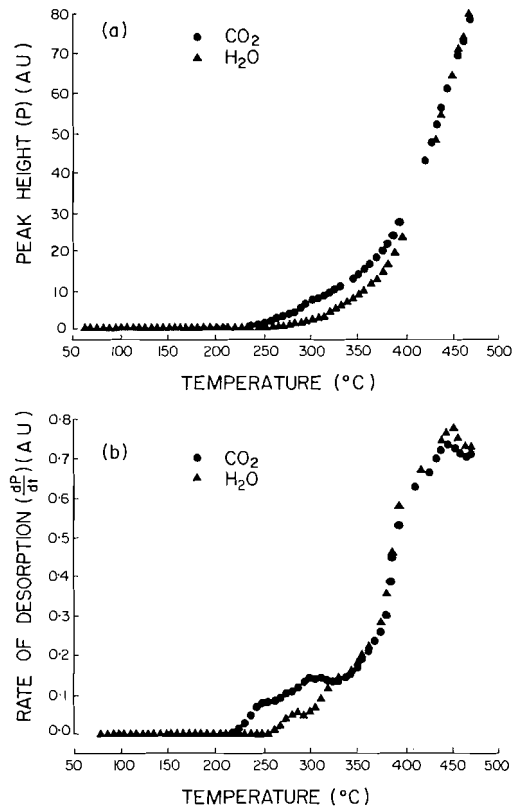

FIG. 5. Thermal desorption of adsorbed species on Californian chrysotile before pretreatment with sulfur dioxide.

which were desorbed from Californian chrysotile preheated under standard conditions, on increasing the temperature of the adsorbent from 50 to 450°C (au = arbitrary units). Figure 5*b* shows the rates of desorption of the species with respect to the substrate temperature. Only carbon dioxide and water were desorbed under these conditions. The figure indicates three distinct temperatures at which the rate of desorption of carbon dioxide maximizes, but there are only two such temperatures for the water component. The maximum at ~460°C in the carbon dioxide pattern coincides with the second maximum in the water desorption rate.

Figures 6*a* and *b* show the relative amounts of species desorbed and the rates of desorption, respectively, with temperature of substrate from Californian chrysotile after pretreatment with sulfur dioxide. In addition to sulfur dioxide, which exhibited four rate-of-desorption maxima, carbon dioxide and water were also desorbed (Fig. 6*b*). Comparison of Figs. 5 and 6 indicates that the desorption temperatures for carbon dioxide and water decrease considerably as a result of the pretreatment. Figure 6*b* further shows that, at a given temperature, more than one adsorbate can be desorbed. Thus,

Can. J. Chem. Downloaded from www.nrcresearchpress.com by 210.87.254.5 on 09/05/12
For personal use only.

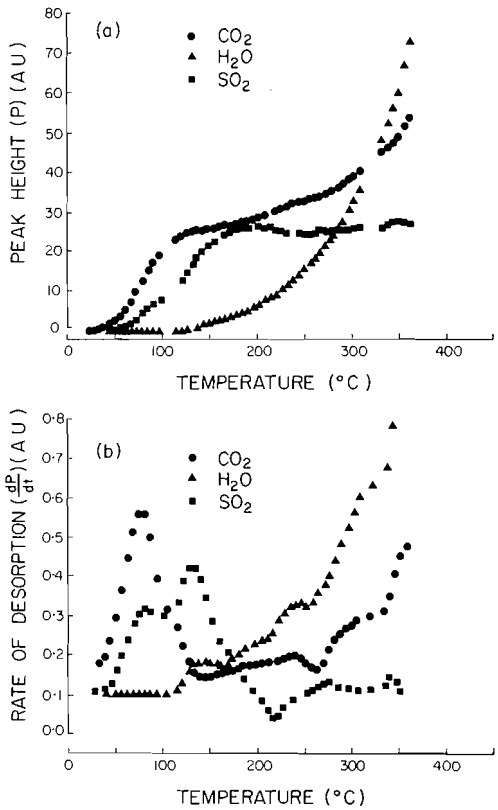

FIG. 6. Thermal desorption of adsorbed species on Californian chrysotile after pretreatment with sulfur dioxide.

for example, at 75°C both sulfur dioxide and carbon dioxide were desorbed, at 130°C both sulfur dioxide and water, and at 235°C both water and carbon dioxide.

These results suggest that co-desorbed sulfur dioxide and water and also carbon dioxide and water may exist as single species on the surface, perhaps as (H_2SO_3) and (H_2CO_3) respectively, or that the desorbed gases were attached to the surface in a very similar way. Cracking pattern studies tend to suggest that both phenomena occur. Thus sulfur dioxide and water desorbed at 135°C and the carbon dioxide and water desorbed at 235°C arise from (H_2SO_3) and (H_2CO_3), respectively, whereas all other species are desorbed as individual molecules from the surface.

Discussion

Previous work on magnesia (10), alumina (17), and silica (24) yielded values of 80, 20 to 50, and <10 kcal mol^{-1} for the heats of adsorption at surface coverages of 1 μmol m^{-2} in this temperature range. The alumina heat values were clearly related to the 'previous history' of the samples and the decrease in the heats over the oxide set was related to the decrease in ionicity of the oxides and to their ability to form compounds with sulfur dioxide.

The present results are generally consistent with these conclusions. Thus, Figs. 2 and 4 indicate that significant changes in the adsorbate–adsorbent interactions have occurred over the coverage range from chemisorption reactions, substantially exothermic, to a weaker chemisorption mode at 2–5 μmol m^{-2}.

These changes can be further emphasized by a comparison of the values of the calculated differential molar entropies. These were large and negative at low coverages (-80 to -40 cal deg^{-1} mol^{-1} at 100 Torr), increasing with increased coverage to values (4.0 cal deg^{-1} mol^{-1} at 600 Torr) close to the configurational entropy ($\sim$1.5 cal deg^{-1} mol^{-1}) in the case of Californian chrysotile and to values ($\sim$25 cal deg^{-1} mol^{-1} at 600 Torr) between the configurational entropy ($\sim$2.0 cal deg^{-1} mol^{-1}) and the entropy of a two dimensional 'mobile' film for the Quebec material.

The heat values for the highest coverages studied were still much higher than the heat of condensation of sulfur dioxide, $\sim$1.2 to 5 kcal mol^{-1}, at these temperatures, whence some form of hydrogen bond formation may be indicated (18).

The tendency of the heats of adsorption vs. coverage profiles to merge at higher substrate temperatures, Figs. 2 and 4, is consistent with the observation that above 100°C the sulfur dioxide which is most weakly bound to the surface, for example that desorbed at 75°C in Fig. 6, will not be retained and its contribution to the adsorption heats will be lost.

Figures 1 and 3 show that the chrysotiles exhibit similar isotherm patterns, with the Californian material having the larger adsorption capacity. The capacity differences shown by the lower temperature isotherms are almost directly proportional to the surface areas of the solids, 60 and 40 m^2 g^{-1} for the Californian and Quebec chrysotiles (13), respectively. At 373 and 423 K, the isotherms, as well as the adsorption heat profiles, for both materials show similar values suggesting that the extra capacity of the Californian asbestos at low temperatures is almost entirely achieved through the uptake of sulfur dioxide in a less strongly bound condition.

The thermal desorption results, Figs. 5*a* and *b*, may be usefully compared with De Vleesschauwer's (21) report that nesquehonite ($MgCO_3 \cdot 3H_2O$) under dynamic heating conditions similar to those used in the present study decomposes thus:

$$[1]\quad MgCO_3 \cdot 3H_2O \xrightarrow{\sim 150^\circ C} MgCO_3 \cdot H_2O \xrightarrow{\sim 400^\circ C} MgO + CO_2 + H_2O$$

Further it has been reported (21, 22) that in similar conditions nesquehonite yields some basic magnesium carbonate ($4MgO \cdot 3CO_2 \cdot 3H_2O$). These data suggest that perhaps a carbonate, similar to nesque-

Can. J. Chem. Downloaded from www.nrcresearchpress.com by 210.87.254.5 on 09/05/12
For personal use only.

honite or the monohydrate dehydration product of nesquehonite, may be present as a trace impurity in Californian chrysotile.

This would also account for carbon dioxide and water desorption at 400°C and above. The remaining very minor carbon dioxide peaks could then be due to desorption of carbon dioxide with water or perhaps to the decomposition of a small amount of basic carbonate impurity.

Figure 6*b* shows that as the substrate temperature of the sulfur dioxide treated Californian chrysotile was increased both carbon dioxide and sulfur dioxide were desorbed simultaneously at approximately 75°C indicating that both were weakly chemisorbed to the surface perhaps by hydrogen bonding through mono- or bidentate complexes similar to those suggested for sulfur dioxide adsorbed on magnesia (23). With further increase in substrate temperature, sulfur dioxide and water were desorbed simultaneously. Sulfurous acid may have formed on the surface:

$$[2] \qquad 2SO_2 + Mg(OH)_2 \rightarrow MgSO_3 + H_2SO_3$$

$$\Delta H_{298} = -24 \text{ kcal mol}^{-1}$$

Sulfite ions were detected by chemical tests of the chrysotile even at temperatures >300°C. This sulfite was not present solely as sulfurous acid since this would not be present on the surface above 135°C. Further, analyses of the mass spectral cracking patterns in the temperature region where the sulfur dioxide and water were desorbed indicated that the sulfur dioxide was 'complexed' to the water and not in the 'free' state.

Raising the substrate temperature to 240°C resulted in the simultaneous desorption of carbon dioxide and water. Thus carbonic acid may also be a surface product:

$$[3] \qquad MgCO_3 \cdot xH_2O + SO_2 \rightarrow MgSO_3 + (CO_2 + xH_2O)$$

$$\Delta H_{298} \sim 0$$

$$MgCO_3 \cdot xH_2O + H_2SO_3 \rightarrow MgSO_3 + (CO_2 + yH_2O)$$

$$\Delta H_{298} \sim 0$$

Further increase to 275°C resulted solely in the desorption of sulfur dioxide. This may be explained by the decomposition of the surface sulfite complex already postulated as the product of a number of adsorbate–adsorbent interactions ([2] and [3]) in agreement with Goodsel *et al.* (23) who observed the decomposition of a bidentate sulfite complex of magnesium at ~300°C.

The remaining desorption products identified at higher temperatures would result from decomposition of unreacted carbonate residue and a more strongly bound surface sulfite. A comparison of the relative amounts of carbon dioxide and water desorbed above 300°C, Fig. 6*b*, from both untreated and treated chrysotiles, shows that the ratio $[CO_2]/[H_2O]$ is much smaller in the latter case in support of the hypothesis that all the carbon dioxide desorbed at 75 and 240°C originates from one source.

The adsorption of sulfur dioxide on Californian chrysotile tends to destabilise the residue of the carbonate impurity to thermal decomposition by as much as 50°C, Fig. 6*b*, again indicating that the carbonate is a surface species since a bulk carbonate impurity would be expected to show some residue of unreacted carbonate not affected by the adsorption of sulfur dioxide.

It now seems reasonable to suggest that sulfur dioxide may be adsorbed, perhaps by hydrogen bonding, on an adjacent site to the carbonate and that it can act to destabilise the carbonate to a greater or lesser extent. The former would be expected to result in carbon dioxide desorption while the simultaneous desorption of carbon and sulfur dioxides at 75°C, Fig. 6*b*, suggests that the decomposition of a surface complex involving the two species has occurred.

The high initial heats of adsorption, Figs. 2 and 4, may be related to surface heterogeneity but a scheme consistent with the observed surface dehydration reaction can also accommodate these features. It would result in the formation of magnesium sulfate and sulfur. Although the presence of trace quantities of elemental sulfur were indicated[1] by mass spectroscopy and electron microscopy, chemical tests for both materials were inconclusive. However, the presence of sulfate under very similar experimental conditions has previously been reported for sulfur dioxide on magnesia (10) where heats of adsorption were also in this region.

These various conclusions and hypotheses may be summarised (Scheme 1).

Thermodynamic analyses of possible contributing steps and a comparison with the measured heats of adsorption indicates that simple acid–base type reactions do not account for the high heats of adsorption measured at very low coverages. Summation of the heats of all of these possible steps, guided by the thermal desorption results, would account for only ~35 kcal mol^{-1} thus lending additional credibility to the postulate regarding sulfur formation at low surface coverages which would then yield overall heats of adsorption values ~90 kcal mol^{-1}.

The rapid decrease in the heats of adsorption with increased coverage indicates that the major continuing contribution to the heat values lies with interactions such as sulfite formation. However, in continuing these investigations we hope to clarify

[1]W. J. Murphy and R. A. Ross. Unpublished data.

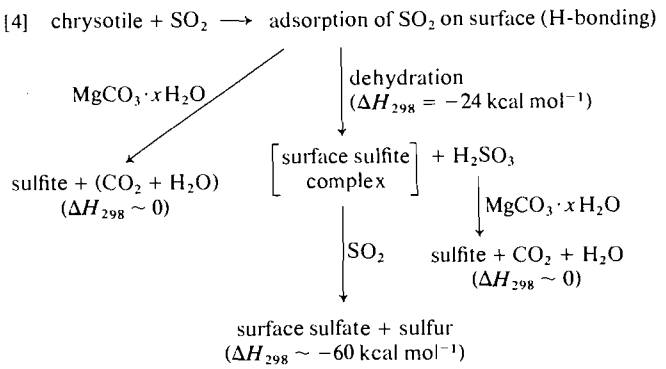

SCHEME 1

some of these features by providing further specialised evidence from both the thermodynamic and kinetic work on these and related surfaces.

Acknowledgement

We wish to acknowledge assistance from S. Spivak.

1. R. CHAMBON and P. CHAMBON. Lyon Pharm. **24**(5), 627 (1973).
2. Applicability of Metal Oxides to the Development of New Processes for Removing SO_2 from Flue Gases. Vol. II(8), Contract PH 86-68-68, Tracor. 1969.
3. Applicability of Inorganic Solids other than Oxides to the Development of New Processes for Removing SO_2 from Flue Gases. Contract PH 22-68-57, FMC Corporation. 1969.
4. J. C. GIBSON. Composites, **3**(2), 57 (1972).
5. J. R. KRAMER, O. MUDROCH, and S. TIHOR. Asbestos in the environment. Report to Environment Canada, May 1974.
6. Report of the Advisory Committee on Asbestos Cancers. Br. J. Ind. Med. **30**, 180 (1973).
7. G. W. WRIGHT. Statement before U.S. Dept. of Labour, Occupational Safety and Health Hearing on Proposed Occupational Asbestos Standard, March 6, 1972. p. 3; as in J. L. MYERS. Soc. Plast. Eng. Tech. Pap. 20, 207 (1974).
8. I. J. SELIKOFF, E. C. HAMMOND, and J. CHENG. J. Am. Med. Assoc. **204**(2), 104 (1968).
9. E. C. HAMMOND and I. J. SELIKOFF. *In* Biological effects of asbestos. Proceeding of Working conference at the I.A.R.C. Lyon, France. 1973. p. 312.
10. R. W. GLASS and R. A. ROSS. Can. J. Chem. **50**, 2451 (1972).
11. W. J. MURPHY, R. A. ROSS, and R. W. GLASS. Ind. Eng. Chem. Prod. Res. Dev. **16**, 69 (1977).
12. W. J. MURPHY and R. A. ROSS. J. Phys. Chem. **81**, 1078 (1977).
13. W. J. MURPHY and R. A. ROSS. Clays Clay Miner. **25**, 78 (1977).
14. E. ROBINSON and R. A. ROSS. J. Chem. Soc. A, 2521 (1969).
15. W. R. SMITH and D. G. FORD. J. Phys. Chem. **69**, 3587 (1965).
16. C. KEMBALL. Adv. Catal. **2**, 233 (1950).
17. R. W. GLASS and R. A. ROSS. J. Phys. Chem. **77**, 2571 (1973).
18. J. M. THOMAS and W. J. THOMAS. Introduction to the principles of heterogeneous catalysis. Academic Press, London. 1967.
19. A. A. HODGSON. Fibrous silicates. Royal Institute of Chemistry Lecture Ser. No. 4. 1965.
20. G. K. BORESKOV and V. V. POPOVSKII. Kinet. Catal. **1**, 530 (1960).
21. W. F. N. M. DE VLEESSCHAUWER. Physical and chemical aspects of adsorbents and catalysts. *Edited by* B. G. Linsen. Academic Press, London. 1970. Chapt. 6.
22. L. WALTER-LEVY. Ann. Chim. **7**, 216 (1937).
23. A. J. GOODSEL, M. T. D. LOW, and N. TAKEZAWA. Environ. Sci. Technol. **6**(3), 268 (1972).
24. R. W. GLASS and R. A. ROSS. Can. J. Chem. **49**, 2832 (1971).

Can. J. Chem. Downloaded from www.nrcresearchpress.com by 210.87.254.5 on 09/05/12
For personal use only.

Vapour pressures of $CaCl_2$–NaCl–H_2O and $MgCl_2$–NaCl–H_2O at 25°C. Prediction of the water activity of supersaturated NaCl solutions

DOAN THI AN, TJOON TOW TENG,[1] AND JAMES MALCOLM SANGSTER[2]

Département de Génie Chimique, Ecole Polytechnique, Campus de l'Université de Montréal, C.P. 6079, Succursale "A", Montréal (Qué.), Canada H3C 3A7

Received November 28, 1977

DOAN THI AN, TJOON TOW TENG, and JAMES MALCOLM SANGSTER. Can. J. Chem. **56**, 1853 (1978).

Vapour pressures of concentrated solutions (up to $I = 14$) of the systems $CaCl_2$ + NaCl + H_2O and $MgCl_2$ + NaCl + H_2O have been measured at 25°C by the static method. By means of reverse application of the Reilly–Wood–Robinson and Zdanovskii–Stokes–Robinson equations to these data, water activities of supersaturated NaCl solutions up to ~15 *m* have been deduced, and are represented in polynomial form.

DOAN THI AN, TJOON TOW TENG et JAMES MALCOLM SANGSTER. Can. J. Chem. **56**, 1853 (1978).

Les pressions de vapeur des solutions concentrées (jusqu'à $I = 14$) des systèmes $CaCl_2$ + NaCl + H_2O et $MgCl_2$ + NaCl + H_2O ont été mesurées à 25°C au moyen de la méthode statique. L'application à rebours des équations de Reilly–Wood–Robinson et de Zdanovskii–Stokes–Robinson à ces données a été effectuée pour calculer les valeurs de l'activité de l'eau de solution aqueuses sursaturées du NaCl jusqu'aux concentrations ~15 fois molales. Les résultats sont présentés en forme d'un polynome.

Introduction

In previous work (1, 2) the equations of Reilly–Wood–Robinson (RWR) and Zdanovskii–Stokes–Robinson (ZSR) have been used in reverse on water activity (a_w) data of mixed aqueous solutions to obtain supersaturated a_w's of single solutes. The calculations were done on existing data of various mixed solutions for certain electrolytes beyond their individual solubility limits.

Sodium chloride has been known to be salted-in by certain solutes in water (3), especially solutes with the common anion. In the present work, $MgCl_2$ and $CaCl_2$ have been chosen as partner solutes. Water activities of these systems have been measured by the static method to concentrations higher than those previously reported in the literature. The reverse calculation procedures introduced previously (1, 2) have been used here to extend supersaturated a_w values for NaCl up to ~15 *m*.

Experimental

Chemicals

NaCl (Anachemia, reagent) was dried at 100°C and used without further treatment. $MgCl_2.6H_2O$ (B.D.H Anala R) and $CaCl_2.2H_2O$ (Anachemia reagent) were treated (3*c*) to remove any superficial water. Distilled water was degassed by double distillation *in vacuo*.

Apparatus

The apparatus was similar to that described previously (4), except that the transducer and servo pressure controller were omitted.

Procedure

The salts were weighed into the sample flask through a capped side arm, after which water was distilled in through the vacuum manifold. The weight of water was determined by difference. A series of measurements were taken, starting with a dilute solution and concentrating it after a vapour pressure measurement by evaporating some solvent. Otherwise the manipulations were as previously described (4).

Results and Discussion

NaCl Alone

The apparatus and technique were first tested by measuring the vapour pressure of water and aqueous NaCl solutions at 25°C. The results for NaCl below saturation, expressed as osmotic coefficients, are shown in Fig. 1. This compares our measurements with those of Gibbard *et al.* (5), using as reference the standard data of Robinson and Stokes (taken from the equation parameters of Childs *et al.* (6)). Corrections for non-ideality of the vapour phase were not made in the present work, as these were usually less than the deviations shown in Fig. 1.

Mixed Electrolytes

Tables 1 and 2 present our experimental data of the mixed systems $CaCl_2$ + NaCl + H_2O and $MgCl_2$ + NaCl + H_2O at 25°C. Measurements were taken on both sides of the saturation limit of NaCl, at which $a_w = 0.75$ and $I = 6$. The solute mole fraction of NaCl was kept small for the special purposes of this work, i.e. to make I as large as possible (or a_w as small as possible) without precipitating the salts.

ZSR Equation

The application of this equation with corrections

[1]Present address: School of Applied Sciences, Universiti Sains Malaysia, Minden, Penang, Malaysia.

[2]To whom correspondence should be addressed.

Can. J. Chem. Downloaded from www.nrcresearchpress.com by 210.87.254.42 on 09/05/12
For personal use only.

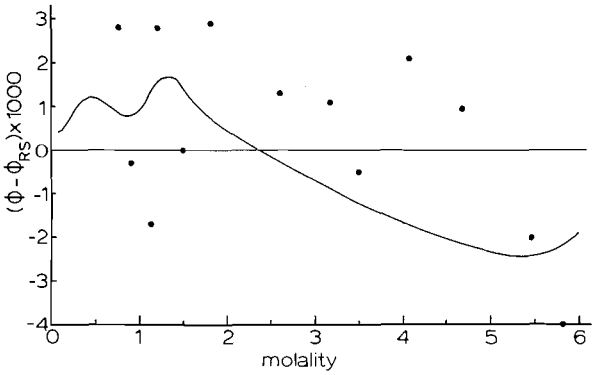

FIG. 1. Measured osmotic coefficients (ϕ) of aqueous NaCl solutions at 25°C relative to the standard data of Robinson and Stokes (ϕ_{RS}). Points: this work. Curve: ref. 5.

TABLE 1. Water activities and osmotic coefficients for the system $MgCl_2(1) + NaCl(2) + H_2O$ at 25°C

m_1	m_2	a_w	ϕ*
2.0468	0.2339	0.8289	1.5763
2.3841	0.2851	0.7895	1.6993
2.5851	0.3092	0.7645	1.7800
2.4982	0.5231	0.7590	1.7918
2.7478	0.5733	0.7214	1.9293
2.8715	0.3434	0.7209	1.9529
3.0905	0.1954	0.7026	2.0274
2.9571	0.6192	0.6914	2.0259
3.1582	0.4797	0.6772	2.0735
3.2366	0.3871	0.6682	2.1350
3.1670	0.6631	0.6590	2.1377
3.4266	0.5205	0.6397	2.1908
3.5435	0.3015	0.6335	2.2558
3.5166	0.7363	0.6071	2.3043
3.7352	0.3179	0.6047	2.3581
3.6499	0.5544	0.6038	2.3227
3.8070	0.3240	0.5942	2.3944
3.8415	0.2429	0.5932	2.4135
3.9493	0.3361	0.5736	2.4641
4.0669	0.3461	0.5567	2.5218
4.2068	0.3580	0.5369	2.5887
4.3245	0.3680	0.5201	2.6467
4.5172	0.2856	0.4966	2.7514

*In this paper the fourth decimal place figure in ϕ is given for rounding-off purposes only.

for Zdanovskii non-ideality (1, 2) is valid for mixed solutions whose $a_w < 0.75$. In the present work we have calculated a ZSR deviation factor b_Z for solutions of $a_w > 0.75$ (3*b*, *c*, 7, 8) and for these systems it was found that b_Z could be represented empirically by the equation

$$[1] \qquad b_Z = b_0 + b_1 a_w + b_2/y_1 y_2$$

where the y's are solute molality fractions and b_0, b_1, and b_2 are constants. Equation [1] was assumed to be extrapolatable into the supersaturation region. Those pertinent data in Tables 1 and 2 were used to

TABLE 2. Water activities and osmotic coefficients for the systems $CaCl_2(1) + NaCl(2) + H_2O$ at 25°C

m_1	m_2	a_w	ϕ
1.5446	0.1316	0.9054	1.1249
1.4943	0.1933	0.9025	1.1693
1.5287	0.1977	0.8978	1.2008
1.6167	0.1424	0.8976	1.1673
1.5696	0.2030	0.8950	1.2040
1.7375	0.1530	0.8862	1.2151
1.6612	0.2149	0.8858	1.2437
1.7348	0.2244	0.8790	1.2668
1.8561	0.1635	0.8751	1.2565
1.8898	0.1665	0.8728	1.2579
1.8375	0.2377	0.8679	1.3130
1.9336	0.2501	0.8581	1.3487
2.1429	0.1888	0.8488	1.3374
2.0509	0.2653	0.8461	1.3883
2.2198	0.2871	0.8278	1.4504
2.3501	0.3040	0.8136	1.4955
2.3187	0.2042	0.8110	1.5786
2.5526	0.2248	0.7964	1.5600
2.5103	0.3247	0.7952	1.5549
2.6816	0.3468	0.7746	1.6224
2.9785	0.2624	0.7576	1.6289
2.8597	0.3699	0.7524	1.6943
3.0420	0.3595	0.7478	1.6388
3.0142	0.3899	0.7330	1.7552
3.1608	0.3735	0.7325	1.6893
3.1915	0.4128	0.7112	1.8193
3.3228	0.4298	0.6949	1.8658
3.5253	0.4560	0.6688	1.9440
3.6708	0.4748	0.6502	1.9979
4.0121	0.3534	0.6339	1.9860
3.8657	0.5000	0.6245	2.0745
4.1824	0.3684	0.6121	2.0493
4.1572	0.4913	0.6100	2.0391
4.3211	0.5107	0.5902	2.0933
4.3896	0.3867	0.5878	2.1145
4.6536	0.4099	0.5566	2.1986

calculate supersaturated a_w's as before (1, 2). The results appear in Tables 3 and 4 and are incorporated in Fig. 2.[3]

RWR Equation

The application of this equation, with corrections (2), is valid for mixed solutions whose $I > 6$. The corresponding RWR deviation factors (2) were found for solutions at $I < 6$ (3*b*, *c*, 7, 8) and could be represented as functions of a_w or I:

$$[2] \qquad b_{RWR} = c_0 + c_1 a_w$$

or

$$[3] \qquad b_{RWR} = d_0 + d_1 I$$

where the c's are independent of a_W and the d's inde-

[3]Tables 3 and 4 are available upon request, at a nominal charge, from the Depository of Unpublished Data, CISTI, National Research Council of Canada, Ottawa, Ont., Canada K1A 0S2.

Can. J. Chem. Downloaded from www.nrcresearchpress.com by 210.87.254.42 on 09/05/12
For personal use only.

Can. J. Chem. Downloaded from www.nrcresearchpress.com by 210.87.254.42 on 09/05/12
For personal use only.

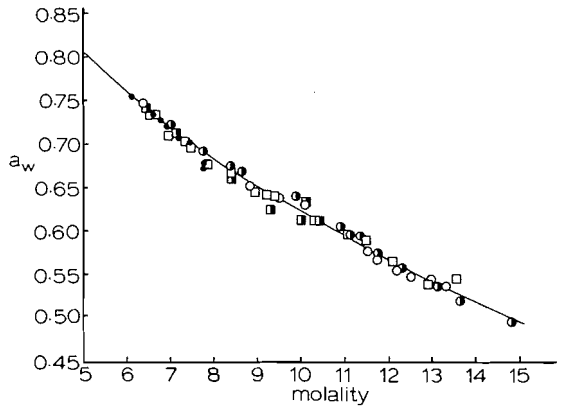

FIG. 2. The water activity of supersaturated aqueous solutions of NaCl at 25°C, as calculated by reverse RWR (○, □) and ZSR (◑, ◨) methods. (In order to avoid undue clutter, not all points are shown.) ●, ref. 2; ◑, ○, from data on the system $MgCl_2$–NaCl–H_2O; ◨, □ from data on the system $CaCl_2$–NaCl–H_2O; —, eq. [4].

pendent of I. The choice between eqs. 2 and 3 was made according to the closeness of fit for each system, and these equations were assumed to extrapolatable into the supersaturation region. Those pertinent data in Tables 1 and 2 were again used for reverse calculation as before (2). The results appear in Tables 3 and 4 and are incorporated in Fig. 2.[3]

Final Combined Results for NaCl

The a_w supersaturated values from both reverse methods have been combined and fitted to the polynomial (9)

$$[4] \qquad a_w = 1 + \sum_1^9 A_i m^i$$

whose A_i values are given in Table 5, together with limits of applicability and the standard deviation.

TABLE 5. A_i parameters for the equation $a_w = 1 + \sum_1^9 A_i m^i$ for the water activity of NaCl solutions at 25°C in the range $0.49 < a_w < 1$ or $0 < m < 15$. $\sigma(a_w) = 0.0075$

i	A_i
1	-4.03987×10^{-2}
2	6.76209×10^{-3}
3	-2.37823×10^{-3}
4	2.51691×10^{-4}
5	-3.61478×10^{-6}
6	-7.65032×10^{-7}
7	5.08006×10^{-8}
8	-2.48762×10^{-9}
9	7.84928×10^{-11}

TABLE 6. Water activities and osmotic coefficients of supersaturated NaCl solutions at 25°C at rounded molalities

m	a_w	ϕ
6.5	0.7382	1.2961
7.0	0.7170	1.3191
7.5	0.6973	1.3342
8.0	0.6792	1.3421
8.5	0.6628	1.3430
9.0	0.6480	1.3380
9.5	0.6347	1.3284
10.0	0.6221	1.3174
10.5	0.6100	1.3066
11.0	0.5977	1.2986
11.5	0.5846	1.2956
12.0	0.5702	1.2993
12.5	0.5543	1.3102
13.0	0.5372	1.3267
13.5	0.5198	1.3452
14.0	0.5040	1.3584
14.5	0.4937	1.3511
14.8	0.4918	1.3309

Values of a_w and osmotic coefficient at round molalities are given in Table 6.

Figure 2 shows that both reverse methods yield concordant results (open symbols), independent of the mixed solute system. Also shown in this figure are data (closed symbols) from a previous work (2) using still different mixed solute systems. The whole suggests that the reverse calculation method is generally valid, when used as described.

Acknowledgment

T.T.T. wishes to thank the Computer Unit of Universiti Sains Malaysia for use of computing facilities.

1. J. SANGSTER, T. T. TENG, and F. LENZI. Can. J. Chem. **51**, 2626 (1973).
2. F. LENZI, T. T. TRAN, and T. T. TENG. Can. J. Chem. **53**, 3133 (1975).
3. (*a*) R. A. ROBINSON and C. K. LIM. Trans. Faraday Soc. **49**, 1144 (1953); (*b*) Y. C. WU, R. M. RUSH, and G. SCATCHARD. J. Phys. Chem. **72**, 4048 (1968); (*c*) R. F. PLATFORD. J. Phys. Chem. **72**, 4053 (1968); (*d*) J. C. DOWNES. J. Chem. Eng. Data, **18**, 412 (1973).
4. M. C. TRUDELLE, M. ABRAHAM, and J. SANGSTER. Can. J. Chem. **55**, 1713 (1977).
5. H. F. GIBBARD, G. SCATCHARD, R. A. ROUSSEAU, and J. L. CREEK. J. Chem. Eng. Data, **19**, 281 (1974).
6. C. W. CHILDS, C. J. DOWNES, and R. F. PLATFORD. Aust. J. Chem. **26**, 863 (1973).
7. A. N. KIRGINTSEV and A. V. LUK'YANOV. Russ. J. Phys. Chem. **39**, 389 (1965).
8. R. A. ROBINSON and V. A. BOWER. J. Res. Natl. Bur. Stand. **70A**, 313 (1964).
9. T. T. TENG and F. LENZI. Can. J. Chem. Eng. **52**, 387 (1974).

Intermediates in the γ-radiolysis of divalent sulfur compounds in dilute glass matrices

FRANK CUTHBERT ADAM, GLENN EDWARD SMITH, AND ALLEN JOHN ELLIOT
Department of Chemistry, University of Calgary, Calgary, Alta., Canada T2N 1N4

Received September 7, 1977

FRANK CUTHBERT ADAM, GLENN EDWARD SMITH, and ALLEN JOHN ELLIOT. Can. J. Chem. **56**, 1856 (1978).

The optical spectra of the charged ions obtained from γ-irradiation of dilute alkyl mercaptans, sulfides, and disulfides in a variety of dilute rigid glasses are measured at 77 K. The photochemical stability of these ions is determined. A new photochromic species has been found. It is derived from a mercaptan dimer cation and is analogous to the photochromic anion produced from alkyl disulfides. The results of γ-radiation are compared to the uv photolysis of similar matrices, and it is found that the thiyl (RS·) and perthiyl radicals (RS_2·) are not generally in evidence in γ-irradiated matrices although they may be obtained by appropriate annealing or photobleaching of the irradiated matrix. The ions which have been characterized optically are RSH^+, RSH^-, $RSSR^+$ or their dimers, and RSS(H)R. The relative stabilities of these species in the low temperature glasses are determined.

FRANK CUTHBERT ADAM, GLENN EDWARD SMITH et ALLEN JOHN ELLIOTT. Can. J. Chem. **56**, 1856 (1978).

On a obtenu les spectres optiques d'ions portant des charges; ceux-ci ont été préparés par irradiation γ d'alkyl-mercaptans, de sulfures d'alkyle, de disulfures d'alkyle dilués dans un certain nombre de verres rigides à 77 K. On a déterminé la stabilité photochimique de ces ions. On a trouvé une nouvelle espèce photochromique. Elle dérive d'un cation dimère du mercaptan et elle est analogue à l'anion photochromique obtenu à partir des disulfures d'alkyle. On a comparé les résultats obtenus par irradiation γ à ceux obtenus par photolyse uv de matrices semblables et on a trouvé que les radicaux thiyl (RS·) et perthiyl (RS_2·) ne se retrouvent généralement pas dans les matrices ayant subit une irradiation γ quoiqu'elles peuvent être obtenues si l'on recuit ou si l'on fait subir une photodécoloration appropriée à la matrice irradiée. Les ions que l'on a caractérisés d'une façon optique sont RSH^+, RSH^-, $RSSR^+$ ou leurs dimères ainsi que RSS(H)R. On a déterminé les stabilités relatives de ces espèces dans des verres à basse température.

[Traduit par le journal]

Introduction

By currently held views in radiation biology, much of the damage caused by high energy radiation incident on living materials results not so much from primary effects but rather from secondary attack by ionized electrons and radicals produced in the surrounding medium, usually water (1). The target molecules themselves are usually present in a high state of dilution so that primary effects are minimal. It is also known that damage may eventually become localized within the target molecules at sites containing sulfur atoms (2). By way of example, disulfide linkages show a high cross-section for capture of mobile electrons, forming an anionic adduct (3) which may dissociate to give the thiyl radical RS·

$$e_m + RSSR \rightarrow RSSR^- \rightarrow RS^- + RS\cdot$$

Thiols act as efficient radical scavengers (4) also giving rise to the thiyl radical

$$RSH + X\cdot \rightarrow RS\cdot + HX$$

Depending upon the identity of R and X, the mercaptans may act to 'sensitize', 'protect against', or 'repair' damage to the substrate molecules. In any event, the transient common to most of these systems is the relatively unreactive thiyl radical and its presence is generally inferred by the detection of disulfides not present before irradiation and which result from the recombination of two such thiyl radical residues.

Earlier work done in this laboratory (5) has shown that in certain model systems which mimic the in vivo situation there were few similarities between the epr spectra of the γ-radiolysed and uv photolysed systems, both of which were purported to form the ubiquitous thiyl radical. This has resulted in much more detailed investigation of the uv photolysis of simple aliphatic mercaptans (6), sulfides, and disulfides (7), dissolved at low concentration in rigid organic glasses maintained at low temperatures. In such rigid media, diffusion controlled processes (such as thiyl recombination) can be retarded so that the metastable intermediates can be studied by conventional optical and epr techniques. The uv photolysed glasses have led to a characterization of the thiyl radical RS·, of the perthiyl radical RS_2·, and of other relevant species which may be of interest as possible intermediates in the γ-radiolysis of the same systems.

Can. J. Chem. Downloaded from www.nrcresearchpress.com by 210.87.254.6 on 09/05/12
For personal use only.

Can. J. Chem. Downloaded from www.nrcresearchpress.com by 210.87.254.6 on 09/05/12
For personal use only.

It is the aim of the present study to determine the nature of the metastable transients formed by γ-radiolysis and compare them, when possible, to those obtained by photolysis.

Three solvents are of particular utility in the present work in that each will form, at 77 K, a rigid transparent glass suitable for most optical studies, but will differ in the nature of the ionic transients that they will stabilize. These three solvents are MTHF (2-methyl tetrahydrofuran), 2-BuCl (2-chlorobutane), and 3MP (3-methyl-pentane) and because of their high concentration will sustain most of the radiation damage by the general reaction [1].

$$[1] \qquad MH \rightarrow MH^+ + e$$

In MTHF, the solvent cation rapidly disproportionates to give the solvent radical M· and a solvated proton. The ejected electron is either trapped in the matrix or adds to a suitable solute acceptor to give a stabilized anion species (8). On the other hand, 2-BuCl suffers dissociative electron capture to give immediately chloride ion and the corresponding butyl radical, while the cation in this case can oxidize a solute molecule to give a stabilized solute cation (9). The hydrocarbon glass 3MP stabilizes neither the free electron nor the MH^+ ion, so that both cationic and anionic solute species may be observed, along with any neutral radical entities which may result from ion recombinations and solvent decomposition (10).

Experimental

The general procedures have been described earlier (6, 7) and are analogous to those used in photolysis experiments. The solvents were purified by passage through activated silica gel columns and freshly distilled before use. The mercaptans were distilled under dry nitrogen gas at ambient pressure. The sulfides and disulfides were distilled at reduced pressure before use. All samples were prepared under high vacuum conditions with optical samples being in 15 mm id sealed suprasil ampoules while epr samples were in 3 mm id suprasil tubes. Both epr and optical samples were held within 2°C of the boiling point of liquid nitrogen and warmed by adjustment of the gas flow rate (epr) or liquid refrigerant level in a special optical Dewar. A Gates P-109 high pressure 100 W mercury lamp (for uv) or 500 W tungsten projection lamp (for visible light) were used for photobleaching experiments, although in some cases the Beckmann DU-2400 spectrophotometer provided sufficient intensity at the appropriate wavelength to effect the bleaching transformations. Otherwise the above sources were used in conjunction with those Corning Glass Co. filters required to isolate the spectral region of interest.

It was difficult with the large optical cells to produce clear glasses which did not shatter during the protracted times required to carry out some of the experiments. For this reason 20% by volume 3MP was added to all MTHF and 2-BuCl glasses. These modified glasses had all of the radiolytic properties associated with the pure matrices, so the mixtures will accordingly be referred to as 'MTHF' or '2-BuCl' in the following text.

The irradiation source was a ^{60}Co Gammacell 220 unit from Atomic Energy of Canada Ltd. and the dose rate was approximately 8×10^4 rad/h. It was necessary to irradiate the smaller samples used for epr study about 5–10 times longer than was required to obtain satisfactory spectra from the optical samples (i.e. with absorbancies in the 0.1 to 1.0 range).

Results

The optical spectra are described for the different substrates in Sections *A–C* dealing with the sulfides, disulfides, and mercaptans respectively. These are further subdivided according to the solvents used; first described are 2MTHF glasses which preferentially stabilize the ionized electrons, or substrate anions. Solute cations should not form in this glass except under very unusual circumstances. Secondly, the results for γ-irradiated 2BuCl glasses are described. In this matrix one expects absorptions from solvent or solute cations and nothing from the anionic species. Finally the spectra of irradiated 3MP glasses are considered. Absorptions due to both cationic and ionic substrate radical ions should be present, and each would be expected to tally (separately) with the absorptions observed in the other two solvents.

In each of the above glasses there will be, along with other non-absorbing species, solvent radicals resulting from the γ-irradiation.

A. Alkyl Sulfides

(1) 2MTHF Glasses

A γ-irradiation of a 0.1 *M* EtSEt/MTHF glass at 77 K produces only the blue coloration typical of the solvent trapped electron. This color may be bleached away with ir light giving rise to no new optical absorptions above 350 nm. The coloration fades on warming the matrix.

(2) 2BuCl Glasses

A γ-irradiated 0.1 *M* Et_2S/2BuCl glass gives an optical absorption at 475 nm, suggesting that this peak is due to a cation. An additional peak at 375 nm is also observed. Neither peak is affected by photobleaching and both disappear as the matrix is warmed to the melting point.

(3) 3MP Glasses

The corresponding 3MP glasses give an optical absorption at 475 nm, in addition to that observed in the MTHF glass. The latter transition is removed by an ir bleach or by thermal annealing of the matrix, during which the 475 nm peak is unaffected. The absorption at 375 nm of the BuCl glass is absent in 3MP, however.

The rose colored 0.1 *M* Et_2S/3MP glass is not readily altered by illumination at wavelengths longer than 254 nm, but fades irreversibly when warmed to 88 K to give pale yellow glass.

Can. J. Chem. Downloaded from www.nrcresearchpress.com by 210.87.254.6 on 09/05/12
For personal use only.

B. Alkyl Disulfides

(1) 2MTHF Glasses

As has been noted with other primary or secondary alkyl disulfides (11), EtSSEt exhibits photochromic behavior when γ-irradiated in MTHF glasses at 77 K. The absorption immediately following irradiation is at 420 nm and the glass is yellow. Bleaching with light in the 380–480 nm range gives the simultaneous diminution of the 420 nm peak and growth of a double peak in the near ir at 700 and 880 nm. Bleaching with 700–1000 nm light restores the original absorption at 420 nm. In the following text, the yellow form will be referred to as 'A' while its photochromic partner will be 'B'. All disulfides exhibit the initial 'A' absorption, but tertiary butyl disulfide cannot be converted to the 'B' form.

The photochromes 'A' and 'B' are bleached by near uv radiation to give weak absorptions near 400 nm and 520 nm.

(2) 2BuCl Glasses

All alkyl disulfides have absorptions near 720 nm in BuCl glasses (11) at 77 K. These glasses also have absorptions near 440 nm, as does the irradiated pure 2BuCl glass at 77 K. The 720 nm peak is stable to illumination at this wavelength, but photolysis of the 440 nm peak causes a reduction in its magnitude with concomitant growth of the 720 nm peak. This process is not reversible, and is not photochromic. It has been attributed (11) to the process

$$RSSR + BuCl^+ \xrightarrow{h\nu} BuCl + RSSR^+$$

wherein $BuCl^+$ absorbs at 440 nm and $RSSR^+$ absorbs at 720 nm.

(3) 3MP Glasses

Photochromism is observed in disulfide–3MP glasses; a 0.1 *M* Et_2S_2/3MP glass gives with γ-radiation one peak at 420 nm and a second peak at 720 nm as in Fig. 1*a*. The latter peak is stable to prolonged photolysis in the 720 nm region. On the other hand, photobleaching the 420 nm peak causes loss of this 'A' peak and growth of the 'B' peaks, superimposed on the cation absorption at 720 nm as in Fig. 1*b*. The 'A' ↔ 'B' transformations of Figs. 1*a* and *b* can be cycled several times without affecting the cation absorption intensity.

As far as the relative peak heights of the 420 and 720 nm absorptions are concerned, the spectrum of the 0.1 *M* Et_2S_2/3MP glasses in Fig. 1*a* is very similar to that obtained from irradiated pure *n*-amyl disulfide at 77 K (12). Since the latter compound scavenges both electrons and positive charges equally effectively, one must conclude that Et_2S_2 in 3MP does too. The ratio OD(anion)/OD(cation) is about 4 in each case. For 0.1 *M* t-Bu_2S_2/3MP glasses the

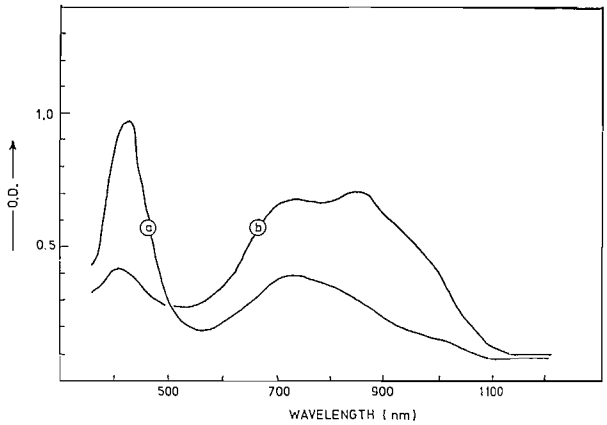

FIG. 1. Photochromic behavior of γ-radiolysed 0.1 *M* ℓ^{-1} Et_2S_2/3MP glass. (*a*) Initial spectrum, dose 1.6×10^{18} eV g^{-1} at 77 K and showing $Et_2S_2^-$ (420 nm) and $(Et_2S_2)_2^+$ at 720 nm. (*b*) Following 10 min 360–485 nm photobleach showing $(Et_2S_2)^+$ at 420 nm, EtSS(H)Et at 700–820 nm. A 800 nm photobleach will restore (*a*).

anion peak occurs at 430 nm and the cation peak occurs at 720 nm; the absorbance for the anion peak is roughly the same (at equivalent dose) for both the ethyl and *tert*-butyl derivatives, while the cation absorption is decreased by a factor of 6 for the *tert*-butyl disulfide. One can conclude from this that the efficiency of cation transfer from the solvent to the solute is much lower for *tert*-butyl derivatives than for the other alkyl disulfides. This is perhaps due to the 'shielding' of the disulfide linkage by the bulky tertiary alkyl groups.

As was also found for the pure *n*-amyl disulfide system (12) following γ-radiation, there was a gradual decay of the 'A' photochrome in the Et_2S_2/3MP system. Only a part of this decay can be accounted for by a slow 'A' → 'B' dark reaction. The decay can be accelerated by photobleaching with light in the 300–400 nm region, a result in accord with the work of Milliken *et al.* (13) who observed the effect in pure polycrystalline ethyl disulfide. In the 3MP matrix, the cation absorption at 720 nm is not materially affected by this photobleach (14).

C. Alkyl Mercaptans

(1) 2MTHF Glasses

When a 0.1 *M* EtSH/MTHF glass is irradiated, one obtains a greenish-blue glass which shows a solvent trapped electron absorption near 1150 nm, and a weak peak near 408 nm. An ir photobleach removes the former absorption while at the same time the 408 nm peak grows in intensity, with the result that the glass becomes yellow in color. A photobleach in the 400 nm region produces no immediate change (i.e. no photochromism) although prolonged bleaching causes the peak to shift to

Can. J. Chem. Downloaded from www.nrcresearchpress.com by 210.87.254.6 on 09/05/12
For personal use only.

395 nm. The effect of a 300–400 nm bleach is similar. Clearly the original 408 nm absorption is due to an electron adduct to RSH, or is a product formed from RSH^- (15).

(2) 2BuCl Glasses

The γ-radiolysis of the 0.1 *M* EtSH/2-BuCl system produces a yellow glass. The peak located at 400 nm is not photochromic and there is no absorption in the 800 nm region. An identical absorption is obtained by 253.7 photolysis of the EtSH/BuCl glass (following slight warming) and can be attributed to the thiyl radical. It can arise in the γ-radiolysed system by a deprotonation reaction.

$$RSH^+ \rightarrow RS\cdot + H^+$$

$$H^+ + Cl^- \rightarrow HCl$$

(3) 3MP Glasses

The γ-irradiation of a 0.1 *M* EtSH/3MP glass produces a yellow–green coloration in the matrix at 77 K. This is due to an absorption at 420 nm and a double peak at 700 and 880 nm as in Fig. 2*a*. A short photobleach of the 420 nm peak produces no change, while a similar exposure to 800 nm radiation produces a marked increase in the absorption at 420 nm and total loss of absorption at 700 and 880 nm. This can be seen in curve *b* of Fig. 2. Illumination of this yellow matrix with 420 nm light restores the original spectrum of curve *a*. This photochromic behavior is also observed with isopropyl mercaptan/3MP glasses but not with the 0.1 *M* *tert*-butyl derivative, which gives a single nonphotochromic peak at 430 nm. There are quite apparently two species which may absorb in the 400 nm region, one of which is photochromic and the other of which is not. Furthermore the two photochromic species observed with EtSH appear identical in all ways to the corresponding 'A' and 'B' modifications observed with ethyl disulfide glasses.

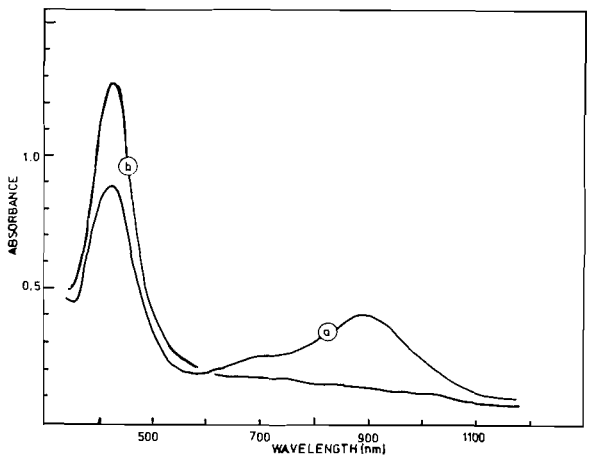

FIG. 2. Photochromic behavior of a γ-radiolysed 0.1 *M* ℓ^{-1} EtSH/3MP glass at 77 K. (*a*) Initial spectrum, dose 3.0×10^{18} eV gm^{-1} showing $(EtSH)_2^-$ at 420 nm, EtSS(H)Et at 700–820 nm. (*b*) Following 10 min >750 nm photobleach showing $Et_2S_2^-$ and $(EtSH)_2^-$ at 420 nm. A 420 nm photobleach will restore (*a*).

If the irradiated glass is stored overnight at 77 K, or subjected to a 300–400 nm photobleach, the 420 peak shifts to ~405 nm, and all absorptions in the 720–880 nm region are lost. The species produced may be the thiyl radical EtS· which is known to absorb at 405 nm in this particular matrix (6, 7). It is known that 300–400 nm light will not itself induce photolysis of the substrate RSH.

Discussion

There are complicating factors in the analysis and assignments in the optical spectra of irradiated and/or photolysed divalent sulfur compounds. For instance S_3 (16), S_8, RS·, RS_2·, and $RSSR^-$ are known to absorb in the spectral region between 380 and 425 nm as does, apparently, the electron adducts to mercaptans in nonpolar glasses. It would therefore be quite easy to make erroneous assignments to absorptions occurring in this region. Another difficulty arises because many of the radicals or radical ions of interest here can be produced by a variety of means under different experimental conditions. This has resulted in a number of entirely divergent assignments having been made to ostensibly the same species. We will try to reconcile some of these differences in the following discussion.

The particular advantage of working with low concentrations of sulfur substrates in rigid organic glasses is that the unstable transients can only react with their nearest neighbors, which are usually solvent molecules. Photolysis studies (7) have shown that sulfur atoms, for instance, do not migrate in 3MP at 77 K but only become mobilized as the temperature of the medium is warmed to ~85 K. As a result, species such as S_3 and S_8 can be logically eliminated as being present in the γ-radiolysed systems just described. Migration of smaller species such as protons are not ruled out however. Photolysis studies (7) have also shown that solute–solute interactions are not completely eliminated at the concentrations used here (0.1 mol dm^{-3}). These solutions are not sufficiently dilute to completely prevent association of the solute molecules as the liquids are frozen to the glassy state and some dimers are unquestionably present as the glasses finally harden. Once formed, however, no further changes in molecular distribution are possible. Dilute glasses are therefore intermediate between liquid phase studies where diffusion is unrestricted, and the solid crystalline state where there is no diffusion but where

Can. J. Chem. Downloaded from www.nrcresearchpress.com by 210.87.254.6 on 09/05/12
For personal use only.

short range solute–solute reactions may occur with ease.

(1) The Photochromic Process

Without a doubt the most intriguing aspect of the present radiolytic studies in the glassy phase is the photochromic transformation and the observation of this phenomenon with dilute mercaptans as well as with disulfides. It seems unlikely that such a close similarity in spectral properties in these two systems could result from 'accidental' coincidences between one-sulfur molecular species derived from a thiol and the two-sulfur species such as would be formed from a disulfide. We thought for some time that the photochromism could only result from the reversible 'pumping' an electron from a monomeric thiol negative ion to a thiocarbonyl molecule.

$$CH_3CH_2SH^- + CH_3CH{=}S \underset{h\nu'}{\overset{h\nu}{\rightleftharpoons}} CH_3CH_2SH + CH_3CH{-}S^-$$

These particular species would have been anticipated to result from a tautomeric disproportionation of $Et_2S_2^-$. The thiocarbonyl, which absorbs weakly at 520 nm (7), has been observed to result from electronically excited RSH and RSSR. Dimeric species were not suspected at that time. Although this mechanism 'explains' why *tert*-butyl derivatives do not undergo photochromism (no α-hydrogen), the scheme suffers from a number of difficulties not the least of which is that aliphatic thioketyl anions have not been found to have optical absorptions in the 600–900 nm region and the proton hyperfine structure which might be expected for a species such as $CH_3\dot{C}HS^-$ is completely lacking in the epr spectrum (17).

On the other hand, the identification of the 'A' photochrome as the disulfide anion appears to be on firm ground. In the pulse radiolysis of aqueous disulfides, an absorption near 410 nm grows in at the same rate as the absorption of the hydrated electron disappears (18). Akasaka *et al.* (19) have also shown that single crystals of cystine hydrochloride turn yellow when γ-irradiated at low temperatures. The n–σ* absorption near 400 nm is associated with an anion with an epr signal containing the proton hyperfine structure characteristic of an intact C—S—S—C skeleton. This identification is consistent with our observation of an optical transition at 420 nm in irradiated Et_2S_2/MTHF and /3MP glasses. This assignment is presumed correct in the following discussion.

The most important feature of the mercaptan photochromism is that it is observed in 3MP but not in MTHF glasses, while disulfides exhibit the effect in both of these matrices. A second distinction is that it is the 'B' photochrome that is formed initially with thiols, while for disulfides it is the 'A' form which is produced during the radiolysis. These data are mutually compatible if the 'A' photochrome can be formed by an electron adduct to disulfide (i.e. $RSSR^-$) and if the 'B' form has a cationic thiol precursor. This precursor cannot be RSH^+ since the butyl chloride glasses give no indication of absorption in the 700–900 nm region and this ion does not meet the requirement of having two sulfur atoms in close proximity, so that $RSSR^-$ may be formed readily by a photochromic transformation. The same objection cannot be raised against a thiol dimer. Both 2-BuCl and 2-MTHF are considerably more polar than 3MP and may not support self-association of thiols to the extent that 3MP does. The presence of thiol dimers has already been established in the uv photolytic studies of the 3MP glass at the same solute concentration (7). In that instance, both the thiyl radical RS· (from the monomer) and the perthiyl radical RS_2· (from the dimer) are formed during the photolysis at 77 K. In the present case, if cationic dimers are indeed involved in the radiolysis then the most probable reaction to occur is the charge transfer process from the solvent cation;

$$(RSH)_2 + MH^+ \rightarrow (RSH)_2^+ + MH$$

The resulting dimer cation is in fact a fully protonated disulfide anion and may be converted to the latter by the successive deprotonations through a sulfenium radical intermediate, RSS(H)R. Thus,

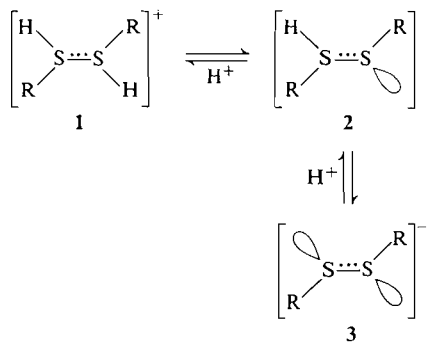

The sulfenium radical **2** has been postulated as an intermediate in pulse radiolysis studies (18). We suggest that the ionized thiol dimer $(RSH)_2^+$ (i.e. **1**) spontaneously deprotonates to give the sulfenium species **2**, and that this is the species 'B' of both the irradiated mercaptan and disulfide systems. This molecule then undergoes photon-assisted deprotonation to give the 'A' modification **3**. The proton remains nearby in the medium because of the negative charge on **3**, but is readily available for the reverse photoinduced protonation 'A' → 'B'.

Can. J. Chem. Downloaded from www.nrcresearchpress.com by 210.87.254.6 on 09/05/12
For personal use only.

The foregoing scheme seems more plausible than that originally suggested (11) to explain the photochromism of the disulfide negative ion. It was thought to arise from photoinduced interchange between geometrical isomers (rotomers) of this ion. However it is difficult to see why mercaptans should give mostly the 'B' conformers while disulfides give the 'A' form. This is especially true for the *tert*-butyl derivatives which would be expected on steric grounds to give the 'B' or '*trans*' form for both thiol dimers and disulfides (11).

The reason that *tert*-butyl mercaptan does not undergo the photochromic reaction may now be ascribed to a lower association constant, to a lower probability of cationic exchange from the solvent radical ion (as was observed with the corresponding disulfide), or to an increased susceptibility for the sulfenium intermediate to decompose either by C—S cleavage, or by ejection of a thermal hydrogen atom. Thus, with the *tert*-butyl derivative

$$RSS(H)R \rightarrow RS_2\cdot + HR$$

or

$$\rightarrow RSSR + H\cdot_{th}$$

The last two reactions may also account for the fact that the sulfenium intermediate 'B' is not observed by photobleaching the 'A' species produced by electron attachment to *tert*-butyl disulfide. The bulky alkyl groups could also hinder any geometrical readjustments which the transformation might require.

(2) Nonphotochromic Anions

Since the photochromism model described above depends on the formation of thiol dimers in 3MP at 77 K, EtSH/3MP glasses have been studied at various EtSH concentrations (0.001 to 0.3 *M*) and different γ-radiolytic doses. The concentrations of the nonphotochromic yellow and photochromic blue species increase linearly with dose, but the relative proportions of each remain roughly the same in all determinations, so there is no systematic variation which will allow us to calculate an association constant. However, if the photochrome 'B' is indeed due to a dimer, then the constancy in relative absorptions between the two products suggests that the anionic species absorbing at 420 nm may also be a dimer ion. Thus,

$$(RSH)_2 + e \rightarrow (RSH)_2^-$$

We have obtained no evidence that the dissociative electron capture reaction

$$RSH + e \rightarrow R\cdot + SH^-$$

has occurred in 3MP matrices where alkyl radicals may be readily detected by epr at 77 K. This contrasts with more polar media (e.g. aqueous) where this reaction occurs readily (20). Although the optical absorptions in the near ir observed with RSH in both 3MP and 2MTHF are similar to those of the solvent trapped electron, we have been unable to get the singlet epr spectrum of this species under conditions where the signal is readily observed with the irradiated pure solvents. This suggests that the electrons are trapped near to mercaptan molecules in the glassy solutions and if indeed the molecular ion RSH^- is formed then it too absorbs in the near ir.

The disulfide negative ion has been discussed in the previous section. Sulfides do not apparently form negative ions, of either a monomeric or dimeric form.

(3) Nonphotochromic Cationic Species

Stable cations are expected to be formed only in BuCl or 3MP glasses.

(a) Sulfide Cations

Two absorptions can possibly be attributed to sulfide cations: that at 475 nm (which is observed in both 3MP and BuCl) and that at 375 nm (which is seen only in BuCl). One must compare these values to those obtained from irradiated single crystals of methionine (21) or *N*-acetylmethimine (22) which absorb in the 600–750 nm region. This absorption is photolabile and has been attributed to both the monomeric cation and to the dimeric cation (23), mostly on the basis of the epr proton hyperfine structure. This latter conclusion has, however, been contested (24). In aqueous sulfide solutions using hydroxyl radicals as oxidant (25) only dimeric cations, $(RSR)_2^+$, are observed, it being thought that the monomer ions are susceptible to deprotonation yielding the α-abstraction radical RSR-(—H). Pulse radiolysis studies (26) demonstrate in a very convincing manner that in aqueous solutions an absorption at 470 nm must be attributed to $(RSR)_2^+$. It has also been suggested that RSR^+ and $(RSR)_2^+$ both absorb at ~470 nm (27). A peak at 375 nm is obtained in pulse radiolysed sulfide aqueous solutions containing halide ion and assigned to the species R_2SCl (28). Since we observe a transition here in the Et_2S/BuCl system (but not in a 3MP glass) we suggest that rather than the formation of RSR^+ by charge transfer, in BuCl,

$$BuCl^+ + RSR \rightarrow R_2SCl + Bu^+$$

while in 3MP

$$MH^+ + RSR \rightarrow MH + RSR(—H) + H^+$$

We therefore assign the 470 nm peak to the dimer cation $(RSR)_2^+$ in agreement with the pulse radiolysis experiments.

TABLE 1. Absorption maxima of charged radicals of saturated divalent sulfur compounds and their photochemical stability. The *hν* refers to bleaching in the 300–400 nm region

	Transient	λ_{max}	Solvent	Remarks
Anions	$EtSSEt^-$	420	2MTHF, 3MP	Photochromic (to EtSS(H)Et)
	$EtSH^-$	~1150 nm	2MTHF, 3MP	Photolabile
	$(EtSH)_2^-$	408	2MTHF	H^+, $h\nu \rightarrow RS\cdot$
	$(EtSH)_2^-$	420	3MP	H^+, $h\nu \rightarrow RS_2\cdot$
Neutrals	$EtS\cdot$	395	2MTHF	Photostable
		400	BuCl	Photostable
		405	3MP	Reference 6
	$EtS_2\cdot$	395	3MP	Reference 6
	EtSS(H)Et	720–880	3MP	Photochromic (to $Et_2S_2^-$) $h\nu \rightarrow RS_2\cdot$
	$CH_3CH{=}S$	520	3MP, 2MTHF	Reference 6
Cations	$(EtSSEt)_2^+$	720	3MP, 2BuCl	Photostable
	$(EtSEt)_2^+$	475	3MP, 2BuCl	Photostable
	$EtSEt^+$	~430	3MP, 2BuCl	—
	$EtSEt^+$	>600(?)	3MP	Photolabile → EtSEt(—H)

(b) Disulfide Cations

There is likewise some question as to the assignment of the disulfide cation absorption. Aqueous pulse radiolysis studies (29) suggest it should lie at ~410 nm. No dimerization is observed. Single crystal studies of cystine (30) indicate a photolabile absorption at 550 nm should be attributed to the disulfide cation. It is likely that in this case the ion is held in a thermally metastable configuration by the crystal host and so the results cannot be compared directly to those obtained in less rigid matrices. As in the case of irradiated sulfide glasses, the formation of disulfide dimers cannot be precluded and the possibility that the absorption at 720 nm is in fact due to $(RSSR)_2^+$ must be considered. As can be seen, a small residual absorption at 420 nm occurs in Fig. 1*b*. This absorption may be due to $RSSR^+$ and it is normally concealed (as in Fig. 1*a*) by the more intense $RSSR^-$ absorption. In RSSR–BuCl glasses, where the latter species is absent, there is also absorption at 440 nm, but the pure irradiated glass also has an optical transition in this region (see Fig. 7 of ref. 11) so that no definitive conclusion can be reached. Until evidence is obtained to the contrary, the 720 nm peak in RSSR–3MP glasses is assigned to a disulfide dimer cation, while the monomeric ion is assumed to absorb near 430 nm.

(c) Mercaptan Cations

As noted in earlier sections, there has been no absorption directly attributable to mercaptan cations. The double peak at 700–820 nm in 3MP is due to sulfenium RSS(H)R and the single peak at 400 nm in BuCl is due to RS·. The precursors of these species are $(RSH)_2^+$ and $(RSH)^+$ respectively. RSH^+ should be stable in 3MP glasses, since this medium lacks strong proton acceptors such as Cl^- as found in BuCl glasses. It is possible that this species absorbs below 350 nm, the lower limit of our determinations. This would then agree with the pulse radiolysis results which place the absorption of aquated (or protonated) thiyl radical at 330 nm (20).

The ultimate assignments will have to await further experiments which are rather more sensitive to the dimer–monomer ratios of these glasses. It is for this reason that our epr experiments have not been particularly helpful. Apart from the many interfering resonances due to solvent radicals, etc., the smaller epr samples may well contain a different dimer–monomer balance due to the fact they freeze much more quickly than the large optical samples. This is especially unfortunate since it would have been a useful ancilliary to optical detection because, as has been mentioned, many irradiated sulfur compounds absorb in the same region of the spectrum. Since several of these compounds may be expected to occur in the same radiolysed system, great care should be taken when analysing the results of, say, pulse radiolysis experiments in nonpolar liquids where an optical method is the sole means used to discriminate between the reactive intermediates present. A summary appears in Table 1.

Acknowledgements

The financial help of the Defense Research Board and National Research Council of Canada is gratefully acknowledged.

1. T. SANNER and A. PIHL. Radiation protection and sensitization. *Edited by* H. L. Moroson and M. Quintiliani. Taylor and Francis, London. 1970. p. 43.
2. W. GORDY, W. B. ARD, and H. SHEILDS. Proc. Natl. Acad. Sci. **41**, 983 (1955).
3. G. E. ADAMS, G. S. MCNAUGHTON, and B. D. MICHAEL. The chemistry of ionization and excitation. *Edited by* G. R.

Can. J. Chem. Downloaded from www.nrcresearchpress.com by 210.87.254.6 on 09/05/12
For personal use only.

A. Johnson and G. Scholes. Taylor and Francis, London. 1967. p. 281.
4. L. ELDJARN and A. PIHL. Mechanism in radiobiology. Academic Press, New York, NY. 1960. p. 23.
5. J. SKELTON and F. C. ADAM. Can. J. Chem. **49**, 2536 (1971).
6. A. J. ELLIOT and F. C. ADAM. Can. J. Chem. **52**, 102 (1974).
7. F. C. ADAM and A. J. ELLIOT. Can. J. Chem. **55**, 1546 (1977).
8. J. P. GUARINO and W. H. HAMILL. J. Am. Chem. Soc. **86**, 777 (1964).
9. T. SHIDA and W. H. HAMILL. J. Chem. Phys. **44**, 4372 (1966).
10. T. SHIDA and W. H. HAMILL. J. Chem. Phys. **44**, 2369 (1966).
11. T. SHIDA. J. Phys. Chem. **72**, 2597 (1968).
12. T. SHIDA. J. Phys. Chem. **74**, 3055 (1970).
13. S. B. MILLIKEN, K. MORGAN, and R. M. JOHNSEN. J. Phys. Chem. **71**, 3238 (1967).
14. F. K. TRUBY. J. Chem. Phys. **40**, 2768 (1964).
15. A. TORIKAI, S. SAWADA, K. FUEKI, and Z. KURI. Bull. Chem. Soc. Jpn. **43**, 1617 (1970).
16. B. MEYER, T. STROYER-HANSEN, and T. V. OOMEN. J. Mol. Spectrosc. **42**, 335 (1972).
17. P. NETA and R. W. FESSENDEN. J. Phys. Chem. **75**, 2277 (1971).
18. M. Z. HOFFMANN and E. HAYON. J. Am. Chem. Soc. **94**, 7950 (1972).
19. K. AKASAKA, S. KOMINAMI, and H. HATANO. J. Phys. Chem. **75**, 3746 (1971).
20. M. Z. HOFFMANN and E. HAYON. J. Phys. Chem. **77**, 990 (1973).
21. S. KOMINAMI. J. Phys. Chem. **76**, 1729 (1972).
22. S. KOMINAMI, K. AKASAKA, H. UMEGAKI, and H. HATANO. Chem. Phys. Lett. **9**, 510 (1971).
23. M. C. R. SYMONS. J. Chem. Soc. Perkin Trans. II, 1618 (1974).
24. H. C. BOX and E. E. BUDZINSKI. J. Chem. Soc. Perkin Trans. II, 553 (1976).
25. B. C. GILBERT, D. K. C. HODGEMAN, and R. O. C. NORMAN. J. Chem. Soc. Perkin Trans. II, 1748 (1973).
26. (*a*) G. MEISSNER, A. HENGLEIN, and G. BACK. Z. Naturforsch. Teil B, **22**, 13 (1967); (*b*) M. BONIFAČIĆ, M. MOCKEL, D. BAHNEMANN, and K.-D. ASMUS. J. Chem. Soc. Perkin Trans. II, 675 (1975).
27. W. BORS, E. LENGFELDER, M. SARAN, C. FUCHS, and C. MICHEL. Biochem. Biophys. Res. Commun. **70**, 81 (1976).
28. K.-D. ASMUS, D. BAHNEMANN, M. BONIFAČIĆ, and H. A. GILLIS. Faraday Discuss. Chem. Soc. **63**, 213 (1977).
29. M. BONIFAČIĆ, K. SCHÄFER, H. MÖCKEL, and K.-D. ASMUS. J. Chem. Phys. **79**, 1496 (1975).
30. K. AKASAKA, S. KOMINAMI, and H. HATANO. J. Phys. Chem. **75**, 3746 (1971).

Can. J. Chem. Downloaded from www.nrcresearchpress.com by 210.87.254.6 on 09/05/12
For personal use only.

Photolyse de l'isoprène gazeux entre son seuil d'absorption (ca. 255 nm) et 147.0 nm

ROSAIRE DEMERS, GUY J. COLLIN[1] ET H. GAGNON-DESLAURIERS (MME)

Département des Sciences Pures, Université du Québec à Chicoutimi, Chicoutimi (Qué.), Canada G7H 2B1

Reçu le 21 octobre 1977

ROSAIRE DEMERS, GUY J. COLLIN et H. GAGNON-DESLAURIERS. Can. J. Chem. **56**, 1864 (1978).

La photolyse de l'isoprène a été étudiée entre son seuil d'absorption, ca. 255 nm, et 147.0 nm à des pressions variant entre 30 et 2660 N m^{-2}. Entre 230 et 255 nm, les produits légers formés ont des rendements qui suivent une loi de type Stern–Volmer. On en conclue que la molécule photoexcitée est stabilisée par collision dans cette région de pression. A 174 nm et à 163.3 nm, l'effet de pression est beaucoup moins important et la totalité des molécules photoexcitées se fragmentent. A 147 nm, aucun effet de pression n'est observable, et le produit majeur est le vinylacétylène ($\Phi = 0.66$). La formation de ce produit est expliquée par la scission de la liaison CH_3—C_4H_5 suivie de la fragmentation du radical C_4H_5* excité. A 174 nm, ce radical peut être stabilisé par collision. Enfin nous avons mesuré le rapport $k(CH_3 + H_2S)/k(CH_3 + \text{isoprène}) = k_1/k_{12}$ et ce rapport est de 41 ± 3.

ROSAIRE DEMERS, GUY J. COLLIN, and H. GAGNON-DESLAURIERS. Can. J. Chem. **56**, 1864 (1978).

We studied the photolysis of isoprene at wavelengths between the absorption threshold (ca. 255 nm) and 147.0 nm. The pressure effect was studied between 30 and 2660 N m^{-2}. At the lower energy, light products are formed and their yields decrease with an increase in the pressure. From Stern–Volmer plots, we have concluded that the photoexcited molecule is collision stabilized at high pressure. Less pressure dependence was observed at 174 and at 163.3 nm. At these energies, and at 147 nm, all of the photoexcited molecules decompose. At 147 nm, no pressure effect was observed, and the main product is vinylacetylene ($\Phi = 0.66$). The formation of this product was explained on the basis of the CH_3—C_4H_5 split followed by the fragmentation of the excited C_4H_5* radicals. At 174 nm, this last radical is collisionally stabilized. Finally we have measured the ratio $k(CH_3 + H_2S)/k(CH_3 + \text{isoprene}) = k_1/k_{12}$ and $k_1/k_{12} = 41 \pm 3$

Introduction

Lors de l'étude de la photolyse des butènes dans la région du l'ultra-violet sous vide, nous avons récemment étudié certains aspects de la chimie des divers radicaux C_3H_5 (1). Nous avons entrepris l'étude de l'isoprène, méthyl-2-butadiène-1,3, afin d'examiner si la scission de la liaison C—C centrale à partir de la molécule photoexcitée se fait avec une fréquence suffisante pour permettre l'étude des radicaux CH_3CCH_2. Nous sommes évidemment intéressés à connaître le comportement de la molécule photoexcitée en comparaison avec ce que nous connaissons des hydrocarbures insaturés (2).

Partie expérimentale

Produits chimiques

L'isoprène est un produit acheté de "Chem. Sample Co." de pureté moléculaire affichée de 99.5%. L'analyse de ce produit montre qu'il contient du méthyl-2-butène-2 (0.14%), du vinylacétylène (0.019%) et du méthyl-2-butène-1 (0.0061%). Un autre échantillon provenant de l' "American Petroleum Institute" de pureté moléculaire affichée à 99.96% a été utilisé à toutes longueurs d'onde. L'analyse n'a montré que la présence de méthyl-3-butène-1 (0.0026%). L'oxygène, 99.99% et l'oxyde nitrique, 99.0%, sont des produits "Matheson of Canada" et sont utilisés tels que reçus. L'iodure d'hydrogène ("anhydrous, Air liquide du Canada") de pureté 99.8% est utilisé après sublimation afin d'éliminer la présence d'iode qui s'accumule lentement dans le réservoir. On en mesure la pression, au moment de l'introduction dans le réacteur, à l'aide d'un manomètre à huile. L'hydrogène sulfuré (99.5%) est un produit de Matheson of Canada Ltd.

Préparation et analyses des échantillons

On a utilisé une rampe à vide munie de robinets en Téflon, de manomètres à membrane métallique, "Wallace et Tiernan", et maintenue à une pression de 5×10^{-6} Torr (6.6×10^{-4} N m^{-2}) ou moins à l'aide d'une pompe à diffusion à huile à deux étages.

Le réacteur est normalement un ballon de 0.5 ℓ en Pyrex attaché directement à la lampe au moyen d'un joint rodé scellé à la cire noire. Dans le cas des irradiations avec la lampe à mercure, on a utilisé un réacteur cylindrique en quartz de 0.75 ℓ situé à quelques cm de la lampe.

Les analyses ont été faites par introduction d'une fraction (5%) des échantillons photolysés dans un chromatographe à gaz équipé d'un double détecteur à flamme ionisante. On a utilisé une colonne de squalane (25%) de 8 m de longueur approximativement (3). Quelques analyses ont été faites avec une colonne d'alumine en programmation de température (30–150°C).

Lampes d'irradiations et actinométrie

La lampe à mercure utilisée est du type haute pression ("Hanovia 679A-36") et est utilisée soit avec un filtre en Vycor qui est complètement opaque en dessous de 229 nm, soit avec un filtre en Corex également opaque en dessous de 230 nm. La

[1]Auteur à qui toute correspondance doit être adressée.

Can. J. Chem. Downloaded from www.nrcresearchpress.com by 210.87.254.105 on 09/05/12
For personal use only.

Can. J. Chem. Downloaded from www.nrcresearchpress.com by 210.87.254.105 on 09/05/12
For personal use only.

lampe à azote a été préparée sur place (4) et produit des photons principalement autour de 174.5–174.3 nm. La lampe à brome a aussi été décrite et produit essentiellement l'émission du brome atomique à 163.3 nm (5). La lampe à xénon est essentiellement monochromatique (147 nm) (6). Tous les spectres des lampes, ainsi que l'absorption par l'isoprène des raies émises par le mercure ont été mesurées à l'aide d'un monochromateur "McPherson 235". On a ainsi observé que l'isoprène commence à absorber vers 255 nm. Par exemple 20 Torr (2660 N m^{-2}) d'isoprène absorbent ca. 10% de la raie située à 253.7 nm. L'absorption est complète vers 236 nm. L'actinométrie a été réalisée par comparaison. Dans le cas des lampes à azote et à brome on a admis que le rendement quantique $\Phi(C_2H_2)$ obtenu dans la photolyse de l'éthylène est de 0.75 (7). Dans le cas de la lampe à xénon, on a admis que le rendement quantique obtenu dans la photolyse du *cis*-butène-2 est de 0.30 (8). Aucune actinométrie n'a été faite avec la lampe à mercure, la difficulté majeure résidant dans le fait que la lampe est loin d'être monochromatique. Notons enfin que l'usage de HI n'est pas sans défaut puisque des traces d'air semblent catalyser l'addition de ce produit sur l'isoprène dans un mécanisme en chaîne (voir plus loin).

Résultats

La formation des produits est rapportée sous forme de rendements quantiques lorsqu'ils sont disponibles. L'incertitude expérimentale dans ce cas est de $\pm 10\%$. Par contre, les rendements des produits relativement les uns aux autres, sont valables à $\pm 5\%$, les analyses par chromatographie, sauf pour les produits de faibles rendements, étant le plus souvent reproductibles à $\pm 2\%$.

Photolyse vers 230–255 nm

On observe que la majorité des produits légers ont des rendements qui croissent entre 30 et 250 N m^{-2} et puis qui décroissent par la suite jusqu'à 2600 N m^{-2}. On trouve dans ce groupe, l'éthylène, l'acétylène, le propyne, l'allène et le pentadiène-1,4. Ces produits ne sont pas affectés par la présence de HI ou de NO. Afin d'alléger le texte on a représenté l'inverse du rendement des produits en fonction de la pression: figs 1 et 2. L'augmentation du rendement à basse pression est due au fait de l'absorption partielle de la lumière vers 230–245.5 nm. Dès que la pression atteint 150 N m^{-2}, l'échantillon absorbait plus de 90% de ce qu'il absorbait à une pression de 2660 N m^{-2}. Les points obtenus à 30, 70 et 150 N m^{-2} ont été corrigés relativement au rendement de l'éthylène en admettant que le rendement de ce produit qui suit une loi de type Stern–Volmer entre 280 et 2660 N m^{-2}, la suive aussi entre 30 et 280 N m^{-2}.

On trouve également dans ce groupe le vinylacétylène dont le rendement est fortement augmenté en présence de NO et de HI (tableau 1). L'addition de HI, augmente en outre les rendements en méthane, butadiène-1,3, méthyl-2-butène-1-yne-3, et fait apparaître d'importantes quantités de méthylbutènes. L'oxyde nitrique fait décroître légèrement le rendement en méthane, fait disparaître celui en éthane, et augmente le rendement en vinylacétylène. Enfin divers produits (figs 3 et 4) ont des rendements qui tantôt croissent, tantôt décroissent avec l'augmentation de la pression. Il faut dire que dans la région du chromatogramme où apparaissent la majorité de ces composés (méthyl-2-butène-2, cyclopentadiène, *trans*-pentadiène-1,4,... (certains se trouvant dans la queue de l'isoprène), l'identification des produits n'est pas absolument certaine. Ces produits ont été identifiés par une astérisque dans les figs 3 et 4. Une série d'expérience faite avec le filtre en Corex diminue l'intensité de la lampe d'un facteur ca. 5. Le maximum des rendements est obtenu vers une pression voisine de 800 N m^{-2}. Par contre la distribution et le comportement du rendement des produits avec la pression, en présence de NO ou de HI est très similaire à celui observé avec le filtre du Vycor. On ne rediscutera plus des résultats obtenus avec ce filtre.

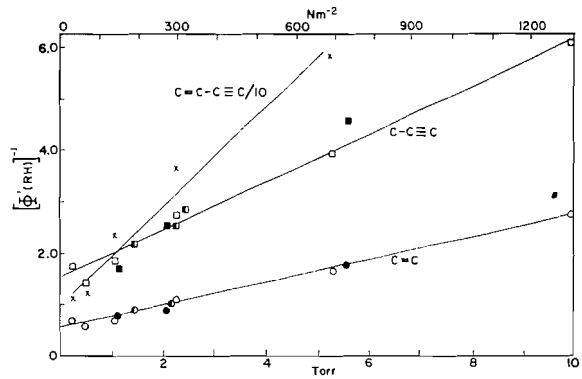

FIG. 1. Variations de l'inverse du rendement absolu (échelle arbitraire) de produits dans la photolyse de l'isoprène entre 230 et 255 nm: ×, ○, □: isoprène pur; ●, ■: isoprène + 10% NO; ◐, ◧: isoprène + 10% HI.

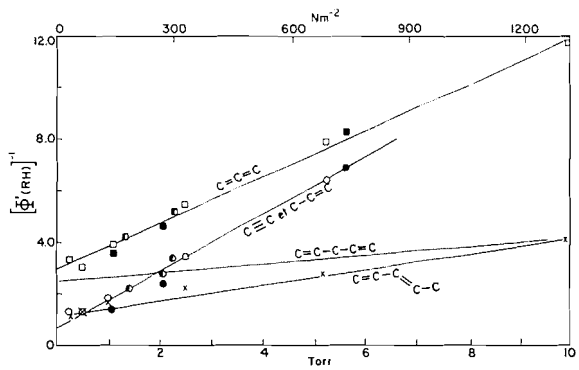

FIG. 2. Varaitions de l'inverse du rendement absolu (échelle arbitraire) de produits dans la photolyse de l'isoprène entre 230 et 255 nm: ×, ○, □: isoprène pur; ●, ■: isoprène + 10% NO; ◐, ◧: isoprène + 10% HI. Pour plus de clarté on n'a pas rapporté les points correspondants pour le pentadiène-1,4 (isoprène pur, en présence de HI).

Can. J. Chem. Downloaded from www.nrcresearchpress.com by 210.87.254.105 on 09/05/12
For personal use only.

TABLEAU 1. Photolyse de l'isoprène vers 230–255 nm. Rendements relatifs[a]

Isoprène (N m^{-2})	155[b]	144	286	192	278	300
Additif: X	—	NO	NO	HI	HI	HI
(N m^{-2})		13	26	14	28	57
Méthane	25	8	10	256	235	nm[c]
Vinylacétylène	8	48	70	150	159	154
Butadiène-1,3 + isobutène + butyne-1	8	15	12	81	83	166
Méthyl-2-butène-1-yne-3	18	11	15	24	118	329
Méthyl-3-butène-1	0	0	0	165	475	1 280
Méthyl-2-butène-1	0	0	0	108	107	775
Méthyl-2-butène-2	90[d]	85[d]	105[d]	1675	4280	10 900

[a]$\phi'(C_2H_2) = 100$; temps d'irradiation: 60 min.
[b]Rapport final C_2H_2/isoprène $= 35 \times 10^{-4}$.
[c]Non mesuré.
[d]Identification incertaine.

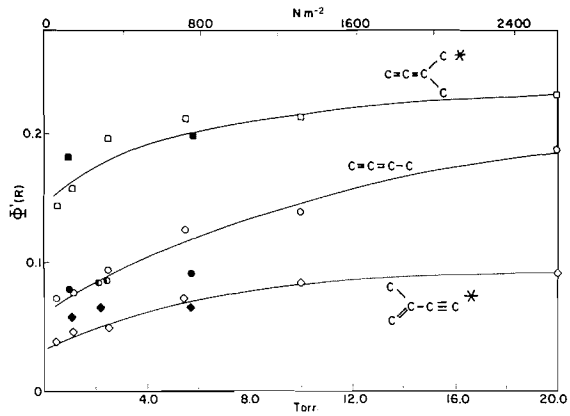

FIG. 3. Variations des rendements absolus (échelle arbitraire) des produits dans la photolyse de l'isoprène entre 230 et 255 nm: ○, □, ◇: isoprène pur; ●, ■: isoprène + 10% NO; ◐, ◧, ◆: isoprène + 10% HI. L'astérisque indique un doute quant à l'identification du produit.

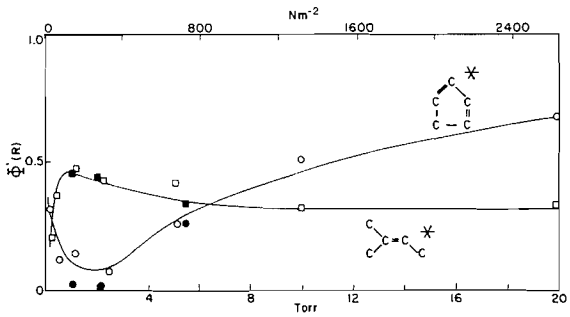

FIG. 4. Voir fig. 3.

Photolyse à 174 nm

Les rendements quantiques des produits sont indiqués dans le tableau 2. L'effet de pression est moindre qu'à plus basses énergie (fig. 5). L'addition de NO est marginale, sauf sur le rendement en éthane qu'il fait disparaître. Par contre, la présence

TABLEAU 2. Photolyse de l'isoprène à 174 nm. Rendements quantiques à 133 N m^{-2} [a]

Additifs		10% O_2	20% H_2S
Méthane	0.020	0.012	0.60
Acétylène	0.030	0.030	0.03
Ethylène	0.10	0.095	0.125
Ethane	0.02	0.00	0.02
Propène	0.03	0.04	nm[b]
Propyne	0.03	0.035	0.03
Allène	0.025	0.025	0.02
Vinylacétylène	0.07	0.07	0.07
Méthyl-2-butène-1-yne-3	0.02	0.02	nm[b]
Cyclopentadiène[c]	0.04	0.04	0.04
Pentadiène-1,3[c]	0.02	0.02	0.02

[a]Temps d'irradiation: 60 min; rapport final C_2H_4/isoprène dans la photolyse de l'isoprène pur: 7.7×10^{-4}. Voir l'effet de pression sur la fig. 5.
[b]Non mesuré.
[c]Identification incertaine.

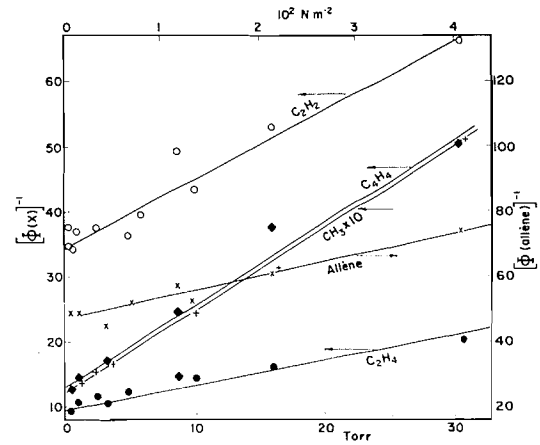

FIG. 5. Variations de l'inverse de rendements quantiques dans la photolyse de l'isoprène à 174 nm en fonction de la pression; ○: C_2H_2; ◆: C_4H_4; +: $CH_3/10$; ×: allène et ●: C_2H_4.

de HI augmente légèrement les rendements en méthane et butadiène-1,3 (fig. 5) et fait apparaître des quantités plus importantes de méthylbutènes. H_2S augmente de façon considérable le rendement en méthane (tableau 2).

Photolyse à 163.3 nm

Les résultats sont similaires à ceux obtenus à 174 nm, avec un effet de pression encore moindre. Les rendements sont indiqués dans le tableau 3, ainsi que l'effet de O_2, H_2S et de HI sur ceux-ci. L'oxygène diminue les rendements en méthane, éthane, vinylacétylène et butadiène-1,3. Au contraire, HI et H_2S augmentent les rendements en méthane, éthane, éthylène et butadiène-1,3.

Une série d'analyses a été faite pour rechercher les produits éventuels des réactions d'addition entre l'isoprène et les radicaux méthyles et les atomes

Can. J. Chem. Downloaded from www.nrcresearchpress.com by 210.87.254.105 on 09/05/12
For personal use only.

TABLEAU 3. Photolyse de l'isoprène à 163.3 nm. Rendements quantiques obtenus à 133 N m^{-2} [a]

Additif		10% O_2	20% H_2S	10% HI
Méthane	0.025	0.015	0.72	0.55
Acétylène	0.095	0.095	0.09	0.09
Ethylène	0.24	0.24	0.27	0.27
Ethane	0.21	0.00	0.12	0.05
Propène	0.095	0.095	0.085	0.085
Propane	Traces	0.00	nm[b]	nm[b]
Propyne	0.095	0.085	0.085	0.085
Allène	0.05	0.05	0.05	0.04
Vinylacétylène	0.15	0.15	0.085	0.10
Butadiène-1,3	0.035	0.015	0.05	0.075
Méthyl-3-butène-1-yne-3	0.04	0.04	0.015	0.025

[a]Temps d'irradiation: 30 min. Le rapport final C_2H_4/isoprène est voisin de 14.7×10^{-4}.
[b]Non mesuré.

d'hydrogène d'une part, et l'isoprène et les atomes d'hydrogène et les radicaux méthyles d'autre part (tableau 4). Ces produits disparaissent en présence d'oxygène.

Photolyse à 147 nm

Les rendements des produits sont indiqués dans les tableaux 4 et 5. On note en plus l'absence d'effet de pression entre 90 et 2150 N m^{-2}. L'oxyde nitrique diminue les rendements en éthane, ainsi que de plusieurs composés en C_6. L'addition de HI ou de H_2S, augmente plusieurs des rendements dont celui du méthane $\Delta\phi(CH_4) = 0.75$, de l'éthylène $\Delta\phi(C_2H_4) = 0.12$, du propène $\Delta\phi(C_3H_6) = 0.09$, des C_3H_4 $\Delta\phi(C_3H_4) = 0.03$, ainsi que des méthylbutènes dans de plus importantes proportions.

Discussion

Bilans de matière et d'énergie

La comparaison des rendements quantiques obtenus à 174, 163.3 et 147 nm sous une pression de 133 N m^{-2} (tableaux 2, 3 et 5) montre une croissance

TABLEAU 4. Photolyse de l'isoprène pur à 163.3 et à 147 nm[a]

Produit	163.3 nm 560	163.3 nm 2050	147 nm 90–2150 N m^{-2}	Note
Diméthyl-3,3-butène-1	0.00	0.00	0.03	[c]
Méthyl-3-pentène-1	0.020	Traces	0.00	[b]
Diméthyl-2,3-butène-1	0.020	0.007	0.04	[c]
Méthyl-2-pentène-1	0.005	Traces	0.00	[b]
Méthyl-2-pentène-2	0.15	0.10	0.14	[b,c]
cis + *trans*-Méthyl-3-pentène-2	0.040	0.041	0.07	[b,c]
Diméthyl-3,3-pentène-1	0.014	0.024	nm[e]	[d]

[a]Tous ces produits disparaissent en présence de 10% de O_2 ou de NO, ou de 20% de H_2S.
[b]Produits de l'addition successive isoprène + CH_3 + H.
[c]Produits de l'addition successive isoprène + H + CH_3.
[d]Produits de l'addition successive isoprène + CH_3 + CH_3.
[e]Non mesuré.

TABLEAU 5. Photolyse de l'isoprène à 147 nm entre 90 et 2150 N m^{-2}. Rendements quantiques[a]

Additif (%)		NO (10)	HI (5–12)	H_2S (20–30)
Méthane	0.02	0.02	0.76	0.77
Acétylène	0.125	0.125	0.125	0.125
Ethylène	0.185	0.207	0.324	0.30
Ethane	0.075	0.00	0.00	<0.01
Propène	0.05	0.04	0.13	nm[b]
Propyne	0.055	0.065	0.087	0.097
Allène	0.082	0.096	0.0109	0.091
Vinylacétylène[c]	0.66	0.66	0.68	0.66
Isobutène	0.02	0.00	0.00	nm[b]
Méthyl-2-butène-1-yne-3	0.092	0.091	0.105	0.09

[a]Temps d'irradiation 30 min.
[b]Non mesuré.
[c]Rapport final C_4H_4/isoprène < 30×10^{-4} à une pression de 115 N m^{-2}.

des rendements avec l'énergie des photons incidents. A 174 nm, le produit "moléculaire", c'est-à-dire formé en présence d'un intercepteur radicalaire tel que l'oxygène ou l'oxyde nitrique, majeur est l'éthylène: $\Phi(C_2H_4) = 0.10$. A 163.3 nm, ce rendement est de 0.25. A 147 nm, le produit majeur est le vinylacétylène: $\Phi(C_4H_4) = 0.66$. Par contre l'usage d'intercepteur radicalaire comme l'hydrogène sulfuré, ou l'iodure d'hydrogène, montre un rendement appréciable en méthane: $\Phi(CH_4) \simeq 0.8$ à chaque cas. En présence de HI, de H_2S, cette formation est liée à la présence de radicaux méthyles (9):

[1] $CH_3 + HX \rightarrow CH_4 + HX$ (où X = HS, I)

Cette observation montre le rôle important de la liaison CH_3—C_4H_5 dans la fragmentation de la molécule photoexcitée.

Il est tentant de mettre en évidence la formation concurrente du radical C_4H_5, à travers une réaction similaire à la réaction [1]. L'augmentation marginale de butadiène-1,3 en présence de HI ou de H_2S, même s'il suggère la présence d'un tel radical est loin de montrer un accord quantitatif entre le rendement en radicaux CH_3 et C_4H_5 (10). Ce dernier radical, très insaturé, n'est probablement pas intercepté par H_2S, tout comme ne le sont pas les radicaux allyles (11). HI a cependant une meilleure efficacité bien qu'incomplète (10) (tableau 1). En outre la réactivité importante de l'isoprène envers les radicaux est un handicap sérieux à leur mesure.

[2] $C_5H_8 + h\nu \rightarrow C_5H_8^{**}$

[3] $C_5H_8^{**} \rightarrow CH_3 + C_4H_5$

$\Delta H = 439$ kJ mol^{-1}

Après scission de la liaison CH_3—C_4H_5, il reste un surplus de l'énergie du photon qu'il faut distribuer entre les deux fragments. Ce surplus est de 22–72 et

Can. J. Chem. Downloaded from www.nrcresearchpress.com by 210.87.254.105 on 09/05/12
For personal use only.

de 246 kJ mol^{-1} à 230–255 et 174 nm respectivement. On ne connaît rien de précis sur cette distribution. Si le radical méthyl emporte ce surplus, il est insuffisemment excité pour se fragmenter: $\Delta H(CH_3 \rightarrow CH_2 + H) = 468$ kJ mol^{-1}. Si le radical C_4H_5 emporte ce surplus, il est possible qu'il se fragmente: $\Delta H(C_4H_5 \rightarrow C_4H_4 + H) = 130$ kJ mol^{-1} à 174 nm. Une réaction globale du type

[4] $$C_5H_8^{**} \rightarrow C_4H_4 + CH_3 + H$$
$$\Delta H = 569 \text{ kJ mol}^{-1}$$

est donc thermiquement acceptable. La formation simultanée de méthane et de vinylacétylène est un processus mineur, puisqu'il y a toujours plus de C_4H_4 que de CH_4 moléculaires. Même vers 230–255 nm, le vinylacétylène formé en présence de NO est $\simeq 7$ fois plus important que le méthane.

A 163.3 et à 147 nm, le surplus d'énergie, après la réaction [3] est 290 et de 368 kJ mol^{-1}. L'augmentation du rendement en vinylacétylène avec l'augmentation d'énergie résiduelle est en faveur de ce mécanisme. Comme les réactions [3] et [4] sont les seules sources de radicaux méthyles (voir plus loin), et la réaction [4], la source de vinylacétylène, le rendement de ces deux produits permet la mesure des réactions [3] et [4].

Les réactions de formation de l'éthylène sont moins évidentes. En effet, il y a toujours moins de C_3H_4 que d'éthylène à être formé, et l'usage de H_2S, ou de HI, ne montre pas de façon évidente les fragments complémentaires de C_2H_4. On note cependant que le rapport C_3H_4/C_2H_4 est de 0.61 ± 0.04 entre 230 et 255 nm, 1.02 ± 0.06 à 174 nm, 0.60 ± 0.04 à 163.3 nm et de 1.5 ± 0.1 à 147 nm.

Dans la région de 230–255 nm, où l'énergie disponible par photon est de 511–461 kJ mol^{-1} une décomposition concertée peut être efficace.

[5] $$C_5H_8^{**} \rightarrow C_2H_4 + C_3H_4$$
$$\Delta H = 165 \text{ kJ mol}^{-1}$$

Cette réaction demande une modification importante de la molécule photoexcitée avec un déplacement de type [1]–[3] d'un atome d'hydrogène avant ou pendant la scission. La décomposition en deux fragments radicalaires, scission de la liaison C—C, avec formation de deux radicaux vinyles et $CH_3—C{=}CH_2$ suivie de la fragmentation du radical C_3H_5 est thermiquement inacceptable. Il en est de même de la fragmentation du radical vinyle.

[6] $$C_5H_8^{**} \rightarrow C_2H_3 + C_3H_4 + H$$
$$\Delta H = 602 \text{ kJ mol}^{-1}$$

[7] $$C_5H_8^{**} \rightarrow C_2H_2 + C_3H_5 + H$$
$$\Delta H = 610 \text{ kJ mol}^{-1}$$

Ces deux réactions ne sont donc acceptables qu'à 174 nm et en dessous. Le fragment C_3H_5 n'a pu être mis en évidence qu'à 147 nm (effet de HI ou de H_2S). Par contre on observe un léger rendement en radicaux vinyles: $\Phi(C_2H_3) = 0.03$ à 174 et à 163.3 nm et 0.11 à 147 nm rend crédible la réaction [6].

La rupture de la liaison centrale, réaction [6], produit le radical C_3H_5 de structure $CH_3—C{=}CH_2$ (en n'admettant aucune réorganisation dans la molécule photoexcitée avant ou pendant la dissociation). On sait que la fragmentation de ce radical lorsqu'il est excité peut conduire à l'allène et au propyne dans le rapport 1.5, en accord avec ce qui est observe à 147 nm (1, 12).

Enfin, un excès d'éthylène est formé. La réaction suivante est proposée pour tenir compte du bilan de matière mais la formation de radicaux C_3H_3 reste à faire (10):

[8] $$C_5H_8^{**} \rightarrow C_3H_3 + C_2H_4 + H$$

On observe à 230–255, 174 et 163.3 nm l'équivalence des rendements en propène et acétylène. Cela suggère la réaction concertée suivante:

[9] $$C_5H_8^{**} \rightarrow C_2H_2 + C_3H_6$$
$$\Delta H = 171.4 \text{ kJ mol}^{-1}$$

Cette réaction est précédée ou se fait de façon concurrente à un déplacement 4–2 d'un atome d'hydrogène dans la molécule photoexcitée. A 147 nm, le manque de propène comparativement à l'acétylène, si la réaction [9] est encore valide, est explicable par la fragmentation plus poussée du propène: l'excès d'énergie à cette longueur d'onde est de 636 kJ mol^{-1}.

Enfin, un dernier composé formé en quantités mineures est le méthyl-2-butène-1-yne-3.

[10] $$C_5H_8^{**} \rightarrow C_5H_6 + H_2 \text{ (2H)}$$
$$\Delta H = 60(540 \text{ kJ mol}^{-1})$$

Un certain nombre de composés en C_5 dont l'identification n'est pas définitive (figs 3 et 4) ont des rendements qui tantôt croissent, tantôt décroissent avec l'augmentation de pression à 230–255 nm et qui ont encore des rendements appréciables à 174 nm (produits formés en présence d'oxygène). Il faut noter ici que la photolyse sensibilisée au mercure ($^3P_1$) de l'isoprène fait apparaître les diméthyl-3,3- et 1,3-cyclopropènes qui ont un rendement dont le comportement est similaire à celui observé du méthyl-2-butène-2 (13). Ces deux composés dérivés du cyclopropène n'ont pas été identifiés, et l'absence de témoin ne permet pas d'éliminer leur formation. La présence de ces produits suggère cependant au moins à 230–255 nm, une réorganisation (isomérisation) de la molécule photoexcitée suivie d'une stabilisation par collision.

Can. J. Chem. Downloaded from www.nrcresearchpress.com by 210.87.254.105 on 09/05/12
For personal use only.

Effet de pression

Les courbes de type Stern-Volmer (figs 1, 2 et 5) illustrent la stabilisation par collision d'intermédiaires photoexcités: la molécule photoexcitée pouvant être l'un d'eux.

[11] $$C_5H_8^{**} + M \rightarrow C_5H_8^{*} + M$$

où $C_5H_8^*$ est une molécule qui ne donne plus lieu à la formation de produit léger. A 230–255 nm, l'augmentation des produits en C_5 est compatible avec la stabilisation de la molécule photoexcitée. A 174 et à 163.3 nm, la situation semble plus complexe. Le fait que les droites $\Phi(C_2H_2)^{-1}$ et $\Phi(C_3H_6)^{-1}$ en fonction de la pression sont confondues justifie la réaction [9]. Puisque le rendement en radicaux méthyles suit aussi une loi du même type, on est tenté d'admettre que même à 163.3 nm, la molécule photoexcitée a un temps de vie suffisemment long pour être stabilisée à haute pression. Cette observation est contraire avec ce qui est observé avec les butènes (1). Le spectre d'absorption de l'isoprène a été discuté (14, 15). Hormis la possibilité d'une absorption partielle par l'isomère *cis* de l'isoprène, les raies à 174 et à 163.3 nm se trouvent dans un région où existent des états Rydberg, états bien connus pour leur temps de vie relativement long.

En tenant compte de ces remarques et en utilisant les rendements obtenus à pression nulle (extrapolation des droites Stern–Volmer), on propose dans le tableau 6 le schémas de fragmentation de la molécule photoexcitée. Cette fragmentation est donc complète à pression nulle à 174 nm.

Réactions radicalaires

Le rendement en éthane, ainsi que celui de plusieurs composés en C_5 et C_6 disparaissent lors de l'addition d'oxygène ou d'oxyde nitrique confirmant ainsi leur origine radicalaire. Il faut tout d'abord noter la faible quantité d'éthane formé dans l'isoprène pur comparativement aux rendements $\Phi(CH_3)$ mesurés à l'aide de H_2S ou de HI_3 (tableaux 2 et 3). Dans ce système, les radicaux méthyles n'ont pas la chance de se recombiner entre eux mais disparaissent principalement par d'autres voies réactionnelles et l'addition directe du radical méthyle sur l'isoprène doit être envisagée. En fait on observe des produits provenant de l'addition successive du radical méthyle et d'un atome d'hydrogène, et l'inverse, sur l'isoprène (tableau 4).

TABLEAU 6. Fragmentation de la molécule isoprène photoexcitée

N°	$C_5H_8^{**} \rightarrow$	Rendements quantiques 174 nm	163.3 nm	147 nm
10	$C_5H_6 + 2H\ (H_2)$	0.02	0.05	0.09
3	$C_4H_5 + CH_3$	0.70	0.60	0.16
4	$C_4H_4 + CH_3 + H$	0.07	0.15	0.50
9	$C_3H_6 + C_2H_2$	0.03	0.095	0.04
7	$C_3H_5 + C_2H_2 + H$	—	—	0.09
5	$C_3H_4 + C_2H_4$	0.03	0.135	0.03
6	$C_3H_4 + C_2H_3 + H$	0.03	0.03	0.12
8	$C_3H_3 + C_2H_4 + H$	0.07	0.105	0.03
	Isomérisation (?)	0.06	<0.01	$\simeq 0.00$
Total:		1.01	1.165	1.06

L'addition d'un atome d'hydrogène sur l'isoprène n'est pas empêchée même par la présence d'oxygène (16). Une fraction des radicaux méthyles se combinent donc aux radicaux C_5H_9 qui en résultent. La somme des rendements en C_6 donne une limite inférieure du rendement en atome d'hydrogène puisqu'il faut tenir compte de la recombinaison des radicaux C_5H_9 entre eux. Le rendement de cette réaction peut être grossièrement évaluée sur la base de la loi statistique habituelle (17):

$$\frac{\Phi(CH_3 + C_5H_9)}{\Phi(CH_3 + CH_3)^{1/2} \cdot \Phi(C_5H_9 + C_5H_9)^{1/2}} = 2$$

Ainsi à 163.3 nm et sous 560 N m^{-2}, le rendement $\Phi(C_5H_9 + C_5H_9)$ peut être estimé à 0.07 et cette valeur atteint 0.3 à 147 nm. Le rendement en atome d'hydrogène est alors tel que $\Phi(H) = 2\Phi(C_5H_9 + C_5H_9) + \Phi(C_6)$. On obtient $\Phi(H) = 0.3 \pm 0.1$ et 0.9 ± 0.2 à 163.3 et à 147 nm respectivement. En outre le rendement en radicaux méthyles peut aussi être évalué de la même façon: $\Phi(CH_3) = 2\Phi(C_2H_6) + \Phi(C_6) + 2\Phi(C_7)$ (le terme $\Phi(C_7)$ tient compte de l'addition successive de deux radicaux méthyles sur l'isoprène). On obtient ainsi $\Phi(CH_3) = 0.68$ et 0.43 à 163.3 et à 147 nm respectivement. Ces valeurs sont sous estimées puisque la mesure systématique des produits en C_7 n'a pas été faite. On note donc une diminution des rendements en atomes d'hydrogène avec une diminution de l'énergie des photons en accord avec la fragmentation proposée de la molécule photoexcitée (tableau 6).

A 174 nm, seul le rendement en éthane intéressant cette cinétique radicalaire a été mesuré et son rendement est relativement bas. Cette observation est probablement reliée au fait que l'intensité de la lampe est plus faible que les deux autres. Il en résulte que les radicaux méthyles disparaissent du réacteur principalement par addition sur l'isoprène. Nous avons tiré avantage de ces conditions expérimentales pour mesurer le rapport des constantes de vitesse des réactions entre le radical méthyle et l'hydrogène sulfuré d'une part, et l'isoprène d'autre part.

[12] $$CH_3 + C_5H_8 \rightarrow C_6H_{11}$$

Les réactions [1] et [12] conduisent à une cinétique

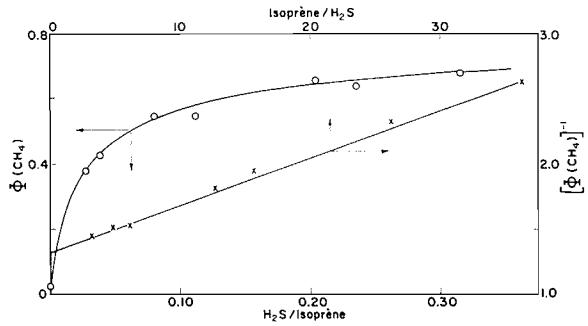

FIG. 6. Variation du rendement en méthane et de son inverse dans la photolyse à 174 nm des mélanges isoprène (5.0 Torr – 665 N m^{-2}): hydrogène sulfuré.

simple:

$$[\Phi(CH_4)]^{-1} = [\Phi(CH_3)]^{-1} + [\Phi(CH_3)]^{-1} \cdot k_{12}/k_1 \cdot [\text{isoprène}]/[H_2S]$$

La fig. 6 montre la linéarité obtenue entre l'inverse du rendement en méthane et la variation du rapport [isoprène]/[H_2S]. D'après la pente de la droite, on a estimé le rapport k_1/k_{12} à 41 $\pm$ 3. Ce rapport est sans doute légèrement sous-estimé puisque l'on a ignoré les réactions du type $CH_3 + CH_3$ et $CH_3 + C_6H_{11}$.

Nota

Dans ce système, l'usage de HI comme intercepteur radicalaire, n'est pas sans défaut. Dans chacun des cas on a noté une augmentation importante du rendement des méthyl-2-butène-2 et, en moindres quantités, méthyl-3-butène-1 (les rendements quantiques pouvaient atteindre 10) (voir aussi tableau 1). On sait que HI s'additionne facilement sur l'isoprène en position 1,4 et qu'il donne lieu à la formation des C_5H_{10} dans un mécanisme en chaîne probablement entretenu par les atomes d'iode (18). Ainsi à 174 nm, on a été incapable de mesurer convenablement le rendement en radicaux méthyles par cette méthode.

Remerciements

Nous voulons exprimer notre gratitude au CNR ainsi qu'au MEQ (programme FCAC) pour l'aide qu'ils nous ont généreusement accordé tout au long de ce travail.

1. G. J. COLLIN et A. WIĘCKOWSKI. J. Photochem. **8**, 103 (1978).
2. G. J. COLLIN. J. Chim. Phys. **74**, 302 (1977).
3. R. A. HIVELY. Anal. Chem. **35**, 1921 (1963).
4. A. WIĘCKOWSKI et G. J. COLLIN. J. Phys. Chem. **81**, 2592 (1977).
5. A. WIĘCKOWSKI et G. J. COLLIN. Can. J. Chem. **56**, 1435 (1978).
6. R. GORDEN, JR., R. E. REBBERT et P. AUSLOOS. NBS Tech. Note 496 (1969).
7. P. POTZINGER, L. C. GLASGOW et G. VON BÜNAU. Z. Naturforsch. Teil A, **27**, 628 (1971).
8. G. J. COLLIN et K. BUKKA. J. Photochem. **6**, 381 (1976/77).
9. G. J. COLLIN, P. M. PERRIN et C. M. GAUCHER. Can. J. Chem. **50**, 2391 (1972).
10. Z. DIAZ et R. D. DOEPKER. J. Phys. Chem. **81**, 1442 (1977).
11. P. AUSLOOS, R. E. REBBERT et S. G. LIAS. J. Photochem. **2**, 267 (1973/74).
12. J. A. HERMAN, K. HERMAN et P. AUSLOOS. J. Chem. Phys. **52**, 28 (1970).
13. S. BOUÉ et R. SRINIVASAN. Mol. Photochem. **4**, 93 (1972).
14. W. C. PRICE et A. D. WALSH. Proc. R. Soc. London Ser. A, **174**, 220 (1940).
15. M. B. ROBIN. *Dans* Higher excited states of polyatatomic molecules. Academic Press, New York, NY. 1975. p. 166 et suivantes.
16. J. A. KERR et M. J. PARSONAGE. *Dans* Evaluated kinetic data on gas phase addition reactions. CRC Press, Cleveland, Ohio. 1972. pp. 370 ainsi que les références qui y sont citées.
17. R. WESTON, JR. et H. A. SCHWARTZ. *Dans* Chemical kinetics. Prentice-Hall, Inc., Englewood Cliffs, NJ. 1972. p. 90.
18. P. J. GORTON et R. WALSH. J. Chem. Soc. Chem. Commun. 782 (1972).

Can. J. Chem. Downloaded from www.nrcresearchpress.com by 210.87.254.105 on 09/05/12
For personal use only.

Apparent molar heat capacities and volumes of aqueous electrolytes at 25°C: Na_2SO_4, K_2SO_4, $Na_2S_2O_3$, $Na_2S_2O_8$, $K_2S_2O_8$, K_2CrO_4, Na_2MoO_4, and Na_2WO_4

INGER V. OLOFSSON,[1] JAN J. SPITZER, AND LOREN G. HEPLER

Department of Chemistry, University of Lethbridge, Lethbridge, Alta., Canada T1K 3M4

Received January 17, 1978

INGER V. OLOFSSON, JAN J. SPITZER, and LOREN G. HEPLER. Can. J. Chem. **56**, 1871 (1978).

We have made heat capacity and density measurements leading to apparent molar heat capacities and volumes for dilute aqueous solutions of Na_2SO_4, K_2SO_4, $Na_2S_2O_3$, $Na_2S_2O_8$, $K_2S_2O_8$, K_2CrO_4, Na_2MoO_4, and Na_2WO_4. We have used these apparent molar quantities to extrapolate to infinite dilution to obtain the corresponding standard state apparent and partial molar quantities. These latter values have been used in calculation of conventional ionic heat capacities and volumes.

INGER V. OLOFSSON, JAN J. SPITZER et LOREN G. HEPLER. Can. J. Chem. **56**, 1871 (1978).

On a effectué des mesures de capacité calorifique et de densité conduisant aux capacités calorifiques et aux volumes molaires apparents de solutions aqueuses diluées de Na_2SO_4, K_2SO_4, $Na_2S_2O_3$, $Na_2S_2O_8$, $K_2S_2O_8$, K_2CrO_4, Na_2MoO_4 et Na_2WO_4. On a utilisé ces quantités molaires apparentes pour effectuer une extrapolation vers une dilution infinie afin d'en tirer les quantités molaires partielles apparentes des états standard correspondants. On a utilisé ces dernières valeurs pour calculer les capacités calorifiques et les volumes ioniques conventionnels.

[Traduit par le journal]

Introduction

As part of our continuing program of measurements leading to thermal and volumetric properties of aqueous solutions, we have made calorimetric measurements leading to apparent molar heat capacities and density measurements leading to apparent molar volumes of eight $(M^+)_2(X^{2-})$ electrolytes at 25°C. Results of these measurements and our thermodynamic calculations are reported in this paper.

Experimental

Our heat capacity measurements have been made with two different Picker flow calorimeters of the same type, as described previously (1). A small systematic error in the measurements with the first calorimeter has been identified and corrected as recently described (2, 3). Tests by Picker and our various comparisons (4–10)[2] of results obtained with several calorimeters have confirmed that the earlier small error is negligible with the new calorimeter.

Densities of solutions have been measured with a flow densimeter that has been described previously (11).

Results of all calorimetric and density measurements refer to 25.00 ± 0.05°C.

Samples of analytical reagent grade Na_2SO_4, K_2SO_4, and K_2CrO_4 were dried to constant mass at 110°C. Solutions were then prepared from dried samples and distilled water by mass.

Reagent grade $Na_2S_2O_8$ and $K_2S_2O_8$ were recrystallized from solutions that were saturated at about 50°C and then cooled to 0°C. Resulting crystals were dried to constant mass over P_2O_5. All solutions for subsequent measurements were prepared by mass of salt and distilled water.

Reagent grade Na_2MoO_4 and Na_2WO_4 were recrystallized from slightly alkaline solutions and dried by heating to constant mass. Solutions for subsequent measurements were prepared by mass of salt and distilled water.

Stock solutions of sodium thiosulfate were prepared from analytical grade $Na_2S_2O_3 \cdot 5H_2O$ and then analyzed by adding excess iodide and titrating with standard KIO_3 solution. Other solutions were prepared by dilution of these stock solutions.

Results and Calculations

Results of measurements with the Picker flow calorimeter are heat capacities per unit volume, which we express in terms of J K^{-1} cm^{-3}. Combination of these heat capacities with the densities and the already known heat capacity of pure water permits calculation and heat capacities of solutions expressed in terms of J K^{-1} (g of solution)$^{-1}$. These latter heat capacities are then used in obtaining the desired apparent molar heat capacities of solutes that we represent by ϕ_C and express in terms of J K^{-1} mol^{-1}. Similarly, densities of the solutions lead to the apparent molar volumes of the solutes that we represent by ϕ_V and express in terms of cm^3 mol^{-1}. For these calculations of apparent molar quantities we have used equations based on

$$[1] \qquad \phi_Y = [Y(\text{solution}) - n_1 Y_1^0]/n_2$$

in which the symbols have the following meanings: Y is the extensive property (heat capacity or volume here) of a specified quantity of solution, n_1 is the number of moles of solvent in this specified quantity of solution, Y_1^0 is the property (heat capacity or volume) of 1 mol of pure solvent, and n_2 is the number of moles of solute in the specified quantity of solution.

[1] Visiting scientist from University of Lund, Lund, Sweden.

[2] E. M. Woolley. Private communication.

Can. J. Chem. Downloaded from www.nrcresearchpress.com by 210.87.254.42 on 09/05/12
For personal use only.

Can. J. Chem. Downloaded from www.nrcresearchpress.com by 210.87.254.42 on 09/05/12
For personal use only.

TABLE 1. Parameters for eq. [2]

Solute	ϕ_C^0 (J K^{-1} mol^{-1})	B_C (J K^{-1} mol^{-2} kg)	ϕ_V^0 (cm^3 mol^{-1})	B_V (cm^3 mol^{-2} kg)
Na_2SO_4	−190.1	133.0	11.4	0.8
K_2SO_4	−251.0	73.6	32.8	2.4
$Na_2S_2O_3$	−163.6	106.0	26.3	3.0
$Na_2S_2O_8$	−29.3	50.9	76.1	−2.4
$K_2S_2O_8$	−84.0	160.0	97.6	−6.9
K_2CrO_4	−235.0	36.6	38.2	0.2
Na_2MoO_4	−122.8	31.1	28.0	−0.5
Na_2WO_4	−110.4	7.8	30.0	−2.8

Our experimental results are finally tabulated in terms of ϕ_C and ϕ_V values at specified molalities.[3] Concentrations of solutions ranged from 0.015 to 0.29 molal.

Apparent molar properties of dilute solutions of strong electrolytes are accurately described by equations of the form

$$[2] \qquad \phi_Y = \phi_Y^0 + A_Y(d_1^0 m)^{1/2} + B_Y m$$

in which ϕ_Y^0 is the value of ϕ_Y at infinite dilution, A_Y is the limiting slope derived from the Debye–Hückel theory, m is the molality, and B_Y is an adjustable parameter. Our principal interest has been in determining the ϕ_Y^0 values that are identical with the corresponding partial molar properties at infinite dilution ($\bar{Y}_2^0$). For calculations leading to these values we have used $A_C(d_1^0)^{1/2} = 150.4$ J K^{-1} mol$^{-3/2}$ kg$^{1/2}$ and $A_V(d_1^0)^{1/2} = 9.72$ cm^3 mol$^{-3/2}$ kg$^{1/2}$. Our ϕ_C^0, B_C, ϕ_V^0, and B_V values based on least-squares fitting of our experimental results to equations of the form of [2] are given in Table 1. Total uncertainties due to chemicals, measurements, and data treatment amount to about ±3 J K^{-1} mol^{-1} in ϕ_C^0 and about ±0.5 cm^3 mol^{-1} in ϕ_V^0.

Results of our work as summarized in Table 1 can be compared with results of earlier investigators as follows. We also present calculations with ionic heat capacities and volumes, based on the common and useful convention that $H^+(aq)$ has $\phi_C^0 = 0$ and $\phi_V^0 = 0$. For these latter calculations we also use $\phi_C^0(Na^+) = 43$ J K^{-1} mol^{-1} and $\phi_C^0(K^+) = 13$ J K^{-1} mol^{-1} from Desnoyers, de Visser, Perron, and Picker (3) along with $\phi_V^0(Na^+) = -1.21$ cm^3 mol^{-1} and $\phi_V^0(K^+) = 9.02$ cm^3 mol^{-1} from Millero (12).

Our $\phi_C^0 = -190.1$ J K^{-1} mol^{-1} for aqueous Na_2SO_4 is in excellent agreement with $\phi_C^0 = -191.7$ J K^{-1} mol^{-1} from the Université de Sherbrooke (3), also obtained by flow calorimetry. Earlier enthalpy of solution measurements at several temperatures in combination with $d\Delta H^0/dT = \Delta C_p^0$ led Gardner, Jekel, and Cobble (13) to $\bar{C}_p^0$ ($= \phi_C^0$) $= -195$ J K^{-1} mol^{-1} for aqueous Na_2SO_4. For aqueous K_2SO_4 we have $\phi_C^0 = -251.0$ J K^{-1} mol^{-1} and also $\phi_C^0 = -254.5$ J K^{-1} mol^{-1} from the Université de Sherbrooke (3). Our ϕ_C^0 values for these two electrolytes in combination with ϕ_C^0 values for $Na^+(aq)$ cited in the paragraph above lead to $\phi_C^0 = -276$ and -277 J K^{-1} mol^{-1} for $SO_4^{2-}(aq)$, while the other ϕ_C^0 values lead to $\phi_C^0 = -278$, -281, and -280 J K^{-1} mol^{-1} for $SO_4^{2-}(aq)$. We now choose an average $\phi_C^0 = -278$ J K^{-1} mol^{-1} (std. dev. = 2) for $SO_4^{2-}(aq)$ and list this value in Table 2.

We do not know of any earlier results leading to ϕ_C^0 values for the other salts we have investigated so we proceed to use our ϕ_C^0 values from Table 1 for calculation of ionic heat capacities.

The ϕ_C^0 for aqueous $Na_2S_2O_3$ leads to $\phi_C^0 = -250$ J K^{-1} mol^{-1} for $S_2O_3^{2-}(aq)$. For $S_2O_8^{2-}(aq)$ we obtain $\phi_C^0 = -115$ J K^{-1} mol^{-1} from the ϕ_C^0 for aqueous $Na_2S_2O_8$, while the ϕ_C^0 for aqueous $K_2S_2O_8$ leads to $\phi_C^0 = -110$ J K^{-1} mol^{-1} for $S_2O_8^{2-}(aq)$. Because we believe that the samples of $K_2S_2O_8$ were purer than the samples of $Na_2S_2O_8$, we choose this latter $\phi_C^0 = -110$ J K^{-1} mol^{-1} as best for $S_2O_8^{2-}(aq)$. The ϕ_C^0 values for aqueous K_2CrO_4, Na_2MoO_4, and Na_2WO_4 lead to the following: $\phi_C^0 = -261$ J K^{-1} mol^{-1} for $CrO_4^{2-}(aq)$, $\phi_C^0 = -209$ J K^{-1} mol^{-1} for $MoO_4^{2-}(aq)$, and $\phi_C^0 = -196$ J K^{-1} mol^{-1} for $WO_4^{2-}(aq)$.

TABLE 2. Conventional [$\phi_Y^0(H^+) = 0$] apparent molar heat capacities and volumes for aqueous ions at 298.15 K

Ion	ϕ_C^0 (J K^{-1} mol^{-1})	ϕ_V^0 (cm^3 mol^{-1})
SO_4^{2-}	−278	13.98[a]
$S_2O_3^{2-}$	−250	28.7
$S_2O_8^{2-}$	−110[b]	79.6[b]
CrO_4^{2-}	−261	20.2
MoO_4^{2-}	−209	30.4
WO_4^{2-}	−196	32.4

[a]From ref. 12.
[b]Based on our results for the potassium salt.

[3]A complete set of the experimental results is available, at a nominal charge, from the Depository of Unpublished Data, CISTI, National Research Council of Canada, Ottawa, Ont., Canada K1A 0S2.

Millero (12) has listed ϕ_V^0 values for aqueous Na_2SO_4 and K_2SO_4 that are almost certainly more accurate than our values for these electrolytes, although the agreement is satisfactory. On the other hand, our ϕ_V^0 values for the other electrolytes we have investigated are probably more accurate than the corresponding values cited by Millero (12). We therefore adopt $\phi_V^0 = 13.98$ cm^3 mol^{-1} for SO_4^{2-}(aq) from Millero (12) and calculate the following ionic volumes from our results. Our ϕ_V^0 values for aqueous $Na_2S_2O_3$, K_2CrO_4, Na_2MoO_4, and Na_2WO_4 lead to $\phi_V^0 = 28.7$ cm^3 mol^{-1} for $S_2O_3^{2-}$(aq), $\phi_V^0 = 20.2$ cm^3 mol^{-1} for CrO_4^{2-}(aq), $\phi_V^0 = 30.4$ cm^3 mol^{-1} for MoO_4^{2-}(aq), and $\phi_V^0 = 32.4$ cm^3 mol^{-1} for WO_4^{2-}(aq). Our ϕ_V^0 values for aqueous $Na_2S_2O_8$ and $K_2S_2O_8$ lead to $\phi_V^0 = 78.5$ and 79.6 cm^3 mol^{-1} for $S_2O_8^{2-}$(aq). As before we select the result from the potassium salt as the most accurate. All of these ionic ϕ_V^0 values are collected in Table 2.

Acknowledgments

We all thank the National Research Council of Canada for support of this research. I.V.O. also thanks the Canada Council for a scholarship.

1. P. Picker, P.-A. Leduc, P. R. Philip, and J. E. Desnoyers. J. Chem. Thermodyn. **3**, 631 (1971).
2. G. Perron, N. Desrosiers, and J. E. Desnoyers. Can. J. Chem. **54**, 2163 (1976).
3. J. E. Desnoyers, C. de Visser, G. Perron, and P. Picker. J. Solution Chem. **5**, 605 (1976).
4. P. P. Singh, E. M. Woolley, K. G. McCurdy, and L. G. Hepler. Can. J. Chem. **54**, 3315 (1976).
5. P. P. Singh, K. G. McCurdy, E. M. Woolley, and L. G. Hepler. J. Solution Chem. **6**, 327 (1977).
6. O. Enea, P. P. Singh, E. M. Woolley, K. G. McCurdy, and L. G. Hepler. J. Chem. Thermodyn. **9**, 731 (1977).
7. P. P. Singh, J. J. Spitzer, R. M. McKay, K. G. McCurdy, and L. G. Hepler. Thermochim Acta. In press.
8. A. Roux, G. M. Musbally, G. Perron, J. E. Desnoyers, P. P. Singh, E. M. Woolley, and L. G. Hepler. Can. J. Chem. **56**, 24 (1978).
9. J. J. Spitzer, P. P. Singh, K. G. McCurdy, and L. G. Hepler. J. Solution Chem. **7**, 81 (1978).
10. L. G. Hepler. To be published.
11. P. Picker, E. Tremblay, and C. Jolicoeur. J. Solution Chem. **3**, 377 (1974).
12. F. J. Millero. *In* Water and aqueous solutions: structure, thermodynamics, and transport processes. *Edited by* R. A. Horne. Wiley-Interscience, New York, NY. 1972.
13. W. L. Gardner, E. C. Jekel, and J. W. Cobble. J. Phys. Chem. **73**, 2017 (1969).

Can. J. Chem. Downloaded from www.nrcresearchpress.com by 210.87.254.42 on 09/05/12
For personal use only.

Synthèse et caractérisation des oxypentafluorouranates(VI) NH_4UOF_5, $KUOF_5$, $RbUOF_5$ et $CsUOF_5$

PHILIPPE JOUBERT ET ROLAND BOUGON[1]

Centre d'Etudes Nucléaires de Saclay, Division de chimie, Département de Génie Isotopique, B.P. n°2, 91190 Gif/Yvette, France

ET

BERNARD GAUDREAU

Université de Limoges, Laboratoire de Chimie Minérale B, 123, rue Albert Thomas, 87060 Limoges Cedex, France

Reçu le 30 septembre 1977

PHILIPPE JOUBERT, ROLAND BOUGON et BERNARD GAUDREAU. Can. J. Chem. **56**, 1874 (1978).

Les oxypentafluorouranates(VI) $MUOF_5$ (M = NH_4, K, Rb, Cs) ont été préparés dans SO_2 liquide par action sur UOF_4 du fluorure d'ammonium ou du fluorure alcalin correspondant. Leur étude par diffraction des rayons-X, par spectroscopie infra-rouge et Raman et une isotypie avec les hexafluorouranates(V) MUF_6 correspondants a permis de mettre en évidence deux types d'environnement de l'uranium: l'environnement pseudooctaédrique constitué des 5 atomes de fluor et de l'oxygène dans $CsUOF_5$ et dodécaédrique pour les autres complexes (M = NH_4, K, Rb). Dans ce dernier cas les dodécaèdres pontés par des fluors forment des chaines infinies.

L'ion UOF_5^- a été caractérisé à l'état solide par spectroscopie vibrationnelle. L'indexation des spectres faite dans l'hypothèse d'une symétrie C_{4v} a été confirmée par un calcul de constantes de force. Selon ces données et contrairement aux valeurs connues pour d'autres oxypentafluoroanions, le fluor axial est moins ionique que les fluors équatoriaux.

PHILIPPE JOUBERT, ROLAND BOUGON, and BERNARD GAUDREAU. Can. J. Chem. **56**, 1874 (1978).

The oxypentafluorouranates(VI) $MUOF_5$, where M = NH_4, K, Rb, Cs, have been synthetized from reaction of UOF_4 with the ammonium or corresponding alkali metal fluoride in liquid SO_2. According to X-ray diffraction, Raman and infrared spectroscopy, and from an isomorphism with the corresponding hexafluorouranates(V) MUF_6, two different environments around the uranium atom are observed. In $CsUOF_5$ the five fluorine atoms and the oxygen around the uranium result in a pseudo-octahedral surrounding whereas for the other complexes (M = NH_4, K, Rb) each uranium is surrounded by eight light atoms forming a dodecahedron. In this structure the dodecahedra are linked together by fluorine atoms to form infinite chains. The UOF_5^- ion has been characterized by vibrational spectroscopy in the solid state. The proposed assignment, which was made with the assumption of a C_{4v} symmetry of the UOF_5^- ion, was confirmed by a force constant calculation. From these data and contrary to the values reported for comparable oxypentafluoroanions, the axial fluorine is found to be less ionic than the equatorial ones.

Introduction

L'étude des oxypentafluorouranates(VI) $MUOF_5$ (M = NO, NH_4, K) que nous avions abordée précédemment (1, 2) a été approfondie avec les composés où M désigne NH_4, K, Rb, Cs.

Partie expérimentale

Réactions

Les mélanges et les broyages des produits solides sont effectués sous atmosphère d'azote sec. Les transferts des produits volatils s'effectuent à l'aide d'une rampe en monel équipée de vannes F.W. Les réactions ont lieu dans des pots en KelF (polymère de monochlorotrifluoréthylène) munis de vannes d'isolement également en KelF.

Produits de départ: préparations

$UOF_4\alpha$ est obtenu par hydrolyse ménagée d'UF_6 (Comurhex) en milieu fluorhydrique (3). KF, RbF (Merck) et CsF (British Drug House) sont déshydratés à 300°C sous vide. NH_4F est obtenu par synthèse à partir de HF (Comurhex), bidistillé sous fluor (Comurhex) et d'ammoniac (Air Liquide) bidistillé sur P_4O_{10}. L'anhydride sulfureux (Matheson) est déshydraté par bidistillation sur P_4O_{10}. SO_2 liquide est condensé sur un mélange équimolaire de $UOF_4\alpha$ et de MF dans un réacteur refroidi à −196°C. Lors du retour à la température ambiante le réacteur est agité, puis SO_2 est évacué par vaporisation et pompage. Dans une précédente publication (1) nous signalions l'utilisation de HF comme milieu réactionnel, mais la présence fréquente d'impureté HMF_2 nous a fait préférer SO_2 liquide. En effet les fluorosulfinates sont thermodynamiquement moins stables que les hydrogénofluorures correspondants (4, 5).

Les résultats des analyses chimiques des produits ainsi obtenus sont reproduits dans le tableau 1. Ils indiquent qu'on a bien formé les composés 1/1 correspondant au mélange initial, et qu'il n'y a pas eu de départ de composé volatil (O_2, UF_6).

Les pentafluorouranates préparés se présentent sous la forme de poudres jaune à jaune-orangé. Ces poudres sont très hygroscopiques et donnent par hydrolyse des composés d'uranyle.

[1]Auteur à qui toute correspondance doit être adressée.

Can. J. Chem. Downloaded from www.nrcresearchpress.com by 210.87.254.42 on 09/05/12
For personal use only.

TABLEAU 1. Résultats des analyses chimiques

	U		M		F		O	
	Exp.	Th.	Exp.	Th.	Exp.	Th.	Dif.	Th.
NH_4UOF_5	65.2	64.85	4.8	4.90	24.0	25.89	5.9	4.36
$KUOF_5$	61.5	61.32	10.0	10.07	23.2	24.48	5.2	4.13
$RbUOF_5$	54.7	54.78	19.2	19.68	21.5	21.86	4.6	3.68
$CsUOF_5$	49.5	49.39	27.3	27.52	19.8	19.71	3.4	3.38

Mesures physiques

Diffractions des rayons-X

Le diagramme Debye–Scherrer des poudres contenues dans des capillaires de Lindemann est réalisé en utilisant la raie Kα du cuivre. Une chambre a été modifiée afin d'enregistrer les spectres entre 77 et 300 K.

Spectres infra-rouges

La poudre est maintenue entre deux fenêtres de AgBr ou de AgCl. Les spectres sont réalisés avec les spectrophotomètres Perkin-Elmer 457 et 225 et Beckman IR9. Un dispositif mis au point au laboratoire permet d'enregistrer les spectres à 90 K.

Spectres Raman

Les échantillons sont contenus dans des capillaires scellés en Pyrex de 2 mm de diamètre. Les spectres sont enregistrés à l'aide d'un spectrophotomètre Coderg T800 équipé d'un laser Spectra-Physics 165-02 à argon–krypton ionisé. La raie utilisée est à 647.1 nm. Un cryostat Coderg à température variable (77–300 K) permet d'enregistrer les spectres Raman à basse température.

Résultats et discussion

Cristallographie

L'existence de grandes analogies entre les spectres de diffraction des rayons-X (RX) des complexes de l'U(V) de formule MUF_6 (M = NH_4, K, Rb, Cs) (6, 7) et les $MUOF_5$ correspondants nous a permis d'indexer ces derniers par isotypie (tableau 2), et de mettre en évidence deux types d'oxypentafluorouranates: orthorhombique si M = NH_4, K, Rb, et rhomboédrique pour $CsUOF_5$. Aucune transformation allotropique n'a pu être observée pour les deux types ($RbUOF_5$ et $CsUOF_5$) entre 300 et 77 K.

$MUOF_5$: M = NH_4, K, Rb

Ces phases sont isotypes des MUF_6 correspondants (6, 7), donc de $RbPaF_6$ (8). La structure de $RbPaF_6$ comprend des piles de dodécaèdres liés par des arêtes le long de l'axe *a*. La formule structurale s'écrit:

$$[Rb(PaF_{4/2}{}^{**}F_4{}^{*})]$$

où *F sont les fluor terminaux appartenant à la même sphère de coordination Pa—F* = 2.09 Å et **F les fluors pontés appartenant à deux sphères de coordination adjacentes le long de l'axe *a* (Pa—F** = 2.34 Å).

En l'absence de monocristal nous ne pouvons déterminer le groupe d'espace dans lequel les composés étudiés cristallisent. A ce stade un désordre oxygène–fluor peut être envisagé sur tous les sites anioniques.

$CsUOF_5$

Ce composé présente un diagramme RX voisin de celui de $CsUF_6$ (6) dont la maille cristalline est rhomboédrique de groupe spatial $R\bar{3}$ (9). Elle se décrit comme un empilement CsCl d'ions Cs^+ et UF_6^-. Par analogie, $CsUOF_5$ serait donc constitué d'ions Cs^+ et UOF_5^-, les 5 atomes de fluor et celui d'oxygène étant distribués statistiquement sur les 6 sites équivalents de groupe $R\bar{3}$.

Spectroscopie vibrationnelle

La différence structurale mise en évidence par RX apparaît aussi dans les spectres vibrationnels (tableau 3) les figs 1 et 2 représentent les spectres ir et Raman obtenus pour $RbUOF_5$ et $CsUOF_5$. Les spectres vibrationnels des sels de potassium et d'ammonium présentent le même aspect que ceux de rubidium exepté pour les vibrations du cation NH_4^+. Par contre $CsUOF_5$ se distingue des autres complexes et les différences les plus sensibles apparaissent pour les vibrations attribuables à l'extension des liaisons U—O et U—F terminale. Un abaissement régulier de ces fréquences est prévisible lorsque l'on passe du sel de potassium à celui du césium comme pour $M_3U^{VI}O_2F_5$ (10), $MU^{VI}F_7$, $M_2U^{VI}F_8$ (11). Cet abaissement se manifeste bien lors du passage du potassium au rubidium mais la fréquence de vibration U—O du sel de césium est supérieure de 10 cm^{-1} à celle de l'oxypentafluorouranate de rubidium. Cette anomalie s'explique par la différence d'environnement de l'uranium mise en évidence par l'étude cristallographique.

Pour le sel d'ammonium on constate une augmentation de la fréquence de vibration U—O. Ce phénomène déjà mis en évidence pour $(NH_4)_3UO_2F_5$ (10) s'interprète par la formation préférentielle de liaison hydrogène avec les atomes de fluor avec en corollaire un renforcement de la liaison U—O.

Les vibrations situées dans le domaine 800–850 cm^{-1} sont attribuées à l'extension de la liaison uranium–oxygène (11), et celles situées dans le domaine 500–600 cm^{-1} correspondent aux vibrations

Can. J. Chem. Downloaded from www.nrcresearchpress.com by 210.87.254.42 on 09/05/12
For personal use only.

Can. J. Chem. Downloaded from www.nrcresearchpress.com by 210.87.254.42 on 09/05/12
For personal use only.

TABLEAU 2. Spectres de diffraction X des complexes $MUOF_5$ (M = NH_4, K, Rb, Cs)

NH_4UOF_5				$KUOF_5$			
	dÅ				dÅ		
hkl	Calc.	Obs.	*I*	*hkl*	Calc.	Obs.	*I*
020	5.80	5.77	100	020	5.64	5.60	60
001	5.77			001	5.55	5.45	70
021	4.08	4.08	45	021	3.958	3.94	95
200	4.05	4.004	20	201	3.253	3.23	100
220	3.317	3.311	35	040	2.821	2.812	50
201	3.311			221	2.818		
040	2.899	2.905	10	041	2.515	2.513	30
221	2.876	2.877	30	202	2.284	2.286	< 5
041	2.591	2.588	20	241	2.131	2.127	60
240	2.356	2.362	10	222	2.117	2.114	60
202	2.347			331	2.029	2.031	20
241	2.181	2.184	40	151	2.023		
222	2.177			400	2.006	2.002	20
042	2.045	2.047	15	042	1.979	1.979	< 5
400	2.022	2.024	10	420	1.890	1.890	40
420	1.909	1.909	20	401	1.887		
401	1.908			421	1.790	1.790	40
421	1.813	1.813	25	113	1.781	1.785	40
152	1.764	1.763	10	061	1.781		
332	1.755	1.752	< 5	023	1.759	1.753	< 5
203	1.737	1.738	5	332	1.715	1.710	10
133	1.684	1.684	5	152	1.711		
351	1.682			203	1.681	1.679	10
223	1.664	1.663	10	440	1.635	1.634	30
440	1.659						
Orthorhombique				Orthorhombique			
$a = 8.08 \pm 0.01$ Å				$a = 8.02 \pm 0.01$ Å			
$b = 11.59 \pm 0.02$ Å				$b = 11.28 \pm 0.02$ Å			
$c = 5.77 \pm 0.02$ Å				$c = 5.55 \pm 0.01$ Å			
$RbUOF_5$				$CsUOF_5$			
	dÅ				dÅ		
hkl	Calc.	Obs.	*I*	*hkl*	Calc.	Obs.	*I*
020	5.87	5.82	50	100	5.30	5.30	< 5
001	5.77			$10\bar{1}$	4.00	3.97	100
021	4.11	4.12	100	110	3.591	3.57	70
220	3.324	3.324	80	$11\bar{1}$	3.200	3.184	< 1
040	2.933	2.929	20	200	2.672	2.666	30
002	2.883	2.880	20	$11\bar{2}$	2.310	2.299	25
221	2.879			210	2.294		
102	2.715	2.724	< 1	$21\bar{1}$	2.222	2.214	70
310	2.622	2.621	< 5	211	2.009	2.000	25
022	2.588	2.590	< 5	$21\bar{2}$	1.874	1.871	< 5
240	2.372	2.378	5	220	1.795	1.791	15
202	2.346	2.345	5	$30\bar{1}$	1.747	1.740	20
				310	1.638	1.637	30
241	2.194	2.189	40	$22\bar{2}$	1.601	1.597	10
222	2.178	2.183	40	$21\bar{3}$	1.512	1.509	30
042	2.056	2.057	20	311	1.511		
400	2.017	2.020	10	$31\bar{2}$	1.486	1.485	15
				$32\bar{1}$	1.418	1.417	10
420	1.908	1.907	10	400	1.336	1.334	< 5
061	1.852	1.855	10	$30\bar{3}$	1.333		

TABLEAU 2 (*Continu et suite*)

$RbUOF_5$				$CsUOF_5$			
	dÅ				dÅ		
hkl	Calc.	Obs.	*I*	*hkl*	Calc.	Obs.	*I*
023	1.827	1.825	10	321	1.321	1.319	<5
421	1.812	1.812	5	$4\bar{1}\bar{1}$	1.316		
260	1.759	1.761	10	$41\bar{1}$	1.267	1.266	<1
203	1.735	1.734	10	$40\bar{2}$	1.250	1.249	<1
261	1.683	1.682	5	330	1.197	1.195	<2
223	1.664	1.663	10	411	1.197		
440	1.662						

Orthorhombique	Rhomboédrique
$a = 8.07 \pm 0.01$ Å	$a = 5.40 \pm 0.01$ Å
$b = 11.73 \pm 0.02$ Å	$\alpha = 95°50 \pm 0.10$
$c = 5.77 \pm 0.01$ Å	

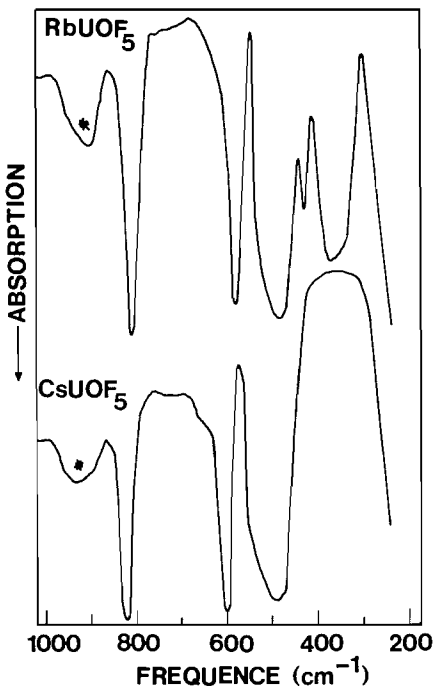

FIG. 1. Spectre infra-rouge de $RbUOF_5$ et $CsUOF_5$ solides. *Uranyle vraisemblablement formé au cours du pastillage.

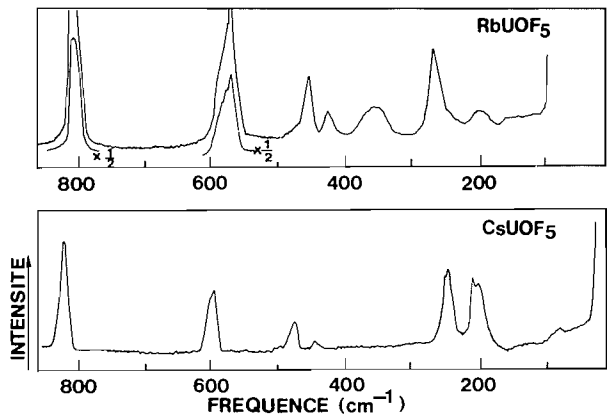

FIG. 2. Spectre Raman de $RbUOF_5$ et $CsUOF_5$ solides.

des fluors terminaux (11, 12). Les différentes études faites sur $UOF_4\alpha$ (11) et sur $UF_5\alpha$ et β (13) ont montré que les fréquences imputables aux vibrations des fluors pontés sont situées aux environs de 380 cm^{-1} ($UOF_4\alpha$ 375 cm^{-1}, $UF_5\alpha$ 388 cm^{-1}, $UF_5\beta$ 390 cm^{-1}).

Pour les phases $MUOF_5$ autres que $CsUOF_5$ il existe plusieurs vibrations dans la zone des 380 cm^{-1} qu'on peut raisonablement attribuer à des fluors pontés. Par contre les oxygènes ne sont certainement pas pontés, en effet la vibration située à 800–830 cm^{-1} correspond à l'extension d'une liaison U—O terminale (11) et l'existence de ponts U—O—U entraînerait la présence d'une bande ir large et intense entre 400 et 600 cm^{-1} (14–16) qui n'est pas observée dans les spectres $MUOF_5$. Les bandes ir vues dans cette région sont selon toute vraisemblance uniquement attribuables aux liaisons U—F. Nous concluons donc que seuls des ponts fluors existent dans les phases $MUOF_5$ pour M = NH_4, K, Rb, et celles-ci doivent s'écrire [$M(UF_{4/2}{**}O, 3F*)$], les astérisques ayant les mêmes définitions que précédemment.

Dans le cas de $CsUOF_5$ il n'y a pas de vibration aux environs de 380 cm^{-1}, donc ni les fluors ni les oxygènes (voir discussion précédente) ne sont pontés. L'existence de l'ion UOF_5^- dans $CsUOF_5$ inférée par les résultats de diffraction X se trouve donc confirmée.

Les spectres vibrationnels obtenus aux environs de 90 K sont identiques à ceux obtenus à température

Can. J. Chem. Downloaded from www.nrcresearchpress.com by 210.87.254.42 on 09/05/12
For personal use only.

Can. J. Chem. Downloaded from www.nrcresearchpress.com by 210.87.254.42 on 09/05/12
For personal use only.

TABLEAU 3. Spectres[a,b] vibrationnels des complexes $MUOF_5$ (M = K, Rb, NH_4, Cs)

$KUOF_5$		$RbUOF_5$		NH_4UOF_5		$CsUOF_5$		$[Ph_4P]UOF_5$[c]		UOF_5^- fréquences calculées	
ir[c]	Raman	ir[c]	Raman	ir[c]	Raman	ir[c]	Raman	ir	Raman		
										161	$\nu_6(b_1)$ pliage ant. sym. hors plan F′—U—F
							182 ep			182	$\nu_4(a_1)$ pliage sym. hors plan F′ U—F
			198(0.6)		195(0.3)		201(4.7)			201	$\nu_{11}(e)$ pliage ant. sym. F—U—F
							209(5.5)			209	$\nu_{10}(e)$ pliage F′—U—F
	270(3)		264(2.9)		260(1.9)		248(6.4)	238		248	$\nu_9(e)$ pliage F—U—O
		350 m			345(0.3)						
	365(2) l	370 m	365(2) l		370(0.8)					283	$\nu_7(b_2)$ pliage sym. dans le plan F—U—F
		390 l									
425 f	425(0.8)	425 f	424(1.1)		415(0.3)						
							445(0.4)			445	$\nu_5(b_1)$ élongation hors phase UF_4
480 F	460(1.5)	455 m	455(2.5)		465(0.9)						
	470 ep	485 l		480 F		481 l, F	480(2.3)	490		480	$\nu_8(e)$ élongation ant. sym. UF_4
510 ep		510				500 ep		505			
585 TF	580(4.4)	583 TF, l	570(5.5)	585 TF	585(5.9)	595 ep	593(5.5)			593	$\nu_3(a_1)$ élongation U—F′
	595 ep		585 ep		598 ep	603 TF	602 ep	595		602	$\nu_2(a_1)$ élongation sym. UF_4
800 ep	800 ep	795 ep	795 ep	825 TF	825(10)	820 TF	820(10)	815	817	820	$\nu_1(a_1)$ élongation U—O
815 TF	815(10)	809 TF	807(10)								
				1415 ep							ν_4 NH_4^+ attribution $\simeq C_{2v}$
				1435 F							
				1690 f							ν_2
				2865 ep, m							$2\nu_4$
				3115 massif							$\nu_2 + \nu_4$
				3220 large							ν_3

[a]Fréquences exprimées en cm^{-1}.
[b]Les valeurs entre parenthèses correspondent aux intensités relatives (non corrigées) abréviations TF très forte; F forte; m moyenne; f faible; l large; ep épaulement.
[c]Fréquences limitées pour l'infra-rouge à la zone d'absorption de AgBr (M = Rb, Cs) et AgCl (M = NH_4, K).
[d]Les conditions expérimentales n'ont pas permis l'obtention du speetre Raman dans ce domaine.
[e]D'après la réf. 27.

TABLEAU 4. Constantes de force calculées pour l'ion UOF_5^- et comparées à celles obtenues pour des espèces homologues (millidynes par Å)

Constante de force	UOF_5^-	IOF_5 (21)	UF_6 gaz (31)	UF_6^- (32)	UOF_5^- (27)	$UO_2F_5^{3-}$ (33)
f_S	5.90	6.99			5.87	5.892
f_R	3.68	4.60				
f_r	2.67	4.42	3.80	2.70		
f_{rr}	0.46	0.18	0.302	0.363		
f'_{rr}	0.47	0.00	−0.202	−0.258		
f_α/r^2	0.22	0.20	0.134	0.115		
f_β/r_R	0.18	0.55				
f_γ/r_S	0.29	0.44				
$f_{\beta\gamma}/r_{RS}^{1/2}$	0.07	0.06				

U—O=S=1.80 Å; U—F_{eq}=r=UF_{ax}=R=2.09 Å

α=F—U—F=90°

β=F—U—F′=90°

γ=F—U—O=90°

ambiante. Ceci implique une conservation de la symétrie des motifs optiques et corrobore les résultats cristallographiques obtenus aux mêmes températures.

Spectres vibrationnels de l'ion UOF_5^- et attribution

La complexité des spectres vibrationnels des phases $MUOF_5$ avec M = NH_4, K, Rb due à la faible symétrie du motif optique (vraisemblablement C_1) n'a pas permis d'approfondir l'analyse vibrationnelle de ces composés. En ce qui concerne $CsUOF_5$, l'indexation des spectres vibrationnels de l'ion UOF_5^- a été faite dans l'hypothèse d'une symétrie C_{4v} à partir de comparaisons avec les spectres des espèces MOF_5^{2-} et MOF_5^-, M = Ta (17), Te (18), Mo, W (2, 19), Re (20) et IOF_5 (21) et à partir des résultats de résonance magnétique nucléaires du ^{19}F (22). Cette dernière a montré que pour $CsUOF_5$ il existait à la température ambiante deux types de fluors dans la proportion 1/4. La raie la plus intense est située vers les hauts champs par rapport à l'autre soit respectivement −285 et −405 ppm par rapport à $CFCl_3$ pris comme référence externe. Dans l'hypothèse d'une symétrie C_{4v} et suivant des observations faites sur des composés semblables (23), le fluor axial serait donc moins ionique que les fluors équatoriaux, contrairement à ce qui a été observé en solution pour les ions $MoOF_5^-$ et WOF_5^- (2). Par contre un ordre identique à celui que nous trouvons pour UOF_5^- a déjà été observé dans le cas de IOF_5 (24).

Il faut noter que cette symétrie C_{4v} n'est qu'une approximation: en effet de par les structures cristallines trouvées pour K_2MoOF_5, H_2O (25) (monoclinique), $AMOF_5$ (A = K, Rb, Cs et M = Mo, W (26)) et $CsUOF_5$ (rhomboédrique) l'atome central est dans un site de symétrie plus basse que C_{4v}. Nous indexons cependant les spectres vibrationnels avec cette symétrie qui est par ailleurs justifiée en première approximation par les résultats de rmn (22) et par le nombre de raies Raman et ir observées,

Pour cette symétrie la théorie des groupes prévoit 11 modes normaux de vibrations soit $4A_1 + 2B_1 + B_2 + 4E$, tous les modes sont actifs en Raman, seuls les modes A_1 et E le sont en ir.

Les indexations ont été faites en considérant les formes et les intensités respectives des différentes bandes des spectres ir et Raman. Pour comparaison, on a fait figurer dans le tableau 3 les fréquences attribuées (27) à l'anion dans le composé $[Ph_4P]UOF_5$.

D'une façon générale, on a observé pour tous les composés une largeur importante des raies du spectre Raman de ces solides même aux environs de 90 K. Ainsi la raie du mode $\nu_1(a_1)$ a une largeur à mi-hauteur $\Delta\bar{\nu}$ de 13 cm^{-1} à 90 K. Cela peut probablement s'interpréter par l'existence d'un désordre cristallin entraînant des élargissements des niveaux vibrationnels (28).

Détermination des constantes de force

Les attributions précédentes ont été confirmées par une analyse en coordonnées normales. Les notations et le champ de force définis par Smith et Begun (21) dans le cas de l'étude de la molécule IOF_5 ont été utilisés. Les calculs de constantes de forces ont été effectués sur un ordinateur IBM 360/91 à l'aide de programmes mis au point par Rousson et coll. (29).

Les angles sont pris égaux à 90° et les distances interatomiques choisies sont déduites des calculs faits à partir des spectres de diffraction de neutrons soit U—O = S = 1.80 Å, U—F_{eq} = r = UF_{ax} = R = 2.09 Å (22). Le fait de prendre des liaisons

Can. J. Chem. Downloaded from www.nrcresearchpress.com by 210.87.254.42 on 09/05/12
For personal use only.

Can. J. Chem. Downloaded from www.nrcresearchpress.com by 210.87.254.42 on 09/05/12
For personal use only.

UF_{eq} et UF_{ax} égales entre elles peut se justifier par le faible écart correspondant de 0.04 Å trouvé (30) par diffraction électronique pour IOF_5.

Sur les 11 fréquences prévues par la théorie des groupes 9 ont été observées; ce qui ne permet pas de calculer tous les termes de la matrice **F**. Il a été admis que tous les termes d'interaction pliage-extension étaient nuls, de même que les interactions entre angles α opposés ($f_{\alpha\alpha}$) et adjacents β et γ ($f_{\beta\beta}$, $f_{\gamma\gamma}$) ainsi que les interactions entre liaisons à 90° sauf la constante f_{rr}'. De même que Smith, un terme non diagonal a été calculé afin d'obtenir des solutions physiquement acceptables et donnant un bon accord entre fréquences observées et calculées (21).

Le calcul de la distribution d'énergie potentielle a montré par ailleurs que les modes ν_9, ν_{10} et ν_{11} de symétrie E étaient fortement couplés.

Les valeurs des constantes de force calculées sont consignées au tableau 4 où figurent à titre de comparaison les valeurs des constantes de forces de UF_6 gaz (31) UF_6^- (32), UOF_5^-(f_{U-O}) (27), $UO_2F_5^{3-}$ (F_{U-O}) (33) et IOF_5 (21): la liaison U—O possède dans UOF_5^- un caractère certain de double liaison, puisque la constante de force correspondante est proche de celle connue pour l'ion $UO_2F_5^{3-}$ (33). Par ailleurs la liaison U—F_{ax} a un caractère de covalence inférieur ou proche de celui de UF_6 (31) tandis que les quatres liaisons du plan équatorial ont un caractère ionique proche de celui trouvé pour l'ion UF_6^- (32). On identifie bien, deux types de liaisons pour UOF_5^- avec une liaison axiale plus covalente que l'équatoriale. Ces résultats sont à rapprocher de ceux trouvés pour IOF_5 d'après les spectres vibrationnels (21) et la rmn du ^{19}F (24). L'ion UOF_5^- dans $CsUOF_5$ solide a une répartition du nuage électronique différente de celle trouvée pour les ions analogues tels que $TeOF_5^-$ (18), $MoOF_5^-$ et WOF_5^- (2, 19, 20), la charge formelle négative serait donc essentiellement répartie dans l'ion UOF_5^-, sur les quatre fluors du plan équatorial. Ces différences de répartition sont peut être attribuables aux effets des orbitales de l'uranium.

Conclusion

Par réaction dans SO_2 liquide entre UOF_4 et des bases de Lewis telles que NH_4F, KF, RbF et CsF, les pentafluorouranates ont été obtenus exempts de composés de composition différente. La connaissance de l'ensemble des spectres de diffraction X, infrarouge et Raman nous permet de dire que les phases $MUOF_5$ s'écrivent $M(UF_{4/2}(O, 3F))$ avec M = NH_4, K, Rb et Cs^+ UOF_5^-. Pour l'ion UOF_5^- les spectres vibrationnels et leur analyse en coordonnées normales qui sont en accord avec une symétrie C_{4v} montrent que le fluor axial possède un caractère plus covalent que les fluors équatoriaux.

1. P. Joubert et R. Bougon. C.R. Acad. Sci. Ser. C, **280**, 193 (1975).
2. R. Bougon, T. Buy-Huy et P. Charpin. Inorg. Chem. **14**, 1822 (1975).
3. P. W. Wilson. Chem. Commun. 1241 (1972).
4. T. C. Waddington. Non-aqueous solvent systems. Rédigé par T. C. Waddington. Academic Press, London, New York. 1965. p. 253.
5. A. V. Nicolaev, A. A. Opalowski, V. E. Fedorov et T. D. Fedotova. J. Therm. Anal. **6**, 461 (1974).
6. R. A. Penneman, G. D. Sturgeon et L. B. Asprey. Inorg. Chem. **3**, 126 (1964).
7. L. B. Asprey, F. H. Kruse, A. Rozenzweig et R. A. Penneman. Inorg. Chem. **5**, 659 (1966).
8. J. H. Burns, H. A. Levy et O. L. Keller. Acta Crystallogr. Sect. B, **24**, 1675 (1968).
9. A. Rozenzweig et D. T. Cromer. Acta Crystallogr. **23**, 868 (1967).
10. Nguyen Quy Dao et H. Knidiri. Spectrochim. Acta, **32A**, 1113 (1976).
11. R. T. Paine, R. R. Ryan et L. R. Asprey. Inorg. Chem. **14**, 1113 (1975).
12. R. Bougon, P. Charpin, J. P. Desmoulin et J. G. Malm. Inorg. Chem. **15**, 2532 (1976).
13. E. Jacob. Z. Anorg. Allg. Chem. **400**, A5 (1973).
14. H. R. Hoekstra. J. Inorg. Nucl. Chem. **27**, 801 (1965).
15. P. Caillet et R. Brochu. Bull. Soc. Chim. 41 (1970).
16. G. Fonteneau. Thèse, Rennes. 1975.
17. G. Pausewang, R. Schmitt et K. Dehnicke. Z. Anorg. Allg. Chem. **408**, 1 (1974).
18. E. Mayer et S. Sladky. Inorg. Chem. **14**, 589 (1975).
19. A. Beuter et W. Sawodny. Z. Anorg. Allg. Chem. **427**, 37 (1976).
20. W. Kuhlmann. Thèse, Ulm. 1976.
21. D. F. Smith et G. M. Begun. J. Chem. Phys. **43**, 2001 (1965).
22. P. Joubert, J. M. Weulersse et R. Bougon. Résultats non publiés.
23. R. Bougon, R. M. Costes, J. P. Desmoulin, J. Michel et J. L. Person. J. Inorg. Nucl. Chem. Suppl. 99 (1975).
24. N. Bartlett, S. Beaton, L. W. Reeves et E. J. Wells. Can. J. Chem. **42**, 2531 (1964).
25. D. Granjean et P. R. Weiss. Bull. Soc. Chim. 3054 (1967).
26. G. B. Hargreaves et R. D. Peacock. J. Chem. Soc. 2170 (1958); 4390 (1958).
27. K. W. Bagnall, J. G. H. la Preez, B. J. Gellatly et J. H. Holloway. J. Chem. Soc. Dalton Trans. 1963 (1975).
28. G. Turrel. Infrared and Raman spectra of crystals. Academic Press, London and New York. 1972. p. 219.
29. R. Rousson, G. Tantot et M. Tournarie. J. Mol. Spectrosc. **59**, 1 (1976).
30. L. S. Bartell, F. B. Clippard et E. J. Jacob. Inorg. Chem. **15**, 3009 (1976).
31. G. Nagarajan et T. S. Adams. Z. Phys. Chem. Leipzig, **255**, 869 (1974).
32. E. Soulie. Thèse Doctorat, Paris. 1977.
33. M. Knidiri. Thèse Doctorat, Paris. 1974.

Ion association in solutions of HCl in DMSO–water mixtures: ultrasonic absorption studies

PEETER KRUUS AND M. JACQUELINE MCGUIRE

Department of Chemistry, Carleton University, Ottawa, Ont., Canada K1S 5B6

Received January 5, 1978

PEETER KRUUS and M. JACQUELINE MCGUIRE. Can. J. Chem. **56**, 1881 (1978).

Ultrasonic absorption measurements are reported for the system HCl – dimethylsulfoxide (DMSO) – water in the frequency range 3.5 to 140 MHz. For all solutions studied, the excess absorption due to the presence of HCl can be fitted well with a single relaxation equation. For 0.10 mol ℓ^{-1} solutions of HCl in DMSO–water mixtures, no further relaxations at higher frequencies are likely. Reasonable results are obtained when the ultrasonic results are analyzed assuming the process responsible for the excess absorption to be the dissociation–association equilibrium of HCl, and using equilibrium constants determined from conductivity (C. Cooke *et al.* Electrochim. Acta, **20**, 591 (1975)). The value of $|\Delta V_{eff}|$ is 20–25 cm^3 mol^{-1} and k_{ass} is approximately 3×10^9 ℓ mol^{-1} s^{-1}, as compared to a value of 10×10^9 ℓ mol^{-1} s^{-1} calculated from limiting conductivities assuming diffusion-controlled rate theory.

PEETER KRUUS et M. JACQUELINE MCGUIRE. Can. J. Chem. **56**, 1881 (1978).

On rapporte des mesures d'absorption d'ultrasons par le système HCl – diméthylsulfoxyde (DMSO) – eau à des fréquences allant de 3.5 à 140 MHz. Pour toutes les solutions étudiées, l'absorption en excès due à la présence de HCl peut être bien exprimée par une seule équation de relaxation. Pour des solutions de 0.10 mol ℓ^{-1} de HCl dans des mélanges de DMSO – H_2O, il ne semble pas y avoir d'autres relaxations à des fréquences plus élevées. On obtient des résultats raisonnables lorsqu'on analyse les résultats d'ultrasons en faisant l'hypothèse que le processus responsable pour l'absorption en excès est dû à l'équilibre association/dissociation de HCl et en faisant appel aux constantes d'équilibre déterminées par la conductivité (C. Cooke *et al.* Electrochim. Acta, **20**, 591 (1975)). La valeur de $|\Delta V_{eff}|$ est 20–25 cm^3 mol^{-1} et k_{ass} est environ 3×10^9 ℓ mol^{-1} s^{-1}; on doit comparer cette valeur à celle de 10×10^9 ℓ mol^{-1} s^{-1}, calculée à partir des conductivités limites en faisant appel à la théorie de la vitesse contrôlée par la diffusion.

[Traduit par le journal]

Introduction

The detailed mechanism of ion pairing has been elucidated to a considerable extent through ultrasonic absorption studies (1). In nearly every case, ultrasonic absorption results suggest that ion pairing occurs through a process involving at least two steps. This is the case for multivalent electrolytes in water (2) and for univalent electrolytes in organic solvents (3, 4).

Results for aqueous solutions of medium strong acids can be explained by a single-step mechanism (5), but the acid dissociation constant obtained in such an analysis is somewhat different from that obtained by other methods, e.g. conductivity. Data on solutions of HCl in dimethylformamide have also been analysed by a single-relaxation mechanism (6).

An ultrasonic study of HCl in dimethylsulfoxide (DMSO) – water solutions was undertaken in order to see if the ion pairing in this system occurs by a single-step mechanism. A thorough conductivity study of this system is available (7), giving the association constants, the limiting conductivities, and the dielectric constants. It is thus also possible to determine whether it is valid to describe the ultrasonic results in terms of simple basic models such as diffusion controlled kinetics.

DMSO is of considerable medical and industrial importance (8), especially in the form of a water–DMSO solvent system. Because of the strong hygroscopic nature of DMSO, it seldom can be used in a completely non-aqueous state (3, 7).

Experimental

Stock solutions of HCl in DMSO were made up by bubbling HCl gas diluted with N_2 through liquid DMSO in a flask swirled in an icebath. The heat of solution is sufficient so that without cooling and dilution of the gas, decomposition of DMSO resulted, as evidenced by the smell of mercaptans. The concentrations of the stock solutions were measured through titration with standardized sodium hydroxide of samples diluted considerably with water; these were at most 0.6 mol ℓ^{-1}. Aliquots of these standard solutions were diluted with DMSO and/or water to make up the solutions used in the study. It was found to be most convenient to express the composition in terms of mole fraction X of DMSO and molarity c of HCl.

Solutions with $X < 0.92$ and $c < 0.3$ were also made up by mixing concentrated aqueous hydrochloric acid with DMSO. The results for solutions made up this way were consistent with results for solutions made up from the stock.

The chemicals used were: Matheson anhydrous HCl, Baker Analyzed Reagent or Fisher Certified DMSO, Linde N_2, and Baker Analyzed Reagent hydrochloric acid. In making up some samples of stock solution, the gas was bubbled through two DMSO samples in series, with only the second sample used. This was to remove any DMSO-soluble impurities in the

Can. J. Chem. Downloaded from www.nrcresearchpress.com by 210.87.254.42 on 09/05/12
For personal use only.

Can. J. Chem. Downloaded from www.nrcresearchpress.com by 210.87.254.42 on 09/05/12
For personal use only.

TABLE 1. Summary of single relaxation curve analysis of ultrasonic absorption data

X_{DMSO}‡	$(c_{HCl})_0$ (mol ℓ^{-1})	Number of points	B*	A (10^{-15} m^{-1} s^2)	σ	ν_r (MHz)	v† (10^5 m s^{-1})	η/ρ† (cstoke)
1.00	0.30	4	51	281	3	32		
1.00	0.30	5	51	275	8	32	1.495†	2.03†
1.00§	0.30	8	51*	383	14	29		
0.977	0.30	4	53	363	13	26	1.500	2.08
0.974§	0.30	4	53	432	10	25	1.502†	2.10†
0.955	0.30	5	56	394	23	27	1.503	2.12
0.947	0.30	5	56	406	13	29	1.504	2.13
0.940	0.30	5	57	416	8	25	1.505	2.15
0.933	0.30	10	58	420	20	26	1.506	2.19
0.926	0.30	9	61*	441	11	28	1.508	2.21
0.919	0.30	10	61	422	15	26	1.510†	2.25†
0.915	0.30	4	61	475	6	29	1.510	2.26
0.912	0.30	5	61	402	26	29	1.516	2.26
0.905	0.30	5	61	428	20	26	1.525	2.28
0.879	0.30	5	62	398	29	29	1.530	2.35
0.853	0.30	4	62	397	10	35	1.543†	2.37†
0.800	0.30	9	63*	306	6	40	1.558	2.58
0.799	0.30	5	62	304	11	40	1.558	2.58
0.791	0.30	4	62	243	15	46	1.560†	2.58†
0.745	0.30	5	62	226	12	45	1.575	2.69
0.651	0.30	4	62	142	4	50	1.585†	2.93†
0.504	0.30	4	56	40	—	>50	1.640	3.20
0.477	0.30	4	56	34	—	>50	1.643	3.58
0.396	0.30	4	54	8	—	>50	1.643	4.00
1.00	0.10	4	33	200	3	25	1.490†	1.88†
1.00	0.10	9	35*	216	4	23		
0.971	0.10	4	33	248	2	27	1.510†	1.97†
0.926	0.10	8	38*	219	5	28	1.53	2.03
0.900	0.10	4	35	211	2	31	1.536†	2.08†
0.807	0.10	4	36	143	4	38	1.557†	2.26†
0.800	0.10	9	35*	136	3	41	1.560	2.30
0.680	0.10	4	36	68	1	54	1.577†	2.55†

*B fixed at values shown except where for * values which were obtained by a 3-parameter fit.
†Only these values were determined experimentally; other values were obtained by interpolation.
‡Braces denote data combined for analysis in Table 3.
§Final results rejected as solutions probably picked up water during transfer from high to medium frequency apparatus.

gas. Results obtained using these solutions were consistent with results from solutions where this precaution was not taken.

Dry-box conditions were not used, but it was attempted to minimize the time of contact of the solutions with the atmosphere. Other steps were taken to minimize water content: the gas mixture was passed through a drying agent before bubbling through DMSO; the DMSO used was taken from freshly opened bottles or decanted from bottles where the DMSO had been standing over molecular sieves. Even though the water content in the Baker DMSO is quoted as $<0.05\%$, previous work (3) suggests that the initial "nonaqueous" DMSO solutions may have had a water content of up to 0.2% by volume, corresponding to $X \simeq 0.99$ or a concentration of water in the order of 0.1 mol ℓ^{-1}. Exposure to the atmosphere would increase the water content even more, as at 20°C, DMSO has an equilibrium moisture content of 10% water (9).

Ultrasonic absorption was measured for all the solutions in the frequency range 10.6 to 52 MHz with the medium frequency apparatus described in ref. 10. Velocities were also measured on this apparatus by the method described in ref. 10, and viscosities with a Cannon–Fenske viscometer.

Absorption at 20, 60, 100, and 140 MHz was measured with apparatus B as described in ref. 10. The signal from the receiving transducer was fed directly into an HP10514 mixer, where it was mixed with a CW signal from an HP VHF signal generator to give a difference frequency of 20 MHz. This signal was then passed through a preamplifier and displayed on an oscilloscope. The absorption was measured by noting the size of the signal on the oscilloscope as the distance travelled by the ultrasound was varied. Any non-linearities in the amplification were corrected for by calibrating the apparatus with liquids of known absorption (carbon tetrachloride, toluene, DMSO, and water).

Analysis of Results by Single Relaxation Equations

Table 1 summarizes the ultrasonic absorption, velocity, and viscosity results obtained.

The absorption data (α/ν^2 as a function of ν) were analyzed in terms of a single relaxation equation, [1]:

$$[1] \qquad \frac{\alpha}{\nu^2} = \frac{A}{1 + (\nu/\nu_r)^2} + B$$

For the cases where high frequency data were available, the data were fitted by eq. [1] with A, B, and ν_r all being adjusted to give a minimum in the standard deviation σ. Examples of two such fits are given in Fig. 1.

Can. J. Chem. Downloaded from www.nrcresearchpress.com by 210.87.254.42 on 09/05/12
For personal use only.

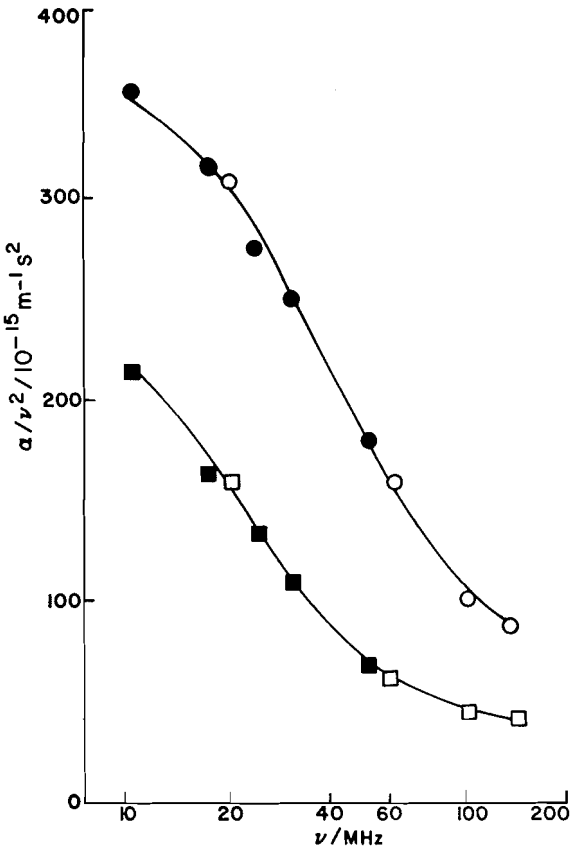

FIG. 1. Single-relaxation curve fitting (A, B, ν_r variable) of experimental data: ●, ○, $c = 0.30$, $X = 0.80$; ■, □, $c = 0.10$, $X = 1.00$. The filled points represent data taken with the medium-frequency apparatus, the empty with the high-frequency.

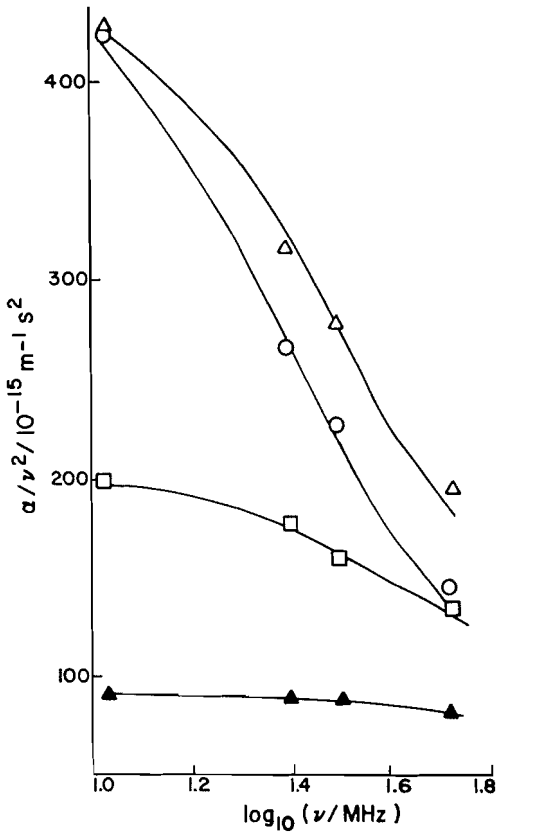

FIG. 2. Single-relaxation curve fitting (A, ν_r variable, B fixed) of experimental data, $c = 0.30$; ○, $X = 0.97$; △, $X = 0.85$; □, $X = 0.65$; ▽, $X = 0.48$.

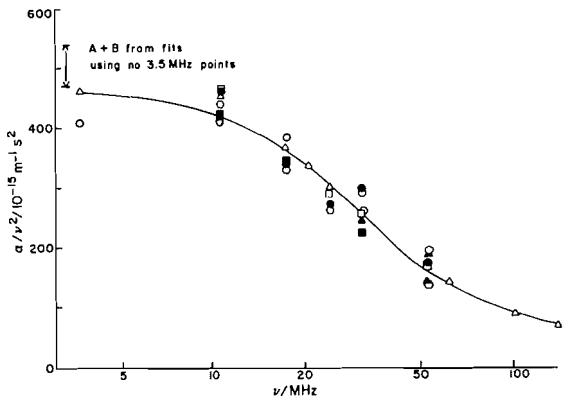

FIG. 3. Single-relaxation curve fitting of data from 7 different runs, $c = 0.3$, $X = 0.92 \pm 0.01$.

In order to obtain a complete frequency range from 10.6 to 140 MHz, two apparatuses had to be used. This involved transfer of the solution and readjustment of the electronic equipment. The majority of the solutions were therefore investigated only in the 10.6 to 52 MHz range. These data were fitted also by eq. [1], but only A and ν_r were adjusted. The value of B was chosen by interpolation from B-values obtained from 3-parameter fits. Figure 2 shows examples of fits where only A and ν_r were varied.

Figure 2 also shows how at lower X values, the relaxation frequency ν_r becomes so great that a meaningful fit of the data in the 10.6 to 52 MHz range by [1] becomes meaningless. In such cases, ν_r cannot be obtained, but the low frequency data can be used to obtain $A + B$ directly ($\nu \ll \nu_r$).

It was in principle possible to make absorption measurements also at 3.5 MHz with the apparatus used. However, the precision of these results was very poor. Even when α/ν^2 is relatively high (of the order of $400 \times 10^{-15}\ m^{-1}\ s^2$), at 3.5 MHz the value of α is so small ($\simeq 4\ m^{-1}$) that meaningful absorption measurements are difficult. Thus the 3.5 MHz values are reported here only for the solution where absorption was highest (Fig. 3). The low α values at 3.5 MHz and the flatness of the α/ν^2 vs. ν graphs at low X values are signs that there are no additional relaxation processes present in these systems with a ν_r in the low MHz range.

Can. J. Chem. Downloaded from www.nrcresearchpress.com by 210.87.254.42 on 09/05/12
For personal use only.

Table 1 contains data on the ultrasonic velocity v and the kinematic viscosity η/ρ for some solutions. The data for other solutions was obtained by interpolation. Data for the pure solvent system DMSO–water is not listed as it was found to be in good agreement (within 1%) of those in ref. 7. These data are needed to calculate the classical absorption α_c, due primarily to viscosity (1):

$$[2] \qquad \frac{\alpha_c}{\nu^2} = \frac{8}{3}\pi^2 \frac{\eta}{\rho} \frac{1}{v^3}$$

Reference 3 contains the (α_c/ν^2) data for the solvent system.

The B values obtained for solutions with $c = 0.10$ are within 1 or 2 units of the values obtained by correcting the absorption of the pure solvent system with changes in (α_c/ν^2) due to changes in v and η/ρ, i.e., setting

$$[3] \quad (B)_{\text{solution}} = (B)_{\text{solvent}} + \left(\frac{\alpha_c}{\nu^2}\right)_{\text{solution}} - \left(\frac{\alpha_c}{\nu^2}\right)_{\text{solvent}}$$

This suggests that in these solutions there are no additional relaxation processes due to the presence of the HCl at higher frequencies; unless, of course, there is a process which has $\Delta V_{eff} = 0$ (see eq. [7]).

The $c = 0.30$ solutions have B values slightly in excess of those predicted from eq. [3], suggesting the presence of another process relaxing at higher frequencies. Such a process could conceivably be the formation of a complex ion HCl_2^-. The Cl^- ion is poorly solvated in DMSO (3, 11) and HCl_2^- has been noted (12). In addition, $AgCl_2^-$ forms readily in DMSO solutions (13). Since the relaxation strength of the process responsible for the high frequency absorption excess is small, further ultrasonic studies (i.e., by variation of c) would be quite imprecise.

Single-relaxation equations fit the experimental data quite well. The relative standard deviations for the $c = 0.10$ data are all below 3% when σ is taken relative to $A/2$. In the case of the $c = 0.30$ solutions, the highest value of $2\sigma/A$ is 15% with typical values more of the order of 5%. The variation of the A and ν_r values obtained by the analysis are presented in Fig. 4.

The validity of the curve-fitting techniques used was tested on a set of data at the experimental frequencies which describe a single-relaxation curve exactly. Table 2 shows that an error of 10% in the choice of B already introduces a relative error of 2.5%. For the type of data obtained in this experiment, the curve-fitting is seen from Table 2 to give more scatter in the ν_r values than in the A values. This may be one cause for the scatter in the ν_r vs. X data in Fig. 4.

An estimate of the variability in the A and ν_r values due to experimental uncertainty is also made in Table 2. The least accurate experimental data used regularly are the α/ν^2 for 10.6 MHz, which may have an uncertainty of 5 to 10%, depending on its absolute value. An error of 5% in the 10.6 MHz data would cause an error of 12% in A and 7% in ν_r, while one of 10% would cause an error of 23% in A and 15% in ν_r. Such uncertainties are consistent with the scatter in Fig. 4.

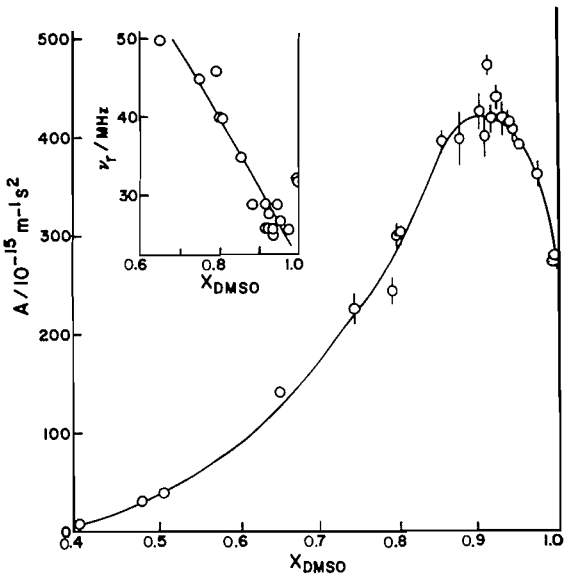

FIG. 4. A vs. X and ν_r vs. X for solutions 0.30 mol ℓ^{-1} in HCl.

Correlation of Ultrasonic and Conductivity Results

HCl is not fully dissociated in DMSO. However, when sufficient water is added, the dissociation becomes in effect complete. As the excess ultrasonic absorption disappears as $X < 0.4$, the process most likely to be responsible for the absorption is:

$$[4] \qquad H^+ + Cl^- \underset{k_{diss}}{\overset{k_{ass}}{\rightleftharpoons}} HCl$$

The activity equilibrium constants K_a for process [4] in DMSO–water mixtures have been measured by conductivity (7). In the range $0.74 < X \leq 1.0$, the measured values of K_a follow the Bjerrum equation quite well, with critical distances of $q = e^2/2\varepsilon kT$ of the order of 0.12 nm.

Analysis of the A and ν_r values from ultrasonics requires a knowledge of the concentration equilibrium constant $K_c = K_a y_\pm^2 / y_{HCl} = K_a y_\pm^2$ assuming $y_{HCl} = 1$. The activity coefficients are available for HCl in DMSO, but only up to 0.05 molal. The Debye–Hückel relation describes the $y_\pm$ well up to 0.01 molal (14). Here the $y_\pm$ was assumed to be

TABLE 2. Sensitivity of curve-fitting

Program used	Points used	A	B	ν_r	σ
FITAB	All	199.7	100.1	25.0	0.37
(A, B, ν_r all variable)	6 points $\nu \geq 24.6$	No convergence			
	6 points $\nu \leq 31.6$	201.1	98.6	25.2	0.48
	6 points $10.6 \leq \nu \leq 51.6$	200.0	99.6	25.1	0.49
FITA	All	199.8	100*	25.0	0.37
(A, ν_r variable;	All	206.4	90*	27.3	4.9
B fixed)	5 points $\nu > 31.6$	196.8	100*	25.3	0.26
	5 points $\nu < 24.6$	199.8	100*	25.0	0.50
	6 points $10.6 < \nu < 51.6$	199.8	100*	25.0	0.43
	6 points $10.6 < \nu < 51.6$	205.1	90*	27.2	2.1
	6 points $10.6 < \nu < 51.6$	195.0	110*	22.9	2.5
	5 points $10.6 < \nu < 51.6$ with 10.6 MHz point 5% high	223.7	100*	23.2	3.7
	5 points $10.6 < \nu < 51.6$ with 10.6 MHz point 10% high	246.2	100*	21.2	2.3

*Fixed values of B. Points used are at 10 experimental frequencies 3.5, 10.6, 17.6, 20.9, 24.6, 31.6, 51.6, 61.0, 101.0, 141.0 MHz for an exact single-relaxation equation with $A = 200$, $B = 100$, $\nu_r = 25$.

given by the Davies form (15):

$$[5]\quad \log_{10} y_{\pm} = \frac{-1.825 \times 10^6 \times (\varepsilon T)^{-3/2} \times \mu^{1/2}}{1 + (50.3 \times 10^8 \times (\varepsilon T)^{-1/2} \times 3.04 \times 10^{-8} \times \mu^{1/2})} + 0.1\mu$$

This assumes the distance of closest approach parameter to be 0.30 nm. The sensitivity of the results of the analysis to the form of the $y_{\pm}$ equation assumed has been investigated previously, although not for cases where concentrations are as high as 0.3 molar (5).

The K_c values can be obtained by an iteration in which K_c is initially assumed equal to K_a. Next the degree of dissociation α can be obtained, and hence the ionic strength $\mu = \alpha c$ for a 1:1 electrolyte. The $y_{\pm}$ is next calculated from [5] and a new value $K_c = y_{\pm}^2 K_a$ is obtained. This iteration is continued until K_c is constant to within 0.1%. Values of $y_{\pm}$, K_c, and α obtained this way are shown in Table 3 together with the K_a and ε values from ref. 7 used in the analysis. It is of interest to note that $y_{\pm}$ varies relatively little with the value of K_a due to counterbalancing effects in [5]. The μ used and the $y_{\pm}$ calculated here do not assume complete dissociation as some listings do. If incomplete dissociations are included in the $y_{\pm}$ value, then the $y_{\pm} = \alpha \times$ the $y_{\pm}$ calculated here.

The quantity A in Table 1 for a process such as that described by [4] is given by (5):

$$[6]\quad A = \frac{\pi(\Delta V_{eff})^2 \rho v}{RT} \left\{ \frac{(2-\alpha)}{\alpha(1-\alpha)c} + \frac{\partial \ln y_{\pm}}{\partial \alpha} \right\}^{-1} \cdot \frac{1}{\nu_r}$$

Here ΔV_{eff} is the effective volume change of [4],

$$[7]\quad \Delta V_{eff} = \Delta V^0 - \frac{\alpha \Delta H^0}{\rho C_p}$$

In [7] α refers to the thermal expansivity. Values of $|\Delta V_{eff}|$ can be calculated from [6] as all other quantities are available. The results are shown in Table 3. Neither the sign of ΔV_{eff} can be determined, nor can the relative contributions to it from ΔV^0 and ΔH^0 (eq. [7]).

The rate constant k_{ass} for the process in [4] can be obtained from values of ν_r through the relation (5):

$$[8]\quad \frac{1}{\tau} = 2\pi\nu_r = k_{diss} + k_{ass}(c_{H^+} + c_{Cl^-}) = k_{ass,\infty} \left\{ \frac{1}{K_a} + (\alpha c)^2 y_{\pm}^2 \left(\frac{2}{\alpha c} + 2\frac{\partial \ln y_{\pm}}{\partial \alpha} \right) \right\}$$

The $k_{ass,\infty}$ calculated in this way is the limiting value at infinite dilution, i.e., as $\mu \to 0$. The values obtained are listed in Table 3. No corrections to k_{ass} have been made due to change in ε with c (15).

The sensitivity of the $|\Delta V_{eff}|$ and k_{ass} values listed in Table 3 to variations is such that if one of ρ, v, or A is changed by 10%, then $|\Delta V_{eff}|$ is altered only by 5% while k_{ass} remains the same. A 10% change in K_a changes $|\Delta V_{eff}|$ by 1% and k_{ass} by 5%, while a 10% change in ν_r changes $|\Delta V_{eff}|$ by 5% and k_{ass} by 10%. Taking account of all possible errors, experimental as well as from analysis, the values of $|\Delta V_{eff}|$ and k_{ass} listed are probably correct to better than 20%. The largest uncertainty is probably the evaluation of activity coefficients, i.e., the use of eq. [5]. Values of $y_{\pm}$ (really $\alpha y_{\pm}$) can in principle be determined experimentally from cell emf values.

Table 3 also shows the results of application of simple diffusion control theory to estimate $k_{ass,\infty}$.

Can. J. Chem. Downloaded from www.nrcresearchpress.com by 210.87.254.42 on 09/05/12
For personal use only.

Can. J. Chem. Downloaded from www.nrcresearchpress.com by 210.87.254.42 on 09/05/12
For personal use only.

TABLE 3. Results of analysis of ultrasonic data

X_{DMSO}	$K_a^* = a_{HCl}/a_{\pm}^2$	ε^*	$y_{\pm}$ (mol ℓ^{-1})	$K_e = K_a/y_{\pm}^2$ (mol^{-1} ℓ)	$\alpha = c_{Cl^-}/(c_{HCl})_0$	$\lvert\Delta V_{eff}\rvert$ (cm^3 mol^{-1})	Λ_∞^* (Ω^{-1} cm^2 mol^{-1})	$k_{ass,\infty}$‡	k_{diff}‡
(*a*) $(c_{HCl})_0 = 0.30$ mol ℓ^{-1}									
†1.00	126	46.6	0.614	47	0.23	21	40.5	3.3	10.7
0.977	102	47.4	0.611	38	0.26	21	39.5	2.4	10.5
†0.95±0.01	80±4	48.2±0.3	0.607	30±2	0.28±0.01	22±1	38.5±0.3	2.3±0.3	9.7±0.1
†0.93±0.01	69±4	49.0±0.3	0.607	26±2	0.30±0.01	22±1	37.9±0.2	2.1±0.1	9.3±0.2
†0.91±0.01	61±3	49.4±0.2	0.607	22±1	0.32±0.01	22±2	37.3±0.2	2.0±0.2	9.0±0.1
0.879	48	50.3	0.604	17	0.35	20	36.7	1.9	8.7
0.853	40	51.0	0.603	15	0.38	22	35.6	2.1	8.5
†0.80±0.01	27.5±0.5	53.1±0.2	0.608	10±0.2	0.43±0.01	19±1	34.4±0.1	2.0±0.2	7.6
0.745	21	55.0	0.615	8	0.47	17	33.6	1.8	7.4
0.651	10	58.3	0.620	4	0.59	14	32.6	1.3	7.1
(*b*) $(c_{HCl})_0 = 0.10$ mol ℓ^{-1}									
†1.00	126	46.6	0.689	60	0.33	24	40.5	3.8±0.2	11.5
0.971	98	47.8	0.688	46	0.37	26	39.3	3.7	11.2
0.926	69	49.0	0.683	32	0.42	24	37.9	3.2	10.1
0.900	56	49.7	0.682	26	0.46	25	37.0	3.2	9.6
†0.80±0.01	28.5±1	52.9±0.2	0.683	13±1	0.56±0.01	22	34.5±0.1	2.8±0.1	8.8±0.2
0.680	12.5	57.3	0.695	6	0.70	19	32.7	2.6	7.8

*Interpolated from data in ref. 7.
†Average of 2 or 3 sets of data from Table 1.
‡In 10^9 ℓ mol^{-1} s^{-1}.

The diffusion controlled rate constants k_{diff} are calculated from the relation (5):

$$[9] \quad k_{diff} = \frac{4\pi(D_+ + D_-)}{1000} Lw(\exp[w/a] - 1)^{-1}$$

Here L is Avogadro's number, and $w = -e^2/\varepsilon kT$ for [+1], [−1] reactions. The sum of diffusion constants can be obtained from conductivity as $D = \Lambda_\infty RT/F^2$ for infinite dilution. A correction for an increased viscosity for $c > 0$ was made, but no correction for any effect of dissolved electrolyte on ε.

A reaction distance a of 0.72 nm was used in applying eq. [9]. This is the distance between a solvent separated ion pair, i.e., (+)DMSO(−). If a = 0.42 nm were used, then the values of k_{diff} would be 85% of those in Table 3, and for a = 0.12 nm, the Bjerrum distance from conductivity (7), 80%. A value 0.72 nm was chosen as it is unreasonable to use a continuum theory for distances less than molecular dimensions.

Discussion

In most ultrasonic studies of ion pairing, the results cannot be fitted by a single relaxation equation in a satisfactory manner. For HCl in DMSO–water, however, the data can be fitted very well by a single-relaxation equation.

The variation of A with X as shown in Fig. 4 shows the relaxation strength to peak at $X \simeq 0.92$. At this solvent composition, $K_a \simeq 65$, giving an optimal degree of dissociation for ultrasonic absorption (eq. [6]). For $X > 0.92$, equilibrium [4] is shifted too far towards products (associated ions), and for $X < 0.92$, too far towards reactants (free ions). In the case of alkali metal halides, the optimal degree of association is never reached, so that any addition of water to a solution of alkali halides in DMSO causes a decrease in ultrasonic absorption (3).

The variation of v_r with X is also shown in Fig. 4. There is definitely an increase in v_r as more water is present. However, the higher v_r values at $X = 1.0$ are not clearly outside the limits of experimental uncertainty. An anomaly might be expected where $c_{H_2O} \simeq c_{Cl^-}$ as Cl^- is poorly solvated by DMSO (11) and might therefore be expected to have strong preferential solvation by H_2O. For solutions 0.3 molar in HCl this condition ($c_{H_2O} = c_{Cl^-} \simeq 0.24 \times 0.3$) would occur already at $X_{DMSO} = 0.995$ (0.13% by volume H_2O) as [DMSO] is 14 mol ℓ^{-1}. Thus even in 'pure' DMSO the mole ratio of H_2O to Cl^- is probably appreciable. No anomalous behaviour of Λ_∞ vs. X or Λ vs. c is apparent in the conductivity data (7), but the concentrations of HCl used in conductivity studies are smaller by more than a factor of 10.

Equation [8] suggests that v_r should increase with c. However, the data in Table 1 show v_r to be about the same for $c = 0.3$ and $c = 0.1$. This is due to the greater degree of dissociation at lower c values, together with a larger value of k_{ass} at lower c values. The $k_{ass,\infty}$ values calculated from the v_r (Table 3) show them to be somewhat greater for $c = 0.1$. It may be that formation of complex ions is non-negligible at $c = 0.30$. Since activity coefficient corrections are more likely to be valid for $c = 0.10$, the values of $|\Delta V_{eff}|$ and $k_{ass,\infty}$ in Table 3 for $c = 0.10$ are more likely to be correct.

The results of an ultrasonic study of HCl in dimethylformamide (6) give $|\Delta V_{eff}|$ and k_{ass} values close to those in Table 3. A distance of closest approach of 1.0 nm is calculated from k_{ass} using diffusion-controlled theory in ref. 6. However $-e^2$ instead of e^2 should have been used in the equation corresponding to [9]. With this correction, the results in ref. 6 are similar to those found here: $k_{ass,\infty}$ is too low to give a physically real value of reaction distance a from eq. [9].

Ultrasonic studies of acids in water give a much larger value of a (5). This is possible because of the possibility of hydrogen-bond jumping in reactions in water involving H^+. The value of $|\Delta V_{eff}|$ ($\simeq |\Delta V^0|$ in aqueous solutions) is about 20 cm^3 mol^{-1}, similar to the values in Table 3. Diffusion-controlled rate theory should be more realistic for the case of the aqueous acid studies (5), as it is used for distances well in excess of a molecular diameter for the solvent H_2O.

Studies of ultrasonic absorption in solutions of 1:1 salts in nonaqueous solvents suggest that a two-step model is more appropriate. Both in the case of DMSO (3) and 2-propanol (4) solutions, experimental data suggested a second relaxation at higher frequencies. A second step may also be possible in the HCl–DMSO–water system when $c = 0.30$. In ref. 4, the high frequency absorption is postulated to be due to a modification of the structure of the solvent by the ions, instead of one of the steps in the 2-step ion pair mechanism proposed. In ref. 3, the insensitivity of the lower v_r ($\simeq$ 5 MHz) with ionic species suggests it to be characteristic of a reaction involving primarily solvent motion, e.g. reaction to form a contact ion pair from a solvent separated ion pair. In the case of a small ion like H^+, the ion may essentially "belong" to only one solvent molecule (16), making it more easily accessible for anions. For larger cations a more structured primary solvent sheath is formed which prevents the anion from immediately contacting the cation, making the solvent-separated ion pair a meaningful entity.

Can. J. Chem. Downloaded from www.nrcresearchpress.com by 210.87.254.42 on 09/05/12
For personal use only.

Can. J. Chem. Downloaded from www.nrcresearchpress.com by 210.87.254.42 on 09/05/12
For personal use only.

Conclusions

The results of the study strongly suggest that the excess ultrasonic absorption observed in this system is due to a single-relaxation process. The process responsible seems quite certainly to be the association–dissociation equilibrium of HCl.

Analysis of the ultrasonic results using the equilibrium constant from conductivity gives $|\Delta V_{eff}|$ values of the order of 20–25 $cm^3\ mol^{-1}$, typical of the ΔV's of ion pairing reactions when hydrogen ions are involved. Moreover, the $|\Delta V_{eff}|$ values obtained are quite consistent with variation in the mole fraction of DMSO even though the relaxation strength and the equilibrium constant vary considerably.

Values of the rate constant for ionic association are of the order of $3 \times 10^9\ \ell\ mol^{-1}\ s^{-1}$, as compared to $10 \times 10^9\ \ell\ mol^{-1}\ s^{-1}$ calculated from diffusion-controlled theory. Such a large discrepancy is not unexpected since k_{diff} is calculated assuming the solvent to be a continuum. Such a model is especially inappropriate in cases where the solvent molecules are large (DMSO has a diameter of approximately 7 Å), as then the distances considered are more likely to be of the order of molecular dimensions. Approximations made in the calculation of $k_{ass,\infty}$ from experimental data may also contribute to the discrepancy. The estimation of activity coefficient effects is especially open to error.

The results for this study differ from results of most other studies of ion-pairing phenomena in that the phenomenon can be explained in a satisfactory manner by a single relaxation process, and in that when the available conductivity equilibrium constant data are used in analysis, the results are very reasonable. For ion pairing processes involving larger cations, at least two equilibria affect the ultrasonic absorption.

This may be because larger cations (e.g. alkali metal or earth ions) may have primary solvation sheaths which contain several quite rigidly held solvent molecules, preventing a contact ion pair from forming readily. Thus a distinct solvent-separated ion pair species exists, and at least two distinct equilibria exist in the process free ions → contact ion pair. In a primarily nonaqueous solution, a smaller ion has fewer molecules in its primary solvation shell (11). The crude model of the solvation of a proton in such solutions may be obtained by considering it as a very small ion. It would then possibly be solvated most strongly by only a single solvent molecule. Thus it is not well shielded geometrically, and direct formation of the contact ion pair is easier.

Acknowledgements

The authors wish to thank Dr. B. E. Poppe for aid with some of the measurements. Financial assistance was provided by the National Research Council of Canada and Carleton University.

1. P. KRUUS. Liquids and solutions: structure and dynamics. M. Dekker, New York. 1977.
2. A. BECHTLER, K. G. BREITSCHWERDT, and K. TAMM. J. Chem. Phys. **52**, 2975 (1970).
3. D. R. DICKSON and P. KRUUS. Can. J. Chem. **49**, 3107 (1971).
4. T. NOVESKE, J. STUEHR, and D. F. EVANS. J. Sol. Chem. **1**, 93 (1972).
5. L. W. GREEN, P. KRUUS, and M. J. MCGUIRE. Can. J. Chem. **54**, 3152 (1976).
6. S. C. CHAN and J. P. VALLEAU. Can. J. Chem. **46**, 853 (1968).
7. C. COOKE, C. MCCALLUM, A. D. PETHYBRIDGE, and J. E. PRUE. Electrochim. Acta, **20**, 591 (1975).
8. S. W. JACOB and R. HERSCHLER (*Editors*). Biological actions of dimethyl sulfoxide. 1975.
9. E. HÄGGLUND, B. LINDBERG, and J. MCPHERSON. Acta Chem. Scand. **10**, 1160 (1946). D. MARTIN, A. WEISE, and H. J. NICLAS. Angew. Chem. **79**, 340 (1967).
10. R. J. FANNING and P. KRUUS. Can. J. Chem. **48**, 2052 (1970).
11. M. S. GOLDENBERG, P. KRUUS, and S. K. F. LUK. Can. J. Chem. **53**, 1007 (1975).
12. C. THOMSON, D. T. CLARK, T. C. WADDINGTON, and H. D. B. JENKINS. J. Chem. Soc. Faraday II, **71**, 1974 (1975).
13. J. C. SYNNOTT and J. N. BUTLER. J. Phys. Chem. **73**, 1470 (1969).
14. S. M. PETROV, Y. I. UMANSKII, I. F. MULLIN, and A. N. TERTICHNIYI. Russ. J. Phys. Chem. **47**, 363 (1973).
15. R. A. ROBINSON and R. H. STOKES. Electrolyte solutions. Revised edition. Butterworths, London. 1968.
16. P. KRUUS and B. E. POPPE. In preparation.

Pulse radiolysis of deuterated aqueous LiCl glasses. Dependence of the yields and rates of reaction of visible and infrared absorbing trapped electrons on LiCl concentration[1]

HUGH A. GILLIS AND GEORGE G. TEATHER

Division of Physics, National Research Council of Canada, Ottawa, Ont., Canada K1A 0R6

AND

GEORGE V. BUXTON

University of Leeds, Cookridge Radiation Research Centre, Cookridge Hospital, Leeds LS16 6QB, England

Received September 30, 1977

HUGH A. GILLIS, GEORGE G. TEATHER, and GEORGE V. BUXTON. Can. J. Chem. **56**, 1889 (1978).

The yields and reactions of trapped electrons which absorb in the visible (e_{vis}^-) and infrared (e_{ir}^-) have been studied by pulse radiolysis in deuterated aqueous 6–15 *M* LiCl glasses at low temperatures. At 76 K $G(e_{vis}^-)$ increases and $G(e_{ir}^-)$ decreases as the concentration of LiCl is increased, but $[G(e_{vis}^-) + G(e_{ir}^-)] \simeq 1.8$ over the whole concentration range. Because the hydration number of Li^+ is 4, $G(e_{ir}^-)/G(e_{vis}^-)$ was plotted against [free D_2O]/[$LiCl \cdot 4D_2O$] and found to give a straight line passing through the origin, for $[D_2O]/[LiCl] > 4$. From this proportionality it is concluded that e_{ir}^- is an electron trapped in a purely amorphous water environment and e_{vis}^- is mainly associated with water bound to Li^+.

The reactions of e_{ir}^- and e_{vis}^- with Cu(II) and SeO_4^{2-} have been investigated. At 138 K the rate of reaction of e_{vis}^- with SeO_4^{2-} increases with decreasing [LiCl] whereas its rate of reaction with Cu(II) is slower and independent of [LiCl]. At 76 K, where the rates of reaction of e_{ir}^- with the scavengers can also be measured, it is found that in each case e_{vis}^- and e_{ir}^- react more slowly in 12 *M* LiCl glass than in 6 *M* LiCl glass, the difference being more marked for SeO_4^{2-}. In the absence of scavenger the electron in the smaller yield decays faster. These observations can be rationalized on the basis that electrons can tunnel in either direction between visible and infrared traps before being scavenged, and it seems they cannot be rationalized in terms of direct tunnelling only.

$G(Cl_2^-)$ is found to be proportional to the electron fraction of $Cl^- \cdot 3D_2O$ in the glass and its extrapolated value for pure $Cl^- \cdot 3D_2O$ is 3.4. It is inferred that Cl_2^- arises mainly from ionization of the D_2O bound to Cl^-.

HUGH A. GILLIS, GEORGE G. TEATHER et GEORGE V. BUXTON. Can. J. Chem. **56**, 1889 (1978).

Les rendements et les réactions d'électrons piégés qui absorbent dans le visible (e_{vis}^-) et dans l'infrarouge (e_{ir}^-) ont pu être étudiés par radiolyse pulsée dans des verres aqueux deutérés de 6 à 15 *M* de LiCl à basse température. A 76 K, $G(e_{vis}^-)$ augmente et $G(e_{ir}^-)$ diminue à mesure que la concentration de LiCl augmente; toutefois $[G(e_{vis}^-) + G(e_{ir}^-)] \simeq 1.8$ à toutes les concentrations. Dû au fait que le nombre d'hydration de Li^+ est 4, on a porté en graphique $G(e_{ir}^-)/G(e_{vis}^-)$ en fonction de [D_2O libre]/[$LiCl \cdot 4D_2O$] et on a trouvé que cette ligne est droite et qu'elle passe à l'origine pour $[D_2O]/[LiCl] > 4$. En se basant sur cette proportionalité, on peut conclure que e_{ir}^- est dû à un électron piégé dans un environnement d'eau purement amorphe alors que e_{vis}^- est associé principalement avec de l'eau liée à Li^+.

On a étudié les réactions de e_{ir}^- et de e_{vis}^- avec Cu(II) et SeO_4^{2-}. A 138 K, la vitesse de la réaction de e_{vis}^- avec SeO_4^{2-} augmente lorsque la concentration de [LiCl] diminue alors que sa vitesse de réaction avec Cu(II) est plus faible et ne dépend pas de la concentration de [LiCl]. A 76 K, température à laquelle les vitesses de réaction de e_{ir}^- avec des piégeurs ont pu aussi être mesurées, on a trouvé que dans chaque cas e_{vis}^- et e_{ir}^- réagissent plus lentement dans des verres de 12 *M* LiCl que dans des verres de 6 *M* LiCl; la différence est la plus marquée avec SeO_4^{2-}. Lorsqu'il n'y a pas de piégeurs, l'électron dans un champ plus faible disparaît plus rapidement. On peut rationaliser ces observations en se basant sur l'hypothèse que les électrons peuvent réagir par une réaction tunnel dans chaque direction entre les pièges du visible et de l'infrarouge avant d'être piégé et il semble que l'on ne peut pas rationaliser les observations en terme uniquement de tunnel direct.

On a trouvé que $G(Cl_2^-)$ est proportionnel à la fraction électronique de $Cl^- \cdot 3D_2O$ dans le verre et sa valeur extrapolée pour $Cl^- \cdot 3D_2O$ pure est de 3.4. On a déduit que Cl_2^- provient principalement de l'ionisation de D_2O lié à Cl^-.

[Traduit par le journal]

Introduction

Trapped electrons which absorb in the infrared, e_{ir}^-, have been observed in a few aqueous glasses, but not in several others (1). These trapped electrons can be produced directly by ionizing radiation (1), or indirectly by photoionization of trapped electrons

[1]NRCC No. 16762.

Can. J. Chem. Downloaded from www.nrcresearchpress.com by 210.87.254.105 on 09/05/12
For personal use only.

Can. J. Chem. Downloaded from www.nrcresearchpress.com by 210.87.254.105 on 09/05/12
For personal use only.

which absorb in the visible, e_{vis}^- (2). The intensities of the infrared and visible absorption bands vary from one glass to another, e.g. the infrared band is much more prominent in 2.5 *M* $MgCl_2$ than in 9.5 *M* LiCl, while the opposite is true for the visible band. We have also observed a similar infrared band in single crystals of ice which we have tentatively assigned to electrons trapped in naturally occurring cavities in the ice structure (3).

These observations suggest that the infrared band in the glasses might also be due to electrons trapped in a purely water environment, and that the higher yields of e_{ir}^- found in particular glasses (1) could be due to these glasses having smaller fractions of their water content involved in hydration, so that the probability of electrons being trapped in a purely water environment would be greater.

To test this idea we chose to investigate the variation in intensity of the infrared and visible bands with composition in the LiCl system because (*a*) it forms good glasses over a wide range of LiCl concentration (4), (*b*) we have already studied this glass extensively for 9.5 *M* LiCl (1, 5, 6), and (*c*) the total hydration number of LiCl has been estimated as 6–8 in one report (4), while more recent work (7) indicates that the hydration number of Li^+ is 4. Thus in glasses containing the lower concentrations of LiCl significant amounts of the water will not be involved in hydration of the ions.

It has also been shown (6) that the rate at which e_{vis}^- reacts with scavengers in 9.5 *M* LiCl glass is consistent with its being transformed into e_{ir}^- before reaction, and in a very recent study (2*b*) strong evidence for the reverse transformation has been obtained. Therefore with the hope of obtaining more information about these conversions, we have also investigated in the present study the effect of the composition of the LiCl glasses on the reactions of e_{vis}^- and e_{ir}^- with chosen solutes.

Experimental

The experiments at 76 K were carried out at the National Research Council of Canada, Ottawa and those at 138 K at the University of Leeds. Details of the pulse radiolysis facilities and techniques used in this work were as described before (1, 5, 6). All optical densities (OD) reported in this paper have been corrected for small absorptions in the Suprasil cells. All samples were prepared in D_2O (99.7 atom% D, from Merck, Sharp and Dohme, or 99.8 atom% D, from Norsk Hydro) which was used as received. Solutes were analytical reagent grade and were also used without further purification.

Results

(1) Spectrum of Trapped Electrons (e_t^-) at 76 K: Dependence on LiCl Concentration

The spectrum of e_t^- was measured at 76 K at the end of a 40 ns pulse in a number of LiCl/D_2O glasses of different compositions. As before (1), the spectrum consists of a band in the visible region with $\lambda_{max} \sim 650$ nm and a second band in the infrared with $\lambda_{max} > 2350$ nm, but the intensities of the two bands depend strongly on the concentration of LiCl in the glass, as can be seen in Fig. 1. However, no effect of LiCl concentration on the positions or shapes of the two bands is seen.

We have shown before (1) that the absorption at 650 nm is due solely to e_{vis}^- and absorption at 2350 nm is similarly due only to e_{ir}^-. The data in Table 1 show how the yields of these species vary with the composition of the LiCl/D_2O glass. The striking feature of these data is the way in which $G(e_{ir}^-)$ increases and $G(e_{vis}^-)$ decreases as the water content of the glass increases, while the sum of the yields remains practically constant.

The values of $G(e_{vis}^-)$ and $G(e_{ir}^-)$ in 9.5 *M* LiCl glass are respectively 29% and 18% lower than the values which were reported before (1). We believe that the discrepancy is associated with dosimetry problems in the earlier work. The values in Table 1 have been confirmed in repeat experiments and are therefore considered to be correct.

(2) Decay of e_t^- at 76 K

The decay of e_{vis}^- and e_{ir}^- at 76 K after a 40 ns pulse was monitored at 650 nm and 2350 nm respectively. The decays are kinetically complex and depend on the composition of the glass. Examples are given in Fig. 2 and Table 2 which show that the rate at which a given band decays increases as the intensity of the band decreases.

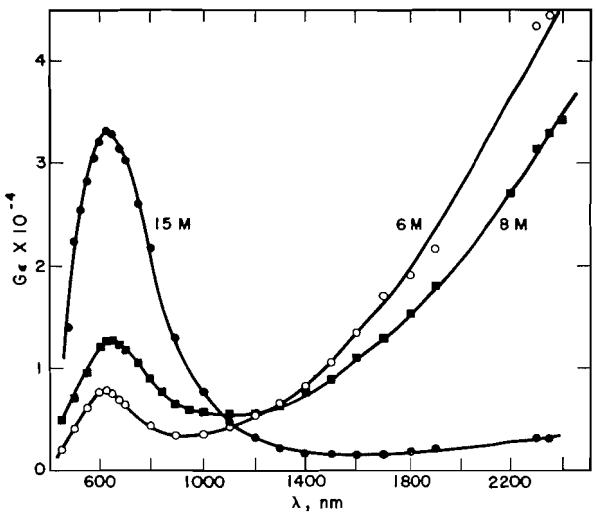

FIG. 1. Dependence of spectrum of e_t^-, measured 100 ns after the start of a 40 ns pulse, on [LiCl] in deuterated aqueous LiCl glasses at 76 K.

Can. J. Chem. Downloaded from www.nrcresearchpress.com by 210.87.254.105 on 09/05/12
For personal use only.

TABLE 1. Yields of e_{vis}^- and e_{ir}^- in LiCl/D_2O glasses

[LiCl] (M)	Density (g/ml)	Moles D_2O / Moles LiCl	$G(e_{vis}^-)^{a,c}$	$G(e_{ir}^-)^{b,c}$	Total G
6	1.210	7.96	0.38	1.46	1.84
7	1.232	6.68	0.43	1.24	1.67
8	1.252	5.71	0.65	1.09	1.74
9.5	1.271	4.56	0.98	0.78	1.76
12	1.321	3.38	1.46	0.39	1.85
15	1.359	2.41	1.65	0.10	1.75

[a] ε_{650} taken as $2 \times 10^4\ M^{-1}\ cm^{-1}$ (1).
[b] ε_{2350} taken as $3.05 \times 10^4\ M^{-1}\ cm^{-1}$ (1).
[c] Corrections have been made for the electron densities of the glasses at 76 K. The yields were measured 100 ns after the start of a 40 ns pulse.

(3) Effect of the Electron Scavengers Cu(II) and SeO_4^{2-}

To investigate further the idea that the reaction of e_{vis}^- with certain solutes proceeds via transformation of e_{vis}^- into e_{ir}^- (6), we have measured the rate at which e_t^- reacts with cupric ion and selenate ion. These solutes were chosen because (*a*) SeO_4^{2-} is a very efficient scavenger of 'dry' electrons, e_{dry}^-, whereas Cu(II) is a very inefficient one (6), (*b*) the opposite holds for e_{vis}^-, and (*c*) there are indications (1, 6) that the reactivity of e_{ir}^- may be similar to that of e_{dry}^-.

(a) Reaction at 138 K

At 138 K no e_{ir}^- are observed (1) and so reaction of e_{vis}^- with Cu(II) and SeO_4^{2-} was followed at 600 nm. The decays of e_{vis}^- following a 10 ns pulse are presented in Figs. 3 and 4 and have been corrected for the decay of e_{vis}^- in the absence of scavenger by dividing $OD/OD_{17\ ns}$ in the presence of scavenger by $OD/OD_{17\ ns}$ in the absence of scavenger. This procedure, used earlier by Miller (8), is valid if the change in OD due to e_t^- is of the form

$$\frac{-d(OD)}{dt} = (k'(t) + k''(t))(OD)$$

where $k'(t)$ and $k''(t)$ are time-dependent first-order rate constants which refer to the decay of e_t^- in the absence of scavengers and reaction of e_t^- with scavengers respectively. In the presence of scavenger the optical density OD_s at time t is given by

$$\ln OD_s = -\int_0^t k'(t)\,dt - \int_0^t k''(t)\,dt$$

when the initial OD_s is taken as unity. Similarly in the absence of scavenger the optical density OD_B at time t is given by

$$\ln OD_B = -\int_0^t k'(t)\,dt$$

Hence

$$\ln (OD_s/OD_B) = -\int_0^t k''(t)\,dt$$

which on differentiation gives

$$\frac{-d(OD_s/OD_B)}{dt} = k''(t)(OD_s/OD_B)$$

Therefore from plots of OD_s/OD_B vs. time as in Figs. 3–6, which have been normalised to unity at the first observation time (17 ns or 100 ns), $k''(t)$ can be calculated at any time.

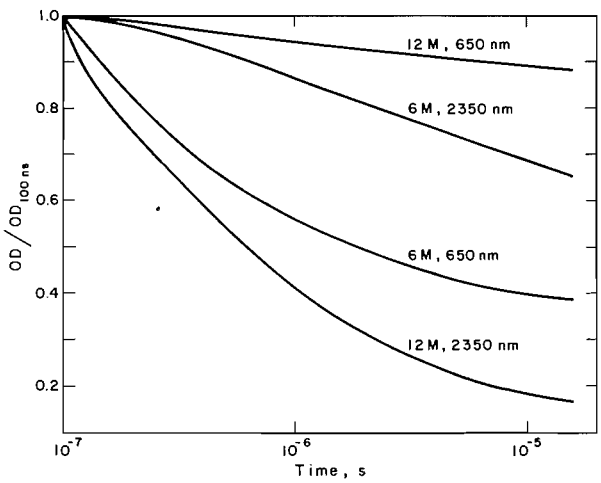

FIG. 2. Decay of e_t^- at 650 nm and 2350 nm at 76 K in 6 M and 12 M LiCl glass, without scavenger. Time is measured from the start of a 40 ns pulse.

TABLE 2. Fractions of e_t^- which do not decay between 100 ns and 10 μs in LiCl/D_2O glasses without scavenger at 76 K

	$OD_{10\ \mu s}/OD_{100\ ns}$	
[LiCl]/M	At 650 nm	At 2350 nm
6	0.39	0.69
9.5	0.89	0.32
12	0.89	0.17
15	0.84	0.20

Can. J. Chem. Downloaded from www.nrcresearchpress.com by 210.87.254.105 on 09/05/12
For personal use only.

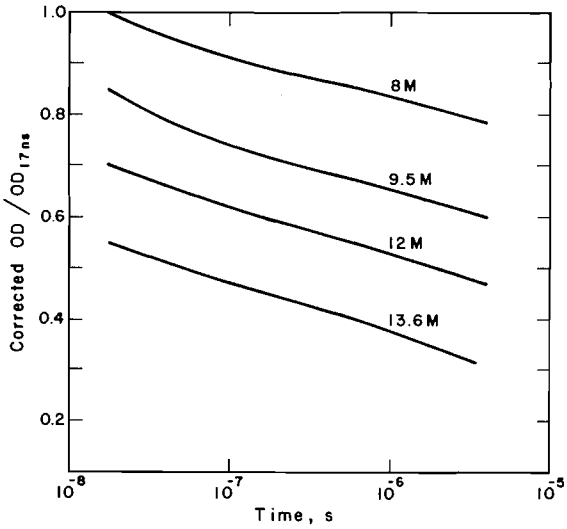

FIG. 3. Effect of [LiCl] on the decay of e_{vis}^- at 600 nm at 138 K in LiCl glass containing 5 m*M* Cu(II). Time is measured from the start of a 10 ns pulse. Each curve has been corrected for the decay of e_{vis}^- in the glass containing no scavenger as described in the text. The lower curves are displaced vertically.

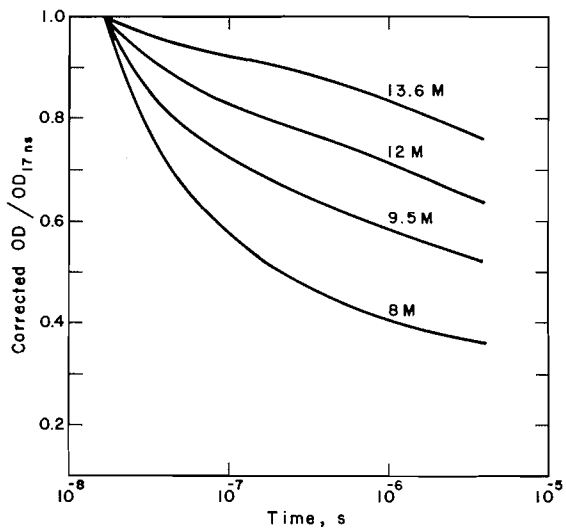

FIG. 4. Effect of [LiCl] on the decay of e_{vis}^- at 600 nm and 138 K in LiCl glass containing 5 m*M* SeO_4^{2-}. Time is measured from the start of a 10 ns pulse. Each curve has been corrected for the decay of e_{vis}^- in the glass containing no scavenger as described in the text.

Noteworthy features of the data in Figs. 3 and 4 are the increase in the rate of reaction of e_{vis}^- with SeO_4^{2-}, and its constant and slower rate of reaction with Cu(II), with decreasing [LiCl].

(b) Reaction at 76 K

At 76 K the decays of e_{vis}^- and e_{ir}^- were followed at 650 nm and 2350 nm respectively. Data for 6 *M* and 12 *M* LiCl glasses containing SeO_4^{2-} or Cu(II) are presented in Figs. 5 and 6. The pulse length was

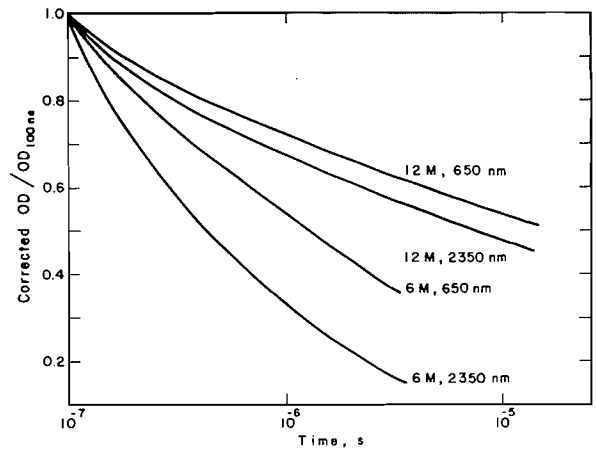

FIG. 5. Effect of [LiCl] on the decay of e_{vis}^- at 650 nm and e_{ir}^- at 2350 nm at 76 K in LiCl glass containing 20 m*M* Cu(II). Time is measured from the start of a 40 ns pulse. Each curve has been corrected for the decay of e_{vis}^- or e_{ir}^- in the glass containing no scavenger as described in the text.

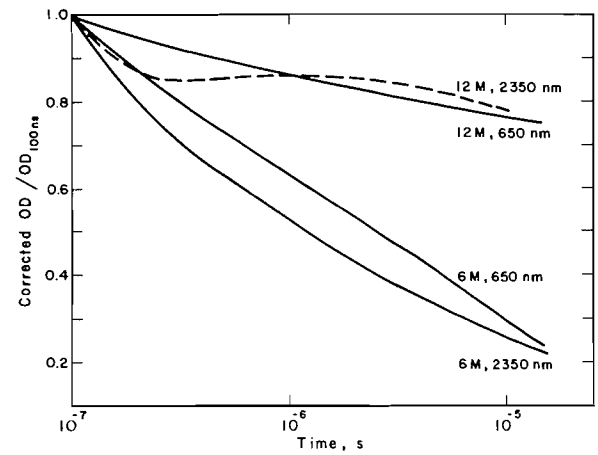

FIG. 6. Effect of [LiCl] on the decay of e_{vis}^- at 650 nm and e_{ir}^- at 2350 nm at 76 K in LiCl glass containing 5 m*M* SeO_4^{2-}. Time is measured from the start of a 40 ns pulse. Each curve has been corrected for the decay of e_{vis}^- or e_{ir}^- in the glass containing no scavenger as described in the text. The data for the 12 *M* glass at 2350 nm are rather uncertain.

40 ns and the decays have been corrected for the decay in the absence of scavenger (see Fig. 2) as described above.

(4) Effect of Scavengers on the Yields of e_{vis}^- and e_{ir}^-

The data in Table 3 show how G/G_0, the ratio of the yields in the presence and absence respectively of Cu(II) or SeO_4^{2-}, measured at the end of the pulse, varied with [LiCl]. At 138 K where only $G(e_{vis}^-)$ could be measured, 5 m*M* Cu(II) scarcely affected G/G_0 in any LiCl glass whereas 5 m*M* SeO_4^{2-} decreased G/G_0 to a larger extent at the lower concentrations of LiCl. At 76 K SeO_4^{2-} was again more effective than Cu(II) in decreasing $G(e_{vis}^-)$ and

TABLE 3. Effect of scavengers on $G(e_{vis}^-)$ and $G(e_{ir}^-)$ in $LiCl/D_2O$ glasses

T (K)	[LiCl] (M)	λ (nm)	G/G_0 5 mM SeO_4^{2-}	G/G_0 5 mM Cu(II)	G/G_0 20 mM Cu(II)
138[a]	8	600	0.37	0.97	
	9.5	600	0.62	0.95	
	12	600	0.72	0.90	
	13.6	600	0.81	1.06	0.74[c]
76[b]	6	650	0.55		0.71
	6	2350	0.25		0.54
	12	650	0.60		0.73
	12	2350	0.44		0.66

[a]Measured at 17 ns after start of 10 ns pulse.
[b]Measured at 100 ns after start of 40 ns pulse.
[c]Measured 35 ns after start of 25 ns pulse.

TABLE 4. Dependence of $G(Cl_2^-)$ on [LiCl] in $LiCl/D_2O$ glasses at 76 K

[LiCl] (M)	$10^{-4}G\varepsilon_{350}$ Measured	Due to e_{vis}^-	Due to Cl_2^-	$G(Cl_2^-)$[a]
6	1.51	0.16	1.35	1.57
7	1.82	0.18	1.64	1.91
9.5	2.62	0.41	2.21	2.57
12	3.16	0.61	2.55	2.97

[a]ε_{350} taken as $8.6 \times 10^3\ M^{-1}\ cm^{-1}$ (9).

$G(e_{ir}^-)$. However, at this temperature G/G_0 for e_{vis}^- was essentially independent of [LiCl].

(5) Yields of Cl_2^-

The maximum in the spectrum of Cl_2^- at 76 K was confirmed as 350 nm for 7 M LiCl glass. The measured yields of Cl_2^- for several different LiCl concentrations are listed in Table 4. We have corrected these yields for the contribution of e_{vis}^- (which cannot be measured) to the total absorption at 350 nm by assuming that the absorption spectra of e_{vis}^- in LiCl glasses and 50% ethylene glycol/D_2O glass, which have virtually identical shapes when $\lambda > 450$ nm (1), are also similar at $\lambda < 450$ nm.

Discussion

(1) Correlation between Glass Composition and Trapped Electron Yields

The dependence of $G(e_{vis}^-)$ and $G(e_{ir}^-)$ on [LiCl] in the glass (see Table 1) strongly suggests that they are correlated. The quantum yields for production of e_{ir}^- by laser bleaching of e_{vis}^- show the same trend with varying [LiCl] as that shown in Table 1; quantum yields for 6.5 and 15 M glasses were measured as 0.018 and 0.004, respectively (2*b*). Conclusions reached about the structure of these glasses from recent nmr studies (7) are that the lithium ion is coordinated to the oxygen atoms of four water molecules in a tetrahedral structure. Three of these are shared with six separate chloride ions in an octahedral arrangement, and the fourth water molecule is unshared. The basic unit is therefore $(Li{\cdot}4H_2O)^+Cl^-$ and the basic structure is believed to be a distorted face-centred cube with the Li^+ and Cl^- arranged octahedrally round one another. Water in excess of that required to form $(Li{\cdot}4H_2O)^+$ does not form further coordination shells and is regarded as being essentially free (7). The structure of this free water is not established but it appears to be amorphous rather than ice-like (7). Angell and Sare (4) similarly concluded that concentrated LiCl solutions around the glass transition temperature consist of two coexisting liquid phases: amorphous water (or very dilute solution) and a salt-rich hydrated ionic liquid. The more dilute of the LiCl solutions which can form glasses show a tendency to phase separate (4). Substitution of D_2O for H_2O is unlikely to change these structures.

On this basis we might expect a correlation of $G(e_{vis}^-)$ and $G(e_{ir}^-)$ with the relative amounts of $LiCl{\cdot}4D_2O$ and free water in the glass. This is borne out by Fig. 7 which shows that $G(e_{ir}^-)/G(e_{vis}^-)$ is proportional to [free D_2O]/[$LiCl{\cdot}4D_2O$]. Such a relationship is expected to hold if pre-existing trapping sites for e_{ir}^- and e_{vis}^- are in competition for mobile electrons which would otherwise recombine with the geminate positive holes (reactions [1]–[3]),

Can. J. Chem. Downloaded from www.nrcresearchpress.com by 210.87.254.105 on 09/05/12
For personal use only.

Can. J. Chem. Downloaded from www.nrcresearchpress.com by 210.87.254.105 on 09/05/12
For personal use only.

[1] $e^- + \text{positive hole} \rightarrow \text{no } e_t^-$

[2] $e^- + \text{infrared trap} \rightarrow e_{ir}^-$

[3] $e^- + \text{visible trap} \rightarrow e_{vis}^-$

These processes are analogous to the competitive scavenging of electrons by two solutes in hydrocarbons (10). The appropriate equations are (10) [4] and [5]

$$[4] \qquad \frac{G(e_{ir}^-)}{G(e_{vis}^-)} = \frac{\alpha_2[\text{ir trap}]}{\alpha_3[\text{vis trap}]}$$

$$[5] \quad G(e_{ir}^-) + G(e_{vis}^-) = G_i \frac{\{\alpha_2[\text{ir trap}] + \alpha_3[\text{vis trap}]\}^{1/2}}{1 + \{\alpha_2[\text{ir trap}] + \alpha_3[\text{vis trap}]\}^{1/2}}$$

where G_i is the initial yield of mobile electrons and α is the reactivity of the electron with the trapping site. Here we assume, by analogy with the situation in liquid hydrocarbons (10), that all the mobile electrons in the glass can be treated as geminate ions. This is reasonable since only the high frequency dielectric constant will apply at this stage. The data in Fig. 7 satisfy eq. [4] if [ir trap] = x[free D_2O] and [vis trap] = y[$LiCl{\cdot}4D_2O$] when the ratio [D_2O]:[LiCl] > 4. Correspondingly the requirement for eq. [5] to be valid is that $\{[\text{free } D_2O] + LiCl{\cdot}4D_2O]\}^{1/2}$ be constant since $[G(e_{ir}^-) + G(e_{vis}^-)]$ is approximately constant (see Table 1) and $x\alpha_2 = y\alpha_3$ (see Fig. 7). In fact $\{[\text{free } D_2O] + [LiCl{\cdot}4D_2O]\}^{1/2}$ decreases by only 29% from 5.45 for 6 *M* LiCl to 3.84 for 9.5 *M* LiCl. The latter concentration corresponds to the lowest nonzero value of [free D_2O]/[$LiCl{\cdot}4D_2O$] in Fig. 7. The lack of any decrease in $[G(e_{ir}^-) + G(e_{vis}^-)]$ between 6 and 9.5 *M* LiCl may be due to a lower yield of unscavenged holes that can undergo reaction [1] at higher $[Cl^-]$ (see section (4) below).

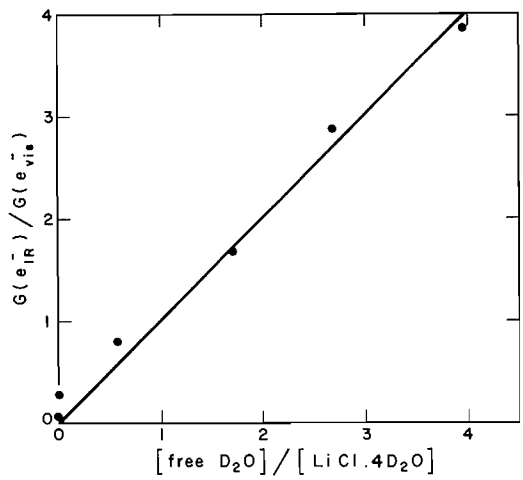

FIG. 7. Dependence of $G(e_{ir}^-)/G(e_{vis}^-)$ on [free D_2O]/[$LiCl{\cdot}4D_2O$] in LiCl glass at 76 K.

So far the simple model of e_{ir}^- and e_{vis}^- being electrons trapped in free water and $LiCl{\cdot}4D_2O$ structures respectively seems to be a reasonable one. However, it is clear from Table 1 and Fig. 7 that $G(e_{ir}^-)$ is still significant at LiCl concentrations of 12 or 15 *M* where little or no free water is expected to be present in the glass. This leads us to conclude that either traps for e_{ir}^- are not exclusively confined to purely water structures, or such structures are by chance still formed when [D_2O]:[LiCl] < 4.

(2) Reaction of e_t^-

Reaction of e_t^- with solutes in rigid glasses is generally accepted to proceed via a tunnelling mechanism. Before discussing the reactions observed in this study it will be helpful to summarise the pertinent features of the two types of tunnelling mechanism which have been postulated, viz. direct tunnelling (11) and trap-to-trap tunnelling (12). The basis of the direct tunnelling model is that the electron tunnels from its trap to the acceptor so that the reaction rate depends upon the concentration of the acceptor but not on the presence of other (empty) traps. In the trap-to-trap tunnelling model it is postulated that the electron tunnels from one trap to another until it finds itself in a trap which is within the reaction distance of the acceptor. In this case the reaction rate depends upon the concentration of traps as well as of acceptor.

Miller's (11) formulation of the direct tunnelling model is as follows: If every trapped electron within the distance a of randomly distributed acceptor S is captured, the probability P that it will have reacted in time t is

$$[6] \qquad P = 1 - \exp(-2.52 \times 10^{-3} a^3[S])$$

where a is the width of the barrier through which the electron tunnels and is given by (8)

$$[7] \qquad a = a_0 + 2.26B^{-1/2}(15 + \log Ft)$$

B is the binding energy of the trapped electron and F is an "inefficiency factor" included by Miller (8) to take account of the observation that tunnelling rates differ from one kind of acceptor to another. Thus, according to the model, the parameters affecting the tunnelling rate are B, F, and [S]. Values of B are not known with any certainty (2*b*) but are probably within a factor of two of 1 eV for aqueous glasses. For 6 *M* NaOH glass Miller (8) assumed B = 1.2 eV and found that F ranged from 10^4 to 10^{-15} depending on the acceptor. The factor F is thought (8) to be associated with Franck–Condon restrictions to the transfer of an electron to the acceptor.

Can. J. Chem. Downloaded from www.nrcresearchpress.com by 210.87.254.105 on 09/05/12
For personal use only.

In the trap-to-trap tunnelling model proposed by Buxton and Kemsley (12), it is assumed that the probability that an electron will have reacted in time t is $P_t \times P_s$, where P_t is the probability that the electron will tunnel to another trap and is given by eq. [6] with [S] replaced by [trap], and P_s is the probability that the electron will be scavenged and is given by eq. [6] with a replaced by r. In this case the tunnelling rate of the electron should depend on [trap], [S], a, and r. For a number of different aqueous glasses, the parameter r varies with acceptor, ranging from 6 Å to 20 Å (12), but for a given acceptor it has about the same value as the reaction distance for solvated electrons obtained from diffusion kinetics measurements in the corresponding aqueous liquid (12). In general these values of r do not change very much from one aqueous liquid to another (6, 12). In this case the variation in r is, presumably, also a reflection of Franck–Condon restrictions to the electron transfer process.

The striking features of the data shown in Figs. 5 and 6 are (*a*) for a particular glass at 76 K e_{vis}^- and e_{ir}^- react at rather similar rates with either SeO_4^{2-} or Cu(II), (*b*) changing [LiCl] markedly affects the reaction rates, and (*c*) SeO_4^{2-} is a very efficient acceptor of e_{vis}^- in the more dilute LiCl glasses (see also Fig. 4) although it is a very poor acceptor in other aqueous glasses (8, 12).

On the face of it these results seem to be the opposite of what one would expect to observe if the direct tunnelling model outlined above was operative. Thus one might anticipate that e_{ir}^- would react much faster than e_{vis}^- since e_{ir}^- would be expected to be much less strongly bound than e_{vis}^-, the respective transition energies at λ_{max} being 0.34 eV and 1.94 eV (1). It could be argued, perhaps, that changes in B are counterbalanced by changes in F, and we have no information about F other than as an adjustable parameter. The effects of [LiCl] on the tunnelling rate are also unexpected since they imply that values of F for both e_{vis}^- and e_{ir}^- change very considerably when [LiCl] is increased from 6 M to 12 M. Such large changes in F appear to be at variance with the spectral data in Fig. 1 which show that the positions and shapes of the bands assigned to e_{vis}^- and e_{ir}^- are independent of [LiCl], which suggests that B for each type of electron does not change very much either. We have no information on the effect of [LiCl] on the energy states of the acceptors, but feel that any changes should be rather small, especially in view of the insensitivity of r for solvated electron reactions to the composition of the aqueous liquid noted above.

A factor which does change with [LiCl] is the trap concentration, as revealed by the values of $G(e_{vis}^-)$ and $G(e_{ir}^-)$ in Table 1 which we have already discussed. Therefore it does appear that there is some sort of influence of trap concentration on tunnelling rates in LiCl glasses and this suggests that trap-to-trap tunnelling may occur. If this is the case can these unusual tunnelling kinetic data be rationalized? As noted above, SeO_4^{2-} is a very poor acceptor of e_{vis}^- although it scavenges e_{dry}^- very efficiently (5, 8), and yet both e_{vis}^- and e_{ir}^- react rapidly with SeO_4^{2-} when the ratio visible traps:infrared traps is low, and they both react slowly when this ratio is high (see Fig. 6 and Table 1). Let us assume that electrons can tunnel between any two traps, and donor and acceptor traps can be either visible or infrared. Then, in 6 M LiCl glass an electron on average would be more likely to tunnel to an infrared trap and conversely, in 12 M LiCl glass tunnelling to a visible trap would be more likely. Thus if SeO_4^{2-} is a better acceptor of e_{ir}^- than e_{vis}^- (i.e. the reaction distance r is larger for e_{ir}^-; see also section 3 below) both e_{ir}^- and e_{vis}^- would appear to react more rapidly in 6 M LiCl glass and less rapidly in 12 M LiCl glass. The same considerations apply to the data in Fig. 4 for 138 K. The less marked effects of [LiCl] in the case of Cu(II) (see Figs. 3 and 5) would then suggest that this acceptor reacts with more nearly the same efficiency with both e_{vis}^- and e_{ir}^-. In other systems Cu(II) reacts much more efficiently than SeO_4^{2-} with e_{vis}^- (6, 11).

Objections which have been raised by the referees to the idea of trap-to-trap tunnelling are that the occupied traps would be deeper than the unoccupied traps, and that infrared traps would be shallower than visible traps. We have observed no signs of trap deepening in this work and we emphasize the fact that e_{ir}^- exists quite separately from e_{vis}^- and there is no evidence that it transforms into e_{vis}^- by deepening its trap. However, if we make the reasonable assumption that tunnelling cannot be endothermic by much more than kT, then the trap-to-trap interpretation requires that a fairly high concentration of visible traps have a ground state energy that is very similar to that of a high concentration of infrared traps, and such a near-coincidence is unexpected in view of quite different energies at λ_{max} of the optical transitions in e_{vis}^- and e_{ir}^-. In terms of e_t^- as a particle in a cubic box, which is undoubtedly a gross over-simplification of the real situation, the near-coincidence in ground state energies would imply that the infrared traps must be $\sqrt{5.7}$ times wider than the visible traps.

In our opinion the present data are more in line with a trap-to-trap tunnelling model than with current direct tunnelling models. However, each model is undoubtedly a very simplified representa-

Can. J. Chem. Downloaded from www.nrcresearchpress.com by 210.87.254.105 on 09/05/12
For personal use only.

tion of the actual processes occurring and further experimental and theoretical work is needed to unravel their complexities. In particular attention should be focussed on the effects of the glass composition and structure on tunnelling kinetics.

(3) Effect of Cu(II) and SeO_4^{2-} on the Yields of e_{vis}^- and e_{ir}^-

It is difficult to evaluate the data in Table 3 quantitatively because of the problem of estimating the amount of decay which occurs during the pulse. However, a number of features deserve comment. First, Cu(II) reduces $G(e_t^-)$ much less effectively than SeO_4^{2-} in agreement with previous conclusions that SeO_4^{2-} is a good dry electron scavenger and Cu(II) is not (6, 12). As proposed before (6), the effect of Cu(II) on $G(e_{vis}^-)$ at 76 K is attributed mainly to formation of encounter pairs. Secondly, $G(e_{ir}^-)$ is decreased more than $G(e_{vis}^-)$, indicating a higher probability of encounter pair formation by e_{ir}^- (1), i.e. a larger value of r. The effect is more marked for SeO_4^{2-}, and supports the conclusions already drawn from the kinetic data about the reactivity of e_{ir}^-. Thirdly, the G/G_0 values for SeO_4^{2-} at 138 K vary much more with [LiCl] than those at 76 K for SeO_4^{2-} or Cu(II). A possible explanation for this is that at 138 K thermal detrapping of e_{ir}^- and efficient scavenging of the resulting mobilised electron by SeO_4^{2-} plays a significant role in the decay of e_{vis}^- at low [LiCl].

(4) Yields of Cl_2^-

Whereas $[G(e_{vis}^-) + G(e_{ir}^-)]$ is independent of [LiCl], $G(Cl_2^-)$ appears to be proportional to [LiCl]. Cl_2^- is likely to be produced by the reaction sequence

$$[8] \qquad (D_2O^+ \ldots Cl^-) \rightarrow D_2O + Cl$$

$$[9] \qquad Cl + Cl^- \rightarrow Cl_2^-$$

where $(D_2O^+ \ldots Cl^-)$ represents ionization of D_2O bound to Cl^-.

If as proposed (7) each Cl^- is bound to six water molecules, each of which is shared with another Cl^-, then $G(Cl_2^-)$ should be proportional to the electron fraction of $Cl^-\cdot 3D_2O$ if ionization of the free D_2O and the D_2O bound only to Li^+ does not contribute significantly to $G(Cl_2^-)$. A plot of $G(Cl_2^-)$ against the electron fraction of $Cl^-\cdot 3D_2O$ is shown in Fig. 8 and implies that $G(Cl_2^-)$ from this entity is 3.4.

The larger yields of Cl_2^- at higher $[Cl^-]$ imply a lower yield of unscavenged holes that can undergo reaction [1], and hence a higher yield of e_t^- through reactions [2] and [3]. This effect could compensate for the lower concentration of electron traps (decrease in $\{[\text{free } D_2O] + [LiCl\cdot 4D_2O]\}^{1/2}$) and account for the observation that $[G(e_{vis}^-) + G(e_{ir}^-)]$ does not decrease at the higher concentrations of LiCl.

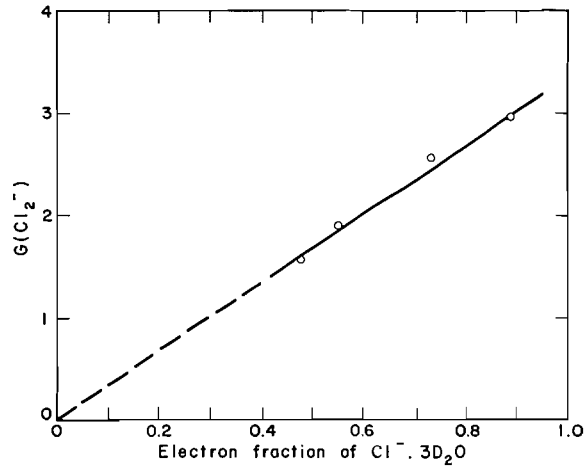

FIG. 8. Dependence of $G(Cl_2^-)$ on the electron fraction of $Cl^-\cdot 3D_2O$ in LiCl glasses at 76 K.

It is perhaps worth noting that in a pulse radiolysis (13) study of aqueous lithium chloride solutions at room temperature it was found that $G(Cl_2^-)$ passes through a maximum at a Cl^- concentration of about 9 *M*. However, there is no evidence that structures such as $Cl^-\cdot 3H_2O$ exist at room temperature, so that similarities with results found in the present work are not expected.

(5) Conclusions

The major conclusions drawn from this work are the following: (*a*) The infrared absorbing trapped electron is mainly associated with a purely water environment, which is in agreement with conclusions from luminescence studies on mixed-solute aqueous glasses (14), and e_{vis}^- is mainly associated with water bound to Li^+. (*b*) The unusual tunnelling kinetics observed in LiCl glasses seem to be associated with the relative concentrations of infrared and visible traps which change with [LiCl].

Acknowledgements

We are indebted to Dr. N. Boden and his coworkers for information and helpful discussions on the structure of LiCl glasses and to Dr. D. C. Walker for providing us with manuscripts before publication.

1. G. V. BUXTON, H. A. GILLIS, and N. V. KLASSEN. Can. J. Chem. **54**, 367 (1976).
2. (*a*) H. A. GILLIS and D. C. WALKER. J. Chem. Phys. **65**, 4950 (1976). (*b*) T. A. NGUYEN and D. C. WALKER. J. Chem. Phys. **67**, 2399 (1977).
3. G. V. BUXTON, H. A. GILLIS, and N. V. KLASSEN. Can. J. Chem. **55**, 2385 (1977).
4. C. A. ANGELL and E. J. SARE. J. Chem. Phys. **52**, 1058 (1970).

5. G. V. BUXTON and K. G. KEMSLEY. J. Chem. Soc. Faraday Trans. I, **71**, 568 (1975).
6. G. V. BUXTON and K. G. KEMSLEY. J. Chem. Soc. Faraday Trans. I, **72**, 1333 (1976).
7. I. C. BAIANU, N. BODEN, D. LIGHTOWLERS, and M. MORTIMER. Chem. Phys. Lett. **54**, 169 (1978).
8. J. R. MILLER. J. Phys. Chem. **79**, 1070 (1975).
9. G. V. BUXTON. *In* Fast processes in radiation chemistry and biology. *Edited by* G. E. Adams, E. M. Fielden, and B. D. Michael. Wiley, London. 1975. p. 95.
10. J. M. WARMAN, K.-D. ASMUS, and R. H. SCHULER. *In* Radiation chemistry – II. Advances in Chemistry Series, Vol. 82. *Edited by* R. F. Gould. American Chemical Society, Washington. 1968. p. 25.
11. J. R. MILLER. J. Chem. Phys. **56**, 5173 (1972).
12. G. V. BUXTON and K. G. KEMSLEY. J. Chem. Soc. Faraday Trans. I, **72**, 466 (1976).
13. R. J. WOODS, B. LESIGNE, L. GILLES, C. FERRADINI, and J. PUCHEAULT. J. Phys. Chem. **79**, 2700 (1975).
14. T. Q. NGUYEN and D. C. WALKER. J. Chem. Soc. Faraday Trans. I, **73**, 1958 (1977).

Can. J. Chem. Downloaded from www.nrcresearchpress.com by 210.87.254.105 on 09/05/12
For personal use only.

Identification of C-24 alkyl epimers of marine sterols by ^{13}C nuclear magnetic resonance spectroscopy[1]

J. L. C. WRIGHT, A. G. MCINNES, S. SHIMIZU, D. G. SMITH, AND J. A. WALTER

National Research Council of Canada, Atlantic Regional Laboratory, 1411 Oxford Street, Halifax, N.S., Canada B3H 3Z1

AND

D. IDLER AND W. KHALIL

Marine Sciences Research Laboratory, Memorial University of Newfoundland, St. John's, Nfld., Canada A1C 5S7

Received January 17, 1978

J. L. C. WRIGHT, A. G. MCINNES, S. SHIMIZU, D. G. SMITH, J. A. WALTER, D. IDLER, and W. KHALIL. Can. J. Chem. **56**, 1898 (1978).

^{13}C nuclear magnetic resonance spectra of diastereomeric C-24 alkyl sterols have been assigned. Differences in the chemical shifts of side-chain carbons permitted the determination of the absolute configuration at C-24 in several sterols since these chemical shifts are insensitive to structural changes remote from the asymmetric centre. An unknown sterol from *Tetraselmis suecica* has been identified as (24*R*)-24-methylcholest-5-en-3β-ol and the configuration assigned from ^1H nmr data to the sterol from *Phaeodactylum tricornutum* has been confirmed. The utility and potential of this method in characterising new sterols and their biological precursors is discussed.

J. L. C. WRIGHT, A. G. MCINNES, S. SHIMIZU, D. G. SMITH, J. A. WALTER, D. IDLER et W. KHALIL. Can. J. Chem. **56**, 1898 (1978).

On a attribué les spectres rmn du ^{13}C de stérols diastéréoisomères en position C-24 de la chaîne alkyle. Les différences dans les déplacements chimiques des carbones de la chaîne latérale permettent de déterminer la configuration absolue au niveau C-24 dans plusieurs stérols puisque ces déplacements chimiques ne sont pas sensibles à des changements structuraux éloignés du centre asymétrique. Un stérol inconnu provenant du *Tetraselmis suecica* a pu être identifié comme étant le méthyl-24 cholesten-5 ol-3β (24*R*) et on a pu confirmer la configuration attribuée à partir de la rmn du ^1H au stérol provenant du *Phaeodactylum tricornutum*. On discute de l'utilité et des potentialités de cette méthode dans la caractérisation de nouveaux stérols et de leurs précurseurs biologiques.

[Traduit par le journal]

Introduction

Many sterols of plants and microorganisms contain a methyl or ethyl group at C-24, and both C-24 diastereoisomers have been found to occur naturally. From the cases that have been examined it appears that the alkyl group is derived biosynthetically by a transalkylation process involving *S*-adenosylmethionine (1). Sterols are vital membrane components of many organisms and presumably their stereochemical features are important in this respect (2–4). Indeed, there appears to be some phylogenetic significance to the configuration at C-24, since, in general, algae and fungi produce sterols with the 24β configuration (24*S* if a saturated side chain, 24*R* if the Δ^{22} derivative) whereas sterols in most vascular plants possess the 24α configuration (1).

In the identification of stereoisomers ordinary X-ray diffraction analysis yields only the relative configurations of chiral centers, although the absolute configurations become accessible if one is already known. Anomalous X-ray scattering is the only method which characterises configurations directly. In contrast indirect methods always involve comparisons with model compounds of known configuration. Those which measure a general property of a molecule, e.g. optical rotation, melting point, retention time in gas–liquid chromatography, are necessarily restricted to the recognition of previously identified compounds, whereas others like nuclear magnetic resonance spectrometry, which provide information on specific sites in a molecule, can be used to identify structural units in unknown compounds.

During the course of our investigations of marine algal products, it occurred to us that the efficacy of ^{13}C nmr spectroscopy to probe stereochemical features (5, 6) might result in a more versatile approach to the identification of C-24 alkyl sterols. Thus chemical shift data obtained for the side-chain carbons of diastereoisomeric model steroids epimeric at C-24 should provide the basis for defining the configuration at this position in unknown steroids with the same side chain, provided changes in molecular structure are remote from the chiral center. Also, as the spin–lattice relaxation times of corresponding carbons in the two epimeric side chains would be

[1]NRCC No. 16610.

Can. J. Chem. Downloaded from www.nrcresearchpress.com by 210.87.254.40 on 09/05/12
For personal use only.

Can. J. Chem. Downloaded from www.nrcresearchpress.com by 210.87.254.40 on 09/05/12
For personal use only.

very similar, the composition of mixtures of stereoisomers can be obtained from the relative intensities of corresponding carbon signals.

Experimental

(24*R*)-24-Methylcholesta-4,22-dien-3-one (**14**) was purchased from Steraloids Inc., Wilton, NH, listed as 4,22-cholestadien-24-methyl-3-one, catalogue No. C2952. 'Campesterol' (**2***b*), from soybean, was obtained from Nutrional Biochemicals, Cleveland, OH, and contained approximately one-third 22,23-dihydrobrassicosterol (**2***a*). Stigmasterol (**11***a*) was purchased from Applied Science Laboratories, State College, PA, and purified by chromatography on alumina and crystallisation.

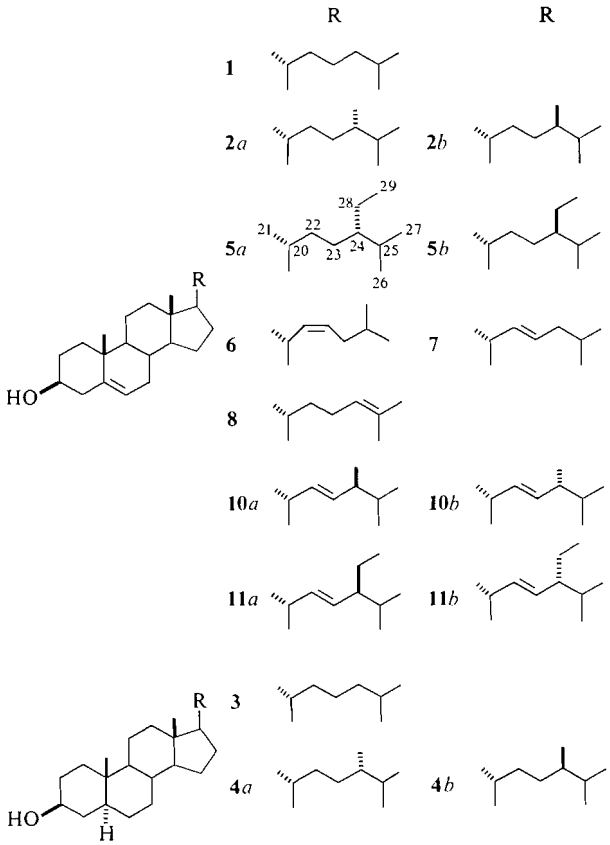

Ergostanol (**4***a*) and 22,23-dihydrobrassicasterol (**2***a*) were obtained by selective reduction (7) of ergosterol (**9**). 24-Methylcholesterol (**2***b*) from *Tetraselmis suecica*, clionasterol (**5***a*) from *Nitella*, poriferasterol (**11***b*) from *Spirogyra*, and 22-dehydrocampesterol (**10***a*) from *Phaeodactylum tricornutum* were obtained from Dr. G. Patterson. The sample of 22-*cis*-dehydrochalesterol was a gift from Dr. J. A. Svoboda. Except as noted elsewhere in the text the remaining sterols were isolated from scallop or prepared from these sterols (8, 9).

^{13}C nuclear magnetic resonance spectra were recorded with a Varian XL-100/15 Fourier transform spectrometer under the following conditions: frequency 25.16 MHz, acquisition time 1.6 s (data accuracy ± 0.3 Hz), spectral width 2560, 4002, or 5120 Hz, flip angle ca. 57°, internal pulse lock to ^2H in C^2HCl_3 (solvent), temperature 30°C, concentration 5–30 mg/ml. For off-resonance decoupling, protons were irradiated at δ_H ca. 6.25 ppm ($\gamma H_2/2\pi$ ca. 1800 or 3800 Hz). Broadband ^1H decoupling was obtained by phase modulation of the decoupling field from 0 to 180° at 150 Hz, with $\gamma H_2/2\pi$ 3800 Hz.

Proportions of diastereoisomers in mixtures were determined by averaging the relative intensity of each pair of ^{13}C resonances for which the chemical shift differed appreciably between epimers (error is standard deviation).

Results

Assignment of Resonances

Sterol Ring System

The original assignments of the resonances in the ^{13}C nmr spectrum of cholesterol (**1**) were made by Reich *et al.* (10) and were later confirmed by Mantsch and Smith (11), although those for C-12, C-16, C-20, C-26, and C-27 were tentative. Subsequent work (12, 13) showed that the assignments for C-12 and C-16 should be interchanged but final confirmation of the assignments arose from an elegant study by Popják and co-workers (14) on cholesterol biosynthesis using singly and doubly ^{13}C-labeled mevalonate. They were also able to establish for the first time that the *pro*-(*S*)-methyl carbon C-27 (derived from C-3′ of mevalonate) resonated at lower field than the *pro*-(*R*)-methyl carbon C-26 (originating from C-2 of mevalonate). Thus all the sterols listed in Table 1 possessing the cholesterol ring system produce easily identifiable signals in their ^1H broadband-decoupled, off-resonance decoupled, and high resolution ^{13}C spectra. Similarly the resonances for C-1 through C-19 in **4***a* and **4***b* were assigned with the aid of recent chemical shift data (15, 16) on 5α-cholestan-3β-ol (**3**) which differed from initial assignments (10) by interchanging those for C-12 and C-16, and C-18 and C-19.

Saturated Side Chain

Resonances for the alkyl side-chain carbons (C-20 through C-28 or C-29) of **2***a*, **2***b*, **4***a*, **4***b*, **5***a*, and **5***b* (see Table 1) were assigned by direct comparison with published spectral data on model alkanes (17), combined with calculations using an improved set of ^{13}C chemical shift additive substituent parameters (18). Space-filling molecular models indicated restricted rotation about the C-24, C-25 bond in these steroids, with H-24 and H-25 antiperiplanar in the most stable conformation, and this conclusion is supported by the X-ray crystallographic data for several ergostane derivatives (19). If this conformation predominates in **2***a* and **4***a*, which have a 24*S*-configuration, it follows that the *pro*-(*R*)-methyl carbon (C-26, δ_C 17.7) attached to C-25 will be synclinal to the C-28 methyl group, and therefore chemically shielded (20) relative to the *pro*-(*S*)-methyl carbon (C-27, δ_C 20.5), whereas the reverse can be expected for **2***b* and **4***b* with a 24*R* configuration (C-26, δ_C 20.2; C-27, δ_C

Can. J. Chem. Downloaded from www.nrcresearchpress.com by 210.87.254.40 on 09/05/12
For personal use only.

TABLE 1. Carbon chemical shifts of C_{27}, C_{28}, and C_{29} sterols

Carbons	**1**	**2***a*	**2***b*	**3***	**4***a*	**4***b*	**5***a*	**5***b*	**6**	**7**	**8**	**9**†	**10***a*	**10***b*	**11***a*	**11***b*	**14**
1	37.29	37.34		37.0	37.07		37.31		37.33	37.29	37.33	37.88	37.36		37.31	37.30	38.61
2	31.69	31.76		31.5	31.58		31.57		31.73	31.70	31.73	28.10	31.69		31.69	31.69	33.97
3	71.81	71.87		71.4	71.40		71.69		71.84	71.82	71.84	72.66	71.76		71.81	71.83	199.48
4	42.34	42.40		38.2	38.28		42.25		42.37	42.33	42.40	36.62	42.30		42.35	42.27	123.77
5	140.78	140.75		44.9	44.92		140.76		140.81	140.77	140.84	138.25	140.79		140.80	140.79	171.52
6	121.71	121.72		28.8	28.79		121.59		121.74	121.70	121.75	120.04	121.60		121.69	121.72	32.94
7	31.93	31.99		32.1	32.14		31.92		31.95	31.92	31.97	116.16	31.97		31.94	31.92	32.05
8	31.93	31.99		35.5	31.57		31.92		31.95	31.92	31.97	141.16	31.97		31.94	31.92	35.63
9	50.18	50.24		54.4	54.43		50.17		50.25	50.19	50.22	46.02	50.27		50.20	50.20	53.86
10	36.52	36.58		35.5	35.57		36.51		36.58	36.53	36.57	37.06	36.58		36.56	36.55	35.70
11	21.11	21.16		21.3	21.30		21.11		21.12	21.09	21.15	21.07	21.13		21.11	21.11	21.03
12	39.82	39.86		40.1	40.10		39.81		39.79	39.70	39.86	39.00	39.77		39.74	39.73	39.53
13	42.34	42.40		42.6	42.64		42.33		42.30	42.26	42.40	42.78	42.35		42.35	42.33	42.30
14	56.80	56.85		56.5	56.56		56.79		56.88	56.87	56.83	54.45	56.96		56.91	56.90	55.98
15	24.31	24.36		24.3	24.25		24.32		24.32	24.30	24.36	23.01	24.39		24.39	24.37	24.16
16	28.24	28.27		28.3	28.27		28.26		28.10	28.57	28.27	28.10	28.86	28.58	28.96	28.82	28.46
17	56.20	56.11	56.21	56.3	56.20	56.31	56.11		56.28	55.95	56.17	55.66	56.06		56.06	56.06	55.98
18	11.87	11.90		12.1	12.10		11.87		12.22	12.07	11.95	12.06	12.09		12.07	12.06	12.18
19	19.41	19.44		12.3	12.35		19.40		19.46	19.43	19.45	16.13	19.42		19.42	19.42	17.38
20	35.81	36.26	35.96	35.8	36.25	35.93	36.29	36.17	34.24	40.13	36.16	40.40	40.33	40.24	40.54	40.45	40.12
21	18.74	18.95	18.77	18.7	18.88	18.68	18.82		20.73	20.87	18.70	21.07	21.06		21.11	20.95	20.90
22	36.22	33.80		36.2	33.74		33.95		137.23	138.12	35.67	135.25	136.05	135.83	138.37	138.28	135.64
23	23.86	30.67	30.37	23.9	30.65	30.35	26.43	26.13	125.46	126.25	24.80	131.76	131.84	131.76	129.32	129.37	131.90
24	39.54	39.17	38.92	39.5	39.13	38.88	46.07	45.85	36.82	41.98	125.29	42.78	43.12	42.90	51.29	51.25	42.81
25	28.02	31.54	32.49	28.0	31.58	32.45	28.98	29.18	28.77	28.64	130.93	33.04	33.28	33.16	31.94	31.87	33.09
26	22.57	17.68	20.26	22.6	17.64	20.22	19.07	19.84	22.41	22.31	17.67	19.96	19.69	20.02	21.26	18.97	19.95
27	22.86	20.56	18.32	22.8	20.53	18.28	19.62	19.07	22.64	22.31	25.74	19.67	20.19	19.69	19.02	21.20	19.63
28		15.51	15.44		15.41		23.09					17.63	18.08	17.68	25.44	25.42	17.61
29							12.32								12.27	12.43	

*These values were reported for 3β-cholestanol in ref. 16.
†These values were reported for ergosterol acetate in ref. 21.

Can. J. Chem. Downloaded from www.nrcresearchpress.com by 210.87.254.40 on 09/05/12
For personal use only.

18.3). The numbering of these methyl carbons conforms with that used for the corresponding carbons in cholesterol (14).

Previously reported (17) chemical shift data for 2,3-dimethyl- (**12**) and 2-methyl-3-ethylpentane (**13**) were used to assign resonances for C-26 and C-27 of **5***a* and **5***b*. Two methyl carbons attached to C-2 in **12** resonated at δ_C 20.0 and δ_C 17.7, whereas similar carbons in **13** were fortuitously chemically equivalent at δ_C 19.0. Thus replacement of the methyl group bonded to C-3 of **13** with an ethyl group deshields one methyl carbon (δ_C 17.7) by 1.3 ppm and shields the other (δ_C 20.0) by 1.0 ppm. The same substituent change at C-24 on going from **2***a* (**2***b*) or **4***a* (**4***b*) to **5***a* (**5***b*) produces a similar shift in resonances, permitting the C-26 (*pro-*(*R*)-methyl) and C-27 (*pro-*(*S*)-methyl) signals for **5***a* and **5***b* to be assigned as shown in Table 1.

Unsaturated Side Chain

Assignment of resonances due to the alkenyl side-chain carbons C-20, C-22 through C-25, and C-28 of

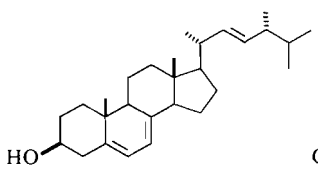

9

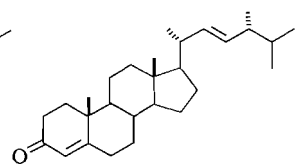

14

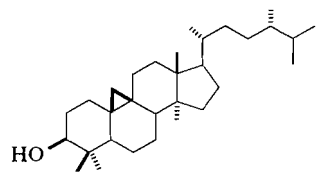

15

10*a* and **10***b* was based on chemical shift data from a recent study by Cushley and co-workers (21) on ergosterol (**9**) labeled from [1-^{13}C]acetate. Their results led to the interchange of previous assignments (10) for the pairs of carbons C-5,C-8; C-12,C-16; C-22,C23, and left only the assignments for C-21, C-26, and C-27 in doubt. The latter were identified as follows. Comparison with published data (22) for (*E*)-(C-6, δ_C 22.36) and (*Z*)-5-methylhex-22-ene (C-6, δ_C 22.42) enabled the resonances of C-26 (δ_C 22.41, 22.31) and C-27, (δ_C 22.64, 22.31), and therefore C-21 (δ_C 20.73, 20.87), to be identified in **6** and **7**. Although the C-21 methyl resonance is insensitive to the stereochemistry of the Δ^{22} double bond the data for desmosterol (**8**) indicates that this carbon, as well as C-26 and C-27, is influenced by the position of the bond. In **9**, **10***a*, and **10***b* the methyl substituent at C-24 would be expected to shield both C-26 and C-27, but not C-21, which would still resonate at ca. δ_C 21.0. Resonances were assigned to C-26 and C-27 on the basis that the most shielded methyl carbon is synclinal to C-28 in the most stable conformation. The chemical shifts of C-26 and C-27 in **9**, **10***a*, and **10***b* are in good agreement with the shift of the fortuitously chemically-equivalent terminal methyl carbons (δ_C 19.78) of 3,4-dimethylpent-1-ene (22). For **11***a* and **11***b*, the assignments for C-20 through C-25, C-28, and C-29 followed from the expected changes in chemical shift due to replacement of the C-24 methyl group of **9**, **10***a*, and **10***b* by an ethyl group. The signals from C-26 and C-27 were assigned as for **5***a* and **5***b*.

Discussion

The absolute configuration at C-20 and C-24 has been deduced for several C-24 alkyl sterols, as a result of chemical (23) and X-ray crystallographic studies (19).

The original ^{1}H nmr study (24) at 60 and 100 MHz showed slight chemical shift differences between the methyl hydrogens of several C-24 alkyl sterols but later studies at 220 MHz (25–29) and 270 MHz (30) permitted a rough quantitative analysis of an epimeric mixture. However it was still difficult to differentiate the epimers of C-24 ethyl sterols and the problem was magnified by the introduction of a *trans* double bond at C-22 (28, 29).

*(24*R*)-24-Methylcholest-5-en-3*β*-ol (**2**b) and (24*S*)-24-Methylcholest-5-en-3*β*-ol (**2**a)*

Four samples were available including authentic 24*R* and 24*S* material, the former from Applied Science Laboratories and the latter obtained by catalytic reduction of ergosterol (**9**). The remaining two were epimeric mixtures, one from soybean and the other from scallop. For these sterols characteristic chemical shifts induced by the C-28 methyl group on other side-chain carbons provide a basis for assigning the configuration at C-24. Thus C-26 has δ_C 17.6 in the 24*S* epimer **2***a* and C-27 has δ_C 18.3 in the 24*R* epimer **2***b*. C-26 and C-27 in the 24*S* diastereoisomer have a chemical shift difference of 2.8 ppm in contrast to a difference of only 1.8 ppm for the 24*R* epimer, although in both cases the average chemical shift of the two carbons is δ_C 19.2 $\pm$ 0.1 ppm. Also C-25 is 1 ppm more shielded in the 24*S* than the 24*R* diastereoisomer. Configurational effects on other side-chain carbons are less pronounced, with C-17 slightly more shielded and C-20, C-21, C-23, and C-24 more deshielded in the 24*S* isomer. This information allowed a 24-methyl cholesterol derivative of unknown configuration from *Tetraselmis suecica* to be identified as campesterol (**2***b*). Intensity measurements established that the soybean mixture contained 34% **2***a* and 66% **2***b*

Can. J. Chem. Downloaded from www.nrcresearchpress.com by 210.87.254.40 on 09/05/12
For personal use only.

(±5%) in contrast to the scallop sample which contained 52% **2***a* and 48% **2***b* (±6%).

*(24*R*)-24-Methyl-5α-cholestan-3β-ol (4*b*) and (24*S*)-24-Methyl-5α-cholestan-3β-ol (4*a*)*

This mixture of diastereoisomers was obtained by catalytic reduction of 24-methyl-22-dehydrocholesterol isolated from scallop. Reduction of the cholesterol nucleus has no effect on the side-chain resonances which display shifts almost identical with those for dihydrobrassicasterol (**2***a*) and campesterol (**2***b*) (Table 1). Analysis of the mixture showed 33% **4***a* and 67% **4***b* (±3%).

*(24*R*)-24-Ethylcholest-5-en-3β-ol (5*b*) and (24*S*)-24-Ethylcholest-5-en-3β-ol (5*a*)*

Three samples were examined: sitosterol (**5***b*) isolated and purified from soybean, clionasterol (**5***a*) obtained from *Nitella* as the acetate (31), and a mixture isolated from scallop.

As discussed in the ^{1}H nmr studies (28, 29), it becomes more difficult to differentiate the C-24 diastereoisomers of C_{29} sterols. With ^{13}C nmr they are more readily distinguishable although the differences are small and it is advisable to have spectra of both epimers for comparison.

For **5***a* and **5***b*, the most substantial chemical shift differences as a result of configuration changes at C-24 occur for C-26 (0.77 ppm more shielded in the *S* isomer), C-27 (0.55 ppm less shielded), C-23 (0.30 ppm less shielded), C-25 (0.20 ppm more shielded), C-24 (0.22 ppm less shielded), and C-20 (0.12 ppm less shielded).

Good quantitative analysis of a mixture is possible: the diastereomeric mixture from scallop shows 33% **5***a* and 67% **5***b* (±2%). Interestingly the sample of 24*S* isomer, clionasterol (**5***a*), isolated from *Nitella* (31) appears to contain a slight amount (~10–15%) of the diastereoisomer, perhaps reflecting a lack of stereochemical control during the biogenesis or epimerisation of a labile biogenetic intermediate.

*(22*E*,24*R*)-24-Methylcholesta-5,22-dien-3β-ol (10*b*) and (22*E*,24*S*)-24-Methylcholesta-5,22-dien-3β-ol (10*a*)*

Two samples were examined: a mixture of C-24 diastereoisomers from scallop and a sample from the diatom *Phaeodactylum tricornutum* reported to be the 24*S* isomer, 22-dehydrocampesterol (**10***a*). Since no authentic sample of the 24*R* isomer was available to us, ergosterol acetate (21) was used as a model compound for the chemical shifts of the side-chain carbons C-20 through C-28 (Table 1).

Differences between the ^{13}C nmr spectra of the epimers were apparent from a comparison of 22-dehydrocampesterol (**10***a*) and the scallop mixture, the most useful for analysis being the resonances of C-28 and C-16, respectively 0.4 and 0.28 ppm more shielded in the 24*R* isomer. Specifically, the resonance for the C-28 methyl carbon appears at a characteristic value of δ_C 17.6 ± 0.1 in the 24*R* epimer. The C-26 resonance in the 24*S* isomer overlaps with that for C-27 in the *R* isomer but δ_C for C-27 (*S*) and C-26 (*R*) differ by 0.17 ppm. Integration of resonances from the scallop mixture indicated that it contained 72% of **10***a* and 28% **10***b* (±2%).

The ^{13}C nmr spectrum of the sterol from *P. tricornutum* was in complete accord with the assignment of the 24*S* configuration by Rubinstein and Goad (27), based on ^{1}H nmr data.

*(22*E*,24*R*)-24-Ethylcholesta-5,22-dien-3β-ol (11*b*) and (22*E*,24*S*)-24-Ethylcholesta-5,22-dien-3β-ol (11*a*)*

Three samples were examined: the two pure diastereoisomers and a mixture from scallop that contained predominantly one epimer.

The ^{13}C chemical shift differences between these diastereoisomers are so small that it is preferable to have the other isomer, or a mixture, for comparison under identical conditions before the configuration of an unknown sterol of this type can be established. From our data (Table 1) the largest chemical shift difference between epimers is at the C-16 resonance (0.14 ppm) and the C-29 resonance (0.16 ppm). Quantitative analysis is still possible, and this mixture from scallop contains 33% **11***a* and 67% **11***b* (±8%).

To improve analysis by ^{1}H nmr Rubinstein *et al.* (28) suggested the unsaturated side chain should be reduced. Although this would assist in the ^{13}C nmr analysis it is not essential. Chiral solvents may help, but shift reagents are unlikely to be useful as they cause negligible shifts in the side-chain resonances (15, 33).

Using our data, it should be possible to identify the configuration of unknown sterols with a side chain common to any of the cases we have analysed in this study. The effect of changing the concentration of various steroid derivatives is small (16) and from the data available it appears that many structural changes in rings A, B, and C of the sterol also have little or no effect on the chemical shift of the side-chain resonances. For example, compare data for **2***a*,**2***b*; **4***a*,**4***b*; **10***a*,**10***b* (Table 1).

The C-28 methyl resonance at δ_C 17.6, characteristic of a 24*R* configuration in sterols possessing an unsaturated side chain, is also found in the cholestadienone derivative **14** (Table 1) and in a variety of ergosterol derivatives (34) despite structural modifications of ring C. Similarly we can assign an *S*

configuration at C-24 of cyclolaudanol (**15**) (35) in spite of the major structural differences between the cholesterol and cycloartenol skeletons. These examples illustrate the potential of this approach in characterising unknown sterols and their biological precursors.

Acknowledgements

We would like to acknowledge the technical assistance of Cheryl Craft at the Atlantic Regional Laboratory and the gift of sterols from Dr. G. W. Patterson, University of Maryland. This work was supported in part by research grant A6732 from the National Research Council of Canada to D.R.I.

1. L. J. GOAD, J. R. LENTON, F. F. KNAPP, and T. W. GOODWIN. Lipids, **9**, 582 (1974).
2. B. A. KNIGHTS. Chem. Br. **9**, 106 (1973).
3. W. R. NES. Lipids, **9**, 596 (1974).
4. E. HEFTMANN. Phytochemistry, **14**, 891 (1975).
5. N. K. WILSON and J. B. STOTHERS. Top. Stereochem. **8**, 1 (1974).
6. A. S. PERLIN. *In* Isotopes in organic chemistry. Vol. 3. *Edited by* E. Buncel and C. C. Lee. Elsevier North-Holland Inc., New York, NY. 1977. p. 171.
7. W. TADROS and A. L. BOULOS. Helv. Chim. Acta, **58**, 668 (1975).
8. G. W. PATTERSON, M. K. KHALIL, and D. R. IDLER. J. Chromatog. **115**, 153 (1975).
9. D. R. IDLER, M. W. KHALIL, J. D. GILBERT, and C. J. W. BROOKS. Steroids, **27**, 155 (1976).
10. H. J. REICH, M. JAUTELAT, M. T. MESSE, F. J. WEIGERT, and J. D. ROBERTS. J. Am. Chem. Soc. **91**, 7445 (1969).
11. H. H. MANTSCH and I. C. P. SMITH. Can. J. Chem. **51**, 1384 (1973).
12. H. EGGERT and C. DJERASSI. J. Org. Chem. **38**, 3788 (1973).
13. J. W. APSIMON, H. BEIERBECK, and J. K. SAUNDERS. Can. J. Chem. **51**, 3874 (1973).
14. G. POPJAK, J. EDMOND, F. A. L. ANET, and N. R. EASTON. J. Am. Chem. Soc. **99**, 931 (1977).
15. D. J. CHADWICK and D. H. WILLIAMS. J. Chem. Soc. Perkin II, 1903 (1974).
16. H. EGGERT, C. L. VAN ANTWERP, N. S. BHACCA, and C. DJERASSI. J. Org. Chem. **41**, 71 (1976).
17. L. P. LINDEMAN and J. Q. ADAMS. Anal. Chem. **43**, 1245 (1971).
18. D. M. GRANT and E. G. PAUL. J. Am. Chem. Soc. **86**, 2984 (1964).
19. C. ROMERS, C. ALTONA, H. J. C. JACOBS, and R. A. G. DE GRAAFF. *In* Terpenoids and steroids. Vol. 4. *Edited* by K. H. Overton. Specialist Periodical Reports. The Chemical Society, London. 1974. p. 531.
20. W. R. WOOLFENDER and D. M. GRANT. J. Am. Chem. Soc. **88**, 1496 (1966); H. BEIERBECK and J. K. SAUNDERS. Can. J. Chem. **54**, 2985 (1976); K. SIEDMAN and G. E. MACIEL. J. Am. Chem. Soc. **99**, 659 (1977).
21. R. J. CUSHLEY and J. D. FILIPENKO. Org. Magn. Reson. **8**, 308 (1976).
22. P. A. COUPERUS, A. D. H. CLAGUE, and J. P. C. M. VAN DONGEN. Org. Magn. Reson. **8**, 426 (1976).
23. C. J. W. BROOKS. *In* Rodds chemistry of carbon compounds. Vol. 2, Pt. D. *Edited by* S. Coffey. Elsevier Publishing Company, New York, NY. 1976. p. 1.
24. M. J. THOMPSON, S. R. DUTKY, G. W. PATTERSON, and E. L. GOODEN. Phytochemistry, **11**, 1781 (1972).
25. L. J. MULHEIRN. Tetrahedron Lett. 3175 (1973).
26. I. RUBINSTEIN and L. J. GOAD. Phytochemistry, **13**, 481 (1974).
27. I. RUBINSTEIN and L. J. GOAD. Phytochemistry, **13**, 485 (1974).
28. I. RUBINSTEIN, L. J. GOAD, A. D. H. CLAGUE, and L. J. MULHEIRN. Phytochemistry, **15**, 195 (1976).
29. W. R. NES, K. KREVITZ, and S. BEHZADAN. Lipids, **11**, 118 (1976).
30. W. SUCROW, M. SLOPIANKA, and H. W. KIRCHER. Phytochemistry, **15**, 1533 (1976).
31. G. W. PATTERSON. Phytochemistry, **11**, 3481 (1972).
32. D. R. IDLER and P. WISEMAN. Comp. Biochem. Physiol. **35**, 679 (1970).
33. W. B. SMITH, D. L. DEAVENPORT, J. A. SWANZY, and G. A. PATE. J. Magn. Reson. **12**, 15 (1973).
34. R. J. ABRAHAM and J. R. MONASTERIOS. J. Chem. Soc. Perkin II, 662 (1974).
35. F. KHUONG-HUU, M. SANGARE, V. M. CHARI, A. BEKAERT, M. DEVYS, M. BARBIER, and G. LUKACS. Tetrahedron Lett. 1787 (1975).

Can. J. Chem. Downloaded from www.nrcresearchpress.com by 210.87.254.40 on 09/05/12
For personal use only.

The X-ray crystal structure of (±)-flavipucine

PETER S. WHITE, JOHN A. FINDLAY, AND WAH HUNG JOHN TAM
Department of Chemistry, University of New Brunswick, Fredericton, N.B., Canada E3B 5A3

Received February 6, 1978

PETER S. WHITE, JOHN A. FINDLAY, and WAH HUNG JOHN TAM. Can. J. Chem. **56**, 1904 (1978).

Synthetic (±)-flavipucine ($C_{12}H_{15}O_4N$) is monoclinic, space group $P2_1/c$, with $a = 11.506(5)$, $b = 8.765(5)$, $c = 11.981(7)$ Å, $\beta = 91.09(2)°$, $Z = 4$. X-ray analysis confirms its structure as **1**, 3′-isovaleryl-6-methyl pyridine-3-spiro-2′-oxiran-2(1*H*),4(3*H*)-dione and reveals the configuration of the oxirane to be *Z*.

PETER S. WHITE, JOHN A. FINDLAY et WAH HUNG JOHN TAM. Can. J. Chem. **56**, 1904 (1978).

La (±)-flavipucine ($C_{12}H_{15}O_4N$) obtenue par synthèse est monoclinique, groupe d'espace $P2_1/c$ avec $a = 11.506(5)$, $b = 8.765(5)$, $c = 11.981(7)$ Å, $\beta = 91.09(2)°$, $Z = 4$. L'analyse par rayons-X confirme que sa structure est celle de **1**, soit l'isovaléryl-3′ méthyl-6 pyridine spiro-3 oxiranne-2′ dione-2(1*H*), -4(3*H*) et révèle que la configuration de l'oxiranne est *Z*.

[Traduit par le journal]

Some time ago on the basis of chemical and spectroscopic data we proposed (1) structure **1**, 3′-isovaleryl-6-methyl pyridine-3-spiro-2′-oxiran-2(1*H*),-4(3*H*)-dione, for flavipucine an antibiotic factor isolated from a strain of *Aspergillus flavipes*. Recently, we developed an efficient two-step synthesis of racemic (±)-flavipucine starting with 4-hydroxy-6-methyl-2-pyridone and isobutyl glyoxal (2). Despite this latter development the relative configuration of the oxirane bridge remained unsolved. Furthermore, direct chemical or spectroscopic evidence for the existence of the epoxide feature was scant. Attempts to solve the structure of natural (−)-flavipucine by X-ray techniques by two different groups failed.[1] Noting that our synthetic racemic (±)-flavipucine had a different melting point (153–155°C) from natural (−)-flavipucine (130–131°C) we considered that its crystals might be more amenable to scrutiny by X-ray methods. Accordingly a sample of synthetic (±)-flavipucine recrystallized from benzene was studied with the following results.

Experimental

A preliminary photographic investigation indicated the space group to be $P2_1/c$. Unit cell dimensions were obtained by a least squares fit of 12 well-centered reflections on a Picker FACS-I diffractometer using graphite monochromated Mo K_α radiation. The relevant crystallographic data are:

$C_{12}H_{15}O_4N$ fw = 237.2
Monoclinic, $P2_1/c$, $a = 11.506(5)$, $b = 8.765(5)$, $c = 11.981(7)$ Å. $\beta = 91.09(2)°$, $V = 1208.0$ Å^3, $D_c = 1.30$, $Z = 4$ (20°C; Mo K_α, $\lambda = 0.71069$ Å), crystal size 0.60 × 0.35 × 0.45 mm.

Intensities were measured on the diffractometer using an $\omega - 2\theta$ scan at a rate of 1° 2θ min^{-1} over a range of 2° 2θ corrected for dispersion of the K_α doublet. A stationary background count of 10 s was made on both sides of each reflection. A standard reflection monitored every 20 reflections throughout data collection showed no systematic change in intensity. After correction for background, reflections with a net intensity of less than 20 counts were classified as unobserved. Data were collected to $2\theta = 50°$ which resulted in 2128 unique reflections of which 1160 were considered observed and used in the refinement of the structure.

Structure Determination and Refinement

The structure was solved by multiple solution direct methods using the computer program MULTAN (3). The set of phases with the highest 'combined figure of merit' was used to produce an *E*-map which was searched for peaks. The program FRAGMENT (4) was used to locate sets of connected peaks consistent with expected bond lengths and angles. The resulting fragment consisted of all the nonhydrogen atoms; the oxygen and nitrogen positions were assigned from a chemical knowledge of the structure (1).

Data reduction and refinement of the structure was performed using the XRAY-76 program package of Stewart (5). The structure was refined by least-squares methods, minimizing the quantity $\sum w(|F_o| - |F_c|)^2$. The weighting scheme was of the form $w = 1/\sigma^2(F)$, with σ estimated from the measured intensity (6). Initial refinement of the nonhydrogen atomic positions with isotropic thermal parameters resulted in an agreement index $R = 0.15$, at this point a difference synthesis was used to locate the hydrogen positions. Inclusion of hydrogens with isotropic thermal parameters and use of anisotropic thermal parameters for all other atoms yielded a final agreement index of $R = 0.062$. Table 1 contains the final atomic positional parameters.[2]

Discussion

The structure of the molecule and the numbering scheme are shown in Fig. 1, hydrogens being numbered after the atom to which they are bonded; bond distances and angles are given in Table 2. The six membered ring is essentially planar with an expected shortening of the bond lengths caused by partial

[1]At the Chemistry Department, University of New Brunswick (1972) and C. G. Casinovi, private communication.

[2]Tables of thermal parameters and structure factors are available, at a nominal charge, from the Depository of Unpublished Data, CISTI, National Research Council of Canada, Ottawa, Ont., Canada K1A 0S2.

Can. J. Chem. Downloaded from www.nrcresearchpress.com by 210.87.254.105 on 09/05/12
For personal use only.

Can. J. Chem. Downloaded from www.nrcresearchpress.com by 210.87.254.105 on 09/05/12
For personal use only.

TABLE 1. Fractional atomic coordinates (esd's)

(*a*) Nonhydrogen atoms ($\times 10^4$)

Atom	*x*	*y*	*z*
N1	5736(3)	6560(4)	9030(3)
C2	4937(4)	6965(5)	8247(3)
O2	4026(3)	7593(4)	8466(2)
C3	5246(4)	6572(5)	7076(3)
C4	6487(4)	6098(5)	6823(3)
O4	6785(3)	6050(4)	5850(2)
C5	7170(4)	5749(5)	7768(4)
C6	6822(4)	5940(5)	8804(3)
C7	7521(5)	5584(7)	9831(4)
O1′	4662(3)	7437(3)	6226(2)
C3′	4321(4)	5903(5)	6356(3)
C1″	3116(4)	5541(5)	6771(4)
O1″	2989(3)	4422(4)	7344(3)
C2″	2171(4)	6532(6)	6328(4)
C3″	969(4)	6206(6)	6738(4)
C4″	64(5)	7024(9)	5980(6)
C5″	838(5)	6649(9)	7926(5)

(*b*) Hydrogen atoms ($\times 10^3$)

Atom	*x*	*y*	*z*
H1	549(3)	679(4)	979(2)
H5	785(3)	533(4)	763(3)
H7(a)	824(3)	525(5)	958(4)
H7(b)	755(4)	631(6)	1035(4)
H7(c)	713(4)	516(7)	1052(5)
H3′	454(3)	516(4)	586(3)
H2″(a)	238(3)	755(4)	647(3)
H2″(b)	223(3)	647(4)	545(3)
H3″	79(3)	498(4)	658(3)
H4″(a)	16(6)	651(8)	518(6)
H4″(b)	32(5)	817(6)	610(4)
H4″(c)	−61(5)	668(7)	626(5)
H5″(a)	84(6)	815(9)	787(6)
H5″(b)	146(6)	646(8)	845(6)
H5″(c)	−6(5)	640(6)	844(5)

delocalization of the π bonds, C3 however, lies 0.23 Å out of the plane (Table 3) on the same side as C3′. The plane of the epoxide ring (C3, O1′, C3′) is inclined at 89.4° to that of the six-membered ring. There are no other unusual features observed in the bond lengths and angles, neither are there any short intramolecular contacts. The shortest intermolecular contact is N1—H1---O1′, N1---O1′ being 3.05 Å. The H1---O1′ distance of 2.10 Å is significantly shorter than the sum of van der Waals' radii of 2.4 Å (7) and may be the result of weak hydrogen bonding.

The clarification of the stereochemistry of flavipucine, showing the oxirane bridge to have a *Z* configuration, sheds light on the question of the mechanism of the flavipucine to (optically inactive) isoflavipucine (9) **4** transformation which we observed to take place when the crystalline material is heated to its melting point or alternatively when heated in non-

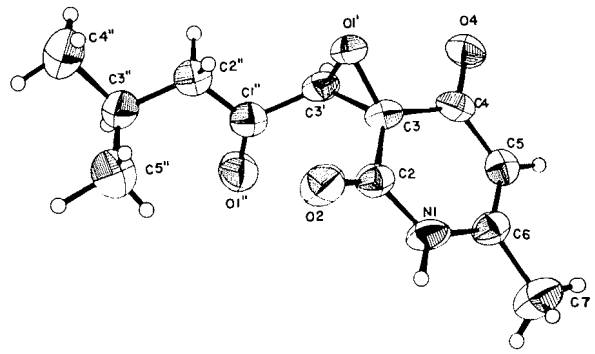

FIG. 1. ORTEP (8) diagram of the molecule with thermal ellipsoids drawn at 50% probability.

TABLE 2. Bond lengths and distances*

Bond	Distance (Å)	Bond	Distance (Å)
N1—C2	1.348(5)	C5—C6	1.321(6)
N1—C6	1.394(6)	C6—C7	1.491(7)
C2—O2	1.216(5)	O1′—C3′	1.410(6)
C2—C3	1.494(6)	C3′—C1″	1.516(6)
C3—O1′	1.427(6)	C1″—O1″	1.208(6)
C3—C3′	1.478(6)	C1″—C2″	1.482(7)
C3—C4	1.523(6)	C2″—C3″	1.504(7)
C4—O4	1.222(5)	C3″—C4″	1.545(8)
C4—C5	1.400(6)	C3″—C5″	1.485(8)

Bonds	Angle (deg)	Bonds	Angle (deg)
C6—N1—C2	124.7(3)	C5—C6—N1	121.3(4)
N1—C2—C3	114.9(4)	C5—C6—C7	125.5(4)
N1—C2—O2	123.2(4)	C7—C6—N1	113.1(4)
O2—C2—C3	121.9(4)	C3—O1′—C3′	62.8(3)
C2—C3—C4	119.4(3)	C3—C3′—O1′	59.1(3)
C2—C3—C3′	117.3(4)	C3—C3′—C1″	123.0(3)
C2—C3—O1′	115.5(3)	O1′—C3′—C1″	119.6(4)
C3′—C3—O1′	58.0(3)	C3′—C1″—C2″	115.4(4)
C3′—C3—C4	116.3(4)	C3′—C1″—O1″	118.5(4)
O1′—C3—C4	115.7(3)	O1″—C1″—C2″	125.7(4)
C3—C4—C5	114.4(4)	C1″—C2″—C3″	116.4(4)
C3—C4—O4	118.7(4)	C2″—C3″—C4″	109.4(4)
O4—C4—C5	126.9(4)	C2″—C3″—C5″	112.0(4)
C4—C5—C6	123.8(4)	C4″—C3″—C5″	111.3(5)

*Estimated standard deviations in parentheses.

TABLE 3. Equation of plane and deviations of atoms (Å) from the plane. Equation: $4.5596x + 8.0465y + 0.0495z = 7.9437$

Atom	Deviation	Atom	Deviation
N1	−0.005	O4	0.047
C2	−0.048	C5	−0.010
O2	0.043	C6	−0.010
C3*	−0.228	C7	0.027
C4	−0.045		

*Atom not used to define the plane.

anhydrous xylene (139°C). Recently we have found that application of synthetic racemic flavipucine to alumina tlc plates and development with benzene – ethyl acetate (7:3) also effects a substantial (35%)

transformation to isoflavipucine **4**. Earlier we had outlined possible mechanisms for this novel reaction, one of which required an *E* configuration for the oxirane bridge. We have now found that synthetic racemic epiflavipucine **2** is transformed (on alumina) into isoflavipucine **4** with equal facility as is flavipucine **1** itself. To accommodate these findings we propose the mechanism portrayed in Scheme 1 in which either **1** or **2** is first transformed into the common achiral intermediate **3**.

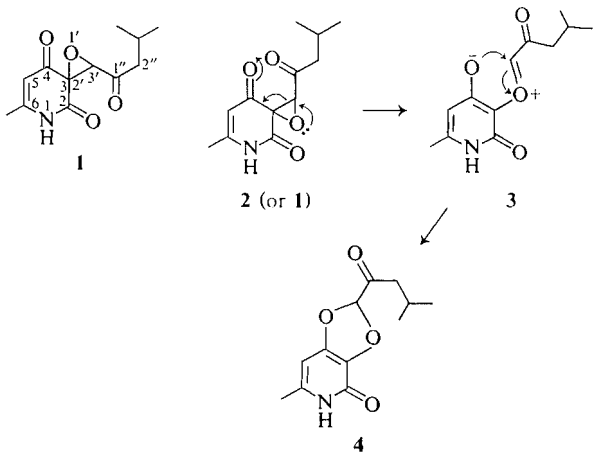

SCHEME 1

Acknowledgment

Financial assistance from the National Research Council of Canada is gratefully acknowledged.

1. J. A. FINDLAY and L. RADICS. J. Chem. Soc. Perkin I, 2963 (1972).
2. J. A. FINDLAY, JOHN WAH HUNG TAM, and JIRI KREPINSKY. Synth. Commun. **7**, 149 (1977).
3. G. GERMAIN, P. MAIN, and M. M. WOOLFSON. Acta Crystallogr. A, **27**, 368 (1971).
4. M. H. J. KOCH. Acta Crystallogr. A, **30**, 67 (1974).
5. J. M. STEWART (*Editor*). Technical Rept. TR446, Computer Science Center, University of Maryland, MD. 1976.
6. P. W. R. CORFIELD, R. J. DOEDENS, and J. A. IBERS. Inorg. Chem. **6**, 197 (1967).
7. I. OLOVSSON and P. G. JÖNSSON. *In* The hydrogen bond. Vol. II. *Edited by* P. Schuster, G. Zundel, and C. Sandorfy. North-Holland Publishing Co., Amsterdam, New York, Oxford. 1976. pp. 393–456.
8. C. K. JOHNSON. Oak Ridge Natl. Lab. Technical Rept. ORNL-3794. 1965.
9. J. A. FINDLAY, JIRI KREPINSKY, ANITA SHUM, C. G. CASINOVI, and L. RADICS. Can. J. Chem. **55**, 600 (1977).

Can. J. Chem. Downloaded from www.nrcresearchpress.com by 210.87.254.105 on 09/05/12
For personal use only.

A new route to 5-bromo-5′-bromomethylpyrromethenes[1]

AREND ROWOLD AND S. FERGUSON MACDONALD

Division of Biological Sciences, National Research Council of Canada, Ottawa, Ont., Canada K1A 0R6

Received February 16, 1978

AREND ROWOLD and S. FERGUSON MACDONALD. Can. J. Chem. **56**, 1907 (1978).

Esters of hitherto inaccessible 5-bromo-5′-bromomethylpyrromethenes, with alternating acetic acid (or methyl) and propionic acid groups in the β positions, are obtained by brominating the appropriate 5-acetoxymethylpyrrole-2-carboxylic acids in ethanol-free chloroform at ≤10°C. The bromomethylpyrromethenes give the corresponding methoxymethylpyrromethenes in methanol at room temperature.

AREND ROWOLD et S. FERGUSON MACDONALD. Can. J. Chem. **56**, 1907 (1978).

On a pu obtenir des esters des bromo-5 bromo-5′ méthylpyrrométhènes qui étaient jusqu'à présent inacessible et qui possèdent en alternance en position β, des groupes acide acétique (ou méthyle) et des groupes d'acide propionique; on a réalisé cette préparation en faisant la bromuration des acides acétoxyméthyl-5 pyrrolecarboxyliques-2 appropriés dans du chloroforme sans éthanol à une température ≤10°C. Les bromométhylpyrrométhènes conduisent au méthoxyméthylpyrrométhènes correspondants par réaction avec le méthanol à la température ambiante.

[Traduit par le journal]

The unavailability of some 5-bromo-5′-bromomethylpyrromethenes has limited the generality of Johnson and co-workers (1) synthesis of porphyrins from 1′-bromo-8′-methylbiladienes-a,c (cf. refs. 2 and 3). We were particularly interested in esters of **4***a* and its isomers, which were also promising intermediates for the synthesis of polypyrranes related to the uroporphinogens (4, 5). A preliminary communication (5) covers the work described below.

2-Methylpyrroles, and their 5-carboxy- (ref. 6*a*) or 5-*tert*-butoxycarbonyl derivatives (7), are brominated to 5-bromo-5′-methylpyrromethenes with alternating β substituents, e.g. **3***a*. 5-Bromo-5′-bromomethylpyrromethenes are obtained in the same way or, with greater formal generality, by brominating 5-bromo-5′-methylpyrromethenes. However, both of these are uncertain routes to the bromomethylpyrromethenes when there are propionic acid groups in the β positions. In particular, the brominations of **3***d*, **3***e* (4), and of **3***j* (8) had failed, although unstable preparations of 5-bromo-5′-bromomethylpyrromethenes had been obtained by brominating the 5′-methylpyrromethenes **7** (9) and **8** (2), and the *tert*-butyl ester **1***l* (10) (see below). In the brominations of **7** and **8**, the 5-bromo-5′-methylpyrromethenes were identified intermediates.

To study the formally more general of the two methods, the bromination of four 5-bromo-5′-methylpyrromethenes under various conditions was followed by the ^{1}Hmr signals of the CH_2Br (or CH_2OMe) and bridge CH groups. The best results were obtained in acetic acid after 45 min on the steam bath, using 2 mol of bromine with **3***h* and **3***k*, and 4 mol with **3***b* and **3***e*. Complete bromination could not be forced because of the instability of the bromomethyl derivatives. The crude products, containing 5′-methyl- and 5′-bromomethylpyrromethenes, were treated with methanol to convert the latter into more stable 5′-methoxymethylpyrromethenes, and those from **3***b* and **3***e* were then dissolved in chloroform–methanol (9:1) and filtered through alumina to remove by-products. The ^{1}Hmr spectra of the products from **3***b*, **3***e*, **3***h*, and **3***k* then indicated conversions of <30, <30, 65, and 85%, respectively. Only the methoxymethylpyrromethene **5***k* (<60%) was obtained crystalline, and this is much more readily obtained otherwise (see below). Other routes to **4***a* and **4***d* or their esters were obviously required, but the ester **3***k* was evidently more readily brominated than the above mentioned free acid **3***j*.

Routes to **4***a* and **4***d* or their esters based on the bromination of 2-methylpyrroles were then considered, although these would be inapplicable to isomers. The familiar mechanism for such halogenations (11) appeared to be an uncertain guide here. Its failure to explain the chlorination of a 2-methylpyrrole to a 5-free-5′-methylpyrromethene (4) is a fundamental defect, and it is not relevant to the threat of more complex reactions (11). However, it had suggested that 5′-bromomethylpyrromethenes would be favoured if 2-methylpyrroles were more completely converted to 2-bromomethylpyrroles before condensing to pyrromethenes; thus 2-methyl-5-*tert*-butoxycarbonylpyrroles were brominated to 5-bromo-5′-bromomethylpyrromethenes (12). With this in mind, we brominated 5-acetoxymethylpyrrole-

[1]NRCC No. 16684.

Can. J. Chem. Downloaded from www.nrcresearchpress.com by 210.87.254.42 on 09/05/12
For personal use only.

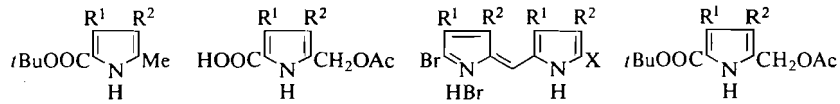

1 **2** **3** X = Me; **4** X = CH_2Br; **5** X = CH_2OMe **6**

R^1,R^2 = (*a*) P,A; (*b*) P^{Me},A^{Me}; (*c*) P^{Et},A^{Et}; (*d*) A,P; (*e*) A^{Me},P^{Me}; (*f*) A^{Et},P^{Et}; (*g*) P,Me; (*h*) P^{Me},Me; (*i*) P^{Et},Me; (*j*) Me,P; (*k*) Me,P^{Me}; (*l*) Me,P^{Et}

7 **8** X = H; **9** X = COO*t*Bu

A = CH_2COOH, A^{Me} = CH_2COOMe, A^{Et} = CH_2COOEt,
P = CH_2CH_2COOH, P^{Me} = CH_2CH_2COOMe, P^{Et} = CH_2CH_2COOEt

2-carboxylic acids **2**, for both a hydroxymethylpyrrole (13) and an ethoxymethylpyrromethene (6*b*) had been converted into their bromomethyl derivatives by hydrogen bromide in acetic acid. This was not considered too promising because the acetoxymethyl groups might well be displaced by bromine before they were locked on as bromomethyl, a process requiring hydrogen bromide formed by the brominative displacement of the carboxyl group.

However, bromine in ethanol-free chloroform at $\leq 10°C$ converted the 2-acetoxymethylpyrrole-5-carboxylic acids **2***c*, **2***f*, **2***i*, and **2***l* into the pure crystalline 5-bromo-5′-bromomethylpyrromethene hydrobromides **4***c*, **4***f*, **4***i*, and **4***l* (55–70%). At room temperature, although this was not at first realized, methanol converted these into the 5-bromo-5′-methoxymethylpyrromethene hydrobromides **5***c*, **5***f*, **5***i*, and **5***l* (80–90%). The methyl ester **4***b* corresponding to the ethyl ester **4***c* was obtained analogously from **2***b*. Some of these bromomethylpyrromethenes do not keep well unless thoroughly purified. Particularly in the case of **4***c*, they are better stored as their methoxymethyl derivatives which appear to be equivalent synthetically. Analyses of 5-methoxymethylpyrromethenes were regarded as more significant than those of 5-bromomethylpyrromethenes, which might not be distinguished by analysis from mixtures of 5-methylpyrromethenes with their perbromides.

The 5-bromomethylpyrromethenes **4***k* and **4***l* are exceptional among those discussed here because they are available, and more easily so, by an earlier method. This is because the *tert*-butyl esters **1***k* and **1***l* not only are obtained directly by ring synthesis, but also give **4***k* and **4***l* on bromination. The two-stage bromination which had converted **1***l* to **4***l* (10) failed with **1***k*, and its bromination in chloroform gave only **3***k*. However, bromine in hot acetic acid converted **1***k* to **4***k* which was isolated as the methoxy methyl derivative **5***k*. In other but related situations *tert*-butyl esters appeared less useful than carboxylic acids or carboxyl-free derivatives. Thus, although 5-bromomethylpyrromethenes were obtained by brominating **8** and **2***l* (see above), we failed to obtain such by brominating the related *tert*-butyl esters **9** and the known **6***k* (14).

It may be noted that all the 5-bromo-5′-methylpyrromethene hydrobromides **3***a*–**3***l* are now known, except **3***f* and **3***l*: **3***a* (4), **3***d* (15), **3***e* (4), **3***g* (6*c*), **3***j* (6*d*), **3***k* (free base (6*d*)); see Experimental for **3***b*, **3***c*, **3***g* (a better preparation), **3***h*, **3***i*, **3***k* (hydrobromide).

Experimental

Preparations are ordered according to the parent pyrrole: **2***b*, **3***b*, **4***b* then **2***c*, **3***c*, **4***c*, **5***c*, etc. Ethanol-free chloroform was used in preparing 5′-bromomethylpyrromethenes: chloroform was washed three times with concentrated H_2SO_4, filtered, stirred with NaOH pellets, filtered, stabilized by adding 5% (v/v) of dry ether, and stored indefinitely in brown bottles. The ^{1}Hmr spectra (in $CDCl_3$, tetramethylsilane as internal standard) were determined on a Varian EM360 (60 MHz) spectrometer; chemical shifts are expressed as ppm (δ).

*5-Acetoxymethyl-3-(2-methoxycarbonylethyl)-4-methoxycarbonylmethylpyrrole-2-carboxylic Acid (***2***b)*

Benzyl 5-acetoxymethyl-3-(2-methoxycarbonylethyl)-4-methoxycarbonylmethylpyrrole-2-carboxylate (16) (6.5 g) was hydrogenated in 250 ml of methanol over 400 mg of 5% Pd–C. The filtrate and washings (hot chloroform) were evaporated and the residue was twice recystallized from chloroform–hexane to give a colourless product (56%), mp 153–157°C. *Anal.* calcd. for $C_{15}H_{19}O_8N$: C 52.78, H 5.61, N 4.10; found: C 53.02, H 5.56, N 3.97.

*5-Bromo-4,3′-bis(2-methoxycarbonylethyl)-3,4′-bismethoxycarbonylmethyl-5′-methylpyrromethene Hydrobromide (***3***b)*

The corresponding tetracarboxylic acid **3***a* (4) (4.69 g) was warmed to solution in 50 ml of methanol containing 2.5 ml of acetyl bromide. After 24 h at 20°C the solution was seeded, left 2 h at 0°C, and the product was separated. After washing with cold methanol it formed brown rods (82%), mp 149–

Can. J. Chem. Downloaded from www.nrcresearchpress.com by 210.87.254.42 on 09/05/12
For personal use only.

Can. J. Chem. Downloaded from www.nrcresearchpress.com by 210.87.254.42 on 09/05/12
For personal use only.

152°C. *Anal.* calcd. for $C_{24}H_{30}O_8N_2Br_2$: C 45.44, H 4.77, N 4.42, Br 25.20; found: C 45.61, H 4.90, N 4.41, Br 25.03.

*5-Bromo-5′-bromomethyl-4,3′-bis(2-methoxycarbonylethyl)-3,4′-bismethoxycarbonylmethylpyrromethene Hydrobromide (**4**b)*

Powdered 5-acetoxymethyl-3-(2-methoxycarbonylethyl)-4-methoxycarbonylmethylpyrrole-2-carboxylic acid (**2***b*, 2.23 g) slurred in 60 ml of ethanol-free chloroform was stirred for 20 min at 10°C after 0.52 ml of bromine had been added at that temperature. The solvent was removed (rotary, then at 0.1 Torr for ½ h), and the residue was stirred with dry ether to give the product (67%) as red needles, mp 124–126°C (dec.); ^{1}Hmr: 2.4–3.3 (8H, m, 2 CH_2CH_2CO), 3.45, 4.00 (4H, 2s, $2CH_2CO$), 3.68, 3.70, 3.77 (12H, 3s, $4CH_3O$), 5.00 (2H, s, CH_2Br), 7.74 (1H, s, bridge CH). *Anal.* calcd. for $C_{24}H_{29}N_2O_8Br_3$: C 40.41, H 4.10, N 3.93, Br 33.61; found: C 40.69, H 4.17, N 3.95, Br 33.12.

In later runs this (unlike the corresponding ethyl ester) did not crystallise readily unless the crude product was swirled mechanically with ether and glass beads.

Benzyl 5-Acetoxymethyl-3-(2-ethoxycarbonylethyl)-4-ethoxycarbonylmethylpyrrole-2-carboxylate

Benzyl 5-methyl-3-(2-ethoxycarbonylethyl)-4-ethoxycarbonylmethylpyrrole-2-carboxylate (17) (12 g) and 15.4 g of lead tetraacetate in 360 ml of acetic acid were stirred at 38°C for 16 h, then for 3 h more after adding 2 g of lead tetraacetate. The solvent was removed below 50°C and 200 ml of water were added to the residue. The mixture was neutralized with sodium bicarbonate, then extracted several times with chloroform. The chloroform (800 ml) was washed with water until the latter was clear and colourless. Evaporating the chloroform left the product which was crystallized from benzene–*n*-hexane as tiny colourless needles (76%), mp 108–110°C (lit. (18) mp 105–106°C). *Anal.* calcd. for $C_{24}H_{29}O_8N$: C 62.73, H 6.36, N 3.05; found: C 63.04, H 6.40, N 2.93.

*5-Acetoxymethyl-3-(2-ethoxycarbonylethyl)-4-ethoxycarbonylmethylpyrrole-2-carboxylic Acid (**2**c)*

The preparation of this from the above 2-benzyl ester followed that of its isomer **2***f* (below) exactly, except that it could be done on a larger (5 g) scale because it was more stable. The recrystallized product (95%) formed colourless needles, mp 148–152°C (dec.). *Anal.* calcd. for $C_{17}H_{23}O_8N$: C 55.28, H 6.28, N 3.79; found: C 55.52, H 6.35, N 3.76.

*5-Bromo-4,3′-bis(2-ethoxycarbonylethyl)-3,4′-bisethoxycarbonylmethyl-5-methylpyrromethene Hydrobromide (**3**c)*

The corresponding tetracarboxylic acid **3***a* (recrystallized (4), 400 mg) was heated to solution in 5 ml of 10% ethanolic HBr (prepared using HBr gas). The solution was kept at 50°C for 5 h, seeded, then 18 h at 20°C, then 2 h at 0°C. After washing with ether the product formed red-brown plates (63%), mp ca. 105°C, changing to needles, mp ca. 113°C. *Anal.* calcd. for $C_{28}H_{38}O_8N_2Br_2$: C 48.71, H 5.55, N 4.06, Br 23.15; found: C 48.74, H 5.57, N 4.01, Br 23.03.

*5-Bromo-5′-bromomethyl-4,3′-bis(2-ethoxycarbonylethyl)-3,4′-bisethoxycarbonylmethylpyrromethene Hydrobromide (**4**c)*

The pyrrole **2***c* (1.4 g) was heated to solution in 35 ml of ethanol-free chloroform. Bromine (0.44 cm^3 in four portions) was added to the stirred solution at 10°C. The solvent was removed (rotary, then 1 h at 0.1 Torr) after 10 min, and the residue was stirred 1 h with 30 ml dry ether. The crystalline product was separated, washed with dry ether, and recrystallized from ethanol-free chloroform–*n*-pentane as red needles (69%), mp 114–115°C (capillary); ^{1}Hmr: 1.10–1.40 (12H, m, 4 CH_2CH_3), 2.5–3.3 (8H, m, 2 CH_2CH_2CO), 3.68 and 4.00 (each 2H, s, CH_2CO at 4′ and 3 respectively), 4.00–4.45 (8H, m, 4 CH_2CH_3), 5.05 (2H, s, CH_2Br), 7.83 (1H, s, bridge CH). *Anal.* calcd. for $C_{28}H_{37}O_8N_2Br_3$: C 43.71, H 4.85, N 3.64, Br 31.16; found: C 43.80, H 4.92, N 3.59, Br 31.02. Store at 0°C as the more stable methoxymethyl derivative.

*5-Bromo-5′-methoxymethyl-4,3′-bis(2-ethoxycarbonylethyl)-3,4′-bisethoxycarbonylmethylpyrromethene Hydrobromide (**5**c)*

The above bromomethyl derivative **4***c* was dissolved in methanol which was then evaporated, all at room temperature. The residue crystallized when ether was added to it. It was recrystallized as orange needles (90%) from chloroform–*n*-pentane, mp 112–113°C (capillary); ^{1}Hmr: 1.08–1.39 (12H, m, 4 CH_2CH_3), 2.5–3.2 (8H, m, 2 CH_2CH_2CO), 3.46 (3H, s, OCH_3), 3.66 and 3.95 (each 2H, s, CH_2CO at 4′ and 3, respectively), 3.85–4.40 (8H, 4q, 4 CH_2CH_3), 5.03 (2H, s, CH_2OCH_3), 7.76 (1H, s, bridge CH). *Anal.* calcd. for $C_{29}H_{40}O_9N_2Br_2$: C 48.34, H 5.60, N 3.89, Br 22.18; found: C 48.18, H 5.59, N 4.12, Br 22.32.

Benzyl 5-Acetoxymethyl-4-(2-ethoxycarbonylethyl)-3-ethoxycarbonylmethylpyrrole-2-carboxylate

The preparation of this from benzyl 5-methyl-4-(2-ethoxycarbonylethyl)-3-ethoxycarbonylmethylpyrrole-2-carboxylate (17) (12 g) followed exactly that of its isomer (β substituents reversed) above. The recrystallized product (74%) formed fine colourless hairs, mp 128–130°C. *Anal.* calcd. for $C_{24}H_{29}O_8N$: C 62.73, H 6.36, N 3.05; found: C 62.94, H 6.47, N 2.95.

*5-Acetoxymethyl-4-(2-ethoxycarbonylethyl)-3-ethoxycarbonylmethylpyrrole-2-carboxylic Acid (**2**f)*

The above benzyl ester (1.58 g) was hydrogenated in 80 ml of ethanol with 120 mg of 5% Pd–C for ½ hr only (uptake 106% theory). The filtrate from the catalyst was evaporated (rotary) and the residue was crystallized three times from chloroform–*n*-hexane (finally at 0°C) to give the cream coloured dimorphic product (80%) as rods, mp ca. 85°C, fine needles, mp 114–117°C. Two further recrystallizations gave the colourless analytical specimen. *Anal.* calcd. for $C_{17}H_{23}NO_8$: C 55.28, H 6.28, N 3.79; found: C 55.09, H 6.35, N 3.69. Larger runs were less successful because the product is rather unstable.

*5-Bromo-5′-bromomethyl-3,4′-bis(2-ethoxycarbonylethyl)-4,3′-bisethoxycarbonylmethylpyrromethene Hydrobromide (**4**f)*

Bromine (0.2 ml) was added over 2 min to a stirred solution of 5-acetoxymethyl-4-(2-ethoxycarbonylethyl)-3-ethoxycarbonylmethylpyrrole-2-carboxylic acid (**2***f*, 700 mg) in 15 ml of ethanol-free chloroform cooled in ice. After 10 min the solvent was removed at 20°C (rotary, then 0.1 Torr for 1 h). The residue was stirred with 15 ml of dry ether and the product filtered off and washed with 5 ml of dry ether. It formed tiny orange-red needles, (62%) as recrystallized from ethanol-free chloroform–*n*-pentane, mp 133–134°C (capillary); ^{1}Hmr: 1.27 (12H, t partly overlapped, 4 CH_2CH_3), 2.67–3.13 or broader (8H, m, 2 CH_2CH_2CO), 3.57 and 3.85 (each 2H, s, CH_2CO at 3′ and 4), 3.94–4.38 (8H, 4q, 4 CH_2CH_3), 5.02 (2H, s, CH_2Br), 7.78 (1H, s, bridge CH). *Anal.* calcd. for $C_{28}H_{37}O_8N_2Br_3$: C 43.71, H 4.85, N 3.64, Br 31.16; found: C 43.81, H 4.98, N 3.67, Br 31.28.

*5-Bromo-5′-methoxymethyl-3,4′-bis(2-ethoxycarbonylethyl)-4,3′-bisethoxycarbonylmethylpyrromethene Hydrobromide (**5**f)*

The preparation of this from **4***f* followed that of its isomer **5***c* above exactly. The recrystallized product (87%) formed orange-brown needles, mp 126–127°C (capillary); ^{1}Hmr: 1.1–1.4 (12H, 4t overlapping, 4 CH_2CH_3), 2.4–3.2 (8H, m, 2

Can. J. Chem. Downloaded from www.nrcresearchpress.com by 210.87.254.42 on 09/05/12
For personal use only.

CH_2CH_2CO), 3.50 (3H, s, OCH_3), 3.56 and 3.87 (each 2H, s, CH_2CO at 3′ and 4, respectively), 4–4.4 (8H, 4q overlapping, 4 CH_2CH_3), 4.98 (2H, s, CH_2OCH_3) 7.72 (1H, s, bridge CH). *Anal.* calcd. for $C_{29}H_{40}O_9N_2Br_2$: C 48.34, H 5.60, N 3.89, Br 22.18; found: C 48.48, H 5.59, N 3.91, Br 21.90.

Ethyl 3-(2-Ethoxycarbonylethyl)-4,5-dimethylpyrrole-2-carboxylate

A solution of ethyl 3-(2-ethoxycarbonylethyl)-5-methylpyrrole-2-carboxylate (20) (40 g) in 200 ml of 67% hydriodic acid, 200 ml of acetic anhydride and 60 ml of 50% hypophosphorous acid was stirred at 25°C while 9 g paraformaldehyde were added in portions. After ¼ h additional stirring at 45°C, 10 ml of hypophosphorous acid were added then, after 1 h, 400 ml of ice water. The precipitate was separated after standing at 0°C and washed with water. More was obtained by concentrating the filtrate to 250 ml (rotary, 30°C) then diluting with 250 ml of water. The dried precipitate was heated to boiling in 100 ml of 10% ethanolic HCl. After 4 h at 20°C and 2 days at 0°C, the product was separated and washed with water; more was obtained by concentrating the ethanolic filtrate. Recrystallization from 400 ml *n*-pentane (thimble) gave colourless prisms (85%), mp 91–91.5° (lit. (19) mp 90.5–91.5°C).

3-(2-Carboxyethyl)-4,5-dimethylpyrrole-2-carboxylic Acid

Ethyl 3-(2-ethoxycarbonylethyl)-4,5-dimethylpyrrole-2-carboxylate (12.5 g) in 40 ml of ethanol was boiled on the steam bath while aqueous NaOH (60 ml of 10% w/v) was added in portions. Boiling was continued ½ h then the ethanol was removed (rotary, 30°C). The residue was made up to 75 ml with water then heated 1 h *in* the steam bath under reflux. The product was precipitated at 0°C by SO_2 (congo red), scratching to ensure a filterable product. It was separated and washed by stirring in 50 ml of ice water, mp 128–131°C (80%). *Anal.* calcd. for $C_{10}H_{13}O_4N$: C 56.86, H 6.20, N 6.63; found: C 56.98, H 6.20, N 6.65.

5-Bromo-4,3′-bis(2-carboxyethyl)-3,4′,5′-trimethylpyrromethene Hydrobromide (3g) (6c)

Powdered 3-(2-carboxyethyl)-4,5-dimethylpyrrole-2-carboxylic acid (1 g) suspended in 3 ml of acetic acid was stirred while 2.5 ml of bromine in acetic acid (15 g of bromine made up to 25 ml) was added in three portions. The solution was seeded then allowed to stand 2 h while protected from moisture before the product was filtered off. After washing with acetic acid then acetic acid – ether it formed red-brown prisms (51%), mp ca. 200°C (dec.). It analysed badly: *Anal.* calcd. for $C_{18}H_{22}O_4N_2Br_2$: C 44.10, H 4.52, N 5.72; found: C 41.03, H 4.59, N 5.46.

5-Bromo-4,3′-bis(2-methoxycarbonylethyl)-3,4′,5′-trimethylpyrromethene Hydrobromide (3h)

This was prepared, like the corresponding ethyl ester **3*i*** below, from **3*g*** and MeOH–AcBr. It formed orange rods (78%), mp ca. 185°C when rapidly heated. *Anal.* calcd. for $C_{20}H_{26}O_4N_2Br_2$: C 46.35, H 5.06, N 5.41, Br 30.84; found: C 46.16, H 5.12, N 5.29, Br 30.66.

Benzyl 3-(2-Ethoxycarbonylethyl)-4,5-dimethylpyrrole-2-carboxylate

Ethyl 3-(2-ethoxycarbonylethyl)-4,5-dimethylpyrrole-2-carboxylate (above, 16 g) was heated 3 h on the steam-bath under a water-pump vacuum with a solution of 2.91 g of sodium in 450 ml of reagent grade benzyl alcohol. The benzyl alcohol was then evaporated (rotary) and the residue was dissolved in 400 ml of water. After the solution was twice washed with ether, it was acidified to congo red at 15°C. The precipitate was recrystallized from aqueous dioxan as fine needles of the monobenzyl ester (free propionic acid), mp 170–173°C. This was esterified in 450 ml of 5% HCl in ethanol to give the product (15.2 g, 77%) as colourless needles, mp 84–85.5°C after recrystallization from hexane (thimble).

Benzyl 5-Acetoxymethyl-3-(2-ethoxycarbonylethyl)-4-methylpyrrole-2-carboxylate

A solution of 5 g of benzyl 3-(2-ethoxycarbonylethyl)-4,5-dimethylpyrrole-2-carboxylate and 7.25 g of lead tetraacetate in 125 ml of acetic acid was stirred 18 h at 41°C while protected from moisture; 1 g more lead tetraacetate was then added and stirring continued for 4 h. Water (250 ml) was added and the mixture was left 2½ h in ice. The precipitate was separated and dissolved in chloroform. The chloroform solution was washed with water, concentrated to 20 ml, diluted with 400 ml of warm *n*-hexane, then left at 0°C. The crystals which separated were recrystallized from benzene–*n*-hexane then from hexane giving colourless needles (75%), mp 94–96°C. For analysis, it was recrystallized from benzene–*n*-hexane, mp 95–96°C. *Anal.* calcd. for $C_{21}H_{25}O_6N$: C 65.10, H 6.50, N 3.62; found: C 65.28, H 6.51, N 3.58. Under other conditions the product obtained was contaminated with the starting material or the aldehyde (^{1}Hmr).

5-Acetoxymethyl-3-(2-ethoxycarbonylethyl)-4-methylpyrrole-2-carboxylic Acid (2i)

The above benzyl ester (1.935 g) was hydrogenated for 3 h in 50 ml of dioxan with 200 mg 5% Pd–C. The filtered solution was concentrated to 10 ml, 10 ml of ether were added, and the solution was left at 0°C overnight. The product separated as colourless prisms (40%), mp 124–130°C. *Anal.* calcd. for $C_{14}H_{19}O_6N$: C 56.56, H 6.44, N 4.71; found: C 56.80, H 6.39, N 4.79. Much more of the product was recovered from the mother liquor.

5-Bromo-4,3′-bis(2-ethoxycarbonylethyl)-3,4′,5′-trimethylpyrromethene Hydrobromide (3i)

The dicarboxylic acid **3*g*** (above) was heated to boiling in 20 ml of ethanolic HBr (prepared from 25 ml ethanol and 1.25 ml of acetyl bromide) then left overnight at 20°C. The mixture was then cooled to 0°C and the product (77%) was separated and washed with cold ethanol, mp 161–162°C. *Anal.* calcd. for $C_{22}H_{30}N_2O_4Br_2$: C 48.36, H 5.54, N 5.13, Br 29.26; found: C 48.50, H 5.57, N 4.98, Br 29.12.

5-Bromo-5′-bromomethyl-4,3′-bis(2-ethoxycarbonylethyl)-3,4′-dimethylpyrromethene Hydrobromide (4i)

This was prepared like **4*f*** using 564 mg of **2*i***, 15 ml of ethanol-free chloroform and 0.2 ml of bromine. After recrystallizing from chloroform–*n*-hexane it formed tiny red needles (70%), dec. >160°C; ^{1}Hmr: 1.23, 1.28 (6H, 2t, 2 $COOCH_2CH_3$), 2.17, 2.50 (6H, 2s, CH_3's at 3 and 4′), 2.5–3.1 (8H, m, 2 CH_2CH_2CO), 4.12, 4.18 (4H, 2q, 2 $COOCH_2CH_3$), 4.94 (2H, s, CH_2Br), 7.56 (1H, s, bridge CH). *Anal.* calcd. for $C_{22}H_{29}O_4N_2Br_3$: C 42.26, H 4.68, N 4.48, Br 38.35; found: C 42.28, H 4.74, N 4.49, Br 38.33.

5-Bromo-5′-methoxymethyl-4,3′-bis(2-ethoxycarbonylethyl)-3,4′-dimethylpyrromethene Hydrobromide (5i)

The preparation of this from **4*i*** was analogous to that of **5*c*** but it was recrystallized from chloroform–*n*-hexane, finally at 0°C. It formed purple needles (82%), mp 125–126°C (capillary); ^{1}Hmr: 1.20, 1.26 (6H, 2t, 2 $COOCH_2CH_3$), 2.16, 2.50 (6H, 2s, CH_3's at 3 and 4′), 2.5–2.9 (8H, m, 2 CH_2CH_2CO), 3.51 (3H, s, CH_2OCH_3), 4.15, 4.20 (4H, 2q, 2 $COOCH_2CH_3$), 4.97 (2H, s, CH_2OCH_3), 7.55 (1H, s, bridge CH). *Anal.* calcd. for $C_{23}H_{32}O_5N_2Br_2$: C 47.93, H 5.60, N 4.86, Br 27.73; found: C 47.60, H 5.69, N 4.94, Br 27.89.

5-Bromo-3,4′-bis(2-methoxycarbonylethyl)-4,3′,5′-trimethylpyrromethene Hydrobromide (3k)

Bromine (4 ml) in 20 ml of chloroform was added over 10 min to *tert*-butyl 4-(methoxycarbonylethyl)-3,5-dimethylpyr-

Can. J. Chem. Downloaded from www.nrcresearchpress.com by 210.87.254.42 on 09/05/12
For personal use only.

role-2-carboxylate **1***k* (7) (10.34 g) in 100 ml of chloroform while stirring at 20°C. Stirring was continued 1 h, the solvent was removed *in vacuo* and the residue was crystallized as red plates (64%) from chloroform–ether, mp >160°C (dec.); ^{1}Hmr: 2.05, 2.43, 2.73 (each 3H, s, CH_3's at 4, 3′ and 5′, respectively), 2.5–3.3 (8H, m, 2 CH_2CH_2CO), 3.62, 3.68 (each 3H, 2s, $2OCH_3$), 7.41 (1H, s, bridge CH). *Anal.* calcd. for $C_{20}H_{26}O_4N_2Br_2$: C 46.35, H 5.06, N 5.41, Br 30.84; found: C 46.47, H 5.16, N 5.40, Br 30.79. The free base has been described (6*d*).

Ni Complex of the Free Base

Red-brown prisms, mp 152–153°C from methanol. *Anal.* calcd. for $C_{40}H_{48}O_8N_4Br_2Ni$: C 51.58, H 5.19, N 6.02, Br 17.16; found: C 51.82, H 5.23, N 6.15, Br 17.17.

*5-Bromo-5′-methoxymethyl-3,4′-bis(2-methoxycarbonylethyl)-4,3′-dimethylpyrromethene Hydrobromide (***5***k)*

A solution of 2.07 g of *tert*-butyl 4-(2-methoxycarbonylethyl)-3,5-dimethylpyrrole-2-carboxylate **1***k* (7) and 1.6 ml of bromine in 6 ml of acetic acid was heated ½ h on the steam bath. The solvent was evaporated and the residue was stirred for a few minutes with warm methanol. The residue left on removing the methanol *in vacuo* crystallized on stirring with 10 ml of ether. Recrystallization from chloroform–ether gave small orange needles (55%), decomposes above 150°C; ^{1}Hmr: 2.10 and 2.43 (each 3H, s, probably 4- and 3′- CH_3, respectively), 2.6–3.1 (8H, m, 2 CH_2CH_2CO), 3.52 (3H, s, CH_2OCH_3), 3.66 and 3.71 (each 3H, s, 2 $COOCH_3$), 4.97 (2H, s, CH_2OCH_3), 7.51 (1H, s, bridge CH). *Anal.* calcd. for $C_{21}H_{28}O_5N_2Br_2$: C 46.00, H 5.15, N 5.11, Br 29.15; found: C 45.94, H 5.21, N 5.09, Br 29.24.

Free Base of the Above

A chloroform solution of the hydrobromide **5***k* was shaken with 5% aqueous NaOH. The chloroform was evaporated and the residue was crystallized from methanol as red-brown plates (75%), mp 90–93°C; ^{1}Hmr: 2.00 and 2.21 (each 3H, s, probably 4- and 3′- CH_3, respectively), 2.3–3.1 (8H, m, 2 CH_2CH_2CO), 3.43 (3H, s, CH_2OCH_3), 3.69 (6H, s, 2 $COOCH_3$), 4.51 (2H, s, CH_2OCH_3), 6.84 (1H, s, bridge CH). *Anal.* calcd. for $C_{21}H_{27}O_5N_2Br$: C 53.97, H 5.82, N 5.99, Br 17.10; found: C 54.02, H 5.77, N 5.93, Br 17.28.

*5-Acetoxymethyl-4-(2-ethoxycarbonylethyl)-3-methylpyrrole-2-carboxylic Acid (***2***l)*

Benzyl 5-acetoxymethyl-4-(2-ethoxycarbonylethyl)-3-methylpyrrole-2-carboxylate (21) (3.87 g) was hydrogenated in 120 ml of dioxan over 500 mg of 5% Pd–C for 1.5 h. The filtrate was concentrated (rotary, 20°C) to 20 ml and 20 ml of ether was added. The colourless needles (71%), mp 117–125°, could not be recrystallized without decomposition and analysed badly. *Anal.* calcd. for $C_{14}H_{19}O_6N$: C 56.56, H 6.44, N 4.71; found: C 58.45, H 6.54, N 4.37.

*5-Bromo-5′-bromomethyl-3,4′-bis(2-ethoxycarbonylethyl)-4,3′-dimethylpyrromethene Hydrobromide (***4***l)*

This was prepared like **4***f* using 564 mg of 5-acetoxymethyl-4-(2-ethoxycarbonylethyl)-3-methylpyrrole-2-carboxylic acid **2***l*, 15 ml of ethanol-free chloroform, and 0.2 ml of bromine. After recrystallization from ethanol-free chloroform–*n*-pentane, it formed small red needles (56%), mp 180–181°C (capillary, dec.) (lit. (10) mp 155°C). *Anal.* calcd. for $C_{22}H_{29}O_4N_2Br_3$: C 42.26, H 4.68, N 4.48, Br 38.35; found: C 42.28, H 4.88, N 4.44, Br 38.51.

*5-Bromo-5′-methoxymethyl-3,4′-bis(2-ethoxycarbonylethyl)-4,3′-dimethylpyrromethene Hydrobromide (***5***l)*

The preparation of this from **4***l* was analogous to that of **5***c* but it was recrystallized from chloroform–ether as orange needles (81%), mp 129–130°C (capillary); ^{1}Hmr: 1.23, 1.28 (6H, 2t, 2 $COOCH_2CH_3$), 2.13, 2.47 (6H, 2s, CH_3's at 4 and 3′), 2.61–3.14 (8H, m, 2 CH_2CH_2CO), 3.54 (3H, s, CH_2OCH_3), 4.16, 4.20 (4H, 2q, 2 $COOCH_2CH_3$), 5.02 (2H, s, CH_2OCH_3), 7.55 (1H, s, bridge CH). *Anal.* calcd. for $C_{23}H_{32}O_5N_2Br_2$: C 47.93, H 5.60, N 4.86, Br 27.73; found: C 47.85, H 5.80, N 4.73, Br 27.93.

tert-*Butyl 5-Formyl-4-methoxycarbonylethyl-3-methylpyrrole-2-carboxylate*

The corresponding 5-methylpyrrole **1***k* (7) (2.81 g) and 4.43 g of lead tetraacetate in 70 ml of acetic acid was stirred vigorously for 1 h at 20–25°C. More lead tetraacetate (4.43 g) was then added and the mixture was heated 1 h on the steam-bath. The solvent was removed *in vacuo* and the residue was extracted several times with chloroform. The extract was well washed with water, dried, and evaporated. When the residue was dissolved in very little methanol, the product crystallized as colourless rods (75%), mp 89–93°C, raised to 94.5–95.5°C (lit. (2) mp 91–94°C) after two recrystallizations from chloroform–*n*-hexane. *Anal.* calcd. for $C_{15}H_{21}O_5N$: C 61.00, H 7.17, N 4.74; found: C 61.16, H 7.21, N 4.69.

tert-*Butyl 3,3′-bis(2-Methoxycarbonylethyl)-4′-methoxycarbonylmethyl-4,5′-dimethylpyrromethene-5-carboxylate Hydrobromide (***9***)*

tert-Butyl 5-formyl-4-(2-methoxycarbonylethyl)-4-methylpyrrole-2-carboxylate (295 mg) and the dimethyl ester of hemopyrroledicarboxylic acid (19), (239 mg) in 10 ml of methanol were treated with six drops of 47% hydrobromic acid. After 1 h the solvent was evaporated and the residue was rubbed with ether to give the product (420 mg). For analysis it was twice recrystallized from chloroform–*n*-hexane, mp 125–128°C; ^{1}Hmr: 1.74 (9H, s, CMe_3), 2.33 (3H, s, CH_3 at 4), 2.6–3.2 (8H, m, 2 CH_2CH_2CO), 2.86 (3H, s, CH_3 at 5′), 3.59 (2H, s, CH_2COOCH_3), 3.68–3.78 (9H, 3 partially overlapping s, 3 OCH_3), 7.00 (1H, s, bridge CH). *Anal.* calcd. for $C_{27}H_{37}O_8N_2Br$: C 54.27, H 6.24, N 4.69, Br 13.38; found: C 54.33, H 6.29, N 4.58, Br 13.21.

Acknowledgement

The authors are grateful to the Deutsche Forschungsgemeinschaft for a stipendium supporting A.R.

1. R. L. N. Harris, A. W. Johnson, and I. T. Kay. J. Chem. Soc. C, 22 (1966).
2. A. R. Battersby, E. Hunt, E. McDonald, J. B. Paine, and J. Saunders. J. Chem. Soc. Perkin Trans. 1, 1008 (1976).
3. A. H. Jackson and K. M. Smith. *In* The total synthesis of natural products. Vol. 1. *Edited by* J. ApSimon. Wiley-Interscience, New York, NY. 1973. p. 184.
4. A. Markovac, B. D. Kulkarni, K. B. Shaw, and S. F. MacDonald. Can. J. Chem. **44**, 2329 (1966).
5. A. Rowold and S. F. MacDonald. Can. J. Chem. **55**, 2916 (1977).
6. H. Fischer and H. Orth. Chemie des pyrrols. Vol. 2/1. Johnson Reprint Corp., New York, NY. 1968: (*a*) p. 71 ff; (*b*) p. 107; (*c*) p. 87; (*d*) p. 86.
7. A. W. Johnson, I. T. Kay, E. Markham, R. Price, and K. B. Shaw. J. Chem. Soc. 3416 (1959).
8. H. Fischer and W. Fröwis. Hoppe-Seyler's Z. Physiol. Chem. **195**, 49 (1931).
9. P. Bamfield, R. Grigg, A. W. Johnson, and R. W. Kenyon. J. Chem. Soc. C, 1259 (1968).
10. A. H. Jackson, G. W. Kenner, and J. Wass. J. Chem. Soc. Perkin Trans. 1, 1475 (1972).

11. A. H. CORWIN and P. VIOHL. J. Am. Chem. Soc. **66**, 1137 (1944).
12. J. ELLIS, A. H. JACKSON, A. C. JAIN, and G. W. KENNER. J. Chem. Soc. 1935 (1964).
13. H. FISCHER and P. ERNST. Ann. Chem. **447**, 139 (1926).
14. P. S. CLEZY and A. J. LIEPA. Aust. J. Chem. **23**, 2443 (1970).
15. S. F. MACDONALD and R. J. STEDMAN. Can. J. Chem. **32**, 896 (1954).
16. A. R. BATTERSBY, M. IHARA, E. MCDONALD, J. SAUNDERS, and R. J. WELLS. J. Chem. Soc. Perkin Trans. 1, 283 (1976).
17. J. M. OSGERBY, J. PLUSCEC, Y. C. KIM, F. BOYER, N. STOJANAC, H. D. MAH, and S. F. MACDONALD. Can. J. Chem. **50**, 2652 (1972).
18. P. S. CLEZY and V. DIAKIW. Aust. J. Chem. **26**, 2697 (1973).
19. M. W. ROOMI and S. F. MACDONALD. Can. J. Chem. **48**, 139 (1970).
20. S. F. MACDONALD and R. J. STEDMAN. Can. J. Chem. **33**, 458 (1955).
21. E. BULLOCK, A. W. JOHNSON, E. MARKHAM, and K. B. SHAW. J. Chem. Soc. 1430 (1958).

Can. J. Chem. Downloaded from www.nrcresearchpress.com by 210.87.254.42 on 09/05/12
For personal use only.

Some reactions of 2-*n*-butyl(phenyl)-1,2-dihydropyridines with isocyanates, pyridyl esters, and diethyl chlorophosphate

THEODORE A. ONDRUS, FRANK M. PASUTTO, AND EDWARD E. KNAUS

Faculty of Pharmacy and Pharmaceutical Sciences, University of Alberta, Edmonton, Alta., Canada T6G 2N8

AND

C. S. GIAM

Department of Chemistry, Texas A&M University, College Station, TX 77843, U.S.A.

Received January 10, 1978

THEODORE A. ONDRUS, FRANK M. PASUTTO, EDWARD E. KNAUS, and C. S. GIAM. Can. J. Chem. **56**, 1913 (1978).

Reaction of the ambident 1-lithio-1,2-dihydropyridines (**1**) and related dienamines (**2**) with several electrophiles has been investigtaed. Reaction of **1** with aliphatic isocyanates occurs predominantly or exclusively at nitrogen, whereas similar reactions employing **2** do not proceed and a dimeric product **8** resulting from self condensation of **2** is obtained. In contrast, reaction of **2***a* with the more electrophilic phenyl isocyanate (**3***c*) gave both *N*-phenylaminocarbonyl-2-*n*-butyl-1,2-dihydropyridine (**4***d*) and 2-*n*-butyl-5-phenylaminocarbonylpyridine (**6***d*) whereas a similar reaction with **1***a* afforded **4***d*, **5***d*, and **6***d*, as well as the stable *N*-unsubstituted-1,2-dihydropyridine **7***d*. Novel 2-*n*-butyl-5-(2-,3-,4-pyridylcarbonyl)-1,2-dihydropyridines **13***a–c* are obtained from reaction of **1***a* with pyridyl esters **12***a–c*. Reaction of **1***a* with diethyl chlorophosphate and ethyl acetate occurs exclusively at nitrogen to afford high yields of **16***a* and **16***b*, respectively. The mechanism for the formation of the 1,5-disubstituted-1,2-dihydropyridines **5** is described.

THEODORE A. ONDRUS, FRANK M. PASUTTO, EDWARD E. KNAUS et C. S. GIAM. Can. J. Chem. **56**, 1913 (1978).

On a étudié la réaction entre divers électrophiles et des lithio-1 dihydro-1,2 pyridines (**1**) et des diénamines (**2**) qui leur sont reliées et qui possèdent deux sites réactifs. La réaction de **1** avec les isocyanates aliphatiques se produit principalement ou exclusivement au niveau de l'azote; des réactions semblables faisant appel à **2** ne se produisent pas et l'on obtient que le dimère **8** résultant de l'autocondensation de **2**. Par opposition, la réaction de **2***a* avec l'isocyanate de phényle qui est plus électrophile (**3***c*) conduit à la *N*-phénylaminocarbonyl *n*-butyl-2 dihydro-1,2 pyridine (**4***d*) ainsi qu'à de la *n*-butyl-2 phénylaminocarbonyl-5 pyridine (**6***d*); une réaction semblable avec la **1***a* fournit **4***d*, **5***d*, **6***d* ainsi que **7***d*, la dihydro-1,2 pyridine non-substituée sur l'azote qui est stable. On a obtenu les nouvelles *n*-butyl-2(pyridylcarbonyl-2 ou -3,-4)-5 dihydro-1,2 pyridines **13***a–c* par réaction de **1***a* avec les esters de pyridyl **12***a–c*. La réaction de **1***a* avec le chlorophosphate de diéthyle et l'acétate d'éthyle se produit exclusivement au niveau de l'azote pour conduire, avec de bons rendements, à **16***a* et **16***b* respectivement. On décrit le mécanisme conduisant à la formation des dihydro-1,2 pyridines disubstituées en 1,5 (**5**).

[Traduit par le journal]

The reaction of the ambident *N*-lithio-1,2-dihydropyridines (**1**), obtained from the reaction of organolithium reagents and pyridines (1), with suitable electrophiles is a versatile procedure for the synthesis of *N*-substituted 1,2-dihydropyridines and/or 3-substituted pyridines which are otherwise difficult to prepare (2). In this way direct methods for the preparation of *N*-acyl(aroyl)-1,2-dihydropyridines (3) and introduction of alkyl, aminoalkyl, arylalkyl, hydroxyalkyl, acyl, amino, halo, and 3-pyridyl substituents into the β position of pyridine were conveniently effected (2–4). The ratio of *N*/*C*-substitution dropped significantly in going from the less reactive to more reactive electrophiles (3). The mesomeric structures of the structurally related dienamines (**2**), obtained from reaction of **1** with 3 equiv. of water (5), strongly suggest that electrophilic attack may also occur either at carbon or nitrogen or both. We now wish to describe the reactions of **1** and **2** with isocyanates, pyridyl esters, and diethyl chlorophosphate.

Reaction of *N*-lithio-2-*n*-butyl-1,2-dihydropyridine

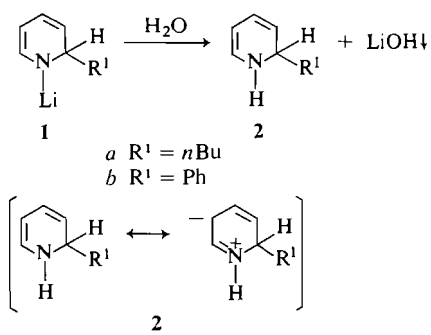

1 **2**

a R¹ = *n*Bu
b R¹ = Ph

2

Can. J. Chem. Downloaded from www.nrcresearchpress.com by 210.87.254.40 on 09/05/12
For personal use only.

Can. J. Chem. Downloaded from www.nrcresearchpress.com by 210.87.254.40 on 09/05/12
For personal use only.

(**1***a*) with ethyl isocyanate (**3***a*) afforded 1-ethylaminocarbonyl-2-*n*-butyl-1,2-dihydropyridine (**4***a*, 51.6%), the 1,5-disubstituted-1,2-dihydropyridine **5***a* (11.8%), and the *C*-substitution product 2-*n*-butyl-5-ethylaminocarbonylpyridine (**6***a*, 14.6%). On the other hand, reaction of **1***b* with **3***a* resulted in exclusive *N*-substitution to yield **4***b* (61%) as the sole product. The reaction of **2***b*, in comparison to **1***b*, with **3***a* was

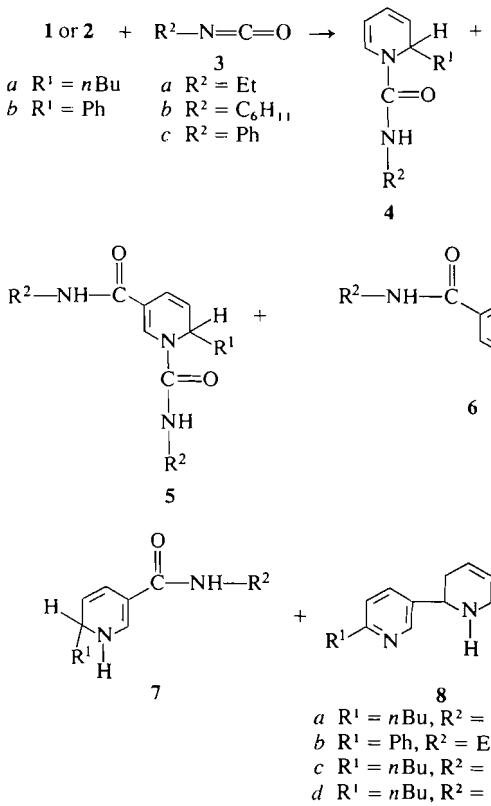

almost negligible since a near quantitative yield of 2-phenylpyridine was obtained together with a trace of **4***b*. Treatment of **2***a* (lithium hydroxide free) with **3***a* afforded **8** (R^1 = Bu, 35.4%) as the only isolable product. The dimeric product **8** (R^1 = Bu) most likely arises from self condensation of **2***a* since repetition of the reaction in the absence of **3***a* gave **8** (R^1 = Bu, 37.3%) and 2-butylpyridine (10.4%). In a related study it was found that 10% of the lithium hydroxide produced upon addition of 1 equiv. water to **1***a* remained in solution.[1] It is essential that solutions of **2** be free of lithium hydroxide which would also be expected to react with isocyanates **3** leading to urea derivatives (6). Lithium hydroxide free solutions of **2***a* are prepared by adding 3 equiv. of water to **1** and drying the ethereal solution with anhydrous sodium sulfate. Reaction of **1***a* with cyclohexyl isocyanate (**3***b*) afforded **4***c* (17%) and **6***c* (14%) whereas the reaction of **2***a* with **3***b* gave rise to **8** (R^1 = Bu, 27.2%) as the only isolable product.

The reaction of **2***a* with phenyl isocyanate (**3***c*) was investigated since an electron-attracting substituent is known to enhance the reactivity of the isocyanate group to a nucleophilic reagent (6). Thus, treatment of **2***a* with the more electrophilic **3***c* afforded the *N*-substituted product **4***d* (30.2%) and the *C*-substitution product **6***d* (15%). The 1,5-disubstituted product **5***d* was not detected. In a similar experiment (see Table 1) reaction of **1***a* with **3***c* gave rise to **4***d* (9.0%), **5***d* (14.8%), **6***d* (29.9%), and the stable *N*-unsubstituted 1,2-dihydropyridine **7***d* (42.8%). The structures assigned to **4**–**8** were assigned on the basis of their ir, ^{1}H nmr, and ms data which is consistent with the spectroscopic data previously reported for reaction of the ambident **1** with other electrophiles (1–3).

One possible pathway for the formation of the 1,5-disubstituted compounds **5***a* and **5***d* could involve reaction of the isocyanate **3** with **9** to give the dihydro intermediate **10**. Proton abstraction of the active C-5 proton by base such as 2-butylpyridine (some of which is always obtained) could give rise to **11** which on further reaction with **3** would afford **5**. It is unlikely that **5** arises from reaction of **4** with **3** since treatment of **4***a* with **3***a* and then 2-butylpyridine failed to yield any of the disubstituted product **5***a*, an observation which is consistent with a previous study (3).

The reaction of *N*-lithio-2-*n*-butyl-1,2-dihydropyridine (**1***a*) with pyridyl esters **12** was examined since it could be a useful procedure to prepare novel diheterocyclic ketones which would be useful medicinal intermediates. Treatment of **1***a* with ethyl

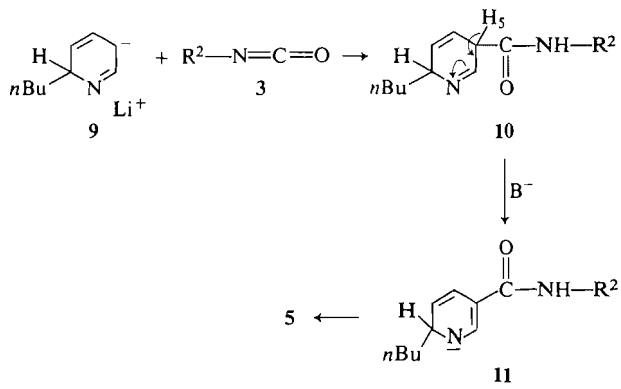

nicotinate (**12***a*) resulted in exclusive *C*-acylation to give **13***a* (39.6%), **14***a* (2.7%) along with some 2-butylpyridine (**15**, 8%). Similar reactions of **1***a* with **12***b* gave **13***b* (47.4%), **14***b* (8.6%), and **15** (4.8%) and with **12***c* afforded **13***c* (47.5%), **14***c* (4%), and **15**

[1] E. E. Knaus and T. A. Ondrus. Unpublished results.

TABLE 1. Reactions of 1,2-dihydropyridines with isocyanates

1,2-Dihydropyridine	Isocyanate 3 R^2	Yield (%) 4	5	6	7	8
1*a*	Et	51.6	11.8	14.6		
1*b*	Et	61.0				
2*a*	Et					35.4[a]
1*a*	C_6H_{11}	17.0		14.0		
2*a*	C_6H_{11}					27.2[a]
1*a*	Ph	9.0	14.8	29.9	42.8	
2*a*	Ph	30.2[a]		15.0[a]		

[a]The solution of the dienamine **2***a* is lithium hydroxide free.

(15.1%). It is expected that **14***a–c* arise from **13***a–c* during tlc purification since the presence of **14** was not evident in the reaction mixture before purification and solutions of **13** in deuteriochloroform

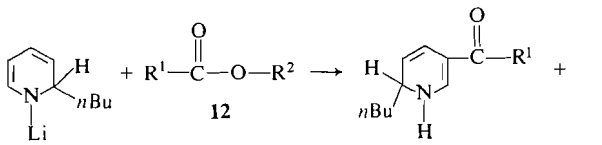

1*a* **12** **13**

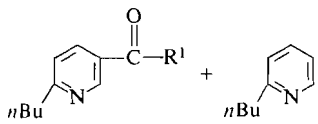

14 **15**

a R^1 = 3-pyridyl, R^2 = Et
b R^1 = 4-pyridyl, R^2 = Me
c R^1 = 2-pyridyl, R^2 = Et

undergo oxidation slowly at 25°C on exposure to air as indicated by ^{1}H nmr. The stability of the 1,2-dihydropyridines **13***a–c* is likely due to the stabilizing effect of the 5-(2-,3-,4-pyridylcarbonyl) substituents (7).

Treatment of **1***a* with diethyl chlorophosphate and ethyl acetate afforded **16***a* (68.3%) and **16***b* (99%), respectively. Further studies involving the chemistry of dienamines **1** and **2** are now in progress in these laboratories.

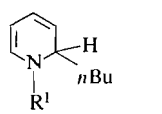

16

a $R^1 = (EtO)_2P(O)$—
b $R^1 = CH_3CO$—

Experimental

Melting points are determined with a Büchi capillary apparatus and are uncorrected. ^{1}H nmr spectra were determined for solutions in deuteriochloroform unless otherwise noted with TMS as internal standard with a Varian EM-360A or A-60 A spectrometer. Infrared spectra were recorded on a Perkin Elmer 267 spectrometer. Mass spectra were measured with an AEI-MS-9 or MS-50 mass spectrometer and these exact mass measurements are used in lieu of elemental analysis.

*1-Lithio-2-*n*-butyl-1,2-dihydropyridine (***1***a) and 2-*n*-Butyl-1,2-dihydropyridine (***2***a)*

General Procedure A

To an ice-cold solution of *n*-butyllithium (1.28 g, 0.02 mol) in 50 ml anhydrous ether, under a nitrogen atmosphere, pyridine (1.58 g, 0.02 mol) was added dropwise with stirring. The resulting dark brown solution containing **1***a* (0.02 mol) was allowed to stir for 35 min at 0°C before use in subsequent reactions.

To the solution of **1***a* (0.02 mol) in 50 ml anhydrous ether described above, under a nitrogen atmosphere, water (1.33 g, 0.074 mol) was added dropwise with stirring at 0°C. The reaction was allowed to proceed for 10 min, anhydrous sodium sulfate (16 g) was added, and the mixture stirred for an additional 15 min at 0°C. The solution was allowed to stand without agitation for 5 min after which an aliquot of the supernatant containing the required amount of **2***a* (lithium hydroxide free) was removed using a syringe under a nitrogen atmosphere.

*1-Lithio-2-phenyl-1,2-dihydropyridine (***1***b)*

General Procedure B

To an ice-cold solution of phenyllithium (1.68 g, 0.02 mol) in 100 ml anhydrous ether, under a nitrogen atmosphere, pyridine (1.58 g, 0.02 mol) was added dropwise with shaking. The resulting yellow precipitate was redissolved by repeated shaking. Upon cooling to 0°C the adduct **1***b* was obtained as a yellow crystalline solid which was washed with 30 ml dry ether and taken up in 100 ml dry tetrahydrofuran. A 2 ml aliquot of the above solution was hydrolyzed with 10 ml water and the concentration determined by titration with hydrochloric acid (8).

*N-Ethylaminocarbonyl-2-*n*-butyl-1,2-dihydropyridine (***4***a), 1,5-Di(ethylaminocarbonyl)-2-*n*-butyl-1,2-dihydropyridine (***5***a), and 2-*n*-Butyl-5-ethylaminocarbonylpyridine (***6***a)*

To a solution of **1***a* (1.53 g, 10.67 mmol) in 125 ml anhydrous ether, under a nitrogen atmosphere at −65°C, a solution of ethyl isocyanate (0.758 g, 10.67 mmol) in 2 ml anhydrous ether was added dropwise with stirring. The reaction was stirred at −65°C for 1.5 h and allowed to return to 25°C over a 0.5 h period after which 50 ml water was added. Extraction with chloroform (3 × 50 ml), drying (sodium sulfate) and removal of the solvent *in vacuo* gave a yellow oil. Preparative tlc was effected on eight 8 × 8 in. silica gel DF-5 plates, 0.75 mm in thicknesss, using benzene–ether (1:3 v/v) as development

Can. J. Chem. Downloaded from www.nrcresearchpress.com by 210.87.254.40 on 09/05/12
For personal use only.

Can. J. Chem. Downloaded from www.nrcresearchpress.com by 210.87.254.40 on 09/05/12
For personal use only.

solvent. Extraction of the band having R_f 0.86 with 100 ml warm methanol afforded **4***a* (1.145 g, 51.6%); ir (neat): 3360 (s, NH), 1642 (s, CO) cm^{-1}; ^1H nmr δ: 0.76–1.82 (m, 12H, $—CH_3$, C_4H_9) 3.33 (m, 2H, $—CH_2—$), 4.72 (m, 1H, H-2), 5.26 (d, $J_{5,6}$ = 8 Hz of d, $J_{4,5}$ = 5 Hz of d, $J_{3,5}$ = 1.5 Hz, 1H, H-5), 5.41–5.82 (m, 2H, H-3, NH, exchanges with deuterium oxide), 5.91 (d, $J_{3,4}$ = 9.5 Hz of d, $J_{4,5}$ = 5 Hz, 1H, H-4), 6.66 (d, $J_{5,6}$ = 8 Hz, 1H, H-6). Exact mass calcd. for $C_{12}H_{20}N_2O$: 208.1571; found (high resolution ms): 208.1581. Similar extraction of the band having R_f 0.2 afforded a yellow oil which was rechromatographed on two 8 × 8 in. silica gel DF-5 plates, 0.75 mm in thickness, using ether–methanol (16:1 v/v) as development solvent. Extraction of the band having R_f 0.78 with 100 ml warm methanol afforded **5***a* (0.175 g, 11.8%); ir (KBr): 3360 (m, NH), 1665 (s, CO), 1655 (s, CO) cm^{-1}; ^1H nmr δ: 0.7–1.81 (m, 9H, C_4H_9), 1.18 (t, J = 7 Hz, 6H, $—CH_3$), 3.38 (m, 4H, $—CH_2—$), 4.79 (m, 1H, H-2), 5.62 (d, $J_{3,4}$ = 9.2 Hz of d, $J_{2,3}$ = 6 Hz, 1H, H-3 and m, 1H, NH, exchanges with deuterium oxide), 6.0 (t, J_{NH-CH_2} = 5 Hz, 1H, NH, exchanges with deuterium oxide), 6.3 (d, $J_{3,4}$ = 9.2 Hz, 1H, H-4), 7.58 (s, 1H, H-6). Exact mass calcd. for $C_{15}H_{25}N_3O_2$: 279.1941; found (high resolution ms): 279.1947. Similar extraction of the band having R_f 0.73 afforded **6***a* (0.322 g, 14.6%); ir (neat): 3340 (m, NH), 1650 (s, CO) cm^{-1}; ^1H nmr δ: 0.79–1.93 (m, 7H, $—CH_2CH_2CH_2CH_3$), 1.2 (t, J = 7 Hz, 3H, $—CH_2CH_3$), 2.79 (t, J = 7 Hz, $—CH_2CH_2CH_2CH_3$), 3.45 (m, 2H, $—CH_2CH_3$), 6.32 (s, 1H, NH, exchanges with deuterium oxide), 7.18 (d, $J_{3,4}$ = 8 Hz, 1H, H-3), 8.01 (d, $J_{3,4}$ = 8 Hz of d, $J_{4,6}$ = 2.5 Hz, 1H, H-4), 8.89 (d, $J_{4,6}$ = 2.5 Hz, 1H, H-6). Exact mass calcd. for $C_{12}H_{18}N_2O$: 206.1415; found (high resolution ms): 206.1412.

*N-Ethylaminocarbonyl-2-phenyl-1,2-dihydropyridine (**4**b)*

To a solution of **1***b* (4.1 mmol) in 20 ml anhydrous tetrahydrofuran, under an atmosphere of nitrogen at −65°C, a solution of ethyl isocyanate (0.291 g, 4.1 mmol) in 2 ml dry tetrahydrofuran was added dropwise with stirring. The reaction was immediately allowed to return to 25°C and stand for 1 h after which 10 ml water was added. Extraction with chloroform (3 × 20 ml), drying (sodium sulfate) and removal of the solvent *in vacuo* gave an orange viscous semisolid. This semisolid was washed with 10 ml cold ether (to remove 2-phenylpyridine) leaving **4***b* (0.551 g, 61%) as a white solid; mp 108–110°C; ir (KBr): 3310 (s, NH), 1640 (s, CO) cm^{-1}; ^1H nmr δ: 1.01 (t, J = 7 Hz, 3H, $—CH_3$), 3.2 (q, J = 7 Hz, 2H, $—CH_2—$), 4.81 (broad s, 1H, NH, exchanges with deuterium oxide), 5.22 (d, $J_{5,6}$ = 7.5 Hz, of d, $J_{4,5}$ = 5.75 Hz, 1H, H-5), 5.4–5.85 (m, 2H, H-2, H-3), 5.96 (d, $J_{3,4}$ = 8.75 Hz, of d, $J_{4,5}$ = 5.75 Hz, 1H, H-4), 6.86 (d, $J_{5,6}$ = 7.5 Hz, 1H, H-6), 7.3 (m, 5H, phenyl). Exact mass calcd. for $C_{14}H_{16}N_2O$: 228.1263; found (high resolution ms); 228.1252.

*6,6′-Di-n-butyl-1,2,3,6-tetrahydro-2,3′-dipyridyl (**8**, R_1 = Bu)*

To a solution of **2***a* (1.462 g, 10.67 mmol) in 80 ml anhydrous ether, under a nitrogen atmosphere at −65°C, a solution of ethyl isocyanate (0.758 g, 10.67 mmol) in 2 ml anhydrous ether was added dropwise with stirring. The reaction was stirred at −65°C for 0.5 h, allowed to return to 25°C and stir for 1.5 h after which 50 ml water was added. Extraction with chloroform (3 × 40 ml), drying (sodium sulfate), and removal of the solvent *in vacuo* gave a viscous yellow oil. Preparative tlc was effected on eight 8 × 8 in. silica gel DF-5 plates, 0.75 mm in thickness, using benzene–ether (1:1 v/v) as development solvent. Extraction of the band having R_f 0.46 with 200 ml warm methanol afforded **8**, R′ = Bu (0.515 g, 35.4%). Identification was based on the spectral properties which were identical to those of an authentic sample (4).

*N-Cyclohexylaminocarbonyl-2-n-butyl-1,2-dihydropyridine (**4**c) and 2-n-Butyl-5-cyclohexylaminocarbonylpyridine (**6**c)*

To a solution of **1***a* (2.72 g, 19 mmol), in 50 ml dry ether, under a nitrogen atmosphere at −65°C, cyclohexyl isocyanate (2.42 g, 19 mmol) was added dropwise with stirring. The resulting solution was allowed to stir at −65°C for 20 min and after warming to 25°C, 20 ml water was added. Extraction with chloroform (3 × 20 ml), drying (sodium sulfate), and removal of the solvent *in vacuo* gave a brown oil. Preparative tlc was effected on six 8 × 8 in. silica gel GFP 254 plates, 0.75 mm in thickness, using benzene – ethyl acetate (1:3 v/v) as development solvent. Extraction of the fraction having R_f 0.95 with 50 ml warm methanol afforded **4***c* (0.846 g, 17%); ir (neat): 3340 (m, NH), 1630 (s, CO), cm^{-1}; ^1H nmr δ: 0.8–2.05 (m, 21H, C_4H_9, C_6H_{11}, NH, exchanges with deuterium oxide), 4.66 (m, 1H, H-2), 5.34 (m, 1H, H-5), 5.64 (m, 1H, H-3), 5.98 (m, 1H, H-4), 6.4 (m, 1H, H-6). Exact mass calcd. for $C_{16}H_{26}N_2O$: 262.2045; found (high resolution ms): 262.2045. Similar extraction of the band having R_f 0.65 gave **6***c* (0.692 g, 14%), mp 103–104°C; ir (chloroform): 3435 (m, NH), 1650 (s, CO), cm^{-1}; ^1H nmr δ: 0.94 (t, J = 7 Hz, 3H, $—CH_3$), 1.1–2.1 (m, 15H, C_6H_{11}, $—CH_2CH_2CH_2CH_3$), 2.29 (broad s, 1H, NH, exchanges with deuterium oxide), 2.82 (t, J = 7 Hz, 2H, $—CH_2CH_2CH_2CH_3$), 7.22 (d, $H_{3,4}$ = 7.5 Hz, 1H, H-3), 8.0 (d, $J_{3,4}$ = 7.5 Hz of d, $J_{4,6}$ = 2.5 Hz, 1H, H-4), 8.84 (d, $J_{4,6}$ = 2.5 Hz, 1H, H-6). Exact mass calcd. for $C_{16}H_{24}N_2O$: 260.1888; found (high resolution ms): 260.1892.

*N-Phenylaminocarbonyl-2-n-butyl-1,2-dihydropyridine (**4**d), 1,5-Di(phenylaminocarbonyl)-2-n-butyl-1,2-dihydropyridine (**5**d), 2-n-Butyl-5-phenylaminocarbonylpyridine (**6**d), and 2-n-Butyl-5-phenylaminocarbonyl-1,2-dihydropyridine (**7**)*

To a solution of **1***a* (1.462 g, 10.67 mmol) in 125 ml anhydrous ether under a nitrogen atmosphere at −65°C, a solution of phenyl isocyanate (1.509 g, 12.67 mmol) in 3 ml anhydrous ether was added dropwise with stirring. The reaction was stirred at −65°C for 0.5 h, allowed to return to 25°C and stir for 1.5 h after which 100 ml water was added. Extraction with chloroform (4 × 50 ml), drying (sodium sulfate), and removal of the solvent *in vacuo* gave an orange semisolid. This semisolid was triturated with 30 ml ether leaving **7** (1.158 g, 42.8%) as a light yellow solid; mp 140–141°C; ir (KBr): 3400 (w, NH), 3280 (w, NH), 1650 (s, CO) cm^{-1}; ^1H nmr (DMSO-d_6) δ: 0.67–1.65 (m, 9H, C_4H_9), 4.18 (m, 1H, H-2), 4.99 (d, $J_{3,4}$ = 10 Hz of d, $J_{2,3}$ = 4 Hz, 1H, H-3), 6.49 (d, $J_{3,4}$ = 10 Hz, 1H, H-4), 6.82–7.83 (m, 7H, H-6, phenyl, NH, exchanges with deuterium oxide), 8.95 (s, 1H, NH, exchanges with deuterium oxide). Exact mass calcd. for $C_{16}H_{20}N_2O$: 256.1571; found (high resolution ms): 256.1573. The ethereal filtrate was evaporated *in vacuo* to give a viscous yellow oil. Preparative tlc was effected on eleven 8 × 8 in. silica gel DF-5 plates, 0.75 mm in thickness using benzene–ether (2:1 v/v) as development solvent. Extraction of the band having R_f 0.98 with 100 ml warm methanol afforded **4***d* (0.246 g, 9.0%) whose spectral properties were identical to those of **4***d* described in the reaction below. Similar extraction of the band having R_f 0.82 afforded **5***d* as a white solid (0.591 g, 14.8%): mp 70°C; ir (KBr): 3330 (m, NH), 1652 (s, CO) cm^{-1}; ^1H nmr δ: 0.63–1.91 (m, 9H, C_4H_9), 4.75 (m, 1H, H-2), 5.6 (d, $J_{3,4}$ = 10 Hz of d, $J_{2,3}$ = 6 Hz, 1H, H-3) 6.39 (d, $J_{3,4}$ = 10 Hz, 1H, H-4), 6.93–7.6 (m, 10H, phenyl), 7.7 (s, 1H, H-6), 8.15 (s, 1H, NH, exchanges with deuterium oxide), 8.22 (s, 1H, NH, exchanges with deuterium oxide). *Anal.* calcd. for $C_{23}H_{25}N_3O_2$: C 73.57, H 6.71, N 11.19; found: C 72.47, H 6.85, N 10.48. Repeated attempts to obtain analytically pure **5***d* were not successful. Similar extraction of the band

Can. J. Chem. Downloaded from www.nrcresearchpress.com by 210.87.254.40 on 09/05/12
For personal use only.

having R_f 0.3 afforded **6***d* (0.81 g, 29.9%) whose spectral properties were identical to those of **6***d* described in the reaction below.

*N-Phenylaminocarbonyl-2-*n*-butyl-1,2-dihydropyridine (**4**d) and 2-*n*-Butyl-5-phenylaminocarbonylpyridine (**6**d)*

To a solution of **2***a* (1.462 g, 10.67 mmol) in 80 ml anhydrous ether, under a nitrogen atmosphere at −65°C, a solution of phenyl isocyanate (1.271 g, 10.67 mmol) in 3 ml anhydrous ether was added dropwise with stirring. The reaction was stirred at −65°C for 0.5 h, allowed to return to 25°C and stir for 1.5 h after which 50 ml water was added. Extraction with chloroform (3 × 40 ml), drying (sodium sulfate), and removal of the solvent *in vacuo* gave a viscous yellow oil. Preparative tlc was effected on 11 silica gel DF-5 plates, 8 × 8 in., 0.75 mm in thickness using benzene–ether (1:1 v/v) as development solvent. Extraction of the band having R_f 0.98 with 100 ml warm methanol afforded **4***d* (0.824 g, 30.2%); ir (neat): 3330 (m, NH), 1655 (s, CO) cm^{-1}; ^1H nmr δ: 0.75–2 (m, 9H, C_4H_9), 4.88 (m, 1H, H-2), 5.49 (d, $J_{5,6}$ = 7.5 Hz of d, $J_{4,5}$ = 5 Hz of d, $J_{3,5}$ = 1.5 Hz, 1H, H-5), 5.8 (m, 1H, H-3), 6.05 (d, $J_{3,4}$ = 9.25 Hz of d, $J_{4,5}$ = 5 Hz, 1H, H-4), 6.61 (d, $J_{5,6}$ = 7.5 Hz, 1H, H-6), 6.78 (s, 1H, NH, exchanges with deuterium oxide), 7.04–7.6 (m, 5H, phenyl). Exact mass calcd. for $C_{16}H_{20}N_2O$: 256.1571; found (high resolution ms): 256.1577. Similar extraction of the band having R_f 0.41 afforded **6***d* (0.405 g, 15.0%); ir (KBr): 3352 (m, NH), 1660 (s, CO) cm^{-1}; ^1H nmr δ: 0.7–1.99 (m, 7H, $—CH_2CH_2CH_2CH_3$), 2.85 (t, J = 7 Hz, 2H, $—CH_2CH_2CH_2CH_3$), 6.9–7.8 (m, 6H, H-3, phenyl), 8.14 (d, $J_{3,4}$ = 8 Hz of d, $J_{4,6}$ = 2.5 Hz, 1H, H-4), 8.56 (s, 1H, NH, exchanges with deuterium oxide), 9.01 (d, $J_{4,6}$ = 2.5 Hz, 1H, H-6). Exact mass calcd. for $C_{16}H_{18}N_2O$: 254.1415; found (high resolution ms): 254.1427.

*2-*n*-Butyl-5-(3′-pyridylcarbonyl)-1,2-dihydropyridine (**13**a) and 2-*n*-Butyl-5-(3′-pyridylcarbonyl)pyridine (**14**a)*

To a solution of **1***a* (1.43 g, 10 mmol) in 60 ml anhydrous ether, under a nitrogen atmosphere at 25°C, a solution of 3-ethoxycarbonylpyridine (1.51 g, 10 mmol) in 5 ml anhydrous ether was added dropwise with stirring. The reaction was stirred at 25°C for 1 h after which 90 ml water was added. Extraction with ether (6 × 30 ml), drying (sodium sulfate), and removal of the solvent *in vacuo* gave a red oil. Preparative tlc was effected on three 8 × 16 in. silica gel DF-5 plates, 0.75 mm in thickness using ether–methanol (9:1 v/v) as development solvent. Extraction of the band having R_f 0.42 with 100 ml warm methanol afforded **13***a* (0.957 g, 39.6%); ir (neat): 3260 (m, NH), 1652 (s, CO) cm^{-1}; ^1H nmr δ: 0.66–1.77 (m, 9H, C_4H_9), 4.29 (m, 1H, H-2), 5.15 (d, $J_{3,4}$ = 10 Hz, 1H, H-3), 6.54 (d, $J_{3,4}$ = 10 Hz, 1H, H-4), 6.94–7.4 (m, 3H, H-5′, H-6, NH, exchanges with deuterium oxide), 7.72 (d, $J_{4',5'}$ = 8.5 Hz of d, $J_{4',6'}$ = 2 Hz of d, $J_{2',4'}$ = 2 Hz, 1H, H-4′), 8.53 (d, $J_{5',6'}$ = 5 Hz of d, $J_{4',6'}$ = 2 Hz, 1H, H-6′), 8.58 (d, $J_{2',4'}$ = 2 Hz, 1H, H-2′). Exact mass calcd. for $C_{15}H_{18}N_2O$: 242.1415; found (high resolution ms): 242.1414. Similar extraction of the band having R_f 1 afforded a dark yellow oil which was rechromatographed on one 8 × 16 in. silica gel DF-5 plate, 0.75 mm in thickness using ether–methanol (20:1 v/v) as development solvent. Extraction of the band having R_f 1 with 100 ml warm methanol afforded 2-*n*-butylpyridine (0.108 g, 8.0%). Similar extraction of the band having R_f 0.95 afforded 3-ethoxycarbonylpyridine (0.408 g, 27.0%). Similar extraction of the band having R_f 0.76 afforded **14***a* (0.064 g, 2.7%); ir (neat): 1670 (s, CO) cm^{-1}; ^1H nmr δ: 0.73–2.17 (m, 7H, $—CH_2CH_2CH_2CH_3$), 2.89 (t, J = 7 Hz, 2H, $—CH_2CH_2CH_2CH_3$), 7.2—7.59 (m, 2H, H-5′, H-3), 7.92–8.24 (m, 2H, H-4′, H-4), 8.7–9.05 (m, 3H, H-2′, H-6′, H-6). Exact mass calcd. for $C_{15}H_{16}N_2O$: 240.1259; found (high resolution ms): 240.1257.

*2-*n*-Butyl-5-(4′-pyridylcarbonyl)-1,2-dihydropyridine (**13**b) and 2-*n*-Butyl-5-(4′-pyridylcarbonyl)pyridine (**14**b)*

To a solution of **1***a* (2.86 g, 20 mmol) in 60 ml anhydrous ether, under a nitrogen atmosphere at 25°C, a solution of 4-methoxycarbonylpyridine (2.74 g, 20 mmol) in 10 ml anhydrous ether was added dropwise with stirring. The reaction was stirred at 25°C for 0.5 h after which 100 ml water was added. Extraction with ether (6 × 100 ml), drying (sodium sulfate), and removal of the solvent *in vacuo* gave a red oil. Preparative tlc was effected on six 8 × 16 in. silica gel DF-5 plates, 0.75 mm in thickness using ether–methanol (15:1 v/v) as development solvent. Extraction of the band having R_f 0.21 with 100 ml warm methanol afforded **13***b* (2.29 g, 47.4%); ir (neat): 3240 (m, NH), 1650 (s, CO) cm^{-1}; ^1H nmr δ: 0.65–1.7 (m, 9H, C_4H_9), 4.27 (m, 1H, H-2), 5.13 (d, $J_{3,4}$ = 10 Hz of d, $J_{2,3}$ = 3.5 Hz, 1H, H-3), 6.49 (d, $J_{3,4}$ = 10 Hz, 1H, H-4), 6.88–7.28 (m, 3H, H-3′, H-5′, H-6), 7.93 (m, 1H, NH, exchanges with deuterium oxide), 8.4–8.62 (m, 2H, H-2′, H-6′). Exact mass calcd. for $C_{15}H_{18}N_2O$: 242.1415; found (high resolution ms): 242.1417. Similar extraction of the band having R_f 0.67 afforded **14***b* (0.41 g, 8.6%); ir (neat): 1670 (s, CO) cm^{-1}; ^1H nmr δ: 0.72–2.07 (m, 7H, $—CH_2CH_2CH_2CH_3$), 2.9 (t, J = 7 Hz, 2H, $—CH_2CH_2CH_2CH_3$), 7.29 (d, $J_{3,4}$ = 8 Hz, 1H, H-3), 7.48–7.65 (m, 2H, H-3′, H-5′), 8.04 (d, $J_{3,4}$ = 8 Hz of d, $J_{4,6}$ = 2.5 Hz, 1H, H-4), 8.72–8.95 (m, 3H, H-2′, H-6′, H-6). Exact mass calcd. for $C_{15}H_{16}N_2O$: 240.1259; found (high resolution ms): 240.1256. Similar extraction of the band having R_f 0.85 afforded 4-methoxycarbonylpyridine (0.449 g, 16.4%). Similar extraction of the band having R_f 0.94 afforded 2-*n*-butylpyridine (0.128 g, 4.8%).

*2-*n*-Butyl-5-(2′-pyridylcarbonyl)-1,2-dihydropyridine (**13**c) and 2-*n*-Butyl-5-(2′-pyridylcarbonyl)pyridine (**14**c)*

To a solution of **1***a* (1.45 g, 10.1 mmol) in 60 ml anhydrous ether, under a nitrogen atmosphere at 25°C, a solution of 2-ethoxycarbonylpyridine (1.53 g, 10.1 mmol) in 5 ml anhydrous ether was added dropwise with stirring. The reaction was stirred at 25°C for 1 h after which 100 ml water was added. Extraction with chloroform (5 × 50 ml), drying (sodium sulfate), and removal of the solvent *in vacuo* gave a red oil. Preparative tlc was effected on eight 8 × 8 in. silica gel DF-5 plates, 0.75 mm in thickness, using ether–methanol (15:1 v/v) as development solvent. Extraction of the band having R_f 0.54 with 100 ml warm methanol afforded **13***c* (1.162 g, 47.5%); ir (neat): 3250 (s, NH), 1648 (s, CO) cm^{-1}; ^1H nmr δ: 0.7–1.95 (m, 9H, C_4H_9), 4.3 (m, 1H, H-2), 5.14 (d, $J_{3,4}$ = 10 Hz, 1H, H-3), 6.7 (d, $J_{3,4}$ = 10 Hz, 1H, H-4), 7.03–8.25 (m, 5H, H-6, H-3′, H-4′, H-5′, NH, exchanges with deuterium oxide), 8.52 (m, 1H, H-6′). Exact mass calcd. for $C_{15}H_{18}N_2O$: 242.1415; found (high resolution ms): 242.1412. Similar extraction of the band having R_f 0.81 afforded **14***c* (0.097 g, 4%); ir (neat): 1670 (s, CO) cm^{-1}; ^1H nmr δ: 0.68–2.24 (m, 7H, $—CH_2CH_2CH_2CH_3$), 2.88 (t, J = 7 Hz, 2H, $—CH_2CH_2CH_2CH_3$), 7.3 (d, $J_{3,4}$ = 8 Hz, 1H, H-3), 7.46–8.22 (m, 3H, H-4′, H-3′, H-5′), 8.4 (d, $J_{3,4}$ = 8 Hz of d, $J_{4,6}$ = 2.5 Hz, 1H, H-4), 8.75 (d, $J_{5',6'}$ = 5 Hz of d, $J_{4',6'}$ = 2 Hz, of d, $J_{3',6'}$ = 1 Hz, 1H, H-6′), 9.36 (d, $J_{4,6}$ = 2.5 Hz, 1H, H-6). Exact mass calcd. for $C_{15}H_{16}N_2O$: 240.1259; found (high resolution ms): 240.1247. Similar extraction of the band having R_f 0.95 afforded 2-ethoxycarbonylpyridine (0.236 g, 15.5%). Similar extraction of the band having R_f 1 afforded 2-*n*-butylpyridine (0.206 g, 15.1%).

*N-Diethylphosphoryl-2-*n*-butyl-1,2-dihydropyridine (**16**a)*

To a solution of **1***a* (2.72 g, 19 mmol) in 50 ml anhydrous

ether, under a nitrogen atmosphere at −65°C, a solution of diethyl chlorophosphate (3.28 g, 19 mmol) in 5 ml dry ether was added dropwise with stirring. The resulting solution was maintained at −65°C for 20 min and after warming to 25°C, 20 ml water was added. Extraction with chloroform (3 × 20 ml) drying (sodium sulfate) and removal of the solvent *in vacuo* afforded a brown oil which was subjected to preparative tlc on six 8 × 8 in. silica gel GFP 254 plates, 0.75 mm in thickness, with benzene–ether (1:1 v/v) as development solvent. Extraction of the band having R_f 0.7 with 50 ml methanol gave **16***a* (3.54 g, 68.3%), ir (neat): 1265 (s, PO) cm^{-1}; ^1H nmr δ: 0.9 (t, J = 7 Hz, 3H, $—CH_2CH_2CH_2CH_3$), 1.0–1.8 (m, 12H, $—CH_2CH_2CH_2CH_3$, $—OCH_2CH_3$), 4.0 (m, 5H, H-2, $—OCH_2CH_3$), 5.25 (m, 1H, H-5), 5.5 (m, 1H, H-3), 5.85 (m, 1H, H-4), 6.1 (m, 1H, H-6). Exact mass calcd. for $C_{13}H_{24}NO_3P$: 273.1494; found (high resolution ms): 273.1494.

N-*Acetyl-2*-n-*butyl-1,2-dihydropyridine* (**16**b)

To a solution of **1***a* (1.36 g, 9.5 mmol) in 50 ml dry ether, under an atmosphere of nitrogen at −65°C, ethyl acetate (0.84 g, 9.5 mmol) was added dropwise with stirring. The resulting solution was maintained at −65°C for 20 min and after warming to room temperature water (25 ml) was added. Extraction with chloroform (3 × 20 ml), drying (sodium sulfate) and removal of the solvent yielded a light yellow oil. Quantitative vpc analysis using a ⅛ × 20 in. column packed with 10% UCW-98 on WAW-DMCS (80–100 mesh) with a helium flow rate of 25 ml/min and a column temperature of 125°C afforded 2-*n*-butylpyridine (0.011 g, 0.8%), retention time of 1.2 min, which showed ir and ^1H nmr spectra identical to those of an authentic sample; and **16***b* (1.74 g, 99%), retention time of 6.1 min; ir (neat): 1655 (s, CO) cm^{-1}; ^1H nmr δ: 0.9 (t, J = 7 Hz, 3H, $CH_2CH_2CH_2CH_3$), 1.0–1.95 (m, 6H, $CH_2CH_2CH_2CH_3$), 2.19 (s, 3H, $COCH_3$), 5.07 (m, 1H, H-2), 5.33 (m, 1H, H-5), 5.67 (m, 1H, H-3), 5.82 (m, 1H, H-4), 6.5 (m, 1H, H-6). Exact mass calcd. for $C_{11}H_{17}NO$: 179.1310; found (high resolution ms): 179.1310.

Acknowledgment

We are grateful to the Medical Research Council of Canada (Grant MA-4888) for financial support of this work.

1. C. S. GIAM and J. L. STOUT. Chem. Commun. 142 (1969).
2. C. S. GIAM, E. E. KNAUS, R. A. LOCKHART, and I. G. KEENER. Can. J. Chem. **53**, 2305 (1975).
3. C. S. GIAM, E. E. KNAUS, and F. M. PASUTTO. J. Org. Chem. **39**, 3565 (1974).
4. E. E. KNAUS, T. A. ONDRUS, and C. S. GIAM. J. Heterocycl. Chem. **13**, 789 (1976).
5. E. E. KNAUS, R. I. MARSTON, I. MEIER, and C. S. GIAM. Can. J. Pharm. Sci. **11**, 73 (1976).
6. S. OZAKI. Chem. Rev. **72**, 457 (1972).
7. U. EISNER. Chem. Commun. 1348 (1969).
8. H. GILMAN and A. H. HAUBEIN. J. Am. Chem. Soc. **66**, 1515 (1944).

Can. J. Chem. Downloaded from www.nrcresearchpress.com by 210.87.254.40 on 09/05/12
For personal use only.

Analyse des malates de cuivre et d'uranyle par potentiométrie, polarimétrie et spectrophotométrie

ILHAM KHALIL,[1] MICHELLE M. PETIT-RAMEL ET CLAUDETTE CHAPELET-BARBIER[2]

Laboratoire de Chimie Minérale I, Université Claude Bernard, Lyon I, 43 Boulevard du 11 novembre 1918, 69621, Villeurbanne, France

Reçu 5 août 1977

ILHAM KHALIL, MICHELLE M. PETIT-RAMEL et CLAUDETTE CHAPELET-BARBIER. Can. J. Chem. **56**, 1919 (1978).

Les constantes de stabilité et constantes optiques des malates de cuivre $[CuH_2Mal]^+$, $[CuHMal]$, $[CuH_2Mal_2]^{2-}$, $[CuMal]^-$, $[Cu_2Mal_2]^{2-}$ et $[CuH_{-1}Mal]^{2-}$ ont été affinées par une méthode de "pit-mapping", qui donne aussi leurs limites de confiance, à partir des mesures potentiométriques, spectrophotométriques visibles et polarimétriques.

Dans le cas des malates d'uranyle, la présence d'espèces polynucléaires, perceptible par potentiométrie, a été confirmée par spectrométrie rmn. Les constantes des espèces $[UO_2HMal]$, $[UO_2Mal]^-$, $[(UO_2)_2Mal_2]^{2-}$, $[(UO_2)_3Mal_5]^{9-}$ et $[(UO_2)_3H_{-2}Mal_5]^{11-}$ ont été calculées d'abord par "pit-mapping", puis par la méthode graphique de Lefebvre. Toute les valeurs sont données à 25°C pour une force ionique de 0.5 en $NaNO_3$.

ILHAM KHALIL, MICHELLE M. PETIT-RAMEL, and CLAUDETTE CHAPELET-BARBIER. Can. J. Chem. **56**, 1919 (1978).

The stability and optical constants of the copper malates $[CuH_2Mal]^+$, $[CuHMal]$, $[CuH_2Mal_2]^{2-}$, $[CuMal]^-$, $[Cu_2Mal_2]^{2-}$, and $[CuH_{-1}Mal]^{2-}$ have been fitted by a pit-mapping method, which also gives their confidence limits, from potentiometric, visible spectroscopic and polarimetric measurements.

In the case of the uranyle malates, the presence of polynuclear species, detectable in the potentiometric study, have been confirmed by nmr spectrocopy. The constants of $[UO_2HMal]$, $[UO_2Mal]^-$, $[(UO_2)_2Mal_2]^{2-}$, $[(UO_2)_3Mal_5]^{9-}$, and $[(UO_2)_3H_{-2}Mal_5]^{11-}$ have been determined, first by a pit-mapping method, then, by the graphical method of Lefebvre. All the values are given at 25°C for an ionic strength of 0.5 in $NaNO_3$.

Bien que, dès 1844 Peligot (1) puis Itzig (2) et Courtois (3) aient décrit la préparation des malates d'uranyle à l'état solide, nous constatons que les malates occupent une place beaucoup moins importante que les complexes d'autres acides-alcools tels les acides tartrique, lactique ou citrique (4–6).

Pour notre part, nous avons utilisé la potentiométrie pour l'interprétation des phénomènes et surtout le calcul des constantes de stabilité, la spectrophotométrie et la polarimétrie pour la confirmation de certains de nos résultats. Enfin la résonance magnétique du proton devrait nous permettre d'élucider les phénomènes d'association métal-coordinat, tout particulièrement dans le cas de l'uranyle.

En ce qui concerne l'acide malique, dont nous ne rappellerons que les résultats définitifs (6), la rmn a permis de mettre en évidence, comme l'avait montré Pachler (23) les variations du déplacement chimique et des constantes de couplage jusqu'au point d'équivalence. Selon le domaine de pH envisagé, l'acide malique existe essentiellement sous deux formes rotamères (*a*) et (*c*), la forme (*a*) devenant prédominante avec l'augmentation de l'alcalinité du milieu (7, 8).

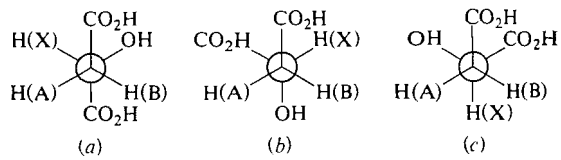

I. Malates d'uranyle

Feldman et coll. (9, 10) ont montré que l'acide malique formait vers pH 2.4, des chélates à prédominance binucléaire par l'intermédiaire de liaisons tridentées. Ces liaisons se produisant par des ponts OH entre les ions uranyle, la formation de ces dimères est suivie à p$H > 4$ de leur hydrolyse et de leur polymérisation, puis de l'apparition du trimère. Rajan et Martell (11) puis Campi et Ginnaro (12) en ont déjà calculé les constantes de stabilité, mais la structure de ces complexes ayant donné lieu à des interprétations diverses nous les discuterons et les comparerons à l'ensemble de nos résultats.

I.1. Mise en évidence des espèces et calcul des constantes

La démarche que nous suivrons découle directement de l'examen des courbes de formation (fig.

[1]Boursière du Centre National de la Recherche Scientifique du Liban.

[2]Laboratoire de Chimie Physique Moléculaire, Université Claude Bernard, Lyon I, 43 Boulevard du 11 novembre 1918, 69621, Villeurbanne.

Can. J. Chem. Downloaded from www.nrcresearchpress.com by 210.87.254.105 on 09/05/12
For personal use only.

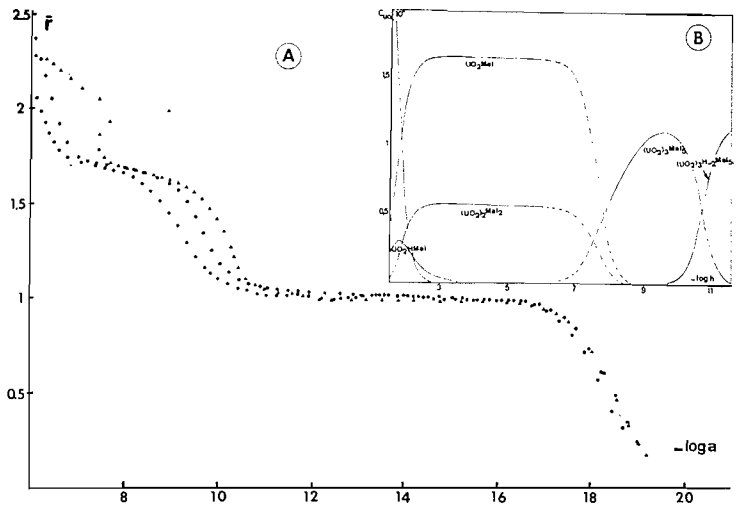

FIG. 1. Uranyl – acide malique. (*a*) Courbes de formation, [Mal] = 6×10^{-2} *M*. ● $[UO_2] = 10^2$ *M*; * $[UO_2] = 2 \times 10^{-2}$ *M*; ▲ $[UO_2] = 3 \times 10^{-2}$ *M*. (*b*) Courbes de répartition. [Mal] = 6×10^{-2} *M*; $[UO_2] = 3.2 \times 10^{-2}$ *M*.

1*a*) sur lesquelles on distingue trois zones bien différenciées:

p*H* < 5 formation de l'espèce UO_2Mal en même temps que des espèces protonées pour des $-\log a > 12$.

6 < p*H* < 10 présence de l'espèce polynucléaire $(UO_2)_3Mal_5$ pour des $-\log a$ compris entre 11 et 7.5. Les courbes sont équidistantes et l'écartement séparant deux courbes est proportionnel à Δm (21).

p*H* > 10 formation d'espèces hydroxydées pour des $-\log a < 7.5$.

Les complexes du milieu acide p*H* < 5 ont pu être abordés facilement par la méthode du "pit-mapping" (13). Pour les p*H* > 5 les espèces ont été mises en évidence spectrophotométriquement par la méthode trichrome (14) et les constantes de stabilité déterminées par la méthode de Lefebvre (4). La polarimétrie sera dans tous les cas un moyen commode de délimiter les zones de formation et même de confirmer certains de nos résultats.

I.1.1. Méthode du "pit-mapping": La comparaison des courbes de titrage normalisées $\bar{q}_{cal}$, $\bar{q}_{exp} = f(pH)$ (fig. 2) pour des p*H* < 5 a permis de calculer les constantes de stabilité des espèces et l'écart-type correspondant. Les valeurs définitives sont rassemblées dans le tableau 2.

I.1.2. Méthode spectrophotométrique: La complexation de l'uranyle par l'acide malique se traduit sur la fig. 3 par un léger déplacement vers les fortes longueurs d'onde. Ce phénomène se reproduit d'ailleurs pour un grand nombre de composés de l'uranyle, en particulier les citrates (15–17) et peut être rapproché de l'effet néphélauxétique observé dans les complexes lanthanidiques colorés (18).

Entre p*H* 2.8 et 5.0 la densité optique ne varie plus

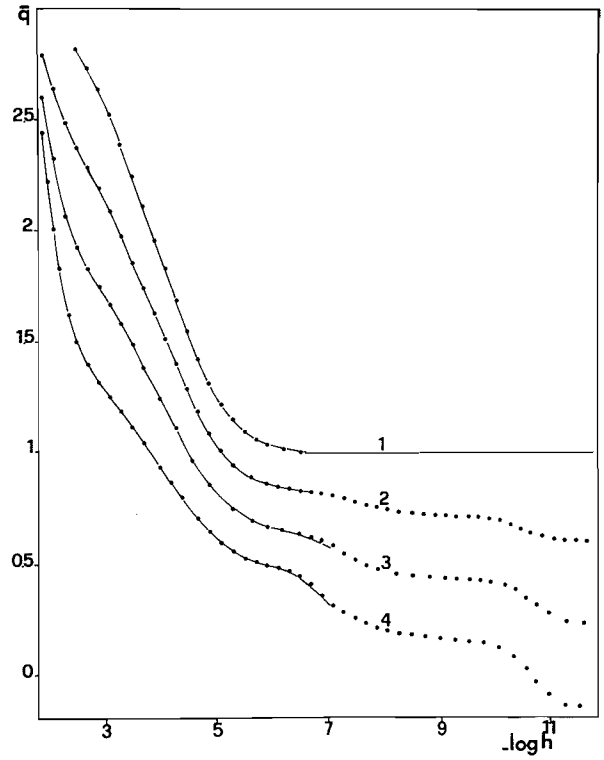

FIG. 2. Uranyle – acide malique. Courbes normalisées $\bar{q} = f(pH)$ [Mal] = 6×10^{-2} *M*. (*1*) $[UO_2] = 0$; (*2*) $[UO_2] = 10^{-2}$ *M*; (*3*) $[UO_2] = 2 \times 10^{-2}$ *M*; (*4*) $[UO_2] = 3 \times 10^{-2}$ *M*.

et les spectres sont confondus. Le ou les complexes formés ont atteint leur maximum de concentration. Au fur et à mesure que le p*H* augmente, une autre espèce apparait et on observe son maximum de formation dans le domaine étroit de p*H* compris entre 9.4 et 10.3. Un léger déplacement a lieu ensuite

Can. J. Chem. Downloaded from www.nrcresearchpress.com by 210.87.254.105 on 09/05/12
For personal use only.

Can. J. Chem. Downloaded from www.nrcresearchpress.com by 210.87.254.105 on 09/05/12
For personal use only.

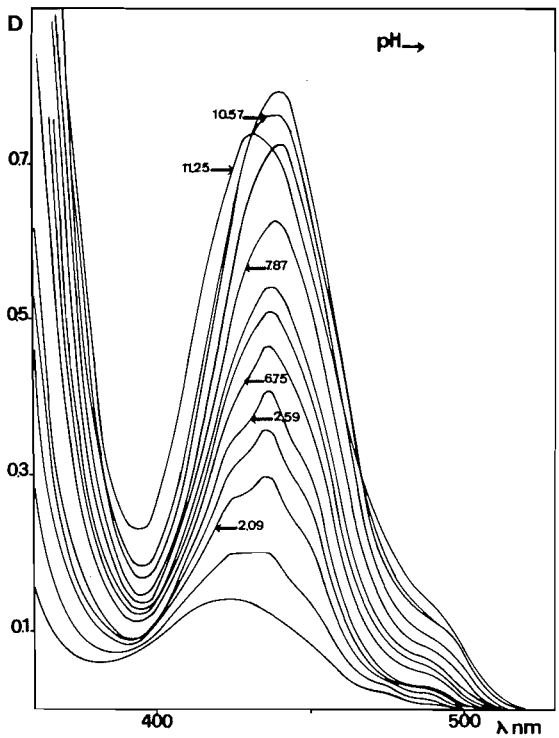

FIG. 3. Uranyle – acide malique. Spectres d'absorption en fonction du pH. [Mal] = 6×10^{-2} M. [UO_2] = 10^{-2} M.

vers les faibles longueurs d'onde et le coefficient d'absorption diminue. L'apparition d'un point isosbestique à 430 nm suppose la présence d'un équilibre entre deux espèces absorbant à cette même longueur d'onde.

L'application de la méthode trichrome (14) aux faisceaux de spectres de la fig. 3 révèle l'existence de plus d'une espèce jusqu'à pH 2.8 (fig. 4). Puis les courbes deviennent parallèles à l'axe des pH et dans le meilleur des cas il y a présence d'une seule espèce absorbant dans ce domaine. Ce parallélisme se retrouve dans un domaine de pH restreint $8.8 < pH < 10.2$ et aux environs de pH 11.7.

L'existence des complexes étant pressentie, nous avons déterminé la formule par application de la méthode des variations continues à pH 9. L'absorption maximum est obtenue pour 37.5% d'uranyle et 62.5% d'acide malique. Ceci exclut, par conséquent le rapport 1:1 acide malique:uranyle au pH envisagé. Ajoutons que si nous mesurons l'écart entre chaque courbe de neutralisation du complexe et celle de l'acide malique et si nous nous reportons aux courbes de formation, nous constatons qu'il correspond à la consommation de 5/3 d'ion OH par atome d'uranyle lorsque $8.8 < pH < 10.2$ et 7/3 d'ion OH dans le domaine $11 < pH < 12$. Cela conduit, en première approximation aux formules $(UO_2)_3Mal_5$

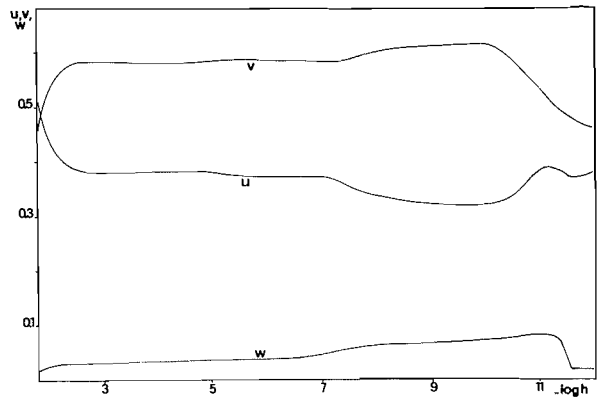

FIG. 4. Uranyle – acide malique. Méthode trichrome.

et $(UO_2)_3H_{-2}Mal_5$ avec

$$3(UO_2)^{2+} + 5(HMal)^{2-} \rightleftarrows ((UO_2)_3Mal_5)^{9-} + 5H^+$$

$$3(UO_2)^{2+} + 5(HMal)^{2-} + 2H_{-1}H^+ \rightleftarrows ((UO_2)_3H_{-2}Mal_5)^{11-} + 7H^+$$

si $H_{-1}H^+ = OH^-H^+$.

I.1.3. Méthode de Lefebvre: Les complexes ci-dessus sont caractérisés successivement par les constantes β_{305} et β_{3-25}, définies par:

$$\beta_{305} = \frac{[(UO_2)_3(Mal)_5]}{[UO_2]^3[Mal]^5}$$

$$\beta_{3-25} = \frac{[(UO_2)_3H_{-2}(Mal)_5]}{[UO_2]^3[H]^{-2}[Mal]^5}$$

et dont la détermination nécessite la connaissance préalable des concentrations de toutes les espèces présentes en solution.

La concentration en ions uranyle est calculée par application de la méthode de Lefebvre (4) puisque $-\log m$ ne nous est pas accessible par mesure directe à l'aide d'une électrode réversible. La méthode consiste à relever, à partir du faisceau de courbes de neutralisation pour différentes valeurs de pH, les volumes de soude correspondants et ceci pour tous les rapports envisagés. On effectue alors le tracé des droites:

$$V_{ml} = f(C_{UO_2}) \quad \text{à différents pH} \qquad \text{(fig. 5}a\text{)}$$

On mesure la pente de chacune de ces droites et on trace:

$$\delta n_{H-1}/\delta n_{UO_2} = f(-\log h) \qquad \text{(fig. 5}b\text{)}$$

Nous remarquons sur la fig. 5*b* un palier, situé entre les pH 8.8 et 10.2 correspondant à une consommation en uranyle proportionnelle au nombre de ml versés. En d'autres termes, nous nous trouvons dans la zone du saut de potentiel coïncidant avec la formation du complexe $(UO_2)_3Mal_5$. La surface

Can. J. Chem. Downloaded from www.nrcresearchpress.com by 210.87.254.105 on 09/05/12
For personal use only.

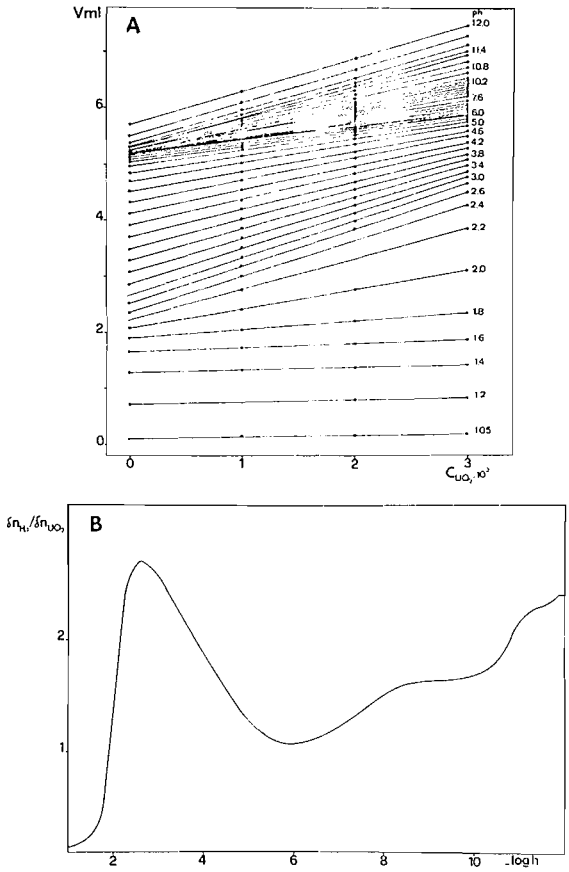

FIG. 5. Uranyle – acide malique. Méthode de Lefebvre.

comprise entre cette dernière courbe et l'axe des pH, ajoutée à $-\log [UO_2]_{initial}$ connu, permet d'obtenir $-\log [UO_2]_{final}$ tout au long de la courbe. Notons que $-\log [UO_2]_{initial}$ est facilement calculé, à partir de la concentration initiale en uranyle, puisque le pH de départ, atteint après addition d'une quantité d'acide nitrique suffisante pour rétrograder l'ionisation de l'acide malique, ne permet pratiquement pas la complexation de l'ion métallique. Ceci se traduit par des courbes de neutralisation relativement confondues au point de départ vers pH = 1.

En ce qui concerne la concentration en ions malates libres, elle est calculée par différence entre la concentration totale en acide malique et la concentration du complexe supposé être entièrement formé dans tout le domaine d'existence précédemment déterminé.

Le même raisonnement est valable pour le domaine des pH, situé aux environs de 11.7.

Nos essais expérimentaux ont été réalisés sur des solutions de compositions suivantes:

Solution n°	1	2	3	4
C_{H_3Mal}	6×10^{-2}	6×10^{-2}	6×10^{-2}	6×10^{-2}
C_{UO_2}	0	10^{-2}	2×10^{-2}	3×10^{-2}

Les valeurs rassemblées dans le tableau 1 permettent le calcul des constantes de stabilité du complexe polynucléaire $(UO_2)_3Mal_5$ puis du complexe $(UO_2)_3H_{-2}Mal_5$. Sur le même tableau nous avons représenté la variation de chacune des constantes des espèces $(UO_2)_3Mal_5$, $(UO_2)_2Mal_3$ et $(UO_2)_3H_{-2}Mal_3$. Pour les premières, la calcul a été fait en écrivant l'acide malique sous la forme H_3Mal alors que pour la dernière, nous nous sommes placés dans les conditions de Rajan et Martell et nous avions considéré l'acide malique comme un diacide. La comparaison de ces valeurs montre bien une constance plus importante pour l'espèce $(UO_2)_3Mal_5$. Ce qui permet, encore une fois, de recouper notre hypothèse.

En procédant de la même façon pour $(UO_2)_3H_{-2}Mal_5$ et $(UO_2)_3H_{-1}Mal_5$, nous sommes amenés à admettre, en définitif, dans chacune des deux zones, les espèces $(UO_2)_3Mal_5$ et $(UO_2)_3H_{-2}Mal_5$ respectivement.

Les constantes calculées pour les espèces précédentes sont obtenues en faisant la moyenne des valeurs du tableau 1

$(UO_2)_3Mal_5$ $8.8 < pH < 10.3$

$$\log \beta_{305} = 79.50 \pm 0.07$$

$(UO_2)_3H_{-2}Mal_5$ $pH > 11$

$$\log \beta_{3-25} = 57.70 \pm 0.10$$

I.1.4. Courbes de répartition: Elles représentent globalement les résultats du "pit-mapping" et de la méthode de Lefebvre (fig. 1*b*). Comme les courbes de répartition, les courbes polarimétriques $\alpha = f(pH)$ (fig. 6) montrent une nette séparation des domaines de formation des espèces. Les constantes optiques ainsi que les constantes de stabilité sont rassemblées dans les tableaux 2 et 3.

I.2. Etude par résonance magnétique du proton

Les premiers travaux de rmn sur le malate d'uranyle ont été effectués par Mariano et Gil (7, 8) sur une solution équimoléculaire 0.2 *M* d'acide malique et d'ion uranyle à pH 3. Nous avons exploré le domaine de pH allant de 3 à 5.6 avec des solutions contenant les mêmes proportions molaires d'acide malique et d'uranyle (0.16 et 0.2 *M*). Tous les spectres observés présentent un caractère commun à savoir la présence de deux parties X distinctes, l'une résolue, l'autre non résolue tandis qu'il n'apparait qu'une seule partie AB. La séparation ainsi que le rapport d'intensité des

TABLEAU 1. $C_{H_3Mal} = 6 \times 10^{-2}\ M$; $C_{UO_2} = 3 \times 10^{-2}\ M$; Mal′ = HMal

$-\log h$	$[UO_2]$	[Mal]	$\log \beta_{305}$	[Mal]	$\log \beta_{203}$	[Mal′]	$\log \beta_{3-23}$
8.80	9.247×10^{-14}	3.242×10^{-9}	79.54	4.864×10^{-9}	49.18	3×10^{-2}	26.72
9.00	4.380×10^{-14}	5.142×10^{-9}	79.51	7.713×10^{-9}	49.23	3×10^{-2}	27.29
9.20	2.070×10^{-14}	8.149×10^{-9}	79.49	1.222×10^{-8}	49.28	3×10^{-2}	27.87
9.40	9.705×10^{-15}	1.291×10^{-8}	79.48	1.937×10^{-8}	49.34	3×10^{-2}	28.45
9.60	4.508×10^{-15}	2.047×10^{-8}	79.48	3.071×10^{-8}	49.40	3×10^{-2}	29.05
9.80	2.079×10^{-15}	3.243×10^{-8}	79.49	4.864×10^{-8}	49.47	3×10^{-2}	29.66
10.00	9.543×10^{-16}	5.142×10^{-8}	79.50	7.713×10^{-8}	49.55	3×10^{-2}	30.27
10.20	4.350×10^{-16}	8.149×10^{-7}	79.52	1.222×10^{-7}	49.63	3×10^{-2}	30.90
10.40	1.948×10^{-16}	1.291×10^{-7}	79.57	1.936×10^{-7}	49.73	3×10^{-2}	31.55

$-\log h$	$[UO_2]$	[Mal]	$\log \beta_{3-25}$	$\log \beta_{3-15}$
11.00	1.284×10^{-17}	5.141×10^{-7}	57.74	69.06
11.20	4.649×10^{-18}	8.149×10^{-7}	57.66	69.18
11.40	1.627×10^{-18}	1.291×10^{-8}	57.63	69.35
11.60	5.622×10^{-19}	2.047×10^{-6}	57.61	69.54
11.80	1.890×10^{-19}	3.242×10^{-6}	57.63	69.76
12.00	6.257×10^{-20}	5.138×10^{-6}	57.67	70.00

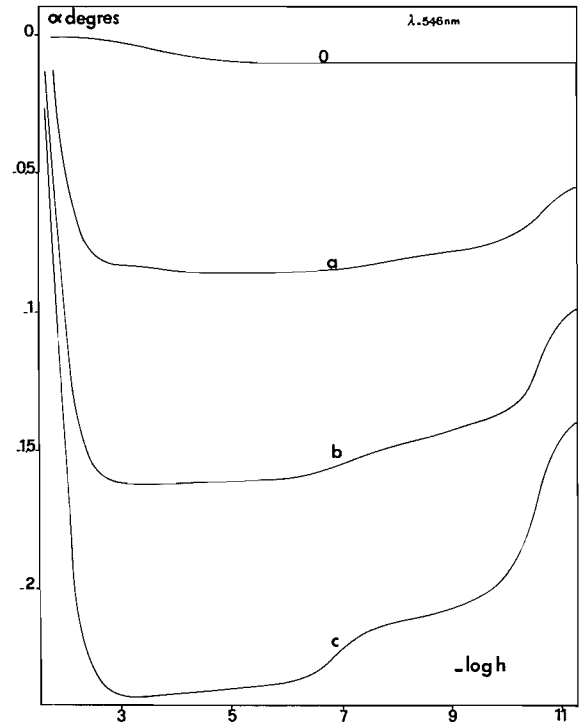

FIG. 6. Uranyle – acide malique. Pouvoir rotatoire en fonction du pH. [Mal] = $6 \times 10^{-2}\ M$. (0) $[UO_2] = 0$; (*a*) $[UO_2] = 10^{-2}\ M$; (*b*) $[UO_2] = 2 \times 10^{-2}\ M$; (*c*) $[UO_2] = 3 \times 10^{-2}\ M$.

deux massifs de la partie X varient avec les conditions de pH et de température. Sur l'un des deux massifs situé du côté des champs faibles, à température ordinaire, (fig. 7) apparait la structure qui nous a servi (avec la partie AB) à évaluer les constantes de couplage. On constate que les paramètres de couplage ainsi que le déplacement chimique entre les noyaux A et B varient peu avec le pH; seule varie de façon appréciable la position relative des deux groupes de raies de la partie X. A pH 5.6 leur séparation de 0.24 ppm devient suffisante pour mesurer le

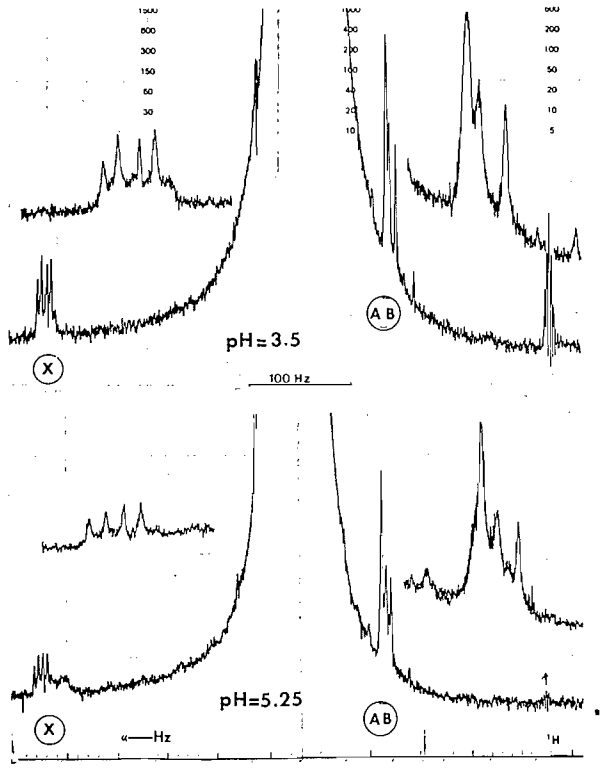

FIG. 7. Uranyle – acide malique; rmn 100 MHz dans D_2O. Parties X et AB agrandies 4 fois.

Can. J. Chem. Downloaded from www.nrcresearchpress.com by 210.87.254.105 on 09/05/12
For personal use only.

Can. J. Chem. Downloaded from www.nrcresearchpress.com by 210.87.254.105 on 09/05/12
For personal use only.

TABLEAU 2. Constantes de stabilité et constantes optiques des malates d'uranyle et de cuivre(I) = 0.5 $NaNO_3$; t = 25°C

Espèce	log β_{nqr}	$\varepsilon_{nqr}\lambda$ = 700 nm	$[m]_{nqr}\lambda$ = 546 nm
H_3Mal log K_3 3.14(0.02); log K_2 4.49(0.01); log K_1 15.46(0.01)			
CuH_2Mal*	22.05(0.03)	74.8	−72
$CuHMal$*	19.08_4(0.015)	19.4	−181
CuH_2Mal_2*	35.98(0.04)	55	−366
$CuMal$*	14.68(0.04)	10	−65
Cu_2Mal_2*	30.27_6(0.055)	279	−29
$CuH_{-1}Mal$	4.081(0.025)	37	1008
Espèce	**log β_{nqr}**	**$\varepsilon_{nqr}\lambda$ = 425 nm**	**$[m]_{nqr}\lambda$ = 546 nm**
UO_2HMal	19.8(0.1)	33	153
UO_2Mal*	18.35(0.03)	8	−801
$(UO_2)_2Mal_2$*	38.03(0.07)	240	−1568
$(UO_2)_3Mal_5$	79.50(0.07)	63	−2079
$(UO_2)_3H_{-2}Mal_5$	57.70(0.10)	69	−1355

*Seules les valeurs notées d'un astérisque peuvent être comparées à celles de nos références bibliographiques. Nous les avons recalculées sans tenir compte de la dissociation alcoolique de l'acide malique (tableau 3).

rapport des intensités ($<1/1.6$), le massif le plus intense se situant du côté des champs forts. Nous donnerons les valeurs des paramètres indépendants du pH et de la concentration (à la précision de nos mesures).

$$J_{AX} = 12.5 \text{ Hz} \qquad J_{BX} = 0.1 \text{ Hz}$$

$$J_{AB} = (-)17.2 \text{ Hz} \qquad \delta_{AB} = 0.07 \text{ ppm}$$

L'influence de la température a été étudiée sur la solution équimoléculaire 0.173 M à pH 5.6. On constate qu'à 10°C, la résolution de la partie X est moins bonne qu'à 30°C, la partie X la mieux résolue se trouvant encore du côté des champs faibles. Tandis qu'à 60°C, les raies X et AB sont nettement plus fines, le massif X non résolu se trouvant cette fois du côté des champs faibles, contrairement aux deux premiers cas.

Il faut admettre, d'après ces observations qu'il existe plusieurs espèces différentes en solution. Aux pH inférieurs à 7, l'existence d'un couplage à longue distance du deuterium alcoolique avec le proton X dans l'une des formes étant exclu on peut avancer l'hypothèse de la présence simultanée de trois espèces: le monomère $(UO_2)Mal$ et deux dimères $(UO_2)_2Mal_2$ de structures différentes **1** et **2**.

Ces trois complexes sont très voisins par leurs systèmes AB, mais l'un d'eux se différencie plus nettement par ses noyaux X. D'après les structures **1** et **2**, on peut en effet attendre des spectres très voisins pour le monomère et le dimère **1**, tandis que la partie X du dimère **2** serait plus affectée par la présence de deux groupements uranyle, les parties AB étant moins sensibles à la différence de structure.

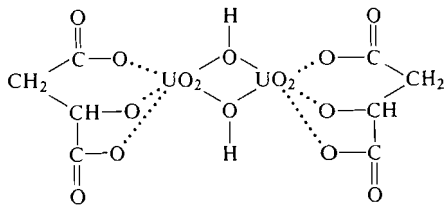

1

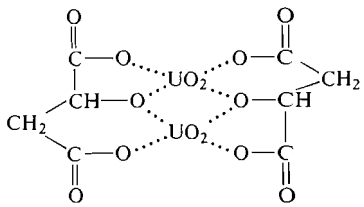

2

II. Malates de cuivre

Delsal (20), Lefebvre (4), Rajan et Martell (5) ont mis en évidence la formation d'un complexe très stable de formule $CuMal$ ou Cu_2Mal_2. La neutralisation progressive de mélanges acide malique–cuivre fait bien apparaître un saut de pH très net après addition de un OH par ion cuivrique. Puis, la précipitation de l'hydroxyde rend les mesures impossibles et l'on ne retrouve pas le deuxième point d'équivalence mis en évidence par Lefebvre, car il est uniquement perceptible en présence d'un grand excès d'acide malique. De plus, l'addition d'ions cuivriques à la solution d'acide malique, modifie très nettement le pouvoir rotatoire, ce qui indique que la complexation a lieu dès le début de la neutralisation. Les variations du pouvoir rotatoire en fonction du pH

TABLEAU 3.

Espèces		Références					
H_3Mal	H_2Mal'	(4)	(25)	(26)	(27)	(5) dimérisé	Nos valeurs
CuHMal	CuMal′	3.40	3.93	3.54	4.22	8.0	3.63
Cu_2Mal_2	$Cu_2Mal_2'H_{-2}$	28.9					28.45
CuMal	$CuMal'H_{-1}$			0.72			0.78
CuH_2Mal	CuHMal				2.83		6.60
CuH_2Mal_2	$CuMal_2$				5.42		5.07

	Références		
	(10)	(11)	Nos valeurs
$(UO_2)_2Mal_2$	7.76		7.11
$K_{ML} = \frac{[UO_2L^-][H^+]^3}{[UO_2^{2+}][H_3L]}$		−5.55	−4.74
$K_D = \frac{[(UO_2)_2L_2^{2-}][H^+]^6}{[UO_2^{2+}]^2[H_3L]^2}$		−7.75	−8.15

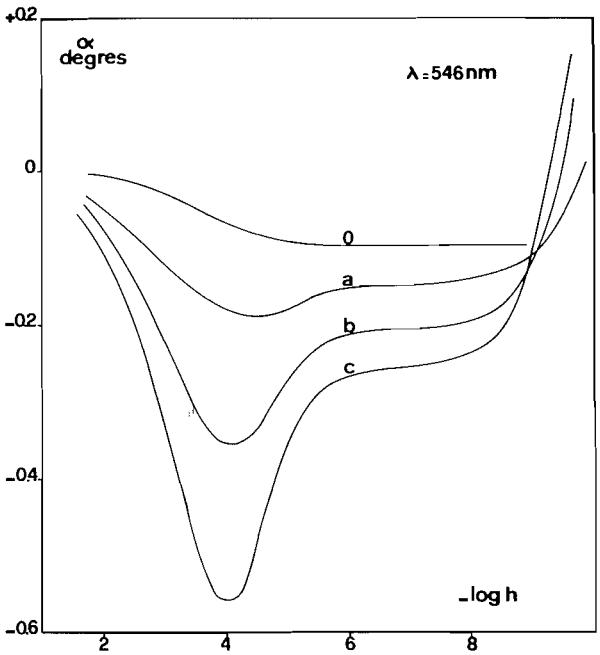

FIG. 8. Cuivre – acide malique. Pouvoir rotatoire en fonction du pH. [Mal] = 6×10^{-2} M. (0) [Cu] = 0; (*a*) [Cu] = 1.035×10^{-2} M; (*b*) [Cu] = 2.070×10^{-2} M; (*c*) [Cu] = 3.105×10^{-2} M.

(fig. 8) laissent prévoir la formation d'au moins quatre espèces.

II.1. Mise en évidence des espèces

L'examen des courbes de formation (fig. 9*a*) montre, pour $10 < -\log a < 15$ (soit $3.3 <$ p$H <$ 7), un déplacement net des $-\log a$ pour des valeurs croissantes en Δm, ce qui suppose, comme dans le cas précédent, la présence d'espèces polynucléaires. En outre $\bar{r}$, tend vers l, deux hypothèses sont possibles: soit formation de la seule espèce Cu_nMal_n, soit présence simultanée du monomère CuMal et du polymère Cu_nMal_n. De part et d'autre de la zone de formation de l'espèce polynucléaire, la présence d'espèces protonées en milieu acide ($-\log a > 15$; p$H < 3.3$) et d'espèces hydroxydées en milieu alcalin ($-\log a < 9$; p$H > 8$) est tout à fait probable.

II.2. Calcul des constantes de stabilité et des constantes optiques

La comparaison des courbes de neutralisation normalisées $\bar{q}$, et par suite la convergence du processus d'affinement conduit aux valeurs des constantes de stabilité rassemblées dans le tableau 2. Pour pouvoir comparer nos résultats aux données bibliographiques, nous représenterons les valeurs calculées avec les constantes d'ionisation carboxyliques seules (22). Les courbes de répartition des malates de cuivre en fonction du pH sont représentées sur la fig. 9*b*.

Le tracé des spectres d'absorption (fig. 10) pour toutes les valeurs de pH dans le domaine des longueurs d'onde 500–900 nm, montre la formation graduelle d'espèces relativement stables qui déplacent le maximum vers les faibles longueurs d'onde. Le point isosbestique vers 780 nm indique la présence de deux espèces en équilibre, CuHMal et CuMal; la contribution de l'espèce $Cu(HMal)_2$ n'intervenant pratiquement pas.

A partir des données précédentes nous avons pu calculer à l'aide du programme ACREF 5A, les pouvoirs rotatoires et les coefficients d'absorbance de

Can. J. Chem. Downloaded from www.nrcresearchpress.com by 210.87.254.105 on 09/05/12
For personal use only.

Can. J. Chem. Downloaded from www.nrcresearchpress.com by 210.87.254.105 on 09/05/12
For personal use only.

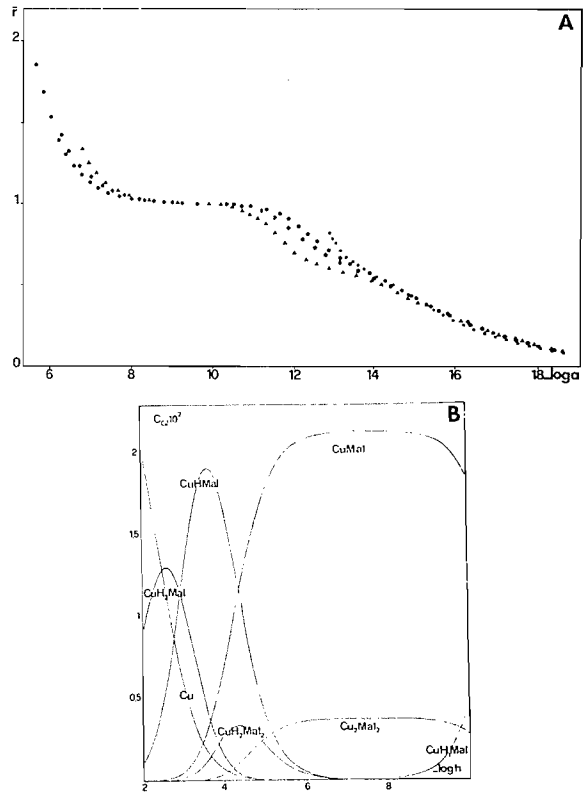

FIG. 9. Cuivre – acide malique. (*a*) Courbes de formation [Mal] = 6×10^{-2} *M*. ▲ [Cu] = 1.035×10^{-2} *M*; * [Cu] = 2.070×10^{-2} *M*; ● [Cu] = 3.105×10^{-2} *M*; · [Cu] = 6.126×10^{-2} *M*. (*b*) Courbes de répartition [Mal] = 6×10^{-2} *M*. [Cu] = 3.105×10^{-2} *M*.

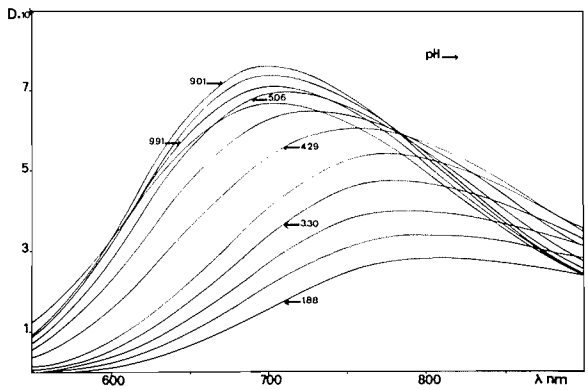

FIG. 10. Cuivre – acide malique. Spectres d'absorption en fonction du p*H*. [Mal] = 6×10^{-2} *M*. [Cu] = 2.054×10^{-2} *M*.

chacune des espèces à la longueur d'onde de 700 nm (tableau 2).

II.3. Résonance magnétique du proton

Le paramagnétisme électronique des ions Cu^{2+} ne nous a pas permis d'envisager une étude quantitative des spectres rmn et nous n'avons pu que suivre l'interaction coordinat – ion métallique en observant l'élargissement progressif des raies de résonance de l'acide malique après addition de cuivre.

Conclusions

Jusqu'à p*H* 5, les malates d'uranyle ont été traités par "pit-mapping". Pour des p*H* plus élevés, la présence d'espèces polynucléaires perceptible sur les courbes de formation, dont le décalage $\Delta(-\log a)$ est proportionnel à l'augmentation de la concentration du métal Δm (6) a été confirmée par spectrophotométrie. Ces constantes de stabilité de ces polymères ont du être calculées par la méthode graphique de Lefebvre. Parmi les trois métaux étudiés, Cu, Y (19) et UO_2, c'est bien l'ion UO_2(VI) qui présente la plus forte tendance à former des complexes polynucléaires. Bien que la plupart des auteurs aient négligé la présence du monomère (UO_2)Mal (10, 11, 24), les études potentiométriques et polarimétriques révèlent la présence simultanée d'un monomère et d'un dimère. En outre, les spectres rmn nous ont permis de visualiser le dédoublement de la partie X correspondant à l'équilibre monomère ⇄ dimère, ce dernier pouvant présenter deux structures différentes.

Au delà de p*H* 6, la rmn se révèle inopérante car les rapports UO_2 : Mal utilisés, voisins de 1, favorisent la précipitation d'hydroxyde insoluble.

En ce qui concerne les malates de cuivre, le décalage $\Delta(-\log a)$ des courbes de formation traduit l'apparition de l'espèce dimérisée Cu_2Mal_2 en concentration faible par rapport au monomère.

Partie expérimentale

Les mesures conjointes de p*H*, de pouvoir rotatoire ou d'absorption ont été réalisées à l'aide d'un compensateur Metrohm E 388 couplé, soit à un spectrophotomètre Beckman DK 2A soit à un polarimètre photoélectrique Perkin-Elmer M141.

Les spectres rmn ont été effectués à 100 MHz sur spectrophotomètres Varian HA 100 et XL 100 en présence d'alcool isobutylique tertiaire comme référence interne. Les échantillons ont été préparés par mise en solution directe dans l'eau lourde, d'acide malique et de nitrate d'uranyle en proportions égales. La recristallisation du malate d'uranyle pour la préparation de l'échantillon, ne modifiant pas le spectre rmn a été abandonnée. Le p*H* a été ajusté et corrigé par addition d'une solution concentrée de NaOD en très faible quantité.

Remerciements

Nous remercions vivement Monsieur le Professeur R. A. Pâris, de l'Université de Lyon, pour ses conseils et pour l'intérêt qu'il a porté à ce travail.

1. E. PELIGOT. Ann. Chim. Phys. **12**, 562 (1844).
2. H. ITZIG. Ber. Dtsch. Chem. Ges. **34**, 3822 (1901).
3. G. COURTOIS. C.R. Acad. Sci. **153**, 245 (1911).
4. J. LEFEBVRE. J. Chim. Phys. **54**, 581 (1957).

5. K. S. RAJAN et A. E. MARTELL. J. Inorg. Nucl. Chem. **29**, 463 (1967).
6. I. KHALIL. Thèse, Lyon. 1976.
7. V. M. S. GIL et J. S. MARIANO. Rev. Port. Quim. **11**, 212 (1969).
8. J. S. MARIANO et V. M. S. GIL. Mol. Phys. **17**, 313 (1969).
9. I. FELDMAN et J. R. HAVILL. J. Am. Chem. Soc. **76**, 2114 (1954).
10. I. FELDMAN, C. A. NORTH et H. B. HUNTER. J. Phys. Chem. **64**, 1224 (1960).
11. K. S. RAJAN et A. E. MARTELL. J. Inorg. Nucl. Chem. **26**, 1927 (1964).
12. E. CAMPI et M. C. GINNARO. Ann. Chim. (Rome), **11–12**, 761 (1974).
13. G. SILLEN. Acta Chem. Scand. 159 (1962).
14. H. FLASCHKA, J. BUTCHER et R. SPEIGHTS. Talanta, **8**, 400 (1961).
15. I. FELDMAN et N. F. NEUMAN. J. Am. Chem. Soc. **73**, 2312 (1951).
16. C. HEITNER et I. ELIEZER. Bull. Soc. Chim. Fr. **23**, 174 (1956).
17. A. M. GUREVICH et N. P. OSICHEVA. Radiokhimiya, **10**, 214 (1968).
18. S. HUBERT, M. HUSSONNOIS et R. GUILLAUMONT. J. Inorg. Nucl. Chem. **35**, 2923 (1973).
19. I. KHALIL et M. M. PETIT-RAMEL. Bull. Soc. Chim. Fr. **11–12**, 1127 (1977).
20. J. L. DELSAL. J. Chim. Phys. **35**, 314 (1938).
21. L. C. VAN POUCKE et H. F. DE BRABANDER. Talanta, **20**, 733 (1973).
22. I. KHALIL et M. M. PETIT-RAMEL. Bull. Soc. Chim. **7–8**, 1255 (1974).
23. K. G. R. PACHLER. Z. Anal. Chem. **224**, 211 (1967).
24. J. D. PEDROSA et V. M. S. GIL. J. Inorg. Nucl. Chem. **36**, 1803 (1974).
25. S. RAMAMOORTHY et M. SANTAPPA. J. Inorg. Nucl. Chem. **30**, 1855 (1968).
26. B. NANDA et S. PANI. J. Indian Chem. Soc. **5**, 355 (1958).
27. V. K. ZOLOTUKHIN, Z. G. GALANETS et V. T. KOROTYA. Ukr. Khim. Zh. **39**, 1059 (1973).

Can. J. Chem. Downloaded from www.nrcresearchpress.com by 210.87.254.105 on 09/05/12
For personal use only.

The reactions of metal acetylacetonates with acids

A. J. C. NIXON AND D. R. EATON

Department of Chemistry, McMaster University, Hamilton, Ont., Canada L8S 4M1

Received January 24, 1978

A. J. C. NIXON and D. R. EATON. Can. J. Chem. **56**, 1928 (1978).

The reactions of a number of metal acetylacetonates with trifluoroacetic acid have been investigated using nmr. The initial reaction involves protonation on the carbon atom of the ligand. In the case of the aluminum compound in coordinating solvents there is further reaction to give cationic complexes. The results are used to reinterpret the kinetics of ligand exchange for this compound. It is argued that, contrary to previous suggestions, the slow step is the breaking of the first metal oxygen bond to form a dangling ligand intermediate. A consequence of this conclusion is that intramolecular rearrangements of Al(III) β diketonates must proceed by twisting rather than by bond rupture mechanisms.

A. J. C. NIXON et D. R. EATON. Can. J. Chem. **56**, 1928 (1978).

Faisant appel à la rmn, on a étudié les réactions d'un certain nombre d'acétylacétonates de métaux avec l'acide trifluoroacétique. La réaction initiale implique la protonation de l'atome de carbone du ligand. Dans le cas du composé de l'aluminium, dans des solvants permettant la coordination, il y a une réaction subséquente conduisant à des complexes cationiques. On a utilisé ces résultats pour réinterpréter la cinétique de l'échange de ligand de ce composé. On présente des arguments qui, contrairement aux suggestions antérieures, suggéreraient que l'étape déterminante correspond aux bris du premier lien métal oxygène pour former un intermédiaire comportant un ligand en suspens. Une conséquence de cette conclusion implique que les réarrangements intramoléculaires de β-dicétonates de Al(III) doivent procéder par des torsions plutôt que par un mécanisme de rupture des liaisons.

[Traduit par le journal]

Introduction

A number of ligand exchange reactions of β diketonate complexes of metal ions have been shown to be catalyzed by acids. In particular the case of aluminum acetylacetonate has been investigated in some detail by Saito and Masuda (1, 2). These authors suggested that protonation occurs on the oxygen of the ligand and results in the formation of a dangling ligand intermediate of "considerably long lifetime". Their interpretation of the data leads to the conclusion that the rate determining step for ligand exchange was the breaking of the second metal–ligand bond. This conclusion has been quoted (3) to support the possibility of bond rupture mechanisms for the intramolecular rearrangement reactions of this and similar chelates. We have recently investigated (4) both the ligand exchange and isomerization reactions of vanadium(III) β diketonates with somewhat similar results. Saito and Masuda's mechanism implies that nmr spectra should provide evidence for the suggested intermediate. Such evidence could take the form of either additional lines in the spectra or of broadening or shifting of the $Al(acac)_3$ resonances due to rapid exchange with another species. The present paper reports nmr studies of the reactions of acids with a number of metal acetylacetonates which were undertaken with the objective of clarifying the ligand exchange mechanisms.[1]

Results

Trifluoroacetic acid has been used in most of these studies. It is a relatively strong acid (pK_a 0.25) which is miscible with most organic solvents. The trifluoroacetic anion is a poor ligand and side reactions such as oxidation are minimal. Sulphuric acid was used in some experiments and gave generally similar results but some charring of the solutions was evident at temperatures greater than 0°C. The reactions with $Al(acac)_3$ (acac = acetylacetonate) have been studied in most detail but results with V, Pd, Pt, Rh, and Co acetylacetonates will also be briefly reported.

The nature of the nmr spectra obtained by adding trifluoroacetic acid to $Al(acac)_3$ depends very markedly on the solvent used. However all the results can be fitted to the following scheme:

$$[1]\quad Al(acac)_3 + CF_3COOH \underset{}{\overset{\text{fast}}{\rightleftharpoons}} Al(acac)_2(acHac)^+ + CF_3COO^-$$

[1] A preliminary account of some of these results has appeared. See ref. 19.

Can. J. Chem. Downloaded from www.nrcresearchpress.com by 210.87.254.105 on 09/05/12
For personal use only.

Can. J. Chem. Downloaded from www.nrcresearchpress.com by 210.87.254.105 on 09/05/12
For personal use only.

[2] $Al(acac)_2(acHac)^+ + S \underset{}{\overset{slow}{\rightleftharpoons}} Al(acac)_2(acacH)S^+$

[3] $Al(acac)_2(acacH)S^+ + S \underset{fast}{\rightleftharpoons} Al(acac)_2S_2^+ + acacH$

In this scheme (acHac) represents the keto form of acetylacetone and (acacH) the enol form. S is a solvent molecule which may in some cases be water which is always present in small amounts. $Al(acac)_2(acacH)S^+$ is a dangling ligand intermediate (2).

In solvents such as dimethyl formamide (DMF) dimethyl sulphoxide (DMSO) and acetone, there are four sets of resonances. One set belongs to $Al(acac)_3$ and two other sets are assigned to the enol and keto isomers of acetylacetone. This assignment is confirmed by adding acetylacetone. All of these lines are sharp and are not shifted from the positions found in the absence of acid. The fourth set is assigned to $Al(acac)_2S_2^+$. The nmr spectrum for this complex (S = DMF) has been reported by Movius and Matwiyoff (5) and the observed chemical shifts are in good agreement with this report. The ionic nature of the product was confirmed by conductivity measurements (in acetone). The addition of $Al(acac)_3$ produced a large increase in the conductivity of trifluoroacetic acid. The ^{19}F nmr spectrum showed only a single line in the position expected for trifluoroacetic acid. A mixture of $Al(acac)_3$ and $Al(CF_3COO)_3$ (in acetone) showed two additional sets of lines, one corresponding to $Al(acac)_2S_2^+$, in good agreement with the additional lines obtained by adding CF_3COOH to $Al(acac)_3$ in acetone, and one corresponding to the complex $Al(acac)S_4^{2+}$ reported by Movius and Matwiyoff (5).

In these solvents, therefore, equilibrium [1] is to the left and equilibrium [3] is to the right. As a result the intermediate species of eqs. [1]–[3] are present only in very low concentrations and the nmr spectra show only the initial reactant ($Al(acac)_3$) and the final products $Al(acac)_2S_2^+$ and acacH.

The situation in non-coordinating solvents such as benzene-d_6 or nitromethane-d_3 is different. The initial effect of adding CF_3COOH is to broaden the CH protons of $Al(acac)_3$. In a solution in benzene 0.5 *M* in CF_3COOH the C—H resonance is ~30 Hz broad (at 100 MHz). At the same time, weak resonances corresponding to acacH appear. The chemical shifts of $Al(acac)_3$ are entirely unaffected by CF_3COOH but those of acacH are significantly changed. In these cases since S is a poor ligand equilibria [2] and [3] are displaced to the left. As a result there is a sufficient concentration of $Al(acac)_2(acHac)$ to cause significant broadening of the C—H resonances. Protonation has occurred on the carbon at a rate moderately fast on the nmr time scale. Only a small amount of acacH has been formed and this appears at an average chemical shift due to equilibrium [3]. Since benzene is unlikely to function even as a poor ligand it is possible that S may represent trace amounts of water in the above case.

Chloroform and methylene chloride show behaviour as solvents which is intermediate between DMF and benzene. There is some broadening of the C—H resonance and new lines attributable to $Al(acac)_2S_2^+$ have appeared. Figure 1 shows a 220 MHz spectrum of the methyl region of $Al(acac)_3$ + CF_3COOH in $CDCl_3$. A small splitting of the resonance assigned to $Al(acac)_2S_2^+$ is apparent with one component being rather broader than the other. By analogy with the results of Movius and Matwiyoff (5) the two lines are assigned as *cis*- and *trans*-$Al(acac)_2S_2^+$ with the *cis* line being broadened by exchange between the two non-equivalent methyl environments. In contrast to the results in DMF and DMSO the free ligand lines show small shifts from their usual positions. These shifts cannot be accounted for by the effect of CF_3COOH alone. In these cases the equilibria [2] and [3] are sufficiently far to the right to give significant amounts of $Al(acac)_2S_2^+$ but the concentrations of intermediates remaining are sufficiently high to give line broadening and shift effects. The observed chemical shifts of the various species in different solvents are summarized in Table 1.

The results for other metal acetylacetonates may be summarized briefly. $Co(acac)_3$ and $Rh(acac)_3$ in $CDCl_3$ showed marked broadening of the C—H resonance but no new lines appeared. We deduce that reaction [1] occurs but that the stability of the complexes is too great to allow reactions [2] and [3] to proceed. With $Pt(acac)_2$ only a small broadening

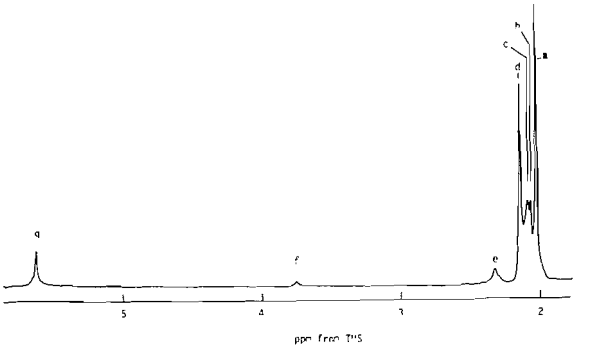

FIG. 1. ^1H 220 MHz nmr spectrum of $Al(acac)_3$ with CF_3COOH in $CDCl_3$ showing resolution of resonance assigned to $Al(acac)_2^+$. Methyl resonances: (*a*) $Al(acac)_3$; (*b*) $Al(acac)_2^+$ S_2 *trans*; (*c*) $Al(acac)_2$ S_2 *cis*; (*d*) Hacac (enol); (*e*) acHac (keto).

TABLE 1. Chemical shifts of acetylacetone and aluminium acetylacetonates in various solvents with and without trifluoroacetic acid*

Species solution	Hacac		acHac		$Al(acac)_3$		$Al(acac)_2^+$	
	CH_3	CH	CH_3	CH_2	CH_3	CH	CH_3	CH
$CDCl_3$/Hacac	2.03	5.50	2.22	3.58	—	—	—	—
$CDCl_3$/$Al(acac)_3$	—	—	—	—	1.99	5.47	—	—
$CDCl_3$/Hacac CF_3COOH 0.5 *M*	2.07	5.55	2.25	3.64	—	—	—	—
$CDCl_3$/$Al(acac)_3$ CF_3COOH 0.5 *M*	2.12	5.57	2.70	3.66	2.03	5.6	2.05	5.62
CD_3NO_2/Hacac	2.00	5.59	2.14	3.60	—	—	—	—
CD_3NO_2/$Al(acac)_3$	—	—	—	—	1.91	5.54	—	—
CD_3NO_2/$Al(acac)_3$ CF_3COOH 0.25 *M*	Some unresolved methyl signals				1.97	5.63 Broad		
C_6D_6/Hacac	1.69	5.12	1.78	3.06	—	—	—	—
C_6D_6/$Al(acac)_3$	—	—	—	—	1.76	5.30	—	—
C_6D_6/$Al(acac)_3$ CF_3COOH 0.25 *M*	1.66	4.98	—	—	1.76	5.30 Broad	—	—
DMF/Hacac	2.03	5.68	2.16	3.74	—	—	—	—
DMF/$Al(acac)_3$	—	—	—	—	1.88	5.56		
DMF/$Al(acac)_3$ CF_3COOH 0.5 *M*	2.03	5.68	2.16	3.74	1.88	5.56	1.92	5.64
DMSO/Hacac	2.02	5.68	2.14	3.69	—	—	—	—
DMSO/$Al(acac)_3$	—	—	—	—	1.88	5.50	—	—
DMSO/$Al(acac)_3$ CF_3COOH 0.25 *M*	2.02	5.68	2.14	3.69	1.88	5.50	1.97	5.64

*Shifts in ppm from TMS, 100 MHz, $T = 27°C$.

of the C—H resonance was observed. This complex is apparently difficult to protonate. The paramagnetic $V(acac)_3$ showed a decrease in the intensity of the CH_3 and C—H resonances with concurrent appearance of free ligand lines. At least one new, but extremely broad, resonance appeared downfield from the CH_3 line, i.e. in a position corresponding to complexed acetylacetone. Superficially at least $V(acac)_3$ behaves similarly to $Al(acac)_3$. The reaction of CF_3COOH with $Pd(acac)_2$ leads to the appearance of a number of new lines, some, but not all, of which can be assigned to free ligand. The ^{19}F spectrum of a solution of $Pd(acac)_2$ with CF_3COOH in $CDCl_3$ shows new resonances 0.71 and 1.44 ppm downfield from CF_3COOH. It appears that CF_3COO^- can replace acac on $Pd(acac)_2$ in a manner analogous to that observed for other anionic ligands (6). A side reaction was also noted which led to loss of the TMS calibrant and the appearance of a new line 0.21 ppm downfield from TMS. At the same time metallic Pd is deposited. This reaction may be analogous to the reaction between lead tetraacetate and TMS in trifluoroacetic acid (7).

Discussion

The above results are not consistent with the mechanism of Saito and Masuda (1, 2) for ligand exchange in $Al(acac)_3$.

The three reactions [1]–[3] provide a pathway for ligand exchange. Modifications are possible, e.g. reaction [2] could occur without transferring the proton from carbon to oxygen. However the three basic steps of (*a*) protonation, (*b*) breaking and reforming the first metal–oxygen bond, and (*c*) breaking and reforming the second metal–oxygen bond must be present. Since the overall reaction is slow at least one of these steps must be slow.

Contrary to the suggestion of Saito and Masuda protonation occurs on the carbon. Brouwer (8) has investigated the protonation of a number of 1,3-dicarbonyl compounds. In some cases the initial protonation is on oxygen and in others it occurs on carbon. Acetylacetone protonates initially on oxygen but substitution of CH_3 by a more electron withdrawing group, e.g. OC_2H_5, leads to carbon protonation. Since the aluminum ion will withdraw electrons from the oxygen, carbon protonation is perhaps not surprising. Protonation is clearly not the slow step.

The following argument shows that reaction [3], the breaking of the second Al—O bond, cannot be slow as was suggested by Saito and Masuda. In THF (the solvent used in ref. 1.) equilibrium [3] is clearly to the right since the nmr spectra show only $Al(acac)_2S_2^+$ and free ligand rather than $Al(acac)_2(acacH)S^+$. If the rate constant for the forward reaction were small, that for the backward reaction would have to be even smaller to give a large equilibrium constant. If this were the case the overall rate

Can. J. Chem. Downloaded from www.nrcresearchpress.com by 210.87.254.105 on 09/05/12
For personal use only.

Can. J. Chem. Downloaded from www.nrcresearchpress.com by 210.87.254.105 on 09/05/12
For personal use only.

of ligand exchange would be determined by the backward reaction and would be proportional to ligand concentration. Saito and Masuda found the rate to be independent of ligand concentration. The nmr results support this conclusion since they indicate that in less strongly coordinating solvents the free ligand is in rapid exchange with another species. Only a reaction involving breaking of the second bond can lead to exchange with free ligand. Breaking of the first Al—O bond (reaction [2] or a modification thereof) must therefore be the slow step.

This conclusion does not represent any disagreement with the experimental results of Saito and Masuda. Their argument in favour of the slow step being the breaking of the second bond was based on the observation that the activation energies were the same for the acid catalyzed and uncatalyzed reactions. They considered that this observation was inconsistent with the breaking of the first bond being the rate determining step. However an examination of Fig. 5 of ref. 2 suggests that their rate constant for acid catalysis also contains a term for water catalysis which may be dominant. In this case the reported activation energies refer to the same reaction. The remainder of their data is entirely consistent with the present interpretation.

The above discussion applies to acid catalyzed ligand exchange reactions. Similar arguments are relevant to the uncatalyzed and water catalyzed pathways. If the rate of breaking the first bond is slow for the protonated complex it will be even slower in the neutral complex. Data in the literature allow an estimate of this rate for some acetylacetonate complexes. Thus Pearson and Anderson (9) have studied the kinetics of the formation of $Cu(acac)^+$ and concluded that the rate determining step is ring closure to form the second M—O bond and the six membered chelate ring. This conclusion is consistent with a great deal of other data on the formation of six membered chelates (10, 11). Since for most acac complexes the equilibrium constant clearly favours the chelate over the dangling ligand isomer it follows that if the formation reaction is slow the dissociation to the dangling ligand must be very slow. The postulation of rapid dangling ligand formation for $Al(acac)_3$ is therefore anomalous. The rate for $Cu(acac)^+$ may be estimated. The formation constant for the complex (14) is $\sim 10^{10}$. For a model monodentate ligand, e.g. propionic acid (14) $K \sim 10^2$. The overall rate of formation (9) is 2×10^4 s^{-1} M^{-1}. Hence the rate for dangling ligand to chelate is $\sim 10^2$ s^{-1} and the equilibrium constant for this reaction is $\sim 10^8$. This gives a rate for the chelate to dangling ligand intermediate of 10^{-6} s^{-1}. Fortuitously this agrees exactly with the rate 6×10^{-5} min^{-1} given by Saito and Masuda for the uncatalyzed ligand exchange of $Al(acac)_3$. Clearly, though, the observed rates are consistent with the rate determining step being the breaking of the first M—O bond. Catalysis by water increases this rate by taking up the sixth coordination position and stabilizing the dangling ligand intermediate. Acid catalysis operates by weakening the M—O bond by protonating either the carbon or the oxygen (indirectly). Evidence for such increased lability is provided by the studies of Cramer and Chudyk (12) and of van Leeuwen and Praat (13) on metal complexes of neutral acetylacetone.

The above conclusion has important consequences in the area of intramolecular rearrangements of Al(III) β diketonates (3). A number of authors (14–16) have discussed such mechanisms in detail but have been unable to reach a definite decision as to whether they involve a bond rupture or a twisting process. The above result eliminates all bond rupture mechanisms. The rate for such a mechanism cannot be faster than ligand exchange which is much slower than rearrangement. By analogy a similar argument may hold for Ga and In β diketonates but cannot be applied directly to V, Zr, and Hf complexes (4, 17) since the rates of ligand exchange reactions of these compounds are not determined by the rates of breaking M—O bonds. However, for the case of $V(acac)_3$ it is interesting to note that there is no acid catalysis of the rearrangement reactions but the ligand exchange is strongly acid catalyzed (4). The present results suggest that $V(acac)_3$ reacts with acids in a manner similar to $Al(acac)_3$. If this is the case, acid catalysis of the rearrangement reactions of V(III) β diketonate complexes would be predicted if they involve metal–oxygen bond breaking. The fact that catalysis is not observed therefore argues against a bond breaking mechanism. Catalysis of ligand exchange in cases where there is a term in the rate equation dependent on ligand concentration can be rationalized by noting that the rate determining step involves reaction of free ligand with $M(acac)_2(acacH)S^+$ or with $M(acac)_2S_2^+$ which require protons for their formation. The above results are therefore also consistent with the reported acid catalysis of ligand exchange of $Pd(acac)_2$ (18).

Experimental

Metal acetylacetonates were obtained from Research Organic/Inorganic Chemical Co. Nuclear magnetic resonance spectra were obtained with a Varian HA 100 spectrometer (probe temperature 27°C) using tetramethyl silane as an internal calibrant. A few samples were examined on a Varian 220 MHz spectrometer to obtain optimum resolution. All solvents were deuterated except DMF.

Acknowledgements

We are indebted to the National Research Council of Canada for financial support of this research. We would also like to thank Dr. A. Gray of the 220 MHz NMR Centre for aid in obtaining 220 MHz spectra.

1. K. SAITO and K. MASUDA. Bull. Chem. Soc. Jpn. **41**, 384 (1968).
2. K. SAITO and K. MASUDA. Bull. Chem. Soc. Jpn. **43**, 119 (1970).
3. N. SERPONE and D. G. BICKLEY. Prog. Inorg. Chem. **17**, 391 (1972).
4. A. J. C. NIXON and D. R. EATON. Can. J. Chem. **56**, 1005 (1978); **56**, 1012 (1978).
5. W. G. MOVIUS and N. A. MATWIYOFF. J. Am. Chem. Soc. **90**, 5452 (1968).
6. R. G. PEARSON and D. A. JOHNSON. J. Am. Chem. Soc. **86**, 3983 (1964).
7. R. O. C. NORMAN and M. PROUSTIE. J. Chem. Soc. C, 196 (1969).
8. D. M. BROUWER. Recl. Trav. Chim. Pay-Bas, **87**, 225 (1968).
9. R. G. PEARSON and O. G. ANDERSON. Inorg. Chem. **9**, 39 (1970).
10. Stability Constants of Metal Ion Complexes. Chem. Soc. Special Publ. #17. 1964.
11. K. KUSTIN, R. F. PASTERNACK, and E. M. WEINSTOCK. J. Am. Chem. Soc. **88**, 4610 (1966).
12. R. E. CRAMER and M. A. CHUDYK. Inorg. Chem. **12**, 1193 (1973).
13. P. W. N. M. VAN LEEUWEN and A. P. PRAAT. Inorg. Chim. Acta, **4**, 101 (1970).
14. J. R. HUTCHISON, J. G. GORDON, and R. H. HOLM. Inorg. Chem. **10**, 1004 (1971).
15. R. C. FAY and T. S. PIPER. Inorg. Chem. **3**, 348 (1964).
16. J. J. FORTMAN and R. E. SIEVERS. Inorg. Chem. **6**, 2022 (1967).
17. A. C. ADAMS and E. M. LARSEN. Inorg. Chem. **5**, 814 (1966).
18. K. SAITO and M. TAKAHASHI. Bull. Chem. Soc. Jpn. **42**, 3462 (1969).
19. D. R. EATON and A. J. C. NIXON. Inorg. Chim. Acta Lett. **25**, L55 (1977).

Can. J. Chem. Downloaded from www.nrcresearchpress.com by 210.87.254.105 on 09/05/12
For personal use only.

Kinetics, medium, and deuterium isotope effects in the alkaline decomposition of quaternary phosphonium salts. IV. Tetraphenylphosphonium chloride in tetrahydrofuran–water mixtures

FAYEZ Y. KHALIL

Chemistry Department, Faculty of Science, Alexandria University, Alexandria, Egypt

AND

GUNNAR AKSNES

Department of Chemistry, University of Bergen, N-5014 Bergen, Norway

Received July 26, 1977

FAYEZ Y. KHALIL and GUNNAR AKSNES. Can. J. Chem. **56**, 1933 (1978).

The third-order rate constants of the reaction between tetraphenylphosphonium chloride and sodium hydroxide in binary tetrahydrofuran–water systems have been determined as a function of temperature. Increasing the THF content of the reaction medium up to 70% (v/v) results in a ca. 10^6-fold rate acceleration at 25°C. This is explained as due to increased desolvation of reactants as well as an opposite effect on the transition-state solvation in THF-rich media. The rate in deuterium oxide is higher than in water and the kinetic isotope factor k'_{DO^-}/k'_{HO^-} depends strongly on temperature. The inverse proportionality of rate to the water concentration of medium showed that a large number of water molecules (about 13) is to be removed from the solvation sheaths of reactants before formation of the activated complex. The thermodynamic activation parameters have been derived and expressed as functions of the composition of the medium. It is found that $\Delta H^{\ddagger}$ decreases by about 17 kcal/mol over the range 0–70% THF, while $\Delta S^{\ddagger}$ decreases by about 29 cal mol^{-1} deg^{-1} over the same range. As a result, $\Delta G^{\ddagger}$ shows a net decrease of 8 kcal/mol indicating partial compensation between $\Delta H^{\ddagger}$ and $T\Delta S^{\ddagger}$.

FAYEZ Y. KHALIL et GUNNAR AKSNES. Can. J. Chem. **56**, 1933 (1978).

On a déterminé, en fonction de la température, les constantes de vitesse du troisième ordre de la réaction entre le chlorure de tétraphénylphosphonium et l'hydroxyde de sodium dans un système binaire tétrahydrofuranne–eau. Une augmentation de la quantité de THF dans le milieu réactionnel jusqu'à environ 70% (v/v) conduit à une augmentation de vitesse, à 25°C, d'environ 10^6. On explique ce résultat sur la base d'une augmentation de la désolvatation de réactifs ainsi que par un effet opposé sur la solvatation de l'état de transition dans un milieu riche en THF. La vitesse dans l'eau lourde est plus grande que dans l'eau et l'effet isotopique k'_{DO^-}/k'_{HO^-} varie d'une façon importante avec la température. Le fait que les vitesses varient d'une façon proportionellement inverse à la concentration d'eau dans le milieu montre qu'un grand nombre de molécules d'eau (environ 13) doivent être enlevées des couches de solvatation des réactifs avant la formation du complexe activé. On a évalué les paramètres d'activation thermodynamique et on les a exprimés en fonction de la composition du solvant. On a trouvé que le $\Delta H^{\ddagger}$ diminue par environ 17 kcal/mol lorsque la quantité de THF varie de 0–70% alors que le $\Delta S^{\ddagger}$ diminue d'environ 29 cal mol^{-1} deg^{-1} aux mêmes concentrations. Il en résulte que le $\Delta G^{\ddagger}$ présente une diminution nette de 8 kcal/mol indiquant une compensation partielle entre le $\Delta H^{\ddagger}$ et le $T\Delta S^{\ddagger}$.

[Traduit par le journal]

Introduction

The solvent effects on the alkaline decomposition of quaternary phosphonium salts have been the subject of our interest in recent years (1–4). Different studies of these reactions have been made before (5); but treatment of the problem from the viewpoint of medium effects is, however, far less exhaustive; it is the aim of our present work to examine these effects. As a representative of this type of reaction we have chosen tetraphenylphosphonium chloride which reacts with sodium hydroxide to give tetraphenylphosphine oxide and benzene. We have studied the reaction both kinetically and thermodynamically in a series of binary organic solvent–water mixtures. The solvents taken were nonpolar as well as dipolar aprotic ones, namely, dioxane–water (2), acetone–water (3), and dimethyl sulphoxide–water (1) mixtures. Because the reaction takes place between two ions, the changes of solvation that reactants exhibit upon transfer from the protic solvent water to a dipolar aprotic solvent such as acetone or dimethyl sulphoxide will have a remarkable effect on rate. Our previous work (1–3) has established that tremendous rate acceleration can be obtained, giving rise to rate factors as large as 9 powers of 10 upon addition of a dipolar aprotic

Can. J. Chem. Downloaded from www.nrcresearchpress.com by 210.87.254.42 on 09/05/12
For personal use only.

Can. J. Chem. Downloaded from www.nrcresearchpress.com by 210.87.254.42 on 09/05/12
For personal use only.

solvent to the reaction medium (1). Such an observation has also been reported for many organic reactions involving anions (ref. 6 and references cited therein and ref. 7) and has often been attributed to changes in solvation of reactant anion as well as the transition state (1, 8–10).

Tetrahydrofuran (THF) is a solvent of low ionising power (11) with a dielectric constant of 7.4 at 25°C, a dipole moment of 1.7 D (12), and a certain hydrogen-bonding ability (13). It is classified as structure making when it is a cosolvent in water (14) and it possesses a suitable range of miscibility with water which allows for preparing binary solvent mixtures varying widely in composition. The present paper deals with a kinetic investigation of the alkaline decomposition of tetraphenylphosphonium chloride in a series of THF–water mixtures at different temperatures in order to accumulate kinetic, thermodynamic, and mechanistic data for confirming the reaction behaviour in protic – dipolar aprotic media. The major effect of THF on rate will be a consequence of the modifying effect on the water structure (15, 16) and hence on the hydrogen-bonding ability of the mixed solvent. The reaction was also studied in a THF–D_2O mixture at several temperatures in conjunction with kinetic solvent isotope effect as well as changes in thermodynamic parameters of activation.

Experimental

Tetraphenylphosphonium chloride (Fluka) was obtained in an adequately pure form and was used without further purification. Tetrahydrofuran (Fluka) was freed of peroxides by treatment with ferrous sulphate and sodium bisulphate, then solid potassium hydroxide, followed by drying and fractional distillation from sodium metal. The pure solvent boiled at 65.2°C (17). The heavy water (Norsk Hydro) used was 99.8% D_2O.

The kinetic procedure for measurement of the reaction rate was based on determination of the amount of sodium hydroxide consumed during the course of the reaction. The reaction mixtures were prepared so as to contain 0.02 mol/ℓ of NaOH in a series of THF–H_2O mixtures. In addition, a solution containing 0.02 mol/ℓ NaOD (prepared by dissolving Na metal in D_2O) in 70% THF–D_2O mixture was prepared. Thermally equilibrated quantities of each solvent mixture were mixed with 0.02 mol/ℓ amounts of the phosphonium salt previously weighed in volumetric flasks. The solutions were thoroughly shaken and immediately placed in a thermostat adjusted to within ±0.05°C. At time intervals accurate samples were taken and rapidly poured into an excess of standard HCl. The resulting solutions were analysed by back titration against standard NaOH to the phenolphthalein end point. Several runs were made in duplicate and the results were concordant within ±2%. The values of the dielectric constant of the mixed THF–water solvents were interpolated from the data reported by Heydtmann and Steiger (18).

Results and Discussion

The rates of the reaction were determined in binary solvent mixtures of THF and water covering the range 0–70% (v/v) in steps of 10%. The temperatures at which the reaction was studied depended on the rates in different media and varied from 20 to 55°C, where each run was carried out at six temperatures. Rate measurements were also made in a medium consisting of 70% THF (v/v) and 30% D_2O using DO^- as the attacking anion. In all cases the reaction was found to obey third-order kinetics in which the rate was first order in the phosphonium cation and second order in the hydroxide or deuteroxide anions, respectively. The specific rate constants were obtained from slopes of the graphical plots, represented in Fig. 1, of $(1/(a-x)^2) - 1/(a^2)$ vs. time in the range below 30% completion in H_2O-rich solvents and 75% completion in THF-rich solvents. The reason for this discrepancy is that in more aqueous media the produced phosphonium oxide precipitated and had a catalysing effect on the reaction causing a marked deviation of the linear third-order plots towards higher rate. In less aqueous media, however, no precipitation of tetraphenylphosphonium oxide took place and the reaction could be followed accurately up to 75% completion. The activation energies were determined from the appropriate Arrhenius plots of log k' vs. $1/T$. The results are set forth in Table 1. The thermodynamic parameters of activation $\Delta G^{\ddagger}$, $\Delta H^{\ddagger}$, and $\Delta S^{\ddagger}$, as well as the preexponential factor log A were obtained from the expressions (19) $k' = (kT/h) \exp(-\Delta G^{\ddagger}/RT)$, $\Delta H^{\ddagger} = E - RT$, $\Delta G^{\ddagger} = \Delta H^{\ddagger} - T\Delta S^{\ddagger}$, and $k' = A \exp(E/RT)$, respectively.

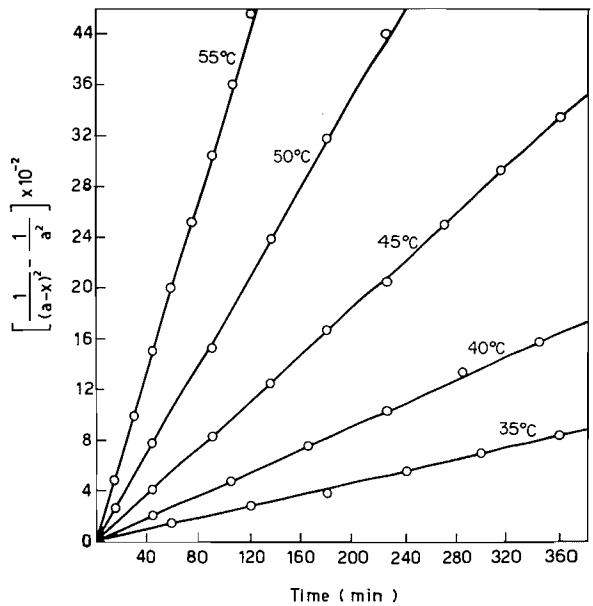

FIG. 1. Representative kinetic plots for the third-order alkaline decomposition of tetraphenylphosphonium chloride in 40% (v/v) THF–H_2O mixture at different temperatures.

TABLE 1. Third-order rate constants k' and activation energies E for the alkaline decomposition of tetraphenylphosphonium chloride in THF–H_2O and THF–D_2O mixtures at different temperatures[a,b]

THF content			k' (ℓ^2 mol^{-2} min^{-1})								E (kcal/ mol)
vol%	wt%	mol%	20°C	25°C	30°C	35°C	40°C	45°C	50°C	55°C	
0	0.00	0.00		5.3×10^{-4}		3.3×10^{-3}	7.9×10^{-3}	1.8×10^{-2}	4.3×10^{-2}	9.6×10^{-2}	33.5
10	8.96	3.00		1.2×10^{-3}		7.1×10^{-3}	1.7×10^{-2}	3.7×10^{-2}	8.4×10^{-2}	1.8×10^{-1}	32.2
20	17.81	5.14		5.5×10^{-3}		2.9×10^{-2}	6.5×10^{-2}	1.4×10^{-1}	2.9×10^{-1}	5.9×10^{-1}	30.4
30	26.89	8.41		3.4×10^{-2}		1.6×10^{-1}	3.3×10^{-1}	6.8×10^{-1}	1.4	2.6	28.6
40	36.42	12.51		2.8×10^{-1}		1.2	2.3	4.6	8.7	16.7	26.3
50	45.85	17.46		2.5		9.3	17.8	33.1	60.0	1.0×10^{2}	24.0
60	55.43	23.70		33.9		1.0×10^{2}	1.7×10^{2}	2.7×10^{2}	4.4×10^{3}	7.0×10^{2}	19.6
70	66.00	32.66	3.8×10^{2}	6.3×10^{2}	1.0×10^{3}	1.6×10^{3}	2.5×10^{3}	3.7×10^{3}			16.6
70–30 D_2O	63.78	32.82	1.7×10^{3}	2.3×10^{3}	3.3×10^{3}	4.5×10^{3}	5.7×10^{3}	8.0×10^{3}			11.8

Parameter	Value				
	20°C	25°C	30°C	35°C	40°C
k'_{DO^-}/k'_{HO^-}	4.5	3.8	3.3	2.8	2.3
$k'_{70\%THF}/k'_{water}$		1.2×10^{6}		4.8×10^{5}	3.2×10^{5}

[a]Equal concentrations of phosphonium and hydroxide or deuteroxide ions (0.02 M) were taken throughout.
[b]Total ionic strength amounts to 0.04. No corrections for zero ionic strength or thermal expansion were made.

Effect of THF Content of the Medium

The gradual addition of THF to water causes a large increase in the rate. Thus, in 70% THF–water (v/v) at 25°C the rate is higher by a factor of 6 powers of 10 than that in water at the same temperature. The plot of log k' vs. the concentration of THF, expressed, in moles per litre of the mixed solvent, shows a relatively slow increase in rate in the water-rich solvents followed by a rapid increase when the THF content exceeds about 30% (v/v) or 4 mol/ℓ (Fig. 2). It is well known that water has an extensive tendency to solvate ions strongly and to form hydrogen bonds with hydroxide anions (20, 21). This is favoured by the high dielectric constant of water which, in turn, is due to the polar nature of this solvent and to the fact that the dimensions of the water molecule favour a tetrahedrally coordinated structure (21). Diluting water with a dipolar aprotic solvent, the solvating power of the medium will decrease progressively until it reaches a minimum in slightly aqueous or nonaqueous solvents. Consequently, the retarding effect of the solvation sheath around the anion will drop causing a large enhancement in the reaction rate. The rate-retarding role of water can be shown; for example, in the alkaline decomposition of some tetraalkylphosphonium ions (22) it was found that the anhydrous compound decomposed within 30 min at 25°C, whereas its aqueous solution was refluxed for 40 h without any appreciable change. It is to be concluded, therefore, that the increase in rate of the present reaction with increasing THF content of the medium is, at least partly, attributable to desolvation of the hydroxide ion. The latter, being the strongest base that can exist in water, and its catalytic activity greatly inhibited by its extensive hydration, will gradually loose its solvation sheath, particularly in high THF contents, and thus will be much more reactive. The effect is, of course, relatively slight at high water concentrations in which there is enough water to hydrate the HO^- anions as well as to form hydrogen bonds with the cosolvent. This explains the initial slow rise in the curves of Fig. 2 followed by a steep increase.[1]

It may be assumed that the inverse proportionality of the reaction rate to the water concentration of the medium can be included in the kinetic equation, shown below, since the removal of the hydration sheaths of reactants is an important process prior to formation of the activated complex:

$$[1] \qquad \frac{dx}{dt} = \frac{k_1}{[H_2O]^n}(a - x)(b - x)^2$$

in which dx/dt, the reaction rate, is assumed to be inversely proportional to the nth power of the molar concentration of water, k_1 being the proportionality constant, $(a - x)$ the concentration of the phosphonium cation, and $(b - x)$ that of the hydroxide anion. Practically, the concentration of water remains constant during the reaction course, and therefore the value $k_1/[H_2O]^n$ will be equal to the specific

[1]Under the conditions of the present experimental technique it was quite difficult to follow the reaction with sufficient accuracy up to more than 70% THF (v/v). The question, therefore, whether the plot of log k' vs. amount of THF added would be expected to level off at higher organic solvent compositions, remains without answer.

Can. J. Chem. Downloaded from www.nrcresearchpress.com by 210.87.254.42 on 09/05/12
For personal use only.

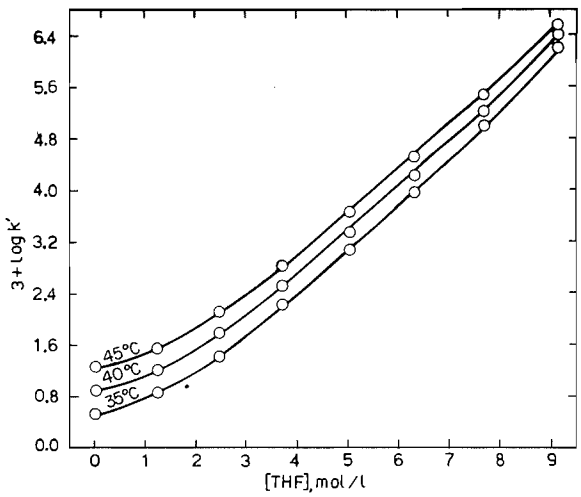

FIG. 2. Plots of the rate constant (log k') for the reaction under investigation vs. the concentration of THF in the medium.

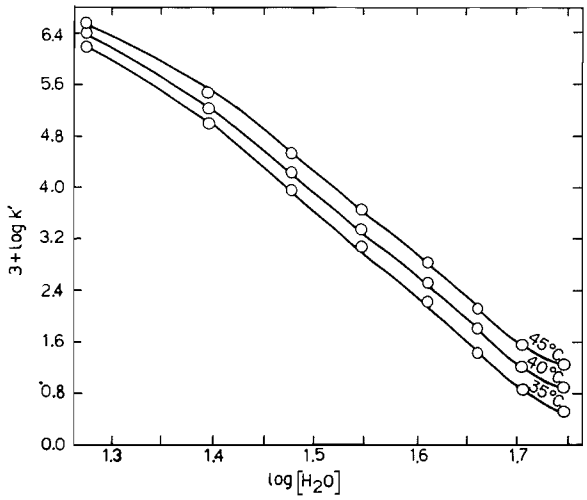

FIG. 3. Variation of the rate constant (log k') for the reaction studied with the concentration of water (log [H_2O]) in the medium at different temperatures.

third-order rate constant k', i.e.,

$$[2] \qquad k' = k_1/([H_2O]^n)$$

and

$$[3] \qquad \log k' = k_2 - n \log [H_2O]$$

where k_2 is another constant. Consequently, the plot of log k' against log [H_2O] should be linear with a negative slope of n. Such plots, illustrated in Fig. 3, gave a linear relationship in the range 10–60% (v/v) THF or 51–25 mol/ℓ of water. The value of n estimated in this way amounts to about 13, confirming our assumption (2) that a large number of water molecules are involved in the activation process. This argument may find further support if one calculates $k'[H_2O]^n$ according to eq. [2], putting, for example, n = 1–12. The resulting values show the same remarkable variation with solvent composition, though decreasing dependence is exerted as n approaches 13. On the other hand, the value $k'[H_2O]^{13}$ was found to be almost constant and independent of the water content or the solvent composition of the medium. Nevertheless, this large value of n is not surprising if one considers that the HO^- anion is, at least, trihydrated in water (23) and that the solvation sheaths around two hydroxide anions and one phosphonium cation have to be disrupted before the formation of the activated complex can take place.

Rate in Deuterium Oxide

The kinetic deuterium isotope effect constitutes an important tool which has found wide application, both kinetically and mechanistically (24). The simple use of such effect involves the determination of whether a bond to a hydrogen or deuterium is broken in the rate-determining step of the reaction, and hence mechanistic information can firmly be established. In the present work, the kinetic solvent deuterium isotope effect was investigated under the same experimental conditions by measuring the rate in 70% THF – D_2O mixture at six different temperatures. In these experiments deuteroxide ion furnished the attacking nucleophile instead of hydroxide ion. The results are included in Table 1, where it is evident that the rate in D_2O is always higher than that in H_2O. The observation confirms that the reaction mechanism does not involve the breaking of any bonds to H or D in the rate-determining step, as shown below.

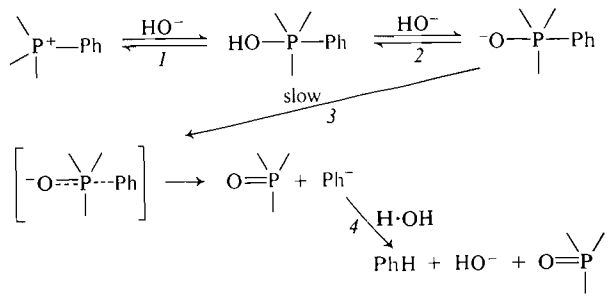

in which preequilibrium *1* is a rapid addition of the HO^- ion to the phosphorus atom of the quaternary salt, whereas preequilibrium *2* involves a rapid formation of the conjugate base of the pentacovalent phosphorus intermediate. This is followed by step *3* which is a slow rate-determining formation of tetraphenylphosphine oxide and the phenyl carbanion. The latter finally takes up a proton in the

Can. J. Chem. Downloaded from www.nrcresearchpress.com by 210.87.254.42 on 09/05/12
For personal use only.

TABLE 2. Comparison of the kinetic isotope effects for the reaction in different solvent systems

Solvent mixture	$D_{25°C}$ (organic solvent)	k'_{DO^-}/k'_{HO^-} (at 25°C)	ΔE $E_{HO^-} - E_{DO^-}$ (kcal mol^{-1})	$t(k'_{DO^-}/k'_{HO^-} = 1)$ (°C)
70% dioxane–D_2O	2.1	2.32	3.83	69
70% THF–D_2O	7.4	3.80	4.80	77
70% acetone–D_2O	20.4	2.19	5.63	52
60% DMSO–D_2O	46.4	1.50	9.89	35

rapid step *4* to give benzene. The formation of a pentacovalent rather than a hexacovalent intermediate, which is formed during the alkoxide-promoted decomposition of phosphonium salts (4), takes place since the ionised phosphorane is sufficiently energetic to expel the phenyl carbanion.[2]

The present isotope effect is, therefore, shown to be a secondary rather than a primary one. This effect, expressed in the kinetic factor k'_{DO^-}/k'_{HO^-}, exhibits a strong dependence on temperature. It amounts to 4.5 at 20°C and drops to 2.3 at 40°C (Table 1). The temperature at which this factor becomes unity, i.e. when the rate in 70% THF – H_2O becomes equal to that in 70% THF–D_2O mixture, is extrapolated to be 77°C. The value of this temperature was found to be 69°C for dioxane–water (2), 52°C for acetone–water (3), and 35°C for dimethyl sulphoxide – water systems (cf. Table 2). Furthermore, although the value of ΔE, which is the difference in activation energies between the hydroxide- and deuteroxide-promoted reactions for the different solvent systems runs parallel to the increase in polarity of the medium, yet the change in the kinetic isotope factor does not follow the same sequence. The anomaly is exhibited by THF–D_2O medium which should have given a value of k'_{DO^-}/k'_{HO^-} between that of dioxane–D_2O and acetone–D_2O mixtures. This variation shows clearly that specific solvent effects play an important role in determining the relative rates in D_2O when mixed with different organic solvents, as compared to the rates in H_2O when mixed with the same solvents. The lower activation energy and the higher reaction rate in the THF–D_2O mixture as compared to those in the corresponding THF–H_2O mixture (Table 1) are attributed partly to the higher basicity of DO^- in D_2O than HO^- in H_2O (25), and partly due to a difference in the stabilities of the internal solvent structure of the two media towards rise in temperature (1, 3). The latter effect, which directly influences the solvating power of the reaction medium as well as the structural stabilities of the solvation shells of initial and transition states, predominates at temperatures higher than 77°C, causing a lower rate in D_2O than in water.

The Role of Changing Dielectric Constant

According to Born's theory (26) the rate of reaction between two ions of opposite sign should show inverse proportionality to the dielectric constant of the medium, where the plot of log k' vs. $1/D$ should be linear with a negative slope. Applying this to the reaction under investigation in the present solvent mixtures gave a straight line only in the high dielectric constant range (Fig. 4). Deviation from linearity towards lower rates starts beyond 40% (v/v) THF and may be attributed to differential solvation effects (19). The slope of the linear portion of the plot gives a value of 0.55 Å for $r^{\neq}$, the radius of the activated complex, which is far below the calculated value (5–6 Å) (2). Treating the solvent as one with a uniform dielectric constant and a zero ionic strength, which is not the case, causes discrepancy and renders the rates of ionic reactions poorly correlatable to the dielectric constant of the medium (27, 28). In other words, the specific solvent effects encountered here add further evidence to the fact that the type of solvent is more important than its polar character, as estimated by the dielectric constant. This furnishes another example violating the

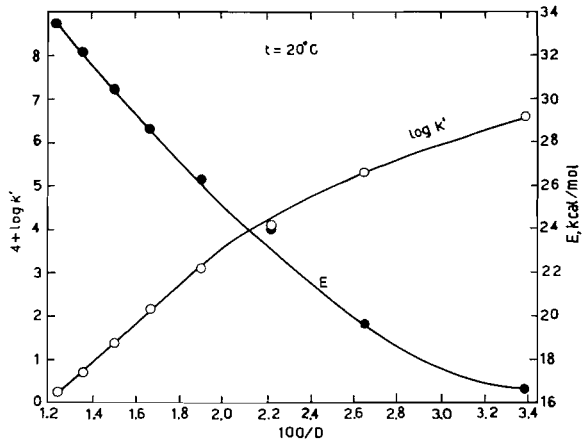

FIG. 4. Dependence of the rate constant (log k') and activation energy E for the present reaction upon the dielectric constant ($1/D$) of the binary solvent mixture.

[2]Further evidence for the pentacovalent intermediate can be found in ref. 38.

Can. J. Chem. Downloaded from www.nrcresearchpress.com by 210.87.254.42 on 09/05/12
For personal use only.

TABLE 3. Thermodynamic activation parameters and preexponential factor at 25°C

THF content		$\Delta G^{\ddagger}$	$\Delta H^{\ddagger}$	$\Delta S^{\ddagger}$	$\log(A)$
vol%	mol%	(kcal/mol)	(kcal/mol)	(cal mol^{-1} deg^{-1})	(ℓ^2 mol^{-2} s^{-1})
0	0.00	24.3	32.9	29.1	19.6
10	3.00	23.8	31.7	26.5	19.0
20	5.14	22.9	29.8	23.3	18.4
30	8.41	21.8	28.0	20.7	17.8
40	12.51	20.6	25.7	17.2	17.0
50	17.46	19.3	23.4	14.1	16.3
60	23.70	17.7	19.0	4.3	14.2
70	32.66	16.0	16.0	−0.1	13.2
70–30 D_2O	32.82	15.2	11.3	−13.3	10.3

Hughes–Ingold theory (29) which simply relates the reaction rate to the polarity of the solvent.

It has been pointed out frequently (8–10) that separation of solvent effects into ground and transition-state contributions in bimolecular reactions involving anions revealed that higher rates and lower activation energies in dipolar aprotic solvents are due also to the increased solvation of transition states in those solvents. Decreasing the polarity, and hence the dielectric constant, leads to more solvation of the transition state, where there is charge dispersal, as the solvent changes from protic to dipolar aprotic (6, 20). As a result, the potential energy of the transition state will decrease (19) and hence the activation energy will drop more and more as the medium is enriched in THF. The drastic lowering (about 17 kcal/mol) of E over the whole range of solvent composition is thus rationalised in terms of some combination of these two factors, namely reactant desolvation and increased transition-state solvation. The latter effect, however, becomes more evident at sufficiently low dielectric constants where the organic cosolvent prevails. In this range of solvent composition there is not enough water to solvate the transition state efficiently and therefore solvation of the latter will take place mainly with the dipolar aprotic solvent. No doubt such a large decrease in E (cf. Fig. 4) manifests the internal structural changes, and hence the alterations in hydrogen-bonding ability, of the solvent mixture as the latter is varied in dielectric constant.

Thermodynamic Activation Terms

Table 3 lists the thermodynamic data of activation ($\Delta G^{\ddagger}$, $\Delta H^{\ddagger}$, and $\Delta S^{\ddagger}$) together with the preexponential factor log A. All parameters show considerable dependence on solvent composition. Thus, the increase in reaction rate is associated with a decrease in activation enthalpy ($\Delta H^{\ddagger}$) by about 17 kcal/mol, which is partially compensated (30–32) through the decrease of $\Delta S^{\ddagger}$ by about 29 cal mol^{-1} deg^{-1} over the whole range of medium composition, thus causing $\Delta G^{\ddagger}$ to decrease only by 8 kcal/mol. The considerable changes in these functions imply that the contributions from relative changes in solvation shells of reactants and transition state during the course of the reaction are very important factors in the rate process. Theoretical calculations and interpretations of such contributions (33, 34) expected of microscopic solvent changes are complicated by the involvement of several steps in the reaction mechanism. However, it is possible to correlate the trend in each of these parameters with the ionising power or hydrogen bonding ability of the solvent system. Thus, the decrease in $\Delta G^{\ddagger}$ with successive addition of THF is a direct consequence of the decrease in the free energy involved in breaking the hydrogen bonds associated with the ground state. The latter energy will definitely decrease as the mixed solvent is made less hydrogen bonding by decreasing its water content. The large decrease in the value of $\Delta H^{\ddagger}$ depicted in Table 3 as the medium composition passes from 0 to 33 mol% THF indicates that in water-rich solvents more energy has to be overcome before the transition state can be formed. The substantial diminution of $\Delta S^{\ddagger}$ values with addition of THF is also indicative of remarkable changes in solvation effects. A solvent-sorting phenomenon is evident in the nonlinear drop of $\Delta S^{\ddagger}$ with changes in solvent composition (35). Opposing the decrease in E, the preexponential factor log A decreases progressively along the same range of solvent composition. However, it is the enormous decrease in E that controls the reaction rate rather than the drop in A.

It is noteworthy that although the trends in the thermodynamic parameters of the reaction in different solvent systems (1–3) appear, at the first glance, to be more or less similar, complications arise upon comparison of the absolute values of these parameters. Such comparison is, however,

Can. J. Chem. Downloaded from www.nrcresearchpress.com by 210.87.254.42 on 09/05/12
For personal use only.

rendered easier if enough data are available concerning the exact specific effects of each binary solvent system as well as the relative hydrogen-bonding energies and other relevant thermodynamic properties of its components (36, 37).

1. PART III, F. Y. KHALIL, and G. AKSNES. Phosphorus Sulphur, **3**, 27 (1977).
2. F. Y. KHALIL and G. AKSNES. Acta Chem. Scand. **27**, 3832 (1973).
3. F. Y. KHALIL and G. AKSNES. Z. Phys. Chem. **97**, 179 (1975).
4. G. AKSNES, F. Y. KHALIL, and P. J. MAJEWSKI. Phosphorus Sulphur, **3**, 157 (1977).
5. K. L. MARSI and J. E. OBERLANDER. J. Am. Chem. Soc. **95**, 200 (1973); S. E. CREMER, B. C. TRIVEDI, and F. L. WEITL. J. Org. Chem. **36**, 3226 (1971); W. E. MCEWEN, G. AXELARD, M. ZANGER, and C. A. VANDER WERF. J. Am. Chem. Soc. **87**, 3948 (1965); K. D. BERLIN and J. B. BUTLER. Chem. Rev. **60**, 243 (1960); H. HOFFMAN. Ann. **634**, 1 (1960).
6. A. J. PARKER. Chem. Rev. **69**, 1 (1969).
7. J. MILLER and A. J. PARKER. J. Am. Chem. Soc. **83**, 117 (1961).
8. C. A. KINGSBURY. J. Org. Chem. **29**, 3262 (1964).
9. P. HABERFIELD, L. CLAYMAN, and J. S. COOPER. J. Am. Chem. Soc. **91**, 787 (1969).
10. R. FUCHS and L. L. COLE. J. Am. Chem. Soc. **95**, 3194 (1973).
11. S. G. SMITH, A. H. FAINBERG, and S. WINSTEIN. J. Am. Chem. Soc. **83**, 618 (1961).
12. C. P. SMYTH. Dielectric behaviour and structure. McGraw-Hill, New York, NY. 1955. p. 299.
13. S. SEARLES and M. TAMRES. J. Am. Chem. Soc. **73**, 3704 (1951); S. SEARLES, M. TAMRES, and E. R. LIPPINGCOTT. J. Am. Chem. Soc. **75**, 2775 (1953).
14. R. E. ROBERTSON and S. E. SAGAMORI. Can. J. Chem. **50**, 1353 (1972).
15. M. J. STACKELBERG and B. METHUEN. Z. Electrochem. **62**, 130 (1958).
16. S. R. GOUGH and D. W. DAVIDSON. Can. J. Chem. **49**, 2691 (1971).
17. M. BRODON, M. TAMRES, and S. SCOTT, JR. J. Am. Chem. Soc. **82**, 2129 (1960).
18. H. HEYDTMANN and H. STEIGER. Ber. Bunsenges. Phys. Chem. **70**, 1095 (1966).
19. S. GLASSTONE, K. J. LAIDLER, and H. EYRING. The theory of rate processes. McGraw-Hill, New York, NY. 1941.
20. A. J. PARKER. Q. Rev. Chem. Soc. 163 (1962).
21. R. A. ROBINSON and R. H. STOKES. Electrolyte solutions. Butterworths, London. 1968.
22. H. R. HAYS and R. G. LAUGHLIN. J. Org. Chem. **32**, 1060 (1967).
23. G. YAGIL and M. ANBAR. J. Am. Chem. Soc. **85**, 2375 (1963).
24. L. MELANDER. Isotope effects on reaction rates. Ronald, New York, NY. 1960.
25. K. WIBERG. Chem. Rev. **55**, 713 (1955).
26. E. S. AMIS. Solvent effects on reaction rates and mechanism. Academic Press, New York, NY. 1966.
27. J. E. POTTS and E. S. AMIS. J. Am. Chem. Soc. **71**, 2112 (1949).
28. E. S. AMIS and G. JAFFÉ. J. Chem. Phys. **10**, 598 (1942).
29. E. S. HUGHES and C. K. INGOLD. J. Chem. Soc. 252 (1935).
30. J. F. BUNNETT. *In* Technique of organic chemistry. Vol. VII, Pt. I, 2nd ed. *Edited by* S. L. Friess, E. S. Lewis, and A. Weissberger. Interscience, New York, NY. 1961.
31. C. D. RICHIE and W. F. SAGER. Prog. Phys. Org. Chem. **2**, 323 (1964).
32. E. BUNCEL and J. P. MILLINGTON. Can. J. Chem. **43**, 556 (1965).
33. O. EXNER. Collect. Czech. Chem. Commun. **37**, 1525 (1972).
34. R. W. ALDER, R. BAKER, and J. M. BROWN. Mechanism in organic chemistry. Wiley-Interscience, London. 1971.
35. R. F. HUDSON and B. SAVILLE. J. Chem. Soc. 4114 (1955).
36. E. TOMMILA and M. L. MURTO. Acta Chem. Scand. **17**, 1947 (1963).
37. E. TOMMILA. Suom. Kemistil. B, **37**, 117 (1964).
38. P. HAAKE and F. H. WESTHEIMER. J. Am. Chem. Soc. **83**, 1102 (1961); M. GRAYSON and P. T. KEOUGH. J. Am. Chem. Soc. **82**, 3919 (1960); M. ZANGER, C. A. VANDER WERF, and W. E. MCEWEN. J. Am. Chem. Soc. **81**, 3806 (1959); L. HEY and C. K. INGOLD. J. Chem. Soc. 531 (1933); C. W. FENTON and C. K. INGOLD. J. Chem. Soc. 2342 (1929).

Can. J. Chem. Downloaded from www.nrcresearchpress.com by 210.87.254.42 on 09/05/12
For personal use only.

Conformational analysis of ketoximes by the application of carbon-13 nuclear magnetic resonance spectroscopy

PATRICK GENESTE, ROBERT DURAND, AND JEAN-MARC KAMENKA
Laboratoire de Chimie Organique Physique Appliquée, Ecole Normale Supérieure de Chimie, 8, Rue Ecole Normale, 34075 Montpellier, France

AND

HELMUT BEIERBECK, ROBERT MARTINO,[1] AND JOHN K. SAUNDERS
Département de Chimie, Université de Sherbrooke, Sherbrooke (Qué.) Canada J1K 2R1

Received July 25, 1977[2]

PATRICK GENESTE, ROBERT DURAND, JEAN-MARC KAMENKA, HELMUT BEIERBECK, ROBERT MARTINO, and JOHN K. SAUNDERS. Can. J. Chem. **56**, 1940 (1978).

The carbon-13 chemical shifts for a number of relatively rigid ketoximes are presented. It is shown that the chemical shift difference, $\Delta\delta$ (*syn–anti*), for the carbons α to the oxime carbon depends on the dihedral angle between the C=N and C_α—H bonds. This stereochemical dependence is then used to determine the preferred conformation of substituted cyclohexanone oximes.

PATRICK GENESTE, ROBERT DURAND, JEAN-MARC KAMENKA, HELMUT BEIERBECK, ROBERT MARTINO et JOHN K. SAUNDERS. Can. J. Chem. **56**, 1940 (1978).

On rapporte les déplacements chimiques du carbone-13 d'un certain nombre de cétoximes relativement rigides. On démontre que la différence des déplacements chimiques, $\Delta\delta$(*syn–anti*), pour les carbones en α du carbone de l'oxime dépend de l'angle dièdre entre les liens C=N et C_α—H. On utilise ensuite cette corrélation stéréochimique pour déterminer la conformation privilégié des oximes de cyclohexanone substitués.

[Traduit par le journal]

Currently, carbon-13 nuclear magnetic resonance spectroscopy (^{13}Cmr) is an informative and important technique for conformational analysis. The shielding parameters have been shown to be very sensitive to environment (1) such that relatively small conformational changes lead to significant chemical shift variations. During a study of the reactivity of ketones and ketoximes, it was necessary to have increased knowledge of their conformations in solution. From earlier reports (2, 3), it appeared that ^{13}Cmr may furnish such information since $\Delta\delta$(*syn–anti*) values for the carbons α to the oxime carbon are significant and hence we undertook a study of the ^{13}Cmr chemical shifts of a number of relatively rigid ketoximes. In this paper we present the results of this study and their subsequent use in the conformational analysis of substituted cyclohexanone oximes.

Results

The ^{13}Cmr spectral data for the ketoximes studied are given in Table 1. The chemical shifts for compounds **1**, **3**, **12**, **13**, **16**, **17**, and **18** have been given elsewhere (3). The two sets of values agree within 0.3 ppm, with the exception of **17** and **18** where slight assignment modifications have been made. The assignments for the remaining compounds were made with the aid of single frequency off-resonance decoupled (sford) spectra, from the chemical shifts for the corresponding ketones (4), and the observation (2, 3) that for carbons α to the C=N bond, the carbon *syn* to the OH group is shielded relative to the *anti* position. Also, for oximes whose corresponding ketones do not have two-fold symmetry, distinguishable isomers exist, which were generally present in unequal amounts. For compound **2**, carbons 1, 2, 4, 6, 7 (the quaternary carbon), and 8 (the CH_3 carbons) were readily assigned from the sford spectrum. The protons on carbon 2 have a chemical shift difference of 1 ppm (5) and thus this carbon appeared in the sford spectrum as the X part of an ABX system, whereas the other methylenes appeared as the normal triplets. The remaining resonances were assigned to carbons 3 and 5 on the basis of the different shifts induced by $Pr(fod)_3$. The signals for **3** could then be assigned using the data for **2** together with the effect of a tertiary butyl group (6). The sford spectra for **4**, **5**, and **6** led to straightforward assignments of carbons 1, 3, and 5 in each compound and for carbon 2 in **4** and **5**. The only ambiguity is the distinction between (*i*) the pairs of carbons β and γ to the oxime and (*ii*) carbons 4 and 8 of compound **4**. The latter were assigned from the corresponding ketone data (4). In **1**, **2**, and **3**, $\Delta\delta$(*syn–anti*) for the β carbon is approximately -1.3 ppm and thus in **4**, **5**, and **6**, the

[1]Permanent address: Université Paul Sabatier, 118, route de Narbonne, Toulouse, France.

[2]Revision received March 14, 1978.

Can. J. Chem. Downloaded from www.nrcresearchpress.com by 210.87.254.5 on 09/05/12
For personal use only.

TABLE 1. Chemical shift data for ketoximes[a]

Compound	δ C-1	C-2	C-3	C-4	C-5	C-6	C-7	C-8	C-9	C-10	$\Delta\delta_\alpha$	θ[b]
1	28.9	166.9	36.3	37.6	28.0	39.0	39.0	28.0	36.7	37.6	−7.4	0
2	160.5	24.4	26.4	47.7	27.6	32.0	32.6	27.6			−7.6	7.5
3	160.4	25.4	25.7	24.4	26.7	31.9					−6.5	7.5
4	34.4	33.1	159.0	38.6	34.9	29.4[c]	28.5[c]	39.3			−5.5	10
5	37.5	29.4	157.7	34.3	38.3	135.4[c]	134.4[c]	42.3			−4.9	15
6	33.6	33.6	17.9	36.1	39.4	25.8	25.7	162.9			−5.8	10
7	167.0	28.8	32.0	21.4	33.5	36.1	33.5	21.4	32.0		−7.3	0
8	26.4	27.5	36.5	161.5	28.4	28.9	31.9	27.9	22.8	24.5	−5.5(C-3)	
9			31.0	162.0								
10	31.6	164.9	31.6	25.6	25.0[c]	25.3[c]	25.3	25.0				60
11	161.8	24.8	25.4	33.8	44.4	34.4	26.8[c]	26.1[c]	26.1[c]	47.8		0
12	38.3	166.4	37.2	35.6	26.0	27.4	38.5				−2.3(C-3)	60,60
13	42.3	167.3	34.9	35.5	27.2	27.9	39.1				−4.0(C-1)	19
14	33.9	164.9	37.2	45.1	31.5	26.3	26.3	31.5	44.5		−3.3	48,78
15	30.5	170.1	34.0	51.1	26.3	27.9	26.3	51.1			−3.5	48,78
16	167.4	27.3	24.4	25.4	30.8						−3.5	48,78
17	163.0	37.1	35.8	24.1	26.2	24.8	16.9					
18	163.6	26.7	31.7	20.6	26.9	28.4	16.4					
19	166.0	26.7	32.0	20.6	36.1	33.2	16.7	16.7				
20	166.0	27.3	31.1	16.4	31.8	34.0	18.3	20.9			−6.7	
21	159.4	37.3	34.2	52.7	34.2	44.8	31.1[c]	30.9[c]	31.1	30.9	−7.5	
22	159.4	35.0	41.1	52.0	32.6	44.8	32.6	34.7	27.7		−6.7(C-2)	
23	160.2	41.7	40.3	52.0	34.1	37.6	32.0	33.8	29.0		−7.2(C-6)	
24	157.8	37.5	36.8	66.1	36.9	44.7	31.8	31.8	24.9[c]	24.6[c]	−7.2	
25	163.0	25.3	40.5	25.4	41.6	28.8	32.7[c]	26.9	33.5[c]	26.9	−3.5	

[a]Relative to TMS as approximately 0.7 *M* $CDCl_3$.
[b]See ref. 5 for the determination of θ.
[c]Could be interchanged.

more shielded β or γ carbon was assigned as the *syn*. The carbon resonances for **7** were assigned in a similar manner.

The twistane isomers were present in unequal amounts. The spectrum of the major isomer, **8**, was assigned from the sford spectrum and by comparison with the corresponding ketone (7). The only carbons of the minor isomer that could be assigned were those corresponding to carbons 3 and 4. For compounds **10–13** use of the sford spectra together with the reported values for the corresponding ketones (4, 8) led to the assignments given in Table 1. The ketone corresponding to **14** gave the following spectrum: 217.1 (C-2), 45.6 (C-1,3), 44.0 (C-4,9), 31.5 (C-5,8), and 26.4 ppm (C-6,7). The spectrum of **14** was then assigned using these values together with the sford spectrum as was the spectrum of **15**.

The two oximes, **17** and **18**, were present in unequal amounts with the major isomer having the CH_3 and the OH groups *anti* (3). From the sford spectrum, carbons 1, 2, and 7 (the CH_3 carbon) of **17** could readily be assigned as could carbon 6 since it appeared as the X part of an ABX system. Carbons 4 and 5 should be little changed from their position in **3** and thus the remaining resonances were assigned. In **18**, the methyl group is axial as evidenced by the chemical shift at 20.6 ppm which can only be assigned to carbon 4. The sford spectrum led to the assignments of carbons 1, 2, and 7 and since C-5 is δ to the CH_3 group it should have about the same chemical shift in **2**, **17**, and **18**. Also C-6 should be shielded by about 4.0 ppm in **18** relative to **2** owing to the axial CH_3 group at C-2. Thus, C-5 absorbs at 26.9, C-6 at 28.4, and C-3 at 31.7 ppm in **18**. These assignments differ from the earlier values (3); for **17**, C-5 and C-6 have been interchanged whereas for **18**, C-3, C-5, and C-6 have been changed.

The assignments of the resonances for compounds **19–25** were straightforward with the aid of sford spectra, and assuming that the $\Delta\delta(syn\text{–}anti)$ for β and γ carbons are negative. In the case of the tetramethyl, trimethylphenyl, and the di-*tert*-butyl compounds, the CH_3 absorptions could not be unambigously assigned.

Discussion

In Fig. 1, the chemical shift difference $\Delta\delta(syn\text{–}anti)$ for the carbons α to the C=N bond is plotted as a function of the dihedral angle (θ)[3] between the C=N and C—H bonds. The plot demonstrates a marked dependence on the value of θ with a maximum

[3]Values of θ were obtained from the literature. The references for the individual compounds are found in ref. 5. Only C—H bonds with θ < 90° are considered.

Can. J. Chem. Downloaded from www.nrcresearchpress.com by 210.87.254.5 on 09/05/12
For personal use only.

Can. J. Chem. Downloaded from www.nrcresearchpress.com by 210.87.254.5 on 09/05/12
For personal use only.

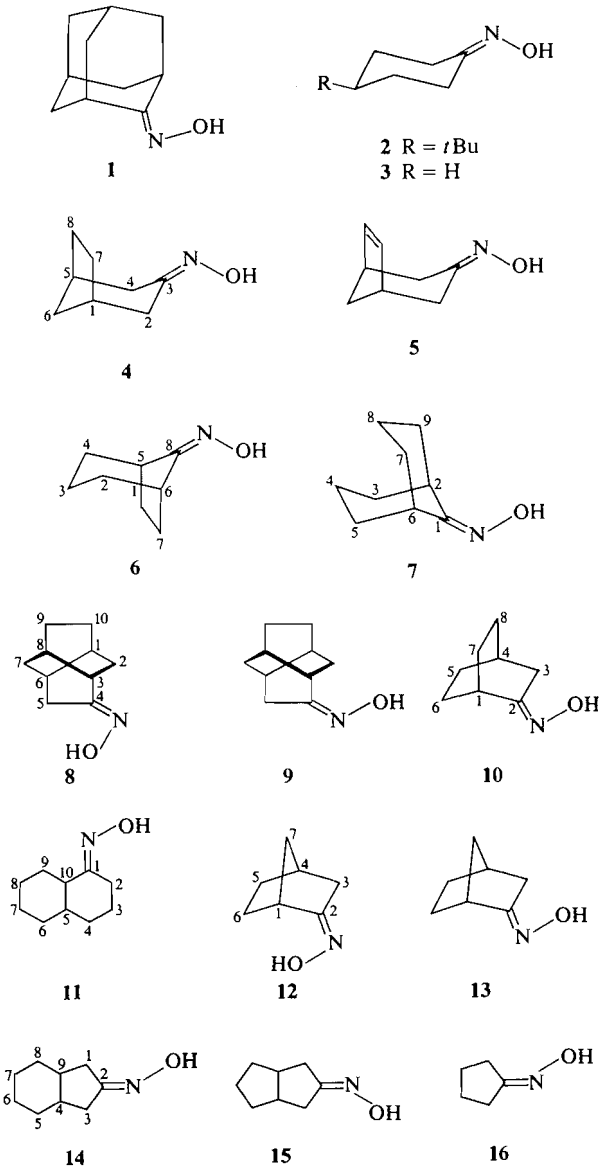

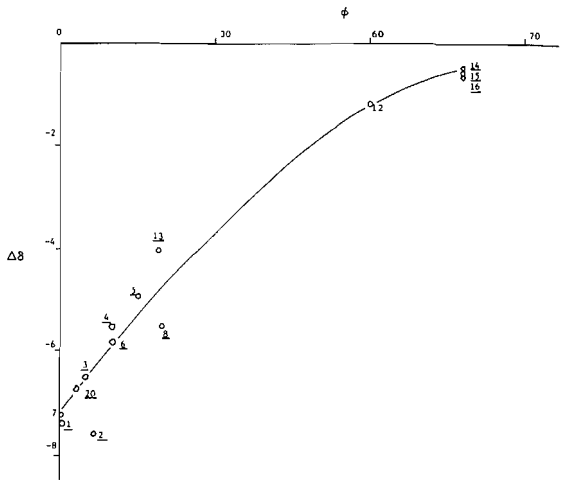

FIG. 1. Plot of $\Delta\delta$(*syn–anti*) vs. dihedral angle for the α carbons of ketoximes.

occurring when θ is 0° and decreasing with increasing angle. The shape of the curve resembles that obtained from the ^{1}Hmr spectra of ketoximes (5). However, the signs of the shift difference are opposite, i.e. whereas in the ^{13}Cmr spectra $\Delta\delta$(*syn–anti*) = −7.5 ppm at 0°, in the ^{1}Hmr spectra $\Delta\delta$ is +1.0 ppm. Such a correlation is also obtained from $\Delta\delta$(*syn–anti*) for the carbon β to the C=N although the variation with angle is much smaller. It is thus apparent from these curves that both the ^{13}Cmr and the ^{1}Hmr $\Delta\delta$ values for the α carbons are sensitive probes for stereochemical information.

The chemical shifts for C-4 of **18** and **19** are identical, and since in **19** the CH_3 group *syn* to OH is axial (5), we can conclude that **18** has the CH_3 axial as was proposed earlier (3).

For compound **20**, $\Delta\delta_\alpha$(*syn–anti*) is −6.5 ppm indicating a dihedral angle of about 10° between the C=N and C_α—H bonds. Also C-4 absorbs at 16.4 ppm, that is, it is shielded by 4.2 ppm relative to C-4 in **19**. This can only be explained by a conformation in which the two methyl groups are axial as was proposed earlier from ^{1}Hmr spectra (5). More recently Fraser and Grindley (9) demonstrated that the two methyl groups in *N*-nitroso-*trans*,*trans*-2,6-dimethyl-4-phenylpiperidine are also axial. Compounds **21**–**24** all have $\Delta\delta_\alpha$ values between −6.7 and −7.2 ppm indicating that these compounds exist in chair conformations since the dihedral angle is close to 0°. This result confirms the most widely held view of the conformations of the starting ketones (5). Finally, compound **25** has a $\Delta\delta_\alpha$(*syn–anti*) value of −3.5 ppm indicating that θ is of the order to 40°. Thus this molecule must exist in a twist boat conformation with the *tert*-butyl groups occupying pseudoequatorial positions in accordance with the twist conformation of the ketone (10).

It has been shown (11) that the effect of methyl group substitution can be ascertained using eq. [1]

$$[1] \qquad \Delta\delta = \eta_{HC}(HC) + \eta_{CC}(CC) + \gamma$$

where HC corresponds to the *gauche* interaction CH_3—C,C—H; CC corresponds to the *gauche* interaction CH_3—C,C—C; γ corresponds to the shielding effect on the carbon γ to the substituted carbon; and η is the number of interactions. The numerical values attributed to each of these is HC = 4.7 ppm, CC = +1.7 ppm, γ = −4.5 ppm when the introduction of the CH_3 group removes a 1,3 diaxial hydrogen–

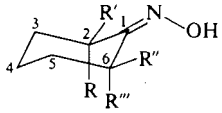

17 R = R″ = R‴ = H; R′ = CH_3
18 R = R′ = R″ = H; R‴ = CH_3
19 R = R″ = H; R′ = R‴ = CH_3
20 R′ = R″ = H; R = R‴ = CH_3

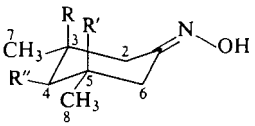

21 R = R′ = CH_3; R″ = H
22 R = CH_3; R′ = ϕ; R″ = H
23 R = ϕ; R′ = CH_3; R″ = H
24 R = R′ = CH_3; R″ = $C(=O)-CH_3$

25

hydrogen interaction and γ = 0 when introduction of the CH_3 group does not remove such an interaction (12). These values were derived from cyclohexane derivatives. In the case of the substituted carbons, α shifts of +5.8 ppm (equatorial) and 1.2 ppm (axial) can be used (13). The chemical shifts for compounds **17–25** can then be predicted using eq. [1], α shifts where necessary, and the data for compound **3** to verify that compounds **17–21** exist in essentially the same conformation as **3** and that **25** is in a different conformation. Compound **19** can be used as an example to illustrate the method of predicting shifts; δ(C-2) = 25.4 + 1.2(α) = 26.6; δ(C-3) = 25.7 + 4.7(HC) + 1.7(CC) = 32.1; δ(C-4) = 24.4 − 4.5(γ) = 19.9; δ(C-5) = 26.7 + 2 × 4.7 (2 × HC) = 36.1; δ(C-6) = 31.9 + 5.8(α) − 4.5(γ) = 33.2. The results given in Table 2 indicate that for compounds **17–21**, the chemical shifts are predicted reasonably well using methyl parameters deduced from cyclohexane derivatives and thus these compounds exist essentially in chair forms. The small discrepancies between the predicted and experimental values are probably due to small distortions which alleviate the axial CH_3,CH_3 interactions. For compound **25**, the lack of correlation between predicted and observed values is confirmation that the compound exists in a conformation other than a chair.

From Table 1, the chemical shifts for the oxime carbons exhibit a consistent behaviour for six-membered rings. The oxime carbon for compounds **2**, **3**, **4**, **21**, **23**, and **24** all absorb at 160 ± 1 ppm. Substitution of one CH_3 group at the α carbon causes a 3 ppm downfield shift as seen for compounds **17** and **18**, whereas with substituents at both α carbons this absorption appears at 167 ± 1 ppm as observed for **1**, **6**, **7**, **19** and **20**. These results imply an additive β effect. However, the oxime carbon in cyclopentanone oxime absorbs at 164.9 ppm whereas in cyclohexanone oxime it absorbs at 160.4 ppm. Grover *et al.* (14) suggested that eclipsing between an α CH and the CO bonds for ketones has an important influence on the shielding of the carbonyl carbon and that the closer the CH and CO bonds are to being eclipsed, the more shielded is the carbonyl carbon. The results presented here for oximes are similar, provided a 3.0 ppm deshielding effect for an axial CH_3 (or CH_2) is included, i.e. the deshielding effect of an axial CH_3 (or CH_2) group appears to be a β effect, whereas the introduction of an equatorial group in six-membered rings can be interpreted in terms of a β effect, removal of an eclipsing C—H bond, or a combination of both. The comparison of the shifts for five- and six-membered rings indicates that the eclipsing interaction has a role in the shielding of the oxime carbon. In fact, with the exception of **5**, the larger the value of $\Delta\delta_\alpha$(*syn–anti*) the more shielded the oxime carbon, after allowing for the effect of axial CH_3 or CH_2 groups. A good example can be seen by comparing **2** and **25** since **2** exists in the chair conformation whereas **25** has been shown to exist as a twist boat. The oxime

TABLE 2. Predicted chemical shifts for methylated cyclohexanone oximes

	C-2		C-3		C-4		C-5		C-6	
Compound	δ	Δδ[a]	δ	Δδ	δ	Δδ	δ	Δδ	δ	Δδ
17	37.7	+0.6	36.1	−0.3	24.4	+0.3	25.7	−0.5	25.4	+0.6
18	26.6	−0.1	32.1	+0.4	19.9	−0.5	26.7	0	27.4	−1.0
19	26.6	−0.1	32.1	+0.1	19.9	−0.7	36.1	0	33.2	0
20	26.6	−0.7	32.1	+1.0	15.4	−1.0	33.1	+1.3	33.2	−0.8
21	39.3	+2.0	32.9	−1.3	32.6	+0.6	32.9	−1.3	46.0	+1.2
25	25.6	+0.3	47.7	+6.0	24.6	−0.8	48.7	+7.1	33.1	+4.3

[a]Δδ = δ(predicted) − δ(observed).

Can. J. Chem. Downloaded from www.nrcresearchpress.com by 210.87.254.5 on 09/05/12
For personal use only.

TABLE 3. Chemical shift difference,[a] ketone oxime

Compound	Substituted carbon	$\Delta\delta_\alpha$(ketone oxime) *syn*	$\Delta\delta_\alpha$(ketone oxime) *anti*	$\Delta\delta_\alpha$(*syn–anti*)	$\Delta\delta_\beta$(ketone oxime) *syn*	$\Delta\delta_\beta$(ketone oxime) *anti*	$\Delta\delta_\beta$(*syn–anti*)	Reference[b]
1	50.5	18.2	10.8	−7.4	1.8	0.4	−1.4	3
2	50.0	17.0	9.4	−7.6	1.6	0.4	−1.4	1
3	49.3	16.1	9.6	−6.5	1.2	−0.1	−1.3	1
4	50.9	17.2	11.7	−5.5	0.9	0.4	−0.5	4
5	52.4	17.0	12.1	−4.9	0.8	0	−0.8	4
6	54.1	11.2	5.4	−5.8	3.4(C-2)	0.9	−2.5	4
					−3.1(C-7)	−3.0	−0.1	4
7	54.7	17.9	10.6	−7.3	2.4	0.9	−1.5	4
8	50.4		11.1	−5.0	1.2(C-6)			7
9		13.8		−5.5		−0.8(C-8)		7
						−1.5(C-3)		
10	51.8	13.0			2.3			14
11	50.1	16.8			0			14
12	51.0	10.2(C-2)	7.9	−2.3	−0.2(C-4)	−0.1	−0.1	14
13	50.0	11.7(C-1)	7.7	−4.0	−2.3(C-6)	−3.2	+0.9	14
14	52.2	11.7	8.4	−3.3	−1.1	−0.5	−0.6	
15	50.1			−3.5				
16	52.2	10.8	7.3	−3.5				1
17	49.9							15
18	49.3							15
19	50.2							15
20	47.6	17.9	11.2	−6.7			−0.7	15
21	52.6	16.5	9.0	−7.5	1.8	1.8	0	15
22	51.8	16.2(C-2)	9.5	−6.7	1.4(C-3)	2.2	−0.8	
23	51.0	16.4(C-6)	9.2	−7.2	1.8(C-5)	1.8	0	
24	52.5	16.3	9.1	−7.2	1.7	1.8	−0.1	
25	51.8	14.6	11.1	−3.5	0.5	−0.6	−1.1	

[a]Positive numbers indicate deshielding.
[b]Reference for ketones.

carbon of **25** is deshielded by 2.5 ppm relative to that in **2**. Also the carbonyl carbon of the ketone analog of **25** is deshielded by 3.3 ppm relative to that observed in **2**. The anomalous high field shift of **5** is due to an interaction between the double bond and the oxime carbon, an interaction shown to shield the carbonyl carbon of the corresponding ketone (4). Thus, as was found in the case of ketones (14), it appears that the eclipsing of the C_α—H and C=N bonds shields the oxime carbon.

Inspection of Table 3, in which the chemical shift differences between the ketoximes and their corresponding ketones are given, permits a number of interesting observations. First of all, the chemical shift differences for the substituted carbons are relatively constant with the exception of **6**, **7**, **18**, and **20**. In the latter two compounds, the preferred conformations of the oximes are different from those observed for the ketones. Methyl groups which were equatorial in the ketone are axial in the oximes. For **6** and **7**, the chemical shift of the substituted carbon is similar to that observed for similar structural units (e.g. ref. 1) whereas in the corresponding ketones, the carbonyl carbon is deshielded by 4 to 5 ppm relative to adamantanone. These results suggest that the parent ketones of **6** and **7** exist in distorted conformations which differ from the conformations of the ketoximes. Secondly, the variation of $\Delta\delta_\alpha$(*syn–anti*) is due to a variation in the shielding of both the *syn* and *anti* carbons. The $\Delta\delta_\alpha$(ketone oxime) for **6** is quite different from values observed in other six-membered ring compounds which supports the proposed conformational change suggested above. Finally, the effect of the oxime group is also transmitted to the β carbons in that both Δδ(ketone oxime) and Δδ(*syn–anti*) differ from zero with the *syn* carbon generally more shielded than the *anti* carbon.

One of the most useful diagnostic tools in ^{13}Cmr is the so called γ effect as has been mentioned and applied earlier. This effect was originally ascribed in the case of axial methylcyclohexane derivatives to a hydrogen–hydrogen steric compression causing electron density to move from the hydrogen to the carbon resulting in a shielding of the carbon and a concomitant deshielding of the hydrogen (16). Recently, other interpretations of the origin of this

Can. J. Chem. Downloaded from www.nrcresearchpress.com by 210.87.254.5 on 09/05/12
For personal use only.

TABLE 4. Calculated angle dependence of the electric effect on the ^{13}C chemical shifts of the α carbon of ketoximes

Angle (deg)	Point dipole 0.7 Å from N on N—O bond			Point dipole 1.4 Å from N on N—O bond		
	δ(*syn*)	δ(*anti*)	Δδ(*syn–anti*)	δ(*syn*)	δ(*anti*)	Δδ(*syn–anti*)
0	−6.0	1.0	−7.0	−6.35	0.65	−7.0
10	−5.82	1.04	−6.86	−6.13	0.65	−6.78
20	−5.37	1.09	−6.46	−5.54	0.67	−6.21
30	−4.71	1.16	−5.89	−4.67	0.72	−5.39
40	−3.9	1.25	−5.15	−3.69	0.77	−4.46
50	−3.0	1.32	−4.37	−2.70	0.81	−3.51
60	−2.2	1.37	−3.57	−1.81	0.86	−2.65
70	−1.41	1.40	−2.81	−1.03	0.89	−1.92
80	−0.72	1.43	−2.15	−0.40	0.91	−1.31
90	−0.13	1.46	−1.59	+0.11	0.93	−0.82
100	−0.33	1.46	−1.13	0.51	0.95	−0.44
110	−0.72	1.46	−0.74	0.82	0.96	−0.14
120	−0.89	1.46	−0.57	1.03	0.97	0.06

effect have been suggested (12, 17). Calculations using equations similar to those derived by Grant and Cheney (16) show that although the steric compression model predicts the trend of the chemical shift difference as a function of dihedral angle for the α carbons, it is not quantitative. Also it does not explain the $\Delta\delta_\beta$(*syn–anti*) values.

Another factor that has been invoked to explain shieldings is the electric field effect (18–20). Using the simplified point dipole approximation and the equation derived by Buckingham (21) calculations of the chemical shifts due to the electric field effect at the α carbons of oximes as a function of dihedral angle are given in Table 4. The calculated stereochemical dependence is similar to that observed experimentally. No attempt was made to obtain a quantitative correlation between predicted and observed shifts since the representation of the electric field as a point dipole is an approximation which should only be employed to show qualitative trends. Also the shift difference for a given angle in ^{13}Cmr should be about 20 times that observed in ^1Hmr since shieldings of about 180 ppm/electron in the former and 8 ppm/electron in the latter have been observed (22). Hence other factors must also be involved in the shieldings. In the *N*-nitroso derivative of piperidine where the dihedral angle between the N—N and the α C—H bonds is 0°, a value of Δδ(*syn–anti*) = −11.0 ppm was observed in ^{13}Cmr whereas in ^1Hmr this difference was only 0.03 ppm (9). In this type of compound both the steric compression model (9) and the electric field effect (20) have been invoked to explain the ^{13}C shifts.

Thus even though both the electric field effect and the steric compression model can explain the observed $\Delta\delta_\alpha$ trends, it is evident that other factors must be taken into account to explain the absolute shifts observed in both ^{13}Cmr and ^1Hmr.

Conclusions

The results presented here demonstrate the dependence, the origin of which is not yet clear, of the chemical shift difference Δδ(*syn–anti*) on the dihedral angle between the C=N and C—H bonds. The observed values of Δδ can be used to estimate this angle and thus to determine the preferred conformation of oximes in solution. It appears that the chemical shift of the oxime carbon depends on the number of C=N, C_α—H eclipsing interactions as well as on the number of axial CH_3 or CH_2 groups. From the observed Δδ(*syn–anti*) values, it has been shown that *cis*-2,6-dimethylcyclohexanone oxime exists in a slightly distorted chair form with the 2-CH_3 group axial, that 3,3,5,5-tetramethyl and 3-phenyl-3,5,5-trimethylcyclohexanone oxime exist in chair conformations whereas the *trans*-3,5-di-*tert*-butyl derivative exists in a twist boat.

Experimental

All compounds were synthesized using methods described in the literature (5). The ^{13}Cmr spectra were recorded on a Bruker HX-90 spectrometer equipped with a Nicolet 1083 computer (8K memory for data) operating in the Fourier transform mode. Sweep widths of 5000 Hz were used with a line broadening factor of 0.5 Hz. The compounds were studied as approximately 0.7 *M* solutions in $CDCl_3$ with internal TMS as reference.

Acknowledgements

We are grateful to the National Research Council

Can. J. Chem. Downloaded from www.nrcresearchpress.com by 210.87.254.5 on 09/05/12
For personal use only.

of Canada for generous financial support and also to the Cooperation Franco–Québécois for a post-doctoral fellowship (R.M.) and for missions of short duration in France (J.K.S.) and in Québec (P.G., J.M.K.). We would like to express our appreciation to two conscientious referees. We thank Professors G. Lamaty and B. Boyer for providing us with samples of oximes **22**, **23**, **24**, and **25**.

1. J. B. STOTHERS. Carbon-13 nmr spectroscopy. Academic Press, New York, NY. 1972.
2. G. C. LEVY and G. L. NELSON. J. Am. Chem. Soc. **94**, 4897 (1972).
3. G. E. HAWKES, K. HERWIG, and J. D. ROBERTS. J. Org. Chem. **39**, 1017 (1974).
4. J. B. STOTHERS, J. R. SWENSON, and C. T. TAN. Can. J. Chem. **53**, 581 (1975).
5. P. GENESTE, R. DURAND, and C. MOREAU. Org. Magn. Reson. **73**, 241 (1971).
6. F. J. WEIGERT and J. D. ROBERTS. J. Am. Chem. Soc. **92**, 1347 (1970).
7. H. BEIERBECK and J. K. SAUNDERS. Can. J. Chem. **55**, 3161 (1977).
8. J. B. GRUTZNER, M. JAUTELAT, J. B. DENCE, R. A. SMITH, and J. D. ROBERTS. J. Am. Chem. Soc. **92**, 7107 (1970).
9. R. R. FRASER and T. B. GRINDLEY. Can. J. Chem. **53**, 2465 (1975).
10. N. L. ALLINGER, H. M. BLATTER, L. A. FREIBERG, and F. M. KARKOWSKI. J. Am. Chem. Soc. **88**, 2999 (1966).
11. H. BEIERBECK and J. K. SAUNDERS. Can. J. Chem. **53**, 1307 (1975).
12. H. BEIERBECK and J. K. SAUNDERS. Can. J. Chem. **54**, 2985 (1976).
13. H. BEIERBECK and J. K. SAUNDERS. Can. J. Chem. **54**, 632 (1976).
14. S. H. GROVER, D. H. MARR, J. B. STOTHERS, and C. T. TAN. Can. J. Chem. **53**, 1351 (1975).
15. J. B. STOTHERS and C. T. TAN. Can. J. Chem. **52**, 308 (1974).
16. D. M. GRANT and B. V. CHENEY. J. Am. Chem.Soc. **89**, 5315 (1967).
17. (*a*) K. SEIDMAN and G. E. MACIEL. J. Am. Chem. Soc. **99**, 659 (1977); (*b*) D. GORENSTEIN. J. Am. Chem. Soc. **99**, 2254 (1977).
18. J. C. BATCHELOR. J. Am. Chem. Soc. **97**, 3410 (1975) and references cited therein.
19. M. W. DUCH. Ph.D. Thesis, University of Utah, Salt Lake City, UT. 1970
20. G. E. ELLIS, R. G. JONES, and M. G. POPADOPAULOS. J. Chem. Soc. Perkin II, 1381 (1974).
21. A. D. BUCKINGHAM. Can. J. Chem. **38**, 300 (1960).
22. T. K. WU and B. P. DAILEY. J. Chem. Phys. **41**, 2796 (1974).

Can. J. Chem. Downloaded from www.nrcresearchpress.com by 210.87.254.5 on 09/05/12
For personal use only.

Application of water nuclear magnetic resonance relaxation times to study of metal complexes of the soluble soil organic fraction fulvic acid[1]

KATALIN DECZKY AND COOPER H. LANGFORD[2]

Metal Ions Group, Chemistry Department, Carleton University, Ottawa, Ont., Canada K1S 5B6

Received August 30, 1977

KATALIN DECZKY and COOPER H. LANGFORD. Can. J. Chem. **56**, 1947 (1978).

The binding of the paramagnetic metal ions Mn^{2+}, Cu^{2+}, and Fe^{3+} to the acid soluble organic fraction of soils, fulvic acid, has been examined. The measurements use effects on paramagnetic ion induced longitudinal (T_1) and transverse (T_2) relaxation in the proton magnetic resonance signal of solvent water. The effects of the fulvic acid sample are compared to model ligand effects. Evidence is developed to suggest that Mn^{2+} forms outer sphere complexes with fulvic acid. On the contrary, Cu^{2+} and Fe^{3+} appear to form inner sphere complexes.

KATALIN DECZKY et COOPER H. LANGFORD. Can. J. Chem. **56**, 1947 (1978).

On a étudié l'adsorption des ions métalliques paramagnétiques Mn^{2+}, Cu^{2+} et Fe^{3+} par l'acide fulvique, la fraction acide organique des sols qui est soluble en acide. Les mesures font appel à la relaxation longitudinale (T_1) et transversale (T_2) induite par l'ion paramagnétique sur le signal de résonance magnétique du proton de la molécule de solvant. On compare les effects de l'échantillon d'acide fulvique avec les effets de ligands modèles. On a observé des données suggérant que le Mn^{2+} forme des complexes périphériques avec l'acide fulvique. Par ailleurs le Cu^{2+} et le Fe^{3+} semblent former des complexes au niveau des sphères intérieures.

[Traduit par le journal]

Introduction

The soil organic fractions, humic acid and fulvic acid, are probably important in a variety of processes in which metals are mobilized in aquatic and soil systems and may play a central role in supplying nutrients to plants. A well characterized sample of a fulvic acid isolated at the Soil Research Institute, Agriculture Canada has received serious attention by titrimetric and ion exchange technique which characterizes its thermodynamics as a ligand (1). (It binds metals in even quite acid media.) Structural modification has provided some evidence of the structure of such complexes (1). The present report is devoted to attempt to come to additional structural conclusions by looking at the effects of fulvic acid on the nmr relaxation times of solvent protons on water molecules which may exchange into the sites in the coordination sphere of dissolved metal ions. In studying fulvic acid complexing, we are driven to means such as solvent nmr by the generally very unfavourable spectroscopic situation which fulvic acids impose. Broad and featureless bands from this structurally complicated material obscure most of the regions of the visible, uv, ir, and Raman spectra which might offer structural guidance. Solvent nmr is a way past this serious barrier. We have chosen to work at acid pH, such as that generated by modest amounts of the relatively strong acid, fulvic acid, in order to minimize extraneous electrolytes in the fulvic acid solutions. (That complexing is sufficient in such media is indicated by the effects of ligands on the interactions between paramagnetic ions and H_2O that we monitor by nmr.)

Some time ago, Mildvan and Cohn (2) demonstrated the utility of solvent nmr relaxation times in the presence of paramagnetic ions for study of the binding of these ions to enzymes. Paramagnetic ions shorten relaxation times of coordinated water molecules. When there is fast chemical exchange of nuclei (protons) of coordinated water molecules with water molecules in the bulk of the solution, the nmr signal is an average between the two environments and the paramagnetic effect is seen in the nmr signal for bulk solvent protons averaged in according to McConnell's fast exchange equation. This is a limiting case of the general treatment of chemical exchange (3):

$$[1] \qquad 1/T_{1,2(\mathrm{obs})} = P_{\mathrm{A}}/T_{1,2\mathrm{A}} + P_{\mathrm{M}}/T_{1,2\mathrm{M}}$$

where $T_{1,2(\mathrm{obs})}$ designates the *observed* relaxation time (T_1 or T_2) for either longitudinal (T_1) or transverse (T_2) relaxation in the proton nmr signal. The subscript A designates the relaxation times characteristic for protons in the bulk solvent environment. The subscript M designates protons in the paramagnetic ion solvation shell. P_{A} is the probability that a proton is in the bulk solvent environment. P_{M} is the probability that a proton is in the coordination sphere of the paramagnetic ion. In a dilute solution, P_{A} is equal to unity to a good approximation. P_{M}

[1]We thank the National Research Council of Canada for support.

[2]To whom correspondence should be addressed.

Can. J. Chem. Downloaded from www.nrcresearchpress.com by 210.87.254.6 on 09/05/12
For personal use only.

Can. J. Chem. Downloaded from www.nrcresearchpress.com by 210.87.254.6 on 09/05/12
For personal use only.

may be expressed in terms of C_M, the concentration of paramagnetic ions and q, the number of water molecules coordinated to the paramagnetic ion. Thus a proportionality may be written:

$$[2] \qquad (1/T_{1,2(obs)} - 1/T_{1,2A}) \propto qC_M/T_{1,2M}$$

If a paramagnetic ion is coordinated only to water, q will be equal to 4–6. (In the case of the present metal ions, the number is 6.) The coordination of the metal ion to a non-solvent ligand must change q to a smaller value but it may simultaneously lead to an alteration of $T_{1,2M}$. As a result, there are three cases. Coordination of a paramagnetic ion to a non-solvent ligand may lead to an increase in observed relaxation rates (of $1/T_{1,2}$) because of a reduction of $T_{1,2M}$. Second, a decrease in observed relaxation rates can be a consequence of reduction of q. The third possibility is decrease of observed relaxation rate because of an increase of $T_{1,2M}$. In studies of interaction of Mn^{2+} with enzymes (2), the most important case is the first where a reduction of $T_{1,2M}$ is observed. Since the simplest measurement is that of T_2 from absorption signal line width ($\pi\Delta\nu = 1/T_{2(obs)}$ where $\Delta\nu$ is the width at half height of the Lorentzian absorption line), the reduction of T_{2M} is associated with *enhanced* line broadening (increased $\Delta\nu$).

The factors which control T_{1M} or T_{2M} are described by the Solomon–Bloembergen equation (3,4). The relaxation of a nucleus is determined by one of the various possible sources of a fluctuating magnetic field which can influence the magnetic state of the nucleus under observation. These are described by τ_R, the rotational correlation time, τ_S, the paramagnetic electron relaxation correlation time, and τ_M, the chemical exchange correlation time. (τ_M cannot control in the fast exchange case of eq. [1], it is included here for completeness.) A simple physical picture of effects on observed T_1 or T_2 depends upon the recognition that both τ_S, the paramagnetic electron relaxation correlation time, and τ_R, the rotational correlation time of the molecule containing the nucleus, are short times compared to the reciprocal of the nmr frequency. They tend to average out the fluctuation of local field to zero. The result is that observed relaxation processes are 'maximally inefficient', governed by the *fastest* correlation time. This curious situation means that as a correlation time shortens, it becomes determining and reduces efficiency of relaxations.

In situations where τ_R is most important, rotation of a metal ion is slowed by complexation to a large molecule (protein or fulvic acid) and the consequence for $1/T$ is increase in relaxation efficiency. For the case of $1/T_2$ enhanced line broadening is observed (2). In situations where τ_S is important, long times are usually associated with high spins and electron configurations in high symmetry environments. These times are reduced by removal of symmetry and the result is less efficient relaxation (line narrowing in the T_2 case).

Two preliminary points remain to be recorded. First, frequently $T_1 \neq T_2$. This can only arise in the fast exchange when τ_S is the important factor and *scalar* coupling is important between the paramagnetic electron and the nucleus (4, 5). As long as magnetic dipolar coupling dominates interactions between the paramagnetic electron and the nucleus under observation, $T_1 = T_2$. (τ_M control also leads to $T_1 = T_2$ but τ_M is not important in fast exchange.) Second, the basic reference point for study of complexes of metal ions with macromolecular ligands is the behaviour of the hexaaquometal ions $M(OH_2)_6^{n+}$ ($n = 2$ or 3). The factors important to water proton relaxation times in the hexaaquometal ions are collected in Table 1.

Experimental

Materials

The fulvic acid sample used in these studies was a generous gift of Dr. D. S. Gamble of The Soil Research Institute, Agriculture Canada. It is an unusually well characterized sample of this poorly understood material which is derived from a Bh horizon podzol from Prince Edward Island. The characteristics of this sample have been reviewed (1). For our purposes, its most important characteristics are 3.3 milliequivalents of phenolic functional groups and 7.7 milliequivalents of carboxylate functional groups per gram of FA (1). This and studies of blocking group inhibitions of the metal complexing functions (1) imply that strong metal complexes are formed with salicylic acid type functionality. All experiments used fulvic acid concentration of 1 mg/ml.

Model ligands were Fisher or Eastman Organic Chemicals of good grades used without purification. Metal ion stock solutions were prepared from suitable reagent grade sulfate or perchlorate salts and standardized by well known titrimetric techniques (11). Fulvic acid solutions at final desired concentrations were brought to pH = 2 with $HClO_4$. Some model ligand studies were carried out in solutions near neutral pH. There were no qualitative differences. In the case of Mn^{2+}, an experiment was also run by neutralization to pH = 4.00 which corresponds to extensive deprotonation of the FA (1).

Equipment

All nmr spectra were those of protons on water (the solvent). Transverse relaxation times were estimated from the width at half height ($\Delta\nu$) of continuous wave absorption signals of Lorentzian shape recorded on Varian T-60, EM360, and HA100 spectrometers. Special attention was directed to signal phasing and operating at low RF power because these are the main sources of line shape distortion. $1/T_{2(obs)}$ was calculated from the relation $\pi\Delta\nu = 1/T_{2(obs)}$. Temperature dependence studies in the 5–40°C range were performed on the Varian EM360 using a Varian temperature control device capable of maintaining constant, known sample temperature of ±1°C. Locking signals were obtained from external D_2O or CH_3CN.

Longitudinal relaxation times were obtained on a Varian XL-100 system with a Nicolet Fourier transform computer. T_1

TABLE 1. Factors important to water proton relaxation times in hexaaquometal ions

Paramagnetic ion	Number of unpaired electrons	τ_S	τ_R	τ_M	Dominating τ	Reference
Mn^{2+}	5	1×10^{-8}	3×10^{-11}	2.5×10^{-7}	τ_R	1, 5, 6
Cu^{2+}	1	10^{-9}	3×10^{-11}	10^{-9}	τ_R	6, 7
Fe^{3+}	3	$\sim 10^{-11}$ to $\sim 10^{-12}$	$\sim 10^{-11}$	10^{-9}	τ_S	8, 9, 10

values were calculated from free induction decay records. The lock was external D_2O and temperature control was similar to that on the EMS60. Pulses ranged from 0.001 to 8 s.

Procedure

Solutions were prepared at constant ligand concentrations and variable metal ion concentration. A pH of 2.00 was used throughout, except in an Mn^{2+} series. It was adjusted with perchloric acid. The model organic ligands were in excess or in a 1:1 relationship to the most concentrated metal ion solutions. As noted above, fulvic acid concentrations were 1 mg/ml. This implies (1) 3.3 milliequivalents dm^{-3} of functionality analogous to salicylic acid. Metal ions were added to FA solutions up to 3.3×10^{-3} M except in the case of Cu^{2+}. In this case, studies of transverse relaxation rates were made using 5×10^{-3} M Cu^{2+} and 5 mg/ml of FA. In this case, dependence of T_2 on model ligand concentration was not followed because of the small values of line widths.

Results and Discussion

Manganese Experiments

The experiments on Mn^{2+} are an extension of those on T_2 reported in a previous publication (12). We reported there that formation of inner sphere complexes between Mn^{2+} and either ethylenediaminetetraacetic acid (EDTA) or bipyridine (bipy) led to a substantial reduction in water line widths, hence $1/T_2$. Line-width changes at 10^{-3} M Mn^{2+} where a factor of 2 with bipy and a factor near 10 for EDTA. This could be attributed to occupation of exchangeable water sites by the ligand and reduction of q of eq. [2]. However, it is also possible that conversion of the essentially octahedral aquo ion Mn^{2+} to a complex of lower symmetry can reduce paramagnetic electron relaxation times (τ_S). (Frequency dependence confirms a role for τ_S.)

In either case, there was a sharp contrast between the effect of these ligands and the effect of sulphosalicylic acid (SSA) which has complexing functionality very similar to that expected to be effective in fulvic acid. SSA had no effect on T_2 values in solutions containing Mn^{2+}. Since SSA is reported to complex divalent metal ions (13), we concluded (12) that the complex was outer sphere with almost no perturbations of q or τ_S. The results with FA are similar to those with SSA but *not* equivalent. At the time of our earlier report, we suggested that the FA complexes of Mn^{2+} which when clearly shown to be present by ion exchange measurements reported in ref. 12 were outer sphere like those of SSA but we were unable to interpret the small decrease in line widths ($1/T_2$) in the presence of FA.

Figure 1 shows water line widths in FA solutions as a function of Mn^{2+} concentrations at two frequencies. The dashed line shows the behaviour in the absence of FA. There is a definite decrease due to FA. The frequency dependence implicates τ_S but the temperature dependence indicated by curves A and G in Fig. 2 indicates that the relaxation mechanism is only slightly different from that in the absence of FA. The situation is clarified in Fig. 3 where $1/T_1$ values are reported. We see that FA has a nearly zero effect on T_1. T_1 is controlled by τ_R (2, 6, 7). Thus, τ_S is more sensitive than τ_R to complexing the large FA molecule.

Although FA does modify water T_2, it is possible that Mn^{2+} complexing is very small at pH = 2.0. Consequently, the experiments were also run at pH = 4.0 where ion exchange experiments (12) have shown extensive Mn^{2+} binding to FA. The Mn^{2+} dependence of relaxation is entirely parallel to the results at pH = 2.0. The only difference is that FA alone causes a little water relaxation itself at pH = 4.0. Some free radical character of FA's has been noted (1).

There is only one straightforward explanation of this combination of circumstances. An outer sphere

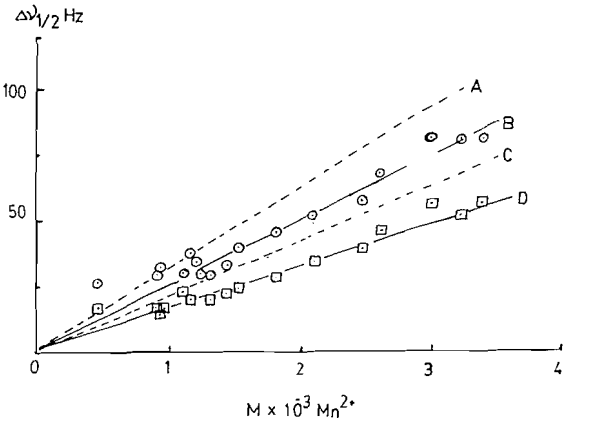

FIG. 1. Concentration dependence of transverse relaxation rates of Mn^{2+}-aquo and FA complexes, at 60 and 100 MHz. Concentration of FA = 1 mg/ml, A = Mn^{2+}-aquo at 100 MHz. B = Mn^{2+}-FA at 100 MHz. C = Mn^{2+}-aquo at 60 MHz. D = Mn-FA at 60 MHz.

Can. J. Chem. Downloaded from www.nrcresearchpress.com by 210.87.254.6 on 09/05/12
For personal use only.

Can. J. Chem. Downloaded from www.nrcresearchpress.com by 210.87.254.6 on 09/05/12
For personal use only.

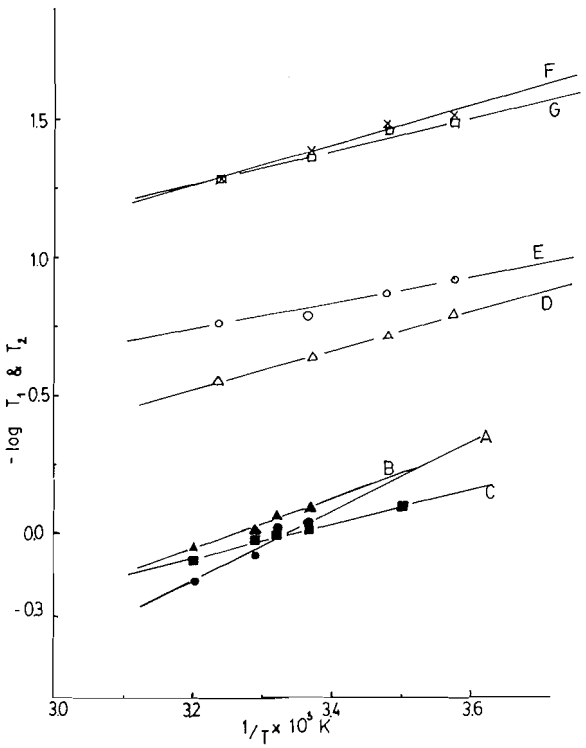

FIG. 2. Temperature dependence of transverse and longitudinal relaxation times of Mn^{2+} and Cu^{2+} complexes. A = longitudinal relaxation times of 1×10^{-4} Mn^{2+} + 1 mg/ml FA solution at pH = 2. B = longitudinal relaxation times of 1×10^{-3} M of Cu^{2+}-aquo complex. C = longitudinal relaxation times of 1×10^{-3} M Cu^{2+} + 1 mg/ml FA solution. D = transverse relaxation times of 5×10^{-3} M Cu^{2+} + 5 mg/ml FA solution. E = transverse relaxation times of 5×10^{-3} M Cu^{2+}-aquo complex. F = transverse relaxation times of 1×10^{-3} M Mn^{2+}-aquo complex. G = transverse relaxation times of 1×10^{-3} M Mn^{2+} + 1 mg/ml FA.

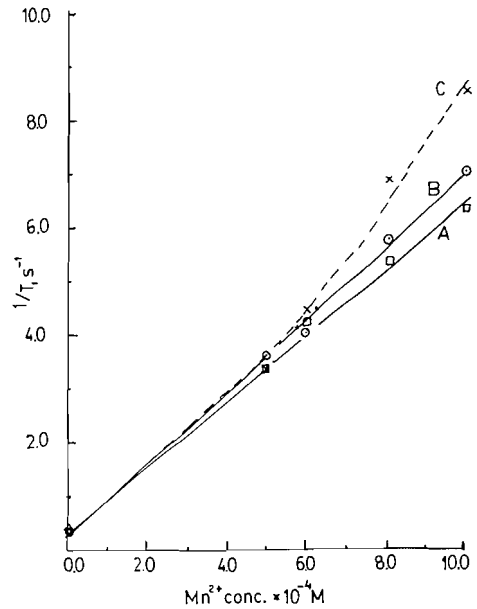

FIG. 3. Longitudinal relaxation rate dependence on the concentration of the Mn^{2+} ion at room temperature. Concentration of FA = 1 mg/ml, of bipy = 6×10^{-3} M. A = Mn–aquo. B = Mn–FA. C = Mn–bipy.

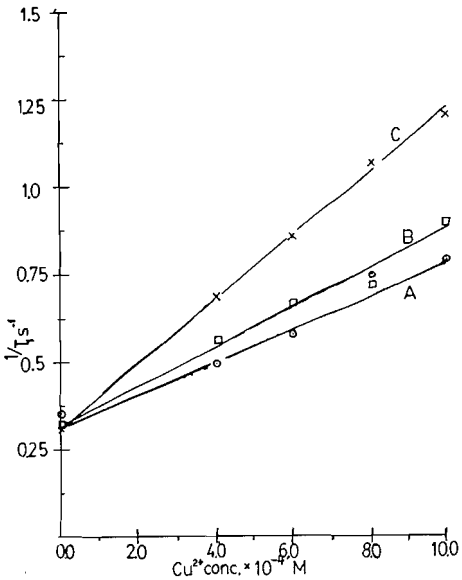

FIG. 4. Longitudinal relaxation rate dependence on the Cu^{2+} ion concentration at room temperature. Concentration of FA = 1 mg/ml of bipy = 1×10^{-3} M. A = Cu^{2+}–bipy. B = Cu^{2+}–aquo. C = Cu^{2+}–FA.

complex forms between the fully hydrated $Mn(OH_2)_6^{2+}$ and FA which can rotate nearly as freely as in water, probably because coordinated water protons H-bond to FA ligand sites more or less as they do to solvent water. (In ref. 12, thermodynamic analyses of Mn^{2+} binding suggested dominance by simple electrostatic interaction.) On the other hand, the $Mn(OH_2)_6^{2+}$ ion does not see a fully symmetric environment and this alters τ_S, and consequently T_2, moderately. (An alternate and structurally similar possibility is H-bonding to FA slowing proton exchanges, but this should initially cause broadening.) This gives us a picture of an ion, fully hydrated, tumbling around on electrostatic binding sites of the ligand. The picture suggests a "caged" ion which is consistent with the Schnitzer–Gamble (1) picture of FA as a three dimensional entity with H-bonding crucial to overall structure.

Copper Experiments

It has been suggested that Cu^{2+} forms an inner sphere bidentate chelate complex with adjacent —COOH and phenolic functional groups of FA (1). The temperature dependence data in Fig. 2 indicate that addition of FA to a Cu^{2+} solution does change the mechanism of proton relaxation significantly. Cu^{2+} concentration dependence of $1/T_1$ is shown in

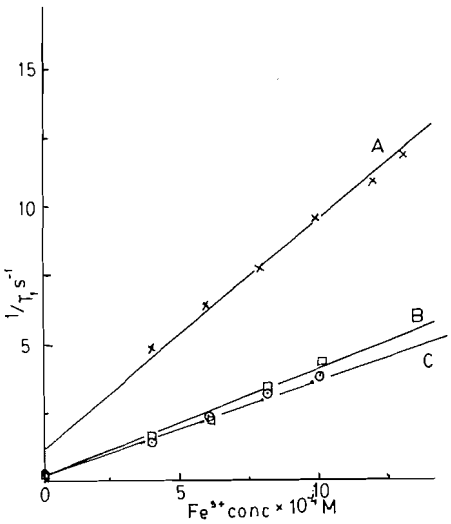

FIG. 5. Longitudinal relaxation rate dependence on the Fe^{3+} ion concentration at room temperature. Concentration of FA = 1 mg/ml, concentration of SSA = concentration of Fe^{3+}. *A* = Fe^{3+}–aquo. *B* = Fe^{3+}–FA. *C* = Fe^{3+}–SSA.

Fig. 4. Data for the complexation of Cu^{2+} by bipy is included for comparison.

Bipy, which is a small molecule, causes a slight decrease in the relaxation rate, $1/T_1$. This is consistent with a reduction in q under circumstances where τ_R is the important relaxation time as it is in the aquo complex in water (7, 8). FA, in contrast, enhances relaxation. This is consistent with τ_R remaining important for an inner sphere complex of Cu^{2+} where rotation requires tumbling of the entire large FA entity. Relaxation enhancement here is very similar to that seen in studies of Mn^{2+} binding to proteins (2) and arises similarly. The contrast to Mn^{2+}–FA behaviour clearly supports assignment of an inner sphere structure to the Cu^{2+} complex and an outer sphere structure to the Mn^{2+} complex. We see clear evidence of real effects in both cases but one is opposite to the other. The implication clearly follows from earlier theory (2).

Iron Experiments

Combination of Fe^{3+} with either FA or the related model SSA causes similar and large reduction of both relaxation rates, $1/T_1$ and $1/T_2$. The T_1 data are shown in Fig. 5. A 'titration' experiment with SSA showed that the largest part of the effect could be produced with one equivalent of SSA per Fe^{3+} and that a second and third SSA had a small effect. Since the 1:1 stoichemistry *requires at least four of the six water molecules coordinated to* Fe^{3+} *to remain. The effect is not on q.* It is only plausible to attribute the effect to a change in τ_S consequent on reduction of the symmetry of the high spin d^5 centre. The case parallels the aquo ion, Fe^{3+} where τ_S (9, 10) was considered dominant. Our earlier paper noted a frequency dependence in T_2 for iron complexes (12). Since the effect is large here, it implies inner sphere complexation.

Concluding Remark

The most useful result of this study may prove to be the recognition of $Mn(OH_2)_6^{2+}$ outer sphere complexes of FA. If such interactions are general in acid solution, the ion may prove to be a useful probe for FA conformational changes.

Acknowledgements

We thank Dr. G. W. Buchanan for his help with T_1 measurements. Dr. D. S. Gamble has contributed continuing valuable commentary.

1. D. S. GAMBLE and M. SCHNITZER. *In* Trace metals and metal organic interactions in natural waters. *Edited by* P. C. Singer. Ann Arbor Sciences, Ann Arbor. 1973. pp. 265–302.
2. A. S. MILDVAN and M. COHN. Biochemistry, **2**, 910 (1963); Adv. Enzymol. **33**, 1 (1970).
3. T. J. SWIFT and R. E. CONNICK. J. Chem. Phys. **37**, 307 (1962).
4. I. SOLOMON. Phys. Rev. **99**, 559 (1955).
5. N. BLOEMBERGEN. J. Chem. Phys. **27**, 572 (1957).
6. G. NAVON. Chem. Phys. Lett. **7**, 390 (1970).
7. N. BLOEMBERGEN and L. O. MORGAN. J. Chem. Phys. **34**, 842 (1961).
8. L. O. MORGAN and A. W. NOLLE. J. Chem. Phys. **31**, 365 (1959).
9. R. HAUSSER and G. LAUKIN. Z. Phys. **153**, 394 (1959).
10. A. W. WISHINIA. J. Chem. Phys. **32**, 891 (1960).
11. L. ERDEY. Bevezetes Kemiai Analizisbe, Tankönyvkiado, Budapest. 1962. pp. 125, 144, 146.
12. D. S. GAMBLE, C. H. LANGFORD, and J. P. K. TONG. Can. J. Chem. **54**, 1239 (1976).
13. L. G. SILLEN (*Editor*). Stability constants of metal ion complexes. Special Publication #17, The Chemical Society, London. 1964.

Can. J. Chem. Downloaded from www.nrcresearchpress.com by 210.87.254.6 on 09/05/12
For personal use only.

Synthèse et propriétés chimiques du phényl-5-octahydro-1,2,3,4,6,7,8,9-dibenzophosphole

FRANÇOIS MATHEY ET DANIEL THAVARD

Equipe IRCHA-CNRS, 2 à 8 rue Henry Dunant, 94320 Thiais, France

Reçu 2 novembre 1977

FRANÇOIS MATHEY et DANIEL THAVARD. Can. J. Chem. **56**, 1952 (1978).

Le phényl-5-octahydro-1,2,3,4,6,7,8,9-dibenzophosphole (L) a été synthétisé en faisant réagir le DBU sur le composé d'addition $PhPBr_2$-bicyclohexenyl-1,1′. Les propriétés chimiques ont été comparées avec celles des phospholes plus classiques. Son oxyde et son sulfure sont monomères. Une double réaction d'expansion de cycle est observée avec le chlorure de benzoyle comme dans le cas des phospholes simples. Au contraire les rendements de la coupure de la liaison P—Ph par K dans le THF sont faibles et l'échange P—Ph → P—*t*Bu par réaction avec *t*BuLi, ne donne aucun résultat. Le phosphacymantrène correspondant est obtenu par réaction avec $Mn_2(CO)_{10}$. Les complexes $\sigma LFe(CO)_4$, $\sigma,\eta LFe_2(CO)_7$ et $\eta LOFe(CO)_3$ ont été préparés par réaction de L ou LO avec $Fe_3(CO)_{12}$.

FRANÇOIS MATHEY and DANIEL THAVARD. Can. J. Chem. **56**, 1952 (1978).

5-Phenyl-1,2,3,4,6,7,8,9-octahydrodibenzophosphole (L) has been synthesized by reacting DBU with the $PhPBr_2$-1,1′-bicyclohexenyl cycloadduct. Its chemical properties have been compared with those of more classical phospholes. Its P-oxide and P-sulfide are monomeric. A double ring-expansion reaction is observed with benzoyl chloride as with simple phospholes. On the contrary we met a limited success with the P—Ph bond cleavage by K in THF and we did not succeed at all when attempting a P—Ph → P—*t*Bu exchange by reaction with *t*BuLi. The corresponding phosphacymantrene has been obtained with $Mn_2(CO)_{10}$. $\sigma LFe(CO)_4$, $\sigma,\eta LFe_2(CO)_7$, and $\eta LOFe(CO)_3$ complexes have been obtained from the reactions of L or its P-oxide with $Fe_3(CO)_{12}$.

Les dibenzophospholes **1** sont probablement les phosphines cycliques les plus utilisées comme coordinats des métaux de transition (voir réf. 1). Leur géométrie rigide et leur demande stérique relativement faible, entraînent la stabilisation de degrés de coordination peu courants (par exemple la coordinance 5 du nickel). D'autre part, de puissants catalyseurs d'hydrogénation, à base de rhodium et de phényl-5-dibenzophosphole, ont été décrits (2). Ces phosphines présentent donc un intérêt tout particulier pour la chimie des métaux de transition. Or, par

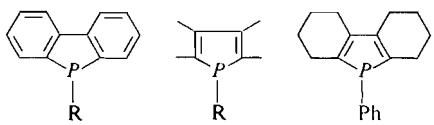

1 **2** **3**

rapport aux phospholes simples du type **2**, les dibenzophospholes se caractérisent essentiellement par deux faits: (*a*) l'intéraction doublet libre du phosphore – système diénique a pratiquement disparu dans **1** (voir les données comparées sur **1** et **2** concernant l'oxydation (3), la déquaternarisation (4) et l'inversion du P (5)). (*b*) Il n'y a pas dans **1** de système diénique "libre" disponible pour fournir des complexes η avec les métaux de transition au contraire de **2** (voir réf. 1).

Pour rétablir l'intéraction doublet libre – système diénique dans **1** et pour "libérer" le motif diénique, tout en conservant une géométrie à peu près équivalente, nous nous sommes donc intéressés au phényl-5-octahydro-1,2,3,4,6,7,8,9-dibenzophosphole **3**. Le phosphole **3** doit a priori fournir des P-complexes plus labiles que ceux de **1** (rétablissement de la délocalisation partielle du doublet libre) et que ceux de **2** (cône d'encombrement plus ouvert selon Tolman (6)) ce qui doit présenter un intérêt particulier pour les catalyseurs d'hydrogénation du type Wilkinson. Par contre, il doit fournir des complexes diéniques plus stables que ceux dérivés de **2** (la tétrasubstitution enrichit en électrons le système diénique). Nous verrons ci-après, que ces conclusions semblent partiellement vérifiées par l'expérience. Nous décrivons ci-contre la synthèse de **3**, l'étude de sa chimie "classique" et quelques-uns de ses complexes avec le fer et le manganèse.

Le composé d'addition de la phényldibromophosphine et du bicyclohexényl-1,1′ a été préparé en s'inspirant du travail de Campbell et coll. (7). Ce produit a été ensuite déshydrohalogéné directement par le DBU suivant la méthode générale que nous avons décrite pour la préparation des phospholes (8).

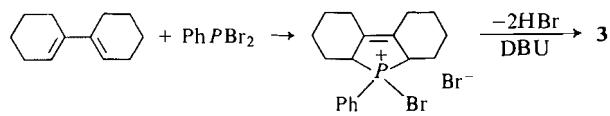

DBU = diaza-1,5-bicyclo[5,4,0]undécène-5

Can. J. Chem. Downloaded from www.nrcresearchpress.com by 210.87.254.40 on 09/05/12
For personal use only.

Can. J. Chem. Downloaded from www.nrcresearchpress.com by 210.87.254.40 on 09/05/12
For personal use only.

Le rendement global de cette séquence peut atteindre 38%. Le phosphole **3** se présente sous la forme d'un liquide visqueux ayant une certaine tendance à la cristallisation à température ambiante. Sa faible volatilité (Eb ~165–170°C/0.1 mm Hg) et probablement aussi l'encombrement du phosphore lui confèrent une assez bonne résistance à l'oxydation par l'air. Son spectre de rmn du proton ($CDCl_3$, TMS interne) se compose d'un pseudo-doublet asymétrique assez fin à 7.26 et 7.19 ppm (Ph) et de deux massifs élargis d'importance égale à 2.28 et 1.67 ppm (CH_2). Le phosphore (δ positif à champ fort, P_4O_6 externe) présente le déblindage caractéristique des phospholes: $\delta^{31}P$ (**3**) = 104.9 ppm. La valeur trouvée est pratiquement identique à celle du phényl-1-phosphole (9). A noter que l'on ne retrouve pas ici le blindage relatif dû à la substitution dialkyl-3,4 dans la famille des phospholes. Le spectre de rmn ^{13}C est évidemment complexe mais il est facile de détecter les trois types de carbones secs. L'interprétation que nous proposons est la suivante: P—*C*(Ph) δ = 133.9 ppm $^1J_{(P-C)}$ = 13.3 Hz; P—*C*(cycle) δ = 138.5 ppm $^1J_{(P-C)} \leq 1$ Hz; P—C—*C*(cycle) δ = 144 ppm $^2J_{(P-C)}$ = 8.9 Hz. Ces valeurs sont compatibles avec les données de la littérature (10, 11). Le couplage $^1J_{(P-C)}$ dans le cycle est cependant exceptionnellement faible, la valeur la plus basse observée précédemment étant celle du phényl-1-diméthyl-3,4-phosphole: $^1J_{(P-C)}$ = 2.8 Hz.

L'oxyde **4**, dérivé de **3**, est préparé classiquement par oxydation de **3** par H_2O_2 dans l'acétone à −30°C; ir: ν(P=O) = 1195 cm^{-1} (KBr). Il est monomère comme l'atteste la rmn du phosphore: $\delta^{31}P$ (**4**) = 66.8 ppm. Il est intéressant de remarquer que c'est le premier oxyde de phosphole monomère ne comportant pas de substituants aryles sur les carbones du noyau. L'absence de dimérisation selon Diels–Alder est probablement due à l'encombrement du système diénique. Le sulfure **5** est également monomère: $\delta^{31}P$ (**5**) = 61.6 ppm.

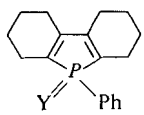

Y = O **4**
Y = S **5**

Nous avons ensuite étudié la coupure de la liaison P—Ph par deux équivalents de potassium dans le THF au reflux, selon la méthode de Braye (12). En méthylant le produit de la réaction par ICH_3, nous avons obtenu le sel de phospholium **6** avec un rendement très modeste toutefois (~15%). Ce sel a été parfaitement caractérisé par une analyse élémentaire complète et par rmn en solution dans $CDCl_3$: ^1H: absence de phényle, doublet $CH_3\overset{+}{P}$ à 2.35 ppm, $^2J_{(H-P)}$ = 14 Hz. ^{13}C: $CH_3\overset{+}{P}$ à 6.6 ppm, $^1J_{(P-C)}$ = 48.4 Hz; Cα à 122.9 ppm, $^1J_{(P-C)}$ = 79.2 Hz; Cβ à 157.1 ppm, $^2J_{(P-C)}$ = 22 Hz. ^{31}P: $\delta^{31}P$ (**6**) = 78.5 ppm.

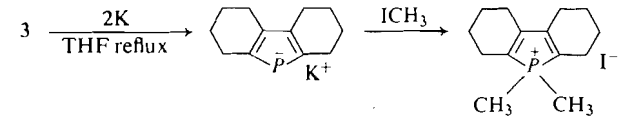

6

Comme le suggère Braye (12), il semble bien que les substituants aryles sur les carbones du noyau jouent un rôle non négligeable dans la stabilisation des anions phospholyles, d'où les rendements élevés des réactions qu'il décrit.

D'autre part, l'échange P—Ph → P—Bu^t par réaction de **3** avec le tertiobutyl-lithium dans l'hexane à température ambiante par analogie avec la réaction du phényl-1-diméthyl-3,4-phosphole (13) a échoué; on obtient un mélange complexe de produits difficilement séparables. L'encombrement stérique du phosphore joue peut être un rôle important dans l'échec de cette réaction.

Au contraire la réaction d'extension de cycle des phospholes par le chlorure de benzoyle (14) est transposable avec **3** mais le rendement reste modeste:

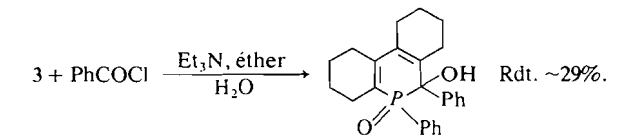

7

Le composé **7** a été caractérisé sans ambiguïté par ir (ν en cm^{-1}, KBr): OH 3160, C=C 1623, 1600, 1580, P=O 1150 et rmn ^1H (DMSO) δ OH 5.73 ppm $J_{(H-P)}$ 14 Hz (voir réf. 14) et ^{13}C ($CDCl_3$, TMS) δ (P—*C*—OH) 45.4 ppm $^1J_{(P-C)}$ 69.9 Hz; δ (P—*C*=C) 76.9 ppm $^1J_{(P-C)}$ 83 Hz.

Il est intéressant de noter que, tout récemment, la même réaction a été appliquée avec succès aux dibenzophospholes (15, 16). A la différence des dibenzophospholes toutefois (16) et de la même façon que les phospholes simples (14) il est également possible de convertir l'hydroxydihydrophosphorine **7** en oxa-1-phospha-2-cycloheptadiène-4,6 **8**.

La disparition du OH dans le composé **8** est visible sur le spectre ir (KBr) qui est comparable à celui des

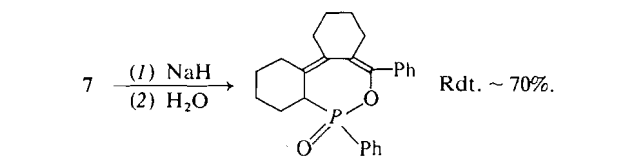

8

Can. J. Chem. Downloaded from www.nrcresearchpress.com by 210.87.254.40 on 09/05/12
For personal use only.

cycles à 7 chaînons analogues (voir réf. 14): C=C 1630, 1599, 1590, P=O 1240, 1230, P—O—C 1048. La rmn ^{13}C ($CDCl_3$) confirme la présence d'un groupe P—CH dans le cycle: δ (P—*C*H) 38.9 ppm $^1J_{(P-C)}$ 84.4 Hz $^1J_{(C-H)}$ 124.4 Hz et la rmn du phosphore ($CDCl_3$, P_4O_6 externe) est compatible avec une structure de phosphinate: $\delta^{31}P$(**8**) = 49.7 ppm.

Nous avons ensuite complété cette étude chimique "classique" de **3** par une étude de quelques-uns de ses complexes.

A 150°C dans le xylène avec une quantité équimoléculaire de $Mn_2(CO)_{10}$, **3** fournit le phosphacymantrène correspondant **9** après coupure de la liaison P—Ph de la même façon que les P-phénylphospholes plus simples (17). Le rendement reste toutefois très modeste et la réaction est peu reproductible.

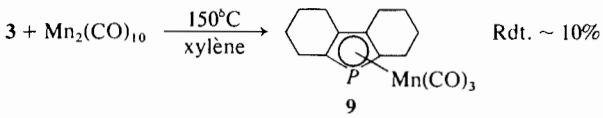

9

Le spectre ir de **9** (décaline) est particulièrement intéressant: ν(CO) = 2018, 1943 et 1930 cm^{-1}. Ces données sont à comparer avec celles du phosphacymantrène lui-même: ν(CO) = 2032, 1958 et 1954 cm^{-1} et celles de son dérivé diméthylé en 3,4: ν (CO) = 2025, 1953 et 1941 cm^{-1}. Elles mettent bien en évidence le caractère η-donneur très accentué du noyau phospholyle de **9**. Le phosphore de **9** est très blindé comme dans tous les produits de cette série (travaux sous presse): $\delta^{31}P$(**9**) = 165.1 ppm (P_4O_6 externe).

Enfin le spectre de masse (70 eV) comprend le moléculaire de *m/e* 330 (*I* = 16%), le pic M-2CO de *m/e* 274 (*I* = 16%) et le pic de base M-3CO de *m/e* 246 ce qui confirme définitivement la formule proposée.

La réaction de **3** avec $Fe_3(CO)_{12}$ nous a fourni, d'autre part, 3 complexes que nous décrivons par ordre de Rf décroissants (gel de silice).

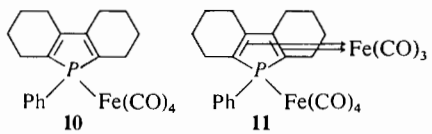

10

11

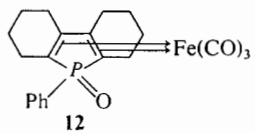

12

Le premier de ces complexes est le classique complexe σLFe$(CO)_4$ **10**. L'analyse ne permet pas de le distinguer du complexe ηLFe$(CO)_3$ (complexation du diène) mais la formule **10** est établie sans ambiguïté par ir: ν(CO) (décaline) = 2053, 1977, 1945 et 1938 cm^{-1}. Ces données sont à comparer avec celles du complexe LFe$(CO)_4$ où L = phényl-1-diméthyl-3,4-phosphole: ν(CO) = 2051, 1979, 1948 et 1939 cm^{-1} (18). Il semble donc que le phosphore de **3** ait un pouvoir donneur–accepteur très voisin de celui du phényl-1-diméthyl-3,4-phosphole ce qui est, somme toute, assez logique. Le complexe LFe$(CO)_4$ dérivé de **1** étant inconnu, nous ne pouvons toutefois pas contrôler nos hypothèses de départ sur ce point. Le spectre de masse de **10** comprend le moléculaire de *m/e* 436 (*I* = 6%), le pic M-2CO de *m/e* 380 (*I* = 16%), le pic M-3CO de *m/e* 352 (*I* = 35%), le pic M-4CO de *m/e* 324 (*I* = 100%) et le pic M-4CO-Fe de *m/e* 268 (*I* = 100%) ce qui parachève l'identification de **10**. Le phosphore apparaît à 37.8 ppm (P_4O_6) ce qui confirme la complexation de P (même déblindage que dans le cas du phényl-1-diméthyl-3,4-phosphole (18)).

Le deuxième complexe est le complexe σ,ηLFe_2-$(CO)_7$ **11** analogue à celui obtenu avec le phényl-1-diméthyl-3,4-phosphole (18). Sa formule est essentiellement établie sur la base du spectre de masse: moléculaire de *m/e* 576 (*I* = 0.6%); présence de tous les pics M-CO, M-2CO, ..., M-7CO, ce dernier assez intense (*I* = 69%); pic de base à *m/e* 268 (M-7CO-2Fe). L'analyse élémentaire C,H,Fe est en bon accord avec la formule proposée et le déplacement chimique du P est compatible avec les données existantes (18): $\delta^{31}P$ (**11**) = 0 ppm (P_4O_6). Le spectre ir est évidemment assez compliqué dans la région des CO: bandes à 2061, 2046, 2023, 2020, 1997, 1988, 1978, 1949 et 1937 cm^{-1} dans la décaline.

Le dernier complexe est le complexe η dérivé de l'oxyde **12**. Il a été authentifié par comparaison avec un complexe préparé directement à partir de **4**. Son spectre ir est caractéristique des systèmes diène–Fe$(CO)_3$: ν(CO) = 2063, 2000 et 1973 cm^{-1} (décaline) et le phosphore est peu affecté par la complexation: $\delta^{31}P$ (**12**) = 59.1 ppm (P_4O_6); ir: ν(P=O) = 1205 cm^{-1} (KBr).

Partie expérimentale

Toutes les chromatographies ont été effectuées sur colonnes de gel de silice 70–230 mesh Merck. Le travail expérimental a été réalisé avec la collaboration de M. M. Longeau. Les auteurs remercient Mme R. Mankowski-Favelier pour les spectres rmn ^{31}P et ^{13}C (Jeol PS 100 F.T.).

I. Synthèse du phényl-5-octahydro-1,2,3,4,6,7,8,9-dibenzophosphole **3**

On laisse réagir à l'abri de la lumière, sous argon et à température ambiante, pendant dix jours, un mélange de bicyclohexenyl-1,1′: 17.8 g (0.1 mol + 10%) et de phényldibromophosphine: 26.8 g (0.1 mol).

L'adduit formé est alors recouvert par 200 cm^3 de benzène sec, refroidi par un bain de glace et traité par une solution de 30.5 g de DBU dans 200 cm^3 de chlorure de méthylène sec. Lorsque tout l'adduit a réagi, on hydrolyse par HCl 0.5 *N*. La

Can. J. Chem. Downloaded from www.nrcresearchpress.com by 210.87.254.40 on 09/05/12
For personal use only.

couche organique est décantée, lavée par une solution de CO_3K_2 et séchée. Les solvants sont évaporés et le phosphole distillé sous pression réduite. Eb 165–170°C/0.1 mm Hg. Rendement maximum obtenu: 38%. *Anal.* calc. pour $C_{18}H_{21}P$: C 80.56, H 7.88; trouvé: C 80.34, H 7.84.

II. Oxyde **4**

A une solution de 5.7 g (0.02 mol) de **3** dans 50 cm³ d'acétone à −30°C, on ajoute 2 cm³ (0.02 mol) de H_2O_2 à 112 vol. On ajoute une pincée de trioxyméthylène et laisse revenir à température ambiante. L'excès de trioxyméthylène est filtré, l'acétone est évaporée. L'oxyde est chromatographié (éluant: AcOEt), puis recristallisé dans l'éther. pf: 141°C; rdt: 44%. *Anal.* calc. pour $C_{18}H_{21}OP$: C 76.03, H 7.44; trouvé: C 75.26, H 7.54.

III. Sulfure **5**

Préparé par action du soufre en excès dans le benzène à l'ébullition pendant 3 h. Le soufre en excès est ensuite filtré. Le benzène est évaporé et le sulfure est recristallisé dans l'hexane. rdt: 70%; pf: 89°C. *Anal.* calc. pour $C_{18}H_{21}PS$: C 71.97, H 7.05; trouvé: C 71.83, H 7.16.

IV. Iodure de diméthyl phospholium **6**

On chauffe à reflux pendant 4 h sous argon: 5.4 g de **3** (0.02 mol), 1.70 g de K (0.04 at.) dans 100 cm³ de THF anhydre. On ajoute alors 5.6 g de ICH_3 (0.04 mol). Au bout de 2 h, on hydrolyse par 10 cm³ d'eau dans 20 cm³ de THF. On évapore à sec; le résidu est repris par un mélange eau–chloroforme. La couche chloroformique est séchée, concentrée. Le produit ainsi obtenu est repris au benzène, l'insoluble est filtré et séché; c'est le sel **6**. rdt: 1 g (15%); pf: 243°C. *Anal.* calc. pour $C_{14}H_{22}IP$: C 48.29, H 6.36, I 36.44, P 8.89; trouvé: C 48.36, H 6.46, I 36.21, P 8.76.

V. Essai d'échange P—Ph → P—tBu dans **3**

A 3.6 g (0.0135 mol) de **3** dans 60 cm³ d'hexane sec, sous argon et à température ambiante, on ajoute 22.5 cm³ de *t*BuLi 0.6 *M*. On laisse agiter pendant 6 h, puis on hydrolyse par 25 cm³ d'eau et neutralise par HCl 2 *N*. La couche organique est séparée, la couche aqueuse est extraite à l'hexane. Les fractions d'hexane réunies sont séchées sur SO_4Na_2 puis distillées. On obtient une fraction $Eb_{0.1}$ = 125–140°C qui est un mélange de **3** et d'autres produits que nous n'avons pu séparer.

VI. Hydroxy-2-dihydro-1,2-phosphorine **7**

Un mélange de 8.1 g de phosphole (0.03 mol) et 30 cm³ de Et_3N dans 170 cm³ d'éther anhydre, on ajoute 9 cm³ (0.06 mol) de chlorure de benzoyle. On chauffe à reflux pendant 4 h, puis on hydrolyse par 100 cm³ d'eau. La couche organique est évaporée à sec. Le résidu est purifié par chromatographie (éluant AcOEt puis AcOEt/MeOH – 90/10). Poids: 3.4 g; rdt: 29%; pf: 181°C. *Anal.* calc. pour $C_{25}H_{27}O_2P$: C 76.90, H 6.97; trouvé: C 76.88, H 6.93.

VII. Oxa-1-phospha-2-cycloheptadiene-4,6 **8**

On agite pendant 48 h à température ambiante, 2 g de **7** dans 50 cm³ de DMF auquels on a ajouté une pincée de NaH. On hydrolyse ensuite par 5 cm³ d'eau, neutralise par HCl 2 *N*, évapore sous vide mécanique et reprend le résidu par un mélange eau–chloroforme. On concentre la couche chloroformique et purifie le produit par chromatographie (éluant AcOEt). Poids: 1.4 g; rdt: 70%; pf: 158°C. *Anal.* calc. pour $C_{25}H_{27}O_2P$: C 76.90, H 6.97; trouvé: C 76.68, H 6.82.

VIII. Phosphacymantrène **9**

On chauffe à reflux pendant 4 h un mélange de 2.7 g (0.01 mol) de **3** et 4 g de $Mn_2(CO)_{10}$ dans 50 cm³ de xylène. On filtre, concentre le filtrat. Le résidu est repris à l'hexane, refiltré, concentré à nouveau et purifié par deux chromatographies successives (la première à l'hexane, la seconde au pentane). Poids: 0.5 g; pf: 61°C. *Anal.* calc. pour $C_{15}H_{16}MnO_3P$: C 54.56, H 4.88; trouvé: C 55.56, H 4.92.

IX. Complexes **10**, **11** *et* **12**

On chauffe à 80°C pendant 3 h 5.4 g (0.02 mol) de **3** et 11 g de $Fe_3(CO)_{12}$. On filtre l'insoluble, concentre le filtrat et chromatographie le résidu. En utilisant d'abord le benzène, on élue ensemble les complexes **10** et **11**; en continuant avec l'acétate d'éthyle on obtient ensuite le complexe **12**. pf: 182°C; rdt: ~15%. *Anal.* calc. pour $C_{21}H_{21}FeO_4P$: C 59.45, H 4.98, Fe 13.16; trouvé: C 60.24, H 5.0, Fe 12.92.

Les complexes **10** et **11** sont ensuite séparés par une nouvelle chromatographie: **10** est élué à l'aide d'un mélange pentane/hexane 50/50 et **11** à l'aide d'un mélange hexane/benzène 70/30. **10**: pf: 84°C; rdt: ~10%. *Anal.* calc. pour $C_{22}H_{21}FeO_4P$: C 60.57, H 4.85, Fe 12.8; trouvé: C 61.28, H 4.95, Fe 13.4. **11**: pf: 135°C (déc.); rdt: ~12%. *Anal.* calc. pour $C_{25}H_{21}Fe_2O_7P$: C 52.12, H 3.67, Fe 19.39; trouvé: C 52.12, H 3.69, Fe 19.68.

Le complexe **12** a été également préparé directement par action du $Fe_3(CO)_{12}$ sur l'oxyde **4** dans les mêmes conditions qu'à partir de **3**: 3 h à reflux dans le benzène et chromatographie (éluant AcOEt). rdt ~50%.

1. D. G. Holah, A. N. Hughes et K. Wright. Coord. Chem. Rev. **15**, 239 (1975).
2. D. G. Holah, A. N. Hughes et B. C. Hui. Can. J. Chem. **50**, 3714 (1972); D. E. Budd, D. G. Holah, A. N. Hughes et B. C. Hui. Can. J. Chem. **52**, 775 (1974); D. G. Holah, I. M. Hoodless, A. N. Hughes, B. C. Hui et D. Martin. Can. J. Chem. **52**, 3758 (1974).
3. A. F. Bedford, D. M. Heinekey, I. T. Millar et C. T. Mortimer. J. Chem. Soc. 2932 (1962).
4. W. B. Farnham et K. Mislow. Chem. Commun. 469 (1972).
5. W. Egan, R. Tang, G. Zon et K. Mislow. J. Am. Chem. Soc. **93**, 6205 (1971).
6. C. A. Tolman. J. Am. Chem. Soc. **92**, 2156 (1970).
7. I. G. M. Campbell, R. C. Cookson, M. B. Hocking et A. N. Hughes. J. Chem. Soc. 2184 (1965).
8. F. Mathey et R. Mankowski-Favelier. Bull. Soc. Chim. Fr. 4433 (1971).
9. F. Mathey et R. Mankowski-Favelier. Org. Magn. Reson. **4**, 171 (1972).
10. T. Bundgaard et H. J. Jakobsen. Tetrahedron Lett. 3353 (1972).
11. L. D. Quin, S. G. Borleske et R. C. Stocks. Org. Magn. Reson. **5**, 161 (1973).
12. E. H. Braye, I. Caplier et R. Saussez. Tetrahedron, **27**, 5523 (1971).
13. F. Mathey. Tetrahedron, **28**, 4171 (1972).
14. F. Mathey. Tetrahedron, **29**, 707 (1973); F. Mathey, D. Thavard et B. Bartet. Can. J. Chem. **53**, 855 (1975).
15. D. W. Allen et A. C. Oades. J. Chem. Soc. Perkin I, 2050 (1976).
16. A. N. Hughes, K. Amornraksa, S. Phisithkul et V. Reutrakul. J. Heterocycl. Chem. **13**, 937 (1976).
17. F. Mathey. Tetrahedron Lett. 4155 (1976).
18. F. Mathey et G. Muller. J. Organometal. Chem. **136**, 241 (1977).

Molecular activation analysis for methylmercury

J.-P. SCHMIT[1] AND D. R. WILES

Chemistry Department, Carleton University, Ottawa, Ont., Canada K1S 5B6

Received January 20, 1978

J.-P. SCHMIT and D. R. WILES. Can. J. Chem. **56**, 1956 (1978).

The principle of molecular activation analysis is described, as well as its unsuccessful application to the species specific determination of methylmercury in fish. The reasons for the failure of the method were determined and are found to be of significance to hot atom chemistry and to possible future use of this principle. The reasons are: (*i*) a matrix dilution of the species sought, (*ii*) a scavenging, probably of methyl groups, by serine or related components of fish powder, and (*iii*) a methylation by some unidentified component associated with the fish fats.

J.-P. SCHMIT et D. R. WILES. Can. J. Chem. **56**, 1956 (1978).

On décrit le principe de l'analyse moléculaire par activation neutronique appliquée au dosage spécifique du méthylmercure dans les poissons. Bien que cette nouvelle méthode n'ait pas réussi dans cette application, les raisons de son insuccès ont été trouvées très significatives dans l'étude de la chemie des atomes chauds et dans son application éventuelle à d'autres problèmes. Ces raisons sont les suivantes: (*i*) la dilution par la matrice de l'espèce étudiée, (*ii*) la reaction de groupes libres methyle avec la serine ou d'autres composés similaires présents dans la chair des poissons, (*iii*) la méthylation du mercure par un composé inconnu associé avec les tissus adipeux des poissons.

Introduction

Recent publications from this laboratory (1–3) have described the principle of "molecular activation analysis", a form of neutron activation analysis in which the specific chemical form of an element can be determined as well as its total quantity. Stemming from developments in the field of hot atom chemistry (4) this method recognizes that a fraction, R, of the molecules will retain their original molecular identity following neutron activation. If the value of R is reliably known, then chemical isolation of the desired compound, with known chemical recovery, q, makes possible the measurement of its radioactivity, so that the usual equation for activation analysis becomes:

$$W_x = \frac{A_x}{qR}\frac{W_r}{A_r}\cdot \phi(t, T)$$

where W and A are respectively the weight and radioactivity of the element present in the compound and a reference sample (denoted by x and r) respectively. The function $\phi(t,T)$ accounts for possible differences in irradiation time t, and decay time T, and can usually be made sensibly equal to 1.00.

In applying this method to the determination of methylmercury in fish, blood, and other materials we first determined the retention, R, of methylmercury in pure crystalline CH_3HgCl:

$$CH_3HgCl(n,\gamma)\ {}^{197}Hg \begin{cases} \nearrow CH_3{}^{197}HgCl \\ \searrow \text{other forms} \end{cases}$$

Results from this experiment were quite satisfactory, as is shown in Table 1. Corresponding determination (2, 3) of the retention in CH_3Hg-doped fish protein concentrate (FPC) led unfortunately to values which were both very low and dependent on the origin of the protein. Values of R ranged from 3% for cod and haddock through 6–8% for tuna and swordfish to 11.8% for seal, as is seen in Table 2. While we were able to develop (3) an alternative method of neutron activation analysis specific for CH_3Hg—, the variability of R clearly means that the intended method is unreliable without a great deal of further work.

In seeking an explanation for the inconsistency of the retention, R, in protein and the wide disparity between these values and that for pure CH_3HgCl, we find several possibilities, any or all of which could be contributing:

(*1*) A matrix effect in the protein concentrate itself. This could result from the wide physical separation of the methylmercury groups from one another, which would make momentum transfer from the activated atom less effective and would cause a reduction of the retention (e.g. from 82% to 12% or to 3%).

TABLE 1. Yields of radioactive mercury from neutron irradiation of crystalline CH_3HgCl

Product isolated	^{197}Hg yield (%)
$(CH_3)_2Hg$	0.1 (ref. 3)
CH_3HgCl	82.0 (ref. 3)
Hg^{2+}	18 (by difference)

[1]Present address: Département de Chimie, Université de Sherbrooke, Sherbrooke (Qué.), Canada J1K 2R1.

Can. J. Chem. Downloaded from www.nrcresearchpress.com by 210.87.254.5 on 09/05/12
For personal use only.

Can. J. Chem. Downloaded from www.nrcresearchpress.com by 210.87.254.5 on 09/05/12
For personal use only.

TABLE 2. Retention of ^{197}Hg as CH_3Hg in fish tissue, each value given is the average of several determinations

Sample	Retention	Reference
Cod, haddock	3.4±0.3	3
Swordfish, tuna	6.6±0.9	3
Seal	11.8	3
Soya flour doped with CH_3HgCl	10.2	This work
Soya flour doped with $HgCl_2$	2.7	This work

(*2*) A 'foreign' compound in the protein causing a further *decrease* in retention (e.g., from 12% to 3%). This could be, for example, a mercury atom scavenger or a methyl radical scavenger.

(*3*) A 'foreign' compound in the protein causing an *increase* in retention (e.g. from 3% to 12%). To judge from the data in Table 2, this would plausibly be related to the fat content. For example, the effectiveness of a typical methylating agent in this case was demonstrated (2) by the substantial increase in retention (from 7% to 22%) on irradiation of a sample of CH_3Hg-doped swordfish protein moistened with 2,2,4-trimethylpentane.

It was with a view to elucidating the cause of this apparent inconsistency in the effect that we undertook the present study, in the hope that even if this method might not be applicable to fish, it might be more reliable when applied to other substrates.

Experimental

Materials and Reagents

Fish samples were obtained from the retail trade as fresh cod filets. Methylmercury chloride was obtained from Strem Chemicals, Inc., and was purified by recrystallization from chloroform. It was kept dry and stored under refrigeration. All other reagents used were Reagent Grade. Solvents were kept air-free and dry by the use of molecular sieves. Soya flour (SF) was obtained as commercial product and washed twice with 25% isopropyl alcohol (IPA) in water, twice with pure IPA, twice with acetone, and once with petroleum ether before being dried and stored at room temperature.

Preparation of Doped Soya Flour

To study the radiochemical retention of methylmercury in the SF 'matrix' we prepared a doped SF by treating purified SF with a solution of methylmercury chloride in chloroform, as was described earlier (2). That the methylmercury is chemically bound to the matrix is shown (5) by the fact that it is completely removed from a chloroform solution on passage of the solution through a 3–5 cm column of soya flour, and is not removed from the column by washing with further chloroform. The nature of this bonding is not known, and we can only surmise that binding is similar to that in other protein-containing substances (6, 7).

Preparation of Fat and the Water Soluble Extract

Fat and other components were extracted from fresh cod filets according to published procedures (8) by means of IPA. After IPA was removed water was added to the residue and the fat extracted with diethyl ether.

(a) Preparation of the fat. After being dried over $CaCl_2$, the crude fat was obtained by removing the ether. A part of the crude product obtained was dissolved in petroleum ether (PE) washed three times with 0.1 *N* HCl to remove the amines and finally with water. The organic layer was then dried and the petroleum ether removed. The crude and the purified fats were kept under refrigeration. The fat was applied to the doped SF as a solution in petroleum ether which was subsequently evaporated.

(b) Preparation of the water soluble extract (WS). The aqueous fraction obtained during the crude fat preparation was separated into two fractions by precipitation with methanol. The precipitate was discarded. The methanol-soluble fraction was evaporated to dryness and the residue (WS) dissolved in 25 ml of a 25% mixture of isopropyl alcohol in water.

Separation Methods

Separation of methylmercury from the SF was done using a modification of the method of Uthe, Solomon, and Grift (9). A few milligrams of nonradioactive methylmercury chloride was added to the aqueous medium to act as a carrier for the radioactive molecules. This method entails the following steps: (*i*) add the neutron-irradiated doped SF to a mixture of 15 ml aqueous solution of 0.1 *M* $CuSO_4$ plus 10 ml of 3 *M* NaBr – 2 *M* H_2SO_4 solution, add about 5 mg CH_3HgCl carrier in 15 ml toluene, shake vigorously for 45 min, let the layers separate, (*ii*) carefully remove the toluene and backwash 3 times by shaking with distilled water, (*iii*) count an aliquot of the toluene solution in a NaI scintillation counter under reproducible geometry.

Radioactivation and Measurements

Neutron irradiations were done using the SLOWPOKE reactor of the Atomic Energy of Canada Ltd., Ottawa, which gave a flux of thermal neutrons of 1.0×10^{12} cm^{-2} s^{-1} and a γ-ray intensity of about 1×10^6 rad h^{-1}. Irradiations were normally of 10 min duration. The reactor temperature at the point of irradiation was about 30–40°C.

Radioactivity measurements were made using a 3 × 3 in. Na(Tl)I scintillation detector coupled to a 512-channel pulse height spectrometer. The 77 keV peak of ^{197}Hg stood out quite clearly above the background. Decay of ^{197}Hg in the samples was corrected for by extrapolating the activities of both the reference sample and the extracted methylmercury sample back to the same time. Counting rates were sufficiently high that statistical errors were small.

We have found that, although pure methylmercury chloride escaped quite readily from polyethylene vials during neutron irradiation (10), methylmercury bound to SF by the doping procedure outlined above did not (3).

Results and Discussion

Among the factors which may perturb the methylmercury retention, the most complex are possible fish protein 'matrix' effects. However, this source of uncertainty can be eliminated by using instead a matrix of soya flour (SF), a similar but more reproducible protein-containing substrate. In fact, on the one hand, soya flour gives retentions comparable to those obtained in protein concentrates and, on the other hand, it is easily obtained pure and does not contain much sodium (whose induced radioactivity interferes with γ-ray measurements). Thus, we have used that new substrate to undertake a systematic study of the factors which may modify the methylmercury retention.

Can. J. Chem. Downloaded from www.nrcresearchpress.com by 210.87.254.5 on 09/05/12
For personal use only.

(a) Influence of Fish Fat

Regarding the influence of fat as a factor expected to increase the methylmercury retention, two principal features deserve consideration. First, previously cited experiments with 2,2,4-trimethylpentane as a methylating agent gave positive results. Second, the retention seems strongly dependent on the normal fat content of the fishes under study, as is seen from the data in Table 2. According to Dambergs, cod protein is produced essentially free of fat, while in other fish, notably herring, the extraction is less effective (8).

In order to understand this anomaly, we prepared a sample of soya flour doped with 158 μg CH_3HgCl per g of SF. To a series of aliquots we added selected amounts of crude fish fat. These samples were then irradiated with neutrons and the retention was measured as described above. The results are shown in Fig. 1. Although, as was expected, the presence of fat increases the retention, it is noteworthy that extrapolation of the observed retention vs. percentage of fat does not lead to the normal 'zero-fat' value of 10.2% for the retention of SF doped only with pure methylmercury. On the other hand, a similar experiment done with fat washed with dilute HCl does lead by extrapolation to the expected value. Moreover, in this experiment the effect of the acid-washed 'pure' fat is strikingly higher than that of the crude product.

A second series of experiments was then undertaken, using SF doped with $HgCl_2$ (172 μg/g SF) instead of methylmercury. The results, shown in Fig. 2, indicate that here again methylmercury is found, in amounts which increase with increasing fat concentration. Since none was present initially, it is clear that in this case the methylmercury has been formed rather than retained. The CH_3 comes presumably from the protein. Moreover, it is noteworthy that with $HgCl_2$-doped SF, both curves, with crude as well as with HCl-washed fat, lead by extrapolation to the expected methylmercury retention of 2.8% for the pure $HgCl_2$-doped SF. As with the methylmercury study, the influence of the HCl-washed fat is stronger than that of the crude fat.

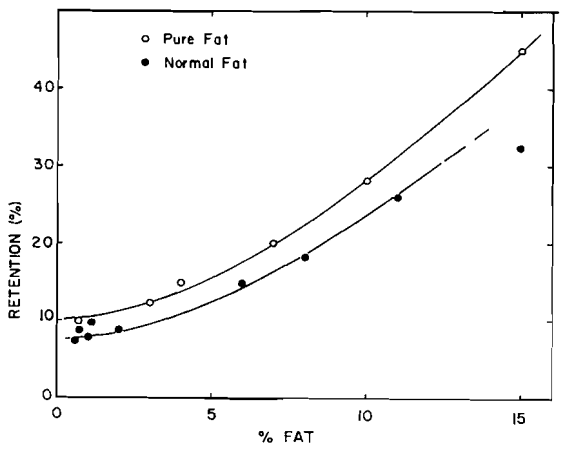

FIG. 1. Variation of retention with fat (CH_3HgCl).

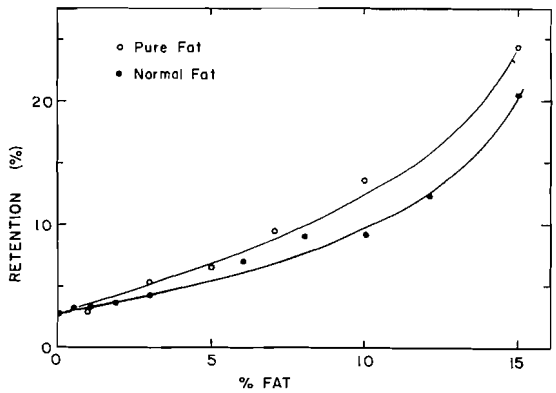

FIG. 2. Variation of retention with fat ($HgCl_2$).

From these observations several features should be noted. First, comparison of the two series of experiments strongly suggests that the phenomenon involves primarily the availability of a reactive methyl group. Indeed, both the 2,2,4-trimethylpentane (2) and the fat can be considered as methylating agents. Thus, these two compounds are able to increase the local concentration of methyl groups and, as a consequence, there is a higher probability for methyl-mercury recombination. Further, the same methylating effect can be observed in the second series of experiments ($HgCl_2$-doped SF) in the absence of initial methylmercury. In this latter case, the only sources of methyl groups are the soya protein, which can be considered constant, and the fat. Thus, it seems that the fundamental mechanism of the variation of retention is more a problem of availability of methyl groups for the recoiling mercury atom than of some inherent properties of that latter. Secondly, the observation that the methylmercury retentions do not extrapolate to the zero-fat value could result from the presence in the fat of another compound which decreases the retention. Thus, one can wonder whether the retention differences in the three classes of fish proteins may be the results of a varying *decrease* (from ~13%) rather than a varying *increase* (from 3%). If this hypothesis is true, then this decreasing factor must act mostly as a methyl radical trap. Moreover, it must be only partly extracted by Damberg's method for FPC preparation, and then must be in higher concentration in the water soluble (acid) fraction. Finally, it must be able

Can. J. Chem. Downloaded from www.nrcresearchpress.com by 210.87.254.5 on 09/05/12
For personal use only.

TABLE 3. Influence of water soluble extracts on retentions in CH_3HgCl-doped soya flour. The fat content is given as weight of added fat as a percent of the weight of soya flour

CH_3HgCl-doped soya flour					
	1 ml WS + fat		3 ml WS + fat		$HgCl_2$-doped soya flour, no fat, retention (%)
No fat retention (%)	Fat (%)	Retention (%)	Fat (%)	Retention (%)	
11.1			0.9	5.5	2.4
9.8			2.2	5.6	2.8
9.8	0.0	5.7	3.0	5.9	2.8
Ave. 10.2 ± 0.4	2.9	7.2	5.0	5.9	Ave. 2.7 ± 0.1
	5.0	9.1	9.9	7.3	
	7.6	9.9			
	10.0	14.3			

to influence the retention even at very low concentration and with very little concentration dependence. This is shown below to be the case.

(b) Retention Decreasing Product (RDP)

Since the very nature of the RDP is unknown, its concentration is also unknown. In a first series of experiments we added different volumes of the methanol fraction of the water soluble extract (WS) to the CH_3HgCl-doped SF. From the results given in Table 3, one can see that: (*i*) the retention is strikingly decreased, even with little volume of WS; (*ii*) the presence of WS delays the increasing effect of fat. On the other hand, irradiation of methylmercury-doped SF fat, followed by separations of fat and SF shows the relative contributions of the two components to the retention, as is seen in Table 4. It is noteworthy that the fat contribution to the total retention and the specific methylmercury retention in fat are not directly related. Moreover, we found that the methylmercury retention in the fat reaches its maximum value at about 15% of fat in the sample, although it is true that for more fat than 15% the results become highly unreliable. The preparation method for doped SF allows the introduction of CH_3HgCl into the protein matrix, while one can expect the fat to be only on the surface, so that beyond a certain fraction (e.g. 1%), addition of fat does not increase the extent of coverage but only the less important depth of coverage. Thus, it is plausible to represent the reaction mixture as a set of CH_3HgCl-doped particles of soya flour coated by layers of fat of various thickness (10–15 monolayers). In that model the role of the fat would be to trap the escaping hot mercury atoms, while the RDP acts as an efficient scavenger for the free methyl radical formed in the soya flour particle. We have no evidence to support this conjecture.

Finally, we conducted a series of experiments in order to elucidate the nature of RDP, if not to determine its exact identity. Of many possible methyl-scavenging compounds, four types are common in fish: amino acids, triglycerides (both saturated and unsaturated), and phospholipids. Of these, the amino acid seemed the most likely to us, because of the demonstrated extractibility of RDP in aqueous HCl. We chose to use serine because of its importance in muscle tissue, along with lecithin (a phospholipid) and triolein and trilaurin (unsaturated and saturated triglycerides, respectively). The results of this experiment are given in Table 5, where it is evident that only the serine has any effect on the retention. The others seemingly have little or no influence on the retention (which also eliminates them as significant methylating agents). The serine gives an immediate distinct reduction in the retention which does not change with a further 1000-fold increase in the serine concentration. This latter behaviour is in keeping

TABLE 4. Distribution of radioactive CH_3Hg— between the soya flour and the fat

		R partial†	
Fat*	*R* total†	SF	Fat
5	7.2%	5.9%	1.3%
10	9.0	7.1	1.9
15	10.1	6.8	3.1

*Weight percent of the soya flour.
†Methylmercury-^{197}Hg as percent of *total* ^{197}Hg.

TABLE 5. Retention of plausible retention decreasing products

Weight mg/g	Retention (%)		Weight mg/g	Retention (%)	
	Serine	Lecithin		Triolein	Trilaurin
7	5.0	11.9	9	12.9	12.4
0.7	5.2	12.0	0.9	12.0	10.8
0.07	5.6	12.5	0.09	11.9	11.3
0.007	5.6	11.8	0.009	11.6	11.2
Blank	10.6	10.6	Blank	10.6	10.6

Can. J. Chem. Downloaded from www.nrcresearchpress.com by 210.87.254.5 on 09/05/12
For personal use only.

with its being a scavenging reaction. The fact that the addition of larger amounts of fat increases the retention after the initial decrease (Fig. 1) suggests that only the original $—CH_3$ is being scavenged while the further methylation does not occur by a scavengeable mechanism.

The slow increase in retention evidently caused by small amounts of the triglycerides, triolein and trilaurin, suggests that one of these compounds (more likely triolein) is responsible for the methylation by added fat.

Conclusions

It now seems that the dependence of the retention on the species of fish is not a matter of a fat-induced increase, as we had initially surmised, but is caused rather by a decrease in retention resulting from the presence of species such as serine and related compounds.

Thus, the main features of the problem can now be explained. The retention of ^{197}Hg in pure crystalline CH_3HgCl is found to be 82.0%, while with methylmercury bound in a protein matrix it is much less: about 11–12%. This marked decrease is doubtless due to a combination of the dilution (by a factor of about 10^4) and the fact that the protein lattice is composed of lighter atoms (C, H, O, N rather than C, H, Hg, and Cl). The latter provides a slightly looser cage for a recoiling mercury atom, so that the atom can somewhat more readily escape from its original ligands. The former ensures that the escaped atom will not be able to react, by exchange, hot reaction or whatever, with a nearby methylmercury, since the nearest one is some 25 molecules away.

This 'standard' protein retention value is then further decreased by the presence, in fish protein concentrate, of methyl scavengers which reduce the probability that the hot mercury atom will remain bound to its original methyl. The identity of these scavenger compounds is not known, although it seems clear from the data in Table 5 that they may be similar to serine. The absence of a concentration dependence shows that the retention difference between one species and another (Table 2) is not a matter of variations of the scavenger concentration among fish species but must rather be a difference in the compound itself.

These experiments show further that the high radiochemical retention in CH_3HgCl must be largely the result of interactions of recoil atoms with neighbouring molecules and does not represent the truest form of retention, in which the original molecule remains intact.

The overall radiochemical reaction involved in the neutron irradiation of CH_3HgCl can now be sketched in terms of three different reactions: (*i*) survival of the molecule intact ('true' retention), 3%; (*ii*) reformation of the original $CH_3—Hg$ bond (scavengeable), 8–9%; (*iii*) formation of CH_3HgCl by reaction with other molecules, 70%; total retention, 82%. Step (*i*) may well include breaking and rapid reformation of the Hg—Cl bond, while step (*iii*) likely includes both hot, epithermal, and thermal reactions.

Clearly, step (*iii*) is not available in pure fish or other protein matrices and step (*ii*) is evidently quenched by acid-extractable compounds such as serine.

Acknowledgements

The authors wish to express their gratitude to Mrs. I. G. deJong, Dr. J. F. Uthe, and Dr. R. G. Ackman for experimental advice and to Environment Canada and the National Research Council of Canada for financial support.

1. I. G. DEJONG, T. OMORI, and D. R. WILES. Chem. Commun. 189 (1974).
2. I. G. DEJONG and D. R. WILES. Radiochem. Radioanal. Lett. **17**, 343 (1974).
3. I. G. DEJONG and D. R. WILES. J. Fish. Res. Board Can. **33**, 1324 (1976).
4. D. R. WILES. Adv. Organomet. Chem. **11**, 207 (1973).
5. I. G. DEJONG and D. R. WILES. Unpublished results.
6. Y. S. WONG, P. C. CHIEH, and A. J. CARTY. Can. J. Chem. **51**, 2597 (1973); Chem. Commun. 741 (1973).
7. D. L. RABENSTEIN. J. Am. Chem. Soc. **95**, 2797 (1973).
8. N. DAMBERGS. J. Fish. Res. Board Can. **26**, 1919 (1969).
9. J. F. UTHE, J. SOLOMON, and B. J. GRIFT. J. Assoc. Off. Anal. Chem. **55**, 583 (1972).
10. L. C. BATE. Radiochem. Radioanal. Lett. **6**, 139 (1971).

Pulse radiolysis: evidence for the reaction of HO_2 with NO_2 in aqueous solution[1]

HARRY CALLENDER SUTTON
Institute of Nuclear Sciences, DSIR, Lower Hutt, New Zealand
AND
WILLIAM ARTHUR SEDDON AND FRED CHARLES SOPCHYSHYN
Physical Chemistry Branch, Chalk River Nuclear Laboratories, Atomic Energy of Canada Limited, Chalk River, Ont., Canada K0J 1J0

Received December 14, 1978

HARRY CALLENDER SUTTON, WILLIAM ARTHUR SEDDON, and FRED CHARLES SOPCHYSHYN. Can. J. Chem. **56**, 1961 (1978).

Nitroform is the major radiation induced species observed after the pulse radiolysis of acidic oxygen saturated solutions of tetranitromethane (TNM) and formic acid. It is formed in three stages, of which a major component at pH < 3 is first order with $t_{1/2} = 49$ s, independent of [TNM] and pH. Evidence is provided for the reactions

$$HO_2 + NO_2 \underset{k_{14}}{\overset{k_3}{\rightleftharpoons}} HO_2NO_2$$

in which $k_{14} = 0.014 \pm 0.002\ s^{-1}$. The data support similar conclusions reached previously in rapid mixing experiments (1) from which it was concluded that $k_3 = 4 \times 10^9\ dm^3\ mol^{-1}\ s^{-1}$.

Analysis of the fastest component of nitroform production over the pH range 1–4 shows that the COOH radical reduces TNM to nitroform with a rate constant about four times greater than that for its reaction with oxygen to produce HO_2.

HARRY CALLENDER SUTTON, WILLIAM ARTHUR SEDDON et FRED CHARLES SOPCHYSHYN. Can. J. Chem. **56**, 1961 (1978).

Lorsque l'on effectue la radiolyse de solutions d'acide formique et de tétranitrométhane (TNM) saturées d'oxygène, le nitroforme est l'espèce la plus importante que l'on observe. Ce composé se forme en trois étapes; la plus importante, qui se produit à un pH < 3, est du premier ordre avec $t_{1/2} = 49$ s et elle est indépendante de [TNM] et du pH. On présente des données concernant les réactions indiquées

$$HO_2 + NO_2 \underset{k_{14}}{\overset{k_3}{\rightleftharpoons}} HO_2NO_2$$

dans lesquelles $k_{14} = 0.014 \pm 0.002\ s^{-1}$. Les données sont en accord avec des conclusions semblables qui ont été obtenues antérieurement lors d'expériences de mélanges rapides à partir desquelles on a conclu que $k_3 = 4 \times 10^9\ dm^3\ mol^{-1}\ s^{-1}$.

L'analyse de la réaction la plus rapide lors de la formation du nitroforme à des pH allant de 1 à 4 montre que le radical COOH réduit le TNM en nitroforme avec une constante de vitesse qui est environ quatre fois plus grande que celle de sa réaction avec de l'oxygène pour fournir du HO_2.

[Traduit par le journal]

Introduction

In a recent study using rapid mixing techniques in a flow system (1), it was concluded that HO_2 produced by the radiolysis of aerated formic acid solution reacts with acid solutions of tetranitromethane (TNM) as follows:

[1] $$HO_2 \rightleftharpoons O_2^- + H^+$$

[2] $$C(NO_2)_4 + O_2^- \rightarrow C(NO_2)_3^- + O_2 + NO_2 \qquad k_2 = 2 \times 10^9\ dm^3\ mol^{-1}\ s^{-1}$$

[3] $$HO_2 + NO_2 \rightarrow HO_2NO_2 \qquad k_3 = 4 \times 10^9\ dm^3\ mol^{-1}\ s^{-1}$$

[4] $$2NO_2 \rightarrow N_2O_4 \qquad k_4 = 10^{10}\ dm^3\ mol^{-1}\ s^{-1}$$

[5] $$N_2O_4 + H_2O \rightarrow HNO_2 + HNO_3$$

[6] $$HO_2NO_2 + C(NO_2)_4 \rightarrow \cdots \rightarrow C(NO_2)_3^-$$

The major feature of this mechanism is that the rapidly formed species HO_2NO_2 (termed peroxynitric acid) reacts slowly with TNM to produce the coloured nitroform anion in [6], in a reaction time which exceeds several seconds but is less than 10 min. In contrast, the nitroform resulting from [2] was produced in less than a second under the conditions studied. Potassium thiocyanate (KCNS) was found to suppress [6] (presumably by decomposing HO_2NO_2) but not [2].

[1]AECL No. 6142. INS Contribution No. 891.

Can. J. Chem. Downloaded from www.nrcresearchpress.com by 210.87.254.105 on 09/05/12
For personal use only.

Can. J. Chem. Downloaded from www.nrcresearchpress.com by 210.87.254.105 on 09/05/12
For personal use only.

We report here studies of the pulse radiolysis of oxygen saturated solutions of formic acid and TNM with results which confirm and extend these conclusions.

Experimental

The basic pulse radiolysis techniques (2) and methods of chemical preparation and analysis (1) have been described previously. Solutions were irradiated in 2 cm cells using 0.5 μs electron pulses from a 2.5 MeV Van de Graaff accelerator. Doses per pulse ranged from 500–900 rads (5–9 Gy).

Slow reactions were recorded on a Tektronix 556 oscilloscope by connecting the external horizontal input to a Wavetek Model 162 function generator and extending the sweep speeds to 24 or 60 s cm^{-1}. In such experiments, photomultiplier fatigue was eliminated using a manually operated light shutter permitting intermittent measurement of the analysing light level at 5–20 s intervals. The pH of solutions was adjusted with H_2SO_4 or KOH, and read on a Fisher Accumet model 320 pH meter.

Results

After pulsing oxygen saturated solutions of 0.01 mol dm^{-3} formic acid containing 155 μmol dm^{-3} TNM at pH 1.85, nitroform was produced in three stages: (i) immediate (complete in 5 μs); (r) rapid, produced in a first order build-up with $k_r = 840\ s^{-1}$ ($t_{1/2} = 0.82$ ms), and (d) delayed, in a first order build-up with $k_d = 0.0144\ s^{-1}$ ($t_{1/2} = 48$ s). Figure 1 shows reproductions of oscilloscope traces which illustrate this behavior. Nitrofrom was, at all stages, the major radiation induced species detectable by light absorption and its spectrum, measured from 270–400 nm, precluded the observation of any other minor species.

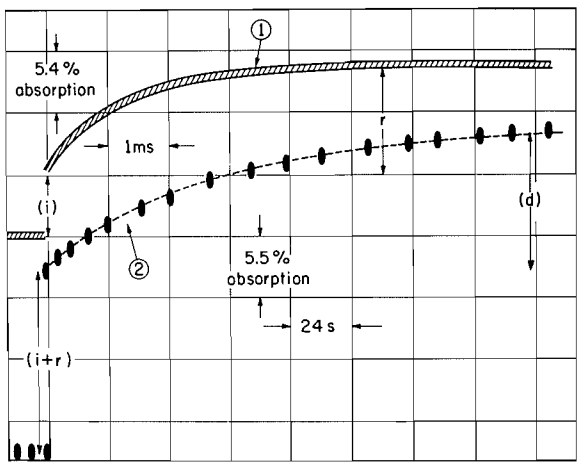

FIG. 1. Reproductions of oscilloscope traces, monitored at 350 nm, showing the formation of nitroform in oxygen saturated solutions of 0.01 mol dm^{-3} HCOOH containing TNM. Concentrations are as given for experiment 8 in Table 1. Dose per pulse, *1* = 810 rads, *2* = 945 rads. The dotted line in trace *2* corresponds to a first order fit with $k_d = 0.0148\ s^{-1}$.

Table 1 summarizes the nitroform yields and kinetic data taking the extinction coefficient at the nitroform band maximim (350 nm) $\varepsilon_{350} = 14\ 400$ $dm^3\ mol^{-1}\ cm^{-1}$ (1). Nitroform yields at each stage (i), (2–5 μs), (r), (4–20 ms), and (d) (300 s) are denoted as G_i, G_r, and G_d respectively, whilst their total is expressed as G_t.

Discussion

The immediate yield of nitroform is partially due to the rapid reaction

[7] $$e_{aq}^- + C(NO_2)_4 \rightarrow C(NO_2)_3^- + NO_2 \qquad k_7 = 4.6 \times 10^{10}\ dm^3\ mol^{-1}\ s^{-1}$$

which competes with

[8] $$e_{aq}^- + O_2 \rightarrow O_2^- \qquad k_8 = 1.9 \times 10^{10}\ dm^3\ mol^{-1}\ s^{-1}$$

and

[9] $$e_{aq}^- + H^+ \rightarrow H \qquad k_9 = 2.3 \times 10^{10}\ dm^3\ mol^{-1}\ s^{-1}$$

for solvated electrons, e_{aq}^-, with $G_{e_{aq}^-} = 2.9$ molecule/100 eV (3). The known rate constants of these reactions (4, 5) imply that about 10% of the immediate yield observed in experiment 11 at pH 1.82 with 582 μmol dm^{-3} TNM ($G_i = 2.28$) is due to reaction [7], and this fraction decreases with decreasing pH.

We attribute the remainder (i.e., most) of the immediate yield to the reactions

[10] $$OH + HCOOH \rightarrow COOH + H_2O$$

[11] $$COOH + C(NO_2)_4 \rightarrow C(NO_2)_3^- + CO_2 + NO_2 + H^+$$

and

[12] $$COOH + O_2 \rightarrow CO_2 + HO_2$$

Reactions analogous to [11] and [12] must be considered in conjunction with the ionised form of the COOH radical, for example

[13] $$CO_2^- + O_2 \rightarrow CO_2 + O_2^-$$

Consequently the apparent rate constants of these reactions are expressed in total radical concentrations as k_{11}^{ap} and k_{12}^{ap}, respectively. Thus, for example, $d([HO_2] + [O_2^-])/dt = k_{12}^{ap}([COOH] + [CO_2^-]) \times [O_2]$ where $k_{12}^{ap} = xk_{13} + (1 - x)k_{12}$ and $x = [CO_2^-]/([CO_2^-] + [COOH])$. Assuming $G_{OH} = 2.7$ (3), independent of pH, then our data conform with this interpretation if $k_{12}^{ap}/k_{11}^{ap} = 0.24 \pm 0.1$. The data do not show any consistent variation of k_{12}^{ap}/k_{11}^{ap} with pH from 1.08 to 4, the values obtained being 0.26 at pH 1.08; 0.26 at 1.32; 0.35 at 1.55; 0.12, 0.14, and 0.27 at 1.82; 0.21 at 1.85; 0.31 at 2.1; 0.27 at 2.85; 0.18 at 3.5; and 0.22 at pH 4.

TABLE 1. Nitroform yields and kinetic data in the pulse radiolysis of oxygen saturated solutions of 0.01 mol dm^{-3} HCOOH containing TNM

Expt. No.	pH	[TNM] (μmol dm^{-3})	G(nitroform) (molecule/100 eV) G_i	G_r	G_d	G_t	k_r (s^{-1})	k_d (s^{-1})
1	6.0[a]	166	$(G_i + G_r) = 5.87$		0	5.87	319 000	—
2	4.0	142	1.58	4.20	?	> 5.78	40 750	—
3	3.50	142	1.64	3.22	0.64	5.50	17 950	0.0174
4	2.85	70	ND[e]	ND	ND	ND	ND	0.0133
5	2.85	147	1.19	3.04	1.10	5.33	5 170	0.0148
6[b]	2.60[b]	162	1.29	2.21	2.12	5.62	2 900	0.0151
7	2.10	148	0.86	1.91	2.64	5.41	1 150	0.0139
8	1.85	155	1.06	1.77	2.49	5.32	840	0.0144
9	1.82	79	0.55	2.45	2.89	5.89	390	0.0116
10	1.82	316	1.79	0.58	3.52	5.89	1 500	0.0154
11	1.82	582	2.28	1.50	2.44	6.22	3 580	0.0142
12	1.55	172	0.82	1.89	2.64	5.35	510	0.0137
13	1.32	157	0.90	1.88	2.72	5.50	330	0.0108
14	1.08	155	0.89	1.73	2.60	5.22	220	0.0119
15[c]	1.50[d]	159	0.92	2.00	3.01	5.93	210	0.0096

[a]Buffered with phosphate.
[b]0.1 mol dm^{-3} HCOOH.
[c]Solution in D_2O.
[d]pD = 1.50 as read on a pH meter. Sam econcentration of H_2SO_4 as for pH = 1.82.
[e]Not determined.

Measurements of the pK of the COOH radical have been reported from 1.4 (6, 7) to 3.9 (8), with recent evidence favouring 1.4 (6). Thus the fraction x defined above cannot exceed 0.32 at pH 1.08 and must increase at least three-fold over the pH range we studied. Fojtik *et al.* (8) report that $k_{11}^{ap} = (4 \pm 1) \times 10^9$ dm^3 mol^{-1} s^{-1}, independent of pH from pH 2 to 7. We conclude, firstly, that $k_{12}^{ap} = (1^{+1}_{-0.5}) \times 10^9$ dm^3 mol^{-1} s^{-1} at $1 < pH \leq 4$, and secondly, that k_{12} must be comparable with k_{13} and probably within the range 10^8 to 10^9 dm^3 mol^{-1} s^{-1}. We are not aware of other measurements of k_{12} but values of k_{13} have been reported as 2.4×10^9 (9) and 2.0×10^9 dm^3 mol^{-1} s^{-1} (10), in reasonable agreement with these conclusions.

The rapid stage, (r), of nitroform production corresponds in rate with that observed after irradiating oxygen saturated TNM solutions (4). It is due to reduction of TNM by O_2^- in [2] at a rate which is approximately expressed by a pseudo first order rate constant of fk_2[TNM] where $k_2 = 2 \times 10^9$ dm^3 mol^{-1} s^{-1} (4), $f = [O_2^-]/([O_2^-] + [HO_2])$, and the p$K$ of the HO_2 radical is 4.88 (11). The observed build-up of nitroform was approximately first order with values of k_r which agree with those calculated as fk_2[TNM] at pH 6 where $f = 1$, but exceed these to an extent increasing with decrease of pH to about three-fold at pH 1.8 and four-fold at pH 1.08.

The mechanism we propose requires that reactions [3] and [4] should compete with [2] for HO_2 and NO_2 in the rapid stage and influence the observed build-up. Computerised calculations of this effect have been made with the rate constants reported previously for k_3 and k_4 (1), taking somewhat uncertain values for $[HO_2]^0$ and $[NO_2]^0$ at the beginning of the rapid stage which are explained and discussed later. On this basis the build-up of nitroform in the rapid stage is calculated to be approximately exponential with a rate constant which exceeds fk_2[TNM] by a factor increasing from 1 to approximately 2 as the pH is lowered from 6 to 1, which is in reasonable agreement with our observations. It seems likely that the effect we describe may have occurred to a smaller extent in the experiments of Rabani *et al.* (4), as these authors also noted a slow build-up of nitroform over some minutes in the pulse radiolysis of oxygen saturated TNM solutions, probably attributable to HO_2NO_2. If so, this would introduce a small error in the estimate of the pK of the HO_2 radical (4.45 ± 0.25) which they deduced from their observations.

The rate of the delayed stage, (d), of nitroform production corresponds with that attributed to [6] (i.e., to peroxynitric acid) in the rapid mixing experiments (1). Delayed yields are also of the same magnitude as in these experiments, amounting to about half the total yield at pH 1.6 and zero at pH 6. Addition of KCNS completely suppressed the delayed reaction both in the rapid mixing experiments and in those reported here. We also found that KCNS partially reduced the immediate and rapid components (G_i and G_r), owing to its competition with [10] for OH radicals (12). However, the delayed formation of nitroform cannot be due to direct re-

Can. J. Chem. Downloaded from www.nrcresearchpress.com by 210.87.254.105 on 09/05/12
For personal use only.

Can. J. Chem. Downloaded from www.nrcresearchpress.com by 210.87.254.105 on 09/05/12
For personal use only.

action of HO_2NO_2 with TNM since the observed build-up is first order with k_d nearly independent of [TNM] and pH.

A possible explanation is that the species HO_2NO_2 slowly decomposes as follows:

[14] $$HO_2NO_2 \rightarrow HO_2 + NO_2$$

so that the NO_2 and HO_2 so evolved at low concentration react nearly quantitatively in [1], [2], [4], and [5]. On this view HO_2NO_2 might be regarded as somewhat analogous to the species H_2O_3 which is formed by reaction of HO_2 with OH (13), but differs from HO_2NO_2 in that it slowly decomposes to unreactive products at a rate which varies with pH. This interpretation implies that the observed $k_d = k_{14} = 0.014 \pm 0.002\ s^{-1}$ and that HO_2NO_2 itself does not react with TNM but is decomposed by KCNS. It also requires that the total or final yield of nitroform (G_t) should be independent of the formation of HO_2NO_2, and therefore constant in all these experiments except for variations of $G_{e_{aq}^-}$ and G_{OH} with pH. In fact, G_t agrees fairly well in most cases with $G(O_2^-) = 6$ at pH ≥ 6 (14), but occasional discrepancies occur in which G_t is smaller by amounts up to 0.7 G units. In the rapid mixing experiments the final yields observed in acid solutions generally exceeded those at pH 7 by about 8% (1).

It is not possible to make reliable kinetic analyses of these yields along the lines given previously (1) because $[HO_2]^0$ at the beginning of the rapid stage (r) can only be inferred indirectly from our observations as the difference between the total and immediate yields of nitroform. This concentration is consistent with the mechanism proposed above and gives calculated values for $[HO_2]^0$ which are typically 3 μmol dm^{-3} at pH ≤ 4. Actual values of $[HO_2]^0$ may exceed those calculated by 0.5 mol dm^{-3} in some cases for reasons given in the preceding paragraph.

Values for $[NO_2]^0$ at the beginning of the rapid stage (resulting from reactions [7] and [11]) may be estimated with less uncertainty as equal to the immediate yield of nitroform, and range from 0.6 to 1.5 μmol dm^{-3} in our experiments. In the rapid mixing experiments, however, $[HO_2]^0$ could be measured directly as typically 7 μmol dm^{-3}, whilst $[NO_2]^0 = 0$. The rapid and delayed yields of nitroform in experiment 9 were $G_r = 2.45$ and $G_d = 2.89$, respectively. These may be compared with those calculated for reactions [2] and [3] (since we assume all the HO_2NO_2 formed in the rapid stage ultimately yields nitroform in a delayed reaction) in competition with reaction [4] as $G[2]_{calcd} = 2.69$ and $G[3]_{calcd} = 2.67$, respectively, adopting the rate constants previously quoted (1) for k_3 (4×10^9 dm^3 mol^{-1} s^{-1}) and k_4 (10^{10} dm^3 mol^{-1} s^{-1}). In this case the apparent mass balance is reasonable, i.e., $G_t = 5.89$, which is close to 6. In experiment 14, $G_t = 5.22$, probably implying that the actual $[HO_2]^0$ considerably exceeds its calculated value. For this experiment $G_r = 1.73$ as compared with $G[2]_{calcd} = 1.94$, and $G_d = 2.60$ as compared with $G[3]_{calcd} = 2.37$, i.e., the calculated yield of HO_2NO_2. In most cases the agreement between observed and calculated yields was within 0.3 G units, and in all cases within 0.6 G units. This appears reasonable in view of the uncertainties in estimating $[HO_2]^0$.

There can be no doubt that a long-lived species such as HO_2NO_2 occurs under the conditions we described, but since we have not observed its absorption spectrum its concentration and properties can be inferred only indirectly. Both the data reported here and previously are consistent with the reaction mechanism discussed in this paper.

1. H. C. Sutton. J. Chem. Soc. Faraday I, **71**, 2142 (1975).
2. W. A. Seddon, J. W. Fletcher, and F. C. Sopchyshyn. Can. J. Chem. **51**, 1123 (1973).
3. B. H. J. Bielski and A. O. Allen. Int. J. Rad. Phys. Chem. **1**, 153 (1969).
4. J. Rabani, W. A. Mulac, and M. S. Matheson. J. Phys. Chem. **69**, 53 (1965).
5. M. Anbar and P. Neta. J. Appl. Radiat. Isotopes, **18**, 493 (1967).
6. E. Heckel. J. Phys. Chem. **80**, 1274 (1976).
7. G. V. Buxton and R. M. Sellers. J. Chem. Soc. Faraday I, **69**, 555 (1973).
8. A. Fojtik, G. Czapski, and A. Henglein. J. Phys. Chem. **74**, 3204 (1970).
9. G. E. Adams and R. L. Willson. Trans. Faraday Soc. **63**, 2981 (1969).
10. G. V. Buxton, R. M. Sellers, and D. R. McCracken. J. Chem. Soc. Faraday I, **72**, 1464 (1976).
11. D. Behar, G. Czapski, J. Rabani, L. M. Dorfman, and H. A. Schwarz. J. Phys. Chem. **74**, 3209 (1970).
12. L. M. Dorfman and G. E. Adams. NSRDS-NBS 46, Library of Congress Cat. No. 72-600321 (1973).
13. G. Czapski and B. H. Bielski. J. Phys. Chem. **67**, 2180 (1963).
14. H. C. Sutton and M. T. Downes. J. Chem. Soc. Faraday I, **68**, 1498 (1972).

Can. J. Chem. Downloaded from www.nrcresearchpress.com by 210.87.254.5 on 09/05/12
For personal use only.

Canadian Journal of Chemistry

Published by
THE NATIONAL RESEARCH COUNCIL OF CANADA

Volume 56 Number 13 August 1, 1978

Journal canadien de chimie

Publié par
LE CONSEIL NATIONAL DE RECHERCHES DU CANADA

Volume 56 numéro 13 1 août 1978

Chemistry and catalytic properties of oxidized rhodium chlorocarbonyl complexes, $Rh_4Cl_4(CO)_4(O_2)_2P_2$; P = tertiary phosphine ligands

WILLIAM R. CULLEN, BRIAN R. JAMES,[1] AND GIORGIO STRUKUL[2]

The Department of Chemistry, University of British Columbia, Vancouver, B.C., Canada V6T 1W5

Received February 7, 1978

WILLIAM R. CULLEN, BRIAN R. JAMES, and GIORGIO STRUKUL. Can. J. Chem. **56**, 1965 (1978).

The reactions of the title complexes $Rh_4Cl_4(CO)_4(O_2)_2P_2$ (where P is a tertiary phosphine type ligand, in particular diphenylisobutylphosphinite) with both dihydrogen and carbon monoxide were studied in solution in the absence and presence of excess P. The reaction stoichiometries, particularly a measured carbon dioxide evolution, confirm the formulation of the reactant tetranuclear complexes. The complexes are effective for catalytic hydrogenation and hydroformylation of olefinic substrates, and the nature of the active catalysts is considered.

WILLIAM R. CULLEN, BRIAN R. JAMES et GIORGIO STRUKUL. Can. J. Chem. **56**, 1965 (1978).

On a étudié les réactions, en solution, des complexes mentionnés dans le titre, $Rh_4Cl_4(CO)_4(O_2)_2P_2$ (où P est un ligand de type phosphine tertiaire en particulier la diphénylisobutylphosphinite), avec l'hydrogène et le monoxyde de carbone en présence et en l'absence d'un excès de P. Les stoechiométries de la réaction, en particulier des mesures d'évolution du dioxyde de carbone, confirment la formule des complexes tétranucléaires réactifs. Les complexes sont efficaces pour effectuer l'hydrogénation et l'hydroformylation d'oléfines et on considère la nature des catalyseurs actifs.

[Traduit par le journal]

Introduction

We recently reported (1) on the synthesis of polynuclear oxygenated rhodium complexes of the type $Rh_4Cl_4(CO)_4(O_2)_2P_2$ (**1**) via O_2 oxidation of the corresponding *trans*-$RhCl(CO)P_2$ complexes (P = PPh_3, PPh_2OBu^i, $PPhEt_2$, PEt_3, and poly-$OPPh_2$ (diphenyl-polymethallylphosphinite)). Their interest stems from their potential as oxygenation catalysts (1). The dioxygen moieties were considered to be present as bridged superoxides. Because of the difficulty in unequivocally demonstrating the oxygen content of such oxidized complexes, we have investigated further the chemistry of **1** (P = $PPh_2(OBu^i)$), especially its reactivity in solution toward H_2 and toward CO, with and without added P; the overall stoichiometries of these reactions confirm the formulation of the oxidized complexes and are of interest in terms of the reactivity of coordinated dioxygen moieties.

In view of the known catalytic activity for some related oxidized rhodium complexes (2), some preliminary studies were then carried out to investigate the catalytic potential of our Rh_4 complexes. The species formed from the H_2 reaction were found effective for the catalytic hydrogenation of olefinic substrates, and those formed from the CO reaction were effective as hydroformylation catalysts.

Experimental Section

Many of the materials and methods used were described in the earlier paper (1). $[RhCl(C_2H_4)_2]_2$, prepared according to the literature (3), was used to synthesize $[RhCl(PPh_2OBu^i)_2]_2$. The ethylene complex (0.3 g) was refluxed with PPh_2OBu^i (0.8 g) in toluene (15 ml) under N_2 for 3 h; after cooling and filtering, the filtrate was concentrated to ~3 ml, and 15 ml of N_2-saturated petroleum ether were then added. The yellow precipitate was collected, washed with petroleum ether, and dried *in vacuo*. Elemental analysis was correct for a chlorobisphosphinite and, on comparison with $[RhCl(PPh_3)_2]_2$, a dimer formulation is assumed (4).

[1]To whom correspondence should be addressed.

[2]On leave from Istituto di Chimica Generale, Universitá di Venezia, Italy.

CO_2 and H_2O were identified by glc using a Hewlett Packard 5750 with Porapak N and 15% FFAP/Chromosorb W columns, respectively.

Olefinic substrates were commercial products, which were passed through alumina to remove peroxides (readily detected by Fe^{2+}/SCN^-) and then distilled under N_2. Hydrogenation procedures have been described elsewhere (5). Hydroformylation reactions were carried out in a stainless steel Parr high pressure bomb (150 ml), thermostatted in an oil-bath; external magnetic stirring was employed. The composition of the final solution was determined by glc or combined glc/mass spectrometry.

Results and Discussion

Reactions of $Rh_4Cl_4(CO)_4(O_2)_2P_2$ with H_2; $P = PPh_3$, PPh_2OBu^i, $PPhEt_2$, PEt_3

The Rh_4 complexes in CH_2Cl_2, chlorobenzene, or *N,N*-dimethylacetamide (DMA) solution, and even in the solid state, decompose quite readily under 1 atm H_2 at 25°C to give metal. We favored the O_2 moiety being bound as bridging superoxide between Rh(I) and Rh(II) centers (1), but in any case treatment with H_2 will lead to formation of Rh(I) (6) and, due to the relatively low number of π-acceptor ligands present per rhodium, hydrogen reduction (or disproportionation) of Rh(I) to metal occurs (7). In the presence of excess P, however, the solution reaction, which takes a few hours at 30°C, results in a color change from deep red to yellow, and no metal is formed; these yellow solutions (CH_2Cl_2) showed single ν(CO) ir bands for P = PPh_3, PPh_2OBu^i, $PhEt_2$, and PEt_3, at 1960, 1980, 1955, and 1950 cm^{-1}, respectively, which correspond to those we measured for the *trans*-$RhCl(CO)P_2$ complexes. Gas liquid chromatographic analysis of the yellow solutions showed the presence of H_2O, and similar analysis of the gas phase above the solution showed CO_2 to be present.

A quantitative study of the H_2 reaction in the presence of excess P proved convenient for the PPh_2OBu^i complex in chlorobenzene solution, and the data are consistent with the overall stoichiometry of reaction [1].

$$[1]\quad Rh_4Cl_4(CO)_4(O_2)_2P_2 + 6P + 3H_2 \rightarrow \underset{\mathbf{1}}{H_2(RhClP_2)_2} + 2RhCl(CO)P_2 + 2H_2O + 2CO_2$$

Solutions of **1** (10^{-2} *M*) containing a six-fold excess of P, when subjected to 1 atm H_2 at 30°C, slowly absorb H_2, and after 8 h the absorption corresponds to 1.0 ± 0.1 mol/mol **1**; in the presence of a sodalime tube, which absorbs the CO_2, the stoichiometry reaches a 3:1 ratio; 2.1 ± 0.2 mol H_2O were also formed per mol of **1**. No phosphine oxide is formed. The $RhCl(CO)P_2$ was detected essentially quantitatively by using the ν(CO) ir band, and was isolated from the yellow solution. The stoichiometry on oxygen can thus be fully accounted for. A small amount of a white solid was also isolated. This solid showed an ir band at 2065 cm^{-1} (Nujol), and in CD_2Cl_2 gave a quartet in the high-field ^1H nmr centered at τ26.6; the same ^1H nmr spectrum was obtained from an authentic sample of $[RhCl(PPh_2OBu^i)_2]_2$ in the presence of H_2, and is attributed to $H_2[RhCl(PPh_2OBu^i)_2]_2$. Such dimer hydrides have been studied by Tolman *et al.* (4) and shown to have structure **2** by the high-field ^1H nmr

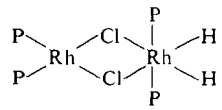

2

which consists of a pair of triplets. However, the coupling of the H to Rh is similar to that of coupling to a *cis*-P, e.g. for the P(*p*-tolyl)$_3$ complex (4) τ26.7, J(Rh–H) = 22 and J(P–H) = 17 Hz, and the quartet observed for our phosphinite complex is accounted for if J(Rh–H) = 21 Hz = J(P–H).

The dimer hydride was not recovered quantitatively and this would be difficult in view of the ready loss of hydrogen from such complexes (4). Nevertheless, taken together with further data below on H_2 uptake, and with data for some CO reactions (following section), the stoichiometry of reaction [1] is considered to be established.

In the presence of a ten-fold excess of P, chlorobenzene solutions of **1** showed a net absorption of ~1.7 mol gas/mol **1**; this is entirely consistent with the expected formation of a tris(phosphinite) complex and its dihydride H_2RhClP_3. The net gas stoichiometry will be governed by equilibria [2]–[4]

$$[2]\quad 2RhClP_3 \rightleftharpoons [RhClP_2]_2 + 2P$$

$$[3]\quad H_2 + RhClP_3 \rightleftharpoons H_2RhClP_3$$

$$[4]\quad H_2 + [RhClP_2]_2 \rightleftharpoons H_2[RhClP_2]_2$$

Data given for the P(*p*-tolyl)$_3$ system (4) indicate that the H_2RhClP_3 complex would not be fully formed for the conditions of our gas uptake experiments (complete formation of $H_2RhCl(PPh_2OBu^i)_3$ requires a net gas absorption of 2.0 mol per mol **1**). H_2 absorption in the presence of less than a five-fold excess of P led to some metal production.

Reaction [1] seemed of interest mechanistically especially in view of the CO_2 production often considered to occur via oxygen atom transfer to coordinated CO (8). Unfortunately, a kinetic investigation by following the gas absorption was thwarted by a lack of reproducibility (typically factors of 2 or 3 for identical runs). Nevertheless, based on some work from this laboratory (9) which showed CO_2 production from reaction of carbonylchlororhodate(I) species with peroxy radicals, and especially a

Can. J. Chem. Downloaded from www.nrcresearchpress.com by 210.87.254.5 on 09/05/12
For personal use only.

Can. J. Chem. Downloaded from www.nrcresearchpress.com by 210.87.254.5 on 09/05/12
For personal use only.

report by Harvie and McQuillin (10) on formation of CO_2 and $[RhCl(PPh_3)_2]_2$ from reaction of $RhCl(CO)(PPh_3)_2$ with *tert*-butylhydroperoxide, reactions [4], [5], and [6] seem reasonable for the overall reaction shown in reaction [1].

[5] $Rh_4Cl_4(CO)_4(O_2)_2P_2 + 6P + 2H_2 \rightarrow 4RhCl(CO)P_2 + 2\text{“}H_2O_2\text{”}$

[6] $2RhCl(CO)P_2 + 2\text{“}H_2O_2\text{”} \rightarrow [RhClP_2]_2 + 2H_2O + 2CO_2$

Sen and Halpern (11) have recently demonstrated the existence of H_2O_2 in some related systems using Pt(0) phosphine complexes for catalytic O_2-oxidation of the phosphine. In our system, H_2O_2 was not detected directly, and the possibility of a rhodium-hydroperoxide intermediate without formation of free H_2O_2 is equally plausible. Nucleophilic attack by free phosphine on coordinated dioxygen can generate peroxide which subsequently oxidizes the phosphine to phosphine oxide (11), and of interest in this respect, addition of excess phosphine to the $Rh_4Cl_4(CO)_4(O_2)_2P_2$ complexes in the *absence of* H_2 leads very slowly (~1 week) to only $RhCl(CO)P_2$ and phosphine oxide, presumably via reaction [7].

[7] $Rh_4Cl_4(CO)_4(O_2)_2P_2 + 10P \rightarrow 4RhCl(CO)P_2 + 4PO$

However, there can be no contribution of such a pathway to reaction [1], the detailed paths of which remain to be elucidated.

Solutions of **1**, especially in DMA where the complexes exist as dinuclear species (1), catalyze the hydrogenation of terminal olefins at 1 atm H_2 and 30°C. With the P = PPh_2OBu^i system, hexene-1, octene-1, and styrene (0.2 *M*) were hydrogenated at maximum rates of $\sim 3 \times 10^{-5}$ *M* s^{-1} using 6.5×10^{-4} *M* **1**. There was no accompanying isomerization. Towards completion of the hydrogenations, metal precipitated and this must result from a lowering of concentration of the olefin which is necessary to coordinate and stabilize rhodium(I). Indeed with more weakly binding substrates such as internal olefins and ketones, metal is formed immediately on exposing the system to H_2. Similar solutions of **1** in the presence of a six-fold excess of P (reaction [1]) effect catalytic hydrogenation of terminal and internal olefins (octene-1, styrene, cyclohexene, diethylmaleate, and acrylamide).

The catalysis could proceed via the $[RhClP_2]_2$ dimer which is known to be a hydrogenation catalyst (4), since the $RhCl(CO)P_2$ systems are ineffective under these conditions (ref. 12, p. 257). In the strongly coordinating DMA solvent, however, solvated $RhClP_2$ monomers will almost certainly be present (cf. reaction [9] below), and the catalysis likely proceeds via such species. Addition of greater than a six-fold excess of P inhibited the hydrogenations which is consistent with mechanistic schemes established for the Wilkinson-type catalysts (4, 13). Augustine and co-workers (2) have used oxidized Rh complexes obtained from $RhCl(PPh_3)_3$ for catalyzing hydrogenation of olefins, but the nature of the catalysts was uncertain.

Reactions of $Rh_4Cl_4(CO)_4(O_2)_2P_2$ with CO

Deep red solutions of the Rh_4 complexes slowly absorb CO at 1 atm and 35°C and become orange; CO_2 is formed. Quantitative gasometric studies in chlorobenzene for the PPh_2OBu^i system show 3.0 mol gas are finally absorbed per mole of **1**, and this ratio becomes 7:1 in the presence of a sodalime tube. Infrared data on the final solutions are given in Table 1, together with data for some $[Rh(CO)_2Cl]_2$ systems; DMA was sometimes used because of the limited solubility of the Rh_4 complexes, although CO absorption studies in this solvent were complicated by an accompanying very slow carbonylation reaction which we have not been able to account for.

The overall process of reaction [8] accounts for the gas stoichiometries and the ir data in CH_2Cl_2:

[8] $Rh_4Cl_4(CO)_4(O_2)_2P_2 + 7CO \xrightarrow{CH_2Cl_2}$ 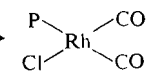 + 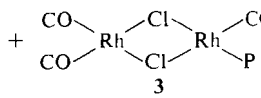 + $\frac{1}{2}[Rh(CO)_2Cl]_2 + 4CO_2$

3

When $[Rh(CO)_2Cl]_2$ and PPh_2OBu^i are mixed in a 1:1 ratio under CO, the ir spectrum is identical to that measured after carbonylation of $Rh_4Cl_4(CO)_4(O_2)_2(PPh_2OBu^i)_2$. Poilblanc and co-workers (14) reported for the $[Rh(CO)_2Cl]_2/PPh_3$ system under CO in octane a very similar spectrum with major ir bands at 2103, 2090, 2032, 2020, and 2000 cm^{-1} and these were due to a mixture of $[Rh(CO)_2Cl]_2$, *cis*-$RhCl(CO)_2P$, and $Rh_2Cl_2(CO)_3P$. We thus formulate reaction [8] as shown; once the coordinated O_2 moieties are converted to CO_2, the system essentially becomes like that of Poilblanc and co-workers, the starting tetranuclear formulation requiring 0.5 mol of $[Rh(CO)_2Cl]_2$ dimer product to balance the reaction.

The simpler spectra measured in DMA are readily accounted for, considering that this coordinating solvent can cleave chloride bridges (1). All the $Rh_4Cl_4(CO)_4(O_2)_2P_2$ complexes after carbonylation give the same two bands as $[Rh(CO)_2Cl]_2$ in DMA;

TABLE 1. Solution infrared data for carbonylated complexes[a]

Complex, solvent	ν(CO), cm^{-1}
$Rh_4Cl_4(CO)_4(O_2)_2(PPh_2OBu^i)_2$ or $[Rh(CO)_2Cl]_2 + PPh_2OBu^i$, CH_2Cl_2	2108, 2091, 2034, 2023, 2004
$Rh_4Cl_4(CO)_4(O_2)_2(PPh_2OBu^i)_2$ or $[Rh(CO)_2Cl]_2 + PPh_2OBu^i$, DMA	2060, 2045, 1978
$Rh_4Cl_4(CO)_4(O_2)_2(PPh_3)_2$, DMA	2060, 2041, 1978
$Rh_4Cl_4(CO)_4(O_2)_2(PPhEt_2)_2$, DMA	2060, 2038, 1978
$Rh_4Cl_4(CO)_4(O_2)_2(PEt_3)_2$, DMA	2060, 2035, 1978
$[Rh(CO)_2Cl]_2$, DMA	2060, 1978
$[Rh(CO)_2Cl]_2$, CH_2Cl_2	2108, 2090, 2033, 2008

[a]A band at 2340 cm^{-1} due to dissolved CO_2 was observed, unless a sodalime tube was present.

these must be due to a *cis*-$Rh(CO)_2Cl(DMA)$ species formed from the dimer according to reaction [9].

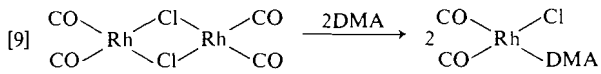

The other product formed in the carbonylation reactions shows a ν(CO) that varies from 2045–2035 cm^{-1} and this must be due to a carbonyl containing the appropriate phosphine. Again the $[Rh(CO)_2Cl]_2/PPh_2OBu^i$ system under CO gives the same spectrum as the $Rh_4Cl_4(CO)_4(O_2)_2(PPh_2OBu^i)_2$/CO solution. We believe that the carbonylphosphine species must be RhCl(CO)P(DMA). The Rh_4 complexes in DMA are known to be dimers (1) of possible configuration **4**, and thus the carbonylation of **1** in DMA may be written as

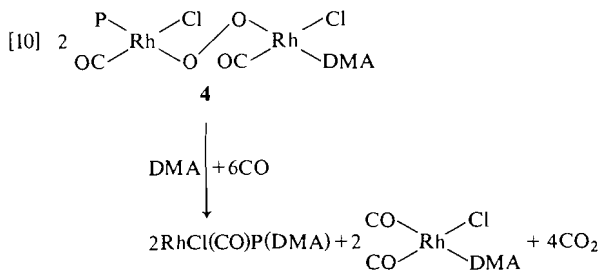

Unfortunately, as mentioned above, we were not able to confirm the net gas absorption in DMA. However, reaction [10] follows rationally from a consideration of reaction [8]: **3** would cleave to give *cis*-$Rh(CO)_2Cl(DMA)$ and RhCl(CO)P(DMA); the $\frac{1}{2}$ mol $[Rh(CO)_2Cl]_2$ would yield *cis*-$Rh(CO)_2Cl(DMA)$; and the *cis*-$RhCl(CO)_2P$ would evolve 1 mol CO in DMA to yield RhCl(CO)P(DMA) (addition of 2 mol of phosphine to 1 mol of $[Rh(CO)_2Cl]_2$ in DMA was found to evolve 2 mol CO). Formation of RhCl(CO)P(DMA) from **3**, **4**, or *cis*-$RhCl(CO)_2P$ could readily yield initially the configuration shown in **5**.

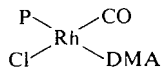

5

The small variation in ν(CO) is certainly consistent with CO being *cis* to P. As with phosphine oxidation, carbonyl oxidation clearly occurs more readily by attack of free rather than ligand CO on the coordinated O_2.

DMA solutions of the Rh_4 complexes catalyzed hydroformylation of terminal olefins under moderate conditions. Data for the PPh_2OBu^i system are given in Table 2. Heptene-1 gave only octanal, 2-methylheptanal, and small amounts of heptane, and the product distribution at 90°C was insensitive to the H_2/CO composition over the range noted at a total pressure of 1000 psi. Diminished activity resulted at lower temperatures but there was little change in the ratio of linear:branched aldehydes (~1.5). Reducing the total pressure increases the selectivity somewhat for linear aldehydes. A similar observation has been reported for rhodium carbonyl catalysts containing phosphites (ref. 12, pp. 262–269, refs. 15, 16) (although the opposite has been observed with phosphines (ref. 12, pp. 262–269, ref. 16)), and this coupled with the relatively high activity of the system indicates that the catalyst contains a PPh_2OBu^i ligand. Better selectivity is also observed on addition of more phosphinite, again typical of rhodium carbonyl systems (ref. 12, pp. 262–269, ref. 16), and in view of the absence of accompanying olefin isomerization, this can be rationalized in terms of more sterically crowded hydridocarbonylphosphine species favoring anti-Markownikov addition of the metal-hydride across the olefinic bond (ref. 12, pp. 262–269, ref. 16). As expected, a $[Rh(CO)_2Cl]_2/PPh_2OBu^i$

Can. J. Chem. Downloaded from www.nrcresearchpress.com by 210.87.254.5 on 09/05/12
For personal use only.

TABLE 2. Data for hydroformylation of hept-1-ene in DMA[a]

CO (psi)	H_2 (psi)	Heptene-1 (%)	Octanal (%)	2-Methyl-heptanal (%)	Heptane (%)
300	700	13	49	34	4
500	500	10	56	34	—
500[b]	500	8	56	36	—
700	300	16	52	32	—
500[c]	500	39	37	20	4
500[d]	500	95	3	2	—
300	300	21	52	27	—
150	150	85	10	4	1
500[e]	500	5	61	34	—
500[f]	500	11	63	26	—
500[g]	500	9	69	22	—

[a]$[Rh_4Cl_4(CO)_4(O_2)_2(PPh_2OBu^i)_2] = 7.5 \times 10^{-4}$ *M*, [heptene-1] = 0.65 *M*, reaction time 24 h, 90°C, unless stated otherwise.
[b]Using 1.5×10^{-3} *M* $[Rh(CO)_2Cl]_2$ and 1.5×10^{-3} *M* PPh_2OBu^i.
[c]At 55°C.
[d]At 20°C.
[e]Added PPh_2OBu^i, 3.9×10^{-3} *M*.
[f]Added PPh_2OBu^i, 1.4×10^{-2} *M*.
[g]Added PPh_2OBu^i, 3.0×10^{-2} *M*.

system (1:1) produced the same hydroformylation catalyst as $Rh_4Cl_4(CO)_4(O_2)_2(PPh_2OBu^i)_2$ (Table 2).

Acknowledgements

We thank the National Research Council of Canada for financial support and Johnson Matthey Ltd. for loan of the rhodium.

1. W. R. CULLEN, B. R. JAMES, and G. STRUKUL. Inorg. Chem. **17**, 484 (1978).
2. R. L. AUGUSTINE, R. J. PELLET, J. F. VAN PEPPEN, and J. P. MAYER. Adv. Chem. Ser. **132**, 111 (1974).
3. R. CRAMER. Inorg. Chem. **1**, 722 (1962).
4. C. A. TOLMAN, P. Z. MEAKIN, D. L. LINDNER, and J. P. JESSON. J. Am. Chem. Soc. **96**, 2762 (1974).
5. B. R. JAMES and G. L. REMPEL. Discuss. Faraday Soc. **46**, 40 (1968); Can. J. Chem. **44**, 233 (1966).
6. B. R. JAMES and G. ROSENBERG. Coord. Chem. Rev. **16**, 153 (1975).
7. B. R. JAMES and F. T. T. NG. J. Chem. Soc. Dalton, 355 (1972).
8. K. R. LAING and W. R. ROPER. Chem. Commun. 1568 (1968); W. O. SIEGL, A. J. LAPPORTE, and J. P. COLLMAN. Inorg. Chem. **10**, 2158 (1971).
9. G. ROSENBERG. Ph.D. Dissertation. University of British Columbia, Vancouver, B.C. 1974.
10. I. J. HARVIE and F. J. MCQUILLIN. Chem. Commun. 369 (1976).
11. A. SEN and J. HALPERN. J. Am. Chem. Soc. **99**, 8337 (1977).
12. B. R. JAMES. Homogenous hydrogenation. Wiley, New York. 1973.
13. J. HALPERN, T. OKAMOTO, and A. ZAKHARIEV. J. Mol. Catal. **2**, 65 (1977).
14. J. GALLAY, D. DE MONTAUZON, and R. POILBLANC. J. Organomet. Chem. **38**, 179 (1972).
15. R. L. PRUETT and J. A. SMITH. J. Org. Chem. **34**, 327 (1969).
16. F. E. PAULIK. Catal. Rev. **6**, 49 (1972).

Can. J. Chem. Downloaded from www.nrcresearchpress.com by 210.87.254.5 on 09/05/12
For personal use only.

The photochemical reactivity of some benzoylthiophenes. IV. The effect of an adjacent methyl group on the excited state reactivity of 3-benzoylthiophene[1]

D. R. ARNOLD AND C. P. HADJIANTONIOU[2]

Photochemistry Unit, Department of Chemistry, The University of Western Ontario, London, Ont., Canada N6A 5B7

Received November 16, 1977

D. R. ARNOLD and C. P. HADJIANTONIOU. Can. J. Chem. **56**, 1970 (1978).

The electronic absorption and phosphorescence emission spectra and the photochemical reactivity of several methyl-3-benzoylthiophenes (2- and 4-methyl-3-benzoylthiophene (**1**, **2**), 2,5-dimethyl-3-benzoylthiophene (**3**), and 3-(2-methylbenzoyl)thiophene (**4**)) have been studied. Partial state diagrams have been constructed. The lowest energy absorption in hexane solution in every case is the carbonyl $n \rightarrow \pi^*$ transition. The two lowest triplet states of these ketones are close in energy and, in fact, the nature of the emitting triplet (n,π^* or π,π^*) depends upon the position of methyl substitution and upon the solvent. The photochemical reactions studied include intramolecular hydrogen abstraction (revealed by deuterium exchange in the adjacent methyl group upon irradiation in perdeuteriomethanol solution), photocycloaddition of dimethyl acetylenedicarboxylate to the thiophene ring, and photocycloaddition of isobutylene to the carbonyl group. Generalizations, potentially useful for predicting photochemical reactivity of these and other aromatic ketones are summarized.

D. R. ARNOLD et C. P. HADJIANTONIOU. Can J. Chem. **56**, 1970 (1978).

On a étudié les spectres électroniques, les spectres d'émission de phosphorescence ainsi que la réactivité photochimique de plusieurs benzoyl-3 thiophènes méthylés (méthyl-2 et -4 benzoyl-3 thiophène (**1**, **2**), diméthyl-2,5 benzoyl-3 thiophène (**3**) et (méthyl-2 benzoyl)-3 thiophène (**4**)). On a pu élaborer des diagrammes partiels des états d'énergie. L'absorption d'énergie la plus basse en solution dans l'hexane correspond, dans tous les cas, à la transition $n \rightarrow \pi^*$ du carbonyle. Les deux états triplets les plus bas de ces cétones ont des énergies semblables et de fait la nature du triplet qui émet (n,π^* ou π,π^*) dépend de la position du substituant méthyle ainsi que du solvant. Les réactions photochimiques étudiées comprennent des réactions d'enlèvement d'hydrogène (mises en évidence par un échange de deutérium dans le groupe méthyle adjacent lorsque l'on effectue une irradiation dans une solution de perdeutériométhanol), une réaction de photocycloaddition de l'acétylène dicarboxylate de diméthyle sur le thiophène et une photocycloaddition de l'isobutylène sur le groupement carbonyle. On donne un résumé des généralisations qui peuvent être utiles pour prédire la réactivité photochimique de ces cétones ainsi que d'autres cétones aromatiques.

[Traduit par le journal]

Introduction

This continuing research program has had two major objectives.[3] The first has been to define generalizations which would be potentially useful for predicting the photochemical reactivity of carbonyl compounds. Such generalizations would ideally be based upon structural considerations and knowledge of the reactivity of model systems alone. Additional knowledge of the electronic configuration of the excited states obtained from absorption and emission studies may be useful and, finally, extrapolation from one type of characteristic excited-state reactivity to another may be required. Predictions have been tested with a series of benzoylthiophenes where the vast knowledge of the photochemical reactivity of alkyl aromatic ketones and benzophenone derivatives serves as the model. In this paper, we focus on the photochemical reactivity of 2- and 4-methyl-3-benzoylthiophene (**1**, **2**), 2,5-dimethyl-3-benzoylthiophene (**3**), and 3-(2-methylbenzoyl)thiophene (**4**); *o*-methylbenzophenone has been extensively studied and is, of course, structurally analogous.

The second objective has been to exploit the unusual reactivity of the excited state of these ketones for synthetic purposes. Utilization of the thiophene ketones should provide not only thiophene derivatives and other sulfur containing products which are difficult to prepare by other methods but also, the reactivity of the thiophene ring in the photoproduct should provide a means of further molecular modification followed perhaps by eventual desulfurization.

Several photochemical reactions have been considered: (*i*) photochemically induced positional isomerization of the thiophene: (*ii*) photoenolization, which might lead to incorporation of deuterium in the adjacent methyl group upon irradiation in deuteriomethanol or to thienocyclobutene systems. Alter-

[1]Contribution No. 179 from the Photochemistry Unit.

[2]On leave from the University of Thessaloniki, Thessaloniki, Greece.

[3]For Part III of this series see ref. 1*c*.

Can. J. Chem. Downloaded from www.nrcresearchpress.com by 210.87.254.5 on 09/05/12
For personal use only.

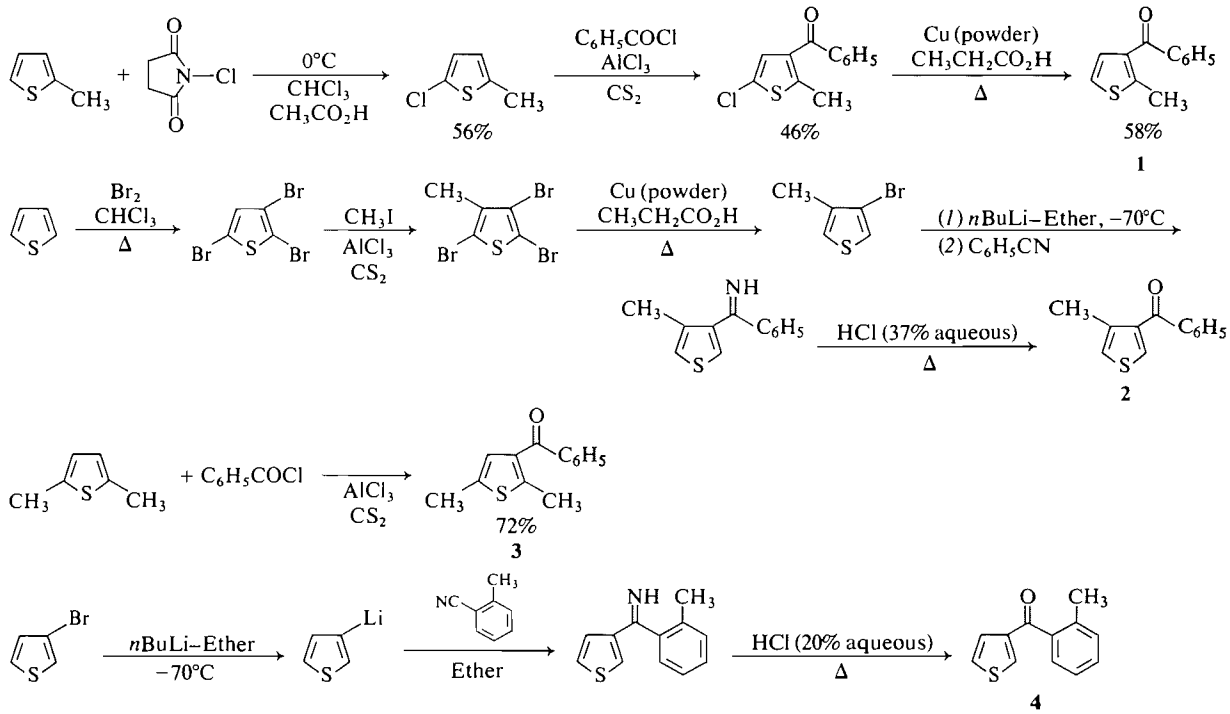

SCHEME 1

natively, the photoenol might be trapped by reaction with dienophiles to afford a useful synthesis of fused bicyclic molecules; (*iii*) photocycloaddition of olefins or acetylenes to the carbonyl group or to the thiophene ring might occur.

The results of these photochemical studies of **1–4** are discussed in connection with the partial state-diagrams for these ketones and for 3-benzoylthiophene (**5**), which can be drawn following the analysis of the absorption and phosphorescence emission spectra.

Results

The procedures used for the preparation of the ketones **1–4** required for this study are summarized in Scheme 1; **1**, **2**, and **4** are new compounds. In our initial attempts to prepare **1**, we used *N*-bromosuccinimide, instead of the *N*-chloro derivative, for the first step. The major brominated product obtained was carried through the Friedel–Crafts benzoylation and debromination and gave 2-benzoyl-5-methylthiophene instead of the desired **1**. In fact, it is known that 2-bromo-5-methylthiophene rearranges to the 4- and 3-bromo-2-methyl derivatives under remarkably mild conditions and the bromo ketone was therefore 5-methyl-4 (or 3) -bromo-2-benzoylthiophene instead of the desired isomer (2). The chloro derivative is much less susceptible to rearrangement. Details are reported in the Experimental.

The ultraviolet absorption spectra of **1–4** and 3-benzoylthiophene (**5**) in hexane and in methanol solution are shown in Figs. 1 and 2. The phosphorescence emission spectra of **1–5** were obtained in several solvents, ethanol–methanol (4:1) (EtOH–MeOH), methylcyclohexane (MCH), ethylene glycol (EG), methylcyclohexane – silica gel (MCH – SG), and diethyl ether – isopentane – ethanol (5:5:2) (EPA), at liquid nitrogen temperature. The triplet energies obtained from the emission spectra are given in Table 1. The shape of the phosphorescence emission varied depending upon the position of the methyl substituent and upon the solvent. Isomers **2**, **4**, and **5** have very similar emission in the same solvent; the variation with solvent for **5** is shown in Fig. 3. No distinct vibrational structure was observed in the emission from either **1** or **3** in any solvent. Except for a significant shift to longer wavelengths (Table 1) for **3**, the spectra were similar to those from **1** as illustrated in Fig. 4.

The rate of phosphorescence decay of ketones **1–5** was briefly studied. It was apparent that, in most solvents, the rate of decay was not a simple exponential function and no attempt was made to determine accurate rate constants. We estimate the lifetimes to be between 10^{-3} – 10^{-1} s in every case.

Irradiations were carried out in Pyrex (100% absorption < 280 nm) tubes kept at 10°C. The source was a 1 kW medium-pressure mercury vapour lamp

Can. J. Chem. Downloaded from www.nrcresearchpress.com by 210.87.254.5 on 09/05/12
For personal use only.

Can. J. Chem. Downloaded from www.nrcresearchpress.com by 210.87.254.5 on 09/05/12
For personal use only.

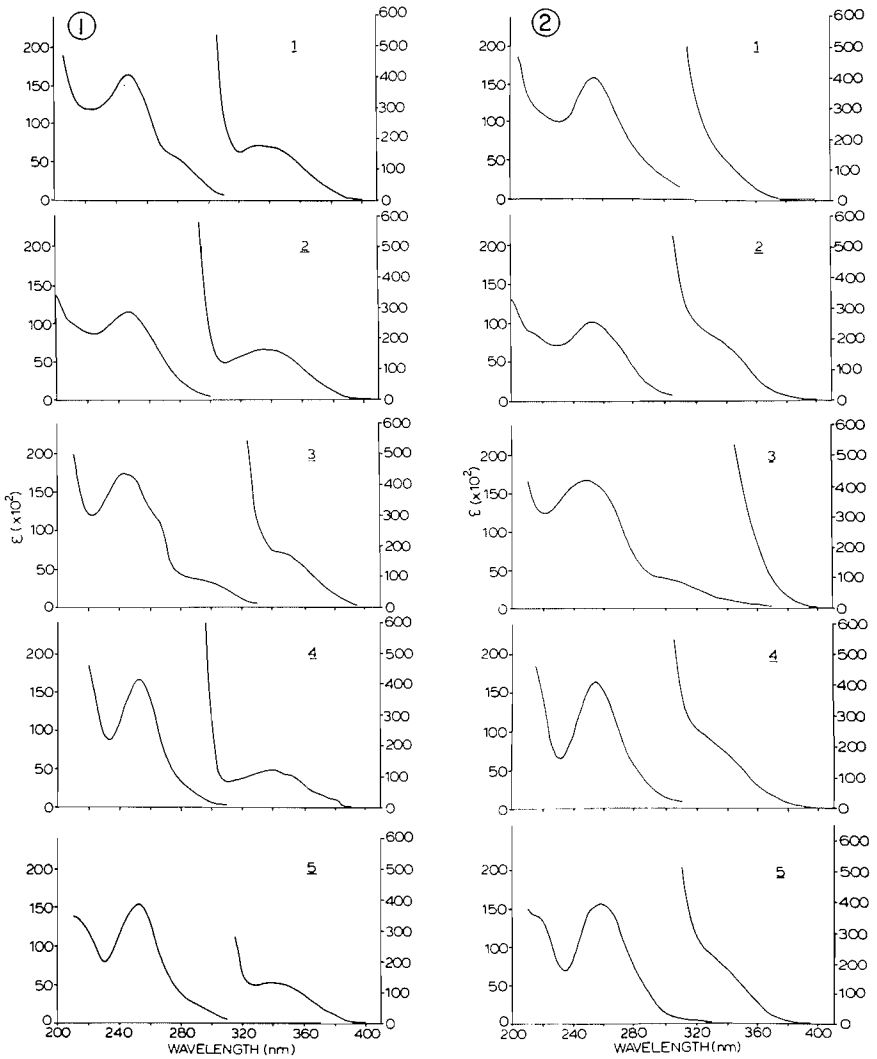

FIG. 1. Ultraviolet absorption spectra of some 3-benzoylthiophenes in hexane solution. The long wavelength region is plotted using the right axis.

FIG. 2. Ultraviolet spectra of some 3-benzoylthiophenes in methanol solution. The long wavelength region is plotted using the right axis.

TABLE 1. Triplet energies of some 3-benzoylthiophenes (**1**–**5**) in various solvents

	E_T (kcal mol^{-1})[a]				
Thiophene	EPA[b]	EtOH–MeOH(4:1)	MCH[c]	Ethylene glycol	MCH – silica gel
1	70.5	69.2	69.1	68.6	67.5
2	70.5	70.2	69.8	69.3	68.0
3	65.0	64.8	64.7	64.0	63.6
4	70.6	71.6	70.8	69.7	69.3
5	70.7[d]	70.6	70.0	68.2	68.6

[a]The position of the O—O band or onset of phosphorescence emission at 77 K.
[b]Diethyl ether – isopentane – ethyl alcohol (5:5:2).
[c]Methylcyclohexane.
[d]Reference 1*a*.

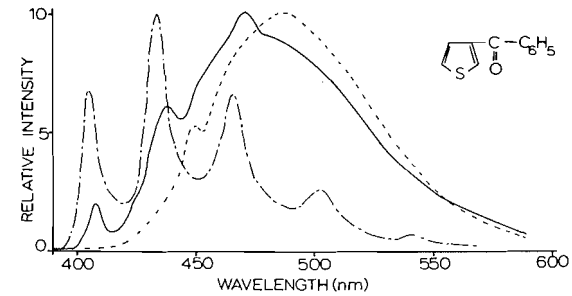

FIG. 3. Phosphorescence emission of 3-benzoylthiophene as afunction of solvent (77 K): — in methylcyclohexane; --- in methylcyclohexane – silica gel, the shape of the spectra taken in ethylene glycol was similar; -·-· in diethyl ether – isopentane – ethanol (5:5:2), the shape of the spectra taken in ethanol–methanol was similar.

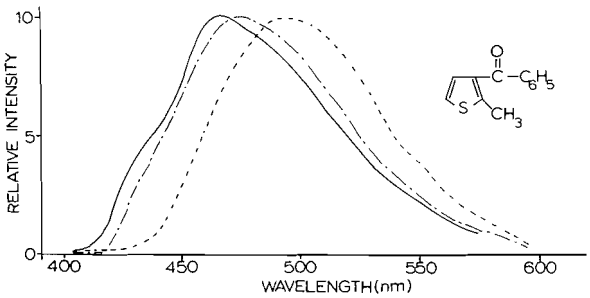

FIG. 4. Phosphorescence emission of 2-methyl-3-benzoylthiophene as a function of solvent (77 K): — in methylcyclohexane; --- in methylcyclohexane – silica gel; -·-· in diethyl ether – isopentane – ethanol (5:5:2).

in a quartz, water-cooled immersion well. Ketones **1–4** were irradiated in perdeuteriomethanol solution. The progress of the reaction was followed by proton nuclear magnetic resonance spectroscopy (^{1}Hmr). During the irradiation the mixture turned dark yellow; however, after 40 h, the starting ketone was largely recovered and purified by column chromatography. There was no evidence of positional isomerization of substituents on the thiophene ring. The extent of deuterium incorporation was determined by mass spectroscopy and in some cases nmr (^{1}H and ^{2}H).

In every case, deuterium (8–20% D_1) was incorporated. The greatest exchange was observed in the case of **3** where the deuterium nmr spectrum indicates deuterium was incorporated in *both* methyl groups. The methyl group which appears at lower field (2.55 ppm) had slightly more exchange than the other methyl group (2.39 ppm): 27% more in a sample which had incorporated 13% of one deuterium. The assignment of the lower field signal to the methyl in the 2 position is consistent with the chemical shift (2.63 ppm) of the methyl in **1**. Furthermore, the higher field methyl signal is broadened as a result of coupling with the proton in the 4 position. No attempt was made to determine the absolute efficiency of these deuterium exchange reactions. A relative estimate of the efficiency was obtained by comparing the extent of deuterium incorporated in *o*-methylbenzophenone under identical conditions. Tubes of *o*-methylbenzophenone and **3**, in perdeuteriomethanol were simultaneously irradiated. After 1 h, the methyl peak of *o*-methylbenzophenone had decreased in area by 25%, after 2 h by 50%; meantime, the peaks due to the methyls in **3** remained essentially unchanged.

The ketones **1–4** were irradiated for 7 h in benzene solution containing an excess of dimethyl acetylenedicarboxylate. Evaporation of the solvent gave a dark oily residue; the ^{1}Hmr spectra indicated considerable starting materials remained and a complex mixture of products had formed. Column chromatography partially separated these mixtures; starting materials were recovered, elemental sulfur was eluted, and in each case a fraction containing major products of the reactions, judging from the correspondence of the ^{1}Hmr spectra with those of the crude reaction mixtures, was obtained.

In each case the ^{1}Hmr and vapour phase chromatography (vpc) indicated this fraction contained at least three compounds. We believe these are positional isomers of benzoyl, methyl, dimethyl phthalates and terephthalates, based upon the ^{1}Hmr, ir, mass spectra, and combustion analysis of the mixtures. Because of the complexity of these mixtures and the large number of possible isomers, no attempts were made to separate and further characterize the products.

When the signals from these keto diesters were subtracted from the ^{1}Hmr spectra of the crude reaction mixtures, another major product was obviously present in each case. These products were not eluted from the column and were unstable in the crude reaction mixtures. Structures consistent with the ^{1}Hmr spectra are the bicyclic adducts (**6–9**) which would result from $2\pi e + 2\pi e$ cycloaddition of the dimethyl acetylenedicarboxylate to the thiophene ring across the 2—3 bond. We found no evidence for any other type of adduct being formed. These irradiations are summarized in Scheme 2.

Obviously the methyl group, present on **1–4**, should not be required for this type of photocycloaddition. To decrease the number of possible isomeric products and provide an analogy for the formation of the keto diesters we studied the irradiation of **5** under these conditions in more detail.

The ^{1}Hmr spectrum of the crude photolysate from

Can. J. Chem. Downloaded from www.nrcresearchpress.com by 210.87.254.5 on 09/05/12
For personal use only.

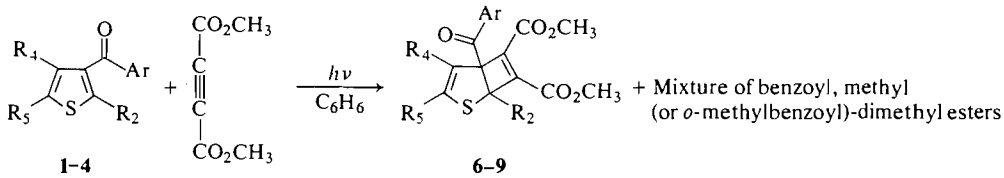

1–4 6–9

1 and **6** $R_2 = CH_3$, $R_4 = R_5 = H$, $Ar = C_6H_5$
2 and **7** $R_4 = CH_3$, $R_2 = R_5 = H$, $Ar = C_6H_5$
3 and **8** $R_2 = R_5 = CH_3$, $R_4 = H$, $Ar = C_6H_5$
4 and **9** $R_2 = R_4 = R_5 = H$, $Ar = C_6H_4(o\text{-}CH_3)$

SCHEME 2

5 and dimethyl acetylenedicarboxylate in benzene had absorptions attributable to the one-to-one adduct, **10**, and three keto diesters (Scheme 3). In this case also, the adduct was not stable; however, a rapid column chromatography provided a fraction, free from starting materials, which contained the adduct and the keto diesters. The analysis of the ^{1}Hmr spectrum of **10**, in comparison with those for the methyl derivatives **6–9**, supports the structural assignments of these compounds. These spectra are summarized in the Experimental. The mass spectrum of the mixture had a peak (*m/e*) equivalent to the molecular weight (exact mass) of adduct **10**. All attempts to obtain the adduct pure led to formation of the keto diester(s). Three keto diesters were separated by column and vapour phase chromatography and their structures established by comparison (ir) with authentic samples obtained by the independent synthesis outlined in Scheme 4.

The thermal Diels–Alder reaction (aluminium trichloride catalyzed (3)) of 2-benzoylthiophene with dimethyl acetylenedicarboxylate was attempted as an alternative approach for the synthesis of **11**; however, the ketone was recovered unchanged and no phthalate could be detected. This reaction was tried for the preparation of the phthalate from ketone **1** and phthalate **12**, also without success.

The ketones **1–4** were irradiated for 1 week in a benzene solution in which isobutylene (30% by weight) was dissolved. Evaporation of the solvent and excess isobutylene left a dark residue. The ^{1}Hmr and vpc of this residue indicated considerable starting ketone remained in every case and several (more than 15) products. There was no evidence in the ^{1}Hmr for the oxetanes. The residues were chromatographed on alumina columns and in every case the first compound to be eluted was the olefin (**14–17**). There was no evidence for the formation of the other possible olefin (i.e., the 1,1-disubstituted ethylene). The ketones **1–4** (60–70%) were eluted after the olefins. We found no indication of positional isomerization of the ketones. None of the other products was identified. These results are summarized in Scheme 5.

The structures of the olefins were firmly established by alternative synthesis: acid-catalyzed dehydration of the alcohol obtained from the Grignard reaction of isopropyl bromide on the ketones **1–4**. The olefin **16** and the alcohol precursor (obtained by the Grignard reaction of phenyl magnesium bromide with 3-isobutyroyl-2,5-dimethylthiophene) have been described previously (4); the olefins **14**, **15**, **17** are new compounds.

Discussion

We have previously reported the ultraviolet absorption and phosphorescence emission spectra of 3-benzoylthiophene (**5**), and constructed a partial state-diagram for this ketone (1*a*). We concluded

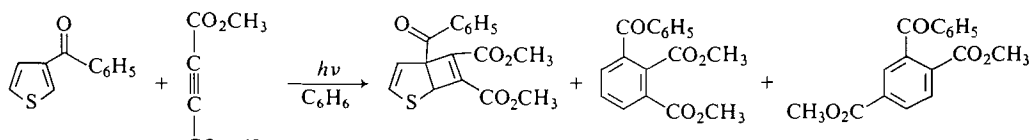

5 **10** **11** (46%) **13** (11.5%)

12 (34%)

SCHEME 3

Can. J. Chem. Downloaded from www.nrcresearchpress.com by 210.87.254.5 on 09/05/12
For personal use only.

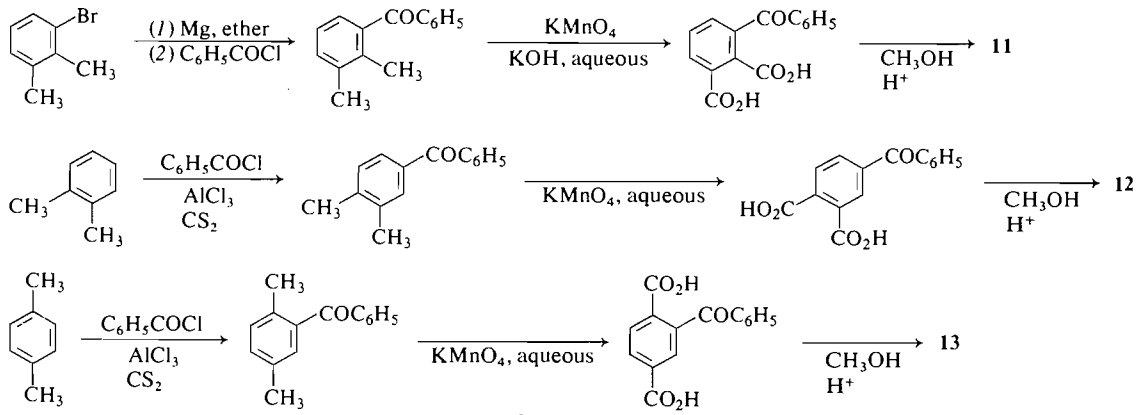

SCHEME 4

that since the lowest energy triplet (in EPA) had n,π* character, **5** would have photochemical reactivity similar to that of benzophenone. What seemed to be a valid extrapolation led to the further prediction (1*c*) that 3-benzoylthiophenes with an adjacent methyl group would react similarly to *o*-methylbenzophenone. We therefore expected that

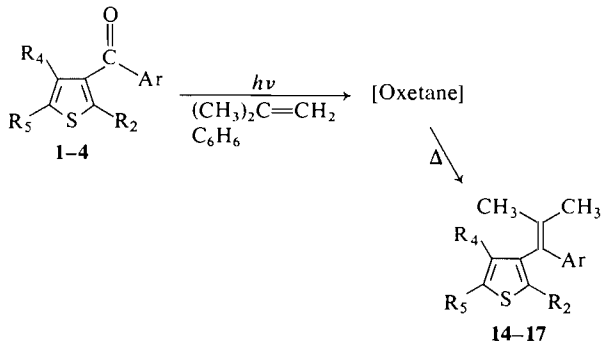

1–4

1 and **14** $R_2 = CH_3$, $R_4 = R_5 = H$, $Ar = C_6H_5$
2 and **15** $R_4 = CH_3$, $R_2 = R_5 = H$, $Ar = C_6H_5$
3 and **16** $R_2 = R_5 = CH_3$, $R_4 = H$, $Ar = C_6H_5$
4 and **17** $R_2 = R_4 = R_5 = H$, $Ar = C_6H_4(o\text{-}CH_3)$

SCHEME 5

ketones **1–4** would undergo efficient intramolecular hydrogen abstraction evidenced by incorporation of deuterium in the adjacent methyl group, upon irradiation in perdeuteriomethanol, and further, that the photoenol might be trapped with a reactive dienophile such as dimethyl acetylenedicarboxylate.[4] These photochemical reactions are well known for *o*-methylbenzophenone (5). Such was not the case; ketones **1–4** do not react photochemically in the expected way. We therefore studied the absorption and phosphorescence emission spectra of **1–5** in more detail in search of an explanation. Since the photochemical reactivity is best discussed in terms of the excited states available to these ketones, we will take up the absorption and emission studies first, construct the partial energy diagrams, and then discuss the photochemical reactivity in light of these results.

The ultraviolet absorption spectra of ketones **1–5** in hexane and in methanol solution are shown in Figs. 1 and 2. The long wavelength (> 320 nm) region of the spectra in hexane solution shows the weak carbonyl n → π* absorptions. This transition is shifted to shorter wavelengths and the shoulder of the adjacent π → π* absorption is shifted to longer wavelengths in methanol solution, so the n → π* absorption is partially obscured in this polar, hydrogen-bonding solvent.

In the spectrum of **5** in hexane, the thienyl, benzoyl, and 3-thienoyl chromophores all contribute to the strong absorption at 252 nm. These bands undergo a bathochromic shift (ca. 10 nm) in methanol as expected for π → π* transitions (1*a*). This region of the spectra of **2** and **4** is similar to that of **5**. There is no evidence for a shift to longer wavelengths of any of the π → π* transitions which could be attributed to an interaction of the methyl substituent.

In contrast, the absorption spectra of **1** has the shoulder at longer wavelengths (275 nm in hexane) indicative of a significant bathochromic shift of a π → π* transition. This shift is even more pronounced (ca. 300 nm in hexane) in the spectrum of **3** (6). The shifts to longer wavelengths of a π → π* transition in the spectra of **1** and **3** gave the first indication of a marked difference between the excited states of these ketones and **2**, **4**, and **5**.

The similarity of the energies of the corresponding singlet states for **2**, **4**, and **5**, reflected in the absorption spectra, extends also to the triplet states. The phosphorescence emission from **2**, **4**, and **5** are similar to one another and behave similarly as a function of solvent. Our interpretation is that the methyl group in the 4 position of thiophene and in the

[4]For a recent review on photoenolization see ref. 5*a*.

Can. J. Chem. Downloaded from www.nrcresearchpress.com by 210.87.254.5 on 09/05/12
For personal use only.

Can. J. Chem. Downloaded from www.nrcresearchpress.com by 210.87.254.5 on 09/05/12
For personal use only.

o-benzoyl position has little effect on either the singlets or the triplets in these compounds. On the other hand, the methyl in the 2 position of **1** and in the 2 and 5 positions of **3** have a pronounced effect on both the singlet and the triplet of these compounds.

The triplet energies, taken from the phosphorescence emission spectra in several solvents, are summarized in Table 1 and typical spectra are shown in Figs. 3 and 4.

In Fig. 3, the phosphorescence emission from **5** in EPA has the vibrational structure characteristic of n,π* carbonyl triplet emission. The separation of the O—O and O—1 bands is 1664 cm^{-1} indicative of the carbonyl bond stretching mode. This 'five fingered' vibrational structure is also observed from **2** and **4** in this medium. The O—O – O—1 band separation is 1654 cm^{-1} for **2** and 1658 cm^{-1} for **4**. The nature of the emissions from **2**, **4**, and **5** changes when MCH is the medium. Still n,π* character is dominant; however, an additional broad structureless emission becomes obvious at longer wavelengths. When the medium is MCH–SG or EG all trace of the structured emission disappears and broad structureless emission is observed from **2**, **4**, and **5**. We assign the structureless emission to a π,π* triplet. This inversion in the order of the n,π* and π,π* triplet of ketones upon changing the solvent from hydrocarbon to polar, hydrogen-bonding solvents is not common but has adequate precedent (7).

The phosphorescence emission from **1** is shown in Fig. 4; **3** behaves similarly except that the emission is at considerably longer wavelengths (Table 1). There is no structured emission from these ketones in any solvents; a regular shift to longer wavelengths, as the solvent polarity is increased, is observed. These features are consistent with the assignment of a π,π* triplet for the lowest triplet of both **1** and **3**.

In their review (7*a*) Nicholls and Leermakers suggest a classification for carbonyl compounds based upon their emissive behaviour as a function of solvent: (I) those ketones with emitting n,π* triplet states in both polar and nonpolar media; (II) those compounds which emit from an n,π* triplet in low polarity solvents but invert to a π,π* state in high polarity media; and (III) ketones for which the lowest-lying triplet is π,π* in all solvents. Using this classification, ketones **2**, **4**, and **5** would be in Group II, whereas **1** and **3** are in Group III. Some acetophenone and benzaldehyde derivatives are also known to be in Group II (7*b*,*d*).

The significant difference in triplet energy and the inversion of the order of triplet state as a function of position of methyl substitution was not anticipated at the onset of this work. In retrospect, the bathochromic shift of a π → π* transition in the absorption spectra of **1** and **3** could have provided insight.

The fact that the methyl group in the 5 position of **3** has a rather large effect, decreasing the π,π* triplet energy by >4 kcal mol^{-1}, while the methyl group in the 4 position of **2** has very little effect, was at first surprising. However, there is a significant effect of a methyl group in the 4 position on the triplet energy (π,π*) of 2-benzoylthiophene where the position of the two groups is interchanged. The triplet energy of 2-benzoylthiophene and 4-methyl-2-benzoylthiophene are 63.5 and 61.5 kcal mol^{-1} (ethanol–methanol (4:1)) (1*c*).

It now seems reasonable that the effect of the methyl(s) lowering the π,π* singlet state in **1** and **3** also affects the corresponding triplet which presumably is associated with the 3-thienoylchromophore.

The partial state-diagrams shown in Fig. 5, are based on the absorption and phosphorescence emission spectra and indicate the energy and order of states in hydrocarbon media. The π,π* singlet energy levels are taken from the maxima or shoulders of the absorption spectra and are therefore maximum values, useful only for comparison. The n,π* singlet energy levels are from the O—O band of the n → π* transitions. The energy of the lowest triplet levels are taken from the O—O band, or high energy onset, of the emission spectra. When the n,π* triplet is the T_2 state (**1** and **3**), its energy has been estimated by assuming the normal ca 2000 cm^{-1} singlet–triplet separation. Obviously, in the case of **2**, **4**, and **5**, where the T_2 state is π,π* (in nonpolar media), the energy gap must be very small (<ca. 4 kcal mol^{-1}) and we estimate a value less than 74 kcal mol^{-1} from the known π,π* triplet energy of the benzoyl chromophore.

It should be pointed out that the triplet energies in Table 1 and Fig. 5 were obtained in rigid media at liquid nitrogen temperatures. The energy, and in fact the order of triplet states, may be different in fluid solutions at the temperature of the irradiations (10°C). What little is known about the effect of these environmental changes on triplet energy indicates the n,π* triplet may be as much as 2 kcal mol^{-1} less in the fluid media at room temperature than that determined in rigid media at −196°C, whereas the π,π* triplet associated with the benzoyl chromophore has virtually the same triplet energy in rigid and nonrigid media (8*a*).

The phosphorescence emission was intense and no fluorescence was observed from **1** – **5** in any solvent. In view of the ordering of states shown in the partial energy-diagrams (Fig. 5), with a lowest n,π* singlet and a lower or near-by π,π* triplet, it seems likely that intersystem crossing will be a rapid process, as it is for most benzophenone derivatives (9).

The first observation regarding the photochemical reactivity of the ketones **1**–**5** is the lack of positional

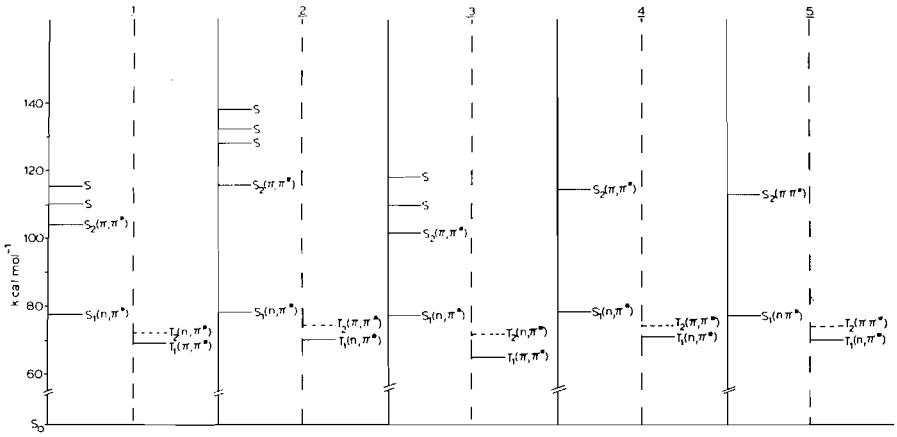

FIG. 5. Partial energy diagrams of 3-benzoylthiophenes **1** – **5**.

isomerization. The interchange of the thiophene carbons 2 and 3 occurs via the intermediate cyclopropenyl thioketone or thioaldehyde and is a fairly general reaction for alkyl- and aryl-substituted thiophenes. This rearrangement appears to involve the lowest singlet π,π^* state and has never been observed when the thiophene is substituted with a carbonyl group; thiophene aldehyde and acetylthiophene also do not rearrange (10). To our knowledge there are no exceptions to this generalization which may, therefore, be useful for predicting photochemical reactivity of other substituted thiophenes.

It is now generally accepted that carbonyl compounds with π,π^* lowest triplets are appreciably less reactive toward both intermolecular and intramolecular (eg. Norrish type II process) hydrogen abstraction (8*a*,*b*). The photoenolization reaction is usually considered as a special intramolecular example of these hydrogen abstractions and, in view of the fact that a 1,4-biradical is known or postulated to be an intermediate, the analogy is justified. An alternative orbital symmetry allowed sigmatropic 1,5-hydrogen shift in the excited state requires an antarafacial hydrogen migration, which seems unlikely, or a sign inversion at one of the incipient double bonds. The latter possibility could lead directly to the formation of the photoenol having the (*E*)-dienol configuration. Since this configuration is frequently the only isomer trapped with dienophiles (5*e*) perhaps the concerted reaction should not be discounted.

In any event, it is certain that an n,π^* state, singlet or triplet, is *not* required for photoenolization. The most convincing evidence for this is the observed photochemical reactivity of the corresponding alkene. Deuterium exchanges between the vinyl and the methyl position of 1,1-dideuterio-2-phenyl-2-(*o*-tolyl)ethylene (11) and the *o*-xylylene has been trapped in a Diels–Alder reaction with cyclohexene (12). Unfortunately, the efficiency (or more to the point, the rate constant) of this reaction has not been measured.

Although it is difficult to estimate the efficiency of the photochemical deuterium incorporation in ketones **1**–**4**, particularly since light absorbing by-products are gradually produced, the comparatively rapid exchange observed with *o*-methylbenzophenone under identical conditions indicates the efficiency of exchange with **1**–**4** is several orders of magnitude *less* than that of the benzophenone derivative.

We are unable to attribute what reactivity does occur to any particular state; the n,π^* singlet and π,π^* and n,π^* triplets are all possibilities. In the case of alkyl phenyl ketones the photochemical reactivity in the Norrish type II reaction (indicated by the rate constant for the hydrogen abstraction step) of those ketones having a lowest π,π^* triplet was attributed to thermal equilibration with the upper reactive n,π^* triplet. The reactivity decreased as the separation between the lowest π,π^* triplet and the upper n,π^* triplet increased (8). Although there is no direct relationship between the efficiency of a photochemical reaction and the reactivity as reflected by the rate constant, we can point out that the most efficient deuterium exchange was observed with **3** where the energy difference between $T_1(\pi,\pi^*)$ and $T_2(n,\pi^*)$ is the largest. However, the observation that deuterium was incorporated in the methyl group in the 5 position of **3** requires that some mechanism in addition to, or perhaps instead of, photoenolization occurs.

There are some features associated with some of the deuterium exchange processes which are worthy of special note. In the case of **2** a simple photoenol intermediate is impossible. The photoenol would have a tetracovalent sulfur structure which would be analogous to the *o*-xylylene intermediate discussed previously in connection with the thermal rearrange-

Can. J. Chem. Downloaded from www.nrcresearchpress.com by 210.87.254.5 on 09/05/12
For personal use only.

Can. J. Chem. Downloaded from www.nrcresearchpress.com by 210.87.254.5 on 09/05/12
For personal use only.

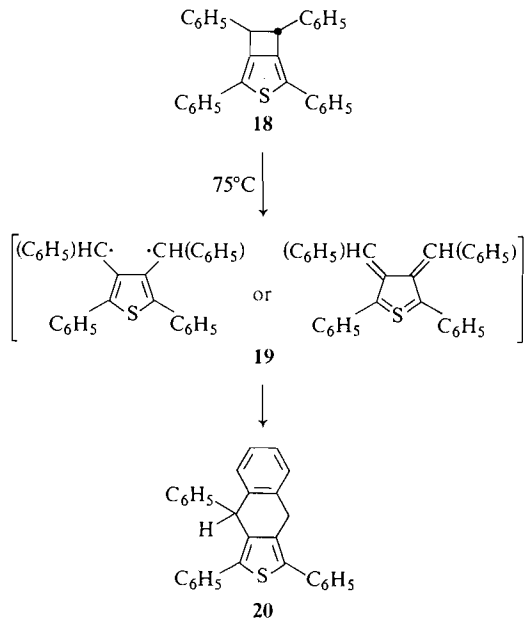

SCHEME 6

ment of thieno[*c*]cyclobutene derivatives (13). For example, **18** rearranges at 75°C to the dihydronaphtho[*c*]thiophene derivative **20** (Scheme 6) (13). We thought it might be possible that irradiation of **2** would yield the thieno[*c*]cyclobuteneol, dihydronaphtho[*c*]thiophene, or other product which would attest to formation of an intermediate similar to **20**; such was not the case. We must, therefore, leave open the question regarding the structure of the intermediate(s) in the deuterium exchange of **2**.

The inefficiency in the exchange process with **4** is significant since the hydrogen being abstracted in this case is benzylic, not thiophenylic, and the photoenol would be an *o*-xylylene analogous to that formed from *o*-methylbenzophenone. The implication is that the inefficiency results from the inherent reactivity of the excited state of the 3-benzoylthiophene chromophore and not the inability to abstract hydrogen from the methyl group on the thiophene.

The question regarding possible conformers of **1–4** should be raised. It has recently been shown that *o*-methylacetophenone has two conformationally related triplets, i.e. where the *o*-methyl group and the carbonyl oxygen are on the same (*syn*) or opposite (*anti*) sides of an approximately planar molecule. These two triplets decay with rates 5×10^9 and 3×10^7 s^{-1} in benzene at room temperature. The longer lived triplet is believed to be the *anti* conformer where the rate of decay is determined by rotation to the *syn* conformer which is then followed by rapid hydrogen abstraction (14). We do not know the preferred conformation of the ground state of **1–4** nor do we know the rate of interconversion of these conformers around the thiophene–carbonyl carbon bond in the excited state. It is, however, unlikely that the preferred orientation or the rate of interconversion is very different from that of *o*-methylacetophenone. This is certainly true for **4** where rotation around the phenyl–carbonyl carbon bond would be involved in an excited state which, from the emission spectrum, appears to be localized predominantly on the 3-thienoyl moiety.

The irradiations of **1–4** in the presence of dimethyl acetylenedicarboxylate were carried out in an attempt to trap the photoenol. The complexity of the reaction mixtures makes it impossible for us to rule out a small amount of this type of reaction; however, we found no evidence for adducts of this type. The products that were characterized indicate the predominant reaction was photocycloaddition to the 2,3 bond of the thiophene. The photocycloaddition of electron-deficient olefins and acetylenes to the excited state of thiophenes and benzothiophenes has been observed previously (15).

A typical known example of this reaction is illustrated in Scheme 7 with 2,5-dimethylthiophene and dimethyl acetylenedicarboxylate (15*a*). These reactions are complicated by the photochemical and thermal instability of the bicyclic adducts. Studies using triplet–triplet transfer sensitizers indicated the cycloaddition reaction can occur with the thiophene triplet. The energy threshold (≥ 62.4 kcal mol^{-1} in benzene solution at room temperature) required to cause reaction with 2,5-dimethylthiophene is somewhat lower than the observed triplet energy of **3** (ca. 65 kcal mol^{-1}, Table 1). It seems improbable that 2,5-dimethylthiophene has a lower triplet energy than **3**; the results more likely indicate the energy transfer process can be endothermic to a small ex-

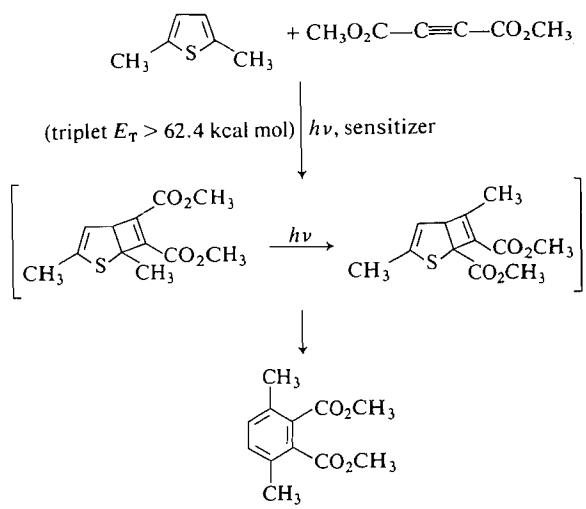

SCHEME 7

Can. J. Chem. Downloaded from www.nrcresearchpress.com by 210.87.254.5 on 09/05/12
For personal use only.

tent. These workers also estimate the triplet energy of thiophene to be ≥ 70 kcal mol^{-1}. This was the first indication of the pronounced effect of the 2,5-methyl groups toward lowering the triplet energy (15*a*).

The formation of adducts **6–10** and the subsequent decomposition of these adducts to diesters, therefore, has adequate precedent and is consistent with a reaction involving the π,π^* triplet of the ketones **1–5**.

The purpose behind the experiments, irradiatngi **1–4** in the presence of isobutylene (Scheme 6), was to test the ability of the excited states of these ketones to undergo photocycloaddition of the olefin to the carbonyl group. It was known that **5** yields the oxetane under these conditions; if intramolecular hydrogen abstraction competes with photocycloaddition, **1–4** would be less prone to yield the oxetanes. The analogous photocycloaddition of *o*-methylbenzophenone is strongly quenched (16). However, *o*-methylbenzaldehyde forms the oxetane with 2,3-dimethyl-2-butene with high efficiency (17).

Following the irradiations, the crude reaction mixtures were quite complex. The oxetanes were not detected; however, the olefins **14–17**, presumably derived from the oxetanes, were separated from the other products and were positively identified. The instability of the oxetanes is not surprising (1*b*,*c*) and the formation of the olefins attests to the fact that **1–4** do indeed undergo photocycloaddition of isobutylene to the carbonyl group. The other products were not identified.

Not too many years ago, it was thought that the first step toward photocycloaddition of the carbonyl group required attack by the nonbonding electron on the oxygen of the carbonyl n,π^* state on the double bond of an electron-rich olefin much like an alkoxy radical would add to an olefin (16). This simple picture no longer adequately explains the results and it is now generally recognized that the first step toward oxetane usually is formation of a complex (or exciplex) between the excited state (n,π^* or π,π^*) of the carbonyl compound and the olefin. The complex then reacts further to give the oxetane, perhaps with the intervention of a diradical intermediate, or deactivates. When the two molecules involved have molecular orbitals which differ in size and shape there may be more than one energy minima on the surface describing the structure of the complex. Whether the product from the excited state of benzoylthiophenes **1–4** with an olefin occurs at the carbonyl group or to the triophene (oxetene or bicyclic adduct upon reaction with dimethyl acetylenedicarboxylate) will then depend upon: (*i*) where complexing occurs, over the carbonyl group or over the thiophene ring; (*ii*) the relative reactivity going on to product vs. the various deactivation pathways for each of the possible orientations of the complex and any other intervening intermediate(s). Stated in this more realistic way it is obvious that predicting the photocycloaddition reactivity of a complex molecule will remain a difficult problem for some time to come.

Conclusions

(*i*) The analysis of the ultraviolet absorption and phosphorescence emission spectra of the 3-benzoylthiophenes **1–5** reveals a pronounced influence of position of methyl substitution and solvent on the energies and relative order of the singlet and triplet states. These data are summarized in Table 1 and in the energy diagrams shown in Fig. 5.

(*ii*) Ketones **1–4** incorporate deuterium in the adjacent methyl group upon irradiation in perdeuterio methanol. Deuterium is also incorporated in the methyl group in the 5 position of **3**. This exchange is much less efficient than that observed for the analogous *o*-methylbenzophenone. A mechanism other than photoenolization may be involved.

(*iii*) Bicyclic[3.2.0] adducts were obtained from the irradiation of ketones **1–5** in the presence of dimethyl acetylenedicarboxylate. These adducts were unstable and decomposed thermally with loss of sulfur to the phthalates and terephthalates. There was no evidence of adducts of the Diels–Alder type involving the photoenol of **1–4**.

(*iv*) The ketones **1–4** undergo photocycloaddition at the carbonyl group with isobutylene. The oxetanes were not characterized; the olefines, formed by loss of formaldehyde from the oxetane, attest to their formation.

(*v*) We found no evidence for photorearrangement of the ketones **1–5**.

(*vi*) The photolysis mixtures were generally complex owing to the photochemical and/or thermal instability of the products. The material balance was therefore poor. The reactions were comparatively inefficient. These factors tend to complicate photophysical and mechanistic studies required to attribute reactivity to a particular excited state. It is clear, however, that these ketones (**1–4**) do not show the expected efficient reactivity of an n,π^* triplet. The available evidence indicates either the π,π^* triplet, or an upper n,π^* triplet, possibly in thermal equilibrium with the π,π^* triplet, is reacting.

Experimental

General

The apparatus and instrumentation for ultraviolet absorption spectra, phosphorescence emission spectra, and life-time measurements were reported in Part I (1*a*). Ultraviolet absorption spectra were obtained in *n*-hexane (BDH, spectral grade)

Can. J. Chem. Downloaded from www.nrcresearchpress.com by 210.87.254.5 on 09/05/12
For personal use only.

and in methanol, which was purified by distillation from magnesium metal, using 1-cm quartz cells. The emission spectra were measured in five different solvents at 77 K after degassing the solutions by three freeze–pump–thaw cycles. Ethanol was purified the same way as methanol, the methylcyclohexane was Eastman Kodak spectro grade, ethylene glycol was from Fisher Scientific, and EPA was from American Instrument Co. All the above solvents showed no emission when irradiated at the wavelength used to obtain the spectra.

Samples used for spectroscopic studies, combustion analyses, and photochemical reactions were purified by semipreparative vpc (Varian, model 920, 10% DEGS Chrom.w, nonacid washed (NAW), 60–80 mesh and 30% SE-30, Chrom.w; NAW, 60–80 mesh).

All irradiations were carried out using a General Electric Co. 1 kW medium-pressure mercury vapour lamp, through a Pyrex filter at 10°C. Samples were not degassed unless stated otherwise. The progress of the reaction was followed by ^{1}Hmr and/or vpc. ^{1}H nuclear magnetic resonance spectra were run in deuteriochloroform solution using tetramethylsilane as internal standard with a Varian HA-100 spectrometer. The chemical shifts are taken as the center of multiplets and the reported coupling constants are the result of a first-order analysis; coupling was confirmed by double irradiation experiments.

The deuterium nmr spectrum of 2,5-dimethyl-3-benzoylthiophene was obtained at 15.4 MHz with a Varian XL-100-15 system in the Fourier transform mode.

Infrared spectra were recorded on a Beckman IR-5A or IR-20A spectrometer and mass spectra on a Varian M-66 or Mat 311A mass spectrometer. Calibration of the ir spectra was done using the 1601.8 cm^{-1} absorption band of polystyrene. The combustion analyses were performed by Chemalytics, Inc., Tempe, Arizona.

3-Methylthiophene, 2,5-dimethylthiophene, 3-bromothiophene, and 3-bromo-*o*-xylene were obtained from Aldrich Chemical Co.

All reported yields are based on isolated products.

Synthesis of Starting Materials

Synthesis of 2-Methyl-3-benzoylthiophene (1)

Preparation of 2-chloro-5-methylthiophene (18)—*N*-Chlorosuccinimide (19) (14.6 g, 10% excess) was added to a solution of 2-methylthiophene (9.8 g, 0.1 *M*) in benzene (60 ml) – acetic acid (60 ml) and stirred for 30 min, refluxed for 1 h, and poured into water. The organic layer was separated, washed with sodium hydroxide (200 ml, 2 *N*) and water and then dried over magnesium sulfate. After three consecutive distillations pure 2-chloro-5-methylthiophene (7.6 g, 58%, bp 155–156°C/760 Torr) was obtained.

Preparation of 5-chloro-2-methyl-3-benzoylthiophene—2-Chloro-5-methylthiophene (4.6 g) and benzoylchloride (4.9 g) were dissolved in carbon disulfide (35 ml) and the solution was cooled in an ice-bath. Aluminum chloride (4.6 g) was added in portions. A slightly exothermic reaction occurred giving a deep red solution which was stirred for 1 h at room temperature and then poured into cold water (200 ml) and extracted with ether. The ether layers were washed with aqueous potassium hydroxide (10%), water (2 × 200 ml), and dried over magnesium sulfate (anhydrous). Evaporation of the solvent and distillation gave 5-chloro-2-methyl-3-benzoylthiophene (3.7 g, 46%, bp 166–167°C/0.15 Torr).

Dechlorination (20) of 5-chloro-2-methyl-3-benzoylthiophene—5-Chloro-2-methyl-3-benzoylthiophene (3.6 g) and activated copper powder (4 g) in propionic acid (10 ml) were refluxed under an argon atmosphere for 24 h. The resulting mixture was poured into water, filtered from solids, neutralized with solid sodium bicarbonate, and extracted with ether. The ether layer was washed with water and dried over anhydrous magnesium sulfate. Removal of ether gave crude product (2.3 g, 73%) which, after distillation, yielded pure 2-methyl-3-benzoylthiophene (1.8 g, 58%, bp 150°C/0.3 Torr); ir (neat) ν: 1660, 1452, 1278, 854, 696, 665 cm^{-1}; ^{1}Hmr ($CDCl_3$) δ (TMS): 7.07 (H-4), 6.95 (H-5), 2.62 ppm (methyl); $J_{4,5}$ = 5.2 Hz; ms (70 eV) *m/e* (relative intensity): 202 (100, M^+), 201 (90), 124 (50), 105 (15), 77 (28). *Anal.* calcd. for $C_{12}H_{10}OS$ (1): C 71.28, H 4.99; found: C 71.09, H 5.08.

Initial attempts to prepare the above thiophene used *N*-bromosuccinimide instead of *N*-chlorosuccinimide. Friedel–Crafts reaction of 2-bromo-5-methylthiophene gave a bromo ketone (mp 93–94°C, recrystallization from hexane); ir (Nujol) ν: 1664, 877, 860, 788, 720, 699, 640 cm^{-1}; ^{1}Hmr ($CDCl_3$) δ (TMS): 7.72 (m), 7.42 (m), 2.40 ppm (s, methyl); ms (70 eV) *m/e* (relative intensity): 282 (8, M^+), 280 (9, M^+), 205 (17), 203 (18), 201 (10), 145 (17), 105 (26), 77 (42), 32 (100), 28 (90). *Anal.* calcd. for $C_{12}H_9BrOS$: C 51.27, H 3.23, Br 28.42; found: C 51.02, H 2.93, Br 28.62.

Debromination of this ketone with activated copper powder yielded 2-benzoyl-5-methylthiophene identified by comparison with the known ir spectrum. Obviously, the 2-bromo-5-methylthiophene underwent isomerization to 4 (or 3) -bromo-2-methylthiophene during the Friedel–Crafts benzoylation and the above bromo ketone (mp 93–94°C) consequently has to be 4-bromo-5-methyl-2-benzoylthiophene or 3-bromo-5-methyl-2-benzoylthiophene instead of the desired 5-bromo-2-methyl-3-benzoylthiophene.

Activated Copper Powder (21)

Oxide free zinc was added to an excess of slightly acidified aqueous cupric sulfate keeping the temperature below 40°C. The precipitated copper was collected, washed with water to remove the remaining cupric sulfate and acid, and finally washed twice with dry acetone and dried for 30 min at 100°C.

Synthesis of 4-Methyl-3-benzoylthiophene (2)

4-Methyl-3-benzoylthiophene was prepared by an adaptation of Gronowitz's method (22), using 3-bromo-4-methylthiophene and benzonitrile.

3-Bromo-4-methylthiophene (23)—2,3,5-Tribromo-3-methylthiophene (24) (12.3 g, 0.037 *M*) was added portionwise to a stirred refluxing mixture of water (75 ml), zinc powder (10.5 g), and acetic acid (7 ml). After addition was complete the mixture was refluxed for 30 h and then distilled from the reaction flask. The aqueous layer of the distillate was separated from time to time from the organic phase and returned to the reaction vessel. The organic phase was washed with sodium carbonate solution then water, dried, and distilled. A crude product (5.5 g, 84%, bp 59–65°C/11 Torr) was obtained. Redistillation gave pure 3-bromo-4-methylthiophene (4.4 g, 68%, bp 179–183°C/760 Torr).

4-Methyl-3-benzoylthiophene (2)—A well dried three-necked round bottom flask with stopper, magnetic stirrer, serum cap, and gas inlet tube was purged with argon for ½ h and cooled in a Dry Ice – acetone bath. The flask was then charged with 3-bromo-4-methylthiophene (1.77 g) and anhydrous ether (4 ml). The etherial solution was stirred for 15 min and then *n*-butyllithium (3.6 ml, 2.77 *M*, in hexanes) was added via a dry syringe, through the serum cap during about 5 min. The light yellow solution was stirred for ½ h and a solution of benzonitrile (1.03 g) in anhydrous ether (2.0 ml) which had been purged with argon and cooled to −78°C, was quickly added to the solution. The resulting orange solution was stirred for 2 h at −78°C and allowed to warm up slowly to −10°C. Then hydrochloric acid (20%, 15 ml) was added via the syringe. The colour changed to brown and then to light yellow while a pre-

Can. J. Chem. Downloaded from www.nrcresearchpress.com by 210.87.254.5 on 09/05/12
For personal use only.

cipitate appeared and redissolved. After 30 min stirring, the organic layer was separated, the ether was evaporated, and the remaining brown oil added to the aqueous layer which was then refluxed with hydrochloric acid (20%, 10 ml) for 10 h. This mixture was extracted with ether (2 × 20 ml), washed with water, saturated aqueous sodium bicarbonate, and dried over anhydrous magnesium sulfate. Evaporation of the solvent gave a dark oil, which was a mixture of the imine and the ketone. These were separated by fractional distillation. The first fraction (bp 170°C/0.05 Torr) yielded 4-methyl-3-benzoylthiophene (1.25 g, 62%); ir (neat) ν: 1645, 1445, 1265, 1180, 895, 870, 816, 790, 747, 730, 712, 693, 668 cm^{-1}; ^{1}Hmr ($CDCl_3$) δ (TMS); 7.58 (H-2, m), 6.98 (H-5, m), 2.42 ppm (CH_3); $J_{2,5}$ = 3.2, J_{5,CH_3} = 1.2 Hz; ms (70 eV) *m/e* (relative intensity): 202 (92, M^+), 201 (100), 124 (38), 105 (9), 77 (15). *Anal.* calcd. for $C_{12}H_{10}OS$ (**2**): C 71.28, H 4.99; found: C 71.28, H 5.10.

Synthesis of 2,5-Dimethyl-3-benzoylthiophene (3)

2,5-Dimethyl-3-benzoylthiophene was prepared (25) by the Friedel–Crafts reaction of 2,5-dimethylthiophene (2.02 g, 0.018 *M*) and benzoyl chloride (2.38 g, 0.017 *M*) in carbon disulfide (25 ml). Anhydrous aluminum chloride (4.53 g, 0.044 *M*) was added in portions and the mixture, after 1 h refluxing, was poured into cold water (1 ℓ) and stirred for 30 min. The organic layer was separated and the aqueous layer was further extracted with carbon disulfide. The combined extract was first washed with aqueous sodium hydroxide (10%, 1 × 200 ml) and then water (3 × 200 ml) and dried over anhydrous magnesium sulfate. Removal of solvent gave a brown viscous oil, which after distillation yielded a clear oil (2.85 g, 72%, bp 185–187°C/10 Torr) that crystallized upon cooling. Recrystallization from methanol gave colourless crystals (mp 44.5–45°C (lit. (4) mp 44°C)).

Synthesis of 3-(2-Methylbenzoyl)thiophene (4)

3-(2-Methylbenzoyl)thiophene was also prepared by an adaptation of Gronowitz's method (22). From 3-bromothiophene (4.06 g) in anhydrous ether (5 ml), *n*-butyllithium (1.25 ml, 2.04 *M*, in hexanes), and *o*-methylbenzonitrile (1.75 g) in anhydrous ether (5 ml), a brown oil (4.62 g crude product, 92%) was obtained. Distillation of the above oil gave two fractions. The first fraction (2.3 g, 46%, bp 114°C/0.03 Torr) was the desired ketone (**4**) and the second fraction (1.8 g, bp 194°C/0.03 Torr) the unhydrolized imine (ir ν: NH 3300, C=N 1602 cm^{-1}) which, upon further refluxing with hydrochloric acid (20%) gave again a mixture of imine and ketone. Isolation of the ketone from the mixture can be achieved by fractional distillation; ir (neat) ν: 1655, 1510, 1417, 1402, 1235, 1150, 970, 862, 825, 738, 662 cm^{-1}; ^{1}Hmr ($CDCl_3$) δ (TMS) 7.76 (H-2), 7.56 (H-4), 7.31 (H-5), 2.39 ppm (methyl); $J_{2,4}$ = 1.4, $J_{2,5}$ = 3.0, $J_{4,5}$ = 5.2 Hz; ms (70 eV) *m/e* (relative intensity): 202 (80, M^+), 201 (40), 185 (17), 169 (100), 157 (9), 141 (72), 119 (19), 111 (56), 91 (52), 83 (25). *Anal.* calcd. for $C_{12}H_{10}OS$ (**4**): C 71.28, H 4.99; found: C 71.48, H 5.07.

Synthesis of 3-Benzoylthiophene (5)

3-Benzoylthiophene was prepared by the method of Hornfeldt and Gronowitz (22) as described in detail in Part I (1*a*).

Irradiation Experiments in Perdeuteriomethanol

A Pyrex ^{1}Hmr tube, containing the 3-benzoylthiophene (100 mg) (**1**–**4**) in perdeuteriomethanol (3 ml) was purged with argon for 10 min, sealed with a serum cap, and irradiated for 40 h. The integrated area and the heights of the ^{1}Hmr peaks due to the methyl group and aromatic protons before and after irradiation indicate a small amount of deuterium incorporation in the methyl group. Evaporation of the solvent in each case gave yellow oils. The mass spectra of samples purified by vpc show ratios of $(M + 1)^+/M^+$ peaks higher than in the corresponding starting materials, evidence indicating deuterium incorporation. The extent of deuteration was calculated using a computer program, and data (peak heights M − 1, M, M + 1, M + 2, M + 3) taken from the mass spectra (14 eV) of the starting and the deuterated compound.

Irradiation of 2-Methyl-3-benzoylthiopene in CD_3OD

Starting material $(M + 1)^+/M^+$ = 0.158; deuterated compound $(M + 1)^+/M^+$ = 0.249 (8.2% mono-D, 0.6% di-D).

Irradiation of 4-Methyl-3-benzoylthiophene in CD_3OD

Starting material $(M + 1)^+/M^+$ = 0.158; deuterated compound $(M + 1)^+/M^+$ = 0.248 (8.2% mono-D, 0.2% di-D).

Irradiation of 2,5-Dimethyl-3-benzoylthiophene in CD_3OD

Starting material $(M + 1)^+/M^+$ = 0.163; deuterated compound $(M + 1)^+/M^+$ = 0.413 (19.3% mono-D, 2.3% di-D).

Irradiation of 2,5-Dimethyl-3-benzoylthiophene in CH_3OD

Starting material $(M + 1)^+/M^+$ = 0.172; deuterated compound $(M + 1)^+/M^+$ = 0.309 (13% mono-D, 0.9% di-D). For the ^{2}H nmr spectrum a mixture of $CHCl_3$ and C_6F_6 (4 : 1, v/v) was used and the instrument locked to the ^{19}F signal with noise modulated proton decoupling at 100 MHz. The shift reagent $Pr(fod)_3$ was used to obtain better dispersion of the ^{2}H resonances but line broadening accompanies the increased dispersion. Line-shape fitting was employed to obtain the relative areas of the individual absorption signals. Shift reagent studies of the proton spectrum of 2,5-dimethyl-3-benzoylthiophene using a Varian XL-100 instrument were also carried out to confirm the assignment of ^{2}H nmr spectrum. With the total deuterium content (13%) as measured by mass spectroscopy deuterium analysis, the relative concentrations of deuterium at individual centers were found 7.3% of D in the methyl group of position 2 (lower field methyl) and 5.7% of D at methyl group of position 5 of the thienyl ring.

Irradiation of 3-(2-Methylbenzoyl)thiophene in CD_3OD

Starting material $(M + 1)^+/M^+$ = 0.160; deuterated compound $(M + 1)^+/M^+$ = 0.320 (14% mono-D, 0.6% di-D).

Irradiation of 3-(2-Methylbenzoyl)thiophene in CH_3OD

Starting material $(M + 1)^+/M^+$ = 0.135; deuterated compound $(M + 1)^+/M^+$ = 0.379 (18% mono-D, 1.9% di-D). The deuterium was clearly in the (2-methylbenzoyl) fragment. Starting material $(119 + 1)^+/(119)^+$ = 0.078; deuterated compound $(119 + 1)^+/(119)^+$ = 0.25 (15% mono-D, 1.1% di-D).

Irradiation Experiments in the Presence of Dimethyl Acetylenedicarboxylate

Irradiation of 3-Benzoylthiophene (5) in the Presence of Dimethyl Acetylenedicarboxylate

Dimethyl acetylenedicarboxylate (376 mg, 0.004 *M*), 3-benzoylthiophene (568 mg, 0.002 *M*), and benzene (6 ml) were placed in a Pyrex irradiation vessel, purged with argon for 15 min, and irradiated for 8 h. The resulting dark brown solution, a complex mixture, was partially separated by column chromatography on silica gel.

3-Benzoylthiophene (283 mg) was isolated from the first fractions eluting with hexane and a mixture of products (145 mg of an orange oil) was obtained from later fractions eluting with 10% benzene in hexane. The ^{1}Hmr and mass spectra of this mixture provided evidence for the formation of a one-to-one adduct. Structure **10** (5-benzoyl-6,7-dicarbomethoxy-2-thiabicyclo[2.3.0]hepta-3,6-diene) was assigned to this adduct; ^{1}Hmr ($CDCl_3$) δ (TMS): 3.85 (s, 3H, methyl), 3.81 (s, 3H, methyl), 4.70 (d, 1H, H-1), 5.93 (d, 1H, H-4), 6.39 (doublet of doublets, 1H, for H_3), 7.68 ppm (complex, 5H, aromatics); $J_{3,4}$ = 6.5, $J_{1,3}$ = 1.5 Hz; ms (70 eV): M^+ 300 (on the mixture). In an attempt to isolate the adduct from this

Can. J. Chem. Downloaded from www.nrcresearchpress.com by 210.87.254.5 on 09/05/12
For personal use only.

mixture by a second column chromatography on silica gel, a mixture containing only aromatic and methyl protons was obtained; no trace of the adduct was eluted. Further separation of this mixture was carried out by semipreparative vpc (10% SE-30, column temperature 210°C). The three major peaks in the vpc were due to isomeric keto diesters. The peak with the shortest retention time corresponds to dimethyl-3-benzoylphthalate (**11**) (48 mg, 46%, mp 125–126°C): ir (neat) ν: 1720, 1660, 1455, 1430, 1300, 1270, 1250, 1145, 1105, 1067, 1002, 932, 830, 822, 795, 787, 772, 750, 723, 702, 697, 652 cm^{-1}; ^{1}Hmr ($CDCl_3$) δ (TMS): 7.74 (complex, 8H, aromatics), 3.91 (s, 3H, methyl), 3.70 ppm (s, 3H, methyl); ms (70 eV) *m/e* (relative intensity): 298 (38, M^+), 267 (56), 239 (18), 221 (100), 207 (8), 105 (82), 77 (33). *Anal.* calcd. for $C_{17}H_{14}O_5$ (**11**): C 68.45, H 4.73; found: C 68.33, H 4.78.

The second peak was dimethyl-2-benzoylterephthalate (**13**) (12 mg, 12%, mp 101–102°C).

Dimethyl-4-benzoylphthalate was the third isomer (36 mg, 34%, mp 82.5–83°C); ir (Nujol) ν: 2940, 1730, 1660, 1600, 1575, 1450, 1290, 1260, 1195, 1158, 1142, 1128, 1065, 982, 948, 926, 868, 840, 825, 800, 792, 785, 768, 745, 722, 700, 674, 662 cm^{-1}; ^{1}Hmr ($CDCl_3$) δ (TMS): 3.92 (s, 3H, methyl), 3.95 (s, 3H, methyl), 7.82 ppm (complex, 8H, aromatics); ms (70 eV) *m/e* (relative intensity): 298 (23, M^+), 267 (35), 239 (7.5), 221 (38), 105 (100), 77 (65). *Anal.* calcd. for $C_{17}H_{14}O_5$ (**12**): C 68.45, H 4.73; found: C 68.34, H 4.82.

The ^{1}Hmr spectra and especially the ir spectra of the keto-diesters (**11–13**) were identical to those of authentic samples obtained by independent synthesis.

Irradiation of 2-Methyl-3-benzoylthiophene (1) in the Presence of Dimethyl Acetylenedicarboxylate

A solution of 2-methyl-3-benzoylthiophene (101 mg, 0.5×10^{-3} *M*) and dimethyl acetylenedicarboxylate (142 mg, 10^{-3} *M*) in benzene (3 ml) was purged with argon for 15 min and irradiated for 8 h; 60% of the starting ketone remained unreacted. Analysis of the ^{1}Hmr spectrum of the crude reaction mixture provided evidence for a one-to-one adduct assigned structure **6**; ^{1}Hmr ($CDCl_3$) δ (TMS): 1.56 (s, 3H, methyl), 6.03 (d, 1H, H-4), 6.45 ppm (d, 1H, H-3); $J_{3,4} = 6$ Hz. The signals for the methyl groups of the carbomethoxyls appear together with other methyl groups in the mixture. Column chromatography on silica gel allowed recovery of the starting materials and a mixture of dimethyl benzoylphthalates (11 mg, 17.5%), showing only aromatic and methyl protons in the ^{1}Hmr spectrum and carbonyl absorption at 1730 and 1670 cm^{-1} in the ir spectrum. *Anal.* calcd. for $C_{18}H_{16}O_5$: C 69.22, H 5.16; found (on the mixture of isomers): C 68.83, H 5.09.

Irradiation of 4-Methyl-3-benzoylthiophene (2) in the Presence of Dimethyl Acetylenedicarboxylate

4-Methyl-3-benzoylthiophene (101 mg, 0.5×10^{-3} *M*) and dimethyl acetylenedicarboxylate (142 mg, 10^{-3} *M*) in benzene (3 ml) solution was purged with argon for 15 min and irradiated for 8 h; 55% of the starting ketone remained unreacted. Structure **7** was assigned to the unstable adduct (4-methyl-5-benzoyl-6,7-dicarbomethoxy-2-thiabicyclo[2.3.0]hepta-3,6-diene) based on the ^{1}Hmr spectrum of the crude reaction mixture. For adduct **7**: ^{1}Hmr ($CDCl_3$) δ (TMS): 3.88 (s, 3H, methyl), 3.80 (s, 3H, methyl), 4.68 (d, 1H, H-1), 1.80 (d, 3H, methyl in position 4), 5.96 ppm (m, 1H, H_3); $J_{3,CH_3} = 1.4$, $J_{1,3} = 1.6$ Hz.

Column chromatography on silica gel gave fractions containing a mixture of dimethyl benzoylphthalates (10 mg, 14%). In the ^{1}Hmr spectrum only aromatic and methyl protons appear and in the ir spectrum carbonyl absorptions at ν 1730 and 1670 cm^{-1} are observed. *Anal.* calcd. for $C_{18}H_{16}O_5$: C 69.22, H 5.16; found (on the mixture of isomers): C 69.40, H 5.15.

Irradiation of 2,5-Dimethyl-3-benzoylthiophene (3) in the Presence of Dimethyl Acetylenedicarboxylate

2,5-Dimethyl-3-benzoylthiophene (**3**) (216 mg, 10^{-3} *M*) and dimethyl acetylenedicarboxylate (284 mg, 2×10^{-3} *M*) in benzene (3 ml) solution were purged with argon for 15 min and irradiated for 8 h; 45% of the starting ketone was recovered. Structure **8** was assigned to the adduct (1,3-dimethyl-5-benzoyl-6,7-dicarbomethoxy-2-thiabicyclo[2.3.0]hepta-3,6-diene); ^{1}Hmr ($CDCl_3$) δ (TMS): 1.56 (s, 3H, methyl), 1.95 (d, 3H, methyl), 5.73 ppm (m, 1H, H-4); $J_{CH_3,4} = 1.5$ Hz. The chemical shifts of methyls in the carbomethoxy groups appear together with other methyl groups present in the reaction mixture. Column chromatography on silica gel gave a mixture of dimethyl benzoylphthalates (32 mg, 18%), showing only aromatic and methyl protons in the ^{1}Hmr spectrum and carbonyl absorptions at 1740 and 1670 cm^{-1} in the ir spectrum. *Anal.* calcd. for $C_{19}H_{18}O_5$: C 69.92, H 5.56; found (on the mixture of isomers): C 70.13, H 5.59.

Irradiation of 3-(2-Methylbenzoyl)thiophene (4) in the Presence of Dimethyl Acetylenedicarboxylate

3-(2-Methylbenzoyl)thiophene (**4**) (101 mg, 0.5×10^{-3} *M*) and dimethyl acetylenedicarboxylate (142 mg, 10^{-3} *M*) in benzene (3 ml) were purged with argon for 15 min and irradiated for 8 h; 50% of the starting ketone remained unreacted. Structure **9** was assigned to the one-to-one adduct (5-(2-methylbenzoyl)-6,7-dicarbomethoxy-2-thiabicyclo[2.3.0]hepta-3,6-diene), based on ^{1}Hmr and double irradiation experiments on the crude reaction mixture; for **9** ^{1}Hmr ($CDCl_3$) δ (TMS): 2.40 (s, 3H, methyl), 4.60 (d, 1H, H-1), 5.66 (d, 1H, H-4), 6.16 (doublet of doublets, 1H, H-3), 7.20 ppm (complex, 4H, aromatics), $J_{1,3} = 1.5$, $J_{3,4} = 6$ Hz. The signals for the methyls of the carbomethoxy groups cannot be assigned as they appear together with other methyl groups present in the mixture. Column chromatography on silica gel gave a mixture of dimethyl- (*o*-methylbenzoyl)phthalates (14 mg, 18%), which was further purified for combustion analysis by vpc. *Anal.* calcd. for $C_{18}H_{16}O_5$: C 69.22, H 5.16; found (on the mixture of isomers): C 69.22, H 5.25. The ir spectrum shows carbonyl absorption at 1730 and 1655 cm^{-1} and in the ^{1}Hmr spectrum only methyl and aromatic protons appear.

The yields in each case were based on the amount of ketone consumed.

Preparation of Dimethyl 3-Benzoylphthalate (11)

2,3-Dimethylbenzophenone (26) (Grignard Reaction)

Magnesium metal (480 mg), 3-bromo-*o*-xylene (500 mg), and anhydrous ether (20 ml) were placed in a dry apparatus and a crystal of iodine was added. An exothermic reaction started and the mixture was gently refluxed. The mixture was stirred and additional 3-bromo-*o*-xylene (totally 3.7 g) in anhydrous ether (20 ml) was added at a rate such that the reflux was maintained (~1 h).

After the addition, the mixture was heated under reflux for ½ h and allowed to cool to room temperature. Then benzoylchloride (2.8 g) in dry ether (10 ml) was added to this solution and the mixture refluxed for 10 h. The resulting mixture was cooled in an ice bath and acetic acid (20 ml, 10%) was slowly added. Water (200 ml) was added and the mixture was extracted (3 × 100 ml) with ether. Evaporation of the solvent and then distillation gave 2,3-dimethylbenzophenone (2.6 g, 62%).

3-Benzoylphthalic Acid

2,3-Dimethylbenzophenone (1 g) and sodium hydroxide (600 mg) in water (100 ml) was heated on a water bath. Potassium permanganate (6 g) was added in four equal portions at 30 min intervals. After 19 h heating, the solution was decolourized with methanol, filtered, and the filtrate acidified

Can. J. Chem. Downloaded from www.nrcresearchpress.com by 210.87.254.5 on 09/05/12
For personal use only.

with concentrated hydrochloric acid. The colourless crystals were recrystallized from water and were 3-benzoylphthalic acid (840 mg, 65%, mp, decomposes giving the anhydride (27)).

*Dimethyl 3-Benzoylphthalate (**11**)*

3-Benzoylphthalic acid (840 mg) in methanol (15 ml) and concentrated sulfuric acid (1 ml) were refluxed overnight. After the work-up and recrystallization of the crude product from chloroform, dimethyl 3-benzoylphthalate (600 mg, 65%, mp 125–126°C) was obtained.

*Preparation of Dimethyl 2-Benzoylterephthalate (**13**)*

2,5-Dimethylbenzophenone (Friedel–Crafts Reaction)

m-Xylene (21.2 g, 0.2 *M*), benzoylchloride (14.0 g, 0.1 *M*), aluminum trichloride (16.0 g, 1.2 *M*), and nitromethane (60 ml) were used. The product 2,5-dimethylbenzophenone (16 g, 40%), was a viscous yellow oil (bp 320°C/760 Torr (lit. (28) bp 317°C/744 Torr).

2-Benzoylterephthalic Acid (29)

2,5-Dimethylbenzophenone (10 g) and potassium permanganate (37 g) in water (250 ml) were refluxed overnight. The resulting diacid (2 g, 42%, based on the consumed ketone) was obtained as colourless crystals (mp 285–286°C, recrystallized from ethanol).

*Dimethyl 2-Benzoylterephthalate (**13**)*

2-Benzoylterephthalic acid (2 g), methanol (30 ml), and concentrated sulfuric acid (2 ml) were refluxed overnight. After the work-up, colourless crystals of dimethyl 2-benzoylterephthalate were obtained (1.4 g, 64%, mp 101–102°C (lit. (30) mp 100-101°C).

*Preparation of Dimethyl 4-Benzoylphthalate (**12**)*

3,4-Dimethylbenzophenone (31) (Friedel–Crafts Reaction)

From *o*-xylene (2.23 g, 0.2 *M*), benzoylchloride (14.05 g, 0.1 *M*), aluminum trichloride (16 g, 1.2 *M*) in nitromethane (60 ml), 3,4-dimethylbenzophenone was obtained (mp 46–48°C (from ethanol), bp 58–60°C/2 Torr).

4-Benzoylphthalic Acid (32)

2,3-Dimethylbenzophenone (10 g) and potassium permanganate (37 g) in water (25 ml) were stirred overnight. The 4-benzoylphthalic acid (150 mg, 23% based on the consumed ketone, mp 173–176°C) was obtained.

*Dimethyl 4-Benzoylphthalate (**12**)*

4-Benzoylphthalic acid (150 mg), methanol (4 ml), and concentrated sulfuric acid (0.5 ml) were refluxed overnight; after the usual work-up, dimethyl 4-benzoylphthalate (99 mg, 60%, mp 82.5–83°C) was obtained.

Irradiation Experiments in the Presence of Isobutylene

A Pyrex irradiation vessel containing the thiophene (**1**–**4**) in benzene was cooled and purged with isobutylene until the maximum amount of isobutylene was dissolved (ca. 25% by volume, 30% by weight). The tube was sealed with a rubber serum cap and irradiated for 190 h. The reaction mixture, after removing the excess isobutylene and the solvent gave a brown oil, which was a complex mixture of products. No ^{1}Hmr absorption was apparent in the region expected for the oxetane methylene protons. The crude reaction mixture was chromatographed on neutral alumina (Fisher, activity 1, 60–200 mesh). Elution with hexanes gave 1-phenyl-1-thienyl-2-methylpropenes (olefins **14**–**17**), with ir spectra identical to those of authentic olefins prepared by a Grignard method given below. Further elution with hexanes–benzene separated unreacted starting ketone. All yields are based on the consumed ketone.

*Irradiation of **1** in the Presence of Isobutylene*

Irradiation of thiophene **1** (100 mg) in a solution of isobutylene in benzene (20 ml) gives a complex mixture. The ^{1}Hmr spectrum has a complex absorption between 2.53–1.33 ppm including singlets at 2.36, 1.83, and 1.63 ppm characteristic of the olefin and at 2.53 for the starting ketone (**1**). After column chromatography, the olefin **14** (6 mg, 11.5%) and the starting thiophene **1** (38 mg), were separated.

*Irradiation of **2** in the Presence of Isobutylene*

Thiophene **2** (60 mg) in a solution of isobutylene in benzene (15 ml) was irradiated. From the resulting mixture, olefin **15** (4 mg, 10.5%) and thiophene **2** (35 mg) were separated.

*Irradiation of **3** in the Presence of Isobutylene*

Thiophene **3** (800 mg) in a solution of isobutylene in benzene (40 ml) was irradiated and a mixture of products was obtained which had complex ^{1}Hmr absorption between 2.5–0.9 ppm, including singlets at 2.00, 1.93, 1.75, 1.60 ppm indicative of the olefin **16** and two singlets at 2.5 and 2.3 ppm for the starting ketone. Chromatography of the crude reaction mixture gave olefin **16** (44 mg, 9%) and starting ketone **3** (428 mg).

*Irradiation of **4** in the Presence of Isobutylene*

Thiophene **4** (160 mg) in a solution of isobutylene in benzene (30 ml) was irradiated. Sharp singlets in the ^{1}Hmr spectrum at 2.01, 1.30, and 1.42 ppm indicated the presence of the olefin **17**. From the crude reaction mixture, olefin **17** (12 mg, 12%) and starting thiophene (72 mg), were separated by column chromatography.

*Synthesis of 1-Phenyl-1-thienyl-2-methylpropenes (Olefins **14–17**)*

Garbish's procedure (33) was followed for the preparation of the olefins **14**–**17**. To a dry flask containing magnesium metal and anhydrous ether, 2-bromopropane in anhydrous ether was slowly added. A crystal of iodine initiated the reaction and the ether was allowed to boil gently until all the magnesium had dissolved. The reaction mixture was heated for 30 min under reflux and was cooled to room temperature. Then thiophene (**1**–**4**) in anhydrous ether was slowly added with stirring. The reaction mixture was stirred overnight and then poured into aqueous ammonium chloride (10%). The resulting layers were separated and the aqueous layer extracted with ether. The combined ether extracts were dried over anhydrous magnesium sulfate and evaporation of the solvent gave a yellow oil, presumably the alcohol, which was not characterized but was taken up in benzene and refluxed for 30 h in the presence of 4-toluenesulfonic acid (trace). The resulting mixture was washed with sodium bicarbonate (10%, aqueous) and dried over magnesium sulfate (anhydrous). Evaporation of the solvent yielded a dark brown oil which was chromatographed on neutral alumina (Fisher, activity 1, 60–200 mesh) to give the olefin (**14**–**17**) upon elution with hexanes.

*Preparation of 1-Phenyl-1-[3-(2-methylthienyl)]-2-methylpropene (**14**)*

Following the above procedure from 2-bromopropane (280 mg) in anhydrous ether (20 ml), magnesium metal (56 mg), and 2-methyl-3-benzoylthiophene (470 mg) olefin **14** (62 mg, 12%) was obtained; ir (neat) ν: 3070, 1520, 1475, 1425, 1340, 1225, 1210, 1050, 930, 977, 848, 750, 666 cm^{-1}; ^{1}Hmr ($CDCl_3$) δ (TMS): 1.69 (s, 3H, methyl), 1.82 (s, 3H, methyl), 2.25 (s, 3H, methyl), 6.65 ppm (d, H-4 of thienyl group; $J_{3,4}$ = 5.5 Hz; ms (70 eV) *m/e* (relative intensity): 228 (100, M^+), 213 (21), 185 (65), 129 (20), 115 (15), 97 (7), 91 (12), 77 (6), 59 (7), 45 (6), 37 (5). *Anal.* calcd. for $C_{15}H_{16}S$ (**14**): C 78.92, H 7.06; found: C 78.91, H 7.11.

*Preparation of 1-Phenyl-1-[3-(4-methylthienyl)]-2-methylpropene (**15**)*

Following the above procedure, from 2-bromopropane (28 mg), magnesium metal (5.6 mg) in anhydrous ether (5 ml) and thiophene **4** (47 mg), olefin **15** (9 mg, 17%) was obtained; ir (neat) ν: 3065, 2960, 1515, 1425, 1224, 1208, 1043, 1030, 928,

Can. J. Chem. Downloaded from www.nrcresearchpress.com by 210.87.254.5 on 09/05/12
For personal use only.

860, 845, 782, 728, 713, 699, 668 cm^{-1}; ^{1}Hmr ($CDCl_3$) δ (TMS): 1.68 (s, 3H, methyl), 1.83 (s, 3H, methyl), 2.66 (s, 3H, methyl), 7.26 – 6.70 ppm (7H, thienyl and aromatic); ms (70 eV) *m/e* (relative intensity): 228 (100, M^+), 213 (30), 185 (78), 165 (36), 129 (39), 115 (54), 91 (15), 77 (19). *Anal.* calcd. for $C_{15}H_{16}S$ (**15**): C 78.92, H 7.06; found C 78.86, H 6.79.

*Preparation of 1-Phenyl-1-[3-(2,5-dimethylthienyl)]-2-methylpropene (**16**)*

Following the above procedure, olefin **16** (71 mg, 12%) was obtained by using 2-bromopropane (280 mg) and magnesium metal (56 mg) in anhydrous ether (20 ml) and 2,5-dimethyl-3-benzoylthiophene (540 mg) also in anhydrous ether (20 ml). This compound was previously prepared (4) by a different route; ir (neat) ν: 3040, 2920, 1615, 1500, 1452, 1380, 1210 cm^{-1}; ^{1}Hmr ($CDCl_3$) δ (TMS): 1.70 (s, 3H, methyl), 1.78 (s, 3H, methyl), 2.18 (s, 3H, methyl), 2.30 (s, 3H, methyl), 6.27 (broad, 1H, H-4) 7.34 – 6.90 ppm (complex, 5H, aromatic); $J_{4,5} < 1$ Hz; ms (70 eV) *m/e* (relative intensity): 242 (100, M^+), 227 (38), 199 (68), 184 (29), 165 (22), 129 (56), 115 (28), 202 (91), 59 (30).

*Preparation of 1-(2-Methylphenyl)-1-(3-thienyl)-2-methylpropene (**17**)*

Olefin **17** (49 mg, 9%) was also prepared by the Garbish procedure (280 mg 2-bromopropene, 56 mg magnesium metal in 20 ml anhydrous ether, and 470 mg of 3-(2-methylbenzoyl)-thiophene (4) in 20 ml anhydrous ether); ir (neat) ν: 3070, 2950, 2870, 1450, 1380, 848, 786, 775, 747, 726, 686, 678 cm^{-1}; ^{1}Hmr ($CDCl_3$) δ (TMS): 1.58 (s, 3H, methyl), 1.98 (s, 3H, methyl), 2.11 (s, 3H, methyl), 7.33 – 6.83 ppm (complex, 7H, aromatic and thienyl); ms (70 eV) *m/e* (relative intensity): 228 (100, M^+), 185 (97), 165 (29), 152 (19), 129 (71), 115 (21), 97 (27), 91 (15), 77 (16). *Anal.* calcd. for $C_{15}H_{16}S$ (**17**): C 78.92, H 7.06; found: C 79.14, H 7.03.

Acknowledgements

This work was supported by a grant from the National Research Council of Canada. We gratefully acknowledge the assistance of Dr. J. B. Stothers in obtaining the deuterium nmr spectra and Ms. H. Schroeder in obtaining the 100 MHz ^{1}Hmr spectra. Some of the preliminary results were obtained by B. M. Clarke, Jr.

1. (*a*) D. R. Arnold and R. J. Birtwell. J. Am. Chem. Soc. **95**, 4599 (1973); (*b*) D. R. Arnold, R. J. Birtwell, and B. M. Clarke, Jr. Can. J. Chem. **52**, 1681 (1974); (*c*) D. R. Arnold and B. M. Clarke, Jr. Can. J. Chem. **53**, 1 (1975).
2. (*a*) R. M. Kellogg, A. P. Schaap, E. T. Harper, and H. Wynberg. J. Org. Chem. **33**, 2902 (1968); (*b*) M. G. Reinecke, H. W. Adidses, and C. Pyun. J. Org. Chem. **36**, 2690 (1971).
3. (*a*) R. Helder and H. Wynberg. Tetrahedron Lett. 605 (1972); (*b*) D. N. Reinhoudt, H. C. Valger, C. G. Kouwenhoven, H. Wynberg, and R. Helder. Tetrahedron Lett. 5269 (1973); (*c*) H. Wynberg and R. Helder. Tetrahedron Lett. 3647 (1972).
4. N. P. Buu-Hoi and Nguyen-Hoan. Recl. Trav. Chim. Pays-Bas, **67**, 309 (1948).
5. (*a*) P. G. Sammes. Tetrahedron, **32**, 405 (1976); (*b*) N. C. Yang and C. Rivas. J. Am. Chem. Soc. **83**, 2213 (1961); (*c*) E. Block and R. Stevenson. J. Chem. Soc. Perkin I, 308 (1973); (*d*) K. R. Huffman, M. Foy, and E. F. Ullman. J. Am. Chem. Soc. **87**, 5417 (1965); **88**, 601 (1966); (*e*) F. Nerdel and N. Brodowski, Chem. Ber. **101**, 1398 (1968).
6. B. Bonini and J. Degani. Bull. Sci. Fac. Chim. Ind. Bologia, **20**, 115 (1962).
7. (*a*) C. H. Nicholls and P. A. Leermakers. Adv. Photochem. **8**, 315 (1971); (*b*) A. A. Lamola. J. Chem. Phys. **38**, 2813 (1963); (*c*) R. D. Rauh and P. A. Leermakers. J. Am. Chem. Soc. **90**, 2246 (1968); (*d*) K. A. Martin, G. Moller, and A. M. Nishimura. J. Phys. Chem. **80**, 2788 (1976); (*e*) R. Rusakowicz, G. W. Byers, and P. A. Leermakers. J. Am. Chem. Soc. **93**, 3263 (1971).
8. (*a*) P. J. Wagner, M. J. Thomas, and E. Harris. J. Am. Chem. Soc. **98**, 7675 (1976); (*b*) P. J. Wagner, A. E. Kemppainen, and H. N. Schott. J. Am. Chem. Soc. **95**, 5604 (1973); (*c*) N. C. Yang, D. S. McClure, S. L. Murov, J. J. Houser, and R. Dusenbery. J. Am. Chem. Soc. **89**, 5466 (1967).
9. M. Batley and D. R. Kearns. Chem. Phys. Lett. **2**, 423 (1968); S. Dym and R. M. Hockstrasser. J. Chem. Phys. **51**, 2458 (1969); A. J. Duben, L. Goodman, and M. Koyanagi. *In* Excited states. Vol. 1. *Edited by* E. C. Lim. Academic Press, New York, NY. 1974. p. 295.
10. H. Wynberg. Acc. Chem. Res. **4**, 65 (1971).
11. F. Scully and H. Morrison. J. Chem. Soc. Chem. Commun. 529 (1973).
12. J. M. Hornback. Tetrahedron Lett. 3389 (1976).
13. M. P. Cava, M. V. Lakshmikantham, and M. Behforouz. J. Org. Chem. **39**, 206 (1974).
14. P. J. Wagner and C.-P. Chen. J. Am. Chem. Soc. **98**, 239 (1976).
15. (*a*) H. J. Kuhn and K. Gollnick. Chem. Ber. **106**, 674 (1973); (*b*) D. C. Neckers, J. H. Dopper, and H. Wynberg. Tetrahedron Lett. 2913 (1969); (*c*) J. H. Dopper and D. C. Neckers. J. Org. Chem. **36**, 3755 (1971).
16. (*a*) D. R. Arnold. Adv. Photochem. **6**, 301 (1968); (*b*) D. R. Arnold, R. L. Hinman, and A. H. Glick. Tetrahedron Lett. 1425 (1964).
17. H. A. J. Carless and H. S. Trivedi. J. Chem. Soc. Chem. Commun. **5**, 81 (1975).
18. F. K. Beilstein. Handbuch der Organischen Chemie. Bd. 17., Hauptwerk, Verlag Springer, Berlin. p. 37.
19. C. A. Grob and H. J. Schmid. Helv. Chim. Acta, **36**, 1763 (1953).
20. D. W. H. MacDowell and F. L. Ballas. J. Org. Chem. **39**, 2239 (1974).
21. M. Donborw. J. Chem. Soc. 1615 (1959).
22. A. Hornfeldt and S. Gronowitz. Acta Chem. Scand. **16**, 789 (1962).
23. S. Gronowitz. Ark. Kemi, **16**, 275 (1960).
24. C. Troyanowsky. Bull. Soc. Chim. Fr. 1424 (1955).
25. A. Kitt. Ber. **28**, 1808 (1895).
26. F. Rekker and W. Nauta. Recl. Trav. Chim. Pays-Bas, **80**, 747 (1961).
27. G. R. Blumenfeld. Ber. **30**, 1115 (1897).
28. K. Elbs and E. Larsen. Ber. **17**, 2847 (1884).
29. K. Elbs and E. Larsen. J. Prakt. Chem. **35**, 479 (1845–1849).
30. F. K. Beilstein. Handbuch der Organischen Chemie. Bd. 10., Hauptwerk, Verlag Springer, Berlin. 1927. p. 881.
31. K. Elbs. J. Prakt. Chem. **35**, 467 (1845–1849).
32. L. Chardonnens and W. Schlapbach. Helv. Chim. Acta, **29**, 1413 (1946).
33. E. W. Garbish. J. Org. Chem. **26**, 4165 (1961).

Polarized fluorescence study of retinals at room temperature

SURAT HOTCHANDANI, PAUL PAQUIN, AND ROGER M. LEBLANC

Groupe de Recherche en Biophysique, Département de Chimie–Biologie, Université du Québec à Trois-Rivières, Trois-Rivières (Qué.), Canada G9A 5H7

Received January 2, 1978

SURAT HOTCHANDANI, PAUL PAQUIN, and ROGER M. LEBLANC. Can. J. Chem. **56**, 1985 (1978).

The solid films of all-*trans*, 9-*cis*, and 13-*cis* retinals have been found to be fluorescent at room temperature. Their polarization study with the aim of understanding the nature of their fluorescent state has also been carried out at room temperature. The high positive polarization of fluorescence with respect to the excitation carried out in the main $^1B_u \leftarrow {}^1A_g$ absorption transition of retinals suggests that their fluorescent state possesses a large amount of ^1B_u character. A vibronic coupling mechanism that suggests the $^1A_g^-$ (a weakly allowed π,π^*) state or $^1n,\pi^*$ state being the lowest singlet state in retinals has also been considered.

SURAT HOTCHANDANI, PAUL PAQUIN et ROGER M. LEBLANC. Can. J. Chem. **56**, 1985 (1978).

A température ambiante, nous observons la fluorescence des isomères de retinal (tout-*trans* 9-*cis* et 13-*cis*) à l'état de film solide. Afin de connaître la nature des états fluorescents, nous avons examiné la polarisation de la fluorescence. La valeur positive de polarisation des retinals lorsque l'excitation est faite dans la transition d'absorption $^1B_u \leftarrow {}^1A_g$ suggère que leur fluorescence possède un fort caractère ^1B_u. La possibilité d'un mécanisme de couplage vibronique a aussi été considérée.

Introduction

During the past couple of years increasing interest in understanding the ordering of the electronic states of retinyl polyenes, the chromophores of the visual pigments, has manifested itself in recent literature (1–10). The phenomenon of electronic relaxation of the singlet states of the polyenes has been, in particular, the topic of active research. The recent discovery (6–8) of a very weakly allowed excited state $^1A_g^-$ (π–π^*) and its contribution to the radiative (fluorescence) properties has also been discussed. The $^1A_g^-$ state, it has been shown, arises due to the inclusion of doubly excited configurations in the calculations of configuration interaction (8), and is considered to be the lowest excited singlet state responsible for fluorescence of polyenes (6, 7, 10). This is in contrast with the usual ^1B_u (π,π^*) assignment of the lowest singlet state for polyenes (11).

The presence of the weakly allowed state $^1A_g^-$ does, however, explain very successfully many discrepancies in fluorescence characteristics of polyenes, for example, (*a*) the radiative fluorescence lifetimes (τ_0) measured experimentally (4, 5, 10) are anomalously longer than those calculated from their respective integrated absorption intensities using Strickler–Berg equation (12), (*b*) the dependence of τ_0 on temperature (5, 10), and (*c*) the different solvent effect on absorption and fluorescence spectra (6).

In retinals (polyene aldehydes) the presence of n,Π^* states (introduced due to nonbonded electrons of heteroatom oxygen) should also be considered in determining their radiative and nonradiative properties. For instance, Abrahamson and Ostroy (1) reported that the retinals but not retinols or retinal Schiff bases have an efficient pathway into the triplet manifold. This unique pathway (channel) by which retinal triplet state is populated has been attributed to the presence of n,π^* singlet states which increase intersystem crossing. This preferential $^1n,\pi \leftrightarrow {}^3\pi$–$\pi^*$ intersystem crossing has also been shown to be responsible for marked dependence of the retinals fluorescence quantum yield, ϕ_f, upon excitation wavelength (2). Although Hochstrasser *et al.* (13) are of the opinion that the triplet precursor lives for about 36 ps and the intersystem crossing process probably involves mixing of σ,π^* and π,π^* states.

In order to characterize the nature of the emitting state, polarization experiments are usually good techniques to look forward to. Moore and Song (*9a*) thus carried out the polarization fluorescence study of all-*trans* retinal in ether at 77 K. Their results did not give any indication of the presence of weakly allowed $^1A_g^-$ (π,π^*) or $^1n,\pi^*$ in the fluorescence state of retinal, and also other isomers were not studied. Since most of the published work on retinals has been carried out at 77 K except for the recent work of Becker *et al.* (2*d*) on all-*trans* retinal, and also since the visual events occur at physiological temperature (which is closer to the room temperature) we have carried out the fluorescence experiments of retinals at room temperature. As an extension of our interest in these molecules (14), we present here the polarized fluorescence study of all-*trans*, 9-*cis*, and 13-*cis* retinals in solid films and at room temperature using photoselection techniques as described by Albrecht (15).

Can. J. Chem. Downloaded from www.nrcresearchpress.com by 210.87.254.42 on 09/05/12
For personal use only.

Can. J. Chem. Downloaded from www.nrcresearchpress.com by 210.87.254.42 on 09/05/12
For personal use only.

Experimental

Materials

The isomeric retinals, namely all-*trans*, 9-*cis*, and 13-*cis* (anhydrous quality), were purchased from Sigma Co., St. Louis, MO, and were stored in the dark at 0°C. The solutions of retinals were made in ether ("ARISTAR" grade, ethanol content 200 ppm, water content 500 ppm) obtained from B.D.H. Chemicals, Montreal. The retinals and solvent ether were used without further purification, and the films were prepared as described elsewhere (14*b*).

Methods and Techniques

Ultraviolet–visible spectra of the films were recorded on Perkin-Elmer 124 spectrophotometer with a HTV R136 photomultiplier. Fluorescence excitation and emission spectra of the films at room temperature were recorded on Perkin-Elmer MPF-2A spectrofluorimeter fitted with excitation and emission monochromators and RCA-136 photomultiplier. The detection of the fluorescence of the films was made by the method as outlined by Leblanc *et al.* (16) and the polarization experiments were carried out as described by Hotchandani and Testa (17). The concentration of the solutions for preparation of the films for recording their fluorescence excitation and emission was $\sim 10^{-5}$ *M*. However, a higher concentration $\sim 10^{-4}$ *M* was used for polarization experiments. All experiments were carried out at room temperature in red light and in nitrogen atmosphere.

Results and Discussion

The solid films of all-*trans*, 9-*cis*, and 13-*cis* retinals have been found to be fluorescent at room temperature. Their absorption, fluorescence excitation, and emission spectra recorded at room temperature are shown in Figs. 1, 2, and 3, respectively. Their polarization curves also recorded at room temperature are shown in the figures. The broad shape, the absence of 0–0 band, and large Stokes shift (3000–3500 cm^{-1}) indicate that the absorption and fluorescence bands of the retinals are severely Franck–Condon forbidden. The broad spectra of retinals are probably due to close lying n,π^* and π–π^* states. Such spectral broadness has also been observed with other polyene aldehydes (18) and many nitrogen heterocyclics (19), and has been attributed to the presence of n,π^* states lying close to π,π^* states.

The fluorescence maxima and other spectral features of the films are presented in Table 1. For comparison the fluorescence maxima of all-*trans* retinal at room temperature (2*d*) and at 77 K (2) are also included. As noted from the table our results for fluorescence maxima of the solid films at room temperature (RT) are at longer wavelengths than those reported at 77 K (2). Judging from the fluorescence maximum of all-*trans* retinal solution (2*d*) at room temperature ($\lambda_{fl} \simeq 600$ nm which is even further displaced to longer wavelengths than the films), one would expect that the fluorescence of

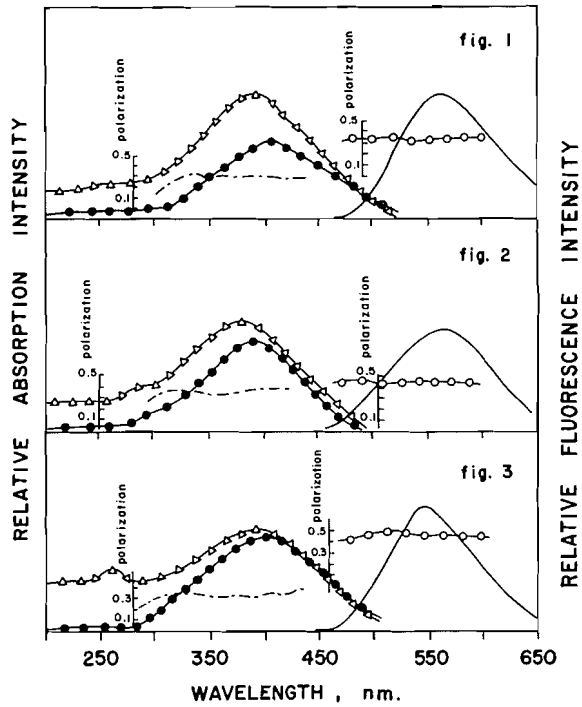

FIG. 1. Absorption spectrum (△), excitation spectrum (●), corrected fluorescence spectrum (—), excitation polarization (·····), and emission polarization (○) of films of all-*trans* retinal at room temperature. The films for excitation and emission were prepared from 500 μl of 3.403×10^{-5} *M* solution in ether. For polarization experiments the films were prepared from 500 μl of 3.403×10^{-4} *M* solution. Monitoring wavelengths for excitation and emission polarization were 550 and 410 nm, respectively.

FIG. 2. Spectra for 9-*cis* retinal films. The films for excitation and emission were prepared from 500 μl of 5.62×10^{-5} *M* solution in ether. For polarization experiments the films were prepared from 500 μl of 5.62×10^{-4} *M* solution. Monitoring wavelengths for excitation and emission polarization were, respectively, 560 and 385 nm. Please refer to Fig. 1 caption for details.

FIG. 3. Spectra of 13-*cis* retinal films. The films for excitation and emission were prepared from 500 μl of 1.258×10^{-5} *M* solution in ether while those for polarization studies were prepared from 500 μl of 1.258×10^{-4} *M* solution. Monitoring wavelengths for excitation and emission, respectively, were 540 and 400 nm. For details, please refer to Fig. 1 caption.

retinals follows the pattern

$$\lambda_{fl}\text{ (Solution at RT, non-rigid system)} > \lambda_{fl}\text{ (Film, rigid system at RT)} > \lambda_{fl}\text{ (Rigid system at 77 K)}$$

such trend has also been observed with other retinyl polyenes (3–5). This shows us that the observed film fluorescence in the present work is due to the retinals and not due to the impurities.

TABLE 1. Fluorescence characteristics of retinals

Compound	Solid films at room temperature (present work)						
	λ_{max} (nm) absorption maximum	λ_{max} (nm) uncorrected excitation	λ_{max} (nm) corrected fluorescence maximum	Fluorescence polarization when excited into the main absorption $^1B_u \leftarrow {}^1A_g$ band	Excitation polarization in the region 320–450 nm	λ_{max} (nm) corrected fluorescence at room temperature	λ_{max} (nm) corrected fluorescence at 77 K (±10 nm)
All-*trans* retinal	395	405	545±10	+0.30–+0.38	+0.25–+0.30	600±25‖ (EPA)	510 (3MP)*†‡ 520 (3MP)§ 540 (EPA)§
9-*cis* retinal	380	390	555±10	~+0.40	+0.30–+0.35		520–525 (3MP)*†‡
13-*cis* retinal	390	400	535±10	~+0.40	+0.30–+0.35		505 (3MP)*†‡

*The values reported are for ordinary retinals in ordinary 3MP where H-bonding is occurring.
†Reference 2*b*.
‡Reference 2*c*.
§Reference 2*e*.
‖Reference 2*d*.

We have also checked qualitatively the excitation wavelength dependence of fluorescence quantum yield of retinals by carrying out excitation at wavelengths (400–450 nm) longer than their respective $^1B_u \leftarrow {}^1A_g$ absorption bands. We definitely have seen an augmentation in the fluorescence intensities as has been reported by others (2) though, of course, the quantitative study was not carried out.

Recently (2 *d*, *e*), it has been shown that the dry retinals in dry hydrocarbon solvents (3MP) or in dry non-hydrogen-bonding polar solvents (dichloromethane) do not fluoresce ($\phi_f < 10^{-4}$) whereas ordinary retinals, in ordinary 3MP (containing trace amounts of water) and in hydrogen-bonding solvents like ethanol, EPA, have been found to fluoresce. This fluorescence was interpreted as due to the hydrogen-bonded retinal species, and that there existed an equilibrium mixture of non-hydrogen-bonded and hydrogen-bonded retinals in hydroxylic solvents explaining the excitation wavelength dependence of ϕ_f of retinals. It is possible that, in the present work, the observed fluorescence of solid films of retinals (prepared from solvent ether containing trace amounts of ethanol and water) is also due to the hydrogen-bonded retinal species, which would then explain the dependence of the fluorescence intensity (or ϕ_f) on excitation wavelength as observed in the present work.

The high positive polarization ($P = +0.40$) for the fluorescence of the isomeric retinals (Table 1) as obtained with the excitation carried out at wavelengths corresponding to the maxima of their respective highly allowed $^1B_u \leftarrow {}^1A_g$ absorption suggests that the absorption and fluorescence correspond to transitions to and from ^1B_u (π,π^*) state or the fluorescent state has large amount of B_u character incorporated in it. The positive polarization for excitation in the wavelength region 320–450 nm further supports it. The declining tendency of the excitation polarization in the wavelength region shorter than 300 nm, as seen from the figures, is possibly due to the onset of second electronic transition of higher energy.

It has been, however, proposed that the $^1A_g^-$ (π,π^*) a very weakly allowed state is the lowest in polyenes, in general, including retinals (6, 7, 10); while others suggest that the $^1n,\pi^*$ is the lowest or is essentially degenerate with the lowest $^1A_g^-$ (π,π^*) state. For example, Song *et al.* (9*b*), in view of their heavy-atom effect results on retinals, suggested that $^1n,\pi^*$ state was above the fluorescing $^1\pi,\pi^*$ state. They, however, did not assign the symmetry (i.e. $^1A_g^-$ or ^1B_u) to this π,π^* fluorescent state of retinals. Becker *et al.* (2 *d*, *e*), on the other hand, while studying the fluorescence of all-*trans* and 13-*cis* retinals in various solvents concluded that the $^1n,\pi^*$ is the lowest excited singlet state in dry alkane nonhydrogen-bonding solvents whereas in hydrogen-bonding solvents $^1\pi,\pi^*$ is the emitting (lowest) state in retinals. The recent two-photon excitation studies of Fang *et al.* (20) on diphenyl octatetraene (DPO) have, however, shown conclusively that $^1A_g^-$ is the emitting state of DPO.

Our results for the positive fluorescence polarization ($P \simeq +0.35–+0.40$) of the solid films of the isomeric retinals at room temperature (when excited into their $^1B_u \leftarrow {}^1A_g$ absorption band), unfortunately, do not seem to be compatible with either $^1\pi,\pi^*$ ($^1A_g^-$), or $^1n,\pi^*$ assignment of the lowest singlet state responsible for retinals fluorescence, but

Can. J. Chem. Downloaded from www.nrcresearchpress.com by 210.87.254.42 on 09/05/12
For personal use only.

on the contrary seem to support that the fluorescent state possesses a large amount of B_u character. A negative or even low positive (+0.00–+0.05) polarization values would have indicated the presence of $^1n,\pi^*$ or $^1A_g^-$ state.

Of course, for hydrogen-bonded retinals as is the case in the present work, the possibility of n,π^*state as the lowest excited singlet state is ruled out. Though, our polarized experiments do not reveal directly the presence of the weakly allowed $^1A_g^-$ state, yet the positive polarization results are in full agreement with the $^1A_g^-$ (π,π^*) assignment of the lowest excited state of retinals. This is due to the fact that $^1A_g^-$ (principally a doubly excited state) has virtually no transition moment of its own to the ground state, and steals all of its intensity from the strongly allowed $^1B_u \leftarrow {}^1A_g$ transition and thus acquires B_u radiative and polarization characteristics. This could occur if the state ^1B_u (π,π^*), $^1A_g^-$ (π,π^*) and, even $^1n,\pi^*$ are energetically very close and are in reality highly mixed due to vibronic interactions.

Acknowledgements

The research was generously supported by the National Research Council of Canada and the Ministère de l'Education du Québec.

1. (*a*) E. W. ABRAHMSON and S. E. OSTROY. Prog. Biophys. Mol. Biol. **17**, 179 (1967); (*b*) E. W. ABRAHMSON and S. M. JAPAR. *In* Handbook of sensory physiology, Vol. VII/1. Photochemistry of vision. *Edited by* H. J. A. Dartnall. Springer-Verlag, Berlin. 1972. p. 1.
2. (*a*) D. E. BALKE and R. S. BECKER. J. Am. Chem. Soc. **90**, 6710 (1968); (*b*) R. S. BECKER, K. INUZUKA, J. KING, and D. E. BALKE. J. Am. Chem. Soc. **93**, 43 (1971); (*c*) W. H. WADDELL, A. M. SCHAFFER, and R. S. BECKER. J. Am. Chem. Soc. **95**, 8223 (1973); (*d*) R. S. BECKER, G. HUG, P. DAS, A. M. SCHAFFER, T. TAKEMURA, N. YAMAMOTO, and W. WADDELL. J. Phys. Chem. **80**, 2265 (1976); (*e*) T. TAKEMURA, P. K. DAS, G. HUG, and R. S. BECKER. J. Am. Chem. Soc. **98**, 7099 (1976).
3. P. E. BLATZ and D. L. PIPPERT. Chem. Commun. 176 (1968).
4. A. J. THOMSON. J. Chem. Phys. **51**, 4106 (1969).
5. J. P. DALLE and B. ROSENBERG. Photochem. Photobiol. **12**, 151 (1970).
6. (*a*) B. S. HUDSON and B. E. KOHLER. Chem. Phys. Lett. **14**, 299 (1972); (*b*) B. S. HUDSON and B. E. KOHLER. J. Chem. Phys. **59**, 4984 (1973).
7. (*a*) R. L. CHRISTENSEN and B. E. KOHLER. Photochem. Photobiol. **18**, 293 (1973); (*b*) **19**, 401 (1974).
8. (*a*) K. SCHULTEN and M. KARPLUS. Chem. Phys. Lett. **14**, 305 (1972); (*b*) K. SCHULTEN, I. OHMINE, and M. KARPLUS. J. Chem. Phys. **64**, 4422 (1976).
9. (*a*) T. A. MOORE and P. S. SONG. Nature New Biol. **243**, 30 (1973); (*b*) P. S. SONG, Q. CHAE, M. FUJITA, and H. BABA. J. Am. Chem. Soc. **98**, 819 (1976).
10. J. B. BIRKS and D. J. S. BIRCH. Chem. Phys. Lett. **31**, 608 (1975).
11. J. R. PLATT. *In* Radiation biology. Vol. 3. Daniel, Davy and Co., Inc. Hartford, CT. 1956. Chapt. 2.
12. J. STRICKLER and K. A. BERG. J. Chem. Phys. **37**, 814 (1962).
13. R. M. HOCHSTRASSER, D. L. NARVA, and A. C. NELSON. Chem. Phys. Lett. **43**, 15 (1976).
14. (*a*) S. HOTCHANDANI, R. M. LEBLANC, and F. BOUCHER. Vision Res. **15**, 605 (1975); (*b*) S. HOTCHANDANI and R. M. LEBLANC. Photochem. Photobiol. **24**, 59 (1976); (*c*) S. HOTCHANDANI, P. PAQUIN, and R. M. LEBLANC. Photochem. Photobiol. **26**, 167 (1977).
15. A. C. ALBRECHT. J. Mol. Spectrosc. **6**, 84 (1961).
16. R. M. LEBLANC, G. GALINIER, A. TESSIER, and L. LEMIEUX. Can. J. Chem. **52**, 3723 (1974).
17. S. HOTCHANDANI and A. C. TESTA. Spectrochim. Acta, **32A**, 1659 (1976).
18. E. R. BLOUT and M. FIELDS. J. Am. Chem. Soc. **70**, 189 (1948).
19. R. M. HOCHSTRASSER. Acc. Chem. Res. **1**, 266 (1968).
20. H. L. B. FANG, R. J. THRASH, and G. E. LEROI. J. Chem. Phys. **67**, 3389 (1977).

Can. J. Chem. Downloaded from www.nrcresearchpress.com by 210.87.254.42 on 09/05/12
For personal use only.

Kinetics and mechanism for the formation of oxygenated products from the photolysis of hexafluoroacetone–methane system

E-CHUNG WU, ROBERT RICHMOND CLARK, AND YI-NOO TANG
Department of Chemistry, Texas A&M University, College Station, TX 77843, U.S.A.

Received October 19, 1977

E-CHUNG WU, ROBERT RICHMOND CLARK, and YI-NOO TANG. Can. J. Chem. **56**, 1989 (1978).

In addition to CF_3H and C_2F_6, four oxygenated products were identified in the photolysis of hexafluoroacetone–methane system: CH_3COCF_3, $(CF_3)_3COH$, $(CF_3)_2(CH_3)COH$, and $(CF_3)_2(CH_3)COCF_3$. The mechanism for the formation of these compounds is discussed, and the activation energies of several of the reactions involved are evaluated from detailed temperature and composition studies.

E-CHUNG WU, ROBERT RICHMOND CLARK et YI-NOO TANG. Can. J. Chem. **56**, 1989 (1978).

Lors de la photolyse du système hexafluoroacétone–méthane, on a identifié quatre produits oxygénés en plus du CF_3H et du C_2F_6; il s'agit de CH_3COCF_3, $(CF_3)_3COH$, $(CF_3)_2(CH_3)COH$ et $(CF_3)_2(CH_3)COCF_3$. On discute du mécanisme de formation de ces composés et on évalue les énergies d'activation de plusieurs réactions impliquées en faisant appel à des études détaillées de température et de composition.

[Traduit par le journal]

Can. J. Chem. Downloaded from www.nrcresearchpress.com by 210.87.254.40 on 09/05/12
For personal use only.

Introduction

During the past twenty years, the various chemical and physical processes associated with the photolysis of hexafluoroacetone (HFA) have been extensively studied (1–7). Although the mechanism of photolysis is quite complicated, the only significant products observed by most of the investigators over a wide range of pressure and temperature were CO and C_2F_6, with the latter being formed from the recombination of CF_3 radicals. Because of the apparent simplicity of the photodecomposition, and the ease of measuring the dissociation yields, HFA has been used as a major source of CF_3 radicals to study their chemical interactions (8).

Hydrogen abstraction of CF_3 in a $(CF_3)_2CO$–CH_4 system has been studied by Ayscough, Polanyi, and Steacie (9), Carmichael and Johnston (10), and Whittle and co-workers (11). An activation energy for this process has been obtained in the range of 10.3–11.5 kcal mol^{-1}. Ayscough (12) has also used this system to estabish the recombination rate of CF_3 radicals. The corresponding reactions with deuterated and partially deuterated methane have been the backbone of the studies of isotopic effects in free radical abstractive interactions (11, 13, 14).

In the pure HFA system, Gordon (7) has also detected an ether as a product which is attributable to the addition of CF_3 to the C=O double bonds of the ketone. He has also evaluated the activation energies for both the addition and reverse decomposition processes. We have performed a detailed study on the interactions of CF_3 radicals with HFA in the presence of methane, and have detected four oxygenated products. The energetics and mechanism for the formation of these four species will be discussed in detail.

Experimental

Hexafluoroacetone obtained from PCR, Inc. was purified by vacuum distillation. Ultra pure grade methane from Matheson with a purity of 99.99% was used directly without further purification. Those compounds used for the purpose of identification, such as CF_3H, C_2F_6 (from Matheson), CF_3COCH_3, $(CF_3)_2CH_3COH$, and $(CF_3)_3COH$ (from PCR, Inc.), were used directly without purification.

The experimental set-up consists of a greaseless vacuum line with two Validyne pressure transducers, a 45 mm × 150 mm long quartz reaction cell in a cylindrical aluminum oven which was regulated by a proportional temperature controller with a temperature fluctuation of ±1.0°C at 300°C, and a Bausch and Lomb monochromator which isolated 313 nm light from an Osram Super-pressure Hg lamp.

HFA was condensed into the reaction cell while CH_4 was transferred by expansion. The reactants were equilibrated at the required temperature for half an hour prior to photolysis. A blank test has shown no dark reaction taking place. Four oxygenated products were observed. Three of them, CF_3COCH_3, $(CF_3)_3COH$, and $(CF_3)_2(CH_3)COH$ were identified by mass spectrometry and further confirmed gas chromatographically using authentic samples. The fourth compound exhibited the following major peaks in its mass spectrum: 181, $(CF_3)_2(CH_3)CO^+$; 145, $(CF_3)_2(CH_3)C^+$; 97, CF_3CO^+; 69, CF_3^+; and 43, CH_3CO^+; no molecular ion is observed. This evidence, coupled with mechanistic expectations, led to the identification of this fourth compound as $(CF_3)_2(CH_3)COCF_3$.

After photolysis, samples were separated into three portions of known ratios which then were analyzed gas chromatographically using three sets of columns: (*1*) a 10 ft × ¼ in. dimethylsulfolane column (23°C) + a 10 ft × ¼ in. molecular seive 5A column (40°C) were used for the analysis of CO and C_2F_6; (*2*) a 50 ft × ¼ in. PCA column (propylene carbonate

Can. J. Chem. Downloaded from www.nrcresearchpress.com by 210.87.254.40 on 09/05/12
For personal use only.

on alumina) at 0°C was used for the analysis of CF_3H and C_2F_6; (*3*) a 30 ft × ¼ in. silicon fluids #96 column (23°C) was used to analyze oxygenated compounds. The peak was measured by (*1*) the product of peak height and half-peak width; and (*2*) the "cut and weigh" method. The results obtained from both methods are in good agreement. Relative thermal conductivities of most of the product compounds were precisely calibrated with authentic samples. The thermal conductivity of $(CF_3)_2(CH_3)COCF_3$ was estimated from those of other oxygenated compounds.

Results and Discussion

Mechanism for Product Formation

The photolysis of HFA in the presence of methane at 313 nm has been studied over a wide pressure and composition range at various temperatures from 298 to 443 K. In most of the samples, the HFA pressure employed is 40 Torr, but the CH_4 pressure varies from 10 to 400 Torr. The products formed are: CO, C_2F_6, CF_3H, $(CF_3)_3COH$, CF_3COCH_3, $(CF_3)_2(CH_3)COH$, and $(CF_3)_2(CH_3)COCF_3$. The yields of CF_3H and CF_3COCH_3 increase, while those of $(CF_3)_3COH$, $(CF_3)_2(CH_3)COH$, and $(CF_3)_2(CH_3)COCF_3$ decrease as the reaction temperature increases. The latter two have a very sensitive temperature dependence. An overall mechanism for the formation of products is proposed as follows:

[1] $(CF_3)_2CO \xrightarrow{h\nu} 2CF_3 + CO$

[2] $2CF_3 \rightarrow C_2F_6$

[3] $CF_3 + CH_4 \rightarrow CF_3H + CH_3$

[4], [−4] $CF_3 + (CF_3)_2CO \rightleftarrows (CF_3)_3CO$

[5] $(CF_3)_3CO + CH_4 \rightarrow (CF_3)_3COH + CH_3$

[6] $CH_3 + (CF_3)_2CO \rightarrow (CF_3)_2(CH_3)CO$

[7] $(CF_3)_2(CH_3)CO \rightarrow CF_3COCH_3 + CF_3$

[8] $(CF_3)_2(CH_3)CO + CH_4 \rightarrow (CF_3)_2(CH_3)COH + CH_3$

[9] $(CF_3)_2(CH_3)CO + CF_3 \rightarrow (CF_3)_2(CH_3)COCF_3$

Another plausible reaction for the mechanism, $(CF_3)_3CO + CF_3 \rightarrow (CF_3)_3COCF_3$, is omitted because the expected ether is not observed as a significant product in the present experiments.

The product, $(CF_3)_3COH$, has never been observed in previous studies. In some earlier work related to the formation and decomposition of $(CF_3)_2(CH_3)CO$ as shown in [6] and [7], Smith and Calvert (15) formed the same radical through reaction [10]

[10] $CF_3 + CH_3COCF_3 \rightarrow (CF_3)_2(CH_3)CO$

by photolyzing a mixture of $CF_3COC_6H_5$ and CF_3COCH_3, but they failed to observe $(CF_3)_2CO$ as a reaction product. This indicated that reaction [−6], the reverse of [6], is not an important decomposition route for this radical. Later, Gile and Whittle (16) studied the photolysis of a mixture of CF_3COCF_3 and CH_3COCH_3, and observed the formation of CF_3COCH_3. With this combined evidence, we have omitted the reverse process [−6] from the mechanism and accepted process [7] as the sole path for the decomposition of $(CF_3)_2(CH_3)CO$. The reason for the domination of process [7] may be attributed to the stronger repulsion between the CF_3 groups and the stabilization of the CH_3 group by hydrogen bonding between H and O atoms in the radical. Besides undergoing decomposition, this radical can either abstract a hydrogen to give an alcohol as in [8], or combine with a CF_3 radical to give an ether as in [9].

Recently, Gordon and co-workers (17) studied the photolysis of a $(CF_3)_2CO$–C_2H_6 mixture and observed $(CF_3)_2(C_2H_5)COH$ as a product. They proposed a mechanism for the formation of this alcohol which involved the H-abstraction from C_2H_6 by electronically excited HFA molecules. This was based on their observations that the CO produced was at the most a few percent of that which would be produced from the unquenched photolysis of HFA, and that considerably more C_2F_6 was observed than would correspond to the observed CO. However, such a chemical quenching mechanism is not significant in the present HFA–CH_4 system because of the following observations. (*i*) The yield of CO from the HFA–CH_4 system is very close to that of the pure HFA system. (*ii*) The product ratio, C_2F_6/CO, is always less than unity. (*iii*) The mass balance between CF_3 and CO for most of the HFA–CH_4 samples (except for those of very high $[CH_4]$) shows a $[C_2F_6 + \frac{1}{2}CF_3H + \frac{1}{2}(CF_3)_3COH - \frac{1}{2}CH_3COCF_3]/CO$ ratio which is around unity.

Evaluation of Activation Energies

From the mechanism postulated above, four quantitative relationships can be obtained as follows:

[11] $k_3/k_2^{1/2} = R_3/R_2^{1/2}[CH_4]$

[12] $R_8/R_7 = (k_8/k_7)\,[CH_4]$

[13] $R_9/R_7 = (k_9/k_7k_2^{1/2})R_2^{1/2}$

[14] $R_3\,[HFA]/R_5 = (k_3/k_4)\,[CH_4] + (k_3/k_4)\,(k_{-4}/k_5)$

where R_i = reaction rate of process i, and [X] = concentration of compound X. The values of $k_3/k_2^{1/2}$ calculated from the right-hand side of eq. [11] are listed in Table 1. At 383 K, a constant value of $R_3/R_2^{1/2}[CH_4]$ was obtained with excellent precision for a thirty-fold variation of the $[CH_4]/[HFA]$ ratio. At 363 K, the data show a slightly larger fluctuation for a ten-fold variation in the $[CH_4]/[HFA]$ ratio due mainly to the smaller yield of CF_3H at this lower

Can. J. Chem. Downloaded from www.nrcresearchpress.com by 210.87.254.40 on 09/05/12
For personal use only.

TABLE 1. The evaluation of the ratio of rate constants, $k_3/k_2^{1/2}$, at various compositions and temperatures

T (K)	$CH_4/(CF_3)_2CO$	$R_2 \times 10^{9}$ [a]	$R_3 \times 10^{10}$ [a]	$[CH_4] \times 10^{3}$ [b]	$(k_3/k_2^{1/2}) \times 10^3$
363	1	2.64	1.27	2.14	1.16
	2	1.38	2.18	4.29	1.37
	3	1.44	3.27	6.45	1.37
	3	2.19	2.11	3.22	1.40
	4	1.31	4.36	8.59	1.40
	5	1.11	3.91	10.73	1.10
	10	1.24	10.05	21.46	1.33
					Ave. 1.29 ± 0.13
383	0.33	4.62	1.91	1.07	2.62
	1	3.42	3.09	2.14	2.47
	2.5	1.41	5.05	5.37	2.51
	3	2.27	3.82	3.22	2.51
	5	1.16	8.53	10.73	2.34
	10	1.05	18.27	21.46	2.64
					Ave. 2.51 ± 0.04
403	1	1.76	3.89	2.14	4.33
423	1	1.42	7.38	2.14	9.16
	1	1.30	6.44	2.14	8.34
443	1	1.14	11.04	2.14	15.30

[a] In mol ℓ^{-1} s^{-1}.
[b] In mol ℓ^{-1}.

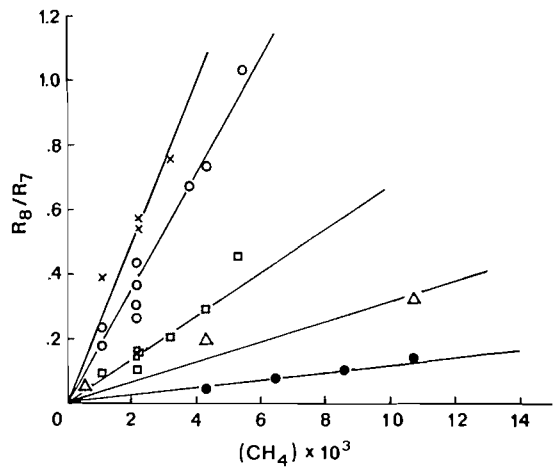

FIG. 1. A plot of R_8/R_7 vs. the concentration of methane at various temperatures. ×, 303 K; ○, 308 K; □, 323 K; △, 343 K; and ●, 363 K.

temperature. Several runs were also carried out at higher temperatures, i.e., 403, 423, and 443 K. An Arrhenius plot for these data gave a value for $E_3 - \frac{1}{2}E_2 = 9.90 \pm 0.34$ kcal mol^{-1}. If we assume $E_2 = 0$, E_3 therefore equals 9.90 kcal mol^{-1}, which is consistent with the value 10.3 kcal mol^{-1} evaluated by Ayscough, Polanyi, and Steacie (9), and the value 9.5 kcal mol^{-1} evaluated by Pritchard, Pritchard, and Trotman-Dickenson (18). Whittle and co-workers (11) have obtained larger values, 11.3, 11.5, while Carmichael and Johnston (10) obtained a value of 11.0 kcal mol^{-1} for E_3. From the Arrhenius plot, a value for log $(A_3/A_2^{1/2}) = 3.05 \pm 0.18$ is obtained where $A_3/A_2^{1/2}$ is in units of $\ell^{1/2}$ mol$^{-1/2}$ s$^{-1/2}$. The corresponding value from ref. 9 is 3.49 and that from ref. 10 is 3.80.

Results related to eqs. [12], [13], and [14] have been calculated. Plots of the ratios R_8/R_7 vs. $[CH_4]$ at various temperatures are shown in Fig. 1 and are linear as required by eq. [12]. The least-squares values of the slopes are 250.3, 177.9, 68.2, 23.44, and 8.44 ℓ mol^{-1} at reaction temperatures of 303, 308, 323, 343, and 363 K, respectively. An Arrhenius plot, shown in Fig. 2(*A*), gave a least-squares value of 12.29 ± 0.09 kcal mol^{-1} for the difference of activation energies, $E_7 - E_8$, and a value of -6.47 ± 0.06 for log (A_8/A_7) where A_8/A_7 is in units of ℓ mol^{-1}.

A plot of R_9/R_7 vs. the square root of R_2 yields the ratio of rate constants, $k_9/k_7k_2^{1/2}$. From Fig. 3 these slopes are 0.495, 0.292, and 0.107 $\ell^{1/2}$ s$^{1/2}$ mol$^{-1/2}$ at 303, 308, and 323 K, respectively. From the Arrhenius plot of these slopes, shown in Fig. 2(*B*), we obtained a least-squares value of -14.53 ± 1.32 kcal mol^{-1} for $E_9 - E_7 - \frac{1}{2}E_2$ and a value of -10.81 ± 0.92 for log $(A_9/A_7A_2^{1/2})$ with the A term in the unit of $\ell^{1/2}$ s$^{1/2}$ mol$^{-1/2}$. If we assume $E_9 = E_2 = 0$ for the radical–radical recombination processes, $E_7 = 14.53$ kcal mol^{-1}. By combining this E_7 value with that of $E_7 - E_8$ determined above, we obtain 2.24 ± 1.32 kcal mol^{-1} for E_8.

The appropriate plot for eq. [14], shown in Fig. 4, yielded least square values of k_3/k_4 from the slopes, 0.094, 0.151, and 0.189 at temperatures 343, 353, and

Can. J. Chem. Downloaded from www.nrcresearchpress.com by 210.87.254.40 on 09/05/12
For personal use only.

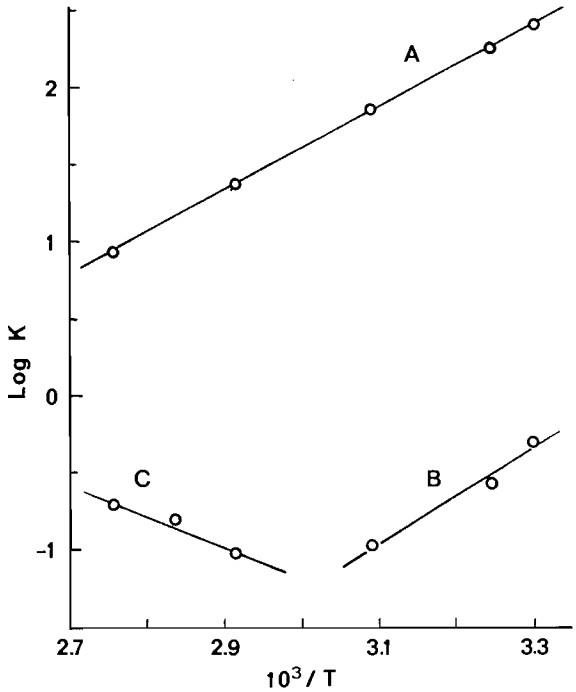

FIG. 2. An Arrhenius plot of log K vs. $1/T$. (A), $K = k_8/k_7$; (B) $K = k_9/k_7k_2^{1/2}$; (C) $K = k_3/k_4$.

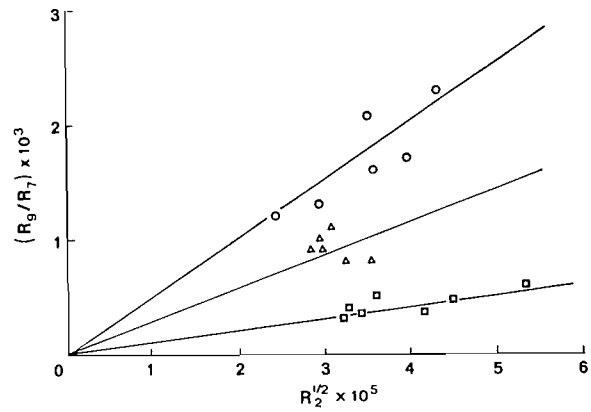

FIG. 3. A plot of R_9/R_7 vs. $R_2^{1/2}$ at various temperatures. O, 303 K; △, 308 K; and □, 323 K.

363 K, respectively; the corresponding values of $k_3k_4/k_{-4}k_5$ from the intercepts are 0.0014, 0.0041, and 0.0054 mol ℓ^{-1} at these three temperatures. The difference of activation energies, $E_3 - E_4$, can thus be obtained as 8.70 ± 1.9 kcal mol^{-1} from the Arrhenius plot shown in Fig. 2(C). The log (A_3/A_4) value is 4.54 ± 1.19. Since E_3 is 9.9 kcal mol^{-1} we can estimate a value of 1.2 kcal mol^{-1} for E_4. The values of k_{-4}/k_5 can also be obtained from the ratios of intercept/slope in Fig. 4 but with higher uncertainties. A least-squares value for $E_{-4} - E_5$ can be estimated as 8.17 ± 3.55 kcal mol^{-1}.

These results are summarized in Table 2.

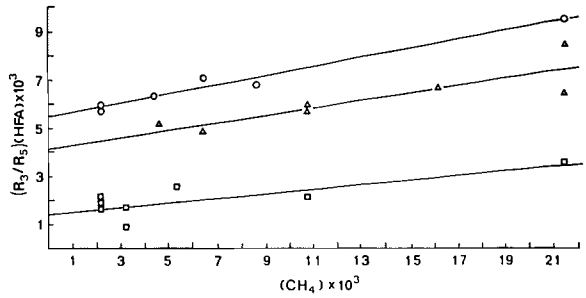

FIG. 4. A plot of R_3[HFA]$/R_5$ vs. the concentration of methane at various temperatures. □, 343 K; △, 353 K; and ○, 363 K.

The CF_3 Addition Process to C=O Bond in HFA

In 1962, Gordon (7) studied the photolysis of HFA at various temperatures and observed the formation of a perfluoro-ether, $(CF_3)_3COCF_3$, as a major product. He proposed that CF_3 radicals formed from the photolysis added to the oxygen end of the C=O bond to give $(CF_3)_2COCF_3$ as shown in [15], which then combined with another CF_3 radical to form the ether as shown in [16].

[15] $$CF_3 + (CF_3)_2CO \rightleftarrows (CF_3)_2COCF_3$$

[16] $$CF_3 + (CF_3)_2COCF_3 \rightarrow (CF_3)_3COCF_3$$

He obtained a value of 9.67 kcal mol^{-1} for E_{15} and a value of 30.6 kcal mol^{-1} for E_{-15}. However, the formation of $(CF_3)_3COH$ and $(CF_3)_2(CH_3)COH$ as major products in our reaction system indicates clearly that the addition should take place at the carbon end of the C=O bond. Therefore, E_{15} obtained by Gordon (7) should be identical to E_4 in our mechanism. We obtained a value of 1.2 kcal mol^{-1} for E_4, which is much smaller than his E_{15} value. We are in favor of this low value because the present experimental results indicate that the rate of formation of $(CF_3)_3COH$ at room temperature is very much higher than that of CF_3H. This indicates that the overall activation energy of processes [4] and [5] should be much less than that of process [3] which is about 10 kcal mol^{-1}. Since the E_a value for [5], the H-abstraction reaction from CH_4 by $(CF_3)_3CO$ radical, should be significant, it renders a 1.2 kcal mol^{-1} E_a value for [4] to be more likely than the 9.67 kcal mol^{-1} value.

Other Kinetic Considerations[1]

As we have discussed above, the values of 8.17 and

[1]Table 3, the dependence of R_8/R_7 on the pressure of methane at various temperatures, and Table 4, composition and temperature dependence of R_2 and R_9/R_7, are both lodged with the Depository of Unpublished Data. Copies of these may be obtained, at a nominal charge, from the Depository of Unpublished Data, CISTI, National Research Council of Canada, Ottawa, Ont., Canada K1A 0S2.

TABLE 2. A summary of the evaluated activation energies of various processes in the mechanism

Processes	Activation energies (kcal mol^{-1})
$CF_3 + CH_4 \xrightarrow{3} CF_3H + CH_3$	$E_3 = 9.90 \pm 0.34$
$CF_3 + (CF_3)_2CO \xrightarrow{4} (CF_3)_3CO$	$E_4 \simeq 1.2$
$(CF_3)_3CO \xrightarrow{-4} (CF_3)_2CO + CF_3$	$E_{-4} - E_5 = 8.17 \pm 3.55$
$CH_4 + (CF_3)_3CO \xrightarrow{5} (CF_3)_3COH + CH_3$	
$(CF_3)_2(CH_3)CO \xrightarrow{7} CF_3COCH_3 + CF_3$	$E_7 = 14.53 \pm 1.32$
$CH_4 + (CF_3)_2(CH_3)CO \xrightarrow{8} (CF_3)_2(CH_3)COH + CH_3$	$E_8 = 2.24 \pm 1.32$

12.29 kcal mol^{-1} have been obtained for $E_{-4} - E_5$ and $E_7 - E_8$, respectively, and we have calculated the value of E_8 from the known value of E_7. If we assume E_5 has a value similar to that of E_8, we are able to estimate a value of 10.4 kcal mol^{-1} for E_{-4}. This value is slightly less than that of E_7. If we compare this estimated E_{-4} value with that of E_{-15} obtained by Gordon (7), again his value is much higher than ours. Our experimental results indicated that in the temperature range of 300–350 K, the stability of these fluorinated *tert*-butoxyl radicals decreases rapidly as temperature increases. Because the stability of these radicals is sensitive to such low temperatures, the activation energies for their decomposition are likely to be rather low. In fact, the decomposition of *tert*-butoxyl radicals has been studied (19, 20): the activation energy is in the range between 11 to 13 kcal mol^{-1} which is consistent with our finding.

There are no values for the Arrhenius parameters of H-abstraction by fluorinated *tert*-butoxyl radical available in the literature. However, it is well known that the *tert*-butoxyl radical needs a much lower activation energy for H-abstraction than does a methyl radical (21). Our low value of E_8, 2.24 kcal mol^{-1}, is therefore consistent with these observations.

By employing the activation energies of eqs. [4] and [−4], we can also evaluate the heat of formation for the $(CF_3)_3CO$ radical. Since we know that $\Delta H_f^0(CF_3,\ 298\ K) = -112.5$ kcal mol^{-1} (22) and $\Delta H_f^0[(CF_3)_2CO,\ 600\ K] = -325.2$ kcal mol^{-1} (23), with the help of the group additivity rule (22) to calculate the required C_p values, we are able to roughly estimate the heat of formation for $(CF_3)_3CO$ as −448 kcal mol^{-1}.

Acknowledgement

The authors acknowledge the kind support provided by the Robert A. Welch Foundation.

1. P. B. AYSCOUGH and E. W. R. STEACIE. Proc. R. Soc. London, A**234**, 476 (1956).
2. (*a*) D. A. WHYTOCK and K. O. KUTSCHKE. Proc. R. Soc. London, A**306**, 503 (1968); (*b*) A. GANDINI and K. O. KUTSCHKE. Proc. R. Soc. London, A**306**, 511 (1968); (*c*) A. GANDINI, D. A. WHYTOCK, and K. O. KUTSCHKE. Proc. R. Soc. London, A**306**, 529 (1968); A**306**, 537 (1968); A**306**, 541 (1968) and references therein.
3. (*a*) P. G. BOWERS and G. B. PORTER. J. Phys. Chem. **68**, 2982 (1964); **70**, 1622 (1966); (*b*) P. G. BOWERS. Can. J. Chem. **46**, 307 (1968).
4. (*a*) W. R. WARE and M. L. DUTTON. J. Chem. Phys. **47**, 4670 (1967); (*b*) W. R. WARE and S. K. LEE. Chem. Phys. **49**, 217 (1968); (*c*) A. M. HALPERN and W. R. WARE. J. Chem. Phys. **53**, 1969 (1970).
5. D. A. KNECHT. Chem. Phys. Lett. **33**, 325 (1975).
6. F. M. SERVIDO and G. O. PRITCHARD. Int. J. Chem. Kinet. **7**, 195 (1975).
7. A. S. GORDON. J. Chem. Phys. **36**, 1330 (1962).
8. P. GRAY, A. A. HEROD, and A. JONES. Chem. Rev. **71**, 247 (1971) and references therein.
9. P. B. AYSCOUGH, J. C. POLANYI, and E. W. R. STEACIE. Can. J. Chem. **33**, 743 (1955).
10. H. CARMICHAEL and H. S. JOHNSTON. J. Chem. Phys. **41**, 1975 (1964).
11. (*a*) W. G. ALCOCK and E. WHITTLE. Trans. Faraday Soc. **61**, 244 (1965); (*b*) R. D. GILE, L. M. QUICK, and E. WHITTLE. Trans. Faraday Soc. **63**, 662 (1967).
12. P. B. AYSCOUGH. J. Chem. Phys. **24**, 944 (1956).
13. R. E. DODD and J. W. SMITH. J. Chem. Soc. 1465 (1957).
14. T. E. SHARP and H. S. JOHNSTON. J. Chem. Phys. **37**, 1544 (1962).
15. R. M. SMITH and J. G. CALVERT. J. Am. Chem. Soc. **78**, 2345 (1956).
16. R. D. GILE and E. WHITTLE. Trans. Faraday Soc. **61**, 1425 (1965).
17. A. S. GORDON, W. P. NORRIS, R. H. KNIPE, and J. H. JOHNSON. Int. J. Chem. Kinet. **7**, 15 (1975).
18. G. O. PRITCHARD, H. O. PRITCHARD, and A. F. TROTMAN-DICKENSON. Chem. Ind. London, 564 (1955).
19. G. R. MCMILLAN. J. Am. Chem. Soc. **82**, 2422 (1960).
20. F. W. BIRSS, C. J. DANBY, and C. N. HINSHELWOOD. Proc. R. Soc. London, A**239**, 154 (1957).
21. P. GARY, R. SHAW, and J. C. J. THYNNE. Prog. React. Kinet. **4**, 63 (1967).
22. S. W. BENSON. Thermochemical kinetics. John Wiley & Son, Inc., New York, NY. 1968.
23. A. S. GORDON. Int. J. Chem. Kinet. **4**, 541 (1972).

Can. J. Chem. Downloaded from www.nrcresearchpress.com by 210.87.254.40 on 09/05/12
For personal use only.

Dehydrogenation of Δ^3-carene over chromia and chromia–alumina catalysts

V. KRISHNASAMY

Alagappa Chettiar College of Technology, University of Madras, Guindy, Madras 600 025, India

Received December 20, 1977

V. KRISHNASAMY. Can. J. Chem. **56**, 1994 (1978).

3-Carene is dehydrogenated over oxidized and reduced chromia and chromia–alumina catalysts at 340 to 500°C, without and with pyridine. Dehydrogenation is found to be more effective over reduced than oxidized catalysts; in either state, however, chromia–alumina is more active than chromia. Pyridine brings down the dehydrogenation ability of chromia and chromia–alumina in both reduced and oxidized states, more markedly in the reduced state. The ratio of *p*-cymene to *m*-cymene at 360 to 425°C is higher over chromia than over chromia–alumina. Increase of temperature from 360°C to higher values decreases the ratio of cymenes over chromia but does not affect the ratio over chromia–alumina. Pyridine has no effect on the ratio of cymenes over chromia; over chromia–alumina, neither, pyridine nor the pretreatment of the catalyst with oxygen or hydrogen has any effect on the ratio.

V. KRISHNASAMY. Can. J. Chem. **56**, 1994 (1978).

Il y a déshydrogénation du carène-3 sur des catalyseurs oxydés et réduits de sesquioxyde de chrome et de sesquioxyde de chrome–alumine à des températures allant de 340 à 500°C avec ou sans addition de pyridine. On a trouvé que la déshydrogénation est plus efficace sur des catalyseurs réduits plutôt qu'oxydés; toutefois, dans chacun des états, le catalyseur sesquioxyde de chrome–alumine est plus actif que le sesquioxyde de chrome. La pyridine abaisse l'habilité à déshydrogéner du sesquioxyde de chrome et du sesquioxyde de chrome–alumine aux états soit réduits ou oxydés; toutefois cet effet est plus marqué dans l'état réduit. Le rapport de *p*-cymène à *m*-cymène à des températures allant de 360 à 425°C est plus élevé lorsque l'on opère sur du sesquioxyde de chrome que dans le cas du sesquioxyde de chrome–alumine. Une augmentation de la température de 360°C vers des valeurs plus élevées provoque une diminution du rapport des cymènes sur le sesquioxyde de chrome mais n'affecte pas le rapport sur le sesquioxyde de chrome–alumine. La pyridine n'a aucun effet sur les rapports de cymènes sur du sesquioxyde de chrome; sur le sesquioxyde de chrome–alumine, ni la pyridine ni un prétraitement du catalyseur avec de l'oxygène ou de l'hydrogène n'affecte ce rapport.

[Traduit par le journal]

Introduction

3-Carene is the major constituent (about 60%) of Indian turpentine oil (1). The oil cannot be stored, as 3-carene readily undergoes aerial oxidation (2, 3) forming resins. Attempts are being made to convert this unstable compound into stable useful intermediates. With this object, chromia and chromia–alumina catalysts which are employed for important industrial reactions (4) have been used in the present investigation for the vapour phase conversion of 3-carene. The observed results are explained in terms of the acidity of the catalyst, the dispersion and oxidation states of chromium ions on the surface of the catalysts, and the poisoning influence of pyridine.

Experimental

Preparation of Materials

Alumina

Alumina was prepared by hydrolysing aluminium isopropoxide with distilled water (5). The precipitated aluminium hydroxide was filtered, washed thoroughly with water, dried at 120°C for 24 h. It was then activated at 500°C in dry air for 24 h, crushed into powder, sieved (100–120 mesh) and used as support for chromia.

Chromia Gel

Chromia gel was prepared and activated according to the procedure described elsewhere (6, 7). The activated material was powdered and pelletized (4 × 4 mm cylindrical size).

Chromia–Alumina

Chromia–alumina (4 × 4 mm cylindrical pellets) was prepared according to the methods of Selwood and Eischens (8) and Yeddanapalli *et al.* (9). The percentage of chromium was estimated to be 5.78.

The surface area measurements of chromia and chromia–alumina were made according to BET method (10) by the adsorption of nitrogen at liquid nitrogen temperature. The experimental procedure and calculations were the same as described by Shoemaker and Garland (11). The values for chromia and chromia–alumina are found to be 14 and 116 m^2/g, respectively.

Prior to each run, the catalyst was reactivated by heating for 8 h in a current of dry air at 500°C until no oxides of carbon were detected in the exit gas; it was then reduced by passing pure dry hydrogen for 6 h at the same temperatures and then brought to the requisite experimental temperature. For conducting runs in the oxidized state, the catalyst was not reduced.

3-Carene

First-quality Indian turpentine oil (Government Turpentine and Rosin Company, Bareilly, India) was used. It contained about 60% 3-carene, the rest being α-pinene and small amounts of β-pinene. 3-Carene was obtained from this oil by fractiona-

Can. J. Chem. Downloaded from www.nrcresearchpress.com by 210.87.254.40 on 09/05/12
For personal use only.

Can. J. Chem. Downloaded from www.nrcresearchpress.com by 210.87.254.40 on 09/05/12
For personal use only.

tion at 10 mm, using a 152 cm glass column packed with stainless steel helices, equivalent to 22 theoretical plates. The purity was found to be better than 99% by gas chromatography.

Pyridine

Analar pyridine (E. Merck) was refluxed over KOH pellets and fractionally distilled with exclusion of moisture, the material distilling at 115.5°/760 mm being collected. Its purity was found to be better than 99% by gas chromatography.

Hydrogen

Hydrogen (Indian Oxygen Co.) was purified by passing successively through a silica gel drying tower, a tube containing freshly reduced copper turnings at 400°C, another silica gel tower, and finally through a trap cooled in liquid oxygen.

Apparatus and Procedure

The reactions were carried out at atmospheric pressure in a fixed bed flow-type reactor. The catalyst (5 g) was placed in a Pyrex reactor tube, 25 cm long and 3 cm internal diameter. Above the catalyst bed, Pyrex glass beads (4 mm diameter) were placed to a height of 5 cm. The tube was inserted into the furnace, a cylindrical steel tube of internal diameter 4 cm, coated with a thin layer of asbestos and wound uniformly with nichrome wire, and heated electrically to the requisite temperature. 3-Carene was passed at a constant rate of 2 cm^3 per gram of catalyst per hour over the catalyst using a constant feed rate syringe pump that could be operated at different feed rates. This procedure was repeated for carene–pyridine mixture also. The hydrogen supply was controlled through precision 'Hoke' valves.

The liquid products collected for the first 15 min of each run, which normally covers an hour, was discarded and analysis was made only of the products collected after this time. This was done to ensure the attainment of a steady state for the reaction over the catalyst and also to eliminate temperature fluctuations, if any, due to the starting of the reaction. After the reaction, the catalyst was regenerated and reduced as described earlier.

The liquid products of dehydrogenation were identified and estimated using a Perkin-Elmer Infracord Model-137 and a Perkin-Elmer Vapour Fractometer Model 154-D. Products other than cymenes were quantitatively estimated by a Perkin-Elmer Column K, consisting of a 2-m column of carbowax on chromosorb. The column temperature for the best resolution within a reasonable time was found to be 115°C with hydrogen inlet pressure of 15 psi. *para* and *meta*-cymenes were separated and estimated in a specially prepared 2-m column filled with 40–60 mesh acid washed kieselguhr, coated with the stationary liquid, consisting by weight of 9% Bentone-34 and 4% Apiezon-L, heated at 108°C with hydrogen passed at a pressure of 28 psi.

For the identification of different peaks in a chromatogram retention times for the different compounds were found by introducing pure substances donated by Hercules Powder Company, U.S.A. For quantitative analysis, synthetic mixtures containing the different compounds in varying proportions were introduced and calibration curves relating the concentration with the peak heights were drawn. Since the peaks obtained were sharp and symmetrical, peak heights were used as a measure of concentration. Initial experiments, in which both peak heights and the total areas were compared using mixtures of known concentrations, gave identical results. Therefore, in subsequent work all analyses were based on comparison of peak heights.

The reaction sequence pertaining to the isomerization of 3-carene to *p*- and *m*-menthadienes and their further dehydrogenation to *p*- and *m*-cymenes is outlined in Scheme 1. The various possible transformations of menthadienes following the isomerization of 3-carene are illustrated in Scheme 2.

Results and Discussion

The results obtained over reduced and oxidized chromia, without and with pyridine, are given in Figs. 1 and 2, respectively. Figures 3 and 4 illustrate

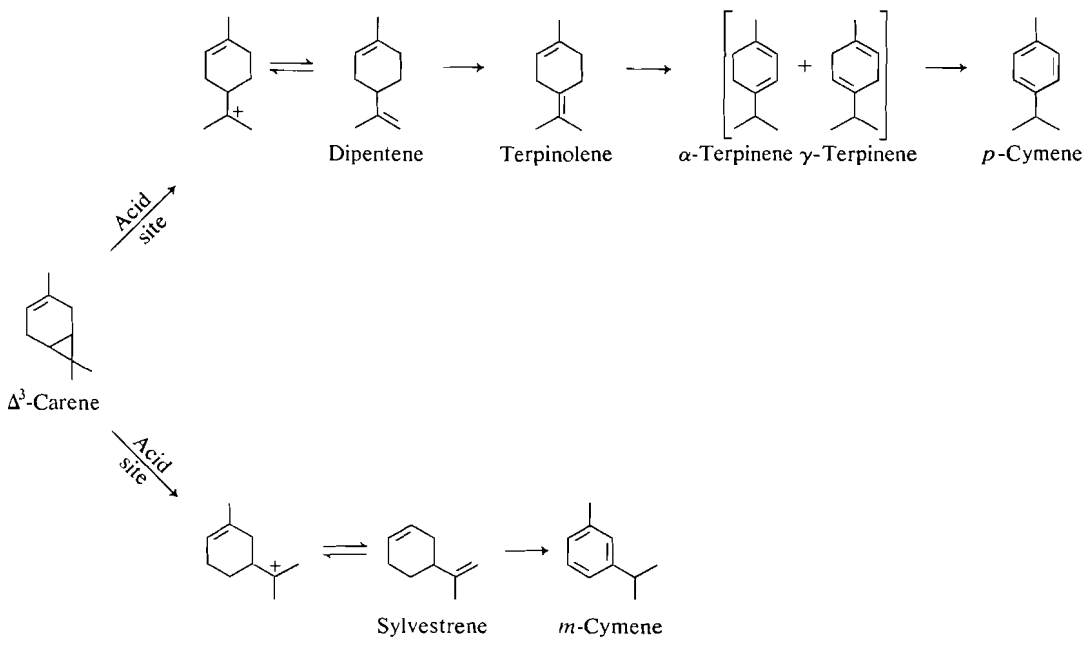

SCHEME 1

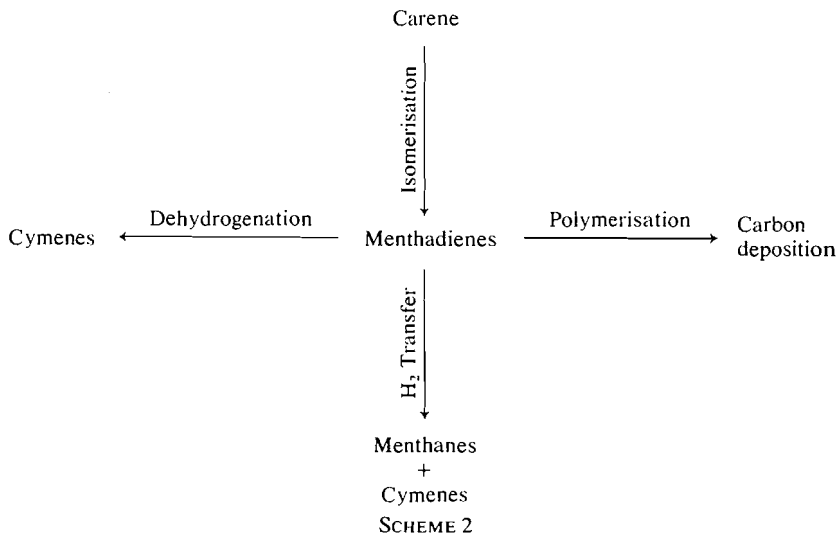

SCHEME 2

the corresponding results over chromia–alumina. The ratios of *p*-cymene to *m*-cymene obtained over chromia and chromia–alumina in both reduced and oxidized states are presented in Fig. 5.

Acidity and Disperison of Chromium Ions

Chromia–alumina in either state is more active than chromia (Figs. 1 to 4). This observation is explained in terms of the acidity of the catalysts and the dispersion of chromium ions. The conversion of 3-carene to cymenes involves two steps (cf. Scheme 1). First, the isomerization of 3-carene to menthadienes and the dehydrogenation of menthadienes to cymenes. The first step requires acid sites and the second step dehydrogenation centres.

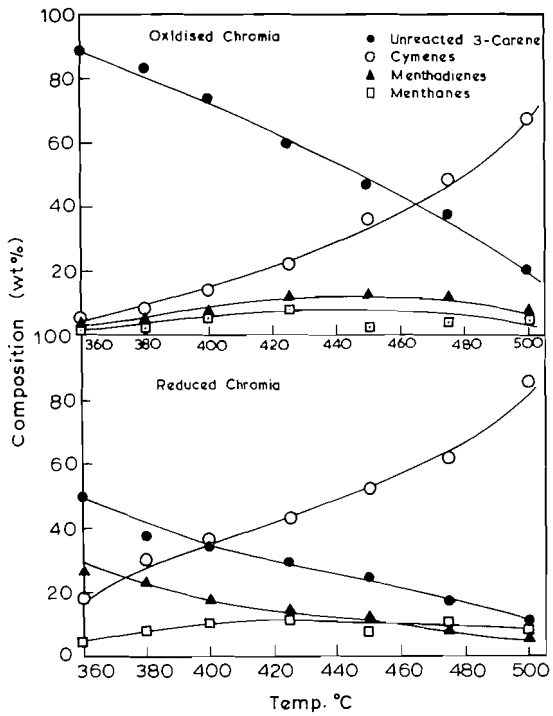

FIG. 1. Dehydrogenation of Δ^3-carene over oxidized and reduced chromia gel at different temperatures. LHSV = 2.

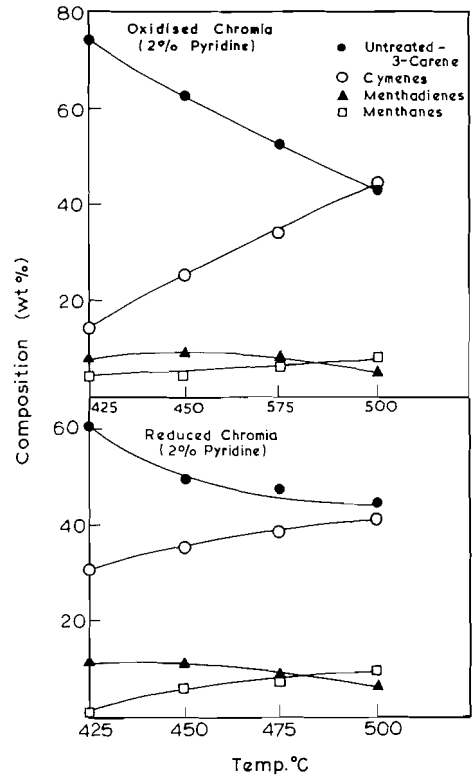

FIG. 2. Dehydrogenation of Δ^3-carene in the presence of 2% pyridine over oxidized and reduced chromia gel at different temperatures. LHSV = 2.

Can. J. Chem. Downloaded from www.nrcresearchpress.com by 210.87.254.40 on 09/05/12
For personal use only.

Can. J. Chem. Downloaded from www.nrcresearchpress.com by 210.87.254.40 on 09/05/12
For personal use only.

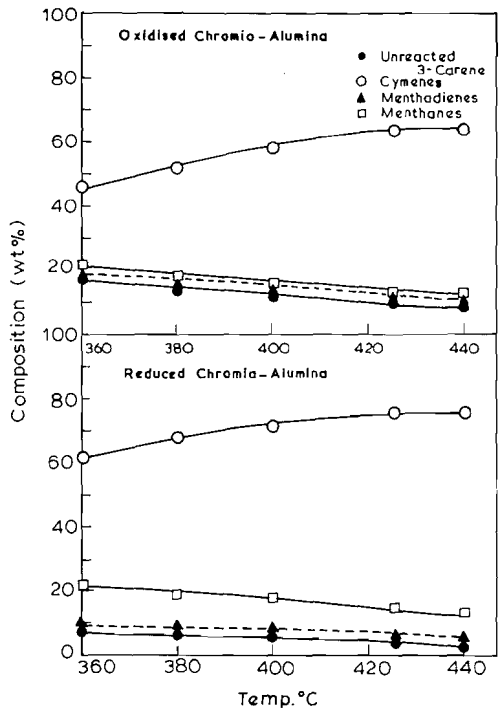

FIG. 3. Dehydrogenation of Δ^3-carene over oxidized and reduced chromia–alumina at different temperatures. LHSV = 2.

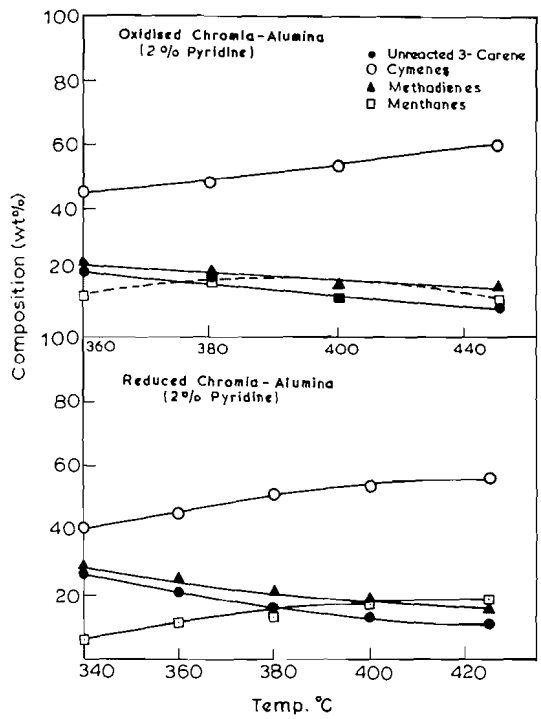

FIG. 4. Dehydrogenation of Δ^3-carene in the presence of 2% pyridine over oxidized and reduced chromia–alumina at different temperatures. LHSV = 2.

The total acidity (12) of chromia–alumina and chromia are 0.64 and 0.14 milliequivalent of *n*-butylamine/g, respectively. The alumina used as a support for chromia in this investigation is found to contain a spectrum of strong, medium, and weak acid sites (13). The acid sites over chromia–alumina are stronger and also more numerous than that over chromia and these decyclise the cyclopropane ring in carene to menthadienes which subsequently get dehydrogenated to cymenes. Such a facile conversion of 3-carene to menthadienes may not be possible over chromia and hence the observed low activity.

The chromia–alumina catalyst employed in this work is an impregnated type, containing less than 6% chromium. The higher dehydrogenation activity of such a catalyst, according to Selwood and Eischens (8) is due to the better dispersion of chromium ions over alumina. It may be mentioned here that in pure chromia the chromium ions occur in the form of isolated clusters, which are not as reactive as the chromium ions dispersed over alumina. When chromia–alumina is used, the menthadienes formed by the isomerization of 3-carene over the acidic sites on alumina also get dehydrogenated over the chromium ions, with the result the menthadienes do not accumulate in the products.

It is of interest to note that chromia–alumina in both reduced and oxidized states favour formation of menthanes, while chromia does not favour their formation (cf. Figs. 1 to 4). This shows that hydrogen is adsorbed strongly over chromia–alumina and hydrogenates the menthadienes adsorbed on the adjacent sites to form menthanes. This observation has also been confirmed by our earlier study (14) of partial pressure of hydrogen over these two catalysts. We have found that an increase of partial pressure of hydrogen increases directly the formation of menthanes over chromia–alumina, but not over chromia. A strong adsorption of hydrogen over chromia–alumina has also been reported by Selwood (15).

Oxidation States of Chromium Ions

Chromia–alumina and chromia are more active in their reduced states than in their oxidized states. It has been reported that chromium in both chromia and chromia–alumina exists as Cr(VI), Cr(V), Cr(III), and, in some cases, Cr(II) states, depending upon the pretreatment (16–21). When the catalyst is treated in an atmosphere of oxygen, it is likely that chromium may be in the Cr(VI), Cr(V), and Cr(III) states. Out of these, only Cr(III) is associated with dehydrogenation activity. On reduction of the catalyst in an atmosphere of hydrogen, all the higher valent chromium ions are reduced to Cr(III) ions and a few may be reduced even further to Cr(II) state,

Can. J. Chem. Downloaded from www.nrcresearchpress.com by 210.87.254.40 on 09/05/12
For personal use only.

both these states being catalytically active. Further, oxidized chromia contains more Cr(VI) ions than oxidized chromia–alumina as found by Soxhlet extraction and hydrogen peroxide decomposition (22). If the higher valent chromium ions other than Cr(III) and Cr(II) are associated with dehydrogenation activity, oxidized chromia and not oxidized chromia–alumina would be more active. Since oxidized chromia is less reactive than oxidized chromia–alumina, the higher valent chromium ions may not be active for the dehydrogenation reactions. Reduction of the catalysts in an atmosphere of hydrogen prior to catalytic reaction creates more chromium ions possessing dehydrogenation activity and, therefore, under reduced catalyst conditions they are more reactive.

Inhibition by Pyridine

Pyridine inhibits the dehydrogenation activity of both oxidized and reduced chromia and chromia–alumina, the poisoning influence being more over reduced catalysts. According to Voltz *et al.* (23), the higher valent chromium ions are more acidic than the lower valent chromium ions. Pyridine being a strong base gets preferentially adsorbed over the strong Lewis acid sites. Since the higher valent chromium ions as explained above are not active for the dehydrogenation of 3-carene, the dehydrogenation activity of oxidized catalysts are less affected.

In the absence of higher valent chromium ions over the reduced catalysts, pyridine may be assumed to be coordinated with lower valent chromium ions; as a result, there is a marked reduction in their activity. This assumption is further supported by a study of heat of adsorption of pyridine over oxidized and reduced chromia by gas chromatography following the methods of Eberly (24). Values obtained are 16.7 and 15.5 kcal/mol for oxidized and reduced chromia (25), respectively. The almost similar values cannot be explained by acidity alone, as a large difference between the oxidized and reduced samples would be expected. The high heat over reduced chromia may be explained if we assume that the exposed Cr(II) ions, being d^4 systems, favour Jahn–Teller distortion of their surroundings so that there are empty coordination sites on which strong adsorption of pyridine can take place. Similar reduction in the activity of reduced chromia by carbon monoxide is also reported (12).

Ratio of p- *to* m-*Cymene*

The ratios of *p*-cymene to *m*-cymene (cf. Fig. 5) over reduced and oxidized chromia at 360°C are 2.6 and 2.0, respectively, which decrease to 0.6 and 1.0 at 500°C. The values for reduced and oxidized chromia with 2% pyridine are about 1.8 and 1.2, respectively, in the temperature range 425 to 500°C. In the case of chromia–alumina, the relative proportion of cymenes is found to be independent of pretreatment of the catalysts and also of the presence of pyridine.

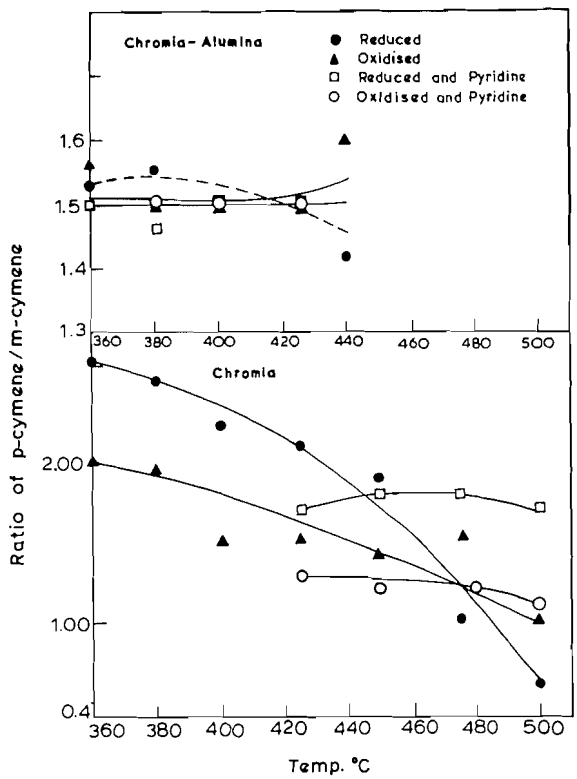

FIG. 5. Ratio of *p*-cymene to *m*-cymene over reduced chromia, oxidized chromia, and in the presence of 2% pyridine; reduced chromia–alumina, oxidized chromia–alumina, and in the presence of 2% pyridine. LHSV = 2.

The decrease in the cymene ratio with increase of temperature is not clearly understood. The possibility of *p*-cymene being converted to *m*-cymene at higher temperatures is ruled out, since separate experiments with pure *p*-cymene fail to isomerize to *m*-cymene. At elevated temperatures, new sites may probably be created which favour the formation of more *m*-menthadienes which are subsequently dehydrogenated to *m*-cymene. When 3-carene mixed with 2% pyridine and passed over these catalysts, the ratio of cymenes remains constant and unaffected by temperature. The new sites assumed to be created as explained above may get deactivated by the presence of pyridine molecules, thereby keeping the cymene ratio constant.

The lower values of *p*-cymene to *m*-cymene over oxidized chromia may be associated with strong acidic sites present in some form over the surface. The higher valent Lewis sites, assumed in an earlier

discussion, may get reduced during the reaction in the presence of 3-carene and their contribution for the lower values of cymene ratio may be insignificant.

The oxygen present initially over the catalyst may oxidize the hydrocarbon to CO which may be coordinated to chromium, giving rise to carboxylate ions, which will increase the surface acidity and hence reduce the cymene ratio. Reduced chromia when pretreated with CO, and also when CO is passed along with 3-carene simultaneously, the cymene ratio is found to be reduced (12). Clark *et al.* (26) has also reported the formation of carboxylate ions over reduced chromia in the presence of CO.

The cymene ratio over chromia–alumina is not affected either by pretreatment of the catalyst or by the presence of 2% pyridine with 3-carene. This shows that the intrinsic acidity of alumina, not affected by the above mentioned factors, decides the cymene ratio. The intrinsic acidity of alumina and chromia–alumina is found to be altered by the incorporation of either alkali metal ions or halide ions (10, 11) and in these cases the cymene ratio is also altered.

Acknowledgement

The author wishes to express his gratitude to Dr. G. S. Laddha, Director, Alagappa Chettiar College of Technology, University of Madras, for the facilities and encouragement given to carry out this work.

1. J. VERGHESE and L. M. YEDDANAPALLI. Chem. Age India, Series 5, 103 (1952).
2. M. G. RAU. Indian For. Res. **11**, 197 (1952).
3. J. OWEN and J. L. SIMONSEN. J. Chem. Soc. 3001 (1931).
4. F. G. CIAPETTA, R. M. DOBRES, and R. W. BAKER. Catalysis. Vol. VI. *Edited by* P. H. Emmett. Reinhold Publ. Corp., New York, NY.
5. H. PINES and W. O. HAAG. J. Am. Chem. Soc. **83**, 2847 (1961).
6. A. STANISLAUS and L. M. YEDDANAPALLI. Can. J. Chem. **50**, 113 (1972).
7. J. TURKEVICH, H. FEHRER, and H. S. TAYLOR. J. Am. Chem. Soc. **63**, 1129 (1941).
8. P. W. SELWOOD and R. P. EISCHENS. J. Am. Chem. Soc. **69**, 1590 (1947); **69**, 2698 (1947).
9. L. M. YEDDANAPALLI *et al.* Symposium on contact catalysis. Calcutta. 1956.
10. P. H. EMMETT (*Editor*). Catalysis. Vol. I. Reinhold Publ. Co., New York, NY. 1954. p. 31.
11. D. P. SHOEMAKER and C. W. GARLAND. Experiments in physical chemistry. McGraw Hill Book Co., New York, NY. 1962. p. 250.
12. V. KRISHNASAMY and L. M. YEDDANAPALLI. Can. J. Chem. **54**, 3458 (1976).
13. V. KRISHNASAMY. Indian J. Chem. **15**, 348 (1977).
14. V. KRISHNASAMY and L. M. YEDDANAPALLI. Can. J. Chem. **55**, 3046 (1977).
15. P. W. SELWOOD. J. Am. Chem. Soc. **88**, 2676 (1966).
16. D. E. O'REILLY and D. S. MACIVER. J. Phys. Chem. **66**, 276 (1962).
17. L. L. VAN REIJEN and P. COSSEE. Actes Deuxieme Congr. Intern. de Catalyse, Paris. Vol. 2. 1960. p. 1679.
18. L. L. VAN REIJEN, P. COSSEE, and H. J. VAN HAREN. J. Chem. Phys. **38**, 572 (1963).
19. D. G. HOWARD and R. H. LINDQUIST. J. Chem. Phys. **38**, 573 (1963).
20. K. I. SOLVETSKAYA and A. M. RUBINSHTEIN. Kinet. Catal. **7**, 316 (1967).
21. E. J. DICKINSON. Trans. Faraday Soc. **40**, 70 (1944).
22. V. KRISHNASAMY, P. RATNASAMY, and L. M. YEDDANAPALLI. Indian J. Chem. **9**, 131 (1971).
23. S. E. VOLTZ, A. E. HIRSCHLER, and A. SMITH. J. Phys. Chem. **64**, 1594 (1960).
24. E. P. EBERLY, JR. Trans. Faraday Soc. **57**, 289 (1961); **57**, 1169 (1961).
25. V. KRISHNASAMY. Ph.D. Thesis, University of Madras. 1968.
26. A. CLARK, J. N. FINCH, and B. H. ASHE. Proc. 3rd Int. Congr. on Catalysis, Amsterdam. 1964. p. 1010.

Can. J. Chem. Downloaded from www.nrcresearchpress.com by 210.87.254.40 on 09/05/12
For personal use only.

Chelates of nickel(II) and copper(II) with tridentate Schiff base formed by the condensation of *S*-benzyldithiocarbazate with benzoin

M. T. H. TARAFDER AND M. AKBAR ALI

Rajshahi University, Rajshahi, Bangladesh

Received August 3, 1977

M. T. H. TARAFDER and M. AKBAR ALI. Can. J. Chem. **56**, 2000 (1978).

New complexes with the Schiff base ligand derived from *S*-benzyldithiocarbazate (NH_2—NH—$CSSCH_2C_6H_5$) have been prepared and characterized by elemental analyses, magnetic, conductometric, ir, and electronic spectral studies. The tridentate ONS Schiff base *S*-benzyl-β-*N*-(phenyl,phenylhydroxymethyl)methylenedithiocarbazate gave mono-ligand complexes with Ni(II) and Cu(II) having the general formula [MligandX] (M = Ni(II) and Cu(II); X = NO_3, Cl, Br, NCS). A proposed square-planar structure for the nickel complexes is supported by magnetic and spectral data. A square-planar structure is also suggested for Cu(II) complexes. The ir results give evidence of the different bondings present in the complexes.

M. T. H. TARAFDER et M. AKBAR ALI. Can. J. Chem. **56**, 2000 (1978).

On a préparé de nouveaux complexes utilisant un ligand comportant une base de Schiff provenant du *S*-benzyldithiocarbazate (NH_2—NH—$CSSCH_2C_6H_5$) et on les a caractérisés par des analyses élémentaires, magnétiques et conductimétriques et par des études de spectres ir et électroniques. La base de Schiff ONS tridentate *S*-benzyl-β-*N*-(phényl,phényl-hydroxyméthyl)méthylènedithiocarbazate réagit avec le Ni(II) et le Cu(II) pour conduire à des complexes ne comportant qu'un ligand ayant des formules générales [MligandX] (M = Ni(II) et Cu(II); X = NO_3, Cl, Br, NCS). La structure plan carré proposée pour les complexes du nickel est en accord avec les données magnétiques et spectrales. On suggère aussi l'existence d'une structure plan carré pour les complexes du Cu(II). L'infrarouge indique les différents types de liaisons qui sont présents dans ces complexes.

[Traduit par le journal]

Introduction

Numerous metal complexes of Schiff base derivatives having nitrogen and sulphur as donors have been investigated extensively (1). However detailed studies of Schiff bases derived from *S*-benzyldithiocarbazate having nitrogen, oxygen, and sulphur as donors are lacking. We present a magnetic and spectroscopic study of Ni(II) and Cu(II) complexes of a ONS Schiff base, i.e., *S*-benzyl-β-*N*-(phenyl,-phenylhydroxymethyl)methylenedithiocarbazate

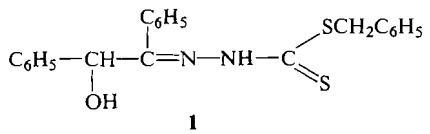

1

derived from *S*-benzyldithiocarbazate.

Experimental

All the chemicals used were reagent grade and were used without further purification. Preparation of the Schiff base, *S*-benzyl-β-*N*-(phenyl,phenylhydroxymethyl)methylenedithiocarbazate (**1**): this compound deposited as yellow crystals after solutions containing *S*-benzyldithiocarbazate (0.1 mol) in 50 ml hot absolute alcohol and benzoin (0.1 mol) in hot alcohol (50 ml) had been heated on the steam bath for a few minutes, mp 205°C. *Anal.* calcd. for $C_{22}H_{20}ON_2S_2$: C 67.33, H 5.1, N 7.1, S 16.3; found: C 67.1, H 5.0, N 6.8, S 15.8. Preparation of complexes: the ONS ligand (0.01 mol) in hot absolute alcohol (300 ml) was mixed with metal (Ni(II) and Cu(II)) salt solution (0.01 mol) in hot absolute alcohol (20 ml). The resulting mixture was kept under reflux for 3 h. The precipitate which settled was filtered, washed several times with hot absolute alcohol so as to remove unreacted Schiff base, and dried *in vacuo* over P_2O_5. The Schiff base yielded complexes having a stoichiometry of 1:1 metal to ligand. The complexes isolated were analyzed as follows. *1. Anal.* calcd. for [Ni(ONS)NO_3]: C 51.58, H 3.7, N 8.2, M 11.47, S 12.5; found: C 51.3, H 3.4, N 8.0, M 11.3, S 12.1. *2. Anal.* calcd. for [Ni(ONS)Cl]: C 54.4, H 3.9, N 5.77, M 12.09, S 13.18; found: C 54.2, H 3.6, N 5.62, M 12.1, S 12.7. *3. Anal.* calcd. for [Ni(ONS)Br]: C 49.8, H 3.58, N 5.28, M 11.08, S 12.08; found: C 49.7, H 3.3, N 5.1, M 11.0, S 11.7. *4. Anal.* calcd. for [Ni(ONS)NCS]: C 54.3, H 3.7, N 8.08, M 11.5, S 18.9; found: C 54.1, H 3.4, N 7.7, M 11.38, S 18.5. *5. Anal.* calcd. for [Cu(ONS)NO_3]: C 51.1, H 3.67, N 8.1, M 12.2, S 12.3; found: C 50.8, H 3.5, N 7.9, M 12.1, S 11.9. *6. Anal.* calcd. for [Cu(ONS)Cl]: C 58.87, H 3.8, N 5.7, M 12.96, S 13.05; found: C 53.65, H 3.5, N 5.35, M 12.8, S 12.7. *7. Anal.* calcd. for [Cu(ONS)Br]: C 49.39, H 3.5, N 5.2, M 11.8, S 11.97; found: C 49.1, H 3.3, N 5.01, M 11.75, S 11.45. The preparation of [Cu(ONS)NCS] was unsuccessful.

Spectra

The solid-state electronic spectra of the complexes were obtained in a Carl Zeiss PMQ II spectrophotometer with a solid-reflectance attachment using MgO as the calibrant. The ir spectral data have been recorded in the range 4000–200 cm^{-1}, with Perkin-Elmer 457 and 225 spectrophotometers, as Nujol mulls between KBr or as KBr discs. The far ir spectra (400–200 cm^{-1}) were recorded as Nujol mulls between polyethylene sheets. The electrical conductance measurements were made at room temperature with a conductivity bridge type E 7566/3 of the M.E.L. Equipment Company Limited,

Can. J. Chem. Downloaded from www.nrcresearchpress.com by 210.87.254.42 on 09/05/12
For personal use only.

TABLE 1. Infrared frequencies (cm^{-1}) of the Ni(II) and Cu(II) complexes and their assignments*

Complex	ν(C=N)	ν(M—N)	ν(C=S)	ν(M—S)	ν(M—O)	ν(M—X)
1. [Ni(ONS)NO_3]	1510	510	950	395 S	550 S	
2. [Ni(ONS)Cl]	1500	530	962	395 S	545	260
3. [Ni(ONS)Br]	1495	515	960	396 S	540	200
4. [Ni(ONS)NCS]	1515	570	955	394 S	550 S	
5. [Cu(ONS)NO_3]	1500	500	955	360	470	
6. [Cu(ONS)Cl]	1505	490 S	965	365	485	320
7. [Cu(ONS)Br]	1505	480	964	370	490	220

*S = strong.

Sussex, using a Griffin and George NO-S75-915/010 conductivity cell with platinum black electrode. Millimolar solutions of the metal-chelates were used. Magnetic susceptibility measurements were made on solid samples at room temperature by the Faraday method. All the values were corrected for diamagnetism according to the method of Selwood (2).

Analysis

Metal analyses were made by means of EDTA titration after decomposing the complexes with a mixture of nitric, sulphuric, and perchloric acids. Carbon–hydrogen–nitrogen analyses were made using microanalytical techniques. The sulphur analysis was carried out according to the method described by Vogel (3).

Results and Discussion

The Schiff base ONS (**1**) was formed by the condensation of *S*-benzyldithiocarbazate with benzoin. With Ni(II) and Cu(II) mono-ligand nitrate, chloride, bromide, and thiocyanate complexes have been assigned the structures [MligandX] on the basis of molecular conductivities and ir absorptions (Table 1). The conductance measurements were done in nitrobenzene medium in which the metal chelates behaved as non-electrolytes because they have very low conductance values, 0–2.5 and 0–2.1 Ω^{-1} cm^2 mol^{-1} for the nickel and copper complexes, respectively, suggesting anion coordination to the metal ion which is also supported by the ir absorptions of the complexes.

The ONS Schiff base *S*-benzyl-β-*N*-(phenyl,phenylhydroxymethyl)methylenedithiocarbazate acts as a tridentate ligand coordinating the metal ion via the β-nitrogen atom, thioketo sulphur, and the oxygen of the hydroxyl group as evident from ir spectral data (Table 1). The C=N stretching vibration in the free ONS Schiff base occurs at ca. 1535 cm^{-1} (4) but on complexation the bands in all the complexes are shifted towards the lower frequency regions (Table 1). This lowering of C=N stretching mode on complexation may tentatively be attributed to a lowering of the C=N bond order as a result of M—N bond formation (5) as evident from the appearance of ν(Ni—N) and ν(Cu—N) bonds at 510–570 (6) and 480–500 cm^{-1} (7) respectively (Table 1). The α-nitrogen atom is not bonded with the metal as ν(N—H) band (ca. 3080 cm^{-1} (8)) of the free ligand does not suffer any shift in the complexes. The ir spectrum of the uncomplexed ligand shows ν(C=S) at ca. 1000 cm^{-1}; it undergoes considerable shift towards lower frequencies in the metal complexes (Table 1). This negative shift of ν(C=S) bands may be taken as an indication of coordination by the thioketo sulphur. This shifting may be due to a lowering of C=S bond order as a result of M—S bond formation.

The far ir spectra of the metal complexes were measured in order to locate metal–sulphur stretching frequencies. The appearance of ν(Ni—S) and ν(Cu—S) bands at ca. 395 cm^{-1} and 360–370 cm^{-1} is indicative of the presence of Ni—S (9) and Cu—S (10) bonds in the nickel and copper complexes. Ali and Livingstone (1) have established in the cases of *S*-methyldithiocarbazate and its various Schiff bases that the thioether sulphur does not coordinate to the metal ion. The disappearance of ν(O—H) observed in the free ligand around 3300 cm^{-1} (11) clearly indicates the loss of the proton from O—H on coordination and formation of a new bond between metal and oxygen as evident from ir spectral data. The absorptions in the region 540–550 and 470–490 cm^{-1} (Table 1) may be due to Ni—O (12) and Cu—O (7) linkages in the nickel and copper complexes respectively. Complex 1 gives ir bands at 1485 and 1260 cm^{-1} indicative that NO_3 occupies one of the stereochemical sites of Ni(II) (13). The complexes [Ni(ONS)X](X = Cl,Br) show ir bands at ca. 260 and 200 cm^{-1} corresponding to ν(Ni—Cl) and ν(Ni—Br) vibrations respectively. The complex [Ni(ONS)NCS] has thiocyanate ν(C—N) absorption at 2105 cm^{-1} suggesting the presence of terminal N-bonded thiocyanate (14). [Cu(ONS)NO_3] gives ir bands at 1480 and 1255 cm^{-1} characteristic of coordinated NO_3. The complexes 6 and 7 display ν(Cu—Cl) and ν(Cu—Br) at 320 and 220 cm^{-1} respectively.

The brown [Ni(ONS)X] complexes are low-spin type (diamagnetic) suggesting square-planar structure. The three coordination positions are occupied

Can. J. Chem. Downloaded from www.nrcresearchpress.com by 210.87.254.42 on 09/05/12
For personal use only.

by the ONS sequence and the fourth coordination site of the Ni(II) ion is occupied by either NO_3, Cl, Br, or NCS. The electronic spectra of the metal complexes provide evidence regarding their structures. The spectra of the nickel complexes give an envelope with a shoulder at 20 000 – 20 100 cm^{-1} which corresponds to $^1A_{2g} \leftarrow {}^1A_{1g}$ transition (15). The other two *d–d* transitions, $^1B_{1g} \leftarrow {}^1A_{1g}$ and $^1E_g \leftarrow {}^1A_{1g}$ (15), in the present cases were not observed but probably were hidden by the charge transfer band. The green paramagnetic copper complexes [Cu(ONS)X] yield magnetic moment (1.8–1.87 BM) corresponding to one unpaired electron. The copper complexes are said to possess square-planar stereochemistry since the copper ion has been found to be reluctant to take up a regular tetrahedral geometry (16). The electronic spectra of the complexes give the two bands at 16 000 – 16 100 cm^{-1} ($^2A_{1g} \leftarrow {}^2B_{1g}$) and 19 000 – 19 600 cm^{-1} ($^2E_{1g} \leftarrow {}^2B_{1g}$) which corresponds to the square-planar stereochemistry (17, 18).

1. M. A. Ali and S. E. Livingstone. Coord. Chem. Rev. **13**, 101 (1974).
2. P. W. Selwood. Magnetochemistry. Interscience, New York, NY. 1956.
3. A. I. Vogel. A text book of quantitative inorganic analysis. Longmans, New York, NY. 1961. p. 467.
4. K. Ueno and A. E. Martell. J. Phys. Chem. **59**, 998 (1955).
5. P. V. Babykutty, C. P. Prabhakaran, R. Anantaraman, and C. G. R. Nair. J. Inorg. Nucl. Chem. **36**, 3685 (1974).
6. K. Ueno and A. E. Martell. J. Phys. Chem. **60**, 1270 (1956).
7. M. N. Patel, C.B. Patel, and R. P. Patel. J. Inorg. Nucl. Chem. **36**, 3869 (1974).
8. L. J. Bellamy. Infrared spectra of complex molecules. John Wiley and Sons, Inc., New York, NY. 1960. p. 227.
9. R. J. Magee, Bookhari Annuar, and J. O. Hill. J. Inorg. Nucl. Chem. **36**, 1255 (1974).
10. B. Singh, Lakshmi, and U. Agarwala. Inorg. Chem. **8**, 2341 (1969).
11. L. J. Bellamy. Infrared spectra of complex molecules. John Wiley and Sons, Inc., New York, NY. 1960. pp. 99–100.
12. Kazuo Nakamoto. Infrared spectra of inorganic and coordination compounds. John Wiley and Sons, Inc., New york, NY. 1962. p. 215.
13. B. M. Gatehouse, S. E. Livingstone, and R. S. Nyholm. J. Chem. Soc. 4222 (1957).
14. Kazuo Nakamoto. Infrared spectra of inorganic and coordination compounds. 2nd ed. John Wiley and Sons, Inc., New York, NY. 1969 p. 188.
15. H. B. Gray and C. J. Ballhausen. J. Am. Chem. Soc. **85**, 260 (1963).
16. A. F. Wells. Structural inorganic chemistry. 3rd ed. University Press, Oxford. 1962; J. D. Duintz and L. E. Orgel. Nature, **179**, 462 (1957).
17. B. N. Figgis. Introduction to ligand fields. Interscience, New York, NY. 1967. p. 316.
18. W. U. Malik, M. P. Teotia, and D. K. Rastogi. J. Inorg. Nucl. Chem. **35**, 4048 (1973).

Can. J. Chem. Downloaded from www.nrcresearchpress.com by 210.87.254.42 on 09/05/12
For personal use only.

pK_a values of protonated α,β-unsaturated cyclic carboxylic acids. Effect of ring size on acidities

S. N. BHAT, RAMA RAO, AND K. RANGANAYAKULU[1]

Department of Chemistry, Banaras Hindu University, Varanasi 221 005, U.P., India

Received December 15, 1977

S. N. BHAT, RAMA RAO, and K. RANGANAYAKULU. Can. J. Chem. **56**, 2003 (1978).

The pK_a values of protonated α,β-unsaturated acids, namely tiglic, cyclopentene carboxylic, cyclohexene carboxylic, and cycloheptene carboxylic acids have been determined spectrophotometrically and the values are −4.08, −4.05, −3.88, and −3.84, respectively. The conjugate acid of tiglic acid is a stronger acid than that of crotonic acid (pK_a −3.94) and the difference in acid strength is explained on the basis of steric inhibition of resonance by the α-methyl group. All the protonated cyclic acids are shown to be somewhat weaker than the corresponding acyclic ones. Several factors have been considered to explain the acid strength of these cyclic α,β-unsaturated acids. It has been shown that the ease of placing the double bond *exo* to the ring system is responsible for the changes in acidity of the above cyclic systems.

S. N. BHAT, RAMA RAO et K. RANGANAYAKULU. Can. J. Chem. **56**, 2003 (1978).

On a déterminé spectrophotométriquement les valeurs de pK_a des acides α,β non saturés protonés suivants: l'acide tiglique et les acides cyclopentène, cyclohexène et cycloheptènecarboxyliques; les valeurs des pK_a sont respectivement de −4.08, −4.05, −3.88 et −3.84. L'acide conjugué de l'acide tiglique est un acide plus fort que l'acide crotonique (pK_a −3.94) et on explique la différence dans la force de l'acide en se basant sur une inhibition stérique à la rèsonance provenant de la présence du groupe méthyle α. On a montré que tous les acides cycliques protonés sont un peu plus faibles que les acides acycliques correspondants. On a considéré plusieurs facteurs pour expliquer la force de l'acide de ces acides α,β non saturés cycliques. On a montré que la facilité de placer la double liaison *exo* dans un système cyclique est responsable des changements d'acidité dans les systèmes cycliques mentionnés ci-dessus.

[Traduit par le journal]

Introduction

The study of the pK_a values of protonated carboxylic acids has attracted many workers lately. Electronic, steric and solvent effects were the most widely studied aspects (1–5). Sorensen (6) considered structure **1** for the protonated crotonic acid on the basis of the symmetrical structure proposed by earlier workers (3, 7) for the protonated carboxyl group. The fact that alkyl substituents at the 3 position remarkably influence the acid strength supports the allylic cation structure **1**. Since resonance

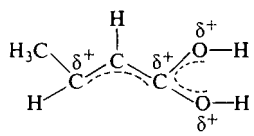

1

participation is more important in the ionic species (**2**) than in the neutral molecule (**3**), the pK_a value is a measure of the stability of the protonated form relative to the unprotonated one. In spite of the large amount of data that are available in the literature on the pK_a values of protonated carboxylic acids (1, 2), there is not much information available so far regarding the acid strength of the cyclic α,β-unsaturated carboxylic acids. We have studied the acid strength of protonated α,β-unsaturated cyclic carboxylic acids **2** (n = 3, 4, 5).[2] Also, the study of the influence of alkyl substitution at the 2 position on the acid strength of protonated crotonic acid was thought to be important since it serves as a model compound for the α,β-unsaturated cyclic carboxylic acids.

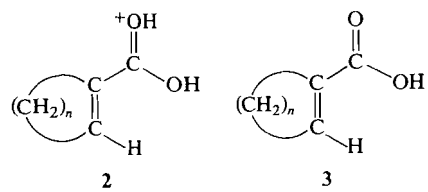

2 **3**

Experimental

Materials and Methods

Cyclopentene, cyclohexene, cycloheptene carboxylic acids, and tiglic acid were prepared according to known methods reported in the literature. Cyclopentene carboxylic acid (8) (mp 123–124°C) was purified by recrystallisation from *n*-hexane – ethyl acetate, and cyclohexene carboxylic acid (9) (bp 103°C/1 Torr), and cycloheptene carboxylic acid (10) (bp 107°C/1 Torr) were purified by distillation. Tiglic acid (11) (mp 63–64°C) was

[1]Author to whom correspondence may be addressed.

[2]We could not determine the pK_a values of other cyclic acids namely, cyclobutene carboxylic acid, cyclopentylidene carboxylic acid, and cyclohexylidene carboxylic acid as these acids are found to be not stable in acidic media.

Can. J. Chem. Downloaded from www.nrcresearchpress.com by 210.87.254.42 on 09/05/12
For personal use only.

Can. J. Chem. Downloaded from www.nrcresearchpress.com by 210.87.254.42 on 09/05/12
For personal use only.

purified by recrystallisation from water. Aqueous sulphuric acid solutions were titrated against standard base. The Hammett acidity functions H_0 and H_A for a given percentage (w/w) of sulphuric acid were available from the literature (12). Although the saturated carboxylic acids act like well behaved Hammett bases in indicator studies (13) and fit the H_0 function, many α,β-unsaturated carbonyl compounds are shown to follow the H_A function (14).[3] We have therefore plotted log Q, i.e. [B]/[BH$^+$], vs. H_A as well as H_0 for the series of α-β-unsaturated carboxylic acids used in the present study and the slopes for both scales are given in Table 1. The actual plot for one of the acids, namely cyclopentene carboxylic acid, is given in Fig. 1. It is clear from the slopes that α,β-unsaturated carboxylic acids have slopes close to unity using the H_A function and we have calculated the data accordingly. The pK_a values of the protonated α,β-unsaturated carboxylic acids using the H_0 function where the slopes of log Q vs. H_0 are not unity, do not represent the true pK_a values. Rather, they are the values at half protonation. However, the order of acidities remains the same in any scale and the same reasoning can be applied to correlate structural effects with acidity.

Various methods, for example potentiometric titrations, conductometric methods, and spectrophotometry, were used earlier to find the dissociation constants or the pK_a values of protonated organic acids in acidic solution. We preferred spectrophotometry for the determination of the pK_a values, since this procedure is reasonably accurate for the determination of the dissociation constants, as long as the different species have different absorptions (15, 16).

Solutions for spectral measurements were made by weighing 0.2–1.0 mg of the organic acid in a small glass boat using a microbalance. The boat was added to the solvent, previously made up to the mark in a standard volumetric flask at 25 ± 0.5°C. A known volume of the solution was further diluted to 10 ml so that the concentration of final solution is $\sim 10^{-5}$ mol/ℓ.

The spectra of the solutions were recorded using a Cary 14-R uv spectrophotometer with a solvent blank as the reference. The temperature did not vary more than 0.5°C during the measurements. Every time a base line correction was made since the absorbance was sometimes very small. The samples were quite stable during the measurements and no irreversible new products were formed.

The dissociation of an acid BH$^+$ in water may be written as

$$BH^+ \rightleftharpoons B + H^+$$

Thus, the pK_a values which are equal to H_A, the Hammett acidity constant, when [BH$^+$]/[B] is equal to unity, were determined.

Results and Discussion

The three cyclic acids, namely cyclopentene (**4**), cyclohexene (**5**), and cycloheptene (**6**) carboxylic acids absorb at 224, 219, and 222 nm, respectively, in water and are in good agreement with the literature data (17). However, the molar extinction coefficients differ slightly. Tiglic acid (**7**) absorbs at 216.5 nm. The transition energies and intensities (oscillator strengths) of these acids show that these are the π–π* transition bands. Our attempts to determine the dissociation constants using n–π* transition bands were not successful as the latter are very weak.

[3]The authors are thankful to one of the referees, who suggested to use the H_A function rather than the H_0 function for the α,β-unsaturated carboxylic acids.

TABLE 1. pK_a values of α,β-unsaturated carboxylic acids using H_A and H_0 functions

Acid	−pK_a*		Slope	
	H_A	H_0	H_A	H_0
Cyclopentene carboxylic acid	4.05	6.47	0.98	0.46
Cyclohexene carboxylic acid	3.88	6.27	0.95	0.48
Cycloheptene carboxylic acid	3.84	6.13	0.96	0.45
Tiglic acid	4.08	6.52	0.94	0.48

*Error limit ±0.10.

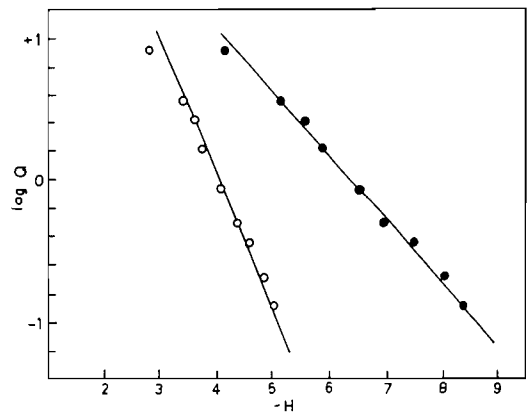

FIG. 1. Plot of log Q, i.e. [B]/[BH$^+$], vs. H for cyclopentene carboxylic acid: (○) using H_A function; (●) using H_0 function.

For the sake of brevity, the variation and the intensity of the band position with the strength of sulphuric acid is given only for cyclopentene carboxylic acid (Table 2). The extent of protonation is determined simply by the decrease in the absorption

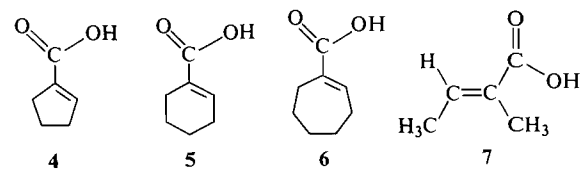

4 **5** **6** **7**

maxima of the free base and the increase in the absorption of the protonated base, the fully protonated base having negligible absorption in the region of maxima. It can be seen from Table 2 that as the concentration of sulphuric acid decreases, that of the protonated species also decreases. The absorption maxima of cyclopentene carboxylic acid shifts from 262.5 to 224 nm, when the medium is altered from 95.32% sulphuric acid to water. Similarly, for the acids **5**, **6**, and **7** the band maxima positions shift

Can. J. Chem. Downloaded from www.nrcresearchpress.com by 210.87.254.42 on 09/05/12
For personal use only.

TABLE 2. The variation of absorption maxima and intensities with the strength of sulphuric acid for cyclopentene carboxylic acid

Strength of sulphuric acid (w/w)	Absorption maxima (nm)	$\varepsilon_{262.5}$ (ℓ mol^{-1} cm^{-1})	ε_{224} (ℓ mol^{-1} cm^{-1})	$\varepsilon_{262.5} - \varepsilon_{224}$
95.32	262.5	10544	907	9637
85.97	260.0	9946	1337	8609
83.72	258.0	9277	2006	7271
80.20	255.0	8371	3111	5260
76.45	251.0	6795	3405	3390
73.67	245.0	4973	4286	687
70.05	240.0	3872	6375	−2503
67.99	238.0	2346	6159	−3813
64.71	236.0	1893	7021	−5128
62.55	236.0	2193	7416	−5223
59.58	234.0	1724	7722	−5998
56.20	232.5	957	7898	−6941
52.13	231.5	707	8274	−7567
39.93	228.5	160	9080	−8920
0.00	224.0	207	7858	−7651

from 256, 256, and 249.5 to 219, 222, and 216.5 nm, respectively. The bands are relatively sharper in pure solvents and then become broad as we approach 50% protonation. The band has its maximum width at this point. The bathochromic shift may be partly due to the effect of change in the dielectric constant of the medium on the π–π* transition of the unprotonated species and partly due to the increased conjugation in the ionic species. The change in half-width of the absorption band also goes in parallel with the above observation. The changes in transition energies when the medium is changed is minimum in case of cyclopentene carboxylic acid and maximum in cyclohexene carboxylic acid.

It was assumed, in general, that displacement of the maximum does not occur as the concentration of sulphuric acid changes when both the forms show clear absorption maxima sufficiently far apart. The superimposed spectra over a range of ionisation ratios should show a clear isobestic point. However, the failure to observe the isobestic points in the present cases shows the 'medium shift' which may be due to the progressive nonavailability of water as the acid strength of the solution is increased. The data are analysed by following the procedure of Davis and Geissman (18). But, as it can be seen from Fig. 2, it is not easy to determine the midpoint of the sigmoid curve, which corresponds to the pK_a value. Therefore, we have used the derivative curve; i.e. dε/dH was plotted against the average H value to get better pK_a values. The values thus obtained are given in Table 1. As the error limit is ±0.10, the above values reported in Table 1 represent the order of acidities rather than the absolute values.

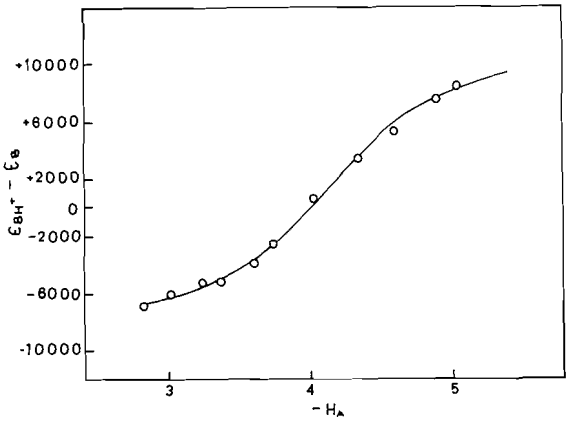

FIG. 2. pK_a calculation using the procedure of Davis and Geissman (18) for cyclopentene carboxylic acid.

Origin of the Differences in pK_a Values

From the data it is clear that the conjugate acid of tiglic acid, with a pK_a value of −4.08 is a stronger acid than crotonic acid (pK_a −3.94), and β,β-dimethylacrylic acid (pK_a −3.55), which were also determined by a similar procedure (ref. 6 and footnote 3). This is in line with the *o*-substituted benzoic acids, where it has been shown that the steric inhibition of resonance by an *ortho* substituent raises the acidity of the conjugated acids (3). Similar trends have also been observed in the dissociation constants of a series of *cis*- and *trans*-methylacrylic acids (19).

In the five-, six-, and seven-membered ring system series, there is a regular decrease in acidity with an increase in ring size. At first glance, the differences in the magnitude of the pK_a values in the cyclic systems may look smaller; however, it is noteworthy that in the benzoic acid series the change in the pK_a value is only 0.18 when the system is changed from benzoic acid to *p*-methylbenzoic acid.[4] All the protonated cyclic acids are weaker than the protonated tiglic acid showing that the protonated species of cyclic systems are stabilized better than that of the open-chain system, presumably due to the absence of the *ortho* effect. As pointed out earlier, resonance interactions are more important in the protonated species (**2**), compared with those of neutral species (**3**), the differences in pK_a in a given series of compounds being a measure of the stability of the protonated form relative to the neutral molecules. Comparison of the acidities in the cyclic system will, therefore, give a measure of the stabilities of the protonated form **2** (n = 3, 4, 5) relative to each other in this series.

Since the difference in these systems is only the

[4]All literature pK_a values are corrected by using the H_A scale of ref. 12.

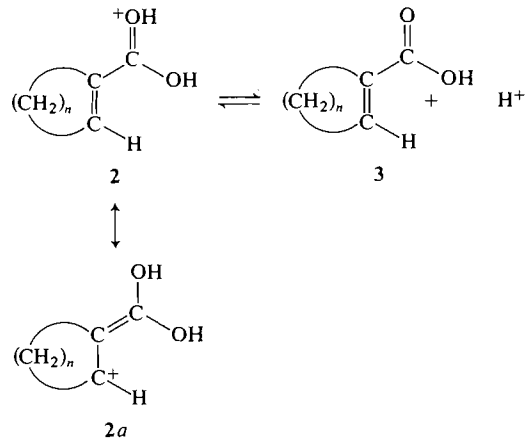

2 3

2a

size of the ring, the following factors could be considered to explain the difference in their acidity.

Solvation

Since smaller ions are solvated better, one would expect the solvation to decrease progressively as the ring size increases, which results in an increase in acidity with increase in the ring size.

Twisting of the Carboxyl Group Out of the Olefinic Plane

In the five-membered ring system the carboxylic group and the double bond are in a single plane, resulting in only small interaction with the C5 hydrogens, whereas in the six-membered ring system, the hydrogens at C6 would push the carboxyl group out of the olefinic plane owing to greater steric interaction, and this results in a weaker conjugative effect in this system. Therefore one would expect considerable increase in the acid strength in the case of six-membered ring system.

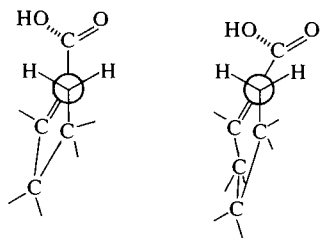

Stabilisation of the Endo *Double Bond vs.* Exo *Double Bond*

One has to consider the resonance forms of the protonated species (structures **2** ↔ **2***a*), which involves placing the double bond *exo* to the ring system.

The first two factors predict the reversal of the order of acidities to those observed. Therefore, we presume that it is the third factor, namely the ease of placing the double bond *exo* to the ring system, which is responsible for changes in acidity in this series. A study of molecular models reveals that in the five-membered ring system, placing a double bond *exo* to the ring leads to a considerable amount of strain and therefore conjugation effects here are less than in the case of six- and seven-membered ring systems, leading to more negative pK_a values. Our observations are parallel to those made by Turner and Garner (20) using the heat of isomerisation values of cycloalkylidene compounds to cycloalkenes. Their studies indicate that an *endo* double bond is more stable in both the five- and six-membered ring systems. But there is a greater difference in the *exo–endo* stability in the five-membered ring system (−3.9 cal/mol) compared to the six-membered case (−2.4 cal/mol). The trend is similar with the seven-membered ring system (−2.32 cal/mol).

The values of the dissociation constants of cyclopentene (0.78), cyclohexene (0.38), and cycloheptene (0.23) carboxylic acids in an ethanol–water system have been determined (21). The larger dissociation constant for cyclopentene carboxylic acid has been attributed to an electron withdrawing effect in the strained five-membered system, which would facilitate the ionisation process and lead to higher acid strength. In the light of our present investigation the differences in the dissociation constants can be attributed to the greater stabilisation of the six- and seven-membered cyclic carboxylic acids by conjugation compared to the five-membered carboxylic acid.

In conclusion, the data presented here on the pK_a measurement of protonated cyclic α,β-unsaturated acids is a direct proof of the greater stability of the *endo* double bond over the *exo* in a five-membered ring system compared to the six-membered one.

Acknowledgements

The authors are thankful to Dr. K. Rajeswari and Dr. R. Balaji Rao for the useful discussions and suggestions, to Professor O. P. Malhotra, Head, Department of Chemistry for providing the facilities, to Mr. Bipin for recording the spectra, and to U.G.C. (India) for supporting the work.

1. M. A. Paul and F. A. Long. Chem. Rev. **57**, 1 (1957).
2. R. F. Cookson. Chem. Rev. **74**, 5 (1974).
3. R. Stewart and K. Yates. J. Am. Chem. Soc. **82**, 4059 (1960).
4. A. R. Goldfarb, A. Male, and N. Gustein. J. Am. Chem. Soc. **77**, 6194 (1955).
5. J. T. Edward and J. C. Wang. Can. J. Chem. **40**, 966 (1962).
6. T. S. Sorensen. Can. J. Chem. **42**, 724 (1964).
7. M. H. Palmer and D. S. Urch. J. Chem. Soc. 174 (1963).
8. A. H. Cook and R. P. Linstead. J. Chem. Soc. 956 (1934).

Can. J. Chem. Downloaded from www.nrcresearchpress.com by 210.87.254.42 on 09/05/12
For personal use only.

9. E. J. BOORMAN and R. P. LINSTEAD. J. Chem. Soc. 258 (1935).
10. S. J. ASSONY and N. KHARASCH. J. Am. Chem. Soc. **80**, 5978 (1958).
11. R. E. BUCKLES and G. V. MOCK. J. Org. Chem. **15**, 68 (1950).
12. (*a*) C. D. JOHNSON and A. R. KATRITZKY. J. Am. Chem. Soc. **91**, 6554 (1969); (*b*) K. YATES and J. B. STEVENS. Can. J. Chem. **42**, 1957 (1964).
13. (*a*) E. M. ARNETT. *In* Progress in physical organic chemistry. Vol. I. *Edited by* S. C. Cohen, A. Streitweiser Jr., and R. W. Taft. Wiley-Interscience, New York, NY. 1963. p. 298: (*b*) S. HOSHINO, H. HOSOYA, and S. NAGAKURA. Can. J. Chem. **44**, 1961 (1966).
14. R. I. ZALEWSKI and G. E. DUNN. Can. J. Chem. **47**, 2263 (1969).
15. A. ALBERT and E. P. SERGENT. The determination of ionization constants. Chapman & Hall, London. 1971.
16. L. P. HAMMETT. Physical organic chemistry. McGraw-Hill, New York, NY. 1970.
17. A. T. NEILSEN. J. Org. Chem. **22**, 1539 (1957).
18. C. T. DAVIS and T. A. GEISSMAN. J. Am. Chem. Soc. **75**, 3507 (1954).
19. E. A. MCCOY and L. L. MCCOY. J. Org. Chem. **33**, 2354 (1968).
20. R. B. TURNER and R. H. GARNER. J. Am. Chem. Soc. **80**, 1424 (1958).
21. O. H. WHEELER and I. LERNER. J. Am. Chem. Soc. **78**, 63 (1956).

Can. J. Chem. Downloaded from www.nrcresearchpress.com by 210.87.254.42 on 09/05/12
For personal use only.

Etude par résonance magnétique nucléaire de composés organiques contenant des chalcogènes. I. L'anisole et ses analogues soufré, sélénié et telluré

GABRIEL LLABRES ET MARCEL BAIWIR[1]

Institut de Physique B5, Université de Liège au Sart Tilman, B-4000 Liège, Belgique

ET

LÉON CHRISTIAENS, JOSÉ DENOEL, LÉOPOLD LAITEM ET JEAN-LOUIS PIETTE

Institut de Chimie organique B6, Université de Liège au Sart Tilman, B-4000 Liège, Belgique

Reçu le 13 decembre 1977

GABRIEL LLABRES, MARCEL BAIWIR, LÉON CHRISTIAENS, JOSÉ DENOEL, LÉOPOLD LAITEM et JEAN-LOUIS PIETTE. Can. J. Chem. **56**, 2008 (1978).

On rapporte les résultats d'une étude par résonance magnétique du proton et du carbone 13 sur l'anisole, le thioanisole, le sélénoanisole et le telluroanisole, ainsi que sur certains de leurs dérivés *para* substitués. Considérés comme des méthyles substitués, ces composés ont un comportement analogue à celui des halogénures de méthyle. On a pu mettre en évidence une relation linéaire entre le déplacement chimique des protons et celui du carbone du méthyle dans la série de l'anisole et dans les halogénures de méthyle à la fois. Si ces résultats s'interprètent le plus souvent à partir d'effets électroniques, un "effet d'atome lourd" doit être invoqué dans le cas des composés tellurés. Les résultats expérimentaux ne sont pas en désaccord avec l'hypothèse d'une configuration plane des composés étudiés.

GABRIEL LLABRES, MARCEL BAIWIR, LÉON CHRISTIAENS, JOSÉ DENOEL, LÉOPOLD LAITEM, and JEAN-LOUIS PIETTE. Can. J. Chem. **56**, 2008 (1978).

Results are reported of a study by ^{1}H and ^{13}C nuclear magnetic resonance of anisole, thioanisole, selenoanisole and telluroanisole as well as of several of their *para*-substituted derivatives. If these compounds are considered as substituted methyl groups, they display a behaviour analogous to that of the methyl halides. It is possible to demonstrate that a linear relation exists between the proton and the carbon chemical shifts in the anisole series as well as in the methyl halides. Although these results most frequently are interpreted in terms of electronic effects, a 'heavy atom effect' must be invoked for the tellurium compounds. The experimental results do not contradict the hypothesis that the compounds studied have a planar configuration [Journal translation]

Introduction

Tant l'anisole que le thioanisole et, dans une mesure moindre, le sénénoanisole ont fait l'objet de nombreux travaux au cours des dernières années (1–4), le problème essentiellement abordé étant celui de la conformation de ces composés et de leurs dérivés substitués. Par contre, aucun travail consacré à la conformation du telluroanisole n'a été publié à ce jour.

Il est généralement admis que les facteurs les plus importants dans ce problème conformationnel sont, d'une part, une éventuelle interaction d'une paire libre de l'hétéroatome avec le système π du cycle et, d'autre part, une interaction stérique entre le groupement méthyle et les hydrogènes aromatiques situés en *ortho*, deux facteurs pouvant influencer de manière assez considérable le spectre rmn de ces composés. En outre, si on admet généralement que la faculté, qu'ont les ponts —O—, —S—, —Se— et —Te— de transmettre des effets électroniques entre deux groupements organiques, aliphatiques ou aromatiques, substitués ou non, décroît dans l'ordre S > Se ≃ — > O (où — désigne le cas où il n'y a pas d'atome liant), ce sujet est malgré tout controversé (5).

Ce sont ces problèmes qui nous ont notamment conduits à entreprendre l'étude par rmn de l'anisole et de ses analogues chalcogénés (fig. 1).

Résultats et discussions

Résonance magnétiques du proton

Le tableau 1 compare les paramètres rmn dans les familles de l'anisole Ph—Y—Me et de l'éther de diméthyle Me—Y—Me, les composés étant considérés comme des méthanes substitués dans les deux cas. L'augmentation des deux paramètres lorsqu'on passe de Me à Ph montre que l'électronégativité de —YPH est supérieure à celle de —YMe quel que soit Y.

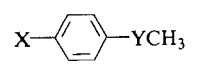

X = H, CH_3, Cl, Br
Y = O, S, Se, Te

FIG. 1. Composés étudiés au cours de ce travail.

[1]Auteur à qui la correspondance doit être adressée.

Can. J. Chem. Downloaded from www.nrcresearchpress.com by 210.87.254.105 on 09/05/12
For personal use only.

Can. J. Chem. Downloaded from www.nrcresearchpress.com by 210.87.254.105 on 09/05/12
For personal use only.

Si on applique les relations empiriques [1] (6) et [2] (7), établies, dans le cas des méthanes substitués, entre les paramètres rmn du méthyle et, d'une part, l'électronégativité E_X du substituant et, d'autre part, la longueur de la liaison r_{C-X}, on obtient le même résultat (tableau 2).

$$[1] \qquad J_{C-H} = 22.6E_X + 40.1r_{C-X} + 5.5$$

$$[2] \qquad \delta_H = 1.667E_X - 2.30$$

L'écart entre les électronégativités calculées dans les deux familles de composés est plus important quand on utilise la relation [2]. Si dans le cas des constantes de couplage [1], les effets électroniques sont de loin les plus influents, dans le cas des déplacements chimiques [2], l'effet de champ, les effets stériques et les effets d'anisotropie magnétique peuvent jouer un rôle important. La mesure des moments dipolaires de Ph_2S et Me_2S (11), d'une part, et l'examen d'un simple modèle géométrique, d'autre part, permettent cependant de négliger pratiquement les deux premiers effets dans la comparaison des deux familles de composés. De fait, le calcul de l'effet de l'anisotropie magnétique à l'aide des tables de Haigh et Mallion (12) permet de rendre compte de façon satisfaisante des différences observées. Il faut signaler que, lors de ce calcul, le meilleur accord a été obtenu en attribuant une configuration plane aux composés. Ce résultat est en accord avec l'étude en température des spectres rmn qui ne montrent aucune variation notoire entre -80 et $+150$°C (tableau 3).

Le tableau 4 montre que les effets sont qualitativement les mêmes dans les halogénures et les chalcogénures de méthyle. Pour les premiers, il existe une relation linéaire ($R = 0.99$) entre l'électronégativité du substituant et le déplacement chimique des protons. Si on interpole les valeurs relatives aux composés chalcogénés sur cette droite, on obtient pour les groupements PhO—, PhS—, PhSe— et PhTe— les électronégativités 3.6, 2.65, 2.55 et 2.45 respectivement (fig. 2), valeurs en bon accord avec celles du tableau 2 et avec celles qu'on attribue généralement aux atomes O, S, Se et Te (10). On peut en conclure que, dans la série de l'anisole, il n'y a pas de changement d'hybridation quand on passe d'un hétéroatome à l'autre.

Le tableau 5 montre que le parallélisme entre les monohalogénures de phényle et les composés étudiés ici est également remarquable tant en ce qui concerne les constantes de couplage que les déplacements chimiques.

La variation des déplacements chimiques en *para*, quand on passe de O à Te (0.3 ppm) et de F à I (0.2 ppm) peut s'interpréter en termes de densité électronique π du carbone lié au proton. L'effet mésomère du substituant diminue quand on passe de F à I et de O à Te. On notera par ailleurs que la délocalisation d'une paire libre du substituant sera maximum dans le cas d'une configuration plane de la molécule. Dans le cas des halogénobenzènes, cette interprétation est corroborée par l'excellente corrélation existant entre le déplacement chimique du proton en *para* et la constante de Taft du substituant (19).

Contrairement à la plupart des benzènes substitués, il n'existe pas de corrélation entre les dé-

TABLEAU 1. Paramètres rmn des protons du méthyle dans les séries de l'éther de diméthyle et de l'anisole

	Ether de diméthyle		Anisole	
Y	δ_{CH_3}	$^1J_{C-H}$	δ_{CH_3}	$^1J_{C-H}$
O	3.24	140.0	3.757	143.5
S	2.08	138.0	2.441	140.0
Se	1.95	140.2	2.302	142.5
Te	1.80	140.7	2.153	143.0

TABLEAU 2. Electronégativités (E) calculées pour le groupement MeY— dans la série de l'éther de diméthyle et le groupement PhY dans celle de l'anisole à partir des relations [1] et [2]

	Ether de diméthyle		Anisole			
Y	E_1	E_2	E_1	E_2	r_{C-Y} (réf.)	E_Y (10)
O	3.438	3.323	3.593	3.633	1.416(8)	3.5
S	2.665	2.627	2.754	2.844	1.802(8)	2.5
Se	2.512	2.549	2.614	2.760	1.943(9)	2.4
Te	2.183	2.459	2.285	2.671	2.141(9)	2.1

TABLEAU 3. Interprétation des différences observées dans le tableau 2 avec indication des distances interatomiques utilisées dans les calculs

	ΔE (ppm)*			
Y	Ce travail	Réf. 12	$r(C_{Ar}—Y)$ (réf.)	$r(C_{Al}—Y)$ (réf.)
O	0.258	0.30	1.36(13)	1.416(8)
S	0.213	0.19	1.76(14)	1.802(8)
Se	0.165	0.17	1.876(15)	1.943(9)
Te	0.165	0.14	2.081(16)	2.141(17)

*$\Delta E = 1.667[(E_2' - E_2) - (E_1' - E_1)]$.

TABLEAU 4. Déplacements chimiques des protons du méthyle dans les halogénures de méthyle (18) et dans la série de l'anisole

X	Y	Me—X	Ph—Y—Me
F	O	4.26	3.757
Cl	S	3.05	2.441
Br	Se	2.68	2.302
I	Te	2.16	2.153

Can. J. Chem. Downloaded from www.nrcresearchpress.com by 210.87.254.105 on 09/05/12
For personal use only.

TABLEAU 5. Paramètres rmn des protons du phényle dans la série de l'anisole* et dans les halogénobenzènes

Y	δ_{ortho}	$\delta_{méta}$	δ_{para}	J_{23}	J_{24}	J_{25}	J_{26}	J_{34}	J_{35}
O	6.749	7.145	6.811	8.41	1.13	0.39	2.60	7.44	1.80
S	7.158	7.143	7.043	8.00	1.03	0.47	2.10	7.46	1.55
Se	7.300	7.152	7.094	7.76	1.23	0.58	1.78	7.44	1.56
Te	7.521	7.099	7.138	7.58	1.19	0.50	1.72	7.47	1.46
X									
F	6.986	7.269	7.054	8.40	1.10	0.42	2.65	7.45	1.74
Cl	7.288	7.240	7.174	8.15	1.14	0.50	2.24	7.57	1.71
Br	7.445	7.161	7.223	8.07	1.10	0.46	2.08	7.49	1.73
I	7.650	7.048	7.260	7.93	1.12	0.47	1.88	7.50	1.74

*On a également mesuré $^2J_{Se-H} = 11.8$ Hz et $^2J_{Te-H} = 22.5$ Hz.

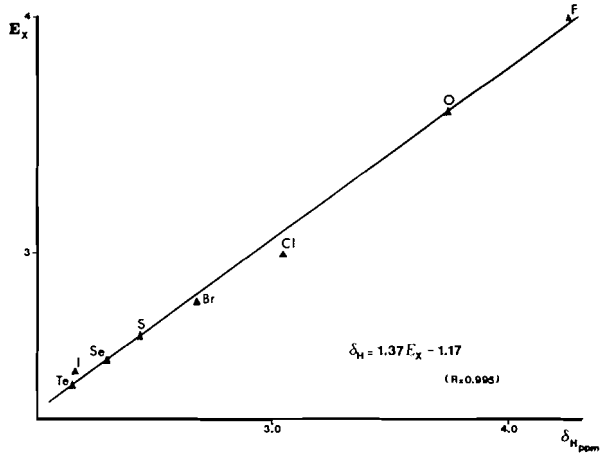

FIG. 2. Corrélation entre le déplacement chimique des protons du méthyle dans les halogénures de méthyle et l'électronégativité du substituant.

placements chimiques des protons en *ortho* et ceux des protons en *para* tant dans les halogénobenzènes que dans nos composés. Dans les deux cas, il s'agit probablement d'une manifestation de l' "effet *ortho*" (20), effet dont la nature n'est pas encore bien définie, mais dans lequel la taille du substituant doit jouer un rôle important.

Notons encore que les constantes de couplage du telluroanisole sont voisines de celles du benzène ($J_o = 7.56$ Hz, $J_m = 1.38$, $J_p = 0.68$ Hz), ce qui peut indiquer que le tellure ne perturberait que faiblement le système électronique du phényle.

Les tableaux 6 et 7 montrent que la substitution d'un chlore ou d'un brome en *para* n'affecte guère que le groupement —TeMe: cette singularité de comportement du tellure est probablement une manifestation d'un "effet d'atome lourd" (21).

Résonance magnétique du carbone 13

Tant dans la série de l'anisole que dans les halogénures de méthyle, le déblindage du carbone du méthyle augmente avec l'électronégativité du substituant (tableau 8). Ce parallélisme se traduit par une

TABLEAU 6. Déplacements chimiques des protons des dérivés *para* substitués dans la série de l'anisole

X	Y	δ_{ortho}	$\delta_{méta}$	δ_{CH_3}(YMe)	δ_{CH_3}
CH_3	O	6.688	6.976	3.72	2.26
CH_3	S	7.083	7.005	2.40	2.295
CH_3	Se	7.258	6.993	2.27	2.305
CH_3	Te	7.431	6.929	2.13	2.32
Cl	O	6.755	7.172		3.755
Cl	S	7.108	7.189		2.430
Cl	Se	7.296	7.178		2.298
Cl	Te	7.49	7.08		2.19
Br	O	6.707	7.304		3.755
Br	S	7.064	7.347		2.428
Br	Se	7.227	7.320		2.298
Br	Te	7.426	7.235		2.194

excellente relation linéaire: $\delta_C{}^X = 1.34\delta_C{}^Y + 2.08$ ($R = 0.999$).

Il faut aussi remarquer que l'effet devient blindant dans les cas du tellure et de l'iode: on retrouve ici l'"effet d'atome lourd" invoqué plus haut (21).

En ce qui concerne les carbones aromatiques, on note à nouveau un parallélisme entre les halogénobenzènes et la famille de l'anisole (tableau 9). Pour C_1 et C_o notamment, il existe des excellentes relations linéaires ($R = 0.999$). L'effet global sur C_1 quand on passe de O à Te est cependant moins marqué que pour le carbone du méthyle (47.4 ppm de variation au lieu de 71.8 ppm). Un carbone aromatique est moins sensible au substituant qu'un carbone aliphatique. Dans le cas de Te, C_1 est blindé par rapport au benzène.

La variation de C_{para} montre une certaine délocalisation de la paire libre du substituant vers le système π du cycle, délocalisation diminuant lorsque la taille de l'hétéroatome augmente.

Quant à C_{ortho}, blindé par rapport au benzène pour O et S, il est déblindé pour Se et Te: l'"effet *ortho*" devrait à nouveau jouer un rôle important.

En résumé, l'effet de substitution des chalcogènes varie de manière importante quand on passe de O à Te. Il dépend grossièrement d'un effet capteur qui

TABLEAU 7. Constantes de couplage des composés du tableau 6

X	Y	J_{23}	J_{25}	J_{26}	J_{35}	$^1J_{C-H}$(YMe)	$^1J_{C-H}$(Me)
H	O	8.40	0.35	2.67	2.42	142.7	125.7
H	S	7.98	0.37	2.33	2.34	140.7	128.0
H	Se	7.88	0.34	2.02	2.02	143.2	127.2
H	Te	7.65	0.40	1.87	1.87	142.5	127.0
Cl	O	8.68	0.16	3.05	2.65		143.3
Cl	S	8.57	0.23	2.74	2.72		141.0
Cl	Se	8.29	0.24	2.47	2.48		143.5
Br	O	8.82	0.23	3.04	2.54		143.2
Br	S	8.31	0.27	2.44	2.34		141.0
Br	Se	8.32	0.30	2.36	2.30		143.5
Br	Te	8.13	0.19	2.04	2.23		142.0

TABLEAU 8. Déplacements chimiques du carbone du méthyle dans la série de l'anisole et dans les halogénures de méthyle

X	Y	Me—X	Ph—Y—Me
F	O	75.4	55.0
Cl	S	25.1	15.8
Br	Se	10.2	7.1
I	Te	−20.5	−16.8
H		−2.1	

TABLEAU 9. Déplacements chimiques des carbones aromatiques dans la série de l'anisole et dans les halogénobenzènes

Y	C_1	C_{ortho}	$C_{méta}$	C_{para}
O	159.9	114.1	129.5	120.8
S	138.6	126.9	128.7	125.0
Se	132.0	130.6	128.9	126.1
Te	112.5	136.7	129.0	127.1
X				
F	163.8	114.6	130.3	124.3
Cl	135.1	126.9	129.7	126.7
Br	123.3	132.0	130.9	127.7
I	96.7	138.9	131.6	129.7

s'estompe au profit d'un effet blindant en carbone 13 (déblindant en proton) de nature mal définie que l'on serait tenté d'appeler "effet d'atome lourd", par analogie avec le comportement des halogénobenzènes.

Si, on considère le carbone et les protons du méthyle à la fois dans la série de l'anisole et dans les halogénures de méthyle, on note une relation linéaire ($R = 0.97$) entre les déplacements chimiques des deux types de noyaux. On est ainsi amené à penser que les mêmes effets agissent sur les deux noyaux, essentiellement effets électroniques et effet d'atome lourd.

Partie expérimentale

Les composés étudiés au cours de ce travail ont été synthétisés dans nos laboratoires, à l'exception des anisoles disponibles commercialement (Aldrich).

Les dérivés séléniés et sulfurés (22) ont été préparés à partir des sélénophénols et thiophénols, eux-mêmes obtenus par réaction entre les magnésiens et le sélénium ou le soufre.

Les dérivés tellurés (23) ont été préparés par réduction des ditellurures et condensation avec l'iodure de méthyle. Ces ditellurures sont obtenus par réaction entre le lithique aromatique et le tellure élémentaire.

Les spectres de résonance magnétique du proton ont été obtenus sur un spectromètre HA100 de Varian. Les paramètres ont été calculés selon la méthode itérative de Johannesen *et al.* (24) à l'aide du programme n° 188 du "Quantum Chemistry Program Exchange." Les déplacements chimiques (référence: TMS) ont été extrapolés pour une dilution infinie. Le solvant utilisé est le tétrachlorure de carbone. Sauf mention contraire, les déplacements chimiques sont exprimés en ppm (±0.003 ppm) et les constantes de couplage en Hz (±0.02 Hz).

Les spectres de résonance magnétique du carbone 13 ont été obtenus sur spectromètre HFX90 de Bruker. Ils ont été enregistrés en transformée de Fourier avec et sans découplage de bruit des protons. Les mesures (à ±0.1 ppm) ont été effectuées à température ordinaire sur des échantillons contenant 1 g de substance pour 2 ml de deutériochloroforme ou à partir de solutions saturées dans le même solvant (référence: TMS).

Remerciements

Nous tenons à remercier Messieurs les Professeurs J. Toussaint et M. Renson pour l'intérêt suivi qu'ils accordent à nos travaux. Nous remercions également le Centre de Résonance Magnétique Nucléaire de l'Université de Liège qui a mis son matériel à notre disposition. L'un de nous (Léopold Laitem) remercie le Fonds National de la Recherche Scientifique de Belgique pour l'octroi d'un mandat d'aspirant.

1. D. G. LISTER et N. L. OWEN. J. Chem. Soc. Faraday Trans. II, **69**, 1304 (1973).
2. N. M. ZARIPOV. Zh. Strukt. Khim. **17**, 741 (1976).
3. P. PALMIERI, F. TULLINI, B. VELINO et C. ZAULI. Gazz. Chim. Ital. **105**, 919 (1975).
4. G. Y. CHERYUKANOVA, G. A. CHMUTOVA et A. N. VERSHCHAGIN. Zh. Fiz. Khim. **49**, 234 (1975).
5. W. F. REYNOLD et R. A. MCCLELLAND. Can. J. Chem. **55**, 536 (1977).
6. N. MULLER et D. E. PRITCHARD. J. Chem. Phys. **31**, 768 (1959).

Can. J. Chem. Downloaded from www.nrcresearchpress.com by 210.87.254.105 on 09/05/12
For personal use only.

7. A. L. ALLRED et E. G. ROCHOW. J. Am. Chem. Soc. **79**, 5361 (1957).
8. J. R. ALLKINS et P. J. HENDRA. Spectrochim. Acta, **22**, 1075 (1966).
9. J. F. BEECHER. J. Mol. Spectrosc. **21**, 414 (1966).
10. L. PAULING. The nature of the chemical bond. Cornell University Press, New York, NY. 1960.
11. L. O. BROCKWAY et H. O. JENKINS. J. Am. Chem. Soc. **58**, 2036 (1936).
12. C. W. HAIGH et R. B. MALLION. Org. Magn. Reson. **4**, 203 (1972).
13. O. KENNARD, F. H. ALLEN et D. G. WATSON (*Editeurs*). International Union of Crystallography. Molecular structures and dimensions. N. V. A. Oosthoek's Uitgevers Mij, Utrecht. 1972.
14. A. C. MCDONALD et J. TROTTER. Acta Crystallogr. **18**, 243 (1965).
15. M. BAIWIR, G. LLABRES, O. DIDEBERG, L. DUPONT et J.-L. PIETTE. Acta Crystallogr. B, **31**, 2188 (1975).
16. M. BAIWIR, G. LLABRES, O. DIDEBERG, L. DUPONT et J.-L. PIETTE. Acta Crystallogr. B, **30**, 139 (1974).
17. J. M. FREEMAN et T. HENSHALL. J. Mol. Struct. **1**, 31 (1967).
18. G. V. D. TIERS. J. Phys. Chem. **62**, 1151 (1958).
19. R. W. TAFT. J. Am. Chem. Soc. **79**, 1045 (1957).
20. W. H. SMITH, D. L. DEAVENPORT et A. M. IHRIG. J. Am. Chem. Soc. **94**, 1959 (1972).
21. G. C. LEVY et G. L. NELSON. Carbon-13 nuclear magnetic resonance for organic chemists. Wiley Interscience, New York, NY. 1972.
22. J. HOUBEN et T. WEYL. Methoden der Organische Chemie. Vol. IX. Georg Thieme Verlag, Stuttgart. 1955.
23. J.-L. PIETTE et M. RENSON. Bull. Soc. Chim. Belges, **79**, 353 (1970).
24. R. B. JOHANNESEN, J. A. FERRETTI, et R. K. HARRIS. J. Magn. Reson. **3**, 84 (1970).

Can. J. Chem. Downloaded from www.nrcresearchpress.com by 210.87.254.105 on 09/05/12
For personal use only.

The synthesis and properties of the hexachloroniobates and hexachlorotantalates of Na, K, Rb, and Cs

DONALD R. SADOWAY[1] AND S. N. FLENGAS

Department of Metallurgy and Materials Science, University of Toronto, Toronto, Ont., Canada M5S 1A4

Received January 16, 1978

DONALD R. SADOWAY and S. N. FLENGAS. Can. J. Chem. **56**, 2013 (1978).

The compounds $NaNbCl_6$, $NaTaCl_6$, $KNbCl_6$, $KTaCl_6$, $RbNbCl_6$, $RbTaCl_6$, $CsNbCl_6$, and $CsTaCl_6$ were synthesized in a closed system by the reaction of $NbCl_5$ or $TaCl_5$ vapour with solid alkali-metal chloride as follows

$$MCl_5(g) + ACl(s) = AMCl_6(l)$$

where M is Nb or Ta, and A is Na, K, Rb, or Cs. The X-ray powder diffraction patterns of these compounds were obtained. Temperatures of various phase transformations were determined cryoscopically.

DONALD R. SADOWAY et S. N. FLENGAS. Can. J. Chem. **56**, 2013 (1978).

On a synthétisé les composés $NaNbCl_6$, $NaTaCl_6$, $KNbCl_6$, $KTaCl_6$, $RbNbCl_6$, $RbTaCl_6$, $CsNbCl_6$ et $CsTaCl_6$ dans un système fermé en faisant réagir du $NbCl_5$ ou du $TaCl_5$ à l'état vapeur avec un chlorure de métal alcalin solide d'après la réaction

$$MCl_5(g) + ACl(s) = AMCl_6(l)$$

où M est soit Nb ou Ta et A est Na, K, Rb ou Cs. On a pu obtenir les spectres de diffraction de rayon-X des poudres de ces composés. On a déterminé les températures de diverses transformations de phase par une méthode cryoscopique.

[Traduit par le journal]

Introduction

The pentachlorides of niobium and tantalum are known to react with alkali-metal chlorides to produce hexachloroniobate(V) and hexachlorotantalate(V) compounds of the general formula, $AMCl_6$, where A is an alkali metal and M is either Nb or Ta. These compounds contain thermodynamically stable forms of the volatile covalently bonded pentachlorides and, as such, are of interest in the extractive metallurgy of niobium and tantalum. Although these compounds have been the subjects of earlier investigations, the results of different studies vary considerably and, in some cases, are contradictory.

In the present investigation the compounds $NaNbCl_6$, $NaTaCl_6$, $KNbCl_6$, $KTaCl_6$, $RbNbCl_6$, $RbTaCl_6$, $CsNbCl_6$, and $CsTaCl_6$ have been synthesized by a method different from those previously employed, as well as, by a conventional technique. The X-ray powder diffraction patterns of these compounds have been obtained. The temperatures of various phase transformations have been determined by cryoscopy.

Experimental

The principal method of compound preparation in this study was the reaction of MCl_5 vapour with ACl powder at a temperature above the melting point of the $AMCl_6$ compound under synthesis. The reaction may be represented as follows:

$$MCl_5(g) + ACl(s) = AMCl_6(l)$$

This was a batch operation conducted in a closed non-isothermal system and was actually a modification of a method used previously in this laboratory to prepare chlorotitanates, chlorozirconates, and chlorohafnates of alkali-metal chlorides and alkaline-earth chlorides (1–3). A variation of this method in which molten $KNbCl_6$ and $KTaCl_6$ are produced in a continuous operation has been reported (4).

The compounds $NbCl_5$ or $TaCl_5$ were obtained from Research Organic/Inorganic Chemical Corporation, Belleville, NJ, U.S.A., and were certified to be of purity 99.99 and 99.9% respectively. Although they were supplied sealed in bottles under a dry nitrogen atmosphere hydrolysis occurred and oxychlorides were present. To purify the salts either of two methods was used. The first method was to sublime the salt in a stream of helium saturated with thionyl chloride as described by Keneshea *et al.* (5). Oxychloride and water reacted according to

$$MOCl_3(g) + SOCl_2(g) \rightarrow MCl_5(g) + SO_2$$

and

$$H_2O(g) + SOCl_2(g) \rightarrow 2HCl + SO_2$$

where M represents Nb or Ta. The purified compounds were sublimed into glass ampoules and sealed under vacuum for storage. The second method, described by Brown (6), was to dissolve the pentachloride compound in freshly distilled thionyl chloride, allow the mixture to digest for 24 h, and filter the solution through a fritted disc having a nominal pore size of 5 μm. The $SOCl_2$ was evaporated from the filtrate and the remaining salt was sublimed in a sealed tube. Reagent grade alkali-metal chlorides were ground to a particle size of −200 mesh. They were dehydrated by exposure to a mixture of chlorine and HCl gases for several hours at 500°C.

[1]Present address: Department of Materials Science and Engineering, Massachusetts Institute of Technology, Cambridge, MA 02139, U.S.A.

Can. J. Chem. Downloaded from www.nrcresearchpress.com by 210.87.254.42 on 09/05/12
For personal use only.

Can. J. Chem. Downloaded from www.nrcresearchpress.com by 210.87.254.42 on 09/05/12
For personal use only.

To prepare the compound, $AMCl_6$, equimolar amounts of ACl and MCl_5 were placed in a borosilicate glass reaction tube, which is shown in Fig. 1. To minimize hydrolysis of the reagents this operation was performed in a glove box filled with anhydrous helium. With its ends stoppered the reaction tube was removed from the glove box and the end nearer the ACl was flame sealed. Next, the reaction tube was evacuated and the ACl was heated to 400°C. During this time the reaction tube was being evacuated to exhaust the gas which was desorbing off the surface of the ACl powder. After 12 h the reaction tube was flame sealed under vacuum. It was placed in a furnace with two independently controlled elements. The MCl_5 was heated to the temperature at which its pressure was approximately 1.5 atm, i.e. 266°C for $NbCl_5$ and 257°C for $TaCl_5$ (7). Except in the case of the NaCl the other alkali chlorides were heated to approximately 10°C above the melting point of the corresponding $AMCl_6$ compound. Reaction times were of the order of several hours. Power to both furnace elements was then disconnected simultaneously and the reaction tube was furnace-cooled. The high pressures over the molten compounds, $NaNbCl_6$ and $NaTaCl_6$, necessitated their preparation in the solid state. Time of reaction was 3 days.

Despite all precautions, a small amount of fibrous white substance remained behind in the MCl_5 part of the reaction tube. This was probably hydrolysed MCl_5. The reaction tube was opened in the glove box and the glass boat was weighed to determine the amount of MCl_5 which had reacted with the ACl and, therefore, the composition of the material in the boat.

For the sake of comparison, some of the compounds were synthesized by precipitation from solutions of $SOCl_2$–ICl (6, 8). Attempts were made to prepare all $AMCl_6$ compounds by this method; however, only $CsNbCl_6$, $CsTaCl_6$, and $RbTaCl_6$ could be produced in quantity.

Other investigators (9–13) have made these compounds by mixing the appropriate quantities of $NbCl_5$ or $TaCl_5$ with ACl and slowly heating the mixture to its melting temperature. The melt is then cooled and the solid product is ground in a dry atmosphere. This method was not used in the present study because it was felt that gas–solid reaction reduces the contamination of the product.

$KNbCl_6$ and $KTaCl_6$ have also been prepared by two other methods. In one, the reaction of a mixture of K_2O and Nb_2O_5 or Ta_2O_5 with CCl_4 is conducted in a sealed ampoule at 400°C (14). In the other, specified amounts of KCl and $NbCl_5$ or $TaCl_5$ dissolved in $SOCl_2$ are heated, excess KCl is removed by filtration, and $SOCl_2$ is evaporated from the filtrate (15). These methods, however, have low yields and are used mainly for the preparation of spectral samples of small mass.

At room temperature the hexachloroniobates are green. Upon heating they turn yellow–orange, and their melts are red. On exposure to moisture for several minutes the solids turn blue, they are white when completely hydrolysed.

The solid hexachlorotantalates and all their hydrolysis products are white. The molten hexachlorotantalates are transparent and have a faint lemon–yellow colour.

Results

X-ray Powder Patterns

The X-ray powder patterns were obtained with a Debye–Scherrer 114.8 mm camera, exposed for 1 h to CuK_α radiation ($\lambda = 1.5418$ Å) filtered through nickel. In a glove box filled with helium the specimens were ground and screened to -200 mesh and hermetically sealed in 0.3 mm quartz glass capillaries.

The results for $NbCl_5$ and $TaCl_5$ which had been purified by precipitation from $SOCl_2$, as described above, agree well with earlier work by Douglass and Staritzky (16) for $NbCl_5$ and Rolsten (17) for $TaCl_5$.

The X-ray patterns of the eight compounds $AMCl_6$, where A is Na, K, Rb, or Cs, and M is Nb or Ta have been obtained. Despite the fact that in some cases the specimens did not consist of exactly equimolar amounts of ACl and MCl_5 extraneous lines which could be attributed to these small variations in composition were not found. Furthermore, in the case of $RbTaCl_6$, $CsNbCl_6$, and $CsTaCl_6$, which were successfully synthesized both by the reaction of MCl_5 vapour with ACl powder and by precipitation from $SOCl_2$–ICl solutions, the two patterns obtained were identical.

Only three X-ray studies of $AMCl_6$ compounds have been reported. Kozhina *et al.* (13) studied $KNbCl_6$ and $KTaCl_6$, Smirnova and Tsintsius (18), $RbNbCl_6$ and $CsNbCl_6$, and Bagnall and Brown (8), $CsNbCl_6$ and $CsTaCl_6$.

There is excellent agreement between the results of this work and that reported by Kozhina *et al.* (13) for $KNbCl_6$ and $KTaCl_6$ respectively.

The results of this work are also in agreement with the main lines obtained by Smirnova and Tsintsius (18) for $RbNbCl_6$.

The results of this study for $CsTaCl_6$ agree with those of Bagnall and Brown (8). The latter prepared their samples by precipitation from $SOCl_2$–ICl solutions; in this study samples were prepared both by that method and by the reaction of CsCl with $TaCl_5$ vapour. Although the pattern by Bagnall and Brown has more lines, both patterns agree on lines of greater intensity. Samples prepared herein by precipitation and by solid–vapour reaction were irradiated; all gave the same results. Furthermore, this powder pattern was successfully indexed. No explanation is given for the extra lines reported by Bagnall and Brown.

The X-ray diffraction patterns for the alkali hexachloroniobate and alkali hexachlorotantalate compounds which have been obtained in this laboratory may be found in the Depository of Unpublished Data, CISTI, at the National Research Council of Canada.[2]

The X-ray diffraction pattern for the compound $CsNbCl_6$ was also obtained. Previous data by Smirnova and Tsintsius (18) and by Bagnall and Brown (8) are contradictory. As seen in Table 1, the present work is in better agreement with the results by Bagnall and Brown (8) who prepared the compound by

[2]Copies of these data are available, at a nominal charge, from the Depository of Unpublished Data, CISTI, National Research Council of Canada, Ottawa, Ont., Canada K1A 0S2.

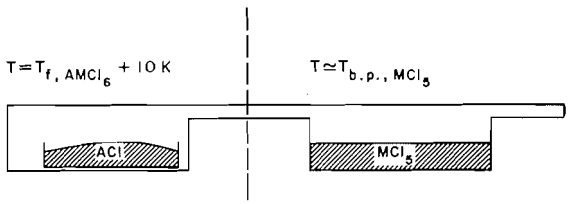

FIG. 1. Reaction apparatus for the synthesis of alkali hexachloroniobate(V) and hexachlorotantalate(V) compounds.

the $SOCl_2$–ICl method as compared to the method of co-melting equimolar amounts of $NbCl_5$ and CsCl used by Smirnova and Tsintsius.

In this study samples which had been prepared both by precipitation from $SOCl_2$–ICl solutions and by the reaction of CsCl with $NbCl_5$ vapour were irradiated. In all cases, the pattern given in Table 1 was obtained. To determine the effect of CsCl on the pattern, a sample of composition $X_{CsNbCl_6} = 0.535$, balance CsCl, was irradiated. The powder pattern was identical with the exception of the reflection at 2.91 Å, the intensity of which had increased with the presence of CsCl. In other experiments with $CsNbCl_6$ two allotropic modifications were detected. Perhaps different investigators have seen different allotropic forms. Nevertheless, five different samples of $CsNbCl_6$ were irradiated in this study, and all five gave the powder pattern in Table 1.

X-ray diffraction patterns for the compounds $NaNbCl_6$, $NaTaCl_6$, and $RbTaCl_6$ also obtained in this laboratory are given in Table 2.

As this study was the first to identify these compounds no comparison can be made with existing data.

Attempts were made to determine the crystal structures of the hexachloroniobate and hexachlorotantalate compounds. Although the data were those of polycrystalline samples, it was possible to test whether the structures were cubic, tetragonal, or hexagonal by means of nomographs. A summary of the results of these calculations is given in Table 3 and the complete indexed X-ray powder patterns and the calculated and experimentally obtained *d*-spacings for $NaNbCl_6$, $KNbCl_6$, $KTaCl_6$, $RbTaCl_6$, and $CsTaCl_6$ may be found at the Depository of Unpublished Data.[2]

Good agreement with the measured pattern of $NaNbCl_6$ was obtained by assuming this compound to have a tetragonal structure.

The measured powder pattern of $KNbCl_6$ is compared with that generated on the assumption that its crystal structure is cubic with a cell dimension $a = 9.80$ Å. The agreement between observed and calculated *d*-spacings is excellent. This confirms a similar conclusion made previously by Kozhina *et al.* (13).

The measured powder patterns of $RbNbCl_6$, $CsNbCl_6$, and $NaTaCl_6$ could not be correlated

TABLE 1. Comparison of powder X-ray diffraction patterns of $CsNbCl_6$

This study		Bagnall and Brown (8)		Smirnova and Tsintsius (18)	
d (Å)	Intensity†	*d* (Å)	Intensity	*d* (Å)	Intensity
				6.45	vs
		5.98	m⁻		
5.55	vw	5.63	m		
		5.32	s⁻	5.37	w
4.86	sm	4.92	s	4.91	vvs
4.73	m	4.79	s		
		4.33	m	4.32	vvw
		3.94	w	3.91	w
3.82	w	3.88	s⁻		
		3.43	s	3.45	s
		3.41	s		
3.39	w	3.38	w⁻		
		3.18	w		
		3.13	m		
		3.02	m⁺		
		2.99	m⁺		
2.91	vw*				
		2.79	vvs	2.80	vvs
2.76	sm	2.77	s⁻		
2.72	m	2.75	s⁻		
		2.68	w	2.67	s
		2.64	m		
		2.49	w⁻		
		2.47	w⁻		
		2.41	w⁻	2.40	w
2.37	w	2.39	m⁺		
2.14	m	2.15	m⁺	2.15	vs
2.12	w	2.12	m		
		2.07	w⁻		
		2.05	m⁻		
		2.04	w⁻		
		2.02	m⁻		
		1.99	w		
		1.97	w		
		1.93	w		
		1.92	w		
		1.90	w		
1.81	w	1.82	m⁺	1.82	vs
1.80	vw	1.80	w		
		1.79	w		
				1.76	vw
		1.70	w		
		1.69	w		
		1.68	w		
1.66	w	1.66	m⁻		
		1.65	m⁻		
		1.59	w⁻		
1.52	vvw			1.53	s
1.51	vvw				
1.46	vvw				

*CsCl gives a reflection at 2.92 Å, $I/I_1 = 100$. s = strong, sm = medium strong, m = medium, w = weak, vw = very weak, vvw = very very weak.

Can. J. Chem. Downloaded from www.nrcresearchpress.com by 210.87.254.42 on 09/05/12
For personal use only.

Can. J. Chem. Downloaded from www.nrcresearchpress.com by 210.87.254.42 on 09/05/12
For personal use only.

TABLE 2. X-ray diffraction powder patterns for the compounds $NaNbCl_6$, $NaTaCl_6$, and $RbTaCl_6$

$NaNbCl_6$ $X_{NbCl_5} = 0.485$ $X_{NaCl} = 0.515$		$NaTaCl_6$ $X_{TaCl_5} = 0.474$ $X_{NaCl} = 0.526$		$RbTaCl_6$ $X_{TaCl_5} = 0.501$ $X_{RbCl} = 0.499$	
d (Å)	Intensity	d (Å)	Intensity	d (Å)	Intensity
6.38	m	5.52	s	5.94	sm
5.55	s	5.24	s	5.18	sm
5.29	s	4.68	s	4.82	s
4.70	s	3.40	vw	4.67	sm
2.89	sm	3.32	w	3.79	m
2.82	sm	2.86	s	3.35	sm
2.34	m	2.80	s	3.03	vvw
2.15	w	2.35	s	2.94	vvw
2.10	w	2.19	vw	2.72	s
2.00	w	2.15	w	2.59	w
1.96	w	2.10	m	2.34	w
1.60	w	1.95	wm	2.10	s
1.26	w	1.89	wm	1.92	vvw
		1.83	wm	1.79	sm
		1.78	wm	1.77	vvw
		1.66	wm	1.57	vvw
		1.60	wm	1.52	vvw
		1.40	wm	1.51	vvw
				1.48	vvw
				1.44	vvw

TABLE 3. Cell dimensions and crystal structures of alkali hexachloroniobate and hexachlorotantalate compounds

Compound	Structure	a (Å)	c (Å)
$NaNbCl_6$	Tetragonal	11.20	10.57
$KNbCl_6$	Cubic	9.80	—
$KTaCl_6$	Hexagonal	11.62	10.97
$RbTaCl_6$	Hexagonal	11.92	14.00
$CsTaCl_6$	Hexagonal	12.60	19.52

without ambiguity to any of the structures considered. This is in contrast with claims by previous investigators that $RbNbCl_6$ and $CsNbCl_6$ are both tetragonal (18). However, these compounds are known to have more than one allotropic modification, and it is possible that the samples prepared herein had different crystal structures.

The measured X-ray powder patterns of $KTaCl_6$, $RbTaCl_6$, and $CsTaCl_6$ corresponded well with those generated by assuming each to possess a hexagonal crystal structure. Previously, Kozhina *et al.* (13) on the basis of their measurements suggested that $KTaCl_6$ was hexagonal. The cell dimensions were given as $a = 11.87$ Å and $c = 10.79$ Å and agree well with estimates of this work, which are, $a = 11.62$ Å and $c = 10.97$ Å. There are no structural data reported in the literature for either $RbTaCl_6$ or $CsTaCl_6$.

Figure 2 shows that the cube root of the volume of the unit cell varies linearly with the radius of the alkali-metal cation, indicating that these three compounds are isostructural.

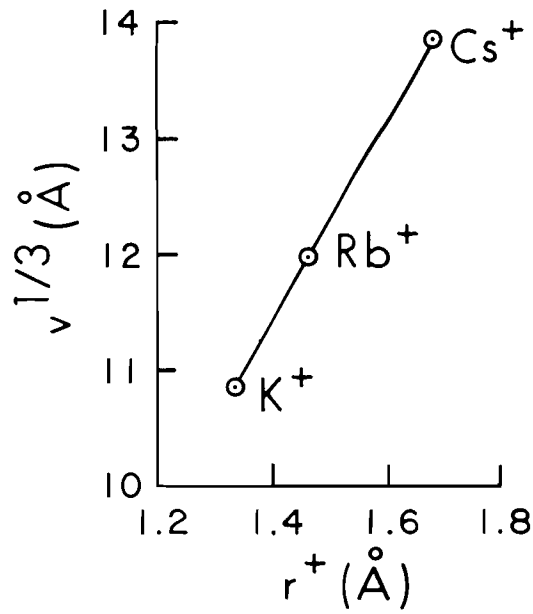

FIG. 2. Variation of cell size with alkali-metal cation radius for the compounds $KTaCl_6$, $RbTaCl_6$, and $CsTaCl_6$.

Cryoscopy

The approximate melting points and temperatures of the solid transformations were found by cryoscopy. Each sample weighed approximately 20 g and was contained in an evacuated fused quartz ampoule. The ampoule contained a glass well which allowed a thermocouple to be placed at the heart of the salt sample. For immersion into a vertical tube furnace the ampoule was contained in a grounded metal sheath which served to prevent induction of spurious voltages in the thermocouple by the ac field of the furnace windings. Furnace temperature was controlled by a variable autotransformer. To maintain a fixed cooling rate an electric motor drove down the variable autotransformer through a variable-ratio gear reductor. Each sample was cooled several times at different rates ranging from 0.5 K/min to 2.5 K/min to obtain data which were free from the effects of undercooling. The thermocouple, 22 gauge, Chromel-P vs. Alumel, ASTM type K, was certified by the Hoskins Manufacturing Co., Detroit, MI, U.S.A., and was checked in this laboratory against a platinum – 13% rhodium vs. platinum standard, manufactured by Egelhard Industries, Carteret, NJ, U.S.A.

The output from the thermocouple was recorded on a multirange chart recorder, Honeywell ElectroniK 193, after compensation by a Sargent zero

TABLE 4. Phase transformations of the alkali-metal hexachloroniobates and hexachlorotantalates

Compound	Melting point (°C)	Eutectic* (°C)	Solid–solid transformations (°C)	Reference
$NaNbCl_6$			299, 245	This work
	444(i)		247	19
	430(i)		256	9
	450(i)		259	12
	468(i)			11
$NaTaCl_6$			225	This work
	484(i)		223	20
	470(i)		232	10
	470(i)			11
$KNbCl_6$	400	370	299	This work
	400	378		11
	396	376	334	12
	396	366	321, 160	19
	394	368		23
	365		156	21
$KTaCl_6$	401	373	311, 138	This work
	410	370	312, 160	20
	420			11
$RbNbCl_6$	380(i)		305	This work
	360(i)			11
$RbTaCl_6$	417		313, 261	This work
	416	382		11
$CsNbCl_6$	535		290	This work
	528	434		11
	528	444	300	21
$CsTaCl_6$	540		296	This work
	548	442	294	22
	555	446		11

NOTE: (i) denotes that the compound melts incongruently.
*The eutectic temperature is that of the ACl–$AMCl_6$ subsystem.

displacement recorder accessory. The results are summarized in Table 4. The most striking feature is that all the $AMCl_6$ compounds proved to be polymorphic in the solid state.

The results of this work for $NaNbCl_6$ and $NaTaCl_6$ agree well with the findings of Palkin and Chikanov (19). Attempts were made to measure the melting points of the incongruently melting compounds. However, the dissociation vapour pressures are so high at this temperature that the fused quartz cells explode. Aside from the well defined solid–solid transformation at 245°C, which occurs with an estimated large enthalpy of transition, $NaNbCl_6$ showed signs of a solid–solid transformation at 299°C, which has not been reported in the literature. It occurs with an estimated very small enthalpy of transition.

$KNbCl_6$ is the most thoroughly studied of all the $AMCl_6$ compounds. Investigators seem to agree that it melts at approximately 395–400°C and that the $KNbCl_6$–KCl eutectic temperature is in the vicinity of 370°C. The solid–solid transformation temperatures vary greatly. Palkin and Chikanov (19) claim two transformations, one at 321°C and another at 160°C, the latter occurring with a large enthalpy of transition. In this investigation, none of the samples of $KNbCl_6$ or $KNbCl_6$–KCl showed any evidence of the latter. Indeed, the transformation reported herein to occur at 299°C is elusive and was observed only in samples whose composition was almost pure $KNbCl_6$.

The results for $KTaCl_6$ agree well with those of Palkin and Chikanov (20) for the $KTaCl_6$–KCl eutectic temperature and the temperature of the $\alpha \rightarrow \beta$ transformation. The latter occurs with an estimated small enthalpy change. Although this study quotes the temperature of the $\beta \rightarrow \gamma$ transformation to be 138°C in contrast to 160°C reported by Palkin and Chikanov (20), both studies estimate the enthalpy change which accompanies this transition to be extremely large. The melting point of $KTaCl_6$, determined herein as 401°C, was a rather elusive quantity to measure because the liquidus from pure $KTaCl_6$ to the $KTaCl_6$–KCl eutectic at 48 m/o $TaCl_5$ is very steep, varying 40–50 K in a composition range of 2 m/o.

Only Huber *et al.* (11) have studied the phase

Can. J. Chem. Downloaded from www.nrcresearchpress.com by 210.87.254.42 on 09/05/12
For personal use only.

changes of $RbNbCl_6$ and $RbTaCl_6$. $RbNbCl_6$ reportedly melts incongruently at 360°C. In this study the liquidus was identified at 380°C; however, there was no thermal arrest at 360°C. The $\alpha \rightarrow \beta$ transformation, which occurs at 305°C with an estimated large enthalpy change, has been discovered in this investigation. Huber *et al.* and this study report effectively identical values for the melting point of $RbTaCl_6$. It appears that this study is the first to discover the $\alpha \rightarrow \beta$ transformation of $RbTaCl_6$. This occurs at 313°C with an estimated large enthalpy change. The cooling curves suggested that there may be still another phase change occurring at 261°C with an estimated small enthalpy change.

The melting point of $CsNbCl_6$ was measured herein to be 535°C, in good agreement with previous estimates (11, 21). The $\alpha \rightarrow \beta$ transition at 290°C with a large enthalpy change has been identified. Morozov in his book (21) reports the existence of a solid–solid transformation at 300°C. Unfortunately, there is no reference to the original study. The measured melting point and temperature of the solid–solid transformation of $CsTaCl_6$ agree well with those determined by Morozov and Simonich (22).

Acknowledgements

The authors wish to thank the National Research Council of Canada for its financial support. The assistance of Mrs. Elke Mutterer for obtaining the X-ray powder patterns and many useful discussions with Professor E. W. Nuffield of the Department of Geology of the University of Toronto are gratefully acknowledged.

1. S. N. Flengas. Ann. N.Y. Acad. Sci. **79**, 853 (1960).
2. R. L. Lister and S. N. Flengas. Can. J. Chem. **41**, 1548 (1963).
3. R. L. Lister and S. N. Flengas. Can. J. Chem. **42**, 1102 (1964).
4. W. Scheller and J. Renard. German patent no. 1136681, September 20, 1962; Chem. Abstr. **58**, 3127 (1963).
5. F. J. Keneshea, D. Cubicciotti, G. Withers, and H. Eding. J. Phys. Chem. **72**, 1272 (1968).
6. D. Brown. Inorg. Synth. **9**, 88 (1967).
7. D. R. Sadoway and S. N. Flengas. Can. J. Chem. **54**, 1692 (1976).
8. K. W. Bagnall and D. Brown. J. Chem. Soc. 581 (1964).
9. I. S. Morozov and B. G. Korshunov. Zh. Neorg. Khim. **1**, 145 (1956); Engl. trans.: Russ. J. Inorg. Chem. **1**(1), 150 (1956).
10. I. S. Morozov, B. G. Korshunov, and A. T. Simonich. Zh. Neorg. Khim. **1**, 1646 (1956); Engl. trans.: Russ. J. Inorg. Chem. **1**(7), 203 (1956).
11. K. Huber, E. Jost, E. Neuenschwander, M. Studer, and B. Roth. Helv. Chim. Acta, **41**, 2411 (1958).
12. A. P. Palkin and N. D. Chikanov. Zh. Neorg. Khim. **4**, 898 (1959); Engl. trans.: Russ. J. Inorg. Chem. **4**, 407 (1959).
13. I. I. Kozhina, V. P. Kustovskaya, I. V. Vasil'kova, and M. P. Susarev. Vestn. Leningr. Univ. Fiz., Khim. **23**(16), 113 (1968).
14. S. M. Horner, R. J. H. Clark, B. Crociani, D. B. Copley, W. W. Horner, F. N. Collier, and S. Y. Tyree, Jr. Inorg. Chem. **7**, 1859 (1968).
15. CIBA, Ltd. British patent no. 876802, September 6, 1961; Chem. Abstr. **56**, 11224 (1961).
16. R. M. Douglass and E. Staritzky. Anal. Chem. **29**, 315 (1957).
17. R. F. Rolsten. ADI 5487, Library of Congress, Washington, DC, U.S.A.
18. E. K. Smirnova and V. M. Tsintsius. Zh. Neorg. Khim. **16**, 566 (1971); Engl. trans.: Russ. J. Inorg. Chem. **16**, 303 (1971).
19. A. P. Palkin and N. D. Chikanov. Zh. Neorg. Khim. **7**, 1370 (1962); Engl. trans.: Russ. J. Inorg. Chem. **7**, 705 (1962).
20. A. P. Palkin and N. D. Chikanov. Zh. Neorg. Khim. **7**, 2388 (1962); Engl. trans.: Russ. J. Inorg. Chem. **7**, 1239 (1962).
21. I. S. Morozov. Primenenie Khlora V Metallurgii Redkikh i Tsvetnykh Metallov, Nauka, Moscow. 1966. p. 222.
22. I. S. Morozov and A. T. Simonich. Zh. Neorg. Khim. **2**, 1907 (1957); Engl. trans.: Russ. J. Inorg. Chem. **2**(8), 311 (1957).
23. O. R. Gavrilov and L. A. Nisel'son. Zh. Neorg. Khim. **11**, 209 (1966); Engl. trans.: Russ. J. Inorg. Chem. **11**, 114 (1966).

Can. J. Chem. Downloaded from www.nrcresearchpress.com by 210.87.254.42 on 09/05/12
For personal use only.

Trimethylene sulfite conformations: Effects of sterically demanding substituents at C-4,6 on ring geometry as assessed by ^1H and ^{13}C nuclear magnetic resonance

GERALD W. BUCHANAN, CATHERINE M. E. COUSINEAU, AND THOMAS C. MUNDELL

Department of Chemistry, Carleton University, Ottawa, Ont., Canada K1S 5B6

Received February 16, 1978

GERALD W. BUCHANAN, CATHERINE M. E. COUSINEAU, and THOMAS C. MUNDELL. Can. J. Chem. **56**, 2019 (1978).

^1H and ^{13}C nmr data for eight phenyl, diphenyl- and di-*tert*-butyl-2-oxo-1,3,2-dioxathianes, substituted at C-4 and/or C-6 are presented. Vicinal couplings obtained from ^1H spectra by iterative computer analysis indicate chair geometries for all materials except *trans*-4,6-disubstituted compounds. ^{13}C chemical shifts are corroborative.

GERALD W. BUCHANAN, CATHERINE M. E. COUSINEAU et THOMAS C. MUNDELL. Can. J. Chem. **56**, 2019 (1978).

On rapporte des données de rmn du ^1H et du ^{13}C relatives à huit phényl-, diphényl- ou di-*tert*-butyl-oxo-2 dioxathianes-1,3,2 substitués en positions 4 et/ou 6. Les valeurs obtenues pour les constantes de couplage vicinales obtenues à partir des spectres du proton par une analyse itérative à l'aide d'un ordinateur indiquent que tous les composés existent dans des conformations chaises à l'exception des composés disubstitués en 4,6 *trans*. Les déplacements chimiques du ^{13}C corroborent ces conclusions.

[Traduit par le journal]

Introduction

For over 15 years, conformational analysis of trimethylene sulfite and its alkyl derivatives has posed an interesting problem in stereochemistry. The literature includes studies by dipole moment measurement (1–3), ultrasonic absorption (4, 5), infrared spectroscopy (1, 6–11), chemical equilibration (12, 13), electron diffraction (14), and ^1H and ^{13}C nmr spectroscopy (6–11), (15–21).

The predominance of an axial S=O function in trimethylene sulfite itself is well established, $-\Delta G^0$ being ca. 2.1 kcal/mol (3). For compounds in which a single substituent can be potentially *syn*-axial to the exocyclic oxygen i.e., *a* (below), the question arises as to whether the ring will change its geometry. If so, does it ring invert to a chair with equatorial S=O or is a twist conformation adopted?

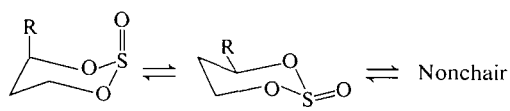

a *b* *c*

On the basis of dipole moments (1–3), ^1H nmr (6–11, 19), and ^{13}C nmr (21) it has been suggested that twist forms are populated appreciably when the possibility of *syn*-axial interaction between the S=O and a single CH_3 group at C-4 or C-6 exists. Recently these interpretations have been questioned by Pihlaja and co-workers (22) who conclude that energy considerations preclude significant contributions from twist forms at least in the case of a single axial CH_3 and an axial S=O group. Their argument is based on rigorous analysis of ^1H spectra and calculations which indicate that the twist chair form of 1,3,2-dioxathiane is ca. 8 kcal/mol less stable than the chair conformer (23, 24).

If the conclusions of Pihlaja and co-workers (22) are valid, then the question arises as to how large a single axial substituent at C-4,6 must be, in order to induce conformational change in sulfites. For 1,2-oxathian-2-oxides we have recently found that even a sterically bulky moiety such as phenyl is insufficient to alter the conformation from a chair with axial S=O (25) i.e.,

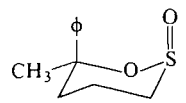

In the case of trimethylene sulfites, no systematic study of compounds having axial functions larger than CH_3 has been reported. Accordingly we have synthesized a series of trimethylene sulfites having potentially axial phenyl and *tert*-butyl functions at C-4,6. These materials have been subjected to ^1H and ^{13}C nmr analysis in order to detect their preferred geometries in solution.

Results and Discussion

^1H Spectra

Table 1 contains the chemical shifts and Table 2 the coupling constants for **1**–**8**. Spectra were analyzed by means of the LAOCN3 program (34) and fitted to an rms error of ± 0.1. In the cases of **4** and **5**, the corresponding 6,6-dideuterio compounds were synthesized, and their spectra employed as a starting

Can. J. Chem. Downloaded from www.nrcresearchpress.com by 210.87.254.40 on 09/05/12
For personal use only.

TABLE 1. ^{1}H chemical shifts for **1–8** (0.1 *M* in $CDCl_3$) ±0.01 ppm

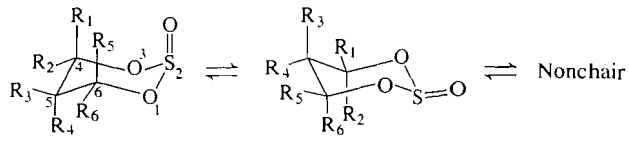

Compound	Substituent	Conformation	δ (ppm) R_1	R_2	R_3	R_4	R_5	R_6
1	$R_2 = R_6 = C(CH_3)_3$	*a*	4.59	0.95	1.64	1.84	4.59	0.95
2	$R_1 = R_5 = C(CH_3)_3$	*b*	1.00	4.02	1.66	1.75	1.00	4.02
3	$R_1 = R_6 = C(CH_3)_3$	*c*	1.00	3.71	1.93	1.81	4.39	1.00
4	$R_2 = \phi$	*a*	5.93	(7.30)	1.78	2.48	5.09	3.92
5	$R_1 = \phi$	*b*	(7.40)	5.43	2.37	1.90	4.54	4.54
		*b**	(7.40)	5.43	2.37	1.90	4.72	4.87
6	$R_2 = R_6 = \phi$	*a*	6.15	(7.39)	2.16	2.54	6.15	(7.39)
7	$R_1 = R_5 = \phi$	*b*	(7.40)	5.60	2.46	2.15	(7.40)	5.60
8	$R_1 = R_6 = \phi$	*c*	(7.42)	5.36	2.99	2.48	5.87	(7.42)

*0.1 *M* in acetone-d_6.

TABLE 2. ^{1}H couplings for **1–8** (±0.1 Hz)

Compound	*J* (Hz) R_1R_3	R_1R_4	R_2R_3	R_2R_4	R_3R_4	R_3R_5	R_3R_6	R_4R_5	R_4R_6	R_5R_6
1	2.2	11.9			−13.5	2.2		11.9		
2			11.3	2.2	−13.9		11.3		2.2	
3			10.0	6.6	−13.3	6.0		10.2		
4	2.6	12.5			−14.6	2.6	1.6	11.8	4.7	−12.2
5			11.5	2.7	−14.0	4.7	11.5	1.9	3.2	−12.1
6	2.3	12.0			−14.5	2.3		12.0		
7			11.7	2.4	−14.7		11.7		2.4	
8			10.2	4.9	−14.4	6.6		6.6		

point for the spectral analysis. For **5**, the protons at C-6 are accidentally isochronous in 0.1 *M* $CDCl_3$ solution, but the spectra recorded in acetone-d_6 show a substantial chemical shift difference between these nuclei. Parenthesized values denote the centre of the phenyl regions which were not analyzed.

The large vicinal couplings observed in **1** and **2** are indicative of chair conformers in which nearly 180° dihedral angles are present between *trans*-diaxial protons. Also in **1**, where the sulfinyl group is *syn*-axial to axial H's on C-4,6 (R_1 and R_5), a pronounced deshielding (0.58 ppm) of these protons is apparent relative to **2** in which the sulfinyl group is equatorial. This difference is close to that found for the corresponding dimethyl compounds (19) and the analogous diphenyl systems **6** and **7** (0.55 ppm). The similarity in the vicinal couplings for **6** and **7** compared to **1** and **2** indicates similar geometries, namely chair forms with axial S=O in **6** and equatorial S=O in **7**.

The ^{1}H spectrum of **3** recorded in CCl_4 and CH_3CN solutions has been analyzed by Cazaux *et al.* (26). Based on Eu(fod)$_3$ experiments and consideration of Karplus curves they concluded that the molecule adopts a twist conformation as shown below.

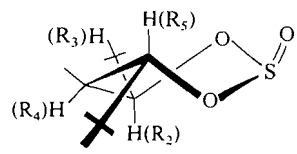

3

Our data for **3** in $CDCl_3$ are in close accord with those reported by the French group. The intermediate couplings of ca. 10 Hz between R_2R_3 and R_4R_5 could arise from dihedral angles near 150° in each case. For couplings involving R_2R_4 and R_3R_5, dihedral angles of ca. 30° may be present, resulting in the smaller couplings of ca. 6 Hz.

Can. J. Chem. Downloaded from www.nrcresearchpress.com by 210.87.254.40 on 09/05/12
For personal use only.

Can. J. Chem. Downloaded from www.nrcresearchpress.com by 210.87.254.40 on 09/05/12
For personal use only.

The other situation which could lead to intermediate J values is a chair–chair equilibrium. If this were the case, the shift difference between R_2 and R_5 of **3** would be considerably less than that between the C-4,6 protons of **1** and **2** (0.58 ppm), since the S=O would be *syn*-axial to R_5 only part of the time. But the observed shift difference between R_2 and R_5 of **3** is large (0.68 ppm), indicating a preference for a conformation such as the twist form above in which the S=O deshields R_5 considerably relative to R_2. Further support for this conclusion comes from the ^{13}C data (*vide infra*). Also, we have carried out low temperature studies (to $-120°C$) on **3** and no spectral changes were found. Although this is not rigorous proof for a twist form, it does mitigate against a chair $\rightleftharpoons$ chair equilibrium with a barrier >10 kcal/mol and appreciable contributions from two chairs.

With regard to the monophenyl systems **4** and **5**, the only previous work published was on a material proposed to be '4-phenyltrimethylene sulfite' by Albriktsen (18). This liquid compound was characterized only by its boiling point. No elemental analysis data were presented. Furthermore *only one isomer* was described. We have now synthesized two isomers of this material, one liquid (**4**) and one solid (**5**) and our nmr results are drastically different from those of Albriktsen *for both isomers*. A further problem with the earlier work was that the spectrum of the neat liquid was analyzed, although it has been clearly demonstrated (27) that sulfites experience strong self association and are likely to be dimers at high solute concentration. In an attempt to determine if the previous liquid (18) was a polymer of our liquid isomer **4**, we have recorded a 60 MHz spectrum of neat **4** and compared it to the 60 MHz spectrum published earlier. The spectra are grossly different and we are forced to conclude that Albriktsen's material was *not* in fact a 4-phenyltrimethylene sulfite at all.

In contrast to Albriktsen's postulate of a twist conformation, the ^1H data clearly show that *both* **4** and **5** are chair forms, with axial and equatorial sulfinyl groups respectively. The large vicinal couplings between potentially diaxial protons suggest chairs, so do the small J's between axial–equatorial and equatorial–equatorial nuclei. The large negative geminal J's are normal, with $J_{5,6}$ being more positive due to the influence of the adjacent electronegative oxygen atom (28).

The substantial deshielding of the axial proton of **4** (i.e. R_5) relative to R_6, is evidence for the axial S=O, whereas in **5**, with the equatorial S=O, R_5 and R_6 have only slightly different chemical shifts (in acetone-d_6).

For the *cis*-diphenyl compounds **6** and **7**, the couplings are remarkably similar to those for the *cis*-di-*tert*-butyl materials **1** and **2**, respectively. Accordingly, we suggest that **6** is a chair conformer with axial S=O, whereas **7** is a chair with an equatorial S=O moiety. The *trans*-diphenyl isomer **8** shows intermediate magnitude for vicinal H–H couplings. We have examined its spectrum to $-120°C$ with no observable changes and therefore conclude that it also most likely adopts a nonchair geometry, with the same provisos re: a possible chair $\rightleftharpoons$ chair equilibrium as stated earlier for **3**.

^{13}C Spectra

Carbon shifts for **1–8** are collected in Table 3. Assignments were straightforward and were verified by selective ^1H irradiation for carbons bearing protons. Aromatic resonances are designated as quaternary, *ortho*, *meta*, and *para*. Peak overlap was evident for *meta* and *para* positions in most materials.

The primary diagnostic tool for ring geometry is the γ effect of the exocyclic oxygen on the C-4,6 resonances. When the S=O is axial in a chair, the *gauche*-γ effect results in a substantial upfield shift at C-4,6 in sulfites (21) relative to instances where the S=O is equatorial in a chair. Analogous findings for isomeric sulfoxides (thiane oxides) have also been published (29). For the 4,6-dimethyl trimethylene sulfites studied earlier (21), results are presented below (9.1 ppm *gauche*-γ effect).

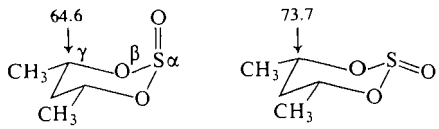

Findings for **1** vs. **2** and **6** vs. **7** are very similar to those for the dimethyl isomers. In **1**, the existence of an axial S=O in the chair shields C-4,6 by 9.6 ppm relative to **2**, whereas in **6** the *gauche*-γ shielding is 8.7 ppm compared to **7**.

For the *trans*-di-*tert*-butyl compound **3** the shift at C-6 is 1 ppm upfield from that found in **1**. This result mitigates against a substantial amount of a chair conformer with equatorial S=O since this would deshield C-6. On the other hand, if **3** was in a chair form with axial S=O, the presence of the axial *tert*-butyl group at C-4 should shield C-6 more than 1 ppm (relative to **1**) owing to the extra *gauche*-γ interaction. We feel the data are best accommodated by the twist boat form of **3** depicted earlier. In this conformation C-6 still experiences a large γ-effect owing to the *pseudo*-axial S=O but the *syn*-axial interaction between the bulky *tert*-butyl group and the exocyclic oxygen is removed.

Can. J. Chem. Downloaded from www.nrcresearchpress.com by 210.87.254.40 on 09/05/12
For personal use only.

TABLE 3. ^{13}C chemical shifts ($\delta_c \pm 0.1$ from TMS) for **1–8** (0.1 *M* in $CDCl_3$)

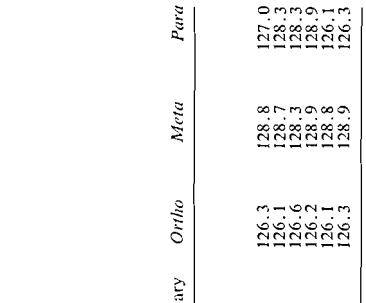

Compound	Substituent	Conformation	C-4	C-5	C-6	R_1	R_2	R_3	R_4	R_5	R_6	$(*CH_3)_3C$	Quaternary	*Ortho*	*Meta*	*Para*
1	$R_2 = R_6 = C(CH_3)_3$	*a*	75.4	26.7	75.4		34.0				34.0	25.3				
2	$R_1 = R_5 = C(CH_3)_3$	*b*	85.0	24.9	85.0	34.7				34.7		25.6				
3	$R_1 = R_6 = C(CH_3)_3$	*c*	80.0	27.7	74.4	34.2					33.7	25.3				
4	$R_2 = \phi$	*a*	68.8	33.5	58.0								138.7	126.3	128.8	127.0
5	$R_1 = \phi$	*b*	78.7	31.8	64.6								138.3	126.1	128.7	128.3
6	$R_2 = R_6 = \phi$	*a*	70.0	41.0	70.0								138.7	126.6	128.3	128.3
7	$R_1 = R_5 = \phi$	*b*	78.7	39.4	78.7								138.0	126.2	128.9	128.9
8	$R_1 = R_6 = \phi$	*c*	74.6	38.8	69.5								138.8	126.1	128.8	126.1
													138.7	126.3	128.9	126.3

In the case of compound **4**, it is instructive to compare the shifts induced by phenyl substitution with those caused by equatorial phenyl substitution at C-6 in 1,2-oxathiane-2-oxides (sultines), which are deemed to be in chair conformations having axial S=O groups (25).

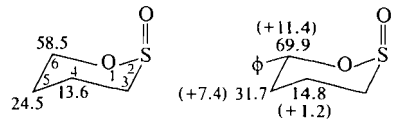

For the above sultines, the α effect is +11.4 ppm, the β effect is +7.4 ppm, and the *trans*-γ shift at C-4 is +1.2 ppm. In the sulfite **4** the α, β, and *trans*-γ effects are +11.7, +7.5, and +0.9 ppm, respectively. The striking correspondence between these substituent parameters suggest that these sultines and sulfites have similar geometries.

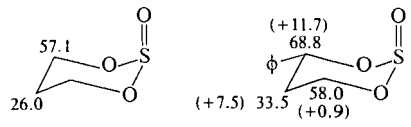

4

The marked downfield shifts at C-4 (10.7 ppm) and C-6 (6.6 ppm) compared to **4** indicate the absence of any substantial amount of axial S=O in **5**, since the *gauche*-γ shieldings are essentially lost. We therefore assign a chair form to **5** with equatorial S=O, although the fact that the changes at C-4 are ca. 4 ppm larger than at C-6 may indicate a minor amount of twist conformer.

For the *trans*-diphenyl material **8**, the ^{13}C shifts at C-4,6, compared with those for the *cis* isomers **6** and **7**, are remarkably similar to the case of the *trans*-di-*tert*-butyl system **3**, when viewed relative to **1** and **2**. Therefore a similar twist geometry is proposed for **8** and **3**.

To conclude, our results show clearly that the introduction of a phenyl or *tert*-butyl group in a potentially *syn*-axial orientation to the S=O of a trimethylene sulfite, causes the ring to invert to a chair with both the S=O and the bulky substituent equatorial. The only cases in which twist geometries are present are in *trans*-4,6-disubstituted systems in which there appears to be a reluctance for the heterocycle to adopt a chair conformation with a purely axial phenyl or *tert*-butyl function at C-4 or C-6.

Experimental

Spectra

The ^1H nmr spectra were obtained as 0.1 *M* solutions in $CDCl_3$ with TMS as internal standard, using a Varian HA-100 nmr spectrometer.

The ^{13}C nmr spectra were recorded as 0.1 *M* solutions in

Can. J. Chem. Downloaded from www.nrcresearchpress.com by 210.87.254.40 on 09/05/12
For personal use only.

$CDCl_3$ with TMS as internal standard, using a Varian XL-100-12 nmr spectrometer equipped with a Nicolet BNC-12 computer (20K memory). The pulsed Fourier transform method was employed at 25.16 MHz with complete proton noise decoupling. The free induction decays were transformed after a sufficient number had been accumulated. Commonly 8192 data points were used in the interferogram. Spectra widths of 5000 Hz were routinely used.

Materials

cis-*4,6-Di*-tert-*butyltrimethylene Sulfites (**1** and **2**)*

To 1.0 g *meso*-2,2,4,4-tetramethyl-3,5-heptanediol (30) in 20 ml dry pyridine and 75 ml dry benzene was added 1.5 ml $SOCl_2$ in 25 ml of benzene, dropwise with stirring and external cooling. The reaction was allowed to run overnight. The organic layer was then filtered to remove the pyridinium hydrochloride and treated with 10% sodium carbonate, washed with water, and dried over sodium sulphate.

After filtration the excess solvent was removed on a rotary evaporator yielding a viscous liquid which solidified immediately. Fractional crystallization from 50:50 pentane–benzene yielded 550 mg of **2**, mp 133–135°C, (lit. (26) 138°C) and 130 mg of **1**, mp 102–103°C. Both compounds gave satisfactory ir spectra, with sulfinyl stretching bands at 1200 cm^{-1} (**1**) and 1220 cm^{-1} (**2**) *Anal.* calcd. for **1**: C 56.37, H 9.47, O 20.48, S 13.68; found: C 56.39, H 9.49, S 13.60.

trans-*4,6-Di*-tert-*butyltrimethylene Sulfite (**3**)*

To 1.0 g racemic 2,2,4,4-tetramethyl-3,5-heptanediol (30) in 100 ml dry benzene and 12 ml dry pyridine was added 1.0 ml $SOCl_2$ in 20 ml benzene, dropwise with external cooling. The reaction was allowed to continue overnight at room temperature. The solution was then filtered and washed in turn with 10% sodium carbonate, 0.1 *N* HCl, and water. Concentration on the rotary evaporator gave 1.0 g viscous yellow liquid which solidified on cooling. Recrystallization from toluene yielded 630 mg of **3**, mp 45–46°C (lit. (26) 46°C). The ir showed S=O stretch at 1215 cm^{-1}.

*4-Phenyltrimethylene Sulfites (**4** and **5**)*

To 2.0 g of 1-phenyl-1,3-propanediol (31) in 50 ml anhydrous ether and 8 ml pyridine was added dropwise with stirring and external cooling, 1.5 ml $SOCl_2$ in 20 ml dry ether. The reaction was allowed to run at room temperature overnight.

After filtering off the pyridine HCl, the organic layer was washed with 5% $NaHCO_3$, 0.1 *N* HCl, and water and dried over sodium sulphate. The solvent was then evaporated and the mixture chromatographed on 50 g of silica gel with benzene as eluent to yield 450 mg of **4** as a clear liquid n_D^{25} 1.5458 and 800 mg of **5** as a white solid, mp 60–61°C. The ir showed characteristic sulfinyl stretching vibrations at 1190 cm^{-1} for **4** and 1220 cm^{-1} for **5** with no OH. *Anal.* calcd. for **4**: C 54.52, H 5.08, S 16.17, O 24.22; Found: C 54.61, H 5.00, S 16.21.

cis-*4,6-Diphenyltrimethylene Sulfites (**6** and **7**)*

To 400 mg of the *meso*-1,3-diphenyl-1,3-propanediol (32) in 10 ml dry benzene and 2 ml dry pyridine was added dropwise with stirring and external cooling 0.5 ml $SOCl_2$ in 5 ml benzene. The reaction was allowed to run at room temperature for 3 h. The hydrochloride salt was then filtered off and the mother liquor washed in turn with sodium carbonate, 10% HCl, and water and dried over magnesium sulphate.

Evaporation of the solvent yielded a white solid which recrystallized from toluene as fibers. This initial product proved to be **7** almost exclusively. It was impossible, however, to completely separate the two isomers by fractional crystallization so it was necessary to chromatograph the products on 50 g of silica gel with benzene as eluent. This gave a total of 120 mg **6**, mp 83–84°C, and 155 mg **7**, mp 123–124°C. The ir contained S=O stretching peaks at 1190 cm^{-1} for **6** and 1220 cm^{-1} for **7** and no OH absorption. *Anal.* calcd. C 65.67, H 5.14, S 11.69, O 17.50; found for **6**: C 65.70, H 5.21, S 11.67; found for **7**: C 67.81, H 5.09, S 11.72.

trans-*4,6-Diphenyltrimethylene Sulfite (**8**)*

To 2.0 g of the racemic 1,3-diphenyl-1,3-propanediol (30) with 10 ml pyridine in 200 ml dry benzene was added dropwise with external cooling 1.6 ml thionyl chloride in 6.5 ml benzene. After 3 h the salt was removed by filtration and the solvent evaporated. Sulfite **8** crystallized directly from the residual pyridine as plates, mp 54–55°C. The ir spectrum contained a characteristic S=O stretching absorption at 1225 cm^{-1} but no OH band. A total of 1.7 g product was obtained. *Anal.* calcd. for **8**: C 65.67, H 5.14, S 11.69, O 17.50; found: C 65.64, H 5.11, S 11.75.

*6,6-Dideuterio-4-phenyltrimethylene Sulfites (**4**-d_2 and **5**-d_2)*

Preparation was identical to that described for **4** and **5**. The required 3,3-dideuterio-1-phenyl-1,3-propanediol was prepared by $LiAlD_4$ reduction of the product of the Reformatsky reaction between benzaldehyde and ethyl bromo acetate (33). Mass spectra (low resolution) of dideuterio-**4**-d_2 and **5**-d_2 gave the following *m/e* values (relative intensities in parentheses), **4**-d_2: parent ion 200(9.0), 136(11.0), 119(4.1), 104(100), 77(30.0), 51(22.0), 43(13.4), and 28(89.0); **5**-d_2: 200(9.8), 136(25.6), 119(5.0), 104(100), 77(26.0), 51(22.0), 43(11.0), and 28(89.0).

Acknowledgements

Financial support from the Carleton University President's Research Fund and the National Research Council of Canada is gratefully acknowledged.

1. H. F. VAN WOERDEN and E. HAVINGA. Recl. Trav. Chim. Pays-Bas, **86**, 341 (1967); **86**, 353 (1967).
2. G. WOOD and M. H. MISKOW. Tetrahedron Lett. 1109 (1969).
3. G. WOOD, J. M. MCINTOSH, and M. H. MISKOW. Can. J. Chem. **49**, 1202 (1971).
4. G. ECCLESTON, P. C. HAMBLIN, R. A. PETHRICK, R. F. M. WHITE, and E. WYN-JONES. Trans. Faraday Soc. **66**, 310 (1970).
5. P. C. HAMBLIN, R. A. PETHRICK, R. F. M. WHITE, and E. WYN-JONES. J. Mol. Struct. **1**, 333 (1968).
6. P. C. LAUTERBUR, J. G. PRITCHARD, and R. L. VOLLMER. J. Chem. Soc. 5307 (1963).
7. C. G. OVERBERGER, T. KURTZ, and S. YAROSLAVSKY. J. Org. Chem. **30**, 4363 (1965).
8. L. CAZAUX and P. MARONI. Tetrahedron Lett. 3667 (1969); Bull. Soc. Chim. Fr. 794 (1972).
9. P. MARONI and P. TISNES. Bull. Soc. Chim. Fr. 780 (1972).
10. L. CAZAUX, G. CHAISSAING, and P. MARONI. Tetrahedron Lett. 2517 (1975).
11. C. H. GREEN and D. G. HELLIER. J. Chem. Soc. Perkin Trans. **2**, 458 (1972).
12. H. F. VAN WOERDEN, H. CERFONTAIN, C. H. GREEN, and R. J. REIJERKERK. Tetrahedron Lett. 6107 (1968).
13. H. F. VAN WOERDEN and A. T. DE VRIES-MIEDEMA. Tetrahedron Lett. 1687 (1971).
14. F. J. MUSTOE and J. L. HENCHER. Can. J. Chem. **50**, 3892 (1972).
15. R. S. EDMUNDSON. Tetrahedron Lett. 1649 (1965).
16. G. WOOD and M. H. MISKOW. Tetrahedron Lett. 4433 (1966).
17. P. ALBRIKTSEN. Acta Chem. Scand. **25**, 478 (1971).
18. P. ALBRIKTSEN. Acta Chem. Scand. **26**, 1783 (1972); **26**, 3678 (1972).

19. G. WOOD, G. W. BUCHANAN, and M. H. MISKOW. Can. J. Chem. **50**, 521 (1972).
20. P. ALBRIKTSEN. Acta Chem. Scand. **27**, 3889 (1973).
21. G. W. BUCHANAN, J. B. STOTHERS, and G. WOOD. Can. J. Chem. **51**, 3746 (1973).
22. H. NIKANDER, V. MUKKALA, T. NURMI, and K. PIHLAJA. Org. Magn. Reson. **8**, 375 (1976).
23. K. PIHLAJA. J. Chem. Soc. Perkin Trans. **2**, 890 (1974).
24. K. PIHLAJA. Kem. Kemi, **1**, 492 (1974).
25. G. W. BUCHANAN, N. K. SHARMA, F. DE REINACH-HIRTZBACH, and T. DURST. Can. J. Chem. **55**, 44 (1977).
26. L. CEZAUX, G. CHASSAING, and P. MARONI. Org. Magn. Reson. **8**, 461 (1976).
27. G. WOOD and M. MISKOW. Tetrahedron Lett. 1775 (1970).
28. K. C. RANEY and J. MESSICK. Tetrahedron Lett. 4423 (1975).
29. G. W. BUCHANAN and T. DURST. Tetrahedron Lett. 1683 (1975).
30. J. DALE. J. Chem. Soc. C, 910 (1960).
31. S. SEARLES, E. K. IVES, and S. NUKINA. J. Org. Chem. **24**, 1770 (1959).
32. R. T. LALONDE, P. B. FERRARA, and A. D. DEBBOLI, JR. J. Org. Chem. **37**, 1094 (1972).
33. C. SCHAAL. Bull. Soc. Chim. Fr. **11**, 3083 (1973).
34. S. CASTELLANO and A. A. BOTHNER-BY. J. Phys. Chem. **41**, 3863 (1964).

Can. J. Chem. Downloaded from www.nrcresearchpress.com by 210.87.254.40 on 09/05/12
For personal use only.

The clathrate hydrate of 2-methylpropanal: dielectric evidence[1]

S. R. GOUGH

Division of Chemistry, National Research Council of Canada, Ottawa, Ont., Canada K1A 0R9

Received March 6, 1978

S. R. GOUGH. Can. J. Chem. **56**, 2025 (1978).

Dielectric relaxation evidence is presented of the encageability of 2-methylpropanal in the structure II clathrate hydrate lattice. The hydrate composition is inferred to be $(CH_3)_2CHCHO \cdot 17H_2O$ and, for the 2-methylpropanal/THF mixed hydrate studied in detail, the activation energy for aldehyde reorientation is shown to be 2.0 kcal/mol. The results suggest that the guest–host interactions may be somewhat different for the two guest species.

S. R. GOUGH. Can. J. Chem. **56**, 2025 (1978).

On présente des données de relaxation diélectrique concernant la possibilité de mettre en cage le méthyl-2 propanal dans un réseau d'hydrate clathratique ayant la structure II. On déduit que la composition de l'hydrate est $(CH_3)_2CHCHO \cdot 17H_2O$ et dans le cas de l'hydrate mixte du méthyl-2 propanal/THF qui a été étudié en détail, l'énergie d'activation de la réorientation de l'aldéhyde est de 2.0 kcal/mol. Les résultats suggèrent que les interactions entre le réseau et les molécules encagées sont quelque peu différentes pour les deux espèces emprisonnées.

[Traduit par le journal]

Recently the properties of aldehyde–water systems have been under scrutiny from a variety of angles (1–4). Phase diagrams have been published for such systems for ethanal (CH_3CHO) (1), propanal (CH_3CH_2CHO) (3), butanal ($CH_3CH_2CH_2CHO$) (2), and 2-methylpropanal ($(CH_3)_2CHCHO$) (2) which indicate the formation of various hydrates for all except butanal. Of these hydrates, X-ray examination (2, 3) showed those of propanal and 2-methylpropanal to be clathrate hydrates of structure II. Elsewhere, concurrent dielectric and nmr experiments (4) showed ethanal and propanal to form unstable clathrate hydrates most probably of structure II. In this note are presented similar dielectric results which demonstrate the encageability of 2-methylpropanal in the structure II lattice and which allow the composition of the hydrate to be estimated. 2-Methylpropanal is a large molecule ($\simeq$6.9 Å) and is enclathrated only with some difficulty as is evidenced below.

Sample Preparation

Initial attempts to prepare the hydrate by dropwise addition of water at 0°C to freshly distilled aldehyde held at temperatures near −25°C (the method of Cohen and van der Horst (4, 5) for "ice VIII") met with only limited success, but nevertheless, sufficient hydrate ($\simeq$8% of the dielectric sample) was obtained to demonstrate its clathrate nature. However, several samples prepared as before (4) by rapidly mixing the precooled liquids, immediately freezing the mixture in liquid nitrogen, and then conditioning at various temperatures for varying periods, showed, by the absence of any low temperature dielectric absorption, the absence of hydrate of the clathrate type. Similarly, attempts to prepare nmr samples in sealed tubes in the absence of air by methods which have previously met with considerable success for other hydrates, proved futile.[2] Probably the 2-methylpropanal hydrate requires the incorporation of a considerable quantity of air as a "Hilfsgas" (7) to ensure its stability relative to ice. Practically quantitative enclathration of the 2-methylpropanal (RCHO) was achieved finally, by promoting formation of the structure II lattice by including a quantity of the well known (8, 9) hydrate former, tetrahydrofuran (THF), in the reaction mixture. Two samples, containing 0.48 and 0.25 mol of THF respectively per $\simeq$ 17 mol of water, were prepared as follows. The appropriate quantities of THF and aldehyde were cooled, mixed with precooled water at 0°C, and shaken using a Vortex mixer to form an emulsion which was then frozen quickly to a solid mass. This was warmed until partially melted and the resultant slurry, after further shaking, was pipetted into the precooled dielectric cell (10) where it was refrozen and then conditioned at $\simeq -10$°C for half an hour before cooling to the required temperature. The stoichiometric composition of the system was $0.52RCHO \cdot 0.48THF \cdot 13.5H_2O$ in the first case and $0.75RCHO \cdot 0.25THF \cdot 16.0H_2O$ in the second, excess of the hydrate formers with respect to the ideal $M \cdot 17H_2O$ requirement being taken in order to suppress the formation of ice. The mixed hydrates proved to be stable over periods of several days (at temperatures as high as −5°C for the 0.52:0.48 sample) with no sign of conversion of the hydrated aldehyde to *gem*-diol and ice. This is in contrast to the results obtained for the hydrates of other aldehydes previously examined (4), which, in the dielectric samples studied, showed considerable rates of decomposition, even at −80°C in one instance.

Results

The dielectric properties of the 2-methylpropanal/THF mixed hydrate of 52:48 mol% guest ratio are illustrated in Fig. 1 for the temperature range where the enclathrated molecules show dielectric relaxation effects at frequencies of 1 MHz and below. At each

[1]NRCC No. 16698.

[2]The author is indebted to J. A. Ripmeester for this observation.

Can. J. Chem. Downloaded from www.nrcresearchpress.com by 210.87.254.40 on 09/05/12
For personal use only.

Can. J. Chem. Downloaded from www.nrcresearchpress.com by 210.87.254.40 on 09/05/12
For personal use only.

TABLE 1. Dielectric relaxation data for hydrates of 2-methylpropanal and tetrahydrofuran

	Permittivity			Temperature (K) of 10 kHz loss max.		Activation energy (kcal/mol)	
	$\varepsilon_{\infty 2}$ at 7 K	ε_{02} at 168 K		$T_{\varepsilon_m''}$ (THF)	$T_{\varepsilon_m''}$ (RCHO)	ΔE (THF)	ΔE (RCHO)
RCHO hydrate	—	—	(8.10)*	—	54.5	—	—
Mixed hydrate (25% THF)	—	—	—	24.0	52.5	—	—
Mixed hydrate (48% THF)	3.35±0.05	6.5±0.1	(6.55)*	24.5	51.1	0.87	2.0_1
THF hydrate	—	—	—	24.2†	—	0.91†	—

*Calculated value, see text.
†Data taken from ref. 8.

frequency two regions of dispersion–absorption are apparent corresponding to the reorientation of the two types of guest molecule present. For the lower temperature region the usual Arrhenius plot yields an activation energy of 0.87 kcal/mol for the THF reorientation process. This value, together with the temperatures at which the loss exhibits maxima, is in agreement with previously published data (8) for the pure THF–water structure II clathrate system. For the higher temperature relaxation region, which can only arise from the molecular reorientation of encaged aldehyde molecules,[3] the corresponding energy is 2.0_1 kcal/mol, a value in accord with those of other molecules of similar size enclathrated in the type II lattice (11). The results, summarized in Table 1, demonstrate the considerably greater reorientational mobility in the clathrate cage of the smaller (≃5.9 Å) THF molecules over the larger (≃6.9 Å), more hindered, aldehyde molecules. This is strikingly illustrated in Fig. 1, where, near 32 K, reorientation of THF may be seen to correspond to frequencies near 1 MHz whereas that for aldehyde corresponds to frequencies near 1 Hz, indicating a difference of $\simeq 10^6$ in reorientation rate for the two guest species at this temperature.

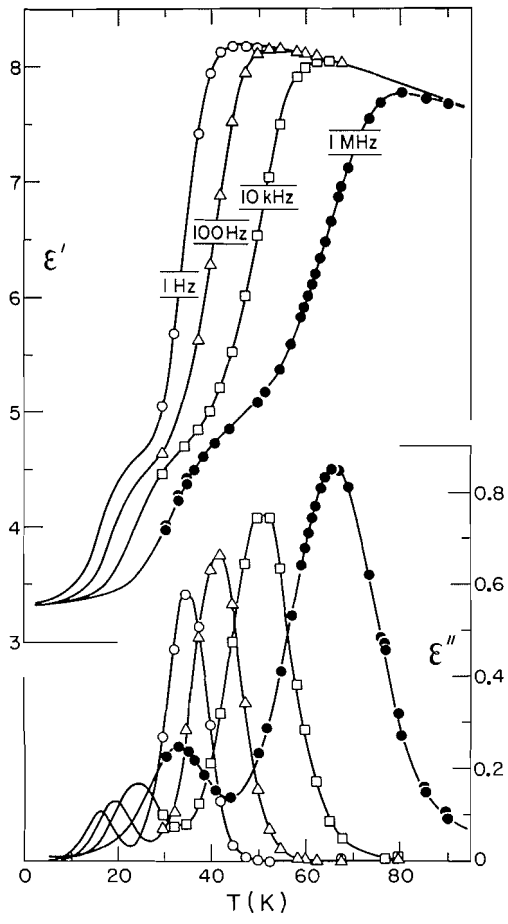

FIG. 1. Guest molecule dispersion–absorption curves for the mixed hydrate of THF and 2-methylpropanal. Data points below 30 K are omitted for greater clarity. Composition is $0.52RCHO{\cdot}0.48THF{\cdot}13.5H_2O$.

Discussion

(a) Permittivity

Previous dielectric studies (8) of clathrate hydrates of type II have shown that the contribution to the permittivity arising from near isotropic reorientation of the guest molecules is well represented by the Onsager spherical cavity model, which in this case may be applied in the form

$$\frac{(\varepsilon_{02}-1)(2\varepsilon_{02}+1)}{3\varepsilon_{02}} = \frac{(\varepsilon_{\infty 2}-1)(2\varepsilon_{\infty 2}+1)}{3\varepsilon_{\infty 2}} + \frac{4\pi N_M}{3kT}\left[\frac{x\mu_{THF}^2}{(1-f_M\alpha_{THF})^2} + \frac{(1-x)\mu_{RCHO}^2}{(1-f_M\alpha_{RCHO})^2}\right]$$

where x and $(1-x)$ represent the relative amounts of THF and RCHO respectively. ε_{02} is the permittivity which includes contributions from reorientation of both guest molecules but not from water

[3]The candidacy of an intramolecular reorientation process for this absorption is eliminated (*a*) by the absence of a third relaxation region at still higher temperatures corresponding to relaxation of the remaining aldehyde dipole component, and (*b*) by the fact that the dielectric increment observed at higher temperatures corresponds (see Discussion) to isotropic reorientation of the total aldehyde dipole.

Can. J. Chem. Downloaded from www.nrcresearchpress.com by 210.87.254.40 on 09/05/12
For personal use only.

molecules and $\varepsilon_{\infty 2}$ is the limiting low temperature permittivity containing no orientational component. N_M is the number density of the guest molecules, μ their dipole moment, and α their polarisability derived from the molar refraction of the respective liquids. The reaction field factor f_M is given by $2(\varepsilon_{02} - 1)/[a^3(2\varepsilon_{02} + 1)]$ where a is the mean free radius (3.2 Å) of the almost spherical clathrate cage. For the sample of 52:48 mol% ratio, $\varepsilon_{\infty 2} = 3.35$ at 7 K, and with $N_M = 1.545 \times 10^{21}$ molecules cm^{-3} (derived from the structure II lattice parameter of 17.3 Å at 168 K) and $\mu_{RCHO} = 2.7$ D (a value typical (12) of similar molecules), ε_{02} is calculated to be 6.5_5 at 168 K, a value which compares well with the experimentally observed one of 6.5 ± 0.1. (For the pure aldehyde hydrate, containing no THF and of composition $RCHO \cdot 17H_2O$, the model predicts ε_{02} at 168 K to be 8.1.) Thus, in agreement with the previously reported X-ray observation (2), it may be concluded from the above and from the observation of rapid molecular motion at low temperatures that molecules of 2-methylpropanal can be incorporated into the large cage of the structure II hydrate lattice, albeit with some difficulty.

(b) Relaxation Times

The apparent variation of guest molecule relaxation time with hydrate composition, as is evidenced by the temperatures at which ε'' shows maxima (Table 1), offers an opportunity to comment on the influence of compositional change on the reorientation of the guest species. The trends, illustrated in Fig. 2, may be rationalized in terms of changes in guest–host interaction as the guest concentration ratio varies. The temperatures of maximum loss are reproducible, and are considered to be accurate, to within 0.1° and are *inversely* related[4] to the reorientation rates of the guest molecules. For RCHO, the increase in relaxation time with increasing aldehyde concentration evident from the figure, points to increasing restriction of the already highly hindered aldehyde molecules. This must arise as a consequence of the increase in net dipole moment per unit volume as THF ($\mu = 1.63$ D) is replaced by RCHO ($\mu \simeq 2.7$ D). At the same time the lattice must expand[5] as more of the larger guest is enclathrated at the expense of the smaller. This expansion apparently dominates the situation in the case of the THF, where, as is reflected in the upper curve of the figure, faster relaxation of the already relatively unhindered THF molecules is seen for the sample of higher aldehyde content.

In the case of the mixed hydrate considered here the interesting possibility arises for the occurrence of some expansion of the cages containing aldehyde at the expense of compression of the adjacent cages containing THF, the overall lattice parameter being little affected at low aldehyde concentrations. The data (Fig. 2) offer some support for this concept in that the THF reorientation is slightly slower for the 50% sample, than for the pure THF hydrate itself. At concentrations of aldehyde greater than $\simeq 50\%$ the effect of the lattice expansion predominates and so the THF relaxation again becomes faster.

The opposite effects observed for the two guest species, as the guest concentration ratio changes, supports the speculation that their guest–host interactions are essentially different in some respects. The extremely rapid THF reorientation probably is controlled predominantly by the small electrostatic fields arising, at the cage centre, from the dipoles of the water molecules forming the cage walls. The much slower (by a factor of $\simeq 10^6$) reorientation of the larger, more restricted, aldehyde molecules, on the other hand, may well be controlled predominantly by forces arising from extensive van der Waals contact with the cage walls and by somewhat shielded interactions with neighbouring guest molecules.

(c) Composition

The composition of structure II clathrate hydrates has been examined in detail twice previously. In the first instance (9) for fifteen type II hydrates it was shown that no statistical evidence of any departure from the ideal $M \cdot 17H_2O$ stoichiometry could be

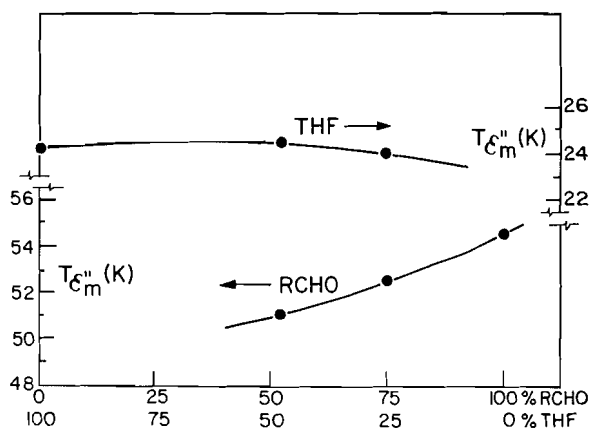

FIG. 2. Dependence of guest molecule reorientation (see text) on relative guest concentration. The datum for THF hydrate is taken from ref. 8.

[4]The inverse relationship between temperature and rate arises simply as a consequence of the method of measurement, i.e., fixed frequency and variable temperature. At constant frequency, relaxation observed at lower temperatures arises from intrinsically faster reorientation processes. The extreme widths of the low temperature absorptions precluded adoption of the more conventional variable frequency, fixed temperature, technique.

[5]Lattice expansion as a function of lattice occupancy factor (6) and of guest size (11) has been well documented previously.

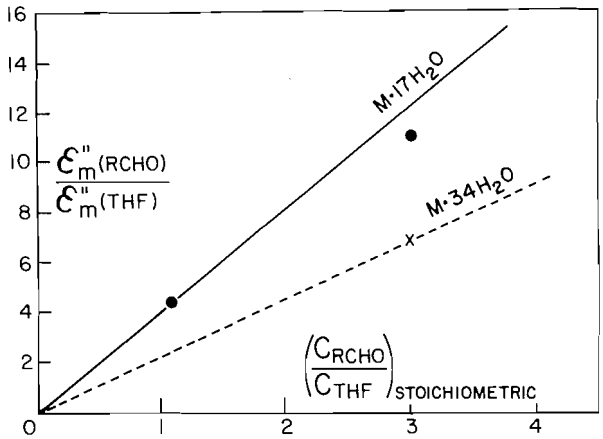

FIG. 3. Dependence of dielectric loss ratio on concentration ratio for the two guest species considered. The lines, drawn for illustrative purposes, refer to hydrate compositions as indicated. The data point at concentration ratio 3:1 falls short of the solid line as a consequence of incomplete conversion to hydrate of the initial components. Point X is derived by simple proportion from the magnitudes of the experimentally observed loss maxima.

demonstrated. The more recent publication (11) discussed (in some detail for the case of 1,3-dioxane hydrate) the evidence against the proposals of Rosso and Carbonnel (refs. 7 and 12 of ref. 11), based on thermal measurements, that the composition of certain hydrates is $M{\cdot}34H_2O$. Those arguments are extended to the hydrates discussed here by means of Fig. 3, in which are compared the relative magnitudes of the 10 kHz loss peaks for aldehyde and THF for the samples studied. The ε_{max}'' ratio shows the proportionality with stoichiometric concentration ratio expected for hydrate compositions near $M{\cdot}17H_2O$, where here M refers to the sum of the RCHO and THF components. Furthermore, for the sample of 75:25 mol% guest ratio the figure clearly demonstrates an aldehyde occupancy factor considerably greater than that required by an $M{\cdot}34H_2O$ composition as indicated by X. It is inferred from these considerations that the composition of the less stable hydrate of 2-methylpropanal itself, containing no other dipolar hydrate former, is also $M{\cdot}17H_2O$ rather than the $M{\cdot}34H_2O$ value, deduced from thermal measurements, which has already been questioned (11).

1. J.-C. Rosso and L. Carbonnel. C.R. Hebd. Seances Acad. Sci. Ser. C, **282**, 395 (1976).
2. J.-C. Rosso, C. Caranoni, and L. Carbonnel. C.R. Hebd. Seances Acad. Sci. Ser. C, **283**, 91 (1976).
3. J.-C. Rosso, C. Caranoni, and L. Carbonnel. C.R. Hebd. Seances Acad. Sci. Ser. C, **283**, 699 (1976).
4. D. W. Davidson, S. R. Gough, and J. A. Ripmeester. Can. J. Chem. **54**, 3085 (1976).
5. E. Cohen and C. J. F. van der Horst. Z. Phys. Chem. B**40**, 231 (1938).
6. J. A. McIntyre and D. R. Petersen. J. Chem. Phys. **47**, 3850 (1967).
7. M. von Stackelberg and W. Meinhold. Z. Electro. Chem. **58**, 40 (1954).
8. S. R. Gough, R. E. Hawkins, B. Morris, and D. W. Davidson. J. Phys. Chem. **77**, 2969 (1973).
9. S. R. Gough and D. W. Davidson. Can. J. Chem. **49**, 2691 (1971).
10. S. R. Gough. Can. J. Chem. **50**, 3046 (1972).
11. D. W. Davidson, S. R. Gough, F. Lee, and J. A. Ripmeester. Rev. Chim. Minérale. **14**, 447 (1977).
12. A. L. McClellan. Tables of experimental dipole moments. Vol. 1. W. F. Freeman and Co. 1963; Vol. 2. Rahara Enterprises. 1974.

Can. J. Chem. Downloaded from www.nrcresearchpress.com by 210.87.254.40 on 09/05/12
For personal use only.

Catalyst modification by metal deposition: the deposition of silver on platinum at underpotential and overpotential

REMIGIO GERMANO BARRADAS, STEPHEN FLETCHER, AND SANDOR SZABO[1]

Department of Chemistry, Carleton University, Ottawa, Ont., Canada K1S 5B6

Received January 1, 1978

REMIGIO GERMANO BARRADAS, STEPHEN FLETCHER, and SANDOR SZABO. Can. J. Chem. **56**, 2029 (1978).

It is demonstrated that platinum catalysts can be modified by electrochemical means. The deposition of silver is described at both underpotential and overpotential. Although the deposition reactions can be quantified, the electrode kinetics cannot be investigated because of the simultaneous formation and reduction of platinum oxides.

REMIGIO GERMANO BARRADAS, STEPHEN FLETCHER et SANDOR SZABO. Can. J. Chem. **56**, 2029 (1978).

On a démontré que les catalyseurs de platine peuvent être modifiés par des méthodes électrochimiques. On décrit la déposition de l'argent à sous-tension et sur-tension. Quoique les réactions de déposition peuvent être quantifiées, on ne peut pas étudier la cinétique à l'électrode à cause de la formation et de la réduction simultanées des oxydes de platine.

[Traduit par le journal]

Can. J. Chem. Downloaded from www.nrcresearchpress.com by 210.87.254.42 on 09/05/12
For personal use only.

Introduction

The deposition of silver on polycrystalline platinum has been studied by several workers (1–8). They have shown that silver may be deposited in two fundamentally different forms. One form is deposited in monolayer quantities at potentials positive to the reversible equilibrium potential (1–6), which is the so-called underpotential deposition. The other form is bulk silver which is deposited at overpotential (7, 8). The processes involved in these depositions are not only of fundamental theoretical interest (9–12), but are also of great practical importance in the modification of the properties of finely dispersed catalytic surfaces (see, for example, refs. 6 and 13). The present study was therefore undertaken with a view to characterizing some of these processes.

According to Stucki (1), measurement of the rate of change of the number of adsorbed hydrogen atoms compared to the number of deposited silver atoms at underpotential indicated that after the deposition of two monolayers the Pt electrode had assumed the properties of bulk silver. Also the stripping curve of the Ag layers showed two peaks, one at +0.73 V and the other at 0.80 V vs. SCE. This compared with the bulk value of 0.35 V.

Hammond and Winograd (14) recently studied X-ray photoelectron spectroscopic evidence of distinctive underpotential deposition states of Ag on Pt substrates. They noted that the formation of "islands" was minimized and that a bulk silver species was formed only after the completion of the first monolayer. The deposit appeared more metallic than ionic in nature and existed as a smooth two-dimensional atomic array in submonolayer quantities.

Some measurements of the charge associated with underpotential deposition were reported by Cadle and Bruckenstein (4). The effect on the adsorption of hydrogen at platinum by the deposition process was also studied. Submonolayer and monolayer amounts of Ag were deposited at +300 mV (vs. SCE) and then the electrode was scanned into the hydrogen adsorption region. It was found that the weakly adsorbed hydrogen was inhibited more than the strongly adsorbed species provided that the surface coverage of Ag was $< 50\%$. A maximum of 368 $\mu C\ cm^{-2}$ was deposited before hydrogen adsorption was completely inhibited. One monolayer of close-packed silver atoms corresponded to 268 $\mu C\ cm^{-2}$ at their electrode.

The deposition of bulk silver has been studied by Pangarov and Velinov (8). They studied the crystal orientation of three-dimensional electrodeposited silver as a function of overpotential, and then correlated their results with work function data. It is clear from the data described above that their work was not so much on a platinum substrate but rather on a substrate considerably modified by underpotentially deposited silver.

In the present work we utilize the linear potential sweep technique, the potential step technique, and rotating disc electrodes in order to investigate this manifestly complex system. The underpotential deposition is considered first.

Experimental

The smooth (polycrystalline) platinum electrodes used in the present work were in the form of small cylinders sealed in Araldite and machined into rotating discs of conventional

[1] On leave from The Central Research Institute for Chemistry of the Hungarian Academy of Sciences, H-1525/17, Budapest, Hungary.

Can. J. Chem. Downloaded from www.nrcresearchpress.com by 210.87.254.42 on 09/05/12
For personal use only.

design (apparent surface area = 0.41 cm^2). Before use the electrodes were rinsed in nitric acid then washed for several hours in triply-distilled water. Electrical contact was made between the electrodes and the instrumentation via Vibrometer mercury slip-ringless transmitters (Rohrbach System). These transmitters succeeded in eliminating almost completely the numerous disadvantages of the usual solid contact transmitters, e.g. variations in insulation and contact resistances and parasitic thermal emf. Contact resistance was $\ll 0.2$ mΩ. Solution resistance was minimized by the incorporation into the cell design of an adjustable luggin reference probe which was connected to a hydrogen electrode in the same solution. The use of the identical solution in the reference and cell compartments of the apparatus hence obviated the need for a frit or liquid junction. All potentials are therefore quoted on the ϕ-potential scale.

The plating solutions consisted of various quantities of ARISTAR silver perchlorate in 1.00 *M* ARISTAR perchloric acid. The cell was cleaned before the commencement of experiments by immersion for several hours in boiling nitric acid. After this treatment the cell was then flushed with boiling triply-distilled water in order to desorb any residual impurities on the surface of the Pyrex glass.

The constant potential source was a PAR 170 potentiostat and appropriate potential waveforms were generated on the same instrument. On short time-scales data were recorded photographically via a Tektronix oscilloscope (type 503).

Deoxygenation was achieved by flushing the apparatus with purified nitrogen from which any residual traces of oxygen were removed by washing with vanadous chloride solutions. The gas was further cleaned by incorporating strongly alkaline (KOH) solutions into the delivery system to eliminate the possibility of contamination of the cell by microtraces of grease from within the nitrogen cylinders and regulation valves. The gas was finally passed through an identical solution to that in the cell to remove any small water droplets carried through from the other purification stages.

Some measurements were also performed on large platinum foils (apparent surface area 4.86 cm^2, 99.999% purity, Koch-Light laboratories) which were sealed into Pyrex glass holders. Where comparison was possible these electrodes produced identical results to the rotating disc electrodes. Hence there was no possibility of contamination from the Araldite mounting in the case of the rotating disc electrodes, which in a separate experiment were found to be stable in perchloric acid media for a period of several months.

Results

(1) The Deposition of Ag at Underpotential on Pt

The effect of cycling the electrode potential linearly over the range +1400 to +50 mV until a pseudo-steady state is reached is shown in Fig. 1. The scan rate is 20 mV s^{-1} at a stationary platinum electrode in 10^{-4} *M* $AgClO_4$. It is immediately apparent that a number of separate processes are occurring. (A) is the bulk deposition of silver in the region of three-dimensional nucleation and growth (8), for which deposition begins at circa +450 mV. The peak marked (B) in the figure is the reverse process of that indicated by (A), namely the dissolution of bulk silver back into solution. At point (C) there is some small indication of the possible oxidation of a weakly adsorbed silver species, and this is followed by the oxidation of the

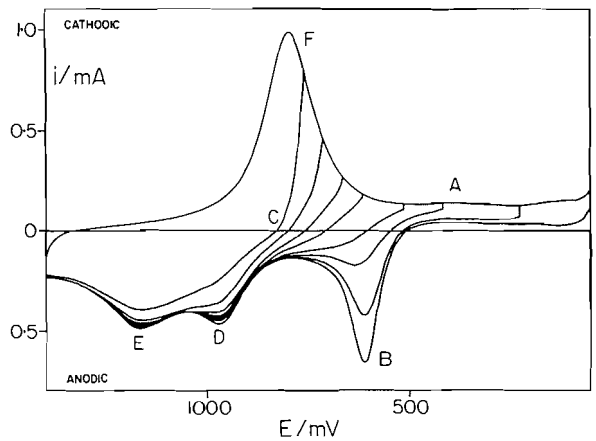

FIG. 1. Effect of linearly scanning the electrode potential at a stationary Pt electrode. v = 20 mV s^{-1}, $[Ag^+] = 10^{-4}$ *M*.

two strongly adsorbed species labelled (D) and (E) at +970 and +1160 mV respectively. Upon reversing the direction of the potential scan the underpotential deposition of Ag can be seen to occur in one broad, unresolved peak (F) at +800 mV. This is a potential region which coincides with the reduction of platinum oxides in the pure base electrolyte. The deposited silver completely inhibits hydrogen adsorption in this case.

By comparing the cyclic voltammogram of Fig. 1 with that of the same electrode in the base electrolyte alone, it is possible to estimate the amount of charge (corresponding to a monolayer) from the charge of the hydrogen adsorption reaction (1). This is shown as the shaded area in the stripping curve (Fig. 2). Unfortunately further quantification does not appear to be possible because some platinum oxides may be formed in the same region at the same time as the silver desorption.

According to the data of Stucki (1) the two strongly adsorbed silver species (our E and D, his I and II) should occur at +450 and +380 mV anodic to the bulk dissolution respectively. In our case, these underpotential values are +560 and +370 mV. We can only conjecture that the differences arise because of the different electrolytes used in the two studies (i.e. 1.0 *M* H_2SO_4 in ref. 1 and 1.0 *M* $HClO_4$ in the present work).

Attempts to locate a very weakly adsorbed species with an underpotential of 80 mV, as reported by Szabo and Nagy (6), proved futile. There are several possible explanations for this discrepancy. The first is that the time-scale of the present work (s) did not allow sufficient resolution of the phenomenon. The second explanation is that the arrest observed on the charging curves of ref. 1 is an artifact produced by the complex diffusion problems nor-

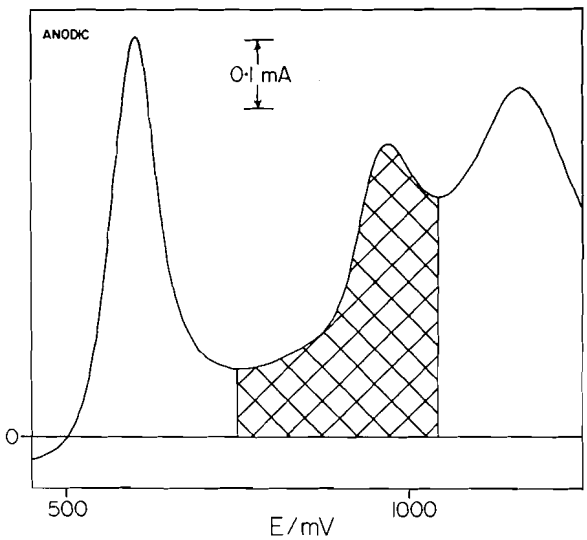

FIG. 2. Typical stripping curve showing bulk silver and two major underpotentially deposited species. The shaded area corresponds to one monolayer of charge at our electrode.

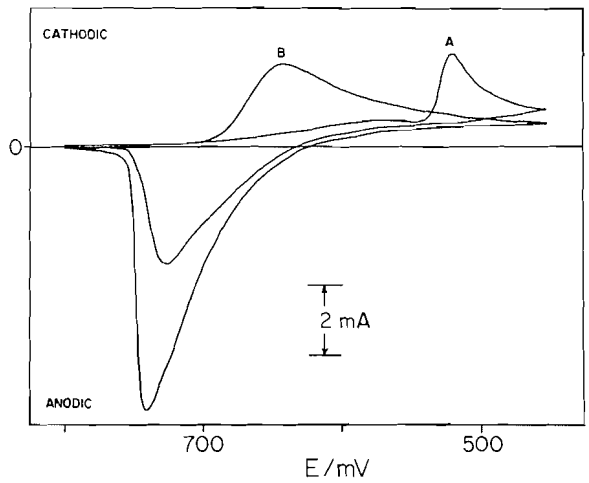

FIG. 3. Continuous cycling of electrode potential following preanodization. Deposition and stripping of bulk silver. v = 50 mV s^{-1}, $[Ag^+] = 10^{-2}$ *M*. (*A*) First cycle, (*B*) pseudo-steady state.

mally associated with finely dispersed surfaces (i.e. platinized platinum). A third possible explanation is the existence of two peaks in the voltammogram corresponding to bulk silver dissolution. Such a phenomenon has been observed, in fact, in the present work (see below).

(II) The Deposition of Ag at Overpotential on Pt

At potentials cathodic to the reversible Nernst potential, silver is deposited in the form of three-dimensional nuclei on the Pt/Ag substrate (8). However it was found that the reaction was not at all straightforward, since the *i–E* and *i–t* curves recorded showed a strong time dependence following surface pretreatment. A good example is shown in Fig. 3. In this case, the electrode was strongly anodized ($E > +1000$ mV) so that all silver deposited on the electrode dissolved into the bulk of solution, leaving the electrode covered with a thick film of platinum oxide. Having rotated the electrode to bring the bulk concentration of electrolyte to the electrode surface, the electrode potential was then continuously cycled (50 mV s^{-1}) between +800 and +450 mV. It was found that the deposition potential slowly shifted by about 300 mV in the anodic direction until a pseudo-steady state had been established. The reason for this must be that the bulk deposition will not proceed in the absence of underpotentially adsorbed silver. Indeed, on the first cycle a broad prepeak may be observed which we attribute to the underpotential deposition reaction. The other reason for the slow attainment of the pseudo-equilibrium is the relaxation of the diffusion regime into which the deposit is growing. Obviously the bulk concentration of Ag^+ close to the electrode surface becomes depleted as the surface deposit grows. The nature of the diffusion zone was therefore the next phenomenon investigated. This was best observed by the use of rotating electrodes.

The result is shown in Fig. 4*a* for a bulk concentration of Ag^+ of 1.0×10^{-2} *M*, using a linear potential scan rate of 50 mV s^{-1}. It is clear that the current rises very rapidly indeed and that eventually a limiting current condition is reached. The limiting currents are plotted as a function of rotation speed in Fig. 4*b*, which are in accordance with the Levich equation

$$[1] \qquad i_{lim} = 0.62nFC_b D_0^{2/3} \nu_k^{-1/6} \omega^{1/2}$$

where i_{lim} is the limiting current density (mA cm^{-2}), n is the number of electrons, F is the Faraday constant, C_b is the bulk concentration (mol ml^{-1}), D_0 is the diffusion coefficient (cm^2 s^{-1}), ν_k is the kinematic viscosity (cm^2 s^{-1}), and ω is the rotation speed. We may therefore apply the Nernst diffusion zone hypothesis and suppose that a semi-infinite *linear* diffusion zone exists at the electrode surface. This contradicts the intuitive notion that each individual (crudely hemispherical) silver nucleus grows into a hemispherical diffusion zone. It is obvious, therefore, that the diffusion zones surrounding each individual nucleus must have overlapped on the time scale of the experiment.

The data of Fig. 4*a* were obtained without a preanodisation, which accounts for the absence of the prepeak so evident in Fig. 3. When a strong anodisation precedes the evaluation of the rotation speed

Can. J. Chem. Downloaded from www.nrcresearchpress.com by 210.87.254.42 on 09/05/12
For personal use only.

Can. J. Chem. Downloaded from www.nrcresearchpress.com by 210.87.254.42 on 09/05/12
For personal use only.

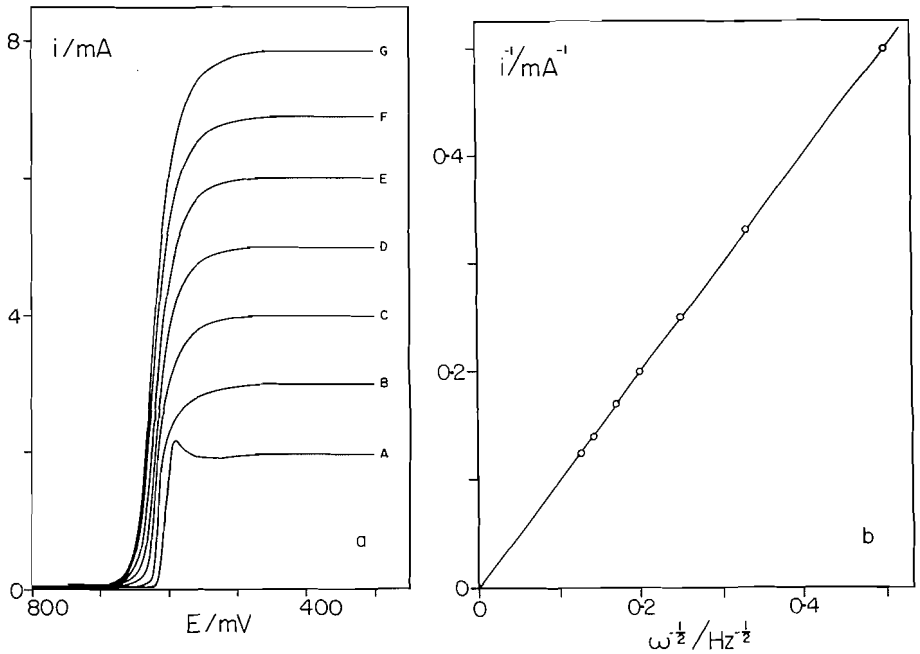

FIG. 4. (*a*) Rotation speed dependence of the bulk deposition reaction, showing attainment of steady state. $v = 50$ mV s^{-1}, $\omega = (A)$ 4, (B) 9, (C) 16, (D) 25, (E) 36, (F) 49, (G) 64 Hz. $[Ag^+] = 10^{-2}$ *M*. (*b*) Test of the Levich equation with the data of Fig. 4*a*.

dependence, the prepeak of course reappears, although this in no way affects the value of the limiting currents. This is because the value of the limiting current is determined purely by the bulk concentration of Ag^+ and the other constants described by [1].

The extraordinary sharp increase in current at short times in Fig. 4*a* arises because of the large dependence of the nucleation and growth parameters on potential. Quantitative estimation of these parameters is usually best obtained by potential step measurements at stationary laminar electrodes. Some of these are illustrated in Fig. 5. Once again it is clear that the rate of growth of the deposit depends very strongly on the residual quantity of platinum oxide from the preanodization. However the approximately linear-rising transient clearly indicates the nucleation and growth nature of the deposition process.

Finally we report a rather novel result. At high ($>10^{-3}$ *M*) bulk concentrations of Ag^+ the amount of underpotentially adsorbed silver becomes negligible compared to the bulk deposit (Fig. 6). The most striking consequence of this increase is that the dissolution peak of bulk silver splits into two peaks. This duplication does not appear if the cycling takes place over the potential ranges +1400 to +400 mV or +1000 to +40 mV, but it appears on the first cycle even over the potential range +800 to +40 mV if the electrode has been anodized before the first

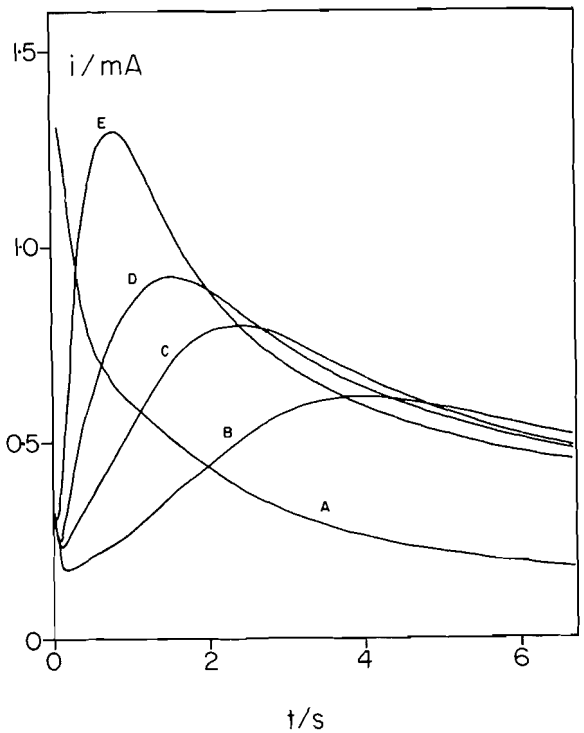

FIG. 5. Repetitive pulses from +800 to +575 mV following a strong anodization. $[Ag^+] = 10^{-2}$ *M*, $\omega = 0$ (A) 1st pulse, (B) 5th pulse, (C) 6th pulse, (D) 7th pulse, (E) 8th pulse.

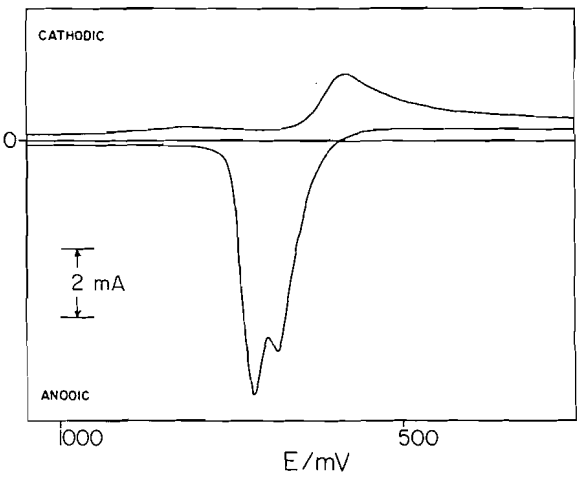

FIG. 6. Splitting of silver bulk dissolution peak under conditions of continuous cycling of electrode potential. Scan from +1250 to +40 mV, $[Ag^+] = 5 \times 10^{-3}$ *M*, $v = 200$ mV s^{-1}, $\omega = 0$.

scan. These experimental observations clearly indicate that the doublet is connected with the reduction of the surface oxides of the platinum. The phenomenon could be best investigated between 10^{-3} and 10^{-2} *M* $AgClO_4$ concentration limits.

We suppose that there are two types of surface oxide on the platinum. These may be adsorbed, for instance, on the 100 and 110 crystal faces of the polycrystalline material, in a similar manner to adsorbed hydrogen (15). If the rate of reduction of surface oxides is different, it follows that after the reduction of the first oxide silver begins to deposit on the free surface and later the reduction of the second oxide provides the silver deposition process with new free surface. The deposition on two 'different' surfaces might then result in two structurally different deposits, which would then dissolve at different potentials.

An alternative explanation is that bulk silver may be deposited in more than one orientation or morphology (as indicated by Pangarov and Velinov (8)) independent of the rate of reduction of the platinum oxides. However, whether such a phenomenon might fully explain the 'splitting' of the dissolution peaks of Fig. 6 is not at present known.

Conclusions

It has been demonstrated that platinum catalysts can easily be modified by electrochemical means. In this instance, various quantities of silver have been deposited and stripped from a (formally) laminar surface. The processes involved have been identified and compared to literature data. A completely quantitative analysis, involving the solution of the electrode kinetics, could not be performed because of the polycrystalline nature of the electrode surface and because of the concurrent formation of platinum oxides in the potential region of interest. Further advances must obviously await parallel investigations on platinum single crystal electrodes (11, 12).

1. S. STUCKI. J. Electroanal. Chem. **80**, 375 (1977).
2. G. W. TINDALL and S. BRUCKENSTEIN. Electrochim. Acta, **16**, 245 (1971).
3. G. W. TINDALL and S. BRUCKENSTEIN. Anal. Chem. **40**, 1051 (1968).
4. S. M. CADLE and S. BRUCKENSTEIN. Anal. Chem. **43**, 1858 (1971).
5. B. J. BOWLES. Electrochim. Acta, **15**, 589 (1970).
6. S. SZABO and F. NAGY. J. Electroanal. Chem. **70**, 357 (1976).
7. V. KLAPKA. Collect. Czech. Chem. Commun. **36**, 1181 (1971).
8. N. A. PANGAROV and V. VELINOV. Electrochim. Acta, **11**, 1753 (1966).
9. K. JUTTNER, G. STAIKOV, W. J. LORENZ, and E. SCHMIDT. J. Electroanal. Chem. **80**, 67 (1977).
10. W. J. LORENZ, M. D. HERMANN, N. WUTHRICH, and F. HILBERT. J. Electrochem. Soc. **121**, 1167 (1974).
11. A. BEWICK and B. THOMAS. J. Electroanal. Chem. **65**, 911 (1975).
12. A. BEWICK and B. THOMAS. J. Electroanal. Chem. **70**, 239 (1976).
13. R. R. ADZIC, D. N. SIMIC, A. R. DESPIC, and D. M. DRAZIC. J. Electroanal. Chem. **80**, 81 (1977).
14. J. S. HAMMOND and N. WINOGRAD. J. Electroanal. Chem. **80**, 123 (1977).
15. E. YEAGER, W. E. O'GRADY, M. Y. C. WOO, and P. HAGANS. J. Electrochem. Soc. **125**, 348 (1978).

Can. J. Chem. Downloaded from www.nrcresearchpress.com by 210.87.254.42 on 09/05/12
For personal use only.

Construction of a novel generator for use in HF adsorption studies

FRANK M. KIMMERLE[1] AND A. ARCHAMBAULT[2]

Department of Chemistry, Université de Sherbrooke, Sherbrooke (Qué.), Canada J1K 2R1

AND

GHYSLAIN DUBE

Arvida Research Center, Aluminum Co. of Canada, Jonquière, P.Q., Canada G7S 4K8

Received January 6, 1978

FRANK M. KIMMERLE, A. ARCHAMBAULT, and GHYSLAIN DUBE. Can. J. Chem. **56**, 2034 (1978).

An HF generator based on the dissociation pressure of an alkali bifluoride is described. Sodium bifluoride salt was found to yield HF pressures of the order of 0.001 to 0.3 mm in the temperature range 60 to 135°C due to the equilibrium $NaHF_2 \rightleftarrows HF + NaF$. The HF generator allows a dry carrier gas (typically N_2) to pass through a thermoregulated chamber filled with the crystalline bifluoride and furnishes HF concentrations from 5 to 1000 ppm at flowrates up to 5 ℓ/min for periods up to one year. The HF concentrations thus generated were stable to within 1% after a 40 min warm up period. Described also is the associated control system which allows the operator to send alternately dry carrier gas with or without trace HF concentration to an external cell or analyser.

FRANK M. KIMMERLE, A. ARCHAMBAULT et GHYSLAIN DUBE. Can. J. Chem. **56**, 2034 (1978).

On décrit un générateur de HF qui est basé sur la pression de dissociation d'un bifluorure alcalin. On a trouvé qu'un sel de bifluorure de sodium fournit des pressions de HF de l'ordre de 0.001 à 0.3 mm à des températures allant de 60 à 135°C dues à l'équilibre $NaHF \rightleftarrows HF + NaF$. Le générateur de HF permet à un gaz porteur sec (N_2) de passer à travers une chambre à température constante remplie de bifluorure cristallin et fournit des concentration de HF de 5 à 1000 ppm à des vitesses d'écoulement allant jusqu'à 5 ℓ/min pour des périodes allant jusqu'à une année. Les concentrations de HF générées de cette manière sont stables à 1% après une période de réchauffement de 40 minutes. On décrit aussi un système de contrôle associé qui permet à l'opérateur d'envoyer d'une façon alternative un gaz porteur sec avec ou sans trace de concentration de HF vers une cellule extérieure ou un analyseur.

[Traduit par le journal]

Introduction

In the course of our research program on the adsorption of HF on alumina powders, we needed a reliable, precise, and inexpensive source of dilute hydrogen fluoride in an appropriate carrier gas. Although dilute gas mixtures were available at relatively low pressures on special order from commercial suppliers of compressed gases, their composition was variable and their cost prohibitive for our purposes. We have succeeded in building a simple generator based on the temperature dependent dissociation of sodium bifluoride

[1] $$NaF \cdot HF \rightleftarrows NaF + HF$$

At HF/NaF mole ratios <1, where no other stoichiometric compounds except $NaHF_2$ and NaF have been reported, the equilibrium vapour pressure of HF should be independent of the quantity of the bifluoride or fluoride present and can be calculated from the equilibrium constant of eq. [1] as

[2] $$\ln P_{HF}\,(\text{atm}) = \ln K_{diss} = \frac{\Delta \bar{G}_{diss}}{RT}$$

This system has been studied by Fisher (1), Froning *et al.* (2), and Miller (3) using, respectively, direct pressure measurements, a transpiration method (both at higher temperatures), and a room temperature effusion method. They calculated K_{diss} and hence P_{HF}, the partial pressure of HF as a function of temperature and their results can be expressed respectively as

At 430–542 K

[3] $$\log P_{HF}\,(\text{atm}) = 6.594 - 3521/T\,(T \text{ in K})$$

At 473–548 K

[4] $$\log P_{HF}\,(\text{atm}) = 5.821 - 3196/T\,(T \text{ in K})$$

At 310–371 K

[5] $$\log P_{HF}\,(\text{atm}) = 6.677 - 3940/T\,(T \text{ in K})$$

At 273 K, eqs. [3], [4], and [5] predict equilibrium values of 5.0×10^{-7}, 1.3×10^{-6}, and 1.8×10^{-8} atm. Extrapolation to 373 K also gives rise to the contradictory values 1.4×10^{-3}, 1.8×10^{-3}, 1.3×10^{-4} atm. Although it is difficult to comment on the validity of the different experimental techniques employed, it has been noted by Miller (3) that the discrepancy may be due in part to the different temperature regions investigated.

[1]To whom correspondence should be addressed.

[2]Present address: Bombardier Ltée, Kingsbury, Québec, Canada.

Can. J. Chem. Downloaded from www.nrcresearchpress.com by 210.87.254.6 on 09/05/12
For personal use only.

Can. J. Chem. Downloaded from www.nrcresearchpress.com by 210.87.254.6 on 09/05/12
For personal use only.

Results reported in this study are based on concentration, not pressure measurements. In the presence of an inert carrier gas of molecular weight M_{CG}, and a total pressure P_T atm, the HF concentration may be conveniently expressed as a weight fraction:

$$[6] \quad [\text{HF}] \text{ in ppm} \simeq \frac{M_{HF}P_{HF} \times 10^6}{M_{HF}P_{HF} + M_{CG}(P_T - P_{HF})}$$

While the apparent molecular weight of hydrogen fluoride gas approaches that of H_6F_6 at very high pressures (4), a value of 20.01 g/mol was used at the low partial pressures prevailing in this present work. On the basis of eqs. [3] to [5] it could therefore be expected that HF/N_2 mixtures (5 ppm to 10%) of fixed compositions should result by passing dry nitrogen gas through a bed of $NaHF_2$ crystals at temperatures in the range 0 to 200°C. A prototype generator based on these thermodynamic predictions was built and, incidentally, numerical results in close agreement with Miller's work were obtained.

Experimental

(1) Reagents

Sodium bifluoride was prepared from Analar hydrofluoric acid 48% and Baker Analyzed Reagent sodium fluoride. HF (230 ml 48%) was added to 235 g NaF dissolved in 3 ℓ of boiling doubly distilled water. The solution was allowed to digest overnight on a steam bath, allowed to cool slowly to 0°C, and then rapidly filtered. The precipitate was recrystallized from doubly distilled water in a similar manner, dried in a dry air stream and finally in a vacuum oven for 12 h at 110°C at 10 mm Hg. All manipulations were carried out using new Nalgene Labware cleaned with live steam and boiling hot distilled water.

A hexamethylenetetraamine (Baker Grade), HMTA, solution was used to absorb HF. This buffer solution was prepared by neutralizing a 1% HMTA aqueous solution to p*H* 5.6 with 6 *M* HCl and adding 2 ml of the surfactant Triton X-100 0.2% in order to lower its surface tension.

(2) Instrumentation

The HF generator consists of the bifluoride reactor, a temperature control system, and a control system for the switching of gas streams. It is designed to be used with an external cell where HF can react or be adsorbed and an external HF analyser where the original or the residual HF concentration can be measured. The entire generating system is constructed from commercially available hardware, SWAGELOK connections, WHITEY and NUPRO valves and metering valves, 1/4 in. and 1/8 in. copper tubing. For the sake of economy all metal parts in contact with the gas stream are copper or brass rather than more resistant metals such as monel. However, after three months of continuous use at temperatures up to 135°C no deterioration due to HF attack was noticeable.

$NaHF_2$ Reactor

The reactor consists of a slightly modified PICKER type 449 TP 11 *M* heat exchanger. Its 48 inner copper tubes were filled with crystalline sodium bifluoride salt. The finely divided salt retained by two copper screens and thin Teflon membranes was compacted by mechanically vibrating the entire structure. One charge of the reactor, about 850 g $NaHF_2$, is theoretically sufficient to furnish over two million litres of HF at a concentration of 100 ppm. Connections to the external system are achieved by two B-14BKM4S4 WHITEY valves which can also be closed to isolate the reactor for repairs or exchange.

Temperature Control

The temperature of the $NaHF_2$ reactor is controlled by circulating oil in the outer jacket of the reactor in a countercurrent direction to the gas flow in the inner tubes. The oil is heated by a 800 W element which is controlled by a Yellow Springs Instrument type 406 thermistor located at the entrance to the reactor. The temperature of the circulating oil is thus controlled to better than 0.1°C at the lower end of the reactor, i.e. the exit of the HF/N_2 gas. The thermistor constitutes part of an electrical bridge and its resistance is continuously compared with one of five reference resistances. The out-of-balance signal controls the heating element whose power can be further adjusted with a variable transformer to yield about 50% utilisation time.

Reactant Controls

The control logic governing the gas flow is schematized in Fig. 1. A stream of carrier gas sent through the network (1 + 2) or a stream passing through the network 3 can be directed to an external cell by means of a fourway valve (S-Reactor). Subsequently either stream can be sent to the external HF analyser or to waste by means of a fourway valve (S-Analyser).

HF Analyser

The gas stream containing concentrations of the order of 10 to 500 ppm HF is contacted in an absorption tower, Fig. 2, with the HMTA absorbing solution. After degassing, the buffered solution is analysed using an Orion fluoride electrode 94-09-A in a manner not unlike that described previously (5). The 4 ml free gas volume of the tower provides a contact time of more than 0.5 s (at flow rates up to 0.5 ℓ/min) with about 0.3 ml of liquid hold up. The volume of the capillary tubing between the tower and the electrodes was kept to 0.2 ml, and the dead space of the electrode compartment to 0.1 ml in order to obtain a response time of less than 30 s.

Results and Discussion

HF Analyser

The electrode response of the analyser was calibrated using NaF solutions 10^{-6} to 10^{-1} *M* F^- in the 0.05 *M* HMTA buffer. These standard solutions were drawn through the electrode compartment by a Technicon Pump at the same rate as the sample solutions, i.e. 1.52 to 1.54 ml min^{-1}. A Nernstian electrode response with a slope −58.5 mV/log $[F^-]$ was observed over the concentration range 10^{-1} to 10^{-4} *M* but slight deviations from linearity became notice-

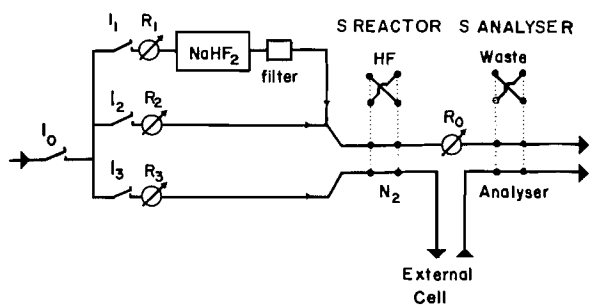

FIG. 1. Control logic HF generator.

Can. J. Chem. Downloaded from www.nrcresearchpress.com by 210.87.254.6 on 09/05/12
For personal use only.

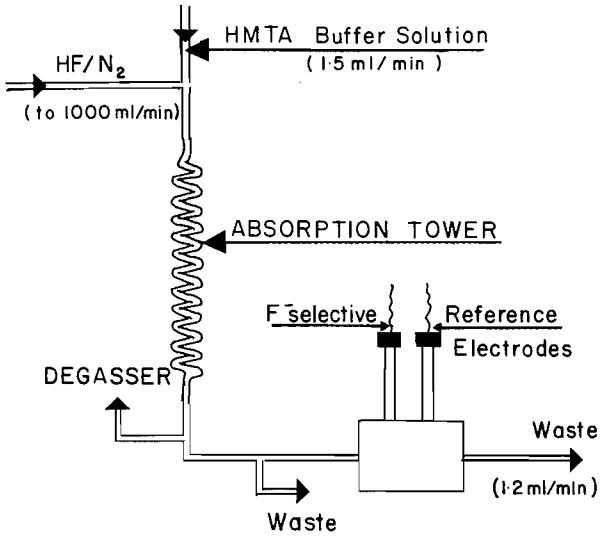

FIG. 2. HF adsorption tower and electrode compartment.

able below 5×10^{-5} *M* F^-. Measurements of HF concentrations in the sample solutions were confined to the range 5×10^{-2} to 10^{-4} *M* F^-.

Evaluation of the efficiency of the scrubbing or absorption tower ideally requires a steady source of a fixed HF concentration in an inert carrier gas and the purpose of this project was precisely to construct such a generator. By allowing the scrubbed nitrogen carrier gas to bubble through a second absorption solution for extended periods of time it was evident that over 99% of the HF was absorbed in the tower for nitrogen flow ranges below 500 ml/min. As the gas flow rate increased further and the residence time in the absorption tower was reduced to less than 0.5 s, the scrubbing efficiency decreased slightly to about 95%. The scrubbing efficiency did not depend on the F^- concentrations except under conditions where the F^- concentration in the absorbing solution exceeded the concentration of the HMTA buffer, i.e., 0.05 *M*.

The HF analyser (i.e. the absorption tower and electrode response) can be evaluated by varying the flow rate of the buffer solution, the flow rate of the HF/N_2 gas, or the concentration of the HF in the carrier gas. The fluoride concentration in the buffer solution should vary as

$$[F^-] = \frac{[\text{ppm HF}]_{N_2}}{20} \times \frac{\text{Nitrogen flow rate}}{\text{Buffer flow rate}} \times \frac{\text{Density of } N_2}{\text{Density of HMTA}} \times 10^{-6}$$

where the density of the nitrogen carrier gas at the temperature of the tower (14°C) can be taken as 1.22 g/ℓ and that of the buffer solution as 1.00 g/ml. Thus, the electrode response should vary in a logarithmic fashion with the nitrogen or the buffer flow rates as well as with the HF concentrations.

The variations of electrode response with the flow rates are summarized in Fig. 3. Curve (*a*) refers to the results obtained by maintaining a constant flow rate and constant pressure in the HF generator, directing part of the gas to waste and allowing a variable amount to pass through the analyser with a flow rate d_{HF/N_2}. A linear relationship is obtained with a slope −57.8 mV/log (flow rate) up to flow rates of 0.5 ℓ min^{-1}. At higher flow rates a non-Nernstian response can be ascribed to a decreased scrubbing efficiency as noted above.

Curve (*b*) refers to the results obtained by maintaining a fixed HF/N_2 flow rate of 280 ml min^{-1}, a fixed concentration of 120 ppm HF, and varying the flow rate of the HMTA buffer from 0.2 to 2 ml min^{-1}. A linear response was obtained with a slope 64 mV/log (flow rate) somewhat greater than the theoretical value of 58.5 mV. This difference is

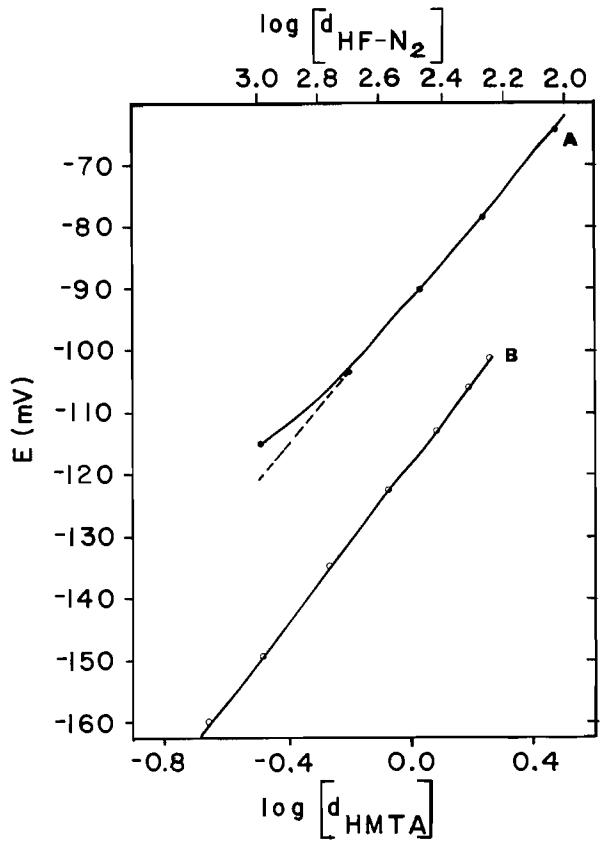

FIG. 3. Electrode response as a function of nitrogen gas and buffer flow rates in the absorption tower. (*A*), Gas flow rate in analyser, d_{HF}/N_2 in ml min^{-1}. Flow rate in generator 1.6 ℓ min^{-1} at 125 ppm HF buffer flow rate 1.53 ml min^{-1}. (*B*), Buffer flow rate in ml min^{-1}. Gas flow rate in analyser and generator 280 ml min^{-1} at 125 ppm HF.

Can. J. Chem. Downloaded from www.nrcresearchpress.com by 210.87.254.6 on 09/05/12
For personal use only.

thought to be due to the streaming potential developed by pumping the low ionic strength HMTA buffer through Teflon tubing. A similar effect was observed when standard NaF solutions were employed. Adding an inert electrolyte such as NaCl or KCl to the buffer has been suggested (6) in order to reduce the streaming potential but may promote crystallization when the analyser is left unattended.

HF Generator

For reasons outlined below, the pressure at the outlet of the bifluoride reactor should be maintained at a constant value if possible, and all flow restrictions with the exception of a 7 micron filter (Nupron B-4FT7-7 $C_V = 0.15$) should be placed upstream. When packed with $NaHF_2$ crystals the columns constitute a major restriction to the gas flow rate and will only allow a flow of about 7 ℓ/min for a 10 psi pressure drop. This gas stream (stream *1*, Fig. 1) can be diluted with pure carrier gas (stream *2*, Fig. 1) yielding a fixed quantity of HF in a variable amount of carrier gas, or a concentration varying according to:

$$[7] \quad [HF]_{1+2} = \frac{[HF]_1 \times \text{Flow rate 1}}{(\text{Flow rate 1} + \text{flow rate 2})}$$

The initial tests on the bifluoride reactor have been confined to studies at low flow rates 1, zero flow rate 2, and such low exit pressures that the value of P_T (eq. [6] can be assumed to equal 1 atm). The steady state values for a gas flow about 350 ml min^{-1} in the reactor are given in Fig. 4 and compared with the predictions of Miller (3) and Fisher (1). A least-squares fit to our data yields the expression

$$[8] \quad \log P_{HF}\,(\text{atm}) = 7.205 - \frac{4013}{T}\,(340 \text{ to } 400\,\text{K})$$

When expressed in terms of a weight fraction in a nitrogen atmosphere eq. [8] becomes:

$$[9] \qquad \log\,(\text{ppm HF}) = 13.072 - \frac{4013}{T}$$

and concentrations between 25 to 1000 ppm HF are available by choosing temperatures between 70 to 125°C.

Our numerical values are almost exactly twice those obtained by Miller (3) and some ten times smaller than those reported by Fisher (1), the latter being the most widely quoted in the literature. Using for reaction [1] the free energy function calculated by Miller (3), we obtain an enthalpy of decomposition of $NaHF_2$ $\Delta H^0_{298} = 18.06 \pm 0.1$ kcal/mol at 25°C. This is in excellent agreement with the theoretical value predicted by Higgins and Westrum (7) as 17.88 ± 0.2 kcal/mol.

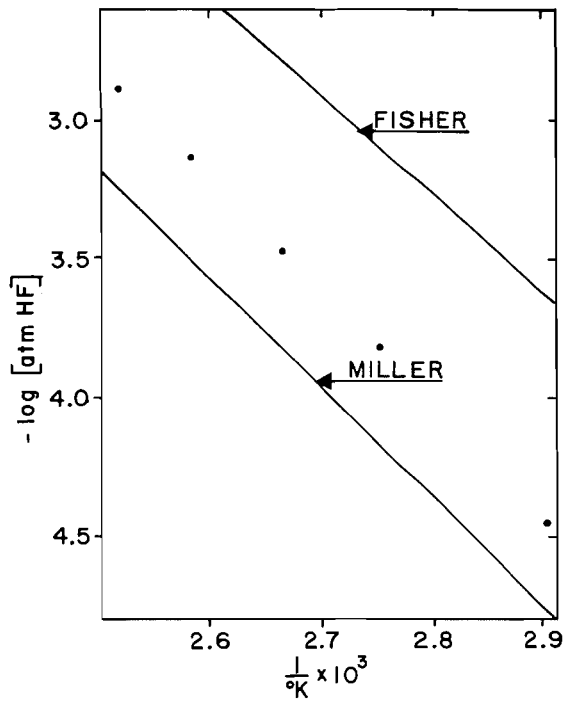

FIG. 4. Partial pressure of HF in the $NaHF_2$ reactor at various temperatures. Included are predictions based on eqs. [3] and [5] and our experimental results.

An appreciable pressure drop in the $NaHF_2$ reactor itself would affect the kinetic response, i.e. the speed with which equilibrium HF concentration is attained at the exit port. Furthermore, according to eq. [6] the pressure at the exit port determines the HF concentration although it does not affect the HF partial pressure. Any flow restriction after the HF reactor, such as the filter or an external reaction cell, will increase P_T at high flow rates and thereby reduce the HF concentration. By deliberately throttling the gas flow using a fine metering valve in place of an external reaction cell we have verified that eq. [6] is obeyed at least up to 40 psi.

The HF concentration in the carrier gas could thus be calculated from eq. [6], the temperature of the bifluoride reactor and a manometer reading at the exit port. A less cumbersome and more direct method is also available. Using the control panel and the metering valve R_0 it is possible to place an equivalent flow restriction in the by-pass of the external reaction cell. Switching the four way valve (S-Analyser) will send either stream (1 + 2) or stream 3 to the analyser without provoking any pressure changes. At all times it is thus possible to measure the HF concentrations directly in the carrier gas before or after the external cell.

The time necessary to attain steady state HF con-

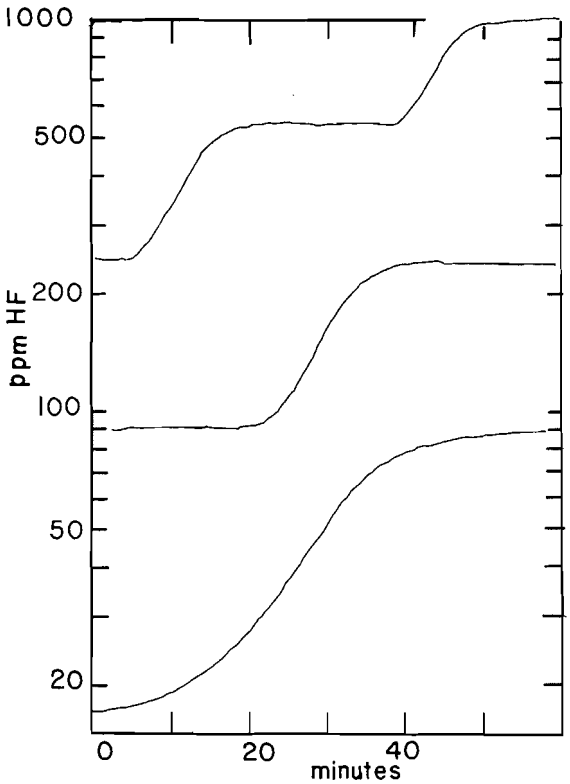

FIG. 5. Time response of the HF generator. Temperature jumps from 72°C to 91°C to 103°C to 116°C to 126°C. Nitrogen flow rate 4.7 ℓ min^{-1}, absorbant flow rate 8.4 ml min^{-1} 2% HMTA solution.

centrations is relatively short. Typical results are illustrated in Fig. 5 for the variation of the HF analyser signal as the temperature of the $NaHF_2$ generator is increased in a stepwise fashion from 72 to 126°C. Since the electrode potential is proportional to log [F^-], the logarithmic chart paper is calibrated to read directly [HF] in ppm. Even at the high nitrogen flow rates employed here (5 ℓ/min) and hence the non-negligible pressure inside the $NaHF_2$ generator, HF concentrations stable to within 1% are rapidly attained. The equilibration time is roughly proportional to the relative HF concentration changes or the temperature increment (about 1 min/°C). It is thus possible to change the HF concentration in the carrier gas from 20 to 1000 ppm within 1 h without changing the gas flow rates or diluting the gas in any manner.

The long term stability of the reactor was evaluated over a 48 h period. The electrode response drifted about 1 mV/day due to temperature changes in the laboratory. When the electrodes were occasionally recalibrated with standard NaF solutions, the potentials remained constant to within ± 0.2 mV.

Conclusions

The HF generator yields very stable concentrations of hydrogen fluoride gas, relatively independent of the nature, or the flow rate of the carrier gas. Unlike the effusion techniques presently employed for calibration of analytical instruments, the generator can furnish high HF concentrations at high flow rates over extended periods of time with approximately the same requirements for temperature control. Also, unlike cylinders of anhydrous HF and associated metering valves, or dilute gaseous mixtures presently used for adsorption studies, the HF generator constitutes a safe, relatively cheap source of dilute gaseous mixtures whose composition is governed by thermodynamic principles.

Acknowledgements

The financial support of the Aluminum Company of Canada and the National Research Council of Canada is gratefully acknowledged. The authors thank W. D. Lamb and K. F. Denning for their suggestions during the pratical evaluation of the generator, the technical assistance of R. Lessard is also appreciated.

1. J. FISHER. J. Am. Chem. Soc. **79**, 6363 (1957).
2. J. F. FRONING, M. K. RICHARDS, T. W. STRICKLIN, and S. G. TURNBULL. Ind. Eng. Chem. **39**, 275 (1947).
3. A. R. MILLER. J. Phys. Chem. 1144 (1967).
4. J. H. SIMONS (*Editor*). Florine chemistry. Vol. 3. Academic Press, New York, NY. 1950. p. 230*ff*.
5. A. S. HALLSWORTH, J. A. WEATHERELL, and D. DEUTSCH. Anal. Chem. **48**, 1660 (1976).
6. P. VAN DER WINKEL, J. MERTENS, and D. L. MASSART. Anal. Chem. **46**, 1765 (1974).
7. T. L. HIGGINS and E. F. WESTRUM, JR. J. Phys. Chem. **65**, 830 (1961).

Can. J. Chem. Downloaded from www.nrcresearchpress.com by 210.87.254.6 on 09/05/12
For personal use only.

Synthesis and vibrational spectra of tin(II) isothiocyanate adducts with some O- and N-donor ligands[1]

TEWFIK B. ABSI, RAMESH C. MAKHIJA, AND MARIO ONYSZCHUK[2]
Department of Chemistry, McGill University, Montreal, P.Q., Canada H3A 2K6

Received June 28, 1977

TEWFIK B. ABSI, RAMESH C. MAKHIJA, and MARIO ONYSZCHUK. Can. J. Chem. **56**, 2039 (1978).

Five new adducts of $Sn(NCS)_2$ have been prepared and characterized: $Sn(NCS)_2 \cdot 2L$ (L = 2,6-dimethyl-γ-pyrone and *N*,*N*-dimethylacetamide), $Sn(NCS)_2 \cdot LL$ (LL = 1,10-phenanthroline and 2,2′-bipyridine), and Sn(NCS)(ox) (ox = 8-hydroxyquinolinate). By comparing their infrared and Raman spectra with those of $SnX_2 \cdot L$ (X = Cl, NCS; L = triphenylphosphine oxide), $SnX_2 \cdot 2L$ (X = Cl, NCS; L = dimethylsulphoxide and pyridine-*N*-oxide), $SnCl_2 \cdot LL$ (LL = 1,10-phenanthroline and 2,2′-bipyridine), and SnCl(ox), assignments have been made for ν(CN), ν(CS), and δ(NCS) vibrations; these suggest the presence of N-bonded and —NCS— bridge-bonded thiocyanate groups. Molecular weight, conductivity, and X-ray powder diffraction data support the conclusion that the adducts with the oxygen donor ligands are molecular with only N-bonded thiocyanate groups. Adducts with the bidentate nitrogen donor ligands are polymeric and have —NCS— bridging and N-bonded thiocyanate.

TEWFIK B. ABSI, RAMESH C. MAKHIJA et MARIO ONYSZCHUK. Can. J. Chem. **56**, 2039 (1978).

On a préparé et caractérisé cinq nouveaux adduits du $Sn(NCS)_2$: $Sn(NCS)_2 \cdot 2L$ (L = diméthyl-2,6 γ-pyrone et *N*,*N*-diméthylacétamide), $Sn(NCS)_2 \cdot LL$ (LL = phénanthroline-1,10 et bipyridine-2,2′) et Sn(NCS)(ox) (ox = hydroxy-8 quinolinate). En comparant leurs spectres infrarouge et Raman avec ceux de $SnX_2 \cdot L$ (X = Cl, NCS; L = oxyde de triphénylphosphine), $SnX_2 \cdot 2L$ (X = Cl, NCS; L = diméthylsulphoxyde et pyridine *N*-oxyde), $SnCl_2 \cdot LL$ (LL = phénanthroline-1,10 et bipyridine-2,2′) et SnCl(ox), on a pu faire des attributions pour les vibrations du ν(CN), ν(CS) et δ(NCS); celles-ci suggèrent la présence de groupes thiocyanates liés par l'azote et pontés par le —NCS—. Les données de poids moléculaires, de conductivité et de diffraction de rayon-X des poudres sont en accord avec la conclusion que les adduits avec les ligands donneurs d'oxygène sont moléculaires et n'impliquent que des groupes thiocyanates liés par l'azote. Les adduits avec les ligands d'azote donneurs bidentates sont des polymères et possèdent des groupes NCS assurant les ponts et des thiocyanates liés par l'azote.
[Traduit par le journal)

Introduction

Although several complex ions (1–3) and neutral adducts (4) of tin(II) thiocyanate have been reported, little is known about their vibrational frequencies and mode of thiocyanate bonding, which may be —NCS, —SCN, —NCS—, or variations of the latter. We have re-examined the previously reported neutral complexes (4) and have made five new ones with the objective of obtaining physical data and vibrational spectra which might reveal the type of thiocyanate bonding.

Experimental

Anhydrous tin(II) thiocyanate (3) and tin(II) chloride (5) were prepared by literature methods. *N*,*N*-Dimethylacetamide (dma) and dimethylsulphoxide (dmso) were dried over a molecular sieve and distilled before use. The crystalline ligands 2,6-dimethyl-γ-pyrone (dmp), 2,2′-bipyridine (bipy), 1,10-phenanthroline (phen), triphenylphosphine oxide (tppo), and 8-hydroxyquinoline (Hox) had the required melting points after commercial samples were dried in a vacuum. All manipulations were done under dry nitrogen in a glove-bag.

Infrared spectra (4000–400 cm^{-1}) of samples as Nujol mulls and ethanol solutions were recorded on a Perkin-Elmer 521 spectrophotometer. Raman spectra (3000–30 cm^{-1}) of powdered samples in sealed capillary tubes at −40°C were recorded on a Jarrell-Ash 25-300 instrument using either 647.1 or 514.5 nm laser excitation. Electrical conductivities[3] at 25°C of freshly prepared ethanol solutions of $Sn(NCS)_2$ and acetone solutions of $Sn(NCS)_2$ adducts with the oxygen donor ligands were made with a Radiometer-Copenhagen Model CDM3 conductivity meter. Molecular weights[3] in acetone solution were determined by vapour pressure osmometry by Galbraith Laboratories Inc., Knoxville, Tennessee. X-ray powder diffraction *d*-spacings[3] were obtained with a Debye-Scherrer camera using Ni-filtered CuK_α radiation (λ = 1.5418 Å). Microanalyses for C, H, and N were done by Chemalytics Inc., Tempe, Arizona. Tin was determined as the oxide after samples were treated with nitric acid and ignited at 800°C. Chlorine was determined gravimetrically as silver chloride.

The adducts $Sn(NCS)_2 \cdot 2dmso$, $Sn(NCS)_2 \cdot tppo$, $SnCl_2 \cdot 2dmso$, $SnCl_2 \cdot 2pno$, $SnCl_2 \cdot bipy$, $SnCl_2 \cdot phen$, and SnCl(ox)

[1]Presented at the 2nd Joint Conference of the Chemical Institute of Canada and the American Chemical Society, Montreal, P.Q., May 30–June 2, 1977.

[2]To whom correspondence should be addressed.

[3]Tables of the results may be obtained, at a nominal charge, from the Depository of Unpublished Data, CISTI, National Research Council of Canada, Ottawa, Ont., Canada K1A 0S2.

Can. J. Chem. Downloaded from www.nrcresearchpress.com by 210.87.254.5 on 09/05/12
For personal use only.

Can. J. Chem. Downloaded from www.nrcresearchpress.com by 210.87.254.5 on 09/05/12
For personal use only.

TABLE 1. Thiocyanate frequencies (cm^{-1}) of $Sn(NCS)_2$ adducts

Compound	ν(CN)		ν(CS)		δ(NCS)	
	Infrared	Raman	Infrared	Raman	Infrared	Raman
$Sn(NCS)_2$	2113 s		804 m	814 m	472 m	477 s
	2080 vs	2075 vs	780 m	785 m	456 m 448 m	457 m
$Sn(NCS)_2$·tppo (1:1)	2078 s	2052 s	828 w	832 w	475 m	483 s
	2046 vs	2035 s		802 m	472 m	474 s
$Sn(NCS)_2$·2pno (1:2)	2055 vs	2049 vs	812 sh	820 m	471 m	455 w
$Sn(NCS)_2$·2dmso (1:2)	2068 s	2092 w	817 w	824 m	474 m	472 m
	2057 s	2060 vvs	810 sh		471 sh	
	2015 w	2013 w				
$Sn(NCS)_2$·2dma (1:2)	2071 s					
	2052 s	2049 vvs	832 m	833 s	482 vs	478 vs
$Sn(NCS)_2$·2dmp(1:2)	2054 m	2025 vs	832 w	828 vs	482 w	480 m
	2028 vs					
		2090 w				
	2073 s	2075 m	822 w	828 w	482 m	490 s
$Sn(NCS)_2$·bipy (1:1)	2055 s	2056 m	806 w	798 w	476 s	480 s
	2043 s	2037 s				
	2060 m	2059 m				
$Sn(NCS)_2$·phen (1:1)	2049 s	2043 s	818 m	821 m	470 sh	470 w
	2008 vs	2001 vs			466 m	
	1960 w					
Sn(NCS)(ox)	2064 s	2053 s	775 vvw	775 m	474 m	470 s
	2052 s	2038 m			468 m	

were prepared as previously reported (4–6). Satisfactory melting points and tin and/or chlorine analyses were obtained in all cases.

$Sn(NCS)_2$·2dma was obtained when water was added dropwise to a solution of $Sn(NCS)_2$ (0.01 mmol, 2.4 g) in dma (20 ml) until white needles precipitated; these were filtered and washed with ether. *Anal.* calcd. for $C_{10}H_{18}N_4O_2S_2Sn$: C 29.36, H 4.43, N 13.70, Sn 29.01; found: C 28.5, H 4.5, N 13.4, Sn 29.9; mp 92°C; yield 63%. After adding a solution of $Sn(NCS)_2$ (0.01 mmol, 2.4 g) in ethanol (20 ml) to a solution of bipy (0.01 mmol, 1.6 g) in ethanol (15 ml), a yellow precipitate formed. This mixture was stirred overnight and the yellow product, *$Sn(NCS)_2$·bipy*, was filtered and washed with ether. *Anal.* calcd. for $C_{12}H_8N_2S_2Sn$: C 36.86, H 2.06, N 14.32, Sn 30.35; found: C 36.6, H 2.4, N 14.5, Sn 30.3; mp 235°C (dec.); yield 81%. The following adducts were prepared similarly: *$Sn(NCS)_2$·phen. Anal.* calcd. for $C_{14}H_8N_4S_2Sn$: C 40.51, H 1.94, N 13.50, Sn 28.60; found: C 41.1, H 2.1, N 13.7, Sn 27.9; mp 252°C (dec.); yield 90%. *Sn(NCS)(ox). Anal.* calcd. for $C_{10}H_6N_2OSSn$: C 37.43, H 1.88, N 8.73, Sn 36.98; found: C 36.9, H 1.7, N 9.0, Sn 36.3; mp 290°C (dec.); yield 83%. *$Sn(NCS)_2$·2dmp. Anal.* calcd. for $C_{16}H_{16}N_2O_4S_2Sn$: C 39.78, H 3.34, N 5.80, Sn 24.57; found: C 39.5, H 3.3, N 5.4, Sn 24.6; mp 154°C; yield 65%; was obtained when $Sn(NCS)_2$ (0.01 mmol) and dmp (0.02 mmol) were combined in ethanol (35 ml).

Results and Discussion

The splitting of the ν(CN) and ν(CS) bands in the infrared spectrum of crystalline $Sn(NCS)_2$ (Table 1) is consistent with the presence of two crystallographically distinct thiocyanate groups as shown recently by an X-ray diffraction crystal structure determination (7). Although each thiocyanate group fulfils a bridging function, the shortest distances (2.20 and 2.27 Å) are Sn—N, mainly covalent, interactions. Therefore, it is not surprising that $Sn(NCS)_2$ is monomeric in acetone solution (M, found: 226; calcd.: 235) and a nonelectrolyte in ethanol solution (molar conductance, $\Lambda(0.0313\ M) = 2.64 \times 10^{-3}$ ohm^{-1} cm^2 mol^{-1}). Retention of N-bonded thiocyanate groups by $Sn(NCS)_2$ in ethanol solution is confirmed by the intensity of ν(CN), measured by Ramsay's direct integration method (8), being $26.5 \times 10^4\ M^{-1}$ cm^{-2} (per thiocyanate group) which is in the range $17–32 \times 10^4\ M^{-1}$ cm^{-2} characteristic of N-bonded transition metal thiocyanates in methanol solution (9). Moreover, the change of the ν(CN) absorption from two peaks at 2113 and 2080 cm^{-1} in the solid state to a single band at 2050 cm^{-1} in ethanol solution is also consistent with the disappearance of thiocyanate bridges and the presence of only N-bonded thiocyanate (9, 10).

The oxygen donor ligands: pno, dmso, dma, and dmp form 1:2 complexes which (*i*) melt sharply at moderate temperatures (90 to 160°C), (*ii*) dissolve readily in such polar solvents as ethanol and acetone, and (*iii*) are highly dissociated in acetone solution (dissociation 40 to 76%, calculated from the molecular weight data) in which they are also nonelectrolytes ($\Lambda = 6.5 \times 10^{-3}$ to 15.8×10^{-3} ohm^{-1} cm^2 mol^{-1}). These physical properties, together with the lowering of the ν(CN) and raising of the ν(CS) frequencies relative to those of $Sn(NCS)_2$, support

the conclusion that these complexes are molecular in the solid state with thiocyanate groups N-bonded. X-ray powder diffraction patterns of the dmso and dma adducts consisted of 21 and 17 sharp lines respectively, indicating low crystal symmetry. The coordination sphere around Sn(II) in 1:2 adducts should be tetrahedral if the lone electron pair is not stereochemically important, or bisphenoid if the lone electron pair occupies an equatorial site in a trigonal bipyramidal arrangement of electron pairs around Sn(II) (11).

The bidentate nitrogen-donor ligands bipy and phen form 1:1 complexes which melt with decomposition at 235 and 250°C, respectively, and are insoluble in common polar and non-polar organic solvents; properties which strongly suggest that they are polymeric. Their ν(CN), ν(CS), and δ(NCS) frequencies are consistent with the presence of both N-bonded and bridging thiocyanate groups, suggesting that units are linked together by thiocyanate bridges. The oxinate Sn(NCS)(ox) also has physical properties and thiocyanate frequencies consistent with a polymeric structure in which thiocyanate groups are bridging.

Acknowledgements

We are grateful for the financial support of the National Research Council of Canada and le Gouvernement du Québec, Ministère de l'Education.

1. A. M. GOLUB and V. M. SAMOILENKO. Ukr. Khim. Zh. **29**, 789 (1963).
2. I. V. KROTOV. C. R. Acad. Sci. U.S.S.R. **3**, 603 (1934).
3. B. R. CHAMBERLAIN and W. MOSER. J. Chem. Soc. A, 354 (1969).
4. J. D. DONALDSON and D. G. NICHOLSON. J. Chem. Soc. A, 145 (1970).
5. J. S. MORRISON and H. M. HAENDLER. J. Inorg. Nucl. Chem. **29**, 393 (1967).
6. M. A. DOSKEY and C. CURRAN. Inorg. Chem. Acta, **3**, 169 (1969).
7. A. G. FILBY, R. A. HOWIE, and W. MOSER. J. Chem. Soc. Dalton, In press.
8. D. A. RAMSAY. J. Am. Chem. Soc. **74**, 72 (1952).
9. R. A. BAILEY, S. L. KOZAK, T. W. MICHELSEN, and W. N. MILLS. Coord. Chem. Rev. **6**, 407 (1971).
10. A. H. NORBURY. Adv. Inorg. Chem. Radiochem. **17**, 231 (1975).
11. R. J. GILLESPIE. Molecular geometry. Van Nostrand Reinhold Company, London. 1972. p. 62.

Can. J. Chem. Downloaded from www.nrcresearchpress.com by 210.87.254.5 on 09/05/12
For personal use only.

Study of the electrolytic reduction of Cr(VI) in aqueous solutions of chromic acid by the rotating disc electrode method

HÉLIO C. CHAGAS

Instituto de Química, Universidade de São Paulo, C. P. 20780, São Paulo, Brasil

Received December 15, 1977

HÉLIO C. CHAGAS. Can. J. Chem. **56**, 2042 (1978).

The Cr^{6+}/Cr^{3+} reduction in aqueous solution is studied in the presence of sulfate and chloride ions by the rotating disc electrode method. In the low chromic acid concentration region, the results exhibit some differences in relation to those obtained using more concentrated solutions. However, it is demonstrated that in the presence of sulfate and chloride ions there is a chemical reaction preceding the electrochemical process, confirming a previous suggestion. Results for Cr^{6+}/Cr^{3+} reduction process in perchloric acid medium at various temperatures are presented and a reduction mechanism is suggested.

HÉLIO C. CHAGAS. Can. J. Chem. **56**, 2042 (1978).

On a étudié la réduction Cr^{6+}/Cr^{3+} en solution aqueuse, en présence d'ions sulfates et d'ions chlorures, en faisant appel à la méthode d'électrode de disque tournant. A de basses concentrations d'acide chromique, les résultats présentent quelques différences par rapport à ceux obtenus dans des solutions plus concentrées. Toutefois, on a démontré lorsque l'on travaille en présence d'ions sulfates et d'ions chlorures, qu'il se produit une réaction chimique précédant le processus électrochimique; cette démonstration confirme une suggestion antérieure. On présente des résultats relatifs au processus de réduction Cr^{6+}/Cr^{3+} en milieu acide perchlorique à diverses températures et on suggère un mécanisme pour la réduction.

[Traduit par le journal]

Introduction

Although the kinetics of the electrolytic reduction of chromium have been extensively studied, a theoretical model which explains all of the available experimental results remains to be formulated. Ryan (1) has reviewed the state of this problem up to 1964.

It is known that the deposition of chromium from aqueous solutions of hexavalent electrolytes occurs only in the presence of certain added ions such as SO_4^{2-}.

Polarization curves for the reduction of chromic acid in the presence of SO_4^{2-} ions exhibit two regions (2–4). In the first region, which has two maxima, a process corresponding to the reduction Cr^{6+}/Cr^{3+} and the formation of a cathode film occur. In the second region, i.e., at more cathodic potentials, three simultaneous processes are observed: the reduction Cr^{6+}/Cr^{3+}, evolution of gaseous hydrogen ($2H^+/H_2$), and deposition of metallic chromium (Cr^{6+}/Cr^0). The SO_4^{2-} ions play a role in the formation of the cathodic film, via which the reduction to metallic chromium takes place.

Various investigators (1, 5, 6) have emphasized the importance of the formation of complex ions in the reduction of chromium. Thus, the intermediate formation of complex chromium–chromate ions at the electrode surface was suggested by Ryan (1) as a possible mechanism through which hexavalent chromium could be deposited electrolytically as metallic chromium.

On the other hand, participation of atomic hydrogen in the reduction Cr^{6+}/Cr^{3+} was pointed out by Usachev (7) and confirmed by Marchenko and coworkers (8). Additional evidence for the role of atomic hydrogen in the reduction Cr^{6+}/Cr^{3+} was obtained by Jones and Saiddington (9) from microscopic studies.

Using the rotating disc electrode method and working at the potential of the first maximum of the polarization curve for the reduction of chromic acid in the presence of SO_4^{2-} ions (region in which only the reduction Cr^{6+}/Cr^{3+} occurs), Budevskii and Toshev (10) demonstrated that a chemical process must occur prior to the electrode process. These authors also noted that phenomena such as dissolution of the cathodic film, formation of electroactive complexes, etc. might also be responsible for the observed behavior.

As has been observed by Biryukov (11), it is difficult to make valid comparisons between the mechanisms of reduction of chromium in stirred and stationary systems. Thus, for example, the cathodic films formed at stationary electrodes in the presence of sulfuric acid at low chromic acid concentrations attain considerable thickness and are visually observable (4); in contrast, film formation could not be visually detected at the rotating disc electrode at velocities above 25 rd/s.

Nevertheless, in addition to other advantages, the well defined hydrodynamic conditions for material transport which are obtained in the rotating disc electrode method justify its application to the eluci-

Can. J. Chem. Downloaded from www.nrcresearchpress.com by 210.87.254.105 on 09/05/12
For personal use only.

Can. J. Chem. Downloaded from www.nrcresearchpress.com by 210.87.254.105 on 09/05/12
For personal use only.

dation of the mechanism of the chromium reduction process.

In the present work, we report the results of a rotating disc electrode study of the effects of SO_4^{2-} and Cl^- ions on the Cr^{6+}/Cr^{3+} reduction process in aqueous solutions of chromic acid. In addition, we utilize the rotating disc electrode method to examine the Cr^{6+}/Cr^{3+} reduction kinetics at various temperatures in perchloric acid medium.

Experimental

The rotating disc electrode apparatus utilized in this work has been previously described (12, 13). Curves of the current as a function of the working electrode potential were automatically recorded for each frequency of electrode rotation. This frequency was varied in integral steps of the square root of the frequency $f^{1/2}$ from 2 to 10 $Hz^{1/2}$.

The electrode potential scan rate was fixed at 10 mV/s in all experiments, curves always being registered from less cathodic to more cathodic potentials.

A gold disc electrode having a diameter of 4.61 mm was employed throughout. This electrode was polished and checked for the existence of leakage in the manner previously described (12). A platinum foil electrode with an approximate area of 12 cm^2 was used as the auxiliary electrode and a saturated calomel electrode (SCE) utilized as the reference electrode.

The electrolytic cell employed was similar to that described by Johnson (14), having a capacity of about 200 ml and an external thermostatable water jacket.

Chromic acid solutions were prepared by dissolution of chromic oxide (Carlo Erba, AR grade) in triply distilled water. Stock solutions of sulfuric, hydrochloric, and perchloric acids were similarly prepared in triply distilled water from analytical grade reagents.

The study of the reduction of hexavalent chromium ions in the presence of sulfate ions was carried out at 25°C employing chromic acid concentrations of 0.1, 0.2, 0.3, and 0.4 *M*. The reduction in the presence of chloride ions was studied at a chromic acid concentration of 0.1 *M*, varying the chloride ion concentration in the range 0.3–2.6 m*M*.

In these experiments, the SO_4^{2-} and Cl^- ion concentrations were varied in increments by addition of aliquots from the appropriate stock solution to the electrolyte present in the electrolytic cell.

In order to obtain reproducible voltammograms, the gold electrode was periodically polished with Buehler 0.05 μm gamma micropolish, and the potential scan limited to the region up to the first maximum of the polarization curve.

In the study of the reduction Cr^{6+}/Cr^{3+} in 0.5 *M* perchloric acid, the hexavalent chromium concentration was varied from 0.10 to 0.29 m*M*, experiments being carried out at 25.0, 30.0, 35.0, and 40.0°C.

Oxygen was eliminated from the solutions by bubbling with purified nitrogen for 30 min and all subsequent manipulations and measurements carried out under a nitrogen atmosphere.

Kinematic viscosities of 0.5 *M* perchloric acid were calculated from density and viscosity measurements at various temperatures.

Results and Discussion

Effect of SO_4^{2-} Ions on the Reduction Cr^{6+}/Cr^{3+}

Curves of the current as a function of the electrode potential for the Cr^{6+}/Cr^{3+} reduction process in the presence of SO_4^{2-} ions exhibit a relatively broad maximum. Denoting the maximum measured current density by i_{lim}, graphs of $i_{lim}/f^{1/2}$ vs. i_{lim} were constructed from the polarization curves. These graphs, which refer to a chromic acid concentration of 0.2 *M*, are shown in Fig. 1. Analogous results were obtained at chromic acid concentration of 0.1, 0.3, and 0.4 *M*.

Within the framework of the theory developed by Vielstich and Jahn (15) the linear behavior of these graphs permits us to infer that the electrochemical process is preceded by a chemical reaction under these conditions.

For a system of the type

$$A_1 \underset{k_2}{\overset{k_1}{\rightleftarrows}} A_2$$

$$A_1 + ne^- \rightarrow P$$

in which a chemical reaction takes place in the solution and a charge transfer reaction occurs at the surface of the rotating disc electrode, Vielstich and Jahn have developed the following expression:

$$[1] \qquad (i_{lim}/\omega^{1/2}) = b + ci_{lim}$$

where $b = 0.62\, nF\nu^{-1/6}D^{2/3}C^0 = i_{lim}{}^d/\omega^{1/2}$, $i_{lim}{}^d$ = limiting diffusion current density, $c = -(1/1.62 D^{1/3}\nu^{1/6})\,(k_1/k_2)\,\delta_k$, and $\delta_k = 1/\sqrt{(k_1 + k_2)/D}$ = thickness of the kinetic layer, and n, F, ν, D, C^0, and ω have the usual significance.

In the limit of $\omega^{1/2} \rightarrow \infty$, eq. [1] permits us to

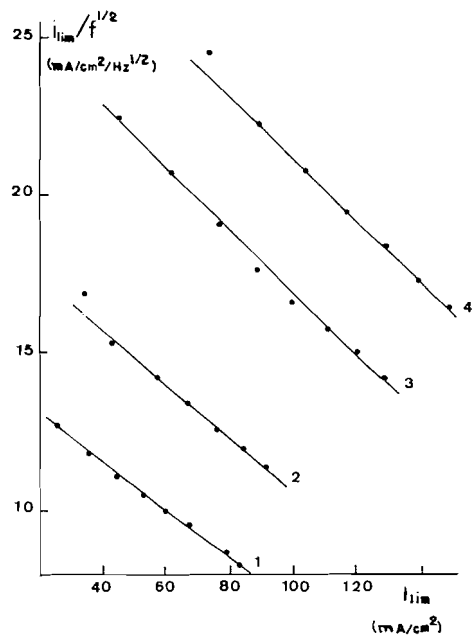

FIG. 1. Plot of $i_{lim}/f^{1/2}$ vs. i_{lim}, $[CrO_3] = 0.2$ *M*. $[SO_4^{2-}]$: (*1*) 1.76 m*M*; (*2*) 2.34 m*M*; (*3*) 3.46 m*M*; (*4*) 4.68 m*M*. $t = 25$°C.

Can. J. Chem. Downloaded from www.nrcresearchpress.com by 210.87.254.105 on 09/05/12
For personal use only.

determine the current density i_k corresponding to the kinetic process

$$[2] \qquad i_k = -(b/c)$$

which should be independent of ω.

Equation [1] can thus be put in the following form:

$$[3] \qquad (1/i_{lim}) = (1/i_{lim}^{d}) + (1/i_k)$$

Equation [3] has been derived by Budevskii (16) for the same mechanistic model and utilized by Budevskii and Toshev (10) in their study of the Cr^{6+}/Cr^{3+} reduction process in 2 *M* chromic acid in the presence of SO_4^{2-} ions.

As shown in Figs. 2 and 3, the values of $i_{lim}^{d}/f^{1/2}$ and i_k, calculated from the plots of $i_{lim}/f^{1/2}$ vs. i_{lim}, depend on the concentration of SO_4^{2-} ions and of chromic acid.

As can be seen in Fig. 2 for 0.1, 0.2, and 0.4 *M* chromic acid solutions, the variation of the ratio $(i_{lim}^{d}/f^{1/2})$ with SO_4^{2-} concentration gives evidence for two linear regions of different slope. Thus, at low sulfate ion concentrations, this ratio is directly proportional to the sulfate ion concentration. The value of the slope in this region varies little with the chromic acid concentration and is larger than that observed at higher SO_4^{2-} concentrations.

Figure 3 demonstrates that at SO_4^{2-} concentrations above 2 m*M*, a linear increase in the kinetic current is observed.

Effect of the Presence of Cl^- Ions on the Cr^{6+}/Cr^{3+} Reduction Process

The study of the effect of Cl^- ions on the Cr^{6+}/Cr^{3+} reduction process was performed in a manner similar to that described for SO_4^{2-} ions.

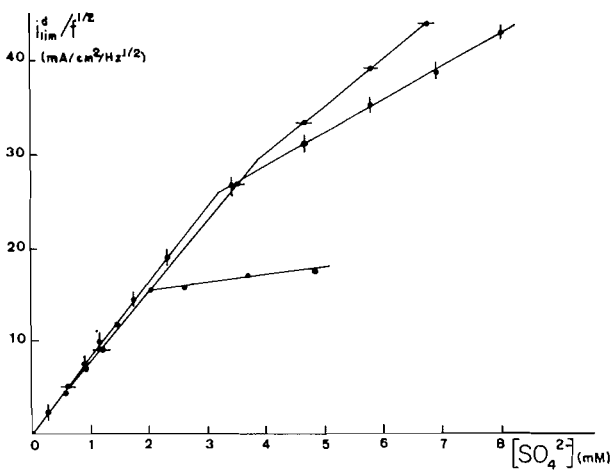

FIG. 2. Plot of $i_{lim}^{d}/f^{1/2}$ vs. $[SO_4^{2-}]$. $[CrO_3]$: ●, 0.1 *M*; ◐, 0.2 *M*; ◒, 0.4 *M*. t = 25°C.

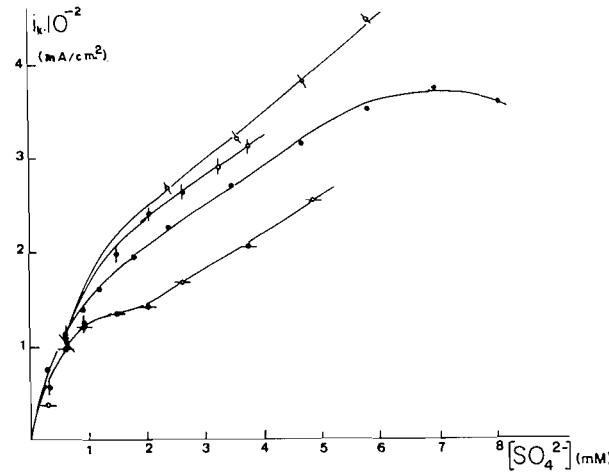

FIG. 3. Plot of i_k vs. $[SO_4^{2-}]$. $[CrO_3]$: ○, 0.1 *M*; ●, 0.2 *M*; ◐, 0.3 *M*; ◒, 0.4 *M*. t = 25°C.

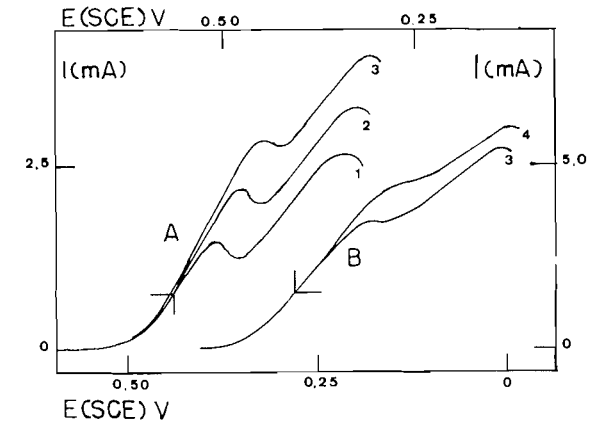

FIG. 4. Voltamograms. *A*, f = 16 Hz; *B*, *f* = 64 Hz. $[Cl^-]$: (*1*) 1.64 m*M*; (*2*) 1.96 m*M*; (*3*) 2.28 m*M*; (*4*) 2.60 m*M*. t = 25°C.

The polarization curves obtained for 0.1 *M* chromic acid solution in the presence of Cl^- ions are shown in Fig. 4. These curves exhibit two waves at potentials more positive than that at which electrode passivation occurs. In contrast to the behavior observed in the presence of SO_4^{2-} ions, the peaks (limiting currents) of the polarization curves are sharp in the presence of Cl^-. At the higher Cl^- concentrations, the first wave again tends to disappear as the velocity of rotation of the electrode is increased.

Graphs of $i_{lim}/f^{1/2}$ as a function of i_{lim} at various Cl^- concentrations for the first and second waves are shown in Figs. 5 and 6, respectively.

The linear behavior of the plots of Fig. 5 indicates that the Cr^{6+}/Cr^{3+} reduction process in the presence of Cl^- ions must also be preceded by a chemical reaction. Plots of values of the ratio $i_{lim}^{d}/f^{1/2}$ and of

Can. J. Chem. Downloaded from www.nrcresearchpress.com by 210.87.254.105 on 09/05/12
For personal use only.

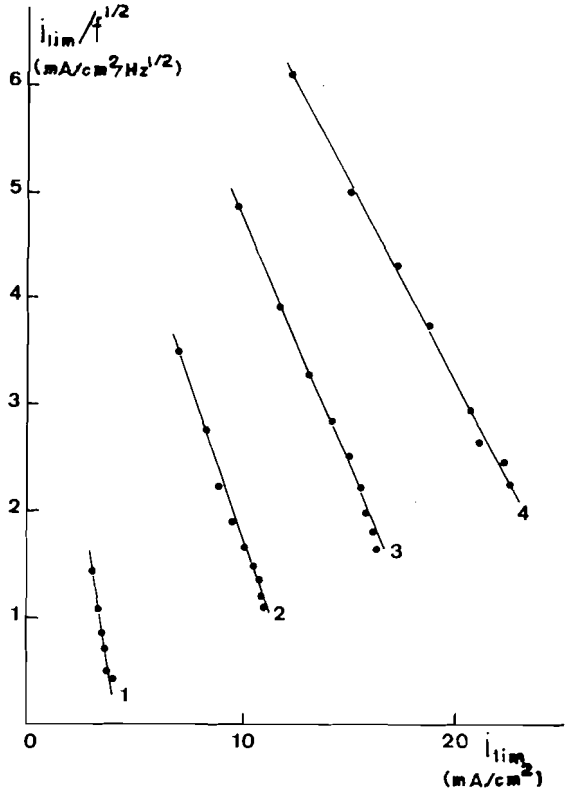

FIG. 5. Plot of $i_{lim}/f^{1/2}$ vs. i_{lim}, t = 25°C for the less cathodic wave. [CrO_3] = 0.1 M and [Cl^-]: (*1*) 1.32 mM; (*2*) 1.64 mM; (*3*) 1.96 mM; (*4*) 2.28 mM. t = 25°C.

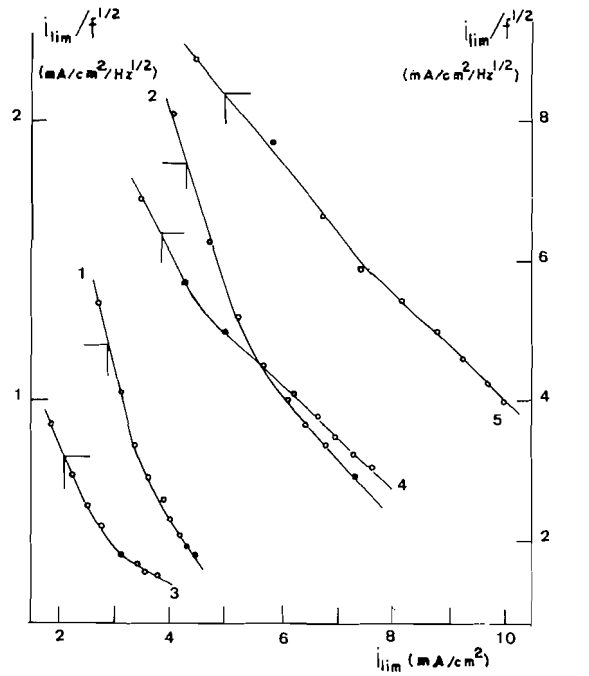

FIG. 6. Plot of $i_{lim}/f^{1/2}$ vs. i_{lim} for the more cathodic wave. [CrO_3] = 0.1 M and [Cl^-]: (*1*) 0.66 mM; (*2*) 0.99 mM; (*3*) 1.32 mM; (*4*) 1.96 mM; (*5*) 2.60 mM. t = 25°C.

the kinetic current density i_k vs. the Cl^- ion concentration are shown in Fig. 7.

Over the small interval of Cl^- concentration in which the first wave could be studied, the kinetic current density i_k is linearly related to the Cl^- concentrations above 1 mM (Fig. 7).

Study of the Reduction Cr^{6+}/Cr^{3+} in 0.5 M Perchloric Acid

At the $Cr_2O_7^{2-}$ concentrations and electrode rotation rates employed, the polarization curves for the reduction Cr^{6+}/Cr^{3+} in 0.5 M perchloric acid exhibit a well-defined plateau corresponding to a limiting diffusion current density i_{lim}^d. These limiting currents obey the Levich equation, being directly proportional to $f^{1/2}$, at the various $Cr_2O_7^{2-}$ concentrations (Fig. 8). Additionally, the ratio $i_{lim}^d/f^{1/2}$ is a linear function of the $Cr_2O_7^{2-}$ concentration throughout the temperature range investigated (Fig. 9).

Table 1 presents data for the kinematic viscosity of 0.5 M perchloric acid at various temperatures, diffusion coefficients obtained by application of the Levich equation to the disc electrode data, and solvodynamic radii calculated from the Stokes-Einstein equation: $(D\eta/T) = k/6\pi r$.

In the experimental temperature range, the diffusion coefficient data exhibit typical Arrhenius behavior ($D \times 10^5$ cm^2/s) = 1153 exp ($-2060/T$) with an activation energy for diffusion of E_D = 4.1 kcal/mol.

The experimental polarization curve data were analyzed in terms of the treatment developed by Opekar and Beran (17), using the following equation

$$[4] \quad \log (I/I_{lim}^d - I) = A - 2.30\,(\alpha_i n_i F/RT)\,(E - E_i^0)$$

In this equation, A is a constant (dependent on $f^{1/2}$), E_i^0 the standard potential, α_i the charge transfer coefficient, and n_i the number of electrons involved in the process.

Curves of log $(I/I_{lim}^d - I)$ as function of the elec-

TABLE 1. Variation of viscosity and diffusion coefficient with temperature

T(°C)	η (cP)	$D \times 10^5$ (cm^2/s)	$r \times 10^8$ (cm)
25.0	0.8863	1.14	2.2
30.0	0.8053	1.32	2.1
35.0	0.7344	1.43	2.1
40.0	0.6715	1.60	2.1

Can. J. Chem. Downloaded from www.nrcresearchpress.com by 210.87.254.105 on 09/05/12
For personal use only.

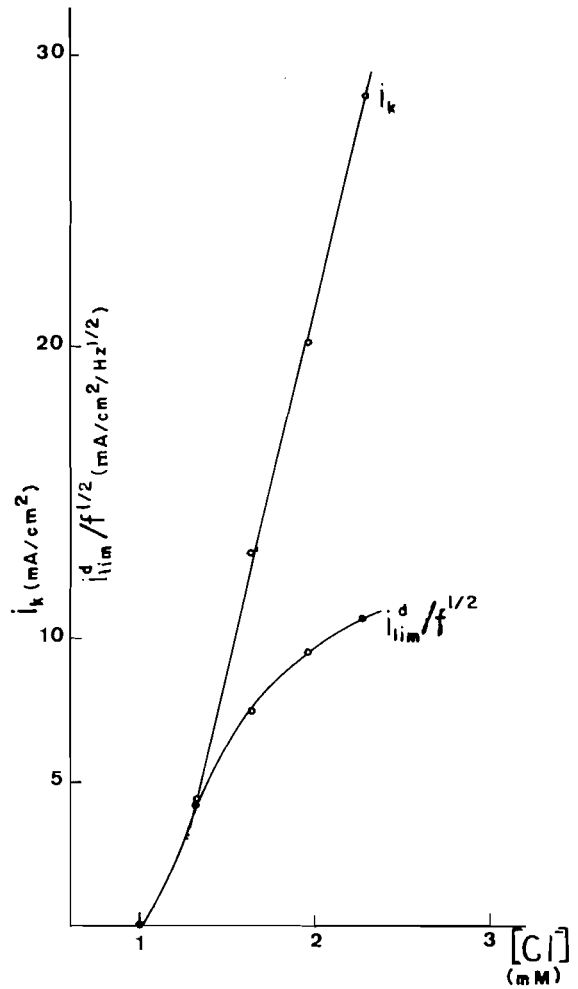

FIG. 7. Plot of $i_{lim}{}^d/f^{1/2}$ and i_k vs. $[Cl^-]$ for the less cathodic wave. $[CrO_3] = 0.1\ M$. $t = 25°C$.

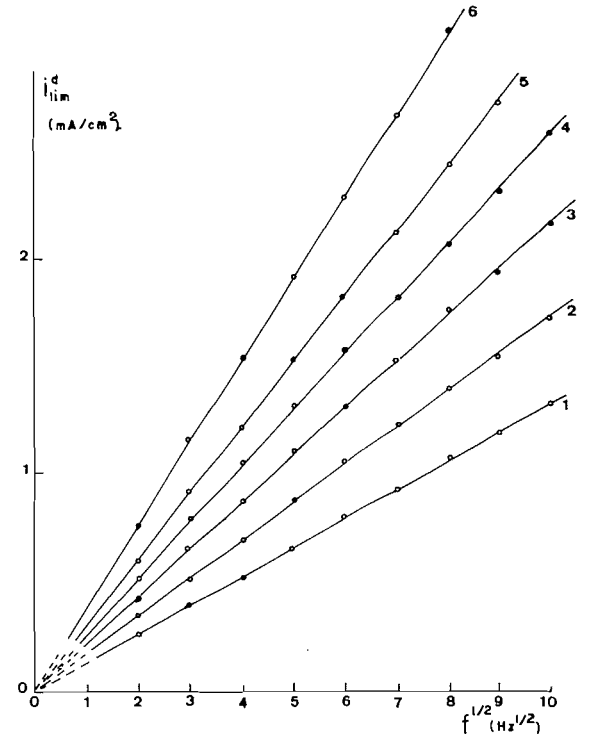

FIG. 8. Plot of $i_{lim}{}^d$ vs. $f^{1/2}$. $t = 40°C$, $[ClO_4^-] = 0.5\ M$; $[Cr_2O_7{}^{2-}]$: (*1*) 0.10 mM; (*2*) 0.13 mM; (*3*) 0.17 mM; (*4*) 0.20 mM; (*5*) 0.23 mM; (*6*) 0.29 mM.

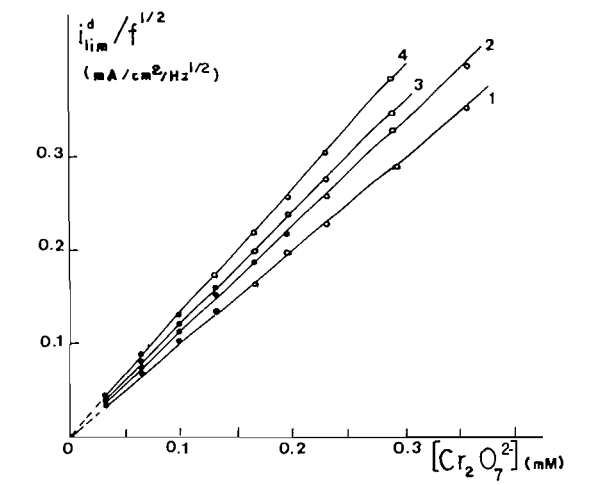

FIG. 9. Plot of $i_{lim}{}^d/f^{1/2}$ vs. $[Cr_2O_7{}^{2-}]$, $[ClO_4^-] = 0.5\ M$. t: (*1*) 25.0°C; (*2*) 30.0°C; (*3*) 35.0°C; (*4*) 40.0°C.

trode potential E at a rotation frequency of $f = 49$ Hz and a $Cr_2O_7{}^{2-}$ concentration of 0.13 mM are shown in Fig. 10.

These curves exhibit two linear portions of different slope at all temperatures investigated, indicating that the reduction Cr^{6+}/Cr^{3+} occurs in two steps. Values of the products $\alpha_i n_i$ calculated from the slopes of Fig. 10 corresponding to the linear regions at less cathodic ($\alpha_1 n_1$) and more cathodic ($\alpha_2 n_2$) potentials are presented in Table 2. In addition, this table contains values of the charge transfer coefficients α_1 and α_2 calculated assuming that n_1 and n_2 refer to one- and two-electron steps, respectively.[1]

[1]In principle the data are not sufficient to eliminate the possibility that the two rate determining steps occur in parallel with $\alpha_2 n_2$ corresponding to a 3-electron process which becomes the faster step at more cathodic electrode potentials.

Conclusions

The present work demonstrates that, in the presence of sulfate ions, the reduction Cr^{6+}/Cr^{3+} must be preceded by a chemical reaction, confirming the previous suggestion of Budevskii and Toshev (10). Our results at low chromic acid concentrations exhibit,

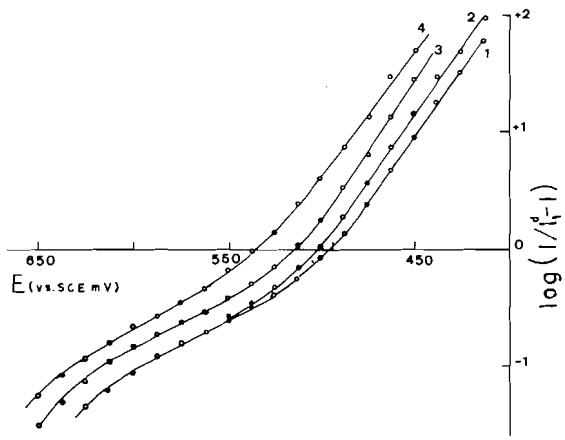

FIG. 10. Dependence of log $I/I_{lim}^{d} - I$ upon electrode potential, $f = 49$ Hz, $[Cr_2O_7^{2-}] = 0.13$ mM. $[ClO_4^-] = 0.5$ M. t: (*1*) 25.0°C; (*2*) 30.0°C; (*3*) 35.0°C; (*4*) 40.0°C.

TABLE 2. Charge transfer coefficients for Cr^{6+}/Cr^{3+} reduction

T (°C)	$\alpha_1 n_1$	n_1	α_1	$\alpha_2 n_2$	n_2	α_2
25.0	0.56	1	0.56	1.28	2	0.64
30.0	0.52		0.52	1.47		0.74
35.0	0.51		0.51	1.36		0.68
40.0	0.56		0.56	1.41		0.71
			$\bar{\alpha}_1 = 0.54$			$\bar{\alpha}_2 = 0.69$

however, several differences in relation to those obtained by these authors. Although the kinetic current i_k does depend on the sulfate ion concentration (see Fig. 3), we do not observe the direct proportionality reported by Budevskii and Toshev using more concentrated solutions.

If we assume that the chemical reaction preceding the electrochemical process is attributable to reduction of hexavalent chromium by atomic hydrogen (8):

$$Cr_2O_7^{2-} + 8H^+ + 6H_{at} \rightarrow 2Cr^{3+} + 7H_2O$$

we can conclude that the generation of atomic hydrogen, catalyzed by the presence of sulfate ions (7) in the cathode film, may be 'inhibited' by excess SO_4^{2-} ions. Such 'inhibition' would lead to a decrease in the kinetic current, of the type observed in Fig. 3 at chromic acid concentration of 0.2 M and for sulfate concentrations above 6 mM. Potential sources of an inhibitory effect of this type would be modifications of the composition and/or structure of the cathode film.

The sulfate concentrations which correspond to the sharp breaks in the curves of $i_{lim}^{d}/f^{1/2}$ vs. SO_4^{2-} concentration (Fig. 2) are approximately those above which a linear relationship is observed between the kinetic current i_k and SO_4^{2-} concentration (Fig. 3). This change in behavior probably bears a relationship as well, to modifications of the cathode film.

Using a value of 1×10^{-5} to 3×10^{-5} cm^2/s for the diffusion coefficient in the Levich equation, and an analysis similar to that employed by Budevskii and Toshev, we calculate that, in the region where $i_{lim}^{d}/f^{1/2}$ is directly proportional to the sulfate concentration, the number of electrons exchanged is of the order of 50–25 per sulfate ion. Since three electrons are consumed in the reduction per molecule of CrO_3, we obtain the result that approximately 17–8 molecules of CrO_3 are reduced per sulfate ion in the cathode film. This latter value is roughly twice that calculated by Budevskii and Toshev.

As can be seen in Figs. 4 and 6 the effect of Cl^- ion on the reduction Cr^{6+}/Cr^{3+} is more complex than that of SO_4^{2-} ions. The two peaks of the curve in Fig. 4 are associated with the formation of cathodic films on the electrode surface at two different potentials. The breaks in the curves of Fig. 6 may be related to the interaction of the effects of these two films on the reduction process.

In the non-complexing perchloric acid medium, the reduction Cr^{6+}/Cr^{3+} occurs in an entirely different manner. Thus, in the range of temperatures studied, the reduction process exhibits a region which is limited by convective diffusion, the calculated activation energy ($E_D = 4.1$ kcal/mol) being within the normal range for a diffusional process. It was additionally verified (Tables 1 and 2) that the solvodynamic radius of the dichromate ion and the charge transfer coefficients α_1 and α_2 are temperature independent.

Taken as a whole, the results indicate that in perchloric acid the Cr^{6+}/Cr^{3+} reduction process occurs in two steps in accord with the following scheme:

$$Cr^{6+} \xrightarrow{1e^-,\ \bar{\alpha}_1 = 0.54} Cr^{5+} \xrightarrow{2e^-,\ \bar{\alpha}_2 = 0.69} Cr^{3+}$$

At less cathodic potentials, the first step is rate limiting and at more cathodic potentials the second step is rate limiting.

Acknowledgements

The author is grateful to FAPESP for financial support of this work (processo 75/1062) and to Dr. Ivo Jordan for his translation of portions of publications not available in English.

1. N. E. RYAN. Met. Finish. **63**, 46 (1965); **63**, 73 (1965).
2. D. N. USACHEV and A. T. VAGRAMYAN. Sov. Electrochem. **11**, 103 (Consultants Bureau, N.Y.) 1961.
3. A. T. VAGRAMYAN and D. N. USACHEV. J. Phys. Chem. USSR, **32**, 1900 (1958).
4. A. T. VAGRAMYAN, Z. A. SOLOV'EVA, and YU. S. PETROVA. Sov. J. Appl. Chem. USSR, **34**, 1907 (1960).

Can. J. Chem. Downloaded from www.nrcresearchpress.com by 210.87.254.105 on 09/05/12
For personal use only.

5. H. GERISCHER and M. KÄPPEL. Zs. F. Elektrochem. **61**, 463 (1957).
6. H. FEIGL and C. A. KNORR. Zs. F. Elektrochem. **63**, 239 (1959).
7. D. N. USACHEV. J. Phys. Chem. USSR, **36**, 711 (1962).
8. N. A. MARCHENKO, S. KH. LIPKO, and F. KHORVATKH. Sov. Electrochem. **10**, 414 (1974).
9. M. H. JONES and J. SAIDDINGTON. 48th Ann. Proc. Am. Electropl. Soc. 32 (1961).
10. E. BUDEVSKII and S. TOSHEV. A. K. Dokl. Nauk SSSR, **130**, 1047 (1960).
11. N. D. BIRYUKOV. Sov. Electrochem. **12**, 1742 (1970).
12. H. C. CHAGAS. Cienc. Cult. **29**, 601 (1977).
13. H. C. CHAGAS. To be published.
14. D. C. JOHNSON. Thesis. University of Minnesota, MN, USA. 1967.
15. W. VIELSTICH and D. JAHN. *In* Advances in Polarography. Vol. 1. *Edited by* I. S. Longmuir. Pergamon Press, New York. 1960. p. 281.
16. E. BUDEVSKII. Izv. Bulg. Akad. Nauk, Sov. Phys. **5**, 89 (1955).
17. F. OPEKAR and P. BERAN. Electrochim. Acta, **22**, 243 (1977).

Can. J. Chem. Downloaded from www.nrcresearchpress.com by 210.87.254.105 on 09/05/12
For personal use only.

Influence des groupes *tert*-butyle, triméthylsilyle et triméthylgermyle sur la stéréochimie de réactions d'addition en série cyclohexénique. II. Epoxydation des dérivés vinyliques et ouverture des époxydes par $LiAlH_4$, $MeOH/H^+$ et H_2O/H^+

JEAN-CLAUDE RICHER ET MARC-ANDRÉ POIRIER

Département de Chimie, Université de Montréal, B.P. 6210, Montréal (Qué.), Canada H3C 3V1

ET

YVETTE MARONI ET GEORGES MANUEL

Département de Chimie, Université Paul Sabatier, 118 Route de Narbonne, 31077 Toulouse Cedex, France

Reçu le 30 janvier 1978

JEAN-CLAUDE RICHER, MARC-ANDRÉ POIRIER, YVETTE MARONI et GEORGES MANUEL. Can. J. Chem. **56**, 2049 (1978).

On présente la réaction d'époxydation des *tert*-butyl-1 (**1***a*), triméthylsilyl-1 (**1***b*) et triméthylgermyl-1 (**1***c*) diméthyl-4,4 cyclohexènes et on examine la stéréochimie de l'ouverture des époxydes correspondants (**3***a*, **3***b*, **3***c*) par l'hydrure double de lithium et d'aluminium, par le méthanol et enfin par l'eau en milieu acidulé; on note que par opposition à la régiochimie de l'ouverture de **3***a*, celle de **3***b* et **3***c* est complètement inversée par les effets électroniques des groupes triméthylsilyle et triméthylgermyle.

JEAN-CLAUDE RICHER, MARC-ANDRÉ POIRIER, YVETTE MARONI, and GEORGES MANUEL. Can. J. Chem. **56**, 2049 (1978).

Epoxidation of 1-*tert*-butyl (**1***a*), 1-trimethylsilyl (**1***b*), and 1-trimethylgermyl (**1***c*) 4,4-dimethylcyclohexenes is described and the stereochemistry of the ring opening of the resulting epoxides (**3***a*, **3***b*, **3***c*) by lithium aluminium hydride as well as methanol and water in acidic medium is examined. The regiochemistry of the ring opening of **3***a* is completely reversed, in the case of **3***b* and **3***c*, by the electronic effects of the trimethylsilyl and trimethylgermyl groups.

Introduction

Dans une publication antérieure (1), on a décrit la synthèse des alcènes vinyliques et allyliques des types **1** et **2**, tout en examinant la stéréochimie de leur réaction d'hydroboration (2).

L'étude d'α,β-époxyvinylsilanes suscite beaucoup d'intérêt (3–7). Dans cette communication, on rapporte les résultats obtenus lors de l'époxydation des alcènes du type **1** par l'acide *m*-chloroperbenzoïque (AMCP) et lors de l'ouverture des époxydes du type **3** par l'hydrure double de lithium et d'aluminium ($LiAlH_4$), par le méthanol et l'eau acidulés. Ces résultats permettent de mettre en évidence les influences relatives des groupes *tert*-butyle et triméthylsilyle (ou germyle).

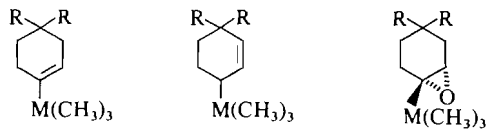

1 **2** **3**

a M = C; R = CH_3
b M = Si; R = CH_3
c M = Ge; R = CH_3

Résultats et discussion

La réaction d'époxydation de l'alcène carboné **1***a* par l'acide *m*-chloroperbenzoïque (AMCP), conduit à l'époxyde **3***a*. L'époxydation de l'alcène silylé **1***b* (8) et germylé (**1***c*) par AMCP conduit d'une façon analogue aux époxydes **3***b* et **3***c*.

TABLEAU 1. Pourcentages relatifs des isomères obtenus par réduction des époxydes du type **3**

	% alcool	
	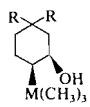	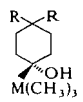
Epoxyde	**4**	**5**
3*a*	0	100
3*b*	99	1
3*c*	96	4

Les résultats obtenus lors de la réduction des époxydes du type **3** par l'hydrure double de lithium et d'aluminium sont rapportés dans le tableau 1. Comme l'indique le tableau 1, l'ouverture de l'époxyde carboné **3***a* par $LiAlH_4$ procède par une ouverture *trans* et diaxiale avec attaque sur le carbone le plus dégagé. En série silylée (**3***b*) et germylée (**3***c*), la régiochimie de la réaction est inversée.

La réduction des époxydes silylé (**3***b*) et germylé (**3***c*), en accord avec les résultats de Robbins et

Can. J. Chem. Downloaded from www.nrcresearchpress.com by 210.87.254.40 on 09/05/12
For personal use only.

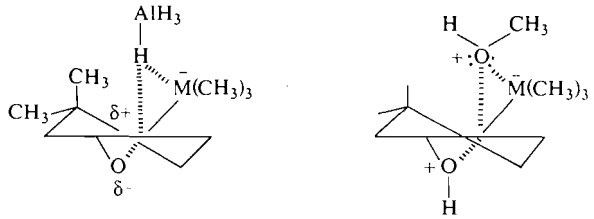

8*a* 8*b*

SCHÉMA 1

Whitham (9), procède par une attaque nucléophile au carbone-1 avec inversion de configuration, conduisant respectivement aux alcools **4***b* et **4***c*. La régiospécificité observée peut être expliquée par un état de transition (schéma 1, **8***a* M = Si, Ge) similaire à celui proposé par Eisch et Trainor (10) dans le cas des α,β-époxyvinylsilanes.

L'effet électronique développé dans cet état de transition par le groupe triméthylsilyle (8) l'emporte sur les fortes interactions pouvant intervenir entre l'un des méthyles du groupe $(CH_3)_3M$ et le réactif. L'hypothèse d'un réarrangement, en présence d'un acide de Lewis (8, 9, 11), des époxydes silylés et germylés en cétone **6** puis réduction de celle-ci ne

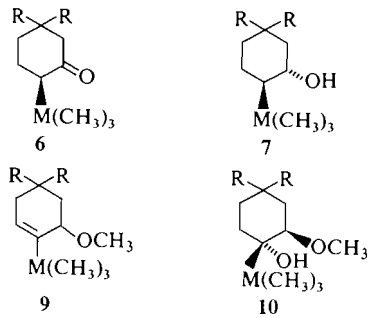

peut être retenue, puisque la réduction de **6***b* par $LiAlH_4$ conduit à 15% de **7***b* et 85% de **4***b* (12) et d'ailleurs la préférence de l'ouverture en α,β-époxysilanes a déjà été observée dans plusieurs travaux (8, 9, 13).

La régiochimie de l'ouverture des époxydes carbonés, silylés et germylés par le méthanol en milieu acide est la même que celle observée lors de leur réduction par $LiAlH_4$. L'ouverture de l'époxyde carboné **3***a* par le méthanol en milieu légèrement acide, conduit à 67% de *tert*-butyl-2 diméthyl-5,5 cyclohexanone **6***a* et à 33% d'éther allylique **9***a*. L'éther allylique **9***a* provient essentiellement de l'hydroxy-éther **10***a* qui se forme d'une façon transitoire et qui se déshydrate facilement en milieu acide (14). On a montré que la cétone **6***a* peut se former par réarrangement de l'éther allylique **9***a* en milieu acide en remettant le mélange **6***a*–**9***a* dans les conditions décrites précédemment et en notant que celui-ci évoluait vers un nouveau mélange constitué presqu'uniquement de cétone **6***a*. On pourrait aussi suggérer que la cétone **6***a* provient d'un réarrangement pur et simple de **3***a* en milieu acide; le fait que l'on n'isole pas de cétone **6***a* par traitement de **3***a* en milieu acide aqueux indique que cette dernière suggestion ne doit pas être retenue.

Plusieurs études concernant l'ouverture d'α,β-époxyvinylsilanes en milieu acide ont été rapportées jusqu'à maintenant (9, 6, 15). Stork et Colvin (14) ont montré que l'ouverture des α,β-époxyvinylsilanes en milieu acide conduit à des composés carbonylés et ils ont suggéré que cette réaction procède suivant le schéma 2. Par ailleurs Hudrlik *et al.* (15) ont

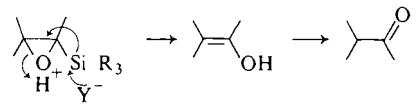

SCHÉMA 2

récemment observé des résultats semblables en série acyclique pour l'hydrolyse catalysée en milieu acide tandis qu'ils notaient la formation de diols en série cyclique.

Dans notre cas, l'ouverture des époxydes **3***b* et **3***c* par le méthanol en milieu acide dilué conduit uniquement aux composés de type **11**, en accord avec les résultats de Robbins et ses collaborateurs (9) et l'obtention de l'hydroxy éther **11** peut être expliquée

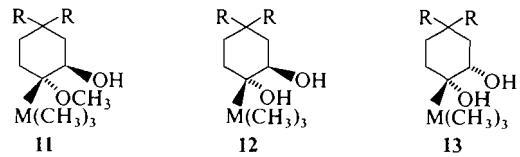

en se basant uniquement sur le fait que les groupes OH et $(CH_3)_3M$ où M = Si, Ge ne peuvent pas adopter la configuration *anti* nécessaire à une β-élimination (15).

La stéréo- et régiospécificité de cette réaction peut être rationalisée d'une façon similaire à celle proposée pour la réduction des époxydes **3***b* et **3***c* par $LiAlH_4$ (voir schéma 1, **8***b*).

On remarque que l'atome de germanium introduit des facteurs stéréoélectroniques comparables à ceux introduits par l'atome de silicium au cours de l'ouverture des époxydes du type **3**.

La stéréochimie de l'ouverture des époxydes **3** par l'eau en milieu acide ressemble beaucoup à celle de l'ouverture par le méthanol en milieu acide (9). Cette dernière nous a permis en premier lieu d'établir le sens de l'ouverture des époxydes du type **3**.

L'ouverture de l'époxyde **3***a* par l'eau en milieu acide conduit uniquement au composé **12***a*. Les résultats peuvent être interprétés par un mécanisme

Can. J. Chem. Downloaded from www.nrcresearchpress.com by 210.87.254.40 on 09/05/12
For personal use only.

Can. J. Chem. Downloaded from www.nrcresearchpress.com by 210.87.254.40 on 09/05/12
For personal use only.

similaire à celui proposé pour l'ouverture par le méthanol acidulé (schéma 1, **8***b*). Le diol **12***a* ne conduit pas à des produits de déshydratation ou de réarrangement et pourrait s'expliquer par des raisons de solubilité dans le milieu réactionnel.

L'ouverture des époxydes **3***b* et **3***c* par l'eau en milieu acide conduit aux diols *trans* **12***b* et **12***c* (9). Dans chacun des cas, seulement un stéréoisomère est isolé. Les configurations ont été déterminées par des méthodes spectrométriques telles que la rmn et par comparaison avec leurs isomères *cis* (**13**) obtenus par action du tétroxyde d'osmium (16, 17) sur les alcènes du type **1**.

Partie expérimentale

Les points de fusion ont été déterminés sur un appareil Cole-Parmer de la compagnie Instrument & Equipment.

Les spectres ir ont été pris sur un spectrophotomètre Beckman modèle IR-8 à double faisceau et sauf indication contraire, tous les spectres ont été pris entre deux plaques de NaCl.

Les spectres de résonance magnétique nucléaire ont été déterminés sur un spectromètre modèle C-60-H de la compagnie JEOL. Le solvant choisi est le $CDCl_3$ pour les séries carbonées et le tétrachlorure de carbone pour les séries silylées et germylées. Les déplacements chimiques sont exprimés en ppm et se réfèrent au tétraméthylsilane utilisé comme référence interne pour les séries carbonées; le chloroforme est utilisé comme référence interne pour les séries silylées et germylées. Les indices de réfraction ont été déterminés à l'aide d'un réfractomètre du type Abbé. La pureté de tous les nouveaux produits décrits dans ce travail a été déterminée par chromatographie en phase gazeuse et leur identité confirmée par spectrométrie de masse à l'aide d'un spectromètre Hitachi-Perkin-Elmer modèle RMU6-D opérant avec une énergie de faisceau d'électrons ionisant de 70eV.

Epoxydation des alcènes

De l'alcène carboné **1**a

Dans un ballon de 50 ml surmonté d'un refrigérant, on introduit (1.0 g) 6 mmol d'alcène **1***a* (18) dilué dans 6 ml de $CHCl_3$ et 12 ml de CH_2Cl_2. A cette solution, on ajoute rapidement 2.0 g (12 mmol) d'acide *m*-chloroperbenzoïque et on chauffe à 40–45°C le ballon sous agitation, pendant 24 h.

Le mélange réactionnel est filtré et le précipité lavé avec du chloroforme. Le filtrat est lavé avec une solution de soude 5% puis à l'eau et la phase organique séchée sur du K_2CO_3, filtrée et concentrée sous vide, conduit à 1.0 g d'époxyde **3***a* (90% du rendement théorique) dont les caractéristiques sont les suivantes: pé 78°C/11 Torr; n_D^{23} 1.4500; ir: 860, 750 (C—O); rmn (CCl_4): 2.92 (C<u>H</u>(O)—C—, m), 0.92 (9 protons du groupe *tert*-butyle, s) 0.87 et 0.82 ppm (6 protons correspondants au *gem*-diméthyle).

Des alcènes silylé **1**b *et germylé* **1**c

On procède comme pour l'époxydation de l'alcène carboné **1***a*, à ceci près que la réaction a lieu à −5°C pendant 45 min. Le mélange réactionnel est extrait comme précédemment et conduit respectivement aux époxydes **3***b* et **3***c* (92% du rendement théorique).

Epoxyde **1**b—pé 28°C/0.25 Torr; n_D^{23} 1.4519; ir 1245 ($SiCH_3$), 980, 960, 830, 740 cm^{-1} (correspondant à la vibration C—O); rmn (CCl_4): 2.83 (C<u>H</u>(O)—C—, m) 0.90, 0.80 (6 protons correspondants au *gem*-diméthyle), 0.03 ppm (singulet 9 protons du $SiMe_3$).

Epoxyde **1**c—pé 88°C/10 Torr; n_D^{18} 1.4721; ir: 1230, 750 (C—O), 820 ($GeMe_3$) cm^{-1}; rmn (CCl_4): 2.80 (correspondant au proton époxyde), 0.90 et 0.83 (6 protons du groupe *gem*-diméthyle), 0.43 ppm (singulet 9 protons du $GeMe_3$).

Réduction par $LiAlH_4$

La réduction des époxydes de type **3** a été réalisée comme suit; dans un ballon de 100 ml refroidi à 0°C, on introduit 0.5 g de $LiAlH_4$ en suspension dans 10 ml d'éther anhydre. Par une ampoule à brome, on ajoute une solution contenant 5.5 mmol d'époxyde dans 10 ml d'éther anhydre. On porte le mélange réactionnel au reflux du solvant pendant 20 h, puis refroidit à 0°C. Après hydrolyse avec une solution de soude 5%, on extrait les produits organiques à l'éther. La phase éthérée est alors séchée sur du Na_2SO_4, filtrée et concentrée sous vide. Les rendements moyens en alcool sont de 85%.

Analyse des produits

Les mélanges d'alcools provenant des réactions de réduction des époxydes par $LiAlH_4$ ont été analysés par chromatographie en phase gazeuse à l'aide d'un chromatographe à ionisation de flamme Research Chromatograph 700 de la compagnie F et M muni d'une colonne de 6 pied × ⅛ po remplie de Diatoport 5750 (80–100) supportant 6% de son poids de LAC 728. Les temps de rétention (en minute) des alcools dans ces conditions sont résumés dans le tableau 2. L'identification des pics a été réalisée par superposition avec des échantillons authentiques préparés par une autre voie (1).

TABLEAU 2. Temps de retention (en min) des alcools

Alcool	Série *a*	Série *b*	Série *c*
5	3.7	3.2	5.3
4	5.5	4.3	6.4
7	7.3	5.1	7.2

Ouverture par le méthanol acidulé

L'ouverture des époxydes du type **3** a été réalisée sur des échantillons de 1.2 mmol d'époxydes en solution dans 14 ml de méthanol anhydre et 0.3 ml d'acide sulfurique. Le mélange réactionnel est agité à 45°C pendant 24 h, refroidi et extrait de la façon habituelle. Les rendements moyens de cette réaction sont de 75%.

L'analyse du mélange de la série a a été effectuée par cpg en utilisant une colonne de 10 pied × ¼ po remplie avec 15% de Carbowax 20 M déposé sur chromosorb W 60–80 mesh, chauffé à 120°C et un débit de 66 ml/mn.

Composé **6**a—Voir réf. 19.

Composé **9**a—ir: 3065 (C=C), 1080 (C—O) cm^{-1}; rmn (CCl_4): 5.30 (C<u>H</u>=C), 3.57 (C<u>H</u>—O), 3.10 (OMe), 0.93 et 0.83 (correspondant à 6 protons du groupe *gem*-diméthyle), 1.03 ppm (9 protons du *tert*-butyle).

Composé **11**b—pé 66–68°C/0.8 Torr; n_D^{20} 1.4735; ir 3480, 2840, 1245, 975 cm^{-1}; rmn (CCl_4): 3.93 (proton carbinolique), 3.23 (OMe), 0.96 (*gem*-diméthyle, s) et 0.13 ppm (Me_3Si); rmn (DMSO-d_6): doublet à 4.43 ppm, J_{H-OH} = 3.60 Hz.

Composé **11**c—pé 80–82°C/0.8 Torr; n_D^{20} 1.4873; ir: 3450, 2840, 1045, 815 cm^{-1}; rmn (CCl_4): 3.83 (proton carbinolique), 3.23 (OMe), 0.93 (*gem*-diméthyle, s) 0.28 (Me_3Ge); rmn (DMSO-d_6): doublet à 4.63 ppm, J_{H-OH} = 3.60 Hz.

Ouverture par l'eau acidulée

D'une façon générale, l'ouverture des époxydes du type **3** a

été réalisée en maintenant un mélange formé de 14 ml d'eau, 0.3 ml H_2SO_4 concentrée et 0.6 g (11 mmol) d'époxyde à 45°C pendant 24 h. Après refroidissement et extraction de la façon habituelle, les diols ont pu être isolés avec des rendements moyens de 50%.

Composé ***12***a—pf 144–145°C; ir (Nujol): 3300 cm^{-1} (O—H); rmn (CCl_4): 3.73 (proton carbinolique), 1.07 (9 protons du *tert*-butyle), 0.77, 0.87 ppm (6 protons du *gem*-diméthyle); rmn (DMSO-d_6): doublet mal résolu à 4.30 ppm et singulet à 3.73 ppm.

Composé ***12***b—pf 78–80°C; ir (Nujol): 3420, 1240 cm^{-1}; rmn (CCl_4): 3.83 (proton carbinolique), 1.19 (*gem*-diméthyle, s), 0.36 ppm (Me_3Si); rmn (DMSO-d_6): doublet à 4.76 ppm, J_{H-OH} = 4.00 Hz et singulet à 3.83 ppm.

Composé ***12***c—pf 92–94°C; ir (Nujol): 3410, 1380, 1370, 840 cm^{-1}; rmn (CCl_4): 3.66 (proton carbinolique), 0.96 (*gem*-diméthyle, s) 0.23 ppm (Me_3Ge); rmn (DMSO-d_6): doublet à 4.56 ppm, J_{H-OH} = 3.90 Hz, singulet à 3.90 ppm.

Obtention des diols cis (***13***)

L'obtention des diols *cis* (**13**) a été réalisée comme suit: dans un ballon de 100 ml à 25°C et à l'obscurité, 30 ml d'éther anhydre et 0.8 g (5 mmol) d'alcène sont introduits. On ajoute 1 g de tétroxyde d'osmium préalablement dissous dans 5–10 ml d'éther, et le mélange réactionnel est maintenu 40 h à 25°C. L'éther est évaporé et le mélange traité par 25 ml d'eau, 5 g de mannitol, 2 g de KOH et 30 ml de CH_2Cl_2. On porte au reflux le mélange réactionnel pendant 5 h puis on extrait à l'éther les produits organiques. Après sublimation, 0.7 g de diol est obtenu. Les rendements moyens de cette réaction sont de 70%.

Composé ***13***a—pf 126–127°C; ir (Nujol): 3340, 1370, 1360, 1060 cm^{-1}; rmn (CCl_4): 3.90 (proton carbinolique), 0.93 et 0.87 (*gem*-diméthyle), 1.03 ppm (9 protons du *tert*-butyle); rmn (DMSO-d_6): doublet mal résolu à 3.83 ppm et singulet à 3.20 ppm.

Composé ***13***b—pf 122–123°C; ir (Nujol): 3350, 1375, 1350, 1040, 960 cm^{-1}; rmn (CCl_4): 3.60 (C*H*—O), 0.93 et 0.86 (*gem*-diméthyle), 0.03 ppm (Me_3Si); rmn (DMSO-d_6): doublet à 4.00 ppm, J_{H-OH} = 6.80 Hz, singulet à 2.97 ppm.

Composé ***13***c—pf 122–123°C; ir (Nujol): 3320, 1380, 1365, 1070, 1050 cm^{-1}; rmn (CCl_4): 3.86 (C*H*—O), 1.23 et 1.16 (*gem*-diméthyle), 0.46 ppm (Me_3Ge); rmn (DMSO-d_6): doublet à 4.03 ppm, J_{H-OH} = 6.80 Hz, singulet à 3.26 ppm.

Remerciements

Les auteurs remercient vivement le Conseil national de recherches Canada, le CNRS français et les autorités chargées d'administrer les accords Franco-Québécois pour l'aide financière apportée sous forme d'octroi de recherches, de bourses d'études et de frais de mission. Les auteurs tiennent à remercier le Dr Pierre Maroni pour l'accueil chaleureux réservé à M. Marc-André Poirier durant son stage à Toulouse. Les auteurs tiennent aussi à exprimer leur reconnaissance aux Dr Mazerolles et Lesbre pour leur compréhension et leurs discussions utiles.

1. C. Freppel, M. A. Poirier, J. C. Richer, Y. Maroni et G. Manuel. Can. J. Chem. **52**, 4133 (1974).
2. H. C. Brown et Z. Zweifel. J. Am. Chem. Soc. **83**, 2544 (1961).
3. H. Sakurai, N. Hayashi et M. Kumada. J. Organometal. Chem. **18**, 351 (1969).
4. A. G. Brook et D. M. Macrae. J. Organometal. Chem. **77**, C19 (1974).
5. L. V. Nozdrina, Ya. I. Mindlin et K. A. Andrianov. Russ. Chem. Rev. **42**, 509 (1973).
6. T. H. Chan, Ming P. Li, W. Mychajlowskij et D. N. Harpp. Tetrahedron Lett. 3511 (1974).
7. R. K. Boeckman, Jr. et K. J. Bruza. Tetrahedron Lett. 3365 (1974).
8. P. F. Hudrlik, R. N. Misra, G. P. Withers, A. M. Hudrlik, R. J. Rona et J. P. Arcoleo. Tetrahedron Lett. 1453 (1976).
9. C. M. Robbins et G. H. Whitham. Chem. Commun. 697 (1976).
10. J. J. Eisch et J. T. Trainor. J. Org. Chem. **28**, 2870 (1963).
11. M. Obayashi, K. Utimoto et H. Nozaki. Tetrahedron Lett. 1807 (1977).
12. M. A. Poirier. Thèse de doctorat, Université de Montréal, Montréal, Qué. 1975.
13. P. F. Hudrlik, D. Peterson et R. J. Rona. J. Org. Chem. **40**, 2263 (1975).
14. G. Stork et E. Colvin. J. Am. Chem. Soc. **93**, 2080 (1971).
15. P. F. Hudrlik, J. P. Arcoleo, R. H. Schwartz, R. N. Misra et R. J. Rona. Tetrahedron Lett. 591 (1977).
16. R. B. Woodward, F. Sondheimer, D. Taub, K. Heusler et W. M. McLamore. J. Am. Chem. Soc. **74**, 4223 (1952).
17. C. W. Davey, E. L. McGinnes, J. M. McKeown, G. D. Meakins, M. W. Pemberton et R. N. Young. J. Chem. Soc. 2674 (1968).
18. J. C. Richer et C. Freppel. Can. J. Chem. **46**, 3709 (1968).
19. M. A. Poirier. Thèse de Maîtrise, Université de Montréal, Montreal, Qué. 1972.

Can. J. Chem. Downloaded from www.nrcresearchpress.com by 210.87.254.40 on 09/05/12
For personal use only.

Solvolysis rates in aqueous – organic mixed solvents. V. Kinetics of the alkaline decarboxylation of trichloroacetate ion in water – ethanol solutions

EL-HUSSIENY M. DIEFALLAH[1] AND A. M. EL-NADI
Department of Chemistry, Assiut University, Assiut, Egypt

Received March 15, 1978

EL-HUSSIENY M. DIEFALLAH and A. M. EL-NADI. Can. J. Chem. **56**, 2053 (1978).

The kinetics of the alkaline decarboxylation of trichloroacetate ion in ethanol–water solutions have been studied over the temperature range 35.0 to 70.0°C. The rate of reaction is first order with respect to the trichloroacetate ion and is independent of the concentration of the hydroxide ion. The reactivity is enhanced by increasing the concentration of ethanol in the water–ethanol solutions and the rate of reaction varies with ethanol addition in a nonlinear manner. The rate of reaction increases with the reciprocal of the dielectric constant of the medium and the plot of log k vs. $1/D$ is approximately linear for solvent mixtures with less than about 0.7 water mole fraction but is strongly curved towards the pure water end. The activation parameters for the reaction show a regular increase in the solvent composition range 0.3 to 1.0 water mole fraction. The results are discussed in terms of the influence of solvent internal pressure and polarity on reactivity and of the increased amount of hydrogen-bonded structure in the water-rich solutions.

EL-HUSSIENY M. DIEFALLAH et A. M. EL-NADI. Can. J. Chem. **56**, 2053 (1978).

On a étudié à des températures allant de 35 à 70°C, la cinétique de la décarboxylation alcaline de l'ion trichloroacétate dans des solutions d'éthanol–eau. La vitesse de réaction est du premier ordre par rapport à l'ion trichloroacétate et elle est indépendante de la concentration de l'ion hydroxyde. Il y a une augmentation de la réactivité lorsque l'on augmente la concentration de l'éthanol dans des solutions d'eau–éthanol et la vitesse de la réaction varie avec l'addition d'éthanol d'une façon qui n'est pas linéaire. La vitesse de réaction augmente d'une façon parallèle à la constante diélectrique du milieu et une courbe de log k en fonction de $1/D$ est approximativement linéaire pour des mélanges de solvants contenant une fraction molaire d'eau plus petite que 0.7; toutefois il se produit une incurvation importante lorsque l'on approache de l'eau pure. Les paramètres d'activation de la réaction augmentent d'une façon régulière lorsque la fraction molaire d'eau dans le solvant varie de 0.3 à 1.0. On discute des résultats en terme d'une part de l'influence de la pression interne du solvant et de la polarité sur la réactivité et d'autre part de l'augmentation de la quantité de structure contenant des ponts hydrogène dans des solutions riches en eau.

[Traduit par le journal]

Introduction

Studies have been undertaken by several investigators to test for different theories accounting for the effect of solvent on the rates of chemical reactions in aquo-organic solvent binaries (1–10). Several factors influence solvent effects on chemical reaction rates; their relative importance seems to be a function of substrate, detailed mechanism of reaction, and experimental conditions. The influence of solvent variation on reaction rates may be examined conveniently in terms of the changes in the activation parameters, $\Delta H^{\neq}$ and $\Delta S^{\neq}$. For some solvolysis reactions in binary alcohol–water systems, changes in the activation parameters upon solvent variation were related to the accompanying solvent reorganization attending the activation process. The effect of solvent structure has been shown to be important in some cases but the sensitivity to solvent structural effects cannot always be demonstrated clearly and is dependent upon the nature of the organic co-solvent and on the temperature and the detailed mechanism of reaction. Dack (11) pointed out that solvent effects can generally be understood in terms of changes in volumes of activation and the cohesive energy density of the molecules of solvent, reactants and activated complex.

We have been undertaking a detailed study of the rates and mechanisms of the alkaline solvolysis of chloroacetate ions (1–4) in water–alcohol solutions, in order to test various theories of solvent effects on chemical reactions in solution. In the present study, we report the results of investigating solvent effects on the rate and mechanism of the alkaline solvolysis of sodium trichloroacetate in water–ethanol solutions.

Experimental

The details of the experimental procedure including methods for the characterization of the products of the reaction are similar to those previously outlined (1). The rate of reaction

[1]To whom all communications should be addressed. Present address: Department of Chemistry, Faculty of Science, King Abdulaziz University, Jeddah, P.O. Box 1540, Saudi Arabia.

Can. J. Chem. Downloaded from www.nrcresearchpress.com by 210.87.254.42 on 09/05/12
For personal use only.

Can. J. Chem. Downloaded from www.nrcresearchpress.com by 210.87.254.42 on 09/05/12
For personal use only.

TABLE 1. Effect of temperature and solvent composition on the rate constants of the alkaline solvolysis of trichloroacetate ion in water–ethanol solutions

Solvent water–ethyl alcohol (v/v)	Water mol fraction	Rate constant, $k \times 10^6$ (s^{-1})				
		35.0°C	45.0°C	50.0°C	56.0°C	70.0°C
Water	1.0	0.0384±0.0003	0.184±0.003	0.399±0.003	0.879±0.003	7.68±0.02
90.5:9.5	0.96	0.102 ±0.002	0.43 ±0.01	0.85 ±0.015	1.49 ±0.03	9.59±0.03
81.0:19.0	0.93	0.144 ±0.002	0.51 ±0.02	1.17 ±0.01	2.13 ±0.035	12.05±0.01
71.5:28.5	0.89	0.206 ±0.001	0.55 ±0.03	1.49 ±0.02	2.98 ±0.01	14.39±0.015
62.0:38.0	0.84	0.278 ±0.002	0.86 ±0.01	1.81 ±0.035	3.41 ±0.015	15.99±0.02
43.0:57.0	0.71	0.352 ±0.002	1.41 ±0.02	2.55 ±0.04	5.12 ±0.02	18.39±0.025
24.0:76.0	0.505	0.576 ±0.003	1.79 ±0.01	3.19 ±0.03	5.76 ±0.02	20.79±0.01
14.5:85.5	0.35	0.704 ±0.003	2.05 ±0.01	3.68 ±0.02	6.39 ±0.05	25.58±0.02

was followed in the temperature range 35.0 to 70.0°C, using a titrimetric method by following the release of chloride ions according to Volhard's technique. The initial concentrations of the trichloroacetic acid were in the range 0.10 to 0.05 mol/ℓ, while the initial concentrations of the base were in the range 0.80 to 0.40 mol/ℓ. In each reaction mixture, the concentration of the base was more than about five times that of the trichloroacetic acid.

Results and Discussion

The kinetics of the alkaline decarboxylation reaction of trichloroacetate ion in ethanol–water solutions showed certain similarities to that in the methanol–water solutions (1). In both cases the rate of reaction was found to be independent of the concentration of hydroxide ion and first order with respect to the trichloroacetate ion. Figure 1 shows typical first-order plots obtained in water–ethanol solutions at 50.0°C. The rate constants were evaluated from the slopes of such linear plots; data obtained with different solvent compositions and at the several temperatures are listed in Table 1. At least four kinetic runs were performed at each combination of reaction temperature and solvent composition.

Figure 2 shows the effect of solvent composition on the rate constants. It can be seen that the reactivity is enhanced by increasing the concentration of ethanol in the solution, and the rate of reaction varies with ethanol addition in a nonlinear manner. The change from methanol to ethanol should not produce a change in mechanism.

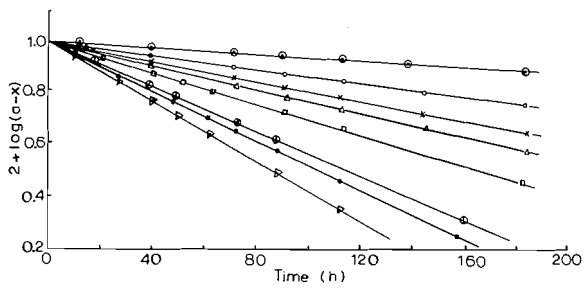

FIG. 1. First-order plots at 50.0°C in water–ethanol solutions. Water mol fraction: ⊙, 1.0; ○, 0.96; ×, 0.93; △, 0.89; □, 0.84; ⊗, 0.71; ●, 0.50; △, 0.35.

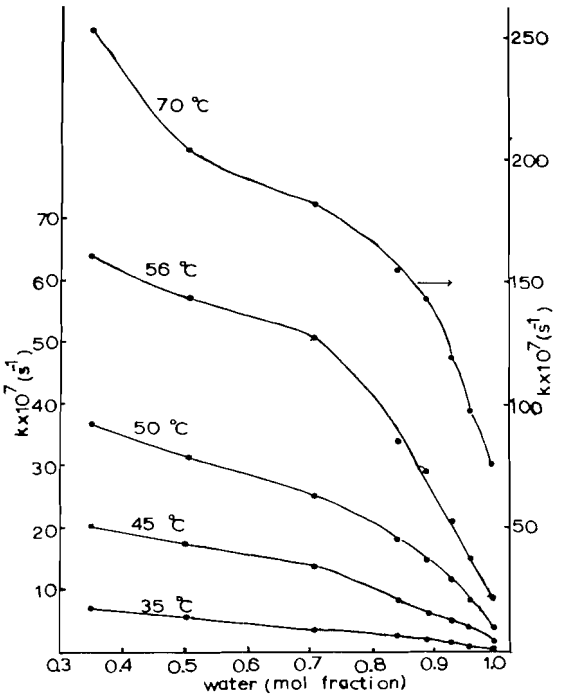

FIG. 2. Dependence of the first-order rate constants on solvent composition.

The kinetics of the reaction suggest a mechanism (12, 13) in which the rate-determining step is the breaking of the carbon–carbon bond with concomitant release of CO_2 and the formation of trichloromethyl carbanion intermediate:

[1] $$Cl_3C—COO^- \rightarrow Cl_3C^- + CO_2$$

The cumulative electron-withdrawing effect of the three chlorine atoms causes the C—C bond to break easily. The carbanion then expels chloride ion to

Can. J. Chem. Downloaded from www.nrcresearchpress.com by 210.87.254.42 on 09/05/12
For personal use only.

form dichlorocarbene:

[2] $$Cl_3C^- \rightarrow Cl_2C: + Cl^-$$

Bigeleisen and Allen (14) determined the relative rates of decomposition of 1-^{12}C and 1-^{13}C trichloroacetate ions in water and showed that the 1-^{12}C ion decomposes 1.0338 times as fast as the 1-^{13}C ion. This has been taken to support rate determining formation of Cl_3C^- but is also in accord with a rate limiting, one step formation of dichlorocarbene:

[3] $$Cl_3C—COO^- \rightarrow Cl^- + CO_2 + CCl_2$$

A choice between [1] and [3] could be made if it were known whether or not the reaction exhibits a chlorine isotope effect but such studies are not available at the present time. It is noted that [3] is a fragmentation process and this would result in an increased $\Delta S^{\ddagger}$ owing to the gain of translational, rotational, and vibrational degrees of freedom (15). In the alkaline decomposition of chloroform it is commonly assumed that the rate-determining step in the reaction is the unimolecular elimination of chloride ion from trichloromethyl anion to form dichlorocarbene (16–19). Measurements of the pressure coefficient of the rate constant (16) strongly suggested that H_2O electrostatically bound to the Cl_3C^- ion is released during the reaction and that the transition state goes on to free CCl_2.

The electrophile dichlorocarbene reacts with base to yield carbon monoxide and formate (17–20). Robinson (20) has proposed on kinetic evidence that carbon monoxide and formate are not formed simultaneously but that carbon monoxide is the primary product from which formate is produced by a subsequent slow reaction with hydroxide ions. Measurement of the concentrations of CO and $H{\cdot}COO^-$ during the course of the alkaline hydrolysis showed that the concentration–time curves are typically those of consecutive reactions. The decomposition of dichlorocarbene therefore includes the following consecutive reactions:

[4] $$CCl_2 \xrightarrow{2OH^-,\ H_2O} CO$$

[5] $$CO \xrightarrow{OH^-\ (slow)} H{\cdot}COO^-$$

Kinetic studies (20) of the reaction in which formate is produced from carbon monoxide and aqueous alkalis suggested that the mechanism involves a direct slow attack by hydroxide ions on the carbon atom in carbon monoxide followed by a prototropic rearrangement to formate. The ultimate end products of the reaction of trichloroacetate ion with base therefore has been identified as salts of hydrochloric, formic and carbonic acids (1).

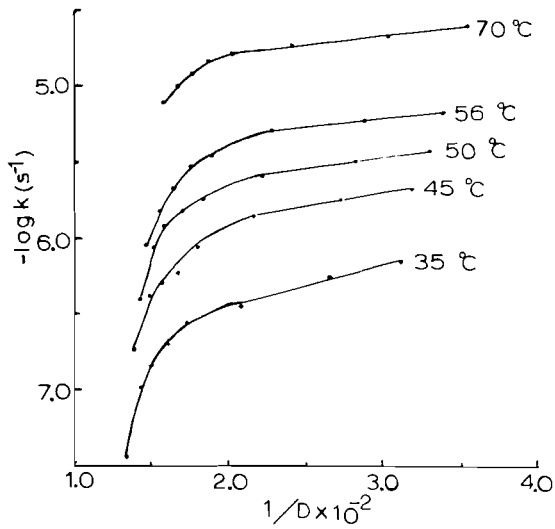

FIG. 3. Dependence of the first-order rate constants on the dielectric constant of the medium.

The rate of the reaction studied here decreases with increasing dielectric constant of the medium and the plot of log k vs. $1/D$ (Fig. 3) is approximately linear for solvent mixtures with less than about 0.7 water mole fraction but is strongly curved toward the pure water end. The use of $(D - 1)(2D + 1)^{-1}$ instead of D^{-1} did not improve the plot.

The enthalpy and entropy of activation for the reaction were calculated making use of the transition state theory (21) and the results together with E_a, the energy of activation and $\Delta G^{\ddagger}$, the free energy of activation are listed in Table 2. Figure 4 shows that $\Delta H^{\ddagger}$ and $\Delta S^{\ddagger}$ increase regularly with increase of water concentration in the solution without extrema or inflection points in the rich-water solvent mixtures (1, 2). The change in $\Delta S^{\ddagger}$ amounts to about 26.8 cal K^{-1} mol^{-1} between 1.0 and 0.35 water mole fraction, and that for $\Delta H^{\ddagger}$ is about 10.1 kcal mol^{-1} in the same composition range. The plot of $\Delta H^{\ddagger}$ vs. $\Delta S^{\ddagger}$ (Fig. 5) gave rise to a linear relationship as might be expected from solvents playing similar roles in the reaction (22).

The volumes of the reactant species and that of the activated complex in a given solvent depend on the structure of the species and on the ability of the solvent to compress this volume by electrostriction (11). In the above mechanism there is a net loosening of bonds in the transition state, so we may expect the volume of activation to be a positive quantity and the internal pressure of the reactant ion to be higher than that of the activated complex. The effect of solvent change on the rate is determined by the influence of solvent internal pressure and polarity on the volume of activation. The increase in solvent

Can. J. Chem. Downloaded from www.nrcresearchpress.com by 210.87.254.42 on 09/05/12
For personal use only.

TABLE 2. Activation parameters (at 50.0°C) for the solvolysis of trichloroacetate ion in water–ethanol solutions

Water mol fraction	E_a (kcal/mol)	ΔH^* (kcal/mol)	ΔS^* (cal deg^{-1} mol^{-1})	ΔG^* (kcal/mol)
1.0	31.65±0.03	31.01±0.03	7.99±0.12	28.43±0.07
0.96	26.93±0.04	26.29±0.04	−5.11±0.15	27.94±0.09
0.93	26.62±0.03	25.98±0.03	−5.46±0.12	27.74±0.07
0.89	26.13±0.07	25.49±0.07	−6.48±0.25	27.58±0.15
0.84	24.50±0.03	23.86±0.03	−11.13±0.12	27.46±0.06
0.71	23.72±0.06	23.08±0.06	−12.87±0.21	27.24±0.12
0.505	21.55±0.02	20.91±0.02	−19.14±0.08	27.10±0.04
0.35	21.57±0.01	20.93±0.01	−18.80±0.06	27.00±0.03

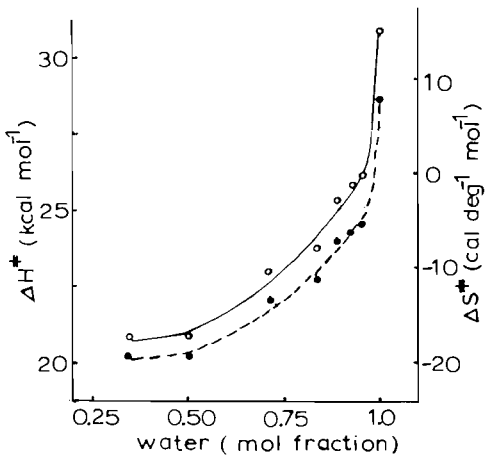

FIG. 4. Dependence of the activation parameters, ΔH^* and ΔS^* on solvent composition: ○, ΔH^*, ●, ΔS^*.

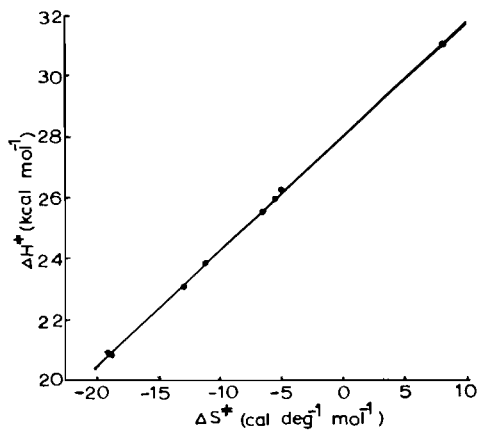

FIG. 5. A plot of ΔH^* vs. ΔS^* for the alkaline solvolysis of trichloroacetate ion in water–ethanol solutions.

polarity increases solvent electrostriction around the reactants relative to the activated complex, thereby causing the activation volume to be more positive and the rate of reaction to decrease. Alternatively, it may be pointed out that, since the transition state is bigger than the ground state and is involving the release of the neutral CO_2 molecule and the delocalization of charge, it is expected to be relatively less solvated by water than the reactant ion as the dielectric constant of the medium increases (16). If the reactants are relatively more solvated than the activated complex, there is an increase in entropy of activation, a decrease in potential energy of the reactants, the activation energy is increased and the reaction rate is consequently diminished.

If a simple electrostatic theory of medium effects (23) is considered, the rate constant of the reaction may be written as:

$$(6)\quad \ln k = \ln k_0 + (Z^2e^2/2D(R/N)T)((1/r) - (1/r^*))$$

where, k_0 can be regarded as the rate constant in a medium of infinite dielectric constant, r and r^* are the radii of the reactant ion and the activated complex; (R/N) is the Boltzmann constant, Z is the valency of the reactant ion, e is the electronic charge, D is the macroscopic dielectric constant, and T is the absolute temperature. Figure 3 shows that a linear relationship between log k and D^{-1} is not strictly obeyed. The main reason for this is that the success of the electrostatic theory has been limited due to its neglect of solvent structural effects, also the macroscopic dielectric constant is not adequate for describing the molecular interactions. However, if we use data obtained at 50.0°C and assume that the trichloroacetate ion has a radius of 3.4 Å (this is about the same value calculated from the average volume occupied per molecule of trichloroacetic acid in the liquid state), then for media with water mole fractions less than about 0.7, eq. [6] gives for the radius of the transition state complex a value of about 5.5 Å, i.e., the volume of the activated complex is about four times that of the reactant ion. In the water-rich region of the composition scale a similar calculation (over the short linear portion of the log $k - D^{-1}$ plot, i.e., 1.0 to about 0.9 water mole fraction) gives $(1/r) - (1/r^*) = 3.26$ Å^{-1}. This value means that both the reactant ion and the activated complex are much compressed by electrostriction in the highly aqueous solutions to the extent that the radius of the reactant ion must be less than

1 Å for eq. [6] to hold. On the basis of the above discussion, one would conclude that the dielectric theory of medium effects does not particularly apply for the water-rich solutions where the structural nature of the solvent and the increased amount of hydrogen-bonded structures play a more important role in the determination of solvent behaviour.

1. EL-H. M. DIEFALLAH and S. A. GHONAIM. J. Chem. Soc. Perkins II, 1237 (1977).
2. EL-H. M. DIEFALLAH. Can. J. Chem. **54**, 1687 (1976).
3. A. M. AZZAM and EL-H. M. DIEFALLAH. Z. Phys. Chem. Leipzig, **91**, 44 (1974).
4. EL-H. M. DIEFALLAH and A. M. KHALIL. Indian J. Chem. **14**A, 1012 (1976).
5. E. F. CALDIN and J. PEACOCK. Trans. Faraday Soc. **51**, 1217 (1955).
6. S. WINSTEIN and A. H. FAINBERG. J. Am. Chem. Soc. **79**, 5937 (1957).
7. E. M. ARNETT, W. G. BENTRUDE, J. J. BURKE, and P. M. DUGGLEBY. J. Am. Chem. Soc. **87**, 1541 (1965).
8. H. S. GOLINKIN and J. B. HYNE. Can. J. Chem. **46**, 125 (1968).
9. J. B. MARTIN and R. E. ROBERTSON. J. Am. Chem. Soc. **88**, 5353 (1966).
10. R. E. ROBERTSON and S. E. SUGAMORI. J. Am. Chem. Soc. **91**, 7254 (1969); Can. J. Chem. **50**, 1353 (1972).
11. M. R. DACK. J. Chem. Educ. **51**, 231 (1974).
12. R. A. FAIRCLOUGH, J. Chem. Soc. 1186 (1938).
13. H. HÖVER. Problems in organic reaction mechanisms. John Wiley & Sons Ltd., New York, NY. 1970. p. 137.
14. J. BIGELEISEN and T. L. ALLEN. J. Chem. Phys. **19**, 760 (1951).
15. B. BUNCEL and J. P. MILLINGTON. Can. J. Chem. **43**, 556 (1965).
16. W. J. LE NOBLE and M. DUFFY. J. Am. Chem. Soc. **86**, 4512 (1964).
17. J. HINE. J. Am. Chem. Soc. **72**, 2438 (1950).
18. J. HINE and A. M. DOWELL, JR. J. Am. Chem. Soc. **76**, 2688 (1954).
19. J. HINE. Divalent carbon. The Ronald Press Company, New York, NY. 1964.
20. E. A. ROBINSON. J. Chem. Soc. 1663 (1961).
21. K. J. LAIDLER. Chemical kinetics. 2nd ed. McGraw-Hill Book Co., New York, NY. 1965.
22. J. E. LEFFLER. J. Org. Chem. **20**, 1202 (1955).
23. I. AMDUR and G. G. HAMMES. Chemical kinetics: Principles and selected topics. McGraw-Hill Book Co., New York, NY. 1966. p. 116.

Can. J. Chem. Downloaded from www.nrcresearchpress.com by 210.87.254.42 on 09/05/12
For personal use only.

Cyclopropanation of steroidal A-ring 2-enol derivatives

JOHN FREELAND TEMPLETON, VOLKER GUSTAV PASLAT, AND CHWI WAN WIE
Faculty of Pharmacy, University of Manitoba, Winnipeg, Man., Canada R3T 2N2

Received November 28, 1977

JOHN FREELAND TEMPLETON, VOLKER GUSTAV PASLAT, and CHWI WAN WIE. Can. J. Chem. **56**, 2058 (1978).

Cyclopropanation of 2-enol derivatives of 17β-acetoxy-5α-androstan-3-one has been studied. The preparation of A-ring cyclopropanol derivatives from the Simmons–Smith reagent or dibromocarbene is described. Long range shielding effects of the cyclopropane ring in the ^{1}Hmr spectrum are discussed.

JOHN FREELAND TEMPLETON, VOLKER GUSTAV PASLAT et CHWI WAN WIE. Can. J. Chem. **56**, 2058 (1978).

On a étudié la cyclopropanation de dérivés énoliques en position 2 de l'acétoxy-17β androstan-5α one-3. On décrit la préparation de dérivés cyclopropanols attachés au cycle A faisant appel à la réaction de Simmons–Smith ou avec du dibromocarbène. On discute des effets de blindage à longue distance du cycle cyclopropane sur les spectres rmn du ^{1}H.
[Traduit par le journal]

Introduction

The synthesis of steroidal cyclopropanol derivatives has been carried out since the development of methylene yielding reagents (1, 2). The iodomethylzinc iodide reagent, prepared from a zinc–copper couple and diiodomethane (3), has been shown to react with enol ethers more rapidly than with the analogous double bond (4) but to be less reactive towards enol acetates (5, 6). Recently, the electron-rich silyl enol ethers have been shown to readily add methylene from this reagent (7). Addition of methylene to an oxygen substituted double bond is a direct way of forming oxygenated cyclopropane derivatives containing an oxygen atom derived from a parent molecule and a method of preparation of methyl substituted carbonyl compounds (8–10). Because cyclopropanols are sensitive to basic and acidic media and to heat, it is necessary that the enolic derivative be easily cleaved. An alternative approach to the direct methylenation of the enolic double bond is the initial addition of a dihalocarbene followed by dehalogenation (11, 12). A number of methods are available for the dehalogenation of unsubstituted dihalocyclopropane derivatives (13).

The addition of methylene, derived from either the Simmons–Smith reagent or via dibromocarbene, to enolic derivatives of 17β-acetoxy-5α-androstan-3-one (**1**) leading to tertiary 3β-oxygen substituted cyclopropanol derivatives has been investigated. A preliminary report has appeared (14).

Results and Discussion

17β-Acetoxy-5α-androstan-3-one (**1**) on treatment with methanol in the presence of acid gave the 3,3-dimethoxy ketal (**2***a*) which, on pyrolysis at reduced pressure, yielded the known methyl enol ether (**3***a*). Addition of methylene to the enolic double bond on treatment with the Simmons–Smith reagent was shown by the presence of high field resonance characteristic of cyclopropyl protons in the ^{1}Hmr spectrum, the absence of the enolic double bond in the ir spectrum, and an increase of 14 amu in the highest mass ion in the mass spectrum of the product. The iodomethylzinc iodide reagent has been shown to be sensitive to steric effects (15); therefore, the presence of the 19-methyl substituent would be expected to cause addition from the α face to give 17β-acetoxy-3β-methoxy-2α,3-cyclopropano-5α-androstane (**4***a*) as in the analogous addition of methylene to steroidal 2-olefins (16). Acidic hydrolysis of the cyclopropyl ether (**4***a*) at room temperature led to the 17β-alcohol (**4***b*) without opening of the cyclopropyl ether. Treatment with dilute acid in methanol at reflux gave 17β-hydroxy-2α-methyl-5α-androstan-3-one (**5**), identified by comparison with an authentic sample.

Treatment of the cyclopropyl ether (**4***a*) with boron trifluoride etherate in acetic anhydride gave the acetoxymethyl derivative (**6***a*). The ^{1}Hmr spectrum showed an olefinic proton and a two-proton singlet assigned to the methylene unit of the acetoxymethyl group. Reaction of the cyclopropyl ether (**4***a*) with boron tribromide gave a monobromo compound (**6***b*) in high yield with no indication of cyclopropanol formation.

Bis(2-chloroethoxy)-5α-androstan-17β-yl acetate (**2***b*) was prepared by azeotropic removal of water from a solution of 17β-acetoxy-5α-androstan-3-one (**1**) in benzene containing *p*-toluenesulfonic acid and 2-chloroethanol. Pyrolysis of the chloroethoxy ketal (**2***b*) gave the 2,3-unsaturated enol ether (**3***b*) of sufficient purity to be used directly in the next reaction with an excess of Simmons–Smith reagent to give the

Can. J. Chem. Downloaded from www.nrcresearchpress.com by 210.87.254.6 on 09/05/12
For personal use only.

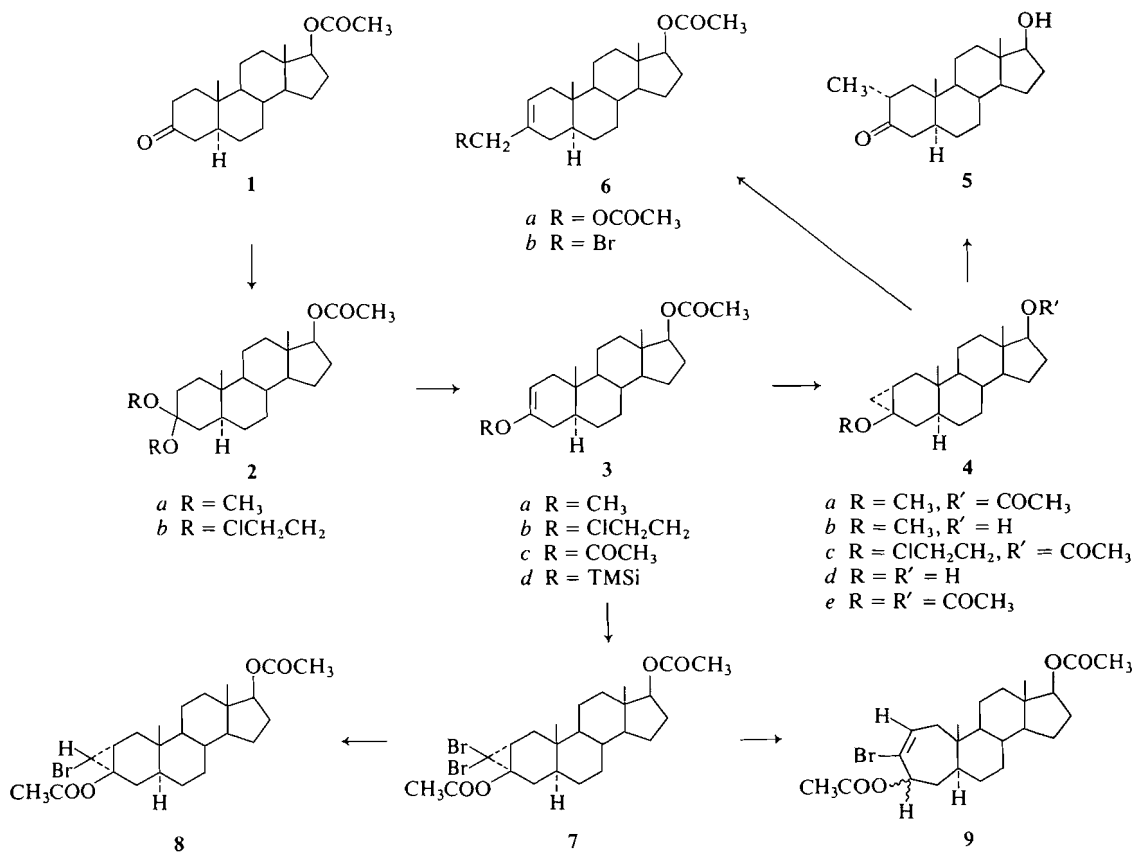

cyclopropyl 2-chloroethyl enol ether (**4***c*). Treatment of this enol ether (**4***c*) with *n*-butyl lithium using the method of Schollköpf *et al.* (17) yield the tertiary cyclopropanol (**4***d*). This heat labile compound gave a melt showing two components on tlc corresponding to the starting material and 17β-hydroxy-2α-methyl-5α-androstan-3-one (**5**). On recrystallization from chloroform, retention of $\frac{1}{2}$ mol of solvent per mole of steroid was shown by ms and elemental analysis. Recrystallization from acetone gave, on the basis of elemental analysis, a hemihydrate. These solvates did not decompose when dried at room temperature under reduced pressure. In the ir the above product showed strong hydroxylic absorption and cyclopropyl C—H stretching and no carbonyl absorption. The ^{1}Hmr spectrum showed high-field resonance consistent with cyclopropyl protons (18). Treatment of the hemihydrate of the cyclopropanol (**4***d*) under either dilute acidic or basic conditions gave 17β-hydroxy-2α-methyl-5α-androstan-3-one (**5**), as shown by comparison of the spectra (ir, ^{1}Hmr, ms) and melting point when mixed with an authentic sample. Acetylation of the cyclopropanol (**4***d*) with acetic anhydride in pyridine gave the diacetate (**4***e*).

The enol acetate (**3***c*) of 17β-acetoxy-5α-androstan-3-one (**1**) was prepared by treatment of the ketone with acetic anhydride in the presence of phosphorous oxychloride. Addition of methylene from an excess of the Simmons–Smith reagent to the 2-enol acetate (**3***c*) gave the diacetate (**4***e*) in low yield. Simmons–Smith addition to the 16-enol acetate has been reported to take place more readily (11, 19), consistent with the greater reactivity of five-membered over six-membered ring olefins (15).

Dibromocarbene addition to the 2-enol acetate (**3***c*) was carried out using the phase-transfer technique (20) to give the expected dibromocyclopropano derivative (**7**). Treatment of the dibromocyclopropano derivative (**7**) with a zinc–copper couple removed the sterically less hindered *exo* bromine to give the *endo*-bromocyclopropane (**8**). The *endo* structure was assigned on the basis of the coupling constant (J = 9 Hz) in agreement with a *cis* cyclopropyl coupling in the monobromocyclopropano derivative (**8**) (21). Hydrogenation of the dibromocyclopropano derivative (**7**) over Raney nickel catalyst also effected removal of the *exo* bromine atom to yield **8**. Further treatment of the monobromocyclopropano derivative (**8**) with either the zinc–copper couple or Raney nickel was unsuccessful

Can. J. Chem. Downloaded from www.nrcresearchpress.com by 210.87.254.6 on 09/05/12
For personal use only.

Can. J. Chem. Downloaded from www.nrcresearchpress.com by 210.87.254.6 on 09/05/12
For personal use only.

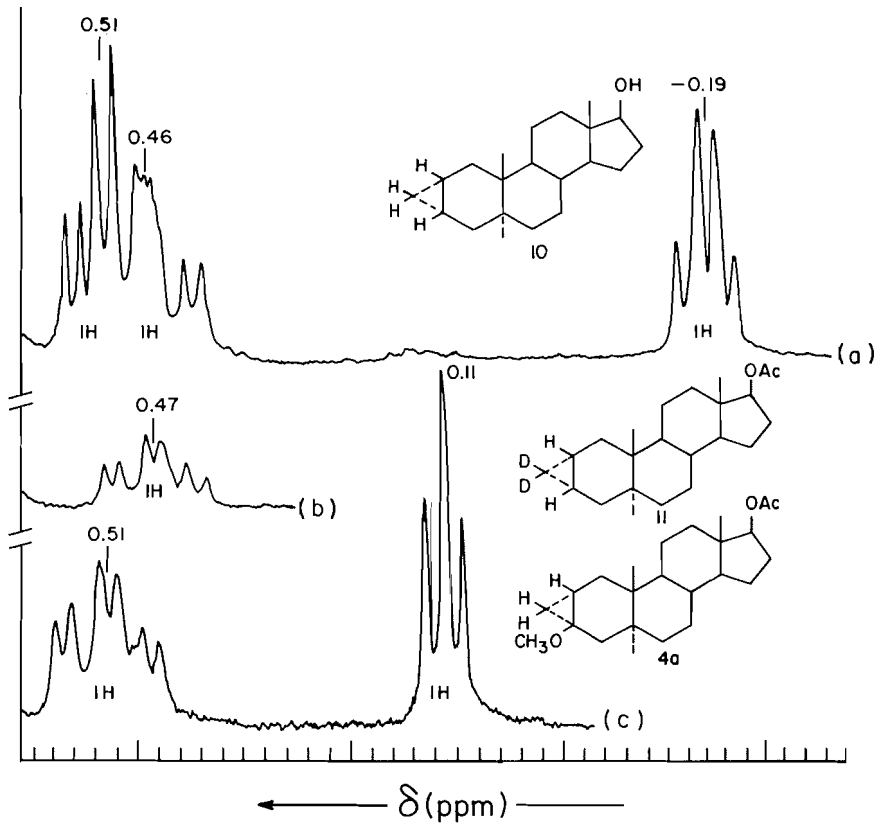

FIG. 1. High-field bands in the 220 mHz ^{1}Hmr spectra of 2α,3α-cyclopropanosteroid derivatives.

in removing the *endo* bromine atom. Lithium aluminium hydride reduction of the dibromocyclopropano derivative (**7**) resulted in the removal of one bromine atom and opening of the cyclopropane ring to yield the A-homoandrostene (**9**) after acetylation. Similar steroid ring enlargements have been observed (12).

The ^{1}Hmr spectrum of the crude reaction product obtained from treatment of the trimethylsilyl derivative (**3***d*) with the Simmons–Smith reagent showed high-field protons corresponding to cyclopropane formation but no crystalline products were obtained from the complex reaction mixture. Olefinic products have been isolated in similar reactions (22).

The ^{1}Hmr spectra of these cyclopropanoandrostanes show the presence of a six-line band at high field which cannot be assigned to a cyclopropyl proton. The spectrum of 17β-hydroxy-2α,3α-cyclopropano-5α-androstane (**10**) has three high-field protons (Fig. 1*a*). Comparison of this spectrum with the dideuterated derivative (**11**) shows the loss of two protons (Fig. 1*b*). These two protons are assigned to the *exo* and *endo* protons which are expected to appear as six- and four-line bands, respectively, as observed, because the *exo* proton undergoes two equivalent *cis* couplings ($J_{exo,2\beta} = J_{exo,3\beta} = 12$ Hz) and one smaller *gem* coupling ($J_{gem} = 5$ Hz) whereas the *endo* proton undergoes three equivalent couplings ($J_{endo,2\beta} = J_{endo,3\beta} = J_{gem} = 5$ Hz) (23). The remaining proton also appears as a six-line band. Examination of the 2β- and 3β-H shows that both are coupled to five protons from which a more complex coupling should result. Deuterium substitution of the 2β- and 4,4-protons does not alter the number of high-field protons observed, thereby eliminating them as the source of this six-line absorption. Substitution of the 3β-proton by an oxygen function causes the loss of one up-field proton leaving a six-line band and a triplet (Fig. 1*c*). The triplet is assigned to the *endo* proton which loses one *trans* coupling and has undergone a shift to lower field. The remaining six-line band is inconsistent with the *exo* proton because that proton should now show one less *cis* coupling and should undergo a shift to lower field. Similar overlapping high-field multiplets are observed in the ^{1}Hmr spectrum of the 4β- and 6α-hydroxyl derivatives of 17β-hydroxy-2α,3α-cyclopropano-5α-androstane (**10**) (24). Further evidence that the six-line proton is not due to a cyclopropyl proton follows from the spectra of the brominated derivatives both

Can. J. Chem. Downloaded from www.nrcresearchpress.com by 210.87.254.6 on 09/05/12
For personal use only.

of which show this signal centered at 0.66 ppm. The 2β-H, like the 1α- and 1β-H to which it is coupled, is expected to appear as a doublet of doublets. Similarly the unaltered coupling observed for the monobrominated derivative is inconsistent with assignment of the six lines to the 2β-proton. Of the remaining protons in the molecule the observed six-line band may arise, on the basis of the coupling constant, from the 9α-,12α-, or 14α-H.

Generally signals which occur at higher field than other alicyclic protons can be assigned to cyclopropyl protons. Bhacca *et al.* (25) has reported the presence of a high-field proton in the ^{1}Hmr spectrum of 3,3′-spirocyclopropano-5α-androstane not present in the spectrum of 5α-androstane which could not be assigned to a cyclopropyl proton. On the basis of the coupling constants, this signal was assigned to a proton at the 6α-,7β-,11α-position resulting from a very long range shielding effect of the cyclopropane ring by an unknown mechanism. The spectra of 2α,3α-cyclopropano-5α-androstane derivatives also show the presence of a high-field signal which cannot be assigned to a cyclopropyl proton and is, therefore, another example of this phenomenon.

These compounds were prepared in connection with studies on the metabolism of 17β-hydroxy-2α,3α-cyclopropano-5α-androstane (**10**) (24).

The above procedures yield 2α,3α-cyclopropano androstane derivatives having either a hydroxyl function at C-3 and C-17, or afforded disubstituted derivatives. A derivative at C-3, which would yield the 3-alcohol and selectively retain the 17-ester function, would give compounds of interest for biological testing, since they avoid the extremes of high and low lipid solubility of the disubstituted and diol compounds (26).

Experimental

For general experimental details of work-up procedures and the acetylation method see ref. 27. Unless otherwise stated, ir (Perkin-Elmer Model 267) and ^{1}Hmr (Varian A56/60A) spectra are recorded in carbon tetrachloride and specific rotations in chloroform. Proton magnetic resonance spectra of compounds **4***a*, **4***c–e*, **6***a–b*, 7, **8**, and **9** were recorded in deuteriochloroform on a Varian HR 220 instrument by the Canadian 220 MHz NMR Centre, Ontario Research Foundation, Toronto, Ontario. Proton magnetic resonance spectra of compounds containing a cyclopropane ring were recorded both with and without the internal TMS standard. Assignment of the six peaks at δ 0.46–0.52 ppm in the ^{1}Hmr spectra of compounds **4***a*, **4***c–e*, and δ 0.66 ppm in compounds 7 and **8** is discussed above. Brockmann Activity II alumina (35–40 × the weight of substance) was used for column chromatography. Neutral alumina was prepared by the ethyl acetate treatment described by Fieser and Fieser (28). Elemental analyses were performed by either Mr. George Crouch, School of Pharmacy, University of London, England, or Pascher and Pascher, Bonn, West Germany.

*3-Methoxy-5α-androst-2-en-17β-yl Acetate (**3**a)*

A flask containing 3,3-dimethoxy-5α-androstan-17β-yl acetate (**2***a*) (29) (7 g) under reduced pressure (water pump) was immersed in an oil-bath (200–210°C). Vigorous reaction ceased after 10 min and the residue was cooled; a drop of pyridine was added, followed by recrystallization from ether–methanol to give the methoxyenol ether (**3***a*) (5 g) mp 122–127°C. Recrystallization gave a sample mp 126.5–129.5°C (lit. (29) mp 127–129°C); ^{1}Hmr δ: 4.28–4.70 (2H, m, vinylic and 17α-protons), 3.44 (s, methoxy), 1.98 (s, 17-acetoxy), 0.78 (s, 18- and 19-methyl) ppm.

*3β-Methoxy-2α,3-cyclopropano-5α-androstan-17β-yl acetate (**4**a)*

The methoxyenol ether (**3***a*) (2.15 g) was treated with the Simmons–Smith reagent as described for the enol ether (**3***b*). Chromatography over alumina gave fractions from petroleum ether which on recrystallization from ether–methanol gave the cyclopropyl ether (**4***a*) (720 mg), mp 138–140°C; $[\alpha]_D^{24}$ +36° (*c* 0.23); ir ν_{max}: 3096 (cyclopropyl C—H), 1730 (ester C=O) cm^{-1}; ^{1}Hmr δ: 4.57 (t, J = 8 Hz, 17α-proton), 3.27 (s, methoxy), 2.04 (s, 17-acetoxy), 0.84 (s, 19-methyl), 0.77 (s, 18-methyl), 0.51 (1H, J = 4.5, 11.5, 12 Hz), 0.11 (1H, dd, $J_{gem} = J_{trans}$ = 5.5 Hz, *endo*-cyclopropyl proton) ppm; ms *m/e*: 360 (M$^+$). *Anal.* calcd. for $C_{23}H_{36}O_3$: C 76.61, H 10.07; found: C 76.39, H 10.28.

*3β-Methoxy-2α,3-cyclopropano-5α-androstan-17β-ol (**4**b)*

The cyclopropyl ether (**4***a*) (463 mg) was dissolved in methanol (22.5 ml) and diethyl ether (27.5 ml) containing concentrated hydrochloric acid (5.4 ml). After 22 h all starting material had disappeared (according to tlc) and a slower fraction had developed. The reaction was worked up to give a crude product which crystallized from petroleum ether 320 mg, mp 105–108°C. Several recrystallizations from petroleum ether gave 3β-methoxy-2α,3-cyclopropano-5α-androstan-17β-ol (**4***b*), mp 109–110°C; $[\alpha]_D^{23}$ +27° (*c* 0.16); ir ν_{max}: 3623 (free O—H), 3480 (bonded O—H), 3067 (cyclopropyl C—H) cm^{-1}; ^{1}Hmr δ: 3.47 (t, J = 8 Hz, 17α-proton), 3.16 (s, methoxy), 0.84 (s, 19-methyl), 0.67 (s, 18-methyl), −0.02 (1H, t, J = 4 Hz, cyclopropyl proton) ppm; ms *m/e*: 318 (M$^+$). *Anal.* calcd. for $C_{21}H_{34}O_2$: C 79.19, H 10.76; found: C 79.05, H 10.87.

*17β-Hydroxy-2α-methyl-5α-androstan-3-one (**5**) from Acid Treatment of the Cyclopropyl Ether (**4**a)*

The cyclopropyl ether (**4***a*) (121 mg) was dissolved in dioxane (4 ml) and methanol (12 ml) containing concentrated hydrochloric acid (1.44 ml). As the starting material decreased (by tlc) two slower fractions developed, the faster corresponding to the 17β-alcohol (**4***b*). After 4½ h only the slower fraction remained. The reaction product was worked up to yield after several recrystallizations from ether – petroleum ether, 17β-hydroxy-2α-methyl-5α-androstan-3-one (**5**) (62 mg), mp 151.5–153°C (lit. (30) 153–154°C); ir ν_{max} (KBr): 3509 (bonded O—H), 1706 (six-membered ring C=O) cm^{-1}; ^{1}Hmr δ: ($CDCl_3$) 3.62 (t, J = 8 Hz, 17α-H), 1.05 (s, 19-methyl), 0.99 (d, J = 6 Hz, 2α-methyl), 0.76 (s, 18-methyl) ppm.

*3-Acetoxymethyl-5α-androst-2-en-17β-yl acetate (**6**a)*

3β-Methoxy-2α,3-cyclopropano-5α-androstan-17β-yl acetate (**4***a*) (120 mg) was dissolved in acetic anhydride (4 ml) and cooled in an ice–salt bath. Boron trifluoride etherate (0.7 ml) was added and the solution allowed to stand at 0°C for 20 h. The reaction mixture was poured into ice-water and extracted with ether; removal of the ether yielded a brown crystalline residue (127 mg). Filtration through neutral alumina in petroleum ether gave fractions (80 mg) from which was obtained on recrystallization from ether–methanol, 3-acetoxymethyl-

Can. J. Chem. Downloaded from www.nrcresearchpress.com by 210.87.254.6 on 09/05/12
For personal use only.

5α-androst-2-en-17β-yl acetate (*6a*) (18 mg), mp 117–119°C C; ir ν_{max}: 1745, 1738 (ester C=O) cm^{-1}; ^{1}Hmr δ: 5.65 (m, olefinic proton), 4.59 (t, J = 8.5 Hz, 17α-H), 4.45 (s, acetoxymethyl protons), 2.07 (s) and 2.05 (s, acetoxy-methylene), 0.78 (s, 19-methyl), 0.73 (s, 18-methyl) ppm; ms *m/e*: 388 (M^+). *Anal.* calcd. for $C_{24}H_{36}O_4$: C 74.19, H 9.34; found: C 74.27, H 9.42.

3-Bromomethyl-5α-androst-2-en-17β-yl acetate (6b)

Boron tribromide (bromine free) (0.6 ml) was added to a solution of the cyclopropyl ether (*4a*) (256 mg) in dichloromethane (10 ml) cooled in a Dry Ice – acetone bath. After 2 h the reaction mixture was poured into ice-water and extracted with dichloromethane to give on recrystallization from dichloromethane–methanol, 3-bromomethyl-5α-androst-2-en-17β-yl acetate (*6b*) (243 mg), mp 158–161°C, recrystallization gave mp 163–164°C; ir ν_{max}: 1736 (ester C=O), 1662 w (C=C) cm^{-1}; ^{1}Hmr δ: 5.78 (br m, olefinic proton), 4.59 (t, J = 8.5 Hz, 17α-H), 3.94 (s, bromomethylene protons), 2.05 (s, 17-acetoxy), 0.79 (s, 19-methyl), 0.73 (s, 18-methyl) ppm; ms *m/e*: 408, 410 (M^+), 329 (M^+ − Br). *Anal.* calcd. for $C_{22}H_{33}O_2Br{\cdot}CH_3OH$: C 62.57, H 8.45; found: C 62.46, H 7.88.

3,3-Bis(2-chloroethoxy)-5α-androstan-17-yl Acetate (2b)

17β-Acetoxy-5α-androstan-3-one (**1**) (1.1 g) was added to a solution of benzene (90 ml) and 2-chloroethanol (10 ml) containing *p*-toluenesulfonic acid monohydrate (100 mg). The solution was fitted with a Dean–Stark apparatus for 3 h of reflux, cooled, and poured into excess cold aqueous sodium bicarbonate, washed with water, dried, and evaporated at reduced pressure with minimal heating. The crude product was recrystallized from ether–methanol containing a trace of pyridine to give the ketal (*2b*) (615 mg), recrystallization gave an analytical sample, mp 94–95°C; $[\alpha]_D^{24}$ +11° (*c* 1.01); ir ν_{max}: 1735 (ester C=O), 671 (C—Cl) cm^{-1}; ^{1}Hmr δ: 4.46 (t, J = 8 Hz, 17α-proton), 3.54 (m, chlorcethoxy protons), 1.93 (s, 17-acetoxymethyl), 0.78 (s, 19-methyl), 0.72 (s, 18-methyl) ppm; ms *m/e*: 474, 476, 478 (M^+). *Anal.* calcd. for $C_{25}H_{40}O_4Cl_2$: C 63.15, H 8.48, Cl 14.91; found: C 62.90, H 8.67, Cl 14.74.

3(2-Chloroethoxy)-5α-androst-2-en-17β-yl Acetate (3b)

A flask containing the ketal (*2b*) (600 mg) was immersed in an oil-bath (200–210°C) under reduced pressure (water pump). After 10 min reaction ceased and the crude product was recrystallized from methanol containing a trace of pyridine to give enol ether (*3b*) (200 mg), mp 123–126°C; $[\alpha]_D^{24}$ +44° (*c* 1.00); ir ν_{max}: 1735 (ester C=O), 1675 (C=C), 671 (C—Cl) cm^{-1}; ^{1}Hmr δ: 4.44 (m, olefinic and 17α-proton), 3.68 (m, chloroethoxy protons), 1.94 (s, 17-acetoxy methyl), 0.75 (s, 18- and 19-methyl) ppm; ms *m/e*: 394 (M^+). *Anal.* calcd. for $C_{23}H_{35}O_3Cl$: C 69.94, H 8.93, Cl 8.96; found: C 70.36, H 9.08, Cl 8.56.

3β(2-Chloroethoxy)-2α,3-cyclopropano-5α-androstan-17β-yl Acetate (4c)

The enol ether (*3b*) (1.6 g) in dry ether (30 ml) was added to a 10 molar excess of the Simmons–Smith reagent prepared from zinc–copper couple (4 g) and methylene iodide (3.32 ml). After 24 h reflux the ir spectrum showed enolic double bond absorption; a second 10 molar excess was added after 48 h and the reaction heated to reflux for a total of 3 days. The reaction product was poured into aqueous sodium bicarbonate and extracted with ether. The residue from the ether extraction was taken up in petroleum ether and chromatographed over neutral alumina. Elution with petroleum ether afforded a major fraction (733 mg) which on crystallization from methanol yielded an analytical sample (433 mg) of the cyclopropyl ether (*4c*), mp 129–130°C; $[\alpha]_D^{24}$ +23° (*c* 1.03); ir ν_{max}: 3075 (cyclopropyl C—H), 1735 (ester C=O), 1235, 1031 (C—O), 669 (C—Cl) cm^{-1}; ^{1}Hmr δ: 4.58 (t, J = 8 Hz, 17α-proton), 3.52–3.82 (m, chloroethoxy protons), 2.04 (s, 17-acetoxy methyl), 0.84 (s, 19-methyl), 0.77 (s, 18-methyl), 0.51 (1H, J = 4, 11.5, 12.5 Hz), 0.15 (1, dd, $J_{gem} = J_{trans}$ = 6 Hz, *endo*-cyclopropyl proton) ppm; ms *m/e*: 408 (M^+). *Anal.* calcd. for $C_{24}H_{37}O_3Cl$: C 70.47, H 9.12, Cl 8.67; found: C 70.38, H 9.28, Cl 8.31.

2α,3-Cyclopropano-5α-androstane-3β,17β-diol (4d)

The 2-chloroethoxycyclopropane ether (*4c*) (1 g) in dry ether (20 ml) was cooled in an ice-bath under a nitrogen atmosphere. *n*-Butyl lithium in petroleum ether (2.3 *M*) (6 ml) was added to the stirred solution and after 15 min the reaction mixture was poured into one equivalent of cold dilute acetic acid (200 ml). The reaction was extracted with ether, the ether was washed with aqueous sodium bicarbonate, water, dried, and evaporated under reduced pressure at room temperature. The crude product was dissolved in acetone at room temperature and concentrated in a stream of nitrogen to yield the cyclopropanol (*4d*) (390 mg), mp 135–144°C. Recrystallization of the heat labile substance from acetone gave a mp 145–155°C. This material showed only one substance on tlc in the following four solvent systems 25% ethyl acetate – petroleum ether, 50% ether–benzene, 5% acetone–chloroform, and 5% methanol – carbon tetrachloride. Analysis by glc as the trimethylsilyl derivative (24) showed one fraction; $[\alpha]_D^{24}$ +18° (*c* 0.963, dioxane); ir ν_{max}: (KBr) 3400 (broad, O—H), 3090 (cyclopropyl C—H), 1058 (C—O) cm^{-1}, heating this disc at 180°C gave a diminished 3400 peak and a new absorption at 1725 (ketone C=O) cm^{-1}; ^{1}Hmr δ: (pyridine-d_5) 3.91 (t, J = 8.5 Hz, 17α-proton), 0.97 (s, 19-methyl), 0.93 (s, 18-methyl), 0.46 (1H, J = 12, 11.5, 4 Hz), 0.35 (1H, t, $J_{gem} = J_{trans}$ = 5 Hz, *endo*-cyclopropyl proton), ppm; ms *m/e*: 304 (M^+). *Anal.* calcd. for $C_{20}H_{32}O_2{\cdot}\frac{1}{2}H_2O$: C 76.62, H 10.61; found: C 76.71, H 10.48. Recrystallization from chloroform, mp 123–128°C. *Anal.* calcd. for $C_{20}H_{32}O_2{\cdot}\frac{1}{2}CHCl_3$: C 67.61, H 9.00, Cl 14.60; found: C 68.60, H 9.11, Cl 12.01.

2α,3-Cyclopropano-5α-androstane-3β,17β-diol Diacetate (4e)

The diol (*4d*) (25 mg) was acetylated (27) and the product (one component on tlc) recrystallized from acetone to give the diacetate (*4e*) (19 mg), mp 162–163°C; $[\alpha]_D^{22}$ +15° (*c* 1.58); ir ν_{max}: 3090 (cyclopropyl C—H), 1735 (ester C=O), 1235, 1176, 1087 (ester C—O) cm^{-1}; ^{1}Hmr δ: 4.55 (t, J = 8 Hz, 17α-proton), 2.03 (s) and 1.96 (s, 3- and 17-acetoxy methyl), 0.91 (s, 19-methyl), 0.77 (s, 18-methyl), 0.52 (1H, J = 12, 11.5, 4.5 Hz), 0.47 (1H, dd, $J_{gem} = J_{trans}$ = 5.5 Hz *endo*-cyclopropyl proton) ppm; ms *m/e*: 388 (M^+) 346 (M^+ − ketene). *Anal.* calcd. for $C_{24}H_{36}O_4$: C 74.19, H 9.34; found: C 74.35, H 9.24.

Acid Treatment of 2α,3-Cyclopropano-5α-androstane-3β,17β-diol (4d)

The diol (*4d*) (170 mg) was dissolved in a solution (17 ml) of concentrated hydrochloric acid in methanol (15% v/v) and heated to reflux for 1 h. The solution was then poured into excess aqueous saturated sodium bicarbonate and extracted with ether to yield a crude product (108 mg) which showed one fraction equivalent to 17β-hydroxy-2α-methyl-5α-androstan-3-one (**5**) on tlc. Recrystallization from acetone gave mp 152.5–153.5°C (lit. (30) mp 152–154°C); mp on admixture with an authentic sample of **5** was not depressed. Spectra (ir, ^{1}Hmr) were identical to those of authentic **5**.

Base Treatment of 2α,3-Cyclopropano-5α-androstane-3β,17β-diol (4d)

The diol (*4d*) (60 mg) was heated under reflux for 2 h with a solution (100 ml) of methanolic potassium hydroxide (2%

Can. J. Chem. Downloaded from www.nrcresearchpress.com by 210.87.254.6 on 09/05/12
For personal use only.

w/v). The reaction, which showed one fraction moving faster than the starting material on tlc, was concentrated and dilute hydrochloric acid was added. Extraction with ether gave a residue which was recrystallized from acetone, mp 146–148°C; ir and ^{1}Hmr spectra were identical to authentic 17β-hydroxy-2α-methyl-5α-androstan-3-one (**5**).

5α-Androst-2-ene-3,17β-diol Diacetate (3c)

Acetic anhydride (10 ml), followed by phosphorous oxychloride (2 ml), were added to a solution of 17β-hydroxy-5α-androstan-3-one (5 g) in dichloromethane (50 ml). The solution was allowed to stand at room temperature overnight and then poured into cold water. The organic layer was separated, washed with water and excess sodium bicarbonate solution, dried over anhydrous sodium sulfate, and evaporated at reduced pressure to yield the diol diacetate (**3c**). Recrystallization from dichloromethane–methanol gave crystals (3.3 g), mp 168–171°C (lit. (31) mp 168–170°C); ir ν_{max}: 1750 (enol acetate C=O), 1735 (17β-acetate C=O), 1695 (C=C) cm^{-1}; ^{1}Hmr δ: 5.25 (m, vinyl proton), 4.62 (t, J = 7 Hz, 17α-proton), 2.08 (s, 3-acetoxy methyl), 2.02 (s, 17β-acetoxy methyl), 0.85 (s, 19-methyl), 0.85 (s, 18-methyl) ppm.

Simmons–Smith Treatment of 5α-Androst-2-ene-3,17β-diol Diacetate (3c)

The enol acetate (**3c**) (1.05 g) was treated with a 10 molar excess of the Simmons–Smith reagent, prepared by the method of Rawson and Harrison (32). After 25 h a second 10 molar excess was added and reflux continued for a further 20 h. Chromatography of the crude product over alumina in petroleum ether gave on elution with 5–25% benzene – petroleum ether fractions (207 mg) from which was obtained on recrystallization from ether the cyclopropyl diacetate (**4e**), mp 163–164°C, identical with the previously prepared cyclopropyl diacetate (**4e**) by comparison of the ir, ^{1}Hmr, and mixture mp.

2α,3α-Dibromocyclopropano-5α-androstane-3β,17β-diol Diacetate (7)

A stirred solution of cetyltrimethylammonium bromide (2 g) in 50% aqueous sodium hydroxide (100 ml) was heated to reflux and a solution of 5α-androst-2-ene-3,17β-diol diacetate (**3c**) (4.6 g) in tribromomethane (25 ml) was added dropwise. After 1 h the exothermic reaction was cooled, diluted with brine, neutralized with 6 *N* sulfuric acid and extracted with chloroform. Evaporation of the chloroform left a dark gummy residue which on filtration through alumina in benzene gave a crystalline product (4 g). Successive recrystallizations from acetone gave the dibromocyclopropanoandrostane (**7**) (1.3 g), mp 199–200°C; $[\alpha]_D^{23}$ +20° (*c* 0.995); ir ν_{max}: 1765 (cyclopropyl ester), 1735 (17β-acetoxy C=O) cm^{-1}; ^{1}Hmr δ: 4.62 (t, J = 8 Hz, 17α-proton), 2.10 (s, 3β-acetoxy), 2.02 (s, 17β-acetoxy), 0.83 (s, 19-methyl), 0.78 (s, 18-methyl), 0.66 (1H, J = 12, 11.5, 4 Hz) ppm; ms *m/e*: 544, 546, 548 (M^+), 502, 504, 506 (M^+ − ketene), 465, 467 (M^+ − Br), 423, 425 [M^+ − (ketene + Br)]. *Anal.* calcd. for $C_{24}H_{34}Br_2O_4$: C 52.76, H 6.27, Br 29.25; found: C 53.04, H 6.36, Br 29.33.

2α,3-(endo)-Bromocyclopropano-5α-androstane-3β,17β-diol Diacetate (8)

(*a*) A stirred mixture of Zn dust (3.3 g) and cuprous chloride (4.9 g) in dry ether (10 ml) were heated to reflux for 30 min to give a zinc–copper couple (32). The dibromocyclopropanoandrostane (**7**) (546 mg) was added and reflux continued for a further 4.5 h. The reaction mixture as poured into aqueous sodium bicarbonate and extracted with ether to give a crude residue (344 mg). Recrystallization from ether–methanol gave the monobromo derivative (**8**), mp 163–164°C; ir ν_{max}: 1752 (cyclopropyl ester), 1735 (17β-acetoxy C=O) cm^{-1}; ^{1}Hmr δ: 4.58 (t, J = 8 Hz, 17α-proton), 3.37 (d, J = 10 Hz, *exo*-cyclopropyl proton), 1.98, 2.03 (2 × s, 3β- and 17β-acetoxy methyl) 0.88 (s, C-19 methyl), 0.77 (s, C-18 methyl), 0.66 (1H, J = 12, 12, 4 Hz) ppm; ms *m/e*: 387 (M^+ − Br), 345 [M^+ − (Br + ketene)], 285 [M^+ − (Br + ketene + HOAc)]. *Anal.* calcd. for $C_{24}H_{35}O_4Br$: C 61.66, H 7.55; found: C 61.87, H 7.59.

(*b*) To a solution of the dibromocyclopropanoandrostane (**7**) (292 mg) in dry dioxane (30 ml) and triethylamine (0.2 ml) was added 2 teaspoonsful of Raney nickel which had been stored under ethanol. This mixture was vigorously stirred under a hydrogen atmosphere for 32 h after which time the catalyst was filtered off and washed with diethyl ether. The ether filtrate was washed with dilute hydrochloric acid, distilled water, and brine. After drying over magnesium sulfate, the ether phase was evaporated at reduced pressure to give a crystalline material (106 mg), mp 160–161°C; recrystallization from hot methanol gave 2α,3-(*endo*)-bromocyclopropano-5α-androstane-3β,17β-diol diacetate (**8**), mp 162–162.5°C; ir ν_{max}: (KBr) 3070 (cyclopropyl, C—H), 1740 (3β-ester, C=O), 1734 (17β-ester, C=O) cm^{-1}; ms *m/e*: 387 (M^+ − Br), 345 [M^+ − (Br + ketene)], 285 [M^+ − (Br + ketene + HOAc)].

3-Bromo-5α-A-homoandrost-2-ene-3aξ,17β-diol Diacetate (9)

A stirred solution of the dibromocyclopropanoandrostane (**7**) (548 mg) and lithium aluminium hydride (500 mg) was heated to reflux in dry ether (15 ml). After 40 h the reaction mixture was poured onto crushed ice and extracted with ether. The crude product was treated overnight at room temperature with acetic anhydride and pyridine. Chromatography of the acetylation product over neutral alumina gave fractions on elution with 5% ether – petroleum ether (77 mg) which on recrystallization from ether – petroleum ether gave the A-homoandrostene (**9**), mp 158–159.5°C; ir ν_{max}: 1740 (3ξ-ester, C=O), 1733 (17β-ester, C=O) cm^{-1}; ^{1}Hmr δ: 6.13 (heptet, J = 10, 6, 2.5 Hz, vinyl proton), 5.50 (d, J = 11 Hz, 3aξ-proton) 4.89 (dd, J = 7, 8.5 Hz, 17α-proton), 2.41 (dd, J = 15, 10 Hz, 1α- or 1β-proton), 2.03, 2.13 (2 × s, 3β- and 17β-acetoxy methyl), 0.75, 0.77 (2 × s, C-18 and C-19 methyl) ppm; ms *m/e*: 466, 468 (M^+), 406, 408 (M^+ − HOAc), 387 (M^+ − Br), 327 [M^+ − (HOAc + Br)].

3-Trimethylsiloxy-5α-androst-2-en-17β-yl Acetate (3d)

The silyl enol ether (**3d**) was prepared by the procedure of House *et al.* (Method A, ref. 33), mp 90–103°C; ir ν_{max}: 1736 (ester C=O), 1669 (enolic C=C cm^{-1}; ^{1}Hmr δ: 4.1–4.6 (m, vinyl and 17α-protons), 1.81 (s, acetoxy), 0.64 (s, C-18 and C-19 methyl), 0 (s, trimethylsiloxy) ppm. *Anal.* calcd. for $C_{24}H_{40}O_3Si$: C 71.24, H 9.96; found: C 71.23, H 10.01.

Simmons–Smith Treatment of 3-Trimethylsiloxy-5α-androst-2-en-17β-yl Acetate (3d)

The silyl enol ether (**3d**) was treated with an excess of the Simmons–Smith reagent as described above for **3c**. The crude product showed the presence of a complex multiplet centered at δ 0.56 ppm (cyclopropyl protons) in the ^{1}Hmr spectrum. Chromatography over alumina gave no clearly defined products or crystalline fractions.

17β-Hydroxy-2α,3α-cyclopropano-5α-androstane (10)

This product was prepared by the Simmons–Smith procedure in ref. 24, mp 129–130°C (lit. (16) mp 130–132°C).

17β-Acetoxy-2α,3α-deuteriocyclopropano-5α-androstane-d_2 *(11)*

Prepared by the procedure in ref. 24, using CD_2I_2, mp 99–101.5°C; ms 98% d_2 (lit. (16) mp 105–106°C).

17β-Hydroxy-2α,3α-cyclopropano-5α-androstane-2β,4,4-d_3

17β-Acetoxy-5α-androstan-3-one-2,2,4,4-d_4 was prepared by

the procedure in ref. 34. Treatment of the crude product with 1 equiv. of bromine in CH_2Cl_2 gave the 2α-bromo derivative which was reduced to the 3ξ-alcohols with sodium borohydride. The epimeric mixture was treated with a zinc–copper couple in acetic acid as in ref. 24 to give 17β-acetoxy-5-androstene-2,4,4-d_3, mp 95–99°C (lit. (35) mp 96°C); ms: d_3 35%, d_2 40%, d_1 21%; ^{1}Hmr the ratio of 17α-H to vinyl proton shows 75% 2β-D. Treatment of the olefin with CH_2I_2 as in ref. 24 gave a product which on hydrolysis yielded 17β-hydroxy-2α,3α-cyclopropano-5α-androstane-2β,4,4-d_3, mp 128–129°C (lit. (16) mp 130–132°C); ms: d_3 24%, d_2 46%, d_1 25%; ^{1}Hmr δ −0.18 (1H, m), 0.50 (2H, m) ppm.

Acknowledgements

We wish to thank Mr. R. C. Linklater, Mr. Dennis Michiel, and Ms. Mohani Singh for their technical assistance and Mr. Mark West for comments on the typescript. Financial assistance from the Faculty of Graduate Studies, Research Board, University of Manitoba, and the Medical Research Council of Canada, is gratefully acknowledged.

1. D. H. Gibson and C. H. DePuy. Chem. Rev. **76**, 605 (1974).
2. V. Schollköpf. Angew. Chem. Int. Ed. Engl. 7, 588 (1968).
3. H. E. Simmons, T. L. Cairns, S. A. Vladuchick, and C. M. Hoiness. Org. React. **20**, (1973).
4. J. H. H. Chan and B. Rickborn. J. Am. Chem. Soc. **90**, 6406 (1968).
5. H. E. Simmons and R. D. Smith. J. Am. Chem. Soc. **81**, 4526 (1959).
6. C. H. DePuy, G. M. Dappen, K. L. Eilers, and R. A. Klein. J. Org. Chem. **29**, 2813 (1964).
7. S. Murai, T. Aya, T. Renge, I. Ryu, and N. Sonoda. J. Org. Chem. **39**, 858 (1974); J. M. Conia and C. Girard. Tetrahedron Lett. 2769 (1973); G. M. Rubottom and M. I. Lopez. J. Org. Chem. **38**, 2097 (1973); R. LeGoaller and J. L. Pierre. Bull. Soc. Chim. Fr. 1531 (1973).
8. E. Wenkert and D. A. Berges. J. Am. Chem. Soc. **89**, 2507 (1967).
9. E. Wenkert, R. A. Mueller, E. J. Reardon, S. S. Sathe, D. J. Scharf, and G. Tosi. J. Am. Chem. Soc. **92**, 7428 (1970).
10. R. E. Ireland, D. R. Marshall, and J. W. Tillery. J. Am. Chem. Soc. **92**, 4754 (1970).
11. W. F. Johns and K. W. Salamon. J. Org. Chem. **36**, 1952 (1971).
12. G. Stork, M. Nussim, and B. August. Tetrahedron, Suppl. 8, Pt. I, **22**, 105 (1966).
13. R. Barlet and Y. Vo-Quang. Bull. Soc. Chim. Fr. 3729 (1969).
14. J. F. Templeton and C. W. Wie. Tetrahedron Lett. 3955 (1971).
15. B. Rickborn and J. H. H. Chan. J. Org. Chem. **32**, 3576 (1967).
16. M. E. Wolff, W. Ho, and R. Kwok. J. Med. Chem. **7**, 577 (1964).
17. V. Schollköpf, J. Paust, A. Al-Azrak, and H. Schumacher. Chem. Ber. **99**, 3391 (1966).
18. W. G. Dauben and W. T. Wipke. J. Org. Chem. **32**, 2976 (1967).
19. K. E. Fahrenholtz, K. P. Meyers, and R. W. Kierstead. J. Med. Chem. **15**, 1056 (1972).
20. K. Skattebøl, G. A. Abskharoon, and T. Greibrokk. Tetrahedron Lett. 1367 (1973).
21. D. Seyferth, H. Yamazaki, and D. L. Alleston. J. Org. Chem. **28**, 703 (1963).
22. I. Ryu, S. Murai, and N. Sonoda. Tetrahedron Lett. 4611 (1977).
23. K. B. Wiberg, D. E. Barth, and P. H. Schertler. J. Org. Chem. **38**, 378 (1973).
24. J. F. Templeton and R. S. Kim. Steroids, **27**, 581 (1976).
25. N. S. Bhacca, M. E. Wolff, and W. Ho. Tetrahedron Lett. 5427 (1968).
26. C. Hansch and J. M. Clayton. J. Pharm. Sci. **62**, 1 (1973).
27. J. F. Templeton and C. W. Wie. Can. J. Chem. **53**, 1693 (1975).
28. L. F. Fieser and M. Fieser. Reagents for organic synthesis. Vol. I. John Wiley and Sons, Inc., New York, NY. 1967. p. 19.
29. G. Karmas. J. Org. Chem. **33**, 2436 (1968).
30. H. J. Ringold, E. Batres, O. Halpern, and E. Necoechea. J. Am. Chem. Soc. **81**, 427 (1959).
31. J. Fajkos. Coll. Czech. Chem. Commun. **25**, 1078 (1960); R. Villotti, H. J. Ringold, and C. Djerassi. J. Am. Chem. Soc. **82**, 5693 (1960); A. Bowers, L. C. Ibanez, E. Denot, and R. Becerra. J. Am. Chem.Soc. **82**, 4001 (1960).
32. R. J. Rawson and I. T. Harrison. J. Org. Chem. **35**, 2058 (1970).
33. H. O. House, L. J. Czuba, M. Gall, and H. D. Olmstead. J. Org. Chem. **34**, 2324 (1969).
34. J. F. Templeton and C. W. Wie. Can. J. Chem. **52**, 517 (1974).
35. R. E. Marker, O. Kamm, D. M. Jones, and L. W. Mixon. J. Am. Chem. Soc. **59**, 1363 (1937).

Can. J. Chem. Downloaded from www.nrcresearchpress.com by 210.87.254.6 on 09/05/12
For personal use only.

Molécules modèles des motifs des poly-1,4-glucosides. I. Synthèse et correspondance configurationelle de diastéréoisomères avec les motifs de la cellulose et de l'amylose

FRANÇOISE LAFUMA ET CLAUDE QUIVORON

Laboratoire de Physico-Chimie Macromoléculaire de l'Université Pierre et Marie Curie (Paris VI), Ecole Supérieure de Physique et de Chimie, 10 rue Vauquelin - 75231, Paris Cedex 05 - France

Reçu le 20 janvier 1977[1]

FRANÇOISE LAFUMA et CLAUDE QUIVORON. Can. J. Chem. **56**, 2065 (1978).

Afin de confirmer ou de préciser les types de chelations les plus probables existant dans les chaînes de cellulose et d'amylose, ainsi que dans les mono- et les disaccharides correspondants, nous avons entrepris des recherches sur des molécules modèles représentant, en partie, les motifs cellobiose et maltose. Ces molécules modèles sont des acétals intra-extracycliques de type cyclohexyloxy-2 tétrahydropyranne, porteurs de groupements hydroxyle primaire ou secondaire, de telle sorte que leurs dispositions covalentes, par rapport à la fonction acétal, soient analogues à celles des groupements (OH)2, (OH)3′, (OH)6 et (OH)6′ de l'amylose et de la cellulose. Vingt et un modèles ont été préparés à partir du dihydro-2,3 pyranne, de l'hydroxyméthyl-2 dihydro-2,3 pyranne ou de leurs époxydes. La plupart des diastéréoisomères correspondant aux modèles possèdant au moins deux atomes de carbone asymétrique, ont été séparés par chromatographie par perméation de gel, en mettant à profit la technique de recyclage. La correspondance configurationnelle de ces diastéréoisomères avec les motifs α-D- et β-D-glucose de l'amylose et de la cellulose, a été étudiée par résonance magnétique nucléaire du proton et du carbone 13. Ce travail d'attribution nous a permis de reconnaître, parmi les 30 diastéréoisomères séparés, 6 représentant les dispositions configurationnelles de l'amylose et 5, celles de la cellulose.

FRANÇOISE LAFUMA and CLAUDE QUIVORON. Can. J. Chem. **56**, 2065 (1978).

To confirm or to elucidate the most probable types of chelation existing in the chains of cellulose or amylose as well as in the corresponding mono- and disaccharides, we have undertaken studies on model molecules which represent, in part, the cellobiose and maltose entities. These model molecules are some intra- extra cyclic acetals of the type 2-cyclohexyloxytetrahydropyran. These molecules contain primary or secondary hydroxyl groups whose covalent dispositions relative to the acetal function are analogous to those of the groups (OH)2, (OH)3′, (OH)6, and (OH)6′, of amylose and cellulose. Twenty-one model compounds have been prepared from 2,3-dihydropyran, 2-hydroxymethyl-2,3-dihydropyran, or their expoxides. Most of the diastereoisomers corresponding to the model compounds containing at least two asymmetric carbon atoms have been separated by gel permeation chromatography using a recycling system to some advantage. The configurational correspondence of the diastereoisomers to the entities α-D- and β-D-glucose of amylose and of cellulose have been studied by proton and carbon-13 nuclear magnetic resonance. These assignments have permitted the recognition, among the 30 diastereoisomers of 6 which have the configuration of amylose and of 5 which have that of cellulose.

[Journal translation]

Introduction

Les interactions hydrogène et, en particulier, les liaisons hydrogène intramoléculaires, qui participent à l'établissement des structures, à l'état solide, de l'amylose, de la cellulose et de leurs mono- et disaccharides, ont fait l'objet d'un grand nombre de travaux expérimentaux et théoriques. En raison de leur insolubilité dans les milieux non aqueux, ces 1,4-glucosides ont été surtout étudiés par diffraction des rayons X. Cependant, les interprétations des clichés obtenus conduisent, notamment dans le cas de la cellulose et de l'amylose, à des systèmes de chélation qui diffèrent, le plus souvent d'un auteur à l'autre. C'est le cas également des divers calculs conformationnels publiés sur ces composés glucosidiques.

En ce qui concerne les monosaccharides comme l'α-D-glucose ou le β-D-glucose, à l'état solide, les auteurs (1, 2) s'accordent à penser qu'il n'existe aucune chélation dans ces composés. Dans le cas des disaccharides et des polysaccharides, les divers travaux théoriques et expérimentaux amènent à considérer des liaisons hydrogène intramoléculaires faisent intervenir des sites situés sur chacun des cycles pyranosidiques. Ainsi, la chélation (OH)3′···O5′ est unanimement admise dans les mailles cristallines du cellobiose (3–5), du méthyl β-cellobioside (6) et de la cellulose (7–12).[2] Divers auteurs proposent, en outre, pour la cellulose deux autres types de chélation qui concernent directement ou indirectement la participation de chaque groupement hydroxyméthylé: ces derniers pourraient être engagés dans une liaison hydrogène intramoléculaire (OH)2···(OH)6′ (12–14)

[1] Revision reçue le 21 mars 1978.

[2] Pour les notations se reporter à la fig. 1.

Can. J. Chem. Downloaded from www.nrcresearchpress.com by 210.87.254.42 on 09/05/12
For personal use only.

Can. J. Chem. Downloaded from www.nrcresearchpress.com by 210.87.254.42 on 09/05/12
For personal use only.

ou ne donner lieu qu'à des liaisons interchaînes (10, 15, 16). Par ailleurs, une troisième chélation: (OH)2···O1 a été proposée par Quivoron *et al.* (17–20), à la suite d'études de chélation, par spectroscopie infrarouge, de molécules modèles représentant partiellement le motif cellobiose.

Pour le maltose (21, 22), le méthyl β-maltoside (23), les cyclodextrines (24, 25) et les différentes variétés cristallines d'amylose (1, 26, 27), la liaison hydrogène intramoléculaire la plus fréquemment citée est la chélation (OH)2···(OH)3′. Quivoron et Néel (19) ainsi que Fialeyre *et al.* (28) sont les seuls à proposer une chélation de type (OH)2····O1, à partir d'études effectuées sur des molécules modèles (17, 18) ou sur le maltose (28) en solution. La liaison hydrogène intramoléculaire (OH)6′····O5 a été, en particulier, suggérée par Quivoron et Néel (19).

Afin de confirmer ou de préciser les types de liaison hydrogène intramoléculaires les plus probables, rencontrés dans la cellulose, l'amylose et dans leurs disaccharides, nous avons entrepris des recherches sur des molécules modèles représentant, en partie, les motifs cellobiose ou maltose, selon la méthode préconisée par Quivoron et Néel (17–19). Ces molécules modèles sont des acétals intra-extracycliques, de type cyclohexyloxy-2 tétrahydropyranne: por-

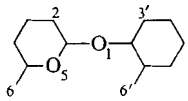

teurs d'un, de deux, voire de trois groupements hydroxyle primaire ou secondaire, de telle sorte que leurs dispositions covalentes, par rapport à la fonction acétal, soient analogues à celles des groupements (OH)2, (OH)3′, (OH)6 et (OH)6′ de l'amylose ou de la cellulose.

Nous exposons dans cette Partie I, la synthèse des molécules modèles retenues, dont la plupart présentent deux atomes de carbone asymétrique. Nous décrivons également la correspondance configurationnelle avec les motifs de la cellulose et de l'amylose, établie pour chacun des racémiques séparés par chromatographie (29). La Partie II (57), est consacrée à l'étude, par spectroscopie infrarouge, des conformations chélatées des diastéréoisomères et à une discussion des résultats, dans le cadre des chélations dans les mono-, di- et poly-1,4-glucosides.

Synthèse des molécules modèles

Les molécules modèles ont été préparées par action du dihydro-2,3 pyranne, de l'hydroxyméthyl-2 dihydro-2,3 pyranne ou de leur époxyde respectif, sur le monoalcool ou sur le diol cyclohexanique approprié. Les modes opératoires sont rapportés dans la partie expérimentale.

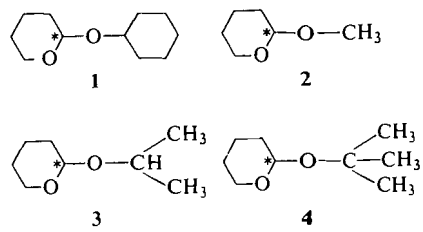

1 2 3 4

Acétals simples

Afin d'obtenir des informations d'ordre conformationnel sur les dérivés monosubstitués du tétrahydropyranne, nous avons synthétisé ces quatre alcoxy-2 tétrahydropyrannes par réaction, en milieu acide, du monoalcool correspondant sur le dihydro-2,3 pyranne (30–33).

Acétal-monoalcools

Les modèles (**5–9**) ont été obtenus par le même type de réaction, en remplaçant le monoalcool par le diol correspondant (17, 34), en grand excès. Pour **8** et **9**, les alcools sont respectivement les cyclohexanediols *cis* et *trans*, préalablement séparés (17).

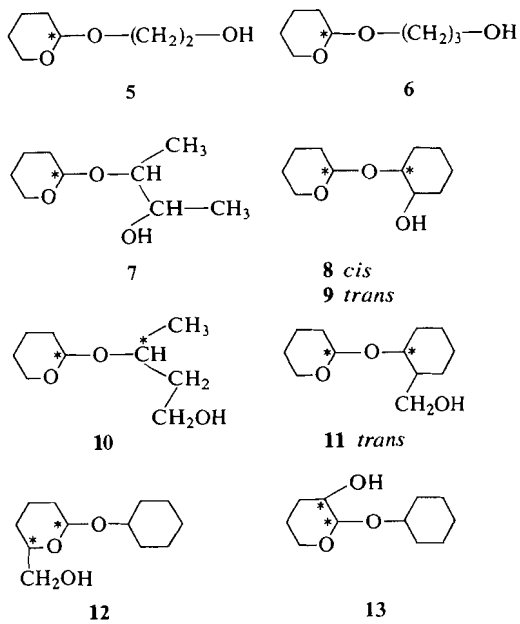

5 6 7 **8** *cis* **9** *trans* 10 **11** *trans* 12 13

Dans le cas des composés **10** et **11**, les diols de départ ont été respectivement le butane-diol-1,3 et le *trans*-hydroxyméthyl-2 cyclohexanol. Afin d'éviter la condensation du dihydro-2,3 pyranne sur la fonction alcool primaire de chacun de ces diols, il s'est avéré nécessaire de bloquer, au préalable, sélectivement celle-ci sous forme de tosylate, puis de régénérer cette fonction après addition du groupement hydroxyle secondaire (voir Partie expérimentale).

De la même façon, le modèle **12** a été obtenu par réaction du cyclohexanol sur l'hydroxyméthyl-2

Can. J. Chem. Downloaded from www.nrcresearchpress.com by 210.87.254.42 on 09/05/12
For personal use only.

dihydro-2,3 pyranne, préparé par réduction du dimère de l'acroléine (35, 36), préalablement acétylé. L'hydrolyse finale de la fonction acétate, à froid en milieu basique, évite toute rupture possible de la liaison acétal formée.

L'acétal-alcool **13** résulte de l'addition du cyclohexanol sur l'époxyde du dihydro-2,3 pyranne. Cet époxyde est préalablement préparé par action de l'acide para-nitroperbenzoïque (37).

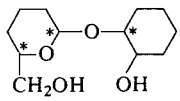

14 *cis*
15 *trans*

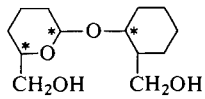

16 *trans*

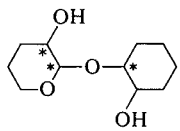

17 *cis*
18 *trans*

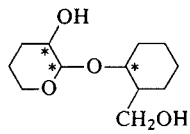

19 *trans*

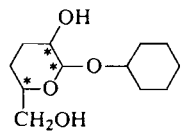

20

Acétal-diols

Les composés **14** et **15** ont été préparés par action respective des cyclohexane-diols-1,2 *cis* et *trans* sur l'hydroxy-méthyl-2 dihydro-2,3 pyranne acétylé (voir modèle **12**). La réaction est analogue dans le cas du modèle **16**, à partir du *trans*-hydroxyméthyl-2 cyclohexanol préalablement tosylé sur la fonction alcool primaire.

Les molécules modèles **17** et **18** sont issues de l'addition des cyclohexane diols-1,2 *cis* et *trans* sur l'époxyde du dihydro-2,3 pyranne (38); le diol de départ est le *trans*-hydroxyméthyl-2 cyclohexanol pour le composé **19**.

L'acétal-diol **20** a été obtenu par addition du cyclohexanol sur l'époxyde de l'acétate de l'hydroxyméthyl-2 dihydro-2,3 pyranne (voir Partie expérimentale).

Acétal-triol

Par analogie avec le modèle précédent (**20**), cet acétal-triol a été préparé par réaction de l'acétate de l'hydroxyméthyl-2 dihydro-2,3 pyranne sur le cyclohexane-diol-1,2 *trans*.

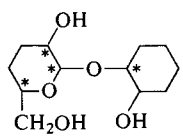

21 *trans*

Séparation chromatographique des diastéréoisomères

Ces séparations ont été réalisées pour la plupart d'entre eux par chromatographie par perméation sur gel en utilisant la technique de recyclage et sont décrites par ailleurs (29, 39).

Le tableau 1 rassemble les différentes fractions obtenues pour les molécules modèles **7**–**20**, c'est à dire comportant deux ou trois atomes de carbone asymétrique. Ces fractions correspondent à des racémiques purs et leur pureté a été caractérisée par spectroscopie, notamment par résonance magnétique nucléaire du proton et du carbone 13. Il ne nous a pas été possible de séparer les diastéréoisomères relatifs au composé **21**, en raison de son insolubilité dans les solvants chromatographiques utilisés (tétrahydrofuranne, éther diisopropylique).

Correspondance configurationnelle de certains diastéréoisomères avec les motifs de la cellulose et de l'amylose

Lorsque l'on considère les diastéréoisomères racémiques correspondant à une même structure covalente, ils diffèrent entre eux par les positions axiales et équatoriales des substituants hydroxyle et des liaisons C—O pontales. Comme dans les chaînes de cellulose et d'amylose, ces groupements O—H et ces liaisons C—O pontales ont des configurations axiales et équatoriales bien déterminées, il convenait, avant l'étude des conformations chélatées (voir Partie II), de déterminer, parmi les diastéréoisomères séparés par chromatographie, ceux qui correspondent aux dispositions configurationnelles des motifs de la cellulose et de l'amylose.

Dans le cas des acétals monohydroxylés de type cyclohexyloxy-2 tétrahydropyranne (deux atomes de carbone asymétrique), certains d'entre eux présentent un racémique possèdant une correspondance configurationnelle avec la cellulose, le second avec l'amylose. A titre d'exemple, les deux racémiques du modèle **9**, que nous avons pu séparer, diffèrent entre eux par les configurations relatives des carbones C1 et C4′. Dans ces conditions, l'un correspond à la disposition (OH)3′/O5 de la cellulose (liaison C1—O1 équatoriale); l'autre a la même disposition dans la chaîne d'amylose (liaison C1—O1 axiale). Dans le cas des acétal-diols qui se présentent, en toute rigueur, sous forme de quatre racémiques diastéréoisomères (trois atomes de carbone asymétrique), l'examen des modèles moléculaires montre qu'excepté les molécules modèles **14** et **17** qui comportent un groupement hydroxyle cyclohexanique *cis*, tous les autres modèles ont chacun un diastéréoisomère décrivant les configurations des hydroxyles cellulosiques et un second spécifique des hydroxyles de l'amylose.

TABLEAU 1. Différentes fractions obtenues par chromatographie pour les molécules modèles **7–20**

Composé	Nombre de C*	Fractions pures	Remarques
7 à **13**	2	Deux fractions notées A et B	
14	3	**14**A, **14**B, **14**C	Absence de **14**D
15	3	**15**A, **15**B, **15**C	Absence de **15**D
16	3	**16**A	**16**B, **16**C, **16**D non résolus
17	3	**17**A, **17**B, **17**C, **17**D	
18	3	**18**A, **18**B, **18**C	**18**D enrichi
19	3	**19**A, **19**B	**19**C, **19**D non résolus
20	3	**20**A, **20**B	**20**C enrichi **20**D non résolu

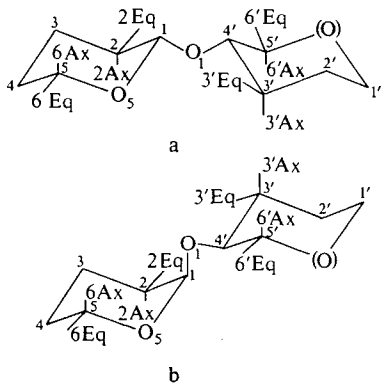

FIG. 1. Correspondance configurationnelle des diastéréoisomères des molécules de type cyclohexyloxy-2 tétrahydropyranne, avec les séquences de la cellulose (*a*) et de l'amylose (*b*).

La fig. 1 indique les structures conformationnelles générales des molécules modèles de type cyclohexyloxy-2 tétrahydropyranne, représentées dans le cadre, soit des séquences de la cellulose, soit des séquences de l'amylose. Ces schémas conformationnels permettent, indépendamment des équilibres de conformations inter-chaises, d'affecter un symbole configurationnel à chaque diastéréoisomère. Ainsi, le diastéréoisomère de type **9** associé à la cellulose (C) sera dénoté: 3′Eq/C; celui de même type associé à l'amylose (A): 3′Eq/A. Avec cette convention de correspondance, l'acétal-diol **18**, par exemple, comportera deux diastéréoisomères intéressants, de symbole: 2 Eq/3′ Eq/C et 2 Eq/3′ Eq/A.

Nous avons proposé, dans le présent travail, une correspondance configurationnelle entre certains des diastéréoisomères séparés et les motifs séquentiels de la cellulose et de l'amylose. Cette correspondance a été étudiée essentiellement à partir des spectres de résonance magnétique nucléaire (rmn) du proton et du carbone 13. Toutefois, pour quelques diastéréoisomères, le profil des bandes infrarouges ν(O—H) de chélation nous a permis d'attribuer leurs configurations.

Equilibres conformationnels des tétrahydropyrannes substitués

Les équilibres de conversion entre formes chaises, qui n'existent pas au niveau des résidus α-D- et β-D-glucose des chaînes d'amylose et de cellulose, sont toujours présents dans les tétrahydropyrannes alcoxylés et compliquent l'interprétation des spectres de rmn. L'analyse des équilibres conformationnels n'est pas simple également dans le cas des cycles au moins disubstitués, tels que les acétal-monoalcools et les acétal-diols, en raison de l'intervention des facteurs classiques de stabilité (40–43).

Si nous considérons, à titre d'exemple, le cas des deux diastéréoisomères du modèle **12**, les équilibres conformationnels sont les suivants:

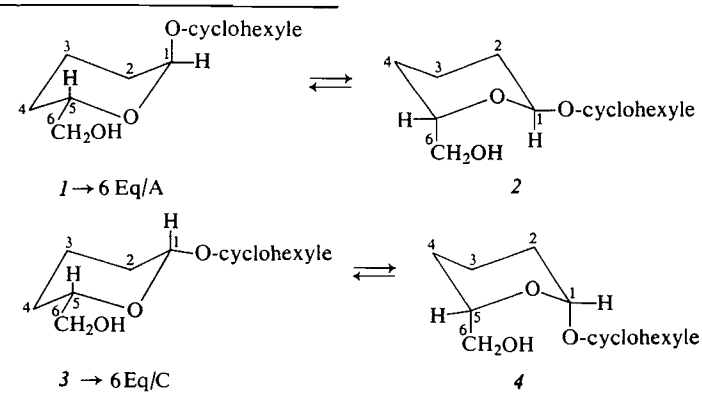

Can. J. Chem. Downloaded from www.nrcresearchpress.com by 210.87.254.42 on 09/05/12
For personal use only.

TABLEAU 2. Différents facteurs jouant un rôle dans la stabilité de chacune des conformations **12**

Conformation	Facteurs de stabilisation	Facteurs de destabilisation
1 → 6 Eq/A	(*1*) Effet anomère (*2*) CH_2OH équatorial	—
2	—	(*1*) Absence d'effet anomère (*2*) CH_2OH axial
3 → 6 Eq/C	CH_2OH équatorial	Absence d'effet anomère
4	Effet anomère	Substituants en 1 et 5 axiaux

Ainsi que le désignent les symboles configurationnels définis précédemment, *1* est le modèle du groupement CH_2OH de l'amylose et *3*, celui correspondant à la cellulose. Le tableau 2 rassemble les différents facteurs jouant un rôle dans la stabilité de chacune de ces conformations. Dans le cas du premier diastéréoisomère *1*/*2*, la conformation la plus probable est donc la conformation *1*, puisqu'il n'apparait aucun facteur d'instabilité alors que la conformation *2* est, au contraire, très défavorisée. Le diastéréoisomère modèle de l'hydroxyle (OH)6 de l'amylose aurait, par conséquent, la même conformation que les résidus d'α-D-glucose (H1 équatorial). Pour le second diastéréoisomère *3*/*4*, le choix est moins évident entre les deux conformations. Nous pensons cependant que la conformation *3*, analogue à celle des résidus celloglucane (H1 axial), est la plus favorisée, en raison du facteur important "1–3 diaxial" qui doit déstabiliser fortement la conformation *4*.

Ce type d'analyses conformationnelles que nous avons effectuées pour les autres diastéréoisomères modèles, nous a permis de faciliter l'interprétation et l'attribution des spectres rmn, dans le but de déterminer les correspondances configurationnelles des diastéréoisomères obtenus par chromatographie, avec les motifs d'amylose et de cellulose.

Détermination des correspondances configurationnelles par résonance magnétique nucléaire du proton

Spectres de résonance magnétique nucléaire du proton des molécules modèles

Les spectres rmn des alcoxy-2 tétrahydropyrannes se présentent, à 60 et à 100 MHz, sous forme de trois massifs distincts et non résolus: le proton "anomère" situé entre 4.5 et 5.0 ppm (en échelle δ par rapport au TMS); les protons portés par des atomes de carbone liés directement à des atomes d'oxygène (3–4 ppm) et les autres protons qui résonent à des champs plus forts (1–2 ppm). La fig. 2*a* représente, à titre d'exemple, le spectre rmn 60 MHz du cyclohexyloxy-2 tétrahydropyranne, molécule modèle **1**. Dans le cas des acétals hydroxylés, les protons des fonctions alcool résonent dans la zone 3–4 ppm.

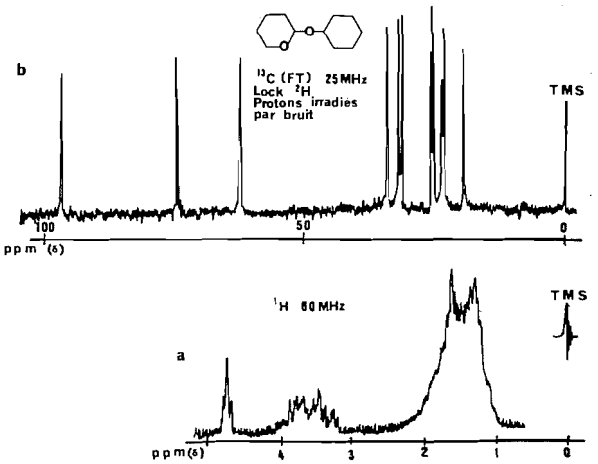

FIG. 2. Spectres de résonance magnétique nucléaire de la molécule modèle **1**: (*a*): spectre de protons enregistré à 60 MHz; (*b*): spectre des carbones 13 enregistré à 25 MHz; solvant: benzène deutérié; référence: tétraméthylsilane.

La seule indication qu'il est possible d'obtenir directement des spectres de ce type, concerne le proton anomère, bien que le déplacement chimique et que le couplage de ce proton soient des moyennes pondérées des deux conformations chaises tétrahydropyranniques. Dans ce type de composé, le proton anomère est préférentiellement en position équatoriale (44).

Outre ces observations liées aux protons anomères, nous nous sommes efforcés de résoudre les massifs des autres protons. Nous avons ainsi étudié, dans un travail annexe, les déplacements chimiques induits, dans les spectres rmn 60 MHz de certains alcoxy-2 tétrahydropyrannes (45) et acétals monohydroxylés (46), par addition de tri(dipivalométhanato) europium $(DPM)_3Eu$, ce qui nous a permis d'attribuer certains protons ou groupes de protons.

*Correspondance configurationnelle des diastéréoisomères de type **12** et **13***

D'une manière générale, les diastéréoisomères correspondant à une même molécule modèle et séparés par chromatographie par perméation de gel, présentent des spectres rmn différents. Cependant, la faible résolution des spectres ne permet pas, en

Can. J. Chem. Downloaded from www.nrcresearchpress.com by 210.87.254.42 on 09/05/12
For personal use only.

Can. J. Chem. Downloaded from www.nrcresearchpress.com by 210.87.254.42 on 09/05/12
For personal use only.

pratique, d'interpréter les différences observées et, de ce fait, d'attribuer les configurations des diastéréoisomères. Dans le cas des acétals monohydroxylés sur le cycle tétrahydropyrannique (molécules modèles **12** et **13**), il nous a toutefois été possible de déterminer la correspondance configurationnelle des quatre diastéréoisomères correspondants.

Nous avons indiqué précédemment que les conformations les plus probables des deux diastéréoisomères de type **12**, étaient vraisemblablement les conformations *1*: 6 Eq/A (proton anomère équatorial) et *3*: 6 Eq/C (proton anomère axial). La fig. 3*a* représente le spectre rmn 60 MHz du mélange des deux diastéréoisomères de type **12**, dans la zone (4–5 ppm) des protons anomères. On observe un signal relativement étroit vers 5 ppm et une résonance large à champ plus fort. La première résonance est due à un proton équatorial (A), la seconde à un proton axial (B) (33, 40, 44). Nous avons ainsi été conduits à attribuer le premier signal à la conformation *1* et le second à la conformation *2*. L'enregistrement séparé des spectres rmn de chacun des deux diastéréoisomères nous a permis, par comparaison avec le spectre du mélange, d'établir la correspondance configurationnelle suivante: **12**A: 6 Eq/A et **12**B: 6 Eq/C.

Nous avons pu obtenir la correspondance configurationnelle des diastéréoisomères **13**A et **13**B, en suivant un raisonnement sensiblement analogue. Le spectre rmn 60 MHz du mélange de diastéréoisomères est reproduit sur la fig. 3*b*. Cette zone 4–5 ppm montre les résonances des deux protons anomères, dont les profils résultent d'un couplage avec le proton vicinal H2 respectif. Par analogie avec les diastéréoisomères de type **12**, la résonance à 4.8 ppm (J = 3 Hz) correspond au proton équatorial; celle à 4.3 ppm (J = 6 Hz), au proton axial. La correspondance configurationnelle des diastéréoisomères séparés par chromatographie est donc: **13**A: 2 Eq/A et **13**B: 2 Eq/C.

Détermination des correspondances configurationnelles par résonance magnétique nucléaire du carbone 13

Il ne nous a pas été possible d'établir, par rmn du proton, les correspondances configurationnelles des diastéréoisomères autres que ceux des type **12** et **13**, en raison de la faible résolution des spectres. Nous avons ainsi été amenés à poursuivre ces analyses configurationnelles par rmn du carbone 13, en utilisant la technique de résonance pulsée par transformée de Fourier. Outre le domaine beaucoup plus important des déplacement chimiques, l'intérêt majeur de cette technique, que nous avons mis à profit dans la détermination des correspondances

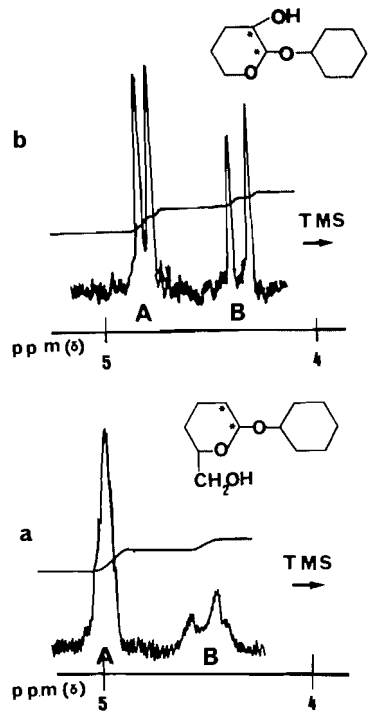

FIG. 3. Spectres de résonance magnétique nucléaire 60 MHz des mélanges de diastéréoisomères de type **12** (spectre *a*) et de type **13** (spectre *b*); solvant: chloroforme deutérié; référence: tétraméthylsilane.

configurationnelles, réside dans la grande sensibilité des déplacements chimiques des ^{13}C, aux effets stériques. La rmn du ^{13}C est, à ce titre, un outil de choix dans l'étude des conformations en série cyclohexanique par exemple (47), où la présence d'un seul substituant suffit souvent à procurer un spectre du premièr ordre (48). Toute contrainte stérique apportée par l'introduction d'un substituant, provoque, en effet, un déplacement vers les champs forts (blindage) de la résonance du carbone qui porte ce substituant (47–50). Ces phénomènes spectraux, propres à la rmn du ^{13}C, ont permis de nombreuses attributions dans la série des inositols (51) et dans celle des monosaccharides (52).

Méthodes d'études utilisées

Les valeurs des déplacements chimiques dans les spectres totalement découplés, permettent de classer les différents carbones dans les trois catégories suivantes:

Carbone anomère C1	:	90 ppm < δ < 110 ppm
Carbone portant un substituant oxygéné (OH ou OR)	:	60 ppm < δ < 85 ppm
Carbone non substitué:		15 ppm < δ < 45 ppm

La fig. 2*b* représente, à titre d'exemple, le spectre

Can. J. Chem. Downloaded from www.nrcresearchpress.com by 210.87.254.42 on 09/05/12
For personal use only.

rmn ^{13}C du cyclohexyloxy-2 tétrahydropyranne (**1**), où l'on remarque que les 11 catégories différentes de ^{13}C donnent 11 raies fines distinctes. Les spectres "off resonance" nous ont, par ailleurs, fourni des données supplémentaires concernant le type de substitution des différents carbones. Enfin, les spectres en présence de $(DPM)_3Eu$ nous ont permis d'obtenir des renseignements complémentaires sur l'attribution des correspondances configurationnelles, compte tenu de ce que nous avions observé en résonance du proton. Cependant, ils n'ont été enregistrés que dans le cas des acétal-monoalcools pour lesquels le site de complexation de l'ion europium est connu (45, 46).

Exemples d'attributions et de correspondances configurationnelles

Il nous a semblé fastidieux de présenter tous les résultats numériques issus des spectres rmn ^{13}C que nous avons enregistrés à partir des 4 acétals simples, des 14 acétal-monoalcools diastéréoisomères et des 17 diastéréoisomères acétals-diols séparés. Nous présentons ici un exemple d'attribution spectrale dans chacun de ces trois cas. D'une manière générale, les attributions des différents ^{13}C des cycles tétrahydropyranniques (P) et cyclohexaniques (C) ont été désignées avec les symboles suivants.

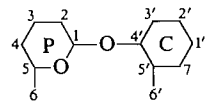

Acétals simples—Nous avons choisi de présenter les attributions spectrales faites à partir du cyclohexyloxy-2 tétrahydropyranne (molécule modèle **1**), étant donné que ce composé constitue le squelette de base des acétal-alcools. De plus, les valeurs numériques des déplacements chimiques de différents ^{13}C dont nous proposons l'attribution, nous ont servi lors de l'interprétation des spectres rmn ^{13}C des acétals mono- et dihydroxylés. Le tableau 3 rassemble les résultats obtenus pour ce composé. La première colonne représente les différents déplacements chimiques mesurés à partir du spectre totalement découplé. ΔEu désigne les différences observées entre les déplacements chimiques mesurés en présence et en absence de $(DPM)_3Eu$ dans le benzène deutérié, extrapolées pour des rapports molaires $(DPM)_3Eu$:soluté égaux à 1 (45, 46). Les natures des différentes contraintes stériques permettant d'attribuer les ^{13}C tétrahydropyranniques et cyclohexaniques, ont été déterminées en fonction des valeurs des déplacements de signaux (47–52).

Acétal-monoalcools—Les spectres rmn ^{13}C des diastéréoisomères correspondants ont été interprétés sur la base des attributions des ^{13}C du cyclohexyloxy-2 tétrahydropyranne (tableau 3). Nous prendrons comme exemple le cas des deux diastéréoisomères de la molécule modèle **13** pour lesquels une correspondance configurationnelle a été proposée par rmn du proton. Le tableau 4 rassemble les résultats obtenus pour les diastéréoisomères **13**A et **13**B, où les déplacements Δδ, exprimés en ppm, sont relatifs aux variations des déplacements chimiques, par rapport aux ^{13}C correspondants du cyclohexyloxy-2 tétrahydropyranne (**1**). Ces valeurs sont affectées d'un signe + lorsqu'ils s'effectuent vers les champs forts et d'un signe −, vers les champs faibles. La comparaison des valeurs Δδ et des contraintes stériques permet de vérifier que le groupement cyclohexyloxy est préférentiellement axial dans **13**A et préférentiellement équatorial dans **13**B. Compte tenu des conformations tétrahydropyranniques les plus favorisées, nous retrouvons ici les correspondances configurationnelles déterminées par rmn du proton: 2 Eq/A pour **13**A et 2 Eq/C pour **13**B. Il a été, de la même façon, possible de confirmer les correspondances configurationnelles des diastéréoisomères **12**A et **12**B, décrites précédemment et de proposer des correspondances pour les autres acétal-monoalcools (voir tableau 6). Dans le cas du couple **9**A, **9**B, les différences de déplacements chimiques des ^{13}C de ces deux diastéréoisomères ne sont pas toujours assez significatives pour préciser avec certitude leurs correspondances configurationnelles. Ces dernières, indiquées dans le tableau 6, ont été, dans ce cas, confirmées à partir des spectres infrarouge de chélation (voir Partie II).

Acétal-diols—Les spectres rmn ^{13}C des diastéréoisomères des différents acétal-diols étudiés, sont

TABLEAU 3. Observations et attributions effectuées à partir du spectre rmn ^{13}C du composé **1**. La nature des différentes contraintes stériques a été déterminée sur la base des résultats bibliographiques (50–53) et les références spectrales sont le déplacement chimique du cyclohexane (δ 27.6 ppm) pour les ^{13}C de type cyclohexanique et ceux du tétrahydropyranne (68.8, 27.4 et 24.3 ppm) pour les ^{13}C tétrahydropyranniques

δ (en ppm)	ΔEu	Nature de la contrainte stérique	Attributions proposées
96.4	27	—	P1
74.1	6.6	—	C4′
61.9	25	(Ax, γ)	P5
34.2	4	(Eq, β)	C5′
32.1	2	(Eq, β)	C3′
31.7	7.2	(Ax, β)	P2
26.15	7.2	(Ax, δ)	P4
26.15	1.6	(Eq, δ)	C1′
24.6	2	(Eq, γ)	C7
24.3	1.6	(Eq, γ)	C2′
19.8	6	(Ax, γ)	P3

TABLEAU 4. Observations et attributions effectuées à partir des spectres rmn du ^{13}C des isomères **13**A et **13**B

δ (en ppm)	ΔEu	Δδ par rapport à **1**	Contrainte stérique supplémentaire par rapport à **1**	Attributions proposées
		Diastéréoisomère ***13***a		
97.2	15	−0.8	(Eq, β)	P1
75.1	10	−1		C4′
68.15	60	−36.5	(Eq, α)	P2
59.5	15	+2.4	(Eq, δ)	P5
33.9	10	+0.3		C5′
32.0	15	+0.1		C3′
28.4	30	−8.6	(Eq, β)	P3
26.0	5	−0.1		C1′
24.9	15	+1.2	(Eq, γ)	P4
24.4	1	+0.2		C7
24.1	3	+0.2		C2′
		Diastéréoisomère ***13***b		
101.7	15	−5.3	(Eq, β) (Eq, α) − (Ax, α)	P1
75.5	10	−1.4		C4′
68.8	65	−37.1	(Eq, α) (Eq, β) − (Ax, β)	P2
63.3	20	−1.4	(Eq, δ) (Eq, γ) − (Ax, γ)	P5
34.1	10	+0.1		C5′
32.1	10	0		C3′
28.6	20	−8.8	(Eq, β) (Eq, γ) − CAx, γ)	P3
26.1	1	0		C1′
24.4	2	+0.2		C7
24.4	5	−0.1		C2′
23.3	20	+2.8	(Eq, γ) (Eq, γ) − (Ax, γ)	P4

d'une interprétation plus délicate en ce qui concerne leurs attributions, en raison de la présence simultanée de deux fonctions alcool sur le squelette cyclohexyloxy-2 tétrahydropyrannique. De plus, il n'est pas significatif, dans ce cas, d'enregistrer les spectres en présence de sels d'europium, ainsi que nous l'avons signalé précédemment.

Les attributions spectrales ont été faites en comparant systématiquement les données avec celles du cyclohexyloxy-2 tétrahydropyranne, d'une part, et avec celles des diastéréoisomères relatifs aux deux acétal-monoalcools correspondants. Ainsi, dans le cas de la molécule modèle **16**, les acétals monohydroxylés parents sont les modèles **11** et **12**. La correspondance configurationnelle d'un diastéréoisomère de type acétal-diol est, par conséquent, une résultante directe des configurations possibles des deux acétal-monoalcools dont il dérive.

Lors des analyses de spectres que nous avons faites, nous avons admis que les effets dûs aux contraintes stériques, au niveau de chaque déplacement chimique de ^{13}C, sont une combinaison linéaire de ceux observés pour les acétals monohydroxylés parents. Cette hypothèse paraît vraisemblable s'il n'y a pas une variation trop importante des équilibres conformationnels, par rapport aux acétals monohydroxylés. Les effets dûs aux contraintes stériques que nous avons été amenés à évaluer, ne tiennent pas compte des nouvelles perturbations apportées par la présence simultanée des deux groupements alcool. Nous ne les avons donc pas considérés comme des valeurs absolues mais ils nous ont permis, dans certains cas, de trancher entre deux structures configurationnelles. De plus, nous avons tenu compte du type de conformation chélatée, déduit par spectroscopie infrarouge (voir Partie II) et de l'examen parallèle des modèles moléculaires qui nous a permis, pour certains diastéréoisomères, d'écarter la ou les structures configurationnelles incompatibles avec le type de chélation observé expérimentalement. Le tableau 5 représente, à titre d'exemple, les déplacements chimiques δ observés pour le diastéréoisomère **15**A ainsi que les déplacements chimiques calculés dans le cas d'une filiation **9**A + **12**A (déplacement

Can. J. Chem. Downloaded from www.nrcresearchpress.com by 210.87.254.42 on 09/05/12
For personal use only.

Can. J. Chem. Downloaded from www.nrcresearchpress.com by 210.87.254.42 on 09/05/12
For personal use only.

TABLEAU 5. Comparaison des déplacements chimiques (δ) observés pour le diastéréoisomère **15A** avec les déplacements chimiques δ_1 et δ_2 calculés pour les couples **9A,12A** et **9A,12B**. Les valeurs δ_1 et δ_2 sont obtenues en ajoutant algébriquement au déplacement chimique d'un carbone donné du composé **1** les valeurs de Δδ (défini dans le texte) observées pour ce même carbone sur le spectre de chacun des composants du couple

Carbone	δ (ppm) observé pour **15A**	δ_1 (ppm) calculé pour la combinaison **9A** + **12A**	δ_2 (ppm) calculé pour la combinaison **9A** + **12B**	$\lvert\delta - \delta_1\rvert$ (ppm)	$\lvert\delta - \delta_2\rvert$ (ppm)
P1	98.6	99.0	104.5	0.4	5.9
P2	32.0	31.3	32.8	0.7	0.8
P3	18.0	18.3	22.6	0.3	4.6
P4	27.3	27.0	26.7	0.3	0.6
P5	70.1	70.5	75.6	0.4	5.1
P6	66.2	66.2	65.7	0.0	0.5
C1′	24.7	24.7	24.7	0.0	0.0
C2′	33.3	32.9	32.8	0.3	0.1
C3′	74.1	73.8	74.1	0.3	0.0
C4′	82.8	83.2	84.6	0.4	1.8
C5′	30.6	31.1	31.4	0.5	0.8
C7	24.3	24.1	22.9	0.2	1.4

TABLEAU 6. Correspondances configurationnelles établies par spectroscopie entre les diastéréoisomères séparés par chromatographie et les séquences d'amylose et de cellulose

Molécule modèle	Diastéréoisomères séparés	Correspondance configurationnelle
8 *cis*	**8A** et **8B**	Aucune correspondance
9 *trans*	**9A**	3′ Eq/A
	9B	3′ Eq/C
11 *trans*	**11A** et **11B**	Pas d'attribution certaine
12	**12A**	6 Eq/A
	12B	6 Eq/C
13	**13A**	2 Eq/A
	13B	2 Eq/C
14 *cis*	**14A**, **14B** et **14C**	Aucune correspondance
15 *trans*	**15A**	6 Eq/3′ Eq/A
	15B	Aucune correspondance
	15C	6 Eq/3′ Eq/C
16 *trans*	**16A**	Aucune correspondance
17 *cis*	**17A**, **17B**, **17C** et **17D**	Aucune correspondance
18 *trans*	**18A**	2 Eq/3′ Eq/A
	18B et **18D**	Aucune correspondance
	18C	2 Eq/3′ Eq/C
19 *trans*	**19A** et **19B**	Pas d'attribution certaine
20	**20A** et **20C**	Aucune correspondance
	20B	2 Eq/6 Eq/A

δ_1) et dans le cas d'une filiation **9A** + **12B** (déplacement δ_2).[3] La comparaison des valeurs $\lvert\delta - \delta_1\rvert$ et $\lvert\delta - \delta_2\rvert$ permet ainsi d'attribuer la correspondance configurationnelle 6 Eq/3′ Eq/A à ce diastéréoisomère. Nous avons rassemblé dans le tableau 6 les correspondances configurationnelles des diastéréoisomères, de type cyclohexyloxy-2 tétrahydropyranne, obtenus par chromatographie. Parmi les 30 diastéréoisomères étudiés, 11 présentent une correspondance configurationnelle saccharidique: 5 avec les

[3]Le type de chélation observé pour le diastéréoisomère **15A** implique en effet une filiation à partir de **9A** tandis que pour les mêmes raisons **15B** et **15C** dérivent de **9B**.

Can. J. Chem. Downloaded from www.nrcresearchpress.com by 210.87.254.42 on 09/05/12
For personal use only.

motifs de la cellulose et 6 avec ceux de l'amylose. Nous décrivons, dans la Partie suivante, les conformations chélateés préférentiellement adoptées par ces diastéréoisomères modèles, dans le but de préciser certaines chélations pouvant survenir dans les polyglucosides.

Partie expérimentale

Molécules modèles

Composés 1–4

Ces composés ont été obtenus suivant le mode opératoire de Parham et Anderson (34) avec un rendement de 80 à 90%: **1**, pé 39–40°C/0.05 Torr (17, 31); **2**, pé 35°C/20 Torr (30); pé 50°C/15 Torr (32); pé 58°C/15 Torr (32).

Composés 5–9

La synthèse de ces molécules modèles a déjà été décrite antérieurement (18). Nous avons légèrement modifié le mode opératoire en effectuant la réaction dans le chlorure de méthylène (250 cm^3 pour 1 mol de dihydropyranne). Les rendements réactionnels sont alors compris entre 48 et 53%: **5**, pé 82°C/1 Torr; **6**, pé 62°C/0.1 Torr; **7**, pé 49°C/0.1 Torr; **8**, pé 120°C/2 Torr; **9**, pé 78°C/0.1 Torr.

Composés 10 et 11

Le transhydroxyméthylcyclohexanol a été préparé suivant le procédé de Smissman et Mode (53). Les monotosylates de ce diol et du butanediol-1,3 ont été obtenus par la méthode de Siegel (54). Ces monotosylates sont des huiles visqueuses légèrement jaunes. Toute purification de ces huiles par distillation est exclue car elles se décomposent vers 90°C même sous atmosphère d'azote. Dans le cas de l'hydroxyméthyl-2 cyclohexanol, l'huile peut cristalliser lentement. Les cristaux obtenus, recristallisés dans l'éther absolu fondent à 75°C.

L'addition sur le dihydropyranne (voir ci-dessus) est effectuée sur l'huile brute. Le produit de la réaction est une huile visqueuse qu'il n'est possible ni de cristalliser, ni de distiller. L'hydrolyse non réductrice du tosylate ayant conduit à des résultats infructueux, nous avons transformé celle-ci en fonction acétate plus facile à hydrolyser en milieu basique. Nous avons suivi un mode opératoire décrit (55) mais dans notre cas particulier, le meilleur rendement en fonctions acétate/tosylate est obtenu au bout de 5 h de reflux (55% pour le dérivé du butanediol-1,3, pé 126°C/10 Torr et 49% pour celui de l'alcool cyclique pé 81°C/0.05 Torr.

L'hydrolyse de la fonction acétate est effectuée à froid par un mélange méthanol anhydre/méthanolate de sodium (56). Après évaporation du méthanol, le résidu est repris à l'eau puis extrait à l'éther. La solution éthérée est séchée sur du sulfate de sodium; l'éther puis l'extrait sont distillés (rendement 97%): **10**, pé 68°/1 Torr (25% par rapport au diol de départ); **11** pé 102°C/0.05 Torr (20% par rapport au diol de départ).

Composés 12, 14–16

L'hydroxyméthyl-2 dihydropyranne, préparé par réduction du dimère de l'acroléine (35, 36), a été acétylé selon la méthode de Zelinski *et al.* (36). Après addition du monoalcool ou du diol correspondant, la fonction acétate est hydrolysée (56) et l'acétal-alcool, purifié: **12**, pé 98°C/0.05 Torr (82% par rapport à l'alcool de départ); **14**, pé 120°C/0.05 Torr (43%); **15**, pé 118°C/0.05 Torr (49%); **16**, ce modèle a été purifié par chromatographie sur gel au cours de la séparation des isomères.

Composés 13, 17–21

A une suspension de 70 g d'acide paranitroperbenzoïque (préparé suivant le procédé de Vilkas (37)) dans 200 ml de chloroforme (sec et débarassé de toute trace d'éthanol par distillation sur de l'anhydride phosphorique), on ajoute progressivement une solution de 0.35 mol de dihydropyranne sec (ou de son dérivé) dans 100 ml de chloroforme sec. La température est maintenue inférieure à 15°C pendant toute l'addition. Lorsque tout le dihydropyranne a été ajouté et que la température n'a plus tendance à s'élever spontanément, on filtre rapidement et l'on rince trois fois au chloroforme pur. La solution chloroformique est alors lavée à la soude pour éliminer toute trace d'acide et séchée sur sulfate de sodium.

La solution précédente est ramenée à 100 ml et on ajoute ensuite 0.3 mol de l'alcool (ou du diol) approprié ainsi que 300 mg d'acide paratoluène-sulfonique. On agite 3 h au reflux, puis on reprend par 200 ml de chloroforme et on lave à la soude normale. La phase organique est ensuite séchée sur sulfate de sodium. On évapore le solvant puis on distille éventuellement le produit obtenu s'il n'est pas trop lourd et surtout s'il ne se dégrade pas trop à la chaleur. Dans le cas des dérivés de l'hydroxyméthyl-2 dihydropyranne, on effectue en dernier lieu une hydrolyse basique de la fonction acétate: **13**, pé 78°C/0.05 Torr; (72% par rapport au dihydropyranne); **17** pé 89°C/0.05 Torr (29%); **18** (38), pé 90°C/0.05 Torr (35%); **19**, pé 120°C/0.05 Torr (16%); **20**, pé 120°C/0.05 Torr (59%); **21**, ce composé n'a pu être purifié ni par distillation, ni par chromatographie en phase liquide, en raison de son insolubilité dans les solvants chromatographiques organiques.

Purification des produits finaux

En raison de la sensibilité à la chaleur de la fonction acétal, il n'a pas toujours été possible de purifier les composés par distillation directe, notamment dans le cas des acétal-diols. La purification a été alors réalisée au cours de la séparation chromatographique des isomères en prélevant les impuretés au fur et à mesure des recyclages (29). Les fractions finales ont toutes été contrôlées par spectroscopie infrarouge et résonance magnétique nucléaire. Ce sont des huiles très visqueuses ou des solides à point de fusion voisin de la température ambiante.

Spectres de résonance magnétique nucléaire

Les spectres des protons ont été enregistrés sur les appareils Varian A60 à 60 MHz, Varian HA 100 ou XL 100 à 100 MHz avec pour référence le tétraméthylsilane (TMS) et pour solvant le chloroforme deutérié, le benzène deutérié ou le tétrachlorure de carbone.

Les spectres en présence de $(DPM)_3Eu$ ont, en particulier, été enregistrés à partir de solutions 0.5 *M* des composés dans le tétrachlorure de carbone en augmentant progressivement la quantité du réactif.

Les spectres des carbones ont été enregistrés à 25 MHz sur les appareils JEOL PS 100 ou Varian XL 100 munis de la transformée de Fourier avec pour référence le TMS et pour solvant le benzène deutérié dont le signal n'interfère en aucun cas avec ceux des composés étudiés. Le signal du deutérium de ce solvant est d'autre part utilisé pour le lock.

1. M. SUNDARALINGAM. Biopolymers, **6**, 189 (1968).
2. G. A. KOGAN, V. M. TUL'CHINSKY, M. L. SHULMAN, S. E. ZURABYAN et A. YA KHORLIN. Carbohydr. Res. **26**, 191 (1973).
3. R. A. JACOBSON, J. A. WUNDERLICH et W. N. LIPSCOMB. Acta Crystallogr. **14**, 598 (1961).
4. C. J. BROWN. J. Chem. Soc. A, 7, 927 (1966).
5. S. S. C. CHU et G. A. JEFFREY. Acta Crystallogr. B, **24**, 830 (1968).
6. J. T. HAM et D. G. WILLIAMS. Acta Crystallogr. B, **26**, 1373 (1970).
7. P. H. HERMANS. Physics and chemistry of cellulose fibers. Elsevier, New York, NY. 1949. p. 3.

8. T. PETITPAS et J. MERING. C. R. Acad. Sci. Paris, **243**, 47 (1956).
9. D. W. JONES. J. Polym. Sci. **32**, 371 (1958); **42**, 173 (1960).
10. C. Y. LIANG et R. H. MARCHESSAULT. J. Polym. Sci. **37**, 385 (1959).
11. N. NORMAN. Text. Res. J. **33**, 711 (1963).
12. A. SARKO et R. MUGGLI. Macromolecules, **7**, 486 (1974).
13. J. MANN et H. J. MARRINAN. J. Polym. Sci. **32**, 357 (1958); **37**, 385 (1959).
14. K. C. ELLIS et J. O. WARWICKER. J. Polym. Sci. **56**, 339 (1962).
15. R. H. MARCHESSAULT et C. Y. LIANG. J. Polym. Sci. **43**, 71 (1960).
16. C. Y. LIANG. J. Polym. Sci. **62**, S5 (1962).
17. C. QUIVORON et J. NEEL. J. Chim. Phys. 1199 (1966).
18. C. QUIVORON et J. NEEL. J. Chim. Phys. 1210 (1966).
19. C. QUIVORON et J. NEEL. J. Chim. Phys. 1223 (1966).
20. C. QUIVORON, J. NEEL et G. CHAMPETIER. Cellul. Chem. Technol. **1**, 3 (1967).
21. C. G. QUIGLEY, A. SARKO et R. H. MARCHESSAULT. J. Am. Chem. Soc. **92**, 5834 (1970).
22. C. G. QUIGLEY. Diss. Abstr. Int. B, **30**, 4590 (1970).
23. S. S. C. CHU et G. A. JEFFREY. Acta Crystallogr. **23**, 1038 (1967).
24. A. HYBL, R. E. RUNDLE et D. E. WILLIAMS. J. Am. Chem. Soc. **87**, 2779 (1965).
25. R. K. MCMULLAN, W. SAENGER, J. C. FAYOS et D. MOOTZ. Carbohydr. Res. **31**, 37 (1973); **31**, 211 (1973).
26. V. S. R. RAO, P. R. SUNDARAJAN, C. RAMAKRISHNAN et G. N. RAMACHANDRAN. *Dans* Conformation of biopolymers. *Edité par* G. N. Ramachandran. Academic Press, New York, NY. 1967. p. 721.
27. B. K. SATHYA NARAYANA et V. S. R. RAO. Biopolymers, **11**, 1379 (1972).
28. M. FIALEYRE, F. LAFUMA et C. QUIVORON. J. Chim. Phys. **74**, 701 (1977).
29. F. LAFUMA, J. LESEC et C. QUIVORON. J. Chromatogr. **138**, 89 (1977).
30. R. PAUL. Bull. Soc. Chim. Fr. **5**, 971 (1934).
31. W. DAUBEN et H. BRADLOW. J. Am. Chem. Soc. **74**, 559 (1952).
32. G. O. PIERSON et O. A. RUNQUIST. J. Org. Chem. **33**, 2572 (1968).
33. A. J. DE HOOG, H. R. BUYS, C. ALTONA et E. HAVINGA. Tetrahedron, **25**, 3365 (1969).
34. W. E. PARHAM et E. L. ANDERSON. J. Am. Chem. Soc. **70**, 4187 (1948).
35. L. CROMBIE, J. GOLD, S. H. HARPER et B. L. STOKES. J. Chem. Soc. 136 (1956).
36. R. ZELINSKI, A. VERBISCAR et H. J. EICHEL. J. Org. Chem. **23**, 184 (1958).
37. M. VILKAS. Bull. Soc. Chim. Fr. 1401 (1959).
38. C. QUIVORON. C. R. Acad. Sci. Ser. C, **266**, 781 (1968).
39. J. LESEC, F. LAFUMA et C. QUIVORON. C. R. Acad. Sci. Ser. C, **278**, 1069 (1974); J. Chromatogr. Sci. **12**, 683 (1974).
40. G. DESCOTES, D. SINOU et J. C. MARTIN. Bull. Soc. Chim. 3730 (1970).
41. A. J. DE HOOG et H. R. BUYS. Tetrahedron Lett. 4175 (1969); M. GELIN, Y. BAHUREL et G. DESCOTES. Bull. Soc. Chim. Fr. 3723 (1970).
42. J. C. MARTIN. Ann. Chim. (Paris), **6**, 205 (1971).
43. R. E. REEVES. J. Am. Chem. Soc. **71**, 215 (1949); **72**, 1500 (1950).
44. R. V. LEMIEUX, R. K. KULLNIG, H. J. BERNSTEIN et W. G. SCHNEIDER. J. Am. Chem. Soc. **79**, 1005 (1957).
45. F. LAFUMA et C. QUIVORON. C. R. Acad. Sci. Ser. C, **272**, 2020 (1971).
46. F. LAFUMA et C. QUIVORON. C. R. Acad. Sci. Ser. C, **276**, 359 (1973).
47. G. W. BUCHANAN, J. B. STOTHERS et D. A. ROSS. J. Am. Chem. Soc. **88**, 4301 (1966); G. W. BUCHANAN et J. B. STOTHERS. Can. J. Chem. **47**, 3605 (1969).
48. D. K. DALLING et D. M. GRANT. J. Am. Chem. Soc. **89**, 6612 (1967).
49. G. W. BUCHANAN, J. B. STOTHERS et S. T. WU. Can. J. Chem. **47**, 3113 (1969).
50. J. D. ROBERTS, F. J. WEIGERT, J. I. KROSCHWITZ et H. J. REICH. J. Am. Chem. Soc. **92**, 1338 (1970).
51. D. E. DORMAN, S. J. ANGYAL et J. D. ROBERTS. J. Am. Chem. Soc. **92**, 1351 (1970).
52. D. E. DORMAN et J. D. ROBERTS, J. Am. Chem. Soc. **92**, 1355 (1970); A. S. PERLIN, B. CASU et H. J. KOCH. Can. J. Chem. **48**, 2596 (1970); E. BREITMAIER, W. VOELTER, G. JUNG et C. TANZER. Chem. Ber. **104**, 1147 (1971).
53. E. E. SMISSMAN et R. A. MODE. J. Am. Chem. Soc. **79**, 3447 (1957).
54. S. SIEGEL. J. Am. Chem. Soc. **75**, 1317 (1953).
55. H. PHILLIPS. J. Chem. Soc. **127**, 2442 (1925).
56. A. THOMPSON et M. L. WOLFROM. Methods Carbohydr. Chem. **2**, 215 (1963).
57. F. LAFUMA et C. QUIVORON. Can. J. Chem. Ce numéro.

Can. J. Chem. Downloaded from www.nrcresearchpress.com by 210.87.254.42 on 09/05/12
For personal use only.

Molécules modèles des motifs des poly-1,4-glucosides. II. Etude, par spectroscopie infrarouge, des conformations chélatées des diastéréoisomères modèles et discussion dans le cadre des chélations glucosidiques

FRANÇOISE LAFUMA ET CLAUDE QUIVORON

Laboratoire de Physico-Chimie Macromoléculaire de l'Université Pierre et Marie Curie (Paris VI), Ecole Supérieure de Physique et de Chimie, 10 rue Vauquelin - 75231, Paris Cedex 05 - France

Reçu le 20 janvier 1977[1]

FRANÇOISE LAFUMA et CLAUDE QUIVORON. Can. J. Chem. **56**, 2076 (1978).

Nous avons étudié, d'une façon systématique, les spectres infrarouges de chélation, dans la région 3700–3300 cm^{-1}, de chacun des 30 diastéréoisomères séparés, en solution diluée dans le tétrachlorure de carbone. Les diastéréoisomères présentant une correspondance configurationnelle avec les chaînes de la cellulose et de l'amylose ont été plus particulièrement examinés. Suivant la structure covalente de la molécule modèle et la configuration du diastéréoisomère, nous avons observé des bandes d'absorption ν(O—H) spécifiques de chélations à 5, 6, 7 et 8 chaînons. Le plus souvent, la géométrie des conformations chélatées varie, pour une même molécule modèle, d'un diastéréoisomère à un autre. Les diastéréoisomères des acétals hydroxylés nous ont permis de connaître ce qui résulte d'une compétition de deux groupements hydroxyle, vis à vis d'un même site accepteur de proton. La discussion de nos résultats expérimentaux dans le cadre des chélations glucosidiques, nous a conduit à proposer les chélations (OH)2···O1; (OH)3′···O5 et (OH)6···O3, pour le cellobiose, le méthyl β-cellobioside et la cellulose. Dans le cas du maltose, du méthyl β-maltoside et de l'amylose, nous avons confirmé la chélation de type (OH)2···(OH)3′, et il nous paraît vraisemblable que la chélation (OH)2···O1 puisse exister dans ces α-1,4-glucosides.

FRANÇOISE LAFUMA and CLAUDE QUIVORON. Can. J. Chem. **56**, 2076 (1978).

We have made a systematic study of the infrared spectra, in the chelation region 3700–3300 cm^{-1}, of each of 30 separate diastereoisomers in dilute solution in carbon tetrachloride. Those diastereoisomers which have configurations corresponding to those of cellulose or amylose were examined more carefully. Depending on the structure of the model molecule and its diastereoisomeric configuration, it was possible to observe absorption bands corresponding to chelation in rings of 5, 6, 7 or 8 members. Most frequently the geometry of the chelated conformations varies from one diastereoisomer to another of a single molecule. The diastereoisomers of hydroxylated acetals have permitted the recognition of the result of a competition between two hydroxyl groups for the same proton accepting site. Discussion of these experimental results in terms of glucosidic chelations have led to the hypothesis that the chelations are (OH)2···O1, (OH)3′···O5 and (OH)6···O3 in cellobiose, in methyl β-cellobioside and in cellulose, respectively. We have confirmed the chelation (OH)2···(OH)3′ in the case of maltose, methyl β-maltoside and amylose and it seems reasonable to suggest that a chelation (OH)2···O1, can exist in these α-1,4-glucosides.

[Journal translation]

Introduction

Nous avons exposé, dans la Partie I précédente (1), la synthèse de diastéréoisomères, modèles des séquences disaccharidiques de la cellulose et de l'amylose ainsi que leurs correspondances configurationnelles avec les motifs α-D- et β-D-glucose (voir tableau 6, Partie I). Dans le présent mémoire, nous avons étudié, d'une façon systématique, les spectres infrarouges, dans la région des vibrations de valence ν(O—H), de chacun de ces diastéréoisomères en solution très diluée dans le tétrachlorure de carbone, afin de connaître la ou les conformations chélatées préférentiellement adoptées par ces diastéréoisomères en solution.

La spectroscopie infrarouge est la méthode de choix pour étudier la formation de liaisons hydrogène intramoléculaires. L'observation la plus caractéristique, dans le spectre d'un soluté se prêtant à une chélation de type O—H···O, est la différence de fréquences Δν (exprimée en cm^{-1}) entre les maximums des bandes de vibration de valence ν(O—H) des groupements hydroxyle "libre" et "chélaté". Les valeurs des différences Δν publiées dans le domaine des diols (2–5), des éther-alcools (6) et des acétal-alcools (7, 8), montrent qu'elles dépendent, d'une manière générale, de la position relative des deux sites donneur et accepteur de proton dans la molécule étudiée. Les différentes catégories de cycles de chélation sont les suivantes, si l'on compte tous les atomes constituant de tels cycles:

[1] Revision reçue le 21 mars 1978.

Can. J. Chem. Downloaded from www.nrcresearchpress.com by 210.87.254.40 on 09/05/12
For personal use only.

Can. J. Chem. Downloaded from www.nrcresearchpress.com by 210.87.254.40 on 09/05/12
For personal use only.

TABLEAU 1. Résultats spectroscopiques relatifs aux acétal-monoalcools

Composé	ν(OH) libre (cm^{-1})	ν_1 (OH lié) (cm^{-1})	$\Delta\nu_1$ (cm^{-1})	Taille du cycle 1	ν_2 (OH lié) (cm^{-1})	$\Delta\nu_2$ (cm^{-1})	Taille du cycle 2	τ
9A	3633[a]	3602	31	5	—	—	—	0[b]
9B	3633[a]	3600	33	5	3434	199	7	3.2[b]
11A	3642	3540	102	6	—	—	—	0.12[c]
11B	3642	3546	96	6	—	—	—	0.58[c]
12A	3644[a]	3606	38	5	—	—	—	—
12B	3646[a]	3602	44	5	—	—	—	—
Hydroxyméthyl-2 tétrahydropyranne	3640[a]	3598	42	5	—	—	—	—
13A	—	3582	51[d]	5	—	—	—	—
13B	3633[a]	3600	33	5	—	—	—	—

[a]Epaulement de faible intensité sur la bande de chélation pentagonale.
[b]Rapport de la densité optique de la bande de chélation *2* à celle de la bande de chélation *1*.
[c]Rapport de la densité optique de la bande de chélation à celle de la bande "OH libre".
[d]Valeur calculée en se référant à la valeur 3633 cm^{-1} pour la fréquence d'absorption (OH) libre.

Cycles à 5 chaînons : $25 < \Delta\nu < 40\ cm^{-1}$

Cycles à 6 chaînons : $75 < \Delta\nu < 110\ cm^{-1}$

Cycles à 7 chaînons : $150 < \Delta\nu < 200\ cm^{-1}$

Cycles à 8 chaînons : $120 < \Delta\nu < 150\ cm^{-1}$

En ce qui concerne la stabilité de ces différents cycles de chélation, il semble qu'elle varie, pour une série homologue de produits, dans l'ordre décroissant (6, 7): 5 > 6 > 7 > 8.

Nous avons étudié les spectres infrarouges de chélation, dans la gamme 3700–3300 cm^{-1}, ainsi que les conformations chélatées, des diastéréoisomères modèles qui ont été séparés par chromatographie (9). Bien que chaque diastéréoisomère ait fait l'objet d'une étude systématique, nous décrivons ci-dessous les résultats obtenus avec ceux présentant une correspondance configurationnelle avec les motifs de la cellulose et de l'amylose.

Dans ce travail, nous avons été amenés à comparer, dans le cas des diastéréoisomères d'une même structure covalente, les densités optiques des bandes ν(O—H) libre et chélaté, dans le but d'estimer qualitativement l'importance des conformations chélatées. Cette comparaison directe suppose que les coefficients d'extinction moléculaire des bandes correspondantes, ne varient sensiblement pas d'un diastéréoisomère à l'autre. Aucune donnée bibliographique n'étant publiée sur ce sujet, nous avons supposé que cette hypothèse pouvait être admise sans trop de réserves.

Conformations chélatées des diastéréoisomères de type acetal-monoalcool

Les molécules modèles **5** et **6**, qui ne sont pas des mélanges de diastéréoisomères (un seul atome de carbone asymétrique), ont déjà fait l'objet d'un travail antérieur (7). Nous n'avons pas rapporté les spectres de chélation des diastéréoisomères **8**A et **8**B qui ne présentent aucune correspondance configurationnelle avec les séquences d'amylose ou de cellulose. Les spectres de chélation des diastéréoisomères des modèles **7**, **10** et **13** sont décrits par ailleurs (10) et montrent une dépendance très notable de la configuration sur la conformation chélatée adoptée, phénomène général que nous avons retrouvé pour la plupart des autres couples de diastéréoisomères étudiés.

Le tableau 1 rassemble les résultats obtenus pour les autres acétal-monoalcools; nous y avons adjoint ceux des diastéréoisomères **13**A et **13**B (10) qui présentent des correspondances configurationnelles avec les séquences d'amylose (**13**A) et de cellulose (**13**B) (1).

Diastéréoisomères 9

Ces deux diastéréoisomères sont d'un grand intérêt, puisque **9**A: 3′Eq/A est un modèle configurationnel de l'amylose et que **9**B: 3′Eq/C est un modèle de la cellulose. Les deux spectres de chélation correspondants sont consignés sur la fig. 1. On observe une différence extrêmement importante entre les deux spectres. Ainsi, le diastéréoisomère **9**A est majoritairement chélaté d'une façon pentagonale sur l'atome d'oxygène pontal, puisqu'il n'est pas possible de mettre en évidence une absorption vers 3400–3450 cm^{-1} qui serait due à une chélation heptagonale sur l'atome d'oxygène cyclique. Au contraire, dans le cas du diastéréoisomère **9**B, les deux types de chélations pentagonale et heptagonale sont présents avec une prépondérance de la conformation chélatée à sept atomes. On constate donc ici une influence notable de la configuration sur les conformations préférentiellement chélatées, tout à fait analogue à celle observée pour le composé 7 (10) qui préfigurait ce modèle.

Nous avons, par ailleurs, décelé des empêchements stériques de formation de chélation, en con-

Can. J. Chem. Downloaded from www.nrcresearchpress.com by 210.87.254.40 on 09/05/12
For personal use only.

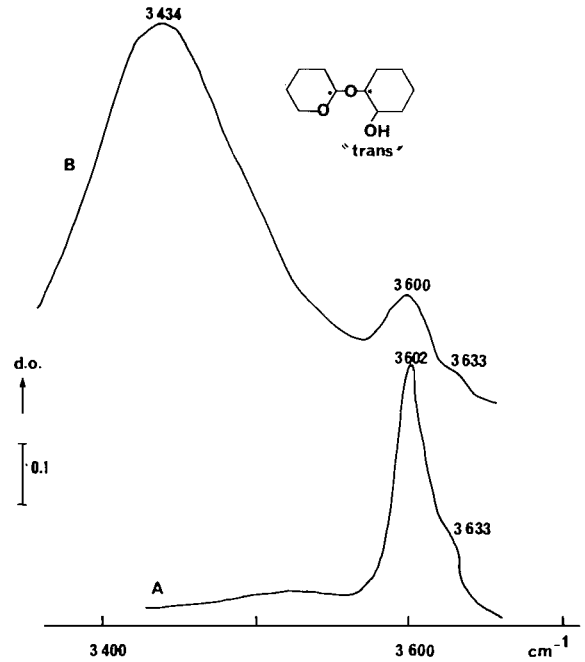

FIG. 1. Spectre infrarouge de chélation des isomères du composé **9**.

struisant les modèles moléculaires des diastéréoisomères **9**A et **9**B. L'examen de ces modèles montre que si la chélation heptagonale est aisée dans le cas de **9**B, elle est exclue, d'un point de vue stérique pour **9**A; ce qui confirme les correspondances configurationnelles proposées (1) et les observations spectroscopiques.

Diastéréoisomères 11

Ces deux diastéréoisomères, dont les correspondances configurationnelles n'ont pas été attribuées d'une façon certaine, ont des spectres infrarouges de chélation qui s'apparentent aux diastéréoisomères de type **10** (10) (voir tableau 1), avec une population en conformation chélatée probablement beaucoup plus grande pour **11**B que pour **11**A.

Diastéréoisomères 12

Le diastéréoisomère **12**A: 6 Eq/A correspond, d'un point de vue configurationnel, aux séquences de l'amylose; **12**B: 6 Eq/C, aux séquences de la cellulose. Ces modèles schématisent donc l'interaction de l'hydroxyle (OH)6 avec la fonction acétal. Les spectres de chélation de ces deux diastéréoisomères sont analogues à celui de l'hydroxyméthyl-2 tétrahydropyranne (tableau 1) et présentent de faibles différences entre eux, en fréquences comme en intensités. Les cycles pentagonaux observés correspondent donc à une chélation sur l'atome d'oxygène tétrahydropyrannique.

Diastéréoisomères 13

Le diastéréoisomère **13**A correspond au groupement (OH)2 des résidus α-D-glucose de l'amylose (2 Eq/A); le diastéréoisomère **13**B à celui des résidus β-D-glucose de la cellulose (2 Eq/C). Ces deux diastéréoisomères sont presque entièrement chélatés en solution. Le diastéréoisomère **13**A, dont le spectre ne fait apparaître aucune absorption ν(O—H) "libre", serait plus chélaté que **13**B.

La comparaison entre les valeurs de Δν observées pour **13**A et **13**B, et les valeurs trouvées par Kuhn (2) pour les cyclohexanediols-1,2, *cis* et *trans* suggère d'apparenter, d'un point de vue configurationnel, le diastéréoisomère **13**A au diol-1,2 *cis* et **13**B au diol-1,2 *trans* (10), ce qui correspond bien aux attributions proposées antérieurement (1).

Conformations chélatées des diastéréoisomères de type acetal-diol

Parmi les 20 diastéréoisomères de type acétal-diol qui ont pu faire l'objet d'une séparation par chromatographie, 5 correspondent à des dispositions configurationnelles de la cellulose ou de l'amylose: **15**A, **15**C, **18**A, **18**C et **20**B. Les diastéréosiomères **19**A et **19**B, effectivement séparés, n'ont pas reçu de correspondance configurationnelle certaine (1). Nous exposons uniquement ci-dessous les résultats obtenus dans le cas de ces diastéréoisomères. La plupart de ces modèles nous ont permis de connaître ce qui résulte d'une compétition entre les chélations de deux hydroxyles sur un même site accepteur de proton d'une fonction acétal, ainsi que cela a lieu au sein des polyglucosides eux-mêmes. Le tableau 2 rassemble les principaux résultats spectroscopiques obtenus pour ces composés.

Diastéréoisomères 15A et 15C

La fig. 2 représente les spectres de chélation de ces deux diastéréoisomères, ainsi, à titre indicatif, que celui du diastéréoisomère **15**B. Le diastéréoisomère **15**A, possèdant une correspondance configurationnelle avec l'amylose (6 Eq/3′ Eq/A), présente, dans son spectre, une bande unique à 3608 cm^{-1}, spécifique de chélations pentagonales. Il est donc vraisemblable d'admettre que sa conformation chélatée prépondérante soit la conformation *1*.

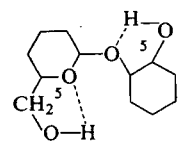

Conformation *1*

Dans le cas du diastéréoisomère **15**C, les deux bandes principales observées sont situées à 3606 cm^{-1}

TABLEAU 2. Résultats spectroscopiques relatifs aux acétal-diols

Composé	ν(OH libre) (cm^{-1})	ν_1(OH lié) (cm^{-1})	$\Delta\nu_1$ (cm^{-1})	Taille du cycle 1	ν_2(OH lié) (cm^{-1})	$\Delta\nu_2$ (cm^{-1})	Taille du cycle 2	ν_3(OH lié) (cm^{-1})	$\Delta\nu_3$ (cm^{-1})	Taille du cycle 3
15A	3644[a]	3608	36	5						
	3630[a]		22	5	—	—	—	—	—	—
15C	3644[a]	3606	38	5	3460	184	7	—	—	—
	3628[a]		22	5		168	7	—	—	—
18A	3628	3592	36	5	3500	128	8	—	—	—
18C	3625[a]	3603	22	5	3468	157	7	—	—	—
19A	3640[a]	3588	[b]	—	3540	100	6	3440	200	7
			42[c]	5		[b]	—		190	7
19B	3640[a]	3604	[b]	—	3538	102	6	—	—	—
	3630[a]		26	5		[b]	—			
20B	3645[a]	3606	39	5	3587	58	5	—	—	—
	3630[a]		24	5		43	5			

[a]Faible épaulement.
[b]Avec ce modèle, il n'est pas possible de construire de cycle 5 chaînons avec le groupement (O—H) primaire ou de cycle à 6 chaînons avec le groupement (O—H) secondaire.
[c]Valeur obtenue en se référant à une valeur de 3630 cm^{-1} pour ν(O—H libre).

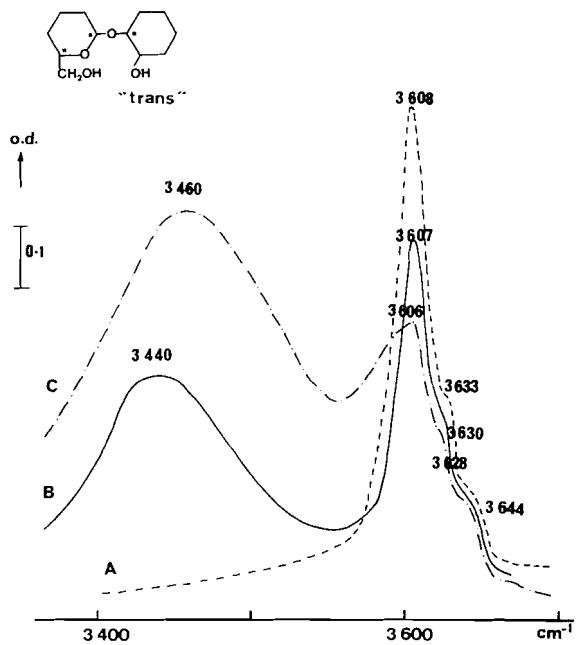

FIG. 2. Spectre infrarouge de chélation des isomères du composé **15**.

(cycle de chélation pentagonale) et à 3460 cm^{-1} (cycle de chélation heptagonale). Il y a donc certainement ici équilibre entre des conformations chélatées de type *1* (voir ci-dessus) et de type *2*.

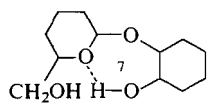

Conformation *2*

Cependant, étant donné la forte absorption à 3460 cm^{-1}, il est possible que les deux conformations chélatées précèdentes soient en équilibre avec la conformation *3*.

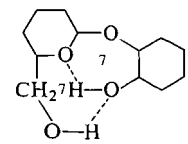

Conformation *3*

qui fait apparaître un second cycle de chélation heptagonale. Cette possibilité est d'autant plus envisageable que le groupement OH secondaire voit son caractère accepteur de proton renforcé par la formation de sa propre chélation.

Diastéréoisomères 18A et 18C

Ces modèles schématisent, par rapport à la fonction acétal intraextracyclique, les hydroxyles (OH)2 et (OH)3′ de l'amylose et de la cellulose: **18**A: 2 Eq/3′ Eq/A et **18**C: 2 Eq/3′ Eq/C. En ce qui concerne le diastéréoisomère **18**A, la présence simultanée de bandes de chélations pentagonale et octogonale, ainsi qu'une absorption non négligeable des vibrateurs O—H "libre", est incompatible avec l'existence d'une seule conformation chélatée. Il est, par conséquent, certain que ce diastéréoisomère soit le siège d'un équilibre entre les conformations chélatées suivantes (schéma 1).

Au contraire, le diastéréoisomère **18**C existerait sous forme de trois conformations chélatées en équilibre entre elles (schéma 2).

Diastéréoisomères 19A et 19B

Deux des quatre diastéréoisomères de la molécule modèle **19**, préparée à partir de l'hydroxyméthyl-2 cyclohexanol *trans*, ont été séparés par chromatographie. Deux diastéréoisomères correspondent, en

Can. J. Chem. Downloaded from www.nrcresearchpress.com by 210.87.254.40 on 09/05/12
For personal use only.

Can. J. Chem. Downloaded from www.nrcresearchpress.com by 210.87.254.40 on 09/05/12
For personal use only.

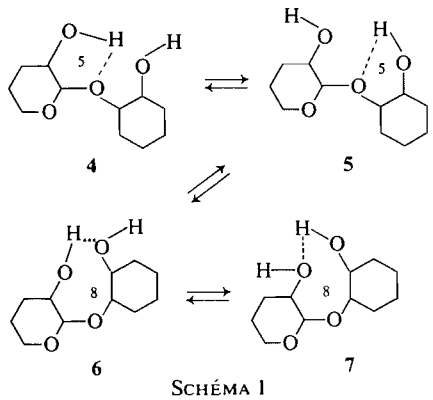

SCHÉMA 1

toute rigueur, à la cellulose et à l'amylose mais n'ont pas été attribués d'une façon certaine.

Nous avons représenté sur la fig. 3 les spectres de chélation du diastéréoisomère pur **19**A, de la fraction enrichie **19**B et celui du mélange **19**C + **19**D. Dans le cas des diastéréoisomère **19**A et **19**B, on observe deux massifs principaux, l'un situé vers 3588–3604 cm^{-1}, l'autre vers 3538–3540 cm^{-1}. Ces deux zones d'absorption sont respectivement spécifiques de chélations pentagonale et hexagonale. Par analogie avec les chélations observées pour les acétals mono-alcools correspondants **11** et **13**, les deux diastéréoisomères **19**A et **19**B seraient le siège d'un équilibre entre formes chélatées (schéma 3).

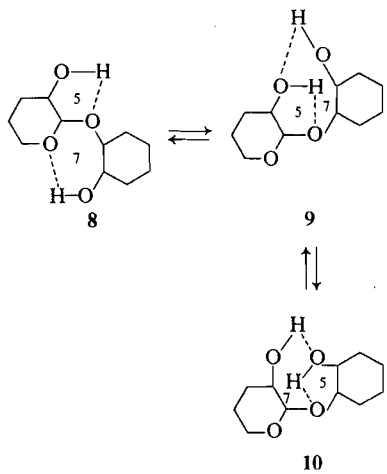

SCHÉMA 2

Le spectre de l'isomère **19**A montre, de plus, une absorption vers 3440 cm^{-1} qui persiste même à haute dilution. Une telle bande, caractérisée par des valeurs $\Delta\nu = 200$ et 190 cm^{-1}, suivant que l'on se réfère aux vibrateurs O—H "libre" primaire ou secondaire, est relative vraisemblablement à une chélation de type heptagonal. Il est possible que cette faible absorption soit due à la chélation, dans la conformation *12*, de l'hydroxyle secondaire sur l'atome d'oxygène de la fonction alcool primaire.

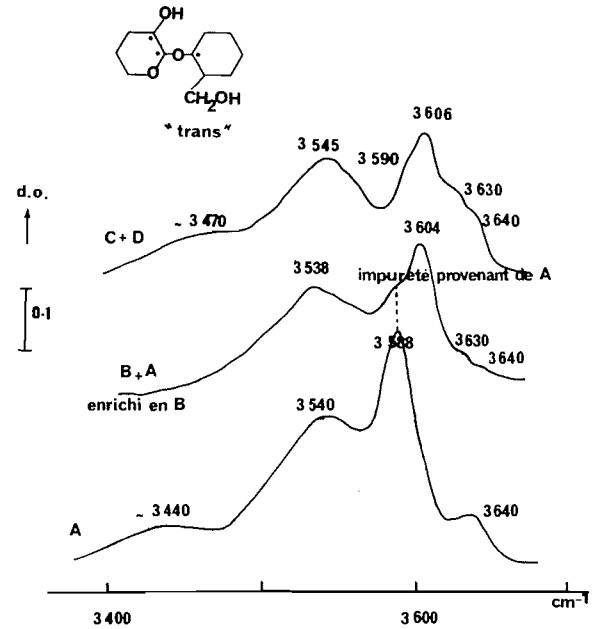

FIG. 3. Spectre infrarouge de chélation des isomères du composé **19**.

Diastéréoisomère 20B

Les fréquences d'absorption (3606 et 3587 cm^{-1}) relevées sur le tableau 2 sont caractéristiques de deux chélations pentagonales différentes. La conformation préférentiellement adoptée par ce diastéréoisomère serait ainsi la suivante.

Discussion des résultats dans le cadre des chélations glucosidiques

La mise en évidence directe de liaisons hydrogène intramoléculaires au sein des chaînes de polysaccharides comme la cellulose et l'amylose est, ainsi que nous l'avons indiqué dans la Partie I (1), difficilement réalisable. Le cas des mono- et des disaccharides n'est guère plus accessible directement: seul Fialeyre *et al.* (11) a pu montrer récemment, par spectroscopie infrarouge, l'existence de cycles pentagonaux de chélation dans certains mono- et disaccharides en solution. L'étude des conformations chélatées des

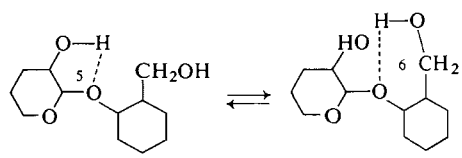

SCHÉMA 3

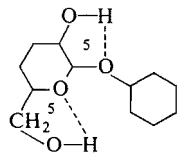

diastéréoisomères modèles correspondant, d'un point de vue configurationnel, aux séquences d'amylose et de cellulose, que nous avons réalisée au cours de ce travail, devrait se révéler très efficace quant aux liaisons hydrogène intramoléculaires, capables de prendre naissance au sein des poly-1,4 glucosides eux-mêmes.

Avant de discuter les résultats expérimentaux obtenus, il convient de faire trois remarques préalables, concernant leur extrapolation au cas de la cellulose, de l'amylose et de leurs mono- et disaccharides. En premier lieu, les diastéréoisomères modèles ne représentent, par principe, que très partiellement les séquences α-D- et β-D-glucosidiques. Cependant, les renseignements issus de la chélation des acétaldiols nous ont permis de connaître ce qui résulte de la compétition de deux fonctions hydroxyle vis à vis d'un même atome d'oxygène acétal. En second lieu, l'étude des conformations chélatées des diastéréoisomères a été effectuée en solution diluée dans un solvant inerte. L'extrapolation des résultats au cas des composés glucosidiques solides ou aux mono- et disaccharides en solution dans l'eau, paraît, dans ces conditions, assez hasardeuse. Nos propres résultats doivent néanmoins permettre de savoir si telle ou telle chélation, proposée dans le cas des composés glucosidiques, par diffraction des rayons X par exemple, est ou non vraisemblable. De plus, nous décrirons ici quelques spectres infrarouges de diastéréoisomères, enregistrés, dans la région ν(O—H), à l'état liquide pur. Ces observations nous ont permis de déceler une persistance de certaines chélations, sous cet état condensé. La troisième remarque concerne les équilibres conformationnels des diastéréoisomères étudiés. Il est, en effet, certain que ces équilibres sont beaucoup plus perturbés en solution qu'à l'état solide (cas des composés glucosidiques). Il en résulte, ainsi que nous l'avons observé, une possibilité d'existence de plusieurs conformations chélatées, pour certains diastéréoisomères. Il nous sera, cependant possible d'écarter certaines des conformations chélatées observées, lorsque ces dernières sont envisagées au sein des chaînes de cellulose et d'amylose, pour des raisons de restriction de liberté de rotation autour des liaisons glucosidiques 1—4′.

Chélations dans les mono- et disaccharides

Les travaux publiés sur les monosaccharides à l'état solide, n'envisagent pas l'existence de liaisons hydrogène intramoléculaires (12, 13). Les réseaux de liaison hydrogène proposés ne font, en effet, intervenir que des interactions intermoléculaires. Dans le cas des disaccharides, la plupart des publications décrivent, en plus des liaisons hydrogène intermoléculaires, des chélations relatives à des sites accepteur et donneur appartenant aux deux cycles pyranosidiques. Ces chélations sont respectivement la liaison (OH)3′···O5 pour le cellobiose (14) et la liaison (OH)2···(OH)3′ pour le maltose (15).

Nous discuterons de la possibilité d'existence de chélations dans les mono- et les disaccharides, dans le cadre de nos propres résultats.

Persistance de chélations dans certains diastéréoisomères à l'état liquide

Afin de tenter de relier les résultats obtenus sur la chélation des diastéréoisomères en solution, avec ceux publiés dans le cas des mono- et des disaccharides en solution ou à l'état solide, nous avons enregistré les spectres infrarouges de certains diastéréoisomères, à l'état liquide pur, dans la gamme 3400–3700 cm^{-1}.

La fig. 4 représente, à titre d'exemple, les spectres obtenus pour les diastéréoisomères **12**A, **12**B, **13**A et **13**B. Chaque spectre présente un large massif vers

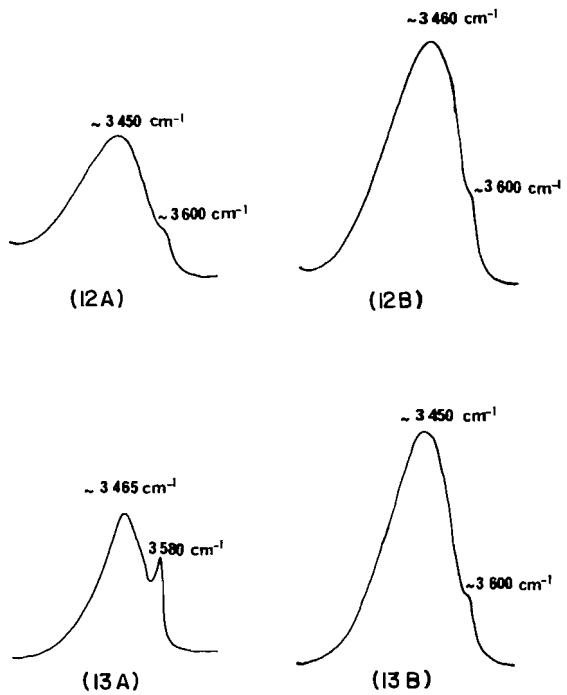

FIG. 4. Spectres infrarouges à l'état liquide pur des isomères des composés **12** et **13** dans la région ν(O—H) 3000–4000 cm^{-1}; appareil Perkin-Elmer 225; faces NaCl.

Can. J. Chem. Downloaded from www.nrcresearchpress.com by 210.87.254.40 on 09/05/12
For personal use only.

TABLEAU 3. Valeurs (en Å) des distances O···O calculées en considérant, dans les mono- et les disaccharides, des couples d'atomes d'oxygène appartenant à un même cycle pyranosidique, d'après les références 15, 18–21

	Distance (Å)											
Sucre	O1···O2	O2···O3	O3···O4	O4···O6	O6···O5	O6···O1	O1′···O2′	O2′···O3′	O3′···O1	O6′···O1	O6′···O5′	O6′···O1′
α-D-Glucose	2.81	2.86	2.91	3.61	2.89	5.16						
β-D-Glucose	2.85	2.90	2.90	3.51	2.81	4.90						
Cellobiose	2.75	2.92	2.86	4.36	2.69	4.71	2.89	2.76	3.00	4.18	2.89	4.89
Maltose	2.85	2.88	2.89	4.25	2.84	4.46	2.82	2.93	2.82	3.54	2.89	5.03
Méthyl β-cellobioside	2.89	2.93	2.94	4.31	2.73	4.70	2.85	2.92	3.08	3.64	2.78	4.90
Méthyl β-maltoside	2.78	2.88	2.84	4.24	2.81	4.48	2.87	2.92	2.79	3.46	2.89	5.01

3450–3465 cm^{-1}, qui est dû aux liaisons hydrogène intermoléculaires. On remarque, vers les hautes fréquences, des faibles épaulements vers 3600 cm^{-1} et une bande de moyenne intensité à 3580 cm^{-1}, dans le cas du diastéréoisomère **13**A. La position en fréquence de ces épaulements et de cette absorption à 3580 cm^{-1}, qui accompagnent le massif des liaisons intermoléculaires, nous a conduit à les attribuer à des liaisons hydrogène intramoléculaires de type pentagonal. En effet, pour le diastéréoisomère **13**A, la bande à 3580 cm^{-1} correspond tout à fait avec celle située à 3582 cm^{-1} pour la solution diluée dans le tétrachlorure de carbone (10) et qui est spécifique d'une chélation de type pentagonal. De la même façon, les épaulements situés vers 3600 cm^{-1} pour les diastéréoisomères **12**A, **12**B et **13**B correspondent à la zone des chélations pentagonales observées en solution.

Nous avons également observé une légère persistance de chélations pentagonales à l'état liquide, dans le cas des diastéréoisomères **15**A et **20**B. Il ne nous a pas été possible de savoir si les autres types de chélation persistent à cet état condensé, car les bandes correspondantes sont situées à des fréquences bien inférieures à 3600 cm^{-1} et sont, si elles existent, masquées par le large massif des interactions intermoléculaires.

Il paraît donc très vraisemblable qu'il existe des liaisons hydrogène intramoléculaires, au moins de type pentagonal, dans les mono- et les disaccharides en solution dans les solvants généralement choisis lors des études antérieures, c'est à dire dans l'eau et dans le diméthylsulfoxyde.

Distances O···O dans les cristaux de mono- et de disaccharides

Bien que la plupart des travaux antérieurs s'accordent à ne pas envisager de chélation dans les monosaccharides à l'état solide, ce problème nous semble toujours posé, en raison de la persistance de certaines chélations, pour les diastéréoisomères en solution ou à l'état liquide. Lorsque l'on détaille les différentes publications, relatives essentiellement à des études radiocristallographiques, on remarque, le plus souvent, qu'elles ne font pas toujours appel à toutes les possibilités d'interactions entre sites oxygénés. En particulier, les atomes d'oxygène acétal, reconnus par Quivoron et Neel (16) comme les sites les plus accepteurs de proton, ne sont pas souvent considérés, sauf pour le cellobiose: chélation (OH)3′···O5.

Dans le but de relier nos propres résultats sur les conformations chélatées des diastéréoisomères, avec des distances O···O privilégiées dans les mono- et les disaccharides à l'état solide, nous avons repris, d'une façon systématique, les données radiocristallographiques antérieures et calculé toutes les distances O···O dans le cas de l'α-D-glucose (17, 18), du β-D-glucose (19), du cellobiose (19), du maltose (15), du méthyl β-cellobioside (20) et du méthyl β-maltoside (21). Le tableau 3 rassemble les valeurs des distances O···O calculées en considérant des couples d'atomes d'oxygène appartenant à un même cycle pyranosidique. Le tableau 4 contient, au contraire, les valeurs des distances O···O, lorsque l'on envisage deux sites "oxygène" situés chacun sur un cycle différent. Ce dernier tableau n'est donc relatif qu'aux quatre disaccharides examinés.

Discussion des résultats

D'une manière générale, les radiocristallographes estiment qu'une liaison hydrogène a une existence "présumée", à l'état solide, lorsque la distance O···O calculée est inférieure ou égale à 2.9–3.0 Å. Le tableau 3 relatif aux chélations au sein d'un même cycle pyranosidique, contient un grand nombre de valeurs inférieures à cette limite, correspondant à des liaisons hydrogène intramoléculaires de type cyclohexanediol-1,2 *cis* ou *trans* ou hydroxyméthyl-2 tétrahydropyranne.

En solution, de telles chélations de type pentagonal sont observées pour les dérivés du cyclohexane (2) et du tétrahydropyranne (3) ainsi que pour nos modèles où elles persistent parfois même à l'état pur. Tous ces éléments nous permettent d'envisager

Can. J. Chem. Downloaded from www.nrcresearchpress.com by 210.87.254.40 on 09/05/12
For personal use only.

Can. J. Chem. Downloaded from www.nrcresearchpress.com by 210.87.254.40 on 09/05/12
For personal use only.

TABLEAU 4. Valeurs (en Å) des distances O···O calculées en considérant, dans le cas de 4 disaccharides, des couples d'atomes d'oxygène situés chacun sur un cycle pyranosidique différent, d'après les références 15, 19–21.

Sucre	Distance (Å)					
	O2···O3′	O6′···O5	O6···O6′	O3′···O5	O6′···O2	O6···O3′
Cellobiose	5.60	6.25	8.41	2.77	4.86	3.14
Maltose	2.79	3.70	4.79	4.91	5.45	7.28
Méthyl β-cellobioside	5.43	5.75	7.85	2.77	4.32	2.96
Méthyl β-maltoside	2.82	3.37	4.23	4.88	5.55	7.26

TABLEAU 5. Chélations mises en évidence, par spectroscopie infrarouge, dans les diastéréoisomères ayant une correspondance configurationnelle avec les séquences de la cellulose

Diastéréoisomère	Modèle de chélation(s)	Observations
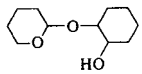 **9B**	(OH)3′···O5 (OH)3′···O1	Chélation heptagonale prépondérante
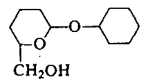 **12B**	(OH)6···O5	Chélation pentagonale prépondérante
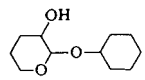 **13B**	OH)2···O1	Chélation pentagonale prépondérante
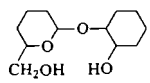 **15C**	(OH)3′···O5 (OH)3′···O1 (OH)6···O5 (OH)6···O3′	Equilibre entre les trois conformations chélatées *1*, *2* et *3*
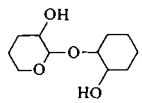 **18C**	(OH)2···O1 (OH)3′···O1 (OH)3′···O5 (OH)3′···(OH)2	Equilibre entre les trois conformations chélatées *8*, *9* et *10*

comme assez vraisemblable, l'existence de liaisons hydrogène intramoléculaires entre sites appartenant à un même cycle pyranosidique, dans les mono- et dans les disaccharides à l'état solide.

En ce qui concerne les chélations faisant intervenir deux sites situés chacun sur un cycle différent (disaccharides du tableau 4), les distances O···O optimales, c'est à dire inférieures ou égales à 2.9–3.0 Å, sont en nombre plus limité. Dans le cas du cellobiose et du méthyl β-cellobioside, les seules distances à retenir sont celles relatives aux chélations (OH)3′···O5 (d = 2.77 Å) et (OH)6···O3′ (d = 2.96–3.14 Å). La première de ces chélations a été proposée, d'une façon unanime, dans les mailles cristallines du cellobiose (14, 19, 22) et du méthyl β-cellobioside (20). Elle se retrouve dans tous les diastéréoisomères en correspondance configurationnelle avec le cellobiose, où elle est susceptible d'exister (**9**B, **15**C, **18**C). L'étude de **18**C montre que sa présence est conjointe à celle d'une chélation (OH)2···O1; lorsqu'il n'y a plus possibilité de rotation autour des liaisons pontales, la conformation *8* serait donc la plus favorisée comme l'ont suggéré Quivoron et Neel (23). La seconde liaison hydrogène intramoléculaire, déduite des valeurs du tableau 4 est l'interaction (OH)6···O3′. Elle a été proposée, en 1970, par Ham et Williams (20) dans la maille cristalline du méthyl β-cellobioside, conjointement avec la chélation (OH)3′···O5 précédente. Le diastéréoisomère **15**C se prête bien à cette double éventualité, comme nous l'avons indiqué précédemment (voir conformation *3*). Il nous semble, en définitive, possible de proposer, dans le cadre de

Can. J. Chem. Downloaded from www.nrcresearchpress.com by 210.87.254.40 on 09/05/12
For personal use only.

TABLEAU 6. Chélations mises en évidence, par spectroscopie infrarouge, dans les diastéréoisomères ayant une correspondance configurationnelle avec les séquences de l'amylose

Diastéréoisomère	Modèle de chélation(s)	Observations
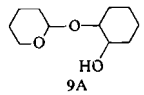 **9A**	(OH)3′···O5 (OH)3′···O1	Chélation pentagonale prépondérante
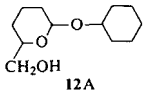 **12A**	(OH)6···O5	Chélation pentagonale prépondérante
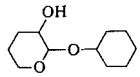 **13A**	(OH)2···O1	Chélation pentagonale prépondérante
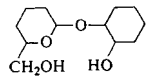 **15A**	(OH)3′···O5 (OH)3′···O1 (OH)6···O5 (OH)6···O3′	Double chélation pentagonale prépondérante
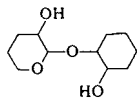 **18A**	(OH)2···O1 (OH)3′···O1 (OH)3′···O5 (OH)3′···(OH)2	Equilibre entre les quatre conformations chélatées *4*, *5*, *6* et *7*
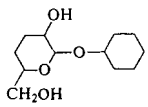 **20B**	(OH)2···O1 (OH)6···O5	Double chélation pentagonale prépondérante

nos résultats expérimentaux, un système de chélations (OH)2···O1, (OH)3′···O5 et (OH)6···O3′, à la fois pour le cellobiose et pour le méthyl β-cellobioside.

En ce qui concerne le maltose et le méthyl β-maltoside, les données du tableau 4 montrent qu'une seule possibilité de chélation peut, a priori, avoir lieu. Il s'agit de la liaison hydrogène (OH)2···(OH)3′: distances O···O de 2.79 et 2.82 Å. Cette liaison hydrogène a, en effet, été proposée pour ces deux disaccharides à l'état solide (15, 21) et en solution (24). L'étude du diastéréoisomère **18**A montre qu'une telle interaction est bien présente dans les conformations chélatées *6* et *7* sans qu'il ne nous soit pour autant possible d'écarter définitivement les conformations *4* et *5*.

Chélations dans les chaînes de cellulose et d'amylose

Parmi l'ensemble des diastéréoisomères étudiés, nous avons attribué, d'un point de vue configurationnel, cinq diastéréoisomères à la cellulose: **9**B, **12**B, **13**B, **15**C et **18**C. Le tableau 5 rassemble les résultats obtenus, par spectroscopie infrarouge, pour ces 5 diastéréoisomères. Une discussion détaillée de ces résultats, dans le cadre des chélations cellulosiques, a été récemment publiée (25). Nous avons proposé, comme dans le cas du cellobiose et du méthyl β-cellobioside, les chélations (OH)2···O1, (OH)3′···O5 et (OH)6···O3′. Ces trois interactions hydrogène pourraient coexister dans les zones désorganisées de la cellulose. Dans les zones cristallines, les groupements (OH)6 pourraient assurer la forte cohésion des chaînes cellulosiques entre elles, par rupture des chélations (OH)6···O3′ et par rotation, perpendiculairement à l'axe des chaînes, des liaisons covalentes O6—H6.

Dans le cas de l'amylose, les diastéréoisomères modèles **9**A, **12**A, **13**A, **15**A, **18**A et **20**B ont permis l'étude, par spectroscopie infrarouge, des chélations pouvant survenir dans les chaînes de ce polysaccharide (voir tableau 6). La discussion de nos résultats expérimentaux, ne dégage pas ici, contrairement au cas de la cellulose (25), de conclusions définitives sur les chélations mises en jeu. Les liaisons hydrogène intramoléculaires que nous pouvons retenir sont les chélations (OH)2···O1, (OH)6···O5 et (OH)2···(OH)3′. Dans le cas de la chélation (OH)6···O5, des travaux effectués par Fialeyre *et al.* (11), à partir de solutions de certains des diastéréoisomères dans des mélanges tétrachlorure de carbone – diméthyl sul-

foxyde, ont montré que cette interaction est moins favorisée que la chélation (OH)2...O1. Il nous semble ainsi vraisemblable qu'il puisse exister, dans les chaînes d'amylose, une double chélation du type:

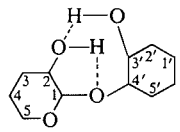

Partie expérimentale

Tous les spectres de chélation ont été enregistrés avec un appareil Perkin-Elmer, modèle 225, à partir de solutions dans le tétrachlorure de carbone de concentrations inférieures dans tous les cas à 5×10^{-3} mol/ℓ, afin d'éviter les associations intermoléculaires.

Dans ces conditions de concentration, il est nécessaire d'opérer avec des cellules suffisamment épaisses pour obtenir des densités optiques mesurables; nos mesures ont été réalisées avec des cuves Infrasil de 2 cm d'épaisseur.

Le tétrachlorure de carbone (produit Prolabo pour spectrophotométrie) a été séché sur des tamis moléculaires 4 Å.

Les spectres sont reproductibles à ± 1 cm^{-1} et les densités optiques ont été mesurées avec une précision de 5%.

1. F. LAFUMA et C. QUIVORON. Can. J. Chem. Ce numéro.
2. L. P. KUHN. J. Am. Chem. Soc. **74**, 2492 (1952); **76**, 4323 (1954).
3. J. S. BRIMACOMBE, A. B. FOSTER, M. STACEY et D. H. WHIFFEN. Tetrahedron, **4**, 351 (1958).
4. M. TICHY. Chem. Listy, **54**, 506 (1960).
5. H. BUC. Ann. Chim. **8**, 409 (1963).
6. L. P. KUHN et R. A. WIRES. J. Am. Chem. Soc. **86**, 2161 (1964).
7. C. QUIVORON et J. NEEL. J. Chim. Phys. 1210 (1966).
8. C. QUIVORON. C. R. Acad. Sci. Ser. C, **266**, 781 (1968).
9. J. LESEC, F. LAFUMA et C. QUIVORON. J. Chrom. Sci. **12**, 683 (1974); J. Chromatogr. **138**, 89 (1977).
10. F. LAFUMA, R. AUDEBERT et C. QUIVORON. C. R. Acad. Sci. Ser. C, **276**, 319 (1973).
11. M. FIALEYRE, F. LAFUMA et C. QUIVORON. J. Chim. Phys. **74**, 701 (1977).
12. M. SUNDARALINGAM. Biopolymers, **6**, 189 (1968).
13. G. A. KOGAN, V. M. TUL'CHINSKY, M. L. SHULMAN, S. E. ZURABYAN et A. YA KHORLIN. Carbohydr. Res. **26**, 191 (1973).
14. R. A. JACOBSON, J. A. WUNDERLICH et W. N. LIPSCOMB. Acta Crystallogr. **14**, 598 (1961).
15. C. G. QUIGLEY, A. SARKO et R. H. MARCHESSAULT. J. Am. Chem. Soc. **92**, 5834 (1970).
16. C. QUIVORON et J. NEEL. J. Chim. Phys. 1199 (1966).
17. R. C. G. KILEAN, W. G. FERRIER et D. W. YOUNG. Acta Crystallogr. **15**, 9113 (1962).
18. E. HOUGH, S. NEIDLE et P. G. H. TROUGHTON. Acta Crystallogr. Sec. B, **29**, 365 (1973).
19. S. S. C. CHU et G. A. JEFFREY. Acta Crystallogr. Sec. B, **24**, 830 (1968).
20. J. T. HAM et D. G. WILLIAMS. Acta Crystallogr. Sec. B, **26**, 1373 (1970).
21. S. S. C. CHU et G. A. JEFFREY. Acta Crystallogr. **23**, 1038 (1967).
22. C. J. BROWN. J. Chem. Soc. A, **7**, 927 (1966).
23. C. QUIVORON et J. NEEL. J. Chim. Phys. 1223 (1966).
24. B. CASU, M. REGGIANI, G. G. GALLO et A. VIGEVANI. Tetrahedron, **22**, 3061 (1966).
25. F. LAFUMA et C. QUIVORON. J. Polymer Sci. Symposium, **52**, 261 (1975).

Can. J. Chem. Downloaded from www.nrcresearchpress.com by 210.87.254.40 on 09/05/12
For personal use only.

Aminoglycoside antibiotics. The total synthesis of 5-deoxykanamycin A

GERRY KAVADIAS,[1] PIERRE DEXTRAZE, ROBERT MASSÉ, AND BERNARD BELLEAU

Bristol Laboratories of Canada, 100 Industrial Boulevard, Candiac, P.Q., Canada J5R 1J1

Received December 16, 1972

GERRY KAVADIAS, PIERRE DEXTRAZE, ROBERT MASSÉ, and BERNARD BELLEAU. Can. J. Chem. **56**, 2086 (1978).

Condensation of 1,6-*N*,*O*-carbonyl-3-*N*-ethoxycarbonyl-2,5-dideoxystreptamine (**7**) with 6-azido-2,3,4-tri-O-benzyl-6-deoxy-α-D-glucopyranosyl chloride by the Koenigs–Knorr reaction produced the α-glycoside **10**. The cyclic carbamate of **10** was opened with ethanol in the presence of sodium ethoxide and the resulting 4-*O*-(6-azido-2,3,4-tri-*O*-benzyl-6-deoxy-α-D-glucopyranosyl)-*N*,*N*′-diethoxycarbonyl-2,5-dideoxystreptamine (**12**) was glycosidated with 3-acetamido-2,4,6-tri-*O*-benzyl-3-deoxy-α-D-glucopyranosyl chloride (**21**) to give the α,α-diglycoside **22**. Hydrogenation of the azido group and removal of the protective groups gave 5-deoxykanamycin A (**25**), an antibiotic with a potency about half that of kanamycin A.

GERRY KAVADIAS, PIERRE DEXTRAZE, ROBERT MASSÉ et BERNARD BELLEAU. Can. J. Chem. **56**, 2086 (1978).

La condensation de la *N*,*O*-carbonyl-1,6 *N*-éthoxycarbonyl-3 didéoxy-2,5 streptamine (**7**) avec le chlorure de l'azido-6 tri-*O*-benzyl-2,3,4 déoxy-6 α-D-glucopyrannosyle, en faisant appel à la réaction de Koenigs–Knorr, conduit à l'α glycoside **10**. On a ouvert le carbamate cyclique de **10** avec de l'éthanol en présence d'éthylate de sodium et la *O*-(azido-6 tri-*O*-benzyl-2,3,4 déoxy-6 α-D-glucopyrannosyl)-4 *N*,*N*′-diéthoxycarbonyl didéoxy-2,5 streptamine (**12**) qui en résulte a été soumise à une réaction de glycosidation avec le chlorure de l'acétamido-3 tri-*O*-benzyl-2,4,6 déoxy-3 α-D-glucopyrannosyle (**21**) pour conduire à l'α,α-diglycoside **22**. L'hydrogénation du groupe azido et l'enlèvement des groupes protecteurs conduit à la déoxy-5 kanamycine A (**25**), un antibiotique dont la puissance est à peu près égale à la moitié de celle de la kanamycine A.

[Traduit par le journal]

In recent years, extensive studies have been carried out on the modification of aminoglycoside antibiotics with the purpose of studying the structure–activity relationship and of producing new antibiotics that are effective against resistant bacteria (1).

Most of the modifications have been directed at the aminosugar part of the molecule and only a few studies have been reported on the relationship between the structural features of the aminocyclitol moiety and the activity of the antibiotics (2).

The present paper describes the synthesis of 5-deoxykanamycin A (**25**) by glucosidation of the readily available and suitably protected 2,5-dideoxystreptamines (3) **7** and **14** by the Koenigs–Knorr reaction and demonstrates the usefulness of **7** and **14** as key intermediates for the synthesis of other 5-deoxyaminocyclitol antibiotics. With the exception of the mutamicins 2 and 2a, no other 5-deoxyaminocyclitol antibiotics have been reported (4). The interesting antibacterial properties of mutamicin 2 was an added incentive in the pursuit of our goals.

In the synthesis of aminoglycosides of 2-deoxystreptamine by the Koenigs–Knorr reaction, mercuric cyanide and dioxane–benzene or dioxane–chloroform are commonly used as catalyst and solvent, respectively (5–13). The role of dioxane in assisting the formation of α-glycosides has been discussed (7). The low solubility of the protected 2-deoxy- and 2,5-dideoxystreptamines in dioxane–benzene solutions led us to examine the use of dimethylformamide as the solvent in this coupling reaction. To establish workable experimental conditions for the synthesis of 5-deoxykanamycin A using dimethylformamide as the solvent, the condensation of **7** and **14** with the readily available 2,3,4,6-tetra-*O*-benzyl-α-D-glucopyranosyl chloride (**6**) (14) was examined first.

Reaction of **7** with **6** in DMF in the presence of mercuric cyanide at 65°C for 24 h gave, after purification on a silica column, 4-*O*-(2,3,4,6-tetra-*O*-benzyl-α-D-glucopyranosyl)-1,6-*N*,*O*-carbonyl-3-*N*-ethoxycarbonyl-2,5-dideoxystreptamine (**8**) in 80% yield. The nmr signal for the anomeric proton in **8** was not clearly defined so that structure **8** could only be inferred. Removal of the protective benzyl groups by catalytic reduction of **8** in the presence of 10% palladium-on-carbon followed by opening of the carbamate ring of **9** with a catalytic amount of sodium in absolute ethanol gave 4-*O*-(α-D-glucopyranosyl)-*N*,*N*′-diethoxycarbonyl-2,5-dideoxystreptamine (**11**). The nmr spectrum of **11** in deuterium oxide showed a doublet at δ 5.08 with a coupling of 2.8 Hz, values which are characteristic of the

[1]Author to whom correspondence may be addressed.

Can. J. Chem. Downloaded from www.nrcresearchpress.com by 210.87.254.40 on 09/05/12
For personal use only.

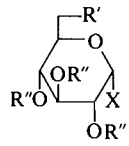

1 R′ = N_3, R″ = Ac, X = OCH_3
2 R′ = N_3, R″ = H, X = OCH_3
3 R′ = N_3, R″ = Bzl, X = OCH_3
4 R′ = N_3, R″ = Bzl, X = OH
5 R′ = N_3, R″ = Bzl, X = Cl
6 R′ = OBzl, R″ = Bzl, X = Cl

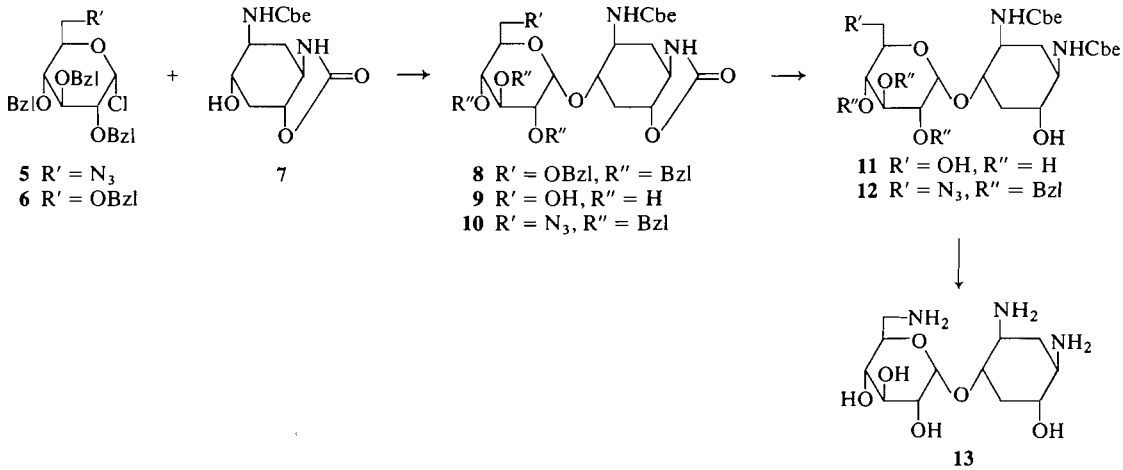

5 R′ = N_3
6 R′ = OBzl

7

8 R′ = OBzl, R″ = Bzl
9 R′ = OH, R″ = H
10 R′ = N_3, R″ = Bzl

11 R′ = OH, R″ = H
12 R′ = N_3, R″ = Bzl

13

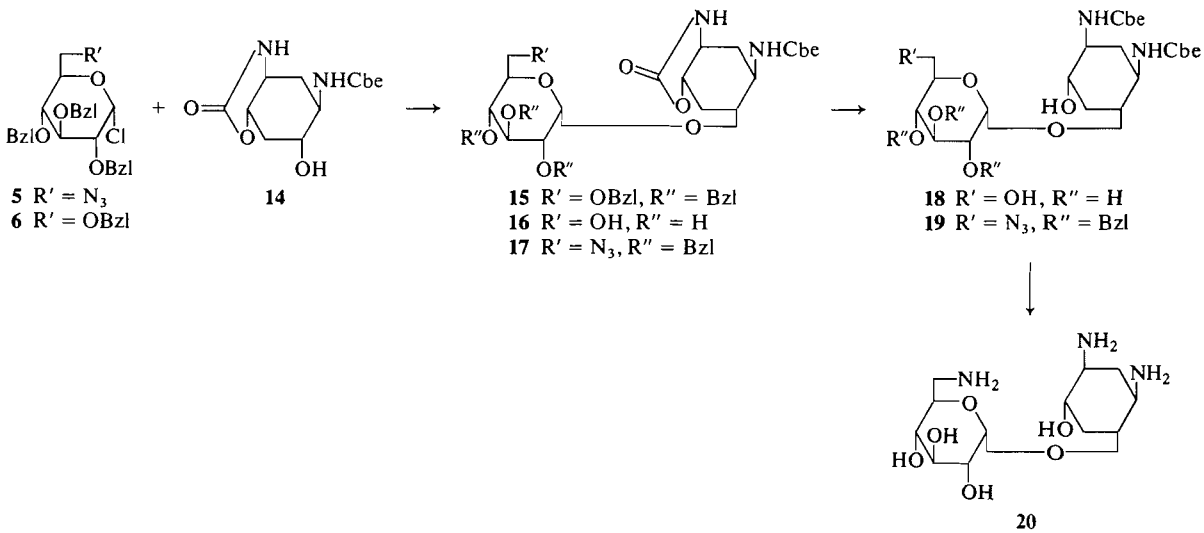

5 R′ = N_3
6 R′ = OBzl

14

15 R′ = OBzl, R″ = Bzl
16 R′ = OH, R″ = H
17 R′ = N_3, R″ = Bzl

18 R′ = OH, R″ = H
19 R′ = N_3, R″ = Bzl

20

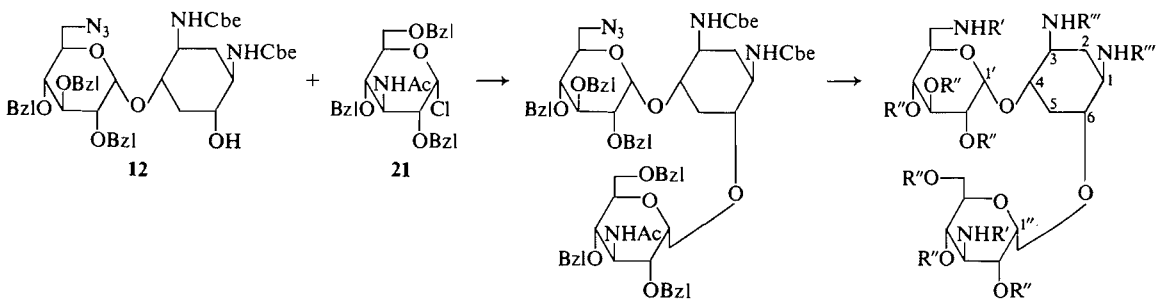

12

21

22

23 R′ = Ac, R″ = Bzl, R‴ = Cbe
24 R′ = Ac, R″ = H, R‴ = Cbe
25 R′ = R″ = R‴ = H

Can. J. Chem. Downloaded from www.nrcresearchpress.com by 210.87.254.40 on 09/05/12
For personal use only.

Can. J. Chem. Downloaded from www.nrcresearchpress.com by 210.87.254.40 on 09/05/12
For personal use only.

expected signal for the anomeric hydrogen of α-D-glucopyranosides.

Condensation of 3,4-*N*,*O*-carbonyl-1-*N*-ethoxycarbonyl-2,5-dideoxystreptamine (**14**) with **6** as described above for the synthesis of **8** afforded 6-*O*-(2,3,4,6-tetra-*O*-benzyl-α-D-glucopyranosyl)-3,4-*N*,*O*-carbonyl-1-*N*-ethoxycarbonyl-2,5-dideoxystreptamine (**15**) as crystals, mp 188–190°C (75.5% yield). To establish the anomeric configuration of this compound, the benzyl protective groups were removed by hydrogenation and the cyclic carbamate opened with sodium in ethanol to give 6-*O*-(α-D-glucopyranosyl)-*N*,*N*′-diethoxycarbonyl-2,5-dideoxystreptamine (**18**) as a crystalline solid, mp 218–220°C, in 84% yield based on **15**. The nmr spectrum of **18** clearly supported the α-glucosidic structure since it exhibited a doublet at δ 5.02 with a coupling of 3.5 Hz for the anomeric hydrogen.

The synthesis of 6-azido-2,3,4-tri-*O*-benzyl-6-deoxy-α-D-glucopyranosyl chloride (**5**) has been reported (15) and the advantages afforded by this intermediate in glycosidation reactions by comparison with the acylamino or aryloxycarbonylamino derivatives of the glycosyl halides have been discussed (8). In this synthesis, 6-azido-2,3,4,-tri-*O*-benzyl-6-deoxy-D-glucose (**4**) (the precursor of **5**) was obtained from the methylglucoside **3** by acid hydrolysis with hydrochloric acid in acetic acid. In our hands, the hydrolysis of **3** by the above method gave poor yields (10–15%) of **4**, the major product being a polar compound with R_f 0 (tlc). The hydrolysis of **3** to **4** was best accomplished by heating **3** in aqueous dioxane in the presence of *p*-toluenesulfonic acid (38% yield). The reaction was slow (5 days) but the only other major component of the reaction mixture was the starting material **3**.

Condensation of 1,6-*N*,*O*-carbonyl-3-*N*-ethoxycarbonyl-2,5-dideoxystreptamine (**7**) with **5** in DMF in the presence of mercuric cyanide at 80–85°C for 24 h produced, after purification on a silica column, 4-*O*-(6-azido-2,3,4-tri-*O*-benzyl-6-deoxy-α-D-glucopyranosyl)-1,6-*N*,*O*-carbonyl-3-*N*-ethoxycarbonyl-2,5-dideoxystreptamine (**10**) in 53.5% yield. The cyclic carbamate of **10** was opened by heating in boiling ethanol in the presence of a catalytic amount of sodium to give 4-*O*-(6-azido-2,3,4-tri-*O*-benzyl-6-deoxy-α-D-glucopyranosyl)-*N*,*N*′-diethoxycarbonyl-2,5-dideoxystreptamine (**12**), mp 167–168°C, in 70% yield. Compound **12** was hydrogenated over palladium hydroxide whereupon the azido group was reduced and the benzyl protecting groups removed. The product was then heated in boiling aqueous barium hydroxide to give 4-*O*-(6-amino-6-deoxy-α-D-glucopyranosyl)-2,5-dideoxystreptamine (**13**), mp 235–237°C with decomposition beginning at 220°C; $[\alpha]_D^{25}$ +83.6°, $[\alpha]_{436}^{25}$ +168°; $\Delta[M]_{TACu}^{16}$ +767.

The observed positive $\Delta[M]_{TACu}^{16}$ for compound **13** shows that it is the 4-isomer and therefore establishes the absolute configuration of **7** as was previously reported (3).

Condensation of **14** with the 6-azido sugar **5** afforded in 55% yield, 6-*O*-(6-azido-2,3,4-tri-*O*-benzyl-6-deoxy-α-D-glucopyranosyl)-3,4-*N*,*O*-carbonyl-1-*N*-ethoxycarbonyl-2,5-dideoxystreptamine (**17**), mp 150–151°C. Reaction of **17** with a catalytic amount of sodium in ethanol gave compound **19**, mp 201–203°C, in 80% yield. The protective groups of **19** were removed as described above for the synthesis of **13**, to give 6-*O*-(6-amino-6-deoxy-α-D-glucopyranosyl)-2,5-dideoxystreptamine (**20**), mp 240–244°C (dec.); $[\alpha]_D^{25}$ +58.3, $\Delta[M]_{TACu}$ −444. The negative $\Delta[M]_{TACu}$ for **20** indicates that it is the 6-isomer and this confirms the assigned absolute configuration of **14** (3).

Condensation of 4-*O*-(6-azido-2,3,4-tri-*O*-benzyl-6-deoxy-α-D-glucopyranosyl)-*N*,*N*′-diethoxycarbonyl-2,5-dideoxystreptamine (**12**) with **21** (17) gave crystalline 4-*O*-(6-azido-2,3,4-tri-*O*-benzyl-6-deoxy-α-D-glucopyranosyl)-6-*O*-(3-acetamido-2,4,6-tri-*O*-benzyl-3-deoxy-α-D-glucopyranosyl)-*N*,*N*′-diethoxycarbonyl-2,5-dideoxystreptamine (**22**), in 70% yield. The azido group of **22** was reduced catalytically and the resulting amino group acetylated to give 4-*O*-(6-acetamido-2,3,4-tri-*O*-benzyl-6-deoxy-α-D-glucopyranosyl)-6-*O*-(3-acetamido-2,4,6-tri-*O*-benzyl-3-deoxy-α-D-glucopyranosyl)-*N*,*N*′-diethoxycarbonyl-2,5-dideoxystreptamine (**23**), mp 210–213°C, in 67% yield. Debenzylation of **23** in the usual manner produced crystalline **24**. The nmr spectrum of the latter showed the signals for the anomeric hydrogens, H-1″ and H-1′, at δ 4.98 and 5.06 with a coupling of 3.5 Hz indicating that both amino sugar units are in the α configuration. Removal of the protective groups of **24** by hydrolysis with aqueous barium hydroxide afforded the desired 5-deoxykanamycin A (**25**). 5-Deoxykanamycin A showed the same spectrum of antibiotic activity as kanamycin A but about half the potency of the latter. Its antibiotic properties are summarized in Table 1.

Experimental

The melting points were determined on a Mel-Temp melting point apparatus and are not corrected. Optical rotations were measured with a Perkin–Elmer Model 141 polarimeter. Nuclear magnetic resonance spectra were taken with a Varian A-60A spectrometer. Tetramethylsilane (for solution other than deuterium oxide) and sodium 4,4-dimethyl-4-silapentane-1-sulfonate (for the solutions of deuterium oxide) were used as internal standards. Thin-layer chromatography (tlc) was carried out on microscope slides coated with silica gel and the spots were visualized with perchloric acid.

Can. J. Chem. Downloaded from www.nrcresearchpress.com by 210.87.254.40 on 09/05/12
For personal use only.

TABLE 1. Minimum inhibitory concentration of 5-deoxykanamycin A against various microorganisms (μg/ml)

Organism	Minimum inhibitory concentration
S. pneum. 9585	125
S. pyogenes 9604[a,b]	125
S. aureus 9537	2
S. aureus 9606	4
S. aureus 20240	>125
E. coli 9632[b]	8
E. coli 21218[b]	>125
E. coli 20895[b]	8
E. coli 20732[b]	125
E. coli 20665[b]	>125
E. coli 20683[b]	>125
E. cloacae 9656	8
E. cloacae 20364[b]	>125
E. cloacae 21006[b]	>125
K. pneum. 9977	1
P. mirab. 9900	32
P. rettgeri 9637	1
P. rettgeri 21207[b]	16
P. stuartii 21210	4
P. stuartii 20894[b]	32
S. marc. 20019	32
S. marc. 20460	>125
P. aerug. 9843A	>125
P. aerug. 20653	>125
P. aerug. 20741	>125
P. aerug. 20717	>125
P. aerug. 20601	>125
P. aerug. 21509	>125

[a]45% antibiotic assay broth, 50% Mueller–Hinton broth, and 5% serum. All others are Mueller–Hinton broth.
[b]10^{-3} organism dilution. All others are 10^{-4} organism dilution.

*Methyl 6-Azido-6-deoxy-2,3,4-tri-*O*-acetyl-α-*D*-glucopyranoside (1)*

This compound was prepared by the method described by Castro *et al.* (18), mp 102–103°C (lit. (19) mp 103°C).

*Methyl 6-Azido-6-deoxy-α-*D*-glucopyranoside (2)*

A solution of 68.2 g methyl 6-azido-6-deoxy-2,3,4-tri-*O*-acetyl-α-D-glucopyranoside in 600 ml dry methanol to which 150 mg sodium hydride had been added (300 mg of 50% NaH–oil suspension washed with benzene), was stirred at room temperature for 45 min and then neutralized with carbon dioxide and the mixture filtered. Evaporation of the filtrate gave 43.3 g of **2** as a syrup; $[\alpha]_D^{22}$ +122° (*c* 1, H_2O) (lit. (15) $[\alpha]_D^{22}$ +122° (*c* 1, H_2O)).

*Methyl 6-Azido-2,3,4-tri-*O*-benzyl-6-deoxy-α-*D*-glucopyranoside (3)*

This compound was prepared from methyl 6-azido-6-deoxy-α-D-glucopyranoside by reaction with benzyl chloride in DMF in the presence of potassium hydroxide according to the published method (15).

*6-Azido-2,3,4-tri-*O*-benzyl-6-deoxy-*D*-glucose (4)*

A solution of 53.5 g (107.3 mmol) of **3** and 81.5 g (430 mmol) *p*-toluenesulfonic acid monohydrate in 430 ml of 70% dioxane–water was heated under reflux for 5 days. After cooling to room temperature, the reaction mixture was poured onto water (500 ml) and the mixture extracted with chloroform (3 × 200 ml). The combined extracts were washed successively with water, aqueous sodium bicarbonate, and water and after drying over sodium sulfate, it was evaporated to dryness. The dark-brown residue showed on tlc (silica, 10% ether–benzene) three spots with R_f values of 0.58 (compound **3**), 0.25 (compound **4**), and 0. The crude product was chromatographed on silica gel (activity II), (300 g, 20 cm × 6.1 cm id) and eluted with 2% ether–benzene. The effluent was collected in 50 ml fractions. Fractions 1–12 were combined and evaporated to dryness to give 23.5 g (44% recovery) of unreacted starting material. Fractions 13–18 gave, after evaporation, 5.0 g of a mixture of starting material **3** and product **4**. The column was then washed with 25% ether–benzene to give 19.3 g (38%) of **4** as a syrup (a mixture of the two anomers) which solidified upon standing at room temperature. This material was used as such in the next reaction.

*6-Azido-2,3,4-tri-*O*-benzyl-6-deoxy-α-*D*-glucopyranosyl Chloride (5)*

This compound was prepared as described by Tagaki *et al.* (15) by reacting **4** with thionyl chloride.

*4-*O*-(2,3,4,6-Tetra-*O*-benzyl-α-*D*-glucopyranosyl)-1,6-*N,*O*-carbonyl-3-*N*-ethoxycarbonyl-2,5-dideoxystreptamine (8)*

To a flame-dried and nitrogen-purged 50-ml three-neck flask fitted with condenser, mechanical stirrer, and nitrogen inlet and outlet tubes was added 2.16 g (8.8 mmol) of **7** (3), 7.3 g of anhydrous calcium sulfate, and 12 ml of dry DMF and the mixture heated to 65°C while stirring under a nitrogen stream. After 1 h, 5.7 g of mercuric cyanide was added together with a solution of 5.5 g (9.8 mmol) of 2,3,4,6-tetra-*O*-benzyl-α-D-glucopyranosyl chloride (**6**) (14) in 15 ml of DMF. The mixture was stirred at 65°C for 27 h and after cooling to room temperature, it was diluted with chloroform (50 ml), filtered, and the solids washed with chloroform (3 × 20 ml). The combined filtrate and washings were washed with water, dried, and evaporated to dryness. The residue was chromatographed on a silica column (240 g, 55 cm × 3.3 cm id) and eluted with MEK–benzene (1:4) to give 5.4 g (80%) of **8** as a homogeneous syrup (tlc on silica, 2% MeOH in $CHCl_3$ as solvent). This material was used as such in the next reaction. A sample was crystallized from isopropyl alcohol – diisopropyl ether and then recrystallized from isopropyl alcohol to give the analytical sample, mp 172–173°C; $[\alpha]_D^{25}$ +38.2 (*c* 1.2, $CHCl_3$); ir (KBr): 1760 (cyclic carbamate) 1700 and 1530 cm^{-1} ($NHCO_2Et$). *Anal.* calcd. for $C_{44}H_{50}N_2O_{10}$: C 68.91, H 6.57, N 3.65; found: C 69.02, H 6.63, N 3.72.

*4-*O*-(α-*D*-Glucopyranosyl)-*N,N'*-diethoxycarbonyl-2,5-dideoxystreptamine (11)*

A solution of 4.46 g (5.8 mmol) of **8** in ethanol (220 ml) was hydrogenated over 10% Pd-on-carbon (0.9 g) under a hydrogen pressure of 3 cm of mercury at room temperature for 48 h. The catalyst was removed, washed with ethanol (2 × 30 ml), and the combined filtrate and washings evaporated to give 2.22 g (94%) of **9** as a syrup. Thin-layer chromatography on silica (chloroform–methanol (3:1)) showed a single spot with R_f 0.39.

Compound **9** (2.22 g) was dissolved in absolute ethanol (115 ml) in which 50 mg of sodium hydride had been dissolved (55% suspension in oil) and the solution heated under reflux for 3 h. After cooling to room temperature, it was neutralized with a cation exchange resin and evaporated to dryness to give crystalline **11**, mp 273–275°C (EtOH), $[\alpha]_D^{25}$ +81.0° (*c*, 0.2, H_2O); nmr spectrum at 80 MHz showed δ: 1.24 and 4.08, (triplet and quartet for N—CO_2Et, J = 7.1 Hz), 5.08 (d, 1, H-1, J = 2.8 Hz). *Anal.* calcd. for $C_{18}H_{32}N_2O_{11}$: C 47.78, H 7.13, N 6.19; found: C 47.65, H 7.11, N 6.35.

Can. J. Chem. Downloaded from www.nrcresearchpress.com by 210.87.254.40 on 09/05/12
For personal use only.

6-O-(2,3,4,6,Tetra-O-benzyl-α-D-glucopyranosyl)-3,4-N,O-carbonyl-1-N-ethoxycarbonyl-2,5-dideoxystreptamine (15)

A quantity of 1.8 g (7.3 mmol) of 3,4-*N,O*-carbonyl-1-*N*-ethoxycarbonyl-2,5-dideoxystreptamine (**14**) (3) was reacted with 5.2 g (9.3 mmol) of **6** in DMF (25 ml) in the presence of mercuric cyanide and anhydrous calcium sulfate as described above for the synthesis of **8**. After work-up, the crude syrupy product crystallized upon exposure to ether. The crystalline product was filtered off to give 3.91 g (70%) of **15**, mp 188–190°C. Thin-layer chromatography on silica (2% methanol in chloroform) showed a single spot with R_f 0.24. The mother liquor was evaporated to dryness and chromatographed on a column of silica (60 g, 12 cm × 3.1 cm id) using MEK–benzene 1:2 as the eluent. The fractions containing **15** were combined and evaporated to dryness to give 470 mg which on trituration with ether gave 300 mg of crystalline **15**, mp 190–192°C. This fraction was combined with the first crop above to give a total of 4.21 g (75.5%). Recrystallization from ethanol gave the analytical sample, mp 190–192°C; $[\alpha]_D^{25}$ +19.9 (*c*, 1.4, $CHCl_3$); ir (KBr): 1770 (cyclic carbamate), 1700 cm^{-1} ($NHCO_2Et$). *Anal.* calcd. for $C_{44}H_{50}N_2O_{10}$: C 68.91, H 6.57, N 3.65; found: C 68.84, H 6.60, N 3.72.

6-O-(α-D-Glucopyranosyl)-3,4-N,O-carbonyl-1-N-ethoxycarbonyl-2,5-dideoxystreptamine (16)

A mixture of 4.0 g (5.2 mmol) of **15** in ethanol (400 ml) was hydrogenated over 0.8 g of 10% Pd/C as described for the synthesis of **11** above. Removal of the ethanol solvent by evaporation gave crystalline **16**. Recrystallization from ethanol gave 2.08 g (88.5%) of crystalline **16** containing **1** mol of EtOH of crystallization, mp 242–243°C; $[\alpha]_D^{25}$ +45.4 (*c*, 2.0, H_2O); ir (KBr): 3320, 1745, 1705, 1690, and 1543 cm^{-1}; nmr (D_2O) δ: 5.02 (d, one proton, H-1, $J_{1,2}$ = 3.5 Hz). *Anal.* calcd. for $C_{18}H_{20}N_2O_{10}\cdot C_2H_5OH$: C 47.78, H 7.13, N 6.19; found: C 47.87, H 7.17, N 6.34.

6-O-(α-D-Glucopyranosyl)-N,N′-diethoxycarbonyl-2,5-dideoxystreptamine (18)

Compound **16** (1.0 g, 2.46 mmol) in absolute ethanol (30 ml) in which a catalytic amount of sodium hydride had been dissolved was heated under reflux for 3 h and the product isolated as described above for the synthesis of **11** to give compound **18** in 95% yield, mp 218–220°C (EtOH); $[\alpha]_D^{25}$ +67.0 (*c*, 0.75, H_2O); ir (KBr): 1695 and 1540 cm^{-1} ($NHCO_2Et$): nmr (D_2O) δ: 5.02 (d, one proton, H-1, $J_{1,2}$ = 3.5 Hz). *Anal.* calcd. for $C_{18}H_{32}N_2O_{11}$: C 47.78, H 7.13, N 6.19; found: C 47.55, H 7.14, N 6.11.

4-O-(6-Azido-2,3,4-tri-O-benzyl-6-deoxy-α-D-glucopyranosyl)-1,6-N,O-carbonyl-3-N-ethoxycarbonyl-2,5-dideoxystreptamine (10)

A flame-dried, nitrogen purged, three-neck flask (100 ml) equipped with a condenser, mechanical stirrer, and nitrogen inlet and outlet tubes was charged with 2.44 g (10 mmol) of (**7**) (3) and 15 ml dry DMF. Under a slow stream of nitrogen, 5.5 g anhydrous calcium sulfate was added and the mixture stirred at room temperature for 30 min followed by heating to 80°C for 15 min. A solution of 5.1 g (10.3 mmol) of 6-azido-2,3,4-tri-*O*-benzyl-6-deoxy-α-D-glucopyranosyl chloride (**5**) in 5 ml dry DMF was then added, followed by the addition of 6.3 g of mercuric cyanide. The mixture was heated at 80–85°C under nitrogen with stirring for 17 h. Fresh mercuric cyanide, 3.0 g was added and heating continued for 3 h. After cooling to room temperature, the reaction mixture was diluted with chloroform (150 ml) and filtered. The solids were washed with chloroform (2 × 10 ml) and the combined filtrate and washings were washed with water (5 × 100 ml), dried, and evaporated to dryness to give a dark brown sticky residue. On tlc (silica, 5% MeOH–$CHCl_3$) it showed five spots with R_f 0, 0.28 (major, compound **10**), 0.38, 0.5, and 0.92, respectively. The crude product was dissolved in 20 ml chloroform and the solution added dropwise with stirring to 175 ml of petroleum ether (bp 40–60°C). The petroleum ether phase was decanted and the residue dissolved in $CHCl_3$ (20 ml) and the latter solution again added to petroleum ether (175 ml). The petroleum ether phase was again decanted and combined with the preceding petroleum ether phase. The residue, 4.1 g, showed on tlc one major spot with R_f 0.28 (compound **10**) and two minor ones with R_f 0 and 0.38, respectively. The petroleum ether phase showed on tlc a small spot for **10** (R_f 0.28) and the spots with R_f 0.38, 0.5, and 0.92 and upon standing at room temperature overnight it deposited 200 mg of compound **10**. The combined yield of **10** was 4.3 g. This material was further purified by passing through a column of silica (activity II) (45 g, 6.5 cm × 4.3 cm id) using 10% methanol in chloroform as the eluent (250 ml). This treatment removed the impurity with R_f 0. The eluent was evaporated to dryness to give 3.75 g (53.5%) of a brown syrup which on tlc showed one major spot with R_f 0.28 (compound **10**) and a trace of a compound with R_f 0.38. This material was used as such in the next reaction.

An analytical sample was obtained by crystallization from ether, mp 75–85°C; $[\alpha]_D^{25}$ +87.4 (*c*, 1.0, $CHCl_3$); ir ($CHCl_3$): 2110 (N_3), 1760 (cyclic carbamate), 1710 and 1520 cm^{-1} (N—CO_2Et). *Anal.* calcd. for $C_{37}H_{43}N_5O_9$: C 63.32, H 6.18, N 9.98; found: C 63.35, H 6.14, N 9.83.

4-O-(6-Azido-2,3,4-tri-O-benzyl-6-deoxy-α-D-glucopyranosyl)-N,N′-diethoxycarbonyl-2,5-dideoxystreptamine (12)

A solution of 3.75 g of the preceding crude **10** in 30 ml absolute ethanol in which 20 mg NaH (55% in oil) had been dissolved was heated under reflux for 3 h with exclusion of moisture. After cooling to room temperature, acetone (35 ml) was added to dissolve the solids and the solution neutralized by passing through a column containing 4.0 g Amberlite IR-120 (H^+ form, washed with water and EtOH). The neutral effluent was evaporated to dryness to give a residue which on tlc (silica; benzene–MEK, 2:1) showed one major spot with R_f 0.39 (compound **12**) and four minor ones with R_f 0, 0.72, 0.89, and 1.0. It was chromatographed through a column packed with 100 g of silica (activity II) (14.5 cm × 4.0 cm id) and the product eluted with benzene–MEK (2:1). Fractions of 20 ml were collected and the material eluted in tubes 6–20. The combined elutes were evaporated, the residue dissolved in 20 ml of boiling ethanol and the mixture filtered. The filtrate was evaporated to dryness to give 2.8 g (70%) of crystalline compound **12**. Recrystallization from ethyl acetate (10 ml) – petroleum ether (20 ml) gave 2.4 g, mp 167–168°C; $[\alpha]_D^{25}$ +77.4° (*c*, 1.0, $CHCl_3$); ir ($CHCl_3$): 2110 (N_3), 1705 and 1520 cm^{-1} (N—CO_2Et). *Anal.* calcd. for $C_{39}H_{49}N_5O_{10}$: C 62.63, H 6.60, N 9.36; found: C 62.28, H 6.54, N 9.04.

4-O-(6-Amino-6-deoxy-α-D-glucopyranosyl)-2,5-dideoxystreptamine (13)

A mixture of 251 mg of **12** in methanol was hydrogenated in a Paar apparatus over 20% $Pd(OH)_2$-on-carbon (200 mg) at room temperature and at an initial hydrogen pressure of 45 psi. After 16 h, the mixture was filtered through a Celite bed and the cake washed with methanol (25 ml). The combined filtrate and washings were evaporated to dryness to give 4-*O*-(6-amino-6-deoxy-α-D-glucopyranosyl)-*N,N′*-diethoxycarbonyl-2,5-dideoxystreptamine as a foam. Thin-layer chromatography on silica with MeOH–$CHCl_3$–NH_4OH (4:1:1) as the solvent showed a single spot (ninhydrin spray). The material was dissolved in water (10 ml), barium hydroxide (1.2 g) was added, and the solution heated at reflux under nitrogen for 22 h. The mixture was diluted with water (20 ml) and the excess barium hydroxide neutralized by passing

Can. J. Chem. Downloaded from www.nrcresearchpress.com by 210.87.254.40 on 09/05/12
For personal use only.

carbon dioxide through the solution. The resulting mixture was heated to boiling and filtered through a bed of Celite and the solids washed with boiling water (2 × 20 ml). The filtrate and the washings were combined and acidified with 1 *N* sulfuric acid to precipitate barium. The mixture was filtered through Celite, the filtrate neutralized with an anion exchange resin (Rexyn 201, OH^- form), and the solution evaporated to dryness to give a syrupy residue which solidified on treatment with methanol. Thin-layer chromatography on silica using $CHCl_3$—MeOH—NH_4OH—H_2O (1:4:2:1) as solvent showed one major spot with R_f 0.40 (ninhydrin spray) and some impurities with lower R_f values. This material was absorbed on a cation exchange resin (Rexyn 102, NH_4^+ form, 3 ml) and the column was first washed with water (50 ml) and then with 0.2 *N* aqueous ammonium hydroxide which after evaporation gave **13** (51 mg, 50%) as a solid, mp 235–237°C (it foamed and decomposed); $[\alpha]_D^{25}$ +83.6 (*c* 0.30, H_2O), $[\alpha]_{436}^{25}$ +168° (*c*, 0.30, H_2O), $[\alpha]_{436}^{25}$ +418 (*c*, 0.35, TACu), $\Delta[M]_{TACu}$ +767.

*6-O-(6-Azido-2,3,4-tri-O-benzyl-6-deoxy-α-D-glucopyranosyl)-3,4-N,O-carbonyl-1-N-ethoxycarbonyl-2,5-dideoxystreptamine (**17**)*

Compound **14** (2.70 g, 11.14 mmol) was reacted with 5.96 g (12.1 mmol) of 6-azido-2,3,4-tri-*O*-benzyl-6-deoxy-α-D-glucopyranosyl chloride (**5**) in dry DMF (23 ml) at 83–85°C, in the presence of mercuric cyanide and calcium sulfate as described above for the synthesis of **10**. After the reaction was completed (20 h) the reaction mixture was cooled to room temperature, diluted with chloroform (150 ml), and filtered. The solids were washed with chloroform (3 × 20 ml) and after combining the washings with the filtrate, the solution was washed with water, dried and evaporated to dryness to give 6.54 g of a brown syrup. Thin-layer chromatography on silica using 5% methanol in chloroform as solvent showed two spots with R_f 0.33 (major, compound **17**) and 0.61 (minor). The crude product was chromatographed on a column of silica (activity III) (150 g, 20 cm × 3.8 cm id) using MEK–benzene (1:4) mixture as the eluent. Fractions of 10 ml were collected and fractions 4–15 contained the compound with R_f 0.61 (silica, 5% MeOH–$CHCl_3$). They were combined and evaporated to dryness to give 1.4 g of a syrup which consisted of 6-azido-2,3,4-tri-*O*-benzyl-6-deoxy-D-glucose (**4**). The fractions 20–98 were combined and evaporated to dryness to give 4.29 g (54.8%) of compound **17** as a syrup. It was crystallized from ethanol–ether to give crystalline **17**, mp 150–151°C; $[\alpha]_D^{25}$ +33.0 (*c*, 1.0, $CHCl_3$); ir (Nujol): 3340 (NH), 2110 (N_3), 1750 (cyclic carbamate) 1710 cm^{-1} (*N*-carbethoxy). *Anal.* calcd. for $C_{37}H_{43}N_5O_9$: C 63.32, H 6.18, N 9.98; found: C 63.35, H 6.15, N 10.16.

*6-O-(6-Azido-2,3,4-tri-O-benzyl-6-deoxy-α-D-glucopyranosyl)-N,N′-diethoxycarbonyl-2,5-dideoxystreptamine (**19**)*

A solution of 2.22 g (3.2 mmol) of **17** in dry ethanol (50 ml) in which 20 mg of sodium hydride (55% oil suspension) had been dissolved was heated under reflux for 3 h. After cooling to room temperature, it was neutralized by treatment with Amberlite IR 120 (H^+ form), the resin filtered off, and the filtrate evaporated to dryness to give 2.4 g (100%) of solid material which on tlc (silica, 5% MeOH–$CHCl_3$) showed one major spot with R_f 0.30 (compound **19**) and traces of a compound with R_f 0.12. Recrystallization from ethanol–ethylacetate (5:1) gave 1.92 g (80.6%) of **19**, mp 201-203°C; $[\alpha]_D^{25}$ +40.2 (*c*, 1.45, $CHCl_3$); ir (Nujol): 3310 (NH, OH), 2110 (N_3), 1690 and 1540 cm^{-1} (*N*-carbethoxy). *Anal.* calcd. for $C_{39}N_{49}N_5O_{10}$: C 62.63, H 6.60, N 9.36; found: C 62.50, H 6.51, N 9.48.

*6-O-(6-Amino-6-deoxy-α-D-glucopyranosyl)-2,5-dideoxystreptamine (**20**)*

A solution of 1.10 g of **19** in methanol (30 ml) was hydrogenated over 1 g of 20% $Pd(OH)_2$-on-carbon as described for the preparation of **13** above. The product was hydrolyzed with aqueous barium hydroxide and purified as described above (compound **13**) to give 252 mg of **20** as an amorphous solid, mp 240–244°C (dec.); $[\alpha]_D^{25}$ +58.3 (*c*, 0.75, H_2O), $[\alpha]_{436}^{25}$ +114 (*c*, 0.75, H_2O), $[\alpha]_{436}^{25}$ −30.8 (*c*, 0.51, in TACu), $\Delta[M]_{TACu}$ −444.5.

*4-O-(6-Azido-2,3,4-tri-O-benzyl-6-deoxy-α-D-glucopyranosyl)-6-O-(3-acetamido-2,4,6-tri-O-benzyl-3-deoxy-α-D-glucopyranosyl)-N,N′-diethoxycarbonyl-2,5-dideoxystreptamine (**22**)*

A flame-dried nitrogen purged 50 ml two-neck flask fitted with mechanical stirrer, condenser, and nitrogen inlet and outlet tubes was charged with 2.99 g (4 mmol) of compound **12** and 10 ml dry DMF and the mixture stirred at room temperature under nitrogen until dissolution was complete. Anhydrous calcium sulfate (3.0 g) was then added and the mixture stirred at room temperature for 30 min. To this was added 1.3 g (4.0 mmol) of 3-acetamido-2,4,6-tri-*O*-benzyl-3-deoxy-α-D-glucopyranosyl chloride (**21**) followed by 3.0 g of powdered mercuric cyanide. The mixture was heated at 80°C while stirring under nitrogen. After 9 h, 1.31 g of **21** and 1.5 g $Hg(CN)_2$ were added, the mixture stirred again at 80°C for 12 h after which time 1.0 g of **21** and 1.0 g $Hg(CN)_2$ were again added. After stirring for 22 h at 80°C, the mixture was cooled to room temperature, diluted with $CHCl_3$ (150 ml), filtered, and the solids washed with $CHCl_3$ (2 × 10 ml). The combined filtrate and washings were washed with water (5 × 150 ml), dried, and evaporated to dryness. Thin-layer chromatography (alumina, 2% MeOH–$CHCl_3$) showed one major spot R_f 0.51 (compound **22**) and three minor ones with R_f values of 0.17, 0.27, and 0.76. The sticky residue on treatment with ethyl acetate – ether crystallized. It was chromatographed through a column packed with alumina (activity II) (150 g) (21.5 cm × 2.8 cm id) and the product eluted in 20 ml fractions with 1% MeOH–$CHCl_3$. Tubes 6–17 were combined and after evaporation gave 4.7 g of a colorless sticky residue which on tlc showed one major spot for **22** and a minor one with R_f 0.76. It was treated with boiling ethyl acetate (40 ml) and the mixture filtered to remove some insoluble solids (220 mg). The filtrate was evaporated to dryness, dissolved into 15 ml of boiling ethyl acetate, and the solution diluted with 30 ml ether. After standing at room temperature overnight, the crystalline product **22** was collected to give 3.40 g (70%), mp 178–188°C. *Anal.* calcd. for $C_{68}H_{80}N_6O_{15}$: C 66.87, H 6.60, N 6.88; found: C 67.28, H 6.67, N 6.57.

*4-O-(6-Acetamido-2,3,4-tri-O-benzyl-6-deoxy-α-D-glucopyranosyl)-6-O-(3-acetamido-2,4,6-tri-O-benzyl-3-deoxy-α-D-glucopyranosyl)-N,N′-diethoxycarbonyl-2,5-dideoxystreptamine (**23**)*

A solution of 3.0 g (2.46 mmol) of **22** in 100 ml of 90% EtOH–water was hydrogenated in a Paar apparatus over Raney nickel at room temperature and at an initial hydrogen pressure of 55 psi. After 3 h, the reaction mixture was filtered and the catalyst washed with EtOH. The combined filtrate and washings were evaporated to dryness to give 2.77 g (94.5%) of a syrup which solidified. Infrared spectroscopy confirmed that hydrogenation was complete (absence of azido band). Thin-layer chromatography on silica (10% MeOH–$CHCl_3$) showed one major spot with R_f 0.43 and four minor ones. The material was dissolved in dry pyridine (10 ml) and acetic anhydride (1.5 ml) was added. After standing at room temperature for 1 h, water (0.5 ml) was added, the solution diluted

Can. J. Chem. Downloaded from www.nrcresearchpress.com by 210.87.254.40 on 09/05/12
For personal use only.

with $CHCl_3$ (150 ml), and washed first with water (3 × 100 ml), then with 5% aqueous HCl (100 ml), and finally with water (100 ml). After drying and removal of the solvent by evaporation, the sticky residue was treated with boiling ethylacetate (25 ml) and the crystalline product **23** collected to give 1.95 g (67%), mp 210–213°C. Recrystallization from EtOH produced an analytical sample; mp 217–218°C. *Anal.* calcd. for $C_{70}H_{84}N_4O_{16}$: C 67.96, H 6.84, N 4.53; found: C 68.09, H 6.90, N 4.57.

4-O-(6-Acetamido-6-deoxy-α-D-glucopyranosyl)-6-O-(3-acetamido-3-deoxy-α-D-glucopyranosyl)-N,N′-diethoxycarbonyl-2,5-dideoxystreptamine (24)

A solution of 700 mg of compound **23** in 80 ml 95% ethanol–water was hydrogenated over 100 mg of Pd/C (10%) at room temperature and at atmospheric pressure for 24 h. The reaction mixture was filtered and the catalyst washed with boiling 70% EtOH–water (4 × 15 ml). The combined filtrate and washings were evaporated to dryness to give 360 mg of crystalline **24**; mp 260–262°C (dec.). The nmr spectrum at 100 MHz in D_2O showed δ: 1.22 and 1.24 (two triplets for CH_3 of $NHCO_2Et$), 4.10 and 4.12 (two quartets for CH_2 of $NHCO_2Et$), 2.03 (s, 6H, NHAc), 4.98 (d, 1, H-1″, $J_{1'',2''}$ = 3.5 Hz) 5.06 (d, 1, H-1′, $J_{1',2'}$ = 3.5 Hz). *Anal.* calcd. for $C_{28}H_{48}N_4O_{16}$: C 48.27, H 6.94, N 8.04; found: C 47.53, H 6.84, N 7.64.

5-Deoxykanamycin A (25)

A solution of 360 mg (0.515 mmol) of **24** in 20 ml of 1 *N* aqueous barium hydroxide was heated at reflux for 24 h while excluding CO_2. It was then diluted with 30 ml water, neutralized with CO_2, heated to boiling, filtered, and the solids washed with boiling water (3 × 30 ml). The filtrate and washings were combined, 5 ml of 1 *N* H_2SO_4 added to precipitate barium, and the solids removed by filtration. The filtrate was passed through a column containing 10 g Rexyn 201 (strongly basic resin in the OH^- form) to remove the acids (H_2SO_4 and AcOH) and the effluent evaporated to dryness to give 200 mg of sticky residue. Thin-layer chromatography on silica (H_2O–MeOH–NH_4OH–$CHCl_3$, 1:4:2:1, ninhydrin spray) showed two spots with R_f 0.19 (major, compound **25**) and R_f 0.49 (probably the cyclic urea). The material was chromatographed using a column packed with Rexyn 102 (NH_4^+ form) (0.9 cm id × 10.2 cm). The column was washed first with water (100 ml), then with 1 *N* ammonium hydroxide (300 ml). The effluent containing compound **25** was evaporated to dryness, the residue dissolved in water and the solution treated with an anion exchange resin (Rexyn 201, OH^- form) to remove some ammonium carbonate. After evaporation of the resin filtrate to dryness, the residue was treated with ethanol and the crystalline material filtered to give 140 mg of **25**, mp 250–255°C (dec.) (decomposition started at 160°C); $[\alpha]_D^{25}$ +101.8 (*c*, 0.33, water). The nmr spectrum at 100 MHz in D_2O showed δ: 5.17 (d, 1, H-1″, $J_{1'',2''}$ = 3.75 Hz), 5.22 (d, 1, H-1′, $J_{1',2'}$ = 3.75 Hz). *Anal.* calcd. for $C_{18}H_{36}N_4O_{10}$: C 46.15, H 7.74; found: C 45.95, H 7.67.

1. (*a*) K. E. Price, J. C. Godfrey, and H. Kawaguchi. Adv. Appl. Microbiol. **18**, 191 (1974); (*b*) S. Umezawa. Adv. Carbohydr. Chem. Biochem. **30**, 111 (1974); (*c*) H. Umezawa. Adv. Carbohydr. Chem. Biochem. **30**, 183 (1974).
2. W. T. Shier, K. L. Rinehart, Jr., and D. Gottlieb. Proc. Natl. Acad. Sci. U.S.A. **63**, 198 (1969); W. T. Shier, S. Ogawa, M. Hichens, and K. L. Rinehart, Jr. J. Antibiot. **26**, 551 (1973).
3. G. Kavadias, S. Velkof, and B. Belleau. Can. J. Chem. **56**, 404 (1978).
4. R. T. Testa, G. H. Wagman, P. J. L. Daniels, and M. J. Weinstein. J. Antibiot. **27**, 917 (1974).
5. S. Umezawa and S. Koto. Bull. Chem. Soc. Jpn. **39**, 2014 (1966).
6. S. Koto, K. Tatsuta, E. Kitazawa, and S. Umezawa. Bull. Chem. Soc. Jpn. **41**, 2769 (1968).
7. A. Hasegawa, N. Kurihara, D. Nishimura, and M. Nakajima. Agr. Biol. Chem. (Tokyo), **32**, 1123 (1968).
8. Y. Nishimura, T. Tsuchiya, and S. Umezawa. Bull. Chem. Soc. Jpn. **44**, 2521 (1971).
9. Y. Nishimura, T. Tsuchiya, and S. Umezawa. Bull. Chem. Soc. Jpn. **43**, 2960 (1970).
10. Y. Nishimura, T. Tsuchiya, and S. Umezawa. Bull. Chem. Soc. Jpn. **46**, 1263 (1973).
11. S. Umezawa, K. Tatsuta, and S. Koto. Bull. Chem. Soc. Jpn. **42**, 533 (1969).
12. S. Umezawa, S. Koto, K. Tatsuta, H. Hineno, Y. Nishimura, and T. Tsumura. Bull. Chem. Soc. Jpn. **42**, 537 (1969).
13. S. Umezawa, S. Koto, K. Tatsuta, and T. Tsumura. Bull. Chem. Soc. Jpn. **42**, 529 (1969).
14. P. W. Austin, F. E. Hardy, J. G. Buchanan, and J. Baddiley. J. Chem. Soc. 2128 (1964).
15. Y. Takagi, T. Tsuchiya, and S. Umezawa. Bull. Chem. Soc. Jpn. **46**, 1261 (1973).
16. S. Umezawa, T. Tsuchiya, and K. Tatsuta. Bull. Chem. Soc. Jpn. **39**, 1235 (1966).
17. S. Koto, T. Tsumura, Y. Kato, and S. Umezawa. Bull. Chem. Soc. Jpn. **41**, 2765 (1968).
18. B. Castro, Y. Chapleur, and B. Gross. Bull. Soc. Chim. Fr. 3034 (1973).
19. F. Gramer, H. Otterbach, and H. Springmann. Chem. Ber. **92**, 384 (1959).

Reaction of 1,1-diphenylpropene with stannic chloride and hydrogen chloride[1]

STANLEY BYWATER AND DENIS J. WORSFOLD

Division of Chemistry, National Research Council of Canada, Ottawa, Ont., Canada K1A 0R9

Received February 15, 1978

STANLEY BYWATER and DENIS J. WORSFOLD. Can. J. Chem. **56**, 2093 (1978).

$SnCl_4$ and HCl have been found to react with 1,1-diphenylpropene to form a small equilibrium amount of the diphenylethylcarbenium ion. No further reaction is detectable, and the equilibrium between the three reactants may be determined from the uv absorption of the ion. The electrical conductances of the solutions have also been measured. The results are consistent with the formation of the salt of this carbenium ion with the $SnCl_5^-$ anion. The salt in the concentrations formed in these experiments (ca. 10^{-5}–10^{-4} M) was nearly all dissociated into free ions in methylene chloride solution. The equilibrium constant for formation of the salt was 2.0 M^{-2} at −30°C, and the dissociation constant into ions 4.4×10^{-4} M. The overall heat of reaction to the carbenium ion salt was 8.8 kcal, most of which is attributed to the initial formation of the undissociated salt.

STANLEY BYWATER et DENIS J. WORSFOLD. Can. J. Chem. **56**, 2093 (1978).

On a trouvé que le $SnCl_4$ et HCl réagissent avec le diphényl-1:1 propène pour conduire, à l'équilibre, à une faible quantité d'ions diphényléthylcarbénium. Il a été impossible de détecter aucune réaction subséquente et l'équilibre entre les trois réactifs peuvent être déterminés à partir de spectre d'absorption uv de l'ion. On a aussi mesuré la conductivité électrique des solutions. Les résultats sont en accord avec la formation du sel de l'ion carbénium avec l'anion $SnCl_5^-$. Aux concentrations de sel formées au cours de ces expériences (environ 10^{-5} à 10^{-4} M), celui-ci est à toutes fins pratiques complètement dissocié en ions libres pour des solutions dans le chlorure de méthylène. La constante d'équilibre pour la formation du sel est de 2.0 M^{-2} à 30°C et la constante de dissociation en ions est de 4.4×10^{-4} M. La chaleur globale de la réaction conduisant au sel des ions carbénium est de 8.8 kcal; on attribue la plus grande partie de cette valeur à la formation initiale du sel non-associé.

[Traduit par le journal]

Several authors have described the reaction of 1,1-diphenylethylene with Friedel–Crafts reagents as a model system for cationic polymerization (1–4), but this reaction has been shown to have several complicating factors. If only the initiation step of cationic polymerization is to be studied, a better model monomer is 1,1-diphenylpropene (DPP). Only the initial cationic centre the diphenylethylcarbenium ion, is formed, and its equilibrium with initiator and monomer may be studied. No dimers or higher molecular weight products are detectable, and the secondary reactions found with 1,1-diphenylethylene are absent. Such a study has already been made on the boron trifluoride – water system, which shows rather complex behavior (5). A system that proved to be uncomplicated and which demonstrates the usefulness of this method of studying the equilibria involved in the initiation reaction is the reaction of the DPP with $SnCl_4$ and HCl, in methylene chloride solution.

Experimental

$SnCl_4$ was fractionally distilled from P_2O_5 and stored on a vacuum rack. It was measured as a vapour in a known volume. HCl gas was dried over P_2O_5 and purified by trap-to-trap distillation. It also was measured as a gas. The reactions were carried out under vacuum in all glass apparatus fitted with breakseals; experimental details are given elsewhere (5). Most reactions were performed at −30°C. The diphenylethylcarbenium ion was measured by uv spectrophotometry (λ_{max}, 438 mμ; ε, 35 000).

Results

In the absence of HCl, methylene chloride solutions of DPP and $SnCl_4$ gave only small uv absorptions due to diphenylethylcarbenium ions (ca. 2×10^{-6} M) at −30°C, presumably caused by residual water. Additions of HCl gave an immediate increase in absorption, the increase being above half power but less than first power in the HCl concentration in the range 1.3–20 $\times 10^{-3}$ M, at three different $SnCl_4$ concentrations.

Solutions of HCl and DPP gave very small concentrations of diphenylethylcarbenium ions. Additions of $SnCl_4$ caused a large increase in ion concentration, again with a dependence slightly greater than half power on the stannic chloride over the range 1.8–28 $\times 10^{-3}$ M. The dependence on the DPP concentration was similar over the range 1.4–6 $\times 10^{-2}$ M.

The concentration of carbenium ions was in the range 10^{-5}–10^{-4} M, dependent on temperature. The concentration decreased reversibly as the tempera-

[1]NRCC No. 16734.

Can. J. Chem. Downloaded from www.nrcresearchpress.com by 210.87.254.105 on 09/05/12
For personal use only.

Can. J. Chem. Downloaded from www.nrcresearchpress.com by 210.87.254.105 on 09/05/12
For personal use only.

ture was raised. From a plot of ln [Ion] vs. $1/T$ over the temperature range $-10°C$ to $-50°C$ the temperature dependence corresponded to an overall heat of reaction of $-8\,800$ cal.

The solutions showed considerable electrical conductance. Solutions of HCl and $SnCl_4$ showed appreciable conductance themselves, although much lower than in the presence of DPP, so that no exact conductiometric analysis of the system was possible. If it is assumed, however, that Λ_0 at 20°C is the same, 89, as that found in the system with BF_3 measured previously, and allowing for the change in viscosity with temperature by Walden's rule, Λ_0 at $-30°C$ can be estimated to be near 60. With this value of Λ_0, solutions having total concentration of diphenylethylcarbenium ions in the region of 10^{-4} M, gave conductances consistent with an ion-pair dissociation constant about 5×10^{-4} M.[2]

Discussion

From these results it is possible to propose the following equilibrium:

$$SnCl_4 + HCl + CH_3CH{=}CPh_2 \underset{}{\overset{K_1}{\rightleftharpoons}} CH_3CH_2\overset{+}{C}Ph_2 \cdot SnCl_5^- \qquad \overset{K_2}{\updownarrow}$$

$$CH_3CH_2{-}\overset{+}{C}Ph_2 + SnCl_5^-$$

If this scheme is valid it is possible to show that if the total ion concentration is small compared with the reactants, as was found (<2%), then the equation

$$\frac{[DPP^+]_{total}}{[HCl]_0[SnCl_4]_0[DPP]_0} = K_1 + \frac{(K_1K_2)^{1/2}}{[HCl]_0^{1/2}[SnCl_4]_0^{1/2}[DPP]_0^{1/2}}$$

should hold. The high degree of dissociation of the initial ion pair leads to the approach to half power dependence of the total ion concentration. $[DPP^+]_{total}$ is the spectroscopically measured diphenylethylcarbenium ion concentration (the sum of the free ion and ion-pair concentrations).

Hence a plot of $[DPP^+]_{total}/[HCl]_0[SnCl_4]_0[DPP]_0$ against $[HCl]_0^{-1/2}[SnCl_4]_0^{-1/2}[DPP]_0^{-1/2}$ should be linear, with an intercept K_1. Then from the slope, $(K_1K_2)^{1/2}$ may be found and hence K_2. This plot is shown in Fig. 1, and from it K_1 is found to be 2.0 M^{-2}, and K_2 is 4.4×10^{-4} M. The value of $K_2 = 4.4 \times 10^{-4}$ M compares well with the approximate value of 5×10^{-4} M found from the conductance data.

[2]Tables of the variation of ion concentration with reagent concentrations may be obtained, at a nominal charge, from the Depository of Unpublished Data, CISTI, National Research Council of Canada, Ottawa, Ont., Canada K1A 0S2.

An alternative scheme whereby the compound $(R^+)_2SnCl_6^{2-}$ is formed which dissociates to $R^+SnCl_6^{2-} + R^+$, when given a similar analysis is not consistent with the experimental data. Neither is the formation of this ion pair followed by a double ionization consistent with the results.

The heat of reaction to form the ionic species, -8.8 kcal, is a composite quantity containing contributions from both K_1 and K_2, the heat of reaction to form the ion pair from the starting reagents and their heat of dissociation into free ions. The proximity of the ionic dissociation constant found here at $-30°C$ to that found in a similar system at $+20°C$ (5) suggests that temperature has only a small effect on the ionic dissociation constant. In fact from the spectroscopic data at $-10°C$, which do however involve rather a long extrapolation, K_2 at this temperature is virtually unchanged. Such a compensation of the effect of the temperature on K_D caused by the change in ε with temperature and the heat of ionic dissociation, is common. Hence the value of -8.8 kcal is probably close to the enthalpy change to form the initial ion pair.

A few experiments were carried out on other initiating systems. When water was used as a co-catalyst, difficulties were encountered from the formation of a white precipitate at appreciable water concentrations. This was aggravated by the low temperature ($-70°C$) needed to obtain reasonable ion concentrations. A temperature dependent equilibrium was

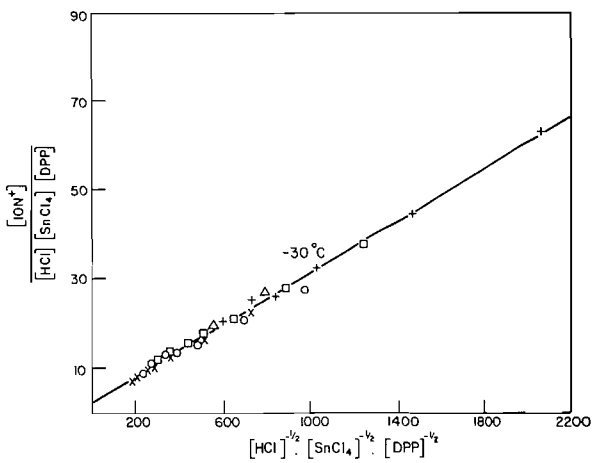

FIG. 1. The concentration of the diphenylethylcarbenium ion as a function of the concentration of HCl, $SnCl_4$, and DPP at $-30°C$. +, $[SnCl_4] = 3.5 \times 10^{-3}$ M, $[DPP] = 5.2 \times 10^{-2}$ M; □, $[SnCl_4] = 1.0 \times 10^{-2}$ M, $[DPP] = 5.1 \times 10^{-2}$ M; ×, $[SnCl_4] = 3.0 \times 10^{-2}$ M, $[DPP] = 5.1 \times 10^{-2}$ M; ○, $[DPP] = 5.8 \times 10^{-2}$ M, $[HCl] = 1.0 \times 10^{-2}$ M; △, $[SnCl_4] = 1.1 \times 10^{-2}$ M, $[HCl] = 1.0 \times 10^{-2}$ M; the other reactant was varied.

found to be established. The presence of excess water over $SnCl_4$ resulted in a decrease in ion formation.

$TiCl_4$ was also used, and it was found that the largest carbenium ion concentrations were produced in the absence of added water. Under these conditions the ion formation was slow, many hours being required to attain equilibrium At low $TiCl_4$ concentrations ($<2 \times 10^{-3}$ M) one diphenylethylcarbenium ion was formed per 2 molecules of $TiCl_4$, when DPP was in large excess. At higher concentrations of $TiCl_4$, ion formation levelled off. Destruction of the ions with methanol regenerated DPP, and no other product could be detected by thin layer chromatography even if 20% of the DPP had been converted to ions. Auto-ionization of the $TiCl_4$ could be suggested to explain these results, but in view of the difficulties Sigwalt (6) has described with the titanium tetrachloride/methylene chloride system, reaction with solvent or impurities could not be discounted.

1. A. G. Evans and E. D. Owens. J. Chem. Soc. 4123 (1959).
2. G. Sauvet, J. P. Vairon, and P. Sigwalt. J. Polym. Sci. Symposium, **52**, 173 (1975).
3. S. G. Entelis and K. S. Kazanskii. Kinet. Katal. **4**, 713 (1963).
4. G. Heublein and M. Helbig. Z. Chem. **9**, 428 (1969).
5. S. Bywater and D. J. Worsfold. Can. J. Chem. **55**, 85 (1977).
6. H. Cheradame and P. Sigwalt. Bull. Soc. Chim. 843 (1969).

Can. J. Chem. Downloaded from www.nrcresearchpress.com by 210.87.254.105 on 09/05/12
For personal use only.

The photochemistry of acrylonitrile vapour at 213.9 nm[1]

A. GANDINI AND P. A. HACKETT

Division of Chemistry, National Research Council of Canada, Ottawa, Ont., Canada K1A 0R6

Received March 20, 1978

A. GANDINI and P. A. HACKETT. Can. J. Chem. **56**, 2096 (1978).

The photolysis of acrylonitrile vapour in the $\pi^* \leftarrow$ n transition was carried out at 213.9 nm. Evidence is presented for two molecular elimination channels, one to yield acetylene and hydrogen cyanide ($\Phi = 0.50$), the other to yield cyanoacetylene and hydrogen ($\Phi = 0.31$). Experiments on acrylonitrile-1-*d* gave evidence that molecular elimination proceeds by α–β elimination following rapid intramolecular scrambling of deuterium by H/D migration in the excited state.

A. GANDINI et P. A. HACKETT. Can. J. Chem. **56**, 2096 (1978).

On a étudié la photolyse de l'acrylonitrile en phase vapeur à 213.9 nm (transition $\pi^* \leftarrow$ n). Les résultats indiquent que la décomposition s'effectue par deux réactions d'élimination moléculaire, une donnant l'acétylène et l'acide cyanidrique ($\Phi = 0.50$), et l'autre donnant le cyanoacetylène et l'hydrogéne ($\Phi = 0.31$). Des expériences avec l'acrylonitrile-1-*d* suggèrent que ces réactions procèdent par l'élimination α–β après une rédistribution intramoléculaire rapide du deuterium par migration H/D dans l'état excité.

Introduction

The photolysis of simple organic nitriles has received little attention. The only thorough investigation in this field is the photolysis of methyl cyanide (1) where both hydrogen atoms and CN radicals were produced in competitive primary steps. However, there have been many studies of the production of $\tilde{A}(^2\Pi_i)$ CN from the photolytic cleavage of a large number of nitriles (2, 3) in which the CN $\tilde{A}(^2\Pi_i) \rightarrow$ CN $\tilde{X}(^2\Sigma^+)$ luminescence was examined.

In a study of the ir laser induced decomposition of acrylonitrile (4) it was found that molecular rather than radical fragments were formed. In order to correlate these results with other studies of the uv and multiphoton ir decomposition of substituted ethylenes we have investigated the photolysis of acrylonitrile vapour in its first excited electronic transition $\pi^* \leftarrow$ n (5).

Experimental

Acrylonitrile (Aldrich) was distilled in a vacuum line from P_2O_5 rejecting generous head and tail portions. Although the purified product polymerised slowly, its purity as shown by glc analysis was not affected. Acrylonitrile-1-*d* (90% D) was prepared by double exchange with D_2O in a basic medium (6).

Photolyses were carried out in a 10 cm long quartz cell provided with 1 in. diameter Suprasil windows. Light from a Philips Spectral zinc resonance lamp, filtered by two 7 mm thick sodium chloride discs and a chlorine filter, was collimated through the cell with a quartz lens and detected by a Hamamatsu R788 solar blind photodiode. Frequent spectral analysis showed that the only line detected by the photodiode and absorbed by the substrate was that at 213.9 nm.

Pressures of products not condensable at -196°C were measured using a MKS Baratron capacitance manometer (1.2 Torr head). Hydrogen content was determined by diffusion through a palladium thimble. Products not condensable at -98°C (acetylene) were analysed by glc. Other products were characterised by mass spectrometry. In the photolysis of acrylonitrile-1-*d* $H_2/HD/D_2$ compositions were determined by glc, using an alumina column, treated with $MnCl_2$, at -196°C (7). Ratios of ethylene-to-acetylene-*d* were also determined by mass spectrometry at low ionisation voltage.

Quantum yields were determined by measuring the hydrogen produced in the photolysis of ammonia-d_3 in the presence of 300 Torr of propane (8).

Results

Four major products were identified, viz. acetylene, hydrogen cyanide, hydrogen, and cyanoacetylene. Experiments at high pressures also produced a white non-volatile polymeric material. No other low molecular-weight products (up to C_4) were detected. An infrared spectrum of polymer formed on the cell walls in a high-pressure photolysis of acrylonitrile-1-*d* was consistent with that of poly(acrylonitrile-1-*d*) (9).

A search was made for luminescence; none was detected.

The quantum yields of hydrogen and of acetylene were both independent of pressure over the range (0–50) Torr, and of D isotope substitution. Their values were measured as $\phi(H_2 + HD) = 0.50 \pm 0.05$ and $\phi(C_2H_2 + C_2HD) = 0.31 \pm 0.03$, while the ratios HD/H_2 and C_2HD/C_2H_2 were both 1.5 ± 0.2. No D_2 was detected.

Discussion

According to Mullen and Orloff (5) the uv absorption spectrum of acrylonitrile contains three transitions $\pi^* \leftarrow$ n (210.7 nm, $\varepsilon \simeq 150$), $\pi^* \leftarrow \pi$ (203.0 nm, $\varepsilon \simeq 2000$), and $\sigma^* \leftarrow \sigma$ (172.5 nm, $\varepsilon \simeq$

[1]NRCC No. 16753.

Can. J. Chem. Downloaded from www.nrcresearchpress.com by 210.87.254.105 on 09/05/12
For personal use only.

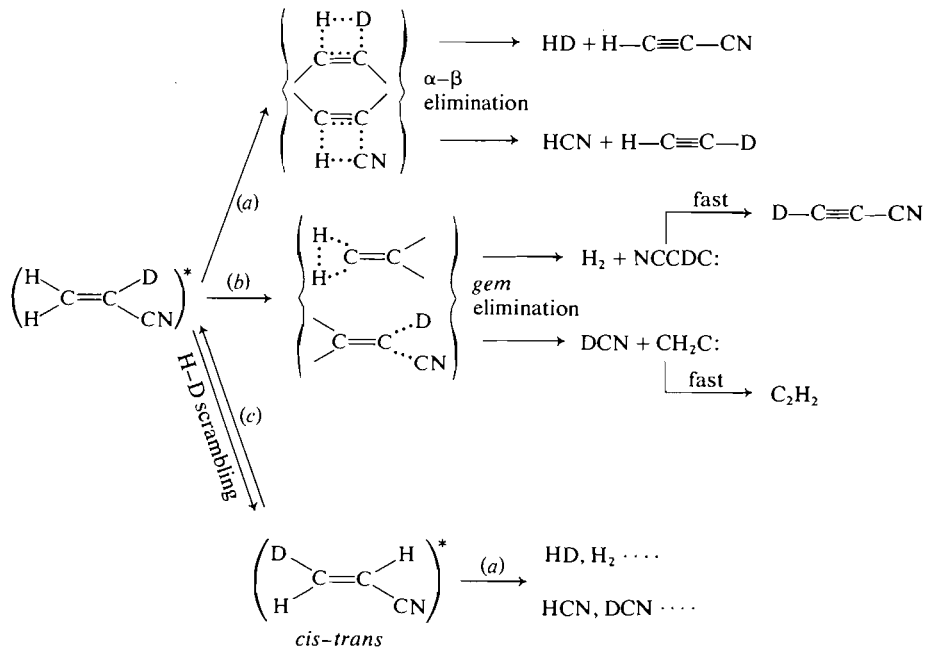

2000). In this context it is interesting to note that we obtained an apparent quantum yield of H_2 at 206.5 nm, using an unfiltered Zn lamp, that was much lower and pressure dependent, in contrast with the results obtained with the 213.9 nm line alone. Whilst this observation seems to confirm the existence of two different electronic states, or the onset of a radical channel at higher energy, we concentrated our efforts on the simpler situation following 213.9 nm excitation only.

The independence of the yield of hydrogen on acrylonitrile pressure and presence of propane (300 Torr) suggests that only molecular elimination is responsible for its formation. This is further confirmed by the presence of equivalent amounts of cyanoacetylene as a product and the absence of products derived from hydrogen atom addition or abstraction reactions. Similarly, the constancy of the acetylene yield and its indifference to the presence of oxygen (10 Torr) suggest a second molecular elimination channel, confirmed by the presence of equivalent amounts of hydrogen cyanide and the absence of products derived from the vinyl radical (e.g. ethylene, butadiene). Therefore the primary steps can be represented as

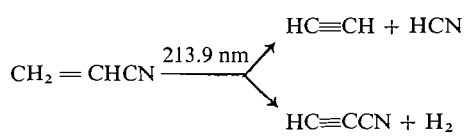

$$\phi_1/\phi_2 = 1.6$$

$$\phi_1{}^{+}\phi_2 = 0.81$$

The quantum yield deficit could be accounted for by polymer formation (from excited acrylonitrile or acetylene) and/or internal conversion, as no luminescence was observed.

The isotopic ratios in the photolysis products of acrylonitrile-1-*d* are interesting. They can be rationalised by either of the following mechanistic reductions, (*a*) a *gem* elimination of H_2 or deuterium cyanide followed by rapid isomerisation of the vinylidene fragment to cyanoacetylene or acetylene, concurrent with α–β elimination of HD or hydrogen cyanide (route *c* not required); in this case αβ eliminations would occur 1.5 times more frequently than αα elimination; (*b*) intramolecular H–D atom scrambling in excited acrylonitrile followed by α–β elimination only (route *b* not required).

Four pieces of evidence favour the second alternative, namely: (*i*) the equality of the ratios HD/H_2 and C_2HD/C_2H_2; (*ii*) the value of these ratios is exactly that expected statistically in the case of α–β elimination from a 90% acrylonitrile-1-*d* mixture in which scrambling of deuterium in the excited molecule is complete; (*iii*) the same value of these ratios is obtained in the multiphoton ir decomposition of acrylonitrile-1-*d* (4); (*iv*) intramolecular atom scrambling has been observed in the gas phase photosensitized reactions of deuterated ethylenes (10–12) and in the matrix isolated uv photolysis (13, 14) and multiphoton ir photolysis (15) of substituted ethylenes.

The absence of free radical formation parallels the results obtained in the multiphoton ir decomposition

Can. J. Chem. Downloaded from www.nrcresearchpress.com by 210.87.254.105 on 09/05/12
For personal use only.

in which the same two channels were observed (4). Whilst it is reasonable to expect that the C—CN bond would not easily be cleaved (2) at this wavelength ($E = 133.7$ kcal) it is surprising that no evidence is found for fission of the C—H bond.

1. D. E. McElcheran, M. J. Wijnen, and E. W. R. Steacie. Can. J. Chem. **36**, 321 (1958).
2. H. Okabe and V.H. Dibeler. J. Chem. Phys. **59**, 2430 (1973).
3. G.A.West and M. J. Berry. J. Chem. Phys. **61**, 4700 (1974).
4. A. Gandini, J. M. Parsons, C. Willis, and R.A. Back. To be published.
5. P. A. Mullen and M. K. Orloff. Theor. Chim. Acta, **23**, 278 (1971).
6. L. C. Leitch. Can. J. Chem. **35**, 345 (1957).
7. T. Terao and R. A. Back. J. Phys. Chem. **73**, 3884 (1969).
8. S. Koda and R. A. Back. Can. J. Chem. **55**, 1380 (1977).
9. H. Tadokova, S. Murahashi, R. Yamadera, and T. Kamei. J. Polym. Sci. A**1**, 3029 (1963).
10. A. B. Callear and R. J. Cvetanovic. J. Phys. Chem. **4**, 873 (1956).
11. S. Tsunashima, S. Hirokami, and S. Sato. Can. J. Chem. **46**, 995 (1968).
12. H. E. Hunziker. J. Chem. Phys. **50**, 1288 (1969).
13. W. A. Guillory and G. H. Andrews. J. Chem. Phys. **62**, 3208 (1975).
14. J. A. Warren, G. R. Smith, and W. A. Guillory. J. Photochem. **7**, 263 (1977).
15. A. Gandini. To be published.

Can. J. Chem. Downloaded from www.nrcresearchpress.com by 210.87.254.105 on 09/05/12
For personal use only.

Canadian Journal of Chemistry

Published by
THE NATIONAL RESEARCH COUNCIL OF CANADA

Journal canadien de chimie

Publié par
LE CONSEIL NATIONAL DE RECHERCHES DU CANADA

Volume 56 Number 16 August 15, 1978

Volume 56 numéro 16 15 août 1978

Can. J. Chem. Downloaded from www.nrcresearchpress.com by 210.87.254.105 on 09/05/12
For personal use only.

Synthesis and coordinating properties of the anionic tridentate ligand, methyl tris(1-pyrazolyl)gallate, $[MeGa(N_2C_3H_3)_3]^-$. X-ray crystal structure of $[MeGa(N_2C_3H_3)_3]Mo(CO)_2(\eta^3\text{-}C_3H_5)$

KENNETH R. BREAKELL, STEVEN J. RETTIG, DOUGLAS L. SINGBEIL, ALAN STORR, AND JAMES TROTTER

Department of Chemistry, University of British Columbia, 2075 Wesbrook Mall, Vancouver, B.C., Canada V6T 1W5

Received March 20, 1978

KENNETH R. BREAKELL, STEVEN J. RETTIG, DOUGLAS L. SINGBEIL, ALAN STORR, and JAMES TROTTER. Can. J. Chem. **56**, 2099 (1978).

The anionic tridentate ligand, $[MeGa(N_2C_3H_3)_3]^-$, has been characterized and its coordinating properties studied. It acts as a six-electron chelating ligand to divalent transition metal ions giving complexes of the type, $[MeGa(N_2C_3H_3)_3]_2M$ (M = Mn, Fe, Co, Ni, Cu, Zn), believed to possess an octahedral MN_6 core. The ligand also forms numerous carbonyl complexes and its coordinating ability in Mo, W, and Mn carbonyl derivatives is compared with that of similar boron ligands and the $\eta^5\text{-}C_5H_5$ ligand. From ir measurements and bond length data it appears that the $[MeGa(N_2C_3H_3)_3]^-$ ligand is superior in creating an electron-rich transition metal centre, and it also affords greater steric protection for the central metal. The expected tridentate chelating nature of the new ligand has been demonstrated through a crystal structure determination of the complex $[MeGa(N_2C_3H_3)_3]Mo(CO)_2(\eta^3\text{-}C_3H_5)$. Crystals of this complex are tetragonal, $a = 26.217(3)$, $c = 10.723(2)$ Å, $Z = 16$, space group $I4_1/a$. The structure was solved by Patterson and Fourier syntheses and was refined by full-matrix least-squares procedures to a final R of 0.030 and R_w of 0.031 for 2582 reflections with $I \geq 3\sigma(I)$.

KENNETH R. BREAKELL, STEVEN J. RETTIG, DOUGLAS L. SINGBEIL, ALAN STORR et JAMES TROTTER. Can. J. Chem. **56**, 2099 (1978).

On a caractérisé le ligand tridentate anionique $[MeGa(N_2C_3H_3)_3]^-$ et on a étudié ses propriétés coordonnantes. Il agit comme ligand chélatant à six électrons vis-à-vis des ions divalantes des métaux de transition qui donnent des complexes du type $[MeGa(N_2C_3H_3)_3]_2M$ (M = Mn, Fe, Co, Ni, Cu, Zn), pour lesquels on croit que le noyau possède une symétrie octaédrique MN_6. Le ligand forme aussi de nombreux complexes carbonyles et on a comparé sa facilité de coordonner dans des dérivés carbonylés du Mo, W et Mn avec celle de ligands semblables de bore et du ligand $\eta^5\text{-}C_5H_5$. En se basant sur des mesures i.r. et des données de longueurs de liaison, il semble que le ligand $[MeGa(N_2C_3H_3)_3]^-$ possède les qualités supérieures pour créer un centre de métal de transition qui est riche en électrons et qu'il fournit aussi une meilleure protection stérique pour le métal central. On a démontré la nature chélatante tridentate attendue du nouveau ligand par une détermination de la structure cristalline du complexe $[MeGa(N_2C_3H_3)_3]Mo(CO)_2(\eta^3\text{-}C_3H_5)$. Les cristaux de ce complexe sont tétragonaux: $a = 26.217(3)$, $c = 10.723(2)$ Å, $Z = 16$, groupe d'espace $I4_1/a$. On a résolu la structure par des synthèses de Patterson et de Fourier et on l'a affinée par la méthode des moindres carrés (matrice complète) jusqu'à une valeur finale de R de 0.030 et R_w de 0.031 pour 2582 réflexions avec $I \geq 3\sigma(I)$.

[Traduit par le journal]

Introduction

Numerous reports (1–4) have described the synthesis and coordination chemistry of the bidentate anionic ligands of the type $Me_2Ga(N_2C_3H_3)_2^-$. The present account details the synthesis of the anionic tridentate chelating ligand, methyl tris(1-pyrazolyl)-gallate, $[MeGa(N_2C_3H_3)_3]^-$, and describes its coordination compounds with transition metal M^{2+} ions (M = Mn, Fe, Co, Ni, Cu, and Zn) and also describes derivatives formed by interaction of the

Can. J. Chem. Downloaded from www.nrcresearchpress.com by 210.87.254.105 on 09/05/12
For personal use only.

TABLE 1. Analytical data for complexes incorporating the $[MeGa(N_2C_3H_3)_3]^-$ ligand

(*a*) $[MeGa(N_2C_3H_3)_3]_2M$ compounds

M	Color	Transition metal precursor	Analysis (%) Found C	Found H	Found N	Calcd C	Calcd H	Calcd N
Mn	White	$MnCl_2$	38.5	4.0	26.9	38.3	3.9	26.8
Fe	Pale yellow	$FeCl_2 \cdot 1.5THF$	38.8	3.9	26.6	38.3	3.9	26.8
Co	Beige	$CoCl_2$	37.9	3.7	26.7	38.1	3.8	26.7
Ni	Lilac	$NiBr_2$	38.3	3.8	26.8	38.1	3.8	26.7
Cu	Blue	$CuBr_2$	37.5	4.0	24.3	37.8	3.8	26.5
Zn	White	$ZnCl_2$	37.9	3.7	26.5	37.7	3.8	26.4

(*b*) Carbonyl compounds, $[MeGa(N_2C_3H_3)_3]X$

X	Color	Analysis (%) Found C	Found H	Found N	Calcd C	Calcd H	Calcd N
$Mo(CO)_2(\eta^3\text{-}C_3H_5)$	Yellow	37.7	3.6	17.3	37.6	3.5	17.5
$Mo(CO)_2(\eta^3\text{-}C_4H_7)$	Yellow	38.8	4.0	17.0	39.0	3.9	17.0
$Mo(CO)_2NO$	Orange	25.8	2.1	17.4	25.9	2.2	17.6
$W(CO)_2(\eta^3\text{-}C_3H_5)$	Yellow	32.1	3.0	15.0	31.8	3.0	14.8
$W(CO)_2(\eta^3\text{-}C_4H_7)$	Yellow	34.7	3.3	14.2	33.1	3.3	14.5
$W(CO)_2NO$	Orange	30.6	2.4	21.1	30.8	2.6	21.0
$Mn(CO)_3$	Pale yellow	36.8	2.7	20.0	36.8	2.8	19.8

ligand with Mo, W, and Mn carbonyl compounds. The tridentate chelating character of the ligand is demonstrated conclusively in the X-ray crystal structure determination of the compound $[MeGa(N_2C_3H_3)_3]Mo(CO)_2(\eta^3\text{-}C_3H_5)$.

Experimental

Starting Materials

Air-sensitive materials were handled in a glove-box under an atmosphere of oxygen-free dry nitrogen or in a nitrogen-blanketed apparatus. Tetrahydrofuran (THF) was dried by refluxing over lithium aluminum hydride and was used immediately following distillation. Pyrazole (K and K laboratories) and sodium hydride (Alfa) were used as supplied. Methyl gallium dichloride was prepared by a standard procedure (5) from gallium trichloride (6) and tetramethylsilane. Molybdenum and tungsten hexacarbonyls were used as supplied (Strem). Manganese pentacarbonyl bromide was prepared from dimanganese decacarbonyl (Strem) by a standard route (7). Allyl bromide and 2-methylallyl chloride were distilled under nitrogen prior to use. $FeCl_2 \cdot 1.5THF$ was prepared as previously described (8). Isoamyl nitrite was used as purchased (MCB).

Preparative Details

Sodium Methyl Tris(1-pyrazolyl)gallate Na^+-$[MeGa(N_2C_3H_3)_3]^-$

$$MeGaCl_2 + 3Na^+(N_2C_3H_3)^- \xrightarrow[\text{r.t.}]{\text{THF}} Na^+[MeGa(N_2C_3H_3)_3]^- + 2NaCl$$

Methyl gallium dichloride (4.761 g, 30.6 mmol) in THF solution was treated with a 3-molar equivalent of sodium pyrazolide (8.262 g, 91.8 mmol) in the same solvent. The mixture was stirred for 2 days and the white precipitate (NaCl) was then filtered off and washed with THF. The filtrate and the washings were made up to a standard volume and aliquots of the resulting solution were employed in subsequent reactions.

Preparation of $[MeGa(N_2C_3H_3)_3]_2M$ Complexes (M = Mn, Fe, Co, Ni, Cu, Zn)

The procedure was similar for each experiment and may be illustrated by describing the preparation of the nickel complex. The transition metal starting materials for all of the preparations are listed in Table 1 along with analytical data for the resulting complexes.

$$NiBr_2 + 2Na^+[MeGa(N_2C_3H_3)_3]^- \xrightarrow{\text{THF}} 2NaBr + [MeGa(N_2C_3H_3)_3]_2Ni$$

An aliquot of the ligand solution, prepared as described above and containing $Na^+[MeGa(N_2C_3H_3)_3]^-$ (1.890 g, 6.12 mmol), was added to a slurry of $NiBr_2$ (0.669 g, 3.06 mmol) in THF. The resulting mixture was stirred overnight and gave a lilac solution and a white precipitate. The precipitate was allowed to settle and the clear lilac solution isolated. The THF solvent was removed under vacuum and the resulting lilac powder was recrystallized from methylene chloride. The product was obtained as air-stable lilac crystals.

Preparation of $[MeGa(N_2C_3H_3)_3]Mo(CO)_2(\eta^3\text{-}C_3H_5)$

Step 1

$$Na^+[MeGa(N_2C_3H_3)_3]^- + Mo(CO)_6 \xrightarrow[\text{reflux}]{\text{THF}} Na^+[MeGa(N_2C_3H_3)_3]Mo(CO)_3^- + 3CO$$

Can. J. Chem. Downloaded from www.nrcresearchpress.com by 210.87.254.105 on 09/05/12
For personal use only.

Step 2

$$Na^+[MeGa(N_2C_3H_3)_3]Mo(CO)_3^- + C_3H_5Br \xrightarrow{THF}$$

$$[MeGa(N_2C_3H_3)_3]Mo(CO)_2(\eta^3\text{-}C_3H_5) + NaBr + CO$$

$Mo(CO)_6$ (1.40 g, 5.30 mmol) in THF and an aliquot of ligand solution containing $Na^+[MeGa(N_2C_3H_3)_3]^-$ (1.890 g, 6.12 mmol) were introduced into two separate parts of a break-seal apparatus. Both solutions were frozen at −196°C and the whole apparatus was evaculated and then sealed off. The apparatus was next warmed to room temperature and the solutions mixed. An immediate yellow coloration developed. The mixture was refluxed for several days after which time the CO evolution was measured (354 ml, 15.8 mmol). The clear yellow–orange solution was then treated with an excess of allyl bromide and the resulting solution refluxed for a few hours. Further gas evolution was noticed. The precipitated NaBr was separated from the solution and the solvent was removed from the latter. The resulting air-stable yellow powder was recrystallized from benzene to yield large golden crystals. Analytical data for this compound and the carbonyl compounds reported below are given in Table 1.

Preparation of $[MeGa(N_2C_3H_3)_3]Mo(CO)_2(\eta^3\text{-}C_4H_7)$

This complex was prepared in a manner similar to the one described above, substituting 2-methylallyl chloride for allyl bromide in step 2 of the synthesis. The product was an air-sensitive bright yellow solid which was purified by vacuum sublimation at 120°C.

Preparation of $[MeGa(N_2C_3H_3)_3]Mo(CO)_2NO$

To a THF solution of $Na^+[MeGa(N_2C_3H_3)_3]Mo(CO)_3^-$ (see above) was added an excess of isoamyl nitrite and the resulting mixture was refluxed briefly. Gas evolution was observed and from the product solution an orange material was obtained. On recrystallization from benzene this gave well-formed bright orange crystals of the desired product.

Preparation of $[MeGa(N_2C_3H_3)_3]W(CO)_2(\eta^3\text{-}C_3H_5)$

Attempts to prepare this complex using the route employed for the analogous Mo compound described above were not successful and the complex was obtained using $(MeCN)_3W(CO)_3$ (9) as starting material.

Step 1

$$(MeCN)_3W(CO)_3 + \text{xs } C_3H_5Br \xrightarrow[\text{r.t.}]{THF}$$

$$(MeCN)_2W(CO)_2(\eta^3\text{-}C_3H_5)(Br) + MeCN + CO$$

Step 2

$$(MeCN)_2W(CO)_2(\eta^3\text{-}C_3H_5)(Br) + Na^+[MeGa(N_2C_3H_3)_3]^- \xrightarrow{THF}$$

$$[MeGa(N_2C_3H_3)_3]W(CO)_2(\eta^3\text{-}C_3H_5) + 2MeCN + NaBr$$

An excess of allyl bromide was added to a slurry of $(MeCN)_3W(CO)_3$ (1.381 g, 3.534 mmol) in THF at room temperature. The color of the mixture changed from yellow to red and the product was a clear solution. $Na^+[MeGa(N_2C_3H_3)_3]^-$ (1.092 g, 3.534 mmol) in THF was added with a concomitant change of color to orange and the formation of a white precipitate. The isolated solution yielded a waxy orange solid which yielded yellow–orange crystals upon recrystallization from benzene.

The $[MeGa(N_2C_3H_3)_3]W(CO)_2(\eta^3\text{-}C_4H_7)$ compound was prepared via a similar route but employing an excess of 2-methylallyl chloride in step 1 of the synthesis in place of allyl bromide.

Preparation of $[MeGa(N_2C_3H_3)_3]W(CO)_2NO$

This compound was prepared using a route similar to that used for the corresponding Mo compound. A THF solution of $Na^+[MeGa(N_2C_3H_3)_3]W(CO)_3^-$ (obtained from $W(CO)_6$ and $Na^+[MeGa(N_2C_3H_3)_3]^-$) was treated with an excess of isoamyl nitrite and the reaction, on work-up, yielded bright orange crystals of the nitrosyl complex.

Preparation of $[MeGa(N_2C_3H_3)_3]Mn(CO)_3$

$$Mn(CO)_5Br + Na^+[MeGa(N_2C_3H_3)_3]^- \rightarrow$$

$$[MeGa(N_2C_3H_3)_3]Mn(CO)_3 + 2CO + NaBr$$

$Mn(CO)_5Br$ (0.774 g, 2.82 mmol) in THF solution and $Na^+[MeGa(N_2C_3H_3)_3]^-$ (0.874 g, 2.83 mmol) in the same solvent were mixed and the resultant combination was refluxed for a few hours. Gas evolution was brisk and at the end of the reaction a pale yellow solution and a white precipitate were obtained. The isolated clear solution gave an off-white solid on removal of the THF solvent. Recrystallization from benzene gave pale yellow crystals of the product.

Spectra

Mass spectra were recorded on a Varian MAT CH4 mass spectrometer at 70 eV with an ion source temperature of 100–180°C. Infrared spectra were recorded on a Perkin Elmer 457 spectrophotometer either as Nujol mulls or as solution spectra in cyclohexane or in benzene solvents. Proton nmr spectra in C_6D_6 were recorded on Varian T60 and XL-100 spectrometers. For complexes of low solubility FT techniques were employed in the recording of their ^1H nmr spectra.

X-ray Crystallographic Analysis of $[MeGa(N_2C_3H_3)_3]Mo(CO)_2(\eta^3\text{-}C_3H_5)$

The crystal (a parallelepiped with (010), (100), (10$\bar{2}$) developed) was mounted with c parallel to the goniostat axis and had dimensions of ca. 0.5 × 0.5 × 0.5 mm. Unit-cell parameters were refined by least squares on 2 sin θ/λ values for 22 reflections measured on a diffractometer with Mo K_α radiation (λ = 0.71069 Å). Crystal data (at 22°C) are:

$C_{15}H_{17}GaMoN_6O_2$ fw = 479.0

Tetragonal, a = 26.217(3), c = 10.723(2) Å, V = 7370(1) Å^3, Z = 16, ρ_c = 1.727 g cm^{-3}, $F(000)$ = 3808, μ(Mo K_α) = 22.3 cm^{-1}. Absent reflections: hkl, $h + k + l \neq 2n$, $hk0$, $h(k) \neq 2n$, and $00l$, $l \neq 4n$ in addition to Laue symmetry $4/m$ determine uniquely the space group $I4_1/a$ (C_{4h}^6, No. 88).

Intensities were measured with zirconium-filtered Mo K_α radiation on a Datex-automated General Electric XRD-6 diffractometer. A θ–2θ scan at 2° min^{-1} over a range of (1.80 + 0.86 tan θ) degrees in 2θ was employed. Background counts (10 s) were measured at each end of the scan. Data were measured to 2θ = 55°. The intensities of the check reflections, measured every 50 reflections throughout the data collection, remained constant to within ±1.5% throughout the data collection. After data reduction, an absorption correction was applied using the Gaussian integration method (10, 11). Transmission factors ranged from 0.346 to 0.427. Of the 4233 independent reflections measured, 2582 (61%) had intensities greater than 3σ(I) above background where $\sigma^2(I) = S + B + (0.02S)^2$ with S = scan count and B = time-averaged background count.

The positions of the molybdenum and gallium atoms were determined from the Patterson function and those of the O, N, and C atoms from a subsequent difference map. After full-matrix refinement of all non-hydrogen atoms with anisotropic thermal parameters to R = 0.037, a difference map gave the positions of all 17 hydrogen atoms, which were subsequently included in the refinement with isotropic thermal parameters. The scattering factors of ref. 12 were used for non-hydrogen atoms and those of ref. 13 for hydrogen atoms. Anomalous scattering factors from ref. 14 were used for the

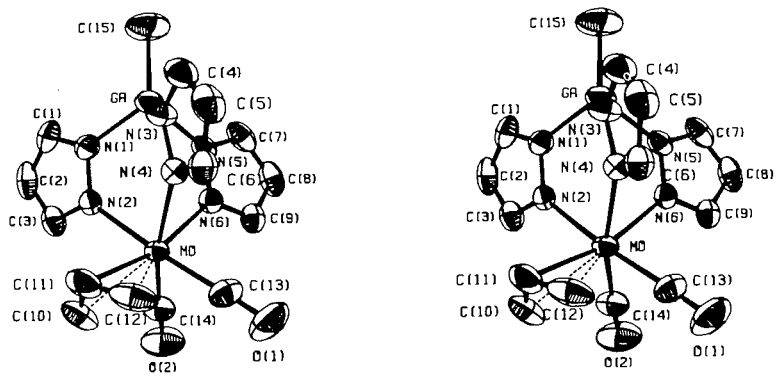

FIG. 1. Stereo view of the dicarbonyl[methyltris(1-pyrazolyl)gallato($N(2)$, $N(2')$, $N(2'')$)](η^3-allyl)molybdenum molecule, 50% ellipsoids are shown for the non-hydrogen atoms. Hydrogen atoms have been omitted for the sake of clarity.

TABLE 2. Final positional parameters (fractional O, N, and C $\times 10^4$, Mo and Ga $\times 10^5$, H $\times 10^3$) with estimated standard deviations in parentheses (origin at $\bar{1}$)

Atom	x	y	z
Mo	12285(1)	17426(1)	35013(3)
Ga	14196(2)	7117(2)	57581(4)
O(1)	1410(2)	1681(2)	651(3)
O(2)	1932(2)	2680(2)	3080(4)
N(1)	1269(1)	1372(1)	6434(3)
N(2)	1275(1)	1785(1)	5661(3)
N(3)	886(1)	620(1)	4562(3)
N(4)	850(1)	950(1)	3581(3)
N(5)	1977(1)	894(1)	4666(3)
N(6)	1918(1)	1260(1)	3766(3)
C(1)	1326(2)	1537(2)	7620(4)
C(2)	1365(2)	2047(2)	7645(5)
C(3)	1341(2)	2190(2)	6408(5)
C(4)	637(2)	184(2)	4265(5)
C(5)	433(2)	230(2)	3110(5)
C(6)	575(2)	708(2)	2710(4)
C(7)	2455(2)	702(2)	4546(5)
C(8)	2702(2)	932(2)	3588(5)
C(9)	2359(2)	1279(2)	3129(4)
C(10)	797(2)	2519(2)	3853(7)
C(11)	468(2)	2113(2)	3687(6)
C(12)	453(2)	1912(2)	2509(7)
C(13)	1334(2)	1693(2)	1720(4)
C(14)	1670(2)	2333(2)	3279(5)
C(15)	1535(5)	157(3)	6930(8)
H(1)	134(2)	135(2)	817(5)
H(2)	140(2)	228(2)	830(5)
H(3)	137(2)	249(2)	605(5)
H(4)	64(2)	−8(2)	486(6)
H(5)	23(2)	−1(2)	269(5)
H(6)	50(2)	86(2)	199(4)
H(7)	254(2)	47(2)	501(4)
H(8)	303(2)	89(2)	336(4)
H(9)	238(2)	151(2)	249(5)
H(10a)	85(2)	270(2)	319(5)
H(10b)	81(2)	266(2)	477(6)
H(11)	27(2)	194(3)	439(6)
H(12a)	50(2)	212(2)	183(5)
H(12b)	27(2)	159(2)	239(5)
H(15a)	168(4)	−12(4)	638(11)
H(15b)	173(3)	26(3)	749(9)
H(15c)	124(4)	7(4)	721(9)

Mo and Ga atoms. The weighting scheme, $w = [1 + \{(|F_o| - 117.5)/47.5\}^2]^{-1}$ and $w = 0.0625$ for the unobserved reflections, gave uniform average values of $w(|F_o| - |F_c|)^2$ over ranges of $|F_o|$ and was employed in the final stages of refinement. A correction for secondary extinction was approximated by basing the least-squares refinement on the minimization of $\Sigma w[|F_o| - |F_c|/(1 + gI)|]^2$ where g is the extinction parameter and I the uncorrected intensity. The final value of g was $5.8(2) \times 10^{-7}$. Convergence was reached at $R = 0.030$ and R_w of 0.031 for 2582 reflections with $I \geq 3\sigma(I)$. For all 4233 reflections $R = 0.069$ and $R_w = 0.040$.

On the final cycle of refinement the mean and maximum parameter shifts corresponded to 0.02 and 0.21σ respectively. The mean error in an observation of unit weight was 2.527. A final difference map showed maximum fluctuations of −1.5 to +0.6 e Å^{-3} near Mo and ±0.3 e Å^{-3} elsewhere. The final positional and thermal parameters appear in Tables 2 and 3 respectively.[1] Measured and calculated structure factors have been placed in the Depository of Unpublished Data.[1]

The ellipsoids of thermal motion for the non-hydrogen atoms are shown in Fig. 1. The thermal motion has been analysed in terms of the rigid-body modes of translation, libration, and screw motion (15) using the computer program MGTLS. The rms standard error in the temperature factors σU_{ij} (derived from the least-squares analysis) is 0.0025 Å^2. Analysis of the entire molecule (rms $\Delta U_{ij} = 0.0074$ Å^2) showed that the atoms O(1), O(2), C(10), C(12), and C(15) exhibit significant independent motion. These atoms were excluded from the rigid-body, resulting in a physically reasonable set of rigid-body thermal parameters (rms $\Delta U_{ij} = 0.0044$ Å^2). The appropriate bond distances have been corrected for libration (16), using shape parameters q^2 of 0.08 for all atoms involved. Corrected bond lengths appear in Table 4 along with the uncorrected values. Corrected bond angles differ by less than 1σ from the uncorrected values given in Table 5.

Results and Discussion

Infrared Spectra

Carbonyl Complexes

The metal carbonyl complexes show important trends in their ir spectra. The wave numbers of ν_{CO} vibrations for the complexes are listed in Table 6

[1]The structure factor table and Table 3 (thermal parameters) are available, at a nominal charge, from the Depository of Unpublished Data, CISTI, National Research Council of Canada, Ottawa, Ont., Canada K1A 0S2.

Can. J. Chem. Downloaded from www.nrcresearchpress.com by 210.87.254.105 on 09/05/12
For personal use only.

TABLE 4. Bond lengths (Å) with estimated standard deviations in parentheses

(*a*) Non-hydrogen atoms

Bond	Length		Bond	Length	
	Uncorr.	Corr.		Uncorr.	Corr.
Mo —N(2)	2.322(3)	2.328	N(5) —N(6)	1.369(4)	1.373
Mo —N(4)	2.303(3)	2.309	N(1) —C(1)	1.351(6)	1.352
Mo —N(6)	2.226(3)	2.232	N(2) —C(3)	1.341(5)	1.342
Mo —C(13)	1.934(5)	1.936	N(3) —C(4)	1.355(6)	1.356
Mo —C(14)	1.947(5)	1.948	N(4) —C(6)	1.341(5)	1.342
Mo —C(10)	2.359(5)	2.360	N(5) —C(7)	1.356(6)	1.357
Mo —C(11)	2.226(5)	2.228	N(6) —C(9)	1.344(5)	1.345
Mo —C(12)	2.336(5)	2.338	C(1) —C(2)	1.341(8)	1.343
Ga —N(1)	1.918(3)	1.922	C(2) —C(3)	1.381(8)	1.382
Ga —N(3)	1.913(4)	1.917	C(4) —C(5)	1.355(8)	1.357
Ga —N(5)	1.934(4)	1.938	C(5) —C(6)	1.376(7)	1.378
Ga —C(15)	1.947(6)	1.947	C(7) —C(8)	1.355(8)	1.357
O(1) —C(13)	1.164(6)	1.166	C(8) —C(9)	1.369(7)	1.372
O(2) —C(14)	1.160(6)	1.162	C(10)—C(11)	1.381(8)	1.383
N(1) —N(2)	1.364(5)	1.368	C(11)—C(12)	1.369(9)	1.371
N(3) —N(4)	1.366(5)	1.371			

(*b*) Bonds involving hydrogen atoms

Bonds	Length (Å)	Mean
C(pyrazolyl)—H	0.77–0.95(4–6)	0.89(6)
C(allyl)—H	0.86–1.05(5–7)	0.97(8)
Me—H	0.84–1.00(9–11)	0.90(8)

together with pertinent ν_{CO} bands for comparable compounds (17, 18). It is noteworthy that the ν_{CO} vibrations for the gallium complexes are consistently ~ 10 cm^{-1} lower than those of the corresponding boron complexes, suggesting a more electron-rich transition metal centre with the introduction of the gallium ligand with consequent increased back-bonding to the carbonyl groups. The results are entirely in agreement with the bond lengths in $[MeGa(N_2C_3H_3)_3]Mo(CO)_2(\eta^3\text{-}C_3H_5)$ and $[HB(N_2C_3H_3)_3]Mo(CO)_2(\eta^3\text{-}C_4H_7)$ (see Crystal Structure section). As with the boron complexes (18), the ν_{CO} values for the gallium complexes decrease by ~ 10 cm^{-1} in going from Mo to W. In the analogous $LMo(CO)_2(\eta^3\text{-}C_3H_5)$ series (where L = $\eta^5\text{-}C_5H_5$, $HB(N_2C_3H_3)_3$, or $MeGa(N_2C_3H_3)_3$), the highest ν_{CO} values occur when L = $\eta^5\text{-}C_5H_5$, the lowest when L = $MeGa(N_2C_3H_3)_3$. Another noteworthy feature is that only in the complex $[MeGa(N_2C_3H_3)_3]W(CO)_2(\eta^3\text{-}C_3H_5)$ do four ν_{CO} bands become apparent, a feature previously reported for the complex $(\eta^5\text{-}C_5H_5)Mo(CO)_2(\eta^3\text{-}C_3H_5)$ (17). This suggests the occurrence of two isomers in the cyclohexane solution of this tungsten complex with the allyl group in one of the isomers rotated in the opposite direction to that depicted in the crystal structure of the Mo derivative (see Fig. 1). The intensities of the two sets of doublets are in approximately a 2:1 ratio suggesting one isomer being preferred over the other. From the crystal structure data in this report, and in the report on the similar boron structure (19), it is apparent that it is preferable for the central atom of the allyl group (whether it bears a hydrogen atom or a methyl group) to orient into the space between the two pyrazolyl groups. Indeed the complex, $[MeGa(N_2C_3H_3)_3]W(CO)_2(\eta^3\text{-}C_4H_7)$, shows only two ν_{CO} bands, suggesting that the C—Me group projecting towards the two CO groups is not energetically favored. The gallium complexes which display just two bands are all thought to be similar, with respect to orientation of their allyl groups, to that illustrated for the $[MeGa(N_2C_3H_3)_3]Mo(CO)_2(\eta^3\text{-}C_3H_5)$ complex (Fig. 1). The larger size of the W atom over the Mo atom may be responsible for the occurrence of a small amount of the less favored isomer in the cyclohexane solution of the $[MeGa(N_2C_3H_3)_3]W(CO)_2(\eta^3\text{-}C_3H_5)$ complex.

The manganese tricarbonyl complex, $[MeGa(N_2C_3H_3)_3]Mn(CO)_3$, showed the expected two ν_{CO} bands in cyclohexane and these occurred at 10 cm^{-1} lower than the ν_{CO} values reported for similar boron complexes (see Table 6) as expected. The Nujol mull spectrum of this complex, however, displayed a split asymmetric ν_{CO} vibration and gave three bands in the ν_{CO} region at 2020, 1922, and 1890 cm^{-1}. Unfortunately the two nitrosyl complexes, $[MeGa(N_2C_3$-

Can. J. Chem. Downloaded from www.nrcresearchpress.com by 210.87.254.105 on 09/05/12
For personal use only.

Can. J. Chem. Downloaded from www.nrcresearchpress.com by 210.87.254.105 on 09/05/12
For personal use only.

TABLE 5. Bond angles (deg) with estimated standard deviations in parentheses

(*a*) Non-hydrogen atoms

Bonds	Angle (deg)	Bonds	Angle (deg)
N(2) —Mo —N(4)	91.7(1)	Ga —N(3) —C(4)	128.1(3)
N(2) —Mo —N(6)	81.8(1)	N(4) —N(3) —C(4)	108.7(4)
N(2) —Mo —C(13)	168.7(2)	Mo —N(4) —N(3)	124.8(2)
N(2) —Mo —C(14)	93.0(2)	Mo —N(4) —C(6)	129.3(3)
N(2) —Mo —C(11)	86.4(2)	N(3) —N(4) —C(6)	105.8(3)
N(4) —Mo —N(6)	80.3(1)	Ga —N(5) —N(6)	121.0(2)
N(4) —Mo —C(13)	92.1(2)	Ga —N(5) —C(7)	131.6(3)
N(4) —Mo —C(14)	167.7(2)	N(6) —N(5) —C(7)	107.3(4)
N(4) —Mo —C(11)	90.3(2)	Mo —N(6) —N(5)	125.5(2)
N(6) —Mo —C(13)	88.4(2)	Mo —N(6) —C(9)	127.8(3)
N(6) —Mo —C(14)	89.1(1)	N(5) —N(6) —C(9)	106.7(3)
N(6) —Mo —C(11)	164.6(2)	N(1) —C(1) —C(2)	110.3(5)
C(13)—Mo —C(14)	81.2(2)	C(1) —C(2) —C(3)	104.4(4)
C(13)—Mo —C(11)	104.2(2)	N(2) —C(3) —C(2)	111.3(5)
C(14)—Mo —C(11)	101.3(2)	N(3) —C(4) —C(5)	109.3(4)
N(1) —Ga —N(3)	102.5(1)	C(4) —C(5) —C(6)	105.0(4)
N(1) —Ga —N(5)	99.3(1)	N(4) —C(6) —C(5)	111.1(4)
N(1) —Ga —C(15)	117.6(3)	N(5) —C(7) —C(8)	110.3(4)
N(3) —Ga —N(5)	100.3(1)	C(7) —C(8) —C(9)	104.8(4)
N(3) —Ga —C(15)	116.9(3)	N(6) —C(9) —C(8)	110.9(5)
N(5) —Ga —C(15)	117.3(4)	Mo —C(10)—C(11)	67.3(3)
Ga —N(1) —N(2)	119.0(2)	Mo —C(11)—C(10)	77.8(3)
Ga —N(1) —C(1)	128.4(3)	Mo —C(11)—C(12)	77.0(3)
N(2) —N(1) —C(1)	108.4(4)	C(10)—C(11)—C(12)	115.6(6)
Mo —N(2) —N(1)	124.5(2)	Mo —C(12)—C(11)	68.2(3)
Mo —N(2) —C(3)	129.8(3)	Mo —C(13)—O(1)	177.2(5)
N(1) —N(2) —C(3)	105.5(4)	Mo —C(14)—O(2)	176.5(5)
Ga —N(3) —N(4)	119.1(2)		

(*b*) Angles involving hydrogen atoms

Bonds	Angle (deg)	Mean (deg)
N—C(pyrazolyl)—H	116–121(3–4)	119(2)
C—C(pyrazolyl)—H	124–134(3–4)	129(3)
C—C(allyl)—H	114–125(3–4)	119(4)
Me—C(allyl)—H	105–115(3–4)	110(4)
H—C(allyl)—H	118(5), 125(5)	122(4)
Ga—Me—H	102–108(6)	106(3)
H—Me—H	110–116(8–9)	113(3)

$H_3)_3]M(CO)_2NO$ (M = Mo, W), were not sufficiently soluble to give spectra in cyclohexane or in CH_2Cl_2. The spectra recorded in Table 6 are taken in Nujol. Four bands (two of strong and two of medium intensity) were found in the ν_{CO} region in each complex and a complex band envelope was observed in the ν_{NO} region of the spectra at $\sim$1650 cm^{-1}. These splittings could well arise from the necessity to use Nujol mull samples, but it is clear that the tungsten complex again displays the lower ν_{CO} frequencies, $\sim$20 cm^{-1} below those for the corresponding molybdenum compound.

[MeGa(N$_2$C$_3$H$_3$)$_3$]$_2$M Complexes (M = Mn, Fe, Co, Ni, Cu, Zn)

The Nujol mull spectra of all six complexes listed in Table 1 were essentially identical, indicating a probable isomorphism in the octahedral complexes. An X-ray structural study of the nickel complex is in progress and should confirm the pseudo-octahedral arrangement of the six ligating nitrogen atoms about the central nickel atom. Such an arrangement has been demonstrated in the crystal structure determination of the boron complex $[HB(N_2C_3H_3)_3]_2Co$ (20).

Two sharp strong bands occurred in the region usually associated with Ga—C stretching vibrations, 628 and 595 cm^{-1}, in each of the spectra. The band at lower frequency is probably the Ga—C stretching vibration for the compounds and the one at 628 cm^{-1}, a little high for a ν_{Ga-C} stretch (21), may be due to a pyrazolyl ring mode.

^{1}H Nuclear Magnetic Resonance Spectra

The ^{1}H nmr results for the 'η^3-allyl' and nitrosyl

Can. J. Chem. Downloaded from www.nrcresearchpress.com by 210.87.254.105 on 09/05/12
For personal use only.

TABLE 6. Metal carbonyl stretching frequencies[a]

Compound	ν_{CO} (cm^{-1})	Reference
$(\eta^5\text{-}C_5H_5)Mo(CO)_2(\eta^3\text{-}C_3H_5)$	1970, 1963, 1903, 1889	17
$HB(N_2C_3H_3)_3Mo(CO)_2(\eta^3\text{-}C_3H_5)$	1959, 1874	18
$BuB(N_2C_3H_3)_3Mo(CO)_2(\eta^3\text{-}C_3H_5)$	1955, 1872	18
$MeGa(N_2C_3H_3)_3Mo(CO)_2(\eta^3\text{-}C_3H_5)$	1948, 1860	This work
$HB(N_2C_3H_3)_3W(CO)_2(\eta^3\text{-}C_3H_5)$	1949, 1862	18
$MeGa(N_2C_3H_3)_3W(CO)_2(\eta^3\text{-}C_3H_5)$	1940, (1904), 1850, (1814)	This work
$HB(N_2C_3H_3)_3Mo(CO)_2(\eta^3\text{-}C_4H_7)$	1958, 1874	18
$MeGa(N_2C_3H_3)_3Mo(CO)_2(\eta^3\text{-}C_4H_7)$	1949, 1863	This work
$HB(N_2C_3H_3)_3W(CO)_2(\eta^3\text{-}C_4H_7)$	1950, 1861	18
$MeGa(N_2C_3H_3)_3W(CO)_2(\eta^3\text{-}C_4H_7)$	1940, 1850	This work
$HB(N_2C_3H_3)_3Mn(CO)_3$	2041, 1941	18
$MeGa(N_2C_3H_3)_3Mn(CO)_3$	2030, 1930	This work
$MeGa(N_2C_3H_3)_3Mo(CO)_2NO$[b]	2018s, 1915s, 1998m, 1896m	This work
$MeGa(N_2C_3H_3)_3W(CO)_2NO$[b]	1995s, 1895s, 1980m, 1870m	This work

[a]Cyclohexane.
[b]Nujol.

TABLE 7. ^1H nmr data for the 'allyl' and nitrosyl complexes in C_6D_6 solvent[d]

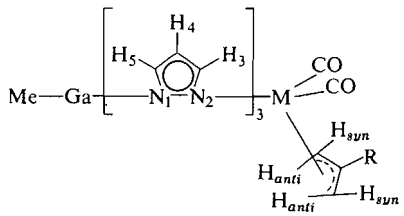

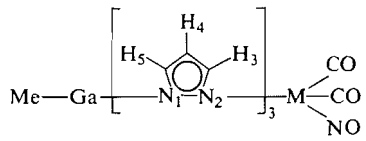

		Allyl compounds			Nitrosyl compounds	
	M = Mo	W	Mo	W	Mo	W
τ ppm	R = H	H	Me	Me	—	—
H_3	1.17d[a](1)	1.17d[a](1)	1.32br(1)	1.32br(1)	2.22d[a](2)	2.11d[a](2)
	2.21d[a](2)	2.05d[a](2)	2.07br(2)	1.97br(2)	2.60d[a](1)	2.50d[a](1)
H_4	4.06t[a](2)	4.15t[a](2)	4.07br(2)	4.15br(2)	4.09t[a](2)	4.15t[a](2)
	4.15t[a](1)	4.27t[a](1)	4.17br(1)	4.32br(1)	4.26t[a](1)	4.33t[a](1)
H_5	2.91d[a](2)	2.98d[a](2)	2.88br(2)	2.96br(2)	2.94d[a](2)	3.02d[a](2)
	3.20d[a](1)	3.32d[a](1)	3.24br(1)	3.36br(1)	3.08d[a](1)	3.18d[a](1)
H_{syn}	6.56d[b](2)	6.76d[b](2)	6.63s(2)	6.86s(2)	—	—
H_{anti}	8.48d[c](2)	8.17d[c](2)	8.51s(2)	8.11s(2)	—	—
R	6.53br(1)	7.18br(1)	8.68s(3)	8.51s(3)	—	—
Ga—Me	10.08s(3)	10.14s(3)	10.08s(3)	10.14s(3)	10.04s(3)	10.08s(3)

[a]$J \approx 2$ Hz.
[b]$J \approx 7$ Hz.
[c]$J \approx 9$ Hz.
[d]τ (TMS) = 10.00 ppm, τ ('C_6D_6') = 2.84 ppm. Relative intensities of signals given in parentheses, s = singlet, d = doublet, t = triplet, br = broad.

complexes of Mo and W are listed in Table 7. All six spectra give signals for the pyrazolyl protons which indicate that two pyrazolyl groups are in like positions whilst the third pyrazolyl group is unique. The assignment of the individual signals to specific pyrazolyl protons follows by analogy with the assignments of Meakin *et al.* for similar boron compounds (22). It is noteworthy that the pyrazolyl protons in $[HB(N_2C_3H_3)_3]Mo(CO)_2(\eta^3\text{-}C_3H_5)$ (22) do not approach the resolution of those in the room temperature spectrum of $[MeGa(N_2C_3H_3)_3]Mo(CO)_2(\eta^3\text{-}C_3H_5)$ until −45°C. In fact, at room temperature, due to a rapid rotation of the $HB(N_2C_3H_3)_3$ moiety about the B...Mo axis, the three pyrazolyl groups appear equivalent. Less severe steric interactions about the molybdenum atom in the boron complex, due to shorter B—N distances relative to Ga—N distances, probably account for the observed difference in the proton nmr spectra. Higher temperature spectra on the gallium complex may demonstrate a similar ability of the $[MeGa(N_2C_3H_3)_3]$ moiety to rotate about the Ga...Mo axis. Comparison of the spectra of the nitrosyl compounds with those of the allyl compounds reveals a significant

Can. J. Chem. Downloaded from www.nrcresearchpress.com by 210.87.254.105 on 09/05/12
For personal use only.

upfield shift of the signal due to the 3-H proton of the unique pyrazolyl group in the nitrosyl compounds. The signals due to the 3-H protons of the two similarly positioned pyrazolyl groups do not change significantly on changing allyl for nitrosyl in the compounds. Both the η^3-allyl groups and the nitrosyl groups are *trans* to the 3-H proton of the unique pyrazolyl group in the pseudooctahedral complexes (see Fig. 1) and it seems possible that some type of *trans* effect is responsible for the observed shift. Another feature of note is that the signals due to the pyrazolyl protons of the η^3-2-methylallyl complexes are not as well resolved as those in the corresponding η^3-allyl complexes. A variable temperature ^{1}H nmr study is being undertaken on these complexes in an attempt to explain these observations.

The allyl protons gave clearly resolved signals except for the unique proton of the η^3-C_3H_5 group. The signals are assigned in Table 7 following assignments for the comparable allyl complexes $(\eta^5$-$C_5H_5)$-$Mo(CO)_2(\eta^3$-$C_3H_5)$ (23, 24) and $(\eta^5$-$C_5H_5)Mo$-$(CO)_2(\eta^3$-$C_4H_7)$ (24) and also using assignments given in ref. 25. Again a variable temperature ^{1}H nmr study would be useful on these complexes in the 'allyl' region of the spectra to determine if rotation of the allyl groups is possible or whether steric interactions restrict the molecular arrangement of these groups to one or the other of the two possible isomers discussed above. A stereochemically rigid system might well be confirmed for the gallium complexes on the nmr time scale within the experimentally accessible temperature range. It is interesting to note that the room temperature ^{1}H nmr spectrum of the complex $[MeGa(N_2C_3H_3)_3]W(CO)_2(\eta^3$-$C_3H_5)$ in C_6D_6 did not indicate the presence of two isomers as suggested by the ir spectrum in cyclohexane solvent. However it is well documented that changing the solvent can radically alter the distribution of isomers in this type of system (26). The ir spectrum of the complex in benzene solvent displayed but two peaks in the ν_{CO} region of the spectrum.

Mass Spectra

$[MeGa(N_2C_3H_3)_3]_2M$ Compounds (M = Mn, Fe, Co, Ni, Cu, Zn)

The mass spectra of all six complexes listed in Table 1 displayed strong signals due to the parent ions and also strong signals corresponding to the $[MeGa(N_2C_3H_3)_3]M^+$ ions. In addition to other weak signals arising from 'mixed metal' ions two strong signals occurred in all six spectra which were assigned to ions containing two gallium atoms, viz. $MeGa_2(N_2C_3H_3)_4^+$ and $Me_2Ga_2(N_2C_3H_3)_3^+$. These ions must arise, after ejection of the transition metal and pyrazolyl groups from the parent species, by a recombination of '$MeGa(N_2C_3H_3)_x$' fragments. It is noteworthy in this regard that a strong signal due to the $MeGa(N_2C_3H_3)^+$ ion occurs in all of the spectra.

Carbonyl Derivatives

Signals due to parent ions were observed in the mass spectra of all seven carbonyl complexes listed in Table 1.

In the spectrum of the manganese compound, $[MeGa(N_2C_3H_3)_3]Mn(CO)_3$, all signals were weak compared to the very strong signal attributable to the $[MeGa(N_2C_3H_3)_3]Mn^+$ ion.

The mass spectra of the three molybdenum derivatives gave well-defined 9-line patterns, of close to the theoretical intensity ratio, for all ions containing both a Ga and a Mo atom. The spectra all displayed as their most intense signal the one arising from the parent ion minus two CO groups. The parent ions themselves gave signals about one-fifth as intense as the above signals.

The mass spectra of the tungsten derivatives gave well-defined 6-line patterns of expected intensity ratio for all ions containing both a Ga and a W atom. The spectrum of the nitrosyl derivative, $[MeGa$-$(N_2C_3H_3)_3]W(CO)_2NO$, displayed as its most intense signal that corresponding to parent ion stripped of two CO groups and a methyl group. The spectra of the tungsten allyl compounds displayed as their most intense signals those arising from parent ions minus two CO groups. In all three tungsten compounds the parent ion signals themselves were about two-fifths as intense as the strongest signals in the spectra. In all six spectra strong signals arising from the $[MeGa(N_2C_3H_3)_3]M^+$ ion (M = Mo or W) were again observed.

In summary, all thirteen complexes listed in Table 1 are sufficiently volatile and stable to give readily observable parent ion signals in their mass spectra. The appearance of signals due to other ions indicates fragmentation patterns which are predictable for these complexes. The intensity ratios of the individual peaks in multi-peak signals agree closely with theoretical predictions based on the percentage isotope compositions of the contributing metal atoms.

Crystal Structure of $[MeGa(N_2C_3H_3)_3]Mo(CO)_2$-$(\eta^3$-$C_3H_5)$

The present structure confirms unequivocally the tridentate chelating character of the new ligand, $[MeGa(N_2C_3H_3)_3]^-$, and warrants close comparison with the structure reported for the similar boron complex, $[HB(N_2C_3H_3)_3]Mo(CO)_2(\eta^3$-$C_4H_7)$ (19). Differences in properties of the compounds are to be expected, due primarily to the much longer mean Ga—N bond distance (1.926(8) Å) compared with the mean B—N distance of 1.545 Å. This difference leads to a greater steric crowding about the Mo atom

Can. J. Chem. Downloaded from www.nrcresearchpress.com by 210.87.254.105 on 09/05/12
For personal use only.

in the gallium complex since the 3-H atoms of the pyrazolyl groups are forced into closer proximity to the Mo atom than in the boron compound. In both structures the M—(N—N)$_2$—Mo (M = B or Ga) boat having the allyl group projecting towards it is flattened compared to the other two such boats having CO groups in close proximity (mean magnitudes of the N—[Mo—N]—N dihedral angles in the present structure are 22.5° for the unique ring and 52.4° for the other rings). The difference is more pronounced in the case of gallium as a result of the greater steric crowding mentioned above. Another noticeable effect of the bulky allyl substituent is that in both structures the shortest Mo—N bond distances are *trans* to the allyl group (2.232(3) vs. 2.309(3) and 2.328(3) Å for the gallium complex and 2.207 vs. 2.312 Å for the boron complex).

Comparison of the Mo—CO and C—O bond distances reveals that the C—O bonds are longer and the Mo—CO bonds significantly shorter in the gallium compound than in the boron compound. This reflects a more electron-rich Mo centre in the gallium complex which may result from an increase in donor strength (or a decrease in acceptor ability) of the gallium ligand over the boron ligand. The bond lengths do reflect an increase in $d\pi$–π^* back-bonding to the CO groups in the gallium complex with concomitant decreases in Mo—CO distances and increases in C—O bond lengths (Mo—CO = 1.959(6) and 1.958(4) Å for B, 1.936(5) and 1.948(5) Å for Ga; C—O = 1.151(7) and 1.150(5) Å for B, 1.162(6) and 1.166(6) Å for Ga). The effect is also reflected in the ν_{CO} vibrations in the ir spectra for the two complexes where the gallium complex exhibits ν_{CO} bands 10 cm^{-1} lower than the boron compound (see above).

The Mo—C—O groupings show a slight deviation from linearity (177.2(5) and 176.5(5)°) which most probably results from local packing forces. The geometry about the Mo atom is distorted octahedral with the η^3-allyl group occupying one of the octahedral positions as a π-donating ligand (Mo—C = 2.228(5), 2.338(5), and 2.360(5) Å). The gallium atom is in a distorted tetrahedral environment with normal Ga—N and Ga—C bond distances (2, 27–35). Other bond lengths and angles in the molecule are as expected. It is interesting that in both the boron structure (19) and the gallium structure the three allyl carbons interacting with the Mo atom occupy the same relative positions, even though in the boron compound the central allyl carbon atom bears a methyl group instead of a hydrogen atom as in the gallium complex.

Steric crowding about the Mo atom results in torsional twists about the pyrazolyl N—N bonds, particularly those *cis* to the allyl group. The Mo—[N—N]—Ga torsion angles (ideally = 0°) are 18.2(2), —18.2(2), and 5.5(2)° respectively for the N(1), N(3), and N(5) pyrazolyl rings. One of the pyrazolyl groups (that containing N(1)) is significantly non-planar (χ^2 = 9.5) while the other two are planar within experimental error. The Ga and Mo atoms are significantly displaced from all three pyrazolyl ring mean planes. The crystal structure consists of well-separated molecules of [MeGa(N$_2$-C$_3$H$_3$)$_3$]Mo(CO)$_2$(η^3-C$_3$H$_5$), the shortest intermolecular distances corresponding to normal van der Waals interactions.

Acknowledgments

We thank the National Research Council of Canada for financial support and the University of British Columbia Computing Centre for assistance. We are grateful to Mr. J. Nip for mass spectra; Mr. P. Borda for C, H, N analyses; and to Dr. S. Chan for nmr spectra.

1. D. F. Rendle, A. Storr, and J. Trotter. J. Chem. Soc. Dalton Trans. 176 (1975).
2. F. G. Herring, D. J. Patmore, and A. Storr. J. Chem. Soc. Dalton Trans. 711 (1975).
3. D. J. Patmore, D. F. Rendle, A. Storr, and J. Trotter. J. Chem. Soc. Dalton Trans. 718 (1975).
4. K. R. Breakell, D. J. Patmore, and A. Storr. J. Chem. Soc. Dalton Trans. 749 (1975).
5. H. Schmidbauer and W. Findeiss. Angew. Chem. Int. Ed. **3**, 696 (1964).
6. N. N. Greenwood and K. Wade. J. Chem. Soc. 1527 (1956).
7. R. B. King. Organometallic synthesis. Vol. 1. Academic Press, New York. 1965. p. 174.
8. M. Aresta, C. F. Nobile, and D. Petruzzelli. Inorg. Chem. **16**, 1817 (1977).
9. D. P. Tate, W. R. Knipple, and J. M. Augl. Inorg. Chem. **1**, 433 (1962).
10. P. Coppens, L. Leiserowitz, and D. Rabinovich. Acta Crystallogr. **18**, 1035 (1965).
11. W. R. Busing and H. A. Levy. Acta Crystallogr. **22**, 457 (1967).
12. D. T. Cromer and J. B. Mann. Acta Crystallogr. Sect. A, **24**, 321 (1968).
13. R. F. Stewart, E. R. Davidson, and W. T. Simpson. J. Chem. Phys. **42**, 3175 (1965).
14. D. T. Cromer and D. Liberman. J. Chem. Phys. **53**, 1891 (1970).
15. V. Schomaker and K. N. Trueblood. Acta Crystallogr. Sect. B, **24**, 63 (1969).
16. D. W. J. Cruickshank. Acta Crystallogr. **9**, 747 (1956); **9**, 754 (1956); **14**, 896 (1961).
17. R. B. King. Inorg. Chem. **5**, 2242 (1966).
18. S. Trofimenko. J. Am. Chem. Soc. **91**, 588 (1969).
19. E. M. Holt, S. L. Holt, and K. J. Watson. J. Chem. Soc. Dalton Trans. 2444 (1973).
20. M. R. Churchill, K. Gold, and C. E. Maw. Inorg. Chem. **9**, 1597 (1970).
21. A. Storr and B. S. Thomas. Can. J. Chem. **48**, 3667 (1970).
22. P. Meakin, S. Trofimenko, and J. P. Jesson. J. Am. Chem. Soc. **94**, 5677 (1972).
23. A. Davidson and W. C. Rode. Inorg. Chem. **6**, 2124 (1967).

24. J. W. FALLER and M. J. INCORVIA. Inorg. Chem. **7**, 840 (1968).
25. M. L. MADDOX, S. L. STAFFORD, and H. D. KAESZ. Adv. Organomet. Chem. **3**, 71 (1965).
26. F. A. COTTON and J. CALDERON. J. Organomet. Chem. **37**, 127 (1972).
27. D. F. RENDLE, A. STORR, and J. TROTTER. J. Chem. Soc. Dalton Trans. 2252 (1973).
28. D. F. RENDLE, A. STORR, and J. TROTTER. Can. J. Chem. **53**, 2930 (1975).
29. D. F. RENDLE, A. STORR, and J. TROTTER. Can. J. Chem. **53**, 2944 (1975).
30. S. J. RETTIG, A. STORR, and J. TROTTER. Can. J. Chem. **53**, 58 (1975).
31. R. T. BAKER, S. J. RETTIG, A. STORR, and J. TROTTER. Can. J. Chem. **54**, 343 (1976).
32. S. J. RETTIG, A. STORR, and J. TROTTER. Can. J. Chem. **53**, 753 (1975).
33. K. S. CHONG, S. J. RETTIG, A. STORR, and J. TROTTER. Can. J. Chem. **55**, 2540 (1977).
34. K. S. CHONG, S. J. RETTIG, A. STORR, and J. TROTTER. Can. J. Chem. **55**, 4166 (1977).
35. K. S. CHONG, S. J. RETTIG, A. STORR, and J. TROTTER. Can. J. Chem. **56**, 1212 (1978).

Can. J. Chem. Downloaded from www.nrcresearchpress.com by 210.87.254.105 on 09/05/12
For personal use only.

Synthèse et identification spectroscopique d'un hydroxylate-3 d'acyl-2 pyridothiazolium

D. TAVERNIER

Laboratorium voor Organische Chemie, Krijgslaan, 271-54 B-9000 Gent, Belgique

ET

J. C. JAMOULLE[1] ET C. L. LAPIÈRE

Laboratoire de Chimie pharmaceutique, U.E.Lg., 5, rue Fusch, B-4000 Liège, Belgique

Reçu le 20 janvier 1978

D. TAVERNIER, J. C. JAMOULLE et C. L. LAPIÈRE. Can. J. Chem. **56**, 2109 (1978).

Lors de la cyclisation de l'acide [(nitro-5 pyridyl-2) amino-3 pyridyl-2]mercaptoacétique, le produit principal de la réaction est constitué par l'hydroxylate-3 de {[(nitro-5 pyridyl-2) amino-3 pyridyl-2]mercaptoacétyl}-2[(nitro-5 pyridyl-2)amino]-8 pyridyl[2,1-*b*]thiazolium (**4**). Sa structure a été déterminée essentiellement par rmn du ^1H et du ^{13}C.

D. TAVERNIER, J. C. JAMOULLE, and C. L. LAPIÈRE. Can. J. Chem. **56**, 2109 (1978).

The principal product from the cyclization of {[3-(5-nitropyridine-2-yl)-amino]pyridine-2-yl}thioacetic acid is 2-{[3-nitropyridine-2-yl)amino]pyridine-2-yl}thioacetyl-8-[(5-nitropyridine-2-yl)amino]-3-oxidopyrido[2,1-*b*]thiazolium (**4**). Its structure was determined primarily by ^1H and ^{13}C nmr.

[Journal translation]

La cyclisation des acides (arylamino-3 pyridyl-2) mercaptoacétiques **1** a été étudiée dans une publication antérieure (1). En choisissant judicieusement les conditions opératoires, cette cyclisation peut être orientée vers la formation et l'isolement de composés pyridothiaziniques **2** ou de dérivés du pyridothiazolium **3**.[2]

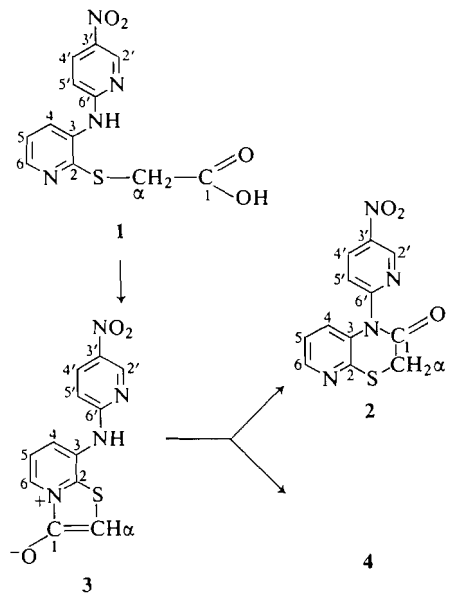

En effectuant l'opération par chauffage à reflux dans le xylène, nous isolons, d'une façon générale, le composé pyridothiazinique par extraction du résidu d'évaporation du xylène, au moyen de méthanol. Dans le cas de l'acide non substitué en α sur la chaîne mercaptoacétique, le rendement en composé pyridothiazinique est faible et le résidu insoluble dans le méthanol est important. Ce résidu peut être recristallisé du nitrobenzène, fournissant ainsi une substance à pf 265–267°C (**4**). L'analyse élémentaire donne des résultats identiques à ceux fournis précédemment par la pyridothiazine et le pyridothiazolium correspondants.

Ce produit présente cependant des caractéristiques physiques et physicochimiques qui le différencient aussi bien du produit de départ que des deux produits de cyclisation isolés antérieurement: il présente une coloration verte; il est pratiquement insoluble dans les solvants usuels; il est chromatographiquement pur et son R_f est différent de ses congénères. La ccm a été réalisée sur plaques de silica gel (Merck 60F, 254), utilisant comme phases mobiles, soit un mélange diméthylformamide–nitrobenzène (1:7), soit un mélange acide acétique – acétate d'éthyle (1:4). Le produit est déposé en solution à 70°C dans la diméthylformamide, et, avant développement, la plaque est séchée à 70°C dans une étuve ventilée; le spectre ir, en pastille de KBr, présente une bande large à 3280 et 3095 cm^{-1} et une bande à 1675 cm^{-1}. On n'observe pas de bande thiocarbonyle vers 1140 cm^{-1}, ni le trio de bandes A, B et C, caractéristique de la fonction acide de départ (3200, 2450 et 1900 cm^{-1}) (2, 3).

La substance a été soumise à la spectrométrie de

[1]Chargé de recherches au F.N.R.S. (Belgique).

[2]La numérotation utilisée est tout à fait arbitraire et s'écarte de toute règle. Elle nous facilitera cependant ultérieurement la comparaison des déplacements chimiques et des constantes de couplage pour atomes correspondants dans les différentes structures.

Can. J. Chem. Downloaded from www.nrcresearchpress.com by 210.87.254.6 on 09/05/12
For personal use only.

Can. J. Chem. Downloaded from www.nrcresearchpress.com by 210.87.254.6 on 09/05/12
For personal use only.

TABLEAU 1. Paramètres spectraux de ^1H de **1**, **3** et **4**

(*a*) Déplacements chimiques

Composé	Hydrogène 4	5	6	2′	4′	5′	NH	α
1	7.76	7.22	8.35	8.91	8.31	6.82	9.79	3.97
4 Fragment A	7.76	7.20	8.34	8.91	8.29	6.82	9.79	4.81
Fragment T	8.69	7.79	8.87	9.03	8.45	7.24	10.70	—
3	8.29	7.67	8.73	9.02	8.43	7.18	10.31	5.41

(*b*) Constantes de couplages des protons en Hz

Composé	*J* 4,5	4,6	5,6	2′,4′	4′,5′
1	7.9	≃1.5	4.7	2.7	9.25
4 Fragment A	7.7	≃1.5	4.7	[a]	[a]
Fragment T	7.5	≃1	6.25	[a]	[a]
3	7.5	≃1	6.5	[a]	[a]

NOTE: Déplacements chimiques en δ par rapport au TMS. Solvant DMSO-d_6. Les spectres ont été enregistrés sur un appareil Varian HR-300 MHz, à la température ambiante, sauf pour 3 (≃60°C). Chacun des quatre cycles pyridiniques porte trois hydrogènes, et l'appartenance de trois hydrogènes à un même cycle a été déduite d'expériences INDOR.

[a]Les constantes de couplage des protons du cycle nitropyridinique sont les mêmes pour **1**, **3** et **4**.

masse afin d'obtenir le poids moléculaire de ce composé. Les informations fournies par cette technique ne sont pas utilisables, car, comme le révèle l'étude thermogravimétrique, le produit se pyrolyse à partir de 150°C avec formation de mercapto-2 nitro-5′ dipyridylamine-3,2′.

Nous nous sommes adressés ensuite à la rmn. En rmn du ^1H il est possible d'attribuer tous les pics enregistrés et de déterminer les constantes de couplage. L'examen spectrométrique indique que **4** contient 12 protons aromatiques différents permettant de conclure à la présence de quatre cycles pyridiniques disubstitués.

On peut reconnaître d'une part deux pyridines-2,3 disubstituées et deux pyridines-2,5 disubstituées. On observe également deux pics différents échangeables par l'eau lourde et attribuables aux hydrogènes mobiles des fonctions diarylamines ainsi que deux protons appartenant à un CH_2 aliphatique déblindé.

Les paramètres spectraux de **1**, **3** et **4** rassemblés dans le tableau 1 mettant bien en évidence que pour les pyridines-2,3 disubstituées, les déplacements chimiques de trois protons pyridiniques présentent des valeurs analogues à celles enregistrées pour le pyridothiazolium **3** tandis que les déplacements chimiques des trois autres protons pyridiniques présentent des valeurs voisines de celles enregistrées pour l'acide de départ. Les valeurs relevées pour cet acide ne présentent rien d'exceptionnel. Notons toutefois, dans le noyau pyridine porteur d'un groupement nitro, l'accroissement du couplage $J_{H_4',H_5'} = 9.25$ Hz par rapport à la pyridine elle-même (7.62 Hz) (4, 5). Cet accroissement est dû au groupement nitro (6, 7). La différence assez marquée des couplages $^3J_{H_5,H_4}$ et $^3J_{H_5,H_6}$ est typique des dérivés pyridiniques.

Les données rmn du noyau pyridinique-2,5 disubstitué pour les composés **4** et **3** sont quasi identiques.

Quand on examine les données spectroscopiques de la pyridine-2,3 disubstituée du pyridothiazolium **3**, on constate un déplacement chimique important des protons (surtout H_4) vers les champs faibles. Quant aux constantes de couplage, $^3J_{H_6,H_5}$ augmente sensiblement tandis que $^4J_{H_6,H_4}$ (8, 9) décroit. Ces variations par rapport au produit de départ peuvent être expliquées par une charge positive sur l'azote pyridinique provoquée par une protonation ou une quaternisation de cet azote. Un phénomène analogue se présente dans **4** pour une des deux pyridines-2,3 disubstitutuées que l'on trouve dans ce composé.

En fonction de ces observations, il est vraisemblable qu'il s'agit de ce qu'on pourrait appeler abusivement un "dimère" asymétrique. La molécule contiendrait une structure pyridothiazolium à côté d'un enchaînement pyridylmercaptoacétyle. Il reste à trouver le mode d'enchaînement des deux "monomères" et leur point d'attache.

En spectrométrie ir, comme nous l'avons déjà fait remarquer, on note une bande νC=O à 1675 cm^{-1} moins intense cependant que celle observée dans la pyridothiazinone **2**. Le trio de bandes A, B et C caractéristique de la fonction acide du dérivé pyridyl-

TABLEAU 2. Paramètres spectraux de ^{13}C de **1** et **4**[a]

Composé		Carbone											
		2	3	4	5	6	2′	3′	4′	5′	6′	α	1
1		154.7	137.0	134.7	120.3	147.1	146.4	132.3	133.3	109.1	160.7	31.96	171.04
4	Fragment A	155.2	136.9	134.4	120.0	146.8	146.2	132.3	133.2	108.9	160.6	37.5	185.7
	Fragment T	155.8*	138.5*	128.5	120.7	133.7†	145.3	134.8	131.0†	111.4	158.8	94.9	170.6[b]

NOTE: Solvant DMSO-d_6. Température 35°C pour **1**, 80°C pour **4**. Les spectres ont été enregistrés sur un appareil Varian XL 100. Déplacements chimiques en δ par rapport au TMS. Le spectre de **1**, totalement couplé avec les hydrogènes, a demandé 103.881 transients, le temps d'acquisition fut 0.533 s, la largeur du spectre était 7500 Hz. Le spectre de **4**, avec couplage partiel des hydrogènes, demandait 52.861 transients dans les mêmes conditions.
[a]Les attributions des carbones marqués* (non fixés à un hydrogène) ou † (carbones fixés à un hydrogène) peuvent être inversés.
[b]Ce carbone ne fut observé qu'après l'addition d'acétylacétonate de chrome(III) et l'emploi d'un champs faible d'irradiation des hydrogènes.

mercaptoacétique est absent. Cette fonction acide est donc engagée dans une liaison où le carbonyle subsiste et d'autre part l'enchaînement entre les deux fragments du "dimère" se fait en toute logique sur le carbone α du thiazolium étant donné que seuls les produits **1** possédant cette position libre donnent lieu à la formation d'un tel produit secondaire. Nous pouvons donc dès à présent proposer la structure **4** pour le JJC 164.

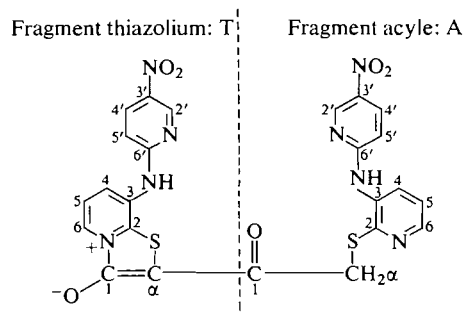

4

La divergence entre le déplacement chimique des protons de **3** et de **4** pour ce qui est de la partie pyridinique *ortho* disubstituée T, serait expliquable par une mésomérie du type **5**, **6** où la délocalisation

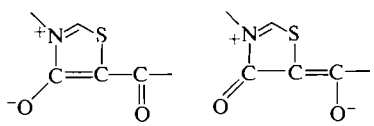

5 **6**

de la charge négative sur l'oxygène du groupe alkyle accentue la charge positive sur l'azote. Ceci peut être responsable d'un déplacement vers les champs faibles, plus prononcé pour les protons de la pyridine-2,3 disubstituée T de **4** que pour les protons de la pyridine-2,3 disubstituée de **3** (10–12).

D'un point de vue chimique, la formation de ce composé peut être considéré comme une condensation apparentée à celle de Friedel et Crafts. Cette condensation se fait entre deux molécules de pyridothiazolium **3**. Il est en effet possible de préparer **4** en mettant en oeuvre le pyridothiazolium **3** seul.

Comme l'instabilité thermique du produit rendait impossible la détermination du poids moléculaire par spectrométrie de masse, il nous a paru prudent de corroborer la structure proposée par spectrométrie de rmn du ^{13}C (tableau 2). Nous trouvons comme prévu 24 carbones dont 11 ne portent pas d'hydrogène. Si ce n'est le pic à 185.7 ppm attribuable à un groupement carbonyle, on constate une coïncidence totale d'une part entre les déplacements chimiques des carbones de **1** et de 11 des carbones de **4** et d'autre part, entre les couplages résiduels de ces 11 carbones en irradiant "off-resonance" les hydrogènes de **1** et **4**. Il est de ce fait intéressant d'attribuer les résonances de l'acide **1** et de transférer ensuite ces attributions à **4**. Les déplacements chimiques et tous les couplages $J_{^{13}C,H}$ de la pyridine sont connus (13, 14). Une première classification ou attribution partielle est possible en admettant une additivité des effets de substituant sur les déplacements chimiques, semblables en série benzénique et en série pyridinique (15*b*), $-NO_2$ (15*a*), —NHR (15*a*), $-SCH_3$ (16).

L'attribution non équivoque est possible grâce à un spectre ^{13}C pris sans découplage des hydrogènes. On sait que les substituants influencent les couplages $J_{^{13}C,H}$ (17–20). Une étude très poussée a été publiée récemment (21). Nous retiendrons de ces travaux qu'un substituant électronégatif diminue le couplage $^3J_{^{13}C,H}$ dans l'unité C=C(X)—C—H et que le couplage $^3J_{^{13}C,H}$ dans l'unité X—C=C—C—H est plus grande pour X = NO_2 que pour X = NH_2. L'application de ces critères permet de discriminer C(2′) de C(6), C(4) de C(4′) et C(3) de C(3′). C(2) est identifié grâce à un couplage triplet avec les deux hydrogènes du groupe —S—CH_2—CO—. Nous n'avons pas observé de couplage avec le proton fixé sur l'azote, ni avec l'azote.

Il n'a pas été possible d'enregistrer un spectre satisfaisant de **4** totalement couplé avec les hydrogènes, la perte d'effet nOe et la solubilité réduite de **4** dépassaient les possibilités du spectromètre. Néanmoins, les couplages résiduels observés en irradiant "off-resonance" les hydrogènes, laissent déjà percer les plus importants des $^nJ_{^{13}C,H}$. Il est

Can. J. Chem. Downloaded from www.nrcresearchpress.com by 210.87.254.6 on 09/05/12
For personal use only.

ainsi possible d'attribuer avec confiance les carbones 5′, 5, 2′, 6′ du fragment de **4T**. Il reste encore à identifier trois carbones directement liés à un atome d'hydrogène, dont seulement un appartient à un cycle nitropyridinique. Il faut constater que les déplacements chimiques de ces carbones protonés se trouvent en moyenne vers les champs forts en comparaison avec **1**. Il est connu que la protonation de la pyridine a pour résultat des changements importants dans les déplacements chimiques, un effet paramagnétique étant observé pour C(3) en C(4), un effet diamagnétique pour C(2) (22, 23). La quaternisation de la pyridine entraîne des changements semblables (24, 25).

Parmi les cinq carbones non identifiés non porteurs d'hydrogène, il y en a deux qui se trouvent en dehors de la région normale des carbones aromatiques l'un à $\delta = 95$, l'autre à $\delta = 170$. L'analogie avec la forme énolique de l'acétylacétone et ses sels métalliques est frappante (15*c* et *d*). L'observation de ces deux fréquences nous fournit donc la preuve la plus directe du cycle pyridothiazolium.

1. J. C. JAMOULLE et C. L. LAPIÈRE. Bull. Soc. Chim. Fr. **34**, 939 (1976).
2. J. C. JAMOULLE. Thèse de doctorat en Sciences pharmaceutiques, Liège. 1977.
3. D. HADZI. Microwave Spectrosc. **14**, 435 (1965).
4. R. L. LICHTER et J. D. ROBERTS. J. Am. Chem. Soc. **98**, 5218 (1971).
5. H. J. BERNSTEIN, J. A. POPLE et W. G. SCHNEIDER. Can. J. Chem. **35**, 1487 (1957).
6. P. F. COX. J. Am. Chem. Soc. **85**, 380 (1963).
7. W. BRÜGEL. Z. Elektrochem. **66**, 159 (1962).
8. J. B. MERRY et J. H. GOLDSTEIN. J. Am. Chem. Soc. **88**, 5560 (1966).
9. T. J. BATTERHAM. NMR spectra of simple heterocycles. Wiley-Interscience, New York, NY. 1973. Chapt. 2, I.
10. T. SCHAEFER et W. G. SCHNEIDER. Can. J. Chem. **41**, 966 (1963).
11. S. CASTELLANO, H. GUNTHER et S. EBERSOLE. J. Phys. Chem. **69**, 4166 (1965).
12. H. GÜNTHER et S. CASTELLANO. Ber. Bunsenges. Phys. Chem. **70**, 913 (1966).
13. P. C. LAUTERBUR. J. Chem. Phys. **43**, 360 (1965).
14. M. HANSEN et H. J. JAKOBSEN. J. Magn. Reson. **10**, 74 (1973).
15. J. B. STOTHERS. Carbon-13 NMR spectroscopy. Academic Press, New York, NY. 1972. (*a*) p. 197; (*b*) p. 252; (*c*) p. 215; (*d*) p. 288.
16. G. W. BUCHANAN, R. ZAMORA et D. E. CLARKE. Can. J. Chem. **52**, 3895 (1974).
17. A. R. TARPLEY et J. H. GOLDSTEIN. J. Phys. Chem. **76**, 515 (1972).
18. A. R. TARPLEY et J. H. GOLDSTEIN. J. Mol. Spectrosc. **37**, 432 (1971); **39**, 275 (1971).
19. Y. TAKEUCHI et K. DENNIS. J. Am. Chem. Soc. **96**, 3657 (1974).
20. C.-J. CHANG. J. Org. Chem. **41**, 1881 (1976).
21. L. ERNST, V. WRAY, V. A. CHERTKOV et N. M. SERGEYEV. J. Magn. Reson. **25**, 123 (1977).
22. R. J. PUGMIRE et D. M. GRANT. J. Am. Chem. Soc. **90**, 697 (1968).
23. H. H. MANTSCH et I. C. P. SMITH. Can. J. Chem. **51**, 1384 (1973).
24. J. A. LEPOIVRE, R. A. DOMMISSE et F. C. ALDERWEIRELDT. Org. Magn. Reson. **7**, 422 (1975).
25. P. VAN DE WEIJER et C. MOHAN. Org. Magn. Reson. **9**, 53 (1977).

Can. J. Chem. Downloaded from www.nrcresearchpress.com by 210.87.254.6 on 09/05/12
For personal use only.

Metabolites of bird's nest fungi. Part 9.[1] Diterpenoid metabolites of *Cyathus africanus* Brodie

WILLIAM A. AYER, TAKASHI YOSHIDA, AND DIRK M. J. VAN SCHIE
Department of Chemistry, University of Alberta, Edmonton, Alta., Canada T6G 2G2

Received March 13, 1978

WILLIAM A. AYER, TAKASHI YOSHIDA, and DIRK M. J. VAN SCHIE. Can. J. Chem. **56**, 2113 (1978).

The diterpenoid metabolites produced when the fungus *Cyathus africanus* Brodie (Nidulariaceae) is grown in liquid culture have been examined. The known compounds cyathin A_3 (**1**) and allocyathin B_3 (**2**) were isolated along with four new diterpenoids which have been named cyafrin A_4, cyafrin B_4, allocyafrin B_4, and cyafrin A_5. The structures of these substances have been determined by chemical and physical methods to be **3***a*, **10***a*, **12***a*, and **15***a*, respectively. Cyafrin A_4 (**3***a*), allocyafrin B_4 (**12***a*), and cyafrin A_5 (**15***a*) have been correlated with cyathin A_3 by chemical transformations. The absolute stereochemistry of cyathin A_3 has been confirmed by the exciton chirality method.

WILLIAM A. AYER, TAKASHI YOSHIDA et DIRK M. J. VAN SCHIE. Can. J. Chem. **56**, 2113 (1978).

On a étudié les métabolites diterpénoïdes qui sont produits lorsque des champignons *Cyathus africanus* Brodie (nidulariaceae) croissent dans des cultures liquides. On a pu isoler les composés connus cyathine A_3 (**1**) et allocyathine B_3 (**2**) de même que quatre nouveaux diterpénoïdes auxquels on a attribué les noms cyafrine A_4, cyafrine B_4, allocyafrine B_4 et cyafrine A_5. On a déterminé, par des méthodes chimiques et physiques, que les structures de ces composés correspondent respectivement à **3***a*, **10***a*, **12***a* et **15***a*. Faisant appel à des transformations chimiques, on a établi une corrélation entre la cyafrine A_4 (**3***a*), l'allocyafrine B_4 (**12***a*) et la cyafrine A_5 (**15***a*) avec la cyathine A_3. On a confirmé la stéréochimie absolue de la cyathine A_3 par la méthode exciton de la chiralité.

[Traduit par le journal]

In 1966, D. Hocking of this university brought from Tanzania two specimens of a bird's nest fungus which he had discovered growing on dead twigs on Mount Kilimanjaro at an altitude of about 8000 ft (2). H. J. Brodie determined this to be a previously unrecognized species of the genus *Cyathus* and named it *Cyathus africanus* (2, 3). We now wish to report on some of the metabolites formed when this species is grown in liquid culture. The crude metabolites were isolated by ethyl acetate extraction of the culture broth obtained after the fungus had grown in still culture on Brodie medium (ref. 3, p. 36) for 30 days. The crude material was separated into its components by column chromatography over silicic acid followed by preparative thin-layer chromatography (ptlc) over silica gel. In this way six different components, A (least polar), B, C, D, E, and F (most polar) were isolated.

Components A and B were shown to be the diterpenoids cyathin A_3 (**1**) (4) and allocyathin B_3 (**2**) (4), respectively, by comparison with authentic samples. These compounds have previously been isolated from *Cyathus helenae* (4, 5). The two other *Cyathus* species which have been investigated, *C. bulleri* (6) and *C. intermedius* (7), have not provided diterpenoids of this or any other type. Cyathin A_3 (**1**) is the most abundant of the metabolites of *C. africanus*, occurring to the extent of about 30 mg/ℓ of culture broth. The next most abundant metabolite is component E, occurring to the extent of about 6 mg/ℓ of culture broth.

Component E was obtained as colorless needles, mp 200–201°C, of molecular formula[2] $C_{20}H_{30}O_4$. This compound has not been isolated previously and has been given the trivial name[3] cyafrin A_4.

Structure **3***a*, which is in tautomeric equilibrium with its internal hemiacetal form **4***a*, is assigned to cyafrin A_4. The solid phase infrared spectrum of cyafrin A_4 does not show carbonyl absorption, indi-

[1]For Part 8, see ref. 1.

[2]Because of the small quantities of pure material available, most molecular formulas have been established by high resolution mass spectrometry (hrms). Eventual correlation with compounds of established molecular formula validates the deductions made in this manner.

[3]The following system of trivial nomenclature, similar to that used for the cyathins (5), has been adopted for those diterpenoid metabolites of *C. africanus* which are not found in *C. helenae*: a cyafrin is a C_{20} compound; cyafrins with 30 hydrogens belong to the A series, those with 28 hydrogens to the B series; the subscript after the letter denotes the number of oxygens present. Isomers of the first isolated cyafrins are placed in the allo series, e.g., both cyafrin B_4 and allocyafrin B_4 are $C_{20}H_{28}O_4$.

Can. J. Chem. Downloaded from www.nrcresearchpress.com by 210.87.254.105 on 09/05/12
For personal use only.

Can. J. Chem. Downloaded from www.nrcresearchpress.com by 210.87.254.105 on 09/05/12
For personal use only.

cating that the compound crystallizes in the hemiacetal form **4***a*. The solution ($CHCl_3$) spectrum, however, shows a broad carbonyl absorption band of medium intensity centered at 1680 cm^{-1} indicating the presence of some of the hydroxyketone tautomer **3***a*. Acetylation of cyafrin A_4 yields a tri-*O*-acetyl derivative **3***b*, which shows absorption for the α,β-unsaturated ketone at 1660 cm^{-1}. The ^{1}Hmr spectrum of **3***b* is strikingly similar to that of *O*,*O*-diacetylcyathin A_3 (**1***b*) with the exception that the spectrum of **3***b* shows an extra acetyl methyl signal and an extra one proton signal at δ 4.89 (apparent triplet, splitting 8 Hz) which may be assigned to a proton geminal to the extra acetoxyl function. This indicated that the extra hydroxyl group in cyafrin A_4 is located at C-1, C-2, C-7, or C-8. C-10 was excluded since the multiplicity of the signal for the proton on C-11 (δ 5.33, apparent triplet, splitting 6.5 Hz) is the same as in cyathin A_3.

To protect the hydroxyl groups on C-11 and C-15 while we explored the environment of the extra hydroxyl function, cyafrin A_4 was treated with 2,2-dimethoxypropane in the presence of *p*-toluenesulfonic acid to give the crystalline acetonide **5***a*. The ^{1}Hmr spectrum of **5***a* is very similar to that of cyathin A_3 acetonide, with the exception that there is a one proton signal at δ 3.88 (apparent triplet, splitting 7 Hz) for the hydrogen geminal to the hydroxyl group. Double irradiation experiments show that this hydrogen is coupled to two hydrogens of chemical shift δ 2.3–2.5. The chemical shift of the latter two hydrogens suggested that they are allylic and thus located at C-2 (the allylic hydrogens of cyclopentene resonate at δ 2.28 (8)) and that the 'extra' hydroxyl group is therefore located at C-1. Oxidation of the acetonide **5***a* with Jones' reagent provided the ketone **6** which shows carbonyl absorption at 1746 cm^{-1}, confirming that the hydroxyl group is in the five-membered ring. The ^{1}Hmr spectrum of **6** shows a new two proton AB quartet at δ 2.99 (J = 19 Hz) attributed to the protons on C-2 which are now both allylic and α to a carbonyl.

To firmly establish the proposed structure we set out to directly correlate cyafrin A_4 with allocyathin B_3 (**2**) or one of its derivatives. Mesylation of the acetonide **5***a* provided the mesylate **5***b*. Attempts to eliminate methanesulfonic acid from **5***b* under a variety of conditions (refluxing lutidine, 1,5-diazabicyclo[5.4.0]undec-5-ene (DBU) in refluxing tetrahydrofuran, DBU in refluxing benzene, potassium *tert*-butoxide in dimethyl sulfoxide) lead to recovery of the mesylate **5***b*. However, treatment of **5***b* with DBU in refluxing dioxane lead to the formation of an isomeric mesylate which is assigned structure **7**, in which the ring C double bond has migrated to the

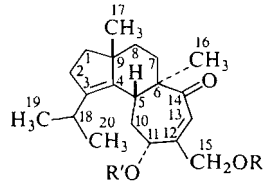

1

a R = R′ = H
b R = R′ = Ac
c R = Ac; R′ = H
d R = Ac; R′ = COPh
e R = Ac; R′ = CO_pBrPh

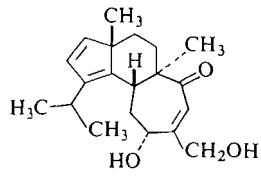

2

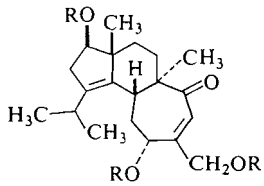

3

a R = H
b R = Ac

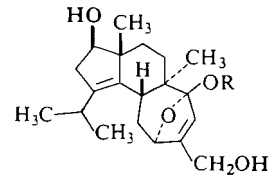

4

a R = H
b R = CH_3

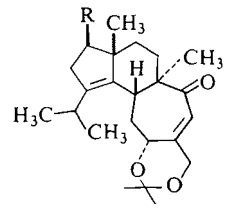

5

a R = OH
b R = OSO_2CH_3
c R = H
d R = OCOPh

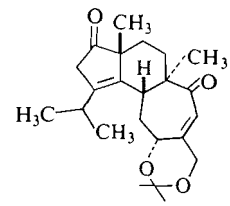

6

β,γ-position. Compound **7** shows carbonyl absorption at 1708 cm^{-1}, no uv absorption for an α,β-unsaturated ketone (**5***a* shows λ_{max} 236 nm (6300)) and a ^{1}Hmr spectrum (see Experimental) consistent with structure **7**. Since it is often possible to replace the mesyloxy group with a hydrogen by reduction with lithium aluminum hydride (LAH), the mesylate **5***b* was treated with methanolic hydrogen chloride which removes the acetonide group and then forms the internal methyl acetal **8**. Reduction of **8** with LAH in tetrahydrofuran led to sulfur–oxygen cleavage to give cyafrin A_4 methyl acetal (**4***b*), identical with a sample prepared by treating cyafrin A_4 (**3***a* ⇄ **4***a*) with methanolic HCl.

Correlation was finally achieved by treatment of *O*-mesylcyafrin A_4 methyl acetal (**8**) for 45 h with DBU in refluxing toluene to give allocyathin B_3 methyl acetal (**9**), identical with an authentic sample (**4**). This correlation confirms the structure and stereochemistry (relative and absolute) of cyafrin A_4 (**3***a* ⇄ **4***a*) except for the stereochemistry of the hydroxyl group at C-1.

Can. J. Chem. Downloaded from www.nrcresearchpress.com by 210.87.254.105 on 09/05/12
For personal use only.

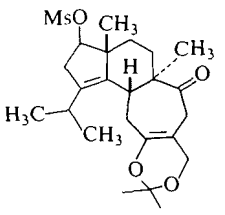

7

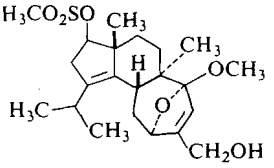

8

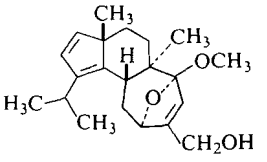

9

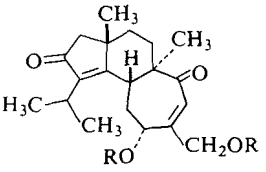

10
a R = H
b R = Ac

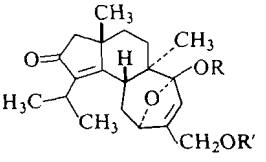

11
a R = R′ = H
b R = CH_3; R′ = H
c R = CH_3; R′ = Ac

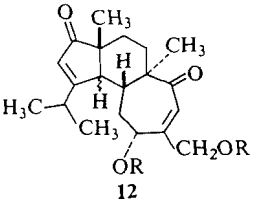

12
a R = H
b R = Ac

The stereochemistry at C-1 was first assigned by ^{1}Hmr spectroscopy using Wenkert's pyridine shift method for determining the dihedral angle between a hydroxyl group and a vicinal methyl group (9). For this purpose the ^{1}Hmr spectra of cyafrin A_4 acetonide (**5***a*) and cyathin A_3 acetonide were recorded in pyridine and in $CDCl_3$. In $CDCl_3$ the methyl at C-9 in cyathin A_3 acetonide appears at δ 1.06 and C-6 methyl at δ 1.10. In pyridine the C-9 methyl is at δ 1.06 and the C-6 methyl at δ 1.18 (C-6 methyl displaced to lower field by contact shift of pyridine with C-14 carbonyl, the spectrum in benzene shows the same shift of the C-6 methyl). Cyafrin A_4 acetonide in $CDCl_3$ shows the C-9 methyl at δ 1.09 and the C-6 methyl at δ 1.00, in pyridine the C-6 methyl appears at δ 1.21 and the C-9 methyl at δ 1.30, thus Δ_{py} for the C-9 methyl is −0.21 ppm, indicative (9) of a *cis* relationship between the C-1 hydroxyl group and the C-9 methyl. Application of Brewster's benzoate rule (10) indicates ($[M]_D$**5***d* − $[M]_D$**5***a* = −62.7) that C-1 has the *R* configuration and thus the hydroxyl group is β (i.e., *cis* to the C-9 methyl). The stereochemistry at C-1 may also be assigned by application of ^{13}Cmr spectroscopy.[4]

Component C, present to the extent of about 4 mg/ℓ of culture broth, has the molecular formula $C_{20}H_{28}O_4$ and thus is named cyafrin B_4. Structure **10***a* ⇄ **11***a* is tentatively assigned to cyafrin B_4 on the following grounds. Acetylation affords an *O*,*O*-diacetyl derivative (**10***b*) the ^{1}Hmr spectrum of which shows appropriate signals for the hydrogens on C-11, C-13, and C-15, as well as signals for the four methyl groups. In addition, a two proton singlet at δ 2.21 is assigned to the C-1 methylene protons. The ir spectrum shows carbonyl absorption at 1695 cm^{-1} and uv absorption at 241 nm which was at first attributed to the ring C unsaturated ketone. However, treatment with methanolic HCl gave a methyl acetal (**11***b*) which also showed carbonyl absorption at 1690 cm^{-1} and uv absorption at 242 nm (ε 13 900) indicating the presence of an α,β-unsaturated keto group in the acetal **11***b*. Both the acetal **11***b* and its *O*-acetyl derivative **11***c* showed a two-proton singlet near δ 2.15 attributable to the C-1 methylene group and the other features of the spectra are consistent with the proposed structure. Attempts to correlate cyafrin B_4 with either cyathin A_3 (**1***a*) or allocyathin B_3 (**2**) via the tosylhydrazone of the methyl acetal **11***b* or by reduction–dehydration of the acetyl derivative **11***c* were unsuccessful, and were abandoned when our supply of cyafrin B_4 was exhausted.

Component D, separated from cyafrin B_4 by preparative tlc was present to the extent of only ca. 0.2 mg/ℓ of broth. High resolution mass spectrometry indicates that this component is isomeric with cyafrin B_4 ($C_{20}H_{28}O_4$) and it is thus named allocyafrin B_4. Structure **12***a* ⇄ **13***a* is assigned to this metabolite. Acetylation provides *O*,*O*-diacetylallocyafrin B_4 (**12***b*), the ^{1}Hmr spectrum of which shows, in addition to the expected methyl signals and signals for the ring C functionality, a singlet at δ 6.00 assigned to the proton on C-2. The uv spectrum of the methyl acetal **13***b* shows a maximum at 235 nm indicative of the ring A unsaturated ketone. This functionality also gives rise to ir absorption at 1700 and 1600 cm^{-1} in **13***b*. Treatment of the acetonide of dehydrocyafrin A_4 (**6**) with methanolic HCl brought about migration of the double bond and cleavage of the acetonide to give allocyafrin B_4 methyl acetal (**13***b*), providing strong support for the structural assignment. The stereochemistry at C-4 has not been established, although we note that 5α-androst-15-en-17-one (**14**) is stable to dilute acid (11), and thus tend to favor a *trans*-AB ring juncture in allocyafrin B_4.

The mother liquors from crystallization of cyafrin A_4 deposited crystals which proved to be co-crystals of cyafrin A_4 and a compound $C_{20}H_{30}O_5$ (component F) which we have called cyafrin A_5. Separation of the two was achieved by ptlc using a solvent system of chloroform–acetonitrile (all solvent systems

[4]Chemical shift assignments for the various cyathins and cyafrin A_4 have been made and are the subject of a forthcoming paper; Can. J. Chem. In press.

Can. J. Chem. Downloaded from www.nrcresearchpress.com by 210.87.254.105 on 09/05/12
For personal use only.

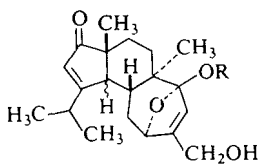

13
a R = H
b R = CH_3

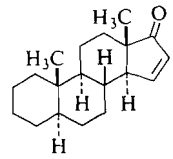

14

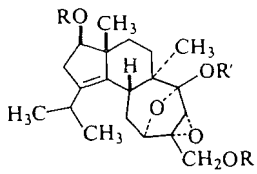

15
a R = R′ = H
b R = Ac; R′ = H
c R = R′ = Ac

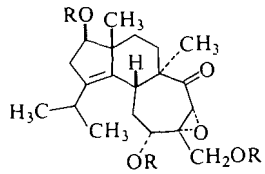

16
a R = H
b R = Ac

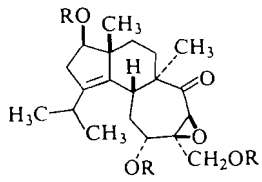

17
a R = H
b R = Ac

containing protic solvents failed to separate the two). Cyafrin A_5 is assigned structure **15***a* on the basis of the following observations. The infrared spectrum, both in the solid state and in solution, does not show carbonyl absorption, indicating that cyafrin A_5 exists mainly in the hemiacetal form **15***a*, with little contribution from the hydroxy ketone form **16***a*. The ^{13}Cmr spectrum does not show carbonyl carbon absorption and reveals the presence of only two olefinic carbons, at δ 138.0 and 136.5, shifts similar to those for C-3 and C-4 (δ 136.7 and 136.3) in cyafrin A_4 methyl ketal (**4***b*). Acetylation of **15***a* under mild conditions (acetic anhydride – pyridine, room temperature) gives the diacetyl derivative **15***b*, which again shows no ketonic carbonyl absorption, but does show hydroxyl absorption. The ^{1}Hmr spectrum of **15***b* shows the expected methyl signals and, in the lower field region, an AB doublet of doublets for the C-15 hydrogens at δ 4.48, a triplet for the C-1 hydrogen at δ 4.90, a multiplet at δ 4.29 for the C-11 hydrogen, and a singlet at δ 3.68 assigned to the C-13 hydrogen. The presence of the epoxide at C-12 and C-13 was first suggested by the observation that in the ^{13}Cmr spectrum of **15***a* the olefinic signals usually associated with these two carbons are replaced by two new signals in the region δ 55–65. When cyafrin A_5 was acetylated in the presence of 4-dimethylaminopyridine (12) a mixture of two triacetyl derivatives, **15***c* and **16***b*, was obtained. The triacetyl derivative **15***c* shows only ester carbonyl absorption (1750 cm^{-1}), whereas the triacetate of the hydroxy ketone form shows, besides ester absorption (1745 cm^{-1}), ketonic carbonyl absorption at 1690 cm^{-1}.

To confirm the structural assignment, cyafrin A_4 (**3***a*) was treated with an alkaline solution of hydrogen peroxide in methanol. The product was a mixture of two crystalline epoxides, the major product being identical with cyafrin A_5. The minor product is the diastereoisomeric epoxide **17***a*, which exists mainly in the hydroxy ketone form (ir absorption at 1710 cm^{-1}). Acetylation of **17***a* provides **17***b*, the triacetyl derivative of the hydroxy ketone form (ir absorption at 1738 and 1710 cm^{-1}).

The assignment of the stereochemistry of the epoxide ring in cyafrin A_5 rests on two pieces of evidence. In cyafrin A_5, the internal hemiacetal form **15***a* is favored over the hydroxy ketone tautomer **16***a*, whereas in the isomeric β-epoxide **17***a* the hydroxy ketone form is favored. Inspection of molecular models reveals that in the hemiacetal form of the β-epoxide there is a serious nonbonded interaction between the oxirane oxygen and the β-hydrogen at C-5 (see **18**), whereas the hydroxy ketone may adopt the strain-free cycloheptanone chair form **19**. In the α-epoxide there appear to be no serious nonbonded interactions in the hemiacetal form **20**, whereas in the hydroxy ketone cycloheptanone chair

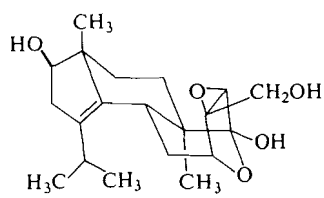

18

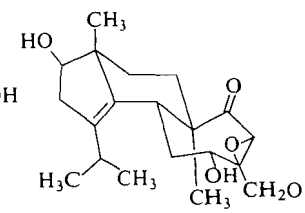

19

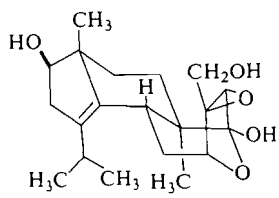

20

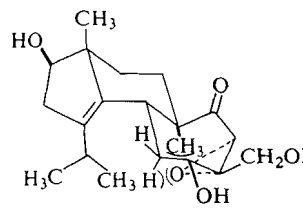

21

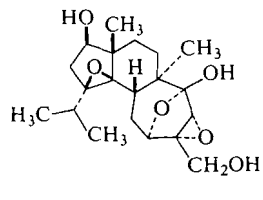

22

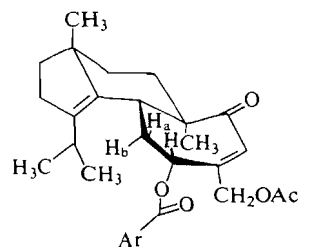

23

Can. J. Chem. Downloaded from www.nrcresearchpress.com by 210.87.254.105 on 09/05/12
For personal use only.

form **21** the oxirane oxygen is close to the methyl at C-6 and to one of the hydrogens on C-10. The second piece of evidence is that epoxidation of both double bonds in cyafrin A_4 (**3***a* ⇄ **4***a*) with *m*-chloroperbenzoic acid gives a diepoxide **22**, identical with the diepoxide obtained when cyafrin A_5 is treated with *m*-chloroperbenzoic acid. It has previously been established (1) that peracid epoxidation of the C-3, C-4 double bond in the cyathins results in the formation of the β-3,4-epoxide. It has been shown that peracid oxidation of allylic alcohols results in an epoxide in which the epoxide oxygen is *cis* to the allylic hydroxyl (13). If the assumption is made that the hydroxyl group at C-11 directs epoxidation of the C-12,C-13 double bond, then the α-12,13-epoxide will be formed from cyafrin A_4. We conclude that the stereochemistry of the epoxide oxygen in cyafrin A_5 is most likely that depicted in **15** and **16**.

The absolute configuration of the cyathins was assigned on the basis of X-ray diffraction studies on the internal hemiacetal form of cyathin A_3 (**1***a*) using the anomalous dispersion resulting from the oxygen atoms.[5] Since the *C. africanus* extracts provided us with a substantial quantity of cyathin A_3 (**1***a*) we have applied the exciton chirality rule (14) to verify this assignment. Since we wished to investigate the dipole–dipole interaction between the ring C enone and a benzoyloxy group at C-11, it was necessary to protect the C-15 hydroxyl group before benzoylation of the C-11 hydroxyl. Treatment of cyathin A_3 (**1***a*) for a short time with a limited amount of acetic anhydride – pyridine in methylene chloride gave the C-15 monoacetyl derivative **1***c*. Benzoylation (benzoyl chloride – pyridine) afforded the C-11 benzoate **1***d* and treatment of **1***c* with *p*-bromobenzoyl chloride in the presence of 4-dimethylaminopyridine (12) furnished the *p*-bromobenzoate **1***e*. In both the benzoate **1***d* and the *p*-bromobenzoate **1***e* the C-11 proton appears as an apparent triplet, splitting 7 Hz. If we make the reasonable assumption that C-11, C-12, C-13, C-14, and C-6 are in the same plane, the coupling constants indicate that ring C adopts the conformation illustrated in **23**, in which the dihedral angle between the C-11 hydrogen and C-10 hydrogen *a* approaches ~20–30°, and the C-11 H, C-10 H_b dihedral angle is 150–160°. The positive Cotton effect (**1***d*, 236 nm; **1***e*, 247 nm) indicates a positive chirality between the axis of the two electric dipole transition moments (14), in agreement with the absolute configuration illustrated in **23**, and thus in **1***d* and **1***e*.

Experimental

High resolution mass spectra were recorded on an A.E.I. MS-50 mass spectrometer coupled to a DS 50 computer. Infrared spectra were recorded on a Unicam SP 1000 or a Nicolet 7199 FT spectrometer. Specific rotations at the D line were determined using a Perkin-Elmer 141 automatic polarimeter and circular dichroism (cd) spectra on a Jasco model SS-20-2 spectropolarimeter. Nuclear magnetic resonance spectra were determined on a Varian HA-100 spectrometer (^{1}Hmr) interfaced to a Digilab FTS/NMR-3 data system and on a Bruker HFX-90 spectrometer (^{13}Cmr), with TMS as internal standard.

Preparative tlc (ptlc) was carried out on 0.75 mm layers of silica gel G (W. Merck, Darmstadt) containing 1% electronic phosphor (General Electric, Cleveland). The solvent systems used were: *A*, Skellysolve B – acetone (3:1); *B*, benzene – acetone – acetic acid (75:25:1); *C*, chloroform–acetonitrile (3:2); *D*, benzene – methanol – acetic acid (18:2:1). Skellysolve B refers to Skelly Oil Company light petroleum, bp 62–70°C. Melting points were recorded on a hot-stage Fisher-Johns apparatus and are uncorrected.

Growth of Cyathus africanus *Brodie*

Slant tubes of *Cyathus africanus* Brodie (strain 66120) were obtained from Prof. H. J. Brodie. The fungus was grown in liquid culture on Brodie medium (3) and the metabolites were isolated as described previously for *C. bulleri* (6). The yield of metabolites was about 0.2 g per litre of culture broth.

Isolation of Metabolites

The crude metabolites (2.7 g) were chromatographed over silicic acid (MN-Kieselgel, 150 g) using chloroform–methanol (19:1) as eluant. Fractions (7 ml) were collected and monitored by tlc (solvent system *B*). Fractions 101–110 contained a mixture of cyathin A_3 and allocyathin B_3 (418 mg) which was separated into its components by ptlc over 10% $AgNO_3$ – silica gel (solvent system *A*) (4). The *cyathin* A_3 (**1**, ~250 mg) and *allocyathin* B_3 (**2**, ~30 mg) isolated were identical (tlc, ir, ^{1}Hmr) with authentic samples. Fractions 123–130 contained cyafrin B_4 and allocyafrin B_4. Separation by ptlc (solvent system *D*) gave *cyafrin* B_4 (R_f 0.6, 49 mg) and *allocyafrin* B_4 (R_f 0.5, 3 mg).[6] Fractions 228–254 yielded crude *cyafrin* A_4 (114 mg) which was purified by recrystallization from acetone.[6] Fractions 255–276 gave a mixture of cyafrin A_4 and cyafrin A_5 which was separated by ptlc (solvent system *C* triple elution). *Cyafrin* A_5 (6 mg) was purified by recrystallization from acetone–benzene.[6]

Cyafrin A_4 (**3**a ⇆ **4**a)

Cyafrin A_4 crystallized from methanol–benzene as colorless needles, mp 200–201°C; $[\alpha]_D^{25}$ −125° (*c* 0.4, CH_3OH); ir (KBr): 3300 (br), no carbonyl; uv: 230 (sh) nm (ε 1500); ^{1}Hmr (pyridine) indicated a mixture of hydroxy ketone and hemiacetal forms. *Exact mass* calcd. for $C_{20}H_{30}O_4$: 334.2144; found (ms): 334.2152.

Cyafrin B_4 (**10**a ⇆ **11**a)

Cyafrin B_4 was obtained as a colorless syrup, $[\alpha]_D^{25}$ −156.5° (*c* 0.34, $CHCl_3$); ir ($CHCl_3$): 3630, 3420, 1695, 1623 cm^{-1}; uv: 241 nm (ε 11 000); ^{1}Hmr, poorly resolved (tautomeric equilibrium). *Exact mass* calcd. for $C_{20}H_{28}O_4$: 332.1988; found (ms): 332.1983.

Allocyafrin B_4 (**12**a ⇆ **13**a)

Allocyafrin B_4 was obtained as a colorless syrup, $[\alpha]_D^{25}$ −157.8° (*c* 0.27, $CHCl_3$); ir ($CHCl_3$): 3600, 3440, 1700, 1680 (sh), 1600 cm^{-1}; uv: 239 nm (ε 16 400); ^{1}Hmr ($CDCl_3$) δ: 1.08 (s, 3H), 1.12 (s, 3H), 1.22 and 1.26 (each 3H, d, J = 7 Hz), 4.42 (m, 3H), 5.98 (bs, 1H), 6.04 (bs, 1H). *Exact mass* calcd. for $C_{20}H_{28}O_4$: 332.1988; found (ms): 332.1985.

Cyafrin A_5 (**15**a)

Cyafrin A_5 was obtained as colorless needles from acetone–benzene, mp 208–209°C; $[\alpha]_D^{25}$ −77.9° (*c* 0.154, CH_3OH); ir

[5]M. J. Bennett and M. Tuggle. Private communication.

[6]Physical data for the new compounds are reported below.

Can. J. Chem. Downloaded from www.nrcresearchpress.com by 210.87.254.105 on 09/05/12
For personal use only.

(film): 3350 (br), 1703 (w); ^{1}Hmr (C_5D_5N + D_2O) δ: 0.88 and 0.99 (each 3H, d, J = 7 Hz, isopropyl methyls), 1.34 (s, 3H), 1.36 (s, 3H), 4.18 (s, 1H), 4.20 and 4.30 (dd, J = 18 Hz), 4.22 (t, 1H, J = 8 Hz), 4.75 (m, 1H); ^{13}Cmr (CD_3OD) δ: 12.3, 17.0, 21.2, 22.5 (CH_3); 28.5, 29.6, 35.6, 37.1, 58.8 (CH_2); 26.4, 40.8, 56.9, 74.0, 82.4 (CH); 43.7, 49.6, 63.9, 164.3 (C); 136.5, 138.0 (C=C). *Exact mass* calcd. for $C_{20}H_{30}O_5$: 350.2092; found (ms): 350.2092.

O,O,O-*Triacetylcyafrin* A_4 (*3*b)

Cyafrin A_4 (60 mg) was dissolved in pyridine (2 ml) and acetic anhydride was added. The solution was allowed to stand overnight at room temperature and then toluene (15 ml) was added and the solvents were removed under reduced pressure. The residue was purified by ptlc (solvent system *A*) to give *O,O,O*-triacetylcyafrin A_4 (*3b*) as a viscous liquid (45 mg); ir: ($CHCl_3$) 1740, 1660 cm^{-1}; ^{1}Hmr ($CDCl_3$) δ: 0.97 and 1.01 (each 3H, d, J = 7 Hz, isopropyl methyls), 1.02 (s, 3H), 1.14 (s, 3H), 2.02 (s, 3H), 2.07 (s, 3H), 2.12 (s, 3H), 4.70 (2H, t, J = 1.5 Hz, C-15 H's), 4.89 (1H, t, J = 8 Hz, C-1 H), 5.33 (1H, t, J = 6.5 Hz, C-11 H), 6.12 (1H, t, J = 1.5 Hz). *Exact mass* calcd. for $C_{24}H_{32}O_5$ (M^+ − HOAc): 400.2250; found (ms): 400.2245.

Cyafrin A_4 *Methyl Acetal* (*4*b)

Cyafrin A_4 (18 mg) was dissolved in a saturated solution of HCl in CH_3OH (0.5 ml) and kept at room temperature for 4 h. The solution was concentrated and the residue dissolved in $CHCl_3$ (10 ml). The $CHCl_3$ solution was washed with saturated $NaHCO_3$, then brine, and evaporated. Purification by ptlc (solvent *B*) gave cyafrin A_4 methyl acetal (*4b*, 7.5 mg), mp 93–94°C (from benzene); $[\alpha]_D^{25}$ −98° (*c* 0.39, $CHCl_3$); ir (film): 3390 cm^{-1}; ^{1}Hmr ($CDCl_3$) δ: 0.87 and 0.96 (each 3H, d, J = 7 Hz), 0.90 (3H, s), 0.96 (3H, s), 3.33 (3H, s, OCH_3), 3.86 (1H, dd, J = 9 and 7 Hz, C-1 H), 4.32 (2H, d, J = 1 Hz, C-15 H's), 4.74 (1H, m, C-11 H), 6.02 (1H, t, J = 1 Hz, C-13 H). *Exact mass* calcd. for $C_{21}H_{32}O_4$: 348.2300; found (ms): 348.2295.

Cyafrin A_4 *Acetonide* (*5*a)

Cyafrin A_4 (20 mg) was dissolved in 2,2-dimethoxypropane (1 ml) and acetone (0.5 ml) containing *p*-toluenesulfonic acid (2 mg). After 1 h at room temperature the reaction mixture was concentrated to half volume and applied to a ptlc plate, which was developed with solvent *B*. The band at R_f 0.42 gave, after elution, cyafrin A_4 acetonide (*5a*), mp 170–171°C (from ether – Skellysolve B) as colorless needles; $[\alpha]_D^{25}$ −58° (*c* 0.4, $CHCl_3$); ir ($CHCl_3$): 3610 (vw), 1658 cm^{-1}; uv (CH_3OH): 236 nm (ε 6300); ^{1}Hmr ($CDCl_3$) δ: 1.00 (3H, s, C-6 methyl) 1.00 (6H, d, J = 7 Hz), 1.09 (3H, s, C-9 methyl) 1.40 and 1.48 (each 3H, s, acetonide methyls), 3.88 (1H, t, J = 7 Hz, C-1 H), 4.30 (3H, m, C-15 and C-11 H's), 5.69 (1H, q, J = 2 Hz, C-13 H); ^{1}Hmr (C_5D_5N) δ: 1.21 (3H, s, C-6 methyl), 1.30 (3H, s, C-9 methyl), 0.91 and 1.01 (each 3H, d, J = 7 Hz, isopropyl methyls). *Exact mass* calcd. for $C_{23}H_{34}O_4$: 374.2457; found (ms): 374.2455.

Dehydrocyafrin A_4 *Acetonide* (*6*)

Cyafrin A_4 acetonide (*5a*, 12 mg) in dry pyridine (0.1 ml) was added to CrO_3 (40 mg) – pyridine (0.4 ml) and the mixture was stirred for ½ h at room temperature, then diluted with water and extracted with $CHCl_3$. The $CHCl_3$ layer was washed with dilute acid, bicarbonate solution, and brine. The residue after removal of $CHCl_3$ was purified by ptlc (R_f 0.5, benzene – ethyl acetate (4:1)) and crystallized from methanol to give dehydrocyafrin A_4 acetonide (**6**) (4.6 mg), mp 144–146°C; $[\alpha]_D^{25}$ −84.25° (*c* 0.4, $CHCl_3$); ir (film) 1746, 1650 cm^{-1}; uv (CH_3OH), 236 nm (ε 8500); ^{1}Hmr ($CDCl_3$) δ: 1.04 and 1.08 (each 3H, d, J = 7 Hz, isopropyl methyls), 1.12 (3H, s), 1.14 (3H, s), 1.41 and 1.48 (each 3H, acetonide methyls), 2.99 (2H, dd, J = 19 Hz, C-2 H's), 4.34 (3H, m, C-11 and C-15 H's), 5.75 (1H, q, J = 1.5 Hz, C-13 H). *Exact mass* calcd. for $C_{23}H_{32}O_4$: 372.2300; found (ms): 372.2299.

Mesylate of Cyafrin A_4 *Acetonide* (*5*b)

Cyafrin A_4 acetonide (*5a*, 13 mg) was dissolved in CH_2Cl_2 (1 ml) and methanesulfonyl chloride (0.01 ml) and triethylamine (0.01 ml) added at 0°C. After 20 min at 0°C, the solution was concentrated to small volume and applied to a ptlc plate which was then developed with solvent system *B*. Elution gave the mesylate *5b* (14 mg) which was crystallized from benzene, mp 159–160°C, $[\alpha]_D^{25}$ −38° (*c* 0.3, $CHCl_3$); ir ($CHCl_3$): 1660 br, 1365, 1340 cm^{-1}; ^{1}Hmr ($CDCl_3$) δ: 1.03 (6H, d, J = 7 Hz, isopropyl methyls), 1.06 (3H, s), 1.10 (3H, s), 1.42 and 1.46 (each 3H, s, acetonide methyls), 3.02 (3H, s, —SO_2—CH_3), 4.30 (3H, m, C-11 and C-15 H's), 4.75 (1H, t, J = 8 Hz, C-1 H), 5.70 (1H, bs, C-13 H).

Rearrangement of 5b *to* **7**

O-Mesylcyafrin A_4 acetonide (*5b*, 7.5 mg) in dioxane (2 ml) containing 1,5-diazabicyclo[5.4.0]undec-5-ene (0.2 ml) was heated to 90°C for 5 h. The reaction mixture was then concentrated, taken up in chloroform, washed with dilute acid and water, dried, and evaporated. The residue was purified by ptlc (solvent *B*, R_f 0.65) to give 7 as a colorless syrup (3 mg); ir ($CHCl_3$): 1708, 1365, 1340 cm^{-1}; uv, no maximum above 210 nm; ^{1}Hmr ($CDCl_3$) δ: 0.99 and 0.97 (each 3H, d, J = 7 Hz, isopropyl methyls), 1.03 (3H, s), 1.15 (3H, s), 1.36 and 1.43 (each 3H, s, acetonide methyls), 3.02 (3H, s, —SO_2—CH_3), 4.03 (2H, bs, C-15 H's), 4.74 (1H, t, J = 8 Hz, C-1 H).

Mesylate of Cyafrin A_4 *Methyl Acetal* (*8*)

O-Mesylcyafrin A_4 acetonide (*5b*, 9 mg) was dissolved in 2.43 *N* hydrogen chloride in methanol (0.5 ml) and left at room temperature for 17 h. The solution was then diluted with $CHCl_3$ and the resulting solution washed with saturated $NaHCO_3$ and then brine. Removal of the chloroform and purification of the residue by ptlc (solvent *B*, R_f 0.55) gave **8** as a colorless oil (5 mg), $[\alpha]_D^{25}$ −82.7° (*c* 0.34, $CHCl_3$); ir ($CHCl_3$): 3610, 1606 (w), 1363 (s) cm^{-1}; ^{1}Hmr ($CDCl_3$) δ: 0.88 and 0.97 (each 3H, d, J = 7 Hz isopropyl methyls), 0.95 (3H, s), 0.98 (3H, s), 2.98 (3H, s, —SO_2—CH_3), 3.28 (3H, s, OCH_3), 4.21 (2H, s, C-15 H's), 4.74 (1H, m, C-11 H), 4.68 (1H, t, J = 9 Hz, C-1 H), 6.01 (1H, bs, C-13 H). *Exact mass* calcd. for $C_{22}H_{34}O_6{}^{32}S$: 426.2076; found (ms): 426.2091.

Allocyathin B_3 *Methyl Acetal* (*9*) *From* **8**

Mesylate **8** (12 mg) was dissolved in toluene (0.8 ml) containing 1,5-diazabicyclo[5.4.0]undec-5-ene (0.2 ml) and the solution was heated under reflux in a nitrogen atmosphere for 45 h. The solution was then diluted with benzene and washed successively with dilute H_2SO_4 and brine. Evaporation and purification by ptlc (solvent *B*, double elution) gave allocyathin B_3 methyl acetal (**9**, 4.5 mg), identical (ir, ^{1}Hmr, tlc, and rotation) with an authentic sample (4).

Benzoate of Cyafrin A_4 *Acetonide* (*5*d)

Cyafrin A_4 acetonide (*5a*, 8 mg) in CH_2Cl_2 (0.4 ml) was treated with benzoyl chloride (0.03 ml) and pyridine (0.03 ml) at room temperature for 30 min. Work-up and purification by ptlc (solvent *A*, double elution) gave the benzoate *5d* as a colorless gum (7 mg), $[\alpha]_D^{25}$ −58.5° (*c* 0.518, $CHCl_3$); ir (CCl_4): 1705, 1650 (br), 1640, 1590 (w) cm^{-1}; uv (CH_3OH): 231 nm (ε 18 400), 280 (sh) (ε 900); ^{1}Hmr ($CDCl_3$) δ: 1.02 and 1.06 (each 3H, d, J = 7 Hz), 1.13 (6H, s), 1.42 and 1.47 (each 3H), 4.33 (3H, m, C-15 and C-11 H's), 5.72 (1H, bs, C-13 H),

Can. J. Chem. Downloaded from www.nrcresearchpress.com by 210.87.254.105 on 09/05/12
For personal use only.

7.48 and 8.06 (5H, m, benzoyl H's). *Exact mass* calcd. for $C_{30}H_{38}O_5$: 478.2719; found (ms): 478.2712.

O,O-*Diacetylcyafrin* B_4 (*10*b)

Cyafrin B_4 (10 mg) was acetylated as described above for cyafrin A_4 to give a colorless oil (8 mg) after purification by ptlc (solvent B); ir ($CHCl_3$): 1740, 1685 cm^{-1}; ^{1}Hmr ($CDCl_3$) δ: 1.17 (3H, s), 1.28 (3H, s), 1.19 and 1.23 (each 3H, d, J = 7 Hz), 2.06 (3H, s), 2.12 (3H, s), 2.21 (2H, s, C-1 H's), 4.70 (2H, m, C-15 H's), 5.41 (1H, t, J = 6 Hz, C-11 H), 6.18 (1H, t, J = 1 Hz, C-13 H). *Exact mass* calcd. for $C_{24}H_{32}O_6$: 416.2199; found (ms): 416.2202.

Cyafrin B_4 *Methyl Acetal* (*11*b)

Cyafrin B_4 (27 mg) was dissolved in a saturated solution of HCl in CH_3OH (0.5 ml) and left overnight at room temperature, then the solution was concentrated and applied to a ptlc plate. Development with solvent B (R_f = 0.46) and elution afforded cyathin B_4 methyl acetal (**11***b*) (16 mg) as a colorless oil, $[\alpha]_D^{25}$ −153.95° (*c* 0.91, $CHCl_3$); ir (film): 3400, 1690, 1615 cm^{-1}; uv (CH_3OH): 242 nm (ε 13 900); ^{1}Hmr ($CDCl_3$) δ: 0.98 (3H, s), 1.16 (3H, s), 1.16 and 1.20 (each 3H, d, J = 7 Hz, isopropyl methyls), 2.14 (2H, s, C-1 H's), 3.31 (3H, s, OCH_3), 4.36 (2H, s, C-15 H's), 4.80 (1H, m, C-11 H), 6.12 (1H, bs, C-13 H). *Exact mass* calcd. for $C_{21}H_{30}O_4$: 346.2144; found (ms): 346.2144.

O,O-*Diacetylallocyafrin* B_4 (*12*b)

Allocyafrin B_4 (3 mg) in CH_2Cl_2 (2 ml) was treated with acetic anhydride (0.05 ml) and pyridine (0.05 ml) for 5 h at room temperature. Addition of toluene and concentration at reduced pressure afforded a crude product which was purified by ptlc (solvent B, R_f 0.47) to give a colorless oil (2 mg); ir (film): 1745, 1698, 1598 cm^{-1}; uv (CH_3OH): 235 nm (ε 12 000); ^{1}Hmr ($CDCl_3$) δ: 1.08 (3H, s), 1.11 (3H, s), 1.16 and 1.23 (each 3H, d, J = 7 Hz, isopropyl methyls), 2.04 (3H, s), 2.08 (3H, s), 4.66 (2H, dd, J = 14 Hz, C-15 H's), 5.48 (1H, m, C-11 H), 6.00 (1H, bs, C-2 H), 6.04 (1H, d, J = 2 Hz). *Exact mass* calcd. for $C_{24}H_{32}O_6$: 416.2198; found (ms): 416.2204.

Allocyafrin B_4 *Methyl Acetal* (*13*b)

Allocyafrin B_4 (3 mg) was treated with methanolic HCl as described above for cyafrin B_4 to give a colorless oil (2.5 mg) after purification by ptlc (solvent *A*); ir (film): 3410, 1700, 1600 cm^{-1}; uv (CH_3OH): 235 nm (ε 9500); ^{1}Hmr ($CDCl_3$): 1.00 (3H, s), 1.16 (3H, s), 1.12 and 1.25 (each 3H, d, J = 7 Hz, isopropyl methyls), 3.30 (3H, s, OCH_3), 4.38 (2H, bs, C-15 H), 4.84 (1H, m, C-11 H), 5.88 (1H, bs, C-2 H), 6.04 (1H, t, J = 2 Hz). *Exact mass* calcd. for $C_{21}H_{30}O_4$: 346.2144; found (ms): 346.2140.

O,O-*Diacetylcyafrin* A_5 (*15*b)

Cyafrin A_5 (2 mg) was acetylated with acetic anhydride (0.3 ml) and pyridine (0.3 ml) at room temperature and worked up in the usual manner. Purification by ptlc (solvent, benzene – ethyl acetate (4:1)) gave a colorless oil (1.3 mg), $[\alpha]_D^{25}$ −40° (*c* 0.1, $CHCl_3$); ir (film): 3420, 1734 cm^{-1}; ^{1}Hmr ($CDCl_3$) δ: 0.94 and 1.00 (each 3H, d, J = 7 Hz), 1.01 (3H, s), 1.03 (3H, s), 2.08 (3H, s), 2.10 (3H, s), 3.68 (1H, s, C-13 H), 4.48 (2H, dd, J = 13 Hz, C-15 H's), 4.90 (1H, t, J = 8 Hz, C-1 H), 4.29 (1H, m, C-11 H). *Exact mass* calcd. for $C_{22}H_{30}O_5$ (M^+ − HOAc): 374.2093; found (ms): 374.2093.

Cyafrin A_5 *Triacetyl Derivatives* ***15***c *and* ***16***b

Cyafrin A_5 (4.7 mg) was dissolved in CH_2Cl_2 (0.3 ml) containing 4-dimethylaminopyridine (10 mg) and acetic anhydride (0.015 ml) added. After 2 h at room temperature CH_2Cl_2 and water were added and the CH_2Cl_2 layer was separated and washed with dilute HCl and brine. After removal of the solvent, the residue was purified by ptlc (solvent *A*, double elution) to yield **15***c* (1.8 mg, R_f 0.28) and **16***b* (2.8 mg, R_f 0.34), both as colorless oils.

Triacetate ***15***c—$[\alpha]_D^{23}$ −21° (*c* 0.12, $CHCl_3$); ir (film): 1750 cm^{-1}; ^{1}Hmr ($CDCl_3$) δ: 0.93 and 1.00 (each 3H, d, J = 7 Hz), 1.01 (3H, s), 1.03 (3H, s), 2.07 (3H, s), 2.11 (3H, s), 2.13 (3H, s), 4.33 and 4.63 (2H, dd, J = 13 Hz, C-15 H's), 4.56 (1H, s, C-13 H), 4.86 (1H, t, J = 9 Hz, C-1 H), 4.33 (1H, m, C-11 H). *Exact mass* calcd. for $C_{24}H_{32}O_6$ (M^+ − HOAc): 416.2199; found (ms): 416.2205.

Triacetate ***16***b—ir (film): 1745, 1690 cm^{-1}; ^{1}Hmr ($CDCl_3$) δ: 0.95 and 1.02 (each 3H, d, J = 7 Hz), 0.97 (3H, s), 1.24 (3H, s), 2.05 (3H, s), 2.06 (3H, s), 2.10 (3H, s), 3.70 (1H, s, C-13 H), 4.07 and 4.43 (2H, dd, J = 12 Hz, C-15 H's), 4.88 (1H, t, J = 8 Hz), 5.19 (1H, dd, J = 10 and 3 Hz, C-11 H). *Exact mass* calcd. for $C_{24}H_{32}O_6$ (M^+ − HOAc): 416.2199; found (ms): 416.2022.

Epoxidation of Cyafrin A_4 *with* H_2O_2

Cyafrin A_4 (**3***a*, 8 mg) was dissolved in CH_3OH (0.3 ml) and 30% H_2O_2 (0.02 ml) and 6 *N* NaOH (0.03 ml) added. The reaction mixture was left at 20°C for 12 h, then it was applied directly to a ptlc plate (solvent C, triple elution). The material (4.7 mg) eluted from the band at R_f 0.33 was crystallized from acetone to give *cyafrin* A_5, mp 210–212°C, identical (ir, tlc, mmp) with an authentic sample. Elution of a band at R_f 0.52 provided the β-epoxide **17***a* (1 mg), mp 201–203°C (from acetone); ir (film): 3380, 1710 cm^{-1}; ^{1}Hmr (C_5D_5N + D_2O) δ: 0.83 and 0.95 (each 3H, d, J = 7 Hz), 1.26 (3H, s), 1.45 (3H, s), 3.91 (1H, m, C-11 H), 4.18 (1H, t, J = 8 Hz, C-1 H), 4.65 and 4.88 (2H, dd, J = 13 Hz, C-15 H's), 4.65 (1H, s, C-13 H). *Exact mass* calcd. for $C_{20}H_{30}O_5$: 350.2093; found (ms): 350.2088.

Triacetate of β-*Epoxide* (*17*b)

β-Epoxide **17***a* (1.3 mg) in CH_2Cl_2 (0.1 ml) was acetylated by treatment with acetic anhydride (0.005 ml) and 4-dimethylaminopyridine (3 mg) at room temperature. The reaction mixture was submitted directly to ptlc (solvent *A*) and the band at R_f 0.26 eluted to give triacetate **17***b* (1.1 mg) as colorless needles, mp 193–195°C (from Skellysolve B – acetone); $[\alpha]_D^{23}$ −54.5° (*c* 0.11, $CHCl_3$); ir (film): 1738, 1710 cm^{-1}; ^{1}Hmr ($CDCl_3$) δ: 0.95 and 1.04 (each 3H, d, J = 7 Hz), 1.01 (3H, s), 1.20 (3H, s), 2.06 (3H, s), 2.10 (3H, s), 2.11 (3H, s), 3.83 (1H, s, C-13 H), 4.34 (1H, m, C-11 H), 4.38 and 4.64 (2H, dd, J = 13 Hz, C-15 H's), 4.88 (1H, t, J = 8 Hz, C-1 H). *Exact mass* calcd. for $C_{24}H_{32}O_6$ (M^+ − HOAc): 416.2199; found (ms): 416.2204.

Epoxidation of Cyafrin A_4

Cyafrin A_4 (5 mg) was added to a solution of *m*-chloroperbenzoic acid (10 mg) in $CHCl_3$ (2 ml) and the reaction mixture was stirred for 2.5 h at room temperature, then washed with saturated $NaHCO_3$ and brine. After evaporation of solvent the residue was subjected to ptlc (solvent *C*, triple elution), and the band at R_f 0.44 eluted to give the diepoxide **22** (1.5 mg) as colorless needles, mp 235–236°C; $[\alpha]_D^{25}$ −47° (*c* 0.14, CH_3OH); ir (film) 3420, 3370 cm^{-1}. *Exact mass* calcd. for $C_{20}H_{30}O_6$: 366.2024; found (ms): 366.2033.

Epoxidation of Cyafrin A_5

A mixture of cyafrin A_5 (0.5 mg) and *m*-chloroperbenzoic acid (1 mg) in $CHCl_3$ (0.1 ml) was left at room temperature for ½ h, then applied to a ptlc plate (solvent *C*, triple elution) to give the diepoxide **22** (0.2 mg), R_f 0.44, identical (tlc, ir) with that obtained from cyafrin A_4.

*15-O-Acetylcyathin A_3 (**1c**)*

Acetic anhydride (0.08 ml) and pyridine (0.3 ml) was added to a solution of cyathin A_3 (40 mg) in CH_2Cl_2 (2 ml). After 40 min the reaction mixture was poured onto ice water and extracted with CH_2Cl_2. The extract was washed with 5% hydrochloric acid, saturated $NaHCO_3$, and brine and then concentrated. The residue was purified by ptlc (solvent *A*) to yield 15-*O*-acetylcyathin A_3 (**1c**, R_f 0.3, 31 mg) and *O*,*O*-diacetylcyathin A_3 (**1b**, R_f 0.4, 8.5 mg). 15-*O*-Acetylcyathin A_3 (**1c**) was obtained as a colorless syrup, $[\alpha]_D^{23}$ −117.3° (*c* 0.358, $CHCl_3$); ir ($CHCl_3$): 3580, 3440 (br), 1740, 1660 cm^{-1}; ^{1}Hmr ($CDCl_3$) δ: 1.02 (6H, d, J = 7 Hz), 0.99 (3H, s), 1.06 (3H, s), 2.11 (3H, s), 4.77 (3H, m, C-11 and C-15 H's), 6.10 (1H, bs, C-13 H). *Exact mass* calcd. for $C_{22}H_{32}O_4$: 360.2301; found (ms): 360.2298.

*15-O-Acetyl-11-O-benzoylcyathin A_3 (**1d**)*

15-*O*-Acetylcyathin A_3 (15 mg) in pyridine (0.5 ml) was treated with benzoyl chloride (0.05 ml) at room temperature for 2 h. The reaction mixture was poured into ice water and extracted with $CHCl_3$ in the usual manner. The product in $CHCl_3$ was filtered through alumina and then further purified by ptlc (solvent *A*) to yield the benzoate **1d** as a colorless gum (7 mg), $[\alpha]_D^{25}$ −40.9° (*c* 0.425, $CHCl_3$); ir ($CHCl_3$): 1745, 1724, 1680, 1665, 1605 cm^{-1}; uv (CH_3OH): 230 (ε 16 800), 274 (sh, ε 1200), 282 nm (sh, ε 980); ^{1}Hmr ($CDCl_3$) δ: 0.98 (6H, d, J = 7 Hz), 1.09 (3H, s), 1.18 (3H, s), 2.06 (3H, s), 4.73 (2H, d, J = 1.5 Hz, C-15 H's), 5.70 (1H, t, J = 7 Hz, C-11 H), 6.20 (1H, t, J = 1.5 Hz, C-13 H), 7.45 (3H, m), 7.99 (2H, dd, J = 8 and 2 Hz); cd (*c* 0.0011 *M*): 236 nm (Δε +13.1). *Exact mass* calcd. for $C_{29}H_{36}O_5$: 464.2563; found (ms): 464.2564.

*15-O-Acetyl-11-O-p-bromobenzoylcyathin A_3 (**1e**)*

p-Bromobenzoyl chloride (200 mg) was added to a solution of 15-*O*-acetylcyathin A_3 (63 mg) and 4-dimethylaminopyridine (111 mg) in CH_2Cl_2 (5 ml). After 15 min at room temperature the solution was diluted with CH_2Cl_2, washed with 5% HCl, saturated $NaHCO_3$, and brine. Evaporation left a colorless syrup which was purified by ptlc (solvent *A*) to give, after crystallization from methanol, 15-*O*-acetyl-11-*O*-*p*-bromobenzoylcyathin A_3 (60 mg), mp 102–103°C, $[\alpha]_D^{23}$ −15.8° (*c* 0.4, $CHCl_3$); ir ($CHCl_3$): 1745, 1720, 1685, 1660 (sh), 1593 cm^{-1}; uv (CH_3OH): 208 (ε 15 900), 246 (ε 18 200), 282 nm (sh, ε 770); ^{1}Hmr ($CDCl_3$) δ: 0.99 (6H, d, J = 7 Hz), 1.10 (3H, s), 1.18 (3H, s), 2.07 (3H, s), 4.72 (2H, s, C-15 H's), 5.67 (1H, t, J = 7 Hz, C-11 H), 6.20 (1H, t, J = 1.5 Hz, C-13 H), 7.71 (4H, dd, J = 9 Hz); cd (*c* 0.0018 *M*, ethanol–dioxane (4:1)): 247 nm (Δε +8.2). *Exact mass* calcd. for $C_{29}H_{35}O_5{}^{81}Br$: 544.1647, for $C_{29}H_{35}O_5{}^{79}Br$: 542.1668; found (ms): 544.1657, 542.1677. *Anal.* calcd. for $C_{29}H_{35}O_5Br$: C 64.08, H 6.49, Br 14.70; found: C 64.02, H 6.53, Br 14.92.

Acknowledgements

We wish to thank Prof. H. J. Brodie for the slant tube culture of *Cyathus africanus* Brodie, Dr. L. M. Browne for assistance in growing the liquid cultures, and the National Research Council of Canada for financial support.

1. W. A. Ayer, L. M. Browne, J. R. Mercer, D. R. Taylor, and D. E. Ward. Can. J. Chem. **56**, 717 (1978).
2. H. J. Brodie. Can. J. Bot. **45**, 1653 (1967).
3. H. J. Brodie. The bird's nest fungi. University of Toronto Press, Toronto, Ont. 1975.
4. W. A. Ayer and H. Taube. Can. J. Chem. **51**, 3842 (1973).
5. A. D. Allbutt, W. A. Ayer, H. J. Brodie, B. N. Johri, and H. Taube. Can. J. Microbiol. **17**, 1401 (1971).
6. W. A. Ayer and M. G. Paice. Can. J. Chem. **54**, 910 (1976).
7. W. A. Ayer and D. R. Taylor. Can. J. Chem. **54**, 1703 (1976).
8. K. Wiberg and B. J. Nist. J. Am. Chem. Soc. **83**, 1226 (1961).
9. P. V. DeMarco, E. Farkas, D. Doddrell, B. L. Mylari, and E. Wenkert. J. Am. Chem. Soc. **90**, 5480 (1968).
10. J. H. Brewster. Tetrahedron, **13**, 106 (1961).
11. C. Djerassi, G. von Mutzenbecker, J. Fajkos, D. H. Williams, and H. Budzikiewicz. J. Am. Chem. Soc. **87**, 817 (1965).
12. W. Steglich and G. Höfle. Angew. Chem. Int. Ed. Engl. **8**, 981 (1969).
13. H. O. House. Modern synthetic reactions. 2nd ed. W. A. Benjamin, Inc. Menlo Park, CA. 1972. pp. 303–306.
14. M. Koreeda, N. Harada, and K. Nakanishi. J. Am. Chem. Soc. **96**, 266 (1974).

Can. J. Chem. Downloaded from www.nrcresearchpress.com by 210.87.254.105 on 09/05/12
For personal use only.

Infrared and laser Raman studies of deuterated model membranes: Phase transition in 1,2-perdeuterodipalmitoyl-*sn*-glycero-3-phosphocholine[1]

S. SUNDER, D. CAMERON, H. H. MANTSCH, AND H. J. BERNSTEIN

Division of Chemistry, National Research Council of Canada, Ottawa, Ont., Canada K1A 0R6

Received February 20, 1978

S. SUNDER, D. CAMERON, H. H. MANTSCH, and H. J. BERNSTEIN. Can. J. Chem. **56**, 2121 (1978).

Raman and infrared spectra of multilayer dispersions of 1,2-perdeuterodipalmitoyl-*sn*-glycero-3-phosphocholine in water are studied as a function of temperature for the CD stretching region. It is found that the bands associated with these vibrations can be used as a sensitive probe to monitor the gel – liquid crystal phase transition which occurs at a lower temperature in the perdeuterated phospholipid than in the corresponding natural (light) lipid.

S. SUNDER, D. CAMERON, H. H. MANTSCH et H. J. BERNSTEIN. Can. J. Chem. **56**, 2121 (1978).

Faisant appel à la spectroscopie Raman et infrarouge, on a étudié, en fonction de la température, les vibrations de valence CD de dispersions de multicouches de perdeutérodipalmitoyl-1,2 *sn* glycérophosphocholine-3 dans l'eau. On a trouvé que les bandes associées avec ces vibrations peuvent être utilisées comme sonde sensible pour évaluer la transition de phase gel – cristal liquide qui se produit à une température inférieure dans le phospholipide perdeutéré par rapport au lipide naturel correspondant (léger).

[Traduit par le journal]

Introduction

Isotopically labelled model compounds are being increasingly used to gain detailed information about the structure and function of biomembranes (refs. 1–20 and references therein). This can supply information about the specific section of the membrane with minimal perturbation. Such systems have been investigated by multinuclear magnetic resonance spectroscopy (1–12) but relatively few studies are available in vibrational spectroscopy (14–20). Isotopic labelling, particularly the replacement of ^1H by ^2H, offers a powerful tool in the study of membranes by vibrational (Raman and infrared) spectroscopy as the mass change causes drastic shifts in the vibrational frequencies with very little change in the chemical nature of the system. In this communication we present a temperature dependence study of the infrared and Raman spectra of 1,2-perdeuterodipalmitoyl-*sn*-glycero-3-phosphocholine as multilayer dispersions in excess water for the temperatures between 20 and 50°C.

Experimental

Material

High purity samples of 1,2-perdeuterodipalmitoyl-*sn*-glycero-3-phosphocholine (DPPC-d_{62}) were obtained from Lipid Specialties Inc., Boston. Thin-layer chromatography showed the absence of any impurity. Polarimetry measurements indicated that the *sn*-3 stereochemistry of the natural glycerophospholipid was retained in the DPPC-d_{62} sample.

[1]NRCC No. 16620.

Method

Infrared Spectroscopy

Multibilayers for infrared measurements were obtained by dissolving about 2 mg of DPPC-d_{62} in chloroform and spreading it on the central area of a freshly cleaned CaF_2 plate (~ 1 cm^2). The chloroform was evaporated under vacuum and the plate soaked in double distilled water for 10 min. The CaF_2 plate bearing the phospholipid film was mounted in a thermostated cell holder and the fully hydrated multibilayers kept at 100% humidity during the measurement. This method of producing planar multibilayers is extensively used in the epr studies of model membranes (21). Temperatures were measured by a Newport digital pyrometer with a thermocouple placed on the CaF_2 plate bearing the film. The temperature reproducibility was estimated to ± 0.05°C. Infrared spectra were obtained with a Perkin-Elmer model 180 grating spectrophotometer at a resolution of ~ 2 cm^{-1}.

Raman Spectroscopy

Samples for Raman studies were prepared by coating the inside of a test tube with the deuterated phospholipid by evaporating a chloroform solution under a gentle stream of nitrogen gas. Last traces of chloroform were removed by placing the tube containing the sample in a vacuum dessicator and pumping over it for more than two hours. Water was added to the sample, followed by shaking on a vortex mixer. The sample was transferred into a glass capillary tube and centrifuged for a few minutes in a table top centrifuge to concentrate the multilayer aggregates. The sample capillary was sealed and placed in a variable-temperature cell described earlier (22). The temperature accuracy for Raman measurements is believed to be ± 1°C.

Raman scattering was obtained by excitation with ~ 300 mW of 514.5 nm radiation from an argon ion gas laser (Coherent radiation model 52). The spectra were recorded at a resolution of ~ 3 cm^{-1} using a Spex 14018 double monochromator, a cooled RCA C31034 photomultiplier, photon counting detection and operating under a Nicolet NIC-1180

Can. J. Chem. Downloaded from www.nrcresearchpress.com by 210.87.254.5 on 09/05/12
For personal use only.

Can. J. Chem. Downloaded from www.nrcresearchpress.com by 210.87.254.5 on 09/05/12
For personal use only.

data system. The spectra were recorded both in analog form with a strip-chart recorder and in digital form in the Nicolet system. Four or more scans were averaged for each spectrum to enhance the signal-to-noise ratio.

Results and Discussion

The infrared and Raman spectra of DPPC-d_{62} multilayer dispersions in the presence of excess water are shown in Figs. 1 and 2, respectively, for the CD stretching region. The frequencies of the observed features are listed in Table 1. The frequency accuracy is believed to be ± 1 cm^{-1} for the infrared spectra and ± 2 cm^{-1} for the Raman spectra. However, the relative displacements of the frequencies of the spectral features could be measured to much better accuracy, up to ± 0.2 cm^{-1} for the infrared and ± 0.5 cm^{-1} for the Raman spectra. The poorer resolution and frequency accuracy for Raman spectra in the present system are due to the presence of fluorescence.

The suggested assignments for the observed features in the infrared and Raman spectra of DPPC-d_{62} are also given in Table 1. These are in agreement with the literature for similar compounds (14–20). The Raman spectrum of polycrystalline DPPC-d_{62} has been recently reported by Bunow and Levin (19). It is interesting to note that the Raman spectrum for the CD stretching region of polycrystalline DPPC-d_{62} and its spectrum as multilayer dispersions at room temperature, in the gel phase, Fig. 2, are very similar. This suggests that the hydrocarbon chains of the phospholipid in the gel phase of the multibilayers have a structure very similar to that in polycrystalline samples.

It has been shown that several spectral parameters derived from the vibrational spectra of phospholipids, such as band intensities, frequency shifts and bandwidths, can be used to follow the structural changes occurring in model membrane systems (14–16, 19, 23–36). Most of this work has been done with 'normal' phospholipids (15, 16, 19). Here we have applied this approach to a deuterated phospholipid and shown that various spectral parameters contained in the infrared and Raman spectra of deuterated lipids can be used to study their phase changes.

Figures 3 and 4 contain the results of a temperature study of the strong bands at ~2089 and ~2194 cm^{-1}, respectively, in the CD stretching region of the infrared spectra of DPPC-d_{62}. These figures contain the absorbance, halfwidth (fullwidth at half height) as well as the frequency maxima for the two infrared bands, plotted as a function of temperature. All three spectral parameters show a phase transition at 37.5 ± 0.5°C in the multilayer dispersions of

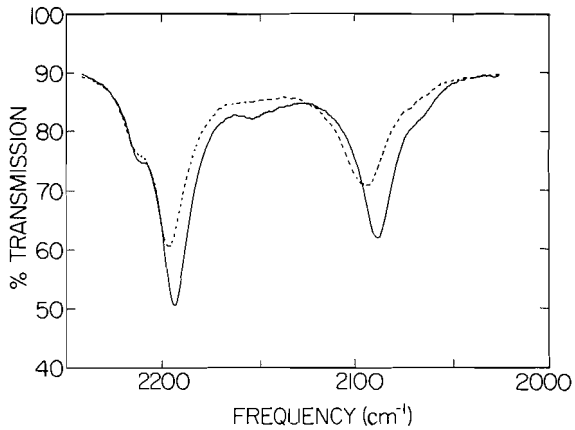

FIG. 1. Infrared spectra of 1,2-perdeuterodipalmitoyl-*sn*-glycero-3-phosphocholine multilayer dispersions in water above (---) and below (—) the gel – liquid crystal phase transition temperature. Spectral slit width ~2 cm^{-1}.

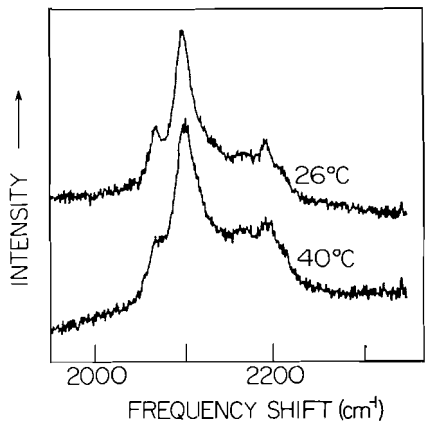

FIG. 2. Raman spectra of 1,2-perdeuterodipalmitoyl-*sn*-glycero-3-phosphocholine multilayer dispersions in water at room temperature (top curve) and at 40°C (bottom curve). Spectral slit width ~3 cm^{-1}. Excitation source ~300 mW of 514.5 nm radiation.

DPPC-d_{62}. This transition is most clearly shown by the absorbance vs. temperature plots (Figs. 3*A* and 4*A*) which indicates a phase transition temperature of 37.5 ± 0.2°C. The uncertainty in the transition temperature reported takes into account the errors in measuring the absolute temperature values; temperature changes in the infrared cell could be measured within an accuracy of ± 0.05°C. It is clear from Figs. 3 and 4 that, in addition to the absorbance, the halfwidths of these bands are also sensitive indicators of the order–disorder transition. Changes in the frequency values of these infrared bands offer additional parameters for following the phase transition with less sensitivity for the 2194 cm^{-1} band than for the 2089 cm^{-1} band.

TABLE 1. Vibrational spectra of 1,2-perdeuterodipalmitoyl-*sn*-glycero-3-phosphocholine for the CD stretching region[a]

Multilayer dispersions in water		Polycristalline solid		
Infrared[b]	Raman[b]	Infrared[b]	Raman[c]	Assignment
2214sh	2214sh	2214sh	2217sh	CD_3 asym st
2194s	2195m	2192s	2198m	CD_2 asym st
	2177m		2178m	
2154br	2165br	2156sh	2165, 2142 br	Overtone and/or combination
	2128sh		2126sh	CD_3 sym st[d]
	2100vs		2103vs	CD_2 sym st (Raman)
2089s		2088s		CD_2 sym st (ir)
2070sh	2070m	2071sh	2073m	CD_3 sym st[d]

[a]All frequencies are in wavenumbers (cm^{-1}). Frequency values are for room temperature spectra. s, m, w, v, sh, and br stand for strong, medium, weak, very, shoulder, and broad, respectively.
[b]This work.
[c]Reference 19.
[d]In Fermi resonance with an overtone and/or combination, see refs. 15 and 20 for a discussion.

Raman spectra were also used to follow the phase changes in the multilayer dispersions of DPPC-d_{62}. Figure 5*A* contains a plot of the bandwidth of the strong Raman band with a maximum around 2100 cm^{-1}. The bandwidths were measured at three-quarter height of the maximum instead of the usual half height to avoid interference from the shoulder around 2130 cm^{-1}. Also shown are plots of the ratio of the intensity of the 2195 cm^{-1} band to the 2100 cm^{-1} band (Fig. 5*B*), and the ratio of the intensity of the 2177 cm^{-1} band to the 2100 cm^{-1} band (Fig. 5*C*) as a function of temperature. Intensities were approximated by peak heights. Both the intensity ratio plots, Figs. 5*B* and 5*C*, and the bandwidth plot, Fig. 5*A*, derived from the Raman spectra, indicate a phase transition at 37 $\pm$ 2°C, in agreement with the value of 37.5$\pm$0.5°C obtained from the infrared studies. The higher uncertainty in the transition temperature obtained by Raman spectra is due to the lower signal-to-noise ratio of the Raman spectra compared with that of the infrared spectra.

The phase transition occurring at 37.5°C as seen in the infrared and Raman spectra is accompanied by the increase in the bandwidths of Raman and infrared bands. This is typical of an order to disorder phase transition (16, 35–37). Bandwidths in vibrational spectra increase with an increase in disorder and/or molecular mobility. The higher bandwidths in the high temperature phase reflect the increased disorder and mobility of the high temperature phase, the liquid crystal phase, compared with the low temperature phase, the gel phase. At present it is difficult to understand the changes in the intensity ratio of these Raman bands. In the light (protonated) lipids in going from gel to liquid crystal phase the intensity of the band assigned to the asymmetric CH_2 vibrations decreases relative to that of the symmetric CH_2 vibrations (16, 29). However, we observe an increase in the corresponding ratio with increasing temperature for the deuterated lipid. Also, it is the band assigned to the CH_2 *asymmetric* mode which is the strongest band in the Raman spectra of the 'light' phospholipids, while it is the band assigned to the *symmetric* vibration which is the strongest in the spectra of deuterated phospholipids. This reversal of the intensity ratio is typical of compounds containing long hydrocarbon chains (15). In spite of the uncertainty about the origin of the changes in the relative intensities of Raman bands, it is clear from Figs. 5*B* and 5*C* that their intensity ratios are a convenient indicator of the phase changes. In the infrared spectra we have used the absorbance of the individual bands (as measured at the peak position) directly. The decrease in the peak absorbance is related to the increase in the halfwidth. Increased disorder in the liquid crystal phase will result in a spread in the density of state vs. frequency curve with the concomitant decrease in the value of peak absorbance (38).

Phase transitions in DPPC-d_{62} multilayer dispersions were also studied by Peterson *et al.* (13) by differential thermal analysis and optical density measurements. They reported a pretransition at 33°C in addition to the main transition at 37.5°C. Our data does not show convincingly the presence of a pretransition but the main transition is clearly seen and is in excellent agreement with their results.

Can. J. Chem. Downloaded from www.nrcresearchpress.com by 210.87.254.5 on 09/05/12
For personal use only.

Can. J. Chem. Downloaded from www.nrcresearchpress.com by 210.87.254.5 on 09/05/12
For personal use only.

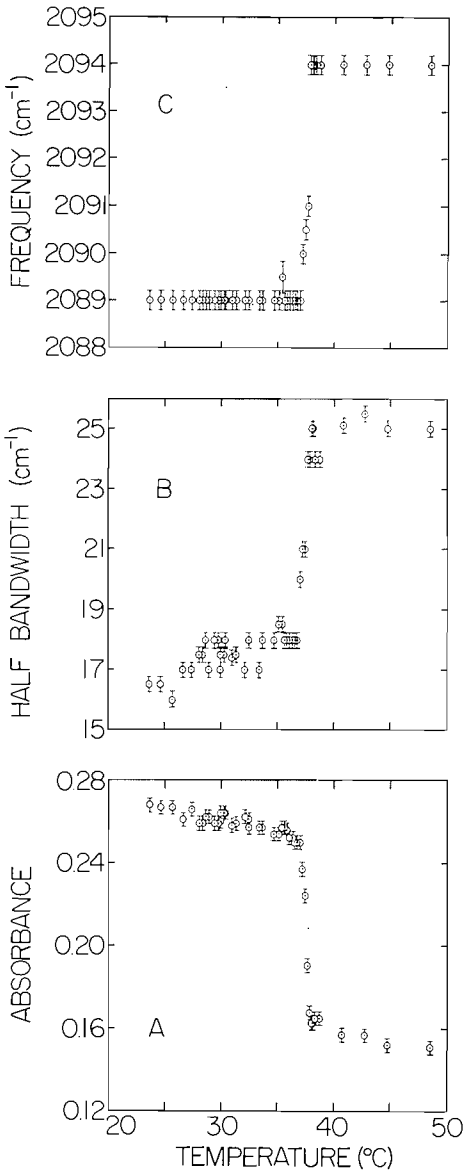

FIG. 3. Temperature dependence of the band with the frequency maximum at ~2089 cm^{-1} in the infrared spectrum of multilayer dispersions of DPPC-d_{62}: (*A*) absorbance; (*B*) halfwidth; (*C*) frequency of the maximum.

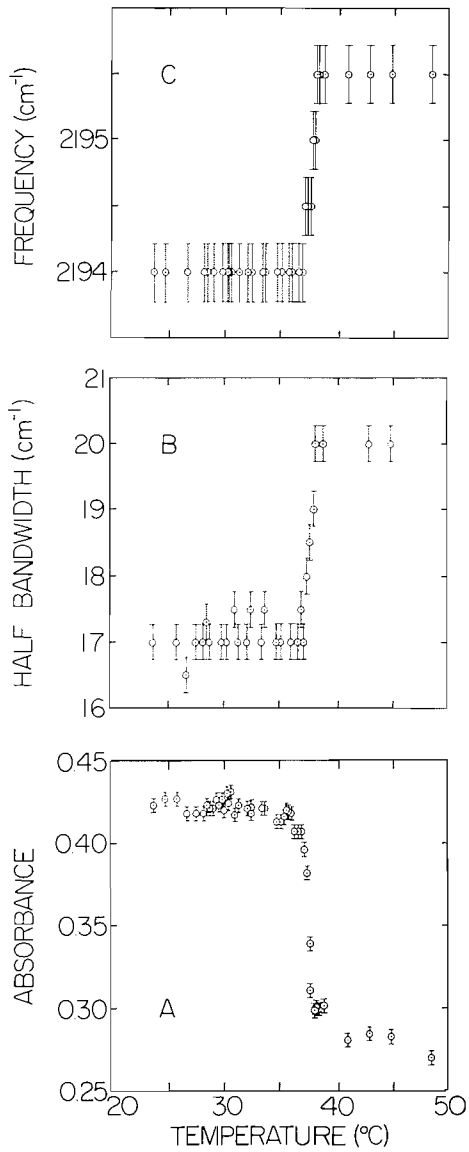

FIG. 4. Temperature dependence of the band with the frequency maximum at ~2194 cm^{-1} in the infrared spectrum of multilayer dispersions of DPPC-d_{62}: (*A*) absorbance; (*B*) halfwidth; (*C*) frequency of the maximum.

We also observe that the main transition is extremely sharp, being essentially complete within seven-tenths of a degree.

The multilayer dispersions of the corresponding light compounds, i.e., DPPC-d_0 also indicated a sharp transition at 41.5 ± 0.2°C in the infrared study. Again the 'pretransition' was not seen very convincingly in the temperature plots. This suggests that at the pretransition the changes in the spectral parameters used here are not much larger than the experimental uncertainty in the present measurements.

The lowering in the phase transition temperature on deuteration is probably related to the slightly lower value of the CD bond length compared with that of the CH bond length. This slightly lowered carbon–hydrogen bond length probably decreases the interlocking of the hydrocarbon chains which facilitates the onset of disorder at lower temperatures.

Here it may be mentioned that a recent study of the

Can. J. Chem. Downloaded from www.nrcresearchpress.com by 210.87.254.5 on 09/05/12
For personal use only.

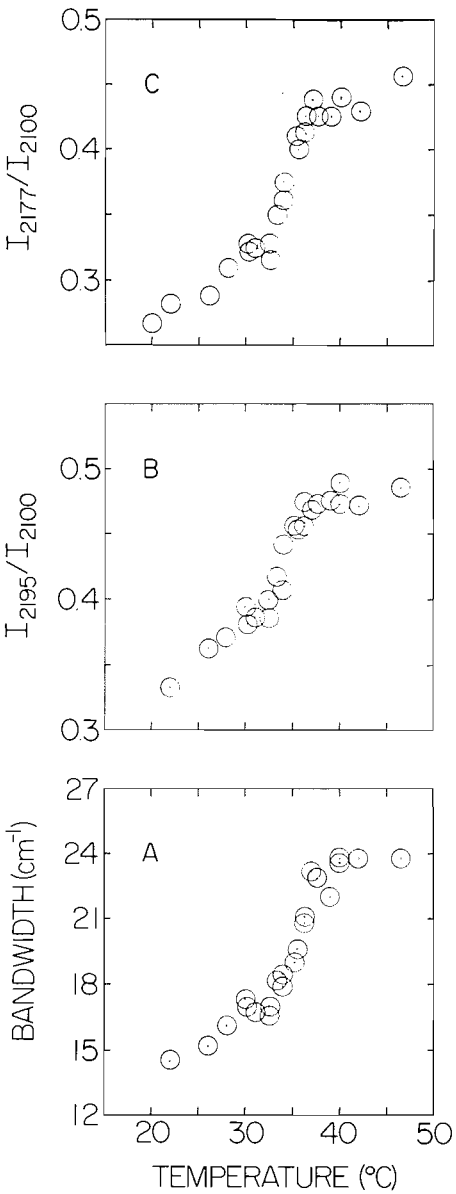

FIG. 5. Temperature dependence of the bands in the CD stretching region of Raman spectrum of multilayer dispersions of DPPC-d_{62}: (*A*) bandwidth of the band ~2100 cm^{-1}; (*B*) ratio of the intensities of bands with maxima at ~2195 and ~2100 cm^{-1}; (*C*) ratio of the intensities of the band with maxima at ~2177 and ~2100 cm^{-1}.

order–disorder phase transition in the molecular crystal charge transfer complex of naphthalene and tetracyanobenzene indicated that when the naphthalene-d_0 is replaced by naphthalene-d_8, the transition temperature is lowered by about 7°C.[2] Although the two systems, glycerophospholipid bilayers and molecular crystal complexes are quite different, the effect of deuteration on the order–disorder transition temperature is in the same direction in both cases. It appears necessary to understand first the effect of deuteration itself on the bilayer structure and the phase transitions before one can confidently use the deuterated derivatives as probe molecules.

[2]S. Sunder, W. F. Murphy, and D. Williams. Unpublished results.

Acknowledgments

We are grateful to Dr. I. C. P. Smith for providing DPPC-d_{62} and for stimulating discussions. We thank Mr. Hector Casal for help in measuring some of the infrared spectra. Thanks are also due to Dr. W. Adams for the loan of his Nicolet system and Dr. W. F. Murphy for help in setting it up.

1. G. W. Stockton, C. P. Polnaszek, A. P. Tulloch, F. Hassan, and I. C. P. Smith. Biochemistry, **15**, 954 (1976).
2. G. W. Stockton, K. G. Johnson, K. W. Butler, A. P. Tulloch, Y. Boulanger, I. C. P. Smith, J. N. Davis, and M. Bloom. Nature, **269**, 267 (1977).
3. J. Seelig, H. Gally, and R. Wohlgemuth. Biochim. Biophys. Acta, **467**, 109 (1977).
4. M. F. Brown and J. Seelig. Nature, **269**, 721 (1977).
5. P. A. Kroon, M. Kainosho, and S. I. Chan. Nature, **256**, 582 (1975).
6. B. Bloj and B. Zilversmit. Biochemistry, **16**, 3943 (1977).
7. R. A. Haberkorn, R. G. Griffin, M. D. Meadows, and E. Oldfield. J. Am. Chem. Soc. **99**, 7353 (1977).
8. C. F. Schmidt, Y. Barenholz, C. Huang, and T. E. Thompson. Biochemistry, **16**, 3948 (1977).
9. G. Arvidson, G. Lindblom, and T. Drakenberg. FEBS Lett. **54**, 249 (1975).
10. B. de Kruyff, A. M. H. P. Van Deen Beselaar, and L. L. M. Van Deenen. Biochim. Biophys. Acta, **465**, 443 (1977).
11. B. de Kruyff and K. W. A. Wirtz. Biochim. Biophys. Acta, **468**, 318 (1977).
12. A. M. W. Lancee-Hermkens and B. de Kruyff. Biochim. Biophys. Acta, **470**, 141 (1977).
13. N. O. Petersen, P. K. Kroon, M. Kainosho, and S. I. Chan. Chem. Phys. Lipids, **14**, 343 (1975).
14. K. Larsson. Chem. Phys. Lipids, **10**, 165 (1973).
15. S. Sunder, R. Mendelsohn, and H. J. Bernstein. Chem. Phys. Lipids, **17**, 456 (1976).
16. R. Mendelsohn, S. Sunder, and H. J. Bernstein. Biochim. Biophys. Acta, **443**, 613 (1976).
17. Y. Koyama, S. Toda, and Y. Kyogoku. Chem. Phys. Lipids, **19**, 74 (1977).
18. S. P. Verma and D. F. Wallach. Biochim. Biophys. Acta, **486**, 217 (1977).
19. M. R. Bunow and I. W. Levin. Biochim. Biophys. Acta, **489**, 191 (1977).
20. R. N. Jones and R. A. Ripely. Can. J. Chem. **42**, 305 (1964).
21. K. W. Butler, A. W. Hanson. I. C. P. Smith, and H. Schneider. Can. J. Biochem. **51**, 980 (1973).
22. S. Sunder and R. E. D. McClung. Chem. Phys. **2**, 467 (1973).
23. J. L. Lippert and W. L. Peticolas. Proc. Natl. Acad. Sci. U.S.A. **68**, 1572 (1971).
24. J. L. Lippert and W. L. Peticolas. Biochim. Biophys. Acta, **282**, 8 (1972).

25. B. J. BULKIN and N. KRISHNAMACHARI. J. Am. Chem. Soc. **94**, 1109 (1972).
26. R. MENDELSOHN. Biochim. Biophys. Acta, **290**, 15 (1972).
27. K. G. BROWN, W. L. PETICOLAS, and E. BROWN. Biochem. Biophys. Res. Commun. **54**, 358 (1973).
28. R. C. SPIKER, JR. and I. W. LEVIN. Biochim. Biophys. Acta, **433**, 457 (1976); **455**, 560 (1976).
29. M. R. BUNOW and I. W. LEVIN. Biochim. Biophys. Acta, **464**, 202 (1977).
30. S. P. VERMA and D. F. H. WALLACH. Proc. Natl. Acad. Sci. U.S.A. **73**, 3558 (1976).
31. R. FAIMAN, K. LARSSON, and D. A. LONG. J. Raman Spectrosc. **5**, 3 (1976).
32. L. J. LIS, S. C. GOHEEN, and J. W. KAUFFMAN. Biochem. Biophys. Res. Commun. **72**, 492 (1977).
33. B. P. GABER and W. L. PETICOLAS. Biochim. Biophys. Acta, **465**, 260 (1977).
34. E. WEIDEKAMM, E. BAMBERG, D. BRDICZKA, G. WILDERMUTH, F. MACCO, W. LEHMANN, and R. WEBBER. Biochim. Biophys. Acta, **464**, 442 (1977).
35. R. MENDELSOHN, S. SUNDER, and H. J. BERNSTEIN. Biochim. Biophys. Acta, **413**, 329 (1975).
36. R. MENDELSOHN, S. SUNDER, and H. J. BERNSTEIN. Biochim. Biophys. Acta, **419**, 563 (1976).
37. J. E. BERTIE and S. SUNDER. J. Chem. Phys. **59**, 3853 (1973).
38. E. WHALLEY and J. E. BERTIE. J. Chem. Phys. **46**, 1264 (1967).

Can. J. Chem. Downloaded from www.nrcresearchpress.com by 210.87.254.5 on 09/05/12
For personal use only.

Excess volumes of chloroform and bromoform mixtures with some *n*-alcohols at 303.15 K

PREM P. SINGH
Department of Chemistry, Punjab Agricultural University, Ludhiana, India
BUTA R. SHARMA
Department of Chemistry, D.A.V. College, Jullundur, India
AND
KULJIT S. SIDHU
Department of Chemistry, Panjabi University, Patiala, India

Received December 5, 1977

PREM P. SINGH, BUTA R. SHARMA, and KULJIT S. SIDHU. Can. J. Chem. **56**, 2127 (1978).

Excess volumes of binary mixtures of chloroform and bromoform with the following *n*-alcohols: methanol, ethanol, and *n*-propanol have been measured as a function of composition at 303.15 K by a dilatometric method.

PREM P. SINGH, BUTA R. SHARMA et KULJIT S. SIDHU. Can. J. Chem. **56**, 2127 (1978).

On a mesuré les volumes d'excès de mélanges binaires de chloroforme et de bromoforme avec les alcools suivants: méthanol, éthanol et propanol; ces mesures ont été effectuées en fonction de la composition à 303.15 K par une méthode dilatométrique.

[Traduit par le journal]

Introduction

Alcohols are strongly self-associated (1) but there is considerable disagreement as to the identification of the predominant associated species (2–5). Furthermore, for binary solution rich in alcohol a three-dimensional network of hydrogen bonded alcohol molecules is believed to be present (6, 7). The purpose of the present investigation is to study the effect of chloroform or bromoform on the excess volumes of their mixtures with some normal alcohols.

Experimental

Materials

Analytical grade chloroform, bromoform, methanol, ethanol, and *n*-propanol were purified by standard procedures (8). Their densities at 298.15 ± 0.01 K (except for chloroform and bromoform for which they were measured at 303.15 ± 0.01 K) agreed within 0.00008 g cm^{-3} with those in the literature (9–11). Excess volumes as a function of composition[1] were determined dilatometrically (12) and are shown in Fig. 1.

Results

The results at 303.15 ± 0.01 K are given in Table 1.[1] The results were fitted to the expression

$$[1]\quad V^E/x_A x_B \text{ cm}^3 \text{ mol}^{-1} = [V_0 + V_1(x_A - x_B) + V_2(x_A - x_B)^2]$$

where V_0, V_1, and V_2 are adjustable parameters and x_A and x_B are the mole fractions of components A and B in the mixture. The parameters were evaluated by fitting experimental values of $V^E/x_A x_B$ to [1] by the method of least-squares. The values obtained are given in Table 2. The standard deviation $\sigma(V^E)$ is also given.

[1]A complete set of the V^E data is available, at a nominal charge, from the Depository of Unpublished Data, CISTI, National Research Council of Canada, Ottawa, Ont., Canada K1A 0S2.

Discussion

The excess volumes V^E for chloroform (A) + methanol (B) and bromoform (A) + methanol (B) are all negative and the curves against x_A are not symmetrical about $x_A = 0.50$. For chloroform + ethanol and bromoform + ethanol, V^E is positive at high mole fractions of chloroform or bromoform in these mixtures but is negative over the rest of the concentration range. Furthermore, V^E is consistently more negative throughout the entire chloroform or bromoform concentration range and the minima shift to still lower x_A when chloroform is replaced by bromoform in its mixture with these alcohols. The V^E data for chloroform + *n*-propanol and bromoform + *n*-propanol are negative to about 50 mol% of chloroform or bromoform and subsequently become positive for solutions rich in chloroform or bromoform. However, V^E is consistently more positive for the latter mixture as compared to the former mixture. Moreover, while for equimolar mixtures or those rich in chloroform or bromoform, V^E increases in the order *n*-propanol > ethanol > methanol, it increases in the order *n*-propanol > methanol > ethanol for solutions for which $x_A = 0.35$.

Numerous studies (12–14) indicate that alcohols are associated through hydrogen-bonded linear chains (with restricted rotation about hydrogen bonds) into variable degrees of polymerisation. The observed V^E data for these mixtures may be explained if it is assumed that (*i*) alcohols have a three-dimensional hydrogen-bonded network and the addition of

Can. J. Chem. Downloaded from www.nrcresearchpress.com by 210.87.254.42 on 09/05/12
For personal use only.

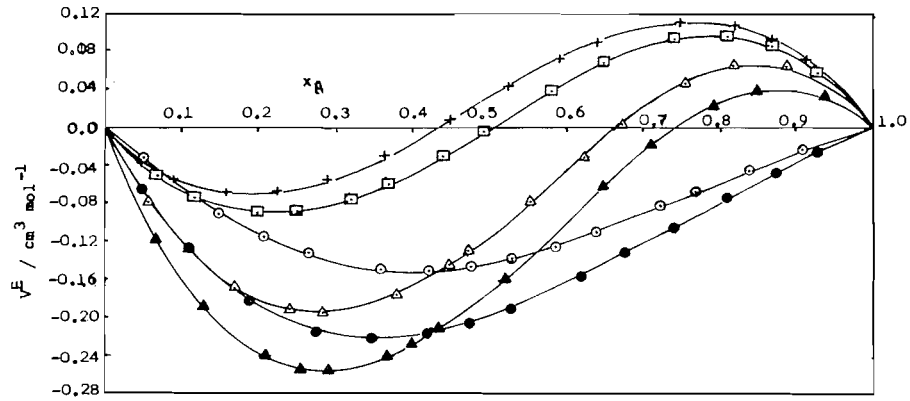

FIG. 1. Volumes of mixing V^E plotted against mole fraction x_A of chloroform or bromoform at 303.15 K for the systems: ○, chloroform + methanol; △, chloroform + ethanol; □, chloroform + *n*-propanol; ●, bromoform + methanol; ▲, bromoform + ethanol; +, bromoform + *n*-propanol.

TABLE 2. Values of the parameters of [1] for the various mixtures at 303.15 K; also given is the standard deviation $\sigma(V^E)$

Mixture	V_0	V_1	V_2	$\sigma(V^E)$ (cm^3 mol^{-1})
Chloroform (A) + methanol (B)	−0.5770	0.2705	0.1055	0.0006
Chloroform (A) + ethanol (B)	−0.4570	1.2639	0.2011	0.0006
Chloroform (A) + *n*-propanol (B)	−0.0050	0.9818	0.0843	0.0005
Bromoform (A) + methanol (B)	−0.8010	0.5625	−0.1023	0.0005
Bromoform (A) + ethanol (B)	−0.6890	1.3479	0.0700	0.0006
Bromoform (A) + *n*-propanol (B)	0.1290	0.9369	−0.0129	0.0007

the second component A causes rupture of some of the hydrogen bonds, (*ii*) the alcohol chain fragments then interact with the component (A) due to specific

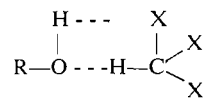

(X = Cl or Br) interactions, and that there is (*iii*) steric repulsion between the alkyl chain of the alcohol and the X (X = Cl or Br) of the CHX_3. The observed V^E would then be the cumulative sum of the contributions due to these factors; the factors (*i*) and (*iii*) require an increase of volume whereas factor (*ii*) requires a decrease. The V^E data for methanol + chloroform and methanol + bromoform suggest that the contribution due to the factor (*ii*) always outweighs those due to the factors (*i*) and (*iii*); consequently V^E is negative throughout the entire concentration range. For other mixtures, depending upon x_A, these factors make appreciable contributions to the volume, so that V^E is either positive or negative. Furthermore, for the same CHX_3, since steric repulsion due to factor (*iii*) mentioned above would increase in the order *n*-propanol > ethanol > methanol, V^E for *n*-propanol + CHX_3 should be positive at a lower x_A as compared to that for ethanol + CHX_3. The V^E data support this conjecture. This scheme of analysis would then expect that V^E should be more positive for *n*-propanol + bromoform as compared to that for *n*-propanol + chloroform as indeed has been observed.

1. F. FRANKS and D. J. G. IVES. Q. Rev. **1**, 20 (1966).
2. G. C. PIMENTAL and A. L. MCCLELLAN. The hydrogen bond. W. H. Freeman, San Francisco, CA. 1960.
3. K. B. WHETSEL and J. H. LADY. Spectrometry of fuels. Plenum Press, New York, NY. 1970. pp. 259–279.
4. E. M. WOOLLEY, J. G. TRAVERS, B. P. ERNO, and L. G. HEPLER. J. Phys. Chem. **75**, 3591 (1971).
5. J. R. JOHNSON, S. D. CHRISTIAN, and H. E. AFFSPRUNG. J. Chem. Soc. A, 764 (1967).
6. J. S. ROWLINSON. Liquid and liquid mixtures. 2nd ed. Butterworths, London. 1969. p. 159.
7. I. PRIGOGINE and R. DEFAY. Chemical thermodynamics. *Translated by* D. H. Evereth. Longman Green & Co., London. 1953. p. 470.
8. A. VOGEL. Practical organic chemistry. Longman Green & Co., London. 1968.
9. T. J. V. FINDLAY and J. L. COPP. Trans. Faraday Soc. **65**, 1463 (1969).
10. D. P. BIDDISCOMBE, E. A. COULSON, R. HANDLEY, and E. F. G. HERRINGTEN. J. Chem. Soc. 1954 (1957).
11. B. E. Trav. Bur. Int. Et. Phys. Chim. Bursselles, J. Chim. Phys. **23**, 733 (1926) quoted from J. Timmerman. Physico-chemical constants of pure organic liquids. Elsevier Publ. Co., Inc., New York, NY. 1950. p. 226.
12. R. K. NIGAM and P. P. SINGH. Trans. Faraday Soc. **65**, 961 (1969).
13. W. H. ZACHARIASEN. J. Chem. Phys. **3**, 158 (1935).
14. R. MECKE. Discuss. Faraday Soc. **9**, 161 (1950).
15. R. MECHE, A. REUTER, and R. SCHUPP. Z. Naturforsch. **49**, 1982 (1949).

Can. J. Chem. Downloaded from www.nrcresearchpress.com by 210.87.254.42 on 09/05/12
For personal use only.

Carbon-13 nuclear magnetic resonance studies of (*Z*)-5-fluoro-2-methyl-1-{[*p*-(methylsulfinyl)phenyl] methylene}-1*H*-indene-3-acetic acid (sulindac) and some related compounds

ALAN WILMOT DOUGLAS

Merck Sharp and Dohme Research Laboratories, P.O. Box 2000, Rahway, NJ 07065, U.S.A.

Received February 20, 1978

ALAN WILMOT DOUGLAS. Can. J. Chem. **56**, 2129 (1978).

Carbon-13 nuclear magnetic resonance spectra have been obtained and fully assigned for a number of 2-methyl-1-{[*p*-(methylthio) or -(methylsulfinyl)phenyl]methylene}-1*H*-indene-3-acetic acid derivatives, including the potent anti-inflammatory compound sulindac, **1***Z*. Paired *E* and *Z* isomers were studied along with the sulindac sodium salt and ethyl ester in the *Z* series. Variations in steric crowding in *E* vs. *Z* isomers produce chemical shift effects which alternate with the number of intervening bonds. Fluorine substituent effects and ^{19}F nuclear spin coupling to ^{13}C nuclei, second-order features in off-resonance proton-decoupled spectra, and values of long-range ^{13}CH nuclear spin coupling constants have been employed in making a complete set of assignments.

ALAN WILMOT DOUGLAS. Can. J. Chem. **56**, 2129 (1978).

On a obtenu les spectres de résonance magnétique nucléaire du carbone 13 et l'on fait des attributions complètes pour un certain nombre de dérivés d'acide méthyl-2 {[*p*-(méthylthio) ou -(méthylsulfinyl)phényl] méthylène}-1*H* indène-acétique-3, dont le composé anti-inflammatoire très efficace sulindac, **1***Z*. On a étudié les paires d'isomères *E* et *Z* de même que les isomères *Z* du sel de sodium du sulindac ainsi que de son ester éthylique. Les variations de l'encombrement stérique dans les isomères *E* en comparaison avec les *Z* conduisent à des effets de déplacements chimiques qui alternent avec le nombre de liens. On a utilisé les effets des substituants fluor, les couplages de spin du ^{19}F avec le noyau ^{13}C, les caractéristiques du second ordre dans le spectre de proton partiellement découplé ainsi que les valeurs à longues distances des constantes de couplage de spin nucléaire ^{13}CH pour faire les attributions complètes.

[Traduit par le journal]

Introduction

In support of the development of a synthetic route (1) to sulindac, (*Z*)-5-fluoro-2-methyl-1-{[*p*-(methylsulfinyl)phenyl]methylene} - 1*H* - indene - 3 - acetic acid, **1***Z*, a potent, nonsteroidal anti-inflammatory agent (1*a*), carbon-13 nmr studies of this and several related compounds were undertaken. As is often the case with large molecules, a number of techniques was required in order to arrive at a complete set of assignments of ^{13}C nmr signals to the structures. In addition to recognition of characteristic chemical shifts (ref. 2, Chapts. 2–5; ref. 3, Chapts. 3, 5, and 8) for saturated, unsaturated, and functional carbons, substituent effects (4, 5; compare ref. 5 with ref. 2, Chapt. 4 and ref. 3, Chapt. 5) in aromatic systems can be useful; effects of fluorine (6), methylthio (7), and methylsulfinyl (7) groups have been employed here. Off-resonance proton-decoupled ^{13}C spectra reveal proton population on carbon atoms as 0, 1, 2, or 3 by the appearance of singlets, doublets, triplets, or quartets, respectively (ref. 2, Chapt. 1; ref. 3, Chapt. 2). Depending upon proton–proton coupling constants, however, certain second-order effects appear in off-resonance decoupled spectra (8–11) and these may be used in distinguishing among possible assignments. In particular, distinction of 'isolated' aromatic ^{13}C—H groups, i.e., those not flanked by other hydrogen atoms, is straightforward in the compounds studied here. Comparison of ^{13}C–F spin coupling constants in the fluorinated indene moiety with those of fluorobenzene (12) was also made. Long range ^{13}C–H coupling constants were used particularly to identify three-bond relationships of carbon nuclei and protons (13, 14) as well as to confirm the *Z* and *E* geometries of benzylidene groups originally assigned from proton nmr considerations (1*b*, 15). Interesting γ-shielding (ref. 3, Chapt. 3) and δ-deshielding (16, 17) effects due to the proximate benzylidene ring occur in the indenyl moiety, and correlation of behavior on *Z* vs. *E* isomers served to complete the assignment process.

Results and Discussion

Carbon-13 chemical shifts have been obtained and assigned for all carbon atoms of *Z* and *E* isomers of the sulfinyl and sulfide compounds **1***Z*, **1***E*, **2***Z*, and **2***E*, as well as for *Z* isomers of the desfluoro and desfluorodesoxy compounds **3** and **4**, respectively, and the sodium salt and ethyl ester of **1***Z*, **5**, and **6**,

Can. J. Chem. Downloaded from www.nrcresearchpress.com by 210.87.254.105 on 09/05/12
For personal use only.

Can. J. Chem. Downloaded from www.nrcresearchpress.com by 210.87.254.105 on 09/05/12
For personal use only.

TABLE 1. Carbon-13 chemical shifts

Compound	Solvent[a]	Concentration (*M*)	1	2	3	4	5	6
1*Z*	D	0.5	140.4	137.8	132.5	106.0	162.5	110.4
1*Z*	C–M	0.5	141.9	138.2	132.4	106.2	163.4	110.7
1*E*	C–M	[b]	141.0	135.2	136.6	106.0	163.5	111.2
2*Z*	D	0.5	139.1	138.0	131.7	105.7	162.4	110.2
2*E*	D	0.2	138.7	134.4	136.2	105.5	162.4	110.5
3	D	0.5	141.6	135.5	133.3	118.4	128.1	124.5
4	D	0.5	140.3	135.7	132.5	118.3	127.8	124.3
5	D	0.25	141.3	134.7	137.5	106.7	162.4	109.6
6	C–M	0.5	141.8	138.4	132.0	106.2	163.5	110.8

[a]D, DMSO-d_6; C–M, ~9:1 $CDCl_3$–CD_3OD.
[b]Saturated solution. Compounds **1***E* and **6** were studied only in the chloroform–methanol medium for convenience in sample recovery; 1*Z* was studied in the same medium for comparison.
[c]Partially obscured by the stronger signal due to C 3′,5′.

respectively. Data are presented in Table 1, where values for **1***Z* are reported for DMSO-d_6 and approximately 9:1 v/v $CDCl_3$–CD_3OD solvents. Compound **1***E* and ester **6** were run only in the mixed solvent; all other compounds were run in DMSO-d_6. Concentrations and solvents are indicated in Table 1. Carbon-13–fluorine nuclear spin coupling constants for **1***Z*, **1***E*, **2***Z*, **2***E*, **5** and **6** are presented in Table 2, where the corresponding values in fluorobenzene (12) also appear. Assignments of C5, C7, C8, and the pair C4 and C6 are firmly established by association of their ^{13}C–F coupling with ^{13}C–F spin coupling in fluorobenzene. Distinction between C4 and C6 was based on off-resonance proton decoupling results (below).

Consideration of ^{13}C–^{19}F coupling alone does not

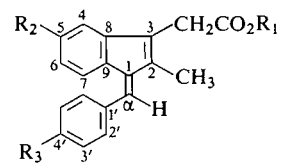

1*Z* $R_1 = H, R_2 = F, R_3 = S(O)CH_3$
2*Z* $R_1 = H, R_2 = F, R_3 = SCH_3$
3 $R_1 = R_2 = H, R_3 = S(O)CH_3$
4 $R_1 = R_2 = H, R_3 = SCH_3$
5 $R_1 = Na^+, R_2 = F, R_3 = S(O)CH_3$
6 $R_1 = C_2H_5, R_2 = F, R_3 = S(O)CH_3$

allow distinction between carbons assigned as C3 and C9 but this choice may be made based upon long-range ^{13}C–H coupling. The fluorine splitting of C3 is in accord with similar ones found in fluorotoluenes (12) or fluorobenzocycloalkanes (18) for a 'zig-zag' path. In benzene (19) or substituted benzenes only the one- and three-bond ^{13}C–H couplings are larger than about 1–2 Hz. In addition to the small fluorine splitting, the pattern observed for the signal assigned to C9 in **1***Z* was a gross quartet due to three non-identical, long-range splittings ascribed to H4, H6, and the benzylidene hydrogen. The sum of the three couplings, all through planar three-bond pathways, was some 24.5 Hz. The appearance of the pattern indicated that one of these couplings was nearly 10 Hz with the other two approximately equivalent at about 7–8 Hz. Carbon 9 is expected to be split by 7–8 Hz by H4 and H6 based on observations in benzene (19) or fluorobenzene (20). For **1***E* a similar quartet of long-range couplings to the carbon signal assigned to C9 is observed, indicating three splittings essentially equivalent at approximately 7 Hz. On the other hand, the proton-coupled pattern of C3 in **1***Z*, although partially obscured, shows no clearly resolved splittings. In **1***E* the proton-coupled signal for C3 is clearly visible and is only a broad multiplet revealing no details of long-range proton coupling.

Values of ~7 and ~10 Hz for the three-bond coupling of C9 to the benzylidene hydrogen in the *E* and *Z* isomers, respectively, are in agreement with the familiar geometrical rules governing ^{13}C–H (and H–H) couplings through olefinic bonds (ref. 21 and references therein) and therefore fully support isomeric structure assignments made earlier on the basis of shielding anisotropy in ^1H nmr spectra (1*b*, 15).

It may be noted in Table 1 that differential shift effects for corresponding *Z* and *E* isomers for C7 and the 2-CH_3 'anticorrelate' with one another, i.e., the isomeric variation which shifts one of these carbons upfield shifts the other down, with the size of the differential shift approximately 3.5 ppm. These are quite reasonable proximity effects (not, it may be noted, anisotropic shielding effects as observed for corresponding protons in earlier ^1H nmr studies (15)) consistent with the established *Z*–*E* isomerism of the compounds. Although it must be emphasized that the complementary behavior of C7 and the 2-CH_3 is the key point, it is of interest to note at least similar deshielding effects upon δ substitution have been observed in 1,8-dimethylnaphthalene (16) as well as in several aliphatic systems (16, 22).

in sulindac and related compounds

7	8	9	Benzal (Cα)	1′	2′,6′	3′,5′	4′	2-CH_3	3-CH_2	Carboxyl	SCH_3
123.1	147.0	129.4	129.4	138.5	129.9	123.9	146.3	10.2	31.1	171.5	43.1
123.7	147.1	129.7	128.0	140.2	130.5	124.1	144.2	10.4	31.7	172.9	43.2
119.7	144.2	132.9	126.8	140.1	130.6	123.5	144.0	14.2	31.6	172.7	43.2
123.0	146.8	129.6	130.4	132.3	129.8	125.5	139.1	10.2	31.1	171.5	14.3
120.0	143.7	133.2	129.4	132.2	130.2	125.1	138.7	14.0	31.2	171.3	14.3
122.0	144.4	133.3	129.2	138.9	129.9	123.8	146.2	10.1	31.3	171.6	43.1
121.9	144.3	133.6	130.2	132.5	129.9	125.5	138.9	10.2	31.3	171.7	14.4
122.5	148.7	129.7	127.0	139.0	129.9	123.8	145.8	10.2	36.1	173.3	43.1
~123.8[c]	147.1	129.7	128.3	140.0	130.5	124.0	144.8	10.5	31.9	170.6	43.5

TABLE 2. ^{13}C–^{19}F nuclear spin couplings[a] in 5-fluoroindene derivatives and fluorobenzene

Compound	Position (coupling type) 3 ($^4J_{CF}$)	4 ($^2J_{CF}$)	5 ($^1J_{CF}$)	6 ($^2J_{CF}$)	7 ($^3J_{CF}$)	8 ($^3J_{CF}$)	9 ($^4J_{CF}$)
1*Z*	2[b] 3[c]	24[b,c]	245[b] 246[c]	23[b,c]	9[b,c]	9[b,c]	3[b,c]
1*E*	2	24	244	24	9	7	2
2*Z*	3	24	243	23	9	9	3
2*E*	2	24	241	23	9	9	3
5	2	23	243	23	8	9	3
6[d]	3	24	247	23	~9	9	3
PhF[e]	—	21	245	21	8	8	3

[a]Values in Hz, ±1 Hz, except $^1J_{CF}$, ±2 Hz.
[b]DMSO-d_6 solution.
[c]~9:1 $CDCl_3$–CD_3OD solution.
[d]$^6J_{CF}$ = 1½ Hz to Cα.
[e]Reference 12.

A similar complementarity must be called upon to distinguish between C1 and C2 of the indene ring system in these molecules, i.e., complementary behavior of C2 and C9 will be anticipated, while the observation of a small, long-range splitting by fluorine is taken as identifying C3. It is observed that C9 exhibits a significant differential shift to lower field upon going from *Z* to *E* isomers in either methylsulfinyl or methylthio derivatives, the differential shifts being 3.3 and 3.6 ppm, respectively. If C2 is assigned at 138.2 ppm in **1***Z*, 135.2 ppm in its *E* isomer, and at 138.1 and 134.5 ppm, respectively, in the *Z*- and *E*-methylthio analogs, the differential shifts of −3.0 and −3.6 may be taken as reflecting the geometrical complementarity of carbons 2 and 9. Proximity shielding by a γ substituent is common in acyclic and simple cyclic systems (3), although it would have been risky to assume direct transferability of such effects into the present, more complicated structural system.

Distinction of C4 and C6, both *ortho* to fluorine and proton bearing, is straightforward when single-frequency off-resonance decoupling (SFORD) is performed at the hydrogen radio frequency (ref. 2, Chapt. 1, ref. 3, Chapt. 2). For C6, which bears a proton strongly coupled to that at C7, a pattern more complex than a simple doublet appears, further split, of course, by ^{19}F. On the other hand, C4 exhibits a simple doublet of doublets, due to the residual ^{13}C–H coupling and the two-bond ^{13}C–F coupling. The complexity or simplicity of SFORD patterns arises from a Bloch–Siegert collapse of the proton chemical shift (23) with the H–H coupling still exerting its full effect (24, 25).

The preceding arguments suffice to allow confident assignment of the nine carbon atoms of the indene ring system itself. Chemical shifts and SFORD multiplicities make assignments of 2-CH_3, 3-CH_2, CO_2H, and —S(O)CH_3 carbons a routine matter, as well as identifying Cα, the benzal carbon, as the only remaining single sp^2-carbon-bearing hydrogen. Assignment of carbons in the sulfur-bearing ring is also straightforward following the work of Buchanan *et al.* (7). The shifts reported for 4-methanesulfinyltoluene in chloroform agree closely with those in Table 1 for carbons 1′ through 6′ of **1***Z* and **1***E* which were obtained in chloroform–methanol solution, the average deviation being only some 0.7 ppm. In fact, if differences of nearly 1.5 ppm are neglected for C1′, attached here to an olefinic rather than an aliphatic carbon, the average disparity falls

Can. J. Chem. Downloaded from www.nrcresearchpress.com by 210.87.254.105 on 09/05/12
For personal use only.

Can. J. Chem. Downloaded from www.nrcresearchpress.com by 210.87.254.105 on 09/05/12
For personal use only.

to slightly less than 0.5 ppm. Agreement is less impressive for sulfides **2***Z* and **2***E*, although the DMSO solvent employed in the present work obviates a strict comparison with the published chloroform solution results (7). In any event, the assignments for the sulfur-bearing ring, although of no critical importance, may be confidently made as in Table 1. Long-range ^{13}C–H coupling constants support the assignments given, in that C3′ and C5′ exhibit only a single long-range splitting larger than 1–2 Hz, while C2′ and C6′ experience approximately 5 Hz long-range couplings to two protons, one located *meta* on the ring and one situated three bonds away at Cα, i.e., the benzylidene hydrogen.

Attention may now be directed to the 'desfluoro' analogs of sulindac, structures **3** and **4**. The very helpful fluorine splittings are now absent but differential shifts based on a fluorobenzene–benzene comparison (6) may be used, along with SFORD results, to lead to a set of assignments. Table 3 presents fluorine differential shift effects for **1***Z* and its desoxy analog, **2***Z*, which result from the choice of assignments made for the corresponding desfluoro compounds. The effect of fluorine substitution on all carbon atoms of the benzylidene group should be insignificant; in fact no observed incremental shift there exceeds 0.3 ppm in either direction with assignments made as given. Small shifts at C1, C2, and C3 are noted, with the effect at C2 being a downfield incremental shift of 2.3 ppm upon fluorine substitution and the effects at C1 and C3 somewhat smaller in magnitude, 0.8 and 1.4 ppm, and in the opposite direction. No significant effect is observed for the 2-methyl, 3-methylene, or carboxyl carbons.

SFORD experiments confirm the assignments of Cα and of C4 and C7 vs. C5 and C6. The use of 'second-order' effects in off-resonance proton decoupled ^{13}C spectra for assigning the α and β carbons of symmetrically *ortho*-disubstituted benzenes has been noted (9). The desfluoro compounds under discussion here do not possess symmetry as far as 'α' and 'β' carbons of the indene portion of the molecules is concerned but the same distinction in terms of general pattern appearance may be expected in view of the large Bloch–Siegert shift compression (23). That is, effective shifts of only a few Hertz should allow comparable domination of the proton–proton spin couplings in the determination of the second-order patterns as if zero shift conditions actually applied. Results for some coumarins indicate this is the case (11) and it is taken to be true here. Proton spectra of the desfluoro compounds indicate that the protons at C4 through C7 are rather closely spaced in chemical shift and the general appearance of off-resonance proton-decoupled ^{13}C patterns is consistent with the assignments made.

TABLE 3. Differential shift effects (fluoro–desfluoro)

	$\Delta\delta^{13}C$		
Carbon	**3** → **1***Z*	**4** → **2***Z*	C_6H_6 → PhF
C4	−12.4	−12.5	−14.1 (*Co*)
C5	+34.5	+34.6	+35.1 (*Ci*)
C6	−14.1	−14.2	−14.1 (*Co*)
C7	+1.2	+2.1	+1.6 (*Cm*)
C8	+2.7	+2.6	+1.6 (*Cm*)
C9	~−3.9	−2.9	−4.4 (*Cp*)

The situation for Cα is straightforward. It is the only single carbon bearing a single, isolated proton in the molecule, and as such, exhibits a simple doublet under SFORD conditions. The only carbon which actually behaved in this way has been assigned to Cα.

Conclusions

In addition to the better known techniques involving ^{13}C chemical shift arguments, ^{13}C spin coupling to ^{1}H and ^{19}F, and the use of first-order SFORD multiplet patterns, extensions of some of these have been used in obtaining complete ^{13}C spectral assignments for sulindac and related compounds. It is of particular interest that the availability of *Z* and *E* isomer pairs allowed the set of molecules serve as its own model system for assignments involving some of the substituted carbon atoms in the indene moiety. It is often worthwhile to attempt to carry out limited chemical transformations in ^{13}C assignment problems, in addition to focusing on physical parameters such as shielding, spin coupling, relaxation, and the like. If a known variation exists in a localized area of a large structure, whether created by the chemist or as a result of biochemical variations in naturally occurring materials, effects at nearby carbons, even if not directly interpretable in terms of γ or δ effects, etc., may frequently distinguish them from otherwise similar carbons. The same principle holds true for ^{13}C observation of evolving chemistry where mechanistic predictions may be tested against observed ^{13}C spectral modifications which arise when reaction intermediates are observed (26, 27). An interplay of chemical insight and physical data is usually more informative than either used alone.

Second-order effects in SFORD spectra should be useful in a wide variety of situations. In addition to giving aromatic substitution information, distinction of axial vs. equatorial C—H groups in pyranoses and related structures and of methyl groups of *C*-ethyl vs. *N*- or *O*-ethyl groups should follow from inspection of SFORD patterns. In certain large molecules where methyl groups attached to olefinic carbons are interspersed in ^{13}C chemical shift with

Can. J. Chem. Downloaded from www.nrcresearchpress.com by 210.87.254.105 on 09/05/12
For personal use only.

others attached to nonfunctionalized methine or methylene groups, distinction of the former by means of the 'pure' quartets they exhibit in SFORD observations may be made.[1] The governing factors here are the existence of large proton–proton spin couplings and the strong Bloch–Siegert compression of an initially not very large proton chemical shift (23–25). Opportunities for exploitation of this phenomenon should be sought. Only a general knowledge or even a good estimate of proton shift separations is needed to make effective use of complexity vs. simplicity in SFORD patterns.

Experimental

Carbon-13 nmr spectra were obtained with a Varian Associates CFT-20 spectrometer. Typical operation involved 4 kHz spectral widths, 0.5 s acquisition times, 30–45° nutation angles, noise-modulated proton decoupling, and weighting of free induction decays by $\exp(-t/0.4)$. Chemical shifts were referenced to tetramethyl silane (TMS), internal, with most runs in DMSO-d_6 using the solvent as secondary reference at 39.5_3 ppm. SFORD and gated decoupling experiments employed 4 kHz spectral widths, 1.0 s acquisition times, and 1.0 s negative exponential weighting constants. Frequency offsets for SFORD experiments were chosen between approximately 400 and 1000 Hz, as necessary to clearly develop second-order features, with irradiation power levels ($\gamma H_2/2\pi$) of approximately 4.8 kHz for 10 mm or 5.6 kHz for 8 mm sample tubes, respectively.

Desfluoro compounds **3** and **4** have not been previously reported. Synthetic and analytical data are available.

Acknowledgements

Mr. Robert Purick is kindly thanked for preparing the 'desfluoro' compounds, **3** and **4**. Dr. S. H. Pines is thanked for helpful discussion and suggestions.

1. (*a*) T.-Y. Shen and C. A. Winter. Adv. Drug Res. **12**, 89 (1977); (*b*) R. F. Shuman, S. H. Pines, W. E. Shearin, R. F. Czaja, N. L. Abramson, and R. Tull. J. Org. Chem. **42**, 1914 (1977).

[1]R. S. Dewey and A. W. Douglas. Unpublished work, Merck Sharp and Dohme Research Laboratories.

2. G. C. Levy and G. L. Nelson. Carbon-13 nuclear magnetic resonance for organic chemists. J. Wiley and Sons, New York, NY. 1972.
3. J. B. Stothers. Carbon-13 nmr spectroscopy. Academic Press, New York, NY. 1972.
4. P. C. Lauterbur. J. Am. Chem. Soc. **83**, 1846 (1961).
5. H. Spiesecke and W. G. Schneider. J. Chem. Phys. **35**, 731 (1961).
6. T. F. Page, Jr. Mol. Phys. **13**, 523 (1967).
7. G. W. Buchanan, C. Reyes-Zamora, and D. E. Clarke. Can. J. Chem. **52**, 3895 (1974).
8. R. A. Newmark and J. R. Hill. J. Am. Chem. Soc. **95**, 4435 (1973).
9. G. Jikeli, W. Herrig, and H. Gunther. J. Am. Chem. Soc. **96**, 323 (1974).
10. J. B. Grutzner. J. Chem. Soc. Chem. Commun. 64 (1974).
11. N. J. Cussans and T. N. Huckerby. Tetrahedron Lett. 2445 (1975).
12. F. J. Weigert and J. D. Roberts. J. Am. Chem. Soc. **93**, 2361 (1971).
13. G. Govil. J. Chem. Soc. A, 1416 (1967).
14. K. N. Scott. J. Am. Chem. Soc. **94**, 8564 (1972).
15. K. Hoogsteen and N. R. Trenner. J. Org. Chem. **35**, 521 (1970).
16. S. H. Grover, J. P. Guthrie, J. B. Stothers, and C. T. Tan. J. Magn. Reson. **10**, 227 (1973).
17. J. B. Stothers and C. T. Tan. Can. J. Chem. **54**, 917 (1976).
18. W. Adcock, B. D. Gupta, T. C. Khor, D. Doddrell, and W. Kitching. J. Org. Chem. **41**, 751 (1976).
19. F. J. Weigert and J. D. Roberts. J. Am. Chem. Soc. **89**, 2967 (1967).
20. L. Ernst, V. Wray, V. A. Chertkov, and N. M. Sergeyev. J. Magn. Reson. **25**, 123 (1977).
21. A. W. Douglas. Org. Magn. Reson. **9**, 69 (1977).
22. J. I. Kroschwitz, M. Winokur, H. J. Reich, and J. D. Roberts. J. Am. Chem. Soc. **91**, 5927 (1969).
23. F. Bloch and A. Siegert. Phys. Rev. **57**, 522 (1940).
24. H. Fritz and H. Sauter. J. Magn. Reson. **18**, 527 (1975).
25. R. Radeglia. Org. Magn. Reson. **9**, 164 (1977).
26. S. H. Pines and A. W. Douglas. J. Am. Chem. Soc. **98**, 8119 (1976).
27. A. W. Douglas. *In situ* ^{13}C FTNMR studies of chemical reactions, presented at the Sixth International Symposium on Magnetic Resonance, Banff, Alberta, Canada, May 22, 1977; to be submitted for publication.

Phase-transfer catalyzed synthesis of activated cyclopropanes[1]

JOHN M. MCINTOSH AND HAMDY KHALIL

Department of Chemistry, University of Windsor, Windsor, Ont., Canada N9B 3P4

Received March 3, 1978

JOHN M. MCINTOSH and HAMDY KHALIL. Can. J. Chem. **56**, 2134 (1978).

The phase-transfer catalyzed condensation of diethyl bromomalonate (*7d*) with Michael acceptors **8**–**12** leads to cyclopropanes in high yields. More hindered acceptors and other haloesters do not react, while condensation of *7d* with crotonaldehyde leads to a 2:1 adduct via a subsequent Darzens condensation. The synthetic potential of the products is also outlined.

JOHN M. MCINTOSH et HAMDY KHALIL. Can. J. Chem. **56**, 2134 (1978).

La condensation, catalysée par transfert de phase, du bromomalonate de diéthyle (*7d*) avec les accepteurs de Michael **8**–**12** conduit à des cyclopropanes avec de bons rendements. Il n'y a pas de réaction avec des accepteurs empêchés ou d'autres esters halogénés; la condensation de *7d* avec le crotonaldéhyde conduit à un adduit 2:1 par l'intermédiaire d'une condensation subséquente de Darzens. On définit le potentiel de synthèse des produits.

[Traduit par le journal]

Recently our interest has been centered on the use of phase-transfer catalysis of reactions between nucleophiles and conjugated carbonyl compounds. This interest was triggered by the observation that, with apparently very little change in reaction conditions, a complete reversal from conjugate to 1,2-addition occurs. For example, reaction of enones with α- or β-mercaptocarbonyl compounds leads exclusively to products derived by 1,4-addition (1), eq. [1], but addition of cyanide ion leads only to 1,2-addition (2), eq. [2]. Furthermore, the cyclodimerization of crotonaldehyde (**1**) leads,[2] by way of **2**, to **3**, eq. [3]. This also involves conjugate addition as the initial step.

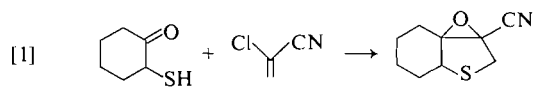

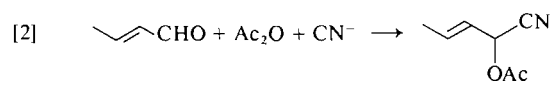

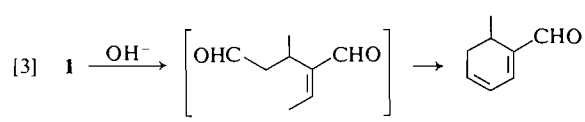

2 **3**

The generally accepted theory of phase-transfer catalysis involves a poorly solvated, tight ion pair (3) as the reactive species. Thus it would appear reasonable that association of the cation Q^+ with the position of highest electron density (the carbonyl oxygen) should lead to preferential 1,2-addition. However, it may be that the nature of the nucleophilic species may play the major role in determining the dominant mode of addition. Thus, soft nucleophiles (e.g., RS^-) would prefer conjugate addition whereas harder ones (e.g., CN^-) would undergo kinetic attack at the carbonyl group (4). To further elucidate the role of the nucleophile, we have investigated some other carbon-based species.

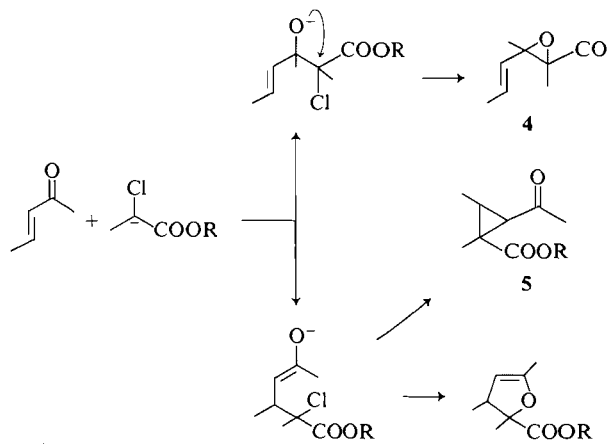

4 **5** **6**

SCHEME 1

The base-catalyzed reaction between α-haloesters and carbonyl groups leads to epoxides (5). This reaction proceeds well under phase-transfer catalysis (1, 6). When conjugated enones are used, three product types (**4**, **5**, or **6**) are possible, depending on the initial mode of addition (Scheme 1). A previous study of this reaction under homogeneous reaction conditions (7) showed that simple α-haloesters afforded products of type **5** under aprotic conditions but not in alcoholic solution. However, using diethyl bromomalonate (DBM, *7d*), the yields of **5** ranged from 45–60% in both protic and aprotic

[1]Phase-transfer catalyzed reactions, Part 3. For Part 2, see ref. 2.

[2]J. M. McIntosh and H. Khalil. Unpublished results.

Can. J. Chem. Downloaded from www.nrcresearchpress.com by 210.87.254.6 on 09/05/12
For personal use only.

Can. J. Chem. Downloaded from www.nrcresearchpress.com by 210.87.254.6 on 09/05/12
For personal use only.

TABLE 1. Phase-transfer reactions

Donor	Acceptor	Product[a]	Yield (%)[b]
$ClCH_2COOEt$ (*7a*)	(**8**)	[c]	—
$BrCH_2COOEt$ (*7b*)	(**9**)	[c]	—
7b	(**10**)	[c]	—
$ClCH_2COOtC_4H_9$ (*7c*)		[c]	—
$BrCH(COOEt)_2$ (*7d*)	**8**	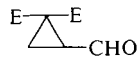 (**18**)[f]	100(70)
7d	**9**	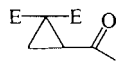 (**19**)[f]	97
7d	**10**	(**20**)	75
7d	(**11**)	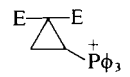 (**21**)	70
7d	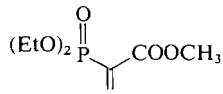 (**12**)	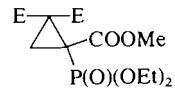 (**22**)	65
7d	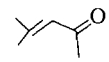 (**13**)	$E_2C{=}CE_2$ (**23**)	[d]
7d	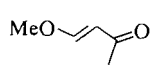 (**14**)	**23**	[d]
7d	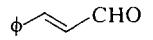 (**15**)	**23**	[d]
7d	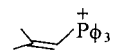 (**16**)	**23**	[d]
7d	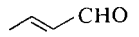 (**1**)	**26**	71(40)[e]

[a]E = COOEt.
[b]Yield quoted is isolated crude yields of greater than 90% purity; values in parentheses are distilled yields.
[c]More than 90% of donor recovered.
[d]Not determined but no other product formed by glc analysis.
[e]Mixture of diastereomers.
[f]See ref. 7.

solvents. In neither case were products of type **4** or **6** reported. In view of the assumed close analogy between phase-transfer and aprotic conditions, we investigated this type of reaction under phase-transfer conditions.

Results and Discussion

The results of the reactions run are summarized in Table 1. Simple α-haloesters ($ClCH_2COOEt$ (*7a*), $BrCH_2COOEt$ (*7b*), and $ClCH_2COOtBu$ (*7c*) did not react at room temperature and could be recovered in high yield. Neither ester hydrolysis nor halogen substitution occurred. In view of the reported (8) successful Darzens condensations using *7c* with unconjugated compounds, it is likely that the anion is being formed but that the reduced electrophilicity of the enone is preventing condensation. Very recent reports (9, 10) of successful cyclopropanations using *7c* show that this reaction will proceed with Michael acceptors which are more stable to the basic reaction conditions (esters, nitriles, sulfones) but these do not address the question of conjugate vs. 1,2-addition.

Reactions of DBM (*7d*) proved more rewarding,

Can. J. Chem. Downloaded from www.nrcresearchpress.com by 210.87.254.6 on 09/05/12
For personal use only.

affording high yields of products of type **5** with acceptors **8–12**, eq. [4]. The only contaminant in

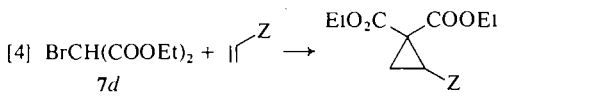

these reactions, aside from some residual starting material, was tetraester **23**. The products were characterized by the lack of a vinyl hydrogen absorption in their nmr spectra. On the other hand, acceptors **13–16** gave **23** as the only isolated product. As in the previous study (7), the presence of two β-substituents completely blocks the conjugate addition but even in these cases no 1,2-addition product was observed.

Condensation of *7d* with acrolein (**8**) occurred normally and afforded **18** in quantitative yield. This could be condensed with a second molecule of *7d* to afford **24**, eq. [5]. However, when crotonaldehyde

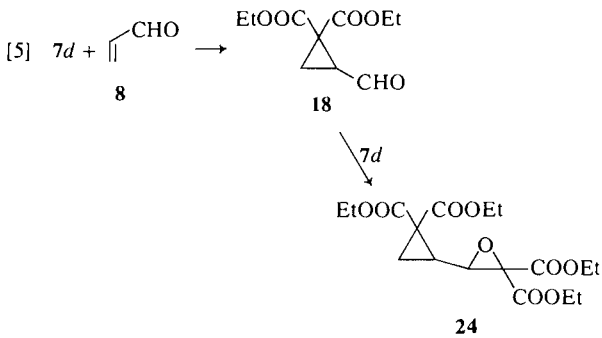

(**1**) was reacted with *7d*, none of the expected **25** could be detected at any time during the reaction, although this is the reported product (7) under homogeneous conditions. The only product formed, in addition to minor amounts of **23**, was **26**, which is analogous to **24**, eq. [6]. To verify the details of

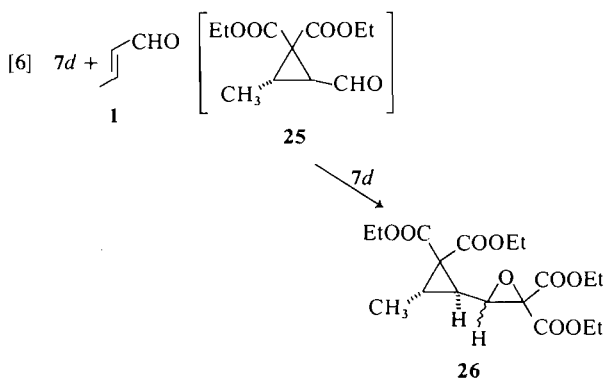

formation of **26**, **25** was prepared (7) and subjected to the usual phase-transfer conditions. An exceptionally rapid reaction occurred, leading exclusively to **26**. It is worthy of mention that a significant by-product in the synthesis of **25** is **26**, which remains as a residue after distillation of **25**. Thus it appears that only the relative rates of the two condensations are different under the two types of reaction conditions.

Both **24** and **26** show a one-proton absorption between δ 3.2–3.6 as a doublet of doublets which we assign to the proton on the oxirane ring. Careful glc analysis indicated the presence of two diastereomers (not separable) in each case. The nmr spectrum of **25** indicates the presence of only one diastereomer (*trans*) and this is supported by its reported transformations (7). Thus further condensation leads to only two diastereomers of **26**. Integration of the doublets at δ 3.47 and 3.27 indicates a 1:2 ratio of diastereomers but the assignment of these is ambiguous. In the case of **24**, the lower field (δ 3.59) doublet is quite sharp but the higher field signal (δ 3.20) is definitely coupled further. In this case the integrated ratios of these two doublets is 2:1.

Although **24** is formed from **18**, we were unable to effect condensation of **19** or simple aldehydes (butanal, cyclohexanecarboxaldehyde) with DBM under comparable conditions! Thus the exclusive formation of **24** remains unexplained.

Another curious result was obtained when we attempted to trap the 1,2-addition product from **1** or **8** and diethyl malonate (**27**) using allyl bromide (2). Reaction of 1 equiv. of each of **27**, **1** (or **8**) and allyl bromide and 10 *N* aqueous sodium hydroxide under the standard conditions led to a rapid disappearance of *all* organic material from the methylene chloride phase. Acidification of the aqueous layer led to moderate yields of the simple Michael addition products **28** and **29**, respectively, eq. [7].

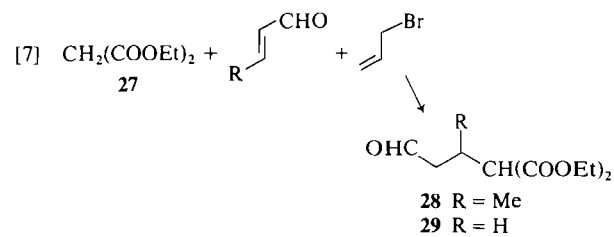

No diethyl allylmalonate was formed. Although it appears that allyl bromide does not enter into this reaction, it is also true that when it is omitted, the yields of **28** and **29** are very substantially reduced and several minor products are also formed. We are unable to offer a reasonable explanation for this result.

TABLE 2. Physical and spectral characteristics of products

Compound	Infrared (cm^{-1})[a]	Nuclear magnetic resonance[b]	Mass spectrum (m/e)[c]
18	1730(b), 1275, 1135, 1320	9.14(d, 1, J = 4 Hz), 4.22 (q, 4, J = 6 Hz), 2.75(m, 1), 2.20–1.70 (m, 2), 1.27 (t, 6, J = 6 Hz)	(214),[d] 29, 140, 169, 86
19	1735, 1720(sh), 1285, 1330	4.20 (q, 2, J = 7 Hz), 4.16 (q, 2, J = 7 Hz), 2.85 (t, 1, J = 7 Hz), 2.33 (s, 3), 1.93 (dd, 1, J = 7.4 Hz) 1.58 (dd, 1, J = 7.4 Hz), 1.25 (t, 3, J = 7 Hz), 1.23 (t, 3, J = 7 Hz)	228, 183, 213, 157, 43
20	1745, 1255, 1380, 1300(d)	4.22 (q, 4, J = 7 Hz), 2.32 (AB q, 2, J = 8 Hz),1.27 (t, 6, J = 7 Hz)	(245),[d,e] 29, 127, 189, 217
21	1740, 1265, 1115, 910	8.0–7.5 (m, 15), 4.35 (q, 2, J = 8 Hz), 3.9–3.25 (m, 3), 2.25–1.68 (m, 1), 1.33 (t, 3, J = 8 Hz), 1.00 (t, 3, J = 8 Hz)	316[f]
22	1745, 1270, 1130, 910	4.55–4.00 (m, 8), 3.75 (s, 3), 2.26 (d, 1, J = 2 Hz), 2.00 (s, 1), 1.6–1.1 (m, 12)	380, 335, 307, 29, 243
26	1740, 1715, 1300, 1240	4.50–4.05 (m, 8), 3.47 and 3.27 (d's, total = 1, J = 5.5 and 8.0 Hz), 2.27–1.48 (m, 2), 1.45–1.01 (m, 15)	(386),[d,e] 281, 28, 282, 283
24	1740, 1715, 1310, 1260	4.51–4.07 (m, 8), 3.59 and 3.20 (d's, total = 1, J = 4.4 and 8 Hz), 2.15–1.10 (m, 15)	(372),[d,e] 29, 169, 140

[a]In chloroform solution; four strongest peaks reported.
[b]Run in $CDCl_3$; tabulation follows the order: chemical shift (δ), multiplicity, number of protons, coupling constant.
[c]Molecular ion followed by four strongest peaks.
[d]Weak or absent.
[e]Confirmed by field ionization experiments.
[f]Run under field desorption conditions (18).

Conclusions

Cyclopropanations of the type reported here appear limited in scope. It appears that synthetically useful yields are obtained only with DBM and unhindered enones. However, only products of 1,4-addition are formed and several of these appear to possess synthetic potential. The recent report (11) of the use of **19** is illustrative. In particular, compounds of type **21** offer the potential of introducing cyclopropylidene residues via the Wittig reaction (12) whereas both **20** and **22** appear to be ideally suited to nucleophilic ring opening (13, 14) with the generation of elaborated olefinic materials. We hope to investigate these in the near future.

On the basis of the available, admittedly incomplete evidence, it appears that the competition between 1,2- and 1,4-addition may be controlled by the hardness of the nucleophilic species (4). The similarity between our results and those of Evans *et al.* (15) using trimethylsilyl cyanide and thiolate in aprotic media is striking and again illustrates the similarity of phase-transfer and aprotic conditions.

Experimental

Nuclear magnetic resonance spectra were run in deuteriochloroform on a JEOL C60HL spectrometer and are reported in ppm downfield from TMS as internal standard; infrared spectra were determined in chloroform solution on a Beckman IR 12 spectrometer. Gas chromatographic analyses were run on an F and M model 720 instrument using a 10 ft column packed with 20% SE 30 on Chromosorb W. Microanalyses were by A. B. Gygli, Microanalyses Laboratory, Toronto, Ont.

Materials

Compounds **9**, **10**, **11**, **13**, **14**, and benzyltriethylammonium chloride were used as purchased. Compounds **1**, **8**, and **15** were distilled before use. Compounds **12** (16) and **16** (17) were prepared as outlined in previous publications.

General Method for Cyclopropanation Reactions

To a mixture of 40 ml of methylene chloride and 4.1 ml of 9.5 *N* aqueous sodium hydroxide (0.04 mol) was added ca. 100 mg of benzyltriethylammonium chloride (TEBAC). The system was purged with nitrogen and cooled to 0°C in an ice–salt bath. To this solution was added a mixture of 0.4 mol of each of the donor and acceptor molecule at 0°C with good stirring. The addition required ca. 10 min. Stirring was continued for 1 h at 0°C and a further 2 h at ambient temperature. The solution was diluted with 35 ml of water, the layers separated, and the organic phase dried over Na_2SO_4. After removal of solvent, anhydrous ether was added and the catalyst removed by filtration. Evaporation afforded an oil which was analyzed by glc. In each case, the product was as shown in Table 1, in some cases contaminated by small amounts (<10%) of tetraester **23**. Products were purified where necessary by chromatography over alumina, using 5% ether – petroleum ether as eluent. Analytical samples were collected from glc. All new compounds gave acceptable elemental analyses; spectral characteristics of the products are presented in Table 2.

1. J. M. McINTOSH and H. KHALIL. J. Org. Chem. **42**, 2123 (1977).
2. J. M. McINTOSH. Can. J. Chem. **55**, 4200 (1977).
3. E. V. DEHMLOW. Angew. Chem. Int. Ed. Engl. **16**, 493 (1977).
4. I. FLEMING. Frontier orbitals and organic chemical reactions. Wiley-Interscience, London. 1976.
5. M. S. NEWMAN and B. J. MAGERLEIN. Org. React. **5**, 413 (1949).
6. A. JONCZYK, M. FEDORYNSKI, and M. MAKOSZA. Tetrahedron Lett. 2395 (1972).

Can. J. Chem. Downloaded from www.nrcresearchpress.com by 210.87.254.6 on 09/05/12
For personal use only.

7. G. VONAVENT, M. CAUSSE, M. GUITARD, and R. FRAISSE-JULIEN. Bull. Soc. Chim. Fr. 2462 (1964).
8. E. D'INCAN and J. SEYDEN-PENNE. C. R. Acad. Sci. Ser. C, **281**, 1031 (1975).
9. A. JONCZYK and M. MAKOSZA. Synthesis, 388 (1976).
10. I. ARTHAUD, J. SEYDEN-PENNE, and P. VIOUT. C. R. Acad. Sci. Ser. C, **283**, 503 (1976).
11. B. M. TROST and W. J. FRAZEE. J. Am. Chem. Soc. **99**, 6124 (1977).
12. E. E. SCHWEIZER, C. J. BERNINGER, and J. G. THOMPSON. J. Org. Chem. **33**, 336 (1968).
13. S. DANISHEFSKY, J. DYNAK, E. HATCH, and M. YANAMOTO. J. Am. Chem. Soc. **96**, 1256 (1974).
14. W. G. DAUBEN and D. J. HART. J. Am. Chem. Soc. **97**, 1622 (1975).
15. D. A. EVANS, L. K. TRUESDALE, K. G. GRIMM, and S. L. NESBITT. J. Am. Chem. Soc. **99**, 5009 (1977).
16. J. M. MCINTOSH and R. A. SIELER. Can. J. Chem. **56**, 226 (1978).
17. J. M. MCINTOSH, H. B. GOODBRAND, and G. M. MASSE. J. Org. Chem. **39**, 202 (1974).
18. G. W. WOOD, J. M. MCINTOSH, and P.-Y. LAU. J. Org. Chem. **40**, 636 (1975).

Can. J. Chem. Downloaded from www.nrcresearchpress.com by 210.87.254.6 on 09/05/12
For personal use only.

Approaches to the synthesis of triterpenoids. IV. The ABC + E ring approach to the pentacyclic triterpene skeleton. Synthesis of a pentacyclic compound suitable for triterpene synthesis[1,2]

JOHN W. APSIMON,[3] SATYANAND BADRIPERSAUD, JOHN W. HOOPER, AND RICHARD PIKE
Department of Chemistry, Carleton University, Ottawa, Ont., Canada K1S 5B6

AND

GEORGE I. BIRNBAUM, CAROL HUBER, AND MICHAEL L. POST
Division of Biological Sciences, National Research Council of Canada, Ottawa, Ont., Canada K1A 0R6

Received January 30, 1978

JOHN W. APSIMON, SATYANAND BADRIPERSAUD, JOHN W. HOOPER, RICHARD PIKE, GEORGE I. BIRNBAUM, CAROL HUBER, and MICHAEL L. POST. Can. J. Chem. **56**, 2139 (1978).

Studies on the ABC + E ring construction of the pentacyclic triterpene skeleton are described. Acid-catalysed cyclisation of the mixture of diastereoisomers **11** led to preferential cyclisation of one isomer to 10-methoxy-2,2,4aβ,6aβ, 12bβ-pentamethyl-1,2,3,4,4a,5,6,6a, 6bα,7,8,12b,13,14-tetradecahydro-1-picenone (**12**). An X-ray analysis was performed on this compound which crystallizes in the monoclinic space group $P2/c$. There are four molecules in the unit cell which has dimensions $a = 6.456(2)$, $b = 42.518(6)$, $c = 8.519(2)$ Å, $\beta = 100.92(3)°$. The structure was solved by direct methods and refined by block-diagonal least-squares to a final R value of 0.042 for all 3234 observed reflections. The molecular structure found by X-ray diffraction confirms the stereochemical reasoning used in the synthetic steps.

JOHN W. APSIMON, SATYANAND BADRIPERSAUD, JOHN W. HOOPER, RICHARD PIKE, GEORGE I. BIRNBAUM, CAROL HUBER et MICHAEL L. POST. Can. J. Chem. **56**, 2139 (1978).

On décrit des études concernant la synthèse des cycles ABC + E du squelette pentacyclique des triterpènes. Une cyclisation acido-catalysée d'un mélange de diastéréoisomères de **11** conduit à la cyclisation préférentielle d'un isomère en méthoxy-10 pentaméthyl-2,2,4aβ,6aβ,12bβ tétradécahydro-1,2,3,4,4a,5,6,6a,6bα,7,8,12b,13,14 picénone-1 (**12**). On a effectué une analyse par rayon X de ce composé qui cristallise dans le groupe d'espace $P2/c$. Il existe quatre molécules par maille de dimension $a = 6.456(2)$, $b = 42.518(6)$, $c = 8.519(2)$ Å, $\beta = 100.92(3)°$. On a résolu la structure par des méthodes directes et on l'a affinée par la méthode des moindres carrés (blocs diagonaux) jusqu'à une valeur finale de R de 0.042 pour les 3234 réflexions observées. La structure moléculaire, qui a été déterminée par diffraction de rayon X, confirme le raisonnement stéréochimique utilisé dans les étapes de la synthèse.

[Traduit par le journal]

We wish to report recent studies aimed at a convergent synthesis[4] of the pentacyclic triterpene system (2) based on an ABC + E ring construction **1**, followed by formation of one bond (dotted in **1**) to

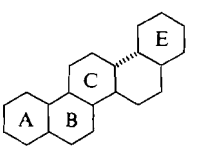

1

yield the polycyclic array. The advantage of this approach lies in the rapid provision of a polycyclic species with preformed stereochemistry, whereas the disadvantage lies in the control of stereochemistry during the vital cyclisation step.

Our basic strategy is outlined in Scheme I. There exists a basic flaw in this plan in that the condensation of two racemates[5] **2** and **3** is unlikely to lead to any chiral induction in view of the distance between the reacting sites and any asymmetry and in fact it is reasonable to expect the production of a 50:50 mixture of the diastereoisomers ***4a***. However, at the outset we felt this route worth pursuing since we were of the opinion from inspection of molecular models and from the belief that the internal aldol-like process (***4b*** → **5**) necessitates a strict stereoelectronic arrangement for cyclisation (3, 4) that one of the diastereoisomers represented as ***4b*** would cyclise preferentially *with respect to* the other, and it ap-

[1]Portions of this work are described in the Ph.D. thesis of S.B. (Carleton University, Ottawa, Ont. 1976). For Part III see ref. 1.

[2]NRCC No. 16712.

[3]To whom inquiries should be directed.

[4]For other successful triterpene syntheses see refs. 4–11 in Part III of this series (1).

[5]With the exception of structure **6**, which represents a natural product, all structures used in this paper represent racemates. Only that enantiomer bearing a direct relationship to the natural series is shown for convenience.

Can. J. Chem. Downloaded from www.nrcresearchpress.com by 210.87.254.5 on 09/05/12
For personal use only.

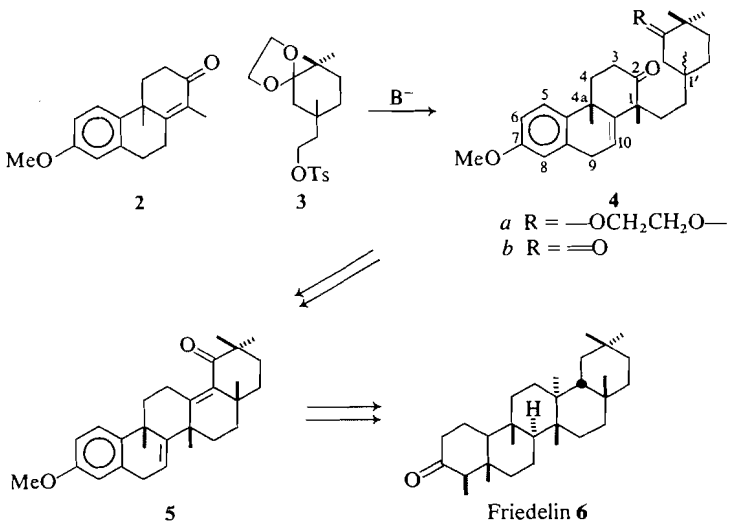

SCHEME 1

peared to us that the isomer cyclising should lead to **5** possessing the correct stereochemistry for further elaboration to friedelin **6**. Thus, although the basic strategy legislated for the loss of 50% of material, the other 50% should consist of a pentacyclic material close in structure to the target molecule. This surmise turned out to be at least partly correct as revealed in the sequel.

As starting material for our work we used tricyclic ketone **2** (5) and the tosylate **3**. The latter compound was available to us from the substituted malononitrile **7** obtained from the potassium fluoride catalysed Michael reaction between 3,3,6-trimethyl-2-cyclohexenone and malononitrile (6). A series of unexceptional steps as outlined in Scheme 2 led to the tosylate **3** in an overall yield of 26% from **7**.

Tricyclic enone **2** was alkylated via its dienolate ion

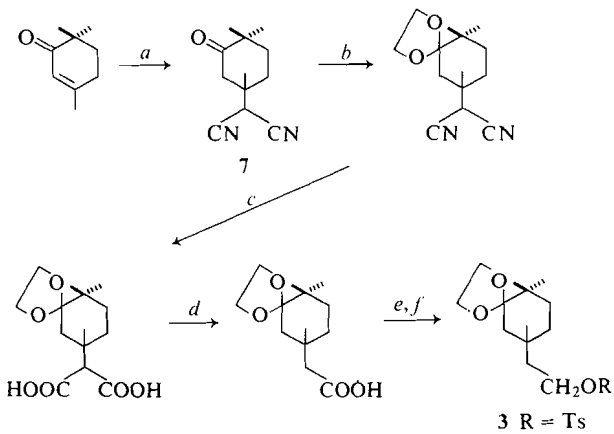

SCHEME 2. Reagents: (*a*) $CH_2(CN)_2$, KF; (*b*) $HOCH_2$-CH_2OH, *p*-TSA–H_2O; (*c*) KOH; (*d*) heat 140–145°C, 2 h; (*e*) $LiAlH_4$; *p*-toluenesulphonyl chloride, pyridine.

generated using potassium *tert*-amyloxide in dry benzene (7), with tosylate **3** to provide **4***a* in 54% yield, which crystallized although nuclear magnetic resonance spectroscopy and thin-layer chromatography indicated a mixture of diastereoisomers to be present. Acid hydrolysis of the ethylene ketal group provided the crystalline mixture of ketones **4***b*. The stereochemistry of the alkylation step at C(1) is based on the observations of previous workers (5,7,8) and on the use of benzene induced shifts of the methyl signals observed in the nmr spectra of our alkylated compounds (5). This assignment is confirmed by the X-ray structure determination quoted later.

Ketone mixture **4***b* was stable in crystalline form but solutions rapidly turned yellow with the formation of another species that was separated by column chromatography on alumina. This material is assigned structure **8** on the basis of its spectroscopic properties[6] including the appearance of the peak at *m/e* 270 in its mass spectrum, arising by cleavage as shown. Compound **8** could also be prepared from **4***b* on oxidation with Jones' reagent indicating the ease of oxidation of the C (9) benzylic-allylic position. Deoxygenated solutions of **4***b* were stable.

We next turned our attention to the cyclisation of the diketone mixture **4***b*. Attempts to effect the intramolecular aldol-like condensation using a variety of bases were singularly unsuccessful under a wide range of conditions. The use of *tert*-butylmagnesium chloride (9) as a cyclisation base at first seemed promising in that one component of the diastereoisomeric mixture reacted (tlc observation) while the other was inert under the conditions used. However, after isola-

[6]For brevity we chose to describe unexceptional spectroscopic values in the experimental section only.

Can. J. Chem. Downloaded from www.nrcresearchpress.com by 210.87.254.5 on 09/05/12
For personal use only.

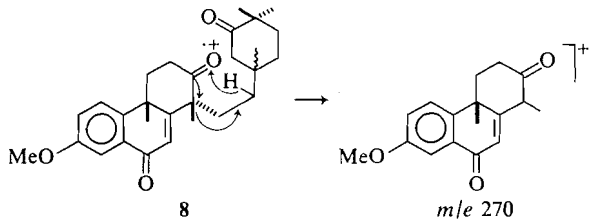

8 *m/e* 270

tion and characterisation it became apparent that simple carbonyl reduction had occurred by hydride transfer from the Grignard reagent (ref. 10 and refs. cited therein) to yield **9** in 39% yield from **4***b* (i.e.,

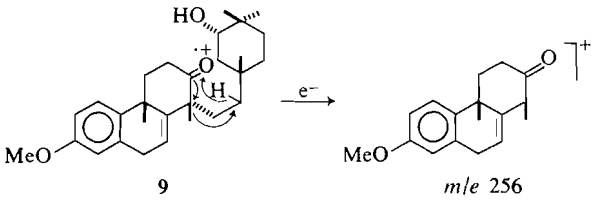

9 *m/e* 256

78% yield based on the reduction of one diastereoisomer). That the ring E carbonyl group had been reduced in this case was supported by the observation that the base peak in the mass spectrum of **9** appears at *m/e* 256 assigned as shown. Further comments on the stereochemistry depicted for **9** are presented later in this report.

With the singular failure of base catalysis to induce cyclisation of **4***b* we next examined acid-induced reactions. In boiling xylene in the presence of *p*-toluenesulphonic acid, **4***b* yields a crystalline product mp 117–121°C whose physical properties indicated a structure far removed from the desired **5**. At first we suspected a simple rearrangement product arising from cation **10** via pathways *a* or *b*. However this

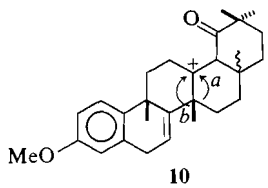

10

proved not to be the case. The structure of this product is discussed in the following paper (11).

It appeared to us that the failure of this cyclisation to provide pentacyclic species could lie in the lability of cation **10** leading to more stable allylic or benzylic species in competing processes. We therefore turned our attention to the cyclisation in the absence of the C(1a)—C(10) double bond in **4***b*. We have previously shown (5, 12) that hydrogenation of compounds related to **4** proceeds stereoselectively depending on the conditions used. In the event, reduction of mixture **4***b* by hydrogen in boiling xylene using palladium-on-charcoal as the catalyst was readily accomplished to yield the mixture of diketones **11**. Once again the stereochemistry assigned (5) to the new chiral centre at C-1a is based on the use of benzene-induced solvent shifts in the nmr spectrum of **11** (See Table 1).

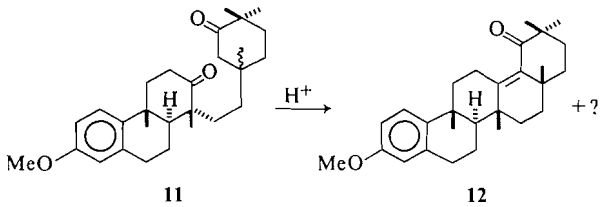

11 12

Reaction of **11** with *p*-toluene sulphonic acid in boiling xylene contradicted our prediction concerning the reactivity of one diastereoisomer compared to the other, since both components of the mixture **11** appeared to cyclise under these conditions. One reaction product crystallised after chromatography on silica gel. This material, mp 182–183°C was obtained in 90% yield based on the cyclisation of one diastereoisomer (i.e., overall 45% yield for this step). The other product from the cyclisation proved more difficult to purify and as yet has not been fully characterised. The crystalline product was assigned structure **12** based on its spectroscopic properties (see Experimental) and was simultaneously analyzed by X-ray diffraction.

Final parameters[7] from this analysis are listed in Tables 2 and 3, and a stereoscopic view of the molecular structure is shown in Fig. 1. This clearly confirms the above assignment, and underlines the sound basis for our other stereochemical predictions in this sequence. Figure 2 shows the final bond lengths, for which the estimated standard deviations are 0.002–0.003 Å. The bond lengths are very much as expected and require no special comments.

Endocyclic torsional angles are shown in Fig. 3. Ring A is approximately (within ±0.007 Å) planar, with distortions giving it a slight boat shape. Rings B and D have half-chair conformations, whereas rings C and E are chair shaped. The B/C ring junction is *trans*. There is some ring flattening in ring C near C(14) and in ring E near C(20). The three methyl groups at ring junctions are mutually *cis* and the ring system is convex toward them (cf. Fig. 1). The 1,3 diaxial methyl groups, C(24) and C(25), are separated by only 3.27 Å and this is despite an angle of 22.9° between the C(9)—C(24) and C(14)—C(25) vectors (which should in an ideal chair be parallel). The re-

[7]Tables of observed and calculated structure amplitudes and of bond angles are available, at a nominal charge, from the Depository of Unpublished Data, CISTI, National Research Council of Canada, Ottawa, Ont., Canada K1A 0S2.

Can. J. Chem. Downloaded from www.nrcresearchpress.com by 210.87.254.5 on 09/05/12
For personal use only.

Can. J. Chem. Downloaded from www.nrcresearchpress.com by 210.87.254.5 on 09/05/12
For personal use only.

TABLE 1. Benzene-induced solvent shifts and methyl group assignments in the nmr spectra of some synthetic compounds*

Compound	Methyl	$\delta CDCl_3$	δC_6D_6	Δ†
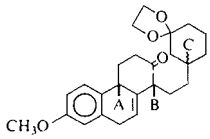	A	80	88	−8
	B	70	65	+5
	C	52	54	−2
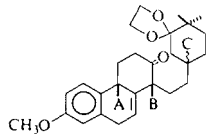	A	81		
	B	70		
	C	51		
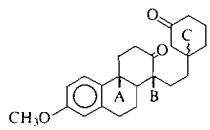	A	71		
	B	62		
	C	50		
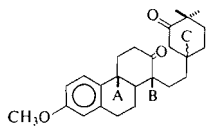	A	75	65	+10
	B	67	62	+5
	C	52	45	+7
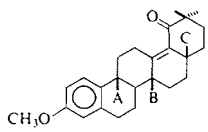	A	79	73	+6
	B	67	60	+7
	C	59	55	+4
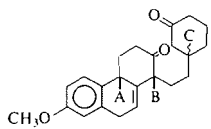	A	80	82	−2
	B	71	64	+7
	C	50	38	+12
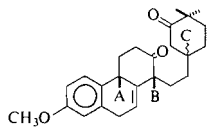	A	80	84	−4
	B	71	63	+8
	C	48	37	+11
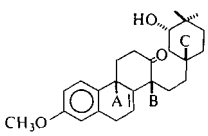	A	80	86	−6
	B	70	65	+5
	C	58	58	0
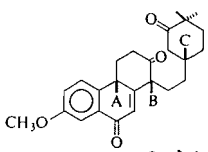	A	86	78	+8
	B	82	58	+24
	C	48	34	+14
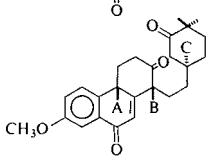	A	86	80	+6
	B	82	59	+23
	C	52	35	+17

*Determined at 60 MHz. Shifts are given in Hz downfield from internal TMS.
†$\Delta = \delta_{CDCl_3} - \delta_{C_6D_6}$.

pulsion between C(24) and C(25) is reflected also in lengthening of the C(9)—C(8) and C(8)—C(14) bonds (to 1.553 and 1.567 Å), and in opening of the C(9)—C(8)—C(14) angle (to 117.7°). C(25) and C(26), however, are 4.69 Å apart, and there is thus probably no repulsion between them. Despite the presence of the C(13)—C(18) double bond in the present compound, which partially flattens the ring C/D/E region, the general shape of this molecule is quite similar to that of epifriedelinol (13) and campanulin (14), another friedelin-type triterpene.

There is no apparent conjugation between the C(13)—C(18) double bond and the C(19)—O(2) carbonyl group; the C(13)—C(18)—C(19)—O(2) torsional angle is −66.7° and the C(18)—C(19) bond, 1.501 Å, is about 0.06 Å longer than expected for a conjugated system. The twist of C(19)—O(2) out of the C(12),C(13),C(18) plane is necessary to avoid too close a nonbonded contact with one of the hydrogen atoms on C(12).

Packing of the molecules in the crystal structure is governed by van der Waals forces; there are no hydrogen bonds or other short intermolecular contacts.

Thus, pentacyclic material **12** is easily obtainable in 16% yield from **2** and **3** and possesses four chiral centres corresponding to friedelin **6**. Work on its conversion to a triterpene as well as other applications of the described intramolecular cyclisation are in progress in our laboratory.

Earlier, structure **9** was assigned to the reduction product of mixture **4***b*, one of the diastereomeric constituents undergoing reduction whilst the other remained unchanged. This latter constituent was separated, hydrogenated and subjected to the acid-catalysed cyclisation process described above. No trace of pentacycle **12** could be detected from this reaction leading us to the conclusion that the C-1′ methyl group in this isomer is α oriented thus the reduction product is assigned a β-methyl group at the same position. The nmr spectrum of **9** exhibits a doublet of doublets at δ 3.40 that is partially hidden by the benzylic proton resonance, which being coupled to the olefinic proton, appears as a doublet. Decoupling of the olefinic proton causes the benzylic protons signal to collapse to a singlet and the doublet of doublets assigned to the carbinol hydrogen becomes clear. The coupling constants observed for this signal are 12 and 6 Hz, corresponding to an axial hydrogen in a cyclohexane flanked by one methylene group. This leads to the conclusion that the hydroxyl group is equatorial and that the complete stereochemical description of **9** is as shown. Attempts to oxidise **9** to the corresponding diketone for conversion to **12** were thwarted by the reactivity of the C-10 benzylic allylic position. Lack of material and other

Can. J. Chem. Downloaded from www.nrcresearchpress.com by 210.87.254.5 on 09/05/12
For personal use only.

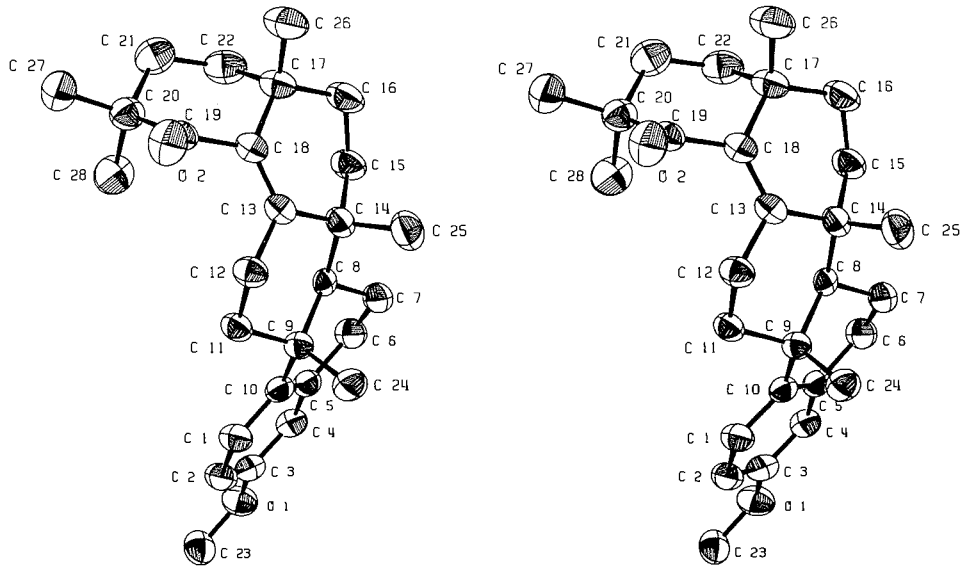

FIG. 1. A stereoscopic view of the compound **12** molecular structure, drawn with the ORTEP program (18). Thermal ellipsoids enclose 50% probability.

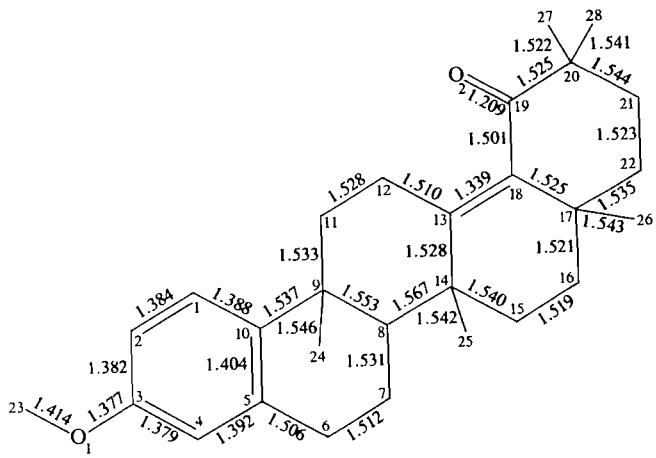

FIG. 2. Final bond lengths. The esd's are 0.002–0.003 Å.

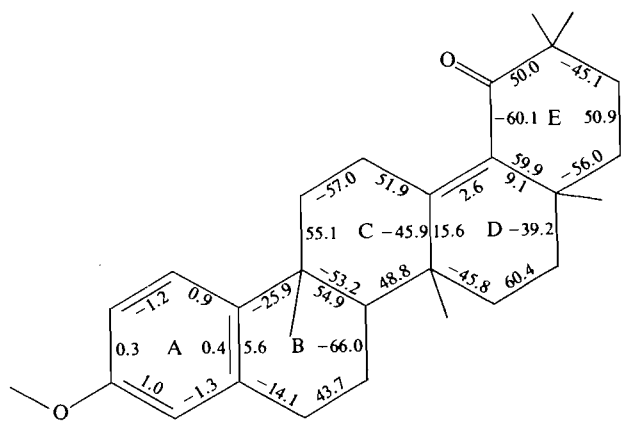

FIG. 3. Endocyclic torsional angles.

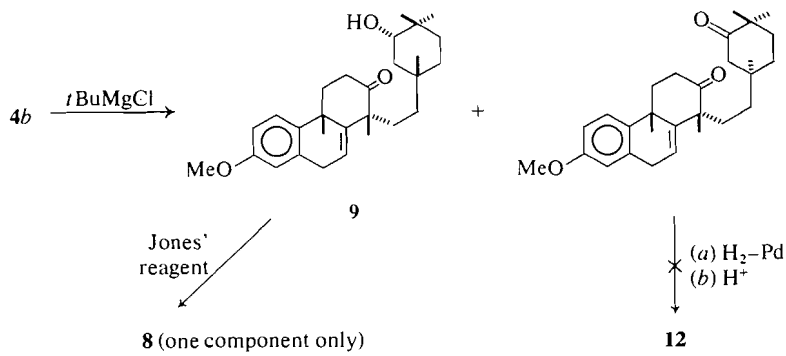

priorities have so far precluded further work on the finer details of this problem.

As already stressed we have often relied on benzene induced solvent shifts of the methyl group resonances in the nmr spectra of synthetic materials for the assignment of stereochemistry (cf. Table 1). In this particular study the spectra of compounds **4**, **8**, **9**, and **11** were complicated in the methyl region because of the presence of the *gem*-dimethyl system in the pendant potential E ring. In order to enable an unambiguous assignment of the methyl signals in the nmr spectra of our intermediate we undertook synthesis of tosylate **13** as outlined in Scheme 3; this, in turn was used to alkylate **2** to yield mixture **14***a* which was deketalised to **14***b* and hydrogenated to **15**. This route is reminiscent of that already described and served to confirm the assignment of nmr signals made previously. We did perform some cyclisation

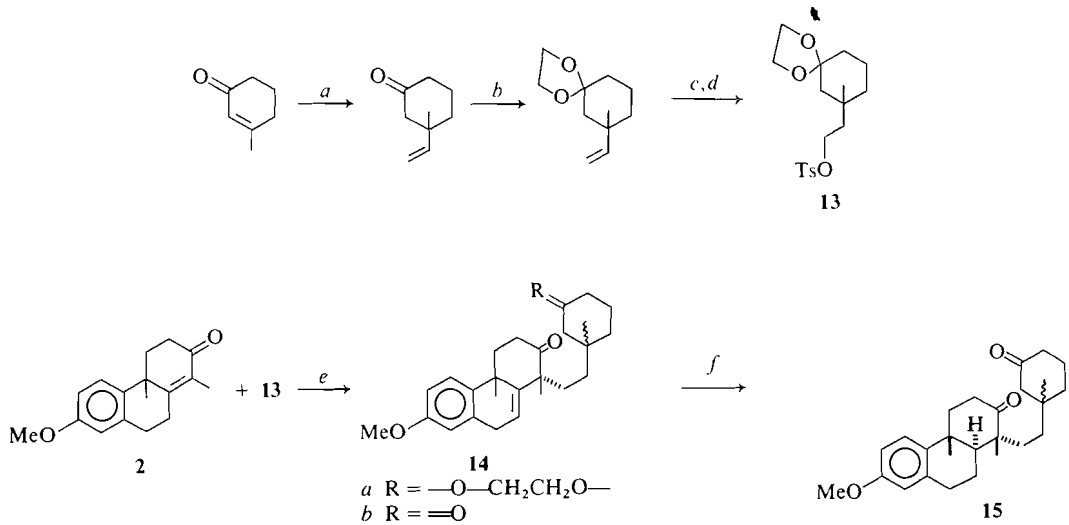

SCHEME 3. Reagents: (*a*) CH_2=CHMgBr, CuI; (*b*) $HOCH_2CH_2OH$, H^+; (*c*) disiamylborane; (*d*) *p*-toluenesulphonyl chloride; (*e*) potassium *tert*-pentoxide; (*f*) Pd/C, H_2, xylene.

attempts on **14***b* and **15** but preliminary indications were not promising. We do not plan any further studies in this particular direction.

The original impetus for the work described herein came from the assumption that the optimum energy pathway for an internal aldol-like cyclisation is that by which the orbital overlap between the enolate π system of one ketone and that of the carbonyl group of the other occurs in a perpendicular manner (see **16**) modified by the suggestions of Burgi *et al.* (ref. 3, see also ref. 4) that nucleophilic attack on the carbon atom of a carbonyl group is directed down 'a funnel of reactivity' whose axis is slightly behind the perpendicular axis of the carbonyl group as in **17**. Inspection of molecular models can often distinguish between two possible modes of attack if severe steric interactions are to be avoided in any transition state assumed to take account of the restrictions summarised in **16** and **17**. In the cases we have reported this is obviously not the complete story but we have detected differences in reactivity toward cyclisation in work that is at present incomplete[8] that can apparently be explained using these concepts. The present

[8]D. T. Tho, A Greaves, and J. W. ApSimon. Unpublished observations.

Can. J. Chem. Downloaded from www.nrcresearchpress.com by 210.87.254.5 on 09/05/12
For personal use only.

Can. J. Chem. Downloaded from www.nrcresearchpress.com by 210.87.254.5 on 09/05/12
For personal use only.

TABLE 2. Final parameters (esd's) for the nonhydrogen atoms. The U_{ij} values are all $\times 10^{4}$*

Atom	x/a ($\times 10^4$)	y/b ($\times 10^5$)	z/c ($\times 10^4$)	U_{11}	U_{22}	U_{33}	$2U_{23}$	$2U_{13}$	$2U_{12}$
O(1)	5758(2)	−3392(3)	8164(1)	655(7)	440(9)	638(7)	−5(11)	430(12)	−161(11)
O(2)	10295(2)	18089(3)	3233(1)	549(7)	769(9)	467(6)	119(11)	363(10)	59(12)
C(1)	8729(3)	2415(4)	6283(2)	545(9)	375(9)	433(8)	−38(13)	286(14)	31(14)
C(2)	7579(3)	−271(4)	6446(2)	551(9)	385(9)	482(9)	−86(14)	216(14)	23(14)
C(3)	6901(2)	−797(3)	7868(2)	405(8)	366(9)	532(9)	95(13)	207(13)	86(12)
C(4)	7375(2)	1367(4)	9089(2)	471(8)	440(9)	464(9)	101(13)	283(13)	119(14)
C(5)	8497(2)	4101(3)	8915(2)	403(8)	394(9)	403(8)	41(13)	142(12)	153(12)
C(6)	8874(3)	6435(4)	10270(2)	642(10)	485(9)	381(8)	27(14)	274(15)	57(15)
C(7)	10487(3)	8936(4)	10110(2)	590(10)	449(9)	348(8)	−40(13)	70(13)	53(14)
C(8)	10129(2)	10177(3)	8394(2)	395(7)	385(9)	341(7)	−54(13)	76(12)	44(12)
C(9)	10575(2)	7519(3)	7251(2)	380(7)	357(9)	386(7)	−68(13)	152(12)	45(12)
C(10)	9206(2)	4658(3)	7480(2)	390(7)	357(9)	391(8)	22(13)	129(12)	176(12)
C(11)	9960(2)	8810(3)	5547(2)	465(8)	366(9)	356(7)	−133(13)	186(12)	−5(12)
C(12)	11076(2)	11894(3)	5309(2)	500(8)	394(9)	392(8)	−81(13)	312(13)	−4(14)
C(13)	10685(2)	14436(3)	6456(2)	376(7)	375(9)	392(7)	−117(13)	177(12)	−102(12)
C(14)	11131(2)	13485(4)	8218(2)	488(9)	403(9)	364(8)	−112(13)	78(13)	−70(14)
C(15)	10038(3)	15815(4)	9181(2)	808(12)	430(9)	369(8)	−153(14)	261(16)	3(16)
C(16)	10365(3)	19228(4)	8762(2)	850(13)	403(9)	475(10)	−258(14)	276(17)	−119(16)
C(17)	9504(3)	19982(3)	7014(2)	585(10)	348(9)	483(9)	−141(13)	326(15)	−34(14)
C(18)	9937(2)	17271(3)	5949(2)	405(8)	366(9)	412(8)	−92(13)	216(12)	−98(12)
C(19)	9165(2)	18006(3)	4214(2)	458(8)	330(9)	415(8)	−54(13)	203(12)	−122(12)
C(20)	6802(2)	18641(4)	3770(2)	434(8)	430(9)	566(10)	29(14)	153(14)	−45(14)
C(21)	6167(3)	21077(5)	4936(2)	559(10)	595(9)	718(12)	41(18)	317(18)	264(18)
C(22)	7106(3)	20484(4)	6690(2)	679(11)	513(9)	656(11)	−99(16)	584(18)	171(16)
C(23)	5318(3)	−5700(4)	6951(2)	670(11)	513(9)	580(11)	67(16)	42(17)	−292(18)
C(24)	12879(3)	6329(4)	7549(2)	428(8)	485(9)	591(10)	−49(14)	175(14)	149(14)
C(25)	13530(3)	13564(5)	8859(2)	556(10)	604(9)	568(11)	−59(16)	−103(16)	−274(16)
C(26)	10613(3)	22977(4)	6569(2)	838(13)	385(9)	633(11)	−123(16)	422(19)	−143(16)
C(27)	6202(3)	19845(5)	2061(2)	644(11)	614(9)	609(11)	132(18)	−103(17)	19(18)
C(28)	5674(3)	15484(5)	3902(3)	454(10)	614(9)	888(14)	218(20)	86(18)	−254(16)

*Thermal factor $\exp[-2\pi^2(U_{11}a^{*2}h^2 + \text{-------} + 2U_{23}b^*c^*kl + \text{-----} + \text{---})]$.

work falls nicely into the framework presented recently by Baldwin and co-workers (19) where orbital overlap considerations have been elegantly summarised in a series of rules for ring closure.

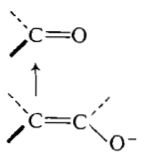

16

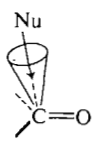

17

Experimental

For general information concerning experimental procedures and spectroscopic analysis see Part III of this series (1).

*2-Keto-1β,4aβ-dimethyl-1α-[2-(1′,4′,4′-trimethyl-3′-ethylenedioxycyclohexyl)ethyl]-7-methoxy-1,2,3,4,4a,9-hexahydrophenanthrene (**4**a)*

The method of Stork and Schulenberg (7) was followed. A mixture of potassium (810 mg, 20.78 mmol), *tert*-amyl alcohol (4 ml), and dry benzene (80 ml) was refluxed under a nitrogen atmosphere to give a solution of potassium *tert*-pentoxide. The tricyclic ketone **2** (5 g, 19.53 mmol) was added to the cooled solution and, while fresh benzene was being added, the reaction mixture was heated for 5 h to distill off a mixture of benzene – *tert*-pentyl alcohol. The resulting green-brown suspension of the potassium salt of **2** was cooled to room temperature and tosylate (solid) **3** (7.2 g, 18.8 mmol) was added. The mixture was refluxed for 2 h and then stirred at room temperature overnight. The greenish black syrupy mixture was poured into an ice–water mixture (250 ml) and acidified with 2 *N* H_2SO_4. The organic material was extracted with ether (×3) washed with ether (×3), washed with saturated sodium chloride solution, and dried over anhydrous magnesium sulphate. Evaporation of the solvent gave a yellow oil which crystallized on standing. Recrystallization of this solid from methanol yielded light yellow crystals (4.58 g, 53.5%), mp 107–115°C. Two more recrystallizations furnished an analytical sample: mp 114–115°C; ir (Nujol): 1705 (C=O) and 1600 cm^{-1} (aromatic); nmr ($CDCl_3$) δ: 0.85 (s, 3, C-1 CH_3), 0.88 (s, 6, *gem*-dimethyl), 1.15 (s, 3, C-4a CH_3), 3.42 (d, 2, J = 4 Hz, C-9 CH_2), 3.78 (s, 3, —OCH_3), 3.83 (s, 4, —OCH_2—CH_2—O), 5.80 (t, 1, J = 4 Hz, C-10 H), and 6.67–7.33 (m, 3, ArH); ms *m/e* (relative intensity): 466 (14), 451 (7), 395 (21), 183 (100). *Anal.* calcd. for $C_{30}H_{42}O$: C 77.21, H 9.07; found: C 77.28, H 9.04.

*2-Keto-1β,4aβ-dimethyl-1α-[2-(3-keto-1,4,4-trimethylcyclohexyl)ethyl]-7-methoxy-1,2,3,4,4a,9-hexahydrophenanthrene (**4**b)*

A solution of ketals **4***a* (4.58 g, 9.82 mmol) in methanol (100 ml) and 5% oxalic acid (enough to make the solution slightly turbid) was refluxed for 2 h. Water was added and the mixture extracted with ether (×3). The ether layer was washed with saturated solution of sodium bicarbonate, then water, and was dried over anhydrous sodium sulphate. Evaporation of the ether under reduced pressure gave a red oil. The oil was dissolved in 20 ml methanol and placed in the refrigerator overnight. The yellow crystals formed were isolated by filtration to give 2.7 g (65%) of the diketones **4***b*: mp 106–112°C; ir (Nujol): 1700 (C=O) and 1610 cm^{-1} (aromatic); nmr ($CDCl_3$) δ: 0.80 (s, 3, C-1′ CH_3), 0.98 (s, 3, C-4′ CH_3), 1.04 (s, 3, C-4′

Can. J. Chem. Downloaded from www.nrcresearchpress.com by 210.87.254.5 on 09/05/12
For personal use only.

TABLE 3. Final parameters (esd's) for the hydrogen atoms*

Atom	x/a ($\times 10^3$)	y/b ($\times 10^4$)	z/c ($\times 10^3$)	B (Å^2)
H(11)	921(2)	271(4)	527(2)	3.0(0.3)
H(21)	725(3)	−168(4)	557(2)	3.8(0.4)
H(41)	695(3)	94(4)	1013(2)	4.2(0.4)
H(61)	928(3)	537(4)	1127(2)	4.1(0.4)
H(62)	753(3)	745(4)	1029(2)	4.3(0.4)
H(71)	1193(3)	800(4)	1038(2)	4.1(0.4)
H(72)	1034(3)	1065(4)	1084(2)	4.3(0.4)
H(81)	852(2)	1051(4)	804(2)	2.6(0.3)
H(111)	841(2)	915(3)	528(2)	2.8(0.3)
H(112)	1027(3)	729(4)	476(2)	3.2(0.3)
H(121)	1069(3)	1255(4)	419(2)	3.5(0.3)
H(122)	1262(3)	1152(4)	545(2)	3.4(0.3)
H(151)	1060(3)	1549(4)	1035(2)	4.7(0.4)
H(152)	847(3)	1534(4)	900(2)	4.1(0.4)
H(161)	1189(3)	1972(5)	897(2)	4.5(0.4)
H(162)	962(3)	2051(5)	940(2)	4.8(0.4)
H(211)	456(4)	2121(5)	480(3)	6.1(0.5)
H(212)	659(3)	2320(5)	461(2)	5.4(0.5)
H(221)	647(3)	1861(5)	711(2)	5.1(0.4)
H(222)	681(3)	2226(5)	736(2)	4.8(0.4)
H(231)	447(4)	−724(5)	740(3)	5.9(0.5)
H(232)	671(3)	−668(5)	673(3)	5.5(0.5)
H(233)	458(4)	−492(5)	592(3)	5.9(0.5)
H(241)	1298(3)	438(5)	690(3)	5.5(0.5)
H(242)	1391(3)	781(5)	730(2)	4.9(0.4)
H(243)	1338(4)	564(5)	866(3)	5.8(0.5)
H(251)	1382(4)	1256(6)	986(3)	7.1(0.6)
H(252)	1442(4)	1248(6)	813(3)	6.5(0.5)
H(253)	1402(3)	1562(4)	895(2)	4.6(0.4)
H(261)	1017(4)	2358(5)	542(3)	5.9(0.5)
H(262)	1218(4)	2260(5)	683(3)	5.9(0.5)
H(263)	1029(3)	2477(5)	725(2)	5.4(0.4)
H(271)	665(4)	1826(6)	131(3)	6.6(0.5)
H(272)	470(4)	2037(7)	185(3)	8.0(0.6)
H(273)	699(4)	2174(6)	189(3)	6.5(0.5)
H(281)	628(4)	1385(6)	322(3)	6.8(0.6)
H(282)	416(4)	1575(5)	360(3)	6.0(0.5)
H(283)	603(4)	1467(5)	503(3)	5.9(0.5)

*Thermal factor exp $[-2\pi^2(U_{11}a^{*2}h^2 + \text{-------} + 2U_{23}b^*c^*kl + \text{-----} + \text{---})]$.

CH_3), 1.18 (s, 3, C-1 CH_3), 1.32 (s, 3, C-4a CH_3), 3.45 (d, 2, J = 4 Hz, C-9 CH_2), 3.84 (s, 3, OCH_3), 5.86 (t, 1, J = 4 Hz, C-10 H), and 6.60–7.40 (m, 3, ArH); nmr (C_6D_6) δ: 0.62 (s, 3, C-1′ CH_3), 0.88 (s, 3, C-4′ CH_3), 0.94 (s, 3, C-4′ CH_3), 1.06 (s, 3, C-1 CH_3), 1.41 (s, 3, C-4a CH_3), 3.24 (d, 2, J = 4 Hz, C-9 CH_2), 3.41 (s, 3, OCH_3), 5.68 (t, 1, J = 4 Hz, C-10 H), and 6.60–7.20 (m, 3, ArH); ms *m/e* (relative intensity): 422 (10), 389 (45), 256 (100). *Anal.* calcd. for $C_{28}H_{38}O_3$: C 79.57, H 9.06; found: C 79.37, H 9.07.

Jones' Oxidation of the Diones 4b

The pair of diastereoisomers, 4*b*, (50 mg) was dissolved in acetone (5 ml) and cooled in an ice-bath. Jones' reagent was added dropwise until an orange colour persisted. There was a green precipitate of chromous salt formed. After stirring for 1 h, water was added and the organic material extracted with ether (× 3). The ether layer was washed with water, saturated brine and dried ($MgSO_4$). Evaporation of the solvent gave 45 mg (90%) of the triones **8**. Two recrystallizations from methanol gave an analytical sample: mp 160–170°C; uv max (95% C_2H_5OH): 362 (10 900), 332 (2300), 224 (18 500), 212 nm (8200); ir (CH_2Cl_2): 1700 (C=O), and 1650 (C=O), 1605 cm^{-1} (aromatic, olefinic); nmr ($CDCl_3$) δ: 0.83 (s, 3, C-1′ CH_3), 1.03 (s, 6, *gem*-dimethyl), 1.37 (s, 3, C-1 CH_3), 1.43 (s, 3, C-4a CH_3), 3.90 (s, 3, O—CH_3), 6.50 (s, 1, C-10 H), 7.00–7.70 (m, 3, ArH); nmr (C_6D_6) δ: 0.62 (s, 3, C-1′ CH_3), 0.88, 0.97 (2 s, 3 each, C-4′ *gem*-dimethyl), 1.00 (s, 6, C-1 and C-4′ CH_3), 1.40 (s, 3, C-4a CH_3), 3.42 (s, 3, OCH_3), 6.55 (s, 1, C-10 H), and 6.71–8.00 (m, 3, ArH); ms *m/e* (relative intensity): 436 (100), 380 (80), 270 (65), 255 (70). *Anal.* calcd. for $C_{28}H_{36}O_3$: C 77.03, H 8.31; found: C 77.04, H 8.28.

The isomer *4b (C-1′ methyl α)* was similarly treated with Jones' reagent as above to give the trione ***8** (C-1′ methyl α)* in 93% yield: mp 183–185°C; ir (CH_2Cl_2): 1700 (C=O), 1650 (C=O), and 1605 cm^{-1} (aromatic, olefin); nmr (C_6D_6) δ: 0.58 (s, 3, C-1′ CH_3), 0.97, 0.98 (2 s, 3 each, C-4′ *gem*-dimethyl), 0.97 (s, 3, C-1 CH_3), 1.33 (s, 3, C-4a CH_3), 3.47 (s, 3, O—CH_3), 6.63 (s, 1, C-10 H), and 6.66–8.00 (m, 3, ArH); nmr ($CDCl_3$) δ: 0.86 (s, 3, C-1′ CH_3), 1.06 (s, 6, *gem*-dimethyl), 1.36 (s, 3, C-1 CH_3), 1.43 (s, 3, C-4a CH_3), 3.90 (s, 3, O—CH_3), 6.47 (s, 1, C-10 H), and 7.00–7.67 (m, 3, ArH); ms *m/e* (relative intensity) 436 (100), 380 (80), 270 (65), 255 (70). *Anal.* calcd. for $C_{28}H_{36}O_3$: C 77.03, H 8.31; found: C 77.15, H 8.29.

Attempted Cyclizations of Diones 4b

A solution of 1.06 g (2.51 mmol) diones **4***b* in 60 ml dimethoxyethane (DME) under an argon sweep, was cooled in a Dry Ice – acetone bath and 14.5 ml of 1.1 *M* (15.95 mmol) *tert*-butylmagnesium chloride in THF was added through a septum by the aid of a syringe. The mixture was stirred for 1 h during which time a white precipitate was formed. This was then refluxed for 1 h and the solution became clear. The mixture was cooled and poured into a beaker containing ice and ammonium chloride (solid). This was extracted with ether (× 3) and the ether layer was washed with water, saturated sodium chloride solution, and dried over anhydrous magnesium sulphate. Evaporation of the solvent gave an oil which, as shown by analytical thin-layer chromatography, contained two products. The mixture was separated by column chromatography using grade III aluminum oxide. Elution with petroleum ether gave compound *4*b *(C-1′ methyl α)* which corresponded to one of the starting diastereoisomers (75% recovery after recrystallization) and elution with 50% petroleum ether in benzene gave the new compound which was found to be the reduced product **9**, mp 133–135°C, 78.8% yield (based on one diastereoisomer). Two further recrystallizations afforded an analytical sample: ir (Nujol): 3450 (OH), 1700 (C=O), and 1605 cm^{-1} (aromatic, olefin); nmr ($CDCl_3$) δ: 0.78, 0.81 (2 s, 3 each, *gem*-dimethyl), 0.97 (s, 3, C-1′ CH_3), 1.23 (s, 3, C-1 CH_3), 1.33 (s, 3, C-4a CH_3), 3.43 (d, 2, J = 4 Hz, C-10 H), 3.40 (d of d, 1, J = 12 and 6 Hz, C-3′ H), 3.80 (s, 3, O—CH_3), 5.90 (t, 1, J = 4 Hz, C-9 H), and 6.67–7.43 (m, 3, ArH); nmr (C_6D_6) δ: 0.70, 0.75 (2 s, 3 each, *gem*-dimethyl), 0.97 (s, 3, C-1′ CH_3), 1.08 (s, 3, C-1 CH_3), 1.43 (s, 3, C-4a CH_3), 3.20 (d, 2, J = 4 Hz, C-9 H), 3.40 (s, 3, O—CH_3), 5.70 (t, 1, J = 4 Hz, C-10 H), and 6.53–7.33 (m, 3 ArH); ms *m/e* (relative intensity): 424 (10), 411 (14), 391 (50), 255 (100). *Anal.* calcd. for $C_{28}H_{40}O_3$: C 79.20, H 9.50; found: C 79.40, H 9.29.

Compound *4*b *(C-1′ methyl α)*: mp 118–122°C; ir: 1700 (C=O) and 1605 cm^{-1} (aromatic, olefin); nmr in $CDCl_3$ and C_6D_6 are identical to that of the mixture of diastereoisomers 4*b*; ms *m/e* (relative intensity): 422 (10), 389 (45), 256 (100). *Anal.* calcd. for $C_{28}H_{38}O_3$: C 79.57, H 9.06; found: C 79.35, H 9.11.

*Hydrogenation of 2-Keto-1,4a-dimethyl-1-[3-keto-1,4,4-trimethylcyclohexylethyl]-7-methoxy-1,2,3,4,4a,9-hexahydrophenanthrene (*4b)

A suspension of 500 mg of 10% palladium-on-charcoal in 15 ml *p*-xylene was hydrogenated at room temperature and atmospheric pressure for 4 h. Olefinic diketones 4*b* (1 g) in

Can. J. Chem. Downloaded from www.nrcresearchpress.com by 210.87.254.5 on 09/05/12
For personal use only.

10 ml *p*-xylene were added and hydrogenated at atmospheric pressure at 140°C for 18 h. The solution was filtered and the *p*-xylene evaporated under reduced pressure. The resulting clear oil was dissolved in methanol and allowed to stand overnight during which time it crystallized to give 600 mg (60%) of the hydrogenated product **12**, mp 108–112°C. Two recrystallizations of a portion gave an analytical sample: mp 117–120°C; ir (Nujol): 1700 (C=O) and 1605 cm^{-1} (aromatic, olefin); nmr ($CDCl_3$) δ: 0.87 (s, 3, C-1′ CH_3), 1.08 (s, 3, C-4′ CH_3), 1.12 (s, 6, C-1, C-4′ CH_3), 1.26 (s, 8, C-4a CH_3), 3.78 (s, 3, —O—CH_3), 6.58 (d, 1, J = 3 Hz (*m*), ArC-8 H), 6.72 (d of d, 1, J = 9 (*o*) and 3 Hz (*m*), ArC-6 H), and 7.26 (d, 1, J = 9 Hz (*o*) ArC-5 H); nmr (C_6D_6) δ: 0.75 (s, 3, C-1′ CH_3), 0.86 (s, 3, C-4′ CH_3), 1.04 (s, 6, C-1, C-4′ CH_3), 1.09 (s, 3, C-4a CH_3), 3.42 (s, 3, O-CH_3), 6.56 (d, 1, J = 3 Hz (*m*) ArC-8 H), 6.74 (d of d, 1, J = 9 (*o*) and 3 Hz (*m*), ArC-6 H), and 6.96 (d, 1, J = 9 Hz (*o*) ArC-5 H); ms *m/e* (relative intensity): 424 (100), 409 (70), 391 (10), 367 (5), 258 (26), 243 (24). *Anal.* calcd. for $C_{28}H_{40}O_3$: C 79.20, H 9.50; found: C 79.24, H 9.59.

2-(3-Ethylenedioxy-1,4,4-trimethylcyclohexyl)malononitrile

Dicyanide **7** (6) (10 g, 0.049 mol) was dissolved in 400 ml benzene containing 15 ml ethylene glycol and 200 mg *p*-toluenesulfonic acid. This solution was refluxed for 24 h. The benzene layer was separated, washed with water, then with saturated sodium chloride solution, and dried over anhydrous magnesium sulphate. After rotary evaporation of the solvent the product crystallized. Recrystallization from hexane yielded 11 g (90%) of the ketal: mp 91–93°C; ir (Nujol): 2250 cm^{-1} (C≡N), no carbonyl absorption; nmr ($CDCl_3$) δ: 0.90, 1.03 (2 s, 3 each, *gem*-dimethyl), 1.60 (s, 3, C-1 CH_3), 3.97 (s, 4, —O—CH_2—CH_2—O—), and 4.73 (s, 1, —$CH(CN)_2$). M^+ calcd. for $C_{14}H_{20}O_2N_2$: 248.1825; found: 248.1832.

2-(3-Ethylenedioxy-1,4,4-trimethylcyclohexyl)ethanoic Acid

A mixture of the above ketal dicyanide (14 g, 0.056 mol), ethylene glycol (32 ml) and potassium hydroxide (50 g, 0.893 mol) in 25 ml water was refluxed for 48 h. The reaction mixture was cooled to room temperature, acidified with cold 3 *N* H_2SO_4 (p*H* 4) and extracted twice with ether. The ether layer was washed with water, saturated sodium chloride, and dried over anhydrous magnesium sulphate. After evaporation of the solvent the crude diacid was decarboxylated by heating at 140–145°C (oil bath) during 2½ h. The nuclear magnetic resonance spectrum of this oil showed that the product had been deketalized. The oil was taken up in benzene; *p*-toluenesulfonic acid (200 mg) and ethylene glycol (15 ml) were added and the mixture refluxed overnight through a Dean–Stark trap. Separation of the benzene layer followed by washing with water, drying ($MgSO_4$), and rotary evaporation of the solvent gave 13.79 g (98%) of the monoacid as an oil. M^+ calcd. for $C_{13}H_{22}O_4$: 242.1518; found (mass spectrum): 242.1457.

2-(3-Ethylenedioxy-1,4,4-trimethylcyclohexyl)ethanol

To a suspension of 6.4 g (0.168 mol) of lithium aluminum hydride in dry diethyl ether (250 ml) was added dropwise 17.2 g (0.071 mol) of the above ketal acid. After completion of addition the mixture was refluxed overnight. The mixture was cooled to ice bath temperature and the excess lithium aluminum hydride was decomposed by careful addition of a saturated solution of Rochelle salt. The ether layer was separated and the aqueous layer extracted twice with ether. The combined ether layer was washed with water, saturated sodium chloride, and dried ($MgSO_4$). Evaporation of the solvent gave 11.8 g of the alcohol which was used in the next reaction without further purification: ir (neat): 3350 cm^{-1} (OH) and no carbonyl absorption; nmr ($CDCl_3$) δ: 0.93 (s, 6, *gem*-dimethyl), 0.98 (s, 3, C-1 CH_3), 3.70 (t, 2, J = 7 Hz, CH_2OH), and 3.92 (s, 4, —O—CH_2—CH_2—O—). M^+ calcd. for $C_{13}H_{24}O_3$: 228.1725; found (mass spectrum): 228.1784.

2-(3-Ethylenedioxy-1,4,4-trimethylcyclohexyl)ethanol Tosylate (3)

The above ketal alcohol (20 g, 0.088 mol) was dissolved in 200 ml dry pyridine and this was cooled in an ice bath. *p*-Toluenesulfonylchloride (purified by recrystallization) (25.5 g, 0.134 mol) was added to the mixture and stirred until dissolved. The reaction mixture was left in the refrigerator overnight. Water was added and the crystals formed (34 g) were collected by filtration. Recrystallization from ether gave 23 g (69%) of pure tosylate **3**: mp 100–104°C; ir (Nujol): 1590 cm^{-1} (aromatic), no carbonyl or hydroxyl absorption; nmr ($CDCl_3$) δ: 0.88 (s, 3, C-1 CH_3), 0.92 (s, 6, *gem*-dimethyl), 2.43 (s, 3, Ar CH_3), 3.83 (s, 4, —O—CH_2—CH_2—O—), 4.08 (t, 2, J = 7 Hz, CH_2—OTs), 7.30 (d, 2, J = 8 Hz, ArH), and 7.75 (d, 2, J = 8 Hz, ArH). *Anal.* calcd. for $C_{20}H_{30}O_5S$ (M^+ 382): C 62.87, H 7.85, O 58.39; found (M^+ 382): C 62.88, H 7.75, O 58.27.

Oxidation of 2-Keto-1β,4aβ-dimethyl-1-(3α-hydroxy-1,4,4-trimethylcyclohexylethyl)-7-methoxy-1,2,3,4,4a,9-hexahydrophenanthrene (9)

Alcohol **9** (50 mg, 0.12 mmol) was dissolved in acetone (5 ml) and cooled in an ice bath. Jones' reagent was added dropwise until a yellow colour persisted. A green precipitate of the chromous salt was formed. After stirring for 1 h at room temperature, water was added and the organic layer extracted with ether (×3). The ether extract was washed with water, saturated sodium chloride solution, and dried over anhydrous magnesium sulphate. Evaporation of the solvent under reduced pressure gave an oil which was crystallized from ether to give 45 mg (90%) of trione **8** (C-1′ methyl β), mp 152–154°C. Two recrystallizations furnished an analytical sample: mp 182–183°C; uv max: 362 (10 900), 332 (2300), 224 (18 500), and 212 nm (8200); ir (CH_2Cl_2): 1700 (C=O), 1650 (C=O), and 1605 cm^{-1} (aromatic, olefin); nmr ($CDCl_3$) δ: 0.80 (s, 3, C-1′ CH_3), 1.03 (s, 6, *gem*-dimethyl), 1.37 (s, 3, C-1 CH_3), 1.43 (s, 3, C-4a CH_3), 1.43 (s, 3, C-4a CH_3), 3.90 (s, 3, OCH_3), 6.47 (s, 1, C-10 H), and 7.33–7.67 (m, 3, ArH); nmr (C_6D_6) δ: 0.57 (s, 3, C-1′ CH_3), 0.86, 0.93 (2 s, 3 each, *gem*-dimethyl), 0.96 (s, 3, C-1 CH_3), 1.30 (s, 3, C-4a CH_3), 3.33 (s, 3, O—CH_3), and 6.66–8.00 (m, 3, ArH). *Anal.* calcd. for $C_{28}H_{36}O_3$ (M^+ 436): C 77.03, H 8.31; found (M^+ 436): C 77.08, H 8.25.

10-Methoxy-2,2,4aβ,6aβ,12bβ-pentamethyl-1,2,3,4,4a,5,6,6a,6bα,7,8,12b,13,14-tetradecahydro-1-picenone (12)

A solution of 200 mg of diketones **11** and 200 mg of *p*-toluenesulfonic acid in 20 ml *p*-xylene under an atmosphere of nitrogen was refluxed for 16 h. Water was added and the benzene layer separated. The aqueous layer was extracted (×2) with ether. The combined extracts were washed with water, saturated sodium chloride solution, and dried over magnesium sulphate (anhydrous). Evaporation of the solvent gave an oil which was chromatographed on silica gel using increasing concentrations of ether in benzene as eluent. The major fraction (100 mg) was crystallized from methanol to give the pentacyclic ketone **12**, mp 145–150°C (45 mg, 47%). Two recrystallizations of a portion gave an analytical sample: mp 156–158°C; ir (neat): 1684 (C=O) and 1625, 1605 cm^{-1} (aromatic, olefinic); nmr ($CDCl_3$) δ: 0.98 (s, 3, C-4a CH_3), 1.04 (s, 3, C-2 CH_3), 1.08 (s, 3, C-2 CH_3), 1.12 (s, 3, C-6a CH_3), 1.31 (s, 3, C-12b CH_3), 3.78 (s, 3, O—CH_3), 7.56 (d, 1, J = 3 Hz (*m*), ArC-9 H), 7.68 (d of d, 1, J = 9 (*o*) and 3 Hz (*m*), ArC-11 H), and 7.70 (d, 1, J = 9 Hz (*o*), ArC-12 H); nmr (C_6D_6) δ: 0.92 (s, 6, C-4a and C-12 CH_3), 1.00 (s, 3, C-6a CH_3), 1.21 (s, 5, C-12 and C-12b CH_3), 3.42 (s, 3, —OCH_3), 6.60 (d, 1, J = 3 Hz (*m*), ArC-9 H), 6.70 (d of d, 1, J = 9 (*o*) and 3 Hz (*m*), ArC-11 H), and 7.03 (d, 1, J = 9 Hz (*o*), ArC-12 H); ms *m/e* (relative intensity): 406 (42), 187 (100). *Anal.* calcd. for $C_{28}H_{38}O_2$: C 82.71, H 9.42; found: C 82.66, H 9.48.

Can. J. Chem. Downloaded from www.nrcresearchpress.com by 210.87.254.5 on 09/05/12
For personal use only.

*1,2,3,4,4a,9-Hexahydro-7-methoxy-1α-[2-(3-ethylenedioxy-1-methylcyclohexyl)ethyl]-1β-dimethyl-2(1H)-phenanthrone (**14**a)*

A mixture of potassium metal (810 mg, 20.78 mmol), *tert*-pentyl alcohol (4 ml), and dry benzene (80 ml) was refluxed (4 h) under a nitrogen atmosphere to give a solution of potassium *tert*-pentoxide. The tricyclic ketone **2** (5 g, 19.53 mmol) was added to the cooled solution and while fresh benzene was being added, the reaction mixture was heated for 5 h to distill off a mixture of benzene – *tert*-pentyl alcohol. The resulting green-brown suspension of the potassium salt of **2** was cooled to room temperature and the tosylate **13** (solid) (6.67 g, 18.84 mmol) was added. The mixture was refluxed for 2 h and then stirred at room temperature overnight. The greenish black syrupy mixture was poured into an ice–water mixture (250 ml) and acidified with 2 *N* H_2SO_4. The organic material was extracted with ether (×3), washed with saturated sodium chloride solution, and dried over anhydrous magnesium sulphate. Evaporation of the solvent gave a yellow oil which solidified on standing. Recrystallization of this solid from methanol yielded light yellow crystals (4.5 g, 53%), mp 88–97°C. Two more recrystallizations provided an analytical sample of the diastereoisomers **14***a*: ir (Nujol): 1700 cm^{-1} (C=O); nmr ($CDCl_3$) δ: 0.86 (s, 3, C-1′ CH_3), 1.16 (s, 3, C-1 CH_3), 1.33 (s, 3, C-1 CH_3), 1.33 (s, 3, C-4a CH_3), 3.47 (d, 2, J = 4 Hz, C-9 H), 3.80 (s, 3, O—CH_3), 5.86 (d, 1, J = 4 Hz, C-10 H), and 6.78–7.43 (m, 3, ArH); nmr (C_6D_6) δ: 0.90 (s, 3, C-1′ CH_3), 1.08 (s, 3, C-1 CH_3), 1.47 (s, 3, C-4a CH_3), 3.23 (d, 2, J = 4 Hz, C-9 H), 3.43 (s, 3, O—CH_3), 3.50, 3.53 (2 s, 4, —OCH_2—CH_2—O—), 5.70 (t, I, J = 4 Hz, C-10 H), and 6.57–7.23 (m, 3, ArH); ms *m/e* (relative intensity): 438 (31), 423 (57), 361 (25), 255 (100). *Anal.* calcd. for $C_{28}H_{38}O_4$: C 76.68, H 8.73; found (M^+ 438): C 76.54, H 8.70.

*3,4,4a,9-Tetrahydro-7-methoxy-1α-[2-(3-keto-1-methylcyclohexyl)ethyl]-1β,4aβ-dimethyl-2(1H)-phenanthrone (**14**b)*

The keto ketals **14***a* (1 g) were dissolved in 25 ml methanol and were heated to near boiling point. A solution of oxalic acid (5%) was added until the mixture was slightly cloudy. This mixture was refluxed for 2.5 h and water was added and the methanol was evaporated under reduced pressure. The aqueous layer was extracted with ether (×3). The ether extract was washed with saturated sodium bicarbonate solution, water and saturated sodium chloride solution and dried over anhydrous magnesium sulphate. Evaporation of the solvent gave an oil (749 mg, 83%) which appeared homogeneous by thin-layer chromatography. Crystallization from methanol gave light yellow crystals, mp 105–109°C. Two recrystallizations from methanol afforded an analytical sample: mp 117–120°C; ir (Nujol): 1700 (C=O) and 1605 cm^{-1} (aromatic, olefinic); nmr ($CDCl_3$) δ: 0.83 (s, 3, C-1′ CH_3), 1.18 (s, 3, C-1 CH_3), 1.13 (s, 3, C-4a CH_3), 3.43 (d, 2, J = 4 Hz, C-9 H), 3.82 (s, 3, OCH_3), 5.88 (t, 1, J = 4 Hz, C-10 H), and 6.73–7.38 (m, 3, ArH); nmr (C_6D_6) δ: 0.63 (s, 3, C-1′ CH_3), 1.07 (s, 3, C-1 CH_3), 1.37 (s, 3, C-4a CH_3), 3.27 (d, 2, J = 4 Hz, C-9 H), 3.47 (s, 3, —O—CH_3), 5.72 (t, 1, J = 4 Hz, C-10 H), and 6.67–7.10 (m, 3, ArH); ms *m/e* (relative intensity): 394 (10), 379 (10), 361 (22), 255 (100). *Anal.* calcd. for $C_{26}H_{34}O_4$: C 79.15, H 8.69; found: C 79.17, H 8.55.

*3,4,4a,9,10aα-Hexahydro-7-methoxy-1α-[2-(3-keto-1-methylcyclohexyl)ethyl]-1β,4aβ-dimethyl-2(1H)-phenanthrone (**15**)*

A suspension of 200 mg of 10% palladium-on-charcoal in 10 ml *p*-xylene was hydrogenated for 2 h at room temperature and atmospheric pressure. The olefinic diketones **14***b* (300 mg) in 10 ml *p*-xylene were added to the suspension of catalyst and the mixture hydrogenated at 140°C and atmospheric pressure for 18 h. The reaction mixture was filtered and the *p*-xylene evaporated under reduced pressure to give an oil (180 mg) homogeneous by thin-layer chromatography. Attempts to induce crystallization failed: ir (neat): 1700 cm^{-1} (C=O); nmr ($CDCl_3$) δ: 0.83 (s, 3, C-1′ CH_3), 1.03 (s, 3, C-1 CH_3), 1.18 (s, 3, C-4a CH_3), 3.70 (s, 3, OCH_3), and 6.50–7.27 (m, 3, ArH); ms *m/e*: 396 (M^+).

3-Methyl-3-vinylcyclohexanone

Copper(I) iodide (3.81 g, 0.02 mol) was suspended in 75 ml of dry ether in a 250 ml three-necked, round-bottomed flask under argon. This suspension was stirred and cooled to −90°C in a Dry Ice – ether bath. Vinyl lithium (18 ml of 2.2 *M* solution, 0.04 mol) was added. The mixture became viscous and yellow. After stirring for 15 min at −90°C, 3-methyl-2-cyclohexenone (3.3 g, 0.03 mol) was added during 5 min. The mixture was stirred for another 5 min and was then quenched with excess methanol. The organic material was extracted three times, each with 50 ml ether, and the combined ether extract was washed successively with water, 5% ammonium hydroxide solution, water, saturated sodium chloride solution, and dried over anhydrous magnesium sulphate. After filtering off the magnesium sulphate, the ether was evaporated under reduced pressure to give an oil. This crude oil was distilled to yield 3.5 g (88%) of the product: bp 40–46°C/0.8 Torr; ir (neat): 1710 (C=O) and 1640, 990 cm^{-1} (—CH=CH_2). M^+ calcd. for $C_9H_{14}O$: 138; found (mass spectrum): 138.

1-Ethylenedioxy-3-methyl-3-vinylcyclohexane

3-Methyl-3-vinylcyclohexanone (13.2 g) was dissolved in 150 ml benzene. Ethylene glycol (10 ml) (excess) and *p*-toluenesulfonic acid (300 mg) were added and the mixture refluxed for 18 h while stirring vigorously. A Dean–Stark trap was used to separate the water formed. After the mixture was cooled, water was added, and the benzene layer was separated. The water layer was extracted with ether (×2) and the benzene and ether extracts were pooled together and washed with water, saturated sodium chloride solution, and dried over anhydrous magnesium sulphate. After removal of the magnesium sulphate by filtration the solvents were distilled at the rotary pump to give an oil. Distillation gave the product in 79% yield: bp 35°C/0.1 Torr; ir (neat): 1635 (C=C), 1065, 1090, 1150, 1180 cm^{-1} (ketal group); nmr ($CDCl_3$) δ: 1.10 (s, 3, CH_3), 3.90 (s, 4, —O—CH_2—CH_2—O—), 5.97 (d of d, 1, J = 18 and 10 Hz, —CH=CH_2), and 4.90 (m, 2, —CH=CH_2); ms *m/e*: 182 (M^+). *Anal.* calcd. for $C_{11}H_{18}O_2$: C 72.49, H 9.95, M^+ 182; found: C 72.56, H 10.06.

2-(3-Ethylenedioxy-1-methylcyclohexyl)ethanol

Disiamylborane was prepared by the method of Brown and co-workers (20). A mixture of sodium borohydride (2.13 g, 0.056 mol) and 2-methyl-2-butene (15.3 ml, 10.2 g, 0.145 mol) in freshly distilled tetrahydrofuran (75 ml) was cooled in an ice bath under a nitrogen atmosphere. Boron trifluoride etherate (9 ml, 10.1 g, 0.07 mol) was added dropwise over a period of 30 min and left stirring for 90 min at 0°C. To this mixture was added the 1-ethylenedioxy-3-methyl-3-vinylcyclohexane (1.47 g, 0.008 mol) very quickly and left to warm to room temperature. After 3 h the flask was cooled in an ice bath and 30.1 ml of 3 *N* NaOH was added followed by 20.0 ml 30% H_2O_2 (cautiously). The tetrahydrofuran was evaporated and the resulting mixture extracted with ether. The ether layer was washed with water, then with saturated sodium chloride solution, and dried over anhydrous magnesium sulphate. After removal of the magnesium sulphate by filtration, the solvent was evaporated under reduced pressure to give an oil which was distilled to yield 0.95 g (58%) of the alcohol: bp 80–85°C/0.01 Torr; ir (neat): 3420 cm^{-1} (OH); nmr ($CDCl_3$) δ: 0.95 (s, 3, CH_3), 3.90 (s, 4, —O—CH_2—CH_2—O—), and 3.67 (t, 2, J = 7 Hz, CH_2—OH); ms *m/e*: 200 (M^+). *Anal.* calcd. for $C_{11}H_{20}O_3$: C 65.97, H 10.07; found: C 65.99, H 10.17.

Can. J. Chem. Downloaded from www.nrcresearchpress.com by 210.87.254.5 on 09/05/12
For personal use only.

2-(3-Ethylenedioxy-1-methylcyclohexyl)ethanol Tosylate (13)

2-(3-Ethylenedioxy-1-methylcyclohexyl)ethanol (10 g, 0.05 mol) was dissolved in 100 ml dry, distilled pyridine and cooled in an ice bath. Solid *p*-toluenesulfonyl chloride (11.2 g, 0.059 mol) was added and the mixture left in the refrigerator overnight. Water was added to this mixture and the crystals formed were collected by filtration (79%). The crude crystals were recrystallized twice from ether to give an analytical sample: mp 66–68°C; ir (Nujol): no hydroxyl or carbonyl absorption, 1590, 1450 cm^{-1} (aromatic); nmr ($CDCl_3$) δ: 1.00 (s, 3, CH_3), 2.53 (s, 3, Ar CH_3), 3.92 (s, 4, —O—CH_2—CH_2—O—), 4.17 (t, 2, J = 7 Hz, CH_2—OTs), 7.43 (d, 2, J = 8 Hz, ArH), and 7.90 (d, 2, J = 8 Hz, ArH); ms *m/e*: 354 (M^+). *Anal.* calcd. for $C_{18}H_{26}O_5S$: C 60.99, H 7.39, S 9.05; M^+ 354; found: C 61.08, H 7.28, S 9.17.

X-ray Data Collection

Compound **12** crystallized from methanol as colourless laths elongated along a^*. The specimen used for data collection was cut to approximate dimensions 0.5 × 0.3 × 0.5 mm, and was mounted with b^* as rotation axis. Crystal data are as follows.

$C_{28}H_{38}O_2$ fw = 406.6
Monoclinic, a = 6.456(2), b = 42.518(6), c = 8.519(2) Å, β = 100.92(3)° (based on λ(CuKα$_1$) = 1.54051 and λ(CuKα$_2$) = 1.54433 Å), V = 2296.1 Å^3. Z = 4, ρ_c = 1.176 g cm^{-3}, space group $P2_1/c$, μ(CuKα) = 5.59 cm^{-1}.

Intensity data were measured with a Picker four-circle diffractometer in the θ/2θ scan mode using scan ranges of 2–3° and a (2θ) scan speed of 2°/min. All measurements were made at room temperature with Ni-filtered Cu radiation. The intensity of a check reflection, monitored at intervals of about 30 reflections, showed only small random fluctuations, and these measurements were used to place all the intensities on a single (arbitrary) scale. All 3908 accessible (2θ ≤ 130°) independent reflections in the *hkl* and $\bar{h}kl$ octants were measured, and of these, 3234 were considered as observed. The remainder, with net counts less than 12 or less than $\frac{1}{10}$ of the total background, were excluded from the least-squares refinement. Structure-factor amplitudes were obtained after applying Lorentz and polarization corrections, and an extinction correction was applied at a later stage. Absorption corrections were considered unnecessary (μ = 5.6 cm^{-1}).

Structure Determination and Refinement

The structure was determined by the symbolic addition procedure, and refinement was by block-diagonal least-squares minimizing $\Sigma w(|F_o| - |F_c|)^2$. The weighting scheme used in the final stages of refinement was of the form:

$$w = w_1 \times w_2$$

where

$$w_1 = 1 \Big/ \left[1 + \left(\frac{F_o - 11.0}{8.0}\right)^2\right]$$

$$1.7 < F_o < 194$$

and $w_2 = 4 \sin^2\theta$ if $\sin^2\theta < 0.25$, otherwise $w_2 = 1$. Hydrogen atoms were all located on a difference map and were subsequently refined isotropically while nonhydrogen atoms were refined anisotropically. Scattering factor values for oxygen and carbon atoms were taken from Hanson *et al.* (15) and for hydrogen from Stewart *et al.* (16). In the final least-squares cycle the mean (shift/estimated standard deviation) was 0.08 and the largest shift was 0.38 σ. The final R value for all 3234 observed reflections was 0.042. A final difference – Fourier map showed no significant features. Computer programs used in the analysis were those of Ahmed *et al.* (17) and Johnson (18).

Acknowledgements

We thank the National Research Council of Canada (Grant in Aid, (J.W.A.), Research Associateship (M.L.P.)) and the Hofmann La Roche Foundation for generous financial assistance and Ms. Sue Macauley for outstanding technical assistance.

1. J. W. APSIMON, S. BADRIPERSAUD, T. T. T. NGUYEN, and R. PIKE. Can. J. Chem. **56**, 1646 (1978).
2. T. K. DEVON and A. I. SCOTT. Handbook of naturally occurring compounds. Vol. II. Academic Press, New York, NY. 1972.
3. H. BURGI, J. D. DUNITZ, J. M. LEHN, and G. WIPFF. Tetrahedron, **30**, 1563 (1974); H. BURGI. Angew. Chem. Int. Ed. Engl. **14**, 460 (1975).
4. W. T. WIPKE and P. GUND. J. Am. Chem. Soc. **98**, 8107 (1976).
5. J. W. APSIMON, P. BAKER, J. BUCCINI, J. W. HOOPER, and S. MACAULAY. Can. J. Chem. **50**, 1944 (1972).
6. J. W. APSIMON, J. W. HOOPER, and B. A. LAISHES. Can. J. Chem. **48**, 3064 (1970).
7. G. STORK and J. W. SCHULENBERG. J. Am. Chem. Soc. **84**, 284 (1962).
8. E. WENKERT, A. ALFONSO, J. BRENDENBERG, C. KANEKO, and A. TAHARA. J. Am. Chem. Soc. **86**, 2038 (1964); R. E. IRELAND and R. C. KIERSTEAD. J. Org. Chem. **31**, 2543 (1966); C. L. GRAHAM and F. J. M. MCQUILLIN. J. Chem. Soc. 4521 (1964); V. PERMUTTI and Y. MAZUR. J. Org. Chem. **31**, 705 (1966); G. JUST and K. ST. C. RICHARDSON. Can. J. Chem. **42**, 464 (1964).
9. H. O. HOUSE, D. S. GRUMRINE, A. Y. TERANISHI, and H. D. OLMSTEAD. J. Am. Chem. Soc. **95**, 3310 (1972); H. O. HOUSE, D. G. MELILLO, and F. J. SANTER. J. Org. Chem. **38**, 741 (1973).
10. W. M. FOLEY, F. J. WELCH, E. M. LACOMBE, and H. S. MOSHER. J. Am. Chem. Soc. **81**, 2779 (1959) and refs. therein.
11. J. W. APSIMON, S. BADRIPERSAUD, M. L. POST, and E. J. GABE. Can. J. Chem. This issue.
12. R. E. IRELAND, D. A. EVANS, D. GLOVER, G. M. RUBOTTOM, and H. YOUNG. J. Org. Chem. **34**, 3717 (1969).
13. M. LAING, M. E. BURKE-LAING, R. BARTHO, and C. M. WEEKS. Tetrahedron Lett. 3839 (1977).
14. F. Mo. Acta Crystallogr. Ser. B, **33**, 641 (1977).
15. H. P. HANSON, F. HERMAN, J. D. LEA, and S. SKILLMAN. Acta Crystallogr. **17**, 1040 (1964).
16. R. F. STEWART, E. R. DAVIDSON, and W. T. SIMPSON. J. Chem. Phys. **42**, 3175 (1965).
17. F. R. AHMED, S. R. HALL, M. E. PIPPY, and C. P. HUBER. NRCC Crystallographic Programs for the IBM/360 System, accession numbers 133–147 *in* J. Appl. Crystallogr. **6**, 309 (1973).
18. C. K. JOHNSON. ORTEP, Report ORNL-3794 (2nd Rev.), Oak Ridge National Laboratory, Oak Ridge, TN. 1970.
19. J. E. BALDWIN. J. Chem. Soc. Chem. Commun. 734 (1976); J. E. BALDWIN. J. Chem. Soc. Chem. Commun. 738 (1976); J. E. BALDWIN and J. A. REISS. J. Chem. Soc. Chem. Commun. 77 (1977); J. E. BALDWIN and L. I. KRUSE. J. Chem. Soc. Chem. Commun. 233 (1977).
20. G. ZWEIFEL, K. NAGASE, and H. C. BROWN. J. Am. Chem. Soc. **84**, 190 (1962).

Approaches to the synthesis of triterpenes. V. An unusual acid-catalysed rearrangement of a β,γ-unsaturated ketone[1,2]

JOHN W. APSIMON[3] AND SATYANAND BADRIPERSAUD
Department of Chemistry, Carleton University, Ottawa, Ont., Canada K1S 5B6
AND
MICHAEL L. POST
Division of Biological Sciences and Chemistry, National Research Council of Canada, Ottawa, Ont., Canada K1A 0R6
AND
ERIC J. GABE
Division of Chemistry, National Research Council of Canada, Ottawa, Ont., Canada K1A 0R6

Received January 30, 1978

JOHN W. APSIMON, SATYANAND BADRIPERSAUD, MICHAEL L. POST, and ERIC J. GABE. Can. J. Chem. **56**, 2150 (1978).

The reaction of 2-keto-1β,4aβ-dimethyl-1α-[2-(3-keto-1,4,4-trimethylcyclohexyl)ethyl]-7-methoxy-1,2,3,4,4a,9-hexahydrophenanthrene **1***a* and *b* with *p*-toluenesulphonic acid in boiling xylene yields the rearranged product, 1,10-dimethyl-2-[2-(3-keto-1,4,4-trimethylcyclohexyl)-ethyl]-7-methoxy-3,4-dihydroanthracene (**3**). Crystals of **3** are monoclinic, space group $P2_1/c$, $Z = 4$, with $a = 7.2684(3)$, $b = 30.942(2)$, $c = 10.5544(7)$ Å, $\beta = 98.24(1)°$. The structure was determined by direct methods from diffractometer data and refined by block-diagonal least-squares to an R of 0.043 for 1810 observed reflections. The molecule exhibits no unusual geometric features, although positional disorder is apparent in the cyclohexanone moiety.

A possible route for the formation of **3** from **1***a* and *b* is presented.

JOHN W. APSIMON, SATYANAND BADRIPERSAUD, MICHAEL L. POST et ERIC J. GABE. Can. J. Chem. **56**, 2150 (1978).

La réaction de l'oxo-2 diméthyl-1β,4aβ [(oxo-3 triméthyl-1,4,4 cyclohexyl)-2 éthyl]-1α méthoxy-7 hexahydro-1,2,3,4,4a,9 phénanthrène (**1***a* et *b*) avec l'acide *p*-toluènesulfonique dans le xylène à l'ébullition conduit au diméthyl-1,10 [(oxo-3 triméthyl-1,4,4 cyclohexyl)-2 éthyl]-2 méthoxy-7 dihydro-3,4 anthracène (**3**), un produit de réarrangement. Les cristaux de **3** sont monocliniques, groupe d'espace $P2_1/c$, $Z = 4$ avec $a = 7.2684(3)$, $b = 30.942(2)$, $c = 10.5544(7)$ Å, $\beta = 98.24(1)°$. On a déterminé la structure par des méthodes directes à partir de données de diffraction de rayon X et on l'a affinée par la méthode des moindres carrés (blocs diagonaux) jusqu'à une valeur de R de 0.043 pour 1810 réflexions observées. La molécule ne présente aucune caractéristique géométrique inhabituelle quoique le désordre de position est apparent dans la portion de la cyclohexanone.

On présente une route possible permettant d'expliquer la formation de **3** à partir de **1***a* et *b*.
[Traduit par le journal]

In the previous paper (1) we described the synthesis of the mixture of substituted reduced phenanthrenes **1***a* and *b* and its conversion into the pentacyclic picenone **2** suitable as an intermediate in triterpene synthesis.

During our studies we noted that the reaction of a mixture of **1***a* and *b* with *p*-toluenesulphonic acid in boiling xylene or benzene gave, after chromatography, a product whose physical properties did not correspond to those expected for a normal cyclisation product of **1***a* and *b* although its molecular weight

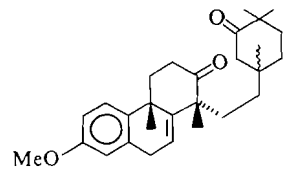

1
a Me group α
b Me group β

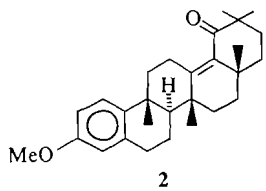

2

(M^+ 404) corresponded to the loss of one molecule of water from **1***a* or **1***b* (M^+ 422). Thus the mass spectrum of the cyclisation product showed a parent ion at *m/e* 404.2717 corresponding to a molecular formula of $C_{28}H_{36}O_2$ and a base peak at *m/e* 237.1264 corresponding to a fragment of structure $C_{17}H_{17}O$. This loss of a fragment $C_{11}H_{19}O$ (mol. wt. 167) suggested that the pendant trimethyl cyclo-

[1]Portions of this work are described in the Ph.D. thesis of S.B. (Carleton University, Ottawa, Ont., 1976). For Part IV see ref. 1.
[2]NRCC No. 16724.
[3]To whom inquiries should be directed.

Can. J. Chem. Downloaded from www.nrcresearchpress.com by 210.87.254.40 on 09/05/12
For personal use only.

TABLE 1. Carbon-13 nuclear magnetic resonance data for **3**

Carbon location*	Chemical shift (δ)	Type of carbon	No. of carbon atoms	No. of protons	No. of oxygen atoms
18	215	C=O	1		1
7	156	O—C=	1		
1,2,1a,4a,5a,8a,10	125.6, 127.0, 128.6 129.9, 133.5, 135.9, 137.4	=C—	7		
5,6,8,9	106.7, 117.3, 118.9, 125.2	=C—H	4	4	
12	55.1	O—CH_3	1	3	1
16,19	39.1, 44.1	—C—	2		
3,4,14,15,16,17,20,21	25.1, 28.7, 29.0 32.5, 36.5, 39.9, 49.8	CH_2	7	14	
11,13	14.3 (2)	=C—CH_3	2	6	
22,23,24	24.8, 25.4 (2)	—C—CH_3	3	9	
		Total	C = 28	H = 36	O = 2

*Carbon locations assigned as shown in Fig. 1.

hexanone ring had been lost together with its side chain:

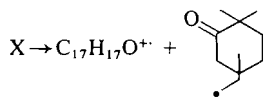

This behaviour is reminiscent of that observed for species such as **1***a* and *b* but not identical since in this latter case a McLafferty-type hydrogen rearrangement (1) is noted.

The 100 MHz proton magnetic resonance spectrum of the product 'X' indicated retention of the phenolic methyl ether system and the presence of two low field methyl groups, present as olefinic or aromatic substituents. The triplet for the olefinic proton appearing at δ 5.86 in the nmr spectrum of **11** was noted to be shifted downfield to δ 7.50 probably attributable to an isolated aromatic proton. The 25.15 MHz carbon-13 nmr spectrum indicated the presence of one carbonyl group (215.7 ppm) as well as eight sp^2 fully substituted carbon atoms. Table 1 summarises the carbon ^{13}C nmr spectrum. A single crystal X-ray structure determination was carried out on this material and revealed its structure to be the dihydroanthracene **3**. All of the spectroscopic properties (see Experimental) accord with this structure.

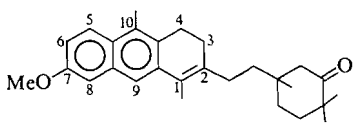

3

A view of the molecule as determined by X-ray diffraction is shown in Fig. 1 and final atomic coordinates and bond lengths and angles for the non-hydrogen atoms are presented in Tables 2 and 3. Full details concerning the H atoms and their bonding geometry have been placed in the Depository of Unpublished Data.[4] The average of all C—H bond lengths is 0.97 Å while that for associated angles is 109° (sp^3) and 119° (sp^2). The geometric features of the molecule show no remarkable deviation from those expected. Thus, the aromatic portion of the anthracene moiety is close to planar (±0.036 Å) and the fused cyclohexene ring, with torsion angles C(1a)—C(1)—C(2)—C(3) and C(1)—C(1a)—C(4a)—C(4) $< \pm 1°$, has a conformation best described as midway between a 'sofa' and a 'boat'. The extended dimethylene bridge, with torsion angles C(1)—C(2)—C(14)—C(15) and C(2)—C(14)—C(15)—C(16) of 95 and 176°, links to the trimethylcyclohexanone ring which is in 'chair' form. The intra-ring bond angle at the carbonyl group(s) approaches sp^2 values. The crystal packing forces in the structure are of the van der Waals type with a majority of the closest intermolecular contacts occurring between the carbonyl O atom(s) and symmetry related H atoms of —CH_2— and —CH_3 groups.

The formation of this species in acid can be explained by the stepwise transformation shown in Scheme 1; for a review of other acid-catalysed ketone rearrangements see ref. 2. It is interesting to note that in the initial rearrangement step it is the equatorial group that migrates rather than the methyl group, although it could be argued that other non-isolated reaction products could arise by an alternate route. We have been unable to detect other species of a similar nature to **3** although, as can be seen from the Experimental, **3** has been isolated in pure form in only about 25% yield. It is also interesting to note

[4]Tables of observed and calculated structure factors, anisotropic thermal parameters, hydrogen atom coordinates, and isotropic thermal parameters together with bond lengths and angles involving the hydrogen atoms are available, at a nominal charge, from the Depository of Unpublished Data, CISTI, National Research Council of Canada, Ottawa, Ont., Canada K1A 0S2.

Can. J. Chem. Downloaded from www.nrcresearchpress.com by 210.87.254.40 on 09/05/12
For personal use only.

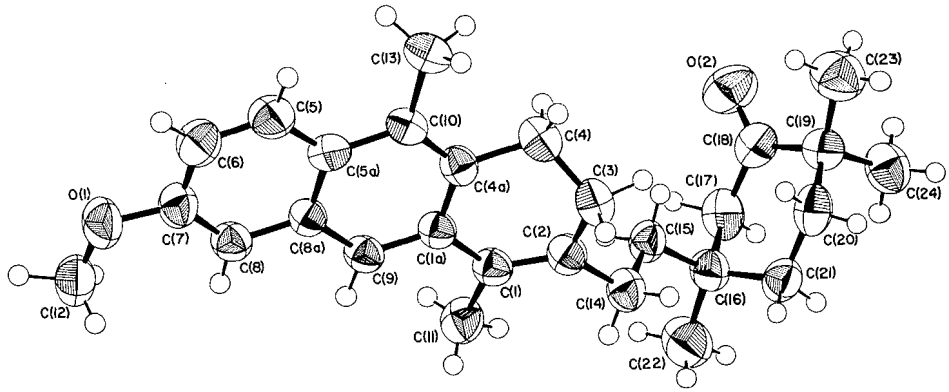

FIG. 1. Perspective view (3) of (**3**) as determined by X-ray analysis. Atom O(2) is shown in its major position (the minor site, O(2′), is on atom C(20)). Nonhydrogen atoms are represented by 50% probability thermal ellipsoids and hydrogen atoms by spheres of arbitrary radius.

TABLE 2. Final atomic coordinates ($\times 10^4$) with estimated standard deviations in parentheses

Atom	*x*	*y*	*z*	Atom	*x*	*y*	*z*
C(1)	5010(4)	384(1)	1473(3)	C(13)	7285(5)	−581(1)	5221(3)
C(1a)	4726(4)	−3(1)	2256(3)	C(14)	7136(5)	940(1)	720(3)
C(2)	6706(5)	554(1)	1495(3)	C(15)	7149(5)	1362(1)	1483(3)
C(3)	8344(5)	354(1)	2306(3)	C(16)	7691(4)	1773(1)	808(3)
C(4)	7863(4)	149(1)	3517(3)	C(17)	7657(5)	2154(1)	1737(4)
C(4a)	6124(4)	−124(1)	3283(3)	C(18)	9168(5)	2130(1)	2866(3)
C(5)	3844(5)	−1085(1)	4559(3)	C(19)	11144(5)	2063(1)	2602(3)
C(5a)	4203(4)	−718(1)	3830(3)	C(20)	11131(5)	1712(1)	1579(3)
C(6)	2247(5)	−1311(1)	4317(3)	C(21)	9683(5)	1747(1)	445(3)
C(7)	839(5)	−1180(1)	3341(3)	C(22)	6280(6)	1861(1)	−400(4)
C(8)	1113(4)	−837(1)	2601(3)	C(23)	12401(6)	1935(1)	3826(4)
C(8a)	2796(4)	−597(1)	2809(3)	C(24)	11818(5)	2491(1)	2100(4)
C(9)	3118(4)	−240(1)	2047(3)	O(1)	−739(3)	−1426(1)	3244(2)
C(10)	5856(4)	−465(1)	4067(3)	O(2)	8812(4)	2182(1)	3923(3)
C(11)	3314(5)	559(1)	633(3)	O(2′)	12282(9)	1462(4)	1702(17)
C(12)	−2279(5)	−1306(1)	2355(4)				

that **3** now contains only one asymmetric centre and is racemic whereas **1***a* and *b* was a mixture of diastereoisomers containing three such centres.

Experimental

For general procedures and details of spectroscopic analyses see Part III of this series (4).

*Acid-catalysed Rearrangement of 2-Keto-1β,4aβ-dimethyl-1α[2-(3-keto-1,4-trimethylcyclohexyl)ethyl]-7-methoxy-1,2,3,4,4a,9-hexahydrophenanthrene (***1***a + b)*

The olefinic diketones **1***a* and *b* (100 mg) were dissolved in 20 ml dry benzene under nitrogen. Solid *p*-toluenesulfonic acid (200 mg) was added and the mixture was refluxed for 7 h. Thin-layer chromatography indicated no loss of the starting material. An additional 200 mg of *p*-toluenesulfonic acid was added and reflux continued overnight. Thin-layer chromatography analysis showed, in addition to starting material, a new product of lesser polarity. After cooling the reaction mixture, water was added and the benzene layer separated. The aqueous layer was further extracted with ether (×3). The combined organic layer was washed with saturated sodium bicarbonate solution, water, saturated sodium chloride solution and dried over magnesium sulphate (anhydrous). Evaporation of the solvent gave an oil which was column chromatographed on silica gel. Elution with benzene gave 25 mg of the rearranged material (**3**) as an oil and further elution with 10% ether in benzene gave the starting diketones (60 mg).

The reaction was repeated under the above conditions except that the benzene was replaced by the higher boiling *p*-xylene. After column chromatography the product was obtained in higher yield (47%) as an oil. Although this material was homogeneous on thin layer chromatography, it was shown by nmr to be a mixture. Crystallization from methanol gave 24 mg of colorless crystals from 45 mg of the oil. The mother liquor appeared to be a mixture of compounds (nmr) which could not be resolved by column or thin-layer chromatography. Recrystallization of the crystalline material gave analytical sample of **3**: mp 117–120°C; uv max (95% C_2H_5OH): 308 (12 900), 295 (14 700), 257 (47 900); ir (Nujol): 1700 (C=O) and 1600 cm^{-1} (aromatic, olefin); nmr ($CDCl_3$) δ: 1.00 (s, 3, CH_3), 1.14 (s, 3, CH_3), 1.16 (s, 3, CH_3), 2.14 (s, 3, C—CH_3), 2.58 (s, 3, =C—CH_3), 3.93 (s, 3, O—CH_3), and 7.00–8.00 (m, 4, ArH); nmr (C_6D_6) δ: 0.82 (s, 3, CH_3), 1.04 (s, 3, CH_3), 1.08 (s, 3, CH_3), 2.18 (s, 3, CH_3), 2.42 (s, 3, CH_3), 2.54 (s, 3, O—CH_3), and 7.00–8.00 (m, 4, ArH); ms *m/e* (relative intensity): 404 (60), 202 (37), 237 (100); high resolution mass spectrum ion 404: mass calcd. for $C_{28}H_{36}O_2^+$: 404.2715; measured 404.2717; ion *m/e* 237; mass calcd. for

Can. J. Chem. Downloaded from www.nrcresearchpress.com by 210.87.254.40 on 09/05/12
For personal use only.

Can. J. Chem. Downloaded from www.nrcresearchpress.com by 210.87.254.40 on 09/05/12
For personal use only.

TABLE 3. Bond distances and angles involving the nonhydrogen atoms

(*a*) Distances: estimated standard deviations $\leq \pm 0.004$Å (except at O(2′) ± 0.01 Å)

Bond	Distance (A°)	Bond	Distance (A°)
C(1)—C(1a)	1.484	C(8a)—C(9)	1.404
C(1)—C(2)	1.338	C(9)—C(1a)	1.371
C(1)—C(11)	1.512	C(10)—C(13)	1.525
C(2)—C(3)	1.496	C(12)—O(1)	1.404
C(2)—C(14)	1.508	C(14)—C(15)	1.531
C(3)—C(4)	1.512	C(15)—C(16)	1.538
C(4)—C(4a)	1.510	C(16)—C(17)	1.536
C(4a)—C(10)	1.373	C(16)—C(21)	1.521
C(4a)—C(1a)	1.426	C(16)—C(22)	1.541
C(5a)—C(10)	1.426	C(17)—C(18)	1.502
C(5a)—C(8a)	1.426	C(18)—C(19)	1.516
C(5)—C(5a)	1.416	C(18)—O(2)	1.191
C(5)—C(6)	1.347	C(19)—C(20)	1.530
C(6)—C(7)	1.404	C(19)—C(23)	1.524
C(7)—C(8)	1.356	C(19)—C(24)	1.533
C(7)—O(1)	1.370	C(20)—C(21)	1.500
C(8)—C(8a)	1.422	C(20)—O(2′)	1.13

(*b*) Angles: estimated standard deviations $\leq \pm 0.3°$ (except at O(2′) $\pm 0.8°$)

Bonds	Angle (deg)	Bonds	Angle (deg)
C(1a)—C(1)—C(2)	120.5	C(4a)—C(10)—C(5a)	120.4
C(1a)—C(1)—C(11)	116.7	C(4a)—C(10)—C(13)	121.5
C(11)—C(1)—C(2)	122.7	C(5a)—C(10)—C(13)	118.1
C(1)—C(1a)—C(4a)	119.6	C(7)—O(1)—C(12)	118.7
C(1)—C(1a)—C(9)	121.7	C(2)—C(14)—C(15)	112.1
C(4a)—C(1a)—C(9)	118.7	C(14)—C(15)—C(16)	116.4
C(1)—C(2)—C(3)	120.3	C(15)—C(16)—C(17)	108.1
C(1)—C(2)—C(14)	124.4	C(15)—C(16)—C(21)	112.4
C(3)—C(2)—C(14)	115.3	C(15)—C(16)—C(22)	110.2
C(2)—C(3)—C(4)	113.2	C(17)—C(16)—C(21)	107.6
C(3)—C(4)—C(4a)	112.8	C(17)—C(16)—C(22)	108.9
C(4)—C(4a)—C(1a)	117.8	C(21)—C(16)—C(22)	109.5
C(4)—C(4a)—C(10)	121.3	C(16)—C(17)—C(18)	113.2
C(1a)—C(4a)—C(10)	120.9	C(17)—C(18)—C(19)	117.7
C(5)—C(5a)—C(10)	124.1	C(17)—C(18)—O(2)	120.2
C(5)—C(5a)—C(8a)	117.0	C(19)—C(18)—O(2)	122.0
C(8a)—C(5a)—C(10)	118.9	C(18)—C(19)—C(20)	108.5
C(5a)—C(5)—C(6)	122.2	C(18)—C(19)—C(23)	110.4
C(5)—C(6)—C(7)	120.5	C(18)—C(19)—C(24)	107.6
C(6)—C(7)—C(8)	120.1	C(20)—C(19)—C(23)	110.9
C(6)—C(7)—O(1)	114.1	C(20)—C(19)—C(24)	109.9
C(8)—C(7)—O(1)	125.8	C(23)—C(19)—C(24)	109.6
C(7)—C(8)—C(8a)	120.6	C(19)—C(20)—C(21)	116.3
C(8)—C(8a)—C(5a)	119.5	C(19)—C(20)—O(2′)	118.4
C(8)—C(8a)—C(9)	121.9	C(21)—C(20)—O(2′)	125.6
C(5a)—C(8a)—C(9)	118.7	C(16)—C(21)—C(20)	113.3
C(8a)—C(9)—C(1a)	122.5		

$C_{17}H_{17}O^+$: 237.1279; measured: 237.1264. *Anal.* calcd. for $C_{28}H_{36}O_2$: C 83.12, H 8.97; found: C 82.95, H 9.12.

X-ray Analysis of **3**

Crystallographic data for crystals of (**3**) are shown below. Preliminary work was carried out with Weissenberg and precession cameras and all intensity and cell data were measured on a Picker diffractometer using a locally written Fortran IV routine (5) on a PDP 8E computer. Accurate orientation and cell parameters were derived with a least-squares treatment of 34 reflections (17 Friedel pairs) with $2\theta > 80°$. The crystal data are as follows

$C_{28}H_{36}O_2$ fw = 404.57

Monoclinic, space group $P2_1/c$ from systematic absences $h0l$ $l = 2n + 1, 0k0$ $k = 2n + 1$; $a = 7.2684(3), b = 30.942(2)$, $c = 10.5544(7)$ Å, $\beta = 98.24(1)°$, $V = 2349.2$Å^3; $\rho_c = 1.14$, $\rho_m = 1.15$ g cm^{-3} (flotation in KCl solution); $Z = 4$. ($F_{000} =$

Can. J. Chem. Downloaded from www.nrcresearchpress.com by 210.87.254.40 on 09/05/12
For personal use only.

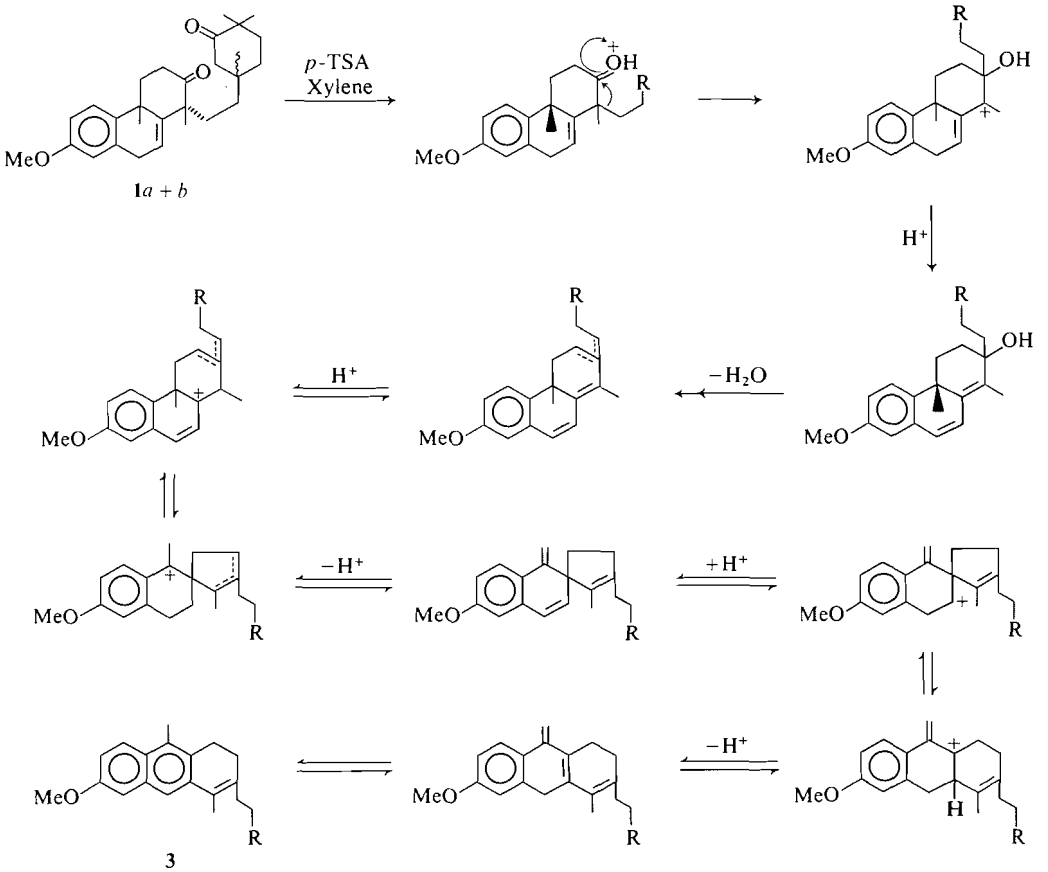

1a + b

3

SCHEME 1

880; CuKα, λ = 1.54056 Å, graphite monochromator; μ = 5.46 cm^{-1}; crystal dimensions 0.27 × 0.29 × 0.07 mm. Data collection details: $2\theta_{max} = 100°$, temperature 23°C, θ/2θ scan at 2° min^{-1} scan speed and background measurements of 21 s at each end of the scan; 2414 unique measured reflections of which 1810 were considered observed at the 2σ level.)

The data collection scheme used was that described by Grant (6) for obtaining a set of controlled precision measurements. A maximum measuring time of 600 s per reflection was allowed and after a preliminary scan the routine decides:

(*i*) Whether the reflection is observed with $I_{net} > 2\sigma(I_{net})$. If not, no further measurement is made and the reflection is considered unobserved.

(*ii*) If it is above this level, can the reflection be measured to 3% statistical accuracy within the allotted time? If it can be so measured, the scan is repeated the required number of times.

(*iii*) If it cannot be measured to 3%, can the reflection be measured to *at least* 15% using the whole of the allotted time? If this precision can be achieved the routine spends the remaining time to do so. If not, no further time is spent on the reflection and it is again considered unobserved. The values 3% and 15% are input parameters to the routine. All unobserved reflections have I_{net} set to $\frac{2}{3}\sigma(I_{net})$.

Three reference measurements were taken after every 50 reflections and no drift was observed. The normal data reduction techniques were used to correct the intensity data to F_o and E values. No absorption corrections were made.

The structure was solved with MULTAN (7) after some initial difficulty. An E-map was computed with $246|E| \geq 1.6$ which showed the 30 nonhydrogen atoms in the top 36 peaks. Refinement was carried out by block-diagonal least-squares methods, and following initial cycles a high thermal parameter on the carbonyl O atom together with evidence from a difference map, indicated positional disorder in the carbonyl group; the major and minor sites being related by a pseudo-mirror plane, defined approximately by the three methyl groups on the cyclohexanone ring. Refinement was continued with both sites included in the structural model. At an R[5] of 15%, 32 of the hydrogen atoms were located in a difference map, the remainder being found at later stages, and following their inclusion with isotropic thermal parameters and anisotropic refinement of the nonhydrogen atoms, convergence was attained at an R of 0.043 for the observed data (R for all data = 0.063)[4] with R_w[5] = 0.043. The goodness of fit[5] values was 1.88. A final difference map showed no peaks > ±0.17 e. The occupancies on the carbonyl sites were 0.85 and 0.21 (i.e., approximately 4:1) and no attempt was made to locate the partially occupied H atoms sites on C(18), any electron density owing to these atoms being compensated by high anisotropy on the adjacent O atom (nb, this also accounts for the sum of occupancies >1.0). Throughout refinement the function minimised was $\Sigma w(|F_o| - |F_c|)^2$ with weights, w, based upon counting statistics. Scattering factor constants were taken from *International Tables for X-ray Crystallography* (8) and were

[5] $R = \Sigma||F_o| - |F_c||/\Sigma|F_o|$; $R_w = \{\Sigma w(|F_o| - |F_c|)^2/\Sigma wF_o^2\}^{1/2}$. Goodness of fit = $\{\Sigma w(|F_o| - |F_c|)^2/(N_o - N_v)\}^{1/2}$ where N_o and N_v are the numbers of observations and variables.

employed in the analytical form: $f_s = c + \sum_{i=1}^{4} a_i \exp(-b_i s^2)$. All calculations were carried out on a PDP-8E computer using mostly locally written programs (9).

Acknowledgements

We thank the National Research Council of Canada for generous financial assistance (J.W.A., S.B.) in the form of a grant-in-aid of research, and a research associateship (M.L.P.). We gratefully acknowledge the aid of Mr. I. Miura, Columbia University, for the determination of some nmr spectra.

1. J. W. APSIMON, S. BADRIPERSAUD, J. W. HOOPER, R. PIKE, and C. HUBER. Can. J. Chem. This issue.
2. A. FRY. *In* Mechanisms of molecular rearrangements. Vol. 4. *Edited by* B. S. Thyagarajan. Wiley Interscience, New York, NY. 1971. p. 113.
3. C. K. JOHNSON. ORTEP II. Report ORNL-3794 (2nd rev.), Oak Ridge National Laboratory, Oak Ridge, TN. 1970.
4. J. W. APSIMON, S. BADRIPERSAUD, T. T. T. NGUYEN, and R. PIKE. Can. J. Chem. **56**, 1646 (1978).
5. D. F. GRANT and E. J. GABE. Am. Crystallogr. Assoc. Meet., Penn. State University, Aug. 1974. Abstr. J3; NRCC Report No. 14325.
6. D. F. GRANT. Acta Crystallogr. Ser. A, **29**, 217 (1973).
7. G. GERMAIN, P. MAIN, and M. M. WOOLFSON. Acta Crystallogr. Sect. A, **27**, 368 (1971).
8. INTERNATIONAL TABLES FOR X-RAY CRYSTALLOGRAPHY. Vol. IV. Kynoch Press, Birmingham. 1974.
9. Y. WANG, E. J. GABE, L. D. CALVERT, and J. B. TAYLOR. Acta Crystallogr. Sect. B, **32**, 1440 (1976).

Can. J. Chem. Downloaded from www.nrcresearchpress.com by 210.87.254.40 on 09/05/12
For personal use only.

Diterpene chemistry. VI. Some chemistry of 8,14-epoxypimaric acid.[1] Comments on the biosynthesis of tetracyclic diterpenes

JOHN W. APSIMON AND STEVEN F. HALL

Department of Chemistry, Carleton University, Ottawa, Ont., Canada K1S 5B6

Received October 14, 1977

JOHN W. APSIMON and STEVEN F. HALL. Can. J. Chem. **56**, 2156 (1978).

The cleavage of methyl pimarate 8,(14) α-epoxide (**4**) was studied with a variety of acidic reagents. The major products observed were the corresponding $\Delta^{7,8}$-14α-alcohol and dienes. Participation of the vinyl group was not detected.

Consideration of the stereoelectronic requirements for cyclisation of olefins with carbonium ions at C-8 of the pimarane skeleton suggest that the pimaranes are not the biogenetic precursors of the tetracyclic diterpenes. A modification of the traditional route is presented as a working hypothesis.

JOHN W. APSIMON et STEVEN F. HALL. Can. J. Chem. **56**, 2156 (1978).

On a étudié la réaction de clivage de l'époxyde-8(14)α pimarate de méthyle (**4**) sous l'influence d'une variété de réactifs acides. Les produits majeurs observés sont le $\Delta^{7,8}$ alcool-14α et des dièns correspondants. On n'a pu détecter la participation du groupe vinyle.

Si l'on considère les facteurs stéréoélectroniques requis pour une cyclisation des oléfines avec les carbocations en C-8 du squelette pimarane, on peut suggérer que les pimaranes ne sont pas les précurseurs biogénétiques des diterpènes tétracycliques. On propose une hypothèse de travail impliquant une modification de la route traditionnelle.

[Traduit par le journal]

As part of our studies of the reactions of certain diterpene epoxides (2, 3) we were intrigued by the possibility that the vinyl group of pimaric acid (**1**) might participate in the opening of an 8,14α-epoxide and thus provide a biomimetic route to the tetracyclic diterpenes (4) as outlined in Scheme 1. This possibility was reinforced by the observations we have already made in the case of ester **2** which is readily converted to hydroxy lactone **3** (2). This route, if successful, could then provide a direct chemical test of the Wenkert proposal (4) for the biosynthesis of the tetracyclic diterpenes from the pimaranes. There have been many unsuccessful attempts at such conversions (5–26, 57).

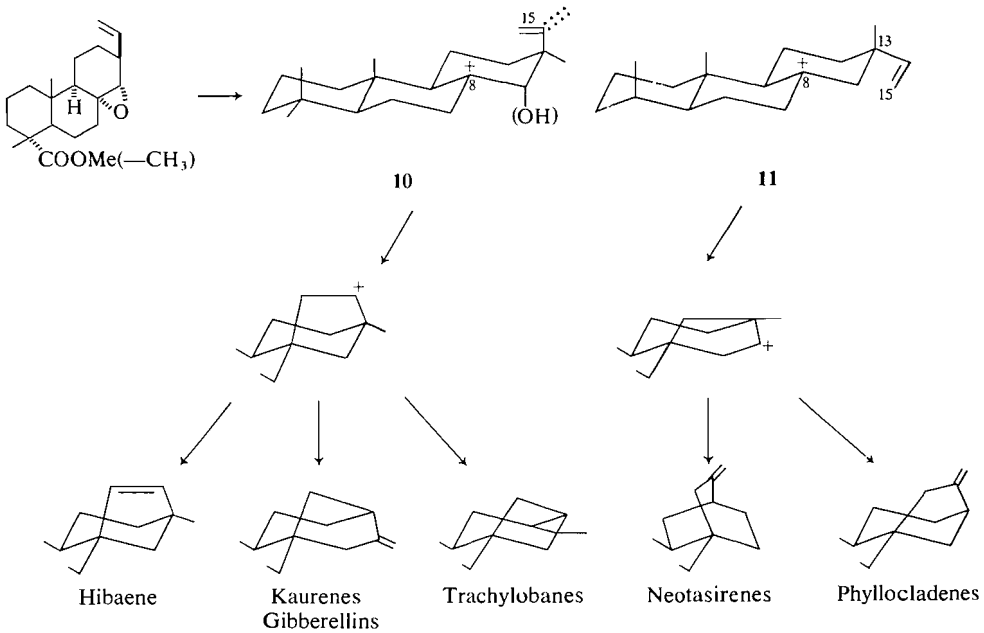

SCHEME 1

[1]For Part V see ref. 1.

Can. J. Chem. Downloaded from www.nrcresearchpress.com by 210.87.254.105 on 09/05/12
For personal use only.

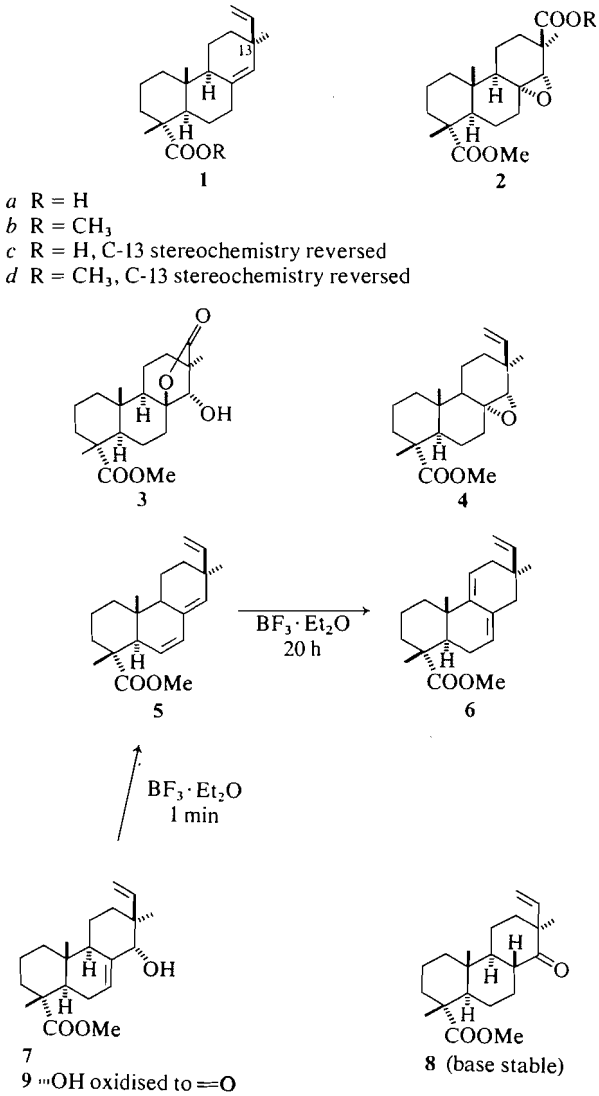

Accordingly, the 8,14α-epoxide of methyl pimarate (**4**) was prepared by treatment of methyl pimarate (**1***a*) with 1.1 equiv. of *m*-chloroperbenzoic acid. Our observations in this and similar experiments correspond to those reported recently (27) for methyl sandarocopimarate (**1***d*). The monoepoxide **4** was reacted with a variety of acidic reagents but we were unable to detect involvement of the vinyl group in the production of cleavage products except in the case of extended treatment with boron trifluoride etherate where a product was observed in which the characteristic proton nuclear magnetic resonance (nmr) signal for the vinyl group had disappeared. However, closer examination of this material indicated the formation of dimeric materials that appeared to be derived from compounds **5** or **6**. All of the cleavage reactions studied led to varying amounts of compounds **5**, **6**, **7**, and **8** depending on the conditions used; the results are summarised in Table 1. The structural elucidation of these compounds is unexceptional and the information is confined to the experimental section of this report.

TABLE 1. Cleavage of methyl pimarate 8(14)α-epoxide (**4**)

Reaction conditions	Product*				
	5	**6**	**7**	**8**	Dimer
Al_2O_3	Trace	Trace	75%		
SiO_2	Trace	Trace	80%		
BF_3–Et_2O, 20 h	~2%	16%		5%	50%
BF_3–Et_2O, 1 min	30%†				
CH_3COOH (1 or 21 h) room temperature			>95%		
$SnCl_4$	80%				Trace

*Isolated yield based on starting epoxide.
†Plus unreacted starting material.

In separate experiments we noted that the allylic alcohol **7** is converted into **5** by acidic reagents and the latter is in turn converted into **6**. It therefore appears that the major pathway for epoxide opening in the case of **4** is by the route *4* → *7* → *5* → *6* (cf. ref. 28). There appears to be no involvement of the vinyl group in an intramolecular sense during this cleavage. The formation of the allylic alcohol **7** rather than the $\Delta^{8,9}$ species suggests a concerted epoxide opening reaction since it is well known that carbonium ions centered at C-8 deprotonate preferentially to provide the tetra-substituted 8,9 double bonds. This observation is then in agreement with our earlier proposition concerning the reactive (and preferred) conformation of α-epoxides in this diterpene series (2, 3). In fact, it was this supposition that led us to believe that some vinyl group participation might be possible in the reactions studied.

That no cyclisation was observed could simply be a matter of the preferred conformation of the vinyl group being that indicated by the dotted lines in structure **10** of Scheme 1, or of the choice of reaction conditions. However, there does rest the possibility that up to this time the reason the lack of in vitro cyclisation in the sense proposed by Wenkert (4) has not been observed is because it is chemically unlikely (ref. 56, p. 164; ref. 57).[2] Thus, in order for bonding to occur between a developing cationic centre (in a chemical or biological sense) and a

[2]It must be stressed that there is an inherent danger in assuming a direct parallel between an in vitro and an in vivo process and using this to make statements concerning actual biosynthetic steps. We do however consider this technique a useful one in suggesting such parallels could exist and in delineating new areas of study.

Can. J. Chem. Downloaded from www.nrcresearchpress.com by 210.87.254.105 on 09/05/12
For personal use only.

Can. J. Chem. Downloaded from www.nrcresearchpress.com by 210.87.254.105 on 09/05/12
For personal use only.

double bond it is necessary for the π bond to overlap with the electron deficient centre. Examination of the pimarene case indicates that such overlap would be very inefficient because of the rigidity of the skeletal system and the stereochemistry of the vinyl group as indicated in **10**. The orthogonal arrangement of the vinyl group π system and the C-8 carbonium ion (or equivalent) suggests that cyclisation of this system is unlikely. The same stereoelectronic argument pertains for the case of the sandoracopimaric acid (**1***c*) derived cation **11**. This being the case, then

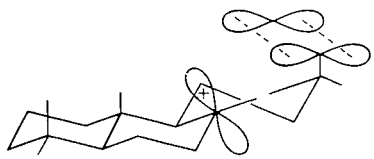

10

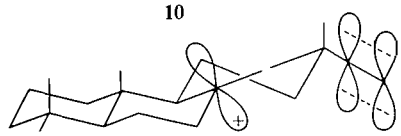

11

it is not surprising that previous in vitro (5–26, see also refs. 40–44) and in vivo (29–39) attempts to imitate the proposed biosynthetic scheme or close models (45, 46) have been unsuccessful. Other cases of cyclisation involving a 1,4 relationship between a carbonium ion centre and a π system have been reported but in all cases the molecules studied either possessed flexible skeletal arrangements allowing efficient overlap or involved hetero atoms in which lone pairs could be involved in the cyclisation process (2, 47–51).

Comments concerning the intermediacy of pimarene derived cations[3] have recently appeared (56, 57) where it is stated that the biosynthetic enzymes could aid in the attainment of the necessary orbital overlap for cyclization, or that some alternative scheme for tetracyclic diterpene biosynthesis via copalyl pyrophosphate (**12**) exists. Other reports have also questioned the traditionally accepted route (32, 52).

At first sight the formal route outlined in Scheme 2 would appear attractive as an alternative mode for tetracyclic diterpene formation. However, as the referees have pointed out[4] this modification does raise other problems that must be answered. Firstly a *trans* → *cis* isomerisation of the side-chain double

[3]In fact the enantiomeric ions to **10** and **11** would be those involved, considering the absolute configuration of the tetracyclic diterpenes observed to date.

[4]We heartily thank both referees for their constructive comments concerning the biosynthetic proposals.

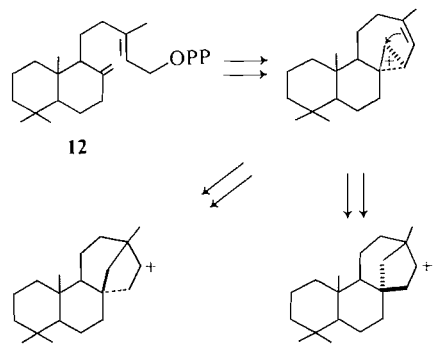

12

SCHEME 2

bond of copalyl pyrophosphate is required before cyclization necessitating an extra step in the biosynthetic pathway and it should be noted that the enzyme kaurene synthetase uses the *trans* isomer as its normal substrate. More serious, however, are the stereochemical implications of this proposal; in particular, if the bridged nonclassical ion indicated in Scheme 2 is the species involved then its trapping should proceed by inversion, a stereoelectronically unlikely step, and trapping by retention has no precedent.[2] These chemical objections can be circumvented by invoking enzyme-stabilised intermediates such as the classical ions **13** and **14**. The immed-

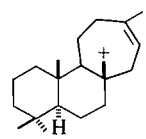

13

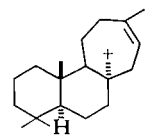

14

iate reaction to this proposal must be that **13** and **14** are primary carbonium ions, albeit neopentyl in nature: species which are traditionally discounted as biosynthetic intermediates. However, it is worth pointing out that at least in one case the primary carbonium ion **15** derived from 29,30-bisnor-2,3-oxidosqualene (synthetic substrate) has been enzymatically converted to 29,30-bisnoramyrin **16** (58),

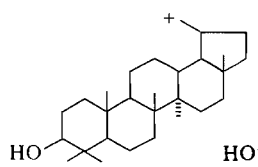

15

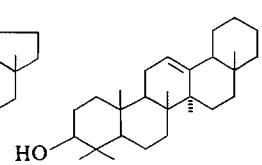

16

indicating that at least in this case that biosynthetic systems can cope with primary carbonium ions, although we stress that the substrate **15** is not natural.

The conjecture raised by Scheme **2** may confuse

Can. J. Chem. Downloaded from www.nrcresearchpress.com by 210.87.254.105 on 09/05/12
For personal use only.

the issue of tetracyclic diterpene biosynthesis[5] yet in view of the apparent need for further work we put forward this proposition especially as it emphasises the importance of considering stereoelectronic aspects of cyclisation processes in both chemical and biochemical cases (cf. ref. 55).

The net effect of the proposed route represents the 'missing-link' in the variety of cyclisation processes leading from labdane precursors to polycyclic diterpenes as outlined in Scheme 3. It must be noted that route *3* in this scheme has been only observed in vitro to date.

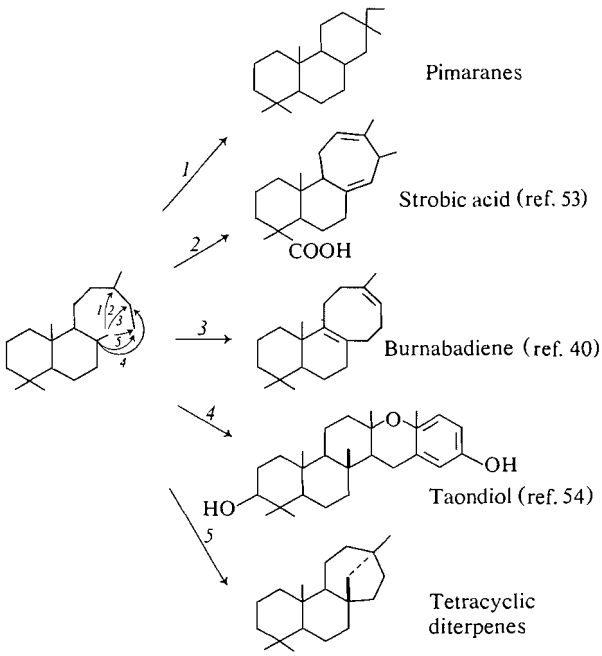

SCHEME 3

Experimental

All melting points were taken on a Kofler hot stage and are uncorrected. Thin-layer chromatography was carried out on precoated silica gel plates obtained from E.M. Reagents (silica gel F-254, 0.25 or 2.0 mm) unless otherwise stated; the plates were developed either by exposure to iodine vapour or by spraying with a solution of ceric sulphate and heating. The nuclear magnetic spectra were obtained on a Varian Model T-60 or Varian H-A 100 spectrometer with tetramethylsilane as internal standard. Chemical shifts are expressed in the δ scale and the usual abbreviations apply. Infrared spectra were determined on a Perkin-Elmer Model 237B grating infrared spectrometer and Beckman AccuLab 2 infrared spectrometer. The ultraviolet spectra were run on a Cary recording spectrometer Model 14 or Perkin-Elmer 202 ultraviolet–visible spectrophotometer. Low resolution mass spectra were obtained on an AEI MS12 instrument at Trent University, Peterborough. Combustion analyses were performed by Spang Microanalytical Laboratory, Ann Arbor, Michigan. Vapour phase chromatographic analyses were performed on a Perkin-Elmer 990 gas chromatograph using a flame ionisation detector and a 5 ft × ¼ in. column packed with 20% DEGS on HMDS treated Chrom W. Methyl pimarate was prepared by the diazomethane treatment of an ethereal solution of pimaric acid.

Methyl Pimarate 8(14)α-Epoxide (4)

To a solution of methyl pimarate (1.46 g, 5 mmol) in dry ether (50 ml) was added *m*-chloroperbenzoic acid (1.2 g, 6.6 mmol) and the reaction mixture was allowed to stir at room temperature for 2 days (protected from light). The reaction mixture was washed with 1% $NaHSO_3$, 5% $NaHCO_3$, and water, dried over anhydrous $MgSO_4$, and evaporated to give a colourless oil (1.595 g) whose nmr showed that the absorption at δ 5.17 (1H, broad singlet) corresponding to the C-14 olefinic proton in the starting material had disappeared and that a new peak at δ 2.73 (1H, sharp singlet) corresponding to the C-14 proton of the 8(14)-epoxide had appeared. The combined products of several epoxidation reactions gave a total of 3.68 g of material which was purified by column chromatography on activity III neutral alumina (250 g, dead volume 250 ml). Methyl pimarate (61 mg) was eluted by 5% benzene in petroleum ether. Benzene in petroleum ether (20:80) eluted a mixture of methyl pimarate 8(14)α-epoxide and a minor amount of two impurities which ran slightly ahead of the epoxide on silica gel tlc plates, eluting with benzene or with 10% ether–benzene (367 mg); 30 through 40% benzene in petroleum ether eluted pure methyl pimarate 8(14)α-epoxide (**4**) (2.117 g); mp 65–67°C; ν_{max}: 1725s, 1245s, 912m cm^{-1}; nmr δ: 2.75 (singlet, 1H), 1.23, 1.10, 0.97 (singlets, $3CH_3$ groups); *m/e* 332 (m^+); $[\alpha]_D^{25}$ −17.4°. *Anal.* calcd. for $C_{21}H_{32}O_3$ (mol. wt. 332.49); C 75.86, H 9.70; found: C 75.82, H 9.61. Benzene eluted methyl pimarate 8(14)α,15-diepoxide (306 mg) (diastereoisomeric mixture); mp 85–86°C; ν_{max}: 1720s, 1250s cm^{-1}; nmr δ: 2.3–3.2 (multiplet, 4H, protons attached to epoxide ring), 1.23, 1.03, 9.98, 9.87 (singlets, $3CH_3$ groups); *m/e* 348 (m^+). *Anal.* calcd. for $C_{21}H_{32}O_4$ (mol. wt. 348.49): C 72.38, H 9.26; found: C 72.35, H 9.18.

Rearrangement of Methyl Pimarate 8(14)α-Epoxide on Alumina

A column was packed from 5 g neutral activity alumina in benzene (dead volume 6.5 ml). Methyl pimarate-8(14)α-epoxide (84 mg) was placed on the column as a solution in the minimum amount of benzene, 1 dead volume of benzene was eluted, and the column allowed to stand overnight. The column was eluted with 4 dead volumes of ether to give a colourless oil (63 mg) which appeared as one major spot on silica gel tlc (20% ether–benzene). This product was purified by preparative tlc on four 20 cm × 20 cm × 2 mm silica gel plates eluting with 20% ether–benzene to give methyl pimara-7,15-diene-14α-olate (**7**) (60 mg); ν_{max}: 3520s, 1725s, 1250s, 920m cm^{-1}; nmr δ: 6.1–4.7 (multiplet, 4H, vinyl group plus one extra vinyl

[5]Obviously this proposition must be considered as a working hypothesis yet in view of our observations and those of others (32, 52, 56, 57) we believe it worthy of examination. In our own laboratory we have commenced a study of the solvolysis of substrates such as **17**.

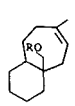

17

Can. J. Chem. Downloaded from www.nrcresearchpress.com by 210.87.254.105 on 09/05/12
For personal use only.

proton), 3.80 (sharp singlet, 1H, H-6—OH), 2.27, 1.08, 0.83 (sharp singlets, $3CH_3$ groups); *m/e*: 332 (m^+). *Anal.* calcd. for $C_{21}H_{32}O_3$ (mol. wt. 332.45): C 75.86, H 9.70; found: C 75.77, H 9.62.

Methyl Pimara-7,15-diene-14-oneate (9)

A solution of methyl pimara-7,15-diene-14α-olate (**7**) (34 mg) in dry petroleum ether (3 ml) was stirred with active MnO_2 (300 mg) at room temperature for 3 days. Thin-layer chromatography on silica gel eluting with 20% ether in benzene showed a single spot at higher R_f than the starting material, of which there was no trace. The reaction mixture was centrifuged, the residue washed with ether, the supernatants combined and evaporated to give a clear oil (19 mg) whose ir spectrum showed no O—H peak. This product was purified by preparative tlc on two 20 cm × 20 cm × 2 mm silica gel plates eluting with 20% ether–benzene to give methyl pimara-7,15-diene-14-oneate (**9**) (10 mg); ν_{max}: 1733s, 1690s cm^{-1}; nmr δ: 6.82 (broad singlet, 1H, H—C=C—C=O), 1.25, 1.08, 0.80 (sharp singlets, $3CH_3$ groups); λ_{max}: 243 nm (calculated value: 242 nm) ε 6020; *m/e* 330 (m^+). *Anal.* calcd. for $C_{21}H_{30}O_3$: C 76.33, H 9.15; found: C 76.22, H 9.07.

Rearrangement of Methyl Pimarate 8(14)α-Epoxide (4) on Silica Gel

A silica gel column was packed from 5 g silica gel in benzene (dead volume 10 ml). Methyl pimarate 8(14)α-epoxide (**4**) (104 mg) was placed on the column as a solution in the minimum amount of benzene and 1 dead volume of benzene was eluted and the column allowed to stand overnight. The column was eluted with 4 dead volumes of ether to give a yellow oil (86 mg). Thin-layer chromatography on silica gel eluting with benzene showed two major spots at lower R_f than the starting material of which there was no trace. The nmr spectrum of this material had no peak at δ 2.75 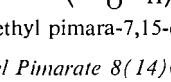 and was similar in all respects to that of methyl pimara-7,15-diene-14α-olate (**7**).

Rearrangement of Methyl Pimarate 8(14)α-Epoxide (4) with $BF_3 \cdot Et_2O$ for 20 h

To a solution of methyl pimarate 8(14)α-epoxide (**4**) (1.982 g) in dry benzene (165 ml) was added freshly distilled $BF_3 \cdot Et_2O$ (1.7 ml) whereupon the reaction mixture turned black. The reaction was stirred at room temperature for 20 h after which time tlc on silica gel plates eluting with benzene or with 10% ether–benzene showed two major spots at higher R_f than the starting material of which there was no trace. Ether (150 ml) was added to the reaction mixture and the solution washed with saturated $NaHCO_3$ solution and with water, then dried over anhydrous $MgSO_4$ and evaporated to give a red gum (2.138 g) of which 1.801 g were separated by column chromotography on silica gel (100 g; dead volume 220 ml) packed in petroleum ether, collecting 25 ml fractions. Petroleum ether eluted fraction *A* (827 mg); 60% benzene – petroleum ether eluted methyl pimara-7,9(11),15-trienoate (**6**) (313 mg) as a colorless oil; uv λ_{max}: 236 (212, 500), 242 (215, 500), 251 (ε 14 000), ir ν_{max}: 1724s, 1245s, 912m cm^{-1}; nmr δ: 6.2–4.6 (multiplet, 5H, vinyl protons) 2.27, 0.98, 0.95 (sharp singlets, $3CH_3$ groups), 2.20–1.85 (multiplet, 6H, H—C—C=C). *Anal.* calcd. for $C_{21}H_{30}O_2$ (M^+ 314): C 80.21, H 9.62; found: C 80.02, H 9.43. Benzene eluted a mixture (110 mg) of methyl pimara-7,9(11),15-trienoate and fraction *A*; 10% ether–benzene eluted fraction *A* (32 mg) and fraction *B* (317 mg).

Fraction A

Thin-layer chromatography on silica gel showed two spots running very close together at R_f 0.36 and 0.40 eluting with benzene and at R_f 0.65 and 0.71 eluting with 10% ether–benzene; ir ν_{max}: 1719 cm^{-1} (no absorption at 900 cm^{-1}); nmr δ: 7.05 (broad singlet, 0.5 H), 3.70 (sharp singlet, 3H, CH_3O_2C—), 1.67 (broad singlet), 1.28 (sharp singlet), 1.23 (sharp singlet), (total integration: δ 2.3–0.1 ≡ 30H: δ 6.5–4.0 ≡ < 0.5H); *m/e* 628 (m^+). This fraction eluded all attempts at further purification and attempts to hydrolyse the carboxymethyl group.

Fraction B

Thin-layer chromatography on silica gel eluting with 10% ether–benzene showed two major spots at R_f 0.50 and 0.39. This fraction was separated by preparative tlc on 11 20 cm × 20 cm × 0.25 mm silica gel plates eluting with 10% ether–benzene. The band at R_f 0.50 gave fraction *A* (24 mg). The band at R_f 0.39 gave methyl pimar-15-ene-14-oneate (**8**) (105 mg); ir ν_{max}: 1725s, 1705s, 1249s, 935m cm^{-1}; nmr δ: 6.3–4.7 (ABX pattern, 3H, vinyl group), 2.85–2.25 (broad multiplet, 1H, H—C—C=O), 1.18, 1.10, 0.97 (sharp singlets, $3CH_3$ groups). M^+ calcd. for $C_{21}H_{32}O_3$: 332.5; found: 332.

Base Treatment of Methyl Pimara-15-ene-14-oneate (8)

A solution of methyl pimara-15-ene-14-oneate (**8**) (25 mg) and sodium methoxide (37 mg) in anhydrous methanol (3 ml) was stirred at room temperature during 22 h. Water (10 ml) was added, the reaction extracted with ether, the extracts combined, washed with water, dried over anhydrous $MgSO_4$, and evaporated to give back methyl pimara-15-ene-14-oneate (**8**) (23 mg). This experiment substantiates the *trans*-BC ring junction.

BF_3–Et_2O Catalysed Rearrangement of Methyl Pimarate (1b)

To a solution of methyl pimarate **1***b* (100 mg) in dry benzene (8 ml) was added freshly distilled $BF_3 \cdot Et_2O$ (100 μl) whereupon the solution darkened. The reaction mixture was stirred at room temperature during 20½ h. Ether (10 ml) was added and the solution washed with saturated $NaHCO_3$ solution then with water, dried over anhydrous magnesium sulphate and evaporated to give pimara-8(9),15-dienoate (93 mg); ν_{max}: 1725s, 1250s, 910m cm^{-1}; nmr δ: 6.2–4.7 (multiplet, 3H, vinyl group), 1.2, 0.98, 0.93 (sharp singlets, $3CH_3$ groups).

Rearrangement of Methyl Pimarate 8(14)α-Epoxide (±) with $BF_3 \cdot Et_2O$ for 1 min in Dilute Solution

To a solution of methyl pimarate 8(14)α-epoxide (**4**) (256 mg) in dry benzene (2500 ml) was added freshly distilled $BF_3 \cdot Et_2O$ (175 μl) and the solution stirred at room temperature during 1 min. The reaction mixture was washed with saturated $NaHCO_3$ solution and water, dried over anhydrous calcium chloride, and evaporated to give a yellow oil (220 mg) whose tlc on silica gel eluting with benzene showed two major spots at R_f 0.062 and 0.375. This crude product was separated by preparative tlc on 17 20 cm × 20 cm × 25 mm silica gel plates eluting with benzene and the band at R_f 0.375 collected to give methyl pimara-6,8(14),15-trienoate (**5**) (80 mg) as a colourless oil; ir ν_{max}: 1730s, 1250s, 920m cm^{-1}; nmr δ: 6.3–4.6 (multiplet, 6H, vinyl group + 3 additional vinyl hydrogens), 1.22, 1.07, 0.75 (sharp singlets, $3CH_3$ groups); λ_{max} 233.8 (ε 9810), 240.5 (ε 10 600), 249.0 nm (ε 7500); ms M^+ calcd.: 314.2246; found: 314.2241. *Anal.* calcd. for $C_{21}H_{30}O_2$ (M^+ 314.5): C 80.21, H 9.62; found: C 79.90, H 9.31.

Rearrangement of Methyl Pimara-7,15-diene-14α-olate (7) with $BF_3 \cdot Et_2O$ for 1 min in Dilute Solution

To a solution of methyl pimara-7,15-diene-14α-olate (**7**) (7.5 mg) in dry benzene (100 ml) was added freshly distilled $BF_3 \cdot Et_2O$ (0.01 ml) and the solution stirred at room temperature for 1 min. The reaction mixture was washed with saturated $NaHCO_3$ solution and water, dried over anhydrous calcium chloride, and evaporated to give a colourless oil (6.5 mg)

Can. J. Chem. Downloaded from www.nrcresearchpress.com by 210.87.254.105 on 09/05/12
For personal use only.

whose tlc on silica gel and on silica gel impregnated with silver nitrate, eluting with benzene, showed one major spot at the same R_f as methyl pimara-6,7(14),15-trienoate (**5**). Peak enhancement by vpc and nmr spectroscopy also indicated that this compound was the major product.

$BF_3 \cdot Et_2O$ Treatment of Methyl Pimara-6,8(14),15-trienoate (5) in Dilute Solution

To a solution of methyl pimara-6,8(14),15-trienoate (**5**) (56 mg) in dry benzene (750 ml) was added freshly distilled $BF_3 \cdot Et_2O$ (7.5 ml) and the solution stirred at room temperature during 30 min. The reaction mixture was washed with saturated $NaHCO_3$ solution and water, dried over anhydrous calcium chloride, and evaporated to give a colourless oil. The above procedure was repeated for further periods of 3, 1, and $15\frac{1}{2}$ h. Nuclear magnetic resonance spectroscopy and peak enhancement by vpc showed a steady decrease in the amount of methyl pimara-6,8(14),15-trienoate (**5**) and a steady increase in the amount of methyl pimara-7,9(11),15-trienoate (**6**) until, after a total of 20 h of reaction, the two compounds were present in approximately equal concentrations.

$BF_3 \cdot Et_2O$-catalysed Rearrangement of Methyl Pimarate 8(14)α-epoxide (4) in Dilute Solution for 20 h

To a solution of methyl pimarate 8(14)α-epoxide (**4**) (99 mg) in dry benzene (1500 ml) was added freshly distilled $BF_3 \cdot Et_2O$ (15 ml) and the solution stirred at room temperature protected from light during 20 h. The reaction mixture was washed with saturated $NaHCO_3$ solution until the washings remained basic, then washed with water and dried over anhydrous $MgSO_4$ to give, after evaporation, a yellow oil (90 mg), whose nmr and ir spectra resembled very closely those of the crude reaction mixture obtained from the more concentrated 20 h reaction. A portion (77 mg) of the reaction product was separated by preparative tlc on five 20 cm × 20 cm × 0.25 mm silica gel plates eluting with benzene and the band at R_f 0.41 was collected to give a clear oil (10 mg) which nmr spectroscopy showed to be an approximately equimolar mixture of methyl pimara-6,8(14),15-trienoate (**5**) and methyl pimara-7,9(11),15-trienoate (**6**). The material on the remaining areas of the plates was recovered to give a yellow oil (50 mg) which was separated by preparative tlc on five 20 cm × 20 cm × 0.25 mm silica gel plates eluting with 10% ether–benzene and the band at R_f 0.63 collected to give a yellow oil (11 mg) which was shown by nmr spectroscopy and by tlc on silica gel plates eluting with 10% ether–benzene to be identical with fraction *A*.

Blank Run of $BF_3 \cdot Et_2O$ Reaction Work-up Procedure on Methyl Pimarate-8(14)α-epoxide (4)

A solution of methyl pimarate-8(14)α-epoxide (62 mg) in benzene (1500 ml) was washed with saturated $NaHCO_3$ solution four times, then with water four times, dried over anhydrous $MgSO_4$, and evaporated to give a clear oil (50 mg) which was shown by ir and nmr spectroscopy and by tlc on silica gel eluting with benzene or with 10% Et_2O–benzene to be methyl pimarate 8,(14)α-epoxide (**4**) indicating that the products detected in the $BF_3 \cdot Et_2O$ catalysed rearrangements are not artifacts of the rearrangement of unreacted starting material during the work-up procedure.

Rearrangement of Methyl Pimarate 8(14)α-epoxide with BF_3 Gas

To a solution of methyl pimarate 8(14)α-epoxide (**4**) (32 mg) in dry benzene (50 ml) was bubbled BF_3 gas for 2 min. The reaction immediately turned cloudy yellow. The solution was stirred at room temperature. After a few minutes this solution went deep red and after about 2 h the solution had gone clear and there was a deep red oil sitting on top of the solution. Stirring was continued for a total of 21 h after which time the solution was clear and a dark red gum adhered to the sides of the flask. The reaction mixture was washed with saturated $NaHCO_3$ solution, the aqueous basic layer washed with benzene, the benzene fractions combined, washed with water, dried over anhydrous $MgSO_4$, and evaporated to give a pale yellow oil (4 mg). The above-mentioned red gum, was dissolved in ether to give a yellow solution which was washed with water, dried over anhydrous $MgSO_4$ and evaporated to give a yellow oil (20 mg) shown by ir and nmr spectroscopy and by tlc on silica gel eluting with benzene or with 10% ether–benzene to consist almost entirely of fraction *A*.

Acetic Acid Catalysed Rearrangement of Methyl Pimarate 8(14)α-Epoxide (4)

A solution of methyl pimarate 8(14)α-epoxide (**4**) (50 mg) in glacial acetic acid (50 ml) was stirred at room temperatures for 1 h, added to water (300 ml), neutralised with Na_2CO_3, and extracted with ether. The ether extracts were combined, washed with water, dried over anhydrous $MgSO_4$, and evaporated to give a colourless oil (45 mg) which was shown by ir and nmr spectroscopy and by tlc on silica gel, eluting with benzene or with 10% ether–benzene, to consist predominantly of methyl pimara-7,15-diene-14α-olate (**7**). No trace of the two isomeric trienes was detected. An identical result was obtained when the reaction was repeated but allowed to run for 21 h.

$SnCl_4$ Catalysed Rearrangement of Methyl Pimarate 8(14)α-Epoxide (4) (1 h)

To a solution of methyl pimarate 8(14)α-epoxide (**4**) (20 mg) in dry benzene (50 ml) was added purified $SnCl_4$ (0.5 ml). The solution was stirred at room temperature and 1 ml samples withdrawn after a total reaction time of 0, 1, 10, and 30 min. During this time the reaction remained a homogeneous clear royal blue solution. The withdrawn samples were evaporated under vacuum and the residue run on silica gel tlc eluting with 10% ether–benzene and the chromatograms were identical showing a single spot at R_f 0.66. The reaction mixture was allowed to stir for a further $\frac{1}{2}$ h and then washed with saturated $NaHCO_3$ solution until the washings remained basic. The aqueous layers were extracted with benzene, the benzene extracts combined, washed with water, dried over anhydrous $MgSO_4$, and evaporated to give a yellow oil (16 mg) which was shown by ir and nmr spectroscopy and by tlc on silica gel eluting with benzene to consist mainly of methyl pimara-6,8(14),15-trienoate (**5**) with a trace of fraction *A* and other unidentified impurities.

Acknowledgements

We thank the National Research Council of Canada for generous financial support and M. Jean Pouydebat, Ets. Granel, Dax, France for generous gifts of pimaric acid.

1. J. W. APSIMON, A. HOLMES, H. BEIERBECK, and J. SAUNDERS. Can. J. Chem. **54**, 418 (1976).
2. J. W. APSIMON and H. KREHM. Can. J. Chem. **47**, 2859 (1969).
3. J. W. APSIMON. Chem. Commun. 83 (1970).
4. E. WENKERT. Chem. Ind. (London), 282 (1955); J. R. HANSON. The tetracyclic diterpenes. Pergamon Press, Oxford. 1968. p. 114.
5. R. A. APPLETON, A. J. MCALEES, A. MCCORMICK, R. MCCRINDLE, and R. D. H. MURRAY. J. Chem. Soc. C, 2319 (1966).
6. G. HUGEL, L. LODS, J. M. MELLOR, and G. OURISSON. Bull. Soc. Chim. Fr. 2894 (1965).

7. G. HUGEL, L. LODS, J. M. MELLOR, D. W. THEOBALD, and G. OURISSON. Bull. Soc. Chim. Fr. 2882 (1965); 2888 (1965).
8. A. H. KAPADI and S. DEV. Tetrahedron Lett. 1255 (1965).
9. C. DJERASSI, P. QUITT, E. MOSETTIG, R. C. CAMBIE, P. S. RUTLEDGE, and L. H. BRIGGS. J. Am. Chem. Soc. **83**, 3720 (1961).
10. B. E. CROSS, J. F. GROVE, and A. MORRISON. J. Chem. Soc. 2498 (1961).
11. B. E. CROSS, J. R. HANSON, and R. N. SPEAKE. J. Chem. Soc. 3555 (1965).
12. A. J. MCALEES, R. MCCRINDLE, and R. D. H. MURRAY. Chem. Ind. (London), 240 (1966).
13. A. H. KAPADI and S. DEV. Tetrahedron Lett. 2729 (1965).
14. R. R. SOBTI and S. DEV. Tetrahedron Lett. 3939 (1966).
15. E. L. GHISALBERTI and P. R. JEFFERIES. Aust. J. Chem. **19**, 1759 (1966).
16. J. R. HANSON. Tetrahedron, **23**, 793 (1967).
17. A. YOSHIKOSHI, M. KITADANI, and Y. KITAHARA. Tetrahedron, **23**, 1175 (1967).
18. P. A. GUNN, R. MCCRINDLE, and R. G. ROY. J. Chem. Soc. C, 1018 (1971).
19. R. A. APPLETON, P. A. GUNN, and R. MCCRINDLE. Chem. Commun. 1131 (1968).
20. R. A. APPLETON, P. A. GUNN, and R. MCCRINDLE. J. Chem. Soc. C, 1148 (1970).
21. J. G. ST. C. BUCHANAN and B. R. DAVIS. Chem. Commun. 1142 (1967).
22. R. M. COATES and E. F. BERTRAM. J. Org. Chem. **36**, 3722 (1971).
23. R. M. COATES and E. F. BERTRAM. Chem. Commun. 797 (1969).
24. R. M. COATES and E. F. BERTRAM. J. Org. Chem. **36**, 2625 (1971).
25. R. D. H. MURRAY, R. W. MILLS, and J. M. YOUNG. Tetrahedron Lett. 2393 (1971).
26. K. M. BAKER, L. H. BRIGGS, J. G. ST. C. BUCHANAN, R. C. CAMBIE, B. R. DAVIS, R. C. HAYWARD, G. A. S. LONG, and D. S. RUTLEDGE. J. Chem. Soc. Perkin I, 190 (1972).
27. B. DELMOND, G. PINTO, J. VALADE, and C. REDIN. C.R. Acad. Sci. Ser. C, **283**, 465 (1975).
28. E. C. LEVY and D. LAVIE. Israel J. Chem. **8**, 677 (1970).
29. A. J. BIRCH, R. W. RICKARDS, H. SMITH, A. HARRIS, and W. B. WHALLEY. Tetrahedron, **7**, 241 (1969).
30. J. R. HANSON and A. F. WHITE. Chem. Commun. 103 (1969).
31. J. R. HANSON and A. F. WHITE. J. Chem. Soc. C, 981 (1969).
32. R. EVANS and J. R. HANSON. J. Chem. Soc. Perkin I, 2382 (1972).
33. B. E. CROSS, R. H. B. GALT, and J. R. HANSON. J. Chem. Soc. 295 (1964).
34. B. E. CROSS, R. H. B. GALT, and J. R. HANSON. J. Chem. Soc. 2937 (1963).
35. D. R. ROBINSON and C. A. WEST. Biochemistry, **9**, 70, 80 (1970).
36. J. E. GRAEBE, D. F. DENNIS, C. D. UPPER, and C. A. WEST. J. Biol. Chem. **240**, 1847 (1965).
37. C. D. UPPER and C. A. WEST. J. Biol. Chem. **242**, 3285 (1967).
38. C. A. WEST and D. T. DENNIS. J. Biol. Chem. **242**, 3293 (1967).
39. R. R. FALL and C. A. WEST. J. Biol. Chem. **246**, 6913 (1971).
40. S. F. HALL and A. C. OEHLSCHLAGER. Tetrahedron, **28**, 3155 (1972).
41. O. E. EDWARDS and R. S. ROSICH. Can. J. Chem. **46**, 1113 (1968).
42. T. MCCREADIE and K. H. OVERTON. Chem. Commun. 288 (1968).
43. T. MCCREADIE and K. H. OVERTON. J. Chem. Soc. C, 312 (1971).
44. E. WENKERT and Z. KUMAZAWA. Chem. Commun. 140 (1968).
45. L. J. DOLBY and R. H. IWAMOTO. J. Org. Chem. **30**, 2420 (1965).
46. D. J. GOLDSMITH and C. J. CHEER. J. Org. Chem. **30**, 2264 (1965).
47. W. HERZ, A. K. PINDER, and R. N. MIRRINGTON. J. Org. Chem. **31**, 2257 (1966).
48. S. K. DASGUPTA, R. DASGUPTA, S. R. GNOSH, and V. R. GHATAK. Chem. Commun. 1253 (1969).
49. L. J. DOLBY, S. ESFANDIARI, C. A. ELLIGER, and K. S. MARSHALL. J. Org. Chem. **36**, 1277 (1971).
50. B. L. SHAPIRO. J. M. GATTUSO, and G. R. SULLIVAN. Tetrahedron Lett. 223 (1971).
51. W. G. DAUBEN and E. I. AOYAGI. J. Org. Chem. **37**, 251 (1972).
52. P. S. MARCHAND and J. F. BLOUNT. J. Chem. Soc. Chem. Commun. 894 (1975).
53. D. F. ZINKEL and B. P. SPALDING. Tetrahedron Lett. 2459 (1971).
54. A. G. GONZALEZ and J. D. MARTIN. Tetrahedron Lett. 2259 (1972).
55. J. E. BALDWIN. J. Chem. Soc. Chem. Commun. 734 (1976).
56. R. M. COATES. *In* Fortschritte der Chemie Organischer Naturstoffe. Vol. 33. *Edited by* W. Herz, H. Grisebach, and G. W. Kirby. Springer-Verlag, New York, NY. 1976.
57. J. W. BLUNT, G. S. BOYD, M. P. HARTSHORN, and M. H. G. MUNRO. Aust. J. Chem. **29**, 987 (1976).
58. E. J. COREY and S. K. GROSS. J. Am. Chem. Soc. **90**, 5045 (1968).

Can. J. Chem. Downloaded from www.nrcresearchpress.com by 210.87.254.105 on 09/05/12
For personal use only.

Organometallic peroxy radicals. 4. Electron spin resonance spectra of the radicals produced by reaction of organophosphorus(IV) and organoarsenic(IV) radicals with ^{17}O-enriched oxygen[1]

J. A. HOWARD AND J. C. TAIT[2]

Division of Chemistry, National Research Council of Canada, Ottawa, Ont., Canada K1A 0R9

Received February 13, 1978

J. A. HOWARD and J. C. TAIT. Can. J. Chem. **56**, 2163 (1978).

It has been shown that some tetra-coordinate phosphorus and arsenic radicals combine with oxygen to give peroxy radicals. The magnitude of the oxygen isotropic and anisotropic hyperfine coupling constants indicates that nearly all the unpaired spin is associated with the two oxygen nuclei with ca. 60% on the terminal oxygen. The large isotropic *g*-factors associated with Group VB peroxy radicals relative to alkylperoxy radicals is attributed to a small change in geometry of the peroxy function.

The radicals with $a_P \sim 9$ G obtained during the reaction of photochemically generated *tert*-butoxy radicals with trialkylphosphites in the presence of oxygen are secondary species which appear to contain only one oxygen atom.

J. A. HOWARD et J. C. TAIT. Can. J. Chem. **56**, 2163 (1978).

On montre que quelques radicaux tétra-coordonnés de phosphore et de l'arsenic se combinent avec l'oxygène pour conduire à des radicaux peroxy. L'amplitude des constantes des couplages isotropes et anisotropes hyperfins de l'oxygène indiquent que pratiquement tout le spin non-pairé est associé avec les deux oxygènes alors qu'environ 60% se retrouve sur l'oxygène terminal. On attribue le fait que les valeurs des facteurs *g* isotropes associés avec les radicaux peroxy du groupe VB sont plus élevées que celles associées aux radicaux alkylperoxy à un petit changement dans la géométrie du groupe peroxy.

Les radicaux avec $a_P \sim 9$ G obtenus par réaction, en présence d'oxygène, de trialkylphosphites avec des radicaux *tert*-butoxy produits photochimiquement, sont des espèces secondaires qui semblent contenir un seul atome d'oxygène.

[Traduit par le journal]

In 1972 two groups of workers (1, 2) reported the detection of tetra-alkoxyphosphoranylperoxy radicals by epr spectroscopy during photolysis of oxygenated solutions of dialkyl peroxide, ROOR, and trialkyl phosphite, $(R'O)_3P$, at low temperatures according to reactions [1]–[3].

$$\text{[1]} \qquad \text{ROOR} \xrightarrow{h\nu} 2\text{RO}^{\cdot}$$

$$\text{[2]} \qquad \text{RO}^{\cdot} + (\text{R}'\text{O})_3\text{P} \rightarrow \text{RO}(\text{R}'\text{O})_3\text{P}^{\cdot}$$

$$\text{[3]} \qquad \text{RO}(\text{R}'\text{O})_3\text{P}^{\cdot} + \text{O}_2 \rightarrow \text{RO}(\text{R}'\text{O})_3\text{PO}_2^{\cdot}$$

where R = *t*-Bu or Et and R′ = Me, Et, *i*-Pr, or *t*-Bu.

The esr spectra of these radicals were characterized by a small phosphorus hyperfine coupling constant (a_P = 8.9–9.45 G) and a high *g*-factor (~2.022). About the same time Furimsky, Howard, and Morton reported that the four-coordinate arsenic radical t-$BuO(Ph)_3As^{\cdot}$ reacts with oxygen to give the peroxy radical t-$BuO(Ph)_3AsO_2^{\cdot}$ (3). In this case hyperfine splitting from the arsenic nucleus (I = 3/2) was not observed while the *g*-factor was similar to the values reported for phosphoranylperoxy radicals.

In an attempt to confirm the structure of these radicals and estimate the influence of the phosphorus and arsenic nuclei on the spin density on the two oxygen atoms we have investigated the esr spectra of the radicals produced by reaction of phosphoranyl and arsanyl radicals with ^{17}O-enriched oxygen. In several cases phosphoranylperoxy and arsanylperoxy radicals have been unambiguously identified. On the other hand this work does cast considerable doubt on the authenticity of previously assigned tetra-alkoxyphosphoranylperoxy radicals.

Experimental

Electron spin resonance spectra were obtained with a Varian E-4 spectrometer equipped with a variable temperature accessory. The microwave frequency was measured with a Syntron-Donner Model 6016 frequency counter which also monitored the frequency of a proton magnetometer used to measure the magnetic field.

Di-*tert*-butyl peroxide (DTBP) was purified by preparative gas liquid chromatography. Triphenylarsine and triphenylphosphine were purified by recrystallization while trimethyl phosphite, triethyl phosphite, and trimethyl arsine were purified by vacuum distillation. The isotopically enriched

[1]NRCC No. 16688.

[2]NRCC Research Associate 1975–1977.

Can. J. Chem. Downloaded from www.nrcresearchpress.com by 210.87.254.5 on 09/05/12
For personal use only.

Can. J. Chem. Downloaded from www.nrcresearchpress.com by 210.87.254.5 on 09/05/12
For personal use only.

oxygen was obtained from Yeda Research and Development Company and its composition was 59.6% ^{17}O and 36.1% ^{18}O.

Results

Trimethylphosphite

The esr spectrum observed during photolysis of solutions of di-*tert*-butyl peroxide and trimethylphosphite in oxygenated cyclopropane at 173 K consisted of two components. A broad singlet, $\Delta H_{ms} \sim 13$ G at $g = 2.033$ (**1**) and a much sharper doublet, $a_P = 9.2$ G, at $g = 2.0213$ (**2**). When the light was shuttered **2** was observed to decay much more rapidly than **1**. If a solution was rapidly cooled immediately after cessation of photolysis the anisotropic spectrum of **1** was obtained; $g_{xx} = 2.0022$, $g_{yy} = 2.0086$, $g_{zz} = 2.0991$, and $g_{ave} = 2.037$.

When these experiments were conducted in the presence of ^{17}O-enriched oxygen the spectrum of **2** consisted of a strong doublet from the species with no magnetic oxygen flanked by a sextet of doublets (**3**), $a_O = 16.4$ G, $a_P = 9.1$ G, $g = 2.0215$. In addition there were weaker transitions from a species **4** with $a_O = 24.2$ G, $a_P = 9.2$ G, and $g = 2.0225$. There was no evidence for a radical with two equivalent or inequivalent oxygen nuclei. The esr spectrum of these species is shown in Fig. 1.

We were not able to produce an isotropic spectrum of **1** labelled with ^{17}O because of the very broad lines associated with this radical. The anisotropic spectrum, obtained upon freezing the solution, contained two sets of equally spaced lines centred about g_{xx} arising from two singly labelled radicals with $A_{xx}(^{17}O) = 76.2$ G and 69.3 G and transitions from the doubly labelled radical. This species is almost certainly a phosphoranylperoxy radical and we are fairly confident that its structure can be represented by

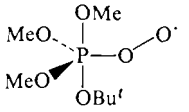

1

a structure that has previously been assigned to **2**, the radical with the 9 G coupling constant (1, 2).

It is possible that **2** is an organophosphorus peroxy radical with magnetically inequivalent oxygens and that **3** and **4** are the radicals with one or other of the oxygen nuclei substituted with ^{17}O. The doubly labelled species would then have to be unresolvable because of very broad lines. There are, however, a number of experimental observations which are not consistent with this assignment. These are: (*i*) the linewidth ($\Delta H_{ms} = 1.8$ G) is uncharacteristically narrow for a peroxy radical; (*ii*) the *g*-factor for **4** is significantly larger than the *g*-factor for **2** and **3**, which is impossible if they are all the same radical; (*iii*) the absence of the spectrum from the doubly labelled species; (*iv*) the relative concentration of **3** and **4** depends on the temperature. Thus at 173 K [**4**]/[**3**] is significantly larger than the ratio at 148 K; and (*v*) there is an induction period before **2** appears upon photolysis of a freshly prepared reaction mixture. The rate of formation of **2** then increases slowly with time and it is present after prolonged photolysis. A concentration time profile of this nature is indicative of a *secondary* species. The rate of production of **2** is much faster for a sample in which **2** has been generated and allowed to decay. If the solution is then warmed to room temperature for a short period of time, cooled, and re-photolyzed the accumulation of **2** again follows a S-shaped concentration–time profile. It would, therefore, appear that **2** is formed from an unstable product of the photochemically initiated autoxidation of $(MeO)_3P$ and contains only *one* oxygen nucleus.

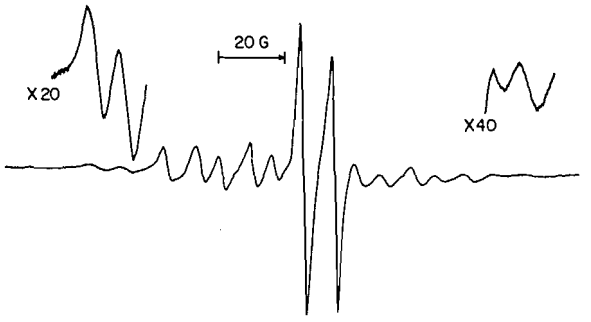

FIG. 1. The esr spectrum of *t*-BuO$(MeO)_3PO^{\cdot}$ enriched with oxygen-17 in cyclopropane at 153 K.

Triethylphosphite

Triethylphosphite behaved just like trimethylphosphite in the presence of photochemically generated *tert*-butoxy radicals and oxygen giving a peroxy radical ($g_{iso} = 2.033$) and species which appeared to contain only one oxygen nucleus ($a_P = 9.4$ G, $g_{iso} = 2.0214$).

Triphenylphosphine

Photolysis of solutions of DTBP and Ph_3P in cyclopropane containing ^{17}O-enriched oxygen at 153 K gave a spectrum consisting of a doublet (~ 3.6 G) at $g = 2.0247$ from a radical with no magnetic oxygen and two sets of sextets with the same *g*-factor (~ 15.5 G and ~ 24.5 G) from radicals containing one ^{17}O nucleus. When the solution containing these radicals was frozen an anisotropic spectrum was observed with $g_{xx} = 2.0022$, $g_{yy} = 2.0079$, and $g_{zz} = 2.0647$ ($g_{ave} = 2.0249$) in which two sets of six equally spaced lines centred about

Can. J. Chem. Downloaded from www.nrcresearchpress.com by 210.87.254.5 on 09/05/12
For personal use only.

g_{xx} were resolved arising from two labelled species ($A_{xx}(^{17}O)$ = 85 G and 70 G).

It has been reported (4) that *tert*-butoxy radicals add to triphenylphosphine to give *tert*-butoxytriphenylphosphoranyl with an approximately tetrahedral disposition of ligands about the phosphorus nucleus. Oxygen must add to the phosphorus nucleus of this radical to give a radical with a pseudo trigonal bipyramidal structure

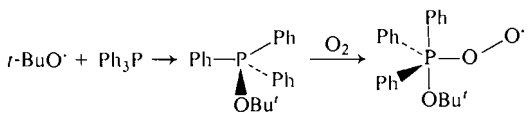

Triphenylarsine

The anisotropic esr spectrum obtained when a solution of DTBP and triphenylarsine in cyclopentane containing ^{17}O-enriched oxygen was photolysed at 193 K and rapidly cooled to 93 K is shown in Fig. 2. Four radicals can easily be identified from this spectrum. A radical with no magnetic oxygen, two radicals containing one ^{17}O nucleus with different hyperfine coupling constants (A_{xx} = 91 G and 61 G), and one radical containing two inequivalent ^{17}O nuclei (A_{xx} = 91 G and 61 G). The average *g*-factors for these four radicals are identical (2.0281) and equal, within experimental error, to the isotropic *g*-factor (2.0274). It is, therefore, quite clear that $Bu^tO(Ph_3)_3As^·$ reacts with oxygen in solution to give $Bu^tO(Ph_3)_3AsO_2^·$.

Trimethylarsine

tert-Butoxytrimethylarsanyl, prepared by reaction of photochemically generated *tert*-butoxy radicals with trimethylarsine (5), reacts with ^{17}O-enriched oxygen in solution to give a broad singlet spectrum (ΔH_{ms} = 7.5 G), centred at g = 2.0278, flanked by two sextets with the same *g*-factor. This spectrum can be analyzed in terms of a peroxy radical containing two inequivalent oxygen nuclei (18.6 and 24.4 G). Neither arsenic hyperfine coupling nor the radical containing two inequivalent oxygen nuclei could be resolved in solution. On the other hand the anisotropic spectrum clearly showed the presence of a radical containing two inequivalent oxygen nuclei in addition to the radicals containing one magnetic oxygen with different coupling constants (A_{xx} = 86.5 and 64.4 G).

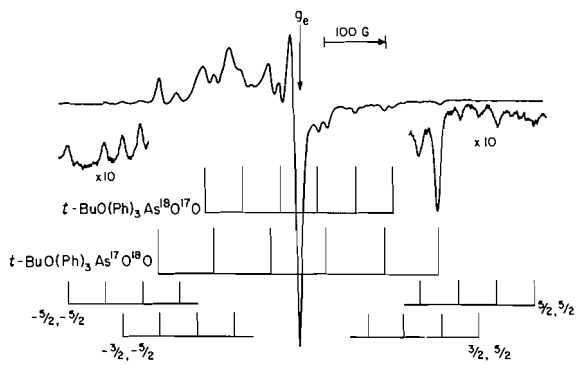

FIG. 2. The esr spectrum of $(CH_3)_3CO(C_6H_5)_3AsO_2^·$ enriched with oxygen-17 in cyclopentane at 93 K.

Discussion

We can conclude unambiguously from this work that four coordinate phosphorus and arsenic radicals react with molecular oxygen to give peroxy radicals that are persistent enough to be studied by esr spectroscopy. In general hyperfine coupling with P and As is not resolved because of the broad lines associated with these radicals although $Bu^tO(Ph)_3PO_2^·$ does exhibit a small isotropic phosphorus coupling constant (~3.6 G). The spin density on phosphorus in this radical, calculated from a_P and A_0 = 13 306 MHz (6), is, however, <0.1%.

All the Group VB peroxy radicals that we have been able to prepare contain magnetically inequivalent oxygen nuclei and strongly anisotropic **g**-tensors implying that the peroxy function is bent. The magnitude of the isotropic oxygen hyperfine coupling constants are very similar to the values for the *tert*-butylperoxy radical (a_{O_1} = 23.87 G, a_{O_2} = 17.63 G). The sums of these coupling constants are close to 41 G and it would appear that all of the unpaired spin is associated with the two oxygen nuclei with 60% on the terminal oxygen (7).

The only significant difference between esr parameters for Group VB organometallic peroxy radicals and alkylperoxy radicals occurs in the magnitude of the isotropic *g*-factor. The *g*-factors for the former radicals are larger solely due to an increase in the *g*-factor associated with the oxygen–oxygen internuclear axis. If, as we have concluded above, the unpaired electron is confined mainly to the oxygen nuclei most of the increase in $g_{||}$ can be attributed to a decrease in the magnitude of θ, the angle between the M—O_2 and O_1—O_2 axes (8). The smaller the angle θ, the less the degeneracy of the oxygen π orbitals will be lifted and the greater will be $g_{||}$.

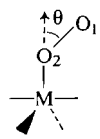

The radicals with phosphorus hyperfine coupling constants of ca. 9 G observed during reaction of photochemically generated *tert*-butoxy radicals with trimethyl phosphite and related compounds in the

presence of oxygen appear to contain only one oxygen nucleus. It is possible that these radicals are tetra-alkoxyphosphoranyloxy radicals analogous to the recently discovered $F_4PO^{\cdot}$ (9). This radical has, however, a smaller *g*-factor (2.01038) and larger phosphorus (41.1 G) and oxygen (22.8 G) hyperfine coupling constants than our species.

The observation of a second, less intense species (**4**) with larger spectral parameters (g and a_0) is somewhat disconcerting. We did consider the possibility that **3** and **4** are different conformations of t-$BuO(MeO)_3PO^{\cdot}$ with **3** having the oxy function in an apical position and **4** having the oxy function in an equitorial position.

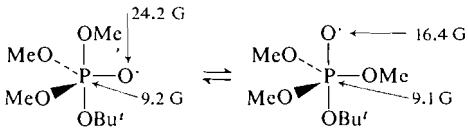

4 **3**

However, as was pointed out by a referee, **3** would almost certainly have C_{3v} symmetry. This would mean that the π-orbitals on oxygen would be degenerate or nearly degenerate and the radical would not be detected in solution because of a line broadening mechanism (10). On the other hand, **3** would have lower symmetry if the *tert*-butoxy ligand occupies an equitorial position.

It could perhaps be argued that **2** really is an organophosphorus peroxy radical (although not t-$BuO(MeO)_3PO_2^{\cdot}$) and because of environmental effects, e.g., association with the parent phosphorus III compound, the lines from the species with the terminal oxygen enriched with ^{17}O are very much broader than the analogous lines from a 'free' peroxy radical. The *g*-factor difference between **3** and **4** is, however, not consistent with this explanation.

In conclusion it would appear that tetra-alkoxyphosphoranyloxy and tetra-alkoxyphosphoranylperoxy can be detected by esr spectroscopy during the reaction of tetra-alkoxyphosphoranyl radicals with oxygen although the identification of the phosphoranyloxy radical is by no means unambiguous.

1. G. B. Watts and K. U. Ingold. J. Am. Chem. Soc. **94**, 2528 (1972).
2. A. G. Davies, D. Griller, and B. P. Roberts. J. Chem. Soc. Perkin, **2**, 993 (1972).
3. E. Furimsky, J. A. Howard, and J. R. Morton. J. Am. Chem. Soc. **94**, 5932 (1972).
4. A. G. Davies, M. J. Parrot, and B. P. Roberts. J. Chem. Soc. Chem. Commun. 973 (1973).
5. A. G. Davies, D. Griller, and B. P. Roberts. J. Organomet. Chem. **38**, C8 (1972).
6. J. R. Morton and K. F. Preston. J. Magn. Reson. In press.
7. E. Melamud and B. L. Silver. J. Phys. Chem. **77**, 1896 (1973).
8. S. A. Fieldhouse, B. W. Fullam, G. W. Neilson, and M. C. R. Symons. J. Chem. Soc. Dalton, 567 (1974).
9. A. R. Boate, J. R. Morton, and K. F. Preston. J. Phys. Chem. **80**, 409 (1976).
10. M. C. R. Symons. J. Am. Chem. Soc. **91**, 5924 (1969).

Can. J. Chem. Downloaded from www.nrcresearchpress.com by 210.87.254.5 on 09/05/12
For personal use only.

An internal coordinate model for molecular vibrations: the energy levels of H_2O and H_2S and related isotopic molecules

JAN BRON

Department of Chemistry, University of Calgary, Calgary, Alta., Canada T2N 1N4

AND

R. WALLACE

Department of Chemistry, University of Manitoba, Winnipeg, Man., Canada R3T 2N2

Received March 15, 1978

JAN BRON and R. WALLACE. Can. J. Chem. **56**, 2167 (1978).

Refinement of a previously described model for describing the anharmonic vibrations of polyatomic molecules is presented. The nonlinear molecules XY_2 (H_2O, D_2O, H_2S, D_2S) are used as examples and it is shown that quite good agreement with the observed spectrum can be obtained for the first twenty vibrational excitations with a six parameter potential function. Apart from its relative simplicity, the main improvement over previously reported work is the inclusion of the bending vibration within the formalism and refinement of the form of potential. It is pointed out that the model is readily extendable to the vibrational analysis of larger molecules.

JAN BRON et R. WALLACE. Can. J. Chem. **56**, 2167 (1978).

On présente un affinement du modèle décrit antérieurement pour décrire les vibrations inharmoniques de molécules polyatomiques. On utilise les molécules non-linéaires XY_2 (H_2O, D_2O, H_2S, D_2S) comme exemples et on montre qu'un très bon accord avec les spectres observés peut être obtenu pour les 20 premières excitations vibrationnelles avec une fonction potentielle contenant six paramètres. En plus de sa simplicité relative, l'amélioration principale par rapport aux travaux rapportés antérieurement est l'inclusion de vibrations de déformation angulaire à l'intérieur du formalisme et un affinement de la forme du potentiel. On peut remarquer que le modèle peut facilement être étendu à l'analyse vibrationnelle de molécules plus grandes.

[Traduit par le journal]

Introduction

A few years ago a paper appeared (1), which presented an alternative to the semi-empirical "local mode" theory of Siebrand and Williams (2) and Henry and Siebrand (3) and the complex normal mode theory, as reviewed by Nielsen (4, 5).

The normal mode theory leads to the following expression for the vibrational energy levels of simple molecules without vibrational degeneracy:

$$[1]\quad E(n_1, n_2, \ldots) = G_0 + \sum_i (v_i + \tfrac{1}{2})\omega_i + \sum_i \sum_j x_{ij}(v_i + \tfrac{1}{2})(v_j + \tfrac{1}{2}) + \text{higher order terms}$$

The unit of energy in [1] is cm^{-1}. The constant term G_0 is of no significance to the vibrational spectroscopist, but is to be considered in statistical mechanical applications (6) of spectroscopy; it cannot be determined experimentally. The quantities x_{ij} are anharmonicity constants, ω_i is the harmonic or normal frequency of vibration, and v_i is a quantum number. The higher order terms in [1] are usually ignored. The expressions, corresponding to [1], for highly symmetric molecules are more complex (7–9). Numerical values for ω_i and x_{ij} may be obtained from an analysis of the vibrational spectrum.

Formulae for G_0 and x_{ij}, in terms of potential constants, rotational and Coriolis constants, have been obtained by means of second order perturbation theory (10). The algebraic complexity of such a perturbation treatment is not trivial. When certain relationships between harmonic frequencies hold, second order perturbation theory may break down, "resonances" occur (4), and further complications may be introduced. Expressions for G_0 and x_{ij} usually involve force constants in dimensionless normal coordinates (5, 11), which are isotope dependent and of limited value. It may be advantageous to obtain, in certain cases, force constants which are independent of isotopic substitution. This can be accomplished by a tedious non-linear transformation of force constants in dimensionless normal coordinates to force constants in internal coordinates (12). Due to limitations of computer time, molecules with more than four or possibly five atoms have not yet been considered. Furthermore, the normal mode theory is so complex that only specialists understand all the details.

In recent publications (1, 13, 14), it has been shown that, in practice, simplification of the vibrational theory of polyatomic molecules is possible. These simplifications come about from the use of an internal coordinate model and the representation of

Can. J. Chem. Downloaded from www.nrcresearchpress.com by 210.87.254.6 on 09/05/12
For personal use only.

Can. J. Chem. Downloaded from www.nrcresearchpress.com by 210.87.254.6 on 09/05/12
For personal use only.

the potential for each internal coordinate by a simple function capable of describing anharmonicity (usually the Morse potential). While previous applications have been restricted to bond stretching coordinates only, the present paper includes the bending coordinate within the same framework. For relatively low excitation of the bending mode this procedure should be satisfactory on account of the empirical nature of the potential. The theory presented below has the following advantages. (*1*) It is readily understood in physical terms. (*2*) The small number of parameters leads to good agreement with observed spectra and can themselves be interpreted physically. (*3*) The need for the tedious transformations, mentioned above, disappears. (*4*) Calculations are fast, computer programs can be short, and the restriction 'for small molecules only' is, in principle, removed. (*5*) The Morse potential can represent the vibrations of other internal coordinates. (*6*) Since no separation of 'modes' is involved, the concept of resonance and associated complications disappear.

Theoretical Considerations

The Hamiltonian operator in terms of internal coordinates, R_i, may be written as (1)

$$[2]\quad \hat{H} = \sum_i \hat{H}_i^{(0)} - \hbar^2 \sum_{i<j}\sum [G_{ij}(\partial^2/\partial R_i \partial R_j) - \hbar^{-2} F_{ij} R_i R_j]$$

in which

$$[3]\quad \hat{H}_i^{(0)} = -\tfrac{1}{2}\hbar^2 G_{ii}(\partial^2/\partial R_i^2) + V_i$$

The quantities G_{ij} are Wilson's **G** matrix elements (15) and F_{ij} is an interaction force constant. The potential energy term in [3] is defined by means of the Morse function (1)

$$[4]\quad V_i = D_i[1 - \exp(-a_i R_i)]^2$$

where D_i and a_i are the Morse parameters for the ith internal coordinate. Compared to the expression used previously (1), [2] contains the additional interaction terms $F_{ij}R_iR_j$, which are necessary to obtain the correct fundamentals and isotope shifts (14). It may be observed that D_i, a_i, and F_{ij} are isotope independent and are, therefore, the same for molecules differing only in isotopic substitution.

The vibrational energy levels of a molecule can be determined by means of [2] and the variation method. A suitable linear variation function has the form

$$[5]\quad \psi = \sum_r c_r \phi_r$$

In [5], the coefficients c_r are parameters to be determined by minimizing the variational integral (16). The functions ϕ_r have been defined as (1)

$$[6]\quad \phi_r = \prod_i |n_i\rangle = |n_1, n_2, \ldots, n_p\rangle$$

There are p or $3N - 6$ (5) internal coordinates that define the vibration of a molecule containing N atoms. The slightly different meaning of the quantum numbers n_i in [6] and v_i in [1] should be noted. As before, $|n_i\rangle$ is the eigenfunction (Morse oscillator function) in the equation

$$[7]\quad \hat{H}^{(0)}|n_i\rangle = [D_i - A_i^{-2}(K_i - n_i - \tfrac{1}{2})^2]|n_i\rangle$$

The constants A_i and K_i are equal to

$$[8]\quad A_i = (2/G_{ii})^{1/2}(a_i\hbar)^{-1};\quad K_i = A_i D_i^{1/2}$$

To find the eigenvalues of the secular determinant requires the evaluation of the integrals (16)

$$[9]\quad H_{ij} = \langle\phi_i|\hat{H}|\phi_j\rangle = H_{ji}$$

and

$$[10]\quad S_{ij} = \langle\phi_i|\phi_j\rangle = S_{ji} = \delta_{ij}$$

In [10], δ_{ij} is the Kronecker δ. The utility of the above method will be illustrated by means of examples.

Examples

The calculations of the vibrational energy levels of the non-linear molecules YX_2 will serve as examples. More specifically, the vibrational energy levels of H_2O, D_2O, H_2S, and D_2S will be evaluated. For YX_2 the matrix elements H_{ij} can now be written as

$$[11]\quad H_{ij} = \langle n_1^{(i)}, n_2^{(i)}, n_3^{(i)}|\hat{H}|n_1^{(j)}, n_2^{(j)}, n_3^{(j)}\rangle$$

where

$$[12]\quad \hat{H} = (\hat{H}_1^{(0)} + \hat{H}_2^{(0)} + \hat{H}_3^{(0)}) - \hbar^2[G_{12}(\partial^2/\partial R_1\partial R_2) + G_{13}(\partial^2/\partial R_1\partial R_3) + G_{23}(\partial^2/\partial R_2\partial R_3)] + F_{12}R_1R_2 + F_{13}R_1R_3 + F_{23}R_2R_3$$

The internal coordinates R_i for YX_2 have been defined in Table 1. It may be readily seen that

$$[13]\quad \langle\phi_i|\hat{H}_i^{(0)}|\phi_i\rangle = \langle n_1^{(i)}, n_2^{(i)}, n_3^{(i)}|\hat{H}_i^{(0)}|n_1^{(i)}, n_2^{(i)}, n_3^{(i)}\rangle$$

are the only non-zero matrix elements of this type and that [13] *and* H_{ii} are equal to

$$[14]\quad H_{ii} = \sum_{j=1}^{3} [D_j - A_j^{-2}(K_j - \tfrac{1}{2} - n_j^{(i)})^2]$$

Division by (hc) converts the units of H_{ii} to wavenumbers (cm^{-1}).

Let us calculate for YX_2 the energies of the states

Can. J. Chem. Downloaded from www.nrcresearchpress.com by 210.87.254.6 on 09/05/12
For personal use only.

generated by $n_1, n_2, n_3 = 0, 1, 2, 3$. The corresponding functions ϕ_i are then defined as follows

[15]

Excitations	States	Permutations
0	$\|000\rangle$	1
1	$\|100\rangle$	3
2	$\|200\rangle$	3
2	$\|110\rangle$	3
3	$\|300\rangle$	3
3	$\|111\rangle$	1
3	$\|012\rangle$	6

Hence, there are a total of 20 states and **H** is a (20 × 20) matrix, leading to a secular determinant of order 20. In the evaluation H_{ij} $(i \neq j)$, it will be assumed that matrix elements that vanish according to *harmonic oscillator* selection rules will be taken as zero. This is justified by the parametric character of our approach and the fact that, if matrix elements are zero when evaluated by means of harmonic oscillator functions, they are small when determined by means of the (proper) Morse oscillator functions, *if* the quantum numbers n_i are not too large. Additional reasons are that the algebra and the number of matrix elements to be evaluated are greatly reduced. Expressions for **G** matrix elements can be found in ref. 15.

The required harmonic oscillator matrix elements can be obtained by means of the recursion relationships

$$[16] \quad [(n_i + 1)h\nu_i]^{1/2}|n_i + 1\rangle - (n_i h\nu_i)^{1/2}|n_i - 1\rangle + \hbar(2G_{ii})^{1/2}\left(\frac{d}{dR_i}\right)|n_i\rangle = 0$$

and

$$[17] \quad [(n_i + 1)h\nu_i]^{1/2}|n_i + 1\rangle + (n_i h\nu_i)^{1/2}|n_i - 1\rangle - (8/G_{ii})^{1/2}\,\pi\nu_i R_i|n_i\rangle = 0$$

In [16] and [17] the frequency ν_i can be expressed in terms of the Morse parameters a_i and D_i. The frequency, ν_i, is equal to

$$[18] \quad \nu_i = (2\pi)^{-1}(f_i G_{ii})^{1/2}$$

The force constant, f_i, can be written as a function of the Morse parameters by differentiating [4] twice and evaluating (17) this second derivative at $R_i = 0$. The result is

$$[19] \quad f_i = 2a_i^2 D_i; \quad a_i = +(f_i/2D_i)^{1/2}$$

and

$$[20] \quad \nu_i = (a_i/2\pi)(2D_i G_{ii})^{1/2}$$

All off-diagonal matrix elements are of the type

$$[21] \quad H_{ij} = \langle n_i^{(i)}, n_2^{(i)}, n_3^{(i)}\,|\hat{P}|n_1^{(j)}, n_2^{(j)}, n_3^{(j)}\rangle$$

where $\hat{P}$ is defined by [2]

$$[22] \quad \hat{P} = \hat{H} - \textstyle\sum_i \hat{H}_i^{(0)} = -\hbar^2 \sum_{i<j}\sum[G_{ij}(\partial^2/\partial R_i \partial R_j) - \hbar^{-2}F_{ij}R_i R_j]$$

Since off-diagonal **H** matrix elements will be evaluated by means of *harmonic* oscillator functions, harmonic oscillator matrix elements are needed. These can be obtained by multiplication of [16] and [17] by $\langle n_i + 1|$, to give the results

$$[23] \quad \langle n_i + 1\left|\frac{d}{dR_i}\right|n_i\rangle = -[(n_i + 1)(f_i/G_{ii})^{1/2}(2\hbar)^{-1}]^{1/2} = -\langle n_i\left|\frac{d}{dR_i}\right|n_i + 1\rangle$$

and

$$[24] \quad \langle n_i + 1|R_i|n_i\rangle = [\tfrac{1}{2}\hbar(n_i + 1)(f_i/G_{ii})^{-1/2}]^{1/2} = +\langle n_i|R_i|n_i + 1\rangle$$

For YX_2, [15] shows that there are 190 off-diagonal matrix elements to be determined. It is not too difficult to write a computer program that evaluates these matrix elements in seconds. After **H** has been determined it should be diagonalized in order to find the 20 energy levels, after diagonalization, the zero point energy (lowest energy level) is subtracted from the other energy levels found after diagonalization, in order to determine the fundamental and other bands.

How to determine H_{ij} $(i \neq j)$ will be shown by means of a few examples:

(A) $H_{ij} \equiv \langle 000|\hat{P}|101\rangle$

$$= -\hbar^2 G_{13}(hc)^{-1}\langle 000|\partial^2/\partial R_1 \partial R_3|101\rangle + F_{13}(hc)^{-1}\langle 000|R_1 R_3|101\rangle$$

$$= -\hbar^2 G_{13}(hc)^{-1}\langle 00|\partial^2/\partial R_1 \partial R_3|11\rangle + F_{13}(hc)^{-1}\langle 00|R_1 R_3|11\rangle$$

$$= -\hbar^2 G_{13}(hc)^{-1}\langle 0\left|\frac{d}{dR_1}\right|1\rangle\langle 0\left|\frac{d}{dR_3}\right|1\rangle + F_{13}(hc)^{-1}\langle 0|R_1|1\rangle\langle 0|R_3|1\rangle$$

$$= -\hbar^2 G_{13}(hc)^{-1}(2\hbar)^{-1}(f_1/G_{11})^{1/4}(f_3/G_{33})^{1/4} + F_{13}(hc)^{-1}(\tfrac{1}{2}\hbar)(f_1/G_{11})^{-1/4}(f_3/G_{33})^{-1/4}$$

This final expression can be evaluated by means of the constants given in Table 1 and the following expressions for the required **G** matrix elements (15) for YX_2:

Can. J. Chem. Downloaded from www.nrcresearchpress.com by 210.87.254.6 on 09/05/12
For personal use only.

TABLE 1. Values for various parameters used in calculations

Parameters	H_2O	H_2S
Bond angle: $\alpha \equiv 1—3—2$	104.5°	92.2°
Bond length (Å): $r = r_{13} = r_{23}$	0.95721	1.336
$f_1 = f_2$ (10^5 dyn cm^{-1})	8.45400	4.14832
f_3 (10^{-11} dyn cm)	0.69250	0.73278
F_{12} (10^5 dyn cm^{-1})	−0.092	−0.012
$F_{13} = F_{23}$ (10^{-3} dyn)	0.0	0.0
$D_1 = D_2$ (10^{-11} erg)	0.81804	1.12812
D_3 (10^{-11} erg)	0.48490	1.18199
R_1 (stretching)	Δr_{13}	Δr_{13}
R_2 (stretching)	Δr_{23}	Δr_{23}
R_3 (bending)	$\Delta\alpha$	$\Delta\alpha$

$$G_{11} = m_1^{-1} + m_3^{-1} = G_{22} = m_2^{-1} + m_3^{-1}$$

$$G_{33} = (m_1 r_{13}^2)^{-1} + (m_2 r_{23}^2)^{-1} + [r_{13}^{-2} + r_{23}^{-2} - 2(r_{13}r_{23})^{-1}\cos\alpha]/m_3$$

$$G_{12} = m_3^{-1}\cos\alpha$$

$$G_{13} = G_{23} = -(r_{23}m_3)^{-1}\sin\alpha$$

The factor $(hc)^{-1}$ has been introduced to change the units of H_{ij} from ergs to cm^{-1}. The mass of the ith atom is m_i.

(B) $$H_{ij} \equiv \langle 101|\hat{P}|103\rangle = 0$$

This matrix element vanishes because the harmonic oscillator selection rule, $\Delta n_i = \pm 1$, is not obeyed.

(C) $$H_{ij} \equiv \langle 000|\hat{P}|111\rangle = 0$$

This matrix element vanishes because the coordinates R_i and R_j in $\hat{P}$ occur only in pairs (R_iR_j or $\partial^2/\partial R_i\partial R_j$) and the eigenfunctions $|n_k\rangle$ are orthonormal.

The force constant f_i is related to the Morse parameter a_i by [19]. Therefore, the matrix elements [23] and [24] can also be expressed in terms of a_i. However, f_i is preferred to a_i, because f_i has a greater physical meaning. Also, [8] and [14] can be expressed in terms of f_i.

As has been discussed before (13), the parameters $f_1 = f_2$, $D_1 = D_2$ and F_{12} can be determined from the (observed) fundamentals. Similarly, the parameters f_3 and D_3 can be evaluated from the bands ν_2, $2\nu_2$ (XY_2), or by ν_2 (H_2Y) and ν_2 (D_2Y) and the (mass) relationships for isotopic molecules implied in the above equations. We found that satisfactory values for f_3 and D_3 can be obtained from observed frequencies, the equation (see [14])

[25] $$E_n - E_0 = (A_3^2 hc)^{-1}(2n_3K_3 - n_3 - n_3^2)$$

and $F_{13} = F_{23} = 0$. It has been assumed that A_3 and K_3 have been expressed, via [8] and [19], in terms of f_3 and D_3.

Results and Discussion

The computational results, based on the data given in Table 1, are presented in Tables 2 and 3. Agreement with observed values is good and on the average to within 0.5%. The observed values for H_2O, D_2O, and H_2S generated by means of [1] and the harmonic frequencies and anharmonicity constants given by Kuchitsu and Morino (18). Similarly the observed bands for D_2S have been based on the

TABLE 2. Observed and calculated frequencies for water and deuterium oxide

State			H_2O			D_2O		
v_1	v_2	v_3	Calcd.	Obsd.	Δν (%)	Calcd.	Obsd.	Δν (%)
1	0	0	3658	3656	0.05	2685	2671	0.52
0	7	0	1597	1597	0.00	1175	1179	−0.34
0	0	1	3756	3754	0.05	2791	2788	0.10
1	0	1	7234	7247	−0.18	5386	5372	0.26
1	1	0	5258	5237	0.40	3868	3843	0.65
0	1	1	5355	5331	0.45	3970	3959	0.35
2	0	0	7184	7227	−0.59	5308	5297	0.21
0	2	0	3140	3160	−0.63	2325	2340	−0.65
0	0	2	7457	7414	0.58	5543	5523	0.36
3	0	0	10560	10713	−1.43	7877	7878	−0.01
0	3	0	4629	4689	−1.28	3450	3482	−0.93
0	0	3	11057	10978	0.72	8256	8206	0.61
1	1	1	8833	8805	0.32	6564	6532	0.49
0	1	2	9071	8970	1.13	6747	6681	0.98
0	2	1	6901	6873	0.41	5124	5106	0.35
1	0	2	10871	10738	1.24	8079	8020	0.73
1	2	0	6805	6784	0.31	5024	4996	0.56
2	1	0	8796	8792	0.04	6511	6461	0.77
2	0	1	10551	10650	−0.93	7905	7911	−0.08

Can. J. Chem. Downloaded from www.nrcresearchpress.com by 210.87.254.6 on 09/05/12
For personal use only.

TABLE 3. Observed and calculated frequencies for hydrogen and deuterium sulphide

State			H_2S			D_2S		
v_1	v_2	v_3	Calcd.	Obsd.	$\Delta\nu$ (%)	Calcd.	Obsd.	$\Delta\nu$ (%)
1	0	0	2616	2615	0.04	1891	1898	−0.37
0	1	0	1182	1183	−0.08	850	855	−0.59
0	0	1	2627	2627	0.00	1901	1909	−0.42
1	0	1	5177	5147	0.58	3757	3758	−0.03
1	1	0	3798	3778	0.53	2743	2743	0.00
0	1	1	3809	3789	0.53	2751	2754	−0.11
2	0	0	5180	5179	0.02	3760	3769	−0.24
0	2	0	2353	2354	−0.04	1695	1705	−0.59
0	0	2	5180	5207	−0.52	3796	3794	0.05
3	0	0	7791	7693	1.26	5649	5615	0.60
0	3	0	3512	3514	−0.06	2536	2548	−0.47
0	0	3	7812	7738	0.95	5666	5653	0.23
1	1	1	6361	6289	1.13	4610	4592	0.39
0	1	2	6429	6347	1.28	4649	4627	0.47
0	2	1	4980	4939	0.82	3597	3592	0.14
1	0	2	7673	7632	0.53	5590	5594	−0.07
1	2	0	4970	4929	0.82	3589	3582	0.20
2	1	0	6362	6322	0.63	4611	4604	0.15
2	0	1	7673	7617	0.73	5589	5581	0.14

data given by Miller *et al.* (19). As is usual for the Morse oscillator, the agreement with observed values gets worse when v_1, v_2, and v_3 increase, if the force constants and D_i have been obtained by fitting to the bands of lower excitation, such as the fundamentals. Although the results have not been given, the vibrational energy levels for HDO, HDS, and all other possible isotopic variants of H_2O and H_2S, have also been calculated and, again, agreement between observed and calculated band positions was excellent.

Table 4 lists the harmonic frequencies and anharmonicity constants for H_2O and H_2S. The calculated values for ω_i were obtained by Wilson's (15) **F**, **G** matrix theory and the data in Table 1. The force constants f_i were taken as the diagonal **F** matrix elements. These values for ω_i were then used, together with the frequencies corresponding to the first six states given in Tables 1 and 2, in [1] to solve for the six anharmonicity constants. It may be seen that agreement with 'experimental' values is reasonable, especially for ω_i and x_{ii}. A redetermination of the frequencies by means of the calculated values of ω_i and x_{ij} *may* lead to improvement in agreement with the observed values. For example, the observed, calculated, and recalculated values for the frequency defined by the state $|002\rangle$ are 7414, 7457, and 7418 cm^{-1}, respectively. This improvement cannot always be expected to occur, but it is not unreasonable to expect it to happen when agreement of the calculated first six frequencies with the experimental values is good.

The results given in Table 2 can be compared with the values obtained by Smith and Overend (20), who used the standard normal mode theory (4, 5). The agreement these workers obtained with experimental values is impressive. But it should be realized, however, that Smith and Overend used for H_2O a 19 parameter potential function and that their method cannot be used, in practice, for larger molecules. Our six parameter potential function and simpler theory can readily be applied to larger molecules. It is for larger molecules, containing five or more atoms, that the model presented in this paper becomes more useful. Furthermore, as has been shown for UF_6 (14), our approach to the vibrational problem yields the splitting of overtone and combination levels by numerical analysis, without the explicit use of group theory.

TABLE 4. A comparison of observed and calculated harmonic frequencies (ω_i) and anharmonicity constants (x_{ij})

	H_2O		H_2S	
cm^{-1}	Calcd.	Obsd.	Calcd.	Obsd.
ω_1	3842	3842	2679	2722
ω_2	1654	1648	1194	1215
ω_3	3941	3943	2690	2733
x_{11}	−47.9	−42.6	−15.5	−25.1
x_{22}	−29.5	−16.8	−6.2	−5.7
x_{33}	−47.5	−47.6	−15.4	−24.0
x_{12}	+3.1	−15.9	+0.4	−19.7
x_{13}	−179.6	−165.8	−65.2	−94.7
x_{23}	+1.34	−20.3	0.0	−21.1
ZPE[a]	4664	—	3404	—

[a]Zero-point energy.

1. R. WALLACE. Chem. Phys. **11**, 189 (1975).
2. W. SIEBRAND and D. F. WILLIAMS. J. Chem. Phys. **49**, 1860 (1968).
3. B. R. HENRY and W. SIEBRAND. J. Chem. Phys. **49**, 5369 (1968).
4. H. H. NIELSEN. Rev. Mod. Phys. **23**, 90 (1951).
5. H. H. NIELSEN. *In* Handbuch der physik. *Edited by* S. Flugge. Springer, Berlin. 1959. Chapt. 37/1; p. 173.
6. M. WOLFSBERG, CHEN FEE CHANG, and J. BRON. Z. Naturforsch. **28**A, 129 (1973).
7. G. HERZBERG. Molecular spectra and molecular structure. Vol. II. van Nostrand, New York. 1955.
8. A. G. ROBIETTE, D. L. GRAY, and F. W. BIRSS. Mol. Phys. **32**, 1591 (1976).
9. K. T. HECHT. J. Mol. Spectrosc. **5**, 355 (1960).
10. W. H. SHAFFER and R. P. SCHUMAN. J. Chem. Phys. **12**, 504 (1944).
11. M. WOLFSBERG, A. A. MASSA, and J. W. PYPER. J. Chem. Phys. **53**, 3138 (1970).
12. A. R. HOY, I. M. MILLS, and G. STREY. Mol. Phys. **24**, 1265 (1972).
13. J. BRON and R. WALLACE. Can. J. Chem. **56**, 379 (1978).
14. J. BRON and R. WALLACE. J. Chem. Soc. Faraday Trans. 2, **74**, 611 (1978).
15. E. B. WILSON, J. DECIUS, and P. C. CROSS. Molecular vibrations. McGraw-Hill Book Company, Toronto, Ontario. 1955.
16. I. N. LEVINE. Quantum chemistry. Vol. I. Allyn and Bacon, Boston. 1970.
17. H. S. JOHNSTON. Gas phase reaction rate theory. The Ronald Press Company, New York. 1966.
18. K. KUCHITSU and Y. MORINO. Bull. Chem. Soc. Jpn. **38**, 814 (1965).
19. R. E. MILLER, G. E. LEROI, and D. F. EGGERS, JR. J. Chem. Phys. **46**, 2292 (1967).
20. D. FOSS SMITH, JR. and J. OVEREND. Spectrochim. Acta, **28**A, 471 (1972).

Can. J. Chem. Downloaded from www.nrcresearchpress.com by 210.87.254.6 on 09/05/12
For personal use only.

Some empirical observations concerning the liquid scintillation counting of coloured solutions[1]

DONALD C. WIGFIELD AND CATHERINE M. E. COUSINEAU
Department of Chemistry, Carleton University, Ottawa, Ont., Canada K1S 5B6

Received July 29, 1977

DONALD C. WIGFIELD and CATHERINE M. E. COUSINEAU. Can. J. Chem. **56**, 2173 (1978).

The colour quenching capabilities of nine dyes have been examined, and compared with the visible absorption spectra of the dyes in toluene solution. From these data an empirical relationship is derived, from which the liquid scintillation counting efficiency is estimated simply from the λ_{max} (wavelength of maximum absorption) of the dye and its absorption, A, at that wavelength. For the particular instrument, window settings, and scintillator solutions used in this work the relationship was

$$\% \text{ efficiency} = A[0.75(\lambda_{max} - 380) - 143] + 84.5$$

Colour quenching agents are classified as severe (λ_{max} 380–480 nm), moderate (λ_{max} 480–520 nm), light (λ_{max} 520–560 nm), or zero (λ_{max} > 560 nm).

The normal external standard channels ratio method for obtaining counting efficiency of chemically quenched samples has been applied to samples that contain colour quenchers and various combinations of colour and chemical quench. The results are in excellent agreement with the actual counting efficiencies; this result is in direct contrast to current views on the matter. It appears, therefore, that the counting of samples quenched both chemically and by colour may not always be impossible and the user is well advised to investigate his own system to evaluate whether results within acceptable error may be obtained.

DONALD C. WIGFIELD et CATHERINE M. E. COUSINEAU. Can. J. Chem. **56**, 2173 (1978).

On a examiné les aptitudes de neuf colorants à agir comme inhibiteurs et on les a comparés avec les spectres d'absorption visibles des colorants en solution dans le toluène. A l'aide de ces données, on a pu tirer une relation empirique à partir de laquelle on peut évaluer l'efficacité de comptages par scintillation liquide en se basant uniquement sur le λ_{max} (longueur d'onde d'absorption maximum) du colorant et son absorption, A, à cette longueur d'onde. Pour notre instrument avec son arrangement des fenêtres et les solutions de scintillateurs utilisés dans ce travail, la relation est

$$\% \text{ efficacité} = A[0.75(\lambda_{max} - 380) - 143] + 84.5$$

On a classifié les colorants comme inhibiteurs sévère (λ_{max} 380–480 nm), modéré (λ_{max} 480–520 nm), léger (λ_{max} 520–560 nm) ou zéro (λ_{max} > 560 nm).

On a appliqué la méthode habituelle des rapports des canaux standards externes pour obtenir l'efficacité du comptage d'échantillons soumis à une inhibition chimique, qui contenaient des colorants inhibiteurs ou diverses combinaisons d'inhibiteurs chimiques et de colorants. Les résultats sont en accord avec les efficacités réelles des comptages; ces résultats sont en opposition directe avec les vues actuelles sur ce sujet. Il semble donc qu'il soit quelquefois possible de faire le comptage d'échantillons soumis à des inhibitions soit chimique soit par colorants et qu'il serait avantageux pour les usagers de bien étudier leur propre système pour évaluer si des résultats à l'intérieur d'erreurs acceptables peuvent être obtenus.

[Traduit par le journal]

The view that the counting efficiency of samples containing both colour and chemical quench cannot be obtained accurately by the conventional external standard ratio method was put forward by Neary and Budd a number of years ago (1). This view is widely held, and was strongly reiterated recently by Stanley (2). Nevertheless, the need for counting coloured solutions (presumably also with their share of chemical quench) frequently arises, especially in the biological and medical sciences, and, despite the fact that in these applications a modest error or uncertainty is often tolerable, there seems to be little tangible advice in the literature on how to handle these solutions or on the extent of inaccuracy incurred if conventional quench correction methods are applied to them. Clearly some colours will be more severe quenchers than others. In this paper we report (*a*) a reinvestigation of the relationship between the optical properties (absorbance, wavelength) of the liquid scintillation counting solutions and their counting efficiency, partly as an independent means of measuring the decrease in counting efficiency as a result of colour quenching, but most importantly to be able to generate some empirical

[1]Studies in liquid scintillation, Part 8. For Part 7, see ref. 8.

Can. J. Chem. Downloaded from www.nrcresearchpress.com by 210.87.254.105 on 09/05/12
For personal use only.

Can. J. Chem. Downloaded from www.nrcresearchpress.com by 210.87.254.105 on 09/05/12
For personal use only.

TABLE 1. Absorption characteristics of the dyes

Dye	Form	λ_{max} (nm)	$\varepsilon_{max} \times 10^{-4}$ (M^{-1} cm^{-1})	Correlation coefficient, r for eff. vs. A plot
Methyl violet	Basic	600	7.26	0.985
Methyl red	Basic	470	—	—
	Acidic	520	6.22	0.936
Methyl orange	Basic	480	1.56	0.998
	Acidic	520	2.66	0.844
Orange G	Acidic	480	1.42	0.988
Methylene blue	Acidic	550	1.25	0.995
		660	8.98	0.982
Crystal violet	Basic	540	4.14	0.931
		610	6.98	0.927
Bromphenol blue	Basic	540	1.50	0.980
		620	—	—
Cresol red	Basic	440	1.06	0.981
Thymol blue	Acidic	410	0.78	0.989

rules concerning the severity of quenching for various types of coloured solutions, and (*b*) an investigation of the actual errors incurred by using the conventional external standard ratio method for quench correction on samples of various degrees of chemical and colour quench.

Results and Discussion

Relationship between Counting Efficiency and the Absorbance Characteristics of Solutions

1. Selection of Dyes

In order to draw conclusions relevant to a variety of coloured solutions, nine dyes were selected giving a range of λ_{max} (wavelength of maximum absorption) from 410 to 660 nm. These dyes, together with their absorption characteristics of methanolic solutions (100 μl) in toluene (15 ml), are listed in Table 1. Toluene solution was employed to ensure that the optical data obtained would be relevant to the subsequent liquid scintillation counting data. Most, but not all, of the absorbance bands gave linear Beer's law plots. The extinction coefficients obtained are all large and within an order of magnitude of each other (10^4–10^5); thus the quantity of dye present in counting solutions is small and relatively constant. Since also the structures of the dyes are chemically rather similar, it is unlikely that the counting differences are to any extent due to chemical quenching. The chemical quenching of 100 μl of methanol is almost unnoticeable.

2. Relationship between Absorbance and Counting Efficiency

A series of counting samples were prepared, using 1-^{14}C-hexadecane as the radio-active source, containing various quantities of each dye. For each sample both the absorbance and the counting efficiency were recorded. These results are presented graphically in Fig. 1 and Table 2. Clearly there is, in most cases, a good linear relationship between counting efficiency and the quantity of dye present, as noted previously by Ross and Yerick (3), using three coal-tar dyes. Also, the slopes (dQ/dA, counting efficiency vs. absorbance) of the lines depend markedly on the wavelength of the dye, and all intersect at the efficiency in the absence of added quench;[2] in this case 84.5% ± 0.5%.

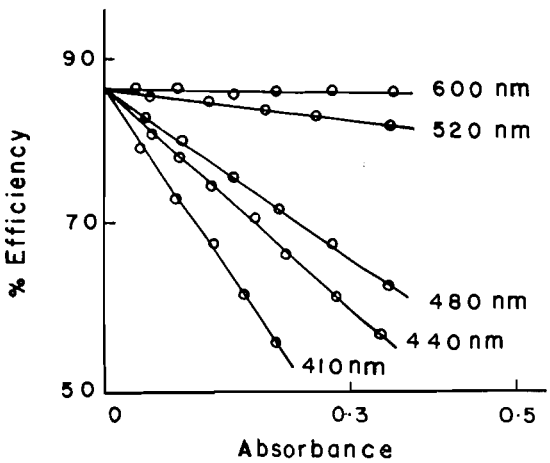

FIG. 1. Examples of relationships between counting efficiency and absorbance at various λ_{max} wavelengths.

3. Effect of Wavelength

The lines of Fig. 1 may be represented mathematically by

$$[1] \qquad \% \text{ efficiency} = (dQ/dA)A + 84.5$$

[2]Refers to normally prepared (as opposed to argon-flushed) samples. The counting efficiency of 84.5% as opposed to the more usual value of ≃90% is a reflection of the lower discriminator set higher than usual, a practice used in these laboratories to avoid phosphorescence complications (see Experimental).

TABLE 2. Dependence of quenching on wavelength difference between λ_{max} of the dye and maximum emission wavelength of the fluor ($\Delta\lambda$)

Dye	Form	$\Delta\lambda_{max}$ (nm)	Slope (dQ/dA)	r (plots of Fig. 1)	Intercept
Methyl violet	Basic	220	−2.02	0.667	83.8
Methyl red	Basic	90	−86.09	0.934	84.0
	Acidic	140	−60.41	0.992	84.0
Methyl orange	Basic	100	−39.95	0.869	83.6
	Acidic	140	−11.18	0.862	84.2
Orange G	Acidic	100	−68.19	0.979	85.2
Methylene blue	Acidic	170	−14.92	0.827	84.8
Crystal violet	Basic	160	−2.19	0.412	84.8
Bromphenol blue	Basic	160	−60.70	0.841	85.3
Cresol red	Acidic	60	−78.10	0.981	84.7
Thymol blue	Acidic	30	−142.9	0.991	85.0
					Ave. 84.5

where the value of (dQ/dA), the slope of the plot of counting efficiency vs. absorbance, is clearly some function of the wavelength of absorption. It seemed worth testing whether the value of (dQ/dA) could be usefully treated as a simple linear function of λ_{max}, within certain limits. The fluors used in this study were a mixture of 2,5-diphenyloxazole (PPO) and 1,4-bis[2-(5-phenyloxazolyl)]-benzene (POPOP) (as noted in the Experimental section) with wavelengths of maximum emission of 380 and 440 nm respectively. Since increase in quench continues as the wavelength of dye absorption decreases between 440 nm and 380 nm, the wavelength parameter used, $\Delta\lambda$, the difference in wavelength between colour quencher and fluor, is ($\lambda_{max} - 380$). A plot of (dQ/dA) as a function of this $\Delta\lambda$ is shown in Fig. 2. Although there is considerable scatter, there is clearly a relationship from $\Delta\lambda = 0$ to $\Delta\lambda = 180$ nm, beyond which there is evidently insufficient spectral overlap between dye and fluor for quenching to occur. Considering that no effect of band width or band shape of the absorption spectra of the dye have been taken into consideration, the scatter in Fig. 2 is remarkably small.

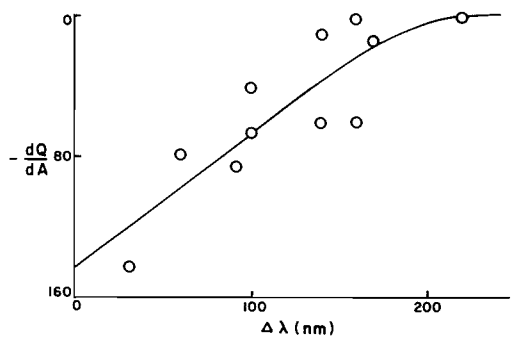

FIG. 2. Relationship of dQ/dA on wavelength difference between fluor and dye.

4. Calculation of Counting Efficiency from the Absorption Spectrum

The linear portion of Fig. 2 is represented by

[2] $$(dQ/dA) = 0.75(\Delta\lambda) - 143$$

for $0 < \Delta\lambda < 180$ nm. Combining eqs. [1] and [2], one obtains

[3] $$\% \text{ efficiency} = A[0.75(\lambda - 380) - 143] + 84.5$$

Clearly eq. [3] allows simple calculation of the counting efficiency change caused by colour quenching purely from the absorption spectrum of the solution.[3] For example, if a solution has $\lambda_{max} = 440$ nm, with $A = 0.22$, the counting efficiency is given by

$$\% \text{ efficiency} = 0.22[0.75(60) - 143] + 84.5$$
$$= 63\%$$

In order to exemplify how the scatter of Fig. 2 is translated into counting efficiency error, comparisons of calculated and observed counting efficiencies for various solutions are shown in Table 3.

These results indicate that the agreement between calculated and observed counting efficiencies is within 3%.[4] This method represents a simple alternative to the Ross and Yerick calculation (3), using essentially the same approach. As Ross and Yerick (3) have pointed out, in order to obtain more accurate estimations of the colour quenching a more detailed computer approach taking into account the entire absorption spectrum, and not just the absorbance at λ_{max}, would be required. Since this present approach was merely to provide some rules for

[3]Clearly this particular equation is applicable only to solutions of this particular fluor.

[4]A 3% error in absolute efficiency can cause a considerably larger error in computing the activity, especially at very low counting efficiencies.

Can. J. Chem. Downloaded from www.nrcresearchpress.com by 210.87.254.105 on 09/05/12
For personal use only.

Can. J. Chem. Downloaded from www.nrcresearchpress.com by 210.87.254.105 on 09/05/12
For personal use only.

TABLE 3. Typical counting efficiencies observed and calculated using eq. [3] to correct for colour quench

Dye added, λ_{max} (nm)	Absorbance	% Efficiency		Difference (%)
		Actual	Calculated	
Methyl red, 470 (basic)	0.14	71.9	73.9	+2.0
	0.27	61.3	64.1	+2.8
Methyl red, 520 (acidic)	0.44	67.3	67.8	+0.5
Methyl orange, 480 (basic)	0.09	80.6	78.4	−2.2
Methyl orange, 520 (acidic)	0.14	81.8	79.2	−2.6
Bromphenol blue, 540	0.07	80.7	82.9	+2.2
Cresol red, 440	0.04	83.0	80.6	−2.4
	0.09	76.9	75.7	−1.2
Thymol blue, 410	0.03	79.0	80.9	+1.9
	0.09	72.1	73.7	+1.6

guidance concerning levels of quench to be expected, such a detailed approach would not seem justified.

5. Empirical Rules concerning the Counting of Coloured Solutions

The above data quantitate the decreasing severity of colour quenching as the wavelength of absorbance of the coloured solution moves away from the wavelength of the fluor. It may be useful to classify coloured solutions in the following manner as quenchers of the PPO system: (*a*) *severe quenchers*: λ_{max} 380–480 nm, e.g., in a solution with λ_{max} 430 nm, $A = 0.5$, the counting efficiency will be reduced to 35%; (*b*) *moderate quenchers*: λ_{max} 480–520 nm, e.g., in a solution with λ_{max} 500 nm and $A = 0.5$, the efficiency will be 61%; (*c*) *light quenchers*: λ_{max} 520–560 nm, e.g., in a solution with λ_{max} 540 nm and $A = 0.5$, the efficiency will be 75%; (*d*) solutions with $\lambda_{max} > 560$ nm do not colour quench the PPO–POPOP system.

TABLE 4. Examples of observed and calculated counting efficiencies using external standard channels ratio

Chemical quench[a] (μl)	Colour quench[b] (μl)	% Efficiency	
		Actual	Calculated
Moderate Chemical – Moderate Colour			
25	20[c]	81.6	80.5
50	40[c]	79.1	78.0
75	60[c]	75.6	74.0
100	100[c]	71.8	69.2
Moderate Colour – Extreme Chemical			
200	100[c]	60.4	57.7
400	100[c]	56.1	54.0
600	100[c]	39.4	38.2
800	100[c]	38.8	38.2
1000	100[c]	32.5	32.2
Moderate Chemical – Extreme Colour			
20	50[d]	61.2	57.5
40	50[d]	57.5	53.5
68	50[d]	54.9	50.9
80	50[d]	52.4	48.5
100	50[d]	49.4	46.2
Extreme Chemical – Extreme Colour			
200	50[d]	38.5	35.7
400	50[d]	27.2	25.0
600	50[d]	19.9	17.0
800	50[d]	14.5	11.0
1000	50[d]	10.4	9.0

[a]Volume of $CHCl_3$ in 15 ml counting solution.
[b]Volume of dye stock solution (1% w/v) in 15 ml counting solution.
[c]Thymol blue.
[d]Methyl red (basic form).

External Standard Ratio Calibration Curves for Chemical and Colour Quench

Because of the doubts concerning the counting of solutions with both colour and chemical quench, we planned to make some comparative measurements of counting efficiency of coloured solutions using both the optical method described above, and the external standard channels ratio method, using a calibration curve based on standard samples with chemical quench. To our surprise, it was immediately apparent that there was excellent agreement between the actual counting efficiency and that obtained by the external standard channels ratio method. Thus, on our Beckman LS system[5] with the discriminator settings used and for the dyes examined, reliable counting efficiencies for solutions of pure colour quench are ap-

[5]Examination of the equations governing liquid scintillation counting suggests that the origin of the obvious difference between our results and those of others may lie in the difference between the logarithmic amplification of the Beckman instruments and the linear amplification of other instruments. Details of this are given in the M.Sc. thesis of Catherine M. E. Ashley, Carleton University (1977). A referee has suggested that the raising of the lower level discriminator may also be a contributing factor (cf. footnote 2).

Can. J. Chem. Downloaded from www.nrcresearchpress.com by 210.87.254.105 on 09/05/12
For personal use only.

parently obtained using the usual calibration curve for chemical quench, in direct contrast with the report of Stanley (2). To examine whether the same agreement would be obtained with solutions containing both chemical and colour quench, a series of such solutions were prepared and examined. As indicated in Table 4, the agreement between actual efficiency and that obtained by the External Standard Channels Ratio method is excellent, with the mean deviation being only 1.7%, and all determinations being within 4% even when very low counting efficiencies were being examined.[4] Few determinations require accuracy higher than this, and, on the Beckman LS system it is clear that, unless higher accuracy is being looked for, the determination of counting efficiency of samples having both chemical and colour quench is simply not a practical problem. Clearly it may be a worthwhile study for the user to investigate whether results on his particular instrument are satisfactory in this regard.

Conclusions

Several previous workers have found that colour and chemical quench correction curves differ significantly and that therefore quench correction of samples quenched both by colour and chemically can be subject to dangerous error. Among these workers, Stanley (2), Bush (5), and Noujaim and co-workers (6) have used Searle, Nuclear Chicago, and Picker Nuclear instruments respectively. Rapkin, on the other hand, has claimed that a single calibration curve is valid for all quenching agents (6, 7). The instrumental difference has generally been ignored in considering this problem, but appears to be an important factor. The present results, obtained on a Beckman LS150 instrument, clearly demonstrate that the accurate counting of solutions quenched both chemically and by colour is not always impractical, and the user is well advised to investigate his particular instrument with mixed chemical, and colour, quenched samples to evaluate whether on his system results of sufficient accuracy are obtained. The dogma that it is impossible to get satisfactory results should be abandoned and replaced by one of individual assessment.

Experimental

Liquid Scintillation counting measurements were obtained on a Beckman LS 150 Liquid Scintillation Counter, with samples prepared in low background glass spectravials (Amersham-Searle) with Spectrafluor solution (Amersham-Searle) diluted as recommended (PPO 4 g/ℓ; POPOP 50 mg/ℓ) with freshly distilled spectral grade toluene. The volume of the counting solution was kept constant at 15 ml by means of an automatic tilting dispenser. Carbon-14 activities were measured using the modified[6] ^{14}C channel, discriminator values 150–500.

Absorption spectra were recorded using a Beckman-25 spectrophotometer calibrated using a holmium oxide standard.

Purification of Dyes

All dyes were recrystallized three times from the appropriate solvent, rinsed with ether and benzene, and dried. Dyes were dissolved in absolute methanol (100 µl) and diluted to 15 ml with toluene for absorption measurements.

Quenched Samples

These were prepared by the addition of varying amounts of chloroform (chemical quench) or dye solution (colour quench) to the counting solution. The ^{14}C standard used was 1-^{14}C-hexadecane (New England Nuclear) delivered to the solutions by means of a Hamilton syringe. Activities per sample were generally kept in the neighbourhood of 50 000 dpm. Total counts accumulated were approximately 160 000 per sample (0.5% (2 σ) error).

Acknowledgment

The financial support of the National Research Council of Canada is gratefully acknowledged.

1. N. P. Neary and A. L. Budd. *In* The current status of liquid scintillation counting. *Edited by* E. D. Bransome. Grune and Stratton, New York. 1970. pp. 273–282.
2. P. E. Stanley. *In* Liquid scintillation science and technology. *Edited by* A. A. Noujaim, C. Ediss, and L. I. Wiebe. Academic Press, Inc., New York. 1976. pp. 103–116.
3. H. H. Ross and R. E. Yerick. Anal. Chem. **35**, 794 (1963).
4. D. C. Wigfield. Anal. Biochem. **59**, 11 (1974).
5. E. T. Bush. Anal. Chem. **35**, 1024 (1963).
6. A. Noujaim, C. Ediss, and L. Wiebe. *In* Organic scintillators and liquid scintillation counting. *Edited by* D. L. Horrocks and C. T. Peng. Academic Press, Inc., New York. 1971. pp. 705–717.
7. E. Rapkin. Picker nuclear laboratory scintillator, **11**, 1L (1966).
8. D. C. Wigfield. *In* Liquid scintillation science and technology. *Edited by* A. A. Noujaim, C. Ediss, and L. I. Wiebe. Academic Press, Inc., New York. 1976. pp. 295–298.

[6]See footnote 3 of ref. 4.

Liquid crystal/glass interface effects on the orientation of lyotropic liquid crystals in magnetic fields

FRED Y. FUJIWARA[1] AND LEONARD W. REEVES[2]

Department of Chemistry, University of Waterloo, Waterloo, Ont., Canada N2L 3G1

Received March 13, 1978

FRED Y. FUJIWARA and LEONARD W. REEVES. Can. J. Chem. **56**, 2178 (1978).

Lyotropic mesophases of both positive (type I) and negative (type II) diamagnetic anisotropy have been prepared. The deuterium magnetic resonance signal from D_2O in the sample has been studied during the process of orientation in a magnetic field. A type II mesophase oriented by a magnetic field in a cylindrical tube perpendicular to the lines of force does not achieve a uniform distribution of directors in a plane perpendicular to the field. The re-orientation of a type I mesophase after an initial displacement of the director at an angle to the field has been studied. Previous equations derived for thermotropic liquid crystals are applicable but the velocity of re-orientation was found to be an inverse function of the radius, for nmr tubes of less than 4 mm in diameter, indicating that liquid crystal/glass interface effects are important.

FRED Y. FUJIWARA et LEONARD W. REEVES. Can. J. Chem. **56**, 2178 (1978).

On a préparé des mésophases lyotropes d'anisotropie diamagnétique positive (type I) ainsi que négative (type II). On a étudié le signal de résonance magnétique du deutérium provenant du D_2O dans l'échantillon au cours du processus d'orientation dans le champ magnétique. Une mésophase du type II orientée par un champ magnétique dans un tube cylindrique perpendiculaire aux lignes de force ne produit pas une distribution uniforme des directeurs dans un plan perpendiculaire au champ. On étudié la réorientation d'une mésophase du type I après un déplacement initial du directeur à un angle par rapport au champ. On peut appliquer les équations dérivées antérieurement pour des cristaux liquides thermotropes; toutefois on a trouvé que la vitesse de réorientation est une fonction inverse du rayon des tubes de rmn de moins de 4 mm de diamètre ce qui indique que les effets d'interfaces cristal liquide/verre sont importants.

[Traduit par le journal]

Introduction

The lyotropic liquid crystals, based on water and amphiphiles, in certain systems have a significant property that they spontaneously orient in magnetic fields (1). Both positive (type I) and negative (type II) diamagnetic anisotropies occur for these lyotropic uniaxial fluids (2, 3) and a considerable amount of chemical work has been done to extend the number of known systems which have this useful property (2–7). The chemical flexibility includes variations of the counter ion, added electrolytes, detergents, and amphiphiles as well as solubilizates of various kinds.

The dynamics of the orientation process in these lyotropic mesophases in magnetic fields has not been previously reported in any detail. This contrasts with the extensive number of studies reported for thermotropic nematic mesophases. The dynamical properties of nematics has been formalized in a chapter in the recent book of de Gennes (8). Since the pioneering studies of Tsvetkov (9, 10) there have been several recent studies of the behaviour of nematic mesophases in rotating magnetic fields (11–19). These mesophases which have a positive diamagnetic anisotropy ($\Delta\chi = \chi_{\parallel} - \chi_{\perp}$, where $\chi_{\parallel}$ and $\chi_{\perp}$ are the diamagnetic susceptibilities measured, respectively, parallel and perpendicular to the optic axis) orient with the optic axis direction parallel to the magnetic field. In a rotating magnetic field (or in the equivalent case where the sample is rotated in a magnetic field) the director (optic axis) assumes an angle ϕ from the magnetic field direction such that the frictional torque and the magnetic torque, $(1/2)\Delta X B^2 \sin 2\phi$, balance. The following equation, derived from the continuum theory model (13), expresses the relationship between the phase lag, ϕ, and the angular frequency, ω:

$$[1] \qquad -\lambda_1\omega = (1/2)\Delta\chi B^2 \sin 2\phi$$

where B is the magnetic field strength and λ_1 is a twist viscosity coefficient taken to be negative (13). The theoretical analysis, which neglects surface effects, predicts that at angular velocities greater than the critical value $\omega_c = -\Delta X B^2/2\lambda_1$ the director will rotate with respect to the magnetic field direction.

Measurements of the angle ϕ as a function of ω,

[1]Present address: Instituto de Quimica, Universidade Estadual de Campinas, Caixa Postal 1170, 13100 Campinas (SP), Brasil.

[2]To whom all correspondence should be addressed.

Can. J. Chem. Downloaded from www.nrcresearchpress.com by 210.87.254.40 on 09/05/12
For personal use only.

Can. J. Chem. Downloaded from www.nrcresearchpress.com by 210.87.254.40 on 09/05/12
For personal use only.

by electron spin resonance (esr) and nuclear magnetic resonance (nmr) spectroscopy (12–14, 16–19), were accurately described by eq. [1] except in the region near the critical velocity. The angle observed was smaller than predicted and an inhomogeneity in the director alignment developed which increased smoothly until at high speeds ($\omega > \omega_c$) the directors adopt an isotropic distribution in the plane containing the magnetic field (16). The rotation of the director was observed but the homogeneity of the alignment decayed quickly (13). This dispersion of the director alignment at angular velocities greater than ω_c has been recently studied in very low magnetic fields (18). In the magnetic fields employed (a few hundred gauss) the rate of the director dephasing process at high angular velocities was very much slower and could be followed in the esr spectra of a paramagnetic probe dissolved in the mesophase. From the dependence of this rate on the angular velocity and the field strength, the authors concluded that the motion of the sample cell surface relative to the mesophase creates twist walls at the interface (8) which propagate towards the nematic bulk.

The lyotropic mesophases provide an opportunity to study the behaviour in magnetic fields of another uniaxial fluid with a completely different composition and internal structure. At present the shapes and long range organization of the surfactant micelles in these systems is not well understood. However, the evidence available indicates that neither the type I nor the type II mesophases belong to the classical lamellar or hexagonal systems.

Qualitatively it has been apparent (1, 2) that the velocity with which initially random directors become oriented to a macroscopically oriented liquid crystal in a magnetic field is considerably slower than for the thermotropic nematic mesophases so far encountered. The rotating magnetic field experiments can be repeated for lyotropic media but in a static rather than dynamic form. The purpose of the present paper is to present a survey of the deuterium magnetic resonance lineshapes encountered during the orientation process of lyotropic mesophases as well as to investigate the influence of glass/liquid crystal interface effects on the kinetics and consequent director angle distributions of type I and type II mesophases.

Experimental

The preparation of the surfactants used have been previously reported (2, 3). The surfactants were recrystallized two to three times and dried under vacuum at 60°C. The Pyrex nmr sample tubes were cleaned with Teepol detergent, thoroughly rinsed with distilled water, and dried at 120°C. The internal diameters of the tubes were determined from volume–weight measurements using water or mercury. For the standard 5 and 10 mm tubes, the manufacturer's specifications were taken.

The samples were prepared by weighing the components into test tubes containing a narrow constriction. After the tubes were sealed the samples were centrifuged back-and-forth until the samples were homogeneous. The type I mesophases studied were ternary systems composed of detergent/heavy water/electrolyte. The detergents used were sodium decylsulfate (SDS), cesium decylsulfate (CDS), and potassium laurate (KL). In the absence of the electrolyte, the binary systems in the concentration region used are known to be hexagonal mesophases (20), which will not orient in the magnetic field presumably because of their very high viscosities. The addition of electrolyte induces a first order phase change to produce the type I mesophases used here. A report of the phase diagrams of these systems is being prepared. The composition of the samples prepared are as follows (compositions given in weight %): sample A, 47.77% D_2O, 50.21% CDS, 2.01% Na_2SO_4; sample B, 64.56% D_2O, 33.22% KL, 2.21% KCl; sample C, 55.69% D_2O, 39.77% SDS, 4.54% Na_2SO_4; and sample D, 63.76% D_2O, 33.98% KL, 2.27% KCl. The type II mesophase used had the composition: 51.71% D_2O, 6.25% decanol, 37.48% SDS, 4.28% Na_2SO_4.

The spectrometer used was a Bruker SXP-60 externally locked to a proton signal in water at 60 MHz. The deuterium frequency occurs at 9.21 MHz. Each of the spectra taken over the course of a kinetic study was obtained in a period of less than 5 s using 1 to 10 pulses.

Results and Discussion

The orientation of the mesophase director can be conveniently monitored by the deuterium nmr spectrum of the D_2O. The deuterium quadrupole splitting $\Delta\nu$ is given by

$$[2] \qquad \Delta\nu = \tfrac{3}{2}QS_{zz}\tfrac{1}{2}(3\cos^2\Omega - 1)$$

where Q is the quadrupole coupling constant, S_{zz} is the degree of order with respect to the director of the principal axis of the electric field gradient, and Ω is the angle between the director and the magnetic field direction. If the directors of the mesophase are randomly oriented in three dimensions (powder pattern) the line shape can be approximated by (21):

$$[3] \qquad g(\nu) = N\left(1 \pm \frac{2\nu}{c}\right)^{-1/2}$$

where $c = \frac{3}{2}QS_{zz}$ and $-c \leq \nu \leq c/2$ for the negative sign and $-c/2 \leq \nu \leq c$ for the positive sign combination. N is a normalization constant.

A relevant equation is that describing the line shape for a mesophase in which the directors are randomly oriented in a plane which includes the magnetic field direction (two dimensional powder pattern) and is given by:

$$[4] \qquad g(\nu) = N'(\sin 2\Omega)^{-1}$$

N' is similarly a normalization constant. In this case $0 \leq \Omega \leq \pi$ represents the angle between the directors and the magnetic field, and $\nu = \frac{3}{8}QS_{zz}$

Can. J. Chem. Downloaded from www.nrcresearchpress.com by 210.87.254.40 on 09/05/12
For personal use only.

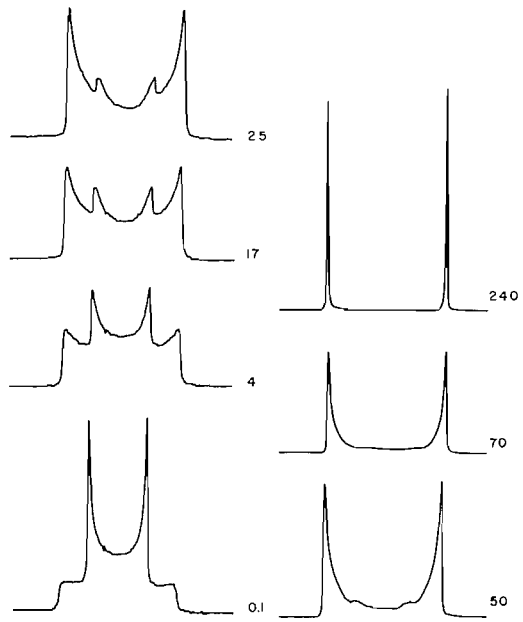

FIG. 1. Deuterium nmr spectra of D_2O in a type I mesophase after various times, given in minutes, in the magnetic field. The doublet separation of the oriented sample was 593 Hz at 30.6°. The composition is listed in the Experimental section as sample A.

$(3\cos^2\Omega - 1)$. In eqs. [3] and [4] the effect of the linewidth is neglected.

In Fig. 1 the line shapes observed for the orientation process of a type I mesophase prepared from the cesium decylsulfate detergent are shown. The sample illustrated had not achieved complete orientation after 240 min. At equilibrium the quadrupole splitting was 592.8 Hz and the linewidth at half-height was 3.9 Hz, approximately 1 Hz greater than the peak for pure D_2O. After only 4 min the intensity of the signals from the directors at $\Omega = 0°$ (the extremes of the spectra) become accentuated and continuously grow at the expense of all other angles as the experiment proceeds. The magnetic torque on a diamagnetic anisotropy ΔX has a sin 2Ω dependence and is a maximum for directors at 45° to the field (8). It becomes zero at 0° and 90°. The persistence of observable intensity for directors at 90° to the magnetic field is clearly seen for the deuterium magnetic resonance spectrum recorded at 70 min after immersion in the field. The theoretical description of the line shape evolution with lack of definite solutions of the dynamic equations for $\Omega > 45°$ (13) is complicated and not necessary since the velocity constant of orientation can be obtained from the following type of experiment.

The dynamic spinning experiments used to study thermotropic nematic mesophases (12, 13, 16, 17) are impractical for the study of these lyotropic mesophases because of the very slow spinning speeds required. However, the same information can be obtained from a static experiment. A type I mesophase was first allowed to orient fully in a magnetic field and subsequently rotated by a fixed angle about an axis perpendicular to the field. The orientation of the director to the static field and the angular distribution in the directors can be monitored as a function of time from the deuterium nmr spectrum. Equation [1] can be integrated to express the instantaneous angle Ω between the director and the magnetic field as a function of time t and the initial sample rotation angle Ω_0. This equation is,

$$[5] \qquad \ln \tan \Omega = -kt + \ln \tan \Omega_0$$

where the rate constant $k = -\Delta\chi B^2/\lambda_1$, the symbols having the same meanings as in eq. [1].

This equation was found to describe the experimental results with an extremely high correlation when the sample was rotated by less than ca. 25°. A typical plot of the experimental data is shown in Fig. 2. During the course of the reorientation the distribution of the directors was observed to be homogeneous; the linewidth of the D_2O doublet increased slowly by only 3 to 4 Hz and then sharpened as the directors approached the equilibrium alignment parallel to the field. For larger rotation angles (but less than 45°) the directors initially rotate with the same rate constant but then began to deviate from the behaviour predicted by eq. [5]. As the process progressed the rate constant gradually increased and this was accompanied by an increase in the director distribution. This behaviour appears to be completely analogous to that observed for the

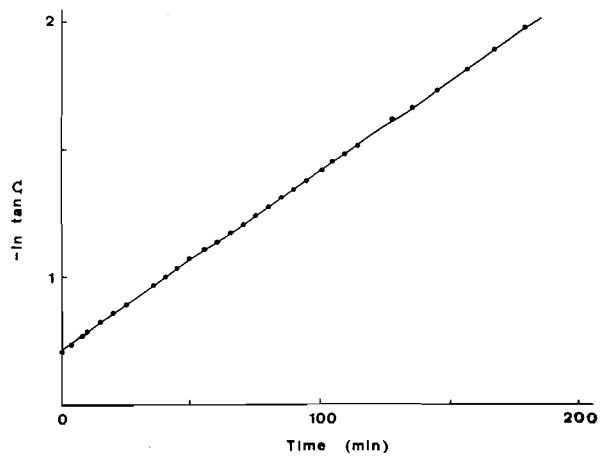

FIG. 2. The dependence of the angle Ω between the magnetic field direction and the director as a function of the time after an initial rotation of 26.3°. The angle was determined from the quadrupole splitting of the D_2O in the mesophase (sample C in Experimental section).

Can. J. Chem. Downloaded from www.nrcresearchpress.com by 210.87.254.40 on 09/05/12
For personal use only.

dynamic sample spinning experiments based on eq. [1] for the thermotropic mesophases. The phase lag ϕ was observed to be smaller than expected and a broad distribution of director directions developed at higher angular velocities.

In order to investigate the possible effects of the glass/liquid crystal interface, the angular velocity constant, k, was determined in cylindrical Pyrex sample tubes of different diameter in the same magnetic field strength, with the same sample at the same temperature. The internal diameters of the tubes varied between 1.3 and 9.07 mm. In all cases the form of eq. [5] accurately described the kinetics for initial rotation angles of less than ca. 25°. However, as indicated in Fig. 3 the observed rate constant k is a strong linear function of the inverse radius of the tube up to ca. 4 mm in diameter. For larger tubes the velocity of orientation is slower and independent of the tube radius. The surprising result is that the smaller the tube diameter the higher the velocity of orientation in the magnetic field and that these effects are evidently provoked by liquid crystal/surface interface forces. While the theory responsible for eqs. [1] and [5] does not admit surface effects the results nevertheless obey the form of the equation accurately for all tube sizes. The behaviour observed here for lyotropic mesophases is in contrast to that for thermotropic mesophases where no dependence on the sample size was observed for tubes of 1 to 5 mm diameters (16).

The effect of the composition of the sample tube was investigated using a cylindrical Teflon tube. The rate constant measured for a sample in this tube was identical to that for the same sample in a Pyrex tube.

The effect on a type I mesophase of rapid spinning about a perpendicular axis to the field was investigated. The sample was first allowed to orient in the magnetic field and then was subject to spinning about the nmr tube axis in the normal way at about 5 Hz for several hours. Immediately on cessation of spinning a deuterium spectrum, shown at the top of Fig. 4, was observed which clearly results from a random orientation of directors in a plane containing the magnetic field (eq. [4]). The act of spinning at an angular velocity greater than the re-orientation rate of the mesophase directors (which is ca. 3×10^{-4} s^{-1} for this sample) leads to randomization in the plane perpendicular to the axis of spinning and parallel to the field. While spinning, the modulations of frequency because of variations of the angles Ω result in extensive side band frequencies which mask the true angular distribution of director angles.

The behaviour of the lyotropic mesophases in these experiments parallels that of the thermotropic mesophase in almost every aspect in spite of the differences in chemical composition. The major exception is the

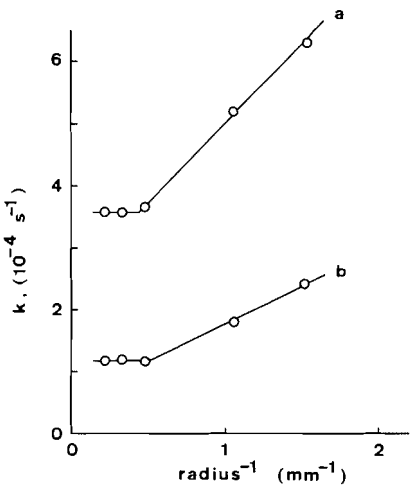

FIG. 3. The dependence of the rate constant on the sample tube size for the reorientation of the director of type I mesophases: curve *a*: a potassium laurate mesophase (sample B in Experimental section) measured at 30.0°, curve *b*: a sodium decylsulfate mesophase (sample C in Experimental section) studied at 29.1°C. The quadrupole splittings were 601 and 723 Hz, respectively.

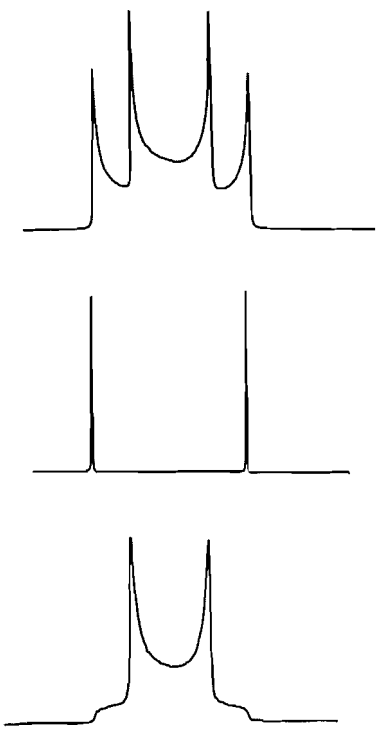

FIG. 4. Deuterium nmr spectra of a potassium laurate type I mesophase (sample D in Experimental section); bottom: immediately after the sample was placed in the probe, middle: after several hours, top: immediately after the sample was stopped after spinning at 5 Hz for several hours. The quadrupole splitting of the oriented sample was 657 Hz at 30.3°C.

Can. J. Chem. Downloaded from www.nrcresearchpress.com by 210.87.254.40 on 09/05/12
For personal use only.

increased reorientation rate observed in small tubes for the lyotropic media. Equation [5] appears to accurately describe the behaviour of the lyotropic mesophases in large samples when the initial angular displacement is not too large. Consequently these experiments provide a convenient method for the determination of the ratio $\Delta\chi/\lambda_1$. The rate constants in the limiting regions for the two samples shown in Fig. 3 are $1.17 \times 10^{-4}\ s^{-1}$ and $3.57 \times 10^{-4}\ s^{-1}$ in a field of 14.1 kG. The ratios of $\Delta\chi/\lambda_1$ of 5.89×10^{-13} and 1.80×10^{-12} (in cgs units) for these two lyotropic mesophases are 4 to 5 orders of magnitude smaller than for the thermotropic mesophases. Typical values of this ratio for the nematic mesophases MBBA (11), PAA (11), and Merck Phase IV (13) are 1.12×10^{-7}, 1.4×10^{-8}, and 2.24×10^{-8} respectively. This large difference must be due to the combined effects of a much smaller diamagnetic anisotropy as well as perhaps a larger viscosity coefficient.

The enhanced reorientation rate constant observed in small tubes probably reflects the effects of twist walls created at the interface between the homogeneously oriented bulk medium and the layer strongly anchored at the surface (8, 22). The coherent length (23) of this surface layer is small compared to the dimensions of the samples studied here. However de Gennes (ref. 8, p. 177) has postulated that the dissipation measured in these rotating field measurements may be influenced by nucleation, migration, and annihilation of the defects produced by the rotation of the directors in the bulk relative to the surface layer. This effect has not been observed for nematic mesophase in samples down to 1 mm in diameter at low angular velocities (16). Presumably in lyotropic mesophases with their much larger viscosity coefficient this relaxation mechanism becomes apparent in much larger samples.

The distribution of director angles in an oriented type II lyotropic mesophase was also investigated. The sample, in a 10 mm nmr tube, was allowed to orient and then was rotated by 90°. The results of this experiment are illustrated in Fig. 5. The initial powder pattern spectrum is replaced by a sharp doublet equal to the separation of the powder pattern maxima. After rotation of the sample tube by 90° the distribution of the directors in the perpendicular plane can be monitored and this is shown in the spectrum recorded at the head of Fig. 5. The result is not a truly random distribution in the plane of the magnetic field as described by eq. [4]. The non-random distribution of directors must originate from the effects of the liquid crystal/glass interface. In the stationary type II mesophase the directors assume a 90° orientation to the field with a high degree of homogeneity. However, in this plane perpendicular

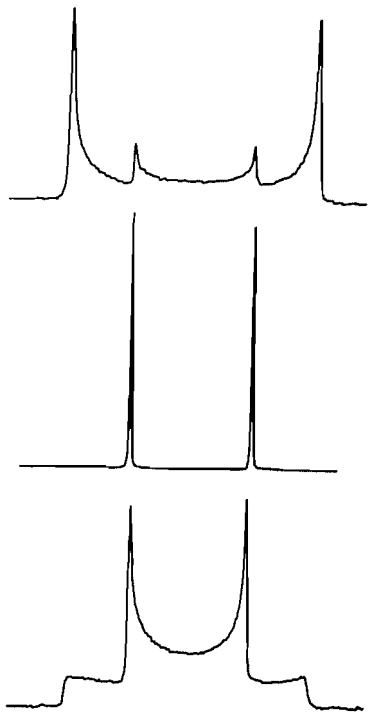

FIG. 5. Deuterium nmr spectra of a sodium decylsulfate type II mesophase (composition given in Experimental section) containing D_2O; bottom, immediately after being placed in the magnet; middle, after the sample was allowed to orient without sample spinning; top, immediately after the oriented sample was rotated 90°. The doublet separation of the oriented sample was 522 Hz at 31°C.

to the field the directors tend to adopt a perpendicular alignment to the cylinder walls in preference to the direction parallel to the tube axis. From the experiment performed here it is evident that the interface effects are propagated into the body of the liquid crystal over distances of several millimetres. These long range interface effects are of course weaker than the magnetic torque exerted on the director in these samples since continuous spinning results in an alignment of the directors parallel to the tube axis with a high degree of homogeneity.

The orientation of the director perpendicular to the surface in the type II mesophases is consistent with our limited knowledge of the micellar structure in these mesophases. The orientation of amphiphilic solutes in these systems indicates that the director is perpendicular to the aqueous/hydrophobic interface. In both lamellar and hexagonal mesophases, this interface is known to align parallel to glass surfaces (24).

Acknowledgments

We are grateful to the National Research Council of Canada for its financial support of this work.

1. K. D. LAWSON and T. J. FLAUTT. J. Am. Chem. Soc. **89**, 5489 (1967).
2. K. RADLEY, L. W. REEVES, and A. S. TRACEY. J. Phys. Chem. **80**, 174 (1976).
3. D. M. CHEN, F. Y. FUJIWARA, and L. W. REEVES. Can. J. Chem. **55**, 2396 (1977).
4. L. W. REEVES, J. SANCHES DE CARA, M. SUZUKI, and A. S. TRACEY. Mol. Phys. **25**, 1481 (1973).
5. L. W. REEVES, A. S. TRACEY, and M. M. TRACEY. J. Am. Chem. Soc. **95**, 3799 (1973).
6. R. C. LONG. J. Magn. Reson. **12**, 216 (1973).
7. F. Y. FUJIWARA and L. W. REEVES. **98**, 6790 (1976).
8. P. G. DE GENNES. The physics of liquid crystals. Clarendon Press, Oxford, England. 1974.
9. V. N. TSVETKOV. J. Exptl. Theoret. Phys. (U.S.S.R.), **9**, 602 (1939); Acta Physicochim. U.R.S.S. **11**, 537 (1939).
10. V. N. TSVETKOV and A. SOSNOVSKII. J. Exptl. Theoret. Phys. **13**, 353 (1943); Acta Physicochim. U.R.S.S. **18**, 358 (1943).
11. H. GASPAROUX and J. PROST. J. Phys. **32**, 953 (1971).
12. A. N. KUZNETSOV and V. A. RADTSIG. Zh. Strukt. Khim. **13**, 802 (1972).
13. F. M. LESLIE, G. R. LUCKHURST, and H. J. SMITH. Chem. Phys. Lett. **13**, 368 (1972).
14. J. W. EMSLEY, J. C. LINDON, and G. R. LUCKHURST. Chem. Phys. Lett. **19**, 345 (1973).
15. V. N. TSVETKOV, I. P. KOLOMIETS, E. I. RYUMTSEV, and F. M. ALIEV. Dokl. Akad. Nauk S.S.S.R. **209**, 1074 (1973); Sov. Phys. Dokl. **18**, 247 (1973).
16. S. G. CARR, G. R. LUCKHURST, P. POUPKO, and H. J. SMITH. Chem. Phys. **7**, 278 (1975).
17. J. PIRS, P. UKLEJA, and J. W. DOANE. Solid State Commun. **19**, 877 (1976).
18. R. CASINI, S. FAETTI, M. MARTINELLI, S. SANTUCCI, and M. GIORDANO. J. Magn. Reson. **26**, 201 (1977).
19. R. M. HORNREICH. Phys. Rev. A**15**, 1767 (1977).
20. A. E. SKOULIOS and V. LUZZATTI. Acta Crystallogr. **74**, 278 (1961).
21. G. E. PAKE. J. Chem. Phys. **16**, 327 (1948).
22. P. G. DE GENNES. J. Phys. **32**, 789 (1971).
23. P. G. DE GENNES. Mol. Cryst. Liq. Cryst. **7**, 325 (1969).
24. B. MELY, J. CHARVOLIN, and P. KELLER. Chem. Phys. Lipids, **15**, 161 (1975).

Can. J. Chem. Downloaded from www.nrcresearchpress.com by 210.87.254.40 on 09/05/12
For personal use only.

The nonstereospecific addition of benzeneselenenyl chloride to 3,4-dihydro-2*H*-pyran

DENNIS G. GARRATT

Department of Chemistry, University of Ottawa, Ottawa, Ont., Canada K1N 6N5

Received January 19, 1978

DENNIS G. GARRATT. Can. J. Chem. **56**, 2184 (1978).

The addition of benzeneselenenyl chloride to 3,4-dihydro-2*H*-pyran in methylene chloride at 25°C gives 65% of the *trans* and 35% of the *cis* Markownikoff adduct: 2-chloro-3-phenylselenotetrahydropyran under conditions of kinetic control. The above reaction was observed to be reversible, the adducts subsequently reacting with the benzeneselenenyl chloride under conditions similar to those used for the reaction with 3,4-dihydro-2*H*-pyran to give diphenyl diselenide and 2,3-dichlorotetrahydropyran in good yield. There was no evidence for the formation of 3-chloro-2-phenylselenotetrahydropyran under conditions of either kinetic or thermodynamic control. Kinetic studies support a mechanism involving a seleniranium ion that opens to an oxacarbonium ion before the product determining step.

DENNIS G. GARRATT. Can. J. Chem. **56**, 2184 (1978).

L'addition du chlorure de benzènesélénenyle au dihydro-3,4 2*H*-pyranne, dans le chlorure de méthylène à 25°C, conduit, dans des conditions favorisant le contrôle cinétique, à l'adduit prévu par la règle de Markownikoff soit le chloro-2 phényl-3 sélénotétrahydropyranne contenant 65% de produit *trans* et 35% de produit *cis*. On a observé que cette réaction est réversible; les adduits réagissent ultérieurement avec le chlorure de benzènesélénenyle, dans des conditions semblables à celles utilisées pour la réaction du dihydro-3,4 2*H*-pyranne, pour conduire au disélénure de diphényle et au dichloro-2,3 tétrahydropyranne avec de bons rendements. Il n'y a aucune indication à l'effet que du chloro-3 phényl-2 sélénotétrahydropyranne pourrait se former dans des conditions de contrôle soit cinétique soit thermodynamique. Les résultats des études cinétiques sont en accord avec un mécanisme impliquant un ion séléniranium qui s'ouvre pour conduire à un ion oxacarbonium avant l'étape déterminant la nature du produit.

[Traduit par le journal]

Introduction

The reaction of areneselenenyl chlorides with alkenes has been found to be a stereospecific *anti* addition by numerous workers (1). This observation in addition to supplementary kinetic evidence has been used as the basis for postulating a mechanism involving a seleniranium ion **1** intermediate before

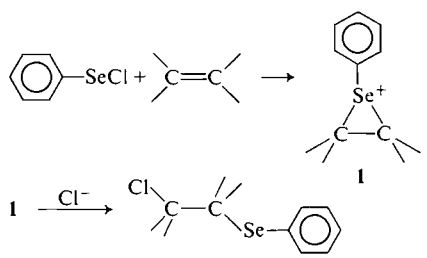

the product forming step (2). Since general mechanistic conclusions are too often drawn from the data of a reaction of an electrophile with alkenes of only one structural type or from a limited number of compounds (3), it seemed advisable to study the reaction of a selenenyl chloride with an olefinic species where a suitable open carbonium ion might be generated during the course of the reaction. We have previously reported the reaction of 2,4-dinitrobenzeneselenenyl chloride with *cis*- and *trans*-1-phenylpropene to be *anti*-stereospecific (4). The major significance of this work rests on the premise that the two nitro groups destabilize the development of positive charge on selenium, thus promoting the formation of an open benzylic carbonium ion. The absence of *non*stereospecific addition therefore is taken as indicative of the greater stability of seleniranium ions relative to benzylic carbonium ions under these conditions. It was clear from this work that an olefinic precursor to a more stable carbonium ion would be necessary if nonstereospecific addition were to be observed.

We wish to report the first case of a nonstereospecific addition of an areneselenenyl chloride to an olefin and discuss its mechanistic implications.

Results

Product Studies

The addition of benzeneselenenyl chloride to 3,4-dihydro-2*H*-pyran in methylene chloride solution gives two products, **2** and **3**, in 35 and 65% yields, respectively. No difference in products was observed in the presence of added oxygen, isoamyl nitrite, or in the presence or absence of light. The reaction was investigated over a wide temperature range −60 to 30°C. The product distribution was observed to be essentially invariant over this range indicating that the *cis* and *trans* adducts are configurationally stable under these reaction conditions. Furthermore it was

Can. J. Chem. Downloaded from www.nrcresearchpress.com by 210.87.254.5 on 09/05/12
For personal use only.

Can. J. Chem. Downloaded from www.nrcresearchpress.com by 210.87.254.5 on 09/05/12
For personal use only.

found that the reaction products are unstable in methylene chloride eliminating HCl or reacting further with benzeneselenenyl chloride in a slow reaction to yield diphenyl diselenide and a 1:2 mixture of *cis*- and *trans*-2,3-dichlorotetrahydropyran. Despite numerous attempts **2** and **3** could not be obtained in their pure state. Control experiments indicated that although the initial reaction proceeded essentially to completion there was in fact an equilibrium between adduct and starting material. Benzeneselenenyl chloride, formed as a result of this reversibility, reacts quantitatively with the adducts **2** and **3**. A similar result has been previously observed with respect to the adduct of benzeneselenenyl chloride with 2,3-dimethyl-2-butene (2).

Structural assignments were based on the 80 and 100 MHz ^{1}H nmr spectra of the crude product mixtures. The chlorine atom at the newly developed anomeric center (C-2) is axial as is predicted by the anomeric effect and confirmed by ^{1}H nmr analysis since the vicinal coupling constants are small (J_{ea} = 3.1 Hz, *cis* isomer and J_{ee} = 4.3 Hz, *trans* isomer (5)). The *cis* and *trans* adducts were assigned using ^{1}H nmr spectroscopy via the criteria that the equatorial anomeric proton at C-2 for the *cis* diastereomer is, in general, shifted further downfield than that of the corresponding *trans* isomer (5). A comparison of ^{1}H nmr parameters of **2** and **3** with the previously published data for the analogous Markownikoff and anti-Markownikoff phenylthio and ethylthio chlorotetrahydropyrans clearly shows them to have the Markownikoff regiochemistry (ref. 5*a*, p. 2152; ref. 6). Thus compounds **2** and **3** may be assigned as *cis*- and *trans*-2-chloro-3-phenylselenotetrahydropyran, respectively.

Kinetic Studies

The rate of the addition of benzeneselenenyl chloride to 3,4-dihydro-2*H*-pyran in methylene chloride at 25°C was followed by the stopped-flow technique using a Durrum–Gibson stopped-flow spectrophotometer. The rate of disappearance of benzeneselenenyl chloride was followed by measuring the decrease in its absorption at 433 nm. The addition was found to exhibit second-order kinetics, first order in olefin and first order in selenenyl chloride to at least 80% completion of the reaction. No correlation was found between the raw kinetic data and integrated first- or third-order rate expressions. The results are given in Table 1.

TABLE 1. Specific rate constants for the addition of benzeneselenenyl chloride to 3,4-dihydro-2*H*-pyran in methylene chloride solution at 25 ± 0.03°C

$[PhSeCl]_0$ (mol ℓ^{-1})	$\left[\bigcirc\!\!\!\!\bigcirc\!\!\!\!\bigcirc\right]_0$ (mol ℓ^{-1})	k_2 (M^{-1} s^{-1})
0.00127	0.2581	496
0.00127	0.0752	502
0.00127	0.0283	499
0.000632	0.0283	513
0.000632	0.00103	488
0.000632	0.000751	492
		Average 498

TABLE 2. A comparison of the specific rate constants for the reactions of benzeneselenenyl chloride and 4-chlorobenzenesulphenyl chloride to a series of simple alkenes

Alkene	k_2 (M^{-1} s^{-1}) ArSCl[a]	PhSeCl[b]
$H_2C{=}CH_2$	65.1	498
Z-$CH_3CH{=}CHCH_3$	1340	1870
E-$CH_3CH{=}CHCH_3$	434	1040
⬡	292	272
⬡O	6980	498
⬡–		216

[a]See ref. 12; kinetic runs carried out in 1,1,2,2-tetrachloroethane.
[b]See ref. 2; kinetic runs carried out in methylene chloride.

Discussion

From the data presented it is clear that the addition of benzeneselenenyl chloride to 3,4-dihydro-2*H*-pyran is nonstereospecific. These results are in contrast to the stereospecific *anti* additions observed for the reaction of ArSeX species to simple alkenes. Despite this change in the degree of stereospecificity, simple second-order kinetics are observed in analogy with previously studied systems.

Considering the nature of the rate determining transition state, it is clear from the data given in Tables 1 and 2 and that available elsewhere (2) that electron donating groups enhance the rate of reaction compared to ethylene. The reaction may thus be considered to be Ad_E2 in nature (7). It is thus somewhat surprising initially that cyclohexene reacts at only half the rate of ethylene and that 3,4-dihydro-2*H*-pyran reacts at a rate equivalent to that of ethylene. A priori one might have expected cyclohexene and *Z*-2-butene to have similar reactivity and to observe a dramatic increase in reactivity for 3,4-dihydro-2*H*-pyran based on its potential for delocalizing charge development on carbon and the increased nucleophilicity of its double bond. Such a postulate would

Can. J. Chem. Downloaded from www.nrcresearchpress.com by 210.87.254.5 on 09/05/12
For personal use only.

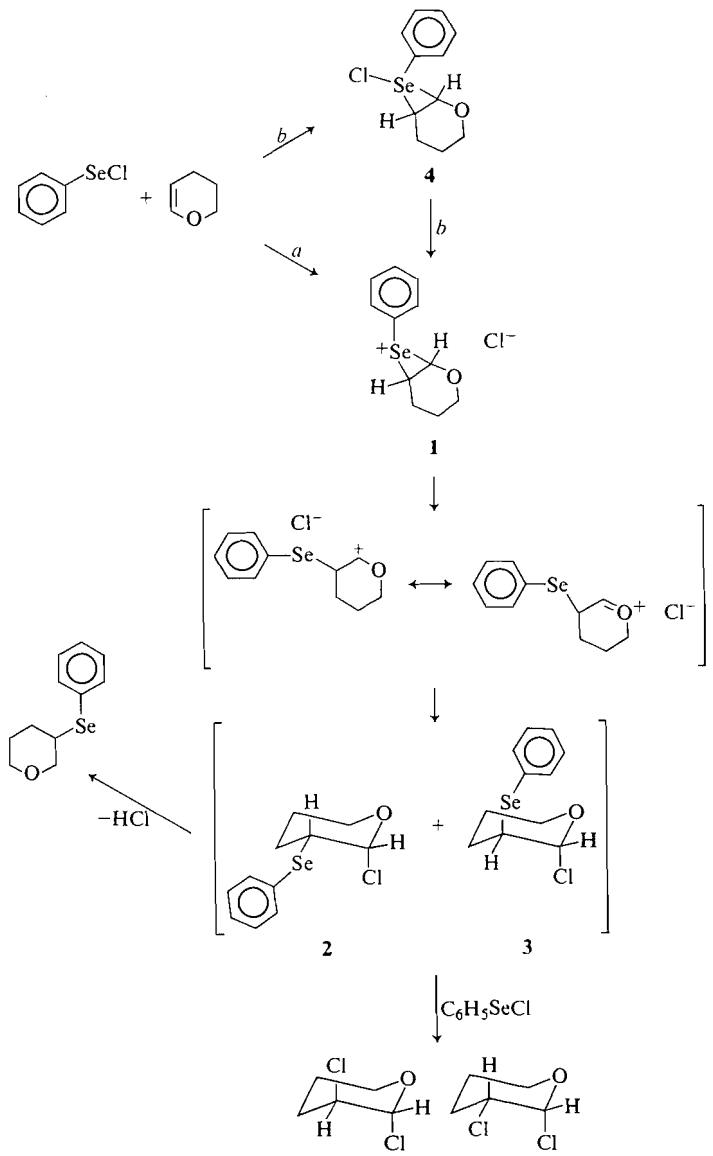

SCHEME 1

be readily supported by the observed *non*stereospecific addition which clearly involves an open carbonium ion rather than a bridged ion intermediate prior to the product determining step. In fact such a variation in reaction rates had been observed for the analogous reactions of 4-chlorobenzenesulphenyl chloride to these alkenes under similar reaction conditions (see Table 2). Furthermore the stereochemistry of the addition of sulphenyl chlorides to 3,4-dihydro-2*H*-pyran is stereospecific *anti*! Consequently it appears increasingly unlikely that an open carbonium ion can be the first formed intermediate.

The equivalency of the rates of reaction of benzeneselenenyl chloride with ethylene and 3,4-dihydro-2*H*-pyran plus the two-fold decrease in reactivity for cyclohexene and 1-methylcyclohexene suggest the presence of a large steric retardation effect which counteracts the expected rate enhancements through electron donation. Alternatively these results might be explained by charge delocalization almost entirely on selenium plus a steric interaction mechanism of somewhat lesser importance.

The mechanism most consistent with these facts involves a bridged transition state in the rate determining step leading to a seleniranium ion **1** intermediate which then opens to an oxacarbonium ion intermediate. In this mechanism only the product determining transition state resembles the open carbonium ion intermediate. A variant of the first mechanism (Scheme 1, route *a*) involving an episelenurane 'like'

Can. J. Chem. Downloaded from www.nrcresearchpress.com by 210.87.254.5 on 09/05/12
For personal use only.

transition state or intermediate **4** is also consistent with our data (Scheme 1, route *b*) and may explain the observed steric effects in the rate determining transition state somewhat better (8).

Although steric crowding and ring strain in the seleniranium ion or the episelenurane can be relieved by opening to the carbonium ion, this does not appear to be the major driving force for the reaction with 3,4-dihydro-2*H*-pyran. Such a scenario would require that the ether oxygen is sterically more bulky than a methylene group, comparing the reactions of cyclohexene and 3,4-dihydro-2*H*-pyran which seems unlikely. A more suitable explanation appears to be that under our reaction conditions an oxacarbonium ion is more stable than a seleniranium ion which is correspondingly more stable than either a secondary or tertiary carbonium ion. It is noted here that the addition of benzeneselenenyl chloride to both cyclohexene and 1-methylcyclohexene is stereospecific *anti*.

In summary we conclude on the basis of the available data that our experimental results for the addition of areneselenenyl chloride to alkenes are consistent with the formation of a bridged rate determining transition state followed by either a seleniranium ion or open carbonium ion intermediate prior to the product determining transition state depending upon the structure of the alkene.

Experimental

General

All melting and boiling points are uncorrected. Nuclear magnetic resonance spectra were recorded on Varian Associates CFT80 and HA-100 spectrometers using TMS as internal reference. Microanalysis was carried out by Scandinavian Microanalysis Laboratories, Herlev, Denmark. 3,4-Dihydro-2*H*-pyran was obtained commercially from Aldrich and purified before use by distillation, bp 85.6–86.2°C (lit. (9) bp 86–87°C). *Benzeneselenenyl chloride* was similarly obtained from Aldrich and recrystallized before use from methylene chloride, mp 63.7–64.5°C (lit. (10) mp 64°C); uv (n → π* Se—Cl); λ max: 433 nm (ε 264 ℓ mol^{-1} cm^{-1}).

Product Studies

Reactions were carried out in both the presence and absence of light, oxygen and/or isoamyl nitrite. No difference in product composition was observed with respect to these variables. Because of the propensity for the adducts **2** and **3** to react with benzeneselenenyl chloride it was necessary to add solutions of the selenenyl chloride to the alkene.

General Procedure

To a quantity (2.185 g, 0.0260 mol) of 3,4-dihydro-2*H*-pyran in 25 ml of methylene chloride was added dropwise a solution of 4.971 g (0.0260 mol) of benzeneselenenyl chloride in 25 ml of methylene chloride. The reaction was carried out in a 125 ml three-neck flask equipped with a gas inlet for nitrogen and a magnetic stirrer. All nitrogen was predried and deoxygenated before use. The reaction was thermostated in a water bath at 25 ± 0.03°C. Removal of the solvent by rotary evaporation at room temperature gave the mixture of **2** and **3** as a light yellow oil. At elevated temperatures substantial decomposition was observed giving mixtures of *cis*- and *trans*-2,3-dichlorotetrahydropyran and an elimination product *5-phenylseleno-3,4-dihydro-2H-pyran*. *cis*-2-Chloro-3-phenylselenotetrahydropyran (**2**): ^{1}H nmr (CD_2Cl_2) δ: 6.31 (d, J = 3.1 Hz (*CH*Cl), anomeric proton), 3.1–4.1 (broad multiplet), 1.5–2.4 (broad multiplet), 7.2 (m (3H)), 7.4 (m (2H)). *trans*-2-Chloro-3-phenylselenotetrahydropyran (**3**): ^{1}H nmr (CD_2Cl_2) δ: 6.24 (d, J = 4.3 Hz (*CH*Cl) anomeric proton), 7.2 (m (3H)), 7.4 (m (2H)). Attempts to isolate **2** and **3** via preparative tlc on silica gel were unsuccessful. 5-Phenylseleno-3,4-dihydro-2*H*-pyran: ^{1}H nmr ($CDCl_3$) δ: 6.88 (s, (1H) olefinic proton), 3.5–4.2 (broad multiplet), 1.5–2.2 (broad multiplet), 7.2 (m (3H)), 7.4 (m (4H)). The *cis* and *trans* isomers of 2,3-dichlorotetrahydropyran were prepared by the published procedures (5*a* and *d*): ^{1}H nmr ($CDCl_3$) anomeric protons *cis* δ 6.01; *trans* δ 5.95.

Kinetic Procedure

All kinetic runs were carried out on a Durrum-Gibson stopped-flow spectrophotometer as previously described (11).

Acknowledgement

Continued financial support from the National Research Council of Canada and the University of Ottawa is gratefully acknowledged.

1. (*a*) D. G. GARRATT and G. H. SCHMID. J. Org. Chem. **42**, 1776 (1977); (*b*) G. H. SCHMID and D. G. GARRATT. Tetrahedron Lett. 3991 (1975); (*c*) K. B. SHARPLESS and R. F. LAUER. J. Org. Chem. **39**, 429 (1974); (*d*) H. J. REICH. J. Org. Chem. **39**, 428 (1974); (*e*) W. JENNY. Helv. Chim. Acta, **36**, 1278 (1953); (*f*) W. JENNY. Helv. Chim. Acta, **41**, 593 (1958); (*g*) F. LAUTENSCHLAEGER. J. Org. Chem. **34**, 4002 (1969); (*h*) S. RAUCHER. J. Org. Chem. **42**, 2950 (1977).
2. D. G. GARRATT. Ph.D. Thesis, University of Toronto, Toronto, Ont. 1975.
3. G. H. SCHMID and D. G. GARRATT. *In* The chemistry of double bonded functional groups. Supplement A, Part 2. *Edited by* S. Patai. Wiley, New York, NY. 1977. p. 892.
4. D. G. GARRATT and G. H. SCHMID. Can. J. Chem. **52**, 3599 (1974).
5. (*a*) T. E. STONE and G. D. DAVES, JR. J. Org. Chem. **42**, 2151 (1977); (*b*) G. E. BOOTH and R. J. OUELLETTE. J. Org. Chem. **31**, 544 (1966); (*c*) G. DESCOTES, D. SINON, and J. C. MARTIN. Bull. Soc. Chim. Fr. 3730 (1970); (*d*) R. U. LEMIEUX and B. FRASER-REID. Can. J. Chem. **43**, 1460 (1965); (*e*) N. S. ZEFIROV and N. M. SHEKHTMAN. Dokl. Chem. (Eng. Transl.), **177**, 1110 (1967); (*f*) A. J. DUGGAN and S. S. HALL. J. Org. Chem. **42**, 1057 (1977).
6. (*a*) M. J. BALDWIN and R. K. BROWN. Can. J. Chem. **45**, 1195 (1967); (*b*) M. J. BALDWIN and R. K. BROWN. Can. J. Chem. **46**, 1093 (1968).
7. C. K. INGOLD. Structure and mechanism in organic chemistry. 2nd ed. Cornell University Press, Ithaca, NY. 1969.
8. D. G. GARRATT and G. H. SCHMID. Can. J. Chem. **52**, 1027 (1974).
9. R. C. YEAST (*Editor*). Handbook of chemistry and physics. 49th ed. The Chemical Rubber Company, Cleveland, OH. 1968. p. C-515.
10. D. G. FOSTER. J. Am. Chem. Soc. **55**, 822 (1933).
11. (*a*) G. H. SCHMID and D. G. GARRATT. Chem. Scr. **10**, 76 (1976); (*b*) G. H. SCHMID, V. M. CSIZMADIA, V. J. NOWLAN, and D. G. GARRATT. Can. J. Chem. **50**, 2457 (1972).
12. (*a*) G. H. SCHMID and D. G. GARRATT. Can. J. Chem. **51**, 2463 (1973); (*b*) G. H. SCHMID, C. L. DEAN, and D. G. GARRATT. Can. J. Chem. **54**, 1253 (1976); (*c*) C. L. DEAN and D. G. GARRATT. Unpublished results.

Further studies of the specificity of carboxypeptidase A towards hippuric acid esters

JOHN W. BUNTING AND SAMUEL S.-T. CHU

Department of Chemistry, University of Toronto, Toronto, Ont., Canada M5S 1A1

Received February 13, 1978

JOHN W. BUNTING and SAMUEL S.-T. CHU. Can. J. Chem. **56**, 2188 (1978).

The kinetics of hydrolysis of a series of 10 new hippurate esters ($C_6H_5CONHCH_2CO_2CRR_1CO_2H$ (I)) by bovine pancreatic carboxypeptidase A have been investigated at pH 7.5, 25°C, and ionic strength 0.5. Pronounced substrate inhibition was displayed by I: R = H, $R_1 = C_6H_5(CH_2)_2$, 3-indolylmethyl, 4-$HOC_6H_4CH_2$, and 4-FC_6H_4 whereas pronounced substrate activation was observed for I: R = H, R_1 = 4-$CH_3C_6H_4$, 4-$C_2H_5C_6H_4$, 4-C_6H_5-C_6H_4, 1-naphthyl, 2-naphthyl, and R = $R_1 = C_2H_5$. In all cases substrate activation and substrate inhibition were shown to be consistent with ES_2 complex formation similar to that previously observed for other hippurate esters. Kinetic parameters were evaluated for each ester and it is noted that all 13 hippurate esters now known to display substrate inhibition have $k_{cat}/K_m > 10^6\ M^{-1}\ min^{-1}$, whereas $k_{cat}/K_m < 10^6\ M^{-1}\ min^{-1}$ for all 9 hippurate esters known to display substrate activation. The enzymic specificity for the R_1 unit of I suggests binding of R_1 in a 'bent' hydrophobic pocket having a restricted entrance.

JOHN W. BUNTING et SAMUEL S.-T. CHU. Can. J. Chem. **56**, 2188 (1978).

On a étudié, à un pH de 7.5, à 25°C et à une force ionique de 0.5, la cinétique de l'hydrolyse d'une série de 10 nouveaux esters hippuriques ($C_6H_5CONHCH_2CO_2CRR_1CO_2H$) (I) par la carboxypeptidase A du pancréas des bovins. Il y a une inhibition marquée du substrat par I: R = H, $R_1 = C_6H_5(CH_2)_2$, indolylméthyl-3, $OHC_6H_4CH_2$-4 et FC_6H_4-4 alors qu'il existe une activation importante du substrat pour I: R = H, $R_1 = CH_3C_6H_4$-4, $C_2H_5C_6H_4$-4, $C_6H_5C_6H_4$-4, naphtyl-1, naphtyl-2 et R = $R_1 = C_2H_5$. Dans tous les cas d'inhibition et d'activation du substrat, on a montré qu'il y a concordance avec la formation d'un complexe ES_2 semblable à celui observé antérieurement pour d'autres esters hippuriques. On a évalué les paramètres cinétiques pour chaque ester et on a noté que les 13 esters hippuriques qui sont maintenant connus et qui montrent une inhibition du substrat ont $k_{cat}/K_m > 10^6\ M^{-1}\ min^{-1}$ alors que les neuf esters connus présentant une activation du substrat possèdent un $k_{cat}/K_m < 10^6\ M^{-1}\ min^{-1}$. La spécificité enzymatique pour le groupe R_1 de I suggère que l'attachement de R_1 se fait dans une couche hydrophobe incurvée ayant une entrée restreinte.

[Traduit par le journal]

Introduction

The kinetics of the hydrolysis of hippurate esters (**I**) by bovine pancreatic carboxypeptidase A are

$$C_6H_5CONHCH_2CO_2CRR_1CO_2H$$
I

complicated by substrate activation and/or substrate inhibition (1–9). Considerable progress has been made in quantitatively describing these phenomena and it has been shown that both substrate activation and substrate inhibition can be ascribed to the formation of 1:2 enzyme–substrate complexes (ES_2) via Scheme 1 (7–10). Some progress has been made in elucidating the relationship between the structure of the alcohol moiety of the ester (i.e., the nature of R and R_1 in **I**) and the occurrence of substrate activation or substrate inhibition; however, more detailed studies are necessary to confirm these ideas. A further complication arises from the observation that there are apparently two different types of ES_2 complex which can lead to substrate activation (7, 9). Furthermore, there are several esters which are known to display both substrate activation and substrate inhibition (7).

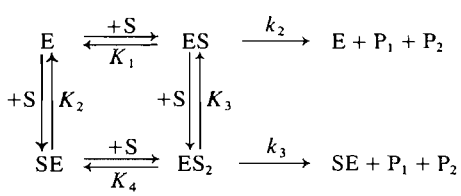

SCHEME 1

In the present work, we have studied the hydrolysis of a further 10 hippurate esters by carboxypeptidase A. Detailed analyses of the kinetics of the enzymic hydrolysis of these esters confirm the interpretations previously made on the basis of more limited data. The current data also considerably extend the knowledge of the specificity of carboxypeptidase A for the alcohol moiety of ester substrates and, in combination with literature data for peptide substrates, allow a comparison of the specificity of this enzyme for specific ester and peptide substrates.

Experimental

α-Hydroxy Acids

DL-3-Indolelactic acid and 2-ethyl-2-hydroxybutanoic acid were obtained commercially.

Can. J. Chem. Downloaded from www.nrcresearchpress.com by 210.87.254.42 on 09/05/12
For personal use only.

Can. J. Chem. Downloaded from www.nrcresearchpress.com by 210.87.254.42 on 09/05/12
For personal use only.

TABLE 1. Characterization of hippurate esters (I)

Ester	R	R_1	Solvent[a]	Melting point (°C)	^{1}H nmr spectrum (CF_3CO_2H), δ (ppm)
1	H	$C_6H_5(CH_2)_2$	CH_3CN–CCl_4(1:1)	150–151	2.4 (2H, t, J = 6 Hz), 2.8 (2H, m), 4.5 (2H, broad), 5.35 (1H, t, J = 6 Hz), 7.2 (5H, s), 7.4–7.8 (6H, m)
2	H	3-Indolylmethyl	$CH_3CO_2C_2H_5$–C_6H_{14}(1:1)	150–151	3.4 (2H, broad), 4.4 (2H, broad), 5.6 (1H,t, J = 6 Hz), 7.1–7.8 (12H, m)
3	H	4-$HOC_6H_4CH_2$	$CH_3CO_2C_2H_5$–C_6H_{14}(1:1)	108–110	3.4 (2H, m), 4.55 (2H, d, J = 4 Hz), 5.55 (1H, t, J = 6 Hz), 6.8 (2H, d, J = 9 Hz), 7.2 (2H, d, J = 9 Hz), 7.5–7.9 (6H, m)
4	H	4-FC_6H_4	CH_3CN–CH_2Cl_2(1:1)	172–173	4.6 (2H, d, J = 4 Hz), 6.25 (1H, s), 7.0–8.0 (10H, m)
5	H	4-$CH_3C_6H_4$	CH_3CN–CH_2Cl_2(1:1)	173–174	2.35 (3H, s), 4.6 (2H, broad), 6.25 (1H, s), 7.3–8.0 (10H, m)
6	H	4-$C_2H_5C_6H_4$	$CH_3CO_2C_2H_5$	179–180	1.25 (3H, t, J = 7 Hz), 2.7 (2H, q, J = 7 Hz), 4.6 (2H, broad), 6.2 (1H, s), 7.3–7.8 (10H, m)
7	H	4-$C_6H_5C_6H_4$	CH_3COCH_3	191–192	4.65 (2H, broad), 6.35 (1H, s), 7.3–7.9 (15H, m)
8	H	1-Naphthyl	$CH_3CO_2C_2H_5$–C_6H_{14}(1:1)	171–172	4.55 (2H, broad), 6.95 (1H, s), 7.3–8.2 (13H, m)
9	H	2-Naphthyl	CH_3OH	194–195	4.65 (2H, broad), 6.4 (1H, s), 7.4–8.0 (13H, m)
10	C_2H_5	C_2H_5	C_2H_5OH	149–150	1.0 (6H, t, J = 8 Hz), 2.2 (4H, q, J = 8 Hz), 4.5 (2H, broad), 7.5–7.9 (6H, m)

[a]Recrystallization solvent.

DL-3-(*p*-Hydroxyphenyl)lactic acid was prepared from 5-(*p*-hydroxybenzylidene)hydantoin (11, 12) as follows. A solution of 5 *M* sodium hydroxide was deoxygenated by purging with nitrogen. This alkaline solution (180 ml) was added to 5-(*p*-hydroxybenzylidene)hydantoin (6.5 g, 0.032 mol) and the solution heated at reflux for 3 h under an atmosphere of nitrogen. The solution was cooled to room temperature. A deoxygenated solution of sodium borohydride (1.22 g, 0.032 mol) in 2% sodium hydroxide (50 ml) was added dropwise over 15 min and the mixture stirred under nitrogen at room temperature for 2 h. Concentrated hydrochloric acid (80 ml) was added slowly and the solution filtered free of white solid and allowed to stand overnight. The solution was acidified with concentrated hydrochloric acid (10 ml), extracted with ether (800 ml), and the ether solution dried over anhydrous magnesium sulfate. Removal of the ether under reduced pressure yielded DL-3-(*p*-hydroxyphenyl)lactic acid (4.6 g, 79%) as a pale yellow, almost colourless solid, mp 106–110°C (dec.).

The remaining α-hydroxy acids were synthesized from the appropriate aldehydes by the general method of Vogel (13).

Synthesis of Esters

All esters were synthesized via the pyridine-catalyzed esterification of hippuryl chloride and the appropriate α-hydroxy acid as previously described (7). The crude products were recrystallized several times to give analytically pure esters. Table 1 contains melting point and ^{1}Hmr spectral data for each ester.

Kinetic Studies

Preparation of enzyme and substrate stock solutions and all kinetic details are as previously described (8, 14). All kinetic data are for pH 7.5, 25°C, and ionic strength 0.5. All calculations are in terms of the concentrations of the L-ester of racemic mixtures. It is well established that the D-esters are neither substrates nor competitive inhibitors for the hydrolysis of the L-esters by carboxypeptidase A (1, 2, 4, 8, 15).

Results

For each of the esters in Table 1, the initial velocity of enzymic hydrolysis was measured at pH 7.5, 25°C, and ionic strength 0.5 over a range of substrate concentration (S) of approximately 0.1–100 mM.

The esters **1–3** displayed substrate inhibition (8, 9). The experimental data for each of these esters were fitted to eq. [1] by the iteration technique

$$[1] \qquad \frac{v}{E} = \frac{k_2^{app}S + k_3S^2/K_{SS}^{app}}{K_S^{app} + S + S^2/K_{SS}^{app}}$$

previously described (16) and the values obtained for the parameters in this way are given in Table 2.

Ester **4** (**I**: R = H, R_1 = 4-FC_6H_4) also displayed substrate inhibition; however, attempts to fit the experimental data for this ester to eq. [1] gave multiple sets of solutions, all of which require K_S^{app} > 2 mM and have k_2^{app}/K_S^{app} = 1.3 × 10^6 M^{-1} min^{-1}. This result is consistent with the observation that the velocity is proportional to the substrate concentration up to S = 2 mM, with $k_{cat}/K_m = k_2^{app}/K_S^{app}$ = 1.3 × 10^6 M^{-1} min^{-1}. In the region where substrate inhibition occurs, v/E is linear in $1/S$ over the range S = 8–50 mM and this allows evaluation of k_3 = 860 min^{-1} and $k_2^{app}K_{SS}^{app}$ = 14 M min^{-1} from the ordinate intercept and slope, respectively, of eq. [2].

$$[2] \qquad v/E = (k_2^{app}K_{SS}^{app}/S) + k_3$$

The esters **5–10** displayed substrate activation (7).

Can. J. Chem. Downloaded from www.nrcresearchpress.com by 210.87.254.42 on 09/05/12
For personal use only.

TABLE 2. Parameters for hydrolysis of hippurate esters (**I**) by carboxypeptidase A[a]

Ester	R	R_1	k_2^{app}(min^{-1})	K_S^{app}(mM)	k_2^{app}/K_S^{app}(M^{-1}min^{-1})	K_{SS}^{app}(mM)	k_3(min^{-1})	$K_S^{app}K_{SS}^{app}$(M^2)
1	H	$C_6H_5(CH_2)_2$	$(4.9\pm0.1)\times10^4$	3.5 ± 0.3	1.4×10^7	1.2 ± 0.1	$(2.1\pm0.1)\times10^3$	4.2×10^{-6}
2	H	3-Indolylmethyl	$(2.52\pm0.04)\times10^4$	0.80 ± 0.02	6.3×10^7	4.1 ± 0.1	$(3.4\pm0.2)\times10^3$	3.3×10^{-6}
3	H	$4\text{-}HOC_6H_4CH_2$	$(1.15\pm0.02)\times10^4$	0.15 ± 0.01	7.7×10^7	5.8 ± 0.4	$(2.0\pm0.3)\times10^3$	8.7×10^{-7}
11[b]	H	$C_6H_5CH_2$	3.8×10^4	0.17	2.2×10^8	0.83	2.2×10^3	1.4×10^{-7}
12[b]	H	C_6H_5	1.1×10^4	1.2	9.2×10^6	1.2	490	1.4×10^{-6}
13[c]	H	$4\text{-}ClC_6H_4$	(55)[d]	[e]	1×10^4	[e]	900	2×10^{-4}
4	H	$4\text{-}FC_6H_4$	$>3\times10^3$	>2	1.3×10^6	[e]	860	1.1×10^{-5}
5	H	$4\text{-}CH_3C_6H_4$	[e]	[e]	2.5×10^3	[e]	310	2.8×10^{-4}
6	H	$4\text{-}C_2H_5C_6H_4$	[e]	[e]	2.1×10^3	[e]	300	2.9×10^{-4}
7	H	$4\text{-}C_6H_5C_6H_4$	[e]	[e]	2.3×10^3	[e]	71	2.4×10^{-4}
8	H	1-Naphthyl	[e]		2.7×10^4	[e]	430	2.2×10^{-5}
9	H	2-Naphthyl	[e]	[e]	<260	[e]	25	2.8×10^{-4}
10	C_2H_5	C_2H_5	[e]	[e]	1.7×10^4	[e]	3.0×10^3	9.4×10^{-4}
14[c]	CH_3	CH_3	[e]	[e]	3×10^5	[e]	8×10^3	6×10^{-5}

[a]At pH 7.5, 25°C, ionic strength 0.5.
[b]From ref. 8.
[c]From ref. 7.
[d]See text.
[e]Not experimentally determinable.

For esters **5–8** and **10**, Lineweaver–Burk plots are linear at the lowest substrate concentrations investigated and values of $k_2^{app}/K_S^{app}(=k_{cat}/K_m)$ may thus be evaluated (Table 2). Ester **9** is an extremely poor substrate and substrate activation is apparent at even the lowest substrate concentrations that are experimentally accessible. Thus only a maximum value of k_2^{app}/K_S^{app} may be estimated in this case. For each of esters **5–10**, values of k_3 and $K_S^{app}K_{SS}^{app}$ were evaluated from plots of S^2E/v against S^2 according to eq. [3] (7). Such plots are linear over at least a five-fold range in substrate concentration in the vicinity of

$$[3] \qquad S^2E/v = k_3S^2 + K_S^{app}K_{SS}^{app}/k_3$$

the maximum rates observed in this work. Parameters obtained for esters **5–10** are summarized in Table 2.

For ester **8**, substrate inhibition was observed in the range $S = 20$–50 mM, however solubility limitations prevented a detailed investigation of this phenomenon.

Discussion

The results summarized in Table 2 for the esters **1–10** extend our earlier studies (7, 8) of the specificity of carboxypeptidase A for the R and R_1 substituents of the alcohol moiety of hippurate esters (**I**). It has recently been shown (17) that the specificity of carboxypeptidase A for hippurate esters, as measured by k_{cat}/K_m $(=k_2^{app}/K_S^{app})$, is typical of the specificity of this enzyme for the alcohol moiety of other specific ester substrates. Thus the values for k_2^{app}/K_S^{app} in Table 2, in conjunction with our earlier data (7, 8, 10, 17), may be used as a guide for the prediction of the relative reactivities of a wide range of ester substrates towards hydrolysis by carboxypeptidase A.

Esters **1–4**, which display substrate inhibition, are the most rapidly hydrolyzed of the new substrates reported in this work, and have specificity constants (k_2^{app}/K_S^{app} in Table 2) in the same range (3×10^6–2×10^8 M^{-1} min^{-1} (8)) as those hippurate esters which have previously been shown to display substrate inhibition.

Esters **5–10** which display substrate activation are quite poor substrates, having $k_2^{app}/K_S^{app} < 10^5$ M^{-1} min^{-1}. The most reactive hippurate ester known to display substrate activation is *O*-hippuryl-2-methyllactic acid (ester **15** in Table 2) having $k_2^{app}/K_S^{app} = 3\times10^5$ M^{-1} min^{-1} (7). On the basis of the data now available, there is a clear relationship between the reactivity of hippurate esters towards enzymic hydrolysis and the occurrence of substrate activation or substrate inhibition. Thus all 13 hippurate esters which display pronounced substrate inhibition have $k_2^{app}/K_S^{app} > 10^6$ M^{-1} min^{-1}, whereas all 9 hippurate esters which display pro-

Can. J. Chem. Downloaded from www.nrcresearchpress.com by 210.87.254.42 on 09/05/12
For personal use only.

nounced substrate activation have $k_2^{app}/K_S^{app} < 10^6$ M^{-1} min^{-1}. Interestingly, slight activation followed by pronounced inhibition has been suggested (8) for *O*-hippuryl-L-lactic acid, which has $k_2^{app}/K_S^{app} = 3 \times 10^6$ M^{-1} min^{-1} and thus seems to be a borderline case in terms of the above ranges. However, in the present study we could not detect any evidence of substrate activation for ester **4** which has $k_2^{app}/K_S^{app} = 1.9 \times 10^6$ M^{-1} min^{-1} and so is also a borderline case.

In terms of Scheme 1, the parameters in eq. [1] are given by eqs. [4]–[6].

$$[4] \qquad k_2^{app} = k_2/(1 + K_1/K_2)$$

$$[5] \qquad K_S^{app} = K_1/(1 + K_1/K_2)$$

$$[6] \qquad K_{SS}^{app} = K_3(1 + K_1/K_2)$$

Equation [1] predicts (7) that substrate activation will be observed when

$$[7] \qquad K_S^{app} > (k_2^{app}/k_3 - 1)S$$

whereas substrate inhibition will be observed if

$$[8] \qquad K_S^{app} < (k_2^{app}/k_3 - 1)S$$

All substrates that are known to display substrate inhibition have $k_2^{app} > k_3$ (e.g., esters **1–4**, **11**, **12** in Table 2) so that, consistent with inequality [8], substrate inhibition is observed for substrate concentrations $S > K_S^{app}/(k_2^{app}/k_3 - 1)$. Inequality [7] may also be satisfied for $k_2^{app} > k_3$ provided that K_S^{app} is quite large (case *i*). However, if $k_2^{app} < k_3$, then inequality [7] is satisfied for all values of S irrespective of the size of K_S^{app} (case *ii*). Case *i* arises if productive binding of the first substrate molecule to the enzyme is weak, whereas case *ii* suggests a situation in which the rate of hydrolysis within an ES complex is much smaller than within an ES_2 species. Clearly, both case *i* (large K_S^{app}) and case *ii* (small k_2^{app}) predict much smaller values for k_2^{app}/K_S^{app} for esters which display substrate activation than for those which display substrate inhibition. This prediction is consistent with the relationship mentioned above between the size of k_2^{app}/K_S^{app} and the occurrence of substrate activation or substrate inhibition.

For *O*-hippuryl-L-*p*-chloromandelic acid (ester **13** in Table 2), it was originally suggested (7) that case *i* was probably applicable. However, more recent comparative studies of the enzymic hydrolysis of other *O*-acyl-L-*p*-chloromandelic acids, which are not as prone to substrate activation as the hippurate ester, and the corresponding *O*-acyl-L-mandelic acids are now available (17). These studies indicate that the introduction of the *p*-chloro substituent results in a dramatic 200-fold decrease in k_2^{app} but only a modest two- to fivefold increase in K_S^{app}. Such data imply that substrate activation in the enzymic hydrolysis of *O*-hippuryl-L-*p*-chloromandelic acid actually arises via case *ii* rather than via case *i*. Consistent with this suggestion, prediction of k_2^{app} for this ester as 1/200 of k_2^{app} for *O*-hippuryl-L-mandelic acid gives $k_2^{app} = 1.1 \times 10^4/200 = 55$ min^{-1} which is considerably less than the observed value of 900 min^{-1} for k_3 for this ester (7) and so is consistent with case *ii*.[1]

Whereas **II**: X = H and **II**: X = F both display substrate inhibition, all other esters **II** in Table 2 are

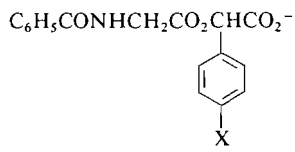

II

much poorer substrates and display substrate activation (X = Cl, CH_3, C_2H_5, C_6H_5). A similar dramatic influence of a substituent X on a phenyl ring has also been observed for *para*-substituted benzoate ions (**III**) acting as reversible inhibitors of the hydrolysis of hippurate esters by carboxypeptidase A (18). Small X groups lead to competitive inhibition by **III** of

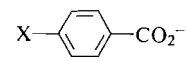

III

hippurate ester hydrolysis, whereas large X groups lead to noncompetitive inhibition. The simplest explanation for these results is in terms of competitive inhibition by **III** requiring the phenyl ring to bind in a hydrophobic pocket which has a geometry that will not accommodate large X groups. The similar dramatic effects of the size of X on the enzymic hydrolysis of **II** (cf. F vs. Cl and H vs. CH_3 in Table 2) strongly suggest that the same steric constraint influences the binding of **II** and **III**. This is consistent with the considerable experimental evidence (8, 19, 20) that points towards the hydrophobic groups of simple competitive inhibitor carboxylate ions binding to the same hydrophobic region of the enzyme as the hydrophobic side chains of the alcohol moieties of ester substrates.

There is not, however, a 1:1 correspondence between the observation of substrate activation or substrate inhibition for X in **II** and the induction of noncompetitive or competitive inhibition by X in **III**. In particular, the hydrolysis of **II** appears to be even

[1]The earlier estimates (7) of $k_2^{app} > 200$ min^{-1} and $K_S^{app} > 50$ mM for *O*-hippuryl-L-*p*-chloromandelic acid are probably in error as a result of an incorrect assumption as to the acceptable range of values for K_{SS}^{app} for this ester.

Can. J. Chem. Downloaded from www.nrcresearchpress.com by 210.87.254.42 on 09/05/12
For personal use only.

more sensitive to the size of X than does the binding of the competitive inhibitors **III**. Thus, whereas **III**: X = CH_3 is a competitive inhibitor (K_i = 8.8 mM) that binds only slightly more weakly than **III**: X = H(K_i = 6 mM), the ester **II**: X = CH_3 is almost a 4000-fold poorer substrate (based on k_2^{app}/K_S^{app}) than **II**: X = H. If it is assumed that the binding of **II** and **III** to the enzyme requires interaction of the carboxylate anion with the same enzymic site, then the greater sensitivity to the size of X in the hydrolysis of **II** than in the binding of **III** can be readily ascribed to the greater distance of X from the terminal carboxylate group in **II** than in **III**.

It seems reasonable to assume that the conclusion reached above for case *ii* being applicable for the hydrolysis of **II**: X = Cl should also be applicable to the other *para*-substituted mandelic acid derivatives (**II**) in Table 2. Case *ii* indicated that the reduced reactivity for large X groups in **II** is predominantly a rate phenomenon (k_2^{app}) rather than a binding phenomenon (K_S^{app}). This suggests that the steric interactions of large X groups with the enzyme can be overcome by reorientation of the substituted phenyl ring by making use of the conformational flexibility provided by the presence of the saturated α-carbon atom of the alcohol moiety. However, this orientation relative to the unsubstituted derivative (**II**: X = H) comes at the expense of the orientation of the hydrolyzable ester bond relative to the catalytically active functional group(s) of the enzyme, and so results in a diminished value for k_2^{app}. This hypothesis suggests that less reorientation should be required for **II**: X = F than for **II**: X = Cl, and thus k_2^{app} is predicted to be larger for X = F than for X = Cl. This prediction is consistent with the experimental observation (Table 2).

The observed enzymic specificity for R_1 in Table 2 may be used to approximately map the enzymic hydrophobic region in which R_1 is bound. The strong binding of esters **2**, **3**, and **11** clearly indicates that the hydrophobic region must be large enough to readily accommodate the 3-indolylmethyl and *p*-hydroxybenzyl groups. The ability of the enzyme to readily accommodate this latter *para*-substituted benzyl group, whereas the *para*-substituted phenyl groups of **II** seem to experience serious steric interactions which result in displaced binding (see above), can be best explained in terms of a 'bent' hydrophobic pocket having a restricted entrance. The conformational flexibility that the β-methylene groups give the *p*-hydroxybenzyl and 3-indolylmethyl groups allows these R_1 groups to position themselves in the pocket without serious interactions with the enzyme 'wall.' However, the rigid R_1 = 4-XC_6H_4, 1-naphthyl, and 2-naphthyl groups encounter serious interactions with the 'wall' near the pocket entrance in attempts to bind so that the hydrolyzable bond is optimally oriented for maximum catalytic effectiveness. As discussed above, these serious interactions can apparently be overcome by a reorientation of the molecule relative to the catalytically active functional groups of the enzyme, which allows a deeper penetration of the R_1 group into the hydrophobic pocket. The shape of the hydrophobic region is also reflected by the much greater reactivity of the α-naphthalene derivative, ester **8**, than the isomeric β-naphthalene derivative, ester **9**. The very low k_2^{app}/K_S^{app} for ester **9** stresses the steric constraints that exist in the vicinity of the hydrophobic pocket entrance, and the requirement for a 'bent' pocket in order to allow for the ready accommodation of the 3-indolylmethyl unit of ester **2**.

The ester **1**, $R_1 = C_6H_5(CH_2)_2$, is an interesting case, since it has the largest k_2^{app} value of any hippurate ester yet studied, and yet K_S^{app} is 100-fold larger than for the most strongly bound hippurate ester known (for $R_1 = (CH_3)_2CHCH_2$, K_S^{app} = 0.021 mM, k_2^{app} = 4400 min^{-1} (8)). The lower homolog, ester **11**, appears to bind about 10-fold more strongly than ester **1** and this suggests that the phenethyl group cannot be accommodated in the hydrophobic pocket in its energetically most favourable conformation. The relationship between esters **1** and **11** should be compared with the corresponding *p*-nitrobenzoate esters (**IV**). For these

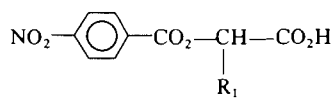

IV

latter esters, K_S^{app} for $R_1 = C_6H_5(CH_2)_2$ is also much larger than for $R_1 = C_6H_5CH_2$ but unlike esters **1** and **11**, this homologation is also accompanied by a 30-fold decrease in k_2^{app} (21).

The similarity of the k_3 values for the fluoro- and chloromandelic acid derivatives further reinforces the conclusion that equivalent ES_2 complexes are responsible for substrate activation and substrate inhibition in these hippuric acid derivatives, and that the observation of one or the other of these phenomena is simply a matter of the relative values of the parameters leading to consistency with inequality [7] or inequality [8]. It is interesting that for **II**, the values of k_3 are in the order Cl ≈ F > H > CH_3 ≈ C_2H_5, which is the order expected based on the electronic effects of these X substituents. Thus the large variations in the rate (k_2^{app}) of hydrolysis of

the ES complexes of these esters appear to have been eliminated in the hydrolysis of the ES_2 species.

The ester **10** has not been considered in any of the above discussion. For the related ester **14**, it has been argued (7, 9) on the basis of the large k_3 value, an enhanced k_3/k_{OH} ratio and the pH dependence of k_3, that substrate activation in the enzymic hydrolysis of this ester arises via an ES_2 complex that is not equivalent to the ES_2 complex involved in substrate activation for *O*-hippuryl-L-*p*-chloromandelic acid. The value of $k_3 = 3000$ min^{-1} for ester **10** is also much larger, relative to the other k_3 values in Table 2, than can be accounted for on the basis of simple substituent effects. In particular, for **I**: R = H, $R_1 = C_2H_5$, k_3 is only 200 min^{-1} (8) and so nonequivalent ES_2 complexes are indicated for this ester and ester **10**. It thus appears that for those hippurate esters that do not have a hydrogen atom on the α-carbon atom of the alcohol moiety, an alternative mode of substrate activation is available other than that discussed in connection with case *ii* above.

It is interesting that the specific ester substrates having R = $C_6H_5CH_2$, 4-$HOC_6H_4CH_2$, and 3-indolylmethyl are among the best ester substrates for carboxypeptidase A. It is noteworthy, that these side chains are those present in phenylalanine, tyrosine, and tryptophan, respectively, and that the best peptide substrates for this enzyme have one of these three amino acids present at the C-terminus. Although it is tempting to suggest that this indicates that the C-terminal side chains of productively bound ester and peptide substrates interact with the same hydrophobic region of the enzyme, such a conclusion is inconsistent with a growing body of experimental evidence that is most simply reconciled in terms of distinct productive binding sites for ester and peptide substrates (15, 22–24). In particular, the observation that the 3-phenylpropanoate and 3-indolylacetate ions are competitive inhibitors of esterase activity (19, 23) but noncompetitive inhibitors of peptidase activity (23, 25) is not readily rationalized in terms of common binding sites for the C-terminal sidechains of ester and peptide substrates.

Acknowledgements

We appreciate the continued support of this work by the National Research Council of Canada. Several of the α-hydroxy acids were originally synthesized by Dr. J. Murphy and Dr. S. H. Kabir.

1. J. E. Snoke and H. Neurath. J. Biol. Chem. **181**, 789 (1949).
2. W. O. McClure, H. Neurath, and K. A. Walsh. Biochemistry, **3**, 1897 (1964).
3. E. T. Kaiser, S. Awazu, and F. W. Carson. Biochem. Biophys. Res. Commun. **21**, 444 (1965).
4. J. R. Whitaker, F. Menger, and M. L. Bender. Biochemistry, **5**, 386 (1966).
5. S. Awazu, F. A. Carson, P. L. Hall, and E. T. Kaiser. J. Am. Chem. Soc. **89**, 3627 (1967).
6. R. C. Davies, J. F. Riordan, D. S. Auld, and B. L. Vallee. Biochemistry, **7**, 1090 (1968).
7. J. Murphy and J. W. Bunting. Can. J. Chem. **52**, 3829 (1974).
8. J. Murphy and J. W. Bunting. Can. J. Chem. **53**, 283 (1975).
9. J. W. Bunting and S. S.-T. Chu. Biochemistry, **15**, 3237 (1976).
10. J. W. Bunting and S. S.-T. Chu. Biochim. Biophys. Acta, **524**, 142 (1978).
11. E. C. Wagner and J. K. Simons. J. Chem. Educ. **13**, 265 (1936).
12. G. Billek. Org. Synth. **43**, 49 (1963).
13. A. I. Vogel. A textbook of practical organic chemistry. 3rd ed. Longmans, Green & Co., London. 1959. p. 774.
14. J. W. Bunting and J. Murphy. Can. J. Chem. **52**, 2640 (1974).
15. L. G. Lange, D. S. Auld, and J. F. Riordan. Biochemistry, **13**, 1983 (1974).
16. J. W. Bunting and J. Murphy. Can. J. Biochem. **50**, 1369 (1972).
17. J. W. Bunting and S. S.-T. Chu. Biochim. Biophys. Acta, In press.
18. J. W. Bunting and C. D. Myers. Can. J. Chem. **53**, 1984 (1975).
19. J. W. Bunting and C. D. Myers. Can. J. Chem. **51**, 2639 (1973).
20. J. W. Bunting and C. D. Myers. Can. J. Chem. **52**, 2053 (1974).
21. J. W. Bunting and S. H. Kabir. J. Am. Chem. Soc. **99**, 2775 (1977).
22. J. F. Riordan. Biochemistry, **12**, 3915 (1973).
23. D. S. Auld and B. Holmquist. Biochemistry, **13**, 4355 (1974).
24. J. W. Bunting and Ç. D. Myers. Can. J. Chem. **53**, 1993 (1975).
25. D. S. Auld and B. L. Vallee. Biochemistry, **9**, 602 (1970).

Can. J. Chem. Downloaded from www.nrcresearchpress.com by 210.87.254.42 on 09/05/12
For personal use only.

Oxidative cyclization of carbonyl derivatives. 5-Imino-Δ^1-1,2,4-triazolines from alkylideneimino guanidines

LUBOMIRA M. CABELKOVA-TAGUCHI AND JOHN WARKENTIN

Department of Chemistry, McMaster University, Hamilton, Ont., Canada L8S 4M1

Received February 10, 1978

LUBOMIRA M. CABELKOVA-TAGUCHI and JOHN WARKENTIN. Can. J. Chem. **56**, 2194 (1978).

Treatment of 2-propylideneimino guanidinium acetate with lead tetraacetate, in methylene chloride containing solid sodium carbonate, afforded the previously unknown 3,3-dimethyl-5-imino-Δ^1-1,2,4-triazoline. Similarly, *N,N'*-diphenyl-*N''*-(2-propylideneimino)guanidinium acetate afforded *Z*-4-phenyl-5-phenylimino-Δ^1-1,2,4-triazoline as the major oxidation product and the corresponding *E* isomer as a minor product. Stereochemistry was established spectrophotometrically and also by isomerizing the minor (*E*) isomer to the major (*Z*) isomer.

LUBOMIRA M. CABELKOVA-TAGUCHI et JOHN WARKENTIN. Can. J. Chem. **56**, 2194 (1978).

La réaction de l'acétate de propylidèneimino-2-guanidinium avec le tétraacétate de plomb dans le chlorure de méthylène contenant du carbonate de sodium solide conduit à la diméthyl-3,3 imino-5 Δ^1 triazoline-1,2,4 qui était inconnue. De la même manière, l'acétate du *N,N'*-diphényl *N''*-(propylidèneimino-2) guanidinium conduit à la phényl-4 phénylimino-5 Δ^1 triazoline-1,2,4(*Z*) comme produit d'oxydation majeur alors que l'isomère *E* correspondant est le produit mineur. On a établi la stéréochimie d'une façon spectrophotométrique et aussi par isomérisation de l'isomère (*E*) en isomère majeur (*Z*).

[Traduit par le journal]

Oxidation of ketone semicarbazones (**1***a*), either with lead tetraacetate (LTA) (1) or by air in the presence of neutral alumina (2), leads to cyclization products **2** and **3**, respectively. Analogous oxidation

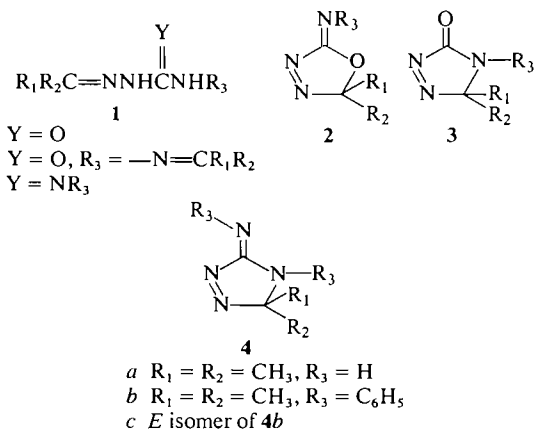

a Y = O
b Y = O, R_3 = —N=CR_1R_2
c Y = NR_3

1 **2** **3**

4

a $R_1 = R_2 = CH_3$, R_3 = H
b $R_1 = R_2 = CH_3$, $R_3 = C_6H_5$
c *E* isomer of **4***b*

of carbohydrazones (**1***b*) yields **2** (R_3 = —N=CR_1R_2) (3) which are of some interest as precursors of diazetidinium hydroxide inner salts (4, 5). As part of a continuing study of the chemistry of cyclic azo systems (5–9), we investigated the oxidation of alkylideneimino guanidines (guanyl hydrazones) (**1***c*) to iminotriazolines **4**, which were unknown. Other Δ^1-1,2,4-triazoline systems were scarce too[1] although there were many examples of 1,2,4-triazoles in the literature. Moreover, we were interested in the stereochemistry of cyclization of **1***c* to **4** because of our earlier finding that **1***a* is oxidized selectively to the *Z* isomer of **2** (10).

Results and Discussion

Oxidation of 2-propylideneimino guanidine[2] (**1***c*, $R_1 = R_2 = CH_3$, R_3 = H) with LTA in CH_2Cl_2 gave 5-imino-3,3-dimethyl-Δ^1-1,2,4-triazoline (**4***a*) in 28% yield. Oxidation with bromine in acetic acid gave the same product in 17% yield. In either case there were numerous by-products which were not identified. The gross structure of **4***a* was established from analytical and spectral data; the strong ir band at 1680 cm^{-1}, characteristic of the exocyclic C=N function (11), was taken as evidence for the imine structure rather than the tautomeric amine structure. Attempts to detect and to separate both *E* and *Z* isomers of **4***a* were unsuccessful. Iminotriazoline **4***a* is readily decomposed by dilute acid or by water to yield acetone. We were unable to find **3**[3] ($R_1 = R_2 = CH_3$, R_3 = H) or the amino tautomer of **4***a*[4] among the products.

Oxidation of *N,N'*-diphenyl-*N''*-(2-propylidene-

[1]The only examples that we were able to find were 1,2,4-triazolinones (**3**) (2).

[2]We assume that it is the free guanidine, not the guanidinium ion, which is oxidized.

[3]Our experience with **3** ($R_1 = R_2 = CH_3$, $R_3 = C_6H_5$), suggests that **3** ($R_1 = R_2 = CH_3$, R_3 = H) would have survived the procedure.

[4]The formation of this tautomer as an intermediate is not precluded, of course, for it may undergo rapid subsequent reactions.

Can. J. Chem. Downloaded from www.nrcresearchpress.com by 210.87.254.40 on 09/05/12
For personal use only.

Can. J. Chem. Downloaded from www.nrcresearchpress.com by 210.87.254.40 on 09/05/12
For personal use only.

imino)guanidine (**1***c*, $R_1 = R_2 = CH_3$, $R_3 = C_6H_5$) with LTA in CH_2Cl_2 afforded **4***b* (40%) and its *E* isomer (1%). These isomers have indistinguishable ^{1}Hmr and ^{13}Cmr spectra and both have ir bands at 1680 (C=N) and 1590 (N=N) cm^{-1}. Assignment of stereochemistry was based on their uv spectra and on the result of an isomerization experiment.

The uv spectra, λ_{max} (95% ethanol) 410 and 395 nm, for the major and minor isomers, respectively, indicate that the latter is less conjugated than the former. Nonbonded interactions between proximate phenyl groups of the *E* isomer, forcing them out of the plane of the triazoline ring, is the only obvious conjugation-inhibiting feature. The minor isomer was therefore assigned the *E* geometry and the major isomer the *Z* geometry (**4***b*, as drawn).

Partial inhibition of resonance because of steric hindrance between phenyl groups of the *E* isomer should mean that its ground state energy is higher than that of the *Z* isomer. Treatment of the minor isomer with aniline–anilinium buffer converted it (50% yield) to the major isomer, under conditions which left a trace of the minor isomer. Thus, the minor isomer is less stable, thermodynamically, than the major isomer and the assignment based on uv data is supported.

Experimental

3,3-Dimethyl-5-imino-Δ^1-1,2,4-triazoline

LTA Method

2-Propylideneimino guanidinium acetate, mp 221–222°C (lit. (12) mp 222°C) was prepared in 78% yield from aminoguanidine bicarbonate (12). To the acetate (1.7 g, 0.01 mol) in 75 ml of ice-cold dichloromethane was added anhydrous sodium carbonate (2.1 g, 0.025 mol) and the mixture was stirred under nitrogen for 3 h. Lead tetraacetate (2.2 g, 5 mmol, washed with petroleum ether) was added and the resulting yellow slurry was stirred for 10 min before a cold solution of sodium bicarbonate (5.0 g in 20 ml of water) was added. The brown slush which formed was stirred for 15 min and then filtered through Celite. The organic layer was separated and washed three times with ice water before it was dried over magnesium sulfate. Evaporation of dichloromethane at ca. 10°C in a rotary evaporator left a crude solid from which **4***a* (0.25 g, 28%) was obtained by sublimation at room temperature and 10^{-2} Torr: mp 70°C (d); ir 3550, 3490 (NH), 1680 (C=N) cm^{-1}; ^{1}Hmr δ: 1.5, s; uv, λ_{max} (95% ethanol): 285 (2.375). *Anal.* calcd. for $C_4H_8N_4$: C 42.86, H 7.16, N 50.00; found: C 42.80, H 7.09, N 50.11.

Br_2 Method

2-Propylideneimino guanidinium acetate (1.7 g, 0.01 mol) in 50 ml of anhydrous methanol was stirred with anhydrous sodium carbonate (2.1 g, 0.025 mol) for 1 h at ice bath temperature. Bromine (0.60 g, 7.5 mmol) was added dropwise and the yellow solution was stirred for 15 min after addition of Br_2 was complete. Filtration and evaporation of the solvent left a solid which was dissolved in water (25 ml). Extraction with ether (25 ml), washing with water, drying, removal of the ether, and sublimation of the solid residue as described above gave **4***a* (0.15 g) in 17% yield.

3,3-Dimethyl-4-phenyl-5-phenylimino-Δ^1-1,2,4-triazolines (4b and the E *Isomer)*

Acetone-4-phenylthiosemicarbazone (**5**) (13) was methylated by a procedure modelled after Kirsten and Smith's methylation of thioureas (14). To an ice-cold solution of **5** (21 g, 0.1 mol) in 200 ml of absolute ethanol was added methyl iodide (15 g, 0.1 mol) and the resulting solution was stirred for 3 h at ice temperature and subsequently for 12 h at room temperature. During this time, a white suspended solid dissolved leaving a clear yellow solution. Most of the ethanol was evaporated with a rotary evaporator and the resulting viscous, yellow oil was chromatographed on silica gel (80–200 mesh) with 1:1 petroleum ether in CCl_4. From the second fraction was obtained, after recrystallization from alcohol, *N*-phenyl-*N'*-(2-propylideneimino)-*S*-methylisothiouronium iodide (**6**) (16.5 g, 79%) as white crystals: mp 43–44°C; ^{1}Hmr δ: 2.05 (s, 3H), 2.10 (s, 3H), 2.40 (s, 3H), 7.25 (s, broad, 5H), 8.20 (s, broad, 1H).

The salt **6** (18 g, 0.05 mol) was heated on a steam bath under an air condenser with aniline (4.65 g, 0.05 mol, freshly distilled) in 50 ml of dry benzene. When the evolution of methanethiol was no longer detectable by odour (about 24 h), the benzene was removed with a rotary evaporator to leave *N,N'*-diphenyl-*N''*-(2-propylideneamino)guanidinium iodide (**7**) as a syrup (87% yield). This product was used directly in the next step.

The procedure for oxidation of **7** with LTA was analogous to that described above. Evaporation of dichloromethane in the work-up procedure left a dark brown oil which was stirred for 12 h with 50 ml of 1:1 petroleum ether in ether. The orange solvent layer was decanted and the extraction was repeated twice more. Evaporation of the combined extracts left a gummy orange residue which was chromatographed on silica gel (80–200 mesh) using petroleum ether (30–60°C) in ether (4:1) as eluent. Crystallization of the main orange fraction afforded 1.2 g (40%) of **4***a* as orange crystals: mp 89.5–90°C (dec.); ^{1}Hmr δ: 1.66 (s, 6H), 7.16 (s, broad, 5H), 7.3 (s, broad, 5H); ^{13}Cmr δ: 156.11, 147.53, 135.79, 129.55, 128.44, 127.40, 126.78, 123.73, 123.37, 102.60, 24.06; ir: 1680 (s, C=N), 1590 (m, N=N) cm^{-1}; uv λ_{max} (95% ethanol): 410 (3.38), 345 (3.67), 235 (4.11) nm; ms: 264 (molecular ion). *Anal.* calcd. for $C_{16}H_{16}N_4$: C 72.73, H 6.10, N 21.19; found: C 72.97, H 6.45, N 20.97.

A yellow to orange lead fraction from the column gave yellow crystals of **4***c* (0.03 g, 1%): mp 93–94°C; ir ^{1}Hmr, and ^{13}Cmr data identical to those listed above; uv λ_{max} (95% ethanol): 395 (3.88), 338 (3.93), 230 (4.69) nm; ms: 264 (molecular ion). *Anal.* calcd. for $C_{16}H_{16}N_4$: N 72.73, H 6.10, N 21.19; found: C 72.75, H 6.38, N 20.86. Mixture mp (**4***a* and **4***b*): 85–87°C.

Isomerization of 4c *to* 4b

To freshly distilled aniline (10 ml) were added 3 drops of concentrated HCl and **4***c* (0.08 g). The solution was kept at ca. 45°C for 4 h, together with a control sample containing only aniline and HCl. The uv spectrum of a portion of the first solution showed a new absorption band at 410 nm which was not present in the uv spectrum of the control sample. Vacuum distillation of the aniline from the test solution and thin layer chromatography of the residue showed that compounds with the R_f values of **4***b* and **4***c* were present. Column chromatography on silica gel afforded **4***b* (0.041 g, 50%): mp 89–90°C; spectra identical to those of **4***a* obtained by oxidation of **7**.

Acknowledgement

The authors wish to thank the National Research

Council of Canada for a grant in support of this work.

1. (*a*) A. M. CAMERON, P. R. WEST, and J. WARKENTIN. J. Org. Chem. **34**, 3230 (1969); (*b*) S. L. LEE, G. B. GUBELT, A. M. CAMERON, and J. WARKENTIN. Chem. Commun. 1074 (1970); (*c*) S. L. LEE, A. M. CAMERON, and J. WARKENTIN. Can. J. Chem. **50**, 2326 (1972).
2. J. K. LANDQUIST. J. Chem. Soc. (C), 63 (1970).
3. P. R. WEST and J. WARKENTIN. J. Org. Chem. **33**, 2089 (1968).
4. K. RAMAKRISHNAN, J. B. FULTON, and J. WARKENTIN. Tetrahedron, **32**, 2685 (1976).
5. P. C. IP, K. RAMAKRISHNAN, and J. WARKENTIN. Can. J. Chem. **52**, 3671 (1974).
6. S. L. LEE, P. KNITTEL, and J. WARKENTIN. Can. J. Chem. **50**, 3248 (1972).
7. (*a*) P. KNITTEL and J. WARKENTIN. Can. J. Chem. **53**, 2275 (1975); (*b*) P. KNITTEL and J. WARKENTIN. Can. J. Chem. **54**, 1341 (1976).
8. D. C. FROST, N. P. C. WESTWOOD, N. H. WERSTIUK, L. M. CABELKOVA-TAGUCHI, and J. WARKENTIN. Can. J. Chem. **55**, 3677 (1977).
9. P. R. WEST and J. WARKENTIN. J. Org. Chem. **34**, 3233 (1969).
10. A. PRAKASH, C. CALVO, A. M. CAMERON, and J. WARKENTIN. J. Cryst. Mol. Struct. **3**, 71 (1973).
11. (*a*) H. NAJER, J. MENIN, and J. F. GIUDICELLI. C. R. Acad. Sci. **258**, 4579 (1974); (*b*) H. NAJER, J. MENIN, and J. F. GIUDICELLI. C. R. Acad. Sci. **259**, 2868 (1964); (*c*) J. F. GUIDICELLI, J. MENIN, and H. NAJER. C. R. Acad. Sci. **260**, 4538 (1965); (*d*) H. NAJER, R. GIUDICELLI, J. MENIN, and J. LOISEAU. C. R. Acad. Sci. **254**, 2175 (1964); (*e*) G. L. SCHMIR and B. A. CUNNINGHAM. J. Am. Chem. Soc. **87**, 5693 (1965); (*f*) H. PETER, M. BRUGGER, J. SCHREIBER, and A. ESCHENMOSER. Helv. Chim. Acta, **46**, 577 (1963); (*g*) M. KURHARA and N. YODA. Tetrahedron Lett. 2597 (1965).
12. F. BAIOCCHI, C. C. CHENG, W. J. HAGGERTY, JR., L. R. LEWIS, T. K. LIAO, W. H. NYBERG, D. E. O'BRIEN, and E. G. PODREBARAC. J. Med. Chem. **6**, 431 (1963).
13. F. J. WILSON and R. BURNS. J. Chem. Soc. **121**, 871 (1922).
14. G. W. KIRSTEN and G. B. L. SMITH. J. Am. Chem. Soc. **58**, 800 (1936).

Can. J. Chem. Downloaded from www.nrcresearchpress.com by 210.87.254.40 on 09/05/12
For personal use only.

Metabolites of bird's nest fungi. Part 10.[1] Carbon-13 nuclear magnetic resonance studies on the cyathins

WILLIAM A. AYER, THOMAS T. NAKASHIMA, AND DALE E. WARD
Department of Chemistry, University of Alberta, Edmonton, Alta., Canada T6G 2G2

Received April 5, 1978

WILLIAM A. AYER, THOMAS T. NAKASHIMA, and DALE E. WARD. Can. J. Chem. **56**, 2197 (1978).

The carbon-13 magnetic resonance spectra of cyathin A_3 and several related compounds have been measured and the chemical shifts have been assigned. The chemical shift data have been used to determine the stereochemistry at C-1 in cyafrin A_4 and to determine the position of the bromine in 1-bromoallocyathin A_3 methyl acetal.

WILLIAM A. AYER, THOMAS T. NAKASHIMA et DALE E. WARD. Can. J. Chem. **56**, 2197 (1978).

On a mesuré les déplacements chimiques et on a fait les attributions pour des spectres de résonance magnétique du ^{13}C de la cyathine A_3 et de plusieurs composés qui lui sont reliés. On a utilisé les données concernant les déplacements chimiques afin de déterminer la stéréochimie en C-1 de la cyafrine A_4 ainsi que la position du brome dans le méthylacétale de la bromo-1 allocyathine A_3.

[Traduit par le journal]

Introduction

The cyathins are a group of diterpenoids first discovered several years ago in these laboratories (2). In 1972 we showed that cyathin A_3, a metabolite of the bird's nest fungus *Cyathus helenae*, possessed structure **1***a* (in tautomeric equilibrium with **1***b*) and thus represented a new structural type among the diterpenoids (3). Since that time the structures of several other metabolites of *C. helenae* possessing the same cyathane carbon skeleton **2** have been elucidated (4–6) and related compounds have been obtained from *C. africanus* (1) and *C. earlei*.[2] As a prelude to the investigation of the biosynthesis of the cyathins and cyafrins, which all contain the cyathane skeleton **2**, and as an aid in assigning structures to newly discovered members of this class of diterpenoids, we have studied the carbon-13 nuclear magnetic resonance (^{13}Cmr) spectra of representative compounds and wish to report here the results of this study. These results are then used to assign the relative stereochemistry at C-1 and C-9 in cyafrin A_4 (1), and to assign the position of a bromo substituent in one of the transformation products of cyathin A_3 (6).

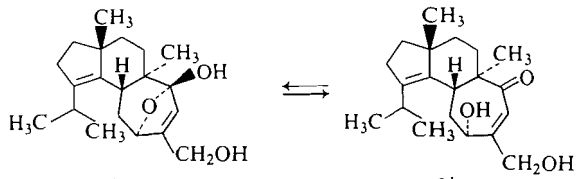

1*a* **1***b*

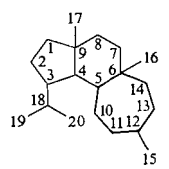

2

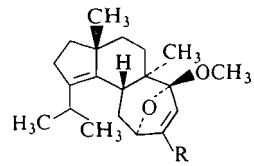

3 R = CH_2OAc
5 R = CH_2OH
6 R = CHO

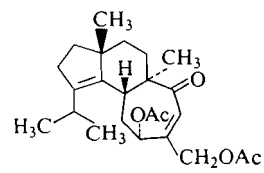

4

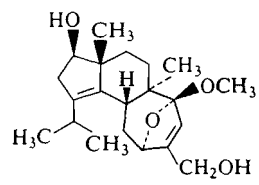

7

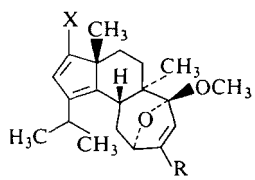

8 X = H, R = CH_2OH
9 X = H, R = CHO
10 X = Br, R = CH_2OAc

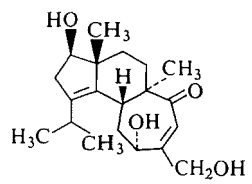

11

Experimental

The ^{13}Cmr spectra were obtained on natural abundance samples at a concentration of approximately 0.2–0.5 *M* in $CDCl_3$ – 5% TMS at a frequency of 22.63 MHz (Bruker HFX-90) and at 15.08 MHz (Bruker WP-60) in 10 mm sample tubes. For those samples (**8**, **9**, and **10**) of limited quantity, a 1.7 mm microinsert was used. Cyclohexane (~2 μl) was used as the

[1]For Part 9 see ref. 1.
[2]W. A. Ayer and S. P. Lee. Unpublished results.

Can. J. Chem. Downloaded from www.nrcresearchpress.com by 210.87.254.40 on 09/05/12
For personal use only.

TABLE 1. Carbon-13 chemical shifts[a] of several cyathins

Carbon	1*a*	1*b*	3	4	5	6	7	8	9	10
1	40.1	37.9	40.0	38.0(0.2)[b]	40.0(0.4)	40.0	81.9	144.3(0.3)	144.3	133.5
2	28.9	28.6	28.7	28.8(0.3)	28.8(0.3)	28.8	35.3	127.9(0.2)	128.0	128.5
3[d]	139.5	140.5	139.3	140.7(0.6)	139.3(0.7)	140.2	136.7	142.5(0.6)	141.5	143.3[c]
4	136.6	136.3	136.5	135.5(0.4)	136.5(0.7)	135.5	136.3	141.0(0.6)	141.4	141.6
5	39.8	38.5	39.6	38.7(1.2)	39.8(0.6)	39.7	40.7	39.3(1.3)	39.2	40.1
6	42.2	54.8	42.2	54.3(1.3)	42.2(1.5)	42.0	41.8	44.6	44.2	45.3
7	30.5	34.6	30.3	34.7(1.9)	30.3(1.2)	30.6	29.9	29.1(0.9)	29.4	28.8
8	37.3	36.1	37.2	36.2(0.6)	37.2(0.6)	37.1	36.3	31.4(0.5)	31.2	31.5
9	48.3	49.4	48.2	49.3(0.4)	48.2(0.6)	48.1	49.0	54.1(0.4)	54.0	55.7
10	26.8	35.6	26.9	31.7(1.2)	27.0(1.7)	26.7	27.4	25.8(1.4)	25.6	25.9
11	78.9	71.9	78.9	72.0(1.9)	78.4(2.5)	76.8	78.6	78.4(1.1)	76.8	78.6
12	147.9	153.9	143.2	143.4(3.2)	148.5(1.5)	148.6	149.3	148.4(1.2)	148.4	143.5
13	123.2	126.0	127.7	127.4(3.3)	123.9(3.7)	147.9	123.2	123.8(2.7)	147.8	127.4
14	110.6	211.0	114.4	208.7	114.4(3.2)	114.7	114.7	114.7	114.7	114.3
15	58.4	64.8	60.0	64.7(2.4)	59.0(13.0)	186.7	58.1	58.6(10.0)	186.5	59.7
16	11.6	15.5	11.9	14.8(1.7)	11.9(1.1)	11.8	11.6	11.8(0.8)	11.8	11.8
17	24.3	24.1	24.0	24.0(0.3)	24.2(0.5)	24.0	16.4	20.6(0.5)	20.7	20.5
18	26.5	27.1	26.4	27.2(0.4)	26.4(0.3)	26.4	26.6	25.8(0.3)	25.7	25.9
19[d]	22.4	22.0	22.3	21.7(0.2)	22.4(0.2)	22.3	21.7	22.8(0.2)	22.7	22.7
20	21.3	21.5	21.4	21.7(0.2)	21.3(0.1)	21.2	20.4	22.7(0.2)	22.7	22.7
—OCH_3			51.1		51.0(1.4)	51.7	50.0	50.9(1.2)	51.7	51.0
—CO_2—			170.4	170.1						170.2
				169.8						
—O_2CCH_3			20.7	20.8(1.5)						20.8
				20.8(1.6)						

[a]All values from TMS. Accurate to ±0.1 ppm.
[b]Values in parentheses indicate $Eu(fod)_3$ induced shifts.
[c]May be interchanged with C-12.
[d]Signals for C-3 and C-4 may be interchanged, as may those for C-19 and C-20.

internal reference in these cases and the data converted to the TMS scale ($\delta_{C_6H_{12}} = 27.7$). All the chemical shifts obtained in this manner appeared to be too high by an average of 0.9 ppm; consequently the reported values in Table 1 have been corrected. For the shift reagent study, $Eu(fod)_3$-d_{10} (Norell Chemical Company, Inc.) was added stepwise, up to 0.0168 g of reagent to 0.020 g of **4**, 0.192 g of reagent to 0.130 g of **5**, and 0.075 g of reagent to 0.050 g of **8**. ^{1}Hmr spectra were obtained in $CDCl_3$ on a Varian HA-100. Cyathin A_3 (**1***a* ⇄ **1***b*) was isolated as previously described (4). The preparation of **3**, **4** and **5** has been described (4) as has the preparation of **6**, **8**, **9**, and **10** (6). Compound **7** was prepared by Dr. T. Yoshida from cyafrin A_4 as previously described (1).

Results and Discussion

The ^{13}C chemical shifts of **1** and **3**–**10** are summarized in Table 1. The ^{13}C spectrum of **1** resulted in 40 distinct carbon resonances due to the slow interchange (on the nmr time scale) between hemiacetal and hydroxy ketone forms, which are represented by structures **1***a* and **1***b*, respectively. The complete analysis of this spectrum proved to be difficult so a number of derivatives of **1**, in which the molecular framework is 'locked' in either the open (hydroxy ketone) or closed (acetal) form, were prepared and their ^{13}Cmr spectra obtained. A comparison of the ^{13}C shieldings of **1** with those obtained for **4** and **5** reveals a one to one correspondence of the ^{13}C resonances (except for carbons α and β to a substituent change, e.g., an —OH replaced by an —OAc group) of both closed forms (**1***a* and **5**) and both open forms (**1***b* and **4**). That is, the ^{13}C spectrum obtained from the tautomeric mixture (**1***a* and **1***b*) can be 'synthesized' by combining the spectra obtained for **4** and **5**. Thus, assignments of the ^{13}C resonances of **4** and **5**, along with the other derivatives, leads to the separate assignments of **1***a* and **1***b*.

Assignments of the ^{13}C resonances were made in the following manner. The carbon shieldings may be grouped into approximately four regions (7): (*i*) those corresponding to carbonyl carbons at ~190 ppm; (*ii*) those to olefinic carbons at ~130 ppm; (*iii*) those to carbons bound to oxygen at ~60 ppm; and (*iv*) those to saturated carbons at ~30 ppm. The carbonyl carbon resonances were readily assigned. In the second group, proton selective (for **3**, **4**, and **5**) and off-resonance decoupling (for **3**–**6**) unambiguously distinguished the resonances of C-13 from those due to C-3, C-4, and C-12. The shielding of C-13 is decreased by ~20 ppm upon introduction of —CHO (**6** and **9**) in place of —CH_2OH (**5**, **7**, and **8**) or —CH_2OAc (**3**, **4**, and **10**) as expected (7). The resonances due to C-12 may be separated from those due to C-3 and C-4 by additivity (β acetoxy in **3** vs. β hydroxy in **5**; **3** → **5** for C-12, ~ +5 ppm). For **8**, **9**, and **10** two additional signals due to C-1 and C-2 appear in this region and the more shielded carbon is assigned to C-2 (8).

Can. J. Chem. Downloaded from www.nrcresearchpress.com by 210.87.254.40 on 09/05/12
For personal use only.

Can. J. Chem. Downloaded from www.nrcresearchpress.com by 210.87.254.40 on 09/05/12
For personal use only.

The third group, C-11, C-14, C-15, and the $-OCH_3$ were assigned unambiguously based on their characteristic shieldings and multiplicity in the off-resonance spectrum.

In the fourth group, the resonances due to C-6 and C-9 were separated on the basis of their multiplicities obtained in the off-resonance spectrum. Little change in shielding is expected for C-9 upon ring closure (**4** → **3**) and on this basis the resonances of C-6 and C-9 were assigned. Selective proton decoupling (for **3**, **4**, and **5**) unambiguously assigned the resonance due to C-18; the remaining methine carbon in this region is due to C-5. The shieldings of these carbons should remain relatively constant for this series of compounds. Selective proton irradiation on **3**, **4**, and **5** allowed the assignment of C-2; again no change in shielding is expected for this carbon in **1** and **3–6**.

Turning to the methyl carbons, C-16 is expected to be the most shielded due to its crowded environment. It also shows the largest shift on ring closure (i.e., **4** → **3**). C-17 is assigned to the least shielded of the methyl resonances because of the higher degree of α and β branching. The acetyl methyls in **3** and **4** were assigned by selective proton decoupling.

The remaining methylene carbons in **1** and **3–6** (C-1, C-7, C-8, and C-10) were assigned in the following manner. Examination of Table 1 shows good agreement of the resonances for **4** and **5** when compared to those obtained for the tautomeric mixture, **1***a* and **1***b*. The only discrepancy in this region occurs at δ 31.7 for **4** when compared to δ 35.6 for **1***b*. The only expected change in shielding should occur at C-10 for which a β-hydroxyl group in **1***b* is replaced by a β-acetyl group in **4** (for C-10; **1***b* → **4**, −5 ppm (7)). Changing from the open form (e.g., **1***b* or **4**) to the closed form (e.g., **1***a* or **5**) causes two of the methylene carbons to become slightly less shielded (~1 ppm) and the other two to become more shielded (~−5 ppm). In **5**, one of the protons of C-10 is in a *syn*-axial orientation with respect to C-16; thus, C-10 is assigned to the most shielded of the methylene carbons. The other methylene carbons which might be affected by internal acetal formation would be C-7 *or* C-8; the close approach of the C-10 proton to those of C-16 could result in a large perturbation on C-8. Alternatively the shielding of C-7 could be influenced, either electronically or sterically, depending upon the functionality at C-14.

To explore this point further a $Eu(fod)_3$ shift study was undertaken to distinguish between C-1, C-7, and C-8 (as well as to confirm some of the other assignments) in **4**, **5**, and **8** and the results are summarized in Table 1. It is well established that lanthanide induced shifts are quantitatively reproduced by the pseudo contact or dipolar shielding term given by (9):

$$\Delta_i = C(1 - 3\cos^2\theta_i)/R_i^3$$

where Δ_i is the induced shift at nucleus i, C is a constant at a given temperature, $(1 - 3\cos^2\theta_i)$ is an orientational factor and R_i is the distance of the shift reagent to nucleus i. The equation is known to break down for carbons α and β to the complexing site (generally a Lewis base) because of the presence of a contact interaction contribution to the shielding (9). Thus, for **4**, **5**, and **8** the shielding of C-7 is expected to be more sensitive to the addition of $Eu(fod)_3$ than C-8 which in turn should be more sensitive than C-1 and the signals were assigned accordingly. The $Eu(fod)_3$ induced shifts for the other carbons in **4**, **5**, and **8** are consistent with the previous assignments.

The stereochemistry of the hydroxyl group at C-1 in cyafrin A_4 (**11**) was originally assigned by application of the pyridine shift (^{1}Hmr) method and by application of Brewster's benzoate rule (1). Examination of the ^{13}Cmr shift data for cyafrin A_4 methyl acetal (**7**) in Table 1 dramatically confirms this assignment. Thus, the C-9 methyl signal is shifted upfield by ca. 8 ppm in **7** relative to **5**, demonstrating the γ-*gauche* relationship between the C-1 hydroxyl and C-17.

In an earlier paper we described the conversion of cyathin A_3 (**1**) into allocyathin B_3 (hydroxy ketone form of acetal **8**) via the monobromo compound **10**. The method of preparation of **10** did not allow us to determine whether the bromine is located at C-1 or C-2. Examination of the ^{13}Cmr spectrum of **10** (Table 1) shows that C-1 is strongly shielded in **10** (relative to **8** and **9**) which is consistent with the location of the bromine at C-1 (10).

Acknowledgements

We wish to thank the National Research Council of Canada for financial support and Dr. T. Yoshida for the preparation of compound **7**.

1. W. A. Ayer, T. Yoshida, and D. M. J. Van Schie. Can. J. Chem. This issue.
2. A. D. Allbutt, W. A. Ayer, H. J. Bordie, B. N. Johri, and H. Taube. Can. J. Microbiol. **17**, 1401 (1971).
3. W. A. Ayer and H. Taube. Tetrahedron Lett. 1917 (1972).
4. W. A. Ayer and H. Taube. Can. J. Chem. **51**, 3842 (1973).
5. W. A. Ayer and L. L. Carstens. Can. J. Chem. **51**, 3157 (1973).
6. W. A. Ayer, L. M. Browne, J. R. Mercer, D. R. Taylor, and D. E. Ward. Can. J. Chem. **56**, 717 (1978).
7. J. B. Stothers. Carbon-13 nmr spectroscopy. Academic Press, New York, NY. 1972.
8. R. A. Friedel and H. L. Retcofsky. J. Am. Chem. Soc. **85**, 1300 (1963).
9. J. W. ApSimon, H. Beierbeck, and J. K. Saunders. Can. J. Chem. **51**, 3874 (1973).
10. G. E. Maciel. J. Phys. Chem. **69**, 1947 (1965).

Stereochemical analysis of aromatic oximes. ^{13}C–^{15}N nuclear spin coupling and ^{13}C shieldings as conformational probes

GERALD W. BUCHANAN AND BRIAN A. DAWSON

Department of Chemistry, Carleton University, Ottawa, Ont., Canada K1S 5B6

Received January 2, 1978

GERALD W. BUCHANAN and BRIAN A. DAWSON. Can. J. Chem. **56**, 2200 (1978).

^{13}C nmr chemical shifts and ^{13}C–^{15}N spin couplings over one, two, and three bonds are reported for six aromatic oximes including two benz annelated compounds. Preferred geometries have been calculated via the GEMO program. Fermi contact contributions to carbon–nitrogen coupling have been evaluated and, in general, agreement between experimental and theoretical values is poor. Vicinal ^{13}C–^{15}N couplings are shown to depend on both dihedral angle and oxime valence angle. Oxime carbon chemical shifts do not provide a measure of deviation from planarity between the oxime group and the aromatic ring.

The sign of $^1J_{CN}$ in *E*-benzaldoxime has been determined to be negative.

GERALD W. BUCHANAN et BRIAN A. DAWSON. Can. J. Chem. **56**, 2200 (1978).

On rapporte les déplacements chimiques en rmn du ^{13}C et les couplages de spin ^{13}C–^{15}N à travers une, deux et trois liaisons dans six oximes aromatiques incluant deux composés benz-orthocondensés. On a calculé les géométries préférentielles à l'aide du programme GEMO. On a évalué les contributions des contacts de Fermi aux couplages carbone–azote; d'une façon générale, l'accord entre les valeurs expérimentales et théoriques est mauvais. On montre que les couplages ^{13}C–^{15}N vicinaux dépendent à la fois de l'angle dièdre et de l'angle de valence de l'oxime. Les déplacements chimiques du carbone de l'oxime ne fournissent pas une mesure de la déviation de la planarité entre le groupe oxime et le cycle aromatique.

On a déterminé que le signe $^1J_{CN}$ dans le (*E*)-benzaldoxime est négatif.

[Traduit par le journal]

Introduction

A number of recent studies have focussed on the theory and calculations of ^{13}C–^{15}N nuclear spin couplings in simple organic molecules (1, 2). Over the past three years work in this laboratory (3, 4) has dealt with the application of ^{13}C–^{15}N coupling as a tool for spectral assignment in aromatic oximes (3) and with the use of geminal ^{13}C–^{15}N *J* values as a configurational probe (4). We now wish to report data for a series of six aromatic oximes in which detailed experimental and theoretical work has been carried out, with a view to establishing the potential of vicinal ^{13}C–^{15}N coupling as a conformational probe and the possibility of using oxime carbon shifts as indicators of steric inhibition of resonance.

To date, no ^{13}C–^{15}N coupling calculations have been published for oximes other than those derived from formaldehyde (5) and acetaldehyde (1). In the present work, the conformational energy minimization of the six aromatic oximes has been accomplished using the GEMO (6) program. Subsequently the optimized geometries have been used to calculate the Fermi contact contribution to ^{13}C–^{15}N couplings over one, two, and three bonds. Results are compared with experimental data. Where possible, the relative signs of $J_{^{13}C^{15}N}$ have been determined by the off resonance ^1H decoupling procedure (4).

Results and Discussion

Coupling Constants

Direct Couplings

Observed and calculated values are presented in Table 1.

Until now, no sign determination of $^1J_{CN}$ has been carried out for oximes, although the sign has been suggested to be negative based on results for related materials (2, 7). For formaldoxime, $^2J_{NH}$ is +2.68 for H_A whereas $^2J_{NH}$ for H_B is −13.88 Hz (8). In the case of *E*-benzaldoxime, $^2J_{NH}$ is nearly identical to $^2J_{NH_A}$ above, namely 2.80 Hz.

Formaldoxime *E*-Benzaldoxime

Assuming that the sign of this coupling is also positive, one can determine the relative sign of $^1J_{CN}$ using off-resonance decoupling (4). The technique is applicable for determining the relative sign of $^nJ_{CX}$ and the corresponding $^{n+1}J_{HX}$ coupling, where X is a spin $\frac{1}{2}$ nucleus, i.e., ^{15}N. Use is made of the *difference* observed for residual splittings, $J_{residual(CH)} = 2\pi\Delta\nu J_{CH}/\gamma H_2$ in the ^{13}C spectrum of the $J_{^{13}C-X}$ doublet. For *E*-benzaldoxime, off-resonance ^1H decoupling on the high-field side ($\Delta\nu$ = 65 Hz, γH_2 = 1600), caused a reduction in the residual splitting

Can. J. Chem. Downloaded from www.nrcresearchpress.com by 210.87.254.40 on 09/05/12
For personal use only.

TABLE 1. Observed* and calculated† coupling constants between ^{13}C and ^{15}N (±0.1 Hz)

Compound	^1J	^2J	^3J
1	3.9 (−14.8)	N—C_1—C_2 = 9.1 (+1.4) N—C_1—C_8 = +1.0 (+7.4)	N—C_1—C_2—$C_{3,7}$ = 2.9 (−8.4)
2	3.1 (−15.4)	N—C_1—C_2 = 1.8 (+9.8) N—C_1—C_8 = −11.6 (−6.1)	N—C_1—C_2—$C_{3,7}$ peak overlap, not observable (−8.1)
3	3.8 (−8.5)	N—C_1—C_2 = 8.8 (−0.3) N—C_1—C_8 < 0.6 (+5.4)	N—C_1—C_2—C_3 = 1.1 (−5.9) N—C_1—C_2—C_7 = 1.2 (−8.5)
4	3.3 (−8.7)	N—C_1—C_2 = 8.0 (+7.4) N—C_1—C_8 < 0.6 (+6.5)	N—C_1—C_2—$C_{3,7}$ = 1.2 (−7.3)
5	3.8 (−11.6)	N—C_1—C_2 = 9.2 (+1.8) N—C_1—C_9 = +0.9 (+7.2)	N—C_1—C_2—C_3 = 0.7 (−6.8) N—C_1—C_9—C_8 nr‡ (+1.2) N—C_1—C_2—C_7 = 2.4 (−6.9)
6	4.2 (−16.0)	N—C_1—C_2 = 8.6 (+2.5) N—C_1—C_{10} = +1.4 (+6.7)	N—C_1—C_2—C_3 = 3.8 (−8.5) N—C_1—C_{10}—C_9 nr (−2.3) N—C_1—C_2—C_7 2.9 (−8.5)

*Absolute values unless otherwise specified.
†Calculated values are in parentheses.
‡Nonresolvable (i.e. <0.6 Hz).

for the low-field lines, indicating $^1J_{CN}$ and $^2J_{H-C-N}$ have opposite signs.

As a check, off-resonance decoupling on the low-field side caused a reduction in the residual J_{CH} on the high-field side. Therefore $^1J_{CN}$ and $^2J_{HCN}$ do indeed have opposite signs and $^1J_{CN}$ is negative.

There is poor agreement between calculated and observed magnitudes of $^1J_{CN}$, although the predicted and observed signs are consistent. It has been calculated (1) that the N lone pair makes a *positive* contribution to $^1J_{CN}$. Assuming that $^1J_{CN}$ is negative for acetophenone oximes as well as the benzaldoxime (9), it is interesting to compare results for **1** and **2**.

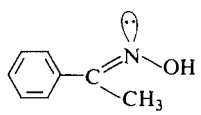

1
$^1J_{CN} = -3.8$ Hz

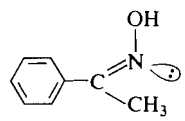

2
$^1J_{CN} = -3.1$ Hz

The phenyl group has a larger effective size than the CH_3. This is reflected in the observation that **1** is considerably more stable than **2**. Accordingly in **1**, the bulky phenyl moiety, being *cis* to the lone pair, will sterically perturb the lone pair relative to **2**. Therefore, there will be less lone pair (positive) contribution to $^1J_{CN}$ in **1** and the enhanced negative value is found.

Geminal Couplings

Earlier experimental results from this laboratory (4) demonstrated that $^2J_{^{13}C-C-^{15}N}$ is large and negative in sign when the N lone pair is *cis* to the CH_3 group (i.e., in **2**) whereas the geminal coupling is small and positive in sign when the N lone pair is *trans* to the CH_3 group (i.e., in **1**). It is interesting to note that calculations for **1** and **2**, based on the Fermi contact mechanism, are consistent with the experimental findings with respect to sign, although the magnitudes are not predicted by the theory. For compounds **3** and **4**, the observed geminal couplings between ^{15}N and the oxime CH_3 are not resolvable (i.e., <0.6 Hz). In **5** and **6**, where larger values are found, we have now determined the signs to be positive using the off-resonance ^1H decoupling procedure (4). Thus for all cases to date, geminal ^{15}N-C–CH_3 J values are positive in situations where the N lone pair is *trans* to the CH_3.

As our procedure for relative sign determination depends on the coupling carbon having a directly

Can. J. Chem. Downloaded from www.nrcresearchpress.com by 210.87.254.40 on 09/05/12
For personal use only.

TABLE 2. Angular dependence of vicinal $^{13}C^{15}N$ coupling

Compound	Path*	Dihedral angle (θ) (deg)	Valence angle (ϕ) (deg)	^3J (Hz) ± 0.1
1	N,1,2,3	0.7	119.5	2.9
	N,1,2,7	179.4		
3	N,1,2,3	0.6	121.9	1.1
	N,1,2,7	179.5		1.2
4	N,1,2,3	35.5	119.5	1.2
	N,1,2,7	144.1		
5	N,1,2,3	0.3	123.2	0.7
	N,1,2,7	179.7		2.4
	N,1,9,8	179.7		nr†
6	N,1,2,3	0.4	119.5	3.8
	N,1,2,7	180.0		2.9
	N,1,10,9	150.8		nr*

*Numbered as in Fig. 1.
†Nonresolvable J < 0.6 Hz.

bonded proton, no sign determinations have been done for the geminal interactions to the C-2 (aromatic carbon) of **1**–**6**. Experimentally these values are rather large (range 8.0 → 9.2 Hz) for **1**, **3**, **4**, **5**, and **6**, again indicating that the presence of the *cis* lone pair on N enhances the absolute value of ^2J (11).

Vicinal Couplings

Three bond ^{13}C–^{15}N J values were observed in all materials except **2** where peak overlap precluded the measurements. Data for the remaining compounds are presented in Table 2 along with the dihedral angles (θ) and the 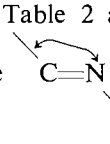 valence angles (ϕ)

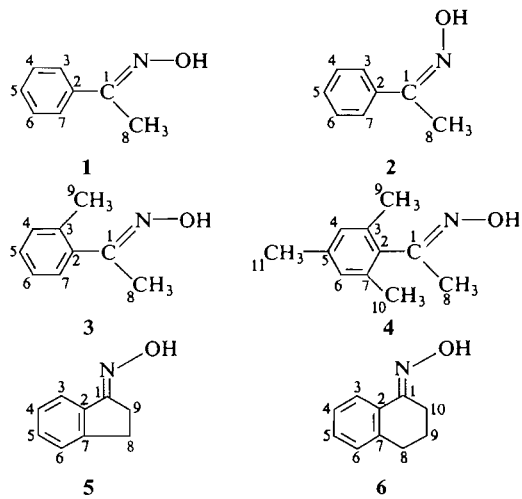

FIG. 1. Structures and numbering scheme for aromatic oximes **1**–**6**.

obtained from GEMO. For **1**, which is calculated to be nearly planar, ^3J is 2.9 Hz. This represents an average value over the two planar conformations, since rotation about the aryl–oxime bond is fast even at −100°C. We have not yet been able to freeze out this process.

In the case of the *ortho*-methyl derivative **3**, the dihedral angles are very similar to **1** but the vicinal couplings are reduced to ca. 1 Hz. A rationale for this reduction comes from examination of the valence angles ϕ. In **3**, the molecule distorts, to reduce steric interactions between the oxime and the *o*-CH_3, by expansion of ϕ to 121.9°, compared to 119.5° in **1**. This expansion renders the N lone pair of electrons more distant from the vicinal carbon in **3** and thus may lead to reduced coupling. Certainly for *geminal* interactions, the coupling has maximum absolute value when the N lone pair is spatially proximate to the coupled carbon (3, 4).

For **4** the coupling of 1.2 Hz is identical to that found for the corresponding 2,4,6-trimethylbenzaldoxime (10). The GEMO calculations suggest that the steric congestion between the oxime function and the two *o*-CH_3 groups is reduced by a deviation from planarity of ca. 36° between the plane of the aromatic ring and the oxime group. It is interesting to note that the ϕ value of **4** is identical to **1**, since **4** escapes steric compression by altering θ. Therefore, for a common ϕ, it appears that there *is* a dihedral angle dependence of ^3J, with maximal coupling found in planar or near planar situations.

The dihedral dependence of $^3J_{CN}$ in **5** and **6** is interesting, albeit unexplained, at present. In **5**, coupling to the *trans*-coplanar carbon (C-7) is considerably larger than that to the *cis*-coplanar carbon (C-3). By

Can. J. Chem. Downloaded from www.nrcresearchpress.com by 210.87.254.40 on 09/05/12
For personal use only.

Can. J. Chem. Downloaded from www.nrcresearchpress.com by 210.87.254.40 on 09/05/12
For personal use only.

contrast in **6**, the coupling to the *cis*-coplanar carbon (C-3) is 3.8 Hz, whereas that to the *trans*-coplanar carbon (C-7) is only 2.9 Hz.

Chemical Shifts

Results for **1** and **2** have been discussed in detail earlier (4). In the case of the *ortho*-alkylated systems **3** and **4**, we wished to explore the possible existence of steric inhibition to resonance, which has been amply demonstrated for the related ketones (12–14). Deviations in planarity between the carbonyl group and the aromatic ring in *ortho*-alkylated acetophenones are known to induce substantial deshielding of the carbonyl group due to less efficient resonance overlap between the phenyl and carbonyl moieties.

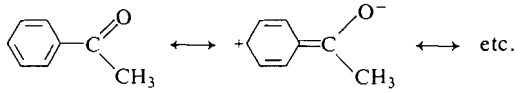

In the present molecules the oxime carbon shift could, in principle, be used to monitor such effects. For the planar system **1**, the C=N resonates at $\delta = 155.9$ ppm, whereas in **3** and **4** there is a minor deshielding (ca. 2 ppm) at this site (Table 3). The effects are much less pronounced than in the corresponding ketones, where the C=O of mesityl methyl ketone is ca. 10 ppm deshielded relative to that of acetophenone (12, 13). Furthermore, examination of the GEMO results indicates that the dihedral angles θ are essentially identical in **3** to those of **1**, only the oxime valence angle ϕ expands in **3** as was noted earlier. In **4** the deviation from planarity is ca. 36° between the oxime function and the aromatic ring but the oxime shift is nearly identical to that of **3**. Clearly the oxime shifts do not provide a mechanism for estimation of torsional angles between the aromatic ring and the substituent group. A factor which may complicate the present situation is a second type of resonance interaction, shown below, which is available to oximes but not to ketones.

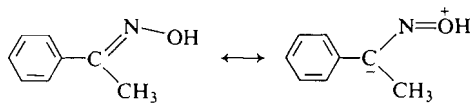

In view of these results, it is useful to compare the oxime shifts of the benz-fused compounds **5** and **6** with those for cyclopentanone and cyclohexanone oxime, respectively (15). For **5**, there is a 2.7 ppm shielding of the oxime resonance compared to the alicyclic case, whereas in **6** the upfield shift due to benz annelation is 5.0 ppm. Therefore there is apparently some conjugative electron release by the aromatic ring into the oxime functions of **5** and **6**. The calculated torsional angles between the oxime group and the aromatic ring of **5** and **6** are nearly identical. This suggests that more subtle bond angle influences may be present to account for the differential shielding in **5** and **6** as a function of ring size.

For *E*-cyclohexenone oxime (below) the oxime carbon is deshielded by only 1 ppm relative to **6**.[1] Thus the electron release from a single conjugated double bond into the oxime moiety appears to be similar to that from an aromatic ring.

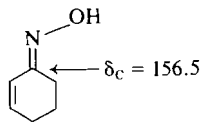

Experimental

Spectra

^{13}C spectra were recorded at 25.16 MHz using a Varian XL-100-12 nmr spectrometer equipped with a Nicolet TT-100 Fourier transform data system. Samples were examined as 0.1 *M* solutions in $CDCl_3$ solution in 5 mm sample tubes. For coupling constant determinations spectral widths were commonly 1000 Hz and a minimum of 8K data points were employed. For chemical shift measurements, spectra widths of 5000 Hz were used. Relative signs of $J_{^{13}C^{15}N}$ were determined as described earlier (4).

Calculations

The initially specified molecular geometries for the oximes, used as input for the GEMO program (6) were derived from standard parameters (16). Subsequently GEMO carries out a systematic variation of bond lengths, bond angles and torsional angles to minimize the conformational energy of the molecule. Parameters were iterated until a convergence criterion of 0.01 kcal/mol was met. The barrier to rotation about the aryl–oxime bond was taken as 9.0 kcal/mol by analogy with results from similar molecules (17). Constants for the van der Waals interactions were taken from COMOL, a program written for conformational energy calculations, by Michel H. J. Koch, Laboratoire de Chimie Physique et de Cristallographie, Universite de Louvain-Belgium. In the present treatment, methyl hydrogens on a given carbon atom are considered equivalent.

The ^{13}C–^{15}N couplings were calculated using the finite perturbation calculation procedure outlined by Pople *et al.* (18), with a program obtained from Quantum Chemistry Program Exchange #224, Bloomington, Indiana.

Materials

The synthesis and properties of **1** and **2** were reported earlier (3, 4). Below are described synthetic procedures for the other materials.

E-o-*Methylacetophenone Oxime* (*3*)

o-Methylacetophenone (0.150 g), $^{15}NH_2OH{\cdot}HCl$ (0.100 g), and KOH (0.20 g) were added to 3 ml EtOH (95%) and the solution was refluxed for 4 h. The solution was then poured into 15 ml cold water, neutralized with 1 *N* HCl, and placed in a freezer for 1 h. The solid was collected and recrystallized from EtOH–H_2O; mp 61–62°C (lit. (19) mp 64.5–65.5°C).

E-*Mesityl Methyl Ketoxime* (*4*)

This compound was prepared according to the procedure of Hauser and Hoffenberg (20) using 95% ^{15}N-enriched hydroxylamine hydrochloride obtained from Merck, Sharpe, and

[1]R. L. Lichter. Private communication.

TABLE 3. ^{13}C chemical shifts for aromatic oximes (δ_C from TMS ± 0.1)*

Compound	C-1	C-2	C-3	C-4	C-5	C-6	C-7	C-8	C-9	C-10	C-11
1	155.9	136.5	126.0	128.5	129.1	128.5	126.0	12.4			
2	154.3	134.0	128.0	128.0	129.0	128.0	128.0	21.4			
3	157.8	137.4	135.7	(128.6)	(130.3)	125.8	128.3	15.9	20.0		
4	157.5	134.1	135.6	128.3	137.7	128.3	135.6	15.9	19.4	19.4	
5†	164.4	135.1	122.0	(125.6)	(127.1)	130.8	148.8	28.5	26.3		
6	155.4	130.2	124.2	126.5	(128.7)	(129.3)	139.9	29.8	21.3	24.0	

*Solutions 0.1 *M* in $CDCl_3$. Values in parentheses denote possible interchange of assignments.
†Solutions 0.1 *M* in DMSO-d_6.

Dohme (Canada); mp 105–107°C (lit. (20) mp 98–99°C; lit. (21) mp 104–105°C).

E-*1-Indanone Oxime* (*5*) *and* E-α-*Tetralone Oxime* (*6*)

Ketone (0.001 mol), $NH_2OH{\cdot}HCl$ (0.100 g), and anhydrous sodium acetate (0.40 g) were added to 1 ml of 95% EtOH and 0.3 ml H_2O and the solution refluxed on a steambath for 1 h and then poured into 5 ml H_2O and placed in a freezer for 1½ h. The solid was collected and recrystallized from an appropriate solvent: **5**, recrystallized from $CHCl_3$, mp 153–154°C (lit. (22) mp 145–146°C) and **6**, recrystallized from *n*-hexane, mp 101–102°C (lit. (23) mp 102–103°C).

Acknowledgements

We wish to thank the National Research Council of Canada and the Carleton University President's Computer Fund for financial assistance. Also, we thank Dr. J-P. Schmidt for his aid with the GEMO program.

1. J. M. SCHULMAN and T. VENANZI. J. Am. Chem.Soc. **98**, 4701 (1976).
2. R. WASYLISHEN. Can. J.Chem. **54**, 833 (1976).
3. G. W. BUCHANAN and B. A. DAWSON. Can. J. Chem. **54**, 790 (1976).
4. G. W. BUCHANAN and B. A. DAWSON. Can. J. Chem. **55**, 1437 (1977).
5. R. L. LICHTER, D. E. DORMAN, and R. WASYLISHEN. J. Am. Chem. Soc. **96**, 930 (1974).
6. N. C. COHEN. Tetrahedron, **27**, 789 (1971).
7. N. J. KOOLE, D. KNOL, and M. J. A. DEBIE. J. Magn. Reson. **21**, 499 (1976).
8. D. CREPAUX, J. M. LEHN, and R. R. DEAN. Mol. Phys. **16**, 225 (1969).
9. G. BINSCH, J. B. LAMBERT, B. W. ROBERTS, and J. D. ROBERTS. J. Am.Chem. Soc. **86**, 5564 (1964).
10. M. CHRISTL, J. P. WARREN, B. L. HAWKINS, and J. D. ROBERTS. J. Am. Chem.Soc. **95**, 4392 (1973).
11. S. BERGER and J. D. ROBERTS. J. Am. Chem. Soc. **96**, 6757 (1974).
12. K. S. DHAMI and J. B. STOTHERS. Can. J. Chem. **43**, 479 (1965).
13. K. S. DHAMI and J. B. STOTHERS. Tetrahedron Lett. 631 (1964).
14. G. W. BUCHANAN, G. MONTAUDO, and P. FINOCCHIARO. Can. J. Chem. **51**, 1053 (1973).
15. G. E. HAWKES, K. HERWIG, and J. D. ROBERTS. J. Org. Chem. **39**, 1017 (1974).
16. J. A. POPLE and D. L. BEVERIDGE. Approximate molecular orbital theory. McGraw-Hill Book Co., New York, NY. 1970. pp. 111–112.
17. H. KESSLER and K. O. KALINOWSKI. *In* Topics in stereochemistry. Vol. 7. *Edited by* N. L. Allinger and E. L. Eliel. Interscience, New York, NY. 1972.
18. J. A. POPLE, J. W. MCIVER, JR., and N. S. OSTLUND. J. Chem. Phys. **49**, 2960 (1968); **49**, 2965 (1968).
19. D. E. PEARSON and W. E. COLE. J. Org. Chem. **20**, 488 (1955).
20. C. R. HAUSER and D. S. HOFFENBERG. J. Am. Chem. Soc. **77**, 4885 (1955).
21. B. J. GREGORY, R. B. MOODIE, and K. SCHOFIELD. J. Chem. Soc. B, 338 (1970).
22. K. HAFNER and K. GOLIASCH. Chem. Ber. **94**, 2909 (1961).
23. G. BADDELEY and R. WILLIAMSON. J. Chem. Soc. 4647 (1956).

Can. J. Chem. Downloaded from www.nrcresearchpress.com by 210.87.254.40 on 09/05/12
For personal use only.

Studies with model membranes. Part XXIV. Evaluation of thermodynamic activation parameters, effective fixed charge density, and test of the theory of bi-ionic potential based on the thermodynamics of irreversible processes

FASIH A. SIDDIQI, M. NASIM BEG, M. IBADUR RAHMAN KHAN, ABDUL HAQ, S. K. SAKSENA, AND BADRUL ISLAM

Membrane Research Laboratory, Department of Chemistry, Aligarh Muslim University, Aligarh, 202001 India

Received November 3, 1976[1]

FASIH A. SIDDIQI, M. NASIM BEG, M. IBADUR RAHMAN KHAN, ABDUL HAQ, S. K. SAKSENA, and BADRUL ISLAM. Can. J. Chem. **56**, 2205 (1978).

The various ionic processes in the membrane system, notably (*a*) ionic transport, (*b*) membrane potential, (*c*) electrical conductivity, (*d*) ionic distribution equilibria, and (*e*) spatial distribution of ions and the potential within the membrane have been thoroughly studied with parchment-supported membranes. By applying the theory of absolute reaction rate, various thermodynamic parameters, namely, enthalpy of activation ΔH^*, energy of activation ΔF^*, and entropy of activation ΔS^* were evaluated. The ΔS^* values were found to be negative, indicating that diffusion takes place with partial immobilization in the membrane phase. A formal relation between $\Delta H_{\text{hydration}}$, $\Delta F_{\text{hydration}}$, and $\Delta S_{\text{hydration}}$ of cations with corresponding values of ΔH^*, ΔF^*, and ΔS^* for diffusion was also worked out. Thermodynamically fixed charge density was evaluated using methods based on thermodynamics of irreversible processes. Potentiometric selectivity and recent theory of bi-ionic potential based on nonequilibrium thermodynamics was tested and found applicable to parchment membranes.

FASIH A. SIDDIQI, M. NASIM BEG, M. IBADUR RAHMAN KHAN, ABDUL HAQ, S. K. SAKSENA et BADRUL ISLAM. Can. J. Chem. **56**, 2205 (1978).

On a étudié d'une façon extensive, à l'aide de membranes supportées par des parchemins, les divers processus ioniques des systèmes de membranes, à savoir: (*a*) le transport ionique, (*b*) le potentiel de la membrane, (*c*) la conductivité électrique, (*d*) les équilibres de distributions ioniques, (*e*) la distribution spatiale. Une application de la théorie des vitesses absolues a permis d'évaluer divers paramètres thermodynamiques, à savoir l'enthalpie d'activation ΔH^*, l'énergie libre d'activation ΔF^* et l'entropie d'activation ΔS^*. On a trouvé que les valeurs de ΔS^* sont négatives; ceci indique que la diffusion a lieu par une immobilisation partielle dans la phase de la membrane. On a aussi pu établir une relation formelle entre les $\Delta H_{\text{hydratation}}$, $\Delta F_{\text{hydratation}}$ et $\Delta S_{\text{hydratation}}$ des cations avec les valeurs correspondantes de ΔH^*, ΔF^* et ΔS^* pour la diffusion. On a évalué la densité de charge fixe thermodynamique en faisant appel à des méthodes basées sur la thermodynamique de processus irréversibles. On a évalué la sélectivité potentiométrique et la théorie récente du potentiel bi-ionique, basée sur la thermodynamique des phénomènes irreversibles, et on a trouvé qu'on peut l'appliquer aux membranes de parchemin.

[Traduit par le journal]

Introduction

We have been engaged in the studies of (*a*) parchment-supported, (*b*) polymeric-composite, and (*c*) polystyrene-based ion exchange membranes (1–8) which can serve as models for biological systems. Membrane theories of Kedem and Katchalsky (9), Spiegler (10), Scathchard (11), Scattergood and Lightfoot (12), etc., have been used to evaluate various membrane parameters.

This article deals with the following aspects of parchment-supported membranes: (*A*) application of Nernst–Planck flux equations and Fick's diffusion law (13) and evaluation of various thermodynamic activation parameters, (*B*) evaluation of thermodynamically effective fixed charge density by the most recent methods of Nagasawa and co-workers (14, 15) and others (16–21) based on thermodynamics of irreversible processes, and (*C*) evaluation of potentiometric selectivity coefficient and test of the most recent theories of membrane potential and bi-ionic potential developed by Toyoshima and Nozaki (22) based on non-equilibrium thermodynamics.

Experimental

Preparation of Parchment-supported Membranes

The membranes of silver tungstate and chromic ferricyanide were prepared by the method of interaction suggested by Weiser (23) and Siddiqi *et al.* (2). First parchment was soaked in distilled water for about 2 h and then tied carefully to the flat mouth of a beaker in which 0.2 *M* solution of $AgNO_3$ was taken. This was suspended for about 72 h in a 0.2 *M* sodium tungstate solution. The temperature was kept at 25°C. The two solutions were interchanged and kept for another 72 h.

[1]Revision received April 20, 1978.

Can. J. Chem. Downloaded from www.nrcresearchpress.com by 210.87.254.105 on 09/05/12
For personal use only.

Can. J. Chem. Downloaded from www.nrcresearchpress.com by 210.87.254.105 on 09/05/12
For personal use only.

In this way fine deposition of silver tungstate was obtained on the surface of parchment paper. Similar procedure was adopted for chromic ferricyanide membrane by taking 0.2 *M* solutions of chromic chloride and potassium ferricyanide. The temperature maintained in this case was kept at 72°C and the time for deposition was 3 h. Both the membranes thus prepared were well washed with deionized water for the removal of free electrolytes. The vegetable parchment paper was supplied by M/S Baird and Tatlock (London) Ltd.

Part A. Studies of Diffusion of Electrolytes Through Parchment-supported Silver Tungstate Membrane

The apparatus and procedures used to measure membrane potential $\Delta\phi_m$, membrane resistance R_m, and electrolyte concentrations are those described by Siddiqi *et al.* (2–4). The half cells contained 125 ml of the electrolyte solutions while the capacity of each of the cells holding the membrane was about 130 ml. Initially the concentrations C_1 and C_2 across parchment-supported silver tungstate membrane were 0.001 *M* and 0.1 *M* of the same electrolyte, respectively. Each of the half cell was fitted with two platinized platinum electrodes firmly fixed to follow concentration changes and two anion reversible Ag–AgCl electrodes: one a disc type to pass a small d.c. current and the other a J-shaped wire electrode placed very near the membrane surface to measure membrane potential (by Pye Precision Potentiometer No. 7568) and changes in membrane potential following current flow. The solutions in both the half cells were kept well stirred by magnetic stirrers. The whole cell assembly was immersed in a water thermostat maintained at 10, 15, 20, 25, and 30°C (±0.1°C).

The changes in conductance on the dilute solution side was followed by means of the conductivity bridge (Cambridge Instrument Co., England, No. L-350140). The exact concentration of the solution at any given time was estimated from a calibration curve. The membrane resistance was determined by applying an external emf to the disc-type Ag–AgCl electrodes and measuring the change in potential across the membrane using J-type wire electrodes. The current passed through the membrane system was determined by measuring *IR* drop across a precision Kilo-Ohm resistor. The current was kept very low in order to minimize the ion transfer during the period (2–3 min) required for each resistance measurement. The direction of current flow was reversed in each successive measurement. The surface of the membrane was controlled during membrane resistance measurements but on account of the changes in salt concentration due to diffusion on the dilute solution side, the control was not 100% perfect. However, reproducible results were obtained during resistance measurements. The d.c. current densities at the electrode and membrane surfaces were also determined in mA cm^{-2}. The resistance measurements gave a value of the entire system, namely,

Electrolyte film – Membrane – Electrolyte film

In order to measure R_m directly the wire electrodes should be placed strictly on the membrane surfaces. When this was done, membrane resistance values were not 100% reproducible. The value of membrane resistance determined in this way includes additional film (very thin) resistance which is outside of the membrane itself. Although the membrane potential could be measured to a better accuracy than ±1%, the estimation of membrane resistance was accurate to ±4%.

Part B. Membrane Potential Measurements

Separate measurements of membrane potentials were carried out by setting another electrochemical cell of the following type

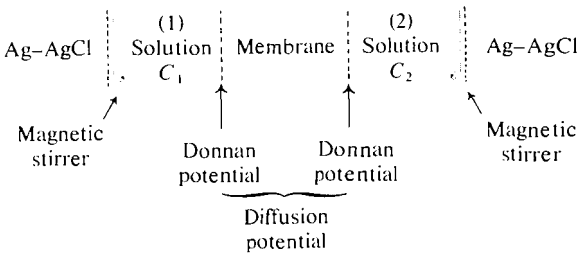

with fixed concentration ratio $C_1/C_2 = \sigma = 10$ throughou the experiment (concentration varied from 1.0 *M* to 1.0 × 10^{-3} *M*). The temperature was kept constant at 25 ± 0.1° and the solutions were vigorously stirred. The membran potentials were measured for parchment-supported silve tungstate and chromic ferricyanide membranes.

Part C. Bi-ionic Potential Measurements

The measurements were recorded by constructing anothe new electrochemical cell of the following type

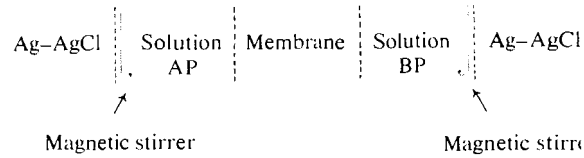

In this cell concentrations of both AP and BP types of elec trolyte solutions (KCl–NaCl, KCl–LiCl, and KCl–NH_4C were kept the same on both sides of the membrane (parch ment-supported silver tungstate membrane only). The bi-ioni potentials were measured at 25°C (±0.1°C) across the parch ment-supported silver tungstate membrane using KCl–NaC KCl–LiCl, and KCl–NH_4Cl electrolyte sets in each successiv measurement. The solutions were vigorously stirred by mear of the magnetic stirrers on both sides of the membrane. Th measurements were recorded when three changes in the te solutions did not lead to potential variation ±0.2 mV. A least two membranes were utilized in each experiment. Th membrane potential measurements with silver tungstate men brane were further carried out to obtain two membrane paran eters V_N and θ/K_N (N = A, B) which are required for th evaluation of theoretical values of bi-ionic potentials. Th membrane potentials were measured by constructing a cell the type described in Part B. The concentration ratio σ w kept constant at 10 for each electrolyte solution (e.g. KC NaCl, LiCl, NH_4Cl etc.) used in the present investigation.

Results and Discussion

Part A. Evaluation of Activation Parameters, Namely, ΔH^*, ΔF^*, and ΔS^* for Diffusion of Various Electrolytes through Parchment-supported Silver Tungstate Membrane

When an ionic gradient is maintained using tw solutions of different concentrations of the sam electrolyte on either side of the membrane, diffusio of electrolytes from the region of higher concentr tion takes place. These transport phenomena a often described by some extended form of Nerns Planck flux equation (24). Evaluation of flows r quire integration of these flux equations under sui able boundary conditions governing the behavi

Can. J. Chem. Downloaded from www.nrcresearchpress.com by 210.87.254.105 on 09/05/12
For personal use only.

of the membrane–electrolyte system. Kittelberger (25) from the simple laws of electrolysis developed the following equation [1] for the evaluation of diffusion rates through membranes. This equation is found to be applicable as is evident from Fig. 1 to the system of parchment-supported silver tungstate membrane.

$$[1] \quad \frac{dQ_+}{dt} = \frac{1}{Z_+ F R_m}\left[\frac{RT}{Z_+ F}\ln\frac{a_2}{a_1} - \Delta\phi_m\right] \times \left[\frac{Z_+ Z_-}{Z_+ + Z_-}\frac{\Delta\phi_m}{(RT/F)\ln a_2/a_1} + \frac{Z_+}{Z_+ + Z_-}\right]$$

where Q_+ is the milliequivalents of cation diffusing in time t s, Z_+ and Z_- are the valencies of the cation and anion, respectively. R_m is the resistance in ohms of the membrane, $\Delta\phi_m$ is the membrane potential in mV, a_1 and a_2 are the activities of the two electrolyte solutions on either side of the membrane, R, T, and F have their usual meanings.

The rates at which various electrolytes diffuse through the membrane were calculated at different temperatures from eq. [1]. The calculated values of diffusion rate (dQ/dt) or D_r in mol/s at 25 ± 0.1°C are given in Table 1. The changes in R_m and $\Delta\phi_m$ and electrolyte flux (dQ/dt) or D_r through silver tungstate membrane are shown in Fig. 2. The diffusion rate derived electrometrically or conductometrically determined changes in the salt concentration of the test solution C_1 is called 'observed' diffusion rate while the values computed from the measured concentration potential and electrolytic resistance of the membrane is designated the 'computed' diffusion rate. The observed and computed diffusion rates are plotted against time (Fig. 1) for various electrolytes diffusing through silver tungstate membrane at 25 ± 0.1°C. It is found that the two methods show somewhat systematic deviations. The reason for these deviations probably has its origin in additional film resistances to mass transfer which are outside of the membrane itself. It was also noted that very small error in the measured salt concentration can produce a large error in the 'observed' diffusion rate. The physical imperfections in the membranes can also contribute towards the deviation.

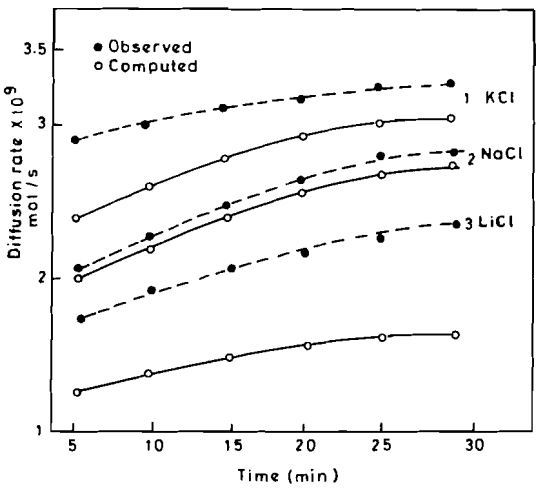

FIG. 1. Plots of observed and computed diffusion rates against time for diffusion of electrolytes through silver tungstate membrane.

The emf measured across the membrane using J-type Ag–AgCl electrodes is made up of two components. The first is the electrode potential difference $\Delta\phi_c$ due to the Ag–AgCl electrodes existing in two chloride solutions of different activities a_1 and a_2 of the same electrolyte and second is due to the membrane potentials $\Delta\phi_m$ arising across the membrane due to flow of electrolyte through it.

$\Delta\phi_c$ is given by the following equation:

$$[2] \quad \Delta\phi_c = (RT/Z_- F)\ln(C_2\gamma_2)/C_1\gamma_1)$$

where γ_1 and γ_2 are the activity coefficients of the electrolyte solutions on either side of the membrane (taken from the literature). Since Z_- is always unity and $C_1\gamma_1(a_1)$ and $C_2\gamma_2(a_2)$ are known, $\Delta\phi_c$ can be computed. As $(\Delta\phi_c + \Delta\phi_m)$ is measured directly, the value of $\Delta\phi_m$ can be evaluated by subtraction.

$\Delta\phi_m$ values for various electrolytes display a very interesting phenomena. In the case of 1:1 electrolytes, the values are all positive indicating that the membrane is cation selective. On the other hand, for 2:1 and 3:1 systems of electrolytes $\Delta\phi_m$ changes sign. It means that the membrane is now anion selective. This change in the selectivity character of the membrane is evidently due to adsorption of multivalent ions leading to a state where a net positive charge is

TABLE 1. Experimental activation energies and the activation parameters derived from transition state theory of rate process for diffusion of various electrolytes by the end of 2 h periods at 25 ± 0.1°C through parchment-supported silver tungstate membrane

	Parameters			
Electrolytes	$D_r \times 10^9$ (mol/s)	$D \times 10^7$ (cm²/s)	E_a (kcal/mol)	d.c. density (mA/cm²)
KCl	2.96	3.90	6.21	4.08×10^{-3}
NaCl	2.09	2.49	5.98	3.46×10^{-3}
LiCl	1.77	2.02	5.75	3.40×10^{-3}
$BaCl_2$	1.56	1.16	4.83	4.42×10^{-3}
$CaCl_2$	2.14	1.97	5.53	4.40×10^{-3}
$MgCl_2$	2.01	1.64	5.18	3.72×10^{-3}
$AlCl_3$	0.94	0.45	6.44	2.67×10^{-3}

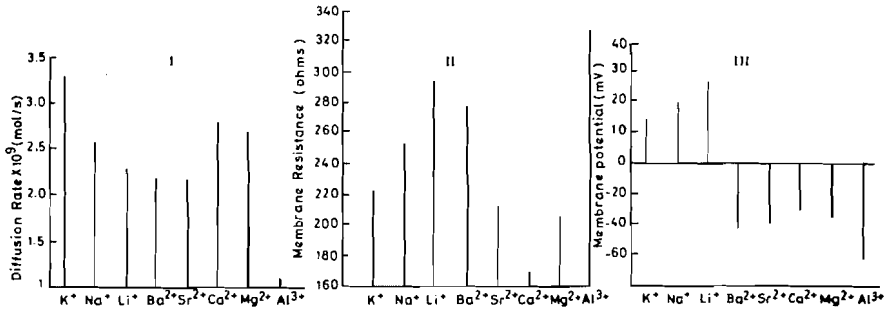

FIG. 2. Plots of diffusion rates, membrane resistance, and membrane potential through silver tungstate membrane against various cations.

left on the membrane surface making it anion selective. Adsorption of Al^{3+} makes the membrane more anion selective than it is with the adsorption of divalent cations. At any given time the membrane resistance R_m increases in the following order

$$LiCl > NaCl > KCl$$

and

$$BaCl_2 > SrCl_2 > MgCl_2 > CaCl_2$$

for 1:1 and 2:1 electrolytes and 3:1 system of electrolyte produces the highest value for membrane resistance.

The rate of flow measured for different electrolytes through silver tungstate membrane follows the sequence

$$KCl > NaCl > LiCl$$

and

$$CaCl_2 > MgCl_2 > SrCl_2 > BaCl_2$$

for 1:1 and 2:1 systems of electrolytes. The diffusion rates are calculated at different temperatures through the investigated membrane and are plotted against $1/T$ (K) (Fig. 3).

The theory of absolute reaction rates has been applied to diffusion by several investigators (26–28). According to Laidler and co-workers (27, 28) the integral diffusion coefficient D is given by

$$[3] \qquad D = Ae^{-E_a/RT}$$

where E_a is the observed activation energy for diffusion and A is the frequency factor. Thus if $\log D_r$ is plotted against $1/T$ (K), the slope gives the value of E_a. The values derived in this way for E_a are given in Table 1 at 25 ± 0.1°C. The derived values of D from eq. [3] are also given in Table 1. Various thermodynamic activation parameters, namely, enthalpy of activation, ΔH^*, entropy of activation, ΔS^*, and free energy of activation, ΔF^*, are also calculated with the help of Gibbs Helmholtz equations. The derived values of ΔH^*, ΔS^*, and ΔF^* are given in Table 2. The values of ΔS^* are found to be negative.

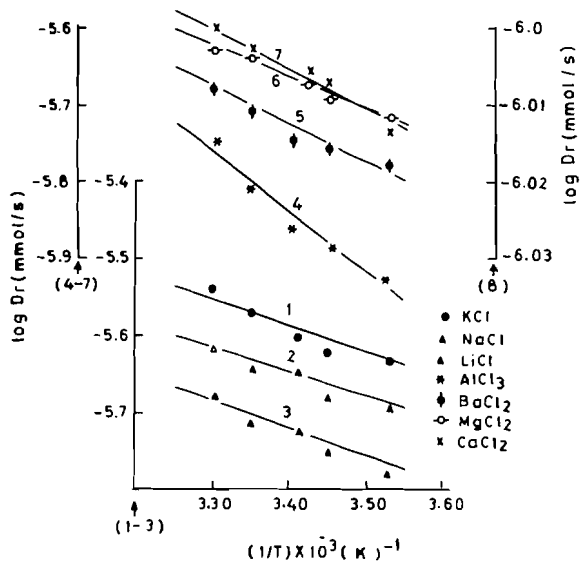

FIG. 3. Plots of diffusion rates of various electrolytes against different temperatures through silver tungstate membrane.

TABLE 2. The thermodynamic activation parameters calculated from the transition state theory of rate processes for electrolyte diffusion at 25 ± 0.1°C through silver tungstate membrane

Electrolytes	ΔH^* (kcal/mol)	ΔS^* (eu)	ΔF^* (kcal/mol)
KCl	5.62	−0.12	5.66
NaCl	5.39	−1.79	5.93
LiCl	5.16	−2.98	6.06
$BaCl_2$	4.24	−7.13	6.37
$CaCl_2$	4.97	−3.83	6.09
$MgCl_2$	4.59	−5.46	6.22
$AlCl_3$	5.85	−3.82	6.99

The negative ΔS^* indicates that the electrolyte dif fusion is taking place with the partial immobilizatio in the membrane phase (28). This partial immobilit increases in a relative manner with increase in th

Can. J. Chem. Downloaded from www.nrcresearchpress.com by 210.87.254.105 on 09/05/12
For personal use only.

Can. J. Chem. Downloaded from www.nrcresearchpress.com by 210.87.254.105 on 09/05/12
For personal use only.

valence of ions constituting the electrolyte with parchment-supported silver tungstate membrane.

Part B. Evaluation of Thermodynamically Effective Fixed Charge Density by the Use of Membrane Potential Values

Both the most recent method by Nagasawa and co-workers (14, 15) as well as the method developed by Kobatake and co-workers (16–21) are based on thermodynamics of irreversible processes applied here for the evaluation of fixed charge density of membranes.

The Method by Kobatake and Co-workers

The following expression used for charge density evaluation is given by Kobatake and co-workers (16–21):

$$[4] \quad \Delta\phi = -\frac{RT}{F}\left[\frac{1}{\beta}\ln\frac{C_2}{C_1} - \left(1 + \frac{1}{\beta} - 2\alpha\right) \times \ln\frac{C_2 + \alpha\beta\theta}{C_1 + \alpha\beta\theta}\right]$$

where

$$[5] \quad \alpha = [u_+/(u_+ + u_-)]$$

and

$$[6] \quad \beta = [1 + (KF\theta/u_+)]$$

The symbols u_+ and u_- represent the molar mobilities of positive and negative ions; K is a constant which is considered to depend upon the viscosity of the solution and the structural details of the polymer network of which the membrane is composed; θ is the fixed charge density (in equivalent/ℓ) of the membrane; C_1 and C_2 are the concentrations of electrolyte solutions across the membrane; R, T, and F have their usual meanings.

Kobatake and co-workers (16–21) have derived two limiting forms of eq. [4] useful for the analysis of experimental data on membrane potential. These are

(*a*) When C_2 becomes sufficiently small with σ fixed, eq. [4] may be expanded to give

$$[7] \quad |\Delta\phi_r| = \frac{1}{\beta}\ln\sigma - \left(\frac{\sigma - 1}{\alpha\beta\sigma}\right)\left(1 + \frac{1}{\beta} - 2\alpha\right)\frac{C_2}{\theta}$$

where $|\Delta\phi_r|$ is the absolute value of reduced membrane potential defined by

$$[8] \quad |\Delta\phi_r| = F\Delta\phi/RT$$

Equation [7] indicates that the value of β and a relation between α and θ may be obtained by determining the intercept and the initial slope of a plot for $|\Delta\phi_r|$ against C_2. The value of intercept is given by $(1/\beta) \times \ln\sigma$ from which β may be evaluated.

(*b*) In the region of high concentration the apparent transference number $t_{-\text{app}}$ is defined by

$$[9] \quad |\Delta\phi_r| = (1 - 2t_{-\text{app}})\ln\sigma$$

Substituting for $|\Delta\phi_r|$ in eq. [4] and expanding the resulting expression for $1/t_{-\text{app}}$ in powers of $1/C_2$ gives

$$[10] \quad \frac{1}{t_{-\text{app}}} = \frac{1}{1 - \alpha} + \frac{(1 + \beta + 2\alpha\beta)(\sigma - 1)\alpha\theta}{2(1 - \alpha)^2(\ln\sigma)C_2}$$

Equation [10] indicates that the intercept for a plot of $1/t_{-\text{app}}$ against $1/C_2$ at fixed σ allows the value of α to be determined. For the evaluation of α from eq. [10], plots of $1/t_{-\text{app}}$ against $1/C_2$ for various electrolytes through parchment-supported silver tungstate and chromic ferricyanide membranes are drawn (Fig. 4). The value of intercept is given by $1/(1 - \alpha)$ from which α is evaluated. Therefore from the predetermined β and α values, θ is evaluated and its values are given in Table 3 for various electrolytes with investigated membranes.

Test of the Kobatake Theory

Kobatake and co-workers (16–21) also suggested the following procedure for comparison of the theory

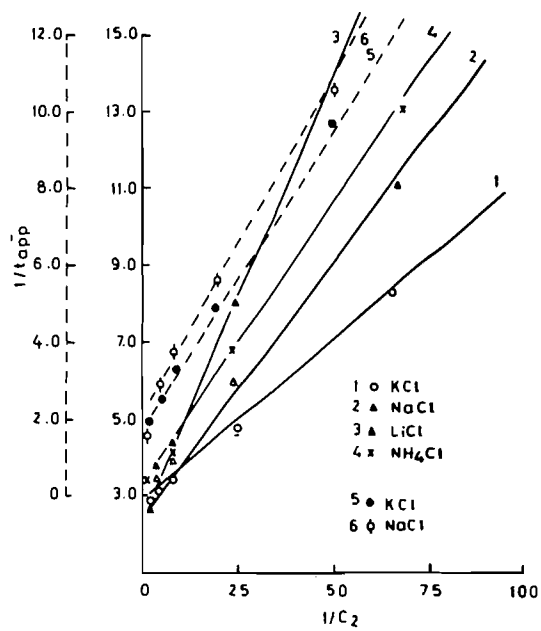

FIG. 4. Plots of $1/t_{-\text{app}}$ against $1/C_2$ for various electrolytes through (*i*) — silver tungstate and (*ii*) --- chromic ferricyanide membranes. (*i*) KCl (○), NaCl (△), LiCl (▲), and NH_4Cl (×); (*ii*) KCl (●), NaCl (ϕ).

TABLE 3. Values derived for thermodynamically effective fixed charge density θ (in equiv./ℓ) of parchment-supported membranes at σ = 10

	Membranes			
	Silver tungstate		Chromic ferricyanide	
Electrolytes	Kobatake method	Nagasawa method	Kobatake method	Nagasawa method
KCl	0.0557	0.032	0.045	0.020
NaCl	0.0813	0.032	0.031	0.080
LiCl	0.0610	0.024	—	—
NH_4Cl	0.0730	0.048	—	—

and experiment by taking the following expressions

$$[11] \qquad (\sigma - e^q)/(e^q - 1) = Z$$

where

$$[12] \qquad q = \frac{|\Delta\phi_r| + (1 - 2\alpha)\ln\sigma}{1/\beta + 1 - 2\alpha}$$

and

$$[13] \qquad Z = C_2/\alpha\beta\theta$$

Thus if eq. [4] is valid, the values of $(\sigma - e^q)/(e^q - 1)$ calculated from measured $\Delta\phi$ and predetermined α, β, and θ values at a known value of σ (= 10) must fall on a straight line which has a unit slope and passes through the origin when plotted against log Z. Figure 5 demonstrates that the theoretical prediction from membrane potential equation is borne out quite satisfactorily by our experimental results with these investigated membranes.

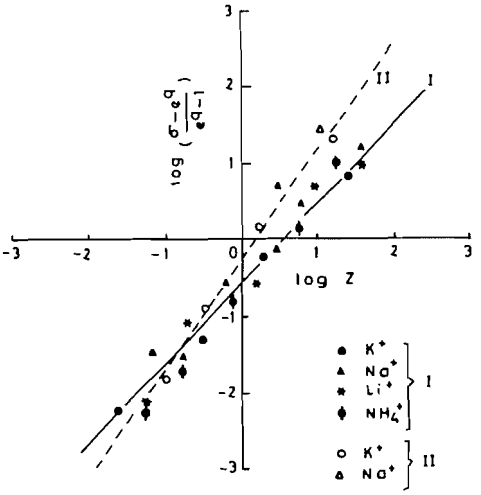

FIG. 5. Plots of log $(\sigma - e^q)/(e^q - 1)$ against log Z for various electrolytes through (*i*) — silver tungstate and (*ii*) --- chromic ferricyanide membranes. (*i*) KCl (●), NaCl (▲), LiCl (*), and NH_4Cl (◆); (*ii*) KCl (○), NaCl (△).

The Method of Nagasawa and Co-workers

Nagasawa and co-workers (14, 15) used the following equations by making various assumptions for activity and mobility of small ions, which are applied here. The membrane potential equation is given by

$$[14] \qquad -\Delta\phi = \frac{RT}{F}\frac{\theta}{2}\frac{\sigma - 1}{\sigma}\frac{1}{C_2} + \frac{RT}{F}\frac{u_+ - u_-}{u_+ + u_-}\frac{\left[1 - \dfrac{\theta J_0}{RT\bar{C}_0(u_+ - u_-)K}\right]}{\left[1 - \dfrac{\theta J_0}{2RT\bar{C}_0 u_- K}\right]}\ln\sigma + \frac{RT\theta}{2Fu_+u_-}\left(\frac{J_0}{RT\bar{C}_0K}\right)^2\frac{\left[1 - \dfrac{\theta J_0(u_+ + u_-)}{4RT\bar{C}_0u_+u_-K}\right]}{\left[1 - \dfrac{\theta J_0}{2RT\bar{C}_0u_-K}\right]}(\sigma - 1)C_2$$

where J_0 is the flux of water, θ is the thermodynamically effective fixed charge density, $\bar{C}_0$ is the concentration of water in the membrane phase, u_+ and u_- are the cation and anion mobilities in the membrane phase, σ is the concentration ratio equal to C_1/C_2, K is a constant defined by

$$[15] \qquad K = \frac{1}{\delta}\left\{\bar{C}_{-(2)} - \bar{C}_{-(1)} - \frac{\bar{C}_{-(2)} + \bar{C}_{-(1)}}{2RT\bar{C}_0u_-} + \frac{\theta^2J_0}{4RT\bar{C}_0(\bar{C}_{-(2)} - \bar{C}_{-(1)})}\ln\frac{\bar{C}_{-(2)} + \frac{\theta}{2}}{\bar{C}_{-(1)} + \frac{\theta}{2}}\right\}$$

Can. J. Chem. Downloaded from www.nrcresearchpress.com by 210.87.254.105 on 09/05/12
For personal use only.

Can. J. Chem. Downloaded from www.nrcresearchpress.com by 210.87.254.105 on 09/05/12
For personal use only.

where $\bar{C}_{-(1)}$ and $\bar{C}_{-(2)}$ are the anionic concentrations in the membrane phase for ions 1 and 2 on two sides 1 and 2 of the membrane; δ is the thickness of the membrane (in cm). At significant electrolyte concentration eq. [14] reduces to

$$[16] \qquad -\Delta\phi = \frac{RT}{F}\frac{\theta}{2}\frac{\sigma - 1}{\sigma}\frac{1}{C_2}$$

except at extremely high concentrations where the potential is significantly affected by J_0. The plots of $[\Delta\phi/\{(\sigma - 1)/\sigma\}]$ against $1/C_2$ are drawn (Fig. 6) for the evaluation of θ, the thermodynamically effective fixed charge density of membrane. The slope of eq. [16] is given by

$$[17] \qquad \frac{RT}{F}\cdot\frac{\theta}{2}$$

This was equated to the graphical value of the slope obtained from Fig. 6. The values of θ thus determined are given in Table 3 for various electrolytes through the investigated membranes.

Part C. Determination of Potentiometric Selectivity Coefficient K_A^{Pot} and Test of Nozaki's Theory of Bi-ionic Potential (BIP)

The mechanism of bi-ionic potential has been considered in detail by a number of workers (29–35). Sollner (35) found that not only the mobility of counter ions is important but the selectivity of the membrane material plays a significant role in the development of BIP. The relations of selectivity of membranes to the various physicochemical parameters have also been given by a number of investigators. The selectivity of membrane is governed by both the mobility of ions in the membrane phase and the equilibrium that exists at the membrane–solution interfaces (e.g., partition coefficients, ion-exchange equilibrium constants). The various factors responsible for the selectivity of the parchment membrane arising from differences in the mobilities of the ions in the membrane are described here. The factors controlling or responsible for the membrane selectivity due to physicochemical equilibrium conditions have been analysed by Reichenberg (36) and intensively pursued by Eisenman and co-workers (37–43). The important facts emerging from the studies of investigators are that (*i*) the pattern of selectivity is predominantly governed by field strength, (*ii*) the number of water molecules in the neighbourhood of the cationic and anionic sites influences only the magnitude and not the sequence of selectivity, and (*iii*) the spatial distribution of anionic site influences the selectivity through the overlap of electrostatic forces.

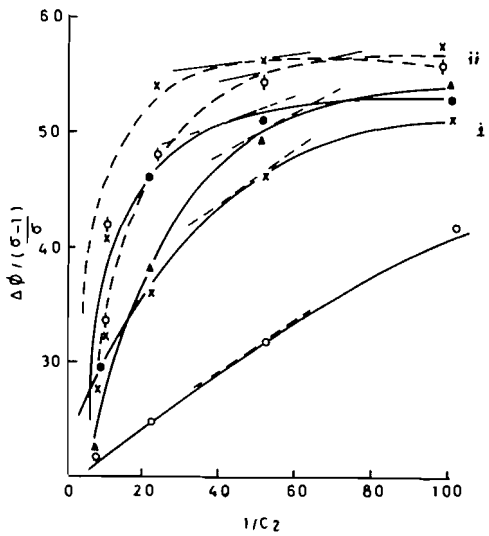

FIG. 6. Plots of $\Delta\phi\sigma/(\sigma - 1)$ against $1/C_2$ for various electrolytes through (*i*) silver tungstate (—) and (*ii*) chromic ferricyanide (---) membranes. (*i*) KCl (●), NaCl (×), LiCl (○), and NH_4Cl (▲); (*ii*) KCl (ϕ), NaCl (×).

Marshall and Krinbill (44) developed the following equation [18] for the bi-ionic potential

$$[18] \qquad \Delta\phi_{BIP} = (RT/F)\ln(a_A\bar{u}_A/a_B\bar{u}_B)$$

where $(\bar{u}_A/\bar{u}_B)$ is the mobility ratio in the membrane phase of the two ions. The values derived for mobility ratios across silver tungstate membrane for 1:1 set of electrolytes are given in Table 4. The BIP values are related to the potentiometric selectivity coefficient K_{BA}^{Pot} by the following relation:

$$[19] \qquad \Delta\phi_{BIP} = \text{constant} + (nRT/F) \times \ln[a_A^{1/n} + (K_{BA}^{Pot}a_B)^{1/n}]$$

which is the extended form of Nicolsky's equation (45–51), with n, R, T, and F having their usual meanings. Super Pot signifies potentiometric selectivity coefficient. According to an IUPAC report # 43, January 1975 on nomenclature for ion selective electrodes, the potentiometric selectivity coefficient is designated K_{BA}. However, the present existing litera-

TABLE 4. Values derived for mobility ratios (u_A/u_B) across silver tungstate membrane

	u_A/u_B		
Concentration	KCl–NaCl	KCl–LiCl	KCl–NH_4Cl
0.1/0.1	1.27	1.22	1.14
0.05/0.05	1.30	1.25	1.19
0.02/0.02	1.35	1.29	1.24
0.01/0.01	1.38	1.30	1.26
0.005/0.005	1.41	1.36	1.35
0.002/0.002	1.43	1.41	1.40
0.001/0.001	1.47	1.54	1.50

TABLE 5. Values derived for K_{BA}^{Pot} for different sets of electrolytes across silver tungstate membrane at 25 ± 0.1°C

KCl–NaCl	KCl–LiCl	KCl–NH_4Cl
1.131	1.096	1.131

ture uses the nomenclature above almost exclusively (52). Conti and Eisenman (53–55) and others (56, 57) have given most complete derivation and analysis of various equations involving the term potentiometric selectivity for permeable ions of the same sign through membranes containing a distribution of fixed sites, including the usual uniform distribution. The various values of BIP obtained with silver tungstate membrane are plotted against mean ion activities and straight lines as shown in Fig. 7 are obtained. From the slopes of the lines the values of K_{BA}^{Pot} are thus obtained and are given in Table 5 for various 1:1 sets of electrolytes (KCl–NaCl, KCl–LiCl, and KCl–NH_4Cl) through silver tungstate membrane.

More recently Toyoshima and Nozaki (22) derived various theoretical equations for membrane potential and bi-ionic potential based on thermodynamics of irreversible processes which are applied and tested here with parchment-supported silver tungstate membrane. The various assumptions for the concentration dependence of u_i and a_i of ion i ($i = +, -$) in the membrane phase are as follows:

$$[20] \qquad u_+C_+ = u_+^0C_+(C_- + \theta)$$

$$[21] \qquad u_-C_- = u_-^0C_-$$

$$[22] \qquad a_+ = \gamma_i^0(C_- + \theta)$$

$$[23] \qquad a_- = \gamma_-^0C_-$$

Here u_i^0 and γ_i^0 are the mobility and activity coefficients of ion i in the free solution. The quantity θ is the thermodynamically effective fixed charge density of the membrane.

According to Toyoshima and Nozaki (22) the system studied consists of two kinds of 1:1 electrolytes (KCl and NaCl) separating a negatively charged membrane. No electric field is applied externally across the membrane, and no electric charge is transported from one side of the membrane to the other. The theoretical equation eq. [24] for bi-ionic potential using variables which contains four parameters (V_{K^+}, V_{Na^+}), (θ/K_{K^+}, θ/K_{Na^+}), (g_{K^+}/g_{Na^+}) and (K_{K^+}/K_{Na^+}) is given by

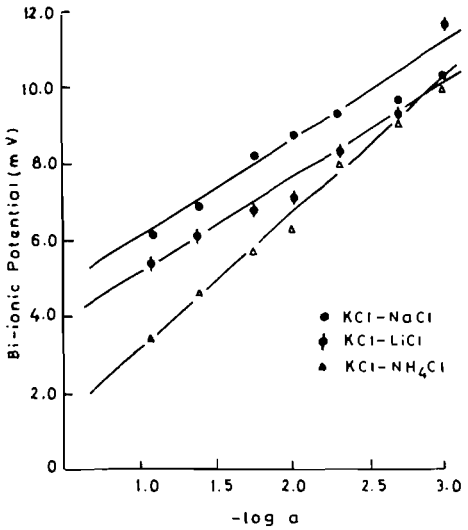

FIG. 7. Plots of observed bi-ionic potential (mV) against $-\log a$ through silver tungstate membrane for various sets of electrolytes at 25 ± 0.1°C.

$$[24] \qquad \Delta\phi_{BIP} = \left(2 \ln \frac{K_{K^+}}{K_{Na^+}} + \ln \frac{JV_{K^+} + 1}{JV_{Na^+} + 1}\right) \frac{F}{RT}$$

where (K_{K^+}/K_{Na^+}) is the selectivity constant of a membrane for positive ion species K^+ to Na^+.

$$[25] \qquad V_{K^+} = 1 + (u_{K^+}^0/u_{Cl^-}^0)$$

and

$$[26] \qquad V_{Na^+} = 1 + (U_{Na^+}^0/U_{Cl^-}^0)$$

For the evaluation of flux J of ion species, Toyoshima and Nozaki (22) gave the following equation [27] which is also used in the present investigation

$$[27] \qquad (2J + 1) \ln \frac{g_{K^+} + 2J}{g_{Na^+} + 2J} - \ln \frac{JV_{K^+} + 1}{JV_{Na^+} + 1} - \ln \frac{g_{K^+}}{g_{Na^+}} = 0$$

where

$$[28] \qquad g_{K^+} = 1 + [1 + (2K_{K^+}C/\theta)^2]^{1/2}$$

and

$$[29] \qquad g_{Na^+} = 1 + [1 + (2K_{Na^+}C/\theta)^2]^{1/2}$$

In order to evaluate (V_{K^+}, V_{Na^+}), (θ/K_{K^+}, θ/K_{Na^+}) for KCl–NaCl set of uni-univalent electrolytes, the following equation [30] given by Toyoshima and Nozaki (22) for membrane potential, $\Delta\phi$, is utilized here.

Can. J. Chem. Downloaded from www.nrcresearchpress.com by 210.87.254.105 on 09/05/12
For personal use only.

Can. J. Chem. Downloaded from www.nrcresearchpress.com by 210.87.254.105 on 09/05/12
For personal use only.

For KCl electrolyte

$$[30]\quad \Delta\phi_{KCl} = -\ln\sigma - \frac{1.2}{V_{K^+}}\ln\frac{[1+(2C_2K_{K^+}/\theta)^2]^{1/2}+(1-2/V_{K^+})}{[1+(2C_1K_{K^+}/\theta)^2]^{1/2}+(1-2/V_{K^+})} + \ln\frac{[1+(2C_2K_{K^+}/\theta)^2]^{1/2}+1}{[1+(2C_1K_{K^+}/\theta)^2]^{1/2}+1}\frac{RT}{F}$$

For NaCl electrolyte

$$[31]\quad \Delta\phi_{NaCl} = -\ln\sigma - \left(1-\frac{2}{V_{Na^+}}\right)\ln\frac{[1+(2C_2K_{Na^+}/\theta)^2]^{1/2}+(1-2/V_{Na^+})}{[1+(2C_1K_{Na^+}/\theta)^2]^{1/2}} + \left(1-\frac{2}{V_{Na^+}}\right)\ln\frac{[1+(2C_2K_{Na^+}/\theta)^2]^{1/2}+1}{[1+(2C_1K_{Na^+}/\theta)^2]^{1/2}+1}\left(\frac{RT}{F}\right)$$

where C_1 and C_2 are the concentrations of electrolyte solution on two sides of the membrane in each case

$$[32]\quad \sigma = C_1/C_2$$

Expanding eqs. [30] and [31] in powers of $1/C_2$ with fixed σ yields:

For KCl electrolyte

$$[33]\quad \Delta\phi_{KCl} = -\left(1-\frac{2}{V_{K^+}}\right)\ln\sigma - 2\left(1-\frac{1}{V_{K^+}}\right)\left(\frac{1}{V_{K^+}}\right)\left(1-\frac{1}{\sigma}\right)\left(\frac{\theta}{K_{K^+}}\right)\left(\frac{1}{C_2}\right)$$

For NaCl electrolyte

$$[34]\quad \Delta\phi_{NaCl} = -\left(1-\frac{2}{V_{Na^+}}\right)\ln\sigma - 2\left(1-\frac{1}{V_{Na^+}}\right)\left(\frac{1}{V_{Na^+}}\right)\left(1-\frac{1}{\sigma}\right)\left(\frac{\theta}{K_{Na^+}}\right)\left(\frac{1}{C_2}\right)$$

The transference number t_{-app} for anion is defined by eq. [9]. Introducing eq. [33] into eq. [9] and eq. [34] into eq. [9] and expanding separately $1/t_{-app}$ as a power series in $1/C_2$, the following expressions are obtained.

For KCl electrolyte

$$[35]\quad \frac{1}{t_{-app}} = V_{K^+} + (V_{K^+}-1)\left(\frac{\sigma-1}{\sigma\ln\sigma}\right) \times \left(\frac{\theta}{K_{K^+}}\right)\left(\frac{1}{C_2}\right)$$

For NaCl electrolyte

$$[36]\quad \frac{1}{t_{-app}} = V_{Na^+} + (V_{Na^+}-1)\left(\frac{\sigma-1}{\sigma\ln\sigma}\right) \times \left(\frac{\theta}{K_{Na^+}}\right)\left(\frac{1}{C_2}\right)$$

The above equations, [35] and [36], were used for the evaluation of V_{K^+}, V_{Na^+}, θ/K_{K^+}, and θ/K_{Na^+} in the following way:

The different values of $1/t_{-app}$ were plotted against $1/C_2$ (Fig. 4) for KCl and NaCl electrolytes through silver tungstate membrane at fixed $\sigma = 10$. Equations [35] and [36] indicate that the intercept of a plot of $1/t_{-app}$ against $1/C_2$ at fixed σ allows the values of V_{K^+} and V_{Na^+} to be determined. For the evaluation of θ/K_{K^+} and θ/K_{Na^+}, the slopes of eq. [35] and eq. [36] are given by the following factors.

For KCl electrolyte

$$[37]\quad \left[\frac{(V_{K^+}-1)(\sigma-1)}{\sigma\ln\sigma}\right]\left(\frac{\theta}{K_{K^+}}\right) = \text{Slope}_{K^+}$$

For NaCl electrolyte

$$[38]\quad \left[\frac{(V_{Na^+}-1)(\sigma-1)}{\sigma\ln\sigma}\right]\left(\frac{\theta}{K_{Na^+}}\right) = \text{Slope}_{Na^+}$$

are first determined. The graphical values of slopes evaluated from Fig. 4 are equated with the above factors, [37] and [38], and then by substituting V_{K^+} and V_{Na^+}, the values of θ/K_{K^+} and θ/K_{Na^+} are evaluated. The same procedures were employed for the other sets of electrolytes (KCl–LiCl and KCl–NH_4Cl); V and θ/K thus determined for various electrolytes, namely KCl, NaCl, LiCl, and NH_4Cl and the values are given in Table 6. The values of g (for K^+, Na^+, Li^+, and NH_4^+) were calculated by substituting θ/K in eq. [28] and eq. [29] for KCl and NaCl electrolytes and the values of g are given in Table 7. The same method was adopted for NH_4Cl and LiCl and the values of g are given in Table 7. The theoretically determined values of BIP from eq. [24] are plotted against log C (Fig. 8) (for KCl–NaCl set). For comparison the observed values of BIP are plotted in the same figure with silver tungstate membrane. For other sets (KCl–LiCl, and KCl–NH_4Cl) the calculated and observed BIP were also plotted in Fig. 8. It is quite evident from Fig. 8 that

Can. J. Chem. Downloaded from www.nrcresearchpress.com by 210.87.254.105 on 09/05/12
For personal use only.

TABLE 6. Values derived for V and (θ/K) for different electrolytes across silver tungstate membrane

Electrolytes	V	(θ/K)
KCl	2.56	0.0984
NaCl	2.82	0.1120
LiCl	2.40	0.0625
NH_4Cl	2.80	0.0682

TABLE 7. Values derived for g with different electrolytes across silver tungstate membrane

Concentration (equiv./ℓ)	g			
	KCl	NaCl	LiCl	NH_4Cl
0.01	2.01	2.01	2.03	2.00
0.02	2.07	2.05	2.24	2.01
0.05	2.40	2.28	2.55	2.08
0.10	3.23	2.97	4.01	2.29
0.20	5.10	4.70	6.78	2.94

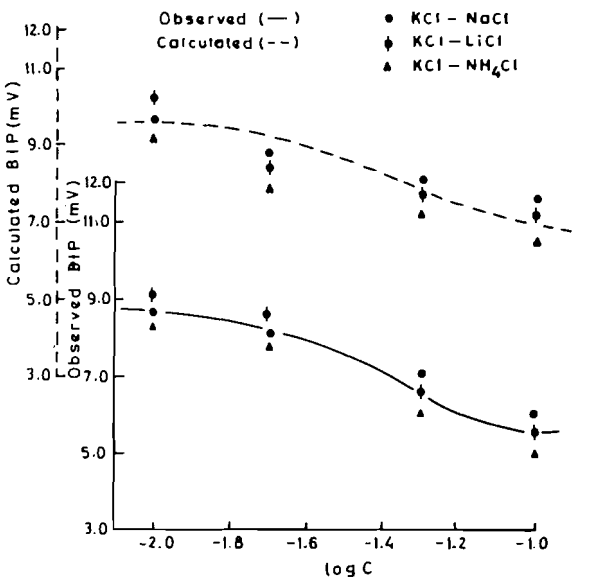

FIG. 8. Plots of observed and theoretically calculated BIP values against log C for various sets of electrolytes through silver tungstate membrane at 25 ± 0.1°C.

the agreement between the observed and theoretical values of BIP are quite fair and it may be concluded that the theory of BIP developed by Toyoshima and Nozaki (22) based on thermodynamics of irreversible processes is applicable to the system of parchment-supported membrane.

Acknowledgements

The authors are grateful to Professor Wasi-ur-Rahman, Head, Department of Chemistry, Aligarh Muslim University, India, for providing research facilities and also to C.S.I.R. (India) for the award of fellowships to M.I.R.K., A.H., and B.I.

1. F. A. SIDDIQI and S. PRATAP. J. Electroanal. Chem. **23**, 137 (1969).
2. F. A. SIDDIQI, N. LAKSHMINARAYANAIAH, and S. K. SAKSENA. Z. Phys. Chem. Frankfurt, **72**, 298 (1970).
3. F. A. SIDDIQI, N. LAKSHMINARAYANIAH, and M. N. BEG. J. Polym. Sci. **9**, 2853 (1971); **9**, 2868 (1971).
4. N. LAKSHMINARAYANAIAH and F. A. SIDDIQI. Biophys. J. **11**, 603 (1971).
5. N. LAKSHMINARAYANAIAH and F. A. SIDDIQI. Biophys. J. **11**, 617 (1971); **12**, 540 (1972).
6. N. LAKSHMINARAYANAIAH and F. A. SIDDIQI. *In* Membrane processes in industry and biomedicine. *Edited by* M. Bier. Plenum Publishing Corporation, New York. 1971. p. 301.
7. W. U. MALIK and F. A. SIDDIQI. Proc. Indian Acad. Sci. A**56**, 206 (1962).
8. N. LAKSHMINARAYANAIAH and F. A. SIDDIQI. J. Polym. Sci. **8**, 2949 (1970); Z. Phys. Chem. Frankfurt, **78**, 150 (1972).
9. O. KEDEM and A. KATCHALSKY. Trans. Faraday Soc. **59**, 1918 (1963); **59**, 1931 (1963); **59**, 1941 (1963).
10. K. S. SPEIGLOR. Trans. Faraday Soc. **54**, 1408 (1958).
11. G. SCATCHARD. Discuss. Faraday Soc. **21**, 30 (1956).
12. E. M. SCATTERGOOD and E. N. LIGHTFOOT. Trans. Faraday Soc. **64**, 1135 (1968).
13. M. PLANCK. Ann. Phys. **39**, 161 (1890); **40**, 561 (1890).
14. M. NAGASAWA and Y. KOBATAKE. J. Phys. Chem. **56**, 1017 (1952).
15. M. TASAKA, N. AOKI, Y. KONDO, and M. NAGASAWA. J. Phys. Chem. **79**, 1307 (1975).
16. Y. KOBATAKE and H. FUJITA. J. Phys. Chem. **72**, 2871 (1968).
17. N. KAMO, M. OIKAWA, and Y. KOBATAKE. J. Phys. Chem. **77**, 92 (1973).
18. Y. KOBATAKE, N. TAKEGUCHI, Y. TOYOSHIMA, and H. FUJITA. J. Phys. Chem. **69**, 3981 (1965).
19. N. KAMO, Y. TOYOSHIMA, and Y. KOBATAKE. Kolloid Z. Z. Polym. **249**, 1061 (1971).
20. N. KAMO, Y. TOYOSHIMA, H. NOZAKI, and Y. KOBATAKE. Kolloid Z. Z. Polym. **248**, 914 (1971).
21. Y. TOYOSHIMA, M. YUASA, Y. KOBATAKE, and H. FUJITA. Trans. Faraday Soc. **63**, 2803 (1967); **63**, 2814 (1967).
22. Y. TOYOSHIMA and H. NOZAKI. J. Phys. Chem. **74**, 2704 (1970).
23. H. B. WEISER. J. Phys. Chem. **34**, 335 (1930); **34**, 1826 (1930).
24. R. SCHLÖGL. Stofftransport durch Membrane Steinkopff. Darmstadt, 1964; Ber. Bunsenges. Phys. Chem. **70**, 400 (1966).
25. W. W. KITTELBERGER. J. Phys. Chem. **53**, 392 (1949).
26. B. J. ZWOLINSKI, H. EYRING, and C. E. REESE. J. Phys. Chem. **53**, 1426 (1949).
27. S. GLASSTONE, K. J. LAIDLER, and H. EYRING. The theory of rate processes. McGraw-Hill, New York. 1941. p. 525.
28. K. E. SHULER, C. A. DAMES, and K. J. LAIDLER. J. Chem. Phys. **17**, 860 (1949).
29. T. TEORELL. Proc. Soc. Exptl. Biol. Med. **33**, 282 (1935); Proc. Natl. Acad. Sci. U.S. **21**, 152 (1935).
30. T. TEORELL. Z. Elektrochem. **55**, 460 (1951).
31. T. TEORELL. Prog. Biophys. Chem. **3**, 305 (1953).
32. K. H. MEYER and J. F. SIEVERS. Helv. Chim. Acta, **19**, 649 (1936); **19**, 665 (1936); **19**, 987 (1936).

33. A. ILANI. Biochim. Biophys. Acta, **94**, 415 (1965).
34. K. SOLLNER, S. DRAY, E. GRIM, and R. NEIHOF. *In* Ion transport across membranes. *Edited by* H. T. Clarke and D. Nachmanshon. Academic Press, New York. 1954. p. 144; *In* Electrochemistry in biology and medicine. *Edited by* T. Shedlovsky. Wiley, New York. 1955. p. 65.
35. K. SOLLNER. J. Phys. Chem. **53**, 1211 (1949); **53**, 1226 (1949); *In* Encyclopedia of electrochemistry. *Edited by* C. A. Hampel. Reinhold, New York. 1964. p. 806.
36. D. REICHENBERG. *In* Ion-exchange. Vol. 1. *Edited by* J. A. Marinsky. Dekker, New York. 1968. p. 227.
37. G. EISENMAN. Bol. Inst. Estud. Med. Biol. (Univ. Nac. Auton Mex.) **21**, 155 (1963); Proc. Int. Congr. Physiol. Sci. 23rd, Tokyo. 1965. p. 489.
38. G. EISENMAN, D. O. RUDIN, and J. U. CASBY. Science, **126**, 831 (1957).
39. G. EISENMAN. Biophys. J. Suppl. **2**, 314 (1962).
40. G. EISENMAN (*Editor*). Glass electrodes for hydrogen and other cations, principles and practice. New York. 1967.
41. G. EISENMAN. Adv. Anal. Chem. Instrum. **4**, 213 (1965); also reprinted in G. Eisenman, R. Bates, G. Mattock, and S. M. Friedman. The glass electrode. Wiley, Interscience, New York. 1966.
42. G. EISENMAN. *In* Ion selective electrodes. *Edited by* R. A. Durst. Natl. Bur. of Std. Spec. Publ. 314, Washington, DC. 1969. p. 1.
43. G. EISENMAN. *In* Symp. membrane transport metabolism. *Edited by* A. Kleinzeller and A. Kotyk. Academic Press, New York. 1961. p. 163.
44. C. E. MARSHALL and C. A. KRINBILL. J. Am. Chem. Soc. **64**, 1814 (1942).
45. B. P. NICOLSKY. Acta Physicochim. URSS, **7**, 597 (1937).
46. R. M. GARRELS, M. SATO, M. E. THOMPSON, and A. H. TUESDELL. Science, **135**, 1045 (1962).
47. E. PUNGOR. Anal. Chem. **39**, 28A (1967).
48. E. PUNGOR and K. TOTH. Anal. Chim. Acta, **47**, 291 (1969).
49. E. PUNGOR and K. TOTH. Analyst, **95**, 625 (1970).
50. H. R. WUHRMAN, W. E. MORF, and W. SIMON. Helv. Chim. Acta, **56**, 1011 (1973).
51. W. E. MORF, D. AMMAN, E. PRETSCH, and W. SIMON. Pure Appl. Chem. **36**, 421 (1973).
52. R. P. BUCK. Critical reviews in analytical chemistry. 1976. pp. 342–382.
53. F. CONTI and G. EISENMAN. Biophys. J. **5**, 247 (1965); **5**, 511 (1965).
54. G. EISENMAN (*Editor*). Membranes. Vol. 1. Dekker, New York. 1972. Vol. 2, New York. 1973.
55. F. CONTI and G. EISENMAN. Biophys. J. **6**, 227 (1966).
56. F. HELFFERICH and H. D. OCKER. Z. Phys. Chem. Frankfurt, **10**, 213 (1957); Discuss. Faraday Soc. **21**, 83 (1956); **21**, 133 (1956).
57. W. R. J. WYLLIE and S. L. KANAAN. J. Phys. Chem. **58**, 73 (1954).

Can. J. Chem. Downloaded from www.nrcresearchpress.com by 210.87.254.105 on 09/05/12
For personal use only.

Effects of potassium ion on the electron-transfer reaction between $Fe(CN)_6^{4-}$ and TCNQ or chloranil

SADAYUKI MATSUDA AND AKIHIKO YAMAGISHI

Department of Chemistry, Faculty of Science, Hokkaido University, Sapporo 060, Japan

Received September 29, 1977

SADAYUKI MATSUDA and AKIHIKO YAMAGISHI. Can. J. Chem. **56**, 2216 (1978).

The effects of potassium ion on the electron-transfer reactions between $Fe(CN)_6^{4-}$ and 7,7,8,8-tetracyanoquinodimethane (TCNQ) or chloranil (QCl_4) were studied with temperature-jump equipment; $Fe(CN)_6^{4-}$ + TCNQ (or QCl_4) $\rightleftharpoons$ $Fe(CN)_6^{3-}$ + $TCNQ^-$ (or QCl_4^-). The solvent was a 1:1 (v/v) mixture of acetonitrile–water. In both systems, the forward rate constants (k_f) were unaffected by the addition of KCl; $k_f(Fe(CN)_6^{4-}/TCNQ) = (2.9 \pm 0.2) \times 10^6\ M^{-1}\ s^{-1}$, and $k_f(Fe(CN)_6^{4-}/QCl_4) = (5.2 \pm 0.4) \times 10^4\ M^{-1}\ s^{-1}$. On the other hand, the backward rate constants (k_b) increased with the increase of the KCl concentration. The results are interpreted in terms of ion-pairing equilibria of $Fe(CN)_6^{4-}$ and $Fe(CN)_6^{3-}$.

SADAYUKI MATSUDA et AKIHIKO YAMAGISHI. Can. J. Chem. **56**, 2216 (1978).

Faisant appel à un appareil de saut de température, on a étudié l'effet des ions potassium sur les réactions de transferts d'électrons entre le $Fe(CN)_6^{4-}$ et le tétracyano-7,7,8,8 quinodiméthane (TCQD) ou le chloranil (QCl_4); $Fe(CN)_6^{4-}$ + TCNQ (ou QCl_4) $\rightleftharpoons$ $Fe(CN)_6^{3-}$ + $TCNQ^-$ (ou QCl_4^-). On a utilisé un mélange 1:1 (v/v) d'acétonitrile–eau comme solvant. Dans chacun des systèmes, les constantes de vitesse vers la droite ne sont pas affectées par l'addition de KCl; $k_f(Fe(CN)_6^{4-}/TCNQ) = (2.9 \pm 0.2) \times 10^6\ M^{-1}\ s^{-1}$ et $k_f(Fe(CN_6^{4-}/QCl_4) = (5.2 \pm 0.4) \times 10^4\ M^{-1}\ s^{-1}$. Par ailleurs, il y a augmentation des constantes de vitesses inverses avec une augmentation de la concentration de KCl. On interprète les résultats en termes d'équilibres d'ions $Fe(CN)_6^{4-}$ et $Fe(CN)_6^{3-}$ en paires.

[Traduit par le journal]

Introduction

It has been reported by several authors that the rates of electron-transfer reactions between negatively charged metal complexes are remarkably accelerated by the presence of alkali metal cations (1, 2). For example, alkali metal ions and tetraalkylammonium ions enhance the electron-exchange rates between $Fe(CN)_6^{4-}$ and $Fe(CN)_6^{3-}$ in the order of $Cs^+ > K^+ > NH_4^+ > Li^+$ (1). It is not reasonable to ascribe the effects to the ion-pair formation of $M^+Fe(CN)_6^{4-}$ or $M^+Fe(CN)_6^{3-}$, since the rate enhancement was observed in such a low concentration of cations there was no appreciable amount of ion-paired species present. Based on the fact that the above order agrees with the lability of desolvation of cation, it is proposed that in a transition state a naked cation, M^+, is shared by two electron-exchanging anions (3)

$$[1] \qquad Fe(CN)_6^{4-} \text{ --- } M^+ \text{ --- } Fe(CN)_6^{3-}$$

This structure is considered to decrease the activation free energy of reaction, because the positive charge of M^+ shields the electrostatic repulsion between reacting anions.

Recently the extension of the above effects to the heterogeneous electron-transfer from organic crystal to $Fe(CN)_6^{3-}$ was reported (4). In this system, the electron-transfer rate was accelerated by alkali metal cations in the order of $Cs^+ > K^+ > Li^+$. These facts suggest that alkali cations play a similar role in the electron–transfer involving organic compounds.

At this stage, it is worthwhile to elucidate the role of cations in homogeneous electron-transfer between an organic molecule and $Fe(CN)_6^{4-}$;

$$[2] \qquad Fe(CN)_6^{4-} + R \rightleftharpoons Fe(CN)_6^{3-} + R^-$$

where R denotes an organic compound with appropriate electron-affinity.[1] The main objective to examine this system is to see if a cation decreases the activation free energy of reaction by forming the transition state,

$$[1'] \qquad Fe(CN)_6^{4-} \text{ --- } M^+ \text{ --- } R$$

which is the analogy of [1].

The present work describes the temperature-jump study of the electron-transfer between $Fe(CN)_6^{4-}$ and 7,7,8,8-tetracyanoquinodimethane (TCNQ) or chloranil. The rate was measured in the presence of potassium chloride in a 1:1 (v/v) mixture of acetonitrile–water. The role of K^+ in electron-transfer was established by obtaining the K^+ effect on both the forward and backward rates.

[1]Although there are a few works concerning the reactions of type (2), no special attentions have been paid to the role of cations (6).

Can. J. Chem. Downloaded from www.nrcresearchpress.com by 210.87.254.6 on 09/05/12
For personal use only.

Can. J. Chem. Downloaded from www.nrcresearchpress.com by 210.87.254.6 on 09/05/12
For personal use only.

Experimental

7,7,8,8-Tetracyanoquinodimethane (TCNQ) and chloranil (QCl_4) were sublimed *in vacuo*. Potassium salt of TCNQ (K^+TCNQ^-) was prepared by reducing TCNQ with potassium iodide in acetonitrile. Potassium salt of QCl_4 ($K^+QCl_4^-$) was prepared similarly in acetone. $K_3Fe(CN)_6$ of G.R. grade was used without further purification. KCl was recrystallized once from an aqueous HCl solution. Acetonitrile of G.R. grade was used without further purification. Water was deionized and distilled. Solvent used was a 1:1 (v/v) mixture of water and acetonitrile.

The electronic spectra were taken at 15°C with a Hitachi EPS-3T spectrophotometer. The rate was measured with a Union Giken temperature-jump apparatus. The application of the present apparatus to the reactions in organic solvents was described elsewhere (5). The reaction was monitored by the transmittance change at 739 nm (λ_{max} of $TCNQ^-$). The sample solution was thermostated at 10°C before the temperature-rise. The temperature-rise was about 5°C, thus both the equilibrium and kinetic results were obtained at 15°C.

Results

(a) $Fe(CN)_6^{4-}$/TCNQ System

When $K_3Fe(CN)_6$ (ca. 10^{-2} *M*) was added to a solution of TCNQ (ca. 10^{-4} *M*), K^+TCNQ^- (ca. 10^{-5} *M*), and KCl (ca. 10^{-2} *M*), the absorbance at 840 nm (λ_{max} of $TCNQ^-$) decreased, depending on the added amount of $K_3Fe(CN)_6$. This indicated the establishment of the following equilibrium.

$$[3] \quad Fe(CN)_6^{4-} + TCNQ \rightleftharpoons Fe(CN)_6^{3-} + TCNQ^-$$

The apparent equilibrium constant of the above reaction defined by

$$K_{ap} = \frac{[TCNQ^-][Fe(CN)_6^{3-}]_t}{[TCNQ][Fe(CN)_6^{4-}]_t}$$

was determined spectrophotometrically in the following way. Here subscript t denotes the total concentration of a bracketed species, considering the fact that $Fe(CN)_6^{4-}$ and $Fe(CN)_6^{3-}$ are at least partially associated with K^+ (7). $[TCNQ^-]$ was determined from the absorbance at 840 nm ($\varepsilon = 4.33 \times 10^4$). [TCNQ] was obtained from the mass balance of

$$[TCNQ]_0 + [TCNQ^-]_0 = [TCNQ] + [TCNQ^-]$$

where subscript zero denotes the initial concentration of a bracketed species before $K_3Fe(CN)_6$ was added. $[Fe(CN)_6^{4-}]_t$ was equated to the decrease of $[TCNQ^-]$. $[Fe(CN)_6^{3-}]$ was equated to the initial value, since it was present in large excess over other species. The calculated K_{ap} was constant at 56 ± 5 for 0.012 *M* of $K_3Fe(CN)_6$ and 0.019 *M* of KCl, where the ratio of [TCNQ] to $[K^+TCNQ^-]$ was varied more than five times in the ranges of $1.0–2.0 \times 10^{-4}$ *M* of TCNQ and $0.3–1.6 \times 10^{-5}$ *M* of K^+TCNQ^-, respectively.

When the concentrations of $K_3Fe(CN)_6$ and KCl were varied, K_{ap} was found to be no longer a constant value. The dependence of K_{ap} on the total concentration of K^+, $[K^+]_t$, is shown in Fig. 1, where $[K^+]_t$ was equated to $3[K_3Fe(CN)_6]_t + [KCl]$. The interpretation of this result is given in the following discussions.

The rates of electron-transfer were measured with a temperature-jump apparatus. The reaction was studied under the conditions of large excess of $K_3Fe(CN)_6$, TCNQ, and KCl over K^+TCNQ^- and $K_4Fe(CN)_6$. Under this condition, it was expected that the forward and backward rates of reaction [3] were mainly determined by the concentration of TCNQ and $K_3Fe(CN)_6$, respectively. At temperature-rise, the exponential decrease of transmittance was observed at 739 nm (λ_{max} of $TCNQ^-$). In order to establish the mechanistic aspects of the reaction [3], the following three series of experiments were performed: (*i*) The relaxation time, τ, was obtained by changing the concentration of TCNQ at the constant concentration of $K_3Fe(CN)_6$ and KCl. The results are displayed in Fig. 2; (*ii*) τ was obtained by changing the concentration of $K_3Fe(CN)_6$ ($0.5–1.2 \times 10^{-2}$ *M*), keeping the concentration of KCl and TCNQ at 0.17 *M* and 7.1×10^{-5} *M*, respectively. τ^{-1} was found to follow the equation,

$$[4] \quad \tau^{-1} = (7.5 \pm 5) \times 10^4 [K_3Fe(CN)_6]_t \ s^{-1}$$

(*iii*) τ was obtained by varying the concentration of KCl at the constant amounts of TCNQ (7.1×10^{-5} *M*) and $[K_3Fe(CN)_6]_t$ (0.012 *M*). The results are shown in Fig. 3, where $[K_3Fe(CN)_6]_t\tau$ is plotted against the reciprocal of $[K]_t$.

Summarizing the above results, the following kinetic expression was obtained.

$$[5] \quad \tau^{-1} = k_1[TCNQ] + k_2[K_3Fe(CN)_6]_t \times [K^+]_t/(1 + A[K^+]_t)$$

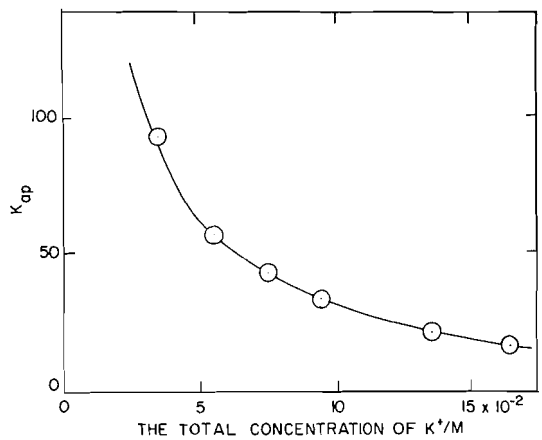

FIG. 1. Dependence of K_{ap} on the total concentration of K^+ for the system of TCNQ/$Fe(CN)_6^{4-}$.

Can. J. Chem. Downloaded from www.nrcresearchpress.com by 210.87.254.6 on 09/05/12
For personal use only.

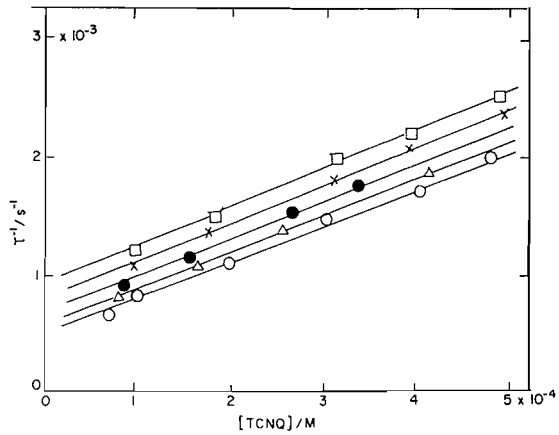

FIG. 2. Dependence of $1/\tau$ on [TCNQ] at various concentrations of $[K^+]_t$; $[K^+]_t$ = (□) 17 × 10^{-2} M, (×) 14 × 10^{-2} M, (●) 9.6 × 10^{-2} M, (△) 5.6 × 10^{-2} M, and (○) 3.6 × 10^{-2} M.

where $k_1 = (2.9 \pm 0.2) \times 10^6\ M^{-1}\ s^{-1}$, $k_2 = (9.9 \pm 1.0) \times 10^5\ M^{-1}\ s^{-1}$, and $A = (9 \pm 2)\ M^{-1}$. The interpretation of this expression is given in the Discussion section.

(b) $Fe(CN)_6^{4-}/QCl_4$ System

The apparent equilibrium constant of the following reaction was determined spectrophotometrically in

$$Fe(CN)_6^{4-} + QCl_4 \rightleftharpoons Fe(CN)_6^{3-} + QCl_4^-$$

a similar way to system (*a*). In this case, the decrease of the absorption peak at 450 nm due to QCl_4^- was measured as the function of the added amount of $K_3Fe(CN)_6$ (ca. 10^{-4} M), QCl_4 (ca. 10^{-4} M), and KCl (ca. 10^{-2} M). The dependence of K_{ap} on the total concentration of K^+ is shown in Fig. 4, in

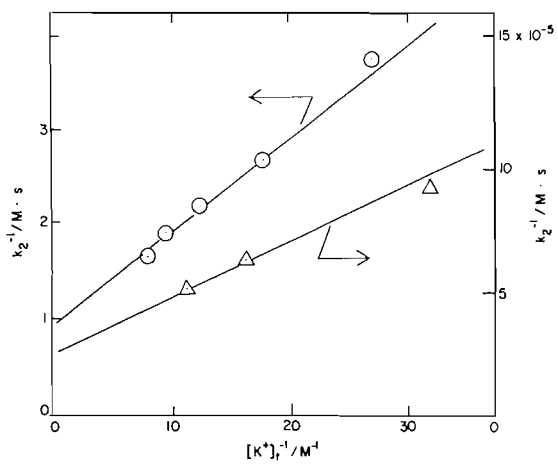

FIG. 3. Dependence of the reciprocal of backward rate, i.e. $[K_3Fe(CN)_6]_t\tau$ on the reciprocal of $[K^+]_t$; (○) TCNQ/$Fe(CN)_6^{4-}$ and (△) $QCl_4/Fe(CN)_6^{4-}$.

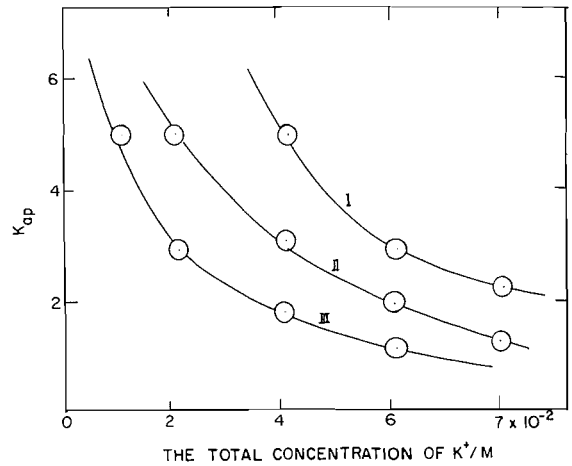

FIG. 4. Dependence of K_{ap} on the total concentration of K^+ for the system of $QCl_4/Fe(CN)_6^{4-}$; solvents are (I) 1:1, (II) 2:1, and (III) 3:1 (v/v) acetonitrile–water.

which K_{ap} was determined for three kinds of mixed solvents.

The temperature-jump measurements were performed for a solution containing the excess amount of $K_3Fe(CN)_6$ and QCl_4 over $K_4Fe(CN)_6$ and $K^+QCl_4^-$, respectively. This simplifies the interpretation of kinetic results as in system (*a*). The experiments similar to system (*a*) lead to the following kinetic expression (Figs. 3 and 5).

$$[6] \quad 1/\tau = k_1[QCl_4] + k_2[K_3Fe(CN)_6]_t \times [K^+]_t/(1 + A[K^+]_t)$$

where $k_1 = (5.2 \pm 0.1) \times 10^4\ M^{-1}\ s^{-1}$, $k_2 = (4 \pm 1) \times 10^{-5}\ M^{-1}\ s^{-1}$, and $A = (10 \pm 4)\ M^{-1}$. The interpretation of this result is given in the following section.

Discussion

To interpret the present equilibrium and kinetic results, we assume the following scheme:

$$[7] \quad \begin{array}{ccc} & \overset{K_0}{} & \\ Fe(CN)_6^{4-} + TCNQ & \rightleftharpoons & Fe(CN)_6^{3-} + TCNQ^- \\ K^+ \Big\downarrow\Big\uparrow K_{II} & & K^+ \Big\downarrow\Big\uparrow K_{III} \\ K^+Fe(CN)_6^{4-} + TCNQ & \rightleftharpoons & K^+Fe(CN)_6^{3-} + TCNQ^- \end{array}$$

where K_{II} and K_{III} are the equilibrium constants of association of $Fe(CN)_6^{4-}$ and $Fe(CN)_6^{3-}$ with K^+, respectively, and K_0 the equilibrium constant of eq. [2]. Under the above reaction scheme, the experimentally obtained K_{ap} is related to K_0, K_{II} and K_{III} as below.

$$[8] \quad K_{ap} = K_0(1 + [K^+]_f K_{III})/(1 + [K^+]_f K_{II})$$

where $[K^+]_f$ denotes the concentration of free K^+

Can. J. Chem. Downloaded from www.nrcresearchpress.com by 210.87.254.6 on 09/05/12
For personal use only.

TABLE 1. The summary of the equilibrium and kinetic results

System	$k_f'/(M^{-1}\,s^{-1})$	$k_b'/(M^{-1}\,s^{-1})$*	k_f'/k_b'	K_{III}†	K_{II}‡
(*a*) $Fe(CN)_6^{4-}$/TCNQ	$(2.9\pm0.2)\times10^6$	$(1.1\pm0.1)\times10^5$	26 ± 3	9 ± 2	130 ± 60
(*b*) $Fe(CN)_6^{4-}$/QCl_4	$(5.2\pm0.4)\times10^4$	$(4.0\pm1)\times10^4$	1.3 ± 0.3	10 ± 4	140 ± 70

*Obtained from the intercept of a straight line in Fig. 3.
†Obtained by dividing the intercept by the slope of a straight line in Fig. 3 (see eqs. [5] and [10]). The observed agreement of this quantity between systems (*a*) and (*b*) supports the validity of eqs. [9] and [10].
‡Obtained by multiplying K_{III} by the quantity, K_{II}/K_{III}, which was determined from Figs. 1 and 4 (see text).

ion.[2] When we compared this relation with the results in Figs. 1 and 4, the following results are obtained: $K_0 = K_{ap}$ (at $[K^+]_f = 0) = (2 \pm 0.5) \times 10^2$ and 15 ± 5 for $Fe(CN)_6^{4-}$/TCNQ and $Fe(CN)_6^{4-}$/QCl_4, respectively. $K_{III}/K_{II} = K_{ap}$ (at $[K^+]_f \to \infty)/K_0 = (7 \pm 3) \times 10^{-2}$ for both $Fe(CN)_6^{4-}$/TCNQ and $Fe(CN)_6^{4-}$/QCl_4. The larger value of K_0 for $Fe(CN)_6^{4-}$/TCNQ as compared to $Fe(CN)_6^{4-}$/QCl_4 reflects the higher electron affinity of TCNQ. The fact that both systems (*a*) and (*b*) give the similar value of K_{III}/K_{II} supports the validity of the above reaction scheme.[3]

Under the above scheme, the relaxation time is related to the forward (k_f) and backward (k_p) rate constants of electron transfer as shown below.

$$[9]\quad \tau^{-1} = \left(k_f \frac{1}{1 + [K^+]_f K_{II}} + k_f' \frac{[K^+]_f K_{II}}{1 + [K^+]_f K_{II}}\right)[R] + \left(k_b \frac{1}{1 + [K^+]_f K_{III}} + k_b' \frac{[K^+]_f K_{III}}{1 + [K^+]_f K_{III}}\right)[Fe(CN)_6^{3-}]_t$$

where k_f, k_b and k_f', k_b' denote the rate constants of electron-transfer reactions involving free and ion-paired ions, respectively. In deriving the above equation, we use the experimental conditions of $[R] \gg [Fe(CN)_6^{4-}]_t$ and $[Fe(CN)_6^{3-}]_t \gg [R^-]$. It is assumed also that the ion-pairing equilibria of $Fe(CN)_6^{4-}$ and $Fe(CN)_6^{3-}$ proceed much faster than the electron-transfer equilibria. When we compare

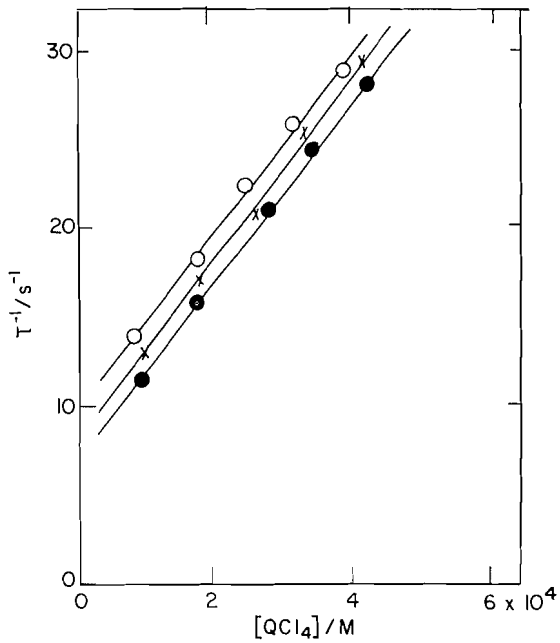

FIG. 5. Dependence of $1/\tau$ on $[QCl_4]$ at various concentrations of $[K^+]_t$; $[K^+]_t$ = (○) 9.0×10^{-2} *M*, (×) 6.0×10^{-2} *M*, and (●) 3.0×10^{-2} *M*.

the theoretical expression [9] with the experimental results [5] and [6], we arrived at the conclusion that [9] becomes identical with [5] and [6] under the conditions of $1 \ll [K^+]_f K_{II}$ and $k_f \ll k_f'[K^+]_f K_{II}$. If this is the case, the following simple relations are obtained:

$$[10]\quad k_1 = k_f' \qquad k_2 = k_b' K_{III} \qquad A = K_{III}$$

In other words, $Fe(CN)_6^{4-}$ is mostly present in the form of $K^+Fe(CN)_6^{4-}$ and the electron-transfer occurs by way of this ion-paired species. In Table 1, the numerical values of equilibrium and rate constants are summarized. It should be noted that the condition, $[K^+]_f K_{II} \gg 1$, assumed for deriving the above relations is satisfied under the present condition. The following points are noted for the present results: (*i*) k_f' for $Fe(CN)_6^{4-}$/TCNQ is much faster than that for $Fe(CN)_6^{4-}$/QCl_4. This corresponds to

[2]The deviation of $[K^+]_t$ from $[K^+]_f$ arises mainly from the association of K^+ with Cl^-. The association constant of K^+ and Cl^- in the present solvent (dielectric constant 54) is concluded to be less than 1, since the association constants in 44% ethanol/water (dielectric constant 42) and 38% ethanol/water (dielectric constant 56) are 1.2 and 0.3, respectively (7). Therefore $[K^+]_t$ is almost equal to $[K^+]_f$ provided that $[K^+]_t$ is less than 0.1 *M*.

[3]The association constants of K^+ with $Fe(CN)_6^{4-}$ and $Fe(CN)_6^{3-}$ in water are reported to be 31 and 7.0 at $\mu = 0.1$ and 35°C, respectively (8). The association of K^+ with $TCNQ^-$ was neglected.

the larger electron affinity of TCNQ than QCl_4. In other words, the electron-transfer rate is influenced by the free energy change of reaction, as is well established in the electron-transfer reaction between metal ions (9). This result is in marked contrast with what was previously observed for the electron-transfer reaction between organic compounds, e.g., $TCNQ^-$/substituted quinone systems (5). In the latter systems, the rate is always nearly a diffusion-controlled one provided that the free energy change of the reaction is negative. Therefore the present results suggest the interaction for the electron-transfer between $Fe(CN)_6^{4-}$ and TCNQ is more similar to the metal ion – metal ion interaction than for organic molecule – organic molecule interactions. (*ii*) The ion-paired species are more reactive in electron-transfer than free ions: i.e. $k_f \ll k_f' \times [K^+]_f K_{II}$. At first glance, this fact seems to support the view that K^+ plays the role of a bridging ion between $Fe(CN)_6^{4-}$ and R (eq. [1′]). If this were correct, however, $[K^+]_t$ would enhance both the forward (k_f') and backward (k_b') reaction rates. It has already been established that k_f' is unaffected by $[K^+]_t$ (eq. [10]). Therefore K^+ does not play a catalytic role as in the reaction of $Fe(CN)_6^{4-}$/$Fe(CN)_6^{3-}$. Consequently the transition state suspected in the Introduction (eq. [I′]) is not realized in the present systems.

1. M. SHPORER, G. RON, A. LOWEWNSTEIN, and G. NARON. Inorg. Chem. **4**, 361 (1965).
2. R. J. CAMPION, C. F. DECK, P. KING, and A. C. WAHL. Inorg. Chem. **6**, 672 (1967).
3. A. C. WAHL. Z. Electrochem. **60**, 90 (1960).
4. G. SCHERER and F. WILLIG. Ber. Bunsenges. Phys. Chem. **78**, 1253 (1974).
5. A. YAMAGISHI. J. Phys. Chem. **80**, 1271 (1976).
6. (*a*) J. H. BAXENDALE *et al.* Trans. Faraday Soc. **47**, 963 (1951); (*b*) S. A. LEVINSON and R. A. MARCUS. J. Phys. Chem. **72**, 358 (1968).
7. G. J. TANG and R. P. T. TOMKINS. Nonaqueous electrolyte handbook. Academic Press, New York. 1972.
8. R. W. CHLEBECK and M. W. LISTER. Can. J. Chem. **44**, 437 (1966).
9. F. BASOLO and R. G. PEARSON. Mechanism of inorganic reactions. Wiley, New York. 1967.

Can. J. Chem. Downloaded from www.nrcresearchpress.com by 210.87.254.6 on 09/05/12
For personal use only.

Synthesis of a 4,5-unsaturated-3-keto sugar (methyl 2-*O*-benzoyl-4-deoxy-6-*O*-triphenylmethyl-α-D-*glycero*-hex-4-enopyranosid-3-ulose)[1]

MARK BERNARD YUNKER AND BERT FRASER-REID

Guelph–Waterloo Centre for Graduate Work in Chemistry, Waterloo Campus, University of Waterloo, Waterloo, Ont., Canada N2L 3G1

Received March 16, 1978

MARK BERNARD YUNKER and BERT FRASER-REID. Can. J. Chem. **56**, 2221 (1978).

An approach to the synthesis of the hex-4-enopyranosid-3-ulose **5** has been investigated. The readily available 3-keto derivative **8** is easily debenzylidinated but the resulting diol is benzoylated preferentially at carbon 4 rather than at the primary position. However, tritylation occurs at the primary position and the product is sulfonylated to give the 4-*O*-methylsulfonyl derivative (**11***b*). Iodinolysis of this α-ketosulfonate did not follow an S_N2 course giving the desired axial iodide **14***b*. Instead a course of reductive elimination was observed involving the presumed intermediacy of an enolic hypoiodite. β elimination of methanesulfonic acid from **11***b* was in fact possible by using diazabicyclononene in benzene–tetrahydrofuran solution. The process undoubtedly involves epimerisation, and the product consists of a mixture of the desired **5** (R = CPh_3) and its 2-epimer **22**. These enones are prone to base-catalysed decomposition so that although the three steps from the starting ketone **8** to the sulfonate **11***b* can each be carried out in excellent yield, the final elimination proceeds in 39% yield after isolation.

MARK BERNARD YUNKER et BERT FRASER-REID. Can. J. Chem. **56**, 2221 (1978).

On a étudié une approche à la synthèse des hexèno-4 pyrannosiduloses-3 (**5**). On peut facilement enlever le groupe benzylidène du dérivé céto-3 (**8**) facilement accessible mais le diol qui en résulte est benzoylé préférentiellement au niveau du carbone-4 plutôt que dans la position primaire. Toutefois la tritylation se produit en position primaire et le produit peut être sulfonylé pour obtenir le dérivé *O*-méthylsulfonyl-4 (**11***b*). L'iodolyse de cet α-cétosulfonate ne se produit pas suivant un mécanisme S_N2 pour conduire à l'iodure axial désiré (**14***b*). Il se produit plutôt une élimination réductrice impliquant vraisemblablement un hypoiodure énolique comme intermédiaire. L'élimination β de l'acide méthanesulfonique à partir de (**11***b*) est possible si l'on fait appel au diazabicyclononène dans une solution de benzène–tétrahydrofuranne. Le processus implique sans aucun doute une épimérisation et le produit comporte un mélange du produit (**5**) désiré (R = CPh_3) et de son épimère-2 (**22**). Ces énones peuvent subir facilement des décompositions catalysées par les bases; ceci implique que même si trois étapes peuvent être effectuées, avec de bons rendements, à partir de la cétone (**8**) pour conduire au sulfonate (**11***b*), l'élimination finale ne se produit qu'avec un rendement de 39% en produit isolé.

[Traduit par le journal]

The synthesis and reactions of unsaturated pyranosides have long been an area of interest in this laboratory (1) and in pursuing this interest we have developed and published preparative procedures for the enones **1** (2*a*; see also 2*b* and earlier work by P. M. Collins), **2** (3), and **3** (4). The unsaturated lactone **4** has also been prepared in our laboratory[2] and hence the potential exists for carrying out conjugate addition reactions at carbons 1, 2, 3, and 4. Indeed many of these enones have been utilized in this way, having been proved of value for the syntheses of branched-chain (5, 6) and amino (7) sugars as well as for photoalkylation (8) and cycloaddition (9) reactions.

The enone **5** is the only missing member of the series and for this reason we decided to attempt its synthesis. Like compound **1**, compound **5** is a vinylogous ester but experience with **1** has shown that these systems undergo conjugate 1,4-additions in good yield (5, 6*a*, 10). Thus availability of **5** would open the possibility of preparing pyranosides with a variety of substituents at carbon 5.

Apart from the foregoing reasons, methods for introducing olefinic unsaturation between carbons 4 and 5 are of interest since this feature is present in at least two antibiotics. The first reported was sisomicin (11) and more recently the antibiotic from *Oospora virescens* has also been found to be a hex-4-enopyranoside (12).

Of the existing methods for introducing unsaturation between carbons 4 and 5, β elimination from aldehydes or uronate derivatives such as **6** (X = H or *O*-alkyl) is the most frequently encountered (13).

[1]Taken from the Ph.D. Thesis of M.B.Y., University of Waterloo (1975). Present address: Department of Chemistry, University of Victoria, Victoria, British Columbia, V8W 2Y2.

[2]M. B. Yunker, J. L. Primeau, and B. Fraser-Reid. Unpublished results.

Can. J. Chem. Downloaded from www.nrcresearchpress.com by 210.87.254.5 on 09/05/12
For personal use only.

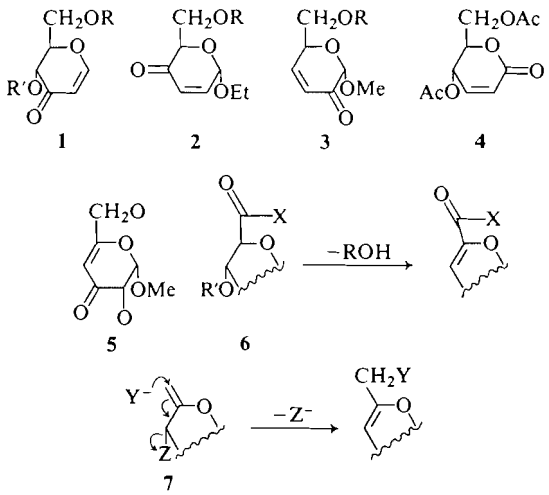

However S_Ni reactions of hex-5-enopyranosides **7** bearing a good leaving group (e.g., Z = OTs) (14) have been observed. Cope and Hofmann eliminations from an *N*-oxide and quaternary ammonium salt, respectively, have been carried out by Stevens and Chitharanjan (15).

For our study, the starting material was the ketone **8** which is available in good yield in three steps from methyl α-D-glucopyranoside (16). The conversion of **8** into **5** was conceived to involve the axial iodide (cf. **14***a*) from which β elimination of hydrogen iodide should be a facile process. In pursuit of this idea, the diol **9**, prepared by acid-catalysed debenzylidination of **8**, was treated with benzoyl chloride at low temperature in the hope of obtaining the primary benzoate **12***a*. In the event, a dibenzoate was produced (in addition to some tribenzoate **10***b*), which was sulfonylated, the expected product being the mesylate **11***a*. Iodinolysis gave a crystalline iodide of correct elemental composition but which could not be dehydrohalogenated using a variety of organic or inorganic bases.

To confirm its structure the iodide was hydrogenolysed using Raney nickel. The nmr spectrum of the product contained a methyl doublet at 1.47 ppm with a coupling constant of 6 Hz which showed immediately that we had prepared the 6-deoxy substance **13***b* rather than a 4-deoxy isomer **14***b*. Thus monobenzoylation of the diol **9** had not occurred at the primary position giving **12***a* but rather at the secondary giving **10***a*, the latter then giving rise to the sulfonate **10***c* and thence the iodide **13***a*.

This unexpected course of selective benzoylation suggested that the 4-hydroxyl group was unusually acidic. This could probably be the result of the hydrogen bonding expressed in **15**. In this connection it is conceivable that **15** could undergo an ene–diol rearrangement giving **16** so that the product from the above series of transformations would be the

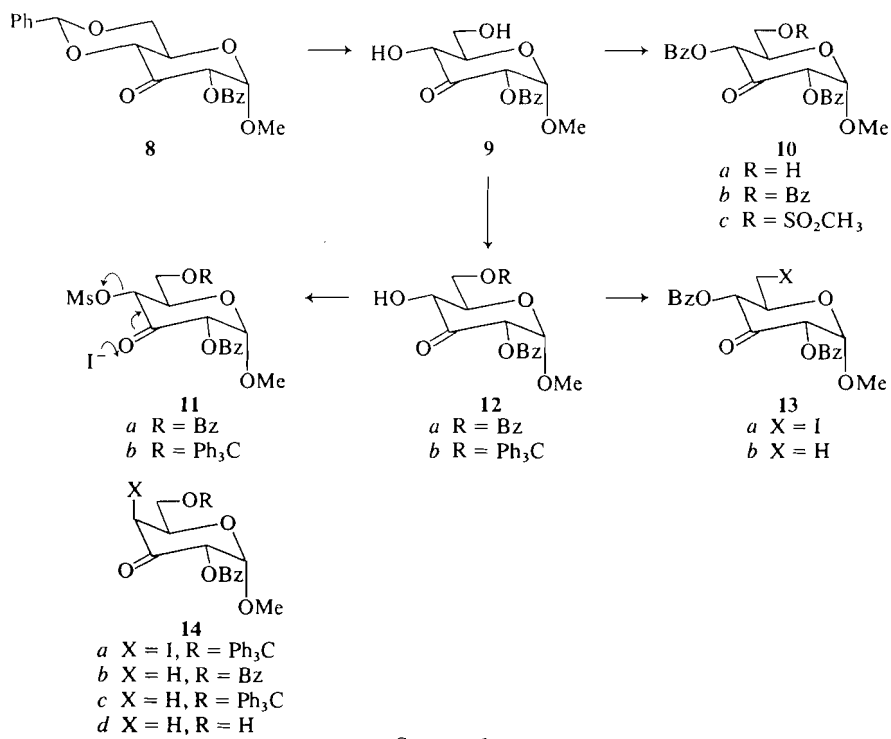

SCHEME 1

Can. J. Chem. Downloaded from www.nrcresearchpress.com by 210.87.254.5 on 09/05/12
For personal use only.

Can. J. Chem. Downloaded from www.nrcresearchpress.com by 210.87.254.5 on 09/05/12
For personal use only.

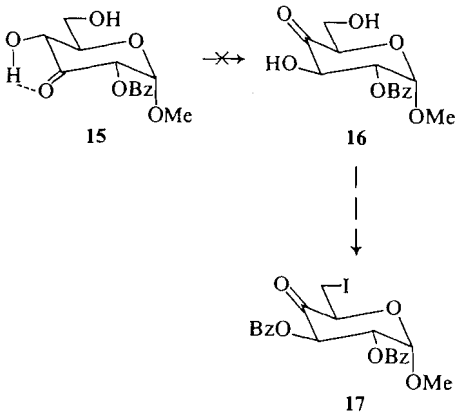

iodide **17** rather than **13***a*. This possibility was readily discounted by examining the 220 MHz nmr spectrum of the crystalline iodide (see Experimental). The signal for H-5 at 4.16 ppm was a triplet of doublets with spacings of 2.5, 7.3, and 10.0 Hz. The first two are assignable as couplings to H-6 and H-6′, whereas the last is clearly a *trans*-diaxial coupling as required by J_{45} of **13***a*. Structure **17** was therefore ruled out.

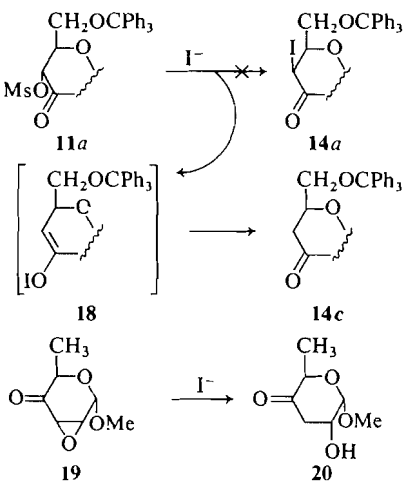

SCHEME 2

Selective protection of the primary hydroxyl group of **9** was in fact accomplished by tritylation giving **12***b*. Presumably the greater steric requirements of the triphenylmethyl group ensures reaction at the primary position, the greater acidity of the C-4 hydroxyl (cf. **15**) notwithstanding.

Sulfonylation of **12***b* proved to be problematic. With *p*-toluenesulfonyl chloride, the reaction proceeded in low yield and was not reproducible. On the assumption that this was due to steric hindrance of the hydroxyl group of **12***b* the procedure for hindered alcohols using methanesulfonyl chloride and triethylamine in methylene chloride (17) was tried. This reaction however took an unexpected course giving a sultone (18). However upon treatment with methanesulfonyl chloride and pyridine in the usual way, **11***b* was obtained in quantitative yield.

Iodinolysis of **11***b* with sodium iodide in methyl ethyl ketone gave two products which were poorly resolved on tlc but a sodium fusion test on the mixture indicated that neither contained iodine. Removal of the trityl group gave separable products, and the major one was judged to be **14***d* on the basis of the mass spectrum and elemental analysis of its *p*-nitrobenzoate. In confirmation of this the 220 MHz nmr spectrum of **14***c* (see Experimental) showed the C-4 methylene protons, identifiable by double irradiation of H-5.

The process of reductive elimination presumably involves the enolic hypoiodite **18**. A comparable process has recently been reported by Paulsen and co-workers (19) for conversion of the oxirane **19** into the alcohol **20**.

In light of the failure to obtain the iodide **14***a* by iodinolysis of **11***b* it was decided to see whether the desired β elimination could be carried out on the sulfonate **11***b* itself. It was reasoned that since carbon 4 is an enolisable centre, treatment with base could cause epimerisation to **21**, and β elimination should then follow since the entities to be eliminated are in the desired antiparallel geometry.

In the event, when the sulfonate **11***b* was treated with diazabicyclononene in tetrahydrofuran–benzene solution at room temperature, the starting material disappeared after 15 min. The product obtained in 39% yield after chromatography, proved to be a mixture of the α-D-*glycero* (**5**) and β-L-*glycero* (**22**) derivatives. Obviously the desired elimination had occurred but had been accompanied by extensive epimerisation at carbon 2. The low yield was in part due to the fact that considerable detritylation occurred during the reaction judging from the amount of triphenylcarbinol detected on tlc. How-

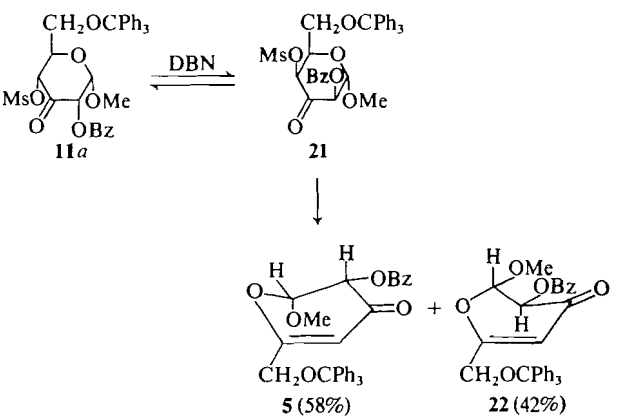

SCHEME 3

Can. J. Chem. Downloaded from www.nrcresearchpress.com by 210.87.254.5 on 09/05/12
For personal use only.

ever there was no evidence for detritylated **5** or **22** among the substances isolated from the chromatographic column. If the reaction was allowed to go for 30 min, the enones **5** and **22** were completely destroyed.

It proved impossible to resolve **5** and **22** using a variety of solvent systems. However the infrared spectrum of the mixture showed, apart from the benzoate absorption at 1735 cm^{-1}, absorptions at 1696 and 1603 cm^{-1} for the α-enone chromphore. In the α-enone **1** the corresponding absorptions are at 1700 and 1600 cm^{-1} (2).

The 220 MHz nmr spectrum (see Experimental) of the mixture showed clearly two sets of signals for the protons on carbons 1, 2, 4, and 6 for the epimers **5** and **22**. The two doublets at 5.44 and 5.86 ppm with a common coupling constant of 3.5 Hz was readily recognized as belonging to H-1 and H-2 of **5** in view of the similarity of these parameters to those of **13***a* (H-1 at 5.40, H-2 at 5.75; J_{12} = 4.0 Hz). A second pair of doublets at 5.34 (H-1) and 5.57 ppm (H-2) with a common coupling of 9.0 Hz indicated that epimerisation had occurred at carbon 2 and that the conformation of the substance, **22**, was as indicated in the drawing (Scheme 3). In both **5** and **22**, an allylic coupling of 1 Hz was observed between H-4 and H-6.

The methoxyl signals of **5** and **22** were clearly resolved at 3.48 and 3.55 ppm, respectively, the assignment being made by comparing their integrated intensities with those of the ring protons described in the preceding paragraph. The ratio of **5** and **22** was thereby determined as 1.4:1.

The mass spectrum of the mixture of **5** and **22** (see Experimental) showed a parent ion of 520.18948 in excellent agreement with the calculated value of 520.18860. The peak for $M^+ - OCH_3$ also showed good correspondence, 489.16542 vs. 489.17021.

In summary, although the first three steps (see Scheme 1) **8** → **9**, **9** → **12***b*, and **12***b* → **11***b* could be carried out in 93%, 77%, and quantitative yields, respectively, conditions could not be found for carrying out the β elimination smoothly. The iodinolysis of **11***b*, instead of giving **14***a*, took an alternative course (Scheme 2) and although treatment with base did afford the desired enone **5**, epimerisation giving **22** also occurred. In addition these enones **5** and **22** proved to be quite labile to base.

Studies aimed at overcoming the problems encountered in the preparation of **5** are currently underway.

Experimental

General

Melting points were determined on a Fischer-Johns heating stage or a Mel-Temp apparatus and are uncorrected. The ^{1}Hmr spectra were determined, unless otherwise stated, in deuteriochloroform containing 1% tetramethylsilane as internal standard with either a Varian T-60 or a Varian HA 100. Coupling constants were obtained by measuring spacings of spectra judged to be first order.

Thin-layer chromatography (tlc) was performed on glass plates coated with silica gel (HF-254, E. Merck) to a thickness of 0.3 mm. The chromatograms were first viewed under ultraviolet light, then exposed to iodine vapor, and finally sprayed with concentrated sulfuric acid. Heating in an oven was required for complete visualization. For column chromatography, E. Merck silica gel (0.05–0.20 mm, 70–325 mesh A.S.T.M.) was used.

*Methyl 2-*O*-Benzoyl-*α*-*D*-ribo-hexopyranosid-3-ulose (**9**)*

Methyl 2-*O*-benzoyl-4,6-*O*-benzylidene-α-*D*-*ribo*-hexopyranosid-3-ulose, **8** (16) (6.4 g, 17.2 mmol) was dissolved in dioxane (0.25 ℓ), heated to 50°C in an oil bath, and 1% sulfuric acid (52 ml) was then added with stirring. After 8 h barium carbonate (35 g) was added and the suspension stirred until the pH was 7, whereupon the salts were removed by filtration through Celite. After concentration of the filtrate the residue was chromatographed on a 1 ft silica column to give 4.7 g (93%) as a syrup; R_f (EtOAc – petroleum ether 1:1) 0.09; nmr ($CDCl_3$) δ: H-1, 5.34 (1H, d, J_{12} = 4 Hz); H-2, 5.68 (1H, broad d); H-4, 4.55 (1H, broad d, J_{45} = 9 Hz); H-5, H-6, H-6′, OH, 3.3–4.3 (5H, m, 2 hydrogens exchange D_2O); OMe, 3.42 (3H, s); OBz centered at 7.5, 8.1 (5H, m).

*Methyl 2,4-Di-*O*-benzoyl-*α*-*D*-ribo-hexopyranosid-3-ulose (**10**a)*

The diol **9** (4.7 g, 15.9 mmol) was dissolved in 1:1 dry pyridine – methylene chloride (100 ml) and cooled to below −40°C in a Dry Ice – 2-propanol bath. Benzoyl chloride (2.00 ml, 15.9 mmol) was diluted with dry methylene chloride (20 ml) and added dropwise to the cold solution over 2.5 h. After 1 additional hour the flask was placed in the freezer compartment of the refrigerator for 2 days. Then, water (15 ml) was added and most of the pyridine was removed on a rotary evaporator. The residue was taken up in ether (150 ml) and washed successively with water, dilute HCl, water, and saturated sodium bicarbonate. The first water wash yielded 0.59 g of unreacted diol. The dried (Na_2SO_4) organic layer yielded a colourless syrup which upon tlc (EtOAc – petroleum ether 1:1) showed two products with R_f 0.52 and 0.23. These were isolated by silica column chromatography in 1.3 and 3.1 g, respectively, and shown to be the tribenzoate (**10***b*) and dibenzoate (**10***a*). Spectral data for **10***a*: nmr ($CDCl_3$) δ: H-1, 5.38 (1H, d, J_{12} = 4 Hz); H-2, 5.78 (1H, d); H-4, 5.85 (1H, d, J_{45} = 10 Hz); H-5, 4.27 (1H, broad d); H-6, H-6′, 3.94 (2H, broad s); OH, 3.3 (1H, broad s) exchangeable with D_2O, OMe, 3.45 (3H, s); OBz centered at 7.5 and 8.1 (10H, m). Irradiation at 5.8 δ (H-4 and H-2) collapses H-5 and H-1 to singlets.

*Methyl 2,4-Di-*O*-benzoyl-6-*O*-methanesulfonyl-*α*-*D*-ribo-hexopyranosid-3-ulose (**10**c)*

The dibenzoate **10***b* (0.72 g, 1.8 mmol) was dried by azeotropic distillation with toluene on a rotary evaporator. Dry pyridine (12 ml) was added and the solution cooled in ice and methanesulfonyl chloride (0.43 ml, 5.4 mmol) was added over 15 min. After 4 h at 0°C, water was added and the mixture was processed in the usual way. A homogeneous, mobile syrup **10***c* 0.65 g, R_f 0.29 (EtOAc – petroleum ether 1:4) was thereby obtained. Spectral data: nmr ($CDCl_3$) δ: H-1, 5.40 (1H, d, J_{12} = 4 Hz); H-2, 5.79 (1H, d); H-4, 5.71 (1H, d, $J_{45} \simeq$ 10 Hz); H-5, H-6, H-6′ centered at 3.57 (3H, broad s); OCH_3, 3.51 (3H, s); OMs, 3.05 (3H, s); OBz centered at 7.5 and 8.1 (10H, m).

Can. J. Chem. Downloaded from www.nrcresearchpress.com by 210.87.254.5 on 09/05/12
For personal use only.

*Methyl 6-Deoxy-2,4-di-*O*-benzoyl-6-iodo-*α*-*D*-ribo-hexopyranosid-3-ulose (**13**a)*

The syrupy sulfonate **10***b* (0.615 g, 1.25 mmol) was dissolved in methyl ethyl ketone and sodium iodide (0.364 g, 2.3 mmol) added. Thin-layer chromatography after 8 h refluxing showed only the iodide **13***a* and so the solution was filtered and the solvent removed. The ethereal solution (150 ml) of the residue was washed twice with aqueous sodium thiosulfate, once with aqueous sodium bicarbonate and water (100 ml portions), and the solution was then allowed to stand over decolourizing carbon and sodium sulfate. Syrupy **13***a* was obtained in quantitative yield, R_f 0.27 (EtOAc – petroleum ether 1:4) and crystallization was effected from methanol. After one recrystallization from methanol: mp 123.5–124°C; $[\alpha]_D^{23}$ +63.5°, (*c* 3.67, $CHCl_3$); spectral data: nmr 220 MHz ($CDCl_3$) δ: H-1, 5.401 (1H, d, J_{12} = 4.0 Hz); H-2, 5.750 (1H, dd, J_{24} = 1.0 Hz); H-4, 5.495 (1H, dd, J_{45} = 10.0 Hz); H-5, 4.16 (1H, ddd, J_{56} = 2.5 Hz, $J_{56'}$ = 7.3 Hz); H-6′, 3.436 (1H, dd, H-6, H-6′ form an AB, $J_{66'}$ = 11.0 Hz); H-6, 3.60 (1H, dd); OMe, 3.53 (3H, s); OBz centered at 7.39, 7.53, and 8.03 (10H, m). *Anal.* calcd. for $C_{21}H_{19}O_7I$: C 49.42, H 3.75, I 24.87; found: C 49.35, H 3.58, I 25.07.

*Methyl 6-Deoxy-2,4-di-*O*-benzoyl-*α*-*D*-ribo-hexopyranosid-3-ulose (**13**b)*

The iodide **13***a* (0.10 g, 0.19 mmol) was dissolved in acetone, (20 ml) an excess of W2 Raney nickel (20) added and the suspension was refluxed with stirring. After 25 h the solution was filtered and the solvent removed to give 0.075 g of **13***b* as a syrup. Thin-layer chromatography showed one spot of R_f 0.59 (EtOAc – petroleum ether 1:1). Spectral data: nmr ($CDCl_3$) δ: H-1, 5.30 (1H, d, J_{12} = 4 Hz); H-2, 5.72 (1H, d); H-4, 5.35 (1H, d, J_{45} = 10 Hz); H-5, 4.33 (1H, dq, J_{56} = 6 Hz); C—C—$H_{3'}$, 1.47 (3H, d); OMe, 3.49 (3H, s); OBz centered at 7.5 and 8.1 (10H, m). The mass spectrum shows a *m/e* 384 parent ion (0.05% of the *m/e* 105 base peak) and loss of methoxy (31) to give *m/e* 353 (0.3%; metastable at *m/e* 324.5) and benzoic acid (122) to give *m/e* 231 (0.8%).

*Methyl 2-*O*-Benzoyl-6-*O*-trityl-*α*-*D*-ribo-hexopyranosid-3-ulose (**12**b)*

The diol **9** (19.8 g, 67 mmol) was dissolved in pyridine (130 ml) and trityl chloride (20.5 g, 73.5 mmol) was added. The solution was stirred at room temperature for 4 days when more trityl chloride (2.1 g, 7.5 mmol) was added. After 2 additional days when only a trace of **9** remained, the pyridine was removed by evaporation and the residue was taken up in a mixture of ether and water. The ether layer was washed with aqueous solutions of hydrochloric acid, sodium chloride, and sodium bicarbonate and then dried and decolourized. After filtration and concentration the residue was chromatographed on a silica column to give 17.4 g (77%) of compound **12***b*; R_f 0.23 (EtOAc – petroleum ether 1:4); nmr ($CDCl_3$) δ: H-1, 5.41 (1H, d, J_{12} = 4 Hz); H-2, 5.75 (1H, dd, J_{24} = 1.5 Hz); H-4, 4.52 (1H, broad d, J_{45} = 10 Hz); H-5, 3.87 (1H, ddd, $J_{56} \simeq$ 2.5 Hz); H-6, H-6′, OH, 3.2–3.6 (3H, m) changeable with D_2O; OMe, 3.48 (3H, s); $OCPh_3$, OBz, 7.0–7.6, 8.2 (20H, m).

*Methyl 2-*O*-Benzoyl-4-*O*-methanesulfonyl-6-*O*-triphenylmethyl-*α*-*D*-ribo-hexopyranosid-3-ulose (**11**b)*

The tritylate **12***b*, sulfonylated as described above for compound **10***a*, gave the desired substance **11***b* in essentially quantitative yield; R_f 0.17 (EtOAc – petroleum ether 1:4). Crystallisation was effected from methanol: mp 189–189.5°C; $[\alpha]_D^{23}$ +1.09°, (*c* 3.54, $CHCl_3$); spectral data: nmr ($CDCl_3$) δ: H-1, 5.35 (1H, d); H-2, 5.72 (1H, broad d, J_{12} = 4 Hz); H-4, 5.45 (1H, broad d, J_{45} = 10 Hz); H-5, 4.10 (1H, ddd, J_{56} = 2 and 4 Hz); H-6, H-6′, 3.5 (2H, broad s); OMe 3.48 (3H, s); OMs 3.05 (3H, s); $OCPh_3$, OBz, 7.1–7.7, 8.2 (20H, m). The mass spectrum showed a faint parent ion at *m/e* 616 and loss of phenyl (77) to give *m/e* 539 (1.3% of base peaks at *m/e* 105). *Anal.* calcd. for $C_{34}H_{32}O_9S$: C 66.217, H 5.231, S 5.200; found: C 66.23, H 5.27, S 5.08.

*Methyl 2-*O*-Benzoyl-4-deoxy-6-*O*-triphenylmethyl-*α*-*D*-erythro-hexopyranosid-3-ulose (**14**c)*

The sulfonate **11***b* (0.370 g, 0.6 mmol) was dissolved in methyl ethyl ketone (15 ml) and sodium iodide (0.166 g, 1.1 mmol) was added. After 2 days tlc showed the disappearance of the starting material and the solution was evaporated to dryness. The residue was taken up in ether and washed with sodium bicarbonate and water before being dried (Na_2SO_4). There was obtained 0.295 g of a foam whose nmr spectrum indicated a mixture of products. These were not well resolved on tlc but after chromatography of a small portion of the mixture on successive silica gel columns, the 4-deoxy compound **14***c* was isolated; R_f 0.32 (EtOAc – petroleum ether 1:4); $[\alpha]_D^{23}$ 26.4° (*c* 9.66, $CHCl_3$); spectral data: ir (CH_2Cl_2): 1730 (OBz), 1715 cm^{-1} (sh, ketone); nmr 220 MHz ($CDCl_3$) δ: H-1, 5.314 (1H, d, J_{12} = 4.0 Hz); H-2, 5.571 (1H, dd, J_{24a} = 0.75 Hz); H-4a, 2.709 (1H, ddd, J_{4a4e} = 14.0 Hz, J_{45} = 11.25 Hz, H-4a,4e form an AB); H-4e, 2.525 (1H, dd, J_{45} = 3.0 Hz); H-5, 4.211 (1H, dddd, J_{56} = 4.1 Hz, $J_{56'}$ = 5.1 Hz); H-6,6′ centered at 3.320 (2H, d-AB); OMe, 3.46 (3H, s); OBz, $OCPh_3$ centered at 7.29, 7.45, 8.11 (20H, m). Irradiation of H-4a changes H-5 to a narrow multiplet and collapses H-2 to a doublet and of H-4e changes H-5 to a ddd (5 lines). The mass spectrum shows a weak parent ion at *m/e* 522 which loses phenyl (77) to give *m/e* 445 (1.4% of the *m/e* 243 (trityl) base peak) and then C_6H_4 (76) to give *m/e* 369 (0.4%).

*Methyl 2-*O*-Benzoyl-4-deoxy-*α*-*D*-erythro-hexopyranosid-3-ulose (**14**d)*

A portion of the tritylate (0.170 g, 0.33 mmol) **14***c* was dissolved in chloroform (10 ml) and cooled to −10°C in an ice–salt bath. Chloroform (5 ml) was cooled separately and hydrogen chloride was bubbled in for 1 min. Both solutions were then mixed and allowed to stand at −10°C. After 30 min tlc indicated that detritylation was complete and ammonia was bubbled into the solution. The precipitated ammonium chloride was removed by filtration through Celite and the filtrate evaporated to dryness. Chromatography on a short column of silica gel afforded the desired compound **14***d* (0.068 g, 75%); R_f 0.17 (EtOAc – petroleum ether 1:1); spectral data: nmr ($CDCl_3$) δ: H-1, 5.33 (1H, d, J_{12} = 4 Hz); H-2, 5.60 (1H, d); H-4a, H-4e, OH centered at 2.6 (3H, m); H-5, 4.27 (1H, m); H-6, H-6′ centered at 3.77 (2H, broad s); OMe, 3.45 (3H, s) OBz centered at 7.6 and 8.2 (5H, m).

The compound was characterized as the *p*-nitrobenzoate and recrystallized from methanol (small needles); mp 134-134.5°C. *Anal.* calcd. for $C_{21}H_{19}O_9N$: C 58.740, H 4.460, N 3.262; found: C 58.65, H 4.53, N 3.27.

*Methyl 2-*O*-Benzoyl-4-deoxy-6-*O*-triphenylmethyl-*α*-*D*-glycero-hex-4-enopyranosid-3-ulose (**5**) and Methyl 2-*O*-Benzoyl-4-deoxy-6-*O*-triphenylmethyl-*β*-*L*-glycero-hex-4-enopyranosid-3-ulose (**22**)*

The sulfonate **11***b* (0.306 g, 0.5 mmol) was dried by azeotroping twice with dry benzene using a rotary evaporator. The flask was transferred to a dry box and a solution (3.4 ml, 0.5 mmol) of diazabicyclononene (2.0 g) in dry tetrahydrofuran (100 ml) was added. A precipitate formed rapidly and after 5 min dry benzene (5 ml) was added and the solution was stirred under an atmosphere of nitrogen for 10 min. Saturated aqueous ammonium chloride (20 ml) and ether were added and the aqueous phase separated and extracted with chloroform. The combined organic layers were dried (Na_2SO_4) and

processing afforded 0.271 g of material which was chromatographed on a silica column using EtOAc – petroleum ether (1:4). A substance (0.100 g) of R_f 0.30 was obtained whose 220 MHz nmr spectrum *vide infra* showed it to contain the α-D-*glycero* (**5**) and β-L-*glycero* (**22**) enones in 58 and 42%, respectively. Spectral data: ir (CH_2Cl_2): 1735 (OBz), 1696 (C=O); 1630 (Ph_3C); 1603 cm^{-1} (C=C); nmr 220 MHz ($CDCl_3$) δ for **5**: H-1, 5.44 (1H, d, J_{12} = 3.5 Hz); H-2, 5.86 (1H, d); H-4, 6.00 (t, J_{46} = 1 Hz); H-6, 3.79 (2H, d); OCH_3, 3.48 (3H, s); for **22**: H-1, 5.34 (1H, d, J_{12} = 9.0 Hz); H-2, 5.57 (1H, d); H-4, 6.07 (1H, t, J_{46} = 1 Hz); H-6, 3.85 (2H, bs); OCH_3, 3.55 (3H, s); for both: OBz, $OCPh_3$, 7.2–7.6 and centered 8.1 (20H, m). For the mass spectrum: (*m/e*): 520 (0.17% of 105 base; calcd. for $C_{33}H_{28}O_6$: 520. 18860; found: 520. 18948; 20.0 rings and double bonds); 489 (0.25%; calcd. for $C_{32}H_{25}O_5$: 489.17021; found: 489.16542; loss of OCH_3 from 520); 447 (12%; calcd. for $C_{30}H_{33}O_4$: 447.15964; found: 447.15898; loss of C_2H_2O from 520); 443 (0.25%; loss of Ph from 520); 338 (0.86%; calcd. for $C_{20}H_{18}O_5$: 338.11543; found: 338.11617; loss PhCO from 443); 243 (80%; CPh_3); 105 (base; PhCO).

Acknowledgements

We are grateful to the National Research Council of Canada and Bristol Laboratories (Syracuse) for financial support.

1. B. FRASER-REID. Acc. Chem.Res. **8**, 192 (1975).
2. (*a*) B. FRASER-REID, D. L. WALKER, S. Y-K. TAM, and N. L. HOLDER. Can. J. Chem. **51**, 3950 (1973); (*b*) P. M. COLLINS, P. GUPTA, and R. IYER. Carbohydr. Res. **11**, 125 (1969).
3. B. FRASER-REID, A. MCLEAN, and E. W. USHERWOOD. J. Am. Chem. Soc. **91**, 5292 (1969); B. FRASER-REID. A. MCLEAN, E. W. USHERWOOD, and M. YUNKER. Can. J. Chem. **48**, 2877 (1970).
4. N. L. HOLDER and B. FRASER-REID. Can. J.Chem. **51**, 3357 (1973); see also E. F. L. J. ANET. Carbohydr. Res. **1**, 348 (1966); K. BOCK and C. PEDERSEN. Tetrahedron Lett. 2983 (1969).
5. (*a*) D. L. WALKER and B. FRASER-REID. J. Am. Chem. Soc. **97**, 6251 (1975); (*b*) D. L. WALKER, B. FRASER-REID, and J. K. SAUNDERS. J. Chem. Soc. Chem. Commun. 319 (1974).
6. (*a*) H. PAULSEN, K. RODEN, and V. SINNWELL. Chem. Ber. **110**, 2146 (1977); (*b*) H. PAULSEN and N. KOEBERNICK. Chem. Ber. **110**, 2127 (1977).
7. J. CLEOPHAX, S. D. GERO, and J. LEBOUL. J. Chem. Soc. Chem. Commun. 710 (1973); J. CLEOPHAX, J. LEBOUL, A. OLESKER, and S. D. GERO. Tetrahedron Lett. 4911 (1973).
8. B. FRASER-REID, N. L. HOLDER, D. R. HICKS, D. L. WALKER, and M. B. YUNKER. Can. J. Chem. **55**, 3978 (1977); B. FRASER-REID, R. C. ANDERSON, D. R. HICKS, and D. L. WALKER. Can. J. Chem. **55**, 3986 (1977).
9. R. M. SRIVASTAVA, B. J. CARTHY, and B. FRASER-REID. Tetrahedron Lett. 2175 (1974).
10. M. B. YUNKER, D. E. PLAUMANN, and B. FRASER-REID. Can. J. Chem. **55**, 4002 (1977).
11. H. REIMANN, R. S. JARET, and D. J. COOPER, J. Chem. Soc. C, 925 (1971); P. L. J. DANIELS, M. UGELMAN, A. K. MALLAMS, R. W. T. KACH, H. F. VERNAY, J. WEINSTEIN, and A. YEHASKE. J. Chem. Soc. Chem. Commun. 1629 (1971).
12. N. CAGNOLI-BELLAVITA. U.S. Patent 3,855,067; Chem. Abstr. **83**, 7126t (1975).
13. G. O. ASPINALL and P. E. BARRON. Can. J. Chem. **50**, 2203 (1972); C. M. MACKIE and A. S. PERLIN. Carbohydr. Res. **24**, 67 (1972); S. HANESSIAN and G. RANCOURT. Can. J. Chem. **55**, 1111 (1977).
14. M. BROCKHAUS and J. LEHMANN. Ann. 1675 (1974); M. BROCKHAUS, W. GORATH, and J. LEHMAN. Ann. 89 (1976).
15. C. L. STEVENS and D. CHITHARANJAN. J. Org. Chem. **40**, 2474 (1975).
16. K. ONODERA and N. KASHIMURA. Methods Carbohydr. Chem. **6**, 331 (1972).
17. R. K. CROSSLAND and K. L. SERVIS. J. Org.Chem. **35**, 3195 (1970).
18. M. B. YUNKER and B. FRASER-REID. J. Chem. Soc. Chem. Commun. In press.
19. H. PAULSEN, K. EBERSTEIN, and W. KOBERNICK. Tetrahedron Lett. 4377 (1974).
20. R. GRAF. Chem. Ber. **96**, 56 (1963).

Can. J. Chem. Downloaded from www.nrcresearchpress.com by 210.87.254.5 on 09/05/12
For personal use only.

Can. J. Chem. Downloaded from www.nrcresearchpress.com by 210.87.254.105 on 09/05/12
For personal use only.

COMMUNICATION

Carbon-13 enrichment in the room temperature multiphoton decomposition of CF_3Br [1]

M. GAUTHIER, P. A. HACKETT, M. DROUIN,[2] R. PILON, AND C. WILLIS

Chemistry Division, National Research Council of Canada, Ottawa, Ont., Canada K1A 0R6

Received June 13, 1978

M. GAUTHIER, P. A. HACKETT, M. DROUIN, R. PILON, and C. WILLIS. Can. J. Chem. **56**, 2227 (1978).

High isotopic selectivities have been observed in the multiphoton decomposition of CF_3Br at room temperature. Photolysis of natural abundance CF_3Br gives C_2F_6 enriched to 42% in carbon-13. This is higher than observed for CF_3I even at very low temperatures.

M. GAUTHIER, P. A. HACKETT, M. DROUIN, R. PILON et C. WILLIS. Can. J. Chem. **56**, 2227 (1978).

La décomposition multiphotonique du CF_3Br à la tempèrature de la piéce conduit à une grande sélectivité isotopique. Le C_2F_6, obtenu par la photolyse du CF_3Br d'abondance isotopique naturelle, est enrichi de 42% en carbone-13. Cette sélectivité est supérieure à ce qui a été observé dans le cas du CF_3I même à très basse tempèrature.

Isotopic selectivity in the multiphoton decomposition of CF_3I induced by focussed infrared radiation from a CO_2-laser has been investigated by measuring the depletion in carbon-12-bearing substrate (1). At room temperatures, the process is virtually non-selective but at $-80°C$ selectivities in the range 10–40 were inferred. The loss of selectivity is most probably a result of the iodine atom abstraction reaction,

$$[1] \qquad {}^{12}CF_3 + {}^{13}CF_3I \rightarrow {}^{12}CF_3I + {}^{13}CF_3$$

which, at room temperature, scrambles the primary selectivity. A comparison of halogen atom transfer reactions involving CF_3 radicals (2) shows that the rate constants at room temperature are in the order

$$k_I \simeq k_{Br} \times 10^3 \gg k_{Cl}.$$

This suggested to us that the multiphoton decomposition of CF_3Br and CF_3Cl would be more tractable systems than CF_3I. We have now shown that the multiphoton decomposition of CF_3Br is highly isotopically selective at room temperature: in fact we observe selectivities higher than those observed in CF_3I even at the lowest temperatures studied. Because of the obvious topicality of this we offer preliminary data here.

All experiments reported here were made using a Lumonics 103 TEA-CO_2 laser. The central portion of the beam was passed through a 1.4 cm diameter aperture and focussed at the centre of the Pyrex reaction cell with a 10 cm focal length germanium lens. Samples of CF_3Br (PCR incorporated) were irradiated and the resultant mixture analysed by glc and mass spectrometry. An isopentane slush bath ($-160°C$) prevented bromine from entering the mass spectrometer. The only product observed was C_2F_6. Since the conversions were small in all cases ($\leq 1\%$) the isotopic composition of the C_2F_6 produced was used to derive primary α-values,

$$[2] \qquad \alpha = \frac{{}^{13}C/{}^{12}C \text{ ratio in products}}{{}^{13}C/{}^{12}C \text{ ratio in starting material}}$$

Peaks at m/e 119, 120, 121 were used, as $C_2F_5^+$ is the most abundant ion in the mass spectrum of C_2F_6.

The α-values observed in the photolysis of 0.19 Torr of CF_3Br are shown in Fig. 1 as a function of laser wavelength, together with a low intensity ir spectrum of the ν_1 band of CF_3Br. As the wavelength of the laser line chosen moves to the low frequency side of the absorption band, the selectivity towards C-13 enriched products continues to increase and is $\alpha = 65$ for the P(26) line of the 9.4 μm band. Beyond this, the yields become small and the measured α-values though high are imprecise. Use of the R lines of the 9.4 μm band of the CO_2 laser shows a strong selectivity towards C-12 enriched products, so strong that we were unable to detect C-13 product ions from the C_2F_6 produced from natural abundance CF_3Br and hence cannot report α-values here.

The pressure dependence of the selectivity was investigated using the P(24) line of the 9.4 μm band of the CO_2 laser. Figure 2 shows α to be strongly pressure dependent. We interpret this loss of selectivity at higher pressures as the result of energy transfer reactions.

Very recently, Letokhov and co-workers (3) reported product enrichment in the multiphoton

[1]NRCC No. 16852.

[2]NRCC Summer Student 1978.

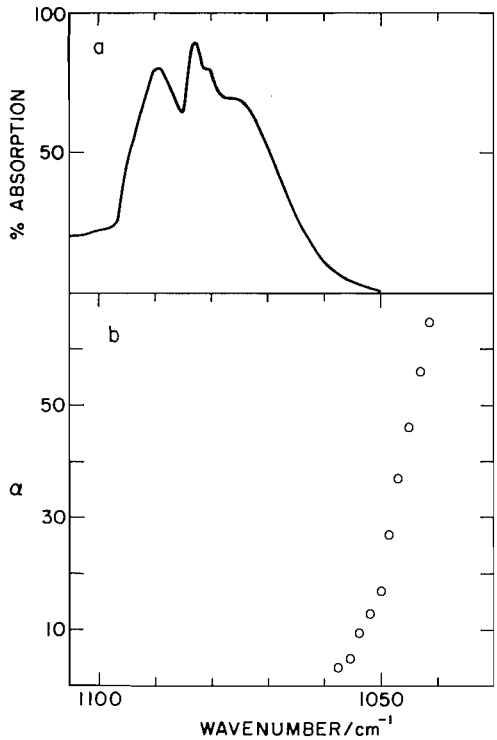

FIG. 1. (*a*) Low resolution, low intensity infrared spectrum of CF_3Br (room temperature, 10 cm cell, 1 Torr). (*b*) α-Values as a function of photolysing wavelength, at 0.19 Torr of CF_3Br at room temperature. α-Values were determined from product C-13 enrichment (see text), the incident fluence depended on the laser line used but was in the range $2 \rightarrow 0.2$ J cm^{-2}; 400 pulses were used on the stronger lines, 2000 on the weakest.

decomposition of CF_3I. At $-40°C$ they observed C_2F_6 enriched to about 20% in carbon-13. Although detailed comparison of the two systems must await

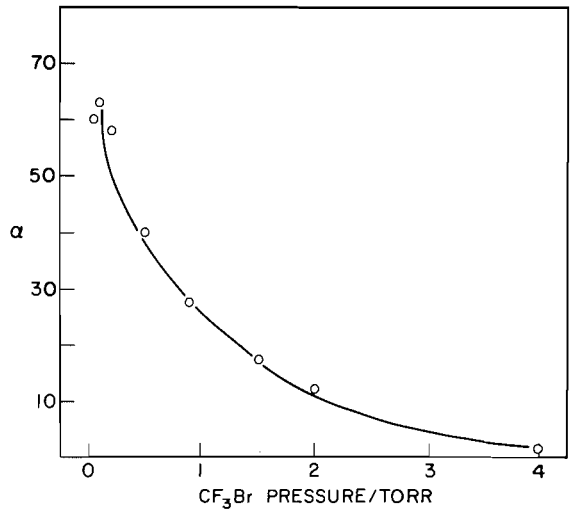

FIG. 2. α-Values as a function of CF_3Br pressure. Photolyses were carried out at room temperature using the P(24) line of the 9.4 μm band; 400 pulses at an incident fluence of 1 J cm^{-2} were used.

full publication, the preliminary data suggest that the selectivity from CF_3Br is at least as good as from CF_3I with the added advantage that the process is selective without cooling.

1. S. BITTENSON and P. L. HOUSTON. J. Chem. Phys. **67**, 4819 (1977).
2. A. F. TROTTMAN-DICKENSON and G. S. MILNE. National Standard Reference Data Series, National Bureau of Standards, Vol. 9. 1967. pp. 59–60.
3. R. V. AMBARTZUMIAN, V. S. LETOKHOV, G. N. MAKAROV, and A. A. PURETZKY. Xth International Quantum Electronics Conference, Atlanta, Georgia, 29th May – 1st June, 1978. Paper N-8.

Can. J. Chem. Downloaded from www.nrcresearchpress.com by 210.87.254.105 on 09/05/12
For personal use only.

Canadian Journal of Chemistry
Published by
THE NATIONAL RESEARCH COUNCIL OF CANADA

Journal canadien de chimie
Publié par
LE CONSEIL NATIONAL DE RECHERCHES DU CANADA

Volume 56 Number 17 September 1 1978

Volume 56 numéro 17 1 septembre 1978

The preferred conformations in solution and rotational barriers of the phenyl moiety in 3,5-dichlorobenzyl derivatives of ammonia, dimethylamine, and dimethylarsine

TED SCHAEFER, WERNER DANCHURA, AND WALTER NIEMCZURA
Department of Chemistry, University of Manitoba, Winnipeg, Man., Canada R3T 2N2

Received March 2, 1978

TED SCHAEFER, WERNER DANCHURA, and WALTER NIEMCZURA. Can. J. Chem. **56**, 2229 (1978).

The long-range spin–spin coupling constants between methylene protons and ring protons are measured in 3,5-dichlorobenzylamine, 3,5-dichlorobenzyldimethylamine, and in 3,5-dichlorobenzyldimethylarsine. The couplings over six bonds are used to derive internal barriers to rotation about the carbon–carbon bond to the phenyl ring. In the above order, they are 0.3 ± 0.3, 0.8 ± 0.2, and 3.0 ± 0.5 kcal/mol. The conformation of lowest energy in the arsine is that in which the CH_2—X bond lies in a plane perpendicular to the benzene plane.

TED SCHAEFER, WERNER DANCHURA et WALTER NIEMCZURA. Can. J. Chem. **56**, 2229 (1978).

On a mesuré les contantes de couplage spin–spin à longue distance entre les protons du méthylène et les protons du cycle dans la dichloro-3,5 benzylamine, la dichloro-3,5 benzyldiméthylamine et la dichloro-3,5 benzyldiméthylarsine. On a utilisé les couplages à travers six liaisons pour déterminer les barrières internes à la rotation autours des liens carbone–carbone conduisant au noyau aromatique. Dans l'ordre mentionnée plus haut, ces valeurs sont respectivement de 0.3 ± 0.3, 0.8 ± 0.2 et 3.0 ± 0.5 kcal/mol. La conformation de plus basse énergie dans l'arsine est celle dans laquelle la liaison CH_2—X se trouve dans un plan perpendiculaire au plan du benzène.

[Traduit par le journal]

Introduction

A recent theoretical and photoelectron spectroscopic study (1) of benzyldimethylarsine concludes that the stable conformation is **1** (X = $As(CH_3)_2$)

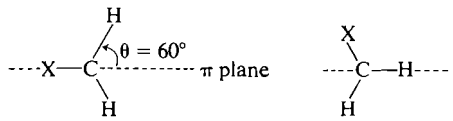

1

2

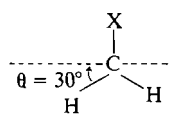

3

instead of **2** or **3**, as would be expected on steric grounds. On the other hand, when X = Cl, Br, or I the *J* method indicates that **3** is preferred by 2 kcal/mol or more (2). The long-range spin–spin coupling constant, ${}^6J_p^{H,CH_2}$, between the methylene protons and the ring proton in the *para* position obeys a $\sin^2\theta$ relationship, where θ is the angle by which the C—H bond on the side chain is twisted out of the plane of the benzene ring (3–6).

For example, in toluene ${}^6J_p^{H,CH}$ ($\theta = 90°$) ≡ ${}^6J_{90}$ is −1.24 Hz (7). For the arsine, having conformation **1**, the observed ${}^6J_p^{H,CH_2}$ should be near −1.24 ($\sin^2 60°$) = −0.93 Hz if **1** is more than 4 kcal/mol more stable than **2** or **3**, as calculated by CNDO/2 (1). If **3** were the stable form, ${}^6J_p^{H,CH_2}$ would be less than 0.6 Hz in magnitude and would approach −1.24 ($\sin^2 30°$) = −0.31 Hz for a high two-fold barrier to rotation about the phenyl-CH_2X bond.

For somewhat lower twofold barriers to rotation, a hindered rotor treatment yields average values of $\sin^2\theta$ as a function of the barrier, the reduced moment of inertia and the temperature. If the stable form is **1**, $\langle\sin^2\theta\rangle$ spans 0.5 and 0.75; if **2**, 0.5 and 0.375; and if **3** is the stable form, $\langle\sin^2\theta\rangle$ lies between 0.5 and 0.25. In toluene, where the internal barrier is negligible in this context, $\langle\sin^2\theta\rangle$ can be taken as 0.5.

Can. J. Chem. Downloaded from www.nrcresearchpress.com by 210.87.254.105 on 09/05/12
For personal use only.

TABLE 1. Proton chemical shifts[a] and spin–spin coupling constants[b] for 3,5-di-chlorobenzyl-X compounds

Parameter	Value		
	X = NH_2 10 mol%, C_6D_6	X = $N(CH_3)_2$ 5 mol%, CS_2	X = As $(CH_3)_2$ 5 mol%, CS_2
ν_{CH_3}	73.7[c]	218.48	89.05
ν_{CH_2}	325.243(3)	331.23	265.95
$\nu_{2,6}$	691.940(3)	714.711(4)	687.065(4)
ν_4	705.753(3)	712.041(5)	702.828(3)
$^4J_o^{H,CH_2}$	−0.773(3)	−0.732(6)	−0.492(5)
$^6J_p^{H,CH_2}$	−0.579(4)	−0.512(7)	−0.391(4)
$^4J_m^{H,H}$	1.943(3)	1.961(4)	1.896(3)
Root mean square deviation	0.012_7	0.012_1	0.008_8

[a]In Hz at 100 MHz to low field of internal tetramethylsilane and at 305 K.
[b]In Hz, numbers in parentheses giving the standard deviation in the last place.
[c]For NH_2 protons.

Accordingly, the surprising conclusion for the arsine was reinvestigated by the *J* method. In addition, the X = $N(CH_3)_2$ and X = NH_2 compounds were studied for purposes of comparison. Attempts at the synthesis of X = $P(CH_3)_2$ ended in failure. Because the phenyl proton region in benzyl compounds is too complex for a precise analysis of its ^1H nmr spectrum, the compounds contained chlorine substituents at the *meta* positions. There is no evidence that these substituents alter the conclusions to be arrived at below (6, 8).

Experimental

3,5-Dichlorobenzylbromide was prepared from the corresponding commercial benzoic acid by standard methods. Dimethylamine was bubbled through a benzene solution of the bromide to yield a precipitate of 3,5-dichlorobenzyl dimethylamine, which was purified and gave a satisfactory ^1H nmr spectrum. 3,5-Dichlorobenzyldimethylarsine was prepared from the bromide and dimethyliodoarsine by the methods in ref. 1 and gave the correct ^1H nmr spectrum. It melted under vacuum between 48 and 52°C (no stem correction) and probably contained some impurity. The 3,5-dichlorobenzylamine had a commercial origin.

Degassed solutions of these compounds (see Table 1) contained internal tetramethylsilane. Their ^1H nmr spectra were repeatedly calibrated at 5 Hz intervals on an HA100 spectrometer at a probe temperature of 305 K. Sweep rates in the frequency-sweep mode were 0.01 and 0.02 Hz/s at a sweep width of 1 Hz/cm.

Results and Discussion

Spectral Analyses

Performed with the computer program LAME (9, 10), the analyses yielded the spectral parameters set out in Table 1. The standard deviations in these parameters were all well below 0.01 Hz, suggesting an accuracy of perhaps 0.02 Hz.

The Internal Rotational Barriers

3,5-Dichlorobenzylamine

If $^6J_{90}$ is −1.24 Hz as in toluene, then $\langle \sin^2 \theta \rangle$ equals $0.59_7/1.24$, or 0.46_7. Taking the reduced moment of inertia as 0.6×10^{-38} g cm^2 (the barrier is fairly insensitive to variations in this quantity), a temperature of 305 K, and conformation **3** as most stable, yields a barrier of 0.4 ± 0.1 kcal/mol. If **2** is the stable form, the barrier rises to about 0.5 kcal/mol.

However $^6J_{90}$ depends somewhat on the electronegativity, E_X, of the substituent X; in this case X = NH_2. Previous work (2) suggests that the magnitude of $^6J_{90}$ sinks to −1.14 Hz when $E_X = 3.0$. Photoelectron spectroscopy (11) indicates that E_{NH} is about the same as that of sulfur, $E_S = 2.5$ on the Pauling scale, whereas $E_N = 3.0$. Assuming E_{NH_2} to be 2.75, together with a linear interpolation between −1.14 and −1.24 Hz at $E_H = 2.1$, yields $^6J_{90}$ as −1.17 Hz. It follows that $\langle \sin^2 \theta \rangle = -0.57_9/-1.17 = 0.49_5$ and that the internal barrier is 0.05 ± 0.05 kcal/mol if **3** is most stable; the assumption that **2** is most stable does not alter the barrier significantly.

It is clear that the barrier is small and, considering measurement errors and the assumption concerning the dependence of $^6J_{90}$ on E_X, a value for the twofold barrier of 0.3 ± 0.3 kcal/mol appears as a sensible compromise. Conformation **1** follows as the high energy form.

An *ab initio* molecular orbital calculation at the STO 3G level (12) gave 2.2 kcal/mol for the barrier in the isolated molecule of benzylamine, **3** most stable. No optimization of the geometry was undertaken. It may be noted that a partial optimization of the geometry in ethylbenzene reduced the corresponding barrier from 4.7 to 2.2 kcal/mol (12), whereas the *J* method yielded 1.2 kcal/mol (8). If a barrier of 2 kcal/mol existed in 3,5-dichlorobenzylamine in solution, $^6J_p^{H,CH_2}$ would lie near −0.4 Hz instead of −0.6 Hz, as observed. Furthermore, an approximate empirical correlation of V_2 with

Can. J. Chem. Downloaded from www.nrcresearchpress.com by 210.87.254.105 on 09/05/12
For personal use only.

Can. J. Chem. Downloaded from www.nrcresearchpress.com by 210.87.254.105 on 09/05/12
For personal use only.

$^4J_o^{H,CH_2}$ for similar compounds (2) predicts a very small barrier for the amine.

3,5-Dichlorobenzyldimethylamine

The reduced moment of inertia varies between 1.2 and 1.9 $\times$ 10^{-38} g cm^2 for various probable conformations, a variation to which the derived barrier is insensitive compared with its sensitivity to an error in ^6J. Under the assumption that $^6J_{90}$ has the same value as in toluene, $\langle \sin^2 \theta \rangle = -0.51_2/-1.24 = 0.41_3$. The barrier is then 1.0 $\pm$ 0.1 kcal/mol. On the other hand, the barrier becomes 0.7 $\pm$ 0.1 kcal/mol if $^6J_{90}$ is -1.17 Hz, corresponding to equal electronegativities for the NH_2 and $N(CH_3)_2$ groups. A suitable value appears to be 0.8 $\pm$ 0.2 kcal/mol, **3** being stable.

If **2** were the ground state conformation, V_2 would be considerably larger. This possibility is considered unlikely because the empirical correlation mentioned above then suggests a modulus of about 0.5 Hz for $^4J_o^{H,CH_2}$ instead of the measured 0.7 Hz.

3,5-Dichlorobenzyldimethylarsine

The reduced moment of inertia ranges between 2.4 and 3.1 $\times$ 10^{-38} g cm^2. The electronegativities of arsenic and hydrogen are nearly equal, so that $^6J_{90}$ can be taken as -1.24 Hz. The observed $^6J_p^{H,CH_2}$ of -0.39_1 Hz leads to a V_2 of 3.0 $\pm$ 0.3 kcal/mol. It seems likely that a barrier of 3.0 $\pm$ 0.5 kcal/mol encompasses the possibilities. It is clear that **3** is the stable conformer. For, if **1** were the stable form, $^6J_p^{H,CH_2}$ would be larger than 0.6 Hz in the presence of a finite barrier. If **2** were the stable form, ^6J would lie between -0.46 and -0.62 Hz for a finite barrier.

Comparisons with Other Methods

In view of the disagreement with the photoelectron results for the arsine derivative, it may be useful to present a comparison of some barriers and conformations previously derived by the *J* method with those deduced by other means.

Phenylethane

Low resolution microwave spectroscopy indicates **3** as the preferred conformation (13). If this is true, then heat capacity data can be fitted by assuming a V_2 of 1.16 kcal/mol (14) for the rotation of the ethyl group. In solution the *J* method yields V_2 as 1.2 kcal/mol for the 3,5-dibromo derivative and **3** is again indicated as the low energy conformation (8). The agreement is rather good, although the internal rotation possibly may be affected by fields from neighbouring molecules and perhaps by a small perturbation from the *meta* substituents in the derivative to which the *J* method was applied. A high resolution microwave investigation of phenylethane would be of interest.

Benzyl Chloride

A recent discussion (15) of electron diffraction data concludes that **3** is the stable conformation and that V_2 is 1.5 kcal/mol, although values as low as 1.0 and as high as 2.7 kcal/mol may not be completely unlikely. The *J* method for the 3,5-dichloro derivative, again in solution, gives 2.1 $\pm$ 0.4 kcal/mol, **3** being stable (2).

Styrene and Isopropyl Benzene

The *J* method (16) yields 1.6 $\pm$ 0.3 kcal/mol for V_2 whereas heat capacity data suggest 2.2 kcal/mol (17) and a recent gas phase, torsional overtone measurement finds 1.8 kcal/mol (18).

There are no data on isopropylbenzene itself. Hyperfine proton coupling in the neutral *p,p',p''*-triisopropyltrityl radical in toluene solution implies that V_2 is 2.1 kcal/mol (19). Hyperfine coupling to the methyl carbon nuclei in *p*-isopropylaniline nickel acetylacetonate complexes suggests 1.5 kcal/mol, whereas the temperature dependence of the methyl carbon spin–lattice relaxation times for *p*-isopropylaniline in chloroform solution indicates 2.8 kcal/mol for V_2 (20). (In our opinion the latter value suffers from the lack of a clear separation between overall and internal reorientational motions.) The *J* method gives 2.0 $\pm$ 0.2 kcal/mol for V_2 in the 3,5-dibromo derivative in CS_2 solution (21).

Conclusions

It would seem that the *J* method, although based on various approximations, arrives at reasonable values for rotational barriers and that, for some benzyl derivatives at least, it also indicates the correct ground state conformations; agreeing with those found in the vapor phase.

Therefore it appears unlikely that a solvent effect would alter the present conclusion about the stable conformation of 3,5-dichlorobenzyldimethylarsine.

Acknowledgments

We are grateful to a referee for helpful comments, to Dr. D. W. Scott for information on phenylethane, and to the National Research Council of Canada for financial support.

1. H. Schmidt, A. Schweig, and H. Vermier. J. Mol. Struct. **37**, 93 (1977).
2. T. Schaefer, L. J. Kruczynski, and W. J. E. Parr. Can. J. Chem. **54**, 3210 (1976).
3. C. J. Macdonald and W. F. Reynolds. Can. J. Chem. **48**, 1002 (1970).
4. R. Wasylishen and T. Schaefer. Can. J. Chem. **50**, 1852 (1972).
5. J. B. Rowbotham and T. Schaefer. Can. J. Chem. **52**, 489 (1974).
6. H. Rottendorf and S. Sternhell. Aust. J. Chem. **17**, 1315 (1964).

7. M. P. WILLIAMSON, R. J. KOSTELNIK, and S. M. CASTELLANO. J. Chem. Phys. **49**, 2218 (1968).
8. T. SCHAEFER, L. KRUCZYNSKI, and W. NIEMCZURA. Chem. Phys. Lett. **38**, 498 (1976).
9. S. CASTELLANO and A. A. BOTHNER-BY. J. Chem. Phys. **41**, 3863 (1964).
10. C. W. HAIGH and J. M. WILLIAMS. J. Mol. Spectrosc. **32**, 398 (1969).
11. R. GLEITER, M. KOBAYASHI, J. SPANGET-LARSEN, S. GRONOWITZ, A. KONAR, and M. FARNIER. J. Org. Chem. **42**, 2230 (1977).
12. W. J. HEHRE, L. RADOM, and J. A. POPLE. J. Am. Chem. Soc. **94**, 1496 (1972).
13. M. S. FARAG. Diss. Abstr. Int. B, **35**, 1594 (1974).
14. A. MILLER and D. W. SCOTT. J. Chem. Phys. **68**, 1317 (1978).
15. L. V. VILKOV, N. P. PENIONZHKEVICH, J. BRUNVOLL, and I. HARGITTAI. J. Mol. Struct. **43**, 109 (1978).
16. T. SCHAEFER and W. J. E. PARR. J. Mol. Spectrosc. **61**, 479 (1976).
17. K. S. PITZER, L. GUTTMAN, and E. F. WESTRUM, JR. J. Am. Chem. Soc. **68**, 2209 (1946).
18. L. A. CARREIRA and T. G. TOWNS. J. Chem. Phys. **63**, 5283 (1975).
19. N. L. BAULD, C. E. HUDSON, and J. S. HYDE. J. Chem. Phys. **54**, 1834 (1971).
20. C. CHACHATY, A. FORCHIONI, and J. C. RONFARD-HARET. Mol. Phys. **31**, 325 (1976).
21. T. SCHAEFER, W. J. E. PARR, and W. DANCHURA. J. Magn. Reson. **25**, 167 (1977).

Can. J. Chem. Downloaded from www.nrcresearchpress.com by 210.87.254.105 on 09/05/12
For personal use only.

Proton magnetic resonance spectra of 3-fluorotoluene and 2-chloro-5-fluorotoluene. The sign and coupling mechanism of $^5J_m{}^{F,CH_3}$

TED SCHAEFER, WERNER DANCHURA, AND WALTER NIEMCZURA
Department of Chemistry, University of Manitoba, Winnipeg, Man., Canada R3T 2N2

Received March 23, 1978

TED SCHAEFER, WERNER DANCHURA, and WALTER NIEMCZURA. Can. J. Chem. **56**, 2233 (1978).

A full analysis of the proton magnetic resonance spectra of 3-fluorotoluene and of 2-chloro-5-fluorotoluene, as 10 mol% solutions in CS_2, demonstrates that the long-range spin–spin coupling constant over five bonds between methyl protons and fluorine-19 is negative. The coupling mechanism consists of a large positive σ electron component and a negative π electron component. The negative sign of the π electron contribution arises from a spin density in the $2p_z$ orbital at carbon-3, which is opposite in sign to that of the spin densities at C-2 and C-4. Combined with positive hyperfine interaction constants, Q_{CCH} and Q_{CF}, the consequence is a negative π electron component.

TED SCHAEFER, WERNER DANCHURA et WALTER NIEMCZURA. Can. J. Chem. **56**, 2233 (1978).

Une analyse complète des spectres de résonance magnétique nucléaire du proton des fluoro-3 et chloro-2 fluoro-5 toluènes en solutions à 10 mol% dans le CS_2, démontre que la constante de couplage spin–spin à longue distance à travers cinq liaisons entre les protons du méthyle et le fluor-19 est négative. Le mécanisme de couplage comporte une composante importante positive due aux électrons σ et une composante négative provenant des électrons π. La valeur négative de la contribution provenant des électrons π est due à une densité de spin dans l'orbitale $2p_z$ au niveau du carbone-3 qui est de signe opposé à celle des densités de spin au niveau des carbone-2 et -4. Si l'on combine ces valeurs avec les constantes d'interactions hyperfines positives, Q_{CCH} et Q_{CF}, la conséquence est une composante négative pour les électrons π.

[Traduit par le journal]

Introduction

The long-range spin–spin coupling constants between methyl protons and ring protons in toluene and its derivatives have been thoroughly examined both experimentally and theoretically (refs. 1–11 and footnote 1). In terms of a σ–π model it was shown that the coupling over six bonds, $^6J_p{}^{H,CH_3}$, is dominated by the π electron contribution and that, indeed, it provides the basis for a determination of small barriers to internal rotation in α-substituted toluene derivatives (8, 10, 12, 13). The other two couplings, $^5J_m{}^{H,CH_3}$ and $^4J_o{}^{H,CH_3}$, contain appreciable contributions from both of the σ and π electron systems.

The analogous long-range couplings in fluorotoluene derivatives, $^6J_p{}^{F,CH_3}$ and $^4J_o{}^{F,CH_3}$, have also been discussed in some detail (2, 14, 15). For example, on the very reasonable assumption (10, 14) that $^6J_p{}^{F,CH_3}$ is dominated by a π electron mechanism, one may write $^\pi J_p{}^{F,CH_3} \propto Q_{CF}\, Q_{CCH}$ in *p*-fluorotoluene. Q_{CF} and Q_{CCH} are the isotropic hyperfine interaction constants between an electron in a π orbital on carbon and the contiguous fluorine nucleus or methyl proton, respectively. Q_{CF} and Q_{CCH} are positive (16–19), so that $^6J_p{}^{F,CH_3}$ is also positive. Similarly, $^4J_o{}^{F,CH_3}$ must have a large positive π electron contribution but there exist complications from σ electron and the socalled through-space mechanisms (15).

In 4-amino-5-bromo-3-fluorotoluene, $^5J_m{}^{F,CH_3}$ was determined to be −0.4 Hz (2). It is quite likely that this relatively small magnitude ($^6J_p{}^{F,CH_3}$ is +1.15 Hz in *p*-fluorotoluene (14) and $^4J_o{}^{F,CH_3}$ is +2.1 Hz in 4-chloro-2-fluoro-5-nitrotoluene (2)) arises from a near cancellation of a positive, highly stereospecific, σ electron component by a negative π electron component. The negative π component can arise if a negative π spin density exists at the carbon of the C—F bond.

The negative sign of $^5J_m{}^{F,CH_3}$ has been questioned in a discussion of $^5J_m{}^{F,CH_3}$, apparently preferred positive (20), in 2-chloro-5-fluorotoluene, **2**. Accordingly, this paper briefly reports the analyses of the ^{1}Hmr spectra of 3-fluorotoluene, **1**, and of **2**. The sign of $^5J_m{}^{F,CH_3}$ is negative in **1** and **2**. A discussion of the coupling mechanism in terms of a σ–π model is given in connection with an INDO MO FPT (21) calculation of $^5J_m{}^{F,CH_3}$, using a standard geometry (22).

Experimental

Degassed, 10 mol% solutions of **1** and **2** in CS_2 contained a small amount of internal tetramethylsilane. The proton magnetic resonance spectra were recorded in the frequency sweep mode at 305 K on an HA100 spectrometer. The spectra

[1] C. Fallick and S. Sternhell. Private communication of results to be published.

Can. J. Chem. Downloaded from www.nrcresearchpress.com by 210.87.254.42 on 09/05/12
For personal use only.

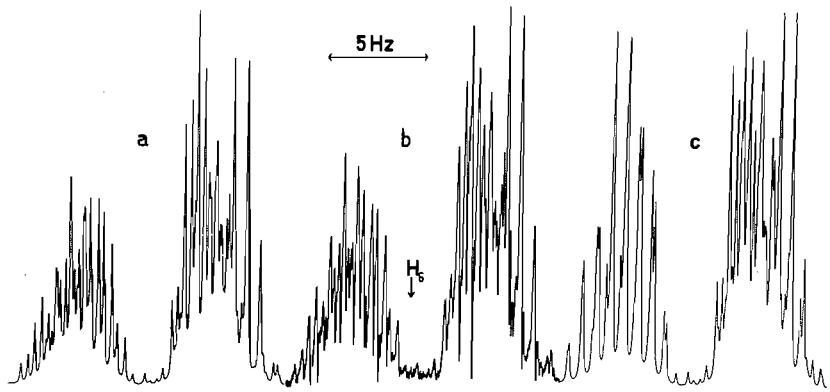

FIG. 1. Part of the H_6 region, from 674.0 to 687.5 Hz at 100 MHz to low field of internal tetramethylsilane, for a 10 mol% solution of 3-fluorotoluene, **1**, in CS_2 solution at 305 K is shown in each of *a*, *b*, and *c*. In *a* the spectrum is that calculated with the parameters in Table 1, i.e., with $^5J_p^{H,F} = 0.144$ Hz. In *c* the calculated spectrum assumes $^5J_p^{H,F} = -0.144$ Hz. These calculated spectra may be compared to the observed spectrum in *b*, particularly to the left-hand multiplet.

were repeatedly calibrated by reading the sweep and manual oscillator frequencies for markers placed at intervals of approximately 5 Hz. Sweep rates were 0.02 and 0.01 Hz/s. The spectral dispersion amounted to 1 Hz/cm. The ring proton spectra of **1** were also calibrated while decoupling the methyl protons.

The signs of $^5J_m^{F,CH_3}$ in **1** and **2** were determined by weak irradiation experiments (23–25) on HA100 and WH-90 spectrometers.

Results and Discussion

Spectral Analyses

These were carried out with the computer program LAME (26, 27). The single resonance spectra were completely insensitive to the sign of $^5J_m^{H,CH_3}$ but were sensitive to the sign of $^5J_p^{H,F}$ in **1**. Figure 1 displays a part of the resonance peaks arising from H_6, illustrating the positive sign of $^5J_p^{H,F}$.

An example of the results of weak irradiation experiments is shown in Fig. 2, whose caption should be read. The theoretical methyl proton spectrum of **1** under conditions of double irradiation was calculated with a version of the computer program DOR (28), modified to accommodate an eight-spin system.

Table 1 gives the spectral parameters for **1** and **2**. It may be noted that the standard deviations of the parameters for the fully coupled spectrum of **1** happen to be 0.004 Hz or less, suggesting an accuracy of perhaps 0.01 to 0.02 Hz. The Bloch–Siegert shift (29) is evident in the shift parameters for coupled and decoupled spectra (Table 1).

$^1H,^1H$, and $^1H,^{19}F$ Couplings Within the Ring

The signs and magnitudes of these couplings have been extensively discussed for related compounds (14, 30–33). It may be noted that, of some 20 $^5J_p^{H,F}$ values, ranging from +0.3 to −2.7 Hz, only those in fluorobenzene and in **1** are positive (14, 31, 34).

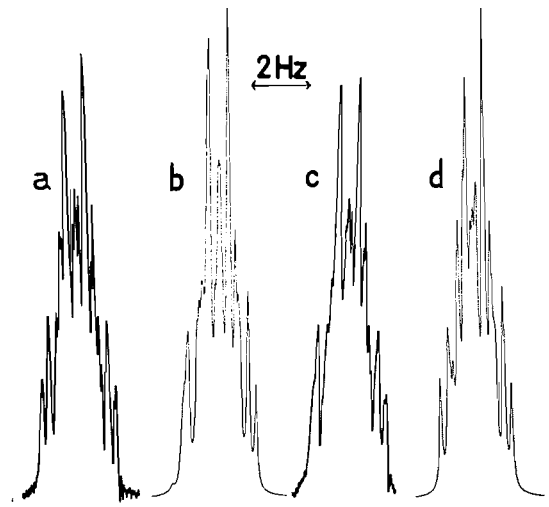

FIG. 2. The methyl proton spectrum for the same sample as in Fig. 1. In *a* the single resonance observed spectrum may be compared with the double resonance spectrum observed in *c* under conditions of weak irradiation at 697.22 Hz to low field of the lock signal. In *b* the calculated double resonance spectrum assumes $^5J_m^{F,CH_3} = -0.253$ Hz and $\gamma H_2 = 0.279$ Hz, where H_2 is the amplitude of the second rf field. In *d* the calculated double resonance spectrum assumes $^5J_m^{F,CH_3} = 0.253$ Hz and $\gamma H_2 = 0.279$ Hz, the other parameters being those in Table 1. Note that the outer two pairs of peaks in the single resonance spectrum would collapse in the absence of $^5J_m^{F,CH_3}$. The calculated spectra had linewidths of 0.10 Hz. The assumed strength of the irradiating field may not match exactly the experimental conditions. The reader is reminded that this figure represents results from only one of a series of double resonance experiments on **1** and **2**.

The Sign of $^5J_m^{F,CH_3}$

$^5J_m^{F,CH_3}$ is −0.25 and −0.23 Hz in **1** and **2** respectively. An interpretation goes as follows. Large positive σ contributions to ^5J can be anticipated for coplanar or near coplanar conformations of the

Can. J. Chem. Downloaded from www.nrcresearchpress.com by 210.87.254.42 on 09/05/12
For personal use only.

TABLE 1. Spectral parameters for 3-fluorotoluene, **1**, and 6-chloro-3-fluorotoluene, **2**, as 10 mol% solutions in CS_2

Parameter[a,b]	Value 1[c]	Value 2[d]		Parameter[a,b]	Value 1[c]	Value 2[d]	
ν_{CH_3}	—	228.361(1)	230.491(3)	$^5J_{25}$	0.397(9)	0.377(4)	0.336(5)
ν_2	672.631(5)	672.374(2)	681.710(4)	$^5J_{36}$	0.143(8)	0.144(3)	—
ν_4	670.987(5)	670.739(2)	672.446(3)	$^4J_o^{H_2,CH_3}$	—	−0.693(2)	−0.700(3)
ν_5	707.677(2)	707.342(1)	715.847(3)	$^4J_o^{H_6,CH_3}$	—	−0.701(2)	—
ν_6	681.623(4)	681.351(2)	—	$^5J_m^{H,CH_3}$	—	0.300(1)	0.355(3)
$^3J_{23}$	9.737(8)	9.732(3)	8.858(7)	$^5J_m^{F,CH_3}$	—	−0.253(2)	−0.226(6)
$^3J_{34}$	8.512(7)	8.529(3)	7.735(6)	$^6J_p^{H,CH_3}$	—	−0.593(2)	−0.626(3)
$^3J_{45}$	8.257(9)	8.279(4)	8.743(5)	rms error	0.013	0.013	0.019
$^3J_{56}$	7.590(5)	7.583(2)	—	Peaks observed	66	164	—
$^4J_{24}$	2.596(6)	2.589(2)	3.037(4)	Transitions calculated	76	595	—
$^4J_{26}$	1.594(5)	1.594(2)	—				
$^4J_{46}$	0.995(6)	1.001(2)	—	Transitions			
$^4J_{35}$	6.017(6)	6.008(2)	5.169(7)	assigned	68	424	—

[a]Shifts at 100.001 MHz to low field of internal TMS at 305 K.
[b]Coupling constants in Hz, numbers in parentheses giving the standard deviation in the last place.
[c]For spectra with methyl protons decoupled and coupled in the two columns.
[d]The numbering for 2 according to the name in the title of the table.

H—C—C—C—C—F fragment in **1** or **2**, particularly in the all-*trans* arrangement. For example, in 3-fluorobenzaldehyde, $^5J_m^{F,CHO}$ is +1.8 Hz, an average for the two planar conformations of the molecular (35). It turns out that INDO MO FPT calculations (35) reproduce this value reasonably well.

In Table 2, the INDO MO FPT values for $^5J_m^{F,CH_3}$ in **1** are tabulated as a function of the angle, θ, by which the C—H bond twists out of the aromatic plane. Figure 3 presents a plot of $^5J_m^{F,CH_3}$ vs. θ, the conformations also being defined there. Note that $^5J_m^{F,CH_3}$ is calculated as positive for planar conformations of the coupling fragment. Furthermore, $^5J_m^{F,CH_3}$ is calculated as large and negative for θ values near 90°, precisely as expected for a negative π electron contribution, which follows a $\sin^2\theta$ law (10). Because Q_{CCH} and Q_{CF} are both positive, this result means that the spin density in the π orbital (or the $2p_z$ orbital) at C-3 is negative. The negative spin density is easily understood as a consequence of electron correlation, the spin densities at C-2 and C-4 being positive[2] (such a result can be deduced from the INDO MO FPT open shell molecular orbitals, the convention being that the proton magnetic moment of a methyl group induces a negative spin density in its *s* orbital).

An instructive comparison can be made with the INDO MO FPT results (10) for $^5J_m^{H,CH_3}$ in toluene, also sketched in Fig. 3. Here the π electron component is positive because Q_{CH} is negative, while the spin density at C-3 is negative, as in **1**. Consequently $^5J_m^{H,CH_3}$ is positive, as observed (7). $^5J_m^{H,CH_3}$ and

TABLE 2. INDO MO FPT values for $^5J_m^{F,CH_3}$ in 3-fluorotoluene

θ (deg)[a]	$^5J_m^{F,CH_3}$ (Hz)	θ (deg)[a]	$^5J_m^{F,CH_3}$ (Hz)
0	0.57	105	−0.81
15	0.42	120	−0.14
30	0.03	135	0.69
45	−0.48	150	1.48
60	−0.95	165	2.04
75	−1.22	180	2.25
90	−1.19		

[a]θ = 180° defines the all-*trans* arrangement of the bonds in the H—C—C—C—C—F fragment; see Fig. 3.

$^5J_m^{F,CH_3}$ are overestimated somewhat in the calculations. Because the barrier to methyl group rotation in 3-fluorotoluene is only 0.042 kcal/mol (38)[3], an average of the 13 calculated values can be reasonably taken and is +0.21 Hz. Clearly, a slight negative shift in the theoretical values would yield a negative coupling.

Conclusions

$^5J_m^{F,CH_3}$ is negative in 3-fluorotoluene and two derivatives as well as in some pyridine derivatives (39). $^5J_m^{F,CH_3}$ is a composite of a positive σ electron contribution and of a negative π electron contribution, the latter attaining its maximum magnitude for conformations in which the side-chain C—H bond is twisted by about 90° out of the aromatic plane. The σ–π model is adequate for a discussion of long-range couplings between methyl protons and ring protons or fluorine nuclei if it is remembered that induced

[2]In terms of a valence bond formulation (36), the spin correlation function for atoms belonging to different classes (starred, unstarred) is negative.

[3]The present calculation gave 0.018 kcal/mol, C—H in plane as most stable, and a dipole moment of 1.87 D, the measured value being 1.85 D (38).

Can. J. Chem. Downloaded from www.nrcresearchpress.com by 210.87.254.42 on 09/05/12
For personal use only.

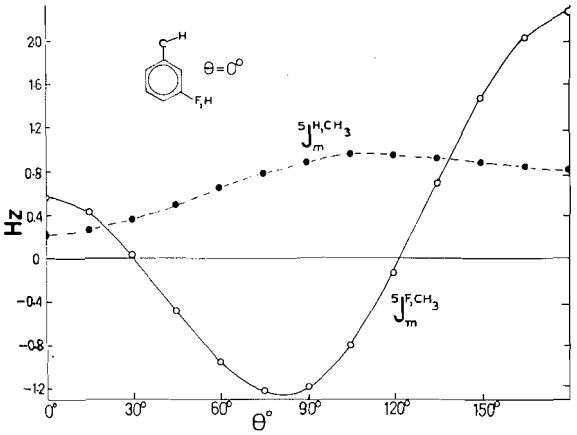

FIG. 3. The open circles are the values of $^5J_m^{F,CH_3}$ in 3-fluorotoluene in Hz calculated by INDO MO FPT as a function of the angle of twist, θ, of the C—H bond in a methyl group. For an all-*trans* arrangement of the intervening bonds, θ = 180°. The solid circles give the calculations for $^5J_m^{H,CH_3}$ in toluene.

spin densities, in π molecular orbitals of benzene derivatives, can have different signs at different sites.

Acknowledgments

We are grateful to the National Research Council of Canada for financial support. Dr. W. J. E. Parr and Dr. R. Wasylishen were generous in their calculational assistance.

1. R. A. HOFFMAN. Mol. Phys. **1**, 326 (1958).
2. D. J. BLEARS, S. S. DANYLUK, and T. SCHAEFER. J. Chem. Phys. **47**, 5037 (1967).
3. G. P. NEWSOROFF and S. STERNHELL. Aust. J. Chem. **21**, 747 (1968).
4. H. ROTTENDORF and S. STERNHELL. Aust. J. Chem. **17**, 1315 (1964).
5. S. STERNHELL. Quart. Rev. **23**, 236 (1969).
6. M. BARFIELD and B. CHAKRABARTI. Chem. Rev. **69**, 757 (1969).
7. M. P. WILLIAMSON, R. KOSTELNIK, and S. M. CASTELLANO. J. Chem. Phys. **49**, 2218 (1968).
8. C. J. MACDONALD and W. F. REYNOLDS. Can. J. Chem. **49**, 94 (1971).
9. J. B. ROWBOTHAM and T. SCHAEFER. Can. J. Chem. **52**, 489 (1974).
10. R. WASYLISHEN and T. SCHAEFER. Can. J. Chem. **50**, 1852 (1972).
11. T. SCHAEFER and W. J. E. PARR. J. Chem. Phys. **65**, 1197 (1976).
12. T. SCHAEFER and W. J. E. PARR. J. Chem. Soc. Faraday Trans. II, **73**, 1501 (1977).
13. W. J. E. PARR and T. SCHAEFER. J. Am. Chem. Soc. **99**, 1033 (1977).
14. R. WASYLISHEN and T. SCHAEFER. Can. J. Chem. **49**, 94 (1971).
15. R. E. WASYLISHEN and M. BARFIELD. J. Am. Chem. Soc. **97**, 4545 (1975).
16. T. M. MCKINNEY and D. H. GESKE. J. Am. Chem. Soc. **89**, 2806 (1967) and references therein.
17. D. LAZDINS and M. KARPLUS. J. Am. Chem. Soc. **87**, 920 (1965).
18. D. R. EATON, A. D. JOSEY, R. E. BENSON, W. D. PHILLIPS, and T. L. CAIRNS. J. Am. Chem. Soc. **84**, 4100 (1962).
19. W. G. ESPERSON and R. W. KREILICK. Mol. Phys. **16**, 577 (1969).
20. P. ALBRIKTSEN and G. HANSEN. Acta Chem. Scand. **26**, 2511 (1972).
21. J. A. POPLE, J. W. MCIVER, JR., and N. S. OSTLUND. J. Chem. Phys. **49**, 2960 (1968); **49**, 2965 (1968).
22. J. A. POPLE and M. S. GORDON. J. Am. Chem. Soc. **89**, 4253 (1967).
23. J. P. MAHER and D. F. EVANS. Proc. Chem. Soc. 208 (1961).
24. R. FREEMAN and D. H. WHIFFEN. Mol. Phys. **4**, 321 (1961).
25. R. FREEMAN and W. A. ANDERSON. J. Chem. Phys. **37**, 2053 (1962).
26. S. CASTELLANO and A. A. BOTHNER-BY. J. Chem. Phys. **41**, 3863 (1964).
27. C. W. HAIGH and J. M. WILLIAMS. J. Mol. Spectrosc. **32**, 398 (1969).
28. G. GOVIL and D. H. WHIFFEN. Mol. Phys. **12**, 449 (1967).
29. W. A. ANDERSON. Phys. Rev. **102**, 151 (1956).
30. V. WRAY, and D. N. LINCOLN. J. Magn. Reson. **18**, 374 (1975) and references therein.
31. V. WRAY, L. ERNST, and E. LUSTIG. J. Magn. Reson. **27**, 1 (1977).
32. A. R. TARPLEY and J. H. GOLDSTEIN. J. Phys. Chem. **76**, 515 (1972).
33. H. M. HUTTON, B. RICHARDSON, and T. SCHAEFER. Can. J. Chem. **45**, 1795 (1967).
34. J. E. LOEMKER and J. H. GOLDSTEIN. Spectrosc. Lett. **1**, 153 (1968).
35. R. WASYLISHEN and T. SCHAEFER. Can. J. Chem. **49**, 3216 (1971).
36. H. M. MCCONNELL. J. Chem. Phys. **30**, 126 (1959).
37. J. SUSSKIND. J. Chem. Phys. **53**, 2492 (1972).
38. E. M. MOORE and M. E. HOBBS. J. Am. Chem. Soc. **71**, 411 (1949).
39. J. B. ROWBOTHAM and T. SCHAEFER. Can. J. Chem. **50**, 2344 (1972).

Can. J. Chem. Downloaded from www.nrcresearchpress.com by 210.87.254.42 on 09/05/12
For personal use only.

On spin trapping hydroxyl and hydroperoxyl radicals

EDWARD G. JANZEN, DALE E. NUTTER, JR.,[1] EDWARD R. DAVIS, AND BARRY J. BLACKBURN[2]

Guelph–Waterloo Centre for Graduate Work in Chemistry, Department of Chemistry, University of Guelph, Guelph, Ont., Canada N1G 2W1

AND

J. LEE POYER AND PAUL B. MCCAY

Biomembrane Research Laboratory, Oklahoma Medical Research Foundation, Oklahoma City, OK 73104, U.S.A.

Received February 13, 1978

EDWARD G. JANZEN, DALE E. NUTTER, JR., EDWARD R. DAVIS, BARRY J. BLACKBURN, J. LEE POYER, and PAUL B. MCCAY. Can. J. Chem. **56**, 2237 (1978).

The assignments of the hydroxyl, hydroperoxyl, and alkylperoxyl radical spin adducts of α-phenyl *N-tert*-butyl nitrone (PBN) are discussed. Results of new experiments designed to test the assignments of the first two are described. It is concluded that the hydroxy adduct assignment is correct. The relationship between a_β^H and a_N is

$$a_\beta^H = 0.60a_N - 6.5$$

This equation gives a good fit for the seven pairs of constants reported for the hydroxy adduct. The assignments for the hydroperoxy adduct may be correct but no proof is yet available for this assignment.

EDWARD G. JANZEN, DALE E. NUTTER, JR., EDWARD R. DAVIS, BARRY J. BLACKBURN, J. LEE POYER et PAUL B. MCCAY. Can. J. Chem. **56**, 2237 (1978).

On discute des attributions des adduits de spin radicalaire de l'hydroxyle, de l'hydroperoxyle et de l'alkylperoxyle avec l'α-phényl *N-tert*-butyl nitrone (PBN). On décrit les résultats des nouvelles expériences effectuées pour valider les attributions des deux premiers. On en conclut que l'attribution pour l'adduit hydroxy est correcte. La relation entre a_β^H et a_N est:

$$a_\beta^H = 0.60a_N - 6.5$$

Cette équation donne une bonne corrélation pour sept paires de constantes rapportées pour l'adduit hydroxyle. Les attributions pour l'adduit hydroperoxyle sont peut être correctes mais on n'a pour l'instant aucune preuve de cette attribution.

[Traduit par le journal]

Introduction

Since difficulties are encountered in the direct detection of oxy radicals by esr (1, 2) the method of spin trapping (3) would seem to be well suited for investigations involving the detection of oxy radicals (4). However, it is very important that assignments of the spin adducts are correct and that as many as possible of the reactions leading to the formation of the spin adducts are at least recognized if not understood.

In this paper the spin trapping chemistry of hydroxyl and hydroperoxyl radicals will be reviewed. Results from new investigations will be presented which confirm the previous assignment of the hydroxy adduct of PBN (5). However, the assignment of the hydroperoxy adduct of PBN still remains an open question.

The Hydroxyl Radical Spin Adduct

In an early survey of reactions of potential radical producing systems with PBN (6) the photolysis of small amounts of hydrogen peroxide in benzene containing PBN was investigated. After 20 min irradiation a spectrum consisting of a triplet of doublets was observed: a_N = 14.12, a_β^H = 2.01 G. After further irradiation a second set of doublets appeared: a_N = 13.4, a_β^H = 4.7 G. These spectra could not be assigned at the time.

In a study of the kinds of radicals produced in a microwave discharge of H_2O (7) the reaction of the effluent gases with powdered PBN produced a spectrum (in benzene) consisting of a triplet of doublets (a_N = 14.63, a_β^H = 2.88 G) and a triplet of triplets (a_N = 14.98, a_β^H = 7.50 (2H) G; from D_2O: a_N = 14.70, a_β^H = 2.61 and a_N = 14.94, a_β^H = 7.66, a_β^D = 1.14 G). The former was assigned to the hydroxy adduct (there is some doubt as to the correctness of this assignment; see Fig. 1 discussed later) and the latter to the hydrogen atom adduct.

An effort was made to obtain spectra of the hydroxy adduct from alternate sources. Benzyl alcohol was reacted in the absence of light with *tert*-butoxy radicals from di-*tert*-butyl peroxyoxalate

[1]Present address: Mead Corporation, Chillicothe, Ohio.

[2]Present address: Department of Chemistry, University of Winnipeg, Winnipeg, Manitoba.

Can. J. Chem. Downloaded from www.nrcresearchpress.com by 210.87.254.105 on 09/05/12
For personal use only.

Can. J. Chem. Downloaded from www.nrcresearchpress.com by 210.87.254.105 on 09/05/12
For personal use only.

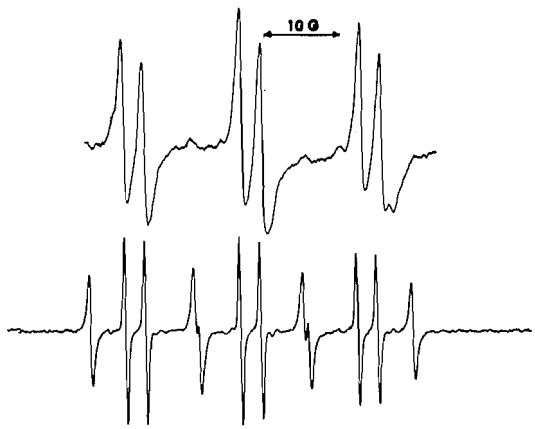

FIG. 1. (*a*) Top spectrum from 5×10^{-2} *M* H_2O_2, 2×10^{-5} *M* $FeCl_3$, 8×10^{-4} *M* ADP, and 0.1 *M* PBN in water. (*b*) Bottom spectrum from 0.01 *M* $(NH_4)_2S_2O_8$ and 0.1 *M* PBN in water; note the strong set of four (actually 2×3) lines between the doublets due to *tert*-butyl hydronitroxide ($(CH_3)_3NHO\cdot$) from hydrolysis of PBN frequently seen when persulfate is used.

(DBPO) in benzene containing 2-methyl-2-nitrosopropane. Di-*tert*-butyl nitroxide, *tert*-butoxy *tert*-butyl nitroxide, and *tert*-butyl hydronitroxide were detected. No clear triplet of doublets was seen. The reaction expected to produce the hydroxy adduct of PBN apparently generates *tert*-butyl hydronitroxide by either electron or hydrogen atom transfer:

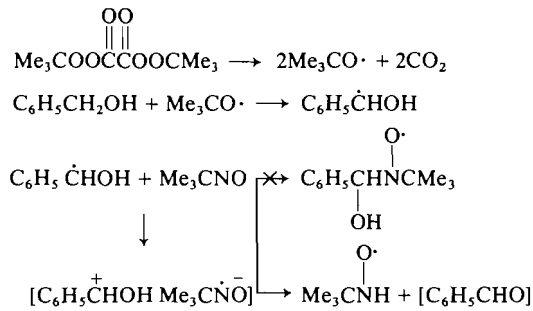

The photolysis of benzophenone in benzene in the presence of benzyl alcohol and 2-methyl-2-nitrosopropane gave only di-*tert*-butyl nitroxide. Eventually on continuous photolysis another signal appeared which would seem to be an aromatic *tert*-butyl nitroxide. Perhaps the α-hydroxybenzyl or the hydroxydiphenylmethyl radical was trapped in the *para* position: e.g.,

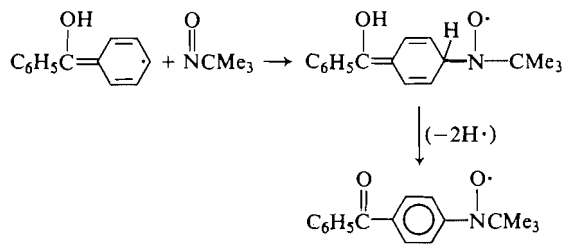

Phenoxy radicals apparently are trapped in a similar manner (8).

Other possible methods of producing hydroxyl radicals or the hydroxy radical spin adduct were investigated (see Table 1). γ-Radiolysis of PBN in water gave a triplet of doublets (a_N = 15.98, a_β^H = 3.12 G) and the hydrogen atom adduct (a_N = 16.57, a_β^H = 10.50 (2H) G). Photolysis in a basic aqueous solution (NaOH) of PBN produced a triplet of doublets (a_N = 15.57, a_β^H = 4.03 G) and the hydrogen atom adduct (a_N = 16.42, a_β^H = 10.34 (2H) G). Photolysis of the sodium salt of 1-anthraquinone sulfonic acid in an aqueous solution of PBN produced a triplet of doublets (a_N = 15.13, a_β^H = 2.63 G). According to a plot of a_β^H vs. a_N (discussed later) it appears that the first and last of the above spectra can be assigned to the hydroxy adduct of PBN but the remaining spectrum is not understood at this time.

A solution of ferric chloride and hydrogen peroxide in water (Fenton's reagent) gave only a triplet due to benzoyl *tert*-butyl nitroxide with PBN. The same result was obtained with $TiCl_3$ and hydroxylamine hydrochloride in water containing PBN. However a solution of ferric chloride chelated with adenosine diphosphate (ADP) to which a small amount of hydrogen peroxide is added gives a triplet of doublets (a_N = 15.49, a_β^H = 2.74 G). The latter appears to be the hydroxy adduct of PBN (see Fig. 1*a*). Both sodium and ammonium persulfate in water containing PBN produce spectra consisting of a triplet of doublets (a_N = 15.13, a_β^H = 2.63 G; a_N = 15.23, a_β^H = 2.60 G, respectively) (see Fig. 1*b*).

Preliminary results with α-(4-pyridyl-*N*-oxide) *N*-*tert*-butyl nitrone (4-POBN) and sodium persulfate in water indicate that the hydroxy adduct is detected in this system. The assignment is based on the detection of an extra splitting of about 0.3 G which is absent in D_2O. The small splitting is probably due to the γ-hydrogen on the hydroxy group (Fig. 2).

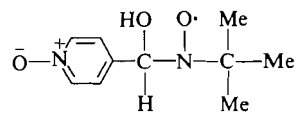

The lack of consistency in splitting constants obtained from different apparent sources of hydroxy radicals is discouraging at first glance. However a plot of one splitting constant (a_β^H) against the other (a_N) as shown in Fig. 3 suggests a grouping of points with a straight line relationship for the values obtained from γ-radiolysis of water, photolysis of sodium anthraquinone sulfate in water, ADP chelated $FeCl_3$ plus H_2O_2 in water, persulfate in water, and one set of values reported by Harbour *et al.* (5) obtained from the photolysis of aqueous

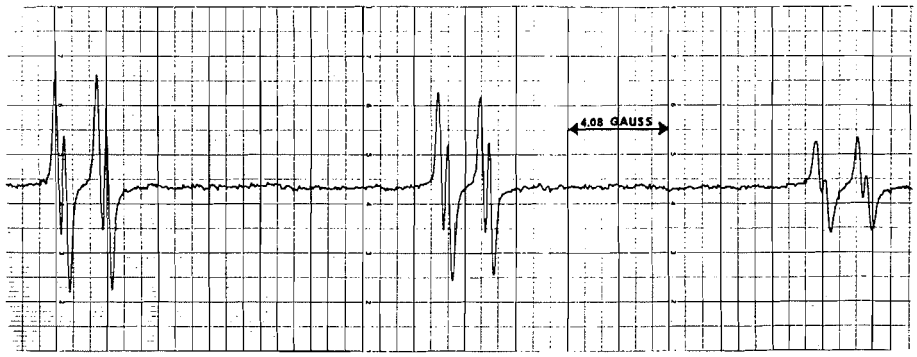

FIG. 2. Electron spin resonance spectrum of the hydroxy adduct of 4-pyridyl-*N*-oxide *N*-*tert*-butyl nitrone produced from sodium persulfate in water: $a_N = 15.03$, $a_\beta^H = 1.67$, $a_{OH}^H = 0.36$ G.

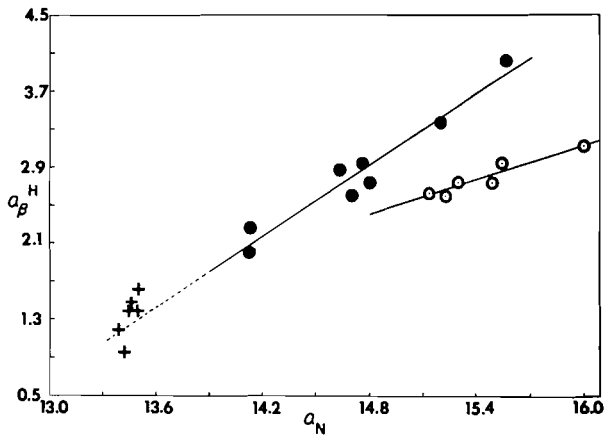

FIG. 3. Plot of the nitrogen and β-hydrogen hyperfine splitting constants for the nitroxides assumed to be hydroxy (○), hydroperoxy (●) and alkylperoxy (×) adducts of PBN (see Table 1).

H_2O_2 and PBN ($a_N = 15.30$, $a_\beta^H = 2.75$; $a_N = 15.55$, $a_\beta^H = 2.95$ G from this study, *vide infra*). Since one point is almost certainly due to the hydroxy adduct (based on the results from sodium persulfate in water with 4-POBN) it can be asserted that the spin adducts whose splitting constants fall on the straight line which passes through this point all have the same structure, namely α-hydroxybenzyl *tert*-butyl nitroxide:

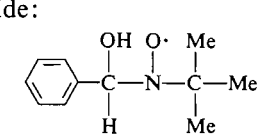

The line drawn through the seven points mentioned shown in Fig. 3 is a computer least-squares best fit. The correlation coefficient is 0.948. The equation of the line is:

$$a_\beta^H = 0.604a_N - 6.53$$

A feel for the 'goodness-of-fit' can be obtained by calculating the expected a_β^H from the measured a_N using the above equation.

Experiment No.	a_N	a_β^H Calcd.	a_β^H Exptl.	Error
5	15.98	3.12	3.12	0.00
7	15.13	2.61	2.63	−0.02
8	15.49	2.83	2.74	+0.09
9	15.13	2.61	2.63	−0.02
10	15.23	2.67	2.60	+0.07
12	15.30	2.71	2.75	−0.04
14	15.55	2.86	2.95	−0.09
			Average	±0.05

As can be seen from the above, the maximum deviation in any given pair of experiments is almost 0.1 G. The average error is about 0.05 G. From experience with many spin trapping experiments one finds repeatability to be of the order of ±0.05 G for single spectra. For spectra with overlapping peaks a maximum deviation of 0.1 G is quite possible. Thus one can conclude that the above equation relates a_N and a_β^H for the hydroxy adduct of PBN with approximately the same error as one can expect from experimental measurements taken by different workers with different instruments in different solvents and different solution compositions.

With ammonium persulfate in water 5,5-dimethyl-pyrroline-*N*-oxide (DMPO) gives a 1:2:2:1 pattern of four lines which can be interpreted in terms of equivalent hyperfine splitting from both the β-hydrogen and the nitroxide nitrogen atom ($a_N = a_\beta^H = 14.77$ G; see Fig. 4*a*). Because this system gives a spectrum with splitting from the hydroxy hydrogen in the adduct of 4-POBN it is assumed that the 1:2:2:1 spectrum is due to the hydroxy adduct of DMPO. However there is no proof of this assignment.

ADP chelated ferric chloride plus hydrogen peroxide gives the same spectrum with DMPO

Can. J. Chem. Downloaded from www.nrcresearchpress.com by 210.87.254.105 on 09/05/12
For personal use only.

Can. J. Chem. Downloaded from www.nrcresearchpress.com by 210.87.254.105 on 09/05/12
For personal use only.

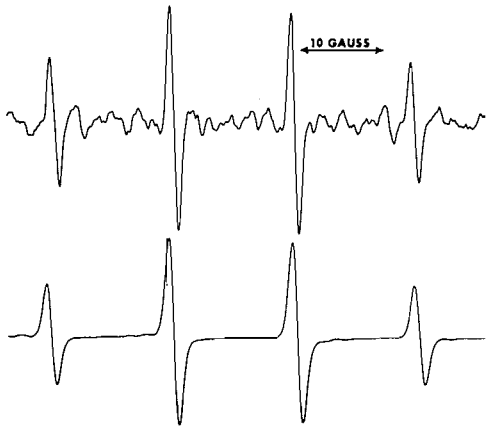

FIG. 4. (*a*) Top spectrum from 0.01 *M* $(NH_4)_2S_2O_8$ and 0.1 *M* DMPO in water; (*b*) Bottom spectrum from 5×10^{-2} *M* H_2O_2, 2×10^{-5} *M* $FeCl_3$, 8×10^{-4} *M* ADP and 0.14 *M* DMPO in water.

($a_N = a_\beta^H = 14.83$ G; see Fig. 4*b*). Floyd and Soong (9) have reported $a_N = a_\beta^H = 14.9$ G for a spectrum assigned to the hydroxy adduct of DMPO. The same spectrum was obtained by Harbour *et al.* (5) from photolysis of low concentrations of hydrogen peroxide and high concentrations of DMPO ($a_N = a_\beta^H = 15.3$, $a_\gamma^H = 0.61$ (1H), 0.25 (1H) G).

The Question of the Hydroperoxyl Radical Spin Adduct

When 0.1 *M* PBN is dissolved in 30% H_2O_2 no signal is detected. Apparently the nitrone does not react so as to produce spin adducts spontaneously by an induced decomposition mechanism i.e., *no* evidence was found for the following possible reactions:

$$H_2O_2 + PBN \longrightarrow C_6H_5CH(OOH)N(OH)CMe_3$$

$$C_6H_5CH(OOH)N(OH)CMe_3 + H_2O_2 \swarrow$$

$$C_6H_5CH(OOH)\overset{O\cdot}{\underset{|}{N}}CMe_3 + HO\cdot + H_2O$$

$$HO\cdot + PBN \longrightarrow C_6H_5CH(OH)\overset{O\cdot}{\underset{|}{N}}CMe_3$$

Upon uv irradiation first a weak signal due to a triplet of doublets with further splitting in the wing doublets is seen. Since the center wing of the nitrogen triplet does not show this splitting the spectrum must be due to two spin adducts with the same β-hydrogen splitting and the same *g*-value but with different nitrogen hyperfine splittings. This spectrum is the same as observed by Harbour *et al* (5). The values obtained here are $a_N = 15.55$, $a_\beta^H = 2.95$ G and $a_N = 14.76$, $a_\beta^H = 2.95$ G (see Fig. 5). The former has been assigned to the hydroxy adduct by Harbour *et al.* (5) and confirmed in this paper. The latter also has been assigned to the hydroperoxy adduct by Harbour *et al.* (5) but there is no proof of this assignment.

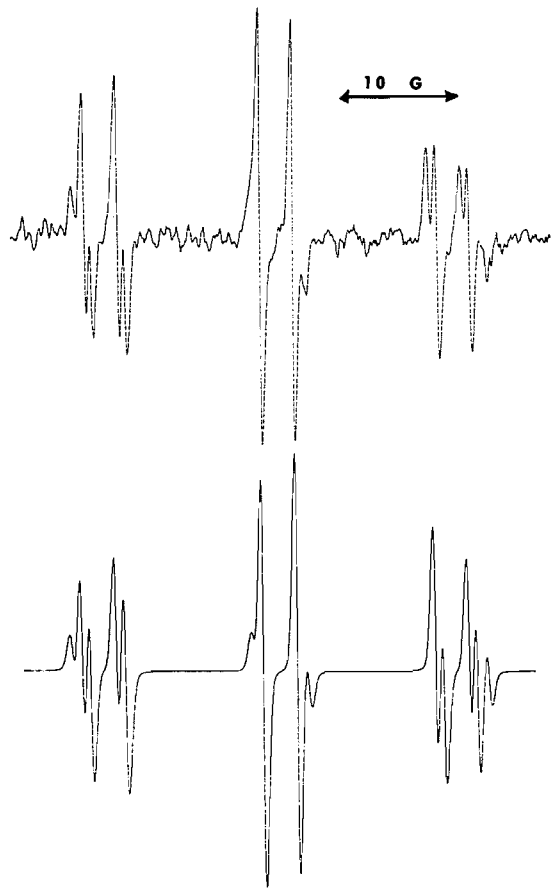

FIG. 5. Top spectrum obtained from uv irradiation of 0.1 *M* PBN in 30% H_2O_2. Bottom spectrum is a computer simulation of the following three sets of parameters in an intensity ratio of 1:1:0.3 $a_N = 15.55$, $a_\beta^H = 2.95$, line width = 0.57 G; $a_N = 14.76$, $a_\beta^H = 2.95$, line width = 0.38 G; $a_N = 15.55$, $a_\beta^H = 4.75$, line width = 0.65 G; *g*-value shift to higher field is 0.15 G.

Upon further photolysis another triplet of doublets not reported by Harbour *et al.* (5) with a relatively large β-hydrogen splitting and a slightly smaller *g*-value is observed ($a_N = 15.55$, $a_\beta^H = 4.75$ G). The complete spectrum can be computer simulated using a ratio of peak intensities of 1:1:0.3 (ratio of areas is 1:1:0.5) as shown in Fig. 5.

Konaka and Mizuta[3] obtained a triplet of doublets from H_2O_2 and *tert*-butyl alcohol – benzene ($a_N = 14.13$, $a_\beta^H = 2.26$ G). In pyridine containing PBN

[3]R. Konaka and K. Mizuta. Unpublished results.

Can. J. Chem. Downloaded from www.nrcresearchpress.com by 210.87.254.105 on 09/05/12
For personal use only.

TABLE 1. Hyperfine splitting constants of PBN spin adducts

		a_N	a_β^H
1	H_2O_2 in benzene	14.12	2.01
2	As above, later	13.4	4.7
3	H_2O microwave discharge	14.63	2.88 (H_2O)
4	(Spin adducts in benzene)	14.70	2.61 (D_2O)
5	γ-radiolysis of H_2O	15.98	3.12
6	Photolysis of OH^-/H_2O	15.57	4.03
7	Photolysis of H_2O–sensitizer*	15.13	2.63
8	$FeCl_3$–ADP and H_2O_2 in H_2O	15.49	2.74
9	$Na_2S_2O_8$ in H_2O (pH > 7)	15.13	2.63
10	$(NH_4)_2S_2O_8$ in H_2O (pH < 7)	15.23	2.60
11	As above, later	15.50	4.83
12	Photolysis of 1% H_2O_2	15.30	2.75 (ref. 5)
13	Photolysis of 30% H_2O_2	14.8	2.75 (ref. 5)
14	Photolysis of 30% H_2O_2	15.55	2.95
15	As above, later	14.76	2.95
16	As above, later	15.55	4.75
17	H_2O_2 in benzene – *tert*-butyl alcohol	14.13	2.26 (footnote 3)
18	H_2O_2 in pyridine	15.20	3.38 (footnote 3)
19	*t*BuOOH, $Pb(OAc)_4$ in CH_2Cl_2 at −80°C	13.39	1.19 (ref. 10)
20	*s*BuOOH, as above	13.50	1.40 (ref. 10)
21	$nC_5H_{11}OOH$, as above	13.44	1.39 (ref. 10)
22	$C_6H_5CMe_2OOH$, as above	13.46	1.47 (ref. 10)
23	$C_{18}H_{37}OOH$, as above	13.50	1.61 (ref. 10)
24	*t*BuOO· in toluene at −80°C	12.85	< line width (ref. 11)
25	*t*BuOO· in toluene at −20°C	13.42	0.95 (ref. 11)

*Saturated sodium salt of 1-anthraquinone sulfonate.

the addition of H_2O_2 also produced a triplet of doublets $a_N = 15.20$, $a_\beta^H = 3.38$ G.

If the magnitude of the β-hydrogen and nitroxide nitrogen hyperfine splittings are plotted against each other for the spectra from the photolysis of H_2O_2 in 30% H_2O_2, H_2O_2 in benzene, H_2O_2 in *tert*-butyl alcohol – benzene, and H_2O_2 in pyridine a reasonable linear relationship is obtained (Fig. 3). The correlation coefficient of the computer least squares fit is 0.9716. The equation of the line is

$$a_\beta^H = 1.26a_N - 15.7$$

The calculated values for a_β^H are compared with the experimental values below. Also included are the splitting constants obtained from the microwave discharge of H_2O and D_2O, and the photolysis of PBN in basic solution.

Experiment No.	a_N	a_β^H Calcd.	a_β^H Exptl.	Error
1	14.12	2.09	2.01	+0.08
13	14.8	2.95	2.75	+0.20
15	14.76	2.90	2.95	−0.05
17	14.13	2.10	2.26	−0.16
18	15.20	3.45	3.38	+0.07
3	14.63	2.73	2.88	−0.15
4	14.70	2.82	2.61	+0.19
6	15.57	3.91	4.03	−0.12
			Average	±0.13

The fit is not nearly as good for the presumed to be hydroperoxy adducts obtained from solutions containing H_2O_2 as for the hydroxy adducts discussed earlier. The results obtained from microwave discharge or photolysis of basic solutions of PBN fit about as well as the rest. At this time it seems impossible to say whether all eight pairs of constants belong to the same spin adduct, and if so, whether this nitroxide is the hydroperoxy spin adduct.

The triplets of doublets with a relatively large β-hydrogen splitting (a_β^H = 4.7–4.8 G) may be due to the benzoyl spin adduct since *tert*-butyl hydronitroxide is also often detected under these conditions:

$$PBN + H_2O \xrightarrow{H^+} C_6H_5CHO + Me_3CNHOH$$

$$Me_3CNHOH \xrightarrow{RO\cdot} Me_3CNHO\cdot$$

$$C_6H_5CHO \xrightarrow{RO\cdot} C_6H_5\dot{C}{=}O$$

$$PBN + C_6H_5\dot{C}{=}O \longrightarrow C_6H_5CH(C_6H_5CO)-N(O\cdot)-CMe_3$$

Spin Adducts of Alkylperoxyl Radicals

Recently Merritt *et al.* (10) reported the detection at low temperatures (−80°C in CH_2Cl_2) of signals assigned to alkylperoxy spin adducts of PBN. The peroxy radical was itself detected first from the

Can. J. Chem. Downloaded from www.nrcresearchpress.com by 210.87.254.105 on 09/05/12
For personal use only.

$Pb(OAc)_4$ oxidation of the hydroperoxide. Upon addition of PBN the spectrum of a nitroxide spin adduct appeared. For the *tert*-butylperoxy radical adduct: $a_N = 13.39$, $a_\beta^H = 1.19$ G (see Table 1 for other examples *19–23*). Only the octadecylperoxy spin adduct was stable at room temperature. A substantial increase in β-hydrogen hyperfine splitting was observed at higher temperatures for this spin adduct. Thus $a_N = 13.50$, $a_\beta^H = 1.17$ G at $-80°C$ and $a_N = 13.50$, $a_\beta^H = 1.61$ G at room temperature.

More recently Howard and Tait (11) repeated these experiments in the absence of $Pb(OAc)_4$ with *O–17* labelled oxygen. They found the following values for the *tert*-butylperoxy adduct of PBN: at $-80°C$, $a_N = 12.85$, a_β^H not detected; at $-20°C$, $a_N = 13.42$, $a_\beta^H = 0.95$, $a_\beta^O = 2.9$ G (*O–17* value obtained at $-60°C$). The β-hydrogen splitting increased with increase in temperature whereas the β-oxygen splitting decreased simultaneously. It is of interest to note that the β-hydrogen splittings of the various alkylperoxy spin adducts at different temperatures plotted against the magnitudes of the nitrogen splittings fall well into a region extrapolated to by the line defined for the same parameters for the hydroperoxy adducts. The peroxy radical adducts of PBN are not stable above 0°C (10, 11). Why the hydroperoxy adduct should be more stable is not understood. Perhaps intramolecular H-bonding plays a role in stabilizing the adduct.

All experiments described here were carried out at room temperature using procedures described before (6).

NOTE: A referee has drawn attention to a recent paper by Ohto *et al.* (12) which describes a study of the autoxidation of various hydrocarbons (cumene, tetralin, ethylbenzene, and cyclohexa-1,4-diene) in the presence of PBN. It is claimed that the corresponding peroxy radicals were trapped and detected in the case of *tert*-butylperoxy at room temperature. This conclusion would seem to be at variance with at least two independent studies (10, 11).

Of direct interest to this paper is the report of an adduct detected in the autoxidation of both 2-propanol and cyclohexa-1,4-diene with the following hyperfine splitting parameters: $a_N = 14.25$, $a_\beta^H = 2.23$ G. This spectrum is assigned to the hydroperoxy adduct. These values fall on the line assigned to the hydroperoxy adduct on the plot of a_β^H vs. a_N (Fig. 3). The calculated value for a_β^H using the equation given before is in excellent agreement with the reported value ($a_\beta^H = 1.26a_N - 15.7 = 1.26(14.25) - 15.7 = 2.28$ G; error +0.05).

Acknowledgements

This research was supported by the Petroleum Research Fund administered by the American Chemical Society and the National Research Council of Canada. Grateful acknowledgement is hereby made.

1. J. A. HOWARD. *In* Advances in free-radical chemistry. Vol. 4. *Edited by* G. H. Williams. Elek Science, London. 1972. p. 49.
2. (*a*) S. WEINER and G. S. HAMMOND. J. Am. Chem. Soc. **91**, 2182 (1969); (*b*) M. C. R. SYMONS. J. Am. Chem. Soc. **91**, 5924 (1969).
3. E. G. JANZEN. Acc. Chem. Res. **4**, 31 (1971).
4. (*a*) E. G. JANZEN, C. A. EVANS, and Y. NISHI. J. Am. Chem. Soc. **94**, 8236 (1972); (*b*) E. G. JANZEN and C. A. EVANS. J. Am. Chem. Soc. **95**, 8205 (1974).
5. J. R. HARBOUR, V. CHOW, and J. R. BOLTON. Can. J. Chem. **52**, 3549 (1974).
6. E. G. JANZEN and B. J. BLACKBURN. J. Am. Chem. Soc. **90**, 5909 (1968); **91**, 4481 (1969).
7. E. G. JANZEN, T. KASAI, and K. KUWATA. Bull. Chem. Soc. Jpn. **46**, 2061 (1973).
8. S. TRABE, K. KURUMA, and R. KONAKA. Chem. Lett. 115 (1972).
9. R. A. FLOYD and L. M. SOONG. Submitted for publication.
10. M. V. MERRITT and R. A. JOHNSON. J. Am. Chem. Soc. **99**, 3713 (1977).
11. J. A. HOWARD and J. C. TAIT. Can. J. Chem. **56**, 176 (1978).
12. N. OHTO, E. NIKI, and Y. KAMIYA. J. Chem. Soc. Perkin Trans. II. 1770 (1977).

Proton magnetic resonance studies on short duplexes. I. Helix formation by the duplex set GpApGpC:GpCpUpC

DONALD W. HUGHES AND RUSSELL A. BELL[1]
Department of Chemistry, McMaster University, Hamilton, Ont., Canada L8S 4M1
AND
THOMAS E. ENGLAND[2] AND THOMAS NEILSON[1]
Department of Biochemistry, McMaster University, Hamilton, Ont., Canada L8S 4J9
Received January 19, 1978

DONALD W. HUGHES, RUSSELL A. BELL, THOMAS E. ENGLAND, and THOMAS NEILSON. Can. J. Chem. **56**, 2243 (1978).

Proton magnetic resonance has been used to investigate the double stranded RNA helix GAGC:GCUC, whose sequence corresponds to the duplex neck region of several tRNAs, a possible aminoacyl-tRNA synthetase recognition site. The nonexchangeable base and ribose anomeric resonances of the separate tetranucleotides were characterized by linear and predominantly upfield chemical shift changes as the temperature was decreased from 65 to 15°C. When these strands were mixed nonlinear, sigmoidal shift changes consistent with base pairing were observed. The melting temperature of the duplex was determined to be 42 ± 1°C which was in excellent agreement with the value obtained from optical methods. This is the first ^{1}Hmr study of a non-self-complementary duplex prepared from synthetic tetraribonucleotides.

DONALD W. HUGHES, RUSSELL A. BELL, THOMAS E. ENGLAND et THOMAS NEILSON. Can. J. Chem. **56**, 2243 (1978).

On a utilisé la résonance magnétique du proton pour étudier la double hélice GAGC:GCUC de RNA dont la séquence correspond à la région duplex du cou de plusieurs tRNA, un site de reconnaissance possible de l'aminoacyl-tRNA synthétase. On a pu caractériser les résonances de la base qui ne peut être échangeé et du ribose anomère des tétranucléotides séparés en faisant appel aux changements dans les déplacements chimiques qui sont linéaires et d'une façon générale vers les hauts champs à mesure que la température est abaissée de 65 à 15°C. Lorsque l'on mélange ces segments, des changements des déplacements de nature sigmoidale non-linéaire, en accord avec un pairage des bases, ont pu être observés. On a déterminé que la température de fusion du duplex est de 42 ± 1°C; cette valeur est en excellent accord avec la valeur obtenue à partir de méthodes optiques. Cette étude rmn du ^{1}H est la première étude d'un duplex qui n'est pas auto-complémentaire et qui a été préparé à partir de tétraribonucléotides de synthèse.

[Traduit par le journal]

Considerable effort has been expended on the detailed nuclear magnetic resonance analysis of the pairing of short strands of nucleic acid sequences (1–5). In this paper we wish to report a proton magnetic resonance investigation of duplex formation by the complementary nucleotides GAGC and GCUC.[3] The two sequences chosen are important because they correspond to natural sequences common to several tRNA molecules; in particular they represent a proposed partial recognition site for yeast phenylalanyl-tRNA ligase (6). In addition the duplex formed by the GAGC:GCUC set is the first simple example of a duplex formed from tetramers containing an internal A·U base pair.

England and Neilson (7) have used ultraviolet and circular dichroism studies on these two tetranucleotide sequences to show that duplex formation occurs and the authors have employed melting temperature (T_m) vs. concentration studies to evaluate the enthalpy change occurring for the single strands to the helix–coil transition.

In principle the chemical shift, coupling constant, and relaxation time data obtainable from the nmr spectrum of a molecule contain all the information necessary to define the geometric and motional behaviour of the molecule. However, the researcher's current ability to obtain this information is limited by the complexity of the tetranucleotide molecules and our inaccurate theoretical knowledge of the

[1]Authors to whom correspondence should be addressed.
[2]Present address: School of Chemical Sciences, University of Illinois, Urbana, IL 61801, U.S.A.
[3]Abbreviations used: GAGC ribosyl 5′-GpApGpC-3′. Oligonucleotides are written in the normal 5′ → 3′ sequence and in the duplex the bases are numbered from left to right and an arrow is used to indicate the direction of the 5′ → 3′ sequence: GAGC
1 2 3 4
CUCG.

Can. J. Chem. Downloaded from www.nrcresearchpress.com by 210.87.254.42 on 09/05/12
For personal use only.

Can. J. Chem. Downloaded from www.nrcresearchpress.com by 210.87.254.42 on 09/05/12
For personal use only.

TABLE 1. Chemical shifts[a] and coupling constants[b] for the derivatives and mixture of GAGC and GCUC at 65°C

	Value				
Parameter	GA[c]	GAG[c]	GAGC	GCUC	GAGC:GCUC
δG(1)H-8	7.789	7.802	7.871		7.870
δA(2)H-2	8.243	8.252	8.146		8.142
δA(2)H-8	8.347	8.393	8.257		8.264
δG(3)H-8		7.948	7.890		7.890
δC(4)H-6			7.738		7.729
δC(1)H-6				7.779	7.786
δU(2)H-6				7.829	7.829
δC(3)H-6				7.779	7.786
δG(4)H-8				7.965	7.965
δG(1)H-1′	5.734	5.752	5.729		
δA(2)H-1′	6.102	6.129	5.983		
δG(3)H-1′		5.916	5.870		
δC(4)H-1′			5.780		
δC(4)H-5			5.848		
$J_{1',2'}$G(1)	6.0	5.0[d]	4.1		
$J_{1',2'}$A(2)	5.2	5.5[d]	3.8		
$J_{1',2'}$G(3)		6.0[d]	3.4		
$J_{1',2'}$C(4)			5.1		
$J_{5,6}$C(4)			7.5		

[a]Chemical shifts in ppm relative to DSS using *tert*-butyl alcohol-OD as an internal reference (± 0.005 ppm).
[b]± 0.2 Hz.
[c]From spectra recorded at 220 MHz.
[d]Couplings not well resolved and accurate to ± 0.5 Hz.

myriad factors that affect the observed chemical shift of a given nucleus. Even more limiting are the relatively high concentrations, from a biological viewpoint, necessary to obtain adequate spectra for most magnetically active nuclei. In consequence nmr studies on oligonucleotides have been limited to ^{1}H spectroscopy and then only to those protons that are the most strongly deshielded in the molecule (4, 8). At low temperatures the N—H protons of N-3 (uracil) and N-1 (guanine) involved in the hydrogen bonding of base pair formation, show pronounced downfield chemical shifts and their shift changes with respect to temperature have, for simple self-complementary nucleotides, given useful information on the helix–coil transition (1, 3). At higher temperatures chemical exchange causes extensive line broadening and the utility of the N—H protons as probes is lost.

More recently the pioneering work of Borer *et al.* (2) on the self-complementary hexanucleotide AAG-CUU has shown that the carbon bound protons of the bases and the anomeric protons of the ribofuranoside ring may be used to define the helix–coil transition. Moreover, the observed chemical shift changes of the base protons were consistent with the duplex adopting either A- or A′-RNA helical structure. In the present paper, because the proton spectra were obtained at 90 MHz, it was only possible to assign fully the downfield aromatic protons of GCUC; the anomeric ribose ring protons were too complex to resolve adequately. It was possible however to completely assign the aromatic protons and the anomeric protons for all four units in GAGC at 65°C.

Results

To assign the downfield proton resonances in the spectrum of GAGC, obtained at 65°C to avoid inter- and intra-strand effects, the spectra of GA and GAG were obtained at the same temperature. These data together with the shifts of GCUC are recorded in Table 1 and summarized in diagrammatic form in Fig. 1.

Before recording the spectrum of the mixture of the tetranucleotides, the temperature dependence of the aromatic resonances in each tetranucleotide were obtained over the range 65–15°C. These data are shown in Fig. 2. All the aromatic protons showed a small and dominantly *linear* variation in chemical shift over this temperature range and in the GAGC moiety the A(2)H-8, A(2)H-2, G(3)H-8, and C(4)H-6 protons showed an upfield shift at low temperatures while the G(1)H-8 proton showed a downfield shift. Of the anomeric protons only A(2)H-1′ and G(3)H-1′ could be observed at low temperature. There was a considerable reduction in the magnitude of $J_{1',2'}$ for all these resonances until at 15°C they appeared as broad singlets (Table 2). The GCUC strand exhibited more variable changes with the U(2)H-6 and C(3)H-6 protons barely moving, G(4)H-8 moving downfield at low temperatures and C(1)H-6 moving

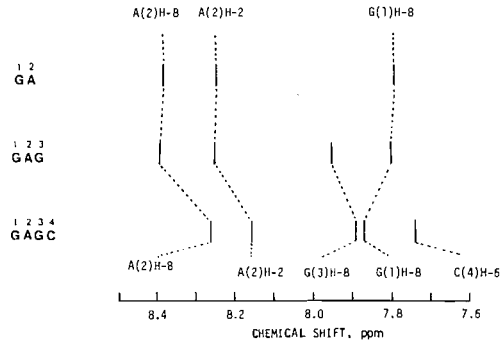

FIG. 1. The incremental assignment scheme for the base proton resonances for the tetranucleotide GAGC.

TABLE 2. GAGC ribose ring $J_{1'2'}$ coupling constant changes with respect to temperature

Temperature (°C)	Ribose, $J_{1'2'}$[a] (Hz)			
	G(1)	A(2)	G(3)	C(4)
65	4.1	3.8	3.4	4.7
55	3.5	3.8	3.0	4.0
45	—[b]	2.9	2.5	—[b]
35	—	2.2	2.4	—
15	—	< 1.0	< 1.0	—

[a] ± 0.2 Hz.
[b] Lines too broad for coupling to be observed.

upfield. Presumably a process such as intermolecular end-to-end base stacking is responsible for these latter shifts. It is noteworthy that the low temperature spectra of GCUC showed the separation of the C(1)H-6 and C(3)H-6 resonances and thereby confirmed their degenerate status in the higher temperature spectra.

The chemical shifts for the combined tetranucleotides at 65°C were identical with those recorded for each individual tetranucleotide and show the absence of inter-strand effects at this temperature. Spectra recorded at lower temperatures showed a marked *nonlinear* variation of the shifts and a rapid broadening of the absorption lines. Thus a spectrum which bore a satisfactory signal-to-noise ratio at 65°C could be accumulated in some 250 pulses but required over 2000 pulses at 25°C. The A(2)H-2 proton remained relatively sharp throughout the entire temperature range but the remaining aromatic protons showed line broadening at the lower temperatures of the order of 5–20 Hz. It was only by comparison of the spectra where the G(1)H-8, A(2)H-8, G(3)H-8, and G(4)H-8 protons had been replaced by deuterium (9) to the spectra of the fully protiated species that reasonable assignments of the remaining lowfield protons could be made. The shift changes with respect to temperature of the mixed tetranucleotides are shown in Fig. 3.

The melting temperature, T_m, of the GAGC:GCUC duplex was estimated from the midpoint of the chemical shift – temperature curves, when they were reasonably complete, in the usual fashion. The values all lay within the range 42 ± 1°C which is in remarkable agreement with the T_m value of 43.5°C predicted by extrapolation of the data for the concentration dependence of T_m obtained from ultraviolet absorption studies (7).

Discussion

The assignment of the lowfield resonances of GAGC was undertaken following the commonly employed method of 'incremental assignment' (2). This method assumes that as fragments are added to a molecular species, the chemical shifts of the protons already present will remain essentially constant. That this assumption is reasonably valid in the present example is evident from the diagrammatic representation of the chemical shifts of GA, GAG, and GAGC shown in Fig. 1. The shift assignments for the G and A residues in GA were consistent with those reported by Lee *et al.* (10) and the positions of G(1)H-8 and A(2)H-8 were confirmed by a deuterium isotope exchange experiment (9). In GAG three of the signals in the aromatic region were virtually identical with those of GA and the new signal at 7.948 ppm therefore assigned to G(3)H-8. Further confirmation of this assignment was obtained from a relaxation time measurement (T_1) with the line at 7.948 ppm showing a shorter relaxation time (ca. 3 s) than the signal at 8.252 ppm (ca. 5 s) which was assigned to A(2)H-2 (11). Similarly the anomeric proton doublet of G(3)H-1′ was clearly discernible at 5.916 ppm ($J_{1',2'}$ = 6.0 Hz) in the presence of the doublets for G(1)H-1′ and A(2)H-1′.

The anomeric region of GAGC was complicated by the overlap of the C(4)H-5 doublet at 5.848 ppm onto both of the C(4)H-1′ and G(3)H-1′ doublets. However, the lowfield C(4)H-6 doublet at 7.725 ppm ($J_{5,6}$ = 7.5 Hz) was well separated from the remaining four aromatic signals and a double irradiation experiment was sufficient to locate clearly the C(4)H-5 doublet.

The reduction of $J_{1',2'}$ for A(2)H-1′ and G(3)H-1′ as the temperature was decreased was attributed to base-stacking forcing the ribose rings into the ^3E or *C*-3′ *endo* conformation. This was consistent with the molecule adopting the A- or A′-RNA structure. Although the anomeric protons were not adequately resolved in GCUC and the duplex, it is expected that the ribose conformational changes in these systems will parallel the trend observed in GAGC.

The anomeric region (5.5–6.0 ppm) of the spectrum of the tetranucleotide GCUC showed a com-

Can. J. Chem. Downloaded from www.nrcresearchpress.com by 210.87.254.42 on 09/05/12
For personal use only.

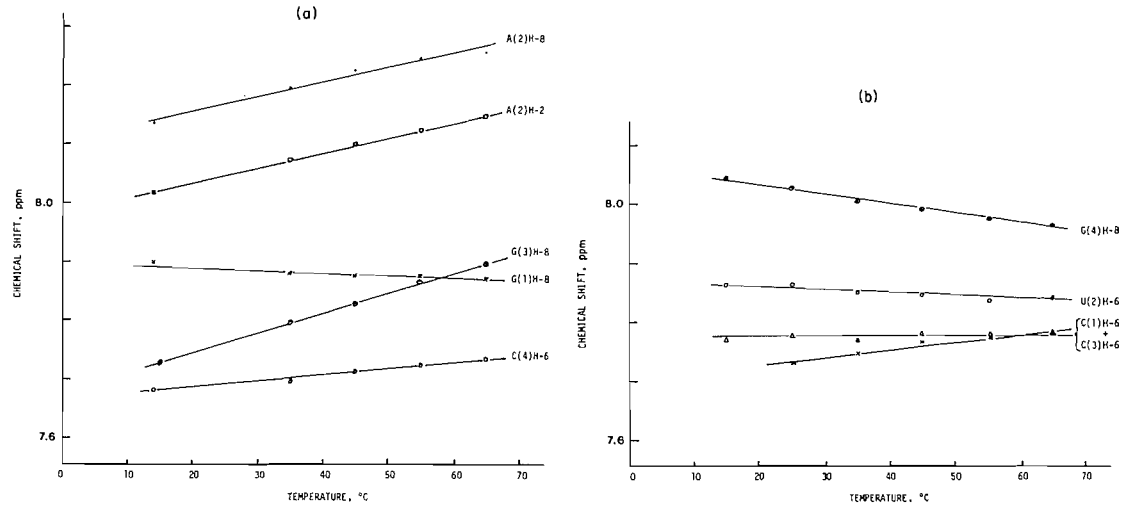

FIG. 2. Variable temperature versus chemical shift plots for: (*a*) GAGC base protons (concentration 6.1 × 10^{-3} *M*) and (*b*) GCUC base protons (concentration 7.3 × 10^{-3} *M*).

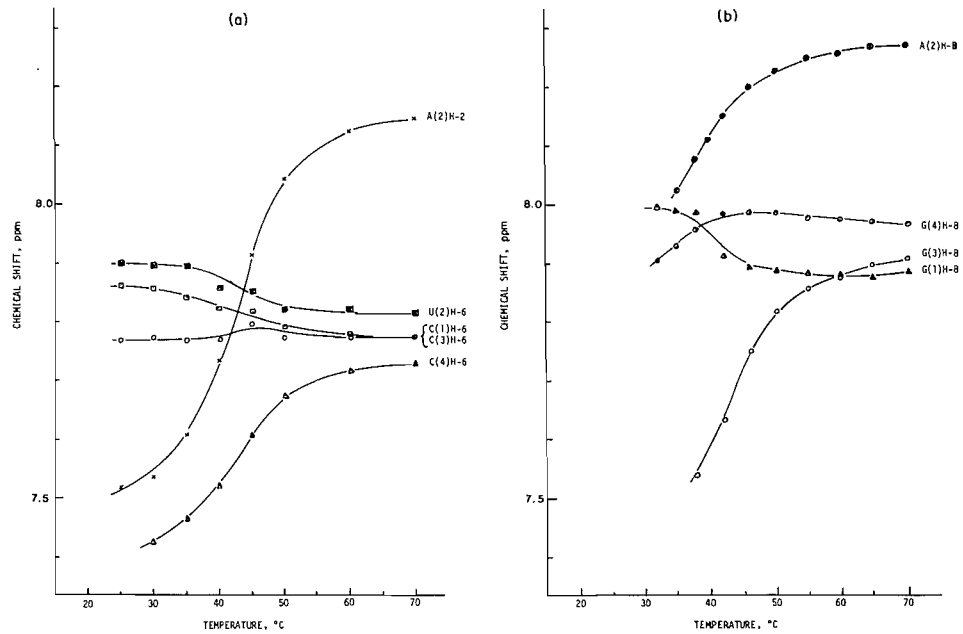

FIG. 3. Temperature dependence of the chemical shifts of the base protons of the duplex GAGC–GCUC (concentration 6.1 and 7.3 × 10^{-3} *M* in 1.0 *M* NaCl and 0.01 *M* sodium phosphate, pD 7.0): (*a*) the nonexchangeable protons A(2)H-2, U(2)H-6, C(1)H-6, C(3)H-6, and C(4)H-6; (*b*) the exchangeable protons A(2)H-8, G(4)H-8, G(3)H-8, and G(1)H-8.

plex overlapping set of lines derived from the four anomeric protons plus the three H-5 protons of C(2), U(3), and C(4) and assignment of the resonances was not attempted. The aromatic region however was simpler and showed only a singlet at 7.965 ppm (assigned G(4)H-8) and four lines between 7.7 and 7.9 ppm. The intensity ratios and coupling constants expected for uracil and cytosine residues led to the assignment of U(2)H-6 at 7.839 ppm ($J_{5,6}$ = 7.6 Hz) and C(3)H-6 and C(1)H-6 at 7.780 ppm ($J_{5,6}$ = 7.4 Hz). The superposition of the C(3)H-6 and C(1)H-6 signals was removed at lower temperatures when one of the protons showed an upfield shift whilst the other showed virtually no chemical shift changes (see Fig. 2*b*). Unfortunately no unambiguous assignment of C(3)H-6 and C(1)H-6 at the lower temperatures could be made but it is probable that the signal showing the greater upfield shift at lower temperatures (7.729 ppm at 25°C) belongs to C(3)H-6 as any stacking interaction

Can. J. Chem. Downloaded from www.nrcresearchpress.com by 210.87.254.42 on 09/05/12
For personal use only.

Can. J. Chem. Downloaded from www.nrcresearchpress.com by 210.87.254.42 on 09/05/12
For personal use only.

between G(4) and C(3) would be expected to result in a diamagnetic shift of the C(3) protons.

The spectrum of the GAGC:GCUC duplex at 65°C was astonishingly close to the sum of the spectra of the two separate strands and emphasised the complete absence of inter- and intra-strand effects at this temperature. The shifts of the various aromatic protons with decreasing temperature varied widely with those of A(2)H-2 being the most dramatic. Unfortunately, because of the severe line broadening experienced at lower temperatures, the full sigmoidal shape of the protons C(1)H-6, G(1)H-8, A(2)H-2, U(2)H-6, C(3)H-6, and C(4)H-6 was only visible. However, these lines with perhaps the exception of C(3)H-6 which showed a most curious temperature behaviour, all gave T_m values lying within the range 42 $\pm$ 1°C. The agreement between this T_m and the extrapolated value expected on the basis of variable concentration – uv studies (7) is remarkable but in conjunction with the similar correspondence in T_m values noted by Borer *et al.* (2) from their studies on the self-complementary A_2GCU_2 system, we must conclude that the nmr method appears to be a valid analytical tool for the measurement of T_m values.

The three protons A(2)H-8, G(3)H-8, and G(4)H-8 whose line positions could not be followed down to 25°C because of excessive line broadening coupled with the problem of line intensity loss arising from the H-8 to D-8 exchange process, showed a curious differential behaviour. The line for G(3)H-8 probably has a T_m close to 43°C but both A(2)H-8 and G(4)H-8 had barely begun the expected upfield movement at 42°C. This suggests that the T_m for these protons is much below 40°C. For the present duplex, these two low T_m values may appear at first sight to be rather unusual, particularly that of A(2)H-8. However, it is a pointed reminder that in observing the shift changes of these aromatic protons we are monitoring a plethora of local diamagnetic and paramagnetic effects which are exerting their influence over a spatial region that is very proximate to each of the protons. Factors such as base ring current shieldings or deshieldings, furanose ring conformations, glycosyl-base ring conformations, phosphate group anisotropies as well as inter-strand hydrogen bondings are all contributing to the screening constant of each hydrogen. Moreover, as we proceed through the T_m region, there is the additional averaging effect arising from the dynamic interconversion between the various intermediate states where only some of the bases are hydrogen bonding. With these points in mind it is not so much surprising that A(2)H-8 and G(4)H-8 show low T_m values but rather that the remaining seven protons should show T_m values so closely grouped together.

From the data presented here on the GAGC:GCUC duplex, there is no evidence of the fraying process noted by Borer *et al.* (2) and Ts'o *et al.* (12) in their examination of the self-complementary A_2GCU_2. It is reasonable to suggest that with the weaker A·U interaction being an interior one in the present duplex, the tendency for a G·C end fraying is much reduced. It is pertinent to note here that preliminary studies in our laboratories of the self-complementary tetramer CAUG shows a general lowering of the T_m values as is consistent with the presence of two A·U pairs but no evidence for terminal fraying of the stronger binding G·C pairs.

The line broadening effects noted for the present duplex appears to be typical of oligonucleotide sequences at relatively high concentrations. We are in full agreement with Borer *et al.* (2) that the principal line broadening factor is interduplex end-to-end stacking. The rate at which the various protons of the duplex broadened was also consistent with this view. Thus the end C(4)H-6 doublet broadened rapidly whereas the A(2)H-2 singlet remained relatively sharp until well below the T_m value. In addition the samples as a whole became distinctly turbid at temperatures below 25°C, and this was taken as evidence that polyduplex stacking was occurring.

Experimental

The compounds used in this study, GA, GAG, GAGC, and GCUC were all synthesised by procedures reported by England and Neilson (13).

The majority of the proton magnetic resonance data was collected on a Bruker WH-90 spectrometer operating in the Fourier transform mode. Temperatures were maintained to within $\pm$1°C by a Bruker B-ST 100/700 variable temperature unit and were calibrated by thermocouple measurements. Some spectra, mainly for confirmation purposes, were recorded at 220 MHz at the Canadian 220 MHz Centre, University of Toronto, Toronto, Ontario. The spectra were referenced to internal DSS (2,2-dimethyl-2-silapentan-5-sulphonate) by using the methyl line of *tert*-butyl alcohol-OD at 1.231 ppm as an internal standard. Chemical shifts were found to be reproducible to better than $\pm$0.005 ppm and coupling constants to less than $\pm$0.2 Hz. All samples were lyophilised twice from D_2O before use and they were taken up in 100% D_2O which was 1.0 *M* in sodium chloride and 0.01 *M* in sodium phosphate buffer (pD 7.0). Concentrations varied from 6.1 to 7.3 $\times$ 10^{-3} *M* and the spectra reported here are the result of three runs on the duplex sample.

Acknowledgement

We thank the National Research Council of Canada for financial support.

1. D. B. ARTER, G. C. WALKER, O. C. UHLENBECK, and P. G. SCHMIDT. Biochem. Biophys. Res. Commun. **61**, 1089 (1974).
2. P. N. BORER, L. S. KAN, and P. O. P. TS'O. Biochemistry, **14**, 4847 (1975).
3. L. S. KAN, P. N. BORER, and P. O. P. TS'O. Biochemistry, **14**, 4864 (1975).

4. T. R. KRUGH, J. W. LAING, and M. A. YOUNG. Biochemistry, **15**, 1224 (1976).
5. D. R. KEARNS. Annu. Rev. Biophys. Bioeng. **6**, 477 (1977).
6. B. DUDOCK, C. DIPERI, K. SCILEPPI, and R. RESZELBACK. Proc. Natl. Acad. Sci. U.S.A. **68**, 681 (1971).
7. T. E. ENGLAND and T. NEILSON. Can. J. Biochem. **55**, 365 (1977).
8. D. R. KEARNS and R. G. SHULMAN. Acc. Chem. Res. **7**, 33 (1974).
9. J. A. ELVIDGE, J. R. JONES, C. O'BRIEN, E. A. EVANS, and H. C. SHEPPARD. J. Chem. Soc. Perkin Trans. II, 1889 (1973); 2138 (1973); 174 (1974).
10. C.-H. LEE, F. S. EZRA, N. S. KONDO, R. H. SARMA, and S. S. DANYLUK. Biochemistry, **15**, 3627 (1976).
11. P. O. P. Ts'o, J. C. BARRETT, L. S. KAN, and P. S. MILLER. Ann. N.Y. Acad. Sci. **222**, 290 (1973).
12. P. O. P. Ts'o, J. L. ALDERFER, P. N. BORER, and L. S. KAN. *In* Structure and conformation of nucleic acids and protein – nucleic acid interactions. *Edited by* M. Sundaralingam and S. T. Rao. University Park Press, Baltimore, MD. 1975.
13. T. E. ENGLAND and T. NEILSON. Can. J. Chem. **54**, 1714 (1976).

Can. J. Chem. Downloaded from www.nrcresearchpress.com by 210.87.254.42 on 09/05/12
For personal use only.

Proton magnetic resonance studies on short duplexes. II. The self-complementary oligoribonucleotide CpApUpG[1]

PAUL J. ROMANIUK AND THOMAS NEILSON[2]
Department of Biochemistry, McMaster University, Hamilton, Ont., Canada L8S 4J9
AND
DONALD W. HUGHES AND RUSSELL A. BELL[2]
Department of Chemistry, McMaster University, Hamilton, Ont., Canada L8S 4M1
Received January 24, 1978

PAUL J. ROMANIUK, THOMAS NEILSON, DONALD W. HUGHES, and RUSSELL A. BELL. Can. J Chem. **56**, 2249 (1978).

Proton nuclear magnetic resonance was used to examine double helix formation in the self-complementary oligoribonucleotide CAUG in neutral D_2O containing 1.0 *M* NaCl. Using the procedure of incremental assignment all the nonexchangeable base and ribose anomeric protons could be assigned and were observed over the temperature range of 70 to 4°C. The chemical shift changes that occurred over this temperature range were sigmoidal in nature which is indicative of base-pairing. From the plot of chemical shift vs. temperature a T_m of 24 ± 1°C was determined. This is the first nmr study of a duplex formed from tetranucleotides which contains two internal A·U base pairs.

PAUL J. ROMANIUK, THOMAS NEILSON, DONALD W. HUGHES et RUSSELL A. BELL. Can. J. Chem. **56**, 2249 (1978).

On a utilisé la résonance magnétique nucléaire du proton pour examiner la formation de doubles hélices dans l'oligoribonucléotide auto-complémentaire CAUG dans du D_2O neutre contenant du NaCl à 1.0 *M*. Faisant appel à la méthode des attributions par augmentation, on a pu identifier, à des températures allant de 70 à 4°C, tous les protons de la base non échangeable et du ribose. Les changements dans les déplacements chimiques qui se produisent dans cet intervalle de température sont de nature sigmoidale et ils indiquent la présence d'un pairage des bases. A partir de la courbe des déplacements chimiques en fonction de la température, on a pu déterminer un T_m de 24 ± 1°C. Ceci est la première étude rmn de la formation d'un duplex à partir de tétranucléotides qui contiennent deux paires de base A·U internes.
[Traduit par le journal]

Introduction

Nuclear magnetic resonance spectroscopy of short oligoribonucleotides has been utilized to probe the physical properties of helix formation of nucleic acids (1–5). Of the several methods available to study these properties, nmr is capable of providing information on the conformational and environmental changes that occur during duplex formation. As well, there have been reports of good correlations between melting temperatures determined by nmr experiments and those predicted by optical methods (1, 2). This was further demonstrated by a study employing both optical methods and nmr of the interaction between the non-self-complementary sequences GAGC and GCUC (6, 7).[3] This was the first report of a duplex between tetraribonucleotides which contained one internal A·U base pair.

Self-complementary sequences are particularly suited for study by nmr since the symmetry of the duplex reduces the number of resonances and therefore complete chemical shift assignments of the base and ribose anomeric protons can usually be made. In addition, chemical synthesis of oligoribonucleotides by the phosphotriester method (8, 9) allows a variety of sequences to be prepared in high yield. In some cases, multi-stranded aggregates are formed by short oligoribonucleotides (10) although this has not yet been observed with a self-complementary sequence. We now report an nmr study on CAUG, a self-complementary tetraribonucleotide which forms a duplex containing two internal A·U base pairs. We intend to use this short helix as a reference for studies on the effect dangling bases and bulge loops have on the stability of RNA secondary structure.

Experimental

The 90 MHz proton nuclear magnetic resonance spectra were recorded in the Fourier transform mode on a Bruker WH-90 spectrometer equipped with quadrature detection. Probe temperatures were maintained to within ±1°C by a Bruker B-ST 100/700 variable temperature unit and were calibrated by thermocouple measurements. Samples were dissolved in 100% D_2O which contained 1.0 *M* sodium chloride and 0.01 *M* sodium phosphate buffer (pD = 7.0).

[1]For Part I, see Ref. 7.
[2]Authors to whom correspondence should be addressed.
[3]Abbreviations used: CAUG, ribosyl 5′-CpApUpG-3′ (all oligonucleotides are written in the 5′ → 3′ sequence).

Can. J. Chem. Downloaded from www.nrcresearchpress.com by 210.87.254.40 on 09/05/12
For personal use only.

Can. J. Chem. Downloaded from www.nrcresearchpress.com by 210.87.254.40 on 09/05/12
For personal use only.

tert-Butyl alcohol-OD was used as an internal reference and the chemical shifts are reported relative to DSS (2,2-dimethyl-2-silapentan-5-sulphonate). The deuterium signal of D_2O provided the field-frequency lock.

The compounds used in this study were prepared by standard procedures: CA, CAU, CAUG, and AUG by the methods of ref. 11.

Results

The low-field proton resonances of CAUG were assigned by comparison with the spectra of CA, CAU, and AUG all of which were recorded at 70°C. These data are presented in Tables 1 and 2. Figure 1 contains the 90 MHz spectra of CAUG at 70°C to illustrate the chemical shift assignments.

The effect of temperature variation on the proton resonances of CAU and AUG was examined, and the results are summarized in Figs. 2 and 3. The resonances of the trinucleotides varied linearly with temperature over the range of 17 to 70°C. For CAU all the protons displayed upfield shifts with decreasing temperature, except for CH-6 which was deshielded. Similar results were obtained for AUG with all the resonances being shielded. At high temperatures the UH-1′ and GH-1′ signals were

TABLE 1. Chemical shifts[a] of the oligoribonucleotides in D_2O[b] at 70°C

	δ			
Proton	CA	CAU	CAUG	AUG
CH-6	7.660	7.687	7.662	
AH-8	8.377	8.382	8.346	8.276
AH-2	8.260	8.250	8.196	8.198
UH-6		7.744	7.692	7.730
GH-8			7.962	7.963
CH-1′	5.779	5.768	5.765	
AH-1′	6.093	6.088	6.039	6.024
UH-1′		5.856	5.845	5.841
GH-1′			5.813	5.841
CH-5	5.958	5.925	5.912	
UH-5		5.746	5.738	5.772

[a]Chemical shifts are in ppm relative to DSS using *tert*-butyl alcohol-OD as an internal reference and are accurate to ±0.005 ppm.
[b]pD = 7.0; concentrations: CA, 1.6×10^{-2} *M*; CAU, 1.0×10^{-2} *M*; AUG, 1.3×10^{-2} *M*; CAUG, 9.2×10^{-3} *M*.

TABLE 2. Coupling constants for the oligoribonucleotides at 70C°

	$J_{1',2'}$			
Proton	CA	CAU	CAUG	AUG
CH-1′	4.4	4.0	3.8	
AH-1′	4.6	3.7	4.4	5.0
UH-1′		4.6	4.8	4.6
GH-1′			5.3	4.6

[a]Accurate to ±0.2 Hz.

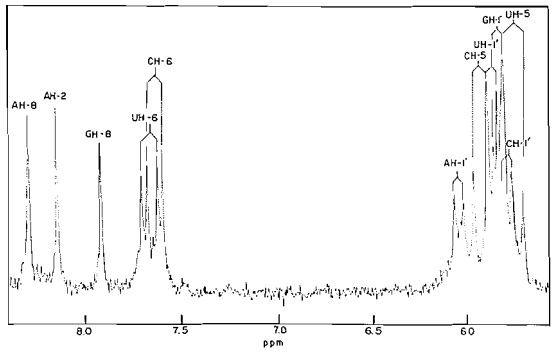

FIG. 1. The assignments of the base and anomeric protons in the ^{1}Hmr spectrum at 70°C of CAUG (concentration 9.2×10^{-3} *M* in 1.0 *M* NaCl and 0.01 *M* sodium phosphate, pD 7.0). Chemical shifts are relative to internal DSS.

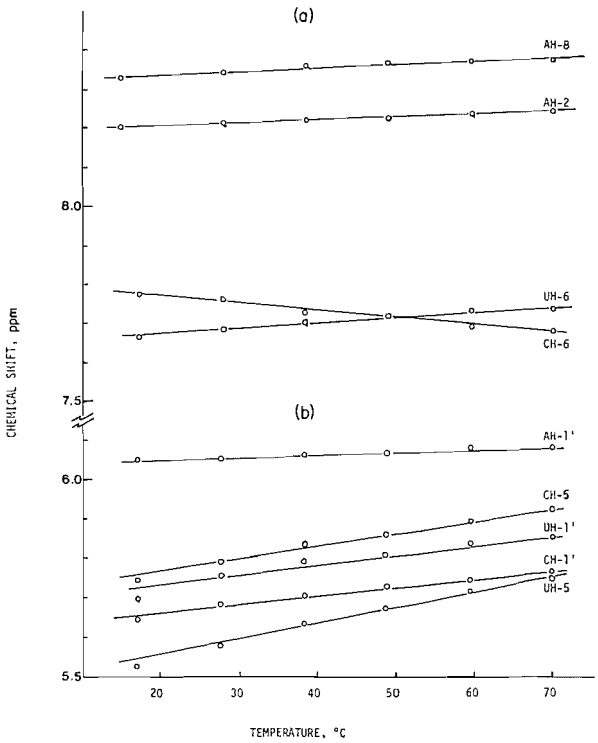

FIG. 2. Chemical shift vs. temperature plots for (*a*) the base and (*b*) the anomeric protons of CAU (concentration, 1.0×10^{-2} *M* in 1.0 *M* NaCl and 0.01 *M* sodium phosphate, pD 7.0). Chemical shifts are relative to internal DSS.

equivalent but began to separate near 50°C with UH-1′ being tentatively assigned to the more shielded resonance.

The proton spectrum of CAUG at high temperatures showed essentially a linear variation with temperature but at 45°C and lower, nonlinear behaviour was observed (Fig. 4). There was a rapid broadening of the resonances as the temperature was decreased below 35°C. The AH-2 signal showed the

Can. J. Chem. Downloaded from www.nrcresearchpress.com by 210.87.254.40 on 09/05/12
For personal use only.

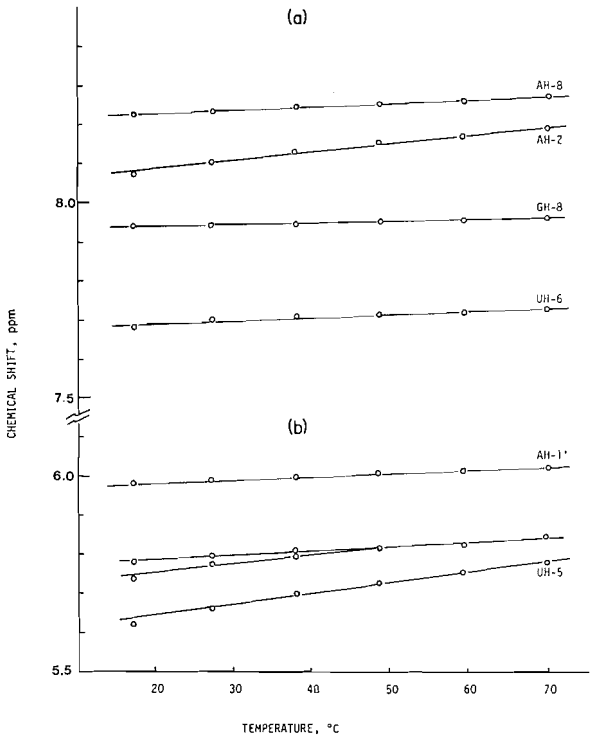

FIG. 3. Chemical shift vs. temperature plots for (*a*) the base and (*b*) the anomeric protons of AUG (concentration, 1.3×10^{-2} *M* in 1.0 *M* NaCl and 0.01 *M* sodium phosphate, pD 7.0). Chemical shifts are relative to internal DSS.

greatest chemical shift change and also remained relatively sharp throughout the temperature range. A large reduction in the magnitude of the H-1′, H-2′ coupling constant was observed until at 20°C these resonances appeared as broad singlets.

The average melting temperature, T_m of the CAUG duplex as determined from the temperature–chemical shift curves of AH-8, AH-2, and GH-8 was found to be 24 ± 1°C.

Discussion

Chemical shift assignments were determined by the standard technique of incremental analysis (2, 12) in which the base and ribose anomeric protons of CA, CAU, and AUG were correlated with those of CAUG. The CA shifts were in agreement with the results published by Ezra *et al.* (13). Addition of the uridine moiety to form CAU resulted in three new doublets appearing at 7.744 (UH-6, $J_{5,6}$ = 8.2 Hz), 5.746 (UH-5, $J_{5,6}$ = 8.2 Hz), and 5.856 ppm (UH-1′, $J_{1',2'}$ = 4.6 Hz). The cytidine and uridine aromatic protons were differentiated by the magnitude of the H-5 and H-6 coupling constant, cytidine, $J_{5,6}$ = 7.6 Hz; uridine, $J_{5,6}$ = 8.2 Hz. The uridine H-5 resonance was distinguished from the anomeric protons by irradiation of H-6 which caused the collapse of the doublet at 5.746 ppm.

The low-field signals of AUG were assigned by comparison to AU and UG (13). The anomeric region of the high temperature spectrum was complicated by the overlap of the UH-1′ and GH-1′ doublets and it was only at lower temperatures that these resonances separated. The lower field signal was tentatively assigned to GH-1′ since this proton should only be slightly shielded due to the weak stacking interaction between the U and G bases (13).

Using the chemical shift assignments of the trimers, the aromatic resonances of CAUG could be readily determined (Table 1 and Figure 1). Assignment of the anomeric protons was made difficult by the overlap of CH-5 (5.912 ppm) and UH-1′ (5.845 ppm), and GH-1′ (5.813 ppm), CH-1′ (5.765 ppm), and UH-5 (5.738 ppm). The observa-

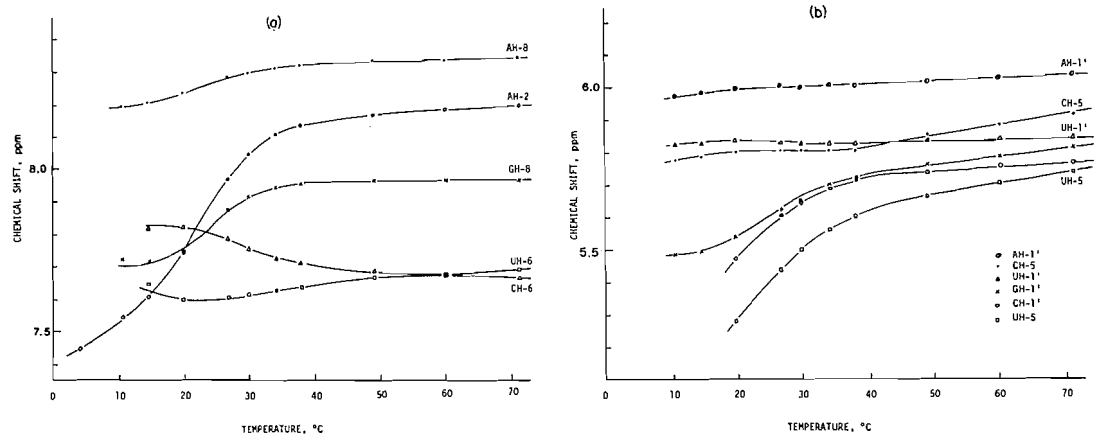

FIG. 4. Dependence of the chemical shift on temperature for the tetranucleotide CAUG (concentration, 9.2×10^{-3} *M* in 1.0 *M* NaCl and 0.01 *M* sodium phosphate, pD 7.0). Some points were not measurable below 20°C because of excessive line broadening. Chemical shifts are relative to internal DSS.

Can. J. Chem. Downloaded from www.nrcresearchpress.com by 210.87.254.40 on 09/05/12
For personal use only.

tion that CH-6 and UH-6 become equivalent near 60°C permitted the simultaneous irradiation of both pyrimidine H-6 resonances and the collapse of both H-5 doublets facilitated the analysis of the anomeric region of the spectrum. A direct result of this double irradiation experiment was that the UH-1′ and GH-1′ signals were found to be nonequivalent in the tetranucleotide as they were in AUG.

The effect of temperature variation on the proton resonances of CAU and AUG was linear and predominantly upfield (Figs. 2 and 3). These shift changes that were observed for the trimers were the result of intramolecular base stacking and were not characteristic of base pairing (1, 2, 7). The degree of base stacking was indicated by the reduction in the value of $J_{1',2'}$ (13 and 15). This corresponds to a shift in the ribose conformational equilibrium towards the ^3E or *C*-3′ *endo* structure. CAU showed the largest conformation changes since at 17°C all the anomeric proton doublets had collapsed to broad singlets with $J_{1',2'}$ less than 1.0 Hz. In contrast, the AUG anomeric couplings at 17°C were still well resolved with a range of 2.0 to 4.5 Hz. This difference in the degree of base stacking in these trimers is currently under further investigation.

The behaviour of the CAUG resonances with respect to temperature was dramatically different to that of the trimers. Above 45°C there was a linear change with respect to temperature for the base and anomeric protons and this is attributed to single strand intramolecular base stacking. Below 45°C there was a general nonlinear variation which is associated with the formation of the following base-paired duplex:

5′-CpApUpG-3′
. . . .
3′-GpUpApC-5′

Of the aromatic protons, AH-8, AH-2, and GH-8 all produced well defined sigmoidal curves. The average T_m was determined to be 24 ± 1°C. It is interesting to note that the pyrimidine H-6 resonances follow essentially the same trend that was observed in CAU. This appears to be a result of the similarity in base-stacking interactions in CAU and CAUG. In the anomeric region of the spectrum the AH-1′, CH-5, and UH-1′ resonances all undergo relatively small shielding changes when compared to GH-1′, CH-1′, and UH-5. Although the curve for GH-1′ is not as well defined as those of the aromatic protons, a T_m of 26 ± 1°C was estimated which is close to the value obtained for the aromatic protons.

Two aspects on the stability of the duplex formed by CAUG arise from these data. The first is the similarity in the T_m values for the majority of resonances of both the terminal and interior base pairs. This may be an indication that the presence of terminal G·C base pairs reduced any effects of fraying. Secondly, increasing the number of A·U base pairs in the interior of the duplex causes a lowering of the T_m value. This is demonstrated by comparison to the duplex formed by GAGC:GCUC (T_m = 42 ± 1°C) which has only one interior A·U base pair (7).

The large reduction in the coupling constant of the anomeric protons as the temperature was lowered ($J_{1',2'}$ less than 1.0 Hz at 20°C) is indicative of a high percentage of the C-3′ endo conformation of the ribose rings. This is consistent with the helical duplex having either the A- or A′-RNA conformation. It appears that base stacking is an integral process involved in double helix formation and may make a significant contribution to the helix stability (16).

Acknowledgements

We thank the National Research Council of Canada for financial support. One of us (P.J.R.) is a grateful recipient of an Ontario Graduate Scholarship.

1. D. B. Arter, G. C. Walker, O. C. Uhlenbeck, and P. G. Schmidt. Biochem. Biophys. Res. Commun. **61**, 1089 (1974).
2. P. N. Borer, L. S. Kan, and P. O. P. Ts'o. Biochemistry, **14**, 4847 (1975).
3. L. S. Kan, P. N. Borer, and P. O. P. Ts'o. Biochemistry, **14**, 4864 (1975).
4. T. R. Krugh, J. W. Laing, and M. A. Young. Biochemistry, **15**, 1224 (1976).
5. D. R. Kearns. Annu. Rev. Biophys. Bioeng. **6**, 477 (1977).
6. T. E. England and T. Neilson. Can. J. Biochem. **55**, 365 (1977).
7. D. W. Hughes, R. A. Bell, T. E. England, and T. Neilson. Can. J. Chem. This issue.
8. T. E. England and T. Neilson. Can. J. Chem. **54**, 1714 (1976).
9. E. S. Werstiuk and T. Neilson. Can. J. Chem. **54**, 2689 (1976).
10. S. R. Jaskunas, C. R. Cantor, and I. Tinoco, Jr. Biochemistry, **7**, 3164 (1968).
11. M. C. Ganoza, A. F. Fraser and T. Neilson. Biochemistry. In press.
12. P. O. P. Ts'o, J. L. Alderfer, P. N. Borer, and L. S. Kan. *In* Structure and conformation of nucleic acids and protein – nucleic acid interactions. *Edited by* M. Sundaralingam and S. T. Rao. University Park Press, Baltimore, MD. 1975. p. 193.
13. F. S. Ezra, C.-H. Lee, N. S. Kondo, S. S. Danyluk, and R. H. Sarma. Biochemistry, **16**, 1977 (1977).
14. C. Altona. *In* Structure and conformation of nucleic acids and protein – nucleic acid interactions. *Edited by* M. Sundaralingam and S. T. Rao. University Park Press, Baltimore, MD. 1975. p. 613.
15. C.-H. Lee, F. S. Ezra, N. S. Kondo, R. H. Sarma, and S. S. Danyluk. Biochemistry, **15**, 3627 (1976).
16. D. W. Appleby and N. R. Kallenbach. Biopolymers **12**, 2093 (1973).

A ^{19}F nuclear magnetic resonance and Raman spectroscopic investigation of the reaction of iodine oxide pentafluoride with the Lewis acids, antimony and arsenic pentafluoride

MORLEY BROWNSTEIN, RONALD J. GILLESPIE, AND JOHN P. KRASZNAI
Department of Chemistry, McMaster University, Hamilton, Ont., Canada L8S 4M1

Received September 20, 1977

MORLEY BROWNSTEIN, RONALD J. GILLESPIE, and JOHN P. KRASZNAI. Can. J. Chem. **56**, 2253 (1978).

The reactions of IOF_5 with SbF_5 and with AsF_5 have been investigated at low temperature by ^{19}F nmr and Raman spectroscopy. It was found that SbF_5 forms labile 1:1 and 2:1 complexes whereas AsF_5 forms only a 1:1 complex. The IOF_5 is bound through its oxygen atom to the Lewis acids AsF_5, SbF_5, or $(SbF_5)_2$.

MORLEY BROWNSTEIN, RONALD J. GILLESPIE et JOHN P. KRASZNAI. Can. J. Chem. **56**, 2253 (1978).

Les réactions entre IOF_5 et SbF_5 ou AsF_5 ont été étudiées à basse température par spectroscopie rmn (^{19}F) et Raman. Dans le cas de l'antimoine la formation de complexes labiles 1:1 et 2:1 a été mise en évidence. Par contre avec l'arsenic seul le complexe 1:1 se forme. Le IOF_5 est lié par son atome d'oxygène aux acides de Lewis AsF_5, SbF_5 ou $(SbF_5)_2$.

Can. J. Chem. Downloaded from www.nrcresearchpress.com by 210.87.254.42 on 09/05/12
For personal use only.

Introduction

It has been shown by Bartlett and Beaton (1) that IOF_5 does not react with SbF_5 even at elevated temperature and pressure to give the IOF_4^+ cation. We have used ^{19}F nmr and laser Raman spectroscopy to investigate the interaction of IOF_5 with SbF_5 and AsF_5 and we have obtained evidence for the formation of donor–acceptor complexes in which the Lewis acid is coordinated to the oxygen of IOF_5. Similar complexes have been observed previously (2, 3) between SbF_5 or AsF_5 and weak bases such as SO_2ClF, SOF_2, CH_3SO_2F, and SO_2 and it was shown that in all of these complexes the base is coordinated to the Lewis acid via the oxygen. SO_2F_2, on the other hand, was found to be too weak a base to interact with SbF_5 or AsF_5 even at very low temperatures and, hence, it was used as an inert low temperature solvent for the present work.

Results and Discussion

The IOF_5–AsF_5 System

The room temperature ^{19}F nmr spectrum of a solution of IOF_5 and excess AsF_5 in SO_2F_2 shows in addition to the solvent peak a very broad line with a linewidth at half height of 1040 Hz at 61 ppm upfield from external $CFCl_3$ which can be assigned to the F-on-As resonance and a rather broad and weak peak at −66 ppm which can be assigned to IOF_5. As the sample is cooled to −110°C, the F-on-As resonance sharpens and the previously collapsed spectrum of IOF_5 becomes well resolved to give a second order AB_4 multiplet. Figure 1 shows the spectrum of a solution containing IOF_5 and excess AsF_5 in SO_2F_2 at −110°C, and Table 1 lists the nmr parameters. The AB_4 multiplet of the IOF_5 spectrum shows all nine of the expected transitions (4) for the A spin system. The second order transitions for the B spin system are not observed because the lines are rather broad and the linewidth is comparable with the expected separation of the lines. The AB_4 spectrum differs from that of a solution of IOF_5 in SO_2F_2 (Fig. 2) in both chemical shift and F—F coupling constant and the linewidth is reduced from 180 to 50 Hz in the presence of AsF_5. These observations suggest that there is complex formation between IOF_5 and AsF_5 at these low temperatures. This complex formation is responsible for the change in the chemical shift and coupling constant of IOF_5 and it also increases the rate of quadrupole relaxation of the iodine by making the electric field gradient around the iodine nucleus less symmetrical and thus

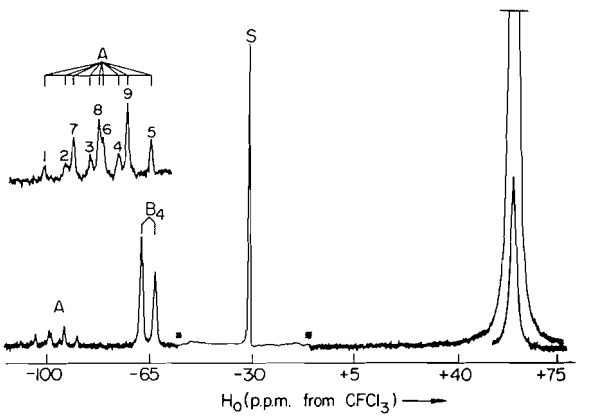

FIG. 1. The ^{19}F nmr spectrum of a solution of IOF_5 and excess AsF_5 in SO_2F_2(S) at −110°C; *, change in spectrometer gain.

Can. J. Chem. Downloaded from www.nrcresearchpress.com by 210.87.254.42 on 09/05/12
For personal use only.

TABLE 1. Chemical shifts (ppm from $CFCl_3$) and coupling constants J (Hz) for the IOF_5:AsF_5:SO_2F_2 system

		IOF_5			AsF_5	
Temp. (°C)	IOF_5:AsF_5	A	B_4	J^a	Shift	Width[b]
+26	1:5	n.o.[c]	−66.3	n.o.	60.9	1040
−110	1:5	−96.8	−65.9	253	57.9	220
−110	1:0[d]	−106.9	−69.1	271	—	—

[a]Coupling constant obtained by comparison with theoretical AB_4 spectra (ref. 4).
[b]Linewidth at half height.
[c]Under these conditions, neither the peak A nor the fine structure of peak B are observed.
[d]Solution of IOF_5 in SO_2F_2 (see Fig. 2).

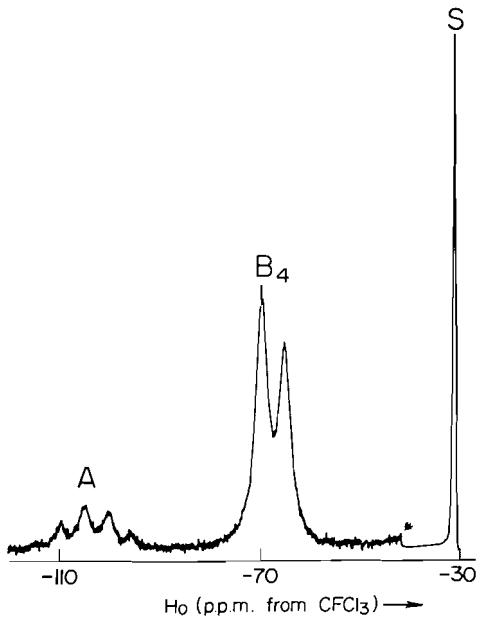

FIG. 2. The ^{19}F nmr spectrum of a solution of IOF_5 in SO_2F_2(S) at −110°C; *, change in spectrometer gain.

decreasing the linewidths. Similarly, the sharpness of the F-on-As peak indicates a much greater rate of quadrupole relaxation of the ^{75}As ($I = \frac{3}{2}$) nucleus than in AsF_5 alone. This would be expected since the electric field gradient about the arsenic will be greater in the complexed molecule than in uncomplexed AsF_5. Although free AsF_5 has a trigonal bipyramidal structure, very rapid intramolecular exchange of the fluorine atoms (pseudorotation) causes a rapid averaging of the electric field gradient to a low value. This very much decreases the rate of quadrupole relaxation and an extensively but incompletely collapsed multiplet spectrum is observed as a rather broad single line. In complexed AsF_5, although there is apparently a more symmetric octahedral arrangement of bonds about arsenic, five are strong As—F bonds while the sixth is a weak As—O bond. The resultant electric field gradient and, hence, the rate of quadrupole relaxation would be expected to be greater for complexed AsF_5 than for uncomplexed AsF_5 giving rise to a sharper line for the former.

The Raman spectrum of the 1:1 adduct is shown in Fig. 3*A* and Table 2 lists the frequencies and approximate descriptions of some of the vibrational modes for both the AsF_5 and SbF_5 adducts, together with pure IOF_5, AsF_5, and SbF_5 at −100°C. The IOF_5 group of the complex retains C_{4v} symmetry on the nmr time scale in SO_2F_2 solution at −100°C. However, this symmetry is probably lowered in the solid and since there are 13 atoms in the complex, a maximum of 33 fundamental modes are expected in the vibrational spectrum. Clearly it is not possible to assign all of these peaks with certainty but since the I=O stretching mode has the highest frequency in free IOF_5 we can at least assign the IO stretch in the complex with confidence. The peak at 921 cm^{-1} is the IO stretch of free IOF_5 (5, 6) which is produced by partial dissociation of the complex: (eq. [1])

$$[1] \qquad IOF_5 \cdot AsF_5 \rightleftarrows IOF_5 + AsF_5$$

The intensity of this peak increases at the expense of the peak at 853 cm^{-1} as the temperature is raised from −100°C and, therefore, we assign the peak at 853 cm^{-1} to the IO stretch of the complexed IOF_5. The reduction in the IO stretching frequency on complexation is consistent with a contribution from a single bonded resonance structure **2** to the structure

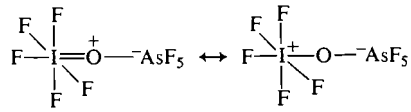

1 **2**

of the complex. A separate AB_4 spectrum is not observed for the uncomplexed IOF_5 and since the peaks of the complex are reasonably sharp we conclude that even at −100°C there is fast exchange between the complex and its components. A similar observation was made in the SOF_2–AsF_5 system (3) where at −100°C only one sharp peak was observed in the F-on-S region of the nmr spectrum. The AsO stretching frequency is difficult to assign due to the

Can. J. Chem. Downloaded from www.nrcresearchpress.com by 210.87.254.42 on 09/05/12
For personal use only.

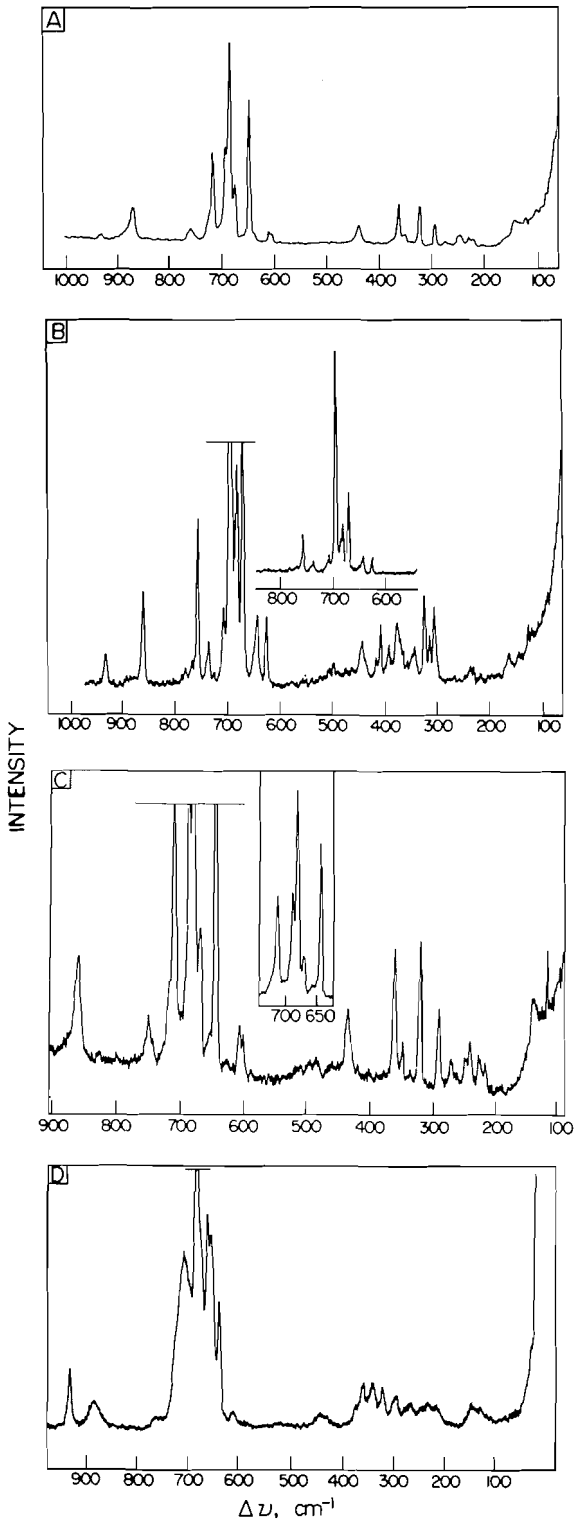

FIG. 3. Raman spectra of: (*A*) $IOF_5 \cdot AsF_5$ at −100°C; (*B*) $IOF_5 \cdot SbF_5$ at −100°C; (*C*) $IOF_5 \cdot 2.2SbF_5$ at −83°C; (*D*) $IOF_5 \cdot 2.2SbF_5$ at 25°C.

complexity of the Raman spectrum but in the ions AsF_5OH^- and $AsF_4(OH)_2^-$ it has been found at 562 and 554 cm^{-1} respectively (7). However, in the spectrum of the adduct no peaks are observed between 500 and 600 cm^{-1}. The IO stretching frequency of 853 cm^{-1} indicates considerable double bond character in the IO bond as the frequency is close to that of IO_4^- (838 cm^{-1}) (8). Hence, one might expect that the AsO bond will be correspondingly weak. Therefore, we tentatively assign the peak at 438 cm^{-1} to the AsO stretching frequency.

The IOF_5–SbF_5 System

The room temperature ^{19}F nmr spectrum of solutions of IOF_5 and SbF_5 in SO_2F_2 as solvent exhibit very broad lines for the F-on-I(VII) and F-on-Sb(V) regions of the spectrum. However, on cooling the solution to about −100°C fine structure is observed. Figure 4 shows the spectrum of an equimolar solution of IOF_5 and SbF_5 in SO_2F_2 at −110°C and the various parameters derived from the spectrum are summarized in Table 3. The spectrum shows in addition to the solvent peak, S, several complex multiplets in the F-on-I(VII) and F-on-Sb(V) regions.

We interpret the spectrum in terms of free IOF_5 and 1:1 and 1:2 IOF_5–SbF_5 complexes **3** and **4**.

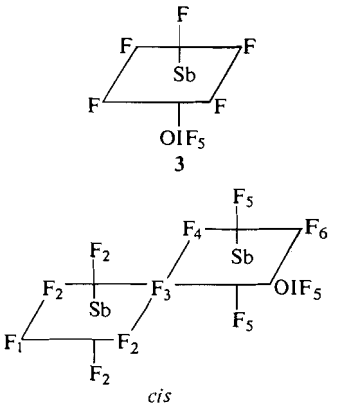

3

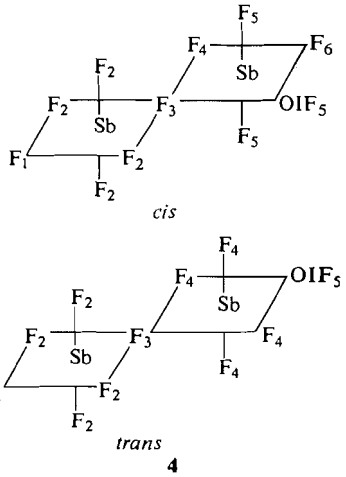

4

Furthermore, the spectrum is only consistent with the IOF_5 coordinating to SbF_5 through oxygen and not through fluorine. The five fluorines on Sb in structure **3** are expected to give rise to an AX_4 spectrum as observed for the multiplets labelled G.

Can. J. Chem. Downloaded from www.nrcresearchpress.com by 210.87.254.42 on 09/05/12
For personal use only.

TABLE 2. Raman spectra of $IOF_5 \cdot MF_5$ complexes and AsF_5, IOF_5, and SbF_5

$IOF_5 \cdot AsF_5$[a] (1:1)	AsF_5[b,d]	IOF_5[a]	SbF_5[c,f]	$IOF_5 : SbF_5$[a] (1:1)	$IOF_5 \cdot SbF_5$[e,f] (1:2.2)		Assignment
921(4)	—	920(23)	—	918(2)	—	920(19)p	I = 0 str. (free IOF_5)
—	—	—	—	872(sh)	875(sh)	873(9)p	I = 0 str. (1:2 complex)
853(8)	—	—	—	864(16)	858(13)	—	I = 0 str. (1:1 complex)
752(17)	—	—	—	752(6)	748(17)	757(4)dp	
—	—	—	745(m)	—	—	—	
730(4)	734(100)	—	736(w)	—	—	—	
—	—	722(1)	723(m)	—	—	—	
—	—	—	717(vs)	717(45)	715(49)	703(57)p	
701(8)	—	—	712(m)	—	—	—	
—	—	692(2)	693(w)	691(sh)	689(50)	—	
691(100)	—	—	—	684(100)	682(100)	—	
682(sh)	—	—	—	—	—	—	
677(22)	—	677(100)	—	677(sh)	671(19)	678(100)p	
—	—	—	668(vs)	—	—	—	
664(36)	—	—	—	—	—	—	
646(sh)	642(10)	—	—	647(70)	653(6)	652(64)p	
638(8)	—	638(85)	—	638(sh)	646(75)	637(42)p	
622(7)	629(40)	—	—	610(5)	606(5)	608(6)dp	
—	—	508(2)	—	—	—	—	
438(3)	—	—	—	438(9)	438(9)	439(4)p	(As)Sb···O str.
402(7)	400(s)ir[d]	—	—	—	—	—	
385(2)	382(16)	—	—	—	—	—	
369(7)	375(s)ir[d]	376(7)	—	—	—	373(sh)dp	
366(sh)	366(5)	—	—	—	—	—	
360(sh)	—	—	—	360(20)	360(18)	360(14)dp	
—	—	—	—	349(7)	348(6)	340(14)dp	
336(3)	—	336(19)	—	—	—	—	
318(11)	—	—	—	323(19)	320(20)	321(12)dp	
304(6)	—	—	—	—	—	—	
—	—	302(7)	—	—	—	298(10)dp	
296(10)	—	—	—	291(10)	289(11)	292(10)dp	
—	—	—	268(m)	268(2)	265(3)	265(10)dp	
—	—	—	241(m)	241(5)	243(5)	245(7)?	
224(1)	—	—	—	221(2)	224(4)	231(7)dp	
—	—	[205(2)]	217(m)	217(2)	213(3)	211(7)dp	
—	—	—	—	—	—	145(7)p	
—	—	—	—	—	—	126(5)p	

[a]This work. Spectrum recorded at −100°C.
[b]G. J. Schrobilgen, unpublished work (solid spectrum).
[c]Reference 16.
[d]Reference 17. Infrared spectrum.
[e]Left-hand column refers to spectrum at −83°C, right-hand column at room temperature.
[f]p = polarised, dp = depolarised, m = medium, vs = very strong, w = weak.

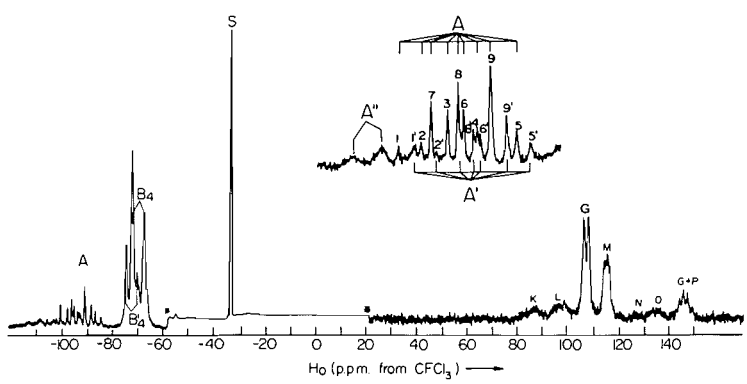

FIG. 4. The ^{19}F nmr spectrum of a solution of $IOF_5 \cdot SbF_5$ in SO_2F_2(S) at −110°C; *, change in spectrometer gain. The region of the spectrum between −80 and −115 ppm is shown in detail.

TABLE 3. ^{19}F nmr parameters[a] for an equimolar mixture of IOF_5 and SbF_5 in SO_2F_2 at −110°C

	F-on-I(VII)			F-on-Sb(V)							
	A	B_4	J	F_1	F_2	F_3	F_4	F_5	F_6	$J_{F_1-F_2}$	$J_{F_2-F_3}$
$IOF_5 \cdot 2SbF_5$	−91.2	−71.2	257	146.1	114.9	87.2	134.5	97.2	127.3	90	49
	A	B_4	J	A	X_4	J					
$IOF_5 \cdot SbF_5$	−94.0	−68.7	278	146.1	106.9	91					
	A	B_4	J								
Uncomplexed IOF_5	−106.7	n.o.[b]	271								

[a]Chemical shifts (ppm from $CFCl_3$) converted from SO_2F_2 internal reference ($\delta_{SO_2F_2} = \delta_{CFCl_3} + 32.04$ ppm) coupling constants (J) in Hz.
[b]B spin system for uncomplexed IOF_5 is obscured by those of the 1:1 and 1:2 complexes.

The fluorines F_2 in the *cis* bridged structure **4** are expected to be the most intense part of the spectrum for this complex and to be a doublet of doublets from coupling to both F_1 and F_3 and therefore M is assigned to fluorines F_2. Double resonance experiments by Dean and Gillespie (2) for the SO_2ClF–SbF_5 system where the profile of the Sb region is very similar to that in the IOF_5–SbF_5 system showed that the peaks labelled K, L, N, O, and P may be assigned to the fluorines F_3, F_5, F_6, F_4, and F_1, respectively. F_3 is coupled to fluorines F_2, F_4, F_5, and perhaps F_6 and is, therefore, expected to give rise to a broad unresolved line as seen for resonance *K*. F_1 is expected to be a quintet provided $J_{F_1-F_3}$ is zero as in $Sb_2F_{11}^-$ (9) by coupling to the four equivalent fluorines F_2. The fluorines F_4, F_5, and F_6 are expected to give rise to complex multiplets by coupling to F_3 and with each other. There is no evidence from the ^{19}F nmr spectrum for the *trans* bridged structure although the $Sb_3F_{16}^-$ anion, which is isoelectronic with the 1:2 complex, has been shown (10) to be *cis* bridged in solution and *trans* fluorine bridged in the solid (11).

In the F-on-I(VII) region, we assign the second order AB_4 multiplet to the fluorines on iodine in the 1:1 complex and the $A'B'_4$ multiplet to those in the 1:2 complex; the approximate ratio of the intensities of AB_4:$A'B'_4$ is 1:0.5 which is in excellent agreement with the approximate intensities of the resonances in the F-on-Sb region which give a mole ratio of **3**:**4** = 1:0.5. However, since the original solution was equimolar in IOF_5 and SbF_5, the presence of **4** indicates that there must also be some free IOF_5 in the solution. The two broad weak lines at −106.7 and −112 ppm (A″) are assigned to two transitions of the A spin system of free IOF_5 ($A''B''_4$), the remaining lines being hidden under the A and A′ resonances whilst the B″ doublet of free IOF_5 is hidden under the B and B′ doublets of the 1:1 and 1:2 complexes (Fig. 4).

The Raman spectra of an equimolar mixture of IOF_5 and SbF_5 as well as a mixture with excess SbF_5 were recorded at low temperature in the absence of a solvent (Fig. 3*B*, *C*, *D*). The IO region of the spectrum showed three peaks for the equimolar solution but only two for the solution containing excess SbF_5. The peak at 918 cm^{-1} can be unambiguously assigned to the IO stretch of free IOF_5 (5, 6) and the peaks at 872 and 864 cm^{-1} to the 1:2 and 1:1 complexes of IOF_5 with SbF_5 respectively. The nmr spectrum of an equimolar solution in SO_2F_2 showed that the 1:1 complex was present in higher concentration than the 1:2 complex at low temperature and this formed the basis for the assignment of the more intense peak at 864 cm^{-1} to the 1:1 complex and the shoulder at 872 cm^{-1} to the 1:2 complex. For the sample which contained excess SbF_5, the Raman spectrum at −83°C showed only the peaks attributable to the complexes, i.e. at 858 and 875 cm^{-1}. As this solution was warmed the peak at 875 cm^{-1} increased in intensity at the expense of the one at 858 cm^{-1} and dissociation to free IOF_5 occurred as evidenced by the appearance of the peak at 920 cm^{-1}. At room temperature the peak at 858 cm^{-1} had disappeared completely. This dissociation can be expressed by [2].

$$[2] \qquad 2IOF_5 \cdot SbF_5 \rightleftarrows IOF_5 \cdot 2SbF_5 + IOF_5$$

At low temperature there is an appreciable quantity of the 1:1 complex which dissociates until at room temperature the equilibrium lies predominantly to the right. The shift of the IO stretching mode to lower frequency is consistent with complexation through the oxygen and, furthermore, the shift of about 60 cm^{-1} indicates a relatively weak interaction. The SbO stretching mode is found at a frequency of 553 cm^{-1} in $SbF_5(OH)^-$ (7) and for the same reasons as were discussed earlier for the AsF_5 complex, we assign the polarised band at 438 cm^{-1} in the SbF_5 adduct to the SbO stretching frequency. However, if two different IO stretches are observed for the 1:1 and 1:2 complexes then two separate SbO stretches should also be observed. The position of the peak at 438 cm^{-1} does not change as the sample is warmed to room temperature and we must conclude that the two SbO stretching fre-

Can. J. Chem. Downloaded from www.nrcresearchpress.com by 210.87.254.42 on 09/05/12
For personal use only.

Can. J. Chem. Downloaded from www.nrcresearchpress.com by 210.87.254.42 on 09/05/12
For personal use only.

quencies for the 1:1 and 1:2 complexes are coincident. These assignments should, however, be regarded as tentative since in practice it is very difficult to distinguish between SbF, IF, and SbO stretching frequencies in complex molecules such as these.

Conclusions

SbF_5 forms 1:1 and 2:1 complexes with IOF_5. Because AsF_5 shows very little tendency to form polymeric As_nF_{5n} units, it forms only a 1:1 adduct. In all of these complexes the IOF_5 is oxygen bridged to the Lewis acid. This bridge in the 2:1 complex is shown to be *cis* to the fluorine bridge of the Sb_2F_{10} unit. Since both the 1:1 and 2:1 complexes exist in solution together with uncomplexed IOF_5, the Lewis basicity of the 1:1 complex must be comparable to that of IOF_5 itself.

It is interesting that IOF_5 is not a fluoride ion donor whereas IF_7 loses a fluoride to a strong Lewis acid such as SbF_5 to give the IF_6^+ cation. Christe has pointed out that highly symmetrical (i.e., octahedral and tetrahedral) fluorides and oxyfluorides (15) are frequently poorer fluoride ion donors than similar compounds of lower symmetry.

Experimental

Preparation of IOF_5

IOF_5 was prepared by the partial hydrolysis (12) of IF_7 in a Kel-F trap containing a small amount of sodium fluoride to remove the HF produced.

IF_7 was prepared by the high pressure, high temperature fluorination (13, 14) of iodine pentafluoride (Matheson) in a welded Monel can connected via $\frac{1}{4}$ in. Monel tubing to a Monel vacuum line. Excess fluorine was removed by pumping the vessel at −196°C.

Antimony pentafluoride was obtained from the Ozark Mahoning Co., and triply distilled in an atmosphere of dry air using an all-glass apparatus.

Arsenic pentafluoride was obtained from the Ozark Mahoning Co., and used directly.

Sulfuryl fluoride (Matheson of Canada) showed only one line in the ^{19}F nmr spectrum and was used without further purification.

Nuclear Magnetic Resonance Measurements

Fluorine nmr spectra were measured using a Varian DA-601L spectrometer operating at 58.3 MHz and modified as described previously (2) to record spectra from the first upper side band in the field sweep unlock mode.

Raman Spectra

Raman spectra were obtained using a Spex Industries Model 1400 spectrometer utilizing the 5145 Å radiation from a Spectra Physics model 164 argon ion laser. Spectra were recorded at −100°C by placing the sample tube inside a glass tube surrounded by an evacuated jacket, silvered except at the centre. Liquid N_2 was boiled off from a Dewar flask and passed through the tube. The temperature was monitored with a copper–constantan thermocouple positioned in the stream just ahead of the sample region. The Raman shifts are estimated to be accurate to $\pm 2\ cm^{-1}$.

Sample Preparation

All manipulations were carried out under anhydrous conditions on a vacuum line constructed from Monel, Kel-F, and Teflon or in a dry box. All preparative work was done in 15 cm × 2 cm od Kel-F tubes (Argonne National Laboratory) equipped with Kel-F heads and Teflon valves.

The nmr and Raman samples were prepared and vacuum sealed in 5 mm od medium wall Pyrex nmr tubes attached to Teflon valves with $\frac{1}{4}$ in. Teflon nuts and ferrules. The SbF_5 samples were prepared by distilling an appropriate quantity of IOF_5 onto a known amount of SbF_5 and then distilling in an excess of SO_2F_2. The AsF_5 samples were prepared similarly except that the AsF_5 was distilled onto a known amount of IOF_5 and then the solvent, SO_2F_2, was added.

Acknowledgement

We thank the National Research Council of Canada for financial support of this work.

1. S. P. Beaton. Ph.D. Thesis, University of British Columbia, Vancouver, B.C., Canada. 1966. *Quoted by* N. Bartlett and F. O. Sladky. J. Am. Chem. Soc. **90**, 5316 (1968).
2. P. A. W. Dean and R. J. Gillespie. J. Am. Chem. Soc. **91**, 7260 (1969).
3. M. Brownstein and R. J. Gillespie. J. Am. Chem. Soc. **92**, 2718 (1970).
4. J. W. Emsley, J. Feeney, and L. H. Sutcliffe. High resolution nuclear magnetic resonance spectroscopy. Vol. 1. Pergamon Press, 1965.
5. D. F. Smith and G. M. Begun. J. Chem. Phys. **43**, 2001 (1965).
6. J. H. Holloway, H. Selig, and H. H. Claassen. J. Chem. Phys. **54**, 5305 (1971).
7. L. Kolditz and K. Bauer. Z. Chem. **3**, 312 (1963).
8. H. Siebert. Z. Anorg. Allg. Chem. **273**, 21 (1953).
9. R. J. Gillespie and K. C. Moss. J. Chem. Soc. A, 1170 (1966).
10. J. Bacon, P. A. W. Dean, and R. J. Gillespie. Can. J. Chem. **48**, 3413 (1970).
11. A. J. Edwards, G. R. Jones, and R. J. C. Sills. Chem. Commun. 1527 (1968).
12. N. Bartlett, S. P. Beaton, L. W. Reeves, and E. J. Wells. Can. J. Chem. **42**, 2531 (1964).
13. R. J. Gillespie and J. W. Quail. Can. J. Chem. **42**, 2671 (1964).
14. N. Bartlett and L. E. Levchuk. Proc. Chem. Soc. 342 (1963).
15. K. O. Christe, C. J. Schack, and D. Pilipovich. Inorg. Chem. **11**, 2205 (1972).
16. P. A. W. Dean and R. J. Gillespie. Can. J. Chem. **49**, 1736 (1971).
17. L. C. Hoskins and R. C. Lord. J. Chem. Phys. **46**, 2402 (1967).

Distillation extractive. II. Etude de l'interaction entre carbures insaturés et solvants dipolaires

CLAUDE WAKSELMAN ET MICHEL BOUQUET
C.N.R.S.-C.E.R.C.O.A. 2 à 8, rue Henry Dunant, 94320 Thiais, France

Reçu le 2 novembre 1977[1]

CLAUDE WAKSELMAN et MICHEL BOUQUET. Can. J. Chem. **56**, 2259 (1978).

La nature des interactions entre hydrocarbures insaturés et solvants aprotiques dipolaires, intervenant dans la distillation extractive, a été étudiée par rmn du ^{13}C, mesure de constantes diélectriques et de moments dipolaires. Les résultats de ces différentes techniques sont en accord avec des interactions de type dipolaire.

CLAUDE WAKSELMAN and MICHEL BOUQUET. Can. J. Chem. **56**, 2259 (1978).

The nature of the interactions between unsaturated hydrocarbons and dipolar aprotic solvents, which occur in the extractive distillations, has been studied by ^{13}C nmr, dielectric constant, and dipole moment measurements. The results of these different methods are in agreement with dipolar interactions.

I. Introduction

Bien que la distillation extractive soit un procédé très utilisé en pétrochimie, la nature du phénomène mis en jeu est encore mal connue.

La séparation d'un mélange de monooléfines, de dioléfines et de parafines d'une coupe d'hydrocarbures en C_4 ou C_5 peut être effectuée par introduction en haut d'une colonne à distiller d'un complexant spécifique des carbures non saturés. Ce complexant est en général un solvant aprotique dipolaire tel que l'acétonitrile, le diméthylsulfoxide ou la *N*-méthyl pyrrolidone (NMP). Il apparaît que les meilleurs complexants présentent un fort dipole et un faible volume molaire (1). La valeur des volatilités relatives des différents hydrocarbures, à dilution infinie dans les solvants, peut être déterminée par chromatographie en phase vapeur, en utilisant une colonne imprégnée par le complexant. La sélectivité (2) d'un solvant peut être caractérisée par la séparation qu'il opère sur le couple d'hydrocarbures de référence isoprène/méthyl-2 butène-2. Cette définition est effectivement utilisée en France par les spécialistes de pétrochimie pour caractériser les complexants.[2]

Une étude (3) par rmn du proton a été effectuée récemment. Elle décrit une tentative de corrélation entre les variations de déplacement chimique des hydrogènes de l'isoprène et du méthyl-2 butène-2, induites par différents solvants dipolaires aprotiques, et les volatilités relatives de ces hydrocarbures. Il nous est apparu que les résultats obtenus par cette technique sont peu cohérents; nous avons alors abordé ce sujet à l'aide de la rmn du ^{13}C (communication préliminaire (4)), et par le calcul de moments dipolaires.

II. Méthodes expérimentales

1. Préparation des solvants et solutés

La N-méthylpyrrolidone (NMP), l'hexaméthylphosphotriamide (HMPT), le carbonate d'éthylène (CE) et la γ butyrolactone (γB) sont des produits commerciaux (Merck) qui ont été redistillés et conservés sur tamis moléculaire.

Dérivés de l'oxo-2 méthyl-3 oxazaphospholane-1,3,2. Leurs synthèses s'effectuent en deux étapes: formation d'un chlorure d'acide $ZP(O)Cl_2$ (Z = R, OR, NR_2) puis cyclisation avec le méthyl-2 aminoéthanol. Les chlorures pour lesquels Z = NR_2 et Z = OCH_3 ont été préparés selon Walsh et Toy (5); celui pour lequel Z = CH_3 a été obtenu selon Kinnear (6). Cyclisation par l'aminoéthanol: dans un tricol d'un litre équipé d'une agitation mécanique, on place 75 g (1 mol) de méthyl-2 aminoéthanol, 100 g (1 mol) de triéthylamine et 700 ml de benzène. Le mélange est refroidi à 0°C et agité. On ajoute goutte à goutte le dichlorure (0.5 *M*). Après addition, l'agitation est poursuivie pendant 5 h en laissant le mélange revenir à température ambiante. Le chlorhydrate de triéthylamine est filtré sur buchner et le solvant, ainsi que les excès de réactifs sont évaporés à pression réduite. Le produit final de condensation est distillé sous pression réduite (tableau 1).

La synthèse de la *NN'*-diméthylpyrrazolidinone-3 (NNMP) a été effectuée selon Kornet et Tan (7). La *N*-méthyloxazolidone-2 (NMPO) et la *N,N'*-diméthylimidazolidinone-2 (NMPN) ont été préparées en adoptant la méthode de Newman et Kutne (8). La synthèse de la *N*-méthyloxazolidinone-3 (ONMP) a été effectuée par extension du mode opératoire de Shunk, Bachelor et Folkers (9) à la méthylhydroxylamine. Ses caractéristiques physiques sont analogues à celles décrites par Petrus et coll. (10). Les hydrocarbures sont des produits commerciaux (Aldrich) de qualité "puriss" conservés au froid et distillés avant usage.

2. Résonance magnétique nucléaire du ^1H

Les spectres de rmn du proton des différents mélanges d'hydrocarbures et de solvants dipolaires, en proportions variables, ont été enregistrés à 60 MHz sur un spectromètre JEOL C-60-HL à la température de 37°C avec 5% molaire de tétraméthylsilane pour référence interne. Les couplages

[1]Révision reçue le 2 mai 1978.
[2]Ces mesures ont été effectuées par Monsieur V. Corso (Compagnie Française de Raffinage, Harfleur) que nous remercions vivement.

Can. J. Chem. Downloaded from www.nrcresearchpress.com by 210.87.254.42 on 09/05/12
For personal use only.

Can. J. Chem. Downloaded from www.nrcresearchpress.com by 210.87.254.42 on 09/05/12
For personal use only.

TABLEAU 1. Solvants phosphorés: caractéristiques et dénominations

	Solvant	Z	Eb
	W1	$-N(CH_3)_2$	112°C/1 Torr
	W9	—N⟨ ⟩	140°C/1 Torr
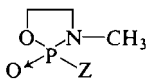	W8	—N⟨ ⟩	146°C/1 Torr
	W2	$-OCH_3$	93°C/1 Torr
	W5	$-CH_3$	92°C/0.5 Torr

multiples entre les protons et le mode d'enregistrement des spectres limitent la précision à 1 Hz malgré l'utilisation d'un fréquencemètre digital RACAL 801-R2. Les spectres de plus grande dilution correspondent à des concentrations de 5% molaire en soluté. L'attribution des signaux, pour les différents hydrocarbures, a été faite selon la littérature (11–14).

3. Résonance magnétique nucléaire de ^{13}C

Les spectres de rmn du ^{13}C des différents mélanges ont été enregistrés à 20 MHz sur un spectromètre Varian CFT-20 à la température de 37°C. Les tubes de 10 mm de diamètre contiennent les échantillons de mélange avec 5% molaire de cyclohexane utilisé comme référence interne. Un tube coaxial, maintenu par un dispositif en Téflon, contient du benzène-d_6 pour assurer la stabilisation en fréquence de l'appareil. L'étendue spectrale est de 4000 Hz et la résolution de 1 Hz. Les spectres sont obtenus en découplage total des protons. Les solutions les plus diluées nécessitent 50 000 accumulations pendant 15 h. Les déplacements chimiques sont exprimés en ppm par rapport au tétraméthylsilane (TMS). Le choix du cyclohexane pour référence interne a été fait selon Bacon et Maciel (15) car ce produit présente moins d'effet de solvant que le TMS. Nous l'avons d'ailleurs vérifié en étudiant les variations de déplacement chimique de solutions de cyclohexane (de 3 à 20% molaire) dans les solvants extracteurs par rapport au pic central de résonance du benzène d_6 contenu dans le capillaire coaxial. L'effet chimique des solvant sur le cyclohexane est ainsi mis en évidence: l'écart maximum, à dilution infinie et sans correction de susceptibilité magnétique, est inférieur à 0.3 ppm à bas champ par rapport au cyclohexane pur.

L'effet de solvant sur le déplacement chimique de la référence interne est d'ailleurs annulé lorsque nous effectuons des calculs de différence d'incréments. Outre son rôle de référence interne, le cyclohexane a été utilisé comme solvant inerte de dilution pour les hydrocarbures (ce choix est logique car la distillation extractive consiste bien à effectuer la séparation entre carbures saturés et non saturés). L'attribution des signaux a été faite suivant la littérature (16–19).

La marge d'erreur de 1 Hz sur l'attribution des déplacements chimiques des signaux est la même pour la rmn du ^1H et du ^{13}C. Toutefois, la gamme des déplacements ne dépasse pas 9 Hz pour le proton alors qu'elle atteint 30 Hz pour le carbone. Il apparaît donc que la précision relative est trois fois plus grande par rmn du ^{13}C.

4. Constante diélectrique

La recherche d'une relation possible entre la sélectivité des complexants et leurs caractéristiques physiques nous a conduit à la mesure de leurs constantes diélectriques et au calcul de leurs moments dipolaires. Ces mesures ont été faites de préférence sur les complexants pris purs, en considérant la réalité de la distillation extractive dans laquelle les oléfines sont extraites avec un excès de solvant spécifique.

Deux séries de mesure des constantes diélectriques ont été effectuées sur deux appareils: le "Dipolmeter W.T.W. DM 01", qui permet de mesurer avec précision des constantes inférieures à 3, a été utilisé pour les complexants dilués dans des solutions benzéniques; un tube EM4 de précision moyenne permet d'accéder aux valeurs de constante diélectrique supérieures à 3 et a été employé pour les solvants purs.

Chaque mesure a été effectuée plusieurs fois et la moyenne des essais a été retenue. Les constantes diélectriques de référence qui servent à l'étalonnage sont celles de l'air, assimilé au vide et du benzène. Les appareils sont thermostatés et les résultats indiqués pour la température de 24°C.

Les valeurs de la densité d ont été mesurées au picnomètre et confirmées par ailleurs.[3] Les indices de réfraction corrigés η_∞ ont été mesurés au réfractomètre O.P.L. et corrigés pour les raies D du sodium au prisme d'Amici. Les constantes diélectriques ε déterminées avec le tube EM 4 sur le solvant pur permettent d'accéder, selon la théorie d'Onsager qui tient compte des interactions dipole–dipole dans les liquides purs, à la valeur du moment dipolaire du complexant pur:

$$\mu = 0.218\left[\frac{M}{d}\frac{(2\varepsilon + \eta_\infty{}^2)(\varepsilon - \eta_\infty{}^2)}{\varepsilon(\eta_\infty{}^2 + 2)^2}\right]^{1/2}$$

Les mesures des constantes diélectriques de solutions benzéniques contenant le complexant à des concentrations variables ne dépassant pas 1% molaire ont été effectuées au "dipolmeter WTW". Nous extrapolons la polarisation molaire à dilution infinie, et calculons la réfraction molaire dans les mêmes conditions, selon la théorie de Debye. Ces extrapolations font intervenir les formules de Clausius–Mossotti et de Debye (20).

$$\tfrac{4}{3}\pi N\alpha = \frac{\varepsilon - 1}{\varepsilon + \eta}\frac{M}{d}$$

$$\mu = 0.0127[(P - R_M)T]^{1/2}$$

avec α polarisabilité totale, N nombre d'Avogadro, P polarisation molaire et R_M réfraction molaire. Le moment dipolaire obtenu est celui du complexant infiniment dilué dans un solvant non polaire. Pour confirmer les résultats obtenus par la théorie d'Onsager sur les complexants purs, nous avons utilisé les mesures de constante diélectrique employées dans la théorie de Debye, en estimant la polarisation comme une grandeur additive. A faible concentration du soluté dans le benzène, nous avons calculé la contribution du soluté dans la mesure de la constante diélectrique du mélange. Les résultats obtenus ont confirmé les mesures effectuées dans le cadre de la théorie du modèle d'Onsager (résultats donnés à ± 0.1 Debye).

III. Résultats

1. Résonance magnétique nucléaire du ^1H

Yablonskii et coll. (3) ont enregistré les spectres rmn du ^1H de l'isoprène et du méthyl-2 butène-2 dans les solvants extracteurs. Ils ont déterminé des différences d'incréments, à dilution infinie, par comparaison entre deux protons de position analogue sur le squelette carboné de ces deux hydrocarbures.

[3]Nous remercions Monsieur V. Corso pour ces mesures.

Can. J. Chem. Downloaded from www.nrcresearchpress.com by 210.87.254.42 on 09/05/12
For personal use only.

Les différences d'incrément sont inférieures à 7 Hz. Ces auteurs ont classé les complexants dans l'ordre de selectivité suivant: acétonitrile < diméthylacétamide < diméthylformamide < diméthylsulfoxide < *N*-méthylpyrrolidone (NMP) < héxaméthylphosphotriamide (HMPT). L'écart dans lequel se situent les différences d'incréments induits ne dépasse pas en fait 3 Hz, fourchette assez restreinte pour permettre une telle classification. L'effet de solvant sur la référence interne n'est pas discuté. Finalement, ces résultats n'ont pas permis à leur auteurs de conclure clairement sur la nature du phénomène mis en jeu dans la distillation extractive.

Nous avons tenté de reproduire l'étude précédente. Les spectres des hydrocarbures en C_5 (isoprène, méthyl-2 butène-2, pentadiène-1,4, pentane) à dilutions variables dans un solvant polaire (NMP ou HMPT) ou dans le cyclohexane ont été enregistrés. Le cyclohexane a été choisi comme solvant inerte de dilution. Nous avons d'abord étudié l'effet de ces solvants sur la référence interne et constaté qu'il était important (21). Le déplacement chimique des protons du tétraméthylsilane, en solution à 5% molaire dans les différents solvants, a été mesuré par rapport au tétraméthylsilane pur placé dans un capillaire coaxial central. Le déblindage observé, sans correction de susceptibilité magnétique, est de 12 Hz dans le cyclohexane, 16 Hz dans la NMP et 22 Hz dans le HMPT. Cet effet de solvant sur la référence interne est annulé quand nous procédons à des différences d'incréments de déplacement chimique du proton entre deux hydrocarbures à dilution infinie dans les solvants. Nous avons comparé nos résultats (tableaux 2),[4] dont un exemple est donné sur la fig. 1, à ceux de la littérature (3). La comparaison des déplacements chimiques des hydrogènes placés sur des sites analogues dans la molécule d'isoprène et dans celle du méthyl-2 butène-2 permet de calculer des incréments, d'importance variable selon le solvant. Il s'avère que le classement de ces solvants est différent selon le site observé, et imprécis car les écarts sont faibles (voir tableau 3). Une classification de complexants basée sur ces résultats semble donc très aléatoire. L'efficacité du HMPT, selon la littérature (3), est d'ailleurs très surestimée et en contradiction avec les mesures de C.P.V.[5]

Pour compléter ces résultats, on peut ajouter les valeurs des différences d'incréments de déplacement chimique pour le couple pentadiène-1,4/*n* pentane

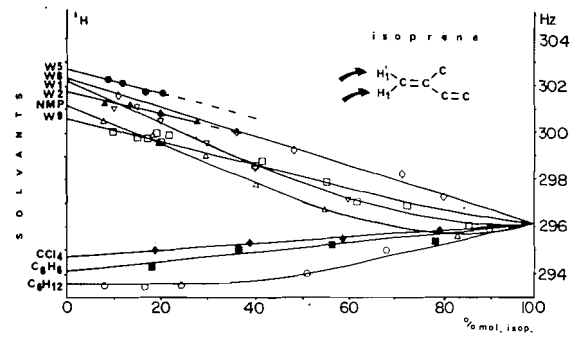

FIG. 1. Déplacements chimiques des protons de l'isoprène: H_1, H_1'.

TABLEAU 3. Différence d'incréments proton (Hz) isoprène/méthyl 2-butène 2

Hydrocarbures sites 1, 3, 4, 5

isoprène

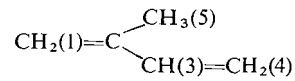

méthyl 2-butène 2

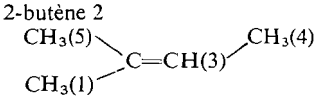

Site	NMP	HMPT	Classement
1	6.3*	7.4*	NMP < HMPT*
	7.7	7.8	NMP ≃ HMPT
3	5.7*	6.0*	NMP < HMPT*
	6.6	6.8	NMP ≤ HMPT
4	8.0	7.8	NMP ≥ HMPT
5	1.9	2.1	NMP < HMPT
Sélectivité†	2.15	1.80	NMP ≫ HMPT

*Valeurs indiquées dans la réf. 4.
†Sélectivités déterminées par CPV (3).

dans la NMP (tableau 4):[4] 4 Hz pour le carbone 1 et 8 Hz pour le carbone 2. Il n'a pas été possible de relier les volatilités des hydrocarbures que nous avons examinés, aux différences d'incrément chimique du proton, calculées par comparaison entre sites analogues, ou par sommation sur l'ensemble des sites. Par contre, d'autres remarques relatives à ces spectres de proton peuvent être formulées. Il s'agit en observant les amplitudes relatives des déplacements sur les courbes de dilution, de comparer les protons homologues des différents hydrocarbures, à dilution infinie dans les solvants. Les signaux des groupes méthyles et méthyléniques ne présentent pas de déplacements importants (3 Hz). Les signaux des protons éthyléniques subissent des déblindages plus marqués. Le groupe $=CH_2$ varie de 7 à 9 Hz dans l'isoprène, de 3 à 4 Hz dans le pentadiène-1,4. Le groupe =CH— varie, dans les deux exemples de

[4]On peut obtenir les données expérimentales de rmn (tableaux 2, 4, 5, 6) mises en dépôt, à un prix nominal, en s'adressant au Dépôt de données non publiées ICIST, Conseil national de recherches du Canada, Ottawa (Ont.), Canada K1A 0S2.

[5]Mesures faites par Monsieur V. Corso.

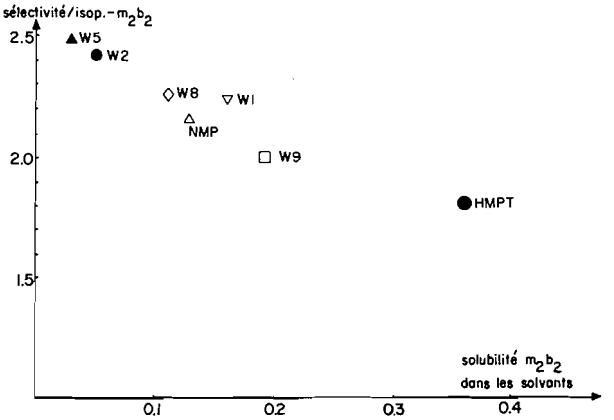

FIG. 2. Sélectivité des solvants.

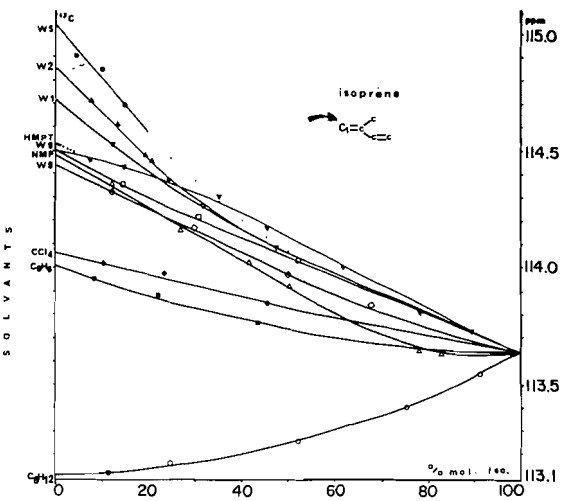

FIG. 3. Déplacements chimiques ^{13}C: carbone C_1 de l'isoprène.

6 Hz. Il y a donc une différence de "sensibilité" des protons à l'effet des solvants, selon la conjugaison de la dioléfine. De façon générale, il apparaît que l'effet de milieu se traduit, pour les différents solvants (NMP, HMPT, solvants phosphorés cycliques W) par un déblindage des protons des hydrocarbures. Par ailleurs, aucun déplacement sur les signaux des protons des solvants n'est observé, quelles que soient les proportions relatives d'hydrocarbures et de complexants.

2. Résonance magnétique nucléaire du ^{13}C

Il nous est apparu que la rmn du ^{13}C est une méthode (22)[6] plus appropriée pour l'étude de l'interaction entre complexants et carbures insaturés. En effet, les valeurs des déplacements chimiques sont plus grandes que celles enregistrées en rmn du proton. Les problèmes de couplage ne se posent plus. Les variations de déplacement chimique sont plus importantes et le classement des solvants est plus précis. De plus, les déplacements ^{13}C sont moins sensibles aux effets d'anisotropie magnétique (importants en rmn du proton) et reflètent plus la structure électronique interne des molécules (23–25).

Nous disposons pour cette étude d'une famille de solvants phosphorés ne différant entre eux que par la nature d'un seul substituant, mais présentant une gamme de sélectivité très étendue (26) (voir fig. 2). Rappelons, à ce sujet, qu'un solvant est caractérisé par sa sélectivité et son pouvoir solubilisant vis-à-vis d'un couple d'oléfines. Les meilleurs complexants (W1, NMP) sont ceux qui possèdent de bonnes valeurs pour les deux critères.

Les spectres des différents hydrocarbures (*n* pentane, isopentane, pentène-1, méthyl-2 butène-2, pentadiène-1,4, isoprène) ont été enregistrés dans des mélanges de cyclohexane et de solvants extracteurs W en proportions variables (tableaux 5).[4]

Les courbes de dilution correspondant aux signaux des différents carbones de ces hydrocarbures ont été tracées et les déplacements chimiques δ à dilution infinie dans les solvants ont été déterminés par extrapolation. L'ensemble des signaux des carbures insaturés est déplacé vers les bas champs par rapport à celui observé dans le cyclohexane (voir fig. 3). L'écart des déplacements chimiques entre les solvants polaires et le cyclohexane est très variable et peut dépasser 1.5 ppm. Nous remarquons que les groupes méthyles sont affectés de façon semblable (0.5 ppm) quel que soit le site et le degré d'insaturation du substrat (isoprène, méthyl-2 butène-2, pentane, isopentane). Les déplacements chimiques des groupes méthyléniques du pentadiène-1,4, du pentane et de l'isopentane ne varient guère (glissement inférieur à 0.1 ppm). Il en est de même pour le carbone tertiaire de l'isopentane. Les carbones oléfiniques présentent plus d'intérêt car ils subissent un déblindage très net qui affecte de façon dissymétrique les doubles liaisons. Pour le pentène-1, les carbones subissent un déplacement à bas champ, respectivement de 0.4 et 0.6 ppm pour le C_1 et 0.8 ppm pour le C_2 dans les solvants NMP et W1 (voir fig. 4). Le pentadiène-1,4, dioléfine non conjuguée, se comporte dans les mêmes conditions comme deux monooléfines terminales simplement reliées par un pont méthylénique; l'amplitude et la dissymétrie du déblindage sont analogues à celles du pentène-1. Il apparaît donc que dans le cas des oléfines terminales le carbone sp^2 le plus substitué est le plus "sensible" aux effets de milieu, même si celui-ci est peu polaire (22).[6] Pour le méthyl-2 butène-2, le C_2 (quaternaire sp^2) subit un

[6]Pour une étude de l'influence des solvants peu polaires sur les spectres rmn ^{13}C des oléfines, voir réf. 22.

Can. J. Chem. Downloaded from www.nrcresearchpress.com by 210.87.254.42 on 09/05/12
For personal use only.

Can. J. Chem. Downloaded from www.nrcresearchpress.com by 210.87.254.42 on 09/05/12
For personal use only.

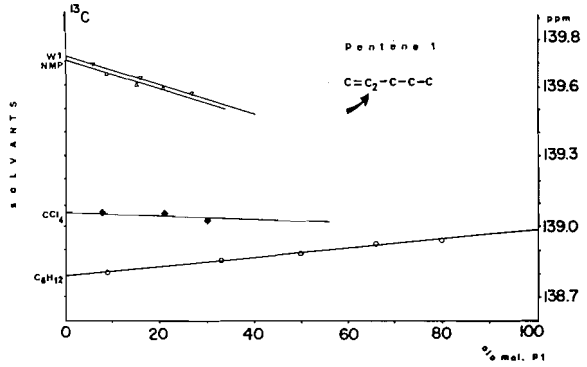

FIG. 4. Déplacements chimiques ^{13}C: carbone C_2 du pentène-1.

déblindage très marqué de 0.8 ppm tandis que le C_3 (CH sp^2) paraît presque insensible aux solvants (voir fig. 5). Les carbones quaternaire C_2 et tertiaire C_3 de l'isoprène se comportent d'une manière analogue à ceux du méthyl-2 butène-2 avec des amplitudes d'increments plus réduites (0.6 et 0.3 ppm). Mais à la différence du pentadiène-1,4 et des monooléfines, ce sont les carbones terminaux (C_1 et C_4) qui enregistrent les plus forts déblindages (1.5 et 1.2 ppm). La sensibilité particulière aux effets de milieu (22)[6] des carbones sp^2 internes n'est donc pas un phénomène général. Les raisons de ces différences de sensibilité n'étant pas évidentes, nous avons préféré examiner par la suite l'influence des solvants sur l'ensemble des carbones des hydrocarbures insaturés.

Nous pouvons remarquer que l'effet de dilution dans le cyclohexane n'est pas ressenti dans le déplacement chimique des carbones des hydrocarbures saturés et monoléfiniques. Seuls les carbones portant les insaturations des dioléfines subissent un blindage par dilution dans le solvant cyclohexanique; cela peut s'interpréter par la rupture progressive des interactions intermoléculaires de type π–π entre oléfines.

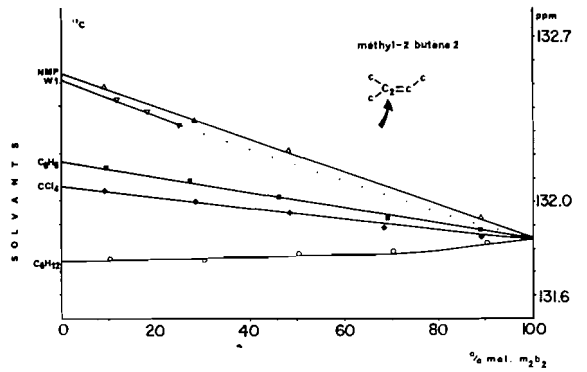

FIG. 5. Déplacements chimiques ^{13}C: carbone C_2 du méthyl-2 butène-2.

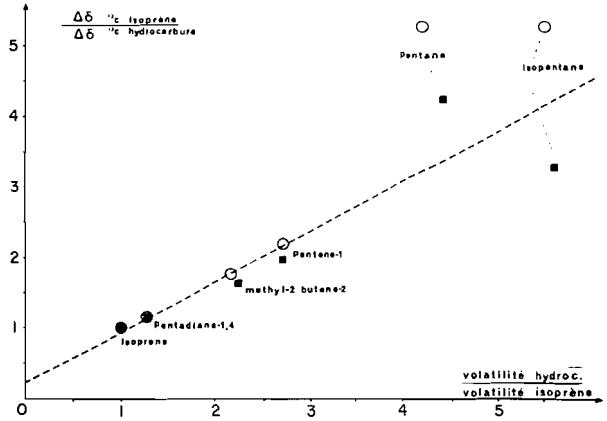

FIG. 6. Incrément chimiques ^{13}C total et volatilité (solvants: ○, NMP; ■, W1).

Incréments chimiques ^{13}C

Nous avons d'abord considéré que l'effet de solvant était un phénomène qui concerne globalement la molécule et que la somme des $\Delta\delta$ induits sur l'ensemble des carbones du soluté, à dilution infinie, pouvait être une mesure de l'influence du complexant:

$$\Delta\delta = (\delta_{C_1} + \ldots + \delta_{C_5})_{solvant} - (\delta_{C_1} + \ldots + \delta_{C_5})_{cyclohexane}$$

(δ_{C_i} représente le déplacement chimique ^{13}C du carbone i d'un carbure).

Il apparaît que l'ordre des valeurs de $\Delta\delta$ pour les différents hydrocarbures est sensiblement parallèle à celui de l'inverse de leurs volatilités dans les solvants (voir fig. 6).

Nous avons ensuite comparé les variations de déplacement chimique des carbones des alcènes, à celles des carbones ayant une position similaire sur le squelette carboné de l'alcane correspondant, ce que nous exprimons pour le carbone i ($i = 1, 2, \ldots, 5$) par:

$$\Delta(\Delta C_i) = (\delta C_{i_{solv.}} - \delta C_{i_{cycloh.}})_{alcène} - (\delta C_{i_{solv.}} - \delta C_{i_{cycloh.}})_{alcane}$$

Ce calcul se traduit, avec les mesures à dilution variables, par des courbes (voir fig. 7) mettant en évidence les effets des solvants NMP et W1 sur l'insaturation des solutés (tableaux 6).[4]

Les valeurs de $\Delta(\Delta C_i)$ sont indépendantes de la référence interne de déplacement chimique choisie pour cette étude. Pour le pentène-1 et le pentadiène-1,4, les valeurs de $\Delta(\Delta C_2)$ et $\Delta(\Delta C_1)$ sont, respectivement, 1.0 et 0.3 ppm. L'effet de solvant sur l'insaturation est nettement marqué par un déblindage en C_2. Pour le méthyl-2 butène-2, l'influence sur le carbone le plus substitué est également mise en évidence. Pour l'isoprène, les quatre carbones portant les insatura-

Can. J. Chem. Downloaded from www.nrcresearchpress.com by 210.87.254.42 on 09/05/12
For personal use only.

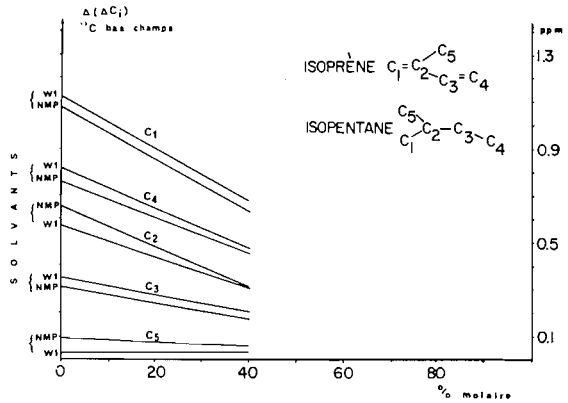

FIG. 7. Différence d'increments ^{13}C, isoprène − isopentane.

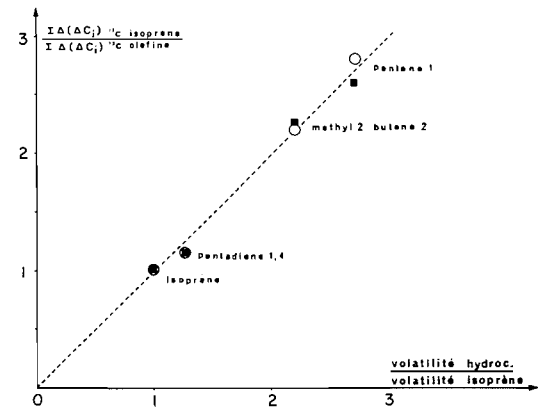

FIG. 8. Incrément ^{13}C d'insaturation et volatilité (solvants: ○, NMP; ■, W1).

tions sont affectés de façon variable, les carbones terminaux étant les plus "sensibles": $\Delta(\Delta C_1) > \Delta(\Delta C_4) > \Delta(\Delta C_2) > \Delta(\Delta C_3)$. Ce mode de calcul révèle les sites les plus perturbés par les solvants. L'effet de solvant est enregistré principalement sur les carbones portant les insaturations; le déblindage affecte de façon différente les deux carbones d'une double liaison. Cette dissymétrie peut s'expliquer, en partie, par la dissymétrie des molécules concernées. L'effet de conjugaison d'une dioléfine se traduit de façon particulière: à l'inverse du pentadiène-1,4, l'isoprène est plus déblindé sur ses carbures sp^2 terminaux.

Les résultats précédents nous ont conduits à calculer la somme

$$\sum_{i=1}^{i=5} \Delta(\Delta C_i)$$

sur les cinq carbones d'un carbure insaturé et à la relier à la volatilité de celui-ci dans les solvants polaires (voir fig. 8). La relation est linéaire pour l'ensemble des oléfines qui ont été étudiées et pour les deux solvants NMP et W1. Ceci met en évidence de façon qualitative le rôle des doubles liaisons dans le mécanisme de la complexation entre solutés et solvants, et de façon quantitative la relation linéaire entre la volatilité d'un soluté et le déplacement chimique ^{13}C vers les bas champs.

L'étude rmn du ^{13}C a également porté sur l'influence des différents solvants vis-à-vis du couple d'hydrocarbures isoprène/méthyl-2 butène-2, qui sert de référence aux pétrochimistes pour déterminer la sélectivité S des complexants par chromatographie en phase vapeur.[7] Comme précédemment, les valeurs de $\Delta\delta$ pour les deux oléfines ont été calculées, à dilution infinie dans les solvants. Les différences d'incréments $(\Delta\delta_{isop.} - \Delta\delta_{m2b2})$, exprimées en ppm sont en relation avec les sélectivités S (voir fig. 9). Nous observons, en effet, la correspondance: $S = \text{Cte} \times (\Delta\delta_{isop.} - \Delta\delta_{m2b2})$. A partir de la famille des solvants phosphorés W et de la NMP, il a été établi que cette constante est de $1.36\ ppm^{-1}$. Nous montrons également qu'il est possible de prévoir la sélectivité d'autres solvants dipolaires à partir des mesures de rmn du ^{13}C avec une bonne précision (voir tableau 7). Les mesures par CPV ont été effectuées postérieurement aux mesures de rmn et montrent un bon accord entre ces deux méthodes. Nous en avons déduit le classement suivant, dans l'ordre de sélectivité décroissante:

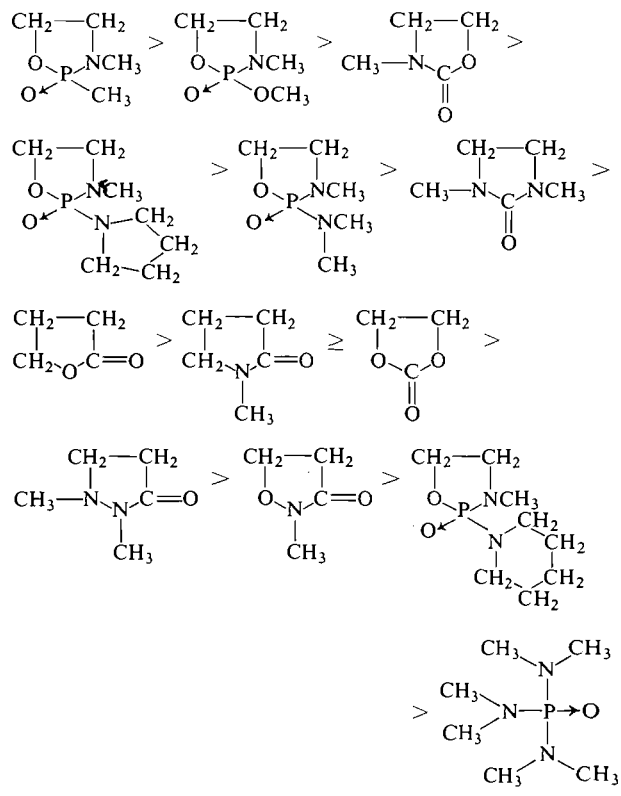

[7]Ce couple d'hydrocarbures a été utilisé comme référence par Monsieur V. Corso pour ses mesures de sélectivité par chromatographie en phase vapeur.

Can. J. Chem. Downloaded from www.nrcresearchpress.com by 210.87.254.42 on 09/05/12
For personal use only.

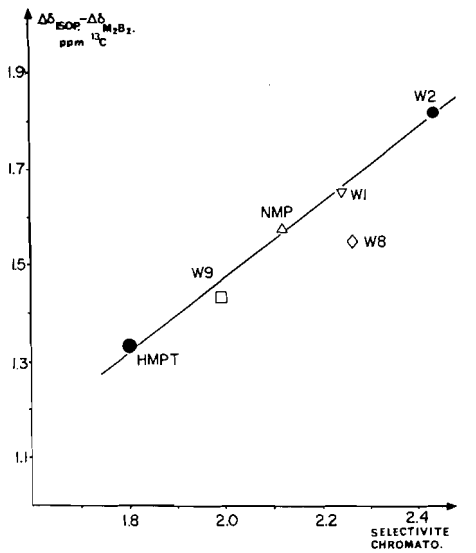

FIG. 9. Correlation Δδ et sélectivité.

TABLEAU 7. Sélectivité des solvants dipolaires à partir des mesures de rmn ^{13}C

Solvant	$\Delta^{13}C$*	Sélectivité ^{13}C†	Sélectivité CPV
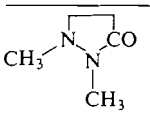	1.53	2.08	2.12
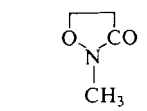	1.43	1.95	1.99
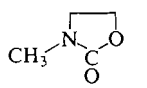	1.82	2.47	2.37

*$(\Delta\delta_{isop.} - \Delta\delta_{m2b2})$ en ppm.
†$1.36 \times \Delta^{13}C$.

Les déplacements chimiques Δδ, les écarts $(\Delta\delta_{isop.} - \Delta\delta_{m2b2})$ et les variations $\sum\Delta(\Delta C_i)$ à bas champs traduisent un appauvrissement en électrons du squelette carboné des hydrocarbures insaturés, au niveau des doubles liaisons. Les signaux des complexants, par contre, ne sont pratiquement pas affectés, quelles que soient d'ailleurs les proportions relatives de solvant et d'hydrocarbures. Pour les oléfines, les variations de déplacement chimique peuvent difficilement s'expliquer par des modifications des angles de valence et de torsion. On constate l'existence d'un effet de solvant assez important pour la molécule de méthyl-2 butène-2 dont le squelette est rigide. Pour la molécule d'isoprène, en très grande majorité s-transoïde (27, 28), l'isomérisation en s-cisoïde se traduirait, en raison d'un accroissement de la compression stérique, par un déplacement chimique vers les hauts champs des carbones terminaux, dans le sens opposé au phénomène enregistré. L'existence d'une forme gauche s'accompagnerait d'un affaiblissement de la conjugaison, et par conséquent d'une diminution de la sélectivité de la séparation entre l'isoprène et les autres carbures insaturés. Nous pouvons plutôt interpréter les variations observées par une interaction de type dipolaire, entre le solvant et les hydrocarbures polarisables (29), dont l'amplitude varie suivant la nature du complexant et le degré d'insaturation des oléfines.

Par ailleurs, des mesures d'enthalpie d'excès de mélange (30) de la NMP avec différents hydrocarbures en C_6 (utilisés pour des raisons techniques parce qu'ils sont moins volatils que leurs homologues en C_5)[8] nous ont permis de relier les chaleurs de mélange avec les volatilités relatives des carbures. Nous enregistrons les plus grandes variations d'enthalpie d'excès pour les diènes conjugués.

3. Constantes diélectriques, moments dipolaires des solvants

Bien que certains auteurs (2, 31) aient nié l'existence d'une relation entre la sélectivité (S) des complexants et leurs grandeurs physiques (densité, constante diélectrique ε, moment dipolaire μ), nous avons tenté de mettre en évidence une formule empirique qui lie S, ε, μ et le volume molaire V des complexants.

Il a été possible de dresser un tableau de valeurs pour les différents solvants étudiés en posant en première approximation $S = K\mu/V$ dans laquelle μ est le moment dipolaire du complexant pur. Cette formule suppose, à priori, une relation directe entre la sélectivité et le rapport μ/V de chacun des solvants. Il faut souligner le fait que nous utilisons les moments dipolaires des solvants purs, en estimant que ces valeurs correspondent à la réalité de la distillation extractive dans laquelle les hydrocarbures sont extraits avec un large excès de complexant. Le volume molaire de la NMP est pris pour unité. La valeur de K (voir tableau 8) est constante pour la famille des dérivés phosphorés W et met en évidence le rôle du volume molaire des solvants (voir fig. 10). Cependant, les dérivés non phosphorés de structure proche de celle de la NMP, avec un cycle pentagonal, présentent des valeurs de K dont la dispersion est assez nette pour mettre en doute la généralité de la formule citée ci-dessus. Nous avons alors tenté de relier la valeur de K pour les deux familles de complexants, à celle de μ/ε. Les résultats obtenus (fig. 11) permettent d'écrire: $K = K_1 + K_2\mu/\varepsilon$. La mise en équation de la sélectivité se fait alors selon: $S = K_1\mu/V + K_2\mu^2/\varepsilon V$. Pour les phosphoramides

[8]Nous remercions M. H. V. Kehiaian et J. P. E. Grolier pour la communication de leurs mesures.

Can. J. Chem. Downloaded from www.nrcresearchpress.com by 210.87.254.42 on 09/05/12
For personal use only.

TABLEAU 8. Constantes physiques des complexants

Solvant	ε	μ*	μ*/V	S	K†
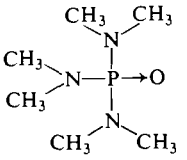	28	5.2	2.86	1.80	0.627
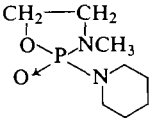	37	6.0	3.17	1.99	0.627
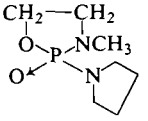	42	6.1	3.59	2.26	0.627
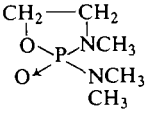	36	5.2	3.61	2.24	0.627
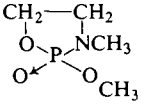	31	4.7	3.64	2.42	0.66
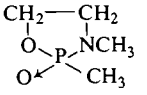	35	4.8	3.97	2.45	0.627
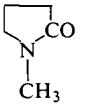	33	4.1	4.1	2.15	0.524
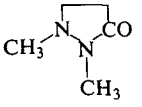					
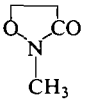	12	2.4	2.6	1.99	0.765
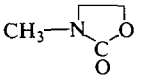	35	4.1	4.55	2.37	0.520
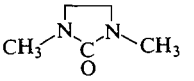	25	3.8	3.37	2.21	0.655
	39	4.1	5.12	2.18	0.426
	89	5.9	8.53	2.15	0.252

*En Debye, à 26°C.
†$S = K\mu/V$.

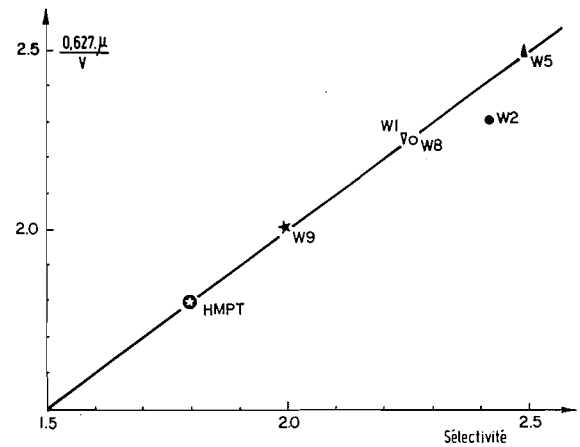

FIG. 10. Solvants phosphoramides, sélectivité et $k\mu/V$.

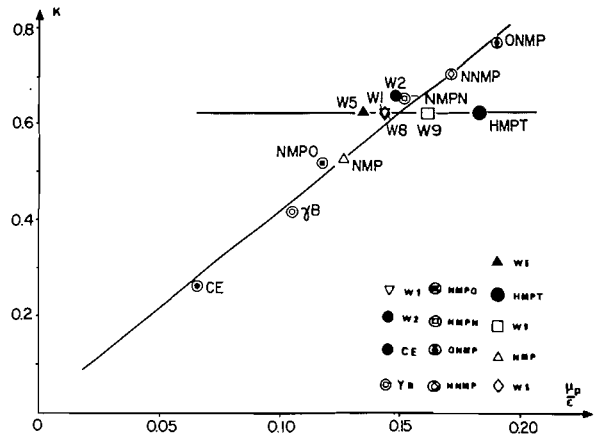

FIG. 11. K fonction de μ_P/ε.

$K_1 = 0.627$, $K_2 \simeq 0$; pour les composés cycliques non phosphorés $K_1 = 0.02$, $K_2 = 3.9$.

Cette formule empirique qui fait correspondre à la sélectivité un phénomène énergétique d'interactions dipolaires (dipole–dipole et dipole–dipole induit) est satisfaisante pour l'ensemble des solvants étudiés. La mise en équation de la sélectivité suggère, dans cette hypothèse d'interactions dipolaires, une orientation privilégiée des molécules de solvants proches de l'oléfine. Une couche de solvatation est occupée par des molécules complexantes orientées par rapport au soluté. Au-delà, il n'y a pas d'orientation préférentielle et l'effet d'écran est introduit par la constante diélectrique. Pour les solvants de très fort dipole, les associations moléculaires sont importantes, le milieu est relativement structuré, et le terme $K_1\mu/V$ est grand. Si le solvant possède un dipole moyen, la structuration du milieu est moins perceptible, l'influence vient de la zone non orientée, et le terme $K_2\mu^2/\varepsilon V$ est important. Dans ce cas, la valeur de la constante diélectrique ne doit pas être trop élevée, pour obtenir une bonne sélectivité, car elle figure au dénominateur de la relation empirique. Les deux modes d'action sont efficaces et peuvent concourir à la sélectivité du complexant. Les constantes K_1 et K_2 paraissent liées à la structure des molécules de solvant, à la nature et à l'accessibilité de leurs dipoles. Elles dépendent, en outre, des caractéristiques physiques (dipole, polarisabilité) des oléfines qui servent de référence pour le critère de sélectivité. La détermination des valeurs de K_1 et K_2 d'après les mesures de sélectivité par CPV pour l'un des membres d'une famille de solvants permet, en principe, de prévoir la sélectivité des autres membres à partir de leurs constantes diélectriques et leurs volumes molaires. Ainsi, nous avions pu estimer les sélectivités de la γ butyrolactone et du carbonate d'éthylène avant de les connaître par CPV. Il apparaît qu'un assez bon accord existe entre ces prévisions, les calculs d'incréments par rmn du ^{13}C et les mesures de sélectivité par chromatographie.

IV. Discussion

Différentes hypothèses peuvent être formulées sur la nature de l'interaction entre solvants et composés non saturés: liaison hydrogène, complexe par transfert de charge, changement conformationnel, interaction dipolaire. L'hypothèse d'une liaison hydrogène ne peut être retenue que pour les carbures acétyléniques. Les mono et di-oléfines ne possèdent pas d'hydrogène acide et les solvants étudiés sont du type dipolaire aprotique. L'amplitude des déplacements chimiques observés par rmn du ^1H est trop faible pour correspondre à ce type d'interaction.

Il ne nous a pas été possible de mettre en évidence, par des mesures en ultra-violet, entre 200 et 400 nm, l'existence de véritables complexes par transfert de charge. De plus, la rmn du ^{13}C montre que les signaux du complexant ne sont pas affectés par la présence des composés non saturés.

Les déplacements chimiques ^{13}C, induits par les complexants, pourraient être interprétés par une modification conformationnelle des molécules d'hydrocarbure. Cependant, une telle interprétation ne rend pas compte des déplacements importants observés pour la molécule de méthyl-2 butène-2 relativement rigide.

Nous avons plutôt retenu une interprétation du phénomène basée sur des interactions de Van der Waals. Nous pouvons considérer à la fois les forces de Keesom (orientation entre deux dipoles permanents) bien que les hydrocarbures ne possèdent

Can. J. Chem. Downloaded from www.nrcresearchpress.com by 210.87.254.42 on 09/05/12
For personal use only.

que des moments dipolaires faibles, et les forces de Debye (interaction d'un dipole permanent et d'un dipole induit par le premier dans une molécule voisine). Cette interprétation est justifiée par les résultats obtenus par la rmn du ^{13}C et par la formule empirique reliant la sélectivité aux caractéristiques physiques des solvants.

Remerciements

Nous remercions la Compagnie Française de Raffinage pour son soutien financier et tout particulièrement Monsieur J. Grosmangin et Monsieur V. Corso pour les mesures chromatographiques.

Nous remercions le Professeur J. Cantacuzene pour l'intérêt qu'il a porté à cette étude et le Professeur J. J. Basselier pour ses conseils et l'utilisation de ses appareils de mesure.

1. J. M. Prausnitz et R. Anderson. A. I. Ch. E. J. **71**, 96 (1961).
2. P. Vernier, C. Raimbault et H. Renon. J. Chim. Phys. **66**, 429 (1969).
3. O. P. Yablonskii, S. Yv. Pavlov, L. F. Lapuka et N. M. Rodionova. Neftekhimiya, **14**, 158 (1974).
4. M. Bouquet et C. Wakselman. Tetrahedron Lett. 2281 (1977).
5. E. N. Walsh et A. D. F. Toy. *Dans* Inorganic syntheses. Vol. 7. *Rédigé par* J. Kleinberg. McGraw-Hill Book Company, New York 1963. p. 69.
6. A. M. Kinnear. J. Chem. Soc. 3437 (1952).
7. M. J. Kornet et S. I. Tan. J. Heterocycl. Chem. **5**, 397 (1968).
8. M. S. Newman et A. Kutne. J. Am. Chem. Soc. **73**, 4202 (1951).
9. C. H. Shunk, F. W. Bachelor et K. Folkers. J. Org. Chem. **22**, 76 (1957).
10. R. Jacquier, J. L. Olive, C. Petrus et F. Petrus. Bull. Soc. Chim. Fr. 1651 (1974).
11. E. Diez et M. Rico. Anal. Fis. **67**, 25 (1971).
12. D. F. Foster et A. Danti. J. Phys. Chem. **69**, 486 (1965).
13. E. Melendez. An. Quim. **64**, 365 (1968).
14. K. W. Bartz et N. F. Chamberlain. Anal. Chem. **36**, 2151 (1964).
15. M. R. Bacon et J. E. Maciel. J. Am. Chem. Soc. **95**, 2413 (1973).
16. G. J. Martin, M. L. Martin et S. Odiot. Org. Magn. Reson. **7**, 2 (1975).
17. R. A. Friedel et H. L. Retcosfky. J. Am. Chem. Soc. **85**, 1300 (1963).
18. A. R. N. Wilson, L. F. van de Ven et J. W. de Maan. Org. Magn. Reson. **6**, 601 (1974).
19. P. A. Couperus, A. D. H. Clague et J. P. C. M. van Dongen. Org. Magn. Reson. **8**, 426 (1976).
20. V. I. Minkin, O. A. Osipov et Y. A. Zh Danov. *Dans* Dipole moments in organic chemistry. Plenum Press, New York, London. 1970.
21. R. Foster. *Dans* Molecular complexes. Vol. 2. Elek Science, London. 1973. p. 137.
22. D. Cans, B. Tiffon et J. E. Dubois. Tetrahedron Lett. 2075 (1976).
23. J. W. Emsley. High resolution NMR spectroscopy. Pergamon Press, Oxford. 1966. p. 988.
24. J. B. Stothers. ^{13}C NMR spectroscopy. Academic Press, New York, NY. 1972. p. 104.
25. K. Seidman et G. E. Maciel. J. Am. Chem. Soc. **99**, 3254 (1977).
26. M. Atlani, V. Corso et C. Wakselman. Brevet C.F.R.-A.N.V.A.R., déposé le 25.6.1974 sous le N° 74-22115.
27. S. Dzhessati, A. R. Kyazimova, V. I. Tyvlin et Yv. A. Pentin. Vestn. Mosk. Univ. Khim. **23**, 19 (1968).
28. D. A. C. Compton et W. O. George. J. Chem. Soc. Perkin Trans. II, 1666 (1976).
29. K. S. Solovev, S. Yv. Pavlov, P. A. Serafimov, G. A. Kirillova, L. L. Karpacheva et V. A. Gorchkov. Zh. Fiz. Khim. **51**, 1060 (1977).
30. P. P. S. Salvja, T. M. Young, R. F. Rodewald, F. H. Fuchs, D. Kohli et R. Fuchs. J. Am. Chem. Soc. **99**, 2949 (1977).
31. P. Vernier. Thèse, Université de Paris. 1967.

Can. J. Chem. Downloaded from www.nrcresearchpress.com by 210.87.254.42 on 09/05/12
For personal use only.

Reduction of some organic compounds by electrochemically generated titanium(III)

OLYMPIA CHRISTOFIS, JACOB J. HABEEB, RICHARD S. STEEVENSZ, AND DENNIS G. TUCK

Department of Chemistry, University of Windsor, Windsor, Ont., Canada N9B 3P4

Received March 31, 1978

OLYMPIA CHRISTOFIS, JACOB J. HABEEB, RICHARD S. STEEVENSZ, and DENNIS G. TUCK. Can. J. Chem. **56**, 2269 (1978).

The electrochemical oxidation of titanium metal in the presence of an essentially non-aqueous electrolyte phase yields titanium(III) species in solution. It has been shown that this method of generating TiX_3 (X = balancing anion) forms the basis of a convenient way of reducing *in situ* certain organic functional groups (sulfoxide, oxime, haloketone, vinyl dicarboxylic acid, and nitro aromatics). The stoichiometry of the reaction has been established in each case, and corresponds to the oxidation of TiX_3 and the formation of the appropriate organic compound. The yields are comparable to those reported in experiments using aqueous titanous chloride.

OLYMPIA CHRISTOFIS, JACOB J. HABEEB, RICHARD S. STEEVENSZ et DENNIS G. TUCK. Can. J. Chem. **56**, 2269 (1978).

L'oxydation électrochimique du titane sous forme métallique en présence d'une phase électrolytique essentiellement non-aqueuse conduit à des espèces titane(III) en solution. On a montré que cette méthode de produire du TiX_3 (X = un anion) peut servir de base pour une méthode convenable de réduire in situ un certain nombre de groupes fonctionnels organiques (sulphoxyde, oxime, halocétone, acide dicarboxylique vinylique et nitro-aromatique). On a établi la stoechiométrie de la réaction dans chaque cas et elle correspond à l'oxydation de TiX_3 et à la formation du composé organique approprié. Les rendements sont comparables avec ceux rapportés dans des expériences faisant appel à du chlorure titaneux en solution aqueuse.

[Traduit par le journal]

Introduction

The use of an aqueous solution of titanium(III) chloride as a mild reducing agent in organic chemistry was first described by Knecht and Hibbert (1, 2) at the beginning of the century. The revival of interest in this method in recent years has been discussed by McMurry (3), whose review demonstrates the range of functional groups which have been reduced, and gives references to specific experimental procedures.

In the course of work on the electrochemical oxidation of titanium in non-aqueous solution, we observed that depending on the reaction conditions, the products contained this element in either +III or +IV states. In particular, the anionic halide complexes of $TiBr_4^-$ and $TiBr_6^{2-}$ were synthesised in separate experiments (4), while the electrochemical reaction of titanium metal with 2,4-pentanedione (Hacac) (5) in the absence of oxygen gave as product $Ti(acac)_3$, which on exposure to air went rapidly to $TiO(acac)_2$ (cf. ref. 6). We subsequently found that the addition of reducible organic compounds would also discharge the deep blue colour of $Ti(acac)_3$, and that this behaviour was not restricted to systems involving acetylacetone. We have therefore carried out a short investigation of the conditions under which electrochemically generated titanium(III) may be used for the *in situ* reduction of suitable organic functional groups. Since the results show that this technique gives good yields of the reduced compounds, it appears that this electrochemical method is a useful and convenient way of carrying out the titanium(III) reduction reaction.

Experimental

Materials and Apparatus

Titanium metal sheet was *m2N7* purity. Organic compounds used as starting materials were reagent grade and were used as received.

The electrochemical cell consisted of 100 cm^3 tall form beaker, capped with a tightly fitted rubber bung through which passed wire leads for the anode and cathode, as well as gas inlet and outlet tubes. The titanium anode was formed into a cylinder (4.5 cm diameter, 4.5 cm high), which surrounded the central titanium cathode, shaped in an oblong propeller form (4.0 cm high, 3.5 cm wide). Potential was applied from a Coutant LQ 50/50 D.C. power pack. No unique advantages are claimed for this experimental design, which must certainly be capable of improvement.

General Procedure

All electrochemical experiments were carried out under nitrogen. The compound (10 mmol) to be reduced was placed in the electrochemical cell, which contained 25 cm^3 methanol, 25 cm^3 acetonitrile, 25 cm^3 glacial acetic acid, 2 cm^3 water, and approximately 0.5 g of tetraethylammonium chloride.

The effective completion of the reaction was marked both by a decrease in current and by the appearance of a permanent blue colour in the solution, although we observed that in some of the electrolytic reductions (e.g., diphenylsulfoxide and nitrobenzene), this blue colour developed in the solution

Can. J. Chem. Downloaded from www.nrcresearchpress.com by 210.87.254.40 on 09/05/12
For personal use only.

TABLE 1. Products and yields in reductions using electrochemically generated titanium(III)

Starting material[a]	Product	Time of electrolysis (h)	Titanium dissolved		Amount of product		Mole ratio Ti dissolved	Yield[b] (%)
			In g	In mmol	In g	In mmol	product	
$(C_6H_5)_2SO$	$(C_6H_5)_2S$	24	0.91	19	1.39	7.4	2.6	74
$C_6H_5C(NOH)CH_3$	$C_6H_5COCH_3$	24	0.70	14	0.96	8.0	1.8	80
$C_6H_5COCH_2Br$	$C_6H_5COCH_3$	18	0.54	11	0.70	5.8	1.9	58
C_7H_9OCl	$C_6H_{10}O$	18	0.70	15	0.72	6.5	2.3	65
Maleic acid	Succinic acid	20	0.55	11	0.70	5.9	1.9	59
Fumaric acid	Succinic acid	24	0.74	15	0.90	8.7	1.7	87
$C_6H_5NO_2$	$C_6H_5NH_2$	36	1.50	31	0.40	4.3	7.2	43

[a]10 mmol in each case.
[b]Based on quantity of starting material.

within the first few hours, indicating that Ti^{III} was being produced faster than it was being consumed. The amount of titanium dissolved was determined from the weight loss at the anode, and the products were identified by spectroscopic comparison with authentic samples. Overall product yields, the amounts of titanium dissolved, and electrolysis times are shown in Table 1.

The reduction appeared to be best carried out with currents below 100 mA, since at higher currents, excessive heating occurred, resulting in loss of solvent and/or possible decomposition of any labile product present. High current also appeared to cause corrosion of the metal anode surface, which developed a grey coating, while at the same time small particles of titanium metal were deposited on the floor of the cell. Cooling the electrolytic cell in an ice-bath reduced the current drastically. The voltages required to achieve an adequate current were in the 1–10 V range.

It was also observed that the rate of the reaction tripled when the surface area of the anode was increased fivefold. Titanium metal was also suitable as a cathode, since it could be formed into a convenient shape of large surface area, but the chemical nature of the cathode is not apparently critical. After each electrochemical reduction, the titanium electrodes were thoroughly cleaned by immersing them in boiling aqueous oxalic acid, thus allowing the continued use of the same electrode, free of surface impurities such as oxides.

Diphenylsulfoxide Reduction

After electrolysis, the contents of the cell were concentrated and about 50 cm^3 of water was added. The aqueous layer was extracted twice with petroleum-ether (30–60°C bp), the organic layer dried over anhydrous sodium sulfate, and solvent removed by evaporation. The nmr and ir spectra, and the glc retention time were identical with those of an authentic sample of diphenylsulfide.

Acetophenone Oxime Reduction

After electrolysis, the contents of the cell were filtered and concentrated. The yellow oily product was washed 3 times with water, and the aqueous layer extracted twice with petroleum-ether (30–60°C bp). The organic extracts were combined and washed with water, dried over anhydrous sodium sulfate, and the volume reduced to ca. 10 cm^3. The crude product was isolated and purified by column chromatography (neutral alumina).

1-Bromoacetophenone Reduction

The electrolysed solution was filtered and the volume reduced by evaporation. Water (50 cm^3) was added, and the resultant solution extracted three times with ether; the combined extracts were washed (10% aqueous sodium bicarbonate), dried (anhydrous sodium sulphate), and evaporated to yield acetophenone.

3-Chloro-2-Norbornanone Reduction

The reduction, and isolation of norcamphor, were similar to the procedures described in the preceding paragraph.

Fumaric Acid Reduction

The electrolytic solution was concentrated to dryness, yielding a white precipitate which was washed with hot chloroform, filtered, and oven dried. The melting point and nmr spectra corresponded to those of succinic acid.

Maleic Acid Reduction

The reduction of maleic acid and isolation of succinic acid followed the procedure for fumaric acid.

Nitrobenzene Reduction

After filtering the electrolysed solution, 150 cm^3 of 12 *M* hydrochloric acid was added and the aqueous layer extracted twice with chloroform. The aqueous layer was then neutralised with NaOH pellets and the free aniline extracted with chloroform. Aniline was the only organic species present in the final extract.

Results and Discussion

Solution Composition, Experimental Design

The reaction medium used in the present work represents a compromise between various requirements, including conductivity, solubility of reagents, adequate rate of formation of TiX_3, adequate rate of reduction, etc. Water must be present in small quantities, as shown by the equations set out below. A solvent mixture of methanol, acetonitrile, and glacial acetic acid in the ratio of 1:1:1 was found to be the most efficient. By contrast, a solvent ratio 2:2:1 gave product yield reduced by 50% based on the starting material. The small amounts (ca. 10 mg) of tetraethylammonium chloride used initially also gave poor yields of the reduced product, but this was overcome by using larger quantities (ca. 500 mg) of the salt.

Reaction Mechanism and Stoichiometry

The experiments described above show that the electrochemical generation of titanium(III) species provides a convenient and clean technique for the

Can. J. Chem. Downloaded from www.nrcresearchpress.com by 210.87.254.40 on 09/05/12
For personal use only.

Can. J. Chem. Downloaded from www.nrcresearchpress.com by 210.87.254.40 on 09/05/12
For personal use only.

reduction of a number of typical organic compounds. In general, the examples chosen are those for which reduction via titanium(III) chloride has already been reported (3).

In view of other work in this laboratory on the electrochemical oxidation of metals (4, 5, 7, 8), we have investigated the stoichiometry of the reaction, and have drawn certain conclusions as to the mechanism. We first note that the formation of the solutions in such reactions is indicative of the production of titanium(III) species, which we generalise as TiX_3 (X = balancing anion). The electrode reactions, following our work on metal chelate complexes (5), are then

Cathode:

[1] $$3e^- + 3HX \rightarrow 3X^- + \tfrac{3}{2}H_2(g)$$

Anode:

[2] $$3X^- + Ti(m) \rightarrow TiX_3 + 3e^-$$

and in keeping with this scheme we have confirmed that hydrogen is indeed formed at the cathode. The reactions of TiX_3 with the organic substrates then follows reactions [3]–[7], in which the final titanium product is written as $TiOX_2$ (see below), although the stoichiometry is not affected by reformulating the product as TiX_4.

[3] $$Ph_2SO + 2TiX_3 + H_2O \rightarrow Ph_2S + 2TiOX_2 + 2HX$$

[4*a*] $$R_2CNOH + 2TiX_3 + H_2O \rightarrow R_2CNH + 2TiOX_2 + 2HX$$

[4*b*] $$R_2CNH + H_2O \rightarrow R_2CO + NH_3$$

[5] $$RCOCH_2X + 2TiX_3 + 2H_2O \rightarrow RCOCH_3 + 2TiOX_2 + 3HX$$

[6] $$RCHCHR + 2TiX_3 + 2H_2O \rightarrow RCH_2CH_2R + 2TiO_2 + 2HX$$

[7] $$PhNO_2 + 6TiX_3 + 4H_2O \rightarrow PhNH_2 + 6TiOX_2 + 6HX$$

For reactions [3]–[6], the formation [2] and subsequent oxidation of TiX_3 should give the mole ratio Ti dissolved:product = 2, and the results in Table 1 for these reactions indeed give this ratio as 2.0 ± 0.3, showing that the principal reactions are those described. For the reduction of the ketoxime, the proposed two step process, [4*a*] + [4*b*], involving hydrolysis of the imine intermediate should lead to the formation of ammonia, which is trapped in our reaction conditions as ammonium acetate, and in one experiment was released by the addition of excess caustic soda after electrolysis. The mole ratio Ti dissolved:NH_3 released was 2.3 (0.83 g, 17 mmol Ti; 7.3 mmol NH_3), in reasonable agreement with the value of 2.0 required by reactions [4*a*] and [4*b*].

For nitrobenzene reduction, the experimental ratio Ti dissolved:aniline recovered is 7.2, somewhat higher than the theoretical value of 6.0 (reaction [7]). The reduction of nitrobenzene by titanium(III) has been the subject of earlier investigation (e.g., ref. 9), which showed that here, as in electrochemical reduction at an inert cathode, a variety of species may be formed, depending on the reaction conditions and in particular on the acidity. With the mildly acidic solution used in the present experiments, aniline is the only product isolated, in keeping with earlier findings (9, 10). The quantity of nitrobenzene is substantially lower than in other systems studied, and this must be due in part to the large amounts of TiX_3 required per mole $PhNO_2$, since for a given rate of TiX_3 generation less $PhNO_2$ will be reduced than (say) Ph_2SO.

In addition to the organic compounds isolated, there is also formed a white solid. Analysis shows that a typical sample contained 32% Ti, had infrared absorptions at, *inter alia*, 1040 (ν(Ti=O), cf. ref. 6) and 1715 cm^{-1} (ν(C=O)), and lost approximately 60% weight on heating to 850°C. Given the nature of the reaction mixture, a number of titanium(IV) species are possible; for example, a mixture of $TiO_2 \cdot 2H_2O$ and $TiO(OAc)_2$ in a 1:3 ratio would have Ti 32%, and would lose 48% weight on complete conversion to TiO_2. In general, the results confirm that the final titanium(IV) species can reasonably be formulated as $TiOX_2$, as in reactions [3]–[9].

Aldoxime, Glyoxime, Phosphine Oxide Studies

When attempts were made to produce species such as 2-pyridinaldehyde from 2-pyridinaldoxime, the yields were very low. For example, even after 50 h electrolysis of the aldoxime, only 0.3 g (7 mmol) of titanium metal had been dissolved, and the total product yield was only 7% (0.7 mmol) based on starting oxime. Polymeric decomposition products were also isolated but not identified.

Attempts to reduce dimethyl- and diphenylglyoxime were unsuccessful, in that neither the mononor the di-ketones were isolated from the cell. Spectral (ir, nmr) studies, and attempts to isolate a 2,4-dinitrophenylhydroazine derivative, failed to indicate the presence of any carbonyl groups.

Finally we note that despite a number of attempts, we have been unable to reduce triphenylphosphine oxide by the electrochemical generation of titanium(III).

General Comment

The procedures described use titanium metal as a

convenient source of Ti^{III}, and simple apparatus for the electrochemical reactions involved. The yields and rate of reduction are comparable with those using aqueous titanium(III) chloride. Thus, while the reduction of either diphenylsulfide or α-haloketones is less efficient than the 70–100% yield reported by Ho and Wong (11) using aqueous titanium(III) chloride under reflux, the reduction of maleic acid gives a higher yield than the 45% achieved in a 24 h reaction with the aqueous reagent at room temperature (12). The convenience of the electrochemical method, and the ability to operate the cell at room temperature, may prove advantageous in certain cases.

Finally we may note that vanadium can also be oxidised electrochemically to yield either vanadium(III) (5) or vanadium(II) (7) species, and that the behaviour of $V(acac)_3$ is similar to that of $Ti(acac)_3$ in that aerial oxidation produces $VO(acac)_2$. We therefore investigated the use of vanadium electrodes in the reactions reported above, but found no evidence of vanadium being consumed. Apparently, therefore, electrochemical oxidation of vanadium is not a satisfactory source of lower oxidation state species, despite the similarity between titanium(III), vanadium(II), and chromium(II) noted by Timms and Wildsmith (13).

Acknowledgement

This work was supported in part by Operating Grants from the National Research Council of Canada.

1. E. KNECHT and E. HIBBERT. Chem. Ber. **36**, 166 (1903).
2. E. KNECHT and E. HIBBERT. Chem. Ber. **40**, 3819 (1907).
3. J. E. MCMURRY. Acc. Chem. Res. **7**, 281 (1974).
4. J. J. HABEEB, F. F. SAID, and D. G. TUCK. Can. J. Chem. **55**, 3882 (1977).
5. J. J. HABEEB, D. G. TUCK, and F. H. WALTERS. J. Coord. Chem. **8**, 27 (1978).
6. C. C. BARRACLOUGH, J. LEWIS, and R. S. NYHOLM. J. Chem. Soc. 3352 (1959).
7. J. J. HABEEB, L. NEILSON, and D. G. TUCK. Can. J. Chem. **55**, 2631 (1977).
8. J. J. HABEEB and D. T. TUCK. J. Organometal. Chem. **134**, 363 (1977).
9. S. A. NEWTON, S. J. STUBBS, and C. J. HINSHELWOOD. J. Chem. Soc. 3384 (1953).
10. N. V. SIDGWICK. The organic chemistry of nitrogen. 3rd ed. *Edited by* I. T. Millar and H. D. Springall. Oxford University Press. 1966. p. 141, pp. 387–391.
11. T.-S. HO and C. M. WONG. Syn. Commun. **3**, 37 (1973); **3**, 273 (1973).
12. J. E. MCMURRY and J. MELTON. J. Org. Chem. **39**, 259 (1974).
13. G. H. TIMMS and E. WILDSMITH. Tetrahedron Lett. 195 (1971).

Can. J. Chem. Downloaded from www.nrcresearchpress.com by 210.87.254.40 on 09/05/12
For personal use only.

The effect of diluent gases on ion formation in hydrocarbon flames[1]

BRENDA L. CHAWNER AND ARTHUR T. BLADES
Alberta Research Council, Edmonton, Alta., Canada T6G 2C2

Received November 29, 1977

BRENDA L. CHAWNER and ARTHUR T. BLADES. Can. J. Chem. **56**, 2273 (1978).

It has been demonstrated that the addition of N_2, CO, Ne, Ar, Kr, Xe, CO_2, and CF_4 to a H_2-air diffusion flame containing He and traces of CH_4 enhances the level of ion formation. This enhancement is proportional to the concentration of both CH_4 and the diluent gas, consistent with the proposition that the diluent gas participates in the ion formation process.

BRENDA L. CHAWNER et ARTHUR T. BLADES. Can. J. Chem. **56**, 2273 (1978).

On a démontré que l'addition de N_2, CO, Ne, Ar, Kr, Xe, CO_2 et CF_4 à une flamme de diffusion H_2 air contenant du He et des traces de CH_4 augmente le niveau de formation d'ions. Cette augmentation est proportionnelle à la concentration à la fois du CH_4 et du gaz utilisé comme diluant ce qui est en accord avec la proposition à l'effet que le gaz diluant participe au processus de formation d'ions.

[Traduit par le journal]

Introduction

It is now generally accepted that ions arise in hydrocarbon flames in the chemi-ionization reaction (1–4).

[1] $$CH + O \rightarrow CHO^+ + e$$

This process forms the basis of the flame ionization detector as used in gas chromatography (5) where organic eluates are burned in a hydrogen-air diffusion flame. With suitable polarizing and collecting electrodes, the ion current is the rate of ion formation and about one in 10^6 carbon atoms introduced into the flame results in the formation of an ion (6). The response of the detector is rigorously linear in CH_4 concentration over several decades, in keeping with the mechanism of ion formation.

In the normal use of the detector, it is frequently the practice to use He, N_2, or Ar as the carrier gas for the chromatography and to add a constant flow of H_2 to the column eluate to maintain the flame in the detector. In this regime, the detector sensitivity is dependent on the composition of the carrier gas and maximum sensitivity is achieved with approximately equal flow rates of H_2 and carrier gas (6). This behavior implies that, up to a point, the addition of the carrier gas enhances the formation of ions, contrary to experience with premixed flames where N_2 additions may result in decreased ion formation (7).

Several attempts have been made to explain this 'carrier gas effect' in terms of the physical properties of the diluent gases (6, 8), the increase in ion formation being fundamentally attributed to a temperature increase. These explanations have been challenged (9–11) and it has been postulated that the carrier gas stimulates ion formation by the additional mechanism (11),

[2] $$CH + O + X \rightarrow CHO \cdot X^+ + e$$

Such a reaction is reasonable if ion formation occurs stepwise,

[3] $$CH + O \rightarrow CHO^*$$

[4] $$CHO^* \rightarrow CHO^+ + e$$

and

[5] $$CHO^* + X \rightarrow CHO \cdot X^+ + e$$

Reaction [5] would be expected, on the basis of the dissociation energies of $CHO \cdot H_2^+$ (0.17 eV) (12), and of $CHO \cdot CO^+$ (0.47 eV) (13), to have an energetic advantage over [4]. On the other hand, the low dissociation energies imply rapid decomposition of the ions in high temperature flames and it is therefore not surprising that these primary ions have not been observed mass spectrometrically. In low temperature atomic flame systems, the ions would have a longer thermal lifetime but their formation would be impeded by the low pressure and, if observed, their origin could be the association reaction,

[6] $$CHO^+ + X \rightarrow CHO \cdot X^+$$

While direct observation of the primary ions may be difficult and of dubious merit, occurrence of reactions [2] or [5] would require that the additional ionization attributable to the carrier gas be first order in CH, or its single carbon precursor, e.g. CH_4, and in the carrier X. Herein, these kinetic orders have been established by the operation of a flame ionization detector with a constant flow of H_2 and He, a continuous but variable addition of CH_4 to the H_2

[1]Alberta Research Council Contribution No. 900.

Can. J. Chem. Downloaded from www.nrcresearchpress.com by 210.87.254.6 on 09/05/12
For personal use only.

Can. J. Chem. Downloaded from www.nrcresearchpress.com by 210.87.254.6 on 09/05/12
For personal use only.

and periodic additions of low concentrations of various 'carrier' gases to the He at constant total flow.

Experimental and Results

In order to demonstrate the magnitude of the carrier gas effect, a flame ionization detector was operated with a constant flow of air (800 ml/min) and of H_2 or D_2 containing 6.2×10^{-3}% CH_4 (30 ml/min). Variable flows of reagent grade He, Ar, and N_2 were then added to the H_2 stream and the relative responses, as shown in Fig. 1, were observed.

The flame ionization detector was then set up with equal flows of H_2 and He (30 ml/min) with provision for the continuous addition of CH_4 (<0.3%) to the H_2. Before mixing with the H_2, the He flowed through a 60 cm long, 14 mm od glass tube fitted with injection ports and then through a katharometer. This arrangement allowed the introduction of diffusion-spread pulses of the test gases at concentrations up to 5% in the He but at constant total 'carrier' flow rate.

The test gases were reagent grades except for CF_4 and CO_2 and chromatographic purification of these gases on a 450 cm *n*-octane/porasil C column at 0°C revealed the presence of ion-producing impurities. These compounds were therefore routinely injected into the system through the chromatographic column. In order to demonstrate the type of response if the test gas contained a hydrocarbon impurity, a set of experiments was carried out with N_2 containing 0.015% CH_4.

The data in Figs. 2, 3, and 4 indicate the response to a constant injection (500 μl) of the test gases at

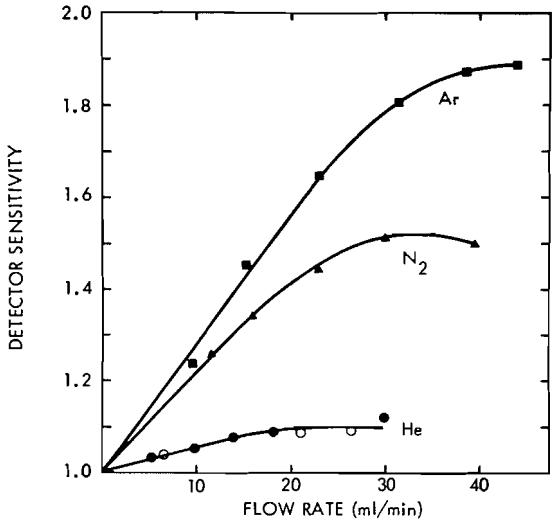

FIG. 1. The effect of flow rate of various diluent gases on the detector sensitivity; H_2, 30 ml/min; air, 800 ml/min; CH_4, 1.9×10^{-3} ml/min. ●, He in H_2; ○, He in D_2; △, N_2 in H_2; □, Ar in H_2.

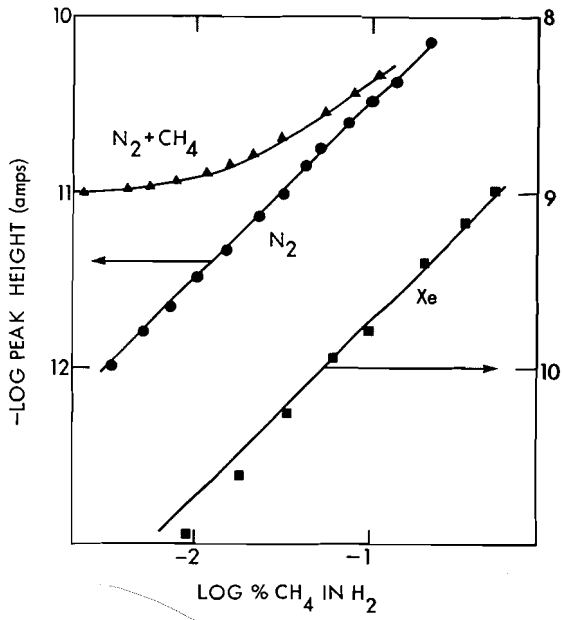

FIG. 2. The effect of CH_4 concentration on the increase in ion formation from a 500 μl slug of Xe, N_2, and N_2 contaminated with CH_4.

variable CH_4 concentrations in the H_2. In Fig. 2, the unit slope for pure N_2 indicates a rate of ion formation due to the presence of N_2, first order in CH_4 over a hundred-fold concentration range. The CH_4-contaminated N_2, on the other hand, indicates a transition from near zero order at low CH_4 concentrations to near first order at high $[CH_4]$; this represents a transition from a response to the CH_4 in the N_2 independent of the CH_4 content of the H_2, to a response to the N_2 dependent on the first order of the CH_4 content, as with the pure N_2. This demonstrates that the effect being observed with the pure test gases is not due to organic impurities therein. In Figs. 2, 3, and 4, the test gases Ar, Kr, Xe, CO, and CO_2 also indicate first order response over the full range of CH_4 concentrations. The data for CF_4 in Fig. 4, however, display a response similar to the impure N_2 in Fig. 2, indicating the presence of an impurity or a partial decomposition of CF_4, but also a rate of ion formation, first order in CH_4.

The data in Figs. 5 and 6 indicate the response to variable injections of the test gases at a constant CH_4 concentration in the H_2 (0.025%). The unit slope for each of the test gases implies that the additional ion formation in their presence is also first order in the test gas concentration.

The test gases were ranked according to their tendency to stimulate the excess ion formation by equal injections (500 μl) of each at a constant CH_4

Can. J. Chem. Downloaded from www.nrcresearchpress.com by 210.87.254.6 on 09/05/12
For personal use only.

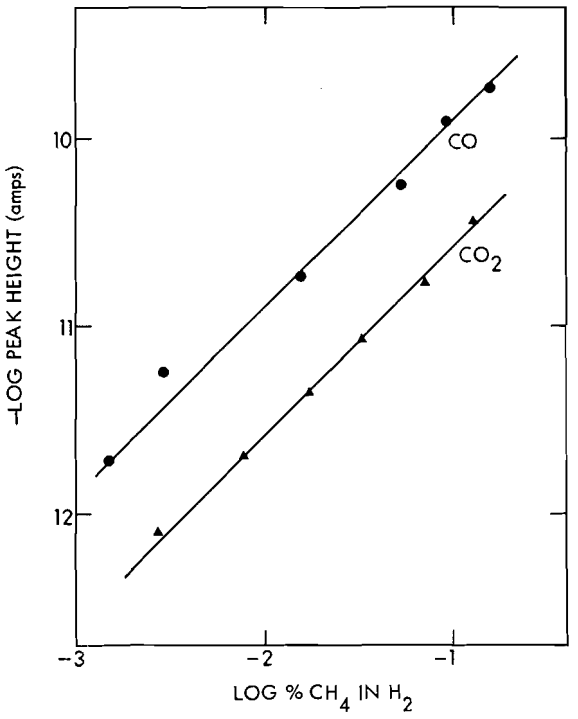

FIG. 3. The effect of CH_4 concentration on the increase in ion formation from a 500 μl slug of CO and CO_2.

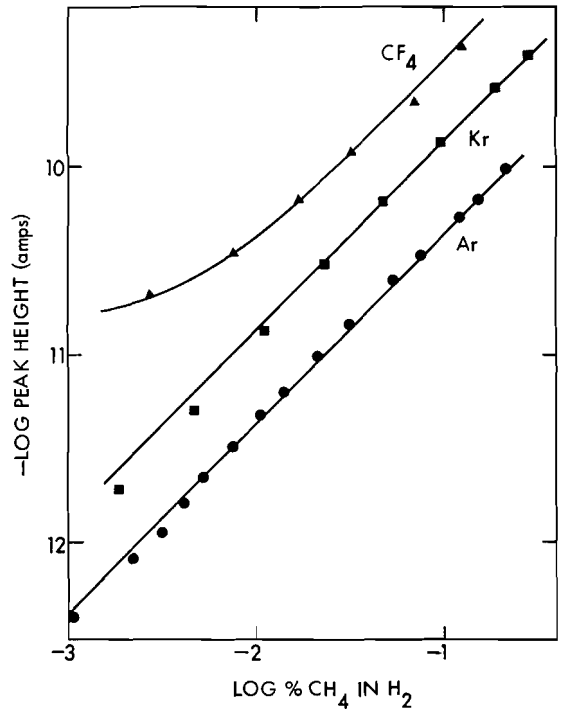

FIG. 4. The effect of CH_4 concentration on the increase in ion formation from a 500 μl slug of CF_4, Kr, and Ar.

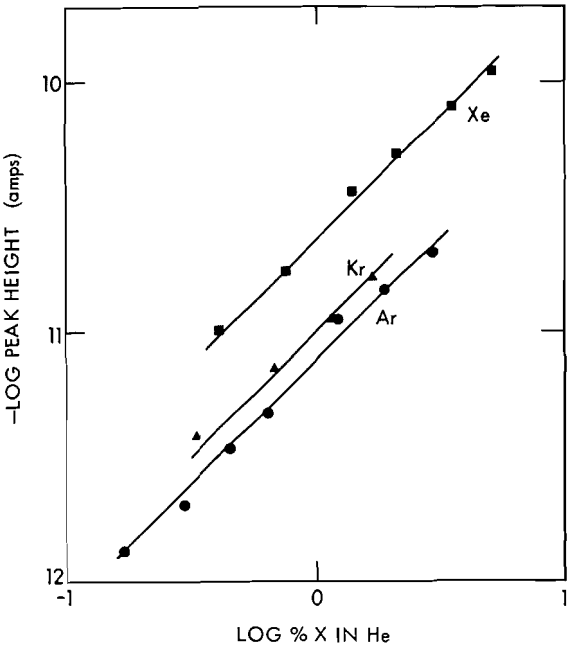

FIG. 5. The effect of the concentration of the test gases Ar, Kr, and Xe on the increase in ion formation at constant CH_4 concentration (0.025% in H_2).

concentration (0.3% in H_2) and measurement of the peak areas. Their efficiencies relative to He were $Ne \approx CO_2 < N_2 < Ar < CO < Kr < Xe \approx CF_4$.

Discussion

Insofar as the purpose of these studies was to obtain kinetic orders for the mutual stimulation of ion formation by CH_4 and the diluent gas, the data presented in Figs. 2, 3, 4, 5, and 6 indicate first order in each, as required by the overall process [2]. However, since this is the only evidence indicating the possibility of such an associative chemi-ionization process in hydrocarbon combustion, it is desirable to examine the system in detail to seek alternate explanations for the observations.

A suitable model for the effect must justify the increase in ion formation, the relative tendencies of the various diluents to promote ion formation and the observed kinetic orders. Physical involvement of the diluent might be expected to arise from simple dilution, temperature effects, or interference with the inter-diffusion of the reacting gases. Simple dilution effects can be ruled out since all diluents would have given the same effect. Likewise, the identical heat capacities of the noble gases would imply equal temperature effects for these gases, which does not correlate with their ion formation enhancement. The possibility that the diluent gas effect might arise in the inter-diffusion of the reacting

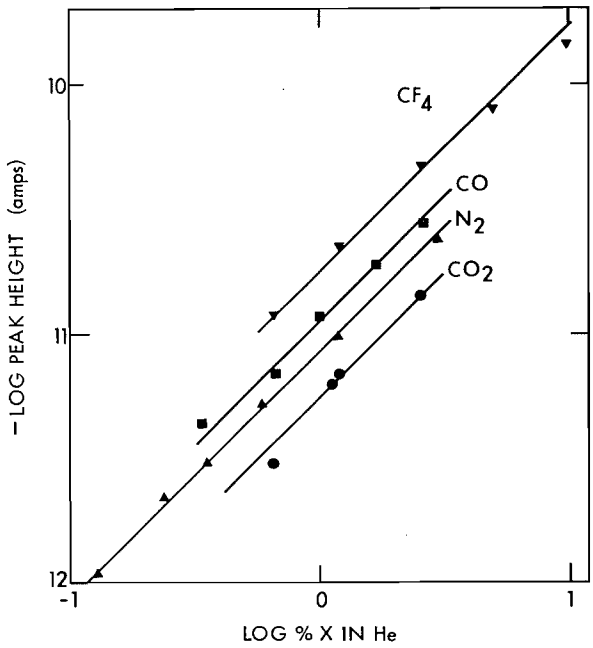

FIG. 6. The effect of the concentration of the test gases CF_4, CO, N_2, and CO_2 on the increase in ion formation at constant CH_4 concentration (0.025% in H_2).

gases is appealing since diffusion depends on molecular weight and the collision cross section and would therefore justify, at least approximately, the relative order of effectiveness of the diluent gases, it being assumed that restricted interdiffusion would promote ion formation. This explanation would also justify the difference in behavior of premixed and diffusion-flames in regard to diluent gases (7). The fact, however, that He gives about the same enhancement of ion formation in both the H_2 and the D_2 flames, as indicated in Fig. 1, implies that the molecular weight of the diluent in relation to that of the H_2 is not crucial. In addition, the enhancement of ion formation from cyano compounds is substantial for most diluent gases but is negative at all flow rates for He (11); it is inconceivable that the same diluent could behave so differently in the two systems if the effect arose only from diffusional differences.

A correlation of the effect with molecular weight and/or collision cross-section might arise in a specific third body process, critical to ion formation. Fontijn *et al.* (14–16) have observed C_2F_4-stimulated ion formation in the O-atom, N-atom flame system which they attribute to enhancement of the concentration of electronically excited N_2 or NO by the C_2F_4 acting as a catalyst in their formation. The comparable process in a hydrocarbon flame might be

$$[7] \qquad CH + O + X \rightarrow CHO^* + X$$

the enhanced ion formation arising from the greater efficiency of formation of the stabilized CHO*. In the combination of N and N or N and O, a third body may carry off some or all of the vibrational energy of the newly-formed, electronically excited N_2 and/or NO but still leave adequate energy for subsequent ion formation. With CHO, the overall exothermicity of reaction [1] is only 0.17 eV (17) and therefore the exact amount of energy removed would be crucial as far as ion formation is concerned. Under these circumstances, the atomic and molecular diluents might have been expected to behave quite differently, the latter potentially carrying off sufficient energy from the CHO to preclude ion formation. Of the diluents investigated, only CO_2 suggests this behavior but this may well have arisen from its involvement in the chemistry of the H_2–O_2 flame.

Other catalytic effects of the diluent gases might arise if a weakly-bound collision complex were formed with CHO, thereby suppressing the formation of the alternate products, CO and H-atoms. The resulting complex might then ionize and dissociate

$$[8] \qquad CHO{\cdot}X^* \rightarrow CHO^+ + e + X$$

or ionize

$$[9] \qquad CHO{\cdot}X^* \rightarrow CHO{\cdot}X^+ + e$$

the enhanced ion formation being due to the formation of $CHO{\cdot}X^*$ and/or to the energetic advantage associated with the formation of the composite ion. Unfortunately, the available evidence is inadequate to give clear preference to either of these pathways or to exclude reactions [5] and [7]. It is therefore only reasonable to modify the mechanism of ion formation in a very general fashion, implying the potential involvement of the diluent gases,

$$[10] \qquad CH + O\ (+X) \rightarrow CHO^+ + e\ (+X)$$

During the preparation of this paper, Vinckier, Gardner, and Bayes (18) have reported enhanced ion formation in the reaction of O atoms with acetylene when diluent He is replaced by other inert gases (Ar, N_2, CO, CF_4, and CO_2). Their order of effectiveness is dramatically different from the flame ionization detector system and is explained on the basis of specific reactions of C_2H_2 in its conversion to CH, three potential excited species being postulated in the reaction scheme. In the flame ionization detector, it has been postulated that organic constituents in general are totally converted to CH_3 prior to oxidation (10) and it is conceivable that the diluent gas effect therein might be explained by a similar generalized mechanism wherein the conversion of CH_3 to CH is subtly enhanced by the diluent. It is noteworthy, however, that the same pattern of effects in the ionization detector is observed with C_2N_2 (19) (wherein CH is not the ion

Can. J. Chem. Downloaded from www.nrcresearchpress.com by 210.87.254.6 on 09/05/12
For personal use only.

precursor) and this origin of the diluent effect with hydrocarbons is therefore highly unlikely.

Acknowledgements

The authors wish to acknowledge useful discussions with Drs. T. M. Sugden and P. Kebarle.

1. W. J. MILLER. XIV Symposium (Internat.) on Combustion. Combustion Institute. 1973. p. 397.
2. A. FONTIJN. Progress in reaction kinetics. Vol. 6. *Edited by* K. R. Jennings and R.B.Cundall. Pergamon Press. 1971. p. 75; A. FONTIJN. Pure Appl. Chem. **39**, 287 (1974).
3. H. F. CALCOTE and W. J. MILLER. Chemical reactions under plasma condition. Vol. 2. *Edited by* M. Venugopalan. Interscience Publishers, 1971. p. 327.
4. W. J. MILLER. Oxid. Combust. Rev. **3**, 97 (1968).
5. I. G. MCWILLIAM. J. Chromatog. **6**, 110 (1961).
6. J. C. STERNBERG, W. S. GALLAWAY, and D. T. L. JONES. Gas chromatography. *Edited by* N. Brenner, J. E. Callen, and M.D. Weiss Academic Press, New York. 1962. p. 231.
7. J. PEETERS, J. F. LAMBERT, P. HERTOGHE, and A. VAN TIGGELEN. XIIIth Symposium (Internat.) on Combustion. Combustion Institute. 1971. p. 321.
8. R. L. HOFFMANN and C. D. EVANS. Science, **153**, 172 (1966).
9. D. A. THOMBS. Chromatographia, **6**, 111 (1973).
10. A. T. BLADES. J. Chromatog. Sci. **11**, 251 (1973).
11. A. T. BLADES. J. Chromatog. Sci. **14**, 45 (1976).
12. P. KEBARLE and K. HIRAOKA. J. Chem. Phys. **63**, 1688 (1975).
13. M. MOET-NER and F. H. FIELD. J. Chem. Phys. **61**, 3742 (1974).
14. A. FONTIJN and P. H. VREE. XIth Symposium (Internat.) on Combustion. The Combustion Institute. 1966. p. 343.
15. A. FONTIJN and R. ELLISON. J. Phys. Chem. **72**, 3701 (1968).
16. A. FONTIJN, R. ELLISON, W. H. SMITH, and J. E. HESSER. J. Chem. Phys. **53**, 2680 (1970).
17. C. S. MATTHEWS and P. WARNECK. J. Chem. Phys. **51**, 854 (1969).
18. C. VINCKIER, M. P. GARDNER, and K. D. BAYES. J. Phys. Chem. **81**, 2137 (1977).
19. B. L. CHAWNER and A. T. BLADES. Can. J. Chem. This issue.

Can. J. Chem. Downloaded from www.nrcresearchpress.com by 210.87.254.6 on 09/05/12
For personal use only.

The effect of diluent gases on ion formation in C_2N_2 flames[1]

BRENDA L. CHAWNER AND ARTHUR T. BLADES
Alberta Research Council, Edmonton, Alta., Canada T6G 2C2

Received November 29, 1977

BRENDA L. CHAWNER and ARTHUR T. BLADES. Can. J. Chem. **56**, 2278 (1978).

Ion formation from traces of C_2N_2 in a H_2 + He-in-air diffusion flame is enhanced by the presence of traces of Ne, Ar, Kr, Xe, N_2, CO, CO_2 and CF_4. The enhancement is proportional to the concentration of both C_2N_2 and the diluent gas and the relative efficiencies are identical to those observed when hydrocarbons are the source of ionization. The observations are consistent with the involvement of the diluent in ion formation, parallel to the hydrocarbon system.

BRENDA L. CHAWNER et ARTHUR T. BLADES. Can. J. Chem. **56**, 2278 (1978).

La formation d'ions à partir de traces de C_2N_2 dans une flamme de diffusion H_2 + He dans l'air est augmentée par la présence de traces de Ne, Ar, Kr, Xe, N_2, CO, CO_2 et CF_4. Cette augmentation est proportionnelle à la concentration à la fois de C_2N_2 et du gas diluant et les efficacités relatives sont identiques à celles observées lorsque les hydrocarbures sont utilisés comme source d'ionisation. Ces observations sont en accord avec une implication du diluant dans la formation d'ions qui est parallèle à celle observée dans le système d'hydrocarbures.

[Traduit par le journal]

Introduction

An examination of the effect of the diluent gases on the rates of ion formation in an H_2–air diffusion flame containing traces of CH_4 has revealed strong evidence for the participation of the diluent in ion formation (1). This has been tentatively attributed to an associative chemi-ionization reaction (2).

[1] $$CHO^* + X \rightarrow CHO.X^+ + e$$

but other variations of the same overall process cannot be excluded on the basis of existing evidence (1).

Similar diluent gas effects are known to occur during C_2N_2 combustion in the same flame system (2). The mechanism of ion formation in this system is not well established but recent evidence has been interpreted (3) as favoring the reaction

[2] $$N(^2P, ^2D) + O \rightarrow NO^+ + e$$

over

[3] $$CN + O + O \rightarrow CO + NO^+ + e$$

The former has been cited as the origin of ions in NH_3 flames (4) while the latter fails to justify the large overall activation energy (111 kJ mol^{-1}) or the high rate of ion formation (3). Nevertheless, it is of interest to examine the diluent gas effect on the C_2N_2 system both in relation to diluent gas effects in general and the mechanism of ion formation.

Experimental and Results

A flame ionization detector having constant flows of H_2 (30 cc/min), He (30 cc/min), and air (800 cc/min) was used. C_2N_2 was continuously added to the H_2 stream giving concentrations up to 0.15% in H_2. The test gases, Ne, Ar, Kr, Xe, N_2, CO, CO_2, and CF_4 were injected into the He stream and allowed to mix with the He by passage through a 60 cm long, 14 mm od glass tube before reaching the flame ionization detector. The CO_2 and CF_4 contained hydrocarbon impurities and were routinely purified by passage through 0.45 m *n*-octane/porasil C column at 0°C before injection. Test gas concentrations (< 5% in the He) were monitored by thermal conductivity and their relative effects were established by the addition of equal amounts of each to the He flow at a constant C_2N_2 concentration. The order of effectiveness was $Ne < CO_2 < N_2 < Ar < CO < Kr < Xe$.

The data in Figs. 1 and 2 were obtained by injecting variable quantities of the test gases at a constant C_2N_2 concentration in the H_2; the slope of unity indicates that the response is first order in the test gas concentration. Figures 3 and 4 show the data resulting from a constant injection of the test gases with variable C_2N_2 concentrations. The slope shows the response to be first-order in C_2N_2 concentration, except in the case of CF_4. The CF_4 curve is nearly zero-order at low C_2N_2 concentrations, but subtraction of the zero order component gives the first-order line, Δ-CF_4.

Discussion

The effects of diluent gases on the rates of ion formation from C_2N_2 are virtually identical to their effects on ion formation from hydrocarbons (2). The increase in ion formation in the presence of the test gases is first order in both the test gas (Figs. 1 and 2), and C_2N_2 concentrations (Figs. 3 and 4), and the

[1]Alberta Research Council Contribution No. 901.

Can. J. Chem. Downloaded from www.nrcresearchpress.com by 210.87.254.105 on 09/05/12
For personal use only.

Can. J. Chem. Downloaded from www.nrcresearchpress.com by 210.87.254.105 on 09/05/12
For personal use only.

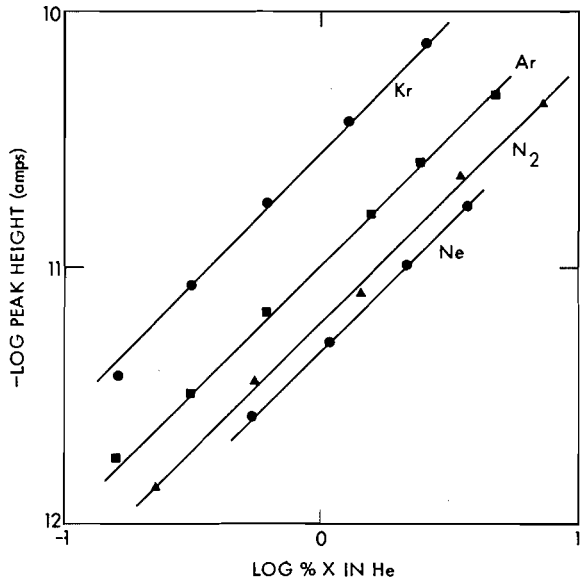

FIG. 1. The effect of the concentration of the test gases Ne, N_2, Ar, and Kr on the increase in ion formation at constant C_2N_2 concentration (0.1% in H_2).

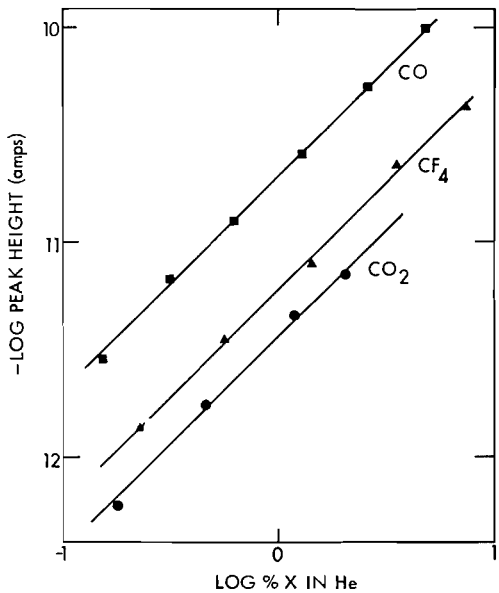

FIG. 2. The effect of the concentration of the test gases CO, CF_4, and CO_2 on the increase in ion formation at constant C_2N_2 concentration (0.1% in H_2).

order of effectiveness of the test gases in stimulating excess ion formation is identical to that in the hydrocarbon system. The one difference is that He may not be effective in increasing ion formation with C_2N_2, as may be inferred from the observation that He addition causes a monotonous decline in the rate of ion formation (2). In any case, there is no reason to

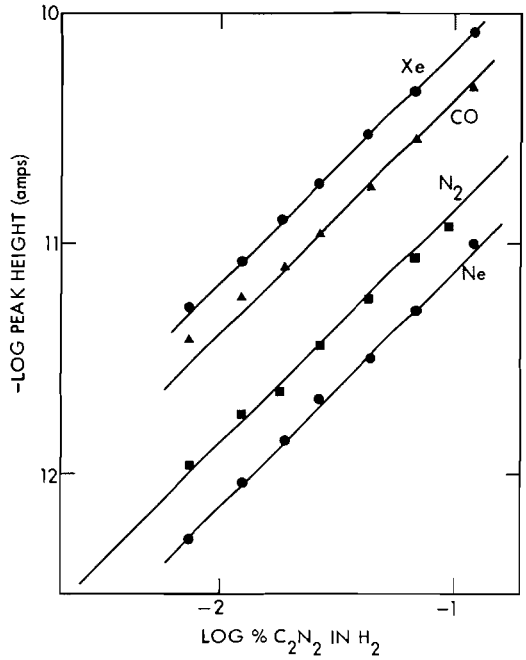

FIG. 3. The effect of C_2N_2 concentration on the increase in ion formation from a 500 μl slug of Ne, N_2, CO, and Xe.

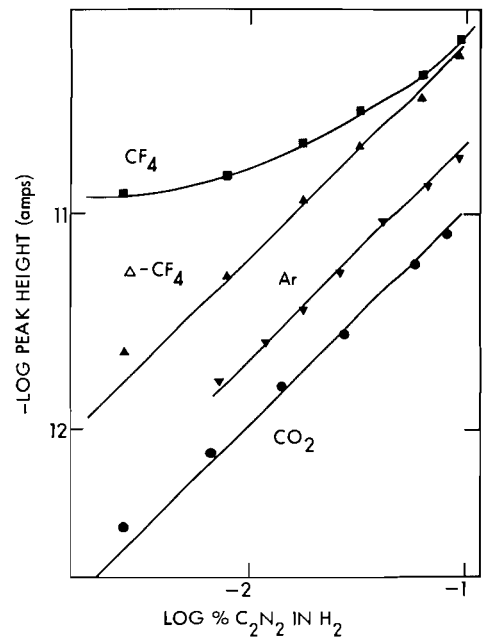

FIG. 4. The effect of C_2N_2 concentration on the increase in ion formation from a 500 μl slug of CO_2, Ar, and CF_4. The ΔCF_4 points are the result of a subtraction of a zero order component of 10^{-11} A.

believe that there is any fundamental difference between the origin of the effect in the two systems.

Since the details of the mechanism of ion formation from C_2N_2 are not well established, it is difficult

to speculate how the diluent gas may affect the rate of the process. Both reactions [2] and [3] depend on the interaction of CN and two O atoms and NO^+ is generally conceded to be the ion first observable or the 'primary' ion; it is therefore reasonable to propose, by analogy with the hydrocarbon system, that the diluent catalyzes the formation of NO* or assists in its ionization. No substantial evidence exists on which a choice could be based and the only conclusion to be reached from the present research is that the reaction

$$CN + O + O + X \rightarrow CO + NO^+ + e + X$$

may be a contributor to ion formation in cyanogen-containing flames.

1. B. L. CHAWNER and A. T. BLADES. Can. J. Chem. This issue.
2. A. T. BLADES. J. Chromatog. Sci. **14**, 45 (1976).
3. M. A. BREDO, P. J. GUILLAUME, and P. J. VAN TIGGELEN. XV Symposium (Internat.) on Combustion, The Combustion Institute. 1975. p. 1003.
4. C. BERTRAND and P. J. VAN TIGGELEN. J. Phys. Chem. **78**, 2320 (1974).

Can. J. Chem. Downloaded from www.nrcresearchpress.com by 210.87.254.105 on 09/05/12
For personal use only.

Preparation of some cyclopentadienyl platinum (IV) complexes

ALAN SHAVER

Department of Chemistry, McGill University, 801 Sherbrooke Street, W., Montreal, P.Q., Canada H3A 2K6

Received January 6, 1978

ALAN SHAVER. Can. J. Chem. **56**, 2281 (1978).

Two routes to the synthesis of $(\eta^5\text{-}C_5H_5)PtR_1R_2R_3$, where R_1, R_2, and R_3 are not all CH_3, were explored. The complexes $[PtR_1R_2R_3X]_4$, where $R_1 = R_2 = CH_3$, $R_3 = C(O)CH_3$, C_2H_5; $R_1 = R_2 = C_2H_5$, $R_3 = CH_3$, $C(O)CH_3$; $R_1 = CH_3$, $R_2 = C_2H_5$, $R_3 = C(O)CH_3$; X = Cl or I, were prepared and treated with TlCp to give $(\eta^5\text{-}C_5H_5)PtR_1R_2R_3$. The latter are the first polyfunctionalized cyclopentadienyl platinum(IV) complexes. Conformational isomerism about the platinum to acetyl–carbon bond was detected by infrared spectroscopy. The cleavage of a Pt—CH_3 or Pt—$C(O)CH_3$ bond in $CpPt(CH_3)_2R$ using the reagents HCl, $HgCl_2$, or I_2 was not successful; the appropriate $[Pt(CH_3)_2RX]_4$ being isolated instead. The chiral nature of $(\eta^5\text{-}C_5H_5)Pt(CH_3)(C_2H_5)[C(O)CH_3]$ is noted.

ALAN SHAVER. Can. J. Chem. **56**, 2281 (1978).

On a exploré deux routes pouvant conduire à la synthèse de $(\eta^5\text{-}C_5H_5)PtR_1R_2R_3$ où R_1, R_2 et R_3 ne sont pas tous des CH_3. On a préparé les complexes $(PtR_1R_2R_3X)_4$ où $R_1 = R_2 = CH_3$, $R_3 = C(O)CH_3$, C_2H_5; $R_1 = R_2 = C_2H_5$, $R_3 = CH_3$, $C(O)CH_3$; $R_1 = CH_3$, $R_2 = C_2H_5$, $R_3 = C(O)CH_3$; X = Cl ou I et on les a traités avec TlCp pour conduire à $(\eta^5\text{-}C_5H_5)PtR_1R_2R_3$. Ces derniers sont les premiers complexes polyfonctionnallisés du cyclopentadiényle platine IV. On a pu détecter, par spectroscopie infrarouge, l'isomérie conformationnelle autour du lien platine–carbone de l'acétyle. On n'a pas pu réussir à cliver les liens Pt—CH_3 ou Pt—$C(O)CH_3$ des $CpPt(CH_3)_2R$ en faisant appel aux réactifs HCl, $HgCl_2$ ou I_2; on a plutôt isolé les complexes $[Pt(CH_3)_2RX]_4$ appropriés. On a noté la nature chirale du $(\eta^5\text{-}C_5H_5)Pt(CH_3)(C_2H_5)[C(O)CH_3]$.

[Traduit par le journal]

Cyclopentadienyltrimethylplatinum(IV), $CpPtMe_3$, was prepared in 1963 by Robinson and Shaw (1). The other molecules of this type differ only by containing substituted cyclopentadienyl ligands such as methylcyclopentadienyl (2), **1***b*, and hydropentalenyl (3), **2**. There are no examples where the platinum is tri- or tetrafunctionalized such as **3** and **4**. The pseudo-

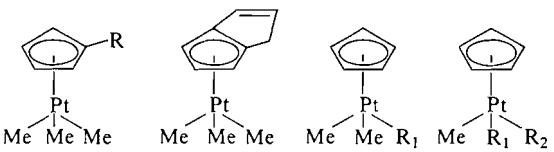

1*a* R = H
b R = Me

2 **3** **4**

tetrahedral or piano stool arrangement of ligands in **4** results in optical isomerism. Chiral organometallics are of interest as a source of fundamental knowledge (4) and as potential catalysts in asymmetric organic synthesis (5, 6). These considerations led to attempts to synthesize **3** and **4**. As will be reported below, the successful preparation of the first polyfunctionalized platinum(IV) cyclopentadienides was achieved, including the chiral molecule η^5-cyclopentadienylmethylethylacetylplatinum(IV), CpPtMeEtAcyl.

Experimental

Nuclear magnetic resonance (^{1}H nmr) spectra were obtained on a Varian T-60 instrument, using tetramethylsilane (TMS) as internal standard. Melting points were determined in open capillaries in a Thomas Hoover Uni-Melt apparatus and are uncorrected. Infrared spectra were taken on a Perkin-Elmer 520 Grating Spectrophotometer. Elemental analyses were performed by Midwest Microanalytical, Indianapolis, Indiana.

Inert atmosphere techniques were used for all preparations. THF, benzene, and toluene were distilled from sodium benzophenone just before use. K_2PtCl_4 was prepared (7) from platinum metal (Engelhard Industries of Canada). $PtMe_2$(COD), where COD = 1,5-cyclooctadiene, was prepared by reported procedures (8). TlC_5H_5, obtained commercially or prepared as described (9), was purified by sublimation (0.01 Torr, 80–90°C) and stored under nitrogen in the dark. Reagent grade CH_3I and CH_3COCl were used without further purification. $[PtMe_3I]_4$, $[PtMe_2AcylCl]_4$, Acyl = $C(O)CH_3$, and $[PtMeEt_2I]_4$ were prepared as described (8). The new compound $[PtEt_2AcylCl]_4$ was prepared by a similar method (i.e. the oxidative-addition of CH_3COCl to $PtEt_2$(COD) (8)).

Preparation of New Platinum(IV) Cubane Type Complexes

A. Ethylmethyl-1,5-cyclooctadieneplatinum(II), PtEtMe(COD), 5

PtEtCl(COD) (8), 2.2 g (6.0 mmol), in 100 ml diethylether at −78°C, was treated with CH_3Li, 7 ml (1.3 *M*, 1.5 equiv.). The acetone – dry ice cooling bath was removed and the reaction mixture allowed to warm to room temperature and stirred for a further 2 h. After hydrolysis and work up (8), 1.6 g (77% yield of PtEtMe(COD) was isolated as a clear, colourless oil. The analytical sample was distilled (40°C, 10^{-2} Torr) in a short path distillation apparatus (Bantam-Ware K-284500). ^{1}H nmr ($CDCl_3$): δ 0.73 (t, 3H, CH_3, J(Pt—H) = 83 Hz), 0.4–1.7 (m, 5H, CH_2CH_3), 2.3 (bs, 8H, CH_2), 4.7 ppm (bt, 4H, CH, J(Pt—H) = 38 Hz). ^{13}C nmr ($CDCl_3$, shifts are referenced to TMS): δ 7.7 (t, CH_3, J(Pt—C) = 828 Hz), 17.0 (t, CH_2—CH_3, J(Pt—C) = 793 Hz), 15.8 (t, CH_2—CH_3, J(Pt—C) = 30 Hz),

Can. J. Chem. Downloaded from www.nrcresearchpress.com by 210.87.254.40 on 09/05/12
For personal use only.

Can. J. Chem. Downloaded from www.nrcresearchpress.com by 210.87.254.40 on 09/05/12
For personal use only.

99.8 and 97.4 (t, CH, J(Pt—C) = 40.4 and 62.5 Hz respectively), 29.9 and 29.5 ppm (t, CH_2 of COD, J(Pt—C) = 5.9 Hz, the coupling constant for the second peak was too small to be observed). *Anal.* calcd. for $C_{11}H_{20}Pt$: C 38.04, H 5.76; found: C 38.3, H 5.81.

B. Ethyldimethyliodoplatinum(IV), [PtEtMe$_2$I]$_4$, 6

CH_3I, 5.5 ml (8.9×10^{-2} mol), was added to PtEtMe(COD), 1.0 g (2.9 mmol) in 5 ml toluene. The reaction solution was kept at 80°C for 2.5 h (air condenser), then allowed to cool and was stripped to dryness. The grey oily solid was taken up in a minimum of CH_2Cl_2 and passed through a small (5 mm × 60 mm) column of florisil (CH_2Cl_2 eluant).

The solution was stripped and the residue was recrystallized from $CHCl_3$/acetone to give 0.44 g (40% yield) white crystals, which decompose above 180°C. Nmr ($CDCl_3$): δ 0.83 (tt, 3H, CH_2CH_3, J(H—H) = 7.5 Hz, J(Pt—H) = 76 Hz), 1.7 (t, 6H, CH_3, J(Pt—H) = 77 Hz), 2.4 ppm (q, 2H, CH_2CH_3, J(Pt—H) = 114 Hz). *Anal.* calcd. for $C_4H_{11}IPt$: C 12.60, H 2.89, Pt 51.18; found: C 12.6, H 2.88, Pt 51.5 (residue).

C. Ethylmethylacetylchloroplatinum(IV), [PtEtMeAcylCl]$_4$, 7

PtEtMe(COD), 0.29 g (0.84 mmol) was dissolved in 2.5 ml of reagent grade $CHCl_3$ which had been passed through a column of basic alumina in order to remove ethanol (monitored by nmr). CH_3COCl, 0.057 ml (0.80 mmol) was added by means of a 0.1 ml microsyringe. After mixing, the reaction solution was allowed to stand for 24 h. The solvent was stripped and the product was recrystallized from ether–hexane to give white crystals, which decompose >160°C. Yield is dependent on the scale of the reaction (in this case greater than 80%); large scale reactions (0.62 g PtEtMe(COD)) give significantly lower yield. Nmr ($CDCl_3$): δ 0.70 (t, 3H, CH_2CH_3, J(H—H) = 7.0 Hz), 1.65 (t, 3H, CH_3, J(Pt—H) = 86 Hz), 2.43 ppm (t, 3H, C(O)CH_3, J(Pt—H) = 15 Hz), CH_2CH_3 obscured by peaks due to C(O)CH_3. *Anal.* calcd. for $C_5H_{11}ClOPt$: C 18.90, H 3.46; found: C 18.5, H 3.54.

Preparation of Cyclopentadienylplatinum(IV) Complexes

CAUTION: These complexes are volatile and care should be exercised to avoid inhalation.

D. η^5-Cyclopentadienyltrimethylplatinum(IV), CpPtMe$_3$, 1a

[$PtMe_3I$]$_4$, 0.92 g (2.5 mmol), was dissolved in 5 ml 2-methylpyridine. THF (30 ml) were added and TlCp, 0.68 g (2.5 mmol), was added to the clear solution. A yellow precipitate formed immediately. The slurry was stirred for 2 h, filtered, and stripped to yield an oily solid. A sublimation probe was inserted and the rest of the 2-methylpyridine was pumped off after which there sublimed white crystals of $CpPtMe_3$, 0.38 g (50% yield) mp = 103–104°C, lit = 65°C (1), 108.5 (10), 104–104.5 (11). The reported value of 65°C is apparently incorrect.

E. η^5-Cyclopentadienyldimethylacetylplatinum(IV), CpPtMe$_2$Acyl, 8

[$PtMe_2AcylCl$]$_4$, 0.40 g (1.3 mmol), in 30 ml THF was treated with TlCp, 0.36 g (1.3 mmol) for 1 h. After work up and sublimation (30°C, 0.02 Torr), **8** was isolated as white crystals, 0.24 g (55%) mp = 67°C. Nmr ($CDCl_3$): δ 1.13 (t, 6H, CH_3, J(Pt—H) = 84 Hz), 2.42 (t, 3H, C(O)CH_3, J(Pt—H) = 6.0 Hz), 5.7 ppm (t, 5H, C_5H_5, J(Pt—H) = 5.8 Hz). Ir(CCl_4) ν(C=O): 1663 (m), 1693 (s). *Anal.* calcd. for $C_9H_{14}OPt$: C 32.43, H 4.2; found: C 32.7, H 4.31.

F. η^5-Cyclopentadienyldiethylmethylplatinum(IV), CpPtEt$_2$Me, 9

To [$PtEt_2MeI$]$_4$, 0.60 g (1.5 mmol) in 30 ml CH_2Cl_2 was added TlCp, 0.40 g (15 mmol) and the slurry was stirred for 5.5 h. After filtering and stripping the solvent, a yellow oil remained. This was distilled in the short path apparatus to give **9**, 0.42 g (83%). Nmr ($CDCl_3$): δ 0.85 (t, 3H, CH_3, J(Pt—H) = 83.2 Hz), 1.9–0.77 (m's, 10H, CH_2CH_3), 5.57 ppm (t, 5H, C_5H_5, J(Pt—H) = 5.9 Hz). *Anal.* calcd. for $C_{10}H_{18}Pt$: C 36.04, H 5.41; found: C 36.5, H 5.40.

G. η^5-Cyclopentadienyldiethylacetylplatinum(IV), CpPtEt$_2$Acyl, 10

As above [$PtEt_2AcylCl$]$_4$, 0.74 g (2.2 mmol) reacted with TlCp, 0.61 g (2.3 mmol) in 25 ml THF. Distilled in the short path apparatus (50°C/0.02 Torr). Nmr ($CDCl_3$): δ 1.27 (tt, 6H, CH_2CH_3, J(H—H) = 6.8 Hz, J(Pt—H) = 66 Hz), 2.5 (t, 3H, C(O)CH_3, J(Pt—H) = 5.2 Hz), 5.8 ppm (t, 5H, C_5H_5, J(Pt—H) = 5.2 Hz), CH_2CH_3 obscured by overlap. Ir(hexane) ν(C=O): 1699 (s) 1668 (m). *Anal.* calcd. for $C_{11}H_{18}OPt$: C 36.6, H 4.99; found: C 37.34, H 5.34.

H. η^5-Cyclopentadienylethyldimethylplatinum(IV), CpPtEtMe$_2$, 11

The amounts were: [$PtEtMe_2I$]$_4$, 0.50 g (1.3 mmol), TlCp, 0.39 g (1.4 mmol) in 40 ml CH_2Cl_2; the slurry was stirred for 14 h. Distilled as before; **11** 0.075 g (18%). Nmr ($CDCl_3$): δ 0.83 (t, 6H, CH_3, J(Pt—H) = 82 Hz), 2.0–1.1 (m's, 10H, CH_2CH_3), 5.7 ppm (t, 5H, C_5H_5, J(Pt—H) = 5.8 Hz). *Anal.* calcd. for $C_9H_{16}Pt$: C 33.9, H 5.02; found: C 34.3, H, 4.83.

I. η^5-Cyclopentadienylethylmethylacetylplatinum(IV), CpPtEtMeAcyl, 12

[$PtEtMeAcylCl$]$_4$, 0.76 g (2.4 mmol) and TlCp 0.58 g (2.2 mmol) were stirred in 30 ml THF for 3.5 h. Distilled (40°C/0.02 Torr) to give 0.73 g (88%). Nmr ($CDCl_3$): δ 1.12 (t, 3H, CH_3, J(Pt—H) = 87 Hz), 1.33 (tt, 3H, CH_2CH_3, J(H—H) = 7.0 Hz, J(Pt—H) = 66 Hz), 2.03 (m, 2H, CH_2CH_3), 2.51 (t, 3H, C(O)CH_3, J(Pt—H) = 6.0 Hz), 5.84 ppm (t, 5H, C_5H_5, J(Pt—H) = 5.6 Hz). Ir(CCl_4) ν(C=O): 1690 (s), 1662 (m). *Anal.* calcd. for $C_{10}H_{10}PtO$: C 34.58, H 4.61; found: C 34.6, H 4.70.

Reactions of CpPtMe$_3$ (1a) and CpPtMe$_2$Acyl, 8, with HCl, HgCl$_2$ and I$_2$

In a typical reaction **1a**, 0.16 g, was treated with 1 equiv. of HCl (generated from CH_3COCl in $MeOH/CH_2Cl_2$). The reaction was stirred overnight. A white precipitate was isolated and shown to be [$PtMe_3Cl$]$_4$ on the basis of its nmr spectrum in $CDCl_3$. In all other cases, (except **5** with I_2 which decomposes), the appropriate platinum tetramer was isolated.

Results and Discussion

Initial attempts to synthesize complexes of type **3** and **4** were directed at functionalizing the Pt—CH_3 bond in $CpPtMe_3$. The complex was treated with the electrophilic cleavage reagents (12) HCl, $HgCl_2$, and I_2. However, instead of attack at the Pt—CH_3 bond, the C_5H_5 ring was displaced and [$PtMe_3X$]$_4$ where X = Cl, Cl, and I respectively, was identified. Scheme 1 depicts the probable products. Since the platinum-containing materials were of primary interest the organic products were not identified, but those depicted are reasonable. The reactions are smooth and give high yields of tetramer. No evidence for any CpPt complexes could be detected in the nmr.

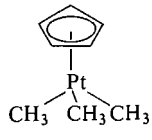

$+ HCl \rightarrow (PtMe_3Cl)_4 + C_5H_6$
$+ HgCl_2 \rightarrow (PtMe_3Cl)_4 + CpHgCl$
$+ I_2 \rightarrow (PtMe_3I)_4 + C_5H_5I$

SCHEME 1

Can. J. Chem. Downloaded from www.nrcresearchpress.com by 210.87.254.40 on 09/05/12
For personal use only.

Upon isolation of $CpPtMe_2Acyl$, (**8** reported below), it was treated with the same reagents and a similar displacement of the C_5H_5 ring occurred with HCl and $HgCl_2$ (Scheme 2).

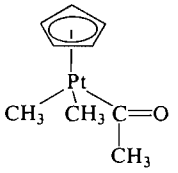

$+ HCl \rightarrow (PtMe_2AcylCl)_4$
$+ HgCl_2 \rightarrow (PtMe_2AcylCl)_4$
$+ I_2 \rightarrow$ dec.

SCHEME 2

Perhaps these reactions are not surprising if, as has been postulated (13), the first step is the oxidation of the metal atom followed by bond cleavage. The platinum in these molecules is in the +4 oxidation state and will not oxidize to higher states with these reagents (14). On the basis of the products produced, it is reasonable to propose that electrophilic attack at the C_5H_5 ring has occurred giving a cationic platinum(IV) cyclopentadiene complex which rapidly loses the diene and condenses to the tetramer.

The failure to functionalize Pt—C bonds in these complexes led to attempts to prepare suitably substituted starting materials. Robinson and Shaw used $[PtMe_3I]_4$ (1). This complex plus $[PtMe_2AcylCl]_4$ and $[PtEt_2MeI]_4$ have been prepared (8) by oxidative addition reactions of the appropriate dialkyl complex $PtR_2(COD)$, R = CH_3, C_2H_5. The complex $[PtEt_2AcylCl]_4$ was prepared by the oxidative addition of CH_3COCl to $PtEt_2COD$. In order to prepare $[PtEtMe_2I]_4$ and $[PtEtMeAcylCl]_4$ it was necessary to prepare PtEtMeCOD. Treatment of PtMeClCOD with excess EtMgBr resulted in high yields of $PtEt_2COD$ with none of the desired mixed alkyl being detected by nmr. Obviously alkyl exchange has occurred. This could happen in two ways (Scheme 3):

$$CODPtMeCl + EtMgBr \rightleftharpoons \begin{matrix} CODPtMeEt \\ CODPtEt_2 \end{matrix}$$

$$Cl—Pt—CH_3 + Br—Mg \rightarrow Cl—Pt—Br + CH_3—Mg \quad \ldots 1$$

$$Cl—Pt—CH_3 + Cl—Pt—CH_3 \rightarrow Cl—Pt—Cl + CH_3—Pt—CH_3 \quad \ldots 2$$

SCHEME 3

the Pt—CH_3 bond could alkylate the Mg—Br bond (*1*) or the Pt—Cl bond (*2*). Alkylation of a Pt—Cl bond results in retention of the methyl group in the platinum-containing products. Since no material containing a Pt—CH_3 bond could be detected, alkylation of a MgBr bond probably occurs. The CH_3—Mg species formed would then be 'lost' in the large excess of EtMgBr used in the preparation, resulting in complete exchange and isolation of $PtEt_2COD$ only. Such exchanges have been observed before between platinum alkyls and magnesium dihalides (15). Exchange between platinum dialkyls and platinum dihalides has also been reported (16).

The problem of preparing PtEtMeCOD was approached by the alternate route of methylating PtEtClCOD. Treatment of PtEtClCOD with excess methyl lithium gave PtEtMeCOD with only a trace of $PtMe_2COD$. The ^{13}nmr data for PtEtMeCOD[1] proved it to be a unique complex and not a 50:50 mixture of $PtMe_2COD$ (17) and $PtEt_2COD$ (18).

The oxidative addition of CH_3I to PtEtMeCOD required heating to 80°C in toluene solution. This is unusual since both the dimethyl and the diethyl complex react at room temperature. The preparation of $[PtEtMeAcylCl]_4$ by the oxidative addition of CH_3COCl is extremely sensitive to reaction conditions. The presence of CH_3CH_2OH in reagent grade $CHCl_3$ causes the reaction of CH_3COCl with PtEtMeCOD to proceed by a different pathway and give a mixture of PtEtClCOD and PtMeClCOD, identified by comparison of the ^{1}H nmr spectrum to those of authentic samples. The high yield of this mixture rules out the simple hydrolysis of a Pt—C bond due to the formation of HCl by the reaction of CH_3COCl with the small amount of CH_3CH_2OH present. The use of ether as a solvent for the oxidative addition results in the isolation of starting material. Reaction occurs in toluene and CH_2Cl_2 to give PtMeClCOD, PtEtClCOD, and some of the desired $[PtEtMeAcylCl]_4$, while CCl_4 gives only the latter in fair yield. The reaction proceeded cleanly in $CDCl_3$ and gave the tetramer in high yields. $CHCl_3$, which had been treated to remove CH_3CH_2OH, duplicated the $CDCl_3$ results. However, attempts to scale up the reaction always led to reduced yields, 0.2 g of PtEtMeCOD being optimum. These results imply free radicals may be involved in this reaction, as has been postulated in other oxidative additions (19).

Other oxidative additions were attempted but were not successful. For example, $Pt(C_6H_5)_2COD$ and $Pt(C_6H_5)(CH_3)COD$ did not react with CH_3I. It has been reported that no reaction occurs between $PtMe_2COD$ and ethyl iodide or benzoyl chloride (8). However, in view of the above, the selection of alternative reaction conditions might result in successful syntheses.

The three new complexes reported here: $[PtEt_2AcylCl]_4$, $[PtEtMe_2I]_4$, **6**, and $[PtEtMeAcylCl]_4$, **7**, are colourless solids. They are much more soluble in organic solvents than the parent complex $[PtMe_3I]_4$, **7** being soluble in ether. Their assignments as tetramers is based on the structure of the parent complex (20). The formation of these complexes probably involves an initial oxidative addition to

[1]Obtained on a Bruker WH-90 by Dr. Gordon Hamer of this department.

Can. J. Chem. Downloaded from www.nrcresearchpress.com by 210.87.254.40 on 09/05/12
For personal use only.

form unstable monomeric species i.e. $PtEt_2AcylCl$-COD. Olefin complexes of platinum(IV) do not exist and rapid loss of COD and condensation to a cubane tetramer occurs. The nmr spectra for these complexes are sharp and give no indication of the presence of geometrical isomerism. It seems unlikely that only one isomer of **7** would be formed. Since the platinum atoms are separated by 3.9 Å from each other (20) it is probable that the arrangement of ligands on one platinum atom has little effect on the arrangement or chemical shift of ligands on another. The possibility of a rearrangement occurring rapidly on the nmr time scale which would average the magnetic environment is considered unlikely but cannot be excluded. One can, however, rule out inter- or intra-molecular alkyl exchange since only one cyclopentadienyl derivative is isolated from each tetramer.

The cyclopentadienylplatinum complexes **1***a*, **8**–**12** result from the treatment of the appropriate tetramer with TlCp. **1***a* was originally prepared from $[PtMe_3I]_4$ and NaCp in 20% yield. The use of carefully purified TlCp results in 50% yield (unmaximized). The use of even a slight excess of TlCp should be avoided since yields appear to be badly reduced. The new complexes **9**–**12** are all clear liquids while **8** is a solid. They are quite volatile and possess a characteristic mushroom odor. As with all organometallic complexes, care should be taken to minimize exposure. They are stable to air but some do tend to turn yellow when distilled.

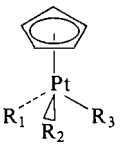

1*a* $R_1 = R_2 = R_3 = CH_3$
8 $R_1 = R_2 = CH_3$, $R_3 = C(O)CH_3$
9 $R_1 = R_2 = C_2H_5$, $R_3 = CH_3$
10 $R_1 = R_2 = C_2H_5$, $R_3 = C(O)CH_3$
11 $R_1 = R_2 = CH_3$, $R_3 = C_2H_5$
12 $R_1 = CH_3$, $R_2 = C_2H_5$, $R_3 = C(O)CH_3$

The complexes show no tendency to undergo reductive elimination reactions at room temperature and can be distilled intact. Other monomeric platinum(IV) alkyl complexes eliminate (21, 22) alkane or alkyl halide to give stable platinum(II) complexes. However, elimination of ethane from **1***a* would give $CpPtCH_3$ which would be predicted to be coordinatively unsaturated and unstable.[2] No evidence for elimination of C_2H_5 with the concomitant formation of a platinum(IV) hydride was detected. Similarly, the acetyl derivatives were stable to decarbonylation. The necessary condition for such reactions is the existence or creation of a vacant coordination site (24–26). This would be expected to be very difficult since platinum(IV) complexes are invariably six-coordinate; hence **1***a*, **8**–**12** are coordinatively saturated. Since there are no neutral two electron donors such as carbonyls or phosphines, the formation of a coordinatively unsaturated species will be a high energy process (10). Studies on the high temperature reactions of these complexes are planned. The reactions of **1***a* and **8** with electrophiles have already been discussed.

The complexes were characterized by infrared and ^1H and ^{13}C nmr spectroscopy (27). The postulated piano stool structure (28) is consistent with these data. As reported in the experimental section, the infrared spectra of **8**, **10**, and **12** have two bands in the acyl stretching region regardless of the supporting medium: neat (**10**, **12**), Nujol (**8**), hexane or CCl_4. However, the relative intensities of the two bands are dependent on the medium. Similar splitting is observed for $[HB(C_3H_3N_2)_3]$ $[C(O)CH_3](CO)_2Fe$ (29), $(\eta^5\text{-}C_5H_5)[C(O)CH_3](R_2NPF_2)(CO)Fe$ (29), and *trans*-$(\eta^5\text{-}C_5H_5)[C(O)CH{=}CH(C_6H_5)](CO)_2Fe$.[3] As in these complexes, we explain the splitting in terms of isomers related by internal rotations of the acetyl group about the Pt—C bond. Three possible conformers are illustrated below. Although there are only two peaks in the infrared spectrum, indicating only two isomers are present, the presence of the third cannot be ruled out (29). Since the nmr spectrum is very sharp it is reasonable to conclude that the isomers interconvert rapidly on the nmr timescale.

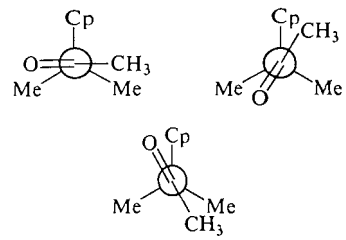

Compounds **8**–**12** are the first cyclopentadienyl complexes of platinum(IV) that have groups other than CH_3 as 'legs' in the piano stool structure. **12** is of interest as a chiral example of this class. The absence of ligands such as phosphines, olefins, or carbonyls makes this complex well suited for model studies, some of which will be reported in the future.

Acknowledgements

The financial support of the National Research

[2]The complex $(\eta^5\text{-}C_5H_5)(CH_3)(CO)Pt$ is known, ref. 23.

[3]S. Quinn and A. Shaver. Unpublished result.

Council of Canada is gratefully acknowledged. The author thanks Dr. Gordon Hamer for the ^{13}C nmr spectrum of PtEtMeCOD.

1. S. D. Robinson and B. L. Shaw. Z. Naturforsch. B18, 507 (1963); J. Chem. Soc. 1529 (1965).
2. H. P. Fritz and K-E. Schwarzhans. J. Organomet. Chem. 5, 181 (1966).
3. T. J. Katz and J. J. Mrowca. J. Am. Chem. Soc. 89, 1105 (1967).
4. H. Brunner. Top. Current Chem. 56, 67 (1975).
5. A. Davison and N. Martinez. J. Organomet. Chem. 74, C17 (1974).
6. G. Jaouen and A. Meyer. J. Am. Chem. Soc. 97, 4667 (1975).
7. G. Brauer. Handbook of preparative inorganic chemistry. Vol. 2. 2nd ed. Academic Press, New York, NY. 1965. pp. 1569, 1571; Inorganic syntheses. Vol. 7. McGraw-Hill, New York, NY. 1963. p. 232; Inorganic syntheses. Vol. 2. McGraw-Hill, New York, NY. 1946. p. 247.
8. H. C. Clark and L. E. Manzer. J. Organomet. Chem. 59, 411 (1973).
9. F. A. Cotton and L. T. Reynolds. J. Am. Chem. Soc. 80, 269 (1958).
10. K. W. Egger. J. Organomet. Chem. 24, 501 (1970).
11. V. A. Semion, A. Z. Rubeznov, Yu. T. Struckov, and S. P. Gubin. Zh. Strukt. Kim. 10, 151 (1969).
12. D. A. Slack and M. C. Baird. J. Am. Chem. Soc. 98, 5539 (1976).
13. T. C. Flood and D. L. Miles. J. Organomet. Chem. 127, 33 (1977).
14. F. R. Hartley. The chemistry of platinum and palladium. John Wiley and Sons. 1973.
15. J. Chatt and B. L. Shaw. J. Chem. Soc. 705 (1959).
16. R. J. Puddephatt and P. J. Thompson. J. Chem. Soc. Dalton Trans. 1810 (1975).
17. H. C. Clark, L. E. Manzer, and J. E. H. Ward. Can. J. Chem. 52, 1165 (1974).
18. M. H. Chisholm, H. C. Clark, L. E. Manzer, J. B. Stothers, and J. E. H. Ward. J. Am. Chem. Soc. 97, 721 (1975).
19. J. S. Bradley, D. E. Connor, D. Dolphin, J. A. Labinger, and J. A. Osborn. J. Am. Chem. Soc. 94, 4043 (1972); J. A. Labinger, A. V. Kramer, and J. A. Osborn. J. Am. Chem.Soc. 95, 7908 (1973).
20. G. Donnay, L. B. Coleman, N. G. Krieghoff, and D. O. Cowan. Acta Crystallogr. B24, 157 (1968).
21. J. D. Ruddick and B. L. Shaw. J. Chem. Soc. A, 2969 (1969).
22. T. G. Appleton, H. C. Clark, and L. E. Manzer. J. Organomet. Chem. 65, 275 (1974).
23. H. C. Clark and A. Shaver. Can. J. Chem. 54, 2068 (1976).
24. D. L. Reger and E. C. Culbertson. J. Am. Chem. Soc. 98, 2789 (1976).
25. J. J. Alexander and A. Wojcicki. Inorg. Chem. 12, 74 (1973).
26. A. Wojcicki. Adv. Organomet. Chem. 11, 87 (1973).
27. G. Hamer and A. Shaver. To be published.
28. G. W. Adamson, J. C. J. Bart, and J. J. Daly. J. Chem. Soc. A, 2616 (1971).
29. F. A. Cotton, B. A. Frenz, and A. Shaver. Inorg. Chim. Acta, 7, 161 (1973).

Can. J. Chem. Downloaded from www.nrcresearchpress.com by 210.87.254.40 on 09/05/12
For personal use only.

The syntheses and properties of *C*-silylimines and their thermal rearrangements to *N*-silylenamines

ADRIAN G. BROOK, CARLO GOLINO,[1] AND EBERHARD MATERN[2]

University of Toronto, Toronto, Ont., Canada M5S 1A1

Received February 27, 1978

ADRIAN G. BROOK, CARLO GOLINO, and EBERHARD MATERN. Can. J. Chem. **56**, 2286 (1978).

C-Silylimines have been synthesized by silylation of lithioaldimines prepared from isonitriles. Their ultraviolet and C=N infrared absorptions show bathochromic shifts relative to related aldimines or ketimines and the nmr spectra show the presence of *syn–anti* isomers, probably due to nitrogen inversion. The silylimines undergo intramolecular thermal rearrangements at about 200–235°C yielding *N*-silylenamines, which have been characterized.

ADRIAN G. BROOK, CARLO GOLINO et EBERHARD MATERN. Can. J. Chem. **56**, 2286 (1978).

On a synthétisé des *C*-silylimines par silylation des lithioaldimines préparés à partir des isonitriles. Leurs absorptions dans l'ultraviolet et l'infrarouge pour le C=N présentent des déplacements bathochromes par rapport aux aldimines ou aux cétimines qui leur sont reliés et les spectres rmn montrent la présence des isomères *syn* et *anti* probablement due à une inversion au niveau de l'azote. Les silylimines subissent des transpositions thermiques intramoléculaires entre 200–235°C conduisant aux *N*-silylénamines qui ont été caractérisés.

[Traduit par le journal]

Acylsilanes have been shown to rearrange both photochemically and thermally. Under the former circumstances (1) a siloxycarbene having significant nucleophilic character has been proposed as an intermediate, whose most studied behaviour has been its facile insertion into bonds bearing acidic hydrogen.

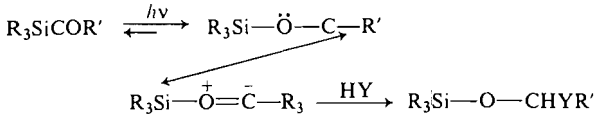

Siloxycarbenes have also been proposed as intermediates in thermal rearrangements, where the sole observed behaviour has involved insertion into an adjacent CH bond (2).

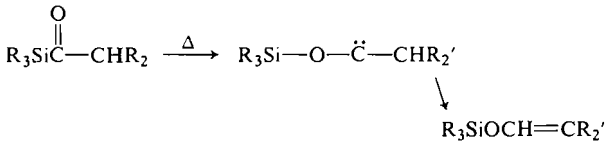

Although these proposals for the thermal rearrangement adequately explain the experimental observations, many (but not all) of the results could be equally well explained by a dyotropic rearrangement of the isomeric enolic form of the acylsilane.

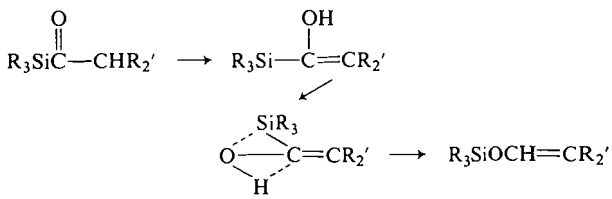

Reetz *et al.* (3) have made a series of elegant studies on variants of related rearrangements generally involving silicon–oxygen species.

We sought to learn more about the generality of the types of rearrangements described above and to this end have investigated some *C*-silylimines, nitrogen analogs of acylsilanes. Of several synthetic routes attempted (which included reactions of acylsilanes with primary amines or amide ions under various conditions, reactions of silyllithium reagents with isonitriles followed by alkylation or silylation, and reaction of amines with α,α-dibromobenzylsilanes) only the addition of organolithium reagents to isonitriles as originally described by Walborsky *et al.* (4), followed by silylation was reasonably successful and several *C*-silylimines were prepared in a pure state by this route.

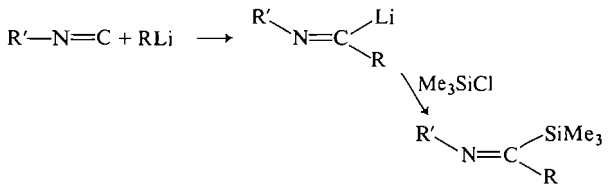

R′ = 2,6-Dimethylphenyl, *t*Octyl, *t*Bu
R = Me, Et, *i*Pr, *n*Bu, *t*Bu

[1]Dow Corning Postdoctoral Fellow, 1971–1972. Present address: Corning Glass Works, Corning, NY.

[2]Present address: Institut für Anorganische Chemie der Universität, Karlsruhe, Germany.

Can. J. Chem. Downloaded from www.nrcresearchpress.com by 210.87.254.105 on 09/05/12
For personal use only.

TABLE 1. Physical properties of *C*-silylimines

	Compound	% yield	Boiling point (°C/Torr)*	Analysis (%) Calculated C	H	N	Found C	H	N
1	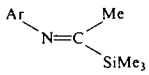	41	52–60/0.1	71.16	9.65	6.38	71.11	9.61	6.38
2	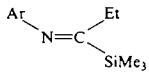	41	74–76/0.3	†					
3	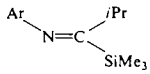	52	89–98/0.5‡	72.80	10.18	5.66	72.97	10.06	5.68
4	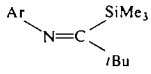	73	103–108/0.2§	73.49	10.41	5.36	73.39	10.25	5.45
5	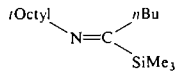	51	88–90/1.4‖	71.29	13.09	5.20	71.39	13.05	5.16
6	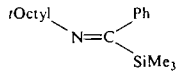	30	95–97/0.3	74.66	10.79	4.84	75.27	10.81	4.76
7	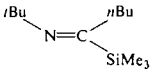	31	52–54/0.8¶	67.53	12.76	6.56	67.47	12.96	6.56

NOTE: Ar = 2,6-dimethylphenyl; *t*Octyl = 2,4,4-trimethyl-2-pentyl.
*All compounds were purified by glc on 20% SE-30 on Chromosorb W at temperatures from 155–200°C.
†Materials only about 95% pure.
‡mp 23°C, from isopropyl alcohol – pentane.
§mp 27°C, from isopropyl alcohol – pentane.
‖n_D^{20} 1.4546.
¶n_D^{20} 1.4340.

Only isonitriles with bulky groups containing no α-hydrogen (*tert*-octyl, *tert*-butyl, 2,6-dimethylphenyl) were successfully employed, less bulky groups (e.g. Ph) or those with α-hydrogen undergoing additional reactions and yielding little if any silylimines. Even then, with 2,6-dimethylphenylisonitrile, low temperature (−80°C) addition of the organolithium reagent was desirable, since even at 0°C an alternative pathway occurred, which probably involved radical anions, as suggested by the intense purple colour observed. Under the most favourable conditions (which we have not optimized) the yields of silylimines were not high. *N*-Alkyl-*C*-silylimines are fairly readily hydrolyzed by water or methanol, yielding the corresponding aldimine by loss of the silyl group. On the other hand, *N*-arylsilylimines such as **1** or **4** (see Table 1) are reasonably stable at room temperature but react at about 80°C with methanol or methanol–HCl to yield 2,6-dimethylaniline and methoxytrimethylsilane.

Like their acylsilane analogs (5) *C*-silylimines have C=N absorption in the infrared region at considerably longer wavelengths than their carbon analogs. Table 2 indicates that the C=N absorption of silylimines generally occurs in the region 6.23–6.30 μ, whereas related carbon analogs (*t*Bu(Me)C=NPh, 6.06 μ (6); Me_2C=N-*n*Pr, 6.02 μ; $(CH_2)_5C$=NPh, 6.04 μ (7)) absorb at shorter wavelengths. The related aldimines *n*BuN=CH-*t*Bu (8), ir 6.02 μ, and *t*Bu-N=CH-*n*Bu, ir 5.95 μ, and *t*octyl-N=CH-*n*Bu, ir 6.00 μ, derived from methanolysis of silylimines **8** and **5**, respectively, similarly absorb at much shorter wavelengths than their silyl precursors.

It is difficult to judge the effect of silyl groups on the ultraviolet absorption of imines because good data is scarce. Imines have both π–π* and *n*–π* absorptions but with *N*-arylketimines the *n*–π* absorption has generally not been observed, presumably because it falls within the envelope of the intense π–π* absorption. It is probably appropriate to compare $Me_3Si(nBu)C$=N-*t*Bu, **2** (λ_{max} 302 nm) with Me_2C=N-*n*Bu (λ_{max} 246 nm) (9) which suggests a bathochromic shift of about 56 nm on replacing alkyl by trimethylsilyl. If the absorption reported at 323 nm in Ph(Me)C=N-2,6-$Me_2C_6H_3$ is the *n*–π* transition, it appears at 25 nm shorter wave-

Can. J. Chem. Downloaded from www.nrcresearchpress.com by 210.87.254.105 on 09/05/12
For personal use only.

Can. J. Chem. Downloaded from www.nrcresearchpress.com by 210.87.254.105 on 09/05/12
For personal use only.

TABLE 2. Spectroscopic properties of *C*-silylketimines*

	Compound	Infrared (C=O) μ	Ultraviolet (solvent) λ_{max} (ε)	Nuclear magnetic resonance δ (ppm)						
				Aromatic	$Me_2C_6H_3$	H_a CH_n—C=N	H_b CH_3—C—C=N	Me_3Si		Proportions
1	Ar, Me[a], N=C, SiMe$_3$	6.28		7.07	2.10	*anti* 1.83		0.47 at 35°C		95
						syn		0.03		5
2	Ar, $CH_2^aCH_3^b$, N=C, SiMe$_3$	6.28	(C_6H_{12}): 211(15 400), 233(10 000), 275(1120), 324(359), 348(s)	7.03	2.04	*anti* 2.25	0.90	0.38	35°C	
						syn ?	1.47	−0.05		
				7.08	2.05	*anti* 2.23	0.88	0.37	3°C	80
						syn 2.62	1.34	−0.07		20
				7.00	2.11	2.34(q)	1.09(t)	0.27(s)	126°C	
3	Ar, $CH^aMe_2^b$, N=C, SiMe$_3$	6.29 (*anti*) 6.19 (*syn*?)		6.95	2.14	*anti* 2.86(b)	1.29(b)	0.48(b)		
						syn		0.10(b)		
				7.02	2.07	*anti* 2.59	1.13	0.43		50
						syn 3.07	1.33	−0.05		50
4	Ar, tBu^b, N=C, SiMe$_3$	6.23 (*syn*)?	(C_6H_{12}): 214(13 650), 244(9180), 282(1120), 348(220) (*i*PrOH): 212(11 820), 242(8850), 281(1160), 343(195)	6.95	2.10		1.39	0.13		95+

	Compound	Infrared (C=O) μ	Ultraviolet (solvent) λ_{max} (ε)	Nuclear magnetic resonance δ (ppm)
5	*t*Octyl, *n*Bu, N=C, SiMe$_3$	6.24		2.37(CH_2—C=N, m), 1.8–1.0(24H, m), 0.10(Me_3Si)
6	*t*Octyl, Ph, N=C, SiMe$_3$	6.28	(C_6H_{12}): 214(7340), 239(2980), 305(284) (*i*PrOH): 212(7950), 239(3100), 306(250)	7.1(Ph), 1.6(CH_2, m), 1.0(15H, m), 0.00(Me_3Si)
7	*t*Bu, *n*Bu, N=C, SiMe$_3$	6.23	(C_6H_{12}): 210(1990), 225(1500), 302(82)	2.35(CH_2—C=N, m), 1.65–0.7 (16H, m), 0.10(Me_3Si)

**Syn–anti* is relationship of Me_3Si to *N*-aryl group.

TABLE 3. Properties of *N*-silylenamines*

	Compound	Infrared (μ)	Nuclear magnetic resonance δ (ppm) Aromatic	$Me_2C_6H_3$	Other
8	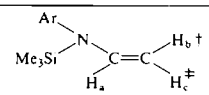	6.11	7.01	2.21	6.40 (H_a, d of d), 3.68 (H_b, d) 3.27 (H_c, d) (J_{ab} = 19, J_{ac} = 10.8, J_{bc} = 0 Hz) 0.20 ($SiMe_3$)
9	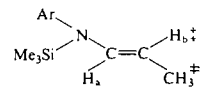	6.05, 10.39	6.98	2.20	6.15 (H_a, d, (br)), 3.72 (H_b, overlapping q), 1.55 (Me_c, d of d) (J_{ab} = 13.6, J_{bc} = 6.8, J_{ac} = 1.4 Hz), 0.15 ($SiMe_3$)
10	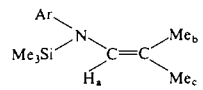	6.03	6.96	2.26	5.83 (H_a, m(br)), 1.63 (Me_c, d), 0.88 (Me_b, d) (J_{ab} = 1, J_{ac} = 0.7 Hz‖), 0.17 ($SiMe_3$)

NOTE: Ar = 2,6-dimethylphenyl.
*All compounds purified by glc on SE-30 on Chromosorb W at 170–180°C.
†*Anal.* calcd. for $C_{13}H_{21}NSi$: C 71.16, H 9.65, N 6.38; found: C 71.04, H 9.74, N 6.74.
‡*Anal.* calcd. for $C_{14}H_{23}NSi$: C 72.03, H 9.93, N 6.00; found: C 72.07, H 9.80, N 6.09.
§*Anal.* calcd. for $C_{15}H_{25}NSi$: C 72.80, H 10.18, N 5.66; found: C 73.02, H 10.04, N 5.70. Yield 75%.
‖Doublets only partially resolved at ambient temperature.

length than the long wavelength absorption of the silyl compounds Me_3Si(Et or *t*Bu)C=N-2,6-$Me_2C_6H_3$, **2** or **4** which have λ_{max} 348 nm. In acylsilanes, bathochromic shifts relative to carbon analogs are of the order of 100 nm (5) but in acylsilanes, the long wavelength absorption is now considered better described as a σ–π* transition in view of the character of the HOMO (10). Whether this is true in silylimines is unknown. Like the acylsilanes, the long wavelength absorption of silylimines shows a small blue shift on changing to more polar solvents.

Although the nmr spectra of the *N*-alkylsilylimines show the presence of only one isomer, those of the *N*-arylsilylimines show the presence of *syn–anti* isomers and the proportion of isomers appears to be determined by steric effects. The spectra are consistently interpretable on the reasonable assumption that whichever group is *syn* to the aryl group suffers significant shielding relative to the situation when that group is *anti* in the other isomer. When R = Me,

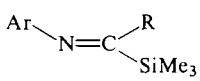

anti

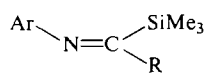

syn

the compound exists largely as the *anti* species, a small upfield Me_3Si peak (≃5%) suggesting the presence of a small amount of *syn* isomer. When R = ethyl, the *anti* isomer predominates (80% at 35°C) but the signals for the *anti* and *syn* trimethyl or ethyl protons are not sharp or well resolved. At −10°C the signals are sharper and the proportions are about 80% *anti* and 20% *syn* isomers. When R = *i*Pr, the signals are only very broad and diffuse at 35°C, but at −5°C they are significantly sharper, and the properties of *anti* and *syn* isomers are essentially equal. The silicon coalescence temperature appears to be about 39°C, and the data suggests that the $\Delta G^{\ddagger}$ for nitrogen inversion is about 14.8 kcal/mol. This may be compared to the value of 20.3 kcal/mol reported for *N*-phenyldimethylimine (11). Finally, when R = *t*Bu, the position of the Me_3Si resonance, 0.13 ppm, is consistent with the isomer present having the *syn* configuration, presumably because the longer Si—C bond (relative to C—C) results in the isomer being relatively the less sterically strained.

The thermal behaviour of the silylimines depends on their structure. The *N*-alkyl compounds decompose slowly when heated above 200°C to a complex mixture of olefins and other unidentified compounds which were not further studied. Compound **4**, the only *N*-aryl compound which lacked hydrogen α to the C=N, failed to rearrange even after 90 h at 225–250°C. By contrast **1**, **2**, and **3** rearranged fairly cleanly at 200–235°C at rates comparable to the isomeric *N*-silylenamines, with relative rates **1** > **2** > **3**. The *N*-silylenamines, **8–10**, were readily isolated by glc, and were characterized by analysis and spectroscopy (see Table 3).

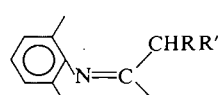

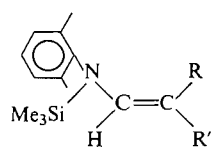

The structural and spectral assignments for the *N*-silylenamines **8** and **9** are based on the expected *trans* proton–proton spin coupling constants. Compound **9** has the sterically less-strained *trans* configuration, with its '*trans*' alkyl methyl group out of

Can. J. Chem. Downloaded from www.nrcresearchpress.com by 210.87.254.105 on 09/05/12
For personal use only.

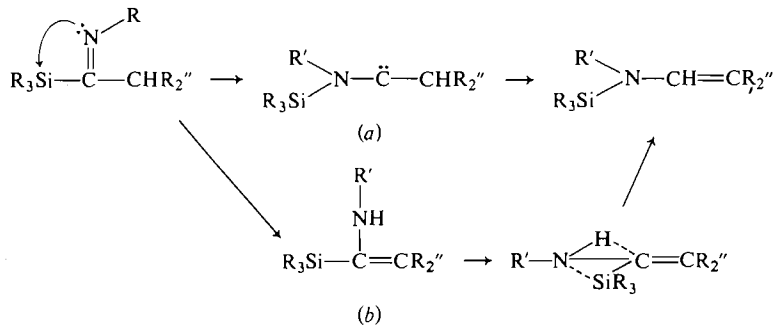

the field of the arylamino group. Its resonance position is therefore significantly downfield (0.75 ppm) relative to the '*cis*'-methyl group in **10**, which is more shielded. It is noteworthy that in the known *N*-methyl-*N*-phenyl-*cis*- or -*trans*-propenylamines or *N*-ethyl-*N*(*o*-tolyl)-*cis*- and -*trans*-propenylamines, the *trans*-methyl groups in each case are, respectively, 0.13 and 0.26 ppm to lower field than the *cis* methyl groups (12).

The *N*-silylenamines were very hydrolytically unstable and rapidly reacted in methanol to give cleavage products and not the enamine. Thus the silylenamine **8** obtained from thermolysis of **1** gave dimethylaniline and methoxytrimethylsilane on treatment with methanol, as shown by its nmr and ir spectra.

A kinetic study of the thermal rearrangement of the methyl-*C*-silylimine **1** showed the reaction to be cleanly first order over several half lives, with E_a = 30.4 kcal/mol and $\Delta S^{\ddagger} = -20.6$ eu. For **2** and **3**, less reliable kinetics suggested that E_a decreased with increasing size of R while $\Delta S^{\ddagger}$ became increasingly negative. (It seems probable that these rearrangements were being carried out above the isokinetic temperature estimated as 137°C from limited data, and hence the influence of $\Delta S^{\ddagger}$ dominates.) The rates of rearrangements were not significantly affected by the addition of traces of base or acid. Attempts to effect the rearrangement photochemically, neat or in hexane, using either long wavelength (λ_{max} 360 nm) or medium pressure mercury lamps, were unsuccessful, only small amounts of decomposition products being observed after hours of photolysis. Photolysis of the *C*-silylimines in carbon tetrachloride occurred to give trimethylchlorosilane, probably by a radical process, as the only silicon-containing species.

While the failure of the silylimines to undergo photochemical rearrangement is unlike the behaviour of the related acylsilanes, their thermal behaviour closely parallels that of the acylsilanes. Thus a mechanism can be written parallelling that proposed for the acylsilanes, in which a silylaminocarbene (*a*) is formed which subsequently inserts into the adjacent CH bond. However, the extent by which the silyl migration preceeds the hydrogen migration is not established and the two migrations may be concerted. It must also be recognized that while the enamine tautomer (*b*) cannot be detected at room temperature, at elevated temperatures it could be the reactive form through which rearrangement, possibly of the dyotropic type, occurs. Certainly the observed entropy of activation indicates considerable loss of freedom of motion in the transition state, consistent with a concerted process.

Experimental

Organometallic reactions were carried out in dried solvents under dry nitrogen. Chromatographic analyses or purifications were done on 5 ft 20% SE-30 on Chromosorb W columns at appropriate temperatures. Nuclear magnetic resonance and infrared spectra were normally run in CCl_4.

Analyses were carried out by A. B. Gygli, Toronto.

Preparation of N-*2,6-Dimethylphenyl(trimethylsilyl)-ethylimine (2)*

To 7.88 g (0.060 mol) of 2,6-dimethylphenylisonitrile in 350 ml of ether at −75°C (some isonitrile began to precipitate out) was added 49 g (55 ml, 0.068 mol) of ethyllithium in benzene over 25 min giving a deep red-brown solution. After 10 min stirring, 8.8 ml (0.068 mol) of trimethylchlorosilane was added over 10 min, while the temperature remained below −70°C. After stirring for 3.5 h at −75°C the reaction mixture was allowed to warm to 25°C during which time it became deep purple. Because of the sensitivity of some silylimines to hydrolysis, filtration of the lithium salts was not carried out but instead the solvent was removed under reduced pressure to give a thick red oil, distilled through a short Vigreaux column to yield 5.70 g (41%) of pale yellow silylimine, shown by glc to be at least 95% pure. Purification was effected by glc on a 20% SE-30 on Chromosorb W column at 200°C.

If instead the isonitrile was treated with ethyllithium at 0°C, a deep purple solution was obtained. Treatment at 0°C with trimethylchlorosilane, followed by slow warming to 25°C gave a dark brown undistillable resin, which appeared to be polymeric, and from which little or no silylimine could be distilled.

The methyl- and *iso*-propylimines were similarly prepared using the appropriate organolithium reagent.

Preparation of N-*2,6-Dimethylphenyl(trimethylsilyl)*-tert-*butylimine (4)*

To a solution of 32 g (0.244 mol) of 2,6-dimethylphenylisonitrile in 1500 ml of dry ether at −78°C was added 224 ml

Can. J. Chem. Downloaded from www.nrcresearchpress.com by 210.87.254.105 on 09/05/12
For personal use only.

Can. J. Chem. Downloaded from www.nrcresearchpress.com by 210.87.254.105 on 09/05/12
For personal use only.

of a 1.3 *M* solution (0.29 mol) of *tert*-butyllithium in pentane over 0.75 h. After addition was complete, the orange solution was stirred at −78°C for 25 min, and then 29.2 g (0.29 mol) of trimethylchlorosilane was added dropwise, followed by 4 h stirring at −78°C. After warming to 25°C overnight, the supernatant was decanted from the lithium salts and was distilled to give 46 g (73%) of a viscous yellow liquid, bp 103–108°C/0.2 Torr. Crystallization from 1:1 2-propanol–pentane gave pure material, mp 26–27°C.

Preparation of N-tert-*Butyl(trimethylsilyl)*-n-*butylimine (7)*

To 15 ml (0.145 mol) of *tert*-butylisocyanide in 150 ml of anhydrous ether at −5°C was added 93 ml (0.147 mol) of *n*-butyllithium in hexane over about 5 min. The reaction mixture turned orange during 15 min stirring at 0°C and then 20.5 ml (0.156 mol) of trimethylchlorosilane was added over 10 min, as a white precipitate formed. After 20 min stirring at 0°C, the reaction was warmed to room temperature over 2 h. After filtration of the solid the filtrate was concentrated under reduced pressure and then was distilled through a 10 cm Vigreaux column to give 9.5 g (31%) of colourless silylimine, **7**, bp 52–54°C/0.8 Torr, purified for analysis by glc.

When **7** was dissolved in methanol, it was 70% hydrolyzed over 10 min to methoxytrimethylsilane, and *N*-(*tert*-butyl)-*n*-butylaldimine, identified by nmr and ir spectra.

Thermal Isomerizations of the C-*Silylimines, Yielding* N-*Silylenamines*

A 0.8 g sample of the ethyl compound **2** was heated in an evacuated sealed nmr tube at 235°C while the course of the reaction was monitored periodically by its nmr spectrum. This provided data which followed first-order kinetics. The compound was 47% rearranged after 6.7 h and after 56 h less than 5% starting material remained. Chromatography showed 86% of *trans*-*N*-trimethylsilyl-*N*-2,6-dimethylphenyl-1-propenylamine, **9**, obtained as a colourless liquid together with 4% starting material and four minor products.

Similar treatment of **3**, the isopropylimine, for 42 h at 277°C (36% rearrangement) followed by 27 h at 290°C led to complete disappearance of the starting material and a 75% yield of the *N*-trimethylsilylenamine, **10**.

When **4**, the *tert*-butylimine, was heated for 62 h at 225°C no change was observed. After a further 28 h at 250°C, a small amount of decomposition was observed but no vinylic protons could be detected.

The rate constants for the thermal rearrangement of **1** at several temperatures were determined: $k = 8.64 \times 10^{-6}$ (202°C); 2.78×10^{-5} (214°C); 4.89×10^{-5} (229°C); 7.61×10^{-5} (236°C) s^{-1}. Four runs at each temperature were made, using nmr data to determine relative concentrations every ½ h or 1 h as appropriate. Plots of ln *c* against time were good straight lines, and the results of different runs agreed closely. A plot of ln *k* against $1/T$ gave a good straight line.

Methanolysis of N-*Isobutenyl*-N-*trimethylsilyl-2,6-dimethylaniline (10)*

A sample of **10** in carbon tetrachloride was treated with 20 equiv. of methanol. After 10 min, the nmr spectra indicated the compound was 90% converted to methoxytrimethylsilane and *N*-2,6-dimethylaminoisopropylaldimine; nmr δ: 7.49 (1H, d, $J = 5$ Hz, H—C=N) 6.94 (3H, m, aryl), 2.6 (1H, m, $CH\text{Me}_2$), 2.02 (6H, s, $Me_2C_6H_3$), 1.20 (6H, d, $J = 6.8$ Hz, $CHMe_2$)ppm. Removal of the volatiles at 70°C under reduced pressure removed the methoxytrimethylsilane but caused extensive decomposition of the aldimine.

Under similar conditions **4**, the precursor of **10**, suffered no hydrolysis after 20 min at 25°C.

Temperature Dependence of the Nuclear Magnetic Resonance Spectra of the C-*Silylimines*

Isopropylimine 3

At 35°C, the nmr spectrum of **3**, (see Table 1) had broad singlets at δ 2.86 (Me_2CH) and 1.29 (Me_2CH) ppm and a partially coalesced doublet δ 0.29 (Me_3Si) ppm. At −5°C these signals were separated into sharp signals at δ 3.07 (m, Me_2CH, *anti* to aryl), 2.59 (m, Me_2CH, *syn* to aryl), and 1.33 (d, $J = 6.5$ Hz, Me_2CH, *anti* to aryl), 1.13 (d, $J = 7.0$ Hz, Me_2CH, *syn* to aryl), and 0.43 (s, Me_3Si, *anti* to aryl) and 0.05 (s, Me_3Si, *syn* to aryl), each signal being of approximately equal intensity (*syn* and *anti* isomers present in equal proportions). At 92°C, the spectrum of a neat sample showed a single septet for Me_2CH, a single doublet for Me_2CH, and a single sharp singlet for Me_3Si. At 39°C, the Me_3Si signals were a coalesced broad flat-topped singlet, peak width at half height = 31 Hz. The trimethylsilyl signals had a maximum separation of 29 Hz (−5°C).

Ethylimines 2

At 35°C two Me_3Si signals could be clearly seen at about 0.43 and 0.00 ppm in the ratio of about 80:20. At −10°C the signals were much sharper, while at 126°C, the two trimethylsilyl signals had collapsed to a single sharp singlet.

Acknowledgements

The authors are grateful to the National Research Council of Canada who supported the research, to Dow Corning Corporation for a Postdoctoral Fellowship to C.G., and to Mr. John Lennon for experimental assistance.

1. J. M. Duff and A. G. Brook. Can. J. Chem. **51**, 2869 (1973).
2. A. R. Bassindale, A. G. Brook, and J. Harris. J. Organometal. Chem. **90**, C6 (1975).
3. (*a*) M. T. Reetz, M. Kliment, M. Plachky, and N. Greif. Chem. Ber. **109**, 2728 (1976); (*b*) M. T. Reetz. Chem. Ber. **110**, 965 (1977).
4. H. M. Walborsky, W. H. Morrison, and G. E. Niznik. J. Am. Chem. Soc. **92**, 6675 (1970).
5. A. G. Brook. Adv. Organomet. Chem. **7**, 95 (1968).
6. D. Y. Curtin, E. J. Grubbs, and C. G. McCarty. J. Am. Chem. Soc. **88**, 2775 (1966).
7. H. Saito and K. Nukada. Tetrahedron, **22**, 3313 (1966).
8. R. Bonnett. J. Chem. Soc. 2313 (1965).
9. D. A. Nelson and J. J. Worman. Tetrahedron Lett. 507 (1966).
10. B. G. Ramsey, A. G. Brook, A. R. Bassindale, and H. Bock. J. Organometal. Chem. **74**, C41 (1974).
11. D. Wurmb-Gerlich, F. Vögtle, A. Mannschreck, and H. A. Staab. Justus Liebigs Ann. Chem. **708**, 36 (1967).
12. M. Rivière and A. Lattes. Bull. Chem. Soc. Fr. 2539 (1967).

Hétérobicycles oxygénés.[1] Synthèse d'alkyl-3,6,8-trioxabicyclo[3.2.1]octanes et d'alkyl-3,7,9 et -4,7,9-trioxabicyclo[4.2.1]nonanes

PIERRE CALINAUD[2] ET JACQUES GELAS

Université de Clermont-Ferrand, Laboratoire de Chimie Organique 1, Ensemble Scientifique des Cézeaux (Ecole Nationale Supérieure de Chimie), BP 45, 63170 Aubière, France

Reçu le 22 mars 1978

PIERRE CALINAUD et JACQUES GELAS. Can. J. Chem. **56**, 2292 (1978).

La cyclisation en milieu basique de 1,3-dioxolannes chloroalkylés en 2 (ou en 4) et hydroxyalkylés en 4 (ou en 2) mène à des acétals bicycliques, intéressants intermédiaires de synthèse (pouvant notamment conduire à des 1,4-dioxannes fonctionnalisés) les 3,6,8-trioxabicyclo-[3.2.1]octanes. Les spectres de rmn de ces hétérobicycles sont étudiés: les constantes de couplage entre protons géminés permettent de différencier le cycle à cinq maillons du cycle à six maillons; la mise en évidence de couplages à longue distance (^4J et ^5J) apporte des arguments concernant la conformation du modèle bicyclique.

Deux séries isomères d'acétals bicycliques alkylés, les 3,7,9- et 4,7,9-trioxabicyclo[4.2.1]-nonanes sont accessibles par (*a*) l'addition intramoléculaire d'un groupement 4-hydroxyalkyle sur la double liaison éthylénique portée par l'atome de carbone en α de C-2 de 1,3-dioxolannes; (*b*) la déchlorhydratation de 2-chlorométhyl-4-hydroxyalkyl-1,3-dioxolannes; (*c*) la déshydratation de dioxolannes-diols. Le principal intérêt de ces hétérobicycles est de présenter un cycle à sept maillons et de pouvoir mener à des 1,4-dioxépannes fonctionnalisés.

PIERRE CALINAUD and JACQUES GELAS. Can. J. Chem. **56**, 2292 (1978).

The cyclization in a basic medium of 2 (or 4)-chloroalkyl-4 (or 2) -hydroxyalkyl-1,3-dioxolanes leads to bicyclic acetals, the 3,6,8-trioxabicyclo[3.2.1]octanes, which are useful intermediates for synthesis, yielding notably functionalized 1,4-dioxanes. The nmr spectra of these heterobicyclics were studied. The geminal proton coupling constants permit one to distinguish between five- and six-membered rings and the determination of couplings over several bonds (^4J and ^5J) yields information concerning the conformation of the model bicyclics.

Two isomeric series of alkylated bicyclic acetals (3,7,9- and 4,7,9-trioxabicyclo[4.2.1]nonanes) are accessible by the following routes: (*a*) the intramolecular addition of a 4-hydroxyalkyl group to the ethylenic double bond on the carbon atom α to C-2 in the 1,3-dioxolanes; (*b*) the dechlorohydration of 2-chloromethyl-4-hydroxyalkyl-1,3-dioxolanes; (*c*) the dehydration of dioxolane-diols. The main interest in these heterobicyclics is to prepare a seven-membered ring and to be able to prepare functionalized 1,4-dioxepanes.

[Journal translation]

Ces dernières années notre laboratoire a été notamment engagé dans l'étude de réactions d'hétérobicyclisation de 1,3-dioxolannes et de 1,3-dioxannes bifonctionnels. Un certain nombre de synthèses de composés bicycliques comportant trois hétéroatomes (oxygène ou azote ou soufre) ont été ainsi mises au point (2). Nous décrivons ici la synthèse et l'étude spectrographique d'alkyl 3,6,8-trioxabicyclo-[3.2.1]octanes.

Lorsque fut entreprise au laboratoire (2*a*) l'étude de tels bicycles, seul le dérivé non substitué avait été préparé par Hallonquist et Hibbert (3). Cette étude concernait uniquement des trioxabicyclooctanes substitués en position 4 et 5 par des groupements alkyle (2*b*), ou un groupement chlorométhyle en 5 ou un atome de chlore en 4 (2*c*). La synthèse du dérivé non substitué, puis celle du composé phényl-5 ont été reprises par la suite respectivement par Baggett *et al.* (4) et Inch et Williams (5). Ces travaux ont été étendus plus récemment (2*f*) à l'étude d'une lactone (4-oxo 5-méthyl trioxabicyclooctane) et d'hémiacétals (4-hydroxy 5-méthyl et 4-hydroxy 4,5-diméthyl trioxabicyclooctanes et leurs dérivés alkoxylés) appartenant à la même série. L'ensemble de ces composés ainsi décrits *dérive uniquement du glycérol.* Nous avons envisagé de préparer des trioxabicyclooctanes substitués en 1, 2 et 7 par un ou plusieurs groupements méthyle en particulier pour les raisons suivantes: (*i*) tout d'abord, ces groupements méthyle peuvent constituer des "pseudo-marqueurs" susceptibles de faciliter l'étude de la fragmentation sous l'impact électronique de tels bicycles, étude réalisée par ailleurs (6); (*ii*) en outre, ils autorisent une étude des couplages protoniques observés en rmn dont la connaissance a été utile dans la détermination (7) de

[1] Recherches dans la série des acétals cycliques: Partie XXIV; Partie XXIII: voir réf. 1.

[2] Ce mémoire constitue une partie de la Thèse d'Etat soutenue par P.C. le 10 septembre 1977 (Clermont-Ferrand No E 248). Il est dédié à Monsieur le Professeur René Rambaud, Ancien Directeur de l'ENSCC, en l'honneur de son départ à la retraite.

Can. J. Chem. Downloaded from www.nrcresearchpress.com by 210.87.254.6 on 09/05/12
For personal use only.

Can. J. Chem. Downloaded from www.nrcresearchpress.com by 210.87.254.6 on 09/05/12
For personal use only.

TABLEAU 1. Alkyltrioxa-3,6,8-bicyclo[3.2.1]octanes

Composés	R-1	R-2éq	R-2ax	R-4éq	R-4ax	R-5	R-7*exo*	R-7*endo*
1	Me	H	H	H	H	H	H	H
2	Me	H	H	H	H	Me	H	H
3	Me	H	H	H ou Me		Me	H	H
4	Me	H	H	Me	Me	Me	H	H
5	H	H	H	Me	Me	H	H	H
6	Me	H	H	Me	Me	H	H	H
7	H	Me ou H		H	H	H	H	H
8	H	Me ou H		H	H	Me	H	H
9	H	Me ou H		Me	Me	H	H	H
10	H	Me ou H		Me	Me	Me	H	H
11	H	H	H	Me	Me	Me	Me ou H	
12	H	H	H	Me	Me	Me	Me	Me

la structure du trioxabicyclooctane (7(*S*)-acétoxy 2(*S*)-méthoxy 3,6,8-trioxabicyclo[3.2.1]octane) obtenu par oxydation périodique du méthyl-β-L-arabinopyranoside.

D'une façon générale, un intérêt de l'étude de trioxabicyclooctanes est que ces composés possèdent une analogie étroite avec des substances naturelles homologues dioxygénés (6,8-dioxabicyclo[3.2.1]-octanes) appartenant notamment à la série des glucides (anhydropyranoses) et à la famille des phéromones (hormones sexuelles des insectes) telles que la frontaline (8), la brévicomine (9) ou la multistriatine (10).

Enfin, signalons que la réaction d'hydrogénolyse des trioxabicyclooctanes constitue un mode d'accés intéressant à des 1,4-dioxannes fonctionnalisés (11).

Il était intéressant de comparer cette étude avec celle de séries homologues supérieures, les *trioxabicyclo[4.2.1]nonanes*. En effet, ces derniers présentent un cycle à sept maillons du type 1,4-dioxépanne, cycle sur lequel la littérature ne posséde que peu d'éléments et qui est facilement accessible par hydrogénolyse de la fonction acétal des bicycles (11).

La synthèse de dioxolannes bifonctionnels (12) permettait d'envisager l'accès à deux séries isomères: les *3,7,9-* et les *4,7,9-trioxabicyclo[4.2.1]nonanes*. Tous les composés correspondant décrits dans le présent mémoire ont été par ailleurs étudiés en spectrographie de masse, afin d'évaluer les possibilités d'utiliser des groupements méthyle comme marqueurs de la fragmentation (13).

Synthèse d'alkyltrioxabicyclooctanes

Les 1,3-dioxolannes chloroalkylés en 2 (ou en 4) et hydroxyalkylés en (4 ou en 2) (**A**, schéma 1) dont la synthèse et l'étude spectrographique ont été décrites précédemment (12) sont soumis à des réactions de déchlorhydratation soit par la potasse en poudre, soit par le *tert*-butylate de potassium en solution dans le *tert*-butanol. (La soude même concentrée et à reflux dans un solvant à haut point d'ébullition est inopérante.) Les trioxabicyclooctanes **B** ainsi obtenus sont rassemblés dans le tableau 1 et ont été identifiés par spectrographie ir et de rmn.[3]

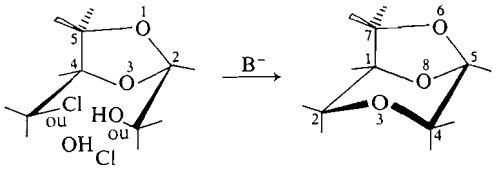

A **B**

SCHÉMA 1

Si l'on considère les dispositions spatiales respectives des substituants halogénés et hydroxylés, les dioxolannes de départ (préparés en milieu acide, donc dans des conditions d'équilibration thermodynamique) sont en fait un mélange de deux stéréoisomères *cis* et *trans*. La cyclisation ne met en jeu que les isomères *cis* (**A** seuls représentés sur le schéma 1) et, à cause de l'absence d'équilibration *cis-trans* en milieu basique, les isomères *trans* sont en principe non attaqués. L'utilisation du *tert*-butylate de potassium dans le *tert*-butanol permet en effet le plus souvent de retrouver ces derniers en fin d'opération. Ce n'est pas cependant toujours le cas car une réaction de β-élimination de l'acide chlorhydrique reste possible; elle mène à des 4-méthylène 1,3-dioxolannes (2*b*, 14). Il n'en reste pas moins que le fait que l'atome d'halogène des dérivés *trans* ne soit pas souvent touché dans la réaction, pourrait indiquer que la cyclisation est une réaction intramoléculaire d'un type pouvant se rapprocher de celui de la réaction S_N2. Si tel est le cas, on doit pouvoir observer une inversion de configuration au niveau de l'atome de carbone portant un atome d'halogène.

[3]Les bicycles **5**, **6** et **9** ont été préparés par une réaction de déchloracylation déjà décrite (2*h*); leurs caractéristiques spectrales n'avaient pas été données et sont seules discutées ici.

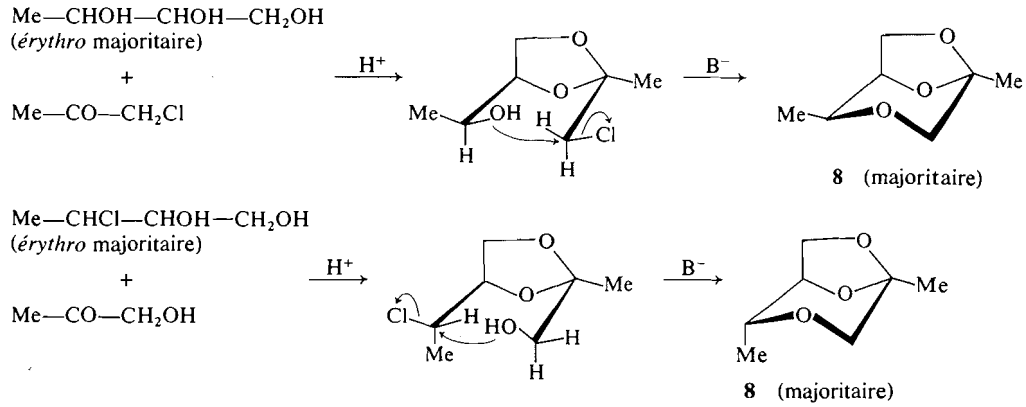

SCHÉMA 2

Nous donnons dans le schéma 2 un exemple relativement en faveur de cette hypothèse: le trioxabicyclooctane **8** peut être obtenu selon deux voies similaires: (*i*) soit à partir du 1,2,3-butanetriol essentiellement *érythro* (préparé (12) par action de l'eau oxygénée en présence d'acide tungstique sur le 2-butène 1-ol essentiellement *trans*); (*ii*) soit à partir du 3-chloro 1,2-butanediol essentiellement *érythro* (préparé (12) par action de l'acide hypochloreux sur le 2-butène 1-ol essentiellement *trans*).

Pour chacune de ces deux manipulations on détecte par chromatographie en phase vapeur deux pics dont les proportions respectives sont inversées (successivement 70:30 et 30:70); ils correspondent aux bicycles ayant une stéréochimie majoritaire conforme soit à un maintien de la chiralité de l'atome C-4′ (attaque de l'atome C-2′), soit à une inversion de cette chiralité (attaque de l'atome de carbone en cause).

Cette observation a été vérifiée chaque fois que l'analyse des spectres de rmn des bicycles obtenus permet une attribution sûre de leur stéréochimie. C'est notamment le cas du bicycle **10** (schéma 3)

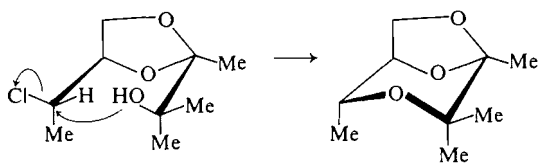

10

SCHÉMA 3

pour lequel le groupement méthyle existe à plus de 90% en position axiale.

On peut remarquer que la stéréochimie du produit obtenu n'est jamais unique. Ceci peut être partiellement expliqué par le fait que la chlorhydrine et le triol *érythro* de départ sont contaminés par la présence de leurs isomères *thréo*. Cependant la proportion de ces derniers ne dépasse guère 5 à 7% (12).

L'importante quantité d'isomère axial obtenue pour le trioxabicyclooctane **8** (schéma 2) pourrait être due soit au fait que le mécanisme invoqué n'est pas unique, soit à une équilibration thermique partielle du mélange obtenu. Il est possible d'équilibrer en milieu acide les bicycles obtenus: dans tous les cas l'isomère équatorial est thermodynamiquement favorisé. Nous ne pouvons malheureusement en tirer de conclusions quantitatives n'ayant pu obtenir de résultats cohérents selon le catalyseur utilisé (acide *p*-toluènesulfonique, éthérate de trifluorure de bore, chlorure d'aluminium, etc...).

Un problème théorique reste pour l'instant sans solution définitive: il a été observé depuis longtemps (2*b*, 15, 16) que l'atome d'halogène en 4′ de 1,3-dioxolannes n'est pas substituable (schéma 4) par les

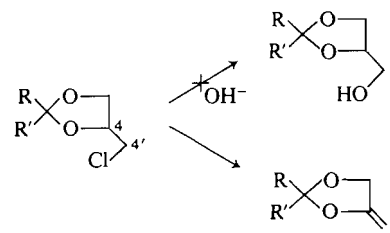

SCHÉMA 4

alcools ou les alcoolates (réaction *inter*moléculaire). Inversement, la réaction *intra*moléculaire (qui mène aux trioxabicyclooctanes) est pourtant assez facilement réalisable comme nous le montrons ici.

Identification des alkyl 3,6,8-trioxabicyclooctanes

Par spectrographie ir on note la disparition de l'absorption correspondant au groupement hydroxyle (ou au groupement acétoxyle pour les composés **5**, **6** et **9**). Les raies indiquées pour la fonction acétal (COCOC) se situent (17) dans l'intervalle 1000–1200 cm^{-1}, mais sont plus nombreuses que celles correspondant aux acétals de départ. Une ou plusieurs bandes apparaissent dans la région 640–680 cm^{-1} (2*b*).

Can. J. Chem. Downloaded from www.nrcresearchpress.com by 210.87.254.6 on 09/05/12
For personal use only.

TABLEAU 2. Déplacements chimiques et constantes de couplage en rmn des trioxabicyclooctanes[a]

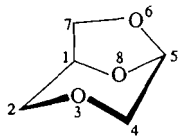

Composés	R-1	R-2éq	R-2ax	R-4éq	R-4ax	R-5	R-7*exo*	R-7*endo*	*J*(Hz)
									6.8[b]
1	s 1.23(3)	d 3.34(1)	d 3.61(1)	m 3.46(2)		s 5.18(1)	d 3.41(1)	d 4.14(1)	11.1[c]
									0.5[d]
2	s 1.20(3)	s 3.45(2)		s 3.36(2)		s 1.28(3)	d 3.41(1)	d 4.13(1)	6.1[b]
	s 1.20(3)	d 3.21(1)	dd 3.65(1)	d 1.00(3)	q 3.41(1)	s 1.23(3)	dd 3.36(1)	d 4.04(1)	6.3[b]
3[h]									11.0[c]
	s 1.20(3)	d 3.21(1)	dd 3.65(1)	q 3.48(1)	d 1.18(3)	s 1.23(3)	dd 3.36(1)	d 4.04(1)	1.5[e]
									6.2[b]
4	s 1.24(3)	d 3.27(1)	dd 3.69(1)	s 1.07(3)	s 1.12(3)	s 1.24(3)	dd 3.34(1)	d 4.00(1)	11.2[c]
									1.5[e]
5	m 4.30(1)	m 3.24–4.18(2)		s 1.05(3)	s 1.21(3)	d 4.83(1)	m 3.24–4.25(2)		1.1[d]
									6.1[b]
6	s 1.21(3)	dd 3.25(1)	dd 3.37(1)	s 1.03(3)	s 1.16(3)	s 4.76(1)	dd 3.25(1)	d 4.00(1)	11.2[c]
									1.1,[d] 1.4[e]
7	m 4.15(1)	d 1.00(3)	q 3.89(1)	s 3.47(2)		s 5.15(1)	m 3.30–4.10(2)		
	m 4.13(1)	d 1.01(3)	q 3.70(1)	s 3.39(2)		s 1.26(3)	m 3.70–4.00(2)		6.4[f]
8[h]									
	m 4.13(1)	m 4.13(1)	d 1.41(3)	s 3.39(2)		s 1.26(3)	m 3.70(2)		
	m 3.40–4.38(2)		d 1.36(3)	s 0.96(3)	s 1.23(3)	s 4.76(1)	m 3.40–4.38(2)		
9[h]									6.8[f]
	m 3.78(1)	d 1.33(3)	m 3.78(1)	s 1.23(6)		s 4.33(1)	m 3.98–4.18(2)		
	m 3.44(1)	d 1.16(3)	m 4.03(1)	s 1.26(6)		s 1.33(3)	m 3.72–4.30(2)		6.4[f]
10									1.6[e]
	m 4.46–3.50(2)		d 1.42(3)	s 1.08(3)	s 1.28(3)	s 1.28(3)	m 3.50–4.46(2)		
11	m 3.53(1)	m 3.75–4.16(2)		s 1.26(3)	s 1.26(3)	s 1.34(3)	m 3.90(1)	d 1.16(3)	
12	t[i] 3.33(1)	t[i] 4.08(2)		s 1.25(3)	s 1.25(3)	s 1.30(3)	s 1.10(3)	s 1.26(3)	1.6[g]

[a]Spectres en solution dans le tétrachlorure de carbone.
[b]$^2J_{7,7}$.
[c]$^2J_{2,2}$.
[d]$^5J_{2eq,5}$.
[e]$^4J_{2ax,7exo}$.
[f]$^3J_{Me\text{-}2ax\ ou\ eq}$.
[g]$^3J_{1,2ax}$ et $^3J_{1,2eq}$.
[h]Mélange de deux stéréoisomères (Me axial ou Me équatorial).
[i]En réalité doublet de doublet avec $J_{1,2ax} \simeq J_{1,2eq}$.

Les caractéristiques des spectres de rmn sont données dans le tableau 2. Seules les observations importantes sont commentées ici.

Constantes de couplage entre protons géminés[4]

Dans beaucoup de cas les protons géminés sur C-4 donnent un singulet et seuls ceux géminés sur C-2 sont différenciés. Ceci peut s'interpréter par l'influence exercée par la nature acétalique de l'atome de carbone C-5.

L'analyse au premier ordre des signaux correspondant à CH_2-7 et CH_2-2 permet de mesurer des constantes de couplage entre protons géminés (^2J) respectivement de 6.1–6.8 et de 11.0–11.2 Hz. Cahill *et al.* (18) indiquent que pour des protons méthylèniques en α d'un hétéroatome un des principaux facteurs affectant la valeur de J_{gem} est la donation en retour de la paire libre à l'orbitale antisymétrique du groupement méthylène. Ce phénomène est lié à la conformation des paires libres par rapport aux atomes d'hydrogène. Si l'on admet une conformation chaise pour le cycle 1,4-dioxanne, l'examen des modèles moléculaires permet de constater (fig. 1) que les paires libres de O-6 sont pratiquement éclipsées pour les deux atomes d'hydrogène sur C-7 (cycle à cinq maillons) et que les paires libres

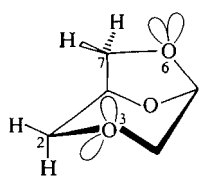

FIG. 1. Modèle moléculaire pour les trioxabicyclooctanes.

[4]Ces constantes de couplage sont indiquées en valeur absolue et sont très vraisemblablement négatives.

Can. J. Chem. Downloaded from www.nrcresearchpress.com by 210.87.254.6 on 09/05/12
For personal use only.

Can. J. Chem. Downloaded from www.nrcresearchpress.com by 210.87.254.6 on 09/05/12
For personal use only.

de O-3 sont décalées par rapport aux deux atomes d'hydrogène portés par C-2 (cycle à six maillons).

Constantes de couplage[5] *entre protons vicinaux*

Lorsque un proton en 5 se trouve en α d'un groupement méthylène en 4 (par exemple pour le bicycle **1**) aucun dédoublement du signal n'est relevé mais sa largeur indique la présence d'un couplage de valeur inférieure à 1 Hz. Pour l'autre position du pont il est possible de détecter un couplage (1.6 Hz) entre H-1 et les protons portés par C-2. Ce signal, qui apparait comme un triplet, pourrait être significatif de la similitude entre les couplage vicinaux éq–éq et éq–ax. La différence entre les positions 1 et 5 sur le bicycle peut être attribuée de son côté à une déformation du cycle à six maillons due au fait que la liaison C-5—O-6 est plus courte que la liaison C-1—C-7.

Couplages à longue distance ^{4}J *et* ^{5}J

Le seul couplage ^4J nettement observé est celui entre l'atome d'hydrogène axial sur C-2 et l'atome d'hydrogène *exo* sur C-7 (^4J 1.5 Hz). D'un point de vue qualitatif on peut remarquer que l'arrangement spatial de ces protons est très près d'une forme W quand le cycle 1,4-dioxanne adopte une conformation chaise légèrement aplatie dans la région C-2—O-3—C-4 de la molécule. Ceci est en accord avec l'hypothèse formulée précédemment pour la conformation des trioxabicyclooctanes (2*f*, 11), probablement proche de celle de l'homobicycle correspondant, le bicyclo[3.2.1]octane (19). L'effet anti-réflexe (20) qui a été mis en évidence dans cette série (2*c*), pourrait être la cause principale de cet aplatissement du cycle.

L'existence de ce couplage est particulièrement utile pour l'attribution de la stéréochimie de groupements portés par les atomes de carbone en cause. C'est notamment sa présence (ou son absence) qui permet de définir la position équatoriale (ou axiale) du groupement méthyle en C-2 sur les bicycles **8** et **10** (schémas 2 et 3).

Le spectre du composé **6** (fig. 2)[6] est un bon exemple d'un groupement méthylène (^2J = 11.2 Hz) où un proton est engagé dans un couplage à travers quatre liaisons (^4J = 1.4 Hz), l'autre proton étant couplé à travers cinq liaisons (^5J = 1.1 Hz) avec un atome d'hydrogène distinct (interprétation confirmée par irradiation des protons en cause et par disparition du couplage en remplaçant H-1 par un groupement méthyle). Un ^5J similaire a été observé dans le spectre du 7(*S*)-acétoxy 2(*S*)-méthoxy 3,6,8-trioxabicyclo[3.2.1]octane obtenu par oxydation périodique du méthyl-β-L-arabinopyranoside (7). De tels couplages ne sont pas aussi fréquents que les ^4J. Cependant, dans les séries qui se rapprochent des trioxabicyclooctanes on trouve des valeurs de 0.1 Hz pour un anhydropyranose (21), 0.6 Hz pour l'α-D-idopyranose (22), 0.7 Hz pour un orthoester cyclique de sucre (23) et 0.9 Hz pour un 1,4-dioxanne (24). La valeur élevée de la constante observée dans notre cas peut s'interpréter par l'aplatissement du cycle 1,4-dioxanne qui tend à rendre coplanaires les cinq atomes impliqués. Plus encore, l'introduction d'hétéroatomes sur le chemin du couplage et la multiplication des chemins possibles (ici deux chemins sont possibles à travers un atome d'oxygène) sont connues pour augmenter la valeur de ^5J. Ainsi des valeurs de 1.25 et 1.7 Hz ont été observées pour des molécules oxygénées bi- et tricycliques (25).

Synthèse d'alkyl-3,7,9-trioxabicyclo[4.2.1]nonanes

Il a été montré au laboratoire (2*a*) que les 4-hydroxyméthyl-1,3-dioxolannes porteurs d'une double liaison en α de l'atome de carbone 2 du cycle, subissent, en milieu acide, une addition intramoléculaire du groupement hydroxyle sur la double liaison. Dans tous les cas étudiés, la formation exclusive (ou nettement préférentielle) de trioxabicyclononanes a été observée. Etant donné que cette étude n'avait concernée que le seul glycérol (atomes de carbone 1, 2 et 8 du bicycle formé non substitués) nous nous sommes proposé d'envisager l'éventuelle influence de groupements méthyle en position 4 ou 4′ ou 5 sur les dioxolannes de départ.

En portant à reflux dans le benzène, en milieu acide, des triols et des cétones éthylèniques appropriées, on obtient des mélanges de dioxolannes éthyléniques et de trioxabicyclononanes définis dans le schéma 5. L'équilibration *cis–trans* en milieu acide des dioxolannes entraîne la réaction quasi-totale du mélange.

La réaction d'addition est régiospécifique: seuls les trioxabicyclononanes sont isolés et la formation éventuelle concurrente de trioxabicyclo*octanes* n'est pas observée dans les cas étudiés ici. Ceci est sans doute dû au fait que la formation d'un carbocation en α de l'atome de carbone acétalique est un processus défavorisé. La protonation de la double liaison s'effectue donc en α du groupement acétal et entraîne l'attaque du groupement hydroxyle en β.

[5]Dans tout ce mémoire nous indiquons des constantes de couplage mesurées directement sur le spectre après analyse du premier ordre. Il s'agit donc d'espacements plutôt que de véritables *J*. Lorsque les effets du second ordre deviennent évidents, la valeur de l'espacement n'est pas indiquée dans le tableau 2.

[6]On peut obtenir la fig. 2 et les tableaux 5 et 6, à un prix nominal, en s'adressant au Dépôt de données non publiées, ICIST, Conseil national de recherches du Canada, Ottawa, Ont., Canada K1A 0S2.

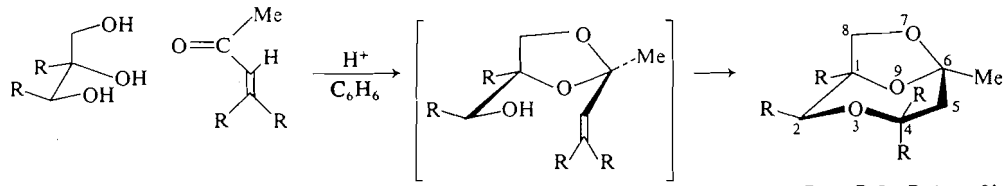

	R-1	R-2	R-4	%
13	Me	H	H	80
14	H	Me	H	90
15	Me	H	H,Me	80
16	Me	H	Me	98

SCHÉMA 5. Acétalisation de triols par des cétones α-éthyléniques. (Pourcentage mesuré par chromatographie en phase vapeur sur le produit brut de la réaction; la différence avec 100 représente le pourcentage de dioxolannes intermédiaires présents dans le mélange; les rendements en produits isolés sont indiqués dans le tableau 3).

Identification des 3,7,9-trioxabicyclo[4.2.1]nonanes

Les particularités présentées par les spectres ir (partie expérimentale) sont les mêmes que celles données plus haut pour les trioxabicyclooctanes.

Le tableau 3 rassemble les spectres de rmn des composés préparés. Nous en commentons seulement les points essentiels.

Constantes de couplage entre protons géminés

Les différences relevées entre les valeurs des constantes de couplage entre protons géminés (s'ils existent) en position 2 ou 5 ou 8 sont dues à la taille du cycle (5 ou 7 maillons) et sont comparables (fig. 3) à celles relevées pour les trioxabicyclooctanes. Pour les protons en 8 une conformation éclipsée des paires libres de O-7 facilite la donation en retour des électrons des paires à l'orbitale antisymétrique du groupement méthylène en 8. Il n'y a pas de différence notable entre le modèle à six maillons (trioxabicyclooctane) et celui à sept maillons (trioxabicyclononane).

Constantes de couplage à longue distance

La conformation en W des protons H-2 axial et H-8 *exo* pour lesquels (fig. 3) on observe un couplage ^4J, est d'autant mieux respectée que le cycle dioxépanne adopte une conformation chaise aplatie. L'effet anti-réflexe, qui joue un rôle dans la conformation des trioxabicyclooctanes est vraisemblablement responsable de l'aplatissement du cycle.

Pour le composé **3** le signal de H-5 équatorial montre un couplage ^5J à travers O-3 avec H-2 équatorial. La valeur relativement élevée de ce couplage (1.2 Hz) peut être justifiée comme précédemment pour les trioxabicyclooctanes.

TABLEAU 3. Déplacements chimiques en rmn des protons des 3,7,9-trioxabicyclo[4.2.1]nonanes

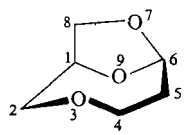

Composés	R-1	R-2ax	R-2éq	R-4ax	R-4éq	H-5ax	H-5éq	Me-6	H-8*endo*	H-8*exo*
13	s 1.18(3)	m 3.45(2)		m 3.60(2)		m 1.91(2)		s 1.38(3)	d 3.96(1) $J = 6.8^a$ $J = 0.5^b$	dd 3.46(1)
14	m 4.10(1)	m 3.73(1)	d 0.98(3)	m 3.73(2)		m 2.13(2)		s 1.36(3)	m 3.73(2)	
15	s 1.17(3)	d 3.60(1) $J = 12^e$	dd 3.30(1)	q 3.68(1) $J = 6.3^d$	d 1.08(3)	d 2.00(1) $J = 11.8^f$	d 1.75(1)	s 1.38(3)	d 3.94(1) $J = 6.6^a$ $J = 1.1^c$	d 3.43(1)
	s 1.23(3)	d 3.66(1) $J = 12^e$	dd 3.50(1)	d 1.10(3) $J = 6.3^d$	q 3.75(1)	d 1.81(1) $J = 9.3^f$	d 1.58(1)	s 1.35(3)	d 3.90(1) $J = 7.1^a$ $J = 1.1^c$	d 3.65(1)
16[g]	s 1.16(3)	dd 3.50(2) $J = 12.8^e$		s 1.13(3)	s 1.31(3)	d 2.03(1) $J = 14.3^f$	d 1.73(1)	s 1.35(3)	d 4.03(1) $J = 6.3^a$ $J = 1.2^b$	dd 3.56(1)

NOTE: Solvant: CCl_4.

[a] $^2J_{8endo,exo}$.
[b] $^4J_{8exo,2ax}$.
[c] $^5J_{2éq,5éq}$.
[d] $^3J_{H\text{-}Me}$.
[e] $^2J_{2ax,2éq}$.
[f] $^2J_{5ax,5éq}$.
[g] $^5J_{2éq,5éq}$ non observé.

Can. J. Chem. Downloaded from www.nrcresearchpress.com by 210.87.254.6 on 09/05/12
For personal use only.

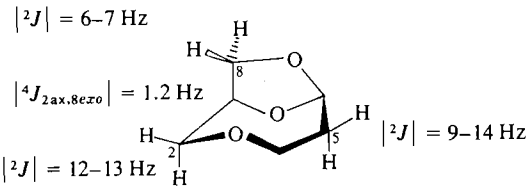

FIG. 3. Les constantes de couplage pour les trioxabicyclononanes.

Synthèse d'alkyl-4,7,9-trioxabicyclononanes

Ces bicycles isomères de ceux décrits dans le paragraphe précédent, sont obtenus selon les mêmes méthodes de cyclisation permettant d'accéder aux trioxabicyclooctanes (homologues inférieurs) à partir de dioxolannes bifonctionnels: (*i*) déchlorhydratation d'acétals halogénés et hydroxylés où l'atome d'halogène est en β de l'atome de carbone C-4 du dioxolanne (schéma 6, méthode *a*) selon le procédé décrit plus haut; (*ii*) déshydratation d'acétals-diols (schéma 6, méthode *b*), selon une méthode mise au point pour les trioxabicyclooctanes.[7]

Les rendements de ces cyclisations sont pour la plupart acceptables. Ces méthodes paraissent donc être des synthèses convenables de bicycles comportant un cycle à sept maillons.

Identification des 4,7,9-trioxabicyclononanes

Les spectres ir des composés présentent essentiellement les caractéristiques décrits pour les trioxabicyclooctanes. Les spectres de rmn sont présentés dans le tableau 4.

En conclusion, nous avons montré que la préparation de trioxabicyclooctanes et de deux séries isomères de trioxabicyclononanes était relativement aisée.

L'intérêt en synthèse de tels bicycles réside principalement dans le fait qu'ils permettent l'accès à des 1,4-dioxannes et des 1,4-dioxépannes fonctionnalisés par un groupement hydroxyméthyle; il est en effet notamment possible d'hydrolyser la fonction acétal ou de l'ouvrir par les hydrures mixtes (11) ou les réactifs de Grignard.[8]

Partie expérimentale

Les analyses par chromatographie en phase vapeur ont été réalisées sur un appareil Hewlett-Packard modèle 5750, équipé d'une colonne Carbowax 20 M (3 mm × 3 m) et d'un détecteur à catharomètre (gaz vecteur: 30 ml d'hydrogène par minute). Les séparations d'échantillons par chromatographie ont été effectuées sur un appareil Varian-Aerograph 705 N, muni d'une colonne Carbowax 20 M (9 mm × 6 m) et d'un détecteur à ionisation de flamme (gaz vecteur, 120 ml d'azote par minute).

Les spectres de rmn ont été réalisés sur un appareil Varian T-60; les abréviations utilisées dans la description de ces spectres sont: s, singulet; d, doublet; t, triplet; q, quadruplet; et m, multiplet; les déplacements chimiques sont indiqués en ppm par rapport au tétraméthylsilane; l'intensité relative de chaque signal est indiquée entre parenthèses; les constantes de couplage indiquées sont les espacements de signaux mesurés sur les agrandissements et sont exprimés en Hz.

Les spectres ir ont été enregistrés sur un appareil Beckman IR 8.

La préparation et l'identification des triols, des chlorhydrines et des dioxolannes de départ ont été précédemment décrites (12, 26).

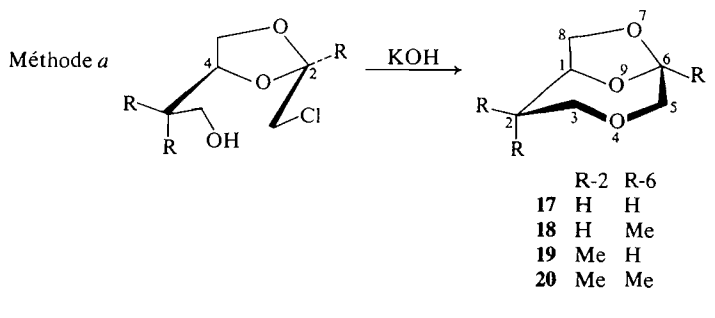

	R-2	R-6
17	H	H
18	H	Me
19	Me	H
20	Me	Me

	R-2	R-5	R′-5
21	H	Me	H
22	H	Me	Me
23	Me	Me	H
24	Me	Me	Me

SCHÉMA 6

[7]J. Gelas et M. Teppaz-Misson. Résultats inédits.
[8]J. Gelas et P. Calinaud. Résultats inédits.

Can. J. Chem. Downloaded from www.nrcresearchpress.com by 210.87.254.6 on 09/05/12
For personal use only.

TABLEAU 4. Déplacements chimiques en rmn des protons des 4,7,9-trioxabicyclo[4.2.1]nonanes

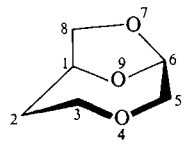

Composés	H-1	R-2ax	R-2éq	H-3ax	H-3éq	R-5ax	R-5éq	R-6	R-8*endo*	R-8*exo*
17	m 4.53–4.03(1)	m 2.13–1.70(2)		m 4.53–3.40(2)		m 4.53–3.40(2)			m 4.53–3.40(3)	
18	m 4.70–4.37(1)	m 2.12–1.70(2)		m 4.20–3.13(2)		d 3.68(1) $J = 12.3$[a]	d 3.23(1)	s 1.27(3)	m 4.20–3.13(2)	
19	m 4.08(1)	s 1.13(3)	s 0.87(3)	m 4.03–3.13(2)		d 3.58(1) $J = 12.4$[a]	d 3.08(1)	m 5.30(1)	m 4.00–3.13(2)	
20	m 4.18(1)	s 1.03(3)	s 0.83(3)	d 3.65(1)	d 3.28(1)	d 3.55(1) $J = 12.4$[a]	d 3.22(1)	s 1.25(3)	m 4.05–3.72(2)	
21	m 4.95–4.33(1)	m 2.20–1.40(2)		m 4.18–3.50(2)		d 1.16(3)	q 3.26(1)	s 1.20(3)	m 4.18–3.50(2)	
	m 4.43(1)	m 2.20–1.40(2)		m 3.97–3.40(2)		q 3.60(1)	d 1.06(3)	s 1.18(3)	m 3.97–3.40(2)	
22	m 4.37(1)	m 2.17–1.67(2)		m 4.00–3.33(2)		s 1.23(3)	s 1.13(3)	s 1.23(3)	m 4.00–3.33(2)	
23	m 4.00–3.87(2)	s 1.13(3)	s 0.73(3)	m 4.00–3.00(2)		q 3.67(1)	d 1.08(3)	s 1.28(3)	m 4.00–3.00(2) $J = 10.6$[b]	
	m 4.53(1)	s 1.08(3)	s 0.85(3)	m 4.33–3.15(2)		d 1.15(3)	q 3.58(1)	s 1.28(3)	m 4.33–3.15(2)	
24	m 4.30–3.50(1)	s 1.05(3)	s 1.00(3)	m 4.30–3.50(2)		s 1.05(3)	s 1.00(3)	s 1.30(3)	m 4.30–3.50(2)	

[a] $^2J_{5ax,5éq.}$
[b] $^2J_{8endo,8exo.}$

Synthèse des trioxabicyclooctanes

Déchlorhydratation par la potasse en poudre

L'acétal (0.1 ou 0.2 mol) est placé dans un ballon de Claisen avec un excès de potasse en poudre et quelques fragments de marbre destinés à offrir un support à la base. Après avoir maintenu la température vers 100°C durant environ 15 min on chauffe progressivement. Le distillat (qui passe à partir de 100°C et jusqu'à environ 180°C) est ensuite repris par 100 ml d'éther, la solution éthérée est séchée (Na_2SO_4), l'éther chassé et le résidu est distillé sous vide réduit.

Déchlorhydratation par le tert*-butylate de potassium*

Une quantité stoechiométrique de potassium en fins morceaux est attaqué par le minimum de *tert*-butanol anhydre. L'acétal en solution dans le *tert*-butanol est mélangé goutte à goutte à la solution d'alcoolate. On porte à reflux environ 24 h. On ajoute lentement de l'eau glacée (100 ml environ pour 0.1 mol d'acétal mis en jeu), extrait à l'éther, lave à l'eau, séche, chasse les solvants et distille sous pression réduite.

Les rendements de ces préparations ainsi que les constantes physiques des trioxabicyclooctanes obtenus sont rassemblés dans le tableau 5.[6]

Synthèse des 3,7,9-trioxabicyclo[4.2.1]nonanes

On place 0.1 mol de triol et 0.1 g d'acide *p*-toluènesulfonique dans un Erlenmeyer contenant 500 ml de benzène, placé sur un agitateur magnétique chauffant et surmonté d'un piège de Dean–Stark muni d'une dérivation fermée par une ampoule à brome. La suspension benzénique est fortement agitée et portée à reflux tandis que l'on rajoute au moyen de l'ampoule 0.1 mol de la cétone éthylénique appropriée (les cétones utilisées ici sont commerciales). Après obtention de la quantité d'eau correspondant à l'acétalisation (0.1 mol), on maintient le reflux durant environ 4 h. Après refroidissement, on neutralise (Na_2CO_3), chasse le benzène et distille le résidu.

Les constantes physiques des composés obtenus (**13–16**) ainsi que les rendements en composé isolé pur sont indiqués dans le tableau 6.[6]

Synthèse des 4,7,9-trioxabicyclo[4.2.1]nonanes

Déshydratation de dioxolannes-diols

Le matériel décrit ci-dessus est utilisé; le triol (0.1 mol) est porté à reflux dans le xylène (500 ml) en présence d'acide *p*-toluènesulfonique (1 g) sous une forte agitation, tandis que la cétone hydroxylée (les cétones utilisées sont commerciales) est ajoutée goutte à goutte. Lorsque la quantité d'eau attendue est obtenue (0.2 mol d'eau pour 0.1 mol de triol) on traite comme précédemment. On obtient ainsi les bicycles **21–24** (tableau 6).

Déchlorhydratation par la potasse d'acétals halogénés et hydroxylés

La méthode utilisé est celle décrite dans un paragraphe précédent; elle mène aux bicycles **17–20** (tableau 6).

1. P. CALINAUD, J. GELAS, D. HORTON et J. D. WANDER. Org. Mass Spectrom. Sous presse.
2. (*a*) J. GELAS. Bull. Soc. Chim. Fr. 3721 (1970); 4041 (1970); (*b*) 4046 (1970); (*c*) 4465 (1970); (*d*) J. GELAS. Tetrahedron Lett. 509 (1971); (*e*) J. GELAS et D. PETREQUIN. Bull. Soc. Chim. Fr. 3471 (1972); (*f*) J. GELAS et A. THIALLIER. Carbohydr. Res. **30**, 21 (1973); (*g*) P. CALINAUD, J. GELAS et D. PÉTREQUIN. Abstr. Papers 4th Int. Congr. Heterocycl. Chem. 187 (1973); (*h*) P. CALINAUD et J. GELAS. Bull. Soc. Chim. Fr. 1155 (1974); P. CALINAUD et J. GELAS. Abstr. Papers 5th Int. Congr. Heterocycl. Chem. 314 (1975).
3. E. G. HALLONQUIST et H. HIBBERT. Can. J. Res. **8**, 129 (1933).
4. N. BAGGET, J. M. DUXBURY, A. B. FOSTER et J. M. WEBBER. J. Chem. Soc. C, 208 (1966).
5. T. D. INCH et N. WILLIAMS. J. Chem. Soc. C, 263 (1970).
6. P. CALINAUD, J. GELAS, D. HORTON et J. D. WANDER. J. Chem. Soc. Perkin Trans. II, 1145 (1974).
7. J. GELAS, D. HORTON et J. D. WANDER. J. Org. Chem. **39**, 1946 (1974).
8. (*a*) G. W. KINZER, A. F. FENTIMAN, JR., T. E. PAGE, JR., R. L. FOLTZ, J. P. VITÉ et J. B. PITMAN. Nature, **221**, 477 (1969); (*b*) B. P. MUNDY, K. B. LIPKOWITZ et G. W. DIRKS. Synthetic Commun. **5**, 7 (1975) et références citées.
9. (*a*) R. M. SILVERSTEIN, R. G. BROWNLEE, T. E. BELLAS, D. L. WOOD et L. E. BROWNE. Science, **159**, 889 (1968); (*b*) W. E. GORE, G. T. PEARCE et R. M. SILVERSTEIN. J. Org. Chem. **41**, 603 (1976) et références citées.
10. (*a*) G. T. PEARCE, W. E. GORE, R. M. SILVERSTEIN, J. W. PEACOCK, R. A. CUTHBERT, G. N. LANIER et J. B. SIMEONE. J. Chem. Ecol. **1**, 115 (1975); (*b*) W. E. GORE, G. T. PEARCE et R. M. SILVERSTEIN. J. Org. Chem. **40**, 293 (1975).
11. J. GELAS et S. VEYSSIÈRES-RAMBAUD. Carbohydr. Res. **37**, 293 (1974).
12. P. CALINAUD et J. GELAS. Bull. Soc. Chim. Fr. 1228 (1975).

Can. J. Chem. Downloaded from www.nrcresearchpress.com by 210.87.254.6 on 09/05/12
For personal use only.

13. P. CALINAUD, J. GELAS, D. HORTON et J. D. WANDER. Org. Mass Spectrom. **11**, 1037 (1976).
14. P. CALINAUD, J. GELAS et S. VEYSSIÈRES-RAMBAUD. Bull. Soc. Chim. Fr. 2769 (1973).
15. H. O. L. FISCHER, E. BAER et L. FELDMANN. Ber. **63B**, 1722 (1930).
16. G. FARGES. Thèse Docteur-Ingénieur, ID 21, Clermont-Ferrand. 1962.
17. (*a*) E. D. BERGMAN et S. PINCHAS. Recl. Trav. Chim. Pays-Bas, **71**, 161 (1952); (*b*) S. A. BARKER, E. J. BOURNE et D. H. WIFFEN. Methods Biochem. Anal. **3**, 219 (1956); (*c*) R. S. TIPSON, H. S. ISBELL et J. E. STEWART. J. Res. Natl. Bur. Stand. **62**, 257 (1959).
18. R. CAHILL, R. C. COOKSON et T. A. CRABB. Tetrahedron, **25**, 4681 (1969).
19. (*a*) A. J. BARETTA, C. W. JEFFORD et B. WAEGELL. Bull. Soc. Chim. Fr. 3899 (1970); (*b*) J. FOURNIER et B. WAEGELL. Tetrahedron, **28**, 3407 (1972).
20. (*a*) C. SANDRIS et G. OURISSON. Bull. Soc. Chim. Fr. 1524 (1958); (*b*) B. WAEGELL et C. W. JEFFORD. Bull. Soc. Chim. Fr. 844 (1964).
21. L. D. HALL, J. F. MANVILLE et A. TRACEY. Carbohydr. Res. **4**, 514 (1967).
22. N. S. BHACCA, D. HORTON et H. PAULSEN. J. Org. Chem. **33**, 2484 (1968).
23. J. C. JOCHIMS, G. TAIGEL et W. MEYER ZU RECKENDORF. Tetrahedron Lett. 3227 (1967).
24. (*a*) K. C. KRAMEY et J. MESSIK. Tetrahedron Lett. 4423 (1965); (*b*) J. DELMAU et J. C. DUPLAN. Tetrahedron Lett. 559 (1966).
25. E. J. BOROS, K. J. KOSKRAN, K. W. KING et J. G. VERKADE. J. Am. Chem. Soc. **88**, 1140 (1966).
26. P. CALINAUD et J. GELAS. Bull. Soc. Chim. Fr. 1237 (1975).

Can. J. Chem. Downloaded from www.nrcresearchpress.com by 210.87.254.6 on 09/05/12
For personal use only.

Utilization of trimethylsilylpropyne as an acetonyl unit in the synthesis of cyclopentenones. Applications to the synthesis of jasmone and dihydrojasmone

PHAIK-ENG SUM AND LARRY WEILER[1]

Department of Chemistry, University of British Columbia, Vancouver, B.C., Canada V6T 1W5

Received March 9, 1978

PHAIK-ENG SUM and LARRY WEILER. Can. J. Chem. **56**, 2301 (1978).

The dianion of β-keto esters are alkylated at the γ-carbon with 3-bromo-1-trimethylsilyl-1-propyne. The resulting alkynes are hydrated (H_3O^+, Hg^{2+}) and cyclized (OH^-) to the corresponding cyclopentenones, jasmone and dihydrojasmone. The failure to obtain cyclopentanones from the acid- and base-catalyzed cyclizations of 6-substituted 3-keto esters may be rationalized by Baldwin's rules for cyclization.

PHAIK-ENG SUM et LARRY WEILER. Can. J. Chem. **56**, 2301 (1978).

Il y a alkylation du dianon des β-cétoesters au niveau du carbone-γ si l'on fait appel au bromo-3 triméthylsilyl-1 propyne-1. L'alcyne qui en résulte peut être hydraté (H_3O^+, Hg^{2+}) et cyclisé (OH^-) pour conduire aux cyclopentanones correspondantes, jasmone et dihydrojasmone. Le fait que l'on ne puisse pas obtenir des cyclopentanones par cyclisations catalysées par les acides ou les bases des céto-3 esters substitués en position 6 peut être rationalisé à l'aide des règles de Baldwin sur les cyclisations.

[Traduit par le journal]

For several years we have been interested in utilizing the dianion of β-keto esters (1) in the preparation of cyclopentanones as outlined in eq. [1].

[1] 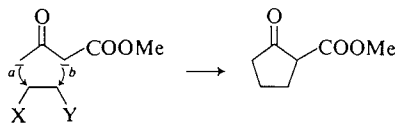

The application of such a cyclization in the synthesis of natural products, for example prostaglandins, rethrolones, and jasmones, is fairly obvious. The initial step *a* in eq. [1] proceeded without complication for a wide range of alkylating agents. However, the second step *b* was singularly unsuccessful under a wide variety of acid- and base-catalyzed conditions, when the carbon bearing the leaving group Y is sp^3 hybridized.[2] In light of Baldwin's suggestion (2) that the cyclization step *b* suffered from a stereoelectronic barrier imposed on it, all of our earlier failures could be rationalized but our synthetic goal remained unattained.

One of the more striking examples of the failure to observe cyclopentanone formation involved the treatment of methyl 6-hydroxy-3-oxoheptanoate (**1**), which is readily prepared from the dianion of methyl acetoacetate and propylene oxide (3), with boron trifluoride to produce the tetrahydrofurylidene (**2**) in greater than 80% yield. Under these same conditions ethyl acetoacetate is alkylated with 2-propanol to give ethyl α-isopropylacetoacetate in 60–67% yield (4).

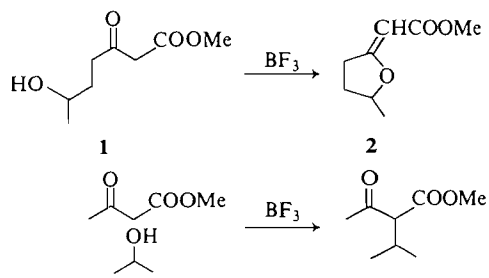

Cyclizations analogous to step *b* (eq. [1]) are known when the electrophilic carbon is sp^2 hybridized (5). This type of cyclization to an sp^2 carbon does not violate Baldwin's rules (2) and there are a number of examples of this cyclization leading to formation of cyclopentenones (6) as shown in eq. [2]. We have

[2] 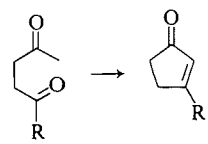

combined this cyclization of a 1,4-diketone with the alkylation of the dianion of β-keto esters to effect a synthesis of cyclopentenones which is detailed below for the preparation of jasmone (**3**) and dihydrojasmone (**4**).

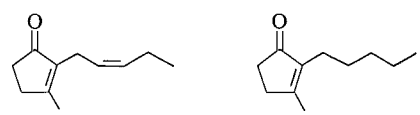

Initially we investigated the utility of a number of acetonyl units as shown in eq. [3]. The reaction of the

[1]Author to whom correspondence may be addressed.

[2]S. N. Huckin, G. R. Rickards, F. W. Sum, and P. E. Sum. Unpublished results 1972–1976.

Can. J. Chem. Downloaded from www.nrcresearchpress.com by 210.87.254.5 on 09/05/12
For personal use only.

Can. J. Chem. Downloaded from www.nrcresearchpress.com by 210.87.254.5 on 09/05/12
For personal use only.

[3] 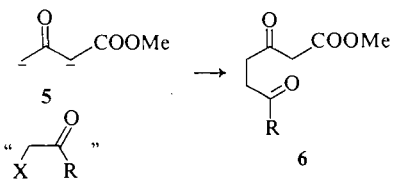

dianion **5** with α-halo ketones led to a mixture of several products which were not further characterized. Dianion **5** did not react with the α-bromo ketal of acetone. Treatment of dianion **5** with 2-methoxyallyl bromide (7) lead to formation of the γ-bromo-β-keto ester. This is consistent with the several other reports of bromine transfer in the reaction of β-substituted bromoalkanes and reactive nucleophiles (see for example ref. 8). However, we were able to prepare the desired 1,4-diketones **6** using 3-bromo-1-trimethylsilyl-1-propyne (9) as outlined in Scheme 1.

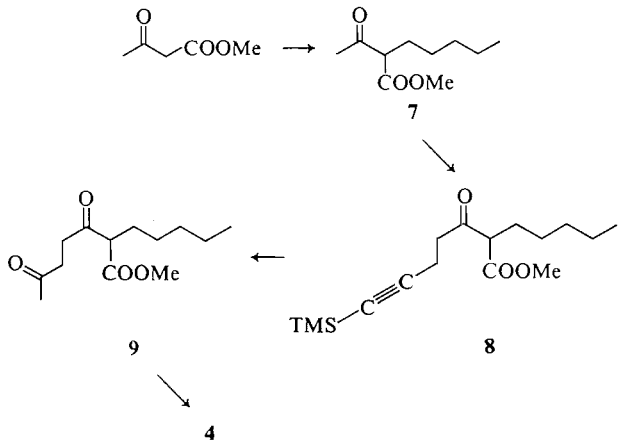

SCHEME 1. Synthesis of dihydrojasmone (**4**).

Methyl acetoacetate was alkylated with 1-bromopentane to give the β-keto ester **7**. The dianion of ester **7** was prepared in the usual fashion (1) and alkylated with 3-bromo-1-trimethylsilyl-1-propyne (9) to yield the monoalkylation product **8** in greater than 90% yield. The trimethylsilylalkyne **8** was cleaved and hydrated in aqueous acid using Hg^{2+} catalyst (10) to yield the 1,4-diketone **9** in almost 80% yield. This product **9** was hydrolyzed, decarboxylated, and cyclized by aqueous base to yield dihydrojasmone (**4**) in greater than 75% yield. Because we did not isolate any intermediates in this transformation we do not know the exact sequence of these steps.

This represents one of the few examples of the utilization of the trimethylsilylpropyne group as the precursor of the acetonyl unit of a 1,4-diketone in the generation of cyclopentenones.[3] Ho (6*b*) reports an unpublished example of an unsubstituted acetylene serving such a purpose in his review of early jasmone syntheses and recently McCrae and Dolby (10*b*) have utilized this same methodology to synthesize a spirocyclopentenone in their efficient synthesis of acorone.

Using a route similar to the above we have also synthesized *cis*-jasmone (3) as shown in Scheme 2. Alkylation of methyl acetoacetate with 1-bromo-2-pentyne (13) gave the acetylene **10** which was partially hydrogenated to the *cis*-alkene **11** using Pd-on-$BaSO_4$ (14). The dianion of **11** was generated and alkylated with 3-bromo-1-trimethylsilyl-1-propyne. Hydration of **12** and cyclization as before gave jasmone **3**[3] in greater than 40% overall yield from methyl acetoacetate.

In summary we find that the alkylation of simple β-keto ester dianions with 3-bromo-1-trimethylsilyl-1-propyne followed by hydration of the alkyne and subsequent cyclization leads to an efficient synthesis of cyclopentenones.

Experimental

All ir spectra were recorded in $CHCl_3$ solution using a Perkin-Elmer Model 700 spectrophotometer and were calibrated with the 1601 cm^{-1} band of polystyrene. The ^1H nmr spectra were recorded in $CDCl_3$ solution on either a Varian model T-60 or HA-100 spectrometer. The signal positions are reported using the δ scale with tetramethylsilane as internal standard. The multiplicity, coupling constants, and integrated peak areas are indicated in parentheses after each signal. The mass spectra were obtained using an Atlas CH-4B mass spectrometer and high resolution determinations were obtained using an AEI MS-9 or MS-50 mass spectrometer. Both instruments were operated at an ionizing potential of 70 eV. The silica gel used was obtained from E. Merck and that used for thin-layer chromatography (tlc) was the grade PF_{254}, whilst that used for column chromatography was the grade finer than

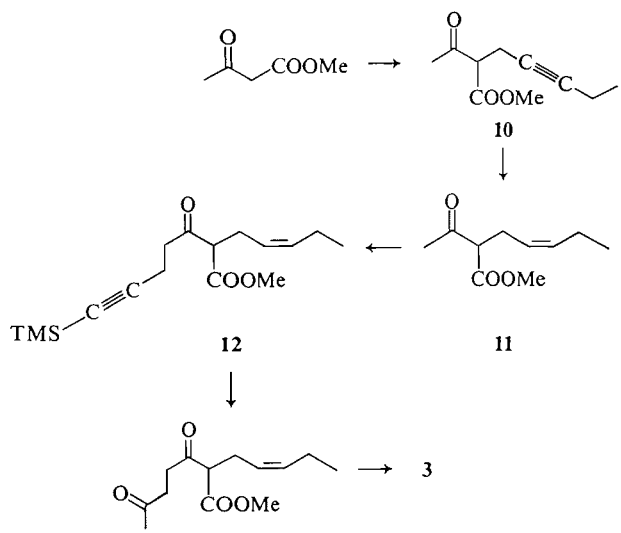

SCHEME 2. Synthesis of jasmone (**3**).

[3]For a review of the numerous syntheses of jasmones see ref. 6 for those published before 1974, ref. 11 for those published between 1974 and 1977, and ref. 12 for some recent syntheses.

Can. J. Chem. Downloaded from www.nrcresearchpress.com by 210.87.254.5 on 09/05/12
For personal use only.

200 mesh ASTM. Elemental microanalyses were performed by Mr. Peter Borda, University of British Columbia.

Methyl 2-Acetylheptanoate (7)

Methyl acetoacetate (5.80 g, 0.050 mol) was alkylated with sodium methoxide, prepared from dry methanol and sodium (1.25 g, 0.050 mol), and 1-bromopentane (8.15 g, 0.054 mol) in refluxing dry methanol (ca. 125 ml) to yield 5.4 g (58%) of keto ester **7**, bp 68°C/0.9 Torr: ir: 1710 and 1740 cm^{-1}; nmr δ: 0.7–1.1 (m, 3H), 1.1–1.5 (bd m, 6H), 1.6–2.1 (m, 2H), 2.18 (s, 3H), 3.37 (t, J = 7 Hz, 1H), and 3.68 (s, 3H); ms (*a*): high resolution calcd. for $C_{10}H_{18}O_3$: 186.1244 amu; found: 186.1241; (*b*) low resolution *m/e* (relative intensity): 43 (96), 55 (28), 87 (90), 101 (58), 116 (100), 117 (20), 129 (16), 144 (64), 155 (12), 186 (8). *Anal.* calcd. for $C_{10}H_{18}O_3$: C 64.49, H 9.74; found: C 64.38, H 9.70.

6-Carbomethoxy-1-trimethylsilyl-1-undecyn-5-one (8)

The ester **7** (0.93 g, 0.0050 mol) was dissolved in dry tetrahydrofuran (THF) and treated with 0.27 g of sodium hydride, which was washed with dry THF, and 3.12 ml of 1.6 *M* *n*-butyllithium all at 0°C. The resulting dianion was alkylated with 0.98 g (0.0052 mol) of 3-bromo-1-trimethylsilyl-1-propyne (9). After stirring for 2 h at 0°C the reaction mixture was quenched with saturated ammonium chloride, extracted with ethyl ether (Et_2O), washed with brine, and dried over sodium sulfate. The solvents were removed under reduced pressure to yield 1.6 g of crude **8** which was homogeneous by chromatography and spectroscopy. This crude compound **8** was used directly in the next step and the compound was characterized by the following data: ir: 1715, 1740, and 2195 cm^{-1}; nmr δ: 0.25 (s, 9H), 0.8–1.2 (m, 3H), 1.2–1.6 (m, 6H), 1.7–2.1 (m, 2H), 2.5–3.0 (m, 4H), 3.5 (m, 1H), and 3.73 (s, 3H); ms (*a*) high resolution calcd. for $C_{16}H_{28}O_3Si$: 296.1804 amu; found: 296.1803; (*b*) low resolution *m/e* (relative intensity): 41 (20), 43 (28), 55 (24), 73 (96), 89 (42), 139 (30), 153 (100), 154 (15), 169 (18), 195 (14), 209 (10), 211 (10), 221 (8), 223 (7), 225 (11), 236 (8), 237 (11), 249 (11), 265 (9), 281 (68), 296 (3).

6-Carbomethoxy-2,5-undecanedione (9)

A solution of 0.16 g of mercuric oxide (HgO) in 0.26 ml of concentrated sulphuric acid and 6 ml water was added to 100 ml THF and warmed to ca. 60°C. A solution of 2.96 g of crude acetylene **8** in 10 ml of THF was added to the mercuric oxide solution. This resulting solution was cooled and was stirred at ca. 40°C for 2 h. The reaction mixture was quenched with water and extracted with Et_2O. The extracts were dried over sodium sulfate and the solvents removed under reduced pressure. The crude oil was distilled at 118°C/0.4 Torr to yield 1.91 g (79% from **7**) of diketo ester **9**: ir: 1715 and 1740 cm^{-1}; nmr δ: 0.7–1.0 (m, 3H), 1.1–1.5 (m, 6H), 1.7–2.0 (m, 2H), 2.15 (s, 3H), 2.72 (bd s, 4H), 3.45 (t, J = 7 Hz, 1H), and 3.68 (s, 3H); ms (*a*) high resolution calcd. for $C_{13}H_{22}O_4$: 242.1503 amu; found: 242.1506; (*b*) low resolution *m/e* (relative intensity): 43 (50), 55 (14), 71 (10), 87 (10), 99 (100), 140 (11), 172 (20), 211 (5), 242 (0.1). *Anal.* calcd. for $C_{13}H_{22}O_4$: C 64.44, H 9.15; found: C 64.33, H 9.25.

Dihydrojasmone (4)

A solution of 0.24 g (0.0010 mol) of diketo ester **9** in 8 ml of 3% aqueous sodium hydroxide was stirred at ca. 70°C for 5½ h. After cooling to room temperature, the reaction mixture was acidified to pH 4 with 25% aqueous sulfuric acid and extracted with Et_2O. The extracts were dried over magnesium sulfate and the solvents removed under reduced pressure. The crude yellow oil was distilled (Kugelrohr) at 85°C/0.4 Torr to yield 0.12 g (72%) dihydrojasmone (**4**) which was homogeneous by tlc analysis and had spectral data identical to that of an authentic sample of dihydrojasmone.

Methyl 2-Acetyl-4-heptynoate (10)

A 1.8 g sample of KH in mineral oil (ca. 0.010 mol) was washed with dry THF and suspended in 25 ml dry THF. Then 1.16 g (0.010 mol) of methyl acetoacetate was added and the solution of the monoanion was cooled to 0°C and alkylated with 1.75 g (0.012 mol) of 1-bromo-2-pentyne (13). The reaction mixture was stirred at room temperature for 4 h, diluted with Et_2O, washed with water, and dried. The solvents were removed under reduced pressure and the alkylated ester **10** distilled at 78°C/0.1 Torr to yield 1.27 g (70%) of product: ir: 1715, 1740, and 2275 cm^{-1}; nmr δ: 1.07 (t, J = 7 Hz, 3H), 1.8–2.3 (m, 2H), 2.27 (s, 3H), 2.4–2.8 (m, 2H), 3.60 (t, J = 7 Hz, 1H) and 3.72 (s, 3H); ms (*a*): high resolution calcd. for $C_{10}H_{14}O_3$: 182.0922 amu; found: 182.0918; (*b*) low resolution *m/e* (relative intensity): 43 (60), 79 (22), 106 (23), 123 (15), 139 (100), 140 (10), 151 (6), 167 (2), 182 (4). *Anal.* calcd. for $C_{10}H_{14}O_3$: C 65.92, H 7.74; found: C 66.21, H 7.87.

Z-Methyl 2-Acetyl-4-heptenoate (11)

A mixture of 3.64 g (0.20 mol) of acetylene **10**, 0.12 g of 5% Pd on barium sulfate (14), and 6 drops of distilled quinoline in 125 ml dry methanol (MeOH) was hydrogenated at atmospheric pressure. After ca. 1 h 1 equiv. of hydrogen was absorbed, the mixture was filtered, and the MeOH was removed under reduced pressure. The crude product was dissolved in Et_2O, and washed with aqueous acid and brine. The ethereal solution was dried over magnesium sulfate and the solvents removed under reduced pressure. The crude product was distilled at 75°C/0.1 Torr to yield 3.26 g (89%) alkene **11**: ir: 1710 and 1740 cm^{-1}; nmr δ: 0.95 (t, J = 7 Hz, 3H), 1.7–2.2 (m, 2H), 2.22 (s, 3H), 2.57 (m, 2H), 3.43 (t, J = 7 Hz, 1H), 3.70 (s, 3H), and 4.9–5.6 (m, 2H); ms (*a*): high resolution calcd. for $C_{10}H_{16}O_3$: 184.1096 amu; found: 184.1095; (*b*): low resolution *m/e* (relative intensity): 43 (100), 68 (45), 81 (33), 95 (25), 109 (30), 125 (15), 137 (7), 141 (85), 152 (10), 166 (5), 184 (10). *Anal.* calcd. for $C_{10}H_{16}O_3$: C 65.19, H 8.75; found: C 65.37, H 8.67.

Z-6-Carbomethoxy-1-trimethylsilyl-8-undecen-1-yn-5-one (12)

The ester **11** (1.84 g, 0.010 mol) was dissolved in dry THF and treated with 0.55 g of oil-free sodium hydride and 4.8 ml of 2.1 *M* *n*-butyllithium at 0°C. The resulting dianion was alkylated with 2.28 g (0.012 mol) of 3-bromo-1-trimethylsilyl-1-propyne (9). This reaction mixture was stirred at 0°C for 3 h and then at room temperature for 2 h. The reaction was quenched with saturated ammonium chloride, extracted with Et_2O, washed with brine, and dried over sodium sulfate. The solvents were removed under reduced pressure to yield 3.00 g of crude **12** which was used directly in the next step. The alkylation product **12** was homogeneous by chromatography and it was characterized by the following spectral data: ir: 1720, 1745, and 2200 cm^{-1}; nmr δ: 0.20 (s, 9H), 1.00 (t, J = 7 Hz, 3H), 1.8–2.9 (m, 8H), 3.53 (t, J = 7 Hz, 1H), 3.70 (s, 3H), and 5.1–5.7 (m, 2H); ms (*a*): high resolution calcd. for $C_{16}H_{23}O_3Si$: 294.1641 amu; found: 294.1636; (*b*): low resolution *m/e* (relative intensity): 41 (40), 43 (40), 73 (100), 89 (26), 141 (35), 193 (11), 235 (22), 279 (10), 294 (3).

Z-6-Carbomethoxy-8-undecen-2,5-dione (13)

The crude trimethylsilylalkyne **12** (1.47 g, 0.0050 mol) was hydrolyzed with HgO (0.076 g) in sulfuric acid, water, and THF under the same conditions as those reported above for the hydrolysis of **8**. The crude product was distilled (Kugelrohr) at 125°C/0.5 Torr and chromatographed on silica gel tlc plates (solvent: CCl_4–Et_2O 4:1) to yield 1.2 g (80%) of dione **13** which had the following spectral properties: ir: 1715 and 1745 cm^{-1}; nmr δ: 0.93 (t, J = 7 Hz, 3H), 1.7–2.2 (m, 2H), 2.17 (s, 3H), 2.57 (m, 2H), 2.73 (br s, 4H), 3.52 (t, J = 7 Hz, 1H), 3.70 (s, 3H), and 5–5.7 (m, 2H); ms (*a*): high resolution calcd. for $C_{13}H_{20}O_4$: 240.1376 amu; found: 240.1373; (*b*): low

resolution *m/e* (relative intensity): 41 (33), 43 (100), 81 (25), 99 (90), 109 (50), 127 (29), 129 (18), 141 (71), 151 (21), 172 (10), 183 (15), 190 (13), 208 (10), 209 (11), 222 (18), 240 (10). *Anal.* calcd. for $C_{13}H_{20}O_4$: C 64.98, H 8.39; found: C 64.70, H 8.45.

Jasmone (3)

A sample of 0.48 g (0.0020 mol) of diketo ester **13** was hydrolyzed and cyclized with 16 ml of 3% aqueous sodium hydroxide using the same procedure as that used in the synthesis of dihydrojasmone (**4**) above. The crude product was distilled (Kugelrohr) to yield 0.28 g (85%) of jasmone (**3**) which was homogeneous by tlc analysis and had spectral data identical to that of an authentic sample of jasmone.

Acknowledgements

We are grateful to the National Research Council of Canada and the University of British Columbia for financial support of this work.

1. (*a*) S. N. Huckin and L. Weiler. J. Am. Chem. Soc. **96**, 1082 (1974); (*b*) L. Weiler. J. Am. Chem. Soc. **92**, 6702 (1970).
2. (*a*) J. E. Baldwin. J. Chem. Soc. Chem. Commun. 734 (1976); (*b*) J. E. Baldwin and L. T. Kruse. J. Chem. Soc. Chem. Commun. 233 (1977).
3. (*a*) P. E. Sum. M.Sc. Thesis, University of British Columbia, Vancouver, B.C. 1976; (*b*) T. A. Bryson. J. Org. Chem. **38**, 3428 (1973).
4. J. T. Adams, R. Levine, and C. R. Hauser. Organic Syntheses. Coll. Vol. III. John Wiley and Sons, New York, NY. 1955. p. 405.
5. G. R. Rickards. M.Sc. Thesis, University of British Columbia, Vancouver, B.C. 1977.
6. (*a*) R. A. Ellison. Synthesis, 397 (1973); (*b*) T. L. Ho. Syn. Commun. **4**, 265 (1974).
7. R. M. Jacobson, R. A. Raths, and J. W. McDonald III. J. Org. Chem. **42**, 2545 (1977).
8. A. E. Greene, J. C. Muller, and G. Ourisson. J. Org. Chem. **39**, 186 (1974).
9. R. B. Miller. Syn. Commun. **2**, 267 (1972).
10. (*a*) G. W. Stacy and R. A. Mikulec. Organic Syntheses. Coll. Vol. IV. John Wiley and Sons, New York, NY. 1963. p. 13; (*b*) D. A. McCrae and L. Dolby. J. Org. Chem. **42**, 1607 (1977).
11. T. L. Ho. Syn. Commun. **7**, 351 (1977).
12. (*a*) A. E. Greene and P. Crabbé. Tetrahedron Lett. 4867 (1976); (*b*) P. Bakuzis and M. L. F. Bakuzis. J. Org. Chem. **42**, 2362 (1977); (*c*) S. Torii, W. Tanaka, and Y. Kobayasi. J. Org. Chem. **42**, 3473 (1977); (*d*) W. J. Manteiro. J. Org. Chem. **42**, 2324 (1977); (*e*) S. Takano, T. Sugahara, M. Isgiguro, and K. Ugasawara. Heterocycles, **6**, 1141 (1977); (*f*) S. Torii, W. Tanaka, and Y. Tomotaki. Bull. Chem. Soc. Jpn. **50**, 537 (1977); (*g*) E. Keinan and Y. Mazen. J. Am. Chem. Soc. **99**, 3861 (1977); (*h*) W. C. Still. J. Am. Chem. Soc. **99**, 4836 (1977).
13. K. E. Schulte and W. Engelhardt. Arch. Pharm. **287**, 495 (1954).
14. R. Mozingo. Organic Syntheses. Coll. Vol. III. John Wiley and Sons, New York, NY. 1955. p. 685.

Can. J. Chem. Downloaded from www.nrcresearchpress.com by 210.87.254.5 on 09/05/12
For personal use only.

Concerning the spectra and solvation process of electrons in liquid butanols[1]

KIYOSHI OKAZAKI AND GORDON R. FREEMAN

Chemistry Department, University of Alberta, Edmonton, Alta., Canada T6G 2G2

Received February 27, 1978

KIYOSHI OKAZAKI and GORDON R. FREEMAN. Can. J. Chem. **56**, 2305 (1978).

The optical absorption spectra of electrons injected into the isomeric butanols settle into that of the equilibrium solvated state at rates that decrease in the order 1-butanol > isobutyl alcohol > 2-butanol at a given temperature. The relative rates reflect the dipolar reorientation times in the liquids. The Arrhenius temperature coefficients of the rates of spectral changes are ~30 kJ/mol. The distribution of dipolar reorientation times overlaps that of geminate reaction times of the charges in an irradiated alcohol, so a significant fraction of the electrons undergoes geminate reaction before they are able to become fully solvated. At $T < 200$ K the fraction increases with decreasing temperature. The concurrence of the solvation process and geminate reaction implies that the former involves, at least in part, electron migration from shallower to deeper traps.

There is an indication of structure in the absorption band at low temperatures and short times. The infrared peak converts to one with a maximum at ~780 nm. The latter slides gradually into the shape of the spectrum of the equilibrium solvated state.

For the spectra of the equilibrium solvated state, the energies at the absorption maxima are given by $E_{\varepsilon_{max}}$ (eV) = 3.10 − 0.0038T in isobutyl alcohol and 2.93 − 0.0044T in 2-butanol, between 170 and 300 K. The respective band widths at half heights are 1.53 ± 0.04 and 1.59 ± 0.04 eV, independent of temperature within an uncertainty of 1 meV/K.

KIYOSHI OKAZAKI et GORDON R. FREEMAN. Can. J. Chem. **56**, 2305 (1978).

Les spectres d'absorption optique d'électrons injectés dans des butanols isomères à une température donnée se stabilisent dans l'état solvaté, en équilibre thermique avec le milieu à des vitesses qui décroissent dans l'ordre butanol-1 > l'alcool isobutylique > butanol-2. Les vitesses relatives sont un reflet des temps de réorientation dipolaire dans les liquides. Les coefficients de température d'Arrhénius pour les vitesses des changements dans les spectres sont ~30 kJ/mol. Les distributions des temps de réorientation dipolaire recouvrent celles des temps de réaction géminée de charge dans un alcool irradié, ce qui implique qu'une fraction importante des électrons subit une réaction géminée avant d'être capable de devenir complètement solvatée. A une température plus basse que 200 K, la fraction augmente avec une diminution de la température. Le fait que le processus de solvatation et la réaction géminée se produisent d'une façon concurrente implique que le premier processus comporte au moins en partie une migration d'électrons d'un piège peu profond vers d'autres plus profonds.

Il existe une indication de structure dans la bande d'absorption à basses températures et à temps courts. La bande infrarouge se transforme en une avec un maximum à environ 780 nm. Cette dernière se déplace graduellement pour prendre la forme du spectre de l'état solvaté en équilibre thermique avec le milieu.

Les énergies à l'absorption maximum de l'état solvaté sont données par $E_{\varepsilon_{max}}$ (eV) = 3.10 − 0.0038T dans l'alcool isobutylique et 2.93 − 0.0044T dans le butanol-2 entre 170 et 300 K. Les largeurs des bandes à demi-hauteur sont respectivement de 1.53 ± 0.04 et 1.59 ± 0.04 eV et ne dépendent pas de la température, avec une incertitude de 1 meV/K.

[Traduit par le journal]

Introduction

The mechanism of electron energy degradation in irradiated fluids continues to attract interest (1) after many years of investigation (2–8). Events at energies $\gtrsim$10 eV are moderately well understood (1–4). At lower energies indirect information can be obtained from the thermalization ranges of the secondary electrons (4–8). In polar and many nonpolar liquids the electrons ultimately become localized and, through further energy loss processes, settle into the solvated state, which is in thermal equilibrium with the medium. Information about the last step may be obtained by measuring the time dependence of spectral changes that take place as the electrons settle from the initial localized levels into the solvated state (9–13).

In this paper, spectral changes in the optical absorption of electrons in 2-butanol and 2-methyl-1-propanol (isobutyl alcohol) are reported as functions of time and temperature. Reactions of the electrons are also discussed.

Experimental

Materials

The 1-butanol and isobutyl alcohol were spectranalyzed grade from Fisher Scientific Co. The 2-butanol was analytical

[1]Assisted financially by the National Research Council of Canada.

Can. J. Chem. Downloaded from www.nrcresearchpress.com by 210.87.254.105 on 09/05/12
For personal use only.

Can. J. Chem. Downloaded from www.nrcresearchpress.com by 210.87.254.105 on 09/05/12
For personal use only.

reagent grade from BDH Chemical Co. The alcohols were further purified as follows. To 1 ℓ of alcohol was added 1 g of sodium borohydride (Terochem Laboratories Ltd.). The solution was bubbled with UHP argon (Matheson Co.) then heated to ~70°C with the argon continuing to flow. This caused a gentle refluxing, which was continued for ~20 h. The alcohol was then distilled through an 85 × 2 cm column packed for 65 cm with 3 mm id glass helices. The alcohol was collected and stored under argon.

Techniques

Alcohol was transferred to the Spectrosil cell (Thermal Syndicate Ltd., optical path 1.35 cm) with a syringe, then bubbled for 20 min with UHP argon. The cell was then sealed with a flame by a technique that prevented alcohol vapor from contacting the hot glass (14).

The radiation was a 100 ns pulse of 1.7 MeV electrons, delivering a dose of 2×10^{16} eV/g. Dosimetry was by oxygen-saturated aqueous KSCN (15).

The optical system and the visible light detector were described in ref. 16, and the uv detector in ref. 15. The response time of the visible light measurement system was determined by comparing the Čerenkov light signal with the known shape of the electron pulse (measured by charge collection on a gold target, response time < 10 ns). The total rise plus fall time of the visible light system was 200 ns for a 100 ns square pulse. The 3–97% rise time for a 10 ns wide step function was 100 ± 10 ns. The latter for the uv measurement system was 70 ns with the 5 MHz filter and 15 ns at full bandwidth.

Results

The optical absorption signals were of the types illustrated in Figs. 3 and 13 of ref. 16. Semilog plots of the absorbance against time after a pulse were often of the type shown in Fig. 17 of ref. 16; the decay became first order after an initial growth or decay of complex order.

To emphasize processes that occur on the low energy side of the absorption spectrum, $G\varepsilon$ is plotted against wavelength, λ (nm) = 1240/$h\nu$ (eV). The quantity $G\varepsilon$ is the product of the electron yield G (electrons/100 eV absorbed) and the decadic molar absorbance ε (M^{-1} cm^{-1}).

The response characteristics of the measuring circuit were such that the optical absorption signal reached a maximum ~150 ns after the start of the 100 ns pulse, when decay after the pulse was fast. This was therefore the shortest time at which spectra were recorded. Signal growth and decay kinetics were complex at short times, so no corrections were made to the measured absorbances.

The freezing point of 1-butanol (184 K) is higher than those of 2-butanol (158 K) and isobutyl alcohol (165 K). The absorption spectrum of electrons in 1-butanol reached its equilibrium shape within the 150 ns resolution time of the measurement at all temperatures down to the freezing point. This means that relaxation of the electrons into the solvated state could not be followed as a function of time in 1-butanol, so experiments with that alcohol were not pursued.

2-Butanol

Optical absorption spectra taken 150 ns after the beginning of the 100 ns pulse are shown in Fig. 1. Time was measured from the beginning of the pulse because that was the only consistent anchor point at all wavelengths. At $T \geq 211$ K the observed spectrum decayed uniformly at all wavelengths, which means that the electrons had relaxed to the equilibrium solvated state within the resolution time of the measurement. The wavelength at the absorption maximum, $\lambda_{G\varepsilon max}$, decreased and the value of $G\varepsilon$ at the peak, $(G\varepsilon)_{max}$, increased with decreasing temperature down to 211 K (Fig. 1). On going from 211 to 183 K the spectrum shift reversed to a larger $\lambda_{G\varepsilon max}$ and lower $(G\varepsilon)_{max}$ (Fig. 1). However, the spectrum at 183 K shifted with time to lower wavelengths and at 2 μs had reached a steady state location and shape with $\lambda_{G\varepsilon max} = 590$ nm and $(G\varepsilon)_{max} = 2.08 \times 10^4$ electrons/100 eV M cm. Thus $\lambda_{G\varepsilon max}$ for the steady state spectrum continued to decrease with temperature, but $(G\varepsilon)_{max}$ passed through an extremum.

Changes in the spectrum shape with time were more clearly measurable at lower temperatures. At 171 K there were two absorption peaks at 150 ns; one at ~920 nm and another at ~800 nm (Fig. 2). The peak at 920 nm decayed rapidly, while the other grew and shifted to lower wavelengths. After 1 μs the change at 920 nm was 80% of the way towards the complete solvation value and the peak was at ~700 nm. This was followed by a slower settling of the long wavelength side of the band towards that of equilibrium solvated electrons, while the short wavelength side changed only slightly (Fig. 2). The equilibrium spectrum had $\lambda_{G\varepsilon max} = 565$ nm.

At 162 K the absorption band at 150 ns contained

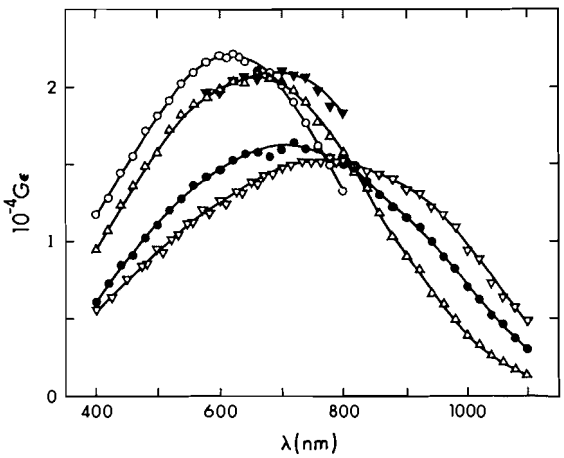

FIG. 1. Optical absorption spectrum of localized electrons in 2-butanol at several temperatures, 150 ns after the start of the 100 ns radiation pulse. $G\varepsilon$ has units of electrons/100 eV M cm. ▽, 299 K; ●, 271 K; △, 240 K; ○, 211 K; ▼, 183 K. The spectra at $T \geq 211$ K are of the equilibrium solvated state.

Can. J. Chem. Downloaded from www.nrcresearchpress.com by 210.87.254.105 on 09/05/12
For personal use only.

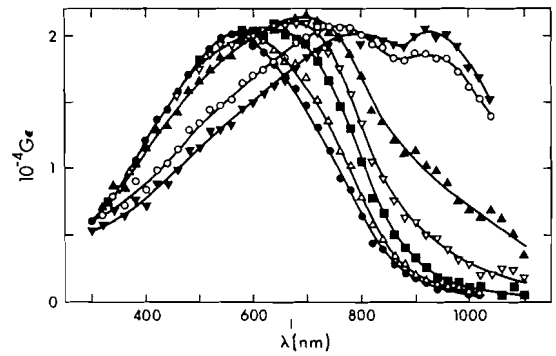

FIG. 2. Absorption spectrum of localized electrons in 2-butanol at 171 K at several times after the start of the 100 ns pulse. The times (μs) are: ▼, 0.15; ○, 0.20; ▲, 0.50; ▽, 1.0; ■, 2.0; △, 5.0; ●, 10.

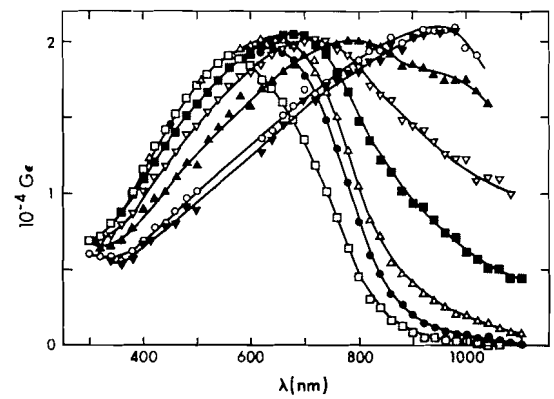

FIG. 3. Absorption spectrum of localized electrons in 2-butanol at 162 K at several times after the start of the 100 ns pulse. The times (μs) are: ▼, 0.15; ○, 0.20; ▲, 0.50; ▽, 1.0; ■, 2.0; △, 5.0; ●, 10; □, 45.

only one peak, at ~960 nm (Fig. 3). As at 171 K, decay of the long wavelength absorption caused growth of the absorption at shorter wavelengths, with a band maximum at ~700 nm after 2 μs. There was then a slower decay of the long wavelength side of the band with relatively little increase of absorption at shorter wavelengths. The time required for the latter decay at 162 K was three- to fourfold longer than that at 171 K, indicating an Arrhenius temperature coefficient of ~30 kJ/mol. The rates of rapid growth at 500 nm and decay at 1000 nm also displayed Arrhenius temperature coefficients of ~30 kJ/mol.

Comparison of Figs. 2 and 3 indicates that the double peak at 150 ns and 171 K is due to spectral shifts that occurred during the 150 ns resolution time.

Isobutyl Alcohol

Spectra recorded 150 ns after the start of the 100 ns pulse in isobutyl alcohol at 299, 243, and 212 K are shown in Fig. 4. The spectra decayed with equal

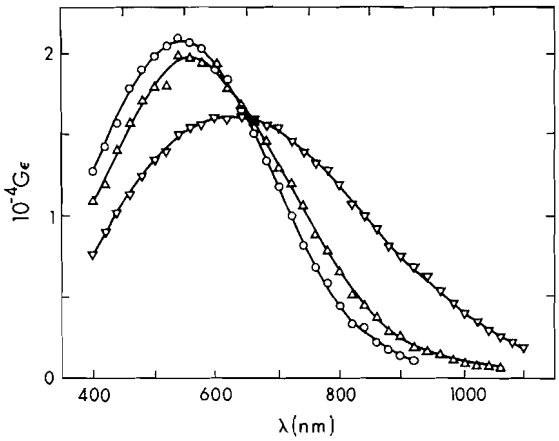

FIG. 4. Absorption spectrum of solvated electrons in isobutyl alcohol at several temperatures, 150 ns after the start of the 100 ns radiation pulse. ▽, 299 K; △, 243 K; ○, 212 K.

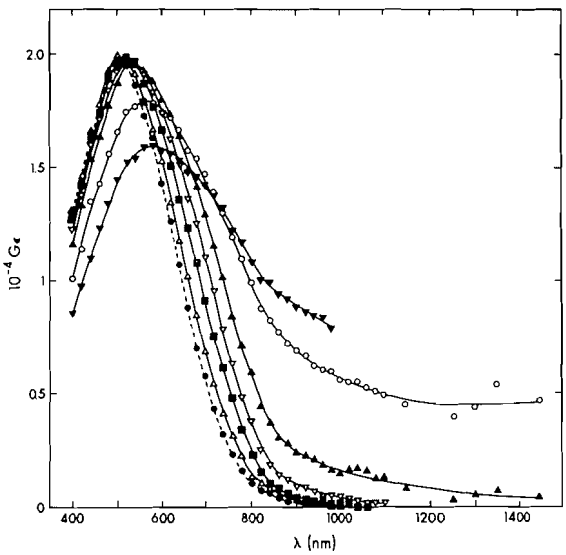

FIG. 5. Absorption spectrum of localized electrons in isobutyl alcohol at 167 K at several times after the start of the 100 ns pulse. The times (μs) are: ▼, 0.15; ○, 0.20; ▲, 0.50; ▽, 1; ■, 2; △, 5; ●, 10.

relative rates at all wavelengths, so correspond to absorption by the equilibrium solvated state. $(G\varepsilon)_{max}$ increased and $\lambda_{G\varepsilon max}$ decreased monotonically with decreasing temperature.

At 183 K the spectrum decayed at long wavelengths and grew at short wavelengths until the equilibrium shape was reached at 1 μs. The spectrum then decayed uniformly at all wavelengths. The equilibrium shape was attained approximately twofold more quickly in isobutyl alcohol than in 2-butanol at the same temperature.

At 167 K the equilibrium shape was attained in ~7 μs (Fig. 5), indicating an Arrhenius tempera-

Can. J. Chem. Downloaded from www.nrcresearchpress.com by 210.87.254.105 on 09/05/12
For personal use only.

ture coefficient of ~30 kJ/mol for the relaxation process.

Discussion

The changes in the optical absorption band of electrons with time in these butanols may be divided into two periods: (*a*) decay of the infrared end and growth of the blue end of the initial band, culminating in the spectrum of the equilibrium solvated state; (*b*) uniform decay of the solvated state spectrum.

(*a*) *Transformation of the Initial Spectrum*

The distribution of times required for dipolar reorientation about the newly created charges in an irradiated alcohol intersects that of the geminate reaction times of the charges (17–20). The reaction rates of the charges are altered by the polarization of the medium that surrounds them, and are therefore affected by the time dependence of the polarization (17–20). It was expected that the changes in polarization about the localized electron would create a time dependence of its optical absorption spectrum, and such was found to be the case (21–24).

The dipolar orientation times are smaller than the principal dielectric relaxation times τ_1 measured at constant field (25) due to: (*a*) the fact that relaxation occurs in the presence of constant charge rather than constant field (17); (*b*) the torque provided by the charge–dipole interaction (18, 19); and (*c*) the nullification by the excess electron of hydrogen bonds in its vicinity. There is a fair correlation between the spectral shift times (11, 26, 27) and the intermediate dielectric relaxation time τ_2 in the alcohols at room temperature (25), but the correlation is less good at low temperatures (9, 12).

The rate of decay of the optical absorption at 1040 nm in the butanols is about half the rate of approach to the maximum absorption at $\lambda \leq \lambda_{G\varepsilon max}$ (Fig. 6). This agrees with the observations of Chase and Hunt (11) for electrons in ethanol, 1-propanol, and 1-butanol. They observed that the rate of decay at 1300 nm equalled the rate of approach to the maximum absorption at 600 nm. The observed decay or growth rate at a given wavelength is the difference between the true decay rate and the rate of formation of that state from other states. If the equality of the rates of decay at 1300 nm and remaining growth at 600 nm is not a coincidence, the decay rate at a longer wavelength, say 1600 nm, should equal that at 1300 nm. This would imply that the same state absorbs at 1600 and 1300 nm. The longer apparent decay time at 1040 nm indicates that an intermediate state absorbs at this wavelength; the state is formed from those that absorb at longer wavelengths and decays to others that absorb at shorter wavelengths. Present equipment is not adequate to test the hypothesis at 1300 and 1600 nm.

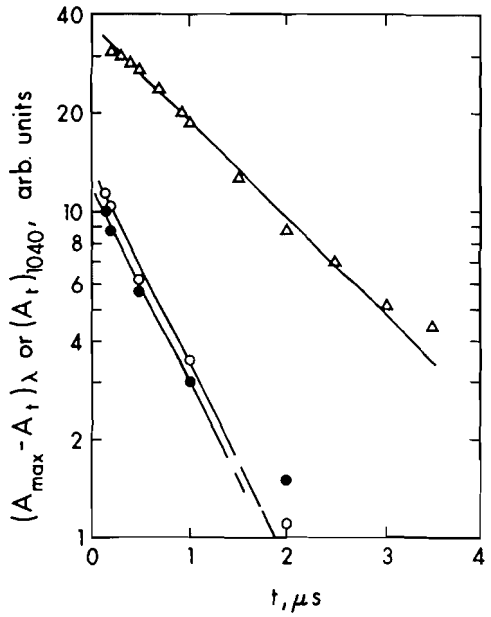

FIG. 6. Decay of absorbance A_t at λ = 1040 nm (△) and remaining growth of absorbance at λ = 560 nm (○) and 450 nm (●) in 2-butanol at 162 K. The remaining growth is a measure of the approach to the maximum absorbance at that wavelength $(A_{max} - A_t)_\lambda$. Time is measured from the beginning of the 0.10 μs pulse. $\lambda_{G\varepsilon max}$ = 560 nm for the equilibrium solvated state.

Another contribution to the wavelength dependent kinetics might be a decrease of the decay rate with increasing depth of the electron trap (28).

Changes in absorbance with time at different wavelengths are shown in Fig. 7 for electrons in 2-butanol at several temperatures. The final band maximum occurs at 560–590 nm at all these temperatures. At $\lambda \leq \lambda_{G\varepsilon max}$ there is growth due to the shift in spectrum, followed by decay due to reaction of the electrons. At ~700 nm there is growth due to the spectral shift, followed by decay due to further spectral shift and to reaction. At λ > 900 nm on the timescale of the present experiments there is only decay, attributed to both spectral shift and reaction.

Behavior is similar for electrons in isobutyl alcohol, although the data for that solvent are more limited (Fig. 8).

Solvation Time τ_s

The time required for newly injected electrons to attain the equilibrium solvated state may be characterized approximately by the time τ_s in eq. [1] for $\lambda \leq \lambda_{G\varepsilon max}$:

$$[1] \qquad (A_{max} - A_t)_\lambda = (A_{max} - A_0)_\lambda \, e^{-t/\tau_s}$$

where A_0 and A_t are the optical absorbances at times

Can. J. Chem. Downloaded from www.nrcresearchpress.com by 210.87.254.105 on 09/05/12
For personal use only.

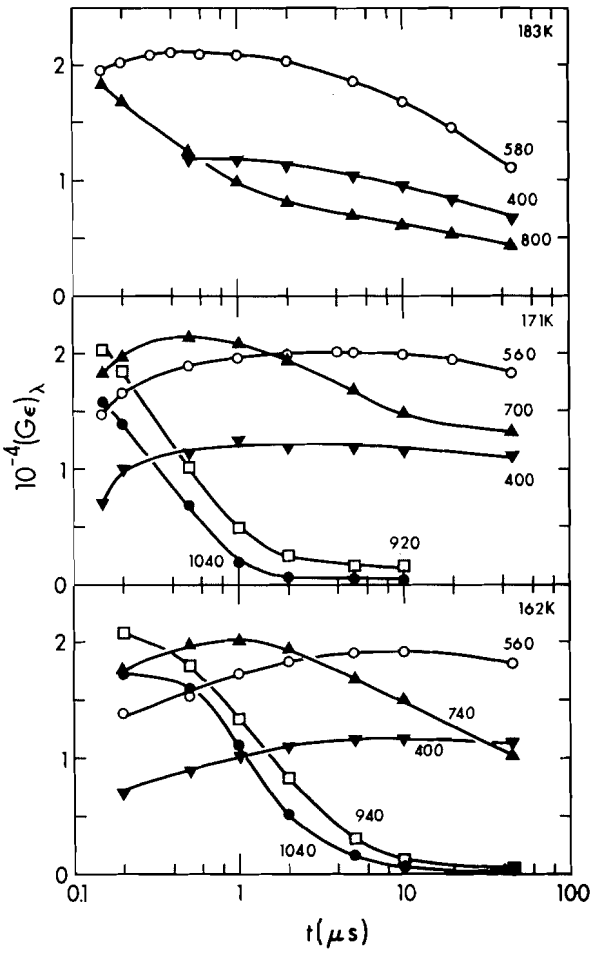

FIG. 7. Time dependence of $(G\varepsilon)_\lambda$ for electrons in 2-butanol at several temperatures. The units of $G\varepsilon$ are (100 eV M cm)$^{-1}$. The wavelengths λ (nm) are indicated on the curves. The values of $\lambda_{G\varepsilon max}$ for the equilibrium solvated state are 590 nm at 183 K, 565 nm at 171 K, and 560 nm at 162 K.

zero and t, respectively, and A_{max} is the maximum attained at that wavelength (see Fig. 7, where $G\varepsilon$ may be substituted for A). The plot of eq. [1] for electrons in 2-butanol at 162 K in Fig. 6 gives $\tau_s = 0.73$ μs. Other values of τ_s obtained in this way for 2-butanol and isobutyl alcohol are shown in Fig. 9.

The time τ_d required for the absorbance at 1000 nm to decay to e^{-1} of its maximum value is about double the τ_s value measured at $\lambda < \lambda_{G\varepsilon max}$ (Fig. 9).

Values of the intermediate dielectric relaxation time τ_2 fall in the order isobutyl alcohol > 1-butanol (29), but the value for 2-butanol is not available. However, the relative values of the principal relaxation time τ_1 are in the order 2-butanol > isobutyl alcohol > 1-butanol (29), so one may assume that τ_2 is also greatest for the 2-isomer. Recalling that τ_s

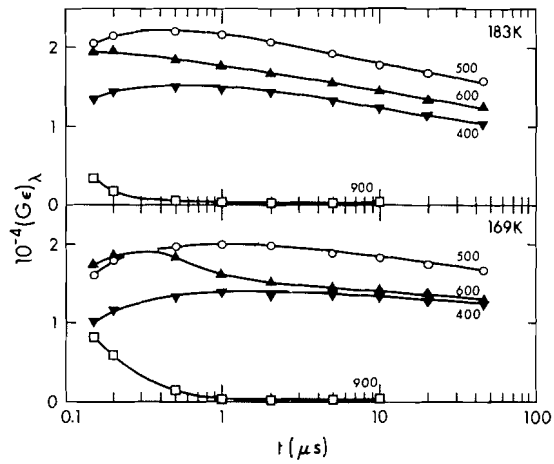

FIG. 8. Time dependence of $(G\varepsilon)_\lambda$ for electrons in isobutyl alcohol at 169 K and 183 K. The wavelengths λ (nm) are indicated on the curves. The values of $\lambda_{G\varepsilon max}$ for the equilibrium solvated state are 515 nm at 183 K and ~505 nm at 169 K.

was too short to measure in 1-butanol with the present system, the previously mentioned correlation between the values of τ_2 and τ_s exists also for the isomeric butanols (Fig. 9). We pick τ_2 simply because it is smaller than τ_1 not because one would expect τ_s to equal τ_2. The temperature dependence of τ_s is similar but not equal to that of τ_2 (Fig. 9).

There is a question about whether the shift of the spectrum is due to dipolar reorientation about a localized electron site, or whether the electron migrates from shallower to deeper traps (12, 23, 30). Both processes are probably involved, because they would be interconnected in a polar liquid. The migration mechanism would be accompanied by a certain amount of electron loss due to geminate reaction, especially at very short times, corresponding to small electron–ion separation distances (19, 20). A significant amount of loss occurs in alcohols at low temperatures (12, 19, 20), where the dipole reorientation times are relatively long.

The amount of electron loss by reaction during the spectrum shift was estimated by integration of plots of $G\varepsilon$ against photon energy, assuming the oscillator strength to remain constant during the shift. In 2-butanol at 171 K, most of the decay in the infrared that occurred between 0.2 and 1.0 μs appeared as growth at higher energies. However, comparison of the shape of the spectrum at 150 ns in Fig. 2 with those of electrons in 1-propanol at low temperatures immediately following a 20 ns pulse (Figs. 4 and 5 of ref. 12) indicates that considerable decay had occurred in the infrared of the present spectrum during the response time of the measuring system. Most of the electron loss apparently occurs

Can. J. Chem. Downloaded from www.nrcresearchpress.com by 210.87.254.105 on 09/05/12
For personal use only.

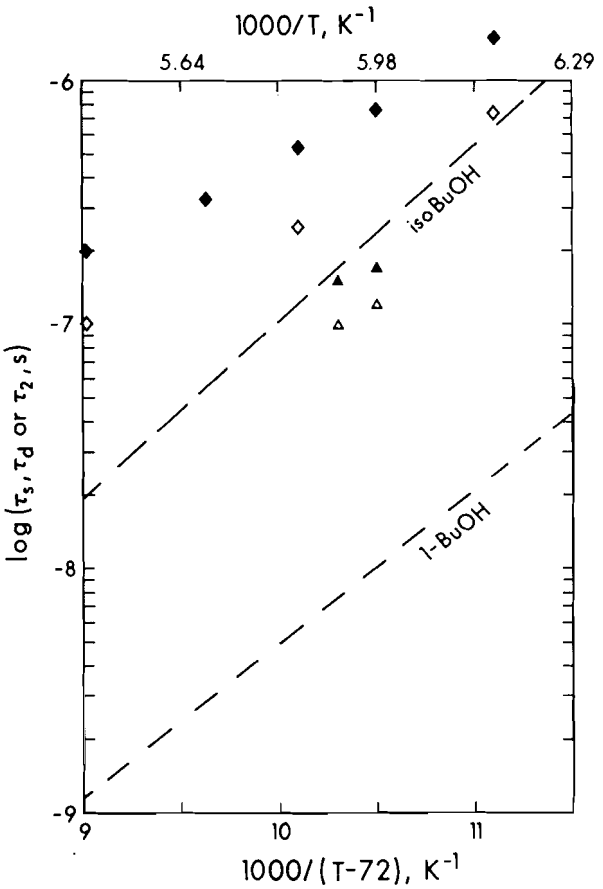

FIG. 9. Electron solvation times τ_s ($\lambda = 500$ nm, open points) and decay times τ_d ($\lambda = 1000$ nm, full points) compared with the second dielectric relaxation times τ_2 (---) in butanols. ◇, ◆, 2-butanol; △, ▲, isobutyl alcohol. The τ_2 lines are labelled and are extrapolations of data for the supercooled liquids (ref. 29). The temperature axis is labelled for both Cole–Davidson and Arrhenius plots.

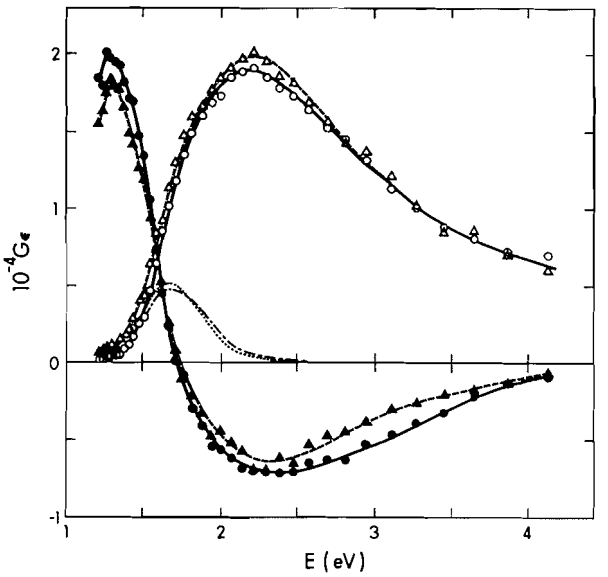

FIG. 10. Comparison of the spectral shift from the infrared to the visible (full points) with the spectrum of the equilibrium solvated state (open points) of extra electrons in liquid 2-butanol. 162 K: ○, equilibrium solvated state spectrum at 45 μs; ····, (10 μs) − (45 μs) subtraction spectrum; ●, (0.2 μs) − (10 μs) subtraction spectrum. 171 K: △, equilibrium state spectrum at 10 μs; ···, (2 μs) − (10 μs) subtraction spectrum; ▲, (0.15 μs) − (2 μs) subtraction spectrum. The small peaks without experimental points represent the shift that occurred during the time gap between the full and open points. Algebraic addition of the three spectra gives the initial spectrum at each temperature.

at very short times (12). At times between 1 and 10 μs (Fig. 2) the red side of the band continued to decay, while the blue side remained virtually unchanged. This is attributed to a continuing blue shift of the spectrum combined with a general loss of electrons to geminate neutralization. The approximate constancy of the blue side of the band between 1 and 10 μs is due to the cancellation of growth from the blue shift and decay by geminate reaction. The rate of decay of the red side is the sum of the rates of the two processes. At times >10 μs the spectrum decays uniformly at all wavelengths and at 45 μs has decreased by 8%.

The behavior was similar in 2-butanol at 162 K, but the timescale was approximately fourfold longer than at 171 K.

The above discussion supports the suggestion of Gilles *et al.* (28) that the equality of the rates of decay at 1300 nm and remaining growth at 600 nm, reported for electrons in ethanol and 1-propanol (11), may be fortuitous. The rate of approach to the maximum $G\varepsilon$ at $\lambda \leq \lambda_{G\varepsilon max}$ gives an upper limit to the solvation rate (lower limit of τ_s).

The spectrum shifts without much electron loss at intermediate times because, for the remaining electrons, fewer diffusion steps are needed to reach a deeper trap than to reach a geminate ion.

Intermediate Spectra

There is an indication of structure in the absorption band of electrons in 2-butanol at low temperatures and short times (Figs. 2 and 3). There is one peak at ~930 nm and another at ~780 nm. The former decays to the latter, and the latter slides gradually into the final shape of the spectrum of the equilibrium solvated state. The two peaks probably indicate two types of electron localization site, the one at longer wavelength involving fewer OH groups in the first coordination sphere. The shifting of the peak at shorter wavelengths corresponds to polarization/migration, as a result of which the electron finds itself in a progressively more polarized site.

Subtraction of a later spectrum from the one at 0.2 μs does not give the spectrum of the species that decayed, because the initial and final bands probably

Can. J. Chem. Downloaded from www.nrcresearchpress.com by 210.87.254.105 on 09/05/12
For personal use only.

overlap. Furthermore, growth in a portion of the original spectrum appears as a negative peak in the subtraction spectrum. The over-all subtraction spectrum illustrates the location and magnitude of the spectral shift. The first spectrum to be subtracted was chosen such that the infrared peak had decayed nearly completely. This corresponded to times of 2 μs at 171 K and 10 μs at 162 K in 2-butanol. The decay and growth that occurred during these periods are shown in Fig. 10. The spectra of the equilibrium solvated state were reached at 10 μs at 171 K and ≥45 μs at 162 K (Fig. 10). The subtraction spectra of the intervening time periods, 2–10 μs at 171 K and 10–45 μs at 162 K, correspond to a relatively small amount of decay in the red and near infrared (Fig. 10). The decays of these small 'subtraction peaks' had Arrhenius temperature coefficients of ~30 kJ/mol.

For a given temperature, summation of the series of subtraction spectra plus the final spectrum gives the initial spectrum.

(b) Decay of the Spectrum of the Solvated State

In isobutyl alcohol at 212 K the optical absorption spectrum reached its equilibrium shape within the 0.15 μs response time of the equipment (Fig. 4). The geminate neutralization reaction in this system continued for more than 50 μs (Fig. 11). Assuming that the dielectric constant of the liquid between a geminate pair of charges attains its static value shortly after the electron reaches its equilibrium state of solvation, the dielectric constant may be taken to be independent of time over the range displayed in Fig. 11. Under these circumstances the rate of the geminate reaction is described by eq. [2] (31).

$$[2] \quad G(e_s^-)_{gi,t} = G(e_s^-)_t - G(e_s^-)_{fi} = Bt^{-1/2}$$

where $G(e_s^-)_{gi,t}$ is the portion of the solvated electron yield surviving at time t that will undergo geminate reaction with ions and radicals in spurs, and it is assumed that the portion that will become free ions, $G(e_s^-)_{fi}$, does not react appreciably on this timescale; B is a proportionality constant. However, in the present systems the solvated electrons undergo a pseudo first order reaction with impurities or the solvent on a timescale that overlaps the tail of the geminate reaction, so one may write:

$$[3] \quad G(e_s^-)_t = (Bt^{-1/2} + G(e_s^-)_{fi})e^{-kt}$$

where k is the first order rate constant. The curve in Fig. 11 is of this form and has the equation:

$$[4] \quad 10^{-4}G\varepsilon_{540} = (0.55t^{-1/2} + 1.22)\exp(-7.2 \times 10^{-3}t)$$

where t is in μs. The first order half life is 96 μs.

The widths of the absorption bands at half height are $W_{1/2} \approx 1.6$ eV at all temperatures in the liquid butanols (Figs. 1–3), so one may take $\varepsilon_{max} \approx 1.0 \times 10^4\ M^{-1}\ cm^{-1}$ (14, 15). This would give $G(e_s^-)_{fi} = 1.2$ in isobutyl alcohol at 212 K (eq. [4]), and a total solvated electron yield observed at 150 ns of 2.1 (Figs. 4 and 11). The initial ionization yield in a number of organic liquids, including saturated hydrocarbons and alcohols, is $G(e^-)_{init} \approx 5$ (32, 33). Approximately half of the initial ion–electron pairs, therefore, undergo geminate neutralization during the first 150 ns in isobutyl alcohol at 212 K.

One may use similar arguments to estimate the fraction of electrons that undergo geminate neutralization before the equilibrium solvated state is reached at lower temperatures. At $T \leq 183$ K in 2-butanol and isobutyl alcohol the time required to reach the equilibrium state was greater than the response time of the system, so $[G(e_s^-)_{max}\varepsilon_{max}]$ could be measured. This quantity decreases with decreasing temperature (Fig. 12*B*), which indicates that a greater fraction of electrons undergoes geminate reaction before reaching the solvated state as the temperature is lowered. Lowering the temperature slows intermolecular rearrangements in the liquid, and hence the solvation process. Similar observations and conclusions were made earlier for electrons in other polar systems (12, 16, 34, 35).

The decrease in $G(e_s^-)\varepsilon_{max}$ with increasing temperature observed at $T \geq 210$ K (Fig. 12*B*) is due to the increasing amount of geminate reaction that occurs during the 150 ns response time of the measurement.

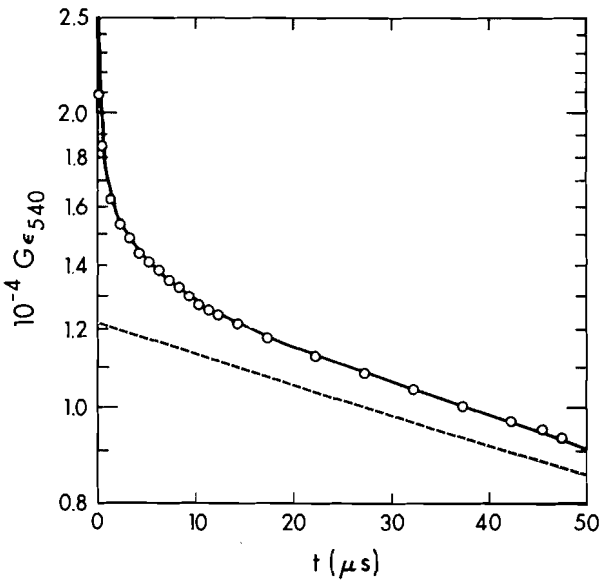

FIG. 11. Decay of the optical absorption at 540 nm of electrons in isobutyl alcohol at 212 K. The full line represents eq. [4]. The dashed line is an extrapolation of the free ion portion from longer to shorter times.

Can. J. Chem. Downloaded from www.nrcresearchpress.com by 210.87.254.105 on 09/05/12
For personal use only.

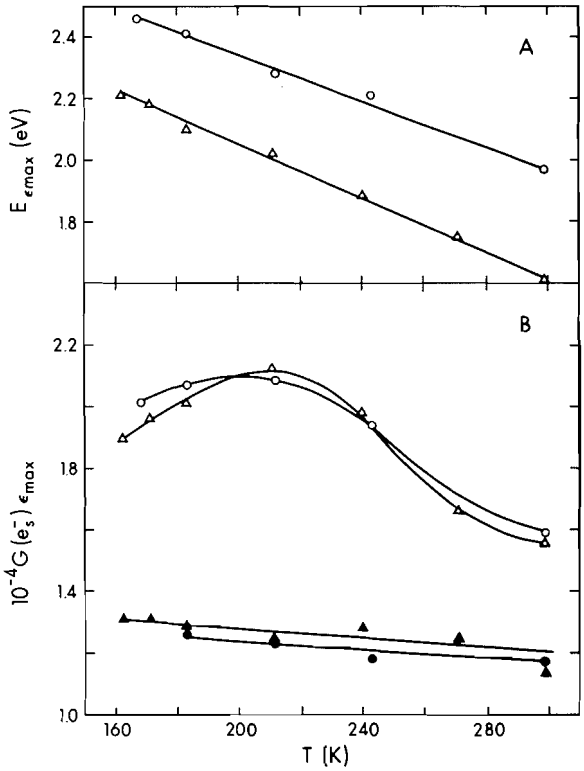

FIG. 12. *A*: Variation of $E_{\epsilon max}$ with temperature, for solvated electrons in isobutyl alcohol (○) and 2-butanol (△). *B*: Variation $G(e_s^-)_{max}\varepsilon_{max}$ (open points) and $G(e_s^-)_{fi}\varepsilon_{max}$ (full points) with temperature in isobutyl alcohol (○, ●) and 2-butanol (△, ▲). At $T > 200$ K the observed values of $G(e_s^-)_{max}\varepsilon_{max}$ are limited by the 150 ns response time of the measurement.

Equations analogous to eq. [4] were used to analyze the decay at each temperature. The values of $G(e_s^-)_{fi}\varepsilon_{max}$ so obtained increased by $\lesssim 10\%$ as the temperature was reduced from 299 to 165 K (Fig. 12*B*).

Temperature Dependence of $E_{\epsilon max}$ *and* $W_{1/2}$

For the spectra of the equilibrium solvated state, the energy at the absorption maximum, $E_{\epsilon max}$, is greater in isobutyl alcohol than in 2-butanol (Fig. 12*A*). The difference may be attributed qualitatively to a difference in the packing of molecules, particularly of H—O—dipoles, around the electron site. The temperature coefficient of $E_{\epsilon max}$ is -3.8 meV/K in isobutyl alcohol and -4.4 meV/K in 2-butanol. The corresponding values in methanol and ethanol are -2.6 and -3.2 meV/K, respectively (14). The magnitude of the coefficient tends to increase with increasing size of the alkyl group.

Within an uncertainty of 1 meV/K the widths of the absorption bands at half height, $W_{1/2}$, are independent of temperature. The values are 1.53 ± 0.04 eV in isobutyl alcohol and 1.59 ± 0.04 eV/K in 2-butanol between 170 and 300 K. The ratio of the portions of the widths on the blue and red sides of the maximum, W_b/W_r, is approximately equal to 1.7 in isobutyl alcohol and 2.3 in 2-butanol, independent of temperature.

1. K. OKAZAKI, M. YAMABE, and S. SATO. Bull. Chem. Soc. Jpn. **50**, 1409 (1977).
2. H. A. BETHE and J. ASKIN. *In* Experimental nuclear physics. Vol. 1. *Edited by* E. Segré. Wiley, New York. 1953. pp. 166–357.
3. R. L. PLATZMAN. Int. J. Appl. Radiat. Isot. **10**, 116 (1961).
4. A. MOZUMDER and J. L. MAGEE. J. Chem. Phys. **47**, 939 (1967).
5. G. R. FREEMAN. J. Chem. Phys. **39**, 1580 (1963).
6. W. F. SCHMIDT and A. O. ALLEN. J. Chem. Phys. **52**, 2345 (1970).
7. J.-P. DODELET, K. SHINSAKA, U. Kortsch, and G. R. FREEMAN. J. Chem. Phys. **59**, 2376 (1973).
8. J.-P. DODELET. Can. J. Chem. **55**, 2050 (1977).
9. J. H. BAXENDALE and P. WARDMAN. J. Chem. Soc. Faraday I, **69**, 584 (1973).
10. G. V. BUXTON, H. A. GILLIS, and N. V. KLASSEN. Chem. Phys. Lett. **32**, 533 (1975).
11. W. J. CHASE and J. W. HUNT. J. Phys. Chem. **79**, 2835 (1975).
12. J. H. BAXENDALE and P. H. G. SHARPE. Int. J. Radiat. Phys. Chem. **8**, 621 (1976).
13. R. S. DIXON, V. J. LOPATA, and C. R. ROY. Int. J. Radiat. Phys. Chem. **8**, 707 (1976).
14. K. N. JHA, G. L. BOLTON, and G. R. FREEMAN. J. Phys. Chem. **76**, 3876 (1972).
15. F.-Y. JOU and G. R. FREEMAN. J. Phys. Chem. **80**, 909 (1977).
16. F.-Y. JOU and G. R. FREEMAN. Can. J. Chem. **54**, 3693 (1976).
17. R. SCHILLER. J. Chem. Phys. **47**, 2278 (1967).
18. G. R. FREEMAN. Adv. Chem. Ser. **82**, 339 (1968).
19. K. N. JHA and G. R. FREEMAN. J. Chem. Phys. **48**, 5480 (1968).
20. K. N. JHA and G. R. FREEMAN. J. Chem. Phys. **51**, 2839 (1969).
21. J. T. RICHARDS and J. K. THOMAS. J. Chem. Phys. **53**, 218 (1970).
22. J. H. BAXENDALE and P. WARDMAN. Chem. Commun. 429 (1971); Nature, **230**, 449 (1971).
23. L. KEVAN. Chem. Phys. Lett. **11**, 140 (1971).
24. H. HASE, M. NODA, T. HIGASHIMURA, and K. FUEKI. J. Chem. Phys. **55**, 5411 (1971).
25. S. K. GARG and C. P. SMYTH. J. Phys. Chem. **69**, 1294 (1965).
26. G. A. KENNEY-WALLACE and C. D. JONAH. Chem. Phys. Lett. **39**, 596 (1976).
27. G. A. KENNEY-WALLACE. Can. J. Chem. **55**, 2009 (1977).
28. L. GILLES, M. R. BONO, and M. SCHMIDT. Can. J. Chem. **55**, 2003 (1977).
29. W. DANNHAUSER and R. H. COLE. J. Chem. Phys. **23**, 1762 (1955).
30. M. TACHIYA and A. MOZUMDER. J. Chem. Phys. **63**, 1959 (1975).
31. G. R. FREEMAN. Int. J. Radiat. Phys. Chem. **4**, 237 (1972).
32. G. R. FREEMAN and T. E. M. SAMBROOK. J. Phys. Chem. **78**, 102 (1974).
33. T. E. M. SAMBROOK and G. R. FREEMAN. Can. J. Chem. **53**, 1521 (1975).
34. G. V. BUXTON, F. C. R. CATTELL, and F. S. DAINTON. Trans. Faraday Soc. **67**, 687 (1971).
35. R. S. DIXON and V. J. LOPATA. J. Chem. Phys. (*a*) **62**, 4573 (1975); (*b*) **63**, 5149 (1975).

Scavenging of electrons prior to solvation in liquid alcohols[1]

KIYOSHI OKAZAKI AND GORDON R. FREEMAN
Chemistry Department, University of Alberta, Edmonton, Alta., Canada T6G 2G2

Received March 28, 1978

Can. J. Chem. Downloaded from www.nrcresearchpress.com by 210.87.254.105 on 09/05/12
For personal use only.

KIYOSHI OKAZAKI and GORDON R. FREEMAN. Can. J. Chem. **56**, 2313 (1978).

A solvent effect similar to that reported earlier (J. Am. Chem. Soc. **98**, 6825 (1976)) has been found for the rates of reaction of solvated electrons with benzene and toluene in a series of alcohols. The value of the rate constant for benzene at 299 K increases abruptly from 1.0 ($10^6\ M^{-1}\ s^{-1}$) in methanol to 6.8 in ethanol, then increases only slightly to 7.0 in 1-propanol and 8.4 in 1-butanol. A further large increase occurs on going to a secondary alcohol solvent: 42 ($10^6\ M^{-1}\ s^{-1}$) in 2-propanol and 69 in 2-butanol. The activation energies are ~30 kJ/mol in all cases, so the rate constants reflect different entropies of activation. The entropies are affected by the solvation energies of the species.

The reactions of benzene and toluene with electrons prior to solvation show relatively little solvent effect, due to their higher energy state. In 2-butanol at 163 K, reactions of quasifree, localized (absorbing in the infrared), and equilibrium solvated electrons have been distinguished. Reactions of e_{qf}^- obey the relation $(A_{i0}/A_i)_{qf} \approx 1 + [P/(1-P)]f_{qf}N_s$, where A_i/A_{i0} is the fraction of electrons that have not been scavenged up to time i, and N_i is the mol fraction of scavenger. See text for remaining symbols. Reactions of e_{loc}^- obey the relation $(A_i/A_{i0})_{loc} \approx \exp(-nf_{loc}N_s)$. The total probability that electrons reach the equilibrium solvated state is $A_i/A_{i0} \approx \exp(-nf_{loc}N_s)/\{1 + [P/(1-P)]f_{qf}N_s\}$. Both diffusion and tunneling may contribute to scavenging of e_{loc}^-. The contribution of these processes, compared to the amount of scavenging e_{qf}^-, increases with increasing scavenger concentration and decreasing temperature.

The parameters $f_{qf}P/(1-P)$ and nf_{loc} each vary approximately as T^{-4}, which is equivalent to an Arrhenius temperature coefficient of about −8 kJ/mol. The negative temperature coefficients could imply either that the scavenging step has a negative temperature coefficient, or that the lowering of the electron energy state has a positive temperature coefficient.

KIYOSHI OKAZAKI et GORDON R. FREEMAN. Can. J. Chem. **56**, 2313 (1978).

On a trouvé un effet de solvant semblable à celui rapporté antérieurement (J. Am. Chem. Soc. **98**, 6825 (1976)) pour les vitesses de réaction entre des électrons solvatés et le benzène et le toluène dans une série d'alcools. Il y a une augmentation rapide de la valeur de la constante de vitesse pour le benzène à 299 K allant de 1.0 ($10^6\ M^{-1}\ s^{-1}$) dans le méthanol à 6.8 dans l'éthanol et des augmentations graduelles jusqu'à 7 dans le propanol-1 et 8.4 dans le butanol-1. Il y a une autre augmentation substantielle lorsque le solvant est un alcool secondaire: 42 ($10^6\ M^{-1}\ s^{-1}$) pour le propanol-2 et 69 pour le butanol-2. Les énergies d'activation sont d'environ 30 kJ/mol dans tous les cas, ce qui indique que les constantes de vitesse sont un reflet de différentes entropies d'activation. Les entropies sont affectées par les énergies de solvatation des espèces.

Les réactions du benzène et du toluène avec des électrons avant la solvatation ne présentent que des effets de solvant relativement faibles dus à leurs états d'énergie plus élevé. Dans le butanol-2 à 163 K, on a pu distinguer les réactions des électrons pratiquement libres, (qf), localisés (loc, qui absorbent dans l'infrarouge) et des électrons solvatés (solv) en équilibre. Les réactions des e_{qf}^- s'effectuent suivant la relation $(A_{i0}/A_i)_{qf} \approx 1 + [P/(1-P)]f_{qf}N_s$ où A_i/A_{i0} est la fraction non-piégée jusqu'au temps i et N_s est la fraction molaire de piège. On retrouvera dans le texte la signification des autres symboles. Les réactions des e_{loc}^- obéissent à la loi $(A_i/A_{i0})_{loc} \approx \exp(-nf_{loc}N_s)$. La probabilité totale que les électrons puissent atteindre un état d'équilibre solvaté est de $A_i/A_{i0} \approx \exp(-nf_{loc}N_s)/\{1 + [P/(1-P)]f_{qf}N_s\}$. La diffusion ainsi que l'effet de tunnel peuvent contribuer au piégeage des e_{loc}^-. La contribution de ces processus comparée à la quantité de piégeage e_{qf}^- augmente avec l'augmentation de la concentration des pièges et la diminution de la température.

Les paramètres $f_{qf}P/(1-P)$ et nf_{loc} varient en fonction de T^{-4} ce qui est équivalent à un coefficient de température d'Arrhénius d'approximativement −8 kJ/mol. Les coefficients de température négatifs peuvent impliquer soit que l'étape du piège a un coefficient de température négatif ou que l'abaissement de l'état d'énergie de l'électron a un coefficient de température positif.

[Traduit par le journal]

---

[1]Assisted financially by the National Research Council of Canada.

Can. J. Chem. Downloaded from www.nrcresearchpress.com by 210.87.254.105 on 09/05/12
For personal use only.

Introduction

Information about the behavior of electrons during their last stages of de-energization in irradiated polar liquids can be obtained from studies of: (*a*) temporal shifts in their optical absorption spectra (1–10), and (*b*) changes of chemical reactivity with energy state (1–3, 5, 6, 11–17). The present work is a contribution to the latter.

The initial yield of solvated electrons in irradiated liquids such as alcohols can be reduced by the addition of a high concentration of scavenger. The electrons can be captured prior to solvation, and there is a competition between localization traps (potential wells in the liquid) and scavenger molecules. In some instances the competition may be represented by a simple logarithmic function of the scavenger concentration (15), while in others it may not (16). Both types of behavior may be represented by a single model (16, 17). However, the model contains three adjustable parameters, which make it more arbitrary than one would like. To obtain more information about scavenging of electrons prior to solvation, we have studied the effects of alcohol molecular structure and temperature.

Experimental

Materials

The methanol was spectrophotometric reagent grade from Baker Chemical Co.; ethanol was absolute reagent grade from U.S. Industrial Chemical Co.; *n*-propanol, certified grade, Matheson, Coleman & Bell Co.; isopropanol, spectrophotometric grade, Aldrich Chemical Co.; 1-butanol, spectranalyzed grade, Fisher Scientific Co.; 2-butanol, analytical reagent grade, BDH Chemical Co.

Ethanol was used without further purification, because it is the highest purity that has been obtained by any method in this laboratory (18). The other alcohols were purified by the procedure reported earlier for the butanols (10).

Benzene and toluene (Phillips Research Grade) were purified under vacuum by stirring for 1–2 days with each of the following: lithium aluminum hydride powder (Alfa Inorganic Ventron Co.), conc. sulfuric acid (Baker Chemical Co.), potassium hydroxide pellets (American Drug and Chemical Co.), and sodium–potassium alloy (Na (dry) and K, Laboratory Reagent, from BDH Chemical Co.).

Solutions were prepared with the aid of syringes and bubbled with UHP argon (Matheson Co.) to free them from oxygen.

Techniques

The radiation, dosimetry, and optical systems were described earlier (10). Briefly, a 100 ns pulse of 1.7 MeV electrons delivered a dose of 2×10^{16} eV/g to the sample. Optical measurements were made at the absorption maximum λ_{emax} of the solvated electron band at each temperature, unless otherwise noted.

Results

Rate Constants, k($e_{solv}^- + S$)

Electrons in their equilibrium solvated state (10) react by pseudo-first order kinetics with solute S in the alcohol. The pseudo-first order rate constants were plotted against the solute concentration and the value of the second order rate constant $k(e_{solv}^- + S)$ obtained from the slope. At least five different concentrations were used for each solute.

Rate constants for reaction with benzene and toluene were measured in a number of alcohols at temperatures ranging from 200 to 300 K. Values of the Arrhenius parameters, $k = A \exp(-E_a/RT)$, and the rate constant at 299 K are listed in Table 1. The values of k for benzene in methanol and ethanol reported in refs. 14 and 16 were slightly larger than those obtained under the same conditions in the present work.

The rate constants are all at least two orders of magnitude below the diffusion controlled limit $\sim 10^{10}\ M^{-1}\ s^{-1}$ at 299 K (19). The activation energies are all ~ 30 kJ/mol and do not reflect the two-fold variation in the activation energies of dielectric relaxation or viscosity (Table 1). Activation energies of diffusion of the reactants are probably similar to the last two quantities.

The values of the rate constants increase by nearly two orders of magnitude on going from methanol to 2-butanol solvent and the change appears in the frequency factor A (Table 1). This is a solvent effect similar to that reported earlier (20). It will be investigated further. The A factor for reaction with benzene and toluene appears to increase with increasing size of the alkyl group on the alcohol and with decreasing solvation energy of the electron. The latter is reflected by $E_{\epsilon max}$ (Table 1). The larger alkyl groups may lower the energy state of the hydrocarbon solute and anion.

Scavenging of Electrons Prior to Solvation

Addition of > 1 mol% of benzene or toluene to an alcohol reduced the initial yield of solvated electrons. Where necessary, the absorption signal of solvated electrons was corrected for pseudo-first order reaction with the solute during the 0.1 μs pulse (16) to obtain the initial absorbance A_i. The ratio A_i/A_{i0} was plotted against solute concentration, where A_{i0} is the absorbance in pure alcohol (Fig. 1). By contrast with the earlier work where only the free ion portion of the signal was used (16), we used the total absorbance at the end of the pulse, including any geminate solvated electrons that might remain at that time. Virtually the same values of A_i/A_{i0} were obtained whether the geminate electrons were excluded or not, but their inclusion avoided a possible extrapolation error.

As the temperature of the solvent methanol was lowered, benzene became more efficient at decreasing the solvated electron yield (Fig. 1). The efficiency increased six-fold between 299 and 183 K.

Can. J. Chem. Downloaded from www.nrcresearchpress.com by 210.87.254.105 on 09/05/12
For personal use only.

TABLE 1. Rate constants of reaction between e_{solv}^- and benzene or toluene in several alcohols

Solvent	$\kappa^{a,b}$	E_{max} (eV)[a,c]	Benzene $10^{-6}k$ (M^{-1} s^{-1})[a]	Benzene log A (M^{-1} s^{-1})	Benzene E_a (kJ/mol)	Toluene $10^{-6}k$ (M^{-1} s^{-1})[a]	Toluene log A (M^{-1} s^{-1})	Toluene E_a (kJ/mol)	E_{τ_1} (kJ/mol)[i]	E_η (kJ/mol)[o]
Methanol	32.5	1.95[d]	1.0	11.50	30.1	1.6	11.71	31.4	15.5[j]	10.9
			1.4[h]	10.51[h]	25.1[h]					
Ethanol	24.4	1.79[d]	6.8	12.04	29.7	5.1	11.08	24.7	18.4[j]	13.8
			7.2[h]	11.20[h]	25.1[h]					
1-Propanol	20.1	1.92[e,f]	7.0	11.79	28.4	6.6	11.84	28.8	24.2[j,k,l]	17.1
2-Propanol	19.7	1.51[f]	42	12.81	29.7	42	12.59	28.4	26.8[j,m]	21.3
1-Butanol	17.3	1.93[e,f]	8.4	12.77	33.4	7.7	12.73	33.4	26.8[l,n]	20.1
2-Butanol	16.4	1.63[g]	69	13.65	33.4	65	13.67	33.4	~27[n]	18.4

[a]Value at 299 K.
[b]Dielectric constant, ref. 35.
[c]Energy at the maximum of the optical absorption spectrum of solvated electrons.
[d]Reference 36.
[e]Reference 37.
[f]Reference 38.
[g]Reference 10.
[h]Reference 16.
[i]Activation energy of solvent dielectric relaxation near 300 K.
[j]Reference 39.
[k]Reference 40.
[l]Reference 41.
[m]Reference 42.
[n]Reference 43.
[o]Activation energy of shear viscosity near 300 K, ref. 44.

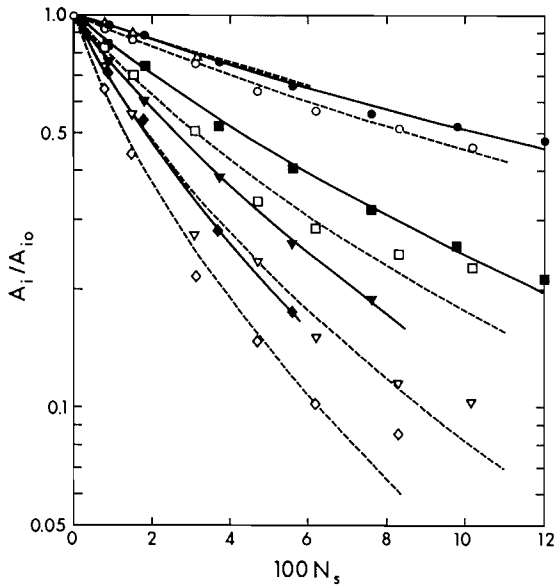

FIG. 1. Effects of benzene (full points) and toluene (open points) on the initial absorbance A_i of solvated electrons after a 100 ns pulse of radiation in methanol. A_{io} is the initial absorbance in the absence of scavenger and N_s is the mol fraction of scavenger. The temperatures (K) were: △, 333; ●, ○, 299; ■, □, 243; ▼, ▽, 213; ◆, ◇, 183. The curves — for benzene and - - - for toluene were calculated from eq. [4] using parameter values from Table 2.

Toluene was slightly more efficient than benzene at reducing the electron yield (Fig. 1).

The electron yield was reduced somewhat more easily in ethanol than in methanol (compare Figs. 1 and 2).

Measurements were made for benzene and toluene in each alcohol. To prevent congestion, the points for only one or the other of the scavengers are shown for ethanol, 1-propanol, 2-propanol, 1-butanol, and 2-butanol (Figs. 2–6). The efficiency of scavenging electrons prior to their solvation changes relatively little from one alcohol to another, by comparison with the large changes in efficiency of reaction after solation (Table 1).

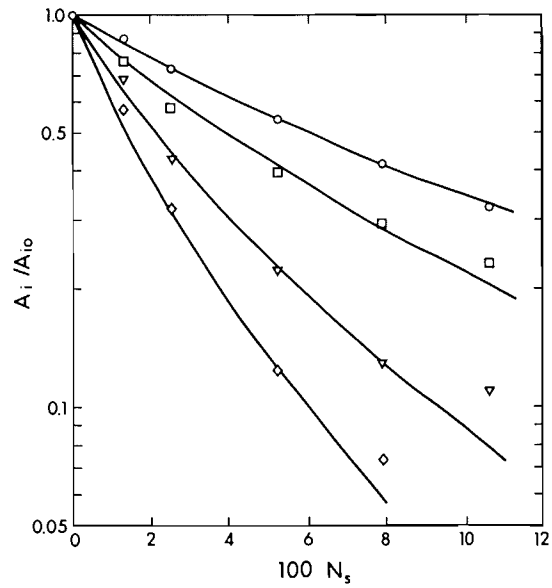

FIG. 2. Effect of benzene on the initial absorbance of solvated electrons after a 100 ns pulse of radiation in ethanol. N_s is the mol fraction of benzene. ○, 298 K; □, 243 K; ▽, 213 K; ◇, 183 K. The curves were calculated from eq. [4] using parameter values from Table 2.

Can. J. Chem. Downloaded from www.nrcresearchpress.com by 210.87.254.105 on 09/05/12
For personal use only.

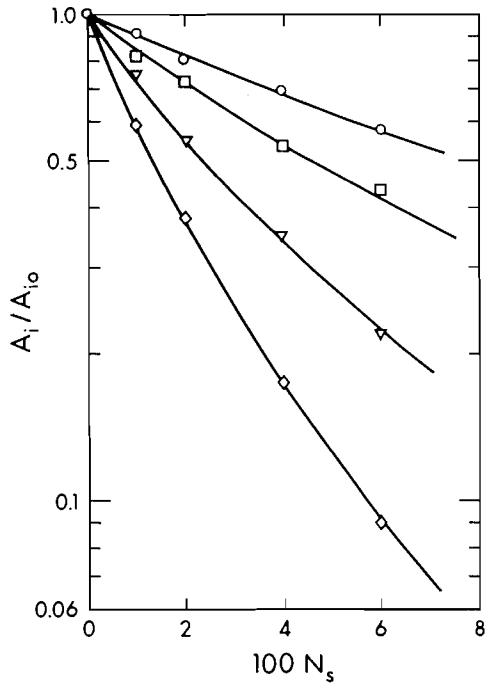

FIG. 3. Effect of toluene on the initial absorbance of solvated electrons after a 100 ns pulse of radiation in 1-propanol. N_s is the mole fraction of toluene. ○, 299 K; □, 243 K; ▽, 213 K; ◇, 183 K. The curves were calculated from eq. [4] using parameter values from Table 2.

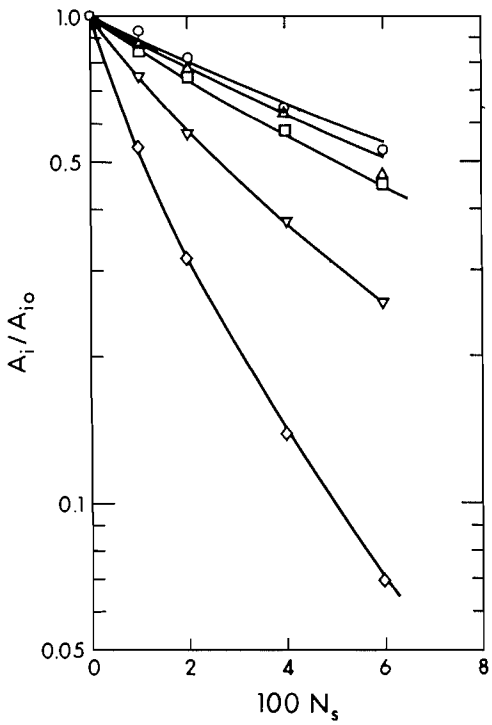

FIG. 4. Effect of toluene on the initial absorbance of solvated electrons after a 100 ns pulse of radiation in 2-propanol. N_s is the mole fraction of toluene. ○, 299 K; △, 273 K; □, 248 K; ▽, 218 K; ◇, 188 K.

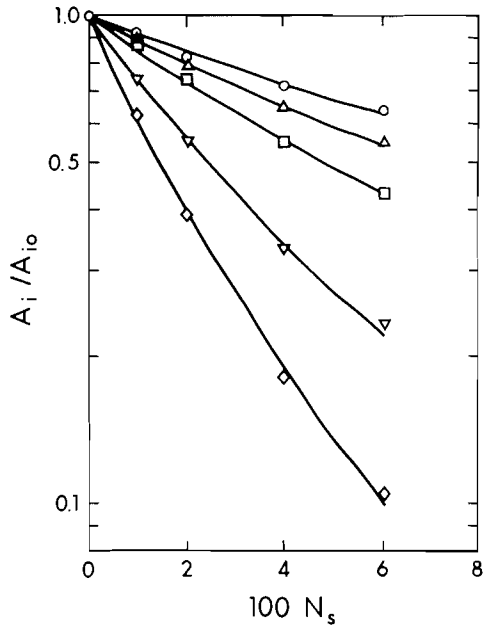

FIG. 5. Effect of toluene on the initial absorbance of solvated electrons after a 100 ns pulse of radiation in 1-butanol. N_s is the mole fraction of toluene. ○, 299 K; △, 273 K; □, 248 K; ▽, 218 K; ◇, 188 K.

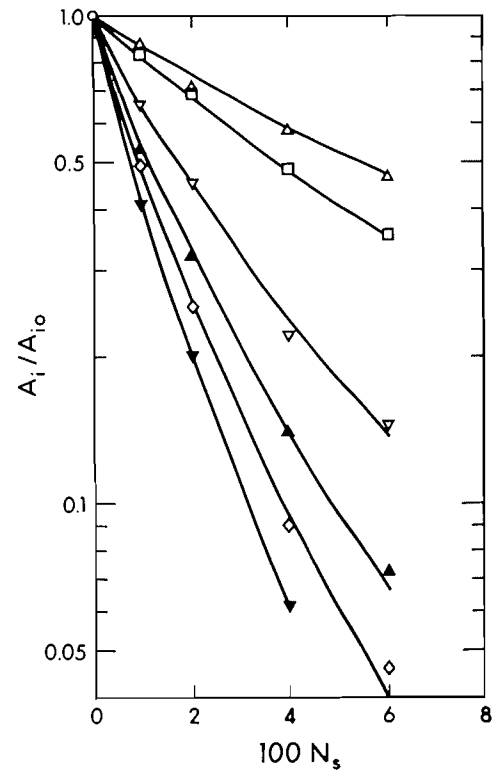

FIG. 6. Effect of benzene on the initial absorbance of solvated electrons after a 100 ns pulse of radiation in 2-butanol. N_s is the mol fraction of benzene. △, 273 K; □, 243 K; ▽, 213 K; ▲, 198 K; ◇, 183 K; ▼, 163 K. The curves were calculated from eq. [4] using parameter values from Table 2.

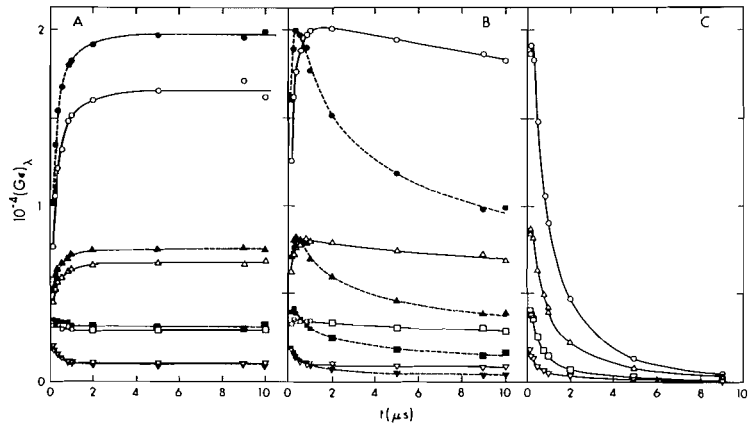

FIG. 7. Optical absorption, plotted as $(G\varepsilon)_\lambda$, as a function of time at different wavelengths and benzene concentrations (mol%) in 2-butanol at 163 K. ○, ●, 0%; △, ▲, 1.0%; □, ■, 2.0%; ▽, ▼, 4.0%. *A*: open points, $\lambda = 500$ nm; closed points, 570 nm. *B*: open, 670 nm; closed, 780 nm. *C*: 1000 nm.

Reaction Rates Measured at Different Wavelengths

At $T > 183$ K electron solvation reached the equilibrium state within the 140 ns time resolution of the measuring equipment (10). Electron reaction rates measured at $\lambda = 500$–1000 nm were therefore independent of wavelength at those temperatures. However, in 2-butanol at 163 K the solvation process was slow enough that reaction rates of electrons in different energy states could be measured.

Five experimental parameters are useful in the description of reaction rates measured at different wavelengths at constant temperature: (*a*) the product of the yield G of species that absorb at wavelength λ and the average decadic molar absorbancy ε at that wavelength, $(G\varepsilon)_\lambda$; (*b*) λ; (*c*) time, t; (*d*) solute concentration; and (*e*) A_{i}/A_{i0}. To present the required portions of this five dimensional situation we used a series of two dimensional plots.

Benzene was the solute. It will be useful to recall that the absorption maximum of the equilibrium solvated state of electrons in 2-butanol at 163 K occurs at $\lambda_{\varepsilon max}(e_{solv}^-) = 560$ nm and that this state is reached ~ 50 μs after injection of the electrons into the liquid (10). Time was measured from the beginning of the 0.10 μs pulse, because that was the only suitable anchor point at all wavelengths.

Consider first the electrons in the deeper traps, $\lambda \leq \lambda_{\varepsilon max}$. In the pure alcohol the absorbance increased by a factor of 2.1 during the period 0.14–4 μs, then remained constant for at least 45 μs (Fig. 7*A* and ref. 10). Addition of 1 mol% benzene reduced the initial absorbance at 0.14 μs to 54% of the value in pure alcohol, and the subsequent growth was only a factor of 1.5 (Fig. 7*A*). The presence of 2% benzene reduced the initial absorbance further and prevented the growth altogether; in fact, 10% decay occurred between 0.14 and 2 μs, then the signal remained constant (Fig. 7*A*). Four mol% benzene reduced the initial absorbance to 23% of that in the pure alcohol, and the signal decayed by half again during the next 2 μs (Fig. 7*A*). These results demonstrate that benzene scavenges electrons both prior to and subsequent to their forming localized states in the fluid.

At $\lambda_{\varepsilon max} < \lambda \leq 1000$ nm the absorbance first grew then decayed. The relative amount of growth decreased and the relative amount of subsequent decay over 10 μs increased with increasing wavelength (Figs. 7 *B* and *C*). The relative effects of 1–4% mol benzene were similar to those observed at $\lambda \leq \lambda_{\varepsilon max}$. The main cause of the decay at $t > 0.2$ μs at $\lambda = 1000$ nm is due to the blue shift of the absorption spectrum as the electron settles into the equilibrium solvated state (10).

Figure 8 shows the shift of the absorption band with time when different amounts of benzene were

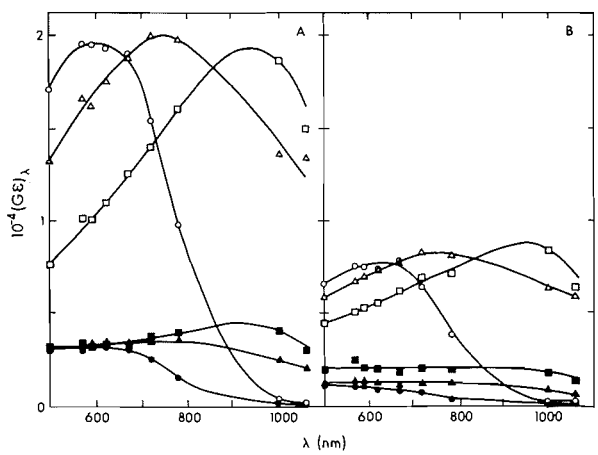

FIG. 8. Optical absorption as a function of wavelength in solutions of benzene in 2-butanol at 163 K, at different times. □, ■, 0.14 μs; △, ▲, 0.54 μs; ○, ●, 9 μs. *A*: open points, pure alcohol; closed points, 2.0 mol% benzene. *B*: open points, 1.0% benzene; closed points, 4.0% benzene.

Can. J. Chem. Downloaded from www.nrcresearchpress.com by 210.87.254.105 on 09/05/12
For personal use only.

Can. J. Chem. Downloaded from www.nrcresearchpress.com by 210.87.254.105 on 09/05/12
For personal use only.

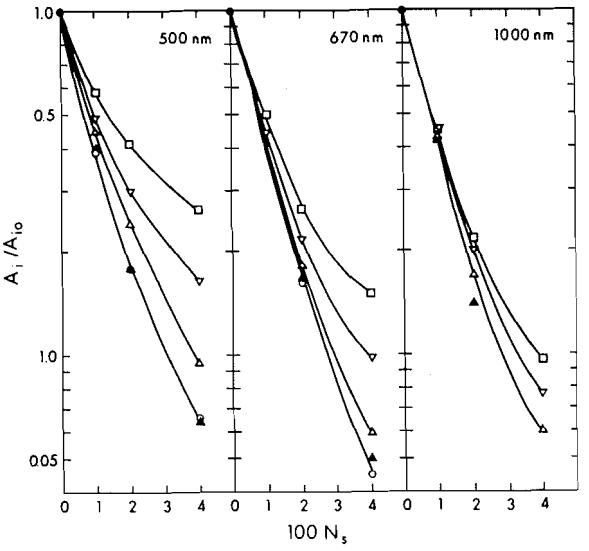

FIG. 9. Effect of benzene concentration on the fractional initial absorbance A_i/A_{io} of electrons in 2-butanol at 163 K, at different times and wavelengths. □, 0.14 μs; ▽, 0.24 μs; △, 0.54 μs; ▲, 2.0 μs; ○, 9 μs. * = △, ▲, and ○ superimpose.

present. The curves for 0.14 μs show that scavenging at short times preferentially decreases the absorption at long wavelengths. The peak at ~950 nm is virtually destroyed by 4% benzene. However, as time progresses there is less distinction between the fractional reductions at different wavelengths (Fig. 9). At times greater than or equal to that required for electrons to reach their equilibrium solvated state, the fractional decrease of absorbance caused by a scavenger is independent of wavelength. In 2-butanol at 163 K this would be $t \geq 50$ μs (10).

Discussion

Scavenging of Electrons Prior to their Solvation

The electrons under consideration are not in thermal equilibrium with the medium. For this reason the usual chemical concept of a rate constant does not apply to their reactions, although as we shall show later, equations that have approximately the correct form can be derived from a rate constant approach. The problem is one of nonhomogeneous kinetics and can be handled by a stochastic model (16, 17, 21, 22). Unfortunately, the language and formalism of statistics do not appeal to one's sense of beauty in simplicity, so simpler versions have been used (13, 15, 23).

As an electron is being de-energized by collisions in the liquid, it becomes scavengeable after the energy has been decreased below some value of the order of 1 eV. The specific upper threshold value depends upon the scavenger. In general, scavenging is possible during the last train of collisions that the quasifree electron undergoes prior to localization. Reaction may also occur if the initial localization site contains a scavenger molecule. In liquids that can form deep traps, electrons that are initially in shallow traps might migrate and react before settling into the equilibrium solvated state. The probability of reaction per encounter depends upon the energy of the encounter pair. However, the energy dependences of the encounter efficiencies f_{qf} and f_{loc} are not known, so average values are used as adjustable parameters. The subscripts qf and loc refer to quasifree[2] and localized electrons, respectively.

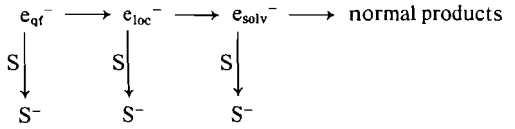

The ratio A_i/A_{io} expresses the fraction of electrons that have not been scavenged up to the time represented by i. For the quasifree regime, P represents the average probability that an electron does not become localized at a given collision and $(1 - f_{qf}N_s)$ is the average probability per collision that it does not react with scavenger which is present at mol fraction N_s. The fraction of electrons that survive the quasifree period is therefore:

$$[1] \quad (A_i/A_{i0})_{qf} = \sum_{m=1}^{\infty} (1 - P)[P(1 - f_{qf}N_s)]^{m-1}$$

where the summation index m represents the number of collisions. Upon inversion eq. [1] reduces to (24):

$$[2] \qquad (A_{i0}/A_i)_{qf} \approx 1 + \left(\frac{P}{1 - P}\right) f_{qf}N_s$$

Equation [2] is only an approximation because P and f_{qf} are not constants, but we approximate them by average values.

After localization there is a further probability that the electron will be scavenged prior to reaching the equilibrium solvated state. This process involves the probability that the initial localization site includes a scavenger molecule, and the probability that the electron migrates or tunnels to a scavenger during the time between localization and equilibration with the medium. We now speak of the probability f_{loc} of reaction per encounter, rather than per collision, because a localized electron has an extended interaction with each of the molecules in its localization site. The localized → solvated time regime also involves a series of electron energies and correspond-

[2]The term quasifree is not restricted to thermal electrons, but simply implies that the electron is not localized and is not in free space.

Can. J. Chem. Downloaded from www.nrcresearchpress.com by 210.87.254.105 on 09/05/12
For personal use only.

ingly varying numbers n of encounters and values of f_{loc}; we again use averages. The probability that localized electrons survive unscavenged to reach the solvated state is:

$$[3] \quad (A_i/A_{i0})_{loc} \approx (1 - f_{loc}N_s)^n \approx \exp(-nf_{loc}N_s), \quad \text{when } 1 \gg f_{loc}N_s$$

The total probability that electrons survive both periods is given by [4]:

$$[4] \quad \frac{A_i}{A_{i0}} \approx (1 - f_{loc}N_s)^n \Big/ \left[1 + \left(\frac{P}{1-P}\right) f_{qf}N_s\right] \approx \exp(-nf_{loc}N_s) \Big/ \left[1 + \left(\frac{P}{1-P}\right) f_{qf}N_s\right]$$

Experimentally, $fN_s \ll 1$, under which circumstances many mathematical functions are approximately equivalent to [2], [3], or [4].[3] Furthermore, depending on the scavenger and solvent, either the [2] or [3] portion may dominate in [4]. For this reason different authors have arrived at various expressions that are all approximations of [4], for example, eq. [5] in ref. 13, [5] and [6] in ref. 14, [7], [9], and [10] in ref. 15, [2] in ref. 23, [4] in ref. 25, [3] in ref. 26, [8] in ref. 27, and the equation in ref. 28. The integral form of [1] (16, 17) leads to

$$[5] \quad A_i/A_{i0} \approx (1 - f_{loc}N_s)^n \ln P / \ln [P(1 - f_{qf}N_s)]$$

which is equivalent to [4] in that the values of P and $(1 - f_{qf}N_s)$ are each only slightly less than unity, in which case $\ln x \approx x - 1$.

Equation [4] was fitted to the scavenging data, examples of which are shown in Figs. 1–6. Equations [2] and [3] are limiting cases of [4] and under most conditions were not valid. However, for benzene in 2-butanol at 163 K, 0.14 μs and $\lambda < 600$ nm eq. [2] is a good approximation (Fig. 10). Recall that $\lambda_{emax} = 560$ nm for the equilibrium solvated state under these conditions, and migration from states at $\lambda \leq \lambda_{emax}(e_{solv}^-)$ is negligible at very short times. This is as close as we have been able to come to the isolation of scavenging from the quasifree state. The slopes of the lines at 0.14 μs in Fig. 10 give $f_{qf}P/(1 - P) = 70$ at 500 nm and 97 at 570 nm. The true amount of increase of the quantity with increasing wavelength may be somewhat smaller than that indicated by the change of slope, because the factor $(1 - f_{loc}N_s)^n$ might make a more significant contribution at the longer wavelength. Both values are actually upper limits. The upward curvature at $\lambda > 600$ nm indicates an increasing contribution of

[3]For example, eq. [5] in ref. 13, [6] in ref. 14, [7] in ref. 15, [14] in ref. 16, [4] in ref. 17, [2] in ref. 23, [4] in ref. 25, [8] in ref. 27 and the equation in ref. 28.

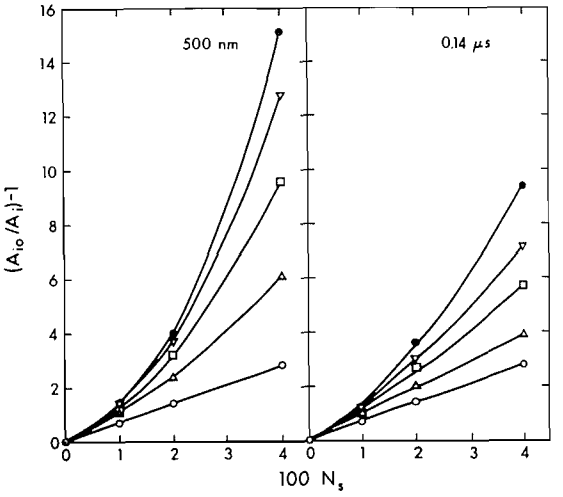

FIG. 10. Results for benzene in 2-butanol at 163 K plotted according to eq. [2]. At 500 nm: ○, 0.14 μs; △, 0.24 μs; □, 0.54 μs; ▽, 0.84 μs; 0.84 μs; ●, 45 μs. At 0.14 μs: ○, 500 nm; △, 570 nm; □, 670 nm; ▽, 780 nm; ●, 1000 nm.

the latter factor with increasing wavelength at short times (Fig. 10, 0.14 μs). This factor also becomes more important at longer times (Fig. 10, 500 nm, increasing curvature with time).

The value of the factor $(1 - f_{loc}N_s)^n \approx \exp(-nf_{loc}N_s)$, and hence of nf_{loc}, can be estimated from the data in 2-butanol at 163 K by plotting $\log[(A_i/A_{i0})_t/(A_i/A_{i0})_{0.14\ \mu s}]$ against N_s for $\lambda < 600$ nm. This is equivalent to dividing eq. [4] by [1]. Such plots for different times t are shown in Fig. 11. The values of nf_{loc} obtained in this way are lower limits, because $(A_i/A_{i0})_{0.14\ \mu s}$ gives an upper limit for eq. [1]. The value of nf_{loc} increases with time, due to electron diffusion and tunneling, reaching ~35 at 5 μs (Fig. 11). By this time relaxation towards the solvated state is well advanced, with decay of the infrared band virtually complete (Fig. 8). However, shifting of the red side of the band in the visible continues for ≥45 μs (10), with negligible further scavenging by benzene. This early scavenging apparently occurs from the infrared band, but not from the band in the visible. The value of f_{loc} would decrease with increasing electron trap depth, and nf_{loc} is negligible for electrons in the visible band. The decrease in the absorption ratio at 500 nm caused by benzene (Fig. 11) was caused by prevention of growth, that is, by capture of electrons as they moved from the shallow traps of the infrared band towards the deeper traps of the band in the visible.

Solvated electrons in liquid ammonia absorb in the infrared and have been reported to have a "solvation number" of 30 ± 10 molecules (29). One wonders whether the value $nf_{loc} \approx 35$ for electrons

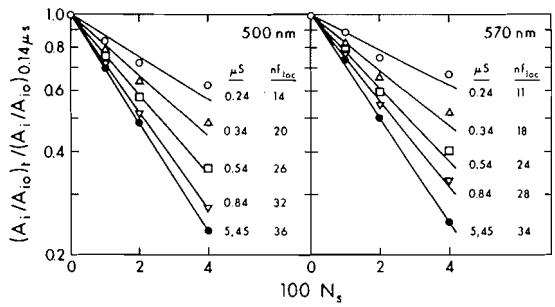

FIG. 11. Plots of log $[(A_i/A_{i0})_i/(A_i/A_{i0})_{0.14\ \mu s}]$ against N_s for benzene in 2-butanol at 163 K. The times and wavelengths at which the A values were determined are indicated in the figure, along with the values of nf_{loc} devised from the slopes.

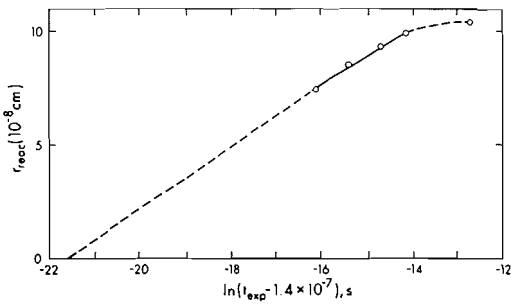

FIG. 12. Plot of the effective reaction radius of the localized electrons as a function of time. See text.

in the infrared band in 2-butanol is related to the "solvation number".

The value of nf_{loc} can be converted to an effective reaction radius, and its time dependence can be compared with that in a tunneling model. A_i/A_{i0} may be interpreted as the probability that there is no scavenger molecule within the effective reaction radius r_{reac} of an electron, that is, within the effective reaction volume $\frac{4}{3}\pi r_{reac}^3$. Using a stochastic approach one may write:

$$[6] \qquad A_i/A_{i0} = (1 - \tfrac{4}{3}\pi r_{reac}^3)^{n_s}$$

where n_s is the number of scavenger molecules/cm^3. Since $1 \gg \frac{4}{3}\pi r_{reac}^3$, [6] is equivalent to [7].

$$[7] \qquad A_i/A_{i0} = \exp(-\tfrac{4}{3}\pi r_{reac}^3 n_s)$$

Comparing [3] with [7] we obtain

$$[8] \qquad nf_{loc}N_s = \tfrac{4}{3}\pi r_{reac}^3 N_A N_s/\bar{V}$$

where N_A is Avogadro's number and $\bar{V}$ is the molar volume (81 cm^3 for 2-butanol at 163 K). Hence,

$$[9] \qquad r_{reac} = 3.2 \times 10^{-8}(nf_{loc})^{1/3}$$

Using a one-dimensional tunneling model and matched energy states on the two sides of the barrier, and equating r_{reac} to the tunneling range, a value for the tunneling barrier height $(V_0 - E_0)$ can be estimated from eq. [10] (25, 30).

$$[10] \quad r_{reac} = \left[\ln t + \ln\left(\nu \frac{16E_0(V_0 - E_0)}{V_0^2}\right)\right] \times \frac{\hbar}{2[2m(V_0 - E_0)]^{1/2}} = \frac{1.23 \times 10^{-14}}{(V_0 - E_0)^{1/2}} \times \left[\ln t + \ln\left(\nu \frac{16E_0(V_0 - E_0)}{V_0^2}\right)\right]$$

where ν is the frequency factor, V_0 (ergs) is the depth of the potential well, E_0 is the kinetic energy of the localized electron, and m is the electron mass.

The values of nf_{loc} were measured from the experimental time 0.14 μs, so the t in eq. [10] is $(t_{exp} - 1.4 \times 10^{-7})$ s. The plot of r_{reac} against ln $(t_{exp} - 1.4 \times 10^{-7})$ in Fig. 12 gives $(V_0 - E_0) \approx 8 \times 10^{-13}$ erg, or 0.5 eV. Taking $V_0 \approx 1$ eV, a long and uncertain extrapolation to $r_{reac} = 0$ in Fig. 12 gives $\nu \approx 6 \times 10^8\ s^{-1}$. A normal frequency factor for the electron might be expected to have a value similar to $E_0/\hbar$, which is $\sim 10^{15}\ s^{-1}$. However, the net rate of tunneling is greatly affected by the degree of mismatch of the energies and densities of states on the two sides of the barrier, and by the rate of removal of electron density from the product side. The latter corresponds to the rate of relaxation of the initial product state by way of physical and chemical processes. The efficiency factor $F = \nu/10^{15}$ (26) indicates the importance of state mismatch and relaxation in limiting the rate. For the present reaction of the infrared-absorbing electrons with benzene in 2-butanol at 163 K $F = 10^{-6}$. The value of F depends on the electron state and the solute, and on factors which affect them, such as the solvent, temperature, and time. In aqueous 6 M sodium hydroxide glass at 77 K, using measurements over the range 10^{-6}–10^2 s, estimated values of F range from 10^4 to 10^{-15} (26). The tunneling factor F is analogous to the stochastic factors f_{loc} and f_{qf}.

The curve in Fig. 12 reaches an upper limit because the time available for reaction is limited by the lifetime of the infrared (shallow trap) state. Relaxation of the electron state increases the barrier $(V_0 - E_0)$ and thereby restricts the growth of r_{reac}.

It is worthwhile to remember that the final electron transfer step to a reactant can always be considered to occur by tunneling. In fluids both diffusion and tunneling contribute to nf_{loc} and both display the same type of kinetics. When the electron and molecule diffusion coefficients are negligible, as in rigid, alkaline glasses at 77 K, tunneling may dominate.

Can. J. Chem. Downloaded from www.nrcresearchpress.com by 210.87.254.105 on 09/05/12
For personal use only.

TABLE 2. Parameter values for eq. [4]

Solvent	T (K)	Benzene $\frac{P}{1-P} f_{qf}$	Benzene nf_{loc}	Benzene $\frac{S_{qf}{}^a}{S_{loc}}$	Toluene $\frac{P}{1-P} f_{qf}$	Toluene nf_{loc}	Toluene $\frac{S_{qf}{}^a}{S_{loc}}$
Methanol	333	—	—		6.2	1.5	3.9
	299	5.7	2.1	2.6	8.0	2.0	3.7
	243	14	5.1	2.5	22	5.4	3.4
	213	23	8.4	2.3	37	9.0	3.1
	183	33	12	2.2	54	13	2.9
Ethanol	298	9.8	3.6	2.5	9.2	2.6	3.3
	243	15	5.6	2.4	23	6.4	3.0
	213	28	10	2.3	39	11	2.7
	183	44	16	2.1	52	15	2.5
1-Propanol	299	6.9	2.8	2.3	7.6	2.8	2.6
	243	14	5.6	2.3	13	4.8	2.5
	213	25	10	2.1	25	9.2	2.3
	183	38	16	1.9	46	17	2.0
2-Propanol	299	—	—		8.6	2.8	2.9
	273	—	—		9.8	3.2	2.8
	248	12	4.4	2.5	12	4.0	2.7
	218	25	9.2	2.3	23	7.6	2.6
	188	51	19	2.0	57	18	2.2
1-Butanol	299	5.2	3.2	1.6	5.7	2.8	2.0
	273	—	—		7.7	3.8	1.9
	248	9.7	6.0	1.5	11	5.4	1.7
	218	19	12	1.4	22	11	1.7
	188	28	17	1.4	37	18	1.6
2-Butanol	299	—	—		4.9	2.5	1.9
	273	9.8	4.9	1.9	—	—	
	243	14	7.0	1.8	14	7.0	1.8
	213	31	15	1.7	31	15	1.7
	198	46	23	1.5	—	—	
	183	57	28	1.5	53	26	1.5
	163	70	35	1.4	—	—	

[a]Fraction scavenged from the qf state ÷ fraction scavenged from the loc state when $N_s = 0.01$.

We cannot estimate the relative contributions of the two mechanisms in the present work.

At higher temperatures in 2-butanol and at all temperatures in the other alcohols, the relaxation processes were so fast that the scavenging of quasifree and localized electrons could not be measured separately. We therefore fitted eq. [4] to the results by using two adjustable parameters, $[f_{qf}P/(1-P)]$ and $[nf_{loc}]$. The values of the parameters increased to similar extents with decreasing temperature. Possible differences in the temperature coefficients were hidden by the experimental scatter. To permit an orderly analysis of the results it was assumed that the temperature coefficients of the two parameters were equal, although it is improbable that this is exactly true. The values obtained for benzene and toluene in each of the alcohols are listed in Table 2.

The relative contributions of scavenging from the quasifree and localized states, S_{qf}/S_{loc}, can be compared at different temperatures and scavenger concentrations.

$$[11] \quad S_{qf}/S_{loc} = \left(1 + \frac{1-P}{Pf_{qf}N_s}\right)^{-1} \times [1 - \exp(-nf_{loc}N_s)]^{-1}$$

Benzene and toluene scavenge quasifree more readily than localized electrons. The value of this ratio at 1 mol% benzene is 2–3 in each of the alcohols at 299 K and decreases gently with temperature (Table 2). The ratio is usually slightly larger for toluene than for benzene (Table 2). Scavenging of the localized state increases in importance with increasing scavenger concentration. For example, benzene in 2-butanol at 163 K gives $S_{qf}/S_{loc} = 1.4$ at 1 mol% and 1.0 at 4%.

The observed effects of temperature and concentration on the value of the ratio are in the expected direction.

Temperature Coefficients of Scavenging Prior to Solvation

The parameters $f_{qf}P/(1-P)$ and nf_{loc} each vary

Can. J. Chem. Downloaded from www.nrcresearchpress.com by 210.87.254.105 on 09/05/12
For personal use only.

approximately as T^{-4}, which is equivalent to an Arrhenius temperature coefficient of about −8 kJ/mol. Arrhenius plots of the data in Table 2 are slightly concave towards the T^{-1} axis, and they are more so when T^{-1} is replaced by $(T - T_\infty)^{-1}$ (31, 32). The temperature dependences are similar in all the alcohols, and for both benzene and toluene. The negative values reflect differences in the following sequences:[4]

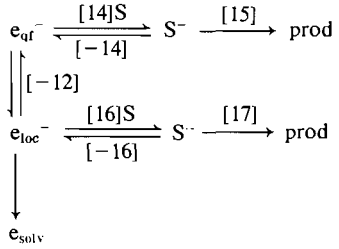

where prod may be a stabilized anion or the product of a further reaction such as protonation.

The similarity of the temperature coefficients of scavenging e_{qf}^- and e_{loc}^- reflects a similarity in the competitive sequences [12] against [14], [15]; and [13] against [16], [17]. Scavenging is more efficient at low temperatures, which seems to imply that: (*a*) [15] and [17] are less important than [14] and [16] in setting the temperature dependence; and (*b*) $E_{12} - E_{14} \approx E_{13} - E_{16} \approx 8$ kJ/mol. Extrapolation of data in ref. 10 indicates that $E_{13} \approx 15$ kJ/mol in this temperature region, so E_{16} is positive. The value $E_{12} - E_{14} \approx 8$ kJ/mol could be explained by a positive E_{12} or a negative E_{14}. The localization sites involved in [12] are potential fluctuations created by irregular molecular orientations that occur naturally in the liquid. A positive temperature coefficient of [12] could refer to the inelastic scattering cross section that de-energizes the electron into the localized state; the cross section might depend on the ease of molecular motion, reflected by τ_2 or τ_3 (33). A negative value of E_{14} would be attributed to the greater stability of the aromatic anion at low temperatures (34).

The reaction rates of solvated electrons with benzene and toluene vary much more from solvent to solvent and with temperature than do those of e_{qf}^- and e_{loc}^- (Tables 1 and 2). This is attributable to the lower energy state of e_{solv}^-.

[4]This reaction scheme is adequate when measurements are confined to the absorbances of e_{loc}^- and e_{solv}^-. If S^- or prod were also measured, it would be necessary to include steps for the reaction of e_{qf}^- and e_{loc}^- with geminate ions and radicals, because not all of the e_{qf}^- ultimately become e_{solv}^- in the irradiated pure solvent (10, 14).

Comparison with Homogeneous Kinetics

Part of the reaction scheme in the previous section can be treated by homogeneous kinetics to give an equation equivalent to [2] (14). Considering only reactions [12] and [14] one may write

$$[18] \qquad A_{i0}/A_i \approx 1 + (k_{14}[S]/k_{12})$$

where $k_{12} = k_{12}'[\text{trap}]$. The trap concentration is characteristic of the solvent at a given temperature and pressure, and is assumed to be independent of solute concentration in dilute solutions. Equation [18] is equivalent to [2], with $10^3 k_{14}/k_{12}\overline{V} = f_{qf}P/(1 - P)$ when [S] is in mol/ℓ.

However, eqs. [3] and [4] cannot be obtained by homogeneous kinetics.

Acknowledgement

We would like to thank the staff of the Radiation Research Centre for aid with the electronics.

1. J. T. Richards and J. K. Thomas. J. Chem. Phys. **53**, 218 (1970).
2. J. H. Baxendale and P. Wardman. (*a*) Chem. Commun. 429 (1971); (*b*) Nature, **230**, 449 (1971); (*c*) J. Chem. Soc. Faraday I, **69**, 584 (1973).
3. L. Kevan. Chem. Phys. Lett. **11**, 140 (1971).
4. H. Hase, M. Noda, T. Higashimura, and K. Fueki. J. Chem. Phys. **55**, 5411 (1971).
5. G. V. Buxton, F. C. R. Cattell, and F. S. Dainton. Trans. Faraday. Soc. **67**, 687 (1971).
6. G. V. Buxton, H. A. Gillis, and N. V. Klassen. Chem. Phys. Lett. **32**, 533 (1975).
7. W. J. Chase and J. W. Hunt. J. Phys. Chem. **79**, 2835 (1975).
8. J. H. Baxendale and P. H. G. Sharpe. Int. J. Radiat. Phys. Chem. **8**, 621 (1976).
9. R. S. Dixon, V. J. Lopata, and C. R. Roy. Int. J. Radiat. Phys. Chem. **8**, 707 (1976).
10. K. Okazaki and G. R. Freeman. Can. J.Chem. Submitted for publication.
11. W. H. Hamill. J. Chem. Phys. **49**, 2446 (1968).
12. H. B. Steen. J. Phys. Chem. **74**, 4059 (1970).
13. H. Ogura and W. H. Hamill. J. Phys. Chem. **78**, 504 (1974).
14. D. Ražem and W. H. Hamill. J. Phys. Chem. **81**, 1625 (1977).
15. K. Y. Lam and J. W. Hunt. Int. J. Radiat. Phys. Chem. **7**, 317 (1975).
16. G. L. Bolton, K. N. Jha, and G. R. Freeman. Can. J. Chem. **54**, 1497 (1976).
17. G. R. Freeman and G. L. Bolton. Fourth Symposium on Radiation Chemistry (1976), Akadémiai Kiadó, Budapest, 1978. pp. 999–1008.
18. S. M. S. Akhtar and G. R. Freeman. J. Phys. Chem. **75**, 2756 (1971).
19. K. N. Jha, G. L. Bolton, and G. R. Freeman. Can. J. Chem. **50**, 3073 (1972).
20. G. L. Bolton and G. R. Freeman. J. Am. Chem. Soc. **98**, 6825 (1976).
21. G. R. Freeman. J. Chem. Phys. **43**, 93 (1965); **46**, 2822 (1967).

Can. J. Chem. Downloaded from www.nrcresearchpress.com by 210.87.254.105 on 09/05/12
For personal use only.

22. L. G. WALKER. Ph.D. Thesis, University of Alberta, Edmonton, Alta. 1967.
23. R. K. WOLFF, M. J. BRONSKILL, and J. W. HUNT. J. Chem. Phys. **53**, 4211 (1970).
24. R. C. WEAST (*Editor*). Handbook of chemistry and physics. 48th ed. Chemical Rubber Co., Cleveland, OH. 1967. p. A-245.
25. J. R. MILLER. J. Chem. Phys. **56**, 5173 (1972).
26. J. R. MILLER. J. Phys. Chem. **79**, 1070 (1975).
27. G. CZAPSKI and E. PELED. J. Phys. Chem. **77**, 893 (1973).
28. D. RAŽEM and I. DVORNIK. Proc. 3rd Tihany Symp. Radiat. Chem. Akadémiai Kiadó, Budapest, 1972. p. 223.
29. R. A. PINKOWITZ and T. J. SWIFT. J. Chem. Phys. **54**, 2858 (1971).
30. W. KAUZMANN. Quantum chemistry, an introduction. Academic Press, New York, NY. 1957. Chapt. 6.
31. F. X. HASSION and R. H. COLE. J. Chem. Phys. **23**, 1756 (1955).
32. W. DANNHAUSER and R. H. COLE. J. Chem. Phys. **23**, 1762 (1955).
33. S. K. GARG and C. P. SMYTH. J. Phys. Chem. **69**, 1294 (1965).
34. T. R. TUTTLE, JR. and S. I. WEISSMAN. J. Am. Chem. Soc. **80**, 5342 (1958).
35. J. A. RIDDICK and W. B. BUNGER. Organic solvents, physical properties and methods of purification. 3rd ed. Wiley-Interscience, New York, NY. 1970. Chapt. 3.
36. K. N. JHA, G. L. BOLTON, and G. R. FREEMAN. J. Phys. Chem. **76**, 3876 (1972).
37. F.-Y. JOU and G. R. FREEMAN. J. Phys. Chem. **80**, 909 (1977).
38. F.-Y. JOU, A. D. LEU, and G. R. FREEMAN. To be published.
39. F. BUCKLEY and A. A. MARYOTT. NBS Circular 589, U.S. Dept. of Commerce, Washington, DC. 1958.
40. R. H. COLE and D. W. DAVIDSON. J. Chem. Phys. **20**, 1389 (1952).
41. S. K. GARG and C. P. SMYTH. J. Chem. Phys. **69**, 1294 (1965).
42. F. X. HASSION and R. H. COLE. J. Chem. Phys. **23**, 1756 (1955).
43. W. DANNHAUSER and R. H. COLE. J. Chem. Phys. **23**, 1762 (1955).
44. R. W. GALLANT. Physical properties of hydrocarbons. Vol. 1. Gulf Publishing Co., Houston, TX. 1968.

Can. J. Chem. Downloaded from www.nrcresearchpress.com by 210.87.254.105 on 09/05/12
For personal use only.

Gas phase ion–molecule reactions of dimethylsulphoxide

JOHN EDWARD FULFORD, JOSEPH WAYNE DUPUIS, AND RAYMOND EVANS MARCH

Department of Chemistry, Trent University, Peterborough, Ont., Canada K9J 7B8

Received December 3, 1976[1]

JOHN EDWARD FULFORD, JOSEPH WAYNE DUPUIS, and RAYMOND EVANS MARCH. Can. J. Chem. **56**, 2324 (1978).

The gas phase ion-chemistry of dimethylsulphoxide (DMSO) and deuterated dimethylsulphoxide (DMSO-d_6) has been examined using a quadrupole ion store (QUISTOR) as an ion–molecule reaction chamber. The QUISTOR results are compared with those obtained by ion trapping and high pressure mass spectrometry as reported by other workers. The performance of the QUISTOR demonstrates the versatility of the technique for ion–molecule reaction studies with variation of ambient pressure and duration of ion storage.

JOHN EDWARD FULFORD, JOSEPH WAYNE DUPUIS et RAYMOND EVANS MARCH. Can. J. Chem. **56**, 2324 (1978).

On a étudié, faisant appel à un réservoire d'ions quadrupolaires (QUISTOR) sous forme de chambre de réaction ion–molécule, la chimie ionique en phase gazeuse du diméthylsulphoxyde (DMSO) et du diméthylsulphoxyde deutéré (DMSO-d_6). On compare les résultats QUISTOR avec ceux obtenus par spectrométrie de masse avec piégeage ionique et à haute pression tels que rapportés par d'autres auteurs. Le bon succès de QUISTOR démontre la versatilité de la technique pour des études de réactions ion–molécule avec variation de la pression ambiante et de la durée de l'entreposage des ions.

[Traduit par le journal]

Introduction

The ion-chemistry described here has been observed with a novel system in which ions may be created and stored in a three-dimensional quadrupole ion store QUISTOR (1) and mass analysed by subsequent ejection into a quadrupole mass filter. When the QUISTOR is used as a storage device and reactor for the study of chemical processes (e.g. ion–molecule and charge transfer reactions) a knowledge of ion energies is essential.

In consideration of ion kinetic energies within the QUISTOR, a distinction must be made between primary ions which are formed initially by electron impact throughout the effective reactor volume and secondary ions formed in subsequent ion–molecule reactions. Attempts have been made to calculate primary ion kinetic energies in collision-free systems (2–4) and secondary ion kinetic energies pertaining after several collisions (5–7). There is good agreement among the estimates of mean primary ion energies in a collision-free system. Recent simulation studies (7) indicate that although a fraction of secondary ions may have several eV of kinetic energy, rapid energy dissipation is effected in the first 6–10 collisions so that after 15 collisions the mean ion energy is <1 eV. A brief account is given below of the examinations of several well characterized chemical systems by quadrupole ion storage mass spectrometry which were carried out in order to ascertain effective ion energies in the QUISTOR.

The ammonia system has been investigated with this technique (8) as a means of estimating the primary ion mean kinetic energies. The experimentally determined rate constants of the principal ion–molecule reactions occurring in ammonia were compared with literature values: from this comparison it was concluded that the primary ion kinetic energies are of the order of 1–3 eV.

The thermal energy reactions of methane have been studied extensively; more than twenty references are cited by Henchman (9) for the production of CH_5^+ which is an agent for chemical ionization. The occurrence of endothermic reactions requiring a primary ion kinetic energy threshold of 1.5 eV for the ground state ion provides an opportunity for assessment of primary ion energies in the QUISTOR. Anders (10) had reported that the reaction producing $C_2H_3^+$ is endothermic by 1.6 eV which is in good agreement with the observations of Harrison *et al.* (11), who found that the $C_2H_3^+$ intensity exceeded that of $C_2H_5^+$ for reactant ion energies in excess of 3 eV. Clow and Futrell (12) have reported however that the $C_2H_3^+$ peak intensity was less than the $C_2H_5^+$ peak intensity for ion energies up to 10 eV. Rate constants for the methane system have been obtained with the QUISTOR (8) and are in good agreement with literature values. Comparison was made also of the ratio of $C_2H_3^+$ and $C_2H_5^+$ inten-

[1]Revision received May 5, 1978.

Can. J. Chem. Downloaded from www.nrcresearchpress.com by 210.87.254.5 on 09/05/12
For personal use only.

Can. J. Chem. Downloaded from www.nrcresearchpress.com by 210.87.254.5 on 09/05/12
For personal use only.

sities as a function of ion energy, the primary ion kinetic energy being varied within the QUISTOR by operation with rf potentials between 800 and 1600 (peak-to-peak).

The results of a QUISTOR study of the water system (8) show very good agreement with those collected by Huntress and Pinnizzotto (13). Comparison of the observed ratio of 1.6 for $K_{H_3O^+}/K_{H_2O^+}$ with Ryan's tabulation (14) of this ratio against ion energy yielded a primary ion kinetic energy of between 1 and 2 eV.

The observation of CH_5^+ in the QUISTOR study of the methane system[2] indicated that chemical ionization should be realizable at extended storage times. This was demonstrated (16) with a methane–methanol (400:1) mixture at a pressure of 10^{-4} Torr. Chemical ionization in the QUISTOR has been observed in this laboratory for a number of alcohols (17), amines, mercaptans, explosives (18), and a miscellany of compounds including ketene (19).

The simulation studies mentioned earlier indicate that the kinetic energy of secondary ions is less than 1 eV. This is supported strongly by the chemical ionization observations in that little, if any, fragmentation of the protonated species occurs in near thermoneutral reactions, hence there has been no enhancement of the exothermicity of the proton transfer reaction by reactant ion kinetic energy. An example may serve to demonstrate further that energies of ions stored in the QUISTOR for periods in excess of ca. 0.5 ms are near thermal energy. The proton affinity (PA) of ketene was determined by the 'bracketing' technique wherein proton transfer equilibrium was approached from both directions. Dimethyl ether and 2-propanol were employed, wherein the proton affinities are less than and in excess of that of ketene, respectively. As our value for the PA of ketene has since been confirmed by the ICR technique (20) and as no fragmentation of the equilibrated $(M + 1)^+$ species was observed, it is concluded that the protonated species were thermalized. At long storage times, multiply-solvated protons have been observed together with dissociation products of these adducts. Consequently, it is possible to obtain information on collisional stabilization of excited addition ions and relative rates of dissociation and deactivation.

While CH_5^+ is the most widely applied chemical ionization agent and has been studied in the QUISTOR, the presence of such an agent is not necessary for the formation of protonated parent molecules, per se. Ionic species of this type are produced in ion confinement devices by auto-chemical ionization through mechanisms which involve the reaction of parent molecules with primary ions formed initially by electron impact. Thus the ion-chemistry of a given compound may be described in terms of the concurrent mechanisms of this type.

Previous workers have shown that the ion-chemistry of simple aliphatic alcohols (21) is characterized by associative complexes leading to the formation of solvated protons and multiply-solvated protons. In the aliphatic alcohols, dissociation of the complex may result in the elimination of water or alkene. This mode of reaction requires an electronegative atom (oxygen) to which is attached a labile hydrogen atom. Recent reports on the ion-chemistry of sulphur (H_2S, CH_3SH, $(CH_3)_2S$ (21) and CH_3SH, CD_3SH (23, 24)) and nitrogen (25–27) analogues show that similar reactions, at least in part, occur in these systems also.

The basic features of the quadrupole ion storage technique are virtually identical with those of the ICR ion trapping technique and the data reported here are similar to those obtained with ICR ion trapping devices. The basic difference arises in the mode of trapping, as Lawson and Todd (28) have explained: in the QUISTOR, a net restoring force experienced by the ions attracts them to the centre of the device due to their motion in the inhomogeneous oscillating electric fields, while in the ICR cell, confinement occurs through the combination of a magnetic field with an inhomogeneous static electric field. In both techniques the space charge potential within the ion cloud determines the maximum density of trapped ions, and this appears to be some two or three orders of magnitude greater in the QUISTOR.

The data reported here are similar also to those obtained from high pressure mass spectrometry but extended to a much longer time scale. It is customary in presenting high pressure mass spectrometry data to display plots of ion intensities as a function of pressure and from such plots conclusions are drawn concerning ion–molecule mechanisms. These conclusions are based on observations of the decay of primary ion intensities as a function of pressure and the concurrent appearance of secondary and higher order ions. Similar conclusions may be drawn from plots of ion intensities as a function of time at a fixed pressure in ion trapping devices such as are used in ICR mass spectrometry (29), beam trapping (24), and QUISTOR studies (8). Furthermore, the temporal dependences of ion intensities obtained with ion confinement techniques may be observed over a range of pressures. Brupbacher *et al.* (25)

[2]A similar observation has been made recently with a cylindrical device (15).

Can. J. Chem. Downloaded from www.nrcresearchpress.com by 210.87.254.5 on 09/05/12
For personal use only.

have shown that as a result of ionization of a substrate material, R, several different primary ions, P_i^+ and neutrals, N_i, may result from the process

$$R \xrightarrow{e^-} \sum_{i=1}^{n} P_i^+ + \sum_{i=1}^{n} N_i$$

Once formed, each of these primary ions may undergo ion–molecule reactions with the substrate. The reactions of one particular primary ion can be summarized as follows:

$$\begin{aligned} P_i^+ + R &\xrightarrow{k_1} S_1^+ + N_1 \\ P_i^+ + R &\xrightarrow{k_2} S_2^+ + N_2 \\ &\vdots \\ P_i^+ + R &\xrightarrow{k_L} S_L^+ + N_L \end{aligned}$$

where S_i^+ represents the various secondary ions formed. For this reaction scheme, the rate of loss of a specific primary ion, P_i^+, is given by

$$[1] \qquad d[P_i^+]/dt = -[R][P_i^+] \sum_{j=1}^{L} k_j$$

where $\sum_{j=1}^{L} k_j$ represents the total rate constant, k_T, for the loss of P_i^+ by reaction with R. Integration of eq. [1] over reaction time, t, gives the expression

$$[2] \qquad \ln \frac{[P_i^+]_t}{[P_i^+]_0} = -k_T[R]t$$

which describes the real kinetic surface for the reaction of P_i^+ with substrate R. High pressure mass spectrometry data yield ion intensity vs. pressure profiles of the kinetic surface for a given reaction time, while ion trapping data yield ion intensity vs. time profiles of the surface for a given pressure.

In the identification of a chemical system, on which the application of quadrupole ion storage devices for the study of ion-chemistry may be demonstrated, the following factors were considered: (*i*) As the identification of ions is facilitated by comparison of the ion-chemistry of a given substance and the fully deuterated analogue, the ready availability of the compounds was essential. (*ii*) The existence of previous studies of the ion-chemistry carried out by ICR technique and high pressure mass spectrometry. (*iii*) The system should exhibit an associative ion-chemistry. (*iv*) The existence of some degree of ambiguity in the studies reported.

Thus dimethyl sulphoxide was selected for this demonstration.

Experimental

The apparatus, which is depicted schematically in Fig. 1, consists of a three-dimensional quadrupole ion store (QUISTOR) mounted in place of the ion source of a conventional quadrupole mass filter (Vacuum Generators Q7B).

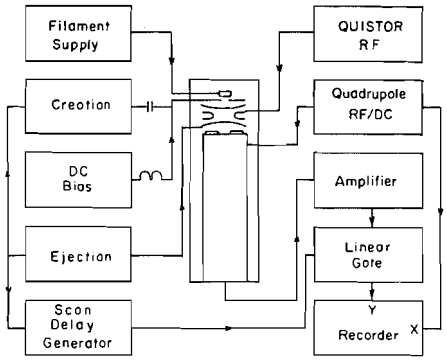

FIG. 1. Schematic diagram of apparatus.

The geometry of the QUISTOR is that of a hyperboloid of one sheet combined with a hyperboloid of two sheets forming the ring and end-cap electrodes, respectively; these are fabricated from stainless steel with $r_0 = 1$ cm and are separated by lava spacers, the whole assembly being machined and mounted with a tolerance of 0.001 in. A simple electron gun is employed comprising a spiral filament made of 0.008 in. tungsten wire and a perforated stainless steel plate, which allows the electron beam to be gated as desired. The QUISTOR/quadrupole combination is mounted vertically inside a stainless steel vacuum system, pumped by a 4-in. oil-diffusion pump, which is connected to a diffusion-pumped, unheated glass inlet system through a needle valve. An rf voltage supply, capable of providing up to 800 V at 1.6 or 2.5 MHz, is connected to the ring electrode, the end-caps being earthed except when ion ejection pulses are applied to the lower one (Fig. 1). In operation the electron gate is made a few volts more negative than the filament, so that the electron beam is turned off, and a positive pulse periodically applied to permit passage of the beam through the QUISTOR with consequent formation of ions. The ionizing beam in this work is directed along the symmetry axis of the device, rather than radially (30), since in this manner the electrons are not influenced by the rf voltage until after they have entered the device, with correspondingly better control of the electron energy. The ions, having been created inside the device, are stored under the influence of the field for a variable time before extraction by a negative pulse applied to the lower end-cap (Fig. 1) and subsequent mass analysis. This is represented in Fig. 2 which shows the typical pulse train; a trigger pulse from the internally triggered ejection generator (Hewlett Packard 214A), triggers the Boxcar Detector (Brookdeal Ortec Scan Delay Generator 9425A (SDG) and Linear Gate 9415 (LG)) and the creation pulse. The dead time is adjusted by the pulse delay circuitry of the creation generator and the storage time may be adjusted up to 100 ms by the pulse repetition control on the ejection generator.

The pulsed ion signal from the electron multiplier is passed to an amplifier which is an integral part of the quadrupole control unit, the Boxcar Detector and thence to the *Y*-drive of an *X*–*Y* recorder (Hewlett-Packard Model 7044A), the *X*-drive of which is furnished by the quadrupole control unit. The major purpose of the amplifier is to serve as an impedence matching unit between the high (ca. 100 MΩ) output impedence of the boxcar detector, although additional gain can be introduced at this point. Inclusion of the linear gate achieves two results; firstly, since it may be triggered when desired, only stored ions (i.e. those which appear coincidentally with the extraction pulse) give rise to a signal at the recorder and any ions which might appear coincident with the creation pulsed (owing to their creation in unstable positions, etc.) are ignored;

Can. J. Chem. Downloaded from www.nrcresearchpress.com by 210.87.254.5 on 09/05/12
For personal use only.

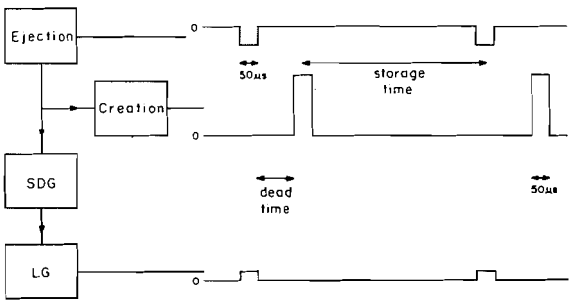

FIG. 2. Pulse train employed under typical operating conditions.

secondly the level recorded during the time that the gate is open is maintained at the output until the next pulse is due, so ensuring that any averaging effect, caused by applying a pulsed signal to the pen recorder, is avoided.

In order to study the ionic reactions occurring in a particular system, the pressure of the compound in the vacuum system is increased to ca. 10^{-4} Torr, and a series of mass spectra observed at several storage times. For each storage time the intensity of each peak is normalized by expressing it as a percentage of the total intensity for that time; this enables comparison between spectra by allowing for fluctuations in ion currents owing to ion-loss processes, etc. It must be emphasized that ion intensities have not been corrected for mass discrimination either in the QUISTOR or in the quadrupole mass filter. The QUISTOR is operated with zero dc bias on the electrodes, hence ions of all mass-to-charge ratios should be stored. Furthermore there is substantial agreement between the ion profiles observed here and those reported by Nixon *et al.* (31) after allowance has been made for the difference in operating pressures. Mass discrimination can be brought about in the QUISTOR so that the device may be operated in a mass spectrometric mode (32); mass spectrometric operation has been effected in the cylindrical storage device also (33).

Electrons with a nominal energy of 55 eV were admitted axially to the QUISTOR in pulses 50 μs wide, and ions ejected after a variable storage time by application of a pulse of −20 V magnitude to the end-cap adjacent to the quadrupole mass filter. It can be shown from the theory of operation of the QUISTOR (34, 35) that when a radio-frequency voltage only is applied to the ring electrode the *m/e* values stable within the trap are given by

$$m/e = \frac{2V_0}{q_z 4\pi^2 f^2 z_0^2}$$

where V_0 is the amplitude of the oscillating potential (radial frequency $2\pi f$ radians s^{-1}) applied between the end-cap electrodes and the ring, z_0 is half the closest distance between the end-caps, and q_z has values between 0 and 0.9. The value of f was fixed at 1.6 MHz and V_0 at 600 V. During individual experiments the source pressure was kept constant and during most experiments this pressure was 2.45×10^{-4} Torr, as measured by the M.K.S. Baratron. At constant pressure, ion–molecule reactions may be studied in the QUISTOR as a function of storage time only.

The DMSO was obtained from the Fischer Scientific Company, dried over molecular sieves, and dissolved gases were removed by freeze–pump–thaw cycles. The DMSO-d_6 was obtained from Stohler Isotope, Montreal and contained traces of mixed deuterated and hydrogenated molecules; the sample was used as obtained.

The progress of the ion–molecule reactions occurring in each sample is illustrated graphically as a plot of the logarithm

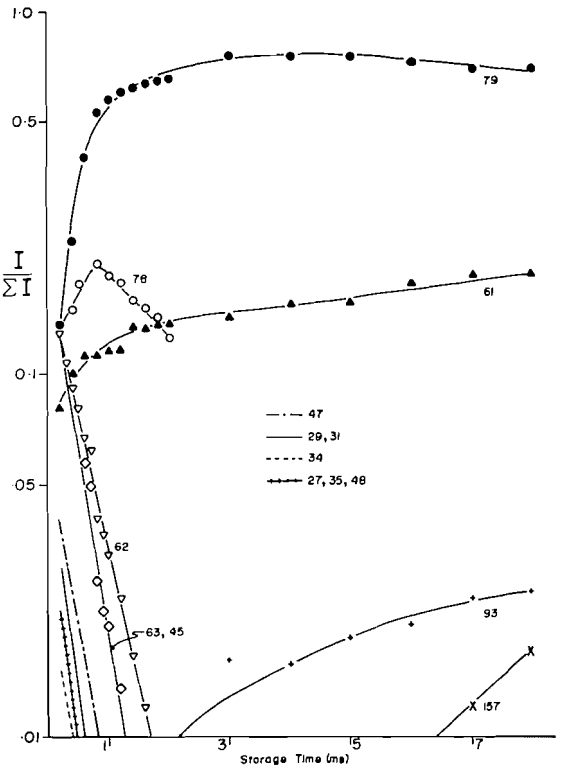

FIG. 3. Variation in the logarithm of normalized ion abundances in DMSO with storage time; 0–8 ms, 1.67 MHz, 600 V(p-p), 2.45×10^{-4} Torr.

of relative ion abundance vs. storage time for each of the reaction products. Some experimental points have been omitted to prevent confusion.

Results and Discussion

While the uses of DMSO vary widely and occur in many fields (36), there are but four studies of the gas phase ion-chemistry: Blais *et al.* (37) studied the formation of positive and negative ions in DMSO; Mackenzie Peers and Muller (38) measured the disappearance rate constants of some primary ions in DMSO; more recently, McAllister (39) and Nixon *et al.* (31) have reported on ICR studies of DMSO.

The DMSO mass spectrum obtained under conditions of continuous ionization and zero storage is in excellent agreement with the electron impact mass spectrum at 10^{-5} Torr reported earlier (37). The ion profiles for DMSO are shown in Fig. 3 for the storage time range 0.2–8 ms, and in Fig. 4 for 0.2–70 ms. Ions of *m/e* 12, 13, 14, 15, 16, 17, 18, 26, 28, 32, 33, and 46 which are not shown in Fig. 3 and Fig. 4 reacted completely in less than 400 μs by charge or proton exchange reactions to produce the parent (M^+) or protonated parent ($(M + 1)^+$) ions. The rapid relative increase in M^+ (*m/e* 78) and $(M + 1)^+$ (*m/e* 79) is shown in Fig. 3. Other fragment or pri-

Can. J. Chem. Downloaded from www.nrcresearchpress.com by 210.87.254.5 on 09/05/12
For personal use only.

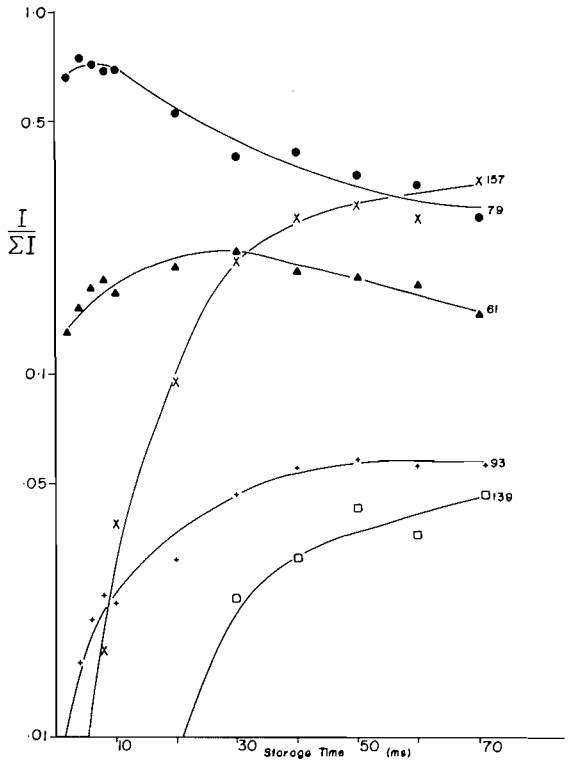

FIG. 4. Variation in the logarithm of normalized ion abundances in DMSO with storage time; 0–70 ms, 1.67 MHz, 600 V (peak to peak), 2.45 × 10^{-4} Torr.

TABLE 1. Ions observed in DMSO and DMSO-d_6 together with structure assignment

m/e in DMSO	*m/e* in DMSO-d_6	Structures	Reference
12	12	C^+	37
13	14	CH^+	37
14	16	CH_2^+	37
15	18	CH_3^+	37
26	28	$C_2H_2^+$	37
27	30	$C_2H_3^+$	37, 40
28	28, 32	CO^+, $C_2H_4^+$	37, 40
29	30, 34	CHO^+, $C_2H_5^+$	37, 40
31	34	H_3CO^+	37
32	32	S^+	37
33	34	HS^+	37
34	36	H_2S^+	37
35	38	H_3S^+	37
45	46	$HC{\equiv}S^+$	37, 40
46	48	H_2CS^+	37
47	50	$[CH_3S]^+$	37
61	66	$[CH_3SCH_2]^+$	37, 40
62	68	$[CH_3SCH_3]^+$	37, 40
63	66	$[CH_3{-}S^+{=}O]$	37, 40
78	84	$[(CH_3)_2SO]^+$	37, 40
79	86	$[(CH_3)_2SOH]^+$	
93	102	$[(CH_3)_2SOCH_3]^+$	
139	150	$[C_4H_{11}S_2O]^+$	
157	170	$[((CH_3)_2SO)_2H]^+$	

mary ions of *m/e* 27, 29, 31, 34, 35, 45, 47, 62, and 63 react more slowly as shown in Fig. 3 and involve proton or charge exchange with parent molecules. The ion-chemistry of a given compound is characterized by the reactivity, with parent molecules, of secondary ions and those primary ions which show an increase in relative concentration due to ion–molecule reactions. In DMSO, the ion-chemistry determining ions are of *m/e* 61, 63, 78, 79, 93, 139, 141, and 157.

The *m/e* 61 ion, which is predominantly $C_2H_5S^+$ (31, 37), was observed to become one of the more abundant species at the longest storage time used in this study, and the observation of *m/e* 66 in DMSO-d_6 supports the assignment of Table 1. In the sole reference to the role of *m/e* 61 (39) it is indicated, from ICR double resonance experiments, that *m/e* 61 is a product ion from a reaction of *m/e* 78.

In this study, growth of the parent ion (*m/e* 78) during the initial 800 μs of storage time was due to charge exchange from fragment ions. Reactions of the parent ion during the subsequent 2 ms (i.e. until the ion intensity could no longer be determined with precision due to the intensity increase of *m/e* 79) are given in Table 2.

The mechanisms for the formation of the $(M + 1)^+$ ion, of *m/e* 79, have been proposed on the basis of ICR double resonance experiments (31, 39) or appearance potential measurements (37). Observation of the $(M + 15)^+$ ion of *m/e* 93 is of interest in this system. It is produced by methyl cation transfer from parent ions (37, 39), a reaction which is not observed in acetone. The *m/e* 102 ion was observed in DMSO-d_6. No reactions have been proposed for *m/e* 93, $[(CH_3)_3SO]^+$, which persists at long storage time and it is concluded from a comparison with the persistence of $(CH_3)_3O^+$ and $(C_2H_5)_3O^+$ (26) that it is a stable and unreactive ion.

In the four studies reported on DMSO, Mackenzie Peers and Muller (38) observe only the disappearance of reacting ions of *m/e* 78 and below without specifying products; Blais *et al.* (37) observe only those reactions which produce ions of *m/e* greater than 78; in the concurrent ICR studies, McAllister (39) reports on double resonance experiments and gives three mass spectra, while Nixon *et al.* (31) report on double resonance experiments, give an ion profile at unspecified pressure, a mass spectrum at unspecified time, and some rate data. Within the four studies the principal inconsistency arises from the observations of high *m/e* ions.

The *m/e* 139 ion, $(M + 61)^+$, was reported by Blais *et al.* (37) and was observed in this work but was not observed in either of the ICR studies. The appearance potential method (37) indicated the formation of *m/e* 139 from parent ion. However, in

TABLE 2. Ion–molecule reactions occurring in DMSO. The parent molecule $(CH_3)_2SO$ is understood as a reactant in each reaction

m/e	Ionic reactants	*m/e*	Products	Reference
141	$[(CH_3)_2SOOSCH_3]^+$	157	$[((CH_3)_2SO)_2H]^+$, CH_2SO	31, 39
79	$[(CH_3)_2SOH]^+$	157	$[((CH_3)_2SO)_2H]^+$	31, 39
78	$[(CH_3)_2SO]^{+\cdot}$	155*	$[C_4H_{11}S_2O_2]^+$, H_2	37
78	$[(CH_3)_2SO]^{+\cdot}$	141*	$[(CH_3)_2SOOSCH_3]^+$, $CH_3\cdot$	31, 39
78	$[(CH_3)_2SO]^{+\cdot}$	139	$[C_3H_7S_2O_2]^+$, $(CH_5\cdot)$	37
78	$[(CH_3)_2SO]^{+\cdot}$	93	$[(CH_3)_2SOCH_3]^+$, $CH_3SO\cdot$	37, 39
78	$[(CH_3)_2SO]^{+\cdot}$	79	$[(CH_3)_2SOH]^+$, $[CH_3SOCH_2]\cdot$	31, 37, 39
78	$[(CH_3)_2SO]^{+\cdot}$	61	$[C_2H_5S]^+$	39
63	$[CH_3SO]^{+\cdot}$	79	$[(CH_3)_2SOH]^+$, $CH_2SO\cdot$	31, 37, 39
63	$[CH_3SO]^{+\cdot}$	78	$[(CH_3)_2SO]^{+\cdot}$	39
62	$[(CH_3)_2S]^{+\cdot}$	79	$[(CH_3)_2SOH]^+$, $[CH_2SCH_3]\cdot$	31, 39
61	$[CH_3SCH_2]^{+\cdot}$	139	$[C_4H_{11}S_2O]^{+\cdot}$	
47	$[CH_3S]^{+\cdot}$	79	$[(CH_3)_2SOH]^+$, $CH_2S\cdot$	39
45	$[CHS]^{+\cdot}$	79	$[(CH_3)_2SOH]^+$, $CS\cdot$	39

*Not observed in this work.

this study, the initial appearance of the *m/e* 139 ion is coincident with the maximum intensity of the *m/e* 61 ion. The ion profiles suggest that in a high pressure domain the *m/e* 139 ion may arise as a collisionally stabilized product of an associative reaction of *m/e* 61 with parent molecule. Blais *et al.* (37) found that the ion intensity of the *m/e* 139 ion could be due to $C_4H_{11}S_2O^+$ and $C_3H_7S_2O_2{}^+$. From a comparison of the experimental and theoretical ratios for the *m/e* 139 to *m/e* 140 peaks they concluded that the ion must be $C_3H_7S_2O_2{}^+$. However in this study, the observation of the *m/e* 150 ion in DMSO-d_6 indicates that the ion is $C_4H_{11}S_2O^{+\cdot}$. As mentioned previously, there is little commentary on the *m/e* 61 ion in the ICR studies.

By way of compensation, the *m/e* 141 ion $(M + 63)^+$ was observed only in the ICR studies and was confirmed (39) by adding xenon with isotopes *m/e* 129–136 for mass calibration.

Double resonance experiments indicated that *m/e* 141 is a product of a reaction involving parent ions

$$[3]\quad \underset{m/e\ 78}{[(CH_3)_2SO]^{+\cdot}} + (CH_3)_2SO \rightarrow \underset{m/e\ 141}{[(CH_3)_2SOCH_3SO]^+} + CH_3\cdot$$

and reacts to form protonated dimer

$$[4]\quad \underset{m/e\ 141}{[(CH_3)_2SOCH_3SO]^+} + (CH_3)_2SO \rightarrow \underset{m/e\ 157}{[((CH_3)_2SO)_2H]^+} + CH_2SO$$

As an unsuccessful search for *m/e* 141 was made in this study, it is suggested that reaction [4] may be endothermic for thermal ions. The explanations offered for the above inconsistencies are not incompatible with a consideration of the operative conditions pertinent to each technique.

The observation of the *m/e* 155 ion (37) has not been confirmed in any subsequent study. The proton bound dimer, *m/e* 157 was observed in the ICR studies and in this study, and is the dominant ion at long storage times. Double resonance experiments indicated that it was a product of reactions involving *m/e* 78 and *m/e* 79. Pressure variation in the QUISTOR indicated unit increase in the order of reaction with respect to DMSO concentration for *m/e* 157 relative to *m/e* 79.

Conclusion

The ion-chemistry of DMSO is understood to be characterized by rapid simple proton transfer and by other processes which are relatively slow. At long reaction times, the thermodynamically favoured species appears to be the associative ion, the proton-bound dimer. While some inconsistency remains to be resolved concerning principally the ions of *m/e* 139, 141, and 155, there is considerable agreement among the results obtained by high pressure mass spectrometry, in cyclotron resonance and quadrupole ion storage techniques. The measure of agreement serves to demonstrate the applicability of quadrupole ion storage mass spectrometry to the study of ion–molecule reactions though with some reservation concerning the definition of ion energy. Previous workers (41, 42) indicate that the energy of a small fraction (<0.1%) of ions in a QUISTOR may be enhanced and open additional endothermic reaction channels.

Acknowledgements

The authors acknowledge gratefully the financial assistance of Trent University and the National Research Council of Canada.

Can. J. Chem. Downloaded from www.nrcresearchpress.com by 210.87.254.5 on 09/05/12
For personal use only.

Can. J. Chem. Downloaded from www.nrcresearchpress.com by 210.87.254.5 on 09/05/12
For personal use only.

1. G. LAWSON and J. F. J. TODD. Mass spectrometry group meeting, Bristol, U.K. 1971. Absts. No. 44.
2. H. G. DEHMELT. Adv. At. Mol. Phys. **5**, 109 (1969).
3. F. G. MAJOR and H. G. DEHMELT. Phys. Rev. **170**, 91 (1968).
4. G. LAWSON, J. F. J. TODD, and R. F. BONNER. *In* Quadrupole mass spectrometry and its applications. *Edited by* P. H. Dawson. Elsevier, Amsterdam. 1976. Chapt. VIII.
5. P. H. DAWSON. Int. J. Mass Spectrom. Ion Phys. **24**, 447 (1977).
6. R. F. BONNER, R. E. MARCH, and J. DURUP. Int. J. Mass Spectrom. Ion Phys. **22**, 17 (1976).
7. R. F. BONNER and R. E. MARCH. Int. J. Mass Spectrom. Ion Phys. **25**, 411 (1977).
8. G. LAWSON, R. F. BONNER, R. E. MATHER, J. F. J. TODD, and R. E. MARCH. J. Chem. Soc. Faraday Trans. 1, **72**, 545 (1976).
9. M. J. HENCHMAN. Ion–molecule reactions. Vol. 1. *Edited by* J. Franklin. Butterworth, London. 1972. pp. 174–175.
10. L. ANDERS. J. Phys. Chem. **73**, 469 (1969).
11. A. G. HARRISON, G. P. NAGY, M. S. CHIN, and A. A. HEROD. Int. J. Mass Spectrom. Ion Phys. **9**, 287 (1972).
12. R. P. CLOW and J. H. FUTRELL. Int. J. Mass Spectrom. Ion Phys. **4**, 165 (1970).
13. W. T. HUNTRESS, JR. and R. F. PINNIZZOTTO, JR. J. Chem. Phys. **59**, 4742 (1973).
14. K. R. RYAN. J. Chem. Phys. **52**, 6009 (1970).
15. R. F. BONNER, J. E. FULFORD, and R. E. MARCH. Int. J. Mass Spectrom. Ion Phys. **24**, 255 (1977).
16. R. F. BONNER, G. LAWSON, J. F. J. TODD, and R. E. MARCH. *In* Advances in mass spectrometry. Vol. 6. *Edited by* A. R. West. Inst. Petroleum, London. 1974. p. 377.
17. R. E. MARCH and R. F. BONNER. Final Report DSS Contract No. OSU4-0092, June 1975.
18. R. E. MARCH and R. F. BONNER. Final Report NRCC Contract No. 031-1077, March 1976.
19. G. B. DEBROU, J. E. FULFORD, E. G. LEWARS, and R. E. MARCH. Int. J. Mass Spectrom. Ion Phys. **26**, 345 (1978).
20. P. AUSLOOS and S. G. LIAS. Chem. Phys. Lett. **51**, 53 (1977).
21. J. L. BEAUCHAMP, M. C. CASERIO, and T. B. MCMAHON. J. Am. Chem. Soc. **96**, 6243 (1975).
22. W. E. W. RUSKA and J. L. FRANKLIN. Int. J. Mass Spectrom. Ion Phys. **3**, 221 (1969).
23. G. P. NAGY, J. C. J. THYNNE, and A. G. HARRISON. Can. J. Chem. **46**, 3609 (1968).
24. B. H. SOLKA and A. G. HARRISON. Int. J. Mass Spectrom. Ion Phys. **14**, 295 (1974).
25. J. M. BRUPBACHER, C. J. EAGLE, and E. TSCHUIKOW-ROUX. J. Phys. Chem. **79**, 671 (1975).
26. T. B. MCMAHON and J. L. BEAUCHAMP. J. Phys. Chem. **81**, 593 (1977).
27. J. E. FULFORD, R. F. BONNER, and R. E. MARCH. Unpublished data.
28. G. LAWSON and J. F. J. TODD. Anal. Chem. **49**, 1619 (1977).
29. R. R. CORDERMAN, P. R. LEBRETON, S. E. BUTTRILL, JR., A. D. WILLIAMSON, and J. L. BEAUCHAMP. J. Chem. Phys. **65**, 4929 (1976); T. B. MCMAHON. Can. J. Chem. **56**, 670 (1978).
30. R. F. BONNER, G. LAWSON, and J. F. J. TODD. Int. J. Mass Spectrom. Ion Phys. **10**, 193 (1972/73).
31. W. B. NIXON, W. S. WOODWARD, M. M. BURSEY, and J. D. HENION. Int. J. Mass Spectrom. Ion Phys. **26**, 115 (1978).
32. R. E. MATHER, R. M. WALDREN, and J. F. J. TODD. Int. J. Mass Spectrom. Ion Phys. To be published.
33. R. E. MARCH, R. E. MATHER, R. M. WALDREN, and J. F. J. TODD. Int. J. Mass Spectrom. Ion Phys. To be published.
34. G. LAWSON, R. F. BONNER, and J. F. J. TODD. J. Phys. E, **6**, 357 (1973).
35. P. H. DAWSON and N. R. WHETTEN. Adv. Electron. Electron Phys. **27**, 59 (1969).
36. S. W. JACOB, E. E. ROSENBAUM, and D. C. WOOD (*Editors*). Dimethyl sulphoxide. Vol. 1. M. Dekker, New York. 1971.
37. J. C. BLAIS, M. COTTIN, and B. GITTON. J. Chim. Phys. Physiochim. Biol. **67**, 1475 (1970).
38. A. MACKENZIE PEERS and J. C. MULLER. Int. J. Mass Spectrom. Ion Phys. **16**, 321 (1975).
39. T. MCALLISTER. Int. J. Mass Spectrom. Ion Phys. **25**, 353 (1977).
40. H. BUDZIKIEWICZ and C. DJERASSI. Mass spectrometry of organic compounds. Holden-Day Inc., London. 1967.

Cadmium complexation by soil fulvic acid

BILL BRADY AND GORDON K. PAGENKOPF[1]

Department of Chemistry, Montana State University, Bozeman, MT 59717

Received February 6, 1978

BILL BRADY and GORDON K. PAGENKOPF. Can. J. Chem. **56**, 2331 (1978).

A soil fulvic acid has been characterized and the complexation stability constants with cadmium have been evaluated. The average gram formula weight of the fulvic acid is 2775. Three complexes of stoichiometry CdFA, Cd_2FA, and Cd_3FA have been observed. The respective conditional stability constants at pH 5.7 are $10^{5.3}$, $10^{9.8}$, and $10^{14.0}$; at pH 6.7 they are $10^{5.6}$, $10^{10.6}$, and $10^{15.5}$; and at pH 7.7 they are $10^{6.0}$, $10^{10.7}$, and $10^{15.4}$.

BILL BRADY et GORDON K. PAGENKOPF. Can. J. Chem. **56**, 2331 (1978).

On a caractérisé un acide fulvique provenant du sol et on a évalué ses constantes de stabilité de complexation avec le cadmium. Le poids formulaire gramme moyen de l'acide fulvique est de 2775. On a observé trois complexes de stoechiométrie CdFA, Cd_2FA et Cd_3FA. Les constantes de stabilité conditionelle respectives à un pH de 5.7 sont $10^{5.3}$, $10^{9.8}$ et $10^{14.0}$; à un pH de 6.7, elles sont $10^{5.6}$, $10^{10.6}$ et $10^{15.5}$ et à un pH de 7.7 elles sont $10^{6.0}$, $10^{10.7}$ et $10^{15.4}$.
[Traduit par le journal]

Can. J. Chem. Downloaded from www.nrcresearchpress.com by 210.87.254.40 on 09/05/12
For personal use only.

The nature and extent of the interactions between trace metals and naturally occurring complexing ligands such as fulvic and humic acids has been and continues to be investigated by an ever-expanding number of research groups. Objectives of some of these studies focus on the role played by chelating agents in the transport of trace metals through natural water systems.

Techniques that establish the complexing capacity of natural waters include copper precipitation (1, 2), copper removal by a chelating resin (3), and oxidation of complexed cobalt(II) (4). Anodic stripping voltammetry (5, 6), differential pulse polarography (7, 8), and ion selective electrodes (9, 10), have also been utilized to determine the degree of trace metal complexation in a variety of waters.

A variety of models have been advanced to rationalize the complexation of metal ions by humic and fulvic acids (11–21). Most of these propose complexation by carboxylic acid groups, phenolic oxygen groups, or a combination similar to that observed in salicylic acid. A spatial arrangement of donors similar to that in catechol has also been suggested. Some studies have provided conditional stability constants and gram formula weights of the complexing agents (6, 10).

This report presents the characterization of a fulvic acid isolated from soil. Included in the characterization is an evaluation of average gram formula weight, pK_a's of ionizable protons, and conditional stability constants for cadmium complexation.

Experimental Section

The fulvic acid used in this study was extracted from a coastal Oregon soil provided by Dr. Jerry Simonson, Department of Plant and Soil Science, Oregon State University. Approximately 200 g of the soil were extracted with 0.1 *N* HCl for 12 h. The solution was filtered through Whatman 42 and 0.45 μm paper, and the filtrate was passed through a Dowex 50 (hydrogen form) cation exchange column. The solution was evaporated to dryness under vacuum, 15 mm. Additional drying was obtained over calcium chloride. The yield was approximately 0.5 g with a 7% ash content. The ash was found to be primarily sodium. Elemental analysis of the isolated fulvic acid provided 44.4% carbon, 4.1% hydrogen, and 45.2% oxygen.

Total acidity was determined by the barium precipitation method (22–24) and found to be 97.9 g/equiv. Carboxyl acidity was determined by the calcium acetate method (25) and found to be 142.2 g/equiv. An ebullioscopic determination using water solvent provided a g-equiv. wt. of 126.

Potentiometric titration data were obtained using 75–300 mg/l fulvic acid solutions. Volumes, ranging from 50–100 ml, were titrated using standard sodium hydroxide solutions. Ionic strength was maintained at 0.01 *M* with NaCl and the temperature was 25.0°C. The electrode system was a glass and an asbestos junction SCE coupled to a Radiometer M26 or Seargent Welch NX. Cadmium ion activity in solution was monitored by an Orion 94–48 cadmium ion selective electrode and an Orion double junction Ag/AgCl reference electrode. The titration cell was designed to permit simultaneous monitoring of hydrogen and cadmium ion activity. The concentrations of cadmium were also monitored with a Princeton Applied Research Model 374 electrochemical analyzer using hanging drop mercury electrode and anodic stripping voltammetry. Doubly-distilled water was used to prepare all solutions and inorganic salts were recrystallized to remove impurities. Computer programs COMICS (26), p-BAR (27), and pHPLOT-2 were used to facilitate data analysis.[2]

Results and Discussion

Cadmium Complexation

Fulvic acid has been titrated, at constant pH, with cadmium in an attempt to establish the stoichiometry

[1]Author to whom correspondence should be addressed.

[2]From C. Whitworth, Department of Chemistry, Montana State University, Bozeman, MT. 1977.

Can. J. Chem. Downloaded from www.nrcresearchpress.com by 210.87.254.40 on 09/05/12
For personal use only.

of the complexation reaction(s), an apparent average gram formula weight of fulvic acid, and an evaluation of the conditional stability constants. The general complexation reaction is shown in reaction [1].

[1] $$n\mathrm{Cd}^{2+} + m\mathrm{H}_y\mathrm{FA} \rightleftarrows \mathrm{Cd}_n\mathrm{H}_{y-x}\mathrm{FA}_m + mx\mathrm{H}^+$$

where H_xFA represents fulvic acid that has some unknown number of bound protons and $0 \leq x \leq 2n$. No ionic charges have been specified, however, in some cases these may be fairly high. At low concentrations of total metal and total ligand it is likely that the predominant complex will be of 1:1 stoichiometry. The specific complexation reaction is shown in reaction [2].

[2] $$\mathrm{Cd}^{2+} + \mathrm{H}_x\mathrm{FA} \rightleftarrows \mathrm{CdFA} + x\mathrm{H}^+$$

and the equilibrium expression is

[3] $$\beta_1 = \frac{[\mathrm{CdFA}][\mathrm{H}^+]^x}{[\mathrm{H}_x\mathrm{FA}][\mathrm{Cd}^{2+}]}$$

where β_1 is the stability constant. The mass balance equations are:

[4] $$[\mathrm{Cd}]_t = [\mathrm{Cd}^{2+}] + [\mathrm{CdFA}]$$

and

[5] $$[\mathrm{FA}]_t = [\mathrm{H}_x\mathrm{FA}] + [\mathrm{CdFA}]$$

Combination of eqs. [3] and [5] provides eq. [6].

[6] $$\frac{[\mathrm{FA}]_t}{[\mathrm{CdFA}]} = 1 + \frac{[\mathrm{H}^+]^x}{\beta_1[\mathrm{Cd}^{2+}]}$$

The concentration of fulvic acid is $[FA]_t$ = g FA/l/GFW where GFW is the gram formula weight of fulvic acid.

Substitution into eq. [6] gives

[7] $$\frac{\text{g FA/l}}{[\mathrm{CdFA}]} = \mathrm{GFW} + \frac{(\mathrm{GFW})[\mathrm{H}^+]^x}{\beta_1[\mathrm{Cd}^{2+}]}$$

Monitoring of a titration of fulvic acid with a cadmium ion selective electrode, at constant pH, provides the Cd^{2+} and CdFA concentrations. A plot of g FA/l/[CdFA] vs. $1/[Cd^{2+}]$ should be linear over the concentration range where only the 1:1 complex forms. Extrapolation to infinite Cd^{2+} concentration provides the average gram formula weight of fulvic acid and $\beta_1/[H^+]^x$ may be calculated from the slope. This AGFW is for complexation and may differ from values obtained by other procedures if the fulvic acid exhibits sizeable polydispersion. In addition, some FA molecules may contain no complexation sites; however, this is doubtful.

Such a plot for the titration of 12.5 mg/l at pH 6.7 is shown in Fig. 1. From the intercept GFW = 2775 and $\beta_1/[H^+]^x = 4.4 \times 10^5\ M^{-1}$.

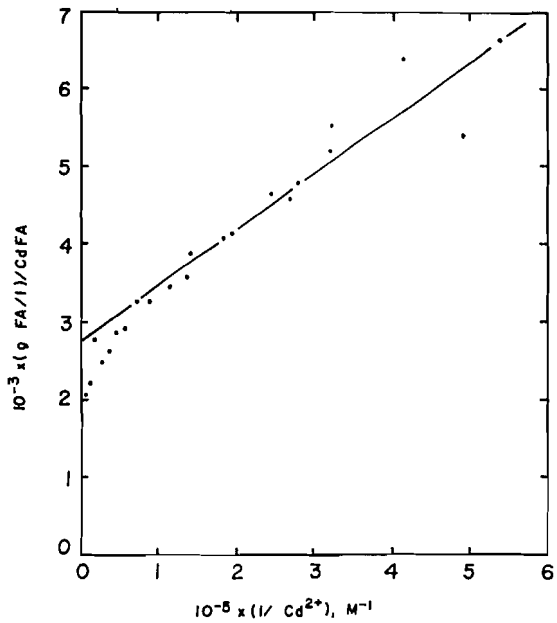

FIG. 1. Evaluation of the average gram formula weight and $\beta_1/[H^+]^x$ at pH 6.7.

It should be noted that deviation from linearity is observed at the higher concentrations of free cadmium. This is indicative of a change in stoichiometry and in this case the formation of complexes that have more than 1 cadmium per fulvic acid molecule.

A term $\bar{m}$, the average number of cadmium ions per fulvic acid, has been defined to facilitate the evaluation of the successive β_n values, as in eq. [8].

[8] $$\bar{m} = \frac{[\mathrm{CdFA}] + 2[\mathrm{Cd_2FA}] + 3[\mathrm{Cd_3FA}] + \ldots}{[\mathrm{H}_x\mathrm{FA}] + [\mathrm{CdFA}] + [\mathrm{Cd_2FA}] + [\mathrm{Cd_3FA}] + \ldots}$$

For the 2:1 complex eq. [8] becomes

[9] $$\bar{m} = (1 - \bar{m})[\mathrm{Cd}^{2+}]\beta_1/[\mathrm{H}^+]^x + (2 - \bar{m})[\mathrm{Cd}^{2+}]\beta_2/[\mathrm{H}^+]^{2x}$$

and the values of $\bar{m}$ are calculated from

[10] $$\bar{m} = \frac{[\mathrm{Cd}]_t - [\mathrm{Cd}^{2+}]}{[\mathrm{FA}]_t}$$

The value of $\beta_2/[H^+]^{2x}$ is calculated from the data that provides $\bar{m}$ values in the range of 1.2 to 1.8.

For the 3:1 complex

[11] $$\frac{\beta_3}{[\mathrm{H}^+]^{3x}} = \frac{\bar{m} - \dfrac{(1-\bar{m})[\mathrm{Cd}^{2+}]\beta_1}{[\mathrm{H}^+]^x} - \dfrac{(2-\bar{m})[\mathrm{Cd}^{2+}]^2\beta_2}{[\mathrm{H}^+]^{2x}}}{(3-\bar{m})[\mathrm{Cd}^{2+}]^3}$$

and values of $\bar{m}$ in the range of 2.2 to 2.8 are used to calculate $\beta_3/[H^+]^{3x}$. The values of $\beta_n/[H^+]^{nx}$ are

Can. J. Chem. Downloaded from www.nrcresearchpress.com by 210.87.254.40 on 09/05/12
For personal use only.

TABLE 1. Conditional stability constants for the complexation of cadmium by fulvic acid

	log ($\beta_n/[H^+]^{nx}$)		
n	pH = 5.7	pH = 6.7	pH = 7.7
1	5.3	5.6	6.0
2	9.8	10.6	10.7
3	14.0	15.5	15.4

listed in Table 1. The fulvic acid concentration ranged from 5.05 to 27.2 mg/l and the $[Cd]_t$ ranged from 7.0×10^{-7} to 1.1×10^{-3} M. With this range of ligand and metal concentrations the free cadmium concentration varies from 6.3×10^{-7} to 6.3×10^{-4} M. The concentration of free cadmium may be calculated using the computer program (26) COMICS, total metal, total ligand, and the $\beta_n/[H^+]^{nx}$ values. A plot of $[Cd^{2+}]$ calculated as a function of $[Cd^{2+}]$ observed is shown in Fig. 2. The correlation coefficient is 0.95 which is a good indication of the uncertainty in the respective conditional stability constants.

An average gram formula weight of 2775 is larger than the values reported by Hansen and Schnitzer (28) whose value ranged from 275 to 2110. This value is also greater than values obtained using copper and lead ion selective electrodes (10). A conditional stability constant of 4.4×10^5 M^{-1} at pH 6.7 is comparable to the values observed for the complexation of copper (6, 10) and lead in this pH range (10). The other studies have not reported conditional constants for the complexes containing more than 1 metal per FA.

The same experimental procedure was utilized to obtain $\beta_n/[H^+]^{nx}$ values at pH 5.7 and 7.7 (see Table 1). From these data the apparent value of x is 0.5. A value of 0.6 has been observed in other studies (6, 10), and a value of 1.0 would be expected if the mode of coordination by fulvic acid is similar to that exhibited by salicylic acid where one donor is a carboxyl oxygen and the other is a phenolic oxygen. It is presumed that the pK_a's of the phenolic oxygens will be greater than 8 and thus hydrogen ion dependence should approach unity. This interpretation assumes that the mode of complexation in each fulvic acid molecule is similar and thus can be quantitatively compared to precisely defined complexing agents. The data are presented in Table 2.[3]

Potentiometric Titration of Fulvic Acid

The titration of acidified fulvic acid with sodium hydroxide is shown in Fig. 3. The absence of any intermediate plateau regions indicates an even spacing and central tendency of the pK_a values. The addition of strong acid has repressed the dissociation of the most acidic protons. Using the carboxyl acidity and the average gram formula weight, there appears to be approximately 20 carboxyl groups per molecule. Each one of these will require 0.148 ml of titrant for neutralization. Analysis of the titration curve indicates that 5.36 ml of NaOH is required to neutralize the added HCl, and that ten acidic groups are titrated by pH 4.4. Over the pH range of 5.7 to

[3]Supplementary material listing pCd_t, pCd, and pH is available from the authors upon request.

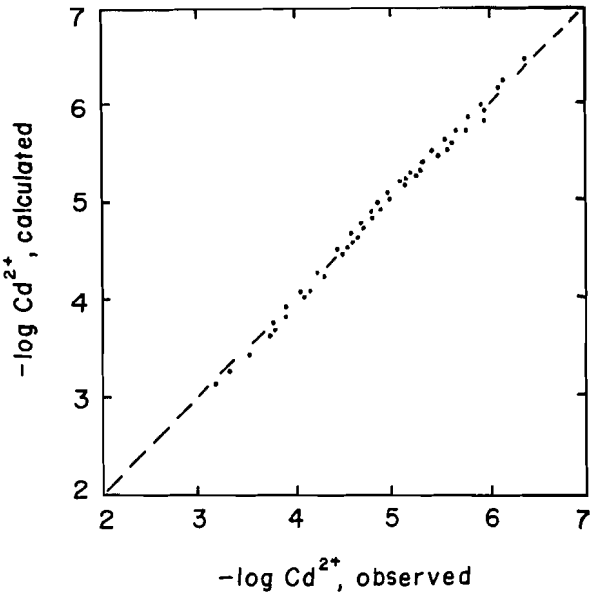

FIG. 2. Correlation between calculated and observed Cd^{2+} concentrations at pH 6.7.

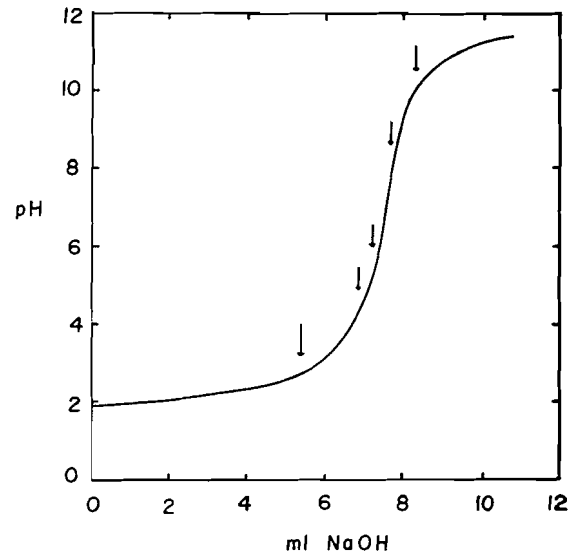

FIG. 3. Titration of acidified fulvic acid with NaOH. $[FA]_t = 3.2 \times 10^{-4}$ M, [HCl] = 0.0117 M, [NaCl] = 0.10 M, [NaOH] = 0.109 M, and total volume = 50.0 ml.

Can. J. Chem. Downloaded from www.nrcresearchpress.com by 210.87.254.40 on 09/05/12
For personal use only.

TABLE 2. Data for complexation of Cd^{2+} by fulvic acid $I = 0.01$ M (NaCl), $T = 25.0°C$, $p(x) = -\log(x)$

(*a*) pH = 5.70

pCd_t	pFA	pCd^{2+}	pCd_t	pFA	pCd^{2+}	pCd_t	pFA	pCd^{2+}
5.29	2.07	5.30	5.41	1.66	5.60	4.59	1.06	5.23
4.99	2.07	5.01	5.36	1.66	5.53	4.51	1.07	5.12
4.82	2.07	4.83	5.27	1.66	5.43	4.45	1.07	5.01
4.70	2.07	4.70	5.20	1.66	5.34	4.39	1.07	4.92
4.52	2.07	4.52	5.11	1.66	5.22	4.34	1.07	4.84
4.40	2.07	4.38	5.01	1.66	5.09	4.30	1.07	4.78
4.26	2.07	4.24	4.92	1.66	4.98	4.22	1.07	4.66
6.02	2.01	6.15	4.82	1.66	4.86	4.16	1.07	4.55
4.41	2.02	4.46	4.74	1.66	4.75	4.10	1.07	4.46
4.11	2.02	4.16	5.23	1.37	5.72	4.05	1.07	4.39
3.82	2.02	3.85	4.96	1.37	5.37	4.01	1.07	4.33
3.65	2.03	3.68	4.80	1.38	5.14	3.97	1.07	4.29
3.43	2.03	3.46	4.68	1.38	4.98	3.93	1.07	4.22
3.15	2.05	3.16	4.59	1.38	4.85	3.90	1.07	4.17
2.96	2.07	2.96	4.52	1.38	4.76	3.86	1.08	4.13
6.02	2.01	6.13	4.45	1.38	4.67	3.84	1.08	4.09
5.72	2.01	5.85	4.30	1.38	4.48	3.81	1.08	4.05
5.54	2.01	5.59	4.13	1.38	4.26	3.78	1.08	4.03
5.32	2.01	5.43	4.00	1.38	4.11	3.75	1.08	3.97
5.06	2.01	5.14	3.91	1.38	4.01	3.70	1.08	3.91
4.74	2.01	4.80	3.76	1.38	3.85	3.66	1.08	3.86
4.41	2.02	4.46	3.65	1.38	3.72	3.62	1.08	3.80
4.02	2.02	4.06	3.61	1.38	3.68	3.54	1.08	3.71
6.01	1.66	6.29	3.53	1.38	3.59	3.48	1.08	3.64
5.84	1.66	6.10	3.46	1.38	3.52	3.42	1.08	3.56
5.71	1.66	5.96	3.36	1.38	3.41	3.33	1.09	3.45
5.61	1.66	5.86	3.27	1.38	3.32	3.21	1.09	3.34
5.54	1.66	5.77	3.19	1.38	3.24	3.15	1.09	3.26
5.47	1.66	5.68	3.14	1.38	3.17			

(*b*) pH = 6.7

pCd_t	pFA	pCd^{2+}	pCd_t	pFA	pCd^{2+}	pCd_t	pFA	pCd^{2+}
6.02	2.31	6.14	4.75	1.92	4.85	4.96	1.57	5.55
5.72	2.31	5.91	4.67	1.92	4.76	4.80	1.57	5.28
5.54	2.31	5.70	4.58	1.92	4.66	4.68	1.57	5.10
5.32	2.31	5.43	4.50	1.92	4.56	4.59	1.57	4.97
5.17	2.31	5.26	4.37	1.92	4.42	4.51	1.57	4.86
5.06	2.31	5.14	4.17	1.93	4.20	4.45	1.57	4.78
4.90	2.31	4.94	4.02	1.93	4.05	4.39	1.57	4.69
4.79	2.32	4.81	3.88	1.93	3.90	4.34	1.57	4.62
4.62	2.32	4.64	3.73	1.94	3.75	4.30	1.57	4.57
6.02	1.92	6.37	5.31	1.83	5.73	4.22	1.57	4.47
5.74	1.92	6.08	5.20	1.83	5.57	4.07	1.57	4.27
5.59	1.92	5.90	5.11	1.83	5.45	3.96	1.57	4.15
5.47	1.92	5.75	4.92	1.84	5.21	3.63	1.58	3.76
5.37	1.92	5.61	4.54	1.86	4.71	3.41	1.58	3.51
5.28	1.92	5.51	4.37	1.87	4.52	3.24	1.58	3.32
5.17	1.92	5.38	4.16	1.87	4.28	3.12	1.58	3.20
5.09	1.92	5.28	3.96	1.87	4.07	4.83	1.92	4.95
5.00	1.92	5.16	3.77	1.87	3.87	5.22	1.57	5.95
4.92	1.92	5.07	3.62	1.88	3.71			

(*c*) pH = 7.7

pCd_t	pFA	pCd^{2+}	pCd_t	pFA	pCd^{2+}
6.02	2.31	6.32	4.66	2.32	4.71
5.72	2.31	5.99	4.45	2.32	4.50
5.44	2.31	5.61	4.24	2.32	4.27
5.29	2.31	5.43	4.02	2.32	4.04
5.17	2.31	5.29	3.72	2.32	3.74
4.98	2.32	5.07	3.43	2.33	3.45
4.84	2.32	4.91			

Can. J. Chem. Downloaded from www.nrcresearchpress.com by 210.87.254.40 on 09/05/12
For personal use only.

TABLE 3. Stability constants of selected ligands with Cd^{2+} (29)

Ligand	log K_1
Acetate	1.7
Oxalic	4.0
Phthalic	2.5
Malonic	3.3
Glycinate	4.8
N-methyliminodiacetate	6.8
Nitrilotriacetate	9.8

7.7 an additional 2.5 acidic groups are neutralized and twenty protons are neutralized by pH 10.1.

These results suggest that this fulvic acid possesses a high negative charge in the pH range often encountered in natural waters. Over the pH range of cadmium complexation, 5.7–7.7, there is a net change of approximately 2.5 units. This is an average change and thus it is unlikely that all are directly involved in the preferred coordination sites. As a consequence, the conditional stability constants have less than unity dependence upon hydrogen ion concentration.

The presence of twenty carboxylic groups and an additional eight phenolic oxygen requires a minimum of 27.7% oxygen by weight. Elemental analysis indicated 45.2% oxygen and thus there is ample functional group oxygen and an additional 17% remains for bridging and other groups.

The stability constants measured in this study are indicative of the sites that have the proper spatial orientation to form chelate rings when coordinated to cadmium. Stability constants for the complexation of cadmium with a variety of carboxylate type ligands are listed in Table 3. These data indicate that formation of a five-membered chelate ring adds from 2 to 2.5 log units to the stability constant. On the basis of this cadmium should be coordinated to at least three donors of the fulvic acid molecule.

One of the most popular models for complexation by naturally occurring ligands is similar to that of salicylic acid, which involves a carboxyl group and a phenolic oxygen. The change in the conditional stability constant over the pH range of 5.7 to 7.7 is approximately one log unit for each of the three $\beta_n/[H^+]^{nx}$ values. If phenolic coordination is involved the pK_a of the phenolic groups would have to be less than 6.7. The majority of the pK_a values for characterized phenolic hydrogens is greater than 9. Many metal ions do displace phenolic hydrogens upon complexation, however, the conditional stability constants decrease rapidly as the hydrogen ion concentration increases and thus it is questionable if this mode of complexation exhibits sufficient stability to be important in the near neutral pH region. In addition at least three cadmium ions can coordinate to FA which is greater than the net proton-level change in the pH range of 5.7–7.7. The large negative charge on the ligand will add stability to the complexes by reducing the rate of complex dissociation and enhanced rate of complex formation.

The magnitude of the successive stability constants indicates that this fulvic acid contains several subunits of similar complexing capability. Subsequent degradation of the molecule could provide a ligand exhibiting comparable complexation stability, however, the apparent gram formula weight would be less.

The stoichiometry of these complexes is opposite to those reported in other studies (10), but it is consistent with the observations that fulvic and humic acids can be precipitated from solutions with high concentrations of transition metals. Another report has alluded to the formation of complexes that contain more than one metal (30).

Acknowledgements

This research was funded in part by the U.S. Environmental Protection Agency, Research Grant No. R803950, Duluth, Minnesota and Research Grant No. R-803727-01-1, Cincinnati, Ohio.

1. S. E. MANAHAN and R. A. KUNKEL. Anal. Chem. **45**, 1465 (1973).
2. D. R. JONES IV and S. E. MANAHAN. Anal. Chem. **49**, 10 (1977).
3. R. J. STOLZBERG and D. ROSIN. Anal. Chem. **49**, 226 (1977).
4. K. W. HANCK and J. W. DILLARD. Anal. Chem. **49**, 404 (1977).
5. T. A. O'SHEA and K. H. MANCY. Anal. Chem. **48**, 1603 (1976).
6. M. S. SHUMAN and G. P. WOODWARD, JR. Environ. Sci. Technol. **11**, 809 (1977).
7. J. G. OSTERYOUNG and R. A. OSTERYOUNG. Am. Lab. **4**(7), 8 (1972).
8. R. ERNST, H. E. ALLEN, and K. H. MANCY. Water Res. **9**, 969 (1975).
9. J. GARDNER. Water Res. **8**, 23 (1974).
10. J. BUFFLE, F. GRETER, and W. HAERDI. Anal. Chem. **49**, 216 (1977).
11. F. L. HIMES and S. A. BARBER. Soil Sci. Soc. Am. Proc. **21**, 368 (1957).
12. R. S. BECHWITH. Nature, **184**, 745 (1959).
13. M. SCHNITZER and S. I. M. SKINNER. Soil Sci. **96**, 86 (1963); **99**, 278 (1965).
14. S. S. KHANNA and F. J. STEVENSON. Soil Sci. **93**, 298 (1962).
15. M. SCHNITZER and E. H. HANSEN. Soil Sci. **109**, 333 (1970).
16. D. S. GAMBLE, M. SCHNITZER, and I. HOFFMAN. Can. J. Chem. **48**, 3197 (1970).
17. P. G. MANNING and S. RAMAMOORTHY. J. Inorg. Nucl. Chem. **35**, 1577 (1973).
18. V. CHEAM and D. S. GAMBLE. Can. J. Soil Sci. **54**, 413 (1974).
19. F. J. STEVENSON. Soil Sci. **123**, 10 (1977).
20. D. S. GAMBLE. Can. J. Chem. **51**, 3217 (1973).
21. J. B. GREEN and S. E. MANAHAN. Can. J. Chem. **55**, 3248 (1977).
22. J. D. BROOKS and STERNHILL. Aust. J. Appl. Sci. **8**, 206 (1957).

23. I. V. AVGUSHEVICH and N. M. KARAVAYER. Sov. Soil Sci. **4**, 416 (1965).
24. M. SCHNITZER and U. C. GUPTA. Soil Sci. Soc. Am. Proc. **29**, 274 (1965).
25. M. SCHNITZER and S. U. KAHN. Humic substances in the environment. Marcel Dekker, Inc., New York, NY. 1972. 327 pp.
26. D. D. PERRIN and I. G. SAYCE. Talanta, **14**, 833 (1967).
27. A. CORSINI and E. J. BILLO. J. Inorg. Nucl. Chem. **32**, 1241 (1970).
28. E. H. HANSEN and M. SCHNITZER. Anal. Chem. Acta, **46**, 247 (1969).
29. L. G. SILLEN and A. E. MARTELL. Stability constants supplement No. 1. Special Publication 25, The Chemical Society, London, 1971.
30. M. ADHIKARI and G. C. HAZRA. J. Indian Chem. Soc. **49**, 947 (1972).

Can. J. Chem. Downloaded from www.nrcresearchpress.com by 210.87.254.40 on 09/05/12
For personal use only.

Ion mobilities in gaseous ammonia

ERIC S. SENNHAUSER AND DAVID A. ARMSTRONG
Department of Chemistry, University of Calgary, Calgary, Alta., Canada T2N 1N4

Received March 16, 1978

ERIC S. SENNHAUSER and DAVID A. ARMSTRONG. Can. J. Chem. **56**, 2337 (1978).

Gaseous ammonia at pressures in the range 200 to 1200 Torr was subjected to continuous irradiation by 40 kVp X-rays and the mobilities of the positive and negative ions (μ_+ and μ_-, respectively) were determined by a pulsed-drift method. The averages of μ_+ and μ_- agreed well with results obtained by another method. The magnitude of μ_+ varied from 3.2 ± 0.2 cm^2 V^{-1} s^{-1} at 200 Torr to 0.53 ± 0.04 cm^2 V^{-1} s^{-1} at 1200 Torr. While μ_- converged to the same value at 1200 Torr, it was slightly higher, 3.3 ± 0.2 cm^2 V^{-1} s^{-1}, at 200 Torr. The pressure dependence and actual magnitudes of μ_+ were found to be in good agreement with theoretical predictions based on ion–molecule collision rate theory for $NH_4^+ \cdot xNH_3$ clustered ions of known x.

ERIC S. SENNHAUSER et DAVID A. ARMSTRONG. Can. J. Chem. **56**, 2337 (1978).

On a soumis de l'ammoniac gazeux, à des pressions allant de 200 à 1200 Torr, à une irradiation continue par 40 kVp de rayons-X et on a déterminé les mobilités des ions positif et négatif (μ_+ et μ_- respectivement) par la méthode de la diffusion pulsée. Les moyennes des valeurs μ_+ et μ_- sont en bon accord avec les résultats obtenus par une autre méthode. La grandeur de μ_+ varie de 3.2 ± 0.2 cm^2 V^{-1} s^{-1} à 200 Torr jusqu'à 0.53 ± 0.04 cm^2 V^{-1} s^{-1} à 1200 Torr. Alors que la valeur de μ_- converge vers la même valeur à 1200 Torr, elle est légèrement plus élevée, 3.3 ± 0.2 cm^2 V^{-1} s^{-1}, à 200 Torr. On a trouvé que les valeurs réelles de μ_+ de même que sa relation avec la pression sont en accord avec les prédictions théoriques basées sur la théorie des vitesses des collisions ion–molécule pour des agrégats d'ions $NH_4^+ \cdot xNH_3$ où x est connu.

[Traduit par le journal]

Introduction

The measurement of ion mobilities can provide information on ion–molecule collision frequencies, and is also a potential means of identifying different long-lived ions in gases subjected to ionising radiation at normal pressures. More specifically, mobilities are required for the calculation of three body ion neutralization rate coefficients (1), which are of interest to us (2). A recent publication from this laboratory (2) reported the measurement of μ, the average of the positive and negative ion mobilities, in ammonia vapour which contained traces of the electron scavenger nitrous oxide and was irradiated at pressures in the range 100 to 1200 Torr. In this paper a drift technique for measuring the individual ion mobilities μ_+ and μ_- is described and applied to the ammonia system. The average of μ_+ and μ_- at pressures in the range 200 to 1200 Torr was found to be in good agreement with the values of μ previously reported for that pressure range. Also the values of μ_+ were briefly compared with predictions based on ion–molecule collision rate theory.

Experimental

Materials

Sample preparation and material purification were performed in a mercury-free vacuum line. Electronic grade ammonia (99.999% min. purity, Matheson Co.) was sublimed from one trap to another at 77 K and noncondensibles were continuously pumped off. After this it was condensed in a trap containing a freshly sublimed mirror of sodium, and then stored at 77 K. Nitrous oxide (98.0% min. purity, Matheson Co.) was thoroughly degassed and distilled several times from one trap to another at 77 K, the last fractions of the distillates being discarded. It was also stored at 77 K.

Apparatus

The irradiation cell was of cylindrical design (Fig. 1) with plane parallel electrodes enclosed in a Pyrex glass envelope. The end electrodes were made of nickel and had a diameter of 6 cm. The two inner grid electrodes consisted of nickel mesh (70 wires/inch, Buch Bee-Mars) sandwiched between two thin concentric nickel rings. The circular mesh area had a diameter of 3 cm. The distances between the electrodes of the first, second, and third cell compartments were 1, 4, and 1 cm, respectively. These are subsequently referred to as d_1, d_2, and d_3.

The space between the first two electrodes on the left is referred to as the radiation compartment, and was subjected to a continuous X-ray beam collimated to 4 or 7 mm in width. The X rays were generated by a Muller MG 150 unit and their peak energy could be varied. Low X-ray energies gave rise to lower background currents (see later) and a peak voltage of 40 kV was normally used.

High voltage (HV) pulses of selectable duration were generated from a dc voltage supply (Harrison 6525A power module) controlled by a switching device, which consisted of high voltage transistors arranged in series and driven by an optical isolator/coupler through an appropriate bias network. The trigger input was from a Tektronix PG 501 pulser and this determined the frequency of the HV pulses applied to the irradiated compartment. The resistors R_1 and R_2 (Fig. 1) were selected from six serially arranged 50 kΩ resistors (OMI, 1%, inductionless) to provide the desired potential gradients

Can. J. Chem. Downloaded from www.nrcresearchpress.com by 210.87.254.40 on 09/05/12
For personal use only.

Can. J. Chem. Downloaded from www.nrcresearchpress.com by 210.87.254.40 on 09/05/12
For personal use only.

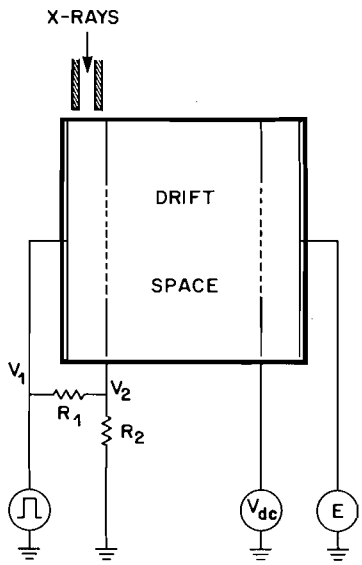

FIG. 1. Cylindrical irradiation–drift cell. V_1 and V_2, pulsed high voltage applied to electrodes bounding the radiation compartment; V_{dc}, steady voltage applied to second grid at end of drift space; E, electrometer; R_1 and R_2, resistors.

in the radiation compartment and drift space. The second grid was connected to a Fluke 412B DC power supply and throughout the experiment it remained at a constant potential V_{dc}, which had the same polarity as the pulsed potentials V_1 and V_2 in Fig. 1. The magnitude of V_2 was always greater than V_{dc} and during the 'on' period for V_1 and V_2 the difference $(V_2 - V_{dc})$ determined E_d, the field across the drift space, while $V_1 - V_2$ determined E_r, the field in the radiation compartment.

For positive potentials positive ions would be swept out of the radiation compartment and across the drift space. All ions crossing the drift space during the 'on' period for V_1 and V_2 would pass through the second grid and be collected. The current due to these was measured on a Victoreen 475A dynamic capacitor electrometer. During the 'off' period positive ions in the drift space were pushed back into the radiation volume or collected on the first grid electrode. Negative ions, which might enter the drift space in the 'off' period and cross it, could not reach the collecting electrode because of the opposing potential on the second grid. For negative applied potentials the situations for positive and negative ions are of course reversed. During an experiment the length of the HV pulse (i.e. the 'on' period) was varied, but the number of pulses per second, v ($\sim$(75 ms)$^{-1}$), was held constant, and adjusted so that steady state conditions would be established in the radiation compartment during the 'off' period.

Results

Drift Current Profiles and Data Analysis

In an experiment, the current was measured as a function of the HV pulse length, t, which was generally varied over the range 0 to 20 ms. Plots of ion drift current vs. t for a sample of 200 Torr NH_3 with 5 Torr N_2O as electron scavenger (3) are shown in Fig. 2. The current I is seen to remain at the background level for some period, then rise rather steeply, bend over, and finally rise linearly with a much smaller slope.

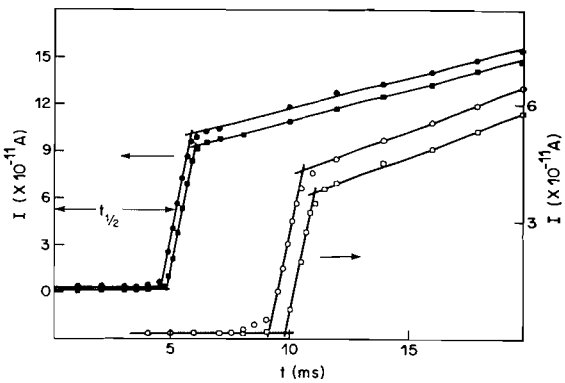

FIG. 2. Plots of ion current vs. time of application of high voltage. ● and ■, E_r = 300 V cm^{-1}, E_d = 250 V cm^{-1}; ○ and □, E_r = 450 V cm^{-1}, E_d = 125 V cm^{-1}. Circles, negative ions; squares, positive ions.

The equation for the drift current vs. t plots can be derived readily if the positive and negative ions are assumed to be present at steady state concentration n_{ss} in the whole volume of the radiation compartment before the high voltage pulse is applied. This assumption is reasonably valid because the 'off' time of the HV pulse was long enough for the spreading of secondary electrons from the collimated X-ray beam and diffusion of the ions toward the electrodes to reach steady state. A second simplifying assumption, namely that the ion concentrations are uniform, is a much more serious approximation, but, does not have a major bearing on the interpretation of the data since it is the time of drift of the center of the ion distribution that was measured. Based on the foregoing assumptions η_+, the number of ions per cm^2 arriving at the grid electrode of the radiation compartment during the application of positive fields for a time t, is

$$\eta_+ = \left\{ n_{ss}\frac{t}{\tau_+} + R\left(\frac{\mu_-}{\mu_- + \mu_+}\right)\frac{t^2}{2\tau_+}\right\} d_1 \qquad \text{for } 0 < t < \tau_+$$

$$\eta_+ = \left\{ n_{ss} + R\left(\frac{\mu_-}{\mu_- + \mu_+}\right)\frac{\tau_+}{2} + R(t - \tau_+)\right\} d_1 \qquad \text{for } t > \tau_+$$

In these expressions $\tau_+ = d_1/\mu_+ E_r$ is the clearing time for positive ions and R the rate of ion pair production in the radiation compartment in ion pairs cm^{-3} s^{-1}. Ion recombination is taken as ceasing when the ion clouds are separated (2).

Allowing for $\tau_+{}^d (= d_2/\mu_+ E_d)$, the time to cross

TABLE 1. Summary of mobilities

$p(NH_3)$ (Torr)	$p(N_2O)$ (Torr)	E_r (V cm^{-1})	E_d (V cm^{-1})	μ_+ (cm^2 V^{-1} s^{-1})	μ_- (cm^2 V^{-1} s^{-1})	μ_+^{av} (cm^2 V^{-1} s^{-1})*	μ_-^{av} (cm^2 V^{-1} s^{-1})*
200	5	450	337.5	3.18	3.26		
		300	250	3.24	3.38		
		200	150	3.22	3.33		
		450	125	3.17	3.37	3.20±0.03	3.34±0.05
350	5	450	450	1.90	1.90		
		450	450	1.93	1.93		
		450	450	2.02	2.04		
		900	337.5	1.88	1.90		
		300	250	1.96	2.02		
		200	150	2.05	2.18	1.96±0.07	2.00±0.10
760	5	450	450	0.82_5	0.83_5	0.83	0.84
1200	5	450	450	0.54	0.53		
		450	450	0.56	0.56		
		450	450	0.54	0.55		
		450	300	0.49	0.50		
		800	300	0.51	0.53	0.53±0.03	0.53±0.02

*The ± figures in these columns are standard deviations. The overall uncertainty was estimated to be ≲7%.

the drift space, the number of ions per cm^2 arriving at the second grid and ultimately being collected is

$$\eta_+^{\,1} = 0 \qquad \text{for } t < \tau_+^{\,d}$$

$$\eta_+^{\,1} = \left\{ n_{ss}\left(\frac{t-\tau_+^{\,d}}{\tau_+}\right) + R\left(\frac{\mu_-}{\mu_- + \mu_+}\right)\frac{(t-\tau_+^{\,d})^2}{2\tau_+}\right\} d_1$$

$$\text{for } \tau_+^{\,d} < t < \tau_+^{\,d} + \tau_+$$

$$\eta_+^{\,1} = \left\{ n_{ss} + R\left(\frac{\mu_-}{\mu_- + \mu_+}\right)\frac{\tau_+}{2} + R(t - \tau_+^{\,d} - \tau_+)\right\} d_1$$

$$\text{for } t > \tau_+^{\,d} + \tau_+$$

The drift currents are obtained from the values of $\eta_+^{\,1}$ by multiplying by evA, where A is the area of the transmission grids and e the electron charge.

The conditions used in the present work were such that the term containing $R\mu_-/(\mu_- + \mu_+)$ was always negligible. Therefore based on the assumptions made $\eta_+^{\,1}$ is initially zero, then rises linearly for t in the range $\tau_+^{\,d}$ to $\tau_+^{\,d} + \tau_+$ to n_{ss}. For $t > \tau_+^{\,d} + \tau_+$, η^1 rises linearly with slope equal to R. The current forms in Fig. 2 reproduce this behaviour rather well. The slight curvature at the points of inflection can be attributed to the following factors: (*a*) as soon as the positive and negative ion clouds are separated mutual repulsion causes spreading (4) and this continues as the ions cross the drift space, (*b*) during this period spreading by diffusion also occurs (4), (*c*) the ion distributions in the radiation compartment fall off near the walls, since the collimated X-ray beam does not completely fill the radiation compartment. Experiments without the collimator caused high background currents and other problems due to electrons and secondary X-rays scattered into the drift space. Collimators were chosen for the pressures used to give reasonably sharp rises in I as in Fig. 2. Calculations based on formulae in ref. 4 showed that the effects of (*a*) and (*c*) above correspond to a spreading of about 1 mm. Also the breadth of the regions of sharp rise in Fig. 2 corresponded to initial ion distributions being reasonably uniform to within 1 mm of the electrode surfaces of the radiation compartment.

Since the ionization region is centred in the radiation compartment, the ion mobilities were determined from $t_{1/2}$, the time to achieve one half of the steep rise due to the arrival of the steady state ion concentration n_{ss}. Linear extrapolations, as in Fig. 2, were used in finding n_{ss} and mobilities were calculated by means of eq. [1]. The position of $t_{1/2}$

$$[1] \qquad \mu = t_{1/2}^{\,-1}\left(\frac{d_1}{2E_r} + \frac{d_2}{E_d}\right)$$

is shown for the top line in Fig. 2. The equation assumes that ion spreading is symmetric in the drift direction and that lateral spreading has no effect on $t_{1/2}$. These assumptions appear to be quite valid, since variations in the numbers of ions n_{ss} or in the time ions spend in the radiation or drift compartments did not alter μ (see below).

Mobilities

The experimental values of μ_+ and μ_- obtained with various applied fields at several ammonia pressures are summarized in Table 1. The standard deviations at each pressure are 6% or less, and there was no dependence of $\mu_\pm$ on E_r or E_d. At higher

Can. J. Chem. Downloaded from www.nrcresearchpress.com by 210.87.254.40 on 09/05/12
For personal use only.

Can. J. Chem. Downloaded from www.nrcresearchpress.com by 210.87.254.40 on 09/05/12
For personal use only.

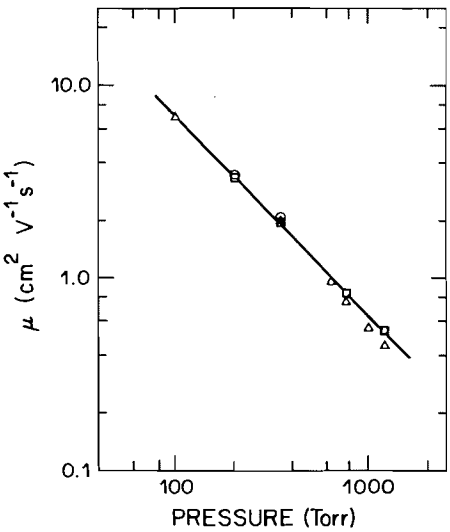

FIG. 3. Pressure dependence of mobilities. □ and ○, μ_+ and μ_-, this study. △, $(\mu_+ + \mu_-)/2$ from ref. 2.

pressures μ_+ and μ_- are equal within experimental error, but at lower pressures μ_- becomes larger. The overall experimental uncertainty was estimated to be $\pm 7\%$.

The pressure dependence of the ion mobilities is presented in Fig. 3. The solid line is drawn through the experimental points for μ_+, and the linearity over the pressure range 200 to 1200 Torr is clearly demonstrated. Over this range the slope gives $\mu \propto (\text{pressure})^{-1.03}$.

Since the magnitudes of μ_+ and μ_- are actually quite similar, comparison with μ, the average of μ_+ and μ_-, at each pressure is valid. The values of μ from ref. 2 are shown by the triangles in Fig. 3. The probable uncertainty of these results ($\sim 10\%$) is larger than for the present ones and there appears to be a small systematic error, which causes the values of μ to fall off faster than μ_+ and μ_- above 600 Torr (e.g. at 1200 Torr $\mu = 0.45$ as opposed to 0.53 for μ_+ and μ_-). However, over most of the pressure range, and particularly below 600 Torr, the agreement is very good. As a point of interest, the values of μ in ref. 2 were found to be constant at field strengths of 1 V cm^{-1} and below. The drift field strengths used here were 90 to 500 V cm^{-1}. Thus the mobilities of the ions in irradiated ammonia are independent of field strength over a very wide range (~ 0.1 to 100 V cm^{-1}).

Discussion

Recent publications (5, 6) dealing with ion–molecule collision rates have drawn attention to the relationship between the mobility of an ion and ξ, the collision frequency for transfer of momentum to the neutral molecules of the gas through which it moves (see also equation 9-4-2 of ref. 4). Taking m as the ion mass and assuming a unit electron charge e, the relation is

$$[2] \qquad \mu = e/m\xi$$

Also to a good approximation ξ is given by [3], in which nk_c is

$$[3] \qquad \xi = nk_cM(M + m)^{-1}$$

the orbiting collision frequency of ion molecule reaction rate theory, and M and n are respectively the molecular mass and number per unit volume of the neutrals. These relationships make it possible to write down the corresponding equations for mobility and k_c for a given type of ion–molecule interaction potential $V(r)$. If hard sphere or r^{12} (r = ion–molecule separation) repulsive interactions are neglected and μ_D is the dipole moment of the neutral, the potential for an ion – polar molecule interaction is of the form (7, 8)

$$[4] \qquad V(r) = \frac{-e^2\alpha}{2r^4} - \frac{e\mu_D \cos\theta}{r^2}$$

where α is the polarisability of the molecule.

Starting with an r-dependent average orientation angle $\bar{\theta}$, Su and Bowers (7, 9) have calculated values of a parameter C, which varies between zero and unity and allows for the effectiveness of the dipole 'locking in' to the charge. The magnitude of k_c and the corresponding mobility are then given by

$$[5] \qquad k_c = \frac{2\pi e}{M_r^{1/2}}\{\alpha^{1/2} + C\mu_D(2/\pi kT)^{1/2}\}$$

and

$$[6] \qquad \mu = [2\pi n M_r^{1/2}\{\alpha^{1/2} + C\mu_D(2/\pi kT)^{1/2}\}]^{-1}$$

where M_r is the reduced mass of the system.

For the case where $C = 0$ these reduce to $k_c = 2\pi e(\alpha/M_r)^{1/2}$ and $\mu = \{2\pi n(M_r\alpha)^{1/2}\}^{-1}$ respectively. The latter differs from the detailed theory of Langevin, which gives $\mu = \{2.210\pi n(M_r\alpha)^{1/2}\}^{-1}$ for a pure polarization potential (4, 6). The reason lies in the

TABLE 2. Percentage distribution of cluster sizes for $NH_4^+ \cdot x(NH_3)$ ions in ammonia*

p (Torr)	% for x = 3	4	5	6
200	0.7	60.1	31.0	8.1
350	0.3	42.8	38.9	18.0
760	—	20.3	39.8	39.8
1200	—	11.1	34.5	54.4

*Calculated from ref. 10.

TABLE 3. Mobilities of $NH_4^+ \cdot xNH_3$ ions in ammonia at 298 K

Pressure (Torr)	Mobility									
	$x = 4$		$x = 5$		$x = 6$		Weighted averages*			
	SB	LD	SB	LD	SB	LD	SB	LD	BR	Experimental
200	5.5	2.1	5.4	2.1	5.3	2.0	5.4_1	2.0_6	3.1_0	3.20±0.03
1200	0.91	0.35	0.90	0.34	0.89	0.34	0.89	0.34	0.52	0.53±0.03

*At 200 Torr $x = 4$ dominates and at 1200 Torr $x = 6$ dominates (see Table 2). All mobilities in $cm^2\ V^{-1}\ s^{-1}$.

fact that k_c counts only 'orbiting collisions' and is about 10% low (ref. 4, p. 446). For the calculation of mobilities we therefore modified [6] to:

$$[7] \quad \mu = [2.210\pi n M_r^{1/2}\{\alpha^{1/2} + C\mu_D(2/\pi kT)^{1/2}\}]^{-1}$$

so that it would correspond to the Langevin formula for $C = 0$. The case for $C = 1$ is referred to as the 'locked dipole' or LD case.

The distribution of cluster sizes for the positive ions in ammonia at our pressures is presented in Table 2. Mobilities were calculated for each of these at 200 Torr and 1200 Torr using eq. [7] for the LD case and for $C = 0.22$, which is appropriate for ammonia molecules at 298 K (9). The results are given in Table 3. The dependence of μ on the number of clustering molecules x in this range is small, because the mass dependence is $M_r^{1/2}$ and the value of M_r is close to 17 for all x. This being the case the dependence on pressure arises primarily from the inverse dependence on n in eq. [6], and the experimental pressure exponent of -1.03 is well justified.

Since the drift time is long relative to the life times for clustering and declustering (10, 11), the cluster size distributions will be maintained as the ions cross the cell. Thus we have calculated weighted average mobilities for comparison with the experimental values in column 11. The experimental results lie between the values derived from the LD approximation and with Su and Bowers' average dipole orientation (see under LD and SB).

Barker and Ridge (8) have recently obtained normalized collision densities, $\xi m/n(M_r\alpha)^{1/2}$, by calculating directly the average energy of interaction for the ion and dipole, a procedure which differs from that of Su and Bowers. Using the $\mu_D/\alpha^{1/2}$ appropriate to ammonia and interpolating from their Fig. 2, we obtained values of μ_+ for the ions in Table 2 and calculated the weighted mean mobilities shown under the heading BR in column 10 of Table 3. The agreement with experimental mobilities is very good, as has been the case for the comparison of Barker and Ridge's collision density calculations with other data (8). Neglect of the repulsive hard sphere interaction does not seem to have caused serious error for the present conditions. However, for the large clustered ions involved here ($D_{m-M} \simeq 4.5$ Å) this point deserves further attention.

As stated elsewhere (2) the exact identity of the long-lived negative ions formed by radiation in ammonia vapour with N_2O present is unknown. However, the similarity of μ_- and μ_+ in the 200 to 1200 Torr range shows that they are clustered, though possibly not as heavily as the positive ions.

1. M. R. FLANNERY. Case Stud. At. Phys. **2**, 3 (1972).
2. E. S. SENNHAUSER and D. A. ARMSTRONG. Radiat. Phys. Chem. **11**, 17 (1978).
3. L. G. CHRISTOPHOROU. Atomic and molecular radiation physics. Wiley, New York. 1971. p. 473.
4. E. W. MCDANIEL. Collision phenomena in ionized gases. Wiley, New York, NY. 1964.
5. D. WOBSCHALL, R. A. FLUEGGE, and J. R. GRAHAM, JR. J. Chem. Phys. **47**, 4091 (1967).
6. D. P. RIDGE and J. L. BEACHAMP. J. Chem. Phys. **64**, 2735 (1976).
7. T. SU and M. T. BOWERS. J. Chem. Phys. **58**, 3027 (1973).
8. R. A. BARKER and D. P. RIDGE. J. Chem. Phys. **64**, 4411 (1976).
9. T. SU and M. T. BOWERS. Int. J. Mass. Spectrom. Ion Phys. **12**, 347 (1973).
10. M. R. ARSHADI and J. H. FUTRELL. J. Phys. Chem. **78**, 1482 (1974).
11. C. E. YOUNG and W. E. FALCONER. J. Chem. Phys. **57**, 918 (1972); F. C. FEHSENFELD and E. E. FERGUSON. J. Chem. Phys. **59**, 6272 (1973).

Can. J. Chem. Downloaded from www.nrcresearchpress.com by 210.87.254.40 on 09/05/12
For personal use only.

Hydrolysis of esters of oxy acids: pK_a values for strong acids; Brønsted relationship for attack of water at methyl; free energies of hydrolysis of esters of oxy acids; and a linear relationship between free energy of hydrolysis and pK_a holding over a range of 20 pK units

J. PETER GUTHRIE[1]

Department of Chemistry, University of Western Ontario, London, Ont., Canada N6A 5B7

Received October 26, 1977[2]

J. PETER GUTHRIE. Can. J. Chem. **56**, 2342 (1978).

By combining various kinds of evidence from the literature it is possible to derive an internally consistent set of pK_a values for the strong mineral acids and the arenesulfonic acids; the values are referred to dilute aqueous solution as standard state and are expected to be correct within 0.5 log unit. Using these pK_a values and literature data for hydrolysis of methyl esters of acids of the type Y—XO_3Me_n, where Y is O, OH, OMe, alkyl, or aryl and X is Cl, S, or P, a Brønsted plot can be constructed with slope equal to 1.02 ± 0.04. From the free energies of hydrolysis for dimethyl sulfate and the methyl phosphates it is possible to calculate rate constants for the microscopic reverse reaction. These define a Brønsted line of slope 0.27 ± 0.3, from which rate constants for the formation of the esters of perchloric and various sulfonic acids may be estimated. This permits calculation of free energies of hydrolysis for these esters.

Thermochemical data in the literature permit calculation of the free energies of hydrolysis of dimethyl sulfate, trimethyl arsenite, and tetraethyl orthosilicate. In the case of dimethyl sulfate the calculation (using the previously reported eq. [1]) leads to a pK_a value in close agreement with theoretical expectation, confirming that eq. [1] is valid for acids of p$K_a \geq -3$. For tetraethyl orthosilicate the thermochemical data are less precise but are in satisfactory agreement with the predictions of eq. [1]. The free energies of hydrolysis derived from the Brønsted correlations are also in good agreement with expectation based on eq. [1].

For acids where resonance phenomena are important either in the acid itself (boric acid) or in the anion (nitric acid, nitrous acid, carboxylic acids) the experimental free energies of formation fall far from the line defined by eq. [1]. It is concluded that eq. [1] is limited to species where there is no π delocalization involving the reacting oxygen, but where this condition is satisfied, the equation holds over the entire accessible range of oxy acid pK_a values, i.e., from −6.4 to 16.

J. PETER GUTHRIE. Can. J. Chem. **56**, 2342 (1978).

En combinant divers types de données provenant de la littérature, il est possible d'obtenir une série autocohérente de valeurs de pK_a pour les acides inorganiques forts et les acides arènesulfoniques; les valeurs se refèrent aux solutions aqueuses diluées comme état de référence et on les croit correctes à ±0.5 unités log. Faisant appel à ces valeurs de pK_a et aux données de la littérature pour l'hydrolyse des esters méthyliques des acides du type Y—XO_3Me_n, où Y = O, OH, Me, alkyle ou aryle, et X = Cl, S ou P, on peut établir une droite de Brønsted avec une pente égale à 1.02 ± 0.04. Utilisant les énergies libres d'hydrolyse du sulfate du méthyle et des phosphates de méthyle, il est possible de calculer les constantes de vitesses pour la réaction microscopique inverse. Ces valeurs définissent une droite de Brønsted de pente 0.27 ± 0.3, à partir de laquelle on peut évaluer des constantes de vitesse pour la formation des esters des acides perchloriques et de divers acides sulfoniques. Ces valeurs permettent de calculer les énergies libres d'hydrolyse de ces esters.

Les données thermochimiques retrouvées dans la littérature permettent de calculer les énergies libres d'hydrolyse du sulfate de diméthyle, de l'arsenite de triméthyle et de l'orthosilicate de tétraéthyle. Dans le cas du sulfate de diméthyle, les calculs (utilisant l'éq. [1] rapportée antérieurement) conduisent à une valeur de pK_a qui est raisonnablement près de la valeur attendue d'une façon théorique; ceci confirme que l'éq. [1] est valide pour les acides de p$K_a \geq -3$. Dans le cas de l'orthosilicate de tétraéthyle, les données thermochimiques sont moins précises mais elles présentent une concordance satisfaisante avec les prédictions de l'éq. [1]. Les énergies libres d'hydrolyse obtenues à partir des corrélations de Brønsted sont aussi en bon accord avec les valeurs attendues en se basant sur l'éq. [1].

Dans le cas des acides où le phénomène de la résonance est important, soit dans l'acide lui-même (acide borique) ou dans l'anion (acide nitrique, acide nitreux, acides carboxyliques), les énergies libres obtenues expérimentalement pour la formation sont très loin de la ligne définie par l'éq. [1]. On en conclut que l'éq. [1] est limitée à des espèces où il n'y a pas de délocalisation pi impliquant l'oxygène qui réagit; toutefois dans le cas où cette condition est satisfaite, l'équation est valable pour la gamme complète des valeurs de pK_a des acides oxygénés soit de −6.4 à 16.

[Traduit par le journal]

[1]Alfred P. Sloan Fellow, 1975–1979.

[2]Revision received May 17, 1978.

Can. J. Chem. Downloaded from www.nrcresearchpress.com by 210.87.254.5 on 09/05/12
For personal use only.

Can. J. Chem. Downloaded from www.nrcresearchpress.com by 210.87.254.5 on 09/05/12
For personal use only.

Introduction

Recently (1) we reported a linear correlation between the free energy change for replacing a hydroxyl group in a molecule by an alkoxyl group and the electronic properties of the rest of the molecules. Initially (1) this was done for ethers using the σ^* values for the substituents on the carbon atom bearing OH or OR, but this has since been extended to other classes of compound by using the pK_a of the OH compound as a measure of the electron withdrawing properties of the rest of the molecule (2). Equation [1] gives the relationship between the free

$$[1] \qquad \Delta G'' = -4.78(\pm 0.28) + 0.336(\pm 0.024)pK_a$$

energy change, corrected for any steric or symmetry effects and the pK_a of the hydroxyl compound for process [2]. Since this correlation worked well for

$$[2] \qquad X\text{—}OR + H_2O = XOH + HOR$$

phosphate esters it seemed worthwhile to see how far it could be extended and what limitations exist for it. Accordingly we wish to report the results of an examination of the hydrolysis equilibria for several esters of inorganic acids. The correlation appears to be useful for any acids where resonance is unimportant in stabilizing the anion but does not work at all for acids for which resonance plays a role.

To extend the method to acids stronger than phosphoric, it was necessary to have pK_a values for strong mineral acids such as sulfuric and perchloric acid, since from these pK_a values and previously reported kinetic studies of the hydrolysis of the methyl esters of these acids it would be possible to make indirect estimates of the free energies of hydrolysis of the esters which could be compared with the predictions of eq. [1]. A review of the data in the literature permits the calculation of a mutually consistent set of pK_a values for acids as strong as fluorosulfonic acid, referred to dilute aqueous solution as standard state. These pK_a values permit construction of a Brønsted plot for rates of hydrolysis of methyl esters of tetracoordinate oxy acids, which serves as an additional test of the correctness of the pK_a values deduced for the strong acids. A much less satisfactory Brønsted plot can be constructed for the (unobservable) reverse reaction, but the number of points is inadequate to specify the line very well. Nevertheless, this line permits the calculation of the rate constants for the reverse reactions, and so the calculation of the equilibrium constants for hydrolysis of the esters. These equilibrium constants are in agreement with the values anticipated from the linear free energy relationship between the free energy of hydrolysis and the pK_a of the acid. Thus the results in this paper demonstrate that the free energy relationship which we have reported covers the entire accessible range of acids which can exist in aqueous solution and within its range of applicability can be used with confidence to estimate unknown equilibrium constants.

Results and Discussion

Thermodynamic properties for all compounds discussed in this paper (including quantities calculated in this work) are found in Table 1. Literature data were supplemented where necessary by estimated quantities calculated using accepted procedures. Details are found in the Appendix.

pK_a Values for Strong Acids

For acids with pK_a values lower than -2 there is no generally satisfactory way to measure the pK_a, referred to aqueous solution. Table 2 summarizes various values which have been suggested. Attempts have been made using nmr data (3–5) but these methods involve severe assumptions and long extrapolations, and generally lead to values for the pK_a which seem unduly high. Although Raman (6, 7) and infrared (8, 9) measurements can lead to concentrations of undissociated acid even for perchloric (6) and sulfuric acids (7–9), these measurements are only possible in very concentrated acid solutions, so that a long and uncertain extrapolation would be needed to refer them to dilute aqueous solution. Direct measurements on dilute aqueous solutions of very strong acids seem unlikely to lead to pK_a values unless some new technical breakthrough occurs.

Attempts have been made to calculate pK_a values for the strong mineral acids using a number of approaches. Pauling's rules (ref. 10, cited in ref. 25) and some elaborations of them (11) are empirical correlations which work well for acids with pK_a values in the measurable range. Pauling's rules are: (*a*) $pK_1 = 7 - 5n$, where n is taken from the structural formula $XO_n(OH)_a$; (*b*) K_1, K_2, K_3, etc., are in the ratio $1:10^{-5}:10^{-10}$. Use of the first rule suggests that for H_2SO_4, $pK_1 = -3$, and for $HClO_4$, $pK_1 = -8$.

Slightly more elaborate was the attempt to calculate pK_a values for inorganic acids reported by Kossiakoff and Harker (12), who employed a simple electrostatic model based on the distribution of formal charges deduced from the octet rule. Their calculations were remarkably successful and led to predicted pK_a values of -3.0 for H_2SO_4 and -7.3 for $HClO_4$. Schwartzenbach (13) employed a similar model to calculate pK_a values for these acids and supported his results by consideration of the series HPO_4^{2-}, $pK = 12.3$; HSO_4^-, $pK = 1.9$; $HClO_4$, $pK = -8.6$; similarly, $H_2PO_4^-$, $pK = 7.2$; H_2SO_4, $pK = -3.1$. Thus for each increase of the formal charge on the central atom by 1 unit, the pK decreases by about 10 units.

TABLE 1. Thermodynamic data for compounds discussed in this paper[a]

(*a*) Compounds for which free energies of formation have not been reported

Compound	ΔH_f°(g)[b]	S°(g)[c]	ΔG_f°(g)[b]	ΔH_v[b,d]	ΔH_f°(l)[b]	ΔG_f°(aq)[b,e]
CH_3ONO	−15.79(0.25)[f]	66.81(0.67)[g]	+0.09(0.32)[h]			−0.89(1.05)[i]
CH_3ONO_2	−29.11(0.30)[f]	80.97(0.1)[j]	−10.15(0.30)[h]	8.15(0.10)[f]	−37.26(0.32)[f]	−9.06(0.38)[k]
$(CH_3O)_2CO$	−136.3(1.0)[l]	83.25(2.0)[m]	−110.07(1.16)[h]			−111.84(1.27)
$(CH_3O)_2SO_2$	−164.1(0.5)[f]	90.15(2.0)[m]	−130.76(0.78)[h]	11.6(0.4)[f]	−175.23(0.23)[f]	−133.88(0.79)
$(CH_3O)_3As$	−131.1(0.4)[f]	103.86(3.0)[m]	−94.66(0.98)[h]	10.1(0.3)[f]	−141.2(0.3)[f]	−97.44(1.10)
$(CH_3O)_3B$	−214.6(0.7)[f]	95.24(2.0)[m]	−177.53(0.92)[h]	8.3(0.5)[f]	−222.9(0.5)[f]	−179.31(1.36)
$(CH_3CH_2O)_4Si$	−326.28(2.1)[n]	157.75(2.0)[m]	−250.54(2.1)[h]	11.56(0.5)[o]	−337.84(2.0)[p]	−251.35(2.2)

(*b*) Compounds for which free energies of formation in aqueous solution have been reported

Compound	ΔG_f°(aq)	Compound	ΔG_f°(aq)	Compound	ΔG_f°(aq)
"$HClO_4$"[q]	−2.57[r]	H_3BO_3	−230.24[r]	CH_3COOH	−94.21[u]
HNO_2	−12.82[s]	H_3PO_4	−274.22(0.48)[t]	$HCOOCH_3$	−73.38[w]
"HNO_3"[q]	−26.43[r]	H_4SiO_4	−312.57[u]	CH_3CH_2OH	−43.31[v]
H_2O[x]	−56.69[r]	CO_2	−92.31[r]	$CH_3CH_2OPO_3H_2$	−257(1)[t]
"H_2SO_4"[q]	−179.94[r]	HCOOH	−88.83[r]	CH_3COOCH_3	−78.43[w]
H_3AsO_3	−152.94[r]	CH_3OH	−41.88[r]	$(CH_3CH_2O)_2PO_2H$	−241(2)[t]
				$(CH_3CH_2O)_3PO$	−223(2)[t]

(*c*) Compounds for which the free energies of formation in aqueous solution have been calculated in this work

Compound	ΔG_f°(aq)	Compound	ΔG_f°(aq)	Compound	ΔG_f°(aq)
$HClO_4$	+4.26[x]	CH_3OClO_3	+25.27[y]	$CH_3CH_2OSiO_3H_3$	−299[y]
HNO_3	−24.65[x]	CH_3OSO_3H	−155.49[y]	$(CH_3CH_2O)_2SiO_2H_2$	−283[y]
H_2SO_4	−176.12[x]	$(CH_3O)_2AsOH$	−116[y]	$(CH_3CH_2O)_3SiOH$	−267[y]
$(CH_3O)As(OH)_2$	−134[y]	$(CH_3O)_2BOH$	−196[y]	H_2CO_3	−144.10[x]
$(CH_3O)B(OH)_2$	−213[y]				

[a]At 25°C, standard states are ideal gas at 1 atm, pure liquid, and 1 *M* aqueous solution with an infinitely dilute reference state, unless otherwise noted.
[b]In kcal mol^{-1}.
[c]In cal deg^{-1} mol^{-1}.
[d]Heat of vaporization.
[e]Unless otherwise noted, calculated from ΔG_f°(g) and the ΔG_t value in Table 6.
[f]Reference 55.
[g]Reference 56.
[h]Calculated from other values in this table.
[i]Calculated using a value for ΔG_t estimated as described in the Appendix.
[j]Reference 57.
[k]Calculated using the entropy of liquid methyl nitrate (58) and the solubility of the liquid in water (59).
[l]Reference 60.
[m]Calculated using the atomic contributions method of Benson and Buss (51).
[n]Calculated using the bond contributions given in ref. 52.
[o]Calculated from the vapour pressure data given in ref. 61, using data for pressures between 1 and 40 Torr; Bradley *et al.* (62) report ΔH_v = 11.25 kcal mol^{-1} but did not specify the pressure range employed.
[p]Recalculated from the data of Flitcroft and Skinner (42) using the modern value for ΔH_f° of amorphous SiO_2 (63).
[q]Free energy of formation of H^+ and the monoanion.
[r]Reference 53.
[s]Reference 64.
[t]Reference 2.
[u]Reference 41.
[v]Reference 65.
[w]Reference 37.
[x]Calculated from the free energy of formation of the anion and the pK_a (Table 2).
[y]Calculated as described in the text.
[z]Standard state is the pure liquid.

All of these calculations are based upon considerations of formal charge; although this approach has been very successful at least for acids of measurable pK_a, including bisulfate, extension to perchlorate involves a particular kind of extrapolation unique to this system and therefore not generally recognized, namely the assumption that a formal charge of plus three can be interpreted in the same sense as one of plus two, i.e., that the electronic effects of the central atom continue to be linear in the formal charge even when this is three. The possibility that nonlinearity might set in seems not to have been considered. The electronegativity of the central chlorine would be so drastically increased by the formal charge of plus three (14) that charge redistribution by inductive withdrawal from the neighboring oxygens could well lead to a smaller than anticipated increment in effective charge on the central atom upon changing from S^{VI} to Cl^{VII}. This effect need not be dependent upon π bonding involving *d* orbitals, although the orbital contracting effect of a large formal charge could well make such π bonding more important in ClO_4^- than in other oxy acids of the nonmetals.

Of these various predictions, that which seems to be on the firmest ground is the prediction of the pK_a of H_2SO_4 by Kossiakoff and Harker (12), although in fact the other methods lead to very similar values. The reason for preferring Kossiakoff and Harker's value is that from their table of predicted p*K* values one can see that they can predict the difference between successive pK_a values within one log unit for those cases which are well behaved acids (without resonance or tautomerization effects to confuse the

Can. J. Chem. Downloaded from www.nrcresearchpress.com by 210.87.254.5 on 09/05/12
For personal use only.

TABLE 2. pK_a values which have been reported for strong acids

Acid	pK_a	Reference	Method
$HClO_4$	−9.9	34	Based on pK in sulfuric acid
	−8.6	13	Theoretical
	−7.3	12	Theoretical
	−7.7	32	Based on pK in organic solvents
	−2.7	4	Nuclear magnetic resonance
	−1.6	3	Nuclear magnetic resonance
p-TsOH	−5.4	32	Based on pK in organic solvents
	−4.1	66	Solubility
	−6.2	67	Spectrophotometric; based on H_0[a]
	−1.3	68	Nuclear magnetic resonance
H_2SO_4	−4.0	34	Based on pK in formic acid
	−3.1	13	Theoretical
	−3.0	12	Theoretical
	−6.0	32	Based on pK in organic solvents
	−9.4	69	Based on acidity function
	−8.3	70	Curve fitting to nmr data

issue), and that they successfully predicted the second pK_a of sulfuric acid. Thus it seems reasonable to expect that the first pK_a of sulfuric acid will be -3 ± 1.

It was also desirable to have pK_a values for a number of sulfonic acids, referred to dilute aqueous solution. Organic folklore suggests that FSO_3H, CF_3SO_3H, and the various arenesulfonic acids have very negative pK_a values. However, consideration of both theoretical expectations and experimental results shows that even FSO_3H is unlikely to have a pK_a less than -7.5.

The starting point for the theoretical argument is the experimental value for the pK_a of methanesulfonic acid in water, which has been measured as -1.92 ± 0.01 (15). In the same investigation the pK_a value for ethanesulfonic acid was found to be -1.68 ± 0.02.

As a model for the effect of substituents upon the pK_a, we consider the behavior of phosphonic acids; Kresge and Tang (16*a*) have reported that for the thermodynamic second pK_a values of alkyl phosphonates, there is a good correlation with σ^*:

$$pK_a = (8.10 \pm 0.10) - (1.26 \pm 0.07)\sigma^*$$

Martin and Griffin (16*b*) have reported a similar correlation with $\rho^* = 1.12$ for the first ionization but they used apparent pK_a values measured at unspecified ionic strength, and it is not clear whether the techniques used to determine these rather low pK_a values were adequate. Although it is quite possible to measure pK_a values less than 2.5 in water by titration, it is imperative to correct for titration of H^+ either by calculation (17) or by differential titration (18). pK_2 values for some arenephosphonic acids are available but only for benzene phosphonic acid is there a thermodynamic value. Mäkitio and Kontinen (19) report that pK_2 is 6.99 at an ionic strength of 0.1 *M* and 7.43 at zero ionic strength. Jaffé *et al.* (20) have reported apparent pK_a values for a number of arenephosphonic acids, including benzenephosphonic acid for which they give $pK_2 = 7.07$. Their values were corrected making the assumption that $pK_a - pK_a'$ will be the same for all arenephosphonates. σ^* values for substituted aryl groups can be calculated from the pK_a values of the appropriate arylacetic acids (21) using the equation reported by Charton (22); (σ_I was converted to σ^* using the standard factor of 6.23 (22)). The pK_a values of Jaffé *et al.* (20) fall very close to the line defined by Kresge's data when these σ^* values are used (see Fig. 1). We conclude that the second pK_a values of both alkyl and arylphosphonic acids can be correlated and presumably predicted by the same equation and that it is very probable that the thermodynamic first pK_a will show a very similar ρ^*. Thus the preferred method for predicting the pK_a values of sulfonic acids should be to use a ρ^* value of 1.26, and extrapolate from the known value for methanesulfonic acid. The value of ρ^* for sulfonic acids should not be expected to be exactly equal to that for phosphonic acids but consideration of the range of ρ^* values encountered for various classes of acids Y—X—OH suggests that it is extremely unlikely to vary by more than ± 0.5. Although this uncertainty could give rise to a range of ± 1.5 in pK_a for $\sigma^* = 3$, it still places stringent limits on the reasonable values for the pK_a of, for example, FSO_3H, for which $\sigma_F^* = 3.24$ (23) and excludes any value for pK_a more negative than -7.5.

If the apparent pK_2 values for phosphate monoesters (2, 19) (including phosphoric acid with a suitable symmetry correction) are similarly plotted against σ^* values for the alkoxy or aryloxy (calculated from pK_a values for the aryloxyacetic acids (24)) substituents, a good linear correlation is obtained,

Can. J. Chem. Downloaded from www.nrcresearchpress.com by 210.87.254.5 on 09/05/12
For personal use only.

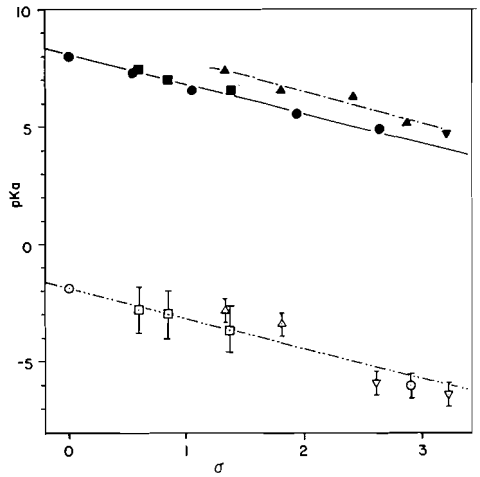

FIG. 1. Dependence of pK_a upon σ^* for phosphonic and sulfonic acids: (———) least-squares line for alkyl phosphonic acid pK_2 (16*a*), (●) alkyl phosphonic acids, (■) aryl phosphonic acids (ref. 20; see text); (– – –) least-squares line for phosphate monoesters pK_2, (▲) monoesters (ref. 2; see text), (▼) monofluorophosphoric acid (ref. 82); (– – – –) predicted line for sulfonic acids; (○) alkylsulfonic acids, (□) arylsulfonic acids, (▽) halosulfonic acids, (△) sulfuric acid and monomethyl sulfate; see text for sources of pK_a values.

with $pK_2 = 9.27 - 1.36\sigma^*$. It should be noted that carbon and oxygen substituents give different though rather similar lines; thus we must not expect to find sulfate esters or sulfuric acid itself falling on the line for sulfonic acids. The pK_a for fluorophosphate falls between the lines for phosphate esters and phosphonic acids.

The considerations discussed above lead to predicted values for the pK_a values of sulfonic acids as follows (error limits are imposed by the assumed uncertainty of 0.5 in ρ^* or are set at 0.5 log unit, whichever is larger): Ph—SO_3H, -2.7 ± 0.5; *p*Br—C_6H_4—SO_3H, -3.0 ± 0.5; *p*NO_2—C_6H_4—SO_3H, -3.6 ± 0.7; Cl—SO_3H, -5.2 ± 1.3; CF_3SO_3H, -5.2 ± 1.3; FSO_3H, -6.0 ± 1.6.

Measurements in 100% sulfuric acid as solvent have led to dissociation constants of 1.0×10^{-4} *m* for $HClO_4$ (25), 8.0×10^{-4} *m* for CF_3SO_3H (26), 2.3×10^{-3} *m* for FSO_3H (27), and 9.0×10^{-4} *m* for $ClSO_3H$ (27). These results lead to pK_a values relative to $HClO_4$ (the weakest acid in the series) of -1.4 for FSO_3H, -1.0 for $ClSO_3H$, and -0.9 for CF_3SO_3H. For a series of structurally similar acids it seems reasonable to expect that relative ionization constants in highly ionizing solvents such as water or sulfuric acid will be closely similar; this is equivalent to assuming that the only significant difference in the two solvents is the dramatic difference in solvent basicity.

Bessière (28, 29) has determined the ionization constants for sulfuric and perchloric acids in trifluoroacetic acid as solvent; his values for pK_i are 2.4 and 0.8, respectively. It must be borne in mind that trifluoroacetic acid is a solvent of low dielectric constant ($\varepsilon = 8.4$) (28), and that the processes of ionization, i.e., heterolytic cleavage of the H—X bond must be considered separately from dissociation to give free ions, the latter being quite unfavorable. Bessière has also reported 'global dissociation constants' for formation of free ions from ion pairs plus unionized acid; the corresponding pK values are 4.5 for perchloric acid, 6.3 for sulfuric acid, and 7.1 for methanesulfonic acid (28). Kolthoff and Bruckenstein (30) have reported the ionization constant for perchloric acid in acetic acid as $pK_i = 1.0$ and have reported pK values for global ionization of 4.87 for perchloric acid, 7.24 for sulfuric acid, and 8.46 for toluenesulfonic acid (31). The global ionization constants seem to be more widely dispersed in acetic acid; unfortunately, there seems to have been no determination of a value of pK_i for sulfuric acid in acetic acid. The values of pK_i, since they refer to a single process, are to be preferred as a measure of acidity; these values lead to a pK_a difference of 1.6 between perchloric and sulfuric acids.

From a study of the reaction I + HA = IHA, where I is an indicator, Bessière (20) has constructed a scale of relative acidities in trifluoroacetic acid; this scale places sulfuric acid 1.7 log units less acidic than perchloric acid and both methanesulfonic acid and *p*-toluenesulfonic acid 2.3 log units less acidic than perchloric acid. (Chlorosulfonic acid is placed slightly less acidic than sulfuric acid but in the absence of control experiments to demonstrate that chlorosulfonic acid is the actual acid species in mixtures of chlorosulfonic and trifluoroacetic acids, this can not be considered definitely established. In sulfuric acid as solvent, chlorosulfonic acid is stronger than sulfuric acid (27).) Since these acidities are based on experiments which do not distinguish between unionized acid, HA, and the ion pair, H^+A^-, the interpretation is less clear than would be desirable. Furthermore, it is not entirely clear how the relative acidities reported were actually calculated; if the data for indicators only are employed (Tables III and IV of ref. 29) somewhat different values are obtained, namely pK_a differences relative to perchloric acid of 1.9 for sulfuric acid and 3.1 for methanesulfonic acid and *p*-toluenesulfonic acid.

The agreement between different approaches to these pK_a differences is considerably less perfect than might be desired but all available data can be summarized by stating that sulfuric acid is 2.0 ± 0.4 pK units less acidic than perchloric acid and that methanesulfonic acid and toluenesulfonic acids (which appear indistinguishable in these experiments) are 3.1 ± 0.5 pK units less acidic than perchloric acid.

Can. J. Chem. Downloaded from www.nrcresearchpress.com by 210.87.254.5 on 09/05/12
For personal use only.

Can. J. Chem. Downloaded from www.nrcresearchpress.com by 210.87.254.5 on 09/05/12
For personal use only.

TABLE 3. pK_a values for acids discussed in this paper[a]

Acid	pK_a	Acid	pK_a
H_3O^+	−1.74	H_3AsO_3	9.29[h]
$CH_3OH_2^+$	−2.18[b]	$CH_3OAsO_2H_2$	8.58[d]
		$(CH_3O)_2AsOH$	7.99[d]
$CH_3CH_2SO_3H$	−1.68(0.02)[c]		
CH_3SO_3H	−1.92(0.01)[c]	H_4SiO_4	9.93[i]
$C_6H_5—SO_3H$	−2.8(1.0)[d]		($pK_2 = 11.69$[i])
pBr—$C_6H_4—SO_3H$	−3.1(1.0)[d]	$(C_2H_5O)SiO_3H_3$	7.27[d]
pNO$_2$—$C_6H_4—SO_3H$	−4.0(1.0)[d]	$(C_2H_5O)_2SiO_2H_2$	8.61[d]
$CF_3—SO_3H$	−5.9(0.5)[d]	$(C_2H_5O)_3SiOH$	7.95[d]
Cl—SO_3H	−6.0(0.5)[d]		
F—SO_3H	−6.4(0.5)[d]	HNO_3	−1.3[h]
$HClO_4$	−5.0(0.5)[d]	HNO_2	3.29[e]
		H_2CO_3	3.58[e]
H_2SO_4	−2.8(0.5)[d]	CH_3OCO_2H	2.92[d]
CH_3OSO_3H	−3.4(0.5)[d]	HCOOH	3.77[e]
		CH_3COOH	4.76[e]
H_3PO_4	2.12[e]		
	($pK_2 = 7.21$[e])		
$(CH_3O)PO_3H_2$	1.50[f]		
	($pK_2 = 6.58$[f])		
$(CH_3O)_2PO_2H$	0.76[g]		

[a]In H_2O at 25°C.
[b]Reference 71.
[c]Reference 17.
[d]Estimated as described in the text.
[e]Reference 72.
[f]Reference 73.
[g]Reference 74.
[h]Reference 75.
[i]Reference 33.

It is somewhat surprising that toluenesulfonic acid and methanesulfonic acid appear so similar, since both on theoretical (σ^* values) and experimental (leaving group behavior) grounds one expects toluenesulfonic acid to be the stronger. However, measurements of ion pair formation could well be perturbed by noncovalent interactions involving the benzene rings of the indicator bases and the toluenesulfonic acid. Thus the relative acidity of toluenesulfonic acid must be considered less reliable.

We now have enough information to construct a scale of acidity values. Starting with methanesulfonic acid, which has a well-established pK_a of −1.92, we can calculate that sulfuric acid has a pK_a of -2.8 ± 0.5, and that perchloric acid has a pK_a of -5.0 ± 0.5 from the data in acetic and trifluoroacetic acids. Then from the data in sulfuric acid we can calculate that the pK_a of chlorosulfonic acid is -6.0 ± 0.5, that of trifluoromethanesulfonic acid is -5.9 ± 0.5, and that of fluorosulfonic acid -6.4 ± 0.5. These pK_a values, and all others used in this paper, are found in Table 3.

Figure 1 shows that these values are in good agreement with the predicted line, which increases our confidence in the assignment. For the arenesulfonic acids, there is actually increased uncertainty, because of the apparent near identity of the pK_a values of methane- and toluenesulfonic acids; for the moment the best estimates for the pK_a of the arenesulfonic acids seem to be those based on the predicted line; to allow for the inconsistent result in acetic and trifluoroacetic acids the error limits are increased to ± 1.0 pK_a unit.

Bessière (32) has proposed a rather different set of pK_a values based upon his data; this scale is determined by the choice of HCl as reference acid, and by the choice of the pK_a for aqueous HCl. There appear to be three fundamental objections to these choices: (*a*) the pK_a of HCl in aqueous solution is imperfectly defined, and values very different from that chosen by Bessière (33) have been proposed;[3] (*b*) Cl^- is quite different in structure and presumably in solvation from the $Y—XO_3^-$ ions used in this work to construct a scale, so that the danger of serious

[3]Bessière chose a value of −3.7 for the pK_a of HCl in water; this value is derived from a scale of acidity in absolute ethanol (34). The scale for absolute ethanol has been based on 'global ionization constants,' which in the case of weak acids such as acetic acid are probably very similar to ionization constants but which may be very different for strong acids which will ionize to give ion pairs in a solvent of low polarity such as ethanol; since the apparent ionization constants for HCl and for CsCl are very similar in ethanol (35), it seems probable that the global ionization constant for HCl is really measuring dissociation of an ion pair. This argument would lead to a much more negative scale based on Bessière's data if HCl is used as reference acid; using the more generally accepted value of −7 for the pK_a in water of HCl (33), the pK_a in water for $HClO_4$ becomes −11. This value is rejected for reasons discussed in the text.

Can. J. Chem. Downloaded from www.nrcresearchpress.com by 210.87.254.5 on 09/05/12
For personal use only.

variations in solvation effects is considerable; in particular, the balance between ionization and dissociation constants is likely to be quite different and thus the meaning of the global ionization constant will not be the same for different structural types; (*c*) it has not been demonstrated as far as one can tell that HCl in trifluoroacetic acid is actually HCl and has not to some considerable extent undergone covalent addition to the acid. HCl has a significant tendency to add to carbonyl groups as shown by chloroalkyl ether formation (36), when the equilibrium is not shifted by dissociation into H^+ and Cl^-, and trifluoroacetic acid is far more prone to undergo nucleophilic addition than are less electron deficient carboxylic acids (37).

Sulfuric Acid and its Methyl Esters

It is possible to test the pK_a value derived for sulfuric acid in aqueous solution by comparing the value of the free energy of hydrolysis of dimethyl sulfate derived from this pK_a, using eq. [1] with the value which can be deduced from the heat of formation of the ester. (Whether this is best regarded as a test of the pK_a value or of eq. [1] depends upon which is considered the better established but in any case serious disagreement would cast doubt on one if not both.)

Equation [1] predicts the free energy of hydrolysis, for the process converting an ester to the unionized acid in aqueous solution. Since sulfuric acid and its monoesters are strong acids the available thermodynamic data refer to the ions. A pK_a value for sulfuric acid in aqueous solution has been derived; it now remains to correct for the effect of replacing OH by OR, in order to estimate a value for the pK_a of monomethyl sulfate. This was done by a modification of a method which we have previously employed (2). The effect was assumed to be the same as the average (symmetry corrected) change in pK_a observed for phosphoric acid and its mono and dimethyl esters, using data collected in ref. 2. This effect is 0.89 in pK_a; this value was used to estimate the other pK_a values for inorganic esters reported in Table 3.

For the overall hydrolysis, the thermodynamic data in Table 1 lead to a free energy change of -12.82 kcal mol^{-1}.

[3] $MeO—SO_2—OMe + 2H_2O \rightleftharpoons 2MeOH + H_2SO_4$

When free energies of hydrolysis for the two stages of hydrolysis are calculated using eq. [1], the values obtained are -6.74 and -5.72 kcal mol^{-1}, respectively, with a total of -12.46 kcal mol^{-1}, in excellent agreement with the thermochemical value.

[4] $MeO—SO_2—OMe + H_2O \rightleftharpoons MeOH + MeO—SO_2—OH$

[5] $MeO—SO_2—OH + H_2O \rightleftharpoons MeOH + H_2SO_4$

Brønsted Correlations for Methyl Ester Formation and Solvolysis

It is possible to test the entire set of pK_a values for strong acids derived above, by taking advantage of the large amount of work which has been done studying the kinetics of hydrolysis of the methyl esters of these acids. A plot of log k vs. pK_a (a Brønsted plot) is expected to show a simple relationship provided that the pK_a values are correct but should show no pattern or a physically unreasonable one if they are seriously in error.

It is quite generally found that rates of nucleophilic substitutions are related to the pK_a of the nucleophile and leaving group and give linear Brønsted plots, provided that the reactions correlated all have the same rate determining step and provided that the variable reagents are of similar structural type (44). This approach has been more frequently employed in substitution at carbonyl (45), phosphoryl (46), or sulfonyl (47) centres than at aliphatic carbon simply because of the scarcity of data satisfying the second criterion. A set of data now exists, as a result of the present work and recent work from this laboratory, and Fig. 2*a* shows that a good Brønsted correlation exists for the rate constants for uncatalyzed hydrolysis of methyl esters of acids of the type $Y—XO_3H_n$ but that methyl nitrate deviates badly. Unlike the other acids nitric acid derives some considerable part of its acidity from resonance stabilization of the anion.

The observation that the points for the esters of the strong acids fall within their uncertainty limits of the line determined by methyl mesylate and trimethyl phosphate constitutes a strong confirmation of the assignment of pK_a values to these acids. Had these acids been as strong as has sometimes been suggested (see Table 2) then a straight line Brønsted plot could not have been obtained. For example, had perchloric acid had a pK_a of ca. -10 as has been suggested, then the average slope of the Brønsted plot from methanesulfonate to perchlorate as leaving group would have been -0.3, corresponding to a marked curvature. Although curved Brønsted plots are by no means unknown (44), it is without precedent to have curvature so extreme at such low values of the observed rate constant, when there is no preequilibrium process preceding a fast rate determining step. The reactions being considered here are believed to be simple S_N2 solvolyses (79), so no such explanation is possible. Thus a linear Brønsted plot is what would be expected.

Although it is possible to construct a Brønsted plot

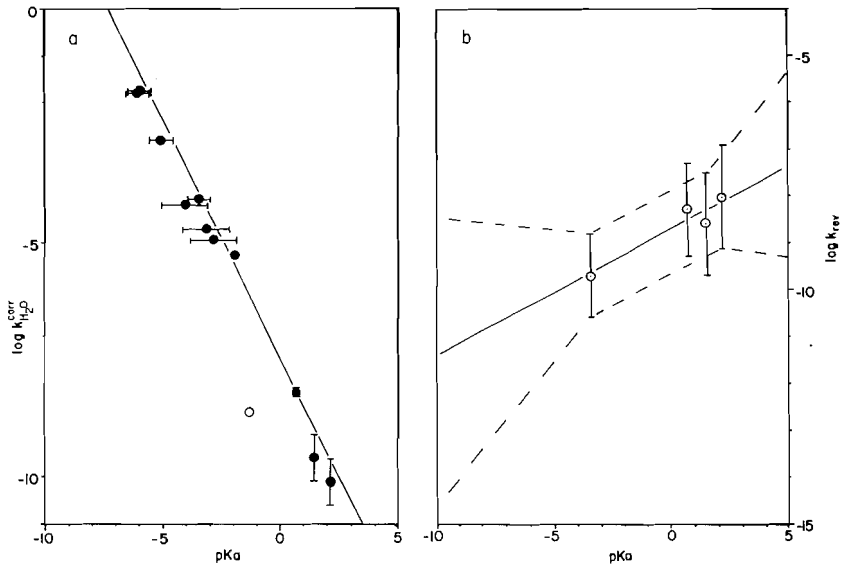

FIG. 2. (*a*) Brønsted plot for hydrolysis of methyl esters of oxy acids, (●) acids without resonance effects, (○) methyl nitrate. The line was determined by weighted least squares: $\log k_{H_2O} = -7.39(\pm 0.09) - 1.02(\pm 0.04)pK_a$. (*b*) Brønsted plot for the calculated rate constants for formation of methyl esters by attack of oxy anions upon protonated methyl. The best line as well as the extreme lines allowed by the data are shown.

for the reverse reaction this is less satisfactory because the available points do not cover a wide enough range. Since the rate determining step for the hydrolysis is attack of water on the methyl carbon leading to protonated methanol as the initial product along with the leaving group as anion, the rate constants for ester formation should be calculated for the microscopic reverse of this reaction, i.e., attack of the anion on protonated methanol. For all of the cases where the rate of hydrolysis is measureable, the equilibrium lies far on the side of hydrolysis; however, the rate constant for ester formation can be calculated if the rate constant and the equilibrium constant for hydrolysis are known. This condition is satisfied for dimethyl sulfate and the methyl phosphates. Since the equilibrium constants are calculated from thermochemical data and so are imprecise, the rate constants for ester formation are subject to uncertainties of at least an order of magnitude. Figure 2*b* shows this Brønsted plot and also the extreme lines which are allowed by the error limits on the data points. The extreme lines are drawn so that they will just pass within the error bars for the data; these lines are used to assess the error bounds for extrapolations of the line beyond the range specified by the data. Within this range, it was assumed that the bounds on the line were the same as the bounds on the data, and lines parallel to the best line were drawn. Rate constants for the formation of the esters for which hydrolysis rate constants are available were taken from this correlation line, with error limits taken from the extreme lines; these rate constants and free energies of hydrolysis derived from them are found in Table 4. Although these values are subject to much greater uncertainty than is desirable, there has been to our knowledge no other method reported to give *any* information concerning these free energies of hydrolysis.

The Brønsted line for the attack of oxy anions on $CH_3OH_2^+$ has a rather small slope, subject to large uncertainties. Unfortunately there do not seem to be any other studies of the kinetics of nucleophilic attack of a series of oxygen monoanions on a cationic substrate, so that it is difficult to assess the reasonableness of the result. One related study is by Kevill and Wang (48*a*) of the nucleophilic attack of a series of arenesulfonate anions upon methyl triflate in acetonitrile. Using the pK_a values for arenesulfonates derived in this work, Kevill's ρ value can be converted to a Brønsted slope of +0.69; this is similar to the upper limit for the slope of Fig. 2*b*. Since Kevill's data refer to a reaction with a neutral substrate in a dipolar aprotic solvent, rather than a cationic substrate in a protic solvent, it is not clear how similar the slopes should be expected to be. A somewhat more analogous system is the reaction of anions with *S*-(2-chloroethyl)thiironium ion (48*b*); from the data in ref. 48*b* it may be calculated that for sulfate and phosphate dianions, the Brønsted slope for nucleophilic attack is +0.23. This is also an imperfect model since the reaction is one of dianions with a highly strained substrate but it is encouraging

Can. J. Chem. Downloaded from www.nrcresearchpress.com by 210.87.254.5 on 09/05/12
For personal use only.

TABLE 4. Data for Brønsted plots

Ester	pK_a of acid[a]	log k_{H_2O}[b]	log k_{rev}[c]	ΔG_{hydrol}[d]	ΔG^{Oe}
CH_3OSO_2Cl	−6.0(0.5)	−1.78[f]	−10.4(1.7)[k]	−11.8(2.3)	−6.6(2.4)
$CH_3OSO_2CF_3$	−5.9(0.5)	−1.76[g]	−10.4(1.7)[k]	−11.8(2.3)	−6.7(2.4)
CH_3OClO_3	−5.0(0.5)	−2.82[h]	−10.2(1.5)[k]	−10.1(2.0)	−6.2(2.1)
$CH_3OSO_2OCH_3$	−3.4(0.5)	−4.08[i]	−9.69(0.90)[l]	−7.7(1.2)	−6.8(1.0)
$CH_3—OSO_2—C_6H_4—NO_2$	−4.0(1.0)	−4.20[j]	−9.9(1.2)[k]	−7.8(1.6)	−5.3(1.7)
$CH_3—O—SO_2—C_6H_4—Br$	−3.1(1.0)	−4.71[j]	−9.6(1.0)[k]	−6.7(1.4)	−5.4(1.6)
$CH_3—O—SO_2—C_6H_5$	−2.8(1.0)	−4.93[j]	−9.6(1.0)[k]	−6.4(1.4)	−5.5(1.6)
$CH_3—OSO_2CH_3$	−1.92	−5.29[j]	−9.3(1.0)[k]	−5.5(1.4)	−5.8(1.6)
$(CH_3O)_3PO$	0.76	−8.2(0.1)[j]	−8.3(1.0)[l]	−0.1(1.3)	−4.1(1.3)
$(CH_3O)_2PO_2H$	1.50	−9.6(0.5)[j]	−8.6(1.1)[l]	+1.4(1.3)	−3.6(1.3)
$CH_3OPO_3H_2$	2.12	−10.1(0.5)[j]	−8.0(1.1)[l]	+2.9(1.3)	−3.0(1.3)
CH_3ONO_2	−1.3	−8.60[i]	—	—	—

[a]From Table 3.
[b]Pseudo-first-order rate constant for hydrolysis in water at 25°C (s^{-1}) divided by the number of hydrolyzable methyl groups.
[c]Second-order rate constant for attack of the anion upon protonated methanol.
[d]Free energy change for the process: $XOCH_3 + H_2O = XO^- + H_2OCH_3^+$; the standard state for water is the pure liquid, and for solutes is 1 *M* aqueous solution.
[e]Free energy change for the process: $XOCH_3 + H_2O = XOH + HOCH_3$.
[f]Reference 76.
[g]Estimated from rate constants for the ethyl ester at 25°C in 100 and 80% aqueous ethanol, (77) assuming that log *k* was linear in Y and that the methyl to ethyl ratio was the same as for $ROSO_2Cl$ (76).
[h]Reference 78.
[i]Reference 79.
[j]Reference 2.
[k]Values taken from the best line in Fig. 2*b*; error limits taken from the extreme lines.
[l]Calculated from k_{H_2O} and equilibrium constant, as described in the text.

that a reaction with similar charge types and the same solvent shows a similar Brønsted slope.

Free Energies of Hydrolysis of Some Other Esters

To supplement the set of compounds X—O—R which can be used to test the range of applicability of eq. [1] some further free energies of hydrolysis for esters of acids of known pK_a can be derived from thermochemical data in the literature.

Arsenious Acid and its Methyl Esters

Arsenious oxide (As_2O_3) is sparingly soluble in water and it is considered that in aqueous solution "... the predominant species is probably $As(OH)_3$" (38). The acid species does not have an As—H bond by contrast to H_3PO_3 (38). The heat of hydrolysis of trimethyl arsenite has been measured and it is reported that the ester hydrolyzed extremely rapidly in water (39). Thus in calculating the free energy of formation of the ester in aqueous solution it was necessary to estimate the free energy of transfer as described in the Appendix. In the absence of experimental knowledge concerning the thermodynamics of solution of organic arsenic compounds there is unavoidably some additional uncertainty in the numerical value of the free energy of formation of the ester in solution. The thermodynamic data in Table 1 lead to an overall free energy of hydrolysis of −11.03 ± 1.69 kcal mol^{-1}. Application of eq. [1] leads to

$$(MeO)_3As + 3H_2O \rightleftharpoons 3MeOH + H_3AsO_3$$

the following values for the first, second, and third stages of hydrolysis: −2.46, −2.46, and −2.42 kcal mol^{-1} or −7.34 kcal mol^{-1} overall. The discrepancy is disturbingly large, amounting to 3.7 kcal overall, or somewhat over 1 kcal per step. However, it is probably unrealistic to expect predictions to be much better than to within a kcal for the extent of structural variation involved in extending a relationship originally derived for carbon compounds to an arsenic derivative. Furthermore the thermodynamic data upon which the 'experimental' free energy of hydrolysis is based are subject to more than the usual uncertainty because of our imperfect knowledge of the solution chemistry of arsenic. It seems not unreasonable to conclude that eq. [1] gives a useful, albeit imprecise, estimate of the free energy of hydrolysis even for an arsenic derivative.

Silicic Acid and its Ethyl Esters

It is now accepted that the species in solutions of SiO_2 or its hydrates at low pH is $Si(OH)_4$ (40), with free energy of formation equal to −312.57 kcal mol^{-1} (41). The heat of hydrolysis of tetraethyl

Can. J. Chem. Downloaded from www.nrcresearchpress.com by 210.87.254.5 on 09/05/12
For personal use only.

Can. J. Chem. Downloaded from www.nrcresearchpress.com by 210.87.254.5 on 09/05/12
For personal use only.

orthosilicate in acidic solution has been measured (42) but is subject to an uncertainty of 2 kcal mol^{-1} because of uncertainty concerning the nature (colloidal solution or amorphous precipitate) of the silica produced (42). The first pK_a for silicic acid is reported to be 9.93 (43); this is in fair agreement with expectations from Pauling's rule and the discrepancy can be rationalized in terms of the low electronegativity of the central atom. If pK_a values for the mono-, di-, and triesters are estimated as already described, the free energies of hydrolysis can be calculated for each step. Steric effects are expected to be small, and for lack of any better approach were estimated on the assumption that they would be the same as for tetraethyl orthocarbonate. The predicted value for the overall free energy of hydrolysis for process [6] is

[6] $$(EtO)_4Si + 4H_2O \rightleftharpoons Si(OH)_4 + 4EtOH$$

-8.75 ± 0.71 kcal mol^{-1}, which is to be compared with the experimental value of -6.31 ± 2.3 kcal mol^{-1}. The agreement is within the uncertainties of the quantities concerned. We conclude that eq. [1] is valid for orthosilicic acid and its esters. Free energies of formation of the mono-, di-, and triesters were calculated using eq. [1] and are included in Table 1.

Methyl Borate

From the free energies of formation for trimethyl borate and boric acid in Table 1 and the usual assumption concerning the acid strengthening effect of replacing hydroxyl by methoxyl, use of eq. [1] leads to a predicted pK_a for boric acid of 9.6. It should be noted that this refers to the hypothetical process shown in eq. [7] and not to the process shown in eq. [8] which is believed to represent what

[7] $$H_3BO_3 \rightleftharpoons H^+ + H_2BO_3^-$$

[8] $$H_3BO_3 + H_2O \rightleftharpoons H^+ + B(OH)_4^-$$

actually happens in aqueous solution (33). The calculated pK_a is close to the observed value but this is probably accidental. Just as eq. [1] leads to anomalously high pK_a values for acids for which the anion shows increased resonance, so it should lead to anomalously low pK_a values for acids, such as boric, which should show a decrease in resonance upon ionization. Using one third of the observed free energy change for complete hydrolysis as the free energy change per step, free energies of formation of mono and dimethyl borate in aqueous solution were calculated. These species are obligatory intermediates in the hydrolysis of trimethyl borate, but nothing seems to be known about their stability.

Methyl Nitrite

Although the free energy of formation of the gaseous ester is well defined, it is necessary to estimate the free energy of transfer because of the rapid hydrolysis of alkyl nitrites. (Transesterification in neutral alcohol is reported to be very fast (49).) From the free energies of formation of the gaseous acid (50) and the hypothetical aqueous acid (calculated from the free energy of formation of nitrite ion and the pK_a reported for nitrous acid) a value of the free energy of transfer of the acid could be obtained; it was then assumed that the increment in ΔG_t on going from acid to ester would be the same as for formic acid. This procedure, though plausible, must lead to considerable uncertainty in the final value of the free energy of formation of the aqueous ester. From the values in Table 1, a free energy of hydrolysis of $+0.78$ kcal mol^{-1} can be obtained, which leads to a pK_a of 15, which is markedly different from the observed value of 3.3. The difference of 12 log units may be attributed to the effect of resonance delocalization in the anion upon the acidity of nitrous acid.

Methyl Nitrate

The data in Table 1 lead to free energy of hydrolysis of -0.78 kcal mol^{-1} and a calculated pK_a of 11.9 for nitric acid; this differs from the observed pK_a value of -1.4 by 13.3 log units, which is a measure of the importance of resonance delocalization upon the acidity of nitric acid.

Methyl Esters of Carboxylic Acids

Equilibrium constants for hydrolysis of methyl formate and acetate have been measured. These lead to pK_a values of 11.3 and 11.6, respectively. Data from the literature permit the calculation of the overall free energy of hydrolysis of dimethyl carbonate as -2.64 kcal mol^{-1}. This leads to a pK_a of 11.8.

Correlation of Free Energy of Ester Hydrolysis with Acid pK_a

The free energies of hydrolysis derived in this work (Table 5), as well as those reported earlier, are plotted as a function of the pK_a of the acid produced on hydrolysis in Fig. 3. Clearly, for those acids where resonance effects are not important, the fit to the previously reported line is very good. Equally clearly, the deviations for those acids which *do* have important resonance effects are very substantial. The correlation holds for the entire range of pK_a values for Brønsted oxygen acids which can exist in water and therefore it seems appropriate to conclude that we have a general method for calculating the equilibrium constant for a defined, and large, class of hydrolysis reactions.

Free Energies of Transfer for Inorganic Acids

From thermodynamic data for the gaseous acids (50) and free energies of formation of the aqueous acids from the present work, the following values for

Can. J. Chem. Downloaded from www.nrcresearchpress.com by 210.87.254.5 on 09/05/12
For personal use only.

TABLE 5. Data for Fig. 3

X—OH	pK_a	$\Delta G''^a$
CH_3OH^b	15.49	$+0.75 \pm 1$
$EtOH^b$	15.93	$+0.07 \pm 1$
$iPrOH^b$	16.10	-0.39 ± 1
$tBuOH^b$	16.04	$+1.35 \pm 1$
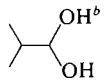	13.77	−0.00
	13.57	−0.00
	13.27	−0.33
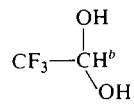	10.20	−1.75
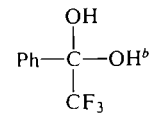	10.00	−1.49
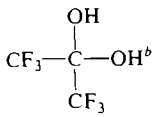	6.58	−2.35
$(HO)_2PO—OH^b$	2.12	−3.12(1.29)
$HOPO_2^-—OH^b$	7.21	−2.01(1.29)
$PO_3^{2-}—OH^b$	12.67	−0.74(1.29)
$(EtO)_3SiOH^{c,d}$	7.95	−1.36(1.0)
$ClO_3—OH^c$	−5.0(0.5)	−5.8(2.1)
$CH_3OSO_2—OH^{c,d}$	−3.4(0.5)	−5.9(1.0)
$CH_3SO_2—OH^c$	−1.92	−5.4(1.6)
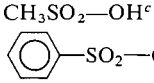	−2.8(1.0)	−5.1(1.6)
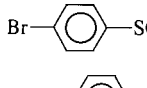	−3.1(1.0)	−5.0(1.6)
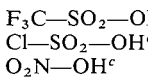	−4.0(1.0)	−4.9(1.6)
$F_3C—SO_2—OH^c$	−5.9(0.5)	−6.3(2.4)
$Cl—SO_2—OH^c$	−6.0(0.5)	−6.2(2.4)
$O_2N—OH^c$	−1.3	−0.37(0.47)
$ON—OH^c$	3.29	+1.19(1.05)
$MeOCO—OH^{c,d}$	2.92	−0.50(1.27)
$HCOOH^c$	3.77	−0.97(0.09)
CH_3COOH^c	4.76	−0.89(0.04)

[a]Free energy of hydrolysis, with neutral reactants and products, in aqueous solution, corrected for steric and symmetry effects.
[b]Reference 2.
[c]This work.
[d]Average $\Delta G''$ per step based on ΔG_f^0 values.

the free energies of transfer from the gas phase to aqueous solution can be calculated: $HClO_4$, -21 ± 4 kcal mol^{-1}; H_2SO_4, -19 ± 2 kcal mol^{-1}; HNO_3, -7.0 kcal mol^{-1}. (The uncertainties reflect the uncertainty in ΔH_f^0(g).) These values are much more negative than the values for the corresponding methyl esters and must reflect the very powerful hydrogen bonding of strongly acidic protons to water.

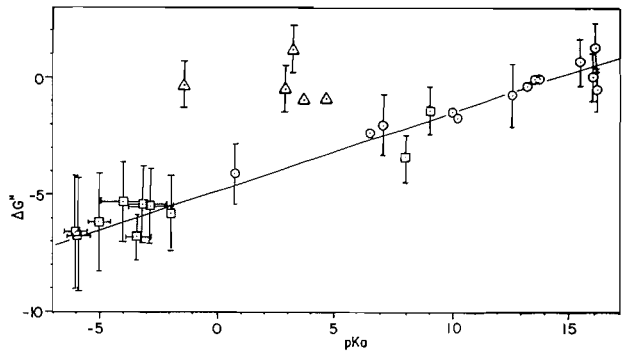

FIG. 3. Test of eq. [1]; the line is calculated using the slope and intercept reported in ref. 2: (○) points for compounds previously reported in ref. 2, (□) points for inorganic acids without resonance, (△) points for acids in which resonance is important.

Experimental

The solubility of dimethyl carbonate in water at 25°C was determined by nmr analysis of a saturated solution, integrating the methyl signal relative to the solvent peak. The solvent was 0.001 *N* aqueous HCl.

Equilibrium constants for ester formation in water at 25°C were determined by nmr analysis as previously described (83); values of the equilibrium constant of 0.097 ± 0.015 M^{-1} for formic acid plus methanol (lit. (84) value 0.122 ± 0.003 M^{-1}) and 0.111 ± 0.006 M^{-1} for acetic acid plus methanol were obtained.

Acknowledgements

Financial assistance from the National Research Council of Canada and the Alfred P. Sloan Foundation is gratefully acknowledged. I thank Dana Zendrowski for technical assistance.

1. J. P. GUTHRIE. Can. J. Chem. **53**, 898 (1975).
2. J. P. GUTHRIE. J. Am. Chem. Soc. **99**, 3991 (1977).
3. G. C. HOOD and C. A. REILLY. J. Chem. Phys. **32**, 127 (1960).
4. R. W. DUERST. J. Chem. Phys. **48**, 2275 (1968).
5. G. C. HOOD and C. A. REILLY. J. Chem. Phys. **27**, 1126 (1957).
6. J. W. AKITT, A. K. COVINGTON, J. G. FREEMAN, and T. M. LILLEY. Trans. Faraday Soc. **65**, 2701 (1969).
7. (*a*) T. F. YOUNG and J. E. WALRAFEN. Trans. Faraday Soc. **57**, 34 (1961); (*b*) N. G. ZARAKHANI and M. I. VINNIK. Russ. J. Phys. Chem. **37**, 260 (1963).
8. V. D. MAIOROV and N. B. LIBROVICH. Russ. J. Phys. Chem. **47**, 989 (1973).
9. V. D. MAIOROV and N. B. LIBROVICH. Russ. J. Phys. Chem. **47**, 1295 (1973).
10. L. PAULING. General chemistry. Freeman, San Francisco, CA. 1947. p. 394.
11. J. E. RICCI. J. Am. Chem. Soc. **70**, 109 (1948).
12. A. KOSSIAKOFF and D. HARKER. J. Am. Chem. Soc. **60**, 2047 (1938).
13. G. SCHWARTZENBACH. Z. Phys. Chem. **176**, 133 (1936).
14. (*a*) R. T. SANDERSON. J. Chem. Educ. **31**, 2 (1945); (*b*) J.

Can. J. Chem. Downloaded from www.nrcresearchpress.com by 210.87.254.5 on 09/05/12
For personal use only.

HINZE, M. A. WHITEHEAD, and H. H. JAFFÉ. J. Am. Chem. Soc. **85**, 148 (1963).
15. A. K. COVINGTON and R. THOMPSON. J. Solution Chem. **3**, 603 (1974).
16. (*a*) A. J. KRESGE and Y. C. TANG. J. Org. Chem. **42**, 757 (1976); (*b*) D. J. MARTIN and C. E. GRIFFIN. J. Organomet. Chem. **1**, 292 (1964).
17. A. ALBERT and E. P. SERJEANT. Ionization constants of acids and bases. Methuen, London. 1962.
18. T. V. PARKE and W. W. DAVIS. Anal. Chem. **26**, 642 (1954).
19. O. MÄKITIO and V. KONTTINEN. Acta Chem. Scand. **23**, 1459 (1969).
20. H. H. JAFFÉ, L. D. FREEDMAN, and G. O. DOAK. J. Am. Chem. Soc. **75**, 2210 (1953).
21. J. F. J. DIPPY and F. R. WILLIAMS. J. Chem. Soc. 161 (1934).
22. M. CHARTON. J. Org. Chem. **29**, 1222 (1964).
23. R. W. TAFT, E. PRICE, I. R. FOX, I. C. LEWIS, K. K. ANDERSON, and G. T. DAVIS. J. Am. Chem. Soc. **85**, 709 (1903).
24. N. V. HAYES and G. E. K. BRANCH. J. Am. Chem. Soc. **65**, 1555 (1943).
25. R. J. GILLESPIE. J. Chem. Soc. 2537 (1950).
26. D. G. RUSSELL and J. B. SENIOR. Can. J. Chem. **52**, 2975 (1974).
27. R. J. GILLESPIE, T. E. PEEL, and E. H. ROBINSON. J. Am. Chem. Soc. **93**, 5083 (1971).
28. J. BESSIÈRE. Bull. Soc. Chim. Fr. 3353 (1969).
29. J. BESSIÈRE. Bull. Soc. Chim. Fr. 3356 (1969).
30. I. M. KOLTHOFF and S. BRUCKENSTEIN. J. Am. Chem. Soc. **78**, 1 (1956).
31. S. BRUCKENSTEIN and I. M. KOLTHOFF. J. Am. Chem. Soc. **78**, 2974 (1956).
32. J. BESSIÈRE. Anal. Chem. Acta, **52**, 55 (1970).
33. R. P. BELL. The proton in chemistry. 2nd ed. Cornell University Press, Ithaca, NY. 1973.
34. G. CHARLOT and B. TRÉMILLON. *Translated by* P. J. J. Harvey. Chemical reactions in solvents and melts. Pergamon Press, Oxford. 1969.
35. A. M. ELAGGAN, D. C. BRADLEY, and W. WARDLAW. J. Chem. Soc. 2092 (1958).
36. R. LEIMER and P. SALOMAA. Acta Chem. Scand. **1**, 353 (1947).
37. J. P. GUTHRIE. Can. J. Chem. **54**, 202 (1976).
38. J. D. SMITH. *In* Comprehensive inorganic chemistry. Vol. 2. *Edited by* A. F. Trotman-Dickenson. Pergamon Press, Oxford. 1973. p. 608.
39. T. CHARNLEY, C. T. MORTIMER, and H. A. SKINNER. J. Chem. Soc. 1181 (1953).
40. V. A. POPEIKIN and A. S. MIKHAILOV. Dokl. Akad. Nauk SSSR, **191**, 917 (1970); Chem. Abstr. **73**, 39220d (1970).
41. H. C. HELGESON. Am. J. Sci. **267**, 729 (1969).
42. T. FLITCROFT and H. A. SKINNER. J. Chem. Soc. 3355 (1956).
43. B. N. RYZHENKO. Geochem. Int. **4**, 99 (1967).
44. W. P. JENCKS. Catalysis in chemistry and enzymology. McGraw-Hill, New York, NY. 1969. p. 81.
45. W. P. JENCKS. Catalysis in chemistry and enzymology. McGraw-Hill, New York, NY. 1969. pp. 511 and 533.
46. (*a*) W. P. JENCKS. Catalysis in chemistry and enzymology. McGraw-Hill, New York, NY. 1969. p. 83; (*b*) A. J. KIRBY and M. YOUNAS. J. Chem. Soc. B, 1165 (1970); (*c*) S. A. KHAN and A. J. KIRBY. J. Chem. Soc. B, 1172 (1970).
47. O. ROGNE. J. Chem. Soc. B, 1855 (1971); O. ROGNE. J. Chem. Soc. B, 727 (1970).
48. (*a*) D. N. KEVILL and A. WANG. J. Chem. Soc. Chem. Commun. 618 (1976); (*b*) C. G. SWAIN and C. B. SCOTT. J. Am. Chem. Soc. **75**, 141 (1953).
49. S. COFFEY (*Editor*). Rodd's chemistry of carbon compounds. 2nd ed. Vol. 1B. Elsevier, Amsterdam. 1965. p. 57.
50. S. W. BENSON. Thermochemical kinetics. 2nd ed. Wiley, New York, NY. 1976.
51. S. W. BENSON and J. H. BUSS. J. Chem. Phys. **29**, 546 (1958).
52. H. E. O'NEAL and M. A. RING. Inorg. Chem. **5**, 435 (1966).
53. F. D. ROSSINI, D. D. NAGMAN, W. E. EVANS, S. LEVINE, and I. JAFFE. Natl. Bur. Stand. (U.S.) Circ. 500 (1952).
54. N. C. DENO and H. E. BERKHEIMER. J. Chem. Eng. Data, **5**, 1 (1960).
55. J. D. COX and G. PILCHER. Thermochemistry of organic and organometallic compounds. Academic Press, New York, NY. 1970.
56. J. D. RAY and A. A. GERSHON. J. Phys. Chem. **66**, 1750 (1962).
57. J. D. RAY and R. A. OGG, JR. J. Phys. Chem. **63**, 1522 (1959).
58. P. GRAY and P. L. SMITH. J. Chem. Soc. 2380 (1953).
59. G. DESSEIGNE. Mem. poudres, **30**, 59 (1948); Chem. Abstr. **44**, 7221c (1950).
60. J. HINE and A. W. KLUEPPEL. J. Org. Chem. **96**, 2924 (1974).
61. D. R. STULL. Ind. Eng. Chem. **39**, 517 (1947).
62. D. C. BRADLEY, R. C. MEHROTRA, J. D. SWANICH, and W. WARDLAW. J. Chem. Soc. 2025 (1953).
63. J. B. PEDLEY and B. S. ISAND. CATCH tables for silicon compounds. University of Sussex, Brighton. 1972.
64. W. M. LATIMER. The oxidation states of the elements and their potentials in aqueous solution. 2nd ed. Prentice Hall, Engelwood Cliffs, NJ. 1952.
65. J. P. GUTHRIE. J. Am. Chem. Soc. **95**, 6999 (1973).
66. J. HORYNA. Coll. Czech. Chem. Commun. **24**, 1596 (1959).
67. H. CERFONTAIN and B. W. SCHNITGER. Recl. Trav. Chim. **91**, 199 (1972).
68. R. H. DINIUS and G. R. CHOPPIN. J. Phys. Chem. **66**, 268 (1962).
69. S. K. HALL and E. A. ROBINSON. Can. J. Chem. **42**, 1113 (1964).
70. E. HÖGFELDT. Acta Chem. Scand. **17**, 785 (1963).
71. L. S. LEVITT and B. W. LEVITT. Tetrahedron, **27**, 3777 (1971).
72. W. P. JENCKS and J. REGENSTEIN. *In* Handbook of biochemistry. 1st ed. H. A. Sober (*Editor*). Chemical Rubber Publishing Co., Cleveland, OH. 1968.
73. C. A. BUNTON, D. R. LLEWELLYN, K. G. OLDHAM, and C. A. VERNON. J. Chem. Soc. 3574 (1958).
74. C. A. BUNTON, M. M. MHALA, K. G. OLDHAM, and C. A. VERNON. J. Chem. Soc. 3293 (1960).
75. R. M. SMITH and A. E. MARTELL. Critical stability constants. Vol. 4. Plenum Press, New York, NY. 1976.
76. E. C. F. KO and R. E. ROBERTSON. Can. J. Chem. **50**, 434 (1972).
77. A. STREITWIESER, JR., C. L. WILKINS, and E. KIEHLMANN. J. Am. Chem. Soc. **90**, 1598 (1968).
78. R. E. ROBERTSON, A. ANNESSA, and J. M. W. SCOTT. Can. J. Chem. **53**, 3106 (1975).
79. R. E. ROBERTSON. Prog. Phys. Org. Chem. **4**, 213 (1967).
80. BEILSTEIN. Handbuch der organischen Chemie. (*a*) Ser. II, Vol. 1, p. 272 (1941); (*b*) Ser. II, Vol. 1, p. 271 (1941); (*c*) Ser. III, Vol. 1, p. 1198 (1958); (*d*) Ser. IV, Vol. 1, p. 1259 (1973).
81. S. H. WEBSTER and L. M. DENNIS. J. Am. Chem. Soc. **55**, 3233 (1933).
82. I. G. RYSS and V. B. TULCHENSKII. Russ. J. Inorg. Chem. **6**, 947 (1961).
83. J. P. GUTHRIE. Can. J. Chem. **55**, 3562 (1977).
84. A. R. FERSHT. J. Am. Chem. Soc. **93**, 3504 (1971).

TABLE 6. Free energies of transfer from the gas phase to aqueous solution

Compound	Solubility (M)	Vapor pressure (Torr)	ΔG_t (kcal mol^{-1})
$(CH_3O)_2SO_2$	0.22[a]	0.36[b]	−3.20
$(CH_3O)_3As$	1.35[c]	9.45[d]	−2.78
$(CH_3O)_3B$	3.5[c]	132[e]	−1.78
$(CH_3CH_2O)_4Si$	0.0096[f]	1.92[g]	−0.79
$(CH_3O)_2CO$	1.59[h]	61.5[i]	−1.77

[a]Reference 80.
[b]Calculated by extrapolation of a line through vapor pressure data from Beilstein (80*b* and *c*).
[c]Calculated as described in the text, using $CH(OCH_3)_3$ (65) as the model for evaluating the effect of hydrogen bonding.
[d]Calculated from the equation relating log p and T given in ref. 39.
[e]Calculated from the equation relating log p to T given in ref. 81.
[f]Calculated as described in the text, using $C(OCH_2CH_3)_4$ (2) as the model for evaluating the effect of hydrogen bonding.
[g]Interpolated from a plot of ln p vs. $1/T$ based on data from ref. 61.
[h]This work, see Experimental.
[i]Estimated as described in the Appendix.

Appendix

Estimation of Entropies

Standard entropies for the gaseous esters had to be estimated in most cases; this was done using the additivity schemes proposed by Benson and Buss (51); wherever possible this was done using bond contributions (51, 52) but in some cases no parameters were available and it was necessary to employ the atomic contributions scheme (51). For this purpose terms for tetracoordinate chlorine, tricoordinate boron, and tricoordinate arsenic were needed; these were calculated from the available entropy data (51, 53) (for perchloric acid, BCl_3 and BF_3, and $AsCl_3$ and AsF_3) and are −35.3, −13.7, and −5.2 cal deg^{-1} mol^{-1}, respectively.

Estimation of Solubilities

Since many of these inorganic esters hydrolyze rapidly, it is not possible to determine their solubilities experimentally. Solubilities were estimated employing a modification of the method of Deno and Berkheimer (54). This method is based upon a relationship between solubility and the parachor expressed as

$$\log (c_1/c_2) = 0.013P - E_A$$

where c_1 is the concentration of the liquid solute in itself, c_2 is the molar solubility in water, P is the parachor of the solute, and E_A is a correction for hydrogen bond formation between solute and water. For each inorganic ester of the $M(OR)_n$ type, E_A was assumed to be equal to the value calculated from the solubility and parachor for the analogous orthoester, $C(OR)_n$ or $HC(OR)_n$, with the same R and n. Parachor values were calculated from density and surface tension data found in Beilstein. The solubility values so estimated are found in Table 6.

Estimation of Vapor Pressures

The vapor pressures of the esters were taken wherever possible from published equations relating log p to T. For the cases of dimethyl sulfate and tetraethyl orthosilicate it was necessary to draw the best lines through plots of ln p vs. $1/T$ (in the case of tetraethyl orthosilicate using only data at low pressure) and so estimate the vapor pressure at 25°C. In the case of dimethyl carbonate, only the boiling point at atmospheric pressure was available so that it was necessary to estimate the vapor pressure using the heat of vaporization (60) and the heat capacity of vaporization taken as −12 cal deg^{-1} mol^{-1} (54*b*).

The vapor pressures are found in Table 6.

Can. J. Chem. Downloaded from www.nrcresearchpress.com by 210.87.254.5 on 09/05/12
For personal use only.

The conformational preferences and the rotational barriers of some simple cyclopropylcarbinyl cations

NANCY OKAZAWA AND TED S. SORENSEN

The Department of Chemistry, University of Calgary, Calgary, Alta., Canada T2N 1N4

Received April 24, 1978

NANCY OKAZAWA and TED S. SORENSEN. Can. J. Chem. **56**, 2355 (1978).

The ground-state rotamer conformations of a series of 'bisected' dicyclopropylcarbinyl cations, cyclopropylallyl cations, and phenylcyclopropylcarbinyl cations have been systematically investigated for the first time, employing ^1H and ^{13}C nmr spectroscopy. In the absence of significant steric factors, these cations adopt conformations involving the 'most extended conjugation.' However, this preference is not overwhelming because, in the presence of other substituents of only modest bulk, other less extended conformations exist. Cation systems, where two of these conformations are observable, have been found for each of the three major types described above. From an nmr line-broadening analysis, the populations of the two conformers and the energy barrier interconverting them have been obtained. In phenyldicyclopropylcarbinyl cations, at least one of the conformers involves a nonplanar phenyl ring.

NANCY OKAZAWA et TED S. SORENSEN. Can. J. Chem. **56**, 2355 (1978).

On a étudié, pour la première fois, faisant appel à la spectroscopie rmn du ^1H et du ^{13}C, les divers rotamères de l'état fondamental d'une série de cations dicyclopropylcarbinyle, cyclopropylallyle et phénylcyclopropylcarbinyle "bisectés." En l'absence de facteurs stériques importants, ces cations adoptent des conformations impliquant la "conjugaison la plus délocalisée." Toutefois cette préférence n'est pas de plus importante; en effet, en présence d'autres substituants de grosseur même modeste il existe d'autres conformations de conjugaison moins étendue. On a trouvé des systèmes cationiques où deux de ces conformations peuvent être observées pour chacun des trois types majeurs décrits plus haut. Faisant appel à une analyse de l'élargissement des raies en rmn, on a pu déterminer les populations des deux conformères et la barrière d'énergie d'interconversion entre eux. Dans les cations phényldicyclopropylcarbinyles, au moins un de ces conformères implique un noyau phényle nonplanaire.

[Traduit par le journal]

Introduction

A large body of experimental evidence has now been accumulated (1) to show that secondary and tertiary cyclopropylcarbinyl cations adopt the 'bisected' geometry depicted in **1**, where overlap is possible between the empty C^+ p_z orbital and the filled antisymmetric Walsh orbital (2). A 'top view' of this same geometry is depicted in **2**, where the upper edge of the cyclopropyl ring plane is outlined.

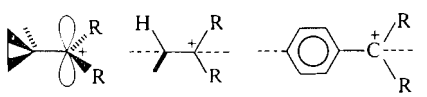

1 **2** **3**

Structure **2** also illustrates a basic feature of a 'bisected' cyclopropylcarbinyl system, viz., the lack of a symmetry plane through the C^+–cyclopropane bond. This feature can be contrasted to that of a planar phenyl-ring-substituted carbocation, as in **3**.

In this study, we have looked at a second conformational feature which arises in cyclopropylcarbinyl type cations in which a second (or even a third) conjugating substituent is joined to the C^+ carbon. For example, when two cyclopropyl rings are present, one has the possibility of three different bisected conformations, i.e. **4***a*, **4***b*, and **4***c*. In addition we

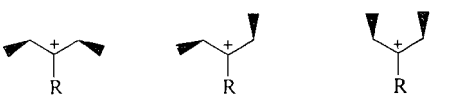

4*a* **4***b* **4***c*

have looked at cyclopropylcarbinyl cations substituted with either conjugating phenyl or alkene groups. The conformational possibilities in these cases will be discussed under the same heading describing the experimental observations.

No comprehensive study concerning the conformational preferences and the rotation barriers of these systems has been reported.

Results and Discussion

Di- and Tricyclopropylcarbinyl Cations

There are three possible bisected conformations in the dicyclopropyl case if the R substituent is symmetric with respect to the R—C^+ bond, structures **4***a–c*. Molecular model studies show that a bisected conformer **4***c* is sterically quite crowded, because of the ring–ring β-CH_2 interaction. Therefore, this

Can. J. Chem. Downloaded from www.nrcresearchpress.com by 210.87.254.5 on 09/05/12
For personal use only.

Can. J. Chem. Downloaded from www.nrcresearchpress.com by 210.87.254.5 on 09/05/12
For personal use only.

conformer will not be considered further in this and the following case (R = CH_3 and H). This neglect of conformer **4***c* is also entirely consistent with the experimental results. In structure **4***a*, both cyclopropyl rings are equivalent, whereas in **4***b* they are not. *If* the barrier for the rotational process interconverting **4***a* and **4***b* can be slowed down on an nmr time scale, then the assignment of the observed spectrum to either **4***a* or **4***b* should be straightforward, because of the symmetry differences. The problem then is in knowing what this rotational barrier would be so that one could appropriately cool the sample to the point where the interconversion rate would be calculated to be slow.

Fortunately, it has been found that when R = CH_3, two conformers are present in appreciable amounts and one can directly determine the activation barrier for the interconversion rotation process. Armed with this, one can then treat two other cation cases where *only one* conformer is observed.

The 1,1-Dicyclopropylethyl Cation **4** *(R = CH_3)*

This cation was prepared from the corresponding alcohol and exhibits a proton spectrum at −40°C similar to that previously reported (3). This spectrum shows a single methyl peak, and a rather complex multiplet appropriate for an $(AA'BB'X)_2$ splitting pattern. The ^{13}C nmr spectrum was also obtained[1] and at −35.5°C shows only four peaks, for C^+, CH_3, and the α and β carbons of the cyclopropyl ring. However, even at this temperature, the CH_3 signal is very broad, indicating that a conformational averaging process is already being slowed down. On further cooling, both the ^1H and ^{13}C nmr spectra exhibit the typical line broadening, coalescence, and resharpening into two sets of peaks, one set characteristic of conformer **4***a* (R = CH_3). The nmr data are collected together in Table 1. The ^{13}C spectra are the most definitive for assignment purposes and a set of these are shown in Fig. 1. The symmetrical conformer **4***a* (R = CH_3) can be assigned to the major isomer (65%) and the *four* ^{13}C peaks of this species are marked in the top spectrum of Fig. 1. The minor isomer **4***b* (R = CH_3) (35%) is characterized by *six* peaks and these are also shown in Fig. 1. This definitive assignment allows one to make several general comments: (*i*) The CH_3 carbon (and the protons) in **4***a* is much more shielded than in **4***b*. This general observation, that groups in the face of a cyclopropane ring are shielded, has been noted many times (5). (*ii*) The α-CH carbons (and protons) in **4***b* have distinctly different chemical shifts and one can very confidently assign the lower field peak to that

[1]The averaged ^{13}C nmr spectrum (partly misassigned) has been reported (4).

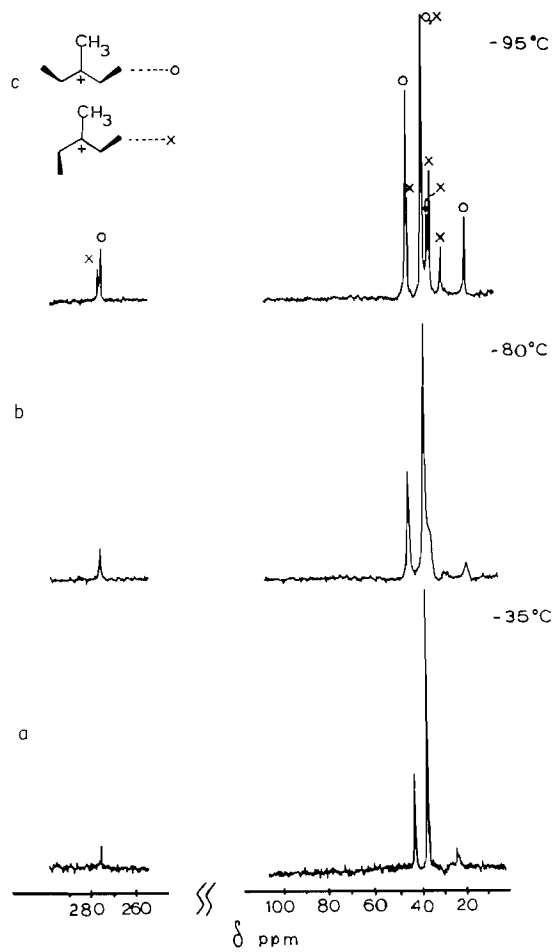

FIG. 1. (*a*) Averaged ^{13}C spectrum of cation **4** (R = CH_3); (*b*) broadened spectrum; (*c*) 'frozen-out' spectrum showing the two conformers.

CH which is not in the face of the other ring and vice versa. In conformer **4***a*, both CH carbons are equivalent and very similar to the lower field one in **4***b*, as expected.

From an nmr lineshape analysis, the **4***a* (R = CH_3) $\underset{k_f}{\rightleftarrows}$ **4***b* (R = CH_3) rate is ca. 145 s^{-1} at −75°C, $\Delta G^{\ddagger}$ = 9.4 kcal/mol.

The 1,1-Dicyclopropylmethyl Cation **4** *(R = H)*

This cation has been reported previously (4, 6). Over the temperature range −50 to −90°C, there is no noticeable line broadening in the ^1H nmr spectrum. The barrier to rotation in this cation should be as large as (or larger than) that found in the previous case (R = CH_3) and we are therefore confident that the absence of line broadening at the lowest temperatures simply reflects a very small population of the second conformer. This single

Can. J. Chem. Downloaded from www.nrcresearchpress.com by 210.87.254.5 on 09/05/12
For personal use only.

observable conformer has the **4***a* (R = H) structure, previously deduced from coupling constant and chemical shift comparisons (6). Therefore, our only contribution in this case is to rule out the possibility of any detectable conformational averaging with **4***b* (R = H). One can estimate (7), assuming that the $^{+}$C—H proton in **4***a* (R = H) and **4***b* (R = H) might be separated by about 100 Hz (see above case), that a 'no-line-broadening observation' means that the maximum possible population of **4***b* (R = H) would be about 1.6% at −75°C.

The Attempted Preparation of the α,α'-Dimethylcyclopropylmethyl Cation 5 and the α,α'-Dimethylcyclopropylethyl Cation 6

To try to systematically vary the conformational preferences in these cations, it was considered that an α-methyl substitutent might have a rather profound effect, perhaps leading exclusively to conformer **5***b* or **6***b* or even **5***c* or **6***c*, or plausibly even to nonbisected conformations:

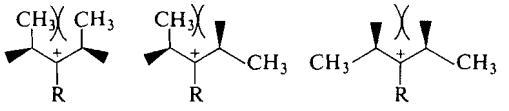

5*a* R = H **5***b* R = H **5***c* R = H
6*a* R = CH_3 **6***b* R = CH_3 **6***c* R = CH_3

The starting alcohols **7** and **8** were prepared as shown in Scheme 1.

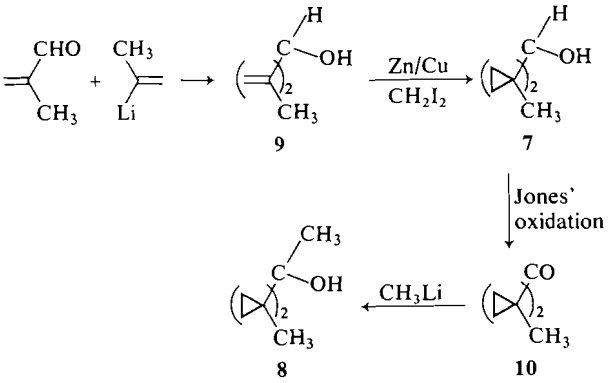

SCHEME 1

However, addition of alcohols **7** or **8** to FSO_3H–SO_2ClF at about −140°C and proton nmr measurements at −120°C showed no evidence of the expected ions. In the case of alcohol **8**, a complex spectrum was obtained and none of the peaks could be identified. In the case of **7**, the observed cation can be assigned the single cyclopropane ring-opened structure **11**, since a spectrum of the authentic cation was available (8). It has generally been observed that α-methylcyclopropylcarbinyl cations are less stable than α-H analogs but they can be prepared,

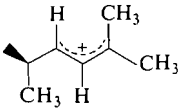

11

e.g., cation **11**. Part of the instability associated with the cations **5** and **6** may be due to the steric problems implicit in any of the bisected conformers.

The mechanism by which alcohol **7** yields cation **11** is not clear since one does not know whether cation **5** is even an intermediate in this transformation.

The Tricyclopropylmethyl Cation 12

This well-known carbocation (6, 9) can exist in two possible bisected conformers **12***a* and **12***b*. In this work, the ^{13}C nmr spectrum of **12** (4) was measured down to −137°C and no evidence for exchange linebroadening was obtained. Conformer **12***a* has previously been proposed as the stable con-

12*a* **12***b*

former (6, 10) and our goal in this instance was simply try to assure ourselves that there was no detectable population of conformer **12***b* (or nonbisected conformers). To do this, one needs to have an *estimate* for the rotational barrier in **12**. One approach is to extrapolate the change in $\Delta G^{\ddagger}$ in the following series:

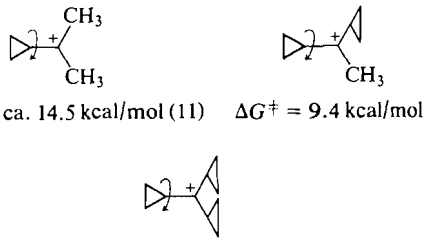

$\Delta G^{\ddagger}$ = ca. 14.5 kcal/mol (11) $\Delta G^{\ddagger}$ = 9.4 kcal/mol

$\Delta G^{\ddagger}$ estimated as 4.5 kcal/mol

For a barrier of 4.5 kcal/mol, the absolute rate expression gives a rate constant at −137°C of 1.7×10^5 s^{-1}, which does not correspond to 'frozen-out' conditions in nmr spectroscopy. Actually, our suspicions are that the $\Delta G^{\ddagger}$ barrier has been estimated too low but this remains just that.

Cyclopropyl-substituted Allyl Cations (or Vinyl-substituted Cyclopropylcarbinyl Cations)

We now consider our second broad category, i.e., with a double bond substituent. For the simple case, these are four possible conformers **13***a–d*. However, none of our examples involve the rather unstable *syn* substitution of the allyl cation, i.e., **13***c*

Can. J. Chem. Downloaded from www.nrcresearchpress.com by 210.87.254.5 on 09/05/12
For personal use only.

TABLE 1. ^1H and ^{13}C nmr parameters for the cations (^1H data in parentheses)

Cation	T (°C)	C⁺ or 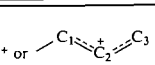	—CH_3, —CH_2—	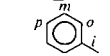	α – Cp	β – Cp
4*a*, R = CH_3	−95	276.1	19.2		45.4	38.1
	(−90)		(2.17)		(3.61)	[b]
4*b*, R = CH_3	−95	277.0	29.5		35.8	34.7
	(−90)		(3.25)		(3.61)	[b]
					44.8	38.1
					(2.59)[a]	[b]
14*a*	−97	C_1 243.0, C_2 137.0, C_3 182.9	C_4 30.5, C_5 20.5, C_6 29.9		43.9	40.2
	(−75)	C_2-H (7.69),[c] C_3-H (8.44)	[g] C_6-H_2 (2.12)		[g]	[g]
14*b*	−97	C_1 246.0, C_2 128.2, C_3 185.3	C_4 30.5, C_5 20.5, C_6 41.5		40.9	40.2
	(−75)	C_2-H (6.89),[c] C_3-H (8.44)	[g] C_6-H_2 (2.12)		[g]	[g]
14$_{average}$	−12	C_1 244.2, C_2 133.6, C_3 183.6	C_4 29.9, C_5 20.1, C_6 34.5		42.7	39.9
	(+10)	C_2-H (7.44),[c] C_3-H (8.50)[d]	[f] C_6-H_2 (2.21)[e]		[f]	[f]
15*a*	−110	C_1 235.7, C_2 138.4, C_3 204.2	C_1-Me 23.3, C_4 35.7, C_5 29.2		42.7	33.3
	(−100)	C_2-H (7.92)	(2.62) $C_{4,5}$ (2.87)		(3.16)	[j]
15$_{average}$	−51	C_1 236.6, C_2 137.5, C_3 204.7	C_1-Me 24.5, C_4 35.0, C_5 28.5		42.2	34.4
	(−40)	C_2-H (7.79)	(2.78) (2.94) (2.91)		(3.23)	[j]
16*a*	−130	C_1 235.0, C_2 136.0,[k] C_3 204.2	C_1-Me 22.3,[k] C_4 29.5, C_5 25.4		46.9	43.0[k]
	(−110)	C_2-H (7.91)	(2.72) $C_{4,5}$ (2.91)			[l]
			C_α-Me 36.0			
			(1.98)			
16$_{average}$	−71	C_1 236.1, C_2 135.2, C_3 203.2	C_1-Me 21.5, C_4 29.0, C_5 25.7		47.0	43.5
	(−55)	C_2-H (7.84)	(2.80) $C_{4,5}$ (2.92)			[l]
			C_α-Me 35.2			
			(1.93)			
17*a*	(−124)	C_2-H (7.77)	$C_{4,5,6}$ [l]		[l]	[l]
17*b*	(−124)	C_2-H (7.00)	$C_{4,5,6}$ [l]		[l]	[l]
17$_{average}$	−67[h]	$C_{1,3}$ 218.8, C_2 128.8	$C_{4,6}$ 30.3, C_5 20.8		31.0	25.5
	(−70)	C_2-H (7.45)	(2.04–2.21)		(3.15)	(2.68)
18*b*	−115	247.7	22.4	C_i 139.9, C_o 135.5, C_o' 134.8 C_m 131.6, C_p 146.0	45.0	44.1
20*b*	−114	260.0		$C_{o,i}$ 130.3, C_m 129.7, C_p 137.9	35.5	35.5
					39.6	38.2

Can. J. Chem. Downloaded from www.nrcresearchpress.com by 210.87.254.5 on 09/05/12
For personal use only.

TABLE 1 (*Concluded*)

Cation	T (°C)	C^+ or C_1	$-CH_3$, $-CH_2-$		α – Cp	β – Cp
20*d*	−114	266.7		C_o 129.3, C_m 126.5, C_p 129.7 C_i 137.3	47.2	38.2
20$_{average}$	−73	262.2		C_o 129.6, C_m 128.0, C_p 135.9 C_i 134.8	41.5	35.7
21*d*	−80	270.2	18.7	C_o 131.7, C_o-Me 134.2, C_m 125.7, C_p 132.2, C_i 128.2	47.3	40.7 37.5
21$_{average}$	−33	[m]	18.7	C_o 131.9, C_m 126.0, 125.5, C_p 132.8 [m]	45.8	38.6
22[n]	−50 (−46)	275.1	C_o-Me 19.5, C_p-Me 20.6 (2.34) (2.49)	C_o 133.4, C_m 130.1, C_p 143.2 (7.21)	49.4	41.5

[a] Tentative assignment.
[b] The β-proton peaks in both conformers appear in a complex arrangement between δ 2.68 and 2.94.
[c] Doublet, $J_{3,4} = 9$ Hz.
[d] Quintet, $J_{3,4} = 9$ Hz, $J_{4,5} = 4.2$ Hz.
[e] Quintet, $J = 6.4$ Hz.
[f] All other signals in the proton spectra are contained in one complicated arrangement from δ 2.84–3.25.
[g] See footnote *f*, except that the range is now δ 2.63–3.56.
[h] This cation was prepared in CF_3COOH (SO_2ClF) since it was too unstable in FSO_3H in the relatively large concentrations necessary for ^{13}C nmr spectroscopy.
[i] At this low temperature, all upper field signals from δ 3.14–1.03 are very broad and unresolved and thus could not be identified.
[j] The β-protons seem to be buried in the methyl signals.
[k] At −130°C, this signal is showing very definite signs of broadening.
[l] The β-protons appear to be buried under the $C_{5,6}$ methyl signals.
[m] The quaternary carbons are too weak to be observed at this temperature.
[n] This ion gave poor quality spectra and the assignments are therefore somewhat tentative.

13*a* **13***b* **13***c* **13***d*

and **13***d*. Previously, we have described (8) two examples where cyclopropyl-substituted allyl cations appeared to exist as a mixture of conformers **13***a* and **13***b* but this deduction was made on the basis of somewhat subtle nmr line-broadening changes, since only one conformer could be directly observed under 'frozen-out' nmr conditions.

Fortunately, a search for a more clearcut example was successful. The 1-cyclopropylcyclohexenyl cation **14** shows sharp ^1H and ^{13}C nmr signals at 0°C.

14*a* **14***b*

However, at lower temperatures, these broaden and finally separate out into two distinct sets of peaks appropriate for the bisected conformers **14***a* and **14***b*. A series of the ^1H peaks involving only the H-2 proton region is shown in Fig. 2. These conformers can be distinguished in the nmr spectra from the H-2 or C-2 chemical shifts, which differ by 0.8 ppm in the ^1H case and 8.8 ppm in the ^{13}C case (see Table 1), owing to the shielding present in conformer **14***b*. At −75°C, the ratio of **14***a* to **14***b* is about 2:1 and the rotation barrier at −45°C is **14***a* $\underset{k_f}{\rightleftarrows}$ **14***b* = ca. 110 s^{-1}, $\Delta G^{\ddagger} = 11.1$ kcal/mol.

The above result puts the previous results involving cations **15** and **16** on a much firmer basis. We have also extended the previous ^1H study by measuring the ^{13}C nmr spectra over a range of temperatures. In the cation **15** case, both the ^1H and ^{13}C spectra show

15*a* R = H **15***b* R = H
16*a* R = CH_3 **16***b* R = CH_3

nmr line broadening and resharpening which is typical of the presence of one major and one minor conformer (7). We have not succeeded in directly observing this minor conformer in the low temperature spectra but using estimated chemical shifts derived from **14**, one can calculate that conformer **15***b* contributes less than 10% of the mixture at −100°C. Both the position of the H-2 or C-2 signal in the 'frozen-out' spectrum and the direction in which the averaged signal moves (upfield) with increasing temperature can be used to assign **15***a* as the major

Can. J. Chem. Downloaded from www.nrcresearchpress.com by 210.87.254.5 on 09/05/12
For personal use only.

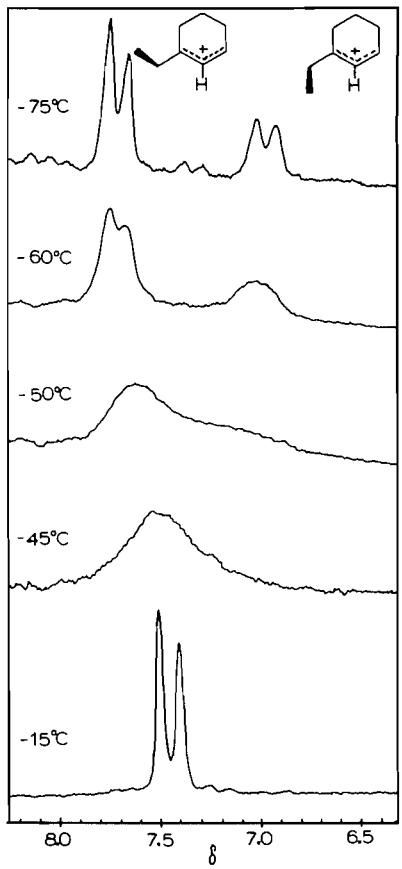

FIG. 2. Proton nmr spectrum of cation **14** (H-2 peak only) showing the progression from an averaged spectrum to one showing both conformers.

conformer. For the **15***a* $\underset{k_f}{\rightleftarrows}$ **15***b* case, the rate constant is ca. 240 s^{-1} at −85°C, $\Delta G^{\ddagger}$ = 7.9 kcal\mol. In the case of cation **16**, a similar situation exists except that the rotation barrier is much smaller. At −130°C, the ^{13}C nmr spectrum shows the C-2, CH_3 on C-1, and the β-CH_2 carbons as very broad peaks compared to the rest. However, this is the lowest temperature for which reasonable spectra were obtained and we therefore cannot be certain of the proportions of **16***a* and **16***b*, except that they appear more nearly equal.

A comparison of the $\Delta G^{\ddagger}$ conformer rotation results for **14**, **15**, and **16** shows some obvious trends. In the cyclohexenyl cation **14**, the allyl cation entity is not fully alkyl substituted and hence is less stable than in **15** or **16**. The conjugation involving the cyclopropyl ring is consequently stronger and the rotational barrier larger. In the case of **15** and **16**, the α-methyl substitution on the cyclopropyl ring seems to be destabilizing, perhaps for steric reasons.

Dicyclopropyl-substituted Allyl Cations

If one puts cyclopropyl groups on both *anti* ends of the allyl system (12), there are three possible bisected conformations, represented by cations **17***a–c*. The ^1H nmr spectrum of cation **17** shows

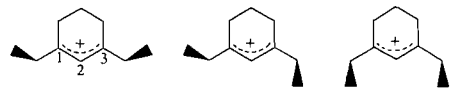

17*a* **17***b* **17***c*

initial broadening of the H-2 proton at about −85 to −90°C (vs. −10°C in the monocyclopropyl case **14**. Maximum broadness occurs at −110°C and by −125°C, two distinct H-2 peaks are observed, in a ratio of about 2:1, assigned to conformers **17***a* and **17***b*, respectively, since the minor H-2 peak occurs 0.79 ppm upfield from the major peak. This chemical shift difference is almost identical to that found in the monocyclopropyl case **14**. At −110°C, the rotation barrier **17***a* $\underset{k_f}{\rightleftarrows}$ **17***b* was k_f = ca. 120 s^{-1}, $\Delta G^{\ddagger}$ = 7.8 kcal/mol. This much smaller barrier for **17**, compared to **14**, is expected because of the more extended conjugation present in the former ion.

Phenylcyclopropylcarbinyl Cations

With one phenyl group and one cyclopropyl group, there are two possible planar-bisected conformers **18***a* and **18***b*. We have looked at the system where R = CH_3. Both this cation and the system with R = H have been previously reported (4, 6). The ^{13}C nmr spectrum of cation **18** has been measured down to −126°C in this study and we have noted no line broadening involving the cyclopropyl or methyl carbons. However, the C^+–phenyl rotation can be slowed down on the nmr time scale since one notes a broadening of the averaged *ortho*-phenyl carbons starting at about −90°C and eventual separation into two peaks at −107°C. The rate for this degenerate process (see **18***b*) is ca. 35 s^{-1} at

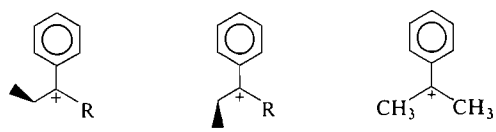

18*a* R = CH_3 **18***b* R = CH_3 **19**

−102°C, $\Delta G^{\ddagger}$ = 8.6 kcal/mol. Our work on the dicyclopropylethyl cation **4** (R = CH_3) suggests that the C^+–cyclopropane rotation will be completely 'frozen-out' by −126°C and the lack of carbon line broadening in the methyl and cyclopropane carbons indicates that *only one* conformer is present in detectable amounts. We assign this conformation to **18***b* (R = CH_3) because this provides

Can. J. Chem. Downloaded from www.nrcresearchpress.com by 210.87.254.5 on 09/05/12
For personal use only.

the least steric interaction (conformer **18***a* (R = CH_3) has a serious interaction between the β-CH_2 cyclopropane protons and the *o*-phenyl protons). Also, the chemical shift similarity of the two *ortho* carbons in **18** seems to be more consistent with **18***b* (R = CH_3).

Since we will have occasion to discuss nonplanar phenyl rings, it should be noted that the distinctive features of the ^{13}C nmr spectrum of the planar **18***b* (R = CH_3) are a relatively shielded C^+ resonance (247.1 ppm) and a large *ortho–para* difference, the *para* carbon being deshielded by about 11 ppm. These features are reasonably similar to those reported for planar cation **19**, δ C^+ = 240.4 ppm and the *ortho–para* difference is 13.5 ppm (4).

Phenyldicyclopropylcarbinyl Cations

With two cyclopropyl rings and one symmetrical phenyl ring, there are three possible planar-bisected conformers **20***a–c*.

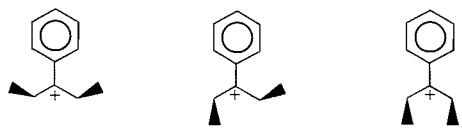

20*a* **20***b* **20***c*

At −70°C, the ^{13}C nmr spectrum of this cation shows only one set of peaks, in reasonable agreement with the reported spectrum (4). However, these are averaged peaks since further cooling of the sample results in line-broadening and then a doubling of most of the signals. Two extreme spectra are shown in Fig. 3. At first sight, the logical choices would appear to be conformers **20***a* and **20***b*, since, as mentioned previously, conformers like **20***c* appear to be very sterically hindered. On further analysis however, we believe that the two conformers have the cyclopropane rings oriented as in **20***a* and **20***b* but that, at least in the **20***a* case, the phenyl ring is substantially nonplanar. This will be designated **20***d*.

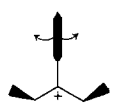

20*d*

From Fig. 3, one can compare the ^{13}C spectra of the two conformers: (*a*) the C^+ signals are separated by 6.7 ppm but both are lower than in **18**; (*b*) one phenyl carbon *in one conformer* is about 8 ppm to lower field than any of the others; (*c*) one α-CH carbon *in one conformer* is about 8 ppm to lower field than any of the other cyclopropyl carbons.

We assign the major conformer to structure **20***b*. From observation *b*, this low-field peak appears to

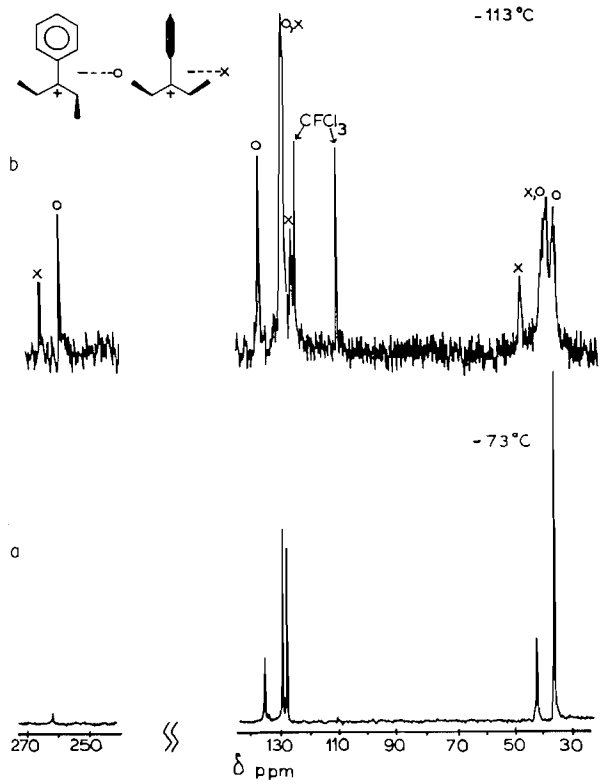

FIG. 3. (*a*) Averaged ^{13}C spectrum of cation **20**; (*b*) 'frozen-out' spectrum showing the two conformers.

be associated with a *conjugated para*-phenyl carbon. The relatively large δ C^+ difference is also consistent with one planar and one nonplanar conformation; these terms however should not be taken too literally (see later). As evidence for a nonplanar conformer **20***d*, one can note the similarity between the low field α-CH carbon assigned to this conformer (47.2 ppm) and the value in the related dicyclopropyl cation **4** (R = CH_3) (45.8 ppm). Furthermore, the phenyl carbons are much more similar than one expects for a conjugated phenyl ring.

The ratio of conformer **20***b* to **20***d* is ca. 2:1 and the interconversion rate at −100°C is $k = 230\ s^{-1}$, $\Delta G^{\ddagger} = 8.1$ kcal/mol.

The above assignments need further verification. Adding an *ortho*-methyl group to the phenyl ring would serve two purposes: (*a*) The conformer **20***b* would logically be further destabilized because of the interaction with the α-CH cyclopropyl proton (see **21***b*). There is also an unfavorable entropy factor. (*b*) There would no longer be a symmetry plane bisecting both cyclopropyl rings as in conformer **20***d* and hence the two β carbons of each ring would now be *nonequivalent* (but *only* in a nonplanar con-

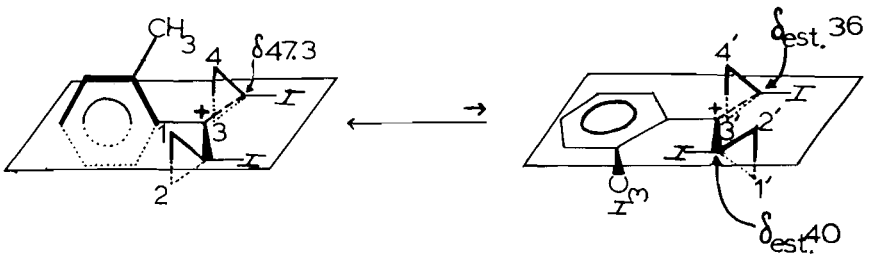

by symmetry
1 = 4
2 = 3

by symmetry
1′ = 2′
3′ = 4′

overall 1 = 2 = 3 = 4
for rapid interconversion

Above coalescence, the α-CH peak chemical shift will be given by the expression

$$\delta_{\alpha\text{-CH average}} = P_{21d} \cdot (47.3) + P_{21b} \cdot ((40 + 36)/2)$$

where P_{21b} will increase as the temperature increases (Boltzmann distribution), i.e., $\delta_{\alpha\text{-CH average}}$ shifts to higher field (P = population).

FIG. 4. Analysis of the nmr line broadening and temperature dependent peak shifts which occur with ion **21**.

formation). These features are shown in structures **21***b* and **21***d*.

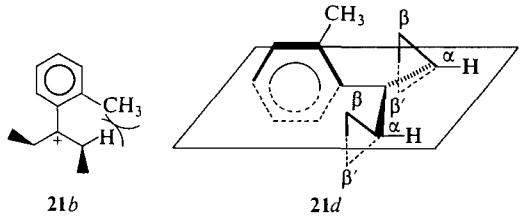

21*b* **21***d*

The ^{13}C nmr spectrum of cation **21** is fully in accord with these expectations. There is one very dominant conformer which can be 'frozen-out' at −80°C. This conformer shows *two distinct* β-CH_2 carbon signals but only *one* α-CH carbon signal, the latter at 47.3 ppm (cf. discussion of **20***d*). The carbons assigned to the *ortho*-CH carbon and the *para* carbon are very similar and finally, the C^+ peak occurs at δ 270.2 ppm, even lower field than the related carbon peak assigned to conformer **20***d*. Thus this conformer is logically **21***d*. A second (minor) conformer is not observed in the −80°C 'frozen-out' spectrum under our S/N conditions but a second conformer *must* be present to explain some of the line broadening and chemical shift movement as one warms the sample up. It can be shown that these results are completely consistent with **21***b* being the minor conformer.

The line broadening observations are these: (*a*) the α-CH carbon peak shifts to higher field with increasing temperature and also broadens; (*b*) the two β-CH_2 carbon peaks broaden and collapse to a single peak at the same temperature as the observation in *a*. The reason for these observations will be apparent if one looks at the equilibrium process involved, i.e., **21***d* ⇄ **21***b*. One sees broadening of the α carbon peak because there is an averaging of this peak in conformer **21***d* with at least one α-CH carbon in conformer **21***b* having a considerably different chemical shift. Since the β carbon symmetries in conformer **21***b* are different from **21***d*, conversion of **21***d* to **21***b* (or *vice versa*) automatically causes all β carbons to become equivalent. These features are illustrated in Fig. 4.

In the 'nonplanar' conformers **20***d* and **21***d*, the phenyl group is presumably twisted to one side or the other as far as steric interactions allow. This could result in some phenyl conjugation but the barrier to a side to side flip process would likely be very small and for nmr symmetry purposes, one can treat the system as having an orthogonal phenyl group. The situation in the so-called 'planar' conformers **20***b* and **21***b* may be similarly complicated; however, we would contend that these conformers have a considerably more planar phenyl ring. With an *ortho*-methyl substituent, the phenyl π-overlap in the 'nonplanar' conformer **21***d* should be further reduced because of the added steric interactions. To accentuate this effect, an attempt was made to prepare the mesityldicyclopropylcarbinyl cation **22**.

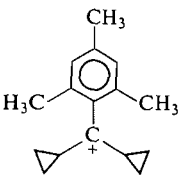

22 (no conformation implied)

Can. J. Chem. Downloaded from www.nrcresearchpress.com by 210.87.254.5 on 09/05/12
For personal use only.

Can. J. Chem. Downloaded from www.nrcresearchpress.com by 210.87.254.5 on 09/05/12
For personal use only.

This cation is rather unstable but the indications are that the C^+ resonance is further lowered, δ 275 ppm vs. 270 ppm in the **21***d* case and 266.7 ppm in the phenyl case **20***d* (however an *ortho* methyl is a γ-substituent with respect to the C^+ nucleus and some *shielding* effect (13) from this may also be present). For two cyclopropyl rings and a methyl substituent, the δ C^+ value is 276 ppm so that, although the carbon C^+ substitution is different, the indications are that the mesityl group is behaving electronically much more like a methyl group than a conjugating phenyl ring.

The interconversion barrier between conformers **21***b* and **21***d* is ca. 11 kcal/mol (k_f for **21***b* ⇄ **21***d* = ca. 90 s^{-1} at −48°C). We picture this process as essentially a rotation of one of the C^+–cyclopropane bonds in **21***d*, this 'freeing' the phenyl ring to rotate to a much more planar, if not planar, situation. Based on the **18***b* (R = CH_3) cation results, such a C^+–phenyl rotation would be expected to be very rapid, i.e., not rate determining.

Olah and Spear (14) and Farnum (15) have suggested that the phenyl rings in the diphenylcyclopropylcarbinyl cation **23** have different degrees of

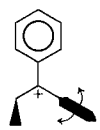

23

planarity and these authors further stress the importance of steric factors in determining the electronic structure of tertiary cations having multiple phenyl rings. Based on the present work, it seems probable that cation **23** would have the specific conformation shown.

One definite generalization can be made concerning the conformational preferences of the cations in this study, namely, *in the absence of steric effects*, they prefer the most 'extended' conjugation (shown below). This effect has been often noted in other conjugated systems; in carbocations, most notably in pentadienyl systems (ref. 16 and footnote 2).

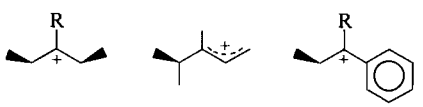

most favored if R is small — most favored — most favored if R is small

Conclusions

Three excellent examples, cations **4** (R = CH_3), **14**, and **20** (see Figs. 1–3), have been found to illustrate that cyclopropylcarbinyl cations conjugated, respectively, with another cyclopropane ring, a vinyl group, or a phenyl ring, are capable of existing in two observable conformations. The structure of these conformers and the height of the interconversion barriers are deduced from the ^1H and ^{13}C nmr spectra.

[2]E. Wagner and T. S. Sorensen. Unpublished results.

Experimental

Mass spectra were obtained using a Varian-Atlas CH-5. Infrared spectra were recorded on a Perkin-Elmer, model 467 spectrophotometer. ^1H nmr spectra were obtained on a Varian Assoc. HA-100 or Bruker WH-90 instrument, reporting in brackets the area of the peak, followed by the multiplicity, s = singlet, d = doublet, t = triplet, q = quartet, c = complex. Organic reactions, particularly those involving lithium, were conducted under a nitrogen atmosphere.

Alcohol Preparations

Dicyclopropylmethanol, dicyclopropylphenylcarbinol, and cyclopropylmethylphenylcarbinol are commercially available. The alcohols, 2-cyclopropyl-4-methyl-3-penten-2-ol and 2-[1-(1-methylcyclopropyl)]-4-methyl-3-penten-2-ol, used to prepare cations **15** and **16**, were prepared as described (8, 17). Tricyclopropylcarbinol (18) and 1,1-dicyclopropylethanol (19) are known.

Bis-(α-methylcyclopropyl)methanol (7)

The lithium analog of 2-bromopropene (20.0 g, 0.165 mol) was prepared and reacted with methacrolein (11.6 g, 0.165 mol), at 0°C, to give 2,4-dimethyl-1,4-pentadien-3-ol, in 23% yield. A Zn/Cu couple (20) (15.6 g) was refluxed with methylene iodide (37.5 g, 0.14 mol) and several iodine crystals in diethyl ether for 40 min before adding the carbinol (3.9 g, 0.035 mol). A second treatment was required for complete cyclopropanation. The product had bp 78–80°C/21 Torr; yield 2.1 g (43%); ^1H nmr δ: 2.74 (1H, s), 1.84 (1H, s), 1.05 (6H, s), 0.53 (4H, c), and 0.18 (4H, c). The mass spectrum showed no parent ion but a large *m/e* = 122 (*M* − 18).

1,1-Bis-(α-methylcyclopropyl)ethanol (8)

Alcohol **7** (1.0 g, 7.14 mmol) was oxidized with Jones' reagent at 20°C to the corresponding ketone, which was characterized by ^1H nmr spectroscopy but not further purified. Methyllithium (3.6 ml of 2.0 *M* solution) was then reacted with the crude ketone. After hydrolysis and extraction, the product was distilled at 75°C/19 Torr; yield 0.15 g (14% overall); ^1H nmr analysis δ: 1.11 (6H, s), 0.90 (3H, s), 0.73 (5H, including OH, c), and 0.14 (4H, c). The mass spectrum showed no parent ion but revealed a large *m/e* = 136 (*M* − 18).

1-Cyclopropyl-2-cyclohexen-1-ol

This alcohol was prepared from cyclopropyllithium and 2-cyclohexen-1-one in 66% yield, bp 94–95°C/17 Torr; ^1H nmr δ: 5.82 (1H, doublet of triplets, J_{23} = 10.1 Hz, J_{34} = 3.2 Hz), 5.46 (1H, doublet of triplets, J_{24} = 2.1 Hz, J_{23} = 10.1 Hz), 2.29 (1H, s), 1.97 (2H, br s), 1.75–1.68 (4H, c), 1.12–0.82 (1H, c), and 0.55–0.23 (4H, c). The mass spectrum showed a parent ion at *m/e* = 138.

1,3-Dicyclopropyl-1,3-cyclohexadiene

The synthetic procedure followed was similar to that reported for the related 5,5-dimethyl system (12). Cyclopropyllithium (from 5.0 g, 0.041 mol of bromide) was reacted with 3-ethoxy-2-cyclohexen-1-one (5.75 g, 0.041 mol) in ether at

Can. J. Chem. Downloaded from www.nrcresearchpress.com by 210.87.254.5 on 09/05/12
For personal use only.

25°C. Following hydrolysis, the product (a mixture of 3-cyclopropyl-2-cyclohexen-1-one and 1,3-dicyclopropyl-1,3-cyclohexadiene) was retreated with the same quantity of cyclopropyllithium. After dilute acid hydrolysis, the product was distilled at 118–122°C/18 Torr; yield 2.1 g (32% overall); ^{1}H nmr analysis δ: 5.43 (1H, s), 5.24 (1H, t, J_{45} = 4.5 Hz), 1.90 (2H, t, J_{56} = 5.0 Hz), 1.95 (2H, q), 1.27 (2H, c), and 0.71–0.30 (8H, c); ir: peaks at 3080, 3010, 1660, and 1605 cm^{-1} are characteristic for cyclopropane rings and a diene. The mass spectrum showed the parent ion at m/e = 160.

o-Tolyldicyclopropylcarbinol

o-Tolyllithium (from 10.0 g, 0.058 mol of the bromide) was reacted in ether at 25°C with dicyclopropyl ketone (6.4 g, 0.058 mol). After work-up, the product was distilled at 105–106°C/0.5 Torr to yield 8.6 g (73%) of the alcohol; ^{1}H nmr analysis δ: 7.18–7.70 (4H, c), 2.65 (3H, s), 1.36 (1H, s), 1.02–1.57 (2H, c), and 0.72–0.26 (8H, c). The mass spectrum showed the parent ion at m/e = 202.

Mesityldicyclopropylcarbinol

Mesityllithium (from 8.0 g, 0.04 mol of the bromide) was reacted with dicyclopropyl ketone (4.4 g, 0.04 mol). The solution was gently refluxed for 3 h. After work-up, the product was distilled at 120–124°C/0.075 Torr, yielding 5.6 g (60%) of the title alcohol; ^{1}H nmr showed δ: 6.64 (2H, s), 2.58 (6H, s), 2.23 (3H, s), 1.38 (1H, s), 1.60–1.14 (2H, c), and 0.48–0.29 (8H, c). The mass spectrum showed the parent ion at m/e = 230.

Ion Preparations

Except for cation **17**, the starting material was the corresponding alcohol. For ^{13}C nmr spectroscopy, the alcohol (150–200 mg in ca. 200 μl of $CFCl_3$) was added slowly with stirring to 3 ml of the precooled acid solution (−80°C, −120°C in the case of cations **16** and **17**, or in the case of the attempted preparation of cations **5** and **6**, at about −140°C) contained in a 10 mm nmr tube. The solvent mixture was normally 1:4 (v/v) FSO_3H–SO_2ClF except for cations **14** and **18** where a 1:2 mixture was used. For ^{1}H nmr spectra, 40–50 mg of the alcohol in a few drops of $CFCl_3$ was added to 0.5 ml of the acid solution in a 5 mm tube. The mesityldicyclopropyl cation **22** preparation (for ^{13}C nmr) was not very successful with the standard solvent systems. Attempts were made to prepare this cation in neat FSO_3H, CF_3COOH or CF_3COOH–SO_2ClF and also the weight of alcohol used was varied from 100–200 mg. Only dilute solutions in neat FSO_3H (no $CFCl_3$ used) gave useful spectra. The dicyclopropylcyclohexenyl cation **17** also presented difficulties and a ^{13}C spectrum was not obtained in the FSO_3H solvent mixtures. In CF_3COOH solvent, the diene precurser gave cation **17** mixed with what appears to be 1,3-dicyclopropylbenzene. For the attempted preparation of cations **5** and **6** for ^{1}H spectra, an acid solution consisting of FSO_3H–SO_2ClF–SO_2F_2 (ca. 1:4:4) was used, and the amount of alcohol was 25 mg. A similar procedure was used for the successful experiments with cation **17**.

Nuclear Magnetic Resonance Spectroscopy

^{13}C nmr spectra (^{1}H broadband decoupled) were recorded on a Bruker WH-90 spectrometer. The temperature was measured before and after each spectrum using a dummy stainless steel tube containing silicone oil and a thermocouple. For critical spectra involving line broadening, the before and after reading was within 1°C, otherwise the results were discounted. The SO_2ClF solvent provided the ^{19}F lock system. All ^{13}C chemical shifts were referenced with respect to internal $CFCl_3$, previously determined as δ 117.9 with respect to external TMS and are reported in Table 1. Multiplicities were determined, where possible, by off-resonance decoupling. ^{1}H nmr spectra were recorded with the same instrument, employing the same temperature calibration procedure. The field-frequency lock was TMS-d_{12} (including a small concentration of TMS-h_{12} for reference purposes) contained in an external capilliary. Below −90°C, a dimethyl ether-d_6 lock was used. Chemical shifts and coupling constants are reported in Table 1.

Acknowledgement

We thank the National Research Council of Canada for generous financial support.

1. H. G. Richey, Jr. *In* Carbonium ions. Vol. 3. *Edited by* G. A. Olah and P. von R. Schleyer. Wiley-Interscience, New York, NY. 1972. Chapt. 25; K. B. Wiberg, B. A. Hess, Jr., and A. J. Ashe III. *In* Carbonium ions. Vol. 3. *Edited by* G. A. Olah and P. von R. Schleyer. Wiley-Interscience, New York, NY. 1972. Chapt. 26.
2. R. Hoffmann and R. B. Davidson. J. Am. Chem. Soc. **93**, 5699 (1971).
3. N. C. Deno, J. S. Liu, J. O. Turner, D. N. Lincoln, and R. E. Fruit, Jr. J. Am. Chem. Soc. **87**, 3002 (1965).
4. G. A. Olah and P. W. Westerman. J. Am. Chem. Soc. **95**, 7530 (1973).
5. L. M. Jackman and S. Sternhell. Applications of nuclear magnetic resonance spectroscopy in organic chemistry. 2nd ed. Pergamon Press, Oxford. 1969. p. 99.
6. C. U. Pittman, Jr. and G. A. Olah. J. Am. Chem. Soc. **87**, 2998, 5123 (1965).
7. N. Okazawa and T. S. Sorensen. Can. J. Chem. In press.
8. K. Rajeswari and T. S. Sorensen. J. Am. Chem. Soc. **95**, 1239 (1973).
9. N. C. Deno, H. G. Richey, Jr., J. S. Liu, J. D. Hodge, J. J. Houser, and M. J. Wisotsky. J. Am. Chem. Soc. **84**, 2016 (1962).
10. N. C. Deno. Progr. Phys. Org. Chem. **2**, 148 (1964).
11. D. S. Kabakoff and E. Namanworth. J. Am. Chem. Soc. **92**, 3234 (1970).
12. N. C. Deno, H. G. Richey, Jr., J. S. Liu, D. N. Lincoln, and J. O. Turner. J. Am. Chem. Soc. **87**, 4533 (1965).
13. J. B. Stothers. Carbon-13 nmr spectroscopy. Academic Press, New York, NY. 1972.
14. G. A. Olah and R. J. Spear. J. Am. Chem. Soc. **97**, 1539 (1975).
15. D. G. Farnum. Adv. Phys. Org. Chem. **11**, 123 (1975).
16. R. Bladek and T. S. Sorensen. Can. J. Chem. **50**, 2806 (1972).
17. T. S. Sorensen and K. Rajeswari. J. Am. Chem. Soc. **93**, 4222 (1971).
18. H. Hart and J. M. Sandri. Chem. Ind. (London), 1014 (1956).
19. H. Hart and J. Sandri. J. Am. Chem. Soc. **81**, 320 (1959).
20. R. S. Shank and H. Schechter. J. Org. Chem. **24**, 1825 (1959).

Some reactions of 10-methyl-10*H*-pyrido[3,2-*b*][1,4]benzothiazine-*n*-butyllithium adduct with electrophiles

FRANK M. PASUTTO and EDWARD E. KNAUS

Faculty of Pharmacy and Pharmaceutical Sciences, University of Alberta, Edmonton, Alta., Canada T6G 2N8

Received February 2, 1978

FRANK M. PASUTTO and EDWARD E. KNAUS. Can. J. Chem. **56**, 2365 (1978).

Reaction of 10-methyl-10*H*-pyrido[3,2-*b*][1,4]benzothiazine (**4**) with *n*-butyllithium affords a mixture of the C-4 proton abstraction product **5***a* and 2-*n*-butyl-4a-lithio-10-methyl-2,4a-dihydropyridyl[3,2-*b*][1,4]benzothiazine **6***a* which results from nucleophilic addition at the C-2 position. Treatment of **5***a* and **6***a* with deuterium oxide gave the deuterated products **5***c* and **6***c* in a ratio of 1:4.4 whereas reaction with diethyl chlorophosphate afforded a mixture of the 4-substituted product **5***d*, 4a-ethyl derivative **6***e*, oxidation product **7** as well as the *N*-substituted-1,2-dihydropyridyl derivative **13**. The stability of the 4a-lithio-2,4a-dihydropyridyl adduct **6***a* is attributed to the ability of sulfur to stabilize an adjacent carbanion. The mechanism for the formation of **6***e* is described.

FRANK M. PASUTTO et EDWARD E. KNAUS. Can. J. Chem. **56**, 2365 (1978).

La réaction de la méthyl-10 10*H*-pyrido[3,2-*b*][1,4]benzothiazine (**4**) avec le *n*-butyllithium conduit à un mélange de produit **5***a* provenant de l'enlèvement du proton en C-4 et de la *n*-butyl-2 lithio-4a méthyl-10 dihydro-2,4a pyridyl[3,2-*b*][1,4] benzothiazine **6***a* qui provient de l'addition nucléophile en position C-2. La réaction de **5***a* et de **6***a* avec l'eau lourde conduit aux produits deutérés **5***c* et **6***c* dans un rapport de 1:4.4 alors que la réaction avec le chlorophosphate de diéthyle conduit à un mélange d'un produit substitué en position 4 (**5***d*) et d'un dérivé éthylé en 4a (**6***e*), d'un produit d'oxydation **7** ainsi que le dérivé dihydro-1,2 pyridyle *N*-substitué (**13**). La stabilité de l'adduit lithio-4a dihydro-2,4a pyridyle (**6***a*) est attribuée à la possibilité qui existe pour le soufre de stabiliser un carbanion adjacent. On décrit le mécanisme de formation de **6***e*.

[Traduit par le journal]

Pyridobenzothiazines are analogs of phenothiazine in which an annular nitrogen atom forms part of the ring structure. Although all four isomeric monopyridobenzothiazines are known the pharmacological actions of the 10*H*-pyrido[3,2-*b*][1,4]benzothiazines have been most significant and a number of these are used clinically such as Prothipendyl (**1***a*), Isothipendyl (**1***b*), Pipazethate (**1***c*), and Pervetral (**1***d*) (1).

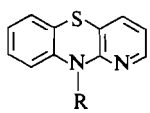

1

a R = $-(CH_2)_3N(Me)_2$
b R = $-CH_2-CH(CH_3)-N(Me)_2$
c R = $-CO_2-(CH_2)_2-O-(CH_2)_2-N$ (morpholine)
d R = $-(CH_2)_3-N$ (piperazine) $-(CH_2)_2OH$

The reaction of *N*-lithio-1,2-dihydropyridines **2**, obtained from reaction of organolithium reagents and pyridines (2), with suitable electrophiles (E) is a versatile procedure for the synthesis of *N*-substituted-1,2-dihydropyridines **3** (3,4). It was therefore of interest to use these procedures to determine what effect elaboration of the pyridyl ring of pyridobenzothiazines had on pharmacological activity. We now wish to describe the preparation of 10-methyl-10*H*-pyrido[3,2-*b*][1,4]benzothiazine-*n*-butyllithium adduct **6***a* and its reaction with water, deuterium oxide, and diethyl chlorophosphate.

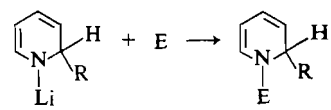

2 **3**

a R = *n*Bu
b R = Ph

Reaction of 10-methyl-10*H*-pyrido[3,2-*b*][1,4]-benzothiazine (**4**) with *n*-butyllithium afforded a mixture of **5***a* and **6***a* which on quenching with water gave rise to a mixture of **5***b* and **6***b* in a ratio of 1:4.4.[1] All efforts to obtain pure **6***b* were unsuccessful. Thin-layer chromatography on silica gel or fractional crystallization of a mixture of **5***b* and **6***b* resulted in aromatization of **6***b* to **7**. Reduction of the imine double bond of **6***b* using sodium cyanoborohydride, sodium borohydride, and lithium aluminium hy-

[1]Spectral determinations were made using a mixture of **5***b* and **6***b* which were present in a ratio of 1:4.4, respectively as determined from the integrals of the H-2 absorption of **5***b* at 8.08 δ and the H-3, H-4 absorptions of **6***b* at 5.6–6.35 δ. The mixture of **5***c* and **6***c* was similarly found to be in the ratio of 1:4.4.

Can. J. Chem. Downloaded from www.nrcresearchpress.com by 210.87.254.105 on 09/05/12
For personal use only.

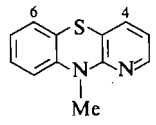

4

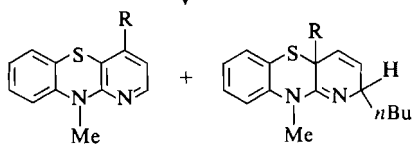

5 6

a R = Li
b R = H
c R = D
d R = P(O)OEt$_2$
e R = Et

dride was equally unsuccessful. All spectral determinations were therefore made using a mixture **5***b* and **6***b*. The presence of **5***b* was evident in the ^{1}H

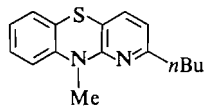

7

nmr spectrum of the mixture and was isolated after preparative tlc of the mixture. The ^{1}H nmr spectrum of this mixture exhibited the characteristic *n*-butyl absorption indicating that nucleophilic addition had occurred. Absorptions in the ir spectrum (cm^{-1}) at 1676 (C=N) and 1640 (C=C) substantiated the presence of a reduced pyridyl ring. Nucleophilic attack by *n*-butyllithium is expected (2) to occur at C-2 of **4** to give one of the three possible isomers **8***a*, **8***b*, or **6***b*.

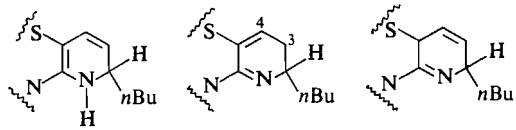

8*a* 8*b* 6*b*

Isomer **8***a* can be eliminated since the ir spectrum did not exhibit an NH absorption and addition of deuterium oxide had no effect on the ^{1}H nmr spectrum. The absence of a one-hydrogen multiplet in the 5–6 δ region expected for the C-4H and a two-hydrogen multiplet in the 2–2.5 δ region due to the allylic C-3H was not consistent with structure **8***b*. The two-hydrogen multiplet at 5.6–6.35 δ due to the C-3H and C-4H and the one-hydrogen multiplets at 4.2 and 3.64 δ due to the C-2H and C-4aH are consistent with structure 2*n*-butyl-10-methyl-2,4a-dihydropyridyl[3,2-*b*][1,4]benzothiazine (**6***b*). These assignments were confirmed by double resonance studies.

Treatment of the **5***b*–**6***b* mixture with heat followed by preparative tlc on silica gel afforded **5***b* (25.1%) and **7** (9.6%). Exposure to oxygen also effects oxidation of **6***b* to **7**. The isolation of **7** confirms the presence of the *n*-butyl substituent at C-2.

Treatment of a mixture of **5***a* and **6***a* with deuterium oxide gave rise to **5***c* and **6***c* as shown by ^{1}H nmr. Purification of this mixture by preparative silica gel tlc gave **5***c* (13.9%) and **7** (6.7%) since 2*n*-butyl-4a-deuterio-10-methyl-2,4a-dihydropyridyl[3,2-*b*]-[1,4]benzothiazine **6***c* undergoes aromatization to **7** during purification. The structure of **6***c* was assigned on the basis of the ^{1}H nmr spectrum of a mixture of **5***c* and **6***c*. The ^{1}H nmr spectrum of **6***c* was simplified relative to **6***b* due to the incorporation of deuterium at C-4a and the assignments are consistent with double irradiation studies.

The formation of the 4a-lithio-2,4a-dihydropyridyl adduct **6***a* rather than the expected *N*-lithio-1,2-dihydropyridyl adduct (2) may be ascribed to the ability of sulfur to stabilize an adjacent carbanion (4). The utility of 2-lithio-1,3-dithianes (**9**) as organolithium reagents (5) is dependent on this stabilizing effect and at least one report (6) suggests the possibility of π bonding between the sulfur and the bridgehead carbanions of **10**. Although 2,5-dihydropyridines have been postulated as intermediates in the synthesis of 2,5-disubstituted pyridines their instability does not permit isolation (3,7,8). The stable 2,5-dihydropyridine **11** was recently obtained from re-

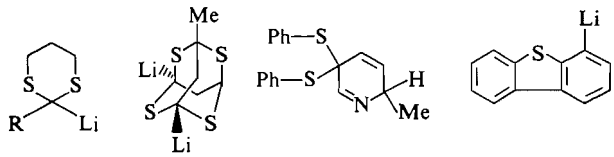

9 10 11 12

action of *N*-lithio-2-methyl-1,2-dihydropyridine with phenyl disulfide (9).

The isolation of **5***c*, which results from reaction of **5***a* with deuterium oxide, represents the first example of proton abstraction from C-4 in any of our studies involving pyridines and organolithium reagents (2,3,7,8). Abstraction of the C-4 rather than the C-2 proton of **4** may be explained in view of the known *ortho*-directing influence of a sulfur atom since dibenzothiophene is easily metalated by *n*-butyllithium to give **12** (10,11). Metalation of **4** appears to be regiospecific since proton abstraction at C-6 was not observed.

Reaction of **4** with *n*-butyllithium and diethyl chlorophosphate afforded **5***d* (17.9%), **6***e* (8.3%), **7** (3%), the *N*-substituted-1,2-dihydropyridine **13** (24.8%), and unreacted **4** (6.6%). The most plausible mechanism for the formation of **6***e* involves nucleophilic attack by the C-4a carbanion of **6***a* at the ethyl

Can. J. Chem. Downloaded from www.nrcresearchpress.com by 210.87.254.105 on 09/05/12
For personal use only.

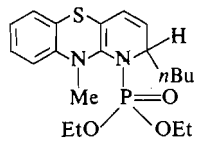

13

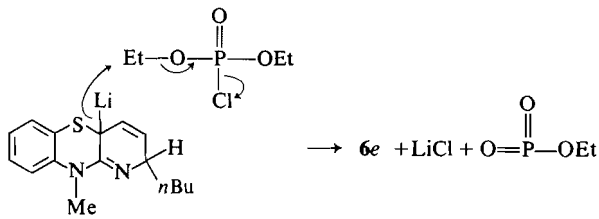

6a

group of diethyl chlorophosphate as illustrated below. The isolation of **6e** provides further confirmation for the structure assigned to **6a–c**.

The reaction of other 10*H*-pyrido[3,2-*b*][1,4]-benzothiazines **1** having varied functionality at the N-10 position with *n*-butyllithium and other electrophiles are now in progress.

Experimental

Melting points were determined with a Büchi capillary apparatus and are uncorrected. Nuclear magnetic resonance spectra were determined for solutions in deuterochloroform with TMS as internal standard with a Varian EM-360A spectrometer. Infrared spectra (film unless otherwise noted) were taken on a Unicam SP-1000 or Perkin Elmer 267 spectrometer. Mass spectra were measured with an AEI-MS-50 mass spectrometer and these exact mass measurements are used in lieu of elemental analyses. All of the products described gave rise to a single spot on tlc using a solvent system less polar and more polar than the specific solvent system described for purification of the reaction mixture. No residue remained after combustion of the products purified by tlc. Kieselgel silica gel DF-5 (Camag) was used for preparative thin-layer chromatography using 20 × 20 cm plates 0.75 mm in thickness.

*4-Lithio-10-methyl-10*H*-pyrido[3,2-*b*][1,4]benzothiazine (**5**a) and 2-*n*-Butyl-4a-lithio-10-methyl-2,4a-dihydropyridyl-[3,2-*b*][1,4]benzothiazine (**6**a)*

General Procedure

To a solution of **4** (1.07 g, 5 mmol) in 125 ml anhydrous tetrahydrofuran, under a nitrogen atmosphere at 0°C, *n*-butyllithium (0.32 g, 5 mmol) was added dropwise with stirring. The reaction was stirred at 0°C for 0.5–1 h to afford a golden brown solution of **5***a* and **6***a* in a 1:4.4 ratio, respectively, as determined after quenching with water.[1] This mixture of **5***a* and **6***a* was then treated with an electrophile as described in individual cases.

*10-Methyl-10*H*-pyrido[3,2-*b*][1,4]benzothiazine (**5**b) and 2-*n*-Butyl-10-methyl-2,4a-dihydropyridyl[3,2-*b*][1,4]-benzothiazine (**6**b)*

To a solution of **4** (1.07 g, 5 mmol) in 125 ml anhydrous tetrahydrofuran, under a nitrogen atmosphere at 0°C, *n*-butyllithium (0.32 g, 5 mmol) was added dropwise with stirring. The reaction was stirred at 0°C for 0.5 h and allowed to warm to 25°C over a 10 min period. The resulting gold-brown solution was treated with water (50 ml), extracted with dichloromethane (3 × 50 ml), dried (sodium sulfate), and the solvent removed *in vacuo* to give a yellow oil (1.36 g) composed of a mixture of **5***b* (18.6%), whose ^{1}H nmr characteristics were identical to those described in the experiment below, and **6***b* (81.4%)(12); ir: 1676 (m, C=N) and 1640 cm^{-1} (s, C=C); ^{1}H nmr δ: 0.74–2 (m, 9H, C_4H_9), 3.41 (s, 3H, NCH_3), 3.64 (m, 1H, H-4a), 4.2 (m, 1H, H-2), 5.6–6.35 (m, 2H, H-3, H-4), 6.6–7.3 (m, 4H, phenyl).

*10-Methyl-10*H*-pyrido[3,2-*b*][1,4]benzothiazine (**5**b) and 2-*n*-Butyl-10-methyl-10*H*-pyrido[3,2-*b*][1,4]benzothiazine (**7**)*

The mixture of **5***b* and **6***b* (0.4 g) described above was heated at 140°C for 1 h and at 170°C for 0.5 h. The resulting dark brown oil was subjected to preparative thin-layer chromatography on six silica gel plates using benzene – ethyl acetate (20:1 v/v) as the development solvent. Extraction of the band having R_f 0.95 with 100 ml warm methanol afforded **7** as a light yellow oil (0.038 g, 9.6%); ^{1}H nmr δ: 0.68–2 (m, 7H, $-CH_2-CH_2CH_2CH_3$), 2.64 (t, J = 7 Hz, 2H, $-CH_2CH_2CH_2CH_3$), 3.44 (s, 3H, NCH_3), 6.5–7.39 (m, 6H, phenyl, H-3, H-4). *Exact mass* calcd. for $C_{16}H_{18}N_2{}^{32}S$: 270.1187; found (high resolution ms): 270.1190. Similar extraction of the band having R_f 0.67 afforded **5***b* (0.079 g, 25.1%); mp 84°C (lit. (12) mp 86°C); ^{1}H nmr δ: 3.44 (s, 3H, NCH_3), 6.6–7.29 (m, 5H, phenyl, H-3), 7.29 (d, $J_{3,4}$ = 8 Hz of d, $J_{2,4}$ = 1.75 Hz, 1H, H-4), 8.08 (d, $J_{2,3}$ = 5 Hz of d, $J_{2,4}$ = 1.75 Hz, 1H, H-2).

*4-Deuterio-10-methyl-10*H*-pyrido[3,2-*b*][1,4]benzothiazine (**5**c) and 2-*n*-Butyl-4a-deuterio-10-methyl-2,4a-dihydropyridyl[3,2-*b*][1,4]benzothiazine (**6**c).*

To a solution of **4** (0.107 g, 5 mmol) in 10 ml anhydrous tetrahydrofuran, under a nitrogen atmosphere at 0°C, *n*-butyllithium (0.64 g, 1 mmol) was added dropwise with stirring. The reaction was stirred at 0°C for 1 h and then stirred at 25°C for 3 h. The resulting brown solution was treated with deuterium oxide (0.04 g, 2 mmol), dried (sodium sulfate), and the solvent removed *in vacuo* to give a light yellow oil (0.141 g) composed of a mixture of **5***c* (18.6%) whose ^{1}H nmr characteristics were identical to those described in the experiment below, and **6***c* (81.4%) (12); ir: 1676 (m, C=N) and 1640 cm^{-1} (s, C=C); ^{1}H nmr δ: 0.65–2 (m, 9H, C_4H_9), 3.42 (s, 3H, NCH_3), 4.16 (m, 1H, H-2), 5.42–6.24 (m, 2H, H-3, H-4), 6.62–7.36 (m, 4H, phenyl).

*4-Deuterio-10-methyl-10*H*-pyrido[3,2-*b*][1,4]benzothiazine (**5**c) and 2-*n*-Butyl-10-methyl-10*H*-pyrido[3,2-*b*]-[1,4]benzothiazine (**7**)*

The mixture of **5***c* and **6***c* described above (0.13 g) was subjected to preparative tlc on two silica gel plates using benzene – ethyl acetate (10:1 v/v) as development solvent. Extraction of the band having R_f 0.58 with 100 ml warm methanol afforded **5***c* as a yellow semisolid (0.015 g, 13.9%); ^{1}H nmr δ: 3.45 (s, 3H, NCH_3), 6.68–7.3 (m, 5H, phenyl, H-3), 8.02 (d, $J_{2,3}$ = 5 Hz, 1H, H-2). *Exact mass* calcd. for $C_{12}H_9DN_2{}^{32}S$: 215.0626; found (high resolution ms): 215.0620. Similar extraction of the band having R_f 0.97 afforded **7** (0.009 g, 6.7%) identical (^{1}H nmr) with the sample prepared above.

*1-Diethylphosphoryl-2-n-butyl-10-methyl-1,2-dihydropyridyl-[3,2-*b*][1,4]benzothiazine (**13**), 4-Diethylphosphoryl-10-methyl-10*H*-pyrido[3,2-*b*][1,4]benzothiazine (**5**d), 2-*n*-Butyl-4a-ethyl-10-methyl-2,4a-dihydropyridyl-[3,2-*b*][1,4]benzothiazine (**6**e), and 2-*n*-Butyl-10-methyl-10*H*-pyrido[3,2-*b*][1,4]benzothiazine (**7**)*

To a solution of **4** (1.07 g, 5 mmol) in 125 ml anhydrous tetrahydrofuran, under a nitrogen atmosphere at 0°C, *n*-butyllithium (0.32 g, 5 mmol) was added dropwise with stirring. The resulting gold-brown solution was stirred at 0°C for

Can. J. Chem. Downloaded from www.nrcresearchpress.com by 210.87.254.105 on 09/05/12
For personal use only.

Can. J. Chem. Downloaded from www.nrcresearchpress.com by 210.87.254.105 on 09/05/12
For personal use only.

1 h, cooled to −77°C and a solution of diethyl chlorophosphate (0.95 g, 5.5 mmol) in 2 ml anhydrous tetrahydrofuran was added dropwise with stirring. The reaction was stirred at −77°C for 1.5 h and allowed to warm to 25°C over a 2 h period. The resulting light orange solution was treated with water (50 ml), extracted with dichloromethane (3 × 50 ml), and dried (sodium sulfate). Removal of the solvent *in vacuo* gave a dark reddish-brown oil. Preparative tlc was effected on 10 silica gel plates using benzene – ethyl acetate (5:1 v/v) as the development solvent. Extraction of the band having R_f 0.95 with 100 ml warm methanol afforded **7** (0.019 g, 3%) identical (^{1}H nmr) with the previous characterized sample. Extraction of the band having R_f 0.41 afforded **13** as a bright yellow oil (0.237 g, 24.8%) ir: 1273 (s, PO), 1630 (m, C=C), and 1567 cm^{-1} (m, C=C); ^{1}H nmr δ: 0.58–1.92 (m, 15H, C_4H_9, $(OCH_2CH_3)_2$), 3.36 (s, 3H, NCH_3), 3.59–4.52 (m, 5H, H-2, $(OCH_2CH_3)_2$), 5.32–5.91 (m, 2H, H-3, H-4), 6.68–7.35 (m, 4H, phenyl). *Exact mass* calcd. for $C_{20}H_{29}N_2O_3P^{32}S$: 408.1630; found (high resolution ms): 408.1635. Extraction of the band having R_f 0.18 afforded **5***d* as a bright yellow oil (0.147 g, 17.9%); ir: 1265 cm^{-1} (s, PO); ^{1}H nmr δ: 1.36 (t, J = 7 Hz, 6H, $(OCH_2CH_3)_2$), 3.44 (s, 3H, NCH_3), 4.25 (m, 4H, $(OCH_2CH_3)_2$), 6.72–7.3 (m, 5H, H-3, phenyl), 8.14 (t, $J_{2,3} = J_{2,^{31}P}$ = 5 Hz, 1H, H-2). *Exact mass* calcd. for $C_{16}H_{19}N_2O_3P^{32}S$: 350.0850; found (high resolution ms): 350.0846. Extraction of the silica gel fraction R_f 0.86 gave a light yellow oil which was rechromatographed on one silica gel plate using benzene – ethyl acetate (10:1 v/v) as the development solvent. Extraction of the band having R_f 0.65 gave **6***e* as a yellow oil (0.058 g, 8.3%); ir: 1677 (w, C=N) and 1631 cm^{-1} (s, C=C); ^{1}H nmr δ: 0.7 (t, J = 7 Hz, 3H, CH_2CH_3), 0.59–2 (m, 11H, C_4H_9, CH_2CH_3), 3.58 (s, 3H, NCH_3), 4.18 (m, 1H, H-2), 5.64 (d, $J_{3,4}$ = 10 Hz of d, $J_{2,3(4)}$ = 2 Hz, 1H, H-3 or H-4), 6.12 (d, $J_{3,4}$ = 10 Hz of d, $J_{2,3(4)}$ = 1.75 Hz, 1H, H-3 or H-4), 6.68–7.44 (m, 4H, phenyl). *Exact mass* calcd. for $C_{18}H_{24}N_2{}^{32}S$: 300.1655; found (high resolution ms): 300.1651. Extraction of the band having R_f 0.5 afforded **4** (0.033 g, 6.6%) identical (mp, ^{1}H nmr) with an authentic sample.

Acknowledgment

We are grateful to the Medical Research Council of Canada (Grant MA-4888) for financial support of this work.

1. C. O. Okafor. Int. J. Sulfur Chem. **B**, **6**, 237 (1971).
2. C. S. Giam and J. L. Stout. Chem. Commun. 142 (1969).
3. C. S. Giam, E. E. Knaus, and F. M. Pasutto. J. Org. Chem. **39**, 3565 (1974).
4. J. M. Brown. Chem. Ind. (London), 454 (1972).
5. E. J. Corey and D. Seebach. Angew. Chem. Int. Ed. Engl. **4**, 1075 (1965); **4**, 1077 (1965).
6. K. C. Bank and D. L. Coffen. Chem. Commun. 8 (1969).
7. C. S. Giam, E. E. Knaus, R. A. Lockhart, and I. G. Keener. Can. J. Chem. **53**, 2305 (1975).
8. E. E. Knaus, T. A. Ondrus, and C. S. Giam. J. Heterocycl. Chem. **13**, 789 (1976).
9. N. Finch and C. W. Gemenden. J. Org. Chem. **40**, 569 (1975).
10. H. Gilman and D. L. Esmay. J. Am. Chem. Soc. **75**, 233 (1953).
11. H. Gilman and S. Gray. J. Org. Chem. **23**, 1476 (1958).
12. W. A. Schuler and H. Klebe. Justus Liebigs Ann. Chem. **653**, 172 (1962); Chem. Abstr. **57**, 9843 (1962).

Fluorinated alkoxides. Part XII. Studies on potentially tridentate fluorinated diols; zwitterionic and five-coordinate complexes of Ni^{2+} and Cu^{2+}

STEPHEN J. LOEB, JOHN W. L. MARTIN, AND CHRISTOPHER J. WILLIS
Chemistry Department, University of Western Ontario, London, Ont., Canada N6A 5B7

Received October 20, 1977

STEPHEN J. LOEB, JOHN W. L. MARTIN, and CHRISTOPHER J. WILLIS. Can. J. Chem. **56**, 2369 (1978).

The complexing ability towards Ni^{2+} and Cu^{2+} of the potentially tridentate ligands $HOC(CF_3)_2CH_2C(O)CH_2C(CF_3)_2OH$, $HOC(CF_3)_2CH_2CH(OH)CH_2C(CF_3)_2OH$, and $HOC(CF_3)_2CH_2CH_2N{:}C(CH_3)CH_2C(CF_3)_2OH$ has been studied. The first two act as bidentate ligands, uninegative or dinegative according to the extent of ionization of the fluorinated alcohol groups; when both were ionized, the complexes had a zwitterionic structure. The third ligand was exclusively tridentate in its complexes; this difference is ascribed to its greater flexibility. Both four- and five-coordinate complexes of nickel were observed, the latter being produced either by choice of co-ligands or by solvation, but no six-coordinate complex was formed in this series. Limitations on coordination for the metal are ascribed to steric effects.

STEPHEN J. LOEB, JOHN W. L. MARTIN et CHRISTOPHER J. WILLIS. Can. J. Chem. **56**, 2369 (1978).

On a étudié la capacité complexante vers le Ni^{2+} et le Cu^{2+} de ligands qui ont la potentialité d'être tridentates: $HOC(CF_3)_2CH_2C(O)CH_2C(CF_3)_2OH$, $HOC(CF_3)_2CH_2CH(OH)CH_2C(CF_3)_2OH$ et $HOC(CF_3)_2CH_2CH_2N{:}C(CH_3)CH_2C(CF_3)_2OH$. Les deux premiers réagissent comme ligands bidentates qui sont uninégatifs et dinégatifs selon le niveau d'ionisation des groupes alcooliques fluorés; si les deux sont ionisés les complexes ont des structures zwitterioniques. Le troisième ligand est uniquement tridentate dans ses complexes; on attribue cette différence à sa flexibilité plus développée. On a observé des complexes du nickel qui sont quatre- ou cinq-coordonnés; on peut produire ces derniers par le choix de co-ligands ou par solvatation. On n'a observé aucun complexe six-coordonné dans cette série. On attribue les limitations de la coordination du métal aux effets stériques.

[Traduit par le journal]

In previous parts of this series, we have shown that an ionized fluorinated tertiary alkoxy grouping, $-C(CF_3)_2O^-$, will readily form a stable complex by coordination to a transition metal ion, provided that it forms part of a chelate ring system. The second donor site in the chelating molecule may be another fluorinated alcohol, as in perfluoropinacol (1, 2), a carboxylic acid (3), a carbonyl oxygen (4), an amino-nitrogen (5), or an imino-nitrogen (6). It would seem reasonable to suggest that a molecule in which two terminal $-C(CF_3)_2OH$ groups are separated by a chain of carbon atoms carrying a central donor atom should be capable of coordination to a metal ion from three positions, giving a tridentate, dinegative, ligand.

Potential Ligand Molecules

In this paper, we describe studies on three molecules of this type, the central potential donor site being a carbonyl oxygen, an unfluorinated alcohol, and an imino-nitrogen; their structures are shown as **1**–**3** respectively.

Of these three, **1** is a known compound produced by the addition of hexafluoroacetone to acetone (7), while **2** was prepared by the reduction of **1**. Compound **3** was not isolated in the free state, but was

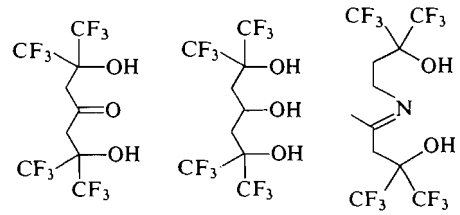

1 **2** **3**

produced in the coordinated form by the template condensation of hexafluorodiacetone-alcohol (HFDA), $HOC(CF_3)_2CH_2COCH_3$, with the known amino-alcohol $NH_2CH_2CH_2C(CF_3)_2OH$ in the presence of Ni^{2+} ions.

It is clear that two six-membered chelate rings will be formed if the three potential donor sites in any of the above molecules are coordinated to the same metal ion. However, the presence of a central sp^2 hybridized carbon atom in compound **1** will obviously reduce the flexibility of the chain, and the examination of molecular models shows such a mode of attachment is unlikely. By conversion of this central atom to sp^3 hybridization, as in compound **2**, this restraint is somewhat reduced, but the chelating ability is still restricted by the requirement that the two chelate rings must share *two* sides. With com-

Can. J. Chem. Downloaded from www.nrcresearchpress.com by 210.87.254.40 on 09/05/12
For personal use only.

Can. J. Chem. Downloaded from www.nrcresearchpress.com by 210.87.254.40 on 09/05/12
For personal use only.

pound **3**, the flexibility of the system is greater, as the two potential chelate rings are fused along one side only, and we therefore expected that, of the three systems studied, compound **3** would be the most likely to act as a tridentate ligand.

Formation of Metal Complexes

In practice, the keto-diol **1** proved to be exclusively bidentate. However, the loss of two protons from the $-C(CF_3)_2OH$ groups gave a dinegative species which combined with suitable metal ions (Ni^{2+}, Cu^{2+}) to give neutral complexes of unusual structure. When the two remaining coordination sites on the metal ion were filled by a neutral bidentate nitrogen donor, such as *N,N,N',N'*-tetramethylethylenediamine (TMED), the product was a neutral species in which the metal atom was clearly four-coordinate, the Ni^{2+} complex being red and diamagnetic. We suggest a zwitterionic structure for these compounds in which the carbonyl oxygen and *one* of the two ionized alkoxy groups are coordinated to the metal, the second alkoxy group being ionized but not coordinated, as in structure **4**.

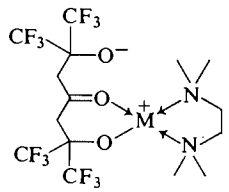

4*a* (M = Ni^{2+})
4*b* (M = Cu^{2+})

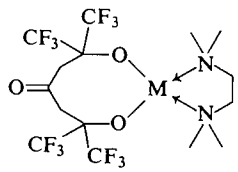

5

This mode of attachment is preferred over the alternative structure **5**, in which the two alkoxy groups coordinate leaving the carbonyl free, on two grounds; the well-known greater stability of six-, rather than eight-membered, chelate rings, and the appearance of the infrared spectra. We have previously demonstrated that an ionized keto-alcohol may act as a bidentate ligand by preparing a stable cationic complex (**7**) of Ni^{2+} with HFDA, the co-ligand being the tridentate macrocycle **6** (abbreviated to [12]-ene-3):

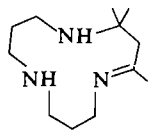

6

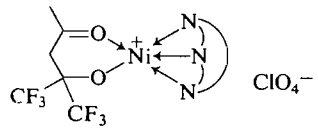

7

In compound **7**, the carbonyl stretching frequency is lowered to 1690 cm^{-1} from 1730 cm^{-1} in the free ligand. We now see shifts from 1720 cm^{-1} in the free ligand to even lower carbonyl frequencies at 1650 cm^{-1} (**4***a*) and 1646 cm^{-1} (**4***b*) which we assign to coordinated carbonyl groups in which the bond has been further weakened by the influence of the negative charge on the adjacent uncoordinated $-C(CF_3)_2O^-$ group. Such shifts would not be expected for structure **5**, in which the carbonyl group is not involved in coordination to the metal ion.

Evidence from ^{19}F nmr spectra, which might have been expected to distinguish **4***a* from **5**, was not helpful. The spectrum of **4***a* showed four peaks, of approximately equal intensity, suggesting that four non-equivalent trifluoromethyl groups were present. However, because of the conformation of chelate rings, such non-equivalence can be found in a variety of possible structures for these complexes and cannot be taken as supporting any one of the postulated modes of attachment of the ligand.

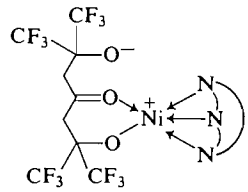

8

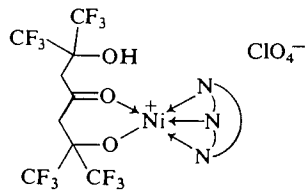

9

In **8**, the carbonyl frequency was at 1640 cm^{-1}, similar to **4**. However, by control of the pH at which the complex precipitated, we were able to protonate **8** to give the cationic complex **9**. In the latter, the carbonyl frequency is at 1699 cm^{-1}, very similar to that in the coordinated HFDA complex **7**, and this change on protonation supports our suggestion that the unusually low carbonyl stretching frequencies in **4** and **8** result from the presence of the adjacent uncoordinated anion within the ligand molecule.

It was not possible to isolate a stable, protonated, cationic form of **4***a* analogous to **9**; the acidification of the solution of the complex merely leading to decomposition. This we ascribe to the greater susceptibility of the four-coordinate metal ion in a cation complex to nucleophilic attack, whereas the five-coordinate metal in **9** is relatively shielded. It is also significant that, using HFDA, which we have found to be a weak ligand giving a very limited range of complexes (6), we were able to isolate a stable five-coordinate nickel complex with [12]-ene-3 as co-ligand, but we could not prepare a stable four-coordinate nickel complex using TMED as co-ligand.

We therefore conclude that the ionized keto-diol **1** acts as a chelating, dinegative, bidentate ligand forming complexes in which considerable charge separation remains. It is peculiarly suited to coordination to dipositive ions, giving neutral, zwitterionic, structures.

Similar behaviour was found for the fluorinated

TABLE 1. Visible spectra

Compound	Absorption maxima (cm^{-1}) (ε)	Solvent†
4*a*	19 300(100)	d
4*b*	16 300(107)	m
7	8 500(17); 11 000(8); 12 800(9); 16 100(46); 26 900(102)	m
8	7 480(24); 12 000(6); 13 000(6); 16 500(44); 26 800(151)	m
9	7 070(13); 7 840(13); 16 100(34); 23 500(101)	m
10	19 650(74)	d
12	19 500(80)	m
13	7 400(9); 11 500(sh); 14 700(27); 24 400(68)	m
14	7 700(10); 8 160(8); 11 700(10); 12 900(9); 15 600(22); 26 250(70)	m/py
15	19 500(77)	m

†m = methanol, d = dichloromethane, py = pyridine.

triol **2**, although it was a poorer donor than the keto-diol. Using TMED as co-ligand, a neutral nickel complex was prepared, to which structure **10** is tentatively given.

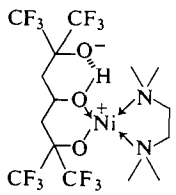

10

This structure, in which chelation occurs through the central, un-ionized, hydroxyl and one of the terminal, ionized, $-C(CF_3)_2O^-$ groups, is preferred by analogy with the keto-diol complex **4***a*. However, a structure in which chelation occurs through the two terminal groups, analogous to **5**, cannot be ruled out on present evidence. The charge separation in **10** may be reduced by hydrogen-bonding between the two oxygen atoms. However, although reduction of the ketone has increased the flexibility of the ligand at the central carbon atom, it is still not able to act in a tridentate fashion. In an effort to reduce steric hindrance offered by the co-ligand, we briefly investigated complexes in which TMED was replaced by *N*,*N*′-dimethylethylenediamine or by ethylenediamine. In neither case was a five-coordinate nickel complex detected.

As mentioned above, complexes of the imino-diol **3** were prepared by template synthesis without isolation of the free ligand. We have previously shown (5) that the amino-alcohol **11** will form complexes with a variety of metal ions, acting as a bidentate, uninegative, ligand. On reacting **11** with Ni^{2+} ions in the presence of HFDA, condensation occurred to produce the neutral mixed-ligand complex **12**. This in turn reacted with nitrogen donors, such as TMED or pyridine, to displace the amino-alcohol and produce neutral four- or five-coordinate complexes in which **3** was acting as a tridentate ligand. The mode of attachment of the ligand, and the coordination number of the metal, are shown by the appearance of the visible spectra (Table 1), where well-defined differences between four- and five-coordinate nickel(II) are shown.

Since five-coordination on Ni^{2+} was readily achieved in **13**, the reason why the similar complexes **4***a* and **10** remained four-coordinate (despite the attraction of the separated charge and the potential formation of another chelate ring) would appear to be in the unfavorable geometry of the ligands, rather than in steric hindrance at the metal.

Of the three potential ligands studied, therefore, we have found that only **3**, the most flexible, is capable of tridentate chelation to Ni^{2+}. We conclude that, for such a mode of action in a donor of this type, the third potential coordinating site in the molecule should be included in the chain of atoms connecting the two $-C(CF_3)_2O^-$ groups, rather than be a substituent on this chain.

Solvation and Five-coordinate Nickel

We have previously demonstrated (2, 6) that many of the four-coordinate fluorinated alkoxy-complexes of Ni^{2+} and Cu^{2+} become five-coordinate by the addition of a donor solvent molecule, although, probably for steric reasons, a further increase to six-coordination is not seen. Of the compounds included in the present study, none of those which were five-coordinate reacted with donor solvent (e.g. pyridine) to become six-coordinate. Of the red, four-coordinate, nickel species, compounds **4***a*, **10**, and **15** readily reacted with pyridine to give green, five-coordinate, adducts, the addition being reversed by moderate heating *in vacuo*. The presence of five-coordination was established from the similarity of the visible spectra to those we have described before (2).

Compounds **12** and **13** are of some interest in this connection. In the latter, five-coordination is achieved, although we have previously found (2) that,

Can. J. Chem. Downloaded from www.nrcresearchpress.com by 210.87.254.40 on 09/05/12
For personal use only.

Can. J. Chem. Downloaded from www.nrcresearchpress.com by 210.87.254.40 on 09/05/12
For personal use only.

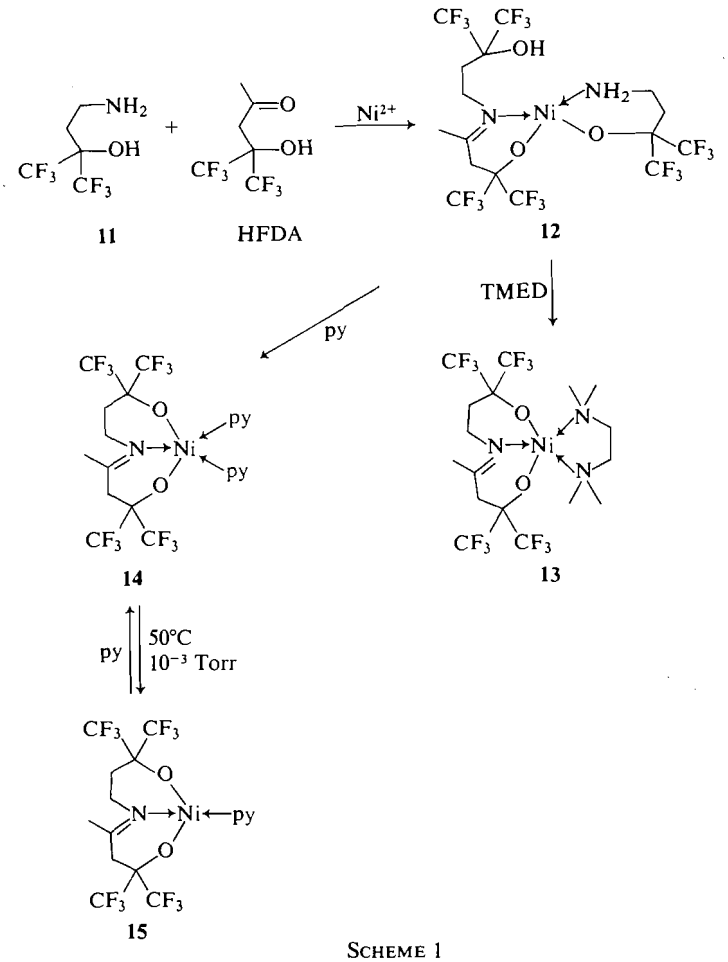

SCHEME 1

for steric reasons, the perfluoropinacol complex **16**, whose four donor groups are all present in **13**, will not react with pyridine or other donors.

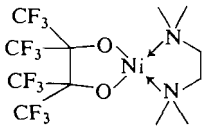

16

Presumably the formation of the additional chelate ring in **13** provides the impetus necessary to overcome this barrier. In compound **12**, five-coordination could be achieved by coordination of the unionized $-C(CF_3)_2OH$ group, but this does not occur. This may be partly due to the weak donor ability of this group, compared to ionized $-C(CF_3)_2O^-$ or a nitrogen base, but it is also consistent with steric hindrance. Whereas in **13** the five-coordinate nickel is surrounded by two fluorinated alkoxy groups and three nitrogen donors, it would be necessary for three bulky fluorinated alkoxy groups to coordinate in order for **12** to become five-coordinate.

Experimental

General

Volatile compounds were handled in a conventional vacuum system. Infrared spectra were recorded on a Perkin-Elmer 621 instrument, visible spectra on Cary 14 and Cary 118 spectrometers. Microanalyses (Table 2) were performed by Alfred Bernhardt Laboratories, West Germany.

1,1,1,7,7,7-Hexafluoro-2,6-bis(trifluoromethyl)-2,6-dihydroxyheptane-4-one (1)

This compound was prepared by the reaction of hexafluoroacetone with acetone, as reported previously (7). In a typical preparation, 20 g of hexafluoroacetone was heated with 20 ml of dry acetone (spectroscopic grade solvent, used without further purification) at 135°C for 4 days in a sealed Carius tube. After removal by distillation of excess acetone and HFDA, **1** remained as a solid. It was purified by recrystallization from ethanol; mp 74–75°C (lit. mp 74–75°C). The yield was about 40% based on hexafluoroacetone.

1,1,1,7,7,7-Hexafluoro-2,6-bis(trifluoromethyl)heptane-2,4,6-triol (2)

A solution of the keto-diol **1** (7.8 g, 20 mmol) in anhydrous diethyl ether (40 ml) was added dropwise to a slurry of lithium tetrahydridoaluminate (0.76 g, 40 mmol) in ether. After refluxing for 1 h, excess hydride was destroyed by the cautious addition of water. The solution was acidified with 30%

TABLE 2. Analytical data and magnetic moments

Compound	Formula	Carbon		Hydrogen		Nitrogen		$\chi_g \times 10^6$ cgse (294 K)	μ_{eff} (BM)
		Calcd.	Found	Calcd.	Found	Calcd.	Found		
2	$C_9H_8F_{12}O_3$	27.6	27.4	2.06	2.13	58.1†	58.4	—	—
4*a*	$C_{15}H_{20}F_{12}N_2NiO_3$	32.0	32.0	3.58	3.61	4.97	5.08	—	*
4*b*	$C_{15}H_{20}CuF_{12}N_2O_3$	31.7	31.8	3.55	3.55	4.93	4.87	1.86	1.74
8	$C_{21}H_{29}F_{12}N_3NiO_3$	38.3	37.5	4.44	4.56	6.38	6.81	4.87	2.88
9	$C_{21}H_{30}ClF_{12}N_3NiO_7$	33.2	33.2	3.99	3.99	5.54	5.64	5.88	3.17
10	$C_{15}H_{22}F_{12}N_2NiO_3$	31.9	31.8	3.93	3.95	4.96	4.95	—	*
12	$C_{16}H_{16}F_{18}N_2NiO_3$	28.0	27.3	2.35	2.32	4.09	4.29	—	*
13	$C_{17}H_{25}F_{12}N_3NiO_2$	34.6	34.6	4.27	4.19	7.12	7.03	7.07	3.26
14	$C_{21}H_{19}F_{12}N_3NiO_2$	39.9	39.8	3.03	3.04	6.64	6.66	7.25	3.42
15	$C_{16}H_{14}F_{12}N_2NiO_2$	34.7	34.5	2.55	2.58	5.06	5.17	—	*

*Diamagnetic.
†Fluorine content.

aqueous sulfuric acid, extracted with ether, and the ether extract dried and evaporated to yield the triol **2**, recrystallized from ethanol, mp 70–71°C, in essentially quantitative yield.

Metal Complexes

The nickel complex **4***a* was prepared by dissolving nickel(II) chloride hexahydrate (2.37 g, 10 mmol) and TMED (1.74 g, 15 mmol) in ethanol and adding an ethanolic solution of **1** (3.90 g, 10 mmol) and potassium hydroxide (1.12 g, 20 mmol) with slight warming. The solution was then cooled to 0°C and precipitated potassium chloride removed by filtration. After removal of solvent, the residue was recrystallized from dichloromethane to give **4***a* as red crystals.

The copper complex **4***b* was prepared by the same method using copper(II) chloride; purple crystals from dichloromethane.

The analogous nickel triol complex, **10**, was prepared by the same procedure, using the triol **2**; red crystals from dichloromethane.

For the [12]-ene-3 complexes, the starting material was the cationic hydroxo-complex $[Ni_2([12]\text{-ene-}3)_2(OH)_2](ClO_4)_2$, whose preparation has been described previously (6, 8).

Ligand **1** was added to this in a 2:1 molar ratio in hot methanol and the solution filtered and evaporated to give complex **8**, recrystallized from ether/hexane. When dilute aqueous perchloric acid was added to **8** in methanol in a 1:1 molar ratio and the solution filtered and evaporated, complex **9** was obtained.

For the series of complexes **12**–**15**, the starting material was the amino-alcohol **11**, prepared as described previously (5). To a solution of nickel chloride hexahydrate (2.73 g, 10 mmol) in ethanol was added **11** (2.11 g, 10 mmol) followed by HFDA (2.24 g, 10 mmol) and potassium hydroxide (1.12 g, 20 mmol). Precipitated KCl was removed by filtration and the solution evaporated to yield the mixed complex **12**; red crystals from dichloromethane.

Addition of TMED (1.74 g, 15 mmol) to a solution of **12** (6.55 g, 10 mmol) in ethanol, followed by filtration and evaporation, gave the TMED complex **13**, green crystals from ether/hexane. Similarly treatment of **12** with pyridine in ethanol gave the dipyridine complex **14**, green crystals from pyridine/ethanol. The latter was converted to the red monopyridine complex **15** by maintaining at 50°C *in vacuo* for 48 h with intermittent grinding.

Infrared spectra of the complexes showed, in addition to carbonyl absorptions discussed above, typical imino C=N absorptions in the region 1645–1665 cm^{-1} for compounds **7**–**15**. All complexes showed strong C—F absorption at 1150–1250 cm^{-1}; **7** and **9** also showed strong, broad absorption due to ClO_4^- at 1100 cm^{-1}.

Acknowledgment

Financial support for this work was provided by the National Research Council of Canada.

1. M. ALLAN and C. J. WILLIS. J. Am. Chem. Soc. **90**, 5343 (1968).
2. W. S. CRIPPS and C. J. WILLIS. Can. J. Chem. **53**, 809 (1975).
3. J. T. PRICE, A. J. TOMLINSON, and C. J. WILLIS. Can. J. Chem. **50**, 939 (1972).
4. C. MACDONALD and C. J. WILLIS. Can. J. Chem. **51**, 732 (1973).
5. I. S. CHANG and C. J. WILLIS. Can. J. Chem. **55**, 2465 (1977).
6. J. W. L. MARTIN and C. J. WILLIS. Can. J. Chem. **55**, 2459 (1977).
7. L. A. SIMONYAN, N. P. GAMBARYAN, and I. L. KNUNYANTS. Zh. Vses. Khim. Ova. **11**, 467 (1966); Chem. Abstr. **65**, 18489c (1966).
8. N. F. CURTIS and D. A. HOUSE. J. Chem. Soc. 5502 (1965).

Can. J. Chem. Downloaded from www.nrcresearchpress.com by 210.87.254.40 on 09/05/12
For personal use only.

Canadian Journal of Chemistry
Published by
THE NATIONAL RESEARCH COUNCIL OF CANADA

Journal canadien de chimie
Publié par
LE CONSEIL NATIONAL DE RECHERCHES DU CANADA

Volume 56 Number 18 September 15, 1978

Volume 56 numéro 18 15 septembre 1978

Can. J. Chem. Downloaded from www.nrcresearchpress.com by 210.87.254.105 on 09/05/12
For personal use only.

Réduction électrolytique de l'aluminium en milieu organique. Caractérisation de l'électrolyte

R. LAFORTUNE, J. T. BOURRET ET G. A. CAPUANO
Département de chimie, Université du Québec à Montréal, Montréal (Qué.), Canada H3C 3P8

Reçu le 16 novembre 1977

R. LAFORTUNE, J. T. BOURRET et G. A. CAPUANO. Can. J. Chem. **56**, 2375 (1978).

Différents électrolytes à base d'alkylbenzène utilisés dans la réduction électrolytique de l'aluminium ont été analysés par chromatographie en phase gazeuse. Aucun produit de réduction ou d'oxydation des solvants organiques n'a été decélé dans les conditions d'électrolyse habituelles. Les solvants tels que toluène, éthylbenzène et diéthylbenzène subissent en présence de bromure d'aluminium des réactions de dismutation. Avec ou sans électrolyse, les électrolytes à base d'éthylbenzène–toluène 1:1 et de diéthylbenzène–toluène 1:4 tendent vers des compositions d'équilibre très voisines expliquant de ce fait pourquoi des revêtements électrolytiques d'aluminium de qualité semblables sont obtenus.

L'effet de la teneur en eau sur la qualité des revêtements d'aluminium obtenus par réduction électrolytique a été étudié. L'étude nous a révélé que les meilleurs revêtements sont obtenus lorsque les solvants organiques sont utilisés "tels que reçus". Ceci nous évite tout traitement de deshydratation ou d'hydratation de ces solvants.

R. LAFORTUNE, J. T. BOURRET, and G. A. CAPUANO. Can. J. Chem. **56**, 2375 (1978).

Various alkylbenzene-based electrolytes used in the electrolytic reduction of aluminum were analyzed by gas phase chromatography. Neither oxidation nor reduction products could be detected in the usual electrolysis conditions. Solvents such as toluene, ethylbenzene, or diethylbenzene undergo dismutation reactions in the presence of aluminum bromide. With or without electrolysis, electrolytes based on 1:1 ethylbenzene/toluene and 1:4 diethylbenzene/toluene tend toward nearby equilibrium compositions. This fact explains why electrolytic aluminum coatings of similar quality are obtained.

The effect of water content on the quality of aluminum coatings obtained by electrolytic reduction was studied. The study revealed that better coatings are obtained if the organic solvents are used 'as received'. Thus it was possible to avoid the pretreatments of drying or hydrating these solvents.

[Journal translation]

Introduction

L'électrodéposition de l'aluminium sur du cuivre ou de l'acier est possible en milieu non-aqueux. Récemment, Capuano et coll. (1, 2) ont réussi, par réduction électrolytique en milieu d'alkylbenzène, à obtenir des revêtements d'aluminium adhérents, ductiles et cohérents, d'une épaisseur de 2 mil (0.05 mm) avec des rendements anodiques et cathodiques (3) de 100%. L'électrolyte le plus fréquemment utilisé (mélange éthylbenzène–toluène 1:1 en volume contenant 50% $AlBr_3$ en poids) diffère des autres électrolytes rapportés dans la littérature (4, 5) du fait que solvants et solutés sont de qualité commercial et qu'en plus, les solvants peuvent être directement utilisés sans traitement de déshydratation. Il a été récemment (3) observé que les électrolytes de diéthylbenzène–toluène 1:4 volume, fournissent des rendements cathodiques et des dépôts d'aluminium identiques à ceux obtenus par l'éthylbenzène–toluène 1:1 volume.

Les conditions d'électrolyse de l'aluminium dépendent beaucoup de la nature de l'électrolyte. Deux paramètres particulièrement importants pour la réussite d'un revêtement de qualité font l'objet de la

Can. J. Chem. Downloaded from www.nrcresearchpress.com by 210.87.254.105 on 09/05/12
For personal use only.

TABLEAU 1. Description des principaux électrolytes utilisés (electrolytes contenant 50% $AlBr_3$ en poids)

Electrolytes	Hydrocarbures utilisés	Durée du vieillissement	Durée de l'électrolyse (h)
A_1	Ethylbenzène	1 jour	0
A_2	Ethylbenzène	7 jours	0
A_3	Ethylbenzène	84 jours	0
A_4	Ethylbenzène–toluène (1:1)	56 jours	0
B_1	Ethylbenzène–toluène (1:1)	57 h	57
B_2	Diéthylbenzène–toluène (1:4)	365 jours	400
B_3	Phase surnageante de l'échantillon B_2 (couche de solvant)	365 jours	400

présence étude: la composition du mélange d'alkylbenzènes et sa teneur en eau.

Partie expérimentale

En ce qui concerne d'abord le mélange d'alkylbenzène, deux séries d'électrolytes sont préparées. Dans la série A, (voir tableau 1) on se préoccupe principalement de l'effet de vieillissement de l'électrolyte sans aucune électrolyse et dans la série B, on étudie le vieillissement de l'électrolyte sous les conditions habituelles d'électrolyse (1–3), ainsi que la composition de sa phase surnageante. La préparation des électrolytes des séries A et B est analogue à celle décrite précédemment (3).

Dans un deuxième temps, l'effet de l'addition d'eau aux solvants utilisés pour la préparation de l'électrolyte a été étudié. Par rapport à un électrolyte organique rigoureusement exempt d'eau (1) de couleur rouge–orange, peu conducteur et ne produisant aucun revêtement d'aluminium, un électrolyte préparé d'un solvant de qualité commerciale contenant une faible quantité d'eau produit un mélange d'une couleur allant du brun au noir dont la conductivité est légèrement plus élevée et les revêtements électrolytiques obtenus sont de haute qualité.

De tous les mélanges d'alkybenzènes que nous avons examinés (1), l'électrolyte d'éthylbenzène–toluène 1:1 s'est révélé le plus avantageux et a été choisi pour l'étude de l'effet de l'eau. Le rôle de l'eau dans l'électrolyse de l'aluminium a donc été évalué lors de trois expériences réalisées selon la procédure déjà décrite: (*a*) l'électrolyse en milieu d'éthylbenzène–toluène anhydre, (*b*) l'électrolyse en milieu d'éthylbenzène–toluène de qualité commerciale et (*c*) l'électrolyse en milieu d'éthylbenzène–toluène partiellement saturé d'eau.

(a) Analyse chromatographique des électrolytes

Réactifs

Cyclohexane; *n*-hexane; méthylcyclohexane; éthylcyclohexane; tetrachlorure de carbone (Fisher grade A.C.S.). Benzène; *para*-xylène; *méta*-xylène; *ortho*-xylène (reactif analytique Baker). Méthyl-1 cyclohexadiène-1,4; triméthyl-1,3,5 benzène; éthyl-1 méthyl-2 benzène; triméthyl-1,2,4 benzène; diéthyl-1,2 benzène; diéthyl-1,3 benzène; diéthyl-1,4 benzène; diéthyl-1,3 méthyl-5 benzène; triéthyl-1,3,5 benzène; éthyl-1 méthyl-3 benzène (Chemical Samples Co., Columbus, Ohio); bromobenzène (Aldrich Chemical, Milwaukee, Wisconsin).

Ces produits ont été utilisés tels que reçus. Cependant une analyse chromatographique en phase gazeuse de traces a démontré que la pureté de chacun était de 99.6+%.

Appareils

Lors de l'analyse par chromatographie en phase gazeuse nous avons utilisé un appareil Perkin-Elmer Modèle 990 à programmation de température et à détecteur à ionisation de flamme, muni d'une colonne de 6 pieds de Carbowax 20M à 5% sur Chromosorb W. L'azote utilisé comme éluant s'écoule à 300 ml/min: la température du collecteur et celle de la chambre d'injection sont à 225°C: les échantillons de 1.0 µl sont élués à une température initiale de 60°C durant 3 min puis dans un gradient de température de 6°/min jusqu'à 150°C maintenue durant 8 min. On a estimé à ±2% la précision par chromatographie en phase gazeuse. La préparation de solutions étalons a permis, par l'établissement de droites de calibration, de préciser davantage les données de l'analyse semi-quantitative et d'obtenir des valeurs quantitatives de concentration des produits tels que benzène, éthylbenzène, diéthylbenzène et triéthylbenzène.

Traitement des échantillons

Une portion de 25 ml d'électrolyte est ajoutée à 75 ml d'eau distillée glacée. Après une agitation vigoureuse, la solution est décantée et la couche organique est séchée sur Na_2SO_4. Une portion de 5.00 ml de cette phase organique est transférée dans un ballon jaugé de 50 ml. On ajoute 0.5 ml de bromobenzène (référence interne de l'analyse chromatographique) et le volume est complété avec du CCl_4. Il a préalablement été établi que l'échantillon ne contenait pas de bromobenzène.

La concentration des produits est déterminée par la méthode de triangulation; le rapport R est calculé selon l'équation suivante:

$$[1] \quad R = \frac{\text{Surface du pic du produit}}{\text{Surface du pic de l'étalon interne}} = \frac{\text{Conc. du produit}}{\text{Conc. de l'étalon int.}}$$

La concentration de l'étalon interne étant de 1.00% v/v, et le facteur de dilution de l'échantillon étant de 10, le pourcentage en volume du produit analysé est donné par l'équation simplifiée:

$$[2] \quad \text{Concentration (\% v/v)} = 10.0R$$

L'analyse quantitative s'effectue avec des solutions standards de chacun des produits contenant 1.00% de bromobenzène comme étalon interne. En même temps que l'analyse chromatographique, une portion de l'électrolyte a été prélevé pour une hydrolyse et une distillation fractionnée. Chacun des consti-

Can. J. Chem. Downloaded from www.nrcresearchpress.com by 210.87.254.105 on 09/05/12
For personal use only.

TABLEAU 2. Analyse chromatographique semi-quantitative des électrolytes*

Produit	Temps de rétention (min)	Concentration des produits de dismutation (% v/v)						
		A_1	A_2	A_3	A_4	B_1	B_2	B_3
Benzène	1.4	21.8	22.1	20.2	24.0	15.8	7.79	10.2
Toluène	2.3				30.0	28.8	26.6	35.8
Ethylbenzène	3.6	54	53	48	14.0	17.3	9.74	10.6
Méta-xylène	3.7						3.98	5.36
Ortho-xylène	4.8					0.33	1.30	1.34
Ethyl-1 méthyl-3 benzène	5.7				5.94	10.7	17.9	25.0
Ethyl-1 méthyl-2 benzène	6.2				0.75	0.97	1.83	2.28
Diéthyl-1,3 benzène	7.4	21.7	23.6	25.9	0.83	3.41	3.20	2.70
Diéthyl-1,2 benzène	8.0				2.00	3.65	4.63	<0.05
Diéthyl-1,3 méthyl-5 benzène	9.5				15.2	12.8	7.79	1.79
Triéthyl-1,3,5 benzène	11.0	2.50	3.86	4.29	1.67	1.95	<0.05	

NOTE: Les analyses chromatographiques et spectroscopiques n'ont révélé aucune trace des produits suivants dont on soupçonnait la présence: cyclohexane; *n*-hexane; méthylcyclohexane; éthylcyclohexane; *para*-xylène; méthyl-1 cyclohexadiène-1,4; triméthyl-1,3,5 benzène; triméthyl-1,2,4 benzène; diéthyl-1,4 benzène.
*Composition des électrolytes établie au tableau 1.

tuants analysés par chromatographie a été d'abord identifié par spectrométrie de masse.

(b) Dosage de l'eau (méthode Karl Fisher)

Appareils

Le titrage a été effectué à l'aide d'un titrimètre Fisher Modèle 35. Deux électrodes de platine fixées dans le couvercle de la cellule de titrage sont branchées au titrimètre et placées sous une tensions de polarisation de 0.65 V.

Réactifs

Le tartrate de sodium dihydraté et le méthanol (0.05% H_2O) (produits de Anachemia Chemicals); les desséchants: P_2O_5, le chlorure de calcium et le réactif Karl Fisher (SOK-3) (produits de Fisher) ont été utilisés sans purification.

Etalonnage des réactifs

Le réactif Karl Fisher est étalonné à l'aide de tartrate de sodium dihydraté ou de chlorure de calcium. Une fois étalonné ce réactif sert à son tour à standardiser la solution méthanol–eau. Cette dernière est utilisée comme liquide de fond et comme titrant de retour dans l'analyse des solvants.

Etalonnage des réactifs (Karl Fisher et méthanol–eau)

On ajoute 70 ml de méthanol–eau dans la cellule de titrage et on titre avec le réactif Karl Fisher au point nul. On ajoute ensuite de 0.05 à 0.15 g de tartrate de sodium dihydraté et après dissolution du sel on titre à nouveau avec le même réactif au même point nul. Les burettes sont toutes protégées de l'humidité de l'atmosphère par un tube desséchant (P_2O_5) intallé à leur extrémité supérieure.

Dosage de l'eau dans les solvants

Le toluène et l'éthylbenzène (reactif analytique Baker) ont été utilisés à trois degrés d'hydratation: (*a*) asséché, (*b*) tel que reçu et (*c*) partiellement saturé d'eau.

(*a*) Dans le premier cas, les solvants ont été asséchés (0.005% H_2O) par reflux en présence de P_2O_5 pendant 3 h, suivi d'une distillation (la première et la dernière partie du distillat ont été rejetées). Après que leur température a atteint 25 ± 0.1°C une partie du solvant distillé a été transférée à vase clos dans la cellule de titrage et une partie dans la cuve d'électrolyses. Le transvasement est effectué à l'aide d'une pression imposée par l'argon sec. (*b*) Les solvants utilisés "tels que reçus" n'ont subi aucun traitement. (*c*) Les solvants "partiellement saturés" ont été préparés en y faisant barbotter de l'azote humidifié pendant une heure à 25°C. L'humidification du gaz a été effectuée par le passage de ce dernier dans l'eau déionisée et distillée.

De 10 à 20 ml de solvant asséché par reflux en présence de P_2O_5, distillé et stabilisé à 25°C sont transférés dans la burette reliée à la cellule de titrage contenant 70 ml de méthanol–eau préalablement neutralisé au point nul par le réactif Karl Fisher. Une fois le solvant introduit dans la cellule, le titrage est répété avec le même réactif suivi d'un titrage de retour par la solution méthanol–eau.

Les autres solvants "tels que reçus" et "partiellement saturés" après avoir été conditionné sont directement versés dans une burette reliée à la cellule de titrage et analysés de la même façon que le solvant asséché.

Résultats et discussion

L'examen de la composition chimique résiduelle des trois électrolytes utilisés dans la réduction de l'aluminium a révélé des modifications importantes dans la nature des composés présents. Ces changements dans la composition du mélange électrolytique ne sont imputables ni a l'oxydation ni à la réduction des solvants organiques, mais ils résultent plutôt de réactions de dismutation.

Electrolyte d'éthylbenzène

A partir du tableau 2, on peut noter les faits suivants relatifs aux échantillons A_1, A_2 et A_3. Du volume inital d'éthylbenzène, près de la moitié de ce solvant est modifié pour donner d'égales quantités de benzène et de diéthylbenzène et quelques pourcents de triéthylbenzène et ce, en moins de 24 h et sans électrolyse. Laissé au repos pendant trois mois, la composition de ce mélange ne varie alors que très peu.

Dans le but d'établir les constantes d'équilibre des réactions de dismutation, l'analyse quantitative des consituants de l'électrolyse dans l'éthylbenzène a été réalisée. Les fractions molaires rapportées au tableau 3 montrent que 47% de l'éthylbenzène est modifié en moins de 24 h et que la réaction évolue très lentement après sept jours (48% en fraction molaire). En trois mois, l'équilibre est presque atteint et la

TABLEAU 3. Analyse quantitative de l'électrolyte éthylbenzène–$AlBr_3$*

Produit	Temps de rétention (min)	Concentration (% v/v)			Fraction molaire		
		A_1	A_2	A_3	A_1	A_2	A_3
Benzène	1.4	15.6	15.9	15.2	0.218	0.214	0.222
Ethylbenzène	3.6	53	52	47	0.540	0.52	0.50
Diéthylbenzène	7.4	24.3	26.4	29.0	0.217	0.229	0.240
Triéthylbenzène	11.0	3.10	4.78	5.32	0.025	0.037	0.038

*Composition des électrolytes établie au tableau 1.

concentration molaire est de 50%. On a observé que l'éthylbenzène se dismute en benzène, en diéthylbenzène et en triéthylbenzène. D'une façon analogue les électrolytes d'éthylbenzène–toluène 1:1 et diéthylbenzène–toluène 1:4 produisent par dismutation des mélanges d'alkylbenzènes de compositions très semblables.

L'obtention d'un mélange d'alkylbenzène à partir d'éthylbenzène provient de deux types de réactions: (*1*) isomérisation: migration intramoléculaire de type 1,2 de groupements alkyles; (*2*) dismutation: migration intermoléculaire de groupes alkyles.

Les premières observations de la dismutation de l'éthylbenzène en présence d'halogénure d'aluminium ($AlCl_3$) ont été faites par Anschütz (6) en 1886.

La réaction de dismutation de l'éthylbenzène en présence de $HF–BF_3$ a été étudiée par Lien et McCaulay (7). Les produits de cette réaction sont le benzène, le diéthyl-1,3 benzène et la constante d'équilibre de ce système est donnée par la réaction [3] et l'éq. [4].

[3] $$2C_6H_5C_2H_5 \rightleftarrows C_6H_6 + C_6H_4(C_2H_5)_2$$

[4] $$K = \frac{[\text{benzène}][\text{diéthylbenzène}]}{[\text{éthylbenzène}]^2} = 0.22$$

En se rapportant au tableau 3, on peut voir que, en ignorant la faible quantité de triéthylbenzène, le calcul de la constante d'équilibre à partir des fractions molaires de l'échantillon A_3 est 0.21. D'après Lien et McCaulay (7) les migrations intermoléculaires des méthyles sont presque inexistantes et seule l'isomérisation est possible.

La réaction de dismutation de l'éthylbenzène et la cinétique de cette réaction ont été étudiées par McCaulay et Lien (7, 8). La cinétique (7) de cette réaction semble être du second ordre. Le mécanisme proposé par Roberts, Ropp et Neville (9) fait intervenir une migration intermoléculaire des groupes éthyles par l'intermédiaire d'une liaison partielle du ^{14}C en α du cycle avec une molécule d'éthylbenzène.

Electrolyte d'éthylbenzène–toluène 1:1

Dans le cas des échantillons A_4 et B_1 préparés à partir d'un mélange 1:1 volume d'éthylbenzène et toluène, 85 et 70% respectivement des volumes de chacun des solvants de départ ont participé à des réactions de dismutation après trois mois avec ou sans électrolyse.

En comparant les échantillons A_4 avec les trois premiers (A_1, A_2 et A_3), on peut voir, que les quantités de benzène sont demeurées semblables et que celles du diéthylbenzène sont réduites par un facteur de 10 au profit des éthylméthylbenzènes et du diéthylméthylbenzène. Le triéthylbenzène subit aussi une baisse. Il est à remarquer que cette comparaison est également valable pour les échantillons B_1 et ceux de A_1, A_2 et A_3. De ce fait, la présence de toluène accélère la dismutation de l'éthylbenzène.

Le fait qu'aucune différence significative n'ait été trouvée dans les compositions des échantillons A_4 et B_1 (électrolytes d'éthylbenzène–toluène avec et sans électrolyse) illustre clairement que l'électrolyse ne fournit aucun produit de réduction ou d'oxydation du solvant tels que méthyl ou éthylcyclohexane ou autres; les produits identifiés dans tous les échantillons ne proviennent que d'équilibres chimiques entre divers alkylbenzènes en présence du catalyseur de bromure d'aluminium.

Electrolyte de diéthylbenzène–toluène 1:4

Il a été observé par Capuano et coll. (3) que les électrolytes d'éthylbenzène–toluène 1:1 et diéthylbenzène–toluène 1:4 fournissaient les mêmes rendements cathodiques et d'excellents dépôts d'aluminium. Le tableau 2 montre clairement la similitude des compositions chimiques des électrolytes à l'équilibre (échantillons B_1 et B_2); les concentrations de diéthylbenzène sont identiques.

On notera que certains résultats des échantillons B_1, B_2 et B_3 doivent être examinés à la lumière de deux faits expérimentaux: le premier étant que ces électrolytes ont subi de fréquentes additions de leurs solvants respectifs afin d'en maintenir le bon rendement lors des électrolyses; le second fait étant que la circulation de l'argon sec visant à conserver l'électrolyte à l'abri de l'humidité favorise l'élimination

Can. J. Chem. Downloaded from www.nrcresearchpress.com by 210.87.254.105 on 09/05/12
For personal use only.

Can. J. Chem. Downloaded from www.nrcresearchpress.com by 210.87.254.105 on 09/05/12
For personal use only.

des constituants les plus volatils tels que le benzène et le toluène.

Compte tenu de la précision de la méthode d'analyse et des faits expérimentaux mentionnés plus haut, on voit que les concentrations des produits des échantillons A_4 et B_1 sont très voisines, les concentrations des échantillons B_2 et B_3 sont aussi très voisines à l'exception du benzène et éthyl-1 méthyl-3 benzène qui sont plus riches dans l'échantillon B_3 tandis que diéthyl-1,2 benzène et diéthyl-1,3 méthyl-5 benzène ont des concentrations plus élevées dans B_2.

Finalement, une comparaison des échantillons B_1 et B_2 peut révéler certains résultats intéressants tels que l'égalité des concentrations de diéthylbenzène, l'apparition de *m*-xylène et la baisse de diéthyl-1,3 méthyl-5 benzène dans l'échantillon B_2.

Phase surnageante (couche de solvant)

Lors de l'électrolyse, le mélange électrolytique se sépare en deux phases. La phase surnageante comportant presque exclusivement le solvant et la phase sous-jacente qui constitue l'électrolyte proprement dit.

La comparaison des constituants de l'électrolyte et ceux de la couche de solvant peut nous renseigner sur l'importance de certains équilibres et la nature des complexes du $AlBr_3$ avec les divers alkylbenzènes. Les produits suivants se retrouvent en plus grande concentration dans la phase solvant: éthyl-1 méthyl-3 benzène; *méta*-xylène; éthyl-1 méthyl-2 benzène alors que le diéthyl-1,3 méthyl-5 benzène et le diéthyl-1,2 benzène se retrouvent en plus grande proportion dans l'électrolyte.

Les différences de concentrations de certains produits dans l'électrolyte et dans la phase surnageante ont été observées par McCaulay et Lien (10). Selon eux, les molécules se partagent entre les deux phases selon leur basicité respective à l'égard du proton telle qu'illustré au tableau 4. Ce phénomène se vérifie également dans nos électrolytes.

L'effet de l'eau

Les résultats ayant trait à la concentration de l'eau dans les solvants organiques sont résumés au tableau 5. On notera ici que les valeurs de saturation en eau des solvants saturés proviennent de la littérature (12, 13). Tel que mentionné dans la partie expérimentale nos premiers résultats nous avait révélé qu'un électrolyte exempt d'eau (0.005% H_2O) ne produisait aucune électrolyse (1). Suite à cette constatation nous avions sugéré (2) de saturer partiellement le solvant d'eau afin de favoriser l'électrolyse. Le présent travail nous a révélé cependant que parmi les trois mélanges à teneur en eau différente examinés, les meilleurs revêtements sont obtenus lorsque le solvant contient environ 25% de son taux de saturation en eau. Cette performance optimale correspond à celle obtenue avec le produit commercial tel que reçu. Cette constatation entraîne des avantages économiques, si on considère que les manipulations de séchage ou d'hydratation comportent un coût considérable dans l'utilisation du procédé à l'échelle industrielle.

TABLEAU 4. Basicités des alkylbenzènes relatives au *p*-xylène selon McCaulay et Lien (10)

Produit	Basicité relative
Toluène	0.01
p-Xylène	1.0
o-Xylène	3.0
m-Xylène	9
Ethylbenzène	—
Triméthyl-1,2,4 benzène	18
Triméthyl-1,2,3 benzène	18
Tétraméthyl-1,2,3,4,5 benzène	60
Tétraméthyl-1,2,3,4 benzène	85
Triéthyl-1,3,5 benzène	433
Diéthyl-1,3 méthyl-5 benzène	865
Triméthyl-1,3,5 benzène	1400
Tétraméthyl-1,2,3,5 benzène	2800
Pentaméthylbenzène	4350
Hexaméthylbenzène	44500

Un mécanisme a déjà été proposé (1) pour expliquer l'effet de l'eau sur la réaction aux électrodes. Nos travaux se poursuivent afin de déterminer la composition des complexes d'aluminium formés en milieu organique. Il serait intéressant aussi de déterminer la corrélation entre les complexes en milieu anhydre (électrolyte rouge–orange) et ceux en milieu plus hydraté (électrolytes brun–noirs).

Conclusions

L'analyse chromatographique en phase gazeuse d'électrolytes servant à la réduction électrolytique de l'aluminium nous a démontré que: (*1*) La réduction électrolytique de l'aluminium ne donne lieu à aucune réaction secondaire d'oxydation ou de réduction des solvants organiques dans les conditions d'électrolyse habituelles (densité de courant: 0–20 mA/cm^2). (*2*) L'électrolyte à base d'éthylbenzène–toluène 1:1 se dismute partiellement en benzène; diéthyl-1,3 méthyl-5 benzène; éthyl-1 méthyl-3 benzène; éthyl-1 méthyl-2 benzène; diéthyl-1,2 benzène; diéthyl-1,3 benzène; et triéthyl-1,3,5 benzène. (*3*) L'électrolyte à base de diéthylbenzène–toluène 1:4 contient les mêmes produits que l'électrolyte précédent et en plus, des xylènes. (*4*) Les compositions d'équilibre de dismutation très voisines de ces deux électrolytes expliquent la qualité comparable des revêtements d'aluminium de l'un et de l'autre.

Une étude de l'effet de la teneur en eau sur la qualité des revêtements d'aluminium par réduction

TABLEAU 5. Concentration d'eau dans les solvants choisis et effet de l'eau sur les revêtements d'aluminium

Solvant ou électrolyte contenant 50% $AlBr_3$ en poids	% H_2O (poids) 25°C	Degré de saturation en eau des solvants (%)	Qualité des revêtements d'aluminium
Toluène	0.005	10	
Toluène qualité commerciale (tel que reçu)	0.013	24	
Toluène partiellement saturé	0.034	63	
Toluène saturé (12)	0.054*	100	
Ethylbenzène asséché	0.005	15	
Ethylbenzène qualité commerciale (tel que reçu)	0.009	27	
Ethylbenzène partiellement saturé	0.024	73	
Ethylbenzène saturé (13)	0.0327*	100	
Electrolyte d'éthylbenzène–toluène 1:1 volume (asséché)		13	Aucun revêtement
Electrolyte d'éthylbenzène–toluène 1:1 volume qualité commerciale (tel que reçu)		26	Revêtement excellents
Electrolyte d'éthylbenzène–toluène 1:1 volume (partiellement saturé en eau)		69	Revêtements partiellement recouverts d'arborescences

*Données tirées de la littérature.

électrolytique nous a révélé: (*a*) que lorsque les solvants et le soluté sont séchés il ne se produit aucune électrolyse d'aluminium; (*b*) que les solvants organiques "tels que reçus" produisent les meilleurs revêtements d'aluminium alors que la teneur en eau de ces solvants est environ 25% de leur taux de saturation.

Remerciements

Les auteurs sont reconnaissants d'un octroi de recherche du Conseil national de recherches du Canada et d'un octroi du Conseil de Recherches pour la Défense.

Nous remercions Monsieur B. Altshuller de la compagnie Alcan pour nous avoir gracieusement fourni l'aluminium de haute pureté utilisé dans la préparation des électrolytes.

Nous tenons également à remercier le Dr. D. Vocelle et le Dr. A. Hade pour des discussions fructueuses et pour l'intérêt qu'ils ont porté à ce travail.

1. G. A. CAPUANO et W. G. DAVENPORT. J. Electrochem. Soc. **118**, 1688 (1971).
2. G. A. CAPUANO et W. G. DAVENPORT. Plating, **60**, 251 (1973).
3. G. A. CAPUANO, R. LAFORTUNE et G. GOBEIL. Plating and surface finishing. Novembre 1977. p. 49.
4. D. E. COUCH et A. BRENNER. J. Electrochem. Soc. **39**, 163 (1952).
5. I. A. MENZIES et D. B. SALT. Trans. Inst. Met. Finish. **43**, 186 (1965).
6. R. ANSCHÜTZ. Ann. **189**, 235 (1886).
7. A. P. LIEN et D. A. MCCAULAY. J. Am. Chem. Soc. **75**, 2407 (1953).
8. D. A. MCCAULAY et A. P. LIEN. J. Am. Chem. Soc. **75**, 2411 (1953).
9. R. M. ROBERTS, G. A. ROPP et O. K. NEVILLE. J. Am. Chem. Soc. **77**, 1764 (1955).
10. D. A. MCCAULAY et A. P. LIEN. J. Am. Chem. Soc. **73**, 2013 (1951).
11. G. A. OLAH. Friedel-Crafts and related reactions. Interscience Publ. Co., New York, NY. 1963.
12. P. K. GLASOE et S. D. STULTZ. J. Chem. Eng. Data, **17**, 66 (1972).
13. H. STEPHEN et T. STEPHEN. Solubility of inorganic and organic compounds. Vol. 1. MacMillan Co., New York, NY. 1963. Part 1, pp. 498–499 et pp. 860–862.

Can. J. Chem. Downloaded from www.nrcresearchpress.com by 210.87.254.105 on 09/05/12
For personal use only.

Polarographic investigation of electron donor–acceptor complexes

LOUIS RAMALEY AND SONIA GAUL[1]

Department of Chemistry, Dalhousie University, Halifax, N.S., Canada B3H 4J3

Received September 29, 1977[2]

LOUIS RAMALEY and SONIA GAUL. Can. J. Chem. **56**, 2381 (1978).

Using a computer-controlled precision polarograph the formation constants of electron donor–acceptor (EDA) complexes formed from aromatic hydrocarbons and nitrofluorene derivatives have been determined in acetonitrile. The EDA interactions are of the same magnitude in this solvent as in less polar solvents. The strength of the complexes is related to the reduction potential (or electron affinity) of the acceptors and the size of the π system of the donors. Spectra of the complexes were computed from spectra of mixtures of acceptor and donor with the help of the polarographic data. No relationship between the molar absorptivity of the charge-transfer band and the formation constant was apparent from these spectra.

LOUIS RAMALEY et SONIA GAUL. Can. J. Chem. **56**, 2381 (1978).

Faisant appel à un polarographe de précision contrôlé par un ordinateur, on a déterminé, dans l'acétonitrile, les constantes de formation des complexes donneurs d'électrons accepteurs (DEA) qui se forment entre des hydrocarbures aromatiques et des dérivés du nitrofluorène. Les interactions DEA sont du même ordre de grandeur dans ce solvant que dans des solvants moins polaires. La force des complexes est reliée au potentiel de réduction (ou électroaffinité) des accepteurs et à la grandeur du système pi des donneurs. On a évalué les spectres des complexes à partir des spectres de mélanges de donneurs et d'accepteurs à l'aide de données polarographiques. Il ne semble exister aucune relation entre l'absorbance molaire de la bande de transfert de charge et la constante de formation si l'on se base sur ces spectres.

[Traduit par le journal]

Introduction

An electron donor–acceptor (EDA) complex results when a molecule of low ionization potential (electron donor, D) interacts with a molecule of high electron affinity (electron acceptor, A). Promotion of an electron from one of the upper filled orbitals of the donor to an unfilled acceptor orbital gives rise to one or more electron absorption bands not observed in the donor or acceptor spectra. These are usually termed charge-transfer (CT) bands and EDA complexes are classified according to the types of orbitals involved in the CT interaction (1). The molecules involved in this study form π–π EDA complexes which are usually reversibly and rapidly formed and exhibit low energies of interaction. Mulliken and Person (1) have published a thorough treatment of EDA interactions and an excellent review of EDA complexation has been produced by Foster (2).

Various correlations between properties of the donor or acceptor and the energy of the CT band have been demonstrated (2). Attempts at correlations involving the formation constant and other properties of EDA complexes or their components have been less successful. For example, the intensity of the CT band often decreases rather than increases as the formation constant increases. One reason postulated for this behaviour is that CT transitions can occur in the absence of a stable complex (3, 4), a phenomenon referred to as contact charge-transfer. A second reason is the difficulty in obtaining accurate values of formation constants for comparison. Various solvents and experimental procedures have been employed, different concentration units are encountered and these are sometimes not clearly specified. There are also certain inherent problems with the measurement methods themselves.

Optical and nuclear magnetic resonance spectroscopy are the most widely used methods for evaluating formation constants. In both methods two unknown properties of the complex must be determined from the data, the formation constant and molar absorptivity for optical spectroscopy or chemical shift for nmr spectroscopy. Usual data analysis methods treat only 1:1 complexes; however, more sophisticated data treatments are available (2) if 2:1 complexes are suspected.

Polarography and other electrochemical techniques have been employed less often in such studies. Peover (5, 6) has studied CT complexes in solvents of low dielectric constant. Holm *et al.* (7) have attempted to compare polarographic and spectrophotometric methods of study and Bonnaterre and Cauquis (8) have used voltammetry in studies of the kinetics of EDA complexation.

A mathematical treatment for the study of com-

[1]Present address: Agricultural Experimental Station, Kentville, Nova Scotia.

[2]Revision received May 15, 1978.

Can. J. Chem. Downloaded from www.nrcresearchpress.com by 210.87.254.40 on 09/05/12
For personal use only.

Can. J. Chem. Downloaded from www.nrcresearchpress.com by 210.87.254.40 on 09/05/12
For personal use only.

plexation by polarography has been presented by De Ford and Hume (9). For the electrochemically reversible reduction of a complex

$$[1]\quad \exp\left[\frac{nF}{RT}[(E_{1/2})_A - (E_{1/2})_C] + \ln\left(\frac{i_A\eta_A{}^{1/2}C_C}{i_C\eta_C{}^{1/2}C_A}\right)\right] = 1 + K_1[D] + K_1K_2[D]^2 + \ldots$$

where the subscript A refers to solutions containing acceptor only and C refers to solutions containing both donor and acceptor, $E_{1/2}$ is the polarographic half-wave potential, i the diffusion limited current, η the viscosity of solution, C the analytical concentration of acceptor, and the other symbols have their usual meaning. The equilibrium constants K_1 and K_2 refer to the following reactions respectively:

$$[2]\quad A + D \rightleftarrows AD$$

$$[3]\quad AD + D \rightleftarrows AD_2$$

Equation [1] assumes that the concentration of donor is constant from the electrode surface to the bulk of solution and that activities are equivalent to concentrations. The first assumption requires that the analytical concentration of donor be much higher than that of the acceptor. This treatment does not take into account the possibility of a termolecular complex of the type A_2D.

In aprotic solvents many electron acceptors are reduced reversibly in one electron steps:

$$[4]\quad A + e^- \rightarrow A^-$$

$$[5]\quad A^- + e^- \rightarrow A^{2-}$$

An EDA complex formed from A and D can also be reduced

$$[6]\quad AD + e^- \rightarrow A^- + D$$

resulting in the dissociation of the complex. Upon addition of D to A the half-wave potential of the first reduction wave shifts to more negative values, the half-wave potential for the second wave, eq. [5], does not. If the diffusion coefficients of A and AD are equal and all diffusion coefficients remain constant, the shift in half-wave potential is equal to the shift in standard potential and is directly related to the free energy of formation of the complex. The term $\ln (i_A\eta_A{}^{1/2}C_C/i_C\eta_C{}^{1/2}C_A)$ from eq. [1] corrects the measured half-wave potentials for changes in diffusion coefficients. The viscosity correction, which did not appear in the original treatment (9), corrects for variations in the diffusion coefficient of A^- caused by changes in viscosity upon addition of large amounts of donor.

Holm *et al.* (7) have suggested that, when complexation occurs, measured polarographic half-wave potentials should be corrected for changes in the energy of the lowest vacant molecular orbital of the acceptor as indicated by a spectral shift, even though such corrections created an anomalous gap in their data. Since shifts in reversible polarographic half-wave potentials properly corrected for changes in diffusion coefficients are equivalent to shifts in standard potentials, such spectral corrections are unnecessary and incorrect.

Polarographic studies of EDA complexation provide formation constants without the need to simultaneously determine some other system parameter. The effect of certain types of termolecular complexes is easily assessed. However, the shifts in half-wave potential are rather small for weak complexes so that the method is less sensitive than optical spectroscopy. Experiments are best done in relatively polar solvents, require a background electrolyte to suppress migration currents and a relatively high donor concentration. Great attention must be paid to experimental detail.

This study was undertaken to examine EDA complexation in a fairly polar solvent, acetonitrile, to determine whether termolecular complexes might exist in this medium, and to attempt to calculate spectra of EDA complexes using formation constant data from a non-spectral source. The acceptors used were 2,4,7-trinitro-9-fluorenone (TNF) (**1**), 9-dicyanomethylene-2,4,7-trinitrofluorene (CNTNF) (**2**),

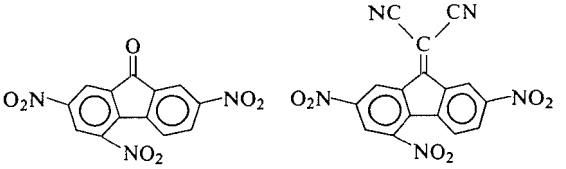

1 **2**

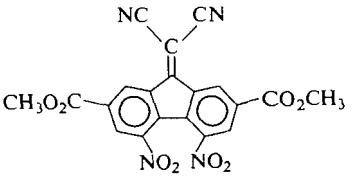

3

and dimethyl-4,5-dinitro-9-dicyanomethylene fluorene-2,7-dicarboxylate (CNDNFDMC) (**3**). The first two compounds are stable, form fairly strong EDA complexes and have found use as analytical reagents. The third compound is also reputed to form strong complexes and might prove useful in the synthesis of CT polymers (10).

Aromatic hydrocarbons were used as donors;

Can. J. Chem. Downloaded from www.nrcresearchpress.com by 210.87.254.40 on 09/05/12
For personal use only.

however, the choice is limited by solubility in the polar solvent since the donor must be in large excess. The compounds selected were naphthalene, phenanthrene, pyrene (**4**), triphenylene (**5**), biphenyl, *o*-

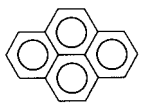

4

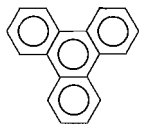

5

terphenyl (1,2-diphenyl benzene), and *m*-terphenyl (1,3-diphenyl benzene).

Experimental

Reagents

Since attempts at further purification produced little change in such characteristics as melting point, colour, or crystallinity, the following were used as received from the manufacturers: naphthalene (Fisher Scientific Co.); phenanthrene (98+%), pyrene (purris), triphenylene (98%), TNF and CNTNF (Aldrich Chem. Co.); and *m*-terphenyl (Eastman Organic Chemicals). Orthoterphenyl and biphenyl (Eastman) were recrystallized from petroleum ether. CNDNFDMC was synthesized according to the method of Sulzberg and Cotter (10).

Bulk reagent grade acetonitrile (Matheson, Coleman and Bell or Fisher Scientific) was purified by method B of Walters and Ramaley (11). The supporting electrolyte, tetrabutyl ammonium perchlorate (TBAP) was prepared by precipitation using tetrabutyl ammonium bromide (Eastman) and reagent grade perchloric acid. The product was repeatedly recrystallized from a water–ethanol mixture until the filtrate gave no precipitate on addition of silver nitrate. The resulting TBAP was dried at 110°C under vacuum.

Thallium metal (99.998%, Alfa Inorganics) was used as received. Distilled mercury was acid washed with dilute nitric acid for 12 h. Thallous perchlorate was prepared from thallous nitrate (Alfa) and perchloric acid by evaporation to dryness followed by three recrystallizations from water. The final product was dried at 120°C.

Polarographic Measurements

A highly precise, digitally controlled potentiostat (12) and sweep generator (13) were used as the polarographic instrumentation. These were controlled by a Hewlett-Packard 2114B minicomputer through a general purpose interface similar to that described by Ramaley and Wilson (14). Included in the computer system were paper tape and magnetic tape peripherals and a point plotter.

A thermostated three electrode cell was used in all measurements. Dry nitrogen could be bubbled through the working compartment which contained the dropping mercury electrode (dme) and a platinum wire counter electrode. The reference was a Tl(Hg)|$TlClO_4$ electrode prepared from a 0.79 wt.% thallium amalgam and a solution of 0.100 *M* TBAP saturated with $TlClO_4$. The reference electrode was separated from the working compartment by two frits and a salt bridge filled with 0.100 *M* TBAP. This electrode was chosen to minimize the liquid junction potential and its change with time since all solutions in the cell were also 0.100 *M* in TBAP. Using the data of Coetzee and Campion (15, 16) the potential of this electrode vs. an aqueous saturated calomel electrode was calculated to be −0.34 V. Experimental measurements produced the same value. The reference electrode was stable for periods of a few days; however, the thallium amalgam slowly decomposes requiring that fresh electrodes be prepared often.

The cell was placed in a small, nitrogen filled dry box during all measurements. The solutions were prepared and stored in the same dry box. Viscosities were determined using an Ostwald viscometer. All measurements were made at 25 ± 1°C.

The potentiostat was programmed to perform tast polarography. In this technique the current is measured at only one time during drop life rather than continuously. This time is usually chosen to be late in drop life when the Faradaic current is high and the background double layer charging current is low for improved sensitivity. With the instrumentation used tast polarography provides almost ideal polarograms since potential is constant during drop life (until after current measurement) and changes in drop time caused by the variation of potential have no effect.

Spectroscopic Measurements

All spectra were recorded using a Cary 14 visible–ultraviolet spectrophotometer also interfaced to the same computer system used for the electrochemical measurements (17).

Data Treatment

All data were recorded on magnetic tape for ease of storage and digital data analysis. Polarographic data analysis is usually done using eq. [7].

$$[7] \qquad E_{dme} = E_{1/2} + \frac{RT}{nF} \ln (i_d - i)/i$$

where i is the current measured at some potential E_{dme} and i_d is the current on the diffusion limited portion of the wave. The half-wave potential and n are determined from a linear least-squares analysis of a plot of E_{dme} vs. ln $(i_d - i)/i$. This suffers from the disadvantage that only points on the rising portion of the wave can be used and the precision of the calculated parameters is not easily determined. Since currents in polarography are additive

$$[8] \qquad i_t = i_b + i_1 + i_2 + \ldots$$

where i_t is the total current, i_b is the current flowing before the first polarographic wave, i_1 is the current for the first wave, etc. If one solves for the currents of the individual waves and substitutes into eq. [8], one obtains

$$[9] \quad i_t = i_b + \frac{(i_d)_1}{1 + \exp[(n_1F/RT)(E - (E_{1/2})_1)]} + \frac{(i_d)_2}{1 + \exp[(n_2F/RT)(E - (E_{1/2})_2)]} + \ldots$$

The values of i_b, $(i_d)_1$, $(i_d)_2$, n_1, n_2, $(E_{1/2})_1$, $(E_{1/2})_2$, etc. can be obtained from eq. [9] by non-linear least-squares analysis (18). This approach has the advantages that the diffusion currents also come from the analysis, more than one wave can be analyzed at a time and the waves can overlap, all the data are used and the precision of the calculated parameters comes directly from the analysis.

Programs were written for the Hewlett-Packard 2114B computer to subtract the background (a polarogram run of a solution of 0.100 *M* TBAP in acetonitrile) from all other polarograms and to determine the diffusion currents and half-wave potentials using eq. [9]. Another program was written to calculate the formation constants by linear least-squares analysis using eq. [1]. The data were analyzed by this program assuming first only a 1:1 complex and then assuming both 1:1 and 2:1 complexes. All concentrations were in mol/ℓ and thus the units of the formation constants are ℓ/mol.

Can. J. Chem. Downloaded from www.nrcresearchpress.com by 210.87.254.40 on 09/05/12
For personal use only.

The spectra of the EDA complexes were computed by another program from spectra of the donor, the acceptor, and a mixture of the two assuming that Beer's law was obeyed. Using the formation constants determined polarographically the concentrations of all species in the mixture were calculated. The spectral contributions of the uncomplexed donor and acceptor were then determined and subtracted from the spectrum of the mixture to produce the spectrum of the complex. The validity of this computed spectrum depends directly on the accuracy of the formation constants; however, high accuracy is more important in the cases where very little complex is formed and the contribution of the free acceptor to the total spectrum of the mixture is large (the free donors contributed very little to these spectra in the visible and near ultraviolet).

All programs were written in Hewlett-Packard assembly language for the particular magnetic tape operating system used.

Results and Discussion

All polarograms obtained showed two one-electron reversible waves between +0.4 V and −0.4 V vs. the $Tl(Hg)|TlClO_4$ reference electrode used. Further reduction waves, the characteristics of which were dependent on solvent purity, were observed at more negative potentials. Reversibility was indicated since the values of n obtained from the data analysis were always close to unity. However, staircase cyclic voltammetry with variation in sweep rate was used to confirm reversibility. The cathodic and anodic peaks obtained were ideal in shape and shifted very little with sweep rate up to values of 6 V/s. The differences in cathodic and anodic peak potential were always very close to the theoretical value of 58 mV for a one-electron reversible reaction. Figures 1 and 2 show typical polarograms obtained in this study. No significant change in half-wave potential for either the first or second reduction wave of TNF was observed upon addition of biphenyl in Fig. 1. The diffusion current decreases due to the increase in viscosity as the concentration of biphenyl increases. The colour of solution changed slightly upon addition of biphenyl, as it did in every case studied, indicating an interaction between donor and acceptor. However, any complex formed was too weak to be detected polarographically.

In Fig. 2 the half-wave potential for the first reduction wave of TNF shifts negatively upon addition of pyrene, whereas the second wave does not shift. Table 1 shows the results obtained by non-linear least-squares analysis for the first wave. The precision of all the half-wave potentials determined from a single experiment by the least-squares data analysis was 300 μV or better. The reproducibility of these values from one experiment to another was 4 mV or better. This loss in precision is probably due to changes in the reference electrode potential with time. The average half-wave potentials for the three acceptors examined are listed in Table 2.

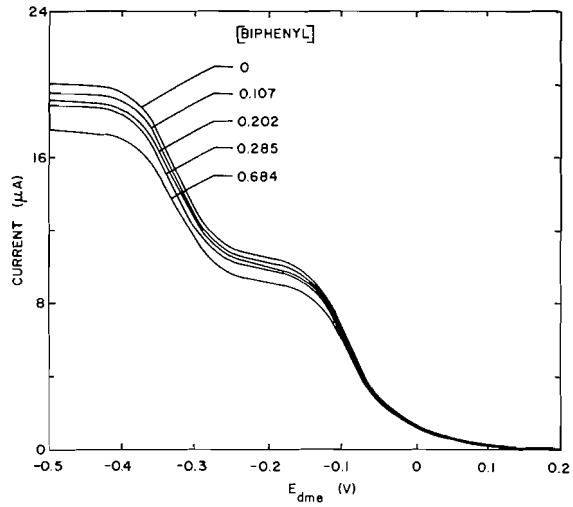

FIG. 1. Polarograms of 9.55×10^{-4} M TNF in acetonitrile and 0.100 M TBAP supporting electrolyte with biphenyl as donor.

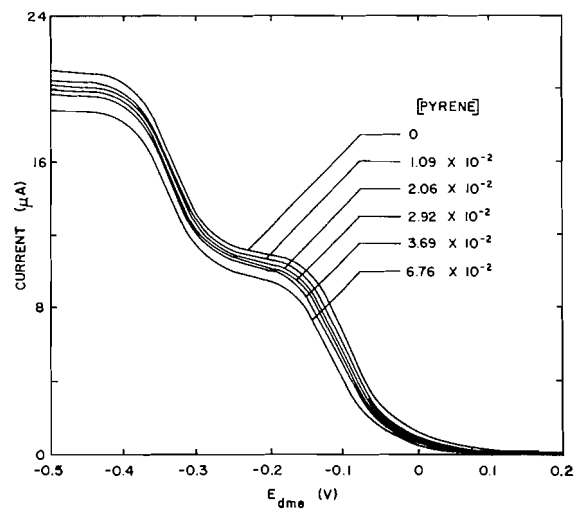

FIG. 2. Polarograms of 9.38×10^{-4} M TNF in acetonitrile and 0.100 M TBAP supporting electrolyte with pyrene as donor.

Table 3 presents the formation constant data for the EDA complexes. The absence of an entry indicates that any complex formed was too weak to be determined polarographically. The data were treated assuming that only a 1:1 complex formed and that both 1:1 and 2:1 complexes formed. When the two-complex model was used, K_2 was negative for eight of the 17 systems studied, indicating that random variation in the data caused a negative curvature. The nine cases where K_2 was positive were subjected to an analysis of variance on the sum of the squared residuals (19) to test whether the two-complex model produced a significantly better fit than the single

Can. J. Chem. Downloaded from www.nrcresearchpress.com by 210.87.254.40 on 09/05/12
For personal use only.

TABLE 1. Half-wave potentials of 9.55×10^{-4} *M* TNF in acetonitrile with 0.100 *M* TBAP as supporting electrolyte

Pyrene concentration (mol/ℓ)	$E_{1/2}$ vs. Tl(Hg)|$TlClO_4$ (V)
0.0000	-0.0923 ± 0.0003
0.0109	-0.0963 ± 0.0003
0.0206	-0.1005 ± 0.0003
0.0293	-0.1035 ± 0.0003
0.0369	-0.1060 ± 0.0003
0.0676	-0.1141 ± 0.0003

TABLE 2. Half-wave potentials of acceptors vs. Tl(Hg)|$TlClO_4$

Acceptor	First wave (V)	Second wave (V)
TNF	−0.090	−0.335
CNTNF	0.326	−0.250
CNDNFDMC	0.313	−0.266

TABLE 3

(*a*) Formation constants of EDA complexes (ℓ/mol) assuming only a 1:1 reaction

	Value of constant		
Donor	TNF	CNTNF	CNDNFDMC
Naphthalene	1.0 ± 0.1	5.2 ± 0.2	7.5 ± 0.5
Phenanthrene	8.7 ± 0.6	78 ± 3	57 ± 3
Pyrene	24.1 ± 0.3	285 ± 17	249 ± 49
Triphenylene	18 ± 7	241 ± 27	247 ± 22
Biphenyl	—	1.7 ± 0.1	2.95 ± 0.04
o-Terphenyl	—	—	0.38 ± 0.07
m-Terphenyl	—	4.9 ± 0.2	7.1 ± 0.1

(*b*) Formation constants of phenanthrene EDA complexes (ℓ/mol) assuming both a 1:1 and a 2:1 reaction

	Value	
Constant	TNF	CNTNF
K_1	5.3 ± 0.8	57 ± 4
K_2	1.7 ± 0.5	1.0 ± 0.2

complex model. At the 95% confidence level only two systems, both with phenanthrene as donor, produced results in which the two-constant model gave a significantly better fit. No obvious reason presents itself to justify 2:1 complexes for phenanthrene (with only two of the three acceptors) and not for the other donors. This behaviour may thus be just due to chance irregularities in the data.

The standard deviations shown in Table 3 are a function of the magnitude of shift in half-wave potential which in turn is a function of both the strength of the complex and the quantity of the donor added. Thus the standard deviation of K_1 for the triphenylene–TNF complex is much higher than that for the pyrene–TNF complex even though the constants are about equal because triphenylene is much less soluble than pyrene in acetonitrile and the resulting shifts in $E_{1/2}$ are much less for triphenylene. In the case of the complexes of pyrene and triphenylene with CNTNF and CNDNFDMC, a precipitate was formed when donor and acceptor were mixed. These solids were still sufficiently soluble to allow determination of half-wave potentials. Since reversible half-wave potentials are independent of concentration, data analysis using eq. [1] could still be carried out. However, the changes in diffusion current that would have occurred in the absence of precipitation had to be estimated from the data for the TNF complexes. For this reason the values of formation constants for these complexes should be considered less certain.

A comparison of the half-wave potentials of the acceptors shows that CNTNF and CNDNFDMC should be about equal in electron affinity but much greater than TNF. The formation constants of CNTNF and CNDNFDMC are also about equal but much greater than those of TNF as expected. The constants for the condensed ring hydrocarbons are much larger than for biphenyl and the terphenyls. In both cases the constants increase as the size of the donor π system increases. The one exception to this is *o*-terphenyl which has a much smaller constant than *m*-terphenyl. This is probably due to steric hindrance in *o*-terphenyl which prevents proper overlap of the π systems of the donor and acceptor.

Although TNF and CNTNF are widely used reagents, few data are available regarding their complexes. The formation constant of the TNF–naphthalene complex determined by spectrophotometric measurement has been reported as 0.97 ℓ/mol in acetic acid at about 20°C (20), as 0.69 ℓ/mol in $CHCl_3$ at 18°C (21), and as 0.75 ℓ/mol in $CHCl_3$ at 20°C (22). Although these values and that obtained in the present work are nearly identical, it is difficult to make comparisons because of differences in solvent and solution components.

Dewar and Thompson (23) have studied the EDA complexes of tetracyanoethylene (TCNE) spectrophotometrically in $CHCl_3$ at 25°C with the same donors as used above. Their results are presented in Table 4. The first half-wave reduction potential for TCNE vs. the Tl(Hg)|$TlClO_4$ reference electrode used in this study is about +0.58 V and thus it should be an even better acceptor than either CNTNF or CNDNFDMC. In general as the solvent becomes more polar, EDA complexes become weaker due to competition from solvent molecules. Thus it would be expected that the EDA complexes studied here would be less stable than those of TCNE in $CHCl_3$. The trends observed by Dewar and Thompson are similar

Can. J. Chem. Downloaded from www.nrcresearchpress.com by 210.87.254.40 on 09/05/12
For personal use only.

TABLE 4. Formation constants of EDA complexes of TCNE at 25°C in $CHCl_3$ from ref. 23

Donor	K_1
Naphthalene	1.01
Phenanthrene	2.16
Pyrene	2.79
Triphenylene	3.52
Biphenyl	0.67
o-Terphenyl	0.15
m-Terphenyl	0.64

to those observed here but the changes in formation constants between donors appear to be much greater in acetonitrile and most of the constants are also greater in acetonitrile. Holm *et al.* (7) have noted that EDA formation constants measured polarographically are considerably larger than those measured by optical spectroscopy. This appears to be the case here also. No satisfactory explanation is presently available for this phenomenon.

Figure 3 shows the spectra of some EDA complexes in the region of the charge-transfer band computed as described above. Pyrene is the only donor of those studied that produces a well defined CT band. The others appear as shoulders on the first absorption band of the acceptor. With these complexes there appears to be no relationship between the formation constants of the complexes and their molar absorptivities. This is not unusual for this type of complex (ref. 1, p. 30).

Figure 4 shows the effect of complexation on the first acceptor band in the complex. In general the energy of this transition changes very little, but the molar absorptivity is decreased and the vibrational fine structure is affected as might be expected.

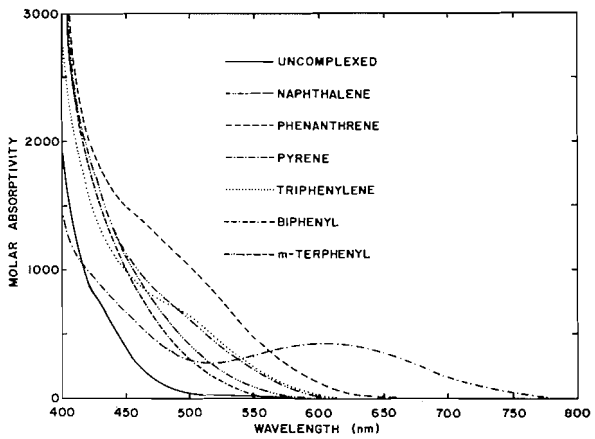

FIG. 3. Spectra of EDA complexes of CNDNFDMC in the charge-transfer region.

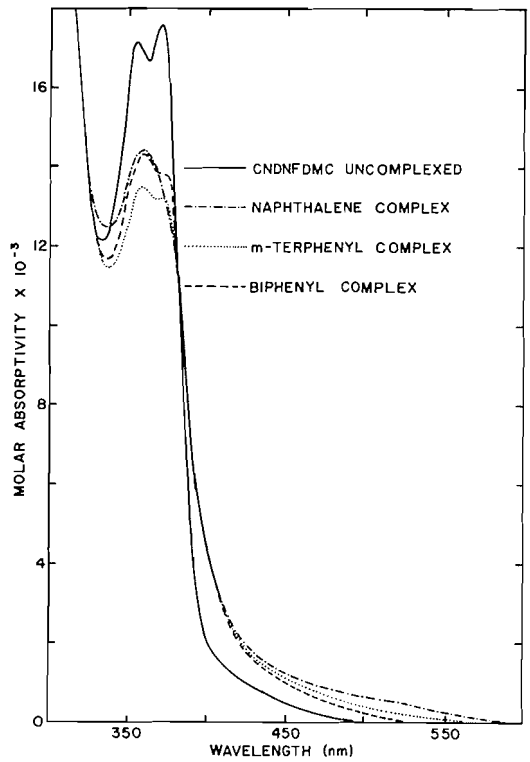

FIG. 4. Acceptor contribution to the spectra of EDA complexes of CNDNFDMC.

Any contribution of contact charge-transfer is included in the spectra of Figs. 3 and 4.

Acknowledgements

The authors wish to thank Sharon Sobel for performing the viscosity measurements and the National Research Council of Canada for financial support.

1. R. S. MULLIKEN and W. B. PERSON. Molecular complexes. Wiley-Interscience, New York. 1969.
2. R. FOSTER. Organic charge-transfer complexes. Academic Press, London. 1969.
3. L. E. ORGEL and R. S. MULLIKEN. J. Am. Chem. Soc. **79**, 4839 (1957).
4. J. N. MURRELL. J. Am. Chem. Soc. **81**, 5037 (1959).
5. M. E. PEOVER. Proc. Chem. Soc. 167 (1963).
6. M. E. PEOVER. Trans. Faraday Soc. **60**, 417 (1964).
7. R. D. HOLM, W. R. CARPER, and J. A. BLANCHER. J. Phys. Chem. **71**, 3960 (1967).
8. R. BONNATERRE and G. CAUQUIS. Bull. Soc. Chim. Fr. 3297 (1972).
9. D. D. DE FORD and D. D. HUME. J. Am. Chem. Soc. **73**, 5321 (1951).
10. T. SULZBERG and R. J. COTTER. J. Org. Chem. **35**, 2762 (1970).
11. M. WALTER and L. RAMALEY. Anal. Chem. **45**, 165 (1973).
12. L. RAMALEY. Chem. Instrum. **6**, 119 (1975).
13. L. RAMALEY. Chem. Instrum. **2**, 415 (1970).

14. L. RAMALEY and G. S. WILSON. Anal. Chem. **42**, 606 (1970).
15. J. F. COETZEE and J. J. CAMPION. J. Am. Chem. Soc. **89**, 2513 (1967).
16. J. F. COETZEE and J. J. CAMPION. J. Am. Chem. Soc. **89**, 2517 (1967).
17. H. LONGERICH and L. RAMALEY. Anal. Chem. **46**, 2067 (1974).
18. J. R. WOLBERG. Prediction analysis. D. VanNostrand Co. Inc., Princeton. 1967.
19. J. R. GREEN and D. MARGERISON. Statistical treatment of experimental data. Elsevier, Amsterdam. 1977. Chapt. 15, Section 7.4.
20. L. H. KLEMM, J. N. SPRAGUE, and H. ZIFFER. J. Org. Chem. **20**, 200 (1955).
21. A. S. BAILEY and J. R. CASE. Tetrahedron, **3**, 113 (1958).
22. N. CHRISTODOULEAS and S. P. MCGLYNN. J. Chem. Phys. **40**, 166 (1964).
23. M. J. S. DEWAR and C. C. THOMPSON, JR. Tetrahedron Supp. **7**, 97 (1966).

Can. J. Chem. Downloaded from www.nrcresearchpress.com by 210.87.254.40 on 09/05/12
For personal use only.

Density and temperature effects on electron mobilities in gaseous, critical and liquid *n*-hexane, cyclohexane, and cyclopentane[1]

SAM S.-S. HUANG AND GORDON R. FREEMAN

Chemistry Department, University of Alberta, Edmonton, Alta., Canada T6G 2G2

Received April 10, 1978

SAM S.-S. HUANG and GORDON R. FREEMAN. Can. J. Chem. **56**, 2388 (1978).

In the low density vapors the density normalized mobilities μn of thermal electrons decreased in the order *n*-hexane > cyclopentane > cyclohexane, although the differences were only ~10%. The mobilities began to increase at electric field strengths $E/n > 0.4$ *Td* in cyclopentane, > 0.5 *Td* in cyclohexane and remained independent of field strength up to 1.5 *Td* in *n*-hexane. The ratio of the threshold drift velocity for electron heating to the speed of low frequency sound in the gas, v_d(threshold)/c_0 = 11 in cyclopentane, 14 in cyclohexane, and is > 35 in *n*-hexane; it increases with decreasing sphericity of the molecules. The electrons are cooled mainly by inelastic collisions with the hydrocarbon molecules. The temperature coefficients of mobilities in the low density gases increase as the molecules become more globular, which could reflect the participation of either low lying transient negative ion states or a Ramsauer–Townsend effect in the scattering processes. The normalized mobilities μn in the saturated vapors began to decrease at $n = 4 \times 10^{19}$ molecules/cm^3 in *n*-hexane, 13×10^{19} in cyclohexane, and 30×10^{19} in cyclopentane. It appears that the minimum size of molecular cluster required for electron quasilocalization is smaller in *n*-hexane than in cyclohexane, and larger in cyclopentane. Electron localization interactions are weaker for more globular molecules.

Mobilities in the critical fluids were 16 cm^2/V s in *n*-hexane, 23 in cyclohexane, and 22 in cyclopentane.

Mobilities in the liquids were independent of field up to the highest value used, which was 1.5 *Td* in the hexanes and 0.9 *Td* in cyclopentane. The mobilities and their temperature dependences were interpreted in terms of a model.

SAM S.-S. HUANG et GORDON R. FREEMAN. Can. J. Chem. **56**, 2388 (1978).

A des densités de vapeurs faibles, la mobilité normalisée pour la densité (μn) des électrons thermiques diminue dans l'ordre de *n*-hexane > cyclopentane > cyclohexane, quoique les différences soient d'environ 10%. Les mobilités commencent à augmenter à une force de champ électrique $E/n > 0.4$ *Td* dans le cyclopentane, > 0.5 *Td* dans le cyclohexane et demeurent indépendants de la force du champ jusqu'à 1.5 *Td* dans le *n*-hexane. Le rapport de la vitesse minimale de diffusion pour le chauffage des électrons à la vitesse de son de basse fréquence dans les gaz v_d(seuil)/c_0 = 11 dans le cyclopentane, 14 dans le cyclohexane et est de > 35 dans le *n*-hexane; cette valeur augmente avec la diminution de la sphéricité des molécules. Les électrons sont refroidis principalement par des collisions inélastiques avec des molécules d'hydrocarbures. Les coefficients de température des mobilités à des faibles densités gazeuses augmentent à mesure que les molécules deviennent plus globulaires ce qui est un reflet de la participation soit d'états ioniques négatifs transitoires de basses énergies ou un effet de Ramsauer–Townsend dans les processus de dispersion. Les mobilités normalisées μn dans des vapeurs saturées commencent à diminuer à $n = 4 \times 10^{19}$ molecules/cm^3 dans le *n*-hexane, 13×10^{19} dans le cyclohexane et à 30×10^{19} dans le cyclopentane. Il semble que la grosseur minimale d'une aggrégation moléculaire nécessaire pour une quasilocation électronique soit plus faible dans l'hexane que dans le cyclohexane et plus grande dans le cyclopentane. Les interactions de localisation électronique sont plus faibles pour des molécules qui sont plus globulaires.

Les mobilités dans des fluides critiques sont 16 cm^2/V s dans le *n*-hexane, 23 dans le cyclohexane et 22 dans le cyclopentane.

Les mobilités dans les liquides sont indépendantes du champ jusqu'aux valeurs les plus élevées utilisées soit 1.5 *Td* dans les *n*-hexanes et 0.9 *Td* dans le cyclopentane. On a interprété les mobilités et leurs relations avec la température en terme d'un modèle.

[Traduit par le journal]

Introduction

Thermal electron mobilities in liquid hydrocarbons have been extensively investigated during the last decade (1–14). To get a better understanding of electron transport in fluids we have recently been doing measurements through the critical and supercritical regions (15–17). Mobilities in dense methane gas have also been reported (18).

In liquid alkanes electron mobilities increase with increasing sphericity of the molecules (1, 5, 10). For example, electrons are more mobile in neopentane

[1]Assisted financially by the National Research Council of Canada.

Can. J. Chem. Downloaded from www.nrcresearchpress.com by 210.87.254.42 on 09/05/12
For personal use only.

Can. J. Chem. Downloaded from www.nrcresearchpress.com by 210.87.254.42 on 09/05/12
For personal use only.

than in *n*-pentane; low mobility, localized states of electrons in liquid alkanes are less stable when the polarizabilities of the molecules are more nearly isotropic (10). In the low density gas, where an electron interacts with essentially one molecule at a time, the mobility is greater in *n*-pentane than in neopentane (19). This is the reverse of the high density behavior, and the cross-over occurs at $\sim 0.7\ d_c$, where d_c is the critical density. To extend this density study to other molecular structures, measurements have now been made in *n*-hexane, cyclohexane, and cyclopentane to determine the effect of cyclization.

Experimental

Materials

The hydrocarbons were Phillips Research Grade. They were further purified by stirring with concentrated sulfuric acid for at least 4 days, decanted into a bulb that was attached to a vacuum system and contained potassium hydroxide pellets. The hydrocarbon was degassed and stirred for 12 h, then distilled onto lithium aluminum hydride, degassed further and stirred for 1 day, then distilled onto sodium/potassium alloy and stirred for 5 days, followed by several freeze–pump–thaw degassing cycles.

Conductance Cells

The cell used at low temperatures was similar to that described in ref. 20. The cells used at high temperatures were similar to the heavy walled cell described in ref. 16. The gap between the parallel plate electrodes was in all cases 0.29–0.34 cm, while the effective areas of the collecting electrodes ranged from 1.9 to 7.8 cm^2.

The heavy walled cells were heated under evacuation to 60 K above the highest temperature at which they would be used, to degas the metal electrodes and interior glass.

Temperature Control

The cooling system was similar to that described earlier (17).

The heating system was similar to that in ref. 16. However, the temperature was measured with two calibrated copper–constantan thermocouples, one attached to the cell near the electrodes and the other to the opposite end of the cell. A third thermocouple in the Dewar vessel was placed near to the cell and connected to the temperature controller. The glass heatpipe was adjusted to minimize temperature gradients in the cell.

The heating and cooling systems were placed in well grounded Faraday cages.

Determination of Mobility μ

The 1.7 MeV X-ray pulse lengths were 0.03, 0.10, and 1.0 μs. The respective doses were ~ 0.01, 0.1, and 1×10^{11} eV/g.

Mobilities were usually measured by a time of flight method described elsewhere (21). In liquid *n*-hexane at low temperatures the flight times were so long that electron scavenging by trace impurities caused interference. Under these circumstances mobilities were determined by an electron conductance technique (10).

Physical Properties of the Fluids

The densities *d* were obtained from refs. 22 and 23. The critical properties of the hydrocarbons are summarized in Table 1. The dielectric constants were calculated from the Clausius–Mossotti equation (24), using molar polarization values from refs. 25 and 26.

TABLE 1. Critical properties of the hydrocarbons*

Hydrocarbon	T_c (K)	P_c (atm)	d_c (g/cm^3)	ε_c†
n-Hexane	508	29.9	0.232	1.26
Cyclohexane	554	40.6	0.272	1.29
Cyclopentane	512	44.6	0.270	1.29

*Reference 22.
†See text.

Results

The vapor densities were varied from the critical d_c to 0.01 d_c and the temperature from about 298 K to 1.12 T_c, where T_c is the critical temperature. Liquid *n*-hexane and cyclohexane were measured from near their melting points to T_c under their vapor pressures. Previous results for liquid cyclopentane (16) are also included.

Effect of Electric Field Strength

Electron mobilities in *n*-hexane were independent of field strength over the range used, 0.1–1.5 *Td* (10^{-17} V cm^2/molecule), in the gas and liquid phases. A field of 1 *Td* in the normal liquid corresponds to ~ 50 kV/cm. The field independence in the gas phase applies both to the vapor in equilibrium with the liquid and to vapor heated well above the coexistence curve.

In cyclohexane and cyclopentane liquids the mobilities were also independent of field strength to the maximum used, which was 1.5 *Td* in the former and 0.9 *Td* in the latter (16). In the vapors, however, the mobilities increased slightly at fields >0.5 *Td* in cyclohexane and >0.4 *Td* in cyclopentane (Fig. 1). All mobilities reported hereafter are low field values.

In the low density vapors the density normalized mobilities μn decreased in the order *n*-hexane > cyclopentane > cyclohexane (Fig. 1).

Effect of Temperature

(a) Liquid Hydrocarbons

Electron mobilities in *n*-hexane increased continuously with temperature from 182 K to T_c, and in the supercritical gas (Fig. 2). The Arrhenius temperature coefficients were 0.11, 0.20, and 0.54 eV at 210, 320, and 455 K, respectively. The mobility increased by four orders of magnitude, from 0.0026 cm^2/V s at 182 K to 16 cm^2/V s in the critical fluid.

The mobility in cyclohexane passed through a maximum, $\mu = 26$ cm^2/V s, about 7 K below T_c (Fig. 3). The temperature coefficients were 0.17, 0.24, 0.48, and -0.63 eV at 330, 430, 525, and 553 K, respectively.

A maximum also occurs in an Arrhenius plot of the mobilities in liquid cyclopentane (16). The behavior is similar to that in Fig. 3.

Can. J. Chem. Downloaded from www.nrcresearchpress.com by 210.87.254.42 on 09/05/12
For personal use only.

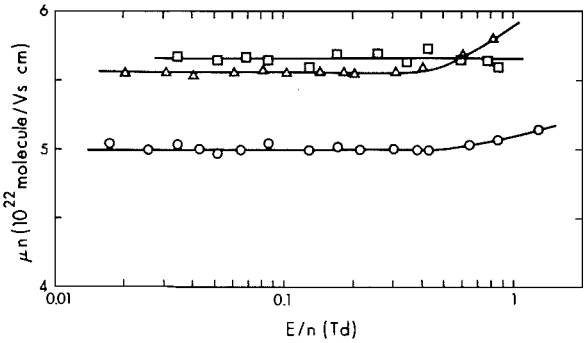

FIG. 1. Density normalized mobilities μn in hydrocarbon vapors as functions of the normalized electric field strength E/n ($Td = 10^{-17}$ V cm^2/molecule). □, *n*-hexane, 364 K, 4.1×10^{19} molecules/cm^3; △, cyclopentane, 410 K, 1.71×10^{20} molecules/cm^3; ○, cyclohexane, 403 K, 6.9×10^{19} molecules/cm^3. The vapors are in equilibrium with the liquid.

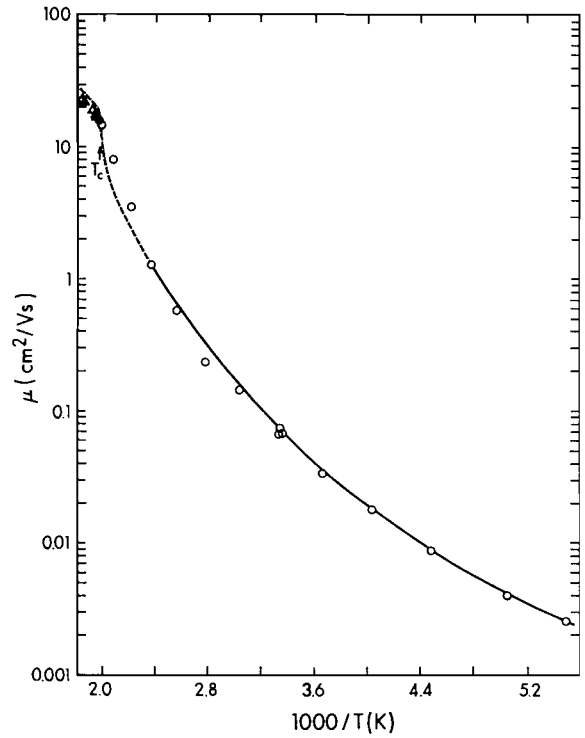

FIG. 2. Arrhenius plot of electron mobilities in *n*-hexane: ○, liquid; ●, critical; △, supercritical. The curve was calculated from eqs. [7]–[12], using the parameter values in Table 3. The dashed portion is inadequate.

(b) Gaseous Hydrocarbons

Electron mobilities were measured as functions of temperature at several fixed densities of the gases.

Arrhenius plots of the mobilities in *n*-hexane at densities from the critical d_c to 0.02 d_c are shown in Fig. 4. The low temperature boundary of the plots corresponds to the mobilities in the saturated vapor along the gas–liquid coexistence curve. The mobility

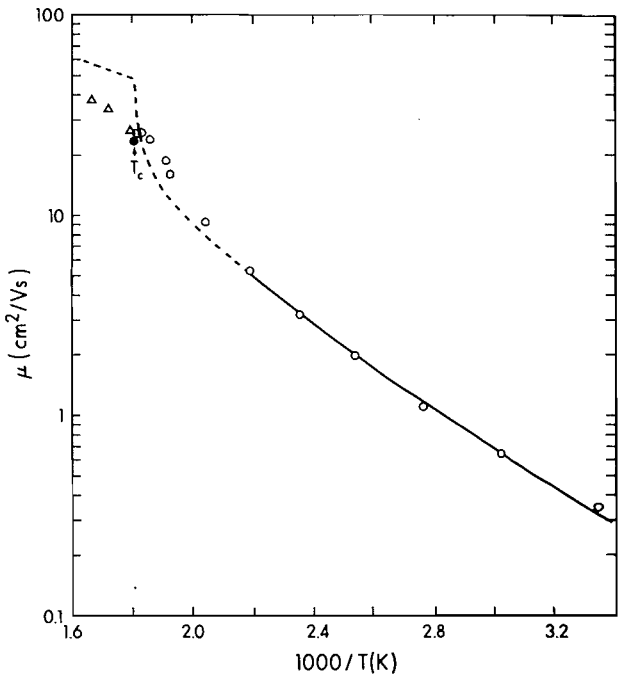

FIG. 3. Arrhenius plot of electron mobilities in cyclohexane. ○, liquid; ●, critical; △, supercritical. The curve was calculated from eqs. [7]–[12], using the parameter values in Table 3. The dashed portion is inadequate.

shows a minimum at the critical point. The temperature coefficients near the coexistence curve were 0.33, 0.38, 0.26, 0.10, 0.04, and 0.00 eV at 1.00, 0.80, 0.50, 0.25, 0.10, and 0.021 d_c, respectively. The coefficients decreased with increasing temperature at constant density.

In cyclohexane vapor the mobility had a positive temperature coefficient even at the lowest density (Fig. 5). The coefficients near the coexistence curve were 0.53, 0.26, 0.10, 0.064, 0.014, and 0.015 eV at 1.00, 0.50, 0.25, 0.10, 0.045, and 0.012 d_c, respectively, and decreased with increasing temperature.

The behavior in cyclopentane vapor (Fig. 6) was similar to that in cyclohexane. The Arrhenius coefficients near the coexistence curve were 0.72, 0.24, 0.091, 0.032, and 0.015 eV at 1.00, 0.50, 0.25, 0.10, and 0.021 d_c, respectively.

Electron mobilities in the critical fluids were 16, 23, and 22 cm^2/V s in *n*-hexane, cyclohexane, and cyclopentane, respectively.

Effect of Density

In low density cyclohexane vapor the density normalized mobility was $\mu n = 5.1 \times 10^{22}$ molecules/cm V s (Fig. 7). At $n > 1.3 \times 10^{20}$ molecules/cm^3 the normalized mobility decreased somewhat, passed through a minimum of 3.8×10^{22} molecules/cm V s at 9×10^{20} molecules/cm^3, increased to a maximum

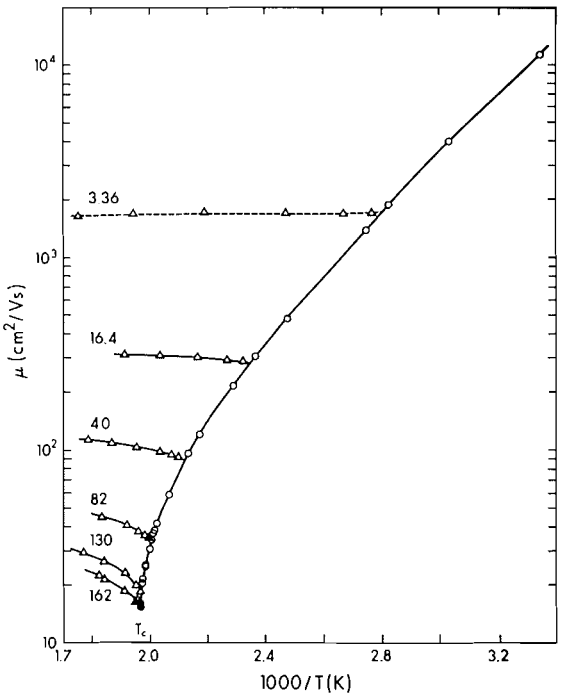

FIG. 4. Arrhenius plots of thermal electron mobilities in *n*-hexane vapor at different constant densities (△). The numbers labelling the lines are the densities (10^{19} molecules/cm^3). ○, Mobilities in gas along the vapor–liquid coexistence curve. ●, Mobility at the critical point. The dashed line was calculated from eqs. [2]–[4], using values of n, α, and A_α from Table 2.

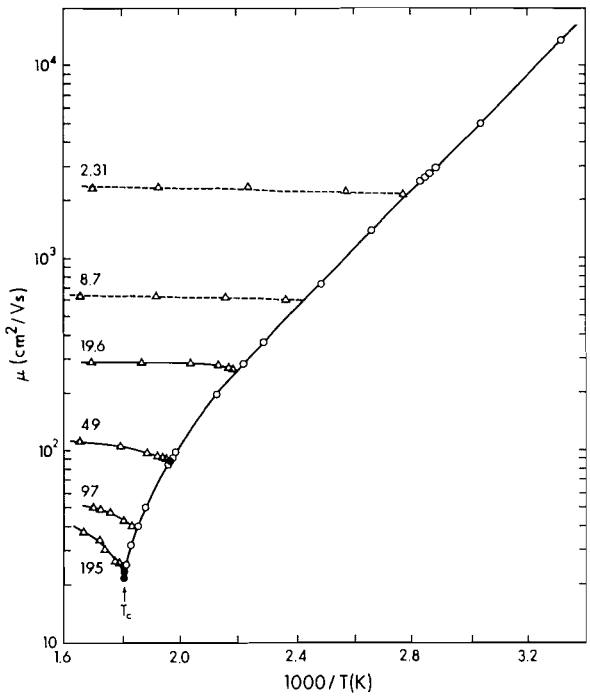

FIG. 5. Arrhenius plots of thermal electron mobilities in cyclohexane vapor at different constant densities (△). The numbers labelling the lines are the densities (10^{19} molecules/cm^3). ○, Mobilities in gas along the vapor–liquid coexistence curve. ●, Mobility at the critical point. The dashed lines were calculated from eqs. [2]–[4], using values of n, α, and A_α from Table 2.

of 7.5×10^{22} molecules/cm V s at 3×10^{21} molecules/cm^3, then decreased as the density was increased further. The critical density n_c lies between the mobility maximum and minimum (Fig. 7).

The behaviors in *n*-hexane and cyclopentane were similar to that in cyclohexane (Fig. 7). The low density values of μn were respectively 5.8, 5.5, and 5.1 (10^{22} molecules/cm V s). However, the ratio of mobilities at the liquid phase maximum and gas phase minimum, μ_{max}/μ_{min}, decreased from 2.1 in cyclopentane to 2.0 in cyclohexane and 1.3 in *n*-hexane. The density at which μn ceases to be independent of n follows the same trend, being respectively 3×10^{20}, 1.3×10^{20}, and 4×10^{19} molecules/cm^3. The mobilities in the liquids at 299 K fall in the same order, 1.1, 0.35, and 0.07 cm^2/V s, respectively.

Discussion

Electric Field Effect

At low applied field strengths the electrons make a negligible net gain of energy from the field and they are in thermal equilibrium with the medium. When the field is increased, as long as the mobility remains independent of the field strength it is assumed that the electrons remain in thermal equilibrium with the medium. The energy gained by acceleration in the field between collisions is lost to the medium during collisions. At sufficiently high fields more energy is gained than is lost, the electrons become 'heated' and the mobility becomes field dependent.

When elastic collisions are the dominant process that moderate the electron energy, the upper limit of the drift velocity at which the electrons remain thermal is equal to the low frequency limit of the velocity of sound, c_0, in the system (27–30). The value of c_0 in a gas is given by (31):

$$[1] \qquad c_0 = (\gamma P/d)^{0.5}$$

where $\gamma = C_p/C_v$ is the heat capacity ratio and P (dyn/cm^2) is the pressure. At low densities, where the gas is nearly ideal, one has $\gamma \approx (C_p/[C_p - R]) \approx 1.1$ and $c_0 \approx 198$ m/s in cyclopentane and 180 m/s in the hexanes at 300 K. The threshold drift velocities for electron heating are v_d(threshold) ≈ 2.2 km/s in cyclopentane, 2.5 km/s in cyclohexane (Fig. 1), and >6 km/s in *n*-hexane vapor. The respective values of v_d(threshold)/c_0 are therefore 11, 14, and >35. These high values imply that the electrons are cooled

Can. J. Chem. Downloaded from www.nrcresearchpress.com by 210.87.254.42 on 09/05/12
For personal use only.

Can. J. Chem. Downloaded from www.nrcresearchpress.com by 210.87.254.42 on 09/05/12
For personal use only.

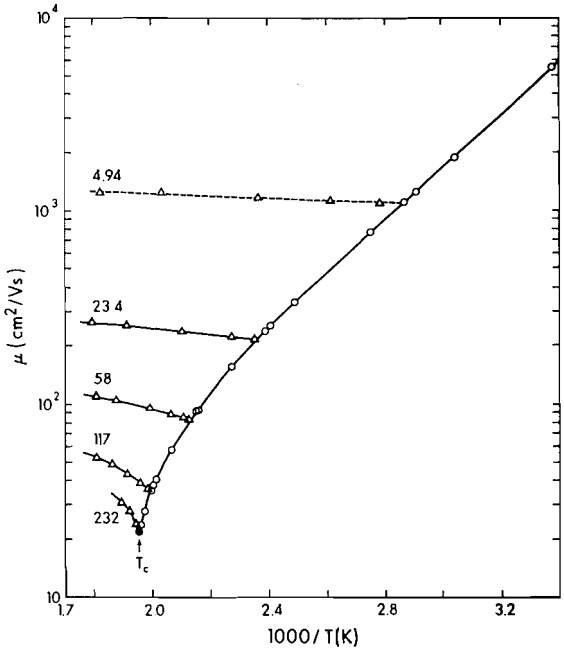

FIG. 6. Arrhenius plots of thermal electron mobilities in cyclopentane vapor at different constant densities (△). The numbers labelling the lines are the densities (10^{19} molecules/cm^3). ○, Mobilities in gas along the vapor–liquid coexistence curve. ●, Mobility at the critical point. The dashed line was calculated from eqs. [2]–[4], using values of n, α, and A_α from Table 2.

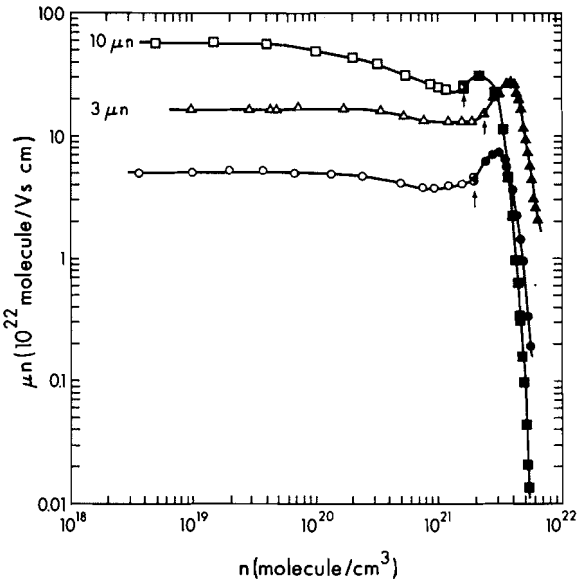

FIG. 7. Plot of μn against n for electrons in fluid cyclohexane (circles), cyclopentane (triangles), and n-hexane (squares). The open symbols represent gases along the vapor–liquid coexistence curves and the closed symbols represent the liquids. The half-closed symbols and the arrows indicate the critical fluids. To prevent congestion, the cyclopentane points are displaced vertically by a factor of 3 and those for n-hexane by a factor of 10.

predominantly by inelastic collisions with the hydrocarbons, in contrast to the behavior with the monatomic molecules of xenon (21).

The value of the ratio v_d(threshold)/c_0 increases with decreasing sphericity of the gas molecules: xenon 0.7 (21), neopentane 5 (19), cyclopentane 11, cyclohexane 14, isopentane 15 (19), n-pentane > 100 (19), and n-hexane probably also > 100.

Scattering Cross Sections of the Low Density Gases

The energy dependences of the cross sections were estimated from the variation of the mobilities with temperature (Figs. 4–6). The magnitudes of the temperature coefficients in the low density gases fell in the same order as the field dependences: cyclopentane $\gtrsim$ cyclphexane $>$ n-hexane.

The mobility μ_{ld} of electrons in a low density gas can be expressed as (32, 33):

$$[2] \qquad \mu_{ld} = -\frac{4\pi}{3}\frac{e}{mn}\int_0^\infty \frac{v^2}{\sigma_v}\frac{df_0}{dv}\,dv$$

where e and m are the charge and mass of the electron, respectively, n is the number of molecules/cm^3, v is the relative velocity of the electrons with respect to the molecules, σ_v is the scattering cross section of the molecules for electrons of velocity v, and f_0 is the spherically symmetric term in the series expansion of the electron velocity distribution function. Thermal electrons have a Maxwellian distribution:

$$[3] \qquad f_0 = \left(\frac{m}{2\pi kT}\right)^{3/2}\exp\left(-\frac{mv^2}{2kT}\right)$$

where k is Boltzmann's constant.

Over a limited range of v the scattering cross section can be approximated by eq. [4] (34):

$$[4] \qquad \sigma_v = A_\alpha v^{-\alpha}$$

where the value of the constant A_α depends on that of α. These two quantities were estimated by fitting eqs. [2]–[4] to mobilities obtained at $n < 10 \times 10^{19}$ molecules/cm^3 (Figs. 4–6). The values are listed in Table 2. The dashed lines in Figs. 4–6 correspond to mobilities calculated from these parameters.

Quantum mechanical theory of electron scattering predicts that for charge/induced dipole and charge/permanent dipole interactions the respective values of α are 2/3 and 2 (35, 36). Classical theory gives $\alpha = 1$ and 2, respectively (34). The experimental value $\alpha = 1.5$ for low density cyclopentane vapor is significantly different from the value 0.67–1.0 expected for scattering by a nonpolar, polarizable particle. Furthermore, the average value of the cross section at 500 K, 22 Å^2 (Table 2), is an order of magnitude smaller than that estimated from the classical theory of scattering by a polarization

TABLE 2. Scattering parameters of the low density gases

Compound	n (10^{19} molcules/cm^3)	α	A_α (cm$^{2+\alpha}$/s$^\alpha$)	$\sigma_{ave,\ 500\ K}$ (10^{-15} cm^2)
n-Hexane	3.36	0.9	4.6×10^{-9}	1.6
c-Hexane	2.31	1.3	4.6×10^{-6}	2.0
	8.73	1.2	8.5×10^{-7}	2.0
c-Pentane	4.94	1.5	1.15×10^{-4}	1.8(2.0[a])

[a]σ_{ave} increased by an arbitrary molecular weight factor $(C_6/C_5)^{2/3}$ to adjust for the physical size of the molecules and facilitate comparison with the hexanes. It is assumed that the molecular volumes of the hydrocarbons are proportional to the molecular weights, and that the physical cross sectional areas are proportional to $MW^{2/3}$.

potential (34). Thus, scattering involves more than the simple polarization field.

Mobility is proportional to σ_v^{-1}, so the average cross section of interest is some function of σ_v^{-1}. Taking σ_{ave} as an effective cross section that is assumed to be independent of v one obtains

$$[5]\quad \sigma_{ave} = \langle v\rangle/\langle v/\sigma_v\rangle = 2(kT/m)^2 A_\alpha \Big/ \int_0^\infty v^{3+\alpha} \times \exp(-mv^2/2kT)\, dv$$

which reduces to

$$[6]\quad \sigma_{ave} = A_\alpha (m/2kT)^{\alpha/2}/\Gamma\left(2+\frac{\alpha}{2}\right)$$

Values of σ_{ave} at 500 K are listed in Table 2.

Although the value $\alpha = 0.9$ for n-hexane (Table 2) is within experimental uncertainty of that expected for scattering by a polarization potential, the cross section itself is an order of magnitude smaller than expected from the classical model.

The value of α for cyclohexane is intermediate between those for n-hexane and cyclopentane (Table 2). The values of σ_{ave} at 500 K are similar for the three compounds. If σ_{ave} for cyclopentane were increased[2] by $(84/70)^{2/3}$ to account for the smaller physical size of the molecule the values of σ_{ave} for the two cyclo compounds would be the same.

As the molecules become more globular, α increases (Table 2). This trend extends to neopentane, for which $\alpha = 3.2$ (19). Two possible interpretations are: (*a*) the scattering displays a Ramsauer–Townsend effect (34), and the scattering minimum moves to lower energy as the degree of sphericity of the molecules decreases; (*b*) a transient negative ion state lying near zero energy makes a stronger contribution to scattering from the more spherelike molecules (37).

High Density Gases

At $n \gtrsim 10\times10^{19}$ molecules/cm^3 μn decreases (Fig. 7), corresponding to an increase in σ_{ave}. The change is due to multibody effects. The temperature coefficients also increase at the higher densities (Figs. 4–6), which correspond to larger apparent values of α. However, A_α might be temperature dependent for multibody interactions, which would vitiate the simple form of [4]. Furthermore, the occurrence in the dense gases of molecular clustering and consequent electron quasilocalization renders [2] inadequate.

The Arrhenius plots at high densities are curved, with slopes decreasing as the temperature is increased above the coexistence region (Figs. 4–6). The curvature is qualitatively attributed to a reduced tendency for the molecules to cluster in the heated gas, hence a reduced contribution from quasilocalization.

The normal boiling point of cyclohexane (354 K) is greater than that of n-hexane (332 K), indicating stronger intermolecular attractive forces in the former. In the saturated vapors at a given density, one might therefore expect the degree of molecular clustering to be at least as great in cyclohexane as in n-hexane. However, the density at which μn becomes density dependent is threefold greater in the former than in the latter (Fig. 7). This means that smaller clusters are needed for electron quasilocalization in n-hexane than in cyclohexane. The electron localization interactions are therefore stronger with the open chain compound.

The values of n (10^{19} molecules/cm^3) at which μn becomes density dependent are ~4 in n-hexane, 13 in cyclohexane, 30 in cyclopentane, and 80 in neopentane (19). As the molecules become more globular the electron localization interactions become weaker. The same conclusion is drawn from the relative mobilities in the normal liquids (Fig. 7 and ref. 38).

The increase of slope as the gas density approaches the critical (Fig. 7) indicates interference of the scattering interactions, beginning the formation of a conduction band.

Liquids

Electron transport in the liquids is thermally activated. One model that is consistent with the results utilizes transitions between localized and extended states, with transport occurring mainly in the latter. To conserve space we list here the relevant

[2]See footnote to Table 2.

Can. J. Chem. Downloaded from www.nrcresearchpress.com by 210.87.254.42 on 09/05/12
For personal use only.

TABLE 3. Parameter values for eqs. [7]–[12][a]

Solvent	a (meV/K)	$\sigma(0)$ (meV)	b (meV/K)	$\left(\frac{E_0}{\sigma}\right)_{300\ K}$	$\mu_{300\ K}$ ($cm^2/V\ s$)
2,3-Dimethylbutane[b]	1.17	49	0.43	1.4	1.2
Cyclopentane[c]	1.06	190	0.047	1.4	1.1
2-Methylbutane[d]	1.13	133	0.14	1.5	0.94
Cyclohexane	0.99	152	0.075	1.7	0.36
3-Methylpentane[b]	0.95	95	0.24	1.9	0.25
n-Pentane[e]	1.02	145	0	2.0	0.13
n-Hexane	0.89	150	0	2.2	0.07
trans-Butene-2[e]	1.08	117	0	2.4	0.07
Butene-1[e]	0.96	49	0.35	2.0	0.20
Isobutene[e]	0.86	8	0.97	1.2	1.9
cis-Butene-2[e]	0.98	0	1.08	0.9	2.8

[a]Assume $\mu_{il}^0 = 0.1\ cm^2/V\ s$, $E_{il} = 0.07$ eV, $E(0) = 0.60$ eV, and $\mu_{ref}^0 = 30\ cm^2/V\ s$ at $T_{ref} = 295$ K for all liquids.
[b]Reference 40.
[c]Parameters obtained by fitting μ at $T < 430$ K; data from ref. 16.
[d]Reference 19.
[e]Reference 17.

equations and refer to an earlier article (17) for discussion of them.

$$[7] \quad \mu_{liq} = (1 - \chi)\mu_{il}^0 \exp(-E_{il}/kT) + \chi\mu_h^0$$

where χ is the fraction of electrons that are in the high mobility state with mobility μ_h^0, and μ_{il}^0 and E_{il} are respectively the pre-exponential factor and activation energy of mobility in the localized (ion-like) state.

$$[8] \quad \chi = \int_{-\infty}^{\infty} N(E)[1 + \exp(E/kT)]^{-1}\,dE$$

$$[9] \quad N(E) = \pi^{-1/2}\sigma^{-1} \exp[-(E - E_0)^2/\sigma^2]$$

$$[10] \quad E_0 = E(0) - aT$$

$$[11] \quad \sigma = \sigma(0) + bT$$

$$[12] \quad \mu_h^0 = \mu_{ref}^0 (d_{ref}/d_T)^2(T_{ref}/T)$$

In systems where the ion-like mechanism makes an appreciable contribution it is possible to determine the values of μ_{il}^0 and E_{il} explicitly (17, 39). Although the mechanism is negligible in the present systems, the approximate values $\mu_{il}^0 = 0.1\ cm^2/V\ s$ and $E_{il} = 0.07$ eV were inserted for completeness.

Equations [10]–[12] are adequate as long as localization is the dominating factor governing electron migration (17, 39). They usually break down near the critical region (Figs. 2, 3, and ref. 17). We therefore focus attention on the normal liquids.

The five parameters in eqs. [10]–[12] are not yet separately determinable. To reduce the plasticity of the calculations and facilitate comparison of several systems, all variability was arbitrarily forced in to a, $\sigma(0)$, and b. The degree of success is displayed in Figs. 2 and 3 and Table 3. The constraints on the calculations are such that the only parameter that shows a regular variation is E_0/σ, which increases as μ decreases (Table 3). A larger E_0/σ indicates a deeper trap.

It was suggested earlier (17) that the apparent insensitivity of σ to temperature in *trans*-butene-2 might be due to the localized state being a molecular anion. It is difficult to understand the similarity of behavior in *trans*-butene-2, *n*-pentane, and *n*-hexane (Table 3).

Acknowledgement

We wish to thank the staff of the Radiation Research Center for help with the electronics.

1. P. H. TEWARI and G. R. FREEMAN. J. Chem. Phys. **49**, 4394 (1968).
2. R. M. MINDAY, L. D. SCHMIDT, and H. T. DAVIS. J.Chem. Phys. **50**, 1473 (1969).
3. W. F. SCHMIDT and A. O. ALLEN. J. Chem. Phys. **50**, 5037 (1969).
4. E. E. CONRAD and J. SILVERMAN. J. Chem. Phys. **51**, 450 (1969).
5. W. F. SCHMIDT and A. O. ALLEN. J. Chem. Phys. **52**, 2345 (1970).
6. W. F. SCHMIDT and A. O. ALLEN. J. Chem. Phys. **52**, 4788 (1970).
7. R. M. MINDAY, L. D. SCHMIDT, and H. T. DAVIS. J. Chem. Phys. **54**, 3112 (1971).
8. W. F. SCHMIDT and G. BAKALE. Chem. Phys. Lett. **17**, 617 (1972).
9. P. G. FUOCHI and G. R. FREEMAN. J. Chem. Phys. **56**, 2333 (1972).
10. J.-P. DODELET and G. R. FREEMAN. Can. J. Chem. **50**, 2667 (1972).
11. A. O. ALLEN and R. A. HOLROYD. J. Phys. Chem. **78**, 796 (1974).
12. A. O. ALLEN, T. E. GANGWER, and R. A. HOLROYD. J. Phys. Chem. **79**, 25 (1975).
13. H. T. DAVIS and R. G. BROWN. *In* Advances in chemical physics. Vol. 31. *Edited by* I. Prigogine and S. A. Rice. Wiley, New York. 1975.
14. J. M. L. ENGELS and A. J. M. VAN KIMMENADE. Phys. Lett. **59A**, 43 (1976).
15. J.-P. DODELET and G. R. FREEMAN. J. Chem. Phys. **65**, 3376 (1976).

Can. J. Chem. Downloaded from www.nrcresearchpress.com by 210.87.254.42 on 09/05/12
For personal use only.

16. J.-P. DODELET and G. R. FREEMAN. Can. J. Chem. **55**, 2264 (1977).
17. J.-P. DODELET and G. R. FREEMAN. Can. J. Chem. **55**, 2893 (1977).
18. N. E. CIPOLLINI, R. A. HOLROYD, and M. NISHIKAWA. J. Chem. Phys. **67**, 4636 (1977).
19. I. GYÖRGY and G. R. FREEMAN. Phys. Rev. Submitted.
20. J.-P. DODELET, K. SHINSAKA, U. KORTSCH, and G. R. FREEMAN. J. Chem. Phys. **59**, 2376 (1973).
21. S. S.-S. HUANG and G. R. FREEMAN. J. Chem. Phys. **68**, 1355 (1978).
22. R. W. GALLANT. Physical properties of hydrocarbons. Vols. 1 and 2. Gulf Publishing Co., Houston, TX. 1968.
23. (*a*) J. TIMMERMANS. Physical chemical constants of pure organic compounds. Elsevier Publishing Co., Amsterdam, Vol. 1, 1950; Vol. 2, 1965; (*b*) R. R. DREISBACH. Adv. Chem. Ser. **15**, (1955); **22**, (1959).
24. N. E. HILL, W. E. VAUGHAN, A. H. PRICE, and M. DAVIES. Dielectric properties and molecular behavior. Van Nostrand Reinhold Co., Toronto. 1969. p. 268.
25. LANDOLT-BÖRNSTEIN. Zahlenwerte und Funktionen aus Physik. Chemie. Astronomie. Geophysik und Technik. 6 Auflage, 1 Band, 3 Teil, Springer-Verlag, Berlin. 1951. pp. 509–512.
26. A. I. VOGEL. J. Chem. Soc. 1323 (1938).
27. F. B. PIDDUCK. Proc. London Math. Soc. **15**, 89 (1916).
28. B. DAVYDOV. Phys. Z. Sowjetunion, **8**, 59 (1935); **12**, 269 (1937).
29. J. LEKNER. Phys. Rev. **158**, 130 (1967).
30. M. H. COHEN and J. LEKNER. Phys. Rev. **158**, 305 (1967).
31. E. HAUSMANN and E. P. SLACK. Physics. Van Nostrand Co., New York. 1944. p. 412.
32. W. P. ALLIS. *In* Handbuch der Physik, Vol. 21. *Edited by* S. Flügge. Springer-Verlag, Berlin. 1956. p. 383.
33. J. L. PACK and A. V. PHELPS. Phys. Rev. **121**, 798 (1961).
34. E. W. MCDANIEL. Collision phenomena in ionized gases. Wiley, New York. 1964. Chapts. 3 and 9.
35. H. S. W. MASSEY and C. B. O. MOHR. Proc. R. Soc. London, A**144**, 188 (1934).
36. S. ALTSHULER. Phys. Rev. **107**, 114 (1957).
37. T. L. COTTRELL and I. C. WALKER. Trans. Faraday Soc. **63**, 549 (1967).
38. J.-P. DODELET, K. SHINSAKA, and G. R. FREEMAN. Can. J. Chem. **54**, 744 (1976).
39. J.-P. DODELET, F.-Y. JOU, and G. R. FREEMAN. J. Phys. Chem. **79**, 2876 (1975).
40. T. G. RYAN and G. R. FREEMAN. J. Chem. Phys. In press.

Can. J. Chem. Downloaded from www.nrcresearchpress.com by 210.87.254.42 on 09/05/12
For personal use only.

Phenyl phosphorodichloridate in the synthesis of cyclic phosphate diesters of biological interest

C. L. PENNEY AND B. BELLEAU

Department of Chemistry, McGill University, 801 Sherbrooke Street W., Montreal, P.Q., Canada H3A 2K6

Received April 12, 1978

C. L. PENNEY and B. BELLEAU. Can. J. Chem. **56**, 2396 (1978).

The general usefulness of phenyl phosphorodichloridate (PPDC) in the synthesis of non-nucleoside cyclic phosphates is described. The method is illustrated with several examples including cyclic phosphates incorporating six to nine members. However, the reagent could not be used for the preparation of five-membered cyclic phosphates or 3′,5′-cycloadenylic acid (cAMP) from adenosine. Based on a number of observations, the conclusion was reached that PPDC cannot be used for the synthesis of strained or reactive cyclic phosphates. A convenient synthesis of *cis*- and *trans*-2-hydroxycyclopentanemethanol and a simple, quantitative method of separation of the two isomers is described. A number of cyclic phosphates were tested as substrates and inhibitors for cyclic purine phosphodiesterase and protein kinase.

C. L. PENNEY et B. BELLEAU. Can. J. Chem. **56**, 2396 (1978).

On décrit l'utilité générale des phényl phosphorodichloridates (PPDC) dans la synthèse des phosphates cycliques non-nucléosides. On illustre la méthode grâce à plusieurs exemples incluant des phosphates cycliques incorporant des cycles de six à neuf membres. Toutefois le réactif ne peut pas être utilisé pour la préparation des phosphates cycliques à cinq membres ou de l'acide cycloadénilique-3′,5′ à partir de l'adénosine. En se basant sur un certain nombre d'observations, on a tiré la conclusion que le PPDC ne peut pas être utilisé pour la synthèse de phosphates cycliques tendus ou réactifs. On décrit une synthèse facile des *cis* et *trans* hydroxy-2 cyclopentane-méthanols et une méthode simple et quantitative de séparation des deux isomères. On a effectué des essais sur un certain nombre de phosphates cycliques comme substrats inhibiteurs de la phosphodiestérase purine cyclique et de la kinase protéine.

[Traduit par le journal]

Introduction

The biological importance of cyclic phosphate diesters is best illustrated by cyclic adenosine and guanosine monophosphate (cAMP and cGMP) which are key regulators of cell function. Little is known as yet about the possible role of nonnucleoside cyclic phosphates. The abnormally high enthalpy and free energy of hydrolysis of cAMP and cGMP (1) is mystifying and the role of these high transfer potentials in metabolic regulation is conjectural. This thermochemical behavior has prompted us to synthesize a variety of simple, nonnucleoside cyclic phosphates in order to evaluate the effects of structural and geometrical factors on the heats of hydrolysis of six-membered cyclic phosphates. In this communication we describe synthetic methodologies for relevant cyclic phosphates. The thermodynamics of their hydrolysis will be described separately.

The most general procedure for the synthesis of cyclic phosphates is that of Khorana and co-workers (2, 3) and involves the cyclization of an acyclic monophosphate with dicyclohexyl carbodiimide (DCC). The method is especially useful for small scale preparations but specific experimental conditions are often required in order to avoid major side reactions. Cyclization of an acyclic intermediate to the corresponding cyclic phosphotriester was accomplished with aqueous base (2), conditions under which hydrolytic pathways compete with ring closure. Because of this limitation, potassium *tert*-butoxide in dimethylsulfoxide (DMSO) was used to effect cyclization (4, 5) but this technique is inconvenient on a large scale, lengthy and costly chromatographic separations being necessary.

In principle, the simplest method would entail the direct formation of a cyclic phosphate from a suitable diol through reaction with phosphorous oxychloride. In practice, however, this approach is generally unsuitable (6, 7) although a few successes have been reported as for the special cases of 2,2-dimethyl-1,3-propanediol and 2,2′-dihydroxybiphenyl (8,9). The practical potential of phenyl phosphorodichloridate (PPDC) for the preparation of cyclic phosphate diesters was explored by Baddiley *et al.* (10, 11) who used the reagent to prepare the cyclic phosphates of certain glycosides as well as pantothenic acid. The low yields reported may have discouraged further development of this approach. Only a few superficial studies of the reagent's ability to form six-membered cyclic phosphate phenyl esters were subsequently reported (12–15) and attention was

Can. J. Chem. Downloaded from www.nrcresearchpress.com by 210.87.254.5 on 09/05/12
For personal use only.

Can. J. Chem. Downloaded from www.nrcresearchpress.com by 210.87.254.5 on 09/05/12
For personal use only.

focused mainly on the spectroscopic properties of the products. We felt it appropriate to carry out a systematic investigation of the potential usefulness of this reagent PPDC in cyclic phosphate syntheses. As it turned out, the reagent proved to be most useful and convenient for the large scale preparation of the desired substrates.

Results and Discussion

The relevant cyclic phosphates were prepared according to general Scheme 1. The use of PPDC in this scheme proved to be widely applicable but with limitations. Thus, cyclic triester intermediates were readily obtained in good yields from the following starting diols: 1,3-propanediol, 1,4-butanediol, 1,5-pentanediol, 1,6-hexanediol, 1,3-butanediol, 2-methyl-1,3-propanediol, 2,2-dimethyl-1,3-propanediol, 2-methyl-2-nitro-1,3-propanediol, 2-methoxy-1,3-propanediol, diethylene glycol, *trans*- and *cis*-2-hydroxycyclopentanemethanol.[1] However, the corresponding phosphotriesters of glycerol, ethylene glycol, 1,2-propanediol, adenosine, ethanolamine, 3-amino-*n*-propyl alcohol, and 1,3-diaminopropane could not be obtained using the same techniques.

The PPDC reagent was found generally superior to phosphorous oxychloride which failed to yield cyclic phosphates in all those cases where PPDC also failed. However, whereas phosphorous oxychloride failed to give the cyclic phosphate of 1,3-propanediol under a variety of conditions, PPDC gave the expected cyclic phosphate in 90% yields. On the other hand, both reagents gave high yields of cyclic phosphate with 2,2-dimethyl-1,3-propanediol as substrate. It is likely that the so-called '*gem*-dialkyl effect' (16) intervenes in this facilitation of ring formation. Perhaps for the same reason, 2-methyl-2-nitro-1,3-propanediol behaved similarly (17).

An interesting and useful discriminatory capability of phosphorous oxychloride was its ability to form selectively the cyclic phosphate of *cis*-2-hydroxycyclopentanemethanol but not so with the *trans* isomer (acyclic high molecular weight diesters being presumably formed). This selectivity allowed the ready separation of the *cis*-phosphate starting from a mixture of the *cis*- and *trans*-diols. In sharp contrast, PPDC gave the cyclic phosphates of both geometrical isomers equally well. It appears then that PPDC exhibits an increased tendency to yield cyclic phosphates. This tendency is best illustrated by the fact that even in the presence of a 2.2-fold excess of 1,3-propanediol, the cyclic phosphate was still formed in 90% yield. Even more striking was the ready preferential formation (60% yield) of the nine-membered ring phosphate from 1,6-hexanediol and the eight-membered analogs from 1,5-pentanediol and diethylene glycol. In the case of 1,5-pentanediol, the cyclic phosphate was contaminated to the extent of 15% with acyclic phosphates as ascertained by nmr spectroscopy. No such contaminants were present in the case of the product derived from diethylene glycol. The phenyl triester intermediate from 2-methoxy-1,3-propanediol and PPDC was obtained readily in 66% yield, thus showing that the inductive effect of the methoxy group on the nucleophilicity of the hydroxyl groups has little influence on the cyclization reaction. This observation taken in conjunction with the fact that *trans*-2-hydroxycyclopentanemethanol readily gave the expected cyclic phosphate with PPDC, leads to the conclusion that the reagent's failure to give a cyclic phosphate with adenosine cannot be attributed to an inductive effect of the ether ring oxygen of the ribose moiety.

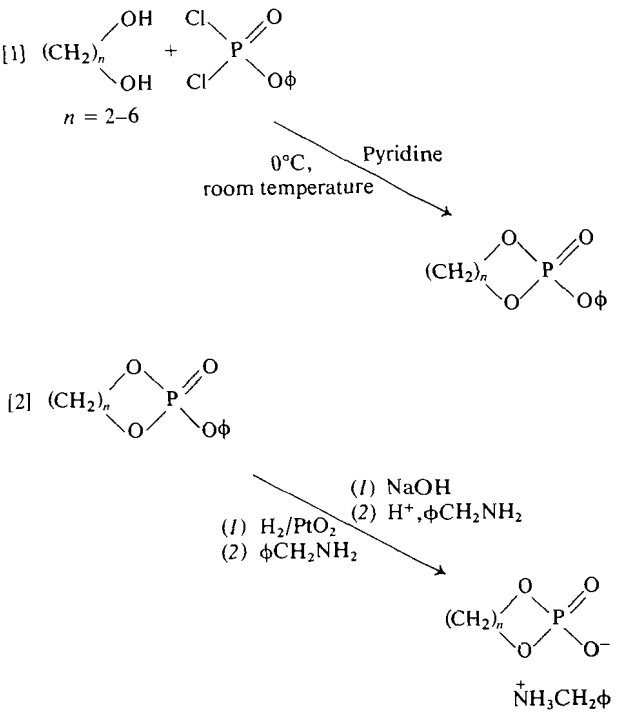

SCHEME 1

Interestingly, the observed tendency of PPDC to form cyclic phosphates did not apply to five-membered rings. Under a variety of conditions, acyclic mono- and bisphosphates accompanied by polymer formation was observed. In addition, phosphorous oxychloride gave only polymers (6). This behavior may be explained on the basis that five-membered

[1]See Experimental for a new convenient synthesis of these substrates and for a simple, quantitative method of isomer separation.

Can. J. Chem. Downloaded from www.nrcresearchpress.com by 210.87.254.5 on 09/05/12
For personal use only.

cyclic phosphates are strained, hence too reactive and unstable to resist decomposition under the experimental conditions for preparation and/or isolation. We have observed in fact that whenever the formation of six-membered ring phosphates (which are more stable) was allowed, polymer formation was difficult to achieve under conditions especially favorable for polymerization. Thus, a mixture of PPDC in 1,3-propanediol as the solvent gave mostly the cyclic phosphate after standing at room temperature for 50 h. Under the same conditions, ethylene glycol gave only polymers over a shorter period of time. It may be that it is the relative stability of the cyclic intermediates that determines polymer formation because they themselves may behave as phosphorylating agents. However, polymer formation is not limited to 1,2-diols as substrates because under harsh conditions (absence of solvent, presence of acid, long reaction times, etc.), 1,5-pentadiol and diethylene glycol also yielded polymers (18, 19) rather than cyclic phosphates as was the case under mild conditions.

The fact that glycerol gave only polymers again suggests that a strained five-membered intermediate leading to polymerization may be initially formed. Should any 1,3-cyclic phosphate ester be formed, we would expect it to be stable and isolatable since the analogous 2-methoxy-1,3-cyclic phosphate could be readily obtained. With amino alcohols or diamines any intermediate cyclic phosphoramidate will behave as a reactive phosphorylating agent (20) which accounts for the observation of exclusive polymer formation in these cases. In fact, the phosphoramidate derived from PPDC and aniline has been used as a phosphorylating agent in the synthesis of phosphotriesters (21).

It is worth noting that the solvent pyridine appeared to have a beneficial effect on cyclic phosphate formation. Thus, the phenyl ester of trimethylene phosphate was obtained in 90% yield in this solvent but the yield dropped to 50% in dioxane containing 2 equiv. of triethylamine. Addition of PPDC to pyridine gave deeply colored solutions, indicating that the reactive species is probably a pyridine complex.

Finally, conversion of the phenyl cyclic phosphate triesters to the cyclic diesters was readily accomplished either by base-catalyzed hydrolysis or hydrogenolysis over platinum. The latter method was preferred for those phenyl triesters carrying electronegative substituents on carbon-2 of the 1,3-diol phosphates because significant ring opening occurred under basic conditions. No useful results were obtained by reacting the phenyl triesters with methanolic ammonia or ammonium hydroxide. However, treatment with tetraethylammonium fluoride in acetonitrile afforded the expected cyclic phosphodiesters in agreement with expectations based on recent observations (22–24). For large scale preparations however, this method was uneconomical and troublesome at the stage of isolation.

The cyclic phosphate diesters were crystallized as their benzylammonium salts rather than cyclohexylammonium salts as is the common practice because their nmr spectra were amenable to much easier interpretation and also allowed ready detection of acyclic phosphate contaminants.

Conclusions

(*a*) Reaction of a 1,3-diol with phosphorous oxychloride will result in cyclic phosphate formation provided the substrate has a favorably constrained geometry and if the substrate has low reactivity (enthalpy of hydrolysis less than -6 kcal/mol as an index for instance). Hence, the usefulness of phosphorous oxychloride for the synthesis of cyclic phosphates is limited. Examples include those noted earlier (substituted 2,2′-biphenyl diols, 2,2-disubstituted-1,3-diols, *cis*-2-hydroxycyclopentanemethanol), *cis*-1,3-cyclohexanediol (25), and xylofuranosyladenine (26). The cyclic phosphate of 1,3-propanediol, if formed, would also be of low reactivity (enthalpy of hydrolysis of trimethylene phosphoric acid is -3.5 kcal/mol (27)) but 1,3-propanediol suffers little conformational constraints relative to the above diols.

(*b*) The same applies to PPDC except that the diol need not be geometrically constrained. Hence, this reagent may be used for the synthesis of cyclic phosphates, including large ring compounds, from unsubstituted alkyl diols. The cyclic phosphate of 1,4-butanediol, like 1,3-propanediol, is of low reactivity (enthalpy of hydrolysis of tetramethylene phosphoric acid is -2.6 kcal/mol (27)).

(*c*) In all those cases where the cyclic phosphate may be expected to have high reactivity (enthalpies of hydrolysis exceeding -6 kcal/mol) PPDC led mostly to decomposition products after work-up (as was the case for instance with ethylene glycol and 1,2-propanediol). This appears to be a special characteristic of PPDC because the analogous ethyl and methyl phosphorodichloridates react with ethylene glycol to give good yields of the expected cyclic triesters (28, 29). The corresponding phenyl cyclic triester can nevertheless be formed under controlled conditions[2] but the product is highly reactive and sensitive to moisture. The enthalpy of hydrolysis of

[2]Private communication from R. Kluger, University of Toronto: ethylene glycol was reacted with PPC using 2,6-lutidine as an acid absorber. The crystalline product was isolated by chromatography and was observed to be highly reactive.

Can. J. Chem. Downloaded from www.nrcresearchpress.com by 210.87.254.5 on 09/05/12
For personal use only.

ethylene phosphate is −6.8 kcal/mol (27) and that of methyl-α-D-glucopyranoside-4,6-cyclic phosphate is −6.3 kcal/mol (30). Hence, the low yield of product upon reaction of the sugar with PPDC (10–20% (10)) may indicate that the cyclic phosphate was readily formed but that only 10–20% of the product survived during work-up. To the best of our knowledge, a successful synthesis of 3′,5′-cyclic phosphate phenyl triesters has not been described using PPDC. The cyclic product would be expected to be most reactive, the enthalpies of hydrolysis for nucleoside 3′,5′-cyclic phosphates being in the range of −10 to −14 kcal/mol (31).

However, the 3′,5′-cyclic phosphate phenyl triester of uridine has been prepared by a *tert*-butoxide-catalyzed cyclization of the appropriate intermediate and was observed to be very moisture sensitive (5). Accordingly, we suggest that PPDC is unsuitable for the preparative synthesis of strained or reactive cyclic phosphates but ideally suited for less reactive ones.

The cyclic phosphate diesters listed in Table 3, as well as trimethylene and tetramethylene phosphoric acid were tested as potential substrates or inhibitors of the mammalian (beef heart) cyclic purine phosphodiesterase and the mammalian (bovine brain) protein kinase. None of these cyclic phosphates exhibited any substrate or inhibitory activities. These enzymes exhibit a strict requirement for a purine base and/or a 2′-hydroxyl function, without which binding on the protein cannot occur. Indeed, most modifications of the purine base of cAMP and cGMP are detrimental to biological activity and the fact that the recognition sites of the proteins can discriminate between adenine and guanine rings further demonstrates the essentiality of the purine base. However, the cyclic phosphates described above were good substrates for the phosphodiesterase from *Aerobacter aerogenes* (27). The results will form the subject of a forthcoming communication.

Experimental

Melting points were determined on a Gallenkamp apparatus and are uncorrected. For tlc, pre-coated silica gel thin-layer sheets (J. T. Baker) with fluorescent indicator were used. Visualization was accomplished with iodine or phosphomolybdate spray (J. T. Baker). For preparative tlc, silica gel from Brinkmann Instruments (Canada) Ltd. was used. Paper chromatography was performed with Whatman No. 1 filter paper, using solvent *A* (7:2:1 isopropyl alcohol – water – ammonium hydroxide). Visualization was accomplished with Hanes–Isherwood spray (32) followed by drying and irradiation with a sunlamp.

Mass spectra were measured on a AEI-MS-902 spectrometer at 70 eV using a direct insertion probe. Infrared spectra were measured on a Perkin Elmer 257 grating infrared spectrophotometer. Nuclear magnetic resonance spectra were recorded on a Varian T-60 spectrometer. Chemical shifts are given in δ values relative to tetramethylsilane. Resonance signals are described using the following format; ^{1}Hmr (solvent), chemical shift, (peak multiplicity, number of protons, and coupling constant (Hz)). Abbreviations: (s), singlet; (d), doublet; (t), triplet; (q), quartet; (m), multiplet; (b), broad. ^{13}C nmr spectra were recorded on a Bruker WH!90FT spectrometer, operating frequency 22.63 MHz.

Elemental analyses (C, H, and N) of cyclic phosphate diesters were performed by Spang Microanalytical Laboratory (Ann Arbor, Michigan). Inorganic phosphate analysis of cyclic phosphate diesters were carried out as previously described (33).

General Synthesis of Cyclic Phenyl Phosphate Triesters

To the appropriate diol (0.11 mol) in 60 ml of anhydrous pyridine (dried 1 week over Linde 4 Å molecular sieves) was added over a 1 h period distilled phenyl phosphorodichloridate (0.10 mol, 15 ml), while maintaining the temperature at ~10°C (ice bath). The mixture was stirred for 20 h at room temperature, the precipitated salts removed by filtration and washed with a little benzene. The combined filtrate and washings were evaporated *in vacuo* (<44°C) and the residue was consecutively washed with 50 ml water, 50 ml saturated $NaHCO_3$, 50 ml water, and finally taken up in benzene or benzene–chloroform (100–350 ml) depending on the solubility of the residue. The solution was stirred for 30 min (with gentle warming, if necessary, to keep the product in solution), dried over sodium sulfate, and evaporated *in vacuo* to give either a crystalline (six-membered triesters) or an oil (larger ring analogs) residue. The phenyl triesters thus prepared gave intense molecular ion peaks characteristic of the cyclic products. The properties of the triester products are summarized in Table 1.

General Preparation of Cyclic Phosphate Diesters

By Hydrolysis

The phenyl phosphate triester (50 mmol) was dissolved in 60 ml dioxane and to this was added 2 *N* NaOH (30 ml). The mixture was allowed to stir at room temperature for 70 h and then extracted with 3 × 50 ml portions of ether and the aqueous phase passed through a column of Dowex-50W-X8 [H^+] resin (25 g, previously washed with three portions of distilled water and with 100 ml of spectrograde methanol) and the column washed with 100 ml of methanol. Appearance of the cyclic phosphoric acid in the effluent was monitored with pH paper. The effluent was brought to pH ~7.5 with benzylamine and the solvent evaporated *in vacuo* to give a residue which was taken up in a minimum amount of warm methanol. Crystallization was induced by the addition of acetone or ether. Recrystallization (several times) was achieved using cold methanol–ether.

By Hydrogenolysis

The phenyl phosphate triester was dissolved in spectrograde methanol or absolute ethanol and the solution shaken in a Parr apparatus over Adams' catalyst (100 mg PtO_2 per gram of triester) under an atmosphere of hydrogen at 50 psi for 15 h. The catalyst was removed, washed with alcohol and the solvent evaporated *in vacuo*. The acidic residue was taken up in a small amount of methanol, the pH of the solution adjusted to ~7.5 with benzylamine, and crystallization induced by the addition of acetone or ether. The product was recrystallized several times from methanol–ether. Properties of the cyclic phosphates are assembled in Tables 2 and 3.

Phosphorylation of 1,2-Diols

A solution of ethylene glycol (0.10 mol, 5.6 ml) in 50 ml cold (0°C) anhydrous pyridine was treated over 1 h with phenyl phosphorodichloridate (0.10 mol). After stirring for 20 h at room temperature, the pyridinium salts were collected and washed with a little benzene. The filtrate and washings were

TABLE 1. Properties of the phenyl phosphate triesters[a]

Phenyl phosphate triester (parent alcohol)	% yield	Melting point (°C)	^{1}Hmr data
1,3-Propanediol	77[b]	73–74	1.6–2.6 (m, 2H)
		(lit. 75)	4.0–4.8 (m, 2H)
		Crystalline	7.3 (s, 5H)
1,4-Butanediol	55	62–64	1.7–2.2 (m, 4H)
		(lit. 61–63)	4.0–4.6 (m, 4H)
		Crystalline	7.3 (s, 5H)
1,5-Pentanediol	50	Viscous oil	1.2–2.0 (m, 6H)
		85% purity[c]	3.9–4.4 (q, 4H)
			7.3 (s, 5H)
			3.4–3.7 (t, 2H)[c]
1,6-Hexanediol	60	Viscous oil[d]	1.2–2.2 (m, 8H)
			3.9–4.4 (q, 4H)
			7.3 (s, 5H)
Diethylene glycol	50	Viscous oil	3.4–3.8 (t, 4H)
			4.0–4.5 (m, 4H)
			7.2 (s, 5H)
1,3-Butanediol	65	79–80	1.5 (q, 3H)
		Crystalline	1.7–2.3 (m, 2H)
			4.2–5.2 (m, 5H)
			7.3 (s, 5H)
2-Methyl-1,3-propanediol	66	85–87	1.0 (q, 3H)
		Crystalline	1.8–2.2 (b, 1H)
			3.8–4.8 (m, 4H)
			7.3 (s, 5H)
2,2-Dimethyl-1,3-propanediol	62	134–136	1.0 (s, 3H)
		(lit. 133–135)	1.4 (s, 3H)
		Crystalline	3.7–4.6 (m, 4H)
			7.3 (s, 5H)
2-Methyl-2-nitro-1,3-propanediol	47	135–137	1.6 (s, 3H)
		Crystalline	4.8–5.3 (m, 4H)
			7.2 (s, 5H)
2-Methoxy-1,3-propanediol	66	105–108	3.5 (s, 4H)
		Crystalline	4.2–4.8 (m, 4H)
			7.2 (s, 5H)
trans-2-Hydroxycyclopentanemethanol	78	83–85	1.3–2.6 (m, 7H)
		Crystalline	3.8–4.7 (m, 3H)
			7.1 (d, 5H)
2:1 *trans*- and *cis*-2-Hydroxycyclopentanemethanol	71	Undefined mp	1.3–2.6 (m, 7H)
			3.8–5.0 (m, 3H)
			7.1 (d, 5H)

[a]All ^{1}Hmr are recorded in $CDCl_3$ and $CDCl_3$–D_2O. Chemical shifts are given in δ values relative to tetramethylsilane (see Experimental).
[b]90% yield when 0.22 mol (19 ml) 1,3-propanediol in 50 ml anhydrous pyridine was treated with 0.10 mol (15 ml) phenylphosphorodichloridate, with the reaction at 0°C, for 1 h.
[c]Acyclic impurity identified by mass spectrometry and ^{1}Hmr. Triplet at 3.4–3.7 indicative of primary hydroxymethyl function. *m/e* = 395. Mol. wt. (cyclic phosphate triester) = 242.
[d]Mol. wt. (cyclic phosphate triester) = 256; *m/e* = 256.

evaporated *in vacuo*, the residue taken up in 100 ml of water, the solution concentrated *in vacuo*, and 150 ml of benzene added. The benzene extract was dried, the salts washed with methanol, and the benzene filtrate and washings were evaporated separately *in vacuo*. The benzene solution gave 2.7 g of a dark brown oil which proved to be the bisphosphorylated ethylene glycol (4 methylene protons to 10 phenyl protons in the ^{1}Hmr spectrum). The methanol solution gave 4.3 g of a light brown oil which proved to be hydroxyethyl phosphorochloridate (four methylene protons to five phenyl protons to one hydroxyl proton in the ^{1}Hmr spectrum): ^{1}Hmr ($CDCl_3$ and $CDCl_3$–D_2O): (*i*) 4.3 (s, 4H), 7.2 (s, 10H); (*ii*) 4.2 (s, 4H), 5.6 (s, 1H), 7.1 (s, 5H).

Application of the above procedure to 1,2-propanediol (0.10 mol, 7.3 ml) again gave two fractions (5 g each) consisting of acyclic mono- and diphosphorylated diol.

The absence of pyridine as solvent, in the above reaction, led to a clear glass.

Phosphorylation of Glycerol

Using pyridine as the solvent and applying the protocol for ethylene glycol, glycerol gave an orange-colored glass insoluble in organic solvents but soluble in hot water. In dry dioxane containing 2 equiv. pyridine, a glassy polymer was also obtained.

Phosphorylation of Adenosine

A number of modifications of the general procedure for cyclic phosphate formation were applied. Included was a known procedure for the reaction between phenylphosphorodichloridate and a nucleoside (benzylidene uridine (34)). Thus, adenosine (20 mmol, 5.35 g dried *in vacuo* over P_2O_5) was dissolved in 150 ml dry pyridine and while stirring, the phenyl phosphorodichloridate (30 mmol, 4.5 ml) was added over a 10 min period. The following experimental variables were examined: (*a*) temperature of addition, 0°C; time of reaction, 20 or 90 h at room temperature; (*b*) prior addition of KCl (1 g), addition of reagent at room temperature, heating

Can. J. Chem. Downloaded from www.nrcresearchpress.com by 210.87.254.5 on 09/05/12
For personal use only.

Can. J. Chem. Downloaded from www.nrcresearchpress.com by 210.87.254.5 on 09/05/12
For personal use only.

TABLE 2. Properties of the phosphate diesters[a]

Cyclic phosphate diester (parent alcohol)	% yield	Melting point (°C)	^{1}Hmr data
1,3-Propanediol[b]	65	102–104 (lit. 102–103) Crystalline	1.7–2.2 (m, 2H) 4.1–4.5 (m, 4H)
1,4-Butanediol[c,e]	76	127–129 (lit. 128–129) Crystalline	1.6–2.0 (m, 4H) 3.7–4.3 (m, 4H)
1,6 Hexanediol[d,e]	60	Brown gum	1.2–1.8 (m, 8H) 3.5–3.9 (m, 4H) 4.0 (s, 2H) 7.3 (s, 5H)
1,3-Butanediol	64	160–161 Crystalline	1.1 (q, 3H) 1.1–1.7 (m, 2H) 4.7–5.3 (m, 3H) 4.0 (s, 2H) 7.3 (s, 5H)
2-Methyl-1,3-propanedio	61	158–160 Crystalline	0.7 (d, 3H, J = 7 Hz) 1.5–2.1 (m, 1H) 3.5–4.1 (m, 4H) 4.0 (s, 2H) 7.3 (s, 5H)
2,2-Dimethyl-1,3-propanediol[e]	79	146–148 Crystalline	3.3 (s, 4H) 4.0–4.4 (m, 4H) 4.1 (s, 2H) 7.4 (s, 5H)
trans-2-Hydroxycyclopentanemethanol	60	153–155 Crystalline	1.4–2.5 (m, 7H) 4.3 (s, 2H) 7.5 (s, 5H)
2:1 *trans*- and *cis*-2-Hydroxycyclopentanemethanol[e]	84	95–98 Crystalline	^{1}H and ^{13}C nmr as expected for *trans–cis* mixture

[a]All ^{1}Hmr were recorded in D_2O. Chemical shifts are given in δ values relative to tetramethylsilane (see Experimental). All compounds are benzylammonium salts, unless otherwise indicated.
[b]Isolated and purified as the free phosphoric acid as both the benzylammonium and cyclohexylammonium salts proved quite hygroscopic. Recrystallized from boiling THF and acetonitrile–ether (2).
[c]Isolated and purified as the free phosphoric acid. Recrystallized from boiling THF and benzene (30). The literature synthesis of this phosphoric acid involved reaction with DCC and barium salt intermediates which becomes especially tedious for large scale preparations.
[d]Could not be crystallized from a variety of solvents as the benzylammonium, cyclohexylammonium, sodium, or barium salts, or as the free acid.
[e]Phenyl group removed by hydrogenolysis in addition to hydrolysis.

TABLE 3. Analytical data for new six-membered cyclic phosphates[a]

Cyclic phosphate diester (parent alcohol)	R_f		Calculated			Observed		
	Paper	Thin layer	C	H	N	C	H	N
trans-2-Hydroxycyclopentanemethanol	0.68	0.70	54.73	7.07	4.91	54.77	7.01	4.86
cis-2-Hydroxycyclopentanemethanol[b]	0.68	0.70	54.73	7.07	4.91	54.80	7.03	4.99
1,3-Butanediol	0.60	0.67	50.96	7.00	5.40	50.96	6.98	5.48
2-Methyl-1,3-propanediol	0.63	0.67	50.96	7.00	5.40	51.03	6.91	5.55
2,2-Dimethyl-1,3-propanediol	0.68	0.75	52.74	7.38	5.13	52.56	7.34	5.19
2-Methoxy-1,3-propanediol	0.47	—	48.00	6.59	5.09	48.03	6.56	5.07

[a]All are benzylammonium salts. Paper chromatograms were developed in 7:2:1 isopropyl alcohol – water – ammonium hydroxide. Thin-layer chromatograms were developed in methanol (see Experimental). All compounds were analyzed for inorganic phosphate, as described (33), and found to contain less than 0.1% free phosphate contaminant.
[b]Synthesized from the reaction of the *trans–cis*-diol with $POCl_3$ (see Experimental).

(reflux) for 6 h then 20 h at room temperature or 90 h at 55°C; (*c*) see ref. 4. With method: (*a*) little phosphorylation was obtained; (*b*) base-catalyzed hydrolysis of the crude product gave phenyl phosphate (identified by ^{1}H and ^{13}C nmr); (*c*) base-catalyzed hydrolysis gave adenosine phenyl phosphate (identification by ^{13}C nmr). No evidence (paper chromatography) for the formation of cyclic phosphate was obtained.

Triester to Diester Conversion

The possibility that the phenyl function could be removed by other methods than hydrolysis and hydrogenolysis was investigated. The attempted procedures involved formation of active intermediates, phosphorofluoridates, acetyl phosphate triester, phosphoroamidates; 10 mmol (2.42 g) of the phenyl phosphate triester of 2,2-dimethyl-1,3-propanediol was used

Can. J. Chem. Downloaded from www.nrcresearchpress.com by 210.87.254.5 on 09/05/12
For personal use only.

as starting material: (*a*) tetraethylammonium fluoride (2 equiv.) in dry acetonitrile led to a 50% removal of the phenyl group after 3 days at room temperature; (*b*) ammonium hydroxide (3.0 ml) in dioxane (30 ml) and water (27 ml) gave back starting material after three days at room temperature. Anhydrous ammonia in dioxane or benzylammonium acetate in acetonitrile at 50°C gave similar results.

cis-*2-Hydroxycyclopentanemethanol Cyclic Phosphate*

To a cold (0°C) solution of 2-hydroxycyclopentanemethanol (a 2:1 *cis–trans* mixture; see below) (50 mmol or 5.8 g) in 100 ml anhydrous pyridine, was added phosphorous oxychloride (55 mmol or 5 ml). After stirring at 0°C for a few minutes and 20 h at room temperature, water (1.5 ml, 83 mmol) was added and stirring continued for 15 h. The pyridinium salts were collected and washed with a little benzene. The filtrate and washings were evaporated *in vacuo* and the residue dissolved in 10 ml of water. The solution was passed through a Dowex-50W-X8 [H^+] column (50 g resin) that was previously washed with distilled water and methanol. The column was washed with 150 ml of methanol and the effluent evaporated *in vacuo*, the dark residue diluted with 100 ml methanol and just enough water to dissolve such a quantity of NaOH that brought the pH to ~7. The solvent was evaporated and to the residue was added 100 ml absolute ethanol. The suspension was stirred a few minutes, the sodium chloride collected, and the filtrate evaporated to give 3.6 g of residue which was dissolved in a little methanol. The solution was passed through 30 g of Dowex resin (as above) and the pH of the methanolic effluent adjusted to ~7 with benzylamine. The solvent was evaporated and crystallization induced by the addition of ether; yield, 1.9 g of crude white product (38% yield) which after two recrystallizations from methanol–ether gave 1.3 g of white lustrous plates, mp 170–172°C; ^{1}Hmr (D_2O): 1.3–2.0 (m, 7H), 3.7–4.3 (m, 3H), 3.9 (s, 2H), 7.4 (s, 5H). See Table 3 for analytical data.

Commercial Diols

Ethylene glycol, 1,2- and 1,3-propanediol, 1,3- and 1,4-butanediol, 1,5-pentanediol, 1,6-hexanediol, diethylene glycol, 2,2-dimethyl-1,3-propanediol, 2-methyl-2-nitro-1,3-propanediol, and glycerol were commercially available. Other 1,3-diols were synthesized as described below.

2-Methyl-1,3-propanediol

Reduction of diethyl methyl malonate by $LiAlH_4$ in dry ether was carried out according to the literature (35). However, the following modification was applied for decomposition and work-up: the cooled reduction mixture initially containing 0.5 mol (19 g) of $LiAlH_4$ was carefully treated sequentially with 20 ml water, 20 ml 17% aqueous NaOH, and 60 ml water. After stirring for a few minutes, the solids were collected and leached for 1 h with 250 ml ether. The combined and dried filtrates were evaporated *in vacuo* to give 12.5 g of light yellow diol (63% yield). Its ir spectrum showed no carbonyl absorption. The diol was distilled *in vacuo* to give 9.9 g of colorless oil, bp 67–69°C/0.6 Torr; ^{1}Hmr (D_2O): 0.8 (d, 3H, J = 6 Hz), 1.7 (m, 1H), 3.4 (d, 4H, J = 6 Hz).

2-Methoxy-1,3-propanediol

1,3-Benzylidene glycerol was prepared according to the literature (36). To a suspension of sodium hydride (0.50 mol, 25 g) in 500 ml tetrahydrofuran (THF) was added under nitrogen 1,3-benzylidene glycerol (0.40 mol, 72 g) in 150 ml THF. After completion of the addition (45 min), stirring was continued for 45 min. To the cooled mixture (ice) was added methyl iodide (0.60 mol or 38 ml) over a 30 min period. The suspension was stirred for 15 h under nitrogen at room temperature, the solids removed by filtration, and the filtrate evaporated *in vacuo*. The residue was taken up in 500 ml of warm benzene, the precipitated sodium iodide removed by filtration, and the solvent evaporated to give 58 g of an oil which upon standing solidified to long brownish needles (75% yield), mp 50–52°C (lit. (36) mp 52°C); ^{1}Hmr ($CDCl_3$): 3.1 (s, 1H), 3.4 (s, 3H), 4.1 (q, 4H), 5.1 (s, 1H), 7.3 (m, 5H).

The product (0.30 mol, 58 g) was dissolved in a mixture of 200 ml tetrahydrofuran and 100 ml water, and 20 g of Dowex-50W-X8) (H^+) resin, previously washed with distilled water, was added. The mixture was heated under reflux for 2 h, the resin filtered off, washed with water, and the filtrate concentrated to about 250 ml *in vacuo* and extracted with 4 × 100 ml of ether. The aqueous phase was evaporated to give 23.8 g of a yellow oil (75% crude yield) which was distilled to give 19.8 g of an oil, bp 80–83°C/1 Torr; ^{1}Hmr ($CDCl_3$): 3.4 (s, 3H), 3.6 (d, 5H), 4.1 (s, 2H).

trans-*2-Hydroxycyclopentanemethanol*

Cyclopentene (0.74 mol, 50 g), paraformaldehyde (24 g), and glacial acetic acid (150 ml) were mixed and the mixture cooled to 0°C. Concentrated sulfuric acid (11.3 ml) was then added dropwise over a period of 1 h. The mixture was stirred at room temperature for 18 h and poured onto a mixture of ice (450 g) and anhydrous sodium carbonate (150 g). After neutralization was complete, the mixture was repeatedly extracted with 150 ml portions of ether and the organic layers combined, dried, and evaporated to give 90 ml of a dark liquid. This procedure was repeated 11 times and the crude products combined to give a total of 1 ℓ of mixed acetates. The crude product was distilled through a Vigreux column then four times through a Widmer column, and finally through a spinning band column (Nester/Faust) to give 80 g of the *trans*-diacetate of 2-hydroxycyclopentanemethanol and 8 g of a 1:1 mixture of *cis*- and *trans*-diacetates as judged by ^{1}Hmr; R_f (tlc) 0.74 (1:1 cyclohexane ethyl acetate) with a trace contaminant with R_f 0.87; ^{1}Hmr (neat): 1.6–2.4 (m, 7H), 2.1 (d, 6H), 4.2 (d, 2H, J = 5 Hz), 5.1 (q, 1H).

The *trans*-diacetate (0.38 mol, 75 g) was dissolved in 1 ℓ of reagent grade methanol. To this was added 50 g of Dowex-50W-X8 [H^+] resin (previously washed three times with methanol) and the mixture heated under reflux for 70 h. The resin was filtered off, washed with methanol, and the filtrate evaporated. The ir spectrum indicated the presence of a trace of diacetate. This product was re-treated as above with 25 g of resin in 500 ml methanol. After 15 h of heating, the product was isolated as above to yield 40 g (91%) of light yellow oil which after distillation yielded 30 g of colorless oil; bp 80–86°C/0.3 Torr; ^{1}Hmr ($CDCl_3$): 1.0–2.3 (m, 7H); ^{13}C nmr (see Table 4) indicated the presence of approximately 5% of contaminating *cis*-diol.

2-Hydroxymethyl Cyclopentanone

(*A*) 2-Hydroxymethylcyclopentanone ethylene ketal was prepared according to the literature (37), except that work-up was as described above for 2-methyl-1,3-propane diol. The distilled ketal (0.20 mol, 31.6 g) was dissolved in 175 ml each of THF and water and after addition of 18 g Dowex-50W-X8 [H^+] resin previously washed with distilled water, the mixture was stirred for 20 h at room temperature. The resin was collected, washed with a little water, and the filtrate and washings concentrated *in vacuo* to one-third its volume, then mixed with 200 ml of saturated saline followed by extraction with 8 × 100 ml ether. The combined extracts were dried and evaporated to give 13.0 g of light yellow oil. The aqueous fraction was concentrated *in vacuo* to approximately 100 ml, extracted with 3 × 100 ml ether, and after drying and evaporation of the ether gave an additional 3.0 g of product. Distillation gave 13.7 g of oil; bp 72–74°C/0.3 Torr (60% yield); ir

TABLE 4. ^{13}C chemical shifts of *trans*- and *cis*-2-hydroxycyclopentanemethanol and their cyclic phosphate diesters (benzylammonium salts)[a]

Diol assignment	*trans*-Diol	*cis*-Diol	*trans*-Phosphate	*cis*-Phosphate
$(CH_2)_3$	22.9	22.4	19.8 (s)	22.5 (s)
	27.8	26.6	21.7 (s)	25.7 (s)
	34.9	35.2	29.8 (d, J = 8 Hz)	34.5 (d, J = 9 Hz)
CH	50.4	47.7	43.8 (d, J = 7 Hz)	41.0 (d, J = 5 Hz)
CH_2OH	64.9	62.6	43.8 (s)	44.0 (s)
CHOH	76.4	74.5	71.8 (d, J = 6 Hz)	67.7 (d, J = 4 Hz)
			83.7 (d, J = 5 Hz)	83.3 (d, J = 6 Hz)
			129.7 (s)	129.7 (s)
			130.1 (s)	130.1 (s)

[a]All spectra were recorded in D_2O. Chemical shifts are given in ppm relative to tetramethylsilane. Format for the resonance signals is the same as for ^{1}Hmr (see Experimental). Assignment of diol primary carbons was based on partially coupled spectra.

(carbonyl), 1720 cm^{-1}; ^{1}Hmr ($CDCl_3$): 1.6–2.6 (m, 7H), 3.7 (d, 2H), 3.9 (s, 1H). Other procedures for the removal of the ketal group, using tartaric and hydrochloric acid were reported to give similar results (37).

(*B*) Aldol condensation method: A modification of the method of Gault *et al.* (38) improved the yield significantly. Thus, cyclopentanone (3 mol, 265 ml) was cooled to 0°C and treated over a period of 1 h with a mixture of 20 ml water, anhydrous K_2CO_3 (2.5 g), and 36–38% aqueous formaldehyde (2 mol, 180 ml). The yellow solution was stirred for 30 min at 4°C and 15 min at room temperature and 50 ml of 0.5 *N* cold aqueous HCl added (final pH ~6). The solution was then saturated with sodium chloride and extracted with 5 × 100 ml portions of ether. The combined extracts were dried after the addition of 100 ml of methyl acetate. The solvent was evaporated *in vacuo* and the residue distilled *in vacuo* to give a small amount of cyclopentanone followed by 38.4 g of light yellow oil, bp 82–88°C/0.7 Torr (17% yield). The spectral properties were identical to the material obtained above.

cis- *and* trans-*2-Hydroxycyclopentanemethanol*

2-Hydroxymethylcyclopentanone (0.175 mol, 20.1 g) was dissolved in 250 ml of absolute ethanol and the mixture hydrogenated over Adams' catalyst (PtO_2, 1 g) in a Parr apparatus under 50 lb of hydrogen. After 24 h, the catalyst was filtered off and the solvent removed *in vacuo* to give 19.4 g of lightly colored oil containing only a trace of ketone as ascertained by ir (96% yield). Distillation gave 14.6 g of clear, viscous oil, bp 101–105°C/1 Torr. No carbonyl absorption detectable by ir. The ^{13}C nmr spectrum indicated the ratio of *trans* to *cis* isomer to be 2:1; see Table 4 for spectra of the pure isomers.

Separation of trans–cis *Isomers*

Separation was readily accomplished by selective acetonide formation (common fractionation techniques proved unworkable for preparative purposes). The mixture of isomers (39 mmol, 4.5 g) was dissolved in 100 ml of dry acetone and to this was added freshly prepared, powdered anhydrous cupric sulfate (4.5 g). After stirring at room temperature for 22 h, the solids were collected, washed with acetone, and the combined filtrate and washings evaporated *in vacuo* to give 4.3 g of a light yellow oil, whose ^{1}Hmr spectrum indicated that the *cis* isomer had been quantitatively converted to the corresponding acetonide. Distillation gave 2.3 g of acetonide, bp 26–28°C/1 Torr followed by 1.7 g of the *trans*-diol, bp 96–99°C/1 Torr (58% yield). This latter fraction was identical in every respect with the *trans*-diol obtained from cyclopentene as described above. The *cis*-diol acetonide (2.3 mmol, 240 mg) was dissolved in a mixture of 10 ml THF and 10 ml water and 1.5 g of Dowex-50W-X8 [H^+] resin, previously washed with distilled water was added. After stirring for 44 h at room temperature, the resin was collected and washed with a little water. The filtrate and washings were evaporated *in vacuo* to give 220 mg of the pure *cis*-diol as a light oil (82% yield); ^{1}Hmr (D_2O): 1.3–2.3 (m, 7H), 3.6 (q, 2H), 4.2 (b, 1H).

Biological Testing

Cyclic Purine Phosphodiesterase Assay

The assay mixture (final volume, 1.0 ml) consisted of (*a*) 200 µl substrate, 0.1 µ*M* cAMP or 2.0 µ*M* of test substrate; (*b*) 500 µl buffer (50 m*M* Tris-Cl, pH 7.8); (*c*) 50 µl $MgCl_2$ (20 m*M*); (*d*) 50 µl water or 0.5 µ*M* inhibitor; (*e*) 50 µl beef heart phosphodiesterase solution. The stock enzyme solution was prepared by dissolving 50 mg of enzyme (Sigma) to 10 ml of distilled water. The assay mixture was incubated in at 30°C for 20 min and then 50 µl of alkaline phosphatase solution added (*E. coli*, Type III-S, Sigma Chemical Co.; stock solution prepared by adding 11 mg of enzyme to 10 ml of water) and the incubation continued for another 40 min. The reaction was terminated by the addition of 100 µl of cold 1.25 *N* HCl and a 200 µl aliquot of the solution withdrawn for phosphate analysis (34). All analyses were performed in duplicate. Small quantities of the corresponding acyclic phosphate monoesters of the test substrates (unpublished results) and 5′-AMP were tested and observed to be substrates for alkaline phosphatase as expected.

Protein Kinase

The assay was performed as described in the literature (39).

Acknowledgements

This work was generously supported by the National Research Council of Canada. The collaboration of Dr. Francis Schuber, Université Louis Pasteur, in the initial phases of this work is gratefully acknowledged. We are thankful to Professor P. Greengard and Dr. T. Ueda, Yale University for the protein kinase results and to Dr. T. H. Chan and Miss M. DiStefano for the tetraethylammonium fluoride results.

1. P. GREENGARD, S. A. RUDOLPH, and J. M. STURTEVANT. J. Biol. Chem. **244**, 4798 (1969).
2. H. G. KHORANA, G. M. TENER, and J. G. MOFFATT. J. Am. Chem. Soc. **79**, 430 (1957).

Can. J. Chem. Downloaded from www.nrcresearchpress.com by 210.87.254.5 on 09/05/12
For personal use only.

3. M. SMITH, G. I. DRUMMOND, and H. G. KHORANA. J. Am. Chem. Soc. **83**, 698 (1961).
4. R. K. BORDEN and J. SMITH. J. Org. Chem. **31**, 3247 (1966).
5. J. H. VAN BOOM, P. M. J. BURGERS, P. VAN DEURSEN, and C. B. REESE. Chem. Commun. 618 (1974).
6. R. S. EDMUNDSON. Chem. Ind. (London), 1828 (1962).
7. M. YOSHIKAWA, T. KATO, and T. TAKENISHI. Tetrahedron Lett. **50**, 5065 (1967).
8. R. I. MCCONNELL and H. W. COOVER. J. Org. Chem. **24**, 630 (1959).
9. S. VAN DER MEER and H. POUWELS. J. Med. Chem. **12**, 534 (1969).
10. J. BADDILEY, J. G. BUCHANAN, and L. SZABO. J. Chem. Soc. 3826 (1954).
11. J. BADDILEY and E. M. THAIN. J. Chem. Soc. 3421 (1951).
12. A. M. MESTON. J. Chem. Soc. 6059 (1963).
13. J. P. MAJORAI, A. MUNOZ, and J. NAVECH. C.R. Acad. Sci. Ser. C, **266**, 235 (1968).
14. L. D. HALL and R. B. MALCOLM. Chem. Ind. (London), 92 (1968).
15. L. D. HALL and R. B. MALCOLM. Can. J. Chem. **50**, 2092 (1972); **50**, 2102 (1972).
16. S. MILSTIEN and L. A. COHEN. J. Am. Chem. Soc. **94**, 9158 (1972).
17. J. H. BILLMAN, J. L. MEISENHEIMER, and R. F. MAY. J. Med. Chem. **9**, 772 (1966).
18. U. D. MAIBORODA and L. A. DATSKEVICH. S. Vysokomol. **6**, 1907 (1964).
19. H. W. COOVER and R. L. MCCONNELL. U.S. Patent No. 2,952,666 (September, 1960); Chem. Abstr. **55**, 3086f (1961).
20. D. M. BROWN. Adv. Inorg. Chem. **3**, 75 (1963).
21. W. S. ZIELINSKI and Z. LESNIKOWSKI. Synthesis, **3**, 185 (1976).
22. K. ITAKURA, N. KATAGIRI, C. P. BAHL, R. H. WIGHTMAN, and S. A. NARANG. J. Am. Chem. Soc. **97**, 7327 (1975).
23. K. K. OGILVIE, S. L. BEAUCAGE, and D. W. ENTWISTLE. Tetrahedron Lett. **16**, 1255 (1976).
24. K. K. OGILVIE and S. L. BEAUCAGE. Chem. Commun. 443 (1976).
25. D. M. BROWN and H. M. HIGSON. J. Chem. Soc. Part I, 2034 (1957).
26. M. HUBERT and L. GOODMAN. Chem. Commun. 740 (1969).
27. J. M. STURTEVANT, J. A. GERLT, and F. H. WESTHEIMER. J. Am. Chem. Soc. **95**, 8168 (1973).
28. J. P. VIVES, A. MUNOZ, J. NAVECH, and F. MATHIS. Bull. Soc. Chim. Fr. 2544 (1965).
29. R. KLUGER, F. COVITZ, E. DENNIS, G. D. WILLIAMS, and F. H. WESTHEIMER. J. Am. Chem. Soc. **91**, 6066 (1969).
30. J. A. GERLT, F. H. WESTHEIMER, and J. M. STURTEVANT. J. Biol. Chem. **250**, 5059 (1975).
31. S. A. RUDOLPH, E. M. JOHNSON, and P. GREENGARD. J. Biol. Chem. **246**, 1271 (1971).
32. C. S. HANES and F. A. ISHERWOOD. Nature, **164**, 1107 (1949).
33. C. L. PENNEY. Anal. Biochem. **75**, 201 (1976).
34. J. M. GULLAND and H. SMITH. J. Chem. Soc. 1532 (1948).
35. W. J. BAILEY, M. E. HERMES, and W. A. KLEIN. J. Org. Chem. **28**, 1724 (1963).
36. H. S. HILL, M. S. WHELEN, and H. HIBBERT. J. Am. Chem. Soc. **50**, 2235 (1928).
37. T. TAKAHASHI, A. KATO, S. MATSUOKA, and Z. YAKUGAKU. Chem. Abstr. **79**, 1087 (1959).
38. H. GAULT and J. SKODA. Bull. Soc. Chim. Fr. 316 (1946).
39. T. UEDA, I. UNO, and P. GREENGARD. J. Biol. Chem. **252**, 5155 (1977).

Can. J. Chem. Downloaded from www.nrcresearchpress.com by 210.87.254.5 on 09/05/12
For personal use only.

ESCA studies of the uracil base. The effect of methylation, thionation, and ionization on charge distribution

JAMES PEELING,[1] FRANK E. HRUSKA, DAVID M. MCKINNON, AND MOHENDER S. CHAUHAN

Chemistry Department, University of Manitoba, Winnipeg, Man., Canada R3T 2N2

AND

N. STEWART MCINTYRE

Analytical Science Branch, Whiteshell Nuclear Research Establishment, Pinawa, Man., Canada R0E 1L0

Received November 30, 1977

JAMES PEELING, FRANK E. HRUSKA, DAVID M. MCKINNON, MOHENDER S. CHAUHAN, and N. STEWART MCINTYRE. Can. J. Chem. **56**, 2405 (1978).

ESCA core line spectra have been obtained for uracil, the thiouracils, and some 1-methyl and 3-methyl analogues. In addition, anions of the mono methyl derivatives have been prepared and studied. Core line binding energy shifts for all solid compounds, ionic and neutral, are found to correlate reasonably with CNDO/2 charge distributions calculated for the free molecules. The correlation line for ionic molecules is offset from that for neutrals by a constant factor ascribed to an intermolecular potential term. Specific effects of methylation, thionation, and ionization on the charge distribution are described. Methylation at either nitrogen leads to electron release from the nitrogen into the ring. Thionation results in a decrease in the charge at the site of thionation, while the electron density at adjacent atoms increases. The alterations in charge density are somewhat different for neutral and ionic compounds. Upon ionization of either N(1) or N(3) sites, much of the residual charge is located on the keto oxygens. The presence and position of the thionated carbon during ionization mainly affects the change in electron density at the C(6) position.

JAMES PEELING, FRANK E. HRUSKA, DAVID M. MCKINNON, MOHENDER S. CHAUHAN et N. STEWART MCINTYRE. Can. J. Chem. **56**, 2405 (1978).

On a obtenu les spectres ESCA des électrons internes de l'uracile et de thiouracile et de quelques analogues méthylés en 1 ou en 3. De plus on a préparé et étudié les anions de dérivés monométhylés. Il y a un déplacement chimique des énergies d'ionization des électrons internes de tous les composés solides, ioniques et neutres, et on a trouvé qu'il existe une corrélation raisonnable avec les distributions de charge calculées par la méthode CNDO/2 pour les molécules libres. La ligne de corrélation pour les molécules ioniques est déplacée par rapport à celle des composés neutres par un facteur constant attribué à un terme de potentiel intermoléculaire. Les effets spécifiques de la méthylation, de la thionation et de l'ionisation sur la distribution de charge sont décrits. La méthylation au niveau de l'un ou l'autre des azotes conduit à une mise en disposition des électrons de l'azote vers le cycle. La thionation conduit à une augmentation de la charge au nive au du site de la thionation alors que la densité électronique au niveau des atomes adjacents augmente. Les modifications de la densité de charge sont légèrement différentes pour les composés neutres ou ioniques. L'ionisation des sites soit N(1) ou N(3) conduit à une charge résiduelle située au niveau des oxygènes cétoniques. Lors de l'ionisation la présence et la position d'un carbone thionaté affecte principalement le changement dans la densité électronique au niveau de la position C(6).

[Traduit par le journal]

Introduction

Sulfur-substituted pyrimidine bases are minor constituents of *t*RNA molecules. For example, 4-thiouridine (1) and 2-thiocytidine (2) are thionucleosides identified in *E coli*. Why such modifications to the normal bases are required is not understood, but undoubtedly the influence of sulfur substitution on the electronic properties of the bases is an important factor. This influence on electronic structure is manifested particularly well by the increases in acidity of the imino protons of the bases, the first pK_a values, being, for example, 9.5 and 8.0 (25°C) for uracil and 4-thiouracil, respectively (3). Consequently, at physiological pH, the thio bases are ionized to a greater extent than the corresponding oxo derivatives.

It seems, therefore, that an understanding of the electronic properties of the neutral, as well as the anionic, forms of sulfur-substituted uracils would provide insight into their biological function. One technique, which can provide information on the

[1]Present address: University of Petroleum and Minerals, Dhahran, Kingdom of Saudi Arabia.

Can. J. Chem. Downloaded from www.nrcresearchpress.com by 210.87.254.5 on 09/05/12
For personal use only.

Can. J. Chem. Downloaded from www.nrcresearchpress.com by 210.87.254.5 on 09/05/12
For personal use only.

electronic structures of materials, is X-ray photoelectron spectroscopy (XPS or ESCA). This method has recently been used to study several purine and pyrimidine bases and a number of their modified analogues (4). It was shown that changes originating in structural modifications could, for the pyrimidines, be analysed quantitatively, but spectral resolution problems presented some difficulties in the more complex purine bases.

In this paper the core electron spectra of uracil, 2-thio, 4-thio, and 2,4-dithiouracil, all their 1-methyl analogues, and some 3-methyl analogues are described. In order to study the effects of ionization on the electron distributions, the sodium salts of the methylated compounds have been prepared, and their ESCA spectra obtained. The measured binding energies are used, along with the results of CNDO/2 (5) molecular orbital calculations, to examine the effect of sulfur substitution, methylation, and ionization on the charge distributions in these bases.[2]

Experimental

Commercial samples of uracil (Eastman Organic Chemicals), 2-thiouracil, 2,4-dithiouracil (Aldrich Chemical Co.), 1-methyluracil, and 3-methyluracil (Vega-Fox Biochemicals) were examined without further purification. Literature procedures were followed in the preparation of 4-thiouracil (6), 1-methyl-2-thiouracil (7), 1-methyl-4-thiouracil (8), 1-methyl-2,4-dithiouracil (9), and 3-methyl-2-thiouracil (7). The sodium salt of each of the methyluracils was prepared by dissolving the pure methyluracil (~0.2 g) in dry methanol (~5 mL) containing an exactly equivalent amount of sodium methoxide. The resulting solution was evaporated by heating to 60°C in a stream of dry nitrogen leaving the crystalline sodium salt. The purity was verified by monitoring the C:O:N:S intensity ratios in the ESCA spectrum of each salt.

The samples were examined as powders, either mounted on the spectrometer probe using double-sided tape, or pressed into finely grooved copper flats fixed to the probe. A McPherson ESCA-36 photoelectron spectrometer, calibrated as described previously (10), was used to obtain spectra of the C_{1s}, N_{1s}, O_{1s}, and S_{2s} or S_{2p} core levels for each sample, using $MgK_{\alpha_{1,2}}$ radiation (1253.6 eV). All the samples were inspected visually, and most were examined over extended periods of time in the spectrometer to check for radiation damage. No damage was evident visually, and the constancy of the spectral band positions and intensities showed that no substantial radiation damage occurred.

Computer deconvolution utilizing the peak fitting routine described by Bancroft *et al.* (11) was applied to determine peak positions in partially resolved bands. Bands were defined according to their energy, intensity, width, and shape (normally an equal combination of Gaussian and Lorentzian shapes). A best fit was obtained using a least-squares analysis. An important feature of this program is the ability to constrain, within limits, certain peak parameters while allowing others to vary freely. In this study the peak intensities were constrained to give areas proportional to those required by the molecular formula. C_{1s} peak widths were constrained to half-widths (FWHM) between 1.4 and 1.6 eV since preliminary examination showed that peak widths for all carbon sites investigated fell in this range. Binding energies were measured relative to the C_{1s} peak ascribed to hydrocarbon contamination and assigned a value of 285.0 eV (12). This peak gradually increased in intensity with time as residual hydrocarbons deposited on the sample surface.

[2]U, m^1U, and m^3U represent uracil and its N(1) and N(3) methylated derivatives. The prefixes s^2 and s^4 indicate sites of thionation, while a superscripted negative sign indicates ionization of an imino nitrogen, e.g. $m^1s^2U^-$.

Results and Discussion

(a) ESCA Spectral Data

Table 1 lists the binding energies for the compounds studied. Figure 1 shows, as examples of deconvoluted spectra, the C_{1s} bands of uracil and the three thiouracils. The accuracy of the binding energy data in Table 1 was assessed by repeated measurements of the core levels in several samples for a number of the compounds. For all the core levels of uracil and the thiouracils, and the N_{1s}, O_{1s}, S_{2s}, and S_{2p} levels of the other compounds, the standard deviations in the binding energies of any peak did not exceed 0.15 eV. For the methylated uracils and the ions, the standard deviations for the C_{1s} levels were found to be ± 0.20 eV. This increased uncertainty is a consequence of the greater number of peaks under the C_{1s} spectral envelopes and, for the ionic species, of the smaller range in C_{1s} binding energies.

Separate N_{1s} binding energies for the two nitrogen sites could be determined only for the ions. In Fig. 2, N_{1s} spectra are shown for the neutral 1-methyluracil and its anionic analogue. The low binding energy peak evident in the spectrum for the ionic compound is ascribed to the ionized nitrogen. Similar N_{1s} spectra were observed for all ionic compounds studied. It was not possible to resolve the O_{1s} peaks in the di-keto derivatives or the S_{2s} and S_{2p} peaks in the di-thio derivatives.

The assignment of the C_{1s} core level peaks of uracil has been discussed previously (4). For the other compounds, peaks were assigned using known substituent effects on the core electron binding energies (13). Assignments reached by this method were confirmed by a quantitative analysis of the data in Table 1 using the charge potential model.

(b) The Charge Potential Model for C_{1s} Binding Energy Shifts

The charge potential model (14) describes the binding energy E_i in terms of the charge q_i on atom i and the charges q_j on the other atoms situated at distances r_{ij} from i, through eq. [1].

$$[1] \qquad E_i = E_i^0 + kq_i + \sum_{j \neq i} q_j/r_{ij}$$

E_i^0 is a reference level and k is a constant. For a variety of molecular solids (14–16), including a series of nucleic acid bases (4), eq. [1] has been

Can. J. Chem. Downloaded from www.nrcresearchpress.com by 210.87.254.5 on 09/05/12
For personal use only.

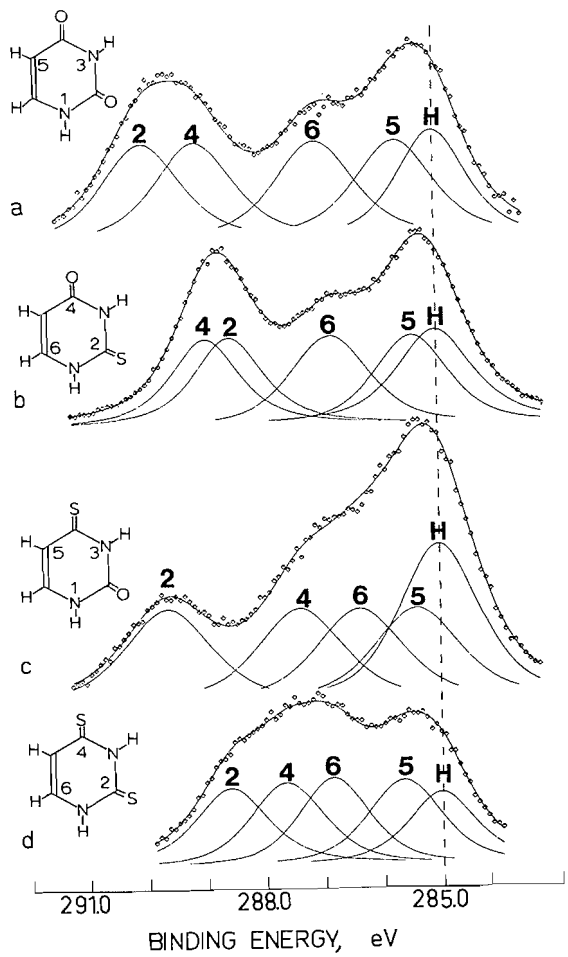

FIG. 1. The C_{1s} spectra of (*a*) uracil, (*b*) 2-thiouracil, (*c*) 4-thiouracil, (*d*) 2,4-dithiouracil. The peak assigned to hydrocarbon contamination and used for an energy reference (285.0 eV) is indicated.

shown to provide a quantitative rationalization of ESCA chemical shifts when the summation extends over a single molecule. When dealing with ionic compounds, the application of eq. [1] is not so straightforward. Intermolecular lattice effects can, in these instances, become important, and the last term in eq. [1] must now, in principle, be extended to a summation over the entire lattice. This is seldom practicable, even where the crystal structure is known; in the case of an unknown crystal structure such as is the situation here,[3] such a procedure is impossible. We therefore proceed as follows: the summation term in eq. [1] is divided into an *intramolecular* potential term, which can be calculated, and an *intermolecular* potential term, P, which cannot be calculated.

[3]To date no crystal structure of an anionic pyrimidine has been reported.

TABLE 1. Core electron binding energies (eV) for uracil, the thiouracils, the 1- and 3-methyl analogues and the anions of the methyl derivatives

Compound	C_{1s}							N_{1s}		O_{1s}	S_{2s}	$S_{2p3/2}$
	$C_2{=}O$	$C_2{=}S$	$C_4{=}O$	$C_4{=}S$	C(5)	C(6)	CH_3	N(1)	N(3)			
Uracil	289.7_5	—	288.9_5	—	285.6_5	286.8_5	—	400.7_0	400.7_0	531.8_5	—	—
2-Thiouracil	—	288.5_0	288.9_5	—	285.5_5	286.9_0	—	400.9_5	400.9_5	532.0_0	227.0	—
4-Thiouracil	289.6_0	—	—	287.3_5	285.5_0	286.5_5	—	400.7_0	400.7_0	532.0_0	226.8	—
2,4-Dithiouracil	—	288.5_0	—	287.4_0	285.6_5	286.6_5	—	400.7_5	400.7_5	—	226.9	—
1-Methyl-uracil	289.4_5	—	288.7_0	—	285.5_0	286.6_5	286.3_5	400.7_5	400.7_5	531.8_5	—	—
1-Methyl-2-thiouracil	—	288.2_5	288.6_0	—	285.7_5	286.7_0	286.4_5	400.8_5	400.8_5	531.8_5	226.9	162.5_5
1-Methyl-4-thiouracil	289.4_5	—	—	287.3_0	285.7_0	286.7_0	286.3_0	400.9_0	400.9_0	531.9_0	226.8	162.3_5
1-Methyl-2,4-dithiouracil	—	288.1_0	—	287.0_5	285.6_0	286.5_0	286.1_0	400.9_5	400.9_5	—	226.8	162.4_5
3-Methyl-uracil	289.4_5	—	288.6_5	—	285.9_0	286.8_0	286.2_5	400.8_5	400.8_5	531.8_5	—	—
3-Methyl-2-thiouracil	—	288.1_5	288.6_5	—	285.7_5	286.7_0	286.0_5	400.8_5	400.8_5	531.8_0	226.6	162.3_0
1-Methyl-uracil ion	288.8_5	—	288.0_0	—	285.1_5	286.5_5	285.7_5	400.7_0	398.6_5	531.0_0	—	—
1-Methyl-2-thiouracil ion	—	287.4_5	287.9_0	—	285.3_5	286.5_5	286.0_0	400.7_0	398.5_5	531.1_5	—	161.9_0
1-Methyl-4-thiouracil ion	288.9_5	—	—	286.8_0	285.4_0	286.2_5	286.0_0	400.8_0	398.8_5	531.2_0	—	162.0_0
1-Methyl-2,4-dithiouracil ion	—	287.4_5	—	286.5_0	285.4_5	286.5_0	285.5_5	400.8_0	398.7_5	—	—	161.9_0
3-Methyl-uracil ion	288.8_5	—	288.2_0	—	285.8_0	286.4_0	286.0_0	398.7_0	400.7_0	531.1_0	—	—
3-Methyl-2-thiouracil ion	—	287.5_0	288.1_5	—	285.7_5	286.4_0	285.8_5	398.7_5	400.8_0	531.3_0	—	161.9_0

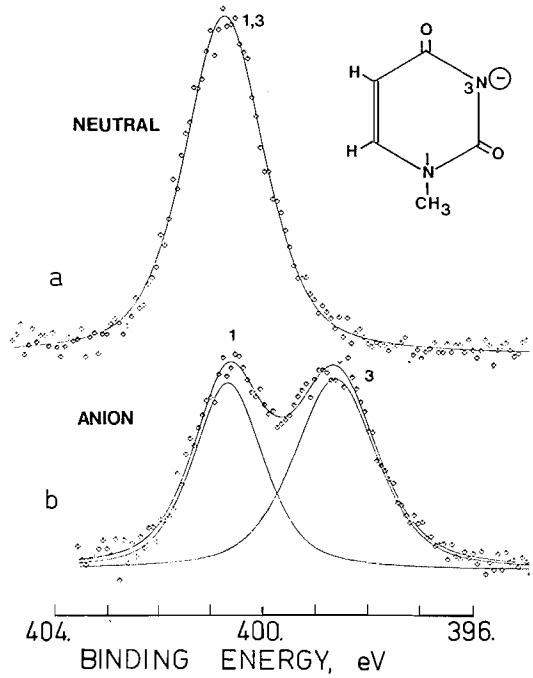

FIG. 2. N_{1s} spectra of (*a*) 1-methyluracil and (*b*) 1-methyluracil anion. The peak at low binding energy in the anion is assigned to the nitrogen at the site of ionization.

$$[2] \qquad E_1 = E_i^0 + kq_i + \left(\sum_{j \neq 1} q_j/r_{ij}\right)_{\text{intramol}} + P$$

Using an average geometry (17) for the uracil derivatives, CNDO/2 molecular orbital theory calculations yielded atomic charges for the neutral and ionized species. The atomic charges were used with the same average geometries to calculate the intramolecular potentials. The charges were then plotted against the experimental C_{1s} binding energies which were corrected for the intramolecular terms. The result is shown in Fig. 3.

The C_{1s} data points in Fig. 3 clearly fall into two linear sets: one for the neutral and one for the ionic compounds. Hollander *et al.* (18) have noted a similar division in a collection of neutral and anionic inorganic compounds. Least-squares analyses of our data yield similar slopes (22.6 ± 0.8 for the neutral molecules; 23.5 ± 1.5 for the ions), but quite different intercepts (284.8 ± 0.2 for neutral molecules vs. 290.7 ± 0.4 eV for the ions).

The slope in each case gives the constant k. From Koopman's theorem this parameter can be related to the one-centre Coulomb integral between a core and valence electron. It is interesting that the value of k should be the same for both neutral and ionic series. However, the intercept in each case incorporates the intermolecular potential term P, and this is expected to be quite different in the two series

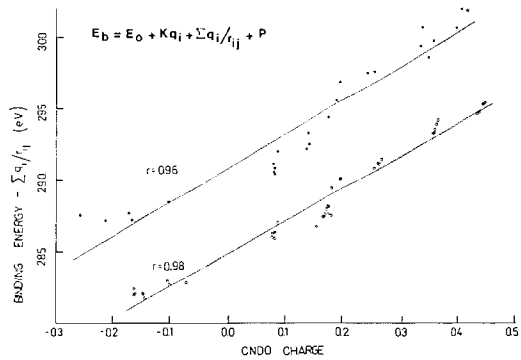

FIG. 3. Plots of calculated atomic charge vs. the experimental binding energies corrected for the intramolecular potential, for the C_{1s} levels of the neutral uracils and methyluracils (○) and the methyluracil anions (*). The linear least-squares fits are shown.

of molecules. In the case of the neutral uracil derivatives, the intercept is in accord with the results of studies on a variety of molecular solids, which yielded values for the intercept closely grouped around 285.0 eV (14–16). If there were a significant intermolecular potential P contributing to the measured binding energies in these systems, it would be the same in all of them, and in view of the diversity of the systems studied this is unlikely to be the case. It follows that for these neutral solids, including our neutral uracil derivatives, the contributions of an intermolecular potential to the core electron binding energies are insignificant, i.e., $P \approx 0$.

On the other hand, in the case of the anionic uracils, the intercept differs markedly from that observed for neutral organic molecules. We attribute this 5.9 eV difference entirely to the intermolecular potential P. Since the C_{1s} data in Fig. 3 define straight lines, P must be approximately the same at all sites in a given ion, and, furthermore, must have approximately the same value for all the ions studied here. If P were to vary with site, considerable scatter could be expected about the line in Fig. 3 for the ions, or if P varied in a systematic fashion with q_i, the slope of the least-squares line for the ions would differ from that for the non-ionized compounds. This is an important result since it means that experimental binding energy shifts in the methyluracil anions are related to the ionic charge distributions in a manner analogous to that for neutral solids. The constancy of P through this series of ions is perhaps an indication that the crystal structures for this series of closely related ions are similar.

The increase in electron density upon ionization at N(1) or N(3) in any of the methyluracils results in a decrease of about 2.1 eV in the binding energy of the nitrogen ionized (Table 1). In a study of hetero-

Can. J. Chem. Downloaded from www.nrcresearchpress.com by 210.87.254.5 on 09/05/12
For personal use only.

Can. J. Chem. Downloaded from www.nrcresearchpress.com by 210.87.254.5 on 09/05/12
For personal use only.

TABLE 2. Changes in experimental and calculated atomic charges of modification of the uracils*

Compound	Atomic charges								
	C(2)	C(4)	C(5)	C(6)	$-CH_3$	N(1)	N(3)	O(2)	O(4)
					(1) Methylation				
(a) Methylation at N(1)									
(i) Uracil	−0.01(0)	−0.01(0)	−0.01(0)	0 (0)	—	+0.05(+0.04)	+0.01(−0.02)	0 (0)	0 (0)
(ii) 2-Thiouracil	0.0 (0)	−0.01(0)	+0.02(0)	0 (0)	—	+0.05(+0.04)	0 (0)	0 (0)	0 (0)
(iii) 4-Thiouracil	−0.01(0)	0 (0)	+0.02(0)	+0.02(0)	—	+0.07(+0.04)	+0.01(0)	0 (0)	0 (0)
(b) Methylation at N(3)									
(i) Uracil	−0.01(0)	−0.01(0)	+0.01(0)	0 (0)	—	+0.01(0)	+0.06(+0.04)	0 (0)	0 (0)
(ii) 2-Thiouracil	0 (0)	−0.01(0)	+0.02(0)	−0.01(0)	—	0 (0)	+0.06(+0.04)	0 (0)	0 (0)
					(2) Thionation				
(a) Thionation at C(2) (neutral)									
(i) Uracil	−0.19(−0.19)	−0.03(0)	−0.02(+0.02)	−0.02(+0.01)	—	+0.06(+0.08)	+0.06(+0.08)	—	0 (+0.01)
(ii) 1-Methyluracil	−0.18(−0.19)	−0.03(0)	+0.01(+0.02)	+0.01(+0.01)	—	+0.06(+0.08)	+0.06(+0.08)	—	+0.01(+0.01)
(iii) 3-Methyluracil	−0.18(−0.19)	−0.03(0)	−0.01(+0.02)	−0.04(+0.01)	—	+0.05(+0.08)	+0.06(+0.08)	—	+0.01(+0.01)
(b) Thionation at C(2) (ion)									
(i) 1-Methyluracil	−0.19(−0.17)	−0.06(0)	−0.02(+0.01)	−0.04(0)	—	+0.04(+0.08)	+0.05(+0.12)	—	−0.01(+0.03)
(ii) 3-Methyluracil	−0.18(−0.17)	−0.05(0)	−0.01(+0.01)	−0.05(0)	—	+0.06(+0.12)	+0.04(+0.08)	—	—
(iii) 1-Methyl-4-thiouracil	−0.17(−0.17)	−0.07(0)	−0.01(+0.01)	−0.03(0)	—	—	—	—	—
(c) Thionation at C(4) (neutral)									
(i) Uracil	−0.03(−0.01)	−0.18(−0.16)	+0.02(+0.06)	−0.03(0)	—	−0.01(+0.01)	+0.05(+0.08)	0 (0)	—
(ii) 1-Methyluracil	−0.03(−0.01)	−0.17(−0.16)	+0.05(+0.06)	−0.02(0)	—	0 (+0.02)	+0.06(+0.08)	0 (+0.1)	—
(d) Thionation at C(4) (ion)									
(i) 1-Methyluracil	−0.06(−0.01)	−0.16(−0.14)	+0.04(+0.07)	−0.06(0)	—	−0.02(+0.02)	+0.06(+0.12)	—	—
(e) Thionation at C(2) and C(4) (neutral)									
(i) Uracil	−0.21(−0.20)	−0.21(−0.19)	+0.03(+0.09)	−0.06(−0.02)	—	—	—	—	—
					(3) Ionization				
(a) Ionization at N(1)									
(i) 3-Methyluracil	+0.01(−0.03)	−0.02(0)	−0.03(−0.05)	+0.05(+0.02)	−0.05(0)	−0.16(−0.25)	−0.01(−0.01)	—	—
(ii) 3-Methyl-2-thiouracil	+0.01(−0.01)	+0.04(−0.01)	−0.03(−0.06)	+0.04(+0.01)	−0.05(0)	−0.15(−0.21)	−0.04(−0.02)	—	—
(b) Ionization at N(3)									
(i) 1-Methyluracil	+0.01(−0.04)	+0.02(−0.01)	0 (−0.01)	−0.03(−0.03)	−0.06(0)	−0.01(−0.01)	−0.14(−0.24)	−0.14(−0.12)	−0.15(−0.12)
(ii) 1-Methyl-2-thiouracil	0 (−0.02)	−0.01(−0.02)	−0.03(−0.02)	−0.05(−0.02)	−0.05(0)	−0.03(−0.01)	−0.14(−0.20)	—	−0.15(−0.10)
(iii) 1-Methyl-4-thiouracil	−0.02(−0.04)	+0.03(0)	−0.01(0)	−0.07(−0.04)	−0.07(0)	−0.03(−0.01)	−0.13(−0.20)	—	—

*Values calculated by CNDO/2 formalism are given in parentheses.

Can. J. Chem. Downloaded from www.nrcresearchpress.com by 210.87.254.5 on 09/05/12
For personal use only.

cyclic dinitrogen bases (19), protonation of one of the nitrogens was found to cause a similar increase in the N_{1s} binding energy (1.7–2.2 eV).

(c) Binding Energy and Charge Shifts

The change in electron density at the carbon, nitrogen, and oxygen atoms has been determined systematically for modification of the uracil structure by methylation, thionation, and ionization (Table 2). Experimental charges were calculated using the charge potential model (eq. [1]). For both neutral and ionic species, k values of 22.6 ± 0.8, 18.5 ± 2.5, and 16.1 ± 4 were adopted for carbon (14), nitrogen (4), and oxygen (14), respectively. E_0 values of 284.8 eV, 399.7 eV, and 532.6 eV were taken for carbon, nitrogen, and oxygen, respectively, in neutral molecules, and for the ions these values were adjusted by 5.9 eV to account for the intermolecular potential. Although the precision of the charges determined for any one atomic site is estimated to be ±0.03 electrons for carbon and ±0.08 electrons for nitrogen, the *change* in site electron density as a result of structural modification is considerably more precise (±0.01 electrons).

(i) Methylation

Methyl substitution at either N(1) or N(3) results in a net decrease in negative charge density, ~0.06 electrons, at the methylated nitrogen. Net charge densities calculated for each site by CNDO/2 formalism are also included in parentheses in Table 2 for comparison, and in the case of the charge decrease on the methylated nitrogen, agreement with our experimental value is reasonable. Although the effect of a methyl group might intuitively be thought of as electron donating, our analysis of its electron withdrawing effect at the nitrogen is supported by previous SCF studies (20). Any other charge redistributions which occur in the molecule upon methylation are too small to be considered significant. To the extent that *N*-methylation is analogous to ribosylation, these results suggest that no major reorganization of the electronic structure of a pyrimidine occurs upon incorporation into a nucleoside.

(ii) Thionation

Thionation of uracil, the methyl uracils, or the methyluracil ions, has the effect of reducing substantially the C_{1s} binding energy of the substituted carbon atom (Table 1). The only other consistent binding energy shift evident in Table 1 is the increase in the binding energy of the remaining oxygen atom. On the other hand, the shifts in experimental charge density exhibit a number of clear trends. Thionation at C(2) in the neutral atom results in an *increase* of electron density at C(2), which agrees well with that predicted by our CNDO/2 calculations. Both adjacent nitrogen atoms undergo a *loss* of electron density. The absolute value of the charge change on the nitrogen is, however, smaller than that experienced by C(2). C(4) and C(6) carbons, two atoms removed from the sulphur modification, again exhibit an *increase* in electron density. Thus, the induced charges alternate in a decaying manner, a trend consistent with the CNDO/2 predictions (and discussed earlier by Pople and Beveridge (21) for simple hydrocarbons). The experimental results suggest that the alternation effect is more extensive than predicted by calculation. Thionation at C(4) results in an almost identical pattern of alternating charge density changes at adjacent centres. Thionation of the m^1U and m^3U anions at C(2) or C(4) also results in decaying charge alternation. However, the magnitude of the effect of thionation is clearly dependent on whether the base is neutral or anionic. For example, 2-thionation of m^1U and m^1U^- leads to a decrease of 0.03 and 0.06 electrons, respectively, at the C(4) position. This is not indicated by our CNDO/2 calculations.

(iii) Ionization

Ionization at N(1) or N(3) results in increases of 0.14–0.16 electrons at the ionized nitrogen site. In addition, increases in charge occur at the keto oxygens. Theoretical and experimental studies of the ionization of thymine (22) have indicated that, upon ionization, carbonyl groups are important in delocalizing the ionic charge in this molecule.

Some of the other trends in charge redistribution following ionization are not predicted by theoretical calculations and are more difficult to understand. For example, the increase in negative charge (0.05 electrons), which occurs at the N(1) or N(3) methyl upon ionization of the other nitrogen, was unexpected in view of the smaller increase at the methylated nitrogen itself. Also unexpected is the *decrease* in negative charge at C(6) upon ionization at N(1). Ionization at N(3), conversely, appears to lead to a charge *increase* at C(6), and the magnitude of this increase is dependent on the presence and position of the substituted thionyl group.

Acknowledgement

The financial support of the National Research Council of Canada is greatly appreciated.

1. M. N. LIPSETT. J. Biol. Chem. **242**, 4067 (1967).
2. J. CARBON, H. DAVID, and M. H. STUDIER. Science, **161**, 1146 (1968).
3. A. PSODA, Z. KAZIMIERCZUK, and D. SHUGAR. J. Am. Chem. Soc. **96**, 6832 (1974).
4. J. PEELING, F. E. HRUSKA, and N. S. MCINTYRE. Can. J. Chem. **56**, 1555 (1978).
5. J. A. POPLE and G. A. SEGAL. J. Chem. Phys. **44**, 3289 (1966).

6. Y. MIZUNO, M. IKEHARA, and K. A. WATANABE. Chem. Pharm. Bull. **10**, 647 (1962).
7. R. N. WARRENER and E. N. CAIN. Aust. J. Chem. **24**, 785 (1971).
8. J. J. FOX, D. VAN PRAAG, I. WEMPEN, I. L. DOERR, L. CHEONG, J. E. KNOLL, M. L. EIDINOFF, A. BENDICK, and G. B. BROWN. J. Am. Chem. Soc. **81**, 178 (1959).
9. B. CHATAMRA and A. S. JONES. J. Chem. Soc. 811 (1963).
10. N. S. MCINTYRE and M. G. COOK. Anal. Chem. **47**, 2208 (1975).
11. G. M. BANCROFT, I. ADAMS, L. L. COATSWORTH, C. D. BENNEWITZ, J. D. BROWN, and W. D. WESTWOOD. Anal. Chem. **47**, 586 (1975).
12. G. JOHANSSON, J. HEDMAN, A. BERNDTSSON, M. KLASSON, and R. NILSSON. J. Electron Spectrosc. Relat. Phenom. **2**, 295 (1973).
13. U. GELIUS, P. F. HEDEN, J. HEDMAN, B. J. LINDBERG, R. MANNE, R. NORDBERG, C. NORDLING, and K. SIEGBAHN. Phy. Scr. **2**, 70 (1970).
14. D. T. CLARK. *In* Electron emission spectroscopy. *Edited by* W. Dekeyser *et al.* R. Reidel Publ. Co., Dordrecht, Holland. 1973. p. 373.
15. D. T. CLARK, J. PEELING, and L. COLLING. Biochim. Biophys. Acta, **453**, 533 (1976).
16. D. T. CLARK and H. R. THOMAS. J. Polym. Sci. Polym. Chem. Edit. **14**, 1671 (1976).
17. J. S. KWIATKOWSKI and B. PULLMAN. Adv. Heterocycl. Chem. **18**, 199 (1975).
18. J. M. HOLLANDER, D. N. HENDRICKSON, and W. L. JOLLY. J. Chem. Phys. **49**, 3315 (1968).
19. L. E. COX, J. J. JACK, and D. M. HERCULES. J. Am. Chem. Soc. **94**, 6575 (1972).
20. W. J. HEHRE and J. A. POPLE. Tetrahedron Lett. **34**, 2959 (1970).
21. J. A. POPLE and D. L. BEVERIDGE. Approximate molecular orbital theory. McGraw-Hill, New York. 1970. p. 122.
22. L. C. SNYDER, R. G. SHULMAN, and D. B. NEUMANN. J. Chem. Phys. **53**, 256 (1970).

Can. J. Chem. Downloaded from www.nrcresearchpress.com by 210.87.254.5 on 09/05/12
For personal use only.

Temperature dependence of adiabatic compressibilities of and sound velocities in *p*-dioxane–water mixtures

NERIYANURI MANOHARA MURTHY AND SARASWATULA VENKATA SUBRAHMANYAM

Department of Physics, Post-graduate Centre, Anantapur 515003, India

Received March 4, 1978

NERIYANURI MANOHARA MURTHY and SARASWATULA VENKATA SUBRAHMANYAM. Can. J. Chem. **56**, 2412 (1978).

The effect of *p*-dioxane on the temperature of adiabatic compressibility minimum (TACM) and sound velocity maximum (TSVM) in water have been studied. Both the structural shifts, $[\Delta T_{\beta\ str}]_{exp}$ and $[\Delta T_{u\ str}]_{exp}$, are found to be positive, increasing with concentration and reaching maximum values around $X_2 \simeq 0.015$. These results have been explained as due to the formation of hydrates of dioxane of varying composition indicating the existence of long range order in the water + *p*-dioxane system in the water-rich region.

NERIYANURI MANOHARA MURTHY et SARASWATULA VENKATA SUBRAHMANYAM. Can. J. Chem. **56**, 2412 (1978).

On a étudié l'effet du *p*-dioxanne sur la température de compressibilité minimale adiabatique (TCMA) et la vitesse maximale du son (TVMS) dans l'eau. On a trouvé que les deux déplacements dus à des structures $[\Delta T_{\beta\ str}]_{exp}$ et $[\Delta T_{u\ str}]_{exp}$ sont positifs lorsqu'on augmente la concentration alors qu'elles atteignent des valeurs maximales autour de $X_2 \simeq 0.015$. On a expliqué ces résultats grâce à la formation d'hydrates du dioxanne de compositions variables indiquant la présence d'un ordre à longue distance dans le système eau + *p*-dioxanne dans la région riche en eau.

[Traduit par le journal]

Introduction

Though the system water + *p*-dioxane has been extensively studied from different angles, divergent views exist on the behaviour of the system in the water-rich region. The heat of mixing (1, 2) in the water-rich region of aqueous *p*-dioxane is negative, indicating the establishment of some long range order in the aqueous solutions of *p*-dioxane. The negative values of heat of mixing in the water-rich region have been explained by Goates and Sullivan (2) as indicative of the existence of short range structures ranging in composition from $1C_4H_8O_2:3H_2O$ to $2C_4H_8O_2:1H_2O$. Geddes (3) reported the presence of $C_4H_8O_2 \cdot 5H_2O$ from his viscometric results. Nuclear magnetic resonance and proton spin relaxation studies (4) on this system in the water-rich region indicate an increase in the degree of hydrogen-bonding in water. But the excess partial molal heat capacities of Bu_4NBr (5) and $n\text{-}Am_4NBr$ (6) in the water + *p*-dioxane system indicate structure rupture by *p*-dioxane even at low concentrations. Infrared studies by Fratello and Luongo (7) indicate considerable reduction in hydrogen-bonding present in pure water upon dilution by *p*-dioxane. Dielectric polarization studies by Tourky *et al.* (8) also indicate that the association of water decreases rapidly with increasing concentration of *p*-dioxane and in solutions containing large amounts of *p*-dioxane, water association is completely broken down. From the studies of ionic mobilities in the *p*-dioxane + water system, Kay and Broadwater (9) also point out that dioxane does not enhance long range order in water. However, ultrasonic velocity (10) and absorption (11) data support the contention that long range order persists in water-rich *p*-dioxane solutions.

In view of the divergent opinions existing on the solution structure of the water + *p*-dioxane system in the water-rich region, we have taken up a systematic study of the effect of *p*-dioxane on the temperature of adiabatic compressibility minimum (TACM) and sound velocity maximum (TSVM) of water, to understand the structural properties of this solute, since such studies (12, 13) have been found to be very useful in predicting whether a solute promotes or disrupts the hydrogen bonded structure of water.

Experimental

A.R. grade *p*-dioxane (BDH) used in the present study was purified as per the following procedure. It was first allowed to stand over sodium hydroxide pellets for several hours and then refluxed for 4 h. The material was then distilled and the middle fraction that boiled from 101 to 101.5°C was collected. It was again refluxed for 6 h with metallic sodium and then distilled using a fractionating column. The sample that had a boiling point of 101.4°C was collected. The density of the purified liquid, determined using a bicapillary type pycnometer with an accuracy of 2 parts in 10^5, was found to be 1.02811 g cm^{-3} at 25°C and this value is in good agreement with literature data (14). Ultrasonic velocities in pure components and aqueous *p*-dioxane solutions were determined using a single crystal variable path interferometer working at 3 MHz with an accuracy of $\pm 0.003\%$. The details of the experimental technique and the method of measurement of velocity and temperature of the experimental liquid were reported in our earlier communication (12).

Can. J. Chem. Downloaded from www.nrcresearchpress.com by 210.87.254.105 on 09/05/12
For personal use only.

Can. J. Chem. Downloaded from www.nrcresearchpress.com by 210.87.254.105 on 09/05/12
For personal use only.

Triple distilled degassed water was used to prepare solutions of aqueous *p*-dioxane of varying concentrations. Ultrasonic velocities in the solutions were determined at $\simeq 2°C$ intervals over a range of 5°C on either sides of T_β and T_u where T_β and T_u represent the temperatures corresponding to the adiabatic compressibility minimum and sound velocity maximum of the solution respectively. The experimental ultrasonic velocities were corrected for diffraction effects following the procedure developed by Subrahmanyam *et al.* (15). Densities of pure components and aqueous *p*-dioxane solutions were determined at $\simeq 2°C$ intervals. The adiabatic compressibilities were calculated using the standard formula, i.e. $\beta = u^{-2}\rho^{-1}$ which are accurate to $\pm 5 \times 10^{-15}$ cm²/dyn. At low concentrations of the organic solute, the temperature dependences of the adiabatic compressibility of and sound velocity in the solution are similar to those of the curves for pure water. Hence templates of the curves for pure water were employed to fix T_β and T_u. The accuracy in fixing T_β is $\pm 0.4°C$ and that of T_u is $\pm 0.2°C$. Since $d\beta/dt = 0$ at $t = T_\beta$ of the aqueous solution, a graphical method was also employed to fix T_β at which

$$\left|\frac{1}{\rho}\frac{d\rho}{dt}\right| = \left|\frac{2}{u}\frac{du}{dt}\right|$$

T_β evaluated by this method is also accurate to $\pm 0.4°C$.

Results

The results on the measurement of adiabatic compressibility and ultrasonic velocity as a function of temperature at different concentrations of dilute aqueous *p*-dioxane[1] are shown graphically in Figs. 1 and 2 respectively. It is worth while to note that the exact temperature range over which velocity measurements have to be carried out to fix T_u is generally higher than that necessary to fix T_β.

The water + *p*-dioxane system is known to exhibit ultrasonic relaxation (16), the relaxation frequency increasing with rise in temperature and concentration of *p*-dioxane. For example at $X_2 \simeq 0.025$, the lower relaxation frequencies at 10 and 25°C respectively are about 60 and 120 MHz. Since the temperature range of the present work is much higher (50 to 80°C) the relaxation frequencies will be definitely much higher than 3 MHz. Hence the velocity dispersion, which is probably negligible even at the relaxation frequency does not affect the present velocity measurements carried out at 3 MHz.

Discussion

The adiabatic compressibility of an aqueous solution can be represented by

$$[1] \qquad \beta = \phi_1\beta_1 + \phi_2\beta_2 + \beta^E$$

where β_1, β_2 and ϕ_1, ϕ_2 refer to the adiabatic compressibilities and volume fractions of water and the organic solute respectively and β^E represents the excess adiabatic compressibility. β_1 and β_2 may be written as

$$[2] \qquad \beta_1 = 42.208 + 0.0016\,(t - 64)^2$$

$$[3] \qquad \beta_2 = \beta_2^0 + \alpha_\beta t + \alpha_\beta' t^2$$

where β_2^0 represents the extrapolated value of the adiabatic compressibility of the organic solute at 0°C, α_β and α_β' are constants, and t represents the temperature in °C. The velocity data of Greenspan and Tschiegg (17) and density data from literature (18) have been used to evaluate the adiabatic compressibility of water at different temperatures and eq. [2] represents the least-squares fit of the above data. Substitution of eqs. [2] and [3] in eq. [1], differentiation of the resulting equation with respect to temperature and using the condition $(d\beta/dt)_{t=T_\beta} = 0$, we get the following expression for T_β of the solution

$$[4] \quad T_\beta = \left[64 - \frac{\phi_2}{\phi_1}\frac{\alpha_\beta}{0.0032}\right]\left(1 + \frac{\phi_2}{\phi_1}\frac{\alpha_\beta'}{0.0016}\right)^{-1} - \frac{d\beta^E}{dt}\left(1 + \frac{\phi_2}{\phi_1}\frac{\alpha_\beta'}{0.0016}\right)^{-1}(\phi_1 \times 0.0032)^{-1}$$

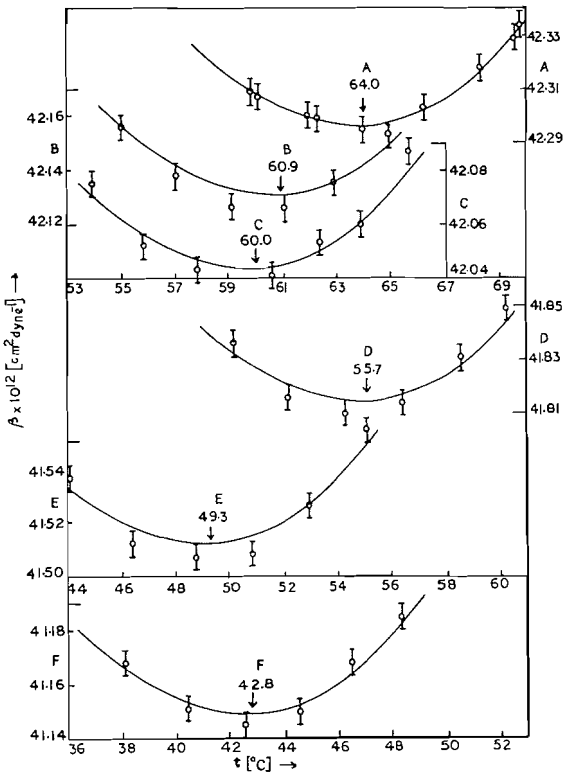

FIG. 1. Adiabatic compressibility, β, vs. temperature of solutions of aqueous *p*-dioxane. *A*, $X_2 = 0.0000$; *B*, $X_2 = 0.0041$; *C*, $X_2 = 0.0063$; *D*, $X_2 = 0.0121$; *E*, $X_2 = 0.0196$; *F*, $X_2 = 0.0280$.

[1]Complete set of the experimental data may be obtained, at a nominal charge, from the Depository of unpublished data, CISTI, National Research Council of Canada, Ottawa, Ont., Canada K1A 0S2.

Can. J. Chem. Downloaded from www.nrcresearchpress.com by 210.87.254.105 on 09/05/12
For personal use only.

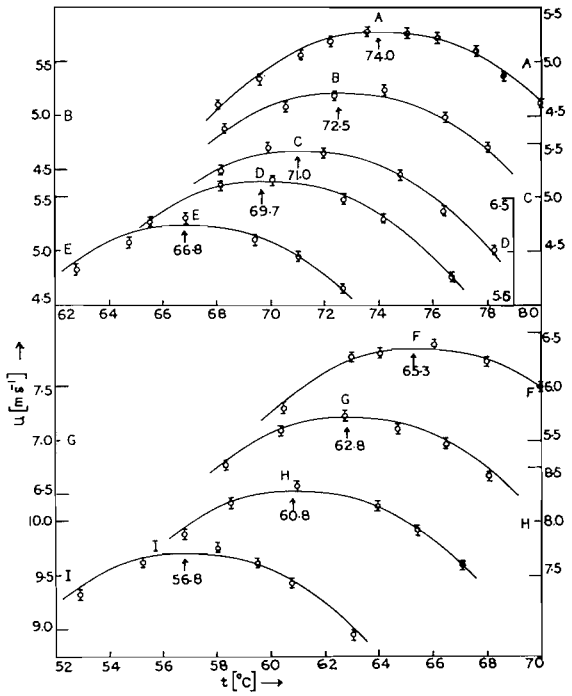

FIG. 2. Ultrasonic velocity vs. temperature in solutions of aqueous *p*-dioxane. The values given on the ordinate have to be added to 1550 ms^{-1}. *A*, $X_2 = 0.0000$; *B*, $X_2 = 0.0020$; *C*, $X_2 = 0.0036$; *D*, $X_2 = 0.0053$; *E*, $X_2 = 0.0090$; *F*, $X_2 = 0.0110$; *G*, $X_2 = 0.0143$; *H*, $X_2 = 0.0170$; *I*, $X_2 = 0.0225$.

Since

$$[5] \qquad \beta = \frac{1}{u^2\rho}$$

where u is the ultrasonic velocity and ρ the density, we can rewrite eq. [1] as

$$[6] \qquad \frac{1}{u^2} = \frac{\phi_1^2}{w_1 u_1^2} + \frac{\phi_2^2}{w_2 u_2^2} + \rho\beta^E$$

where w_1 and w_2 refer to the weight fractions of water and the organic solute respectively in the solution. It may be mentioned here that there is no need to replace ρ by

$$[7] \qquad \rho = \phi_1\rho_1 + \phi_2\rho_2 + \rho^E$$

since the effect of ρ^E, the excess density, on the velocity of the solution is negligibly small. According to Willard (19) the velocity in pure water conforms to the relation

$$[8] \qquad u_1 = 1557 - 0.0245\,(74 - t)^2$$

and over a small range of temperature the sound velocity in the organic solute is given by

$$[9] \qquad u_2 = u_2^0 - \alpha_u t$$

where α_u is the temperature coefficient of sound velocity in solute and u_2^0 is the linearly extrapolated velocity of the solute at 0°C. Substitution of eqs. [8] and [9] in eq. [6], differentiation of the resulting equation with respect to temperature, and using the condition $(du/dt)_{t=TSVM} = 0$, we get the following expression for T_u of the solution

$$[10] \quad T_u = \left[74 - \left(\frac{\phi_2}{\phi_1}\right)^2\left(\frac{w_1}{w_2}\right)\left(\frac{\alpha_u}{0.049}\right)\left(\frac{u_1}{u_2}\right)^3\right] - \left(\frac{w_1}{\phi_1^2}\right)\left(\frac{u_1^3}{0.098}\right)\left[\rho\frac{d\beta^E}{dt} + \beta^E\frac{d\rho}{dt}\right]$$

The values of β_2^0, α_β, α_β', u_2^0, and α_u for *p*-dioxane evaluated using the experimentally determined ultrasonic velocity and density data at different temperatures are respectively 45.979×10^{-12} cm^2/dyn, 0.241×10^{-12} $cm^2/dyn\ °C$, 0.003×10^{-12} $cm^2/dyn\ °C^2$, 1452.42 m/s, and 4.33 m/s °C.

The shifts produced, $\Delta T_\beta = (T_{\beta\ sol} - T_{\beta\ water})$ and $\Delta T_u = (T_{u\ sol} - T_{u\ water})$, may be thought of as arising from two effects; dilution effect and structural effect. The dilution effect is always negative. But the structural effect can either be positive or negative indicating either structure promotion or structure disruption by the solute.

The structural shifts $\Delta T_{\beta\ str}$ and $\Delta T_{u\ str}$ can be obtained either by employing the second terms on rhs of eqs. [4] and [10] respectively, or by using the following relations

$$[11] \qquad [\Delta T_{\beta\ str}]_{exp} = T_{\beta\ exp} - T_{\beta\ id}$$

$$[12] \qquad [\Delta T_{u\ str}]_{exp} = T_{u\ exp} - T_{u\ id}$$

where $T_{\beta\ id}$ and $T_{u\ id}$ are given by the first terms on rhs of eqs. [4] and [10] respectively. These temperatures correspond to those at which the adiabatic compressibility minimum of and sound velocity maximum in the solution would take place if ideal mixing occurs, i.e. β^E is zero. Since the temperature dependence of ϕ_1 and ϕ_2 is very small, ϕ_1 and ϕ_2 used to determine $T_{\beta\ id}$ and $T_{u\ id}$ were those calculated at the T_β and T_u of the solution found experimentally. Successive approximation method was employed for evaluation of $T_{u\ id}$.

$[\Delta T_{\beta\ str}]_{exp}$ and $[\Delta T_{u\ str}]_{exp}$ at each concentration of *p*-dioxane were evaluated using eqs. [11] and [12]. $T_{\beta\ exp}$ used is the average value of T_β obtained from both the template and graphical methods. The values of $[\Delta T_{\beta\ str}]_{exp}$ and $[\Delta T_{u\ str}]_{exp}$ at different mole fractions of *p*-dioxane are presented in Tables 1 and 2 respectively. Plots of $[\Delta T_{\beta\ str}]_{exp}$ and $[\Delta T_{u\ str}]_{exp}$ vs. X_2 of *p*-dioxane are shown in Fig. 3. Both the structural shifts are positive and increase with increasing concentration of *p*-dioxane reaching maximum values around $X_2 \simeq 0.015$ and thereafter the

Can. J. Chem. Downloaded from www.nrcresearchpress.com by 210.87.254.105 on 09/05/12
For personal use only.

TABLE 1. $T_{\beta\ id}$, $T_{\beta\ exp}$, and $[\Delta T_{\beta\ str}]_{exp}$ at different mole fractions, X_2, of *p*-dioxane

X_2	$T_{\beta\ id}$ (°C)	$T_{\beta\ exp}$ (°C) Template method	$T_{\beta\ exp}$ (°C) Graphical method	$[\Delta T_{\beta\ str}]_{exp}$ (°C)
0.0041	60.2	60.9	60.8	+0.7±0.4
0.0063	58.3	60.0	60.0	+1.7±0.4
0.0121	53.3	55.1	55.1	+1.8±0.4
0.0196	48.0	49.3	49.3	+1.3±0.4
0.0280	42.5	42.8	42.5	+0.2±0.4

TABLE 2. $T_{u\ id}$, $T_{u\ exp}$, and $[\Delta T_{u\ str}]_{exp}$ at different mole fractions, X_2, of *p*-dioxane

X_2	$T_{u\ id}$ (°C)	$T_{u\ exp}$ (°C)	$[\Delta T_{u\ str}]_{exp}$
0.0020	71.9	72.5	+0.6±0.2
0.0036	70.1	71.0	+0.9±0.2
0.0053	68.4	69.7	+1.3±0.2
0.0090	64.9	66.8	+1.9±0.2
0.0110	63.0	65.3	+2.3±0.2
0.0143	60.3	62.8	+2.5±0.2
0.0170	58.1	60.8	+2.7±0.2
0.0225	54.5	56.8	+2.3±0.2

structural shifts decrease. This trend is an indication of stabilization of water structure by dioxane molecules in accordance with the nuclear magnetic resonance and proton spin relaxation data (4) on this system. Studies on the apparent molal volumes and heat capacities of *p*-dioxane in water at 25°C by Kiyohara *et al.* (20) indicate that *p*-dioxane is a weakly hydrophobic solute supporting the results of the present study. But the temperature of density maximum studies by Wada and Umeda (21) on this system show negative values for the structural contribution to the shift in the temperature of maximum density of water indicating disruption of hydrogen bonded structure of water by the addition of *p*-dioxane.

The present ultrasonic studies on the water + *p*-dioxane system support the idea that small amounts of dioxane due to the hydrophobic nature of its methylene groups enhance the strength of water–water hydrogen bonds in its vicinity, possibly permitting the water molecules to become organized into clusters which envelope dioxane molecules. Above $X_2 \simeq 0.015$, there starts the breakdown of the three dimensional structure of these clusters. In view of this the positive structural shifts may be thought of as due to ordering of water structure owing to the formation of hydrates of dioxane as reported in literature (2, 3, 16).

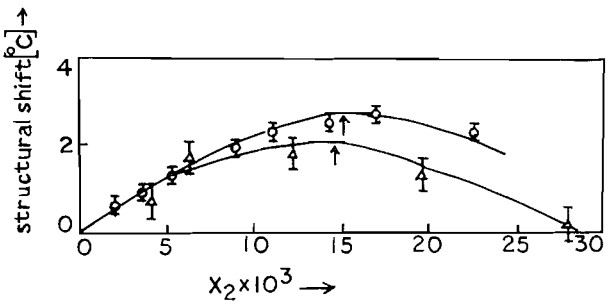

FIG. 3. Structural shifts vs. mole fraction X_2 of *p*-dioxane. △, $[\Delta T_{\beta\ str}]_{exp}$; ○, $[\Delta T_{u\ str}]_{exp}$.

It is also possible to evaluate $\Delta T_{\beta\ str}$ and $\Delta T_{u\ str}$ using the second terms of eqs. [4] and [10], respectively, where we need only the velocity in and density of the solution at different temperatures for the evaluation of $d\beta^E/dt$ and $d\rho/dt$. Evaluation of the structural shifts in this way will serve as a check on the sign and magnitude of the structural shifts obtained using eqs. [11] and [12]. In fact the sign of $d\beta^E/dt$ itself will indicate whether the structural interactions are promotive or disruptive, i.e., positive sign indicating structure disruption and negative sign indicating structure promotion (13). $d\beta^E/dt$ with the probable error has been calculated at each concentration by evaluating β^E at different temperatures and fitting the data to a straight line by least-squares fit method since β^E was found to vary linearly with temperature within the limits of the experimental error. Values of u_1, ρ, β^E, and $d\rho/dt$ at $t = T_{u\ id}$ were used in the calculation of $\Delta T_{u\ str}$. In order to distinguish the structural shifts calculated using the second terms on the rhs of eqs. [4] and [10] respectively from those obtained by using eqs. [11] and [12], the former values may be denoted as $[\Delta T_{\beta\ str}]_{the}$

TABLE 3. Comparison of experimental and theoretical structural shifts

X_2	$\frac{d\beta^E}{dt} \times 10^{15}$ (cm²/dyn)	$\Delta T_{\beta\ str}$ (°C) Expt.	$\Delta T_{\beta\ str}$ (°C) Theoretical	$\Delta T_{u\ str}$ (°C) Expt.	$\Delta T_{u\ str}$ (°C) Theoretical
0.0041	−2.3±1.3	+0.7±0.4	+0.7±0.4		
0.0121	−5.7±2.8	+1.8±0.4	+0.7±0.8		
0.0280	−3.7±1.9	+0.2±0.4	+1.0±0.5		
0.0020	−0.9±0.5			+0.6±0.2	+0.2±0.2
0.0225	−3.5±1.8			+2.3±0.2	+2.3±0.8

and $[\Delta T_{u\ str}]_{the}$ although u and ρ used in the evaluation are the experimental ones. In this method it is not necessary to determine u and ρ at very narrow temperature ranges in as much as they are essential for fixing T_β or T_u. The structural shifts evaluated by the use of either of the methods are compared in Table 3 at representative concentrations and the agreement is quite good.

1. G. N. MALCOLM and J. C. ROWLINSON. Trans. Faraday Soc. **53**, 921 (1957).
2. J. R. GOATES and R. SULLIVAN. J. Phys. Chem. **62**, 188 (1958).
3. J. A. GEDDES. J. Am. Chem. Soc. **55**, 2264 (1936).
4. C. J. CLEMENT. J. Chem. Soc. A**458**, 761 (1969).
5. R. K. MOHANTY, T. S. SARAMA, S. SUBRAMANIAN, and J. C. AHLUWALIA. Trans. Faraday Soc. **67**, 305 (1971).
6. R. K. MOHANTY and J. C. AHLUWALIA. J. Solution Chem. **1**, 531 (1972).
7. A. FRATELLO and J. P. LUONGO. J. Am. Chem. Soc. **85**, 3073 (1963).
8. A. R. TOURKY, H. A. REZK, and Y. M. GIRGIS. J. Phys. Chem. **65**, 40 (1961).
9. R. L. KAY and T. L. BROADWATER. Electrochem. Acta, **16**, 667 (1971).
10. C. J. BURTON. J. Acoust. Soc. Am. **20**, 186 (1948).
11. K. ARAKAWA and N. TAKENAKA. Bull. Chem. Soc. Jpn. **42**, 5 (1969).
12. S. V. SUBRAHMANYAM and N. MANOHARAMURTHY. J. Solution Chem. **4**, 347 (1975).
13. N. MANOHARAMURTHY and S. V. SUBRAHMANYAM. Bull. Chem. Soc. Jpn. **50**, 2589 (1977).
14. H. SCHOTT. J. Chem. Eng. Data, **6**, 19 (1961).
15. S. V. SUBRAHMANYAM, V. HYDERKHAN, and C. V. RAGHAVAN. J. Acoust. Soc. Am. **46**, 272 (1969).
16. G. G. HAMMES and W. KNOCHE. J. Chem. Phys. **45**, 4041 (1964).
17. M. GREENSPAN and C. E. TSCHIEGG. J. Res. Natl. Bur. Stand. **59**, 249 (1957).
18. E. W. WASHBURN (*Editor*). International critical tables of numerical data. Physics, chemistry and technology. McGraw Hill Book Co. Inc., New York. 1928.
19. G. WILLARD. J. Acoust. Soc. Am. **19**, 236 (1947).
20. O. KIYOHARA, G. PERRON, and J. E. DESNOYERS. Can. J. Chem. **53**, 2591 (1975).
21. G. WADA and S. UMEDA. Bull. Chem. Soc. Jpn. **35**, 1797 (1962).

Can. J. Chem. Downloaded from www.nrcresearchpress.com by 210.87.254.105 on 09/05/12
For personal use only.

Mixed oxidation state compounds of antimony: a ^{121}Sb Mössbauer study of some antimony–fluorine systems

JACK G. BALLARD, THOMAS BIRCHALL, RONALD J. GILLESPIE, EDWARD MAHARAJH, DAVID TYRER, AND JOHN E. VEKRIS

Department of Chemistry, McMaster University, Hamilton, Ont., Canada L8S 4M1

Received April 7, 1978

JACK G. BALLARD, THOMAS BIRCHALL, RONALD J. GILLESPIE, EDWARD MAHARAJH, DAVID TYRER, and JOHN E. VEKRIS. Can. J. Chem. **56**, 2417 (1978).

Antimony-121 Mössbauer spectra for $[Sb_2F_4^{2+}][SbF_6^-]_2$ and three compounds containing the $[Sb_3F_{14}^-]$ ion are reported. The Mössbauer data are discussed in relation to their known structures. Two of the compounds give spectra which, on analysis, give η values of unity.

JACK G. BALLARD, THOMAS BIRCHALL, RONALD J. GILLESPIE, EDWARD MAHARAJH, DAVID TYRER et JOHN E. VEKRIS. Can. J. Chem. **56**, 2417 (1978).

On rapporte les spectres de Mössbauer de l'antimoine 121 pour le $[Sb_2F_4^{2+}][SbF_6^-]_2$ et trois composés contenant l'ion $[Sb_3F_{14}^-]$. On discute des données de Mössbauer en terme de leurs structures connues. Deux des composés donnent des spectres qui par analyse donnent des valeurs η sont égales à l'unité.

[Traduit par le journal]

Can. J. Chem. Downloaded from www.nrcresearchpress.com by 210.87.254.5 on 09/05/12
For personal use only.

Antimony pentafluoride forms adducts with a variety of Lewis bases. Of particular interest to us have been those which contain antimony in its two oxidation states, III and V. Antimony-121 Mössbauer spectroscopy has been particularly useful in characterizing a number of such mixed oxidation state compounds (1–4). This technique, along with Raman spectroscopy, provided the first spectroscopic evidence for "SbF_4" (5). Two forms of "SbF_4" were shown to exist and were called forms A and B. Both compounds were shown to contain antimony in the III and V oxidation states. Subsequently Edwards and Slim (6) were able to show that form B was in fact $[Sb_6F_{13}^{5+}][SbF_6^-]_5$. Recently Gillespie *et al.* (7) have characterized, by X-ray crystallography, a 1:1 adduct of SbF_3 with SbF_5 and shown it to be $[Sb_2F_4^{2+}][SbF_6^-]_2$. These workers also presented Raman evidence to show that $[Sb_2F_4^{2+}][SbF_6^-]_2$ was in fact $SbF_3 \cdot SbF_5$ (A). Since the earlier $SbF_3 \cdot SbF_5$ Mössbauer spectra were only obtained at liquid nitrogen temperature it seemed worthwhile recording the spectrum of $[Sb_2F_4^{2+}][SbF_6^-]_2$ at 4 K in order to obtain a better quality spectrum from a well characterized material.

Gillespie and co-workers (8–10) have recently prepared compounds containing the $[Sb_3F_{14}^-]$ anion and here we present data for these compounds which have rather unusual Mössbauer spectra. Mössbauer data are also presented for some other adducts of antimony pentafluoride.

Experimental

$AsF_3 \cdot SbF_5$ was prepared by the slow evaporation of liquid SO_2 from a solution of antimony pentafluoride and excess arsenic trifluoride in liquid SO_2. The white solid was washed with successive amounts of liquid SO_2. $SbF_5 \cdot SO_2$ was obtained by the slow evaporation of SO_2 from a solution of pure antimony pentafluoride in liquid sulphur dioxide. Raman spectroscopy was used to show that these compounds were pure (11, 12). The preparations of the remaining compounds have all been described (8–10).

Mössbauer spectra were recorded at liquid helium temperatures, on samples containing 8–10 mg cm^{-2} of Sb, using a $Ba^{121}SnO_3$ source at room temperature, on apparatus previously described (13). Isomer shifts were measured with respect to InSb at liquid helium temperatures. Spectra were computer fitted by procedures already described (14–16). However, no single programme was available which could treat the spectra of $[Sb_3F_{14}^-]$ which has more than one antimony site, and where the asymmetry parameter η was not equal to zero and had to be varied. In these cases the Sb(III) resonance was fitted separately from that of the antimony(V) using the transmission integral procedure of Cranshaw (16).

Results and Discussion

The data are summarised in Table 1 and the simpler adducts will be discussed first. The adduct formed between SbF_5 and AsF_3 gives only one resonance at 10.9 mm s^{-1} with a negligibly small quadrupole coupling constant. This is what one would expect from an $[SbF_6^-]$ species. Edwards and Sills have shown that this adduct can indeed be considered as having an important contribution from the ionic structure $[AsF_2^+][SbF_6^-]$ (11). They also found that there was a slight distortion of the $[SbF_6^-]$ octahedron, but this does not result in a measurable quadrupole coupling constant.

For $SbF_5 \cdot SO_2$ a less positive isomer shift was obtained indicating a slightly higher *s* electron density at the antimony. This value agrees well with that reported by Carter *et al.* (17). These workers also

Can. J. Chem. Downloaded from www.nrcresearchpress.com by 210.87.254.5 on 09/05/12
For personal use only.

TABLE 1. ^{121}Sb Mössbauer parameters for $SbF_5 \cdot X$; adducts and related anions at 4 K

Compound	I.S. (mm s^{-1} ± 0.1)	eQ_gV_{zz} (mm s^{-1} ± 0.5)	η	Γ	Reference
$[Se_2Te_2^{2+}]$ $[SbF_6^-]$ $[Sb_3F_{14}^-]$	11.0	0	—	2.9	
	−6.5	14.1	0.49±0.1	3.8	
$[Se_{2/3}Te_{3.1/3}^{2+}]$ $[SbF_6^-]$ $[Sb_3F_{14}^-]$	10.9	0	—	3.5	
	−7.3	18.9	0.99±0.1	3.0	
$[S_4N_4^{2+}]$ $[SbF_6^-]$ $[Sb_3F_{14}^-]$	11.1				
	−7.6	17.8	1.0 ±0.2		
$[Sb_2F_4^{2+}]$ $[SbF_6^-]_2$	11.0	4.6		3.0	
	−7.9	14.1		3.9	
$[Sb_6F_{13}^{5+}]$ $[SbF_6^-]_6$	11.2	5.4			5
	−7.5	18.3			
$AsF_3 \cdot SbF_5$	10.9	—		3.3	
$SbF_5 \cdot SO_2$	10.7	−6.3		2.3	
	10.56	—		—	17

reported the presence of a small quadrupole coupling constant but gave no indication of the sign of this interaction. We find a value of −6.3 mm s^{-1}. The negative sign is consistently obtained from our computer fitting procedures no matter what sign was given to the initial estimates for the fitting procedure. Moore *et al.* (18) have shown that the antimony environment consists of five fluorines at 1.85 Å with the sixth coordination position being completed by a longer interaction with one of the SO_2 oxygens (the Sb—O bond length being 2.13 Å). The negative value for the quadrupole coupling constant indicates a reduced electron density along the direction of V_{zz} and suggests that this is collinear with the F—Sb—O axial direction in the molecule.

The spectrum of the 1:1 SbF_3:SbF_5 adduct is shown in Fig. 1 and there are clearly two antimony environments present. The narrow absorption at +11 mm s^{-1} is characteristic of antimony(V) in a near regular octahedron of six fluorines; $[Sb(V)F_6^-]$ salts have isomer shifts of this magnitude (5, 17). At ∼−8 mm s^{-1} a broad asymmetric resonance is observed which is characteristic of antimony(III) in a distorted environment of fluorines. These data are similar to those reported earlier by Birchall *et al.* (5) who isolated two forms for the $SbF_3 \cdot SbF_5$ adduct, which were called forms A and B. Form B was subsequently shown to be $[Sb_6F_{13}^{5+}][SbF_6^-]_5$ (6) and Gillespie and co-workers have recently shown that the compound discussed here is identical to form A (7). In view of the fact that the earlier spectra were only recorded at 80 K, rather than 4 K, the agreement between the two sets of data is acceptable, though the present results must be more accurate considering the improved quality of the spectrum and the more reliable fitting procedures used here.

Gillespie *et al.* (7) have shown that this adduct $SbF_3 \cdot SbF_5$ (A) should be formulated as $[Sb_2F_4^{2+}][SbF_6^-]_2$. They showed that there is a significant interaction between the anions and cation via Sb(V)—F . . . Sb(III) fluorine bridges. This results in a range of Sb(V)—F bond lengths (1.84–1.92 Å) in the hexafluoroantimonate(V) anions and this is undoubtedly the origin of the small quadrupole coupling constant found for the antimony(V) sites. The parameters listed in Table 1 for the Sb(III) site clearly indicate the presence of a stereochemically active *5s* electron pair. The positive value for the quadrupole coupling constant suggests that V_{zz} lies through this lone pair of electrons. However, a simple interpretation of the Sb(III) resonance is not possible. It has been shown that the $[Sb_2F_4^{2+}]$ cation can be approximately described as an SbF_3 molecule linked to an $[SbF^{2+}]$ ion. Further fluorine bridging results in an infinite chain cation $[Sb_2F_4^{2n+}]_n$. One antimony has an environment similar to that in SbF_3 (19), but with one additional long Sb—F contact, while the other antimony has one short Sb—F bond (1.85 Å) and five longer

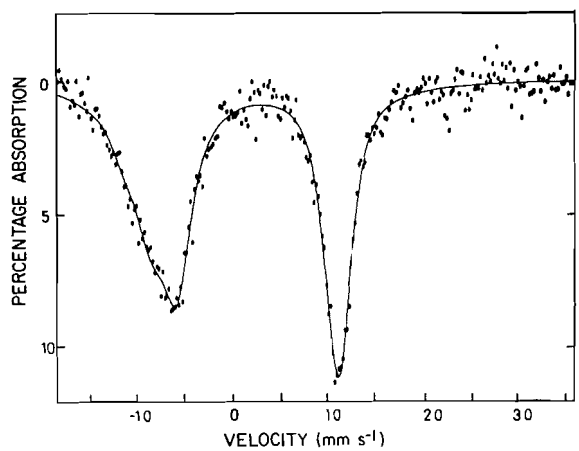

FIG. 1. The ^{121}Sb Mössbauer spectrum of $[Sb_2F_4^{2+}][SbF_6^-]_2$ at 4 K.

Can. J. Chem. Downloaded from www.nrcresearchpress.com by 210.87.254.5 on 09/05/12
For personal use only.

contacts (2.10–2.42 Å). The antimony(III) environments are clearly different yet separate Mössbauer resonances are not resolved. Attempts were made to fit this region of the spectrum to two sites, but meaningful results were not obtained. However, the line width obtained for the Sb(III) site is much larger than normally expected and perhaps can be taken as indicating the presence of more than one Sb(III) site. The data therefore only establish the presence of the lower oxidation state of antimony in a distorted environment. A similar situation pertains in $[Sb_6F_{13}^{5+}][SbF_6^-]_5$ ($SbF_3 \cdot SbF_5$(B)), where again more than one Sb(III) environment is present (6) but not resolved (5).

The remaining compounds in Table 1 contain two anions, namely, $[SbF_6^-]$ and $[Sb_3F_{14}^-]$. This latter anion consists, in all cases, of two $Sb(V)F_6$ octahedra linked by fluorine bridges to an $Sb(III)F_2$ group. Gillespie and co-workers have shown (8–10) that, in these anions, the bridging fluorine atoms are closer to the antimony(V) atoms than to the central antimony(III) atom. Thus $[Sb_3F_{14}^-]$ can be approximately described as an $[Sb(III)F_2^+]$ ion linked by fluorine bridges to two $[Sb(V)F_6^-]$ ions. In all of these compounds, these antimony(V) environments and that of the independent $[SbF_6^-]$ anion are slightly distorted from octahedral geometry.

All three compounds exhibit absorption in both the Sb(III) and Sb(V) regions of the spectrum. The sharp resonance at 11 mm s^{-1} in each spectrum is characteristic of an antimony(V) coordinated by six fluoride ions. The slight distortion present in these $[Sb(V)F_6^-]$ species (8–10) is not evident from the Mössbauer spectrum, nor are the two types of $[Sb(V)F_6^-]$ resolved. The other resonance absorptions in each of these spectra occur at negative velocities with respect to InSb. In the case of $[Te_2Se_2^{2+}]$-$[SbF_6^-][Sb_3F_{14}^-]$ this resonance is broad and very asymmetric, which is typical of the very distorted environments found in SbF_3 and its adducts (e.g. Fig. 1). The distorted environment is attributed to the influence of a stereochemically active electron pair. The isomer shift value of −6.5 mm s^{-1} indicates that there is considerable *s* character to the Sb(III)—F bonds. In fitting this Sb(III) resonance absorption it was necessary to include a variable asymmetry parameter ($\eta = (V_{xx} - V_{yy})/V_{zz}$) in order to obtain a satisfactory fit: the best η value was found to be 0.49. Normally antimony(III) spectra have a zero, or small, value for η, which is usually attributed to the principal component of the electric field gradient tensor, V_{zz}, being coincident with the symmetry axis through the active electron pair and bisecting the angles formed by the normally three short Sb(III)—X bonds, as in SbF_3 (20). A large η value signifies that these axes are not coincident or that the three-fold symmetry axis has been destroyed. Gillspie and co-workers (8) have shown that the immediate antimony(III) environment consists of two short Sb—F distances (1.91 Å) and two somewhat longer ones (2.18 Å); the coordination sphere is completed by four much longer Sb—F contacts. There is no three-fold axis and one would therefore expect a nonzero value for η.

The resonance absorptions at negative velocities for the $[Se_{0.7}Te_{3.3}^{2+}]$ and $[S_4N_4^{2+}]$ compounds are rather unusual for an Sb(III) species. Figure 2 shows the spectrum for $[Se_{0.7}Te_{3.3}^{2+}][SbF_6^-][Sb_3F_{14}^-]$. The resonance in the Sb(III) region appears as a symmetrical doublet. This region can be fitted to two antimony(III) environments with cubic environments having isomer shift values of −5.1 and −8.8 mm s^{-1}. These parameters are rather unrealistic for Sb(III)—F systems. Furthermore it is known that there is only one antimony(III) environment in these compounds which is very distorted from cubic symmetry (9, 10). It has been shown that the ^{121}Sb spectrum becomes more symmetrical as $\eta \rightarrow 1$, and when $\eta = 1$ it has the appearance of a symmetrical doublet (4). Our spectra were fitted with a variable η value and both gave $\eta = 1$, though admittedly the

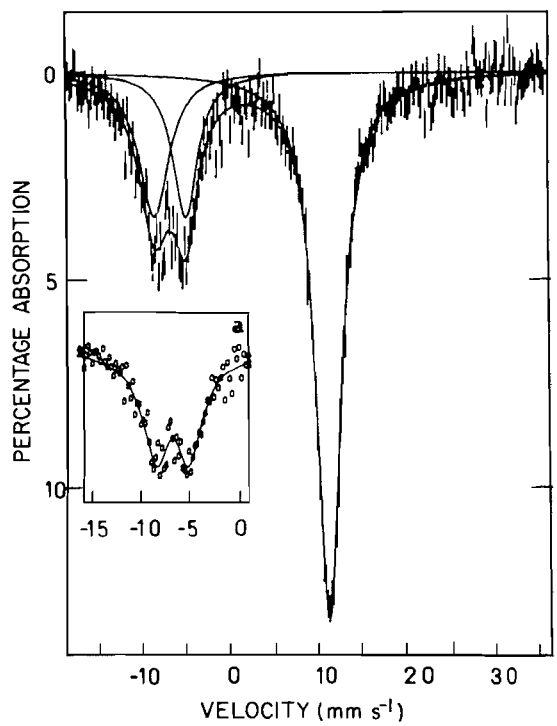

FIG. 2. The ^{121}Sb Mössbauer spectrum of $[Se_{0.7}Te_{3.3}^{2+}]$-$[SbF_6^-][Sb_3F_{14}^-]$ at 4 K. Insert (*a*) Sb(III) region fitted to an eight-line quadrupole pattern with variable η value.

TABLE 2. Antimony(III)–fluorine bond distances in the $[Sb_3F_{14}^-]$ ion

Compound	Distance
$[Se_2Te_2^{2+}]$ $[SbF_6^-]$ $[Sb_3F_{14}^-]$	2 × 1.91; 2 × 2.18; 2 × 2.59; 2.94; 3.07
$[Se_{0.7}Te_{3.3}^{2+}]$ $[SbF_6^-]$ $[Sb_3F_{14}^-]$	1.89; 1.91; 2.19; 2.25; 2.63; 2.77; 2.83; 2.92
$[S_4N_4^{2+}]$ $[SbF_6^-]$ $[Sb_3F_{14}^-]$	1.89; 1.91; 2.27; 2.29; 2.72; 2.73; 3.00; 3.01

error on this value is large. Nevertheless the Sb(III) region of the spectra does have the appearance of symmetrical doublets consistent with this value. Such spectra are rather unusual and few examples are known. The first reported case was for $[(C_6H_5)_2Sb]_2O$ which had $\eta = 0.89$ (21). Alkyl antimony(III) halides also give a similar doublet-like spectrum and have $\eta = 0.9$ (22) though these compounds were not isolated in pure form. These were the only antimony(III) cases known until now. Recently Greenwood and co-workers (23) reported an example for Sb(V) and Ruddick and Sams (24) reported a case where $\eta = 0.75 \pm 0.06$. In this latter case no spectrum was shown so presumably a doublet-like structure was not observed. In all of the previous cases where $\eta \rightarrow 1$, the ligands bonded to the antimony varied considerably in relative electronegativities, i.e. C and O (21), C and Cl (22), C and N or O (23). The examples reported here are the first to show this phenomenon where all of the ligands bonded to the antimony are the same kind, in these cases, fluorine.

A comparison of the parameters for the three $[Sb_3F_{14}^-]$ compounds shows that the $[Se_2Te_2^{2+}]$ compound has a more positive isomer shift, a smaller quadrupole coupling constant and a lower η value than the $[Se_{0.7}Te_{3.3}^{2+}]$ and $[S_4N_4^{2+}]$ analogues. These differences indicate a lower *s* electron density at antimony and a slightly more symmetrical environment. The most intriguing change is the increase in η from 0.49 to 1, since the basic geometry about the central antimony(III) in the $[Sb_3F_{14}^-]$ ion is not dramatically different for the three compounds. In all cases the antimony(III) is surrounded by eight fluorines, to form a distorted monocapped square antiprism, with the lone pair occupying the capped position (Fig. 3). The relevant bond lengths are summarised in Table 2. In the $[Se_2Te_2^{2+}]$ compound there are two equal short Sb—F lengths at 1.91 Å whereas the other compounds have unequal short Sb—F bonds and the two next nearest interactions are also different at 1.89 Å and 1.91 Å. While these are small differences they are real and destroy the plane of symmetry existing in the $[Sb_3F_{14}^-]$ ion in the $[Se_2Te_2^{2+}]$ compound. Presumably the large asymmetry parameter is due to the complete lack of symmetry at the antimony(III) and to the large percentage change in Sb—F distance for the closest

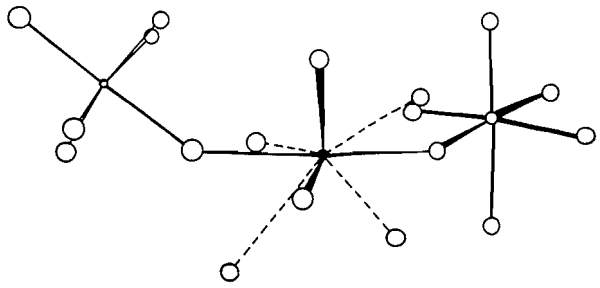

FIG. 3. The $[Sb_3F_{14}^-]$ anion in $[S_4N_4^{2+}][SbF_6^-][Sb_3F_{14}^-]$. --- Long contacts to neighbouring F atoms. ● Sb(III); ○ Sb(V); ○ F.

interactions. Increases in Sb—F distance undoubtedly reflect a lower involvement of 5*s* electrons or increasing *p* character in these bonds which will influence the Mössbauer parameters. If one compares the average Sb—F bond length in the three anions one finds that the order of increasing Sb—F (average) distance follows the change in isomer shift. The anion with the longest Sb—F (ave) bond length has the most negative isomer shift, the highest *s* electron density at antimony and therefore less average *s* character in the Sb—F bonds.

Acknowledgement

The National Research Council of Canada is thanked for financial support.

1. T. BIRCHALL and B. DELLA VALLE. Chem. Commun. 675 (1970).
2. G. G. LONG, R. J. TULBANE, and L. H. BOWEN. Abstracts 158th Am. Chem. Soc. Meeting, New York, Sept. (1969).
3. T. BIRCHALL, B. DELLA VALLE, E. MARTINEAU, and J. B. MILNE. J. Chem. Soc. A, 1885 (1971).
4. J. D. DONALDSON, M. J. TRICKER, and B. W. DALE. J. Chem. Soc. Dalton Trans. 893 (1972).
5. T. BIRCHALL, P. A. W. DEAN, B. DELLA VALLE, and R. J. GILLESPIE. Can. J. Chem. **51**, 667 (1973).
6. A. J. EDWARDS and D. R. SLIM. J. Chem. Soc. Chem. Commun. 178 (1974).
7. R. J. GILLESPIE, D. R. SLIM, and J. E. VEKRIS. J. Chem. Soc. Dalton Trans. 971 (1977).
8. R. J. GILLESPIE, E. MAHARAJH, and D. R. SLIM. Unpublished work.
9. R. J. GILLESPIE, E. MAHARAJH, and D. R. SLIM. Unpublished work.
10. R. J. GILLESPIE, D. R. SLIM, and D. TYRER. J. Chem. Soc. Chem. Commun. 253 (1977).
11. A. J. EDWARDS and R. J. C. SILLS. J. Chem. Soc. A, 942 (1971).

Can. J. Chem. Downloaded from www.nrcresearchpress.com by 210.87.254.5 on 09/05/12
For personal use only.

12. D. M. BYLER and D. F. SHRIVER. Inorg. Chem. **15**, 32 (1976).
13. T. BIRCHALL and A. F. REID. J. Solid State Chem. **13**, 351 (1975).
14. G. K. SHENOY, J. M. FRIEDT, H. MALETTA, and S. L. RUBY. Mössbauer effect methodology, **9**, 277 (1974).
15. G. M. BANCROFT, W. K. ONG, A. G. MADDOCK, R. K. PRINCE, and A. J. STONE. J. Chem. Soc. A, 1966 (1967).
16. T. E. CRANSHAW. J. Phys. E, **7**, 1 (1974).
17. H. A. CARTER, J. M. RUDDICK, J. R. SAMS, and F. AUBKE. Inorg. Nucl. Chem. Lett. **11**, 29 (1975).
18. J. W. MOORE, H. W. BAIRD, and H. B. MILLER. J. Am. Chem. Soc. **90**, 1385 (1968).
19. A. J. EDWARDS. J. Chem. Soc. A, 2751 (1970).
20. J. G. BALLARD, T. BIRCHALL, R. FOURCADE, and G. MASCHERPA. J. Chem. Soc. Dalton Trans. 2409 (1976).
21. L. H. BOWEN, G. G. LONG, J. G. STEVENS, N. C. CAMPBELL, and T. B. BRILL. Inorg. Chem. **13**, 1787 (1974).
22. J. P. DEVORT, J. P. SANCHEZ, J. M. FRIEDT, and G. K. SHENOY. J. Phys. Coll. C6 **35**, C6-225 (1974).
23. N. BERTAZZI, F. DIBIANCA, T. C. GIBB, N. N. GREENWOOD, H. A. MEINEMA, and J. G. NOLTES. J. Chem. Soc. Dalton Trans. 957 (1977).
24. J. N. R. RUDDICK and J. R. SAMS. Inorg. Nucl. Chem. Lett. **11**, 229 (1975).

Can. J. Chem. Downloaded from www.nrcresearchpress.com by 210.87.254.5 on 09/05/12
For personal use only.

The chlorination of sulfides: A reassessment of product controlling factors

TERENCE PATRICK AHERN, DENIS GEORGE KAY, AND RICHARD FRANCIS LANGLER[1]

Department of Chemistry, Dalhousie University, Halifax, N.S., Canada B3H 4J3

Received April 3, 1978

TERENCE PATRICK AHERN, DENIS GEORGE KAY, and RICHARD FRANCIS LANGLER. Can. J. Chem. **56**, 2422 (1978).

A reexamination of previous proposals for the prediction of regioselectivity in sulfide chlorinations has found them to be unsatisfactory. A new basis for such predictions is advanced viz. the electronegativity difference (ΔX_p) of the substituents attached to the α- and α′-carbon atoms of the sulfide substrate. Upon establishing that the new basis for these predictions is satisfactory, it is successfully applied to the problem of predicting reactivity differences in isomeric sulfide chlorinations. The formation of isomeric sulfonium ions is used to establish the failure of possible isomerization processes to occur under normal reaction conditions.

TERENCE PATRICK AHERN, DENIS GEORGE KAY et RICHARD FRANCIS LANGLER. Can. J. Chem. **56**, 2422 (1978).

Après un réexamen des propositions antérieures concernant la prédiction de la régiosélectivité des chlorations de sulfures, on peut les considérer comme non-satisfaisantes. On propose une nouvelle base pour de telles prédictions, à savoir la différence électronégativité (ΔX_p) des substituants attachés sur les atomes de carbones α et α′ du substrat sulfuré. Après avoir établit que la nouvelle base pour ces prédictions est satisfaisante, on l'applique avec succès aux problèmes de la prédiction des différences de réactivité lors des chlorations de sulfures isomères. On utilise la formation d'ions sulfonium isomères pour établir le fait que des processus d'isomérisation, possibles dans des conditions normales de la réaction, ne se produisent pas.

[Traduit par le journal]

Introduction

A substantial number of reports (1–21) which deal with the chlorination of sulfides has appeared in the literature. These reports have led to a somewhat confusing view of the product controlling factors.

The chlorination of sulfides[2] proceeds as depicted in Scheme 1. The mechanism for the Pummerer re-

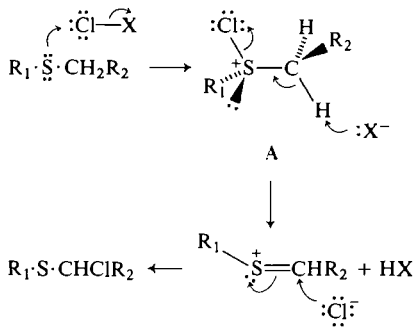

SCHEME 1

arrangement of chlorosulfonium salts **A** is due to Wilson and Huang (11) who examined the chlorination of some benzylic sulfides and concluded that the reactions proceed through a "relatively central E2 elimination." This mechanism appears to be quite general since even sulfides with an α-carbonyl group fail to deuterate when the reactions are conducted in a deuterated medium (21).

In one of the earlier papers attempting to deal with regioselectivity in chlorosulfide product formation, Paquette *et al.* (18) examined the reaction of a series of substituted benzyl chloromethyl sulfides with sulfuryl chloride. The results are shown below.

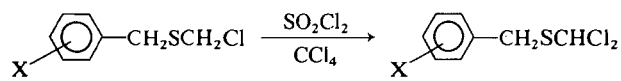

1 **2**

a X = H, *b* X = *p*-Cl, *c* X = *p*-F, *d* X = *m*-CF_3

When the substituent on the phenyl group was changed to a *p*-nitro group the following results were obtained.

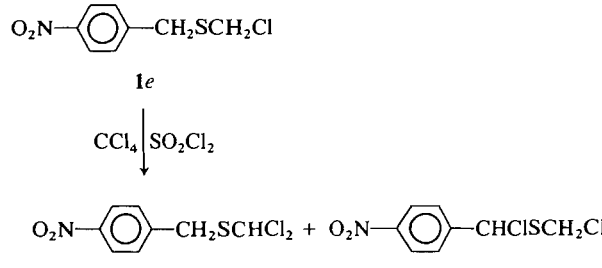

2*e* (40%) **3** (60%)

On the basis of these results it was suggested that pursuant to chlorosulfonium salt formation (**A**,

[1]To whom all correspondence should be addressed.

[2]Sulfuryl chloride, *N*-chlorosuccinimide, and molecular chlorine are all presumed to form chlorosulfonium salts (**A**) as shown in Scheme 1.

Can. J. Chem. Downloaded from www.nrcresearchpress.com by 210.87.254.40 on 09/05/12
For personal use only.

Can. J. Chem. Downloaded from www.nrcresearchpress.com by 210.87.254.40 on 09/05/12
For personal use only.

TABLE 1. ΔpK_a values* of chlorine and phenyl substituted acids*

Parent acid	Substituted acid	ΔpK_a (ref.)†
CH_3CCH_3 (O)	CH_3CCH_2Ph (O)	7.2 (22)
$CH_3SO_2CH_3$	$CH_3SO_2CH_2Ph$	5.8 (22)
CH_3CCH_3 (O)	CH_3CCH_2Cl (O)	3.5 (23)
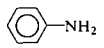	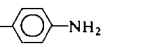	8.5 (24)

*pK_a of parent acid less pK_a of substituted acid.
†pK_a values from ref. 22 determined in DMSO; pK_a values from ref. 23 determined in H_2O.

Scheme 1) "the most acidic α-hydrogen is subject to abstraction and the resulting ylid is transformed to the observed α-chlorosulfide" (18).

Table 1 presents ΔpK_a values for selected acids. These values indicate that all of the benzylic sulfides **1***a* → **1***e* would form chlorosulfonium salts in which the thermodynamic acidity of the benzylic protons would be greater than that of the chloromethyl protons. To find support for expected differences in these thermodynamic acidities, we decided to perform a pair of deuterium exchange experiments. Although sulfoxides are the direct oxy analogues of chlorosulfonium cations,[3] we have chosen sulfone substrates on the grounds that the relative acidities of α- and α′-protons in sulfoxides and sulfones are similar and that sulfones exchange α- and α′-protons under significantly milder conditions than do sulfoxides.

When an equimolar mixture of chloromethyl methyl sulfone and benzyl methyl sulfone was treated with ethanol-*d* in the presence of dilute NaOD catalysis, the product obtained was benzyl methyl sulfone (ca. 25% deuterated, exclusively at the benzylic carbon) and chloromethyl methyl sulfone (ca. 60% deuterated, exclusively at the chloromethyl carbon).

Reflux of a neutral solution of *p*-nitrobenzyl chloromethyl sulfone in ethanol-*d*–D_2O furnished the starting sulfone exclusively deuterated at the benzylic carbon (ca. 75%).

The results indicate that the chlorosulfonium cations (derived from **1***a* and **1***d*) have chloromethyl protons which are similar in thermodynamic acidity to simple benzylic protons and very much less acidic than *p*-nitrobenzylic protons, as expected from the ΔpK_a values in Table 1. Presuming that (*i*) the kinetic acidity of these protons parallels their thermodynamic acidity and that (*ii*) the kinetic acidity of the α- and α′-protons in the chlorosulfonium cations controls regioselectivity in the chlorinations of **1***a* → **1***d*, then mixtures of the regioisomeric dichlorosulfides should have been observed with increasing chlorination at the benzylic carbon as one proceeds through the series. No such result was observed, but instead the progressively increasing acidity of the benzylic protons had no effect on the regioselectivity for the dichlorosulfide products. Furthermore, the chlorination of **1***e* should have furnished **3** regiospecifically, when in fact, the reaction was hardly even regioselective. Consequently, it now appears that the acidity of α-hydrogens does not control regioselectivity in sulfide chlorinations.

Another approach to predicting regioselectivity in sulfide chlorinations may be advanced on the basis of a consideration of the two major resonance contributors (**B** and **C**) for sulfonium ions.[4,5]

$$R_1—\overset{+}{\underset{\cdot\cdot}{S}}=CHR_2 \longleftrightarrow R_1—\overset{\cdot\cdot}{\underset{+}{S}}—\overset{+}{C}HR_2$$

B **C**

Contributor **C** would be stabilized by electron-releasing groups and therefore an analysis of substituent effects on carbonium ion stability might be fruitful in attempting to anticipate regioselectivity in sulfide chlorinations.

One of the earlier reports concerning asymmetric sulfide chlorinations (20) appears to offer some support for this view.

$$CH_3SCH_2CH_3 + Cl_2 \xrightarrow{0°C} CH_3SCHClCH_3$$

Tuleen and Stephens (17) have extended these results and have shown that in general the chlorination of asymmetric dialkyl sulfides with NCS or SO_2Cl_2 gives products chlorinated preferentially in the more substituted alkyl group. They propose that E2 elimination of HCl from the chlorosulfonium salt (**A**, Scheme 1) produces a *carbonium ion* and that differences in chlorinations with SO_2Cl_2 and NCS are dictated by carbonium ion stability. To rationalize the observation that α-chlorodialkyl sulfides preferentially chlorinate in the chloroalkyl group, they suggested that there might be "stabilization of an incipient carbonium ion by a resonance

[3]Chlorosulfonium cations are unstable reactive intermediates and would be unsuitable substrates for exchange experiments.

[4]Throughout this paper the designation of these ions will be restricted to 'sulfonium ions' rather than 'carbonium-sulfonium ions' or 'sulfo-carbonium ions' because the latter names do not appear to be in keeping with the electronic nature of these ions.

[5]Discussions concerning the nature of π bonding in sulfonium ions have appeared previously (25–29).

Can. J. Chem. Downloaded from www.nrcresearchpress.com by 210.87.254.40 on 09/05/12
For personal use only.

interaction involving electron donation from chlorine to carbon" (17). Such a proposal is clearly unsatisfactory since (*i*) a chlorine atom directly attached to a positively charged carbon atom provides "added destabilization of . . . . [a] carbonium ion" (19) and (*ii*) regioselectivity derived from carbonium ion stability would require, for example, that the chlorination of **1***a* furnish predominantly the cross-chlorinated sulfide which is in fact, not formed at all.

Consequently, incipient carbonium ion stability does not control regioselectivity in sulfide chlorinations.

Results and Discussion

In the introduction we have attempted to show that regioselectivity exhibited in the chlorination of asymmetric sulfides cannot be predicted by considering the relative acidities of α-hydrogens or by analyzing incipient carbonium ion stability.

A recent paper by Csizmadia *et al.* (28) has been most helpful in dealing with this problem. They have shown, on the basis of nonempirical SCF-MO computations, that for CH_2OH^+ there is a *net electron donation from oxygen to carbon of 0.03 electron* and for CH_2SH^+ there is a *net electron donation from sulfur to carbon of 0.68 electron*. They have also found that the *CS π overlap is substantially greater than the CO π overlap*.

The implication of their calculations, for resonance theory, is that the importance of the resonance contributor **B** is much greater than had been believed previously (25–29). If one makes the assumption that the resonance contributor **C** has minor significance for the sulfonium ion and that **B** is essentially a complete description of the ion, then substituent effects are readily predicted. Electron-withdrawing substituents attached to the carbon of the CS π bond would assist electron transfer from sulfur to carbon, whereas electron-withdrawing substituents attached to the other carbon atom which is attached to sulfur would resist electron transfer from sulfur to carbon. Therefore the more stable regioisomeric sulfonium ion would have the electron-withdrawing substituent attached to the carbon of the CS π bond. Substituent effects would be expected to alter the transition state energy for the E2 elimination (see **A**, Scheme 1) in the same way, on the grounds that the transition state energy will be sensitive to the nature of the developing CS π bond.

An immediate consequence of this postulate is that regioselectivity in the chlorination of asymmetric sulfides is subject to control by the electronegativity difference between the substituents on the α- and α′-carbon atoms attached to sulfur. Chlorination will go into the group which has the more electronegative substituent on the grounds that such a group will maximize electron transfer from sulfur to carbon in the E2 transition state and in the intermediate sulfonium ion and thereby minimize the energies of both species.

To test our hypothesis we have employed the elegant and versatile method of Huheey (30, 31) for the calculation of group electronegativities. A selection of relevant group electronegativities appears in Table 2. The application of group electronegativities to the prediction of regioselectivity in virtually every known asymmetric sulfide chlorination is shown in Table 3. Table 3 shows that *the electronegativity difference* (ΔX_p) *qualitatively predicts the observed regioselectivity in every case*, independent of chlorinating agent, solvent or sulfide substrate. Table 3 also shows the results for calculations on Paquette's systems and offers a rationale for the failure of **1***a* → **1***d* to furnish regioisomeric dichlorosulfides as well as for the slight regioselectivity observed upon the chlorination of **1***e*. Subsequent to the development of our view of product controlling factors vis à vis regioselectivity in the chlorination of sulfides, we have turned our attention to another problem.

Some time ago we had observed that the chlorination of chlorodimethylsulfide with molecular chlorine in carbon tetrachloride, or in glacial acetic acid would not proceed past the formation of tetrachlorodimethyl sulfide (33). The lack of reactivity of the tetrachlorosulfide was clearly due to the

TABLE 2. Group electronegativities*

Group	Pauling electronegativity (X_p)	*a*	*b*
H—	2.20	—	—
CH_3—	2.27	—	—
CH_3CH_2—	2.28	—	—
Cl—	2.94	—	—
NC—	3.84	—	—
Cl_3C—	2.84	—	—
Ph—	2.49	—	—
ClC_6H_4—	2.56	—	—
FC_6H_4—	2.55	—	—
$O_2NC_6H_4$—	2.98	—	—
EtO(O)C—	2.94	—	—
CH_3SO_2—	3.10	—	—
$PhSO_2$—	2.90	—	—
$CH_3SO_2CH_2$—	2.85	9.11	1.35
CH_3SO_2CHCl—	2.93	9.34	1.33
$CH_3SO_2CCl_2$—	3.00	9.57	1.31
CH_3CHCl—	2.39	7.74	1.81
$ClC_6H_4(O)C$—	2.72	8.70	1.03
$CF_3C_6H_4$—	2.75	8.80	0.99

*Group electronegativities without *a* and *b* values are taken from Huheey's data (30, 31). Group electronegativities where *a* and *b* values are supplied were calculated using Huheey's method.

Can. J. Chem. Downloaded from www.nrcresearchpress.com by 210.87.254.40 on 09/05/12
For personal use only.

failure of the corresponding chlorosulfonium chloride salt to undergo Pummerer rearrangement since chlorination of tetrachlorosulfide in dilute aqueous acetic acid furnished the corresponding tetrachlorosulfoxide.[6] A summary of the relevant information appears below.

$$Cl_3C{\cdot}S{\cdot}CH_3 \xrightarrow[HOAc]{Cl_2} Cl_3C\overset{+}{\underset{\cdot\cdot}{S}}{=}CH_2 + Cl^- \longrightarrow Cl_3C{\cdot}S{\cdot}CH_2Cl$$

I

$$Cl_3C{\cdot}S{\cdot}CH_2Cl \xrightarrow[HOAc]{Cl_2} Cl_3C\overset{+}{\underset{\cdot\cdot}{S}}{=}CHCl + Cl^-$$

II

In considering the activation energies for the formation of **I** and **II**, two factors should be examined. Firstly, **II** contains one more chlorine atom than **I**. The additional chlorine atom will increase the demand for electron density on the positively charged sulfur atom, thereby increasing the transition state energy for the formation of **II** as compared to that for the formation of **I**. Secondly, since the electronegativity difference of the substituents in **II** is smaller[7] than it is for the substituents in **I**, **II** should form the more favourable π bond with a resultant lowering in the activation energy for the formation of **II**. From the order of reactivities of the two chlorinated dimethyl sulfides, the inductive effect of an additional chlorine atom in destabilizing the sulfonium ion by increasing charge concentration on sulfur is more important than its stabilizing effect which operated by enhancing the CS π bond. Clearly, then if we were to establish reactivity as support for our view of the product controlling factors in sulfide chlorinations, we needed a pair of *isomeric* sulfides in which the overall demand for electron density is the same for the sulfur atom but the nature of the CS π bonds would be very different.

In pursuit of such a system, we have prepared and chlorinated the mesylsulfide **4**.

$$CH_3SO_2CH_2SCH_2CH_3 \xrightarrow[CCl_4]{Cl_2} CH_3SO_2CCl_2SCH_2CH_3$$

4 **5**

After bubbling chlorine gas into the reaction mixture for 10 min, the entire sample had been cleanly converted into the mesyldichlorosulfide **5**. Additional chlorination for 4 h effected no further change.

[6]Details of the chlorination reactions of sulfides and sulfoxides in aqueous media have been published previously (34). Sulfoxide formation has been used to confirm the formation of a chlorosulfonium chloride salt (13).

[7]Since the electronegativity differences in these cases disfavour further reaction, the smaller ΔX_p, the more favourable reaction should become.

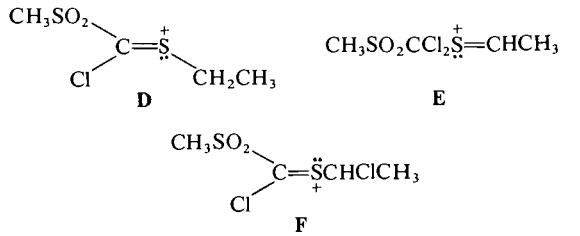

The chlorination of **4** must have successfully produced the sulfonium ion **D** in order for **5** to form. The failure of **E** to form could be anticipated on the basis of the large electronegativity difference between the α- and α'-substituents which disfavors the formation of **E** from the corresponding chlorosulfonium chloride salt. However, **F** would be expected to have a much lower activation energy for formation than **E**, since the destabilizing inductive demands on sulfur are essentially the same in **E** and **F**, but the CS π bond in **F** would be much better than in **E**.

To test this hypothesis, we have synthesized the appropriate mesylchlorosulfide **6** as shown in Scheme 2. The chlorination of **6** furnished the

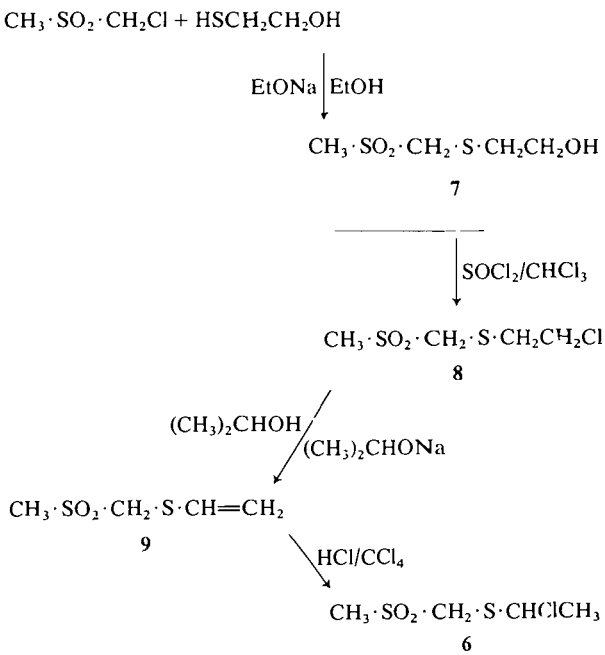

SCHEME 2

mesyltrichlorosulfide **10** in the same chlorination time per gram employed for the conversion of **4** into **5**.

$$CH_3SO_2CH_2SCHClCH_3 \xrightarrow[CCl_4]{Cl_2} CH_3SO_2CCl_2SCHClCH_3$$

6 **10**

Thus, we have experimentally demonstrated the facile formation of **F** under conditions which would

Can. J. Chem. Downloaded from www.nrcresearchpress.com by 210.87.254.40 on 09/05/12
For personal use only.

not furnish **E**. Therefore, as we have predicted on the grounds of CS π bond strengths, the activation energy for the formation of **F** is substantially lower than the activation energy for the formation of **E**. To our knowledge, this constitutes the first report that the *extent* of chlorine incorporation is a function of the substitution pattern of the sulfide substrate.

A fundamental problem connected with studies of sulfide chlorinations has been the unsupported assumption that the carbon bearing chlorine in the product was the carbon atom from which the proton was initially abstracted in the E2 elimination (see Scheme 1). In other words it has been tacitly assumed that sulfonium ions are unable to isomerize under normal reaction conditions. Our results provide a good test of this assumption. The chlorination of **4** must proceed to furnish **12** which is converted into **5** as described previously.

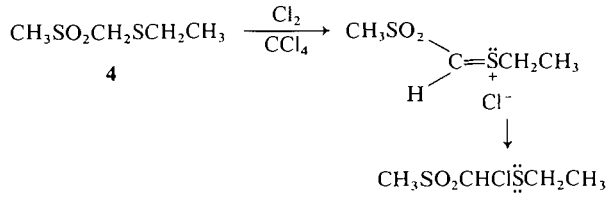

4 **12**

The reaction of alkene **9** with HCl (*vide* Scheme 2) must proceed through the isomeric sulfonium ion as shown below.

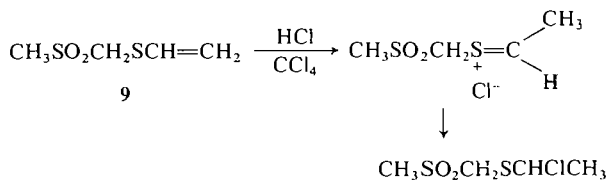

9 **6**

TABLE 3. Regioisomeric chlorosulfides from sulfide chlorinations

Sulfide substrate ($R_1CH_2SCH_2R_2$)	Chlorosulfide products: Major (% yield)	Chlorosulfide products: Minor (% yield)	ΔX_p* ($X_{R_1} - X_{R_2}$)	Reference
	Reagent: SO_2Cl_2			
$PhCH_2SCH_3$	$PhCHClSCH_3$ (100%)	—	0.29	18
	(100%)	—	0.22	18
$pClC_6H_4CH_2SCH_2Ph$	$pClC_6H_4CHClSCH_2Ph$ (62%)	$pClC_6H_4CH_2SCHClPh$ (38%)	0.07	18
$ClCH_2SCH_2Ph$	Cl_2CHSCH_2Ph (100%)	—	0.45	18
$ClCH_2SC_6H_{11}$	$Cl_2CHSC_6H_{11}$ (100%)	—	0.60	18
$ClCH_2SCH_2C_6H_4pF$	$Cl_2CHSCH_2C_6H_4pF$ (100%)	—	0.39	18
$ClCH_2SCH_2C_6H_4pCl$	$Cl_2CHSCH_2C_6H_4pCl$ (100%)	—	0.38	18
$ClCH_2SCH_2C_6H_4mCF_3$	$Cl_2CHSCH_2C_6H_4mCF_3$ (100%)	—	0.19	18
$pO_2NC_6H_4CH_2SCH_2Cl$	$pO_2NC_6H_4CHClSCH_2Cl$ (60%)	$pO_2NC_6H_4CH_2SCHCl_2$ (40%)	0.04	18
$pO_2NC_6H_4CHClSCH_2Cl$	$pO_2NC_6H_4CCl_2SCH_2Cl$ (100%)	—	0.78	18
$Cl_2CHSCH_2C_6H_4pNO_2$	$Cl_3CSCH_2C_6H_4pNO_2$ (100%)	—	0.70	18
$Cl_2CH{\cdot}S{\cdot}CH_3$	Cl_3CSCH_3 (100%)	—	1.48	32
Cl_2CHSCH_2Cl	Cl_3CSCH_2Cl (97%)	$Cl_2CHSCHCl_2$ (3%)	0.74	32
$pClC_6H_4C(O)CH_2SCH_3$	$pClC_6H_4C(O)CHClSCH_3$ (100%)	—	0.45	21
$EtOC(O)CH_2SCH_3$	$EtOC(O)CHClSCH_3$ (100%)	—	0.67	21
$NCCH_2SCH_2Ph$	$NCCHClSCH_2Ph$ (100%)	—	1.35	21
$PhSO_2CH_2SCH_2Ph$	$PhSO_2CHClSCH_2Ph$ (100%)	—	0.41	21

TABLE 3 (*Concluded*)

Sulfide substrate ($R_1CH_2SCH_2R_2$)	Chlorosulfide products: Major (% yield)	Chlorosulfide products: Minor (%	ΔX_p* ($X_{R_1} - X_{R_2}$)	Reference
$CH_3SO_2CH_2SCH_2Ph$	$CH_3SO_2CHClSCH_2Ph$ (100%)	—	0.61	1
$CH_3SO_2CHClSCH_2Ph$	$CH_3SO_2CCl_2SCH_2Ph$ (100%)	—	1.35	1
	Reagent: NCS			
$CH_3CH_2SCH_3$	$CH_3CHClSCH_3$ (77%)	$CH_3CH_2SCH_2Cl$ (23%)	0.07	17
$CH_3CH_2CH_2SCH_3$	$CH_3CH_2CHClSCH_3$ (79%)	$CH_3CH_2CH_2SCH_2Cl$ (21%)	0.08	17
$(CH_3)_2CHSCH_3$	$(CH_3)_2CClSCH_3$ (91%)	$(CH_3)_2CHSCH_2Cl$ (9%)	0.14	17
$(CH_3)_2CHSCH_2CH_3$	$(CH_3)_2CClSCH_2CH_3$ (71%)	$(CH_3)_2CHSCHClCH_3$ (29%)	0.07	17
$ClCH_2SCH_2CH_3$	$Cl_2CHSCH_2CH_3$ (96%)	$ClCH_2SCHClCH_3$ (4%)	0.67	17
$ClCH_2SCH(CH_3)_2$	$Cl_2CHSCH(CH_3)_2$ (89%)	$ClCH_2SCCl(CH_3)_2$ (11%)	0.60	17
$NCCH_2SCH_2CH_3$	$NCCHClSCH_2CH_3$ (100%)	—	1.58	17
$PhCH_2SCH(CH_3)_2$	$PhCHClSCH(CH_3)_2$ (77%)	$PhCH_2SCCl(CH_3)_2$ (23%)	0.15	17
$p CH_3C_6H_4CH_2SCH(CH_3)_2$	$p CH_3C_6H_4CHClSCH(CH_3)_2$ (68%)	$p CH_3C_6H_4CH_2SCCl(CH_3)_2$ (32%)	0.10	17
$p ClC_6H_4CH_2SCH(CH_3)_2$	$p ClC_6H_4CHClSCH(CH_3)_2$ (86%)	$p ClC_6H_4CH_2SCCl(CH_3)_2$ (14%)	0.22	17
	Reagent: $SOCl_2$			
$ClCH_2SCH_3$	Cl_2CHSCH_3 (100%)	—	0.74	32

*In cases where there is more than one substituent on either side the electronegativities were summed and the differences of the sums reported.

Since neither reaction produces any observable amount of the other regioisomeric chlorosulfide (i.e., no **6** from **4** and no **12** from **9**) it is clear that nucleophilic attack by chloride ion on the sulfonium ion is much faster than any available isomerization process. Thus conclusions drawn regarding preferred proton abstraction in the E2 elimination step which are based on locating the chlorine atom in the α-chlorosulfide products are indeed correct.

In conclusion then, (*i*) sulfide chlorinations appear to proceed in general by chlorosulfonium ion formation, followed by E2 elimination of HCl which affords a sulfonium ion (normally attacked by chloride ion on carbon). (*ii*) Which of the regioisomeric sulfonium ions will form predominantly subsequent to E2 elimination from the chlorosulfonium ion can be anticipated on the basis of the electronegativity difference (ΔX_p) of the substituents attached to the α- and α′-carbon atoms. (*iii*) Reactivity differences in isomeric sulfide chlorinations can be predicted on the basis of the ΔX_p of the α- and α′-substituents in conjunction with a consideration of the total electronegativities of all substituents adjacent to sulfur in the starting sulfide.

Further experiments are already underway to examine sulfide chlorinations in terms of regioselectivity as a function of α-substituent electronegativities. As well, a test of this criterion for predicting regioselectivity in the chlorination of sulfoxides is also in progress.

Experimental

General

The ir spectra were recorded on a Perkin-Elmer 237B grating spectrophotometer. The nmr spectra were recorded on a Varian T-60 instrument using TMS as the internal standard. The mass spectra were recorded on a Dupont-CEC model 21-104 mass spectrometer. The samples were directly introduced using an all glass probe and the spectra run at 30 eV with a source temperature of 150°C. Melting points were determined on a Fisher-Johns melting point apparatus and are uncorrected.

Chlorinations

Details have been provided previously (34).

Preparation of $CH_3SO_2CH_2SCH_2CH_2OH$ (7)

Sodium metal (3.460 g) was dissolved in absolute ethanol

Can. J. Chem. Downloaded from www.nrcresearchpress.com by 210.87.254.40 on 09/05/12
For personal use only.

Can. J. Chem. Downloaded from www.nrcresearchpress.com by 210.87.254.40 on 09/05/12
For personal use only.

(250 ml). 2-Mercaptoethanol (11.768 g) and chloromethyl methyl sulfone (35) (20.002 g) were added and the reaction mixture refluxed for 24 h. The reaction mixture was cooled and the ethanol evaporated. Water (10 ml) was added to the concentrate and the pH adjusted to ca. 4 with glacial acetic acid. Chloroform (500 ml) was added and the solution dried and concentrated. The crude concentrate was dissolved in 95% ethanol (15 ml), stored at −20°C overnight and seeded.[8] Filtration afforded clean sulfone-sulfide-alcohol (7) (17.89 g, mp 37–39°C); ir ($CHCl_3$): 3540, 1310, and 1140 cm^{-1}; nmr ($CDCl_3$) δ: 2.26 (1H, s), 3.02 (5H, m), 3.86 (2H, t), and 4.00 (2H, s); ms *m/e*: 170 (M^+, 2.1%), 91 (92.7%), 61 (100%), and 45 (89.1%). *Anal.* calcd. for $C_4H_{10}O_3S_2$: C 28.21, H 5.92; found: C 27.93, H 5.88.

Preparation of $CH_3SO_2CH_2SCH_2CH_2Cl$ (8)

A solution of the alcohol (7) (4.998 g) in chloroform (15 ml) was brought to gentle reflux and a solution of $SOCl_2$ (3.504 g) in chloroform (10 ml) added dropwise over 10 min. Upon completion of the addition, the mixture was refluxed for 2 h. The chloroform was evaporated and the residue chromatographed on silica gel (500 g). The column was washed with diethyl ether (50 100-ml fractions). Fractions 20–50 were combined and concentrated affording clean chlorosulfone sulfide (**8**) (2.047 g, mp 40–43°C); ir ($CHCl_3$): 1320 and 1140 cm^{-1}; nmr ($CDCl_3$) δ: 3.06 (3H, s), 3.26 (2H, t), 3.80 (2H, t), and 4.00 (2H, s); ms *m/e*: 190 (1.7%), 188 (M^+, 5.4%), 111 (33.2%), and 109 (100%). *Anal.* calcd. for $C_4H_9ClO_2S_2$: C 25.46, H 4.80; found: C 25.58, H 4.75.

Preparation of $CH_3SO_2CH_2SCH{=}CH_2$ (9)

Sodium metal (0.120 g) was added to 2-propanol (5 ml) and the mixture refluxed until all the sodium dissolved. A solution of the chlorosulfonesulfide (**8**) (1.002 g) in 2-propanol (5 ml) was added to the sodium isopropoxide solution and the reaction mixture stirred at ambient temperature for 1 h. Water (50 ml) was added and the resultant mixture washed with chloroform (four 50 ml aliquots). After drying and concentration the chloroform solution furnished crude sulfone vinylsulfide (0.687 g). After recrystallization[9] from 95% ethanol the alkene (**9**) had mp 50–52°C; ir ($CHCl_3$): 1595, 1320, 1140, and 960 cm^{-1}; nmr ($CDCl_3$) δ: 3.03 (3H, s), 4.10 (2H, s), 5.50, and 6.50 (3H, $J_{AB} \sim 0$, $J_{AC} \sim 16$ Hz and $J_{BC} \sim 11$ Hz); ms *m/e*: 152 (M^+, 9.2%), 73 (69.2%), and 45 (100%). *Anal.* calcd. for $C_4H_8O_2S_2$: C 31.55, H 5.29; found: C 31.50, H 5.30.

Preparation of $CH_3SO_2CH_2SCHClCH_3$ (6)

The alkene-sulfone-sulfide (**9**) (1.001 g) was added to carbon tetrachloride (35 ml). HCl gas (ca. 200 ml/min) was bubbled into the mixture for 2 h. As the reaction proceeds the alkene goes into solution. About 10 min before completion of the reaction the chlorosulfone sulfide (**6**) begins to precipitate from solution. Sufficient chloroform to just dissolve precipitated product was added, the reaction mixture filtered, and the solvent evaporated affording clean chlorosulfone sulfide (**6**) (1.0648 g). After recrystallization from carbon tetrachloride the product had mp 56–59°C. This compound is unstable at room temperature and should be used within a week after preparation; ir ($CHCl_3$): 1340 and 1145 cm^{-1}; nmr ($CDCl_3$) δ: 1.93 (3H, d, $J = 7$ Hz), 3.10 (3H, s), 4.00 (1H, d, $J = 15$ Hz), 4.33 (1H, d, $J = 15$ Hz), and 5.77 (1H, q, $J = 7$ Hz); ms *m/e*: 190 (2.9%), 188 (M^+, 8.9%), 111 (31.3%), 109 (94.0%), 73 (77.6%), 47 (83.5%), and 45 (100%).

The corresponding β-disulfone was prepared from the chlorosulfone-sulfide (**6**) (1.004 g) in standard fashion (36) using CrO_3/HOAc which furnished 0.718 g of clean chlorodisulfone after recrystallization from 95% ethanol. The disulfone had mp 117–119°C; ir ($CHCl_3$): 1345, 1330, and 1160 cm^{-1}; nmr ($CDCl_3$) δ: 1.90 (3H, d, $J = 7$ Hz), 3.33 (3H, s), 4.50 (1H, d, $J = 15$ Hz), 5.10 (1H, d, $J = 15$ Hz), and 5.50 (1H, q, $J = 7$ Hz); ms *m/e*: 94 (100%), 79 (40.3%), and 63 (59.6%). *Anal.* calcd. for $C_4H_9ClO_4S_2$: C 21.76, H 4.11; found: C 21.85, H 4.24.

Preparation of $CH_3SO_2CH_2SCH_2CH_3$ (4)

The preparation and properties of this compound have been described elsewhere (37).

Chlorination of 4

The sulfone-sulfide (**4**) (1 g) in carbon tetrachloride (5 ml) was quantitatively converted into the dichlorosulfone-sulfide (**5**) upon treatment with Cl_2 (ca. 200 ml/min) for 10 min. Further chlorination for 3h and 50 min effected no further change. The solvent was evaporated and the crude dichlorosulfone-sulfide **5** characterized; ir ($CHCl_3$): 1330 and 1150 cm^{-1}; nmr ($CDCl_3$) δ: 1.37 (3H, t), 3.30 (2H, q), and 3.40 (3H, s); ms *m/e*: 147 (11.1%), 145 (66.6%), 143 (100%), 81 (30%), and 79 (90%).

Treatment of crude **5** (0.720 g) with CrO_3/HOAc (37) furnished clean dichlorodisulfone (0.532 g, mp 90–92°C) after recrystallization from 95% ethanol; ir ($CHCl_3$): 1360, 1350, and 1150 cm^{-1}; nmr ($CDCl_3$) δ: 1.57 (3H, t), 3.50 (3H, s), and 3.80 (2H, q); ms *m/e*: 165 (11.1%), 163 (66.6%), 161 (100%), 77 (54.9%), and 64 (61.9%). *Anal.* calcd. for $C_4H_8Cl_2O_4S_2$: C 18.83,H 3.16; found: C 18.78, H 3.07.

Chlorination of 6

The chlorosulfone-sulfide (**6**) (0.5 g) in carbon tetrachloride (5 ml) was quantitatively converted into the trichlorosulfone-sulfide (**10**) upon treatment with Cl_2 (ca. 200 ml/min) for 5 min. The solvent was evaporated and the crude trichlorosulfone-sulfide **10** characterized; ir ($CHCl_3$): 1345 and 1150 cm^{-1}; nmr ($CDCl_3$) δ: 2.00 (3H, d, $J = 6$ Hz) 3.25 (3H, s), and 5.85 (1H, q, $J = 6$ Hz); ms *m/e*: 183 (0.9%), 181 (9.0%), 179 (29.0%), 177 (29.0%), 81 (20.0%), 79 (60%), 65 (33%), and 63 (100%).

Treatment of **10** (0.680 g) with CrO_3/HOAc (37) furnished the corresponding trichlorodisulfone (0.362 g, mp 60–61°C) after recrystallization from 95% ethanol; ir ($CHCl_3$): 1360, 1350, and 1155 cm^{-1}; nmr ($CDCl_3$) δ: 2.03 (3H, d, $J = 6$ Hz), 3.45 (3H, s), and 5.90 (1H, q, $J = 6$ Hz); ms *m/e*: 165 (9.9%), 163 (59.8%), 161 (89.7%), 65 (33%), and 63 (100%). *Anal.* calcd. for $C_4H_7Cl_3O_4S_2$: C 16.59, H 2.43; found: C 16.60, H 2.42.

Selective Deuteration of p*-Nitrobenzyl Chloromethyl Sulfone*

p-Nitrobenzyl chloromethyl sulfone (0.050 g) (18) was dissolved in a solution of ethanol-*d* (3 ml) and D_2O (5 drops) and the reaction mixture was refluxed for 2 h. The solvent was evaporated and the residue established as partially deuterated at the benzylic position only by nmr viz. 77% removal of signal at δ 4.53 (benzylic methylene (18)). The mass spectrum indicated d_0, 6.6%, d_1, 38.4%, d_2 53.3% for the nitrobenzyl group observed at *m/e* 136.

Competitive Exchange for $PhCH_2SO_2CH_3$ and $ClCH_2SO_2CH_3$

A mixture of benzyl methyl sulfone (0.057 g) and chloromethyl methyl sulfone (0.043 g) was dissolved in a solution of hot ethanol-*d* (3 ml) and NaOD (0.025 *N* in D_2O) (3 drops). The reaction mixture was refluxed 1 h. Methylene chloride (50 ml) was added, the solution washed with water (25 ml) and the organic layer concentrated.

[8]Initially pure sulfone-sulfide-alcohol was obtained by column chromatography of a small sample of crude on silica gel with ether elution followed by acetone elution.

[9]One recrystallization is not adequate for long-term storage. The alkene (**9**) tends to polymerize upon standing unless it has been twice recrystallized.

The nmr indicated 25% deuteration at the benzylic carbon only in the benzylmethyl sulfone and 60% deuteration at the chloromethyl carbon only in the chloromethyl methyl sulfone. The mass spectrum indicated the following results $PhCH_2SO_2CH_3$: d_0 71.6%, d_1 15.3%, d_2 12.9%; $ClCH_2SO_2CH_3$: d_0 24.0%, d_1 21.6%, d_2 52.4%, d_3 1.8%.

Acknowledgements

The authors are indebted to Mr. J. Hancock and Mr. M. Mason for some technical assistance. We thank Dr. J. H. Kim for running the mass spectra and Dr. J. A. Pincock for helpful discussions. We are grateful to Dalhousie University for financial support in the form of a grant from the Research Development Fund.

1. W. R. HARDSTAFF, R. F. LANGLER, J. LEAHY, and M. J. NEWMAN. Can. J. Chem. **53**, 2664 (1975).
2. H. KWART and L. J. MILLER. J. Am. Chem. Soc. **80**, 884 (1958).
3. J. M. STEWART and H. P. CORDTS. J. Am. Chem. Soc. **74**, 5880 (1952).
4. J. M. STEWART and C. H. BURNSIDE. J. Am. Chem. Soc. **75**, 243 (1953).
5. F. G. BORDWELL and B. M. PITT. J. Am. Chem. Soc. **77**, 572 (1955).
6. H. BÖHME, H. FISHER, and R. FRANK. Ann. **563**, 54 (1949).
7. H. KWART and R. K. MILLER. J. Am. Chem. Soc. **78**, 5008 (1956).
8. H. KWART and R. W. BODY. J. Org. Chem. **30**, 1188 (1965).
9. H. KWART and P. S. STRILKO. Chem. Commun. 767 (1967).
10. H. KWART, R. W. BODY, and D. M. HOFFMAN. Chem. Commun. 765 (1967).
11. G. E. WILSON, JR. and M. G. HUANG. J. Org. Chem. **35**, 3002 (1970).
12. G. E. WILSON, JR. and R. ALBERT. J. Org. Chem. **38**, 2161 (1973).
13. G. E. WILSON, JR. and M. Y. CHANG. J. Am. Chem. Soc. **96**, 7533 (1974).
14. D. L. TULEEN and V. C. MARCUM. J. Org. Chem. **32**, 204 (1967).
15. D. L. TULEEN. J. Org. Chem. **32**, 4006 (1967).
16. D. L. TULEEN and T. B. STEPHENS. Chem. Ind. (London), **37**, 1555 (1966).
17. D. L. TULEEN and T. B. STEPHENS. J. Org. Chem. **34**, 31 (1969).
18. L. A. PAQUETTE, L. S. WITTENBROOK, and K. SCHREIBER. J. Org. Chem. **33**, 1080 (1968).
19. L. A. PAQUETTE. J. Am. Chem. Soc. **86**, 4089 (1964).
20. H. BOHME and H. J. GRAN. Ann. **577**, 68 (1952).
21. W. G. PHILLIPS and K. W. RATTS. J. Org. Chem. **36**, 3145 (1971).
22. F. G. BORDWELL, J. E. BARES, J. E. BARTMESS, G. J. MCCOLLUM, M. VAN DER PUY, N. R. VANIER, and W. S. MATTHEWS. J. Org. Chem. **42**, 321 (1977).
23. D. J. CRAM. Fundamentals of carbanion chemistry. Academic Press, New York, NY. 1965.
24. J. B. HENDRICKSON, D. J. CRAM, and G. S. HAMMOND. Organic chemistry. 3rd ed. McGraw-Hill, New York, NY. 1970.
25. H. GROSS and E. HOFT. Angew. Chem. Int. Ed. Engl. **6**, 335 (1967).
26. C. C. PRICE and S. OAE. Sulfur bonding. Ronald Press, New York, NY. 1962.
27. F. G. BORDWELL and P. J. BOUTON. J. Am. Chem. Soc. **78**, 854 (1956).
28. F. BERNARDI, I. G. CSIZMADIA, H. B. SCHLEGEL, and S. WOLFE. Can. J. Chem. **53**, 1144 (1975).
29. E. A. NOE. J. Am. Chem. Soc. **99**, 2803 (1977).
30. J. E. HUHEEY. J. Phys. Chem. **69**, 3284 (1965).
31. J. E. HUHEEY. J. Phys. Chem. **70**, 2086 (1966).
32. W. E. TRUCE, G. H. BIRUM, and E. T. MCBEE. J. Am. Chem. Soc. **74**, 3594 (1952).
33. R. F. LANGLER. Ph.D. Thesis, Dalhousie University, Halifax, N.S. 1975.
34. J. S. GROSSERT and R. F. LANGLER. Can. J. Chem. **55**, 407 (1977).
35. W. R. HARDSTAFF and R. F. LANGLER. Org. Mass Spectrom. **10**, 215 (1975).
36. R. F. LANGLER, W. S. MANTLE, and M. J. NEWMAN. Org. Mass Spectrom. **10**, 1135 (1975).
37. R. F. LANGLER and J. A. PINCOCK. Can. J. Chem. **55**, 2316 (1977).

Can. J. Chem. Downloaded from www.nrcresearchpress.com by 210.87.254.40 on 09/05/12
For personal use only.

Porphyrin syntheses requiring negative substituents[1]

HIROSHI KOBAYASHI,[2] JOHN L. ARCHIBALD,[3] AND S. FERGUSON MACDONALD
Division of Biological Sciences, National Research Council of Canada, Ottawa, Ont., Canada K1A 0R6

Received April 19, 1978

HIROSHI KOBAYASHI, JOHN L. ARCHIBALD, and S. FERGUSON MACDONALD. Can. J. Chem. **56**, 2430 (1978).

Syntheses which convert pyrromethenes, pyrromethanes, or pyrroles to porphyrins in one step are limited by the necessity of avoiding inseparable mixtures of products. Such mixtures from pyrromethenes or pyrromethanes may become separable, and those from pyrroles avoided, if the products bear appropriate negative substituents.

It would appear that isomeric porphyrins with two negative substituents, on adjacent and on opposite rings, respectively, do not form mixed crystals (solid solutions) and are easily separated by crystallization.

HIROSHI KOBAYASHI, JOHN L. ARCHIBALD et S. FERGUSON MACDONALD. Can. J. Chem. **56**, 2430 (1978).

Les synthèses qui permettent de transformer les pyrrométhènes, les pyrrométhanes ou les pyrroles en phorphyrines en une étape sont limitées par la nécessité d'éviter des mélanges de produits qui soient inséparables. De tels mélanges, provenant de pyrrométhènes ou de pyrrométhanes, peuvent devenir séparables et ceux provenant du pyrroles peuvent être évités si le produit porte des substituants négatifs appropriés.

Il semblerait que des porphyrines isomères portant deux substituents négatifs respectivement sur les cycles adjacents et opposés ne forment pas de cristaux mixtes (solutions solides) et peuvent être facilement séparés par cristallisation.

[Traduit par le journal]

Introduction

Although often more convenient, porphyrin syntheses from pyrromethenes, pyrromethanes, or pyrroles lack the formal generality of those from linear tetrapyrroles. This is because they can lead only to inseparable mixtures in some cases. However, familiar effects of negative substituents on the reactivity of pyrroles and on the properties of porphyrins suggest methods for avoiding such mixtures or making them separable.[4] These methods are curious because negative substituents are commonly inimical in porphyrin syntheses and because they suggest that Hans Fischer would have synthesized hemin, even if it had been derived from protoporphyrin 7, 10, or 15.

The primary limitations on syntheses of porphyrins from pyrromethenes or pyrromethanes are illustrated by Hans Fischer's methods (2*a*) (Scheme 1). Porphyrins with the elements of symmetry indicated could be made by method A(*a*) or B(*a*). All others had to be made by A(*b*) and this involved separating the unsymmetrical product from two centrosymmetric by-products formed as in A(*a*). If two isomeric pyrromethenes were used in A(*b*), it was generally impossible to separate the resulting isomeric porphyrins or (if this were possible) to determine which was which. Method A(*b*) was thus inapplicable if the required pyrromethenes were isomers or too closely related. Consequently this method usually required a characteristic substituent (usually a propionic acid group) in one of the pyrromethenes so the three products could be separated by hydrochloric acid fractionation and identified by combustion analysis. It is immaterial here that one of the centrosymmetric by-products could sometimes be avoided: if 5-bromo-5′-bromomethyl- and 5-free-5′-methyl pyrromethenes were available, these were used and only the former self-condensed.

The porphyrins from chlorophylls were fortunately monopropionic acids, available in principle by A(*b*). This method was also applicable to all those mesoporphyrins which had propionic acid groups on adjacent rings, including all those Fischer obtained by B(*a*). However, unlike B(*a*), A(*b*) was inapplicable to any etioporphyrins or coproporphyrins, and the generalities of these two methods are incommensurable. Fischer could and did synthesize 12 of the 15 mesoporphyrins but not the mesoporphyrins 7, 10, and 15 because these are unsymmetrical and have their propionic acid groups on opposite rings. Their syntheses from linear tetrapyrroles would of course be straightforward, cf. that of mesoporphyrin 10 (3). Yet Fischer could have obtained them indirectly from synthetic monopropionic acids, as in the con-

[1]Issued as NRCC No. 16796.
[2]NRCC Postdoctorate Fellow 1963–1965.
[3]NRCC Postdoctorate Fellow 1960–1962.
[4]Some of this work has been briefly reported (1).

Can. J. Chem. Downloaded from www.nrcresearchpress.com by 210.87.254.105 on 09/05/12
For personal use only.

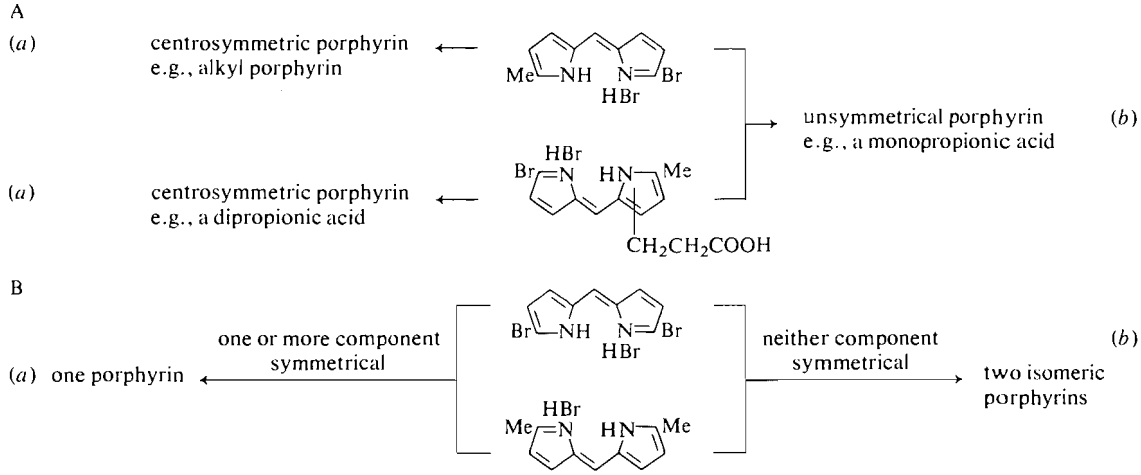

SCHEME I

version of pyrroporphyrin 15 to mesoporphyrin 9 (2*b*), e.g., mesoporphyrin 10 from the known pyrroporphyrin 12 (2*c*). However, as generally understood, Fischer's methods apparently offered no routes to the corresponding deuteroporphyrins 7, 10, and 15, and the problem is fairly represented by these.

The solution to this problem was implicit in Fischer's work. His synthesis of 2-desethylpyrroporphyrin 15 was that of a monopropionic acid by method A(*b*) (Fig. 1; the broken line indicates the pyrromethenes used but bromine is ignored). That of 2-desethylrhodoporphyrin 15 (4) may also have been so regarded but it should be considered as a modification of A(*b*) wherein COOEt replaces CH_2CH_2COOH (Scheme 1). The three products should then differ in the number of their ring carboxyl groups, be separable by hydrochloric acid fractionation and be identifiable by their visible spectra. This modification would be general for monocarboxylic acids and for porphyrins obtainable from them by removing or replacing the carboxyl group. Thus, deuteroporphyrin 10 (Fig. 1) could not have been synthesized like 2-desethylpyrroporphyrin 15 but its 6-carboxylic acid could have been synthesized like 2-desethylrhodoporphyrin 15. In Fischer's synthesis of this last, the yield was 0.05% and partial decarboxylation might have invalidated the method. These difficulties would be avoided if 5-free-5′-formylpyrromethanes replaced his 5-bromo-5′-methylpyrromethenes.

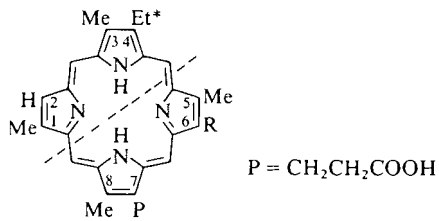

R = H: 2-Desethylpyrroporphyrin 15
R = COOH: 2-Desethylrhodoporphyrin 15
R = H (P for Et*): Deuteroporphyrin 10
R = COOH (P for Et*): 6-Carboxydeuteroporphyrin 10

Fig. 1. Deuteroporphyrin 10 and related porphyrins.

A related modification of A(*b*) (Scheme 1) employed Br instead of either CH_2CH_2COOH or COOEt. This was restricted because bromine was too readily lost under Fischer's conditions. As a convenient and general route to heptasubstituted porphyrins, wherein the loss of bromine is immaterial (cf. pyrroetioporphyrin 5 (4)), it would yield desethylmesoporphyrins from which mesoporphyrin 10 etc., could be obtained.

Method B(*b*) (Scheme 1) had not been used because two isomeric porphyrins necessarily result. However, if each pyrromethene bore a carbethoxy group, these would appear on adjacent rings in one of the products and on opposite rings in the other. The isomers would then be easily distinguished by visible spectra of the 'etio' and 'oxorhodo' type respectively. The effect of the carbethoxy groups on the yield would presumably render this synthesis impracticable, but the equivalent synthesis from a 5,5′-free- and a 5,5′-diformylpyrromethane (Scheme 2) would not be adversely affected by such groups, at least when they were on the 3- or 3′-positions of the pyrromethanes (5).

The problem of separating isomers like the dicarboxydeuteroporphyrins 4 and 5 (Scheme 2) remained. There appeared to be a surprising difference between the hydrochloric acid numbers of the diacetyldeuteroporphyrins 3 and 9 (Fig. 2) reported to be 7 (2*d*) and 3 (2*e*), respectively. This suggested that isomeric porphyrins, in which two negative

Can. J. Chem. Downloaded from www.nrcresearchpress.com by 210.87.254.105 on 09/05/12
For personal use only.

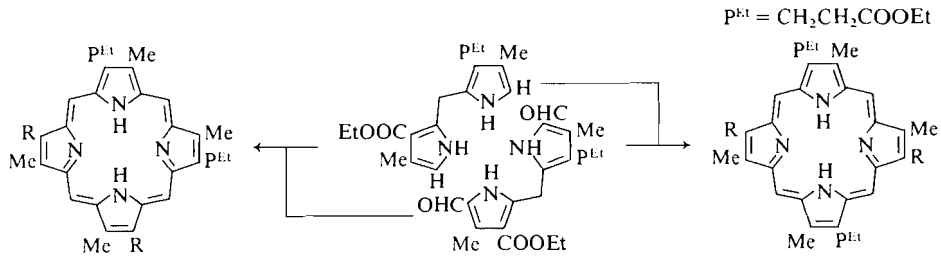

SCHEME 2

groups were differently situated with respect to each other, might be separated by hydrochloric acid fractionation. As a model, we used methyl esters of the diacetyldeuteroporphyrins 2 and 9 (Fig. 2), which have acetyl groups on opposite and adjacent rings, and spectra of the 'oxorhodo' and 'etio' type, respectively. These were synthesized for the purpose from the corresponding deuteroporphyrins. Their insolubility made them ill adapted to hydrochloric acid fractionation, and their hydrochloric acid numbers were both about 8. Although considerable separations were accomplished despite this, we now attribute these to the unexpected and unnoticed crystallization of one isomer or the other.

It was then accidentally found that the diacetyldeuteroporphyrin 2 and 9 esters were easily separated by crystallization from undisturbed solutions in acetone. As crystallized from a 1:1 mixture and recrystallized once, the pure components were recovered in over 80% yield. The separation of a pure porphyrin from a gross mixture of isomers by any method is still exceptional, however lax the criteria of purity. Crystallization had separated uroporphyrin 2 from its more soluble and lower melting isomers but this was tedious and wasteful, apparently because mixed crystals (solid solutions) were formed (6). In the present case diacetyldeuteroporphyrin 2 was the less soluble isomer but the separation reveals and depends on the fact that the two do not form mixed crystals. The idea that the two dicarboxydeuteroporphyrins (Scheme 2) would behave likewise, was encouraged by the notion that negative groups might determine association or packing in such cases. Either isomer could be stacked so that these groups were symmetrically disposed but this was not true of mixtures of the two.

The pyrromethanes (Scheme 2) were ethyl rather than methyl esters, so the resulting porphyrin esters would be relatively low melting. Charring often obscures porphyrin melting points at about 300°C and is not prevented by determining the melting points in capillaries sealed off under high vacuum. When the two pyrromethanes were condensed in AcOH–HI (cf. ref. 5) a roughly 1:1 mixture of the dicarboxydeuteroporphyrin 4 and 5 ethyl esters crystallized ($\geq 43\%$). A considerable separation was effected when the centrifuge brought down only the larger crystals consisting largely of the latter. Chloroform solutions of the two resulting fractions were filtered through alumina and the solvent displaced by acetone. The dominant porphyrins then crystallized from the undisturbed solutions: the ethyl ester of dicarboxydeuteroporphyrin 4 from one, that of dicarboxydeuteroporphyrin 5 from the other.

These two porphyrins were easily distinguished by their melting points and identified by their characteristic visible spectra. Their identity and purity was confirmed by decarboxylating them to the deuteroporphyrins and comparing these with the authentic deuteroporphyrins 4 and 5, which we

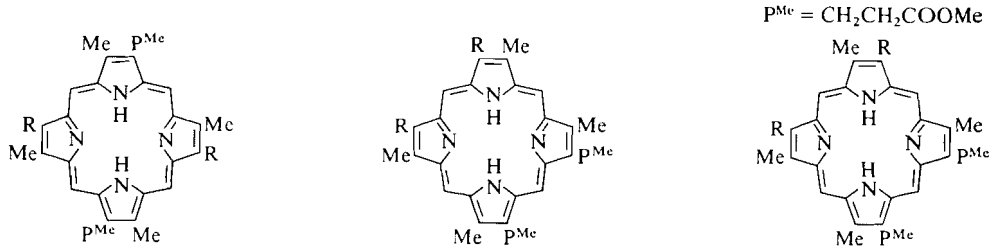

Fig. 2. Deuteroporphyrins and their diacetyl derivatives.

Can. J. Chem. Downloaded from www.nrcresearchpress.com by 210.87.254.105 on 09/05/12
For personal use only.

Can. J. Chem. Downloaded from www.nrcresearchpress.com by 210.87.254.105 on 09/05/12
For personal use only.

prepared by Fischer's usual methods. (Note: This would not have been possible had we worked with the more interesting isomers of types 7, 10, or 15.) In both cases the ethyl esters and their copper complexes agreed in melting point and mixture melting point, but only with deuteroporphyrin 5 did we get identical X-ray powder photographs. This was disappointing but hardly surprising. Specimens of polymorphic substances do not give identical photographs unless they are in the same form or mixture of forms and we had spent a year getting synthetic cytodeuteroporphyrin to photograph like Warburg's analytical specimen (7).

In the methods discussed above, negative groups are used to make multiple products of rational porphyrin syntheses separable and identifiable. In the synthesis which follows, they are used to prevent the irrational formation of isomers through the 'scrambling' of intermediates: ionic redistribution reactions of α-pyrryl and hydroxy groups about the methylene groups. This is apparent when 2-acetoxymethylpyrrole-5-carboxylic acids condense to mixtures of isomeric porphyrins rather than to those of type I (8). However, particularly under mild conditions, it seemed likely that a type I porphyrin would result if the pyrrole bore a 3-acetyl group. This would maintain the integrity of the original 2-pyrryl–CH_2 links by suppressing their fission to the derived 2-pyrryl anion. In fact, formic acid at 25–40°C in the presence of air converted 2-ethoxymethyl-3-acetyl-4-methylpyrrole-5-carboxylic acid into the type I porphyrin (Scheme 3). There was only one meso ^{13}CH signal (CH flanked by Me and Ac) in the nmr spectrum; more than ca. 5% of other isomers would have been revealed by signals from ^{13}CH flanked by 2 Me and by 2 Ac.

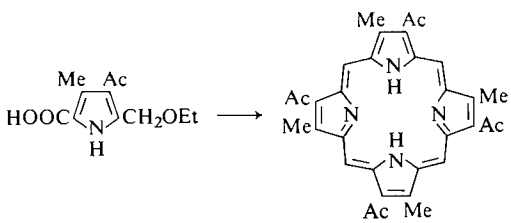

SCHEME 3

Experimental

Diacetyldeuteroporphyrin 9 Methyl Ester (cf. Fig. 2)

Crude diacetyldeuterohemin 9 was heated in HBr–AcOH for 60 h at 40°C (cf. ref. 2*f*). The solution was poured into 40 vol. of water and heated to coagulate the precipitated porphyrin. The latter was separated, washed, dried, and extracted into methanolic HCl (thimble). Water and chloroform were added to the extract and the chloroform layer was washed, dried, and filtered through alumina (Woelm, grade 3), eluting with 5% methanol in chloroform. The filtrate was concentrated and chloroform was displaced by adding hot methanol to the boiling solution. A chloroform solution of the resulting crystals was filtered through alumina, concentrated, and hot acetone added. The product separated overnight from the undisturbed solution as large black leaflets (25% from deuterohemin), mp 244–246°C (lit. (9) mp 244–246°C); λ_{max} in $CHCl_3$ (ε): 519 (14 900), 553 (8200), 588 (7000), 642 nm (3800), i.e., $\varepsilon_{553}/\varepsilon_{519} = 0.55$; hydrochloric acid number ca. 8 (lit. (2*e*) ca. 3). *Anal.* calcd. for $C_{36}H_{38}O_6N_4$: C 69.43, H 6.15, N 9.00; found: C 69.73, H 6.09, N 9.32.

Deuteroporphyrin 2 Methyl Ester

Crude deuteroporphyrin 2 from 3,5-dibromo-4,3′,5′-trimethylpyrromethene-4′-propionic acid hydrobromide, as obtained by treating the melt with aqueous sodium acetate (2*g*), was dried and left 4 days in 5% methanolic HCl. The resulting ester was twice purified by filtering its chloroform solution through alumina then crystallizing from methanol displacing chloroform. It formed purple rods (4%), mp on pre-heated stage 295–297°C (dec.) (lit. (2*g*) mp 285 or 291°C).

Diacetyldeuteroporphyrin 2 Methyl Ester (cf. Fig. 2)

Deuterohemin 2 methyl ester (ref. 2*g*) (200 mg) was acetylated (cf. ref. 2*f*) with 20 ml of acetic anhydride and 1.5 ml of $SnCl_4$ in an ice-bath for 8 min. The diacetyldeuterohemin 2, obtained by pouring the mixture into ice-water, was added to 20 ml of ice-cold concentrated H_2SO_4, then stirred 1¾ h at 20°C. The resulting diacetyldeuteroporphyrin 2, precipitated by adding water, was centrifuged, dried and extracted into 150 ml of 5% methanolic HCl (thimble, 2 h); more of the product was extracted by boiling the insoluble material in methanolic HCl. The resulting methyl ester of diacetyldeuteroporphyrin 2 was brought into chloroform (cf. its isomer above), filtered through alumina, and crystallized by adding much hot acetone to the concentrated chloroform solution. The filtration and crystallization were repeated twice to yield purple needles (43%), mp on stage pre-heated to 290°C, 304–305°C (dec.) (lit. (10) mp 310–315°C (dec.)); λ_{max} in $CHCl_3$ (ε): 521 (8300), 564 (19 200), 588 (11 600), 646 nm (1700), i.e., $\varepsilon_{564}/\varepsilon_{521} = 2.30$. *Anal.* calcd. for $C_{36}H_{38}O_6N_4$: C 69.43, H 6.15, N 9.00; found: C 69.10, H 5.91, N 9.48.

Separating the Methyl Esters of the Diacetyldeuteroporphyrins 2 and 9

The dimethyl esters of diacetyldeuteroporphyrin 2 (9.5 mg; $\varepsilon_{564}/\varepsilon_{521} = 2.23$; decomposes at 301°C after sintering at 298°C) and diacetyldeuteroporphyrin 9 (9.8 mg; $\varepsilon_{553}/\varepsilon_{519} = 0.535$; mp 241–244°C) were dissolved in 5 ml of chloroform which was then displaced by adding hot acetone to the boiling solution. The acetone solution (45 ml) was left undisturbed in the dark at 20°C. The first crop (8.6 mg; $\varepsilon_{564}/\varepsilon_{521} = 2.20$; decomposes from 294°C) separated overnight as purple rods. The concentrated mother liquor (7 ml) was left overnight as above to give the second crop as black rods (9.9 mg; $\varepsilon_{553}/\varepsilon_{519} = 0.58$; mp 242–245°C, sintering from 238°C, a few crystals remained and decomposed above 290°C). A solution of the first crop in chloroform was filtered through alumina, concentrated, and the chloroform was displaced by acetone. The acetone solution (40 ml) deposited the dimethyl ester of diacetyldeuteroporphyrin 2 as purple rods (8.0 mg, 84%), mp 300–303°C (dec.); $\varepsilon_{564}/\varepsilon_{521} = 2.23$. The second crop was purified likewise, crystallizing from 7 ml of acetone, to give the dimethyl ester of diacetyldeuteroporphyrin 9 as black leaflets (7.8 mg, 80%); mp 244–246°C (dec.); $\varepsilon_{553}/\varepsilon_{519} = 0.54$.

Benzyl 2-Chloromethyl-3-carbethoxy-4-methylpyrrole-5-carboxylate

Benzyl 2,4-dimethyl-3-carbethoxypyrrole-5-carboxylate (3.01 g) (11) in 25 ml of chloroform (free of ethanol, stabilized

Can. J. Chem. Downloaded from www.nrcresearchpress.com by 210.87.254.105 on 09/05/12
For personal use only.

with 5% dry ether) was stirred at 20°C while 0.85 ml of sulfuryl chloride in 10 ml of chloroform was dropped in. Two hours later the solvent was evaporated and the residue was crystallized from ether–hexane as colourless needles (64%), mp 137–140°C. *Anal.* calcd. for $C_{17}H_{18}O_4NCl$: C 60.80, H 5.40, N 4.17, Cl 10.55; found: C 61.17, H 5.58, N 4.11, Cl 10.71.

2-Benzyloxycarbonyl-3-methyl-4-(2-carbethoxyethyl)-pyrrole-5-carboxylic Acid

2-Benzyloxycarbonyl-3,5-dimethyl-4-(2-carbethoxyethyl)-pyrrole (12) (49.4 g) in 600 ml of dry ether was treated with 36.6 ml of sulfuryl chloride over 30 min while cooling in water. Next day the solution was refluxed for 1 h, the ether was evaporated, and more ether was added and evaporated. Sodium acetate (120 g) in 1 ℓ of boiling water was added to the residue, the mixture was boiled and stirred for 15 min, and then cooled. The solid, together with the ether extract of the aqueous layer, was extracted with aqueous sodium carbonate. The carbonate solution was washed with ether, cooled in ice, and saturated with SO_2. The precipitated product was recrystallized from aqueous ethanol as pink plates (74%), mp 148–152°C. The recrystallized analytical specimen formed colourless plates, mp 150–152°C. *Anal.* calcd. for $C_{19}H_{21}O_6N$: C 63.50, H 5.89, N 3.90; found: C 63.24, H 5.78, N 4.11.

2-Benzyloxycarbonyl-3-methyl-4-(2-carbethoxyethyl)-5-iodopyrrole

A hot solution of iodine (1.88 g) in 30 ml of ethanol was gradually added to 2.65 g of the above pyrrole 5-carboxylic acid and 1.48 g of potassium bicarbonate in 25 ml of water on the steam bath. When the solution decolorized, it was poured into water. The product separated at 0°C as colourless needles (87%), mp 82–84°C. The analytical sample, mp 85–86°C, had been recrystallized from aqueous ethanol then from hexane (thimble). *Anal.* calcd. for $C_{18}H_{20}O_4NI$: C 48.99, H 4.57, N 3.17, I 28.76; found: C 49.61, H 4.95, N 3.02, I 28.89.

Benzyl 3-Methyl-4-(2-carbethoxyethyl)pyrrole-2-carboxylate

The above 5-iodopyrrole (1 g) in 5 ml of dimethylformamide was stirred overnight with 2 g of zinc dust and a little anhydrous copper sulfate. Chloroform was added and the filtered solution was washed with dilute HCl and with water. The chloroform was evaporated and the residue was distilled (150–155°C, 1×10^{-4} Torr) to give the product (90%) as a colourless oil. *Anal.* calcd. for $C_{18}H_{21}O_4N$: C 68.55, H 6.71, N 4.44; found: C 68.99, H 6.96, H 4.58.

The product could be crystallized at 0°C and then, after draining in tile, could be recrystallized at 0°C from pentane as long colourless needles, mp 33–35°C. Catalytic reduction, in ethanol over platinum oxide in the presence of sodium acetate, was equally satisfactory.

Dibenzyl 4,4′-Dimethyl-3-carbethoxy-3′-(2-carbethoxyethyl)-pyrromethane-5,5′-dicarboxylate

Benzyl 2-chloromethyl-3-carbethoxy-4-methylpyrrole-5-carboxylate (5.14 g) and benzyl-3-methyl-4-(2-carbethoxyethyl)pyrrole-2-carboxylate (4.83 g) were boiled for 70 min in 30 ml of acetic acid containing 1.27 g of anhydrous sodium acetate. Water then precipitated an oil which solidified on standing. The product formed colourless crystals from ethanol (64%), mp 137–138.5°C. The analytical specimen was purified by column filtration and crystallized from benzene–hexane, mp 139–140°C. *Anal.* calcd. for $C_{35}H_{38}O_8N_2$: C 68.39, H 6.23, N 4.56; found: C 68.25, H 6.22, N 4.81.

4,4′-Dimethyl-3-carbethoxy-3′-(2-carbethoxyethyl)-pyrromethane-5,5′-dicarboxylic Acid

The above pyrromethane benzyl ester (6.4 g) was hydrogenated in dioxane (350 ml) over Pd-on-C (500 mg). The resulting mixture was heated to dissolve the product before filtering. Most of the product separated from the filtrate; a second crop, obtained by concentrating the mother liquor, was recrystallized; total yield 70%. For analysis, it was recrystallized from ethanol (thimble), mp 225°C (dec.). *Anal.* calcd. for $C_{21}H_{26}O_8N_2$: C 56.08, H 6.03, N 6.45; found: C 58.23, H 6.08, N 6.51.

4,4′-Dimethyl-3-carbethoxy-3′-(2-carbethoxyethyl)-pyrromethane (cf. Scheme 2)

The above dicarboxylic acid (570 mg) was heated *in vacuo* (5×10^{-4} Torr). Decarboxylation started at 155°C and was completed at ca. 160°C. The product then distilled at 170°C as a colourless oil which crystallized on rubbing with ether; yield 75%, mp 114–116°C. The analytical specimen, mp 116.5–117.5°C had been repeatedly recrystallized from ether. *Anal.* calcd. for $C_{19}H_{26}O_4N_2$: C 65.87, H 7.57, N 8.09; found: C 66.03, H 7.63, N 8.07.

4,4′-Dimethyl-3-carbethoxy-3′-(2-carbethoxyethyl)-5,5′-diformylpyrromethane (cf. Scheme 2)

Dimethylformamide (450 mg) was shaken and cooled in ice while 0.56 ml of $POCl_3$ were dropped in; after 1 h at 20°C, this was dissolved in 4 ml of 1,2-dichloroethane. This solution was cooled in ice while the above 5,5′-free pyrromethane (250 mg) in 3 ml of dichloroethane was added dropwise. After standing 7 days at 20°C while protected from moisture, the mixture was stirred with aqueous sodium acetate. A solution of the colourless precipitate in much ether was washed with aqueous sodium carbonate and with water, then evaporated. The residue crystallized from aqueous ethanol to give the product (50%), mp 158–159°C. The analytical sample, mp 159–162°C, had been repeatedly crystallized from ethanol. *Anal.* calcd. for $C_{21}H_{26}O_6N_2$: C 62.67, H 6.51, N 6.96; found: C 62.83, H 6.40, N 7.14.

Diethyl 1,4,5,8-Tetramethyl-2,7-bis(2-carbethoxyethyl)-porphin-3,6-dicarboxylate (Ethyl Ester of Dicarboxydeuteroporphyrin 4) and Diethyl 1,4,5,8-Tetramethyl-2,6-bis(2-carbethoxyethyl)porphin-3,7-dicarboxylate (Ethyl Ester of Dicarboxydeuteroporphyrin 5) (cf. Scheme 2)

Hydriodic acid (0.18 ml of 56%) in acetic acid (9 ml) was added to a solution of the 5,5′-free pyrromethane (21 mg) and its dialdehyde (24 mg) (Scheme 2) in acetic acid (27 ml). After 25 min, anhydrous sodium acetate (600 mg) in acetic acid (9 ml) was added and the solution was aerated for 1 day in the dark.

Centrifuging then separated only the larger crystals and these (6 mg) were purified by filtering their chloroform solution through alumina (grade 3), concentrating the filtrate to 5 ml, and displacing the chloroform with acetone at the boil (final volume 40 ml). The solution was filtered hot and allowed to stand undisturbed overnight. The ethyl ester of dicarboxydeuteroporphyrin 5 (6 mg, 14%) separated as purple needles, mp 265–271°C. For analysis, it was recrystallized as above, mp 275–277.5°C; λ_{max} in $CHCl_3$ (ε): 518 (9200), 561 (21 200), 586 (10 800), 641 nm (2600), i.e., $\varepsilon_{561}/\varepsilon_{518} = 2.30$. *Anal.* calcd. for $C_{40}H_{46}O_8N_4$: C 67.59, H 6.52, N 7.88; found: C 67.80, H 6.79, N 7.99.

The acetic acid, in which the remainder of the product was suspended, was diluted with water, neutralized with sodium bicarbonate, and extracted with chloroform. The washed and dried chloroform solution was filtered through alumina, concentrated, and the chloroform was displaced by methanol. The crystals which separated (12.5 mg) were dissolved in chloroform, then filtered through alumina and crystallized from 40 ml of acetone like the isomer above. The ethyl ester of dicarboxydeuteroporphyrin 4 separated as black plates (5 mg,

Can. J. Chem. Downloaded from www.nrcresearchpress.com by 210.87.254.105 on 09/05/12
For personal use only.

12%), mp 241–242.5°C; λ_{max} in $CHCl_3$ (ε): 514 (14 800), 550 (7500), 584 (6800), 638 nm (3300), i.e., $\varepsilon_{550}/\varepsilon_{514} = 0.51$. *Anal.* calcd. for $C_{40}H_{46}O_8N_4$: C 67.59, H 6.52, N 7.88; found: C 67.48, H 6.61, N 7.86.

4,4′-Dibromo-3,5,3′,5′-tetramethylpyrromethene Hydrobromide (cf. ref. 13)

Bromine (3.52 g) in 14 ml of acetic acid was added in two portions to a stirred solution of 3,5,3′,5′-tetramethyl-pyrromethene hydrochloride (13) (2.36 g) in 20 ml of hot acetic acid. The mixture was heated 10 min in the steam bath then allowed to cool. The product which separated was recrystallized from 150 ml of 98% formic acid as dark red prisms (3.33 g). *Anal.* calcd. for $C_{13}H_{15}N_2Br_3$: C 35.59, H 3.43, N 6.39, Br 54.60; found: C 35.83, H 3.59, N 6.30, Br 54.48.

1,4,5,8-Tetramethyl-2,7-bis(2-carbethoxyethyl)porphin (Ethyl Ester of Deuteroporphyrin 4) (cf. Scheme 2)

(a) By Direct Synthesis

A well-ground mixture of methylsuccinic acid (14) (2 g), 4,4′-dibromo-3,5,3′,5′-tetramethylpyrromethene hydrobromide (220 mg), and 5,5′-dibromo-3,3′-dimethyl-4,4′-bis(2-carboxyethyl)pyrromethene hydrobromide (15) (280 mg) was heated for ½ h at 180°C. The partially cooled melt was extracted and washed with acetic acid – concentrated HCl (60:40). The extract was diluted with water, neutralized (NaOH then Na_2HPO_4), and heated to coagulate the precipitate. The latter was separated (centrifuge), washed with dilute acetic acid and with methanol, and dissolved in concentrated HCl. The pigment was transferred to ether (using sodium tartarate), thence into 2% HCl, back into ether, then into 0.01% ammonia, and again into ether (using citric acid). The washed and dried ether solution was evaporated and the residue was left overnight in 5% ethanolic HCl. The pigment was brought into chloroform. The washed and dried solution was filtered through alumina (grade 3) and the pigment was crystallized by adding ethanol to the hot concentrated filtrate. It was recrystallized several times from dry ethanol displacing chloroform, finally by allowing the solution (50 ml) to stand undisturbed overnight. It formed red needles, mp 236–240.5°C; it is evidently polymorphic for it once melted and resolidified to plates at 228°C before melting at 235–240°C; λ_{max} in $CHCl_3$ (ε): 499 (14 200), 532.7 (8300), 569 (6400), 622.5 nm (3900). *Anal.* calcd. for $C_{34}H_{38}O_4N_4$: C 72.06, H 6.76, N 9.89; found: C 71.85, H 6.96, N 10.01. The copper complex formed red needles, mp 235–239°C.

(b) From the Ethyl Ester of Dicarboxydeuteroporphyrin 4

The ethyl ester of dicarboxydeuteroporphyrin 4 was decarboxylated in AcOH–HCl at 200°C like its isomer below. The resulting ethyl ester of deuterioporphyrin 4 formed flat red needles, mp 235–241°C after a solid phase change at 230°C, mixture mp with the product of *a* above 236.5–241°C; λ_{max} in $CHCl_3$ (ε): 499 (14 000), 532.2 (8000), 569 (6200), 622.6 nm (3900). The copper complex formed red needles, mp 235–239°C, unchanged when mixed with that obtained in *a* above.

There were slight differences between the X-ray powder photographs of the products of *a* and *b*, both as esters and as copper complexes.

1,4,5,8-Tetramethyl-2,6-bis(2-ethoxycarbonylethyl)porphin (Ethyl Ester of Deuteroporphyrin 5) (cf. Scheme 2)

(a) As a By-product in the Synthesis of δ-Phylloporphyrin 15 (16, 17)

The dicarboxylic acids (37 mg) were brought from 0.01% ammonia into ether, from which 1% hydrochloric acid extracted deuterioporphyrin 5 and 14% hydrochloric acid extracted its bromo derivatives. The deuterioporphyrin 5 was brought into ether, the ether was evaporated, and the residue was esterified in ethanolic HCl. The ester was brought into chloroform, and the solution was filtered through alumina. The ethyl ester of deuteroporphyrin 5 separated as needles (6 mg) from ethanol displacing chloroform, mp 259–263°C; λ_{max} in $CHCl_3$ (ε): 499 (13 900), 532 (8000), 568.7 (6400), 622 nm (3900). The analytical specimen was recrystallized. *Anal.* calcd. for $C_{34}H_{38}O_4N_4$: C 72.06, H 6.76, N 9.89; found: C 71.84, H 6.88, N 9.76. (The methyl ester has been described (*2h*).) The copper complex formed needles, mp 287.5–289°C.

The bromo-deuteroporphyrins in the 14% hydrochloric acid were dehalogenated by the method of Busch (cf. the dehalogenation of bromo-α-phylloporphyrin 15 in ref. 16). The resulting deuteroporphyrin 5 was purified by extraction from ether into 1% hydrochloric acid and worked-up as above to give the ethyl ester of deuteroporphyrin 5 (8 mg), mp and mixture mp with the above 259–263°C.

(b) From the Ethyl Ester of Dicarboxydeuteroporphyrin 5

A solution of the ethyl ester of dicarboxydeuteroporphyrin 5 in acetic acid – concentrated hydrochloric acid (20:1) was deaerated in a tube by heating 1 h at 100°C, evacuating the tube for 2 h while cooling it in liquid nitrogen, then sealing it off at 1×10^{-4} Torr. The tube was then brought to 200–210°C over 2 h, then held at that temperature for 5 h. The solution was diluted with water and neutralized to precipitate the porphyrin. The latter was purified by extraction from ether into 2% hydrochloric acid, then esterified by ethanolic HCl. The ester, in ether, was passed through a column of 2% hydrochloric acid on silica gel. The eluant of the only moving band was washed with water, evaporated, and a chloroform solution of the residue was filtered through alumina (grade 3). After the chloroform was displaced by ethanol at the boil, the product separated overnight as purple needles, mp 256–261°C, 259–263°C when mixed with the product of *a*; λ_{max} in $CHCl_3$ (ε): 499 (13 300), 532 (7600), 568.5 (6100), 622 nm (3700). X-ray powder photographs of the esters under *a* and *b* were identical.

The copper complex formed needles, mp 283–283.5°C, 283.5–286.5°C when mixed with that obtained as in *a*. The X-ray powder photographs of the two specimens were identical. They were thus in the same crystallographic form. However, they apparently change more or less completely into another form before melting, for *b* changes visibly at about 240°C. Further, it melted at 287–292°C when recrystallized in the presence of seed, obtained by heating it to 270°C. We had previously seen no evidence of polymorphism among copper complexes; cf. the methyl esters of coproporphyrin 3 and 4 (15).

2-Ethoxymethyl-3-acetyl-4-methylpyrrole-5-carboxylic Acid (cf. Scheme 3)

The corresponding ethyl ester (18) (2.53 g) was refluxed in 10 ml of 10% NaOH and 10 ml of ethanol for 1.5 h in the steam bath. The solution was then concentrated to ¼ vol. *in vacuo*, diluted to 25 ml with water, filtered with Darco, and acidified with 10% sulfuric acid (Congo red). The product separated as colourless crystals (80%). For analysis, it was repeatedly recrystallized from acetone–water, mp 167°C (dec.). *Anal.* calcd. for $C_{11}H_{15}O_4N$: C 58.65, H 6.71, N 6.22; found: C 58.58, H 6.72, N 6.30.

1,3,5,7-Tetramethyl-2,4,6,8-tetraacetylporphin (cf. Scheme 3)

2-Ethoxymethyl-3-acetyl-4-methylpyrrole-5-carboxylic acid (1 g) was stirred for 7 days at about 38°C with 50 ml of 98% formic acid in a loosely-covered 250 ml beaker. The crystalline product (14%) was separated (centrifuge) and washed with 75% formic acid, with acetic acid, and with acetone. For analysis, it was recrystallized from boiling nitrobenzene

(thimble) as tiny rods, mp > 350°C. It formed green solutions in strong acids but was otherwise very insoluble. To measure the visible spectrum, a boiling chloroform solution was cooled, so the concentration was unknown; λ_{max} (relative density): 526 (1.0), 562 (0.48), 602 (0.40), 659 nm (0.26); ^{13}C nmr (on CFT 20, in trifluoroacetic acid, TMS) δ: 114.8 and 161.9 (TFA centres), 13.86 (ring CH_3), 31.79 (acetyl CH_3), 105.21 (meso CH), 136.37, 142.27, 143.70 and 146.93 (4 pyrrole C), 203.71 ppm (CO). *Anal.* calcd. for $C_{32}H_{30}O_4N_4$: C 71.89, H 5.66, N 10.48; found: C 71.97, H 5.61, N 10.57.

1. S. F. MacDonald, H. D. Mah, and M. F. Chen. Ann. N.Y. Acad. Sci. **244**, 396 (1975).
2. H. Fischer and H. Orth. Die Chemie des Pyrrols. Vol. 2, pt 1. (*a*) p. 160ff, (*b*) p. 444, (*c*) p. 340, (*d*) p. 303, (*e*) p. 304, (*f*) p. 305, (*g*) p. 410, (*h*) p. 412.
3. A. H. Jackson, G. W. Kenner, and K. M. Smith. J. Chem. Soc. C, 502 (1971).
4. H. Fischer and S. Böckh. Ann. Chem. **516**, 177 (1935).
5. G. P. Arsenault, E. Bullock, and S. F. MacDonald. J. Am. Chem. Soc. **82**, 4384 (1960).
6. S. F. MacDonald and K. H. Michl. Can. J.Chem. **34**, 1768 (1956).
7. G. S. Marks, D. K. Dougall, E. Bullock, and S. F. MacDonald. J. Am. Chem. Soc. **82**, 3183 (1960).
8. W. Siedel and F. Winkler. Ann. Chem. **554**, 162 (1943).
9. P. S. Clezy and V. Diakiw. Aust. J. Chem. **28**, 2703 (1975).
10. J. L. Davies. J. Chem. Soc. C, 1392 (1968).
11. A. W. Johnson, E. Markham, R. Price, and K. B. Shaw. J. Chem. Soc. 4254 (1958).
12. E. Bullock, A. W. Johnson, E. Markham, and K. B. Shaw. J. Chem. Soc. 1430 (1958).
13. A. H. Corwin and R. H. Kreible. J. Am. Chem. Soc. **63**, 1829 (1941).
14. E. J. Tarleton, S. F. MacDonald, and E. Baltazzi. J. Am. Chem. Soc. **82**, 4389 (1960).
15. F. Morsingh and S. F. MacDonald. J. Am. Chem. Soc. **82**, 4377 (1960).
16. H. Fischer, W. Siedel, and L. Le Thierry d'Ennequin. Ann. Chem. **500**, 137 (1933).
17. J. L. Archibald, D. M. Walker, K. B. Shaw, A. Markovac, and S. F. MacDonald. Can. J. Chem. **44**, 345 (1966).
18. H. Fischer and E. Adler. Hoppe-Seyler's Z. Physiol. Chem. **210**, 139 (1932).

Can. J. Chem. Downloaded from www.nrcresearchpress.com by 210.87.254.105 on 09/05/12
For personal use only.

Derivatives of porphobilinogen and isoporphobilinogen[1]

GUENTER UFER,[2] SIOE S. TJOA, AND S. FERGUSON MACDONALD
Division of Biological Sciences, National Research Council of Canada, Ottawa, Ont., Canada K1A 0R6

Received April 19, 1978

GUENTER UFER, SIOE S. TJOA, and S. FERGUSON MACDONALD. Can. J. Chem. **56**, 2437 (1978).

One of the more convenient syntheses of porphobilinogen has been adapted to that of isoporphobilinogen and extended to the lactams of both. Aminomethylation of appropriate 2-free pyrroles by the Tscherniac-Einhorn method gives derivatives of porphobilinogen and isoporphobilinogen. A method for aminomethylating reactive pyrroles is illustrated by the conversion of 2,4-dimethylpyrrole into its 5-*N*-acetylthiocarboxamide, then into its 5-acetylaminomethyl derivative, using acetyl isothiocyanate then Raney nickel, both at $\leq 20°C$.

GUENTER UFER, SIOE S. TJOA et S. FERGUSON MACDONALD. Can. J. Chem. **56**, 2437 (1978).

On a adapté une des méthodes de synthèse les plus efficaces pour la porphobilinogène à la synthèse de l'isoporphobilinogène et on l'a étendue à la préparation des lactames de chacun de ces composés.

L'aminométhylation de pyrroles appropriés ne portant pas de substituants en position 2, à l'aide de la méthode Tscherniac–Einhorn, conduit aux dérivés porphobilinogène et isoporphobilinogène.

On a illustré une méthode pour effectuer l'aminométhylation de pyrroles réactifs en transformant le diméthyl-2,4 pyrrole en son *N*-acétylthiocarboxamide-5 puis en son dérivé acétylaminométhyl-5 à l'aide de l'isothiocyanate d'acétyle et du nickel de Raney; les deux réactions sont effectuées à des températures inférieures à 20°C.

[Traduit par le journal]

Introduction

We report here incomplete work on three routes to 2-aminomethylpyrroles, particularly porphobilinogen and isoporphobilinogen. In the first of these, a known route to isoporphobilinogen is shortened, making it fully analogous to one of the more convenient syntheses of porphobilinogen; it is then modified to give the lactams of both. The other two routes involve aminomethylations by the Tscherniac–Einhorn reaction, or by a new and milder method.

Critical steps in nearly all syntheses of porphobilinogen, isoporphobilinogen, and their lactams are the removal of a 5-carboxylic acid group and (in the case of isoporphobilinogen lactam) the closure of the lactam ring. The decarboxylation of 5-carboxy-2-aminomethylpyrroles is impracticable and this decarboxylation is usually carried out on their acylamino derivatives, particularly the lactams (1), which decarboxylate in water at 100°C. However, one convenient synthesis of porphobilinogen (Scheme 1) depends on the easy decarboxylation of the oxime **8***a*, a transitory intermediate in the conversion of **1***a* to **2***a* (2). A similar synthesis of isoporphobilinogen was less direct in that **1***d* was converted to the 5-iodo-2-aldehyde and thence into **2***d*. This was because the **2***d* produced directly from **1***d* could not be isolated (2). This difficulty has now been overcome, and both porphobilinogen and isoporphobilinogen are obtained as in Scheme 1 (see Experimental).

Isoporphobilinogen lactam, which we required, has not been obtained directly from isoporphobilinogen. It had been obtained from appropriate 5-benzyloxycarbonylpyrroles in which the critical lactamization was effected. This involved the propionic acid group as its acid chloride (3) or methyl ester, i.e. 5-benzyloxycarbonylisoporphobilinogen dimethyl ester was cyclized by boiling with α-pyridone in dioxan for 25 h (4). This suggested a route to isoporphobilinogen lactam through **2***d* (Scheme 1), based on the lactamization of the ester of isoporphobilinogen itself and avoiding the backtracking associated with the use of the above benzyl esters. Porphobilinogen lactam, too, would then become available analogously through **2***a*.

Although isoporphobilinogen had been esterified in 90% yield, the reduction of the oximes **2***a* and **2***d* to porphobilinogen and isoporphobilinogen must be carried out in dilute solution to avoid by-products (2). To avoid this necessity, these oximes were first esterified then reduced. The oxime **2***a* had been converted to **4***b* in methanolic HCl (2) and **2***d* was now converted analogously into **4***e* and **4***f*. The ester hydrochlorides of the oximes were then reduced in appropriate alcohols to those of porphobilinogen and isoporphobilinogen, **5***b*, **5***e*, **5***f*, but only **5***f* was isolated (see below).

[1]Issued as NRCC No. 16795.
[2]NRCC Research Associate 1977–1978.

Can. J. Chem. Downloaded from www.nrcresearchpress.com by 210.87.254.6 on 09/05/12
For personal use only.

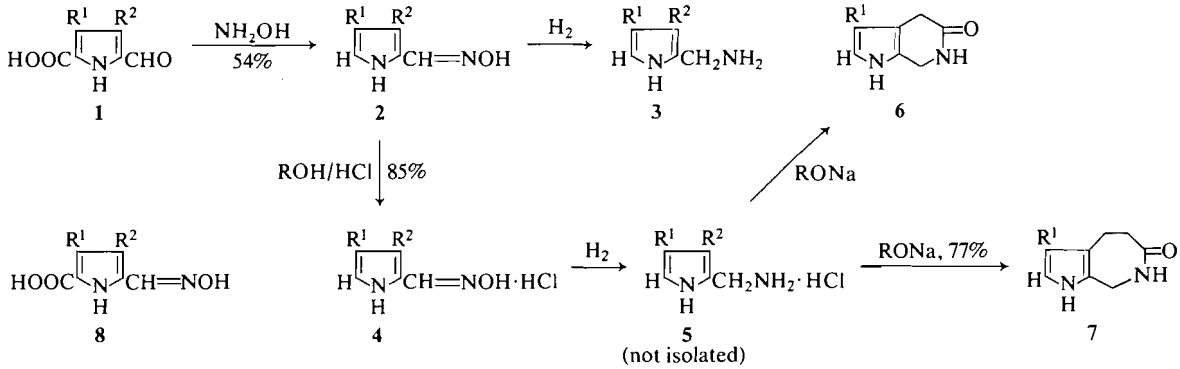

a $R^1 = CH_2CH_2COOH$, $R^2 = CH_2COOH$
b $R^1 = CH_2CH_2COOMe$, R_2 (if present) $= CH_2COOMe$
c $R^1 = CH_2CH_2COOEt$, $R^2 = CH_2COOEt$
d $R^1 = CH_2COOH$, $R^2 = CH_2CH_2COOH$
e $R^1 = CH_2COOMe$, R^2 (if present) $= CH_2CH_2COOMe$
f $R^1 = CH_2COOEt$, R^2 (if present) $= CH_2CH_2COOEt$

SCHEME 1. The yields refer to the methyl ester of isoporphobilinogen lactam.

The reduction of the 5-carbethoxy derivative of **4***c* to the diethyl ester of 5-carboxyporphobilinogen lactam in dilute ammonia (1) implied the lactamization of porphobilinogen esters by a weak base. This suggested the lactamization of isoporphobilinogen esters by a stronger one, particularly sodium alkoxide as used in the familiar preparation of barbituric acid. In the event, the lactams **6***b* (79%), **7***e* (77%), and **7***f* resulted when alcoholic solutions of **5***b*, **5***e*, and **5***f*, as obtained by reducing the oxime esters, were treated with an excess of the appropriate sodium alkoxide at 20°C. Although the ethyl ester of isoporphobilinogen lactam was formed quantitatively (tlc) several methods of isolation gave yields of only 23–42% because the apparent solubilities of the crude product were not consistent.

It should be mentioned here that the methyl and ethyl esters of porphobilinogen lactam melt higher than reported if their melting points are determined in capillaries which have been sealed off under vacuum (1×10^{-5} Torr) to avoid decomposition. The esters of isoporphobilinogen lactam are stable on the shelf and distill unchanged under high vacuum. The methyl ester melted higher than reported but, although we found no indication of the lower of the two melting points reported, a solid phase-change or partial melting represented the higher (see Experimental).

We were also interested in aminomethylation as a source of porphobilinogen derivatives not easily accessible by other methods, or labelled in the aminomethyl group. One of the latter, the ^{13}C-porphobilinogen, had been obtained in eight steps starting with the reductive methylation of **9***a* (R = H) to **9***a* ($R = {}^{13}CH_3$) with $^{13}CH_2O$ (5). Using unlabelled formalin, we have explored the more direct route to promising intermediates offered by the Tscherniac–Einhorn reaction (6). *N*-Hydroxymethylchloroacetamide is only one of the possible reagents here but it is obtained nearly quantitatively from formalin and chloroacetamide. H. Fischer had condensed it with 2,4-dimethyl-3-carbethoxypyrrole in boiling ethanol – concentrated hydrochloric acid and obtained the expected 5-chloroacetylaminomethyl derivative but with some other pyrroles it gave pyrromethanes or mixtures (7).

We found that *N*-hydroxymethylchloroacetamide condensed with **9***a*, **9***b*, **10***a*, **10***b* (R = H) in hot strong absolute ethanolic HCl to give the expected 2-chloroacetylaminomethyl derivatives **9***a*, **9***b*, **10***a*, **10***b* ($R = ClCH_2CONHCH_2$—). The last of these, a derivative of isoporphobilinogen, was obtained in 82% yield, and was reduced to 2-acetylaminomethyl-3-(2-ethoxycarbonylethyl)-4-ethoxycarbonylmethylpyrrole-5-carboxylic acid (98%). Unfortunately, 2.5–3 mol of *N*-hydroxymethylchloroacetamide were used arbitrarily in these experiments.

The scope of this reaction is further illustrated by the conversion of 2,4-dimethyl-5-carbethoxypyrrole into its 3-chloroacetylaminomethyl derivative and 2-methyl-3-carbethoxypyrrole into its 5-chloroacetylaminomethyl derivative. Mono substitution in the latter case was gratifying but when 2 mol of the reagent were used under more vigorous conditions the analyses and molecular weight of the product showed it to be a bis(chloroacetylaminomethyl)-pyrromethane.

We were also interested in the monoaminomethylation of 3,3′-bis(methoxycarbonylmethyl)-4,4′-bis-

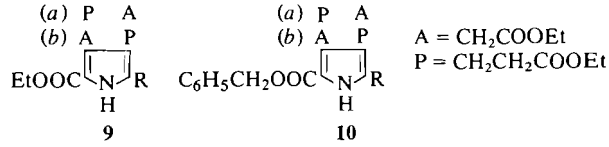

FIGURE 1

Can. J. Chem. Downloaded from www.nrcresearchpress.com by 210.87.254.6 on 09/05/12
For personal use only.

Can. J. Chem. Downloaded from www.nrcresearchpress.com by 210.87.254.6 on 09/05/12
For personal use only.

(2-methoxycarbonylethyl)pyrromethane, which is easily available (8). This would yield products similar to that obtained more indirectly from isoporphobilinogen lactam (3). Preliminary experiments on the aminomethylation of the above symmetrical pyrromethane by the Tscherniac–Einhorn method were, as expected, unsatisfactory. However, before work in this direction ceased, we had developed a method which might prove useful here.

It was suggested by the following. With $AlCl_3$, phenylacetyl isothiocyanate gives the thiohomophthalimide, from which tetrahydroisoquinolone-3 is obtained with Raney nickel (9). At 100°C, but without a catalyst, reactive pyrroles are *C*-thioacylated by phenyl isothiocyanate (10). Solutions of acetyl isothiocyanate are obtained from acetyl chloride and metal thiocyanates in solvents such as acetone. Whether isolated or not, acetyl isothiocyanate reacts easily with aniline, etc., but thioacylation is not always the dominant reaction (11).

This last proved no difficulty and a solution of acetyl chloride and potassium thiocyanate in dimethylformamide at 10°C converted 2,4-dimethylpyrrole into its stable 5-*N*-acetylthiocarbamide **11** (69%) (Scheme 2). Raney nickel at 20°C converted this into the 5-acetylaminomethylpyrrole **12** (52%).

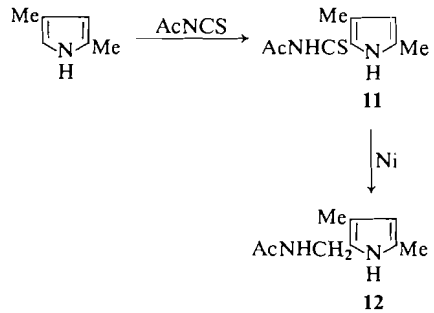

SCHEME 2

Experimental

*2-Formyl-3-carboxymethyl-4-(2-carboxyethyl)pyrrole-5-carboxylic Acid (**1**a) and 2-Formyl-3-(2-carboxyethyl)-4-carboxymethylpyrrole-5-carboxylic Acid (**1**d)*

The crude products (2, 12) may be contaminated with their acid sodium salts, which are insoluble in acetone, so any acetone-insoluble material is dissolved in alkali and reprecipitated as the acid. These salts and discoloration are minimized by adjusting the pH of the hydrolysates (2, 12) to 4.5 before concentrating them; the acids are then precipitated at pH 1. In the case of **1***d*, the crude acid is readily purified by crystallizing from dioxane (Darco); the resulting crystals contain dioxane (ca. 1 mol) from which they are freed by recrystallization from acetone (thimble).

The esters can also be hydrolysed in boiling alcoholic KOH. This is convenient because the acids are precipitated as potassium salts which are insoluble in alcohol.

*2-Oximinomethyl-3-(2-carboxyethyl)-4-carboxymethylpyrrole (**2**d)*

Hydroxylamine hydrochloride (32 g) and 2-formyl-3-(2-carboxyethyl)-4-carboxymethylpyrrole-5-carboxylic acid (**1***d*, 12 g) in 200 ml of water, 128 ml of 10% NaOH (w/v), and 13 ml of ammonium hydroxide (pH of solution ca. 7.0; ammonia minimized discoloration) were heated under reflux for 10½ h. The solution was then concentrated to <100 ml (rotary, 40°C bath), diluted to 200 ml, brought to pH 2.5 at <10°C and seeded. After 2 h at 0°C, the grey crystalline product (54%) was separated and washed with 200 ml of water, mp 175–177°C (lit. (2) mp 178–180°C). For analysis it was twice recrystallized from water. *Anal.* calcd. for $C_{10}H_{12}O_5N_2$: C 50.00, H 5.04, N 11.66; found: C 50.18, H 4.99, N 11.47, ash 0.0.

The unrecrystallized product is suitable for esterification even though it sometimes contains ca. 10% of the 5-carboxylic acid (tlc). If present, the latter is completely removed by recrystallization from 10 parts of water (75% recovery). The yield is considerably increased by completely recycling all mother liquors.

*2-Oximinomethyl-3-(2-methoxycarbonylethyl)-4-methoxycarbonylmethylpyrrole Hydrochloride (**4**e)*

The powdered oxime (**2***d*, 2.118 g) was dissolved in 10 ml of 5% methanolic HCl at 20°C. After ½ h the esterification was complete (tlc) and the solution was seeded if necessary. The red product which separated was washed with ether and more was obtained by adding ether to the mother liquor. As recrystallized from chloroform–pentane it formed flesh coloured plates (85%), mp 120–140°C (dec.). *Anal.* calcd. for $C_{12}H_{17}O_5N_2Cl$: C 47.29, H 5.62, N 9.19, Cl 11.64; found: C 47.39, H 5.64, N 9.31, Cl 11.81.

*2-Oximinomethyl-3-(2-ethoxycarbonylethyl)-4-ethoxycarbonylmethylpyrrole Hydrochloride (**4**f)*

The oxime (**2***d*, 1 g) was warmed to solution in 10 ml of 5% ethanolic HCl. After ½ h at 20°C and 3 h at −20°C the product was separated as flesh coloured needles (82%) which were washed with ether, chloroform, and acetone successively, mp 115–140°C (dec.). *Anal.* calcd. for $C_{14}H_{21}O_5N_2Cl$: C 50.52, H 6.36, N 8.42, Cl 10.65; found: C 50.35, H 6.20, N 8.38, Cl 10.58.

*2-Aminomethyl-3-(2-ethoxycarbonylethyl)-4-ethoxycarbonylmethylpyrrole Hydrochloride (Ethyl Ester of Isoporphobilinogen Hydrochloride) (**5**f)*

The oxime ester **4***f* was reduced in ethanol over 5% Pd-on-carbon. The colourless product crystallized when the residue left after the removal of the catalyst and solvent was seeded. It was recrystallized from ethanol–ether as prisms (65%), mp 95.5–98.5°C (lit. (2) mp 99–100°C). Its X-ray powder photograph was identical with that of material prepared by esterifying isoporphobilinogen (2). *Anal.* calcd. for $C_{14}H_{23}O_4N_2Cl$: C 52.74, H 7.27, N 8.79, Cl 11.12; found: C 52.61, H 7.40, N 8.69, Cl 11.28.

*Lactam of 2-Aminomethyl-3-carboxymethyl-4-(2-methoxycarbonylethyl)pyrrole (Methyl Ester of Porphobilinogen Lactam) (**6**b)*

The oxime ester hydrochloride (**4***b* (2), 1.65 g) in 50 ml of methanol was hydrogenated over 500 mg of 5% Pd-on-carbon. The filtrate and washings were treated with 2.5 ml of sodium in methanol (0.5 g in 10 ml) at 20°C, apparent pH 9.6. After 1 h at 20°C (reaction complete) and 1 h at 0°C the pH was brought to 4.5 with 0.1 ml of acetic acid. The crystalline product (some obtained by filtration, the rest by evaporating the mother liquor) was washed with water and with chloroform. It was recrystallized from 75 ml of methanol (thimble,

Can. J. Chem. Downloaded from www.nrcresearchpress.com by 210.87.254.6 on 09/05/12
For personal use only.

a second thimble below this contained Darco) as colourless crystals (79%); small amounts sublime quantitatively at ca. 190°C (5×10^{-5} Torr). *Anal.* calcd. for $C_{11}H_{14}O_3N_2$: C 59.45, H 6.35, N 12.60, OMe 13.96; found: C 59.34, H 6.23, N 12.69, OMe 13.83.

Behaviour on heating. At about 200°C, the prisms (from methanol) change to plates (stage) which melt with decomposition at 245–265°C (stage or capillary), depending on the rate of heating (lit. (13) mp 240–242°C, (14) mp 248–251°C). The plates obtained from water melt as above without the initial phase change. In capillaries sealed off at 5×10^{-5} Torr, the prisms melt at 277–278°C, mp of yellow resolidified melt 275°C; the phase change would not have been observable in the capillary.

*Lactam of 2-Aminomethyl-3-carboxymethyl-4-(2-ethoxycarbonylethyl) pyrrole (Ethyl Ester of Porphobilinogen Lactam) (**6**c)*

The melting point (stage or capillary) is uncertain (lit. (2) mp 239–244°C). In an evacuated capillary sealed off at 5×10^{-5} Torr, the melting point is 261°C.

Lactam of 2-Aminomethyl-3-(2-carboxyethyl)-4-methoxycarbonylmethylpyrrole (Methyl Ester of Isoporphobilinogen Lactam) (7e)

The oxime methyl ester hydrochloride **4***e* (1.833 g) in 40 ml of methanol was hydrogenated for 12 h over 700 mg of 5% Pd-on-carbon. Sodium (0.1 g) in methanol was added to the filtrate and washing from the catalyst (pH then 9.8–10 on wet indicator paper). After 3 h the reaction was complete (tlc), 0.4 ml of acetic acid was added (pH then 4.5), and the solvent was removed (rotary, 20°C bath, then oil pump). The powdered residue was extracted into 60 ml of ether (thimble, 3 days) from which the product separated as cream coloured microcrystals (77%), tlc: one spot, mp 158–167°C (lit. (3) mp 135–138°C, (4) mp 156–157.5°C); apparently one form, mp ca. 158°C, was more or less completely converted into a second form, mp ca. 170°C. After distillation in small amounts (180°C, 5×10^{-5} Torr) it formed colourless needles, mp 168–170°C. ^{1}Hmr (pyridine-d_5, Varian EM60) δ: 2.95 (4H, s, CH_2CH_2CO), 3.57 (2H, s, CH_2CO), 3.65 (3H, s, OCH_3), 4.42 (2H, d, J = 5 Hz, CH_2N), 6.83 (1H, s, pyrrole CH), 8.36 (1H, t, J = 5 Hz, NH.CO), 11.23 ppm (1H, br, pyrrole NH). *Anal.* calcd. for $C_{11}H_{14}O_3N_2$: C 59.45, H 6.35, N 12.60; found: C 59.23, H 6.47, N 12.44.

Lactam of 2-Aminomethyl-3-(2-carboxyethyl)-4-ethoxycarbonylmethylpyrrole (Ethyl Ester of Isoporphobilinogen Lactam) (7f)

The oxime ethyl ester hydrochloride **4***f* (1.013 g) in 50 ml of dry ethanol was hydrogenated for 12 h over 300 mg of 5% Pd-on-carbon. Sodium (0.1 g) in ethanol was added to the filtrate and washings from the catalyst (pH 9.8–10). After $3\frac{1}{2}$ h the reaction was complete and Dry Ice was added. The solvent was evaporated (rotary, 20°C bath, then oil pump), adding Dry Ice periodically to keep the pH at 7–8. The residue was extracted with warm ethyl acetate, the insoluble matter was dissolved in water, and this solution extracted with more ethyl acetate. The combined extracts were washed with 10 ml of water, dried ($MgSO_4$) and evaporated. The residue was washed with ether leaving the colourless product (42%), mp 162–164°C, tlc: one spot. Small amounts distilled quantitatively (175°C, 1×10^{-4} Torr) as colourless needles, melting point unchanged; ^{1}Hmr (pyridine-d_5) δ: 1.15 (3H, t, CH_2CH_3), 3.02 (4H, s, CH_2CH_2CO), 3.62 (2H, s, CH_2CO), 4.18 (2H, q, CH_2CH_3), 4.48 (2H, d, J = 5 Hz, CH_2N), 6.92 (1H, s, pyrrole CH), 8.61 (1H, t, J = 5 Hz, NH.CO), 11.32 ppm (1H, br, pyrrole NH). *Anal.* calcd. for $C_{12}H_{16}O_3N_2$: C 61.00, H 6.83, N 11.86; found: C 60.98, H 6.71, N 12.02.

*Benzyl 3-Ethoxycarbonylmethyl-4-(2-ethoxycarbonylethyl)-pyrrole-5-carboxylate (**10**a, R = H)*

This preparation followed that of the 2-methyl homologue (15). The triethyl ester **9***a* (R = H) (8.08 g) (16) with 1.72 g of sodium in 220 ml of pure benzyl alcohol gave the 5-benzyl ester of the tricarboxylic acid. This was esterified in ethanolic HCl to the product, colourless needles (2.83 g) from pentane (thimble), mp 63–64°. *Anal.* calcd. for $C_{21}H_{25}O_6N$: C 65.10, H 6.50, N 3.62; found: C 65.02, H 6.29, N 3.49.

*Benzyl 3-(2-Ethoxycarbonylethyl)-4-ethoxycarbonylmethyl-pyrrole-5-carboxylate (**10**b, R = H)*

This was obtained from **9***b* (R = H) (16) like the isomer above. The crude noncrystalline product was distilled (178°C, 5×10^{-4} Torr), crystallized from ether–pentane, then recrystallized by extraction into pentane (thimble), mp 55.5–57.5°C. *Anal.* calcd. for $C_{21}H_{25}O_6N$: C 65.10, H 6.50, N 3.62; found: C 65.20, H 6.56, N 3.52.

*Ethyl 2-Chloroacetylaminomethyl-3-ethoxycarbonylmethyl-4-(2-ethoxycarbonylethyl)pyrrole-5-carboxylate (**9**a, R = $ClCH_2CONHCH_2$—)*

The pyrrole **9***a* (R = H) (333 mg) was heated to boiling in 2 ml of ethanolic HCl (dry ethanol, saturated warm with HCl). *N*-Hydroxymethylchloroacetamide (333 mg) was added and the solution was boiled for 1 min, seeded, and allowed to cool. The product was separated, washed with cold 80% ethanol, and recrystallized from 80% ethanol (7 ml, cooling very slowly). It formed colourless needles (69%), mp 139–141.5°. *Anal.* calcd. for $C_{19}H_{27}O_7N_2Cl$: C 52.96, H 6.32, N 6.50, Cl 8.23; found: C 53.20, H 6.40, N 6.59, Cl 8.41.

*Ethyl 2-Chloroacetylaminomethyl-3-(2-ethoxycarbonylethyl)-4-ethoxycarbonylmethylpyrrole-5-carboxylate (**9**b, R = $ClCH_2CONHCH_2$—)*

Using **9***b* (R = H), this was obtained like the isomer above as colourless needles (73%), mp 151.5–152°C. *Anal.* calcd. for $C_{19}H_{27}O_7N_2Cl$: C 52.96, H 6.32, N 6.50, Cl 8.23; found: C 53.11, H 6.40, N 6.42, Cl 8.39.

*Benzyl 2-Chloroacetylaminomethyl-3-ethoxycarbonylmethyl-4-(2-ethoxycarbonylethyl)pyrrole-5-carboxylate (**10**a, R = $ClCH_2CONHCH_2$—)*

The pyrrole **10***a* (R = H) (333 mg) was warmed to solution in 2 ml of ethanolic HCl (dry ethanol saturated with HCl at 0°C). N-Hydroxymethylchloroacetamide (333 mg) was added and warmed to solution. The solution was boiled 1 min, cooled in ice, and seeded. The crystals were separated and recrystallized from ethanol as colourless needles (78%), mp 138.5–140.5°C. For analysis, it was recrystallized from ether (thimble), then from ethanol, mp 141.5–142.5°C; ^{1}Hmr ($CDCl_3$) δ: 1.22, 1.26 (6H, 2t, CH_2CH_3), 2.40–3.22 (4H, m, CH_2CH_2CO), 3.52 (2H, s, CH_2CO), 4.03 (2H, s, CH_2Cl), 4.10, 4.12 (4H, 2q, CH_2CH_3), 4.45 (2H, d, J = 6 Hz, CH_2N), 5.32 (2H, s, $CH_2C_6H_5$), 7.42 (5H, m, C_6H_5), 7.57 (1H, t, J = 6 Hz, NHCO), 9.95 ppm (1H, br, pyrrole NH). *Anal.* calcd. for $C_{24}H_{29}O_7N_2Cl$: C 58.47, H 5.93, N 5.68, Cl 7.19; found: C 58.21, H 5.94, N 5.59, Cl 7.31.

*Benzyl 2-Chloroacetylaminomethyl-3-(2-ethoxycarbonylethyl)-4-ethoxycarbonylmethylpyrrole-5-carboxylate (**10**b, R = $Cl \cdot CH_2CONHCH_2$—)*

This was prepared from **10***b* (R = H) exactly as its isomer above. After washing with 80% ethanol (4 × 1 ml), it formed colourless needles (82%), mp 141–143°C. For analysis, it was recrystallized from ether (thimble), melting point unchanged; ^{1}Hmr ($CDCl_3$) δ: 1.22 (6H, t, CH_2CH_3), 2.38–2.92 (4H, m CH_2CH_2CO), 3.82 (2H, s, CH_2CO), 4.07 (2H, s, CH_2Cl) 4.10 (4H, q, CH_2CH_3), 4.46 (2H, d, J = 6 Hz, CH_2N), 5.3(

Can. J. Chem. Downloaded from www.nrcresearchpress.com by 210.87.254.6 on 09/05/12
For personal use only.

(2H, s, $CH_2C_6H_5$), 7.42 (5H, m, C_6H_5), 7.57 (1H, t, J = 6 Hz, NHCO), 9.68 ppm (1H, br, pyrrole NH). *Anal.* calcd. for $C_{24}H_{29}O_7N_2Cl$: C 58.47, H 5.93, N 5.68, Cl 7.19; found: C 58.29, H 5.94, N 5.61, Cl 7.31.

2-Acetylaminomethyl-3-(2-ethoxycarbonylethyl)-4-ethoxycarbonylmethylpyrrole-5-carboxylic Acid

The benzyl ester (**10***b*, R=$ClCH_2CONHCH_2$—; 295 mg) was hydrogenated for 24 h in 22 ml of dioxane with 100 mg of sodium acetate trihydrate and 55 mg of 5% Pd-on-carbon. The filtrate (Celite) and washings were evaporated (rotary, 20°C) and the residue was washed with water to leave the product (98%) as colourless needles, mp 141–144°C (dec.); longer needles (mp 145–146°C) formed in the melt. The analytical specimen was rapidly crystallized from hot water. *Anal.* calcd. for $C_{17}H_{24}O_7N_2$: C 55.43, H 6.56, N 7.61; found: C 55.25, H 6.55, N 7.49.

Ethyl 2,4-Dimethyl-3-chloroacetylaminomethylpyrrole-5-carboxylate

2,4-Dimethyl 5-carbethoxypyrrole (1 g) was heated to solution in 6 ml of 10% ethanolic HCl. N-Hydroxymethylchloroacetamide (1 g) was added and the solution was heated 5 min on the steam bath. The product (35%) was separated and washed with 50% ethanol, mp 215–217°C. Recrystallization from 50 ml of 60% ethanol gave colourless needles, mp 217–218°C. *Anal.* calcd. for $C_{12}H_{17}O_3N_2Cl$: C 52.84, H 6.28, N 10.27, Cl 13.01; found: C 52.67, H 6.31, N 10.19, Cl 12.92.

Ethyl 2-Chloroacetylaminomethyl-5-methylpyrrole-4-carboxylate

2-Methyl-3-carbethoxypyrrole (1 g) and *N*-hydroxymethylchloroacetamide (0.8 g, 1 mol) were rubbed to solution in 10 ml of ethanol and 2.2 ml of ethanolic HCl. After 1 day at 20°C, the solution was seeded and the product (31%) was separated 2 days later, mp 199.5–201.5°C. For analysis, it was recrystallized from much water as colourless needles, melting point unchanged. *Anal.* calcd. for $C_{11}H_{15}O_3N_2Cl$: C 51.07, H 5.84, N 10.83, Cl 13.71; found: C 50.96, H 5.83, N 10.79, Cl 13.66.

When the pyrrole was boiled 1 min with 2 mol of the reagent in ethanolic HCl (saturated at 20°C), the product was evidently a dipyrrylmethane, colourless prismatic needles (8%) from acetone, mp 255–257.5°C. *Anal.* calcd. for $C_{23}H_{30}O_6N_4Cl_2$: C 52.17, H 5.71, N 10.58, Cl 13.41; found: C 52.08, H 5.65, N 10.56, Cl 13.35. *Mol. wt.* calcd.: 529.5; found: (osmometer): 534.

*2,4-Dimethylpyrrole-5-*N*-acetylthiocarbamide (**11**)*

A solution of potassium thiocyanate (12.7 g) in 75 ml of dimethylformamide was stirred in an ice bath while acetyl chloride (8.7 g) was dropped in at 20°C. The solution was then diluted to 100 ml with dimethylformamide and allowed to stand ½ h at 0°C. 2,4-Dimethylpyrrole (5 g) was dropped into 75 ml of this solution at 10°C. After ½ h at 0°C, the solution was diluted with 700 ml of ice water, seeded, and left 2 days at 10°C. The product which separated, orange needles (69%), mp 141–142.5°C, showed traces of impurities (tlc). The pure product was obtained as light-brown needles, mp 145–146°C, from water (650 ml, Celite); it sublimes at ca. 130°C (1×10^{-4} Torr) as bright orange prisms. *Anal.* calcd. for $C_9H_{12}ON_2S$: C 55.09, H 6.17, N 14.28, S 16.31; found: C 54.87, H 6.14, N 14.12, S 16.10.

*2,4-Dimethyl-5-acetylaminomethylpyrrole (**12**)*

Raney nickel (W. R. Grace and Co., No. 28, 20 ml) was washed six times with commercial absolute ethanol (centrifuge), suspended in 50 ml of ethanol, and added to a solution of 1 g of **11** in 50 ml of ethanol. The mixture was shaken for 1 h, allowed to stand overnight, then shaken 2 h. A drop of ammonium hydroxide was added to the filtrate (to stabilize the product) which was then evaporated (rotary, 20°C). The residue was distilled into a tube containing seed crystals (125°C, 5×10^{-4} Torr). While standing overnight under vacuum, the product solidified to yellow crystals (52%), mp 65.5–66.5°C; ^{1}Hmr ($CDCl_3$) δ: 1.97, 2.02 (6H, 2s, 2 ring CH_3), 2.20 (3H, s, $COCH_3$), 4.23 (2H, d, J = 6 Hz, CH_2N), 5.65 (1H, m, pyrrole CH), 6.27 (1H, br, NHCO), 8.58 (1H, br, pyrrole NH). *Anal.* calcd. for $C_9H_{14}ON_2$: C 65.03, H 8.49, N 16.85; found: C 64.90, H 8.42, N 17.01.

1. A. H. Jackson and S. F. MacDonald. Can. J. Chem. **35**, 715 (1957).
2. G. P. Arsenault and S. F. MacDonald. Can. J. Chem. **39**, 2043 (1961).
3. A. Valasinas, E. S. Levy, and B. Frydman. J. Org. Chem. **39**, 2872 (1974).
4. A. R. Battersby, J. F. Beck, and E. McDonald. J. Chem. Soc. Perkin 1, 160 (1974).
5. A. R. Battersby, E. Hunt, E. McDonald, and J. Moron. J. Chem. Soc. Perkin 1, 2917 (1973).
6. H. E. Zaugg and W. B. Martin. Org. React. **14**, 52 (1965).
7. H. Fischer and C. Nenitzescu. Ann. Chem. **443**, 123 (1925).
8. G. P. Arsenault, E. Bullock, and S. F. MacDonald. J. Am. Chem. Soc. **82**, 4384 (1960).
9. Y. C. Kim. Can. J. Chem. **47**, 3259 (1969).
10. E. Bullock and R. J. Abraham. Can. J. Chem. **37**, 1391 (1959).
11. A. E. Dixon and J. Hawthorne. J. Chem. Soc. 469 (1905).
12. D. M. MacDonald and S. F. MacDonald. Can. J. Chem. **33**, 573 (1955).
13. B. Frydman, S. Reil, A. Valasinas, R. B. Frydman, and H. Rapoport. J. Am. Chem. Soc. **93**, 2738 (1971).
14. A. R. Battersby, D. A. Evans, K. H. Gibson, E. McDonald, and L. Nixon. J. Chem. Soc. Perkin 1, 1546 (1973).
15. J. M. Osgerby, J. Pluscec, Y. C. Kim, F. Boyer, N. Stojanac, H. D. Mah, and S. F. MacDonald. Can. J. Chem. **50**, 2652 (1972).
16. E. J. Tarlton, S. F. MacDonald, and E. Baltazzi. J. Am. Chem. Soc. **82**, 4389 (1960).

Concerning the extension of the *J* method for internal barriers to six-bond couplings to ^{19}F in the 4-fluorophenyl fragment

TED SCHAEFER, WERNER DANCHURA,
WALTER NIEMCZURA, AND JAMES PEELING

Department of Chemistry, University of Manitoba, Winnipeg, Man., Canada R3T 2N2

Received March 10, 1978

TED SCHAEFER, WERNER DANCHURA, WALTER NIEMCZURA, and JAMES PEELING. Can. J. Chem. **56**, 2442 (1978).

The long-range coupling constants over six bonds from the side-chain protons to the fluorine nucleus on the ring are extracted from the proton magnetic resonance spectra of *p*-fluorobenzyl cyanide, chloride, and bromide; of *p*-fluorobenzal chloride; and of *p*-fluoroisopropylbenzene. On the assumption that these couplings are transmitted via a σ–π mechanism, a hindered rotor treatment yields the barriers to internal rotation about the carbon–carbon bond which attaches the substituent to the benzene ring. These barriers, when compared to those derived from the analogous proton–proton coupling constants, apparently are accurate enough for the determination of ground state conformations and for a rough assessment of the energetics of conformational interconversions.

TED SCHAEFER, WERNER DANCHURA, WALTER NIEMCZURA et JAMES PEELING. Can. J. Chem. **56**, 2442 (1978).

Faisant appel aux spectres de résonance magnétique nucléaire du proton des cyanure, chlorure et bromure de *p*-fluorobenzyle, du chlorure de *p*-fluorobenzal et du *p*-fluoroisopropylbenzène, on a pu évaluer les constantes de couplage à longues distances à travers six liaisons des protons de la chaîne latérale avec le noyau de fluor du cycle. Si on fait l'hypothèse que ces couplages sont transmis par un mécanisme σ–π, un traitement de rotor empêché fournit les barrières à la rotation interne autour de la liaison carbone–carbone qui attache le substituant au noyau benzénique. Il semble que ces barrières, lorsqu'on les compare à celles obtenues à partir de constantes de couplage proton–proton analogues, soient suffisamment correctes pour permettre la détermination des conformations de l'état fondamental et pour évaluer d'une façon approximative les énergies impliquées dans les interconversions conformationnelles.
[Traduit par le journal]

Introduction

The *J* method of determining small (<4 kcal/mol) twofold barriers to internal rotation about bonds to the benzene ring depends on a knowledge of the dependence on the rotational angle of the spin–spin coupling over six bonds between a ring proton and the proton(s) on the side chain, $^6J_p^{H,XH}$. Combined with a hindered rotor treatment of the internal rotation, a knowledge of the sample temperature and of the reduced moment of inertia about the rotor axis suffices to calculate the expectation value of $^6J_p^{H,XH}$ as a function of the barrier (1, 2). In this way reasonable barriers and ground state conformations have been estimated for rotation about C—C, C—Si, and C—S bonds in a variety of benzene derivatives (3–7).

The rotational angle dependence of $^6J_p^{H,CH}$ can be written (8–10) as $^6J = {}^6J_{90} \sin^2 \theta$, where $^6J_{90}$ is the magnitude of ^6J when $\theta = 90°$ in **1**. There exist data implying that ^6J_o is less than 0.03 Hz (11, 12), while $^6J_{90}$ is -1.24 Hz in toluene (13).

For rotation about C—C bonds the barriers and low energy conformations are such that the observed $^6J_p^{H,CH}$ has magnitudes lying between about 0.1 and

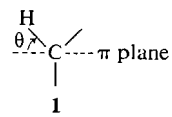

1

0.5 Hz. Although such couplings can be measure to an accuracy of 0.02 Hz, considerable skill an patience is required in their determination, parti ularly when the phenyl proton magnetic resonanc spectra are tightly coupled (3).

Now, it is of interest that $^6J^{H,CF}$ in *p*-fluorotoluer is 1.15 ± 0.02 Hz (14), almost twice the magnitu of $^6J_p^{H,CH}$ in toluene. Furthermore, the same calcul tions (8) which confirm experimental tests th $^6J_p^{H,CH}$ obeys a $\sin^2 \theta$ relationship (9, 10), also predi such a relationship for $^6J_p^{H,CF}$. The presence of C—F bond in the benzene ring considerably simpl fies the spectral analytical procedures and the larg magnitude of $^6J_p^{H,CF}$ makes its accurate determin tion relatively easy. On the other hand, $^6J_p^{H,}$ depends on the σ—π interactions in the C—F bor (15) and these may well be more sensitive to ele tronic perturbations by the side chain of interest th are the σ—π interactions for the C—H bond. other words, $^6J_p^{H,CH}$ is known experimentally (4) a

Can. J. Chem. Downloaded from www.nrcresearchpress.com by 210.87.254.40 on 09/05/12
For personal use only.

Can. J. Chem. Downloaded from www.nrcresearchpress.com by 210.87.254.40 on 09/05/12
For personal use only.

theoretically (8) to be insensitive to intrinsic perturbations from ring substituents, whereas the C—F bond may well alter its partial double bond character in response to substituent perturbations.

In this paper the measurement of $^6J_p^{H,CF}$ and its use in the J method is reported for the *para* fluoro derivatives of toluene; benzyl bromide, chloride, and cyanide; isopropyl benzene; and for benzal chloride. Except for benzyl cyanide, the internal barriers have previously been estimated from $^6J_p^{H,CH}$, so that a comparison can be made with the present approach.

The practice of 'fluorine labelling' of macromolecules (16) invites the speculation that under favorable circumstances the present J method could be applied to the determination of the preferred conformation of the label in large molecules.

Experimental

The fluorine compounds had a commercial origin. All but the *p*-fluorobenzyl cyanide (Parish Chemical Co) came from Aldrich Chemical Co. Any small amounts of impurities did not interfere with the analysis of the ^{1}H nmr spectra. Nuclear magnetic resonance samples were prepared as 10 mol% solutions in CS_2, containing a small amount of tetramethylsilane, and were thoroughly degassed by the freeze–pump–thaw–freeze technique. The ^{1}H nmr spectra were repeatedly calibrated at 5 Hz intervals in the frequency sweep mode of an HA100 spectrometer. The probe temperature was 305 K. The spectral dispersion was 1 Hz/cm and the sweep rates were 0.02 and 0.01 Hz/s. The sign of the long-range coupling over six bonds to ^{19}F, $^6J_p^{H,CF}$, was determined by low-amplitude double irradiation methods (17) and was the same as $^3J^{H,F}$, i.e., positive (18).

Preparation of the 3,5-dichlorobenzyl cyanide proceeded via the benzyl bromide by treatment with KCN in acetone solution. The bromide was prepared from the commercial benzoic acid by reduction to the alcohol, followed by conversion with PBr_3. The cyanide was insufficiently soluble in CS_2 but a mixture of C_6D_6, $CDCl_3$, and CS_2 dissolved enough compound, less than 5 mol%, to allow the recording of good ^{1}H nmr spectra. The compound gave a satisfactory mass spectrum.

The frequencies of the sweep and manual oscillators were recorded with an HP 5323A counter. Peak positions were then interpolated using a vernier and a straight edge. Root-mean-square deviations of peak positions relative to internal tetramethylsilane lay typically in the vicinity of 0.02 Hz. The spectrometer frequency was 100.001_2 MHz.

Results and Discussion

(i) Spectral Analyses

These were undertaken with the computer program LAME (19, 20). A typical analysis gave the results in Table 1, those for 4-fluorobenzyl chloride. The standard deviations in the spectral parameters are 0.004 Hz or less, suggesting an accuracy of at least 0.02 Hz. Figure 1 displays a calculated and an observed spectrum of the side-chain protons in 4-fluorobenzyl bromide. Table 2 contains the spectral parameters of immediate interest, the couplings to the side-chain protons, for the other compounds.

TABLE 1. Proton chemical shifts[a] and coupling constants for 4-fluorobenzyl chloride, 10 mol% in CS_2

Parameter	Value	Parameter	Value
ν_1	724.142(2)[b]	$^5J_{25}^{H,H}$	0.392(3)
ν_2	691.189(2)	$^4J_o^{H,CH}$	−0.492(2)
ν_3	444.945(2)	$^5J_m^{H,CH}$	0.290(2)
$^3J_{23}^{H,H}$	8.535(3)	$^6J_p^{H,CF}$	0.652(4)
$^3J_{34}^{H,F}$	8.416(4)	rms deviation	0.016
$^4J_{26}^{H,H}$	2.770(4)	Transitions calcd.	272
$^4J_{35}^{H,H}$	2.423(4)	Transitions assigned	211
$^4J_{34}^{H,F}$	5.204(4)		

[a]In Hz at 100 M Hz to low field of internal tetramethylsilane at 305 K.
[b]Numbers in parentheses are standard deviations in the last place.

FIG. 1. The calculated (*b*) and observed (*a*) spectra of the side-chain protons of *p*-fluorobenzyl bromide as a 10 mol% solution in CS_2 at 100 MHz and 305 K. The long-range couplings for the calculated spectrum are those in Table 2.

(ii) The Value of $^6J_{90}^{H,CF}$

The barrier to internal rotation in *p*-fluorotoluene is 0.0138 kcal/mol (21). Accordingly, the average value of $\sin^2\theta$ is $\langle\sin^2\theta\rangle = 0.5$. In acetone solution $^6J_p^{H,CF}$ is 1.15 ± 0.02 Hz and is 1.12 Hz in CS_2 solution (Table 2). Although it alters the argument very little, the value of 1.12 Hz will be used because the other compounds were measured in CS_2 solution and because the high dielectric constant of acetone could result in a slightly larger double bond character of the C—F bond (charge separation), leading to a larger $^6J_p^{H,CF}$. It follows that $^6J_{90}^{H,F}$ is 1.12/0.5 or

Can. J. Chem. Downloaded from www.nrcresearchpress.com by 210.87.254.40 on 09/05/12
For personal use only.

TABLE 2. Coupling constants in Hz between the proton(s) on the side-chain and the ring protons or ^{19}F

Compound[a]	$^4J_o^{H,CH}$	$^5J_m^{H,CH}$	$^6J_p^{H,CF}$
$pF—C_6H_4—CH_3$	−0.71	0.36	1.12[b]
$pF—C_6H_4—CH_2Cl$	−0.49	0.29	0.65[c]
$pF—C_6H_4—CH_2Br$	−0.43	0.29	0.54_5
$pF—C_6H_4—CH_2CN$	−0.74	0.33	1.06
$pF—C_6H_4—CHCl_2$	−0.44	0.24	0.22
$pF—C_6H_4—CH(CH_3)_2$	−0.58	0.31	0.56
$3,5\text{-diCl—}C_6H_3CH_2CN$	−0.76	—	−0.60[d]

[a]10 mol% solutions in CS_2.
[b]A 15 mol% solution in acetone-d_6 yielded $^4J_o^{H,CH}$, $^5J_m^{H,CH}$, and $^6J_p^{H,CF}$ as −0.72, 0.34, and 1.15 Hz, respectively (14).
[c]An independent analysis by W. J. E. Parr gave 0.63 Hz.
[d]$^6J_p^{H,CH}$ for a saturated solution in a mixture of C_6D_6, $CDCl_3$, and CS_2.

2.24 ± 0.02 Hz (the standard deviation for $^6J_p^{H,CF}$ was 0.004 Hz).

(iii) Substituent Perturbation of $^6J_p^{H,CF}$

It was argued previously (4) that, in the corresponding toluene derivatives with a hydrogen atom at position 4, $^6J_{90}^{H,CH}$ is reduced in magnitude in the presence of a strongly electronegative substituent in the α position. Thus, for CH_2Cl it was suggested that $^6J_{90}^{H,CH}$ becomes −1.14 Hz, as compared to −1.24 Hz in toluene itself and that, for the $CHCl_2$ group, $^6J_{90}^{H,CH}$ is −1.05 Hz (22). For CH_2Br, $^6J_{90}^{H,CH}$ would be very similar to its value for CH_2Cl and, because bromine is somewhat less electronegative than chlorine, a value of −1.16 Hz appears reasonable. (The barrier for CH_2Br is so large, see below, that a choice of $^6J_p^{H,CH}$ for this group is somewhat academic anyway.) A decrease in $^6J_{90}^{H,CH}$ is supported by INDO MO FPT calculations (1) suggesting polarization of the adjacent C—H bonds by the polar substituent in the side chain. This polarization leads to a decreased overlap between the C—H bond orbitals and the π electron system of the ring (a smaller σ–π interaction).

In the absence of a substituent perturbation of $^6J_p^{H,CF}$, $\langle\sin^2\theta\rangle$ is simply equal to $^6J_{obs}^{H,CF}/2.24$. In presence of a substituent perturbation of the σ–π interaction of a side-chain C—H bond, $\langle\sin^2\theta\rangle$ is obtained from $^6J_{obs}^{H,CF}/(2.24 \times {}^6J_{90}^{H,CH}/1.24)$. The ensuing values of $\langle\sin^2\theta\rangle$ are given in Table 3.

(iv) Derivation of Internal Barriers

Plots of $\langle\sin^2\theta\rangle$ vs. V_2 were constructed for a range of reduced moments of inertia at a temperature of 305 K. If the ground state conformation is **2**, the plot yields a simple curve with a $\langle\sin^2\theta\rangle$ value of 0.5 at a zero barrier; V_2 is the difference in energy between conformations **2** and **3**. At high V_2 values it slowly approaches 0.25 with the consequence that a derived barrier becomes more and more uncertain as it increases above 2.2 kcal/mol.

If the ground state conformation is **3**, $\langle\sin^2\theta\rangle$ falls between 0.75 and 0.5. This conformation need not be considered because the experimental $\langle\sin^2\theta\rangle$ for the benzyl compounds lies between 0.5 and 0.25

For the benzal compounds the ground state conformation is taken as **4**, so that $\langle\sin^2\theta\rangle$ varies between 0.5, for a vanishing barrier, and zero for a very large barrier. For this class of compounds reasonably accurate V_2 numbers are obtainable up to 3 kcal/mol because $\langle\sin^2\theta\rangle$ has twice the range it has for the benzyl compounds.

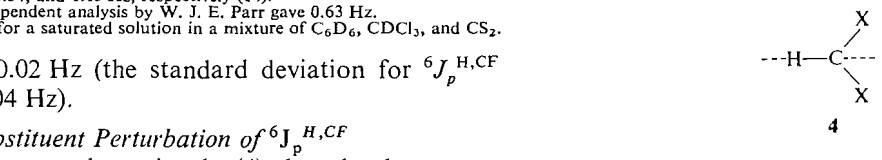

4

The various compounds are now discussed in turn

Benzyl Cyanide Derivatives

In 3,5-dichlorobenzyl cyanide, $^6J_p^{H,CH}$ is −0.60 ± 0.01 Hz. The chlorine substituents do not perturb $^6J_p^{H,CH}$ (4). If $^6J_{90}^{H,CH}$ is −1.24 Hz as in toluene, i.e. if the cyano group does not change the magnitude of the σ–π interaction, then $\langle\sin^2\theta\rangle$ is 0.60/1.24 or 0.48 ± 0.02, where the error allows for measurement errors. From the plots of $\langle\sin^2\theta\rangle$ vs. V_2 a value of 0.2 ± 0.2 kcal/mol is then found on the assumption that **2** is the ground state conformation. However, in 2,6-dichlorobenzyl cyanide, $^6J_p^{H,CH}$ is −0.33 ± 0.0 Hz (23). The barrier is now large, very likely greater than 3 kcal/mol (23), so that $\langle\sin^2\theta\rangle$ is very close to 0.25 ($\sin^2 30°$) because **2** is the predominant conformation. It follows that $^6J_{90}^{H,CH}$ may be 4 × −0.33, or −1.32 Hz, the larger magnitude compared to toluene possibly arising from enhanced hyperconjugation in the presence of the C≡N group. If $^6J_{90}^{H,CH}$ is indeed −1.32 Hz, $\langle\sin^2\theta\rangle$ becomes 0.45_5, corresponding to a barrier of 0.3_5 + 0.2 kcal/mol. The quoted errors assume an error of 0.02 in $\langle\sin^2\theta\rangle$. It seems safe to conclude that the $^6J_p^{H,C}$ method yields a barrier of 0.2_5 ± 0.2 kcal/mol entered in Table 3.

Again, $^6J_p^{H,CF}$ in *p*-fluorobenzyl cyanide is 1.06 Hz and one has $\langle\sin^2\theta\rangle$ as 1.06/2.24, or 0.47, yielding a barrier of 0.3 ± 0.2 kcal/mol. If $^6J_{90}^{H,CH}$ is −1.3 Hz, then the equation in section *iii* implies a $\langle\sin^2\theta$ of 0.44 and a barrier of 0.6 kcal/mol. The mean value of 0.45 ± 0.2 kcal/mol is entered in Table 3.

Apparently, the two approaches yield equa

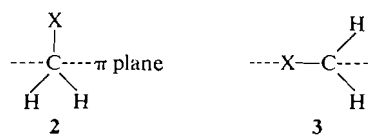

TABLE 3. Comparison of twofold barriers obtained from $^6J_p^{H,CF}$ and $^6J_p^{H,CH}$

Fragment	$\langle \sin^2 \theta \rangle$		V_2 (kcal/mol)		Ref.
	$^6J_p^{H,CF}$	$^6J_p^{H,CH}$	$^6J_p^{H,CF}$	$^6J_p^{H,CH}$	
CH_2CN	0.44(0.47)	0.46(0.48)	0.45±0.2	0.25±0.2	—
CH_2Cl	0.32	0.35	2.7±0.4	2.1±0.4	4
CH_2Br	0.26	0.28	>3	>3	4
$CH(CH_3)_2$	0.25	0.20	1.5±0.2	2.0±0.2	6
$CHCl_2$	0.12	0.20	3.1±0.5	2.2±0.3	22

barrier values to within experimental error. A mean value of 0.35 ± 0.3 kcal/mol may well encompass differences in the solvents and substitution patterns for the two compounds.

The Kerr constant for benzyl cyanide suggests either that the C—CN bond is twisted out of the benzene plane by 44° or that the CH_2CN group rotates freely (24). Our results are consistent with the latter alternative.

Benzyl Chloride and Benzyl Bromide Derivatives

The barriers given in Table 3 assume that $^6J_{90}^{H,CH}$ is −1.14 Hz for CH_2Cl and −1.16 Hz for CH_2Br. For the latter, the J method is very insensitive.

Isopropyl Benzene and Benzal Chloride Derivatives

The barriers in Table 3 are derived on the assumption that $^6J_{90}^{H,CH}$ is −1.24 Hz for $CH(CH_3)_2$ and −1.05 Hz for $CHCl_2$.

(v) Ab initio *Molecular Orbital Calculations*

Previous calculations (4) at the STO 3G level (25, 26) yielded **2** as 2.22 kcal/mol more stable than **3** for benzyl chloride, in good agreement with the present results. Such computations are here extended to benzyl cyanide. A standard geometry (27) gave **2** as 1.98 kcal/mol more stable than **3**. A partial geometry optimization procedure increased the C—C—CN angle to 112.1° for **2** and to 114.4° for **3**, yielding **2** as 0.98 kcal/mol more stable than **3**. These somewhat expensive calculations suggest that a more complete optimization of bond angles and bond lengths could well lead to a barrier in even better agreement with the data in Table 3, viz., about 0.3 kcal/mol.

(vi) Comparison of the Two Sets of Barriers

The barrier values based on $^6J_p^{H,CH}$ are probably more reliable than those based on $^6J_p^{H,CF}$ for the following reasons. First, the tests discussed in the introduction strongly imply that $^6J_p^{H,CH}$ is indeed transmitted via a σ—π mechanism involving a $\sin^2 \theta$ dependence of $^6J_p^{H,CH}$ and that this coupling is negligibly small when $\theta = 0$. For $^6J_p^{H,CF}$, however, one cannot be certain that there exists no contribution in addition to the σ—π mechanism. In fact, in benzal fluoride derivatives, in which the fluorine atom is situated in the side chain, the non σ—π component of $^6J_p^{H,CF}$ is as large as 20% of the σ—π component (22). Second, the σ—π component of $^6J_p^{H,CF}$ in the compounds considered in this paper may be more sensitive to substituent perturbations than is $^6J_p^{H,CH}$ because it depends on the hyperfine interactions in the C—F bond, which apparently vary much more from system to system than the hyperfine interactions in a C—H bond (15, 28). In simpler terms, $^6J_p^{F,CH}$ varies by at least 0.1 Hz from compound to compound (14, 15), whereas any variation in $^6J_p^{H,CH}$ is apparently not detectable (4, 29). It is also conceivable that insertion of a *para* fluoro substituent will cause a change in the magnitude of the barrier, for example, by altering the energy of either the low or high energy conformations. If this alteration occurs, the data in Table 3 suggest that the alterations are such as to increase the barrier when the side chain contains polar substituents and to decrease the barrier when the side chain is relatively nonpolar. A combination of all these factors could well account for the differences in the barriers derived by the two methods.

Nevertheless, the differences are not so great as to eliminate the use of $^6J_p^{H,CF}$ in the determination of ground state conformations or in reaching a rough assessment of the energetics of the internal rearrangements in benzyl or benzal compounds.

Acknowledgment

We are grateful to the National Research Council of Canada for financial assistance.

1. T. SCHAEFER, J. B. ROWBOTHAM, W. J. E. PARR, K. MARAT, and A. F. JANZEN. Can. J. Chem. **54**, 1322 (1976).
2. P. B. AYSCOUGH, M. C. PRICE, and R. E. D. MCCLUNG. Mol. Phys. **20**, 41 (1971).
3. W. J. E. PARR and T. SCHAEFER. J. Am. Chem. Soc. **99**, 1033 (1977).
4. T. SCHAEFER, L. J. KRUCZYNSKI, and W. J. E. PARR. Can. J. Chem. **54**, 3210 (1976).
5. W. J. E. PARR and T. SCHAEFER. Can. J. Chem. **55**, 557 (1977).
6. T. SCHAEFER, W. J. E. PARR, and W. DANCHURA. J. Magn. Reson. **25**, 167 (1977).

Can. J. Chem. Downloaded from www.nrcresearchpress.com by 210.87.254.40 on 09/05/12
For personal use only.

7. W. J. E. PARR and T. SCHAEFER. J. Magn. Reson. **25**, 171 (1977).
8. R. WASYLISHEN and T. SCHAEFER. Can. J. Chem. **50**, 1852 (1972).
9. C. J. MACDONALD and W. F. REYNOLDS. Can. J. Chem. **48**, 1002 (1970).
10. J. B. ROWBOTHAM and T. SCHAEFER. Can. J. Chem. **52**, 489 (1974).
11. J. PEELING, L. ERNST, and T. SCHAEFER. Can. J. Chem. **52**, 849 (1974).
12. J. PEELING, J. B. ROWBOTHAM, L. ERNST, and T. SCHAEFER. Can. J. Chem. **52**, 2414 (1974).
13. M. P. WILLIAMSON, R. KOSTELNIK, and S. M. CASTELLANO. J. Chem. Phys. **49**, 2218 (1968).
14. R. WASYLISHEN and T. SCHAEFER. Can. J. Chem. **49**, 94 (1971).
15. D. J. BLEARS, S. S. DANYLUK, and T. SCHAEFER. J. Chem. Phys. **47**, 5037 (1967).
16. J. T. GERIG. J. Am. Chem. Soc. **99**, 1721 (1977).
17. R. FREEMAN and W. A. ANDERSON. J. Chem. Phys. **37**, 2053 (1962).
18. P. DIEHL and I. GRÄNACHER. J. Chem. Phys. **34**, 1846 (1961).
19. S. CASTELLANO and A. A. BOTHNER-BY. J. Chem. Phys **41**, 3863 (1964).
20. C. W. HAIGH and J. M. WILLIAMS. J. Mol. Spectrosc. **3** 398 (1969).
21. H. D. RUDOLPH and H. SEILER. Z. Naturforsch. **20**, Teil A 1682 (1965).
22. T. SCHAEFER, W. DANCHURA, and W. NIEMCZURA. Can. Chem. **56**, 36 (1978).
23. A. F. JANZEN and T. SCHAEFER. Can. J. Chem. **49**, 181 (1971).
24. K. E. CALDERBANK, R. J. W. LE FÈVRE, and R. K PIERENS. J. Chem. Soc. B, 1463 (1970).
25. W. J. HEHRE, L. RADOM, and J. A. POPLE. J. Am. Chem Soc. **94**, 1496 (1972).
26. W. J. HEHRE, W. A. LATHAN, R. DITCHFIELD, M. D NEWTON, and J. A. POPLE. QCPE, **10**, 236 (1974).
27. J. A. POPLE and M. S. GORDON. J. Am. Chem. Soc. **89**, 425 (1967).
28. W. G. ESPERSEN and R. W. KREILICK. Mol. Phys. **16**, 57 (1969).
29. S. STERNHELL and R. H. ROTTENDORF. Aust. J. Chem. **1** 1315 (1964).

Can. J. Chem. Downloaded from www.nrcresearchpress.com by 210.87.254.40 on 09/05/12
For personal use only.

Reaction of carbon monoxide with nitrous oxide on scandium and magnesium oxides

BORDAN W. KRUPAY[1] AND ROBERT A. ROSS

Department of Chemistry, Lakehead University, Thunder Bay, Ont., Canada P7B 5E1

Received February 15, 1978

BORDAN W. KRUPAY and ROBERT A. ROSS. Can. J. Chem. **56**, 2447 (1978).

The kinetics of the catalytic reaction between carbon monoxide and nitrous oxide has been examined on Sc_2O_3 and MgO in a differential flow reactor at atmospheric pressure. On Sc_2O_3, the apparent activation energy was 126 ± 4 kJ mol^{-1} from 633 to 723 K while a value of 63 ± 4 kJ mol^{-1} was obtained for MgO from 547 to 673 K. On both catalysts, the surface mechanism has been interpreted by a reaction scheme involving each reactant as an adsorbed species with CO and N_2O being further involved in subsequent steps during the course of the surface reaction. The metal/oxygen bond polarization appears to influence both the strength and form of CO adsorption where the reactants interact as surface species each bound to two surface sites on Sc_2O_3 and on one surface site each on MgO.

BORDAN W. KRUPAY et ROBERT A. ROSS. Can. J. Chem. **56**, 2447 (1978).

On a étudié la cinétique de la réaction catalytique entre le monoxyde de carbone et l'oxyde nitreux sur du Sc_2O_3 et du MgO dans un réacteur à flux différentiel, à pression atmosphérique. Sur le Sc_2O_3, l'énergie d'activation apparente est de 126 ± 4 kJ mol^{-1} entre 633 et 723 K alors que l'on a obtenu une valeur de 63 ± 4 kJ mol^{-1} sur du MgO entre 547 et 673 K. Sur les deux catalyseurs, on a interprété le mécanisme de surface par un schéma réactionnel impliquant que chaque réactif est une espèce adsorbée; le CO et le N_2O sont impliqués dans des étapes ultérieures au cours de la réaction de surface. La polarisation de liaison métal/oxygène semble influencer à la fois la force et la forme de l'adsorption du CO au niveau des interactions des réactifs sous forme d'espèces de surface qui sont toutes liées à deux sites de surface du Sc_2O_3 et à un site de surface chacun sur le MgO.

[Traduit par le journal]

Introduction

The kinetics of the catalysed reaction between carbon monoxide and nitrous oxide to yield carbon dioxide and nitrogen has been studied recently on several transition metal oxides (1–4). The course of catalysis on active surfaces, for example cobalt and manganese oxides (4), may be summarised as involving: (*i*) the reaction of carbon monoxide with surface oxygen via a cyclic transition state, (*ii*) the destabilization of an intermediate surface carbonate, and (*iii*) the desorption of carbon dioxide which may occupy two surface sites. Such steps appear to be involved in an apparently complex way in shaping the overall catalytic process.

These features have now been examined in a kinetic study with scandium and magnesium oxides which are not normally associated with high activity in redox-type catalytic reactions (5).

Experimental

The catalytic reaction between carbon monoxide and nitrous oxide was examined in a differential-reactor flow system (6, 7) at atmospheric pressure. High-purity helium was used as the carrier gas in the flow system and Beckman GC-5 gas chromatograph. Nitrogen, carbon monoxide, carbon dioxide, and nitrous oxide were analyzed by a thermal conductivity bridge using stainless steel columns, 183 × 0.32 cm od, packed with 61 cm Carbosieve B and the remainder with Poropak Q at a column temperature of 353 K which was sufficient to resolve all components.

The standard reacting gas mixture consisted of carbon monoxide and nitrous oxide each at a partial pressure of 5.33 kN m^{-2} (40 Torr). 'Blank' runs confirmed that reaction on the quartz wool and reactor walls reached 1% at 853 K which was 130 K above the highest temperature of catalysis. Preliminary experiments with the oxide catalysts established that diffusion phenomena (8, 9) did not influence the rate measurements at a total gas flow rate of 350 ml min^{-1} (N.T.P.).

On scandium oxide (99.90% w/w, Alfa Inorganics Inc.) the CO/N_2O reaction was examined from 633 to 723 K. The conversion level at the highest temperature was 3.7%. The oxide, Sc_2O_3, previously calcined at 873 K for 10 h and stored in a desiccator over P_2O_5, was equilibrated in the standard reacting gas mixture for 5 h at 733 K. Catalysts thus prepared had surface areas of 14 m^2 g^{-1} (krypton; B.E.T.) and a bulk volume of 1.48 cm^3 g^{-1}.

Semi-conductor grade MgO (Research Organic/Inorganic Chem. Corp., batch No. MG13) was heated in the reactor at 873 K for 2 h in air prior to catalysis, cooled to 673 K, and the standard gas mixture introduced. Steady catalytic activity levels were attained after 4.5 h. From 547 to 673 K, the conversion levels ranged from 2.65 to 27.5%. The surface area was 16.6 m^2 g^{-1} and the bulk volume 2.89 cm^3 g^{-1}.

For both Sc_2O_3 and MgO, comparison of the X-ray powder diffraction photographs, taken before and after catalysis, did not reveal any changes as a result of the catalytic reaction.

Carbon monoxide (C.P.; 99.5% minimum), carbon dioxide (Coleman; 99.99%), nitrogen (super-pure; 99.99%), nitrous oxide (99.9% minimum), and helium (high purity; 99.995%) were used as supplied.

[1]Present address: Division of Chemistry, National Research Council of Canada, Ottawa, Ont., Canada K1A 0R9.

Can. J. Chem. Downloaded from www.nrcresearchpress.com by 210.87.254.42 on 09/05/12
For personal use only.

Can. J. Chem. Downloaded from www.nrcresearchpress.com by 210.87.254.42 on 09/05/12
For personal use only.

Results

Reaction Rate Orders on Scandium Oxide

The dependence of the reaction rate upon variations in the carbon monoxide partial pressure was examined from 1.33 to 16.0 kN m^{-2} (10 to 120 Torr) at 673 K with nitrous oxide maintained at 5.33 kN m^{-2} (40 Torr). A non-linear relationship was evident (Fig. 1) where the order of reaction with respect to carbon monoxide increased with partial pressure.

With the carbon monoxide partial pressure fixed at 5.33 kN m^{-2}, the rate was determined in the nitrous oxide partial pressure range from 1.33 to 16.0 kN m^{-2} at 673 K. The data (Fig. 1) were non-linear with a decreasing reaction rate order as the nitrous oxide partial pressure increased.

The partial pressures of carbon monoxide and nitrous oxide were each fixed at 5.33 kN m^{-2} and the carbon dioxide partial pressure was varied from 0.53 to 5.79 kN m^{-2}. Figure 1 indicates that the rate order decreased with increasing carbon dioxide partial pressure. Similarly, the rate order with respect to nitrogen at partial pressures of 2.67, 5.33, and 10.70 kN m^{-2} was zero.

On the basis of these experiments the catalytic reaction rate, r (mol m^{-2} s^{-1}), was expressed as:

$$[1] \qquad r = k\frac{P_{CO}^{0.4}P_{N_2O}^{0.4}}{P_{CO_2}^{0.1}}$$

Reaction Rate Orders on Magnesium Oxide

The reaction rate order with respect to carbon monoxide was determined at 559 K from 4.00 to 13.3 kN m^{-2} with nitrous oxide maintained at 5.33 kN m^{-2}. The results (Fig. 2) show a non-linear relationship and a rate order of 0.6 was calculated at a carbon monoxide partial pressure of 5.33 kN m^{-2}.

With carbon monoxide fixed at 5.33 kN m^{-2}, the partial pressure of nitrous oxide was varied from 4.0 to 13.3 kN m^{-2} at 559 K. The results (Fig. 2) exhibited a similar pattern to those above and a rate order of 0.3 was determined for subsequent rate constant calculations.

Using the same reacting gas mixture as that for scandium oxide, the rate order dependence on carbon dioxide partial pressure was examined in the range 0.33 to 5.79 kN m^{-2} and the results are shown in Fig. 2. As described previously, the reaction rate order determined with respect to carbon dioxide was -0.1. Similarly, variations in the nitrogen partial pressure from 2.67 to 10.7 kN m^{-2} showed a zero order effect on the reaction rate.

The catalytic reaction rate, r (mol m^{-2} s^{-1}), was expressed as:

$$[2] \qquad r = k\frac{P_{CO}^{0.6}P_{N_2O}^{0.3}}{P_{CO_2}^{0.1}}$$

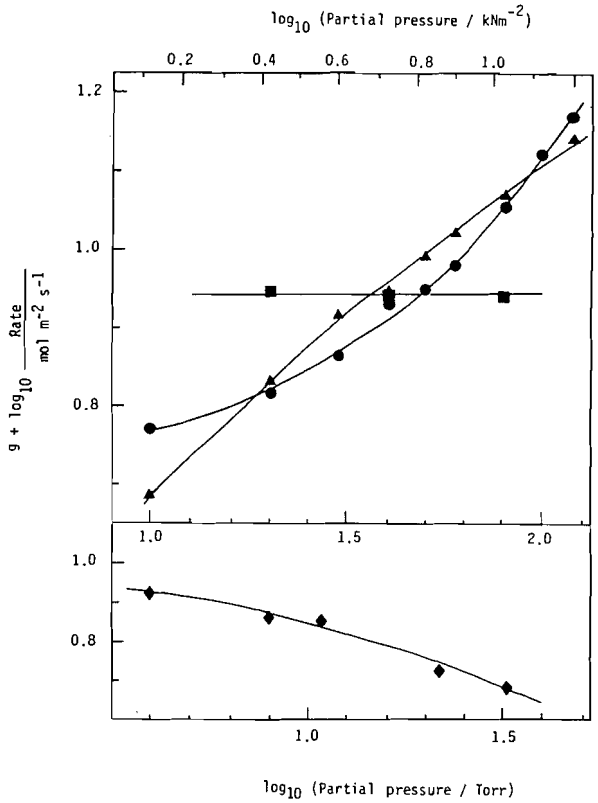

FIG. 1. Reaction rate order measurements for the CO/N_2O reaction on scandium oxide at 673 K for carbon monoxide (●), nitrous oxide (▲), nitrogen (■), and carbon dioxide (◆).

The Effect of Temperature

On scandium oxide, the reaction rate was examined from 633 to 723 K in 10 K intervals after catalyst equilibration for 5 h in the standard reaction mixture at 723 K. Rate constants were calculated by integration of eq. [1] and the Arrhenius plot for these data is shown in Fig. 3. The apparent activation energy was 126 ± 4 kJ mol^{-1}.

Magnesium oxide was equilibrated in the standard gas mixture at 673 K for 4.5 h and the rate of reaction examined from 673 to 547 K. The rate constants calculated from eq. [2] are shown in Fig. 3 whence an apparent activation energy of 63 ± 4 kJ mol^{-1} was obtained.

Discussion

Sc_2O_3 exhibits the largest energy band gap, 5.4 eV, of the first row transition metal oxides (10). The value for magnesium oxide, an insulator, is 8.7 eV. Although Sc_2O_3 is similar in properties to Al_2O_3, its basicity is more akin to that of MgO. Similar catalytic properties for Sc_2O_3 and MgO in the CO/N_2O reaction might then be broadly anticipated as shown, for example, by the temperature range required for the studies, 633 to 723 K, Sc_2O_3, and 601 to 673 K,

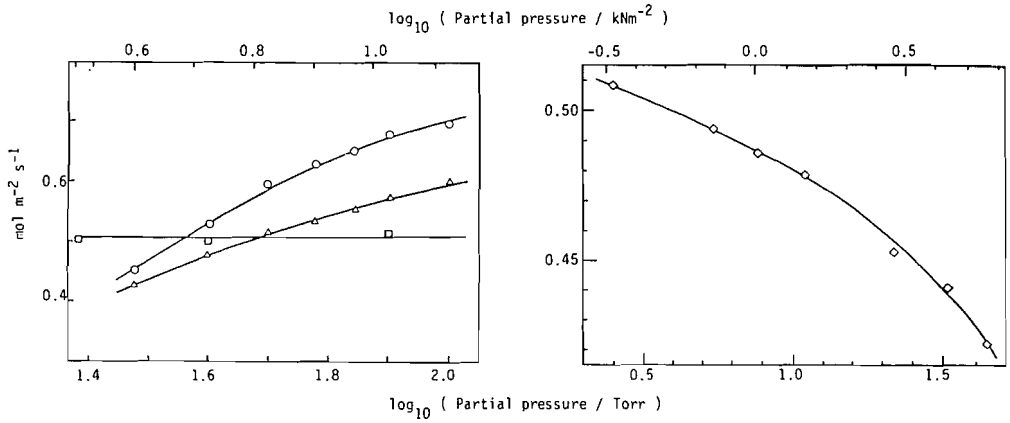

FIG. 2. Effect of variations in the partial pressures of carbon monoxide (○), nitrous oxide (△), nitrogen (□), and carbon dioxide (◇) on the catalytic CO/N_2O reaction on magnesium oxide at 559 K.

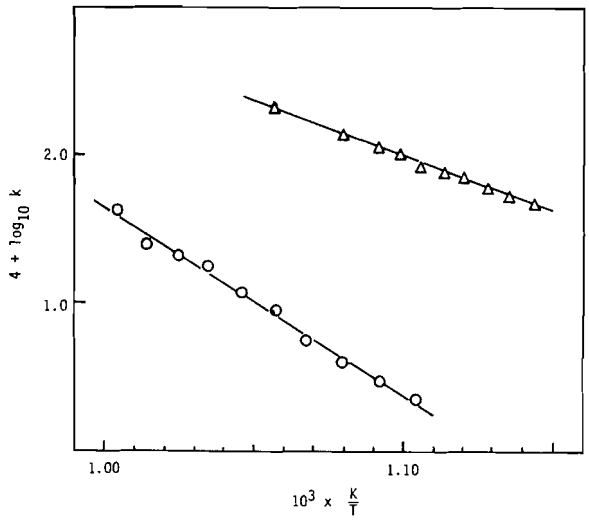

FIG. 3. Arrhenius plots for the catalytic reaction between carbon monoxide and nitrous oxide over magnesium oxide (△) and scandium oxide (○).

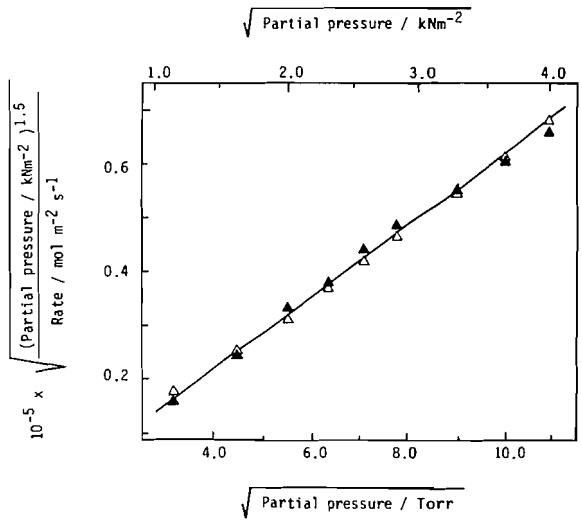

FIG. 4. Reduced plot corresponding to eq. [3] for the carbon monoxide (▲) and nitrous oxide (△) rate orders on scandium oxide at 673 K.

MgO. Further, the reaction rate orders with respect to the reaction components are comparable.

Nitrous oxide decomposition from 673 to 773 K has been proposed (11) to occur through the interaction of defects, such as F-centres, with adsorbed N_2O in the absence of an effective number of impurity states. Such proposals are particularly pertinent to insulator oxides.

The results from the rate order experiments were analyzed by testing various Langmuir–Hinshelwood kinetic expressions (12, 13) and the equations which gave the best statistical correlation coefficients for all the rate order data were adopted as general guides to the nature of the surface reaction (14, 15).

Sc_2O_3

Analysis of the rate order results (Figs. 4 and 5) yielded only one kinetic expression which could accommodate these data:

$$[3]\quad r = \frac{kaP_{CO}^{1/2}bP_{N_2O}^{1/2}}{(1 + aP_{CO}^{1/2} + bP_{N_2O}^{1/2} + cP_{CO_2}^{1/2})^2} \times P_{CO}P_{N_2O}$$

where P represents the partial pressure of the indicated component. The form of this equation suggests that, initially, carbon monoxide and nitrous oxide interact as two adsorbed species (16), each occupying two surface sites. The additional P_{CO} and P_{N_2O} terms in the numerator may be taken to imply that the reaction sequence does not terminate at this stage. A more complex overall surface mechanism would seem likely.

A simple two-stage redox mechanism would not be sufficient to accommodate all parameters and a

Can. J. Chem. Downloaded from www.nrcresearchpress.com by 210.87.254.42 on 09/05/12
For personal use only.

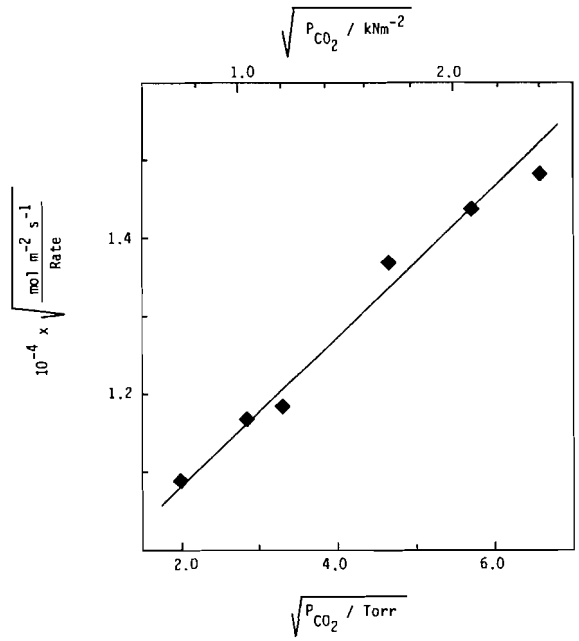

FIG. 5. Reduced plot for the carbon dioxide rate order results on scandium oxide according to eq. [3] at 673 K.

formulation tested to be consistent with the rate order results is:

[4] $$CO + 2S \rightleftharpoons CO(a)$$

[5] $$N_2O + S + CO(a) \rightarrow CO_2{}^*(a) + N_2$$

[6] $$N_2O + CO_2{}^*(a) \rightarrow CO_3(a) + N_2 + S$$

[7] $$CO + CO_3(a) \rightarrow CO_2 + CO_2(a)$$

[8] $$CO_2(a) \rightarrow CO_2 + 2S$$

where S represents a vacant surface site. The square root relationships in eq. [3] with respect to CO, N_2O, and CO_2 are rationalized in steps [4], [5], and [8], respectively, while the P_{N_2O} and P_{CO} terms are interpreted by steps [6] and [7], respectively. With respect to the reaction of nitrous oxide, step [6] would be rate controlling, for carbon monoxide it would be step [7].

Since the continuous addition of carbon dioxide to the reaction gas mixture did not accelerate the catalytic reaction rate, the species $CO_2{}^*(a)$ is proposed which may be regarded as chemically distinct from that arising from carbon dioxide adsorption (17). The structure of the proposed 'carbonate' intermediate in step [6] is not specified but the species is expected to be unstable.

Sc_2O_3 crystallizes in the C-sesquioxide form which is related to the structure of CaF_2 (18). The structure can be regarded as a fluorite lattice with systematic oxygen vacancies and thus the surface process could be:

[9] $CO + N_2O +$ 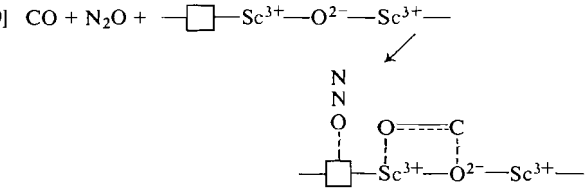

where □ represents an oxygen vacancy. The reactions involving nitrous oxide and carbon monoxide would occur simultaneously, consistent with reactions [4]—[8]. The desorption of carbon dioxide from two surface sites is also accommodated by this scheme.

Previously, cyclic transition states have been proposed (19) for several catalytic redox reactions including the oxidation of carbon monoxide where the surface metal and oxygen sites polarize the CO molecule:

[10] 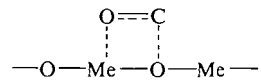

The contribution of polarization effects to the catalytic CO/N_2O reaction was further verified (20) by a relationship between E_A and the charge/radius ratio with respect to the cation (21), a useful indicator of the importance of polarization trends (22).

MgO

The best correlation of the results for carbon monoxide and nitrous oxide (Fig. 6) and carbon dioxide (Fig. 7) was obtained with

$$[11] \quad r = \frac{kaP_{CO}bP_{N_2O}}{(1 + aP_{CO} + bP_{N_2O} + cP_{CO_2}{}^{1/2})^2} \times P_{CO}P_{N_2O}$$

The form of this equation is consistent with the interaction between carbon monoxide and nitrous oxide as adsorbed species (16). The additional P_{CO} and P_{N_2O} terms in the numerator indicate that the reaction sequence does not terminate at this stage, similar to scandium oxide, eq. [3].

A surface scheme consistent with eq. [11] is

[12] $$CO + S \rightleftharpoons CO(a)$$

[13] $$N_2O + S \rightleftharpoons N_2O(a)$$

[14] $$CO(a) + N_2O(a) \rightarrow CO_2{}^*(a) + N_2$$

[15] $$N_2O + CO_2{}^*(a) \rightarrow (CO_3) + N_2$$

[16] $$CO + (CO_3) \rightarrow CO_2(a) + CO_2$$

[17] $$CO_2(a) \rightarrow CO_2 + 2S$$

The rate-determining step with respect to nitrous oxide decomposition is step [15]. A Rideal–Eley type mechanism (16) is not necessarily implied since the weak adsorption of N_2O or CO in steps [15] and [16], respectively, would give the same kinetic ex-

Can. J. Chem. Downloaded from www.nrcresearchpress.com by 210.87.254.42 on 09/05/12
For personal use only.

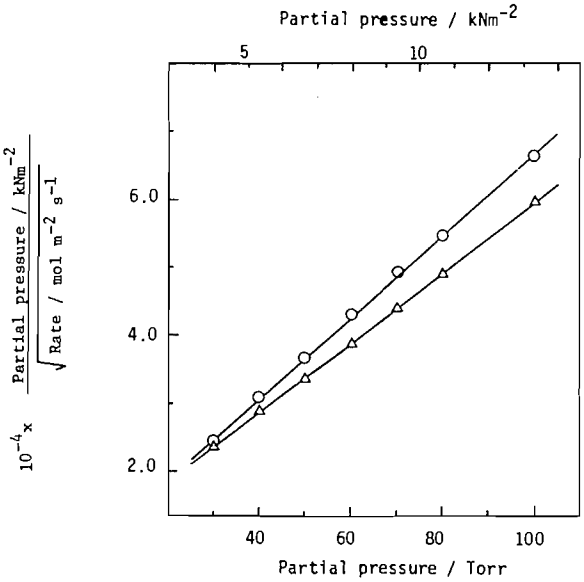

FIG. 6. Carbon monoxide (△) and nitrous oxide (○) rate order results for the catalytic CO/N_2O reaction on magnesium oxide at 559 K plotted according to eq. [11].

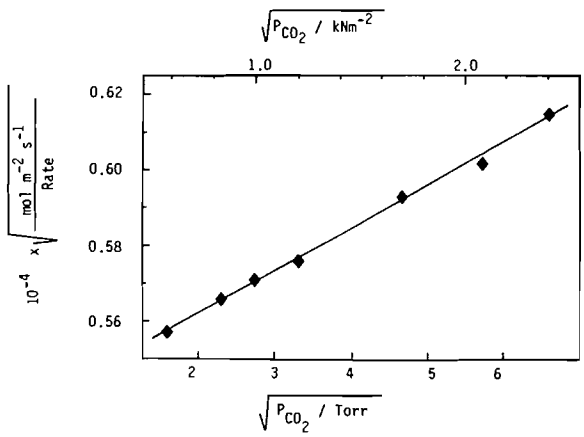

FIG. 7. Carbon dioxide rate order results for the catalytic CO/N_2O reaction on magnesium oxide at 559 K plotted according to eq. [11].

pression. With respect to carbon monoxide, step [16] is rate controlling. The term involving carbon dioxide partial pressure indicates that one of the two product molecules desorbs rapidly while the second is adsorbed more strongly on two surface sites. There would appear again to be a chemical distinction between the surface carbon dioxide species arising from the adsorption of CO_2 and that formed in step [14] since no enhanced catalytic activity resulted with the continuous introduction of carbon dioxide into the reacting gas mixture.

For both oxides, the kinetic equations computed from analysis of the rate order results yielded expressions more complex in nature than those derived for the oxides of manganese and cobalt (4), nickel (3), and vanadium pentoxide melts containing alkali metal sulphate additives (2). This feature may be a consequence of the insulator and near-insulator properties of MgO and Sc_2O_3, respectively. Although the metal/oxygen bond distances are essentially equal (13), polarization is greater in Sc_2O_3 and this might be expected to influence the kinetics of the reaction. Thus, stronger adsorption of CO on Sc_2O_3 would reduce the surface mobility of the adsorbed molecule in comparison to that on MgO in accordance with the slight but reproducible differences in the observed rate order results. It is suggested then that the nature of the surface processes on these oxides may be distinguished by the adsorption of carbon monoxide on two sites on Sc_2O_3 and on one site for MgO with subsequent consequences on the manner of nitrous oxide adsorption which approaches the classical Langmuirian pattern on MgO.

Acknowledgements

The authors thank Imperial Oil Enterprises Ltd., Toronto, Canada, for financial assistance.

1. M. J. FULLER and M. E. WARWICK. J. Catal. **39**, 412 (1975).
2. B. W. KRUPAY and R. A. Ross. J. Catal. **50**, 220 (1977).
3. B. W. KRUPAY and R. A. Ross. Z. Phys. Chem. N. F. **106**, 83 (1977).
4. B. W. KRUPAY and R. A. Ross. Can. J. Chem. **56**, 10 (1978).
5. O. V. KRYLOV. Catalysis by nonmetals. Academic Press, New York and London. 1970.
6. E. F. MCCAFFREY, D. G. KLISSURSKI, and R. A. Ross. Can. J. Chem. **49**, 3778 (1971).
7. B. W. KRUPAY and R. A. Ross. J. Catal. **39**, 369 (1975).
8. C. N. SATTERFIELD. Mass transfer in heterogeneous catalysis. M.I.T. Press. 1970.
9. P. WEISZ and C. D. PRATER. Adv. Catal. **3**, 143 (1951).
10. O. V. KRYLOV. Catalysis by nonmetals. Academic Press, New York and London. 1970. p. 247.
11. W. E. GARNER (*Editor*). Chemistry of the solid state. Butterworths Scientific Publ., London. 1955.
12. K. H. YANG and O. A. HOUGEN. Chem. Eng. Prog. **46**, 146 (1950).
13. O. A. HOUGEN and K. M. WATSON. Chemical process principles. Part III. Wiley, New York and London. 1966.
14. M. BOUDART. A.I.Ch.E. J. **2**, 62 (1956); L. BERÁNEK. Catal. Rev. **16**, 1 (1977).
15. S. W. WELLER. Chemical reaction engineering reviews. *Edited by* H. M. Hulbert. American Chemical Society, Washington, DC. 1975. p. 26.
16. A. CLARK. The theory of adsorption and catalysis. Academic Press, New York and London. 1970. p. 246.
17. W. M. JOHNSON, S. MISRA, and G. H. CADY. Inorg. Chem. **15**, 1227 (1976).
18. A. F. WELLS. Structural inorganic chemistry. 3rd ed. Oxford Clarendon Press. 1962. p. 465; B. I. POPROVSKII and E. V. ISAEVA. Russ. J. Inorg. Chem. Engl. **22**, 1103 (1977).
19. E. C. PITZER and J. C. FRAZER. J. Phys. Chem. **45**, 761 (1941).
20. B. W. KRUPAY and R. A. Ross. Unpublished work.
21. N. N. GREENWOOD. Ionic crystals, lattice defects, and nonstoichiometry. Butterworths, London. 1968.
22. E. F. MCCAFFREY, D. G. KLISSURSKI, and R. A. Ross. Proc. 5th Int. Congr. Catal., Florida (1972), North-Holland Publ. Co., Amsterdam. Paper 3.

Can. J. Chem. Downloaded from www.nrcresearchpress.com by 210.87.254.42 on 09/05/12
For personal use only.

Determination of oxalate by continuous analysis using photochemical oxidation by iron(III) and a CO_2 electrode detector

JEAN MARGARET COOLEY[1] AND BYRON KRATOCHVIL[2]

Department of Chemistry, University of Alberta, Edmonton, Alta., Canada T6G 2G2

Received February 13, 1978

JEAN MARGARET COOLEY and BYRON KRATOCHVIL. Can. J. Chem. **56**, 2452 (1978).

Oxalate concentrations were measured by photochemical oxidation with iron(III) to carbon dioxide. Technicon AutoAnalyzer components were used to automate the sampling and mixing steps, and the carbon dioxide produced in the radiation step was measured with a CO_2 electrode. Variables in the system were evaluated and the optimum conditions identified. A theoretical study was made of the effect on ionic species concentrations of variations in iron(III), acid, and counter ion concentrations. A linear calibration curve could be obtained for oxalate concentrations in the range of 2×10^{-4} to 0.02 *M*; by modifying conditions linearity could be achieved at both higher and lower concentration ranges. Several other acids are partially oxidized under optimum conditions for oxalate. Tartrate, citrate, and malonate introduce errors of 2% or less at concentrations equivalent to oxalate; malate and pyruvate cause errors on the order of 10%. Several small carboxylic acids were found to interfere with the CO_2 electrode.

JEAN MARGARET COOLEY et BYRON KRATOCHVIL. Can. J. Chem. **56**, 2452 (1978).

On a mesuré des concentrations d'oxalate par des oxydation photochimique à l'aide de fer(III) qui conduisent à du dioxyde de carbone. On a utilisé les composantes d'un auto-analyseur Technicon pour automatiser les étapes d'échantillonnages et de mélanges et on a mesuré le dioxyde de carbone qui se produit dans l'étape de la radiation à l'aide d'une électrode de CO_2. On a évalué les variables du système et on a identifié les conditions optimales. On a effectué une étude théorique de l'effet, sur les concentrations des espèces ioniques, de variations dans les concentrations de fer(III), d'acide et de contre ion. On devrait obtenir, une courbe de calibration linéaire pour des concentrations d'oxalate allant de 2×10^{-4} jusqu'à 0.02 *M*; si l'on modifie les conditions, on peut obtenir une linéairité à des concentrations plus élevées ainsi que plus basses. Plusieurs autres acides sont partiellement oxydés sous les conditions optimales pour l'oxalate. Le tartrate, le citrate et le malonate introduisent des erreurs de 2% ou moins à des concentrations équivalentes à celle de l'oxalate; les erreurs introduites par le malate et le pyruvate sont de l'ordre de 10%. On a trouvé que plusieurs petits acides carboxyliques interfèrent avec l'électrode CO_2.

[Traduit par le journal]

Introduction

The determination of oxalate concentrations can be accomplished by a number of procedures. In practical situations, however, the ability to measure this species often is limited due to interferences and detection limits. The classical method is separation by precipitation as calcium oxalate, usually followed by dissolution of the precipitate and determination of either the calcium or oxalate. But the quantitative precipitation of calcium oxalate is slow and not suited to small amounts of oxalate. For trace levels a number of direct and indirect spectrophotometric methods have been suggested (1–6), but all lack high specificity. Enzymatic procedures offer specificity; oxalate decarboxylase, which converts oxalate to formate and carbon dioxide, has been studied for the determination of oxalate in biological fluids (7–9), but since the enzyme is inhibited by sulfate and phosphate and is costly, these methods have not been widely adopted.

In 1955 Rao and Aravamudan utilized the photochemical reaction between iron(III) and oxalate for the determination of oxalate. The resultant iron(II) was titrated with vanadate (10). Riggs and Bricker modified the method by titrating the iron(II) with dichromate or, for smaller amounts of oxalate, by spectrophotometric determination of the iron(II) with 1,10-phenanthroline (11). Any substance that reduces iron(III) or oxidizes iron(II), such as oxygen dissolved in the solution, interferes in these methods.

This paper describes an automated continuous analysis approach to the determination of oxalate using the iron(III) photochemical reaction and measuring carbon dioxide production with a CO_2 electrode. The method is simple, straightforward, and circumvents many of the drawbacks of earlier procedures.

[1]Present address: Syncrude Research, Syncrude Canada Ltd., P.O. Box 5790, Edmonton, Alta., Canada T6C 4G3.

[2]To whom all correspondence should be addressed.

Can. J. Chem. Downloaded from www.nrcresearchpress.com by 210.87.254.40 on 09/05/12
For personal use only.

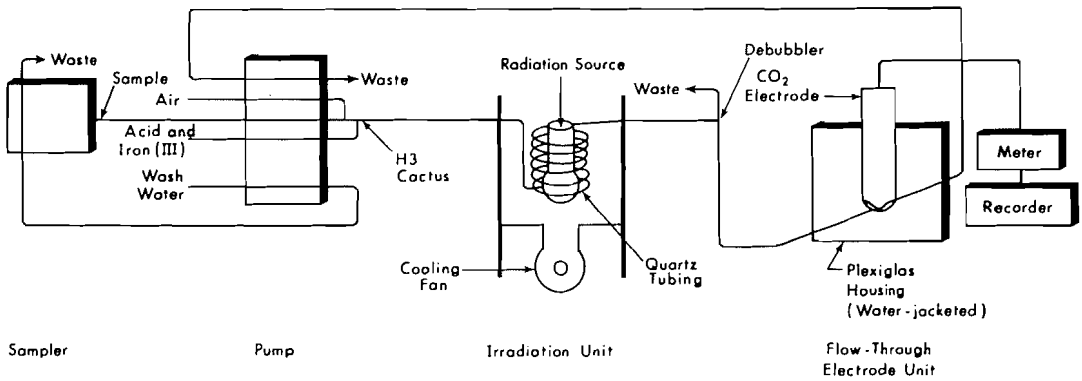

FIG. 1. Schematic diagram of continuous flow system incorporating Technicon AutoAnalyzer sampler and pump units for determination of oxalate.

Experimental

Apparatus

A Technicon single channel AutoAnalyzer Sampler II and Pump I were used to automate the analyses (Fig. 1). In the proportioning pump an acidified solution of iron(III) was mixed with the acidified oxalate samples. Air bubbles were introduced and the solution was then irradiated with a 140-W Hanovia type-30620 ultraviolet mercury lamp during passage through a 12-m coil of 1.65-mm id quartz tubing surrounding the lamp. The lamp–coil unit was cooled from below by a small fan to minimize heating of the solution. A reflecting layer of aluminum foil was placed around the coil to improve efficiency of the radiation source and to protect the operator from ultraviolet radiation. From the coil, the solution passed through a debubbler to a CO_2 electrode (Instrumentation Laboratory) mounted in a flow-through unit constructed from Plexiglas. The bottom of this unit was machined to provide a small volume chamber at the tip of the electrode. The inlet and outlet channels were 1 mm in diameter and were drilled opposite to each other at an upward angle to minimize bubble entrapment in the chamber. Stainless steel fittings were epoxied into the Plexiglas for tubing connections. The electrode, flow-through unit and a portion of the inlet tubing were immersed in a water bath if temperature control was desired. An Orion Model 801 pH meter with a Hewlett-Packard Model 7101BM recorder was used to monitor the electrode potential.

Chemicals

Sodium bicarbonate solutions were prepared in 0.5 *M* NaCl; potassium oxalate solutions were prepared in 0.5 *M* NaCl – 0.1 *M* H_2SO_4. Iron(III) solutions were prepared from the corresponding sulfate or chloride salts in sulfuric or hydrochloric acid. About 0.75 ml of 30% Brij 35 solution was added per litre of iron(III) solution as a wetting agent. The internal filling solution of the CO_2 electrode was varied between 1×10^{-4} and 1×10^{-2} *M* $NaHCO_3$ in 0.5 *M* NaCl saturated with silver chloride. All chemicals were reagent grade or better and were used as received.

Calculations

An IBM 360/67 computer was used to calculate the equilibrium concentrations of species present in various mixtures. The procedure was patterned after the work of Swinnerton and Miller (12), with several modifications. Mass balance and equilibrium equations were written for each solution of interest, then combined to give n equations in n unknowns, n being the number of mass balance equations used. This system was then solved using the Newton–Rapheson method of successive approximations. Stability constants were chosen, whenever possible, at an ionic strength of unity and at 25°C, as this represented the experimental conditions more closely than did standard conditions of zero ionic strength and 0°C.[3]

Results and Discussion

Preliminary Experiments

Initially a series of solutions of acidified oxalate and iron(III) was exposed to ultraviolet radiation. The net reaction may be written as

$$2Fe^{3+} + C_2O_4^{2-} \xrightarrow{h\nu} 2Fe^{2+} + 2CO_2$$

Measurement of the resulting carbon dioxide levels with a CO_2 electrode yielded Nernstian results over the range of 10^{-2} to 10^{-4} *M* oxalate. This approach is not attractive as an analytical method, however, because of loss of carbon dioxide to the atmosphere during irradiation, lack of reproducibility of irradiation conditions, and slowness of the procedure. Therefore, an automated approach was developed that eliminated or diminished appreciably these disadvantages.

Preliminary investigations of the automated system were made using a series of solutions of sodium bicarbonate which were mixed with acid in the pump and analyzed with a CO_2 electrode. One variable studied was the composition of the internal filling solution in the electrode. A 1×10^{-3} *M* $NaHCO_3$ filling solution, 0.5 *M* in NaCl and saturated in AgCl, gave the best compromise between speed and linearity of response. The CO_2 permeable membranes made of Silastic sheeting (0.003 in. from Instrumentation Laboratory) performed acceptably; 0.005 in. and Dacron-reinforced 0.007 in. Silastic sheeting (Dow-Corning) gave similar results. Mem-

[3]The values used for the stability constants are available, at a nominal charge, as Appendix I from the Depository of Unpublished Data, CISTI, National Research Council of Canada, Ottawa, Ont., Canada K1A 0S2.

Can. J. Chem. Downloaded from www.nrcresearchpress.com by 210.87.254.40 on 09/05/12
For personal use only.

Can. J. Chem. Downloaded from www.nrcresearchpress.com by 210.87.254.40 on 09/05/12
For personal use only.

branes prepared from the Dow-Corning material required thorough washing before use to remove the dusting of sodium bicarbonate present on the surface.

Near Nernstian slopes were obtained over a range of 0.1 to 1 × 10^{-4} *M* bicarbonate when the samples were mixed with 2 *M* H_2SO_4 and pumped through the irradiation coil prior to measurement by the CO_2 electrode. A 5 × 10^{-3} *M* $NaHCO_3$ sample was run 5 times at various sampling speeds to test the reproducibility of the system; as sampling speeds were increased from 10 to 20 to 40 samples per hour the standard deviation increased from 0.32 to 0.44 to 1.80 mV. At faster sampling rates successive readings on the same sample increased because equilibrium was not attained. Separation of the samples by use of only every third cup position in the sampler improved precision; accordingly, if time permits, use of one or two empty sample cups following each filled one is recommended.

Oxalate analyses were performed in a similar manner. Samples of 7 to 8 ml were introduced through 0.065-in. id pump tubing, and acidified iron(III) solution through 0.020-in. id tubing. Figure 2 shows a calibration plot for a series of solutions of potassium oxalate. Electrode response for oxalate is linear under these conditions over a range of about 2 × 10^{-4} to 2 × 10^{-2} *M*, but the linear range is increased to that observed for bicarbonate if lower concentrations of iron(III) are used, as is discussed below.

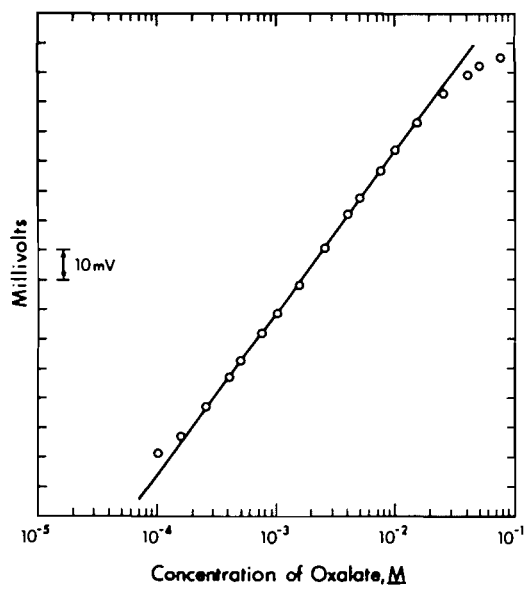

FIG. 2. Calibration plot for a series of oxalate solutions using photochemical oxidation and an IL CO_2 electrode in a continuous-flow mode. Reaction medium under irradiation was 0.05 *M* iron(III) ammonium sulfate, 0.5 *M* sulfuric acid, and 0.5 *M* sodium chloride.

Photochemical decomposition of the iron(III)–oxalate complex yields two moles of carbon dioxide for each mole of oxalate consumed, yet a slope close to 59 mV is obtained experimentally. The Nernst equation for the electrode response can be written in the form

$$E = \text{constant} + \frac{RT}{nF} \log p_{CO_2}$$

$$= \text{constant} + \frac{RT}{nF} \log 2[C_2O_4^{2-}]$$

$$= \text{constant} + \frac{RT}{nF} \log 2 + \frac{RT}{nF} \log [C_2O_4^{2-}]$$

where p_{CO_2} refers to the partial pressure of carbon dioxide in solution. Thus a slope of 59 mV is predicted but the absolute value of the readings for the same concentration of oxalate or bicarbonate will be shifted by a factor of (RT/nF) log 2 or 18 mV. This shift was verified experimentally.

A characteristic of the Severinghaus-type CO_2 electrode used in this work is that equilibrium is reached more quickly with higher concentrations of carbon dioxide than with lower concentrations. Because the continuous system used provides a fixed time interval between samples, nonattainment of equilibrium between samples results in a hysteresis effect. The resulting error may be significant when a sample of low concentration follows one of higher concentration. For example, a 1 × 10^{-4} *M* oxalate sample gave a result 8% higher than the equilibrium value when run immediately after a 1 × 10^{-3} *M* sample. The error becomes significant when the samples cover a wide concentration range.

Effect of Solution Composition

Among the variables investigated in the oxalate system were the effects of acidity, of iron(III) concentration and of several complexing anions. To ascertain the effect of acidity of the reaction mixture on the system, solutions of 0.5 *M* iron(III) ammonium sulfate were prepared in distilled water and in 2 and 4 *M* H_2SO_4. A set of seven solutions ranging from 1 × 10^{-3} to 1 × 10^{-2} *M* in oxalate were run with each iron(III) solution. The concentration of H_2SO_4 in the solutions entering the radiation coil was about 0.1, 0.3, and 0.5 *M* for the three iron(III)–oxalate mixtures. Little difference was found among the three calibrations; standard deviations of the order of 0.36 mV were obtained. Thus adjustment of acidity is not a critical variable for oxalate analysis.

Can. J. Chem. Downloaded from www.nrcresearchpress.com by 210.87.254.40 on 09/05/12
For personal use only.

For practical use the ability to measure a wide range of oxalate concentrations is desirable. Initially a 0.5 *M* iron(III) ammonium sulfate solution was used to ensure an excess of oxidizing agent even at high oxalate concentrations. Riggs and Bricker state that results are independent of iron(III) concentration as long as the ratio of iron(III) to oxalate is 2:1 or greater (11). Rao and Aravamudan maintained iron(III):oxalate ratios of 4:1 or greater in their analyses (10). To ascertain the effect of this ratio on the flow-through system, triplicate portions of 1×10^{-3} *M* potassium oxalate were run with progressively decreasing concentrations of iron(III) ammonium sulfate in 2 *M* H_2SO_4. The analyses were repeated using a 200-W General Electric tungsten lamp and a 12-m Pyrex coil in place of the Hanovia medium pressure mercury lamp and quartz coil so that the effect of radiation conditions also could be studied. At high iron(III) concentrations the quantity of carbon dioxide evolved was greater with the tungsten lamp than with the ultraviolet lamp, but at lower iron(III) to oxalate ratios the ultraviolet lamp gave higher yields. The optimum iron(III):oxalate ratio for irradiation with the ultraviolet lamp is in the range of 5:1 to 0.5:1 (Fig. 3). A similar trend was observed at oxalate concentrations of 1×10^{-4} *M* except that optimum ratios for the ultraviolet system extended to as high as 50:1, while for 1×10^{-2} *M* oxalate a ratio of 0.5:1 iron(III) to oxalate gave maximum carbon dioxide production. Thus, as the oxalate concentration was increased, the ratio of iron(III) to oxalate became more critical, probably because of the fixed time of irradiation and the high absorbance of the solutions. By optimization of the amount of iron(III) used and irradiation conditions the quantity of carbon dioxide produced can be maximized; in this way the limits of linear response of the system are extended.

Since each mole of oxalate requires two moles of iron(III) for complete oxidation to carbon dioxide, ratios below 2:1 indicate iron(II) is being reoxidized to iron(III), apparently by oxygen dissolved in the solutions and present in the air bubbles. When the pump air line was connected to a nitrogen stream, the lower iron(III):oxalate ratios became less favorable; purging the oxalate sample solutions with nitrogen prior to analysis further reduced the electrode readings when iron(III):oxalate ratios below 2 to 1 were used.

Rao and Rao (13, 14) found that hydrochloric acid could be substituted for sulfuric acid in the photochemical oxidation of oxalate without ill effects, but Riggs and Bricker (11) suggested that the use of hydrochloric acid would produce strongly absorbing iron(III)–chloro complexes that would interfere with irradiation efficiency, and recommended that sulfuric acid be used instead. Since chloride is present in many samples this point was investigated. Analysis of oxalate solutions containing chloride gave results similar to those containing sulfate. This observation was shown to be reasonable on the basis of calculations outlined below.

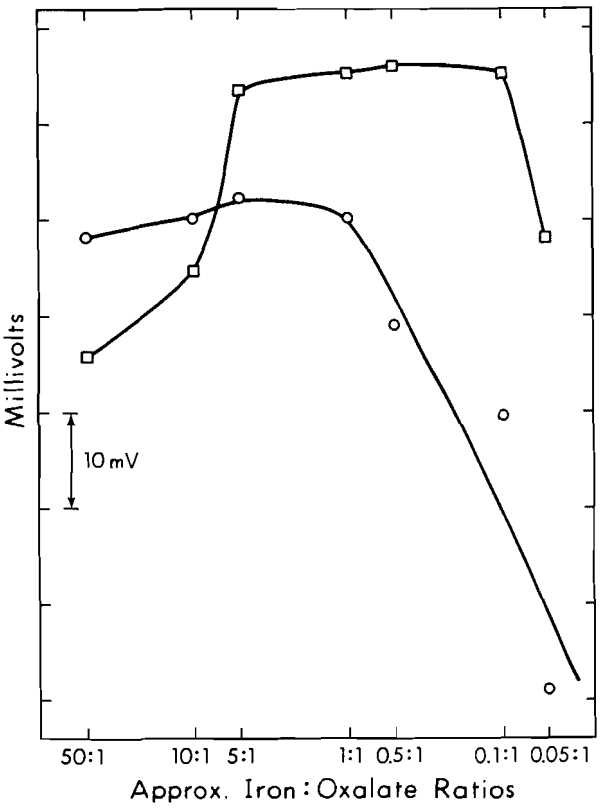

FIG. 3. Effect of iron(III)–oxalate ratio on the oxidation of oxalate at an oxalate concentration of 0.001 *M*. □: Ultraviolet lamp and quartz coil irradiation system. ○: Tungsten lamp and Pyrex coil irradiation system.

The presence of Brij 35 surfactant is recommended for more reproducible response. When a calibration curve for oxalate using 0.5 *M* iron(III) ammonium sulfate in 2 *M* H_2SO_4 was repeated without addition of surfactant the overall standard deviation increased from 0.36 to 0.98 mV.

Calculations

For maximum photochemical conversion of oxalate to carbon dioxide the fraction of oxalate in the form of the iron(III) complex must be maximized. Attainment of this objective is complicated by the large number of species, many highly absorbing, which can form. Determination of the equilibrium concentrations of the species in such systems is most conveniently done by computer. For example,

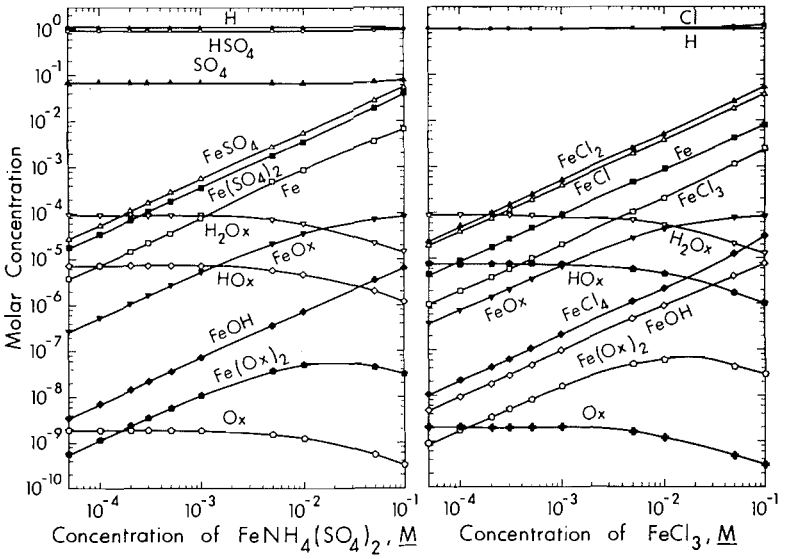

FIG. 4. Left: distribution of species in a solution containing 1×10^{-4} *M* total oxalate and 1 *M* sulfuric acid as a function of iron(III) ammonium sulfate concentration. Right: same, but with 1 *M* hydrochloric acid and iron(III) chloride in place of sulfuric acid and iron(III) ammonium sulfate. Charges omitted for simplicity.

Swinnerton and Miller (12) studied a system containing iron(III), sulfate, hydrogen ion, and oxalate. They omitted the hydrolysis of iron(III) for simplicity and did not consider formation of iron(III)–sulfate complexes. In the calculations reported here hydrolysis to form the $Fe(OH)^{2+}$ complex was taken into account, as was the effect of formation of iron(III)–sulfate complexes. The contribution to the hydrogen mass balance from the hydrolysis of iron(III) was assumed to be small; this amount, for simplicity, was omitted in the value given to the hydrogen mass balance. The validity of this assumption was confirmed for most of the calculations. Further corrections were not added for those cases where the assumption was invalid.

The effect of varying analytical concentrations of iron(III), sulfate, and hydrogen ions on the equilibrium concentrations of various species present was studied. A similar study was undertaken, substituting chloride for the sulfate ions. Uncertainties in some of the results may be moderately large. Double precision was used throughout, but because concentrations and constants often varied widely in magnitude, some truncation errors were likely. Additional uncertainty was introduced because the equilibrium constants used were measured under a wide range of conditions and by different workers. The results, therefore, are not exact, but are useful to indicate trends, to allow calculation of absorbances as a function of solution conditions, and to aid in selecting experimental conditions.

In the first set of calculations, a series of iron(III) ammonium sulfate concentrations ranging from 5×10^{-5} to 0.1 *M* was used in a 1 *M* sulfuric acid and 1×10^{-4} *M* oxalate matrix. The resulting equilibrium concentrations of the various species are plotted in Fig. 4, along with the results of similar calculations with iron(III) chloride, hydrochloric acid, and oxalate.[4]

From these plots it is seen that the concentration of $FeC_2O_4^+$ increases with increasing iron(III) concentrations, as expected. However, the concentrations of the iron(III)–sulfate and –chloride complexes also increase, and since these species absorb significantly in the ultraviolet (15, 16) they interfere with absorption of radiation by the iron(III)–oxalate species, confirming the experimental results. High iron(III) concentrations also lead to the formation of highly absorbing complexes such as $Fe_2(OH)_2^{4+}$ and $Fe_3(OH)_4^{5+}$ (17). Hence high iron(III) concentrations are best avoided. One way of keeping the total iron(III) level low is by the reoxidation of iron(II) with dissolved oxygen, as occurs in this experimental design. This permits the oxidation of oxalate without formation of high concentrations of undesirable iron(III) complexes.

A second set of calculations was performed in which the concentration of sulfuric acid was varied while the total concentration of oxalate and iron(III) ammonium sulfate remained constant. Plots of

[4]An additional plot with only iron(III), hydrogen ion, and oxalate initially present is available as Appendix II from the Depository of Unpublished Data; see footnote 3.

Can. J. Chem. Downloaded from www.nrcresearchpress.com by 210.87.254.40 on 09/05/12
For personal use only.

Can. J. Chem. Downloaded from www.nrcresearchpress.com by 210.87.254.40 on 09/05/12
For personal use only.

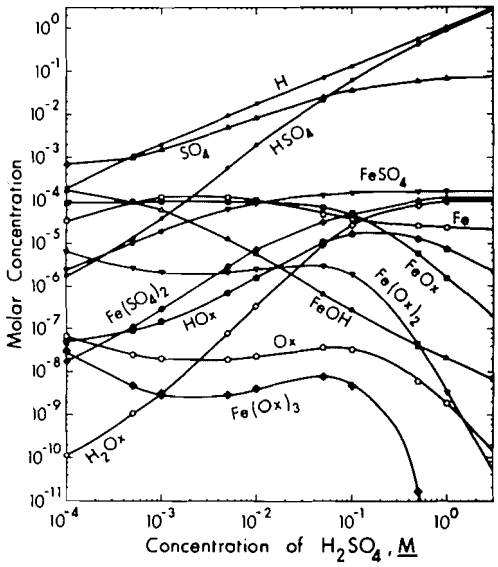

FIG. 5. Distribution of species in a solution containing 1×10^{-4} *M* total oxalate and 3×10^{-4} *M* iron(III) ammonium sulfate as a function of sulfuric acid concentration. Charges omitted for simplicity.

species concentrations as a function of added H_2SO_4 are shown in Fig. 5.[5] These calculations show that in this system the acidity can be varied widely without affecting the fraction of oxalate present as the iron(III)–oxalate monocomplex. This agrees with the experimentally observed results.

A third set of calculations was undertaken in which the stability constants of other iron(III)–carboxylate species and acidity data for these acids were substituted into the program in place of the iron(III)–oxalate formation and acidity constants. Figure 6 shows the variation of the iron(III)–carboxylate species with changing acidity. Oxalate forms the strongest iron(III) complex of the acids studied, hence the importance of acidity control in diminishing interferences due to the presence of other carboxylate anions in an oxalate solution.

Interferences in Determination of Oxalate

Several carboxylic acids other than oxalic acid are photochemically oxidized by iron(III) under certain conditions to produce carbon dioxide. These include citric, tartaric, lactic, maleic, malic, malonic, and pyruvic acids. The error caused by several of these acids in the determination of oxalate is listed in Table 1. As mentioned above, this error can be reduced appreciably in many cases by an increase in sulfuric acid concentration in the sample solution.

[5]Plots of additional sets of calculations in which sulfate is replaced by chloride, and in which neither counter ion is present, are available as Appendix II from the Depository of Unpublished Data; see footnote 3.

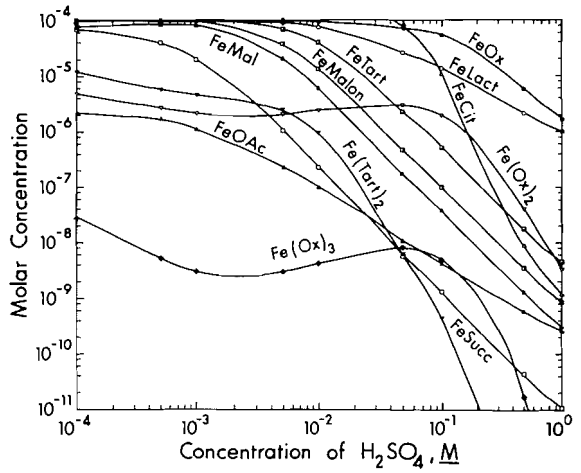

FIG. 6. Effect of sulfuric acid concentration on concentration of iron(III)–carboxylate species for several carboxylate salts. For each carboxylate salt a separate calculation of species distribution similar to Fig. 5 was performed; only the concentration distributions of the iron(III)–carboxylate species are shown here, combined on a single graph for convenient comparison. Cit = citrate, Lac = lactate, Mal = malate, Malon = malonate, Ox = oxalate, Succ = succinate, Tart = tartrate. Charges omitted for simplicity.

TABLE 1. Effect of carboxylic acids on oxalate determination[a]

Oxalate concentration (*M*)	Species added	Species concentration (*M*)	% Error
2.5×10^{-3}	Citrate	2.5×10^{-3}	2
2.5×10^{-3}	Citrate	2.5×10^{-2}	8
2.5×10^{-3}	Tartrate	2.5×10^{-3}	2
2.5×10^{-3}	Tartrate	2.5×10^{-2}	15
5×10^{-4}	Tartrate	5×10^{-4}	0.4
5×10^{-4}	Tartrate	5×10^{-3}	10
5×10^{-4}	Malate	5×10^{-4}	8
5×10^{-4}	Pyruvate	5×10^{-4}	10
5×10^{-4}	Malonate	1×10^{-3}	2

[a]Analyte solutions 0.1 *M* in H_2SO_4; reagent solution 0.5 *M* iron (III) ammonium sulfate in 4 *M* H_2SO_4.

Low molecular weight carboxylic acids such as formic, acetic, and propionic acids were found to interfere with the CO_2 electrode by diffusing across the membrane and causing a change in the pH of the internal filling solution. Diffusion of these acids back across the membrane is slow, and so electrode response to carbon dioxide concentration changes is affected. Acetic acid had been previously reported to interfere in this way (18). Similar but more serious interference was caused by aromatic acids such as benzoic and cinnamic. Soaking of the electrode in water for several hours did not restore the electrode potential to its original value after exposure to these acids and the electrode had to be disassembled and cleaned before it was serviceable again.

Study of Citrate and Tartrate Response

Optimization of conditions for response of the system to citrate and tartrate was examined briefly. Using solutions of sodium citrate or potassium sodium tartrate in 0.5 *M* NaCl with 0.5 *M* $FeNH_4(SO_4)_2$ as reagent, linear calibration plots over the range of approximately 1×10^{-2} to 1×10^{-4} were obtained for both citrate and tartrate using the ultraviolet radiation system.

As with oxalate, linearity at either end of the range can be improved by optimizing the ratio of iron(III) to carboxylate salt. The decomposition of tartrate appears to result in formation of two moles of carbon dioxide per mole of tartrate, while three moles of carbon dioxide appear to be formed per mole of citrate under optimum conditions, as indicated by an experimentally observed displacement of the calibration plot by (RT/nF) log 3, or 28 mV.

In summary, the measurement of carbon dioxide produced upon photochemical oxidation of oxalate by iron(III) provides a method for the determination of oxalate over a useful range of concentrations. The procedure works well in a continuous analysis mode using a carbon dioxide measurement system. An advantage of measuring carbon dioxide rather than iron(II) is that substances that oxidize iron(II) such as dissolved oxygen, or reduce iron(III), such as mannitol, do not interfere. The CO_2 electrode is a simple and convenient detector, but is affected by the presence of low molecular weight aliphatic acids and by aromatic carboxylic acids.

Acknowledgements

Financial support from the National Research Council of Canada and the University of Alberta is gratefully acknowledged.

1. J. BERGERMAN and J. S. ELLIOT. Anal. Chem. **27**, 1014 (1955).
2. Z. D. DRAGANIC. Anal. Chim. Acta, **28**, 394 (1963).
3. F. BURRIEL-MARTÍ, J. RAMÍREZ-MUÑOZ, and E. FERNÁNDEZ-CALDAS. Anal. Chem. **25**, 583 (1953).
4. R. E. NEAS and J. C. GUYON. Anal. Chem. **44**, 799 (1972).
5. D. A. BRITTON and J. C. GUYON. Anal. Chim. Acta, **44**, 397 (1969).
6. V. P. CALKINS. Ind. Eng. Chem. Anal. Ed. **15**, 762 (1943).
7. C. F. KNOWLES and A. HODGKINSON. Analyst, **97**, 474 (1972).
8. P. C. HALLSON and G. A. ROSE. Clin. Chim. Acta, **55**, 29 (1974).
9. J. COSTELLO, M. HATCH, and E. BOURKE. J. Lab. Clin. Med. **87**, 903 (1976).
10. G. G. RAO and G. ARAVAMUDAN. Anal. Chim. Acta, **13**, 415 (1955).
11. W. M. RIGGS and C. E. BRICKER. Anal. Chem. **38**, 897 (1966).
12. J. W. SWINNERTON and W. W. MILLER. J. Chem. Educ. **36**, 485 (1959).
13. G. G. RAO and V. M. RAO. Current Sci. **13**, 317 (1944).
14. G. G. RAO and V. M. RAO. Proc. Natl. Inst. Sci. India, **12**, 217 (1946).
15. R. A. WHITEKER and N. DAVIDSON. J. Am. Chem. Soc. **75**, 3081 (1953).
16. G. A. GAMLEN and D. O. JORDAN. J. Chem. Soc. 1435 (1935).
17. C. F. BAES, JR. and R. E. MESMER. The hydrolysis of cations. John Wiley and Sons, Inc., New York. 1976. p. 257.
18. G. G. GUILBAULT and F. R. SHU. Anal. Chem. **44**, 2161 (1972).

Can. J. Chem. Downloaded from www.nrcresearchpress.com by 210.87.254.40 on 09/05/12
For personal use only.

Rearrangement studies with ^{14}C. XLII. The solvolysis of triphenylvinyl-2-^{14}C bromide in aqueous acetic acid and in 2,2,2-trifluoroethanol

CHOI CHUCK LEE AND ERIC C. F. KO

Department of Chemistry and Chemical Engineering, University of Saskatchewan, Saskatoon, Sask., Canada S7N 0W0

Received February 13, 1978

CHOI CHUCK LEE and ERIC C. F. KO. Can. J. Chem. **56**, 2459 (1978).

Solvolytic studies with triphenylvinyl-2-^{14}C bromide (**1**-Br-2-^{14}C) in HOAc–H_2O and in 2,2,2-trifluoroethanol (TFE) containing 2,6-lutidine were carried out under a variety of conditions. Scramblings of the label from C-2 to C-1 in the reaction product and in the unconsumed reactant were determined. For solvolyses in HOAc–H_2O, scrambling was observed in the product, but not in the recovered reactant. The extent of scrambling was higher when the proportion of H_2O in the solvent was lower. With a given solvent composition, the amount of scrambling did not change with reaction time, the average extents of scrambling being 9.6, 12.7, 15.3, 16.7, and 18.4%, respectively, for solvolysis in 50, 60, 70, 80, and 90% HOAc. With 70% HOAc, the presence of about 3 equiv. of NaOAc or NaBr did not influence the extent of scrambling. For the reactions in TFE, there was scrambling in both the reaction product and the recovered reactant, indicating the occurrence of a return process, The presence of added Et_4NBr did not affect the extent of scrambling, suggesting that the 1,2-phenyl shift occurred in the ion-pair stage and the return is, therefore, an ion-pair return. The amount of scrambling in the product and in the recovered reactant increased with increasing reaction time, but for a given reaction time, the extents of scrambling in the product and in the recovered reactant were the same. The mean values for the scrambling of the label from C-2 to C-1 in the product and the recovered reactant, after a reaction time of 1, 2, 4, and 20 days at 150°C, were 20.1, 30.0, 40.0, and 44.1%, respectively. Mechanistic explanations for both reactions in HOAc-H_2O and in TFE are discussed.

CHOI CHUCK LEE et ERIC C. F. KO. Can. J. Chem. **56**, 2459 (1978).

Des études de solvolyse du bromure de triphénylvinyl-2-^{14}C (**1**-Br-2-^{14}C) dans le trifluoro-2,2,2 éthanol (TFE) contenant de la lutidine-2,6 ont été effectuées dans diverses conditions. On a déterminé l'échange des marqueurs de la position C-2 vers la position C-1 dans le produit de la réaction et dans le réactif qui n'a pas été utilisé. Pour les solvolyses dans HOAc–H_2O, on observe de l'échange dans le produit, ce qui n'est pas le cas pour le réactif récupéré. Le taux d'échange est plus élevé quand la proportion d'eau dans le solvant est plus faible. Pour une composition donnée du solvant, la quantité d'échange n'évolue pas avec le temps de la réaction; les taux moyens d'échange sont 9.6, 12.7, 15.3, 16.7 et 18.4% respectivement pour les solvolyses dans HOAc à 50, 60, 70, 80 et 90%. Dans HOAc à 70%, la présence d'environ 3 équivalents de NaOAc ou de NaBr n'influence pas le taux d'échange. Pour les réactions dans le TFE, on a observé de l'échange à la fois dans le produit de la réaction et dans le réactif récupéré; ceci indique la présence d'un processus de retour. L'addition de Et_4NBr, ne semble pas affecter le taux d'échange suggérant que la transposition-1,2 du phényle se produit au niveau de la paire d'ions et que le retour est donc un retour dans une paire d'ions. La quantité d'échange dans le produit et dans le réactif récupéré augmente avec une augmentation du temps de la réaction mais pour un temps de réaction donné, les taux d'échange dans le produit et dans le réactif récupéré sont les mêmes. Les valeurs moyennes pour l'échange du marqueur de la position C-2 à la position C-1 dans le produit et dans le réactif récupéré après un temps de réaction de 1, 2, 4 et 20 jours à 150°C sont respectivement de 20.1, 30.0, 40.0 et 44.1%. On discute des implications mécanistiques pour les deux réactions soit dans HOAc–H_2O et dans TFE.

[Traduit par le journal]

The generation and reactions of vinyl cations, including rearrangements, have been extensively reviewed by a number of workers active in the field (1–4). The degenerate rearrangement in a triarylvinyl cationic system was first reported from this laboratory in 1974 (5). The work involved a study of the extents of 1,2-phenyl shift across the double bond in the triphenylvinyl cation generated from solvolyses of triphenylvinyl-2-^{14}C triflate (**1**-OTf-2-^{14}C). Subsequently, analogous studies on degenerate rearrangements from 1,2-aryl shifts, using ^{14}C, ^{13}C, or D as label, were carried out in this laboratory (6–9) and by Rappoport and co-workers (10, 11) on triarylvinyl cations with various combinations of phenyl and/or *p*-anisyl as the aryl groups, and these studies have been reviewed by Rappoport (4). Recently, we have also investigated similar degenerate rearrangements in the tri-*p*-tolylvinyl and the 2-phenyl-1,2-di-*p*-tolylvinyl cations generated, respectively, from tri-*p*-tolylvinyl-2-^{13}C bromide and

Can. J. Chem. Downloaded from www.nrcresearchpress.com by 210.87.254.40 on 09/05/12
For personal use only.

Can. J. Chem. Downloaded from www.nrcresearchpress.com by 210.87.254.40 on 09/05/12
For personal use only.

from *cis*- and *trans*-2-phenyl-1,2-di-*p*-tolylvinyl-2-^{13}C bromides (12, 13).

In a study on the formation of vinyl cations from reactions of acids with vinyltriazenes, Jones and Miller (14) made the early observation of rearrangements of less stable to more stable triarylvinyl cations arising from 1,2-aryl shifts. For example, the decomposition of the 1-phenyl-2,2-di-*p*-tolylvinyldiazonium ion generated from the triazene in HOAc gave 20% of the rearranged product, 2-phenyl-1,2-di-*p*-tolylvinyl acetate. This rearrangement, however, could be completely suppressed by the presence of 10 molar equiv. of KOAc. Similarly, in the decomposition of trianisylvinyl-2-^{14}C-phenyltriazene in HOAc, the degenerate rearrangement from 1,2-anisyl shifts in the trianisylvinyl cation gave rise to about 38 and 17% scrambling, respectively, when the reaction was carried out in the absence and in the presence of 1.7 equiv. of NaOAc (9). These results were interpreted as indicating that the rearrangement occurred with the dissociated open triarylvinyl cation. In the presence of added acetate, the rearrangement would compete less effectively with the product forming reaction between the vinyl cation and the acetate anion.

In the solvolyses of **1**-OTf-2-^{14}C in acetic, formic and trifluoroacetic acids, it was found that the presence of added conjugate base of the solvent did not affect the extents of scrambling (5). These findings were interpreted as indicating that the rearrangement took place in the ion-pair stage. An example of such an interpretation can be found in the early, classical work of Young *et al.* (15, 16) on allylic rearrangements through internal return with allylic chlorides, where intimate ion-pairs were involved and the presence of added chloride ions did not affect the rate of rearrangement. If the degenerate rearrangement in the triphenylvinyl cation indeed were to involve ion pairs, a closely related process would be ion-pair return. In the present work, solvolytic studies with triphenylvinyl-2-^{14}C bromide (**1**-Br-2-^{14}C) were carried out with the view of obtaining further information on the role of ion pairs in the rearrangement and return processes.

Results and Discussion

The labelled reactant, **1**-Br-2-^{14}C, was prepared as described previously (5). The reaction of **1**-Br-2-^{14}C or **1**-Br-2-^{13}C with HOAc–AgOAc has been shown to give 6–7% scrambling of the label from C-2 to C-1 (6). When attempts were made to effect the reaction of **1**-Br with glacial HOAc without any Ag salt, the reaction was very slow and extensive decomposition occurred. Hence in the present work, the first series of experiments were carried out by heating **1**-Br-2-^{14}C in HOAc–H_2O at 150°C for different lengths of time. The data are summarized in Table 1. The solvent systems varied from 50% HOAc – 50% H_2O to 90% HOAc – 10% H_2O (by volume). With 70% HOAc, experiments were also carried out in the presence of about 3 equiv. of added NaOAc or NaBr. From the reactions in 50–80% HOAc, the only product obtained was α,α-diphenylacetophenone (**2**). With 90% HOAc, besides **2**, a trace of the acetate product was detectable by nmr.

The reaction product, **2**, was purified by passage through an alumina column before it was degraded (5) by $LiAlH_4$ reduction to 1,2,2-triphenylethanol (**3**), followed by $KMnO_4$ oxidation to benzophenone (**4**). The loss of ^{14}C activity in the conversion of **3** to **4** gave the extent of scrambling of the label from C-2 to C-1. The results are given in Table 1.

In some of the experiments, the unconsumed reactant, **1**-Br-x-^{14}C, was also separated in the alumina column and then subjected to degradation to ascertain whether scramblings arising from return processes have occurred. The method of degradation made use of an earlier finding that the reaction of triphenylvinyl-2-^{14}C-phenyltriazene with aqueous acetone in the presence of $HClO_4$ gave α,α-diphenylacetophenone (**2**) with no isotopic scrambling (9). In the present work, the samples of recovered **1**-Br-x-^{14}C were converted to the Grignard reagent and then treated with phenyl azide to give triphenylvinylphenyltriazene (9). Upon reaction with 90% acetone – 10% H_2O containing 0.1% $HClO_4$, the triazene gave **2** which was in turn reduced to **3** and then oxidized to **4** in the usual way to give the extent of scrambling. The results are also given in Table 1.

As can be seen from Table 1, in the various experiments in which the recovered unconsumed **1**-Br-2-^{14}C was analyzed, there was essentially no isotopic scrambling (0 ± 0.5%), suggesting no ion-pair return or the return process could not compete with rearrangement. Such a finding for solvolytic reactions in a water-containing solvent is not surprising since it is known that, in highly nucleophilic or highly ionizing solvents, the return process competes poorly with the product forming reaction (15, 16). Kinetic studies with **1**-Br by Rappoport and Houminer (17) have also shown that in an aqueous solvent, namely, 60% EtOH – 40% H_2O, the specific rate constant remained unchanged throughout a reaction, indicating no common ion rate depression by the liberated bromide ion.

The extents of isotopic scrambling observed in the reaction product from solvolyses of **1**-Br-2-^{14}C in aqueous HOAc varied depending on the solvent composition (Table 1). For a given mixture of HOAc and H_2O, however, the amount of scrambling

Can. J. Chem. Downloaded from www.nrcresearchpress.com by 210.87.254.40 on 09/05/12
For personal use only.

TABLE 1. Data from solvolyses of triphenylvinyl-2-^{14}C bromide (1-Br-2-^{14}C) in HOAc–H_2O at 150 ± 2°C

Experiment No.	Solvent (% HOAc)	Added salt	Reaction time (days)	Extent of reaction[a] (%)	Specific activity[b] (dpm/mmol)				Scrambling from C-2 to C-1 (%)		
					Reaction product		Recovered reactant		Reaction product	Recovered reactant	k_{SOH}/k_r[e]
					$Ph_2CHCHOHPh$	Ph_2CO[c]	$Ph_2CHCHOHPh$	Ph_2CO[c]			
1	50		1	51(49)	400 000	362 000			9.5		
2	50		2	78(77)	326 000	295 000			9.5		
3	50		2	77	313 000	282 000			9.9(9.6)[d]		8.3
4	60		1	42(40)	762 000	668 000			12.3		
5	60		2	75(75)	225 000	195 000	74 400	74 200	13.3	0.3	
6	60		2	75	540 000	472 000			12.6(12.7)[d]		5.9
7	70		1	28(29)	448 000	384 000			14.3		
8	70		2	61(60)	190 000	161 000	43 100	42 900	15.3	0.5	
9	70	NaOAc	2	65(68)	329 000	280 000	33 200	33 100	14.9	0.3	
10	70	NaBr	2	56(57)	160 000	136 000	12 300	12 300	15.0	0.0	
11	70		8	99(99)	795 000	667 000			16.1		
12	70	NaOAc	8	98(97)	1 130 000	951 000			15.8		
13	70	NaBr	8	98(94)	1 030 000	868 000			15.7(15.3)[d]		4.5
14	80		1	14(13)	250 000	208 000			16.8		
15	80		2	18(16)	726 000	606 000	876 000	870 000	16.5	0.0	
16	80		2	20	897 000	745 000			16.9(16.7)[d]		4.0
17	90		2	9(8)	135 000	110 000	236 000	236 000	18.5	0.0	
18	90		4	15(16)	56 300	46 000			18.3(18.4)[d]		3.4

[a]Estimated by potentiometric titration of the liberated bromide ion; values in parentheses were determined by isotopic dilution.
[b]Measured by a liquid scintillation counter; statistical counting errors were ± 1% or less.
[c]Assayed as the oxime.
[d]Mean values for the corresponding solvent system.
[e]Based on the mean percentage scramblings.

Can. J. Chem. Downloaded from www.nrcresearchpress.com by 210.87.254.40 on 09/05/12
For personal use only.

remained essentially constant, although the reaction time and hence the extent of reaction was changed. In 70% HOAc, the presence of about 3 equiv. of added NaOAc or NaBr also did not influence the degree of rearrangement. From Table 1, it is seen that the mean values for the extents of scrambling of the label from C-2 to C-1 in the reaction products were 9.6, 12.7, 15.3, 16.7, and 18.4%, respectively, for solvolysis in 50, 60, 70, 80, and 90% HOAc.

The above results may be interpreted by the mechanism shown in Scheme 1. Since the presence of NaOAc or NaBr did not materially affect the extent of scrambling (experiments 8–13, Table 1), the previous conclusion (5) that the 1,2-phenyl shift in the triphenylvinyl cation took place in the ion-pair stage has apparently been confirmed. The ion pair may give rise to product directly, or dissociate further before reacting with H_2O to give the products, **2**-*2*-^{14}C and **2**-*1*-^{14}C. The present results cannot differentiate between these two possibilities.

Using the steady state treatment and the method of Bonner and Collins (18), it has been shown (11) that for the mechanism as depicted by Scheme 1, after complete reaction, eq. [1] holds.

$$[1] \qquad [\mathbf{2}\text{-}2\text{-}^{14}C]/[\mathbf{2}\text{-}1\text{-}^{14}C] = 1 + (k_{SOH}/k_r)$$

Similarly, from the steady state treatment, it can be shown that eq. [2] also applies.

$$[2] \qquad \frac{d[\mathbf{2}\text{-}2\text{-}^{14}C]/dt}{d[\mathbf{2}\text{-}1\text{-}^{14}C]/dt} = 1 + (k_{SOH}/k_r)$$

Since the ratio of the rates of formation of the unrearranged and rearranged products is a constant (eq. [2]), the percentage of scrambling should not change with the extent of reaction and this was as observed (Table 1). Utilizing eq. [1] and the mean scrambling value for each solvent system, k_{SOH}/k_r can be calculated and these values are included in Table 1.

From a comprehensive solvolytic study on a series of *cis*- and *trans*-2-aryl-1,2-dimethylvinyl triflates, definitive evidence in support of aryl participation has been obtained by Stang and Dueber (19–21). For example, in the solvolysis of *trans*-1,2-dimethyl-2-phenylvinyl triflate, the phenyl bridged

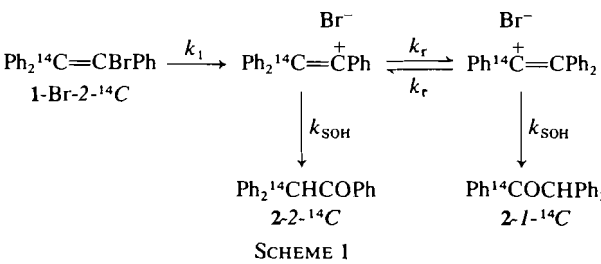

SCHEME 1

vinylidene phenonium ion is shown as a reaction intermediate. On the other hand, there is no phenyl participation or anchimeric assistance in the 1,2-dianisyl-2-phenylvinyl (4, 8, 11) or 2-phenyl-1,2-di-*p*-tolylvinyl (13) cationic systems. It is attractive to consider the possibility that there may be a gradation of mechanisms with the triphenylvinyl case falling into the borderline region, with the observed scramblings attributed to partial phenyl bridging. Such an explanation, however, does not appear to agree with the observed results. From Table 1, it is seen that for a given reaction time (e.g., 2 days), the higher the proportion of H_2O in the HOAc–H_2O solvent, the greater is the extent of the reaction, but the lesser is the degree of scrambling. Assuming that bridging is associated with enhanced rate (21), if borderline behavior and partial bridging were involved, one would expect more scrambling for faster reactions, the opposite of what was observed. Apparently, as depicted in Scheme 1, the product is derived from reaction between the triphenylvinyl cation or ion pair and the more nucleophilic H_2O. The higher the proportion of H_2O in the solvent, the more effectively will the product forming process compete with the 1,2-phenyl shift, hence giving rise to a lesser amount of scrambling. The calculated k_{SOH}/k_r values (Table 1) also reflect this trend.

A kinetic study on the solvolysis of **1**-Br in 2,2,2-trifluoroethanol (TFE), in the presence of 2,6-lutidine, has been reported by Rappoport and Houminer (17). Among the findings was the observation of a common ion rate depression during a given kinetic run or with the presence of added external bromide ion, indicating the occurrence of return processes. In the present work, in order to obtain data on possible scramblings in the recovered reactant arising from returns, a set of experiments was carried out on the solvolysis of **1**-Br-*2*-^{14}C in TFE in the presence of 2,6-lutidine, with or without added tetraethylammonium bromide. Because the product from the trifluoroethanolysis, triphenylvinyl 2,2,2-trifluoroethyl ether (**1**-OTFE), could not be separated from the unreacted **1**-Br by the alumina column, separate experiments for the analysis of the product and the analysis of the unconsumed reactant were carried out with **1**-Br-*2*-^{14}C. The results are summarized in Table 2.

In the analysis of the product, the residue from a given reaction mixture was treated with HOAc–AgOAc (6) in order to convert any unconsumed reactant, **1**-Br-*x*-^{14}C, to **1**-OAc-*x*-^{14}C, which in turn was reduced with $LiAlH_4$ to α,α-diphenylacetophenone (**2**). Ketone **2** could then be separated from the product, **1**-OTFE-*x*-^{14}C, by passage through the alumina column. Since the reaction of the labeled

Can. J. Chem. Downloaded from www.nrcresearchpress.com by 210.87.254.40 on 09/05/12
For personal use only.

TABLE 2. Data from trifluoroethanolysis of 0.12 *M* triphenylvinyl-2-^{14}C bromide (**1**-Br-2-^{14}C) in the presence of 0.36 *M* 2,6-lutidine at 150 ± 2°C with or without added tetraethylammonium bromide

Experiment No.	$[Et_4NBr]$ (*M*)	Reaction time (days)	Extent of reaction[a] (%)	Specific activity[b] (dpm/mmol)				Scrambling from C-2 to C-1 (%)		
				Reaction product		Recovered reactant				
				$Ph_2CHCHOHPh$	Ph_2CO[c]	$Ph_2CHCHOHPh$	Ph_2CO	Reaction product	Recovered reactant	Mean
19	0	1	24			208 000	166 000		20.2	
20	0.19	1	20			261 000	209 000		19.9	20.1
21	0	2	35	96 200	66 900			30.5		
22	0.19	2	31	79 900	55 600			30.4		
23	0	2	35			185 000	130 000		29.7	
24	0	2	34			254 000	177 000		30.3	
25	0.19	2	33			192 000	134 000		30.2	
26	0.38	2	32			313 000	222 000		29.1	30.0
27	0	4	62	144 000	86 600			39.9		
28	0.19	4	54	146 000	88 600			39.3		
29	0	4	62			179 000	107 000		40.3	
30	0.19	4	56			225 000	134 000		40.4	40.0
31	0	20	97	1 910 000	1 050 000			45.0		
32	0.19	20	96	1 640 000	918 000			44.0		
33	0.38	20	96	960 000	545 000			43.2		44.1

[a]Estimated by potentiometric titration of the liberated bromide ion.
[b]Measured by a liquid scintillation counter; statistical counting errors were ± 1% or less.
[c]Assayed as the oxime.

Can. J. Chem. Downloaded from www.nrcresearchpress.com by 210.87.254.40 on 09/05/12
For personal use only.

bromide with HOAc–AgOAc is known to give rise to 6–7% scrambling (6), ketone **2**, recovered from the above treatment, could not be used to determine the extent of scrambling in the recovered reactant. However, the treatment effectively removed the unconsumed reactant from the reaction product. In a control experiment, ordinary **1**-Br, in the presence of **1**-OTFE-*2*-^{14}C, was subjected to the above treatment to give **2** which was found to be nonradioactive, indicating that there was no cleavage of the ether, **1**-OTFE-*2*-^{14}C, during the conversion of **1**-Br to **2**.

In the experiments with **1**-Br-*2*-^{14}C in which the product was analyzed for isotopic scrambling (experiments 21, 22, 27, 28, 31–33, Table 2), after removal of the **1**-Br-*x*-^{14}C as described above, the recovered product, **1**-OTFE-*x*-^{14}C, was hydrolyzed in 70% EtOH containing 0.7 *N* HCl (17) to give **2**, which in turn was degraded in the usual way by reduction to **3** followed by oxidation to **4** to give the extent of scrambling. In another control experiment, it was found that the hydrolysis of **1**-OTFE-*2*-^{14}C in 70% EtOH containing 0.7 *N* HCl gave the unrearranged **2**-*2*-^{14}C, indicating no scrambling during the hydrolysis.

When the unconsumed reactant was analyzed for isotopic scrambling (experiments 19, 20, 23–26, 29, 30, Table 2), the solid residue from each reaction mixture was diluted with ordinary **1**-Br as carrier and then treated in the same way as in the case of the recovered reactant from the solvolyses in HOAc–H_2O. Thus the **1**-Br-*x*-^{14}C was converted to the triazene via the Grignard and then decomposed in acetone–H_2O–$HClO_4$ to give **2**, which in turn was degraded to give the amount of scrambling.

From Table 2, it is seen that unlike solvolyses in HOAc–H_2O, isotopic scrambling was observed in the recovered reactant as well as in the product, and the amount of scrambling was found to increase with an increase in reaction time. Interestingly, for a given reaction time, the extents of scrambling in the product and in the recovered reactant were essentially the same (cf. experiments 21–26 and experiments 27–30, Table 2). The presence of external bromide ion, added as Et_4NBr, did not affect the amount of scrambling in either the product or the recovered reactant, again supporting the earlier conclusion that the scrambling occurred in the ion-pair stage. The return process in the trifluoroethanolysis of **1**-Br-*2*-^{14}C, therefore, is an ion-pair return and not an external ion return. A recent demonstration of an internal return process in a vinyl cationic system was reported by Hanack *et al.* (22) for the solvolysis of (1-bromo-1-methylmethylene)-cyclopropane to give the rearranged product, 1-bromo-2-methylcyclobutene.

The mechanism for the trifluoroethanolysis of **1**-Br-*2*-^{14}C may be depicted by Scheme 2. A steady

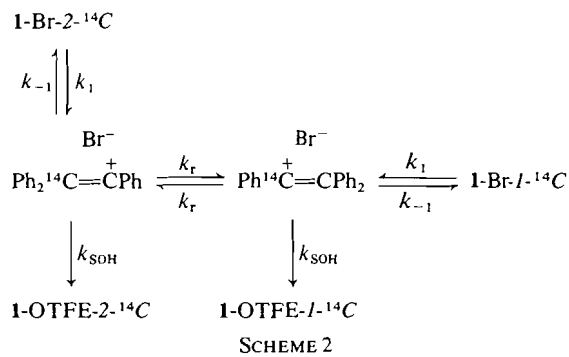

SCHEME 2

state treatment for the processes in Scheme 2 gives the following relationship:

$$\frac{d[\textbf{1}\text{-OTFE-}1\text{-}^{14}C]/dt}{d[\textbf{1}\text{-OTFE-}2\text{-}^{14}C]/dt} = \frac{(k_{-1} + k_{SOH})[\textbf{1}\text{-Br-}1\text{-}^{14}C] + k_r([\textbf{1}\text{-Br-}2\text{-}^{14}C] + [\textbf{1}\text{-Br-}1\text{-}^{14}C])}{(k_{-1} + k_{SOH})[\textbf{1}\text{-Br-}2\text{-}^{14}C] + k_r([\textbf{1}\text{-Br-}2\text{-}^{14}C] + [\textbf{1}\text{-Br-}1\text{-}^{14}C])}$$

Since the formation of the unrearranged and rearranged products would depend on the concentration of the reactant, the extents of scrambling should be different for different extents of reaction, and this was observed (Table 2). If $k_r([\textbf{1}\text{-Br-}2\text{-}^{14}C] + [\textbf{1}\text{-Br-}1\text{-}^{14}C])$ is negligible when compared with $(k_{-1} + k_{SOH})[\textbf{1}\text{-Br-}1\text{-}^{14}C]$ and with $(k_{-1} + k_{SOH}) \times [\textbf{1}\text{-Br-}2\text{-}^{14}C]$, then $[\textbf{1}\text{-OTFE-}1\text{-}^{14}C]/[\textbf{1}\text{-OTFE-}2\text{-}^{14}C] = [\textbf{1}\text{-Br-}1\text{-}^{14}C]/[\textbf{1}\text{-Br-}2\text{-}^{14}C]$, in agreement with the observation in experiments 21–26 and 27–30 that the extent of scrambling was the same in the product and in the recovered reactant. At very early stages of the reaction, the above result may not be observed since $[\textbf{1}\text{-Br-}1\text{-}^{14}C]$ arising from the return process would not have been very high. In experiments 21–30, however, the reaction has proceeded to a significant extent and the concentration of **1**-Br-*1*-^{14}C would have been built up appreciably so that $k_r([\textbf{1}\text{-Br-}2\text{-}^{14}C] + [\textbf{1}\text{-Br-}1\text{-}^{14}C])$ is negligible compared to $(k_{-1} + k_{SOH})[\textbf{1}\text{-Br-}1\text{-}^{14}C]$.

In conclusion, the present work has provided much additional information on the degenerate rearrangement arising from 1,2-phenyl shifts in the triphenylvinyl cationic system. An important role is attributed to ion pairs and ion-pair return is shown to occur in the reaction of **1**-Br-*2*-^{14}C with TFE but not with HOAc–H_2O. The mechanistic processes that take place during the solvolysis of **1**-Br-*2*-^{14}C in

Can. J. Chem. Downloaded from www.nrcresearchpress.com by 210.87.254.40 on 09/05/12
For personal use only.

HOAc–H_2O and in TFE, respectively, are adequately depicted by Schemes 1 and 2.

Experimental

Solvolysis of Triphenylvinyl-2-^{14}C Bromide (1-Br-2-^{14}C) in HOAc–H_2O

1-Br-*2*-^{14}C was prepared as described previously (5). The solvents used were made up of HOAc–H_2O (by volume) in the proportions of 50:50, 60:40, 70:30, 80:20, and 90:10. The reactions were carried out by heating 25–30 m*M* **1**-Br-*2*-^{14}C in sealed tubes at 150 ± 2°C for periods varying from 1–8 days (see Table 1). In 70% HOAc, experiments were also carried out with the presence of about 3 equiv. of NaOAc or NaBr. An illustration of the experimental procedure is given below.

A solution of 210 mg (0.63 mmol) of **1**-Br-*2*-^{14}C and 160 mg (1.96 mmol) of NaOAc in 25 ml of 70% HOAc in a sealed tube was heated in an oil bath at 150 ± 2°C for 2 days. The tube was cooled and opened, and weighed quantities (about 200 mg) of ordinary **1**-Br and α,α-diphenylacetophenone (**2**) were added as carriers. The mixture was extracted with ether (3 × 25 ml) and the extract washed with H_2O. The liberated bromide ion in the combined aqueous phase was determined by potentiometric titration (17) to give the extent of reaction. The ether extract was dried over $MgSO_4$ and the solvent was removed under reduced pressure at room temperature to give an oily residue. Upon passage through an alumina column (2.5 × 25 cm packed with untreated adsorption alumina) and elution with 90% petroleum ether – 10% ether, the unconsumed reactant (**1**-Br-*x*-^{14}C) was separated from the reaction product (**2**-*x*-^{14}C). The **1**-Br-*x*-^{14}C was the first to be eluted, and recoveries of both **1**-Br-*x*-^{14}C and **2**-*x*-^{14}C were aided by monitoring with nmr. A small amount of the product was recrystallized from CH_3OH and its specific activity determined to give the extent of reaction by isotopic dilution calculations. The remainder of the product was diluted further with carrier to give about 1.0 g of material for degradation by $LiAlH_4$ reduction to 1,2,2-triphenylethanol (**3**) and $KMnO_4$ oxidation to benzophenone (**4**) by methods as described previously (5).

The recovered unconsumed reactant, **1**-Br-*x*-^{14}C, was dried overnight in a vacuum desiccator, mixed with more carrier, converted to the Grignard reagent, **1**-MgBr-*x*-^{14}C, and treated with PhN_3 to give the triazene, **1**-NNNHPh-*x*-^{14}C. Decomposition of the triazene in 90% acetone – 10% H_2O containing 0.1% $HClO_4$ gave **2**-*x*-^{14}C which was then degraded in the usual way. The procedures for the conversion of **1**-Br-*2*-^{14}C to **2**-*2*-^{14}C without scrambling by the above series of reactions have been reported in a previous study (9).

Solvolyses of 1-Br-2-^{14}C in 2,2,2-Trifluoroethanol (TFE)

The trifluoroethanolyses were carried out in sealed tubes with 0.12 *M* **1**-Br-*2*-^{14}C, 0.36 *M* 2,6-lutidine, and with the absence or presence of about 1.5 or 3 equiv. of Et_4NBr. The reaction mixtures were heated at 150 ± 2°C for periods varying from 1–20 days. A description of the experimental procedure is given below.

A solution of 200 mg (0.60 mmol) of **1**-Br-*2*-^{14}C, 200 mg (1.8 mmol) of 2,6-lutidine, and 200 mg (0.95 mmol) of Et_4NBr in 5 ml of TFE in a sealed tube was heated in an oil bath at 150 ± 2°C for the desired period. After cooling, the material was poured into 80 ml of ether and the ether solution was washed three times with H_2O. The bromide ion in the aqueous washing was determined by potentiometric titration to give the extent of reaction. The product, triphenylvinyl-*x*-^{14}C 2,2,2-trifluoroethyl ether (**1**-OTFE-*x*-^{14}C) and unconsumed reactant, **1**-Br-*x*-^{14}C, could not be separated by the alumina column. Thus separate experiments were carried out in order to obtain purified α,α-diphenylacetophenone (**2**-*x*-^{14}C) from the product or from the unconsumed reactant.

In order to recover the reaction product, to the washed ether solution of the reaction mixture ordinary **1**-Br and **1**-OTFE (about 200 mg each) were added as carriers. After drying, the solvent was removed and the residue was heated under reflux for 18 h with 10 ml of HOAc containing 200 mg AgOAc. This treatment converted all the **1**-Br-*x*-^{14}C to 1-OAc-*x*-^{14}C, which was worked up and reduced with $LiAlH_4$ as previously described (5) to give **2**-*x*-^{14}C. On passage through the alumina column, the original reaction product, **1**-OTFE-*x*-^{14}C, could be separated by elution with petroleum ether from the **2**-*x*-^{14}C that was derived from the unconsumed reactant, **1**-Br-*x*-^{14}C. After removal of the solvent from the eluate, the residual **1**-OTFE-*x*-^{14}C was hydrolyzed to give another sample of **2**-*x*-^{14}C by refluxing in 14 ml of EtOH and 6 ml of 0.7 *N* HCl for 4 days (17). Nuclear magnetic resonance examination showed that even after 4 days, the hydrolysis was only 75–80% complete. The **2**-*x*-^{14}C so obtained was purified by passage through the alumina column and then degraded, with the aid of carriers if necessary, to **3** and **4** in the usual way.

To obtain a pure sample of **2**-*x*-^{14}C that was derived from the unconsumed reactant, **1**-Br-*x*-^{14}C, the washed ether solution of the reaction mixture was dried over $MgSO_4$. The solvent was removed and the residue was dried overnight in a vacuum desiccator. Inactive **1**-Br was added as carrier and the material was subjected to the same series of reactions as described in the treatment of the recovered **1**-Br-*x*-^{14}C from the solvolysis in HOAc–H_2O. In this way the **1**-Br-*x*-^{14}C was converted via the triazene to **2**-*x*-^{14}C which was purified by passage through the alumina column before it was degraded to **3** and **4**. The purification by column chromatography was necessary because, in this treatment, a small amount of the **1**-Br-*x*-^{14}C remained unreacted and this, together with the reaction product, **1**-OTFE-*x*-^{14}C, and other contaminants such as the excess PhN_3, were separated from the **2**-*x*-^{14}C by the alumina column.

Control Experiments

(*a*) Triphenylvinyl-*2*-^{14}C-phenyltriazene (**1**-NNNHPh-*2*-^{14}C) (9) was treated with TFE containing 0.1% $HClO_4$ to give **1**-OTFE-*2*-^{14}C. Hydrolysis of 200 mg of **1**-OTFE-*2*-^{14}C in 14 ml of EtOH and 6 ml of 0.7 *N* HCl by heating the mixture under reflux for 4 days gave a sample of **2**-*2*-^{14}C without any isotopic scrambling, indicating that the hydrolysis of the ether product did not cause any rearrangement.

(*b*) When ordinary **1**-Br, in the presence of some **1**-OTFE-*2*-^{14}C, was converted to **2** through the triazene as was utilized in the treatment of the recovered unconsumed reactant, the sample of **2** so obtained was not radioactive, indicating no conversion of any **1**-OTFE-*2*-^{14}C to **2**-^{14}C during these treatments.

(*c*) After 200 mg of **1**-OTFE-*2*-^{14}C was heated under reflux for 18 h in 10 ml of HOAc containing 200 mg of AgOAc, it was recovered and then hydrolyzed in EtOH – 0.7 *N* HCl. The product obtained was the unrearranged **2**-*2*-^{14}C, indicating that the treatment with HOAc–AgOAc to destroy the unconsumed reactant did not cause any scrambling in the reaction product.

Acknowledgements

The financial support given by the National Research Council of Canada and valuable comments from Professor R. E. Verrall of this department and Professor Z. Rappoport of the Hebrew University of Jerusalem are gratefully acknowledged.

1. G. MODENA and U. TONELLATO. Adv. Phys. Org. Chem. **9**, 185 (1971).
2. P. J. STANG. Prog. Phys. Org. Chem. **10**, 205 (1973).
3. M. HANACK and L. R. SUBRAMANIAN. J. Chem. Educ. **52**, 80 (1975); M. HANACK. Acc. Chem. Res. **3**, 209 (1970); **9**, 364 (1976).
4. Z. RAPPOPORT. Acc. Chem. Res. **9**, 265 (1976).
5. C. C. LEE, A. J. CESSNA, B. A. DAVIS, and M. OKA. Can. J. Chem. **52**, 2679 (1974).
6. F. H. A. RUMMENS, R. D. GREEN, A. J. CESSNA, M. OKA, and C. C. LEE. Can. J. Chem. **53**, 314 (1975).
7. M. OKA and C. C. LEE. Can. J. Chem. **53**, 320 (1975).
8. C. C. LEE and M. OKA. Can. J.Chem. **54**, 604 (1976).
9. C. C. LEE and E. C. F. KO. Can. J. Chem. **54**, 3041 (1976).
10. Z. RAPPOPORT, E. NOY, and Y. HOUMINER. J. Am. Chem. Soc. **98**, 2238 (1976).
11. Y. HOUMINER, E. NOY, and Z. RAPPOPORT. J. Am. Chem. Soc. **98**, 5632 (1976).
12. C. C. LEE, A. J. PAINE, and E. C. F. KO. Can. J. Chem. **55**, 2310 (1977).
13. C. C. LEE, A. J. PAINE, and E. C. F. KO. J. Am. Chem.Soc. **99**, 7267 (1977).
14. W. M. JONES and F. W. MILLER. J. Am. Chem. Soc. **89**, 1960 (1967).
15. W. G. YOUNG, S. WINSTEIN, and H. L. GOERING. J. Am. Chem. Soc. **73**, 1958 (1951).
16. A. STREITWIESER, JR. Solvolytic displacement reactions. McGraw-Hill, New York, NY. 1962. pp. 86–88.
17. Z. RAPPOPORT and Y. HOUMINER. J. Chem. Soc. Perkin II, 1506 (1973).
18. W. A. BONNER and C. J. COLLINS. J. Am.Chem. Soc. **78**, 5587 (1956).
19. P. J. STANG and T. E. DUEBER. J. Am. Chem. Soc. **95**, 2683 (1973).
20. P. J. STANG and T. E. DUEBER. J. Am. Chem. Soc. **95**, 2686 (1973).
21. P. J. STANG and T. E. DUEBER. J. Am. Chem. Soc. **99**, 2602 (1977).
22. M. HANACK, T. BÄSSLER, W. EYMANN, W. E. HEYD, and R. KOPP. J. Am. Chem. Soc. **96**, 6686 (1974).

Can. J. Chem. Downloaded from www.nrcresearchpress.com by 210.87.254.40 on 09/05/12
For personal use only.

Cancentrine. V.[1] The ^{13}C magnetic resonance spectra of cancentrine and some derivatives; the structure of 10-oxocancentrine

HERBERT L. HOLLAND,[2] DONALD W. HUGHES, AND DAVID B. MACLEAN
McMaster University, Department of Chemistry, Hamilton, Ont., Canada L8S 4M1
AND
RUSSELL G. A. RODRIGO
Wilfrid Laurier University, Department of Chemistry, Waterloo, Ont., Canada N2L 3C5
Received March 30, 1978

HERBERT L. HOLLAND, DONALD W. HUGHES, DAVID B. MACLEAN, and RUSSELL G. A. RODRIGO. Can. J. Chem. **56**, 2467 (1978).

The ^{13}C magnetic resonance spectrum of cancentrine is reported. Assignments of chemical shifts have been made by comparison of the cancentrine spectrum with the published spectra of codeine, codeinone, and cularine and with the spectra reported here for the first time of 9,10-dihydrocancentrine methine-*O*-methyl ether and 10-oxocodeinone. The spectral data so obtained have been used to interpret the ^{13}C spectrum of 10-oxocancentrine, a new alkaloid of the cancentrine family, and to verify the structure deduced for it from ^{1}H nmr, ir, uv, and mass spectral data.

HERBERT L. HOLLAND, DONALD W. HUGHES, DAVID B. MACLEAN et RUSSELL G. A. RODRIGO. Can. J. Chem. **56**, 2467 (1978).

On rapporte le spectre de résonance magnétique nucléaire du ^{13}C de la cancentrine. On a pu faire les attributions des déplacements chimiques par comparaison du spectre de la cancentrine avec les spectres publiés de la codéine, de la codéinone et de la cularine et avec les spectres que l'on rapporte ici pour la première fois de l'éther dihydro-9,10 cancentrine méthine-*O*-méthyle et de l'oxo-10 codéinone. On a utilisé les données spectrales pour interpréter le spectre ^{13}C de l'oxo-10 cancentrine, un nouvel alcaloïde de la famille de cancentrine et pour vérifier la structure déduite à partir de données de rmn ^{1}H, ir, uv et de spectrométrie de masse.
[Traduit par le journal]

The cancentrine alkaloids were first isolated by Manske in 1932 (1) and in 1970 the structure of cancentrine **1***a* was elucidated (2). It is composed of a morphine-like unit and a cularine-like unit which are fused together as shown in Fig. 1. Other alkaloids of established structure in this series are the dehydrocancentrines, A and B (3). They differ from cancentrine in that the former has a double bond between C-8 and C-14 and the latter a double bond between C-31 and C-32. Here, we report a ^{13}C magnetic resonance study of cancentrine, and some model compounds. The ^{13}C information so obtained has been used in the elucidation of the structure of a new alkaloid in this series, 10-oxocancentrine **1***b*.

The interpretation of the ^{13}C spectrum of cancentrine (Table 1) was aided greatly by reference to the published spectra of codeine **2***a* and cularine **3** (Fig. 2 and Table 2). Comparison of the aliphatic region of the codeine (**2***a*) spectrum (4) with that of cancentrine (**1***a*) enabled us to assign the resonances at C-10, C-15, C-16, and N—CH_3 of **1***a*; these assignments were substantiated by examination of the off-resonance spectrum. The high-field resonance of C-10, a benzylic carbon, has been ascribed to a γ steric interaction of the N—CH_3 (4). The other high-field signal in the spectrum of **1***a* at 29.0 ppm has been assigned to C-31 by reference to the cularine **3** spectrum (5). The off-resonance spectrum of **1***a* showed a singlet at 51.4 ppm, a doublet at 46.2 ppm, and a triplet at 40.2 ppm that are attributed to carbon atoms 13, 14, and 8, respectively. The transformation of the six-membered ring C of codeine to the five-membered alicyclic spiro ring present in cancentrine has caused a deshielding of C-13 and C-14 relative to the corresponding carbon atoms of codeine. A similar effect is observed at C-5. The splitting patterns of C-9 and C-32 in the off-resonance spectrum are partially obscured by the overlapping methoxy resonances at 56.5 ppm but the assignment of C-9 to the signal at 58.8 ppm and of C-32 to the signal at 57.8 ppm seem secure in view of the C-9 resonance in codeine at 58.7 ppm. The remaining signal in the aliphatic region at 79.1 ppm is assigned to the spiro carbon, C-6.

The oxygenated aromatic carbon atoms of cancentrine all fall in the range, 135–150 ppm whereas the remaining aromatic carbon atoms, whether substituted with H or carbon, fall in the region 100–130 ppm. By off-resonance decoupling it was

[1]For part IV see ref. 15.
[2]Present address: Department of Chemistry, Brock University, St. Catharines, Ont., L2S 3A1.

Can. J. Chem. Downloaded from www.nrcresearchpress.com by 210.87.254.42 on 09/05/12
For personal use only.

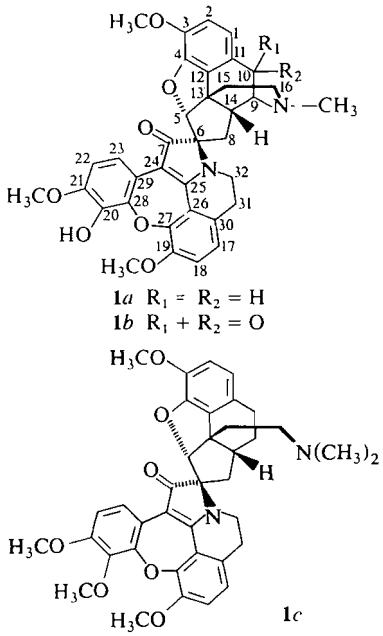

FIG. 1. Structures of cancentrine (**1***a*), 10-oxocancentrine (**1***b*), and 9,10-dihydrocancentrine methine-*O*-methyl ether (**1***c*).

possible in most cases to differentiate the protonated from the nonprotonated carbon atoms. For those cases where overlap of signals made this difficult or impossible the technique of selective enhancement of quaternary carbon signals (6) was used. A low power and modulated decoupling field was applied to the sample, producing essentially a broadband spectrum composed only of the quaternary carbons. From a combination of the low power decoupled and the off-resonance spectra the signal at 119.7 ppm was found to result from the overlap of the signals of both a protonated and a carbon substituted aromatic carbon assigned to C-1 and C-29, respectively, by comparison to the spectra of codeine (**2***a*) and cularine (**3**) (Table 2).

The assignments of carbons 2 through 4 are consistent with the codeine data; however, the similarity in chemical shifts for carbon atoms 11, 12, and 30 did not allow unambiguous assignments to be made. The C-3 and C-4 assignments are in accord with the correlation noted by Terui *et al.* (4) between the peak intensity and the spin–lattice relaxation times, the latter determined by Wehrli for codeine (7). Carbon 4 of **1***a* does not have any neighbouring protons to provide dipolar relaxation and therefore should have a longer T_1 and a lower intensity because of saturation. Accordingly the signal of lower intensity was assigned to C-4.

By reference to the cularine **3** data in Table 2 tentative assignments for the remaining aromatic signals were made. The chemical shifts of C-30 and C-26 were assigned in reverse order to the corresponding cularine carbons, 8a and 4a, because C-26 does not have any neighbouring protons and would be expected to be of lower intensity than the peak assigned to C-30 and this is the case. Of the carbon atoms containing oxygen substituents, C-20 was assigned to the signal at 138.0 ppm because the hydroxy group deshields the directly bonded carbon atom less than a methoxy group (8, 9). Experimental verification is provided in the discussion of **1***c*. The signals of carbons 19 and 23 were differentiated from the remaining low-field aromatic signals by their higher peak intensity. The signals at 194.0, 160.1, and 104.3 ppm are attributed to the carbon atoms of the α,β-saturated carbonyl system, C-7, C-25, and C-24, respectively.

Further evidence for the assignments made in the spectrum of **1***a* was provided by an examination of the spectrum of 9,10-dihydrocancentrine methine-*O*-

TABLE 1. ^{13}C chemical shifts of cancentrine (**1***a*) and two derivatives **1***b* and **1***c*

Carbon	**1***a*	**1***b*	**1***c*
1	119.7	120.2	119.9
2	115.3	115.3	116.0
3	142.7	146.6	142.5
4	145.1	143.3	146.9
5	97.5	96.7	99.3
6	79.1	78.3	79.2
7	194.0	193.2	193.3
8	40.2	40.0	40.1
9	58.8	68.0	23.7
10	20.4	196.3	26.2
11	127.4	124.4	127.3
12	127.7	135.6	128.8
13	51.4	52.5	56.4
14	46.2	48.9	41.9
15	33.2	32.1	33.3
16	46.6	47.3	45.5
17	124.3	124.2	124.2
18	116.3	115.9	116.8
19	149.8	149.5	152.3
20	138.0	137.8	147.8
21	146.8	146.6	151.2
22	109.2	108.9	109.1
23	116.6	115.9	121.1
24	104.3	104.3	104.2
25	160.1	160.4	160.6
26	121.4	121.0	121.8
27	147.7	146.8	147.6
28	140.7	140.5	141.7
29	119.7	119.2	121.0
30	127.8	127.5	128.1
31	29.0	28.8	29.4
32	57.8	57.3	55.8
3 OCH_3	56.5	56.3	56.4
19 OCH_3	56.5	56.3	57.7
20 OCH_3			61.5
21 OCH_3	56.5	56.3	56.7
NCH_3	43.2	43.3	
$N(CH_3)_2$			45.5

Can. J. Chem. Downloaded from www.nrcresearchpress.com by 210.87.254.42 on 09/05/12
For personal use only.

Can. J. Chem. Downloaded from www.nrcresearchpress.com by 210.87.254.42 on 09/05/12
For personal use only.

TABLE 2. ^{13}C chemical shifts of codeine (**2***a*), its derivatives **2***b* and **2***c*, and cularine (**3**)

Carbon	**2***a*[a]	**2***b*[a]	**2***c*	Carbon	**3**[b]
1	119.3	119.7	120.0	1	56.7
2	112.8	114.7	115.0	3	47.5
3	142.0	142.3	149.6	4	26.0
4	146.2	144.6	144.9	4a	126.3
5	91.3	88.0	87.7	5	124.3
6	66.4	194.1	193.2	6	110.4
7	133.2	132.2	132.7	7	148.9
8	128.1	149.1	148.3	8	144.8
9	58.7	58.9	68.5	8a	132.5
10	20.4	20.4	190.4	9	35.3
11	127.0	126.1	125.1	1′	118.3
12	130.9	129.0	137.1	2′	113.6
13	43.0	43.1	44.6	3′	144.8
14	40.7	41.4	44.4	4′	147.3
15	35.8	33.9	33.9	5′	105.1
16	46.4	46.7	47.2	6′	148.4
3 OCH_3	56.2	56.7	56.3	7 OCH_3	55.8
NCH_3	43.0	42.9	43.4	3′ OCH_3	56.0
				4′ OCH_3	56.0
				NCH_3	42.4

[a]Assignments from ref. 4.
[b]Assignments from ref. 5.

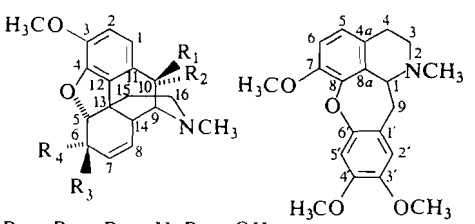

2*a* $R_1 = R_2 = R_3 = H, R_4 = OH$
2*b* $R_1 = R_2 = H, R_3 + R_4 = O$
2*c* $R_1 + R_2 = R_3 + R_4 = O$

3

FIG. 2. Structures of codeine (**2***a*), codeinone (**2***b*), 10-oxocodeinone (**2***c*), and cularine (**3**).

methyl ether (**1***c*) (10). In **1***c* where the N—C-9 bond is broken the chemical shift of C-9 has moved upfield from 58.8 ppm in cancentrine (**1***a*) to 23.7 ppm. Carbon-14 is also shielded relative to **1***a* because of the elimination of the β-nitrogen substituent effect. Carbon-10 is assigned to 26.2 ppm; it is deshielded relative to cancentrine because of the removal of the γ steric interaction with the NCH_3. The chemical shift equivalence of C-16 and the $N(CH_3)_2$ group was confirmed by examination of the off-resonance spectrum in which the methylene triplet of C-16 was centered in the methyl quartet. The off-resonance spectrum also enabled the peak at 61.5 ppm to be assigned to the C-20 methoxy group. This assignment is consistent with other systems containing a sterically crowded methoxy group (11, 12). Carbon-32 could be only tentatively assigned to the signal at 55.8 ppm because of the overlap of its splitting pattern with those of the methoxy carbons in the off-resonance spectrum. By the technique of selective enhancement of quaternary carbons the signal at 56.4 ppm was assigned to C-13.

Using the procedures described in the analysis of the aromatic region of the cancentrine spectrum, the corresponding aromatic carbon atoms of the morphine part of **1***c* were readily assigned. Similarly in the cularine portion of **1***c* the carbon atoms of the ring containing the single methoxy substituent at C-19 remain essentially unchanged relative to **1***a* except for C-19 itself which is deshielded. The conversion of the hydroxy group at C-20 to a methoxy shifted the peak at 138.0 ppm in the spectrum of **1***a* to 147.8 ppm in **1***c*. There was also a deshielding of the resonance for C-23 which now appears at 121.1 ppm. The signals at 151.2 and 152.3 ppm can be assigned either to C-21 or C-19; these signals were more intense than the signals of the other carbons of the cularine portion of the molecule bearing oxygen substituents because of the dipolar relaxation provided by the neighbouring protons on carbons 22 and 18, respectively.

The new cancentrine alkaloid, 10-oxocancentrine has the following spectral properties. Its 220 MHz ^1H nmr spectrum differs from that of cancentrine in several respects. There are no signals at 2.37 and 3.18 ppm corresponding to the 10α and 10β protons, respectively, in cancentrine (2) (Table 3) and there is also a simplification of the multiplet splitting for the C-9 proton now appearing at 3.39 ppm. The aromatic region of the ^1H spectrum of cancentrine (**1***a*) contains three pairs of AB quartets whose chemical shift assignments were determined by both nOe experiments and acetylation shifts (2, 10). In

TABLE 3. 220 MHz ^1H chemical shifts and coupling constants for cancentrine (**1***a*) and 10-oxocancentrine

Proton	**1***a*	**1***b*
H-5	4.88	4.84
H-9	3.41	3.39
H-10α	2.37	
H-10β	3.18	
3-OCH_3	3.97	4.02
19-OCH_3	3.93	3.98
21-OCH_3	3.86	3.85
H-1	6.65	7.45
H-2	6.86	7.00
H-17	6.97	7.03
H-18	7.04	7.09
H-22	6.70	6.67
H-23	7.49	7.49
N-CH_3	2.50	2.53
$J_{10\alpha,10\beta}$	18.5	
$J_{1,2}$	8.8	8.7
$J_{17,18}$	8.5	8.7
$J_{22,23}$	8.4	8.6

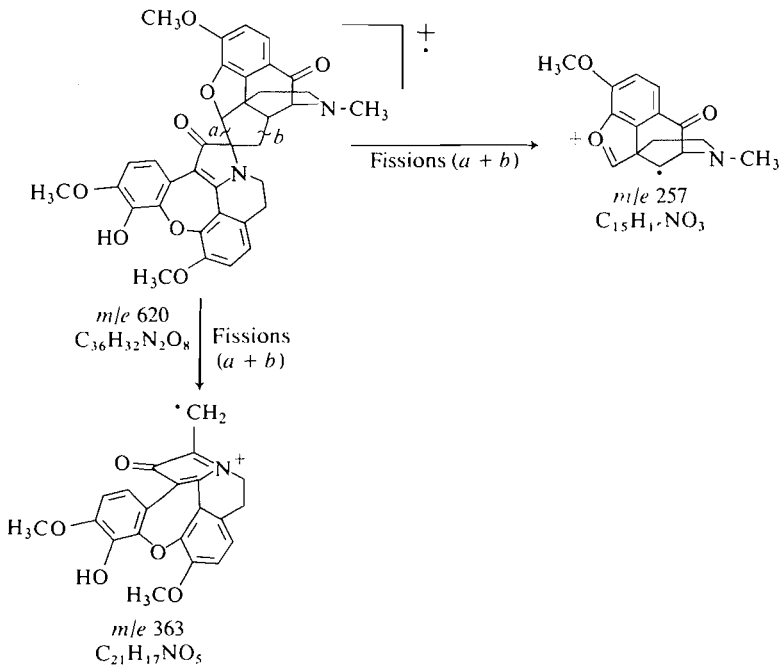

FIG. 3. Fragmentation of 10-oxocancentrine.

cancentrine the two high-field aromatic doublets at 6.65 (J = 8.8 Hz) and 6.70 ppm (J = 8.4 Hz) were assigned to H-1 and H-22, respectively. The spectrum of 10-oxocancentrine (**1***b*) has only one doublet at 6.67 ppm (J = 8.6 Hz) and a doublet centered at 7.45 ppm (J = 8.7 Hz). This new low-field doublet is attributed to H-1 because it is now deshielded by the carbonyl group considered to be situated at C-10. The remaining aromatic resonances of **1***b* show the same spectral pattern as cancentrine except for a slight deshielding (Table 3).

The mass spectrum of **1***b* shows a molecular ion at *m/e* 620 with a composition of $C_{36}H_{32}N_2O_8$. This ion loses CH_3 (*m/e* 605, $C_{35}H_{29}N_2O_8$) and OH (*m/e* 603, $C_{36}H_{31}N_2O_7$). Peaks which provided important structural information occurred at *m/e* 257 and 363 with compositions $C_{15}H_{15}NO_3$ and $C_{21}H_{17}NO_5$, respectively. These fragments in analogy with the mass spectrum of cancentrine (10), are considered to correspond to the morphine (*m/e* 257) and cularine (*m/e* 363) portions of the molecule and result from a fission of the bonds marked *a* and *b* in Fig. 3. Cancentrine undergoes an identical fragmentation to produce ions at *m/e* 243 ($C_{15}H_{17}NO_2$) and *m/e* 363 ($C_{21}H_{17}NO_5$). This difference of 14 mass units in the morphine fragment can be accounted for by the presence of the carbonyl oxygen, replacing the methylene at C-10 of cancentrine.

The ir spectrum was similar to that of the other cancentrine alkaloids (2, 3, 10) showing a phenolic OH stretching at 3450 cm^{-1} and a carbonyl absorption at 1668 cm^{-1}. The single absorption at 1668 cm^{-1} was at first misleading but is not surprising in view of the structure subsequently deduced. Since the ^1H nmr and mass spectral data clearly show a change in functionality only at C-10, structure **1***b* was considered for 10-oxocancentrine.

Further evidence in support of structure **1***b* was gained from a study of its ^{13}C nmr spectrum. The spectrum of the model compound 10-oxocodeinone (**2***c*) was recorded for comparison. The chemical shift assignments of **2***c* were made by comparison to the published spectrum of codeinone (**2***b*) (4). The new carbonyl signal of **2***c* appears at 190.4 ppm indicative of a conjugative interaction with the aromatic ring and this is substantiated by both the ir carbonyl absorption of 1675 cm^{-1} and a deshielding of carbons 3 and 12. The only aliphatic carbons that show a significant change relative to **2***b* are C-9 and C-14 which are deshielded as a result of the α and β substituent effects of the C-10 carbonyl group.

Examination of the aliphatic region of the ^{13}C spectrum of **1***b* showed the absence of a signal at 20.4 ppm corresponding to that of C-10 in cancentrine. There was also a deshielding of the C-9 resonance at 58.8 ppm in cancentrine to 68.0 ppm in **1***b*. The other aliphatic carbons of 10-oxocancentrine are essentially unchanged relative to cancentrine except for a deshielding of C-14 to 48.9 ppm. The deshielding of carbons 9 and 14 is similar in magni-

Can. J. Chem. Downloaded from www.nrcresearchpress.com by 210.87.254.42 on 09/05/12
For personal use only.

Can. J. Chem. Downloaded from www.nrcresearchpress.com by 210.87.254.42 on 09/05/12
For personal use only.

tude to that experienced by the corresponding carbons in **2***c*. These results correlate with the proton data in locating the carbonyl at C-10.

Because of the limited quantities of material the microprobe spectrum of 10-oxocancentrine had a relatively low signal-to-noise ratio for the substituted aromatic carbons and as a result only tentative assignments were made. At the low-field end of the spectrum a pair of signals of approximately equal intensity appear at 193.2 and 196.3 ppm. Since the peak at 193.2 ppm correlates with the chemical shift of C-7 in **1***a* and **1***c*, the other signal at 196.3 ppm was assigned to C-10 even though it is deshielded relative to C-10 in the model **2***c*.

The aromatic carbon chemical shifts for the cularine portion of 10-oxocancentrine were assigned by comparison to **1***a*. The shifts for the codeine substituted aromatic carbons could not be accurately determined but are expected to show a trend similar to those of **2***c* because of the effect of the C-10 carbonyl group.

These studies support the proposed structure **1***b* for 10-oxocancentrine.

Experimental

Apparatus, Methods, and Materials

Natural abundance ^{13}C nuclear magnetic resonance spectra with the exception of **1***b* were recorded on a Bruker WH-90 Fourier transform spectrometer at 22.62 MHz and a probe temperature of +35.0°C. Samples were 0.08–0.15 *M* in $CDCl_3$; TMS was used as an internal reference. Field/frequency locking was provided by the deuterium signal of $CDCl_3$. Spectra were recorded over a 5.0 KHz sweep width in an acquisition time of 1.638 s and using 16 K data points. A 3.7 μs pulse (17° pulse angle) was used. The spectra of **1***a* and **1***c* were obtained in 40 000 transients whereas that of **2***c* required only 3000 scans.

The 220 MHz ^1H magnetic resonance spectra were obtained at the Canadian 220 MHz Centre, University of Toronto, Toronto, Ontario. $CDCl_3$ and TMS were again used as solvent and internal reference, respectively.

Mass spectra were determined on a C.E.C. 21-110B mass spectrometer at an ionizing voltage of 80 eV and a source temperature of 200–250°C. For high resolution work spectra were recorded on plates and accurate mass measurements were made using perfluorokerosene as a marker (13). The composition of all ions discussed in this paper have been checked by high resolution mass spectrometry and agree with calculated values within ±0.005 amu. Infrared spectra were obtained on a Perkin-Elmer 283 spectrometer. A GCA/McPherson Instrument Model 707D spectrometer was used for the uv spectra.

Cancentrine (**1***a*) (1, 3) and 9,10-dihydrocancentrine methine-*O*-methyl ether (**1***c*) (10) have been described previously and 10-oxocodeinone **2***c* (14) was prepared as described below.

10-Oxocancentrine

The isolation and purification of 10-oxocancentrine followed the procedures developed for cancentrine **1***a* (1, 10). In the column chromatograph of the crude mixture of cancentrine alkaloids (silica gel, benzene–acetone–methanol 80:15:5) 10-oxocancentrine is eluted about twice as fast as cancentrine. The compound has the following properties: uv: λ_{max}(EtOH): 268, 284 (sh), 324 (sh), and 436 nm; log ε_{max}: 3.35, 3.34, 2.90, and 2.65, respectively; ir λ_{max}($CHCl_3$): 3450 and 1668 cm^{-1}; ^1H nmr δ: 1.8–3.7 (12H, aliphatic protons), 2.53 (s, 3H, N—CH_3), 3.85 (s, 3H, OCH_3), 3.98 (s, 3H, OCH_3), 4.02 (s, 3H, OCH_3), 4.84 (s, 1H, C—5H), 6.5–7.6 (m, 6H, aromatic protons (assignments given in Table 3)). The molecular formula was established by high resolution mass spectrometry. Calcd. for $C_{36}H_{32}N_2O_8$: 620.216; found: 620.216.

10-Oxocodeinone

A solution of 10-hydroxycodeine (0.5 g) (prepared from codeine phosphate by the procedure of Rapoport and Stevenson (14)) in acetone (50 ml) was cooled to 0°C and then 1.5 ml of standard Jones' reagent was added over 5 min. After stirring for a further 5 min at 0°C, the solution was poured onto 2 *N* $NaHCO_3$ solution (200 ml) and the resulting solution extracted with ether (5 × 75 ml). The ether extract was then dried and evaporated to yield crude 10-oxocodeinone (0.21 g). Recrystallization from anhydrous ether gave a sample melting at 175–178°C. The compound **2***c* had the following properties: uv λ_{max}(EtOH): 237, 287, and 324 (sh) nm; log ε_{max}: 3.25, 3.05, and 2.67, respectively; ir λ_{max} ($CHCl_3$): 1675 and 1620 cm^{-1}; ^1H nmr δ: 2.0–3.5 (6H, aliphatic protons), 2.46 (s, 3H, NCH_3), 3.97 (s, 3H, OCH_3), 4.75 (s, 1H, C—5H), 6.12 and 6.67 (m, 2H, olefinic protons), 6.82 and 7.40 AB (q, J = 8.0 Hz, 2H, aromatic protons). The molecular formula, $C_{18}H_{17}NO_4$, was confirmed by high resolution mass spectrometry.

Acknowledgments

We thank Dr. K. Nakanishi of Columbia University for recording the ^{13}C spectrum of 10-oxocancentrine and the National Research Council of Canada for financial support.

1. R. H. F. Manske. Can. J. Res. B, **7**, 258 (1932).
2. G. R. Clark, R. H. F. Manske, G. J. Palenik, R. Rodrigo, D. B. MacLean, L. Baczynskyj, D. E. F. Gracey, and J. K. Saunders. J. Am. Chem. Soc. **92**, 4998 (1970).
3. D. B. MacLean, L. Baczynskyj, R. Rodrigo, and R. H. F. Manske. Can. J. Chem. **50**, 862 (1972).
4. Y. Terui, K. Tori, S. Maeda, and Y. K. Sawa. Tetrahedron Lett. 2853 (1975).
5. E. Wenkert, B. L. Buckwalter, R. R. Burfitt, M. J. Gasic, H. E. Gottlieb, E. W. Hagaman, F. M. Schell, and P. M. Wovkulick. *In* Topics in carbon-13 nmr spectroscopy. Vol. 2. *Edited by* G. C. Levy. Wiley-Interscience, New York, NY. 1976.
6. I. H. Sadler. J. Chem. Soc. Chem. Commun. 809 (1973).
7. F. W. Wehrli. *In* Topics in carbon-13 nmr spectroscopy. Vol. 2. *Edited by* G. C. Levy. Wiley-Interscience, New York, NY. 1976. p. 343.
8. J. B. Stothers. Carbon-13 nmr spectroscopy. Academic Press, New York, NY. 1972.
9. F. W. Wehrli and T. Wirthlin. Interpretation of carbon-13 nmr spectra. Heyden, London. 1976.
10. R. Rodrigo, R. H. F. Manske, D. B. MacLean, L. Baczynskyj, and J. K. Saunders. Can. J. Chem. **50**, 853 (1972).
11. D. W. Hughes, H. L. Holland, and D. B. MacLean. Can. J. Chem. **54**, 2252 (1976).
12. D. W. Hughes, B. C. Nalliah, H. L. Holland, and D. B. MacLean. Can. J. Chem. **55**, 3304 (1977).
13. K. Biemann. Pure Appl. Chem. **9**, 95 (1964).
14. L. H. Rapoport and G. W. Stevenson. J. Am. Chem. Soc. **76**, 1796 (1954).
15. R. Rodrigo, R. H. F. Manske, D. B. MacLean, and L. Baczynskyj. Can. J. Chem. **50**, 3900 (1972).

Heats and free energies of mixing of tridodecylamine with nine heptane isomers, two octanes, and one hexane. Disorder and steric hindrance contributions

MICHÈLE COUCHON, PHUONG NGUYEN HONG, AND GENEVIEVE DELMAS[1]

Département de chimie, Université du Québec à Montréal, Montréal (Qué.), Canada H3C 3P8

Received April 17, 1978

MICHÈLE COUCHON, PHUONG NGUYEN HONG, and GENEVIEVE DELMAS. Can. J. Chem. **56**, 2472 (1978).

Heats and free energies of mixing have been measured at 298 K for tridodecylamine in n-C_7 and eight branched isomers, n-C_8 and one branched isomer, and a branched hexane. Heats of mixing are such that these systems can be divided in three classes. Class A ($H^E \simeq 90$ J/mol) includes n-C_7 and n-C_8. Class B ($H^E \simeq 295$ J/mol) includes isomers which do not have two substituents on neighbouring carbon atoms, i.e. 2-MeC_6 2,2-diMeC_5, 2,4-diMeC_5, 2,2,4-triMeC_5. Class C which includes isomers having substituents on neighbouring carbon atoms; 2,3-diMeC_5, 2,2,3-triMeC_4, 3-MeC_6, 3,3-diMeC_5, 3-EtC_5, has smaller values of heats of mixing ($H^E \simeq 160$ J/mol). These results are interpreted as not showing an extensive destruction of the correlations of orientations of the dodecyl chains by the linear alkanes of class A. The larger heats of class B are indicative of more disorientations of the long chains by the globular isomers. The smaller values of the heats for class C are seen as the balance of a positive disordering contribution and a negative one. The negative contribution is associated with a sterically hindered character of the compounds having substituents on neighbouring atoms. Free energies of mixing do not separate in the same three classes. This is thought to be due to an enthalpy–entropy compensation in the disordering and steric hindrance contributions. The $X_{12}s_1^{-1}$ parameter of the Flory theory shows the same variation as H^E.

MICHÈLE COUCHON, PHUONG NGUYEN HONG et GENEVIEVE DELMAS. Can. J. Chem. **56**, 2472 (1978).

Nous avons mesuré des chaleurs et énergies libres de mélange à 298 K de la tridodecylamine dans n-C_7 et huit isomères ramifiés, n-C_8 et un isomère ramifié et un hexane ramifié. Les chaleurs de mélange sont telles qu'on peut séparer ces systèmes en trois classes: la classe A ($H^E \simeq 90$ J/mol) comprend n-C_7 et n-C_8. La classe B ($H^E \simeq 295$ J/mol) comprend les isomères ramifiés qui n'ont pas deux substituants sur deux atomes de carbone voisins, i.e. 2-MeC_6, 2,2-diMeC_5, 2,4-diMeC_5, 2,2,4-triMeC_5. La classe C qui comprend les isomères portant des substituants sur des atomes de carbone voisins 2,3-diMeC_5, 2,2,3-triMeC_4, 3-MeC_6, 3,3-diMeC_5, 3-EtC_5 a des chaleurs plus petites ($H^E \simeq 160$ J/mol). Ces résultats sont interprétés comme indiquant une destruction faible des corrélations d'orientations des chaines de la dodecylamine par les alcanes linéaires de la classe A. La destruction de ces corrélations semble bien plus complète par les composés plus globulaires de la classe B. La diminution de H^E pour la classe C serait due à la compensation partielle de deux effets de signe contraire: la chaleur due à la destruction de l'ordre et une contribution négative dite d'empêchement stérique caractéristique des composés substitués plusieurs fois sur le même carbone ou sur des carbones voisins. Les énergies libres de mélange ne se divisent pas apparemment en les mêmes trois classes. Nous pensons que ceci est dû à une compensation entre les contributions enthalpiques et entropiques venant de l'effet de désordre et de celui d'empêchement stérique. Les valeurs calculées du paramètre $X_{12}s_1^{-1}$ de la théorie de Flory varient dans le même sens que les chaleurs.

Heats of mixing of non-polar systems depend on the energy of unlike contacts in relation to that of like contacts. This first contribution H^E(chem) is positive and has been recognized (1). It can be predicted in some cases by current theories based on the analysis of heats of group interactions (2). The second contribution H^E(f.v.) is negative and comes from the difference in degree of thermal expansion or free volume of the two components. H^E(f.v.) can be calculated by the Prigogine–Patterson–Flory theory (3) using an equation of state for the liquids and the solution. Since in non-polar systems, in particular compounds made of CH_3 and CH_2 groups, the difference in cohesive energy between the components is not large, it is quite possible that the negative free volume contribution is larger than the positive H^E(chem) so that the experimental heat is negative. This is indeed the case for mixtures of branched alkanes such as 2,3-dimethylbutane and heptamethylnonane whose H^E(exp.) is equal to -55 J/mol (4). However, when a branched alkane is mixed with a long linear alkane, the heats are always positive, indicating that another positive term has changed the balance of the two cited contributions. An example of such a system is 2,3-dimethylbutane + n-hexadecane for which the H^E(exp.) is equal to 232 J/mol (4).

[1]To whom all correspondance should be addressed.

Can. J. Chem. Downloaded from www.nrcresearchpress.com by 210.87.254.40 on 09/05/12
For personal use only.

Can. J. Chem. Downloaded from www.nrcresearchpress.com by 210.87.254.40 on 09/05/12
For personal use only.

Systematic work on mixtures of globular molecules (SnR_4 (5), NR_3 (22), dibromoethane (6), branched alkanes) with long chain compounds (alkanes, SnR_4, NR_3, alcohol, or halides (10)) has shown positive heat of mixing as a general result. Patterson and coworkers (8) and Turrell and Delmas (9) while studying thermodynamical results and Bothorel (8, 11) while making Rayleigh scattering observations on alkanes and on alkane solutions have made the hypothesis of the existence of order or correlations of orientations in long-chain alkanes of long chain derivatives. Since interactions between aligned chains are energetically more favorable than between randomly oriented chains, an ordered liquid becomes thermodynamically more stable than a non-ordered one. The mixing of an ordered liquid with a non-ordered one destroys the correlations of orientations of the ordered liquid. This destruction of order is accompanied by a positive contribution to the heat of mixing, H^E(dis.). One CH_3 group placed in the middle of the chain significantly prevents the orientations of the chain in the pure liquid. The importance of this effect on the heats can be seen in the following two systems: the heat of mixing of 2,3-dimethylbutane with n-C_{16} is 232 J/mol while it is only 79 J/mol with the 6-methylpentadecane (8*a*). Globular isotropic molecules do not have orientational order.

This third contribution to the heat of mixing does not exist in mixtures of non-ordered globular molecules, it exists in much smaller significance in mixtures of two ordered liquids because of the fitting together of the chains of the two different components (7). Analysis of the heat of mixing of chain-like ordered compounds with globular molecules has shown that the heat of disordering (*a*) in most cases does not depend on the order-breaker used in the mixture, (*b*) increases linearly with the chain length of the chain-like compound (9), (*c*) is quite similar in the SnR_4 or NR_3 compounds having the same chain length but is smaller in alkanes of the same chain length (22), (*d*) is the main contribution to the experimental heat of mixing in many non-polar mixtures of an ordered and non-ordered compound, (*e*) is measurable on mixtures having large heat of mixing as those involving long-chain alcohols or chlorinated compounds (10). The aim of this paper is to investigate another contribution to the heat of mixing, the steric hindrance contribution which will be described in the following paragraph.

H^E(dis.) is found almost independant of the order-breakers but very significant exceptions have been found where H^E(dis.) is much smaller than expected. The order-breaker involved in these cases is either a branched alkane or a tetraalkyl tin derivative or a trialkylamine. For the branched alkane, the effect is larger when the methyl or ethyl substituents on the chain are on the same carbon atom or on neighbouring carbon atoms. For the tin derivatives the effect appears to exist mainly for the propyl and ethyl derivatives (5).

Other investigations made on the heats of mixing of *n*-hexadecane with 21 branched nonanes (8*b*) and mixtures involving tetralkyl or trialkylderivatives (22) have shown that the effect occurs in different systems. To interpret these smaller heats it was assumed that another negative contribution to the heats was present when one of the components of the mixture was sterically hindered. The sign of this contribution is quite unusual for non-polar systems. Its molecular origin is not clearly identified but its sign corresponds to a better packing of the unlike molecules in solution than of the like molecules in the pure liquids. It could also be due to a loss of mobility either of the sterically hindered compounds or of the second component or of both in the solution. This contribution has been called condensation contribution (8*a*) or recently steric hindrance contribution (5). In a later work (22), the magnitude of the steric hindrance contribution has been estimated and found to be, for a given sterically hindered compound, proportional to the volume of the second component. This fourth contribution to the heats, H^E(ster. hind.) can occur in systems where there is no disordering contribution so that the total experimental heat will be negative. A few examples have indeed been found in which the free volume contribution (being negligible) cannot be the origin of the negative experimental heats of mixing. Two remarkable examples can be given: one with a branched alkane 3,3-diethylpentane and the other with tetrapropyl tin as sterically hindered components. The heat of mixing for 3,3-diethylpentane + n-C_8 and tetrapropyltin + heptamethylnonane[2] are respectively -82 (12) and -83 J/mol. As the other contribution in H^E(chem.), H^E(f.v.), H^E(dis.) are not important in these systems, it is likely that the main contribution to the experimental heats is H^E(ster. hind.).

In this work, the steric hindrance contribution to the heat of mixing and free energies will be investigated. A series of branched heptanes was chosen because the different isomers were likely to have different degrees of steric hindrance and also because their vapour pressure at 298 K was high enough for vapour pressure measurements. The second component tridodecylamine was chosen because the steric hindrance effect is known to occur with long-chain compounds and also because its vapour pressure at 298 K is negligible.

The present work gives the values of H^E and G^E

TABLE 1. Parameters for the pure compounds

Compounds	Experimental $d_{25°C}$[a] (g cm^{-3})	Experimental $10^3\alpha_{25°C}$[a] (K^{-1})	Experimental $\gamma_{20°C}$[b] (J cm^{-3} K^{-1})	Calculated V^* (cm^3 mol^{-1})	Calculated P^* (J cm^{-3})	Calculated $s = s/v$ (Å^{-1})
$NDodec_3$	0.82115[c]	0.787[c]	1.104[c]	528.73	475[c]	0.83[c]
n-C_7	0.67951	1.252	0.879	113.70	430	1.01
2,2-Dimethyl C_5	0.66953	1.294	0.790	114.68	394	1.03
2-Methyl C_6	0.67439	1.241	0.821	114.68	416	1.04
2,4-Dimethyl C_5	0.66832	1.312	0.810	114.60	407	1.04
3-Methyl C_6	0.68295	1.224	0.856	113.57	418	1.04
3-Ethyl C_5	0.69395	1.220	0.888	112.90	434	1.00
2,2,3-Trimethyl C_4	0.68588	1.236	0.807	112.89	396	1.04
3,3-Dimethyl C_5	0.68908	1.218	0.835	112.67	415	1.04
2,3-Dimethyl C_5	0.69091	1.209	0.855	112.51	428	1.04
2,3-Dimethyl C_4	0.65702	1.411	—	98.90	379	0.88
2,2,4-Trimethyl C_5	0.68777	1.208	0.798	128.87	389	0.81
n-C_8	0.69849	1.155	0.902	127.90	437	0.99

[a]Reference 18 *a*, *b*.
[b]From compressibilities (18*c*) or directly (18*b*).
[c]Reference 17.

at 298 K of tridodecylamine with the following twelve compounds as second component: (*a*) n-C_7 and eight branched heptanes 2,2-diMeC_5, 2-MeC_6, 2,4-diMeC_5, 2,2,3-triMeC_4, 3-MeC_6, 3-EtC_5, 3,3-diMeC_5, 2,3-diMeC_5, (*b*) one branched hexane 2,3-diMeC_4, (*c*) n-C_8 and one branched octane 2,2,4-triMeC_5. The name tridodecylamine is shortened in the paper to $NDodec_3$.

Experimental

Calorimetry

The heat of mixing was measured with a tilting Tian-Calvet calorimeter. Details of the instrument, the cells, and the calibration can be found in ref. 9. Agreement was better than 2% with the reference system benzene + carbon tetrachloride (13). For each system five to eight runs were made to obtain the maximum and the concentration dependance of the heat of mixing.

Vapour Pressure Measurements

The vapour sorption method was used for the determination of activity coefficients and Gibbs free energy data and hence excess entropies. The vacuum microbalance system was essentially the same as that described by Peterson and Martire (14) or Barbe and Patterson (15). The Setaram (Lyon, France model MTB 10-8) electrobalance was incorporated in a vacuum line for accurate weight determination. The mole fraction of the liquid mixture was then calculated from the increase in weight (measured within ±0.01 mg) of the sample upon introduction of a vapour solute into the system. The pressure of the system was measured with a mercury manometer (±0.08 mm) and corrections were made for the standard conditions of temperature and density of mercury at 0°C as well as for the scale calibration temperature of brass. The sample temperature set at 298 K was measured with a quartz thermometer (model 2801A, Hewlett–Packard Co.) and thermostatted with circulating water within ±0.02 K. Solvents and samples were degassed before each run and equilibrium of the mixing process was achieved when the weight change measured on the Setaram recorder became negligible. Ten to fifteen concentrations were made for each system with the reference system n-C_6 + n-C_{16}; our points agree to within 4% of the published value (16).

Chemicals

Tridodecylamine comes from the same source as in previous work (1, 2), namely, the Eastmann Company. The heptanes come from the Chemical Samples Co. They were distilled in the vacuum system.

Parameters for the Pure Components

The density, expansion coefficient, and thermal pressure coefficient of tridodecylamine were obtained from the previous work (17). The same data on the branched heptanes were obtained from literature (18). Table 1 gives d, α, γ, and the reduced parameter for the volume (V^*) and for the pressure (P^*) calculated with the van der Waals equation of state. The surface-to-volume ratios used in the Flory theory to characterize the shape of the molecules have been calculated as is usually done for the alkanes (3*c*) and are presented in Table 1. In the case of compounds with several methyl or ethyl substituents, a more detailed model with several cylinders rather than one as in the linear alkanes was used. However, the surface-to-volume ratios were not found to be very significantly different. The $X_{12}s_1^{-1}$ parameter calculated below is, in any case, hardly dependant on the surface-to-volume ratio parameter.

Calculation of the Free Volume Contribution

Enthalpy

We have chosen to apply the approximate form (4, 8*a*) of the Prigogine theory which separates the interactional and free volume contributions. H^E(f.v.) is given by eq. [1]

$$[1]\quad H^E(\text{f.v.})/(x_1U_1^* + x_2U_2^*) = \tilde{C}_p(\tilde{T}_U)[\psi_1\tilde{T}_1 + \psi_2\tilde{T}_2 - \tilde{T}_U]$$

Here $\tilde{T}_U$ is an average reduced temperature for the solution appropriate to the energy, U, and is defined by

$$[2]\quad \tilde{U}(\tilde{T}_U) = \psi_1\tilde{U}(\tilde{T}_1) + \psi_2\tilde{U}(\tilde{T}_2)$$

The reducing parameter for the energy U^* ($\tilde{U} = U/U^*$) can be obtained from experimental data since $U^* = P^*V^*$. In the van der Waals model used by Flory $\tilde{U} = -1/\tilde{v}$ so that eq. [2] becomes $1/\tilde{v}_U = \psi_1/\tilde{v}_1 + \psi_2/\tilde{v}_2$. The ψ's are energy fractions, i.e. $\psi_1 = x_1U_1^*/(x_1U_1^* + x_2U_2^*)$. The reduced volume of the

Can. J. Chem. Downloaded from www.nrcresearchpress.com by 210.87.254.40 on 09/05/12
For personal use only.

TABLE 2. Heats of mixing and experimental and calculated parameters for the systems $NDodec_3$ with n-C_7, n-C_8, and different branched heptanes, one branched octane, and two branched hexanes at 298 K

Class	$NDodec_3$ + (component 2)	No.[a]	H^E (max) (J mol^{-1})	x_1 (max)	A_0	A_1	A_2	H_v^E (max) (J cm^{-3})	H^E (f.v.) (J mol^{-1})	$X_{12}s_1^{-1}$ (J cm^{-3} Å)
A	n-C_7	1	90	0.575	355.43	117.79	−51.39	0.310	−83.8	3.45
	n-C_8	10	84	0.550	332.98	95.88	−95.27	0.273	−60.3	2.72
B	2,2-Dimethyl C_5	2	295	0.625	1114.33	572.61	72.20	1.093	−96.28	6.62
	2-Methyl C_6	3	290	0.625	1101.47	481.52	120.67	1.074	−83.76	7.05
	2,4-Dimethyl C_5	4	280	0.625	1059.05	538.02	100.27	1.037	−104.68	7.26
	2,2,4-Trimethyl C_5	11	316	0.625	1200.27	520.17	273.29	1.132	−67.78	7.93
C	3-Methyl C_6	5	166	0.650	618.24	272.55	350.50	0.641	−78.29	4.62
	3-Ethyl C_5	6	170	0.575	644.02	205.87	−2.67	0.588	−68.31	4.82
	2,2,3-Trimethyl C_4	7	180	0.600	667.82	461.16	−208.94	0.637	−78.56	4.82
	3,3-Dimethyl C_5	8	162	0.625	601.62	297.24	76.08	0.603	−74.34	4.52
	2,3-Dimethyl C_5	9	160	0.625	591.81	322.22	110.44	0.596	−73.30	4.46
	2,3-Dimethyl C_4	11	216	0.625	814.24	458.01	−21.75	0.830	−118.75	7.93

[a]Corresponding number on the graphs.

pure components are obtained from their expansion coefficients α and $\tilde{v}^{1/3} = [(4/3)\alpha T + 1]/(\alpha T + 1)$ and their reduced temperature $\tilde{T}_1$ and $\tilde{T}_2$ by $\tilde{T} = \tilde{v}^{-1}(1 - \tilde{v}^{-1/3})\tilde{C}_p(\tilde{T}_U)$ in eq. [1] is $[(4/3)\tilde{v}^{-1/3} - 1]^{-1}$. The interactional contribution expressed in terms of the Flory parameter X_{12} is obtained from the experimental heat and H^E(f.v.).

$$[3]\quad [H^L(\text{exp.}) - H^L(\text{f.v.})]/(x_1U_1^* + x_2U_2^*) = X_{12}\psi_1\frac{\theta_2}{P^*}f(\tilde{v}_U)$$

$f(\tilde{v}_U) = (4\tilde{v}_U - 3\tilde{v}_U^{4/3})^{-1}$ corresponds to $[-\tilde{U}(\tilde{T}_U) + \tilde{T}_U\tilde{C}_p(\tilde{T}_U)]$ in the Van der Waals model. Its value is not far from 1. θ_2 is a surface fraction defined by $x_2V_2^*s_2/(x_2V_2^*s_2 + x_1V_1^*s_1)$. The parameter $X_{12}s_1^{-1}$ has been tabulated instead of X_{12} because it does not depend on which compound has been chosen as the first component ($X_{12}s_1^{-1} = X_{21}s_2^{-1}$).

Entropy

The contribution to the entropy of mixing obtained from the difference in free volume is negative as the enthalpic contribution. It can be calculated in the same way as H^E(f.v.), from the expansion coefficients of the two components and a model:

$$[4]\quad TS^E(\text{f.v.})/(x_1U_1^* + x_2U_2^*) = [\tilde{S}(\tilde{T}_{TS}) + \tilde{C}_p(\tilde{T}_{TS})] \times [\psi_1\tilde{T}_1 + \psi_2\tilde{T}_2 - \tilde{T}_{TS}]$$

Here $\tilde{T}_{TS}$ is very close to $\tilde{T}_U$ defined by eq. [2] and is an average reduced temperature for the solution appropriate to the quantity $\tilde{T}\tilde{S}$ given by:

$$[5]\quad \tilde{T}_{TS}\tilde{S}(\tilde{T}_{TS}) = \psi_1\tilde{T}_1\tilde{S}(\tilde{T}_1) + \psi_2\tilde{T}_2\tilde{S}(\tilde{T}_2)$$

The reduced entropy $\tilde{S}$ is equal to 3 ln $(\tilde{v}^{1/3} - 1)$ in the Flory model.

Results and Discussion

Heat of Mixing

Table 2 summarizes the results of the heats for all the systems. The experimental heats H^E have been fitted to the equation

$$[6]\quad H^E = x_1x_2\sum_{i=0} A_i(x_1 - x_2)^i$$

where x is the mole fraction. The first two columns give the maximum value of the heat of mixing and the concentration at which the maximum occurs, the next six columns list the parameters of eq. [6], the heat per cm^3 H_v^E, the free volume contribution per mole obtained from eq. [1], and the $X_{12}s_1^{-1}$ parameter calculated from eq. [3]. H_v^E is H^E divided by the core volume of the solution ($x_1V_1^* + x_2V_2^*$).

The heat of mixing for the different systems will be discussed in terms of the different contributions such as H^E(chem.), H^E(f.v.), H^E(dis.), and H^E(ster. hind.). H^E(chem) should be small for all the systems because the components are made of the same groups; previous work on $NDodec_3$ having shown that trialkylamine behaves as a long alkane. H^E(f.v.) has about the same value for all the systems involving a heptane because the isomers have similar expansion coefficients. The differences between the experimental heats of mixing (and consequently the X_{12} parameter) are likely to be caused by different values of H^E(dis.) and H^E(ster. hind.) from one isomer to another. The systems can be divided into three classes. Class A is made of two systems: $NDodec_3$ with n-C_7 and n-C_8. The heats of mixing are smaller than that of the other systems because the heptyl and octyl chains are not disturbing too much the orientational order of the dodecyl chains so that H^E(dis.) is relatively small. It is to be noted that although Rayleigh scattering measurements on n-C_7 in the pure state indicate that it is not long enough to have extensive orientational order (11), it behaves in solution more as an ordered compound than an order breaker. Since the sterical hindrance contribution is not known to occur in systems containing long chain compounds and linear alkane it is assumed that, in class A, the steric hindrance contribution is not important. Class B is branched heptanes which do not have two methyl groups on neighbouring carbon atoms, i.e. 2-MeC_6, 2,4-diMeC_5, and 2,2-diMeC_5. The larger heats of

Can. J. Chem. Downloaded from www.nrcresearchpress.com by 210.87.254.40 on 09/05/12
For personal use only.

Can. J. Chem. Downloaded from www.nrcresearchpress.com by 210.87.254.40 on 09/05/12
For personal use only.

mixing are due to H^E(dis.) of $NDodec_3$. H_v^E(1.03–1.10 J/cm^3) compares well to the same quantities for mixtures of $NDodec_3$ with less volatile order breakers such as heptamethylnonane (1.12 J/cm^3) (1). The systems involving 2,2,4-triMeC_5 have been put in the same class because of the position of the groups and the consequently large heats although the value necessary for the comparison with a sterically hindered branched octane has not been measured. Class C composes of the other systems with smaller heats of mixing. It could be possible that these smaller heats are due to incomplete disordering of the dodecyl chains but it does not seem to be the case since Rayleigh scattering measurements on similar branched compounds, a series of branched nonanes, indicate the loss of orientational order of the second component even in solutions which have small heats of mixings (8). The values of the heats in relation to the position of the methyl groups indicate that the steric hindrance is larger when the methyl groups are either on neighbouring C atoms (2,3-diMeC_5 and 2,2,3-triMeC_4) or in the center of the molecule. Note the difference between 3,3-diMeC_5 and 2,2-di-MeC_5. The negative contribution to the heats of mixing seems to be more important when the groups borne by the substituted carbon atom are similar. The same feature gives a large sterically hindered character to the tetraalkyl compounds $SnPropyl_4$ and $SnEthyl_4$. The low unexpected value of the heats for 3-MeC_5 and 3-EtC_5 can perhaps be better understood if these compounds are written as

ethyl—CH—propyl
|
methyl

and $CH(ethyl)_3$ where the similarity of structure with the very sterically hindered compound $C(ethyl)_4$ (usually called 3,3-diethylpentane) is seen. The compounds 2,3-diMeC_4 is put in the sterically hindered compound class since its heat of mixing is about 60 J smaller than the heat of mixing obtained for 2,2-diMeC_4 (measured in this laboratory). The $X_{12}s_1^{-1}$ parameters obtained from eq. [3] reflect the same differences as the heats since their values in J/cm^3 Å^{-1} increase from the ordered systems (about 3) to the order-destroying systems (about 7.5) and decrease again for the sterically hindered compounds (4.6).

A macroscopic estimation of steric hindrance of a given compound is its molar volume, the more sterically hindered component having the smallest volume. Figure 1*a* shows a correlation between the heats and molar volume. Figure 1*b* shows the same correlation with $X_{12}s_1^{-1}$.

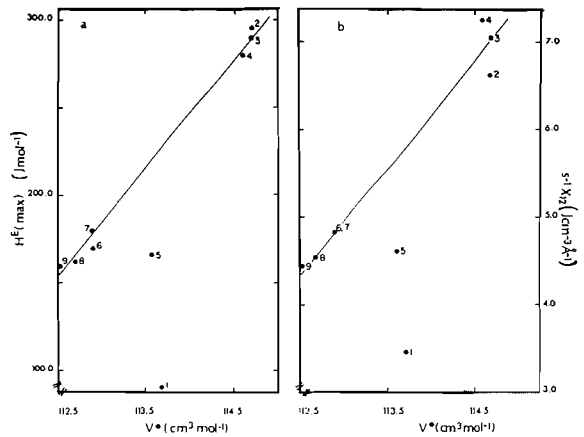

FIG. 1. (*a*) Heats of mixing in J/mol of tridodecylamine with nine heptane isomers vs. the core volume of the heptane. The compounds corresponding to the numbers are listed in Table 2. (*b*) The Flory parameter $X_{12}s_1^{-1}$ vs. the core volume of the heptane. The spread of the X_{12} values corresponds to the inequal magnitude of the disorder and steric hindrance contributions for the different isomers.

Estimation of the Steric Hindrance Contribution

The steric hindrance contribution to the heats can be estimated if one assumes that the system with the highest heat has no steric hindrance contribution and that the free volume and chemical contributions are the same for all the systems. For all the systems, H^E(ster. hind.) is assumed to be 150–280 = −130 J/mol. Similar arguments were used (1) to evaluate H^E(ster. hind.) with other sterically hindered compounds. It was found that for a given sterically hindered compound, H^E(ster. hind.) is proportional to the volume of the second component. The comparison of the values found now and previously indicates that the steric hindrance contribution of the branched heptanes is about the same as that found for $SnPropyl_4$ which is reasonable since the compounds have similar shapes.

Free Energies

The activity coefficient of the volatile component 1, corrected for vapour-phase non-ideality, is given by

$$[7] \quad \ln \gamma_1 = \ln \frac{p_1}{p_1^0 x_1} + \frac{(B_{11} - V_1^0)(p_1^0 - p)}{RT}$$

where p_1 and p_1^0 are the partial pressure and saturated vapour pressure of component 1, p is the equilibrium vapour pressure of the system equal in the present case to p_1, and B_{11} and V_1^0 are the second virial coefficient and liquid molar volume. Values of B_{11} at 25°C were obtained using the empirical correlation of O'Connell and Prausnitz (19). For systems of molecules with a large difference in volume, the

Can. J. Chem. Downloaded from www.nrcresearchpress.com by 210.87.254.40 on 09/05/12
For personal use only.

Flory–Huggins entropy of mixing is more appropriate than the regular solution expression.

$$[8] \qquad TS^E = RT(x_1 \ln \phi_1 + x_2 \ln \phi_2)$$

The change of the solvent chemical potential is related to the configurational entropy of mixing and to the parameter χ by the relation

$$[9] \quad \mu_1{}^E = RT\left[\ln \phi_1 + \left(1 - \frac{V_1^*}{V_2^*}\right)\phi_2 + \chi\phi_2{}^2\right]$$

ϕ_2 is usually the volume fraction. Here, according to Flory, the segment fraction defined as $\phi_1 = x_1V_1^*/(x_1V_1^* + x_2V_2^*)$ is used.

The excess chemical potential of the second component being:

$$\mu_2{}^E = RT\left[\ln \phi_2 - \left(\frac{V_2^*}{V_1^*} - 1\right)\phi_1 + \frac{V_2^*}{V_1^*}\chi\phi_2{}^2\right]$$

The molar free energy of mixing is obtained by

$$[10] \quad G^E = RT\left[x_1 \ln \phi_1 + x_2 \ln \phi_2 + \chi\phi_1\phi_2 \times \left(x_1 + \frac{V_2^*}{V_1}x_2\right)\right]$$

The residual free energy G^E is

$$[11] \qquad G^E(\phi) = RT\chi\phi_1\phi_2\left[x_1 + \frac{V_2^*}{V_1^*}x_2\right]$$

The different symbols $G^E(\phi)$ and $G^E(x)$ correspond respectively to the use of the configurational entropies in ϕ and x. In this work, values of the parameter χ were obtained from the experimental activity coefficients and eqs. [7] and [9]. The residual free energy of mixing is then calculated from eq. [11].

A more usual procedure for mixtures of components having similar size is to obtain G^E by fitting the activity of the volatile component to the following equation (16)

$$[12] \qquad \ln \gamma_1 = x_2{}^2[C_0 + C_1(3 - 4x_2)]$$

The coefficients in this equation come from the Redlich–Kister equation with two coefficients for G^E. The two different expressions for the combinatorial entropies of mixing are

$$[13] \quad G^E(x) = x_1x_2[C_0 + C_1(x_1 - x_2)]$$

$$[14] \quad G^E(\phi) = G^E(x) + [x_1 \ln \phi_1 + x_2 \ln \phi_2 - x_1 \ln x_1 - x_2 \ln x_2]$$

An alternative way to obtain $G^E(\phi)$ is to fit the experimental γ_1 to eq. [12], calculate $G^E(x)$ by eq. [13], and obtain $G^E(\phi)$ by eq. [14]. It has been found that if a sufficient number of points were taken on the $\ln \gamma_1$ vs. x curve in the region of high concentration of the non-volatile component, the values obtained either from eq. [14] or from eq. [11] for $G^E(\phi)$ agree within experimental error, i.e. 10–20 J/mol. If too few points are taken, the $G^E(\phi)$ obtained by eqs. [12]–[14] are higher by 30–40 J than those obtained directly from eq. [11].

Figure 2 gives an example of the variation of χ with the polymer segment fraction. Measurements have been taken between $\phi_2 = 0.95$ and $\phi_2 = 0.45$. The variation of χ does not seem to be regular enough to be ascribed to a concentration dependence so that the listed value of χ is the average value for all the measured concentration range. $G^E(\max)$ is then found for the maximum value of $\phi_1\phi_2(x_1 + (V_2^*/V_1^*)x_2)$. This quantity goes through a maximum for a volume fraction which is slightly dependent on V_2^*/V_1^*, i.e. $\phi(\max) = 0.675$ for the heptanes and octane and $\phi_2 = 0.70$ for 2,3-diMeC$_4$.

The maximum values of $G^E(\phi)$ are given at 25°C by the following relations:

$$[15] \quad G^E(\phi) = \chi M \text{ with}$$

$M = 1155$ J/mol for the heptanes
$M = 1110$ J/mol for the octanes
$M = 1202$ J/mol for 2,3-diMeC$_4$

The concentration dependance of G^E is given by eq. [11]. The maximum is at $\phi_2 = 0.675$ for the heptane systems which corresponds to $x_1 = 0.691$, a value which is not too different from the concentration of the maximum of H^E ($x_1 = 0.62$). The two first columns of Table 3 give, respectively, the χ parameter and the maximum of $G^E(\phi)$; $G^E(x)$ is lower by about 657 J/mol than $G^E(\phi)$ and is consequently negative. On Fig. 3 $G^E(\phi)$ have been plotted like H^E vs. the core volume of the heptanes. One can see that the neat trend of H^E vs. V^* is no longer apparent on G^E.

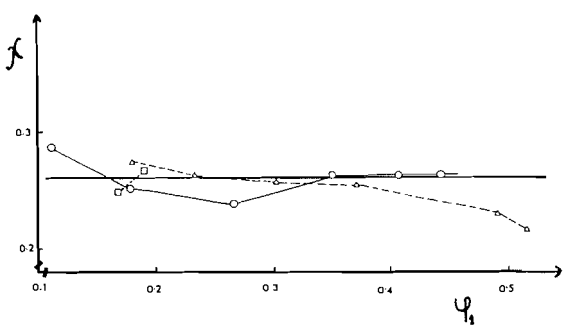

FIG. 2. Typical values of the χ parameter vs. the solvant segment fraction ϕ_1. The data correspond to 2-methyl C_6 and are calculated from eqs. [7] and [9]. □, △, ○ for three runs.

TABLE 3. $G^E(\phi)$ (exp), free volume contribution to the entropy and the non-free volume contributions to H^E and TS^E in J/mol at 25°C

Component + $NDodec_3$	Experimental χ	Experimental $G^E(\phi)^a$ (J/mol)	Experimental $TS^E(\phi)^b$ (J/mol)	Calculated TS^E(f.v.) (J/mol)	Calculated TS^E (dis. + ster. hind.) (J/mol)	Calculated H^E (dis. + ster. hind.) (J/mol)
n-C_7	0.27	312	−222	−264	42	174
2,2-Dimethyl C_5	0.30	347	−52	−289	237	391
2-Methyl C_6	0.26	300	−10	−251	236	374
2,4-Dimethyl C_5	0.33	382	−102	−313	211	385
3-Methyl C_6	0.26	300	−134	−235	101	244
3-Ethyl C_5	0.26	300	−130	−233	103	238
2,2,3-Trimethyl C_4	0.20	231	−51	−233	182	258
3,3-Dimethyl C_5	0.24	278	−116	−227	111	236
2,3-Dimethyl C_5	0.20	231	−71	−225	154	233
n-C_8	0.19	211	−127	−201	74	145
2,2,4-Trimethyl C_5	0.16	173	+143	−226	369	384
2,3-Dimethyl C_4	0.29	335	−119	−346	225	335

[a]The concentration dependance is given by eq. [11]. The concentration of the maximum is $\phi_2 = 0.675$ (or $x_1 = 0.691$) for the heptane systems, see text.
[b]Obtained by the difference between H^E(max) and $G^E(\phi)$(max).

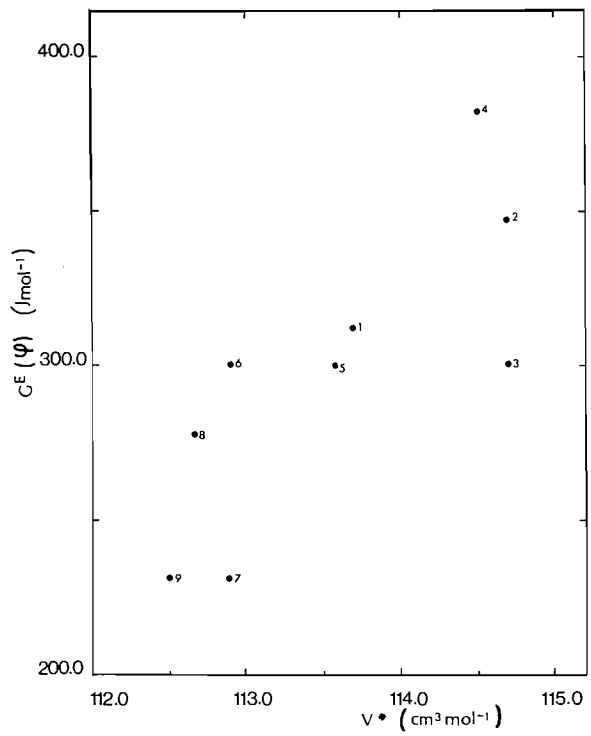

FIG. 3. Excess free energies $G^E(\phi)$ using the Flory–Huggins combinatorial entropy vs. the core volume of the heptane. The compounds corresponding to the numbers are listed in Table 2.

Indeed, five systems out of nine have the same value of G^E within experimental error, i.e. 295 ± 15 J/mol. This is interpreted as an indication of the compensation of the enthalpic and entropic contributions to a given effect. For example, n-C_7, 3-MeC_6, and 2-MeC_6 have the same value of G^E although the heats of mixing indicate the presence of a disordering contribution with 2-MeC_6, of a disordering and steric contribution with 3-MeC_6, and a much smaller contribution with n-C_7. It appears then that the disordering of the long dodecyl chains give a positive contribution to the entropy of mixing so that the net effect in G^E is not large. This result had also been found on the dibromoethane + n- (and branched) alkane systems (21). In the same way, the negative steric hindrance contribution to the heat of mixing in the 3-MeC_6 system must be balanced by a negative entropy term. The systems which have G^E values either larger or smaller than 295 J/mol have several methyl substituents along the chain. It is possible that for these systems, the difference comes from the configurational entropy which may be different from those of the less branched hydrocarbons. It is to be noted that the compensation entropy–enthalpy usually does not exist for the free volume effect which gives an overall positive contribution to G^E. This can be seen (Tables 2 and 3) on the calculated values of H^E(f.v.) and TS^E(f.v.). It is this positive free volume contribution that is the cause of the lower critical solubility temperature observed on systems made of molecules of large free volume differences.

Figure 4 shows the correlation between the part of the heat which is not due to the free volume, H^E(dis. + ster. hind.) and the corresponding entropy terms. H^E(dis. + ster. hind.) = H^E(exp. − H^E(f.v.)).

Interactional Contribution

The line drawn on Fig. 4 through the points corresponding to the different isomers does not extrapolate to zero. This may be due to a contribution coming from the small difference in force field in the the tridodecylamine and the alkanes (or H^E(chem)). From equation of state theories one can calculate

Can. J. Chem. Downloaded from www.nrcresearchpress.com by 210.87.254.40 on 09/05/12
For personal use only.

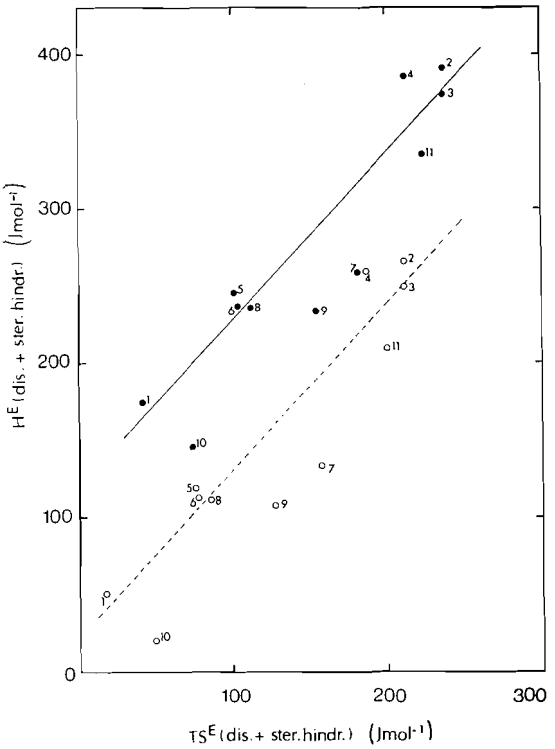

FIG. 4. Enthalpy–entropy compensation for the disorder and steric hindrance contributions. The extrapolated value H^E = 125 J/mol may correspond to H^E (interactional). Dotted line: same plot after subtracting H^E and TS^E (interactional). The compounds corresponding to the numbers are listed in Table 2.

the ratio of the interactional entropy to the interactional enthalpy. From eq. [20] of ref. 3*b*, one finds:

$$[16]\quad \frac{TS^E(\text{interaction})}{H^E(\text{interaction})} = \frac{\tilde{T}\tilde{C}p}{-\tilde{V} + \tilde{T}\tilde{C}p} = \frac{\alpha T}{1 + \alpha T}$$

The above expression in αT has been obtained by the use of the Flory model. Estimation of the interactional contribution to the heat of mixing is given by the extrapolated value of H^E when $TS^E = 0$ on Fig. 4 and the interactional contribution to TS^E is obtained from eq. [5]. With H^E(interaction) = 125 J/mol and $\alpha T = 0.23$ (an average between the αT for the two components)), TS^E(interaction) is found to be 25 J/mol. The dotted line in Fig. 4, obtained by shifting the coordinates of the points by 125 J/mol for H^E and 25 J/mol for TS^E, corresponds to the disorder and steric hindrance contributions for the series of isomers of the heptanes. The slope not too far from 1 indicates a fair compensation between the H^E and TS^E for the disorder and steric hindrance contributions.

One may wish that methods other than the thermodynamics may help to understand, on a molecular level, the difference in the solutions made with, for instance, the 2-Me and the 3-Me hexanes, difference visible by the heats of mixing but not by the free energies.

Acknowledgements

The research was supported by the France–Québec collaboration (M.C.), the Ministry of Education, and the National Research Council of Canada.

1. J. HILDEBRAND R. SCOTT. The solubility of non electrolytes. Dover. 1964. Chapt. VII.
2. J. P. E. GROLIER, K. SOSNKOWSKA-KEHIAIAN, AND H. V. KEHIAIAN. J. Chim. Phys. **70**, 367 (1973).
3. (*a*) I. PRIGOGINE. The molecular theory of solutions. North-Holland, Amsterdam. 1957; (*b*) D. PATTERSON and G. DELMAS. Discuss. Faraday Soc. **49**, 98 (1970); (*c*) P. J. FLORY, R. A. ORWOLL, and A. VRIJ. J. Am. Chem. Soc. **86**, 3507 (1964); **86**, 3515 (1964).
4. P. TANCRÈDE, L. V. LAM, P. PICKER, and D. PATTERSON. J. Chem. Soc. Faraday II, **70**, 1465 (1974).
5. G. DELMAS and NG. T. THANH. J. Phys. Chem. **81**, 1730 (1977).
6. G. DELMAS and P. PURVES. J. Chem. Soc. Faraday II, Part 1, **73**, 1828 (1977).
7. G. DELMAS and NG. T. THANH. J. Chem. Soc. Faraday I, **71**, 1172 (1975).
8. (*a*) P. TANCRÈDE, P. BOTHOREL, and D. PATERSON. J. Chem. Soc. Faraday II, **73**, 29 (1977); (*b*) P. TANCRÈDE, P. BOTHOREL, P. DE SAINT-ROMAIN, and D. PATTERSON. J. Chem. Soc. Faraday II, **73**, 15 (1977).
9. S. TURRELL and G. DELMAS. J. Chem. Soc. Faraday I, **70**, 572 (1974).
10. G. DELMAS and NG. T. THANH. J. Chim. Phys. **72**, 1285 (1975).
11. (*a*) P. BOTHOREL. J. Colloid Sci. **27**, 529 (1968); (*b*) P. BOTHOREL, C. CLEMENT, and P. MARAVAL. C.R. Acad. Sci. **264**, 568 (1967); (*c*) P. BOTHOREL and G. FOECHE. J. Chem. Soc. Faraday Trans. II, **69**, 411 (1973); (*d*) P. BOTHOREL, C. SUCH, and C. CLEMENT. J. Chim. Phys. **70**, 516 (1972); (*e*) H. QUINONES and P. BOTHOREL. C.R. Acad. Sci. **277**, 133 (1973).
12. (*a*) V. MATHOT. Bull. Soc. Chim. Belg. **59**, 111 (1950); (*b*) I. PRIGOGINE and V. MATHOT. J. Chem. Phys. **18**, 765 (1950).
13. K. N. MARCH. Int. Data Ser. A, **1**, 3 (1973).
14. H. T. PETERSON and D. E. MARTIRE. Mol. Cryst. Liq. Cryst. **25**, 89 (1974).
15. M. BARBE and D. PATTERSON. J. Phys. Chem. **82**, 40 (1978).
16. M. L. MCGLASHAN and A. G. WILLIAMSON. Trans. Faraday Soc. **57**, 588 (1961).
17. R. PHILIPPE, M. COUCHON, and G. DELMAS. Can. J. Chem. **56**, 370 (1978).
18. (*a*) R. R. DREISBACH. Physical properties of chemical compounds. Adv. Chem. Ser. Am. Chem. Soc. Washington, DC. 1959; (*b*) Selected values of physical and thermodynamic properties of hydrocarbons and related compounds. API Research Project 44. Carnegie Press, Pittsburgh, PA. 1953; (*c*) G. ALLEN, G. G. D. MANGARAJ, D. SIMS, and C. J. WILSON. Polymer, **1**. 456 (1960).
19. J. P. O'CONNELL and J. M. PRAUSNITZ. Ind. Eng. Chem. Process Des. Dev. **6**, 245 (1967).
20. H. TOMPA. Polymer solutions. Butterworths, London. 1956. Chapt. IV.
21. G. DELMAS and P. PURVES. J. Chem. Soc. Faraday II, Part II, **73**, 1838 (1977).
22. R. PHILIPPE, PHUONG NGUYEN HONG, and G. DELMAS. Can. J. Chem. In press.

Can. J. Chem. Downloaded from www.nrcresearchpress.com by 210.87.254.40 on 09/05/12
For personal use only.

Oxidative ozonolysis of a polyunsaturated fatty acid in BF_3–MeOH medium[1]

J.-L. SEBEDIO AND R. G. ACKMAN[2]

Fisheries and Marine Service, Department of Environment, Halifax Laboratory, Halifax, N.S., Canada B3J 2R3

Received November 15, 1977

J.-L. SEBEDIO and R. G. ACKMAN. Can. J. Chem. **56**, 2480 (1978).

The ozonolysis of the methyl ester of a typical naturally-occurring polyunsaturated acid (linoleic) in BF_3–MeOH medium was investigated. Referring only to difunctional products, yields of the principal reaction product, dimethyl azelate, were approximately 96%. The characteristic secondary product, the dimethyl ester of the acid with one less carbon, was formed only to the extent of 2% or less. Other intermediates and difunctional secondary products which have been identified include the C_9 methyl half-ester, half-aldehyde, and the corresponding dimethyl acetal. Dimethyl malonate was not recovered quantitatively under the conditions employed. Monofunctional products qualitatively and quantitatively duplicated the difunctional products.

J.-L. SEBEDIO et R. G. ACKMAN. Can. J. Chem. **56**, 2480 (1978)

L'ozonolyse de l'ester méthylique d'un acide gras polyinsaturé (linoleique) en milieu BF_3–MeOH donne des rendements de 96% en produit principal de la réaction, l'azélate de méthyle. Le produit secondaire généralement obtenu pour une réaction de ce type à savoir le diester à un carbone de moins n'excède pas 2% du produit principal. Les deux autres produits secondaires identifiés (2 à 3%) sont l'aldehyde-ester en C_9 et l'acétal correspondant. Les conditions expérimentales employeés pour cette reaction ne permettent pas de déterminer la quantité exacte de malonate de méthyle. Les produits monofonctionnels formés reflètent qualitativement et quantitativement les produits difonctionnels.

[Traduit par le journal]

Introduction

In a recent paper (1), it has been shown that the ozonolysis of monoethylenic fatty acids in BF_3–MeOH medium gives good yields ($\geq 98\%$) of the principal diacid product in the form of the dimethyl ester. This technique also restricted the quantity of secondary diester product (i.e., the ester shorter by one carbon) to 1 or at most 2%. A unique advantage of this method is the combining of all steps of the reactions 'in situ' so that the ester products are immediately suitable for recovery and gas–liquid chromatographic (glc) analysis.

To broaden the application of the BF_3–MeOH technique in the fatty acid field, and as an extension of the study of monoethylenic fatty acids, we have now examined the behaviour of a polyethylenic fatty acid. Linoleic (octadeca-9,12-dienoic) acid, an important naturally-occurring fatty acid, was selected for detailed study. Yields of principal dicarboxylic C_9 product ($\sim 96\%$) were as satisfactory as with oleic (octadeca-9-enoic) acid but unexpectedly small proportions of two unknown products were always present. These have been identified as the difunctional C_9 acid–aldehyde and corresponding acetal. The recovery of monofunctional (C_6) products and the two corresponding byproducts is discussed.

[1]Presented in part at the annual conference of the Chemical Institute of Canada, Montreal, May 29th–June 2nd, 1977.

[2]To whom all correspondence shall be addressed.

Results and Discussion

The ozonolysis of methyl linoleate in BF_3–MeOH was first evaluated under the same conditions employed previously (1) with recovery of the mixture of products by extraction with methylcyclohexane and analysis by isothermal glc on open-tubular wall-coated columns (Fig. 1). The products resulting from the oxidative scission of the ethylenic bonds and subsequent esterification should be methyl hexanoate, dimethyl malonate, and dimethyl azelate. The principal products observed (Fig. 1) did not include dimethyl malonate. Possibly there is direct C_3 decomposition during oxidative decomposition of the ozonide. It is also known that dimethyl malonate is susceptible to decomposition during glc analysis and has a low relative molar response in the flame ionization detector (2). However, the water-immiscible extractant employed was the hydrocarbon methylcyclohexane, in which dimethyl malonate was known to have limited solubility. For these reasons no attempt was made initially to investigate the fate of the malonate fragment. The methyl hexanoate is a borderline case for efficient extraction into a hydrocarbon solvent from an aqueous medium and is also volatile enough to be subject to probable losses during solvent removal. Since it was felt that any reaction affecting the C_9 scission fragment would be equally applicable to the C_6 scission fragment, the initial qualitative and quantitative evaluation was based on the percentage of dimethyl azelate (DMC_9)

Can. J. Chem. Downloaded from www.nrcresearchpress.com by 210.87.254.105 on 09/05/12
For personal use only.

Can. J. Chem. Downloaded from www.nrcresearchpress.com by 210.87.254.105 on 09/05/12
For personal use only.

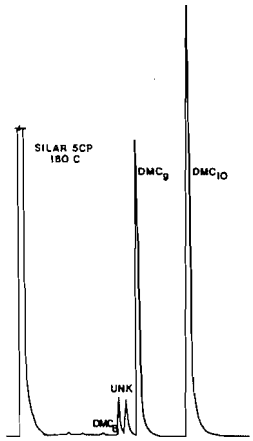

FIG. 1. Isothermal gas–liquid chromatographic analysis of products recovered from an evaluation of the reaction with DMC_{10} added as an internal standard.

formed. An internal standard of dimethyl sebacate (DMC_{10}) was employed and yield calculations were based on 9.7 and 8.7 as relative molar flame ionization responses for the C_{10} and C_9 dimethyl esters analysed on SILAR-5CP open-tubular columns (1). The initial yields of dimethyl azelate were 72% of theory, and in contrast to the results for the monoethylenic acid (1), the principal product was accompanied by two significant unknowns (total ~20%) which appeared to be materials potentially related to DMC_9. The anticipated secondary product, dimethyl suberate (DMC_8), was present (Fig. 1) in the same proportion (~1%) as observed previously. The two unknown products were selected for in-depth study to determine if they were intermediates from incomplete reaction or true secondary reaction products.

The initial study was of the effect of time of reaction at 100°C (Table 1), keeping constant the concentrations of methyl linoleate in BF_3–MeOH, the concentration of BF_3–MeOH employed (7%), and the time of exposure to ozone (1 min). All figures given are normalized to one set of glc-recorder/integrater counts for DMC_{10}. Two additional minor products (unknowns *1* and *2* in Table 1) were observed in early stages of the heating reaction but have not been further studied. They disappear and under the above conditions the other products in the reaction mixture were constant after 60 min. Up to that point, the yield of principal product (DMC_9) increased with time and concurrently the two major unknowns (*3* and *4*) diminished (Table 1). The increase in DMC_9 product could, however, include ester formation from acidic intermediates or products *not* included in the volatile product analysis of Table 1, as well as from the presumed transformations from

TABLE 1. Ozonolysis of 18:2ω6: effect of reaction time at 100°C on hydrocarbon-soluble, glc-volatile, materials

	Peak areas*						
	Unknowns						
Time (min)	*1*	*2*	*3*	*4*	DMC_8	DMC_9	DMC_{10}
0	2	2	30	89	ND	30	500
20	2	2	15	43	3	278	500
60	ND	ND	13	26	4	332	500

*From analyses on SILAR-5CP: areas normalized on basis of DMC_{10} = 500. ND, not detected under analytical conditions employed.

unknowns *3* and *4*. The latter appeared to be intermediates, and not secondary reaction products. Since C_9 chain lengths were implicated, the application of the methods described under Experimental section (*d*) led to the identification of unknown *3* as the C_9 half-ester aldehyde dimethyl acetal $CH_3—O—CO—(CH_2)_7—CH(OCH_3)_2$ and of unknown *4* as the corresponding half-ester aldehyde $CH_3—O—CO—(CH_2)_7—CHO$. A systematic exploration of the ozone exposure and of the concentration of the BF_3—MeOH solution was then instituted to investigate the relationship between these two C_9 compounds and the desired DMC_9 principal product.

The effect of increasing time of exposure to the ozone stream, keeping constant the concentration of BF_3 (7%) and the time of reaction at 100°C (60 min), was to decrease the formation of acetal and aldehyde and thus to increase the yield of DMC_9 product (Table 2). However, the reaction of ozone must be instantaneous and complete as no unaltered 18:2ω6 could be recovered even at 0.5 min. The influence of time of exposure to the ozone stream under these conditions therefore does not alter the stage of electrophilic addition of ozone to the double bonds but does intervene in the transformation of intermediate products (acetal and aldehyde) to acid.

In the next examination, that of the effect of concentration of BF_3 in MeOH (Table 3), it is necessary

TABLE 2. Ozonolysis of 18:2ω6: effect of exposure time to O_2/O_3 on hydrocarbon-soluble, glc-volatile, materials; reaction time 60 min at 100°C

	Area† (%)			
Time* (min)	Acetal + aldehyde	DMC_8	DMC_9	Yield of DMC_9
0.5	25	0.8	74.2	64
1‡	17.6	1	81.4	72
2	7.4	0.7	91.9	92

*Time of exposure to O_3.
†From analyses on SILAR-5CP.
‡See Fig. 1.

TABLE 3. Ozonolysis of 18:2ω6: effect of BF_3 concentration on hydrocarbon-soluble, glc-volatile, materials*

	Area †(%)				
%BF_3 in MeOH	Acetal + aldehyde	DMC_8	DMC_9	Yield range‡	Average‡
2	2.1	0.6	97.3	98	98
7	5.2	0.9	93.9	92–97	94
14	5.9	0.7	93.4	94–96	95

*2 min O_2/O_3, 60 min at 100°C.
†Analyses on SILAR-5CP.
‡One value for 2%, 3 values for 7 and 14%.

to emphasize that the concentrations tested did not produce markedly different results. Possibly, the 2% BF_3 concentration produced slightly higher yields of DMC_9, but in view of potential errors in weighing, extraction, glc, etc., the trend is probably not significant. However, it is possible to say that under these conditions average yields of DMC_9 relative to other glc volatile materials are 96 ± 3%.

It became necessary to investigate the formation and interchange of the aldehyde and acetal intermediates. A suitable mixture (solution A, Table 4) was prepared, containing acetal, aldehyde, DMC_9, and an internal standard of DMC_{10}. Aliquots were examined after heating; B without ozone, or C with ozone. The conversion of acetal and aldehyde to acid clearly requires the oxidizing capacity originating in the ozone/oxygen gas stream. The BF_3 is apparently not a principal reactant. However, it is indispensible for the efficient transformation of these two intermediates into DMC_9 as shown in Table 5 where a similar initial mixture was reacted with ozone in MeOH only or in BF_3–MeOH.

The mechanism generally accepted (3–6) for ozonolysis gives a primary ozonide (Scheme 1, stage *1*) which decomposes to give a zwitterion (stage *2*) and a carbonyl derivative (stage *3*). Two reaction routes are then possible, depending on whether or not one has a participating solvent. The normal route is the formation of an internal ozonide (stage *4*) which is known to be easily decomposed by participating solvents such as MeOH (3, 7) (stage *5*). The alternative, more probably in the presence of MeOH solvent, is the capture of the zwitterion by MeOH (stage *6*) to give methoxyhydroperoxide. The latter is the more widely accepted reaction (8–10).

In respect to the decomposition of the methoxy hydroperoxide (stage *7*) it has been shown by Griesbaum and Keul (10) that this compound decomposes in the presence of HCl by an ionic process. It is reasonable to assume that a mechanism of the same type would apply in the presence of the strongly acidic BF_3.

The intermediates selected for study in the BF_3–MeOH systems were the methyl esters of the difunctional C_9 half-acid aldehyde and corresponding acetal. The aldehyde is generated by the decomposition of the primary ozonides and there is no reason to associate the acetal with any reaction except the normal BF_3-catalysed reaction between MeOH and aldehyde (11). The oxidation of aldehyde (stage *9*) was first thought to be by the intermediary action of one or more oxides of fluorine which are known to be powerful oxidants (12), but this does not seem to be the case. The oxidation appears to conform to literature results based on a simple oxidation process mediated by ozone (13–16). However, we have seen (Table 5) that this conversion of aldehyde to acid is not complete except in the presence of BF_3 which must have some catalytic role.

The equilibrium (*8*) between the aldehyde and acetal will be displaced by the removal of aldehyde by oxidation step (*9*). In this system the ratio of initial intermediate products for aldehyde:acetal is 4:1 (Table 4), but becomes 1:1 after an hour of full reaction (Fig. 1). The initial rapid oxidation of aldehyde to acid (*9*) by O_2/O_3 presumably slows down as oxidant is consumed, permitting the slower acetal formation step (*8*) to come to definite equilibrium.

The suggestion of a limitation of oxidation capacity in our particular system required an investigation of the oxidant capacity. Based on 2 ml of BF_3–MeOH and 2 min of exposure to the O_2/O_3 mixture, it was found that 8–10 mg and 15 mg of linoleic acid gave respective yields of 96 and 97% of DMC_9. At 30 mg the DMC_9 yield dropped to 91% and the acetal +

TABLE 4. Ozonolysis of 18:2ω6: effect of O_2/O_3 on hydrocarbon-soluble, glc-volatile, intermediary reaction products

	Peak areas†			
Reaction*	Acetal	Aldehyde	DMC_9	DMC_{10}
A	21	83	109	500
B	20	62	138	500
C	ND	ND	260	500

*A: initial solution; B:A in BF_3–MeOH, no O_3, 100°C (30 min); C:A in BF_3–MeOH (7%) 2 min O_2/O_3, 100°C (30 min).
†From analyses on SILAR-5CP; areas normalized on basis of DMC_{10} = 500.

TABLE 5. Effect of BF_3 on hydrocarbon-soluble, glc-volatile intermediary reaction materials

	Peak areas†			
Reaction*	Acetal	Aldehyde	DMC_9	DMC_{10}
A	25	163	58	500
B	28	54	51	500
C	ND	ND	347	500

*A: initial solution; B:A in MeOH, 2 min O_3, 100°C (30 min); C:A in BF_3–MeOH (7%), 2 min O_3, 100°C (30 min).
†Analyses on SILAR-5CP: areas normalized on basis of DMC_{10} = 500.

Can. J. Chem. Downloaded from www.nrcresearchpress.com by 210.87.254.105 on 09/05/12
For personal use only.

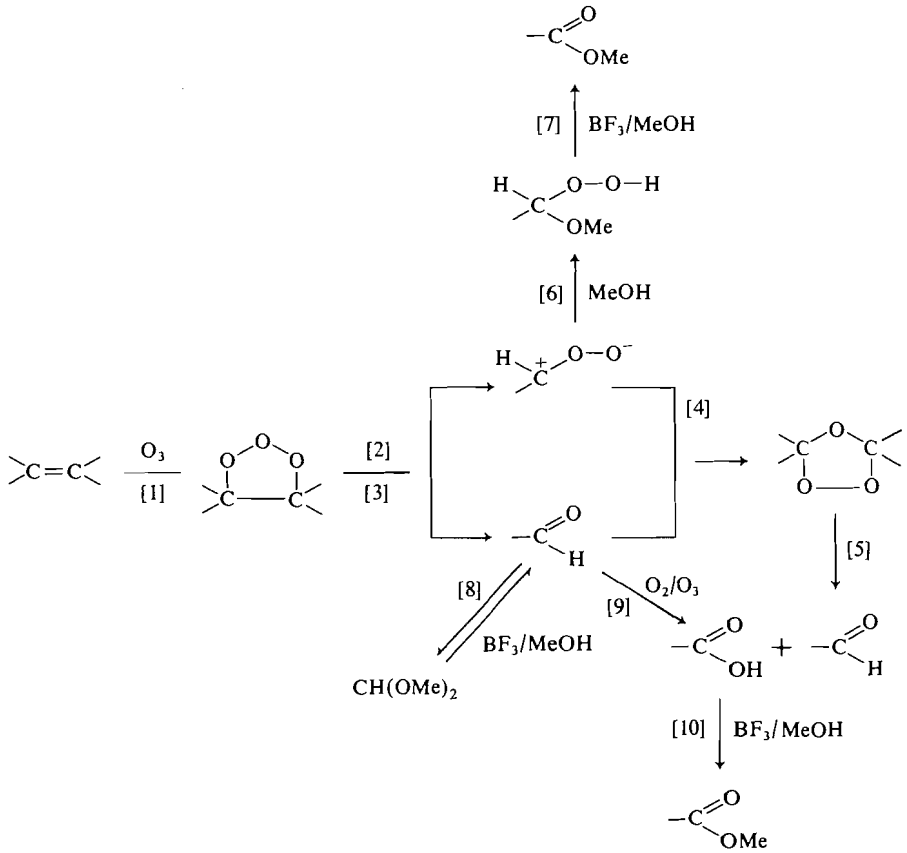

SCHEME 1. General mechanisms of ozonolysis, ozonide decomposition, acetal formation, oxidation, and esterification

aldehyde byproducts rose from 3–4% to 9% of total volatile products. When the system was tested with 60 mg of linoleic acid the ozonolysis itself was incomplete (disappearance of linoleic acid was approximately one half) and the molar proportion of acetal + aldehyde to DMC_9 was 55 to 45. Polyethylenic fatty acids are usually recovered from modern isolation techniques for further study in submilligram amounts. There does not appear to be any problem of scale for oxidative fission of these types of samples with the system described of 2 ml of reactant/solvent in a 10 ml tube and an adequate O_2/O_3 supply.

It is equally possible to pass the ozone into a solution of the reactant unsaturated ester in MeOH and then to add the BF_3. The results obtained are identical to those obtained by adding the ozone to the balance of the reactants except that we have obtained only one reaction intermediate. There is no formation of acetal. It is also possible that BF_3 plays a role in favouring electrophilic addition of ozone to the double bonds, but this effect must be feeble since it does not modify the yield of diacidic products. It is remarkable, in this context, that when monoethylenic acids are ozonized in BF_3–MeOH (1), the aldehyde and corresponding acetal (proportions 4:1) are only detected immediately after the initial ozonolysis and disappear much more rapidly and completely than for the same weight of diethylenic acids. This also emphasizes the importance of an excess of available oxidant.

The primary investigation of the C_9 fragments from linoleic acid was facilitated by the ready solubility of all of the difunctional C_9 products (except free acids) in the hydrocarbon methylcyclohexane. Although chloroform was somewhat more awkward to manipulate, it proved to be very effective in the extraction of both the C_9 difunctional products and the corresponding C_6 monofunctional products from linoleic acid (Table 6). The loss of MMC_6 (methyl hexanoate), relative to MMC_8, was found experimentally to be only 3% in two combined 2 ml chloroform extracts from 2 ml of 7% BF_3/MeOH diluted with 6 ml of H_2O. After applying this correction to a sample exposed to O_2/O_3 for 1 min, the yield of MMC_6 and the related C_6 aldehyde and acetal (Fig. 2) was effectively the same as that for the correspond-

Can. J. Chem. Downloaded from www.nrcresearchpress.com by 210.87.254.105 on 09/05/12
For personal use only.

TABLE 6. Ozonolysis of 18:2ω6, effect of reaction time at 100°C on chloroform-soluble, glc volatile materials

	Peak areas*					
	Expt. 1			Expt. 2		
Time (min)	Aldehyde + acetal (C_6)†	MMC_6	MMC_8	Aldehyde + acetal (C_9)‡	DMC_9	DMC_{10}
1	129	55	820	128	58	900
20	65	252	820	64	318	900
60	52	298	820	51	334	900

*From analyses on SILAR-5CP; areas normalized on basis of MMC_8 = 820 and DMC_9 = 900.
†Respectively peaks 1 and 2 in Fig. 2.
‡Respectively peaks 6 and 7 in Fig. 2.

ing DMC_9 and other difunctional C_9 products. It is thus clear that the reaction, complete or incomplete, is symmetrical and all primary and secondary products are found in equal molar proportions. In many cases of study of the structures of fatty acids it would be sufficient to examine only difunctional and/or longer chain monofunctional products. The use of chloroform for extraction and programmed gas–liquid chromatography (Fig. 2) extends this capability with inclusion of the shorter-chain monofunctional acidic product. No loss of MMC_6 occurred if the chloroform was concentrated 50% for convenience in later analysis.

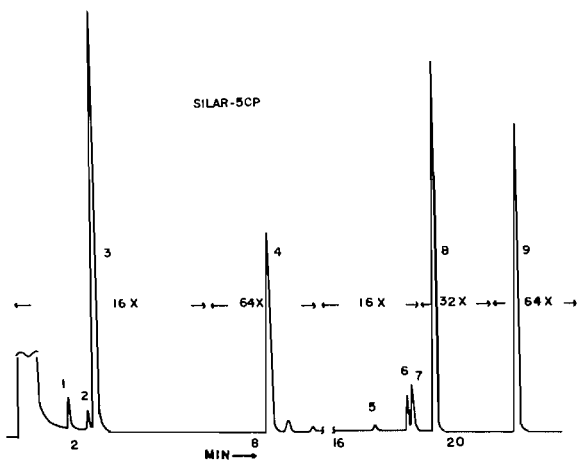

FIG. 2. Programmed-temperature gas–liquid chromatographic analysis of chloroform-soluble products from methyl linoleate recovered from an evaluation of the BF_3/MeOH-ozonolysis reaction, (time 1 min) with added internal standards. Peaks are: (*1*) hexanal, (*2*) hexanal dimethyl acetal, (*3*) methyl hexanoate product, (*4*) MMC_8 (methyl octanoate), internal standard, followed immediately by the small peak for DMC_3, (*5*) DMC_8 (dimethyl hexanedioate), secondary product, (*6*) methyl half ester of C_9 acid-aldehyde dimethyl acetal, (*7*) methyl half ester of C_9 acid-aldehyde, (*8*) DMC_9 (dimethyl heptanedioate) product, and (*9*) DMC_{10} (dimethyl octanedioate) internal standard. Column (see text) was held 80°C for 8 min, programmed at 32°/min to 180°C and then held at 180°C.

A small amount of dimethyl malonate (Fig. 2) was recovered with chloroform as the extractant. The recovery was adequate to act as a qualitative indication of the presence of methylene-interrupted ethylenic bond systems.

When this method of oxidation of products is compared with that formerly applied in this laboratory (17), i.e. ozonolysis in methanol followed by oxidation by a mixture of H_2O_2/HCO_2H, it appears that the BF_3–MeOH method gives less secondary (C_{n-1}) product ($\leq 1\%$ DMC_8 and 3–4% total acetal and aldehyde). It is equally important to note that we have never obtained the secondary (C_n, C_{n-1}) esters observed in certain instances by Pasero and co-workers (18, 19). The formation of these esters has been explained (20) by the transformation of aldehyde and peracid into diacyl peroxides, followed by decarboxylation and formation of the ester. This could well account for the DMC_8 secondary product but the proportion must be extremely small as in BF_3–MeOH medium transesterification would favour conversion to methyl esters.

Materials and Methods

(a) Materials

All solvents were reagent grade and were distilled in glass before use. The BF_3–MeOH (14%) solution was purchased in glass ampoules (Applied Science Laboratories) and these were opened as necessary (any surplus was stored briefly in a screw cap vial with a Teflon liner). The methyl linoleate was prepared by the Hormel Institute and showed only one major component on open-tubular glc. The ampoule, once opened, was immediately flushed with nitrogen and stored under nitrogen to prevent oxidation.

(b) Physico-chemical Apparatus

Gas–liquid chromatographic analyses were carried out in Perkin-Elmer model 900 or 3920 units with flame ionization detectors. Stainless steel wall-coated, open-tubular columns purchased from Perkin-Elmer, Norwalk, CT, were employed, with SILAR-5CP (Applied Science Laboratories) as the liquid phase. The dimensions were 46 m in length × 0.25 mm id, and isothermal operating conditions were 180°C with 60 psi (4 kg/cm²).

Can. J. Chem. Downloaded from www.nrcresearchpress.com by 210.87.254.105 on 09/05/12
For personal use only.

Nuclear magnetic resonance spectra were recorded in $CDCl_3$ on a Varian H.A. 100 spectrometer.

Infrared studies were carried out in a Unicam SP 1000 Infrared Spectrophotometer.

Mass spectral studies were carried out in a DuPont 21.491 mass spectrometer, coupled with a Hewlett-Packard 5750 gas chromatograph; the column was packed with 5% SE-30 M Chromosorb-W.

(c) Ozonolysis Techniques

Typically, appropriate quantities of methyl linoleate (~10 mg) and of dimethyl sebacate (internal standard) were weighed into a leak-tight 10 ml screw cap centrifuge tube. Either BF_3–MeOH, or MeOH if so required, was added (1–2 ml) and ozone in oxygen was bubbled through (total gas flow 250 ml/min) for the required time. The tube was promptly capped (Teflon-faced liner) and inserted into an aluminum heating block (nominally 100°C) for an hour. After cooling, distilled water (6 ml) was added and the products were extracted into methylcyclohexane (two extractions of 2 ml each). If required this extract was concentrated at 100°C with a jet of nitrogen. For chloroform extractions the procedure was the same, the bottom layers being carefully removed with a long slender Pasteur pipette.

Residues of acetone, sometimes used to clean and dry the centrifuge tubes, were found to produce a variety of spurious product peaks and were scrupulously avoided.

(d) Identification of Acetal and Aldehyde

The preparation of the two C_9 compounds was based on their recovery immediately after methyl linoleate was exposed to ozone in BF_3–MeOH. The methylcyclohexane extract, which included a small amount of DMC_9 (any free C_9 acid-ester would be inefficiently extracted under these conditions), was streaked on silicic acid thin-layer plates (Prekotes, Applied Science Laboratories). These were developed in *n*-hexane/diethyl ether (60/40). After spraying with 2′,7′-dichlorofluorescein the bands were located at R_f values, respectively, of 0.41 for half-ester acetal, 0.32 for half-ester aldehyde, and 0.20 for DMC_9. The bands were recovered by extraction with hexane and chloroform. The infrared spectra of the two unknown bands showed intense ester band absorption at 1755 cm^{-1}. The nmr spectra confirmed the ester functions (3.70 ppm singlet in both, 9.76 ppm triplet for the aldehyde, 3.30 ppm singlet for the acetal). The mass spectra gave appropriate and characteristic ester, aldehyde and acetal fragments and confirmed the chain lengths as C_9 through *m/e* of 185 for M − H (aldehyde) and *m/e* of 231 for M − H (acetal). The C_6 acetal was readily prepared from hexanal.

Acknowledgements

The cooperation of the Atlantic Regional Laboratory, National Research Council of Canada, Halifax, in executing the nmr and ms studies is gratefully acknowledged.

1. R. G. ACKMAN. Lipids, **12**, 293 (1977).
2. H. BINDER and W. LINDNER. J. Chromatog. 77, 175 (1973).
3. D. G. M. DIAPER. Oxid. Combust. Rev. **6**, 147 (1973).
4. R. W. MURRAY. Trans. N. Y. Acad. Sci. Ser. II, **29**, 854 (1967).
5. R. CRIEGEE. Angew. Chem. Int. Ed. Engl. **14**, 745 (1975).
6. P. C. HIBERTY. J. Am. Chem. Soc. **98**, 6088 (1976).
7. R. CRIEGEE and H. KORBER. Adv. Chem. Ser. **3**, 22 (1972).
8. E. H. PRYDE, C. M. THIERFELDER, and J. C. COWAN. J. Am. Oil Chem. Soc. **53**, 90 (1976).
9. R. CRIEGEE. Chimia, **22**, 392 (1968).
10. K. GRIESBAUM and H. KEUL. Angew Chem. Int. Ed. Engl. **14**, 716 (1975).
11. W. MORRISON and L. M. SMITH. J. Lip. Res. **5**, 600 (1964).
12. A. G. STRENG. Chem. Rev. **63**, 607 (1963).
13. E. BRINER and G. PAPAZIAN. Helv. Chim. Acta, **23**, 497 (1940).
14. D. SWERN. Organic peroxides. Wiley Interscience ed. 1970.
15. B. I. TARUNIN, M. N. KLIMOVA, and YU. A. ALEKSANDROV. Tr. Khim. Khim. Tekhnol. **5**, 103 (1975); Chem. Abstr. **85**, 108 155*g* (1975).
16. H. M. WHITE and P. S. BAILEY. J. Org. Chem. **30**, 3037 (1965).
17. R. G. ACKMAN, M. E. RETSON, L. R. GALLAY, and F. A. VANDENHEUVEL. Can. J. Chem. **39**, 1956 (1961).
18. D. G. M. DIAPER, J. PASERO, and H. NAUDET. Can. J. Chem. **46**, 2767 (1968).
19. J. PASERO, L. CAMEAU, and M. NAUDET. Bull. Soc. Chim. Fr. 1794 (1963).
20. D. LEFORT, D. TEMPIER, and C. J. SORBA. Bull. Soc. Chim. Fr. 442 (1960).

Can. J. Chem. Downloaded from www.nrcresearchpress.com by 210.87.254.105 on 09/05/12
For personal use only.

Hydrolyse des sels de phospholium monomères: Préparation et propriétés des oxydes de 1,3-diénylphosphines

FRANÇOIS MATHEY ET GEORGES MULLER

Equipe IRCHA–CNRS, 2–8 rue Henri Dunant, B.P. no 28, 94320 Thiais, France

Reçu le 20 mars 1978

FRANÇOIS MATHEY et GEORGES MULLER. Can. J. Chem. **56**, 2486 (1978).

L'hydrolyse des sels de diméthyl-3,4 phospholium par l'éthylate de thallium dans l'alcool fournit dans le cas général, exclusivement les oxydes de diénylphosphines correspondants par ouverture du noyau. Cependant, quand un des substituants du phosphore est le benzyle, l'oxyde de diénylphosphine devient le produit minoritaire, le produit majoritaire étant l'oxyde de méthyl-3 méthylène-4 phospholène-2 qui résulte d'un clivage de la liaison P—CH_2Ph accompagné de l'isomérisation de l'une des doubles liaisons du noyau phosphole. La deutérolyse des sels de benzylphospholium montre que l'isomérisation n'a pas lieu avant l'hydrolyse. Un essai de réduction de la liaison P=O des oxydes de diénylphosphines par le phénylsilane a fourni des produits hydrogénés. Au contraire l'échange P=O → P=S par P_4S_{10} se produit sans destruction du système diénique. La réaction avec $Fe_3(CO)_{12}$ conduit aux complexes diène–$Fe(CO)_3$ avec de hauts rendements. Quand les deux substituants du phosphore sont différents, on obtient deux complexes diastéréoisomères.

FRANÇOIS MATHEY and GEORGES MULLER. Can. J. Chem. **56**, 2486 (1978).

The hydrolysis of 3,4-dimethylphospholium salts by thallium ethylate in alcohol yields exclusively the corresponding dienylphosphine oxides by ring opening in the general case. However when one of the phosphorus substituents is benzyl, the dienylphosphine oxide becomes the minor product of the hydrolysis, the major product being the 3-methyl-4-methylene-2-phospholene oxide which results from the cleavage of the P—CH_2Ph bond with isomerization of one of the double bonds of the phosphole ring. Deuterolysis of benzylphospholium salts shows that the isomerization does not take place before the hydrolysis. Attempted reduction of the P=O bond of dienylphosphine oxides by phenylsilane yields hydrogenated products. On the contrary, the P=O → P=S conversion by P_4S_{10} occurs without destruction of the dienic system. High yields of diene–$Fe(CO)_3$ complexes are obtained by reaction with $Fe_3(CO)_{12}$. When the two phosphorus substituents are different, two diastereoisomeric complexes are obtained.

La voie d'accès normale aux oxydes de 1,3-diénylphosphines a pour point de départ une addition 1,4 du pentachlorure de phosphore sur les diènes conjugués suivie d'une déchlorhydratation 1,4. Les rendements sont souvent modestes; voir réfs 1–3. L'oxyde de (phényl-4-butadiényl)diphénylphosphine a d'autre part été préparé par une réaction de Wittig–Horner entre l'aldéhyde cinnamique et $(Ph_2P(O))_2$-CHK (4). Enfin il a été établi dans deux cas particuliers (5) que l'hydrolyse des sels de phospholium monomères fournissait également des oxydes de 1,3-diénylphosphines avec un rendement quasi-quantitatif. Il nous a donc paru intéressant d'étendre le travail préliminaire de Bergesen à d'autres phospholes et d'étudier quelques propriétés des produits ainsi préparés.

Nous avons choisi d'étudier plus particulièrement l'hydrolyse des sels de type **1**. La substitution diméthyl-3,4 assure la structure monomère des sels, simplifie leur préparation (meilleurs rendements) et facilite l'étude rmn des produits d'hydrolyse.

L'hydrolyse de **1***a* par la soude 2 *N* à chaud nous a fourni en fait un mélange complexe d'isomères non séparables contenant probablement, outre le produit

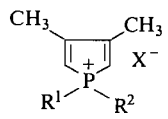

1

a R^1 = Me, R^2 = Ph, X = I
b R^1 = Ph, R^2 = $PhCH_2$, X = Br
c R^1 = *t*Bu, R^2 = Me, X = I
d R^1 = R^2 = Me, X = I
e R^1 = Me, R^2 = $PhCH_2$, X = I
f R^1 = R^2 = $PhCH_2$, X = Br

attendu **2***a*, l'oxyde de phosphine **3** en impureté principale comme en témoigne l'apparition vers 2.95 ppm d'un doublet CH_2P (J_{H-P} = 14 Hz) ($CDCl_3$, TMS externe). Nous avions déjà rencontré un tel problème dans un cas particulier (6). L'apparition de

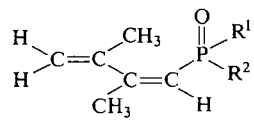

2

(P en *trans* de CH_3 comme dans le cycle phosphole)

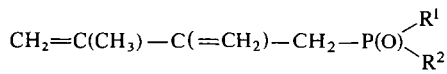

3

produits du type **3** résultant probablement d'une isomérisation de **2***a* en milieu basique à chaud, nous

Can. J. Chem. Downloaded from www.nrcresearchpress.com by 210.87.254.105 on 09/05/12
For personal use only.

Can. J. Chem. Downloaded from www.nrcresearchpress.com by 210.87.254.105 on 09/05/12
For personal use only.

avons mis au point une méthode d'hydrolyse beaucoup plus douce consistant à traiter à froid le sel de phospholium en solution dans l'éthanol par une quantité stoechiométrique d'éthylate de thallium. On obtient alors pratiquement quantitativement l'oxyde **2***a* pur. La méthode est générale et ne fournit qu'un produit quand R^1, $R^2 \neq PhCH_2$.

$$\mathbf{1} \xrightarrow[EtOH,\ 20°C]{EtOTl} \mathbf{2} \quad \text{si } R^1, R^2 \neq PhCH_2$$

Si, par contre, l'un des radicaux R^1 ou R^2 est le benzyle, la réaction d'hydrolyse suit un cours différent: l'oxyde diénique **2** devient alors le produit minoritaire, le produit principal étant l'oxyde de méthylène-4-méthyl-3-phospholène-2 (**4**).

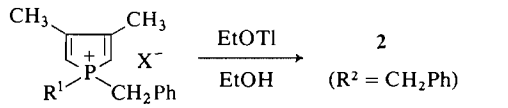

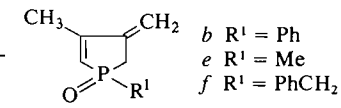

4

Ces deux types de produits sont séparables sans difficulté par chromatographie sur gel de silice. L'obtention de **4** est très surprenante. Logiquement, nous nous attendions en effet à l'obtention d'un oxyde de phosphole se dimérisant instantanément pour fournir un produit du type **5** dont nous ne trouvons pratiquement pas trace.

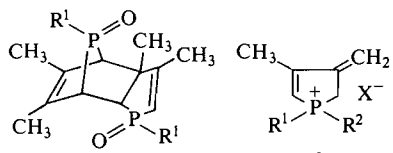

5 **6**

Notons que **4***b* a déjà été préparé par réaction de $CSCl_2$ sur le sulfure de phényl-1-diméthyl-3,4-phosphole (7). La première explication venant à l'esprit, à savoir une isomérisation de **1** en **6** avant hydrolyse, est à rejeter. En effet la deutérolyse de **1***a* ou de **1***f* fournit les oxydes deutériés sur la double liaison **7** et non les produits deutériés sur le méthyle **8** qui proviendraient nécessairement de **6**. Nous ne voyons donc pas d'explication simple du phénomène observé.

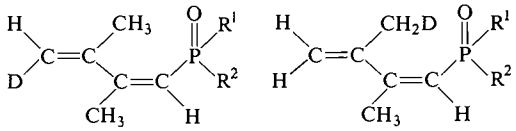

7 **8**

Notons en passant que, comme il semble peu vraisemblable qu'un carbanion vinylique engendré et piégé de façon probablement concertée en milieu protique subisse une isomérisation *cis–trans*, nous admettons que le deutérium est en *trans* du CH_3 dans **7** ce qui nous permet d'attribuer les signaux rmn des deux protons du CH_2 vinylique dans les oxydes **2**. Ces données sont réunies dans le tableau 1. On remarquera que la présence d'un phényle sur le phosphore provoque une forte différenciation des deux méthyles portés par le système diénique ainsi que des deux protons vinyliques du CH_2 en bout de chaîne, effet d'origine vraisemblablement électronique. Le tertiobutyle provoque un effet du même genre mais dans ce cas nous soupçonnons une origine conformationnelle. La répulsion stérique (visible sur le modèle de Dreiding) entre le méthyle en position 3 sur le diène et le groupement phosphorylé porteur du tertiobutyle a probablement pour conséquence une diminution du poids statistique de la conformation transoïde qui est habituellement la plus stable.

Ayant à notre disposition des oxydes diéniques du type **2** nous en avons entrepris l'étude chimique. Nous avons principalement employé **2***a* qui est le plus accessible parmi eux. Nous avons d'abord essayé de préparer les phosphines correspondantes par réduction à l'aide des silanes. En fait, $PhSiH_3$ au lieu de réduire le P=O provoque une hydrogénation-1,4 du système diénique de **2***a*. L'oxyde **9** obtenu n'est pas

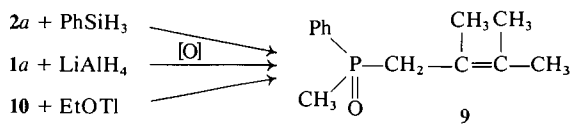

9

très pur mais son identité est indiscutable. On note sur le spectre de rmn du proton ($CDCl_3$) la disparition des protons vinyliques et l'apparition d'un doublet $CH_2P(O)$ à 2.76 ppm (J_{H-P} = 15 Hz). L'identification a été complétée par comparaison des spectres ir et rmn du proton avec un échantillon authentique de **9** préparé par hydrolyse à l'éthylate de thallium du sel de phospholénium **10**.

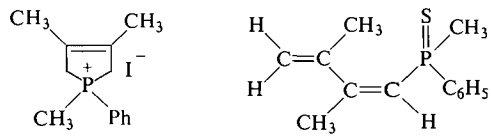

10 **11**

Devant cet échec nous avons étudié la réduction directe du sel de phospholium **1***a* par $LiAlH_4$. Nous avons à nouveau obtenu **9** provenant probablement de la phosphine éthylénique correspondante par suite d'une oxydation durant le traitement hydrolytique du milieu réactionnel. L'obtention du sulfure **11** n'a posé par contre aucun problème particulier. La

TABLEAU 1. Données de rmn* des oxydes diéniques $CH_2{=}C(CH_3){-}C(CH_3){=}CH{-}P(O)\begin{matrix}R^1\\R^2\end{matrix}$

Composé						=CH₂‡				
R^1	R^2	No.	Me—C2†	Me—C4	=CH—P (J_{H-P})	*Trans*	*Cis*	R^1 (J_{H-P})	R^2 (J_{H-P})	$\delta^{31}P$
Me	Ph	**2***a*	1.93	1.55	5.73(22)	5.03	4.80	1.68(11)	7.43	88.8
Ph	$PhCH_2$	**2***b*	1.92	1.50	5.78(23)	5.0	4.70	7.34	7.10 3.25(15)	88.9
*t*Bu	Me	**2***c*	2.38	1.95	5.60(24)	5.33	5.16	1.20(14)	1.50(12)	
Me	Me	**2***d*	1.97	1.92	5.52(20)	5.05	4.98	1.52(13)	1.52(13)	83.9
Me	$PhCH_2$	**2***e*	1.91	1.85	5.45(21)	4.96	4.96	1.33(12)	7.16 3.10(16)	81.9
$PhCH_2$	$PhCH_2$	**2***f*	1.88	1.80	5.26(23)	4.76	4.83	7.11 3.02(14)	7.11 3.02(14)	82.7

*^{1}H: 60 MHz, $CDCl_3$, TMS externe; δ en ppm, *J* en Hz; ^{31}P: P_4O_6 externe, δ positif vers les champs forts.
†Présente un mini-couplage avec le P qui le distingue de Me—C4.
‡Le proton en *trans* du méthyle se présente sous la forme d'un singulet élargi alors que le proton en *cis* se présente sous celle d'un multiplet complexe.

TABLEAU 2. Données de rmn* des complexes $\left[CH_2{=}C(CH_3){-}C(CH_3){=}CH{-}P(O)\begin{matrix}R_1\\R_2\end{matrix}\right]Fe(CO)_3$

Composé						=CH₂‡					
R^1	R^2	No.	Me—C2†	Me—C4	=CH—P (J_{H-P})	*Trans*	*Cis*	$J_{H_t-H_c}$	R^1 (J_{H-P})	R^2 (J_{H-P})	$\delta^{31}P$
Me (1er isomère)	Ph	**12***a*	2.16	2.11	1.90	1.92	3.15	2.8	1.72(12.8)	7.46(*m,p*) 7.57(*o*)	76.0
Me (2ème isomère)	Ph	**12***a′*	2.36	2.25	1.88(~8)	1.93	3.31	~2.5	1.63(12.5)	7.51(*m,p*) 7.70(*o*)	76.2
Me	Me	**12***d*	2.30	2.23	masqué par Me-P	1.92	3.12	2.8	1.45(12.2)	1.53(12.5)	69.6

*^{1}H: 100 MHz avec et sans découplage de ^{31}P, $CDCl_3$, TMS interne; ^{31}P: P_4O_6 externe, δ positif vers les champs forts.
†Plus de mini-couplage avec le P.
‡Le proton en *trans* du méthyle est en *cis* du fer selon la convention de Graf et Lillya (8); le travail de ces auteurs nous a permis d'assigner les signaux sans équivoque.

sulfuration de **2***a* a été réalisée à l'aide de P_4S_{10} dans le toluène à l'ébullition. Les paramètres de rmn du proton de **11** sont très voisins de ceux de **2***a*.

Nous avons voulu enfin vérifier s'il était possible de complexer le système diénique en dépit de sa désactivation par le groupement phosphoryle. La réaction des oxydes **2***a* et **2***d* avec $Fe_3(CO)_{12}$ au reflux du toluène nous a effectivement donné les complexes π attendus **12**. Les complexes **12** ont été caractérisés

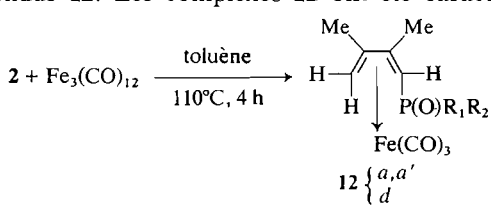

sans ambiguïté par analyse élémentaire C, H, Fe, par ir (présence des trois bandes caractéristiques des complexes diène —$Fe(CO)_3$) et par rmn du proton et du phosphore (tableau 2). Ce sont les premiers complexes π dérivés de diènes phosphorylés ouverts. Auparavant, seuls étaient connus les complexes π des oxydes de phospholes monomères (9, 10). Les données ir ($\nu_{P=O}$) et rmn (δ ^{31}P) semblent indiquer une décroissance de la polarisation du P=O lors de la complexation dûe à un pouvoir attracteur plus grand du diène complexé par rapport au diène libre: par exemple: $\nu_{P=O}$ = 1160 cm^{-1} (**2***d*), 1168 cm^{-1} (**12***d*), 1169 cm^{-1} (**2***a*) et 1177 cm^{-1} (**12***a′*) (produits en pastilles dans KBr). Le même effet a été noté sur le complexe de l'oxyde de diphénylvinylphosphine avec $Fe(CO)_4$ (11). Par contre, une intéraction complexante du fer avec le P=O est exclue car elle se traduirait au contraire par une diminution sensible de la fréquence $\nu_{P=O}$.

Le point le plus intéressant concernant ces complexes réside dans l'obtention de deux isomères à partir de l'oxyde **2***a*. Le carbone diénique lié au phosphore devient tétracoordinné et asymétrique lors de la complexation (substitution fer, carbone, phosphore, hydrogène). Lorsque le phosphore lui-même est asymétrique (cas de **2***a*), il est donc logique d'observer la présence de diastéréoisomères séparables par chromatographie sur colonne. Par contre, lorsque

Can. J. Chem. Downloaded from www.nrcresearchpress.com by 210.87.254.105 on 09/05/12
For personal use only.

Can. J. Chem. Downloaded from www.nrcresearchpress.com by 210.87.254.105 on 09/05/12
For personal use only.

le phosphore n'est plus asymétrique (cas de **2***d*) on n'obtient qu'un seul complexe. Dans ce dernier cas cependant, les deux méthyles portés par le phosphore dans **12***d* sont diastéréotopes. Il est donc normal d'observer un dédoublement du signal Me—P. Néanmoins, l'importance de ce dédoublement nous fait soupçonner un blocage de la rotation du groupement phosphorylé autour de la liaison P–diène qui serait dû à une forte intéraction stérique entre les groupements $P(O)Me_2$ et $Fe(CO)_3$. Nous n'avons toutefois pas pu contrôler cette hypothèse par une étude rmn en température variable par suite de l'instabilité des solutions de **12***d*.

Partie expérimentale

Les spectres rmn ont été enregistrés à 60 MHz sur Perkin-Elmer R 24 A et à 100 MHz sur JEOL PS 100 FT pour le proton ainsi qu'à 40.486 MHz sur JEOL PS 100 FT pour le phosphore.

Purification du phényl-1-diméthyl-3,4-phosphole

Les phospholes de départ ont été obtenus par les méthodes décrites dans la littérature (12–14). La double débromhydratation par le DBU donne des produits de pureté satisfaisante dans le cas du triméthyl-1,3,4-phosphole et du benzyl-1-diméthyl-3,4-phosphole. Par contre, le phényl-1-diméthyl-3,4-phosphole est souvent souillé d'une quantité non négligeable de phényl-1-diméthyl-3,4-phospholène-3 qui ne peut pas être éliminé complètement par simple lavage à l'acide chlorhydrique N (voir réf. 12). Nous avons donc mis au point une méthode de purification plus efficace reposant sur le fait que le tétrachlorure de carbone oxyde préférentiellement le phospholène sans altérer notablement le phosphole lorsque la température est inférieure ou égale à 60°C. Le phosphole impur est dissous dans une quantité égale de tétrachlorure de carbone. On chauffe la solution ainsi obtenue à 60°C pendant 30 min. Il y a formation d'un insoluble jaune plus ou moins huileux. On décante, extrait une fois au tétrachlorure de carbone. On chasse le solvant, reprend le résidu à l'éther ou à l'hexane, élimine l'insoluble par filtration, évapore l'éther et distille. Le phosphole ainsi obtenu ne contient plus de phospholène comme en témoigne la rmn du proton.

Préparation des sels de phospholium

Les sels de phospholium sont obtenus par quaternarisation des phospholes dans l'éther à l'aide d'un large excès d'iodure de méthyle ou de bromure de benzyle. Ainsi, à une solution de 10.5 g de phényl-1-diméthyl-3,4-phosphole dans 50 cm^3 d'éther, on ajoute 10 cm^3 d'iodure de méthyle. On laisse réagir pendant 2 jours à l'abri de l'air et de la lumière. On filtre, rince deux fois à l'éther et sèche sur anhydride phosphorique. Les rendements sont pratiquement quantitatifs.

Hydrolyse des sels de phospholium

A une solution de 0.02 mole de sel de phospholium dans 200 cm^3 d'éthanol absolu, on ajoute rapidement 0.02 mole d'éthylate de thallium sous agitation à température ambiante. Il y a immédiatement formation d'un précipité jaune pour X = I, blanc pour X = Br. On laisse agiter pendant 2 h 30 à température ambiante. On rajoute 200 cm^3 d'éthanol absolu, filtre, rince plusieurs fois, évapore à sec. Les oxydes de diénylphosphines sont purifiés soit par chromatographie sur colonne de silice suivie d'une sublimation, soit par sublimation directe.

R^1 = Me, R^2 = Ph, X = I; éluant AcOEt–MeOH 90:10

Composé **2***a*—rendement 70%; distillation moléculaire 100–110°C/0.1 Torr; pf 82°C; ir (KBr) ν: (C=C) 1600, 1623; (P=O) 1169 cm^{-1}. *Anal.* calc. pour $C_{13}H_{17}OP$: C 70.89, H 7.78; trouvé: C 70.07, H 7.62.

R^1 = tBu, R^2 = CH_3, X = I; éluant AcOEt–MeOH 50:50

Composé **2***c*—R_f 0.5; sublimation 70–80°C/0.05 Torr; ir (KBr) ν: (C=C) 1591; (P=O) 1167 cm^{-1}. *Anal.* calc. pour $C_{11}H_{21}OP$: C 65.97, H 10.57; trouvé: C 65.01, H 10.60.

R^1 = R^2 = CH_3,)X = I; éluant AcOEt–MeOH 60:40

Composé **2***d*—R_f 0.32; rendement 65%; sublimation 50°C/0.05 Torr; pf 76°C; ir (KBr) ν: (C=C) 1595, 1615, 1627; (P=O) 1160 cm^{-1}. *Anal.* calc. pour $C_8H_{15}OP$: C 60.74, H 9.56; trouvé: C 60.79, H 9.53.

Dans le cas où l'un des substituants est le benzyle, il faut obligatoirement chromatographier le mélange brut qui contient deux types d'oxydes (voir la Discussion).

R^1 = Ph, R^2 = $PhCH_2$, X = Br; éluant AcOEt–MeOH 80:20

Composé **2***b*—R_f 0.7; rendement 17%; sublimation 130°C/0.1 Torr; ir (KBr) ν: (C=C) 1601, 1622, 1629; (P=O) 1175–1180 cm^{-1}. *Anal.* calc. pour $C_{19}H_{21}OP$: C 77.01, H 7.14; trouvé: C 76.91, H 6.97.

Composé **4***b*—R_f 0.42; rendement 68%; sublimation 70°C/0.05 Torr. Le produit a été identifié par comparaison avec les données fournies par Kashman *et al.* (7) notamment le spectre de rmn du proton; rmn ^{31}P (P_4O_6 externe) δ: 66.1 ppm; ir (KBr) ν: (C=C) 1622; (P=O) 1211 cm^{-1}.

R^1 = Me, R^2 = $PhCH_2$, X = I; éluant AcOEt–MeOH 60:40

Composé **2***e*—rendement 17%; pf 86°C; ir (KBr) ν: (C=C) 1600, 1628; (P=O) 1173 cm^{-1}. *Anal.* calc. pour $C_{14}H_{19}OP$: C 71.77, H 8.17; trouvé: C 71.81, H 8.08.

Composé **4***e*—rendement 70%; ir (KBr) ν: (C=C) 1620; (P=O) 1210 cm^{-1}; rmn ^1H ($CDCl_3$, 60 MHz, TMS externe) δ: P—CH_3: 1.7 (J_{H-P} = 13 Hz); CH_3: 2.03; P—CH_2: 2.80 (J_{H-P} = 12 Hz); C=CH_2: 5.23, 5.33; P—CH: 6.13 ppm (J_{H-P} = 22 Hz).

R^1 = R^2 = $PhCH_2$, X = Br; éluant AcOEt–MeOH 80:20

Composé **2***f*—rendement 13%; sublimation 110°C/0.05 Torr; pf 120°C. *Anal.* calc. pour $C_{20}H_{23}OP$: C 77.40, H 7.47; trouvé: C 77.36, H 7.49.

Composé **4***f*—rendement 70%; ir (KBr) ν: (C=C) 1623; (P=O) 1208 cm^{-1}; rmn ^1H ($CDCl_3$, 60 MHz, TMS externe) δ: CH_3: 1.96; P—CH_2: 2.70 (J_{H-P} = 12 Hz); PCH_2Ph: 3.26 (J_{H-P} = 15 Hz); C=CH_2: 5.03, 5.16; P—CH: 5.96 (J_{H-P} = 21 Hz); C_6H_5: 7.15 ppm.

Deutérolyse des sels de phospholium

A une solution de 10^{-3} mol de sel de phospholium dans 5 cm^3 de D_2O on ajoute rapidement 10^{-3} mol de TlOEt. Il y a précipitation immédiate. On laisse agiter 1 h, filtre, extrait avec CH_2Cl_2, lave avec 2 cm^3 de D_2O, décante et sèche sur SO_4Na_2. On évapore à sec. Pour R^1 = Me, R^2 = Ph, X = I on obtient directement **7**. Pour R^1 = R^2 = $PhCH_2$, X = Br on chromatographie sur silice avec un mélange AcOEt–MeOH 80:20. Le produit passant en tête est **7** dans lequel R^1 et R^2 sont partiellement deutériés sur les CH_2 benzyliques.

Essais de réduction de **1**a *et* **2**a

Par $PhSiH_3$

Une mixture de 1.5 g de **2***a* et 0.49 g de $PhSiH_3$ est chauffée au bain d'huile à 120–130°C pendant 2 h. Par microdistillation, on obtient à 150–169°C/0.1 Torr un produit dont les spectres ir et rmn correspondent à **9**.

Réduction directe de ***1***a *par* $LiAlH_4$

Dans 125 cm^3 de THF anhydre on met en suspension 8.25 g de **1***a* (0.025 mol) et 0.6 g de $LiAlH_4$. On chauffe à reflux pendant 5 h 30 min. On traite par 100 cm^3 d'une solution à 20% de sel de Seignette. On laisse reposer la nuit. On décante, sèche sur SO_4Na_2, évapore à sec. Le produit distille à 100–110°C/0.2 Torr. Les spectres ir et rmn correspondent à **9**.

Préparation directe de ***9***

On hydrolyse le sel de phospholénium **10** exactement de la même manière que les sels de phospholium; rendement 60%; pf 88°C; distillation moléculaire à 100°C/0.02 Torr; ir (KBr) ν: (P═O) 1166 cm^{-1}; rmn ^1H ($CDCl_3$, 60 MHz, TMS externe) δ: CH_3 massif complexe avec pics à 1.55, 1.65 et 1.75 ppm; P—CH_2: 2.76 ppm $J_{(H-P)}$ 15 Hz; C_6H_5: 7.43 (*m*, *p*), 7.63(*o*) ppm; rmn ^{31}P (P_4O_6 externe) δ: 76.1 ppm. *Anal.* calc. pour $C_{13}H_{19}OP$: C 70.25, H 8.62; trouvé: C 70.23, H 8.62.

Sulfuration de **2**a

A une solution de 2×10^{-2} mol de **2***a* dans 100 cm^3 de toluène sec, on ajoute 2.22 g de P_4S_{10}. On chauffe 1 h à reflux, laisse refroidir, neutralise par une solution saturée de CO_3Na_2. On extrait deux fois la phase aqueuse, lave deux fois à l'eau, décante, sèche sur SO_4Na_2, évapore à sec. Le produit brut cristallise; rendement 55%; pf 86°C (éthanol absolu); distillation moléculaire 90–100°C/0.1 Torr; ir (KBr) ν: (C═C) 1603 cm^{-1}; rmn ^1H ($CDCl_3$, 60 MHz, TMS externe)δ: C—CH_3: 1.53 et 1.88 ppm; P—CH_3: 1.90 ppm $J_{(H-P)}$ 13 Hz; C═CH_2 *cis*: 4.72 ppm, *trans*: 5.03 ppm; P—CH: 5.86 ppm J_{H-P} 22 Hz; C_6H_5: 7.40 (*m*,*p*) et 7.80 (*o*) ppm. *Anal.* calc. pour $C_{13}H_{17}PS$: C 66.07, H 7.25; trouvé: C 65.89, H 7.17.

Complexation de **2** *par* Fe_3CO_{12}

A une solution de 10^{-2} mol de **2** dans 100 cm^3 de toluène sec, on ajoute 10^{-2} mol de Fe_3CO_{12}. On agite à reflux pendant 4 h. On laisse refroidir, filtre, évapore à sec et chromatographie sur colonne de silice.

Le composé **2***a* donne deux produits (R_f 0.42 et 0.25 dans AcOEt–MeOH 95:5).

Composé ***12***a—solide marron; rendement 40%; pf 96°C; ir (décaline) ν: (CO) 2056, 1992, 1976 cm^{-1}. *Anal.* calc. pour $C_{16}H_{17}FeO_4P$: C 53.36, H 4.76, Fe 15.51; trouvé: C 53.40, H 4.79, Fe 15.66.

Composé ***12***a′—solide marron clair; rendement 30%; pf 142°C; ir (décaline) ν: (CO) 2041, 1997, 1975 cm^{-1}. *Anal.* calc.: C 53.36, H 4.76, Fe 15.51; trouvé: C 53.60, H 4.64, Fe 15.63.

Le composé **2***d* donne un seul produit par chromatographie sur silice (R_f 0.5 dans AcOEt–MeOH 70:30).

Composé ***12d***—sublime à 50°C/0.1 Torr; rendement 55%; solide jaune; pf 112°C; ir ($CHCl_3$) ν: (CO) 2061, 1990, 1975 cm^{-1}. *Anal.* calc. pour $C_{11}H_{15}FeO_4P$: C 44.32, H 5.07, Fe 18.74; trouvé: C 44.24, H 5.18, Fe 18.55.

1. L. N. Mashlyakovskii et B. I. Ionin. Zh. Obshch. Khim. **35**, 1577 (1965).
2. L. N. Mashlyakovskii, B. I. Ionin, I. S. Okhrimenko et A. A. Petrov. Zh. Obshch. Khim. **38**, 2124 (1968); **40**, 804 (1970).
3. N. G. Kuzina, L. N. Mashlyakovskii, M. B. Simanovich et B. I. Ionin. Zh. Obshch. Khim. **47**, 1676 (1977).
4. M. I. Kabachnik, T. Ya Medved et E. I. Matrosov. Dokl. Akad. Nauk SSSR, **162**, 339 (1965).
5. K. Bergesen. Acta Chem. Scand. **20**, 899 (1966).
6. F. Mathey, J. P. Lampin et D. Thavard. Can. J. Chem. **54**, 2402 (1976).
7. Y. Kashman, I. Wagenstein et A. Rudi. Tetrahedron, **32**, 2427 (1976).
8. R. E. Graf et C. P. Lillya. J. Organometal. Chem. **122**, 377 (1976).
9. R. C. Cookson, G. W. A. Fowles et D. K. Jenkins. J. Chem. Soc. 6406 (1965).
10. D. G. Holah, A. N. Hughes et B. C. Hui. Can. J. Chem. **50**, 2442 (1972).
11. B. F. G. Johnson, J. Lewis et S. R. Postle. J. Organometal. Chem. **121**, c7 (1976).
12. F. Mathey et R. Mankowski-Favelier. Bull. Soc. Chim. Fr. 4433 (1970); Org. Magn. Reson. **4**, 171 (1972).
13. F. Mathey. Tetrahedron, **28**, 4171 (1972).
14. L. D. Quin, S. G. Borleske et J. F. Engel. J. Org. Chem. **38**, 1858 (1973).

Can. J. Chem. Downloaded from www.nrcresearchpress.com by 210.87.254.105 on 09/05/12
For personal use only.

Can. J. Chem. Downloaded from www.nrcresearchpress.com by 210.87.254.42 on 09/05/12
For personal use only.

The X-ray crystal structure of rapamycin, $C_{51}H_{79}NO_{13}$

D. C. NEIL SWINDELLS, PETER S. WHITE, AND JOHN A. FINDLAY
Department of Chemistry, University of New Brunswick, Fredericton, N.B., Canada E3B 5A3

Received June 23, 1978

D. C. NEIL SWINDELLS, PETER S. WHITE, and JOHN A. FINDLAY. Can. J. Chem. **56**, 2491 (1978).

The antifungal antibiotic Rapamycin crystallises in the orthorhombic space group $P2_12_12_1$ with $a = 34.85(2)$, $b = 13.08(1)$, $c = 12.25(1)$ Å. The molecular structure has been determined by X-ray crystallography to be a completely new type of macrolide antibiotic of formula $C_{51}H_{79}NO_{13}$.

D. C. NEIL SWINDELLS, PETER S. WHITE et JOHN A. FINDLAY. Can. J. Chem. **56**, 2491 (1978).

L'antibiotique antifongique Rapamycine cristallise sous la forme orthorhombique et le groupe d'espace $P2_12_12_1$ avec $a = 34.85(2)$, $b = 13.08(1)$, $c = 12.25(1)$ Å. On a déterminé la structure moléculaire par diffraction des rayons-X; il s'agit d'un antibiotique macrolide d'un type complètement nouveau de formule $C_{51}H_{79}NO_{13}$.

[Traduit par le journal]

Introduction

Rapamycin, an antifungal antibiotic, is the active principle of a strain of *Streptomyces hygroscopicus* which was isolated from an Easter Island soil sample (1). An early report (2) suggested that Rapamycin is a triene of composition $C_{56}H_{89}NO_{14}$. The current investigation has revealed the complete structure to be that of a completely new type of macrolide antibiotic, the molecular formula of which is $C_{51}H_{79}NO_{13}$.

Experimental

The compound was crystallised from a methanol/water mixture. After a preliminary photographic investigation cell dimensions and intensity data were measured using a Picker FACS-I diffractometer. The relevant crystallographic data are:

$C_{51}H_{79}NO_{13}$ fw = 914.2
Orthorhombic, $P2_12_12_1$, $a = 34.85(2)$, $b = 13.08(1)$, $c = 12.25(1)$ Å, $V = 5585.7$ Å^3, $\rho_c = 1.09$, $Z = 4$. Radiation graphite monochromated MoK_α, $\lambda = 0.71069$ Å. Data collected: $2\theta \leq 40°$, 5358 unique reflections, 3118 observed. Crystal size: $0.6 \times 0.4 \times 0.2$ mm.

Initial attempts to solve the structure using the multisolution direct methods program MULTAN (3) proved unsuccessful. However, when a limited amount of structural information was obtained from ^{13}C nmr, it was included in the calculation of the normalised structure factors (E's) and a second attempt was made. The resulting E-map showed four groups of peaks which exhibited bond distances and angles consistent with those expected. These four fragments (32 atoms) were used to phase a Fourier synthesis in which a little more of the structure was discernable. A total of six such syntheses was required before the final structure was obtained.

Initially, all the atoms were assumed to be carbon and the structure was refined by least-squares methods using a block diagonal approximation and unit weights. As the refinement proceeded it was possible to allocate the oxygen and nitrogen positions from bond length and other geometrical considerations. With all non-hydrogen atoms included in the refinement with anisotropic thermal parameters a reliability index, R, of 0.108 has been obtained. A difference synthesis shows no evidence of any further non-hydrogen atoms. With the exception of the direct methods routines the computer programs used have been the X-RAY 76 package of Stewart *et al.* (4).

Discussion

Figure 1 shows the structure assigned to Rapamycin on the basis of this work.[1] The structure includes a thirty-five atom macrocycle, with an amide C16—N17, a lactone C23—O24, and oxygen bridge between C9 and C14 and an additional bond between N17 and C22 to form an α-carbonyl piperidine unit. The triene predicted by Vézina *et al.* is found at C1 through C6.

The nitrogen position was initially located by the short C16—N17 bond length which was unacceptable for a C—C bond. The α-carbonyl piperidine

[1]Tables of atomic coordinates, thermal parameters, bond lengths, and bond angles are available, at a nominal charge, from the Depository of Unpublished Data, CISTI, National Research Council of Canada, Ottawa, Ont., Canada K1A 0S2.

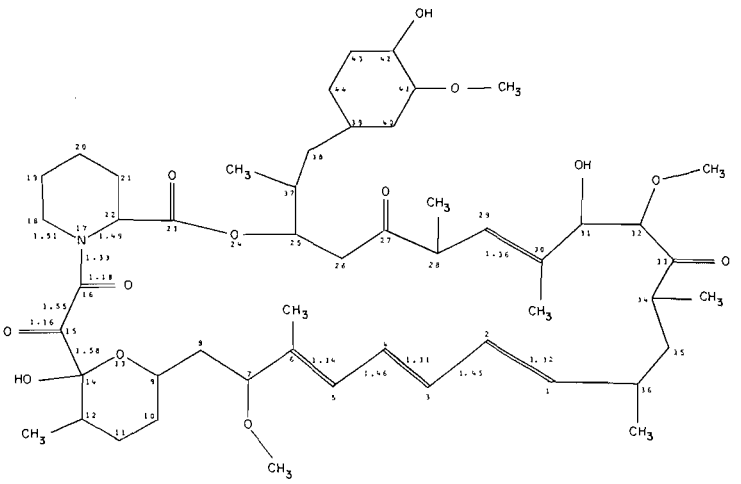

FIG. 1. Molecular structure of Rapamycin showing selected bond lengths (Å, esd, ± 0.02 Å).

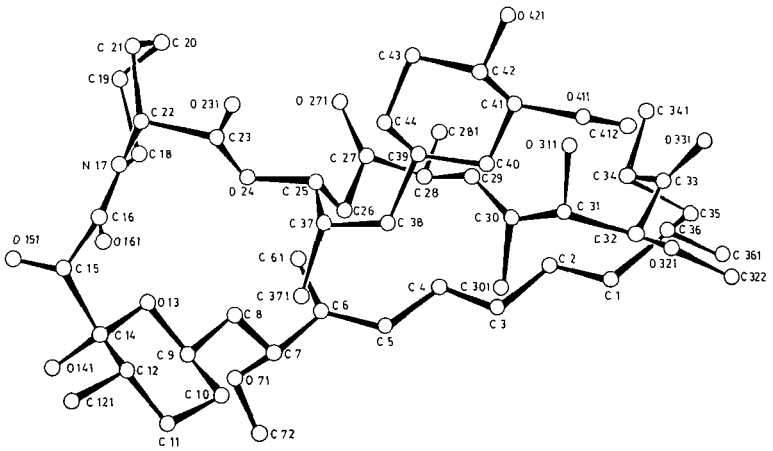

FIG. 2. Perspective view of the Rapamycin molecule.

unit (C15, C16, O161, N17, C18, C22) is essentially planar, thus the nitrogen is sp^2 hybridised and some delocalisation of the carbonyl bond is indicated by a shortening of the C16—N17 bond length, 1.33(2) Å compared to the expected single bond distance of 1.47 Å (5). The two adjacent carbonyl groups (at C15 and C16), on the other hand, are not coplanar and this is reflected in the lack of shortening of the C15—C16 bond (1.55(2) Å).

The triene system exhibits a distinct alternation of bond lengths and although the single bonds, C2—C3 and C4—C5, are shortened to 1.45(2) Å and 1.46(2) Å indicating some double bond character the system is not planar, with a rotation of about 10° occurring about each of the single bonds.

Acknowledgements

The authors are grateful to Ayerst Research Laboratories, Montreal, for suggesting the problem and providing crystalline Rapamycin, to the National Research Council of Canada for financial support and to Dr. J. N. Schoolery, Varian Associates, Palo Alto, California, for providing and commenting on ^{13}C nmr spectra.

1. S. N. SEHGAL, H. BAKER, and CLAUDE VÉZINA. J. Antibiot. **XXVII**, 727 (1975).
2. CLAUDE VÉZINA, ALICIA KUDELSKI, and S. N. SEHGAL. J. Antibiot. **XXVII**, 723 (1975).
3. G. GERMAIN, P. MAIN, and M. M. WOOLFSON. Acta Crystallogr. A**27**, 368 (1971).
4. J. M. STEWART (*Editor*). The X-ray System–Version of 1976. Technical Report TR-446 of The Computer Science Center, University of Maryland, College Park, Maryland.
5. International Tables for X-Ray Crystallography, Vol. 3. The Kynoch Press, Birmingham, England. 1962.

Can. J. Chem. Downloaded from www.nrcresearchpress.com by 210.87.254.42 on 09/05/12
For personal use only.

Canadian Journal of Chemistry
Published by
THE NATIONAL RESEARCH COUNCIL OF CANADA

Journal canadien de chimie
Publié par
LE CONSEIL NATIONAL DE RECHERCHES DU CANADA

Volume 56 Number 19 October 1, 1978

Volume 56 numéro 19 1 octobre 1978

Can. J. Chem. Downloaded from www.nrcresearchpress.com by 210.87.254.5 on 09/05/12
For personal use only.

Heats of vaporization of monoalkylcyclohexanes by the gas chromatography – calorimetry method[1]

RICHARD FUCHS AND L. ALAN PEACOCK
Department of Chemistry, University of Houston, Houston, TX 77004

Received February 27, 1978

RICHARD FUCHS and L. ALAN PEACOCK. Can J. Chem. **56**, 2493 (1978).

A recently developed empirical method for measuring heats of vaporization (ΔH_v^{25}) by a combination of gas chromatography and calorimetric heats of solution in the stationary phase has been applied to a series of 9 monoalkylcyclohexanes having C_1–C_{12} side chains. The uncertainties in the measurements (0.07–0.23 kcal/mol) are critically evaluated. Comparison with literature ΔH_v measurements indicates good agreement for low boiling compounds, and for high boiling compounds, values substantially more reliable than were previously obtained from vapor pressure measurements.

RICHARD FUCHS et L. ALAN PEACOCK. Can. J. Chem. **56**, 2493 (1978).

Une méthode empirique développée récemment pour mesurer les chaleurs de vaporisation (ΔH_v^{25}) en combinant la chromatographie en phase gazeuse et des chaleurs calorimétriques de solution dans une phase stationnaire a été appliquée à une série de 9 monoalkylcyclohexanes portant des chaînes latérales de 1 à 12 carbones. On a évalué d'une façon critique les incertitudes dans les mesures (0.07 à 0.23 kcal/mol). Une comparaison avec des mesures de ΔH_v retrouvées dans la littérature suggère une bonne concordance dans le cas des composés de bas points d'ébullition; dans le cas des composés de points d'ébullition plus élevés on obtient des valeurs beaucoup plus sures que celles obtenues antérieurement à partir de mesures de pression de vapeur.

[Traduit par le journal]

Heats of vaporization (evaporation), ΔH_v^{25}, are essential parameters in thermodynamic studies involving comparisons of gaseous and solution behavior, or interconversion of solution and gaseous data. Some recent examples are the study by Beauchamp and co-workers (1) of carbonium ion solvation in fluorosulfuric acid – antimony pentafluoride (requiring ΔH_v of RBr, RCl), measurements by Arnett *et al.* (2) of pyridinium ion solvation in water (ΔH_v substituted pyridines), conversion of liquid heats of formation to the gaseous state (3, 4) (ΔH_v of ketones), and a study of alkane and alkene solvation in polar and nonpolar solvents (5) (ΔH_v of alkanes, alkenes).

A variety of methods are available for measurement of heats of vaporization, but each has definite limitations. All require specialized apparatus, and most are quite time consuming. Each method is capable of giving good results when properly applied to an appropriate system, but it is quite evident that many literature ΔH_v values have uncertainties (precision) much smaller than the actual errors. For 1-butanol the values 12.19 ± 0.01, 12.27 ± 0.02, and 12.50 ± 0.02 kcal/mol have been reported (6, 7). Clearly at least two of the three measurements must involve substantial errors. Other measurements have been reported (7) which involve even larger errors: methyl tetradecanoate (reported $\Delta H_v = 21.3$ kcal/mol) appears to have a higher value than methyl pentadecanoate (21.0 kcal/mol), in contrast to the widely observed increase of about 1.2 kcal/mol per methylene group in large alkyl chains. For methyl oleate having three additional carbon

[1]This study was supported by the Robert A. Welch Foundation Grant E-136.

Can. J. Chem. Downloaded from www.nrcresearchpress.com by 210.87.254.5 on 09/05/12
For personal use only.

atoms a value of 20.2 kcal/mol has been reported, which is more than 20% (5.1 kcal/mol) below the probable value[2]. These problems may exist because an unsuitable experimental method was used, but more commonly, because an appropriate method was not available.

Of the experimental techniques direct vaporization calorimetry is probably the most accurate (6–9), but its most effective use is restricted to relatively low boiling compounds (bp < ca 150°C). Many of the best literature values have been measured by this method (7). Static vapor pressure measurements at several temperatutes fit by appropriate equations (7) can, in principle, furnish ΔH_v values of both low and high boiling compounds, and some good values for low boiling compounds have been measured by this technique (7, 10). With higher boiling substances having correspondingly lower vapor pressures a small uncertainty in the pressure measurements leads to a rather sizable percentage error, and the method becomes less accurate. Also, at the higher temperatures required to attain measurable vapor pressures, decomposition of the sample becomes a problem (10) which may not be recognized or cannot be avoided, and this leads to erroneous results. For very high boiling liquids non-equilibrium techniques have been used to measure heats of vaporization. The Knudsen effusion method of vapor pressure measurement (11) and the triplet calorimeter technique (12) employ restricted evaporation through orifices at pressures below the equilibrium saturation pressure. The accuracy of values obtained is limited in the former by various factors, particularly the orifice area and depth measurements, and in the latter, by the accuracy of the (PV work) correction to equilibrium conditions, and the availability of the required saturation vapor pressure data at the temperature of measurement. Gas chromatographic determinations of the enthalpy of transfer from solution in a gc stationary phase to the vapor $[-\Delta H(\text{v} \rightarrow \text{S})]$ tend to parallel ΔH_v (13, 14), but the two quantities are equal only if an athermal solution process of the liquid sample in the stationary phase solvent occurs. Since this is seldom the case, measurement of $-\Delta H(\text{v} \rightarrow \text{S})$ is not generally a reliable way to estimate ΔH_v.

A simple method for the measurement of heats of vaporization has recently been developed in this laboratory (15). It has been applied to liquid substances boiling between 65 and 360°C (5, 15), and both lower and higher boiling substances could undoubtedly be handled. Sample size is small (<200–300 μL), and partial decomposition at high temperatures does not affect the results. The method is derived from reported gc determinations of $\Delta H(\text{v} \rightarrow \text{S})$ (16, 17), using DC-200 silicone fluid as the stationary phase – solvent:

$$[1] \qquad \Delta H(\text{v} \rightarrow \text{S}) = -R\frac{\text{d ln } V_g}{\text{d}(1/T)}$$

V_g is the retention volume (18), defined by the equation

$$[2] \qquad V_g = \frac{F_c j}{w_t}(t_r - t_a)\frac{273.15}{T_r P_0}(P_0 - P_w)$$

where F_c is the carrier gas flow rate at room temperature (T_r) and j is the compressibility factor, w_t is the weight of stationary phase, t_r is the sample retention time, t_a is the retention time of air, P_0 is the outlet pressure, and P_w is the vapor pressure of water at room temperature. Extraordinary care and precision in the measurement of these quantities (particularly w_t) have been necessary to obtain meaningful values of V_g (16, 19, 20). Simplification has been possible by our observation (15) that if these quantities are not measured but are held constant, the specific retention volume then equals a constant times the corrected retention time ($\Delta t = t_r - t_a$). In a plot of ln Δt vs. $1/T$ the intercept of the straight line passing through these points differs from that obtained in the plot of ln V_g vs. $1/T$, but the slope is unchanged.

$$[3] \qquad \Delta H(\text{v} \rightarrow \text{S}) = -R\frac{\text{d ln } \Delta t}{\text{d}(1/T)}$$

The resulting enthalpy change ($\Delta H(\text{v} \rightarrow \text{DC-200})$ at the mean value of T) is the same whether Δt or V_g is used. This value is corrected to 25°C using liquid heat capacities ($C_p(\text{l})$) calculated by the group contribution method (21), and gas-phase heat capacities ($C_p(\text{g})$) calculated from the additivity rules of Benson (22), using the equation

$$[4] \qquad \Delta H^{25}(\text{v} \rightarrow \text{S}) = \Delta H^{T_m}(\text{v} \rightarrow \text{S}) + \int_{T_m}^{298.15} (C_p(\text{l}) - C_p(\text{g}))\text{d}T$$

Since

$$[5] \qquad \Delta H_v = \Delta H_s - \Delta H(\text{v} \rightarrow \text{S})$$

the other essential experimental measurement is of ΔH_s, the heat of solution of a liquid sample in the stationary phase (solvent), measured calorimetrically at 25°C. Without this correction $\Delta H(\text{v} \rightarrow \text{S})$ will in general differ appreciably from ΔH_v, particularly for a polar sample in a nonpolar stationary phase.

The experimental procedure used is somewhat empirical in two respects. Rather than the constant

[2] L. A. Peacock, unpublished results.

Can. J. Chem. Downloaded from www.nrcresearchpress.com by 210.87.254.5 on 09/05/12
For personal use only.

flow rate implied by [1] and [2] as the column temperature is changed, constant carrier gas input pressure has been maintained. The flow rate (as indicated by t_a) decreases somewhat with increasing temperature as the carrier gas viscosity increases. Secondly, heat capacity corrections have been made using 25° values of C_p(l) and C_p(g), rather than taking into account the change in these quantities with temperature in [4]. Furthermore (as pointed out by a referee), the partial molal heat capacity is more appropriate than C_p(l) in [4], for the step of the cycle involving the transfer of the solute in DC-200 from T_m to 25°C. However, values of the partial molal quantity (which are not likely to be widely available) probably do not differ greatly from C_p(l).

For these reasons a systematic calibration must be applied. The apparent values of ΔH_v(calorimetric ΔH_s – gc ΔH(v → DC-200)) have been plotted vs. a group of ΔH_v values determined (mainly by direct vaporization calorimetry) with small uncertainties (7, 12). From the slope and intercept of this plot corrected gc–calorimetry values for other substances are calculated. This procedure largely cancels the errors caused by changes in flow rate, C_p(l) and C_p(g) with temperature, since the effects on the calibration compounds and on other substances are similar. A total of nearly 100 nonpolar and moderately polar compounds of various classes have been run by this procedure, and the agreement with carefully measured literature values leaves little doubt of the effectiveness of the calibration procedure.

In the present study we have chosen to examine a series of nine monoalkylcyclohexanes boiling from 100°C to over 330°C. For three of these compounds calorimetric values of ΔH_v have been reported (7), and for four others, values based on static vapor pressure measurements are available (7). Since few available measurements for high boiling substances are believed to be highly reliable, this series offers an additional advantage. For the higher members of the series at least, the usual methylene increment of about 1.2 kcal/mol in ΔH_v is to be expected, and this can serve as the arbiter of any disagreement between the present experimental values and those previously reported.

It is the objective of the present study to compare the results of the gc–calorimetry method for heats of vaporization with those obtained from direct vaporization calorimetry and static vapor pressure methods, and to critically assess the uncertainties in measurements by the new technique.

Experimental

Reagents

The calibration hydrocarbons (*n*-octane, *n*-nonane, mesitylene, *n*-decane, *n*-dodecane, *n*-tetradecane, 1-hexadecene, and *n*-hexadecane) were commercial samples stated to be of 99% or greater purity which was confirmed by gc. The alkylcyclohexanes were obtained from Chemical Samples Co., excepting *n*-butylcyclohexane (Aldrich). All were of 99% or greater purity excepting *n*-dodecylcyclohexane (96%) which was purified by preparative gc to >99% purity. Dow-Corning DC-200 silicone fluid (100cSt) dried with 4A molecular sieve beads was used for calorimetric measurements and column loading.

Gas Chromatography

Retention times were determined using 30 m × 0.5 mm id stainless steel capillary columns over a 50°C range within the temperature interval of 36–200°C. Temperatures were monitored to ±0.1°C with a partial immersion mercury-in-glass thermometer mounted in the gc oven. After each change in temperature the oven and column were equilibrated for 1 h before sample injection. The injection block was maintained about 25°C above the sample boiling point. A heavily loaded column (II) was used for the lower boiling compounds (methyl-, ethyl-, and *n*-propylcyclohexane), and a lightly loaded column (I) was used for the higher boiling members of the series. Dry nitrogen at a pressure of 10.00 ± 0.06 psi was used as the carrier gas. The dead volume time (t_a) was assumed to be equal to the retention time of methane at each temperature. However, a more convenient internal standard, pentane, was routinely used, after the relative retention times of methane and pentane as a function of temperature had been established. Sample retention times relative to pentane were measured and corrected by the addition of the retention time of pentane relative to methane at each temperature. Triplicate retention times at each of six temperatures were measured for each compound.

Calorimetry

Heats of solution of the calibration compounds and the alkylcyclohexanes were determined in DC-200 silicone fluid with apparatus slightly modified from that previously described (5, 15, 25). The vacuum jacketed calorimeter (volume 100 mL) containing 50 mL of DC-200 was stirred with a commercial magnetic bar (12 × 37 mm) using a stirring unit within the constant temperature bath (25.00 ± 0.001°C) powered by a 300 rpm constant speed gear motor. Even with this increased stirring a somewhat longer period of time (2–3 min) was required to reach the final baseline (following sample addition or operation of the calibration heater) than is required with less viscous solvents (5, 25). However, improved sensitivity (200 μV full scale recorder deflection) compared with a previous report (15) is now feasible. Uncertainties in the ΔH_s measurements are estimated to be ±0.02 kcal/mol up to ΔH_s = 1.00, and 2.5% of the heat of solution when ΔH_s > 1.00 kcal/mol, based on the standard deviation of 3–5 ΔH_s measurements. The methylene increment in ΔH_s of the alkylcyclohexanes in DC-200 is 0.09 ± 0.01 kcal/mol per CH_2.

Calculation of Apparent ΔH_v

ΔH(v → DC-200) was calculated (eq. [3]) from the slope of the ln Δt vs. $1/T$ plot. From this quantity at the mean temperature of the Δt measurements ΔH(v → DC-200) at 25°C can be calculated (eq. [4]) by applying the appropriate ΔC_p correction. Apparent ΔH_v^{25} values were calculated from the 25°C values of ΔH_s and ΔH(v → DC-200) (eq. [5]).

Calibration of Columns

A calibration curve was prepared for each DC-200 gc column relating the apparent ΔH_v for each calibration hydrocarbon to the corresponding literature value of ΔH_v (7). For

heavily loaded Column II the values in kcal/mol were: *n*-octane, 9.30 (apparent), (9.92 (7)); *n*-nonane, 10.37 (11.10); mesitylene, 10.64 (11.35); *n*-decane, 11.58 (12.28); and *n*-dodecane, 14.06 (14.65 (12)). Calculation of the slope and intercept provided the equation for Column II (in kcal/mol):

$$[6] \quad \Delta H_v(\text{corr}) = 0.9808\,\Delta H_v(\text{app}) + 0.8907$$

with a correlation coefficient (R) of 0.9997. For Column I the corresponding values were: *n*-octane, 9.30 (9.92); *n*-nonane, 10.44 (11.10); mesitylene, 10.70 (11.35); *n*-decane, 11.62 (12.28); *n*-dodecane, 14.18 (14.65 (12)); *n*-tetradecane, 16.42 (16.99 (12)); 1-hexadecene, 18.62 (19.14); and *n*-hexadecane, 19.05 (19.45 (12)). The resulting equation for Column I (in kcal/mol) is

$$[7] \quad \Delta H_v(\text{corr}) = 0.9793\,\Delta H_v(\text{app}) + 0.8538$$

and the correlation coefficient is 0.9999.

Analysis of Uncertainties

Regression analysis of the ln Δt vs. $1/T$ plot yields, in addition to the slope and intercept, the correlation coefficient and the standard error of the estimate ($S_{y \cdot x}$). Although values of R of 0.9996 or larger were noted for both calibration compounds and alkylcyclohexanes, this can only serve as a rough guide for determining whether data should be rejected, since R increases with slope. The standard error of the estimate may be treated more quantitatively. The standard deviation from regression (S_b) is calculated from $S_{y \cdot x}$ and the sum of the squares of the deviations in x ($x = 1/T$) (26). The uncertainty in the slope may then be expressed as $\pm(t)(S_b)$, where t is the Student t value for a given number of points (6) and confidence level (99%). The calibration curve uncertainty is determined in the same manner.

The total uncertainty in ΔH_v is calculated from the uncertainties in the heat of solution, gc slope, C_p(l), C_p(g), and calibration curve. Each of the component uncertainties (σ) is squared (yielding the variance), and the variances are summed. The square root of the sum of the variances is the total uncertainty in the heat of vaporization.

$$[8] \quad \sigma_{\text{total}} = [\sigma_{\Delta H_s}{}^2 + \sigma_{\text{gc}}{}^2 + \sigma_{C_p(\text{l})}{}^2 + \sigma_{C_p(\text{g})}{}^2 + \sigma_{\text{calibr}}{}^2]^{1/2}$$

Sample Calculation

n-*Butylcyclohexane*

Gas chromatographic data for this compound on Column I was obtained for the temperature range of 39.1 to 80.4°C (Table 1). At each of six temperatures triplicate chromatograms were obtained in the presence of pentane. The retention times vs. pentane were averaged and corrected for the previously determined retention time of pentane vs. methane to give Δt. For each temperature ln Δt was plotted vs. $1/T$ (K), giving the linear regression parameters slope = 5113.64, intercept = −13.3874, correlation coefficient = 0.9999, and standard error of the estimate ($S_{y \cdot x}$) = 0.010. ΔH(v → DC-200) at the mean temperature of the measurement range equals (by [1]) −(5113.64)(1.9872) = −10161.83 cal/mol.

The ΔC_p correction requires estimation of the liquid (23) and gaseous (24) heat capacities. C_p(l) for *n*-butylcyclohexane equals the methyl group contribution (8.70) + eight times the methylene contribution (5 ring, 3 side chain) (8 × 7.323 = 58.58) + the methyne group contribution (4.94) + the cyclohexane ring correction factor (−6.66) = 65.56 cal/mol deg. C_p(g) equals 6.19 + 8(5.50) + 4.54 −6.40 = 48.33 cal/mol deg. $\Delta C_p = C_p$(l) − C_p(g) = 17.2 cal/mol deg. The ΔC_p correction from the mean temperature (333.5 K) to 25°C was calculated using eq. [4], treating C_p(l), C_p(g), and ΔC_p as constant within the temperature range of interest: ΔH^{25}(v → DC-200) = −10.16 ±0.05 + (298.2 − 333.5)(0.0174 ±0.05) = −10.77 ±0.07 kcal/mol. From eq. [5] ΔH_v(apparent) = (0.42 ± 0.02) − (−10.77 ± 0.07) = 11.19 ± 0.07 kcal/mol. The corrected value of ΔH_v(eq. [7]) = 0.979(11.19) + 0.854 = 11.81 ± 0.07 kcal/mol.

Results and Discussion

The heats of vaporization at 25°C of nine mono-*n*-alkylcyclohexanes (alkyl = methyl–heptyl, decyl, and dodecyl) are listed in Table 2. Values for the pentyl and hexyl compounds have not previously been reported. Table 2 also indicates available literature values, and the methylene increment between homologous compounds for both the present experimental and literature values.

Comparison with Previous ΔH_v *Measurements*

The agreement between the present experimental gc–calorimetry values and previous measurements (7) is within the combined uncertainties for the methyl, ethyl, propyl, and decyl compounds, and exceeds this margin by 0.03 kcal/mol for the butyl derivative. The literature values for methyl-, ethyl-, and propylcyclohexane result from vaporization calorimetry measurements (results with propylcyclohexane were later confirmed by vapor pressure measurements), and have stated uncertainties of ±0.01 kcal/mol. One is inclined to consider these the values of choice, although the quite uneven methylene increment should be noted (Me $\xrightarrow{1.22}$ Et $\xrightarrow{1.11}$ Pr). It is likely that at least ΔH_v(Et) is in error by considerably more than the stated uncertainty; a value of ~9.61 kcal/mol would be more in line with the methyl and propyl values. The measured value for heptylcyclohexane seems preferable to the earlier value (determined from vapor pressure measurements) on the basis of a more likely methylene group contribution in the C_7–C_{10} interval (1.19 vs. 1.11 per CH_2). There is excellent agreement in the values for decylcyclohexane. The previously measured (by vapor pressure) ΔH_v of 22.33 ±0.30 kcal/mol for dodecylcyclohexane is more than 1 kcal/mol higher than the new value, and is 3.50 kcal/mol higher than the decylcyclohexane value. The methylene increment of 1.75 kcal/mol per CH_2 is unreasonably large, and this dodecylcyclohexane value should be rejected. (Vapor pressure ΔH_v measurements on the methyl esters of the C_8–C_{15} fatty acids (7) show methylene increments of −0.3 to 1.8 kcal/mol, and uncertainties of 0.3–1 kcal/mol. Our unpublished gc–calorimetry values have increments of 1.12–1.28 kcal/mol, and 0.10–0.22 kcal/mol uncertainties.) It is rather typical of high boiling substances such as dodecylcyclohexane (bp 331°C) that static vapor pressure

Can. J. Chem. Downloaded from www.nrcresearchpress.com by 210.87.254.5 on 09/05/12
For personal use only.

TABLE 1. Gas chromatographic retention time for butylcyclohexane

Column temperature (°C)	Average temperature (K)	Retention time (min)	Average retention time (min)	C_5 vs. C_1 time (min)	Corrected retention time (min)
39.1		19.76			
40.5		18.45			
41.1	313.4	17.89	18.70	0.14	18.84
47.4		12.97			
47.5		12.87			
47.5	320.6	12.89	12.91	0.12	13.03
55.0		8.62			
55.1		8.78			
55.1	328.2	8.86	8.75	0.10	8.85
62.9		6.10			
63.0		6.14			
63.0	336.1	6.14	6.13	0.09	6.22
69.4		4.49			
69.5		4.53			
69.6	342.7	4.51	4.51	0.07	4.58
80.4		2.91			
80.4		2.91			
80.4	353.6	2.89	2.90	0.06	2.96

measurements often lead to quite unsatisfactory values of ΔH_v. The error is in the direction which would be anticipated if slight decomposition were to occur at the higher temperatures of P_v measurement. It should be noted, however, that ΔH_v values of high boiling liquids derived from vapor pressure measurements are sometimes unreasonably low, and this implies that pyrolysis is not the only problem inherent in the method.

Errors in the Gas Chromatography – Calorimetry Method

The uncertainties in the measured ΔH_v values (Table 2) at the 99% confidence level are based on an evaluation of the uncertainties in ΔH_s (calorimetric), $\Delta H(v \rightarrow$ DC-200) (gc), $C_p(l)$, $C_p(g)$, and the calibration line [8]. The accuracy of calibration is an important consideration in determining the overall accuracy of the ΔH_v values. Heavily loaded Column II, which was used principally for compounds boiling below ~175°C was calibrated with mesitylene and the C_8, C_9, C_{10}, and C_{12} *n*-alkanes. Lightly loaded Column I, generally used for compounds of bp 175 – >330°C, was calibrated with the same series of five compounds, and also with *n*-tetradecane, 1-hexadecene, and *n*-hexadecane. The extrapolation of this calibration to even higher values has been verified by measurement of ΔH_v of *n*-heptadecane ($\Delta H_v = 20.58 \pm 0.20$ reported (12), 20.56 ± 0.20 kcal/mol) and of 1-octadecene ($\Delta H_v = 21.32 \pm 0.22$; estimated with methylene group increments of 1.18 kcal/mol per CH_2, 21.50 kcal/mol).

The estimated uncertainties in $C_p(l)$ and $C_p(g)$ are 1 cal/mol deg. (21–24). Temperature variation in these quantities are available for relatively few compounds, so one cannot, in general, make these corrections when using eq. [4]. However, [4] has been applied with C_p temperature corrections to the *n*-alkane calibration compounds, propylcyclohexane, and dodecylcyclohexane. Calculated this way the calibration line for Columns I and II both have slopes of 1.00. Propylcyclohexane and dodecylcyclohexane ΔH_v values are 10.63 and 21.29 kcal/mol, respectively, compared with values calculated assuming constant ΔC_p (Table 2) of 10.68 and 21.25 kcal/mol. It is apparent that omission of the temperature variation in $C_p(l)$ and $C_p(g)$ from consideration has had similar effects on both calibration compounds and alkylcyclohexanes, and has introduced only a minor error. The intercept in eqs. [6] and [7] has been related to variation in the (constant pressure) carrier gas flow with temperature by the observation that the intercept is greatly diminished when a crude flow correction is applied to the retention time data used in eq. [3].

Impurities and partial sample decomposition are normally without effect on the value of $\Delta H(v \rightarrow S)$ obtained by the present method, because gas chromatography is intrinsically a separation, as well as a measuring, procedure. In the calorimetric measurement of ΔH_s sample decomposition is highly unlikely because of the low temperature (25°C) and inert character of the solvent (DC-200 silicone fluid). The presence of a small amount of a highly polar impurity in a much less polar sample (such as 1% of a carboxylic acid in an ester sample) may lead to a

Can. J. Chem. Downloaded from www.nrcresearchpress.com by 210.87.254.5 on 09/05/12
For personal use only.

TABLE 2. Enthalpy data for alkylcyclohexanes in DC-200

Alkyl	ΔH_s[a] (ΔT,K)	ΔC_p[b]	Slope	$-\Delta H$(v → S)[c] T_m(25°C)	R ($S_{y\cdot x}$)	ΔH_v (app)[c]	ΔH_v(corr)[c] (Δ/CH$_2$)[d]	ΔH_v(lit)[e] (Δ/CH$_2$)[f]
Me	0.18	11.8	3583.14	7.12	0.9999	7.72	8.46±0.07	8.45±0.01
	(35.3)			(7.54)	(0.007)		(1.11)	(1.22)
C_2	0.27	13.6	4024.58	8.00	0.9997	8.85	9.57±0.09	9.67±0.01
	(42.3)			(8.58)	(0.014)		(1.11)	(1.11)
C_3	0.35	15.4	4413.46	8.77	0.9997	9.98	10.68±0.09	10.78±0.01
	(55.7)			(9.63)	(0.011)		(1.13)	(1.18)
C_4	0.42	17.2	5113.64	10.16	0.9999	11.19	11.81±0.07	11.96±0.05
	(35.3)			(10.77)	(0.009)		(1.12)	(1.18)
C_5	0.50	19.1	5550.71	11.03	0.9999	12.33	12.93±0.08	—
	(42.0)			(11.83)	(0.011)		(1.16)	
C_6	0.59	20.9	5864.51	11.65	0.9998	13.51	14.09±0.12	—
	(60.6)			(12.92)	(0.015)		(1.14)	
C_7	0.70	22.7	6125.39	12.17	0.9998	14.68	15.23±0.13	15.50±0.05
	(79.7)			(13.98)	(0.013)		(1.19)	(1.11)
C_{10}	0.94	28.2	7065.27	14.04	0.9997	18.33	18.81±0.21	18.83±0.10
	(118.9)			(17.39)	(0.018)		(1.22)	(1.75)
C_{12}	1.14	31.8	7674.32	15.25	0.9997	20.83	21.25±0.23	22.33±0.30
	(139.5)			(19.69)	(0.017)			

[a]In kcal/mol, ±0.02; C_{12}, ±0.03.
[b]In cal/mol deg.
[c]In kcal/mol. Uncertainty calculated by eq. [8].
[d]Methylene increment in ΔH_v, kcal/mol. Average 1.15 ± 0.03 kcal/mol.
[e]In kcal/mol (7).
[f]Average, 1.26 ± 0.24 kcal/mol.

measurable error, but such impurities are readily removed by preparative gc. In the alkylcyclohexane series the presence of $<1\%$ of hydrocarbon impurity has no measurable effect on ΔH_s.

It appears that the gc–calorimetry method gives results with relatively low boiling compounds in good agreement with those obtained by direct vaporization calorimetry. The results with higher boiling compounds show a substantial advantage in reliability of the gc–calorimetry procedure over vapor pressure techniques.

1. R. H. STALEY, R. D. WIETING, and J. L. BEAUCHAMP. J. Am. Chem. Soc. **99**, 5964 (1977).
2. E. M. ARNETT, B. CHAWLA, M. TAAGEPERA, W. J. HEHRE, and R. W. TAFT. J. Am. Chem. Soc. **99**, 5729 (1977).
3. D. HARROP, A. J. HEAD, and G. B. LEWIS. J. Chem. Thermodyn. **2**, 203 (1970).
4. P. SELLERS. J. Chem. Thermodyn. **2**, 211 (1970).
5. P. P. S. SALUJA, T. M. YOUNG, R. F. RODEWALD, F. H. FUCHS, and R. FUCHS. J. Am. Chem. Soc. **99**, 2949 (1977).
6. E. M. ARNETT and D. OANCEA. J. Chem. Educ. **52**, 269 (1975).
7. J. D. COX and G. PILCHER. Thermochemistry of organic and organometallic compounds. Academic Press, New York, NY. 1970.
8. I. WADSÖ. Acta Chem. Scand. **14**, 566 (1960).
9. I. WADSÖ. Acta Chem. Scand. **20**, 536 (1966); **22**, 2438 (1968).
10. D. AMBROSE, J. H. ELLENDER, E. B. LEES, C. H. S. SPRAKE, and R. TOWNSEND. J. Chem. Thermodyn. **7**, 453 (1975).
11. D. P. BACCANARI, J. A. NOVINSKI; Y.-C. PAN, M. M. YEVITZ, and H. A. SWAIN, JR. Trans. Faraday Soc. **64**, 1201 (1968).
12. E. MORAWETZ. J. Chem. Thermodyn. **4**, 139 (1972).
13. S. EVERED and F. H. POLLARD. J. Chromatogr. **4**, 451 (1960).
14. W. E. HAMMERS and C. L. DE LIGNY. Recueil, **88**, 961 (1969); **90**, 819 (1971); **90**, 912 (1971).
15. L. A. PEACOCK and R. FUCHS. J. Am. Chem. Soc. **99**, 5524 (1977).
16. J. F. PARCHER, P. H. WEINER, C. L. HUSSEY, and T. N. WESTLAKE. J. Chem. Eng. Data, **20**, 145 (1975).
17. E. F. MEYER. J. Chem. Educ. **50**, 191 (1973).
18. A. B. LITTLEWOOD, C. S. C. PHILLIPS, and D. T. PRICE. J. Chem. Soc. 1480 (1955).
19. S. H. LANGER and J. H. PURNELL. J. Phys. Chem. **67**, 263 (1963).
20. J. E. OBERHOLTZER and L. B. ROGERS. Anal. Chem. **41**, 1234 (1969).
21. R. SHAW. J. Chem. Eng. Data, **14**, 461 (1969).
22. S. W. BENSON. Thermochemical kinetics. Wiley, New York, NY. 1976.
23. M. LURIA and S. W. BENSON. J. Chem. Eng. Data, **22**, 90 (1977).
24. S. W. BENSON, F. R. CRUICKSHANK, D. M. GOLDEN, G. R. HAUGEN, H. E. O'NEAL, A. S. RODGERS, R. SHAW, and R. WALSH. Chem. Rev. **69**, 279 (1969).
25. R. FUCHS and P. S. SALUJA. Can. J. Chem. **54**, 3857 (1976).
26. W. H. DAVIS, JR. and W. A. PRYOR. J. Chem. Educ. **53**, 285 (1976).

Can. J. Chem. Downloaded from www.nrcresearchpress.com by 210.87.254.5 on 09/05/12
For personal use only.

An esr and CIDEP study of the photoreduction of furil

A. JOHN ELLIOT AND JEFFREY K. S. WAN
Department of Chemistry, Queen's University, Kingston, Ont., Canada K7L 3N6
Received April 7, 1978

A. JOHN ELLIOT and JEFFREY K. S. WAN. Can. J. Chem. **56**, 2499 (1978).

The transient free radicals formed when furil was photoreduced have been characterized by esr and CIDEP. Two furil derived radicals were observed: one was the protonated form of the semidione radical (FH·) while the other was an allyl radical formed by radical addition to the furil ring. Initial polarization was observed for FH· which was consistent with the triplet mechanism and these CIDEP results indicate that phenol is a better chemical quencher of the furil triplet than pentachlorophenol which is in turn more efficient than 2-propanol. A method to estimate relative T_1 of radicals is also described.

A. JOHN ELLIOT et JEFFREY K. S. WAN. Can. J. Chem. **56**, 2499 (1978).

On a caractérisé, par rpe et CIDEP, les radicaux libres transitoires formés lorsqu'on photoréduit le furil. On a observé deux radicaux dérivés du furil: l'un existe sous forme protonée du radical semidione (FH·) alors que l'autre est un radical allyle formé par l'addition radicalaire sur le noyau furil. On a observé la polarisation initiale du FH· qui est en accord avec un mécanisme triplet et ces résultats de CIDEP indiquent que le phénol est un meilleur piège chimique pour le triplet furil que le pentachlorophénol qui est luimême plus efficace que le propanol-2. On décrit une méthode pour évaleur les valeurs T_1 relatives des radicaux.
[Traduit par le journal]

Can. J. Chem. Downloaded from www.nrcresearchpress.com by 210.87.254.42 on 09/05/12
For personal use only.

Introduction

Recently we reported the observation of the zero-field CIDNP when furil was photoreduced in the presence of pentachlorophenol (1). Because zero-field CIDNP studies under suitable conditions can provide some unique insights into cage reactions, the furil–phenol system is being developed as a model to examine the detailed theory involved in zero-field and low-field CIDNP studies. To complement this programme, we have characterized by esr the free radicals generated when furil was photoreduced in the presence of different hydrogen donors. The results of this study are presented here.

Experimental

The chemicals were purchased from: PCR (furil), Baker (phenol), Aldrich (pentachlorophenol), Fisher (2-methylphenol, acetonitrile), and Canlab (2-propanol, toluene, chloroform). Phenol, 2-methylphenol, and 2-propanol were sublimed or distilled before use.

As furil is not very soluble in most of the solvents used in these experiments, its concentration depleted rapidly when static solutions were photolysed directly in the esr cavity of a Varian E-3 spectrometer. To circumvent this problem the solutions (which were deoxygenated by bubbling with nitrogen) were flowed through the cavity. The design of the flow cell was similar to that of a conventional cold trap on a vacuum line except that the solution flowed down the centre tube and back up between this tube and the outer jacket to the outlet at the top. The solutions were accelerated through the system by a pressure differential and the flow rate was controlled by a needle valve. In general the flow rate (1–3 ml/min) was adjusted to optimize signal size. The temperature of the solutions in the cavity were controlled by flowing thermostatted nitrogen gas by the spectrosil flow cell. The 1000 W light source, rotating sector, data acquisition system, and the method used to measure initial polarizations have been described elsewhere (2). The esr simulations were performed on a Nicolet 1180 computer.

Results

Photolysis of Furil: 2-Propanol Solutions

(*a*) No phenols present.

Only the neutral furil radical (FH·) was observed by esr when furil was photoreduced in 2-propanol.

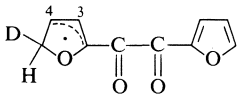

1

The hyperfine coupling constants and their tentative assignments are: $a_3^H = 0.56$ mT; $a_4^H = 0.09$ mT; $a_5^H = 0.47$ mT; $a_{3'}^H = a_{5'}^H = 0.09$ mT; $a_{4'}^H < 0.03$ mT. A temperature-dependent coupling constant (0.09 mT (−30°C), 0.04 mT (0°C), <0.02 mT (20°C)) is assigned to the hydroxyl proton. These constants and assignments differ slightly from those previously published (1). A *g*-factor of 2.0035 was estimated for this radical by comparison to the spectrum of the phenoxy radical whose *g*-factor was assumed to be 2.0048 (3) (see next section).

When the light beam was chopped with the rotating sector, no initial polarization was evident in the CAT traces of the time profile of the furil radical.

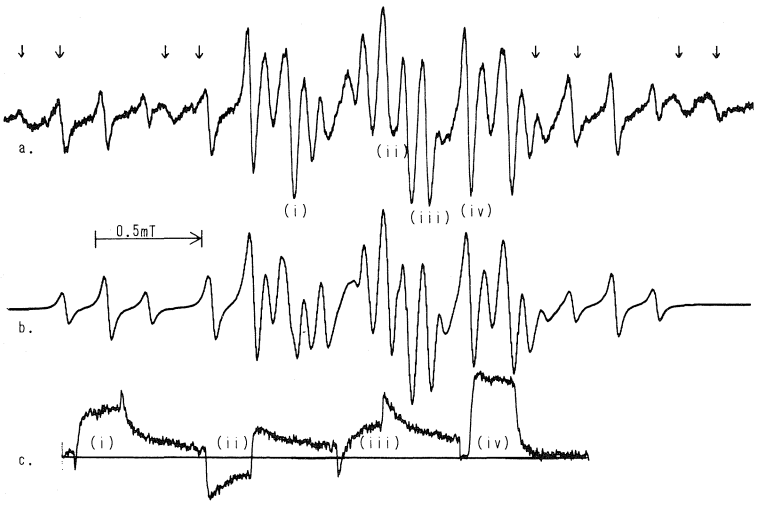

FIG. 1. (*a*) The esr spectrum observed when a furil:2-propanol solution containing 1.28 mol dm^{-3} phenol was photolysed at −30°C. The arrows indicate radical **1**. (*b*) The simulated esr spectrum of furil and phenoxy radical. (*c*) The time profiles of the peaks which are indexed in (*a*).

(*b*) With a phenol present.

When a furil:2-propanol solution containing either phenol, 2-methylphenol, or pentachlorophenol was photolysed, three radicals were always observed: the furil radical, the phenoxy radical, and a third radical (**1**) whose identity we will discuss later.

The spectrum recorded when a furil:2-propanol solution containing 1.28 mol dm^{-3} phenol was photolysed at −30°C is shown in Fig. 1*a*. (The lines from radical **1** are indicated by arrows.) The furil radical spectrum showed strong emissive initial polarization (triplet mechanism) (2, 4) whereas the other two radicals were unpolarized. In fact it was by mapping the polarization of the different peaks (see Fig. 1*c*) that enabled us to assign the furil radical in this overlapped spectrum. A simulated spectrum of just the phenoxy and furil radical is shown in Fig. 1*b*. (It is from the *g*-difference of 0.172 mT (i.e. ΔH) between the two radicals that the furil *g*-factor was estimated in the previous section, from the expression $g = g_{\text{phenol}}(1 - \Delta H/H)$ where H is the magnetic field of the spectrum centre and $\Delta H = 0.172$ mT.) The agreement is very good and what small discrepancies there are arise predominantly from the radical pair polarization which is also present. With radical pair (E–A) polarization the high-field peaks are larger than the corresponding low-field peaks (2, 4).

With 2-methylphenol (1.16 mol dm^{-3}) present in the furil:2-propanol solution, the 2-methylphenoxy radical was observed along with the furil radical and radical **1**. The furil radical was still strongly initially polarized but, in this case, the 2 methylphenoxy radical also shows a small initial polarization. Radical **1** was unpolarized.

With pentachlorophenol, three radicals were again observed. The pentachlorophenoxyl radical appeared as a broad low intensity resonance to the low field side of the furil spectrum, and because it was not obscured by the phenoxy radical, the spectrum of radical **1** could be seen clearly. (These general features can be seen in Fig. 2 although the solvent in this case was 10 vol% 2-propanol:toluene.) At the highest pentachlorophenol concentration studied (1.2 mol dm^{-3}), the furil radical exhibited a small emissive initial polarization.

Photolysis of Furil in Other Solvents

The photoreduction of furil was carried out in a number of other solvent systems. A 10 vol% 2-propanol:toluene system was used because past experience has shown that larger steady-state polarizations are often observed due to the shorter half-life of the radicals (see later). Acetonitrile is a solvent we commonly used in CIDNP experiments but because of its high absorptivity of microwaves at 9.0 GHz it had to be diluted with toluene to recover the cavity *Q*. A 25 vol% acetonitrile:toluene mixture was used. Chloroform solutions were also studied as this solvent is currently used for the CIDNP studies of furil.

(*a*) No phenols present.

Photolysis of furil in all three solvents at −30°C gave the spectrum of the furil radical. (Photolysis of furil alone in toluene gave no observable esr spec-

Can. J. Chem. Downloaded from www.nrcresearchpress.com by 210.87.254.42 on 09/05/12
For personal use only.

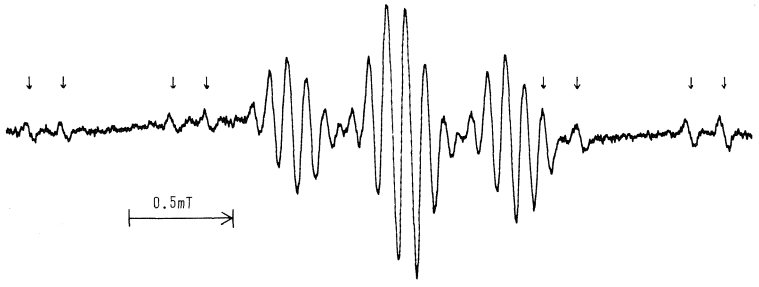

FIG. 2. The esr spectrum observed when a furil:10 vol% 2-propanol:toluene solution containing 0.5 mol dm^{-3} pentachlorophenol was photolysed at $-30°C$. The arrows indicate radical **1**.

trum.) In 10 vol% 2-propanol:toluene, the coupling constants were the same as for the 2-propanol solvent. For the other two solvents, the spectra were weaker than that observed in the 2-propanol:toluene solvent, and the coupling constants for protons 3 and 5 were a little larger ($a_3^H = 0.50$ mT, $a_5^H = 0.59$ mT). When chloroform was the solvent, a second, even weaker, spectrum was detected which was very similar to that of radical **1**.

(*b*) With a phenol present.

In all three solvent systems after the addition of phenol, the unpolarized spectrum of the phenoxy radical and radical **1** were observed along with a strongly emissively polarized furil radical spectrum.

The spectrum observed during the photolysis of a furil:10 vol% 2-propanol:toluene solution containing pentachlorophenol at $-30°C$ is shown in Fig. 2. The intense centre spectrum is that of the furil radical, radical **1** is indicated by the arrows and the pentachlorophenoxy radical by a broad resonance to the lowfield side of the spectrum. In this case none of the radicals were polarized but at higher pentachlorophenol concentration emissive initial polarization was observed in the furil radical spectrum. If 2-propanol was not present in these solutions, the spectrum was weaker and some extra peaks comparable in size to those of radical **1** were observed.

The solubility of pentachlorophenol in chloroform is low but when a 0.1 mol dm^{-1} pentachlorophenol–furil–chloroform solution was photolysed, all three radicals (furil, phenoxy, and **1**) were observed. None were polarized.

Discussion

The observation of initial polarization in the furil radical when phenols were present indicates that a spin polarized triplet state must be involved in the photochemical mechanism (2, 4). If we signify furil as F and the hydrogen donor as HD, the photoreduction can be written as

[1] $$F \xrightarrow{h\nu} {}^1F^* \xrightarrow{ISC} {}^3F$$

[2] $$^3F + HD \rightarrow FH^{\cdot} + D^{\cdot}$$

When HD was 2-propanol, the counter radical D$^{\cdot}$ was not observed because the following reaction (by analogy to biacetyl and pyruvic acid) (5, 6) probably occurred rapidly

[3] $$F + (CH_3)_2\dot{C}OH \rightarrow FH^{\cdot} + (CH_3)_2CO$$

The fate of the counter radicals, D$^{\cdot}$, when phenol, chloroform, or acetonitrile was the hydrogen donor is not certain. In the case when phenol was HD, the half life of the phenoxy radical was far shorter than that of the furil radical (compare, in Fig. 1*c*, trace (*iii*) which is predominantly from FH$^{\cdot}$ to that of (*iv*) of the phenoxy radical). The rate of decay of the phenoxy radical in this system was far greater than when it was generated by photolysing a biacetyl:phenol:2-propanol solution. This suggests that the phenoxy radical reacted through mechanisms other than bimolecular radical–radical reactions. One possibility is the formation of radical **1**.

Provided that only one peak of radical **1** is overlapped by the furil radical spectrum in Fig. 2, its hyperfine coupling constants are: $a^H = 0.17$ mT; 0.67 mT; 2.42 mT. Similar splittings for radical **1** were found regardless which phenol was present or if the reduction of furil was carried out in chloroform alone. A good candidate for **1** is a radical adduct of the form

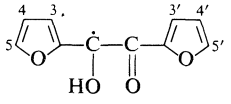

(FH$^{\cdot}$)

where the donor radical has added to the 5 position of the furan ring. These coupling constants are similar to those of related allyl type radical adducts

Can. J. Chem. Downloaded from www.nrcresearchpress.com by 210.87.254.42 on 09/05/12
For personal use only.

formed from substituted furans which have been studied elsewhere (7, 8).

The CIDNP observation (1) suggests that in the primary cage, reaction [4] occurred.

[4] $$FH^{\cdot} + C_4Cl_5O^{\cdot} \rightarrow F + C_4Cl_5OH$$

However, at this point it is not possible to estimate what proportion of radicals underwent this reaction. Presumably the other counter radicals also underwent similar cage reactions.

From the observed electron polarizations, it can be concluded that phenol was a more efficient hydrogen donor than pentachlorophenol which in turn was better than 2-propanol. The basis for this statement is that the enhancement factor V for the polarization generated in the radicals by reaction [2] is given by (2, 4)

[5] $$1/V = 1/V_0 + 1/(V_0{}^3T_1k_q[HD])$$

where V_0 is the enhancement factor at infinite hydrogen donor concentration, ${}^3T_1$ is the spin–lattice relaxation time of the furil triplet, and k_q is the rate constant for reaction [2]. V is related to observed steady state enhancement factor V_{ss} by the relationship

[6] $$V = V_{ss}t_{1/2}/T_1$$

where $t_{1/2}$ is the radical half life and T_1 is the spin–lattice relaxation time. For a given radical and solvent, V_0, ${}^3T_1$, and T_1 are constants, so, for a given hydrogen donor concentration, the HD which generates the larger value of $V_{ss}t_{1/2}$ must have the larger k_q. Because of the severe overlapping of the different spectra, e.g. see Fig. 1*a*, it was impractical to carry out quantitative studies. However, from the magnitudes of the polarizations observed in the furil radical with different hydrogen donors present, it can be said that phenol and 2-methylphenol are comparable as hydrogen donors to the furil triplet and that they are somewhat better than pentachlorophenol which, in turn, is better than 2-propanol.

Some estimate of the *relative* T_1's of the two radicals formed in the photoreduction can be made if the enhancement factor for both radicals can be measured (2). The triplet mechanism predicts that both radicals will be generated with the same V, but the observed V_{ss} of each radical depends on its $t_{1/2}$ and T_1 (eq. [6]). As noted earlier, in these experiments overlapping spectra precluded accurate V_{ss} measurements, but estimates of V_{ss} and $t_{1/2}$ from the CAT traces for the furil radical and 2-methoxyphenoxy radical in 2-propanol indicate that T_1 for the former is about 50 times greater than that for the latter. For the phenoxy radical (in 2-propanol) where no polarization was observed, its T_1 must be at least 100 times less than that of the furil radical. It is not surprising that the T_1 of the 2-methylphenoxy radical is at least twice that of the phenoxy radical as this parallels the behaviour of the T_1 of 2-methylbenzosemiquinone and benzosemiquinone radical anions (9).

Acknowledgements

This research is supported by the National Research Council of Canada. The authors are grateful to Dr. J. deBoer for helpful discussions.

1. H. M. Vyas and J. K. S. Wan. Mol. Phys. **34**, 887 (1977).
2. A. J. Elliot and J. K. S. Wan. J. Phys. Chem. **82**, 444 (1978).
3. P. Neta and R. W. Fessenden. J. Phys. Chem. **78**, 523 (1974).
4. J. K. S. Wan and A. J. Elliot. Acct. Chem. Res. **10**, 161 (1977).
5. K. Y. Choo and J. K. S. Wan. J. Am. Chem. Soc. **97**, 7127 (1975).
6. P. B. Ayscough and R. C. Sealy. J. Chem. Soc. Perkin II, 544 (1973); 1402 (1974).
7. T. Shiga and A. Isomoto. J. Phys. Chem. **73**, 1139 (1969).
8. R. H. Schuler, G. P. Laroff, and R. W. Fessenden. J. Phys. Chem. **77**, 456 (1977).
9. S. K. Rengan, M. P. Khakhar, D. S. Praehananda, and B. Nenkataraman. Pramāna, **3**, 95 (1974).

Can. J. Chem. Downloaded from www.nrcresearchpress.com by 210.87.254.42 on 09/05/12
For personal use only.

An electron spin resonance study of organomercury adducts of phenanthroquinone

KUANG S. CHEN, RICHARD T. SMITH, AND JEFFREY K. S. WAN
Department of Chemistry, Queen's University, Kingston, Ont., Canada K7L 3N6

Received April 26, 1978

KUANG S. CHEN, RICHARD T. SMITH, and JEFFREY K. S. WAN. Can. J. Chem. **56**, 2503 (1978).

The exchange reaction between $M^+PQ^{-\cdot}$ ion-pairs and MeHgCl leads to the formation of $MeHgPQ^{\cdot}$ adduct with a characteristic low *g*-factor of 2.00052 and a small methyl proton splittings of 0.16 G. The dynamic and equilibrium aspects of the exchange depend upon the alkali cation, the concentration of MeHgCl, and for $Na^+PQ^{-\cdot}$ also on temperature. The $MeHgPQ^{\cdot}$ is found to be relatively stable at room temperature and in the presence of water. These results may be of potential value to toxicology studies of methylmercury.

KUANG S. CHEN, RICHARD T. SMITH et JEFFREY K. S. WAN. Can. J. Chem. **56**, 2503 (1978).

La réaction d'échange entre les paires d'ions $M^+PQ^{-\cdot}$ et le MeHgCl conduisent à la formation d'un adduit $MeHgPQ^{\cdot}$ caractérisé par un facteur *g* bas de 2.00052 et un couplage faible du proton méthylique de 0.16 G. Les aspects dynamiques et d'équilibre de l'échange dépendent du cation alcalin, et de la concentration de MeHgCl; dans le cas du $Na^+PQ^{-\cdot}$ ils dépendent aussi de la température. On a trouvé que le $MeHgPQ^{\cdot}$ est relativement stable à la température ambiante et en présence d'eau. Ces résultats peuvent avoir une valeur potentielle pour des études de toxicologie du méthylmercure.

[Traduit par le journal]

Can. J. Chem. Downloaded from www.nrcresearchpress.com by 210.87.254.42 on 09/05/12
For personal use only.

Introduction

The ability of *o*-quinones such as the 9,10-phenanthroquinone (PQ) to form paramagnetic adducts with organometals has recently been emphasized (1). Among the controversial heavy metal environmental contaminants, Pb and Sn adducts with camphorquinone (2) and with PQ (1) have been extensively investigated but few Hg adducts with *o*-quinones had been reported (3). Methylmercury poisoning has generally been acknowledged as an environmental health hazard and in biological systems methylmercury is known to complex with sulfhydryl groups (4). Recent toxicology and biochemical studies (5, 6) show that despite the thermodynamic stability of these diamagnetic methylmercury complexes, ligand exchanges are sufficiently fast so that *N*-acetyl-D,L-penicillamine (5) can be used to extract methylmercury from the red blood cell and tissues. Such chemotherapeutic agents can function as metal regulators if they initially carry essential metals such as Na or K and deliver them to tissues by selectively exchanging and binding the toxic metal which subsequently can be excreted. The present work investigates by esr spectroscopy the specific exchange reactions of paramagnetic alkali–PQ ion-pairs with organomercury compounds leading to relatively stable paramagnetic R—Hg—PQ adducts.

Experimental

9,10-Phenanthroquinone (anthraquinone-free) and $NaBPh_4$ were supplied by Aldrich and the organomercury compounds used were obtained from Alfa. $KBPh_4$ was prepared by the method of Plafaum and Howick (7). Solvents such as tetrahydrofuran (THF), 2-methyltetrahydrofuran (MTHF), and *N*,*N*′-dimethylformamide (DMF) were refluxed over molecular sieves, distilled, and stored over K/Na alloy or molecular sieves under vacuum. Procedures for sample preparations of ion-pairs and the addition of organometals are similar to the method described previously (8). Electron spin resonance spectra were recorded on a Bruker 420 spectrometer with 100 kHz modulation. Magnetic field was monitored by a Bruker nmr oscillator and *g*-factor measurements were made using the potassium naphthalene ion-pair in THF as an external standard (9). Unless otherwise stated, all experiments were carried out at room temperature, 20°C.

Results and Discussion

Most of the previous alkali–PQ ion-pair and their spin adduct studies (1) were carried out in pure THF solvent in which any trace of water had been painstakingly removed. It was demonstrated that in the alkali–PQ ion-pair systems, when THF was pumped off under vacuum and replaced by DMF solvent, the $M^+PQ^{-\cdot}$ ion-pair would dissociate and the radical anion $PQ^{-\cdot}$ (**1**) would be observed. In this study of organomercury–PQ adducts it became desirable that a high concentration of water be present in order to show that mercury–PQ adducts could be observed in biological systems. Therefore, deionized and distilled water was added to THF, wherever desired, to give a 1:5 vol ratio mixture at approximately a pH of 7. A drastic change in the ratio to 3:5 did not appear to affect the esr results. For the $M^+PQ^{-\cdot}$ systems, the addition of water caused the ion-pair to dissociate and the radical anion $PQ^{-\cdot}$ (**2**) to be observed. The

Can. J. Chem. Downloaded from www.nrcresearchpress.com by 210.87.254.42 on 09/05/12
For personal use only.

TABLE 1. Electron spin resonance parameters of anion radicals, ion pairs, and organometal adducts of phenanthroquinone in THF at 20°C[f]

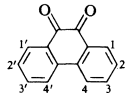

System	g	a_M (G)	$a_{1,1'}$ (G)	$a_{2,2'}$ (G)	$a_{3,3'}$ (G)	$a_{4,4'}$ (G)	a_{CH_3} (G)
MeHgPQ·	2.00052±0.00003		1.69	0.41	1.85	0.41	0.16
Me_3SnPQ·	2.00402	7.05, 7.43[a]	1.84	0.43	1.84	0.43	n.s.
Me_3PbPQ·	2.00433	2.63[b]	1.70	0.41	1.70	0.41	n.s.
Na^+PQ^{-}·	2.00460	0.48[c]	1.43	0.28	1.72	0.43	
K^+PQ^{-}·	2.00464	n.s.	1.43	0.26	1.68	0.44	
PQ^{-}·(I)[d]	2.00485		1.34	0.21	1.67	0.42	
PQ^{-}·(II)[e]	2.00449		1.54	0.32	1.70	0.41	

[a] ^{117}Sn ($I = \frac{1}{2}$, 7.67%), ^{119}Sn ($I = \frac{1}{2}$, 8.68%), $a(^{119}Sn)/a(^{117}Sn) = 1.04$.
[b] ^{207}Pb ($I = \frac{1}{2}$, 21.11%).
[c] ^{23}Na ($I = \frac{3}{2}$, 100%).
[d] In pure DMF.
[e] In mixture of THF and H_2O (volume ratio 5:1).
[f] Hyperfine coupling constants are accurate to ±0.01 G.

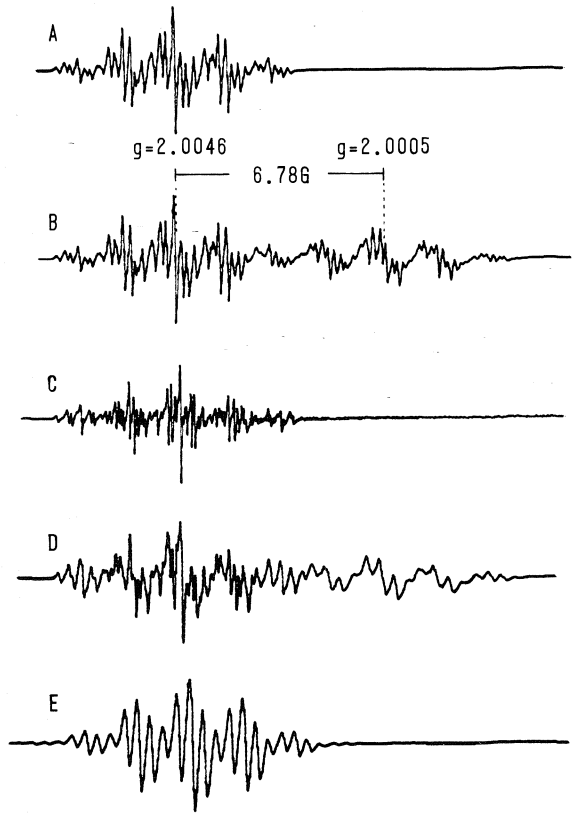

FIG. 1. Electron spin resonance spectra of (*A*) K^+PQ^{-}· ion pair in THF at −30°C, (*B*) K^+PQ^{-}· ion pair and MeHgPQ· adduct in THF at −30°C, (*C*) PQ^{-}·(II) anion radical in the mixture of THF and H_2O (volume ratio 5:1) at −10°C, (*D*) PQ^{-}·(II) anion radical and MeHgPQ· adduct in the mixture of THF and H_2O (volume ratio 5:1), the signal gain of PQ^{-}·(II) anion radical has been attenuated to $\frac{1}{6}$ of that of MeHgPQ· adduct, and (*E*) Me_3PbPQ· adduct in THF at 20°C.

esr parameters of the PQ anion radicals (**1**) and (**2**) are slightly different (Table 1) due to the changes in the solvent. A typical esr spectrum of the K^+PQ^{-}· ion-pair in pure THF is shown in Fig. 1*a* and the same system in THF/H_2O mixture exhibits only the spectrum of PQ^{-}· (**2**) (Fig. 1*c*).

It has been demonstrated (1, 8) in THF that exchanges of cations among alkali–PQ ion-pairs are very specific. For example,

$$[1]\quad K^+PQ^{-}\cdot + NaBPh_4 \xrightarrow{THF} Na^+PQ^{-}\cdot + KBPh_4$$

reaction [1] would proceed instantaneously to completion whereas the exchange involving Na^+PQ^{-}· and $KBPh_4$ in THF would not proceed at all. These specific cation exchange reactions do not appear to be dependent upon the salt concentrations. Exchanges with organometals such as Me_3SnCl and Et_3PbOTf are also rapid and complete at room temperature (1). However, when a trace amount (1 mg or less) of MeHgCl was introduced at room temperature into a THF solution containing the K^+PQ^{-}· ion-pairs, the exchange reaction

$$[2]\quad K^+PQ^{-}\cdot + MeHgCl \xrightarrow{THF} MeHgPQ\cdot + KCl$$

was not complete and the esr spectrum (Fig. 1*b*) clearly showed the coexistence of both the K^+PQ^{-}· and the adduct MeHgPQ·. The concentration of the K^+PQ^{-}· ion-pair was estimated to be about 10^{-2} *M*. When the concentration of the MeHgCl was substantially less than that of the K^+PQ^{-}·, the extent if the exchange as measured by the ratio [MeHgPQ·]/[K^+PQ^{-}·] was not significantly dependent upon temperature (within the experimental range between −67 and 20°C). Addition of more

Can. J. Chem. Downloaded from www.nrcresearchpress.com by 210.87.254.42 on 09/05/12
For personal use only.

MeHgCl (up to 2 mg) would force the exchange to proceed further but slowly to completion, usually upon standing for 3 to 4 h. In another set of experiments in which the initial concentration of MeHgCl was made greater than $K^+PQ^{-\cdot}$ concentration, both $K^+PQ^{-\cdot}$ and $MeHgPQ^{-\cdot}$ were still observable upon mixing but the concentration of $K^+PQ^{-\cdot}$ could be seen slowly decreasing to zero.

The dynamic behaviour of the exchange between $Na^+PQ^{-\cdot}$ and MeHgCl was somewhat different. For example, the addition of 1 mg MeHgCl to a THF solution containing approximately 10^{-2} *M* of $Na^+PQ^{-\cdot}$ at temperatures below $-5°C$ did not lead to any observable exchange. Only when temperature was raised to above $-5°C$ has the esr spectrum of the MeHgPQ· radical become detectable. After an appreciable amount of the adduct MeHgPQ· was formed at higher temperatures, lowering the temperature to $-60°C$ again resulted in the observation of only the $Na^+PQ^{-\cdot}$. This result suggests that the exchange between MeHgCl and $Na^+PQ^{-\cdot}$ is more dependent on temperature.

When water was added to the $K^+PQ^{-\cdot}$ and MeHgPQ· system in THF, the esr spectrum changed from that in Fig. 1*b* to Fig. 1*d*. Careful examination of the spectra showed that upon the addition of water, almost all of the coexisting $K^+PQ^{-\cdot}$ ion-pairs dissociated to solvated K^+ and $PQ^{-\cdot}$ (**2**) but most of the MeHgPQ· adduct remained intact with only some loss of line resolution. It is particularly significant to biological systems which contain large concentration of water at a pH around 7 that the paramagnetic adduct MeHgPQ· can survive under such conditions for at least several days. Furthermore, the concentration of $PQ^{-\cdot}$ (**2**) became significantly larger (about 10 times) than the initial concentration of the precursor $K^+PQ^{-\cdot}$ before water was added. Although a small part of the $PQ^{-\cdot}$ (**2**) concentration may have been derived from the dissociation of the MeHgPQ· adduct in THF/H_2O, the main reason for the observation is probably due to the following equilibrium (10).

[3]
$$\begin{array}{ccc} 2K^+PQ^{-\cdot} & \underset{}{\overset{THF}{\rightleftharpoons}} & (K^+PQ^{-\cdot})_2 \\ \text{paramagnetic} & & \text{diamagnetic} \\ \downarrow +H_2O & & \downarrow +H_2O \\ 2K_{aq}^+ + 2PQ^{-\cdot}(\mathbf{2}) & & 2K_{aq}^+ + 2PQ^{-\cdot}(\mathbf{2}) \end{array}$$

A scheme based upon cation selection of $PQ^{-\cdot}$ (**2**) at $-60°C$ in THF and various exchange reactions can be summarized to account for the aforementioned observations at 20°C:

[4]
$$PQ^{-\cdot}(\mathbf{2}) \xleftarrow[(20°C)]{+H_2O} K^+PQ^{-\cdot} \underset{K^+BPh_4^-}{\overset{Na^+BPh_4^-}{\rightleftharpoons}} Na^+PQ^{-\cdot} \xrightarrow[(20°C)]{+H_2O} PQ^{-\cdot}(\mathbf{2})$$

$$[MeHgPQ^{\cdot} + PQ^{-\cdot}(\mathbf{2})] \xleftarrow[(20°C)]{+H_2O} MeHgPQ^{\cdot} \quad (K^+BPh_4^-,\ MeHgCl) \quad (Na^+BPh_4^-,\ MeHgCl,\ (20°C))$$

The esr spectrum of the MeHgPQ· adduct shown in Fig. 1*b* is clearly different from that of the $K^+PQ^{-\cdot}$ ion-pair. Although the ^{199}Hg ($I = \frac{1}{2}$, 16.86%) and the ^{201}Hg ($I = \frac{3}{2}$, 13.24%) hyperfine splittings were not resolved, the small proton splittings from the methyl group in the MeHg moiety were observed and are reported along with the proton splittings from the PQ moiety in Table 1. The uniquely low *g*-factor of 2.00052 is characteristic of the *o*-quinone–organomercury adducts (4), and this feature affords the possibility of simultaneous quantitative monitoring of the slow exchange between $M^+PQ^{-\cdot}$ and MeHgCl. In order to confirm the assignment of the observed spectrum to MeHgPQ·, a series of separate experiments was performed to generate various organomercury–PQ adducts including the MeHgPQ· by different methods. These can generally be represented by the following reaction scheme (1):

[5]
$$\begin{array}{ccc} PQ + PhHgPh & \underset{\text{or } \Delta}{\overset{h\nu}{\longrightarrow}} & PQ^{-\cdot} + PhHg^{+\cdot}Ph \\ & & \downarrow \\ PhHg\dot{P}Q & \xleftarrow{PQ^{-\cdot}} & PhHg^+ + Ph^{\cdot} \\ (g = 2.00019) & & \end{array}$$

The esr parameters of two of these adducts, PhHgPQ· and $PhCH_2HgPQ^{\cdot}$, are listed in Table 2. The small methylene splittings in the $PhCH_2HgPQ^{\cdot}$ are very similar to the methyl splittings in MeHgPQ·. In the

TABLE 2. Electron spin resonance parameters of mercury, thallium, and lead adducts of phenanthroquinone in MTHF at 20°C[f]

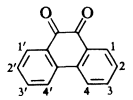

System	g	a_M (G)	$a_{1,1'}$ (G)	$a_{2,2'}$ (G)	$a_{3,3'}$ (G)	$a_{4,4'}$ (G)	a_{CH_2} (G)
$PhCH_2HgPQ^{\cdot}$[a]	2.00023 ± 0.00003		1.85	0.42	1.85	0.42	0.11
$PhHgPQ^{\cdot}$	2.00019	0.83[c]	1.78	0.41	1.78	0.41	
$PhTlPQ^{\cdot}$[b]	2.00331	9.08[d]	1.60	0.38	1.70	0.39	
$Ph_3PbPQ^{\cdot}$	2.00352	3.11[e]	1.77	0.41	1.77	0.41	

[a] In benzene at 15°C.
[b] Data taken from ref. 14.
[c] ^{199}Hg ($I = \frac{1}{2}$, 16.86%).
[d] ^{203}Tl ($I = \frac{1}{2}$, 29.52%), ^{205}Tl ($I = \frac{1}{2}$, 70.48%), $a^{203}Tl/a^{205}Tl = 0.99$.
[e] ^{207}Pb ($I = \frac{1}{2}$, 21.11%).
[f] Hyperfine coupling constants are accurate to ± 0.01 G.

$PhHgPQ^{\cdot}$ adduct, the ^{199}Hg hyperfine splittings were resolved but the ^{201}Hg were not. ^{201}Hg has a nuclear spin of 3/2 and a natural abundance of 13.24% which will render the expected smaller ($a_{^{201}Hg}/a_{^{199}Hg} = -0.37$) splittings too weak for observation.

A detailed accounting of the low g-factor characteristic of all the reported $RHgPQ^{\cdot}$ adducts awaits further theoretical analysis. Nevertheless, we wish to point out here some related experimental observations and some possible empirical approaches.

A d–p π-bonding mechanism has been proposed to explain the observed trend of g-factor for Group IVB-substituted methyl radicals (11) and ethyl radicals (12). Excitation of the unpaired electron into the vacant metal d-orbitals will decrease the g-factor by a value proportional to $\lambda_d/\Delta E$ (13) where λ_d is the one-electron spin–orbit coupling constant of the metal d-orbit and ΔE is the difference in energies between the vacant metal d-orbital and the orbital of the unpaired electron. For comparison, we have prepared the $Me_3PbPQ^{\cdot}$ adduct by a similar exchange reaction with $K^+PQ^{-\cdot}$ and the resulting esr spectrum (Fig. 1*e*) has a g-factor of 2.00433. The $Me_3SnPQ^{\cdot}$ adduct also does not have a *low* g-factor (Table 1). While $PhHgPQ^{\cdot}$ has a low g-factor of 2.00019, $Ph_2TlPQ^{\cdot}$ (14) was reported to have a g-factor of 2.00331 and our experiment showed that $Ph_3PbPQ^{\cdot}$ has a similar high g-factor of 2.00352. Thus, the low g-factor of ~ 2.0002 is truly characteristic of the *organomercury–quinone* adducts. It is perhaps worthwhile to note here that there are many other transition metal complexes in solution which have an isotropic g-factor near or below the free spin value.

Both tin and lead–PQ adducts indeed show a smaller g-factor than the corresponding anion radical but the decrease is far less than that of organomercury PQ adducts. In applying the d–p π-bonding mechanism to $Me_3PbPQ^{\cdot}$, the ΔE represents the difference in energies between the vacant Pb 6d-orbital and the one-electron orbital. With the organomercury–PQ adduct, ΔE is the difference in energies between the one-electron orbital and the vacant Hg 5d-orbital created by the promotion of one 5d electron to 6p orbital. The resulting sp^2 hybrid for the mercury atom enables a coordination number of 3 in forming organomercury–PQ adducts.[1] Such a mechanism will greatly reduce the value of ΔE in the organomercury–PQ adducts which in turn will lower the g-factor.

Conclusion

Paramagnetic $MeHgPQ^{\cdot}$ adducts are stable for several days in THF/H_2O mixture and their uniquely low g-factor affords a potential analytical method for methylmercury in biological systems. The ability of the alkali–PQ ion-pairs to exchange with methylmercury appears to be useful and should be further explored in biological systems.

Acknowledgments

This research is supported by the National Research Council of Canada. The authors are grateful to Dr. M. Singer for some helpful discussion.

1. K. MOCHIDA, J. K. KOCHI, K. S. CHEN, and J. K. S. WAN. J. Am. Chem. Soc. **100**, 2927 (1978).
2. A. HUDSON, R. A. JACKSON, and N. P. C. SIMMONS. J. Chem. Soc. Perkin II, 1633 (1977).
3. G. A. ABAKUMOV, E. N. GLADYSHEV, N. S. VYAZANKIN, G. A. RAZUVAEV, P. YA. BAYUSHKIN, and V. A. MURAEV. J. Organomet. Chem. **64**, 327 (1974).
4. D. D. PERRIN. Top. Current Chem. **64**, 181 (1976).
5. J. AASETH. Acta Pharmacol. Toxicol. **39**, 289 (1976).

[1] A bridged structure has been postulated for phenylmercury alkoxide complexes in which the Hg atom has a coordination number of 3 (15).

Can. J. Chem. Downloaded from www.nrcresearchpress.com by 210.87.254.42 on 09/05/12
For personal use only.

6. D. L. RABENSTEIN and C. A. EVANS. Bioinorg. Chem. **8**, 107 (1978).
7. R. P. PLAFAUM and L. C. HOWICK. Anal. Chem. **28**, 1542 (1956).
8. K. S. CHEN and H. HIROTA. J. Am. Chem. Soc. **94**, 5550 (1972).
9. V. G. WILLIAMS, R. J. PRITCHETT, and G. K. FRAENKEL. J. Chem. Phys. **52**, 5584 (1970).
10. K. MARUYAMA. Bull. Chem. Soc. Jpn. **37**, 553 (1964).
11. J. H. MACKEY and D. E. WOOD. Mol. Phys. **18**, 783 (1970).
12. T. KAWAMURA and J. K. KOCHI. J. Am. Chem. Soc. **94**, 648 (1972).
13. A. J. STONE. Mol. Phys. **6**, 509 (1963); **7**, 311 (1964).
14. H. B. STEGMANN, K. B. ULMSCHNEIDER, and K. SCHEFFLER. J. Organomet. Chem. **101**, 145 (1975).
15. A. J. BLOODWORTH. J. Chem. Soc. C, 2051 (1970).

Can. J. Chem. Downloaded from www.nrcresearchpress.com by 210.87.254.42 on 09/05/12
For personal use only.

A revised structure for aubergenone, a sesquiterpenoid related to eudesmane: synthesis of 4-*epi*-aubergenone

RONALD B. KELLY, SANDRA J. ALWARD, AND K. SURYANARAYANA MURTY
Department of Chemistry, University of New Brunswick, P.O. Box 5050, Saint John, N.B., Canada E2L 4L5
AND
J. B. STOTHERS
Department of Chemistry, University of Western Ontario, London, Ont., Canada N6A 5B7
Received May 11, 1978

RONALD B. KELLY, SANDRA J. ALWARD, K. SURYANARAYANA MURTY, and J. B. STOTHERS. Can. J. Chem. **56**, 2508 (1978).

Syntheses of 4-*epi*-aubergenone, a sesquiterpenoid related to eudesmane, are described. One synthesis afforded this sesquiterpenoid as a racemate (**12**) whereas another, utilizing (+)-carissone as starting material, afforded an enantiomer (**12***a*). The fact that naturally occurring aubergenone is the C(4) epimer of the thermodynamically more stable synthetic **12** was revealed by the discovery that it was completely converted into the latter by treatment with base. This epimeric relationship is substantiated by comparison of the nmr spectra of the two isomers. Evidence requiring the reformulation of the structure of aubergenone as **13** is adduced.

RONALD B. KELLY, SANDRA J. ALWARD, K. SURYANARAYANA MURTY et J. B. STOTHERS. Can. J. Chem. **56**, 2508 (1978).

On décrit la synthèse de l'*epi*-4 aubergénone, un sesquiterpénoïde relié à l'eudesmane. Une synthèse à permis d'obtenir ce sesquiterpénoïde sous forme de racémique (**12**) alors qu'une autre, faisant appel à la (+)-carissone comme produit de départ, conduit à l'énantiomère (**12***a*). Le fait que l'aubergénone naturelle est l'épimère C(4) du produit de synthèse **12** thermodynamiquement le plus stable a été mis en évidence par la découverte qu'il peut être complètement transformé dans ce dernier par traitement avec une base. On a confirmé que ces produits sont des épimères par une comparaison des spectres rmn des deux isomères. On a ajouté des données nécessaires qui permettent de reformuler la structure de l'aubergénone sous forme de **13**.

[Traduit par le journal]

In 1975, the isolation of several metabolites, produced by incubation of eggplant fruit (*Solanum melongena*) with spore suspensions of *Monolinia fructicola* and other fungi, was reported (1). Among the isolated metabolites was a sesquiterpenoid for which the eudesmane related structure **12** was proposed and for which the name aubergenone has since been adopted.

We have completed a synthesis of **12** and found it to be structurally different from aubergenone, although its spectral properties were similar to those of the naturally occurring sesquiterpenoid. However, the availability of the synthetic sesquiterpene **12** led to evidence which revealed that aubergenone is the C(4) epimer of **12** and therefore should be reformulated as **13** (*vide infra*).

We were prompted to undertake a synthesis of **12** by the availability of a supply of the racemic octalone **1** (2) as starting material. Unlike many syntheses in the eudesmane and related fields which originate from enantiomers derived from natural sources (3), our synthesis proceeds from the starting material **1** through a series of racemic intermediates to the racemic end product **12**.

The synthesis of **12**, details of which are given in the Experimental, is outlined in Scheme 1. Since this synthesis is straightforward, a detailed discussion in this section is unnecessary, especially since the last three compounds in the sequence have been correlated with (−)-*trans*-dihydrocarissone (**10***a*) (4) (*vide infra*). It should be mentioned, however, that compounds **8**, **10**, and **12** were unchanged by treatment with base under equilibrating conditions and that the spectral properties and elemental analyses of the compounds shown in Scheme 1 are in agreement with the assigned structures. The properties of the synthetic sesquiterpenoid **12** (ir and nmr spectra, behavior on tlc, and retention time on glc) were not identical to the corresponding properties of aubergenone.

After the completion of the synthesis of **12**, we were afforded the opportunity of substantiating the

Can. J. Chem. Downloaded from www.nrcresearchpress.com by 210.87.254.42 on 09/05/12
For personal use only.

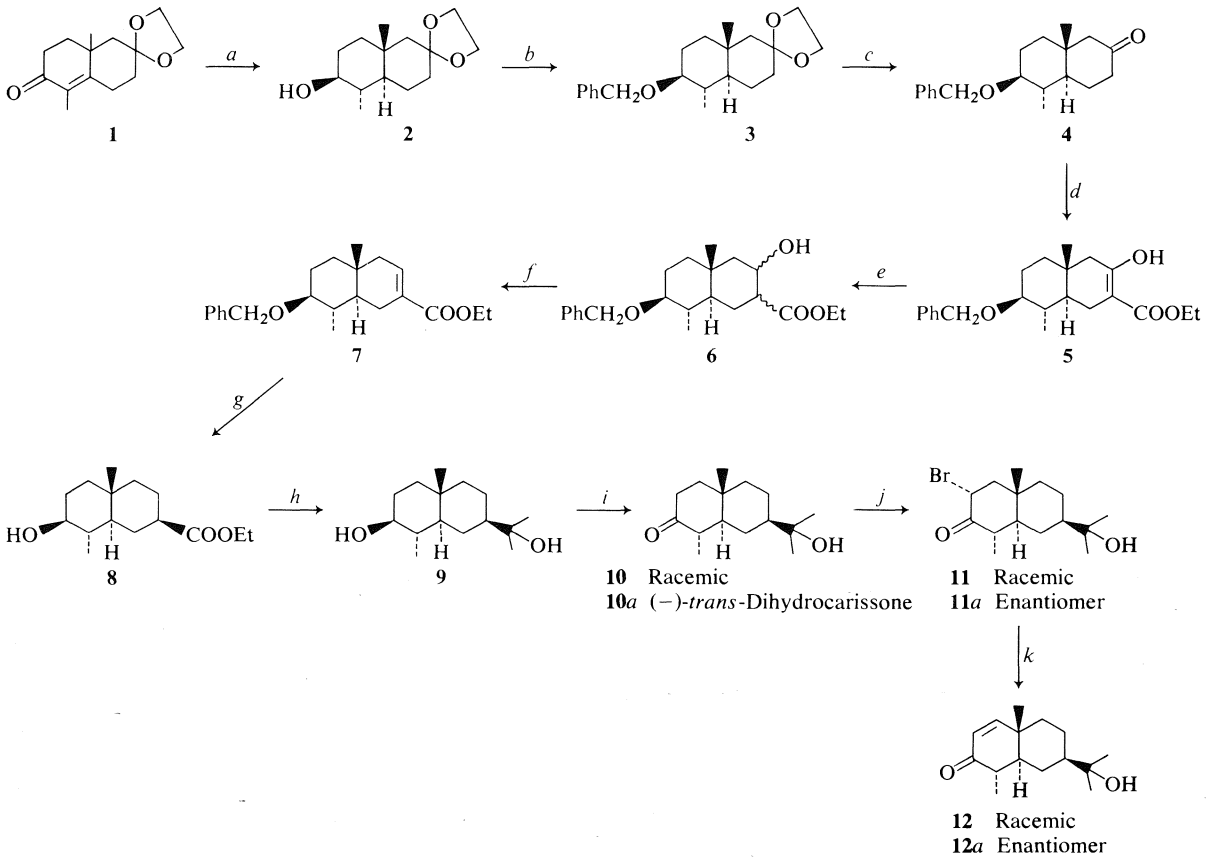

SCHEME 1. Reagents: (*a*) Li, NH_3–EtOH; (*b*) NaH, $PhCH_2Cl$; (*c*) HCl, THF; (*d*) NaH, diethyl carbonate; (*e*) $NaBH_4$; (*f*) $POCl_3$, pyridine; (*g*) H_2, 10% Pd–C; (*h*) MeLi; (*i*) Jones' reagent; (*j*) trimethylphenylammonium tribromide; (*k*) LiBr, Li_2CO_3, DMF.

structures assigned to the last three compounds in Scheme 1 by correlation with (−)-*trans*-dihydrocarissone (**10***a*). The enantiomer **10***a* was prepared from (+)-carissone, kindly provided by Professor Pinder, by a standard procedure (4). It was then converted via the bromide **11***a* into the enantiomer **12***a* by procedures used in the sequence **10** → **11** → **12**. The enantiomers **10***a*, **11***a*, and **12***a* were identical with the corresponding racemic compounds **10**, **11**, and **12** with respect to ir and nmr spectra, behavior on tlc, and retention time on glc. Thus, the validity of the structures **10**, **11**, and **12** was firmly established.

The structural relation of aubergenone to the synthetic sesquiterpenoid **12** was finally revealed when it was discovered that the former was completely transformed into the latter on refluxing with ethanolic potassium hydroxide. This behavior can only be interpreted as the epimerization of the secondary, quasi-axial, methyl group in aubergenone to the thermodynamically more stable quasi-equatorial

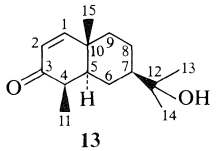

13

orientation as in **12**. The structure **12**, therefore, represents C(4)-*epi*-aubergenone[1] and aubergenone can be assigned structure **13**.

The nmr data for **12** and **13** are listed in Table 1 from which it is apparent that the epimerization of the C(4)-methyl group has relatively little effect on the majority of the shieldings although the observed changes are significant. The most pronounced difference occurred for the angular methyl group whose carbon is deshielded by 3.6 ppm in the natural product. This is another example of the *syn*–axial δ effect which has been noted in a variety of systems

[1]The numbering system shown in **13** is used throughout.

Can. J. Chem. Downloaded from www.nrcresearchpress.com by 210.87.254.42 on 09/05/12
For personal use only.

Can. J. Chem. Downloaded from www.nrcresearchpress.com by 210.87.254.42 on 09/05/12
For personal use only.

TABLE 1. ^1H and ^{13}C mr data[a] for **12** and **13**

	12		**13**	
Position	^{13}C	^1H	^{13}C	^1H
1	160.4	6.74 [10]	160.9	6.77 [10]
2	126.3	5.86 [10]	125.9	5.86 [10]
3	202.3		204.0	
4	42.7	2.27 [6.5, 13]	45.3	2.46 [6.1, 7.8]
5	(48.3)		44.5	
6	25.2		26.1	
7	(48.5)		49.1	
8	21.9		22.4	
9	37.9		40.0	
10	36.2		36.2	
11	11.8	1.14 [6.5]	13.4	1.13 [7.8]
12	72.6		72.6	
13, 14	26.9, 27.6	1.23	27.2, 27.6	1.23
15	17.2	1.07	20.8	1.15

[a]Shieldings given in ppm from internal TMS for $CDCl_3$ solutions; values in parentheses may be interchanged. Proton–proton couplings in Hz are in brackets.

(5). The higher shielding of the carbonyl carbon in **12** relative to that in **13** is indicative of a more effective conjugative interaction in the former which is consistent with a more nearly coplanar enone system. It may be anticipated that the enone moiety in **13** will be twisted to reduce the *syn*–axial interaction between C(11) and C(15). It is interesting that the C(9) shieldings differ by 2.1 ppm in these compounds although this difference is not readily rationalized.

From the proton results it can be seen that only the angular methyl and 4-H shieldings differ significantly in **12** and **13**. The vicinal couplings of the latter are also affected appreciably with the 13 Hz coupling to the ring junction in **12** clearly establishing the antiperiplanar orientation of these protons. The corresponding coupling of 6 Hz in **13** is consistent with some distortion of the half-chair A ring to reduce the methyl–methyl *syn*–axial interaction such that the dihedral angle relating to these protons is significantly smaller than 60°, the value expected for an undistorted arrangement. Since the product obtained by epimerization of natural aubergenone was only available in small quantity (2.3 mg), this sample and a corresponding sample of the synthetic material were examined in CD_2Cl_2 solution using a capillary insert. Both ^1H and ^{13}C spectra of these samples were identical.

Experimental

General

Melting points were determined on a Fisher-Johns apparatus and are uncorrected.

The ir spectra were recorded with a Perkin-Elmer model 237B spectrophotometer. Proton nmr spectra were recorded with Varian XL-100-12 and T-60 instruments and ^{13}C spectra were obtained with a Varian XL-100-15 system operating in the Fourier transform mode. The chemical shifts are expressed in ppm (δ values) relative to TMS as an internal standard. Gas chromatography was performed with a Hewlett-Packard model 5750 instrument fitted with a 6 ft column (diameter 0.25 in.) packed with 10% of UC-W98 on diatoports (80–100 mesh); the temperature was increased from ambient temperature to 250°C at 15°C/min with the helium flow rate at 30 cm^3/min; retention times were compared by coinjection.

Petroleum ether refers to the fraction with boiling point range 30–60°C. Brine refers to a saturated aqueous solution of sodium chloride.

Alcohol 2

A solution of 4.72 g of keto ketal **1** (2) in ether (50 ml) and ethanol (80 ml) was added to 250 ml of liquid ammonia. Lithium (5 g) was added over a period of 1.5 h. The reaction mixture was stirred at reflux for an additional 1.5 h and then treated with 60 g of ammonium chloride. The ammonia was allowed to evaporate overnight and the reaction mixture was worked up in the usual manner with water, brine and ether. The ether extract was dried over sodium sulfate and evaporated to give 4.90 g of crystalline product. Recrystallization from ether – petroleum ether gave 4.00 g (83%) of the alcohol **2**, mp 89°C; ir (Nujol): 3220 cm^{-1} (OH); nmr (CCl_4) δ: 0.89 (s, 3H, angular methyl), 3.00 (m, 1H, *H*—C—OH) and 3.82 (m, 4H, ethylene of ketal). *Anal.* calcd. for $C_{14}H_{24}O_3$: C 69.96, H 10.06; found: C 70.20, H 10.10.

Benzyl Ether 3

A mixture of 1.084 g of alcohol **2**, 400 mg of sodium hydride, and 32 ml of dry benzene was refluxed under a nitrogen atmosphere for 5 h. After cooling to room temperature, the mixture was treated dropwise with 2.0 ml of benzyl chloride and refluxing was continued for 18 h. The cooled reaction mixture was treated with 8 ml of methanol then poured into a mixture of 600 ml of ice and water. Work-up in the usual manner with ether and water yielded 1.10 g (74%) of benzyl ether **3**, mp 98°C; ir (Nujol): shows no OH band; nmr (CCl_4) δ: 0.93 (d, J = 6.5 Hz, 3H, secondary methyl), 0.97 (s, 3H, angular methyl), 2.77 (m, 1H, *H*—C—O), 4.25 and 4.55 (doublets, J = 12 Hz, 1H each, OCH_2Ph), and 7.15 (m, 5H, aromatic protons). *Anal.* calcd. for $C_{21}H_{30}O_3$: C 76.33, H 9.15; found: C 76.25, H 9.38.

Can. J. Chem. Downloaded from www.nrcresearchpress.com by 210.87.254.42 on 09/05/12
For personal use only.

Ketone **4**

A solution of 3.495 g of the benzyl ether **3**, 250 ml of tetrahydrofuran and 210 ml of 1 *M* aqueous hydrochloric acid was left at room temperature under a nitrogen atmosphere for 30 min. The reaction mixture was worked up in the usual manner with chloroform, saturated sodium bicarbonate and brine to give 2.676 g (88%) of ketone **4**, mp 108–109°C; ir (Nujol): 1705 cm^{-1} (ketone); nmr (CCl_4) δ: 0.78 (s, 3H, angular methyl), 0.98 (d, J = 6.5 Hz, 3H, secondary methyl), 2.85 (m, 1H, *H*—C—O), 4.27 and 4.57 (doublets, J = 12 Hz, 1H each, OCH_2Ph), and 7.15 (m, 5H, aromatic protons). *Anal.* calcd. for $C_{19}H_{26}O_2$: C 79.68, H 9.15; found: C 79.51, H 9.23.

Keto Ester **5**

A mixture of 805 mg of sodium hydride and 2.60 g of diethyl carbonate in 15 ml of benzene was brought to reflux temperature under a nitrogen atmosphere. The mixture was treated dropwise, over 1 h, with a solution of 3.20 g of ketone **4** in 18 ml of benzene. Following an additional reflux period of 1 h, the reaction mixture was cooled to room temperature. Excess sodium hydride was destroyed with 2.4 ml of glacial acetic acid followed by 50 ml of ice water. Work-up in the usual manner gave 4.10 g of oil. Column chromatography of the product on 150 g of silica gel, with gradually increasing concentrations of ether in petroleum ether, gave 3.427 g (86%) of the keto ester **5**, mp 55°C; ir (Nujol): 1735, 1705, 1650, and 1610 cm^{-1} (β-keto ester); nmr ($CDCl_3$) δ: 0.85 (s, 3H, angular methyl), 1.03 (d, J = 6.5 Hz, secondary methyl), 1.26 (t, J = 7.0 Hz, 3H, methyl of ester), 4.13 (q, J = 7.0 Hz, 2H, methylene of ester), 4.31 and 4.60 (doublets, J = 11 Hz, 1H each, OCH_2Ph), and 7.20 (m, 5H, aromatic protons). *Anal.* calcd. for $C_{22}H_{30}O_4$: C 73.71, H 8.43; found: C 73.57, H 8.53.

Alcohol **6**

The keto ester **5** (3.40 g) in 43 ml of ethanol was cooled (−15°C) and added to 810 mg of sodium borohydride in 33 ml of ethanol. The mixture was stirred at −15°C for 2.5 h, left at −20°C overnight, then stirred at room temperature for 1 h. Work-up in the usual manner with ether and brine yielded 3.346 g of material which crystallized from ether – petroleum ether to give 2.943 g (86%) of alcohol **6**, mp 70°C; ir (Nujol): 3525 (OH) and 1710 cm^{-1} (ester); nmr ($CDCl_3$) δ: 1.02 (d, J = 6.5 Hz, 3H, secondary methyl), 1.12 (s, 3H, angular methyl), 1.25 (t, J = 7.0 Hz, 3H, methyl of ester), 4.13 (q, J = 7.0 Hz, 2H, methylene of ester), 4.37 and 4.63 (doublets, J = 11 Hz, 1H each, OCH_2Ph), and 7.27 (m, 5H, aromatic protons). *Anal.* calcd. for $C_{22}H_{32}O_4$: C 73.29, H 8.94; found: C 73.65, H 9.03.

α,β-*Unsaturated Ester* **7**

A solution of 2.943 g of the alcohol **6** in 50 ml of pyridine was cooled to 0°C, treated with 4 ml of freshly distilled phosphorus oxychloride and stirred at room temperature in the dark for 2 h. The reaction mixture was diluted with 250 ml of ice water and stirred for 15 min. The cold mixture was worked up in the usual manner with ether, 1 *N* hydrochloric acid, and saturated sodium bicarbonate solution to give 2.70 g of crude product. Purification of the product by column chromatography employing silica gel as adsorbent and ether as eluant gave 2.40 g (86%) of α,β-unsaturated ester **7** as an oil; ir (film): 1710 (ester) and 1650 cm^{-1} (olefin): nmr ($CDCl_3$) δ: 0.82 (s, 3H, angular methyl), 1.05 (d, J = 6.5 Hz, 3H, secondary methyl), 1.27 (t, J = 7.0 Hz, 3H, methyl of ester), 4.13 (q, J = 7.0 Hz, 2H, methylene of ester), 4.35 and 4.63 (doublets, J = 11 Hz, 1H each, OCH_2Ph), 6.80 (m, 1H, vinylic proton), and 7.23 (m, 5H, aromatic protons).

Ester **8**

A solution of 2.15 g of α,β-unsaturated ester **7** in 300 ml of ethanol was hydrogenated over 1.1 g of 10% palladium-on-charcoal catalyst at 2 atm pressure for 3.5 h. The catalyst was filtered off and the solvent evaporated *in vacuo* to give 1.597 g (100%) of ester alcohol **8** as an oil; ir (film): 3400 (OH) and 1725 cm^{-1} (ester); nmr ($CDCl_3$) δ: 0.88 (s, 3H, angular methyl), 0.95 (d, J = 6.5 Hz, 3H, secondary methyl), 1.23 (t, J = 7.0 Hz, 3H, methyl of ester), 3.08 (m, 1H, *H*—C—OH), and 4.10 (q, J = 7.0 Hz, 2H, methylene of ester).

The ester **8** was unchanged with respect to ir and nmr spectra and behavior on tlc after refluxing for 45 min with 1 *M* ethanolic sodium ethoxide.

Diol **9**

To a stirred solution of 40 ml of 1.4 *M* methyl lithium in ether was added a solution of 1.00 g of ester **8** in 8 ml of ether. The solution was stirred at room temperature for 2.5 h then worked up in the usual manner with ether, 3% ammonium chloride solution, and brine to give 945 mg (100%) of the diol **9**, mp 152°C; ir (Nujol): 3330 cm^{-1} (OH); nmr ($CDCl_3$) δ: 0.83 (s, 3H, angular methyl), 0.95 (d, J = 6.5 Hz, 3H, secondary methyl), 1.17 (s, 6H, isopropyl methyls), and 3.10 (m, 1H, *H*—C—OH). *Anal.* calcd. for $C_{15}H_{28}O_2$: C 74.95, H 11.74; found: C 75.27, H 11.78.

Keto Alcohol **10**

A solution of 855 mg of diol **9** in 50 ml of freshly distilled acetone was treated dropwise at 0°C with an 8 *N* solution of Jones' reagent (6) until a persistent orange color was observed. Excess oxidizing agent was destroyed with methanol and the acetone was evaporated *in vacuo*. Work-up in the usual manner with ether, 5% sodium carbonate and brine afforded 688 mg (81%) of **10**, mp 91–93°C; ir (CCl_4): 1715 (ketone), 3500 and 3610 cm^{-1} (OH); nmr (CCl_4) δ: 0.93 (d, J = 6.5 Hz, 3H, secondary methyl), 1.07 (s, 3H, angular methyl), and 1.13 (s, 6H, isopropyl methyls). *Anal.* calcd. for $C_{15}H_{26}O_2$: C 75.58, H 10.99; found: C 75.63, H 11.39.

The keto alcohol **10** was unchanged after refluxing for 2 h with 0.1 *M* ethanolic potassium hydroxide. It was identical with (−)-*trans*-dihydrocarissone, prepared from (+)-carissone by a published method (4), with respect to ir and nmr spectra, behavior on tlc and retention time on glc.

Bromo Ketone **11**

To cold (0°C) stirred solution of 527 mg of the keto alcohol **10** in 16 ml of tetrahydrofuran under a nitrogen atmosphere, was added 833 mg of trimethylphenylammonium tribromide. The solution was stirred for 30 min at 0°C then treated with 9.5 ml of saturated sodium bicarbonate solution. Work-up in the usual manner with ether and brine afforded 712 mg of material which was crystallized from ether – petroleum ether to give 456 mg (65%) of **11**, mp 113–115°C (dec.); ir (Nujol): 3490 (OH) and 1720 cm^{-1} (ketone); nmr ($CDCl_3$) δ: 1.07 (d, J = 6.5 Hz, 3H, secondary methyl), 1.13 (s, 3H, angular methyl), 1.20 (s, 6H, isopropyl methyls), and 4.83 (m, 1H, H—C—Br). The crude product was used directly for conversion into **12**.

The bromo ketone **11** was identical with the bromo ketone **11***a*, prepared from (−)-*trans*-dihydrocarissone (4), with respect to ir and nmr spectra and behavior on tlc.

Bromo Ketone **11**a

Bromination of (−)-*trans*-dihydrocarissone (**10***a*) (4) by the procedure described in the preceding experiment afforded the bromo ketone **11***a*, mp 113–116°C, identical with the racemic bromo ketone **11** (see preceding experiment).

α,β-*Unsaturated Ketone* ***12*** *(4-*epi*-Aubergenone)*

The bromo ketone **11** (220 mg), dissolved in dimethylformamide (11 ml) containing lithium bromide (220 mg) and lithium carbonate (184 mg), was heated under a nitrogen atmosphere at 130°C (bath temperature) for 3 h. Work-up in the usual manner with ether, water and brine, followed by preparative tlc of the crude product on silica gel with ether as solvent afforded 148 mg (90%) of crystalline **12**, mp 130–132°C; ir (CCl_4): 3605 and 3500 (OH), 1680 (unsaturated ketone), and 1615 cm^{-1} (olefin); nmr: see Table 1. *Anal.* calcd. for $C_{15}H_{24}O_2$: C 76.23, H 10.24; found: C 75.87, H 10.41.

The α,β-unsaturated ketone **12** was identical with the enantiomer **12***a* with respect to ir and nmr spectrum, behavior on tlc and retention time on glc. It was unchanged after refluxing with 0.1 *M* ethanolic potassium hydroxide for 3.5 h.

α,β-*Unsaturated Ketone* ***12***a

Dehydrobromination of **11***a* by the procedure described in the preceding experiment afforded the enantiomer **12***a*, mp 95–97°C, identical with the racemic α,β-unsaturated ketone **12** (see preceding experiment).

Epimerization of Aubergenone

Aubergenone (3 mg) was refluxed with 0.1 *M* ethanolic potassium hydroxide for 1 h. Work-up of the reaction solution in the usual manner with ether afforded a product which was identical with 4-*epi*-aubergenone (**12**) with respect to ^{1}Hmr, ^{13}C nmr, and behavior on tlc.

Acknowledgements

We are grateful to Dr A. Stoessl, Agriculture Canada Research Institute, for a sample of aubergenone and to Professor A. R. Pinder, Clemson University, for a sample of (+)-carissone. The financial support of the National Research Council of Canada is gratefully acknowledged.

1. A. Stoessl, J. B. Stothers, and E. W. B. Ward. Can. J. Chem. **53**, 3351 (1975).
2. S. A. Narang and P. C. Dutta. J. Chem. Soc. 2842 (1960).
3. C. H. Heathcock. *In* The total synthesis of natural products. Vol. 2. *Edited by* J. W. ApSimon. John Wiley and Sons Inc., New York, NY. 1973.
4. D. C. Humber, A. R. Pinder, and R. A. Williams. J. Org. Chem. **32**, 2335 (1967).
5. S. H. Grover, J. P. Guthrie, J. B. Stothers, and C. T. Tan. J. Magn. Reson. **10**, 227 (1973); F. W. Wehrli and T. Wirthin. *In* Interpretation of carbon-13 nmr spectra. Heyden and Son Ltd., London, UK. 1976.
6. K. Bowden, I. M. Heilbron, E. R. H. Jones, and B. C. L. Weedon. J. Chem. Soc. 39 (1946).

Can. J. Chem. Downloaded from www.nrcresearchpress.com by 210.87.254.42 on 09/05/12
For personal use only.

Pyrazolato bridged binuclear complexes of palladium and platinum

FLAVIO BONATI[1,2] AND HOWARD C. CLARK

Guelph–Waterloo Centre for Graduate Work in Chemistry, Guelph Campus, University of Guelph, Guelph, Ont., Canada N1G 2W1

Received January 26, 1978

FLAVIO BONATI and HOWARD C. CLARK. Can. J. Chem. **56**, 2513 (1978).

Pyrazolato bridged binuclear complexes of palladium and of platinum, $(C_8H_{12}X)_2M_2(\mu\text{-}Pz_2)$ (X = OCH_3 or pyrazolato), are obtained by reaction of (1,5-cyclooctadiene)dichloro-palladium(II) or -platinum(II) with a 1- unsubstituted pyrazole and sodium hydroxide in methanol.

FLAVIO BONATI et HOWARD C. CLARK. Can. J. Chem. **56**, 2513 (1978).

On a obtenu des complexes binucléaires pontés pyrazolato du palladium et du platine, $(C_8H_{12}X)_2M_2(\mu\text{-}Pz_2)$ (X = OCH_3 ou pyrazolato) en faisant réagir le (cyclooctadiène-1,5)-dichloropalladium(II) ou -platine(II) avec un pyrazole non substitué en 1 en présence d'hydroxyde de potassium dans le méthanol.

[Traduit par le journal]

Can. J. Chem. Downloaded from www.nrcresearchpress.com by 210.87.254.105 on 09/05/12
For personal use only.

Introduction

The pyrazolate anion (Pz^-) can function either as a monodentate or exobidentate ligand. Since the original work by Trofimenko (1) and others (2) on metal poly-1-pyrazolylborates, (e.g. compounds of type A), other elements capable of tetrahedral coordination, such as carbon (2) and gallium (3) have been shown able to replace boron as the coordination centre in A. More recently, neutral bis-1-pyrazolyl derivatives of transition elements, having the square planar geometry, have been obtained, e.g. compounds B where L_2 is 1,2-bis(diphenylphosphino)ethane and Pz^- is monodentate. That these derivatives can themselves behave as bidentate, chelating and metal-containing ligands has been demonstrated by the formation of binuclear complexes C where M is Pt, M′ is Zn, Cd, or Hg, Z is chlorine and $n = 0$, or where M = M′ = Pt, $Z_2 = L_2$ = 1,2-bis(diphenylphosphino)ethane, and $n = 2$ (4, 5). In order to obtain other new binuclear complexes of type C, the preparation of further metal-containing and chelating ligands of type B was undertaken, particularly those containing other ligands L of differing *trans*-influence. Thus, following the preparation of compounds of types B and C where L_2 = α,α′-dipyridyl, other reactions were attempted with diolefin complexes where the products might be either compounds of type B where L_2 is the diolefin, or homobinuclear complexes of type C (M = M′ = Pd or Pt; $L_2 = Z_2$ and $n = 0$), or derivatives of type D where the diolefin has undergone nucleophilic attack by pyrazolate or another nucleophile. As the following results show, the latter has been observed.

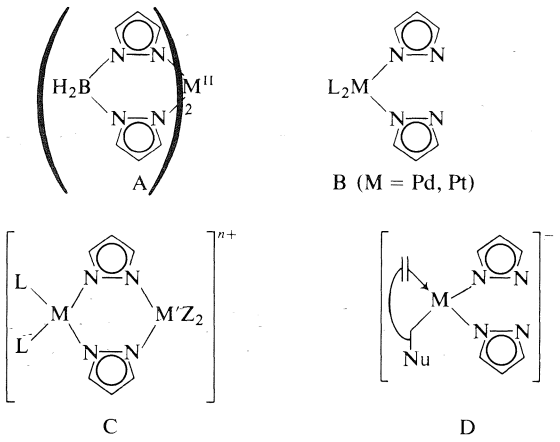

Results and Discussion

(1,5-Cyclooctadiene)dichlorometal (**1** or **2**) and excess pyrazole react in the presence of sodium hydroxide in methanol solution according to one of the following schemes.

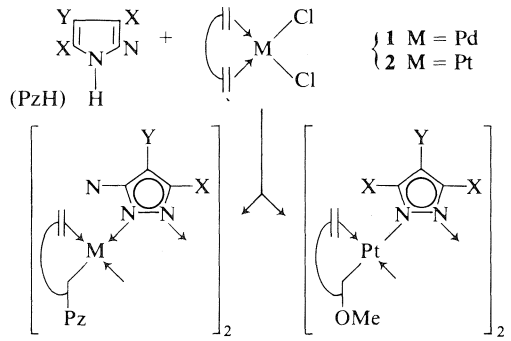

[1]On leave of absence from the University of Camerino, Italy.

[2]Author to whom correspondence should be addressed at Instituto di Chimica Generale, via Venezian 21, 20133 Milano, Italy.

E	No.	X	Y	M
	3	H	H	Pd
	4	Me	H	Pd
	5	Me	I	Pd
	6	H	H	Pt

F	No.	X	Y
	7	Me	Br
	8	Me	I
	9	Me	$N_2C_6H_4Me$

Where the metal is palladium and for pyrazole itself, compound **3** was obtained readily; the same type of pyrazolato-bridged compound, rather than compound D, was obtained even when the heterocyclic ring carried two methyl groups, which should make bridge formation more difficult owing to steric hindrance. Similar results were also obtained when the heterocyclic ring contained another bulky group (compounds **4** or **5** respectively). The compounds were characterized through analytical data, molecular weight determination, infrared and nmr spectra. Additional evidence for the proposed formulation is given by the reaction of a chloroform solution of **3** with hydrochloric acid in methanol to afford the starting compound **1**.

In the case of platinum, compound **6**, belonging to the type E, was obtained with unsubstituted pyrazole, but compounds **7**, **8**, and **9**, belonging to the type F were isolated when variously 4-substituted 3,5-dimethylpyrazoles were allowed to react under similar conditions. In the case of the platinum derivative of 3,5-dimethylpyrazole, the reaction product was a mixture of the two types of compound, E and F. Indeed, the presence of the methoxy group, both here and in the compounds **7**–**9**, is supported by the appearance in the proton nmr spectrum of a singlet at ca. 6.7τ a value to be compared with 6.8τ found (6) in the spectrum of (diphos)Pt[C(OMe)=NAr]$_2$. Infrared evidence for the methoxy group includes a strong band at ca. 1100 cm^{-1}, which, however, falls in the region where another strong band due to the pyrazolate ring is observed. Other infrared bands were observed which are typical of the heterocyclic ligand.[3] They include a strong absorption around 750 cm^{-1} due to the out-of-plane bending of the ring proton(s), a weak band at 3100 cm^{-1} due to the stretching of the C—H bond and observed only in derivatives of the unsubstituted pyrazole, and a weak band(s) in the 1500–1560 region which is connected with the pyrazole ring. All the compounds are thermally fairly stable: decomposition is observed above ca. 170°C.

From the available data, it can be seen that following nucleophilic attack (7) by the methoxide or pyrazolato group, a binuclear system of the type C (M = M′ = Pd or Pt; $L_2 = Z_2$ = cyclooctenyl; $n = 0$) rather than a mononuclear species such as B results. Furthermore, a species like D is not formed perhaps because of the energy gain connected with the formation of a resonance stabilized bis(μ-pyrazolato-*N*,*N*′) bridge between the two metal centres, although the insolubility of the binuclear species may well be a driving force.

In the reaction of the same pyrazole (X = Me; Y = H) with $(C_8H_{12})MCl_2$, a different product is obtained when M = Pd, (**5**), or when M = Pt, (**8**). Hence the different nucleophilic character of the methoxide vs. the pyrazolate anion is not alone responsible for directing the nucleophilic attack. The different behaviour observed here with the various pyrazoles, therefore, is a consequence of some delicate balance between variations in the nucleophilic powers of methoxide and pyrazolates and the properties of the M(II) species.

[3]See ref. 1 and the references cited therein.

TABLE 1. Analytical data[a]

Compound	C	H	N	mw[b]
3	48.05	5.39	15.88	715[c]
	48.0	5.15	16.0	698
4	53.13	6.16	14.10	—
	53.4	6.43	13.85	810
5	32.63	4.08	8.17	—
	32.9	3.65	8.54	1312
6	38.97	4.48	12.84	872[c]
	38.4	4.13	12.82	874
7[d]	33.10	4.42	6.06	971[c]
	33.05	4.13	5.52	1016
8	30.26	3.99	5.01	—
	30.30	3.79	5.05	1110
9	46.74	5.27	11.09	—
	46.2	5.12	10.25	1094

[a]Found/calcd.
[b]By osmometry.
[c]Chloroform solution.
[d]Bromine, 15.26% (calcd. 15.75%).

Experimental

Analyses were carried out by Mr. McKinnon of this department or by M.H.W., Phoenix, Arizona. Molecular weight determinations were carried out by Pascher Microanalytisches Laboratorium, Bonn, West Germany. Infrared spectra were recorded on a Beckman IR-5A instrument; nmr spectra were recorded on a Bruker instrument, operating at room temperature and 60 Mc, by Dr. Albert Woon-Fat of this department; only $CDCl_3$ was used as solvent; values are in τ units. Compounds **1** and **2** are (1,5-cyclooctadiene)dichloropalladium or platinum, respectively (8). Evaporation was always carried out under reduced pressure (water aspirator). The analytical data are reported in Table 1.

Preparation of Compound 3

Compound **1** (507 mg; 1.78 mmol) was suspended in methanol (20 ml) and excess pyrazole (294 mg; 4.32 mmol) was added. Sodium hydroxide (162 mg; 4.05 mmol) in 90% methanol (15 ml) was added dropwise to the solution and a

Can. J. Chem. Downloaded from www.nrcresearchpress.com by 210.87.254.105 on 09/05/12
For personal use only.

white precipitate formed at once, which was filtered and washed with methanol to yield the analytical sample (286 mg; 42%); upon heating it decomposed at ca. 200°C. Additional product could be recovered: the mother liquor was evaporated to dryness, the residue was extracted with methylene chloride (25 ml), the solution was concentrated to a small volume, methanol was added, and the solution again concentrated to a small volume.

The nmr spectrum showed signals at 2.82 (d, J = 2.4 Hz); 2.82 (d, J not determined owing to overlapping but ca. 2 Hz); 2.89 (d, J = 1.9 Hz, 3-H, 5-H, all these signals 8-H); 3.80 (t, J = 2.4 Hz); 3.90 (t, J = 1.9 Hz, 4-H, 2-H each); 4.39 (m, CH—CH—Pd, 4-H); 5.82 (m, 2-H); 6.84 (m, 2(CH=CH)); and 7.2–9.3 (complex, 16-H, methylene protons).

Preparation of Compound ***4***

The reaction was carried out similarly using the stoichiometric quantities of 3,5-dimethylpyrazole and alkali. The residue after evaporation was extracted with chloroform and the residue obtained after evaporation of the extract could be crystallized by concentrating to small volume its methanol solution; upon heating, the sample thus obtained melted into a black liquid at 213°C.

The nmr spectrum showed signals at 4.29 (s) and 4.54 (s, 4-H) and 4.34 (s, CH—CH—Pd), 6.04 (m) and 6.66 (m, CH=CH), 7.70, 7.77, 7.89 and 8.15 (3-Me + 5-Me, all singlets) and at 7.7–9.0 (CH_2).

Preparation of Compound ***5***

The compound was obtained similarly using 3,5-dimethyl-4-iodopyrazole. The crude product (614 mg; 51%) was crystallized by concentrating to half volume its solution in CH_2Cl_2/MeOH (10 + 20 ml). On being heated, the compound turned red and then brown at ca. 170°C.

The nmr spectrum showed 3-Me and 5-Me signals at 7.74 and 7.84 (singlets), and broad signals centred at 3.7, 4.3, 5.3 and in the region 6.3–8.6 due to the alkenyl ligand.

Preparation of Compound ***6***

To a suspension of the compound **2** (538 mg; 1.44 mmol) in methanol (20 ml) pyrazole (300 mg; 4.4 mmol) and, then, sodium hydroxide (197 mg; 4.9 mmol) in wet methanol (22 ml + 3 ml water) were added. The residue left after evaporation was extracted with dichloromethane (5 × 5 ml); after evaporating the extract to dryness the semisolid residue was crystallized twice from diethyl ether/hexane (2/3) to yield the analytical sample.

The nmr spectrum showed complex bands at 2.2–2.9 and at 3.5–3.9 (3-H + 5-H and 4-H of the pyrazolate rings, respectively) and at 6–9.2 and at 4–9.2τ due to the cyclooctenyl ligand.

Preparation of Compound ***7***

To a suspension of compound **2** (258 mg; 0.69 mmol) in methanol (10 ml) 3,5-dimethyl-4-bromopyrazole (241 mg; 1.38 mmol) in the same solvent (5 ml) and, then, sodium hydroxide (60 mg; 1.5 mmol) in 90% methanol (15 ml) were added. The solution was evaporated to dryness and the residue was extracted with benzene (20 ml); after evaporating the extract to dryness, the residue was dissolved in benzene/methanol (20 + 50 ml). The solution was then concentrated till a precipitate appeared, additional methanol (10 ml) was added and the analytical sample, dec. 215°C (225 mg; 64%), was filtered off after further concentration.

In the nmr spectrum, singlets were observed at 7.85 and 7.90 (3-Me + 5-Me), at 6.82 (MeO) while the cyclooctenyl ligand gave a complex absorption stretching from 4.4 to 8.5τ.

Preparation of Compound ***8***

The reaction was carried out similarly using 3,5-dimethyl-4-iodopyrazole. The residue after evaporation was extracted with dichloromethane and the compound was obtained upon addition of methanol. On heating to 215°C, no change was observed in the compound.

In the nmr spectrum, singlets were found at 7.80 (broad) (3-Me + 5-Me), and at 6.77 (MeO), plus a complex absorption between 4 and 9 due to the cyclooctenyl group.

Preparation of Compound ***9***

The reaction was carried out similarly using 3,5-dimethyl-4-(*p*-tolylazo)pyrazole. The residue after evaporation was extracted in dichloromethane; methanol was added dropwise to the concentrated solution whereupon a blackish gum precipitated, which was not examined; upon concentration of the filtered solution, the yellow compound was obtained which, upon heating, decomposed at ca. 170°C.

The nmr spectrum showed singlets at 6.70 (MeO), 7.40, 7.44, 7.47, 7.64 (3-Me + 5-Me + *p*-Me), a pseudoquartet at 2.2–2.30 (C_6H_4) and a broad, complex signal stretching from 4 to 8.7τ due to the cyclooctenyl ligand.

Acknowledgments

One of us (F.B.) thanks the Canada Council for a grant which enabled him to visit the University of Guelph. The continued financial support of the National Research Council of Canada is gratefully acknowledged.

1. S. Trofimenko. Chem. Rev. **72**, 497 (1972).
2. A. G. Shaver. J. Organomet. Chem. Library, **3**, 157 (1977).
3. K. R. Breakell, D. J. Patmore, and A. Storr. J. Chem. Soc. Dalton Trans. 749 (1975).
4. G. Minghetti, G. Banditelli, and F. Bonati. Chem. Ind. 123 (1977).
5. G. Banditelli, F. Bonati, and G. Minghetti. Unpublished results.
6. G. Minghetti, F. Bonati, and G. Banditelli. Inorg. Chem. **15**, 2649 (1976).
7. F. R. Hartley. The chemistry of platinum and palladium. J. Wiley, New York, NY. 1973. Chapt. 13; U. Belluco. Organometallic and coordination chemistry of platinum. Academic Press, London. 1974. Chapt. VI.
8. J. Chatt, L. M. Vallarino, and L. M. Venanzi. J. Chem. Soc. 2496 (1957); 3413 (1957).

Can. J. Chem. Downloaded from www.nrcresearchpress.com by 210.87.254.105 on 09/05/12
For personal use only.

The preparation of platinum(II) complexes with an *ortho*-metallated carbene ligand: the X-ray and molecular structure of $[Pt\{C(NHC_6H_4CH_3)(NHC_6H_3CH_3)\}\{PPh_2(CH_2)_2PPh_2\}]ClO_4$

DAVID F. CHRISTIAN,[1] DAVID A. CLARKE, HOWARD C. CLARK,[2] DAVID H. FARRAR, AND NICHOLAS C. PAYNE[2]

Department of Chemistry, University of Western Ontario, London, Ont., Canada N6A 3K7 and Department of Chemistry, University of Guelph, Guelph, Ont., Canada N1G 2W1

Received February 1, 1978

DAVID F. CHRISTIAN, DAVID A. CLARKE, HOWARD C. CLARK, DAVID H. FARRAR, and NICHOLAS C. PAYNE. Can. J. Chem. **56**, 2516 (1978).

Treatment of PtCl(CNR)(acac) (R = *p*-tolyl; acac = acetylacetonate) with *p*-toluidine gives the carbene compound $PtCl\{C(NHR)_2\}$(acac). Reaction of this complex with a silver salt, followed by treatment with a neutral ligand L, gave *ortho*-metallated species $[Pt\{C(NHC_6H_4CH_3)(NHC_6H_3CH_3)\}L_2]^+$ which have been isolated as crystalline salts. The molecular structure of the ClO_4^- salt with L_2 = bisdiphenylphosphinoethane has been determined by X-ray diffraction. Crystals are monoclinic, space group $P2_1/n$, with four formula units in a cell of dimensions a = 20.370(3), b = 18.116(3), c = 10.770(2) Å, and β = 99.47(6)°. Full matrix least-squares refinement on F using 3252 observations gave a conventional agreement factor R = 0.047. While the formation of these *ortho*-metallated carbene complexes restricts the further extension of this chemistry, the ready reversal by acid treatment is unusual.

DAVID F. CHRISTIAN, DAVID A. CLARKE, HOWARD C. CLARK, DAVID H. FARRAR et NICHOLAS C. PAYNE. Can. J. Chem. **56**, 2516 (1978).

La réaction du PtCl(CNR)(acac) (R = *p*-tolyle; acac = acétylacétonate) avec la *p*-toluidine conduit au composé carbénique $PtCl\{C(NHR)_2\}$(acac). La réaction de ce complexe avec un sel d'argent, suivie par un traitement avec un ligand L neutre, conduit aux espèces orthométalliques $[Pt\{C(NHC_6H_4CH_3)(NHC_6H_3CH_3)\}L_2]^+$ qui ont été isolées sous forme du sels cristallins. On a déterminé la structure moléculaire du sel perchlorique contenant L_2 = bisdiphénylphosphinoéthane en faisant appel à la diffraction de rayons-X. Les cristaux sont monocliniques, groupe d'espace $P2_1/n$ avec quatre formules par maille, a = 20.370(3), b = 18.116(3), c = 10.770(2) Å et β = 99.47(6)°. On a affiné la structure par la méthode des moindres carrés (matrice complète) sur F utilisant 3252 observations avec un facteur conventionnel de R = 0.047. Alors que la formation de ces complexes carbéniques orthométallés réduit l'extension future de sa chimie, le renversement facile par un traitement en milieu acide est inattendu.

[Traduit par le journal]

Introduction

Numerous studies have been reported of isocyanide, carbene, olefin, and related derivations of platinum(II). However, there have been very few reports of compounds containing combinations of such ligands, bound to the same metal centre, thus creating the opportunity for further intra-ligand reactions to occur. For example, it would be particularly interesting to examine the chemistry of a platinum(II) derivative containing an olefin and a carbene bound to the same platinum centre, since the chemical behaviour of such species might provide useful information on the mechanism of olefin dismutation (1). In view of the general stability, and yet substantial reactivity (i.e. reactions occur at moderate but conveniently followed rates) of many related platinum(II) organic derivatives, it might well be feasible to prepare such a Pt(II) species and to find that it displayed an interesting chemistry.

Previously, we have been able to develop the chemistry of cationic isocyanide–platinum(II) species, originally described by Church and May (2) to obtain platinum(II)–formimidoyl complexes by isocyanide insertion into the Pt—H bond (3). These formimidoyl species undergo a reversible protonation with HCl or $HClO_4$ to generate cationic secondary carbene complexes. The reversible nature of this protonation suggested its possible use as the basis of a synthetic route to olefin–carbene complexes of platinum(II).

Acetylacetonate (acac) has been employed here as ligand, the starting material being the complex $K[PtCl(acac)_2]$ (4) prepared from K_2PtCl_4, KOH, and acetylacetone, which affords $H[PtCl(acac)_2]$ on

[1]Present address: New Zealand Steel Ltd., South Auckland, New Zealand.

[2]Authors to whom all correspondence should be addressed.

Can. J. Chem. Downloaded from www.nrcresearchpress.com by 210.87.254.5 on 09/05/12
For personal use only.

Can. J. Chem. Downloaded from www.nrcresearchpress.com by 210.87.254.5 on 09/05/12
For personal use only.

acidification (5). Various compounds of the type PtCl(L)(acac) where L = olefin, acetylene, phosphine, phosphite, etc. have been prepared (6) from the latter by elimination of the C-bound acetylacetonate as acetylacetone on reaction with the neutral ligand. In the present study, PtCl(CNR)(acac) was thus prepared by treatment with *p*-tolylisocyanide (R = *p*-tolyl), and from it PtCl[$C(NHR)_2$]-(acac), **1**, was generated as a colourless precipitate by reaction with *p*-toluidine in benzene.

Results

(a) Chemistry

Removal of the chloride from PtCl{$C(NHR)_2$}-(acac) with silver salts, yields, unexpectedly, a greenish-black powder, **2**. Its solid state infrared spectrum (Table 1) reveals the presence of acetylacetonate, carbene, and, for example, the PF_6 anion. The ^1H nmr spectrum in chloroform-*d* exhibits broad, poorly-resolved signals in the aromatic and methyl regions and was of little further assistance. This compound **2** will be formulated as $[Pt\{C(NHR)_2\}(acac)]^+X^-$ where X = PF_6 etc., although clearly its structure may be more complex. It might, for example, be dimeric with bridging carbene groups.

Compound **2** reacts very rapidly at room temperature with neutral ligands such as *p*-tolyl isocyanide or 1,2-bisdiphenylphosphinoethane, and slowly with coordinating solvents to give pale yellow complexes. An unambiguous assignment of structure was not possible for these species, based upon ir and nmr spectroscopic data. Accordingly a single crystal X-ray analysis was undertaken of the 1,2-bisdiphenylphosphinoethane complex, and this revealed that the compound was in fact an *ortho*-metallated carbene species, of type **3**.

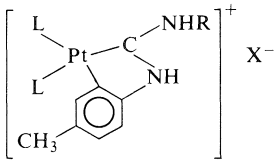

3

The rate of reaction of **2** with solvents is dependent on their coordinating ability, and was observed to be much faster for acetonitrile than acetone. The reactions with these solvents are reversible since stripping the solution to near dryness regenerated the green complex **2**, as the concentration of the higher boiling acetylacetone increased relative to the solvent, S.

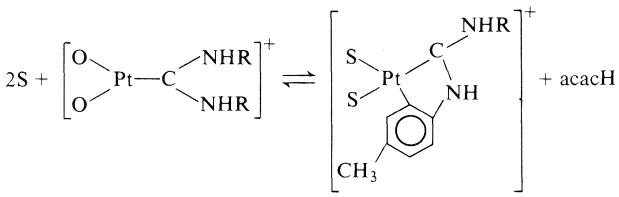

Compound **2** will also react very rapidly at room temperature with one equivalent of sodium diethyldithiocarbamate to give the pale yellow complex **4**

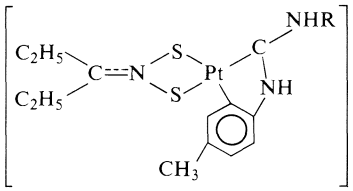

4

Since imidoyl groups, M—$C(R_1)$=NR_2, are known (7) to be reversibly protonated at nitrogen, it is interesting to observe that, following elimination of acetylacetone, *ortho*-metallation, instead of such deprotonation at nitrogen to return a formimidoyl complex, has occurred preferentially. As might be expected, the *ortho*-metallation reaction can be reversed with acids. The addition of hydrochloric acid (CH_3COCl in methanol) to $\{Pt(CNR)_2[C(NHR)(NHC_6H_3CH_3)]\}^+$, $\{Pt(diphos)[C(NHR)(NHC_6H_3CH_3)]\}^+$, and $\{Pt(dtc)[C(NHR)(NHC_6H_3CH_3)]\}$, (dtc = diethyldithiocarbamate) gave a mixture of *cis*- and *trans*-$\{PtCl(CNR)_2[C(NHR)_2]\}^+$, *cis*-$\{PtCl(diphos)[C(NHR)_2]\}^+$, and *cis*-{PtCl(dtc)-$[C(NHR)_2]\}$, respectively.

Subsequent removal of the chlorine from the complex *cis*-$\{PtCl(dtc)[C(NHR)_2]\}$ did not regenerate the original *ortho*-metallated species. Removal of the chlorine from the complex *cis*-$\{PtCl[C(NHR)_2]diphos\}^+$ produced an unidentified complex which gave four phosphorus signals in its ^{31}P nmr spectrum.

(b) Description of the Structure

Selected bond distances and bond angles are presented in Table 2, and some weighted least-squares planes are presented in Table 3. A perspective view of the cation showing the atom numbering scheme is presented in Fig. 1. Only the α-carbon atoms of the phenyl rings are shown. Two of the four sites of a square-planar coordination geometry are occupied by the bidentate phosphine ligand. The remaining two contain the carbene C atom, and an *ortho*-metallated phenyl ring. The crys-

Can. J. Chem. Downloaded from www.nrcresearchpress.com by 210.87.254.5 on 09/05/12
For personal use only.

TABLE 1. Characterization of products*

Parameter	Value					
	1	**2**	**3**	**4**	**5**	**6**
Analyses†C	34.93(34.98)	43.36(44.06)	51.25(50.36)	53.75(53.62)	49.32(49.26)	48.03(47.66)
H	3.16(3.71)	4.18(4.11)	3.98(4.07)	4.29(4.16)	4.03(4.04)	3.46(3.59)
N	3.13(3.19)	5.06(4.96)		3.06(3.06)		7.00(6.87)
Melting point (°C)	> 140 dec.	133–134	158–160	159–161	245–248 dec.	196–197
Nmr parameters						
acac δCH$_3$	2.02s, 2.06s					
acac δH	5.57s					
p-Tolylisocyanide δCH$_3$	2.42s	2.26s	1.71s, 2.20s	1.83s, 2.32s	2.30s	2.30br
p-Tolylisocyanide Phenyl	7.27s		6.70br, 7.20m	7.08m, 8.02m	7.27m	7.13br, m
p-Tolylisocyanide NH						11.76d
						J(HH) = 10 Hz
						J(PtN) = 32 Hz
Diphos phenyl			7.55br	7.72m	7.71m	7.27m
Diphos δCH$_3$						1.17m, 3.50m
Infrared data ν(C≡N)	1520s	1580–1500vs	1543s	1540s	1545s, br	1539m
			1510s		1510s	

*Compound **1** = [PtCl(acac)(CNR)], **2** = [PtCl(acac)(C(NHR)$_2$)], **3** = [Pt(diphos)(C(NHR)(NC$_6$H$_3$CH$_3$))]PF$_6$, **4** = [Pt(diphos)(C(NHR)(NC$_6$H$_3$CH$_3$))]ClO$_4$, **5** = [PtCl(diphos)(C(NHR)$_2$)]PF$_6$, **6** = [Pt(CNR)$_2$(C(NHR)(NC$_6$H$_3$CH$_3$))]CF$_3$SO$_3$.
†Observed values in parentheses.

TABLE 2. Selected interatomic dimensions

(*a*) Bond distance

Bond	Distance (Å)	Bond	Distance (Å)
Pt—P(1)	2.288(4)	C(3)—N(1)	1.29(2)
Pt—P(2)	2.298(4)	C(3)—N(2)	1.31(2)
Pt—C(3)	2.044(14)	N(2)—C(61)	1.39(2)
Pt—C(62)	2.048(13)	C(61)—C(62)	1.43(2)
		C(62)—C(63)	1.37(2)
P(1)—C(11)	1.805(10)	C(63)—C(64)	1.38(2)
P(1)—C(21)	1.814(10)	C(64)—C(65)	1.37(2)
P(1)—C(1)	1.854(15)	C(65)—C(66)	1.38(2)
P(2)—C(2)	1.794(16)	C(61)—C(66)	1.39(2)
P(2)—C(31)	1.787(11)		
P(2)—C(41)	1.819(10)	C(64)—C(67)	1.52(2)
C(1)—C(2)	1.48(2)	N(1)—C(51)	1.43(2)
		C(51)—C(52)	1.40(2)
Cl(1)—O(11)	1.403(13)	C(52)—C(53)	1.39(2)
Cl(1)—O(12)	1.388(15)	C(53)—C(54)	1.39(3)
Cl(1)—O(13)	1.402(14)	C(54)—C(55)	1.36(3)
Cl(1)—O(14)	1.457(16)	C(55)—C(56)	1.37(3)
		C(51)—C(56)	1.32(2)
		C(54)—C(57)	1.50(3)

(*b*) Bond angles

Atoms	Angle (deg)	Atoms	Angle (deg)
P(1)—Pt—P(2)	84.3(1)		
P(1)—Pt—C(62)	97.3(5)		
P(2)—Pt—C(3)	99.1(4)	Pt—C(3)—N(1)	126(1)
C(62)—Pt—C(3)	79.3(6)	Pt—C(3)—N(2)	115(1)
		C(3)—N(2)—C(61)	118(1)
Pt—P(1)—C(11)	110.8(3)	N(2)—C(61)—C(62)	115(1)
Pt—P(1)—C(21)	120.8(4)	N(2)—C(61)—C(66)	124(1)
Pt—P(1)—C(1)	109.1(5)	C(62)—C(61)—C(66)	121(1)
C(11)—P(1)—C(21)	108.1(5)	C(61)—C(62)—Pt	112(1)
C(11)—P(1)—C(1)	104.5(6)	C(61)—C(62)—C(63)	115(1)
C(21)—P(1)—C(1)	102.1(6)	Pt—C(62)—C(63)	132(1)
P(1)—C(1)—C(2)	110(1)	C(62)—C(63)—C(64)	126(1)
P(2)—C(2)—C(1)	112(1)	C(63)—C(64)—C(65)	116(1)
Pt—P(2)—C(2)	107.7(5)	C(63)—C(64)—C(67)	122(1)
Pt—P(2)—C(31)	112.8(4)	C(65)—C(64)—C(67)	122(1)
Pt—P(2)—C(41)	118.6(4)	C(64)—C(65)—C(66)	123(1)
C(2)—P(2)—C(31)	107.2(7)	C(65)—C(66)—C(61)	119(1)
C(2)—P(2)—C(41)	104.0(6)	N(1)—C(3)—N(2)	118(1)
C(31)—P(2)—C(41)	105.7(5)	C(3)—N(1)—C(51)	130(1)
		N(1)—C(51)—C(52)	119(1)
O(11)—Cl(1)—O(12)	115(1)	N(1)—C(51)—C(56)	121(2)
O(11)—Cl(1)—O(13)	111(1)	C(52)—C(51)—C(56)	119(1)
O(11)—Cl(1)—O(14)	102(1)	C(51)—C(52)—C(53)	118(2)
O(12)—Cl(1)—O(13)	116(1)	C(52)—C(53)—C(54)	123(2)
O(12)—Cl(1)—O(14)	102(1)	C(53)—C(54)—C(55)	115(2)
O(13)—Cl(1)—O(14)	108(1)	C(53)—C(54)—C(57)	117(3)
		C(55)—C(54)—C(57)	126(2)
		C(54)—C(55)—C(56)	122(2)
		C(55)—C(56)—C(51)	122(2)

tals are built up from discrete ions, for the shortest cation–anion distance is 2.12 Å between hydrogen atom H1C(66) and atom O(22) in the equivalent position $(1/2 + x, 1/2 - y, 1/2 + z)$.

The coordination geometry about the Pt atom is approximately square planar. The largest deviation from a weighted least-squares plane through the Pt, the two P, the *ortho*-metallated C, and the carbene C atoms is that of C(3) by 0.051(14) Å. The plane through the carbene ligand, defined by the Pt, the

Can. J. Chem. Downloaded from www.nrcresearchpress.com by 210.87.254.5 on 09/05/12
For personal use only.

Can. J. Chem. Downloaded from www.nrcresearchpress.com by 210.87.254.5 on 09/05/12
For personal use only.

TABLE 3. Weighted least-squares planes

Atom	Displacement (Å)	Atom	Displacement (Å)
Equation: $-1.630x + 14.876y + 6.145z - 2.803 = 0$			
Pt	−0.0004(6)	C(3)	0.051(14)
P(1)	0.004(4)	C(62)	0.033(14)
P(2)	0.004(5)		
Equation: $-1.556x + 13.305y + 7.300z - 2.692 = 0$			
C(61)	−0.020(14)	C(64)	0.005(13)
C(62)	0.010(14)	C(65)	−0.004(15)
C(63)	0.000(14)	C(66)	0.021(16)
Equation: $4.194x - 14.47y + 6.372z + 2.283 = 0$			
Pt	0.0000(6)	N(1)	−0.011(14)
C(3)	0.027(14)	N(2)	−0.007(11)

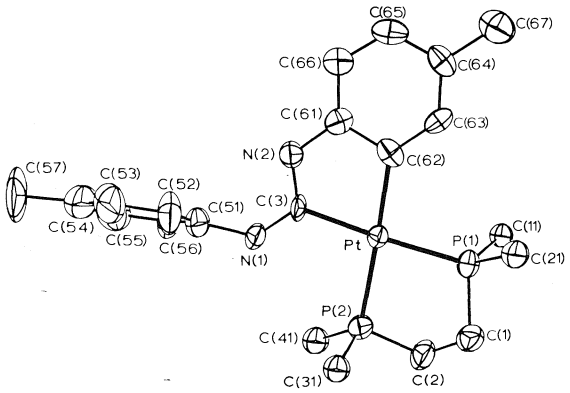

FIG. 1. A perspective view of the cation showing the atom numbering scheme.

carbene C, and the 2 N atoms, is tilted out of the equatorial plane by 7.3°, while the dihedral angle between the equatorial plane and *ortho*-metallated phenyl ring is 8.0° in the opposite direction. By contrast the *p*-tolyl substituent is twisted at an angle of 105.3° to the equatorial plane, thus precluding stabilization of C(3) by electron donation from the ring π-system.

The Pt—C(3) distance of 2.044(14) Å is not significantly different from the value of 2.020(16) Å obtained for *trans*-$[PtCl_2\{C(NC_6H_5)_2C_2H_4\}(P(C_2H_5)_3)_2]$ (8). The Pt—C(62) bond distance of 2.048(13) Å is also equivalent to the Pt—C(3) distance. This indicates that both bonds may be considered as Pt—C(sp^2) single bonds. The geometry about the *ortho*-metallated ring is comparable to those which have been observed in similar structures (9, 10).

The mean C—C bond length for the ring of the *p*-tolyl group is 1.370(29) Å with a mean C—C—C bond angle of 120(3)°. The mean Pt—P bond distance obtained in this structure is 2.293(7) Å. All P—C distances are equivalent, including those to the methylene carbons, with a mean bond distance of 1.812(24) Å. The bond angles around the P atom show it to adopt a distorted tetrahedral geometry (11).

Conclusions

Although the intramolecular reaction between a transition metal and an *ortho* C—H bond on an aromatic substituent on the P ligand is well known (12) and occurs in a variety of complexes, there have been few examples of *ortho*-metallation occurring in carbene complexes. Its occurrence preferentially in these platinum carbene complexes has prevented the preparation of platinum(II) carbene–olefin complexes, but the reversal, by acid treatment, of the *ortho*-metallation reaction is of particular interest.

Experimental

Infrared spectra in the range 4000–400 cm^{-1} were recorded on a Perkin-Elmer grating spectrometer 2, and absorptions are quoted relative to the polystyrene band at 1601.4 cm^{-1}. The ^1H nmr spectra were recorded on a Varian HA-100 spectrometer. Analyses were obtained from Chemalytics Inc. and Midwest Microlab Ltd.

(1) Preparation of K{PtCl(acac)} (4, 13)

Potassium tetrachloroplatinite, K_2PtCl_4 (1.5 g), was dissolved in 4.5 g water in a 25 ml conical flask. The solution was heated to 70°C and 3 ml of acetylacetone and 4.5 ml of KOH solution (1.1 g in water) added. The solution was stirred at 55–60°C for 20 min and then cooled in a refrigerator to produce large yellow crystals of $K\{PtCl(acac)_2\}$ (1.2 g). These were washed with alcohol and ether and dried in a vacuum dessicator.

(2) Preparation of $H\{PtCl(acac)_2\}$ (6)

To a saturated solution of $K\{PtCl(acac)_2\}$ (1 g) in water was added 5 ml of 6 *N* HCl. An immediate dense yellow precipitate was formed, which was filtered, washed with water, and dried under vacuum (0.93 g, 95%).

(3) Preparation of PtCl(CN-p-tolyl)(acac)

To $H\{PtCl(acac)_2\}$ (0.22 g) in benzene (15 ml) was added *p*-tolylisocyanide (1 equiv.) in benzene, producing an immediate lightening of colour. After the solution had been stirred for 20 min, the benzene was evaporated to a small volume and ether was added to produce the crude product, which was recrystallized from acetone–ether (0.20 g, 87%).

(4) Preparation of $[PtCl\{C(NH\text{-}p\text{-}tolyl)_2\}(acac)]$

The complex PtCl(CN-*p*-tolyl)(acac) (0.2 g) was stirred in benzene (15 ml) with excess *p*-toluidine (0.2 g) for 30 min. A white precipitate was obtained, ether being added to ensure complete precipitation. The white micro crystals of the product (0.21 g, 85%) were washed with ether and could be recrystallized for analysis from $CH_2Cl_2/C_6H_6/n$-pentane.

(5) Reaction of $[PtCl\{C(NH\text{-}p\text{-}tolyl)_2\}(acac)]$ with Na(dtc)

$[PtCl\{C(NH\text{-}p\text{-}tolyl)_2\}(acac)]$ (0.2 g) was dissolved in acetone (15 ml) and sodium diethyl dithiocarbamate (Na dtc) (0.085 g) in acetone (5 ml) was added dropwise and stirred. The solution turned a pale yellow colour and a precipitate formed. After being stirred for 3 h, the solution was evaporated to dryness, CH_2Cl_2 added, and filtered. The filtrate was evaporated to a small volume and ether added to produce a yellow crystalline compound identified as $Pt(dtc)_2$ by comparison with an authentic sample.

Can. J. Chem. Downloaded from www.nrcresearchpress.com by 210.87.254.5 on 09/05/12
For personal use only.

(6) Reaction of [PtCl{C(NH-p-tolyl)$_2$}(acac)] with Silver Salts

[PtCl{C(NH-*p*-tolyl)$_2$}(acac)] (0.15 g) in acetone (15 ml) was refluxed for 20 min with 1 equiv. of one of the following silver salts: $AgPF_6$ (0.07 g), $AgSO_3SF_3$ (0.07 g), or $AgClO_4$ (0.06 g). The solution and precipitate were centrifuged to remove any silver chloride formed and the yellow solution was decanted off. Evaporation of the acetone gave dark green/black crystals, formulated as $[Pt\{C(NHR)_2\}(acac)]^+\chi^-$, where $\chi = PF_6$, SO_3CF_3, or ClO_4. Yellow solutions were regenerated when these crystals were dissolved in coordinating solvents such as acetone or acetonitrile.

(7) Preparation of [Pt(CN-p-tolyl)$_2$\{C(NH-p-tolyl)$_2$\}]-SO_3CF_3

[PtCl{C(NH-*p*-tolyl)$_2$}(acac)] (0.2 g) in acetone (15 ml) was refluxed for 20 min with $AgSO_3CF_3$ (0.1 g). The precipitated silver chloride was removed by centrifugation and to the resulting yellow solution was added *p*-tolylisocyanide (0.10 g). The solution was stirred for 15 min, the solvent was removed, and ether added to precipitate the yellow complex [Pt(CN-*p*-tolyl)$_2$\{C(NH-*p*-tolyl)$_2$\}]SO_3CF_3 (0.21 g, 73%).

(8) Preparation of [Pt\{PPh$_2$(CH$_2$)$_2$PPh$_2$\}\{C(NH-p-tolyl)(NHC$_6$H$_3$CH$_3$)\}]χ where $\chi = ClO_4$ or PF_6

[PtCl{C(NH-*p*-tolyl)$_2$}(acac)] (0.15 g) in acetone (15 ml) was refluxed for 20 min with one equivalent of either $AgPF_6$ (0.07 g) or $AgClO_4$ (0.06 g). The precipitated silver chloride was removed by centrifugation, and to the resulting yellow solution was added 1,2-bisdiphenylphosphinoethane (0.12 g). There was an immediate lightening of the colour of the solution; the solvent was evaporated and ether added to produce yellow crystals of [Pt\{PPh$_2$(CH$_2$)$_2$PPh$_2$\}\{C(NH-*p*-tolyl)(NHC$_6$H$_3$CH$_3$)\}]ClO_4 (0.22 g, 88%) or [Pt\{PPh$_2$(CH$_2$)$_2$PPh$_2$\}\{C(NH-*p*-tolyl)(NHC$_6$H$_3$CH$_3$)\}]PF_6 (0.22 g, 84%).

(9) Preparation of [Pt(S$_2$NCEt$_2$)\{C(NH-p-tolyl)(NHC$_6$H$_3$CH$_3$)\}]

[PtCl{C(NH-*p*-tolyl)$_2$}(acac)] (0.15 g) in acetone (15 ml) was refluxed for 20 min with one equivalent of $AgPF_6$ (0.07 g). The precipitated silver chloride was removed by centrifugation and to the resulting yellow solution was added dropwise sodium diethyldithiocarbamate (0.06 g) in acetone (5 ml). The yellow solution immediately turned a paler yellow and a small amount of $NaPF_6$ was precipitated. This was filtered off, the filtrate evaporated to a small volume, and ether added to produce microcrystals of the complex [Pt(S$_2$NCEt$_2$)\{C(NH-*p*-tolyl)(NHC$_6$H$_3$CH$_3$)\}] (0.10 g, 65%).

(10) Preparation of [PtCl\{PPh$_2$(CH$_2$)$_2$PPh$_2$\}\{C(NH-p-tolyl)$_2$\}]PF_6

To [Pt\{PPh$_2$(CH$_2$)$_2$PPh$_2$\}\{C(NH-*p*-tolyl)(NHC$_6$H$_3$CH$_3$)\}]PF_6 (0.21 g) in an acetone–methanol mixture (1:1, 15 ml) was added acetyl chloride (0.02 g). The yellow solution immediately turned white and evaporation of the solvent led to the precipitation of white crystals of the complex [PtCl\{PPh$_2$(CH$_2$)$_2$PPh$_2$\}\{C(NH-*p*-tolyl)$_2$\}]PF_6 (0.20 g, 90%), following recrystallization from acetone–ether.

(11) Preparation of [PtCl(S$_2$NCEt$_2$)\{C(NH-p-tolyl)$_2$\}]

[Pt(S$_2$NCEt$_2$)\{C(NH-*p*-tolyl)(NHC$_6$H$_3$CH$_3$)\}] (0.2 g) in acetone–methanol and acetyl chloride (0.03 g) were mixed and stirred for 15 min. Evaporation of the solvent led to the precipitation of pale yellow microcrystals of the complex [PtCl(S$_2$NCEt$_2$)\{C(NH-*p*-tolyl)$_2$\}] (0.2 g, 94%). This could be recrystallized from CH_2Cl_2/Et_2O.

(12) Reaction of [PtCl\{PPh$_2$(CH$_2$)$_2$PPh$_2$\}\{C(NH-p-tolyl)$_2$\}]PF_6 with $AgPF_6$

[PtCl{PPh$_2$(CH$_2$)$_2$PPh}\{C(NH-*p*-tolyl)$_2$\}]PF_6 (0.2 g) in acetone was allowed to react with $AgPF_6$ for 10 min. The precipitated AgCl was filtered off and the filtrate evaporated to dryness. Recrystallization from CH_2Cl_2/Et_2O led to production of large white crystals of a compound with empirical formula $PtC_{41}H_{40}F_6N_2P_3$ (0.18 g, 91%).

Analytical and spectroscopic data for the above starting materials and reaction products are given in Table 1.

TABLE 4. Crystal data for $C_{41}H_{39}ClN_2O_4P_2Pt$

Parameter	Value
Formula weight	916.27
Space group	$P2_1/n$
a	20.370(3) Å
b	18.116(3) Å
c	10.770(2)
Z	4
β	99.47(6)
Cell volume	3920.2 Å^3
μ	36.0 cm^{-1} for Mo Kα_1

TABLE 5. Experimental conditions for data collection

Radiation: Mo Kα, Nb foil prefilter, 0.07 mm
Takeoff angle: 2.9° (95% of maximum Bragg intensity)
Aperture: 5 mm × 5 mm, 31 cm from crystal
Data collected: $h\ k\ l$ and $\bar{h}\ k\ l$, for $0 < 2\theta < 55°$
Scan: θ–2θ, range 0.9° corrected for dispersion, at 1° min^{-1}
Background: 10 s stationary crystal, stationary counter at limits of scan
Standards: five recorded every 200 observations; 200, 020, 0$\bar{2}$0, 002, and 111

Collection and Reduction of X-ray Data

Prismatic, yellow crystals of [Pt\{C(NH(C$_9$H$_6$))(NH(C$_9$H$_7$))(P$_2$(C$_6$H$_5$)$_4$C$_2$H$_4$)\}]ClO_4 were recrystallized from acetone/ether mixtures. Weissenberg and precession photography using CuKα radiation showed the crystals belonged to the monoclinic system. The systematic extinctions, $h0l$ for $h + l$ odd and $0k0$ for k odd, are consistent only with the space group $P2_1/n$ (alternate setting of $P2_1/c$, C_{2h}^5, No. 14 (14)). The density, 1.56(1) g cm^{-3}, was determined by flotation in a mixture of carbon tetrachloride and *n*-pentane. The calculated density is 1.55 g cm^{-3}, assuming $Z = 4$. Thus no symmetry constraints are imposed on the ions.

The crystal chosen for data collection was of approximate dimensions 0.12 mm × 0.13 mm × 0.16 mm. It was mounted on a Picker FACS-1 computer-controlled diffractometer with [001] offset approximately 20° from coincidence with the spindle axis. The crystal was measured after data collection on a microscope fitted with a filar eyepiece to permit an absorption correction. Eleven faces were identified by optical goniometry as (010) and forms of {10$\bar{1}$}, {100}, {110}, and {101}. Cell constants and an orientation matrix were obtained from a least-squares refinement[3] of the setting angles of 30

[3]The computer programs used in this analysis include local modifications of the following: cell refinement and orientation matrix, PICKTT, from W. C. Hamilton's MODE 1; full-matrix least-squares, J. A. Ibers' NUCLS: Patterson and Fourier syntheses, A. Zalkin's FORDAP; function and errors, W. R. Busing, K. O. Martin, and H. A. Levy's ORFFE; crystal structure illustrations, C. K. Johnson's ORTEP; absorption correction by the analytical method of de Meulanaer and Tompa in the program AGNOST as modified by D. Cahen and J. A. Ibers (21).

Can. J. Chem. Downloaded from www.nrcresearchpress.com by 210.87.254.5 on 09/05/12
For personal use only.

Table 6. Atomic Positional and Thermal Parameters ($\times 10^4$)

Atom	x	y	z	U_{11}[a]	U_{22}	U_{33}	U_{12}	U_{13}	U_{23}
Pt	1839.3(3)[b]	1696.2(3)	941.8(6)	309(3)	339(3)	341(3)	-24(4)	36(2)	91(5)
P(1)	1830(2)	978(2)	2686(4)	465(26)	302(22)	428(27)	1(20)	71(21)	86(20)
P(2)	700(2)	1646(3)	767(4)	354(22)	515(27)	520(28)	-74(25)	48(20)	130(26)
Cl(1)	-1474(3)	825(3)	2915(6)	732(40)	527(35)	787(43)	30(30)	216(34)	34(32)
O(11)	-1725(10)	1494(7)	2377(15)	2547(217)	345(94)	952(128)	114(108)	-249(135)	185(85)
O(12)	-803(8)	829(10)	3431(17)	805(118)	1398(157)	1477(167)	330(116)	112(118)	-359(140)
O(13)	-1692(9)	223(8)	2138(15)	1872(171)	487(95)	942(127)	127(107)	155(119)	-245(96)
O(14)	-1788(8)	774(10)	4034(17)	1142(129)	1514(151)	1151(132)	-564(132)	561(110)	114(138)
C(1)	957(7)	831(8)	2912(15)	479(102)	439(99)	618(121)	38(82)	173(93)	71(92)
C(2)	501(8)	881(10)	1695(16)	489(108)	750(129)	576(123)	-192(96)	31(97)	285(107)
C(3)	1908(8)	2361(8)	-565(13)	469(99)	382(91)	235(89)	45(81)	-23(79)	122(75)
N(1)	1419(6)	2604(7)	-1380(13)	400(81)	601(93)	576(99)	-97(70)	56(75)	281(82)
N(2)	2511(6)	2590(6)	-634(11)	425(82)	398(78)	397(83)	-61(66)	53(70)	-36(67)
C(61)	3040(8)	2273(8)	166(14)	434(101)	499(101)	266(94)	-137(85)	76(81)	-45(83)
C(62)	2851(7)	1776(9)	1073(13)	336(83)	409(94)	354(89)	94(86)	44(71)	-192(93)
C(63)	3366(8)	1422(8)	1813(14)	445(102)	401(92)	433(104)	-54(76)	127(86)	-105(77)
C(64)	4032(7)	1518(8)	1772(15)	402(97)	419(110)	433(104)	112(77)	-34(83)	-132(81)
C(65)	4184(7)	2014(9)	901(17)	296(91)	499(101)	711(132)	-86(80)	111(93)	-177(99)
C(66)	3706(8)	2409(9)	116(15)	419(104)	642(117)	531(117)	-7(92)	146(93)	41(98)
C(67)	4569(8)	1119(9)	2673(17)	533(116)	602(120)	881(149)	-49(95)	-39(109)	19(113)
C(51)	1406(7)	3176(9)	-2305(15)	523(99)	500(129)	348(102)	50(85)	18(79)	108(92)
C(52)	1562(9)	3900(10)	-1916(18)	841(143)	479(118)	736(147)	-56(105)	-130(115)	242(116)
C(53)	1495(10)	4450(10)	-2823(27)	838(156)	442(126)	1499(237)	-93(108)	151(159)	437(154)
C(54)	1316(11)	4306(16)	-4101(24)	694(154)	1339(233)	762(181)	-80(155)	147(134)	515(188)
C(55)	1136(10)	3596(16)	-4390(21)	658(148)	1519(244)	753(170)	37(153)	-35(124)	430(180)
C(56)	1214(9)	3044(9)	-3513(18)	776(133)	642(132)	503(127)	50(99)	121(108)	212(105)
C(57)	1215(13)	4956(13)	-4977(22)	1886(251)	1114(189)	1117(200)	394(184)	444(182)	921(172)

[a] The form of the thermal ellipsoid is given by $\exp[-(\beta_{11}h^2 + \beta_{22}k^2 + \beta_{33}\ell^2 + 2\beta_{12}hk + 2\beta_{13}h\ell + 2\beta_{23}k\ell)]$.
$U_{ij} = \beta_{ij}/2\pi^2 a_i^* a_j^* (\text{Å}^2)$.

[b] Estimated standard deviations are given in parentheses here and in other tables, and refer to the least significant digits.

Can. J. Chem. Downloaded from www.nrcresearchpress.com by 210.87.254.5 on 09/05/12
For personal use only.

Table 8. Derived group atom parameters

Atom	x	y	z	B(Å^2)	Atom	x	y	z	B(Å^2)
PH-1					PH-3				
C(11)	2139(5)[a]	63(4)	2448(10)	2.9(3)	C(31)	357(5)	2455(5)	1362(10)	3.3(3)
C(12)	2433(5)	-383(6)	3438(7)	4.2(4)	C(32)	-121(6)	2432(5)	2149(11)	5.9(5)
C(13)	2685(5)	-1072(6)	3190(9)	5.5(4)	C(33)	-354(5)	3085(8)	2601(10)	7.2(6)
C(14)	2644(5)	-1314(4)	1952(12)	5.3(4)	C(34)	-108(6)	3761(6)	2266(12)	6.6(5)
C(15)	2350(5)	-867(6)	963(8)	5.1(4)	C(35)	369(7)	3784(5)	1479(13)	8.6(6)
C(16)	2098(5)	-179(6)	1211(8)	4.7(4)	C(36)	602(5)	3131(7)	1027(10)	6.4(5)
PH-2					PH-4				
C(21)	2219(5)	1294(6)	4231(8)	3.6(3)	C(41)	208(5)	1483(6)	-776(8)	4.0(4)
C(22)	2056(5)	985(5)	5324(11)	4.5(4)	C(42)	491(4)	1065(6)	-1636(10)	4.4(4)
C(23)	2356(6)	1246(6)	6496(9)	5.5(4)	C(43)	117(5)	886(5)	-2798(9)	5.1(4)
C(24)	2819(6)	1817(7)	6575(8)	5.8(4)	C(44)	-540(5)	1125(6)	-3100(8)	5.0(4)
C(25)	2983(5)	2126(5)	5483(11)	5.8(4)	C(45)	-823(4)	1543(6)	-2240(11)	5.6(4)
C(26)	2683(5)	1865(6)	4310(9)	4.4(4)	C(46)	-449(5)	1722(6)	-1078(9)	4.7(3)
ClO4									
CL(2)	-1461	803	2808	6.99					
O(21)	-2128	1031	2816	6.99					
O(22)	-1027	1192	3754	6.99					
O(23)	-1404	33	3050	6.99					
O(24)	-1285	957	1612	6.99					

[a] Positional parameters x 10^4. Values without esd's were not refined.

Can. J. Chem. Downloaded from www.nrcresearchpress.com by 210.87.254.5 on 09/05/12
For personal use only.

intense, carefully centered reflections with $13° < 2\theta < 27°$. Prefiltered Mo radiation was used, $\lambda = 0.70926$ Å, at 23°C. Crystal data are given in Table 4.

The conditions used for data collection are summarized in Table 5. Several ω scans of intense, low-angle reflections were recorded as a check on crystal mosaicity. The average width at half-height was 0.05°. Measurement of standard reflections during data collection and an examination of crystal mosaicity at the end showed no significant decomposition had occurred.

A total of 6073 reflections was measured. The recorded intensities were corrected for Lorentz and polarization effects. A standard deviation $\sigma(I)$ was assigned to each intensity (I), where $(\sigma(I))^2 = [C + \frac{1}{4}(t_c/t_b)^2(b_l + b_h) + (pI)^2]$ where $I = [C - \frac{1}{2}(b_l + b_h)t_c/t_b]$, C = total count measured in time t_c, and b_l and b_h are background counts each measured in time t_b. P was chosen as 0.02 and then increased to 0.04 for the final cycles of refinement (15). Of the 5888 reflections processed (excluding the standard reflections), 3308 with $I > 3\sigma(I)$ were used in the solution and refinement of the structure.

Solution and Refinement of the Structure

The structure was solved by the heavy atom method, and refined by full-matrix least-squares techniques on F. Scattering factors for neutral non-hydrogen atoms were taken from Cromer and Waber (16), while those for H were from Stewart Davidson, and Simpson (17). The real and imaginary anomalous dispersion corrections of Cromer and Libermann (18) were included for the Pt and P atoms, and in later refinements, for the Cl atom.

The positional parameters for the Pt and two P atoms were determined from a three-dimensional Patterson synthesis. A series of structure factor and difference Fourier synthesis calculations revealed the positions of the remaining 48 non-hydrogen atoms. In the early refinement the C atoms of the four phenyl rings, the six C atoms of the *p*-tolyl ring, and the five atoms of the perchlorate group were constrained as rigid groups. The atoms in the coordinated phenyl ring were treated as individual atoms. The phenyl rings were assumed to have D_{6h} symmetry and a C—C bond length of 1.392 Å (19). The ClO_4 rigid group was given T_d symmetry and a Cl—O distance of 1.42 Å (20). The data were corrected for absorption effects using the analytical method.[3] Transmission coefficients varied from 0.603 to 0.799.

One cycle of refinement varying positional and isotropic thermal parameters for the 16 non-hydrogen atoms, a group origin, three orientation angles, and an overall group thermal parameter for each group gave agreement factors $R_1 = \Sigma||F_o| - |F_c||/\Sigma|F_o| = 0.091$ and $R_2 = (\Sigma w(|F_o| - |F_c|)^2/\Sigma wF_o^2)^{1/2} = 0.099$. The function minimized was $\Sigma w(|F_o| - |F_c|)^2$, and the weight w was calculated as $4F_o^2/\sigma^2(F_o^2)$. In further cycles all non-group atoms were assigned anisotropic thermal parameters. The Cl atom was removed from the perchlorate rigid group, leaving a tetrahedral group of four O atoms. Individual group atom isotropic thermal parameters were varied, and three cycles of refinement converged at $R_1 = 0.057$ and $R_2 = 0.059$.

The 39 H atoms present in the cation were located from a difference Fourier synthesis. Idealized positional coordinates were computed, assuming either sp^2 or sp^3 coordination geometries about the C atoms, and bond distances of 0.95 Å and 1.0 Å, respectively. The hybridization of the N atom is sp^3, with an N—H bond distance of 1.0 Å. All H atoms were assigned isotropic thermal parameters 1.0 Å^2 greater than those of the atoms to which they are bonded. Thereafter the contributions from the H atoms were included in the calculations of F_c and no attempt was made to refine the H atom parameters.

The rigid group constraints were then removed from the four O atoms, and from the six C atoms of the *p*-tolyl group, and the atoms permitted to vibrate anisotropically. After two cycles of refinement (3308 observations and 292 variables) the model converged at $R_1 = 0.049$ and $R_2 = 0.049$.

A subsequent difference Fourier synthesis over the ClO_4 anion region revealed electron density close to O(11), O(12), and O(13) and an additional peak greater than 1.0 e Å^{-3} located at fractional coordinates (−0.119, 0.110, 0.162). These four peaks form a tetrahedral array. This, and the pronounced anisotropic thermal motion of the Cl atom, led us to formulate a disorder model in which two anions occupy the same region in the crystal, but with three of the four O atoms superimposed. The additional peak thus results from the fourth O atom. Refinement of the multiplicity parameter, with appropriate constraints applied to the derivatives, gave a 10(1)% probability of the second orientation. This second group was included thereafter in structure factor calculations, but was not refined. The Cl atom and the four O atoms of the 90% probable orientation were refined anisotropically thereafter.

Two final cycles of refinement with recalculation of H atom parameters (292 variables and 3252 observations with $F^2 > 3\sigma$) converged at residuals of $R_1 = 0.047$ and $R_2 = 0.053$. In the final cycle no positional parameter shift exceeded 0.134 of its estimated standard deviation. The error in an observation of unit weight is 1.11 electrons. A statistical analysis of R_2 over various ranges of $|F_o|$, $\lambda^{-1}\sin\theta$, and diffractometer setting angles χ and ϕ showed no abnormal trends. A comparison of F_o and F_c suggested extinction effects were minimal, and could be ignored. A total difference Fourier synthesis calculated from the final structure factors contained no features of chemical significance. The highest peak, with fractional coordinates (0.135, 0.149, 0.034), located near the Pt atom, had an electron density of 0.95 (16) e Å^{-3}. Final positional and thermal parameters for the non-H atoms are given in Table 6, rigid group parameters in Table 7, derived group atom parameters in Table 8, and hydrogen atom parameters in Table 9. Structure amplitudes are listed in Table 10 as $10|F_o|$ and $10|F_c|$, in electrons, with weights $\times 10^3$.[4]

Acknowledgments

The financial support of this work (to H.C.C. and N.C.P.) by the National Research Council of Canada is gratefully acknowledged.

1. (*a*) N. Calderon. Acc. Chem. Res. **5**, 39 (1972); (*b*) T. J. Katz and J. McGinnis. J. Am. Chem. Soc. **97**, 1592 (1975); (*c*) R. H. Grubbs, P. L. Burk, and D. D. Carr. J. Am. Chem. Soc. **97**, 3265 (1975).
2. M. J. Church and M. J. Mays. J. Chem. Soc. A, 3074 (1968).
3. D. F. Christian, H. C. Clark, and R. F. Stepaniak. J. Organomet. Chem. **112**, 209 (1976).
4. A. A. Grinberg and H. Chaparski. Russ. J. Inorg. Chem. **4**, 137 (1959).
5. D. Gibson, J. Lewis, and C. Oldham. J. Chem. Soc. A, 72 (1967).
6. G. Hulley, B. F. G. Johnson, and J. Lewis. J. Chem. Soc. A, 1732 (1970).

[4]Tables 7, 9, and 10 are available, at a nominal charge, from the Depository of Unpublished Data, CISTI, National Research Council of Canada, Ottawa, Ont., Canada K1A 0S2.

7. D. F. CHRISTIAN, H. C. CLARK, and R. F. STEPANIAK. J. Organomet. Chem. **112**, 227 (1976).
8. K. W. MUIR, R. WALKER, J. CHATT, R. L. RICHARDS, and G. H. D. ROYSTON. J. Organomet. Chem. **56**, C30 (1973); L. MANOJLOVIC-MUIR and K. W. MUIR. J. Chem. Soc. Dalton, 2427 (1974).
9. R. WALKER and K. W. MUIR. J. Chem. Soc. Dalton, 272 (1975).
10. R. J. MCKINNEY, C. B. KNOBLER, B. T. HUIE, and H. D. KAESZ. J. Am. Chem. Soc. **99**, 2988 (1977).
11. T. UCHIDA, Y. UCHIDA, M. HIDAI, and T. KODAMA. Acta Crystallogr. B**31**, 1197 (1975).
12. G. W. PARSHALL. Acc. Chem. Res. **3**, 139 (1970).
13. J. LEWIS. Nature, **195**, 1278 (1962).
14. International Tables for X-Ray Crystallography. Vol. 1. Kynock Press, Birmingham, England. 1969.
15. L. E. MCCANDLISH, G. H. STOUT, and L. C. ANDREWS. Acta Crystallogr. **31**, 245 (1975).
16. D. T. CROMER and J. T. WABER. Acta Crystallogr. **18**, 104 (1965).
17. R. F. STEWART, E. R. DAVIDSON, and W. T. SIMPSON. J. Chem. Phys. **42**, 3175 (1965).
18. D. T. CROMER and D. LIBERMAN. J. Chem. Phys. **53**, 1891 (1970).
19. R. EISENBERG and J. A. IBERS. Inorg. Chem. **4**, 773 (1965).
20. F. S. LEE and G. B. CARPENTER. J. Phys. Chem. **63**, 279 (1959).
21. D. CAHEN and J. A. IBERS. J. Appl. Crystallogr. **5**, 298 (1972).

Can. J. Chem. Downloaded from www.nrcresearchpress.com by 210.87.254.5 on 09/05/12
For personal use only.

Thiosemicarbazide complexes of mercury(II) halides

CHUNG CHIEH, LAURA P. C. LEE, AND CECILIA CHIU

Guelph–Waterloo Centre for Graduate Work in Chemistry, University of Waterloo, Waterloo, Ont., Canada N2L 3G1

Received April 26, 1978

CHUNG CHIEH, LAURA P. C. LEE, and CECILIA CHIU. Can. J. Chem. **56**, 2526 (1978).

Dibromobis(thiosemicarbazide)mercury(II), $HgBr_2(tsc)_2$, is isostructural with dichlorobis(thiosemicarbazide)mercury(II). The crystal is orthorhombic with $a = 8.825(9)$, $b = 8.587(11)$, $c = 15.939(22)$ Å, $z = 4$, space group *Pbcn*. Some bond lengths and angles are: Hg—Br = 2.860(4) Å, Hg—S = 2.45(1) Å, C—S = 1.76(4) Å and $\angle$SHgS = 155°, $\angle$BrHgBr = 97.1°. In both $HgCl_2(tsc)_2$ and $HgBr_2(tsc)_2$, the configuration of the coordinated thiosemicarbazide (tsc) is the same as that of the free molecule. The ir and Raman (R) spectra for the complexes and tsc in the region 300–1600 cm^{-1} are very similar. The strong band at 800 (807 R) cm^{-1} in the tsc due to ν(C—S) is shifted to 773 (796 R), 777 (796 R), and 660 (680 R) cm^{-1} for $HgCl_2(tsc)_2$, $HgBr_2(tsc)_2$, and $HgCl_2(tsc)$ correspondingly. A strong band at 368 (R) cm^{-1} present uniquely for $HgCl_2(tsc)$ can be assigned to ν(Hg—N). The halides in $HgX_2(tsc)_2$ are bonded to one mercury(II) ion and weakly bridged to a neighboring molecule with Hg...Cl = 3.250(3) Å and Hg...Br = 3.436(4) Å. As a result, two Raman bands due to Hg—X are expected. For $HgCl_2(tsc)_2$, the two Raman bands occur at 236 and 166 cm^{-1}, whereas for $HgBr_2(tsc)_2$, one was observed at 190 cm^{-1} but the other was masked by lattice modes. In $HgCl_2(tsc)$, the two Hg—Cl bonds are different and bands at 220 and 190 cm^{-1} are assigned to $\nu(Hg—Cl)_t$.

CHUNG CHIEH, LAURA P. C. LEE et CECILIA CHIU. Can. J. Chem. **56**, 2526 (1978).

Le dibromobis (thiosemicarbazide)mercure(II), $HgBr_2(tsc)_2$, est isostructural avec la dichlorobis(thiosemicarbazide)mercure(II). Le cristal est orthorhombique avec $a = 8.825(9)$, $b = 8.587(11)$, $c = 15.939(22)$ Å, $z = 4$, groupe d'espace *Pbcn*. On a mesuré quelques longueurs et angles de liaison soit: Hg—Br = 2.860(4) Å, Hg—S = 2.45(1) Å, C—S = 1.76(4) Å et $\angle$SHgS = 155°, $\angle$BrHgBr = 97.1°. Dans le $HgCl_2(tsc)_2$ et $HgBr_2(tsc)_2$, la configuration de la thiosemicarbazide (tsc) coordonnée est la même que dans la molécule libre. Les spectres ir et Raman (R) pour les complexes et le tsc dans la région de 300–1600 cm^{-1} sont très semblables. La bande forte à 800 (807 R) cm^{-1} dans le tsc et due à la ν(C—S) est déplacée à 773 (796 R), 777 (796 R) et 660 (680 R) cm^{-1} pour $HgCl_2(tsc)_2$, $HgBr_2(tsc)_2$ et $HgCl_2(tsc)$ respectivement. On peut attribuer à la ν(Hg—N) la bande forte à 368 (R) cm^{-1} qui est présente uniquement dans $HgCl_2(tsc)$. Les halogénures du $HgX_2(tsc)_2$ sont liés à un ion mercure(II) et faiblement pontés à une molécule voisine avec Hg...Cl = 3.250(3) Å et Hg...Br = 3.436(4) Å. Comme conséquence, les deux bandes Raman du Hg—X sont attendues. Pour le $HgCl_2(tsc)_2$, les deux bandes Raman apparaissent à 236 et 166 cm^{-1} alors que pour le $HgBr_2(tsc)_2$ une est observée à 190 cm^{-1} mais l'autre est masquée par les vibrations du réseau. Dans le $HgCl_2(tsc)$, les deux liaisons Hg—Cl sont différentes et on attribue les bandes à 220 et 190 cm^{-1} à la $\nu(Hg—Cl)_t$.

[Traduit par le journal

Introduction

A few group IIB metal complexes of thiosemicarbazide (tsc) have been reported in the literature (1). Compounds $ZnCl_2(tsc)$ and $HgCl_2(tsc)$ are molecular complexes with a bidentate tsc ligand (2, 3). In $HgCl_2(tsc)_2$ and AgCl(tsc), the ligand tsc is monodentate (4, 5). Dibromobis(thiosemicarbazide)-mercury(II) is confirmed to be isostructural with $HgCl_2(tsc)_2$ by crystallographic methods.

Several ir absorption studies of tsc and related compounds have been reported (6–8). However, there is little information about ir or Raman bands in the low frequency region (<600 cm^{-1}) for tsc or its complexes. The difficulty in assigning bands in this region is mainly due to the lack of structural results. For example, the band at 544 cm^{-1} in $HgCl_2(tsc)_2$ was erroneously assigned to ν(Hg—N) (1). The Hg—N bond does not exist in the compound $HgCl_2(tsc)_2$ (4).

Burns reported the ir spectra for AgCl(tsc), $NiCl_2(tsc)_3$, and $Ni(tsc)_2$ in the region 3300–700 cm^{-1} (9). The vibrational assignments by Mashima (8) and the study of spectra in polarized light of orientated tsc crystalline samples by Keresztury and Marzocchi (6) are among those considered to be reliable. These assignments make it possible to analyze the spectra of the complexes. Furthermore there are few metal–ligand vibration assignments in the literature for tsc complexes.

Many characteristic frequencies for (Hg—S)

Can. J. Chem. Downloaded from www.nrcresearchpress.com by 210.87.254.40 on 09/05/12
For personal use only.

Can. J. Chem. Downloaded from www.nrcresearchpress.com by 210.87.254.40 on 09/05/12
For personal use only.

TABLE 1. Atomic parameters for $HgBr_2(tsc)_2$. $\pm(x\ y\ z,\ 1/2 - x\ 1/2 - y\ 1/2 + z,\ 1/2 + x\ 1/2 - y\ \bar{z},\ \bar{x}\ y\ 1/2 - z)$

Atom	x	y	z
Hg	0.5	0.3973(3)	0.25
Br	0.2313(4)	0.1178(5)	0.2090(3)
S	0.4590(9)	0.335(2)	0.3985(6)
N(1)	0.004(5)	0.405(5)	0.386(3)
N(2)	0.163(4)	0.349(4)	0.373(2)
N(3)	0.249(6)	0.474(6)	0.489(3)
C	0.274(4)	0.396(4)	0.421(2)

where S is in the S=C< group, were measured for mercury(II) thiourea (tu) complexes (10), but no measurements have been made for mercury tsc complexes. We now report spectroscopic analyses on the samples used in our X-ray diffraction studies.

Experimental

The compound $HgBr_2(tsc)_2$ was synthesized by mixing stoichiometric $HgBr_2$ and tsc in aqueous solution. However, the reaction mixture was covered with aluminum foil to avoid decomposition by light. The crystals so obtained were colorless.

X-ray diffraction procedures were similar to those carried out for $HgCl_2(tsc)_2$ (4). Crystal data are as follows:

$C_2H_{10}Br_2HgN_6S_2$ fw = 542.7

Orthorhombic, $a = 8.825(9)$, $b = 8.587(11)$, $c = 15.939(23)$ Å; space group *Pbcn*. $D_o = 3.05$ (by flotation), $z = 4$, $D_c = 2.984$ g cm^{-3}. $V = 1207.9$ Å^3, μ(Mo-Kα) = 203.3 cm^{-1}, Systematic absences: $0kl$, $k = 2n + 1$, $h0l$, $l = 2n + 1$, $hk0$, $h + k = 2n + 1$. λ(Mo-Kα) = 0.7107 Å.

The crystal used had a rectangular shape with dimensions of 0.10 × 0.21 × 0.35 mm along [$\bar{1}$01], [101], and [010] directions. It was mounted with b along the ϕ axis of a G.E. XRD-6 automatic diffractometer. Among 855 reflections measured at 25 ± 3°C, 815 with $I > 3\sigma$ were used in the refinement of the structure. The method of data collection was the same as that used for $HgCl_2(tsc)_2$. Absorption corrections were made by the methods of Coppens *et al.* (11). The transmission factor, $A = \int 1/v \exp\{-\mu(r_i + r_d)\}dV$, range is 56 to 6%. Since the Patterson map of $HgBr_2(tsc)_2$ indicated that Hg was located at the same position as that of $HgCl_2(tsc)_2$, atomic parameters from the latter were used in the least-squares refinements. At the final stage, a weighting function $w^{-1} = (40 + F_o + 0.0001F_o^2)$ was used. The final R factor ($= \Sigma||F_o| - |F||/\Sigma|F_o|$) was 0.13. The quality of the data was affected by the absorption. The difference Fourier map showed high background ripple around Hg and Br locations. The atomic parameters are given in Table 1.[1]

Solid state ir spectra were measured on a Beckman IR-10 spectrophotometer. In the region 4000–1200 cm^{-1}, halocarbon mulls in CsI plates were used whereas in 1300–250 cm^{-1} region, Nujol mulls were employed. Polycrystalline Raman spectra were measured on a Jarrell-Ash Model 400 Raman spectrophotometer. The Ar ion laser operated at approximately 350 mW light power.

[1]Copies of the tables of structure factors and temperature parameters may be obtained, at a nominal charge, from the Depository of Unpublished Data, CISTI, National Research Council of Canada, Ottawa, Ont., Canada K1A 0S2.

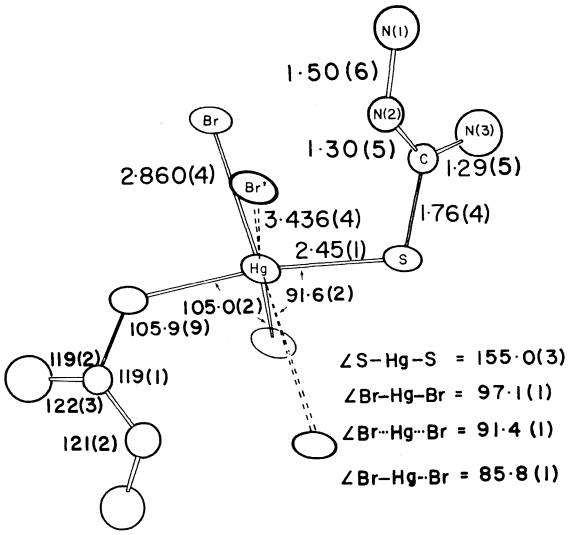

FIG. 1. Important bond distances (Å) and angles (°) for $HgBr_2(tsc)_2$; standard deviations in parentheses.

Results and Discussion

The important bond lengths and angles are given in Fig. 1. The cell constants and Hg—X bond lengths of $HgBr_2(tsc)_2$ are larger than those of $HgCl_2(tsc)_2$ due to the larger size of bromine.

The abilities of tsc to act either as a monodentate or a bidentate ligand have resulted in the formation of $HgX_2(tsc)$ and $HgX_2(tsc)_2$. The configuration of tsc in $HgX_2(tsc)$ is similar to that in $Ni(tsc)_2A$ ($A = SO_4^{2-}$, $2NO_3^-$), or $ZnX_2(tsc)$, whereas in $HgX_2(tsc)_2$ (4) or AgX(tsc) (5) the configuration of the coordinated tsc is not different from that of the free tsc molecule. As a result, ir or Raman spectra of the ligand for monodentate tsc complexes are similar to that of tsc. The spectra of the bidentate tsc complexes belong to a separate category.

In the 1600 cm^{-1} region, two bands were observed for tsc as well as for its complexes. The assignment is given in Table 2.[1] The band due to $\delta(N(3)H_2) + \nu(C—S)$ is shifted to a lower frequency upon coordination. The frequency of the first band, 1618 (1628 R) cm^{-1} of $HgCl_2(tsc)$ is much lower than those of tsc or $HgX_2(tsc)_2$ (1641 (1642 R), ~1650 cm^{-1}) due to the coordination through N(1).

The bands at 1530 (1530 R), 1480 (1500 R), and 1310 cm^{-1} of tsc shift slightly upon complexing in $HgX_2(tsc)_2$. Similar bands in thiourea, *N*-ethylthiourea, and *N,N'*-diethylthiourea complexes showed the same shifts (10, 13, 14).

Bands in the above region depend on the configuration of tsc, which is bidentate in $HgCl_2(tsc)$. The skeletal change gave two bands at 1450 (1456 R) and 1365 (1380 R) cm^{-1}. Nickel and copper com-

TABLE 2. Raman and ir bands (cm^{-1}) for tsc and its complexes*

Band assignment	tsc	$HgCl_2(tsc)_2$	$HgBr_2(tsc)_2$	$HgCl_2(tsc)$	Ref. for assign. in tsc
$\delta(N(1)H_2)$ +	1641 s	1648 s	1650 s	1618 s	6, 12, 15
ν(C—N)	1642 vw R			1628 w R	
$\delta(N(3)H_2)$ +	1618 s	1600 s	1600 s	1600 s	6, 12, 15
ν(C—S)	1614 vw R	1600 w R		1596 w R	
				(1548 m R)	
δ(N(2)H)† +	1530 s	1540 m	1540 m	(1450 m)	6, 9, 15
ν(C—N)	1530 w R	1545 m R		(1456 w R)	
ν(C—N)† +	1480 m	1490 w	1490 w	(1365 m)	6, 9, 15
δ(N(2)H)	1500 w R	1502 w R		(1380 s R)	
ν(C—N) +	1310 sh	1311 sh	1311 sh		6, 9
δ(N(2)H)					
Skeletal +	1285 s	1291 s	1295 s	1290 s	6, 8, 9
ν(C—N) + ν(C—S)	1274 m R	1302 s R	1306 w R	1296 w	
$\rho_r(NH_2)$ +	1162 s	1170 m	1170 m	1170 m	8, 9
$\rho_w(NH_2)$	1170 m R	1188 vw, br R	1176 vw, br R	1196 vw, br R	
$\delta(NH_2)$	1000 vs	1020 sh	1020 sh	1020 s	6, 8
		989 s	990 vs	990 s	
	1008 s R	1016 s R	1016 s R	1038 m R	
				999 m R	
ν(C—S)† +	800 s	773 s	777 s	660 s	6, 9, 15
ν(C—N)	807 s R	796 s R	796 s R	680 s R‡	
$\delta(NH_2)$ +	725 w				6
γ(N(2)H) +	640 m	620 s, br	619 s, br	618 s	
skeletal	590 sh	530 s	531 s	565 s	
	556 s				
	503 w, sp			465 s	
	410 m				
	728 w R				
	638 w R				
	507 s R	496 w R	494 w R	600 w R	
	406 m R	408 s R	393 m R	444 s R	
ν(Hg—N)	—	—	—	368 s R	
ν(C—S)/ν(C—S)	327 m	310 w	309 w	280 m	
+ ν(Hg—S)	288 m R	315 s R	306 s R	302 s R	
$\nu(Hg—Cl)_t$	—	—	—	220 vs R	
				190 s R	
$\nu(Hg—X)_b$	—	236 vs R	190 vs R	—	
Lattice mode	—	198 s R	—	—	
$\nu(Hg...X)_b$	—	166 m R	masked by lattice mode	—	

*δ, deformation; ν, stretching; ρ_r, rocking; ρ_w, wagging; γ, out-of-plane bending; sh, shoulder; br, broad; sp, sharp; vs, very strong; m, medium; w, weak; vw, very weak; R, Raman.
†More contribution from this mode.
‡With ring deformation.

plexes in which the tsc is also bidentate, have bands at ~1450 (1456 R) and ~1370 (1380 R) cm^{-1} (15).

The band at 1162 (1170 R) cm^{-1} was believed to be a rocking and wagging mode of NH_2 (8, 9). In all three complexes, this band occurred at 1170 (1176–1196 R) cm^{-1}. Raman spectra in the region 1100–100 cm^{-1} are given in Fig. 2.

Bands at ~1000 cm^{-1} of tsc and $HgX_2(tsc)_2$ are strong. This band split in two in $HgCl_2(tsc)$ probably because one of the NH_2 groups in the tsc is co-ordinated to mercury.

The band at 800 (807 R) cm^{-1} of the tsc was suggested as mainly a $\rho_w(NH_2)$ by Jensen and Neilson (16). Other authors had assigned it to a combination of ν(C—S) and ν(C—N) mode (6, 9). When complexed, this band appeared at ~773 (796 R) cm^{-1} for $HgX_2(tsc)_2$. This lends further support to the assignment of ν(C—S) with a small contribution from ν(C—N). The corresponding ir bands for $Cu(tsc)_2Cl_2$ and $Ni(tsc)_2Cl_2$ were at 698 (m) and 704 (m) cm^{-1} (15). This suggests further contribution of ring deformation to the bidentate tsc.

The metal-to-ligand or to-halide stretching frequencies are identified in the Raman spectra. A strong Raman band at 368 cm^{-1} found for $HgCl_2$-(tsc), but not for other compounds of Table 2, may

Can. J. Chem. Downloaded from www.nrcresearchpress.com by 210.87.254.40 on 09/05/12
For personal use only.

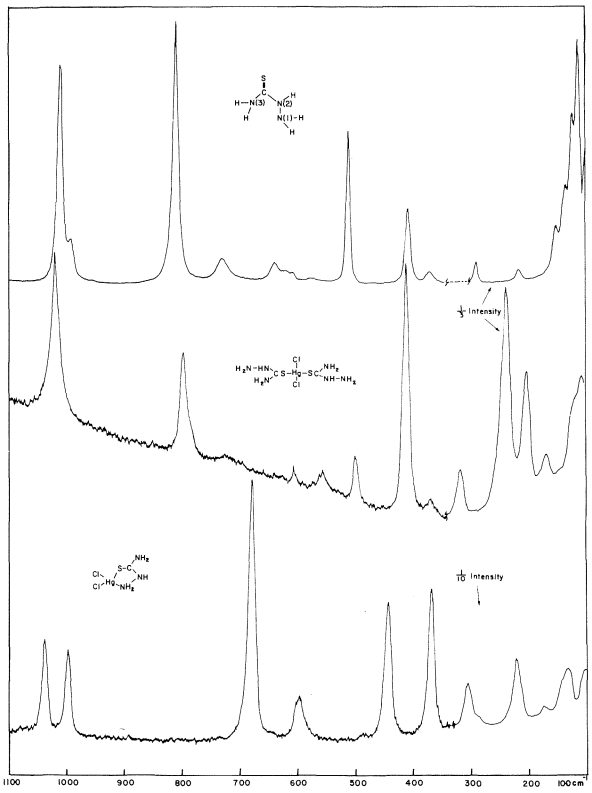

FIG. 2. Raman spectra for tsc and its complexes.

be assigned to ν(Hg—N). Lower frequencies around 340 cm^{-1} were found for mercury(II) halides – morpholine complexes (17).

The medium intense band at 327 (288 R) cm^{-1} for tsc became strong probably as a result of overlapping of ν(C—S) and ν(Hg—S). The latter assignment is supported by a range of mercury(II) halide thiourea and *N*-substituted thiourea complexes by Marcotrigiano *et al.* (13, 14, 18, 19) and Adams and Cornell (20). The frequencies for these complexes range from 200 to 280 cm^{-1}, except those of *N*,*N'*-diethylthiourea complexes, in which case the ranges were from 270 to 350 cm^{-1} in the ir and from 260 to 340 cm^{-1} in the Raman (13). This was the only Raman study for these complexes. The intensity ratio of the two peaks at 408 (R) and 315 (R) cm^{-1} for $HgCl_2(tsc)_2$ is not the same for $HgBr_2(tsc)_2$, however, bands at 310 cm^{-1} are the only common band with comparable intensity and suitable frequency for ν(Hg—S).

Two bands are expected for ν(Hg—X) for all three complexes in Table 2. For $HgCl_2(tsc)$, there are two unequivalent terminal Hg—Cl bonds, $\nu(Hg—Cl)_t$, whereas in $HgCl_2(tsc)_2$, the chloride is asymmetrically bridged to two mercury(II) ions (3, 4). Therefore 220 and 190 cm^{-1} are assigned to $\nu(Hg—Cl)_t$, whereas 236 and 166 cm^{-1} to $\nu(Hg—Cl)_b$. One of the $\nu(Hg—Br)_b$ occurs at 190 cm^{-1} while the other is masked by lattice vibrations. Terminal and bridging halides are also present in the thiourea and *N*-substituted thiourea complexes mentioned earlier. Their vibrational frequencies are comparable to those observed in this study. Mercury(II) halide complexes with nitrogen donor ligands had the same frequency range for Hg—X vibrations (17, 21).

Acknowledgement

This work was supported by the National Research Council of Canada. We thank Dr. S. Y. Tang for his assistance in obtaining the Raman spectra.

1. D. S. MAHADEVAPPA and A. S. A. MURTHY. Aust. J. Chem. **25**, 1565 (1972).
2. M. CAVALCA, M. NARDELLI, and G. BRIANCHI. Acta Crystallogr. **13**, 688 (1960).
3. C. CHIEH and D. H. COWELL. Can. J. Chem. **55**, 3898 (1977).
4. C. CHIEH. Can. J. Chem. **55**, 1583 (1977).
5. G. E. GASPARRI, A. MANGIA, A. MUSATTI, and M. NARDELLI. Acta Crystallogr. B**24**, 367 (1968).
6. G. KERESZTURY and M. P. MARZOCCHI. Chem. Phys. **6**, 117 (1974).
7. R. A. HAINES and K. W. SUN. Can. J. Chem. **46**, 3241 (1968).
8. M. MASHIMA. Bull. Chem. Soc. Jpn. **37**, 974 (1964).
9. G. R. BURNS. Inorg. Chem. **7**, 277 (1967).
10. G. MARCOTRIGIANO and R. BATTISTUZZI. Inorg. Nucl. Chem. Lett. **8**, 969 (1972).
11. P. COPPENS, L. LEISEROWITZ, and D. ROBINOVICH. Acta Crystallogr. **18**, 1035 (1965).
12. D. M. MILLES and T. SUPRUNCHUK. Can. J. Chem. **47**, 1087 (1969).
13. G. MARCOTRIGIANO. Z. Anorg. Allg. Chem. **422**, 80 (1976).
14. G. MARCOTRIGIANO, G. PEYRONEL, and R. BATTISTUZZI. J. Inorg. Nucl. Chem. **37**, 1675 (1975).
15. B. B. KEDZIA. Bull. Acad. Polon. Sci. Ser. Sci. Chim. **6**, 573 (1972); **6**, 565 (1972).
16. K. JENSEN and P. H. NIELSON. Acta Chem. Scand. **20**, 597 (1966).
17. I. S. AHUJA and P. RASTOGI. Inorg. Nucl. Chem. Lett. **5**, 255 (1969).
18. G. MARCOTRIGIANO and R. BATTISTUZZI. J. Inorg. Nucl. Chem. **36**, 3719 (1974).
19. G. MARCOTRIGIANO. Z. Anorg. Allg. Chem. **417**, 75 (1975).
20. D. M. ADAMS and J. B. CORNELL. J. Chem. Soc. A, 884 (1967).
21. I. S. AHUJA and P. RASTOGI. J. Chem. Soc. A, 2161 (1970).

Can. J. Chem. Downloaded from www.nrcresearchpress.com by 210.87.254.40 on 09/05/12
For personal use only.

The formation of propane, propylene, and acetone from 2-propanol over vanadium pentoxide and modified vanadium pentoxide catalysts

DAVID V. FIKIS, WILLIAM J. MURPHY, AND ROBERT A. ROSS
Department of Chemistry, Lakehead University, Thunder Bay, Ont., Canada P7B 5E1

Received April 7, 1978

DAVID V. FIKIS, WILLIAM J. MURPHY, and ROBERT A. ROSS. Can. J. Chem. **56**, 2530 (1978).

The catalytic decomposition of 2-propanol has been studied in a flow system from 200 to 280°C on vanadium pentoxide and modified vanadium pentoxide catalysts. Results were obtained with separate melts of the oxide containing 9.09 mol% of each of the alkali metal sulfates and with individual preparations of the pentoxide containing 1.01, 2.00, and 4.98 mol% potassium sulfate, respectively. In addition to expected dehydration and dehydrogenation reactions, propane was formed over the entire temperature range and became a dominant product at higher temperatures.

Kinetic experiments showed that the dehydration and dehydrogenation reactions were zero order with respect to all components while the propane-forming reaction gave a rate order of 0.3 with respect to 2-propanol concentration. Elimination-type mechanisms have been proposed to explain the results and some evidence of a relationship between catalyst activities and surface acidity is presented. The observed kinetic compensation effect has been shown to compare well with previous work on 2-propanol decomposition on metal oxides.

DAVID V. FIKIS, WILLIAM J. MURPHY et ROBERT A. ROSS. Can. J. Chem. **56**, 2530 (1978).

On a étudié, la décomposition catalytique du propanol-2, dans un système à flux, de 200 à 280°C, sur des catalyseurs de pentoxyde de vanadium et de pentoxyde de vanadium modifié. On a obtenu des résultats avec diverses masses fondues d'oxyde contenant 9.09 mol% de chacun des sulfates de métaux alcalin et avec des préparations individuelles du pentoxyde contenant respectivement 1.01, 2.00 et 4.98 mol% de sulfate de potassium. En plus des réactions de déshydratation et de déshydrogénation attendues, il y a formation de propane à toutes les températures étudiées et ce produit devient le produit majoritaire à des températures plus élevées.

Des expériences de cinétique montrent que les réactions de déshydratation et de déshydrogénation sont d'ordre zéro par rapport à tous les composants alors que l'ordre de la réaction de formation du propane est de 0.3 par rapport à la concentration de propanol-2. On a proposé des mécanismes du type élimination pour expliquer les résultats et on présente quelques données relatives aux activités des catalyseurs et à l'acidité de la surface. On a montré que l'effet de compensation cinétique observée se compare bien avec le travail antérieur sur la décomposition du propanol-2 sur des oxydes métalliques.

[Traduit par le journal]

Introduction

In recent studies (1, 2) of the decomposition of 2-propanol over alkaline earth and transition metal oxides, activity relationships with catalyst oxygen mobilities and contents have been explored. The work has now been extended to include reaction of the alcohol on vanadium pentoxide and separate melts of the oxide containing 9.09 mol% of each of the alkali metal sulfates as additives. Results have also been obtained with individual preparations of the pentoxide containing 1.01, 2.00, and 4.98 mol% potassium sulfate, respectively. Such catalyst preparations appeared to be suitable test vehicles for the earlier hypotheses since the addition of alkali metal sulfates to vanadium pentoxide has a pronounced effect on catalyst activity for sulfuric acid production (3) and also promotes the exchange between molecular oxygen and the oxygen of the metal oxide. These and similar observations have been attributed to changes wrought on the surface mobility of oxygen in the catalyst (4–7).

Specifically, the promoting action for oxygen exchange (4, 5) gave the following additive activity series with vanadium pentoxide catalysts: None < Li_2SO_4 < Na_2SO_4 < K_2SO_4 < Rb_2SO_4 < Cs_2SO_4. Studies of the catalytic activities for sulfur dioxide oxidation showed the same trend (8) and a similar sequence was observed for the present catalysts in the oxidation of carbon monoxide by nitrous oxide (9).

Several studies have also been reported on the influences of various other additives on the activities of metal oxide catalysts in alcohol decomposition reactions (10–12) and the results discussed in terms of relationships with electronic features of the solids.

Experimental Section

Apparatus and Method

The all-glass flow system has been described previously (13, 14). High-purity helium was used as the carrier gas at atmospheric pressure in the flow system and in the Hewlett Packard, Model 5754B gas chromatograph. The analytical columns were constructed from 1.5 m × 0.32 cm od stainless steel tubing packed with "Porapak Q" (150–200 mesh). The column temperature was maintained at 100°C for a post-injection interval of 4 min during which water, propylene, and propane were eluted. The column temperature was then increased by linear temperature programming at 20°C/min to a maximum temperature of 140°C which was then maintained for a further 7 min. During this period, acetone and 2-propanol were eluted. The flow of gas was at a rate of 30 ml min^{-1} (NTP) through the columns. Reaction products were analyzed by both flame ionization (at 175°C) and thermal conductivity detectors (at 200°C, filament current 245 mA).

Surface areas were determined by low-temperature krypton adsorption (BET; −196°C; $\sigma = 21.5$ Å^2).

To establish the experimental conditions for which the reaction rate was not influenced by external or internal diffusion, the influences of space velocity, catalyst mass, and particle size were studied in the usual manner (13). As a result, kinetic measurements were conducted at a total flow rate of 300 ml min^{-1} (NTP) between 200 and 280°C on attainment of a steady catalyst activity level after conditioning for 24 h at 300°C. In all experiments designed to establish kinetic parameters, the steady level conversion maximum was not greater than 10%.

An estimate of the 'apparent acidity' of the catalysts was obtained by agitating 0.2 g of the used solids for 10 min in 40 ml of water, followed by centrifugation and titration of 20 ml of the decanted liquid against standard alkali. The 'apparent acidity' was then taken as directly proportional to the relative amounts of the standard alkali consumed in the neutralization. The results were readily duplicated.

Materials

Vanadium pentoxide was >99.9% pure (Ventron). The samples containing alkali metal sulfates (Ventron, >99.9% pure) were prepared by mixing vanadium pentoxide powder and the corresponding weight of the appropriate sulfate additive in a ball mill for 2 h. This mixture was then heated at 700°C for 4 h in a quartz dish. The liquid melts were cooled rapidly, ground, and pelletized in a 1.27 cm die (ram pressure 3 tons) for 2 min. These pellets, and the pellets of pure vanadium pentoxide which were prepared in a similar manner, were calcined at 500°C for 10 h with the exception of the cesium and rubidium sulfate melts which were calcined at 430°C. The pellets were crushed and sieved to a particle diameter between 0.063 and 0.074 mm for the catalytic studies.

"Spectranalyzed" grade 2-propanol and acetone were supplied by Fisher Scientific. Certified grade helium (>99.9%), hydrogen (99.9%), compressed air, instrument grade propane (99.5%), and C. P. grade propylene (99.0%) were obtained from Canadian Liquid Air Ltd.

Results

The Effect of Exposure Time on the Reaction Products

One gram of catalyst was raised to the reaction temperature in a 300 ml min^{-1} (NTP) stream of helium before admission of 2-propanol to the reactor.

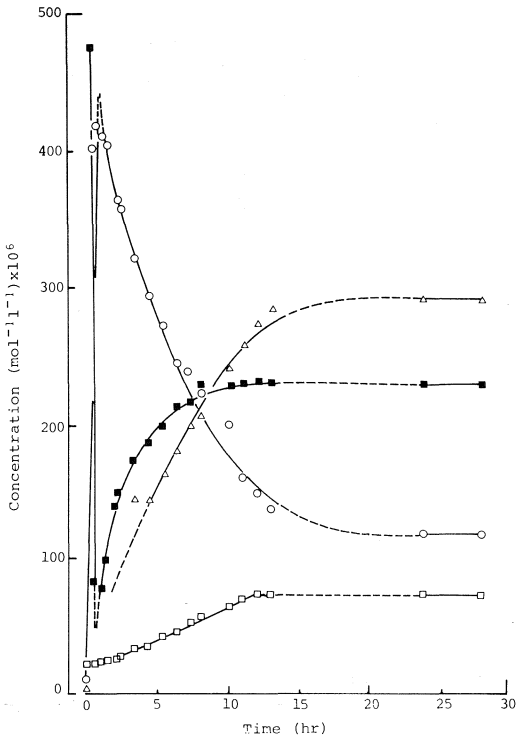

FIG. 1. The effect of exposure time on the reaction components from the decomposition of 2-propanol over V_2O_5: 9.09% K_2SO_4 at 300°C; △ propane; □ acetone; ○ propylene; ■ 2-propanol.

Figure 1 shows the effect of time on the composition of products from 2-propanol decomposition over the catalyst containing 9.09 mol% potassium sulfate at 300°C and 8.84 Torr alcohol partial pressure. Some difficulty was encountered in the quantitative measurement of water produced during reaction due to tailing. Water, however, was always produced and qualitatively paralleled the formation of acetone. Hydrogen was determined in the effluent stream at a level of <5% of the other products of the reaction.

It may be deduced from Fig. 1 that during the initial part of the conditioning period (0–4 h) a distinct inverse relationship exists between 2-propanol decomposition and propylene formation. Further, after a period of approximately 5 h, a similar relationship would appear to exist between the propylene and propane reactions.

Variations of Partial Pressures of 2-Propanol, Acetone, Water Vapour, Molecular Hydrogen, Propylene and Propane

The partial pressure of 2-propanol was varied between 3.37 and 8.84 Torr over V_2O_5:9.09 mol% K_2SO_4 at 230°C and 300 ml min^{-1} (NTP) total

TABLE 1. Apparent activation energies (E_A) and preexponential factors (A) for the decomposition of 2-propanol from 200 to 270°C

Catalyst	2-Propanol decomposition		Acetone formation				Propylene formation		Propane formation	
			270–230°C		220–200°C					
	$\log_{10} A$	E_A (kJ mol^{-1})	$\log_{10} A$	E_A (kJ mol^{-1})	$\log_{10} A$	E_A (kJ mol^{-1})	$\log_{10} A$	E_A (kJ mol^{-1})	$\log_{10} A$	E_A (kJ mol^{-1})
V_2O_5	28.33	88.2	23.08	40.9	20.18	12.9	28.78	95.7	27.92	72.7
V_2O_5:9.09% Li_2SO_4	27.53	84.9	24.64	52.3	20.23	11.3	29.60	115.8	28.06	72.7
V_2O_5:9.09% Na_2SO_4	30.56	104.1	24.33	47.7	21.32	19.2	30.42	115.8	31.10	99.5
V_2O_5:9.09% K_2SO_4	31.35	109.1	24.28	46.0	20.45	7.5	32.10	127.5	31.10	99.5
V_2O_5:9.09% Rb_2SO_4	30.63	109.1	25.42	51.8	21.37	21.3	29.77	115.8	29.11	80.3
V_2O_5:9.09% Cs_2SO_4	32.32	127.5	24.90	54.8	21.73	25.1	31.51	127.5	30.22	95.7
V_2O_5:1.01% K_2SO_4	—	73.9	—	53.5	—	27.2	—	100.0	—	103.3
V_2O_5:2.00% K_2SO_4	—	71.9	—	49.7	—	19.2	—	84.9	—	99.5
V_2O_5:4.98% K_2SO_4	—	76.5	—	52.3	—	25.1	—	100.0	—	103.3

TABLE 2. Effect of conditioning and reaction on the surface areas of the catalysts

Catalyst	Surface area before use* (m^2 g^{-1})	Surface area after conditioning and after reaction (m^2 g^{-1})
V_2O_5	0.93	9.17
V_2O_5:9.09% Li_2SO_4	2.27	12.70
V_2O_5:9.09% Na_2SO_4	0.36	1.11
V_2O_5:9.09% K_2SO_4	0.72	0.83
V_2O_5:9.09% Rb_2SO_4	1.54	2.77
V_2O_5:9.09% Cs_2SO_4	1.14	2.83
V_2O_5:1.01% K_2SO_4	—	8.58
V_2O_5:2.00% K_2SO_4	—	4.88
V_2O_5:4.98% K_2SO_4	—	3.85

*Before conditioning and reaction.

flow. A logarithmic plot of the reaction rate vs. partial pressures of alcohol indicated a reaction order of 0.3 for propane with respect to 2-propanol concentration. Other products showed zero order rate dependencies on the alcohol concentration over the same range.

With the partial pressure of 2-propanol kept constant at 8.84 Torr the reaction rates were unaffected by varying the partial pressures of (*a*) acetone from 0.5 to 3.0 Torr (*b*) water vapour from 0.75 to 3.0 Torr, (*c*) hydrogen from 4.2 to 10.0 Torr, (*d*) propane from 4.2 to 10.0 Torr, and (*e*) propylene from 4.2 to 10.0 Torr.

The Effect of Temperature

Experiments were carried out with 8.84 Torr partial pressure of 2-propanol from 200 to 280°C. The propane-forming reaction was dominant although dehydration to propylene and dehydrogenation to acetone also took place to a significant extent. The contribution of these latter reactions to the overall decomposition decreased at higher temperatures. No other organic compounds could be detected in the temperature range studied.

Table 1 shows the apparent activation energies calculated from experimental rate equations in the usual way (2). The order of reaction for propane with respect to 2-propanol concentration was taken as 0.3 while the net effects of the other components were considered to be zero order.

The surface areas of all catalysts changed significantly during the 24 h conditioning period, Table 2. Little or no change in the values was detected, however, after the reactions had been studied at the steady catalyst activity level. The surface areas determined for the steady level were used in all kinetic calculations.

Plots of $\log_{10} A$ and the apparent activation

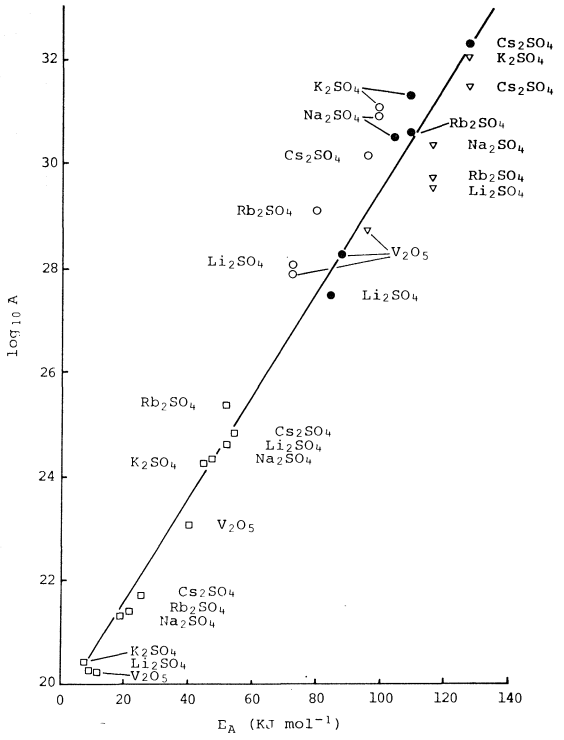

FIG. 2. Compensation effect for V_2O_5 and melts containing alkali metal sulfate additives for various reactions. ● overall 2-propanol decomposition; ▽ propylene formation; ○ propane formation; □ acetone formation.

energies, E_A, for the overall 2-propanol decomposition and for the formation of acetone, propylene, and propane, Fig. 2, indicate that a similar compensation effect is operative in all of these reactions. The values of the constants which define the compensation effect and which were calculated by applying a least-squares analyses of the data to the equation (15):

$$\log_{10} A = \beta + eE_A$$

were found to be 0.1012 ($\sigma = 0.004$) and 19.543 ($\sigma = 0.439$) for e and β respectively; where σ denotes the standard deviations from the mean in each case. The units used for E_A and A were kJ mol^{-1} and molecules m^{-2} s^{-1}, respectively.

All of the catalysts studied, with the exception of that modified with sodium sulfate, were found to be various shades of yellow/orange in color in agreement with literature (16). The sodium sulfate modified catalyst was black which was attributed to the relative ease of this additive in forming vanadium-bronzes when compared with the other components used in the series (17). The black coloration may also indicate a non-stoichiometric deficiency of oxygen in the catalyst (18). All catalysts changed color to black after conditioning and reaction. The onset of this color change took place after 1 to 2 hours into the conditioning period.

Discussion

The effect of catalyst conditioning on product distribution, Fig. 1, suggests that initially, 2-propanol reacts on the surface to produce propylene and acetone. On desorption of these products some surface sites may be occupied by hydrogen and hydroxyl species. Then, as sites become increasingly occupied or blocked, by hydrogen and/or hydroxyl species, propylene production decreases and propane formation becomes evident. Propane may therefore form through hydrogen extraction from the surface. The concept of propane formation by hydrogenolysis of the alcohol rather than by hydrogenation of propylene is supported in some measure by the findings of Balandin *et al.* (19) and by the present observations that changes in the concentration of propylene during conditioning have no effect on the formation of propane.

The nature of the increase in the acetone-formation activity with time during conditioning, Fig. 1, and the qualitative finding that acetone formation runs parallel to water formation may indicate that one of the active adsorption sites is a hydroxyl species as has been identified by X-ray analyses of this catalyst after conditioning (20).

The steady-level values of the reaction rates at any defined temperature did not follow any simple activity series such as those reported by previous workers for various reactions on similar catalysts (4, 5). Attempts to measure the acid/base characteristics of the surfaces by non-aqueous methods (21, 22) were inconclusive, perhaps due to the very dark colorations of the solids. However, a correlation could be established, Fig. 3, between the reaction rates at a given temperature and the 'apparent acidity' of the catalyst surface. This latter term simply indicates the relative ease with which the used catalysts acidified water. Similar correlations were established between the catalyst activity and the equilibrium amounts of vanadate and sulfate anions measured in the aqueous solutions by spectroscopic methods (23). The observed variation in the sulfate and vanadate concentrations is believed to indicate the relative ease or extent with which the alkali metal sulfates and vanadium pentoxide enter into inter-solid reactions in the melt. This hypothesis is supported, in some measure, by the trend of the melting points of the additives which shows a maximum at potassium sulfate.

The steady-level values of the reaction rates, for

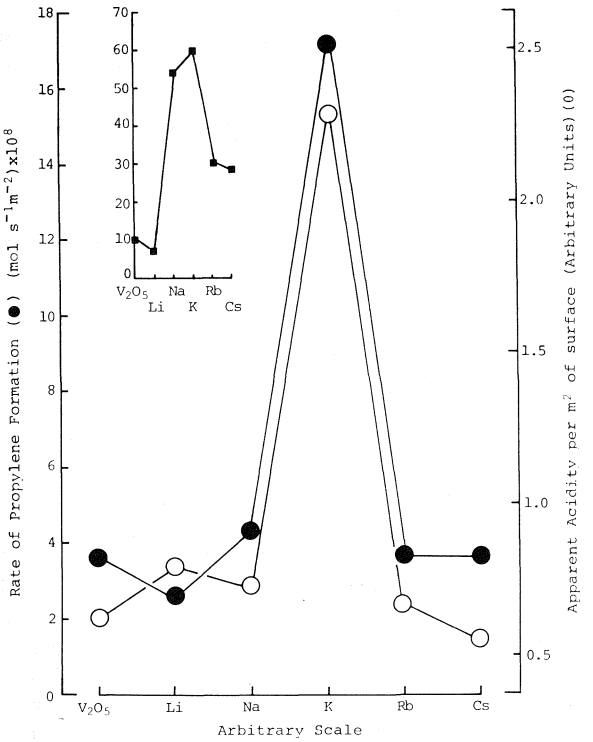

FIG. 3. Effect of variation of alkali metal cation, in catalysts containing 9.09 mol% alkali metal sulfate on, (*a*) rate of propylene formation at 270°C (●) and (*b*) "apparent acidity" (○). Inset: Effect of alkali metal cation variation on rate of overall 2-propanol decomposition. (1 A.U. (arbitrary unit) ≡ 10^{-1} meq. m^{-2}).

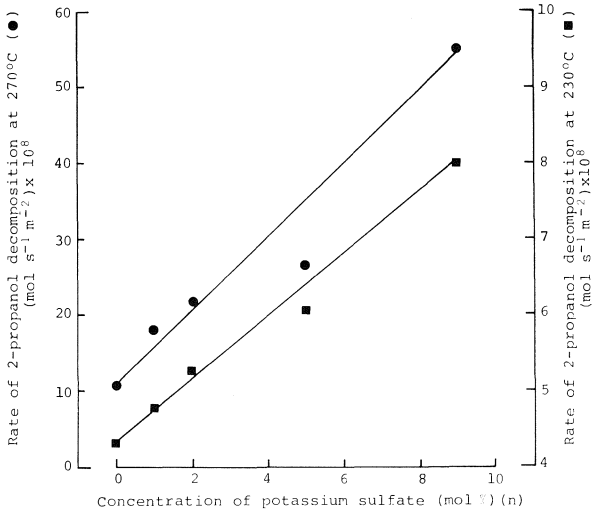

FIG. 4. Rates of 2-propanol decomposition at 270°C (●) and 230°C (■) vs. the concentration of potassium sulfate in V_2O_5:*n* mol% K_2SO_4 catalysts.

the melts containing potassium sulfate, at a given temperature can be expressed as an activity series: 1.01 < 2.00 < 4.98 < 9.09 (mol% K_2SO_4). A linear relationship was established between the overall rate of reaction at a given temperature and the mol percent alkali metal sulfate in the catalyst, Fig. 4. However, a comparison of the magnitudes of the rates of reaction in the present study together with the reported rates for isotopic oxygen exchange, extrapolated to the current working temperatures, indicates that any direct correlation between the oxygen mobility and activity of the catalysts between 200 and 280°C is probably incidental. Further, with the present experimental procedure, most of the active oxygen is probably removed during conditioning (20). 'Apparent acidity' tests could not be performed on the actual catalysts of this series since the samples had been used in other experiments. However, simulated preparations which were shown by both X-ray diffraction and surface area measurements to parallel the experimental samples were examined. The results obtained were encouraging with respect to the hypothesis advanced. The whole aspect of the activity/acidity relationship appears to present a prime area for further study.

In previous work (24) on $V_2O_{(5-x)}$ catalysts, activation energies of 92 and 176 kJ mol^{-1} were determined, respectively, for dehydrogenation and dehydration of 2-propanol from 74 to 104°C. A low selectivity value of 0.11 towards dehydrogenation was observed in terms of dehydration and dehydrogenation rates. Isopropyl ether was a major component also of the reaction products but propane was absent. The marked contrast of these features with the present findings from 200 to 270°C is equated with the lengthy conditioning period at higher temperatures required to attain steady activity levels with the sulfate additives. This same treatment was applied in conditioning the unmodified pentoxide samples.

Thus it might be expected that the O/V ratio would be lowered as a result of conditioning especially since milder reducing treatments will achieve this result (16, 25). A preliminary study of the catalysts after reaction, using X-ray diffraction, has indicated that the solid matrix includes non-stoichiometric oxide and hydroxide phases, two components of which have been tentatively identified as VO_2 and VO(OH) (20).

It appears then, as an initial broad hypothesis, that a decrease in the O/V ratio can influence considerably both kinetic and mechanistic features of catalysis such that results are not inconsistent with earlier studies on $V_2O_{(5-x)}$ (24) and V_2O_3 (26). The

consequences of catalyst-oxygen depletion might be expected to include destabilization of the surface intermediate formed during dehydration through a decrease in the strength of dehydration-center attachment to the surface (27, 28) as may be gauged by the present experimental activation energies which lie from 40 to 60% below the value determined for $V_2O_{(5-x)}$ at lower temperatures.

The apparent activation energy values for acetone formation fall into two distinct regions, Table 1. The low values are somewhat unusual, especially since the acetone reaction was subject to chemical rate control over the entire temperature range covered. However, two such temperature-dependent kinetic regions for acetone formation were established earlier (2) for manganese oxides and related to variations with temperature in the energy of interaction of adsorbate molecules with adsorption sites (29).

The recent work of Galwey (15) shows that a kinetic compensation effect exists for the reactions of 2-propanol on various oxide surfaces (1, 24). The parameters defining this reported effect are slope (0.1012, $\sigma = 0.006$) and the intercept, where $E_A \rightarrow 0$, (15.604, $\sigma = 0.943$). Figure 2 shows that a common compensation effect exists for all the contributing reactions in the decomposition of 2-propanol on the present catalysts. A comparison of the slope, Fig. 2, with that obtained by Galwey shows complete agreement. Thus similarities in both rate-determining steps and reaction mechanisms may be anticipated in the primary surface reactions of 2-propanol over these solids even when some comparative differences exist in the reaction product compositions.

On the basis of a Langmuir–Hinshelwood model, the pseudo-zero order rate dependencies of component concentrations in the dehydration and dehydrogenation reactions may be interpreted in terms of a very rapid saturation of active surface sites amenable to catalysis. Extremely rapid reaction and subsequently fast desorption of the adsorbed species into the gas phase presents an alternative explanation.

The experimental reaction rate data for the propane-forming reaction were treated by statistical analyses in a test/reject fashion to derive rate expressions which might be consistent with the observations. The simple kinetic equations:

$$[1] \qquad r = \frac{kP_{alc}}{1 + kP_{alc}}$$

$$[2] \qquad r = \frac{kP_{alc}^{1/2}}{1 + kP_{alc}^{1/2}}$$

were both applicable; k is the rate constant for the overall decomposition of the alcohol and P_{alc} is the partial pressure of 2-propanol.

Equation 1 (correlation coefficient, 0.998) implies that the rate of reaction is proportional to the amount of alcohol adsorbed on the surface and would be governed by a Langmuir isotherm where the adsorbate occupies one surface site during the rate-determining step (30). Equation 2 (correlation coefficient, 0.993) again invokes Langmuir–Hinshelwood kinetics with the adsorbate occupying two surface sites during the rate-determining step (30). It may be that the observed experimental rate order of 0.3 for the alcohol in the propane reaction implies a mix of the two adsorption modes, which is related to the conditions of catalysis.

The heterogeneous decomposition of 2-propanol has been interpreted in terms of various mechanisms (31–33). Knozinger (34) proposed E-2 type reaction intermediates for the dehydration of primary, secondary, and tertiary alcohols over alumina below 200°C. At higher temperatures, depending on the reactant structure, dehydration was thought to proceed via E-1 type mechanism intermediates (34). Mechanisms for dehydrogenation have been suggested as involving initial adsorption at an electronegative surface site with subsequent two-point adsorption (32).

The reactions involved in the present study may be explained in terms of intermediates typical of such elimination-type mechanisms. Thus, propylene may be formed via an E-2 type mechanism on adjacent vacant surface sites:

[3]

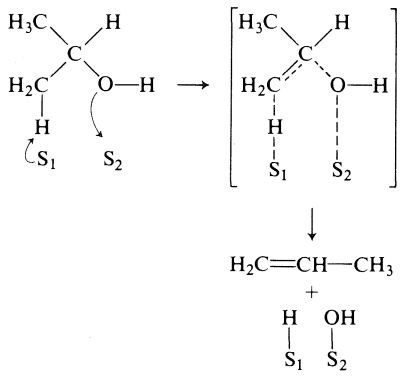

Such an attachment of the alcohol to the surface through the hydroxyl group and a β-hydrogen has been reported to involve little strain even on plane surfaces (35). A mechanism of this type has recently been suggested (36) for dehydration of isopropanol on V_2O_5 and vanadium bronzes in which S_1 and S_2

are V^{4+} and V^{5+} species respectively. In a similar way, acetone could be produced:

[4] 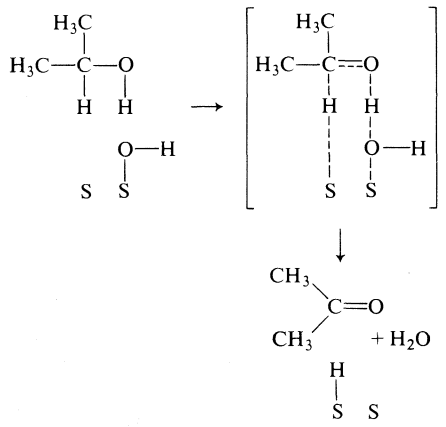

A two-point adsorption intermediate has been reported for acetone formation from 2-propanol (32). The present data suggests that one site is a hydroxyl group which may also form as an adsorbed species resulting from the dehydration reaction.

Both [3] and [4] advocate that some of the original surface sites become occupied by adsorbed hydrogen on dehydration or dehydrogenation and thus as these sites become increasingly occupied, 'dehydration' may become limited to a one-point adsorption center (E-1 type). Propane formation is then linked to the availability of hydrogen on a neighboring adsorption site:

[5] 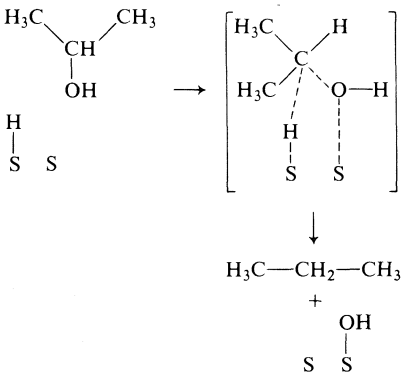

This scheme has features in common with recent work (36) when it was suggested that the alcohol was adsorbed on V^{5+} sites followed by subsequent hydrogen abstraction from the alcohol on a neighboring V^{4+} site to produce propylene resulting in a saturation of adjacent V^{4+} and V^{5+} pairs by H and OH species, respectively. However, there would tend to be an excess of V^{5+} species in all of the catalysts studied, the V^{4+}/V^{5+} ratio increases to as much as 0.5 in V_2O_5 glasses (37), so that alcohol adsorption sites would always be available. Thus the availability of reaction centers would depend solely on the oxidation state and the nature and degree of occupancy of the neighboring vanadium sites by adsorbed species. If the neighboring site is V^{4+}, unoccupied, then dehydration results, but if the site is occupied by hydrogen then propane seems likely to be the product.

In such a mechanism the amount of propane formed would be expected to increase to some limiting value in step with a corresponding decrease in the product concentration of propylene, which is consistent with the trend observed, Fig. 1. Further, since E-1 mechanisms are likely to be favored at higher temperatures (34), the observation that the propane-forming reaction becomes progressively more dominant with temperature increase can also be explained by this proposal.

This study has demonstrated that, while the course of catalysis is related to the availability of oxygenated surface species, a direct link with surface oxygen mobility is improbable. The decomposition results for each of the contributing steps may be explained by elimination-type mechanisms in which intermediate adsorbed species are located at sites offering H or OH. The subsequent measurable acidity may indicate that the activity trends are related to the presence primarily of 'acidic' species in the solid surface.

1. E. F. McCaffrey, T. A. Micka, and R. A. Ross. J. Phys. Chem. **76**, 3372 (1972).
2. E. F. McCaffrey, D. G. Klissurski, and R. A. Ross. J. Catal. **26**, 380 (1972).
3. G. K. Boreskov. Catalysis in sulfuric acid production. Russian State Press for Chemical Literature. 1954.
4. V. N. Bibin and L. A. Kasatkina. Kinet. Catal. **5**, 653 (1964).
5. A. P. Dzisyak, G. K. Boreskov, L. A. Kasatkina, and V. E. Kochurikhin. Kinet. Catal. **2**, 727 (1961).
6. L. A. Kasatkina, G. K. Boreskov, and P. N. Sokolov. Russ. J. Phys. Chem. **34**, 168 (1960).
7. G. K. Boreskov, L. A. Kasatkina, V. V. Popovskii, and Yu. A. Balovnev. Kinet. Catal. **1**, 207 (1960).
8. P. Jiru, D. Tomkova, V. Jara, and J. Wankova. Z. Anorg. Allgem. Chem. **121**, 303 (1960).
9. B. W. Krupay and R. A. Ross. J. Catal. **50**, 220 (1977).
10. A. Bielanski, J. Deren, J. Haber, and J. Sloczynski. Actes du deuxième Cong. Intern. de Catalyse Paris (1960), p. 1653. Technip, Paris (1961).
11. V. M. Frovlov, O. V. Krylov, and S. Z. Roginskii. Dokl. Akad. Nauk SSSR, **126**, 107 (1959).
12. G. M. Schwab, G. Greger, S. Krawczynski, and J. Penzkofer. Z. Phys. Chem., Frankfurt, **15**, 363 (1958).
13. R. A. Ross and B. G. Walsh. J. Appl. Chem. **11**, 469 (1961).
14. A. B. Hart, J. McFadyen, and R. A. Ross. Trans Faraday Soc. **59**, 1458 (1963).

15. A. K. GALWEY. Adv. Catal. **26**, 247 (1977).
16. L. G. MAIDANOVSKAYA and L. M. KURINA. Nauchv. Osnovy Podbara: Proizv. Katalizatorv, Akad. Nauk SSSR Sibirsk. OTD. 232 (1964).
17. R. P. OZEROV. Zh. Neorg. Khim. **4**, 1047 (1959).
18. D. J. HUCKNALL. Selective oxidation of hydrocarbons. Academic Press, London/New York. 1974. p. 153.
19. A. A. BALANDIN, G. V. ISAQULYANTS, N. P. SOKOLOVA, and I. I. ZAKHARYCHEVA. Izv. Akad. Nauk SSSR OTD. Khim. Nauk, 1549 (1961).
20. D. V. FIKIS, W. J. MURPHY, and R. A. ROSS. To be published.
21. T. YAMANAKA and K. TANABE. J. Phys. Chem. **80**, 1723 (1976).
22. O. JOHNSON. J. Phys. Chem. **59**, 827 (1955).
23. A. I. VOGEL. Quantitative inorganic analysis. 3rd ed. Longmans, London. 1970.
24. E. F. MCCAFFREY, D. G. KLISSURSKI, and R. A. ROSS. Proc. 5th Intern. Congr. Catal., Florida, Catalysis, Vol. 1, *Edited by* J. W. Highpower, 3–151 (1973).
25. P. V. GEL'D, S. I. ALYAMEVOKII, and I. I. MATVEENKO. Russ. J. Inorg. Chem. **5**, 815 (1960).
26. A. A. TOLSTOPYATORA, V. A. NAUMOV, and A. A. BALANDIN. Russ. J. Chem. **38**, 879 (1964).
27. D. E. R. BENNETT and R. A. ROSS. J. Chem. Soc. A, 1524 (1968).
28. D. E. R. BENNETT and R. A. ROSS. J. Catal. **18**, 122 (1968).
29. S. J. TEICHNER. J. Catal. **4**, 724 (1965).
30. E. K. RIDEAL. Concepts in catalysis. Academic Press, New York and London. 1968.
31. O. V. KRYLOV. Russ. J. Phys. Chem. **39**, 1422 (1965).
32. O. V. KRYLOV. Russ. J. Phys. Chem. **39**, 1554 (1965).
33. J. C. KURIACOSE, C. DANIEL, and N. BALAKRISHNAN. Indian J. Chem. **7**, 367 (1968).
34. H. KNÖZINGER and A. SCHEGLILA. J. Catal. **17**, 252 (1970).
35. G. FORESTER, H. NOLLER, and K. THOMKE. J. Catal. **44**, 492 (1976).
36. D. K. CHAKRABORTY, D. GUBA, and A. B. BISWAS. J. Solid State Chem. **55**, 263 (1977).
37. M. MUNKATA. Solid-State Electron. **1**, 159 (1960); H. H. NESTER and W. D. KINGERY. *In* VII International Congress on Glass, Brussels. 1965. Paper 106; H. RAWSON. Inorganic glass-forming systems. Academic Press, New York. 1967. p. 195.

Thermodynamic properties of the alkali metal hexachloroniobate and hexachlorotantalate compounds by vapour pressure measurements

DONALD R. SADOWAY[1] AND S. N. FLENGAS

Department of Metallurgy and Materials Science, University of Toronto, Toronto, Ont., Canada M5S 1A4

Received March 14, 1978

DONALD R. SADOWAY and S. N. FLENGAS. Can. J. Chem. **56**, 2538 (1978).

The vapour pressures for the decomposition of the solid and liquid compounds $AMCl_6$ where A = Na, K, Rb, or Cs, and M = Nb or Ta, were measured by a fused quartz Bourdon spiral pressure gauge. The hexachlorotantalates were found to be more stable thermally than the hexachloroniobates. Enthalpies of decomposition were calculated. The dissociation temperatures of each sequence of compounds increase with increasing size of the radius of the alkali-metal cation. Partial pressures of $NbCl_5$ or $TaCl_5$ vapour in equilibrium with solutions representing the binary systems KCl–$KNbCl_6$ and KCl–$KTaCl_6$, respectively, are also reported.

DONALD R. SADOWAY et S. N. FLENGAS. Can. J. Chem. **56**, 2538 (1978).

Faisant appel à une jauge de Bourdon en silice, on a mesuré les tensions de vapeur accompagnant les décompositions des composés solides et liquides $AMCl_6$ où A = Na, K, Rb ou Cs et M = Nb ou Ta. On a trouvé que les hexachlorotantalates sont plus stables du point de vue thermique que les hexachloroniobates. On a calculé les enthalpies de décomposition. Les températures de dissociation pour chaque série de composés augmentent avec une augmentation du diamètre du cation du métal-alcalin. On rapporte aussi les tensions de vapeur partielles du $NbCl_5$ ou du $TaCl_5$ en équilibres respectivement avec des solutions représentant des systèmes binaires KCl–$KNbCl_6$ et KCl–$KTaCl_6$.

[Traduit par le journal]

Introduction

Niobium and tantalum pentachloride vapours react with alkali-metal chlorides to form compounds of the type $[A^+][MCl_6^-]$, where A represents an alkali metal and M represents Nb or Ta. These compounds can melt congruently, as does $KNbCl_6$ (1), or incongruently, as does $NaNbCl_6$ (1). Covalently bonded $NbCl_5$ and $TaCl_5$ melts behave as molecular liquids (2–5); in contrast, solutions of these pentachlorides in molten alkali-metal chlorides are ionic in character, as their electrical conductivities show (6, 7), and thermodynamically stabler than the former, as vapour pressure measurements demonstrate. For example, at 450°C pure $NbCl_5$ has a vapour pressure of 22 atm (8), whilst the partial pressure of $NbCl_5$ over molten $KNbCl_6$ at the same temperature is reported as 0.15 atm (9). These changes in behaviour may be explained by the presence of complex species in the MCl_5–ACl solutions (4, 10, 11).

The compounds $NaNbCl_6$, $NaTaCl_6$, $KNbCl_6$, $KTaCl_6$, $RbNbCl_6$, $RbTaCl_6$, $CsNbCl_6$, and $CsTaCl_6$ were synthesized in this laboratory by the reaction of $NbCl_5$ or $TaCl_5$ vapour with solid alkali-metal chloride under controlled pressure and temperature conditions. The preparation has been described elsewhere (12). The thermodynamic properties of the aforementioned compounds and of solutions of KCl–$KNbCl_6$ and KCl–$KTaCl_6$ were determined by vapour pressure measurements of the following equilibrium:

[1] $AMCl_6$ (s, 1, or solution) $\rightleftharpoons$ ACl (s, 1, or solution) + MCl_5 (vap.)

Experimental

The vapour pressure of $NbCl_5$ or $TaCl_5$ in equilibrium with the compounds $AMCl_6$ or with $AMCl_6$–ACl solutions have been measured by a fused quartz Bourdon spiral pressure gauge contained in a closed apparatus which has been described elsewhere (13).

For these measurements the temperature of the sample container was varied between 190 and 660°C while the upper part of the apparatus containing the Bourdon spiral was maintained at temperatures about 50°C higher than the corresponding normal boiling points of pure $NbCl_5$ and $TaCl_5$.

Samples of the $AMCl_6$ compounds and of their mixtures with alkali-metal chlorides were prepared by methods previously described (12). Materials were handled in a glove box filled with dehydrated helium. Specimens were introduced into the sample container of the apparatus in the form of powders. The part of the cell consisting of the sample container and the Bourdon spiral were sealed under vacuum. It was found that large quantities of adsorbed gas were released from the salt upon heating. This introduced a systematic error into the measurements. Accordingly, an elaborate degassing procedure was employed in which the cell was repeatedly

[1]Present address: Department of Materials Science and Engineering, Massachusetts Institute of Technology, Cambridge, MA 02139.

Can. J. Chem. Downloaded from www.nrcresearchpress.com by 210.87.254.6 on 09/05/12
For personal use only.

Can. J. Chem. Downloaded from www.nrcresearchpress.com by 210.87.254.6 on 09/05/12
For personal use only.

heated, cooled, reopened, and evacuated. When residual gas was no longer present upon cooling, a proper experiment was conducted to measure the vapour pressure of the sample.

Results and Discussion

1. *Properties of the $AMCl_6$ Compounds*

Figures 1–4 display the experimental results for the vapour pressures of the decomposition of the compounds $AMCl_6$, where A is Na, K, Rb, or Cs. Each figure shows the results for both the hexachloroniobate and the hexachlorotantalate of a given alkali metal. The figures also show the results of other investigators. Least-squares lines are given in Table 1.

The shape of the curve of $\ln P_{MCl_5}$ *vs.* $1/T$ may be understood in terms of the equilibrium constant for the decomposition reaction in eq. [1] (14–19). For this reaction

$$[2] \qquad K = P_{MCl_5} \cdot a_{ACl}/a_{AMCl_6}$$

where the standard state for the compounds ACl and $AMCl_6$ is the pure solid at all temperatures, and for MCl_5 is the vapour at a pressure of 1 atm.

In the ACl–$AMCl_6$ subsystem, below the eutectic temperature three phases are present: the pure solids, ACl, and $AMCl_6$, whose activities are unity, and MCl_5 vapour. Therefore, in this region, $K = P_{MCl_5}$.

In the temperature and composition range where molten ACl–$AMCl_6$ solutions are saturated with either ACl or $AMCl_6$ solid, the expression for the equilibrium constant is written as $K = P_{MCl_5}/a_{AMCl_6}$ or $K = P_{MCl_5}a_{ACl}$, respectively. Accordingly, as the activity terms are always less than unity the pressure curves of these solutions are expected to inflect at the eutectic and liquidus temperatures of the corresponding ACl–$AMCl_6$ systems.

The $\ln P_{MCl_5}$ vs. $1/T$ plot is also expected to change slope at temperatures below the eutectic points when the solids present undergo solid–solid transitions.

This is particularly significant for the hexachloroniobate and hexachlorotantalate compounds in which several phase changes in the solid state have been observed.

In connection with this last comment Table 2 is presented as a summary of previously reported results from this laboratory (12). Thus in the present work measurements were taken within temperature ranges for which well defined phases were present.

Figure 1 shows the results for the decomposition of both β-$NaNbCl_6$ and β-$NaTaCl_6$ along with the results of other investigations for these two compounds. It is of interest to note that their decomposition pressures reach 1 atm at temperatures lower than their melting points. Accordingly a plot of $\ln P_{MCl_5}$ vs. $1/T$ should be linear.

TABLE 1. Summary of vapour pressure measurements

Reactions	Temperature range of measurement (T/K)	$\ln P_{MCl_5}$ (atm) $= a_0 + a_1/T$		Standard error of estimate S	ΔH_R^{0*} (K cal/mol)	ΔS_R^{0*} (e. u)
		a_0	a_1			
$NaNbCl_6$ (β-solid) → NaCl(s) + $NbCl_5$ (vap.)	518–561	(8.075)	(−4750)	—	—	—
$NaTaCl_6$ (β-solid) → NaCl(s) + $TaCl_5$ (vap.)	497–650	10.8930 ± 0.2883	−7131.3 ± 163.5	0.0552	14.17 ± 0.32	21.72 ± 0.56
$KNbCl_6$ (β-solid) → KCl(s) + $NbCl_5$ (vap.)	568–643	7.3969 ± 1.7530	−7015.6 ± 1078.7	0.0455	13.94 ± 2.14	14.74 ± 3.50
$KNbCl_6$(l) → KCl (in soln) + $NbCl_5$ (vap.)	673–735	8.1329 ± 0.2019	−6040.1 ± 140.1	0.0238	12.00 ± 0.28	—
$KTaCl_6$(l) → KCl (in soln) + $TaCl_5$ (vap.)	673–805	11.688 ± 0.145	−9316.8 ± 104.8	0.0302	—	—
$RbNbCl_6$ (β-solid) → RbCl(s) + $NbCl_5$ (vap.)	583–632	4.7581 ± 0.0640	−4991.3 ± 38.8	0.0037	9.92 ± 0.08	9.52 ± 0.12
$RbNbCl_6$(l) → RbCl (in soln) + $NbCl_5$ (vap.)	672–852	9.8853 ± 0.3480	−8304.1 ± 261.1	0.0775	—	—
$RbTaCl_6$(l) → RbCl (in soln) + $TaCl_5$ (vap.)	693–848	10.4041 ± 0.2553	−8856.1 ± 192.4	0.0596	—	—
$CsNbCl_6$ (β-solid) → CsCl(s) + $NbCl_5$ (vap.)	670–708	0.4815 ± 0.6533	−2354.9 ± 457.5	0.0290	4.68 ± 0.90	9.63 ± 1.30
$CsNbCl_6$(l) → CsCl (in soln) + $NbCl_5$ (vap.)	822–843	9.9450 ± 0.8453	−8286.2 ± 701.2	0.0176	—	—
$CsTaCl_6$ (β-solid) → CsCl(s) + $TaCl_5$ (vap.)	675–732	0.7937 ± 0.1453	−3095.6 ± 102.2	0.0087	6.15 ± 0.20	1.59 ± 0.29
$CsTaCl_6$(l) → CsCl (in soln) + $TaCl_5$ (vap.)	828–1106	12.8243 ± 0.2572	−11881.6 ± 225.8	0.0320	—	—

*Where $\Delta H_R^0 = a_1 R$ and $\Delta S_R^0 = a_0 R$, where $R = 1.98716$ cal/mol K.

TABLE 2. Characteristic temperatures (12)

Compound	Melting point (K)	Eutectic temperature† (K)	Solid–solid transformation‡ (K)		Comments
			$\alpha \rightarrow \beta$	$\beta \rightarrow \gamma$	
$NaNbCl_6$	(721)*	—	518	572	Incongruently melting
$NaTaCl_6$	(748)*	—	498	—	Incongruently melting
$KNbCl_6$	673	643	572	—	Congruently melting
$KTaCl_6$	674	646	411	584	Congruently melting
$RbNbCl_6$	653	—	578	—	—
$RbTaCl_6$	690	655	534	586	Congruently melting
$CsNbCl_6$	808	(712)*	563	—	—
$CsTaCl_6$	823	(717)*	569	—	Congruently melting

*Average values from several investigations (6, 7, 20, 22, 23, 30).
†Eutectic temperatures corresponding to the ACl–$AMCl_6$ type sub-systems.
‡Systems not yet fully known crystallographically. Solids α, β, and γ simply describe solid–solid transformations observed cryoscopically with increasing temperature. It should be noted that other authors used different symbolism (23, 24, 30).

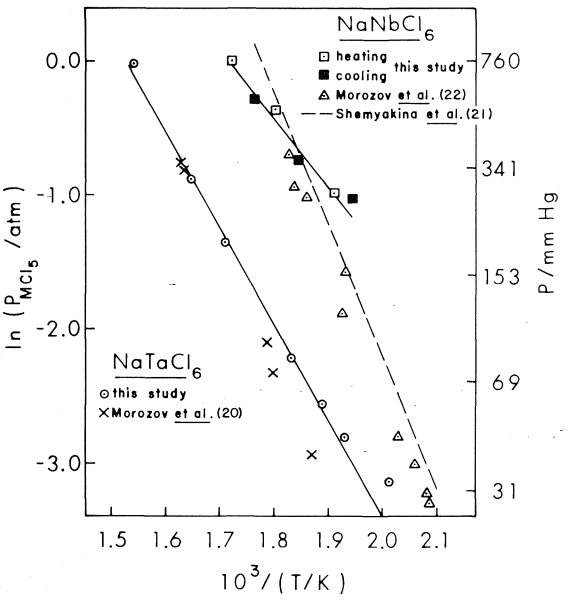

FIG. 1. ln P_{MCl_5} vs. $1/T$ plots for the systems $NaNbCl_6$ and $NaTaCl_6$. Solid lines represent best fit of present data.

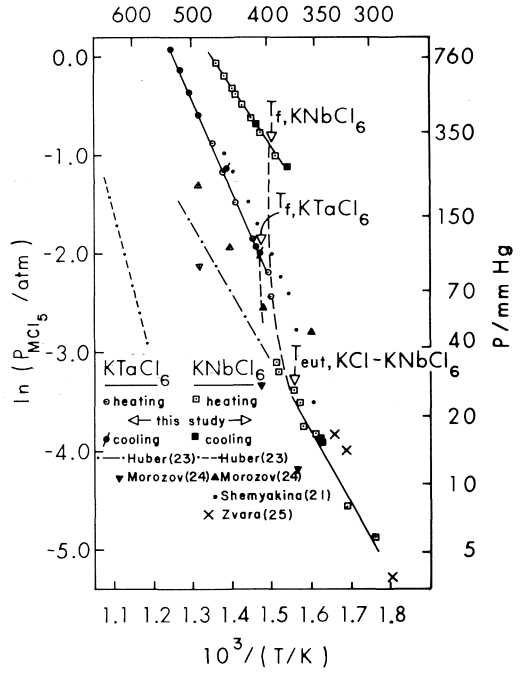

FIG. 2. ln P_{MCl_5} vs. $1/T$ plots for the systems $KNbCl_6$ and $KTaCl_6$. Solid lines represent best fit of present data. Dashed line is simply drawn to link the solid and liquid regions.

In comparison with other vapour pressure studies the results of this work agree well with that of Morozov, Korshunov, and Simonich (20) for the α-$NaTaCl_6$ system. Shemyakina *et al.* (21) and Morozov and Korshunov (22) have measured the decomposition of $NaNbCl_6$ at temperatures lower than that in this investigation, and their values tend to converge at about 518 K which is the transition temperature for its $\alpha \rightarrow \beta$ transformation.

Figure 2 shows the results of both β-$KNbCl_6$ and molten $KTaCl_6$. Data for the decomposition of solid $KTaCl_6$ are not given as the pressures were too low to be measured by the apparatus. Figure 2 also shows the results of other investigations.

The thermal decomposition of $KNbCl_6$ has been studied by Huber *et al.* (23), Morozov and Simonich (24), Shemyakina *et al.* (21), and Zvara and Tarasov (25). The results of the present study for low temperatures agree best with those of Zvara and Tarasov (25), who measured vapour pressures in equilibrium with both α- and β-$KNbCl_6$ solids using a radioactive tracer technique. These authors, however, did not make any comments on the solid–solid transformations occurring during their measurements.

Can. J. Chem. Downloaded from www.nrcresearchpress.com by 210.87.254.6 on 09/05/12
For personal use only.

Can. J. Chem. Downloaded from www.nrcresearchpress.com by 210.87.254.6 on 09/05/12
For personal use only.

Equilibrium pressures reported by both Morozov and Simonich (24) and by Shemyakina *et al.* (21) are not in agreement with values measured in the present study. The former used a transportation technique, while the latter used a null membrane type manometer. Both authors plotted their measured pressures of $NbCl_5$ as a single least-squares line crossing solid–solid transition temperatures and extending into the temperature range for molten $KNbCl_6$. Huber *et al.* (23) measured vapour pressures of $NbCl_5$ in equilibrium with molten $KNbCl_6$ by a transportation method. The results are much lower than those recorded herein. In reports of vapour pressures measured by the transportation technique (23, 24) the authors failed to mention that consideration was given to the problem of depletion of $NbCl_5$ from the $KNbCl_6$ condensed phase as the experiment progressed.

The thermal decomposition of $KTaCl_6$ has been studied by Huber *et al.* (23), Morozov and Simonich (24), and Zvara and Tarasov (25). The results of Huber *et al.* (23) and Morozov and Simonich (24) for molten $KTaCl_6$, both studies having employed transportation techniques, are much lower than those of the present study. No mention was made of the problem of depletion of $TaCl_5$ from the condensed $KTaCl_6$ phase during the course of the experiment. Furthermore, the data of Morozov and Simonich (24), which span the temperature range from solid $KTaCl_6$ to molten $KTaCl_6$, have been represented by a single least-squares line (26).

In Fig. 2 the plot of the ln P_{NbCl_5} vs. $1/T$ for β-$KNbCl_6$ from the results obtained in the present work shows inflections at the eutectic temperature of the KCl–$KNbCl_6$ subsystem and at the melting point of $KNbCl_6$. The curvature of the dotted line joining these two temperatures results from the changing activity of KCl in the melt whose composition varies along the liquidus tie line as temperature is increased. Pressure curves of a similar shape have been recorded in this laboratory for P_{ZrCl_4} and P_{HfCl_4} in equilibrium with K_2ZrCl_6 and K_2HfCl_6, respectively (19).

Figure 3 shows equilibrium vapour pressure measurements for the decomposition of the molten $RbNbCl_6$ and $RbTaCl_6$ compounds. The former reportedly melts incongruently.

Attempts to measure the decomposition of solid $RbTaCl_6$ at temperatures below the melting point were unsuccessful. The equilibrium pressures were low, and despite elaborate degassing there was still enough inert gas present to confound the data.

Huber *et al.* (23) have measured decomposition vapour pressures for both these compounds in the molten state. Figure 3 shows their results for

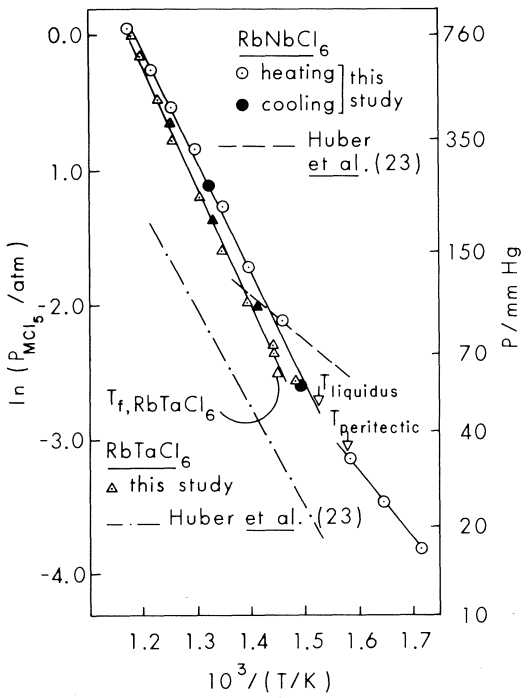

FIG. 3. ln P_{MCl_5} vs. $1/T$ plots for the systems $RbNbCl_6$ and $RbTaCl_6$. Solid lines represent best fit of present data.

$RbNbCl_6$ to be of the same order of magnitude as the results of this study. Their results for $RbTaCl_6$ are lower than in this study. Huber *et al.* (23) employed a transportation technique but did not discuss the effect of the depletion of the volatile pentachloride from the condensed phase during the course of an experiment.

Figure 4 shows the vapour pressures measured for the decomposition of $CsNbCl_6$ and $CsTaCl_6$. Both compounds melt congruently and the $CsMCl_6$–CsCl type phase diagrams indicate simple eutectic melting (23). Therefore, according to the thermodynamic analysis presented earlier, the partial pressure of the pentachloride should be represented on a plot of ln P_{MCl_5} vs. $1/T$ by two linear segments joined by a region of curvature.

These two compounds were extremely difficult to degas, particularly $CsNbCl_6$. This was true both for compounds prepared by precipitation from $SOCl_2$–ICl solutions and for those made by gas–solid reaction. Accordingly the reported vapour pressures over the solid compounds are approximate values and are presented here only for the sake of completeness. Many samples were prepared and studied. The results quoted below were selected as the best because they represent the lowest reproducible pressures measured.

Figure 4 also shows the results of Morozov and

Can. J. Chem. Downloaded from www.nrcresearchpress.com by 210.87.254.6 on 09/05/12
For personal use only.

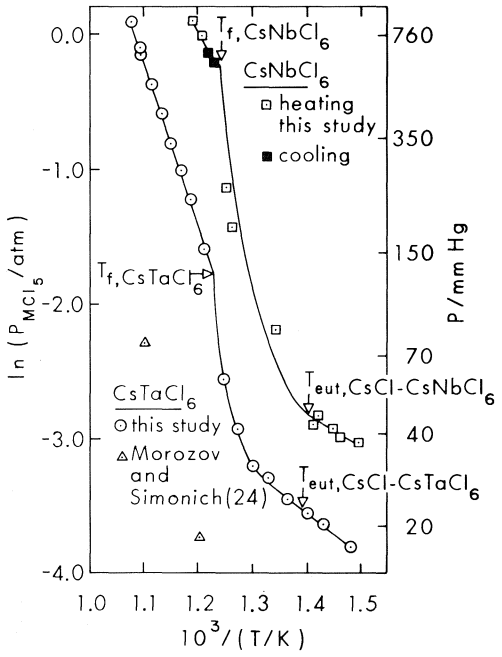

FIG. 4. ln P_{MCl_5} vs. $1/T$ plots for the systems $CsNbCl_6$ and $CsTaCl_6$. Solid lines represent best fit of present data.

Simonich (24) for $CsTaCl_6$. Their equilibrium pressures are lower in magnitude, but the slope of the ln P_{TaCl_5} vs. $1/T$ plot is similar to that recorded herein. Again a transportation technique was used and no explanation was given of effects of depleting $TaCl_5$ from the condensed phase during an experiment.

It appears that this study is the first to report decomposition vapour pressures for $CsNbCl_6$.

2. *Properties of the Solutions of $NbCl_5$–KCl and $TaCl_5$–KCl*

Figures 5 and 6 show the equilibrium vapour pressure measurements for the $NbCl_5$–KCl and $TaCl_5$–KCl systems, respectively. It should be noted that the corresponding phase diagrams show that the composition range of liquid solubility is very narrow. Although the liquid range widens at higher temperatures, the partial pressure of $NbCl_5$ or $TaCl_5$ above these solutions exceeds the upper limit of the pressure gauge used in this investigation. Accordingly, measurements herein were restricted to a narrow range of composition and temperature.

The results for the system $NbCl_5$–KCl shown in Fig. 5 span the concentration range, $0.401 < X_{NbCl_5} < 0.502$. The solution of composition, X_{NbCl_5}

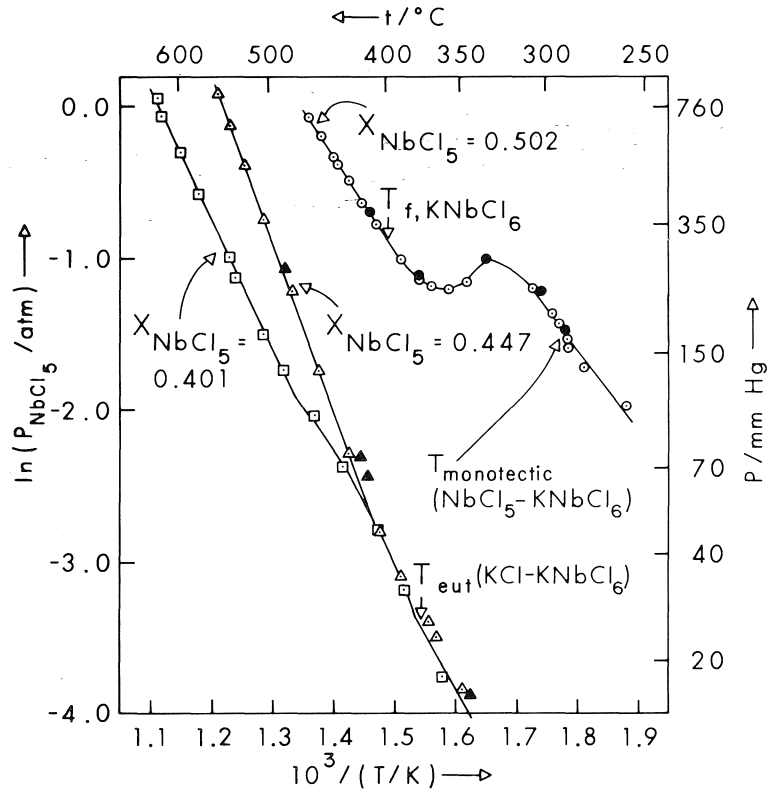

FIG. 5. ln P_{NbCl_5} vs. $1/T$ plots for the binary subsystem KCl–$KNbCl_6$. Solid lines represent best fit of present data. The pressure curve at $X_{NbCl_5} = 0.502$ represents solutions in the $NbCl_5$–$KNbCl_6$ subsystem.

Can. J. Chem. Downloaded from www.nrcresearchpress.com by 210.87.254.6 on 09/05/12
For personal use only.

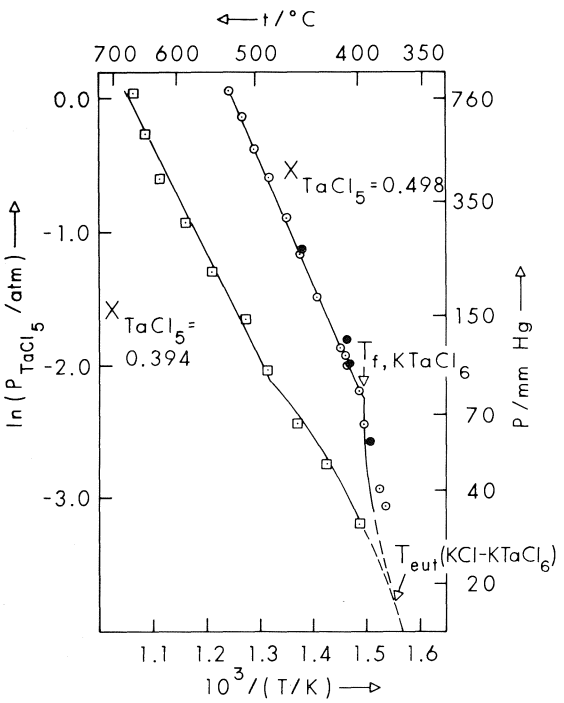

FIG. 6. ln P_{TaCl_5} vs. $1/T$ plots for the binary subsystem $KCl–KTaCl_6$. Solid lines represent best fit of present data.

= 0.502, is part of the $KNbCl_6$–$NbCl_5$ subsystem. As such, its pressure curve is expected to inflect at the monotectic temperature, 285°C (27), and at the liquidus temperature, which in this case is close to the melting point of $KNbCl_6$, which is about 400°C. The solutions of composition, $X_{NbCl_5} = 0.401$ and $X_{NbCl_5} = 0.447$ are part of the $KCl–KNbCl_6$ subsystem. Their pressure curves reveal a common segment at temperatures below the $KCl–KNbCl_6$ eutectic at 370°C (12, 27), as expected. Figure 5 shows a comparison of decomposition pressures between the KCl-rich solutions and the $NbCl_5$-rich solutions. Pressures recorded over the former are much lower and are evidence of the stabilizing effect of the formation of the complex compound $KNbCl_6$.

The results displayed in Fig. 6 are restricted to the $KCl–KTaCl_6$ subsystem. It is interesting to compare the shapes of the curves for the two solutions, as they are found on opposite sides of the $KCl–KTaCl_6$ eutectic composition. Both inflect at the $KCl–KTaCl_6$ eutectic temperature of 370°C (7, 12), and at the corresponding liquidus temperature, which for $X_{TaCl_5} = 0.498$ is almost identical with the melting point of $KTaCl_6$, 401°C (12).

Conclusions

The results of the present study indicate that the thermal stability of the complex compounds $ANbCl_6$ and $ATaCl_6$ is dependent upon the size of the alkali metal cation present.

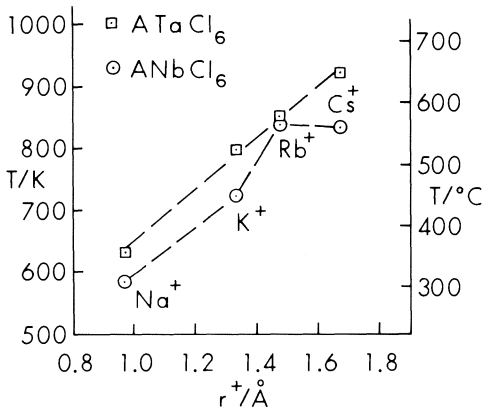

FIG. 7. Dependence of the decomposition temperature of the alkali hexachlorotantalate and hexachloroniobate compounds on the ionic-radii of the alkali metal cations.

Figure 7 shows the dependence of the dissociation temperature of the $AMCl_6$ compounds on the alkali-metal cation radius. The dissociation temperature is defined as the temperature at which the equilibrium pressure P_{MCl_5} becomes 1 atm and, therefore, can be taken as a measure of thermal stability of the $AMCl_6$ compound.

With the exception of $RbNbCl_6$, the results lie on two lines, one for the hexachloroniobates and one for the hexachlorotantalates. The latter have higher dissociation temperatures than their congeners, indicating the greater thermal stability of the hexachlorotantalate compound to the hexachloroniobate alkali-metal compounds. In general complexing for either $NbCl_5$ or $TaCl_5$ results in a dramatic reduction in the pressure of MCl_5 in equilibrium with a compound. For example, at 500°C pure $NbCl_5$ has a vapour pressure of 36 atm (8); in contrast, the partial pressure of $NbCl_5$ over $KNbCl_6$ is 1.43 atm and over $CsNbCl_6$ is 0.37 atm at that temperature.

Secondly, there is a reversal in stability. Pure $TaCl_5$ is more volatile than $NbCl_5$ (13). However, this changes upon formation of the $AMCl_6$ compounds. The partial pressure of $NbCl_5$ over the hexachloroniobate, $ANbCl_6$, is greater than that of $TaCl_5$ over the hexachlorotantalate of the same alkali metal. Nisel'son (28) has reported similar behaviour when $NbCl_5$ and $TaCl_5$ were complexed with $POCl_3$. In this laboratory the same reversal has been observed with $ZrCl_4$, $HfCl_4$, and the complex compounds which they form with the alkali-metal chlorides (14–19).

It is of interest to note that the relative volatility of the two pentachloride vapours is greater over the

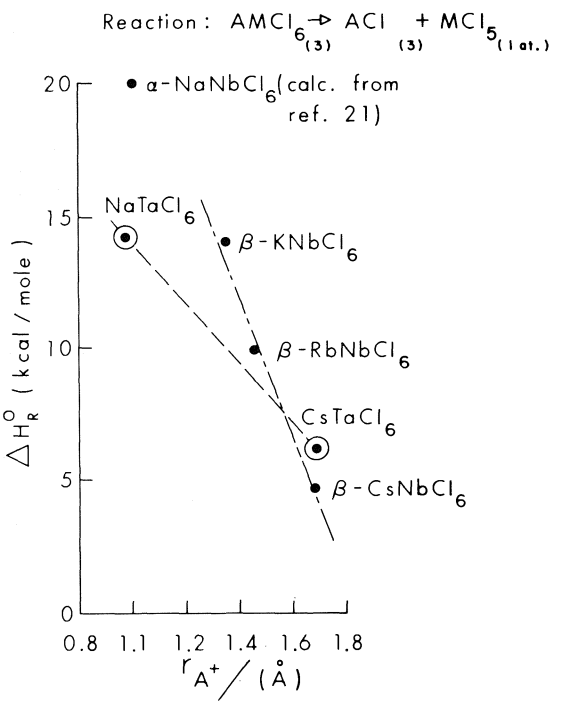

FIG. 8. Plot of ΔH_R^0 vs. the ionic-radii of the alkali metal cations.

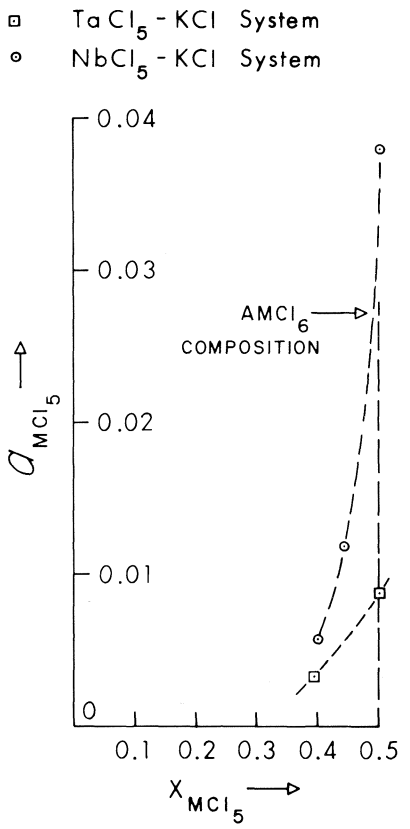

FIG. 9. Activity isotherms for a_{MCl_5} at 496°C for the molten KCl–$KNbCl_6$, and KCl–$KTaCl_6$ solutions.

complex compounds than over the pure pentachloride. At 230°C, $P^0_{TaCl_5}/P^0_{NbCl_5} = 1.42$ (13), while at 500°C over the corresponding potassium complexes, $P_{NbCl_5}/P_{TaCl_5} = 2.10$.

Interesting trends are also seen in the standard enthalpy changes for the decomposition reactions given in Table 1. The data shown in this table provide the temperature dependence of ln P_{MCl_5} and may be used for calculating standard enthalpies in temperature ranges in which the $AMCl_6$ type-compounds are present as single phase solids. The results of these calculations for ΔH_R^0 and ΔS_R^0 are also included in Table 1. A plot of ΔH_R° vs. the alkali metal cation radius, shown in Fig. 8, indicates that reaction enthalpies increase as the size of the alkali metal cation present in the complex compound decreases. The point for $NaTaCl_6$ was calculated from results on α-$NaTaCl_6$ obtained by Shemyakina *et al.* (21) and is expected to deviate from trends followed by the β-phase compounds.

Activity data for MCl_5 calculated from the results on the binary molten solutions of KCl–$KNbCl_6$ and KCl–$KTaCl_6$ indicate a further stabilization for MCl_5 in the presence of excess KCl. Figure 9 shows a plot of the concentration dependence of a_{MCl_5} in molten $NbCl_5$–KCl and $TaCl_5$–KCl solutions at 496°C, where $a_{MCl_5} = P_{MCl_5}/P^0_{MCl_5}$. Values for $P^0_{MCl_5}$ at 496°C were found in the literature: 34.8 atm for $NbCl_5$ (8) and 43.0 atm for $TaCl_5$ (29). As in the case of the pure $AMCl_5$ compounds, the molten hexachlorotantalate solutions are chemically more stable than the molten hexachloroniobates. Figure 9 also illustrates the significantly higher pentachloride activity in solutions whose pentachloride content exceeds the complex composition of 50 mol%.

Acknowledgement

The financial assistance to one of the authors (D.R.S.) by the National Research Council of Canada is gratefully acknowledged.

1. A. P. PALKIN and N. D. CHIKANOV. Zh. Neorg. Khim. **4**, 898 (1959); Russ. J. Inorg. Chem. **4**, 407 (1959).
2. W. BILTZ and A. VOIGT. Z. Anorg. Allg. Chem. **120**, 71 (1922).
3. I. R. BEATTIE, T. R. GILSON, and G. A. OZIN. J. Chem. Soc. A, 2765 (1968).
4. W. BUES, F. DEMIRAY, and H. A. ØYE. Z. Phys. Chem. Frankfurt am Main, **84**, 18 (1973).
5. J. W. JOHNSON and D. CUBICCIOTTI. High Temp. Sci. **2**, 9 (1970).
6. A. P. PALKIN and N. D. CHIKANOV. Zh. Neorg. Khim. **7**, 1370 (1962); Russ. J. Inorg. Chem. **7**, 705 (1962).

Can. J. Chem. Downloaded from www.nrcresearchpress.com by 210.87.254.6 on 09/05/12
For personal use only.

7. A. P. PALKIN and N. D. CHIKANOV. Zh. Neorg. Khim. **7**, 2388 (1962); Russ. J. Inorg. Chem. **7**, 1239 (1962).
8. J. W. JOHNSON, W. J. SILVA, and D. CUBICCIOTTI. High Temp. Sci. **2**, 20 (1970).
9. I. S. MOROZOV and A. T. SIMONICH. Zh. Neorg. Khim. **2**, 1907 (1957); Russ. J. Inorg. Chem. **2**(8), 311 (1957).
10. R. GUT. Helv. Chim. Acta, **43**, 830 (1960).
11. C. M. COOK, JR. J. Am. Chem. Soc. **81**, 535 (1959).
12. D. R. SADOWAY and S. N. FLENGAS. Can. J. Chem. **56**, 2013 (1978).
13. D. R. SADOWAY and S. N. FLENGAS. Can. J. Chem. **54**, 1692 (1976).
14. R. L. LISTER and S. N. FLENGAS. Can. J. Chem. **43**, 2947, (1965).
15. J. E. DUTRIZAC and S. N. FLENGAS. Advances in Extractive Metallurgy Symposium, April 17–20, 1967, The Institution of Mining and Metallurgy, London, England.
16. S. N. FLENGAS, J. E. DUTRIZAC, and R. L. LISTER. Can. J. Chem. **46**, 495 (1968).
17. S. N. FLENGAS and P. PINT. Can. Metall. Q. **8**, 151 (1969).
18. D. A. ASVESTAS, P. PINT, and S. N. FLENGAS. Can. J. Chem. **55**, 1154 (1977).
19. G. J. KIPOUROS and S. N. FLENGAS. Can. J. Chem. **56**, 1549 (1978).
20. L. S. MOROZOV, B. G. KORSHUNOV, and A. T. SIMONICH. Zh. Neorg. Khim. **1**, 1646 (1956); Russ. J. Inorg. Chem. **1**, (7), 203 (1956).
21. T. S. SHEMYAKINA, E. K. SMIRNOVA, T. I. POPOVA, and V. M. KUPTSOVA. Zh. Neorg. Khim, **9**, 2387 (1964); Russ. J. Inorg. Chem. **9**, 1291 (1964).
22. I. S. MOROZOV and B. G. KORSHUNOV. Zh. Neorg. Khim. **1**, 145 (1956); Russ. J. Inorg. Chem. **1**(1), 150 (1956).
23. K. HUBER, E. JOST, E. NEUENSCHWANDER, M. STUDER, and B. ROTH. Helv. Chim. Acta, **41**, 2411 (1958).
24. I. S. MOROZOV and A. T. SIMONICH. Zh. Neorg. Khim. **2**, 1907 (1957); Russ. J. Inorg. Chem. **2**(8), 311 (1957).
25. I. ZVARA and L. K. TARASOV. Zh. Neorg. Khim. **7**, 2665 (1962); Russ. J. Inorg. Chem. **7**, 1388 (1962).
26. I. S. MOROZOV and D. YA. TOPTYGIN. Izv. Akad. Nauk SSSR Ser. Khim. 1920 (1959); Bull. Acad. Sci. USSR, Div. Chem. Sci. 1832 (1959).
27. O. R. GAVRILOV and L. A. NISEL'SON. Zh. Neorg. Khim. **11**, 209 (1966); Russ. J. Inorg. Chem. **11**, 114 (1966).
28. L. A. NISEL'SON. Zh. Neorg. Khim. **2**, 816 (1957); Russ. J. Inorg. Chem. **2**(4), 162 (1957).
29. L. A. NISEL'SON, A. D. PUSTIL'NIK, and T. D. SOKOLOVA. Zh. Neorg. Khim. **9**, 1049 (1964); Russ. J. Inorg. Chem. **9**, 574 (1964).
30. Gmelins Handbuch der anorganischen Chemie, Verlag Chemie GmbH, Weinheim, Fed. Repub. Germany, Tantal, System-Nummer 50, Teil B2, 1971.

Can. J. Chem. Downloaded from www.nrcresearchpress.com by 210.87.254.6 on 09/05/12
For personal use only.

Structural study of the cesium oxypentafluorouranate (VI) $CsUOF_5$

PHILIPPE JOUBERT, JEAN-MARC WEULERSSE, AND ROLAND BOUGON[1]

Centre d'Etudes Nucléaires de Saclay, Division de chimie, Département de Génie Isotopique, B.P. no 2, 91190 Gif/Yvette, France

AND

BERNARD GAUDREAU

Université de Limoges, Laboratoire de Chimie Minérale B, 123, rue Albert Thomas, 87060 Limoges cedex, France

Received March 17, 1978

PHILIPPE JOUBERT, JEAN-MARC WEULERSSE, ROLAND BOUGON, and BERNARD GAUDREAU. Can. J. Chem. **56**, 2546 (1978).

Powder samples of cesium oxypentafluorouranate(VI) were studied by both neutron diffraction and ^{19}F broad line nuclear magnetic resonance.

$CsUOF_5$ crystallises with the $R\bar{3}$ space group, with the parameters $a = 5.41 \pm 0.01$ Å; $\alpha = 95°34' \pm 5'$. The structure, which was found to be unchanged at temperatures as low as 4.2 K, was interpreted by a statistical occupation of six-fold equivalents sites, the occupation rate being 1/6 and 5/6 for oxygen and fluorine, respectively. The nmr study showed that the disorder corresponding to this structure was of dynamic type, and that the UOF_5^- ions were in isotropical rotation. The motion is observable at temperatures as low as 223 K with a characteristic time τ equal to 3×10^{-5} s at 266 K. On the other hand, it was also shown through this nmr study that the point symmetry of the UOF_5^- ion corresponds to the C_{4v} group, with the axial fluorine being more covalent than the equatorial ones. Consistency of the diffraction and nmr results is discussed.

PHILIPPE JOUBERT, JEAN-MARC WEULERSSE, ROLAND BOUGON et BERNARD GAUDREAU. Can. J. Chem. **56**, 2546 (1978).

L'oxypentafluorouranate(VI) de césium $CsUOF_5$ a été étudié sur poudre par diffraction neutronique et résonance magnétique nucléaire du ^{19}F en large bande.

$CsUOF_5$ cristallise dans le groupe spatial $R\bar{3}$ avec les paramètres $a = 5.41 \pm 0.01$ Å; $\alpha = 95°34' \pm 5'$. Il n'y a pas de changement de structure jusqu'à 4.2 K, et celle-ci s'interprète par une occupation statistique de sites à 6 équivalents avec un taux d'occupation respectivement égal à 1/6 et 5/6 pour l'oxygène et le fluor. L'étude rmn montre que le désordre correspondant à cette structure est de type dynamique et que les ions UOF_5^- sont en rotation isotrope. Le mouvement peut-être observé jusqu'à 223 K, avec un temps caractéristique τ de 3×10^{-5} s à 266 K. La rmn montre par ailleurs, que l'ion UOF_5^- possède une symétrie ponctuelle correspondant au groupe C_{4v}, avec un fluor axial plus covalent que les fluors équatoriaux. La cohérence des résultats structuraux obtenus par diffraction et par rmn est discutée.

Introduction

The synthesis and characterization of the oxypentafluorouranates(VI) of monovalent cations $MUOF_5$ (where M = NO, NH_4, K, Rb, Cs) have been described previously (1–3). According to these studies, among the alkaline metals studied only $CsUOF_5$ has been found to contain the UOF_5^- ion. The structure of this ion was further studied by neutron diffraction and ^{19}F nuclear magnetic resonance on a powdered sample. Data from these investigations are presently reported.

Experimental Part

Materials and apparatus were as previously described (3). The powder diffraction patterns were measured at 300 and 4.2 K using thermal neutrons ($\lambda = 1.140$ Å) from the reactor EL3 at Saclay. The ^{19}F nmr were recorded with the spectrometers Varian DP 60 at 11 MHz and Brücker at 76.1 MHz.

[1]To whom correspondence should be addressed.

Results and Discussion

Crystallography

A comparison of the powder X-ray diffraction patterns of $CsUOF_5$ and $CsUF_6$ shows their great similarity (2, 3). To complete the previous studies, and, since it has been found very challenging to obtain and keep single crystals of $CsUOF_5$, further structural investigations were directed towards neutron diffraction on a powdered sample.

The powder neutron diffraction patterns, the lines of which are listed in Table 1, were recorded at 300 and 4.2 K and the corresponding crystal data were found to be as follows

$CsUOF_5$ fw = 481.9

Rhombohedral, $a = 5.41(1)$, $\alpha = 95°34'(5)$, $V = 155.9$ Å^3, $\rho_0 = 5.1(5)$, $z = 1$, $\rho_c = 5.13$ (300 K, neutrons, $\lambda = 1.140$ Å),

$a = 5.33(1)$, $\alpha = 95°52'(5)$, $v = 148.9$ Å^3, $\rho_c = 5.37$ (4.2 K).

Can. J. Chem. Downloaded from www.nrcresearchpress.com by 210.87.254.6 on 09/05/12
For personal use only.

TABLE 1. Neutron powder diffraction data for $CsUOF_5$ at 300 and 4.2 K (rhombohedral cell)

	300 K				4.2 K		
hkl	d_{obsd} (Å)	d_{calcd} (Å)	I_{obsd}	I_{calcd}	d_{obsd} (Å)	d_{calcd} (Å)	I_{obsd}
100	5.36	5.35	51	49	5.27	5.27	36
$10\bar{1}$	4.01	4.01	25	26	3.96	3.96	23
110	3.60	3.59	19	22	3.53	3.53	16
$11\bar{1}$	3.20	3.21	6	7	3.17	3.16	6
111	2.80	2.80	17	14	2.74	2.74	18
200	2.68	2.68	2	2	2.63	2.63	1
$20\bar{1}$	2.50	2.50	54	53	2.47	2.47	58
$11\bar{2}$	—	2.31	5	5	2.29	2.29	8
210	2.30	2.30			2.25	2.25	
$21\bar{1}$	2.22	2.23	100	100	2.19	2.19	100
211	2.01	2.01	7	5	1.98	1.97	2
$20\bar{2}$		2.00				1.98	
$21\bar{2}$	1.87	1.88	5	6	1.86	1.85	5
220	1.78	1.80	18	15			
300		1.78					
$30\bar{1}$	1.75	1.75	6	7	1.73	1.73	3
310		1.64				1.61	
221	1.64	1.63	41	46	1.61	1.60	55
$31\bar{1}$		1.63				1.61	
$22\bar{2}$	1.60	1.60	10	9	1.58	1.58	7
$30\bar{2}$	1.56	1.56	5	5	1.55	1.55	5

The unit cell is very close to that of $CsUF_6$, the space group of which has been found to be $R\bar{3}$ (4, 5). According to this type of structure (6) the only two available sites with one equivalent position (C_{3i}) are occupied by the atoms Cs and U, for $CsUOF_5$ the light atoms have to be placed on six equivalent positions (C_1) with the occupation numbers being 5/6 and 1/6 for F and O, respectively.

This arrangement can be accomplished with only one type of site, identical for F and O, or with two types of sites, one for the F atoms, the other for the O atoms. This last assumption was found to give a slightly better reliability factor $R = 0.06$, compared to $R = 0.10$ for the former.

Thermal motion factors were taken equal to 0.6 Å^2 for Cs and U, and 2.6 Å^2 for F and O. The refinement of the coordinates was made by the least-squares method using a program established[2] at Saclay. At 300 K, the atomic positions in the hexagonal unit cell are given in Table 2.

The uranium–fluorine and uranium–oxygen distances were calculated to be 2.10 ± 0.07 Å and 1.8 ± 0.3 Å, respectively. From these values it is clear that the difference between the oxygen and fluorine positions is hardly significant. From their similar scattering lengths, fluorine and oxygen atoms appear rather as a statistic average for neutron diffraction as well.

[2]P. Meriel, Roche and Rabot, Rapport interne n°116 S.C.E., Commissariat à l'Energie Atomique (1963).

TABLE 2. Final parameters $\times 10^3$

Atom	*x*	*y*	*z*
U	0	0	0
Cs	0	0	1/2
F [5/6]	−50 (5)	171 (5)	−161 (3)
O [1/6]	−64 (22)	171 (23)	−62 (7)

*Estimated standard deviation in parentheses.

According to these data the pseudo-octahedra of the light atoms are elongated along the three-fold axis with a disordered mutual orientation. The angle between the trigonal axis and a U—F bond is found to be 50°, compared to 54°44′ for the undistorted octahedron.

^{19}F Broad Line Nuclear Magnetic Resonance Spectroscopy

Studies of the ^{19}F nmr absorption line-shapes as a function of the temperature are known (7) to give information on solid motions as well as structural data.

The spectra of $CsUOF_5$ were recorded at both low and high field. At low field absorption linewidths are mainly due to the dipolar interaction, whereas at high field it is possible to differentiate non-equivalent atoms by their chemical shifts.

When recorded at low field (11 MHz) between 223 and 300 K the spectrum displayed a rapid change of the second moment M_2 and the half-line width of the absorption line (Fig. 1) which are both indicative of

Can. J. Chem. Downloaded from www.nrcresearchpress.com by 210.87.254.6 on 09/05/12
For personal use only.

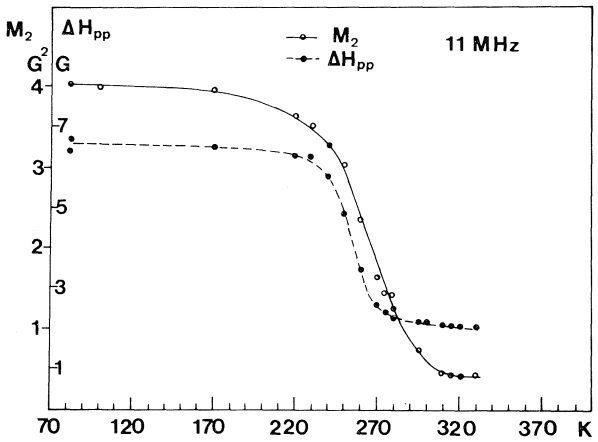

FIG. 1. Data from the ^{19}F nmr spectrum of $CsUOF_5$ at 11 MHz. Variation of the second moment (M_2) and peak-to-peak linewidth (ΔH_{pp}) with temperature.

motion. At high temperature, only an isotropic rotation of the UOF_5^- ion can account for the very low value found for M_2 (0.45 ± 0.1 G^2). From the crystallographic data and the assumption of such an isotropic rotation the value of M_2 was calculated to be 0.54 G^2, in good agreement with the experimental value.

At temperatures less than 223 K, the motion is too slow to narrow the line, the experimental value of M_2 is found to be equal to 4.0 ± 0.1 G^2, again close to the value of 3.8 G^2 calculated with the assumption of a disordered rigid lattice. The correlation time τ of the rotational motion was estimated from the graph M_2 (T) (8). At 266 K where the slope has the largest value, τ was found to be equal to 3×10^{-5} s, with a corresponding activation energy of 6 ± 0.5 kcal mol^{-1}. It is worth remarking that the actual value could be higher since an anisotropy of the UOF_5^- ion rotation or crystalline disorder can spread the correlation time, which in turn results in a broadening of the range of the M_2 variation. The presence of rotational motions confirms the disordered structure proposed above. At low temperature, the motion is dramatically slowed down, the UOF_5^- ions are frozen-like, probably without preferential orientation since no lowering in symmetry was observed by diffraction (down to 4.2 K for neutrons and 77 K for X-rays (3)).

At high field (76.1 MHz) and high temperature, only two lines of relative intensity 1/4 are observed at -405 and -285 ppm downfield from $CFCl_3$ (Fig. 2). This is in full agreement with the vibrational spectroscopy study (3) from which it was concluded that the UOF_5^- ion has the C_{4v} point group symmetry. On the other hand the force constant calculation has shown the axial fluorine atom (*trans* to the oxygen atom) to be less ionic in character than the

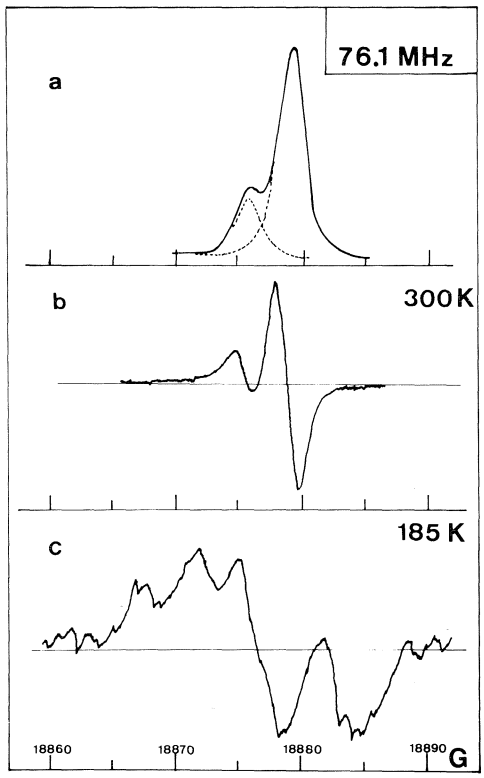

FIG. 2. ^{19}F nmr spectrum of $CsUOF_5$ at 76.1 MHz (ordinate-axis in arbitrary units). (*a*) Integral of the derivative curve recorded at 300 K; (*b*) derivative curve recorded at 300 K; and (*c*) derivative curve recorded at 185 K.

equatorial fluorine atoms. This last conclusion is in turn consistent with the nmr data, since the line of stronger intensity, consequently attributable to the equatorial fluorine atoms, was found to be located 120 ppm highfield from the other line. Such a correlation between ionic character and chemical shift is supported by previous measurements on uranium(VI) related compounds in the solid state, the mean chemical shift of which had been found to be: UF_6, -752 (9, 10); $NOUF_7$, -634; $CsUF_7$, -575; $(NO)_2UF_8$, -555; Cs_2UF_8, -500 (11) (in ppm from $CFCl_3$). Addition of F^- ions to UF_6 is expected to increase the U—F bond polarity and consequently to increase the ionic character of the fluorine atoms, which results in the trend observed for the chemical shifts. The small chemical shifts observed for UOF_5^-, as compared with that of the above-mentioned species, seem also to indicate an increase of the fluorine shielding, which in turn may arise from the substitution of fluorine by a less electronegative ligand. Such an effect has been previously reported (12) for tungsten derivatives.

At lower temperature (Fig. 2), on account of the

Can. J. Chem. Downloaded from www.nrcresearchpress.com by 210.87.254.6 on 09/05/12
For personal use only.

large values of the chemical shift anisotropies (up to 1000 ppm) and, perhaps from octahedral distortion as well, the spectrum was found to be very broad and complex with a second moment equal to 20 ± 1 G^2.

At this stage it is interesting to comment on the apparent discrepancy between the crystallographic data and those obtained by ^{19}F nmr and vibrational spectroscopy (3). The C_{4v} point group symmetry is clearly not rigorously compatible with the $R\bar{3}$ space group found by crystallography. Such a discrepancy has already been found (13) for some hexafluoroanions, which all have shown by nmr a tetragonal distortion of the octahedron whatever the local crystalline symmetry was. Superstructure and disorder which have been proposed (13) to account for the observations made for instance on K_2PtF_6, probably do not stand for $CsUOF_5$ since no superstructure evidence was found by neutron diffraction.

It is certainly more realistic to consider the trigonal distortion in UOF_5^- as being too small to be seen by nmr, especially at high temperature where slight differences in distances are blurred by the motions taking place in the solid. At low temperature, the large chemical shift anisotropies prevent further conclusion regarding the spatial arrangement of the light atoms.

Conclusion

The study of $CsUOF_5$ by both neutron diffraction and ^{19}F nmr allowed a structural model to be proposed for this compound. A disordered structure type is found by diffraction, and nmr has shown it to be of a dynamic type.

Acknowledgments

The authors are indebted to Dr. P. Charpin for helpful discussions and are grateful to Drs. J. Senegas and P. Meriel for their helpful assistance in obtaining nmr and neutron diffraction data in their laboratories.

1. R. Bougon, T. Bui Huy, and P. Charpin. Inorg. Chem. **14**, 1822 (1975).
2. P. Joubert and R. Bougon. C.R. Acad. Sci. Sér. C, **280**, 193 (1975).
3. P. Joubert, R. Bougon, and B. Gaudreau. Can. J. Chem. **56**, 1874 (1978).
4. R. A. Penneman, C. D. Sturgeon, and L. B. Asprey. Inorg. Chem. **3**, 126 (1964).
5. A. Rosenzweig and D. T. Cromer. Acta Crystallogr. **23**, 865 (1967).
6. N. F. M. Henry and K. Lonsdale (*Editors*). International tables for X-ray crystallography. Vol. 1. 2nd ed. T. Kynoch Press, Birmingham, England. 1965.
7. A. Abragam. The principles of nuclear magnetism. Oxford, London. 1961. p. 451.
8. G. R. Murray, Jr. and J. S. Waugh. J. Chem. Phys. **29**, 207 (1958).
9. R. Blinc, V. Marinkovic, E. Pirmajer, and I. Zupanci. J. Chem. Phys. **38**, 1474 (1973).
10. P. Rigny. Exchange reactions. IAEA, Vienna. 1965. p. 399.
11. R. Bougon, R. M. Costes, J. P. Desmoulin, J. Michel, and J. L. Person. Inorg. Nucl. Chem. Suppl. 99 (1976).
12. W. McFarlane, A. M. Noble, and J. M. Winfield. J. Chem. Soc. A, 948 (1971).
13. S. V. Zemskov and S. P. Gaduba. Zh. Struck. Khim. **7**, 904 (1976).

Can. J. Chem. Downloaded from www.nrcresearchpress.com by 210.87.254.6 on 09/05/12
For personal use only.

Electromotive force measurements of the cell: $In/InCl_3/In–Hg$, together with the derived thermodynamic quantities

ALAN N. CAMPBELL

Department of Chemistry, University of Manitoba, Winnipeg, Man., Canada R3T 2N2

Received May 2, 1978

ALAN N. CAMPBELL. Can. J. Chem. **56**, 2550 (1978).

Amalgams containing up to 60 wt.% indium are liquid and homogeneous at room temperature. The emf's of liquid amalgams containing from 10 to 50 wt.% of indium in the cell $In/InCl_3$/amalgam have been determined and from these the quantities ΔG, ΔH, and ΔS for the process In + Hg → amalgam.

ALAN N. CAMPBELL. Can. J. Chem. **56**, 2550 (1978).

Les amalgames contenant jusqu'à 60% en poids d'indium sont liquides et homogènes à la température ambiante. On a déterminé les fem d'amalgames liquides contenant de 10 à 50% en poids d'indium dans une cellule $In/InCl_3$/amalgame et faisant appel à ces données, on a évalué les ΔG, ΔH et ΔS du processus In + Hg → amalgame.

[Traduit par le journal]

Can. J. Chem. Downloaded from www.nrcresearchpress.com by 210.87.254.5 on 09/05/12
For personal use only.

Introduction

Since all amalgams containing less than 60 wt.% indium are liquid at room temperature (1), it was possible to determine the emf of the cell

$$In/InCl_3\,(N)/In–Hg\ amalgam$$

over the concentration range 0–50 wt.% indium and over the temperature range 25–99°C. From these measurements ΔG, ΔS, and ΔH for the process

$$In + Hg \rightarrow amalgam$$

were obtained by the standard methods of thermodynamics.

Experimental

The emf measurements were made with a potentiometer reading to 0.000005 V. The effect of temperature, as well as concentration of indium in the amalgam, of the cell

$$In/InCl_3\,(N)/In–Hg$$

was investigated. The temperature range was 25–99°C and the concentration range 10 to 50 wt.% indium. At concentrations greater than 60 wt.% In, the amalgam is partially solid at room temperature. Between 30 and 40 wt.% In, the emf of the above cell changes only, at 25°C, by 0.0003555 V per 1% by weight of indium.

Results and Discussion

Table 1 gives the emf, temperature coefficient of emf, activity of indium in the amalgam, and the activity coefficient (in terms of atomic fraction) for each concentration of indium. The methods of calculating ΔG, ΔH, and $T\Delta S$ are well known but the reader should perhaps be reminded that the activity of a metal in an amalgam (the other pole of the combination being pure metal) is connected with the emf by the equation:

$$E = (RT/nF) \ln 1/a$$

An inspection of Table 1 shows that E, and there-

TABLE 1. Electromotive force measurements

Wt.% In	x (atom fraction)	T (°C)	E (V)	$\Delta E/\Delta T \times 10^5$	a (activity)	γ (activity coef.)	ΔG_{298} (kcal)	$T\Delta S_{298}$ (kcal)	ΔH_{298} (kcal)
11.8	0.2595	25	0.03088	—	0.02712	0.1096	−2.138	−0.7856	−2.924
		30	0.03108	4.00	0.02813	0.1091			
		50	0.03174	3.44	0.03267	0.1278			
		75	0.03315	4.54	0.03627	0.1284			
		99	0.03360	3.68	0.04307	0.1253			
18.25	0.369	25	0.02507	—	0.0537	0.1455	−1.736	−0.4812	−1.217
		30	0.02520	2.60	0.0553	0.1498			
		50	0.02570	2.52	0.0627	0.1697			
		75	0.02583	1.52	0.0754	0.2044			
		99	0.02706	2.69	0.0794	0.2182			

TABLE 1 (*Concluded*)

Wt.% In	x (atom fraction)	T (°C)	E (V)	$\Delta E/\Delta T \times 10^5$	a (activity)	γ (activity coef.)	ΔG_{298} (kcal)	$T\Delta S_{298}$ (kcal)	ΔH_{298} (kcal)
30.74	0.4362	25	0.01315	—	0.2152	0.4932	−0.9105	−0.2924	−0.6181
		30	0.01320	1.00	0.2194	0.5031			
		50	0.01357	1.48	0.2316	0.5310			
		75	0.01399	1.58	0.2467	0.5655			
		99	0.01439	1.61	0.2600	0.5961			
39.87	0.5367	25	0.009595	—	0.3260	0.6603	−0.6643	−0.5402	−1.2045
		30	0.009714	2.38	0.3191	0.5946			
		50	0.010318	2.89	0.3289	0.9127			
		75	0.010785	2.38	0.3165	0.5897			
		99	0.011683	2.82	0.3544	0.6603			
50.77	0.6431	25	0.00246	—	0.7502	1.167	−0.1703	−0.4496	−0.6199
		30	0.002571	1.10	0.7490	1.165			
		50	0.00303	2.28	0.7214	1.122			
		75	0.00375	2.58	0.6872	1.069			
		99	0.0045	2.76	0.6563	1.021			

fore ΔG, decreases with increasing indium content, presumably becoming zero at about 60 wt.% indium, as it should if the solid phase is pure indium. ΔH and ΔS also decrease but not necessarily to zero.

The temperature coefficients of emf are of the order of 10^{-5} V/deg. The activity coefficient is at first low, about 0.1, but increases with increasing indium content, becoming greater than unity for the highest concentration of indium in the amalgam. It should be pointed out, however, that the activity coefficient has been calculated on the basis of the relation:

$$\gamma = a/\text{atom fraction}$$

Instead of the atom fraction the molality, or the molarity (if the densities of the amalgams were known) could be used. All three definitions seem rather artificial, however, and it is perhaps best to confine the interest to the activity.

1. Constitution of binary alloys. Hansen. Publ. McGraw-Hill, New York. 1958. p. 817; 1st Supplement. 1965. p. 531; 2nd Supplement. 1969. p. 427.

Can. J. Chem. Downloaded from www.nrcresearchpress.com by 210.87.254.5 on 09/05/12
For personal use only.

Production of Ni(I) complexes from reactions between Ni(II) and $NaBH_4$ in the presence of triphenylphosphine and some bidentate phosphines

DAVID G. HOLAH, ALAN N. HUGHES, BENJAMIN C. HUI, AND CHI-TAT KAN
Department of Chemistry, Lakehead University, Thunder Bay, Ont., Canada P7B 5E1

Received January 31, 1978

DAVID G. HOLAH, ALAN N. HUGHES, BENJAMIN C. HUI, and CHI-TAT KAN. Can. J. Chem. **56**, 2552 (1978).

The reactions between a variety of Ni(II) compounds and $NaBH_4$ have been studied in the presence of triphenylphosphine (P) and the bidentate phosphines 1,2-bis(diphenylphosphino)-ethane (diphos), bis(diphenylphosphino)methane (dppm), and *cis*-1,2-bis(diphenylphosphino)-ethylene (vpp). In ethanol, $NiCl_2 \cdot 6H_2O$, P, and $NaBH_4$ give $[Ni(BH_4)P_3]_2$ while NiX_2P_2 X = Cl, Br, I) and $NaBH_4$ produce $Ni(BH_4)P_{1.5}$. Further reactions of the former complex leading to $[Ni_2P_6](PF_6)_2$ and $[NiP_4](PF_6)$ have been studied. Reactions of $Ni(ClO_4)_2 \cdot 6H_2O$, P, and $NaBH_4$ produce $Ni(ClO_4)P_3$ and $[NiP_4](ClO_4)$. The bidentate phosphines, $Ni(ClO_4)_2 \cdot 6H_2O$ and $NaBH_4$ in ethanol all lead to quite different products. For example, with diphos, Ni(II) is stabilized and $[HNi(diphos)_2](ClO_4)$ is formed, but with the other two bidentate phosphines, reduction occurs. With dppm, $[Ni_2(dppm)_4](ClO_4)_2$ is produced, while vpp produces $[Ni(vpp)_2](ClO_4)$. Physical properties, possible structures, and suggested mechanisms of reduction are discussed.

DAVID G. HOLAH, ALAN N. HUGHES, BENJAMIN C. HUI et CHI-TAT KAN. Can. J. Chem. **56**, 2552 (1978).

On a étudié les réactions d'un certain nombre de composés du Ni(II) avec du $NaBH_4$ en présence de triphénylphosphine (P) et des phosphines bidendates, bis(diphénylphosphino-1,2) éthane (diphos), bis(diphénylphosphino) méthane (dppm) et du *cis* bis(diphénylphosphino-1,2) éthylène (vpp). Dans l'éthanol, le $NiCl_2 \cdot 6H_2O$, en présence de P et de $NaBH_4$, conduit au $[Ni(BH_4)P_3]_2$ alors que le NiX_2P_2 (X = Cl, Br, I) et le $NaBH_4$ conduisent au $Ni(BH_4)P_{1.5}$. On a aussi étudié d'autres réactions du premier complexe qui fournissent du $[Ni_2P_6](PF_6)_2$ et dû $[NiP_4](PF_6)$. Les réactions du $Ni(ClO_4)_2 \cdot 6H_2O$ avec la P et le $NaBH_4$ conduisent au $Ni(ClO_4)P_3$ et au $[NiP_4](ClO_4)$. Les phosphines bidentates, en présence de $Ni(ClO_4)_2 \cdot 6H_2O$ et de $NaBH_4$ dans l'éthanol, conduisent à des produits tout à fait différents. Par exemple, avec le diphos, le Ni(II) est stabilisé et il y a formation de $[HNi(diphos)_2](ClO_4)$ mais avec les deux autres phosphines bidentates, il se produit une réduction. Avec le dppm, il y a formation de $[Ni_2(dppm)_4](ClO_4)_2$ alors qu'avec le vpp, il se produit du $[Ni(vpp)_2](ClO_4)$. On discute des propriétés physiques, des structures possibles et des mécanismes suggérés pour la réduction.
[Traduit par le journal]

Can. J. Chem. Downloaded from www.nrcresearchpress.com by 210.87.254.42 on 09/05/12
For personal use only.

Introduction

A convenient route to the preparation of Ni(I) complexes (refs. 1 to 3 and references therein) involves $NaBH_4$ reductions of Ni(II) (4–6). By this method, compounds such as NiL_2X (L = 1,10-phenanthroline, 2,2′-bipyridyl, X = BH_4, PF_6, or BPh_4 (6)) and $[Ni(BH_4)P_3]_2$ (P = triphenylphosphine) (5) have been synthesized. The latter was prepared by the reaction sequence

$$NiCl_2/P/NaBH_4 \rightarrow NiClP_3 \rightarrow [Ni(BH_4)P_3]_2$$

and isolated as a pyrophoric solid which, from its diamagnetism and infrared spectrum, is thought to be a Ni—Ni bonded dimer with bridging BH_4 groups (5). In fact "most known Ni(I) complexes and all isolated Pd(I) and Pt(I) complexes are binuclear in nature, giving diamagnetic metal–metal bonded or ligand-bridged bimetallic species" (3). It has recently been shown (7) that the products formed from $CoCl_2/P/NaBH_4$ reactions which include $Co(BH_4)P_x$ (x = 2 or 3), H_3CoP_3, $HCo(N_2)P_3$, Co(0)—P complexes and P—BH_3, depend essentially on three factors, i.e., the *rate* of addition of $NaBH_4$, the solvent, and the presence or absence of free ligand. In view of the complexity of these Co(II) reactions, the analogous Ni(II) system has been more extensively investigated. This paper reports not only the results of this study of Ni(II) reductions in which a variety of different phosphines have been used, but also some reactions of the interesting complex $[Ni(BH_4)P_3]_2$.

Results and Discussion

$NiCl_2/P/NaBH_4$ Reactions

We have studied the $NiCl_2/P/NaBH_4$ reaction under a wider range of conditions than previously reported (5) and find that, like the analogous reactions involving Co(II) chloride (7), the course of

TABLE 1. Chemical analyses

Complex	Color	Chemical analyses* C	H	Ni
$[Ni_2P_6](PF_6)_2$	Yellow	65.2 (65.5)	4.9 (4.6)	6.1 (5.9)
$[NiP_4](PF_6)$	Yellow	68.9 (69.0)	4.9 (4.8)	4.9 (4.7)
$Ni(BH_4)P_{1.5}$†	Dark green	69.5 (69.4)	5.6 (5.7)	12.6 (12.6)
$Ni(ClO_4)P_3$	Yellow	68.9 (68.6)	5.0 (4.8)	5.9 (6.2)
$[NiP_4](ClO_4)$	Orange	71.3 (71.6)	5.2 (5.0)	4.9 (4.9)
$[HNi(diphos)_2](ClO_4)$	Orange	65.1 (65.3)	5.2 (5.2)	6.0 (6.1)
$[Ni_2(dppm)_4](ClO_4)_2$	Green	65.5 (64.8)	5.2 (4.8)	6.8 (6.3)
$[Ni(vpp)_2](ClO_4)$	Brown	65.6 (65.7)	4.8 (4.7)	6.1 (6.2)

*Calculated values in parentheses.
†P 10.7 (10.0), B (by difference) 2.3 (2.3).

TABLE 2. Electrical conductivities

Complex	Λ_0 ($cm^2\ equiv^{-1}\ ohm^{-1}$)	Slope* ($cm^{1/2}\ equiv^{-1/2}\ ohm^{-1}$) Obsd.	Calcd.	Type
$[HNi(diphos)_2](ClO_4)$†	97.3	232		1:1
$[Ni_2P_6](ClO_4)$†	189.8	400		1:2
$[Ni(phen)_3](ClO_4)_2$†‡		456		1:2
$NaBPh_4$†‡		216		1:1
$[HNi(diphos)_2](ClO_4)$	153.2	428	344	1:1
$[Ni(diphos)_2](ClO_4)_2$	191.8	788	822	1:2
$[Ni_2(dppm)_4](ClO_4)_2$	134.5	716	670	1:2
$[Ni(vpp)_2](ClO_4)$	171.0	317	357	1:1
$[(C_2H_5)_4N]Cl$	171.7	435	357	1:1

*The observed slope is obtained from linear plots of $\Lambda_0 - \Lambda_c$ against $c^{1/2}$ as described previously (9, 19). Slopes from CH_3CN data were calculated according to published procedures (19) and values agree well with those for other complexes (19).
†Measured in CH_3NO_2 at 25°C. All others in CH_3CN.
‡Reference 9.

the above Ni reactions under N_2 depends upon the solvent and on the presence or absence of added ligand. Unlike the cobalt reactions, the results obtained from the Ni system are independent of both time and the rate of addition of $NaBH_4$ and are dependent upon the starting material ($NiCl_2$ behaves differently from $NiCl_2P_2$, see later). Thus, all reactions between $NiCl_2$ and P (minimum molar ratio 1:6) and an excess of $NaBH_4$ in ethanol in the strict absence of oxygen yield $[Ni(BH_4)P_3]_2$ (5) (cf. $CoCl_2$, P, and $NaBH_4$ which give a complex mixture under similar conditions (7)). If all traces of oxygen are not excluded, a mixture of the phosphine oxide, the borane adduct $P{\cdot}BH_3$ and Ni(0)—P complexes are obtained. When less P is used in the above reactions, e.g. Ni:P = 1:2, reduction to Ni(0) is rapid and complete and no intermediate BH_4^- complex could be detected.

All efforts to recrystallize $[Ni(BH_4)P_3]_2$ from organic solvents (benzene, THF, acetonitrile, nitromethane) resulted in decomposition to give $P{\cdot}BH_3$ and Ni(0)—P complexes. It is interesting to note that, while $CoCl_2/P/NaBH_4$ reactions in benzene produce $Co(BH_4)P_2$ (7), the $NiCl_2$–benzene reactions lead only to the above mentioned decomposition products $P{\cdot}BH_3$ and Ni(0)—P complexes. It has not been possible to convert $[Ni(BH_4)P_3]_2$ into any other Ni—BH_4 complex as was the case with Co, i.e. $Co(BH_4)P_3 \rightarrow Co(BH_4)P_2$ (7).

In ethanol, $[Ni(BH_4)P_3]_2$ slowly reacts (2 days) with an excess of $NaPF_6$ to liberate gases and produce, together with unidentified Ni-containing products, a complex of empirical formula NiP_3PF_6 which can be recrystallized from THF (Table 1). The larger the excess of $NaPF_6$ (up to 10 *M*), the higher the yield of product. The fact that a similar reaction with $NaBPh_4$ does not occur tends to rule out a simple substitution of PF_6^- for BH_4^- and the difference in behaviour between $NaPF_6$ and $NaBPh_4$ may be due to the slow hydrolysis of the former to generate HF (8) which would decompose the BH_4^- group.

Like the BH_4^- complex, NiP_3PF_6 is diamagnetic and is probably, therefore, dimeric with a Ni—Ni

Can. J. Chem. Downloaded from www.nrcresearchpress.com by 210.87.254.42 on 09/05/12
For personal use only.

TABLE 3. Physical data

Complex	μ_{eff}	Λ (acetone) M ($\times 10^3$)	Electronic spectra (cm^{-1}) Reflectance	Solution (ε) (acetone)
$[Ni_2P_6](PF_6)_2$	Diamagnetic		28 600	No *d–d* bands, 33 000 – 5 000
$[NiP_4](PF_6)$	2.27	172.5 (0.36)	6 135 ~7 140 (sh) 25 000	6 135 (88.8)(vb)
$[NiP_4](ClO_4)$	2.31	156.3 (0.72)		6 170 (108.9)(vb)
$Ni(ClO_4)P_3$	2.17	135.9 (0.49)	5 460 5 880 (sh) 28 600	5 880 (68.8)(vb)
$[Ni(vpp)_2](ClO_4)$	1.94		~8 000 (sh) 11 050 23 300 (sh) 26 300	10 000 (372.3)
$[HNi(diphos)_2](ClO_4)$	Diamagnetic		7 700 (vb) 24 400	7 700 (9.1)
$[Ni_2(dppm)_4](ClO_4)_2$	Diamagnetic		16 700 (sh) 25 000	17 500 (3770)
$Ni(BH_4)P_{1.5}$	Diamagnetic	0* (2.02)	16 400 25 000	16 400* (900)
$NaPF_6$		162.7 (7.05)		

*THF solution, concentrations based on $[Ni(BH_4)P_{1.5}]_2$.

bond. This is supported by electrical conductivity data (Table 2) in nitromethane solution which confirm that the complex should unequivocally be formulated as a 1:2 electrolyte (9), i.e. $[Ni_2P_6](PF_6)_2$. For comparison, Table 2 also contains data, in nitromethane, on 1:1 and 1:2 electrolytes. The ir spectrum of $[Ni_2P_6](PF_6)_2$ shows the ν_{P-F} vibration at 840 cm^{-1} and there are no bands in its electronic spectrum below 28 000 cm^{-1} (Table 3).

When $[Ni_2P_6](PF_6)_2$ is recrystallized from THF in the presence of an excess of P, the Ni—Ni bond is cleaved and a yellow crystalline solid $[NiP_4](PF_6)$ is formed. This is a paramagnetic, 1:1 electrolyte and its electronic spectrum shows a band with a shoulder in the 6000–7000 cm^{-1} ($\varepsilon \sim 100$) region (Table 3, Fig. 1), consistent with the $^2T_2 \rightarrow {}^2E$ transition of a tetrahedral d^9 configuration. Very recently, the closely related complex $Ni(P(CH_3)_3)_4(BPh_4)$ was accidentally prepared (10) during recrystallization of $[Ni(CH_3)(P(CH_3)_3)_4](BPh_4)$ and this contains (from X-ray data) a distorted tetrahedral Ni(I) ion with electronic properties very similar to those reported above.

It is possible to draw some conclusions about the mechanism of the $NiCl_2/P/NaBH_4$ reactions, the initial product of which is invariably $NiClP_3$ (5). This must clearly be the precursor to the BH_4^- complex. While $NiClP_3$ dissociates in benzene to $NiClP_2$

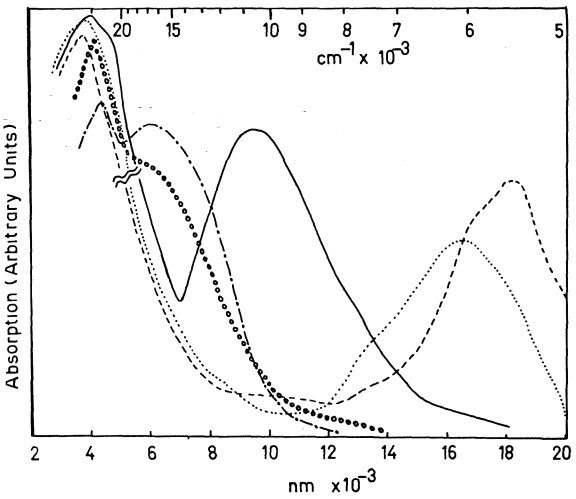

FIG. 1. Reflectance spectra: --- $Ni(ClO_4)P_3$, ··· $[NiP_4](PF_6)$, —$[Ni(vpp)_2](ClO_4)$, -·-·- $Ni(BH_4)P_{1.5}$, ○○○ $[Ni_2(dppm)_4](ClO_4)_2$.

(which has been isolated (2)), it is unlikely that this would occur in ethanol (in which it is less soluble) in the presence of an excess of P. Thus, displacement of Cl^- (and ClO_4^-, see later) by BH_4^- probably results in the initial formation of $P_3Ni—H—BH_3$ followed by rapid dimerization. While all of the complexes listed in the following scheme have not been isolated

Can. J. Chem. Downloaded from www.nrcresearchpress.com by 210.87.254.42 on 09/05/12
For personal use only.

Can. J. Chem. Downloaded from www.nrcresearchpress.com by 210.87.254.42 on 09/05/12
For personal use only.

their probable existence as intermediates is reasonable and compatible with the formation of the complexes that have been obtained. The proposed H-bridged dimer is analogous to the known $[HNi(R_2P(CH_2)_2PR_2)]_2$ (R = C_6H_{11}) species (11).

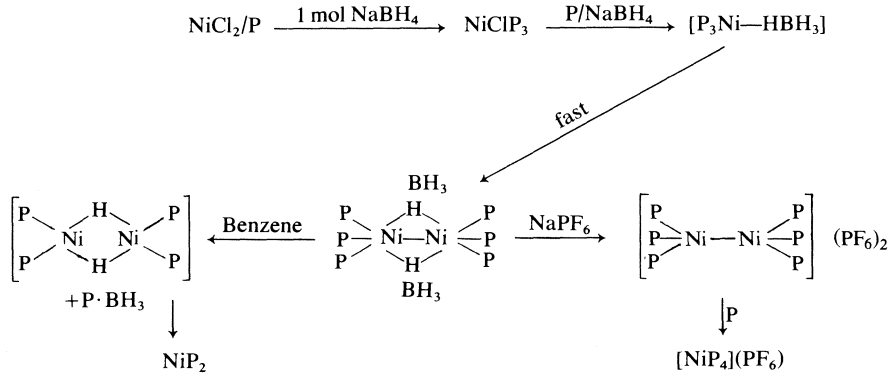

$NiX_2P_2/NaBH_4$ Reactions (X = Cl, Br, I)

As mentioned above, a major difference between Co(II) and Ni(II)/P/$NaBH_4$ reactions is the effect of the nature of the starting material. In the Co reactions, mixtures of $CoCl_2$ and P rapidly produce the $CoCl_2P_2$ complex prior to the addition of the $NaBH_4$, whereas mixtures of $NiCl_2$ and P in ethanol require heating before the formation of $NiCl_2P_2$ occurs. The latter is therefore not present in any significant amount in $NiCl_2/P/NaBH_4$ mixtures at room temperature, and when NiX_2P_2 (X = Cl, Br, I) are used as starting materials, the reactions follow a quite different course.

Related reactions have been studied (12) previously in connection with the preparation of unspecified Ni-catalysts. For example, the reaction sequence

$$NiBr_2(PBu_3^n)_2 \xrightarrow{NaBH_4} HNiBr(PBu_3^n)_2 \longrightarrow Ni(PBu_3^n)_2 + HBr$$

was suggested as preceding further reactions of the Ni(0) complex to form the catalyst (12). It was noted that mixtures of $NiBr_2(PBu_3^n)_2$ and $NaBH_4$ in ethanol under N_2 produce yellow or brown solutions depending upon the amount of $NaBH_4$ added. Similarly, brown solutions from reactions between $NiBr_2P_2$ and $NaBH_4$ under N_2 in THF/ethanol or benzene/ethanol have been studied as catalytic systems (13).

We find that the products from reactions between NiX_2P_2 (X = Cl, Br, I, preferably the last because of its greater reactivity) and $NaBH_4$ in ethanol are critically dependent upon experimental conditions. The major product is a brown, ether-soluble solid which appears to be NiP_2 (12), but under certain conditions a highly crystalline pyrophoric solid with the empirical formula $Ni(BH_4)P_{1.5}$ can be isolated. The addition of free P to this reaction and/or prolonging the reaction time leads only to the coproduction of $P{\cdot}BH_3$ and, as the amount of P is increased, so the borane adduct becomes the major product. Reactions in benzene/ethanol mixtures lead to the production of $P{\cdot}BH_3$ and unidentified Ni complexes. The complex formulated as $Ni(BH_4)P_{1.5}$ can be recrystallized unchanged from cold benzene or THF but decomposes to $P{\cdot}BH_3$ and unidentified Ni complexes in acetonitrile and nitromethane.

The complex is a diamagnetic non-electrolyte in THF solution. There is no evidence in the ^1H nmr spectrum (10–40 τ) in either benzene or THF solution, or in the ir spectrum, for a Ni—H linkage. Regarding the bonding of BH_4, the ir spectrum is consistent with bidentate coordination (14), with bands at 2440 cm^{-1} (ν_{B-H_t}), 1970 cm^{-1} (ν_{B-H_b}), and 1380 cm^{-1} ($\nu_{bridge\ stretch}$) although the expected BH_2 deformation at 1100–1200 cm^{-1} is not identifiable due to ligand vibrations in this region. On deuteration, the ν_{B-D_t} vibration shifts to 1840 cm^{-1} giving ν_D/ν_H as 0.754, similar to values observed previously (7). The main feature of the electronic spectrum of the complex (Table 3, Fig. 1) is a band at 16 400 cm^{-1} with, in THF solution, $\varepsilon \sim 900$, the origin of which is unknown, although it does resemble the spectrum of $Ni(dppm)_2(ClO_4)$ (see later). No meaningful data were obtained from a mass spectrum, which indicated decomposition even under the mild conditions used for recording the spectrum.

There is little we can say about the structure of this peculiar complex. The empirical formula suggests that the complex contains Ni(I) and that, in view of the diamagnetism, it must be at least dimeric. The BH_4 groups may be chelating to one metal or bridging two metals. We are currently attempting to grow crystals suitable for a structure determination.

Can. J. Chem. Downloaded from www.nrcresearchpress.com by 210.87.254.42 on 09/05/12
For personal use only.

The BH_4^- groups are not replaced by PF_6^-, as occurs with $[Ni(BH_4)P_3]_2$ and, as mentioned above, the complex does not react with added P. No reaction has been observed to lead to mixtures of $[Ni(BH_4)P_3]_2$ and $Ni(BH_4)P_{1.5}$ nor have conditions been found which allow the interconversion between the two; therefore the mechanisms for their formation are probably quite different with no common intermediate.

$Ni(ClO_4)_2$/Monodentate Phosphine/$NaBH_4$ Reactions

The reaction between $Ni(ClO_4)_2$, P, and an excess of $NaBH_4$ in ethanol yields $[Ni(BH_4)P_3]_2$ unlike the similar Co reaction which produces $Co(BH_4)P_2$ (7). With much less $NaBH_4$, a mixture of $[Ni(BH_4)P_3]_2$ and $Ni(ClO_4)P_3$ is obtained, the latter being purified by recrystallization from THF/ether. Magnetic and spectral data for $Ni(ClO_4)P_3$ (solution and solid state) (Table 3, Fig. 1) are consistent with a tetrahedrally coordinated Ni(I) system, with the $^2T_2 \rightarrow {}^2E$ transition shifted to lower energy compared to its position for $[NiP_4]^+$, consistent with the fact that a weaker ligand field exists in the former complex. The interaction between the Ni and the ClO_4 group must be very weak since the ir spectrum shows bands at 625 and 1090 cm^{-1} which are the ν_4 and ν_3 bands of an essentially ionic perchlorate (15). Additional evidence for a weak Ni—ClO_4 link comes from the solution properties of the complex. The spectrum in acetone is, as mentioned above, typical of a tetrahedral d^9 configuration but the electrical conductivity is only slightly less than that expected for a 1:1 electrolyte (Table 3) and therefore dissociation of the type

$$Ni(ClO_4)P_3 \underset{}{\overset{\text{solvent}}{\rightleftharpoons}} NiP_3(Acetone)^+ + ClO_4^-$$

probably occurs. In addition, acetone solutions of $Ni(ClO_4)P_3$ react readily with P to produce $[NiP_4](ClO_4)$ with electronic properties (Table 3) very similar to the PF_6^- complex already discussed.

These reactions again serve to illustrate the stepwise mechanism for the formation of BH_4^- complexes, and it is clear that $Ni(ClO_4)P_3$ serves as a precursor in a totally analogous way to $NiClP_3$ as already discussed and as summarized below (reactions in ethanol):

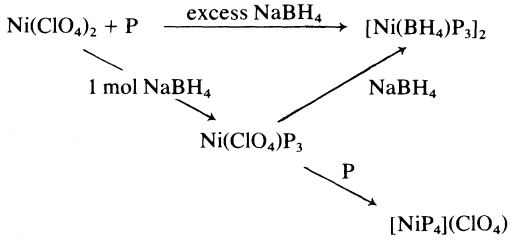

As in the $NiCl_2/P/NaBH_4$ reactions, the solvent plays an important role in determining the reaction products and, for example, mixtures of $Ni(ClO_4)_2$ and P in ethanol/benzene (1:2) react with 1 mol of $NaBH_4$ in ethanol to precipitate immediately orange-red crystals of NiP_3 (16).

As expected, the poorer π-acceptor ligands Ph_3As and Ph_3Sb cannot stabilize Ni(I) and mixtures of $Ni(ClO_4)_2$ and these ligands are immediately reduced to NiL_3 species by 1 mol of $NaBH_4$ in ethanol. Similar results have been observed previously (5, 17).

$Ni(ClO_4)_2$/Bidentate Phosphine/$NaBH_4$ Reactions

We have previously noted (6) that neutral square-planar Ni(II) complexes (e.g. of *N,N*-diethyldithiocarbamate and dimethylglyoxime) are unreactive towards $NaBH_4$ due, presumably, to the stability of the complexes and the reluctance of BH_4^- to interact with the vacant axial coordination sites on the metal. However, cationic square planar Ni(II) species $[Ni(L—L)_2]^{2+}$ (as ClO_4^- salts) should be more vulnerable to BH_4^- attack and, in this connection, three different bidentate phosphines have been studied, namely 1,2-bis(diphenylphosphino)ethane (diphos), bis(diphenylphosphino)methane (dppm), and *cis*-1,2-bis(diphenylphosphino)ethylene (vpp). Results of reactions, in ethanol, between the appropriate starting material, $[Ni(L—L)_2](ClO_4)_2$, prepared *in situ*, and $NaBH_4$ (Ni:$NaBH_4$ = 1:1) are outlined below.

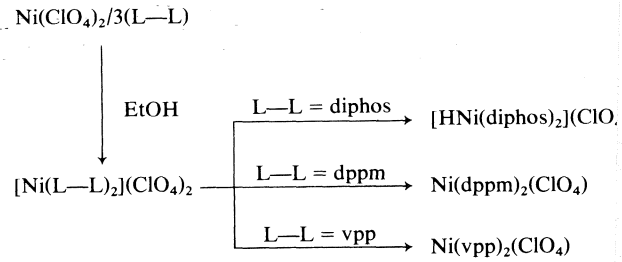

Thus, the red crystalline $[HNi(diphos)_2](ClO_4)$ ($\nu_{Ni—H}$ 1950 cm^{-1}, τ = 23.5 in DMSO-d^6 at 40°C due to Ni—H) is obtained when L—L = diphos. This diamagnetic 5-coordinated Ni(II) cation has previously been reported with a variety of anions (18), generally prepared (e.g. with $AlCl_4^-$, HCl_2^-, BF_4^-) by the protonation of $Ni(diphos)_2$ by strong acids, although the route involving $NaBH_4$ is somewhat simpler and easier.

When L—L is dppm, $NaBH_4$ addition results in the production of the diamagnetic solid $Ni(dppm)_2(ClO_4)$, the dark green color of which is not inconsistent with the presence of a reduced Ni species (cf., $NiX_2P_2/NaBH_4$), particularly in view of the fact that the Ni(II) hydride mentioned above is red. No

Can. J. Chem. Downloaded from www.nrcresearchpress.com by 210.87.254.42 on 09/05/12
For personal use only.

evidence (nmr 10–35 τ, ir) of a Ni—H link could be found, and peaks at 620 and 1100 cm^{-1} (broad) show the presence of ionic perchlorate. The complex is therefore probably dimeric, with a structure corresponding to one of the types shown below:

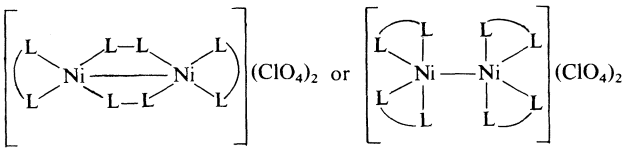

(A) (B)

Conductivity data for this and related complexes are shown in Table 2 from which it can be concluded that the dppm complex is indeed a 1:2 electrolyte. The solid state and solution spectra (Table 3, Fig. 1) are quite similar to those of $Ni(BH_4)P_{1.5}$. Recrystallization from a polar solvent such as CH_3CN in the presence of free dppm or of P results in recovery of starting material, unlike $[Ni_2P_6](PF_6)_2$ which produces $[NiP_4](PF_6)$ as already discussed, and this tends to support the structure with bridging ligands rather than a single Ni—Ni bond as suggested for the PF_6 dimer. However, it should be borne in mind that the Ni—Ni cleavage with P observed for $[Ni_2P_6](PF_6)_2$ occurs with a four-coordinate Ni system whereas in A and B above, the Ni is five-coordinate. In fact, structure A is closely related to the Pt(I) complex $[PtCl(dppm)]_2$ which has bridging phosphine ligands (20).

In theory, it might be possible to distinguish between the above two structural possibilities A and B by ^1H nmr spectral measurements since in A, the methylene protons of the bridging ligands might have a different chemical shift from that of the methylene protons in the chelating ligands. In B, one would expect all of the methylene groups to be magnetically identical.

Examination of the ^1H nmr spectrum of the complex in deuterated acetone at 40°C indeed shows two methylene proton resonances as very broad and poorly defined signals centered on τ 6.96 and τ 7.29 overlapping to some extent at the bases of the signals. However, the two signals are not of equal area and the ratio of the area of the high-field signal to that of the low field signal is 1.3:1. Therefore the spectrum is, apparently, not compatible with either structure.

However, the broadness of the signals and the unusual ratio is suggestive of a temperature-dependent equilibrium between two structures and variable temperature ^1H nmr measurements confirm this. Thus, on cooling the solution of the complex to 0°C, the spectrum modifies such that the lower field signal becomes of much greater area and also becomes considerably sharper while the higher field signal is very greatly reduced in area. This indicates that at 0°C, one species greatly predominates. On the other hand, at 50°C the higher field peak becomes much sharper and of greater area while the lower field peak diminishes. This suggests that at 50°C, the other species predominates.

The spectral changes are reversible on cooling the solution again and the changes in general are consistent with an equilibrium between two structures. However, the broadness of the signals at 40°C suggests that the kind of equilibrium involved is an exchange equilibrium where, at 0°C, essentially all of the ligands are fully coordinated and bidentate (which would give the greatest shift to lower field to the methylene protons) while at 50°C, the exchange is very rapid and the methylene protons are magnetically averaged and more like those in the free ligand. In fact the location of the higher field signal (τ 7.29) is very close to that of the methylene protons of the free ligand (τ 7.21).

It seems then that the ^1H nmr spectrum does not allow us to distinguish between the two possible structures since ligand dissociations in either structure could explain the spectra although the spectrum at 0°C, which shows only one significant methylene absorption (albeit a broad one), might marginally favour structure B.

Finally, when L—L is vpp, the product is the paramagnetic (μ_{eff} = 1.94 BM) complex $[Ni(vpp)_2](ClO_4)$. This is a 1:1 electrolyte (Table 2), has bands in the ir spectrum at 625 and 1100(b) cm^{-1} associated with an ionic ClO_4^- group, and has an electronic spectrum (Table 3, Fig. 1) in which the *d–d* band is shifted by almost 4000 cm^{-1} to higher energy than occurs in the tetrahedral $[NiP_4]^+$ species. This is no doubt due, in part, to a stronger ligand field exerted by the chelating ligand compared with that of triphenylphosphine, but may also reflect considerable distortion from tetrahedral towards a square planar geometry about the nickel.

In these reactions, the probable sequence is:

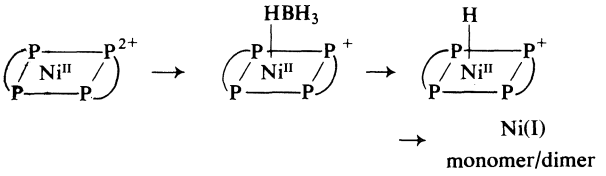

but it is not understood why reactions involving diphos stop at the Ni(II)—H stage while the other two phosphines allow reduction but produce quite different products. Molecular models reveal that all three ligands can adopt configurations where the

P—P 'bite' distances are very similar (although vpp is somewhat different in that it is a very rigid molecule), and therefore the differences are unlikely to be steric in origin. The rigid vpp is also different in that it has an ethylenic π-system which could interact with metal *d*-electrons although whether this plays a unique role is doubtful since both it and dppm allow reduction of the Ni(II).

Experimental

Materials

All chemicals were reagent grade and, with the exception of P which was recrystallized from ethanol, were used without purification. NiX_2P_2 (X = Cl, I) were prepared by literature methods (21). Solvents were distilled, degassed, and stored under N_2 over 4A molecular sieves.

Analyses and Physical Measurements

Samples were suitably protected from atmospheric oxidation during weighing or data collection.

Chemical analyses for C and H were performed on a Perkin-Elmer model 240 analyser and, for $Ni(BH_4)P_{1.5}$, additional C, H together with P and Ni analyses were determined by Dr. F. Pascher, Bonn, W. Germany. Ni was analysed volumetrically by edta after degradation of the complexes by conc. HNO_3.

Infrared studies were carried out on a Beckman IR12 spectrophotometer (calibrated with a polystyrene reference film) using Nujol mulls between NaCl (650–4000 cm^{-1}) or polyethylene plates (200–650 cm^{-1}). Electronic spectra were recorded on a Cary 14 recording spectrophotometer and nmr spectra were obtained using a Varian Associates Model A60-A spectrometer. Magnetic moments were measured in the solid state by the Gouy method and in solution by the nmr method (22). Molar conductivities were measured on a YSI model 31 conductivity bridge at 25°C. Mass spectra were recorded on a Hitachi-Perkin Elmer RMU-7 double focussing mass spectrometer and, for X-ray powder diffraction measurements, samples in Lindeman capillaries were photographed on a Debye–Scherrer type camera using Ni-filtered copper K_α radiation from a Phillips PW1130 X-ray Generator.

Syntheses

All syntheses were carried out under pure N_2 in a glove box.

$[Ni(BH_4)P_3]_2$

This complex is best prepared by a slight modification to the method already described (5). A suspension of $NaBH_4$ (0.2 g, 5.3 mmol) in ethanol (10 ml) was added dropwise to a stirred suspension of $NiCl_2 \cdot 6H_2O$ (0.1 g, 0.4 mmol) and P (0.6 g, 2.2 mmol) in ethanol (25 ml). A gas, presumably H_2, was generated rapidly during the initial stages of addition of the $NaBH_4$ suspension and the color of the mixture changed from green to orange and slowly to reddish brown. The mixture was stirred for 3 h when the yellow brown precipitate was filtered off, washed in sequence with EtOH, H_2O, EtOH, and ether, and dried under reduced pressure for 3 h.

d-*Spacings from X-ray Powder Pattern (Relative Intensities 0–10)*

9.63 (7), 8.92 (10), 7.48 (2), 6.30 (2), 5.42 (2), 4.45 (4), 4.34 (4), 4.04 (2), 3.88 (5), 3.44 (2).

$[Ni_2P_6](PF_6)_2$

A mixture of $[Ni(BH_4)P_3]_2$ (1.5 g, 0.87 mmol) and $NaPF_6$ (2.1 g, 12.5 mmol) was stirred in ethanol (25 ml) for 2 days after which the resulting solid was filtered off and washed with ethanol, water, ethanol, and ether. The crude solid was dissolved in THF, filtered, and the filtrate concentrated to small volume. Addition of ether precipitated the yellow product in ~30% yield. It was again recrystallized from acetone/ether.

$[NiP_4](PF_6)$

$[Ni_2P_6](PF_6)_2$ in the pure state or before recrystallization was dissolved in THF and a six-fold molar excess of P added. The solution was filtered if necessary and the filtrate concentrated to small volume before the addition of ether precipitated the yellow product in ~70% yield.

$Ni(BH_4)P_{1.5}$

A suspension of $NaBH_4$ (0.32 g, 8.41 mmol) in ethanol (7 ml) was added dropwise over a period of 10 min to a stirred suspension of NiI_2P_2 (2.38 g, 3.38 mmol) in ethanol (15 ml). The mixture was stirred for an additional 5 min before the resulting brown solid was filtered off and washed with ethanol, water, ethanol, and finally with ether until the ether washings were colorless. This indicated complete removal of the Ni(0)—P impurity. The green solid which remained was dissolved in benzene (or THF), the solution filtered, and the filtrate concentrated under reduced pressure to ~4/5 of the original volume. Small green crystals were produced overnight and these were washed with benzene and ether and dried under reduced pressure. The yield was ~30% but can be significantly reduced by small changes (e.g. adding the $NaBH_4$ too slowly) in the above experimental conditions. Chemical analyses (Ni, C, H, P, and, by difference, B) were essentially identical for samples recrystallized from both benzene and THF.

d-*Spacings (Relative Intensities 0–10)*

11.81 (3), 9.24 (10), 8.45 (10), 6.96 (1), 6.22 (5), 4.94 (1), 4.79 (1), 4.61 (1), 4.45 (7), 4.10 (6).

$Ni(ClO_4)P_3$ and $[NiP_4](ClO_4)$

A solution of $NaBH_4$ (0.073, 1.93 mmol) in ethanol (15 ml) was added dropwise to a stirred mixture of $Ni(ClO_4)_2 \cdot 6H_2O$ (0.77 g, 2.11 mmol) and P (2.39 g, 9.11 mmol) in ethanol (20 ml). The mixture, which quickly precipitated an orange-yellow solid, was stirred for 1 h before the solid was filtered off and recrystallized from acetone.

Recrystallization of pure $Ni(ClO_4)P_3$ (~3 g) (or the crude product) from acetone/toluene in the presence of P (3 *M* excess) produced $[NiP_4](ClO_4)$ which was washed with toluene (8 ml) and ether (6 × 8 ml).

$[HNi(diphos)_2](ClO_4)$

$Ni(ClO_4)_2 \cdot 6H_2O$ (0.93 g, 2.54 mmol) and diphos (3.04 g, 7.63 mmol) were mixed in ethanol (20 ml) and immediately produced a yellow precipitate of $Ni(diphos)_2(ClO_4)_2$. To this stirred mixture, a suspension of $NaBH_4$ (0.12 g, 3.13 mmol) in ethanol (10 ml) was added dropwise and the color of the mixture turned to orange. Stirring was continued for 1 h before the solid was filtered off and washed with ethanol, water, ethanol, benzene (until the washings were colorless), and ether. The product was recrystallized from THF or acetone. Yield ~90%.

$[Ni_2(dppm)_4](ClO_4)_2$

This complex was prepared in a manner similar to that described above for $[HNi(diphos)_2](ClO_4)$ using $Ni(ClO_4)_2 \cdot 6H_2O$ (0.75 g, 2.06 mmol), dppm (1.61 g, 4.20 mmol), and $NaBH_4$ (0.11 g, 2.89 mmol). The crude product was recrystallized from acetone/ether as dark green crystals and washed with ether. Yield ~50%.

Can. J. Chem. Downloaded from www.nrcresearchpress.com by 210.87.254.42 on 09/05/12
For personal use only.

[Ni(vpp)$_2$](ClO$_4$)

This complex was prepared in a similar way to that described above for [HNi(diphos)$_2$](ClO$_4$) using Ni(ClO$_4$)$_2$·6H$_2$O (0.43 g, 1.17 mmol), vpp (1.61 g, 4.07 mmol), and $NaBH_4$ (0.05 g, 1.31 mmol). The product was recrystallized from acetone (or CH_3CN) and ether in ~50% yield.

Acknowledgments

We thank the National Research Council of Canada and the Ventron Corporation, Beverly, Massachusetts for generous financial support of this work.

1. M. Aresta, C. F. Nobile, and A. Sacco. Inorg. Chim. Acta, **12**, 167 (1975).
2. M. J. Nilges, E. K. Barefield, R. L. Belford, and P. H. Davis. J. Am. Chem. Soc. **99**, 755 (1977).
3. W. E. Geiger, Jr., C. S. Allen, T. E. Mines, and F. C. Senftleber. Inorg. Chem. **16**, 2003 (1977).
4. L. Sacconi and S. Midollini. J. Chem. Soc. Dalton Trans. 1213 (1972); L. Sacconi, A. Orlandini, and S. Midollini. Inorg. Chem. **13**, 2850 (1974); L. Sacconi, C. A. Ghilardi, C. Mealli, and F. Zanobini. Inorg. Chem. **14**, 1380 (1975).
5. D. G. Holah, A. N. Hughes, B. C. Hui, and K. Wright. Can. J. Chem. **52**, 2990 (1974).
6. D. G. Holah, A. N. Hughes, and B. C. Hui. Can. J. Chem. **55**, 4048 (1977).
7. D. G. Holah, A. N. Hughes, B. C. Hui, and C.-T. Kan. Can. J. Chem. **56**, 814 (1978).
8. J. R. Van Wazer. Phosphorus and its compounds. Vol. 1. Interscience, New York. 1958. pp. 808–809.
9. R. D. Feltham and R. G. Hayter. J. Chem. Soc. 4587 (1964).
10. A. Gleizes, M. Dartiguenave, Y. Dartiguenave, J. Galy, and H. F. Klein. J. Am. Chem. Soc. **99**, 5187 (1977).
11. K. Jonas and G. Wilkie. Angew. Chem. Int. Ed. Engl. **9**, 312 (1970).
12. J. Kiji, K. Yamamoto, S. Mitani, S. Yoshikawa, and J. Furukawa. Bull. Chem. Soc. Jpn. **46**, 1791 (1973).
13. C. U. Pittman, Jr. and L. R. Smith. J. Am. Chem. Soc. **97**, 341 (1975).
14. T. J. Marks and J. R. Kolb. Chem. Rev. **77**, 263 (1977).
15. B. J. Hathaway and A. E. Underhill. J. Chem. Soc. 3091 (1961).
16. C. A. Tolman, W. C. Seidel, and D. H. Gerlach. J. Am. Chem. Soc. **94**, 2669 (1972).
17. S. J. Lippard and D. A. Ucko. Inorg. Chem. **7**, 1051 (1968).
18. D. M. Roundhill. Adv. Organomet. Chem. **13**, 273 (1975).
19. A. Davison, D. V. Howe, and E. T. Shawl. Inorg. Chem. **6**, 458 (1967); R. L. Dutta, D. W. Meek, and D. H. Busch. Inorg. Chem. **9**, 1215 (1970).
20. M. P. Brown, R. J. Puddephatt, M. Rashidi, L. Manojlovic-Muir, K. W. Muir, T. Solomun, and K. R. Seddon. Inorg. Chim. Acta, **23**, L33 (1977); M. P. Brown, R. J. Puddephatt, M. Rashidi, and K. R. Seddon. J. Chem. Soc. Dalton Trans. 951 (1977).
21. L. M. Venanzi. J. Chem. Soc. 719 (1958).
22. D. F. Evans. J. Chem. Soc. 2003 (1959).

Can. J. Chem. Downloaded from www.nrcresearchpress.com by 210.87.254.42 on 09/05/12
For personal use only.

Total synthesis of indole and dihydroindole alkaloids. XVI.[1,2] Derivatives of vinblastine and vincristine: change of functionality in the vindoline unit

JAMES P. KUTNEY, JOHN BALSEVICH, TOSHIO HONDA, PING-HUANG LIAO, HERMAN P. M. THIELLIER, AND BRIAN R. WORTH

Department of Chemistry, University of British Columbia, 2075 Wesbrook Place, Vancouver, B.C., Canada V6T 1W5

Received May 23, 1978

JAMES P. KUTNEY, JOHN BALSEVICH, TOSHIO HONDA, PING-HUANG LIAO, HERMAN P. M. THIELLIER, and BRIAN R. WORTH. Can. J. Chem. **56**, 2560 (1978).

Studies describing the preparation of various derivatives of vinblastine and vincristine are presented. Vindoline (**3**) is transformed into a series of derivatives and the latter via Polonovski-type coupling with catharanthine (**2**) provide the bisindole alkaloid derivatives of the vinblastine series. Selective Jones' oxidation transforms the vinblastine family into the corresponding vincristine derivatives.

JAMES P. KUTNEY, JOHN BALSEVICH, TOSHIO HONDA, PING-HUANG LIAO, HERMAN P. M. THIELLIER et BRIAN R. WORTH. Can. J. Chem. **56**, 2560 (1978).

On présente des études décrivant la préparation de divers dérivés de la vinblastine et de la vincristine. On transforme la vindoline (**3**) en une série de dérivés et ces derniers par l'intermédiaire d'un couplage de type Polonovski avec la catharanthine (**2**) fournissent les dérivés de l'alcaloïde bisindole de la série de la vinblastine. Une oxydation sélective de Jones transforme les composés de la famille de la vinblastine en dérivés correspondants de la vincristine.

[Traduit par le journal]

Can. J. Chem. Downloaded from www.nrcresearchpress.com by 210.87.254.6 on 09/05/12
For personal use only.

Earlier reports from these (see ref. 5 for earlier parts of this series) and other (6–8) laboratories have discussed syntheses of various derivatives of the antitumour agent, vinblastine (**1**). The two strategies generally employed; functionalisation of catharanthine (**2**) followed by coupling with vindoline (**3**), or direct coupling of (**2**) and (**3**) with subsequent elaboration of the so formed 3′,4′-dehydrovinblastine (**4**); have provided derivatives with various functionality in the indole (cleavamine) unit. The present work describes the preparation of vinblastine–vincristine derivatives bearing different functions in the vindoline unit of the molecule. To this end both the coupling of vindoline derivatives with catharanthine via the modified Polonovski reaction (6,9) and elaboration of 'dimeric' substrates have been utilized.

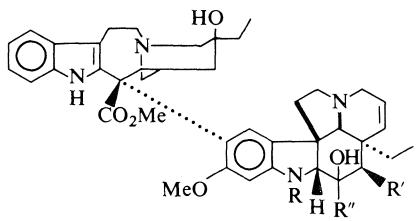

1 R = Me, R′ = OAc, R″ = CO_2Me
14 R = Me, R′ = H, R″ = CO_2Me
22 R = Me, R′ = OH, R″ = $CONH_2$
23 R = CHO, R′ = OAc, R″ = CO_2Me

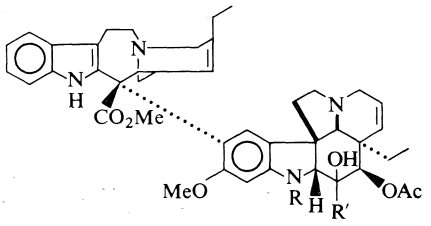

4 R = Me, R′ = CO_2Me
25 R = CHO, R′ = CO_2Me
26 R = Me, R′ = CONHMe
27 R = CHO, R′ = CONHMe

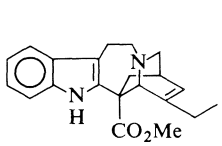

2

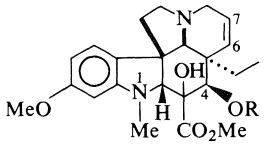

3 R = Ac
5 R = H

Vindoline, a readily available alkaloid from *Catharanthus roseus* G. Don (*Vinca rosea* L.), for which both total (10, 11) and partial (12, 13) syntheses have appeared, was subjected to the transformations depicted in Scheme 1. Reaction of desacetylvindoline (**5**) with *N*,*N*′-thiocarbonyldiimidazole gave a high yield of the thionocarbonate **6** which on treatment with Raney nickel led efficiently to the unsaturated ester **7**. Prolonged reaction of **6** afforded the ring E saturated derivative **8** which was also available from desacetyldihydrovindoline via **9** (14) using a similar reaction sequence. Both esters **7** and **8** were readily converted to the corresponding

[1]For Part XV, see ref. 1.

[2]For preliminary reports on portions of this work see refs. 2–4.

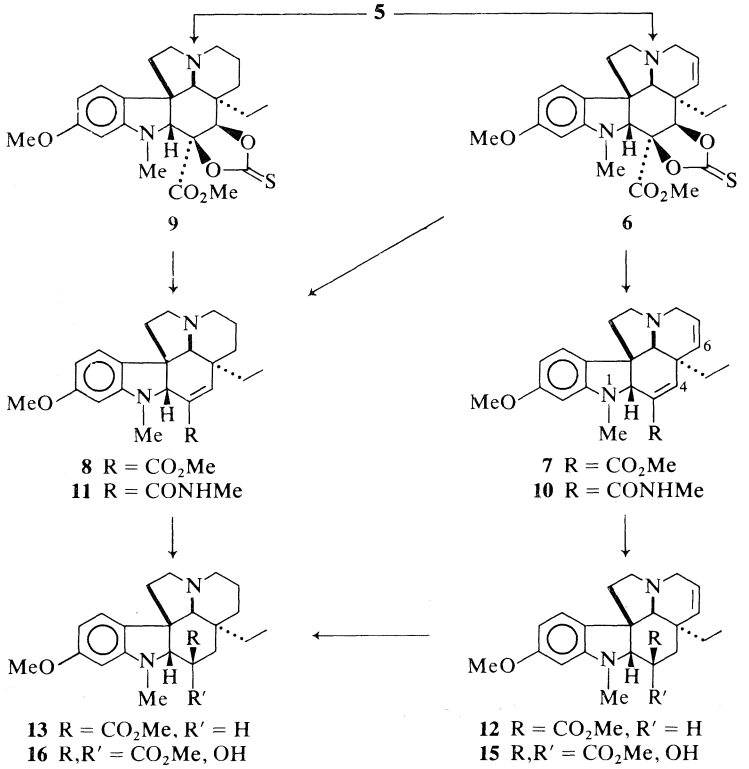

SCHEME 1

TABLE 1. Coupling of vindoline derivatives with the N_b oxide of catharanthine (**2**)

Substrate	Product	Yield (%)
7	**17**	45
8	**18**	30
10	**19**	36
11	**20**	22
15	**21**	32

N-methyl amides **10** and **11** respectively, by the direct action of methylamine. Alternatively, reaction of **7** and **8** with sodium amalgam in methanol solution provided the more favoured 3(*R*)-esters **12** and **13** (11) in high yields. The uncomplicated nature of these reductions may be attributed to severe steric crowding at C4 thus preventing coupling of the presumed radical intermediates.

In view of the recent interest in 4-desacetoxyvinblastine (**14**), isolated from *C. roseus* by the Lilly group (15), it seemed appropriate to synthesize derivatives of this type. Here, α-hydroxylation of the esters **12** and **13** with molybdenum peroxide HMPA pyridine complex (16–18) provided the respective hydroxyesters **15** and **16**. The latter was also available by reaction of **13** with hydrogen peroxide in the presence of potassium *tert*-butoxide. In addition, hydrogenation of **15** gave **16**, demonstrating identical configuration at C3. The data available did not enable unambiguous absolute configurational assignment for these hydroxyesters.

The modified Polonovski reaction has found wide application in the preparation of bisindole derivatives of the vinblastine type. Further exploitation of this method enabled the preparation of 'dimeric' compounds from the vindoline derivatives discussed above. Table 1 summarizes these results. The amide derivatives **19** and **20** and the hydroxyester **21** are of particular interest owing to their similarity to vinblastine amide **22** (19) and 4-desacetoxyvinblastine **14** reported by the Lilly group (15). Notably the efficiency of this coupling reaction is retained with substrates of this type which themselves remain highly nucleophilic at the 15-position, while a report has appeared on the failure of N_a-formyl substrates to react (6). The success of the coupling seems also dependent on the ability of the catharanthine derivative to stabilise the reaction intermediate from C5—C18 cleavage (6, 9).

The interesting biological activity of several 22-oxo-'dimeric' alkaloids and derivatives, e.g., vincristine (**23**), 22-oxoleurosine (**24**) (20), and 3′,4′-dehydrovincristine (**25**) (21), prompted the preparation of a series of synthetic derivatives of this type to complement the biological data already available from the parent amines. Indeed a procedure for the

Can. J. Chem. Downloaded from www.nrcresearchpress.com by 210.87.254.6 on 09/05/12
For personal use only.

Can. J. Chem. Downloaded from www.nrcresearchpress.com by 210.87.254.6 on 09/05/12
For personal use only.

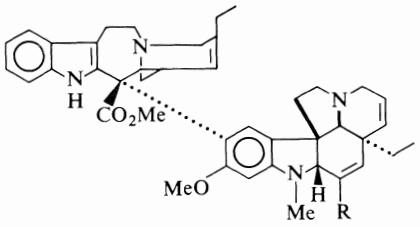

17 R = CO_2Me
19 R = CONHMe

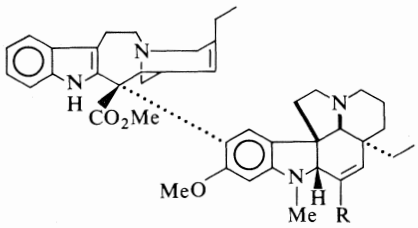

18 R = CO_2Me
20 R = CONHMe

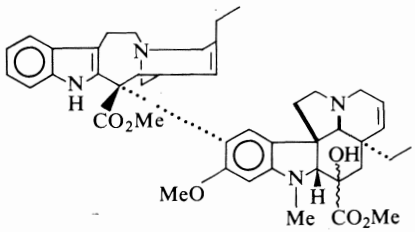

21

TABLE 2. 22-Oxo derivatives via Jones' oxidation

Substrate	Product	Yield (%)
4	**25**	80
26	**27**	53
28	**29**	68
30	**31**	48
32	**33**	63
34	**24**	75
35	**36**	30
	37	17
39	**38**	72

'chromic acid' (CrO_3) oxidation of vinblastine (**1**) to **23** had appeared (22). Although this method was found ineffectual in promoting oxidation of 3′,4′-dehydrovinblastine (**4**), modification of the procedure did enable specific oxidation of the various 'bisindole' derivatives listed in Table 2. Generally, low temperature oxidation with Jones' reagent gave reproducibly high yields of the N_a-formyl compounds. The ease of specific oxidation within these complex molecules is quite remarkable. Oxidations of leurosine (**34**) serve to illustrate this point. Here, treatment of **34** with Jones' reagent at low temperature provided 22-oxoleurosine (**24**) which is presently in clinical use in

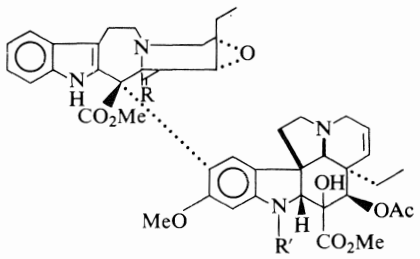

24 R = H_2, R′ = CHO
34 R = H_2, R′ = Me
35 R = O, R′ = Me
36 R = O, R′ = CHO
37 R = O, R′ = H

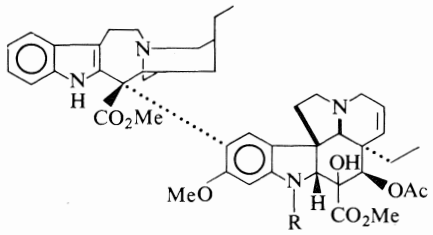

28 R = Me
29 R = CHO

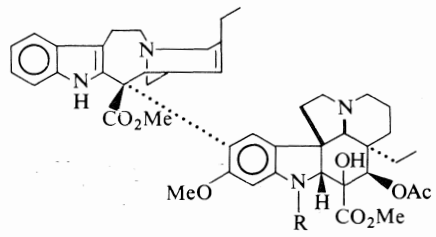

30 R = Me
31 R = CHO

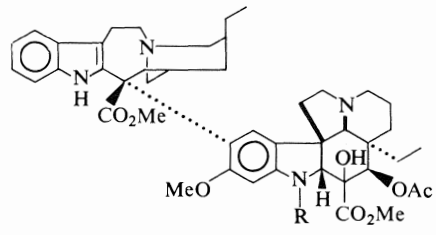

32 R = Me
33 R = CHO

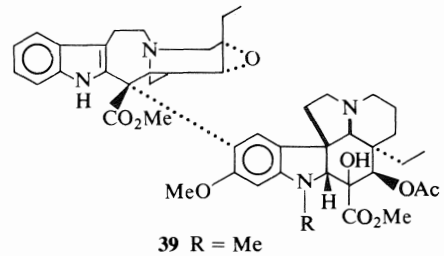

39 R = Me
38 R = CHO

Can. J. Chem. Downloaded from www.nrcresearchpress.com by 210.87.254.6 on 09/05/12
For personal use only.

Hungary (20). Further oxidation with iodine in the presence of sodium bicarbonate afforded the 19′-oxidation product **36**. Alternatively, iodine–bicarbonate oxidation of leurosine and subsequent Jones' oxidation of the product **35**, gave **36** together with the secondary amine **37**. The dihydro derivative **38** was also available from 6,7-dihydroleurosine (**39**), prepared by *tert*-butyl hydroperoxide oxidation of **30** or by hydrogenation of leurosine (**34**). In this latter reaction, products of oxiran cleavage were not observed.

The work described here, together with that reported in previous parts of this series, has allowed the preparation of numerous derivatives of vinblastine and vincristine with the potential of extending this number to provide an effective biological screening program. It is hoped that this program will provide valuable information relating to structure–activity relationships for the bisindole alkaloid oncolytic agents.

Experimental

Melting points were determined on a Kofler block and are uncorrected. Ultraviolet (uv) spectra were recorded on a Cary 15 spectrophotometer in ethanol solution. The wavelengths of absorption maxima are reported in nanometers (nm) with log ε values in parentheses. Infrared (ir) spectra were measured on a Perkin Elmer model 710 or 457 spectrophotometer in chloroform solution. The absorption maxima are reported in wavenumbers (cm^{-1}), calibrated with respect to the absorption band of polystyrene at 1601 cm^{-1}. Proton magnetic resonance (^{1}Hmr) spectra were measured in deuteriochloroform ($CDCl_3$) solution at ambient temperature on either a Varian HA-100 or XL-100 spectrometer. Chemical shift values are given in the δ (ppm) scale relative to tetramethylsilane (TMS) used as internal standard. The integrated peak areas, signal multiplicities, and proton assignments are given in parentheses. Low resolution mass spectra (ms) were determined on either an AEI-MS-902 or an Atlas CH-4B spectrometer. High resolution mass spectra were measured on an AEI-MS-902 instrument. Microanalyses were carried out by Mr. P. Borda of the Microanalytical Laboratory, University of British Columbia.

Thin-layer chromatography (tlc) utilized Merck silica gel G (according to Stahl) containing 2% fluorescent indicator. For preparative layer chromatography (plc), plates (20 × 20 or 20 × 60 cm) of 1 mm thickness were used. Visualization was effected by viewing under ultraviolet light and/or by colour reaction with ceric sulphate spray reagent. Column chromatography utilized Merck silica gel 60 (70–230 mesh) or Merck aluminium oxide 90 (neutral).

As a matter of routine, all reagents and solvents were recrystallized or distilled before use.

The Thionocarbonate ***6***

Thiocarbonyl diimidazole (400 mg) was added to a solution of desacetylvindoline (**5**) (230 mg) in butan-2-one (23 ml) and the resulting solution refluxed under a nitrogen atmosphere for 20 h. The mixture was then cooled, diluted with ethyl acetate, washed with 1 *M* sodium carbonate solution, saturated sodium chloride solution, dried (Na_2SO_4), and evaporated *in vacuo*. Recrystallisation of the residue from ethyl acetate afforded the thionocarbonate **6** (210 mg, 83%), mp 184–186°C; uv λ_{max}: 235 (4.28), 300 (3.64); ir ν_{max}: 1740, 1615, 1610, 1315; ^{1}H nmr δ: 7.02 (1H, d, J = 8 Hz, C14-H), 6.43 (1H, dd, J = 8, 2 Hz, C15-H), 6.16 (1H, d, J = 2 Hz, C17-H), 6.00 (1H, m, C7-H), 4.62 (1H, bd, J = 10 Hz, C6-H), 4.78 (1H, d, J = 2 Hz, C4-H), 3.98 (3H, s, —OCH_3), 3.90 (1H, s, C2-H), 3.82 (3H, s, —OCH_3), 2.63 (3H, s, —NCH_3), 0.30 (3H, t, J = 7 Hz, —CH_2CH_3); ms *m/e*: 456 (M^+), 440, 427, 426, 425, 395, 380, 379 (100%), 349, 295, 188, 174, 135, 121. *Anal.* calcd. for $C_{24}H_{28}SN_2O_5$: C63.13, H6.18, N6.14; found: C63.25, H6.20, N6.42.

The Unsaturated Ester ***7***

The thionocarbonate **6** (200 mg) in dry THF (10 ml) was added to a suspension of Raney nickel (5 g) in dry THF (50 ml). The mixture was refluxed for 1 h and then filtered. The filtrate was evaporated *in vacuo* and the residue chromatographed on silica gel to give **7** (140 mg, 84%) as a colourless foam; uv λ_{max}: 252 (3.91), 307 (3.74); ir ν_{max}: 1705, 1615; ^{1}H nmr δ: 7.26 (1H, s, C4-H), 7.03 (1H, d, J = 8 Hz, C14-H), 6.28 (1H, dd, J = 8, 2 Hz, C15-H), 6.01 (1H, d, J = 2 Hz, C17-H), 5.65–6.00 (2H, m, C6-H and C7-H), 4.26 (1H, s, C2-H), 3.80 (6H, s, 2 × —OCH_3), 2.74 (3H, s, —NCH_3), 1.42 (2H, q, J = 7.5 Hz, —CH_2CH_3), 0.63 (3H, t, J = 7.5 Hz, —CH_2CH_3); ms *m/e*: 380 (M^+), 350, 321, 297, 282, 244, 220, 208, 205, 188, 174, 149. *Mol. wt.* calcd. for $C_{23}H_{28}N_2O_3$: 380.2100; found (high resolution ms): 380.2092.

The Ester ***8***

Reaction of the thionocarbonate (**6**) with Raney nickel in refluxing THF for 20 h gave an almost quantitative yield of the unsaturated ester (11).

The Amide ***10***

The ester **7** (300 mg) in methylamine (10 ml) was heated at 60°C in a sealed tube for 72 h. The solvent was removed *in vacuo*. The residue was dissolved in dichloromethane, washed with water, and dried (Na_2SO_4). Evaporation of the solvent and crystallisation from ethyl acetate – petroleum ether gave the amide **10** (270 mg, 90%), mp 196–198°C; uv λ_{max}: 250 (3.95), 305 (3.73); ir ν_{max}: 3500, 1650, 1620; ^{1}H nmr δ: 7.00 (1H, d, J = 8 Hz, C14-H), 6.48 (1H, s, C4-H), 6.25 (1H, dd, J = 8, 2 Hz, C15-H), 5.98 (1H, d, J = 2 Hz, C17-H), 5.60–6.00 (2H, m, C6-H and C7-H), 4.24 (1H, s, C2-H), 3.77 (3H, s, —OCH_3), 2.87 (3H, d, J = 5 Hz, —$NHCH_3$), 2.76 (3H, s, —NCH_3), 1.40 (2H, q, J = 7.5 Hz, —CH_2CH_3), 0.60 (3H, t, J = 7.5 Hz, —CH_2CH_3); ms *m/e*: 379 (M^+), 321, 188, 174, 149. *Mol. wt.* calcd. for $C_{23}H_{29}N_3O_2$: 379.2260; found (high resolution ms): 379.2262. *Anal.* calcd.: C72.79, H7.70, N11.07; found: C72.64, H7.67, N11.00.

The Amide ***11***

Reaction of the ester **8** with methylamine as described above gave the amide **11** (88%) as a colourless foam; ir ν_{max}: 3500, 1660, 1605; ^{1}H nmr δ: 6.34 (1H, s, C4-H), 4.24 (1H, s, C2-H), 3.72 (3H, s, —OCH_3), 2.88 (3H, d, J = 4 Hz, —$NHCH_3$), 2.74 (3H, s, —NCH_3), 0.60 (3H, t, J = 7 Hz, —CH_2CH_3); ms *m/e*: 381 (M^+), 366, 351, 336, 322, 320, 246, 217, 208, 174, 144, 124 (100%). *Mol. wt.* calcd. for $C_{23}H_{31}N_3O_2$: 381.2416; found (high resolution ms): 381.2412.

The Ester ***12***

An excess of 10% sodium amalgam was added in portions to a solution of the unsaturated ester **7** (100 mg) in methanol (10 ml) at ambient temperature. Stirring was continued for a total of 6 h, the mixture was filtered, and the filtrate concentrated *in vacuo*. Chromatography on silica gel afforded the 3(*R*)-ester **12** (78 mg, 78%); mp (methanol – petroleum ether) 186–188°C; uv λ_{max}: 252 (3.71), 304 (3.55); ir ν_{max}: 1725; ^{1}H nmr δ: 6.90 (1H, d, J = 8 Hz, C14-H), 6.16 (1H, dd, J = 8, 2 Hz, C15-H), 5.95 (1H, d, J = 2 Hz, C17-H), 5.71

Can. J. Chem. Downloaded from www.nrcresearchpress.com by 210.87.254.6 on 09/05/12
For personal use only.

(1H, dd, J = 10, 2 Hz, C7-H), 5.84 (1H, bd, J = 10 Hz, C6-H), 3.87 (1H, d, J = 10 Hz, C2-H), 3.76 (3H, s, —OCH_3), 3.67 (3H, s, —OCH_3), 2.73 (3H, s, —NCH_3), 0.77 (3H, t, J = 7 Hz, —CH_2CH_3); ms *m/e*: 382 (M^+, 100%), 380, 351, 208, 189, 188, 187, 174, 161, 135, 122, 121, 107, 93. *Mol. wt.* calcd. for $C_{23}H_{30}N_2O_3$: 382.2257; found (high resolution ms): 382.2271. *Anal.* calcd. for $C_{23}H_{30}N_2O_3 \cdot \frac{1}{2}H_2O$: C71.89, H7.91, N7.29; found: C71.80, H8.20, N7.01.

The Ester ***13***

Reduction of the ester **8** with 10% sodium amalgam as described above gave the 3(*R*)-ester **13** (82%) identical with an authentic sample (11).

The Hydroxyester ***15***

Diisopropylamine (0.5 ml) and *n*-butyllithium (0.5 ml of a 20% solution in heptane) were stirred at 0°C in dry THF (5 ml) for 15 min. A solution of the ester (**12**) (60 mg) in dry THF (5 ml) was added and the solution stirred at 0°C for 30 min and then at ambient temperature for 1 h. The solution was cooled to 0°C and $MoO_5 \cdot Py \cdot HMPA$ complex (16–18), (80 mg) added. The mixture was stirred at 0°C for 1 h, diluted with water, and extracted with ethyl acetate. The extract was washed with saturated sodium chloride solution, dried (Na_2SO_4), and evaporated. Chromatography on silica gel gave the hydroxyester **15** (22 mg, 35%) as a colourless foam; uv λ_{max}: 252 (3.83), 306 (3.77); ir ν_{max}: 3520, 1720, 1615–1610; ^{1}H nmr δ: 6.88 (1H, d, J = 8 Hz, C14-H), 6.17 (1H, dd, J = 8, 2 Hz, C15-H), 5.98 (1H, d, J = 2 Hz, C17-H), 5.70 (1H, bdd, J = 11, 4 Hz, C7-H), 5.52 (1H, bd, J = 11 Hz, C6-H), 3.92 (1H, s, C2-H), 3.82 (3H, s, —OCH_3), 3.78 (3H, s, —OCH_3), 2.78 (3H, s, —NCH_3), 0.79 (3H, t, J = 7 Hz, —CH_2CH_3); ms *m/e*: 398 (M^+), 382, 338, 296, 224, 189, 136, 135, 121. *Mol. wt.* calcd. for $C_{23}H_{30}N_2O_4$: 398.2205; found (high resolution ms): 398.2183.

The Hydroxyester ***16***

(*a*) Hydroxylation of the ester **13** as described above for the preparation of **15**, gave **16** (32%); uv λ_{max}: 252 (3.73), 305 (3.64); ir ν_{max}: 3550 (br), 1725; ^{1}H nmr δ: 6.85 (1H, d, J = 8 Hz, C14-H), 6.18 (1H, dd, J = 8, 2 Hz, C15-H), 5.98 (1H, d, J = 2 Hz, C17-H), 3.87 (1H, s, C2-H), 3.84 (3H, s, —OCH_3), 3.78 (3H, s, —OCH_3), 2.78 (3H, s, —NCH_3), 0.68 (3H, t, J = 7 Hz, —CH_2CH_3); ms *m/e*: 400 (M^+), 298, 188, 174, 124. *Mol. wt.* calcd. for $C_{23}H_{32}N_2O_4$: 400.236; found (high resolution ms): 400.235.

(*b*) Oxygen gas was passed through a solution of the anion, prepared as in *a* above, for 18 h at ambient temperature. Work-up as before gave the hydroxyester **16** in 30% yield.

(*c*) The unsaturated derivative **15** was hydrogenated over 10% palladium-on-carbon catalyst in ethanol to give (80%) the ester **16** identical with that prepared above.

The 'Dimer' ***17***

Catharanthine **2** (88 mg) and *m*-CPBA (42 mg) were stirred in dry dichloromethane (1.5 ml) at −10 to −15°C for 30 min. The vindoline derivative **7** (50 mg) was added and the solution cooled to −50°C. Trifluoroacetic anhydride (0.13 ml) was added and the mixture stirred at −50°C for 4 h, poured into a cold solution of sodium borohydride in methanol, and extracted with dichloromethane. The extract was washed with water, dried (Na_2SO_4), and concentrated *in vacuo*. Chromatography on silica gel gave **17** (35 mg, 45%) as a colourless foam, uv λ_{max}: 263 (4.40), 287 (4.27), 295 (4.24), 311 (3.98); cd: 208 (−22.0), 221.5 (+12.2); ir ν_{max}: 1720, 1700; ^{1}H nmr δ: 8.07 (1H, s, —NH), 7.20 (4H, m, C4-H and indole aromatic —H), 6.54 (1H, s, C14-H), 6.02 (1H, s, C17-H), 5.6–6.0 (3H, m, C3′-H, C6-H, C7-H), 4.24 (1H, s, C2-H), 3.78 (6H, s, 2 × —OCH_3), 3.62 (3H, s, —OCH_3), 2.83 (3H, s, —NCH_3), 1.04 (3H, t, J = 7.5 Hz, —CH_2CH_3), 0.80 (3H, t, J = 7.5 Hz, —CH_2CH_3); ms *m/e*: 716 (M^+), 657, 536, 534, 464, 451, 393, 380, 353, 336, 277, 237. *Mol. wt.* calcd. for $C_{44}H_{52}N_4O_5$: 716.3937; found (high resolution ms): 716.3948.

The Dimer ***18***

Similarly the ester **8** reacted with catharanthine *N*-oxide to give **18** in 30% yield; uv λ_{max}: 268 (4.31), 284 (4.21), 292 (4.14), 313 (3.87); cd: 207 (−17.4), 222 (+14.0); ir ν_{max}: 1720; ^{1}H nmr δ: 8.04 (1H, s, —NH), 7.10–7.20 (4H, m, C4-H, aromatic —H), 6.60 (1H, s, C14-H), 6.00 (1H, s, C17-H), 5.52 (1H, d, J = 6 Hz, C3-H), 4.24 (1H, s, C2-H), 3.80 (3H, s, —OCH_3), 3.77 (3H, s, —OCH_3), 3.58 (3H, s, —OCH_3), 2.86 (3H, s, —NCH_3), 1.00 (3H, t, J = 7 Hz, —CH_2CH_3), 0.82 (3H, t, J = 7 Hz, —CH_2CH_3); ms *m/e*: 718 (M^+), 704, 659, 593, 534, 464, 451, 393. *Mol. wt.* calcd. for $C_{44}H_{54}N_4O_5$: 718.4094; found (high resolution ms): 718.4109.

The 'Dimer' ***19***

Similarly, the amide **10** was reacted with catharanthine *N*-oxide to give **19** (36%); uv λ_{max}: 267 (4.38), 287 (4.26), 296 (4.17), 312 (3.96); cd: 207.5 (−28.2), 222 (+14.1); ir ν_{max}: 1720, 1660; ^{1}H nmr δ: 8.07 (1H, s, —NH), 6.62 (1H, s, C14-H), 6.36 (1H, s, C4-H), 6.03 (1H, s, C17-H), 5.5–6.0 (3H, m, C3′-H, C6-H, C7-H), 4.24 (1H, s, C2-H), 2.90 (3H, d, J = 6 Hz, —NHCH_3), 2.88 (3H, s, —NCH_3), 1.02 (3H, t, J = 7.5 Hz, —CH_2CH_3), 0.83 (3H, t, J = 7 Hz, —CH_2CH_3); ms *m/e*: 715 (M^+), 686, 656, 624, 534, 533, 393, 336. *Mol. wt.* calcd. for $C_{44}H_{53}N_5O_4$: 715.4096; found (high resolution ms): 715.4053.

The Dimer ***20***

Similarly the amide **11** gave **20** in 22% yield; uv λ_{max}: 261 (4.25), 287 (4.11), 296 (4.07), 312 (3.93); ir ν_{max}: 1720, 1660; ^{1}H nmr δ: 8.02 (1H, s, —NH), 6.60 (1H, s, C14-H), 6.20 (1H, s, C4-H), 5.98 (1H, s, C17-H), 5.50 (1H, m, C3-H), 4.27 (1H, s, C2-H), 3.76 (3H, s, —OCH_3), 3.57 (3H, s, —OCH_3), 2.90 (3H, d, J = 6 Hz, —NHCH_3), 2.87 (3H, s, —NCH_3), 0.99 (3H, t, J = 7 Hz, —CH_2CH_3), 0.86 (3H, t, J = 7 Hz, —CH_2CH_3); ms *m/e*: 717 (M^+), 688, 685, 660, 659, 658, 626, 594, 536, 535, 455, 394, 337, 278. *Mol. wt.* calcd. for $C_{44}H_{55}N_5O_4$: 717.4253; found (high resolution ms): 717.4209.

The Dimer ***21***

Similarly the hydroxyester **15** gave a 32% yield of **21**; uv λ_{max}: 272 (4.27), 286 (4.18), 295 (4.07), 317 (3.80); cd: 208 (−24.3), 222 (+27.7); ir ν_{max}: 3470, 1725; ^{1}H nmr δ: 8.14 (1H, s, —NH), 6.58 (1H, s, C14-H), 6.03 (1H, s, C17-H), 5.54 (3H, bs, C3-H, C6-H, C7-H), 3.84 (3H, s, —OCH_3), 3.80 (3H, s, —OCH_3), 3.58 (3H, s, —OCH_3), 2.81 (3H, s, —NCH_3), 0.88–1.08 (6H, m, 2 × —CH_2CH_3); ms *m/e*: 734 (M^+), 676, 675, 674, 616, 615, 495, 494. *Mol. wt.* calcd. for $C_{44}H_{54}N_4O_6$: 734.4042; found (high resolution ms): 734.4009.

The Dimer ***24***

Jones' reagent (0.5 ml) was added, at −78°C under an atmosphere of dry nitrogen, to a solution of leurosine (**34**) (50 mg) in acetic anhydride (1 ml) and acetone (6 ml). The mixture was stirred at this temperature for 1 h, diluted with concentrated ammonium hydroxide (10 ml), and allowed to warm to ca. 0°C. The mixture was partitioned between 5% sodium bisulphite solution and dichloromethane, the organic layer dried (Na_2SO_4), and concentrated *in vacuo*. Chromatography on silica gel gave 22-oxoleurosine (**24**) (38 mg, 75%), mp (methanol) 212–216°C; uv λ_{max}: 219 (4.68), 253 (4.20), 262 (4.15), 289 (4.18), 296 (4.22); ir ν_{max}: 3470, 1738, 1688; ^{1}H nmr δ: 8.80 and 8.20 (1H, 2 × bs, —NCHO), 8.01

Can. J. Chem. Downloaded from www.nrcresearchpress.com by 210.87.254.6 on 09/05/12
For personal use only.

(1H, bs —N*H*), 6.88 (2H, bs, C14-H, C17-H), 5.94 (1H, dd, J = 10, 4 Hz, C7-H), 5.44 (1H, d, J = 10 Hz, C6-H), 5.26 (1H, s, C4-H), 4.66 (1H, m, C2-H), 3.92 (3H, s, —OCH_3), 3.75 (3H, bs, —OCH_3), 3.71 (3H, s, —OCH_3), 2.09 (3H, s, —$OCOCH_3$), 1.62 (2H, q, J = 7.5 Hz, —CH_2CH_3), 0.97 (3H, t, J = 7.5 Hz, —CH_2CH_3), 0.84 (3H, t, J = 7 Hz, —CH_2CH_3); ms *m/e*: 822 (M^+), 820, 683, 588, 121 (100%), 106. *Mol. wt.* calcd. for $C_{46}H_{54}N_4O_{10}$: 822.3839; found (high resolution ms): 822.3806.

The Dimer ***25***

Similarly, 3′,4′-dehydrovinblastine (**4**) gave **25** in 80% yield; uv λ_{max}: 218 (4.69), 255 (4.20), 296 (4.20); ir ν_{max}: 3460, 1740, 1680; ^{1}H nmr δ: 8.80 (1H, bs, —NCHO), 8.10 (1H, bs, —NH), 6.90 (1H, s, C14-H), 5.93 (1H, m, C7-H), 5.25 (1H, s, C4-H), 5.36–5.58 (2H, m, C3′-H, C6-H), 3.91 (3H, s, —OCH_3), 3.76 (3H, s, —OCH_3), 3.68 (3H, s, —OCH_3), 2.06 (3H, s, —$OCOCH_3$), 1.00 (3H, t, J = 7 Hz, —CH_2CH_3), 0.82 (3H, t, J = 7 Hz, —CH_2CH_3); ms *m/e*: 806 (M^+), 355, 354, 169, 168, 150, 149, 136, 122, 121, 106, 77, 44, 43. *Mol. wt.* calcd. for $C_{46}H_{54}N_4O_9$: 806.3890; found (high resolution ms): 806.3931.

The Dimer ***27***

Similarly the amide **26** gave **27** (53%); ir ν_{max}: 3440, 1730, 1675; ^{1}H nmr δ: 8.80 and 7.92 (1H, 2 × bs, —NCHO), 8.19 (1H, s, —NH), 8.11 (1H, s, —NH), 6.89 (1H, s, C14-H), 5.96 (1H, m, C7-H), 5.7–5.2 (3H, m, C6-H, C4-H, and C3′-H), 4.60 and 4.22 (1H, 2 × s, C2-H), 3.92 (3H, s, —OCH_3), 3.71 (3H, s, —OCH_3), 2.04 (3H, s, —$OCOCH_3$), 1.04 (3H, t, J = 7 Hz, —CH_2CH_3), 0.76 (3H, t, J = 7 Hz, —CH_2CH_3); ms *m/e*: 805 (M^+), 749, 654, 595, 524, 466, 395, 393, 265, 149, 136, 135, 122, 121, 120, 108, 107, 106, 93, 92, 91, 79, 77, 69, 67, 65, 60, 57, 55, 51, 45, 44 (100%), 43. *Mol. wt.* calcd. for $C_{46}H_{55}N_5O_8$: 805.4049; found (high resolution ms): 805.4023.

The 'Dimer' ***29***

Similarly 4′-deoxyleurosidine (**28**) gave the formamide **29** (68%); uv λ_{max}: 218 (4.59), 248 (4.05), 294 (4.07); ir ν_{max}: 3420, 1730, 1680; ^{1}H nmr δ: 8.81 (1H, bs, —OH), 8.22 and 7.85 (1H, bs, —NCHO), 8.02 (1H, bs, —NH), 6.67 (1H, s, C14-H), 5.95 (1H, m, C7-H), 5.42 (1H, d, J = 10 Hz, C6-H), 5.24 (1H, s, C4-H), 4.77 and 4.52 (1H, bs, C2-H), 3.93 (3H, s, —OCH_3), 3.70 (3H, s, —OCH_3), 2.10 (3H, s, —$OCOCH_3$), 0.92 (3H, t, J = 7 Hz, —CH_2CH_3), 0.84 (3H, t, J = 7 Hz, —CH_2CH_3); ms *m/e*: 808 (M^+), 806, 782, 781, 780, 751, 750, 749, 650, 592, 591, 526, 524, 466, 464, 354, 353, 282, 281, 223, 209, 169, 168, 167, 149, 138, 125. *Mol. wt.* calcd. for $C_{46}H_{56}N_4O_9$: 808.4046; found (high resolution ms): 808.4064.

The 'Dimer' ***31***

Similarly, 3′,4′-dehydro-6,7-dihydrovinblastine (**30**) gave **31** (48%), mp 243–246°C; uv λ_{max}: 218 (4.70), 250 (4.21), 292 (4.12); ir ν_{max}: 3460, 1730, 1680; ^{1}H nmr δ: 8.15 (1H, bs, —NH), 6.69 (1H, s, C14-H), 6.15 (1H, m, C3-H), 5.38 (1H, s, C4-H), 3.94 (3H, s, —OCH_3), 3.81 (3H, s, —OCH_3), 3.70 3H, s, —OCH_3), 2.08 (3H, s, —$OCOCH_3$), 1.06 (3H, t, J = 7 Hz, —CH_2CH_3), 0.96 (3H, t, J = 7 Hz, —CH_2CH_3); ms *m/e*: 808 (M^+), 780, 750, 749, 732, 690, 658, 657, 511, 510, 509, 508, 480, 469, 468, 451, 395, 369, 356, 355, 284, 174, 149, 135, 124, 121, 120. *Mol. wt.* calcd. for $C_{46}H_{56}N_4O_9$: 808.4046; found (high resolution ms): 808.4039.

The 'Dimer' ***33***

Similarly 4′-deoxy-6,7-dihydroleurosidine (**32**) gave **33** in 63% yield; mp 198–201°C; uv λ_{max}: 218 (4.51), 248 (3.96), 292 (4.00); ir ν_{max}: 3480, 1730, 1680; ^{1}H nmr δ: 8.01 (1H, bs, —NH), 6.82 (1H, s, C14-H), 5.38 (1H, s, C4-H), 4.61 (1H, s, C2-H), 3.90 (3H, s, —OCH_3), 3.79 (3H, s, —OCH_3), 3.62 (3H, s, —OCH_3), 2.02 (3H, s, —$OCOCH_3$), 0.92 (6H, t, J = 7 Hz, 2 × —CH_2CH_3); ms *m/e*: 810 (M^+), 809, 808, 747, 732, 649, 524, 395, 394, 380, 353, 336, 256, 254, 252, 223, 185, 149, 135, 124, 122. *Mol. wt.* calcd. for $C_{46}H_{58}N_4O_9$: 810.4383; found (high resolution ms): 810.4371.

The 'Dimers' ***36*** *and* ***37***

(*a*) Similarly, 19′-oxoleurosine **35** gave:

(*i*) The 22-oxo derivative **36** (30%); uv λ_{max}: 217 (4.78), 258 (4.24), 280 (4.17), 288 (4.23), 296 (4.27); ir ν_{max}: 3478, 1740, 1678, 1645, 1600; ^{1}H nmr δ: 8.82 (1H, bs, —NCHO), 8.06 (1H, bs, —NH), 7.16 (1H, s, C17-H), 6.93 (1H, s, C14-H), 5.97 (1H, dd, J = 10, 4 Hz, C7-H), 5.47 (1H, d, J = 10 Hz, C6-H), 5.28 (1H, s, C4-H), 4.74 (2H, m, C2′-H, C2-H), 3.95 (3H, s, —OCH_3), 3.78 (3H, s, —OCH_3), 3.68 (3H, s, —OCH_3), 2.10 (3H, s, —$OCOCH_3$), 1.02 (3H, t, J = 7 Hz, —CH_2CH_3), 0.87 (3H, t, J = 7 Hz, —CH_2CH_3); ms *m/e*: 836 (M^+), 834, 820, 777, 761, 677, 661, 636, 121. *Mol. wt.* calcd. for $C_{46}H_{52}N_4O_{11}$: 836.3620; found (high resolution ms): 836.3686.

(*ii*) The secondary amine **37** (17%); uv λ_{max}: 212 (4.70), 224 sh (4.58), 252 (4.10), 279 (4.09), 286 (4.11) 294 (4.07), 314 sh (3.75); ir ν_{max}: 3476, 1735, 1645, 1620; ^{1}H nmr δ: 8.02 (1H, bs, —NH), 6.66 (1H, s, C14-H), 6.30 (1H, s, C17-H), 5.89 (1H, dd, J = 10, 3.5 Hz, C7-H), 5.57 (1H, s, C4-H), 5.34 (1H, d, J = 10 Hz, C6-H), 4.78 (2H, m, C2′-H, —NH), 4.19 (1H, bs, C2-H), 3.81 (6H, s, 2 × —OCH_3), 3.62 (3H, s, —OCH_3), 2.14 (3H, s, —$OCOCH_3$), 1.02 (3H, t, J = 7 Hz, —CH_2CH_3), 0.84 (3H, t, J = 7 Hz, —CH_2CH_3); ms *m/e*: 808 (M^+), 806, 749, 648, 296, 207, 174. *Mol. wt.* calcd. for $C_{45}H_{52}N_4O_{10}$: 808.3593; found (high resolution ms): 808.3618.

(*b*) Iodine (25 mg) was added to a mixture of 22-oxoleurosine (**24**) (34 mg) in THF (5 ml) and sodium bicarbonate (35 mg) in water (2 ml). The mixture was stirred vigorously at ambient temperature for 15 min, poured into saturated sodium bicarbonate solution, and extracted with dichloromethane. The extract was washed with 10% sodium bisulphite solution, dried (Na_2SO_4), and evaporated. Chromatography on silica gel gave **36** (24 mg, 67%).

*3′,4′-Dehydro-6,7-dihydrovinblastine (****30****)*

As described above for the preparation of **17**, dihydrovindoline gave **30** (33%); uv λ_{max}: 213 (4.70), 255 (4.15), 287 (4.10), 295 (4.08), 307 (3.80); cd: 210 (−34.3), 226 (+27.1), 257 (+21.7), 304 (+9.75); ir ν_{max}: 3465, 1735, 1730, 1710, 1610; ^{1}H nmr δ: 7.96 (1H, bs, —NH), 6.52 (1H, s, C14-H), 6.02 (1H, s, C17-H), 5.55 (1H, s, C4-H), 5.41 (1H, bd, J = 8 Hz, C3-H), 3.76 (3H, s, —OCH_3), 3.75 (3H, s, —OCH_3), 3.60 (1H, s, C2-H), 3.52 (3H, s, —OCH_3), 2.58 (3H, s, —NCH_3), 2.02 (3H, s, —$OCOCH_3$), 0.92 (3H, t, J = 7.5 Hz, —CH_2CH_3), 0.73 (3H, t, J = 7 Hz, —CH_2CH_3); ms *m/e*: 794 (M^+), 736, 735, 734, 370, 284, 136, 135, 124, 121 (100%), 120. *Mol. wt.* calcd. for $C_{46}H_{58}N_4O_8$: 794.4254; found (high resolution ms): 794.4275.

*6,7-Dihydroleurosine (****39****)′*

tert-Butyl hydroperoxide (0.3 ml) was added to a solution of **30** (60 mg) in dry THF (3 ml) containing 1% aqueous trifluoroacetic acid (0.3 ml). The solution was stirred at ambient temperature for 9 h, diluted with methanol (1 ml), and partitioned between saturated sodium bicarbonate solution and dichloromethane. The organic layer was dried (Na_2SO_4) and concentrated *in vacuo*. Chromatography on silica gel gave **39** (25 mg, 41%) as a clear glass; uv λ_{max}: 213 (4.68), 260 (4.12), 284 (4.03), 294 (4.00), 310 (3.75); ir ν_{max}: 3478, 1738, 1612; ^{1}H nmr δ: 8.03 (1H, bs, —NH), 6.57

(1H, s, C14-H), 6.13 (1H, s, C17-H), 5.64 (1H, s, C4-H), 3.84 (3H, s, $-OCH_3$), 3.82 (3H, s, $-OCH_3$), 3.73 (1H, s, C2-H), 3.62 (3H, s, $-OCH_3$), 2.68 (3H, s, $-NCH_3$), 2.12 (3H, s, $-OCOCH_3$), 0.98 (3H, t, $J = 7.5$ Hz, $-CH_2CH_3$), 0.82 (3H, t, $J = 7$ Hz, $-CH_2CH_3$); ms *m/e*: 810 (M^+), 808, 671, 453, 106 (100%). *Mol. wt.* calcd. for $C_{46}H_{58}N_4O_9$: 810.4203; found (high resolution ms): 810.4203.

The 'Dimer' 38

Oxidation of **39**, as described above for the preparation of **24**, gave **38** (72%), mp (methanol) 202–205°C; uv λ_{max}: 218 (4.68), 252 (4.20), 287 (4.18), 296 (4.22); ir ν_{max}: 3478, 1738, 1687; ^{1}H nmr δ: 8.00 (1H, bs, —NH), 6.82 (1H, s, C17-H), 5.40 (1H, s, C4-H), 4.67 (1H, bs, C2-H), 3.92 (3H, s, $-OCH_3$), 3.81 (3H, s, $-OCH_3$), 3.66 (3H, s, $-OCH_3$), 2.08 (3H, s, $-OCOCH_3$), 0.99 (6H, t, $J = 7$ Hz, $2 \times -CH_2CH_3$); ms *m/e*: 824 (M^+), 686, 658, 138, 124 (100%), 106. *Mol. wt.* calcd. for $C_{46}H_{56}N_4O_{10}$: 824.3995; found (high resolution ms): 824.3955.

Acknowledgements

Financial aid from the National Research Council of Canada and from Contract NO1-CM-23223, National Cancer Institute, National Institutes of Health, Bethesda, Maryland is gratefully acknowledged. We are grateful to the Lilly Research Laboratories for supplies of vindoline and catharanthine.

1. J. P. Kutney, U. Bunzli-Trepp, T. Honda, J. Katsube, and B. R. Worth. Helv. Chim. Acta. In press.
2. J. P. Kutney, K. K. Chan, W. B. Evans, Y. Fujise, T. Honda, F. K. Klein, and J. P. de Souza. Heterocycles, **6**, 435 (1977).
3. J. P. Kutney, W. B. Evans, and T. Honda. Heterocycles, **6**, 443 (1977).
4. J. P. Kutney, J. Balsevich, T. Honda, P. H. Liao, H. P. M. Thiellier, and B. R. Worth. Heterocycles, **9**, 201 (1978).
5. J. P. Kutney, T. Honda, A. V. Joshua, N. G. Lewis, and B. R. Worth. Helv. Chim. Acta, **61**, 690 (1978).
6. N. Langlois, F. Gueritte, Y. Langlois, and P. Potier. J. Am. Chem. Soc. **98**, 7017 (1976).
7. Y. Langlois, N. Langlois, P. Mangeney, and P. Potier. Tetrahedron Lett. 3945 (1976).
8. Y. Honma and Y. Ban. Tetrahedron Lett. 155 (1978).
9. J. P. Kutney, T. Hibino, E. Jahngen, T. Okutani, A. H. Ratcliffe, A. M. Treasurywala, and S. Wunderly. Helv. Chim. Acta, **59**, 2858 (1976).
10. M. Ando, G. Büchi, and T. Ohnuma. J. Am. Chem. Soc. **97**, 6880 (1975).
11. J. P. Kutney, U. Bunzli-Trepp, K. K. Chan, J. P. de Souza, Y. Fujise, T. Honda, J. Katsube, F. K. Klein, A. Leutwiler, S. Morehead, M. Rohr, and B. R. Worth. J. Am. Chem. Soc. In press.
12. Y. Ban, Y. Sekine, and T. Oishi. Tetrahedron Lett. 151 (1978).
13. S. Takano, K. Shishido, M. Sato, and K. Ogasawara. Heterocycles, **6**, 1699 (1977).
14. M. Gorman, N. Neuss, and K. Biemann. J. Am. Chem. Soc. **84**, 1058 (1962).
15. N. Neuss, A. J. Barnes, and L. L. Huckstep. Experientia, **31**, 18 (1975).
16. E. Vedejs. J. Am. Chem. Soc. **96**, 5944 (1974).
17. H. Mimoun, I. S. de Roch, and L. Sajus. Bull. Soc. Chim. Fr. 1481 (1969).
18. E. Vedejs, D. A. Engler, and J. E. Telschow. J. Org. Chem. **43**, 188 (1978).
19. M. J. Sweeney, G. J. Cullinan, G. A. Poore, and K. Gerzon. Proc. Tenth Ann. Meet. Am. Soc. Clin. Oncology, March 15, 1975.
20. S. Eckhardt, I. Hindy, and E. Farkas. Ninth Int. Congr. Chemother. London, July, 1975. Abstr.
21. J. C. Miller, G. E. Gutowski, G. A. Poore, and G. B. Boder. J. Med. Chem. **20**, 409 (1977).
22. K. Jovanics, K. Szasz, G. Fekete, E. Bittner, E. Dezserl, and J. Eles. U.S. Patent No. 3,899,493 (August, 1975).

Can. J. Chem. Downloaded from www.nrcresearchpress.com by 210.87.254.6 on 09/05/12
For personal use only.

Infrared studies of carboxylic acids and pyridine in chloroform and methanol[1]

B. A. DAWA AND JOAN A. GOWLAND[2]

Department of Chemistry, Ahmadu Bello University, Zaria, Kaduna State, Nigeria

Received February 9, 1978

B. A. DAWA and JOAN A. GOWLAND. Can. J. Chem. **56**, 2567 (1978).

The reactions of acetic, chloroacetic, and trichloroacetic acids with varying relative concentrations of pyridine in chloroform have been reinvestigated using infrared spectroscopy. The same systems have also been studied in methanol. Some different assignments of peaks have been made, and the anomalous infrared results previously observed for trichloroacetic acid in chloroform are explained in terms of charge transfer complex formation.

B. A. DAWA et JOAN A. GOWLAND. Can. J. Chem. **56**, 2567 (1978).

On a réétudié, faisant appel à la spectroscopie infrarouge, les réactions des acides acétique, chloroacétique et trichloroacétique avec diverses concentrations relatives de pyridine dans le chloroforme. On a aussi étudié les mêmes systèmes dans le méthanol. On a fait quelques attributions de bandes différentes et les résultats infrarouges anormaux observés antérieurement pour l'acide trichloroacétique dans le chloroforme peuvent être expliqués en terme de la formation d'un complexe de transfert de charge.

[Traduit par le journal]

Can. J. Chem. Downloaded from www.nrcresearchpress.com by 210.87.254.40 on 09/05/12
For personal use only.

Introduction

Infrared spectroscopy is a very useful tool for studying acid–base equilibria in nonaqueous solvents both to determine the equilibrium constants and to determine the products actually obtained. Since Barrow's paper, in 1954 (1), many studies of carboxylic acid – amine equilibria have been reported in solvents such as carbon tetrachloride, chloroform (1, 2), benzene (3), acetonitrile (4), and ether (5). In all cases there was evidence of 1:1, 2:1, and sometimes 3:1 complex formation involving either hydrogen bonding or proton transfer. Solvent participation varies and this gives rise to significant differences in the spectra obtained for a given acid and base in various solvents.

Where proton transfer is incomplete, the appearance of peaks for both the ionized and H-bonded forms is said to suggest a tautomeric equilibrium. Although infrared studies have thrown much light on the nature of such equilibria, Hilbart and Satchell (5) have commented that the structural details of variously identified adducts in nonaqueous solvent remains very much an open question.

As part of a study of the use of other forms of spectroscopy such as uv and nmr in looking at such equilibria, Barrow's infrared work for acetic, chloroacetic, and trichloroacetic acids and pyridine in chloroform was reinvestigated and then the same systems were studied with methanol as solvent. In methanol, the solvent absorption only allowed study of the region between 1800 and 1500 cm^{-1}.

A reinterpretation of some of the infrared results is given in view of band assignments made since 1954. Also an explanation is offered in terms of charge transfer complex formation for the anomalous behaviour observed for trichloroacetic acid – pyridine in chloroform where the carbonyl "wavelength shift is much less than would be expected for a product with a free symmetric carboxylate group" (2).

Experimental

AnalaR chloroform, methanol, acetic acid, chloroacetic acid, trichloroacetic acid, and pyridine were purified using standard procedures.

Infrared spectra were run on a Pye-Unicam S.P.1200 infrared spectrophotometer. Solution spectra were taken using the same pair of approximately 0.1 mm sodium chloride cells throughout the study. All spectra were calibrated using the polystyrene peak at 1601 cm^{-1}.

Ultraviolet spectra referred to below were run on a Pye-Unicam S.P.8000B instrument.

Stock solutions which were 0.2 and 0.4 *N* in acid or base were prepared for each acid and pyridine in both chloroform and methanol. The pyridine in chloroform solution tended to decompose after approximately a week and therefore its purity was checked before use by running the ultraviolet spectrum of a 2×10^{-4} *N* solution. Just before use, the following solutions were prepared: 0.2 *N* pyridine with 0.05 *N* acid, 0.1 *N* acid, and 0.2 *N* acid; 0.1 *N* acid with 0.02 *N* pyridine; 0.05 *N* pyridine and 0.1 *N* pyridine. Infrared spectra of these solutions as well as the 0.1 *N* acid and 0.2 *N* pyridine solution were taken.

Results and Discussion

Although changes were observed in other regions, discussion will be confined to the infrared region

[1]This paper was presented, in part, at the 1973 Conference of the Science Association of Nigeria.

[2]Present address: Department of Chemistry, University of Toronto, Toronto, Ont., Canada M5S 1A1.

Can. J. Chem. Downloaded from www.nrcresearchpress.com by 210.87.254.40 on 09/05/12
For personal use only.

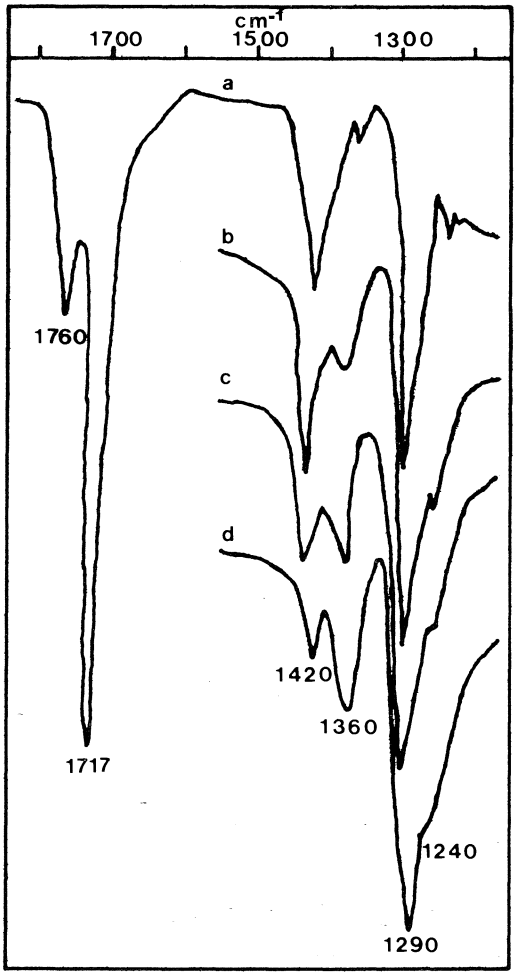

FIG. 1. Acetic acid peaks in infrared spectra of acetic acid – pyridine solutions in chloroform with pyridine peaks omitted; (*a*) 0.1 *N* HOAc in $CHCl_3$; (*b*) 0.1 *N* HOAc + 0.05 *N* pyridine in $CHCl_3$; (*c*) 0.1 *N* HOAc + 0.1 *N* pyridine in $CHCl_3$; (*d*) 0.1 *N* HOAc + 0.2 *N* pyridine in $CHCl_3$.

between 1200 and 1800 cm^{-1}. The wavenumber for all the acid and base peaks for the three acids and pyridine are listed in Table 1.[3] The significant changes will be discussed here and illustrated in Figs. 1–3 as indicated below. Assignment of peaks was facilitated by noting changes when acid or base concentration was varied and base or acid concentration remained constant.

For each acid in chloroform, peaks due to monomer C=O stretch (weak) and dimer stretch were observed as well as the usual combination bands. For acetic acid, the peaks at approximately 1420 and 1290 cm^{-1} are C—O stretch and O—H in-plane deformation combination bands for the dimer, and the much weaker peaks at 1360 and 1240 cm^{-1} are the corresponding bands for the monomer (cf. refs. 6 and 7). The assignment of these bands has been the subject of many studies with the currently accepted assignment being due to the work of Hadzi as discussed in ref. 7. Chloroacetic and trichloroacetic acids show similar combination bands. It is noteworthy and not previously recorded that as the amount of pyridine is increased in acetic acid – pyridine solutions (where no proton transfer occurs) the dimer combination bands decrease in intensity (especially the 1420 band) and the monomer bands increase as shown in Fig. 1. Although not shown, but as Barrow also noted (2), the carbonyl band at about 1717 cm^{-1} also decreases in intensity. These changes are due to the pyridine – acetic acid H-bonded complex formation in which the acetic

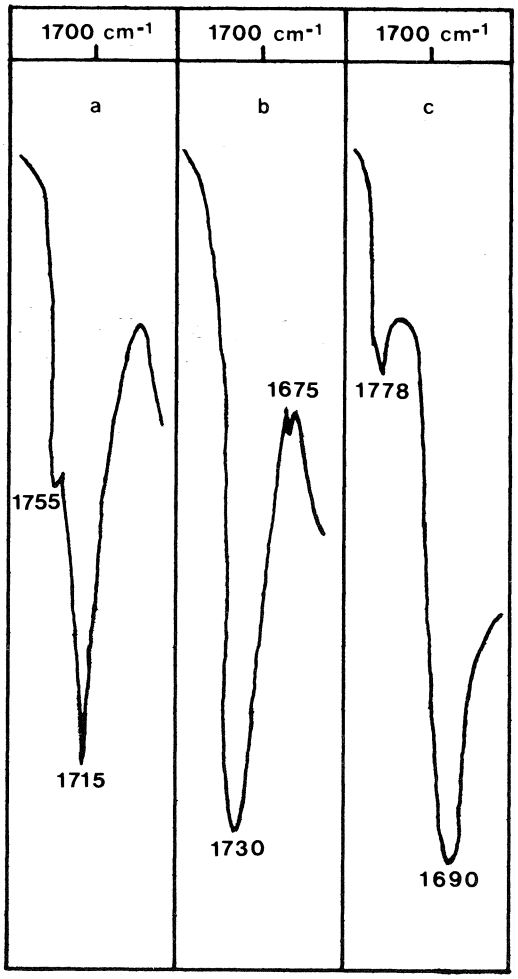

FIG. 2. Acid carbonyl peaks in infrared spectra of 0.2 *N* acid and 0.2 *N* pyridine in MeOH; (*a*) acetic acid; (*b*) chloroacetic acid; (*c*) trichloroacetic acid.

[3]Available, at a nominal charge, from the Depository of Unpublished Data, CISTI, National Research Council of Canada, Ottawa, Ont., Canada K1A 0S2.

Can. J. Chem. Downloaded from www.nrcresearchpress.com by 210.87.254.40 on 09/05/12
For personal use only.

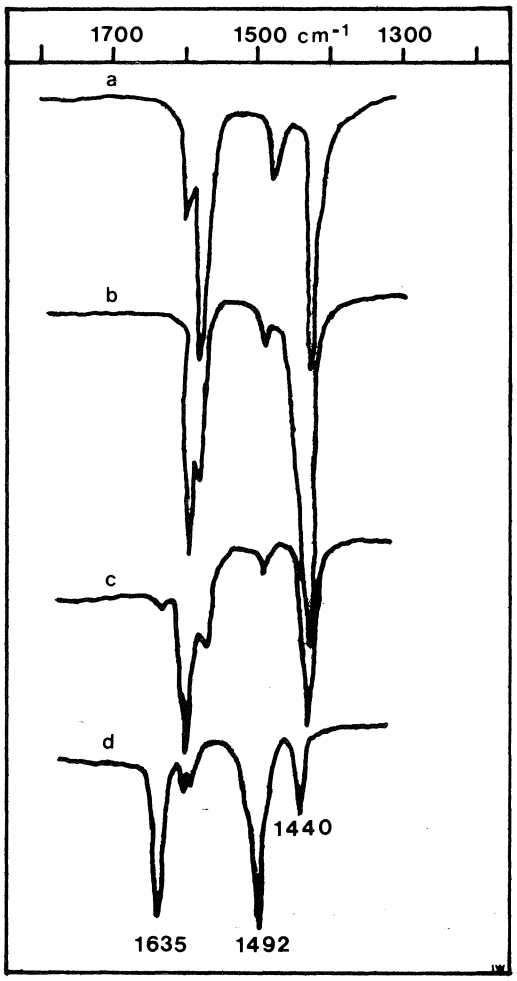

FIG. 3. Infrared spectra of 0.2 *N* acid and 0.2 *N* pyridine in $CHCl_3$ showing only the pyridine peaks; (*a*) with no acid (pyridine only); (*b*) with acetic acid; (*c*) with chloroacetic acid; (*d*) with trichloroacetic acid.

acid appears to have increasingly monomeric properties. Small shoulders at approximately 1690 cm^{-1} in the chloroacetic acid spectra can be assigned to CO_2^- stretch. For some solutions with trichloroacetic acid, shoulders or peaks around 1680 cm^{-1} are due to CO_2^- asymmetric stretch, with the corresponding symmetric stretch at 1360 cm^{-1}. Thus, in agreement with Barrow's work, for acetic acid, H-bonded complex formation with no proton transfer was observed; for chloroacetic acid only a very small amount of proton transfer was observed; but for trichloroacetic acid considerable proton transfer was seen. A similar trend was observed in methanol as seen in Table 2[3] and Fig. 2, which shows almost complete proton transfer for trichloroacetic acid as indicated by the strong CO_2^- band at 1690 cm^{-1}.

The pyridine peaks of interest in this region, at 1592, 1580, 1475, and 1432 cm^{-1} in chloroform

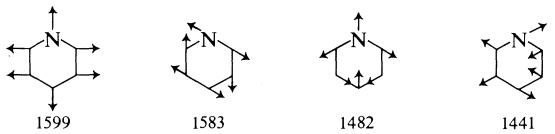

(Fig. 3*a*) have been assigned the following vibrational modes (8), (wavenumbers are for neat pyridine).

In this study shifts of up to 10 cm^{-1} have been observed for these peaks in chloroform solutions with added acid. Methanol absorption in this region does not allow a comparable study. Even more significant is the change in relative intensity of these four peaks in the presence of different acids. This is illustrated in Fig. 3 for solutions 0.2 *N* in acid and 0.2 *N* in pyridine. The additional peak at approximately 1635 cm^{-1} for trichloroacetic acid solution is attributed to the formation of pyridinium ion (2, 8).

A further analysis of these pyridine data in view of Katritzky's work (8) seems in order. Barrow suggested (2) that the peaks at 1480 and 1630 cm^{-1} are characteristic of pyridinium and therefore absent for pyridine, and that the 1430 cm^{-1} peak is present in pyridine spectra but absent in pyridinium spectra. He also says that the shift of the 1580 cm^{-1} peak to 1603 cm^{-1} indicates hydrogen bonding. The data in Table 1 and the spectra in Fig. 3 show some reinterpretation is possible.

First, with respect to the 1480 cm^{-1} peak, this peak shifts from 1475 up to 1492 cm^{-1} with added acid but is definitely present for both pyridine and pyridinium (see change from *a* to *d* in Fig. 3). However, it does decrease in intensity for H-bonded complexes and increases significantly when proton transfer has occurred. This band has been attributed to vibration mode III (above) and the observed behaviour fits in with the corresponding changes in dipole moment with H-bonding or proton transfer.

Consideration of mode IV would lead to the prediction of opposite behaviour for the 1432 cm^{-1} band. This is what is observed, i.e., a marked reduction in intensity upon proton transfer, but some increase with H-bonding.

For pyridine itself (Fig. 3*a*), a doublet of unequal intensity at 1592 (weaker) and 1580 cm^{-1} was observed rather than the single band reported by Barrow (2). But for an H-bonded complex (Fig. 3*b*), e.g., with acetic acid, the 1592 cm^{-1} band becomes more intense rather than the single band observed by Barrow actually shifting. Protonation would lead to a more symmetrical vibration of the molecule, for mode I and II, which would be infrared forbidden or weak (cf. benzene), and indeed in trichloroacetic acid solutions, these peaks are very weak.

Can. J. Chem. Downloaded from www.nrcresearchpress.com by 210.87.254.40 on 09/05/12
For personal use only.

Barrow raises the question of the nature of the equilibrium when there is partial proton transfer, i.e., whether (*i*) there are two reactions to form (*a*) an H-bonded complex and (*b*) a proton-transferred complex; or (*ii*) just one reaction to form some proton transferred complex. His choice of *i* is based on the band assignment quoted above. Consideration of the data in this study, presented above, leads to the same conclusion but on a different basis. From the spectra shown in Fig. 3, an H-bonded complex between acetic acid ($pK_a = 4.74$) and pyridine in chloroform, results in increased intensity of the 1592 cm^{-1} peak relative to the 1580 cm^{-1} peak and increased intensity of the 1432 cm^{-1} peak. Protonation by trichloroacetic acid ($pK_a = 0.70$) leads to appearance of a peak at 1640 cm^{-1}, decreasing intensity of the 1592 and 1580 cm^{-1} peaks, increased intensity of the 1475 cm^{-1} peak, and decreased intensity of the 1432 cm^{-1} peak. For intermediate strength chloroacetic acid ($pK_a = 2.85$) solutions, as shown in Fig. 3*c*, the small peak at 1635 cm^{-1} and the decreased 1432 cm^{-1} peak suggest some protonation but the remaining peaks are similar to Fig. 3*b* rather than Fig. 3*a* therefore suggesting case *i* holds for partial protonation.

Barrow (2) mentions that for trichloroacetic and trifluoroacetic acids and pyridine in chloroform, the "wavelength shift is much less than would be expected for a product with free symmetric carboxylate group ... and that there is an absence of a split between carbonyl and carboxylate absorption." The same phenomena was again observed in this study but in methanol, solutions of the same concentrations as studied in chloroform showed well defined peaks at 1775(w), 1755(w), and 1690(s) cm^{-1} (for C=O monomer, C=O dimer and CO_2^- respectively) (e.g., see Fig. 2*c*). Other workers have studied various alkylamines and trichloroacetic acid in chloroform (9), benzene (3), and ether (5) and have found no absorption above 1700 cm^{-1}. The explanation for the presence of a 'free' carboxylate peak in solvents where ion pair formation is expected, is solvent participation and evidence for this is well documented in refs. 1 and 2.

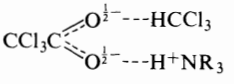

Since trichloroacetic acid gives strong 'free' carboxylate absorption with solvent participation as just shown, when reacted with alkylamines in chloroform (9) in benzene (3), and with pyridine in methanol (Fig. 2), and with *p*-anisidine (a base of similar strength to pyridine in water) in chloroform,[4] it might be concluded that pyridine in chloroform was causing the presence of such a broad medium intensity band between 1720 and 1680 cm^{-1}. A possible explanation of the anomalous behaviour, is the formation of a charge transfer complex between the pyridinium ion and trichloroacetate ion in chloroform.

Pyridinium is well known for formation of charge transfer complexes (10), for example, 1-methylpyridinium iodide forms a charge transfer complex as follows:

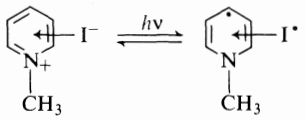

Formation of such complexes is detected by the presence of extra peaks in the ultraviolet absorption spectrum and often by colour formation. 1-Methylpyridinium iodide has charge transfer bands at 294.5 and 379.6 nm (11). The amount of charge transfer complex formation and the position of the charge transfer peaks depend on the solvent. Charge transfer formation with pyridinium salts, in which the complex formed is less polar, decreases as the polarity of the solvent increases.

Ultraviolet spectra of concentrated solutions (2–4 *M*) pyridine in chloroform or methanol show no absorption above 280 nm but such solutions containing equimolar amounts of trichloroacetic acid have shoulders extending to 400 nm. Dilution of the mixtures leads to a nonlinear decrease in absorption for this shoulder. For methanol solutions, this extra absorption had disappeared when pyridine concentration reached 0.4 *N* but was still present as a weak symmetrical band ($\lambda_{max} \simeq 330$ nm) for 0.1 *N* pyridine and 0.1 *N* trichloroacetic acid in chloroform. Hence, in addition to the two equilibria suggested by Barrow, a third equilibrium can be proposed, i.e.

$$Py + CCl_3COOH \rightleftharpoons Py \ldots HOOCCCl_3 \rightleftharpoons$$
$$Py{-}H^+ \ {}^-OOCCCl_3 \rightleftharpoons CCl_3COO^- \cdot Py{-}H^+$$

The structure of such complexes has been suggested to be (11):

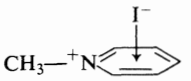

If a similar structure is proposed for trichloroacetic acid, then it could be represented as:

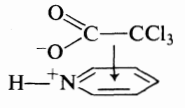

Thus, an unsymmetrical —COO^- could be obtained

[4]Unpublished results (this laboratory).

and absorption in the infrared for C=O, probably at a lower wavenumber than the COOH carbonyl band, would be expected. Judging from the fairly weak ultraviolet absorption, K for the charge transfer complex formation is probably small, and therefore infrared absorption for more than one form of carboxylate should be expected, giving rise to a broad band in the carboxylate–carbonyl region, as is observed.

Acknowledgement

We thank Dr. H. T. Bozimo for useful discussions.

1. G. M. Barrow and E. A. Yerge. J. Am. Chem. Soc. **76**, 5211 (1954).
2. G. M. Barrow. J. Am. Chem. Soc. **78**, 5802 (1956).
3. S. Bruckenstein and A. Saito. J. Am. Chem. Soc. **87**, 689 (1965).
4. S. L. Johnson and K. A. Rumon. J. Phys. Chem. **69**, 74 (1965).
5. F. Hibbert and D. N. P. Satchell. J. Chem. Soc. B, 573 (1968).
6. A. P. Cross. Introduction to practical infrared spectroscopy. Butterworth Scientific Publications, London. 1960. p. 69.
7. C. N. R. Rao. Chemical applications of infrared spectroscopy. Academic Press, New York, NY. 1963. pp. 222–223.
8. A. R. Katritzky. Q. Rev. **13**, 353 (1954).
9. J. W. Smith and M. C. Victoria. J. Chem. Soc. A, 2468 (1968).
10. E. M. Kosower, J. A. Skorcz, W. M. Scharz, Jr., and J. M. Patton. J. Am. Chem. Soc. **82**, 2188 (1960).
11. E. M. Kosower. J. Am. Chem. Soc. **80**, 3253 (1958).

Can. J. Chem. Downloaded from www.nrcresearchpress.com by 210.87.254.40 on 09/05/12
For personal use only.

The reactions of lithioacetonitrile and lithiomethoxyacetonitrile with certain ketones

CHARLES F. BEAM,[1] KEITH D. SHEALY, SHARON A. RISINGER, JANE BROWN, KIMBERLY L. SIDES, CANDACE R. HANBERRY, KATHY P. PAVLAKOVICH, AND STEVEN E. DAVIS

Department of Chemistry, Newberry College, Newberry, SC 29108, U.S.A.

Received March 21, 1978

CHARLES F. BEAM, KEITH D. SHEALY, SHARON A. RISINGER, JANE BROWN, KIMBERLY L. SIDES, CANDACE R. HANBERRY, KATHY P. PAVLAKOVICH, and STEVEN E. DAVIS. Can. J. Chem. **56**, 2572 (1978).

Lithioacetonitrile and lithiomethoxyacetonitrile were condensed with ketones to give either mono- or dialdol condensation products.

CHARLES F. BEAM, KEITH D. SHEALY, SHARON A. RISINGER, JANE BROWN, KIMBERLY L. SIDES, CANDACE R. HANBERRY, KATHY P. PAVLAKOVICH et STEVEN E. DAVIS. Can. J. Chem. **56**, 2572 (1978).

On a condensé le lithioacétonitrile et le lithiométhoxyacétonitrile avec des cétones pour conduire soit à des produits de mono- ou de dicondensations aldoliques.

[Traduit par le journal]

Can. J. Chem. Downloaded from www.nrcresearchpress.com by 210.87.254.42 on 09/05/12
For personal use only.

Introduction

Recently, Kaiser and Hauser (1) and Crouse and Seebach (2) have reported the preparation and condensation of lithioacetonitrile with ketones or aldehydes to give monoaldol products. Improved yields of monoaldol condensation products of lithioacetonitriles have been reported by Cuvigny *et al.* (3). Gornowicz and West (4) and Das and Wilkie (5) have also prepared the lithio salts of simple nitriles such as acetonitrile or phenylacetonitrile. In another account, Kaiser and Hauser (6) describe some of the problems encountered in attempted aldol condensations with lithiophenylacetonitrile. Stork and Maldonado (7) and Hunig and Wehner (8) have cited some monoalkylations of α-cyano ether anions and Hunig and Wehner (9) have isolated aldol products after treating these anions with ketones.

In each report, no mention was made of the isolation of dialdol condensation products. The anions were generally prepared by treating the nitrile with base at lower temperature (e.g., −78°C) followed by condensation with electrophilic reagent and stirring in the cold. The mixture was then allowed to warm to room temperature, and the product isolated. Interestingly, Hauser and coworkers (10) reported isolation of dialdol products resulting from the condensation of benzophenone with another multiple anion. We have also noted that diaroylation occurred when dilithiooximes and dilithiophenylhydrazones were condensed with acid chlorides (11, 12), and dialkylation of C(α)-anions of nitriles has been established (13, 14).

[1]Author to whom correspondence should be addressed.

Results and Discussion

During the preparation and reaction of lithiomethoxyacetonitrile (**1**) we made some expected and unexpected observations. When **1** was treated with benzophenone and 4-methylbenzophenone, the expected aldol products **2** and **3** were isolated in 25 and 20% yields, respectively. When **1** was prepared and condensed with these ketones at −78 or 0°C, the yields of these products (**2** and **3**) were essentially unchanged (ca. 25%); however, **1** condensed with 9-fluorenone to give dialdol product **4** in 36% yield (Scheme 1).

Lithioacetonitrile (**5**), prepared at 0°C, was also found to undergo the same dialdol condensation when treated with benzophenone, 2-benzoylthiophene, 9-fluorenone, and 4-chlorobenzophenone

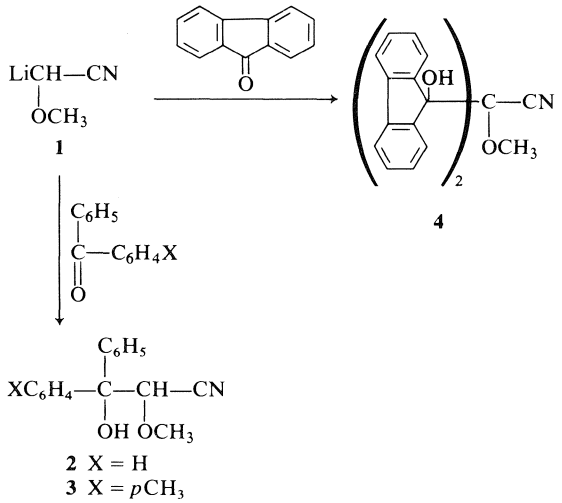

SCHEME 1

Can. J. Chem. Downloaded from www.nrcresearchpress.com by 210.87.254.42 on 09/05/12
For personal use only.

(**6–9** in Table 1) but the monoaldol product **10** was isolated in 45% yield when **5** was condensed with 4-methylbenzophenone (Scheme 2).

Aside from infrared spectra of these products displaying cyanide absorptions from 2222–2290 cm^{-1} and hydroxyl absorptions from 3200–3400 cm^{-1}, monoaldol product (**10**) displayed ^1H nmr methylene absorptions at δ 3.47 ppm whereas dialdol (**6–9**) ^1H nmr spectra contained methine resonances from δ 4.67–5.40 ppm. ^1H nmr spectra of some crude products indicated mixtures of mono- and dialdol products were present. When **5** was prepared from methyllithium and lithium diisopropylamide, the same products listed in Table 1 were isolated. In all condensations of **5** with 4-methylbenzophenone, the monoaldol product was isolated instead of the dicondensation product. We do not have a satisfactory explanation for this result. At the present time, the preparation of dilithioacetonitrile (4) followed by treatment with ketones listed in Table 1 has been unsuccessful.

The condensation of acetonitrile carbanion **5** with the ketone could be attributed to the formation of the weaker base, which would be an alkoxide-type anion **11** (Scheme 3). Since the pK_a of tertiary alcohols is near 19 and that of acetonitrile is 25, the alkoxide ion **11** should be a weaker base than acetonitrile carbanion **5** (15). Then while an equilibrium between alkoxide ion **11** and secondary carbanion **12**, shifted towards **12** may appear less likely, the reaction of **12** with another molecule of benzophenone would result in alkoxide **13**, a monoanion. Since the ketone is being added to acetonitrile carbanion **5**, and **5** is present in excess until addition is complete, alkoxide **11** could react with **5** to give dianion **14** and **14** would condense with benzophenone to give **15**. Secondary carbanion **12** could also react with **5** to give **14** before **12** could react with benzophenone to give **13**. Under the conditions of the reaction (base–nitrile–ketone 1 : 1 : 1), **13** if formed would react with **5** to give **15**. Dianion **15** would result from either route, and upon neutralization would give dialdol nitrile **6**.

Our investigation differs from the reports previously cited (1–3, 9) in that the nitrile carbanion was prepared and condensed with the electrophilic reagent at 0°C instead of lower temperatures (e.g., −78°C, except for **2** and **3** mentioned earlier). The results obtained suggest other equilibrium were involved at 0°C and at lower temperatures they were not as important, as evidenced by the fact that other investigators reported good to excellent yields of monoaldol products.

Experimental

Tetrahydrofuran was distilled from sodium (benzophenone). Nuclear magnetic resonance spectra were obtained on a

TABLE 1. Aldol condensation products of lithioacetonitrile

Compound No.	Empirical formula	Electrophilic reagent	Yield[b] (%)	Melting point[a] (°C)	Elemental analysis						Nuclear magnetic resonance[d] δ(ppm)	Infrared[e] (cm^{-1})
					Calculated			Found				
					C	H	N	C	H	N		
6	$C_{28}H_{23}NO_2$	Benzophenone	53[c]	214–217	82.94	5.72	3.45	83.24	5.80	3.37	4.95(CH)	2290(CN)
7	$C_{24}H_{19}NO_2S_2$	2-Benzoylthiophene	36	170–175	69.03	4.59	3.37	69.33	4.63	3.37	5.40(CH)	2260(CN)
8	$C_{28}H_{21}Cl_2NO_2$	4-Chlorobenzophenone	30	215–220	70.89	4.46	2.93	70.71	4.55	2.78	5.40(CH)	2240(CN)
9	$C_{28}H_{19}NO_2$	9-Fluorenone	52	196–198	83.77	4.77	3.49	83.73	4.97	3.49	4.67(CH)	2240(CN)
10	$C_{16}H_{15}NO$	4-Methylbenzophenone	45	132–133	80.98	6.37	5.90	81.02	6.40	5.66	3.47(CH_2)	2270(CN)[f]

[a]Melting points were taken in a Thomas Hoover melting point apparatus in open capillary tubes and are uncorrected. Analytical samples of dialdol products did not exhibit the sharp melting point (or melting point range) characteristic of monoaldol products.
[b]Yields for dialdol products based upon one half the number of moles of electrophilic reagent used. Yield for monoaldol product **10** based on the number of moles of ketone used.
[c]A 17% yield of monoaldol product was isolated from this reaction. See previous footnote.
[d]DMSO-d_6 for **6–10**.
[e]Nujol mulls **6–9**.
[f]$CHCl_3$ solution.

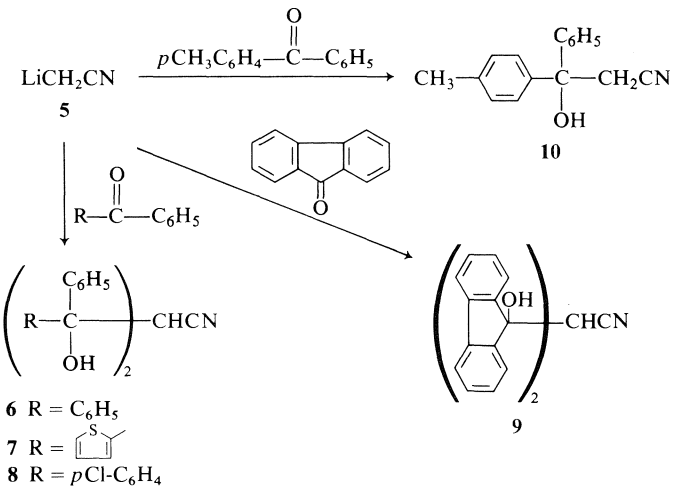

SCHEME 2

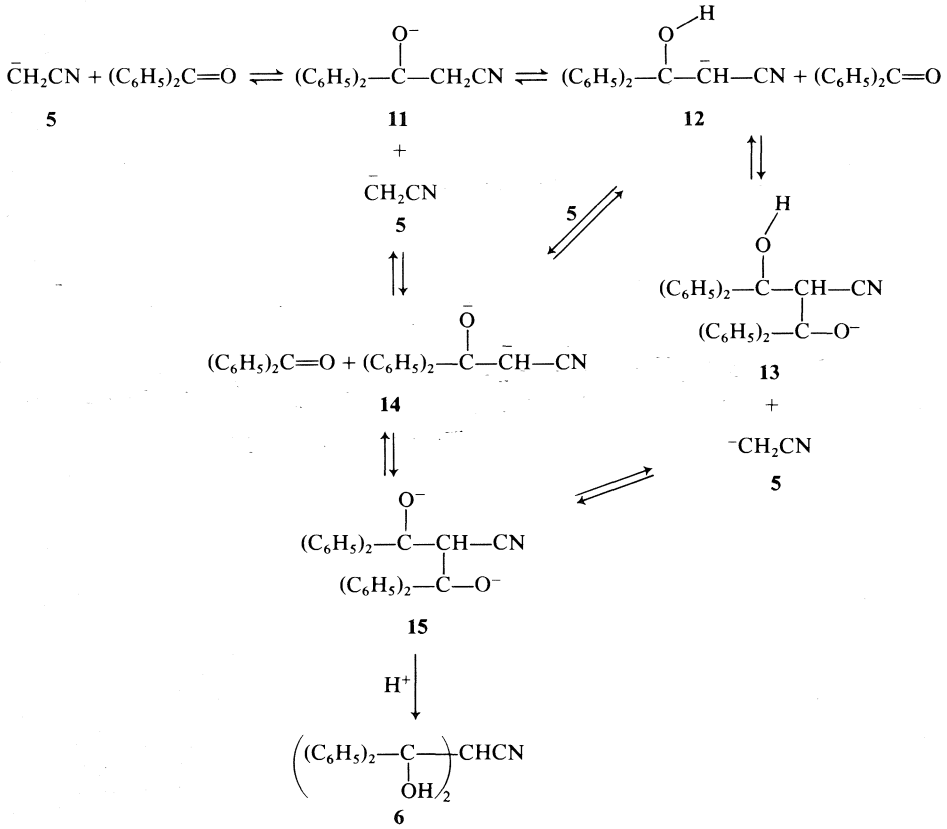

SCHEME 3

Varian Associates EM 300X nmr spectrometer (TMS standard). Infrared spectra were obtained on a Perkin-Elmer 700 infrared spectrometer. Combustion analyses were performed by Robertson's Laboratory, 73 West End Ave., Florham Park, NJ and M-H-W Laboratories, Garden City, MI. *n*-Butyllithium was purchased from Lithium Corporation of America.

Preparation and Reactions of Lithioacetonitrile and Lithiomethoxyacetonitrile

The lithionitriles were prepared by cooling to 0°C (unless specified) and blanketing under nitrogen a solution containing 0.05 mol of nitrile in 100 ml of dry tetrahydrofuran (THF). A 0.055 mol sample of *n*-butyllithium was added dropwise during 5 min and the solution was stirred for 1 h. This was followed by rapid addition of 0.055 mol of ketone dissolved in 50 ml of THF. After 10 min of stirring the mixture was neutralized by pouring into 100 ml of 3 *N* HCl and ice. The layers were separated and 100 ml of ether was added to the aqueous layer and then neutralized with $NaHCO_3$. The organic layers were combined, dried ($MgSO_4$), and concentrated (Rotovac). This

Can. J. Chem. Downloaded from www.nrcresearchpress.com by 210.87.254.42 on 09/05/12
For personal use only.

general procedure was used for the preparation of nitriles **2–4** and **6–10**.

Condensation of Lithiomethoxyacetonitrile with Benzophenone, 4-Methylbenzophenone, and 9-Fluorenone, respectively

Nitrile **2**, 25% from ethanol, mp 120–122°C; ^{1}Hmr ($CDCl_3$) δ: 3.47 (s, 3H, OCH_3), 4.63 (s, 1H, CH), and 6.87–7.47 (broad s, 10H, ArH); ir ($CHCl_3$): 2222 cm^{-1} (CN). *Anal.* calcd. for $C_{16}H_{15}NO_2$ (**2**): C 75.88, H 5.97, N 5.53; found: C 76.03, H 5.96, N 5.47.

Nitrile **3**, 20% from ethanol, mp 144–145°C; ^{1}Hmr ($CDCl_3$) δ: 2.30 (s, 3H, $ArCH_3$), 3.53 (s, 3H, OCH_3), 4.70 (s, 1H, CH), and 6.87–7.63 (m, 9H, ArH); ir ($CHCl_3$): 2225 cm^{-1}. *Anal.* calcd. for $C_{17}H_{17}NO_3$ (**3**): C 76.39, H 6.41, N 5.24; found: C 76.19, H 6.56, N 4.99. (The yields of **2** and **3** were 25% at −78°C.)

Nitrile **4**, 36% from ethanol, mp 254–255°C; ^{1}Hmr ($CDCl_3$) δ: 4.23 (s, 3H, OCH_3) and 6.5–7.4 (m, 8H, ArH); ir (Nujol): 2280 cm^{-1} (CN). *Anal.* calcd. for $C_{29}H_{21}NO_3$ (**4**): C 80.72, H 4.91, N 3.25; found: C 80.60, H 5.11, N 3.00.

Acknowledgement

This project was supported at Newberry College by a grant awarded by the Cottrell Science Grants Program of the Research Corporation.

1. E. M. Kaiser and C. R. Hauser. J. Org. Chem. **33**, 3402 (1968).
2. D. N. Crouse and D. Seebach. Chem. Ber. **101**, 3113 (1968).
3. T. Cuvigny, P. Hullot, and M. Larcheveque. J. Organometal. Chem. **57**, C36 (1973).
4. G. A. Gornowicz and R. West. J. Am. Chem. Soc. **93**, 1714 (1971).
5. R. Das and C. A. Wilkie. J. Am. Chem. Soc. **94**, 4555 (1972).
6. E. M. Kaiser and C. R. Hauser. J. Am. Chem. Soc. **89**, 4566 (1967).
7. G. Stork and L. Maldonado. J. Am. Chem. Soc. **93**, 5286 (1971).
8. S. Hunig and G. Wehner. Synthesis, 181 (1975).
9. S. Hunig and G. Wehner. Synthesis, 391 (1975).
10. R. E. Ludt, G. P. Crowther, and C. R. Hauser. J. Org. Chem. **35**, 1289 (1970).
11. R. M. Sandifer, L. M. Shaffer, W. M. Hollinger, D. C. Reames, and C. F. Beam. J. Heterocycl. Chem. **13**, 607 (1976).
12. C. F. Beam, D. C. Reames, C. E. Harris, L. W. Dasher, W. M. Hollinger, N. L. Shealy, R. M. Sandifer, M. Perkins, and C. R. Hauser. J. Org. Chem. **40**, 514 (1975).
13. W. G. Kenyon, E. M. Kaiser, and C. R. Hauser. J. Org. Chem. **30**, 4135 (1965).
14. A. C. Cope, H. L. Holmes, and H. O. House. Org. React. **9**, 107 (1957).
15. D. J. Cram. Fundamentals of carbanion chemistry. Academic Press Inc., New York, NY. 1965. Chapt. 1.

Can. J. Chem. Downloaded from www.nrcresearchpress.com by 210.87.254.42 on 09/05/12
For personal use only.

^{13}C and ^{2}H spin–lattice relaxation in neopentane-d_{12}

BRIAN A. PETTITT AND RODERICK E. WASYLISHEN
Department of Chemistry, University of Winnipeg, Winnipeg, Man., Canada R3B 2E9
AND
RONALD Y. DONG
Department of Physics, University of Winnipeg, Winnipeg, Man., Canada R3B 2E9
AND
T. PHIL PITNER
Phillip Morris U.S.A. Research Center, P.O. Box 26583, Richmond, VA 23261, U.S.A.

Received April 27, 1978

BRIAN A. PETTITT, RODERICK E. WASYLISHEN, RONALD Y. DONG, and T. PHIL PITNER. Can. J. Chem. **56**, 2576 (1978).

The results of a variable temperature study of the ^{2}H and ^{13}C spin–lattice relaxation times in neopentane-d_{12} are reported along with those for the ^{13}C's in neopentane at a single temperature. Orientational and angular momentum correlation times derived from these T_1's exhibit the following: (*i*) τ_2 is continuous through the melting point with an activation energy of 0.98 kcal/mol, (*ii*) τ_J is more or less constant at 0.33 $\pm$ 0.03 ps within 40 K of either side of the melting point, and (*iii*) they do not conform to the theoretical relationships of extended diffusion, Fokker–Planck, or Langevin theories. The spin–rotation coupling constants are calculated to be -0.69 kHz for neopentane and -0.52 kHz for neopentane-d_{12}.

BRIAN A. PETTITT, RODERICK E. WASYLISHEN, RONALD Y. DONG et T. PHIL PITNER. Can. J. Chem. **56**, 2576 (1978).

On rapporte les résultats d'études à températures variables des temps de relaxation spin–réseau du ^{2}H et du ^{13}C dans le néopentane-d_{12} de même que ceux du ^{13}C du néopentane à une seule température. Les temps de corrélation de moments angulaires et d'orientation que l'on peut tirer de ces valeurs T_1 présentent les caractéristiques suivantes: (*1*) τ_2 est continu au niveau du point de fusion avec une énergie d'activation de 0.98 kcal/mol, (*2*) τ_J est plus ou moins constant à 0.33 $\pm$ 0.03 ps dans des limites de 40 K au-dessous et au dessus du point de fusion et (*3*) ces valeurs ne sont pas conformes avec les relations théoriques des théories de la diffusion étendue, de Fokker–Planck ou de Langevin. On a calculé les constantes de couplage spin–rotation qui s'établissent à -0.69 kHz pour le néopentane et -0.52 kHz pour le néopentane-d_{12}.

[Traduit par le journal]

Introduction

The techniques of spin–lattice and dielectric relaxation, infrared absorption, and Rayleigh–Brillouin, Raman, and neutron scattering continue to add to a considerable body of data on molecular rotations in condensed phases. These data are normally discussed within the theoretical framework of time-dependent correlation functions, thereby concentrating on the characteristic times associated with molecular rotations in an equilibrium ensemble. The dynamics underlying such discussions are generally of two types: hydrodynamical theories providing means to calculate rates of rotational diffusion for 'large' molecules, and quasi-kinetic theories which introduce idealized collision dynamics relating orientational correlation times to rates of angular momentum-changing collisions (1). Theories of the latter type are essential for small molecules, and the widely-used extended diffusion theory of Gordon and McClung has been successful in explaining the rotational characteristics of CF_4, CCl_4, and ClO_3F; for a comprehensive review of the extended diffusion theory and its applications, see ref. 2. Probably the best approximation to the full kinetic formulation is the Fokker–Planck model (3), which has been shown to agree reasonably well with molecular dynamics 'experiments' on rough spheres (4). On the other hand, the Langevin (friction) model (5) is probably the last resort of kinetic theory, yet it is capable of exhibiting some of the details of the more elaborate approaches. All of these procedures are rather crude in comparison to those of quantum statistical mechanics, but they have been useful enough vis-à-vis experiments to deserve attention. At present, it is difficult to say precisely how model-dependent our understanding of molecular rotations in liquids and solids is, and this paper is meant to be a comparison of the above-mentioned approaches as applied to

Can. J. Chem. Downloaded from www.nrcresearchpress.com by 210.87.254.105 on 09/05/12
For personal use only.

Can. J. Chem. Downloaded from www.nrcresearchpress.com by 210.87.254.105 on 09/05/12
For personal use only.

nuclear spin–lattice relaxation in general, and that of ^{13}C and ^{2}H in $C(CH_3)_4$ and $C(CD_3)_4$ in particular.

In addition to its near spherical shape, neopentane has several interesting properties. It undergoes a transition at 140 K from an hexagonal structure in which rotations are not appreciable to a face-centred cubic lattice ($\Delta S_t = 2.21R$) in which rotations are liquid-like, before melting at 257 K ($\Delta S_m = 1.52R$) (6). The liquid boils under atmospheric pressure at 282 K, but can be kept in that phase at higher temperatures in a sealed tube. The solid II → solid I transition is accompanied by an 18% increase in volume (7), the high temperature (solid I) phase being a typical 'plastic crystal' which is easily deformable and has a translational diffusion coefficient about 10^{-4} times that of the liquid near the melting point (8). Livingstone *et al.* (9) studied the rotation of neopentane by infrared and Raman spectroscopy, concluding that the reorientational characteristics are continuous through the melting point and are not in the small step limit of diffusion. Månsson *et al.* (10) concluded from neutron scattering experiments that the molecules rotate more freely in the solid I than the liquid for temperatures near the melting point. This observation is particularly interesting because it was also one of the main conclusions of O'Dell and Berne's study (4) of the molecular dynamics of the rough sphere fluid.

The next section summarizes the experimental procedure used in the determination of ^{13}C and ^{2}H spin–lattice relaxation times, and the final section presents an analysis of the results.

Experimental

Neopentane was obtained from Chemical Samples Company of Columbus, Ohio, and neopentane-d_{12} from Merck, Sharp, and Dohme of Montreal. Neat samples were degassed by the freeze–pump–thaw cycle under vacuum and sealed.

All spin–lattice relaxation times were measured using the inversion-recovery pulse sequence (d–180°–t–90°), where d is a delay time ($d > 5T_1$) and t is a variable time. T_1 values were calculated from the slopes of ln $\{\langle Mz\rangle_0 - \langle Mz\rangle_t\}$ vs. t (11). Deuterium relaxation rates of neopentane-d_{12} were measured at 13.81 MHz with a Bruker SXP pulsed spectrometer. The temperature was maintained with an accuracy of ±0.5 K by a nitrogen gas flow. Proton-decoupled natural abundance ^{13}C spectra were obtained on a Varian CFT-20 spectrometer (8 mm variable temperature probe) and a Varian XL-100 spectrometer. Nuclear Overhauser enhancement factors (nOe's) were measured using the gated proton decoupler on the CFT-20 with $d > 10T_1$ (^{13}C). The temperature was maintained with an accuracy of ±1.0 K by a nitrogen gas flow.

Results and Discussion

The deuterons in neopentane-d_{12} relax by interaction of their electric quadrupole moments with the gradient of the local electric field, which is directed along the C—D bond and therefore has the time dependence of the rotation of that vector. As a result, the spin–lattice relaxation time can be related to τ_2, the orientation correlation time associated with a second order spherical harmonic via (12)

$$[1] \qquad \frac{1}{T_1} = \frac{3\pi^2}{2}\left(\frac{e^2qQ}{h}\right)^2 \tau_2$$

where (e^2qQ/h) is the quadrupole coupling constant here taken to be 174 kHz, the value for cyclohexane (13). Equation [1] is valid for symmetric C—D bonds when τ_2 is small in comparison to the inverse of the deuterium Larmor frequency (extreme narrowing).

The central ^{13}C of neopentane-d_{12} relaxes by coupling of its magnetic moment with the magnetic field generated by the relative rotation of the remaining charges in the molecule (the spin–rotation mechanism). In this case, T_1 is related to the correlation time associated with the molecular angular momentum by (14)

$$[2] \qquad \frac{1}{T_1^{SR}} = \frac{8\pi^2}{h^2} IkTC^2\tau_J$$

where C is the spin–rotation coupling constant, I is the moment of inertia, and the other symbols have their usual meanings. The moments of inertia were calculated from standard geometries, giving $I = 1.89 \times 10^{-38}$ g cm^2 for neopentane and $I = 2.51 \times 10^{-38}$ g cm^2 for neopentane-d_{12}. The spin–rotation coupling constants were calculated from chemical shift data and the experimental value for $^{13}C^{16}O$ by a method summarized in the Appendix, giving $C = -0.69$ kHz for neopentane and $C = -0.52$ kHz for neopentane-d_{12}.

The ^{13}C nuclei of neopentane are relaxed by the spin–rotation mechanism and by the interaction of their magnetic moments with those of the nearest protons, i.e. the intramolecular dipolar mechanism. In principle, the two contributions to the relaxation rates can be separated by measuring the ^{13}C nOe's (15). The dipolar term is related to τ_2 by (12)

$$[3] \qquad \frac{1}{T_1^{d}} = n\left(\frac{\gamma_C\gamma_H\hbar}{r_{CH}^3}\right)^2 \tau_2$$

in the extreme narrowing approximation, where $n = 3$, $r_{CH} = 1.09$ Å for the methyl carbons and $n = 12$, $r_{CH} = 2.16$ Å for the central carbon, and γ_C and γ_H are the gyromagnetic ratios of ^{13}C and protons.

Grant *et al.* (16), by means of inelastic neutron scattering experiments, determined that CH_3 torsional oscillations are restricted by a 3-fold barrier of 5.03 kcal/mol.[1] The Boltzmann distribution indi-

[1]A slightly smaller barrier (4.92 kcal/mol) was reported by Weiss and Leroi (16*b*) from studies of infrared spectra.

Can. J. Chem. Downloaded from www.nrcresearchpress.com by 210.87.254.105 on 09/05/12
For personal use only.

TABLE 1. ^{13}C and ^{2}H relaxation times and rotational correlation times of neopentane-d_{12}

State	T(K)	T_1 (^{2}H)* (s)	T_1^{SR} (central ^{13}C)† (s)	τ_2 (ps)	τ_J (ps)
	301		130	(0.64)‡	0.38
	296	3.32		0.67	
	291	3.25	155	0.69	0.33
Liquid	281	2.97	158	0.75	0.34
	272	2.67	172	0.84	0.32
	260	2.50	184	0.89	0.32
	mp				
	255	2.40	195	0.93	0.30
	250	2.28	195	0.98	0.31
Plastic	239	2.02	192	1.10	0.33
crystal	229	1.78		1.25	
	217		192	(1.42)‡	0.36
	214	1.61		1.39	
	208	1.42		1.57	

*Estimated error: ±5%.
†Estimated error: ±10%.
‡Interpolated value from Fig. 1.

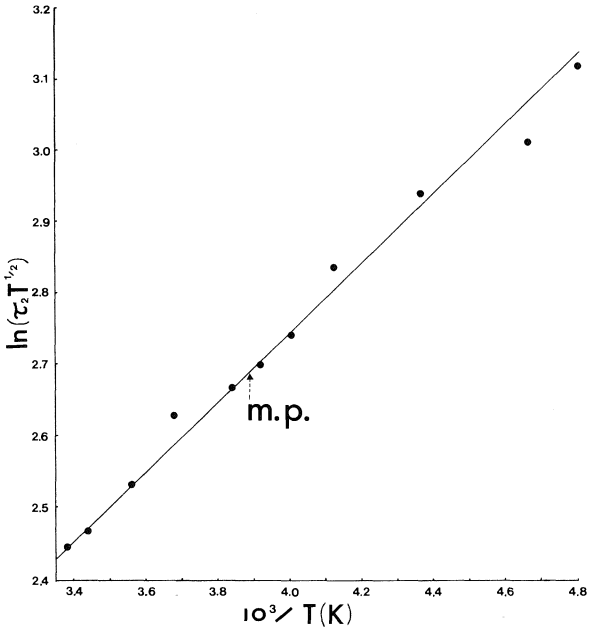

FIG. 1. Graphical summary of the temperature dependence of τ_2 for neopentane-d_{12} in terms of eq. [4]. The slope corresponds to E_a = 0.98 kcal/mol (τ_2 is in ps).

cates that for temperatures below 300 K the molecules are almost all in the bottom 1/10 of the potential wells. It is assumed here that the internal motion associated with this potential does not contribute to the relaxation of the ^{2}H and ^{13}C spins, i.e. the molecules are assumed to be rigid rotors.

Table 1 displays the deuterium and central carbon-13 spin–lattice relaxation times for neopentane-d_{12} at selected temperatures between 208 and 301 K. Also displayed are the τ_2's and τ_J's derived from them via eqs. [1] and [2]. If the rotation was free or only slightly frictionally retarded (17), the τ_2's would have a $T^{-1/2}$ dependence and it is convenient to summarize the results by writing (18)

$$[4] \qquad \tau_2 = CT^{-1/2} \exp(E_a/RT)$$

where the constant depends on how one approaches the free limit ($C = (\pi I/12k)^{1/2}$ for slight frictional damping). That is, the rotation is imagined to be a thermally activated process with 'barrier' E_a. Figure 1 illustrates the τ_2 data of Table 1 as a plot of $\ln(\tau_2 T^{1/2})$ vs. $1/T$, where it can be seen that the data are reasonably well represented by E_a = 0.98 kcal/mol and are continuous across the melting point. Proton T_1's show considerable variation near the melting point because of modulation of the intermolecular dipolar interactions by translational diffusion (19). Table 1 indicates that, whereas τ_2 changes by a factor of about 2.5 over a 100 K temperature range, τ_J is more or less constant within 40 K of either side of the melting point.[2] Relationships between τ_2 and τ_J are at the core of the kinetic treatments mentioned in the Introduction, and the following paragraphs outline their essential features.

In the extended diffusion theory of Gordon and McClung (2), inertial rotational jumps are interrupted by instantaneous collisions at intervals characterized by a Poisson distribution with average value τ_J. In the M-diffusion limit, the direction of the molecular angular momentum is randomized by each collision but the magnitude is unchanged; whereas in the J-diffusion limit both are randomized. Qualitatively, the two models imply 'weak' and 'strong' collisions, respectively. The predicted relationships between τ_2^* and τ_J^* are depicted in Fig. 2 ($\tau^* = \tau(kT/I)^{1/2}$ is a reduced correlation time).

A detailed analysis of the Fokker–Planck fluid of spherical molecules has been presented by Fixman and Rider (3*a*), but the necessary numerical procedures have limited its application. Evans (3*b*) has treated the problem in the high density (liquid) region by regarding the free rotation as a perturbation on the collision dynamics and approximately summing the resulting series. By these means, he was able to obtain the $\tau_l \leftrightarrow \tau_J$ dependency as follows:

$$[5] \qquad \tau_l^* = \frac{1}{l(l+1)\tau_J^*}\{1 + [l(l+1) - \tfrac{1}{2}]\tau_J^{*2}\}$$

This equation is also plotted in Fig. 2 over an

[2]The τ_J data of Table 1 actually exhibit a minimum in the neighbourhood of the melting point, but the error (±10%) is too large to claim this as a real effect.

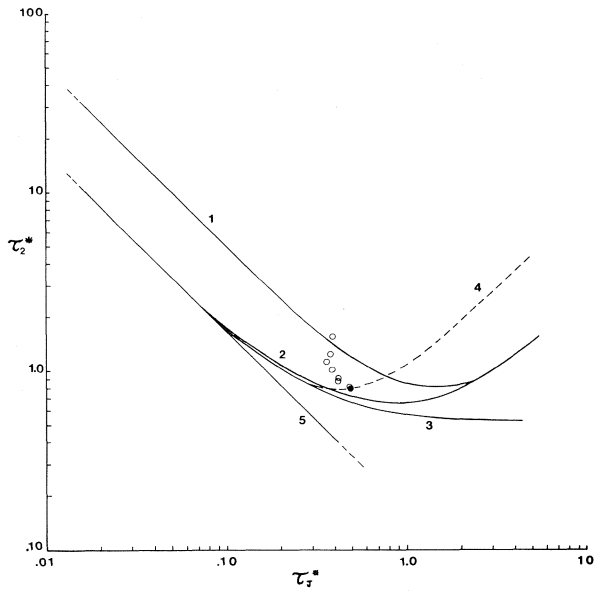

FIG. 2. Interdependence of reduced orientational and angular momentum correlation times: *1*, M-diffusion; *2*, J-diffusion; *3*, Langevin (friction) theory; *4*, approximate Fokker–Planck theory; and *5*, Hubbard relation. The open circles represent the data for neopentane-d_{12} and the closed circle is for neopentane.

extensive range, but is only reliable up to the neighbourhood of its minimum[3] (3*b*).

Kluk and Powles (5) have shown that for spherical and linear molecules in the rotational friction (Langevin) model, the analogous relationship is

$$[6]\quad \tau_l^* = \frac{1}{l(l+1)\tau_J^*} \times M(1, 1 + l(l+1)\tau_J^{*2}, l(l+1)\tau_J^{*2})$$

where $M(\alpha, \gamma, x)$ is the Kummer series,

$$[7]\quad M(\alpha, \gamma, x) = 1 + \frac{\alpha}{\gamma}x + \frac{\alpha(\alpha+1)}{2!\gamma(\gamma+1)}x^2 + \ldots$$

so, to lowest order

$$[8]\quad \tau_l^* = \frac{1}{l(l+1)\tau_J^*}\{1 + l(l+1)\tau_J^{*2} + \ldots\}$$

Equation [6] is also illustrated in Fig. 2, from which it can be seen that the *J*-diffusion, Fokker–Planck, and Langevin models all have as their high density limits the small step diffusion model, which is characterized by the Hubbard relation $\tau_l^*\tau_J^* = [l(l+1)]^{-1}$. In addition, the figure demonstrates (albeit the plot is ln–ln) that the three models predict similar deviations from small step diffusion up to $\tau_J^* \lesssim 0.5$. The accuracy of a particular model is difficult to judge on the basis of correlation times alone because they are essentially features of the short-time part of the correlation functions, the behaviour of which the model may reproduce quite well before deviating at longer times (4).

The data of Table 1 are plotted on Fig. 2 along with the point $\tau_2 = 0.55$ ps and $\tau_J = 0.34$ ps determined from T_1 (methyl ^{13}C) = 23.5 s (nOe = 1.65) and T_1 (central ^{13}C) = 86 s (nOe = 0.48) for neopentane at 291 K. The dipolar contribution to the central carbon's T_1 corresponds to $\tau_2 = 0.66$ ps. Attempts to obtain data for neopentane at other temperatures were frustrated by unreproducible nOe's. The kinetic behaviour of neopentane-d_{12} clearly conforms to none of the predictions, but falls more or less between the two extremes of the extended diffusion theory such that the experimental points at the high temperatures (liquid) lie just above the J-diffusion curve and the ones at low temperature (solid I) are near the M-diffusion curve. The most that can be inferred from this observation is that although the average time between collisions does not change, the collisions weaken as the substance is cooled such that the magnitude of the angular momentum is progressively less affected. This seems reasonable, considering the loss of translational mobility on freezing. However, the interpretation of angular momentum relaxation as a binary collision process (instantaneous or otherwise) is too naive to be applied with confidence to substances near their melting points, where many body processes govern the dynamics. In the Fokker–Planck and Langevin models, many body processes are implicit in average torques and friction coefficients, but these concepts are of limited conceptual value on the picosecond timescale.

As yet there are very little data available on angular momentum relaxation in liquids and virtually none in solids, and the work reported here was conceived as an investigation of the utility of the ^{13}C Fourier transform nmr method in obtaining such information. Orientational relaxation data are demonstrably easier to obtain by this method (20), but less informative with respect to the specific microdynamical events underlying measureable quantities (in this case, T_1's). The only related study that we are aware of, that of Boden and Folland (21) on ^{31}P and ^{2}H relaxation in phosphine (PH_3 and PD_3), serves to highlight the specificity of a molecule's rotational characteristics in the neighbourhood of the melting point demonstrated here for neopentane.

[3]Evans and Keyes (3*c*) turned the perturbation procedure around and examined the low density (gas) limit of the Fokker–Planck model, but results for intermediate densities where inertial and collisional effects are comparable are as yet unavailable in analytical form.

Can. J. Chem. Downloaded from www.nrcresearchpress.com by 210.87.254.105 on 09/05/12
For personal use only.

Can. J. Chem. Downloaded from www.nrcresearchpress.com by 210.87.254.105 on 09/05/12
For personal use only.

They observed a discontinuity in τ_2 but not in τ_J across the melting point and found that τ_2 has a higher activation energy in the liquid than in the plastic solid. They concluded that rotation in the liquid is isotropic and closer to the M-diffusion limit. Based on neopentane and phosphine, we conclude that there is much to learn about molecular rotations in condensed phases.

Acknowledgements

We are grateful to Dr. R. E. D. McClung for a copy of his extended diffusion program, Werner Danchura for a program that calculates moments of inertia, and the National Research Council of Canada and the University of Winnipeg for financial support.

Appendix

Calculated Spin–Rotation Constants of Neopentane and Neopentane-d_{12}

The term in the molecular Hamiltonian responsible for the spin–rotation mechanism can be written as (22)

$$[A1] \qquad H^{SR} = -\hbar^{-2}\hat{S}_\alpha \cdot \mathsf{M} \cdot \hat{J}$$

where $\hat{S}_\alpha$ and $\hat{J}$ are the spin operators for nucleus α and the molecular angular momentum, and $\mathsf{M} = h\mathsf{C}$ is the spin–rotation coupling tensor in units of energy. Ramsey (23) showed that M is related to the average nuclear shielding, σ.

$$[A2] \qquad \sigma = (1/3)(\sigma_{xx} + \sigma_{yy} + \sigma_{zz}) = \sigma_d + \sigma_p$$

where

$$[A3] \qquad \sigma_d = \frac{e^2}{3mc^2}\sum_i \langle 0|r_i^{-1}|0\rangle$$

is the diamagnetic contribution, and

$$[A4] \qquad \sigma_p = \frac{(m'/m)}{3\hbar^2 g_\alpha}\sum_{j=1}^{3} I_j M_j - \frac{e^2}{3mc^2}\sum_{\alpha'}{}' \frac{Z_{\alpha'}}{r_{\alpha'}}$$

is the paramagnetic contribution. $|0\rangle$ is the ground electronic state vector, r_i is the position of electron i with respect to nucleus α, g_α is the nuclear g-factor, I_j is the jth component of the diagonalized moment of inertia tensor, $Z_{\alpha'}$ is the charge of nucleus α' at relative position $r_{\alpha'}$, and m'/m is the proton/electron mass ratio.

The two components of σ_p are denoted σ_p' and σ_N, the latter being due to the nuclear framework only. Clearly, for molecules in which C reduces to a scalar, σ_p' is sufficient to determine its value. This is made possible by an accurate approximation for σ_d due to Flygare and Goodisman (24),

TABLE 2. Spin–rotation constants of neopentane and neopentane-d_{12}

Molecule	δ^{TMS} (ppm)	σ_p' (ppm)	C (kHz)
B = $^{13}C^{16}O$	−182.2*	−256	−32.6†
A = $^{13}C(CH_3)_4$	−27.9‡	−102	−0.69
A = $^{13}C(CD_3)_4$	−27.0§	−101	−0.52

*Reference 27.
†Reference 28.
‡Reference 29.
§Determined from a measurement of $\delta^{TMS}[C(CD_3)_4] - \delta^{TMS}[C(CH_3)_4] = 1.0$ ppm.

$$[A5] \qquad \sigma_d \simeq \sigma_d(\text{atom}) - \sigma_N$$

where σ_d(atom) is the diamagnetic shielding of nucleus α in the free atom. In this approximation,

$$[A6] \qquad \sigma \simeq \sigma_d(\text{atom}) + \sigma_p'$$

Introduction of the chemical shifts of nucleus α in molecules A and B with respect to reference molecule R by

$$[A7] \qquad \delta^R(A) = \sigma(A) - \sigma(R)$$

and a similar expression for B, and use of equation [A6] results in

$$[A8] \qquad \sigma_p'(A) = \sigma_p'(B) - \{\delta^R(B) - \delta^R(A)\}$$

Thus an experimental σ_p'(B) and chemical shift data are sufficient to determine σ_p'(A), A = neopentane or neopentane-d_{12}. Table 2 presents the relevant data based on B = $^{13}C^{16}O$. This procedure was used by Gillen *et al.* (25) for CCl_4 and can be extended to a symmetric top molecule if its chemical shift anisotropy is known (26).

1. W. A. STEELE. Adv. Chem. Phys. **34**, 37 (1976).
2. R. E. D. MCCLUNG. Adv. Mol. Relaxation Interaction Processes, **10**, 83 (1977).
3. (*a*) M. FIXMAN and K. RIDER. J. Chem. Phys. **51**, 2425 (1969); (*b*) G. T. EVANS. J. Chem. Phys. **65**, 3030 (1976); (*c*) G. T. EVANS and T. KEYES. J. Chem. Phys. **67**, 615 (1977); (*d*) G. T. EVANS. J. Chem. Phys. **67**, 2911 (1977).
4. J. O'DELL AND B. J. BERNE. J. Chem. Phys. **63**, 2376 (1975).
5. E. KLUK and J. G. POWLES. Mol. Phys. **30**, 1109 (1975).
6. D. FOX, M. M. LABES, and A. WEISSBERGER (*Editors*). Physics and chemistry of the organic solid state. John Wiley and Sons. 1963. (*a*) Chapt. 1, (*b*) Chapt. 9.
7. R. RUDMAN and B. POST. Mol. Cryst. **5**, 96 (1968).
8. J. E. TANNER. J. Chem. Phys. **56**, 3850 (1972).
9. R. C. LIVINGSTON, W. G. ROTHSCHILD, and J. J. RUSH. J. Chem. Phys. **59**, 2498 (1973).
10. T. MÅNSSON, L. G. OLLSON, and K. E. LARRSON. J. Chem. Phys. **66**, 5817 (1977).
11. T. C. FARRAR and E. D. BECKER. Pulse and Fourier transform nmr. Academic Press, New York. 1971.
12. A. ABRAGAM. The principles of nuclear magnetism. Oxford University Press, London. 1961.
13. J. C. ROWELL, W. D. PHILLIPS, L. R. WHELBY, and M. PANAR. J. Chem. Phys. **43**, 3442 (1965).

14. P. S. HUBBARD. Phys. Rev. **131**, 1155 (1963).
15. J. R. LYERLA and G. C. LEVY. Topics in carbon-13 nmr spectroscopy. Vol. 1. *Edited by* G. C. Levy. Wiley, New York. 1974. Chapt. 3.
16. (*a*) D. M. GRANT, K. A. STRONG, and R. M. BRUGGER. Phys. Rev. Lett. **20**, 983 (1968); (*b*) S. WEISS and G. E. LEROI. Spectrochim. Acta, **25**A, 1759 (1969).
17. W. B. MONIZ, W. A. STEELE, and J. A. DIXON. J. Chem. Phys. **38**, 2418 (1963).
18. P. W. ATKINS, A. LOEWENSTEIN, and Y. MARGALIT. Mol. Phys. **17**, 329 (1969).
19. (*a*) E. O. STEJSKAL, D. E. WOESSNER, T. C. FARRAR, and H. S. GUTOWSKY. J. Chem. Phys. **31**, 55 (1959); (*b*) S. B. W. ROEDER and D. C. DOUGLASS. J. Chem. Phys. **52**, 5525 (1970); (*c*) W. C. ALLEN, N. LIU, and J. JONAS. J. Chem. Phys. **63**, 3317 (1975).
20. R. E. WASYLISHEN and B. A. PETTITT. Mol. Phys. In press.
21. N. BODEN and R. FOLLAND. Chem. Phys. Lett. **32**, 127 (1975).
22. W. H. FLYGARE. Chem. Rev. **74**, 653 (1974).
23. N. F. RAMSEY. Phys. Rev. **78**, 699 (1950).
24. W. H. FLYGARE and J. GOODISMAN. J. Chem. Phys. **49**, 3122 (1968).
25. K. T. GILLEN, J. H. NOGGLE, and T. K. LEIPERT. Chem. Phys. Lett. **17**, 505 (1972).
26. C. DEVERELL. Mol. Phys. **18**, 319 (1970).
27. R. ETTINGER, P. BLUME, A. PATTERSON, and P. C. LAUTERBUR. J. Chem. Phys. **33**, 1597 (1960).
28. I. OZIER, L. M. CRAPO, and N. F. RAMSEY. J. Chem. Phys. **49**, 2314 (1968).
29. J. B. STOTHERS. Carbon-13 nmr spectroscopy. Academic Press, New York. 1972.

Can. J. Chem. Downloaded from www.nrcresearchpress.com by 210.87.254.105 on 09/05/12
For personal use only.

Mechanism of S_Ni reactions. The effect of the base strength of the anionic fragments[1]

D. J. VERRINDER, M. J. HOURIGAN, AND J. M. PROKIPCAK[2]

Department of Chemistry, University of Guelph, Guelph, Ont., Canada N1G 2W1

Received July 4, 1977[3]

D. J. VERRINDER, M. J. HOURIGAN, and J. M. PROKIPCAK. Can. J. Chem. **56**, 2582 (1978).

The kinetics and stereochemical aspects of the thermal decomposition of aralkyl carbonates, thiocarbonates, and carbamates were examined. The rates for the decompositions as well as the rates of loss of optical activity followed first-order kinetics. The decompositions appear to involve the heterolysis of the aralkyl–oxygen bond followed by the breakdown of the subsequent ion pair via a cyclic mechanism. However, it was found that this ion pair could return to covalency without completely decomposing to products leading to the racemization of the starting materials. This type of racemization occurred more readily in the case of the carbamates than in the thiocarbonates and carbonates. The dependence of the decomposition rates and the loss of optical activity on the nature of the hetero atom of the anionic fragment of the starting material is discussed.

D. J. VERRINDER, M. J. HOURIGAN et J. M. PROKIPCAK. Can. J. Chem. **56**, 2582 (1978).

On a étudié la cinétique et l'aspect stéréochimique de la décomposition thermique de carbonates, thiocarbonates et de carbamates d'aralkyles. Les vitesses de décomposition de même que les vitesses de perte d'activité optique suivent une cinétique du premier ordre. Il semble que les décompositions impliquent une hétérolyse du lien oxygène–aralkyle suivie par une décomposition subséquente de la paire d'ions par l'intermédiaire d'un mécanisme cyclique. Toutefois on a trouvé que cette paire d'ions peut effectuer un retour vers une covalence sans se décomposer complètement en produits conduisant à une racémisation des produits de départ. Ce type de racémisation se produit plus facilement dans le cas des carbamates que dans le cas des thiocarbonates et des carbonates. On discute du fait que les vitesses de décomposition et de perte d'activité optique dépendent de la nature de l'hétéroatome de la fraction anionique du produit de départ.

[Traduit par le journal]

Introduction

Previous work (1) has indicated that the thermal fragmentation of aralkyl carbonates followed a path similar to that found for the thermal fragmentation of thiocarbonates (2, 3). Both of these decompositions appear to involve a mechanism involving heterolysis of the aralkyl–oxygen bond with subsequent formation of ion-pair intermediates. Moreover, the dependence of the rates on the nature of the aralkyl group indicates that this cleavage occurs in the transition state of the rate-determining step. The two possible modes of decomposition are outlined in Scheme 1 where B can be S or O. Path *1* which involves two successive bond cleavages (aralkyl–oxygen bond followed by carbonyl–oxygen bond) appears to best accommodate experimental work to date. However consideration must still be given to Path *2* where the two bonds are broken simultaneously. Regardless of whether Path *1* or Path *2* is followed, the overall process is still considered to be an S_Ni reaction since random recombination of the fragments does not occur to any appreciable extent as would be expected if the process were completely ionic in nature (1).

Although the decompositions of carbonates and thiocarbonates have been studied separately, no attempts to compare these decompositions under the same reaction conditions have been found. If one could extend the comparison to include the analogous carbamate series i.e., where B = NH; it would be possible to investigate the effect that the hetero atom B has on the decompositions as B goes from N to O to S. This would lead to some indication of the importance which the nucleophilic character of the anion portion (ϕS^-, ϕO^-, and ϕNH^-) has on the decomposition rates. This report involves a kinetic and stereochemical study of the decompositions of a series of carbonates (**1**), thiocarbonates (**2**), and carbamates (**3**). The required feature of the compounds investigated was the presence of an anisylic group (*p*-methoxybenzyl). This choice was necessary to ensure that all the decompositions would occur at a rate rapid enough to be conveniently measured.

All the decompositions studied did follow first-order kinetics over at least 75% of the reaction. The carbonates and thiocarbonates decomposed reasonably fast at temperature ranges of 100–150 and 70–

[1]Taken from the theses of D. J. Verrinder and M. J. Hourigan presented to the Faculty of Graduate Studies, University of Guelph, Guelph, Ont., as part of the requirements for the degrees of M.Sc.

[2]To whom correspondence should be sent.

[3]Revision received May 2, 1978.

Can. J. Chem. Downloaded from www.nrcresearchpress.com by 210.87.254.105 on 09/05/12
For personal use only.

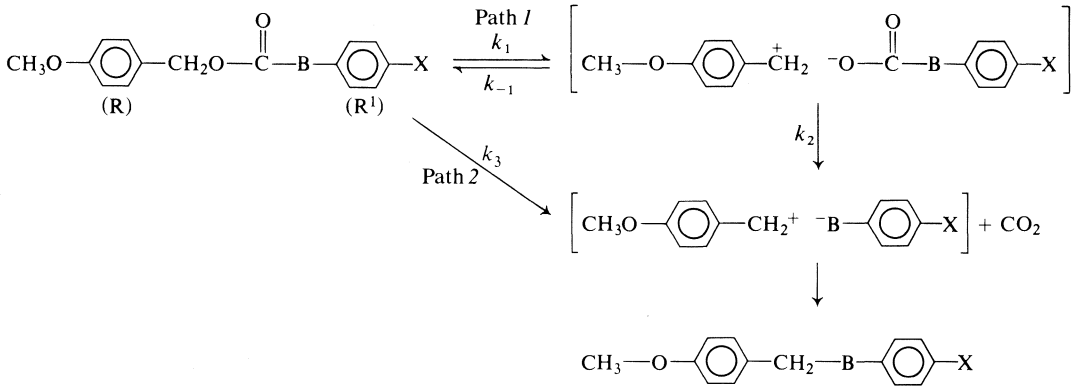

SCHEME 1

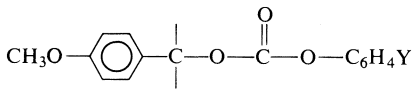

1

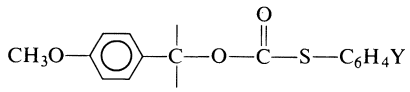

2

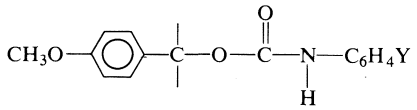

3

130°C, respectively, to give the corresponding ether and thioether. The carbamates however, did require higher temperatures (minimum of 170°C) and product identification was much more difficult because of a greater variety of side products such as ring substituted anilines and diphenyl urea.

The stereochemical studies were carried out on systems where the aralkyl group was *p*-methoxybenzhydryl. The chiral centre was generated by the presence of a phenyl group rather than an alkyl group in order to prevent any complicating elimination reactions from occurring along with the desired decompositions. The variations of the decomposition rates owing to the hetero atom B, the effect of solvent polarity as well as the stereochemistry at the chiral centre was investigated.

Experimental

Synthesis of Carbonates, Thiocarbonates, and Carbamates

Anisyl alcohol was available commercially and was used without any further purification. *p*-Methoxybenzhydryl alcohol was prepared by the reaction of phenyl magnesium bromide with anisaldehyde (4-methoxybenzaldehyde) according to the method of Balfe and co-workers (4). These alcohols were then converted to carbonates by reacting them with phenyl chloroformate (5) and to thiocarbonates by reacting them with phenyl chlorothiolformate (2). The carbamates were made by the well documented reaction of the alcohols with phenyl isocyanate. The physical constants and analyses for previously unreported starting compounds are given in Table 1. All melting points were determined on the Fisher-Johns melting point apparatus and are uncorrected. Information on any compounds used in this study but not appearing in Table 1 can be found in earlier work (1, 5).

Product Identification of the Decomposition Reactions

Experimental data will not be given for the identification of products previously reported, namely the ethers obtained from the decomposition of the carbonates. Decomposition of the carbamates gave products which were not readily isolateable. However mass spectral data and combined chemical reactions indicate the expected *N*-substituted anilines along with ring substituted anilines and diphenyl urea were obtained in the reaction.

The decomposition of the thiocarbonates did give excellent yields of thioethers. Since these thioethers have not been previously reported, the data will be given for them. Decomposition of anisyl phenyl thiocarbonate gave anisyl phenyl thioether, mp 83–84°C, in an 80% yield which had the following spectral data: nmr ($CDCl_3$) δ(ppm): 3.65 (3H singlet, (CH_3O)), 4.89 (2H singlet, methylene), 6.70–7.21 (9H multiplet, aromatic). *Anal.* calcd. for $C_{14}H_{14}OS$: C 73.01, H 6.13; found: C 72.81, H 6.35. Decomposition of *p*-methoxybenzhydryl phenyl thiocarbonate gave *p*-methoxybenzhydryl phenyl thioether, mp 94–96°C, in an 85% yield. The following spectral data was obtained: nmr ($CHCl_3$) δ(ppm): 3.73 (3H singlet, CH_3O), 5.55 (1H singlet, methine), 6.77–7.45 (14H multiplet, aromatic). *Anal.* calcd. for $C_{20}H_{18}OS$: C 78.38, H 5.93; found: C 78.12, H 6.06.

Resolution of 4-Methoxybenzhydrol

A mixture of *dl*-4-methoxybenzhydrol was converted to *dl*-4-methoxybenzhydryl hydrogen phthalate using the method of Balfe *et al.* (4). The following method was used to resolve the *dl* mixture. A slurry of 4-methoxybenzhydryl hydrogen phthalate (100 g, 0.278 mol) in 320 ml of warm ethyl acetate was added to a magnetically stirred suspension of (−)-cinchonidine (83.9 g, 0.285 mol) in 50 ml of ethyl acetate. Recrystallizations from ethyl acetate were carried out until a white powder of cinchonidine (+)-4-methoxybenzhydryl phthalate (35.6 g), mp 138–141°C (lit. (4) mp 143–144°C) was obtained. Removal of the solvent *in vacuo* from the mother liquor yielded a solid which after several recrystallizations from acetone resulted in

Can. J. Chem. Downloaded from www.nrcresearchpress.com by 210.87.254.105 on 09/05/12
For personal use only.

Can. J. Chem. Downloaded from www.nrcresearchpress.com by 210.87.254.105 on 09/05/12
For personal use only.

TABLE 1. The preparation of carbonates, thiocarbonates, and carbamates

Compound	Melting point (°C)	Yield (%)	Analysis (%) C Calcd.	C Found	H Calcd.	H Found	N Calcd.	N Found	S Calcd.	S Found
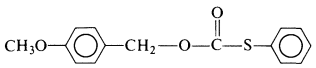	49–50	57	65.66	65.32	5.14	5.28	—	—	11.70	12.16
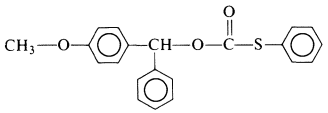	102–103	87	71.97	71.86	5.19	5.22	—	—	9.14	9.02
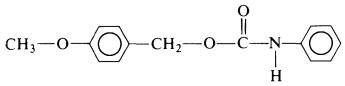	91–92	67	70.02	69.67	5.88	5.82	5.44	5.36	—	—
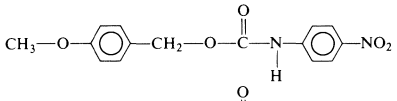	149–151	98	59.60	59.21	4.67	4.41	9.27	9.27	—	—
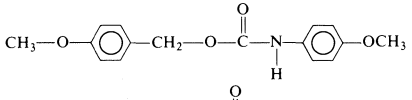	96–98	72	66.88	67.02	5.96	5.96	4.88	4.81	—	—
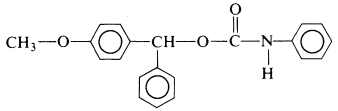	91–93	82	75.65	75.93	5.76	5.54	4.20	4.38	—	—

Can. J. Chem. Downloaded from www.nrcresearchpress.com by 210.87.254.105 on 09/05/12
For personal use only.

a white powder of cinchonidine(−)-4-methoxybenzhydryl phthalate (54.6 g), mp 106–110°C.

The hydrolysis of the cinchonidine salt was carried out in the following manner. A cooled solution of cinchonidine(−)-4-methoxybenzhydryl phthalate (20.0 g, 0.055 mol) in 200 ml benzene was washed with an ice-cold solution of 45 g ammonium chloride in 150 ml of 4% hydrochloric acid. The organic layer was quickly separated and washed with ice-cold water (3 × 150 ml). The benzene layer was dried over anhydrous sodium sulfate. When the solvent was removed *in vacuo*, a white precipitate of (−)-4-methoxybenzhydryl hydrogen phthalate was obtained which was immediately dissolved in 100 ml of anhydrous ether. This ethereal solution was added slowly with stirring to a suspension of lithium aluminum hydride (2.28 g, 0.060 mol) in 100 ml anhydrous ether. After the addition, the reaction mixture was stirred at room temperature for 2 h and was then hydrolyzed by the addition of first 2.3 ml of water, then 2.3 ml of 15% sodium hydroxide, and finally 6.9 ml of water. The reaction mixture was filtered and the solvent removed *in vacuo*. The resultant oil was dissolved in chloroform, dried, and then the solvent removed to give a solid which upon recrystallization from chloroform – petroleum ether (bp 30–60°C) resulted in transparent needle-like crystals, mp 63.0–64.0°C of pure (−)-4-methoxybenzhydrol, $[\alpha]_D^{20}$ −31.6° (*c* 2.31, $CHCl_3$).

The (−)-4-methoxybenzhydrol was converted to the thiocarbonate and carbamate whereas the (+)-4-methoxybenzhydrol was used to prepare the carbonate. These were all prepared using the methods already described and the optical rotations of the final compounds are given for hexamethylphosphoramide (HMP) solutions: (−)-4-methoxybenzhydryl *S*-phenyl thiocarbonate, $[\alpha]_D^{20}$ −24.0°; (+)-4-methoxybenzhydryl phenyl carbonate, $[\alpha]_D^{20}$ +15.9°; (−)-4-methoxybenzhydryl *N*-phenyl carbamate, $[\alpha]_D^{20}$ −14.5°.

Kinetics of the Decompositions

The decompositions of all the anisyl and 3,4-dimethoxybenzyl carbonates, carbamates, and thiocarbonates were followed using nmr techniques outlined in a previous paper (1). However, this method could not be used for the *p*-methoxybenzhydryl system since there was no reasonable separation in the nmr spectrum between the methylene peak of the parent compounds and the corresponding products. Since all the starting compounds had a carbonyl group which gave a strong absorption band in the infrared over the region 1765–1730 cm^{-1} and since this absorption was not close to any other major absorptions, the base-line method was used to analyze each ir spectrum. Furthermore, earlier experiments with standard solutions of the various starting compounds in the various solvents employed for the decompositions showed that, over a convenient range, a plot of absorbance of the carbonyl band versus concentration of solution was satisfactorily linear and thus satisfied Beer's law. A typical kinetic run will be outlined below for the thiocarbonate.

The thiocarbonate (6.68 g, 0.019 mol) was dissolved in HMP to a volume of 10 ml. Ten aliquots (0.40 ml) were placed in tubes and these tubes were simultaneously placed in a thermostatically controlled (90±0.2°C) oil bath. Tubes were removed at specified time intervals and immediately quenched in a Dry Ice – acetone bath. Chloroform (1.0 ml) was added to each tube, each tube was shaken to ensure mixing, and an ir of the carbonyl absorption region (1670–2000 cm^{-1}) was taken. Each solution was run three times against a blank solution of 0.4 ml HMP in 1.0 ml chloroform. The base-line method was used to analyze each spectrum and the average absorbance ($\log P_0/P$) was calculated for each solution. The average absorbance was multiplied by the slope of the Beer's Law plot to give the concentration of the sample. The plot of log concentration vs. time in seconds was made and the method of weighted least squares was used to get the slopes of the lines.

In the case of the stereochemical studies, the samples from the reaction tubes were analyzed on a Beckmann 141 automatic polarimeter, using a 0.1 dm polarimeter cell maintained at 20±0.2°C with a sodium D line (λ = 589 nm) light source. The value for the optical rotation was determined for each sample and then the log of the optical rotation was plotted vs. time in seconds to get the rate of loss of optical rotation.

Results and Discussion

Kinetics

Using the aforementioned method, good first-order kinetics were obtained for all the decompositions and the first-order rate constants were calculated. Table 2 shows the results of the kinetic studies and indicates the dependence of the decomposition rates on the nature of the aralkyl group, on the nature of the phenyl substituents, and on the nature of the hetero atom i.e., S, O, and N attached to the phenyl group.

The nature of the substituent on the phenyl group showed very little effect on the decomposition rates although electron withdrawing groups did enhance the rate constants slightly. This is in accordance with results from previous work (1) which showed that dispersal of a negative charge was involved and any electron-withdrawing group is able to help stabilize the negative species. There was however a more noticeable variation in decomposition rate as the aralkyl group was altered. In all cases when the aralkyl group was changed from anisyl to *p*-methoxylbenzhydryl, the decomposition rates increased appreciably. Except for the unexpected behaviour of the 3,4-dimethoxylbenzyl system, it appears that as the aralkyl group's ability to stabilize an electron deficient centre increased, the decomposition rates increased. This would indicate that an intermediate was involved which had some carbonium ion character.

Finally, as the hetero atom changed from S to O to N, the decomposition rates were greatly reduced and higher temperatures were required to effect decomposition. It would thus seem that the base properties of the hetero atom are important in the rates: the more basic the hetero atom, the slower the decomposition rate.

Solvent Effects

The rates of decomposition were carried out in hexamethylphosphoramide, benzonitrile, and diphenyl ether, solvents with different dielectric constants. In most cases, the rates of decomposition were enhanced by using the more polar solvent indicating some kind of ionization process is occurring. The one discrepancy in the solvent effect studies was the *p*-methoxybenzhydryl *N*-phenyl carbamate which

TABLE 2. Kinetics for the decompositions of carbonates, thiocarbonates, and carbamates

Compound	Temperature (°C)	Solvent*	Rate constant k_1 (s^{-1})	$\Delta H^{\neq}$ (kcal mol^{-1})	$\Delta S^{\neq}$ (eu)
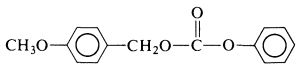	150	HMP	$1.74\pm0.09\times10^{-4}$	29.5±1.4	−6.29±2.25
	150	BN	$2.12\pm0.11\times10^{-4}$†	18.8±1.2	−31.6 ±1.6
	150	DPE	Too slow to measure†		
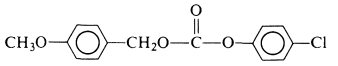	150	HMP	$8.36\pm0.14\times10^{-4}$	24.2±1.2	−15.8 ±1.6
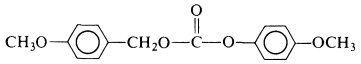	150	HMP	$1.61\pm0.06\times10^{-4}$	20.0±0.9	−29.1 ±1.7
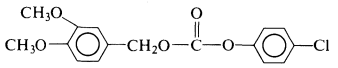	150	HMP	$1.91\pm0.06\times10^{-3}$	19.2±1.0	−26.3 ±1.5
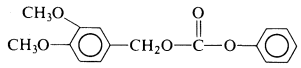	150	HMP	$3.02\pm0.09\times10^{-4}$†		
	150	BN	$5.42\pm0.16\times10^{-5}$†		
	150	DPE	Too slow to measure†		
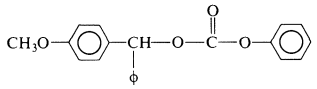	120	HMP	$1.61\pm0.04\times10^{-3}$	27.1±1.1	−2.89±0.87
	120	BN	$1.08\pm0.05\times10^{-2}$		
	120	DPE	$5.24\pm0.36\times10^{-4}$		
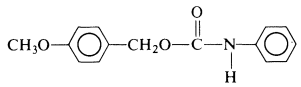	170	HMP	$2.00\pm0.09\times10^{-4}$	30.3±1.4	−7.65±2.09
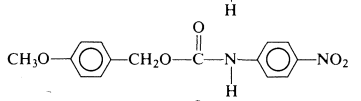	170	HMP	$3.17\pm0.11\times10^{-4}$	20.6±1.4	−28.4 ±2.5
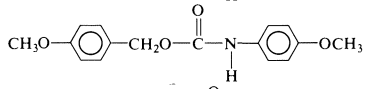	173	HMP	$3.24\pm0.07\times10^{-4}$	26.8±1.4	−14.9 ±2.6
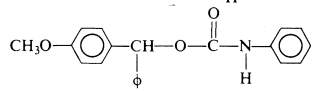	170	HMP	$1.04\pm0.10\times10^{-3}$	30.9±1.6	−7.87±3.16
	170	BN	$5.84\pm0.52\times10^{-4}$		
	170	DPE	$1.46\pm0.13\times10^{-4}$		
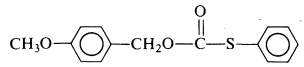	150	HMP	$3.20\pm0.07\times10^{-4}$	15.8±1.0	−33.1 ±1.6
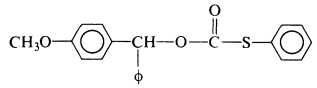	70	HMP	$7.42\pm0.15\times10^{-4}$	21.8±0.5	−9.58±0.93
	70	BN	$1.89\pm0.05\times10^{-3}$		
	70	DPE	$5.25\pm0.22\times10^{-5}$		

*Hexamethylphosphoramide (HMP); diphenyl ether (DPE); benzonitrile (BN).
†Taken from previous work (1) for comparison purposes.

showed no apparent solvent effect. This lack of solvent effect could point to a more concerted mechanism being operative for the carbamate in which the transition state has no appreciable ionic character.

Activation Parameters

The activation parameters for various systems were determined in an attempt to shed some light on the nature of the intermediates involved in the different decompositions. These values were calculated using the method of Purlee *et al.* (6) and are found in Table 2. The $\Delta H^{\neq}$ calculations do indicate that more energy is required to break bonds as we go from S to O to N which coincides with the relative basicities of the three elements. Any other immediate information from the data was not apparent. However when a plot of $\Delta H^{\neq}$ vs. $\Delta S^{\neq}$ was made (Fig. 1), a very interesting correlation was found. All but two of the starting compounds investigated were found to follow a relationship defined by Leffler (7) as the compensation effect. These compounds were found to show a dependence between their entropy and enthalpy values i.e., a large enthalpy value was associated with a low entropy value and vice versa. Furthermore this relationship held in various solvents as well. The fact that the correlation of enthalpy and entropy approaches a linear relationship was thought to be indicative of a series of related reactions which involve a similar transition state. Thus an increased amount of bond stabilization with a subsequent increase in $\Delta H^{\neq}$ leads to an increase in the rigidity of the transition state and subsequently a more negative

Can. J. Chem. Downloaded from www.nrcresearchpress.com by 210.87.254.105 on 09/05/12
For personal use only.

Can. J. Chem. Downloaded from www.nrcresearchpress.com by 210.87.254.105 on 09/05/12
For personal use only.

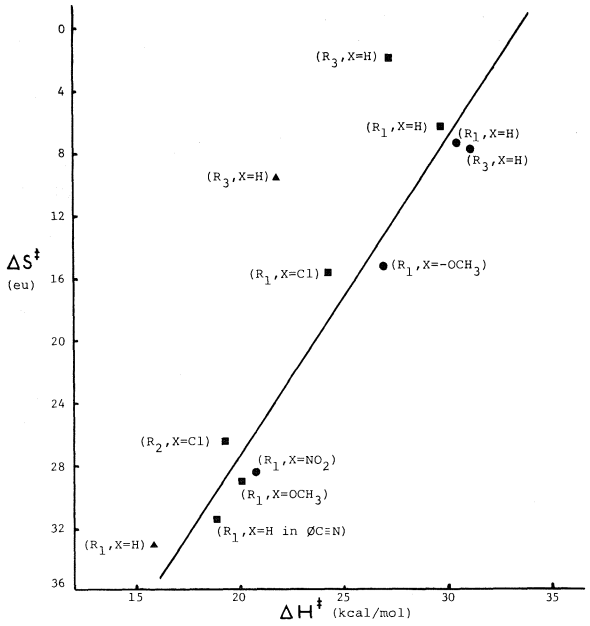

FIG. 1. $\Delta S^{\ddagger}$ values plotted against $\Delta H^{\ddagger}$ values:

carbonates ■ R—O—C(=O)—O—⟨⟩—X,

carbamates ● R—O—C(=O)—N(H)—⟨⟩—X,

thiocarbonates ▼ R—O—C(=O)—S—⟨⟩—X;

$R_1 = CH_3O$—⟨⟩—CH_2—, $R_2 = CH_3$—O—⟨⟩—CH_2— (CH_3O),

$R_3 = CH_3O$—⟨⟩—CH(Ø)—; hexamethylphosphoramide (HMP) was the solvent in all but one case.

$\Delta S^{\ddagger}$ value. These conclusions are consistent with Scheme 1. It is felt that the reason the benzhydryl carbonate and thiocarbonate did not obey the relationship is a direct result of the very stable *p*-methoxybenzhydryl carbonium ion which can form. A more detailed explanation of this is given in the interpretation of the combined kinetic and stereochemical data.

Stereochemical Studies

All previous work (1) thus far appear to point to at least some formation of an aralkyl carbonium ion. Indeed Kice *et al.* (3) found that in the decomposition of 4-chlorobenzhydryl *S*-aryl thiocarbonates, racemization resulting from carbonium ion – carboxylate ion pair formation and recombination was occurring at a faster rate than decomposition. In an effort to see the extent of ion-pair formation, studies were carried out on the carbonates, thiocarbonates and carbamates. The decomposition rates and rates of loss of optical activity were carried out simultaneously. All the compounds studied (Table 3) showed a first-order rate dependence on optical activity.

All the systems were found to racemize at rates faster than their decomposition rates. This racemization process can be accommodated by the mechanism in Scheme 1 where there is heterolysis of the aralkyl bond with formation of ion pairs followed by rapid ion-pair return to reactants. The rates of decomposition of the anisyl and 4-methoxybenzhydryl compounds were quite similar and this coupled with relatively small solvent response is consistent with a cyclic type of transition state proposed for analogous reactions (8).

To interpret the results of the kinetic and stereochemical investigations, and check the validity of the qualitative hypotheses described, Scheme 2 was introduced for the decompositions. This scheme includes optical activity aspects explicitly. The first-order behaviour observed in the stereochemical investigation can be explained as follows.

Optical rotation

$$\alpha = c([(+)R] - [(-)R])$$

where c = constant
thus

$$\frac{d\alpha}{dt} = c\left(\frac{d[(+)R]}{dt} - \frac{d[(-)R]}{dt}\right)$$

$$= c(-k_1[(+)R] + k_{-1}[IP] + k_1[(-)R] - k_{-1}[IP])$$

$$= -k_1 c([(+)R] - [(-)R])$$

$$= -k_1\alpha$$

This allows identification of k_1 and the k_α, the rate constant for loss of optical activity.

The first-order decomposition behaviour can be accounted for by considering the following expressions:

$$d[IP]/dt = k_2[IP]$$

Assuming the steady-state approximation

$$d[IP]/dt = k_1([(+)R] + [(-)R]) - (2k_{-1} + k_2)[IP] \cong 0$$

or

$$[IP] \cong \left(\frac{k_1}{2k_{-1} + k_2}\right)([(+)R] + [(-)R])$$

Thus

TABLE 3. Rates of decomposition and loss of optical activity

Compound	Temperature*	$k_\alpha \times 10^4$† (s^{-1})	$k_d \times 10^4$ (s^{-1})	k_α/k_d
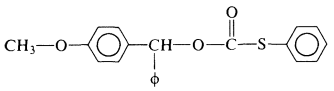	40	1.00	Too slow to measure	3 (approx.)
	60	7.89	2.45	
	70	17.8	7.35	
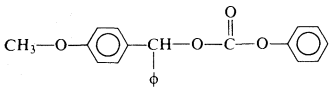	70	0.669	Too slow to measure	5 (approx.)
	90	4.25	0.810	
	100	9.93	2.23	
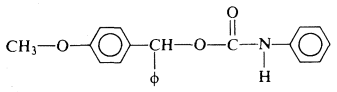	120	Too slow to measure	Too slow to measure	10 (approx.)
	170	12.3	1.23	
	180	24.2	2.49	

*Other temperatures were used but similar results were obtained.
†k_α (rate constant for optical activity loss) had regression coefficients of at least 0.9970.

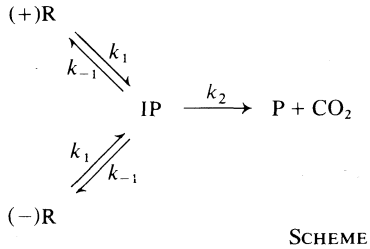

R represents the enantiomers of the carbonate, carbamate, or thiocarbonate
IP represents ion pairs
P represents the products

SCHEME 2

$$\frac{d[IP]}{dt} = \left(\frac{k_1k_2}{2k_{-1} + k_2}\right)([(+)R] + [(-)R])$$

Since the observable used was the carbonyl peak and since this should be proportional to ([(+)R] + [(−)R]), we have a normal first-order rate constant k_d where

$$k_d = k_1k_2/(2k_{-1} + k_2)$$

where

$$k_1 = k_\alpha$$

therefore

$$d[P]/dt = k_d([(+)R] + [(-)R])$$

Furthermore

$$\frac{k_\alpha}{k_d} = \frac{\text{rate of racemization}}{\text{rate of decomposition}}$$

$$= \frac{2k_{-1} + k_2}{k_2}$$

$$= \frac{2k_{-1}}{k_2} + 1$$

But from Table 3 k_α/k_d varies from ≈ 3 to ≈ 5 and thus $2k_{-1}/k_2$ varies from ≈ 1 to ≈ 4. Thus, there is no possibility of reducing the expression for k_d by assuming that $k_{-1} \ggg k_2$.

In the treatment of the stereochemical studies, a slight simplification was made. In the discussion it was assumed that the ion pairs formed in the decompositions could undergo return to substrate equally well with retention and inversion of configuration. However it has been shown (3) that the return of this ion pair is more likely to occur with retention of configuration rather than inversion. This would lead to a racemization rate constant k_α which would be slightly less than the first-order constant k_1 rather than equal to it. This simplification was made to allow less complex rate expressions to be used and does not alter the validity of any of the major conclusions made.

Conclusions

In conclusion, the results from the thermal decompositions of the carbonates, thiocarbonates and carbamates appear to be consistent with a mechanism involving heterolytic aralkyl–oxygen cleavage resulting in an ion-pair formation. The ion pair may return to reactants with loss of optical activity (Path *1* of Scheme 1) or undergo complete decomposition to carbon dioxide and the corresponding ether, thioether, or amine. The ion pair return to reactants occurs more readily in the case of the carbamates and least in the thiocarbonates, whereas complete decomposition to products follows the reverse order.

Can. J. Chem. Downloaded from www.nrcresearchpress.com by 210.87.254.105 on 09/05/12
For personal use only.

The differences in the behaviour for the decompositions can be accounted for by the fact that the ϕS^- and ϕO^- represent much better leaving groups than ϕNH^-, so that in the thiocarbonate and carbonate decompositions, cleavage of $\phi-S-\overset{\overset{O}{\|}}{C}-O^-$ and $\phi-O-\overset{\overset{O}{\|}}{C}-O^-$ to CO_2 and ϕS^- and ϕO^- occurs more readily and leads to products. In the case of the carbamate, cleavage of $\phi NH-\overset{\overset{O}{\|}}{C}-O^-$ to ϕNH^- and CO_2 does not occur as readily and return to reactant occurs more readily. This is expected if one accepts that the differences in stability of the carboxylate anions coincides with the differences in basicity of ϕNH^-, ϕO^-, and ϕS^-. A qualitative indication can be obtained for this if one considers the k_α/k_d ratio. The stronger the base fragment such as ϕNH^- the more likely ion pair will return to reactants and hence k_α/k_d would be larger since $k_\alpha \gg k_d$. Conversely, for a weaker base such as ϕS^-, the more likely decomposition would be faster and k_α/k_d would be smaller in magnitude since $k_\alpha \ll k_d$. Thus the k_α/k_d values of approximately 3,5, and 10 for the thiocarbonate, carbonate, and carbamate appears to coincide with the order of base strengths which in turn parallels the ΔH values for the initial bond cleavage. Therefore it appears the base characteristics of the hetero atom B in Scheme 1 does play an important role in the mode of decompositions.

Acknowledgements

The authors wish to thank the National Research Council of Canada for financial assistance for this research. Also thanks are extended to Dr. R. K. Boyd of this department for his assistance in the development of the rate expressions which were used in this work.

1. J. M. Prokipcak and T. H. Breckles. Can. J. Chem. **50**, 1770 (1972).
2. J. L. Kice, R. A. Bartsch, M. A. Dankleff, and S. L. Schwartz. J. Am. Chem. Soc. **87**, 1734 (1965).
3. J. L. Kice, R. L. Scriven, E. Koubek, and M. Barnes. J. Am. Chem. Soc. **92**, 5608 (1970).
4. M. P. Balfe, M. A. Doughty, J. Kenyon, and R. Poplett. J. Chem. Soc. 605 (1942).
5. J. M. Prokipcak and T. H. Breckles. Can. J. Chem. **49**, 914 (1971).
6. E. L. Purlee, R. W. Taft, Jr., and C. A. De Fazio. J. Am. Chem. Soc. **77**, 837 (1955).
7. J. E. Leffler. J. Org. Chem. **20**, 1202 (1955).
8. E. Dyer and G. C. Wright. J. Am. Chem. Soc. **81**, 2138 (1959).

Can. J. Chem. Downloaded from www.nrcresearchpress.com by 210.87.254.105 on 09/05/12
For personal use only.

The radical addition of *N*-haloamides to 1,6-heptadiene: The transfer step in the photochemical and chromous chloride promoted addition of *N*-haloamides to olefins[1,2]

MARTINE MONDON[3] and JEAN LESSARD

Département de chimie, Université de Sherbrooke, Sherbrooke (Qué.), Canada J1K 2R1

Received April 25, 1978

MARTINE MONDON and JEAN LESSARD. Can. J. Chem. **56**, 2590 (1978).

A study of the photochemical addition of *N*-haloamides (ZCONHX) to 1,6-heptadiene shows that the reactivity of ZCONHX as an halogen-atom donor to an alkyl radical increases with Z in the order $CH_3 < ClCH_2 < OC_2H_5 \leq CCl_3 \sim CF_3$ which indicates a polar character of the transition state. An *N*-bromoamide is shown to be more reactive than an *N*-chloroamide as expected. The chromous chloride promoted addition of *N*-chlorochloroacetamide and *N*-chlorotrichloroacetamide to 1,6-heptadiene is compared with the photochemical addition under similar conditions of solvent and temperature. The better interpretation of the results, for the chromous chloride promoted additions, is in terms of a classical chain mechanism rather than a redox chain mechanism; the latter mechanism cannot be excluded however.

MARTINE MONDON et JEAN LESSARD. Can. J. Chem. **56**, 2590 (1978).

Une étude de l'addition photochimique de *N*-haloamides (ZCONHX) à l'heptadiène-1,6 montre que la réactivité de ZCONHX, en ce qui a trait à l'attaque d'un radical alkyle sur l'halogène, croit avez Z dans l'ordre suivant: $CH_3 < ClCH_2 < OC_2H_5 \leq CCl_3 \sim CF_3$. Ceci indique un certain caractère polaire de l'état de transition. On démontre qu'un *N*-bromoamide est plus réactif qu'un *N*-chloroamide tel que prévu. L'addition du *N*-chlorochloroacétamide et du *N*-chlorotrichloroacétamide, catalysée par le chlorure chromeux, est comparée à l'addition photochimique dans un même solvant et à la même température. Les résultats s'expliquent mieux si les additions catalysées par le chlorure chromeux font intervenir un mécanisme en chaine classique plutôt qu'un mécanisme en chaine de type redox mais n'excluent pas ce dernier.

Introduction

In the chromous chloride promoted addition of *N*-haloamides (ZCONHX) to olefins, we observed that the ratio of 1,2-addition ([2] and [3]) to 1,H-addition ([2] and [4]) was larger for X = Br than for X = Cl and increased with Z in the order $CH_3 < ClCH_2 < C_2H_5O \leq CCl_3 \sim CF_3$ (1). These observations were explained using the mechanistic hypothesis summarized by eqs. [1]–[5] (2).

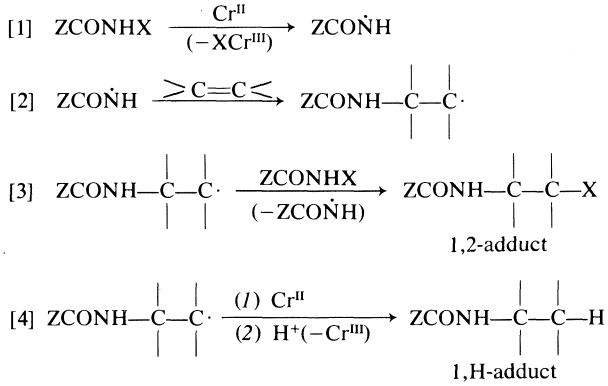

[1] $ZCONHX \xrightarrow[(-XCr^{III})]{Cr^{II}} ZCO\dot{N}H$

[2] $ZCO\dot{N}H + >C=C< \rightarrow ZCONH-\overset{|}{\underset{|}{C}}-\overset{|}{\underset{|}{C}}\cdot$

[3] $ZCONH-\overset{|}{\underset{|}{C}}-\overset{|}{\underset{|}{C}}\cdot \xrightarrow[(-ZCO\dot{N}H)]{ZCONHX} ZCONH-\overset{|}{\underset{|}{C}}-\overset{|}{\underset{|}{C}}-X$ (1,2-adduct)

[4] $ZCONH-\overset{|}{\underset{|}{C}}-\overset{|}{\underset{|}{C}}\cdot \xrightarrow[(2)\ H^+(-Cr^{III})]{(1)\ Cr^{II}} ZCONH-\overset{|}{\underset{|}{C}}-\overset{|}{\underset{|}{C}}-H$ (1,H-adduct)

[5] $ZCO\dot{N}H \xrightarrow[(2)\ H^+(-Cr^{II})]{(1)\ Cr^{II}} ZCONH_2$

The competition between the transfer step [3] and the termination step [4] implies that the better the transfer agent, the larger should be the 1,2-addition to 1,H-addition ratio for a given olefin. Indeed, an *N*-bromoamide (bromide-atom transfer) should be a better transfer agent than an *N*-chloroamide (chlorine-atom transfer). We were then led to hypothesize that the reactivity of the *N*-haloamide as transfer agent would increase with the electron-withdrawing power of the ZCO moiety as a result of an increasing polar contribution to the stabilization of the transition state (2).[4]

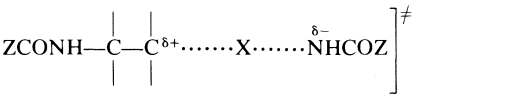

$$\left[ZCONH-\overset{|}{\underset{|}{C}}-\overset{|}{\underset{|}{C^{\delta+}}}\cdots\cdots X\cdots\cdots \overset{\delta-}{N}HCOZ \right]^{\neq}$$

To verify this hypothesis, we studied the photochemical addition of ZCONHX (**1**) to 1,6-heptadiene (**2**) for which the adduct **3** to adduct **4** ratio (Scheme 1) would be expected to increase with the reactivity of ZCONHX as an halogen-atom transfer agent (the photochemical addition of *N*-haloamides to olefins has been shown to proceed by a radical chain mechanism as expected (3)). We also compared the photo-

[1]Abbreviated from the Ph.D. Thesis of M. Mondon, Université de Sherbrooke, 1977.

[2]Presented in part at the 2nd joint Conference, Chemical Institute of Canada – American Chemical Society, Montreal P.Q., June 1977.

[3]Arts Council of Canada Predoctorate Fellow, 1973–1975.

[4]A polar transition state has been proposed for the attack on *C*-halogen bonds by carbon radicals (4).

Can. J. Chem. Downloaded from www.nrcresearchpress.com by 210.87.254.6 on 09/05/12
For personal use only.

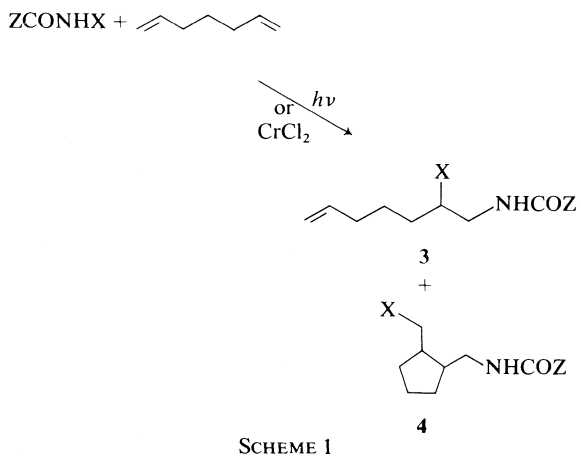

SCHEME 1

chemical and the chromous chloride promoted addition of two *N*-chloroamides to 1,6-heptadiene (**2**), under similar conditions of solvent and temperature, with the aim of gaining some information on the transfer step of the chromous chloride initiated additions. A classical chain mechanism ([2] and [3]) has been considered more probable than a redox chain mechanism ([2] and [6]) mainly on the basis of the low redox potential of the chromic ion (2).

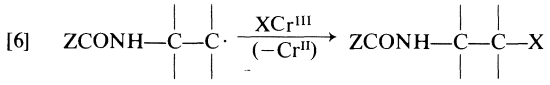

Results and Discussion

The radical addition of *N*-haloamides **1** to 1,6-heptadiene (**2**) was more complicated than shown in Scheme 1 and led to complex mixtures of up to seven different types of adducts, plus products resulting from the halogenation of **2** (except in the chromous chloride initiated reactions), and some dimers and/or telomers. No attempt was made to isolate the products of halogenation and the telomers. The structures of the adducts, determined by ir, ^{1}Hmr, and mass spectrometry (see Experimental) are shown in Scheme 2 with the probable mechanism of their formation: horizontal reactions involve additions of radicals and halogen-atom transfers; vertical reactions involve hydrogen abstraction (RH = **2** and/or solvent) by alkyl radicals and/or their chromium(II) reduction in the chromous chloride promoted additions.[5] The adducts **4** and **6** were obtained as a mixture of *cis* and *trans* isomers (with one isomer predominating) according to vpc analysis, and no attempt was made to separate the two isomers. The ^{1}Hmr spectrum of a mixture of *cis* and *trans* **4** showed either two close doublets or a broadened doublet at ca. 0.9 ppm for the methyl group. In the ^{1}Hmr spectrum of mixtures of *cis* and *trans* **6**, there was no detectable change upon varying the proportions of the two isomers. A similar observation was made by Brace (5) for an analogous compound resulting from the radical addition of carbon tetrachloride to **2**.

The yields of adducts together with the reaction conditions are recorded in Table 1. The adducts **3** and **5** (transfer), and **4** and **6** (rearrangement) account for more than 90% of the addition products. The yields of the two-to-one adduct **5** represent maximum yields since they are based on chromatographic fractions containing **5** as well as dimers and/or telomers from which **5** could be isolated pure in a few cases only (see Table 1, footnote *c*).

The results of Table 1 show that, for the photochemical additions at 15–20°C, the ratio of transfer to rearrangement is larger for X = Br than for X = Cl as expected (compare entries 6 and 4) and increases with Z in the order $CH_3 < ClCH_2 < C_2H_5O \leq CCl_3 \sim CF_3$ (entries 1 to 5). The parallel with the variation of the 1,2-addition to 1,H-addition ratio, for the chromous chloride promoted additions of the same *N*-chloroamides to cyclohexene, is striking. Thus our hypothesis is confirmed: the reactivity of ZCONHX as an halogen-atom donor towards an alkyl radical increases with the electron-withdrawing power of the ZCO moiety. This is shown also by the variation of the relative proportions of adducts **4** and **6**. Adduct **4** results from halogen-atom transfer onto the intermediate radical B whereas adduct **6** results from hydrogen-atom abstraction by radical B (Scheme 2). As the reactivity of ZCONHX as an halogen donor increases, the **4**/**6** ratio should increase, and it does with the electron-withdrawing character of the ZCO moiety (entries 1 to 5).

To see whether or not the nature of the transfer step is the same for the chromous chloride promoted additions and the photochemical additions, we compared the two initiation methods, using *N*-chlorochloroacetamide (**1***b*) and *N*-chlorotrichloroacetamide (**1***d*), under similar conditions of solvent and temperature, that is in methanol–chloroform at ca. −70°C (Table 1, entries 7 to 10). For both methods of initiation, the chain-transfer step is faster with $Z = CCl_3$ than with $Z = ClCH_2$ as shown by the larger transfer to rearrangement and **4**/**6** ratios obtained with **1***d* (compare entries 7 and 8, 9 and 10). We also carried out the photochemical addition of **1***d* in the presence of a stoichiometric amount of chromic chloride and found that, within the limit of experimental errors, the presence of chromic ions had practically no effect

[5] It has been shown by deuterium incorporation experiments that, in the chromous chloride promoted addition of *N*-haloamides to olefins, nonhalogenated adducts, termed 1,H-adducts, result mainly from chromium(II) reduction of an intermediate radical then protonolysis (2).

Can. J. Chem. Downloaded from www.nrcresearchpress.com by 210.87.254.6 on 09/05/12
For personal use only.

Can. J. Chem. Downloaded from www.nrcresearchpress.com by 210.87.254.6 on 09/05/12
For personal use only.

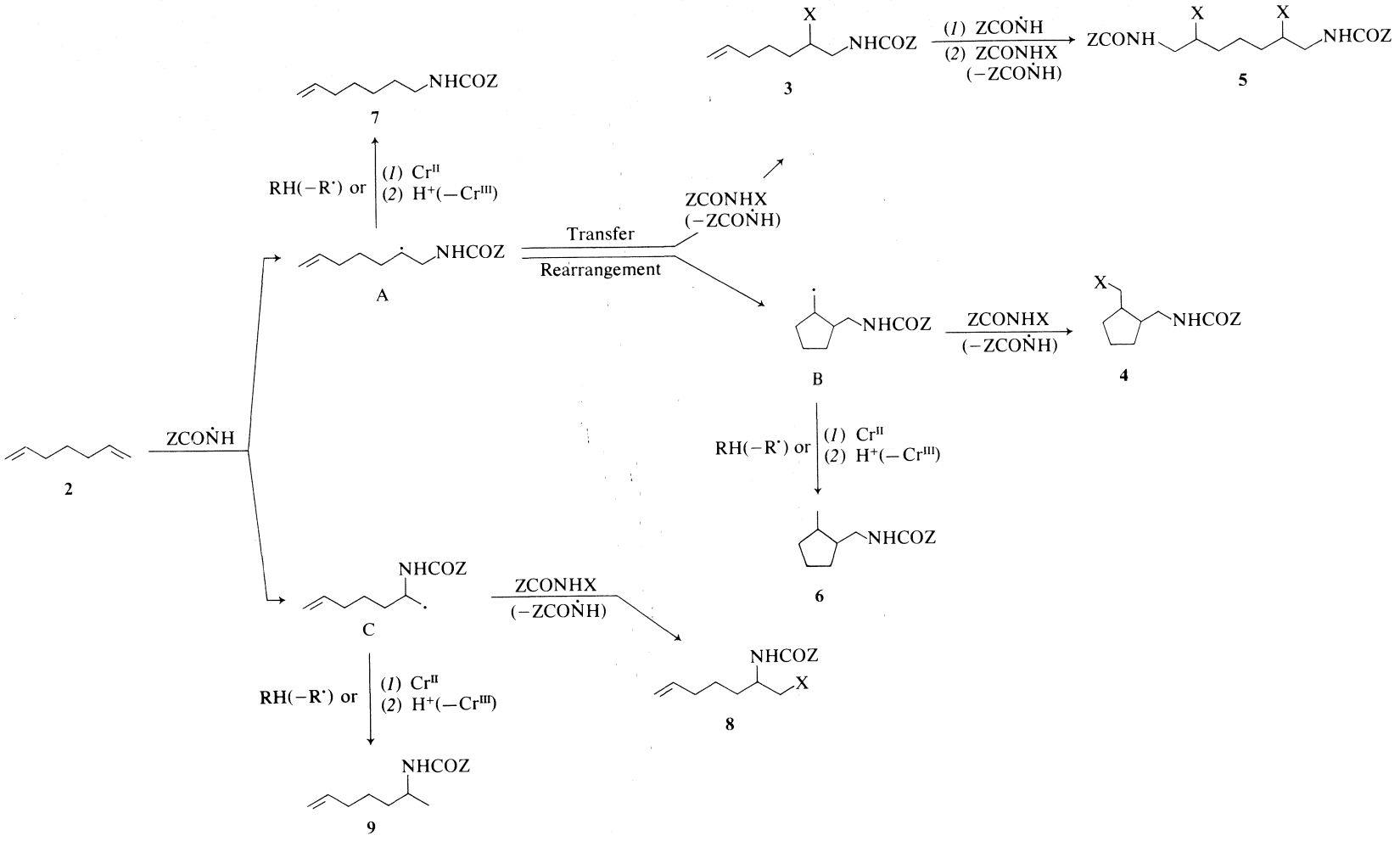

a Z = CH_3, X = Cl
b Z = $ClCH_2$, X = Cl
c Z = C_2H_5O, X = Cl
d Z = CCl_3, X = Cl
e Z = CF_3, X = Cl
f Z = CCl_3, X = Br

SCHEME 2

Can. J. Chem. Downloaded from www.nrcresearchpress.com by 210.87.254.6 on 09/05/12
For personal use only.

TABLE 1. Photochemical and chromous chloride promoted additions of ZCONHX (**1**) to 1,6-heptadiene (**2**) (Scheme 2)

Entry	ZCONHX	Reaction conditions[a] Initiator	T (°C)	Solvent	Yield[b] of addition products (%) 3	5[c]	4	6	7	8	9	Total	4/6	$(3+\frac{1}{2}5)/(4+6)$	t/r[d]	Ratio of 1,2-addition to 1,H-addition[e]
1	$CH_3CONHCl$ (1*a*)	*hv*	15–20	CH_2Cl_2	4		42	20		1		67	2.1	0.06		0.94
2	$ClCH_2CONHCl$ (1*b*)	*hv*	15–20	CH_2Cl_2	8	< 4	45	12				69	3.8	0.18; 0.18[f]		5.8
3	$C_2H_5OCONHCl$ (1*c*)	*hv*	15–20	CH_2Cl_2	20	< 9	51	9				89	5.7	0.41; 0.49[f]		14.5
4	$Cl_3CONHCl$ (1*d*)	*hv*	15–20	CH_2Cl_2	20	< 10	50	4		4		88	12.5	0.46; 0.51[f]		≥28
5	$F_3CONHCl$ (1*e*)	*hv*	15–20	CH_2Cl_2	20	< 12	66			2		100	> 11[g]	0.39; 0.45[f]		31
6	$Cl_3CONHBr$ (1*f*)	*hv*	15–20	CH_2Cl_2	55	< 25	7					87		9.6		
7	$ClCH_2CONHCl$ (1*b*)	$CrCl_2$	—70	$CHCl_3$–CH_3OH	10		5	44	3		2	64	0.11	0.20		
8	$Cl_3CONHCl$ (1*d*)	$CrCl_2$	−70	$CHCl_3$–CH_3OH	23	< 5	7	4		1	4	44	1.8	2.3		
9	$ClCH_2CONHCl$ (1*b*)	*hv*	−70	$CHCl_3$–CH_3OH	4	< 3	9	31		2		49	0.29	0.14		
10	$Cl_3CONHCl$ (1*d*)	*hv*	−70	$CHCl_3$–CH_3OH	22	< 10	19	8		2	2	63	2.4	1.0; 1.1[f]		
11	$Cl_3CONHCl$ (1*d*)	*hv*	−70	$CHCl_3$–CH_3OH–$CrCl_3$	18	< 10	21	7			3	59	3.0	0.82		

[a]To minimize the formation of **5**, an excess of olefin was used. By using 3 mol of **2** per mole of **1**, less than 5% of dimers and/or telomers was formed.
[b]The yields are based on **1** and in many cases represent yields determined by integration of the ^{1}Hmr spectrum of a mixture of two compounds (see the Experimental).
[c]Maximum yields (see the text). Compounds **5***c*, **5***e*, and **5***f* could be isolated pure in 2, 6, and 17% yields, respectively.
[d]t = transfer, r = rearrangement. Half the yield of **5** represents the amount of **3** converted to **5**.
[e]Chromous chloride promoted additions to cyclohexene, taken from ref. 2.
[f]The reaction was carried out twice and the first value corresponds to the experiments described in the Experimental and to the yields given in the table.
[g]The adduct **6***e* was not detected in the chromatographic fractions and we assume that we would have been able to detect 3% of it.

on the transfer to rearrangement and **4**/**6** ratios (compare entries 10 and 11).

The differences in the **4**/**6** ratios observed when comparing the two methods of initiation (entries 7 and 9, 8 and 10) can be accounted for by different mechanisms of formation of **6**. In the chromous chloride promoted additions, **6** is most likely formed by chromium(II) reduction of the intermediate radical B followed by protonolysis of the carbon–chromium bond (Scheme 2). In the photochemical additions, the formation of **6** involves hydrogen-atom abstraction by radical B from the solvent and/or the olefin (Scheme 2). It is noteworthy that the photochemical additions in methylene chloride led to larger **4**/**6** ratios than the photochemical additions in chloroform–methanol and this most probably reflects the fact that chloroform is more reactive towards the alkyl radical B than methylene chloride.[6] In fact the main source of hydrogen in the additions carried out in methylene chloride as solvent could be the allylic hydrogens of **2**.

As for the differences in the transfer to rearrangement ratios observed between the two modes of initiation (compare entries 7 and 9, 8 and 10), we believe they could be attributed to the fact that it was not possible to reproduce exactly the same reaction conditions, even when the photochemical additions were carried out in the presence of chromic chloride. An explanation based on different mechanisms for the chain-transfer step in the two modes of initiation seems less probable. Indeed, if a ligand transfer [6] was involved in the chromous chloride promoted additions, the influence of Z on the rate of the transfer step should have been smaller than in the photochemical additions, even if the halochromic ion participating in the ligand transfer was directly bonded to the amido group as depicted in Scheme 3 (ZCONHX could act as a bidentate ligand in the initiation step (2)); Z would then be farther away from the reacting centers than in an halogen-atom transfer from ZCONHX. In fact, the effect of Z appears to be similar with the two methods of initiation and even somewhat greater with chromous chloride: $CrCl_2$, $t/r(CCl_3) \sim 10 \times t/r(ClCH_2)$; *hv*, $t/r(CCl_3) \sim 7 \times t/r(ClCH_2)$ (see entries 7 to 10).

Conclusion

This work shows that the reactivity of *N*-haloamides as halogen-atom donors to alkyl radicals

[6]Chloroform has been shown to be more reactive towards $CH_3^\bullet$ radicals than methylene chloride (6). As the reactivity of different hydrogen donors towards a given alkyl radical (nonpolar) should depend mainly on D(C—H) of the donor, methylene chloride and methanol might have similar reactivities: D(C—H) $CH_2Cl_2 \sim D$(C—H) $CH_3OH \sim 94$ kcal mol^{-1} (7).

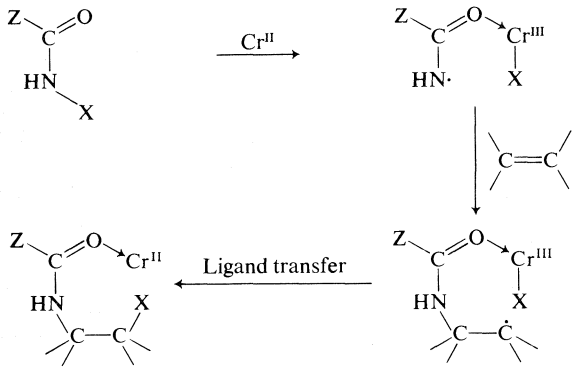

SCHEME 3

increases with the electron-withdrawing power of the acyl moiety, which indicates that the transition state has polar character.

The increase of the rate of the chain-transfer step with the electron-withdrawing character of the acyl group, in the chromous chloride promoted additions, is better interpreted in terms of a classical chain mechanism but offers no conclusive evidence against a redox chain mechanism. Both mechanisms could be involved as already suggested (8).

Experimental

The pertinent general information has been given in ref. 1. Most of the ^{1}Hmr spectra were recorded on a Bruker WP-60 spectrometer.

N-*Haloamides*

The *N*-chloroamides were prepared by the sodium hypochlorite method (9); their iodometric purity will be indicated when lower than 99%. *N*-Bromo-2,2,2-trichloroacetamide (**1***f*) was prepared from trichloroacetamide and acetylhypobromite (10): mp 123–124°C, 99% iodometric purity, 92% yield.

Photochemical Additions

The uv irradiations were carried out in a Rayonnet RPR-100 reactor equipped with 16 2537 Å lamps. For the reactions at 15–20°C, a Vycor cell cooled with tap water was used. The jacketed Vycor cell shown in Fig. 1 was used for the reactions at −70°C, the cooling mixture (methanol saturated with Dry Ice) being placed in the central cavity A. The solvents used were dry: methylene chloride and chloroform freshly distilled from P_2O_5, absolute methanol. Nitrogen was passed through the solution for 10 min before irradiating and a slow stream of nitrogen was maintained throughout the irradiation which was stopped when no more *N*-haloamide was present (negative starch–iodide paper test). The crude product was separated by preparative-layer chromatography (plc) on silica gel using a continuous elution system. Owing to the number of compounds formed and their close R_f values, fractions containing a mixture of two compounds were often obtained. Their relative proportions (molar ratios) were determined by ^{1}Hmr spectroscopy unless otherwise stated. Samples > 95% pure (by tlc and vpc) could be obtained after further separation but not always. Only those compounds which could be readily purified by crystallization were submitted to a microanalysis. Compounds **3***a* and **4***a*, and those resulting from the addition of **1***d* and **1***f* (Z = CCl_3) underwent decomposition upon vpc analysis. The reaction conditions together with the isolation of the various

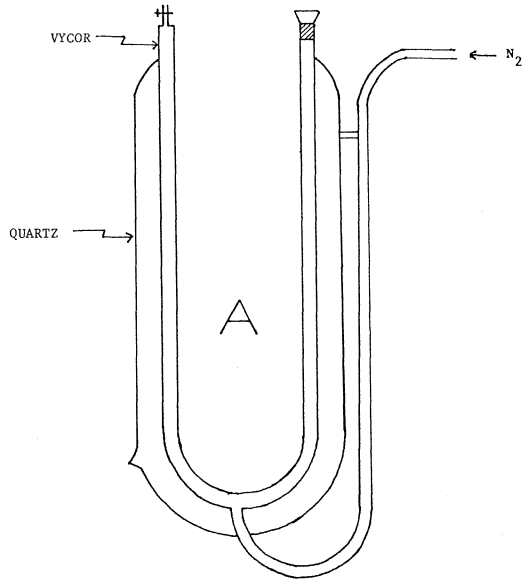

FIG. 1. Cell for low-temperature photolyses.

compounds are described below. The characteristic infrared absorptions and mass spectral data are recorded in Table 2. The ^{1}Hmr spectral data are given below for each compound isolated. The protons on the carbon bearing the amido group were identified by irradiating the NH or by exchanging the NH with D_2O. The CH_2X protons of compounds **4** and **8**, the CH_2N protons of compounds **3**, **4**, and **6**, represent the AB part of an ABX system (with further coupling with the NH for the CH_2N protons). The average chemical shift of both protons is reported together with the number of lines and the apparent *J* values (spectral splittings). When there are a great number of lines as for the CH_2N protons of compounds **3** and **5**, the chemical shift of both extreme lines is given.

N-*Chloroacetamide (1a)*

N-Chloroacetamide (**1***a*) (0.965 g, 97%, 10 mmol) and 1,6-heptadiene (**2**) (2.88 g, 30 mmol) in methylene chloride (100 ml) were irradiated at ca. 15°C for 2 h. The solvent was evaporated and the crude product separated by column chromatography with hexane – ethyl acetate 1:1 to give five main fractions. The first fraction (798 mg) contained halogenated products and was not investigated further. The second fraction (32 mg) was identified as *2-acetylamino-1-chloro-6-heptene* (**8***a*) (1%) by ir, mass, and ^{1}Hmr spectroscopy: δ($CDCl_3$):0.9–1.7 (4H), 2.1 (2H), 3.67 (4 lines, *J* = 3.5 and 4.0 Hz, CH_2Cl), 4.1 (m, H_2), 4.85 (m, H_7), 5.08 (m, H_7), and 5.4–6.2 ppm (H_6 + NH). The third fraction consisted of a mixture which, by further separation by plc (hexane – ethyl acetate 2:1), yielded *1-acetylamino-2-chloro-6-heptene* (**3***a*) contaminated by small amounts of **6***a* (76 mg, ~4%) and *1-(acetylamino)methyl-2-methylcyclopentane* (**6***a*) (78 mg, 5%) characterized by their ir, mass, and ^{1}Hmr spectra: **3***a*, δ($CDCl_3$):0.9–2.7 (6H), 2.03 (s, $COCH_3$), 2.9–4.1 (3H: CH_2N + H_2), 4.85 (m, H_7), 5.10 (m, H_7), 5.4–6.2 ppm (H_6 + NH); **6***a*, δ($CDCl_3$):0.87 (d, *J* = 6.5 Hz, CH_3), 0.92 (d, *J* = 6.5 Hz, CH_3), 1.0–2.2 (8H), 1.97 (s, $COCH_3$), 1.98 (s, $COCH_3$), 3.2 (m, CH_2N), and 5.5 ppm (m, NH). The fourth fraction (935 mg) consisted of a 2.5:1 mixture of **4***a* (37%) and **6***a* (15%, total yield of 20%). The fifth fraction (83 mg) was identified as *1-(acetylamino)methyl-2-chloromethylcyclopentane* (**4***a*) (5%, total yield of 42%) by ir, mass, and ^{1}Hmr spectro-

Can. J. Chem. Downloaded from www.nrcresearchpress.com by 210.87.254.6 on 09/05/12
For personal use only.

Can. J. Chem. Downloaded from www.nrcresearchpress.com by 210.87.254.6 on 09/05/12
For personal use only.

TABLE 2. Characteristic infrared absorptions and mass spectral data

Compound[a]	Infrared absorptions[b] (cm^{-1})							Mass spectral data (*m/e*)
	ν_{N-H}							
	Free	Associated	$\nu_{=C-H}$	$\nu_{C=O}$	$\nu_{C=C}$	δ_{N-H}	$\delta_{=C-H}$	(Molecular ion and/or some characteristic fragments)
3*a*[c]	3450	3330	3070,3010	1670		1510	970,890	189,191 (2.3:1, M^+); 154 (M^+ − Cl); 72 ($CH_3CONHCH_2$)
3*b*	3425		3070,3010	1680	1640(sh)	1530	975,890	223,225 (1.4:1, M^+); 188,190 (2.8:1, M^+ − Cl); 106,108 (2.6:1, $ClCH_2CONHCH_2$)
3*c*	3450		3070,3010	1720	1640	1510	975,890	219,221 (2.8:1, M^+); 184 (M^+ − Cl); 102 ($C_2H_5OCONHCH_2$)
3*d*	3425		3060,3010	1720	1640	1510	975,890	291,293,295,297 (3:6:3:1, M^+);[d] 256,258,260 (3:3:1, M^+ − Cl); 174,176,178 (3.5:3:1, $CCl_3CONHCH_2$)
3*e*	3430		3070,3010	1735	1645	1540	975,890	208 (M^+ − Cl); 207 (M^+ − HCl); 174,176 (2.8:1, M^+ − CF_3); 126 ($CF_3CONHCH_2$)
3*f*	3420		3070,3010	1725	1645	1515	975,890	300,302,304 (1.3:2.2:1, M^+ − Cl);[e] 256,258,260 (3:3:1, M^+ − Br); 174,176,178 (2.8:2.8:1, $CCl_3CONHCH_2$)
4*a*	3450	3330		1665		1515		189,191 (2.8:1, M^+); 154 (M^+ − Cl); 140 (M^+ − CH_2Cl); 72 ($CH_3CONHCH_2$)
4*b*	3420			1675		1530		223,225 (1.5:1, M^+); 188,190 (2.7:1, M^+ − Cl); 174,176 (2.8:1, M^+ − CH_2Cl); 106,108 (2.4:1, $ClCH_2CONHCH_2$)
4*c*	3450			1720		1510		219,221 (2.5:1, M^+); 184 (M^+ − Cl); 183 (M^+ − HCl); 102 ($C_2H_5OCONHCH_2$)
4*d*	3430			1720		1510		291,293,295,297 (4:6:4:1, M^+);[d] 256,258,260 (3:3:1, M^+ − Cl); 242,244,246 (2.8:2.8:1, M^+ − CH_2Cl); 174,176,178 (3:3:1, $CCl_3CONHCH_2$)
4*e*	3430	3330		1730		1545		243,245 (2.2:1, M^+); 208 (M^+ − Cl); 207 (M^+ − HCl); 194 (M^+ − CH_2Cl); 174 (M^+ − CF_3); 126 ($CF_3CONHCH_2$)
5*c*	3450			1725		1510		342,344,346 (8:5:1, M^+); 307,309 (2.7:1, M^+ − Cl); 297,299,301 (9:6:1, M^+ − C_2H_5O); 102 ($C_2H_5OCONHCH_2$)
5*e*	3430			1735		1540		390,392 (1.5:1, M^+); 355,357 (3:1, M^+ − Cl); 321,323 (1.5:1, M^+ − CF_3); 126 ($CF_3CONHCH_2$)
5*f*	3420			1725		1515		539,541,543,545,547,549 (2:6:8:6:3:1, M^+ − Cl);[f] 495,497,499,501,503,505 (3:10:12:8:3:1, M^+ − Br); 457,459,461,463,465,467 (2:7:9:7:3:1, M^+ − HClBr); 174,176,178 (3:3:1, $CCl_3CONHCH_2$)
6*a*	3450	3330		1670		1510		155 (M^+); 140 (M^+ − CH_3); 72 ($CH_3CONHCH_2$)
6*b*	3425			1675		1535		189,191 (2.4:1, M^+); 154 (M^+ − Cl); 140 (M^+ − CH_2Cl); 107,109 (4:1, $ClCH_2CONHCH_3$)
6*c*	3450			1720		1510		185 (M^+); 156 (M^+ − C_2H_5); 102 ($C_2H_5OCONHCH_2$)
6*d*[g]	3430			1720		1510		257,259,261 (2.6:2.6:1, M^+); 222,224 (1.5:1, M^+ − Cl); 175,177,179 (2.8:2.8:1, $CCl_3CONHCH_3$)
7*b*	3430		3060,3010	1675	1640(sh)	1530	975,890	189,191 (2.5:1, M^+); 154 (M^+ − Cl); 140 (M^+ − CH_2Cl); 106,108 (2.5:1, $ClCH_2CONHCH_2$); 107,109 (2.6:1, $ClCH_2CONHCH_3$); 96 (C_7H_{12})
8*a*	3450	3330	3065,3010	1665		1510	975,890	189,191 (2.6:1, M^+); 154 (M^+ − Cl); 140 (M^+ − CH_2Cl)
8*d*[h]	3430		3060,3010	1670	1645(sh)	1510	980,895	256,258,260 (2.5:2.5:1, M^+ − Cl); 242,244,246 (2.4:2.4:1, M^+ − CH_2Cl)
8*e*	3420		3060,3010	1730	1645	1535	975,895	
9*b*	3430		3060,3010	1670	1640(sh)	1530	975,890	189,191 (2.5:1, M^+); 174,176 (2.3:1, M^+ − CH_3); 154 (M^+ − Cl); 120,122 (2.8:1, $ClCH_2CONHCHCH_3$)
9*d*	3440		3060,3010	1720	1640	1510	975,890	257,259,261 (2:1.7:1, M^+);[d] 222,224,226 (7.7:5:1, M^+ − Cl); 188,190,192 (2.7:2.7:1, $CCl_3CONHCHCH_3$)

[a]See Scheme 2 for structural formulae.
[b]The carboethoxy group gives a strong band at 1220–1200 cm^{-1} (**3***c*, **4***c*, **5***c*, and **6***c*) and the CF_3 group, strong bands at 1220 and 1155 cm^{-1} (**3***e*, **4***e*, **5***e*, and **8***e*).
[c]Contaminated by small amounts of **6***a*.
[d]The corresponding $M^+ + 1$ peaks are as intense or more intense than the M^+ peaks.
[e]Weak peaks at *m/e* 336,338,340 (3:5:3, $M^+ + 1$).
[f]Weak peaks at *m/e* 575,577,579,581,587 (1:4:6:5:2, $M^+ + 1$).
[g]Contaminated by small amounts of **8***d*.
[h]Contaminated by small amounts of **6***d*.

Can. J. Chem. Downloaded from www.nrcresearchpress.com by 210.87.254.6 on 09/05/12
For personal use only.

scopy: δ($CDCl_3$):1.0–2.0 (6H), 2.00 (s, $COCH_3$), 2.3 (m, 2H), 3.18 (broad t, J = 6 Hz, $\Delta\nu_{1/2}$ = 14 Hz; CH_2N), 3.52 (3 lines, J = 6 and 7 Hz, CH_2Cl), and 5.9 ppm (m, NH).

N-*Chlorochloroacetamide (**1**b)*

At 15°C in CH_2Cl_2—The *N*-chloroamide **1***b* (330 mg, 2.5 mmol) and **2** (720 mg, 7.5 mmol) in CH_2Cl_2 (25 ml) were irradiated for 1.5 h. Separation by plc (ether – hexane 1:2.5) gave three main fractions. The least polar fraction (102 mg) consisted of a 2:3 mixture of *1-chloroacetylamino-2-chloro-6-heptene* (**3***b*) (8%) and *1-(chloroacetylamino)methyl-2-methylcyclopentane* (**6***b*) (12%). Further separation (ether – hexane 1:5) allowed the isolation of homogeneous samples of **3***b* and **6***b*, both compounds being characterized by their ir, mass, and ^{1}Hmr spectra: **3***b*, δ($CDCl_3$):1.0–2.4 (6H), 3.4–4.2 (CH_2N + H_2), 4.08 (s, $ClCH_2CO$), 4.85 (m, H_7), 5.09 (m, H_7), 5.5–6.05 (H_6), and 6.4 ppm (m, NH); **6***b*, δ($CDCl_3$):0.89 (d, J = 6.5 Hz, CH_3), 1.1–2.4 (8H), 3.28 (broad t, J ~ 5.5 Hz, $\Delta\nu_{1/2}$ = 15 Hz, CH_2N), 4.05 (s, $COCH_2Cl$), and 6.9 ppm (m, NH). The second fraction was identified as *1-(chloroacetylamino)methyl-2-chloromethylcyclopentane* (**4***b*) (249 mg, 45%) by ir, mass, and ^{1}Hmr spectroscopy: δ($CDCl_3$):1.1–2.0 (6H), 2.3 (m, 2H), 3.32 (broad t, J ~ 6 Hz, $\Delta\nu_{1/2}$ ~ 14 Hz, CH_2N), 3.52 (3 lines, J = 6 and 7 Hz, CH_2Cl), 4.05 (s, $COCH_2Cl$), and 6.76 ppm (m, NH). The third fraction (20 mg) was probably a mixture of **5***b* and telomers and was not investigated further.

At −70°C in $CHCl_3$–CH_3OH—The *N*-chloroamide **1***b* (0.517 g, 4 mmol) and **2** (1.15 g, 12 mmol) in a mixture of chloroform (25 ml) and methanol (20 ml) were irradiated at −70°C for 8 h. Since the reaction mixture was acidic, it was washed with a saturated $NaHCO_3$ solution, dried, then the solvent evaporated. The separation led to four main fractions. The least polar fraction (35 mg) consisted of a 1:1 mixture of **6***b* (2%) and most probably *1-chloro-2-(chloroacetylamino)-methyl-6-heptene* (**8***b*) (2%): ν_{max} (CCl_4):3420, 3060, 3010, 1670, 1640 (sh), 1530, 975, and 980 cm^{-1}; δ($CDCl_3$):0.89 (d, J = 6.5 Hz, CH_3 of **6***b*), 3.28 (broad t, J ~ 5.5 Hz, CH_2N of **6***b*), 3.68 (4 lines, J = 3.5 and 4 Hz, CH_2Cl of **8***b*), 4.05 and 4.08 (two s, $ClCH_2CO$), 4.15 (m, H_2 of **8***b*), 4.85, 5.08, and 5.5–6.1 (olefinic H's of **8***b*), and 6.7 ppm (NH). This fraction was not investigated further. The second fraction (218 mg) consisted of a 1:6 mixture of **3***b* (4%) and **6***b* (24%). The third fraction (112 mg) was a 2:1 mixture of **4***b* (9%) and **6***b* (5%, total yield of 31%). Fraction four (23 mg) was probably a mixture of **5***b* and telomers and was not investigated further.

N-*Chlorourethane (**1**c)*

The *N*-chloroamide **1***c* (340 mg, 91%, 2.5 mmol) and **2** (720 mg, 7.5 mmol) in CH_2Cl_2 (25 ml) was irradiated for 1 h at 15°C. Separation of 70% of the crude product (ether – hexane 1:5) gave three main fractions. The least polar fraction (107 mg) consisted of a 2.2:1 mixture of *2-chloro-1-ethoxycarbonylamino-6-heptene* (**3***c*) (20%) and *1-(ethoxycarbonylamino)methyl-2-methylcyclopentane* (**6***c*) (9%). The two products were separated by preparative vpc and characterized by their ir, mass, and ^{1}Hmr spectra: **3***c*, δ($CDCl_3$):1.25 (t, J = 7 Hz, OCH_2CH_3), 1.1–2.3 (6H), 3.0–3.8 (CH_2N), 3.0 (m, H_2), 4.13 (q, J = 7 Hz, OCH_2CH_3), 4.85 (m, H_7), 5.10 (m, H_7 + NH), and 5.5–6.15 ppm (H_6); **6***c*, δ($CDCl_3$):0.89 (d, J = 6.5 Hz, CH_3), 1.24 (t, J = 7 Hz, OCH_2CH_3), 1.0–2.3 (8H), 3.13 (broad t, J ~ 5.5 Hz, $\Delta\nu_{1/2}$ = 14 Hz, CH_2N), 4.10 (q, J = 7 Hz, OCH_2CH_3), and 4.52 ppm (broad t, J ~ 7 Hz, NH). The second fraction consisted of *2-chloromethyl-1-(ethoxycarbonylamino)methylcyclopentane* (**4***c*) (196 mg, 51%) characterized by its ir, mass, and ^{1}Hmr spectra: δ($CDCl_3$): 1.22 (t, J = 7 Hz, OCH_2CH_3), 1.1–2.0 (6H), 2.25 (m, 2H), 3.15 (6 lines, J = 7 Hz, CH_2N), 3.51 (4 lines, J = 6.5 and 7 Hz, CH_2Cl), 4.09 (q, J = 7 Hz, OCH_2CH_3), and 4.98 ppm (m, NH). The last fraction (40 mg) contained telomers and some *1,7-bis(ethoxycarbonylamino)-2,6-dichloroheptane* (**5***c*) which could be isolated (13 mg, 2%) by further separation by tlc, mp 114–117°C. An additional quantity was obtained by carrying out the addition with 5 mmol of **1***c*, and 2.5 mmol of **2**. Recrystallization from methylene chloride – ether afforded the analytical sample, mp 120–121°C; ir and mass spectra, see Table 2; δ($CDCl_3$): 1.25 (t, J = 7 Hz, OCH_2CH_3), 1.7 (m, 6H), 3.45 (m, $\Delta\nu_{1/2}$ ~ 25 Hz, 4H: H_1 + H_7), 4.0 (m, H_2 + H_6), and 5.12 ppm (broad t, J ~ 7 Hz, NH). *Anal.* calcd. for $C_{13}H_{24}Cl_2N_2O_4$: Cl 20.64; found: Cl 20.22.

N-*Chlorotrichloroacetamide (**1**d)*

At 15°C in CH_2Cl_2—The *N*-chloroamide **1***d* (503 mg, 98%, 2.5 mmol) and **2** (720 mg, 7.5 mmol) in CH_2Cl_2 (25 ml) were irradiated for 1 h. Separation of 60% of the crude product (ether–hexane 1:10) gave four main fractions. The first fraction (31 mg) consisted of a 1:1 mixture of *1-chloro-2-trichloroacetylamino-6-heptene* (**8***d*) (4%) and *2-methyl-1-(trichloroacetylamino)methylcyclopentane* (**6***d*) (4%). Further separation of a thin-layer plate gave samples of **8***d* and **6***d* contaminated, respectively, by small amounts (< 10%) of **6***d* and **8***d*. These samples were characterized by ir, mass, and ^{1}Hmr spectroscopy: **8***d*, δ($CDCl_3$):1.1–2.3 (6H), 3.72 (4 lines, J = 3.5 and 4 Hz, CH_2Cl), 4.18 (m, $\Delta\nu_{1/2}$ ~ 23 Hz, H_2), 4.85 (m, H_7), 5.10 (m, H_7), 5.5–6.1 (H_6), and 6.65 ppm (m, NH); **6***d*, δ($CDCl_3$):0.90 (d, J = 6.5 Hz, CH_3), 1.1–2.3 (8H), 3.33 (6 lines, J ~ 6 Hz, CH_2N), and 6.6 ppm (m, NH). The second fraction consisted of *2-chloro-1-trichloroacetylamino-6-heptene* (**3***d*) (85 mg, 20%) characterized by its ir, mass, and ^{1}Hmr spectra: δ($CDCl_3$):1.2–2.4 (6H), 3.20–4.05 (several peaks, CH_2N), 4.1 (m, $\Delta\nu_{1/2}$ ~ 16 Hz, H_2), 4.88 (m, H_7), 5.11 (m, H_7), 5.5–6.13 (H_6), and 7.05 ppm (m, NH). The third fraction consisted of *2-chloromethyl-1-(trichloroacetylamino)methylcyclopentane* (**4***d*), mp 50–63°C (218 mg, 50%). It was recrystallized once from ether, mp 67–71°C: ir and mass spectra, see Table 2; δ($CDCl_3$):1.2–2.0 (6H), 2.36 (m, 2H), 3.35 (t, J = 6 Hz, CH_2N), 3.53 (d, J = 6 Hz, CH_2Cl), and 6.86 ppm (m, NH). *Anal.* calcd. for $C_9H_{13}Cl_4NO$: Cl 48.40; found: Cl 48.56. The last fraction (50 mg) contained trichloroacetamide, telomers, and probably some **5***d* but the latter compound could not be obtained pure upon further separation (ether–hexane 1:1); a mixture of **5***d* and telomers was obtained (37 mg).

At −70°C in $CHCl_3$–CH_3OH—The *N*-chloroamide **1***d* (757 mg, 3.8 mmol) and **2** (1.10 g, 11.4 mmol) in chloroform (25 ml) – methanol (20 ml) was irradiated at −70°C for 4 h. The separation (ether–hexane 1:20) afforded five main fractions. The least polar fraction (34 mg) consisted of a 1:2 mixture of **6***d* (1%) and *2-trichloroacetylamino-6-heptene* (**9***d*) (2%). Further separation on a thin plate afforded an homogeneous sample of **9***d* characterized by its ir, mass, and ^{1}Hmr spectra: δ($CDCl_3$):1.23 (d, J = 6.8 Hz, CH_3), 1.1–1.6 (4H), 2.08 (m, 2H allylic), 3.98 (m, $\Delta\nu_{1/2}$ = 29 Hz, H_2), 4.85 (m, H_7), 5.08 (m, H_7), 5.5–6.15 (H_6), and 6.33 ppm (m, NH). The second fraction (98 mg) consisted of a 1:3.5 mixture of **8***d* (2%) and **6***d* (7%, total yield 8%). The third fraction consisted of **3***d* homogeneous by tlc (248 mg, 22%). The fourth fraction consisted of **4***d* (207 mg, 19%), mp 55–65°C. The more polar fraction (314 mg) was separated further (ether–hexane 1:1) to yield trichloroacetamide and a mixture of telomers containing probably compound **5***d* (99 mg). It was not investigated further.

At −70°C in $CHCl_3$–CH_3OH and in the presence of $CrCl_3$—The *N*-chloroamide **1***d* (498 mg, 92%, 2.3 mmol), **2** (662 mg, 6.9 mmol), and hexahydrated chromic chloride (2.3 ml of a 1 *M* solution in methanol, 2.3 mmol) in chloroform (17 ml) – methanol (11 ml) were irradiated for 8 h. Separation as above gave 66 mg of a mixture of **9***d* (3%) and **6***d* (7%), 115 mg of **3***d* (17%), 144 mg of **4***d* (21%), and 100 mg of a mixture which,

Can. J. Chem. Downloaded from www.nrcresearchpress.com by 210.87.254.6 on 09/05/12
For personal use only.

by further separation, gave a mixture (56 mg) of telomers and **5***d*, and trichloroacetamide.

N-*Chlorotrifluoroacetamide* (*1*e)

The *N*-chloroamide **1***e* (384 mg, 96%, 2.5 mmol) and **2** (720 mg, 7.5 mmol) in methylene chloride (25 ml) were irradiated for 1 h. Separation of 60% of the crude product (ether–hexane 1:5) gave three fractions. The least polar fraction (8 mg) consisted of *1-chloro-2-trifluoroacetylamino-6-heptene* (**8***e*) (2%) characterized by its ir and ^{1}Hmr spectra: δ($CDCl_3$):1.3–2.3 (6H), 3.69 (4 lines, J = 3.5 and 4 Hz, CH_2Cl), 4.23 (m, $\Delta\nu_{1/2}$ = 22 Hz, H_2) 4.85 (m, H_7), 5.09 (m, H_7), 5.5–6.1 (H_6), and 6.45 ppm (NH). The second fraction (312 mg) consisted of 1:3.3 mixture (by ^{1}Hmr and vpc) of *2-chloro-1-trifluoroacetylamino-6-heptene* (**3***e*) (20%) and *2-chloromethyl-1-(trifluoroacetylamino)methylcyclopentane* (**4***e*) (66%). These two compounds were separated by preparative vpc and characterized by their ir, mass, and ^{1}Hmr spectra: **3***e*, δ($CDCl_3$):1.3–2.3 (6H), 3.1–4.3 (3H: CH_2N + H_2), 4.85 (m, H_7), 5.09 (m, H_7), 5.46–6.15 (H_6), and 6.8 ppm (m, NH); **4***e*, δ($CDCl_3$):1.3–2.0 (6H), 2.37 (m, 2H), 3.38 (t, J = 6 Hz, CH_2N), 3.53 (d, J = 6 Hz, CH_2Cl), and 6.8 ppm (m, NH). The third fraction (36 mg) crystallized from a chloroform–ether solution to afford *1,7-bis(trifluoroacetylamino)-2,6-dichloroheptane* (**5***e*) (18 mg, 6%), mp 151–153°C. One recrystallization afforded the analytical sample, mp 153–154°C; ir and mass spectra, see Table 2; δ($CDCl_3$):1.75 (m, 6H), 3.4–3.8 (4H: CH_2N), 4.0 (m, H_2 + H_6), and 7.15 ppm (m, NH). *Anal.* calcd. for $C_{11}H_{14}Cl_2F_6N_2O_2$: Cl 18.13; found: Cl 17.98.

N-*Bromotrichloroacetamide* (*1*f)

The *N*-bromoamide **1***f* (664 mg, 91%, 2.5 mmol) and **2** (720 mg, 7.5 mmol) in methylene chloride (25 ml) was irradiated for 0.75 h. The crude product was taken up in ether and the adduct **5***f* (16 mg, 2%), mp 159–163°C, precipitated out (see below for characterization). Part of the filtrate (50%) was separated (ether–hexane 1:10) into three main fractions. The least polar fraction consisted of *2-bromo-1-trichloroacetylamino-6-heptene* (**3***f*) (232 mg, 55%) characterized by its ir, mass, and ^{1}Hmr spectra: δ($CDCl_3$):1.2–2.3 (6H), 3.3–4.1 (CH_2N), 4.15 (m, CH_2Cl), 3.85 (m, H_7), 5.5–6.3 (H_6), and 7.3 ppm (m, NH). The second fraction (30 mg) contained *2-bromomethyl-1-(trichloroacetylamino)methylcyclopentane* (**4***f*) (7%) contaminated with small amounts of an olefinic compound (most probably **3***f*). It was not purified further: ν_{max} ($CHCl_3$):3430, 1720, and 1515 cm^{-1} (amido group); δ($CDCl_3$):1.2–2.0 (6H), 2.4 (m, 2H), 3.4 (m, $\Delta\nu_{1/2} \sim$ 15 Hz, CH_2Br + CH_2N), 6.8 (m, NH), and very weak absorptions at 4.85 and 5.10 ppm due to the presence of an olefinic compound. From the third fraction (92 mg) *1,7-bis(trifluoroacetylamino)-2,6-dichloroheptane* (**5***f*) (54 mg, 15%), mp 162–165°C, crystallized out from ether. Recrystallization from methylene chloride – ether afforded the analytical sample, mp 167–168°C; ir and mass spectra, see Table 2; δ(CD_2Cl_2):1.80 (m, 6H), 3.5–3.9 (4H: CH_2N), 4.15 (m, H_2 + H_6), and 6.83 ppm (m, NH). *Anal.* calcd. for $C_{11}H_{14}Br_2Cl_6N_2O_2$: Br 27.61, Cl 36.75; found: Br 27.3, Cl 37.1.

Chromous Chloride Promoted Additions

The apparatus as well as the procedure for the chromous chloride promoted addition of *N*-haloamides to olefins have been described in ref. 1. The separations were carried out as described for the photochemical additions.

N-*Chlorochloroacetamide* (*1*b)

The *N*-chloroamide **1***b* (423 mg, 3.3 mmol) and **2** (992 mg, 10 mmol) were dissolved in chloroform (19 ml) and methanol (12 ml) at ca. −70°C. The 1 *M* methanolic chromous chloride solution was added dropwise over 3 h (6.5 ml, 6.5 mmol). Water (20 ml) was added and the mixture was rapidly extracted with ether. The aqueous mixture was kept 20 h at room temperature then extracted with methylene chloride. Separation of the residue (235 mg) from the extraction with ether gave two fractions: (*a*) a 1:2 mixture (150 mg) of **3***b* (7.5%) and **6***b* (15%); (*b*) **4***b* (34 mg, 5%). Separation of the residue (204 mg) from the methylene chloride extraction gave two fractions: (*a*) **6***b* (167 mg, 27%); (*b*) a 1:1 mixture (26 mg) of **3***b* (2%, total yield 10%) and **6***b*, (2%, total yield of 44%). The aqueous phase from the above extractions were continuously extracted with methylene chloride for 3 days. Separation of the residue (97 mg) gave three fractions: (*a*) *2-chloroacetylamino-6-heptene* (**9***b*) (11 mg, 2%) characterized by its ir, mass, and ^{1}Hmr spectra: δ($CDCl_3$):1.17 (d, J = 6.5 Hz, CH_3), 1.2–1.7 (4H), 2.05 (m, 2H), 4.03 (s over a m, respectively $ClCH_2CO$ and H_2), 4.84 (m, H_7), 5.07 (m, H_7), 5.5–6.1 (H_6), and 6.4 ppm (NH); (*b*) *1-chloroacetylamino-6-heptene* (**7***b*) (17 mg, 3%) characterized by its ir, mass, and ^{1}Hmr spectra: δ($CDCl_3$):1.1–1.8 (6H), 2.10 (m, 2H), 3.31 (broad q, $J \sim$ 6.5 Hz, CH_2N), 4.85 (m, H_7), 5.08 (m, H_7), 5.5–6.1 (H_6), and 6.6 ppm (NH); (*c*) chloroacetamide (44 mg, 15%), mp 114–116°C.

N-*Chlorotrichloroacetamide* (*1*d)

The *N*-chloroamide **1***d* (798 mg, 4 mmol) and **2** (1.15 g, 12 mmol) were dissolved in chloroform (25 ml) and methanol (15 ml) at ca. −70°C. The 1 *M* methanolic chromous chloride solution was added over 2 h (5.5 ml, 5.5 mmol). Water (20 ml) was added and the mixture was stirred at room temperature for 1 h then extracted with methylene chloride. Upon evaporating the solvent, trichloroacetamide, mp 140°C, crystallized out (240 mg, 37%). Separation of the filtrate (ether–hexane 1:20) gave five fractions: (*a*) **9***d* (24 mg, 2%); (*b*) a 3:1 mixture (46 mg) of **6***d* (3%) and **8***d* (1%); (*c*) **3***d* (268 mg, 23%); (*d*) **4***d* (78 mg, 7%); (*e*) a mixture (51 mg) of telomers, trichloroacetamide, and probably also **5***d* (not investigated further). Continuous extraction of the aqueous phase by methylene chloride for 3 days afforded an additional amount of **9***d* (22 mg, 2%; total yield, 4%) and **6***d* (11 mg, 1%; total yield of 4%).

Acknowledgements

We are grateful to the 'Ministère de l'Education du Québec' and the National Research Council of Canada for financial assistance. We thank Mr. J. Tamas for the microanalyses.

1. H. Driguez, J. M. Paton, and J. Lessard. Can. J. Chem. **55**, 700 (1977).
2. H. Driguez and J. Lessard. Can. J. Chem. **55**, 720 (1977).
3. D. Touchard. Ph.D. Thesis, Université de Sherbrooke, Sherbrooke, Qué. 1974.
4. C. Walling. Free radicals in solution. John Wiley and Sons, Inc., New York, NY. 1957. p. 158; P. I. Abell. *In* Free radicals. Vol. 2. *Edited by* J. K. Kochi. John Wiley and Sons, Inc., New York, NY. 1973. p. 86; M. L. Poutsma. *In* Free radicals. Vol. 2. *Edited by* J. K. Kochi. John Wiley and Sons, Inc., New York, NY. 1973. p. 124.
5. N. O. Brace. J. Org. Chem. **32**, 2711 (1967).
6. A. F. Trotman-Dickenson. Q. Rev. **7**, 198 (1953).
7. D. M. Golden and S. W. Benson. Chem. Rev. **69**, 125 (1969).
8. J. Lessard, R. Cote, P. Mackiewicz, R. Furstoss, and B. Waegell. J. Org. Chem. In press.
9. C. Bachand, H. Driguez, J. M. Paton, D. Touchard, and J. Lessard. J. Org. Chem. **39**, 3136 (1974).
10. T. R. Beebe and J. W. Wolfe. J. Org. Chem. **35**, 2056 (1970).

^{15}N-Etioporphyrin I and its copper complexes: Proton and electron magnetic resonance characterization

M. MOMENTEAU, J. MISPELTER, B. LOOCK, AND J. M. LHOSTE

Fondation Curie – Institut du Radium, Section de Biologie, Centre Universitaire d'Orsay, Bâtiment 112, 91405 – Orsay, France

Received April 11, 1978

M. MOMENTEAU, J. MISPELTER, B. LOOCK, and J. M. LHOSTE. Can. J. Chem. **56**, 2598 (1978).

^{15}N-Etioporphyrin I was prepared by polycondensation of 5-hydroxymethylpyrrole-2-carboxylic acid, obtained via the Bullock route. This method gives an isomerically pure porphyrin with a high yield. The labelled compound was analyzed by nmr of the free base, of the dicationic form, and of the zinc complex. The spectrum of the free base shows a rapid tautomerism of the NH protons at 34°C which disappears at low temperature. All spectra reveal several long-range proton–nitrogen-15 interactions. The electron spin resonance spectrum of the paramagnetic complex of this porphyrin with copper-63 is readily analyzed. This analysis was extended to the spectra of the complexes obtained with natural copper and with nitrogen-14 porphyrins.

M. MOMENTEAU, J. MISPELTER, B. LOOCK et J. M. LHOSTE. Can. J. Chem. **56**, 2598 (1978).

On a réalisé la synthèse de la ^{15}N-étioporphyrine par polycondensation du pyrrole 2-carboxylique, 5-hydroxyméthyle qui a été préparé par la méthode de Bullock. La porphyrine, isomériquement pure, est obtenue avec un haut rendement. Son analyse par rmn du proton, ainsi que celles de sa forme dicationique et de son complexe de zinc, sont décrites. Le spectre de la base libre révéle un tautomérisme rapide des protons NH à 34°C, qui disparait à basse température. D'autre part tous les spectres montrent des interactions à longue distance entre les protons du cycle tétrapyrrolique et les azotes-15. Le complexe ^{63}Cu – ^{15}N-étioporphyrine I a été également étudié par rpe. A partir de l'analyse de ce spectre, une analyse complète des spectres des complexes obtenus avec le cuivre naturel et avec les porphyrines azote-14 a pu être faite.

Can. J. Chem. Downloaded from www.nrcresearchpress.com by 210.87.254.42 on 09/05/12
For personal use only.

Introduction

Details of the electronic and stereochemical structures of porphyrins and related compounds may be investigated by the appropriate utilization of isotopically substituted compounds in electron or nuclear magnetic resonance experiments. Among the labels in common use, deuterium and carbon-13 are most prevalent (1, 2). Nitrogen-15 ($I = \frac{1}{2}$) appears to be also a favorable label. ^{15}N-enriched porphyrins have been investigated by Boxer *et al.* (2) and Irving and Lapidot (3). The compounds were obtained with a moderate isotopic enrichment via biosynthetic methods. Gust and Roberts (4) have described the chemical synthesis of ^{15}N-mesotetraphenylporphine prepared from enriched pyrrole but highly enriched etio type porphyrins have not yet been reported. The present paper deals with the preparation of ^{15}N-etioporphyrin I and its metallic derivatives. The method derives from that of Bullock *et al.* (5) and Inhoffen *et al.* (6) and produces with high yield a pure isomer I which has been characterized by proton magnetic resonance.

In addition, the paramagnetic copper complex of this enriched porphyrin was studied by esr in dimethylformamide or diluted in the free base at room temperature and at 77 K. The spectra could be readily analyzed using a pure copper-63 complex. A similar study has been performed with enriched and natural copper complexes of ^{14}N-etioporphyrin I, providing a complete set of esr data for copper porphyrins.

Results and Discussion

^{15}N-Etioporphyrin I (1,3,5,7-tetraethyl-2,4,6,8-tetramethylporphyrin) was prepared by polycondensation of 5-hydroxymethylpyrrole-2-carboxylic acid by a procedure based on the synthesis described by Inhoffen *et al.* (6) for the preparation of octaethylporphyrin. 3-Ethyl-2,4-pentanedione (**1**), prepared from ethyl iodide and acetylacetone, was condensed with ethyl 3-oxo-2(^{15}N-hydroxyimino)butanoate (**2**) obtained by a direct reaction of ethyl acetoacetate and sodium ^{15}N-nitrite. This condensation is a variation related to that of Fischer and Fink derived from the well-known Knorr synthesis (7). Treatment of the resulting pyrrole, ethyl 3,5-dimethyl-4-ethylpyrrole-2-carboxylate (**3**), with lead tetraacetate gave the acetoxy derivative from which the 3-methyl-4-ethyl-5-hydroxymethylpyrrole-2-carboxylic acid (**5**) was obtained by basic hydrogenolysis. When a solution of this acid derivative was refluxed with potassium ferricyanide, **6** was formed in good yield (18% based upon **3**, after chromatography on silica gel column). This preparation is detailed in the Experimental.

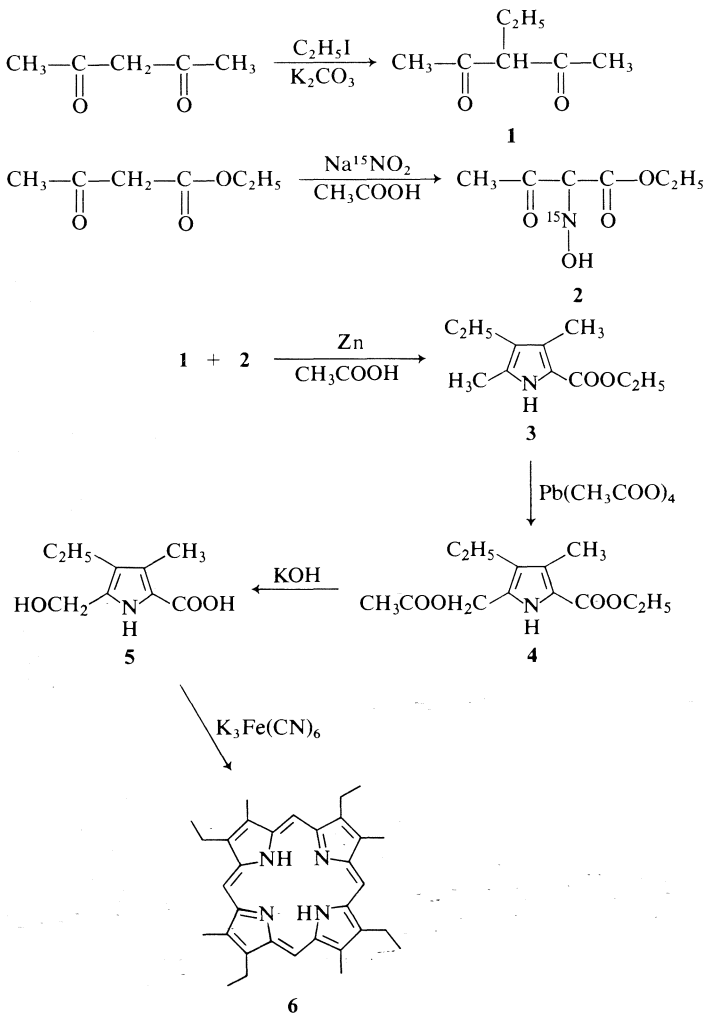

The analysis of the porphyrin (nmr and elemental analysis) confirms that the procedure used has provided a porphyrin of high yield and a single isomer. This is not the case for other methods described for the synthesis of etioporphyrin I (8) or related isomer I porphyrins (9) which gave a mixture of isomers (i.e., I, II, III, IV). The yield of the latter methods of preparation are furthermore much lower. These low yields of cyclization of tetramacrocycle derivatives could be attributed to the formation of linear verdin compounds during the self condensation of the pyrrolic precursors. In addition, Smith (10) has described the preparation of etioporphyrin I from unsymmetrical perbromide pyrromethenes with a high yield but some amounts of verdin were still present. The porphyrin could be also prepared by condensation of a dipyrromethene perbromide and a dipyrromethene hydrobromide obtained from the same pyrrolic derivative **3**, following the method of Rislove *et al.* (11). This more conventional procedure has provided a porphyrin with a lower final yield (12% based upon **3**). Thus, the modifications made in our chemical procedure influence both the yield and the purity of the final product. These two factors are important when the compound is synthesized with isotopically enriched precursors.

^1H *Nuclear Magnetic Resonance Spectra*

The proton nmr spectrum of the ^{15}N-etioporphyrin is shown in Fig. 1. The meso proton resonances centered at 10.08 ppm exhibit a triplet structure whereas those of the ^{14}N-etioporphyrin prepared by identical procedures appear in the same conditions as a single line at 10.08 ppm. The observed splitting (4.55 Hz) in the ^{15}N compound can therefore be attributed to the spin–spin coupling of the meso protons with the nitrogen-15 nuclei of the two adjacent pyrrole rings. Furthermore, the equivalence of the four methine protons establishes the isomeric nature of the porphyrins as etioporphyrin I.

Can. J. Chem. Downloaded from www.nrcresearchpress.com by 210.87.254.42 on 09/05/12
For personal use only.

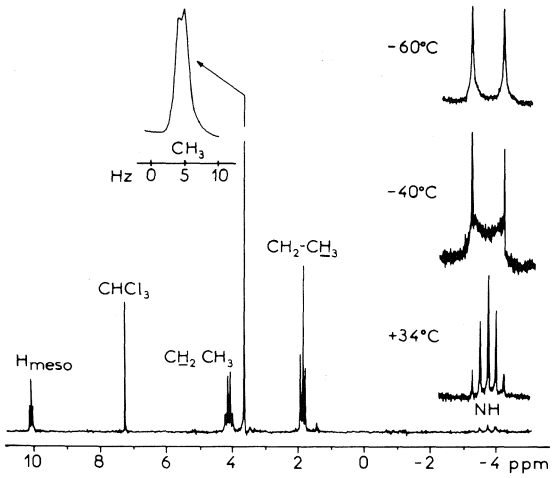

FIG. 1. ^{1}H nuclear magnetic resonance spectrum of ^{15}N-etioporphyrin I in deuteriochloroform at 34°C. On the right side of the figure are shown the NH proton resonances at various temperatures.

The two equivalent pyrrolic NH protons of the free base ^{15}N-porphyrin resonate at -3.7 ppm as a multiplet of relative intensity 1:4:6:4:1 at room temperature. Lowering the temperature to -60°C the multiplet changes into a doublet with a coupling constant of 97.5 Hz equal to the frequency distance of the outer lines in the quintet. This coupling constant is typical of one-bond ^{15}N–^{1}H coupling, as observed in ^{15}N-pyrrole (12) and in pheophytin a (2) and it was also measured in the pyrrolic precursors **3**, **4**, and **5**. The temperature dependence of the multiplet structure of the imino proton resonances of the free base porphyrin is characteristic of an intramolecular exchange process and is essentially identical to that reported for other ^{15}N-labeled porphyrins (3, 13). A particular aspect of the lineshape evolution, not reported until now, is worth further consideration. It can be noted (Fig. 1) that the outer lines of the multiplet do not broaden upon lowering the temperature. The transitions corresponding to these lines connect the energy level with nitrogen spins $\alpha\alpha\alpha\alpha$ and $\beta\beta\beta\beta$ in a X_2ABCD system, where X stands for the protons under observation and ABCD for the nitrogen-15 nuclei. These levels are not modulated in the exchange process at any temperature since the permutation of the A, B, C, and D nuclei leaves the corresponding eigenstate unchanged. These lines should be sensitive only to intermolecular exchange processes, prevented by use of aprotic solvent, or to an intramolecular exchange of the protons between sites having different chemical shift. The latter process should occur in a tautomerism reaction involving adjacent pyrrols, i.e., if the two opposite protons do not jump simultaneously. The lifetime of such an intermediate state appears negligible on the nmr scale down to -60°C in agreement with results obtained by different methods on deuterioporphyrin IX dimethylester (14) and mesotetraphenylporphine (14, 15).

The one-bond $J_{^{15}N,^1H}$ coupling in the dication, obtained by bubbling gaseous hydrochloric acid through the solution, is somewhat smaller (92.5 Hz). This was also observed for other ^{15}N-porphyrin cations (3, 4) and has been interpreted by a change in the nitrogen atom hybridization (3) corresponding to a deformation of the pyrrole rings.

Long-range ^{15}N–^{1}H couplings could also be observed in this porphyrin. The three-bond coupling observed for the methine protons in the free base (4.55 Hz) and in the dication (4.75 Hz) is larger than that previously observed (2) in ^{15}N-labelled pheophytin a and chlorophyll a (3 Hz). We measured also a reduced coupling (2.9 Hz) in the zinc complex of the present porphyrin. These changes could be attributed to structural features but it should be mentioned that we observed a comparable coupling (2.5 Hz) in the starting compounds in which the protons are bonded to a carbon with sp^3 hybridization. The present observations contrast with the strong dependence of $^2J_{^{15}N,^1H}$ and $^3J_{^{15}N,^1H}$ couplings upon protonation of ^{15}N-heterocyclics (16).

Charge dependence is more strictly evidenced in the four-bond nitrogen coupling with the pyrrolic methyl protons. In fact, these protons exhibit a resolved 0.8 Hz splitting (Fig. 1) which could not be assigned by homonuclear decoupling experiments and was assigned to a heteronuclear coupling. A similar four-bond coupling was not resolved in the resonances of the methylene protons of the ethyl groups. However, the linewidth of these latter resonances (2.2 Hz) could mask such an interaction. This coupling disappears in the dication which exhibits a 1.5 Hz splitting of the methyl resonances of the ethyl groups assigned to a five-bond heteronuclear coupling with the nitrogen-15 nucleus.

Pure electronic effects should be at the origin of the still longer range coupling observed in the zinc complex. Indeed, the methine proton resonances exhibit, in addition to the three-bond $^3J_{^{15}N,^1H}$ couplings, a structure consistent with a 1.4 Hz coupling of each proton with two other and still equivalent nitrogen-15 nuclei. Similar couplings have been also observed in chlorophyll a and assigned to a ^5J coupling through the metal ion (2). The lack of sensitivity of this coupling to the nature of the metal ion (Zn or Mg) makes it more plausible to assign it to a ^7J coupling corresponding to a preferred pathway through the porphyrin ring associated with π electron delocalization.

Can. J. Chem. Downloaded from www.nrcresearchpress.com by 210.87.254.42 on 09/05/12
For personal use only.

Electron Spin Resonance Spectra of ^{63}Cu – Etioporphyrin I

The presence of both ^{63}Cu and ^{65}Cu with their slightly different gyromagnetic ratios of 0.709 and 0.759, respectively, gives rise to complicated spectra of copper porphyrins and other tetrapyrrolic compounds due to the superimposition of two hyperfine splitting patterns (17, 18). The esr spectra of copper porphyrins are simplified by the use of isotopically enriched ^{63}Cu complexes (19, 20). They are further better resolved in the ^{15}N-labelled compounds because only a five-line superhyperfine splitting pattern of the copper hyperfine lines should be observed, each nitrogen-15 nuclei having a spin of $\frac{1}{2}$.

Indeed, such a well-resolved structure is observed in the low-field parallel components as well as in the highest field portion of the spectrum (Figs. 2 and 3). These latter resonances arise from a singularity which corresponds to a lack of dependence of the resonance field values upon changes in θ (Fig. 2) for orientations of the magnetic field H_0 which differ from the symmetry axes of the complex (21); (the

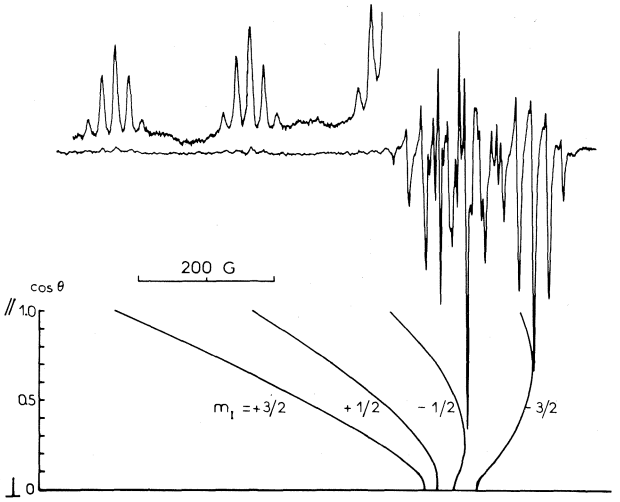

FIG. 2. Electron spin resonance spectrum of $^{63}Cu - ^{15}N$-etioporphyrin I diluted in the free base (1/1000) at 77 K (upper). The resonance fields as a function of $Z = \cos\theta$, where θ is the angle between the magnetic field direction and the symmetry axis of the complex (lower).

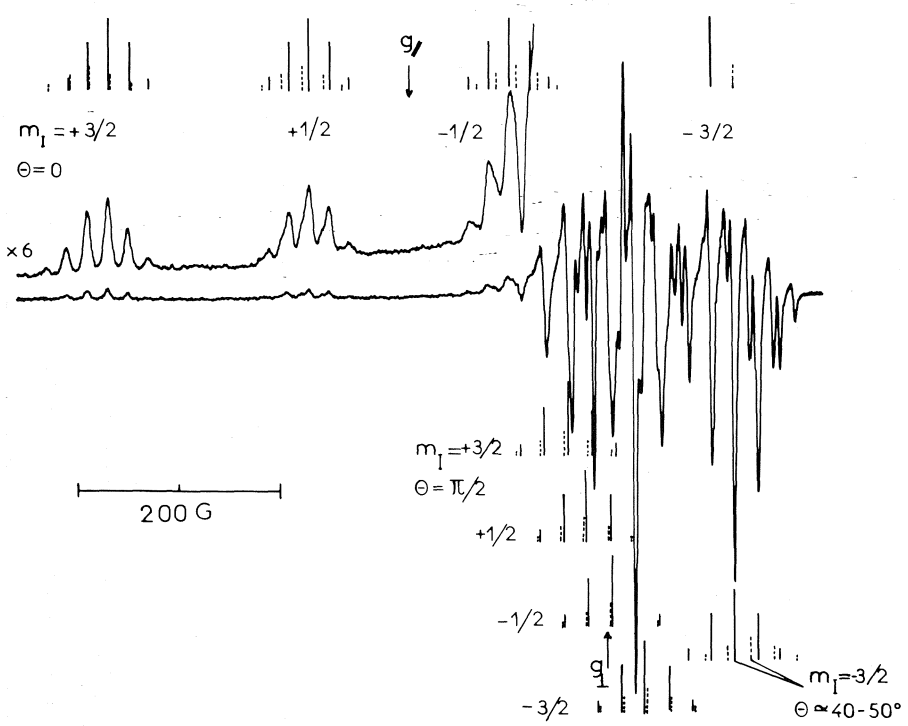

FIG. 3. Electron spin resonance spectrum of natural Cu – ^{15}N-etioporphyrin I diluted in the free base (1/1000) at 77K. The resonance fields indicated as a stick diagram were calculated to second order (22) with parameters of Table 1 and $A(^{65}Cu) = A(^{63}Cu) \times \mu(^{65}Cu)/\mu(^{63}Cu)$. The singularities for noncanonical orientations were obtained from the angular dependence of the resonance fields. The $m_I = -\frac{3}{2}$, $\theta = 0$ resonances were not completely drawn because these lines are completely masked in the experimental spectrum due to their low intensity. Full lines correspond to ^{63}Cu whereas the broken lines correspond to the ^{65}Cu isotope. The intense and sharp line in the high-field part of the spectrum is assigned to the singularity from noncanonical orientation for $m_I = -\frac{1}{2}$ discussed in the text (see also Fig. 2). The corresponding lines are not drawn on this figure.

Can. J. Chem. Downloaded from www.nrcresearchpress.com by 210.87.254.42 on 09/05/12
For personal use only.

Can. J. Chem. Downloaded from www.nrcresearchpress.com by 210.87.254.42 on 09/05/12
For personal use only.

additional structure visible in this high-field part (Fig. 2) is due to a 10% contamination of the enriched sample by ^{65}Cu–^{15}N-porphyrin). On the contrary, the nitrogen superhyperfine structure is unresolved or poorly resolved in the low-field part of the spectra recorded using porphyrins which are not selectively enriched. The apparent good resolution which may be observed however with the latter compounds in the high-field region is due to the fact that the difference between the ^{63}Cu and ^{65}Cu hyperfine components is approximately equal to the superhyperfine structure due to the ^{14}N nuclei (Table 1). This difference is, however, well resolved in the spectrum of the ^{15}N-labelled porphyrin (Fig. 3) and is readily interpreted using ^{65}Cu hyperfine coupling constants calculated from the measured ^{63}Cu constants and the ratio of the magnetic moments of these two isotopes.

The $g_{\parallel}$ part of the spectrum of the ^{63}Cu–^{15}N-porphyrin is easily interpreted owing to the good resolution and to negligible second-order effects. The $g_{\perp}$ part of the spectrum cannot be interpreted so readily since the total number of resolved lines is larger than that expected ($5 \times 4 = 20$ lines). The additional lines are not due to contamination by the ^{65}Cu isotope but probably to a singularity for a non-canonical orientation in the $m_I = -\frac{1}{2}$ resonance fields as already mentioned for the $m_I = -\frac{3}{2}$ components. Indeed, the calculation of the resonance field, including second-order effects (22) with the approximated parameters deduced from the spectrum at 77 K and the isotropic system at 300 K in dimethylformamide (Table 1), shows one that this singularity occurs for a value of the angle of the magnetic field direction with the symmetry axis of about 75° ($\cos\theta = 0.26$) for the $m_I = -\frac{1}{2}$ components and 47° ($\cos\theta = 0.68$) for the $m_I = -\frac{3}{2}$ components (Fig. 2). Furthermore, these calculations reveal that second-order effects result in a non-uniform splitting between the hyperfine lines for the perpendicular orientation of the magnetic field, from 18 G for the two low-field transitions to about 33 G for the two high-field transitions (Figs. 2 and 3).

Conclusion

The isotopic labelling of porphyrins with ^{15}N may be helpful for the elucidation of physicochemical properties involving the mass or the magnetic moment of the nitrogen nuclei. In the present paper, we have described long-range $J_{^{15}N,^{1}H}$ coupling in the nmr spectra which are not resolved using the natural isotope ^{14}N. On the other hand, substitution of selectively enriched ^{63}Cu in the ^{15}N porphyrin has allowed determination of a complete set of esr parameters which can be extended to other isotopic compositions. We shall report in the forthcoming

TABLE 1. g values and coupling constants (in Gauss) for copper – etioporphyrin I at room temperature (average values) and at 77 K. The same coordinates were used for the nitrogen hyperfine structure and the metal fine and hyperfine structures, i.e., the symmetry axes of the molecule

	Solvent	$\langle g \rangle$	$\langle A \rangle$		$g_{\parallel}$	$g_{\perp}{}^{a}$	$A_{\parallel}$		$A_{\perp}{}^{a}$	
			Cu	N			Cu	N	Cu	N
$^{63}Cu-{}^{15}N$-Etio I	Dimethylformamide	2.0940±0.0005	86.8±0.5	22.6±0.3	2.1844±0.0010	2.0488	202.1±0.5	19.8±0.3	25.3	24.1
	H_2-Etio I				2.1887±0.0005		200.5±0.5	19.9±0.15		22.1±0.3
$^{63}Cu-{}^{14}N$-Etio I	Dimethylformamide	2.0943±0.0010	87.2±1.0	16.0±0.3	2.1858±0.0010	2.0486	200.4±1.0	14.2±0.5	26.9	16.9
	H_2-Etio I				2.1891±0.0005		200.5±0.5	14.2±0.2		

[a]Calculated from $<g>$, $g_{\parallel}$, $<A>$, and $A_{\parallel}$; measured in $^{63}Cu-{}^{15}N$-Etio I diluted in H_2-Etio I.

Can. J. Chem. Downloaded from www.nrcresearchpress.com by 210.87.254.42 on 09/05/12
For personal use only.

publication on the nitrogen and metal isotopic effects on the Raman and infrared spectra (23).

Experimental

All starting materials were analytical grade (Merck Company). $^{15}NO_3Na$ and ^{63}Cu were purchased from CEA, France. Dimethylformamide was distilled under reduced pressure of nitrogen and stored on a 0.4 nm molecular sieve. Proton magnetic resonance spectra in deuteriochloroform (CEA, France) were recorded at 100 MHz in the Fourier transform mode using 4 K data points in the frequency domain. Pyridine-d_5 was added to the deuteriochloroform solution of Zn – ^{15}N-etioporphyrin I to destroy the association of the metalloporphyrin molecules. Chemical shifts were referenced to internal tetramethylsilane (TMS). Electron spin resonance spectra were recorded on a Varian 4502 X band spectrometer. The magnetic field strength was calculated from the nuclear resonance frequency of a proton probe located close to the cavity (Varian F8A magnetometer). This frequency was determined with a Hewlett-Packard 5245 L frequency counter. The microwave frequency was measured with a calibrated wavemeter.

*3-Ethyl-2,4-pentadione (**1**)*

This compound was prepared by the method of Johnson *et al.* (24) and was used for the synthesis of 3-acetylhexane-2-one. The desired product was distilled at 176–180°C (71%); nmr (deuteriochloroform) δ: 0.9 (*t*, —CH_2CH_3), 1.9 (q, —CH_2-CH_3), 2.19 (s, —CH_3), 3.54 (t, —CH).

*Ethyl 3,5-Dimethyl-4-ethyl-^{15}N-pyrrole-2-carboxylate (**3**)*

A method analogous to Eisner's preparation of ethyl 4-acetyl-3-ethyl-5-methylpyrrole-2-carboxylate (7) was employed. Ethyl acetoacetate (26 g) in 75 ml of acetic acid was treated with sodium ^{15}N-nitrite (15 g) in 35 ml of distilled water at 0°C during 4 h and kept overnight at room temperature. This solution was added to 3-ethyl-2,4-pentadione (32 g), zinc dust (28 g), and sodium acetate (34 g). The mixture was well stirred and refluxed for 4 h, then poured while hot into ice water. The crude product was filtered off and recrystallized from ethanol (22.2 g, 56%); nmr (deuteriochloroform) δ: 1.05 (t, —CH_2CH_3), 1.34 (t, —OCH_2CH_3), 2.19 (d, $^3J_{N,H}$ = 2.4 Hz, N—C—CH_3), 2.27 (s, —CH_3), 2.37 (q, —CH_2CH_3), 4.28 (q, —O—CH_2CH_3), 8.45 (d, $^1J_{NH}$ = 97, NH). *Anal.* calcd. for $C_{11}H_{17}O_2N$: C 67.35, H 8.67, N 7.65; found: C 67.29, H 8.62, N 7.38.

*Ethyl 5-Acetoxymethyl-3-methyl-4-ethyl-^{15}N-pyrrole-2-carboxylate (**4**)*

To 15.7 g of ethyl 3,5-dimethyl-4-ethyl-^{15}N-pyrrole-2-carboxylate in acetic acid (400 ml), lead tetraacetate (45 g) was added with stirring during 30 min. Stirring was continued for 2 h more. Acetic acid was removed under reduced pressure and the residue was dissolved in chloroform, washed with water, then dried over anhydrous sodium sulfate. The chloroform was evaporated to dryness. The desired product was crystallized from methanol to yield white crystals (12 g, 59%); nmr (deuteriochloroform) δ: 1.08 (t, —CH_2CH_3), 1.35 (t, —O—CH_2CH_3), 2.07 (s, —CO—CH_3), 2.28 (s, —CH_3), 2.46 (q, —CH_2—CH_3), 4.31 (q, —O—CH_2—CH_3), 5.02 (d, $^3J_{N,H}$ = 2.8 Hz, —CH_2—O), 8.95 (d, $^1J_{NH}$ = 97.9 Hz, NH). *Anal.* calcd. for $C_{13}H_{19}NO_4$: C 61.42, H 7.48, N 5.91; found: C 61.28, H 7.27, N 5.79.

*5-Hydroxymethyl-3-methyl-4-ethyl-^{15}N-pyrrole-2-carboxylic Acid (**5**)*

Pyrrolic ester **4** (11 g) in 150 ml of methanol containing 22.5 g of potassium hydroxide was heated under reflux for 4 h. The solution was evaporated under reduced pressure. The solid residue was dissolved in water (100 ml) and the aqueous solution was washed with ether, then acidified with dilute HCl. The precipitated product was filtered, washed with aqueous sodium acetate, and water (6.9 g, 87%); nmr (deuteriochloroform) δ: 1.07 (t, —CH_2—CH_3), 2.32 (s, —CH_3), 2.43 (q, —CH_2—CH_3), 4.42 (d, $^3J_{N,H}$ = 2.4 Hz, —CH_2—OH), 8.90 (d, $^1J_{NH}$ = 97.6 Hz, N*H*).

*^{15}N-Etioporphyrin I (**6**)*

An acetic acid solution (28 ml) containing 6.80 g of pyrrole-carboxylic acid **5** and potassium ferricyanide (1.36 g) was heated under reflux with vigorous stirring for 1 h. The reaction mixture was allowed to stand 3 days. The precipitate was collected, washed with methanol, and dried (2.42 g, 54.3%).

This material was dissolved in a minimal volume of chloroform and applied on an alumina column (neutral, grade I) previously treated with the same solvent. ^{15}N-Etioporphyrin I was eluted with chloroform and recrystallized in chloroform–methanol mixture: 1.57 g (yields: 35.3 and 18%, respectively, based upon **5** and **3**); spectrum (benzene): λ_{max}(nm) (ε(m*M*)): 399 (163), 498 (14.4), 530 (10.5), 568.5 (6.7), 623 (6.3). *Anal.* calcd. for $C_{32}H_{38}N_4$: C 79.67, H 7.88, N 12.45; found: C 80.0, H 7.93, N 12.39.

The structure was confirmed by the nmr spectrum of the solution in deuteriochloroform (see the text).

Synthesis of Metalloderivatives

The zinc and copper porphyrins were prepared from the metal acetates in acetic acid by the method of Fischer and Strangler (8), then purified by chromatography on a silica gel column. The metalloporphyrins were eluted with chloroform. Zn – ^{15}N-etioporphyrin I in benzene: λ_{max}(nm), (ε(m*M*)): 402 (340.7), 531 (15.6), 568 (28.8). Cu – ^{15}N-etioporphyrin I in benzene: λ_{max}(nm) (ε(m*M*)): 398 (291.7), 524.5 (12.6), 561.5 (28.2).

Acknowledgement

This work was supported by Institut National de la Santé et de la Recherche Médicale (C.R.L. No 77-4-091-3).

1. J. A. S. Cavaleiro, A. M. d'A. Rocha Gonsalves, G. W. Kenner, and K. M. Smith. J. Chem. Soc. Perkin I, 1771 (1974).
2. S. G. Boxer, G. L. Closs, and J. J. Katz. J. Am. Chem. Soc. **96**, 7058 (1974).
3. C. S. Irving and A. Lapidot. J. Chem. Soc. Chem. Commun. 184 (1977).
4. D. Gust and J. D. Roberts. J. Am. Chem. Soc. **99**, 3637 (1977).
5. E. Bullock, A. W. Johnson, E. Marklan, and K. B. Shaw. J. Chem. Soc. 1430 (1958).
6. H. H. Inhoffen, J. H. Fuhrhop, H. Voigt, and H. Brockmann. Ann. Chem. **695**, 133 (1966).
7. H. Fischer and E. Fink. Z. Physiol. Chem. **280**, 123 (1944).
8. H. Fischer and G. Stangler. Ann. Chem. **459**, 53 (1927).
9. A. H. Jackson, P. Johnston, and G. W. Kenner. J. Chem. Soc. 2262 (1964).
10. K. M. Smith. Tetrahedron Lett. **25**, 2325 (1971).
11. D. J. Rislove, A. T. O'Brien, and J. M. Sugihara. J. Chem. Eng. Data, **13**, 588 (1968).
12. T. Bundgaard, H. J. Jakobsen, and E. J. Rahkamaa. J. Magn. Reson. **19**, 345 (1975).
13. H. J. C. Yich, M. Sato, and H. Morishima. J. Magn. Reson. **26**, 365 (1977).

14. R. J. ABRAHAM, G. E. HAWKES, and K. M. SMITH. Tetrahedron Lett. 1483 (1974).
15. S. S. EATON and G. R. EATON. J. Am. Chem. Soc. **99**, 1601 (1977).
16. E. W. RANDALL and D. G. GILLIES. Prog. Nucl. Magn. Reson. Spectrosc. **6**, 119 (1971).
17. J. M. ASSOUR. J. Chem. Phys. **43**, 2477 (1965).
18. A. MAC CRAGH, C. B. STORM, and W. S. KOSKI. J. Am. Chem. Soc. **87**, 1470 (1965).
19. Y. HSU. Mol. Phys. **21**, 1087 (1971).
20. C. M. GUZY, J. B. RAYNOR, and M. C. R. SYMONS. J. Chem. Soc. A, 2299 (1969).
21. R. NEIMAN and D. KIVELSON. J. Chem. Phys. **35**, 156 (1961).
22. B. BLEANEY. Philos. Mag. **42**, 441 (1951).
23. P. V. THOAÏ, J. P. LEICKNAM, M. MOMENTEAU, and B. LOOCK. To be published.
24. A. W. JOHNSON, F. MARKHAM, R. PRICE, and K. B. SHAW. J. Chem. Soc. 4254 (1958).

Can. J. Chem. Downloaded from www.nrcresearchpress.com by 210.87.254.42 on 09/05/12
For personal use only.

COMMUNICATION

Base-catalyzed hydrogen isotope exchange of thiocamphor: α-thioenolization rate constants

NICK HENRY WERSTIUK AND PAUL ANDREWS

Department of Chemistry, McMaster University, Hamilton, Ont., Canada L8S 4M1

Received June 29, 1978

NICK HENRY WERSTIUK and PAUL ANDREWS. Can. J. Chem. **56**, 2605 (1978).

The rates of base-catalyzed protium–deuterium exchange (α-thioenolization) of the *exo* and *endo* protons of thiocamphor (**1**), in 2:1 dioxane–D_2O at 25.0 ± 0.5°C, have been determined by monitoring the uptake of deuterium mass spectrometrically. The *exo* and *endo* exchange rate constants, 2.20×10^{-2} and 5.60×10^{-4} M^{-1} s^{-1}, respectively, are 23.2 and 12.3 times larger than the rate constants for *exo* and *endo* exchange in camphor (**2**). Factors which may determine the rate enhancements are discussed.

NICK HENRY WERSTIUK et PAUL ANDREWS. Can. J. Chem. **56**, 2605 (1978).

Faisant appel à la spectrométrie de masse pour évaluer l'absorbtion du deutérium, on a déterminé les vitesses, catalysées par les bases, des échanges protium–deutérium (α-thioénolisation) des protons *exo* et *endo* du thiocamphre (**1**), dans le dioxanne–D_2O 2:1, à 25.0 ± 0.5°C. Les constantes de vitesse d'échange *exo* et *endo*, 2.20×10^{-2} et 5.60×10^{-4} M^{-1} s^{-1} sont respectivement 23.2 et 12.3 fois plus élevées que les constantes de vitesse des échanges *exo* et *endo* du camphre (**2**). On discute des facteurs qui peuvent déterminer les augmentations de vitesse.

[Traduit par le journal]

Thione–thioenol tautomerism was first studied by Reyes and Silverstein in 1958 (1). Since then other workers have attempted to detail the factors which affect the equilibrium (2, 3). However, up to the present time, there have been no reports of studies of acid- or base-catalyzed α-thioenolization of thiones. In this communication, we report the rates of base-catalyzed protium–deuterium exchange of the *exo* and *endo* protons in thiocamphor (**1**) and discuss possible rate-controlling factors.

We chose to study **1** because there is a substantial difference in exchange rates of the diastereotopic protons and the substrate does not undergo trimerization, a reaction which unhindered thiones undergo very readily (4).

The rate constants listed in Table 1 were obtained by the method developed in these laboratories (5). That good first-order kinetics were observed and that analytical gas chromatographic analysis showed no significant conversion of **1** into **2** established that sulfur–oxygen exchange, a potentially complicating process that would decrease the base concentration, is insignificant.

Several factors may contribute to the increase in the α-deprotonation[1] rates of **1** relative to **2**. Because

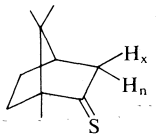

1

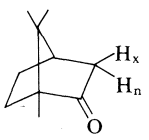

2

oxygen is more electronegative than sulfur and the carbonyl group would be expected to be more electron withdrawing than the thiocarbonyl group, base-catalyzed hydrogen isotope exchange of ketones should be more facile than exchange of thiones. From a survey of carbonyl and thiocarbonyl compounds (8), it is clear that the dipole moments of the thiocarbonyl compounds are close to or greater than the dipole moments of the carbonyl compounds. The

TABLE 1. Second-order rate constants of NaOD-catalyzed deuterium exchange of thiocamphor (**1**) and camphor (**2**) at 25.00 ± 0.05°C in 2:1 dioxane–D_2O

Substrate		k (M^{-1} s^{-1})*	k_{rel}		k_{exo}/k_{endo}
1	*exo*	2.20×10^{-2}	23.2		39.2
	endo	5.60×10^{-4}		12.3	
2	*exo*	9.50×10^{-4}†	1		21.2
	endo	4.46×10^{-5}†		1	

*Second-order rate constants were obtained by dividing the pseudo-first-order rates by the base concentration (0.0099 *M*). The rate constants were reproducible to a maximum deviation of ± 10%.

†The rate constants for exchange of camphor were obtained by Tidwell (6).

[1]We have established through several exploratory runs that β-thioenolization (homothioenolization) of 3,3,6,6-tetramethylbicyclo[2.2.1]heptan-2,5-dithione occurs more readily than β-enolization (homoenolization) of 3,3,6,6-tetramethylbicyclo[2.2.1]heptan-2,5-dione (7).

Can. J. Chem. Downloaded from www.nrcresearchpress.com by 210.87.254.6 on 09/05/12
For personal use only.

near equality of the aromatic solvent-induced shift (ASIS) of the ^{1}Hmr resonances of **1** and **2** determined by Demarco (9) and confirmed in these laboratories, indicates that the dipole moments are nearly identical. Thus the nmr data are in accord with the dipole moments of **1** (2.89 D) and **2** (2.98 D) that were determined by Lumbroso (10). However, it is interesting to note that theoretical calculations by Lumbroso (10) and Julg *et al.* (11) indicate that the thiocarbonyl group, $\overset{\delta-}{\diagdown}\overset{\delta+}{\diagup}C{=}S$, is polarized in the opposite sense to the carbonyl group, $\overset{\delta+}{\diagdown}\overset{\delta-}{\diagup}C{=}O$. Nevertheless, since the C=S and C=O bond moments certainly control the magnitudes of the dipole moments of **1** and **2** and the C=S bond is considerably longer than the C=O bond (12), the carbonyl group is expected to be more polar than the thiocarbonyl group. Thus the electrical effect of the carbonyl group should be greater than its sulfur analog.

That the increase in acidity may be due to a ground state effect, a consequence of the fact that the C=S bond is considerably weaker than the C=O bond (12, 13), is indicated by the following analysis. The energy changes associated with anion formation, as calculated from approximate bond energies for C=S, C=O, C—S, and C—O, assuming that all other effects are common, indicate that α-thioenolization would occur more readily than α-enolization.

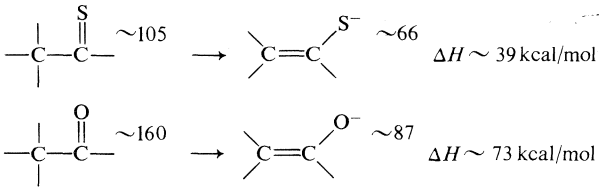

That sulfur acids are more acidic than the corresponding oxyacids is due to two factors: the —S—H bond is longer and weaker, and as established by the electron affinities (EA) of the atoms, sulfur (EA −47 kcal/mol) accomodates a negative charge better than oxygen (EA −34 kcal/mol) (14). The latter effect results from the fact that the additional 3*p* electron on sulfur is more diffuse and less crowded than the additional 2*p* electron on oxygen.

Thus, if the electrical effect of the C=O group is greater than the effect of C=S, then the ground state effect and the ability of sulfur to support a negative charge combine to outweigh the electrical effect and produce the observed increase in rate. It is interesting to note that thioamides are stronger acids ($\Delta pK_a \sim 2$) than amides (15).

Acknowledgements

We thank the National Research Council of Canada for financial support.

1. Z. Reyes and R. M. Silverstein. J. Am. Chem. Soc. **80**, 6367 (1958).
2. S. Bleish and R. Meyer. Chem. Ber. **100**, 93 (1967).
3. F. Duus, P. Kakobsen, and S. O. Lawesson. Tetrahedron, **24**, 5323 (1968).
4. P. S. Fraser, L. V. Robbins, and W. S. Chilton. J. Org. Chem. **34**, 2509 (1974).
5. N. H. Werstiuk, R. Taillefer, and S. Banerjee. Can. J. Chem. **56**, 1140 (1978).
6. T. T. Tidwell. J. Am. Chem. Soc. **92**, 1448 (1970).
7. N. H. Werstiuk. Can. J. Chem. **53**, 2211 (1975).
8. D. Paquer. Int. J. Sulfur Chem. B, **7**, 269 (1972).
9. P. Demarco. Chem. Commun. 1418 (1969).
10. H. Lumbroso. Bull. Soc. Chim. Fr. 3201 (1966).
11. A. Julg, M. Bonnet, and Y. Ozias. Theor. Chim. Acta, **17**, 49 (1970).
12. E. Campaigne. *In* The chemistry of the carbonyl group. Part 1. *Edited by* S. Patai. John Wiley and Sons, Inc., New York, NY. 1966. p. 917.
13. J. March. Advanced organic chemistry; reactions, mechanisms and structure. 2nd ed. McGraw-Hill Inc., New York, NY. 1977. p. 28.
14. I. G. Csizmadia. *In* The chemistry of the thiol group. Part 1. *Edited by* S. Patai. John Wiley and Sons, Inc., New York, NY. 1974. p. 22.
15. W. Walter and R. F. Becker. Ann. Chem. **727**, 71 (1969).

Can. J. Chem. Downloaded from www.nrcresearchpress.com by 210.87.254.6 on 09/05/12
For personal use only.

Canadian Journal of Chemistry
Published by
THE NATIONAL RESEARCH COUNCIL OF CANADA

Journal canadien de chimie
Publié par
LE CONSEIL NATIONAL DE RECHERCHES DU CANADA

Volume 56 Number 20 October 15, 1978 Volume 56 numéro 20 15 octobre 1978

Can. J. Chem. Downloaded from www.nrcresearchpress.com by 210.87.254.6 on 09/05/12
For personal use only.

Appearance potentials of ion fragments of iron pentacarbonyl

B. R. CONARD AND R. SRIDHAR
J. Roy Gordon Research Laboratory, Inco Metals Co., Mississauga, Ont., Canada L5K 1Z9

Received November 7, 1977[1]

B. R. CONARD and R. SRIDHAR. Can. J. Chem. **56**, 2607 (1978).

The previously reported fragments and a new fragment, FeC_2^+, have been observed in the mass spectrum of iron pentacarbonyl. The electron impact appearance potentials for the minor fragments of $Fe(CO)_5$ are (in eV): $FeC_3O_2^+$, 18.2; FeC_2O^+, 20.2; FeC_2^+, 29.9; FeO^+, 22.5; and $Fe(CO)_3^{2+}$, 24.0. Electron energy calibration was carried out using existing data for the major fragments of $Fe(CO)_5$.

B. R. CONARD et R. SRIDHAR. Can. J. Chem. **56**, 2607 (1978).

Un examen du spectre de masse du pentacarbonyle fer révèle la présence des fragments rapportés antérieurement aux côtés d'un nouveau fragment, FeC_2^+. Les potentiels d'apparition des fragments minoritaires sous impact électronique du $Fe(CO)_5$ sont (en eV): $FeC_3O_2^+$, 18.2; FeC_2O^+, 20.2; FeC_2^+, 29.9; FeO^+, 22.5 et $Fe(CO)_3^{2+}$, 24.0. On a calibré les énergies électroniques à l'aide de données existantes pour les fragments principaux du $Fe(CO)_5$.

[Traduit par le journal]

Even though a number of mass spectrometric studies (1–5) have been performed on $Fe(CO)_5$, the appearance potentials of only the most intense ions have been reported. The objective of the present work was to study the fragmentation pattern of iron pentacarbonyl and to measure the appearance potentials of the minor fragments.

The observed fragmentation pattern confirmed the minor fragments of $Fe(CO)_5$ reported by Winters and Collins (3). In addition, a new fragment, FeC_2^+, was observed for the first time and its appearance potential, as well as those of other minor fragments, were measured.

Experimental Methods

The mass spectrometer was an Extranuclear model 162-8 quadrupole instrument. The ion source consisted of two tungsten filaments and the total emission current was regulated. The quadrupole unit was housed in a vacuum system equipped with a 30 ℓ/s Varian ion pump and a 75 ℓ/s Veeco ion pump capable of pumping the system to better than $\sim 10^{-6}$ Pa (10^{-8} Torr).

The carbonyl vapour studied was obtained by room temperature sampling of the vapour in contact with liquid $Fe(CO)_5$, which was obtained from Domtar, Inc.

The ion carbonyl vapours were leaked into the ion source at a constant rate employing a Varian model 451–5100 leak valve. To ensure that carbonyl vapours entered the ion source directly, a 3.2 mm diameter stainless steel tube was attached to the high vacuum side of the leak valve and it extended to the ion source. This system gave very high sensitivity and without it the FeC_2^+ fragment would not have been detected. With time, however, the stainless steel tube, heated by the ion source, caused decomposition of the carbonyl in the tube before reaching the ion source. In general, it took 2 h for the tube to get hot enough to decompose the carbonyl completely and this time was sufficient to carry out numerous measurements. The carbonyl ion signals could be readily restored by turning off the ion source filaments and allowing the ion source to cool. This problem could have been overcome by water cooling the gas admission tube, but it was not necessary for this study.

The leak valve was adjusted to yield a constant total pressure of 1.3×10^{-4} Pa in the vacuum system (as measured by the ion pump current). The leak valve was closed during background measurements.

The Fragmentation Spectrum

Winters and Kiser (1) reported ions formed by the successive loss of CO and measured the appearance potential for $Fe(CO)_5^+$, $Fe(CO)_4^+$, $Fe(CO)_3^+$, $Fe(CO)_2^+$, $Fe(CO)^+$, and Fe^+. In addition to these species, Bidinosti and McIntyre (4) reported FeC^+, FeC_2O^+, FeO^+, and $Fe(CO)_3^{2+}$. The most com-

[1]Revision received June 14, 1978.

Can. J. Chem. Downloaded from www.nrcresearchpress.com by 210.87.254.6 on 09/05/12
For personal use only.

TABLE 1. Appearance potentials of ions observed from $Fe(CO)_5$

Mass	Ion	Relative abundance, this work (58 eV)	Appearance potentials (eV)					
							This work[a]	
			Ref. 1	Ref. 2	Ref. 4	Ref. 5	Regr. result	New
40	C_2O^+	(4)						
42	$Fe(CO)^{2+}$	2.5	30.2				30.24	
56	Fe^+	50	16.1	14.70	15.31	15.99	15.51	
68	FeC^+	7			23.6		23.65	
70	$Fe(CO)_3^{2+}$	2.4						24.0
72	FeO^+	1.2						22.5
80	FeC_2^+	0.17						29.9
84	$Fe(CO)^+$	100	14.0	12.90	13.39	13.76	13.18	
96	FeC_2O^+	0.8						20.2
112	$Fe(CO)_2^+$	25	11.8	10.92	11.27	11.12	11.24	
124	$FeC_3O_2^+$	0.08						18.2
140	$Fe(CO)_3^+$	11.9	10.3	9.89	10.01	10.04	10.08	
168	$Fe(CO)_4^+$	15.4	10.0	8.34	8.73	9.17	9.30	
196	$Fe(CO)_5^+$	5.3	8.53	8.14	8.16	8.40	8.53	

[a]These values were calculated using eq. [1].

plete fragmentation pattern reported to date was by Winters and Collins (3) and included $FeC_3O_2^+$ as well as a number of doubly ionized species.

The ions observed at 58 eV in the present work are listed in Table 1. They were identified by their mass, the isotopic distribution of iron, and their disappearance when the leak valve was closed. The presence of $FeC_3O_2^+$ was confirmed. A new fragment was identified as FeC_2^+ and is analogous to MC_2^+ fragments observed for a number of carbonyl molecules (4, 6).

All fragments (except CO), as well as the parent ion $Fe(CO)_5^+$, were observed to decrease as a function of the time the ion source was on. As noted by Pignataro and Lossing (7) and by Shadskii (8), $Fe(CO)_5$ undergoes decomposition in a hot ion source. In our experiments, as described before, the decomposition probably occurred in the tube leading to the ion source. The only ion observed to increase as a function of time was CO^+, which was consistent with the decomposition of $Fe(CO)_5$. Unfortunately, reliable intensity measurements on CO^+ were not possible due to the large amount of CO initially present in the CO-saturated iron pentacarbonyl sample and C_2O^+ intensities were unreliable due to interference from Ar^+ that was present in the system from previous measurements.

Appearance Potentials

The appearance potential determinations were carried out by the method of linear extrapolation. Data were obtained by focussing on the top of a peak and measuring the ion intensity as a function of increasing electron energy. The electron energy dial (10-turn potentiometer) was calibrated using the appearance potentials of major fragments of $Fe(CO)_5$ determined by a number of other workers who also used electron impact techniques. Their reported values are given in Table 1. A straight-line regression, constrained to go through the origin, was performed on the differences between our eV potentiometer settings and the previous values for the major fragments as a function of the eV potentiometer setting:

$$[1]\quad \Delta eV = (0.225 \pm 0.005) \times \text{potentiometer setting}$$

Using the standard deviation of the slope of this regression we estimate that the electron energies reported here are accurate to within ± 0.5 eV.

Acknowledgements

This work was supported by the National Research Council of Canada under the Industrial Research Assistance Program and the authors thank Inco Metals Ltd, for permission to publish the work. The careful experimental work by Mr. Brian McAneney is gratefully acknowledged.

1. R. E. WINTERS and R. W. KISER. Inorg. Chem. **3**, 699 (1964).
2. A. FOFFANI, S. PIGNATARO, B. CANTONE, and F. GRASSO. Z. Phys. Chem. New. Folge. **45**, 79 (1965).
3. R. E. WINTERS and J. H. COLLINS. J. Phys. Chem. **70**, 2057 (1966).
4. D. R. BIDINOSTI and N. S. MCINTYRE. Can. J. Chem. **45**, 641 (1967).
5. G. A. JUNK and H. J. SVEC. Z. Naturforsch. **236**, 1 (1968).
6. S. M. SCHILDCROUT, G. A. PRESSLEY, JR., and F. E. STAFFORD. J. Am. Chem. Soc. **89**, 1617 (1967).
7. S. PIGNATARO and F. P. LOSSING. J. Organomet. Chem. **11**, 571 (1968).
8. I. P. SHADSKII. Zh. Fiz. Khim. **47**, 2542 (1973).

Kinetics and mechanism of substitution reactions of (*N*,*N*-dimethylformamide)pentaammine–cobalt(III) and –rhodium(III) ions in DMF as solvent

S. T. Danny Lo, Margaret J. Sisley, and Thomas W. Swaddle[1]

Department of Chemistry, The University of Calgary, Calgary, Alta., Canada T2N 1N4

Received April 13, 1978

S. T. Danny Lo, Margaret J. Sisley, and Thomas W. Swaddle. Can. J. Chem. **56**, 2609 (1978).

The exchange of *N*,*N*-dimethylformamide (DMF) between $M(NH_3)_5DMF^{3+}$ and solvent in acidic DMF solutions proceeds with pseudo-first-order kinetics governed by the parameters $k_{ex}(55°C) = 8 \times 10^{-5}$ and 1.1×10^{-4} s^{-1}, $\Delta H_{ex}^* = 113$ and 99 kJ mol^{-1}, $\Delta S_{ex}^* = +22$ and -20 J K^{-1} mol^{-1}, and $\Delta V_{ex}^* = +3.2$ and -1.4 cm^3 mol^{-1} for M = Co and Rh respectively. For M = Co (but not Rh), the exchange rate was much faster in the absence of acid, and reduction of Co(III) to Co(II) was significant at low acidities. Solubility problems precluded the measurement of meaningful rate data for the reactions of $M(NH_3)_5DMF^{3+}$ with nucleophiles X^- in acidic DMF solution except for the case M = Co with X = Br^-, for which a limiting first-order rate coefficient 2.5 times k_{ex} was obtained for the formation of $Co(NH_3)_5Br^{2+}$ at high [Br^-] at 55°C. Despite this last result, the mechanism of simple substitution reactions is evidently dissociative interchange (I_d) for pentaamminecobalt(III) complexes in general, but associative interchange (I_a) for pentaamminerhodium(III) analogues.

S. T. Danny Lo, Margaret J. Sisley et Thomas W. Swaddle. Can. J. Chem. **56**, 2609 (1978).

L'échange de la *N*,*N*-diméthylformamide (DMF) entre le complexe $M(NH_3)_5DMF^{3+}$ et le solvant dans des solutions acides de DMF se produit suivant une cinétique du pseudo-premier ordre pour laquelle les paramètres sont $k_{ex}(55°C) = 8 \times 10^{-5}$ et 1.1×10^{-4} s^{-1}, $\Delta H_{ex}^* = 113$ et 99 kJ mol^{-1}, $\Delta S_{ex}^* = +22$ et -20 J K^{-1} mol^{-1} et $\Delta V_{ex}^* = +3.2$ et -1.4 cm^3 mol^{-1} respectivement pour M = Co et Rh. Dans le cas de M = Co (mais non dans celui de Rh), la vitesse d'échange est beaucoup plus rapide en l'absence d'acide et il se produit une réduction importante de Co(III) en Co(II) à des acidités basses. A cause de problèmes de solubilité, il n'a pas été possible de faire des mesures significatives de vitesse pour les réactions du complexe $M(NH_3)_5DMF^{3+}$ avec des nucléophiles X^- en solutions acides de DMF excepté dans le cas où M = Co avec X = Br^- pour laquelle réaction un coefficient de vitesse limite du premier ordre de 2.5 fois k_{ex} a pu être obtenue pour la formation de $Co(NH_3)_5Br^{2+}$ à concentration élevée de [Br^-] à 55°C. Malgré ce dernier résultat, le mécanisme pour les réactions de substitutions simples est évidemment un échange dissociatif (I_d) pour les complexes pentaamminecobalt(III) d'une façon générale mais d'échange associatif (I_a) pour les analogues pentaamminerhodium(III).

[Traduit par le journal]

Introduction

The purpose of this study was to test the assertion (1) that the mechanism of simple ligand substitution in solution changes from dissociative to associative interchange (I_d to I_a) as one goes from the pentaamminecobalt(III) to the pentaamminerhodium(III) series. Evidence for such a change in reactions [1] and [2]

$$[1]\quad M(NH_3)_5{}^{18}OH_2{}^{3+} + H_2O \xrightarrow{k_{ex}} M(NH_3)_5OH_2{}^{3+} + H_2{}^{18}O$$

$$[2]\quad M(NH_3)_5OH_2{}^{3+} + X^- \overset{K}{\rightleftharpoons} \{M(NH_3)_5OH_2{}^{3+}, X^-\} \xrightarrow{k_i} M(NH_3)_5X^{2+} + H_2O$$

has been found in measurements of k_i relative to k_{ex} (2), but the validity of this approach has recently been questioned (3, 4). A less equivocal case can be built upon the discontinuities in the sequences of values of the activation parameters ΔH_{ex}^*, ΔS_{ex}^*, and ΔV_{ex}^* for reaction [1], and more particularly in the sign of ΔV_{ex}^*, as one goes from M = Co to Rh and Ir (1, 5–7). We have recently advanced further, quite independent evidence favoring this mechanistic dichotomy (8), but, as Moore (9) points out, the question of the mechanism of substitution at rhodium(III) centers remains controversial (3, 10–12).

In this article, we describe attempts to elucidate this problem by changing the solvent to *N*,*N*-dimethylformamide (DMF) (reactions [3] and [4]),

$$[3]\quad M(NH_3)_5{}^*DMF^{3+} + DMF \xrightarrow{k_{ex}} M(NH_3)_5DMF^{3+} + {}^*DMF$$

[1]To whom all correspondence should be addressed.

Can. J. Chem. Downloaded from www.nrcresearchpress.com by 210.87.254.5 on 09/05/12
For personal use only.

Can. J. Chem. Downloaded from www.nrcresearchpress.com by 210.87.254.5 on 09/05/12
For personal use only.

[4] $M(NH_3)_5DMF^{3+} + X^- \overset{K}{\rightleftharpoons} \{M(NH_3)_5DMF^{3+}, X^-\} \xrightarrow{k_i} M(NH_3)_5X^{2+} + DMF$

in which the ion-pair formation constants K were expected to be large enough to permit reliable k_i data to be obtained.

Experimental

Materials

N,N-Dimethylformamide (Baker Analyzed or Fisher Certified Reagent) was purified less than 24 h before use in kinetic or spectroscopic measurements by drying it over a Linde 4A molecular sieve for a day or more, and distilling it fractionally under reduced pressure. Aqueous solutions of the product were neutral to pH paper. The numerical magnitudes of the kinetic results were not significantly dependent upon the source of the DMF or the rigour with which oxygen and moisture were excluded in the distillation, but best precision and reproducibility were obtained using freshly-opened Baker Analyzed DMF and a bleed of dry, oxygen-free nitrogen in the stillpot. DMF-d_7 (99.5% isotopic purity) was supplied by Stohler Isotopes. Trifluoromethanesulfonic acid was purified as previously described (13), but *para*-toluenesulfonic acid monohydrate (Fisher Certified Reagent), tetra-*n*-butylammonium bromide, tetraethylammonium chloride and bromide (Eastman), and perchloric acid (Baker Analyzed) were used without further purification. Potassium trioxalatochromate(III) was prepared by a standard method (14). Potassium thiocyanate was recrystallized from hot acetone by addition of ether.

N,N-Dimethylformamidepentaamminecobalt(III) perchlorate was made from aquopentaamminecobalt(III) perchlorate (15). *Anal.* calcd. for $[Co(NH_3)_5OCHN(CH_3)_2)](ClO_4)_3$: N 16.3, C 7.0, H 4.3, Cl 20.6; found: N 16.4, C 7.1, H 4.1, Cl 20.8. A solution of this compound in DMF ($\sim$0.01 M; M = mol dm^{-3}) showed light absorption maxima at 506 and 349 nm with molar absorptivities ε of 89.6 and 79.9 M^{-1} cm^{-1} respectively. The latter molar absorptivity was reduced to 76.4 M^{-1} cm^{-1} on addition of trifluoromethanesulfonic or *para*-toluenesulfonic acid ($\sim$0.01 M) but the spectrum was otherwise unchanged. These values differ slightly from those reported for the same complex in *aqueous* solution (15). $[Co(NH_3)_5DMF](ClO_4)_3$ containing partially DMF-d_7-labelled DMF was made by a procedure similar to the foregoing, using partially-labelled DMF.

Bromo- and thiocyanato-*N*-pentaamminecobalt(III) perchlorates were made as previously described (16, 17) and their purity was confirmed by elemental microanalysis. Their spectra in DMF ($\sim$0.01 M) in the presence of $\sim$0.01 M *para*-toluenesulfonic acid showed first ligand-field absorption maxima at 550 (ε 63.0) and 501 nm (ε 206.4 M^{-1} cm^{-1}) respectively.

N,N-Dimethylformamidepentaamminerhodium(III) perchlorate was made by dissolving 2.5 g Ag^+-free $[Rh(NH_3)_5OH_2](ClO_4)_3$ (6) in 7–10 cm^3 of DMF, heating the solution at 85°C for 3 h, then cooling the mixture to 0°C and adding 10 cm^3 water followed by a mixture of 5 cm^3 72% $HClO_4$ and 5 cm^3 water. The yellow precipitate was washed with acetone and then ether, recrystallized from a further 10 cm^3 of DMF in the same way, and dried over P_2O_5 under reduced pressure. Yield, 2.2 g.

Anal. calcd. for $[Rh(NH_3)_5DMF](ClO_4)_3$: C 6.4, H 4.0, Cl 19.0; found: C 6.6, H 4.0, Cl 18.9. The 60 MHz ^{1}H nmr spectrum in DMSO-d_6 showed signals of equal intensity at 6.48 and 6.67τ due to the two CH_3 groups, and a resonance at 2.07τ due to the —CHO proton. The uv spectrum at 21°C showed an absorption maximum at 323 nm (ε 216.0 M^{-1} cm^{-1}).

$[Rh(NH_3)_5DMF](ClO_4)_3$ partially labelled with DMF-d_7 was made in the above way, using the partially-labelled solvent. $[Rh(NH_3)_5DMF](BF_4)_3$ was made as above, but using 48% aqueous HBF_4 (Ventron) in place of the diluted $HClO_4$, and ethanol in place of acetone (in which the tetrafluoroborate salt was quite soluble).

Kinetics of the Exchange Reactions

The progress of reaction [3] (M = Co) at atmospheric pressure was followed by chilling aliquots taken from the thermostatted ($\pm$0.02°C) solution of partially ($\sim$7%) DMF-d_7-labelled $[Co(NH_3)_5DMF](ClO_4)_3$ in freshly-distilled DMF to 0°C and adding an equal volume of a cold aqueous solution containing the stoichiometric amount of potassium trioxalatochromate(III), with scratching and cooling. The filtered precipitate of $[Co(NH_3)_5DMF][Cr(C_2O_4)_3]$ was washed with acetone, dried under vacuum at 60°C for 12 h, and the coordinated DMF was recovered on a vacuum line by fusing the precipitate with KNCS. The DMF was analyzed with an Atlas CH-5 mass spectrometer for the ratio R of mass number 80 (DMF-d_7) relative to 74 (DMF-d_1, -$^{13}C_1$, -$^{15}N_1$, and -$^{17}O_1$) (18). The fraction x of the DMF which was d_7-labelled at time t was calculated from the relationship

[5] $$x = [1 + 25.84R^{-1}]^{-1}$$

The pressure dependence of the rate of reaction [1] was followed by withdrawing aliquots from a pressurized ($\pm$0.5 MPa), thermostatted ($\pm$0.1°C) syringe assembly as described elsewhere (17).

The progress of reaction [3] when M was Rh was followed in the same way as for M = Co, except that aliquots were delivered into ice-cold DMF containing an excess of tetraethylammonium chloride, and the precipitated $[Rh(NH_3)_5DMF]Cl_3$ was washed with acetone and dried at 70°C under reduced pressure and decomposed as such at 175 $\pm$ 5°C on the vacuum line.

Kinetics of the Anation Reactions

Typically, a solution containing a $Co(NH_3)_5DMF^{3+}$ or $Rh(NH_3)_5DMF^{3+}$ salt and trifluoromethanesulfonic or *para*-toluenesulfonic acid in freshly-distilled DMF was brought to the desired reaction temperature, and a solution of a salt of the nucleophile X^- in DMF at the same temperature was added to it (the complex and nucleophile salts were dissolved separately to minimize the risk of precipitation of $[M(NH_3)_5DMF]X_3$). The mixture was promptly transferred to an optical cell in an electrically heated aluminum block, the temperature of which was controlled to $\pm$0.1°C with a Melabs CTC-1A proportional controller, and the progress of the reaction was followed spectrophotometrically *in situ* with a Cary Model 17Hc spectrophotometer. In these as in all the other kinetic experiments light was excluded except for purposes of spectrophotometric measurements, and for the latter duplicate determinations were made at different slit widths or wavelengths to check for photochemical effects. For reactions involving cobalt(III), the final solutions were analyzed for cobalt(II) by adding a small amount of *para*-toluenesulfonic acid followed by a large excess of KNCS and determining the $Co(NCS)_4^{2-}$ concentration spectrophotometrically at 625 nm (ε 1890 M^{-1} cm^{-1}).

Can. J. Chem. Downloaded from www.nrcresearchpress.com by 210.87.254.5 on 09/05/12
For personal use only.

TABLE 1. Pseudo-first-order rate coefficients k_{ex} for the exchange of DMF between $Co(NH_3)_5DMF^{3+}$ and DMF solvent

T (°C)	$[Co(NH_3)_5DMF^{3+}]$ (M)[a]	[acid] (M)[b]	P (MPa)	k_{ex} (s^{-1}) × 10^5
30.05	0.0390	0.242	0.1	0.243 ± 0.006
40.06	0.0190	0		≥140
	0.0387	0		~57
	0.0777	0		~38
	0.0390	0.241		1.11 ± 0.02
50.25	0.0192	0.0094		4.46 ± 0.09
	0.0194	0.0194		4.79 ± 0.09
	0.0194	0.0400		4.41 ± 0.08
	0.0194	0.0697		4.53 ± 0.09
	0.0392	0.240		4.42 ± 0.08
	0.0792	0.474		4.30 ± 0.10
55.36	0.0394	0.240		8.94 ± 0.18[g]
	0.0390	0.241		8.44 ± 0.16
	0.0390	0.0460[c]		8.17 ± 0.16
	0.0395	0.219[c]		7.58 ± 0.15
	0.00397	0.00460[d]		8.0 ± 0.3
	0.00404	0.00460[e]		8.5 ± 0.3
	0.00405	0.00460[f]		7.8 ± 0.5
55.4	0.0362	0.236	101	7.59 ± 0.15
	0.0361	0.238	162	6.92 ± 0.11
	0.0366	0.253	222	6.58 ± 0.11
	0.0362	0.263	312	5.80 ± 0.10
	0.0363	0.240	402	5.32 ± 0.10

[a]As ClO_4^- salt.
[b]Unless otherwise stated, *p*-toluenesulfonic acid.
[c]Trifluoromethanesulfonic acid.
[d]$[Br^-] = 2.56 \times 10^{-2}$ M.
[e]$[Br^-] = 5.20 \times 10^{-2}$ M.
[f]$[Br^-] = 0.101$ M.
[g]In the presence of 2% added Co^{2+}.

Results

The $Co(NH_3)_5DMF^{3+}$/DMF Exchange

The exchange of DMF between $Co(NH_3)_5DMF^{3+}$ and DMF solvent followed first-order kinetics

$$[6] \qquad \ln (x_t - x_\infty) = k_{ex}t + \ln (x_0 - x_\infty)$$

to at least 75% completion of reaction in the presence of added *para*-toluenesulfonic acid in six-fold molar excess over the complex, and at least 40% reaction with half as much acid as complex. The rate coefficient k_{ex} was independent of the acid concentration within this range, and was essentially the same whether anhydrous trifluoromethanesulfonic acid or *para*-toluenesulfonic acid monohydrate was used, i.e., neither the nature of the acid anion nor the presence of small amounts of water (presumably as H_3O^+ in this case) affected the exchange rate significantly. In the absence of any added acid, however, the exchange rates were very much higher, not accurately reproducible, and markedly dependent upon the concentration of the complex.

Reduction of cobalt(III) to cobalt(II) became significant at low acid concentrations. For $[Co(NH_3)_5DMF^{3+}] \sim 0.04$ M and [acid] ~ 0.24 M, no cobalt(II) could be detected after 80% completion of exchange at 55.4°C, although 0.9% of the cobalt was present as cobalt(II) after 10 half-periods ($t_{1/2}$) of the exchange reaction and as much as 10% after $50t_{1/2}$, i.e., the redox process was autocatalytic. Reduction was somewhat faster at lower acid concentrations, e.g., for [complex] = [acid] = 0.04 M, traces of cobalt(II) were detectable after $0.6t_{1/2}$ for reaction [1] and 50% Co^{2+} after $50t_{1/2}$. Neither the deliberate addition of cobalt(II) nor the increased importance of spontaneous reduction *per se*, however, had any significant influence upon k_{ex}. Finally, the addition of Br^-, even in concentrations sufficient for almost complete ion-pairing with $Co(NH_3)_5DMF^{3+}$, did not affect k_{ex} within the experimental uncertainty.

Table 1 lists data which illustrate the above generalizations and which give linear plots of $\ln (k_{ex}/T)$ against $1/T$ and of $\ln k_{ex}$ against pressure P (correlation coefficients $r^2 = 0.9998$ and 0.9966 respectively). Values of k_{ex} obtained using ordinary glassware correlate well with those obtained with the pressure apparatus. The corresponding activation parameters are $\Delta H_{ex}^* = 113.4 \pm 1.2$ kJ mol^{-1},

TABLE 2. Pseudo-first-order rate coefficients k_{obsd} for the formation of $Co(NH_3)_5Br^{2+}$ from $Co(NH_3)_5DMF^{3+}$ and Br^- in DMF

T (°C)	$[Co(NH_3)_5DMF^{3+}]$ (M)[a]	[acid] (M)[b]	$[Br^-]$ (M)[c]	k_{obsd} (s^{-1}) × 10^5
55.3	0.00182	0.00297	0.00969	5.08 ±0.11
			0.0198	8.90 ±0.18
			0.0505	11.9 ±0.3
			0.0758	14.2 ±0.3
			0.102	15.4 ±0.3
			0.149	16.0 ±0.3
	0.00400	0.00470	0.0121	4.35 ±0.09
			0.0245	6.82 ±0.14
			0.0397	8.81 ±0.18
			0.0782	12.0 ±0.2
			0.100	13.4 ±0.3
			0.151	14.6 ±0.3
		0.0217	0.0138	3.11 ±0.06
			0.0317	6.06 ±0.12
			0.0497	7.60 ±0.15
			0.0725	9.55 ±0.20
			0.118	12.1 ±0.2
			0.142	13.4 ±0.3
			0.101	11.2 ±0.2
50.2			0.101	5.60 ±0.12
		0	0.0500	35.0 ±0.07
		0	0.0250	32.4 ±0.07
44.9		0.0217	0.101	2.66 ±0.06
40.1				1.29 ±0.03
31.1				0.330±0.006

[a]As perchlorate salt; initial concentration.
[b]*p*-Toluenesulfonic acid monohydrate.
[c]As tetra-*n*-butylammonium salt.

$\Delta S_{ex}^* = +21.6 \pm 3.8$ J K^{-1} mol^{-1}, and $\Delta V_{ex}^* = +3.2 \pm 0.1$ cm^3 mol^{-1} at 55.4°C; these error limits are standard deviations of the linear regressions, and experimental uncertainties are probably twice these values. Assumption of a quadratic dependence of ln k_{ex} upon P gives $(\partial \Delta V_{ex}^*/\partial P)_T = (0.11 \pm 0.17) \times 10^{-2}$ cm^3 mol^{-1} MPa^{-1} over the range 0–400 MPa, which means that the pressure dependence of ΔV_{ex}^* is below the limit of detection and in any event much smaller than the molar compressibility of DMF (5.8×10^{-2} and 2.6×10^{-2} cm^3 mol^{-1} MPa^{-1} at 0.1 and 180 MPa respectively, based on the data of Brummer (19)).

Reaction of $Co(NH_3)_5DMF^{3+}$ with Bromide Ion in DMF

The substitution of DMF in $Co(NH_3)_5DMF^{3+}$ ($\sim 1.8 \times 10^{-3}$ M) by bromide ion in the presence of added *para*-toluenesulfonic acid with DMF as solvent was followed spectrophotometrically at 580 nm (ε = 13.4 and 51.4 M^{-1} cm^{-1} for the DMF and bromo complexes, respectively). At 55.4°C, with $\sim 3.0 \times 10^{-3}$ M acid, the reaction followed pseudo-first-order kinetics (rate coefficients k_{obsd}) with respect to $[Co(NH_3)_5DMF^{3+}]$ for at least $2t_{1/2}$, independently of the initial concentration of this complex, with maintenance of isosbestic points at 440 (ε 61.1) and 422 nm (ε 17.5 M^{-1} cm^{-1}).

For $[Br^-]$ up to 0.051 M, the cobalt content of the reaction mixtures was found to comprise 99% $Co(NH_3)_5Br^{2+}$ and 0.6–0.8% cobalt(II) after $10t_{1/2}$ for the anation reaction, but the amount of cobalt(II) did not increase further, even after $40t_{1/2}$, and it was verified independently that $Co(NH_3)_5Br^{2+}$ did not decompose significantly to cobalt(II) in DMF under these conditions. Cobalt(II), added at the beginning of the anation reaction, had no discernable effect upon the anation rate. At higher $[Br^-]$, $[Co(NH_3)_5Br]Br_2$ precipitated after $3t_{1/2}$, and accordingly the extent of cobalt reduction was not investigated.

Precipitation of bromide salts of either $Co(NH_3)_5DMF^{3+}$ or $Co(NH_3)_5Br^{2+}$ prevented the direct observation of a limiting value k_i of k_{obsd} at high enough $[Br^-]$ to cause substantially complete ion pairing, except at the highest temperature (55.4°C), for which a provisional value of about 2.3×10^{-4} s^{-1} was estimated from limited data. High acid concentrations helped suppress precipitation, but it will be apparent from Table 2 that there is a small retarding effect of acid over and above the much more dramatic retardation brought about even by small additions of acid, relative to the experiments

Can. J. Chem. Downloaded from www.nrcresearchpress.com by 210.87.254.5 on 09/05/12
For personal use only.

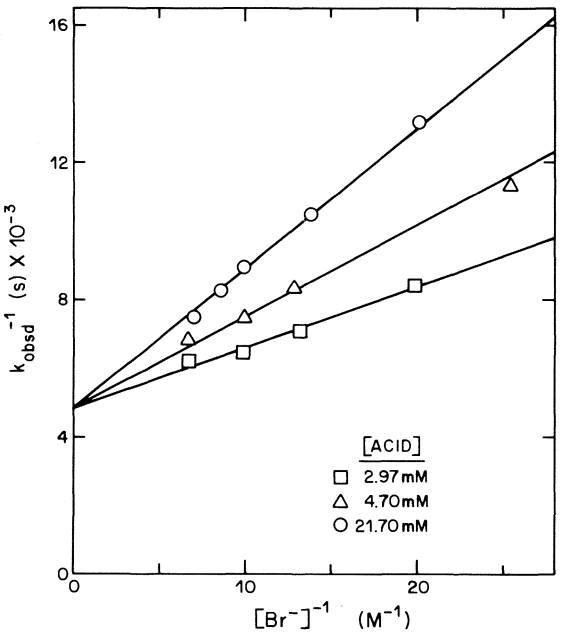

FIG. 1. Dependence of the pseudo-first-order rate coefficient k_{obsd} for the formation of $Co(NH_3)_5Br^{2+}$ from $Co(NH_3)_5DMF^{3+}$ in DMF upon $[Br^-]$ at various concentrations of *para*-toluenesulfonic acid.

without acid. At any one acidity, however, k_{obsd}^{-1} was found to be a linear function of $[Br^-]^{-1}$ to within the experimental uncertainty, and yielded extrapolated values of $k_i = (2.1 \pm 0.1) \times 10^{-4}$ s^{-1} at 55.4°C for three different acidities spanning a concentration range of over sevenfold, as shown in Fig. 1.

Unfortunately, precipitation phenomena precluded similar estimates of k_i at the lower temperatures, and the corresponding activation parameters ΔH_i^* and ΔS_i^* could not be measured. For the single bromide concentration of 0.101 *M*, however, the temperature dependence of k_{obsd} at 21.7 m*M* acid gave $\Delta H_{obsd}^* = 118.6 \pm 0.4$ kJ mol^{-1} and $\Delta S_{obsd}^* = 39.7 \pm 1.4$ J K^{-1} mol^{-1} (error limits are standard deviations; $r^2 = 0.99996$).

Reaction of $Co(NH_3)_5DMF^{3+}$ with Other Anions in DMF

The reaction with chloride ion was forestalled by precipitation of the chloride of the DMF complex. Azide and other basic anions reacted rapidly with $Co(NH_3)_5DMF^{3+}$, presumably by conjugate base pathways. Thiocyanate ion in the presence of added *para*-toluenesulfonic acid (~1.4 m*M*) reacted slowly with $Co(NH_3)_5DMF^{3+}$ (~1.0 m*M*), but a significant amount of cobalt(II) formed even early in the reaction (~1% after 20% completion of the anation, with 0.5 *M* KNCS), and meaningful rate data could not be obtained.

The $Rh(NH_3)_5DMF^{3+}$/DMF Exchange

When M was Rh, reaction [3] followed first-order kinetics (eq. [6]) over the first 80% of exchange at least, and values of k_{ex} are collected in Table 3. Unlike k_{ex} for M = Co (Table 1), k_{ex} for $Rh(NH_3)_5DMF^{3+}$ in DMF is almost unaffected by the presence or absence of added acid. The nature of the anion present does not influence k_{ex}, although a small retardation with increasing complex concentration is discernable. For [complex] = [trifluoromethanesulfonic acid] = 0.245 *M*, we have $\Delta H_{ex}^* = 99.1 \pm 2.0$ kJ mol^{-1} and $\Delta S_{ex}^* = -19.8 \pm 6.0$ J K^{-1} mol^{-1}. For [complex] = [*p*-toluenesulfonic acid] = 0.051 *M*, $\Delta V_{ex}^* = -1.4 \pm 0.2$ cm^3 mol^{-1} at 44.8°C, and the data obtained in the pressure assembly give an extrapolated value of k_{ex} at 0.1 MPa of 3.68×10^{-5} s^{-1}, in good agreement with the experimental value for ordinary glassware. The precision of the data was insufficient to warrant consideration of relationships other than a linear one between ln k_{ex} and *P*.

Reaction of $Rh(NH_3)_5DMF^{3+}$ with Anions in DMF

Precipitation of $[Rh(NH_3)_5DMF]Cl_3$ was immediate on mixing solutions of the perchlorate of the complex (even as dilute as 0.2 m*M*) with Et_4NCl solutions in DMF.

Attempts to follow the reaction of $Rh(NH_3)_5DMF^{3+}$ (0.8 m*M*) with bromide ion (4.0 m*M*) in acidic DMF solution at 55°C *in situ* in the spectrophotometer were complicated by oscillations (with periods of about 1.5 min and remarkably repetitive 'fine structure') of the otherwise progressively increasing optical absorbance at 324 nm. The intensities of these oscillations (but not their period) were smaller at 370 nm, though they increased with time and were not observed at all in DMF solutions of the reactants taken separately. Precipitation of bromide salts, however, ultimately prevented the progress of the presumed anation reaction from being followed even by analyzing samples of the bulk solution (thermostatted with exclusion of light) spectrophotometrically at 370 nm.

The reaction of $Rh(NH_3)_5DMF^{3+}$ with NCS^- in acidic DMF could be followed spectrophotometrically at 300 nm over the first 20–30% reaction at 55°C before precipitation of the product set in, but it became apparent, especially at lower temperatures (down to 15°C), that an initial, somewhat faster, step preceded that which could be conveniently studied. Presumably, the initial step was substitution of coordinated DMF to give thiocyanato-*S*-pentaamminerhodium(III) ion, and the slower process was isomerization of this to the *N*-bonded form which was shown to be the final product. Meaningful rate coefficients for these processes could not be extracted

Can. J. Chem. Downloaded from www.nrcresearchpress.com by 210.87.254.5 on 09/05/12
For personal use only.

TABLE 3. Pseudo-first-order rate coefficients for the exchange of DMF between $Rh(NH_3)_5DMF^{3+}$ and DMF solvent

T(°C)	$[Rh(NH_3)_5DMF^{3+}]$ (M)[a]	[acid] (M)	P (MPa)	k_{ex} (s^{-1}) × 10^{-5}
25.00	0.245	0.245[b]	0.1	0.244±0.009
45.00	0.063	0		3.52 ±0.012
	0.245	0		3.30 ±0.011
		0.245[c]		3.13 ±0.010
55.00	0.031	0		13.2 ±0.2
	0.245			11.3 ±0.3
	0.245[d]			11.3 ±0.3
		0.245[b]		10.6 ±0.3
44.82	0.051	0.051[c]		3.72 ±0.12
			9.2	3.67 ±0.12
			100.5	3.95 ±0.10
			201.2	3.90 ±0.18
			202.0	4.14 ±0.20
			303.4	4.34 ±0.05
			399.5	4.56 ±0.10

[a]Perchlorate salt except as indicated.
[b]Trifluoromethanesulfonic acid.
[c]*Para*-toluenesulfonic acid.
[d]Tetrafluoroborate salt.

from the absorbance data, but the limiting rate for the first at high $[NCS^-]$ was clearly faster, and the rate of the second a little slower, than the $Rh(NH_3)_5DMF^{3+}$/DMF exchange reaction under the same conditions.

Discussion

The positive value of ΔV_{ex}^* for M = Co in reaction [3] contrasts with the negative value for M = Rh, just as for the analogous reaction [1] (5, 6), and can be taken to indicate that I_d processes are rather general for substitution in cobalt(III) ammines and I_a for the rhodium(III) analogues, independent of the nature of the solvent and the ligand being replaced. The lower values of ΔH_{ex}^* and ΔS_{ex}^* for M = Rh (99 kJ mol^{-1} and −20 J K^{-1} mol^{-1}) relative to M = Co (113 kJ mol^{-1} and +22 J K^{-1} mol^{-1}) support these assignments; in particular, it would be very difficult to reconcile these data with a common I_d or D mechanism for the Co and Rh complexes on the basis of any current theory of ligand substitution energetics.

It is perhaps disappointing that the ΔV_{ex}^* value for reaction [3] with M = Rh is not more dramatically negative, so as to make as persuasive a case as possible for an I_a mechanism. We note that steric hindrance to the aquation of $Rh(NH_2CH_3)_5Cl^{2+}$, though again indicative of I_a, is also unspectacular (8), and it may be that much of the current confusion (9) over mechanistic assignments in reactions of rhodium(III) complexes originates in the absence of any truly striking effects which would provide compelling evidence for one mechanism or another. Nevertheless, the acceleration of the $Rh(NH_3)_5DMF^{3+}$/DMF exchange by increasing pressure is unmistakable, and the negative contribution to ΔV_{ex}^* made by transfer of the attacking ligand from the outer to the inner coordination spheres in an I_a process will be partly (but never wholly (20)) compensated by a stretching of the bond to the leaving group and also of the bonds to the other ligands (here, NH_3). At present, there seems to be little prospect of accounting in detail for the numerical magnitude of ΔV_{ex}^*, but the sign of this parameter remains a useful criterion of mechanism.

In the absence of added acid, k_{ex} for the $Co(NH_3)_5DMF^{3+}$/DMF exchange was very high, poorly reproducible, and larger at lower complex concentrations, presumably through the incursion of conjugate-base pathways (4), while low acidities also favored autocatalytic reduction of $Co(NH_3)_5DMF^{3+}$ to cobalt(II). Similar effects and their probable explanations were reported in our article on the analogous reactions of $Co(NH_3)_5DMSO^{3+}$ in dimethylsulfoxide solutions (4). For the $Rh(NH_3)_5DMF^{3+}$/DMF system, however, neither redox phenomena nor acceleration of reaction [3] at low acidities were significant.

For the anation of $Co(NH_3)_5DMF^{3+}$ by Br^-, a small but significant effect of added acid persisted, beyond the suppression of conjugate base pathways. For data measured at a given concentration of acid, however, k_{obsd}^{-1} was a linear function of $[Br^-]^{-1}$ and these functions extrapolated to give the same limiting value k_i (±5%) whatever the acidity (Fig. 1). According to the interchange model (21), the slopes

Can. J. Chem. Downloaded from www.nrcresearchpress.com by 210.87.254.5 on 09/05/12
For personal use only.

Can. J. Chem. Downloaded from www.nrcresearchpress.com by 210.87.254.5 on 09/05/12
For personal use only.

of these linear plots should equal $(k_i K)^{-1}$, so that increasing the acid concentration from 3 to 22 mM evidently decreases the apparent ion pair formation constant K from 27 to 12 M^{-1}, presumably because H^+ competes with $Co(NH_3)_5DMF^{3+}$ and the acid anion with Br^- in ion pairing. A disturbing feature is the apparent constancy of K over a range of ionic strengths I, which casts doubt upon the identification of K with a true ion association constant, but empirically the reciprocal–reciprocal plot affords a satisfactory means of extrapolating k_{obsd} values to their upper limit k_i.

The value of k_i for the reaction of bromide with $Co(NH_3)_5DMF^{3+}$ in DMF is about 2.5 times k_{ex} at 55.4°C. A similar ratio (3.3) was obtained for the corresponding reactions of $Co(NH_3)_5DMSO^{3+}$ in DMSO (4), yet in both these cases there is clear evidence for the operation of an I_d mechanism for the solvent exchange reactions at least, and we have previously pointed out (4) that a modest excess of k_i over k_{ex} is not inconsistent with an I_d mechanism for the anation reaction so long as ΔH_i^* and ΔH_{ex}^* are essentially the same. For the reactions [3] and [4] with M = Co and X = Br, a true ΔH_i^* value could not be obtained because of solubility problems, but for $[Br^-] = 0.101\ M$ we have an apparent ΔH_{obsd}^* of 118 kJ mol^{-1}, as compared with 113 kJ mol^{-1} for ΔH_{ex}^*, and this small difference is attributable to the fact that $Co(NH_3)_5DMF^{3+}$–Br^- ion pairing is barely more than half complete in 0.101 M bromide, since ΔH^0 for the complete formation of the roughly analogous *cis*-$Co(en)_2ClDMF^{2}$–Br^- ion pair in DMF is about +12 kJ mol^{-1} (22). Unfortunately, attempts to measure ΔH_i^* for the reaction of $Rh(NH_3)_5DMF^{3+}$ with Br^- in DMF were foiled by the incursion of an unusual cyclic secondary reaction, while k_i could not be measured for other reactions of the type [4] (M = Co or Rh) because of solubility problems.

To conclude, the evidence presented in this paper, albeit incomplete, supports previous assertions (1–2, 6–8) that reactions of the types [1]–[4] proceed by I_d processes for M = Co but I_a for M = Rh. All the experimental data known to us, including recent work by Heaton *et al.* on substitution reactions of amine complexes of rhodium(III) in water (23), are consistent with an I_a mechanism for simple substitution in the pentaamminerhodium(III) series; van Eldik's assignment (12) of an I_d mechanism to the reactions of $Rh(NH_3)_5OH_2^{3+}$ with various aqueous oxalate species is based on the observation that $k_i < k_{ex}$, but this is also entirely consistent with an I_a process in which oxalate is a less effective nucleophile towards rhodium(III) than is water, even if only for statistical reasons (1), and in any event C—O rather than Rh—O bond forming may be involved.

Acknowledgements

We thank the National Research Council of Canada for financial assistance and Dr. W. L. Reynolds for discussions.

1. T. W. Swaddle. Coord. Chem. Rev. **14**, 217 (1974).
2. H. L. Bott, A. J. Poë, and K. Shaw. Chem. Commun. 793 (1968); J. Chem. Soc. A, 1745 (1970); F. Monacelli. Inorg. Chim. Acta, **2**, 263 (1968).
3. M. J. Pavelich, S. M. Maxey, and R. C. Pfaff. Inorg. Chem. **17**, 564 (1978).
4. S. T. D. Lo, E. M. Oudeman, J. C. Hansen, and T. W. Swaddle. Can. J. Chem. **54**, 3685 (1976).
5. H. R. Hunt and H. Taube. J. Am. Chem. Soc. **80**, 2642 (1958).
6. T. W. Swaddle and D. R. Stranks. J. Am. Chem. Soc. **94**, 8357 (1972).
7. S. B. Tong and T. W. Swaddle. Inorg. Chem. **13**, 1538 (1974).
8. T. W. Swaddle. Can. J. Chem. **55**, 3166 (1977).
9. P. Moore. Inorganic reaction mechanisms (Specialist periodical report). Vol. 5. *Edited by* A. McAuley. The Chemical Society, London. 1977. p. 228.
10. R. J. Buchacek and G. M. Harris. Inorg. Chem. **15**, 926 (1976).
11. M. J. Pavelich. Inorg. Chem. **14**, 982 (1975).
12. R. van Eldik. Z. Anorg. Allg. Chem. **416**, 88 (1975).
13. L. Fabes and T. W. Swaddle. Can. J. Chem. **53**, 3053 (1975).
14. G. Pass and H. Sutcliffe. Practical inorganic chemistry. Chapman and Hall, Ltd., London. 1968.
15. W. L. Reynolds and M. A. Knoll. Int. J. Chem. Kinet. **8**, 389 (1976).
16. A. M. Newton and T. W. Swaddle. J. Phys. Chem. **79**, 795 (1975).
17. W. E. Jones, L. R. Carey, and T. W. Swaddle. Can. J. Chem. **50**, 2739 (1972).
18. S. T. D. Lo and T. W. Swaddle. Inorg. Chem. **14**, 1878 (1975).
19. S. B. Brummer. J. Chem. Phys. **42**, 1636 (1965).
20. V. Gutmann and H. Mayer. Struct. Bonding Berlin, **31**, 49 (1976).
21. C. H. Langford and W. R. Muir. J. Am. Chem. Soc. **89**, 3141 (1967).
22. I. A. Lantzke and D. W. Watts. Aus. J. Chem. **19**, 969 (1966).
23. S. P. Dagnall, M. P. Hancock, B. T. Heaton, and D. H. Vaughan. J. Chem. Soc. Dalton Trans. 1111 (1977).

Phase transformation studies on pure and K-doped Na_2SO_4

RITCHIE MACLAREN MURRAY AND ETALO A. SECCO[1]

Department of Chemistry, St. Francis Xavier University, Antigonish, N.S., Canada B2G 1C0

Received May 24, 1978

RITCHIE MACLAREN MURRY and ETALO A. SECCO. Can. J. Chem. **56**, 2616 (1978).

Phase transformation studies on pure Na_2SO_4 revealed four phases only; phase IV was not observed.

Electrical conductivity measurements have been made on polycrystalline undoped and K-doped Na_2SO_4 and on single crystals of undoped Na_2SO_4. Kinetic measurements on II → III transformation in undoped Na_2SO_4 show rate of conversion to be time independent and inversely related to temperature.

The presence of K in Na_2SO_4 effects a lowering of both the transition temperature and the enthalpy of transition along with an alteration from the "athermal" kinetic behavior to first-order kinetics.

RITCHIE MACLAREN MURRAY et ETALO A. SECCO. Can. J. Chem. **56**, 2616 (1978).

Des études de transformations de phases sur le Na_2SO_4 pur indiquent l'existence d'uniquement quatre phases; on n'a pas pu observer la phase IV.

On a effectué des mesures de conductivités sur du Na_2SO_4 polycristallin non-dopé et dopé par du K ainsi que sur des monocristaux de Na_2SO_4 non-dopés. Des mesures cinétiques sur la transformation II → III du Na_2SO_4 non-dopé indiquent que le taux de conversion est indépendant du temps et inversement proportionnel à la température.

La présence de K dans le Na_2SO_4 diminue la température ainsi que l'enthalpie de transition par une modification du comportement cinétique "athermique" en une cinétique du premier ordre.

[Traduit par le journal]

Introduction

The polymorphism of Na_2SO_4 has been investigated (1–5), and the regions of stability of various modifications have been reported (6). The existence of phase IV and the nature of the stability of phase II in Na_2SO_4 remain as open questions.

Our interest in Na_2SO_4 phase relationships arises from its common isostructural feature with K_2SO_4, orthorhombic at room temperature (7). Furthermore, the recent report citing mixed Na_2SO_4–K_2SO_4 matrix incorporating Tl^+ to give a phosphor (8) prompted us to investigate the phase interrelationships and phase transformation kinetics and to measure the electrical conductivity as a function of temperature in Na_2SO_4 and K-doped Na_2SO_4.

This paper presents the results of such an investigation using X-ray diffractometry, differential scanning calorimetry, and electrical conductivity techniques.

Experimental

Anhydrous Na_2SO_4 was from Fisher Certified stock. Both stock and twice-recrystallized Na_2SO_4 were used in thermal analyses for comparison purposes; in the conductivity measurements of pure Na_2SO_4 only twice-recrystallized material was used. Single crystals of Na_2SO_4 phase V were obtained from aqueous solution (distilled H_2O) at 318–323 K.

K-doped Na_2SO_4 samples were prepared by fusing the requisite composition mixture of the respective sulfates (K_2SO_4 Fisher Certified grade) in a Pt crucible.

The procedure for the electrical conductivity measurements on single crystal or polycrystalline sample has already been described (7).

X-ray diffraction patterns were obtained using a Norelco diffractometer with CuK_α radiation. Diffraction patterns at elevated temperatures were recorded with a Model X-86-N high temperature accessory (Materials Research Corp.) attached to the Norelco unit (9).

DSC traces were recorded on a duPont Model 990 Thermal Analyzer module with the differential scanning calorimeter attachment; samples were encapsulated in Al containers. The instrument was calibrated for enthalpy measurements using the heat of fusion for Sn as reference.

In the DSC kinetic measurements each sample, annealed at 573 K to ensure complete conversion to phase I, was subsequently cooled and maintained at the set temperature for the required time interval. The II/III content was evaluated by comparing the DSC enthalpic peak areas in the heat mode of the individual II → I and III → I transitions in the converted sample relative to the peak areas of their respective transitions in the pure state; the II → III transition was unaffected in the temperature region studied.

Results and Discussion

Our results on the polymorphic behavior in pure Na_2SO_4 can be fitted to four phases in agreement with Eysel (6). The phase relationships with their transition temperatures are presented below:

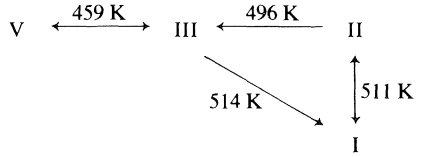

[1]To whom correspondence should be addressed.

Can. J. Chem. Downloaded from www.nrcresearchpress.com by 210.87.254.5 on 09/05/12
For personal use only.

Can. J. Chem. Downloaded from www.nrcresearchpress.com by 210.87.254.5 on 09/05/12
For personal use only.

TABLE 1. Transition ΔH values for pure Na_2SO_4

Transition reaction	ΔH (kcal/mol)	
	This work	Eysel (6)
V → I	2.80	2.59
V → III	1.02	1.01
III → I	1.68	1.58
I → II	1.10	1.08
II → III	0.57	0.54

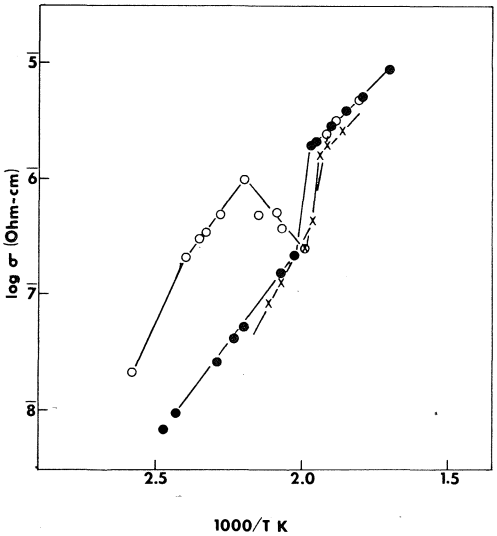

FIG. 1. Logarithm of conductivity, σ, vs. $10^3/T$ (K) for undoped Na_2SO_4 on heat mode in air: ○ single crystal V, ● polycrystalline V, × polycrystalline III.

No evidence for phase IV was found in our study.

The ΔH values accompanying the various transformations as determined by DSC in this study are presented, along with the values from Eysel, in Table 1.

The log σ vs. $1/T$ K plots for undoped Na_2SO_4 in the heat mode are given in Fig. 1. The initial higher conductivity of V in single crystal form declines at 454 K and merges with the polycrystalline curve at 508 K prior to the discontinuity.[2] The sharp rise in conductivity at 514 K for polycrystalline phase III is consistent with III → I phase transition as confirmed by X-ray diffraction.

The conductivity behavior for the high temperature phase I in the cool mode is shown in Fig. 2. The presence of the intermediate phase II was confirmed by X-ray diffraction (6).

Figures 3 and 4 show plots of log σ vs. $1/T$ K for

[2]The V → III transformation proceeds to a significant extent only in coarse Na_2SO_4, cross section >0.3 mm. The single crystal conductivity drop is consistent with DSC thermal anomalies associated with V → III transition in coarse Na_2SO_4 V samples (10, 11).

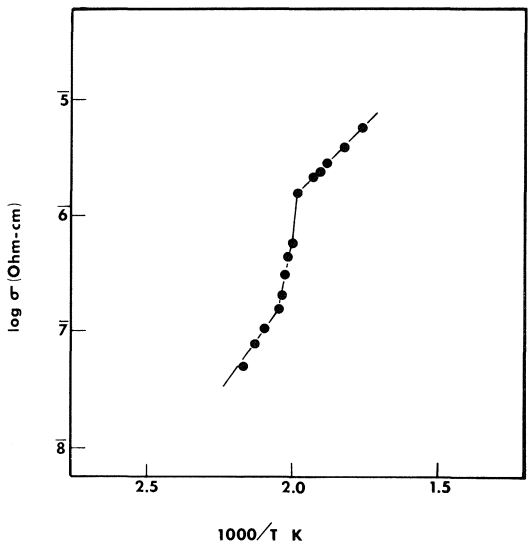

FIG. 2. Logarithm of conductivity, σ, vs. $10^3/T$ (K) for undoped Na_2SO_4 in cool mode in air for polycrystalline I.

0.8 mol% and 4.1 mol% K_2SO_4 in Na_2SO_4, respectively; the conductivity is lower for the richer K_2SO_4 sample. The effect of K_2SO_4 presence on phase transformation temperatures and hysteresis is clearly evident.

The rate of II → III transformation in undoped Na_2SO_4 was determined as a function of temperature in the region 483–503 K. Since the rate of conversion was dependent on particle size we selected the particle sample in the optimum range, viz. 0.04–0.07 mm cross section. The conversion fractions α vs. time for the various temperatures are plotted in Fig. 5. The fraction is independent of time at constant temperature but the fraction is inversely related to temperature. It is evident that the constant fraction

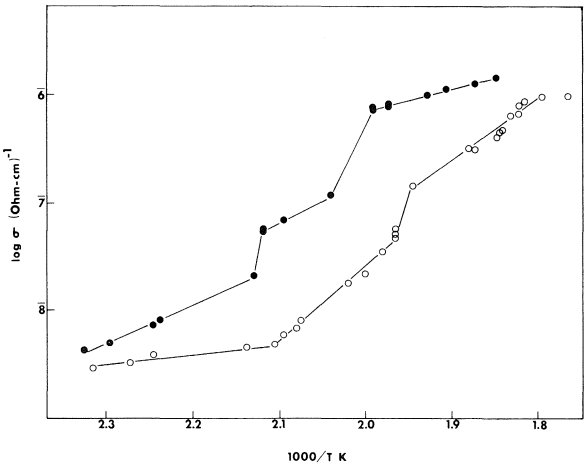

FIG. 3. Logarithm of conductivity, σ, vs. $10^3/T$ (K) for 0.8 mol% K-doped Na_2SO_4 polycrystalline in air: ○ heat mode, ● cool mode.

Can. J. Chem. Downloaded from www.nrcresearchpress.com by 210.87.254.5 on 09/05/12
For personal use only.

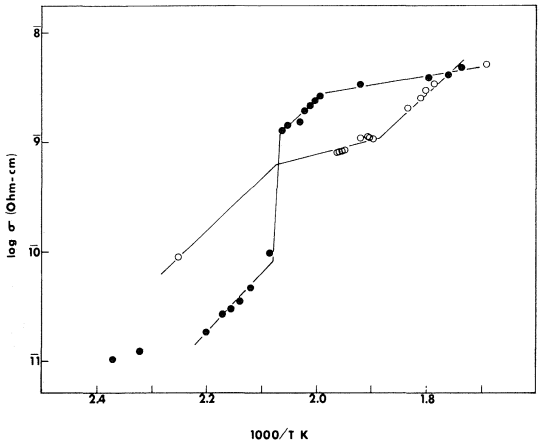

FIG. 4. Logarithm of conductivity, σ, vs. $10^3/T$ (K) for 4.1 mol% K-doped Na_2SO_4 polycrystalline in air: ○ heat mode, ● cool mode.

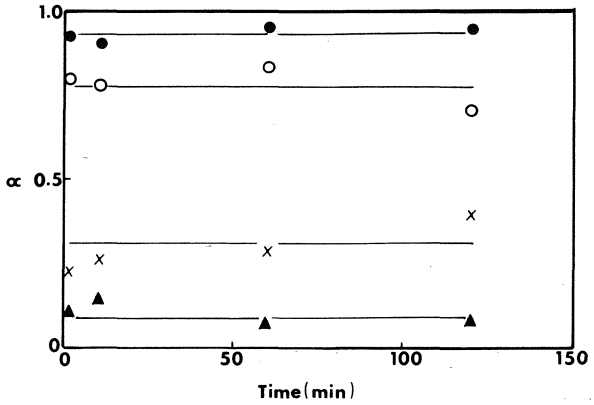

FIG. 5. Fraction of II → III conversion, α, vs. time in undoped Na_2SO_4 at various temperatures: ● 492 K, ○ 494 K, × 496 K, ▲ 498 K.

of II → III inversion is not the consequence of slow rate; the constant fraction most likely represents a stable inter-sublattice coupling. This "athermal" type of behavior has appeared in other systems (12, 13).

Figure 6 presents α vs. t data at various temperatures for 0.8 mol% K_2SO_4 in Na_2SO_4 of 0.04–0.07 mm cross section. The K_2SO_4 presence alters the

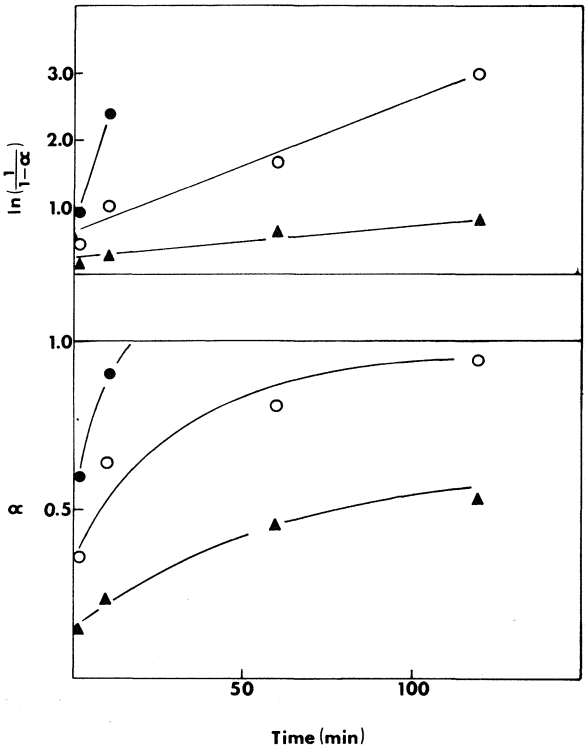

FIG. 6. Fraction of II → III conversion, α, vs. time and ln 1/(1 − α) vs. time in 0.8 mol% K-doped Na_2SO_4 at various temperatures: ● 473 K, ○ 475 K, ▲ 477 K.

kinetic behavior of the II → III transformation from the unusual "athermal" behavior to the more common first-order kinetics while maintaining the inverse temperature dependence.

The ΔH values accompanying the various phase transformations in K-doped Na_2SO_4 samples are given in Table 2. The dopant effected a lowering of both the transition temperature and the enthalpy of transition. The shift to lower values is assigned to the volume effect of the respective phases as tabulated in Table 3 and the larger K^+ radius relative to Na^+, i.e. 1.33 Å vs. 0.95 Å (14). The additional strain energy in K-doped Na_2SO_4 phase III relative to pure Na_2SO_4 phase III is visualized as the main factor in promoting the III → I transition in K-doped samples.

TABLE 2. Transition temperature and ΔH data for K-doped Na_2SO_4

0.8 mol% K_2SO_4		Transition reaction	4.1 mol% K_2SO_4	
T_t (K)	ΔH (kcal/mol)		T_t (K)	ΔH_t (kcal/mol)
506–508	1.48	III → I	494	1.19
499	0.98	II → I	477	0.95
477	0.50	II → III	—	0.24 (calcd.)

TABLE 3. Molar volume data for pure Na_2SO_4 phases

Phase (T, K)	V_M (cm^3)	No. molecules unit cell
V (518)	54.3	8
III (514)	53.3	4
I (514)	55.2	2
II (498)	54.5	4

Acknowledgments

The authors are indebted to the National Research Council of Canada for financial support and to Anthony S. J. Secco for electrical conductivity measurements and drawings.

1. F. C. KRACEK and R. E. GIBSON. J. Phys. Chem. **34**, 188 (1930).
2. E. L. KREIDL and I. SIMON. Nature, **181**, 1529 (1958).
3. C. MAZIÈRES. Ann. Chim. Paris, **6**, 575 (1961).
4. R. MOREAU. Bull. Soc. R. Sci. Liège, **32**, 252 (1963).
5. H. F. FISCHMEISTER. Monatsh. Chem. **93**, 420 (1962).
6. W. EYSEL. Thermal analysis. Vol. 2. Proc. Third ICTA Davos. 1971. p. 179.
7. M. NATARAJAN and E. A. SECCO. Can. J. Chem. **53**, 1542 (1975).
8. M. SAKAGUCHI, M. OHTA, K. NAKAZATO, and T. KONDOH. J. Electrochem. Soc. **124**, 1272 (1977).
9. E. A. SECCO. Can. J. Chem. **42**, 2143 (1964).
10. N. E. SCHMIDT and V. A. SOKOLOV. Russ. J. Inorg. Chem. **6**, 1321 (1961).
11. Q. R. GOYAL, V. V. DESHPANDE, and M. D. KARKHANAVALA. Indian J. Chem. **9**, 1006 (1971).
12. R. C. GARVIN. J. Phys. Chem. **69**, 1238 (1965).
13. A. J. LEADBETTER and A. F. WRIGHT. Philos. Mag. **33**, 105 (1976).
14. L. PAULING. Nature of chemical bond. 3rd ed. Cornell University Press, Ithaca, NY. 1959. p. 514.

Can. J. Chem. Downloaded from www.nrcresearchpress.com by 210.87.254.5 on 09/05/12
For personal use only.

Volatility of amines used for water treatment in steam generating systems

POYILATH VARIETH BALAKRISHNAN
Atomic Energy of Canada Limited, Chalk River Nuclear Laboratories, Chalk River, Ont., Canada K0J 1J0

Received April 18, 1978

POYILATH VARIETH BALAKRISHNAN. Can. J. Chem. **56**, 2620 (1978).

The relative volatilities of cyclohexylamine and morpholine in dilute aqueous solution have been measured in the temperature range 150 to 300°C at the corresponding equilibrium vapour pressure of the solution. Cyclohexylamine strongly prefers the steam phase while morpholine has a relatively volatility close to that of water. In both cases an azeotrope of the amine and water, with a vapour pressure higher than that of either component, must exist; however, with morpholine and water azeotrope formation only occurs above 175°C. The concentration dependence of the distribution between the steam and solution phases of both amines is explained in terms of their partial ionization in solution.

POYILATH VARIETH BALAKRISHNAN. Can. J. Chem. **56**, 2620 (1978).

On a mesuré les volatilités relatives de la cyclohexylamine et de la morpholine dans des solutions aqueuses diluées, à des températures allant de 150 à 300°C et aux tensions de vapeur de la solution correspondante. La cyclohexylamine préfère fortement la phase vapeur alors que la volatilité relative de la morpholine ressemble à celle de l'eau. Dans les deux cas, il doit exister un azéotrope de l'amine et de l'eau alors que la tension de vapeur est plus élevée que celle de chacun des composants; toutefois, dans le cas de la morpholine et de l'eau, la formation de l'azéotrope ne se produit qu'au dessus de 175°C. On explique le fait que la distribution entre les phases vapeur et liquide des deux amines dépend de la concentration en termes de leur ionisation partielle en solution.

[Traduit par le journal]

Can. J. Chem. Downloaded from www.nrcresearchpress.com by 210.87.254.6 on 09/05/12
For personal use only.

Water treatment in nuclear steam generating systems is now based predominantly on alkaline volatile reagents, which neutralize acidity in the water thereby protecting surfaces from corrosion. Acidity in the water is usually caused by carbon dioxide from in-leakage of air or from the decomposition of carbonates in the steam generator. Since carbon dioxide is carried with the steam the carbonic acid in the condensate is best neutralized by a reagent which could also be carried into the steam phase, i.e., a volatile reagent. Thus, common reagents used are amines such as ammonia, morpholine, and cyclohexylamine.

A knowledge of the volatility of the reagent is important for determining the ability of the reagent to protect areas exposed to wet steam as well as for determining the loss of the reagent during the deaeration of the feedwater or by blowdown of the steam generator water. In addition, such knowledge would also be useful in evaluating the chemistry of the steam generator water under 'volatile' treatment; the chemistry will be influenced by the residual amine concentration in the water.

There have been some studies on the volatility of amines. Jones (1) has determined the relative volatility of ammonia in water in the concentration range 2 to 200 μg NH_3/kg water, in the temperature range 150 to 325°C. Berk and Nigon (2) have discussed the volatility of cyclohexylamine and morpholine solutions on the basis of observations in boilers. Albrecht and Schuck (3) and Cuisia (4) have determined the volatility of cyclohexylamine and morpholine, but in these studies the equilibration was done at 1 atm pressure. The present work extends the studies on cyclohexylamine and morpholine to pressures up to the saturation vapour pressure of water corresponding to a temperature of 300°C (i.e. 8.59 MPa).

Experimental

The distribution of morpholine and cyclohexylamine in the temperature range of 150 to 300°C (pressure range 476 kPa to 8.59 MPa) was studied in the apparatus shown in Fig. 1. The system consists of a large (≃8 L) autoclave with an arrangement to draw samples from the liquid and vapour phases. The arrangement also allows the condensed vapour to be circulated back by natural circulation to the liquid phase in the autoclave, thereby allowing more mixing between the two phases. However, during the preliminary experiments, the same results were obtained with the system operating in the dynamic mode with recirculation as when it was operating in the static mode without the recirculation and consequently the latter mode of equilibration was used in the later experiments. When operating in the static mode, the rising portion of the vapour line in the apparatus was made as short as possible to minimize any error due to refluxing.

For each experiment 4 L of demineralized water was put in the autoclave. Nitrogen was bubbled through the water for about 1 h to remove dissolved air. Sufficient amine to give approximately the desired concentration (mg amine/kg water) was added to the water and the autoclave closed. The gas pressure over the solution in the autoclave was reduced by

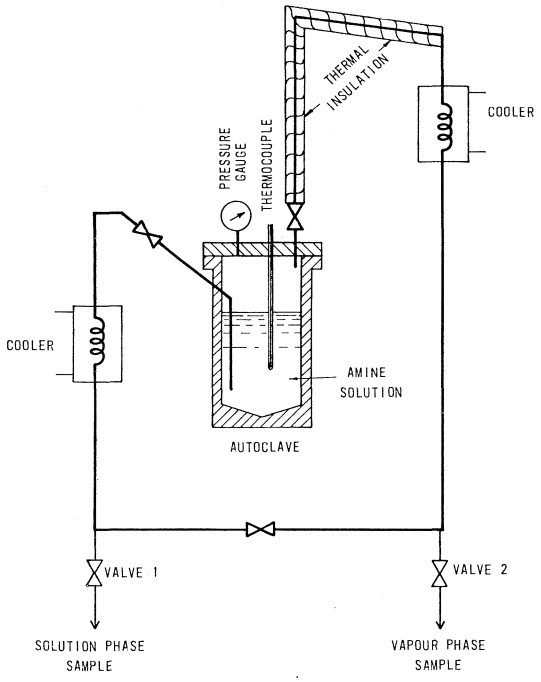

FIG. 1. Apparatus for volatility studies at high temperatures.

pumping off the gas with a vacuum pump for about 15 min. The autoclave was then heated to the desired temperature. Twice during the heating, i.e. when the temperature just exceeded 100°C and when the experimental temperature was reached, some steam (equivalent to $\simeq$100 g water) was blown off via valve 2 to assure complete removal of gases from the system. The system was maintained at the experimental temperature for 4 h and then 20 to 100 g sample of the solution phase and 10 to 50 g sample of steam phase were taken via valves 1 and 2, respectively, for determination of the amine molality in each phase. The size of the sample depended on the amine content in the sample. The sample size was kept to the minimum and the sample was drawn slowly (over a period of 10 min) to minimize the perturbations in the equilibrium. In the preliminary experiments, samples were taken from the autoclave at 2-h intervals over a period of 24 h. Analyses of these samples for amine showed that a steady state with respect to the amine distribution was attained within 4 h. In view of the precautions taken to minimize perturbations in the equilibrium during sampling, this steady state should be close to the equilibrium.

The amine molality in a sample was determined by potentiometric titration of a suitable aliquot against standard hydrochloric acid, with care being taken to exclude air during the analysis by bubbling nitrogen through the solution.

Values for the relative volatility, defined here as the (dimensionless) ratio of the amine molality in the steam sample to that in the water sample, were calculated.

Results and Discussion

The relative volatility values at different amine concentrations (mg amine/kg water) and at different temperatures are given in Table 1 for cyclohexylamine and in Table 2 for morpholine.

The relative volatility of cyclohexylamine was always considerably greater than unity, i.e. the amine molality in the vapour phase was much higher than that in the liquid phase in the temperature and concentration ranges studied. The relative volatility decreased as the temperature increased in the range 175 to 300°C, but increased as the concentration increased.

TABLE 1. Cyclohexylamine: relative volatility and distribution coefficient

Temperature (°C)	Water phase amine conc. (mg amine/kg water)	Relative volatility (RV)	K_a (mol/kg)	K_w (mol^2/kg^2)	Neutral fraction (α)	Distribution coefficient (RV/α)
150	56.1	19.4	3.436×10^{-8}	2.275×10^{-12}	0.711	27.3
150	18.8	12.2	3.436×10^{-8}	2.275×10^{-12}	0.558	21.8
150	10.2	10.7	3.436×10^{-8}	2.275×10^{-12}	0.457	23.4
175	38.2	22.5	9.247×10^{-8}	3.622×10^{-12}	0.722	31.1
175	15.3	22.1	9.247×10^{-8}	3.622×10^{-12}	0.600	36.8
175	9.3	10.6	9.247×10^{-8}	3.622×10^{-12}	0.522	20.3
200	32.9	19.9	2.254×10^{-7}	4.989×10^{-12}	0.773	25.7
200	19.8	18.8	2.254×10^{-7}	4.989×10^{-12}	0.718	26.2
200	8.5	12.8	2.254×10^{-7}	4.989×10^{-12}	0.605	21.1
225	34.7	16.9	5.035×10^{-7}	5.998×10^{-12}	0.832	20.3
225	17.1	14.8	5.035×10^{-7}	5.998×10^{-12}	0.770	19.2
225	10.5	12.1	5.035×10^{-7}	5.998×10^{-12}	0.717	16.9
250	42.3	13.7	1.042×10^{-6}	6.368×10^{-12}	0.887	15.4
250	16.9	10.9	1.042×10^{-6}	6.368×10^{-12}	0.828	13.2
250	10.3	7.4	1.042×10^{-6}	6.368×10^{-12}	0.786	9.4
275	45.6	10.1	2.009×10^{-6}	5.970×10^{-12}	0.923	10.9
275	13.5	8.5	2.009×10^{-6}	5.970×10^{-12}	0.864	9.8
275	7.6	4.8	2.009×10^{-6}	5.970×10^{-12}	0.824	5.8
300	44.5	6.8	3.648×10^{-6}	5.000×10^{-12}	0.946	7.2
300	19.2	5.9	3.648×10^{-6}	5.000×10^{-12}	0.920	6.4
300	6.5	2.5	3.648×10^{-6}	5.000×10^{-12}	0.869	2.9

Can. J. Chem. Downloaded from www.nrcresearchpress.com by 210.87.254.6 on 09/05/12
For personal use only.

TABLE 2. Morpholine: relative volatility and distribution coefficient

Temperature (°C)	Water phase amine conc. (mg amine/kg water)	Relative volatility (RV)	K_a (mol/kg)	K_w (mol²/kg²)	Neutral fraction (α)	Distribution coefficient (RV/α)
158	186	0.86	5.496×10^{-7}	2.685×10^{-12}	0.953	0.90
158	21	0.72	5.496×10^{-7}	2.685×10^{-12}	0.868	0.83
160	448	0.88	5.833×10^{-7}	2.793×10^{-12}	0.970	0.90
180	436	0.98	1.034×10^{-6}	3.908×10^{-12}	0.973	1.01
180	179	1.00	1.034×10^{-6}	3.908×10^{-12}	0.958	1.04
182	25	0.98	1.091×10^{-6}	4.018×10^{-12}	0.893	1.10
200	436	1.01	1.767×10^{-6}	4.989×10^{-12}	0.977	1.03
200	199	1.12	1.767×10^{-6}	4.989×10^{-12}	0.965	1.16
203	21	1.11	1.911×10^{-6}	5.140×10^{-12}	0.900	1.23
230	414	1.31	3.717×10^{-6}	6.138×10^{-12}	0.982	1.33
237	20	1.30	4.372×10^{-6}	6.266×10^{-12}	0.925	1.41
251	20	1.22	5.991×10^{-6}	6.353×10^{-12}	0.935	1.30
255	185	1.33	6.542×10^{-6}	6.339×10^{-12}	0.979	1.36
273	331	1.30	9.563×10^{-6}	6.026×10^{-12}	0.987	1.32
285	22	1.32	1.217×10^{-5}	5.636×10^{-12}	0.959	1.38
300	409	1.33	1.624×10^{-5}	5.000×10^{-12}	0.992	1.34

The relative volatility of morpholine, at temperatures lower than about 175°C, was slightly less than unity. With increasing temperature, relative volatility increased and tended to approach a limiting value of about 1.35.

The effect of amine molality on the relative volatility may be explained on the basis of the limited ionization of the amine in the solution. The equilibrium involved is

$$[1] \qquad BH^+ \rightleftarrows B + H^+$$

where B is the base, cyclohexylamine or morpholine, and BH^+ the conjugate acid, cyclohexylammonium or morpholinium ion. Only the neutral (uncharged) amine is expected to go into the vapour phase. Thus, the equilibrium for the distribution of the amine in the two phases would be

$$[2] \qquad B_{water} \rightleftarrows B_{steam}$$

The equilibrium constant for reaction [2], i.e. the distribution coefficient, is

$$[3] \qquad K_D = [B]_{steam}/[B]_{water}$$

$[B]_{steam}$ may be assumed to be the total amine molality in steam. The molality term $[B]_{water}$ may be calculated from the total amine molality, B_T, in the water phase using the equilibrium constant K_a for reaction [1]

$$[4] \qquad K_a = \frac{[B][H^+]}{[BH^+]} = \frac{\alpha}{1-\alpha}[H^+]$$

where α is the fraction of the total amine that is neutral, i.e.,

$$[5] \qquad \alpha = [B]/B_T$$

For electroneutrality,

$$[6] \qquad [BH^+] + [H^+] = [OH^-] = K_w/[H^+]$$

or

$$[7] \qquad (1-\alpha)B_T = K_w/[H^+] - [H^+]$$

where K_w is the ionic product of water. From eqs. [4] and [7]

$$[8] \qquad K_a(\alpha-1)^2(K_a + \alpha B_T) - \alpha^2 K_w = 0$$

from which α may be evaluated. The distribution coefficient K_D for the amine may then be obtained from the relative volatility values using the relation

$$[10] \qquad K_D = \text{relative volatility}/\alpha$$

For evaluating α the ionization constants, K_a, determined by Mesmer and Hitch (5) were used. The values for ionic product of water, K_w, were chosen from the 'best' set of values listed in the review article by Olofsson and Hepler (6) on the thermodynamics of ionization of water. The calculated values of α and values for K_a and K_w are also listed in Tables 1 and 2. Figures 2 and 3 show plots of the distribution coefficient vs. temperature for cyclohexylamine and morpholine respectively at pressures corresponding to the vapour pressure of the solution at the temperature. The figures show that the description of the system in terms of a distribution coefficient, K_D, for the equilibrium between the neutral amine in the water phase and the amine in the steam phase is satisfactory. The deviation towards lower values for the distribution coefficient in the case of cyclohexylamine at the concentration of

Can. J. Chem. Downloaded from www.nrcresearchpress.com by 210.87.254.6 on 09/05/12
For personal use only.

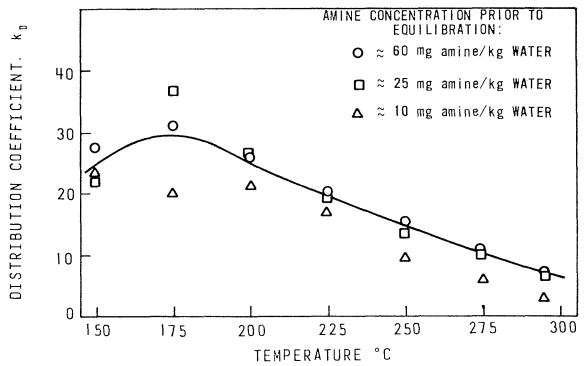

FIG. 2. Distribution of cyclohexylamine between steam and water.

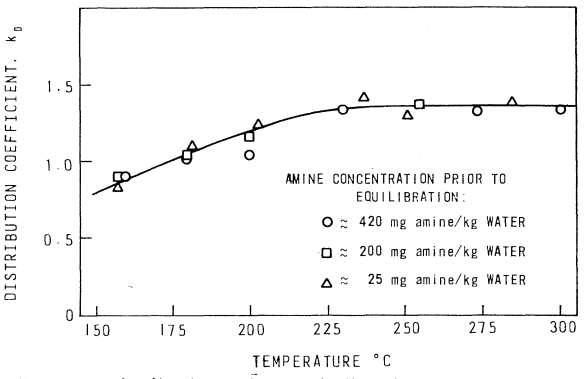

FIG. 3. Distribution of morpholine between steam and water.

≃10 mg amine/kg water before equilibration is probably due to the effect of residual carbon dioxide in the autoclave during the experiment. The residual carbon dioxide may effectively be lowering the volatility of the amine, the effect becoming more significant at lower concentrations of the amine. Also, at lower concentrations of amine, the determination of the amine molality by the titration method becomes more difficult and less accurate.

The distribution coefficient of cyclohexylamine was observed to be greater than unity at all temperatures (Table 1 and Fig. 2). Based on data available for temperatures up to 134°C, the vapour pressure of pure cyclohexylamine may be expected to be lower than that of pure water at all temperatures. The observed volatility behaviour then indicates the existence of an azeotrope of higher vapour pressure than that of either pure component, water or the amine. The azeotrope formation would be at some concentration of amine higher than those studied. The azeotrope must exist throughout the range of temperature and pressure studied (temperature: 150 to 300°C, pressure: the saturated vapour pressure of the solution corresponding to the temperature). Since the vapour pressure of water increases rapidly with temperature, the decreasing trend in the distribution coefficient observed at temperatures higher than 175°C might be reflecting the nature of the cyclohexylamine–water phase diagram, such as a shift in the azeotrope composition towards higher mole fraction of water.

Morpholine is not known to form an azeotrope with water at the low pressures at which it has been studied. The observation of a distribution coefficient less than 1 (Table 2 and Fig. 3) at temperatures lower than 175°C (and correspondingly lower pressures) is thus consistent with the available information. However, with the temperature increasing above 175°C, along with a corresponding increase in the pressure, the distribution coefficient becomes greater than unity and eventually levels off at a value of 1.35. This behaviour may be explained by the existence of an azeotrope of higher vapour pressure than that of either morpholine or water, at temperatures higher than 175°C.

Acknowledgements

B. M. Kent and D. P. Martin, both of Chalk River Nuclear Laboratories, rendered valuable assistance in carrying out the experiments. I thank them.

1. M. E. JONES. J. Phys. Chem. **67**, 1113 (1963).
2. A. A. BERK and J. NIGON. U.S. Bureau of Mines, Technical Paper 714 (1948).
3. S. H. ALBRECHT and J. J. SCHUCK. Mater. Perform. **15**, 23 (1976).
4. G. C. CUISIA. Mater. Perform. **16**, 21 (1977).
5. R. E. MESMER and B. F. HITCH. J. Solution Chem. **6**, 251 (1977).
6. G. OLÓFSSON and L. G. HEPLER. J. Solution Chem. **4**, 127 (1975).

Can. J. Chem. Downloaded from www.nrcresearchpress.com by 210.87.254.6 on 09/05/12
For personal use only.

Influence des composés organiques sur la vitesse d'apparition du complexe de transfert de charge 1Sn(II)–4Sn(IV) dans les bains acides d'étamage brillant[1,2]

GASTON VERVILLE

Division de conversion de l'énergie, Centre de recherches pour la Défense, Ottawa (Ont.), Canada K1A 0Z4

Reçu le 5 janvier 1978

GASTON VERVILLE. Can. J. Chem. **56**, 2624 (1978).

La variation d'absorbance de solutions stanneuses au cours du temps, comparée à la variation d'absorbance de ces solutions en présence de composés organiques nous a permis de montrer l'influence de certains composés organiques sur la vitesse d'apparition du complexe de transfert de charge 1Sn(II)–4Sn(IV) et sur la stabilité des solutions en milieu acide sulfurique. Nous avons distingué trois types de comportement qui nous ont permis de classer les composés étudiés en trois grandes catégories.

L'interprétation des résultats tient compte du fait que l'apparition du complexe 1Sn(II)–4Sn(IV) et la stabilité des solutions stanneuses dépendent de la concentration initiale en impuretés stanniques, de la vitesse d'oxydation des ions stanneux, de l'hydrolyse des ions stanniques et de la stabilité des colloïdes stanniques formés.

GASTON VERVILLE. Can. J. Chem. **56**, 2624 (1978).

The effect of a number of organic compounds on the rate of formation of 1Sn(II)–4Sn(IV) charge transfer complex in acidic stannous sulphate solutions and on the stability of these solutions has been determined by measuring, spectrophotometrically, the change of absorption of these solutions with time. From the results, it is possible to classify these organic compounds into three broad categories in terms of how they affect the formation of the charge transfer complex and the stability of the solution.

These results have been interpreted taking into account that the formation of the 1Sn(II)–4Sn(IV) complex depends on the initial concentration of stannic ions present as an impurity in the stannous sulphate solution, the rate of oxidation of the stannous ions, the rate of hydrolysis of the stannic ions, and the stability of stannic colloids that are formed.

Can. J. Chem. Downloaded from www.nrcresearchpress.com by 210.87.254.6 on 09/05/12
For personal use only.

Introduction

Nos travaux sur les bains acides d'étamage brillant (1) ont montré que les bains modernes d'étamage opèrent en présence de tensides et en présence de colloïdes stanniques qui forment des complexes de transfert de charge *X*Sn(II)–*Y*Sn(IV) avec les ions stanneux. Une étude bibliographique plus approfondie nous a également révélé que les colloïdes stanniques et les complexes *X*Sn(II)–*Y*Sn(IV) s'insèrent dans les mécanismes proposés pour expliquer le fonctionnement des bains sensibilisateurs des surfaces hydrophobes (2, 3). Bien que les complexes *X*Sn(II)–*Y*Sn(IV) aient déjà fait l'objet d'un certain nombre de publications (4–12) et que la nature et le rôle exacts de ces complexes soient encore discutés, il nous est apparu intéressant d'étudier à partir de solutions stanneuses l'effet de divers composés organiques sur la vitesse d'apparition du complexe 1Sn(II)–4Sn(IV). Ce complexe est le complexe de transfert de charge identifié par Paul *et al.* (4) dans la zone d'acidité (0.2–1 *M*) où opèrent les procédés industriels déjà mentionnés.

Le complexe 1Sn(II)–4Sn(IV) n'apparaît que lorsqu'on met en présence des colloïdes stanniques et des complexes stanneux positifs (1, 4). Par ailleurs ce complexe est généralement caractérisé par une absorption intense dans l'uv qui s'étend parfois jusqu'au visible (fig. 1) pour conférer aux mélanges des solutions stanneuses et stanniques une coloration jaunâtre. En partant de solutions de sulfate stanneux, dont l'oxydation à température ambiante produit des colloïdes stanniques, la variation d'absorbance des solutions stanneuses au cours du temps comparée à la variation d'absorbance de ces solutions en présence de composés organiques permet de montrer l'influence de ces composés sur la vitesse d'apparition du complexe 1Sn(II)–4Sn(IV).

Composés étudiés et mode opératoire

Les composés étudiés et leurs concentrations ont été choisis en relation avec leur présence dans les bains acides d'étamage: polypropylène glycol P-400, phénol, acide hydroxyphénol sulfonique, méthanol, éthanol, méthanal, acide formique.

Les composés employés sont de qualité R.P. et ne sont l'objet d'aucune purification. Le sulfate stanneux utilisé contenait 1.5% d'impuretés stanniques.

Les composés choisis sont introduits après dissolution complète de 30 g/ℓ de sulfate stanneux en

[1]Rapport CRDO No 786.

[2]Tiré des résultats du travail de thèse de l'auteur présentés à l'Université Scientifique et Médicale de Grenoble pour obtenir le titre de docteur-ingénieur, Grenoble, France, décembre 1975.

Can. J. Chem. Downloaded from www.nrcresearchpress.com by 210.87.254.6 on 09/05/12
For personal use only.

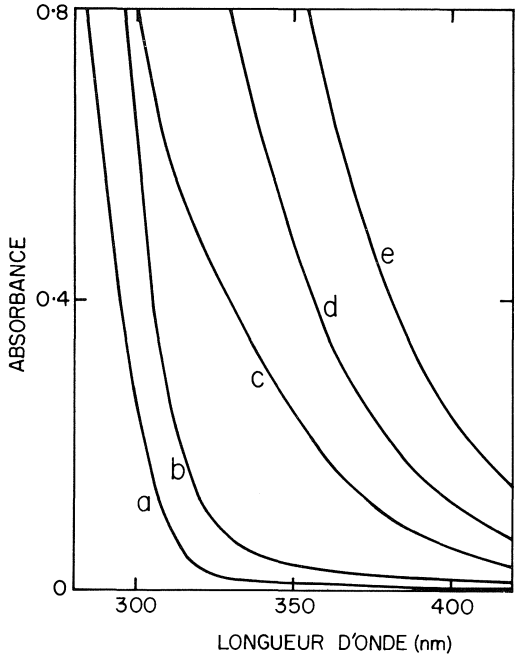

FIG. 1. Spectres d'absorption uv–vis. d'une solution stanneuse, d'une solution stannique et de leurs mélanges en milieu HCl, pH = 0.6: *a*, solution stanneuse fraichement préparée ($SnCl_2 \cdot 2H_2O$, 5×10^{-3} *M*); *b*, solution stannique vieillie pendant 24 h ($SnCl_4 \cdot 5H_2O$, 5×10^{-3} *M*); *c*, mélange équimolaire, 2.5×10^{-3} *M* Sn total; *d*, mélange équimolaire, 5.0×10^{-3} *M* Sn total; *e*, mélange équimolaire, 1.0×10^{-2} *M* Sn total.

milieu acide sulfurique 5 et 10% V. Les solutions résultantes sont ensuite placées dans des erlenmeyers de 250 ml et laissées au repos en contact avec l'air à température ambiante. Les mesures journalières d'absorbance des solutions sont réalisées à l'aide d'un spectrophotomètre SAFAS 1700.

Résultats

Les courbes de la fig. 2 montrent l'évolution au cours du temps d'une solution $SnSO_4$ 30 g/ℓ, H_2SO_4 5%. On remarque un déplacement progressif du seuil d'absorption vers les grandes longueurs d'onde avec le temps. Ce déplacement vers le visible est responsable de l'apparition de la coloration jaune caractéristique des complexes 1Sn(II)–4Sn(IV). Ultérieurement apparaissent l'opalescence de la solution puis la formation d'un précipité. La diffraction des R–X et les analyses par spectrophotométrie ir montrent que ce dernier correspond à du SnO_2 hydraté.

Les figs 3 à 7 illustrent des exemples typiques des courbes obtenues en suivant l'absorbance des solutions à 400 nm en fonction du temps.

Chaque courbe a été divisée en trois périodes: une 1ère période ou période d'induction où l'absorption

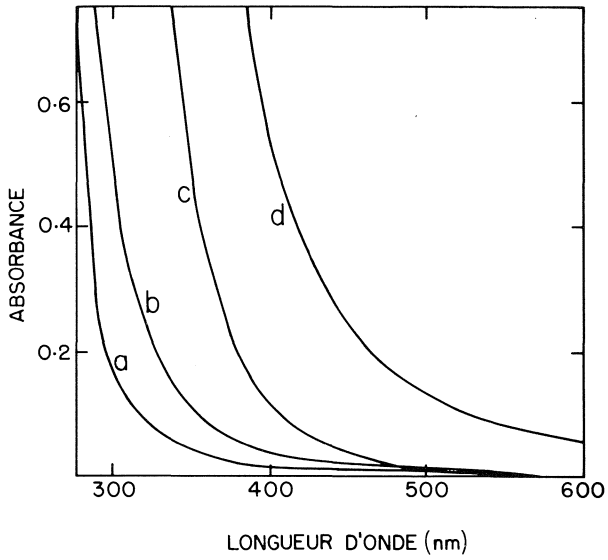

FIG. 2. Evolution au cours du temps d'une solution $SnSO_4$ 30 g/ℓ, H_2SO_4 5%: *a*, solution initiale; *b*, solution après 3 jours; *c*, solution après 5 jours; *d*, solution après 14 jours.

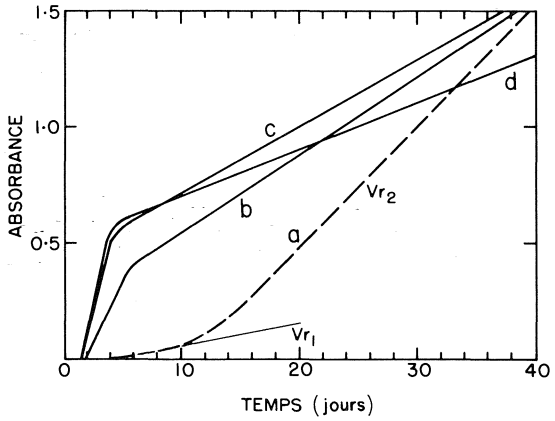

FIG. 3. Influence du méthanol sur l'absorbance des solutions en milieu H_2SO_4 10%: *a*, $SnSO_4$ 30 g/ℓ; *b*, *a* + méthanol (0.25 *M*); *c*, *a* + méthanol (1.25 *M*); *d*, *a* + méthanol (2.5 *M*).

est nulle, une 2ème période où l'augmentation de l'absorption s'effectue à vitesse constante v_1 et une 3ème période où l'augmentation de l'absorption s'effectue à vitesse constante v_2.

La comparaison de la courbe obtenue à partir d'une solution exempte de composé organique avec celle obtenue à partir d'un mélange choisi permet de distinguer trois catégories de composés organiques selon leur influence sur la vitesse d'apparition du complexe.

Classification des composés étudiés

1ère catégorie: méthanol, méthanal, éthanol

Les figs 3 et 4 illustrent les résultats obtenus avec le méthanol. Les composés de cette catégorie

Can. J. Chem. Downloaded from www.nrcresearchpress.com by 210.87.254.6 on 09/05/12
For personal use only.

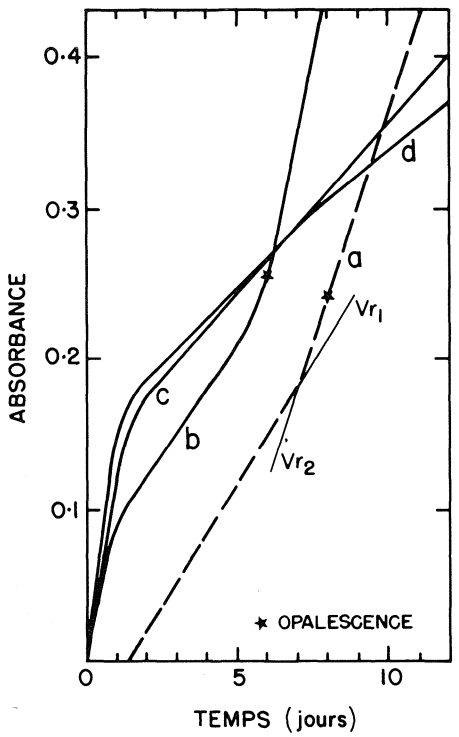

FIG. 4. Influence du méthanol sur l'absorbance des solutions en milieu H_2SO_4 5%: *a*, $SnSO_4$ 30 g/ℓ; *b*, *a* + méthanol (0.25 *M*); *c*, *a* + méthanol (1.25 *M*); *d*, *a* + méthanol (2.5 *M*).

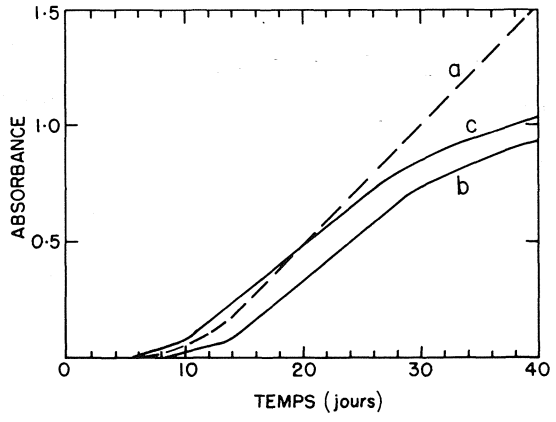

FIG. 5. Influence du polypropylène glycol sur l'absorbance des solutions en milieu H_2SO_4 10%: *a*, $SnSO_4$ 30 g/ℓ; *b*, *a* + polypropylène glycol 2 g/ℓ; *c*, *a* + polypropylène glycol 20 g/ℓ.

diminuent la période d'induction et accélèrent la vitesse d'apparition du complexe durant les premiers jours d'observation. Cette vitesse v_1 augmente avec la concentration des composés. Ces composés ralentissent ensuite la vitesse v_2 d'autant plus que leur concentration est plus élevée. Le tableau 1 présente

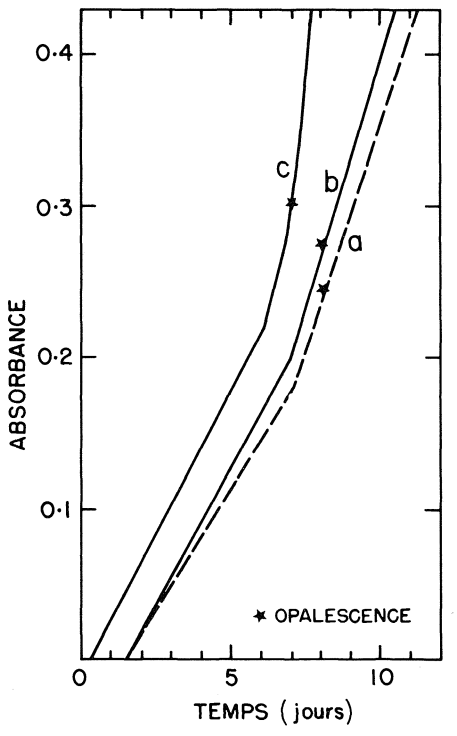

FIG. 6. Influence du polypropylène glycol sur l'absorbance des solutions en milieu H_2SO_4 5%: *a*, $SnSO_4$ 30 g/ℓ; *b*, *a* + polypropylène glycol 2 g/ℓ; *c*, *a* + polypropylène glycol 20 g/ℓ.

les valeurs des vitesses d'apparition tirées des pentes des courbes. A concentration égale, les solutions en présence de méthanol présentent l'activation maximale pour la vitesse v_1.

Le tableau 2 présente les temps compris entre les phases successives qui caractérisent l'évolution des solutions en milieu H_2SO_4 5%. On constate que les composés de la 1ère catégorie augmentent considérablement la durée de vie des solutions[3] ainsi que le temps écoulé entre l'apparition de l'opalescence et la précipitation.

2ème catégorie: polypropylène glycol, acide formique

Les produits de cette catégorie n'influencent pas d'une façon notable la vitesse d'apparition du complexe. A une acidité donnée, leur influence sur la vitesse est indépendante de leur concentration (voir tableau 1). On remarque également qu'une augmentation de leur concentration en solution H_2SO_4 5% se traduit par une diminution de la durée de vie des solutions. Les figs 5 et 6 illustrent les résultats obtenus avec le polypropylène glycol.

[3]Temps écoulé entre la mise en solution et l'apparition d'un précipité au fond des erlenmeyers.

TABLEAU 1. Vitesses d'apparition du complexe 1Sn(II)–4Sn(IV)

Solution		H_2SO_4 10% (absorbance/jour)		H_2SO_4 5% (absorbance/jour)	
		1ère pente (v_1)	2ème pente (v_2)	1ère pente (v_1)	2ème pente (v_2)
$SnSO_4$ (g/ℓ)	30	8.4×10^{-3}	5.3×10^{-2}	3.0×10^{-2}	*
Méthanol (*M*)	0.25	1.1×10^{-1}	3.4×10^{-2}	1.0×10^{-1}	2.6×10^{-2}
	1.25	2.1×10^{-1}	2.9×10^{-2}	1.4×10^{-1}	2.6×10^{-2}
	2.5	2.6×10^{-1}	2.1×10^{-2}	2.0×10^{-1}	2.2×10^{-2}
Méthanal (*M*)	0.25	6.2×10^{-2}	3.8×10^{-2}	1.0×10^{-1}	2.8×10^{-2}
	1.25	1.4×10^{-1}	3.5×10^{-2}	1.2×10^{-1}	2.3×10^{-2}
	2.5	2.1×10^{-1}	2.2×10^{-2}	1.5×10^{-1}	2.1×10^{-2}
Éthanol (*M*)	0.25	7.4×10^{-2}	3.8×10^{-2}	7.6×10^{-2}	3.3×10^{-2}
	1.25	1.1×10^{-1}	3.3×10^{-2}	1.0×10^{-1}	2.4×10^{-2}
	2.5	1.1×10^{-1}	1.8×10^{-2}	1.2×10^{-1}	2.2×10^{-2}
Acide formique (*M*)	0.25	5.8×10^{-3}	2.6×10^{-2}	3.0×10^{-2}	*
	1.25	7.5×10^{-3}	2.5×10^{-2}	3.0×10^{-2}	*
	2.5	†	†	3.0×10^{-2}	*
Polypropylène glycol (g/ℓ)	2	1.2×10^{-2}	4.1×10^{-2}	3.8×10^{-2}	*
	20	1.4×10^{-2}	4.0×10^{-2}	3.8×10^{-2}	*
Phénol (*M*)	0.05	†	†	1.4×10^{-2}	2.6×10^{-2}
	0.25	†	†	1.0×10^{-3}	†
Acide hydroxyphénol sulfonique (*M*)	0.05	†	†	1.7×10^{-2}	*
	0.20	†	†	7.0×10^{-3}	2.0×10^{-2}

*Opalescence.
†Non-déterminée.

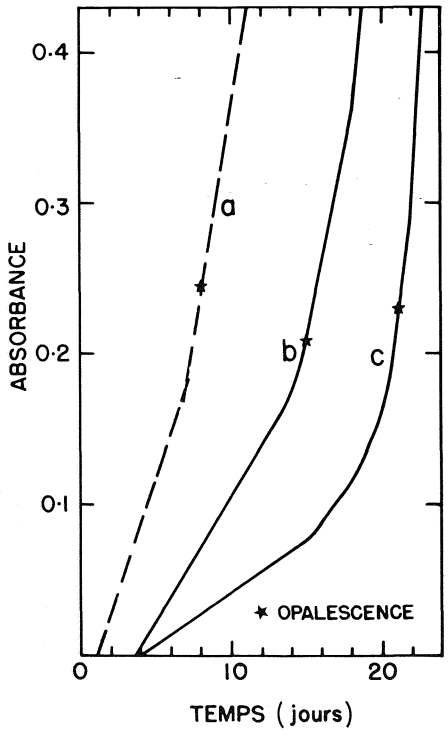

FIG. 7. Influence de l'acide hydroxyphénol sulfonique sur l'absorbance des solutions en milieu H_2SO_4 5%: *a*, $SnSO_4$ 30 g/ℓ; *b*, *a* + acide hydroxyphénol sulfonique 0.05 *M*; *c*, *a* + acide hydroxyphénol sulfonique 0.2 *M*.

3ème catégorie: phénol, acide hydroxyphénol sulfonique

La fig. 7 présente les résultats obtenus avec l'acide hydroxyphénol sulfonique. Les composés de cette catégorie augmentent considérablement la période d'induction; par exemple la période d'induction est supérieure à 40 jours dans les solutions H_2SO_4 10% en présence de 0.2 *M* de ces composés. Ces composés diminuent d'une façon notable les vitesses v_1 et v_2 et ce d'autant plus que leur concentration est plus élevée.

Analyse des résultats

Rappelons que la formation du complexe 1Sn(II)–4Sn(IV) n'intervient que lorsqu'on met des colloïdes d'oxyde stannique en présence de complexes stanneux positifs. Dans l'ensemble les résultats observés s'expliquent à l'aide des deux considérations suivantes: (*1*) La période d'induction et la vitesse d'apparition du complexe 1Sn(II)–4Sn(IV), à partir d'une solution stanneuse, dépend de la concentration initiale en impuretés stanniques (13), de la vitesse d'oxydation des ions stanneux et de l'hydrolyse des ions stanniques. (*2*) L'oxydation des ions stanneux et l'hydrolyse des ions stanniques étant complétées, la stabilité des solutions sera contrôlée par la stabilité des colloïdes stanniques.

Les composés de la 1ère catégorie (méthanol, méthanal, éthanol) sont reconnus pour leur caractère

Can. J. Chem. Downloaded from www.nrcresearchpress.com by 210.87.254.6 on 09/05/12
For personal use only.

TABLEAU 2. Evolution des solutions stanneuses en milieu H_2SO_4 5%

Solution		Période d'induction (jours)	Apparition opalescence (jours)	Apparition suspension (jours*)	Apparition précipité (jours)	Temps total (jours)
$SnSO_4$ (g/ℓ)	30	1	7	7	8	23
Méthanol (*M*)	0.25	0	6	7	10	23
	1.25	0	10	17	21	48
	2.5	0	22	26	105	153
Méthanal (*M*)	0.25	0	6	8	10	24
	1.25	0	10	16	22	48
	2.5	0	22	27	105	154
Ethanol (*M*)	0.25	0	6	8	10	24
	1.25	0	13	18	17	48
	2.5	0	23	25	110	158
Acide formique (*M*)	0.25	1	6	8	9	24
	1.25	1	4	2	4	11
	2.5	1	3	2	4	10
Polypropylène	2	1	7	7	10	25
glycol (g/ℓ)	20	1	6	4	6	17
Phénol (*M*)	0.05	3	9	9	13	34
	0.25	11	20	—	—	—
Acide hydroxy-	0.05	4	11	10	8	33
phénol sulfonique (*M*)	0.20	4	17	11	10	42

*Temps écoulé entre l'apparition de l'opalescence et le moment où on ne peut distinguer un objet sur le plancher en regardant au-dessus des erlenmeyers placés à un mètre du sol.

faiblement réducteur. Il est alors paradoxal de constater une courte période d'induction et une augmentation de la vitesse v_1 lorsque leur concentration augmente car ce comportement indique une augmentation de la vitesse d'oxydation des ions stanneux ou de l'hydrolyse des ions stanniques. Le caractère réducteur de ces composés permet d'écarter la première hypothèse. Il est peu probable également qu'ils facilitent l'hydrolyse étant donné la grande stabilité des solutions en présence de ces composés. Le comportement des produits de cette catégorie s'explique plutôt à partir de la formation de complexes de transfert de charge ayant une composition différente du complexe 1Sn(II)–4Sn(IV) étudié et qui absorberaient également à 400 nm. En effet Meyer *et al.* (7, 8) et De Maine *et al.* (9) ont montré dans leurs travaux que des mélanges de chlorure stanneux et stannique formaient des complexes de transfert de charge en présence de méthanol et d'éthanol purs. Ces auteurs n'ont toutefois pas identifié les constituants stanneux et stanniques des complexes de transfert de charge étudiés.

Le polypropylène glycol et l'acide formique, qui se classent dans la 2ème catégorie, n'influencent pas d'une façon notable la vitesse d'apparition du complexe. Toutefois ils semblent agir sur la stabilité des colloïdes; en trop grande concentration ces produits favorisent la polymérisation des colloïdes stanniques en milieu H_2SO_4 5% et de ce fait diminuent la durée de vie des solutions.

Le phénol et l'acide hydroxyphénol sulfonique, qui se classent dans la 3ème catégorie sont deux antioxydants reconnus. Ils augmentent considérablement la période d'induction et diminuent les vitesses v_1 et v_2 ce qui explique l'augmentation de la durée de vie des solutions. Il est bon toutefois de remarquer que ces composés ne semblent jouer qu'un rôle secondaire sur la stabilité des colloïdes formés car la période comprise entre l'apparition de l'opalescence et l'apparition d'un précipité est sensiblement la même que la solution de référence en milieu H_2SO_4 5%.

Conclusion

Cette étude sur l'influence des composés organiques sur la vitesse d'apparition du complexe 1Sn(II)–4Sn(IV) et la stabilité des solutions stanneuses nous a permis d'une part de distinguer trois types de comportement et d'autre part de faire ressortir l'influence remarquable des composés tels que le méthanol et le méthanal souvent rencontrés dans la composition des bains d'étamage. Ces composés, en plus de faciliter la mise en solution des additifs organiques, augmentent d'une façon notable la stabilité des solutions et interviennent dans la formation de complexes de transfert de charge dont le rôle reste encore à être déterminé.

1. G. VERVILLE. Thèse Docteur-Ingénieur, Université Scientifique et Médicale de Grenoble, Grenoble, France. 1975. No d'ordre: A. O. 11738.

Can. J. Chem. Downloaded from www.nrcresearchpress.com by 210.87.254.6 on 09/05/12
For personal use only.

2. N. FELDSTEIN, J. A. WEINER et G. L. SCHNABLE. J. Electrochem. Soc. **119**, 1486 (1972).
3. R. L. COHEN et K. W. WEST. J. Electrochem. Soc. **119**, 433 (1972).
4. A. D. PAUL, K. I. ROBBINS et C. A. OVERFIELD. Proc. W. Va. Acad. Sci. **38**, 237 (1966).
5. C. I. BROWNE, R. P. CRAIG et N. DAVIDSON. J. Am. Chem. Soc. **73**, 1946 (1951).
6. R. P. CRAIG et N. DAVIDSON. J. Am. Chem. Soc. **73**, 1951 (1951).
7. E. G. MEYER et M. KAHN. J. Am. Chem. Soc. **73**, 4950 (1951).
8. E. G. MEYER et M. A. MELNICK. J. Phys. Chem. **61**, 367 (1957).
9. P. A. D. DE MAINE et M. M. DE MAINE. J. Inorg. Nucl. Chem. **11**, 144 (1959).
10. G. GORDON et C. H. BRUBAKER, JR. J. Am. Chem. Soc. **82**, 4448 (1960).
11. A. VERTES. Radiochem. Radioanal. Lett. **4**, 337 (1970).
12. J. SEDLACEK, A. GOSMAN, P. PODHAJECKY et J. TARASOVA. J. Radioanal. Chem. **30**, 273 (1976).
13. G. VERVILLE. Can. J. Chem. **55**, 3425 (1977).

Can. J. Chem. Downloaded from www.nrcresearchpress.com by 210.87.254.6 on 09/05/12
For personal use only.

Excited radicals in the gas phase photolysis of butene isomers at different photon energies: energy distribution in reaction products

GUY J. COLLIN AND ANDRZEJ WIĘCKOWSKI[1]

Département des Sciences Pures, Université du Québec à Chicoutimi, Chicoutimi (Qué.), Canada G7H 2B1

Received May 9, 1978

GUY J. COLLIN and ANDRZEJ WIĘCKOWSKI. Can. J. Chem. **56**, 2630 (1978).

A systematic study of the pressure effects on the quantum yields of some products between 0.1 and 600 Torr (13 and 80 000 N m^{-2}) was carried out in the 7.6 and 8.4 eV photolysis of normal, iso- and *cis*-2-butenes. The propylene quantum yield (s-C_4H_9* → C_3H_6 + CH_3) decreased with the increase in the *n*-butene pressure and a good linearity of S/D (stabilization/decomposition) vs. pressure plot, over a broad pressure region, was observed. It is concluded that hydrogen atoms involved in the s-C_4H_9* radical formation are produced with a relatively narrow energy distribution. The slope of S/D vs. pressure lines decreased with the increase in photon energy, indicating the trend in the kinetic energy of the H-atoms.

In the case of isobutene and *cis*-2-butene photolysis, the Stern–Volmer plots for allene formation were nonlinear. It is concluded that the formation of two different allene precursors is needed to account for this result. By the use of a simple RRK-type formalism we also conclude that the excess energy of the photon in the primary photoexcited butene molecules is far from being randomized before their fragmentation occurs.

$$C_4H_8 + h\nu \rightarrow C_4H_8^{**} \rightarrow C_3H_5^* + CH_3$$

GUY J. COLLIN et ANDRZEJ WIĘCKOWSKI. Can. J. Chem. **56**, 2630 (1978).

Nous avons étudié systématiquement l'effet de la pression sur le rendement quantique de certains produits entre 0.1 et 600 Torr (13 et 80 000 N m^{-2}) lors de la photolyse des butènes dans la région de 7.6–8.4 eV. La formation du propène décroît avec l'augmentation de pression: s-C_4H_9* → C_3H_6 + CH_3. De l'absence de courbure de la droite S/D (stabilisation/decomposition) en fonction de la pression on conclue que les atomes d'hydrogène sont formés avec une distribution d'énergie plutôt étroite. La pente de cette droite décroît avec l'augmentation de l'énergie des photons montrant l'effet de cette augmentation sur l'énergie cinétique des atomes d'hydrogène produits. Les courbes de type Stern–Volmer du rendement de l'allène avec la pression montrent dans le cas du *cis*-2-butène et de l'isobutène une courbure prononcée à basse pression. Cette courbure ne semble pas être le résultat d'une large distribution d'énergie dans le fragment C_3H_5*. Au contraire, il semble qu'il faille l'expliquer par la formation de deux intermédiaires différents. Les constantes de vitesse de formation de l'allène permettent via une formulation simple du type RRK de conclure que la distribution de l'excès d'énergie dans la molécule photoexcitée n'est pas statistiquement distribuée.

$$C_4H_8 + h\nu \rightarrow C_4H_8^{**} \rightarrow C_3H_5^* + CH_3$$

Introduction

The kinetic study of the photoactivated system provides not only some valuable information about unimolecular processes, but also some unique data on the partitioning of energy among the fragmentation products (1). The advantages of such systems are quite obvious: the internal energy of the excited species may vary along with the changes in photon energy, and the decomposition processes occur at a low temperature, ensuring a smaller spread of internal energies in the species as compared to what is observed in thermally activated systems. However, the Stern–Volmer treatment of the primary photoexcited species is limited to large molecules of numerous oscillators, and/or at relatively low photon energies. For example, the collisional stabilization of photoexcited *cis*-2-butene (C2B) molecules reported to occur at 6.7 eV (2) is no longer observed at 7.1 eV (3).

Another kind of photoexcitation arises when the hydrocarbon fragments produced in the primary photochemical step contain enough internal energy to undergo subsequent unimolecular reactions. As shown by many authors (1), these products are formed with a relatively broad spread in internal energy, and the energy need not be statistically distributed among the internal degrees of freedom. It has previously been reported (2, 4) that the gas phase photolysis of butene isomers leads to the formation of the C_3H_5* radicals

[1] $$C_4H_8^{**} \rightarrow C_3H_5^* + CH_3$$

[1]1976/1977 sabbatical year. Present address: Chemistry Department, University of Warsaw, Zwirki i Wigury 101, 02089, Warsaw, Poland.

Can. J. Chem. Downloaded from www.nrcresearchpress.com by 210.87.254.40 on 09/05/12
For personal use only.

Can. J. Chem. Downloaded from www.nrcresearchpress.com by 210.87.254.40 on 09/05/12
For personal use only.

which may contain a part of the excess energy of the incident photon. In the 7.1 eV photolytic butene systems (nitrogen resonance lines, 174.3–174.5 nm), we have shown that the C_3H_5* radicals decompose, yielding C_3H_4 hydrocarbon products, whose yield is strongly dependent on the total pressure. In particular, the resulting $[\Phi(\text{allene})]^{-1}$ vs. butene pressure plots turn out to be nonlinear, and this observation was attributed to the formation and decomposition of two distinct types of the C_3H_5* radicals of reasonably narrow energy content (3, 5).

In the present study, the decomposition processes of the excited C_3H_5* radicals formed in the gas phase photolysis of normal butene (NB), *cis*-2-butene (C2B), and isobutene (IB) were investigated at two photon energies: at 7.6 eV (a bromine resonance line, 163.3 nm) (6) and at 8.4 eV (a xenon resonance line, 147.0 nm). Some results on the decomposition of the s-C_4H_9* radical (the propylene formation process) are also included. For the purpose of comparison, the earlier data on these systems obtained at 7.1 eV are added and discussed (and partially reinterpreted). The attention is focussed on the implications of the experimental results towards the theory of unimolecular processes of systems activated by the absorption of photons by organic molecules.

Experimental

The design of the resonance lamps as well as the details of the experimental and chromatographical procedure have been given before (3, 5–7). All quantum yields of the products were determined by using ethylene as an actinometer with $\Phi(C_2H_2) = 0.75$ (8).

Results

Before applying a steady-state treatment (Stern–Volmer or S/D vs. pressure plots) to our systems it is necessary to check if the product quantum yields decrease to zero with the increase in pressure or to a constant, pressure independent value. In the 7.1 eV photolysis of C2B, the allene quantum yield was equal to 0.11 at 0.05 Torr against 0.002 at 400 Torr (3). This means that an almost entire deactivation of the allene precursor was attained. Similar observations were made on C2B photolysis at 7.6 eV as well as on IB photolytic system at 7.1 and 7.6 eV, respectively. However, in the case of 8.4 eV photolysis of both C2B and IB, even under the highest reactant pressure applied (600 Torr), the allene quantum yield still represented a substantial fraction of the yields determined at the lowest pressure. Although the drop in the Φ(allene) value was observed over the whole pressure region investigated, a direct evidence that this value would tend to zero was lacking. Thus, the same way of decoding the Φ(allene) against pressure data at three photon energies used (see below) involves the assumption that no other routes of the allene formation process, yielding a pressure independent Φ(allene) contribution, become active in the 7.6–8.4 eV region.

In the NB photolysis at 7.1 and 7.6 eV, respectively, an analysis of the allene quantum yield as a function of NB pressure revealed that at high pressure, a constant, pressure-independent Φ(allene) value was attained. Thus, the rate constants of the decomposition of the C_3H_5* radicals produced in the system studied were determined by using the $[\Phi - 0.02]^{-1}$ vs. pressure plots.

Considering the above remarks, and assuming the steady state conditions for allene and propylene precursors, the Stern–Volmer plots were obtained and they are presented in Figs. 1–6. In the C2B and IB photolytic systems, two pressure regions, low and high, were distinguished and analysed (Figs. 2–5) in the same way as was done in our previous works (3, 5). On the contrary, the good linearity of the plot $[\Phi(\text{allene}) - 0.02]^{-1}$ vs. NB pressure, covering a broad pressure region, was attained (Fig. 1), which made us reinterpret our earlier data on NB photolysis at 7.1 eV (5).

The kinetics of the propylene formation process is analysed (5) by the use of the S/D vs. NB pressure plots (Fig. 6), ($D = \Phi(C_3H_6)$, $S = \Phi^0(C_3H_6) - \Phi(C_3H_6)$, where $\Phi^0(C_3H_6)$ values resulted from the extrapolation of $\Phi(C_3H_6)$ values to zero pressure). These plots are virtually equivalent to the Stern–Volmer ones. A good linearity of these plots over a wide range of pressure should be noted.

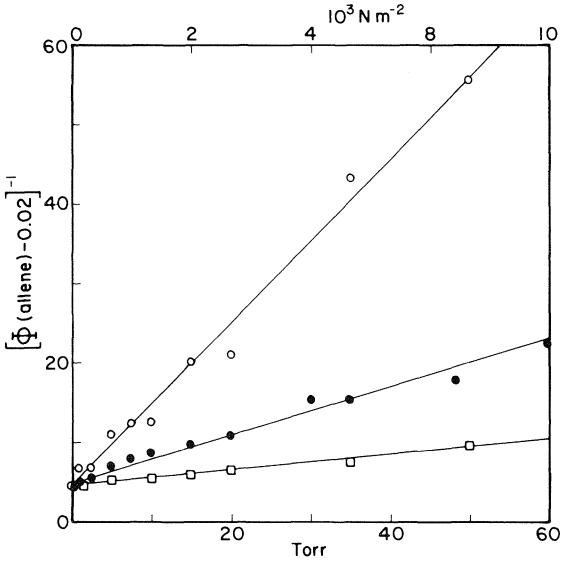

FIG. 1. Photolysis of normal butene at 7.1 eV (○), 7.6 eV (●), and 8.4 eV (□). The $[\Phi(\text{allene}) - 0.02]^{-1}$ vs. pressure.

Can. J. Chem. Downloaded from www.nrcresearchpress.com by 210.87.254.40 on 09/05/12
For personal use only.

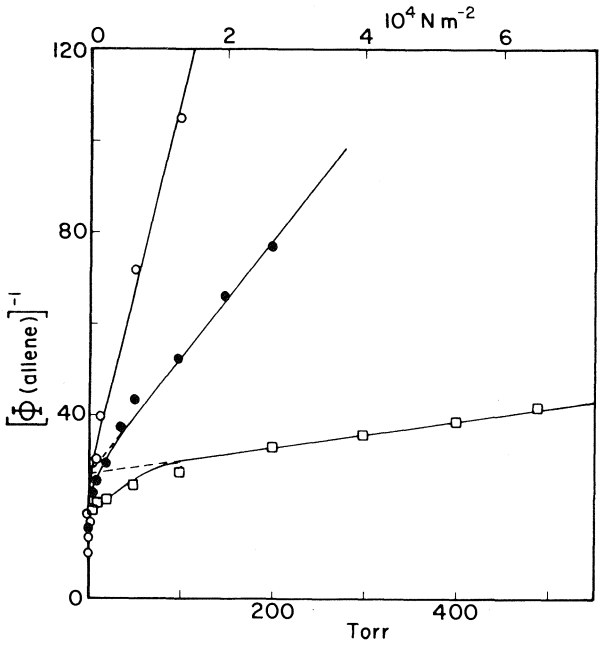

FIG. 2. Photolysis of *cis*-2-butene at 7.1 eV (○), 7.6 eV (●), and 8.4 eV (□). The $[\Phi(\text{allene})]^{-1}$ vs. pressure.

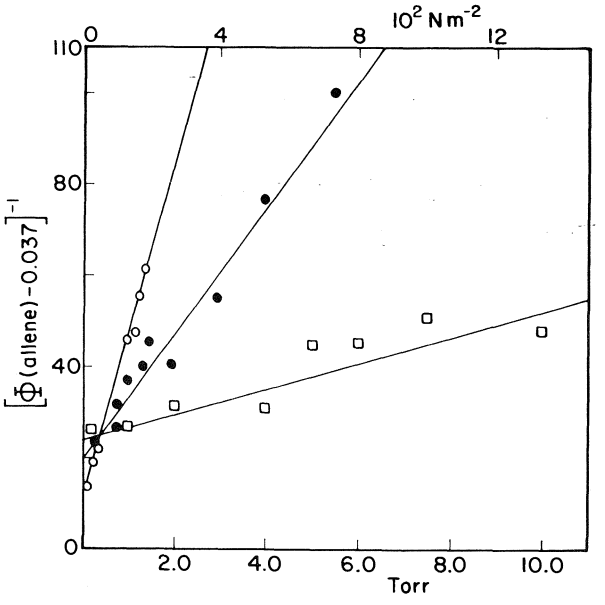

FIG. 3. Photolysis of *cis*-2-butene in the low pressure region (see Fig. 2). The $[\Phi(\text{allene}) - 0.037]^{-1}$ vs. pressure.

The least-squares slopes and intercepts of the lines in Figs. 1–6 were used to determine the decomposition rate constants of the excited radicals (3, 5) and they are given in Table 1. It was assumed that the deactivation of the excited radicals:

[2] $$R^* + M \rightarrow R + M$$

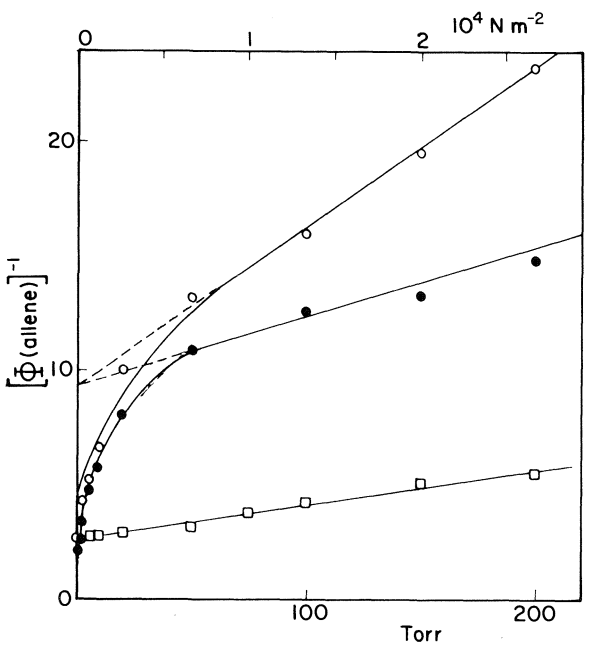

FIG. 4. Photolysis of isobutene at 7.1 eV (○), 7.6 eV (●), and 8.4 eV (□). The $[\Phi(\text{allene})]^{-1}$ vs. pressure.

occurs at each collision, and the collision numbers were calculated in a normal way (9). The radical and molecular diameters used for the calculations are $\sigma C_4H_8 = 0.65$ nm, $\sigma C_4H_9 = 0.65$ nm (10), and $\sigma C_3H_5 = 0.467$ nm (11).

Discussion

(*i*) *The Propylene Formation Process in the NB Photolysis*

Since it is relatively simpler, this problem will be considered first. Propylene is produced from the decomposition of the excited s-C_4H_9* radicals (5). These radicals are formed through the addition of hydrogen atoms, present in the studied photolytic system, to the terminal carbon atom (12) of the parent NB molecules:

[3] $$H + CH_3CH_2CH{=}CH_2 \rightarrow \text{s-}C_4H_9^* \qquad \Delta H = -43 \text{ kcal mol}^{-1}$$

[4] $$\text{s-}C_4H_9^* \rightarrow C_3H_6 + CH_3 \qquad \Delta H = +30 \text{ kcal mol}^{-1}$$

The contribution of some other processes, i.e. the non-terminal H-atom addition and the isomerization of the s-C_4H_9* to n-C_4H_9* radical, which may be followed by the formation of ethylene (12, 13) as well as the hydrogen abstraction process (14), is small and, as such, does not need to be considered.

The decomposition of chemically activated s-butyl radicals, obtained by the addition of virtually thermal H-atoms to C2B molecules, has been studied

TABLE 1. Rate constants[a] of the allene and propylene formations in the far uv photolysis of butenes

Photon energies (eV)	$C_3H_5^* \rightarrow$ allene + H[b]					
		cis-2-Butene		Isobutene		
	n-Butene	LPR	HPR	LPR	HPR	s-$C_4H_9^* \rightarrow C_3H_6 + CH_3$
7.1	7.4	0.45	61	2.4	216	1.9
7.6	27	3.0	201	2.9	670	2.4
8.4	88	14	1520	96	—	3.9

[a] $k^{dec}(10^7\ s^{-1})$.
[b] LPR = low pressure region; HPR = high pressure region.

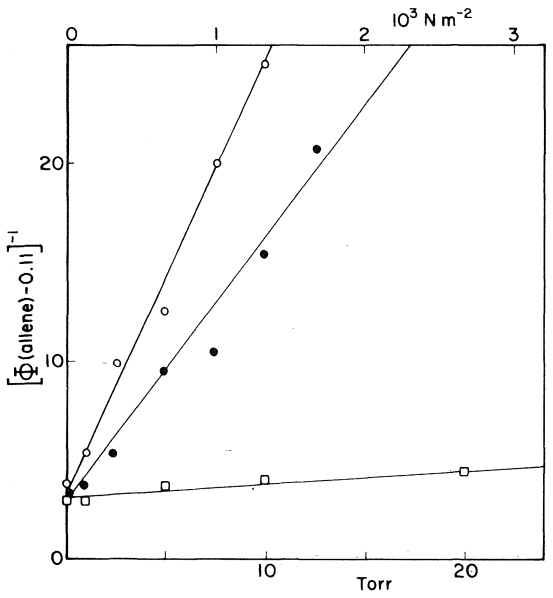

FIG. 5. Photolysis of isobutene in the low pressure region (see Fig. 4). The $[\Phi(\text{allene} - 0.11)]^{-1}$ vs. pressure.

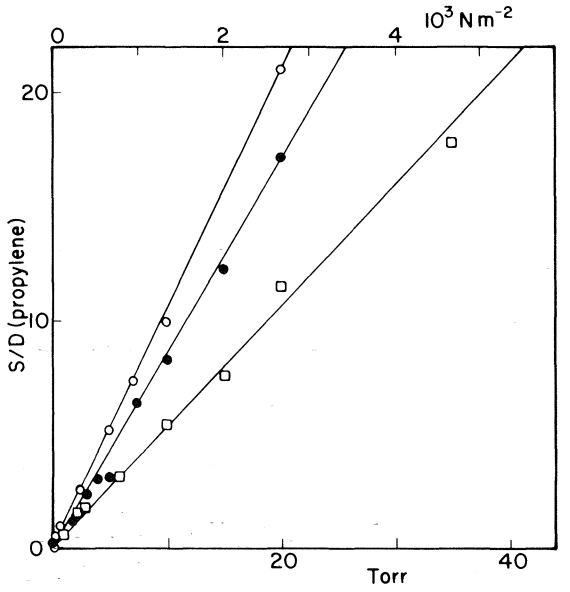

FIG. 6. Photolysis of *n*-butene. The S/D ratio for the propylene formation at 7.1 eV (○), 7.6 eV (●), and 8.4 eV (□).

by Rabinovitch and co-workers (10, 15). The observable unimolecular decomposition rate constant has been shown to depend on the butene pressure reflecting the spread of excitation energies in the reactant produced by the activating reaction (15). The good linearity of the S/D pressure plot in the broad pressure region at the three photon energies studied (Fig. 6) indicates that the energy distribution function of the s-$C_4H_9^*$ species is closer to the δ-function (1) ($f(\varepsilon_{mono}) = 1$ and $f(\varepsilon) = 0$ for all other values of ε) than that in experiments reported by Rabinovitch and co-workers (10, 15). Two factors may be cited to account for this observation: (*i*) virtually monoenergetic H-atoms are produced during the photolysis and (*ii*) the energy of the H atoms is higher than their average thermal energy (5) (the thermal energy distribution of the NB molecules contributes less to the overall energy distribution function of s-$C_4H_9^*$ radicals). The higher excess energy on the s-$C_4H_9^*$ radicals than that expected from the exothermicity process [3], involving thermalized species, has previously been concluded (5). Now, as shown in Fig. 6 and Table 1, this excess energy depends on the photon energy used for the photolysis. The same result was obtained in the *n*-pentene photolysis at 7.1 and 7.6 eV (6). However, in the latter case, the photon energy effect on the decomposition rate of the s-$C_5H_{11}^*$ radicals was found to be stronger than that observed in the present study.

The lack of the curvature of the S/D vs. pressure plots also demonstrates that the "strong collision" assumption made in the Experimental section is valid to a good approximation (the multistep deactivation of the s-$C_4H_9^*$ radicals would yield a curvature of the plot in the low pressure region if the assumption were not valid (1)).

Can. J. Chem. Downloaded from www.nrcresearchpress.com by 210.87.254.40 on 09/05/12
For personal use only.

Can. J. Chem. Downloaded from www.nrcresearchpress.com by 210.87.254.40 on 09/05/12
For personal use only.

(ii) Allene Formation Process in NB Photolysis

The C_3H_5* radical is produced (process [1]) in its allylic form. If not collisionally stabilized (process [2]), it either decomposes, yielding allene, or isomerises to the vinylic structure, which may be followed by propyne formation.

[5] $CH_2CHCH_2^* \rightarrow CH_2{=}C{=}CH_2 + H$

$\Delta H = +57.5$ kcal mol^{-1}

[6] $CH_2CHCH_2^* \rightarrow CH_3CHCH^*$

$\Delta H \rightarrow +15.5$ kcal mol^{-1} (11)

As we have reported previously (5), the last process is a minor one and it will not be discussed in the present paper.

Having determined the three rate constants of the decomposition process of the C_3H_5* radical at different energies (Table 1), one is tempted to draw some semi-quantitative conclusions on the energy dependence of the kinetics of this process. It is well recognized that the three point probe represents the minimum of the one methodically demanded and therefore the simplest theoretical formalism will be applied.

Let us assume that the rate constant of process [5] can be represented by a simple RRK-type equation (1):

[7] $$k^{dec}(\varepsilon) = A[(\varepsilon - \varepsilon_0)/\varepsilon]^{s-1}$$

It has been shown (16) that this form is a good approximation over a reasonable energy range. In this equation, A is a constant (not specified in the present interpretation), s is the number of effective oscillators in the decomposing species, ε_0 is the critical energy for the process, and ε is the active energy of the C_3H_5* radical. Using the data given in ref. 17, the ε_0 value was estimated to be equal to 60 kcal mol^{-1}.

The ε value now remains to be evaluated, and one may expect at first that a simple statistical formulation based on the internal degrees of freedom is held for the energy distribution between the products of process [1]. Thus, the C_3H_5* fragment carries 18/30 of the photon excess energy. The CH_3 fragment carries 6/30 and the remaining are left for relative motion.

[1*a*] $$\underset{30\text{ vib.}}{n\text{-}C_4H_8^{**}} \rightarrow \underset{18\text{ vib.}}{C_3H_5^*} + \underset{6\text{ vib.}}{CH_3}$$

The resulting $<\varepsilon>$ values were used for making a plot log k^{dec} vs. log $<\varepsilon>$, and this is demonstrated in Fig. 7, curve *a*. Although a reasonable linearity of the plot is achieved, the slope of the line yields the s value equal to 3, which is far from the one expected on the assumption of the energy randomization in the decomposing C_3H_5* radicals.

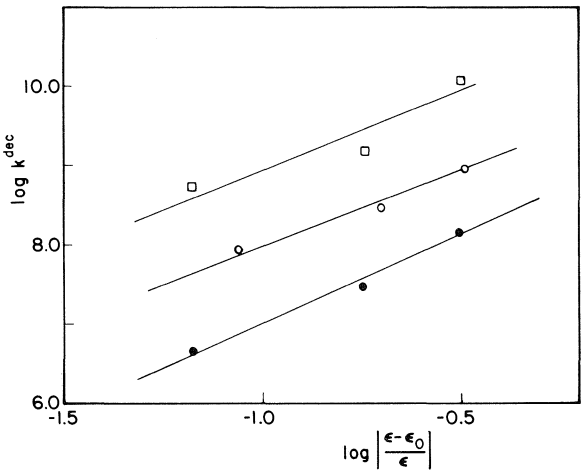

FIG. 7. The logarithmic rate constant of allene formation vs. the logarithmic $(\varepsilon - \varepsilon_0)/\varepsilon$ ratio in the photolysis of *n*-butene (○), *cis*-2-butene: low pressure region (●) and high pressure region (□).

It is easy to show that the required increase in the number of effective degrees of freedom is achieved when one assumes that the fraction of the available energy that the C_3H_5* bears away in process [1] is higher than was predicted by a statistical model for energy partitioning. For example, if all excess energy were to reside in the C_3H_5* radical, the s value obtained from the slope: log k^{dec} vs. log ε_{max} line would be equal to 8 and the linearity of the plot would even be improved. This value could be quite acceptable since the number of effective vibration modes in the excited species is always less than that calculated from the relationship $3N - 6$ (see, e.g., Table III in ref. 18). Our results indicating that a majority of the photoexcitation energy resides on the heavier fragment (C_3H_5* radical) agree with the earlier data of Cambell and Schlag in cyclobutanone photolysis (19):

[8] $$C_4H_6O^{**} \rightarrow c\text{-}C_3H_6^* + CO$$

The authors have found that the cyclopropane contained *far more* internal energy than predicted on the statistical basis, although this difference disappeared at a higher energy. On the other hand, Dorer has investigated the isomerization of methylcyclopropane, produced by the photolysis (313.0 nm) of 4-methyl-1-pyrazoline, to butene isomers (20). He concluded that the fraction of energy carried away by the CH_3—c-C_3H_5* fragment *is less* than would be predicted on the statistical model for energy partitioning. However, Dorer's later study of the photodissociation of cyclobutanone led the author to the conclusion that the available excess energy *is* statistically distributed among the degrees of freedom of the photolytic products (21).

Can. J. Chem. Downloaded from www.nrcresearchpress.com by 210.87.254.40 on 09/05/12
For personal use only.

These few quoted results (for more data: see ref. 1 and the references quoted in Chapt. 9) are sufficient to indicate that the statistical distribution of energy in the photochemically activated system may be observed, but not necessarily always. It probably depends on the system studied and on the photon energy used for the activation.

One more argument may be added in favour of the non-statistical energy partitioning being involved in process [1]. If the majority of the excess energy is carried away by the C_3H_5* radicals, these radicals may be formed with the energy distribution function of a relatively narrow width. This, in turn, may explain why such a good linearity of the Stern–Volmer plots, covering the broad pressure region, is observed (Fig. 1).

(iii) Allene Formation in C2B System

The C_3H_5* radical formed in the decomposition process of the photoexcited C2B molecule may be assumed to be in its vinylic form

[1*b*] $$C2B^{**} \rightarrow CH_3CHCH^* + CH_3$$

It is interesting to note that the decomposition process of this radical does not lead to the formation of propyne (3), whose yield is pressure dependent. Therefore, it has previously been concluded that two other routes are most likely: the isomerization to the allylic structure and the fragmentation into acetylene (3):

[9] $$CH_3CHCH^* \rightarrow CH{\equiv}CH + CH_3$$

A schematic energy diagram which covers the isomerization process followed by the C—H split of the resulting allylic radical is shown in Fig. 8. As seen, for the three photon energies used for the present study, even the excess energy calculated on the statistical basis is sufficient to cause the isomerization as well as the break of the allylic C—H bond.

Now, it is necessary to consider the curvature of the Stern–Volmer plot (3), which, in the kinetic analysis of the allene formation process, made us distinguish two separate pressure regions, and two different rate constants at a given photon energy (Table 1). This curvature may: (*i*) reflect the wide spread in energies of the excited C_3H_5* radicals, (*ii*) indicate that allene is formed from the same C_3H_5* precursor in two distinct energy states, or (*iii*) indicate that allene is formed from chemically different precursors, i.e. either from the C_3H_5* or from the C_4H_7* radicals or from the primary photoexcited C_4H_8** molecules.

The fact that two linear regions of the Stern–Volmer plot could be found suggests that the first alternative is less likely than the remaining two (3). Moreover, the broad energy distribution in the

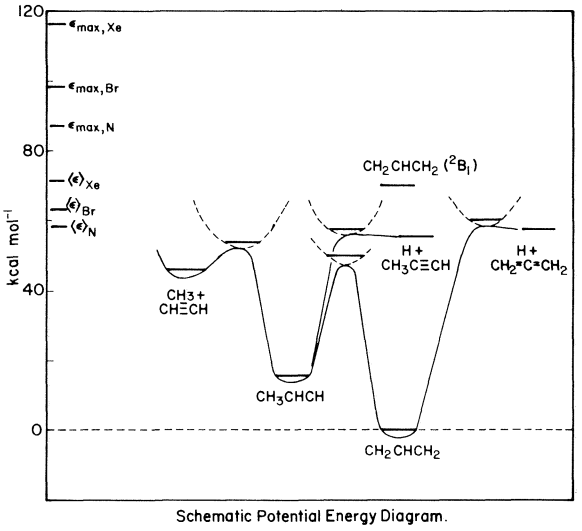

FIG. 8. Schematic potential energy diagram of various routes for the C_3H_5* isomerization and fragmentation processes. Pertinent thermochemical values are taken from refs. 11, 17, 22, and 25.

C_3H_5* radicals might only arise as a result of the decomposition of the energetically randomised C2B** molecules. We may verify if this is the case by applying the RRK-type equation to the rate constants obtained at the three photon energies (Table 1, low pressure region). The log k^{dec} vs. log $<\varepsilon>$ plot (Fig. 7, curve *b*) yields again the *s* parameter equal to 3. In order to get a closer approximation to theory, and in conformity with what was done in the case of the NB photolysis, one must assume that far more energy than predicted on the statistical basis is carried away by the C_3H_5* fragments (the *s* parameter is equal to 8 when the C_3H_5* fragments receive all excess energy). Thus, it is evident that this observation does not match the randomization assumption.

Although the second alternative, i.e. the formation of two energy states of the allylic C_3H_5* radical has been favoured in our earlier papers (3, 5), in the light of the kinetic results presented in Table 1 this view can no longer be sustained. When passing from the low pressure region (LPR) to the high pressure region (HPR), one may note that the unimolecular rate constant of the allene formation process at, e.g. 7.1 eV, increases by ca. two orders of magnitude. This increase is larger than that equal to ca. 30 kcal mol^{-1} (Table 1) brought about by the increase in photon energy from 7.1 to 8.4 eV. On the other hand, the value of $\Delta\varepsilon = \varepsilon_{max} - \langle\varepsilon\rangle$ (Fig. 8) at 7.1 eV is also equal to ca. 30 kcal mol^{-1}. It should be noted that no larger difference in the energy on the C_3H_5* radicals formed at this photon energy can be expected, especially keeping in mind the evidence

against the randomization assumption (see above). If so, the observation:

$$(k_{dec,HPR}/k_{dec,LPR})_{7.1\ eV} = 136 \text{ (Table 1)}$$

cannot be accounted for on a purely energetical basis. Different electronic states cannot be considered either. The first excited electronic state of the allylic radical (3.0 eV) which may be attained upon the fragmentation of the photoexcited C2B molecule (22) is known to be a repulsive one. Thus, the decomposition of this radical occurs within a period of one critical oscillation. The second electronic state (22, 23) has an energy of 5.37 eV, which is higher than the ε_{max} for all photon energies applied in the present work.

Therefore, the nonlinearity of the Stern-Volmer plots (Figs. 2 and 3) appears to reflect the formation of allene from two chemically different precursors. In addition to the C_3H_5* radicals, allene may be formed from C_4H_7* radicals (3) or directly from the photoexcited C_4H_8** molecules:

[10] $$C_4H_7^* \rightarrow C_3H_4 + CH_3$$

[11] $$C_4H_8^{**} \rightarrow C_3H_4 + CH_3 + H$$

The possibility of process [10] in the low pressure region has been eliminated in our earlier work (3). The analysis of the radical–radical processes, which led us to this conclusion, cannot be done in the high pressure region with sufficient accuracy. It should, however, be noted that the absorption spectroscopy of radicals formed in the far uv photolysis of 2-butenes has been interpreted on the basis of the C_4H_7 radical formation (23). The decomposition channels of this radical have not, however, been established.

The formation of allene from the primary photoexcited butene molecules has been reported by Borrel *et al.* (2) and Chesick (4) at the photon energy ≤ 6.7 eV; the quenching of the C_4H_8** molecules has been observed. If this process occurs also at higher photon energies (up to 8.4 eV) and if one recalls that the quantum yields of other primary products have been found not to depend on pressure (3, 5), this result would mean that the fragmentation mode represented by process [11] is the easiest one to be quenched by collisions. So far, however, our experiments cannot provide evidence to distinguish between the last two possibilities.

(iv) In IB Systems

At 7.1 and at 7.6 eV, the results in the IB photolysis are similar to those observed in the C2B photolytic system (see Figs. 2 to 5). A relatively small increase in the rate constant of the allene formation process in this photon energy region is, however, followed by a rapid jump in the k^{dec} value at 8.4 eV (Table 1). In fact, only a small decrease in the quantum yield with IB pressure was observed (detectable at pressures higher than 20 Torr, Fig. 5), which is in agreement with the earlier data reported by Herman *et al.* (24). It is thus concluded that, contrary to what was observed in NB and C2B photolysis, the excess energy on the C_3H_5* radical, formed from the photodecomposition of the IB** molecules, does not increase continuously with the increase in the photon energy but, in the 7.6–8.4 eV energy region, changes by steps. Different electronic (vibronic?) states are probably involved in both photon energy regions. However, more direct data are needed to account for this observation.

Conclusion

The most interesting result obtained in the present study is that the primary photoexcited butene molecules are not energetically randomized before their fragmentation processes (e.g. process [1] or [11]) occur. This conclusion is based on the kinetic analysis of the allene formation process made by the use of the RRK-type equation. Some arguments supporting this view come also from the comparison of the fragmentation patterns of C2B and *trans*-2-butene (T2B) at 7.1 eV (3, 5*b*). Differences, well outside the experimental error may be observed, especially dealing with the ratio of Φ(allene) (extrapolated to zero pressure) to Φ(propyne). This ratio for the C2B and T2B photolysis is equal to 5.0 and 2.3, respectively. Since C2B and T2B are geometric isomers, one might expect that the energy randomization, following the internal conversion to the ground electronic state (4), should lead to the same primary photoexcited C_4H_8** species and would result in the same product distribution. This apparently is not the case.

Acknowledgments

We would like very much to thank the National Research Council of Canada and le Ministère de l'Education du Québec for their financial assistance throughout this work. One of us (A.W.) is pleased to acknowledge helpful discussions with his colleagues, Drs. J. Niedzielski and J. Gawłowski from Warsaw University.

1. W. Forst. *In* Theory of unimolecular reactions. Academic Press, New York, NY. 1973.
2. P. Borrell and F. C. James. Trans. Faraday Soc. **62**, 2452 (1966); P. Borrell, P. Cashmore, A. Cervenka, and F. C. James. J. Chim. Phys. 229 (1970).
3. A. Więckowski and G. J. Collin. J. Phys. Chem. **81**, 2592 (1977).
4. J. P. Chesick. J. Chem. Phys. **45**, 3934 (1966).
5. (*a*) G. J. Collin and A. Więckowski. J. Photochem. **8**, 103

Can. J. Chem. Downloaded from www.nrcresearchpress.com by 210.87.254.40 on 09/05/12
For personal use only.

(1978); (*b*) A. WIĘCKOWSKI and G. J. COLLIN. Can. J. Chem. **55**, 3636 (1977).
6. A. WIĘCKOWSKI and G. J. COLLIN. Can. J. Chem. **56**, 1435 (1978).
7. G. J. COLLIN and K. BUKKA. J. Photochem. **6**, 381 (1976/77).
8. P. POTZINGER, L. C. GLASGOW, and G. VON BÜNAU. Z. Naturforsch. A, **27**, 628 (1971).
9. J. G. CALVERT and J. N. PITTS, JR. *In* Photochemistry. 2nd ed. J. Wiley and Sons, Inc. 1967. p. 605.
10. M. J. PEARSON and B. S. RABINOVITCH. J. Chem. Phys. **42**, 1624 (1965).
11. T. IBUKI, T. MURATA, and Y. TAKEZAKI. J. Phys. Chem. **78**, 2543 (1974).
12. W. E. FALCONER and W. A. SUNDER. Int. J. Chem. Kinet. **III**, 395 (1971).
13. G. J. COLLIN. Can. J. Chem. **51**, 2853 (1973).
14. K. R. JENNINGS and R. J. CVETANOVIĆ. J. Chem. Phys. **35**, 1233 (1961); W. E. FALCONER and W. A. SUNDER. Int. J. Chem. Kinet. **IV**, 315 (1972).
15. B. S. RABINOVITCH and R. W. DIESEN. J. Chem. Phys. **30**, 735 (1959).
16. D. L. BUNKER. J. Chem. Phys. **40**, 1946 (1964).
17. D. M. GOLDEN, A. S. RODGERS, and S. W. BENSON. J. Am. Chem. Soc. **88**, 3196 (1966).
18. T. F. THOMAS, C. I. SUTIN, and C. STEEL. J. Am. Chem. Soc. **89**, 5107 (1967).
19. R. J. CAMBELL and E. W. SCHLAG. J. Am. Chem. Soc. **89**, 5103 (1967).
20. F. H. DORER. J. Phys. Chem. **73**, 3109 (1969).
21. F. H. DORER. J. Phys. Chem. **77**, 954 (1973).
22. C. L. CURRIE and D. A. RAMSAY. J. Chem. Phys. **45**, 488 (1966).
23. A. B. CALLEAR and H. K. LEE. Trans. Faraday Soc. **64**, 308 (1968).
24. J. HERMAN, K. HERMAN, and P. AUSLOOS. J. Chem. Phys. **52**, 28 (1970).
25. P. I. ABELL. *In* Comprehensive chemical kinetics. Vol. 18. 1976. p. 120.

Can. J. Chem. Downloaded from www.nrcresearchpress.com by 210.87.254.40 on 09/05/12
For personal use only.

Reactions of hydrogen atoms with hexafluoroacetone[1]

D. W. GRATTAN[2] AND K. O. KUTSCHKE

Division of Chemistry, National Research Council of Canada, Ottawa, Ont., Canada K1A 0R6

Received August 11, 1977[3]

D. W. GRATTAN and K. O. KUTSCHKE. Can. J. Chem. **56**, 2638 (1978).

Attempts were made to study the kinetics of the reaction of atomic H with $(CF_3)_2CO$ vapour (HFA). Atomic H was generated from H_2 by mercury photosensitization in the presence of C_2H_4 and HFA but the system was complicated by the loss of C_2H_5 radicals by addition to HFA and the kinetic results were intractable. When atomic H was generated from C_3H_8, the kinetics again were obscured by some unidentified reaction(s) which became more important at higher $[HFA]/[C_3H_8]$. An estimate of the rate constant for the addition of H to HFA obtained at low $[HFA]/[C_3H_8]$ yielded $k_9 = 8.5 \times 10^5$ ℓ mol^{-1} s^{-1}. Trifluoroacetaldehyde was identified with some reliability but many of the other heavier products formed in the H_2 + HFA reaction could not be identified. Quenching cross-sections were determined for C_2H_4, C_3H_8, C_4H_{10}, and HFA relative to that for N_2O.

D. W. GRATTAN et K. O. KUTSCHKE. Can. J. Chem. **56**, 2638 (1978).

On a effectué des essais pour étudier la cinétique de la réaction de l'hydrogène atomique avec le $(CF_3)_2CO$ à l'état de vapeur (HFA). On a produit des hydrogènes atomiques à partir de H_2 par photosensibilisation au mercure en présence de C_2H_4 et de HFA mais le système était compliqué par la perte de radicaux C_2H_5, par addition au HFA et les résultats cinétiques ne peuvent être interprétés. Lorsque l'on a produit des hydrogènes atomiques à partir de C_3H_8, la cinétique était à nouveau obscurcie par quelques réactions non-identifiées qui deviennent importantes lorsque $[HFA]/[C_3H_8]$ devient plus grand. On a évalué la constante de vitesse pour l'addition de H à du HFA pour un faible rapport $[HFA]/[C_3H_8]$; alors $k_9 = 8.5 \times 10^5$ mol^{-1} s^{-1}. On a identifié le trifluoroacétaldéhyde avec une assez bonne certitude mais on n'a pas pu identifier les produits plus lourds formés par la réaction de H_2 + HFA. On a déterminé les sections droites de piégage du C_2H_4, du C_3H_8, du C_4H_{10} et du HFA relatives à celle du N_2O.
[Traduit par le journal]

In a system in which trifluoromethyl radicals are generated photochemically in the presence of hydrogen, the apparent value of the rate constant for the abstraction of a hydrogen atom from the molecular species is estimated from the ratio $\rho \equiv R_{CF_3H}/R_{C_2F_6}{}^{1/2}[H_2]$ where R_X is the rate of formation of the product X. It should be noted that ρ is an experimental quantity whose interpretation in terms of rate constants is uncertain by a factor of two depending on the fate of H-atoms produced in the abstraction reaction (1). In some unpublished work,[4] an attempt was made to detect possible variations in ρ by photolyzing hexafluoroacetone at 100°C in the presence of molecular hydrogen. It was anticipated that for conditions associated with large values of $[CF_3]/[H]$ (high $[CF_3COCF_3]$, high light intensity, low $[H_2]$) the H-atoms formed in the abstraction reaction would be scavenged by the CF_3 radicals to yield additional CF_3H so that the value of ρ would be larger (in the limit, larger by a factor of two) than that observed when the converse conditions were employed. In fact, in a series of eight experiments ρ remained constant within $\pm 7\%$ (12.4 ± 0.8 in arbitrary units, total range 11.4 to 13.7 with no trends) even though the conditions noted earlier had been varied sufficiently to cause $R_{C_2F_6}/R_{CF_3H}$ (a crude indication of $[CF_3]/[H]$) to change from 0.0074 to 91. As a consequence these experiments were discontinued.

In those same experiments, however, it was noted that the material balance ratio m ($\equiv(\frac{1}{2}R_{CF_3H} + R_{C_2F_6})/R_{CO}$) increased monotonously from 0.88 for conditions yielding high $[CF_3]/[H]$ to 2.6 at low $[CF_3]/[H]$. It was thought that at low $[CF_3]/[H]$ the H-atom produced in the abstraction reaction might have formed a secondary alkoxyl radical by addition to hexafluoroacetone and that subsequent decomposition of that radical could yield, in part, trifluoroacetaldehyde and a trifluoromethyl radical. In this way, CF_3 radicals might be generated without the formation of carbon monoxide so that the experimental trend in m would be explained, at least qualitatively. Such radical exchange reactions are known to occur in other systems (2) although it had been suggested earlier (3) that H-atoms did not participate in this type of reaction.

The present experiments were undertaken in an attempt to study the addition–exchange reaction of

[1]NRCC No. 16899.
[2]Post Doctoral Fellow 1973–1975.
[3]Revision received July 10, 1978.
[4]J. Klinger and K. O. Kutschke. Unpublished results.

Can. J. Chem. Downloaded from www.nrcresearchpress.com by 210.87.254.6 on 09/05/12
For personal use only.

Can. J. Chem. Downloaded from www.nrcresearchpress.com by 210.87.254.6 on 09/05/12
For personal use only.

H-atoms with hexafluoroacetone in a quantitative way. Hydrogen atoms were generated in the presence of hexafluoroacetone by the mercury-sensitized decomposition of hydrogen or of propane. Attempts were made to evaluate relative rate constants by competitive methods. Each of the competitions studied yielded unexpected kinetic results and possible mechanistic explanations are discussed.

The constants for the quenching of $Hg(^3P_1)$ by ethylene, propane, *n*-butane, and hexafluoroacetone (HFA) were required and were measured with the nitrous oxide method.

Experimental

A conventional photolysis apparatus was employed which contained a quartz reaction cell (200 cm^3, optical path 10 cm) illuminated by a quartz low-pressure mercury lamp (4). Between the lamp and the cell were a shutter and a 2 mm Corning 9-54 filter thus ensuring that the only significant illumination was at 253.7 nm. Mercury condensation in the U bend of the lamp was avoided by using a lamp with electrodes thermostatted at 20°C, and the housing of the lamp at 26°C so that any mercury distillation tended towards the electrodes. The stability of the lamp was checked by means of two phototubes (RCA 935), one of which was placed behind the cell; the other was used to monitor the lamp directly and was connected with the lamp housing by means of a fibre optic.

The cell was mounted in a loop in series with a U-tube, containing a drop of mercury and thermostatted at 20°C, a U-trap, and a glass reciprocating-piston circulation pump; the loop was connected to the vacuum system by three metal Hoke valves, joined at the same point on the loop. These led to vacuum, to the dosing system, and to an analysis line containing, in series, solid and liquid nitrogen traps, a LeRoy still, a diffusion pump, gas burette, and Toepler pumps which in turn led to a gas-chromatographic sampling loop and detachable sample containers for gas chromatography, mass-spectrometry etc.

In the earlier experiments a Perkin Elmer F1 chromatograph with thermistor detectors was used, and during the course of the work this was replaced with a Gow Mac (Model 69-570) dual column instrument, which was also fitted with thermistors. Integration was performed with a disc-integrator.

The HFA (99.9%) was obtained from Matheson and was purified by careful trap-to-trap distillation. Subsequent analysis revealed the presence of 0.01% sulphur dioxide as the only significant impurity. It was stored in darkness and no decomposition was observed over the course of a year.

Propane (Matheson Research Grade) was purified as above and was analyzed especially carefully for traces of olefinic impurities; none were detected by gas chromatography. *n*-Butane and ethylene (99.8% Matheson), Matheson nitrous oxide (98%), and carbon tetrafluoride (99.9%) were purified by careful trap-to-trap distillation and degassing. Although the purity of nitrous oxide was only 98%, the principal impurity was air, and was easily removed. Hydrogen was purified by passage through a heated palladium thimble.

The experimental mixture was prepared by pressurizing calibrated volumes with the gases to be used; pressure was measured with a mercury manometer which was read by a cathetometer. The gases were then condensed into the U-trap of the cell with liquid nitrogen. When hydrogen was used, the condensible gases were first condensed into the U-trap (~¼% of the cell + loop volume) with liquid nitrogen and hydrogen was then admitted to the required pressure. The gases were allowed to warm and were mixed with the circulating pump. The circulating pump did not operate at total pressures below 5 Torr; at these pressures condensible gases were mixed by repeated condensation and evaporation.

Analysis was by low temperature distillation, gas chromatography, and, for part (*iv*), by mass spectrometry; details are placed at the Depository of Unpublished Data.[5]

Results and Discussion

(i) Quenching Constants, with the Nitrous Oxide Method (5, 6)

The rate constant obtained by this treatment, k_q, is a composite quantity which is composed of at least two constants $k_n + k_{na}$. The mechanism for an alkane RH, was regarded by Cvetanović as follows,

$$Hg(^1S_0) + h\nu_{2537} \rightarrow Hg(^3P_1)$$

[1] $$Hg(^3P_1) + N_2O \rightarrow N_2 + O + Hg(^1S_0)$$

[1*a*] $$\rightarrow Hg(^3P_0) + N_2O$$

[2] $$Hg(^3P_1) + RH \rightarrow Hg(^1S_0) + R + H$$

[2*a*] $$\rightarrow Hg(^3P_0) + RH$$

If the metastable mercury atoms do not enter reactions leading directly or indirectly to the formation of nitrogen then [1] is the sole source of nitrogen and a plot of $1/r_{N_2}$ vs. $[RH]/[N_2O]$ will be linear (r_{N_2} is the rate of formation of nitrogen). Moreover, the ratio of the slope to the intercept of this plot yields the quenching ratio, $(k_2 + k_{2a})/(k_1 + k_{1a}) \equiv k_{q2}/k_{q1}$. For work to be discussed later it was necessary to know this ratio for propane. This value had been measured by Rousseau and Gunning (7) but it was redetermined to preserve internal consistency. For accuracy in these determinations it is useful to determine the intercept at $[RH]/[N_2O] = 0$ with as much precision as possible. Thus it was important to obtain more than one curve so that the quenching constant of *n*-butane was also measured. Figure 1 contains the results of the determinations for C_2H_4, C_3H_8, and $n\text{-}C_4H_{10}$. The difference in the intercept for ethylene compared with that for propane and *n*-butane represents the decrease in the lamp output in the eighteen months which elapsed between these determinations.

When the quenching constants of hydrocarbons are measured, the oxygen generated in the decomposition of nitrous oxide is rapidly taken up by reaction with alkanes. With HFA this scavenging might be inefficient so that HgO would be formed and would be deposited on the cell windows as de-

[5]Detailed descriptions of distillation and chromatographic procedures are available, at a nominal charge, from the Depository of Unpublished Data, CISTI, National Research Council of Canada, Ottawa, Ont., Canada K1A 0R6.

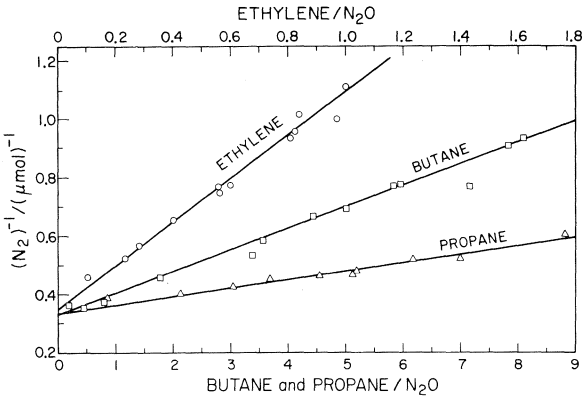

FIG. 1. Quenching plots for C_2H_4, C_3H_8, and n-C_4H_{10}; a constant exposure time was used so that the N_2 yield is proportional to r_{N_2}.

scribed by Cvetanović (8). Therefore the quenching curve for HFA was determined in the presence of ethylene at three ratios of $[C_2H_4]/[N_2O]$. To reactions [1], [1a], [2], and [2a], the following must be added:

$$[3] \qquad Hg(^3P_1) + HFA \rightarrow Hg(^1S_0) + HFA^*$$

$$[3a] \qquad \rightarrow Hg(^3P_0) + HFA$$

The rate of nitrogen formation is now given by the following equation:

$$\frac{I_a}{\gamma_{N_2}} = \frac{k_1 + k_{1a}}{k_1} + \frac{k_2 + k_{2a}}{k_1}\frac{[C_2H_4]}{[N_2O]} + \frac{k_3 + k_{3a}}{k_1}\frac{[HFA]}{[N_2O]}$$

The first two terms on the right may be evaluated from the quenching plot for ethylene obtained in the absence of ketone (filled circles in Fig. 2). The slopes of the other three lines in Fig. 2, together with the intercept, then were used to evaluate $(k_3 + k_{3a})/(k_1 + k_{1a})$. As is required by the mechanism the slopes are independent of the values of the three fixed ratios of $[C_2H_4]/[N_2O]$ used in these experiments.

Table 1 compares the measured values of the k_q determined in this work with the literature values. Although only ratios of quenching constants are determined by the method used (they are process II values in Cvetanović's terminology), individual k_q have been evaluated by using literature values of k_{q,N_2O} (6), or k_{q,C_2H_4} (6), as indicated in the footnotes to Table 1. The agreement among the various values reported is well within experimental error except for the value obtained here for n-C_4H_{10}. As the other values determined in this work agree with the literature there is no obvious explanation for the discrepancy.

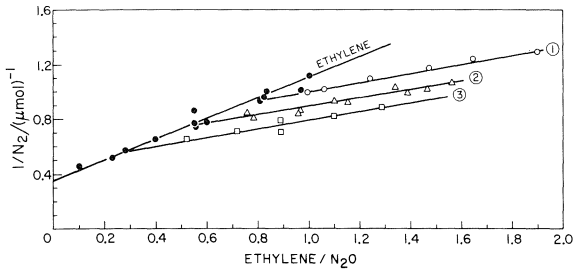

FIG. 2. Quenching plots for HFA. The symbol N_2 represents the amount of nitrogen formed in a fixed time and thus is proportional to r_{N_2}. Line *1*, $[C_2H_4]/[N_2O] = 0.81$; line *2*, $[C_2H_4]/[N_2O] = 0.54$; line *3*, $[C_2H_4]/[N_2O] = 0.27$.

TABLE 1. Quenching constants, k_q

Compound	k_q[a] This work[b]	Others[b]	Others[c]
HFA	13.0	—	—
C_2H_4[h]	31.0	30.0[d]	—
C_3H_8	1.27	1.13[e]	1.28[f]
n-C_4H_{10}	3.35	3.65[d]	3.75[f], 3.83[g]

[a]All k_q in 10^{10} ℓ mol^{-1} s^{-1}.
[b]Based on $k_{q,N_2O} = 14.3$, ref. 6.
[c]Based on $k_{q,C_2H_4} = 30.0$, ref. 6.
[d]Reference 6.
[e]Reference 7.
[f]Reference 9.
[g]Reference 10.
[h]Note that $k_{q,C_2H_4} = 30$ was obtained by substituting $k_{q,N_2O} = 14.3$, into Cvetanović's value of $k_{q,C_2H_4}/k_{q,N_2O} = 2.1$ (6).

The values of individual quenching constants have been obtained relative to the value of $k_{q,N_2O} = 14.3 \times 10^{10}$ ℓ mol^{-1} s^{-1}, which was obtained by Cvetanović. Michael and Suess recently published a higher figure for the latter, of 24.0×10^{10} ℓ mol^{-1} s^{-1}, which would necessitate increasing these values by a factor of 1.68 (10). Since in this work we have only been concerned with the ratios of quenching constants, it is doubtful that the absolute values are of much importance. The latter comment may also be applied to the criticism of the N_2O technique by Vikis *et al.* (9, 11) who explained the divergence between the chemical and physical measurements of k_q by showing that the effect of $Hg(^3P_0)$ had been neglected in the former.

The value of $k_{q,HFA}$ in Table 1 may be compared with the known (12) value of 39×10^{10} ℓ mol^{-1} s^{-1} for acetone. Presumably the greater polarity of the carbonyl group in the fluorinated ketone has decreased the quenching ability of the group.

(ii) The Competition between HFA and Ethylene for Hydrogen Atoms, H + HFA Method I

Following the technique devised by Cvetanović and Doyle to study the relative rates of addition of hydrogen to olefins (12), a large pressure of hydrogen (600 Torr) was used to quench most of the $Hg(^3P_1)$ to

Can. J. Chem. Downloaded from www.nrcresearchpress.com by 210.87.254.6 on 09/05/12
For personal use only.

Can. J. Chem. Downloaded from www.nrcresearchpress.com by 210.87.254.6 on 09/05/12
For personal use only.

give H atoms. In that work (12) the yield of *n*-butane produced by the recombination of the C_2H_5 radicals formed by the addition of hydrogen atoms to ethylene was measured as a function of the ratio of X, the olefin, to ethylene. The mechanism was considered to be the following:

$$Hg(^1S_0) + h\nu_{2537} \rightarrow Hg(^3P_1)$$

$$Hg(^3P_1) + H_2 \rightarrow H + H + Hg(^1S_0)$$

[4] $$H + C_2H_4 \rightarrow C_2H_5$$

[5] $$H + X \rightarrow XH$$

[6] $$2C_2H_5 \rightarrow n\text{-}C_4H_{10}$$

[6*a*] $$\rightarrow C_2H_4 + C_2H_6$$

[7] $$2XH \rightarrow HX{-}XH$$

[7*a*] $$\rightarrow X + XH_2$$

[8] $$C_2H_5 + XH \rightarrow C_2H_6{-}X$$

[8*a*] $$\rightarrow C_2H_4 + XH_2$$

[8*b*] $$\rightarrow X + C_2H_6$$

Solving these equations with the assumption that the radical interaction rates are equal (i.e. $k_6 + k_{6a} = k_7 + k_{7a} = 0.5(k_8 + k_{8a} + k_{8b})$) yields

$$(r_{1,0}^{1/2} - r_1^{1/2})/r_1^{1/2} = k_5[X]/k_4[C_2H_4]$$

where r_1 is the yield of n-C_4H_{10}, and $r_{1,0}$ is its yield when [X] = 0.

If it is assumed that HFA behaves like an olefin, and that the initially formed adduct between H and HFA subsequently decomposes with unit efficiency, then reactions [5], [7], and [8], respectively, would be replaced by:

[9] $$H + HFA \rightarrow HCF_3CO + CF_3$$

[10] $$2CF_3 \rightarrow C_2F_6$$

[11] $$CF_3 + C_2H_5 \rightarrow CF_3C_2H_5$$

[11*a*] $$\rightarrow CF_3H + C_2H_4$$

Making the same assumptions about radical interaction rates a similar equation is obtained.

[12] $$(r_{1,0}^{1/2} - r_1^{1/2})/r_1^{1/2} = k_9[HFA]/k_4[C_2H_4]$$

Ethylene and HFA were used at pressures up to 20 Torr, and since the values of k_q for ethylene, HFA, and hydrogen are 31, 13, and 20 $\times$ 10^{10} ℓ mol^{-1} s^{-1} (6), ethylene and HFA could only account for a maximum of 6.8% of the quenching of $Hg(^3P_1)$. It was argued (12) that any excited species produced in the latter quenching processes would be quickly deactivated at these near-atmospheric pressures to return to the ground state without decomposition. This assumption is now harder to justify as more recent work has shown the quenching of $Hg(^3P_1)$ to $Hg(^3P_0)$ and subsequent quenching of $Hg(^3P_0)$ to be more important than was previously suspected (9). However, if the mechanisms are modified to include the effects of mercury metastables they become intractable.

The competition was studied at four pressures of ethylene, 5, 10, 15, and 20 Torr. Most of the determinations were carried out at 10 Torr. Equation [12] is plotted in Fig. 3. The predicted linear dependence is found but it is also noted that the slope depends on the absolute value of $[C_2H_4]$. This latter result is not compatible with the mechanism.

An important process which has been ignored is undoubtedly the radical exchange reaction between ethyl radicals and HFA; similar reactions are known (2, 3)

[13] $$C_2H_5 + (CF_3)_2CO \rightarrow C_2H_5CF_3CO + CF_3$$

If this reaction is included in the kinetic scheme, and [9] is omitted, and it is assumed again that radical interaction rates are equal, i.e. $2k \equiv 2(k_6 + k_{6a}) = (k_{11} + k_{11a}) = 2k_{10}$, then

[14] $$(r_{1,0}^{1/2} - r_1^{1/2})/r_1^{1/2} = \tfrac{1}{2}k_{13}k_6^{1/2}k^{-1}r_{1,0}^{-1/2}[HFA]$$

In (*iii*) the rate constant for H + HFA is shown to be about 8.5 $\times$ 10^5 ℓ mol^{-1} s^{-1} and that for H + C_2H_4 is known to be 7 $\times$ 10^8 ℓ mol^{-1} s^{-1} (13). Therefore under the above conditions, the reaction of H + HFA is almost negligible and the assumption that reaction [9] may be neglected is justified.This lends some credence to the value of k_{13} obtained below. Note that the concentration of ethylene does not appear in this expression. The assumption has

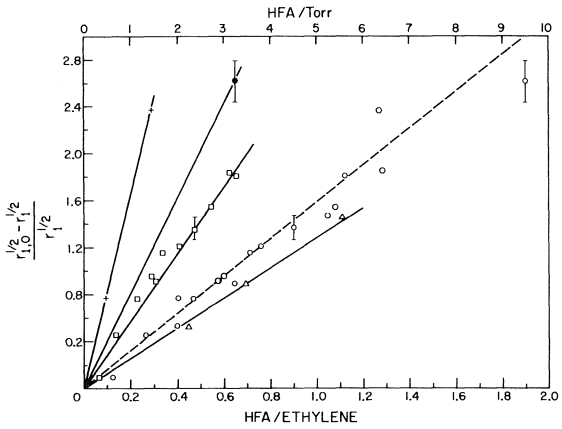

FIG. 3. Plots of eq. [12] with $[C_2H_4]$ = 20 Torr, +; $[C_2H_4]$ = 15 Torr, ●; $[C_2H_4]$ = 10 Torr, □; $[C_2H_4]$ = 5 Torr, △. These plots use the lower abscissa. The broken line is a plot of the same data (open circles) according to eq. [14]; upper abscissa.

Can. J. Chem. Downloaded from www.nrcresearchpress.com by 210.87.254.6 on 09/05/12
For personal use only.

been made that all of the atomic hydrogen reacts with ethylene to give ethyl radicals. The plot of this equation is shown also in Fig. 3 (open circles) and it may be seen that, although there is still some scatter, the points appear to coalesce around a single straight line. On this evidence alone it is not possible to eliminate other mechanistic explanations of the dependence of the results on the absolute pressure.

To evaluate k_{13} it is necessary to make some assumption about the rates of radical interaction. In the book by Kerr and Ratajcjak (14) the rate constants for CF_3 and C_2H_5 combinations are assumed to be 10^{11} and $10^{10.4}$ ℓ mol^{-1} s^{-1}, respectively. Radical interaction for C_2H_5 becomes $1.14 \times 10^{10.4}$ ℓ mol^{-1} s^{-1} if allowance for the disproportionation is made (disproportionation/combination for $C_2H_5 = 0.14$ (15)). We therefore took $k_6 = 10^{10.4}$ ℓ mol^{-1} s^{-1}, and k as $1.14 \times k_{13}$. Since $r_{1,0}$ was measured as 1.27×10^{-8} mol ℓ^{-1} s^{-1}, substitution in [14] gives k_{13} as 3×10^5 ℓ mol^{-1} s^{-1}. There must be a large uncertainty in this value from the above assumptions concerning radical interactions, probably as large as $\pm 50\%$.

A comparison with literature values for similar reactions is shown in Table 2. Two trends may be observed. For methyl or ethyl radical addition to a ketone the addition rate increases with increasing fluorination of the ketone, whereas for trifluoromethyl radical addition the reverse trend is observed. Our result, though high, is compatible with the first of these trends. It would appear that the inductive effect of the fluorine in HFA reduces the electron density on the central carbon atom, enhancing the rate of addition of the electron-rich ethyl radical. The reason for the reverse trend with fluorinated radicals probably derives from the repulsive effect between the highly fluorinated species.

An alternative explanation of the dependence on absolute $[C_2H_4]$ in Fig. 3 might involve a reaction between HFA and ethylene which could alter $[HFA]/[C_2H_4]$ during the photolysis. Several kinds of interaction between these partners are known to occur. For example, it has been shown that triplet HFA reacts with olefins to give oxetanes (25), and that between 0°C to −9°C in solution, HFA and ethylene copolymerize by a free radical mechanism to give what is surmised to be an alternating copolymer (26). If similar or related processes took place, they would cause substantial losses in the absolute amounts of HFA and ethylene and, possibly, changes in their ratio. This possibility was investigated by recovering the HFA and ethylene remaining after photolysis. The photolysis time was increased from 10 to 120 min in these experiments to maximize any such changes. The results were variable but, on the average, for each molecule of HFA lost, 2.6 molecules of ethylene were removed. It is concluded that during the normal 10 min photolysis, no significant alteration in $[HFA]/[C_2H_4]$ could have occurred so that the former explanation is favoured.

TABLE 2. Comparison of rate constants with literature

Radical	Ketone	Rate constant[a]	References
C_2H_5	$(C_2H_5)_2CO$	3.22×10^3	16
C_2H_5	$(C_2F_5)(C_2H_5)CO$	7.9×10^3	17
C_2H_5	$(CF_3)_2CO$	$3 \pm 2 \times 10^5$	This work
CH_3	$(CH_3)_2CO$	2.9×10^1	18
CH_3	$(CHF_2)_2CO$	1.5×10^4	19
CF_3	$(CH_3)_2CO$	3.1×10^3	20
CF_3	$(CF_3)(CH_3)CO$	$2.8, 2.1, 20 \times 10^1$	21, 22, 23
CF_3	$(CF_2H)(CF_3)CO$	2×10^1	24

[a]All rate constants in units of ℓ mol^{-1} s^{-1}.

(iii) The System Propane/HFA; H + HFA Method II

Because of the interference of the reaction between C_2H_5 and HFA, the previous method was not appropriate, so an attempt was made to use a system similar to that devised by Back (27) and developed by Cvetanović *et al.* (28, 29). In this method hydrogen atoms were generated by quenching $Hg(^3P_1)$ with an alkane (Cvetanović *et al.* used *n*-C_4H_{10}, and Back, C_3H_8) and the yield of molecular hydrogen (for a fixed photolysis time) is a function of the stationary state concentration of atomic hydrogen. Any added species which reacts with hydrogen atoms would reduce this stationary state concentration and hence decrease the yield of H_2. In this system it was expected that the H_2 yield would be independent of any interaction between HFA and alkyl radicals. However, it also suffers from two disadvantages: (*i*) since the quenching constant of an alkane is small, the quenching of $Hg(^3P_1)$ by HFA cannot be neglected; (*ii*) as the photolysis proceeds, the disproportionation of the alkyl radical leads to an increasing concentration of alkene, which in turn reacts with hydrogen atoms, so that conversions must be kept small. Propane was used rather than *n*-butane, since the impurity olefin content is stated to be smaller in C_3H_8 than that in *n*-C_4H_{10}.

A pressure of 300 Torr was used to obtain the maximum possible quenching of $Hg(^3P_1)$ by propane. HFA was added in the pressure range 0–45 Torr. A plot of H_2 against photolysis time showed that the generation of H_2 was a reasonably linear function of time for exposures less than 10 min. A photolysis time of 6 min was chosen; this yielded 1.8 μmol of H_2 and corresponded to 0.08% conver-

Can. J. Chem. Downloaded from www.nrcresearchpress.com by 210.87.254.6 on 09/05/12
For personal use only.

sion (Cvetanović *et al.* used a very large reaction volume and recovered 35 μmol of H_2, which corresponded to 0.03% conversion).

The following mechanism, a modified version of that of Cvetanović *et al.*, was used to derive a function relating r_{H_2} to $[HFA]/[C_3H_8]$.

[2] $Hg(^3P_1) + C_3H_8 \rightarrow H + C_3H_7 + Hg(^1S_0)$

[3] $Hg(^3P_1) + HFA \rightarrow HFA^* + Hg(^1S_0)$

[15] $H + C_3H_8 \rightarrow C_3H_7 + H_2$

[9] $H + HFA \rightarrow CF_3 + CF_3CHO$

[16] $2C_3H_7 \rightarrow C_6H_{14}$

[16*a*] $\rightarrow C_3H_6 + C_3H_8$

[17] $C_3H_7 + HFA \rightarrow CF_3 + C_3H_7COCF_3$

[18] $CF_3 + C_3H_7 \rightarrow CF_3H + C_3H_6$

[18*a*] $\rightarrow CF_3C_3H_7$

[10] $2CF_3 \rightarrow C_2F_6$

[19] $HFA^* \rightarrow CO + 2CF_3$

[20] $HFA^* + M \rightarrow HFA + M$

Using the normal stationary-state method, the following relationship was derived:

$$\frac{k_{15}}{k_9}\frac{r_{2,0}}{r_2} = \left(\frac{k_{15}}{k_9} + \frac{[HFA]}{[C_3H_8]}\right)\left(1 + \frac{k_3[HFA]}{k_2[C_3H_8]}\right)$$

In the above expression, k_3/k_2 is the ratio of the quenching constants for HFA and propane (Table 1), r_2 is the yield of hydrogen, $r_{2,0}$ is the yield of hydrogen in the absence of HFA, and k_{15}/k_9 is the ratio of interest. Rearrangement of this equation gives

$$[21]\quad \frac{k_{15}}{k_9} = \frac{[HFA]}{[C_3H_8]}\left\{1 + \frac{k_3[HFA]}{k_2[C_3H_8]}\right\} \times \left\{\frac{(r_{2,0} - r_2)}{r_2} - \frac{k_3[HFA]}{k_2[C_3H_8]}\right\}^{-1}$$

On evaluating k_{15}/k_9 it was found to be a function of the $[HFA]/[C_3H_8]$ ratio; this is shown in Fig. 4. This suggests that a process which has been neglected becomes increasingly important as $[HFA]/[C_3H_8]$ increases. In the initial portion of the curve k_{15}/k_9 is reasonably constant at about 0.15. If Baldwin's value for $H + C_3H_8$ of 1.18×10^5 ℓ mol^{-1} s^{-1} is taken (30), $k_9 = 8.5 \times 10^5$ ℓ mol^{-1} s^{-1}.

Figure 5 shows the variation of r_2 with the ratio $[HFA]/[C_3H_8]$. The broken line represents the rate of formation of H_2, r_3, which may be calculated if reaction [9] were negligibly slow so that only the competitive quenching (reactions [2] and [3]) caused the rate of formation of H_2 to decrease as [HFA] was increased. It is evident from Fig. 5 that competitive quenching alone is insufficient to account for the decrease actually observed and, therefore, that some reaction in addition to [15] consume H atoms. Thus the difference $r_3 - r_2$ is an indirect measure of the contribution of reaction [9] to the rate of decrease in the rate of formation of $[H_2]$; this difference is given in eq. [22].

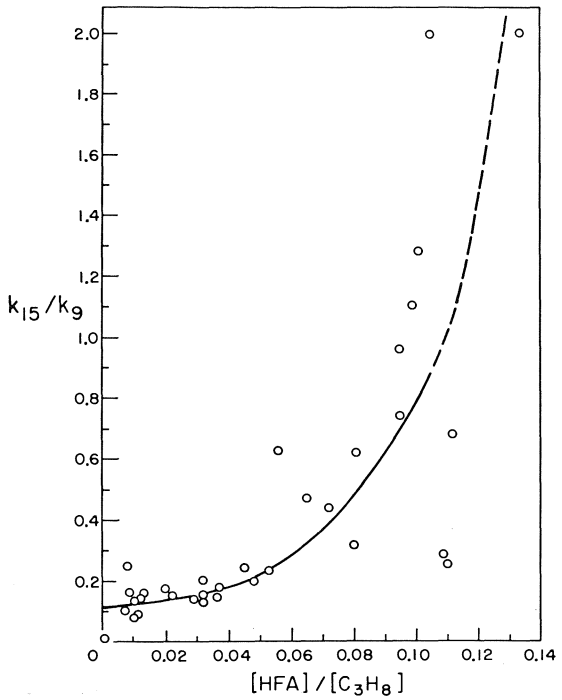

FIG. 4. Variation of the apparent values of k_{15}/k_9, evaluated by eq. [21], with $[HFA]/[C_3H_8]$.

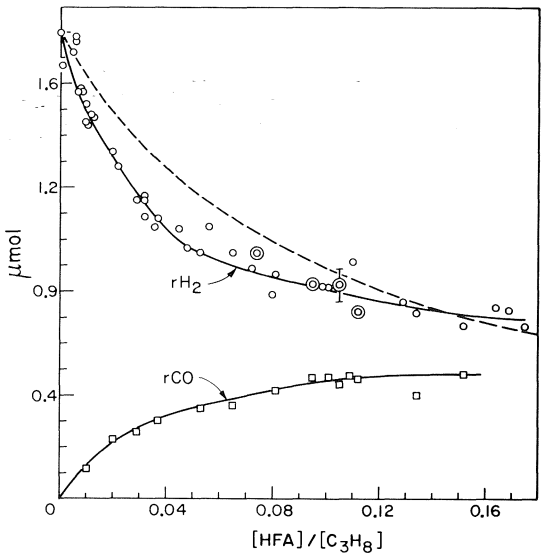

FIG. 5. Variation of r_{H_2} and r_{CO} as a function of $[HFA]/[C_3H_8]$. The broken line is explained in the text.

$$[22]\quad r_3 - r_2 = \frac{r_{2,0}\left(\frac{k_9[\mathrm{HFA}]}{k_{15}[\mathrm{C_3H_8}]}\right)}{\left(1+\frac{k_3[\mathrm{HFA}]}{k_2[\mathrm{C_3H_8}]}\right)\left(1+\frac{k_9[\mathrm{HFA}]}{k_{15}[\mathrm{C_3H_8}]}\right)}$$

If the value of 6.7 is taken for k_9/k_{15}, 10 for k_3/k_2, this function predicts that $r_3 - r_2$ goes to a maximum of 0.36 at $[\mathrm{HFA}]/[\mathrm{C_3H_8}] \simeq 0.12$, whereas the results obtained give a maximum of about 0.25 around $[\mathrm{HFA}]/[\mathrm{C_3H_8}] \simeq 0.04$.

It is evident that the value of k_9 obtained in this work cannot be taken as established. Nevertheless the fact that the data in Fig. 5 follow approximately the predictions of the mechanism gives some credence to the value. Moreover, alternative mechanistic explanations all proved to be untenable; some of those considered are outlined below.

It is conceivable that excited HFA could be quenched by propane so efficiently that sufficient energy transfer would take place to dissociate a C—H bond in propane. If so, then collisional deactivation by a non-reactive body should interfere with this process and reduce the yield of hydrogen. Therefore 300 Torr of CF_4 was added at four higher values of $[\mathrm{HFA}]/[\mathrm{C_3H_8}]$; and as can be seen in Fig. 5 (concentric circles) there was no effect. Thus this explanation was ruled out.

Another possibility was that HFA was quenching $Hg(^3P_1)$ efficiently to $Hg(^3P_0)$, and not effectively quenching the latter. If so, as the HFA concentration increased it would lead to more formation of $Hg(^3P_0)$ which would be quenched by C_3H_8, leading to decomposition. This was tested by using the method of Vikis, Torrie, and LeRoy (9). The production of hydrogen from the non-complete quenching of excited mercury by ethylene was studied as HFA was introduced. The pressure of ethylene used was about 5 Torr and HFA was added in the ratio of 0.7 to 1.3 $[\mathrm{HFA}]/[\mathrm{C_2H_4}]$. If HFA quenches $Hg(^3P_1)$ to $Hg(^3P_0)$ and not the latter, the stationary-state concentration of $Hg(^3P_0)$ should be considerably increased as HFA is added. Since the lifetime of the metastable $Hg(^3P_0)$ is much greater than $Hg(^3P_1)$, the number of collisions between C_3H_8 and excited mercury species will increase and this has been shown to give an increase in the yield of hydrogen. In this instance, as HFA was added the yield of hydrogen decreased, and therefore this explanation too was considered improbable.

(iv) Product Analysis

Attempts were made to detect the heavier products formed in the $Hg(^3P_1)$ sensitized decomposition of H_2 (600 Torr) in the presence of 10–20 Torr of HFA. It was hoped that only those arising as a result of the reaction of H with HFA would be observed, but, as we have shown, this is a rather slow process. As a consequence products arising from the quenching of $Hg(^3P_1)$ by HFA interfered considerably as was evidenced by the appearance of nearly twenty peaks in the gas chromatogram. The identities of several of the product peaks (CO, C_2F_6, CF_3H, C_3F_8, and HFA) were readily established but the assignment of many was not possible even though their mass spectra were taken. Some of these seemed to be fluoroalkyl alcohols of higher molecular weight and one was almost certainly trifluoroacetaldehyde (very strong peaks at *m/e* 20); this latter might well arise from reaction [9].

It is interesting to compare this work to that of Gordon *et al.* (31), who studied the photolysis of HFA in ethane. These workers found various high molecular weight alcohols and derived a mechanism to account for their production. A crucial reaction in this system was the intramolecular hydrogen shift in the alkoxy radical shown below

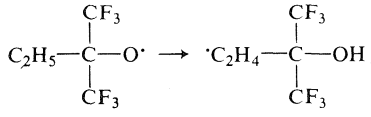

The hydroxylated radical so produced can attack more HFA or recombine. In the system on which we carried out product analysis, this process is ruled out since no α-hydrogens are present and the secondary alkoxy radical can only give β-scission to give an aldehyde or ketone, abstract an H from hydrogen to form an alcohol, or recombine to give a peroxide.

(v) Correlation with the HFA Photolysis in the Presence of H_2

The value of k_9 estimated in (*iii*) may be used to calculate the value of the material balance expected in the experiments described in the Introduction. If reaction [9] is included with the usual reactions forming CF_3H and C_2F_6 in that system (see ref. 1), then the material balance ratio may be expressed as

$$[23]\quad m = 1 + \tfrac{1}{2}k_9k^{-1/2}[\mathrm{HFA}] \times \{(R_{\mathrm{CO}}{}^{1/2} - R_{\mathrm{C_2F_6}}{}^{1/2})/R_{\mathrm{CO}}\}$$

where k is the rate constant for the mutual and cross combination reactions of CF_3 and H in their high pressure limits. Values of m calculated on this basis exceed those found experimentally by an order of magnitude (e.g. for $[\mathrm{HFA}] = 20$ Torr and $[\mathrm{H_2}] =$ 395 Torr, 1.25 μmol CO, and 0.54 μmol C_2F_6 were formed in 1 h in a reaction volume of 0.177 ℓ at 100°C; $m_{\mathrm{calcd}} \simeq 18$, $m_{\mathrm{obsd}} = 1.75$). Moreover, as [9] is expected to require some activation energy, the value of k_9 taken to calculate m should be larger than the room temperature value estimated in (*iii*);

Can. J. Chem. Downloaded from www.nrcresearchpress.com by 210.87.254.6 on 09/05/12
For personal use only.

such a correction could only magnify the disagreement.

It seems unlikely that the assumptions involved in the derivation of [23] could introduce so large an error except that which requires [9] as written to represent the sole interaction between H and HFA. Indeed, the rather large number of heavier products detected in (*iv*) suggests that a substantial portion of the H + HFA interactions proceed to other products. In that event, the rate of H disappearance by reaction with HFA should not be equated to the rate of CF_3 formation in that interaction as was done in the derivation of [23], but rather only some as yet unknown fraction of that rate should be used. It is evident that much more work will be required before a quantitative description of these systems can be given.

1. K. O. KUTSCHKE. Can. J. Chem. **42**, 1232 (1964).
2. A. F. TROTMAN-DICKENSON and G. S. MILNE (*Editors*). Tables of bimolecular gas reactions. National Standard Reference Data Series, National Bureau of Standards, 9, Washington. 1967. p. 128.
3. S. J. W. PRICE and K. O. KUTSCHKE. Can. J. Chem. **38**, 2128 (1960).
4. C. R. MASSON, V. BOEKELHEIDE, and W. A. NOYES. *In* Techniques of organic chemistry. Vol. II. *Edited by* A. Weissberger. Interscience, New York, NY. 1961. p. 276.
5. R. J. CVETANOVIĆ. J. Chem. Phys. **23**, 1208 (1955).
6. R. J. CVETANOVIĆ. *In* Progress in reaction kinetics. Vol. 2. *Edited by* G. Porter. MacMillan Co., New York, NY. 1964. p. 39.
7. Y. ROUSSEAU and H. E. GUNNING. Can. J. Chem. **41**, 465 (1963).
8. R. J. CVETANOVIĆ. J. Chem. Phys. **23**, 1203 (1955).
9. A. C. VIKIS, G. TORRIE, and D. L. LEROY. Can. J. Chem. **50**, 176 (1972).
10. J. V. MICHAEL and G. N. SUESS. J. Phys. Chem. **78**, 5 (1974).
11. G. LONDON, A. C. VIKIS, and D. J. LEROY. Can. J. Chem. **48**, 1420 (1970).
12. R. J. CVETANOVIC and L. C. DOYLE. J. Chem. Phys. **50**, 4705 (1969).
13. J. V. MICHAEL, D. T. OSBORNE, and G. N. SUESS. J. Chem. Phys. **58**, 2800 (1973).
14. J. A. KERR and E. RATAJCJAK (*Editors*). The second supplementary table of bimolecular gas reactions. University of Birmingham, Great Britain. 1971.
15. A. C. FALCONER and W. A. SANDER. Int. J. Chem. Kinet. **3**, 523 (1971).
16. J. C. J. THYNNE. Trans. Faraday Soc. **58**, 676 (1962).
17. R. L. THOMMARSON and G. O. PRITCHARD. J. Phys. Chem. **70**, 230 (1966).
18. H. O. PRITCHARD and G. O. PRITCHARD. Can. J. Chem. **41**, 3042 (1963).
19. G. O. PRITCHARD and R. L. THOMMARSON. J. Phys. Chem. **71**, 1674 (1967).
20. R. A. SIEGER and J. G. CALVERT. J. Am. Chem. Soc. **76**, 5197 (1954).
21. R. M. SMITH and J. G. CALVERT. J. Am. Chem. Soc. **78**, 2345 (1956).
22. E. R. MORRIS and J. C. J. THYNNE. J. Organomet. Chem. **17**, 3 (1969).
23. G. O. PRITCHARD and M. J. PERONA. Int. J. Chem. Kinet. **2**, 281 (1970).
24. T. H. MCGEE and C. E. WARING. J. Phys. Chem. **73**, 2838 (1969).
25. N. E. SHORE and N. J. TURRO. J. Am. Chem. Soc. **97**, 2482 (1975).
26. Y. TABATA, W. ITO, and K. OSHIMA. *In* Polymerization and new polymers. *Edited by* N. A. J. Platzer. Adv. Chem. Ser. 129, Am. Chem. Soc. New York, NY. 1972. p. 190.
27. R. A. BACK. Can. J. Chem. **37**, 1834 (1959).
28. R. J. CVETANOVIĆ, W. E. FALCONER, and K. R. JENNINGS. J. Chem. Phys. **35**, 1225 (1961).
29. K. R. JENNINGS and R. J. CVETANOVIĆ. J. Chem. Phys. **35**, 1233 (1961).
30. R. R. BAKER, R. R. BALDWIN, and R. W. WALTER. Trans. Faraday Soc. **66**, 2812 (1970).
31. A. S. GORDON, W. P. NORRIS, R. H. KNIPE, and J. H. JOHNSTON. Int. J. Chem. Kinet. **7**, 15 (1975).

Can. J. Chem. Downloaded from www.nrcresearchpress.com by 210.87.254.6 on 09/05/12
For personal use only.

Detection of intermediates and isolation of hydroquinone monoacetate in the Dakin oxidation of *p*-hydroxyacetophenone

MARTIN B. HOCKING,[1] MING KO, AND TREVOR A. SMYTH
Department of Chemistry, University of Victoria, Victoria, B.C., Canada V8W 2Y2

Received April 18, 1978

MARTIN B. HOCKING, MING KO, and TREVOR A. SMYTH. Can. J. Chem. **56**, 2646 (1978).

Oxidation of *o*-, *m*-, and *p*-hydroxyacetophenone with peracetic acid or *tert*-butyl hydroperoxide, oxidants relatively readily monitored by nmr, failed to generate isolable intermediates though an intermediate was detected for the *p*-ketone. Attempted oxidation of a number of related ketones under Dakin conditions failed either to react, or to generate a detectable intermediate. However, with delicate adjustment of pH and careful timing of the isolation procedure, hydroquinone monoacetate has for the first time been successfully isolated from an alkaline aqueous hydrogen peroxide oxidation (Dakin oxidation) of *p*-hydroxyacetophenone.

MARTIN B. HOCKING, MING KO et TREVOR A. SMYTH. Can. J. Chem. **56**, 2646 (1978).

L'oxydation des *o*-, *m*- et *p*-hydroxyacétophénones par l'acide peracétique ou l'hydroperoxyde de *tert*-butyle, des oxydants qui peuvent être facilement détectés par rmn, n'ont pas conduit à la formation d'intermédiaires pouvant être isolés, même si on a pu détecter un intermédiaire dans le cas de la cétone *para*. Lors d'essais d'oxydation d'un certain nombre de cétones apparentées, dans les conditions de Dakin, nous n'avons observé aucune réaction et nous n'avons pu générer d'intermédiaires pouvant être détectés. Toutefois en ajustant d'une façon délicate le pH et en minutant correctement le procédé d'isolation, on a pu isoler pour la première fois le monoacétate d'hydroquinone d'une oxydation par le peroxyde d'hydrogène en milieu aqueux alcalin (oxydation de Dakin) d'une *p*-hydroxyacétophénone.

[Traduit par le journal]

Can. J. Chem. Downloaded from www.nrcresearchpress.com by 210.87.254.42 on 09/05/12
For personal use only.

Introduction

Oxidation of hydroxyacyl aromatics with aqueous alkaline hydrogen peroxide to yield dihydroxy aromatics has received significant attention for its synthetic utility (1, 2) and its scope was reviewed some time ago (3). However, the mechanistic pathway followed by this process has received little attention, apart from relatively recent proposals that it proceeds via an ester intermediate (4), frequently by analogy to the better understood though only superficially related Baeyer–Villiger oxidation of bisaromatic ketones.

A series of competitive oxidation hydrolysis experiments with initial simultaneous presence of *p*-hydroxyacetophenone and hydroquinone monoacetate (HMA) substrates showed that loss of ketone was more rapid than of ester, which suggested that ester could not be an intermediate in this process (5). However, ester which may have subsequently formed from ketone made this a potentially ambiguous result though there was no evidence of ester during a reaction in the absence of initial ester (Scheme 1). Kinetic experiments have established a first-order rate dependence on ketone concentration for both *ortho*- and *para*-hydroxyacetophenone but at the same time unexpectedly demonstrated a 1.4 order of dependence in hydrogen peroxide (6), again an inconclusive result. Fortunately, however, during a few of the preliminary runs for the kinetic experiments at lower pH which were monitored by ^{1}H nmr, an occasional fleeting additional proton resonance at about the same shift as would be expected for the acetate methyl of HMA was observed. Here are reported the results of the experiments directed towards establishing conditions which prolonged the lifetime of this and related intermediates to enable more extensive observation of their formation to be made, and eventually to enable procedures to be developed to isolate a key intermediate in this process and prove its identity.

Experimental

Commercial *p*-hydroxyacetophenone was purified by crystallization from water and dried (80°C/24 h) before use. Hydroquinone monoacetate was obtained in poor yield as previously described (6), *m/e* 152. Peracetic acid was freshly prepared on an approximately 2 g scale for each experiment from glacial acetic acid (2.5 g), 90% hydrogen peroxide (1.5 g, FMC; normal precautions (7)), and concentrated sulphuric acid (50 mg) by the method of Greenspan (8). Concentrations of 50–52% were obtained by titrimetric determination (9, 10) and were confirmed by ^{1}H nmr measurements (11). The reported mole ratios of hydrogen peroxide are based on determinations of the nominal 30% material immediately before use (12).

Proton nmr monitoring was carried out and spectra were obtained at 37°C on Perkin-Elmer R-12 or R-32 spectrometers, using 6% TMS in CCl_4 sealed in an axially-positioned thin-wall capillary as external reference for the reported shifts of aqueous solutions. Mass spectra were obtained on Hitachi Perkin-Elmer RMU-6E double focussing and Finnigan

[1]Visiting Professor, 1978–1979, Department of Chemistry, McGill University, Montreal, P.Q. H3A 2A7.

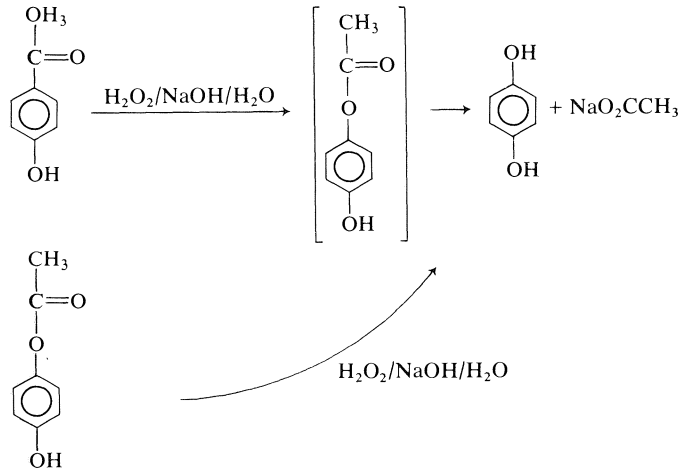

1

SCHEME 1. Competitive oxidation hydrolyses of *p*-hydroxyacetophenone and hydroquinone monoacetate.

quadrupole spectrometers. Analytical and preparative gas–liquid chromatographic (glc) results were obtained on Varian Aerograph Model 920 instruments fitted with flame ionization and thermistor thermal detectors, respectively.

Hydroquinone Monoacetate Hydrolysis Rate Experiments

Hydroquinone monoacetate relative hydrolysis rates were surveyed by small scale experiments using ^{1}H nmr monitoring of the ester and acetate ion resonances at δ 2.72 and 2.35 ppm, respectively.[2] One example where the generation of intermediate peracetic acid was observed is described below.

Hydrogen peroxide (60 mg, 30%) was added to a solution of HMA (5 mg) in 0.5 ml of water thermostatted at 37°C. After 75 min a singlet resonance at 2.53 ppm indicated that about 20% of the residual ester was present, and acetic acid was absent. After 15 h the breakdown of the reaction progress by ^{1}H nmr was approximately: ester, 50%; peracetic acid **2**, 20%; and acetic acid, 30%. By 66 h the ester had hydrolyzed completely.

Extraction Experiments during Hydroquinone Monoacetate Hydrolyses

Hydroquinone monoacetate (44 mg) was dissolved in 0.5 ml of 0.1 *M* sodium hydroxide containing 120 mg of 30% hydrogen peroxide and 2 min later the resulting solution was extracted with 3 ml followed by 1 ml of deuteriomethylene chloride. Examination of the dried extracts by ^{1}H nmr demonstrated the presence of four times as much HMA, at δ 2.20, as intermediate **2**, δ 2.10 ppm, in the first extract, and an HMA concentration of about 0.8 that of the intermediate **2**, in the second; ms (room temperature 70 eV) *m/e*: 167, 152 (HMA); ^{13}Cmr (CD_2Cl_2): two benzene derivatives. The resonance ascribed to the methyl of HMA was confirmed by seeding with genuine material (6). Loss of the ^{1}H nmr resonance at 2.10 ppm occurred on careful evaporation and resolution, or from washing a portion of the extract with 6 drops of water. The original aqueous raffinate contained HMA, intermediate **2** (predominating), and acetate ion, δ ≃ 2.20, 2.10, and 2.00 ppm, respectively.

Seeding experiments with freshly prepared peracetic acid (8) on a new experiment gave peaks which coincided with the singlet for intermediate **2** for both a deuteriochloroform extract and the aqueous raffinate.

Stable Intermediate Experiments

p-*Hydroxyacetophenone with Peracetic Acid*

A solution of *p*-hydroxyacetophenone (97 mg) in 0.46 ml of 1 *M* sodium carbonate at 37°C was rapidly oxidized but failed to show directly any detectable intermediate with peracetic acid (260 mg of 51.5%).

This experiment was repeated and 1 min after mixing was chilled, saturated with sodium chloride, and then extracted with 1 ml deuteriochloroform. The dried extract contained HMA, peracetic and acetic acids, by ^{1}H nmr and ir; ms (room temperature, 70 eV) *m/e*: 152, 111, 109. About 15 mg of impure hydroquinone was isolated from the acidified aqueous reaction solution.

Other experiments conducted are mentioned in the discussion.

Small-scale ^{1}H Nuclear Magnetic Resonance Survey Oxidations of m- and p-*Hydroxyacetophenone*

The hydroxyketone, in varying mole ratios, was dissolved in aqueous solutions of 0.10–0.74 *M* sodium hydroxide or sodium carbonate and the solutions placed in a thermostat bath at 37°C for several minutes. Via a calibrated dropper the desired quantity of stock hydrogen peroxide, also at 37°C, was added to the solution of the ketone and the solution vigorously mixed, and then an aliquot withdrawn and placed in an nmr tube. The region 1 to 4 ppm for protons was then repeatedly scanned for a period of an hour or so, or until there appeared to be no further change, to observe the loss of the ketone methyl singlet and development of an acetate ion singlet plus the appearance of any additional resonances of interest. From a matrix of some 30 experiments of this kind the set of conditions outlined in the procedure below was devised for the *p*-ketone.[2]

Hydroquinone Monoacetate Isolation from a Dakin Oxidation of p-*Hydroxyacetophenone*

To a stirred solution of *p*-hydroxyacetophenone (20.0 g) in 240 ml of 0.4 *M* aqueous sodium carbonate at 37°C was added 20 ml of 36.8 wt.% hydrogen peroxide. Once the solution became homogeneous (about 2 min), the reaction was quenched

[2]A copy of Tables 1 and 2 summarizing the results from 14 experiments in this series is available, at a nominal charge, from the Depository of Unpublished Data, CISTI, National Research Council of Canada, Ottawa, Ont., Canada K1A 0S2.

Can. J. Chem. Downloaded from www.nrcresearchpress.com by 210.87.254.42 on 09/05/12
For personal use only.

Can. J. Chem. Downloaded from www.nrcresearchpress.com by 210.87.254.42 on 09/05/12
For personal use only.

by sharp chilling in a salted ice bath and by the addition of 1.0 *M* sulfuric acid to pH < 3 while simultaneously bubbling excess sulfur dioxide through the solution. The chilled solution was then extracted with 4 × 100 ml and 1 × 100 ml of ether and the two series of extracts dried (Na_2SO_4) and solvent removed to yield 21.92 and 0.84 g of pale brown solid. Gas–liquid chromatography of this material on a 1.3 m × 3 mm, 3% SE30 on 80/100 mesh Chrom P packed column at 164°C, 15 ml/min He carrier, gave retention times for benzoquinone, 1.1 min; hydroquinone, 4.2 min; HMA, 7.0 min; *p*-hydroxyacetophenone, 10.4 min and established that the composition of the larger sample was approximately 16 and 75% of the former two, and 3–4% of each of the latter two compounds.

The combined evaporated crude extracts were triturated with cold benzene (4 × 50 ml) and the combined solutions dried and chilled to 0°C, which brought down 1.58 g of pale yellow crystals, mp 82–105°C, of impure *p*-hydroxyacetophenone (nmr). After drying, the benzene was removed from the filtrate leaving 4.3 g of pale orange crystals in oil. The oil (1.68 g) was filtered off and was then extracted with 3 × 3 ml of benzene. The first extract (0.85 g) contained 38 mol% HMA (plus 58% *p*-hydroxyacetophenone), 4% acetic acid, by ^{1}H nmr, and the second and third extracts contained negligible further HMA. It was not possible to crystallize this extract from a variety of solvents either directly or from combined appropriate fractions, obtained after solvent chromatographing on activated alumina columns twice. However, after successful preliminary separate sublimation tests with authentic HMA and *p*-hydroxyacetophenone, about 130 mg of 86% (^{1}H nmr) HMA was sublimed (90–110°C/15 Torr) from the first extract. Recrystallization from hexane twice, with charcoal, gave a few milligrams of colourless plates (needles occasionally obtained if crystallization was rapid) of HMA, mp 60–63°C; ms, methane chemical ionization, 152, 153 (M + 1), 181 (M + 29), and 193 (M + 41), were obtained both for this material and for authentic hydroquinone monoacetate (6); ir (Nujol) ν_{max}: 3440 (s, OH), 1745 and 1726 (s, C=O); electron impact ms (room temperature, 70 eV) *m/e* (relative intensity >10%): 152(13), 110(100), 109(11), 82(12), 81(19), 55(12), 54(14), 53(18), 43(51), 39(13).

From extracts of later oxidations of *p*-hydroxyacetophenone, HMA was separated with difficulty by preparative glc using 100 μl injections of a 10% ethereal solution onto a 1 m × 6 mm column of 1.5% OV 701 on Chrom G H/P 100/120 at 190°C, 70 ml/min He carrier. Retention times observed were hydroquinone diacetate 1.8 min; HMA, 3.1 min; and *p*-hydroxyacetophenone, 6 min. One recrystallization of the HMA fraction from hexane gave colourless square plates identical to the above, mp 63–64°C (lit. (13) mp 65–66°C).

Results and Discussion

Preliminary nmr tube scale experiments established that HMA alone in water at 37°C remained virtually unchanged even after 17 h although addition of a small amount of sodium hydroxide to the solution brought about hydrolysis in less than 2 min, extremely rapid compared to control experiments with phenyl acetate. Aqueous hydrogen peroxide alone also caused rapid disappearance of the HMA interestingly enough generating peracetic acid, **2**, and possibly a per ortho ester (see Scheme 2) giving a ^{1}H nmr resonance at δ 2.14, which then quite slowly faded to the methyl shift for aqueous acetic acid, plus hydroquinone (not specifically monitored). Eventually conditions were devised prolonging the lifetime of these intermediates to more than an hour. Extraction experiments were successful in obtaining stable methylene chloride solutions of the intermediates in which the presence of peracetic acid was confirmed by seeding experiments. But apart from obtaining mass spectrometric confirmation of the per ortho ester by an *m/e* of 167 it was not possible to further characterize this material.

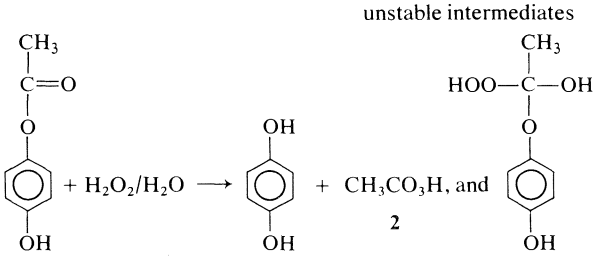

SCHEME 2

The results obtained from the monoester experiments above initially discouraged direct pursuit of the intermediate from alkaline hydrogen peroxide oxidation of *p*-hydroxyacetophenone. It had also been noted that solvent changes, for instance to acetone or pyridine, completely alter the course of the reaction (14). Therefore, consideration was then given to oxidant variants or more stable aryl ketone substrates in an attempt to obtain a somewhat longer-lived and less sensitive intermediate to facilitate isolation.

Peracetic acid oxidation of acetophenone at low pH has been reported to give phenyl acetate, phenol, and benzoic acid (15). Accordingly, peracetic acid oxidations of *p*-hydroxyacetophenone in aqueous sodium carbonate were conducted. Deuteriochloroform extracts gave a ^{1}H nmr singlet resonance coinciding with added HMA, and the correct *m/e* 152, but the solution concentration was low and the experimental procedure was difficult to scale up to permit confirmation of this result by isolation.

tert-Butyl hydroperoxy radical has been used to oxidize aromatic substrates (16) and the hydroperoxide to oxidize aliphatic aldehydes (17, 18). However, even up to five times excess of this oxidant failed to give any detectable (11) oxidation or intermediate formation with *p*-hydroxyacetophenone in aqueous sodium hydroxide, or with the mono- or diacetates of hydroquinone in carbon tetrachloride, either cold or hot. A slow oxidation occurred with *tert*-butyl hydroperoxide and *o*-hydroxyacetophenone at 85°C although it was not possible to detect any intermediate. Possibly the reported inhibiting effect of phenols generally on the decomposition of *tert*-butyl hydroperoxide (19) may be the explanation for this uniformly observed sluggish reactivity.

Can. J. Chem. Downloaded from www.nrcresearchpress.com by 210.87.254.42 on 09/05/12
For personal use only.

Acyl aromatics such as *m*-hydroxyacetophenone and *p*-nitroacetophenone have been reported to be stable to Dakin oxidation conditions (1). If the reaction proceeds via the pathway outlined earlier (4), it was likely that this lack of reactivity was the consequence of the low migratory aptitude of the phenyl group rather than from the reduced nucleophilicity of the carbonyl carbon towards hydroperoxide anion. With this in mind, *m*-hydroxyacetophenone was exposed to Dakin conditions while monitoring by ^{1}H nmr. Small amounts of acetate ion were generated but at no time was there a detectable amount of intermediate. It had been determined that if resorcinol had formed, it would not have been more than slightly affected under the experimental conditions used. Separate parallel experiments were conducted with *p*-methoxyacetophenone, 5-nitrosalicylaldehyde, and 3-nitro-4-hydroxyacetophenone with similar negative results.

Accordingly, a number of small-scale Dakin oxidations of *p*-hydroxyacetophenone were carried out and monitored by ^{1}H nmr to determine whether conditions could be suitably adjusted, not only to generate the same nmr resonance coincident in shift to that of the methyl of HMA fleetingly observed previously, but to extend the lifetime of HMA sufficiently to enable isolation of the material. With two of these, namely these having *p*-hydroxyacetophenone, sodium carbonate, and hydrogen peroxide in the amounts 0.74, 0.12, 0.66 and 1.48, 0.12, 1.41 mmol, respectively, in 1.2 ml of water, an nmr singlet at the desired shift was observed and, for the latter experiment at least, a confirmed lifetime for the desired intermediate of more than an hour was obtained.

From a scaled-up Dakin oxidation of *p*-hydroxyacetophenone, using the conditions established by these small-scale experiments, pure HMA was eventually obtained. Initial difficulties with relatively large quantities of co-produced and easily sublimed benzoquinone were largely avoided by the application of gaseous sulfur dioxide to the quenched reaction solutions early in the work-up. Benzene trituration followed by evaporation served to recover the monoester still associated with ketone but virtually free of associated, less soluble hydroquinone. Either careful sublimation or preparative glc followed by crystallization then gave pure HMA.

Although this first isolation of HMA from a Dakin oxidation of *p*-hydroxyacetophenone certainly implicates the ester as an intermediate in this process, the evidence obtained here is insufficient to establish this as the sole intermediate. Consideration of the kinetic results obtained earlier (6), which were inconsistent with a pathway only involving ester, strengthens this proposal that ester formation is probably accompanied by at least one other pathway for the progression of Dakin oxidation. Evidently further experimental results are necessary before the details of this process can be established with any greater certainty.

Acknowledgements

The authors thank the National Research Council of Canada and the University of Victoria for financial support and D. L. McGillivray for mass spectra.

1. H. D. DAKIN. Am. Chem. J. **XLII**, 477 (1909).
2. W. BAKER, H. F. BONDY, J. GUMB, and D. MILES. J. Chem. Soc. 1615 (1953); W. BAKER, F. J. W. MCOMIE, and T. L. V. ULBRICHT. J. Chem. Soc. 1825 (1952): G. BARGER. J. Chem. Soc. **113**, 219 (1918); cf. W. W. WESTERFELD. J. Biol. Chem. **143**, 177 (1942).
3. M. HUDLICKY. Chem. Listy, **46**, 567 (1952); J. PLIML. Chemie (Prague), **10**, 647 (1958).
4. A. G. DAVIES. Organic peroxides. Butterworths, London. 1961. p. 155; J. B. LEE and B. C. UFF. Q. Rev. Chem. Soc. **21**, 429 (1967); W. A. WATERS. Mechanisms of oxidation of organic compounds. Methuen and Co. Ltd., London. 1964. pp. 47 and 48; L. J. CHINN. Selection of oxidants in synthesis. Marcel Dekker, Inc., New York, NY. 1971. p. 112.
5. M. B. HOCKING. Can. J. Chem. **51**, 2384 (1973).
6. M. B. HOCKING and J. H. ONG. Can. J. Chem. **55**, 102 (1977).
7. Concentrated hydrogen peroxide. Technical Data Bulletin No. 46, FMC Corp., New York, NY. 1975; E. S. SHANLEY and J. R. PERRIN. Jet Propul. **28**, 382 (1968); W. C. SCHUMB, C. N. SATTERFIELD, and R. L. WENTWORTH. Hydrogen peroxide. Reinhold Publishing Corp., New York, NY. 1955. pp. 152–188.
8. F. P. GREENSPAN. J. Am. Chem. Soc. **68**, 907 (1946).
9. J. D'ANS and W. FREY. Ber. **45**, 1845 (1912); J. D'ANS (sic) and W. FREY. Z. Anorg. Chem. **84**, 145 (1913).
10. M. W. C. SMIT. Recl. Trav. Chim. Pays-Bas, **49**, 675 (1930); B. D. SULLY and P. L. WILLIAMS. Analyst (London), **87**, 653 (1962).
11. A. I. VOGEL. A textbook of quantitative inorganic analysis, including elementary instrumental analysis. 3rd ed. Wiley, New York, NY. 1961. pp. 348, 349, and 363.
12. C. A. BUNTON and J. HELLYER. J. Am. Chem. Soc. **89**, 6252 (1967).
13. A. VON WACEK and H. O. EPPINGER. Chem. Ber. **73**, 644 (1940); A. VON WACEK and A. VON BEZARD. Chem. Ber. **74**, 845 (1941).
14. A. BALLIO and L. ALMIRANTE. Ann. Chim. (Rome), **41**, 421 (1951); Chem. Abstr. **46**, 2518 (1952); W. E. VON DOERING and L. SPEERS. J. Am. Chem. Soc. **72**, 5515 (1950); S. L. FRIESS. J. Am. Chem. Soc. **71**, 14 (1949).
15. J. A. HOWARD and J. H. B. CHENIER. J. Am. Chem. Soc. **95**, 3054 (1973).
16. I. SCHLOSSMAN (to Halcon International Inc.). Fr. Patent No. 1,395,951 (April 16, 1965); Chem. Abstr. **63**, 9817g (1965).
17. M. C. V. SAUER and J. O. EDWARDS. J. Phys. Chem. **75**, 3377 (1971).
18. G. A. WARD and R. D. MAIR. Anal. Chem. **41**, 538 (1969); D. S. SWERN, A. H. CLEMENTS, and T. M. JUONG. Anal. Chem. **41**, 412 (1969).
19. E. G. GINTSBERG, V. V. GUR'YANOVA, and B. M. KOVARSKAYA. Zh. Obshch. Khim. **40**, 2319 (1970); Chem. Abstr. **74**, 75841 m (1971).

Water-soluble lysine-containing polypeptides. V. Circular dichroism, electron microscopic, and thermal denaturation studies of the interaction of poly(L-lysyl-L-alanine) and poly(L-lysyl-D-alanine) with calf thymus DNA[1]

SANDRA L. KIELLAND, LEWIS A. SLOTIN,[2] AND ROSS E. WILLIAMS

Division of Biological Sciences, National Research Council of Canada, Ottawa, Ont., Canada K1A 0R6

Received April 6, 1978

SANDRA L. KIELLAND, LEWIS A. SLOTIN, and ROSS E. WILLIAMS. Can. J. Chem. **56**, 2650 (1978).

Turbidity measurements, circular dichroism spectra, electron micrographs and thermal denaturation profiles of complexes between sonicated DNA and either poly(L-lysyl-L-alanine) or poly(L-lysyl-D-alanine) show significant differences which might be related to the primary or secondary structure of the polypeptides.

SANDRA L. KIELLAND, LEWIS A. SLOTIN et ROSS E. WILLIAMS. Can. J. Chem. **56**, 2650 (1978).

Nous avons pris des mesures de turbidité, des spectres du dichroisme circulaire, des micrographies éléctroniques ainsi que des spectres thermo-optique des complexes entre l'ADN (traité aux ultrasons) et poly(L-lysyl-L-alanine) ou poly(L-lysyl-D-alanine). Les différences observées entre les complexes pourraient être attribuables aux structures primaires et secondaires des polypeptides.

[Traduit par le journal]

Introduction

In the living cell many proteins are found in direct association with nucleic acids. Many of these proteins, such as the histones, have cationic regions in them which are found in direct contact with the nucleic acids. Homopolymers, as well as random and sequential copolymers, containing the amino acids arginine or lysine, have been used as models of these cationic regions (see ref. 1 and previous papers in this series, refs. 1–26). Complexes between the polypeptides and the nucleic acids have been formed in one of three different ways: (*i*) by simply mixing the compounds together (2–9); (*ii*) by step-wise dialysis from high concentration salt solutions (10–19); (*iii*) by equilibrium gradient dialysis from high concentration salt solutions (20–26). Of the three, equilibrium gradient dialysis from high concentration salt solutions has proved to be the most easily reproduced (21). Studies in these laboratories have been initiated with the aim of discerning the various factors important to the formation of polypeptide–, and thus protein – nucleic acid complexes.

From amongst the various factors which might be important to the formation of cationic polypeptide – nucleic acid complexes it has been suggested that the conformational flexibility of the polypeptide, i.e., the degrees of freedom possessed by the polypeptide backbone and groups attached to it, might play a role in determining the final form of the complex. The studies which led to this suggestion were those in which the effect of poly(L-lysine) and a set of lysine-glycine sequential copolypeptides on the formation of the aggregated, or ψ-state of calf thymus DNA was studied (25, 26). It was shown that poly(L-lysine) induced maximum formation of ψ-state DNA at lower lysine – DNA phosphate ratios than any of the poly(L-lysine-glycine) sequential copolymers. This difference was attributed, in part, to the fact that poly(L-lysine) was conformationally less flexible than any of the lysine-glycine copolymers. However, the complete separation of the influence of polypeptide conformational flexibility from the other possible factors, such as charge spacing and hydrophobicity, was not possible in these experiments.

Recently we have reported the synthesis of two sequential polypeptides, poly(L-lysyl-L-alanine) (PL-L-Ala) and poly(L-lysyl-D-alanine) (PL-D-Ala) (27). These two polymers have the same interlysine charge spacing, very similar overall hydrophobicities, and have been shown to have different conformational flexibilities (27). In an effort to determine if different polypeptide conformational flexibilities influence polypeptide interaction with DNA we have studied their ability to induce the ψ (or aggregated)-state in calf thymus DNA (CT-DNA). After back dialysis of the components to physiologically-related conditions i.e., pH 7.0, 0.15 *M* NaCl, the formation of ψ-state DNA was examined by solution turbidity measurements, circular dichroism (cd) spectroscopy, and electron microscopy (em). In addition, the effect of

[1]NRCC No. 16844.

[2]NRCC Research Associate, 1975–1977. Present Address: Ministry of State for Science and Technology, 270 Albert Street, Ottawa, Ont., Canada.

Can. J. Chem. Downloaded from www.nrcresearchpress.com by 210.87.254.42 on 09/05/12
For personal use only.

Can. J. Chem. Downloaded from www.nrcresearchpress.com by 210.87.254.42 on 09/05/12
For personal use only.

the polymers on the thermally-induced transition of DNA from its double stranded state to its single stranded state was examined.

Method and Materials

Chemicals used to prepare buffers were commercially available and reagent grade. All water used was deionized and distilled from glass. Specific experimental details have been previously reported for: (*i*) the preparation, purification, sonication, and concentration assays of calf thymus DNA (25, 26); (*ii*) the preparation, characterization, and concentration assays of the poly-L-lysine sample (1×10^4 molecular weight) which was used (25, 26, 28); (*iii*) the preparation, characterization, and concentration assays of poly(L-lysyl-L-alanine) and poly-(L-lysyl-D-alanine) samples which were used (27); (*iv*) the preparation of annealed complexes containing the polypeptide and the 40-s sonicate of calf thymus DNA (DNA molecular weight approximately 500 000) (26).

Instruments used to measure and methods of expressing the results of ultraviolet spectra, solution turbidity, and circular dichroism spectra have been described previously (25). Instrumentation and techniques of preparing grids for electron microscopy have been reported previously (26).

Thermal melting experiments were done using a Cary-Varian spectrophotometer, model 14 equipped with a thermostatted multisample changer. Solutions were contained in Teflon-stoppered quartz cells (internal width, 0.4 cm; path length, 1.0 cm). Solution temperatures were monitored with a thermistor-equipped Telethermometer, Yellow Springs, Ohio, U.S.A. Changes in absorption (A) with temperature (T) were monitored at 260 nm. No corrections for thermal expansion of the solutions were made. The results were plotted as differential absorptions vs. temperature i.e., dA_T/dT_T vs. T where $dA_T = (A_{T+2} - A_{T-2})$, $dT_T = (T_{T+2} - T_{T-2})$, and T = measured temperature in °C. Readings were taken at 2°C intervals only after the constancy of absorption was established. Total hypochromicity of a salt gradient annealed sample of purified calf thymus DNA (40-s sonicate) was 26 ± 2%($10^{-3}M$EDTA, pH 7.0). Hypochromicity is defined as $(A_{260}{}^{95} - A_{260}{}^{25})/A_{260}{}^{95}$ where $A_{260}{}^{T}$ is the solution absorption at 260 nm and 95°C and 25°C, respectively.

Results

Formation of annealed complexes between cationic polypeptides and calf thymus DNA (CT-DNA) by gradient dialysis from high concentrations of salt to physiological conditions (i.e., 0.15 M NaCl, pH 7) results in the appearance of, what has been designated, the ψ-(or aggregated) state of DNA. Poly(L-lysine) and several random and sequential lysine-containing copolypeptides have been shown to induce the formation of this ψ-state in DNA (1). The ψ-state of DNA has been suggested to result from the aggregation of double-stranded regions of the DNA into an ordered (or liquid crystalline) array (29–32). This aggregation could be brought on by solvent exclusion, by induction of long range order into the DNA (21) and, perhaps by phase separation of the components from solution (i.e., coacervate formation) (31, 32).

Experimentally, the formation of the ψ-state results in the formation of a large negative band in the cd spectrum between 260 and 280 nm accompanied by solution turbidity and the formation of aggregates observable by em. Each of these have been examined with complexes containing calf thymus DNA (CT-DNA) and either PL-L-Ala or PL-D-Ala. Thermal denaturation profiles of the complexes have also been determined. The results are given below.

Solution Turbidity

Complex formation results in an increase in solution turbidity at 400 nm (25). The solution turbidity, although not directly connected to ψ-state formation, was shown to be influenced by the structure of the lysine-containing polypeptide and the strandedness of the DNA (26). Solutions containing complexes of CT-DNA and poly(L-lysine) become more and more turbid as the lysine – DNA phosphate (L/P) ratio increases (Fig. 1). The turbidity plateaus at about the same L/P ratio as the maximum in the formation of the ψ-state DNA (26). An increase in solution turbidity with increasing L/P ratio also occurred in solutions of complexes containing either PL-L-Ala or PL-D-Ala; however no plateau was reached even at L/P ratios as high as 2. It was noted that slightly more turbidity was associated with complexes containing PL-L-Ala than those containing PL-D-Ala. The gradual increase of solution turbidity and the lack of a plateau was similar to that found for complexes of poly(L-lysylglycine) (26). It may also be noted that the solution turbidity at an L/P ratio of 1 of complexes containing the lysine–alanine complexes was less than

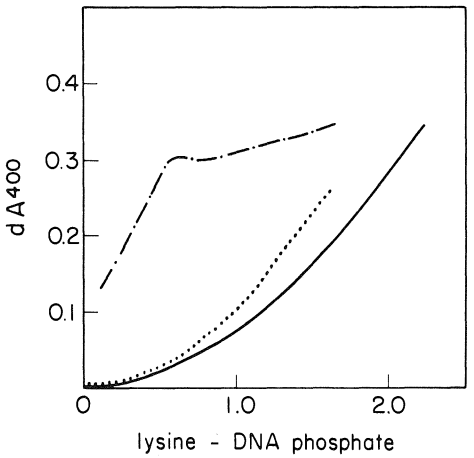

FIG. 1. Variation in sample turbidity dA^{400} with lysine – DNA phosphate ratios in complexes between lysine-alanine polypeptides and sonicated calf thymus DNA: poly(L-lysine)–DNA complexes (- · - · -); poly(L-lysyl-L-ala)–DNA complexes (· · ·); poly(L-lysyl-D-ala)–DNA complexes (———). Experimental conditions: DNA phosphate concentration, 1.77×10^{-4} M; sodium chloride, 0.15 M; sodium cacodylate, 0.001 M; pH 7.0; T = 25°C.

Can. J. Chem. Downloaded from www.nrcresearchpress.com by 210.87.254.42 on 09/05/12
For personal use only.

that found for the solutions of poly(L-lysylglycine)/CT-DNA.

Circular Dichroism Spectra

Complex formation results in changes to the solution cd spectrum of CT-DNA. When complexes are formed with poly(L-lysine) the cd spectrum of CT-DNA changes from one attributed to B-DNA to one representative and diagnostic of ψ-state DNA (Fig. 2) (21, 25, 26). The change in spectrum results in the formation of a large negative band between 260 and 280 nm. Both PL-L-Ala and PL-D-Ala cause the formation of ψ-state DNA when complexes are formed with CT-DNA (Fig. 2).

Plotting the ellipticity generated at 275 nm vs. the L/P ratio (Fig. 3) shows that the maximum formation of the ψ-state occurs around an L/P ratio of 0.6 with poly(L-lysine) and around 1.5 with the two lysine-alanine polymers. The peaking of ellipticity at an L/P ratio around 1.5 was very similar to that observed with the set of lysine-glycine copolymers (25, 26). The production of ellipticity associated with ψ-state formation, however, varied with the L/P ratio and depended upon the polymer incorporated in the complex. At low L/P ratios (less than 1) PL-L-Ala was more effective in causing formation of the ψ-state whereas the reverse was true at high L/P ratios (greater than 1). It would, thus, appear that the DNA in complexes containing low concentrations of PL-L-Ala was more ordered than that in complexes containing PL-D-Ala whereas the reverse would hold for DNA in complexes having higher concentrations of the polypeptides.

Electron Microscopy

Complex formation results in the formation of uranyl acetate stainable aggregates which may be observed in the electron microscope. As the L/P ratio in the complexes increases and approaches the maximum in the formation of the ψ-state large clusters of circular aggregates are formed. Each circle has an apparent diameter of about 6000 Å. An electron micrograph of complexes of poly(L-lysine)/CT-DNA is shown in Fig. 4*a*. This may be compared with the electron micrographs prepared in an identical manner with complexes formed between either PL-L-Ala/CT-DNA (Fig. 4*b*) or PL-D-Ala/CT-DNA (Fig. 4*c*). Aggregates containing PL-L-Ala (Fig. 4*b*) were similar to those incorporating poly(L-lysine) in that they were densely stained and showed a tendency to form clusters, although this tendency was somewhat reduced compared with that of poly(L-lysine). The diminished tendency to form clusters was similar to that observed in the complexes formed between CT-DNA and poly(L-lysylglycine) and the other related lysine-glycine polymers (26). The shape of the complexes, however, was more oval than that

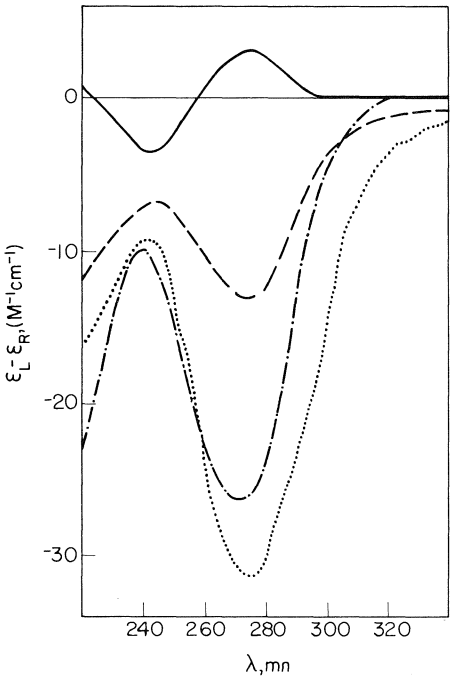

FIG. 2. Circular dichroism spectra of lysine and lysylalanine polypeptides complexed with sonicated calf thymus DNA: sonicated calf thymus DNA (———); poly(L-lysine)–DNA complexes, lysine – DNA phosphate ratio, 0.8 (– · –); poly(L-lysyl-L-alanine)–DNA complexes, lysine – DNA phosphate ratio, 0.92 (· · ·); poly(L-lysyl-D-alanine)–DNA complexes; lysine – DNA phosphate ratio, 1.14 (- - -). Experimental conditions: as for Fig. 1; T = 27°C. No corrections have been made for sample turbidity.

of either the poly(L-lysine) or any of the lysine-glycine copolymers. The complexes were also smaller, i.e., the dimensions of the PL-L-Ala/CT-DNA complexes were approximately 2000 Å by 3000 Å.

The complexes between PL-D-Ala and CT-DNA (Fig. 4*c*) were much less densely stained (more diffuse) than those of PL-L-Ala/CT-DNA and showed no tendency of clustering. They were also oval shaped and had dimensions of approximately 2000 Å by 6000 Å.

Thermal Denaturation Experiments

When the temperature of a solution of double stranded DNA rises the ultraviolet absorption at 260 nm undergoes a relatively abrupt increase (hyperchromism) (33). The temperature at which the transition occurs (T_m) is defined by the ionic composition and strength of the solvent and the nucleic acid base composition of the DNA (34). Positively charged polymers cause a rise in the T_m of native DNA. For example, it has previously been shown that when poly(L-lysine) was complexed with DNA the T_m of native DNA was raised and that the fraction of the DNA involved in the rise depended on the L/P ratio (35, 36).

Can. J. Chem. Downloaded from www.nrcresearchpress.com by 210.87.254.42 on 09/05/12
For personal use only.

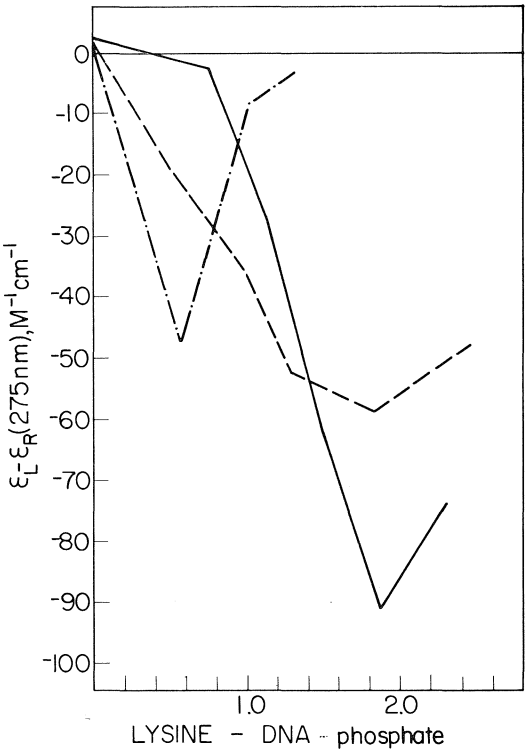

FIG. 3. Variation of the molar ellipticity ($\varepsilon_L - \varepsilon_R$) at 275 nm with the lysine – DNA phosphate ratios in complexes between the lysine and lysylalanine polypeptides and sonicated calf thymus DNA: poly(L-lysine)–DNA complexes (– · –); poly(L-lysyl-L-alanine)–DNA complexes (– –); poly(L-lysyl-D-alanine)–DNA complexes (———). Experimental conditions: as for Fig. 1.

The effect of poly(L-lysine), PL-L-Ala, and PL-D-Ala on the melting behaviour (denaturation) of the purified, sonicated DNA used to form the complexes was determined. Complexes were formed, as in the other experiments, by back dialysis in a linear gradient of decreasing salt concentration until physiological conditions were reached. The complexes were then dialyzed against 10^{-3} *M* ethylenediaminetetraacetic acid (EDTA), pH 7.0, and melted. The derivative melting profile of purified, sonicated DNA has a major T_m centered at 54 ± 2°C (Fig. 5). The transition was relatively broad and asymmetric indicating that the DNA was composed of molecules having different guanine-cytosine (G/C) contents (37, 38). The melting behaviour of complexes of poly(L-lysine) and the DNA, at an L/P ratio where light scatter was negligible, showed two major transitions: one was/centered at 61 ± 2°C while the other was centered at 71 ± 2°C. The major loss of lower melting material from underneath the DNA melting regions could be connected with the adenine-thymine (A/T) specificity of poly(L-lysine) (39). It would be expected that lower melting (A/T rich)

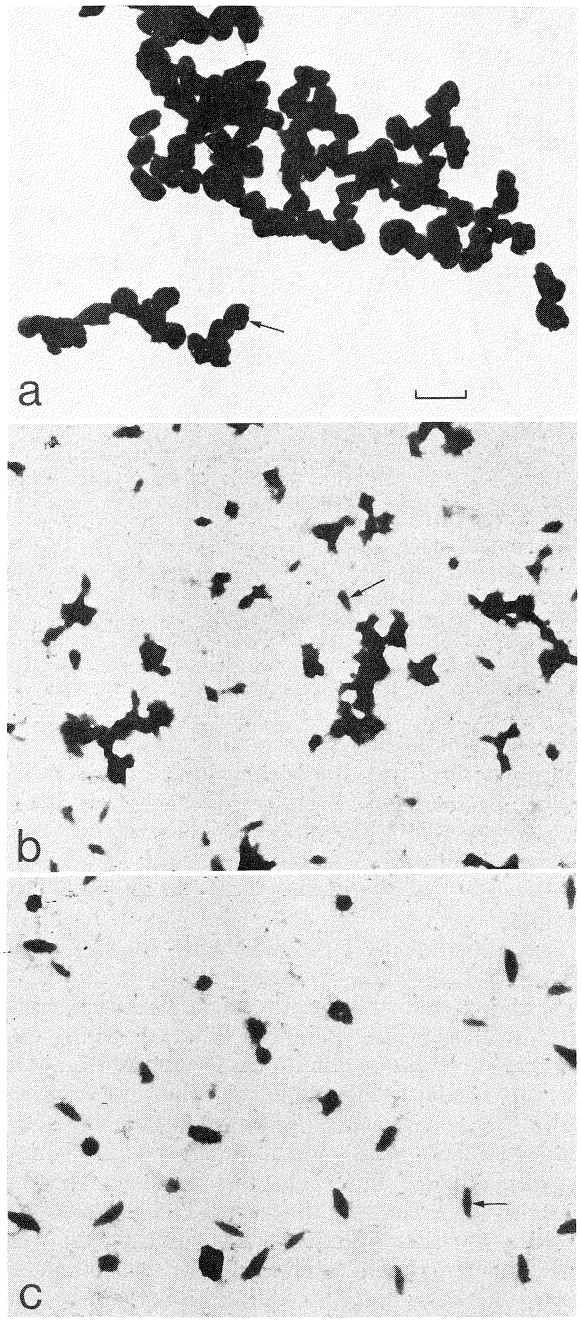

FIG. 4. Electron micrographs of formaldehyde-fixed, dehydrated and stained polypeptide – sonicated DNA complexes: (*a*) poly(L-lysine)–DNA complexes, L/P = 0.64; (*b*) poly(L-lysine-L-alanine)–DNA complexes, L/P = 1.36; (*c*) poly(L-lysine-D-alanine)–DNA complexes, L/P = 1.47. Experimental conditions: DNA-phosphate concentration = 1.77×10^{-4} *M*. Complexes were fixed before drying in 0.15 *M* NaCl, 0.0010 *M* sodium cadodylate, pH 7.0, ~1.0% formaldehyde. Dried complexes were stained with uranyl acetate. The bar indicates a distance of 1 micrometre (μm). All the micrographs have the same magnification. Arrows indicate typical complexes used for dimension determinations.

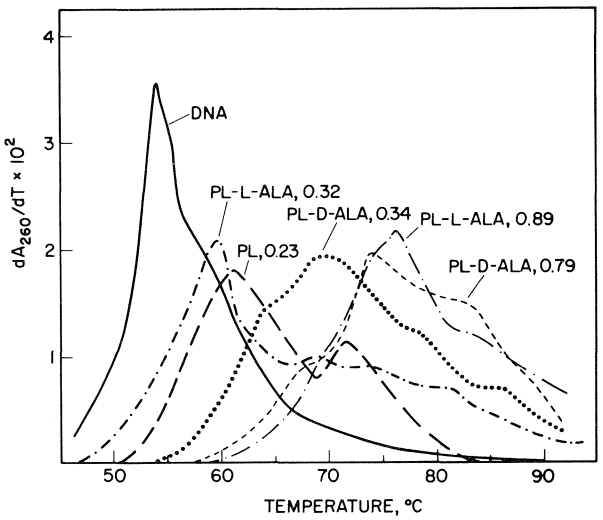

FIG. 5. Derivative absorption melting profiles (dA_{260}/dT vs. T) of purified, sonicated DNA (———) complexed with: (*i*) poly(L-lysine), L/P ratio = 0.23 (- - -); (*ii*) PL-L-Ala, L/P ratio = 0.32 (– · – · –), L/P ratio = 0.89 (— · — · —); (*iii*) PL-D-Ala, L/P ratio = 0.34 (· · · · · · · · ·), L/P ratio = 0.79 (– – – – – – –). Experimental conditions: 1.0×10^{-3} *M* EDTA, pH 7.0; DNA-phosphate concentration, 1.70×10^{-4} *M*.

material would be preferentially complexed and leaving a G/C rich fraction melting in the DNA region. Such a suggestion has previously been made (35). Increasing the L/P ratio in the complex to above 0.5 resulted in large amounts of light scatter and invalidated the measurement of the melting behaviour.

For complexes of DNA with both PL-L-Ala and PL-D-Ala L/P ratios of approximately 0.3 and 0.7 were chosen since light scattering effects were minimal. At an L/P ratio of about 0.3 the melting behaviour of complexes containing DNA and PL-L-Ala was very similar to that seen with poly(L-lysine) complexes. The derivative profile consisted of a T_m centered at 60 ± 2°C and a very broad transition between 65 and 85°C. The loss of lower melting material from beneath the native DNA peak also suggests a similar A/T base specificity for PL-L-Ala. The derivative profile generated by melting complexes containing DNA and PL-D-Ala at an L/P ratio about 0.3 had a broad transition centered at 70°C. None of the lower melting material remained which might suggest that PL-D-Ala has little or no base pair specificity. Thus both polymers caused different thermal melting behaviour at low L/P ratio. At the high L/P ratio, both polymers shifted the center of the transition in the derivative melting profile to temperatures between 75 and 85°C. Both polymers were equally effective at causing the shift in T_m. Both profiles were broadened compared to that of DNA and no significant difference between the profiles was noted.

Discussion

Formation of complexes between CT-DNA and either of the two lysine-alanine copolypeptides, i.e., either PL-L-Ala or PL-D-Ala, results in (*i*) the formation of turbidity in solution; (*ii*) the formation of a cd spectrum characteristic of ψ-state DNA; (*iii*) the formation of aggregates which can be observed, after suitable fixing and staining, in the electron microscope. The present results have shown that the observations are dependent on which of the two polypeptides is incorporated into the complex. For example, the complexation of PL-L-Ala and CT-DNA resulted in slightly more turbid solutions, more distortion to the cd spectrum of DNA at low L/P ratios and less distortion at high L/P ratios and more electron dense, more clustered aggregates than complexation of PL-D-Ala and CT-DNA. In addition, to these results, the thermal melting profiles of the complexes containing the two polypeptides were different when L/P ratios were low indicating that they complexed with DNA in different manners.

Differences in molecular weights between the two polymers might play a role in explaining the results. Although both polymers seem to be equally polydisperse and of similar molecular weight, as indicated by their thin-layer gel filtration profiles (27), they might not, in fact, have the same molecular weights and distribution of molecular weights. Dissimilar solution conformations, as observed by the cd spectra (27), could play an important role in determining the observed molecular weight profiles and thus, make the two profiles seem similar.

However, if one assumes that both polymers are equally polydisperse and have the same molecular weights the differences between the complexes could be ascribed to one of two explanations. The polypeptide conformational flexibility, that is the ability of the polymer to adopt various conformations in solution, might play a role in determining the way in which the polypeptide interacts with the DNA. It has been previously reported that the solution conformations of the two polypeptides respond differently to changes in ionic strength and pH (27). PL-L-Ala has a propensity for adopting an α-helical conformation whereas PL-D-Ala prefers to remain in what appears to be a random conformation. This behavior could be reflected in the complex. On the other hand, the polypeptides could bind to the nucleic acid by adopting the same peptide backbone conformation. The differences between the complexes would then be

Can. J. Chem. Downloaded from www.nrcresearchpress.com by 210.87.254.42 on 09/05/12
For personal use only.

Can. J. Chem. Downloaded from www.nrcresearchpress.com by 210.87.254.42 on 09/05/12
For personal use only.

the result of the switch of the L-amino acid to the D-amino acid and the resulting change in the appearance of the polypeptide surface in contact with the DNA.

Although the simplest explanations seem to be those related to either the solution behaviour of the polypeptides, i.e., conformational flexibility or to molecular weight differences, the present data do not allow a disentangling of the various factors involved in establishing the ψ-state simply because the necessary assessment of the constancy of the polypeptides' conformation in the complex cannot be made and no determination of the actual polypeptide molecular weight is available.

Direct comparison of the results with those reported previously by others also presents some difficulty because of differences in DNA preparations, differences in polypeptide molecular weights and compositions, as well as differences in methods of complex formation. For example, the polypeptide, PL-L-Ala, has been previously prepared by a slightly different route (40). Its interaction with DNA was studied via directly mixed complex formation. In general, it was shown to have A/T specificity similar to that found for poly(L-lysine) (41). Random copolymers of lysine and alanine have been studied by two groups: The one formed complexes by direct mixing of one copolymer with DNA (42, 43) whereas the other formed complexes by annealing a set of copolymers of different composition with DNA (44). In general, the results indicated that the behaviour of the polypeptide in solution influenced its complexation with DNA (44). However, direct attribution of this behaviour to the differences seen was not possible because changes in polypeptide composition accompanied the changes in solution behaviour. A similar problem arises with the interpretation of the results on the study of back-dialyzed complexes formed between DNA and the sequential polypeptides poly(L-lysyl-L-alanyl-glycine) (PL-Ala-Gly) and poly-(L-lysyl-L-alanyl-L-proline) (PL-Ala-Pro) (45). Differences in the solution behaviour of the two polypeptides were used to explain partially the differences in the resulting complexes, i.e., PL-Ala-Gly caused no changes in the DNA cd spectrum whereas PL-Ala-Pro resulted in the formation of the ψ-state DNA spectrum. As was noted, the insertion of a proline in place of the glycine could have altered the hydrophobic nature of the polymer and, thus, altered the mode of interaction. However, a recent report has confounded this interpretation since it was shown that a different preparation of PL-Ala-Gly was able to induce formation of the ψ-state in DNA (24). Either differences in the methods of polypeptide polymer preparation, which might result in more or less chain branching or, alternately, differences in polypeptide molecular weight could explain the results obtained by these two groups.

Acknowledgements

The authors wish to thank Mr. Alex E. Castagne for amino acid analyses, Mr. Lee Sowden for photographing the electron microscopic grids, Mr. Robert Whitehead for preparing photographs, and the drafting staff for preparing the figures.

1. A. J. HOPFINGER. Intermolecular interactions and biomolecular organization. J. Wiley and Sons, NY. 1977.
2. M. TSUBOI, K. MATSUO, and P. O. P. TS'O. J. Mol. Biol. **15**, 256 (1966).
3. M. LENG and G. FELSENFELD. Proc. Natl. Acad. Sci. U.S.A. **56**, 1325 (1966).
4. J. T. SHAPIRO, M. LENG, and G. FELSENFELD. Biochemistry, **8**, 3219 (1969).
5. S. INOUE and T. ANDO. Biochem. Biophys. Res. Commun. **32**, 501 (1968).
6. S. KAWASHIMA, S. INOUE, and T. ANDO. Biochem. Biophys. Acta, **186**, 145 (1969).
7. S. INOUE and T. ANDO. Biochemistry, **9**, 4410 (1970).
8. P. DE SANTIS and M. SAVINO. Biochim. Biophys. Acta, **272**, 518 (1972).
9. P. DE SANTIS, R. RIZZO, and M. SAVINO. Macromolecules, **6**, 520 (1973).
10. D. E. OLINS, A. L. OLINS, and P. H. VON HIPPEL. J. Mol. Biol. **24**, 157 (1967); **33**, 265 (1968).
11. T. Y. SHIH and J. BONNER. J. Mol. Biol. **48**, 469 (1970).
12. M. ZAMA and S. ICHIMURA. Biochem. Biophys. Res. Commun. **44**, 936 (1971).
13. M. ZAMA and S. ICHIMURA. Biochem. Biophys. Acta, **294**, 214 (1973).
14. C. CHANG, M. WEISKOPF, and H. J. LI. Biochemistry, **12**, 3028 (1973).
15. H. J. LI, B. BRAND, and A. ROTTER. Nucl. Acids Res. **1**, 257 (1974).
16. H. J. LI, C. CHANG, M. WEISKOPF, B. BRAND, and A. ROTTER. Biopolymers, **13**, 649 (1974).
17. H. J. LI, B. BRAND, A. ROTTER, C. CHANG, and M. WEISKOPF. Biopolymers, **13**, 1681 (1974).
18. H. J. LI, P. EPSTEIN, S. S. YU, and B. BRAND. Nucl. Acids Res. **1**, 1371 (1974).
19. M. WEISKOPF and H. J. LI. Biopolymers, **16**, 669 (1977).
20. D. CARROLL. Anal. Biochem. **44**, 496 (1971).
21. D. CARROLL. Biochemistry, **11**, 421 (1972).
22. R. MANDEL and G. D. FASMAN. Biochemistry, **15**, 3122 (1976).
23. E. ONG, C. SNELL, and G. D. FASMAN. Biochemistry, **15**, 468 (1976).
24. K. BLAHA, S. STOKROVA, B. SEDLACEK, and J. SPONAR. Coll. Czech. Chem. Commun. **41**, 2273 (1976).
25. R. E. WILLIAMS and S. L. KIELLAND Can. J. Chem. **53**, 542 (1975).
26. S. L. KIELLAND and R. E. WILLIAMS. Can. J. Chem. **54**, 3884 (1976).
27. L. A. SLOTIN, D. R. LAUREN, and R. E. WILLIAMS. Can. J. Chem. **55**, 4257 (1977).
28. J. BROWN, J. R. LANGLOIS, D. R. LAUREN, B. K.

STOOCHNOFF, and R. E. WILLIAMS. Can. J. Chem. **52**, 3140 (1974).
29. G. D. FASMAN, B. SCHAFFHAUSEN, L. GOLDSMITH, and A. ADLER. Biochemistry, **9**, 2814 (1970).
30. J. SPONAR and I. FRIC. Biopolymers, **11**, 2317 (1972).
31. C. F. JORDAN, L. S. LERMAN, and J. H. VENABLE, JR. Nature (London), (New Biol.), **236**, 67 (1972).
32. S.-M. CHENG and S. C. MOHR. Biopolymers, **14**, 663 (1975).
33. J. MARMUR and P. DOTY. J. Mol. Biol. **5**, 109 (1962).
34. J. MARMUR, R. ROWND, and C. L. SCHILDKRAUT. *In* Progress in nucleic acid research. Vol. 1. *Edited by* J. N. Davidson and W. E. Cohn. Academic Press, New York, NY. 1963. p. 231.
35. D. E. OLINS, A. L. OLINS, and P. H. VON HIPPEL. J. Mol. Biol. **24**, 157 (1967).
36. D. E. OLINS, A. L. OLINS, and P. VON HIPPEL. J. Mol. Biol. **33**, 265 (1968).
37. H. J. LI, B. BRAND, and A. ROTTER. Nucl. Acids Res. **1**, 257 (1974).
38. H. J. LI, C. CHANG, and M. WEISKOPF. Biochemistry, **12**, 1763 (1973).
39. M. LENG and G. FELSENFELD. Proc. Natl. Acad. Sci. U.S.A. **56**, 1325 (1966).
40. G. SPACH, A. BRACH, and F. HEITZ. C. R. Acad. Sci. **265**, 19 (1967).
41. J. P. PRIVAT, G. SPACH, and M. LENG. Eur. J. Biochem. **26**, 90 (1972).
42. M. F. PINKSTON and H. J. LI. Biochemistry, **13**, 5227 (1974).
43. M. F. PINKSTON, A. H. RITTER, and H. J. LI. Biochemistry, **15**, 1676 (1976).
44. S. STOKROVA, J. SPONAR, M. HAVRANEK, B. SEDLACEK, and K. BLAHA. Biopolymers, **14**, 1231 (1975).
45. A. M. SCHWARTZ and G. D. FASMAN. Biochemistry, **16**, 2287 (1977).

Can. J. Chem. Downloaded from www.nrcresearchpress.com by 210.87.254.42 on 09/05/12
For personal use only.

Water-soluble lysine-containing polypeptides. VI. A study of annealed complexes between calf thymus DNA and the following copolymers: poly-(L-lysyl-X), where X = Gly, L-Ala, L-Val, L-Leu, and L-Phe[1]

SANDRA L. KIELLAND, LEWIS A. SLOTIN,[2] AND ROSS E. WILLIAMS

Division of Biological Sciences, National Research Council of Canada, Ottawa, Ont., Canada K1A 0R6

Received May 5, 1978

SANDRA L. KIELLAND, LEWIS A. SLOTIN, and ROSS E. WILLIAMS. Can. J. Chem. **56**, 2657 (1978).

Turbidity measurements, circular dichroism spectra, electron micrographs, and thermal–optical measurements have been made on complexes between sonicated DNA and several polypeptides with the following structure: poly-(L-lysine-L-X) where X = Gly, Ala, Val, Leu, Phe. The results are influenced by any method of polypeptide synthesis which results in chain branching of the polypeptide. When polypeptides prepared by the same synthetic route are incorporated into the complexes the results also depend on the polypeptide used. Five possible explanations are offered as sources of the latter observations.

SANDRA L. KIELLAND, LEWIS A. SLOTIN et ROSS E. WILLIAMS. Can. J. Chem. **56**, 2657 (1978).

Nous avons pris des mesures de turbidité, des spectres du dichroisme circulaire, des micrographies éléctroniques ainsi que des spectres thermo-optiques de complexes entre l'ADN (traité aux ultra sons) et plusieurs polypeptides avec les structure suivantes: poly-(L-lysine-L-X) ou X = Gly, Ala, Val, Leu, Phe. Nous avons observé que les résultats sont influencés par la méthode de synthèse ainsi que le polypeptide incorporé dans les complexes. Nous avons donné cinq possibilités afin d'expliquer les résultats.

Introduction

Synthetic polypeptides, i.e. homopolymers and random or sequential copolymers, containing amino acids with positively-charged side chains have been used as models of biologically-significant basic proteins. The polypeptides have been prepared in order to simplify and investigate the effects of amino acid primary and secondary structure on protein – nucleic acid interaction (1–6).

The effect of polypeptide amino acid sequence, charged-group spacing, polymer conformation, and, to some extent, side chain size (or hydrophobicity) has been examined in a series of papers (7–9) which have dealt with the interaction between calf thymus DNA and several sequential polypeptides containing lysine. In the present paper a more extensive study of the effect of increasing the side chain size and, thus, hydrophobicity of the amino acid accompanying lysine will be undertaken. To this end a set of sequential dipeptide copolymers containing lysine and one other amino acid have been synthesized (10). The polypeptides are: poly-(L-lysylglycine)$_n$ (P-Lys-Gly), poly-(L-lysyl-L-alanine)$_n$ (P-LysAla), poly-(L-lysyl-L-valine)$_n$ (P-LysVal), poly-(L-lysyl-L-leucine)$_n$ (P-LysLeu), poly-(L-lysyl-L-phenylalanine)$_n$ (P-Lys-Phe).

The interaction between these polypeptides and a preparation of sonicated calf thymus DNA (the 40 s sonicate) has been studied by preparing complexes using an annealing system in which the components are brought together in a gradient of linearly decreasing salt concentration finally reaching the so-called physiological conditions, i.e. 0.15 *M* NaCl, pH 7. Increases in solution turbidity at 400 nm, as well as the formation of a large negative band at 275 nm in the circular dichroism spectrum have been monitored as a function of the lysine/DNA phosphate (L/P) ratio. The changes in the circular dichroism (cd) spectrum have previously been shown to be connected with the formation of an organized and aggregated state of DNA (the so-called ψ state) (11–14). In addition to the spectroscopic studies, the size and shape of complexes made visible in the electron microscope by fixing and staining have been examined. The effect of the polymers on the thermally-induced transition of DNA from its double stranded state to its single stranded state was also examined.

Studies of the interaction of poly-(L-lysine), a sample of P-LysGly prepared via a dipeptide intermediate and P-LysAla have been previously reported (7). The results of these studies are used here only to put the studies on the remaining polymers into context.

Methods and Materials

Chemicals used to prepare buffers were commercially available reagent grade and used as received. Water used was deionized and distilled from glass.

[1]NRCC 16821.

[2]NRCC Research Associate, 1975–1977. Present address: Ministry of State for Science and Technology, 270 Albert Street, Ottawa, Ont., Canada K1P 5G8.

Can. J. Chem. Downloaded from www.nrcresearchpress.com by 210.87.254.5 on 09/05/12
For personal use only.

Can. J. Chem. Downloaded from www.nrcresearchpress.com by 210.87.254.5 on 09/05/12
For personal use only.

Specific experimental details have been previously published for: (*1*) the preparation, purification, sonication, and concentration assays of calf thymus DNA (15); (*2*) the preparation, characterization, and concentration assay of the poly-(L-lysine) sample (10^4 molecular weight (15)); (*3*) the preparation, characterization, and concentration assay of a P-LysGly sample prepared by dipeptide polymerization (15); (*4*) the preparation, characterization, and concentration assay of the other polymers (10); (*5*) the preparation of annealed complexes containing the polypeptide and the 40 s sonicate of calf thymus DNA (9).

Instruments used to measure and methods of expressing the results of ultraviolet spectra, solution turbidity, and circular dichroism spectra have been described previously (8, 9). Instrumentation and techniques of preparing grids for electron microscopy have been reported previously (8). Details of the thermal melting experiments and methods of expressing the results have also been reported (7).

Reductive alkylations of the lysine polymers were done using conditions previously outlined (16). The polymers (1–2 mg) were dissolved in an ice cold solution (1.0 ml) of borate buffer (0.2 *M*, pH 9.0) containing sodium borohydride (0.5 mg/ml). Aliquots (5 × 5 μl) of a concentrated solution of formaldehyde (37% v/v) were added. The solution was stirred for 30 min and evaporated to dryness. The residue was dissolved in borate–borohydride and treated with formaldehyde as before. After evaporation the residue was hydrolyzed for 24 h at 110°C in 6 *N* HCl (3 ml). The residue, after evaporation, was dissolved in citric acid buffer (0.3 *M*, pH 2.8) and an aliquot analyzed as previously described (17) on a Beckman amino acid analyzer 120C equipped with a short column (0.9 × 10 cm) (PA-35 resin). Elution was with 0.35 *N* sodium citrate buffer, pH 5.2 at 28°C and a flow rate of 50 ml/h.

Results

A. Solution Turbidity

It has previously been shown that, as the lysine – DNA phosphate (L/P) ratio increases in poly-L-Lysine/DNA complexes prepared by back dialysis to physiologically-related conditions, the turbidity of the solution increased and reached a plateau at an L/P ratio of about 0.6 (8) (Fig. 1). Complexes containing DNA and the sequential dipeptide polymers showed no tendency of forming a plateau of solution turbidity at L/P ratios less than 2 (Fig. 1). Turbidity increases were observed, as previously reported (7, 8), for P-LysGly and P-LysAla while no increases in turbidity were observed for P-LysVal, P-LysLeu, and P-LysPhe up to L/P ratios less than 3. In addition to the P-LysGly sample, prepared via a dipeptide intermediate (15), a sample of P-LysGly, prepared via a tetrapeptide intermediate (10), was used to prepare complexes. It was observed that larger L/P ratios were required to produce turbidity equivalent to that produced by the sample of P-LysGly prepared by a dipeptide polymerization. This difference in behaviour was reflected in both the cd studies and in the thermal melting profiles (see below). Dialysis of all the complexes against 10^{-3} *M* ethylenediaminetetra acetic acid (EDTA) resulted in little change in the observed results except that complexes of DNA and P-LysLeu and P-LysPhe developed turbidity under these conditions (dA^{400} approx. 0.1 at an L/P ratio = 2).

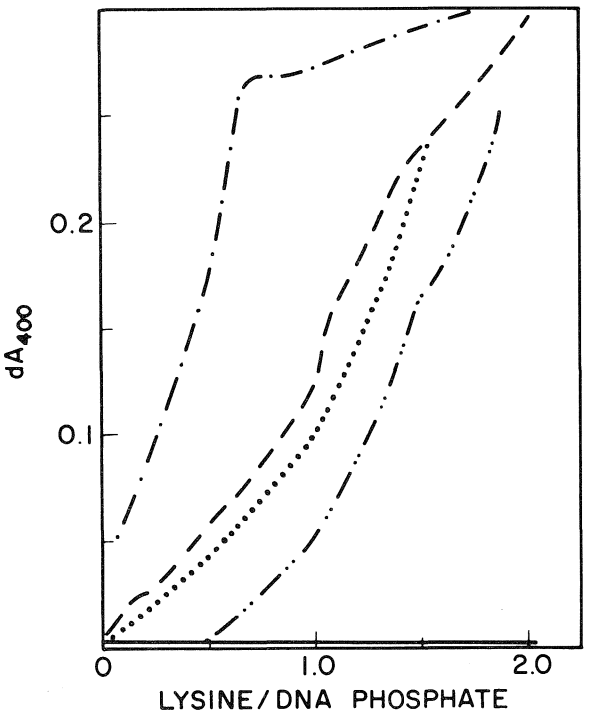

FIG. 1. Variation of solution turbidity (dA^{400}) with lysine/DNA-phosphate ratios in complexes between calf thymus DNA and the following polypeptides: poly-(L-lysine), ·-·-·; poly-(L-lysyl glycine) (via a dipeptide intermediate), ---; poly-(L-lysyl glycine) (via a tetrapeptide intermediate), ·-·-·-·-·; poly-(L-lysyl-L-alanine) · · ·; poly-(L-lysyl-L-X), where X = val, leu, phe, —. Experimental conditions: DNA phosphate concentration, 1.8 ± 0.2 × 10^{-4} *M*; sodium chloride, 0.15 *M*; sodium cacodylate 0.001 *M*, pH 7.0.

B. Circular Dichroism Spectra

Upon forming complexes of poly-L-lysine (P-Lys) and calf thymus DNA by back dialysis to physiologically related conditions the B-structure circular dichroism spectrum of DNA changes into one characteristic of the ψ-state (aggregated state) of DNA (11–14). The spectrum is characterized by the presence of an intense negative band between 260 and 280 nm. Measurement of the ellipticity at 275 nm as a function of the changing L/P ratio shows that a maximum is reached around an L/P ratio of 0.6 (Fig. 2) (8, 9). Two samples of P-LysGly were compared for their ability to produce the ψ-state in DNA. One sample was prepared via a dipeptide intermediate (15), the other via a tetrapeptide intermediate (10). Both samples produced spectra charac-

Can. J. Chem. Downloaded from www.nrcresearchpress.com by 210.87.254.5 on 09/05/12
For personal use only.

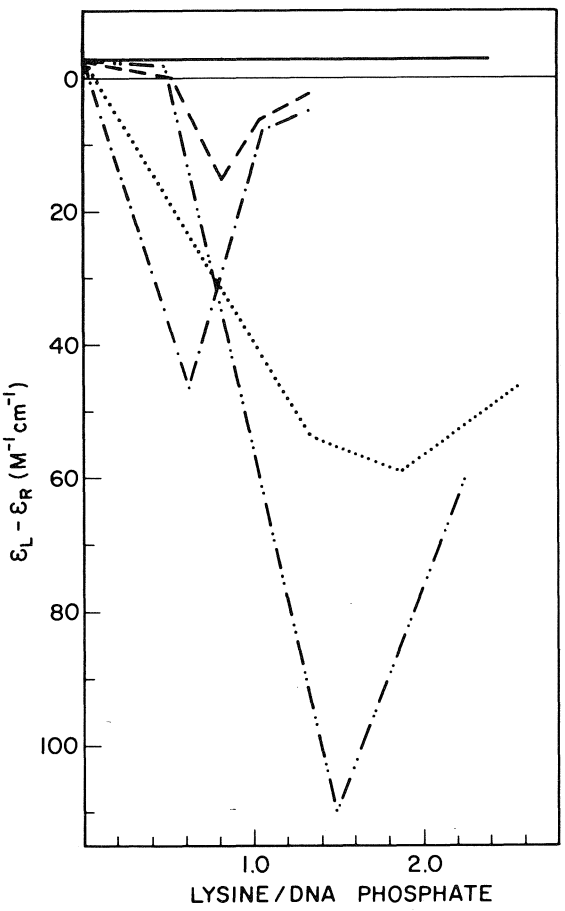

FIG. 2. Variation of the molar ellipticity ($\varepsilon_l - \varepsilon_r$) observed at 275 nm in the circular dichroism spectrum with lysine–DNA phosphate ratios in complexes between sonicated calf thymus DNA and the following polypeptides: poly-(L-lysine), ·····; poly-(L-lysyl glycine) (prepared via a dipeptide intermediate), ---; poly-(L-lysyl glycine) prepared via a tetrapeptide intermediate), ·-·-·-·-·; (poly-(L-lysyl-L-alanine), ···; poly-(L-lysyl-L-X), where X = val, leu, phe, —. Experimental conditions: as given for Fig. 1.

teristic of ψ-state DNA. The results of using the polymer prepared via the dipeptide route have been reported previously (8, 9). Maximum ellipticity was reached at an L/P ratio of about 1.0 and was considerably less than that observed with several other lysine–glycine polymers (8, 9). The polymer produced via the tetrapeptide intermediate promoted maximum ψ-state formation at an L/P ratio of about 1.2. Besides peaking at an L/P ratio of about 1.2 the ellipticity generated at the maximum was considerably greater than that developed by the other P-LysGly sample and more in line with that produced by the set of lysine–glycine polymers studied previously (8, 9). The sample differences were unrelated

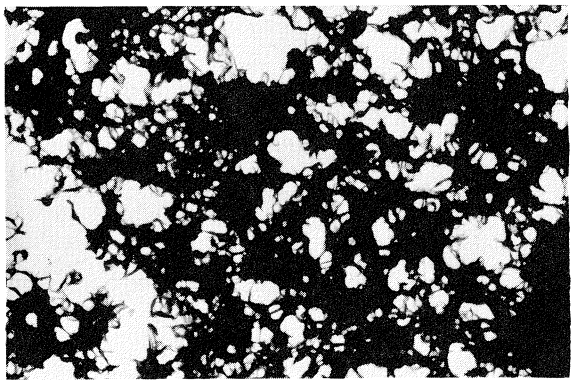

FIG. 3. Electron micrograph of formaldehyde-fixed, dehydrated, and stained complexes of sonicated calf thymus DNA and poly-(L-lysyl-L-leucine) (L/P ratio = 2.8). Complexes used for preparing the micrograph were taken from solutions which had been dialyzed against 10^{-3} *M* EDTA.

to the use of sonicated or unsonicated DNA.[3] The maximum ellipticity generated by the P-LysGly, produced by the tetrapeptide route, was much larger than that produced by complexing P-LysAla with DNA (Fig. 2). This would suggest that DNA in the P-LysGly complexes was more highly ordered. The remaining polypeptides, P-LysVal, P-LysLeu, and P-LysPhe, showed no tendency to promote ψ-state formation, since only minor changes in the cd spectrum were observed up to an L/P ratio of 2 (Fig. 2). Dialyzing the complexes into 10^{-3} *M* EDTA resulted in a loss of ellipticity at the maximum L/P ratios but still left a substantial amount of ψ-state as judged from the cd spectra of P-Lys, P-LysGly, and P-LysAla complexes. Of the remaining polypeptides only P-LysLeu and P-LysPhe exhibited a weak tendency towards ψ-state formation ($\varepsilon_l - \varepsilon_r$ (275 nm) = −10 to −15, at L/P ratios of approximately 2.5).

C. Electron Micrographs

Aggregates of uranyl acetate-stainable material are observed when complexes, which have been back dialyzed to physiological conditions, are formaldehyde fixed and examined in the electron microscope (8). The electron micrographs of complexes of P-Lys and sonicated calf thymus DNA are clustered circles about 6000 Å in diameter (8). Similar electron micrographs are obtained with complexes containing P-

[3]Comparison of the maximum ellipticity generated by the two PL–Gly samples gave the following results: dipeptide route polymer: unsonicated DNA, $\Delta\varepsilon = -3$ (L/P 1.5); sonicated DNA, $\Delta\varepsilon = -16$ (L/P 1.5). Tetrapeptide route polymer: unsonicated DNA, $\Delta\varepsilon = -17$ (L/P 1.5); sonicated DNA $\Delta\varepsilon = -130$ (L/P 1.5).

Can. J. Chem. Downloaded from www.nrcresearchpress.com by 210.87.254.5 on 09/05/12
For personal use only.

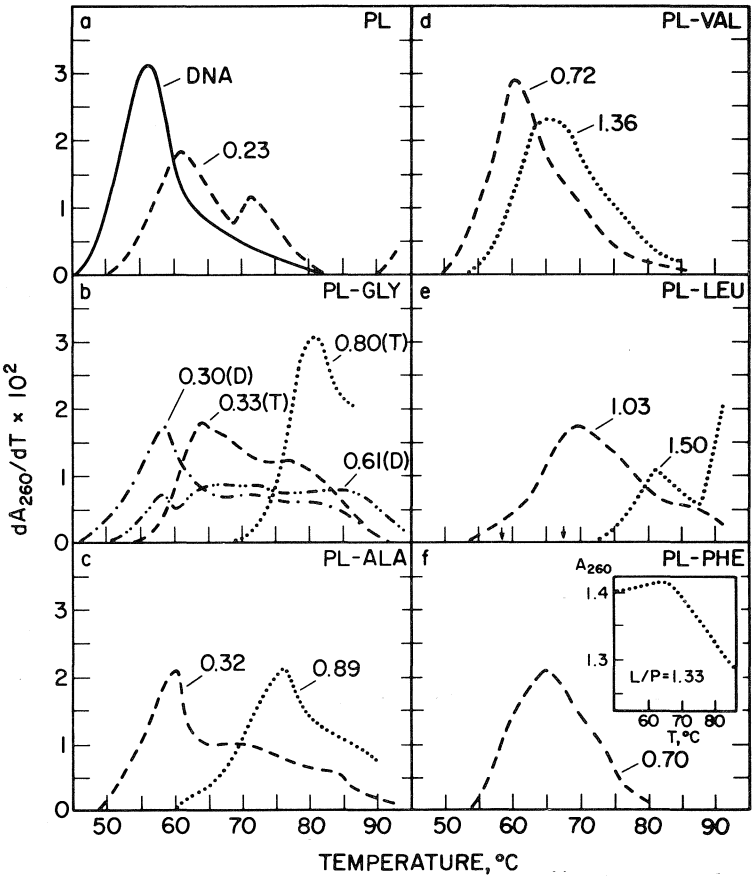

FIG. 4. Derivative absorption melting profiles (dA_{260}/dT vs. T) of purified, sonicated DNA (—) complexed with the following polypeptides (the numbers given in parentheses and on the figure are L/P ratios): (*a*) poly-(L-lysine) (0.23) ---; (*b*) poly-(L-lysyl glycine) (prepared via a dipeptide (D) intermediate) (0.30) -·-·-·-; (0.61) -·-·-·-; and poly-(L-lysyl glycine) (prepared via a tetrapeptide (T) intermediate) (0.33) ---; (0.80) · · ·; (*c*) poly-(L-lysyl-L-alanine) (0.32) ---; (0.89) · · ·; (*d*) poly-(L-lysyl-L-valine) (0.72) ---; (1.36) · · ·; (*e*) poly-(L-lysyl-L-leucine) (1.03) ---; (1.50) · · ·; (*f*) poly-(L-lysyl-L-phenylalanine) (0.70) ---; (inset) absorption (260 nm) vs. temperature (T) measurements. Experimental conditions: sodium EDTA, 10^{-3} M, pH 7.0. DNA phosphate concentrations (1.8 ± 0.2) × 10^{-4} M.

LysGly[4] and P-LysAla although there was less tendency to clustering of the circles (7, 8). No detectable aggregates were present in the electron micrographs of the complexes containing the remaining polymers even when L/P ratios were increased to between 3 and 4. Dialysis of the complexes against 10^{-3} M EDTA resulted in electron micrographs which were unchanged for complexes of P-Lys, P-LysGly, and P-LysAla. Only complexes of DNA and P-LysLeu and P-LysPhe resulted in observable aggregates. They were, in both cases, large and amorphous (for example, see Fig. 3).

[4]There were no observable differences between electron micrographs of complexes of the P-LysGly sample prepared by the tetrapeptide route and the P-LysGly sample prepared by the dipeptide route.

D. Thermal Melting Experiments

The thermal-optical transition of double-stranded DNA to single stranded DNA has been widely used as a method for investigating the interaction of cationic polypeptides with DNA. Studies have been reported on the interaction of step-wise dialyzed complexes of DNA with P-Lys and oligolysine (2, 18). In the present case, the sonicated DNA used to form complexes was dialyzed to physiological-like conditions and then to 10^{-3} M EDTA, pH 7.0. The derivative melting profile of the DNA is given in Fig. 4*a*. As may be noted there is a transition at 56 ± 2°C and it is asymmetric. The asymmetry has been attributed to the presence of G/C- and A/T-rich regions in the DNA (2, 19, 20). The low L/P ratio complex of P-Lys and the sonicated DNA

Can. J. Chem. Downloaded from www.nrcresearchpress.com by 210.87.254.5 on 09/05/12
For personal use only.

had the melting profile in Fig. 4*a*. The profile is biphasic. A substantial fraction of the melting material under the DNA peak has been lost and replaced by two peaks: one, melting at 61°C and the other, melting at 71°C. Complexes containing DNA and P-Lys at higher L/P ratios (i.e. >0.5) had too much light scatter to allow measurements to be made.

Complexes of DNA and P-LysGly, prepared by the dipeptide route, at low L/P ratios had the melting profile given in Fig. 4*b*. The melting profile of low L/P ratio complexes of DNA and P-LysGly, prepared by the dipeptide route, had a peak at 58°C and a broad melting zone between 65 and 85°C. At higher L/P ratios the melting profile became very broad although a peak of material melting at 58°C was still observable.

The melting profile of complexes of DNA and P-LysGly, prepared by the tetrapeptide route, was very similar to that of complexes containing DNA and P-Lys but was shifted to higher temperatures. It was a biphasic melting profile with peaks at 63°C and 77°C (L/P ratio = 0.33). At higher L/P ratios the melting profile had one broad transition at 81°C. It is obvious that the differences between the two P-LysGly preparations which were observed in the turbidity and cd of their complexes with DNA are also reflected in the thermal melting profiles.

Complexes of DNA and P-LysAla at low L/P ratios (L/P ratio = 0.33) had the melting profile given in Fig. 4*c*. The profile had peaks at 60, 70, and 83°C. The lower two peaks occurred at the same temperature as the two peaks seen in DNA/P-Lys complexes. An increase in the L/P ratio resulted in complete loss of material melting at 61°C and the formation of transitions at 77 and 85°C.

Complexes of DNA and P-LysVal at low L/P ratios (i.e. <0.5) had melting profiles which were unchanged from that of DNA (Fig. 4*d*). Only higher L/P ratios caused a shift in the melting profile to occur. At an L/P ratio of 0.7 the melting profile was shifted to higher temperatures and was unchanged in shape or intensity. Raising the L/P ratio still further caused only a small shift in the position of the profile and some broadening.

Complexes of DNA and P-LysLeu had the melting profiles shown in Fig. 4*e*. At low L/P ratios (<0.5) little change in the DNA profile was noted. At an L/P ratio of 1.0 the profile was characterized by a broad melting region centered at 70°C and a small band at 85°C. Increasing the L/P ratio resulted in some solution turbidity which affected measurements in the region between 55 and 70°C (marked by arrows). At higher temperatures a peak at 81°C appeared along with a substantial fraction of material melting at temperatures greater than 90°C.

Complexes of DNA and P-LysPhe had melting profiles shown in Fig. 4*f*. At low L/P ratios (<0.5) the melting profile of DNA was unchanged. At an L/P ratio of 0.7 the melting profile had a broad band centered at 65°C with a slight shoulder at 73°C. Increasing the L/P ratio resulted in light scatter and the thermal optical profile shown (Fig. 4*f*, inset). The observed decrease in absorption could be connected with the loss of light scatter upon melting of the complexes.

From the above results it may be concluded that: (*1*) P-Lys, P-LysGly, and P-LysAla behaved similarly since observable changes occurred in their melting profiles at L/P ratios less than 0.5 (i.e. one amino acid residue per phosphate group). The remaining polymers were effective at changing the melting profile only at L/P ratios above 0.5; (*2*) the melting profiles of P-Lys and P-LysAla were very similar since there seemed to be a small fraction of DNA melting at 60°C which remained uncomplexed; (*3*) the profiles of complexes of DNA and P-LysGly (both samples), P-LysVal, P-LysLeu, and P-LysPhe maintained their general shape and shifted up as the L/P ratio increased.

Discussion

The spectroscopic, electron microscopic (em), and thermal–optical examination of annealed complexes of DNA and the lysine-containing dipeptide copolymers have shown that the observations can be influenced by many different factors. The results can be influenced by the method of polypeptide preparation, i.e. the lysylglycine copolymer results, and the size or type of the aliphatic side chain in the dipeptide copolymers.

A. Synthesis-related Effects

Two samples of P-LysGly, prepared via different routes, were examined for their ability to produce solution turbidity, to induce a ψ-state cd spectrum, to produce observable complexes in the em and to change the melting profile of DNA. Although no differences between the two samples were seen in the e.m., differences were noted in the remaining studies. The differences remained whether sonicated or unsonicated DNA was used.[3] The differences seemed unrelated to molecular weight since the thin-layer gel filtration profiles of the two polymers were the same. In addition, side chain blocking group removal was complete in both polymers and, thus, would be an unlikely cause of the observations.

It is conceivable, however, that the two polymers

Can. J. Chem. Downloaded from www.nrcresearchpress.com by 210.87.254.5 on 09/05/12
For personal use only.

have different amounts of chain branching as a result of ε amino group deblocking during polymer preparation. Therefore, an attempt was made to check for chain branching in each of the polymers. In the absence of chain branching complete reductive alkylation of the ε amino groups of lysine in the polymers by formaldehyde–borohydride treatment would result in no residual lysine being observed after hydrolysis of the polymers. In the presence of chain branching the presence of blocked or masked ε amino groups of lysine at the branch points would result in a residual lysine concentration being observed even after complete reductive alkylation and hydrolysis. Using a procedure which resulted in a residual lysine concentration of 6 ± 2% (i.e. loss of 94% of the lysine) in the P-Lys sample, which had been prepared via *N*-carboxyanhydride polymerization (15), it was found that reductive alkylation and hydrolysis resulted in 3 ± 2% residual lysine in the polymer prepared via the dipeptide route and 7 ± 2% residual lysine in the polymer prepared via the tetrapeptide route (Table 1). This result seems to indicate that different amounts of chain branching are present in the polymers and could be playing an important role in determining the outcome of the experiments.

Residual lysine concentrations in the remaining polymers were also determined (Table 1). As can be seen the remaining polymers had amounts of residual lysine ranging from 10 to 21%. Factors, other than the amount of chain branching are likely to be the cause of not only the amount of the residual lysine but also the variation amongst the polymers. This is best illustrated by the results obtained with P-Lys-L-Ala (Table 1) and P-Lys-D-Ala (results given in parentheses, Table 1). P-Lys-L-Ala had 11% residual lysine whereas P-Lys-D-Ala had 6% residual lysine. Since both polymers had been prepared by the same route, factors other than the method of synthesis are the likely source of the difference. The conformations of the two polymers are likely to be different at the pH used for the treatment since it was found these polymers respond differently to changes in pH (10). The P-Lys-L-Ala polymer would be expected to have a substantial fraction of α-helical structure in it at pH 9. This might block Schiff base formation, inhibit side-chain reduction by the borohydride or promote aggregation of the polypeptide in solution. The results obtained with the other polymers having the larger aliphatic side chains could be the result of a combination of one or more of these factors.

TABLE 1. Residual lysine concentrations observed after reductive alkylation and hydrolysis of the lysine

Sample	Lysine remaining (%) after treatment and hydrolysis[a] (errors given are standard deviations)
P-Lys	6±2
P-LysGly[b]	3±2
P-LysGly[c]	7±2
P-LysAla[c]	11±3 (6±2)[d]
P-LysVal[c]	21±5
P-LysLeu[c]	12±4
P-LysPhe[c]	10±3

[a]Residual lysine concentrations were determined on three samples by formaldehyde–borohydride reductive alkylation, subsequent hydrolysis in 6 *N* HCl and analysis as described in the experimental section. Lysine remaining (%) is defined as $L_r/L_t \times 100$, where L_r is the number of moles of lysine found after treatment and hydrolysis and L_t is total number of moles of lysine in the untreated and hydrolyzed sample.
[b]Prepared via a dipeptide intermediate (15).
[c]Prepared via a tetrapeptide intermediate (10).
[d]P-Lys-D-Ala sample prepared via a tetrapeptide intermediate (10).

It thus appears that an exact measurement of residual lysine content, and, thereby, chain branching, is only possible if the polymer can adopt a truly random conformation in solution and is known to be in an unaggregated state.

B. Side-chain-related Effects

The sequential lysine-containing dipeptide polymers studied here may be divided into two groups: those that promote DNA ψ-state formation (cd experiments) and cause changes in the DNA thermal melting profile at low L/P ratios (<0.5) and those that do not. P-Lys, P-LysGly, and P-LysAla are grouped in the first category whereas P-LysVal, P-LysLeu, and P-LysPhe are grouped in the second.

Several simplistic correlations may be drawn between these two categories and the properties of the polypeptides. It can be suggested that the division is related to:

(*1*) The aggregation of the polypeptides with large, hydrophobic side chains, either in solution before complex formation or on the surface of the DNA after complex formation. The net result of polypeptide aggregation would be an inability to promote the aggregation of the DNA. Aggregation of the polypeptides in solution before complex formation was checked previously. Although thin-layer gel filtration (TLGF) experiments at different salt concentrations suggested that aggregation of P-LysVal, P-LysLeu, and P-LysPhe did not seem to be occurring (10) the reductive alkylation results might suggest otherwise (Table 1).

(*2*) The difference in molecular weights of the various polymer preparations. It would have to be suggested that the lower molecular weight polymers (as assessed by TLGF), i.e. P-LysVal, P-LysLeu, and P-LysPhe, interact with DNA but are of insufficient size to promote ψ-state formation or cause changes in the thermal melting profiles. Indeed, it was observed that the lower molecular weight polymers,

Can. J. Chem. Downloaded from www.nrcresearchpress.com by 210.87.254.5 on 09/05/12
For personal use only.

while they do interact with DNA and promote changes in the thermal melting profiles at higher L/P ratios, caused a shift in the thermal melting profiles similar to that observed with small molecular weight oligolysines, and protamine (18).

(*3*) The size of the aliphatic side chain of the amino acid being varied. It could be suggested that the larger side chain amino acids are prevented from associating with the DNA so as to promote ψ-state formation and changes in the thermal melting profiles. This proposal would require that side chains smaller than valine would be able to effectively promote ψ-state formation and cause changes in the thermal melting profile of DNA. If this factor were the sole determinant then it might be suggested that regions in cationic proteins devoid of large side chain amino acids could readily induce DNA packing much in the same way as that in ψ-state DNA. An example of such a region in a cationic protein is the N-terminal sequence of histone H-4 (21).

(*4*) The different conformational states that can be adopted by each of the polypeptides in solution. Each polypeptide has been found to adopt different conformations depending on the state of charge on the lysine side chain (10). The results are summarized in Table 2. It would appear that no correlation exists between polypeptide conformation and the ability to promote ψ-state formation or, at low L/P ratios, induce changes in the thermal melting profile of DNA when the lysine side chain is charged. When the lysine side chain is uncharged, however, the polypeptides may be grouped into two categories: those that form β-like structures and those that do not. The polypeptides which form β-like structures, i.e. P-LysVal, P-LysLeu, and P-LysPhe, are also those which are unable to promote ψ-state formation and induce changes in the thermal melting profile of DNA at low L/P ratios. It might also be noted that, within the remaining group, P-Lys and P-LysAla cause very similar biphasic changes in the thermal melting profile of DNA and that they both adopt an α-helical conformation when uncharged. From the data gathered in these experiments and the difficulty in separating the DNA cd spectrum from the polypeptide cd spectrum in the complexes it is not possible to tell what conformation the polypeptides adopt in the complex. Thus, it is also not possible to determine if such a correlation is reflected in the polypeptide–DNA complex where it might be expected that the lysine side chains would be neutralized by the DNA phosphate groups.

(*5*) The above noted effects of different amounts of polypeptide chain branching. The results obtained upon reductive alkylation of the P-LysGly sample and the P-Lys-D-Ala sample suggest that the majority of the polypeptides prepared via a tetrapeptide intermediate will have approximately the same amount of chain branching (Table 1) and, thus it would seem that chain branching effects would not contribute appreciably to differences observed among the polypeptides. Our inability to accurately measure the amount of chain branching in all polypeptides, however, leaves this possibility still open.

TABLE 2. Solution conformations adopted by the various dipeptide polymers

Polymer	Solution conformation adopted[a] when side-chain state[b] = Charged[c]	Neutral[d]
P-Lys	Random[e]	α-Helix
P-LysGly	Random	Random
P-LysAla	Random	α-Helix
P-LysVal	Random	β
P-LysLeu	Random	β[f]
P-LysPhe	Random	β

[a]Assignments based on polypeptide cd spectrum under different experimental conditions (10).
[b]Refers to lysine ε amino group.
[c]Data obtained at pH 7, 0.14 *M* NaF.
[d]Data obtained at pH 12, 0.14 *M* NaF.
[e]Also called disordered or extended (22–24), or a 3, helix (25).
[f]Assignment has recently been corroborated (26).

The present studies have implied that one or more of the several factors mentioned above may be important in determining how polypeptides and proteins interact with DNA. Other workers, dealing with back-dialyzed complexes between DNA and both random and sequential (tripeptide) lysine-containing copolymers, have usually used one or two of them in attempts to explain their results (27–33). It is now evident that before the full and separate importance of each of the critical factors involved can be ascertained in a quantitative sense a very much more strict control of the experimental variables will be necessary. Indeed, the control must be much more strict than has, at present, been achieved either in the present set of experiments or those reported elsewhere.

Acknowledgements

The authors wish to thank Mr. Alex E. Castagne for amino acid analyses, Mr. Lee Sowden for photographing the electron microscopic grids, Mr. Robert Whitehead for preparing the photograph, and the drafting staff for preparing the figures.

1. A. J. HOPFINGER. Intermolecular interactions and biomolecular organization. J. Wiley and Sons, New York. 1977.
2. D. E. OLINS, A. L. OLINS, and P. H. VON HIPPEL. J. Mol. Biol. **24**, 157 (1967).
3. M. TSUBOI. *In* Conformation of biopolymers. Vol. 2. *Edited by* G. N. Ramachandran. Academic Press, New York. 1967. p. 689.

4. K. WEHLING, H. A. ARFMANN, K.-H. C. STANDKE, and K. G. WAGNER. Nucleic Acids Res. **2**, 799 (1975).
5. P. H. VON HIPPEL and J. D. MCGHEE. Ann. Rev. Biochem. **41**, 231 (1973) and references therein.
6. K. G. WAGNER and H. A. ARFMANN. Eur. J. Biochem. **46**, 27 (1974) and references therein.
7. S. L. KIELLAND, L. A. SLOTIN, and R. E. WILLIAMS. Can. J. Chem. This issue.
8. S. L. KIELLAND and R. E. WILLIAMS. Can. J. Chem. **54**, 3884 (1976).
9. R. E. WILLIAMS and S. L. KIELLAND. Can. J. Chem. **53**, 542 (1975).
10. L. A. SLOTIN, D. R. LAUREN, and R. E. WILLIAMS. Can. J. Chem. **55**, 4257 (1977).
11. G. D. FASMAN, B. SCHAFFHAUSEN, L. GOLDSMITH, and A. ADLER. Biochemistry, **9**, 2814 (1970).
12. J. SPONAR and I. FRIC. Biopolymers, **11**, 2317 (1972).
13. C. F. JORDAN, L. S. LERMAN, and J. H. VENABLE, JR. Nature (New Biol.), **236**, 67 (1972).
14. S.-M. CHENG and S. C. MOHR. Biopolymers, **14**, 663 (1975).
15. J. BROWN, J. R. LANGLOIS, D. R. LAUREN, B. R. SLOOCHNOFF, and R. E. WILLIAMS. Can. J. Chem. **52**, 3140 (1974).
16. G. E. MEANS and R. E. FEENEY. Biochemistry, **7**, 2192 (1968).
17. W. K. PAIK and S. KIM. Biochem. Biophys. Res. Commun. **27**, 479 (1967).
18. D. E. OLINS, A. L. OLINS, and P. H. VON HIPPEL. J. Mol. Biol. **33**, 265 (1968).
19. H. J. LI, B. BRAND, and A. ROLLER. Nucleic Acids, **1**, 257 (1974).
20. H. J. LI, C. CHANG, and M. WEISKOPF. Biochemistry, **12**, 1763 (1973).
21. S. C. R. ELGIN and H. WEINTRAUB. Ann. Rev. Biochem. **44**, 725 (1975).
22. D. G. DEARBORN and D. B. WETLAUFER. Biochem. Biophys. Res. Commun. **39**, 314 (1970).
23. M. L. TIFFANY and S. KRIMM. Biopolymers, **6**, 1379 (1968).
24. M. L. TIFFANY and S. KRIMM. Biopolymers, **8**, 347 (1969).
25. W. B. RIPPON and R. LAM. Int. J. Poly. Mater. **4**, 25 (1975).
26. S. BRAHMS, J. BRAHMS, G. SPACH, and A. BRACK. Proc. Natl. Acad. Sci. **74**, 3208 (1977).
27. S. STOKROVA, J. SPONAR, M. HAVRANEK, B. SEDLACEK, and K. BLAHA. Biopolymers, **14**, 1231 (1975).
28. R. MANDEL and G. D. FASMAN. Biochemistry, **15**, 3122 (1976).
29. R. MANDEL and G. D. FASMAN. Biopolymers, **14**, 1633 (1975).
30. E. G. ONG, C. SNELL, and G. D. FASMAN. Biochemistry, **15**, 468 (1976).
31. E. C. ONG and G. D. FASMAN. Biochemistry, **15**, 477 (1976).
32. A. M. SCHWARTZ and G. D. FASMAN. Biochemistry, **16**, 2287 (1977).
33. K. BLAHA, S. STOKROVA, B. SEDLACEK, and J. SPONAR. Coll. Czech. Chem. Commun. **41**, 2273 (1976).

Can. J. Chem. Downloaded from www.nrcresearchpress.com by 210.87.254.5 on 09/05/12
For personal use only.

Sterically hindered aromatic compounds. VIII. Comparative photochemistry of 2,4,6-tri-*tert*-butyl- and 2,5-di-*tert*-butylnitrosobenzenes

L. Ross C. Barclay, Derek Leigh Carson, Jean A. Gray, Michael Grossman, Prabhaker G. Khazanie, John R. Milton, and Christopher E. Scott

Department of Chemistry, Mount Allison University, Sackville, N.B., Canada E0A 3C0

Received February 2, 1978

L. Ross C. Barclay, Derek Leigh Carson, Jean A. Gray, Michael Grossman, Prabhaker G. Khazanie, John R. Milton, and Christopher E. Scott. Can. J. Chem. **56**, 2665 (1978).

Ultraviolet irradiation of hydrocarbon solutions of 2,4,6-tri-*tert*-butylnitrosobenzene (**1**) formed Ar—N̈—OH. The initial products were 2-methyl-1-nitroso-2-(3,5-di-*tert*-butyl)-phenylpropane (Ar—$C(CH_3)_2CH_2NO)_2$ (**3**) and a mixed dimer (**4**). Secondary and minor photoproducts isolated included 2-methyl-2-(3,5-di-*tert*-butyl)phenylpropanal oxime (**5**), 2-methyl-2-(3,5-di-*tert*-butyl)phenylpropanal (**6**) derived from **5**, and 1,3,5-tri-*tert*-butylbenzene (**7**). The initial products are explained by formation of a tri-*tert*-butylphenyl radical (**15**), rearrangement of a hydrogen atom from an *ortho tert*-butyl to the ring in **15**, and rapid recombination of the neophyl radical with nitric oxide. Photolysis of 2,5-di-*tert*-butylnitrosobenzene (**2**) initially gave Ar_2N—Ȯ (**10**). Product analysis indicated a comparatively complex mixture including 1,4-di-*tert*-butylbenzene (**11**), 2,5-di-*tert*-butylphenol (**12**), and 2,5-di-*tert*-butylanilino-*p*-(2,5-di-*tert*-butyl)quinone (**13**). Evidence indicates that **12** and **13** form from free radical reactions involving **10** and the 2,5-di-*tert*-butylphenyl radical. The different photochemistry of **1** and **2** is discussed in terms of differential steric and conformational effects on the nitroso function which also is evident in their ultraviolet spectra.

L. Ross C. Barclay, Derek Leigh Carson, Jean A. Gray, Michael Grossman, Prabhaker G. Khazanie, John R. Milton et Christopher E. Scott. Can. J. Chem. **56**, 2665 (1978).

L'irradiation ultraviolette de solutions dans les hydrocarbures du tri-*tert*-butyl-2,4,6 nitrosobenzène (**1**) conduit à la formation de Ar-N̈-OH. Les produits initiaux sont le méthyl-2-nitroso-1 (di-*tert*-butyl-3,5)-2-phénylpropane (Ar—$C(CH_3)_2CH_2NO)_2$ (**3**) et un dimère mixte (**4**). Les photoproduits secondaires et mineurs isolés comprennent l'oxime du méthyl-2 (di-*tert*-butyl-3,5)-2-phénylpropanal (**5**), le méthyl-2 (di-*tert*-butyl-3,5)-2 phénylpropanal (**6**) provenant de **5** et le tri-*tert*-butyl-1,3,5 benzène (**7**). On explique la formation des produits initiaux par la formation d'un radical tri-*tert*-butylphényle (**15**), qui subit une transposition d'un atome d'hydrogène d'un groupe *tert*-butyle *ortho* vers le cycle dans **15** et une recombinaison rapide du radical néophyle avec l'oxyde nitrique. La photolyse du di-*tert*-butyl-2,5 nitrosobenzène (**2**) conduit initialement à Ar_2N—Ȯ (**10**). L'analyse des produits indique la présence d'un mélange relativement complexe comprenant du di-*tert*-butyl-1,4 benzène (**11**), du di-*tert*-butyl-2,5 phénol (**12**) et de la di-*tert*-butylanilino-2,5 *p*-(di-*tert*-butyl-2,5)quinone (**13**). Les données indiquent que **12** et **13** sont formés à partir de réactions radicalaires impliquant **10** et le radical di-*tert*-butyl-2,5 phényle. On discute de la photochimie différence de **1** et de **2** en termes d'effets stériques différentiels et conformationnels sur la fonction nitroso qui est aussi évidentes dans le spectre ultraviolet.

[Traduit par le journal]

Introduction

The photochemistry of aryl nitroso compounds has not been studied as extensively as that of aliphatic *C*-nitroso compounds (ref. 1 and references therein and ref. 2), nitrosamines (3, 4) or aryl nitro compounds (5). Nitroso compounds usually exist as an equilibrium mixture of monomer and dimer forms in solution so that a complex mixture of products can result: for example, from the photolysis of nitrosobenzene (6). The hindered aryl nitroso compounds 2,4,6-tri-*tert*-butylnitrosobenzene (**1**) and 2,5-di-*tert*-butylnitrosobenzene (**2**) are known to exist as monomers in solution and in the preferred out-of-plane and coplanar *anti* conformations shown (7) below.

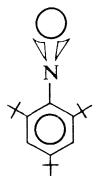

1

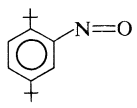

2

These compounds are selected as model monomeric aryl nitroso compounds for exploratory photochemical studies. The reported photostability of **1** (8) is surprising in view of the known reactivity of other monomeric nitroso compounds (9).

*The Photolysis of 2,4,6-Tri-*tert*-butylnitrosobenzene (1)*

Irradiation of **1** (through quartz in cyclopropane

Can. J. Chem. Downloaded from www.nrcresearchpress.com by 210.87.254.42 on 09/05/12
For personal use only.

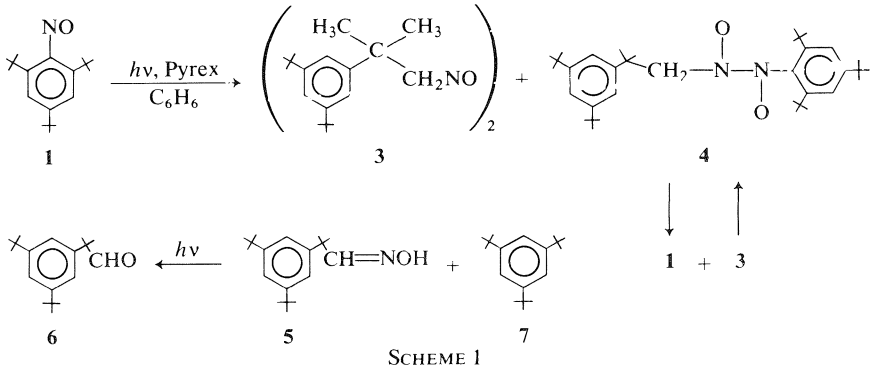

SCHEME 1

in an esr spectrometer and in benzene or cyclohexane through Pyrex) gave persistent esr signals consisting of a sextet of 1:2:1 triplets assigned to Ar—$\dot{N}$—OH, where $a^N \simeq 15$, $a_{OH}^H \simeq 40$, and $a^H_{meta\ H's} \simeq 1$ G. This contrasts with the reported photostability of **1** and lack of esr signals on irradiation (8).

Larger scale photolyses for product analysis by preparative tlc resulted in the products as outlined in Scheme 1.[1] The number and yield of the various photoproducts depended on the photolysis time as summarized in Table 1. Our preliminary studies (10) incorrectly assigned a structure [Ar—$CH_2C(CH_3)_2$-$NO]_2$ for one of the primary products **3** based solely on spectroscopic evidence. The correct structure for **3** is now based on the ready conversion of **3** → **5** → **8** and the synthesis of **8** by mild Friedel–Crafts *tert*-butylation of the known **9** (Scheme 2).

Depending on the percentage conversion, the major photoproduct was the mixed dimer (**4**, lower conversion) or the nitroso dimer **3**. When samples of **1** were photolyzed for different times ($1\frac{1}{2}$–$6\frac{1}{4}$ h), it was found that the mixed dimer **4** could be isolated in 70% yield by shorter photolysis times and then the percentage of **4** decreased with a concomitant increase in **3**. The mixed dimer **4** presumably forms by reaction of **1** with the monomer of **3**. We also observed the formation of **4** in a dark reaction by combining **1** and dimer **3** and observing the interconversion by direct nmr methods. Equal weights of **1** and **3** in benzene initially showed only the nmr peaks for **1** (δ 1.25, *tert*-butyls) and **3** (δ 1.33, s, 18H, *tert*-butyls; δ 1.48, s, 6H, $C(CH_3)_2$; and δ 4.58, s, 2H, methylene). On standing, the peaks for **1** and **3** decreased and new peaks appeared in the methylene region at δ 4.64 and a new $C(CH_3)_2$ signal at δ 1.55 assigned to the mixed dimer **4**. After 24 h, the ratio of **4** to **3** was estimated (nmr) to be 5:1. The ratios

TABLE 1. Product distribution[a] from photolysis of 2,4,6-tri-*tert*-butylnitrosobenzene (**1**)

	% yield	
Product	40% conversion[b]	88% conversion[c]
3	37	40
4	50	16
5	11	7
6	—	6
7	—	2

[a]Yields were determined by preparative tlc.
[b]Photolysis time 2 h. Initial concentration of **1** 3.45×10^{-3} mol L^{-1}. Benzene elution separated the products into four bands which contained the compounds eluted in the order of elution: **1**, **4**, **3**, **5**.
[c]Photolysis time 7 h. Initial concentration of **1** 3.23×10^{-3} mol L^{-1}. Thin-layer chromatographic separation gave six bands as follows: band 1, mixture of **1** and **7** separated by tlc using cyclohexane; band 2, **4**; band 3, **3**; band 4, mixture of **5** and **6** separated by tlc using benzene and ethyl ether (10%); band 5, **5**; band 6, a mixture of **5** and **6** separated by tlc using benzene.

of **3** to **4** observed in the photolysis runs are probably functions of the concentration of **1** remaining as well as the relative stability of **3** and **4**. The mixed dimer **4** dissociated partially into **1** and **3** on attempted isolation and therefore could not be fully characterized. After additional photolysis time, both **3** and **4** were converted to secondary products. A separate experiment on the photolysis of **3** for 3 h (50% conversion) confirmed that it does photodegrade under these conditions. Thin-layer chromatographic analy-

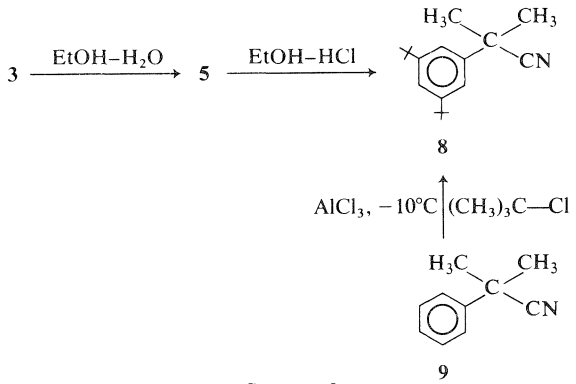

SCHEME 2

[1]The photolysis of **1** was accelerated by benzophenone; however the products shown here were not detected. A cyclic imine also reported earlier (10) from photolysis of **1** is now known to be produced by other (e.g., thermal) reactions. These results will be reported on separately.

Can. J. Chem. Downloaded from www.nrcresearchpress.com by 210.87.254.42 on 09/05/12
For personal use only.

TABLE 2. Products from photolysis of 2,5-di-*tert*-butylnitrosobenzene (**2**)[a]

Photolysis time (h)	% conversion of **2**	% yield of products		
		p-Di-*tert*-butylbenzene (**11**)	2,5-Di-*tert*-butylphenol (**12**)	Anil quinone (**13**)
8	[b]	7	12	13
9¾	43[c]	Not measured	20	9
13	47[d]	6	14	7

[a]The mixture was separated by preparative tlc, using benzene–cyclohexane (70:30), as follows: band 1, a mixture of **11** and an unidentified radical (30 lines, scan range ± 25 g at 3237 g) separated by tlc; band 2, **2**; band 3, a trace of radical **10** mixed with **2**; band 4, **13**; band 5, **12** (compared with an authentic sample); bands 6–9 traces, unidentified; band 10, (the application zone), a dark resin, approximately ¼ of the product.
[b]Recovered **2** not measured. Initial concentration of **2** = 3.84×10^{-3} mL^{-1}.
[c]Initial concentration of **2** = 3.63×10^{-3} mL^{-1}.
[d]Initial concentration of **2** = 7.16×10^{-3} mL^{-1}.

sis indicated a complex mixture of at least six products. The only compound identified was the oxime (**5**, 13%). Photolysis of **5** in turn showed that it was converted to the aldehyde **6** (63% in 2½ h).

*The Photolysis of 2,5-Di-*tert*-butylnitrosobenzene (2)*

Electron spin resonance examination of the solutions (benzene, cyclohexane, or pentane) from photolysis of **2**, after short irradiation times (5 min), showed the presence of a persistent radical which exhibited a triplet (1:1:1) of multiplets assigned to the Ar_2N—$\dot{O}$ radical (**10**) ($a_N = 11.5$, $a_H \simeq 0.5-1$ G, where Ar = 2,5-di-*tert*-butylphenyl). On longer photolysis times, this spectrum was replaced by a more complex set of persistent signals indicative of a mixture of radicals.

Photolysis of **2** for product analysis showed marked differences from that of **1**. During irradiation of **2**, the benzene solutions became red-orange in colour and a comparatively long photolysis time (13 h) was needed to achieve comparable conversions of **2** (40–50%, compare Table 1 and Table 2) since the red product (**13**) acted as an internal filter. The photo mixture from **2** also was much more complicated. At least 10 separate tlc bands were obtained and it was difficult to obtain a material balance since up to one third of the product was a resinous material that did not develop on the tlc. Nevertheless it was possible to characterize the major products of preparative tlc separation (see Scheme 3 and Table 2). The red product was identified as 2,5-di-*tert*-butylanilino-*p*-(2,5-di-*tert*-butyl)quinone (**13**) by its analysis, spectroscopic properties, and synthesis by condensation of 2,5-di-*tert*-butylaniline with 2,5-di-*tert*-butyl-*p*-quinone. There was some indication that the anil quinone (**13**) undergoes photodegradation since its yield decreased on longer photolysis times (Table 2). When some plates containing the separated mixture were allowed to stand exposed to light at least a day, bands 1 and 3 changed to the red colour of **13** (initially found in band 4). These bands were rechromatographed and they did in fact yield some of **13**. This observation indicates that photolabile intermediates are present and these lead to **13** by secondary reactions.

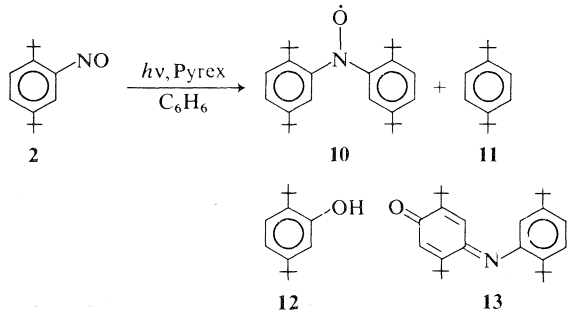

2 **10** **11** **12** **13**

SCHEME 3

Discussion

*The Photorearrangement of 2,4,6-Tri-*tert*-butylnitrosobenzene (1)*

Ayscough *et al.* (11) decided from esr studies and the lack of photosensitization that nitrosobenzene undergoes photodissociation to phenyl radicals and nitric oxide via an excited singlet state. On the other hand Pak and Testa (12) found that nitrosobenzene undergoes photoreduction in 2-propanol to phenylhydroxylamine consistent with reaction through an n,π* triplet. Our observation of the benzophenone acceleration of the photolysis of **1** does not clarify the nature of the reactive state involved because the reaction products were not the same as in the direct photolysis.[1]

The markedly different photochemical behaviour of the structurally similar nitroso compounds **1** and **2** can be accounted for in terms of differential steric and conformational effects. These effects are evident in the electronic absorption spectra of **1** and **2** (Fig. 1) which may give some clue into this different behaviour. Both compounds show the typical visible absorption at 750–800 nm responsible for the green colour and assigned to the $n_N \rightarrow \pi^*$ transition. This

Can. J. Chem. Downloaded from www.nrcresearchpress.com by 210.87.254.42 on 09/05/12
For personal use only.

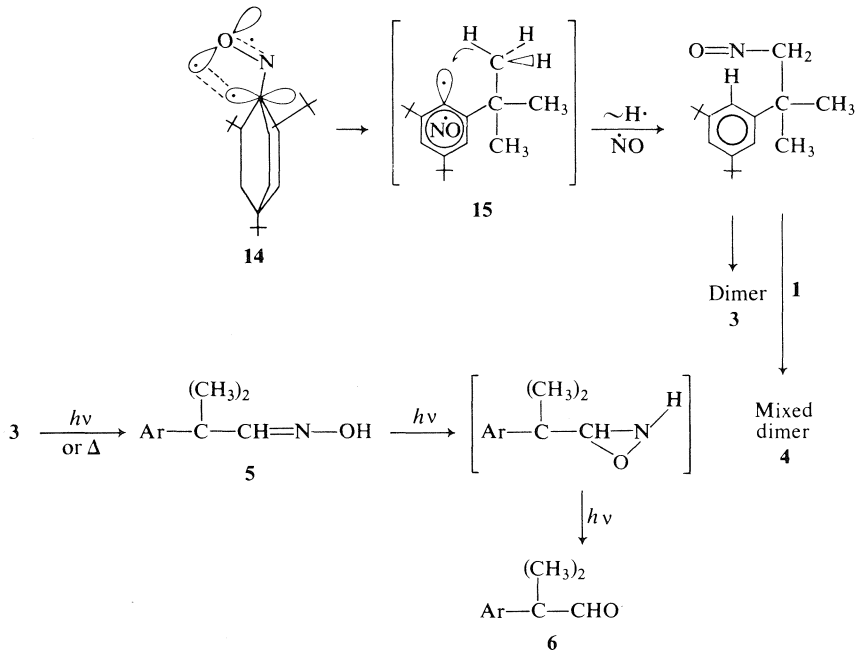

SCHEME 4

band for the more hindered compound **1** is shifted only slightly to shorter wavelength and is more intense. The spectra of **1** and **2** are quite different in the ultraviolet. The coplanar compound **2** shows absorption (λ_{max} 296, ε = 8234 and λ_{max} 317, ε = 5150) very similar to that shown for nitrosobenzene (11). In contrast the usually strong band at 290–300 nm is replaced in **1** by a shoulder with greatly diminished intensity, presumably owing to suppression

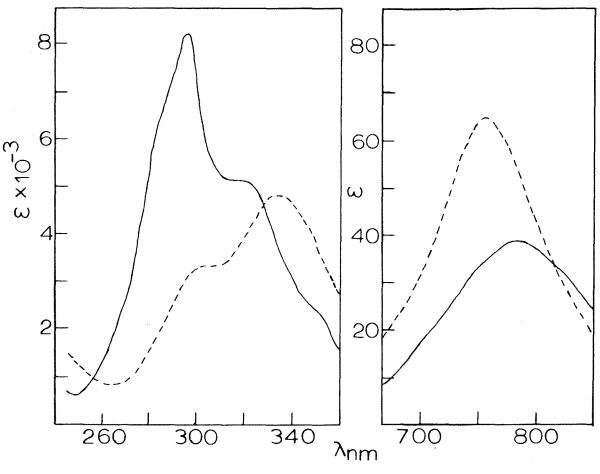

FIG. 1. Ultraviolet–visible spectra in cyclohexane: — 2,5-di-*tert*-butylnitrosobenzene; - - - 2,4,6-tri-*tert*-butylnitrosobenzene.

of the usual $\pi \rightarrow \pi^*$ transition by steric inhibition of coplanarity. On the other hand a new broad band appears in **1** at 320–350 nm (λ_{max} 334, ε = 4800) which would overlap the region for the usually weak band for the $n_O \rightarrow \pi^*$ transition of the nitroso group (13). This absorption is tentatively assigned to an enhanced $n_O \rightarrow \pi^*$ for **1** superimposed on the weakened $\pi \rightarrow \pi^*$ absorption. When the nitroso group is effectively twisted out of plane of the benzene ring by two *ortho tert*-butyls, the unpaired electron in an oxygen 2*p* orbital of the excited state can undergo partial overlap with the aromatic *p*-orbitals (Scheme 4, **14**) with a resulting enhancement of the $n_O \rightarrow \pi^*$ absorption. A similar explanation has been used to account for some enhancement in the $n \rightarrow \pi^*$ absorption of the aryl nitro group by an *o-tert*-butyl group (14) and the steric acceleration of the photorearrangement of aryl nitro to a nitrite (15).

The steric hindrance to coplanarity in **1** is expected to promote the cleavage of the aryl carbon to nitrogen bond in the excited state leading to the aryl radical or radical pair (**15**). We have independently observed that this tri-*tert*-butyl phenyl radical readily abstracts a hydrogen atom from a C—H bond of an *o-tert*-butyl group (16) followed by a neophyl rearrangement. In the present case, the neophyl radical is trapped by rapid recombination with nitric oxide to account for the product of migration of the NO function without rearrangement in the side

Can. J. Chem. Downloaded from www.nrcresearchpress.com by 210.87.254.42 on 09/05/12
For personal use only.

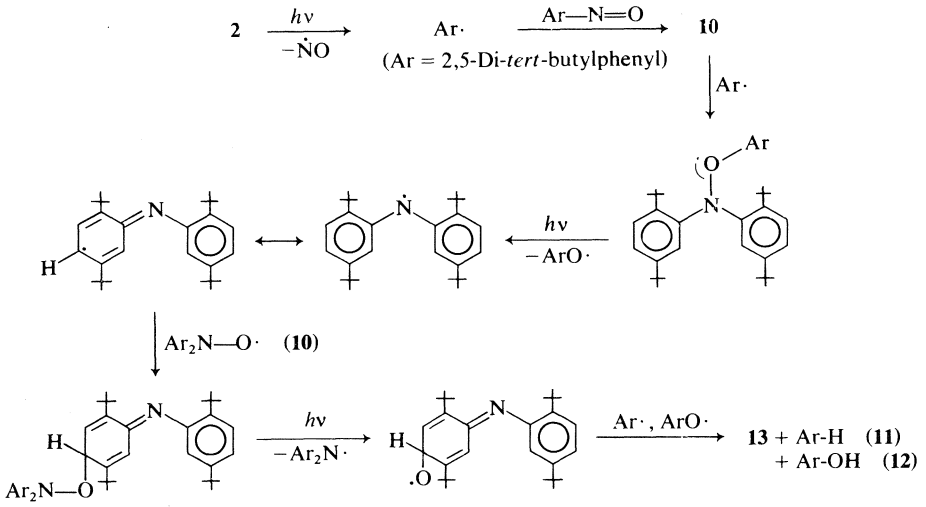

SCHEME 5

chain.[2] The photorearrangement of the aryl nitroso function predominates over other possible reactions. Thus hydrogen abstraction from solvent to form tri-*tert*-butylbenzene (**7**) is a very minor competing reaction. Although **1** is usually an effective spin trapping reagent (8), it fails to trap the reactive aryl radical (**15**) most probably owing to the combined steric effects of *o*-*tert*-butyl groups in **1** and **15**. This steric effect causes a major difference in the photochemistry of **1** vs. **2**. Furthermore the recombination of the neophyl radical with ·NO prevents spin trapping of the rearranged radical. Known secondary reactions account for such minor products as the oxime **3** (9) and the aldehyde **6** (17).

Aromatic nitroso compounds are reported to be stable to irradiation with red light (18) while aliphatic nitroso compounds are reactive. In view of the inhibition of coplanarity and photochemical reactivity of **1**, it was of interest to determine if **1** displays any photochemical reactivity by irradiation with visible light. Compound **1** proved to be stable to prolonged irradiation from a filtered sodium vapor lamp.

[2]The following alternative mechanism for photorearrangement of **1** is consistent with our observation of the Ar—N̈—OH radical

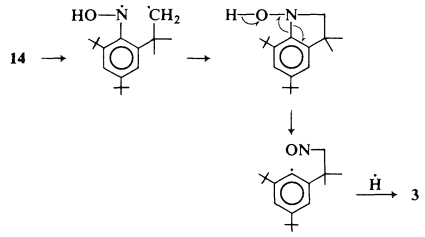

*The Photochemistry of 2,5-Di-*tert*-butylnitrosobenzene (2)*

Although the photolysis of **2** yielded a complex mixture only partially identifiable, the results serve to establish the contrast in photochemical behaviour of **1** and **2**. The formation of the diaryl nitroxide radical (**10**) as the initial detectable product from **2** indicates that it initially follows the usual photochemistry of aryl nitroso compounds (18) (Scheme 5). The formation of such products as a phenol (**12**) and an anil quinone (**13**) does not have precedence in the photochemistry of aryl nitroso compounds although phenol is a known pyrolysis product of nitrosobenzene (19). A possible pathway for the formation of **12** and **13** is outlined in Scheme 5. This involves the combination of **10** with the aryl radical followed by appropriate radical disproportionation reactions leading eventually to **11**, **12**, and **13**. There is some experimental evidence to support this pathway. The 2,5-di-*tert*-butylphenyl radical[3] was generated independently by reaction of 2,5-di-*tert*-butylbromobenzene with trimethyltin radicals (16) and trapped with **2** to form **10**. Then **10** was combined again with more 2,5-di-*tert*-butylphenyl radical followed by thin-layer chromatographic analysis. The formation of the anil quinone (**13**) was qualitatively observed on the tlc plate. This observation does not completely rule out other conceivable modes of formation of **13**. For example the nitroxide radical (**10**) might undergo disproportionation re-

[3]Although this radical cannot be detected directly by esr, there is indirect evidence that it does form by abstraction of the halogen atom by trimethyltin (16).

Can. J. Chem. Downloaded from www.nrcresearchpress.com by 210.87.254.42 on 09/05/12
For personal use only.

Can. J. Chem. Downloaded from www.nrcresearchpress.com by 210.87.254.42 on 09/05/12
For personal use only.

actions (20) leading to **13**. Furthermore sterically hindered phenoxyl radicals are reported to be spin trapped by aryl nitroso compounds at the aryl carbon para to the phenoxyl oxygen thereby forming quinoid systems (21). By analogy spin trapping at the *para* position of 2,5-di-*tert*-butylphenoxyl by **2** (or possibly a reactive state of **2**) could lead to a quinoid system which by a series of dark reactions could form **13**. However, we failed to detect the formation of **13** by the reaction of **2** with 2,5-di-*tert*-butylphenol (**12**) under conditions which generate the 2,5-di-*tert*-butylphenoxyl radical. The properties of the latter are not previously reported. It was generated[4] for characterization by photolysis in the presence of di-*tert*-butylperoxide and found to give an eight-line esr spectrum (two quartets $a^{H_3} = 2.1$, $a^{H_4} = 8.1$, and $a^{H_6} = 6.1$ G; $g = 2.0052$). These signals were rapidly obscured at room temperature by those of a longer lived radical which appeared as two doublets ($a^{H_3} = 1.3$, $a^{H_6} = 5.71$ G; $g = 2.00506$). This result indicates that initially generated **16** rapidly undergoes dimerization (22) as outlined in Scheme 6 to yield a longer lived phenoxyl radical, probably **17**. This reaction may be faster than the trapping of **16** by **2**.

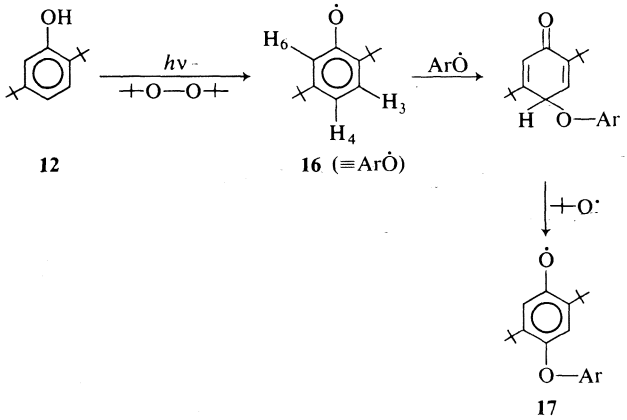

12 **16** (≡ArȮ) **17**

SCHEME 6

Experimental

Details on spectroscopic methods, tlc procedures, and the synthesis of nitroso compounds **1** and **2** were reported earlier (23).

Photolyses Procedures

The initial irradiation and esr studies were carried out by irradiation of a cyclopropane solution of 2,4,6-tri-*tert*-butylnitrosobenzene (**1**) with a 200 W super pressure mercury arc lamp in the cavity of a Varian E-4 Spectrometer.[4] Since the radicals being observed were relatively long lived (e.g., from **1**—Ar—N̈—OH, from **2**—Ar_2—N—O·), they were also observed in samples removed from preparative runs.

[4]This experiment was carried out in the laboratory of Dr. K. U. Ingold, National Research Council of Canada, Ottawa, Ont.

Preparative scale photolyses were generally carried out by irradiation of a benzene solution at 20°C with a 450 W Hanovia high pressure mercury vapor lamp (679A-36) in a Pyrex immersion well reactor. Large scale (2–3 g) photolyses of 2,5-di-*tert*-butylnitrosobenzene (**2**) in a 2-L preparative reactor with a 1000 W mercury vapor lamp (Photochemical Research Associates model R1000) gave similar results as the above lamp. The solvents used (spectral grade benzene or spectral grade cyclohexane) were distilled before use. The solutions were purged with oxygen free nitrogen for at least one hour before irradiation and a slow stream of nitrogen was passed through during photolysis. Photolysis runs to study the effect of irradiation times on product distribution were carried out in Pyrex tubes attached to the immersion well of the 450 W lamp. The effect of added benzophenone was also carried out in this way and the rate of disappearance of the nitroso compound (**1**) in the presence of benzophenone compared with the direct photolysis. A 20-fold molar excess of benzophenone caused a 10-fold increase in the rate of disappearance of **1**. In all runs the progress of the photolysis was conveniently followed by measuring the decrease in the visible absorbance readings at 750 nm for **1** and 790 nm for **2** using a B & L Spectronic 700.

Irradiations with visible light were carried out with a GE Lucalox 400 W high pressure sodium vapor lamp and a potassium dichromate filter (24).

Product Analysis

The solvent was removed from the photolysis mixtures on a rotary evaporator at 25°C. The products were then separated as soon as possible on preparative tlc plates.

*Photolysis Products from 2,4,6-Tri-*tert*-butylnitrosobenzene (1)*

Details on the separation and yields of the various compounds are given in Table 1. Compounds isolated by tlc were further purified for analysis by sublimation under reduced pressure. Data on the products from nitroso compound **1** are given below. Spectroscopic data on compounds **3** and **5** were given earlier (9).

*The photonitroso compound 2-methyl-1-nitroso-2-(3,5-Di-*tert*-butyl)phenylpropane (3). Conversion into oxime 5 and nitrile 8*—The pure compound **3** melted at 146°C. *Anal.* calcd. for $C_{18}H_{29}NO$: C78.49, H10.61, N5.09; found: C78.27, H10.92, N5.33. A sample of 50 mg of **3** dissolved in 15 ml of ethanol containing 10 drops of water was refluxed for 3½ h. Evaporation of the solvent on the rotavac left a colourless solid, mp 94–96°C, identified by its nmr spectrum (10) as the oxime (**5**). A sample of **3** (334 mg) was heated in an atmosphere of nitrogen for 20 min at 145–170°C. At 145–148°C the melted **3** quickly turned green, which colour faded by 151°C (7 min.). On cooling a near colourless solid formed, mp 90–94°C (323 mg, 97%) which proved to be **5**. An attempt at glc analysis of **3** showed that it decomposed during analysis. For example at 155–225°C on a 20% Carbowax column (10 ft × ¼ in.) and 60 cm³/min He it was converted (80%) into the nitrile (**8**) identified by its melting point and ir spectrum on comparison with synthetic **8**.

The mixed dimer (4)—Band 2 from the tlc separation of the photolysis of **1** containing the mixed dimer **4** was initially colourless but slowly turned green and after several hours was deep green. This band was then removed (69 mg) and the tlc repeated and it was found to separate into **1** (19 mg), **4** (32 mg), and **3** (16 mg). This ready dissociation of **4** into a mixture of **1** and **3** precluded its detailed characterization. However its formation from **1** and **3** in a dark reaction could readily be observed by direct nmr observations (e.g., see Results).

Can. J. Chem. Downloaded from www.nrcresearchpress.com by 210.87.254.42 on 09/05/12
For personal use only.

The oxime 2-methyl-2-(3,5-di-tert-*butyl)phenylpropanal oxime (**5**). Conversion into nitrile (**8**) and aldehyde (**6**)*—The purified oxime had a mp 95–96°C. *Anal.* calcd. for $C_{18}H_{29}NO$: C78.49, H10.61, N5.09; found: C78.64, 78.70; H10.48, 10.53; N5.21. The oxime (51 mg) in ethanol (5 ml) containing $\frac{1}{2}$ ml concentrated hydrochloric acid was refluxed overnight. The product was precipitated by adding ice water and extracted with ether to give 40 mg of solid. The ir and nmr spectra indicated that this product was a mixture of the nitrile **8** (mainly) and the aldehyde (**6**). Gas–liquid chromatographic analysis (20% Carbowax, 150–200°C, and 60 cm^3/min He) indicated a mixture of 64% **8** and 36% **6**. The glc peaks were collected and subjected to mass spectroscopic analysis for further identification. Parent masses were obtained at *m/e* 257 for **8** and *m/e* 260 for **6** as calculated. The nitrile was also obtained (92%) when the oxime was subjected to these glc conditions. It was collected from the glc for analysis. It gave a mp 70–71°C. The ir spectrum showed a sharp band at 2230 cm^{-1} for —C≡N. The nmr spectrum had bands at 1.35 (s, 18H, 2 × $(CH_3)_3C$—), 1.78 (s, 6H, $(CH_3)_2C$—) and 7.46–7.58 δ (m, 3H, aryl H's). *Anal.* calcd. for $C_{18}H_{27}N$: C84.07, H10.57, N5.44; found: C84.16, 84.10; H10.47, 10.50; N5.45, 5.38. The minor component from the above acid treatment of the oxime gave a mp 75–76°C. Its structure was assigned as the aldehyde-2-methyl-2-(3,5-di-*tert*-butyl)phenylpropanal (**6**) from spectral data, The ir spectrum had a strong band at 1734 cm^{-1} (—C=O) and weak bands at 2720 and 2820 cm^{-1} (—CHO). The nmr spectrum had bands at 1.37 (s, 18H, 2 × $(CH_3)_3C$—), 1.48 (s, 6H, $(CH_3)_2C$), 7.28 (d, J = 2 Hz, 2H, aryl H's 2 and 6), 7.53 (t, J = 2 Hz, 1H, aryl H-4), and 9.90 δ (s, 1H, —CHO). There was not sufficient **5** for an elemental analysis.

*Photolysis of the Photonitroso Compound (**3**)*

The photonitroso compound (258 mg in 180 ml benzene) was irradiated with the 450 W mercury vapor lamp for 3 h. Preparative tlc separation of the products using benzene as eluent resulted in separation into six bands. Only two of these components could be identified: band 2 yielded 139 mg (54%) of starting compound (**3**) and band 3 yielded the oxime **5** (18 mg, 13%).

*Photolysis of the Oxime (**5**)*

The oxime (20 mg in 20 ml benzene) was irradiated, in a Pyrex tube attached to the immersion well, for 2½ h. The product was applied to a tlc plate, eluted with benzene, and the major band proved to be the aldehyde (**6**) (12 mg, 63%) from its melting point and ir spectrum.

Photolysis of 2,5-Di-tert-*butylnitrosobenzene (**2**)*

In a trial photolysis of **2**, six Pyrex tubes each containing 30 mg of **2** in 30 ml of benzene were attached to the immersion well of the 450 W lamp and irradiated successively for 1½, 3, 4½, 6, 7½, and 9 h followed by tlc analysis of the products from each solution. The solutions were orange and on longer irradiation orange-red in colour. The tlc analysis, even after only 1½ h irradiation (29% conversion), revealed a complex mixture of at least 10 components. The most marked trend was the appearance of a dark red band which increased with the photolysis time as **2** decreased. The results from preparative scale photolysis of **2** for product analysis are summarized in Table 2. *2,5-Di*-tert-*butylanilino*-p-*(2,5-di*-tert-*butyl)quinone (**13**)*, from band 4 consisted of dark red crystals, mp 190–195°C. Spectral data showed ir ν_{max}: 1645 (s, conjugated C=O) and visible–uv: λ_{max} 490 (ε 2256) and λ_{max} 278 nm (ε 10 829). The nmr spectrum (determined on a Varian HA-100) showed four singlets (1.47, 1.31, 1.26, and 1.08 δ) assigned to the four tertiary butyl groups. There were signals for five aromatic protons. Two of these were singlets (6.57 and 6.39 δ) assigned to the two hydrogens (*para*) on the quinoid ring. The other three protons were involved in an ABX system, with the AB section centred at 7.15 δ (ν_{AB} = 21.2, J_{AB} = 8.3 Hz) and the X resonance at 6.13 δ. The X proton was coupled to the upfield B proton of the AB system by 2.0 Hz as shown by a double resonance experiment whereby irradiating the X proton while observing the AB region for 20 scans caused the multiplet for B to collapse into a simple doublet. *Anal.* calcd. for $C_{28}H_{41}NO$ (mol. wt. 407): C82.49, H10.14, N3.44; found (mass spectrum *m/e* 407 (M^+)): C82.27, 82.34; H9.92, 10.04; N3.23, 3.26.

Three of the preparative tlc plates were allowed to stand exposed to air and light for several days. After a day, bands 1 and 3 deepened in colour from yellow to red. After several days, these bands were extracted, reapplied to a preparative tlc plate along with some previously separated anil quinone (**13**) and developed with benzene–cyclohexane (70:30). The result showed that bands 1 and 3 were transformed, at least in part, into **13**.

Attempts to Observe the Anil Quinone in 'Dark Reactions'

Reaction of 2,5-Di-tert-*butylnitrosobenzene (**2**) with the 2,5-Di*-tert-*butylphenyl Radical*

A mixture of 2,5-di-*tert*-butylbromobenzene (100 μL) and hexamethylditin (Aldrich, 100 μL) in 0.5 ml benzene under nitrogen in a quartz tube was irradiated for 10 min with 254/nm light in a Rayonet reactor. The light was turned off and immediately a solution of **2** (0.031 g in 50 μL benzene) was injected through a septum into the mixture which was stirred by purging with nitrogen. This reaction mixture was allowed to stand for 1 h and then it in turn was injected into another freshly photolyzed mixture of 2,5-di-*tert*-butylbromobenzene and hexamethylditin, prepared as described above. This mixture was allowed to stand overnight and then was applied to preparative tlc plates along with small spots of the three starting reagents. Elution with benzene indicated that the mixture contained mainly the starting reagents which eluted rapidly. However a new band appeared which slowly turned red on standing. This band was extracted, reapplied to a tlc plate and developed along with some of the anil quinone (**13**). The result showed that some of **13** was formed in this reaction but there was not sufficient material for further identification.

Generation of the 2,5-Di-tert-*butylphenoxy Radical (**16**) and Attempted Reaction with **2***

A solution of 2,5-di-*tert*-butylphenol (**12**) in di-*tert*-butylperoxide was irradiated (uv) in the cavity of the esr spectrometer.[4] An eight-line spectrum appeared initially and this was assigned to the 2,5-di-*tert*-butylphenoxy radical (**16**) (see Discussion). By the time of a second 4-min scan, the secondary radical (**17**) appeared as two doublets and this grew steadily at room temperature so as to obscure the primary radical. A solution of **12** (0.011 g) and di-*tert*-butylperoxide (50 μL) in 0.20 ml of benzene under nitrogen was photolyzed in a quartz tube with 254 nm light for 45 s. The resulting esr spectrum indicated that a mixture of radicals **16** and **17** was present. A solution of **2** (0.010 g in 0.20 ml of benzene) was immediately injected into the reaction mixture. This mixture was applied to a preparative tlc plate and eluted with benzene–cyclohexane (70:30). There was no evidence for the appearance of the anil quinone (**13**) on the plate immediately after development nor after standing for several days.

Syntheses

α-(3,5-Di-tert-*butyl)phenylisobutyronitrile (**8**). Friedel–Crafts* tert-*Butylation of α-Phenylisobutyronitrile*

α-Phenylisobutyryl chloride (25) was converted into α-phenylisobutyramide (mp 159–160°C, lit. (26) mp 160–

Can. J. Chem. Downloaded from www.nrcresearchpress.com by 210.87.254.42 on 09/05/12
For personal use only.

161.5°C) by treatment with ammonia gas in ethyl ether. The amide was dehydrated by heating with phosphorus pentoxide in tetrachloroethane (27) to yield α-phenylisobutyronitrile (26). The latter had a sharp ir band at 2220 cm^{-1} (—C≡N) and nmr bands at 1.54 (s, 6H, $(CH_3)_2\overset{|}{C}$—CN) and 7.50 δ (m, 5H, aryl H's).

A solution of the nitrile (1.46 g) in 10 ml of *tert*-butyl chloride was cooled to −40°C and anhydrous aluminum chloride (2.0 g) was added over 10 min. The temperature of the mixture was raised to −10°C in 30 min accompanied by evolution of hydrogen chloride. After a total reaction time of 1 h, the reaction was quenched in ice water and extracted with pentane. Gas–liquid chromatographic analysis of the product (10 ft × $\frac{1}{4}$ in. 20% Carbowax, at 175°C and 60 cm^3/min He) revealed two components in the ratio 70:30. Reaction conditions using longer times and additional *tert*-butyl chloride and aluminum chloride had little effect on changing this distribution of products. Analytical samples were obtained by collection from glc separation on a 20% Carbowax column (Aerograph Autoprep.). The minor component (30%) had mp 70°C and proved to be identical to the nitrile **8** as derived from oxime **5** (above) by its ir and nmr spectra.

The major component (70%) from the *tert*-butylation was identified as α-(4-*tert*-butyl)phenylisobutyronitrile according to the following data. It gave mp 56–57°C, an ir band at 2220 for —C≡N and nmr bands at 1.34 (s, 9H, $(CH_3)_3C$—), 1.74 (s, 6H, $(CH_3)_2\overset{|}{C}$—CN), and 7.58 δ (s, 4H, aryl H's). *Anal.* calcd. for $C_{14}H_{19}N$ (mol wt. 201): C.83.53, H9.51, N6.96; found (mass spectrum *m/e* 201(M^+)): C83.62, 83.68; H9.45, 9.45; N6.94, 6.93.

2,5-Di-tert-*butylanilino*-p-(*2,5-di*-tert-*butyl*)*quinone (13)*

Attempts to synthesize the anil quinone (**13**) by condensation of 2,5-di-*tert*-butyl-1,4-benzoquinone with 2,5-di-*tert*-butylaniline using boron fluoride etherate (28) were unsuccessful and yielded unreacted starting materials. The following procedure yielded **13** in low yield. A mixture of the above quinone (1.10 g, 5 mmol), 2,5-di-*tert*-butylaniline (1.03 g, 5 mmol) and *p*-toluenesulfonic acid (0.20 g) in xylene was refluxed for 10 h in an apparatus connected to a water trap. The xylene was distilled under reduced pressure, the residue dissolved in ether and extracted with water. The organic layer was dried, evaporated to a small volume, applied to preparative tlc plates and eluted with benzene–cyclohexane (50:50). The tlc procedure was repeated to completely separate the product **13** from the starting quinone which was the major component. The product (0.144 g, 7.1%) proved identical to the anil quinone (**13**) from the photolysis of **2** by its ir and nmr spectra.

Acknowledgments

The authors are grateful to the National Research Council of Canada for financial support of this research. One of us, John R. Milton, was the recipient of a Shell (Canada) Undergraduate Research Scholarship. We thank Dr. K. U. Ingold of NRCC (Ottawa) for assistance in obtaining the esr data and Mr. D. R. Smith of NRCC (Atlantic Regional Laboratories) for the spin decoupling experiment.

1. J. A. Maassen and T. J. de Boer. Recl. Trav. Chim. Pays-Bas Belg. **92**, 185 (1973).
2. B. G. Gowenlock, J. Pfab, and G. Kresze. Justus Liebigs. Ann. Chem. 1903 (1975).
3. K. S. Pillay, S. C. Chen, T. Mojelsky, and Y. L. Chow. Can. J. Chem. **53**, 3014 (1975).
4. Y. L. Chow. Acc. Chem. Res. **6**, 354 (1973).
5. D. O. Döpp. Top. Curr. Chem. **55**, 49 (1975).
6. R. Tanikaga. Bull. Chem. Soc. Jpn. **42**, 210 (1969).
7. R. Okazaki and N. Inamoto. J. Chem. Soc. (B), 1583 (1970).
8. S. Terabe and R. Konaka. J. Chem. Soc. Perkin II, 369 (1973).
9. A. Mackor and T. J. de Boer. Recl. Trav. Chim. Pays-Bas Belg. **89**, 164 (1970).
10. L. R. C. Barclay and I. T. McMaster. Tetrahedron Lett. 4901 (1973).
11. P. B. Ayscough, R. C. Sealy, and D. E. Woods. J. Phys. Chem. **75**, 3454 (1971).
12. K. Pak and A. C. Testa. J. Phys. Chem. **76**, 1087 (1972).
13. C. N. R. Rao and K. R. Bhaskar. *In* The chemistry of the nitro and nitroso groups. *Edited by* Henry Feuer. Interscience, New York, NY. 1969. Chapt. 3.
14. D. Döpp. Chem. Ber. **104**, 1035 (1971).
15. (*a*) O. L. Chapman, D. C. Heckert, J. W. Reasoner, and S. P. Thackaberry. J. Am. Chem. Soc. **88**, 5550 (1966); (*b*) Y. Kitaura and T. Matsuura. Tetrahedron, **27**, 1583 (1971).
16. G. Brunton, D. Griller, L. R. C. Barclay, and K. U. Ingold. J. Am. Chem. Soc. **98**, 6803 (1976).
17. T. Oine and T. Mukai. Tetrahedron Lett. 157 (1969).
18. H. A. Morrison. *In* The chemistry of the nitro and nitroso groups. *Edited by* H. Feuer. Interscience. 1969. Chapt. 4.
19. A. I. Feinstein and E. K. Fields. J. Org. Chem. **36**, 3878 (1971); **37**, 118 (1972).
20. E. G. Rozantsev. Free nitroxyl radicals. Plenum Press. 1970. Chapt. VI.
21. E. L. Zhuzhgov, N. M. Bazhin, M. P. Terpugova, and Y. D. Tsuetkov. Izv. Akad. Nauk SSSR (English transl.), **11**, 2530 (1974).
22. L. R. Mahoney and S. A. Weiner. J. Am. Chem. Soc. **94**, 585 (1972).
23. L. R. C. Barclay, P. G. Khazanie, K. A. H. Adams, and E. Reid. Can. J. Chem. **55**, 3273 (1977).
24. B. G. Gowenlock, G. Kresze, and J. Pfab. Tetrahedron, **29**, 3587 (1973).
25. L. R. C. Barclay, K. L. Adams, H. M. Foote, E. C. Sanford, and R. H. Young. Can. J. Chem. **48**, 2763 (1970).
26. A. C. Cope, T. T. Foster, and P. H. Towle. J. Am. Chem. Soc. **71**, 3929 (1949).
27. W. S. Bishop. Organic synthesis, Coll. Vol. III. John Wiley and Sons, New York, NY. 1955. p. 584.
28. J. Figueras, P. W. Scullard, and A. R. Mack. J. Org. Chem. **36**, 3497 (1971).

Synthesis and reactions of 2-epoxyethylenepyridine 1-oxide with nitrogen, oxygen, and sulfur nucleophiles

ABRAHAM BENDERLY, GEORGE B. FULLER, EDWARD E. KNAUS, AND KINFE REDDA

Faculty of Pharmacy and Pharmaceutical Sciences, University of Alberta, Edmonton, Alta., Canada T6G 2N8

Received May 5, 1978

ABRAHAM BENDERLY, GEORGE B. FULLER, EDWARD E. KNAUS, and KINFE REDDA. Can. J. Chem. **56**, 2673 (1978).

The reaction of 2-epoxyethylenepyridine 1-oxide (**4**), obtained by *m*-chloroperbenzoic acid oxidation of 2-vinylpyridine (**2**), with nitrogen, oxygen, and sulfur nucleophiles has been investigated. Reaction of **4** with cyclic or acyclic amines affords pyridylethanolamine 1-oxides **8** which on reductive deoxygenation using palladium-on-charcoal and hydrogen give rise to pyridylethanolamines **9**. Similar reactions with sodium ethoxide and sodium thiophenol yield the respective ethyleneglycol **8***f* and thioethanol **8***g* derivatives.

ABRAHAM BENDERLY, GEORGE B. FULLER, EDWARD E. KNAUS et KINFE REDDA. Can. J. Chem. **56**, 2673 (1978).

On a étudié la réaction de l'époxy-2 éthylènepyridine oxyde-1 (**4**), obtenu par oxydation à l'aide d'acide de *m*-chloroperbenzoïque de la vinyl-2 pyridine (**2**), avec des nucléophiles azotés, oxygénés et sulfurés. La réaction de **4** avec des amines cycliques ou acycliques conduit aux pyridyléthanolamineoxides-1 (**8**) qui par désoxygénation réductrice, faisant appel au palladium sur du charbon et de l'hydrogène, donnent naissance au pyridyléthanolamines (**9**). Des réactions semblables avec l'éthylate de sodium et le thiophénolate de sodium conduisent respectivement à des dérivés éthylèneglycol **8***f* et thioéthanol **8***g*.

[Traduit par le journal]

A considerable degree of pharmacological interest has recently been attached to 2-amino-1-hydroxyethyl derivatives **1** of benzene (1), pyridine (ref. 2 and references cited therein) and structurally related systems having rigid (2–4) and semirigid (5) conformations. Derivatives of ethanolamine **1** which

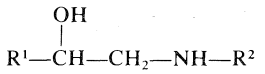

1

R^1 = Ph, 2-, 3-, or 4-Pyridyl
R^2 = *i*Pr, *t*Bu

possess an isopropyl or *tert*-butyl R^2-substituent usually exhibit significant β-adrenoreceptor activity (1–5). Pyridylalkanolamines **1** are obtained from reaction of the appropriate pyridinecarboxaldehyde with nitroalkanes (6) or with isocyanides (2); however neither of these procedures is applicable to the synthesis of the potentially bioisosteric ethanolamines **1** in which the terminal amino nitrogen is part of a heterocyclic ring system. It would be of interest, therefore, to prepare a stable and yet reactive precursor which on reaction with either cyclic or acyclic aliphatic amines would afford the desired ethanolamines **1**. We now describe the synthesis of 2-epoxyethylenepyridine 1-oxide (**4**) and its reaction with nitrogen, oxygen, and sulfur nucleophiles.

Oxidation of 2-vinylpyridine (**2**) with excess *m*-chloroperbenzoic acid (**3**) in methylene chloride at

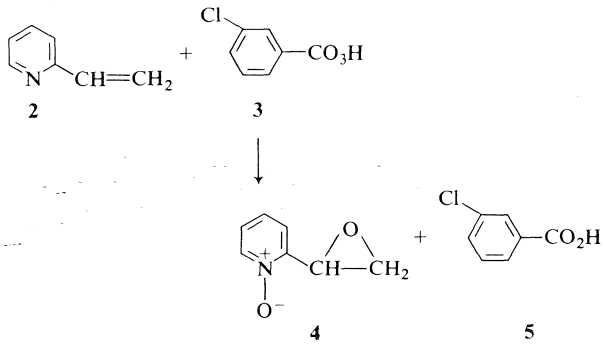

2 **3** **4** **5**

reflux temperature afforded 2-epoxyethylenepyridine 1-oxide (**4**, 60%). The epoxide **4** proved to be very stable and is routinely purified by elution with benzene from a neutral alumina oxide column to remove **3** and **5**. This purification procedure is superior to recrystallization from methylene chloride. 4-Epoxyethylenepyridine 1-oxide (**6**), obtained by a similar oxidation of 4-vinylpyridine, was obtained in 32% yield after neutral alumina oxide chromatography. The epoxide **6** was less stable than **4** and was reacted immediately after purification. An attempt to prepare 2-epoxyethylenepyridine (**7**) by selective

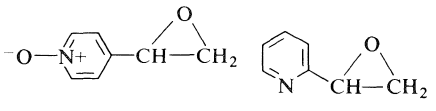

6 **7**

Can. J. Chem. Downloaded from www.nrcresearchpress.com by 210.87.254.105 on 09/05/12
For personal use only.

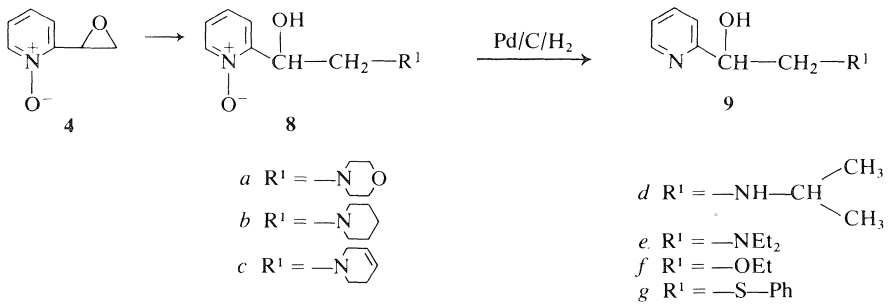

oxidation of the vinyl substituent of **2** using aqueous sodium hypochlorite in the presence of the phase transfer catalyst tetrabutylammonium hydrogen sulfate at pH 8–9 was unsuccessful (7).

Reaction of **4** with 2 equiv. of morpholine in absolute ethanol at 25°C for 12 h afforded the ethanolamine **8***a* (66%). Reductive deoxygenation of **8***a* using 10% palladium-on-charcoal and hydrogen gas at 30 psi gave rise to the desired 1-hydroxy-1-(2-pyridyl)-2-(4-morpholino)ethane (**9***a*, 90%) in which the terminal nitrogen of the ethanolamine system is part of a morpholine ring. The reaction of **4** with amines is general as illustrated by reactions with piperidine, 1,2,3,6-tetrahydropyridine, isopropylamine, and diethylamine (see Table 1). In a related reaction treatment of 4-epoxyethylenepyridine 4-oxide (**6**) with morpholine gave rise to **10** (50.3%).

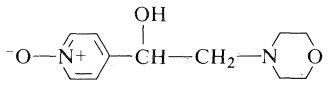

10

The reaction of **4** with oxygen and sulfur nucleophiles was also investigated. For example treatment of **4** with sodium ethoxide gave the ethylene glycol derivative **8***f* (31.6%) while reaction with sodium thiophenol afforded the thioethanol derivative **8***g* (24.9%).

The broad spectrum pharmacological screening of selected ethanolamines is now in progress.

TABLE 1. Reaction of 2-epoxyethylenepyridine 1-oxide with nucleophiles and deoxygenation of 2-pyridylethanolamine 1-oxides using palladium-on-charcoal and hydrogen

Nucleophile (Nu)	**4**:Nucleophile	Product	% yield
Morpholine	1:2	**8***a*	66.4
		9*a*	89.7
Piperidine	1:5	**8***b*	70
		9*b*	80
1,2,3,6-Tetrahydropyridine	1:2	**8***c*	64.1
Isopropylamine	1:4	**8***d*	60
Diethylamine	1:4	**8***e*	31.9
Sodium ethoxide	1:1	**8***f*	31.6
Sodium thiophenol	1:1	**8***g*	24.9

Experimental

Melting points were determined with a Büchi capillary apparatus and are uncorrected. Nuclear magnetic resonance spectra were determined for solutions in deuteriochloroform with TMS as internal standard with a Varian EM-360A spectrometer. Infrared spectra were recorded on an Unicam SP-1000 spectrometer. Mass spectra were measured with an AEI-MS-50 mass spectrometer.

*2-Epoxyethylenepyridine 1-Oxide (**4**)*

To a suspension of *m*-chloroperbenzoic acid (33.95 g of 85%, 164.5 mmol) in dry methylene chloride (250 ml) was added 2-vinylpyridine (5.0 g, 47 mmol) all at once. The mixture was allowed to stir for 30 min at 0–25°C before refluxing for 36 h. The resulting suspension was filtered and the filtrate concentrated *in vacuo*. Elution of the product from a 2.5 cm × 21 cm neutral alumina oxide column using 600 ml benzene gave **4** (3.84 g, 60%) as a white solid; mp 89–90°C; ir (KBr): 1270 (s, *N*-oxide); ^{1}H nmr δ: 2.77 (d, J_{gem} = 5.75 Hz of d, J_{vic} = 2.5 Hz, 1H, 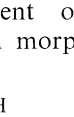), 3.35 (d, J_{gem} = 5.75 Hz of d, J_{vic} = 4 Hz, 1H,), 4.6 (d, J_{vic} = 4 Hz of d, J_{vic} = 2.5 Hz, 1H, —C*H*—CH$_2$—), 7.1–7.6 (m, 3H, H-3, H-4, H-5), 8.3 (m, 1H, H-6). *Exact Mass* calcd. for $C_7H_7NO_2$: 137.0476; found (high resolution ms): 137.0479.

*1-Hydroxy-1-(1-oxido-2-pyridyl)-2-(4-morpholino)ethane (**8**a) General Procedure*

To an ice-cooled solution of **4** (1.02 g, 7.47 mmol) in absolute ethanol (100 ml) was added morpholine (1.3 g, 14.94 mmol). The reaction, after gradual warming to 25°C, was allowed to proceed for 12 h. Removal of the solvent *in vacuo* and extraction of the residue with chloroform (300 ml) gave **8***a* (1.11 g, 66.4%) as a pale yellow solid after recrystallization from benzene; mp 128–130°C; ir (KBr): 3210 (m, OH); ^{1}H nmr δ: 2.6 (t, J = 5 Hz, 4H, H-3, H-5 (morpholine)), 2.83–3.6 (m, 2H, —CH—C*H*$_2$—) 3.73 (t, J = 5 Hz, 4H, H-2, H-6 (morpholine)), 4.93 (s, 1H, OH, exchanges with D_2O), 5.34 (d, J = 8 Hz of d, J = 4 Hz, 1H, —C*H*—OH), 7.08–7.48 (m, 2H, H-3, H-5), 7.48–7.8 (m, 1H, H-4), 8.3 (m, 1H, H-6). *Anal.* calcd. for $C_{11}H_{16}N_2O_3$: C 58.91, H 7.19, N 12.49; found: C 58.95, H 6.91, N 12.37.

*1-Hydroxy-1-(2-pyridyl)-2-(4-morpholino)ethane (**9**a)*

Catalytic hydrogenation of **8***a* (0.432 g, 1.93 mmol) in 95% ethanol (60 ml) was carried out using 10% palladium-on-charcoal (150 mg) and hydrogen gas at 30 psi for 12 h. Removal of the charcoal by filtration and evaporation of the solvent *in vacuo* gave **9***a* (0.36 g, 89.7%) as a white solid; mp 68–70°C; ir (KBr): 3180 (m, OH); ^{1}H nmr δ: 2.6 (t, J = 5 Hz,

Can. J. Chem. Downloaded from www.nrcresearchpress.com by 210.87.254.105 on 09/05/12
For personal use only.

Can. J. Chem. Downloaded from www.nrcresearchpress.com by 210.87.254.105 on 09/05/12
For personal use only.

4H, H-3, H-5 (morpholine)), 2.98 (m, 2H, —CH—CH_2), 3.8 (t, J = 5 Hz, 4H, H-2, H-6 (morpholine)), 4.72 (s, 1H, OH, exchanges with D_2O), 4.96 (d, J = 8 Hz of d, J = 4 Hz, 1H, —C*H*—OH), 7.08–7.65 (m, 2H, H-3, H-5), 7.65–8.0 (m, 1H, H-4), 8.7 (d, $J_{5,6}$ = 6 Hz, 1H, H-6). *Anal.* calcd. for $C_{11}H_{16}N_2O_2$: C 63.44, H 7.74, N 13.45; found: C 63.26, H 7.87, N 13.28.

*1-Hydroxy-1-(1-oxido-2-pyridyl)-2-(1-piperidino)ethane (**8**b)*

To an ice-cooled solution of **4** (1.0 g, 7.3 mmol) in 100 ml absolute ethanol was added piperidine (3.1 g, 36.49 mmol) and the reaction was completed as described under the general procedure. Recrystallization of the product from benzene gave **8***b* (1.134 g, 70%) as a white solid; mp 154–155°C; ir (KBr): 3200 (m, OH), 1215 (s, *N*-oxide); ^{1}H nmr δ: 1.25–2.08 (m, 6H, H-3, H-4, H-5 (piperidine)), 2.18–2.8 (m, 4H, H-2, H-6 (piperidine)), 3.33 (m, 2H, —CH—CH_2), 5.3 (d, J = 8 Hz of d, J = 4 Hz, 1H, —C*H*–OH), 6.15 (s, 1H, OH, exchanges with D_2O), 7.18–7.54 (m, 2H, H-3, H-5 (pyridine-1-oxide)), 7.54–7.81 (m, 1H, H-4 (*N*-oxide)), 8.23 (m, 1H, H-6 (*N*-oxide)). *Anal.* calcd. for $C_{12}H_{18}N_2O_2$: C 64.84, H 8.16; found: C 65.14, H 8.28.

*1-Hydroxy-1-(2-pyridyl)-2-(1-piperidino)ethane (**9**b)*

Catalytic hydrogenation of **8***b* (1 g, 4.5 mmol) in absolute ethanol (100 ml) was effected using 10% palladium-on-charcoal (0.3 g) and hydrogen gas at 38 psi for 12 h. Removal of the catalyst by filtration, evaporation of the solvent *in vacuo*, and recrystallization from benzene–heptane (1:1 v/v) afforded **9***b* (0.742 g, 80%) as a white solid; mp 65–66°C; ir (KBr): 3320 (m, OH); ^{1}H nmr δ: 1.28–2.1 (m, 6H, H-3, H-4, H-5 (piperidine)), 2.35–2.83 (m, 4H, H-2, H-6 (piperidine)), 2.83–3.33 (m, 2H, —CH—CH_2), 4.97 (d, J = 8 Hz of d, J = 4 Hz, 1H, —C*H*—OH), 6.75 (s, 1H, OH, exchanges with D_2O), 7.08–7.6 (m, 2H, H-3, H-5 (pyridine)), 7.6–7.8 (m, 1H, H-4 (pyridine)), 8.48–8.68 (m, 1H, H-6 (pyridine)). *Anal.* calcd. for $C_{12}H_{18}N_2O$: C 69.87, H 8.79; found: C 69.98, H 8.79.

*1-Hydroxy-1-(1-oxido-2-pyridyl)-2-(1-(1,2,3,6-tetrahydropyridino))ethane (**8**c)*

To an ice-cooled solution of **4** (0.77 g, 5.61 mmol) in 120 ml absolute ethanol was added 1,2,3,6-tetrahydropyridine (0.931 g, 11.22 mmol) and the reaction was completed as described under the general procedure. The product was purified by elution from a 2.5 × 21 cm neutral alumina oxide column using chloroform–methanol (1:1 v/v, 500 ml) to afford **8***c* (0.791 g, 64.1%) as a pale yellow crystalline solid; mp 104–106°C; ir (KBr): 3200 (m, OH), 1215 (s, *N*-oxide); ^{1}H nmr δ: 1.9–2.3 (m, 2H, H-3 (tetrahydropyridine)), 2.3–2.95 (m, 4H, H-2 (tetrahydropyridine)), —CH—CH_2—), 2.95–3.35 (2H, m, H-6 (tetrahydropyridine)), 5.45 (d, J = 8 Hz of d, J = 4 Hz, 1H, —C*H*—OH), 5.87 (m, 3H, H-4, H-5 (tetrahydropyridine, OH exchanges with D_2O)), 7.09–7.62 (m, 2H, H-3, H-5 (pyridine 1-oxide)), 7.62–7.91 (m, 1H, H-4 (pyridine 1-oxide)), 8.2–8.49 (m, 1H, H-6 (pyridine 1-oxide)). *Anal.* calcd. for $C_{12}H_{16}N_2O_2$: C 65.43, H 7.32; found: C 65.45, H 7.40.

*1-Hydroxy-1-(1-oxido-2-pyridyl)-2-(isopropylamino)ethane (**8**d)*

To an ice-cooled solution of **4** (1.25 g, 9.11 mmol) in 100 ml absolute ethanol was added isopropylamine (2.15 g, 36.44 mmol) and the reaction was completed as described under the general procedure. The product was purified by elution from a 2.5 × 12 cm neutral alumina oxide column using ether–methanol (10:1 v/v, 450 ml) to give 1.321 g of **8***d* which was recrystallized from ethyl acetate to give **8***d* (1.071 g, 60%); mp 138–140°C; ir (KBr): 3240, 3260 (m, OH, NH); ^{1}H nmr ($CDCl_3$ and DMSO-d_6) δ: 1.1 (m, 6H, Me), 2.73–3.30 (m, 3H, —CH—CH_2, —C*H*—Me_2), 4.41 (br s, 2H, OH, NH, exchanges with D_2O), 5.25 (d, J = 8 Hz of d, J = 4 Hz, 1H, —C*H*—OH), 7.18–7.54 (m, 2H, H-3, H-5), 7.54–7.88 (m, 1H, H-4), 8.3 (m, 1H, H-6). *Anal.* calcd. for $C_{10}H_{16}N_2O_2$: C 61.20, H 8.22; found: C 61.06, H 8.23.

*1-Hydroxy-1-(1-oxido-2-pyridyl)-2-(diethylamino)ethane (**8**e)*

To an ice-cooled solution of **4** (2 g, 14.65 mmol) in absolute ethanol (100 ml) was added diethylamine (4.28 g, 58.6 mmol) and the reaction was completed as described under the general procedure. The product was purified by elution from a 2.5 × 15 cm neutral alumina oxide column using ether–methanol (10:1 v/v, 500 ml) to give **8***e* as a semisolid (1.371 g) which was purified further by preparative tlc on 10 8 × 8 in silica gel GFP 254 plates, 0.75 mm in thickness, using ether–methanol (4:1 v/v) as development solvent. Extraction, with warm methanol (100 ml), of the fraction having R_f 0.38, gave **8***e* (0.981 g, 31.9%) as a semisolid; ir (thin film): 3240 (m, OH), 1230 (s, *N*-oxide); ^{1}H nmr δ: 1.0 (t, J = 7 Hz, 6H, —CH_2CH_3), 2.3–2.9 (m, 4H, CH_2CH_3), 3.2 (m, 2H, —CH—CH_2), 4.9 (s, 1H, OH, exchanges with D_2O), 5.2 (d, J = 8 Hz of d, J = 4 Hz, 1H, —C*H*—OH), 7.03–7.45 (m, 2H, H-3, H-5), 7.45–7.8 (m, 1H, H-4), 8.25 (m, 1H, H-6). *Anal.* calcd. for $C_{11}H_{18}N_2O_2$: C 62.83, H 8.63; found: C 62.54, H 8.51.

*1-Hydroxy-1-(1-oxido-4-pyridyl)-2-(4-morpholino)ethane (**10**)*

To a suspension of *m*-chloroperbenzoic acid (33.95 g of 85%, 164.5 mmol) in dry methylene chloride (200 ml) was added 4-vinylpyridine (5.0 g, 47 mmol) all at once. The mixture was stirred for 30 min at 0–25°C before refluxing for 36 h. The resulting suspension was filtered and the filtrate concentrated *in vacuo*. The reaction mixture was purified by elution from a 2.5 × 11 cm neutral alumina oxide column using benzene (500 ml) on two consecutive columns to give **6** (2.14 g, 32%).

To an ice-cooled solution of **6** (1.2 g, 8.76 mmol) in 80 ml absolute ethanol was added morpholine (0.762 g, 35 mmol) and the reaction was completed as described under the general procedure. The product was purified by elution from a 2.5 × 12 cm neutral alumina column using ether–methanol (10:1 v/v, 300 ml) to yield **10** (0.987 g, 50.3%) as a yellow solid; mp 93–95°C; ir (KBr): 3350 (m, OH), 1245 (s, *N*-oxide); ^{1}H nmr δ: 2.59 (t, J = 5 Hz, 4H, H-3, H-5 (morpholine)), 2.66–3.0 (m, 2H, —CH—CH_2), 3.74 (t, J = 5 Hz, 4H, H-2, H-6 (morpholine)), 4.87 (t, J = 6 Hz, 1H, —C*H*—OH), 5.18 (s, 1H, OH, exchanges with D_2O), 7.46 (d, J = 6 Hz, 2H, H-3, H-5 (pyridine-1-oxide)), 8.23 (d, J = 6 Hz, 2H, H-2, H-6 (pyridine 1-oxide)). *Anal.* calcd. for $C_{11}H_{16}N_2O_3$: C 58.91, H 7.19; found: C 59.14, H 7.31.

*1-Hydroxy-1-(1-oxido-2-pyridyl)-2-(ethoxy)ethane (**8**f)*

To an ice-cooled solution of **4** (0.535 g, 3.9 mmol) in dry tetrahydrofuran (60 ml) was added dropwise a solution of sodium ethoxide (0.266 g, 3.9 mmol) in 20 ml absolute ethanol. The reaction was completed as described under the general procedure. The product was purified on five 20 × 20 cm silica gel PFP 254 plates, 0.75 mm in thickness, using ether–methanol (4:1 v/v) as development solvent. Extraction, with 80 ml warm methanol, the fraction having R_f 0.32 gave **8***f* (0.226 g, 31.6%) as a low melting solid; ir (KBr): 3150 (m, OH), 1210 (s, *N*-oxide); ^{1}H nmr δ: 1.21 (t, J = 6 Hz, 3H, —CH_2CH_3), 3.5 (q, J = 6 Hz, 2H, —CH_2CH_3), 3.7–4.09 (m, 2H, —CH—CH_2—), 4.48 (s, 1H, OH, exchanges with D_2O), 5.24 (t, J = 5 Hz, 1H, —C*H*—OH), 7.09–7.71 (m, 3H, H-3, H-4, H-5), 8.3 (m, 1H, H-6). *Anal.* calcd. for $C_9H_{13}NO_3$: C 59.0, H 7.15; found: C 58.88, H 7.14.

*1-Hydroxy-1-(1-oxido-2-pyridyl)-2-(phenylthio)ethane (**8**g)*

To an ice-cooled solution of **4** (0.58 g, 4.23 mmol) in dry

tetrahydrofuran (80 ml) was added dropwise a solution of sodium thiophenol (0.56 g, 4.66 mmol) in dry tetrahydrofuran (20 ml) and the reaction was completed as described under the general procedure. Purification of the reaction product was effected by preparative tlc on six 8 × 8 in silica gel PFP 254 plates, 0.75 mm in thickness, using ether–methanol (4:1 v/v) as development solvent. Extraction, with 100 ml warm methanol, the fraction having R_f 0.38 afforded **8***g* (0.261 g, 24.9%); mp 136–139°C; ir (KBr): 3100 (m, OH), 1215 (s, *N*-oxide); ^{1}H nmr ($CDCl_3$ + DMSO-d_6) δ: 2.9–3.9 (m, 2H, —CH—CH_2), 5.31 (d, J = 8 Hz of d, J = 4 Hz, 1H, —C*H*—OH), 6.9–7.48 (m, 7H, H-3, H-5, phenyl), 7.48–7.83 (m, 1H, H-4), 8.17 (m, 1H, H-6). *Anal.* calcd. for $C_{13}H_{13}NO_2S$: C 63.14, H 5.30; found: C 62.80, H 5.22.

Acknowledgement

We are grateful to the National Research Council of Canada (Grant A0531) for financial support of this work.

1. T. Jen, J. S. Frazee, C. Kaiser, D. F. Colella, and J. R. Wardell, Jr. J. Med. Chem. **20**, 1029 (1977).
2. T. Jen, J. S. Frazee, M. S. Schwartz, C. Kaiser, D. F. Colella, and J. R. Wardell, Jr. J. Med. Chem. **20**, 1258 (1977).
3. H. Sugihara, K. Ukawa, H. Kuriki, M. Nishikawa, and Y. Sanno. Chem. Pharm. Bull. **25**, 2988 (1977).
4. K. Itoh, M. Motohashi, H. Kuriki, H. Sugihara, N. Inatomi, M. Nishikawa, and Y. Oka. Chem. Pharm. Bull. **25**, 2917 (1977).
5. P. C. Jain, Y. Khandelwal, and O. N. Tripathi. J. Med. Chem. **21**, 68 (1978).
6. F. Zymalkowski. Arch. Pharm. **291**, 12 (1958); **294**, 29 (1961); **295**, 217 (1962).
7. S. Krishnan, D. G. Kuhn, and G. A. Hamilton. J. Am. Chem. Soc. **99**, 8121 (1977).

Can. J. Chem. Downloaded from www.nrcresearchpress.com by 210.87.254.105 on 09/05/12
For personal use only.

Cyclitol analogs of biological interest. Regioselective nucleophilic substitutions of 1,4-cyclohexadiene bisepoxide and bisepisulfide

F. HAVIV[1] AND B. BELLEAU

Department of Chemistry, McGill University, Montreal, P.Q., Canada H3A 2K6

Received May 15, 1978

F. HAVIV and B. BELLEAU. Can. J. Chem. **56**, 2677 (1978).

Reaction of *cis*-1,4-cyclohexadienebisepoxide with aluminium azide afforded the all-equatorial 1,3-diazido-4,6-cyclohexanediol (**2**) through a metal-template mechanism. Hydrogenation of the product gave 2,5-dideoxystreptamine. Synthon **2** underwent normal coupling with 6-deoxy-6-azido-2,3,4-tris(*O*-benzyl)-α-glucosyl chloride and the resulting product gave the expected glucoside, a precursor of 5-deoxyneamine analogs. The *cis*- and *trans*-1,4-cyclohexadienebisepoxides were converted in good yields to the corresponding bisepisulfides and monoepoxide monoepisulfides. Regioselective opening of the *cis*-bisepisulfide with acetyl chloride and mercuric acetate by a metal-template mechanism led to stereochemically defined dithio analogs of cyclitols.

F. HAVIV et B. BELLEAU. Can. J. Chem. **56**, 2677 (1978).

La réaction du *cis*-cyclohexadiène-1,4 bis-époxyde avec l'azoture d'aluminium conduit au diazido-1,3 cyclohexanediol-4,6 complètement équatorial (**2**) par l'intermédiaire d'un mécanisme métal-gabarit. L'hydrogénation du produit conduit à la didéoxy-2,5 streptamine. Le synthon **2** subit le couplage normal avec la chlorure de déoxy-6 azido-6 tris(*O*-benzyl-2,3,4)α-glucosyle et le produit qui en résulte conduit au glucoside attendu, un précurseur des analogues déoxy-5 néamine. Les *cis*- et *trans*-cyclohexadiène-1,4 bis-époxydes peuvent être transformés avec de bons rendements en bis-épisulfures correspondants et en mono-époxyde-mono-épisulfures. L'ouverture régiosélective du *cis*-bis-épisulfure avec le chlorure d'acétyle et l'acétate mercurique par un mécanisme de métal-gabarit conduit à des analogues dithio de cyclitols d'une stéréochimie particulière.

[Traduit par le journal]

Can. J. Chem. Downloaded from www.nrcresearchpress.com by 210.87.254.40 on 09/05/12
For personal use only.

We have recently described the synthesis of 2,5-dideoxystreptamine (1) and derivatives from *cis*-1,4-cyclohexadienebisepoxide (**1**) the preparation of which by an improved process has also been described by us (2). This streptamine analog served as starting material for the total synthesis of the biologically effective 5-deoxykanamycine A analog of the kanamycin class of antibiotics (3). Synthetic endeavors of this kind necessitate the cumbersome and uneconomical protection and deprotection of the substrate amino groups. The best way to circumvent these complications would be to use the 2,5-diazido analog **2** of 2,5-dideoxystreptamine as starting material for glycoside synthesis. Reduction at the last stage would quantitatively transform the azido groups to amine functions. Unfortunately, reaction of the azide anion with bisepoxide **1** gives only the expected 1,4-diazido-3,4-diol **4**.[2] We have now found that the use of aluminium azide in THF leads to the desired 1,3-diazido isomer **2** in low yield. No attempt was made to improve the yield. It appears that the major side reaction involved epoxide degradation by tenacious residual aluminium chloride salts. By analogy with the observations of others (4, 9), formation of the 1,3-diazido isomer is attributable to a template effect brought about by the oxophilic aluminium cation as depicted in **5**. The suitability of this diazidodiol in glycoside synthesis was briefly explored using 6-deoxy-6-azido-2,3,4-tris(*O*-benzyl)-α-glucosyl chloride (5) as the reagent. The expected glycosides were formed and one of the diastereomers isolated in crystalline form (**6**). We have not established which of the diastereomers **6***a* or **6***b* actually crystallized. This glucoside is a precursor of 5-deoxyneamine and kanamycin analogs. The practical potential of synthon **2** is thus established.

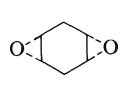

1

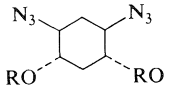

2 R = H
3 R = Ac

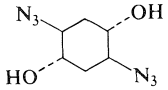

4

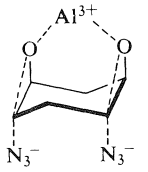

5

Another class of cyclitol analogs of potential interest as precursors of biologically active molecules consists in thiol relatives of defined geometry. The bisepisulfide analogs **7** and **9** and monoepisulfides

[1]Present address: Abbott Laboratories, North Chicago, IL 60064, U.S.A.

[2]G. Kavadias. Unpublished results. We thank Dr. Kavadias of Bristol Laboratories for this information.

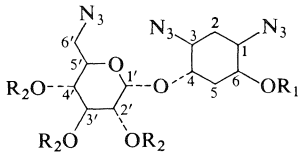

6*a* R_1 = Ac, R_2 = Benzyl
6*b* R_1 and glycosyl are interchanged

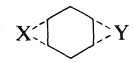

7 X = Y = S
8 X = S, Y = O

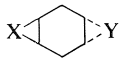

9 X = Y = S
10 X = S, Y = O

8 and **10** of the corresponding bisepoxides appeared attractive as starting materials and accordingly their synthesis from *cis*- and *trans*-1,4-cyclohexadienebisepoxides was investigated. In general, epoxides can be converted to episulfides by reaction with thiocyanate, thioamides, thiourea, thiotriphenylphosphine and related reagents (ref. 6 and references therein). In our hands, the thiourea method proved to be the most effective and reliable. Thus, treatment of the *cis*-bisepoxide **1** with a twofold excess of thiourea in the presence of 2 equiv. of sulfuric acid followed by mild base treatment of the intermediate bisisothiouronium salt **11** gave the crystalline *cis*-bisepisulfide **7** in high yield. On standing, it gradually decomposed and underwent rapid polymerization in protic solvents. When the *cis*- or *trans*-bisepoxides (1) were treated with thiourea in the presence of only 1 equiv. of acid followed by base treatment, the corresponding *cis*- and *trans*-monoepisulfide monoepoxide **8** and **10** could be obtained. The configurational assignments are based on the well-known stereochemical course of epoxide–episulfide conversions (6–8) and were confirmed by ^1H and ^{13}C nmr spectroscopy (Table 1). Under the conditions which allowed the *cis*-bisepoxide to react cleanly in the expected manner with hydrazine (1), the bisepisulfide **7** polymerized instantly. However, it reacted readily with acetyl chloride to give the 1,4-dichlorodiacetyl product **12** (the ^{13}C nmr spectrum showing only one signal at 36.156 ppm for the two methylenes). This result parallels Craig's observations with the corresponding *cis*-bisepoxide (9). Reduction of **7** with lithium aluminium hydride (LAH) gave *cis*-1,4-cyclohexane dithiol which was characterized as the diacetyl derivative **13** (the ^{13}C nmr spectrum showed only one signal for the methylenes at 30.401 ppm). The *cis*-bisepisulfide undergoes 1,4-diaxial attack by LAH whereas the *cis*-bisepoxide is reduced to *cis*-1,3-cyclohexane diol (9). This contrasting behavior can be explained on the basis that a template effect by the aluminium ion (as in the formation of **2**) controls the course of reduction with the bisepoxide

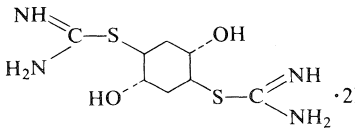

11

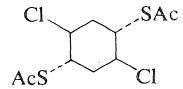

12

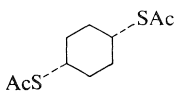

13

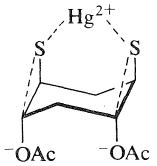

14

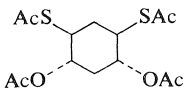

15

(9) but not in the case of the bisepisulfide because of the poor affinity of aluminium for sulfur. However, with a strongly thiophilic salt such as mercuric acetate, a template-directed 1,3-diaxial opening of the bisepisulfide by acetate (as in **14**) now occurred. The product was purified as the tetraacetate **15** and in agreement with the assigned structure, the ^{13}C nmr spectrum of the compound showed two signals for the methylenes at 33.02 and 30.64 ppm. The use of these geometrically defined thiocyclitols in the synthesis of potentially bioactive molecules will be reported later.

TABLE 1. Spectral characteristics of 1,4-cyclohexadiene bisepoxide, bisepisulfides, and mixed monoepoxides monoepisulfides

Compound	Mass *m/e*	^1H nmr ($CDCl_3$), δ (ppm)	^{13}C nmr ($CDCl_3$), δ (ppm)
1	112	2.50 (4H, broad q) 3.09 (4H, broad s)	49.20 (CO) 23.60 (CH_2)
7	144	2.28–3.16 (4H, m) 3.10 (4H, s)	33.60 (CS) 29.60 (CH_2)
8	128	2.25–2.75 (4H, m) 3.10 (4H, m)	48.28 (CO) 30.27(CS) 22.17 (CH_2)
9	144	2.65 (4H, m) 2.95 (4H, m)	31.83 (CS) 29.78 (CH_2)
10	128	2.60 (4H, m) 3.18 (4H, m)	48.00 (CO) 33.80 (CS) 27.20 (CH_2)

Experimental

Melting points were evaluated with a Thomas-Hoover capillary apparatus and are uncorrected. The ^1H nmr spectra were obtained with a Varian T-60 spectrometer using tetramethylsilane as the internal standard. The ^{13}C nmr spectra were obtained with a Brucker HX-90 spectrometer and mass spectra with a Varian Mat-CH-5 single focusing spectrom-

Can. J. Chem. Downloaded from www.nrcresearchpress.com by 210.87.254.40 on 09/05/12
For personal use only.

Can. J. Chem. Downloaded from www.nrcresearchpress.com by 210.87.254.40 on 09/05/12
For personal use only.

eter. Elemental analyses were performed by Sprang Microanalytical Laboratory.

trans-trans-*1,5/2,4-1,5-Diazido-2,4-cyclohexanediol Diacetate (3)*

A solution of anhydrous $AlCl_3$ (5.985 g) in dry THF (90 ml) was added to a suspension of sodium azide (9.65 g) in dry THF (90 ml). The mixture was heated under reflux for 90 min under nitrogen and a solution of the bisepoxide **1** (1) (2 g) in 115 ml THF added dropwise over a 2 h period. Heating under reflux was continued for an additional 2.5 h, the mixture cooled to 0°C, and concentrated HCl (22.5 ml) carefully added followed by a 1:1 mixture of ether–THF (150 ml). The organic phase was separated, washed with aqueous NaCl, dried, and evaporated. The oily residue was treated with excess acetic anhydride in pyridine (room temperature, 17 h), the solution worked up in the usual manner, and the residue purified on thick silica gel plates ($CHCl_3$ as the solvent). The major band yielded an oil which crystallized from hexane–$CHCl_3$ to give 650 mg of crystals, mp 78°C; ir (KBr) 2100, 1740 cm^{-1}; ^1H nmr (CD_3Cl_3) δ: 4.83 (2H, m), 3.55 (2H, m), 2.75–1.20 (4H, m), 2.10 ppm (6H, s); ^{13}C nmr ($CDCl_3$) δ: 169.25 (C—O), 71.46 (C—O), 59.97 (C—N_3), 33.21 and 31.86 (CH_2), 20.43 ppm (CH_3); M^+ 282. *Anal.* calcd. for $C_{10}H_{14}N_6O_4$: C42.55, H5.00, N29.78; found: C42.60, H4.89, N29.78.

trans-trans-*1,5,2/4-1,5-Diazido-2,4-cyclohexanediol (2)*

The preceding diacetate (0.5 g) in methanol (150 ml) was heated under reflux in the presence of the resin Rexyn 101 (2 g) for 3–4 h, the resin removed by filtration, and the filtrate evaporated *in vacuo* to give **2** (323 mg) which after recrystallization from EtOAc–hexane had mp 80–81°C; ir (KBr): 3500–2700, 2080 cm^{-1}. *Anal.* calcd. for $C_6H_{10}N_6O_2$: C36.36, H5.09, N42.41; found: C36.43, H5.12, N42.26.

2,5-Dideoxystreptamine Dihydrochloride

A solution of the preceding diazido diol **2** (0.20 g) in ethanol (10 ml) was shaken under a pressure of 48 psi of hydrogen over Raney Ni at room temperature. After 2 h, the mixture was worked up in the usual manner, the residue treated with ethanolic HCl to give in quantitative yield, the title compound, mp 290–293°C (lit. (4) mp 290–295°C) identical in every respect with an authentic specimen (1).

A solution of the diazido diol **2** (1.265 g) in dry DMF (11.3 ml) was mixed under nitrogen at room temperature with $CaSO_4$ (4.13 g) (preheated to 240°C for 4 h) and after stirring for 10 min, the temperature was raised to 80°C and a solution of 6-deoxy-6-azido-2,3,4-tris(*O*-benzyl)-α-D-glucopyranosyl chloride (3.158 g) (5) in DMF (11.3 ml) added dropwise (30 min) followed by the addition of $Hg(CN)_2$ (4.735 g). The mixture was stirred at 80°C for 23 h, 2.35 g of $Hg(CN)_2$ added, and heating to 87°C maintained for another 7 h. After standing overnight at room temperature, CH_2Cl_2 was added and the precipitate filtered off and the solids washed repeatedly with CH_2Cl_2. The combined filtrate and washings were washed with water, dried and evaporated to yield a dark syrup heterogeneous by tlc. Chromatography on silica ($CHCl_3$–hexane 1:1 as the eluent) gave a crude fraction (3.61 g) R_f 0.14 ($CHCl_3$) which was rechromatographed on thick plates of silica ($CHCl_3$–hexane 1:1). The major band was treated with acetic anhydride in pyridine in the usual manner and after work-up, the product chromatographed on thick plates of silica ($CHCl_3$–hexane 1:1). The band with R_f 0.5–0.6 appeared to consist of the two diastereomers ***6a*** and ***6b*** as judged by nmr spectroscopy. On standing in ethanol one of the isomers crystallized (151 mg), mp 96–97°C; ir (KBr): 2100, 1710 cm^{-1}; ^1H nmr ($CDCl_3$) δ: 7.25 (15H, m, 3 C_6H_5); 5.10–4.25 (8H, m, 3 benzylic-CH_2, H, and 6H), 4.25–2.90 (9H, m, at 2′,3′,4′,5′,6′ and 1,3,4), 2.06 (3H, s, CH_3CO) and 2.90–1.18 (4H, m, at 2,5); $[\alpha]_D^{25}$ 50° (*c* 1, $CHCl_3$). *Anal.* calcd. for $C_{35}H_{39}N_9O_7$: C60.24, H5.63, N18.07; found: C60.30, H5.70, N17.84. It was not possible to obtain the other isomer in crystalline form from the mother liquors.

cis-*4,8-Dithiatricyclo[5.1.0.0^{3,5}]octane (7)* (cis-*1,4-Cyclohexadiene bisepisulfide*)

The bisepoxide **1** (1.12 g) was added at 0°C to a stirred suspension of thiourea (2.064 g) in 2 *N* H_2SO_4 (10 ml) under nitrogen. The icebath was removed and stirring continued for 1 h during which time the product dissolved gradually to be replaced by a white precipitate of the bisisothiouronium salt **11**. Aqueous Na_2CO_3 was added to bring the pH to 8.5 and the mixture immediately extracted with benzene. The combined extracts were dried and evaporated to give the bisepisulfide **7** (1.2 g; 83%), mp 64–65°C (hexane–$CHCl_3$). The spectral characteristics are given in Table 1. *Anal.* calcd. for $C_6H_8S_2$: C49.95, H5.59, S44.45; found: C50.07, H5.58, S44.47.

trans-*4,8-Dithiatricyclo[5.1.0.0^{3,5}]octane (9)* (trans-*1,4-Cyclohexadiene bisepisulfide*)

The preceding procedure was followed using 0.336 g of *trans*-1,4-cyclohexadiene bisepoxide (1) and 0.456 g of thiourea in 3 ml of 2 *N* H_2SO_4. After work-up, **9** was obtained (0.28 g; 64.8%) as an oil which upon sublimation *in vacuo* gave crystals, mp 47–48°C. See Table 1 for spectral data. *Anal.* calcd. for $C_6H_8S_2$: C49.95, H5.59, S44.45; found: C49.97, H5.72, S44.51.

cis-*4-Oxa-8-thiatricyclo[5.1.0.0^{3,5}]octane (8)*

To a suspension of *trans*-1,4-cyclohexadienebisepoxide (1) (0.336 g) and thiourea (0.228 g) in water (9 ml) was added at 5°C under nitrogen 1.5 ml of 2 *N* H_2SO_4. The icebath was removed and after 20 min a white precipitate had separated. Stirring was continued for 20 min, the pH brought to 8.5 with aqueous $NaHCO_3$, and the mixture extracted with benzene. The combined extracts were combined, dried and evaporated to give a semisolid mass which was purified on thick plates of silica ($CHCl_3$–hexane 4:1). The major band yielded 0.158 g (36.5% yield) of the *trans*-bisepisulfide **9** (identical to the above product) and the minor band yielded a 0.047 g (12.3% yield) of **8** as an unstable colorless oil, bp 40°C/0.1 Torr. The spectral characteristics are given in Table 1. Reliable microanalyses could not be obtained because of its instability. Unchanged starting material was recovered in 44.6% yield.

trans-*4-Oxa-8-thiatricyclo[5.1.0.0^{3,5}]octane (10)*

Application of the preceding procedure to 0.896 g of **1** and 0.729 g of thiourea in 4 ml of 2 *N* H_2SO_4, led after work-up and chromatography on thick plates of silica ($CHCl_3$–CH_3OH 96:4) to 0.230 g (20% yield) of **10** which after sublimation had mp 62–63°C. See Table 1 for spectral data. *Anal.* calcd. for C_6H_8OS: C56.24, H6.29, S25.02; found: C56.10, H6.23, S24.53.

trans-trans-*1,4/2,5-2,5-Dichloro-1,4-cyclohexanedithiol Diacetate (12)*

A solution of the bisepisulfide **7** (0.65 g) in acetyl chloride was stirred under nitrogen at room temperature for 17 h after which time the mixture was evaporated *in vacuo*, the residue taken up in CH_2Cl_2, the solution washed with aqueous NaCl, dried, and evaporated. From hexane, crystals mp 89–90°C, were obtained (0.587 g or 43.5% yield); ir (KBr): 1680 cm^{-1}; ^1H nmr ($CDCl_3$) δ: 4.03 (4H, m), 2.70–2.40 (4H, m), 2.40 ppm (6H, s); ^{13}C nmr ($CDCl_3$) δ: 192.55 (C—O), 57.68 (C—Cl), 45.00 (C—S), 36.16 (CH_2), 30.38 ppm (CH_3); M^+ 300. *Anal.* calcd. for $C_{10}H_{14}Cl_2O_2S_2$: C40.05, H4.67, S21.22; found: C40.01, H4.72, S21.21.

cis-*1,4-Cyclohexanedithiol Diacetate (**13**)*

A solution of **7** (1.12 g) in dry THF (30 ml) was added dropwise to a refluxing suspension of LAH (0.5 g) in dry ether (30 ml) under nitrogen and heating continued for 2 h after which time a mixture of aqueous HCl–THF was carefully added while cooling in ice. The organic layer was separated, dried and evaporated to give a colorless oil which was taken up in pyridine–acetic anhydride. After standing at room temperature overnight, the mixture was worked up in the usual manner to yield a semisolid consisting of **13** (0.542 g or 30% yield). Sublimation gave white crystals mp 63–65°C; ir (KBr): 1685 cm^{-1}; ^1H nmr ($CDCl_3$) δ: 3.60 (2H, m), 2.30 (6H, s), 1.80 ppm (8H, m); ^{13}C nmr ($CDCl_3$) δ: 30.401 (CH_2 groups), 30.759 (CH_3), 40.92 (C—S), 195.065 ppm (C=O); M^+ 232. *Anal.* calcd. for $C_{10}H_{16}O_2S_2$: C51.69, H6.94, S27.60; found: C51.60, H6.87, S27.63.

trans-trans-*1,5/2,4-2,4-Dithiol-1,5-cyclohexanediol Tetraacetate (**15**)*

A solution of **7** (0.458 g) in dry THF (80 ml) was heated under reflux for 17 h in the presence of $Hg(OAc)_2$ (2.02 g) under nitrogen. Water (5 ml) was added and a stream of H_2S passed through the mixture until precipitation of HgS was complete. Ethyl acetate (100 ml) was added, the mixture filtered, the filtrate washed with aqueous NaCl, dried and evaporated to give an oil which was taken up in pyridine–acetic anhydride. After 16 h, the solution was worked up in the usual manner and the resulting oil purified on thick plates of silica ($CHCl_3$). The major band yielded 0.24 g (21.7% yield) of **15** which crystallized from hexane–$CHCl_3$; mp 121°C; ir (KBr): 1730, 1690 cm^{-1}; ^1H nmr ($CDCl_3$) δ: 4.93 (2H, m), 3.90 (2H, m), 3.00–1.80 (4H, m), 2.40 ppm (6H, s); ^{13}C nmr ($CDCl_3$) δ: 193.13 (S—CO), 169.61 (O—CO), 70.13 (C—O—), 41.65 (C—S), 33.02 and 30.64 (CH_2), 20.93 ppm (CH_3); *m/e* 289 (M^+ – AcO). *Anal.* calcd. for $C_{14}H_{20}O_6S_2$: C48.27, H5.79, S18.41; found: C48.38, H5.70, S18.47.

Acknowledgements

This work was generously supported by Bristol Laboratories of Canada. We are grateful to Dr. A. Perlin for the ^{13}C nmr spectra.

1. G. KAVADIAS, S. VELKOF, and B. BELLEAU. Can. J. Chem. **56**, 404 (1978).
2. G. KAVADIAS and B. BELLEAU. U.S. Patent No. 4,003,922 (January, 1977).
3. G. KAVADIAS, S. VELKOF, and B. BELLEAU. Can. J. Chem. **56**, 2086 (1978).
4. T. SUAMI, S. OGAWA, H. UCHINO, and Y. FUNAKI. J. Org. Chem. **40**, 456 (1975).
5. Y. TAKAGI, T. TSUCHIYA, and S. UMEZAWA. Bull. Chem. Soc. Jpn. **46**, 1261 (1973).
6. T. H. CHAN and J. R. RINKENBINE. J. Am. Chem. Soc. **94**, 2880 (1972).
7. S. KAGABU and H. PRINZBACH. Angew. Chem. Int. Ed., Engl. **14**, 252 (1975).
8. G. E. MCCASLAND, A. K. H. ANISUZZAMAN, S. R. NAIK, and L. J. DURHAM. J. Org. Chem. **37**, 1201 (1972).
9. T. W. CRAIG, G. R. HARVEY, and G. A. BERCHTOLD. J. Org. Chem. **32**, 3743 (1967).

Can. J. Chem. Downloaded from www.nrcresearchpress.com by 210.87.254.40 on 09/05/12
For personal use only.

Phenol sulfate esters: ultraviolet, infrared, ^1H and ^{13}C nuclear magnetic resonance spectroscopic investigation

MARK A. RAGAN[1]

Institute of Marine Biochemistry, N-7034 Trondheim-N.T.H., Norway

Received April 25, 1978

MARK A. RAGAN. Can. J. Chem. **56**, 2681 (1978).

Renewed interest in naturally occurring phenol sulfate ester salts has necessitated modern spectroscopic investigation of these compounds. Synthetic methods, plus spectroscopic (uv, ir, ^1H nmr, ^{13}C nmr), chromatographic, and electrophoretic properties are given for the potassium salts of phenyl sulfate (**1**), pyrocatechol disulfate (**2**), resorcinol disulfate (**3**), hydroquinone disulfate (**4**), phloroglucinol mono- (**5**), di- (**6**), and tri- (**7**) sulfates, and for the 2-sulfate (**8**) and 2,5-disulfate (**9**) of 1,2,3,5-tetrahydroxybenzene (**10**). ^{13}C nmr chemical shift effects resulting from the replacement of phenolic —OH with —OSO_3K are reported. Spectroscopic properties of the related compounds 1,2,3-tribenzyloxybenzene (**11**), 2,6-dibenzyloxy-1,4-benzoquinone (**12**), 2,6-dimethoxy-1,4-benzoquinone (**13**), 1,3-dibenzyloxy-2,5-dihydroxybenzene (**14**), and of a tentatively identified 1,3-dibenzyloxy-2,5-dihydroxybenzene monoethyl ether (**15**) are available as supplementary material.

MARK A. RAGAN. Can. J. Chem. **56**, 2681 (1978).

Un intérêt renouvelé pour les sels de sulfates d'esters de phénols se retrouvant dans la nature a nécessité une étude spectroscopique moderne de ces composés. On a effectué la synthèse et l'on a déterminé les spectres (uv, ir, rmn du ^1H, rmn du ^{13}C) ainsi que les propriétés chromatographiques et électrophorétiques de sels de potassium du sulfate de phényle (**1**), du disulfate de pyrocatéchol (**2**), du disulfate de résorcinol (**3**), du disulfate d'hydroquinone (**4**) et des mono- (**5**), di- (**6**) et tri- (**7**) sulfates du phloroglucinol ainsi que du sulfate-2 (**8**) et du disulfate-2,5 (**9**) tétrahydroxy-1,2,3,5 benzène (**10**). On rapporte l'influence sur les déplacements chimiques en rmn du ^{13}C, du remplacement du —OH phénolique par un —OSO_3K. Les propriétés spectroscopiques des composés apparentés comme le tribenzyloxy-1,2,3 benzène (**11**), la dibenzyloxy-2,6 benzoquinone-1,4 (**12**), le diméthoxy-2,6 benzoquinone-1,4 (**13**), le dibenzyloxy-1,3 dihydroxy-2,5 benzène (**14**) et le composé identifié d'une façon non-définitive comme étant l'éther méthylique du dibenzyloxy-1,3 dihydroxy-2,5 benzène (**15**) sont disponibles sous forme de données supplémentaires.

[Traduit par le journal]

Introduction

Although it has been recognized for many years that phenols may occur as sulfate ester salts in higher animals and plants (1, 2), until about 1950 these compounds were considered to be of infrequent occurrence and minor importance. Eventually sulfate ester salts were implicated as end products in the detoxification of certain phenols by higher animals (3). More recently, Harborne and co-workers (4) have shown that flavonoids often occur as sulfate ester salts in a wide range of higher plants, particularly those growing in marine, estuarine, or freshwater environments; and Jensen and Ragan (5) have demonstrated the presence of the new natural product 1,2,3,5-tetrahydroxybenzene 2,5-disulfate in the marine brown alga *Ascophyllum nodosum* (L.) LeJol. (Phaeophyceae).

Sulfated anthraquinones (6), betacyanins (7), flavonoids (4), and other polyphenols (5) may occur in only small quantities in the plant source and upon extraction may be very unstable. Hence classical methods for determining the position of sulfate groups, usually requiring moderately large quantities of the sulfate, are ill suited to investigation of their structures. It is now demonstrated that spectroscopic methods, particularly ^{13}C nuclear magnetic resonance spectroscopy, provide a rapid and powerful approach to complete structural determination of phenol sulfate ester salts.

The compounds synthesized for spectroscopic (uv, ir, ^1H nmr, ^{13}C nmr), chromatographic and electrophoretic investigation were the potassium salts of (mono)phenyl sulfate (**1**); the disulfates of pyrocatechol (**2**), resorcinol (**3**), and hydroquinone (**4**); the mono- (**5**), di- (**6**), and tri- (**7**) sulfates of phloroglucinol; and the 2-sulfate (**8**) and 2,5-disulfate (**9**) of 1,2,3,5-tetrahydroxybenzene (**10**). Although not **1** (1, 8–21), or **2** (16), or **4** (22, 23) is a new product, no spectroscopic data have been reported for them; **3**, **5**, **6**, and **7** appear to be new compounds. Some spectroscopic data for **8** and **9** have been reported earlier (5).

Results and Discussion

Of the methods examined for the preparation of phenol sulfate ester salts (1, 8–12, 15, 20, 24, 25), the one found to be most suitable for routine application

[1]Present address: Atlantic Regional Laboratory, National Research Council of Canada, Halifax, N.S., Canada B3H 3Z1.

Can. J. Chem. Downloaded from www.nrcresearchpress.com by 210.87.254.6 on 09/05/12
For personal use only.

TABLE 1. Substituent effects for —OH and —OSO_3K on the benzene ring, and replacement effects for —OH → —OSO_3K. Positive values are downfield from TMS. All data in ppm*

	Column A			Column B			Column C
Position	—OH	—OSO_3K	—OH → —OSO_3K	—OH	—OSO_3K	—OH → —OSO_3K	—OH → —OSO_3K
ipso	+25.5	+22.7	−2.8	+27.1	+22.2	−5.0	−5.8 ± 2.1
ortho	−14.6	−6.8	+7.8	−12.9	−6.6	+6.3	+5.4 ± 0.9
meta	0.0	+1.6	+1.6	+1.1	+1.1	0.0	+0.7 ± 1.1
para	−9.3	−1.9	+7.4	−8.0	−2.4	+5.6	+6.5 ± 1.9

*Values in column A from phenol and **1**; values in column B from resorcinol and **3**; values in column C from **5** and **6** vis-a-vis phloroglucinol; see text.

on the 0.05–0.10 mol scale was a modification of that of Feigenbaum and Neuberg (15), in which the phenol (dissolved in pyridine) was added in one portion to a cooled pyridine solution of the pyridine–SO_3 complex (see Experimental). Compounds **1** → **4** and **7** were white or nearly-white solids which could be crystallized (with slight decomposition) from aqueous methanol or ethanol, and with the exception of **1** were extremely soluble in cool water. The trisulfate **7** was less soluble in methanol or ethanol than were the disulfates **2** → **4**, which were in turn less soluble than **1** or **8**. Although relatively stable at room temperature when dry, in aqueous solution the sulfate salts underwent progressive hydrolysis (12, 26–28). Attempted replacement of the K^+ counterions with H^+ on Dowex 50-W caused considerable decomposition.

Analytical separation of **1** → **9** was carried out more successfully by paper electrophoresis (pH 1.5–5.0, usually pH 4.0) than by paper chromatography (see Experimental). The former method allowed separation of investigated monosulfates ($R_{\text{phloroglucinol trisulfate}} \equiv R_7 = 0.44$–$0.60$) and disulfates ($R_7 = 0.78$–$0.89$) from trisulfates ($R_7$ around 1.00) (4, 25).

The sulfate ester salts exhibited bimodal uv spectra, with aromatic absorption at about 270 nm, together with a characteristic absorption at 220–225 nm not present in the corresponding free phenols and possibly involving the sulfate group(s): compare the 220–225 nm extinction coefficients of **1** vs. **2** → **4**, and of **8** vs. **9**.

In addition to the expected strong ester sulfate ir bands at 1040–1070 (C—O—S) and 1225–1290 (S=O) cm^{-1} (25), additional ir bands not seen with the corresponding free phenols were observed in spectra of *o*- and *p*-sulfate ester salts at 625–640, 685–725, and 840–870 cm^{-1}. Although the precise position of these bands differed for each investigated phenol sulfate ester salt, both monosulfates (**1**, **8**) absorbed at 640 and 690–695 cm^{-1}, and both *p*-disulfates (**4**, **9**) at 620–630 and 850–870 cm^{-1}. The *m*-substituted sulfate ester salts **3** and **7** showed more complex ir bands which could not be easily reconciled with this pattern. No evidence was found for contamination of the preparations with potassium sulfate (found upon addition of potassium sulfate: 1110 and 615 cm^{-1}).

In comparison with ^1H nmr signals of the corresponding free phenols, ring proton signals of **1** → **4** and **7** → **9** appeared farther downfield relative to TMS (solvent: D_2O). The spin–spin systems were in all cases as expected (29).

^{13}C nmr proved to be very useful for detecting the pattern of sulfate substitution. Although the replacement of a phenolic —OH group by —OSO_3K had little effect on either the relative signal intensities per nucleus (and hence on relative relaxation and nuclear Overhauser enhancement) or the magnitude of ^{13}C–^1H coupling constants, the ^{13}C chemical shifts were changed in a predictable manner (Table 1). The replacement effects for conversion of —OH to —OSO_3K were calculated as follows (solvent, D_2O): ^{13}C nmr chemical shifts of phenol itself were assigned from published data (30) and from nondecoupled spectra, enabling signals of **1** to be assigned from chemical shift (C-1), ^{13}C–^1H coupling (C-2,6 vs. C-3,5) and signal intensity (C-1; also C-4 vs. C-2,6) data. Thus substituent effects for —OH (30) and —OSO_3K on the benzene ring could be determined, and the replacement effect for conversion of —OH to —OSO_3K was calculated by subtraction (Table 1, column A). Using these substituent effects, signals in the spectra of resorcinol and of **3** were assigned, and the assignments were again confirmed from nondecoupled spectra. From these shifts, substituent effects for —OH and —OSO_3K were again calculated, and replacement effects for —OH → —OSO_3K determined by subtraction (Table 1, column B). The latter replacement effects were found to be valid for estimation of chemical shifts of sulfate ester salts of all the other simple polyphenols investigated, when calculated from the shifts of the corresponding free phenols.

A further refinement was, however, possible: from these replacement effects (column B), it was possible to assign ^{13}C signals from **5** and **6** in spectra of a mixture containing phloroglucinol, **5**, **6**, and **7**. To the extent possible, these assignments were confirmed (*i*) by proton-decoupled ^{13}C spectra of phloro-

Can. J. Chem. Downloaded from www.nrcresearchpress.com by 210.87.254.6 on 09/05/12
For personal use only.

Can. J. Chem. Downloaded from www.nrcresearchpress.com by 210.87.254.6 on 09/05/12
For personal use only.

glucinol and of **7** individually; (*ii*) by nondecoupled spectra, using convolution difference methods (31) where necessary; and (*iii*) by correlation of relative signal intensity (separately for ^{13}C—H and ^{13}C—O— nuclei) with compound abundance as estimated from paper chromatography and paper electrophoresis. From these eight shifts, the replacement effects for —OH → —OSO_3K were calculated directly for **5** and **6**. Owing to slight inconsistencies between individual substituent effects in **5** and **6**, a rough estimate of the imprecision of the calculated values was also obtained (Table 1, column C).

These replacement effects (Table 1, column C) were used to calculate expected ^{13}C chemical shifts for all possible symmetrical sulfate esters of 1,2,3,5-tetrahydroxybenzene (**10**), allowing the 'phenolic precursor' in exudates of *Ascophyllum nodosum* to be identified as 1,2,3,5-tetrahydroxybenzene 2,5-disulfate; this was confirmed by synthesis (5). It is likely that these replacement effects will in similar fashion prove useful in the eventual assignment of ^{13}C nmr spectra of sulfated flavonoids and related natural products. In favorable situations (such as that reported here with mixtures of phloroglucinol and **5** → **7**), simple mixtures of sulfated polyphenols may be resolved by this approach.

Experimental

Ultraviolet spectra (ε in parentheses) were recorded in methanol (for **10**), 9:1 (v/v) methanol–water (**1**), or 4:1 methanol–water (**2** → **4**, **7**) using a Coleman-Hitachi 124. Infrared spectra were recorded in KBr using a Hitachi Perkin-Elmer 257. Mass spectra were taken at 70 eV using an AEI MS-902 with on-line PDP 8/1 computer. ^1H nmr (99.6 MHz) and ^{13}C nmr (25.05 MHz) spectra of the sulfate ester salts and of the corresponding free phenols were recorded using a JEOL FX-100 operated in FT mode. Proton-decoupled ^{13}C spectra were recorded in D_2O, and non-decoupled ^{13}C spectra (either with or without retention of nOe) in approximately 1:1 (v/v) H_2O–D_2O. Chemical shifts (δ and δ_C) are reported relative to TMS (10% in $CDCl_3$ in a coaxial capillary). Nondecoupled ^{13}C spectra were enhanced, when necessary, by convolution difference techniques (31). The resolution was 1.2 Hz or better for **1** → **10**. Ascending mode paper chromatography was done on Whatman No. 1 paper using 20% (w/v) aqueous KCl (32). Paper electrophoresis was carried out as described earlier (5). Sulfate ester salts were detected on paper by the usual spray reagents (33) applied after mild acid hydrolysis (15% concentrated HCl in ethanol with gentle heating) or with acidic spray reagents such as vanillin–HCl, Ehrlich's reagent, anisaldehyde–HCl, or diazo reagents in excess HNO_2. With vanillin–HCl, the temporal order of color development upon gentle heating was phloroglucinol > **5** > **6** > **7**.

All reagents were AR grade. The pyridine–SO_3 complex was routinely prepared from pyridine and chlorosulfuric acid (9,12) (see below) but for critical small-scale work was instead prepared from solid SO_3 and pyridine (12, 34).

Complete Sulfation of Polyphenols

General procedure (**1** → **4**, **7**): pyridine (ca. 50 ml) was cooled to −20°C and 0.115 mol (7.5 ml) chlorosulfuric acid (chlorosulfonic acid) was added dropwise (CAUTION!) with manual stirring and efficient cooling. After cooling again to −20°C, a solution of the *anhydrous* polyphenol (0.10 mol equiv.) in pyridine (ca. 30 ml) was added in one portion and the solution was stirred overnight at room temperature. Thereafter, excess solvent was evaporated *in vacuo* (<40°C). The syrupy residue was redissolved in distilled water (200 ml) and the pH adjusted to 8.0–8.5 with dilute aqueous KOH. After 10–15 min, the solvent was removed *in vacuo* (<35°C). The residue was redissolved in boiling ethanol (for **1**) or alternatively was washed with boiling ethanol to remove color, filtered immediately (Whatman GF/C), redissolved in boiling, very slightly basic methanol–water (4:1 v/v for **2** → **4**; 7:3 for **7**), and filtered hot (GF/C) before crystallization. With **7**, this entire procedure was repeated once; for **1** → **4**, one sulfation was sufficient and yields were 80–95% of theoretical. Elemental analyses tended to be 5–8% low after crystallization, owing largely to contaminating inorganic salts which, however, did not interfere with spectroscopic investigation.

Attempts to form pyrogallol trisulfate by repeated application of this method were unsuccessful, giving primarily a mixture of mono- and disulfate esters, plus uncharacterized by-products.

Partial Sulfation

Compounds **5** and **6** were synthesized by the above method from phloroglucinol *dihydrate* (0.15 mol equiv.), using only 0.075 mol of chlorosulfuric acid; after work-up (see **7**) the product, which contained contaminating phloroglucinol and **7**, was not purified further but ^{13}C signals of **5** and **6** individually could be identified unambiguously in spectra of the mixture (see text). Compound **9** was synthesized similarly from **8** (5).

Phenyl sulfate, potassium salt (***1***) — λ_{max}: 271 (190), 264 (260), 259 (250), 252 (sh, 200), 221 nm (620); ν_{max}: 640m, 690m, 695m, 720w, 735m, 775ms, 820w, 865ms, 905w, 915w, 1010w, 1020w, 1060s, 1125w, 1160w, 1210m, 1235s, 1255s, 1260s, 1280s, 1450w, 1485m, 1585m, 3060w cm^{-1}; δ: complex, asymmetric multiplet (unlike that of phenol in D_2O), with major signals at 7.29, 7.32, 7.36, 7.40, 7.46 ppm; δ_C and J_{CH}: see Table 2; pc: R_f = 0.81; pe: R_7 = 0.60.

Pyrocatechol (1,2-dihydroxybenzene) disulfate ester, dipotassium salt (***2***) — λ_{max}: 271 (455), 266 (540), 221 (1090), 215 (sh, 1030); ν_{max}: 635m, 725ms, 775ms, 845m, 885w, 895m, 960w, 1040s, 1060s, 1115w, 1165w, 1190w, 1245w, 1270s, 1455w, 1465w, 1495m, 1595w, 1620-1640w cm^{-1}; δ: AA′BB′ system (14 lines resolved), ($\nu_A - \nu_B$) approximately 20–25 Hz, symmetrical around centroid 7.52 ppm; δ_C and J_{CH}: see Table 2; pc: R_f = 0.94; pe: R_7 = 0.89. *Monosulfate, monopotassium salt* (16, 17, 28, 35): pc: R_f = 0.85; pe: R_7 = 0.50.

Resorcinol (1,3-dihydroxybenzene) disulfate ester, dipotassium salt (***3***) — λ_{max}: 271.5 (330), 265 (395), 220nm (1130). ν_{max}: 625w, 680m, 690w, 730m, 760m, 795w, 805w, 845m, 870m, 960ms, 1050s, 1055s, 1070m, 1090m, 1120m, 1225s, 1240s, 1275s, 1290s, 1465w, 1480m, 1590m, 1605m, 3065w, 3125w cm^{-1}; δ: AB_2X system (approximately 25 signals resolved) with major signal at 7.35 ppm; δ_C and J_{CH}: see Table 2; pc: R_f = 0.91; pe: R_7 = 0.84. *Monosulfate, monopotassium salt* (16): pc: R_f = 0.78; pe: R_7 = 0.53.

Hydroquinone (1,4-dihydroxybenzene) disulfate ester, dipotassium salt (***4***) — λ_{max}: 268 (510), 224nm (1280); ν_{max}: 620m, 630ms, 700m, 715ms, 850s, 860s, 870s, 975w, 1010w, 1020wm, 1055s, 1095w, 1100wm, 1190ms, 1240s, 1265s, 1280s, 1285s, 1500s, 1895w, 1930w, 3110w cm^{-1}; δ: 7.38 ppm; δ_C and J_{CH}: see Table 2; pc: R_f = 0.91; pe: R_7 = 0.86. *Monosulfate, monopotassium salt* (16, 18, 19, 22, 36): pc: R_7 = 0.80; pe: R_f = 0.48.

Phloroglucinol (1,3,5-trihydroxybenzene) monosulfate ester, potassium salt (***5***) — δ_C and J_{CH}: see Table 2. In nondecoupled

Can. J. Chem. Downloaded from www.nrcresearchpress.com by 210.87.254.6 on 09/05/12
For personal use only.

TABLE 2. Chemical shifts (δ_C) in ppm and ^{13}C–^{1}H coupling constants in Hz for compounds **1** through **10**

	Chemical shifts					
Compound	C-1	C-2	C-3	C-4	C-5	C-6
1	151.2	121.7	130.1	126.6	130.1	121.7
2	143.4	143.4	123.5	127.4	127.4	123.5
3	151.8	115.3	151.8	119.5	130.7	119.5
4	149.0	123.0	123.0	149.0	123.0	123.0
5	152.9	101.2	158.4	101.4	158.4	101.2
6	152.5	105.6	152.5	107.7	160.2	107.7
7	152.2	113.2	152.2	113.2	152.2	113.2
8	150.0	121.6	150.0	96.0	154.1	96.0
9	150.4	126.2	150.4	103.0	149.5	103.0
10	146.5	125.6	146.5	95.7	149.5	95.7
	Coupling constants, $^{1}J_{CH}$, all doublets					
Compound	C-1	C-2	C-3	C-4	C-5	C-6
1	—	163.6	162.4	163.6	162.4	163.6
2	—	—	164.8	164.8	164.8	164.8
3	—	166.0	—	166.0	166.0	166.0
4	—	166.0	166.0	—	166.0	166.0
5	—	~162	—	~162	—	162
6	—	169.7	—	163.6	—	163.6
7	—	169.7	—	169.7	—	169.7
8	—	—	—	162.4	—	162.4
9	—	—	—	166.2	—	166.2
10	—	—	—	159.3	—	159.3
	Coupling constants, $^{2}J_{CH}$ and/or $^{4}J_{CH}$					
Compound	C-1	C-2	C-3	C-4	C-5	C-6
1	m	m	m	m	m	m
2	d ~3.6	d ~3.6	t ~2.4	m	m	t ~2.4
3	m	m	m	m	m	m
4	m	(+)	(+)	(+)	(+)	(+)
5	(++)	—	m ~4.2	—	m ~4.2	—
6	(++)	—	(++)	—	m ~3	—
7	m ~3.7	—	m ~3.7	—	m ~3.7	—
8	br	—	br	—	t 3.7	—
9	m	—	m	—	t 5.1	—
10	br	—	br	—	t 3.7	—
	Coupling constants, $^{3}J_{CH}$					
Compound	C-1	C-2	C-3	C-4	C-5	C-6
1	m	t ~6.1	d 7.3	t 6.7	d 7.3	t ~6.1
2	t ~7.9	t ~7.9	d ~9.8	d 8.5	d 8.5	d ~9.8
3	m	t 4.9	m	m ~6.1	—	m ~6.1
4	m	(+)	(+)	m	(+)	(+)
5	—	m	—	t ~3	—	m
6	—	t ~4.3	—	t 4.9	—	t 4.9
7	—	t 4.8	—	t 4.8	—	t 4.8
8	—	m ~7	—	d 4.9	—	d 4.9
9	—	t 6.7	—	d 4.4	—	d 4.4
10	—	m ~7	—	d ~5.5	—	d ~5.5

NOTE: (+) $^{n}J_{CH}$ approximately 3.0 Hz but n not determined; (++) see Experimental; m, multiplet; d, doublet; t, triplet; br, broad 'singlet' (multiplicity not resolved).

Can. J. Chem. Downloaded from www.nrcresearchpress.com by 210.87.254.6 on 09/05/12
For personal use only.

spectra (mixtures of phloroglucinol, **5**, **6**, and **7**), the signals from C-1 were partially obscured by those of C-1,3 of **6** and C-1,3,5 of **7**, while signals from C-4,6 of **6** obscured one of the $^1J_{CH}$ doublets of C-4 and of C-2,6; pc: $R_f = 0.81$; pe: $R_7 = 0.78$.

Phloroglucinol disulfate ester, dipotassium salt (***6***) — δ_C and J_{CH}: see Table 2; pc: $R_f = 0.71$; pe: $R_7 = 0.44$.

Phloroglucinol trisulfate ester, tripotassium salt (***7***) — λ_{max}: 270 (170), 266 (180), 215 nm (1260); ν_{max}: 670m, 685m, 715w, 740w, 755m, 805wm, 890wm, 990s, 1055s, 1125wm, 1255s, 1450m, 1605m, 3090w cm^{-1}; δ: 7.39 ppm; δ_C and J_{CH}: see Table 2; pc: $R_f = 0.89$.

1,2,3,5-Tetrahydroxybenzene 2-sulfate ester, potassium salt (***8***) — uv, ir, and ^1H nmr data have been presented earlier (5); δ_C and J_{CH}: see Table 2; pc: $R_f = 0.73$; pe: $R_7 = 0.56$. Most preparations also contained a disulfate of unknown structure as a very minor contaminant: pc: $R_f = 0.85$; pe: $R_7 = 0.83$.

1,2,3,5-Tetrahydroxybenzene 2,5-disulfate ester, dipotassium salt (***9***) — uv, ir, ^1H nmr, and ^{13}C nmr data have been presented earlier (5), see also Table 2; pc: $R_f = 0.87$; pe: $R_7 = 0.76$. Native preparations from *Ascophyllum nodosum* contain a monosulfate of unknown structure presumably based on **10**; pc of monosulfate: $R_f = 0.72$; pe: $R_7 = 0.56$ (compare with **8**). Preparations from *A. nodosum* also contain traces of a disulfate tentatively identified as the 1,3-disulfate ester of **10** (5).

1,2,3,5-Tetrahydroxybenzene (***10***)—Compound **10** was formed by catalytic hydrogenolysis of 2,6-dibenzyloxy-1,4-benzoquinone (**12**) (ref. 37 and footnote 2). In contrast to the report of Baxter and Brown (37), but in agreement with the older literature (see references cited in ref. 37), the product discolored slowly in air, although **12** had been thrice crystallized; mp (capillary, uncorrected) 166–169°C (lit. (37) mp 168–170°C, (38) mp 165–167°C); λ_{max}: 266–290 (broad, flat absorption; 560), 239 nm (550); ν_{max}: 650w, 680w, 790m, 810m, 820w, 835w, 1000ms, 1005ms, 1045s, 1140s, 1155s, 1180s, 1195s, 1300s, 1380m, 1485s, 1520m, 1530s, 1630s, 3280s cm^{-1}; δ: 6.01 ppm. δ_C and J_{CH}: see Table 2. The protons directly bonded to C-4,6 were exchangeable into D_2O, as evidenced by the gradual loss of ^{13}C–^1H couplings during 24 to 48 h (cf. ref. 39); ms (90°C) *m/e*: 142 (M^+; 100%), 141 (6%), 140 (5%), 113 (5%), 96 (31%), 78 (10%), 71 (10%), 69 (13%).

Acknowledgements

T. Anthonsen, H. Grasdalen, A. Jensen, H. Kjøsen, B. Larsen, and T. Painter made helpful suggestions throughout the course of this work. Nuclear magnetic resonance spectra were provided by H. Grasdalen and J. Halvorsen. Professor H. Yoshikawa kindly translated ref. 16. I thank the National Research Council of Canada for financial support.

[2]1,2,3,5-Tetrahydroxybenzene (**10**), required for spectroscopic investigation of **8** and **9**, was synthesized by classical methods from 1,2,3-trihydroxybenzene via 1,2,3-tribenzyloxybenzene (**11**) and 2,6-dibenzyloxy-1,4-benzoquinone (**12**). Comprehensive uv, ir, ^1H nmr and ^{13}C nmr properties of these compounds are described in the supplementary material (available, at a nominal charge, from The Depository of Unpublished Data, CISTI, National Research Council of Canada, Ottawa, Ont. Canada K1A 0S2), as are spectroscopic data of the reference compounds 2,6-dimethoxy-1,4-benzoquinone (**13**), 1,3-dibenzyloxy-2,5-dihydroxybenzene (**14**), and a tentatively identified 1,3-dibenzyloxy-2,5-dihydroxybenzene monoethyl ether (**15**).

1. E. Baumann. Ber. Dtsch. Chem. Ges. **9**, 54 (1876).
2. R. Kawaguchi and K. W. Kim. J. Pharm. Soc. Jpn. **57**, 180 (1937); Chem. Abstr. **33**, 6310/6 (1939).
3. R. T. Williams. *In* Biochemistry of phenolic compounds. *Edited by* J. B. Harborne. Academic Press, London. 1964. pp. 205–248.
4. J. B. Harborne. Progr. Phytochem. **4**, 189 (1977).
5. A. Jensen and M. A. Ragan. Tetrahedron Lett. 847 (1978).
6. J. B. Harborne and N. Mokhtari. Phytochemistry, **16**, 1314 (1977).
7. F. Imperato. Phytochemistry, **14**, 2526 (1975).
8. E. Czapek. Monatsh. Chem. **35**, 635 (1914).
9. A. Verley. Mem. Soc. Chim. Ser. III, **25**, 46 (1901).
10. C. Neuberg and E. Simon. Biochem. Z. **156**, 365 (1925).
11. P. Baumgarten. Ber. Dtsch. Chem. Ges. **59**, 1976 (1926).
12. G. N. Burkhardt and A. Lapworth. J. Chem. Soc. 684 (1926).
13. G. N. Burkhardt. J. Chem. Soc. 337 (1933).
14. G. N. Burkhardt, W. G. K. Ford, and E. Singleton. J. Chem. Soc. 17 (1936).
15. J. Feigenbaum and C. A. Neuberg. J. Am. Chem. Soc. **63**, 3529 (1941).
16. S. Yamaguchi. Nippon Kagaku Zasshi, **80**, 171 (1959).
17. T. Sato, T. Fukuyama, T. Suzuki, and H. Yoshikawa. J. Biochem. **53**, 23 (1963).
18. B. Williams, L. G. Dring, and R. T. Williams. Biochem. J. **127**, 24P (1972).
19. I. D. Capel, M. R. French, P. Millburn, R. L. Smith, and R. T. Williams. Biochem. J. **127**, 25P (1972).
20. J. B. Hawkins and L. Young. Biochem. J. **56**, 166 (1954).
21. K. S. Dodgson, F. A. Rose, and N. Tudball. Biochem. J. **71**, 10 (1959).
22. M. Scalera, W. B. Hardy, E. M. Hardy, and A. W. Joyce. J. Am. Chem. Soc. **73**, 3094 (1951).
23. W. Bradley and J. G. Lee. J. Chem. Soc. 3549 (1957).
24. E. E. Gilbert. Sulfonation and related reactions. Interscience Publishers, New York, NY. 1965. pp. 375–382.
25. D. J. Hearse, A. H. Olavesen, and G. M. Powell. Biochem. Pharmacol. **18**, 173 (1969).
26. G. N. Burkhardt, C. Horrex, and D. I. Jenkins. J. Chem. Soc. 1649 (1936).
27. G. N. Burkhardt, A. G. Evans, and E. Warhurst. J. Chem. Soc. 25 (1936).
28. E. T. Kaiser and O. R. Zaborsky. J. Am. Chem. Soc. **90**, 4626 (1968).
29. J. C. Schug and J. C. Deck. J. Chem. Phys. **37**, 2618 (1962).
30. J. B. Stothers. Carbon-13 nmr spectroscopy. Academic Press, New York, NY. 1972.
31. I. D. Campbell, C. M. Dobson, R. J. P. Williams, and A. V. Xavier. J. Magn. Reson. **11**, 172 (1973).
32. Kjemisk Avdeling av Norsk Institutt for Tang- og Tareforskning. Norsk Inst. for Tang- og Tareforsk. Foreløbige Rapp. **89** (1959).
33. M. A. Ragan and J. S. Craigie. *In* Handbook of phycological methods. Vol. 2. *Edited by* J. Hellebust and J. S. Craigie. Cambridge University Press, London. In press.
34. L. F. Fieser and M. Fieser. Reagents for organic synthesis. Vol. 1. John Wiley & Sons, New York, NY. 1967. p. 1127.
35. G. A. Garton and R. T. Williams. Biochem. J. **43**, 206 (1948).
36. W. Baker and N. C. Brown. J. Chem. Soc. 2303 (1948).
37. R. A. Baxter and J. P. Brown. Chem. Ind. (London), 1171 (1967).
38. T. Posternak. Helv. Chim. Acta, **19**, 1333 (1936).
39. J. S. Craigie, A. G. McInnes, M. A. Ragan, and J. A. Walter. Can. J. Chem. **55**, 1575 (1977).

A facile synthesis of methyl 3,6-dideoxy-α-L-*xylo*-hexopyranoside (colitose)[1]

DAVID R. BUNDLE AND STAFFAN JOSEPHSON[2]

Division of Biological Sciences, National Research Council of Canada, Ottawa, Ont., Canada K1A 0R6

Received May 15, 1978

DAVID R. BUNDLE and STAFFAN JOSEPHSON. Can. J. Chem. **56**, 2686 (1978).

Methyl 3,6-dideoxy-α-L-*xylo*-hexopyranoside (**7**) has been synthesised in four steps from methyl α-L-fucopyranoside. The intermediate methyl 3,4-*O*-benzylidene-α-L-fucopyranoside was separated into the *S* (**1***a*) and *R* (**1***b*) diastereoisomers and the absolute configuration established by proton and carbon-13 nmr spectroscopy. Under the conditions of the Hanessian–Hullar reaction methyl 4-*O*-benzoyl-3-bromo-3,6-dideoxy-α-L-gulopyranoside was the major product. Each diastereoisomer **1***a* or **1***b* gave identical products and product ratios; the stereochemistry and relative proportions of these products were determined by proton and carbon-13 nmr. The synthesis of ascarylose from methyl α-L-rhamnopyranoside by an analogous route is also reported. The bromo deoxy intermediates were reduced to the dideoxy sugars by catalytic hydrogenation with palladium.

DAVID R. BUNDLE et STAFFAN JOSEPHSON. Can. J. Chem. **56**, 2686 (1978).

On a synthétisé le didéoxy-3,6 α-L-*xylo*-hexapyrannoside (**7**) de méthyle en quatre étapes à partir de l'α-L-fucopyrannoside de méthyle. On a séparé l'intermédiaire *O*-benzylidène-3,4 α-L-fucopyrannoside de méthyl en diastéréoisomères *S* (**1***a*) et *R* (**1***b*) et on en a établi la configuration absolue par spectroscopie rmn du proton et du carbone 13. Faisant appel aux conditions de la réaction de Hanessian–Hullar, le produit principal est le *O*-benzoyl-4 bromo-3 didéoxy-3,6 α-L-gulopyrannoside de méthyle. Chacun des diastéréoisomères **1***a* ou **1***b* conduit à des produits et à des rapports de produits identiques; on a déterminé la stéréochimie et les proportions relatives de ces produits par rmn du proton et du carbone 13. On rapporte aussi la synthèse de l'ascarylose à partir de l'α-L-rhamnopyrannoside de méthyle par une voie analogue. On a réduit les intermédiaires bromo-déoxy en sucres didéoxy par une hydrogénation catalytique avec du palladium.

[Traduit par le journal]

Introduction

Colitose, 3,6-dideoxy-L-*xylo*-hexose, is a constituent of several lipopolysaccharides (LPS) (1, 2). Unlike the other 3,6-dideoxyhexoses tyvelose, paratose, and abequose, which also occur in the LPS of various strains of *Salmonella* (1), colitose is the only dideoxy hexose that also occurs in the LPS of *Escherichia coli* (2). Although colitose has been synthesised as a racemic mixture with its optical antipode abequose (3) no practical synthesis of this important sugar has been reported. The synthesis of this sugar for subsequent use in halide ion (4) catalysed glycosylation reactions was necessary to provide a route to artificial antigens. This was achieved starting from readily available L-fucose. To compare certain nmr parameters of the intermediate 3-bromo-3,6-dideoxyhexopyranosides, ascarylose, 3,6-dideoxy-L-*arabino*-hexose was synthesised. This latter synthesis utilised essentially the same route as that reported in a publication that appeared whilst this work was in progress (5).

Results and Discussion

The synthesis of 3,6-dideoxyhexopyranosides in a form suitable for subsequent use in either halide ion (4) catalysed glycosylation or modified Koenigs–Knorr (6, 7) conditions generally proceeds by one of two routes. Either a 3-deoxy-4,6-*O*-benzylidene-hexopyranoside is used to introduce the 6-deoxy function (8), or alternatively a readily available 6-deoxyhexopyranoside possessing either a suitable epoxide (9) or benzylidene acetal of the 1,3-dioxalane type is used to introduce the 3-deoxy function by way of a bromo deoxy derivative (5, 8). In the synthesis reported here we have used the latter route starting from readily available L-fucose (6-deoxy-L-galactose), which provides the title compound (**7**) in five steps from the 6-deoxyaldohexose.

Methyl α-L-fucopyranoside was converted to a mixture of *S* and *R* isomers of the 3,4-*O*-benzylidene acetals, **1***a* and **1***b* using either α,α-dimethoxytoluene (10) or α,α-dibromotoluene in pyridine (11). Although the latter method resulted in the preferential formation of the *S* isomer (H-*endo*) to the extent, **1***a*:**1***b*, 2:1 the product required chromatographic purification before the next step. The acetal exchange method (10), however, provided **1***a* and **1***b* in the ratio 1:1 from which a 15% yield of pure *R* isomer (**1***b*) could be readily crystallised. The remaining mixture of diastereoisomers could be used directly in the next step or resolved by column chromatography after conversion to the *p*-nitrobenzoates **2***a* and **2***b*.

[1]NRCC No. 16861.

[2]NRCC Research Associate.

Can. J. Chem. Downloaded from www.nrcresearchpress.com by 210.87.254.105 on 09/05/12
For personal use only.

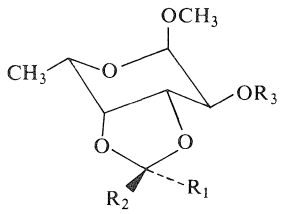

1*a* $R_1 = R_3 = H, R_2 = C_6H_5$
1*b* $R_1 = C_6H_5, R_2 = R_3 = H$
2*a* $R_1 = H, R_2 = C_6H_5, R_3 = p\text{-}NO_2C_6H_4CO$
2*b* $R_1 = C_6H_5, R_2 = H, R_3 = p\text{-}NO_2C_6H_4CO$

Treatment of **1***a* or **1***b* with *N*-bromosuccinimide (NBS) in refluxing carbon tetrachloride (12) yielded the bromo sugar (**3**) in greater than 80% yield. When either the pure *R* or *S* isomer was used as starting material a 5:1 ratio of methyl 4-*O*-benzoyl-3-bromo-3,6-dideoxy-α-L-gulopyranoside (**3**) to methyl 3-*O*-benzoyl-4-bromo-4,6-dideoxy-α-L-glucopyranoside (**4**) was obtained. If the crude syrup obtained from the acetylation step was used directly in the Hanessian–Hullar reaction (12) the ratio of gulopyranoside (**3**) to glucopyranoside (**4**) was found to be 2:1. However, if this syrup was first triturated with Skellysolve B to remove α,α-dimethoxytoluene and other impurities and then dried, the product ratio was again 5:1. Deliberate contamination of crystalline starting material **1***a* or **1***b* with 10% α,α-dimethoxytoluene did not produce the larger proportion of glucopyranoside (**4**) relative to gulopyranoside (**3**), that had been observed for crude syrup. The nature of the impurity causing the change of product ratios remains obscure. Several bromination reactions were conducted using crystalline samples of **1***a*, **1***b*, and mixtures of **1***a* and **1***b*. The reaction products without chromatographic treatment were quantified by ^{13}C nmr spectroscopy and in each case the ratio of gulopyranoside (**3**) to glucopyranoside (**4**) remained 5:1 even for syrups of **1***a* and **1***b*. It should be noted that, whereas crystalline starting material always reacted rapidly in less than 20 minutes under the conditions of the Hanessian–Hullar reaction (12) (a period much shorter than those previously reported (12, 13)), syrups invariably took at least 3 h to react completely.

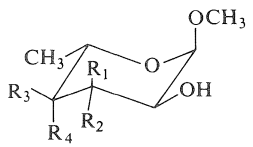

3 $R_1 = Br, R_2 = R_3 = H, R_4 = C_6H_5COO$
4 $R_1 = R_4 = H, R_2 = C_6H_5COO, R_3 = Br$
5 $R_1 = R_2 = R_3 = H, R_4 = C_6H_5COO$
6 $R_1 = R_3 = R_4 = H, R_2 = C_6H_5COO$
7 $R_1 = R_2 = R_3 = H, R_4 = OH$

Proton nmr spectra (Table 1) of compounds **1***a* and **1***b* establish that these acetals exist as distorted $^1C_4$ chairs owing to the constraints imposed by the 1,3-dioxalane ring. Assignment of absolute configuration at the acetal carbon is based on established rules (14, 15) relating relative chemical shifts of benzylic protons to stereochemistry. In contrast, comparison of ^{13}C chemical shifts (Table 2) of the acetal carbon atoms for *R* and *S* isomers shows the reverse order; that is *R* isomer (H-*exo*) at lower field than the *S* isomer (H-*endo*). Although the aforementioned observation is to be expected an additional consequence of the *endo*-phenyl substituent of **1***b* is the deshielding, to the extent of 1.9 ppm of the C-2 resonance, owing presumably to the anisotropic deshielding influence of the phenyl ring. All other ring carbons for both isomers **1***a* and **1***b* possess very similar chemical shifts. Based on these observations, ^{13}C nmr may also be used by analogy with ^1H nmr to assign absolute configuration of acetals.

Despite significant 1,3-*syn*-diaxial interactions present in the $^1C_4$ conformation of the gulopyranoside (**3**), the three-bond coupling constants (Table 1) are consistent with a somewhat distorted $^1C_4$ chair and exclude any of the alternate higher energy boat or skew-boat conformations. The proton, H-5, of the gulopyranoside (**3**) is deshielded by 0.5 ppm relative to the H-5 proton of either the acetal **1***b* or the altropyranoside (**9**), which also possesses a *syn*-axial bromine substituent. However, this deshielding may be attributed to the combined effects of a vicinal *trans*-axial, benzoate group and the *syn*-axial bromine atom (16). The ^1H and ^{13}C nmr parameters for the compounds **1**–**11** (Tables 1 and 2) provide proof of the configuration and conformation assigned to these structures **1**–**11**.

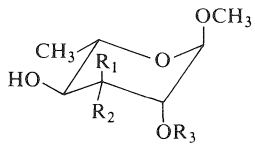

9 $R_1 = Br, R_2 = H, R_3 = C_6H_5CO$
10 $R_1 = R_2 = H, R_3 = C_6H_5CO$
11 $R_1 = R_2 = R_3 = H$

Selective proton decoupling was used to unequivocally assign the ^{13}C resonances in several instances (Table 2). Carbon-13 nmr was most effective in monitoring the regiospecificity of the NBS reaction and in conjunction with the proton–proton coupling constant data of Table 1, clearly show that the stereochemistry of the products of the Hanessian–Hullar reaction is consistent with the mechanism first proposed by Hanessian and Plessas (12). It has been pointed out by Thiem and Elvers (17) that this reac-

Can. J. Chem. Downloaded from www.nrcresearchpress.com by 210.87.254.105 on 09/05/12
For personal use only.

TABLE 1. 79.9 MHz ^{1}H nmr parameters for compounds **1–11***

Compound	Chemical shifts (δ ppm)†							Coupling constants (Hz)				
	H-1	H-2	H-3	H-4	H-5	H-6	PhHC(O)O	$J_{1,2}$	$J_{2,3}$	$J_{3,4}$	$J_{4,5}$	$J_{5,6}$
1*a*	4.78	3.87	4.42	4.07	4.07	1.38	6.17	4.0	6.5	5.5	—	6.5
1*b*‡	4.73	3.82	4.32	4.10	4.17	1.38	5.83	3.9	6.2	5.8	2.2	6.5
2*a*	5.03	5.27	4.77	4.5 –4.0		1.44	6.23	4.0	7.5	—	—	6.5
2*b*	4.98	5.18	4.64	4.4 –3.9		1.48	5.92	4.0	7.5	—	—	6.6
3‡	4.78	4.01	4.48	5.35	4.62	1.22	—	4.2	3.7	3.3	1.5	6.5
4	4.84	3.87	5.56	3.71	4.02	1.48	—	3.8	10	10	10	5.9
5	4.75	4.02	2.36, 1.65	5.18	4.02	1.18	—	3.6	—	—	2.5	6.5
6	4.69	3.70	5.19	2.0, 1.2	3.70	1.12	—	4.0	—	—	—	6.5
7‡	4.66	3.95	2.09, 1.82	3.71	3.86	1.20	—	3.8	—	—	—	6.5
7‡ in D_2O	4.67	4.01	1.94	3.82	3.93	1.16	—	3.9	—	—	—	6.6
9	4.71	5.49	4.51	3.57	4.05	1.45	—	1.8	3.5	3.8	8.0	6.0
10	4.70	5.12	2.15	3.76	3.76	1.40	—	1.8	—	—	—	5.8
11‡	4.44	3.83	2.01, 1.80	3.57	3.57	1.26	—	1.5	—	—	—	5.8
11‡ in D_2O	4.51	3.89	2.04, 1.75	3.61	3.61	1.26	—	1.6	—	—	—	5.8

*Unless otherwise indicated the solvent was $CDCl_3$.
†Chemical shifts are expressed relative to internal 1% TMS and relative to TSP for D_2O solutions.
‡Spectra recorded at 220 MHz.

TABLE 2. Carbon-13 nuclear magnetic resonance parameters for compounds **1–11***

Compound	Chemical shifts (ppm)†							
	C-1	C-2	C-3	C-4	C-5	C-6	Acetal carbon	OCH_3
1*a*	99.0	67.6	76.0	77.5	63.6	16.3	102.9	55.5
1*b*‡	98.7	69.5	76.2	77.6	63.6	16.3	103.9	55.5
3‡	99.3	64.0	50.2	74.7	60.3	16.2	—	55.5
4	99.5	72.6	75.6	52.8	68.2	19.2	—	55.6
5‡	99.6	64.0	32.1	71.7	64.7	16.3	—	55.1
6‡	100.2	72.0	71.8	38.0	63.6	20.7	—	55.2
7	99.4	65.8	34.9	68.9	63.6	16.2	—	55.1
7 in D_2O	100.2	67.3	34.2	69.4	64.1	16.6	—	56.1
9‡	99.0	73.2	52.0	69.6	65.8	17.8	—	55.4
10‡	97.3	71.1	32.7	69.3	68.1	17.8	—	54.7
11	100.1	68.5	35.2	69.6	67.7	17.8	—	54.8
11 in D_2O	100.8	68.4	34.6	70.7	68.0	17.9	—	55.7

*Measured for chloroform solutions unless otherwise indicated.
†Chemical shifts expressed relative to 1% internal TMS in $CDCl_3$ and external TMS for D_2O.
‡Those compounds for which assignments are based on selective decoupling experiments.

tion has received limited application to pyranosides possessing benzylidene acetals of the 1,3-dioxalane type. The example reported here for the pure diastereoisomers **1***a* and **1***b* provide further evidence that the stereochemistry of the benzylidene acetal does not affect the regiospecificity of the Hanessian–Hullar reaction and that the brominated carbon atom experiences inversion of configuration in the absence of neighbouring group participation.

The bromo sugars **3**, **4**, and **9** were readily and cleanly reduced to the respective benzoylated dideoxyhexosides **5**, **6**, and **10** by hydrogenation over palladium in ethanol solution. Compound **11** previously prepared by Florent and co-workers (5) by reduction of **9** with lithium aluminium hydride had similar chemical characteristics to those reported. We have found it more convenient in larger scale work to perform this and related reductions by catalytic hydrogenation. In the case of the 4-*O*-benzoyl-*xylo*-hexopyranoside (**5**) this approach allows selective blocking at C-2 as has been demonstrated by Garegg and co-workers (7).

The specific rotation of methyl 3,6-dideoxy-α-L-*xylo*-hexopyranoside (**7**) was determined in water, −126.0°, and in chloroform, −149.6°, and compares with the value, +148° obtained for the optical antipode, abequose (**9**). The rotation of the methyl glycoside (**11**) of ascarylose exhibits a similar although less marked dependence upon solvent. High resolution 220 MHz proton spectra (Table 1) for the

Can. J. Chem. Downloaded from www.nrcresearchpress.com by 210.87.254.105 on 09/05/12
For personal use only.

Can. J. Chem. Downloaded from www.nrcresearchpress.com by 210.87.254.105 on 09/05/12
For personal use only.

glycosides **7** and **11** both in D_2O and $CDCl_3$ require each compound exist as $^1C_4$ chairs (18). The solvent dependence of optical rotation may be either the result of small conformational distortions or the favouring in aqueous solution of that conformer possessing an antiparallel relationship for the aglyconic carbon and ring oxygen atoms. The dihydric nature of water is known to favour this possibility (19–21). The nmr data available to us at present do not allow a choice between these explanations especially since small changes of the torsional angle, $H_a—C_a—C_b—H_b$, need not result in detectable variations of $^3J_{H_a,H_b}$, particularly for complex multiplets, such as those of the axial and equatorial protons at C-3 (22). Further experiments are in progress in an attempt to distinguish between conformational distortion of the $^1C_4$ chair or specific solvation of aglycon rotamers.

Experimental

Thin-layer chromatography was performed with Merck precoated silica gel 60 F-254 plates, and the detection of compounds was achieved by quenching of uv fluorescence and with 5% sulphuric acid in ethanol. Column chromatography utilised silica gel G60 (70–230 mesh) and redistilled solvents. Skellysolve B refers to hexane supplied by Getty Refining and Marketing Company, Tulsa, Oklahoma. Palladium 10% on charcoal was purchased from Engelhard Industries, Newark, New Jersey. Solvents were purified and dried according to standard procedures (23). Processed solutions were dried over anhydrous sodium sulphate and solvent removal was achieved with bath temperatures 40°C or lower unless otherwise stated. Melting points were determined on a Fisher-Johns apparatus and are uncorrected. Optical rotations at the sodium line were measured in a 1-decimetre cell at room temperature (20–23°C). Carbon-13 and ^1H nmr spectra were recorded at 20 and 79.9 MHz, respectively, in the pulsed Fourier transform mode on a Varian CFT-20 spectrometer. Proton spectra recorded at 220 MHz were purchased from the Canadian 220 MHz NMR Centre, University of Toronto. Proton chemical shifts are expressed relative to 1% tetramethylsilane (TMS) for deuteriochloroform solutions and in the case of deuterium oxide, relative to sodium 3-trimethylsilylpropionate-2,2,3,3-d_4 (TSP) 1 mg/ml. Carbon-13 shifts are expressed relative to internal and external TMS for deuteriochloroform and deuterium oxide solutions. Selective heteronuclear decoupling was used to confirm assignments of ^{13}C resonances and homonuclear spin decoupling was used throughout for ^1H nmr.

*Methyl 3,4-*O*-Benzylidene (*S *and* R*)-*α*-L-*fucopyranoside (**1***a and **1***b)*

Methyl α-L-fucopyranoside (24) (20 g, 115 mmol) was added to a solution of α,α-dimethoxytoluene (28 g, 184 mmol) in dry acetonitrile (200 ml) containing toluenesulphonic acid (200 mg). The solution was stirred overnight and then warmed (~50°C) under reduced pressure to complete the reaction. Triethylamine (2 ml) was added before concentration and the syrup which was dissolved in ethyl acetate (300 ml) was extracted with 5% potassium bicarbonate and water. Solvent removal left a colourless syrup (38.5 g) consisting of both diastereoisomers and α,α-dimethoxytoluene. The syrup was dissolved in ethanol and Skellysolve B was added. After several days at room temperature crystals (4.5 g), of pure *R* (H-*exo*) isomer **1***b* were obtained. Further treatment of the mother liquors gave 6.0 g of a crystalline mixture, consisting of *S* and *R* isomers in the ratio 1:2. Trituration of the concentrated mother liquors, 17 g with Skellysolve B removed impurities of α,α-dimethoxytoluene and provided 12.5 g of a homogeneous syrup containing both isomers **1***a* and **1***b*. The total yield of the title compound was 23 g, 77%.

Conversion of the syrup to the *p*-nitrobenzoates **2***a* and **2***b* allowed separation and recovery of pure **1***a* and **1***b*. Crude syrup (8.8 g) containing **1***a* and **1***b* was dissolved in chloroform (100 ml) containing triethylamine (6 ml), *p*-nitrobenzoylchloride (8.2 g) was added and after 16 h the reaction was worked-up in the usual manner. Thin-layer chromatography in Skellysolve B, ethyl acetate 2:1 showed two spots which were separated by column chromatography utilising 600 g of silica gel and the solvent system used for tlc. The *S* isomer **2***a* eluted first (4.0 g), closely followed by the *R* isomer **2***b* (2.3 g). Although both fractions were homogeneous by tlc neither crystallised and after confirmation of purity by ^1H nmr (Table 1), they were immediately converted to the required acetals **1***a* and **1***b*. The syrups were dissolved in dry methanol (50 ml) to which freshly prepared 0.1 *M* sodium methoxide solution (1 ml) was added. After 16 h transesterification was complete and following deionisation with Rexyn 101 (H^+) resin the syrups were applied to short columns of silica gel (1 × 40 cm) and eluted with Skellysolve B – ethyl acetate 3:1 and then ethyl acetate. Pure H-*endo* (**1***a*) and H-*exo* (**1***b*) were recovered from the ethyl acetate solutions and crystallised spontaneously on concentration. Recrystallisation from ethanol – Skellysolve B (*R* isomer) and ether (*S* isomer) gave analytical samples of **1***a* and **1***b*. The physical and analytical data for each isomer were as follows.

S *Isomer*—mp 92–93°C; $[\alpha]_D$ −148.0° (*c* 0.9, $CHCl_3$). *Anal.* calcd. for $C_{14}H_{18}O_5$: C 63.15, H 6.81; found: C 63.41, H 6.90.

R *Isomer*—mp 104–105°C, $[\alpha]_D$ −105.8° (*c* 1.8, $CHCl_3$). *Anal.* found: C 63.29, H 6.78.

*Methyl 4-*O*-Benzoyl-3-bromo-3,6-dideoxy-*α*-*L*-gulopyranoside (**3***) and Methyl 3-*O*-Benzoyl-4-bromo-4,6-dideoxy-*α*-*L*-glucopyranoside (**4***)*

N-Bromosuccinimide (3.6 g, 20.4 mmol) was added to a crystalline mixture of **1***a* and **1***b* (2:1; 4.1 g, 15.4 mmol) and barium carbonate suspended in 200 ml of carbon tetrachloride. The mixture was refluxed with stirring for 30 min, diluted with methylene chloride (200 ml), and filtered. The filtrate was washed with water and concentrated to a syrup. Thin-layer chromatography (Skellysolve B – ethyl acetate 3:1) showed one major and one minor component. Silica gel chromatography with the same solvent system yielded pure **3** (4.2 g, 79%) as a syrup $[\alpha]_D$ −149.1° (*c* 1.3, $CHCl_3$), R_F 0.37, and pure **4** (0.9 g 17%), mp 143–145°C (recrystallized from ether) $[\alpha]_D$ −69.5° (*c* 1.1, $CHCl_3$), R_F: 0.27. *Anal.* calcd. for $C_{14}H_{17}BrO_5$: C 48.71, H 4.96, Br 23.15; found: C 48.61, H 5.01, Br 23.20.

To establish the ratio of products the reaction was carried out exactly as described above but on a 200–300 mg scale with pure samples of **1***a* and **1***b*. After extraction the recovered syrup was dissolved in deuteriochloroform and the ^{13}C nmr spectrum was recorded. Product ratios were based upon peak heights and integrated peak areas for several resonances.

*Methyl 4-*O*-Benzoyl-3,6-dideoxy-*α*-*L*-xylo-hexopyranoside (**5***)*

The 3-bromo compound (**3**) (2.0 g, 5.8 mmol) was hydrogenated at 65 psi at room temperature with 10% palladium-on-charcoal (0.5 g) in ethanol (100 ml) containing triethylamine (1.0 g 10 mmol) for 16 h.

After filtration and concentration, the crystalline residue was dissolved in methylene chloride, washed with aqueous sodium bicarbonate, water, and dried. The concentrated residue was

purified on 200 g of silica gel with the solvent Skellysolve B – ethyl acetate 3:1 to yield pure **5** (1.1 g, 73% yield), mp 118–119°C (recrystallized from Skellysolve B – ethyl acetate), $[\alpha]_D$ −115.1° (*c* 1.0, $CHCl_3$). *Anal.* calcd. for $C_{14}H_{18}O_5$: C 63.15, H 6.81; found: C 62.96, H 6.78.

*Methyl 3-*O*-Benzoyl-4,6-dideoxy-*α*-*L*-*arabino*-hexopyranoside (**6**)*

The 4-bromo compound (**4**) (0.52 g, 1.5 mmol) was hydrogenated with 10% palladium-on-charcoal (0.2 g) in ethanol (30 ml) containing triethylamine (0.25 g, 2.5 mmol) and worked up in precisely the manner described above for compound **5**.

Column chromatography in similar fashion but with Skellysolve B – ethyl acetate, 2:1 yielded crystalline **6** (0.27 g, 68%) mp 79–81°C, $[\alpha]_D$ −178.3° (*c* 1.0, $CHCl_3$). Recrystallisation was effected from ethyl acetate – Skellysolve B.

*Methyl 3,6-Dideoxy-*α*-*L*-xylo-hexopyranoside (**7**)*

The benzoate (**5**) (0.4 g, 1.5 mmol) in methanol solution (50 ml) was stirred overnight with a catalytic amount of sodium methoxide. Deionisation with Rexyn 101 (H^+) resin provided a residue on concentration, which was purified on a silica gel column using ethyl acetate – methanol – water 85:10:5 as solvent. The title compound **7** was obtained as a homogeneous syrup (0.2 g, 80%) which has resisted attempts at crystallisation; $[\alpha]_D$ −126.0° (*c* 1.0, H_2O), $[\alpha]_D$ −149.6° (*c* 1.0, $CHCl_3$), R_F 0.49 (ethyl acetate – methanol – water 85:10:5).

*Methyl 2,3-*O*-Benzylidene-*α*-*L*-rhamnopyranoside (**8**)*

A solution of methyl α-L-rhamnopyranoside (25) (10.0 g, 56.2 mmol) and α,α-dimethoxytoluene in dry acetonitrile (50 ml) containing 2 g of Rexyn 101 (H^+) resin was rotated under reduced pressure on the rotary evaporator at a temperature of 50°C. The pressure was adjusted so as to avoid excessive evaporation of solvent. After 2 h the acetonitrile was evaporated and the residue dissolved in methylene chloride was filtered, dried, and concentrated. Purification on a silica gel column (Skellysolve B – ethyl acetate 3:1) gave pure **8** (10.1 g, 73%), a 1:1 mixture by ^1H nmr of both diastereoisomers; $[\alpha]_D$ −25.5° (*c* 1.1, $CHCl_3$). *Anal.* calcd. for $C_{14}H_{18}O_5$: C 63.15, H 6.81; found: C 62.98, H 6.89.

*Methyl 2-*O*-Benzoyl-3-bromo-3,6-dideoxy-*α*-*L*-altro-hexopyranoside (**9**)*

The benzylidene acetal (**8**) was subjected to the Hanessian–Hullar reaction in the same molar quantities as were compounds **1***a* and **1***b*. Reaction was complete after 45 min and work-up was conducted in the normal way. Column chromatography silica gel with Skellysolve B – ethyl acetate, 3:1) gave pure **9** (4.5 g, 85%) as a syrup $[\alpha]_D$ +11.3° (*c* 1.3, $CHCl_3$) (lit. (5) $[\alpha]_D^{20}$ +12°).

*Methyl 2-*O*-Benzoyl-3,6-dideoxy-*α*-*L*-arabino-hexopyranoside (**10**)*

The hydrogenation of compound **9** was conducted in a similar manner to that described for the gulopyranoside (**3**). Silica gel column chromatography with Skellysolve B – ethyl acetate 1:1 as solvent gave **10** (1.1 g, 71%) as a homogeneous syrup $[\alpha]_D$ −37.2° (*c* 1.0, $CHCl_3$).

*Methyl 3,6-Dideoxy-*α*-*L*-arabino-hexopyranoside (**11**)*

The benzoate compound (**10**) (0.53 g, 2.0 mmol) was added to a solution of methanol (50 ml) containing a catalytic amount of sodium methoxide. After 16 h the reaction was worked up as described for **7**. Column chromatography in a manner similar to that used for compound **7** gave **11** (0.28 g, 87%), mp 82–84°C, $[\alpha]_D$ −118.7° (*c* 0.9, H_2O), $[\alpha]_D$ −127.7° (*c* 1.0, $CHCl_3$). Recrystallisation was effected from chloroform (lit. (5) mp 80–81°C, $[\alpha]_D^{20}$ −103° (H_2O)).

1. O. Lüderitz, A. M. Staub, and O. Westphal. Bacteriol. Rev. **30**, 192 (1966).
2. I. Ørskov, F. Ørskov, B. Jann, and K. Jann. Bacteriol. Rev. **41**, 667 (1977).
3. O. Westphal and O. Lüderitz. Angew. Chem. **72**, 881 (1960).
4. R. U. Lemieux, K. B. Hendriks, R. V. Stick, and K. James. J. Am. Chem. Soc. **97**, 4056 (1975).
5. J-C. Florent, C. Monneret, and Q. Khuong-Huu. Carbohydr. Res. **56**, 301 (1977).
6. G. Ekborg, P. J. Garegg, and B. Gotthammar. Acta Chem. Scand. B, **29**, 765 (1975).
7. K. Eklind, P. J. Garegg, and B. Gotthammar. Acta Chem. Scand. B, **30**, 300 (1976).
8. K. Eklind, P. J. Garegg, and B. Gotthammar. Acta Chem. Scand. B, **29**, 633 (1975).
9. G. Siewert and O. Westphal. Justus Liebigs Ann. Chem. **720**, 171 (1968).
10. M. E. Evans. Carbohydr. Res. **21**, 473 (1972).
11. P. J. Garegg and C-G. Swahn. Acta Chem. Scand. **26**, 3895 (1972).
12. S. Hanessian and N. R. Plessas. J. Org. Chem. **34**, 1035 (1969).
13. S. Hanessian. Methods Carbohydr. Chem. **6**, 183 (1972).
14. N. Baggett, K. W. Buck, A. B. Foster, M. H. Randall, and J. M. Weber. Proc. Chem. Soc. 118 (1964).
15. N. Baggett, K. W. Buck, A. B. Foster, M. H. Randall, and J. M. Weber. J. Chem. Soc. C, 3394 (1965).
16. R. U. Lemieux and J. D. Stevens. Can. J. Chem. **43**, 2059 (1965).
17. J. Thiem and J. Elvers. Carbohydr. Res. **60**, 63 (1978).
18. D. R. Bundle and R. U. Lemieux. Methods Carbohydr. Chem. **7**, 79 (1976).
19. R. U. Lemieux, A. A. Pavia, J. C. Martin, and K. A. Watanabe. Can. J. Chem. **47**, 4427 (1969).
20. R. U. Lemieux. Pure Appl. Chem. **25**, 527 (1971).
21. R. U. Lemieux. Pure Appl. Chem. **27**, 527 (1971).
22. G. I. Birnbaum and D. R. Bundle. Biophys. Biochim. Acta. In press.
23. D. D. Perrin, W. L. Armarego, and D. R. Perrin. Purification of laboratory compounds. Pergamon Press, London. 1966.
24. U. Zehavi and N. Sharon. J. Org. Chem. **37**, 2141 (1972).
25. G. M. Bebault and G. G. S. Dutton. Can. J. Chem. **50**, 3373 (1972).

Can. J. Chem. Downloaded from www.nrcresearchpress.com by 210.87.254.105 on 09/05/12
For personal use only.

Solvent effects on the structure of S_N2 transition states

KENNETH CHARLES WESTAWAY

Department of Chemistry, Laurentian University, Sudbury, Ont., Canada P3E 2C6

Received April 11, 1978

KENNETH CHARLES WESTAWAY. Can. J. Chem. **56**, 2691 (1978).

Two research groups have used heavy atom leaving group kinetic isotope effects to determine how the structure of an S_N2 transition state is affected by a change in solvent. Two completely different types of behaviour were observed in these studies. In one case, the leaving group kinetic isotope effect, and thus the transition state structure, changed markedly when the solvent was varied over a reasonably narrow range. In the other study, the leaving group kinetic isotope effect (transition state structure) remained constant over a wide range of solvents. A model describing the interaction between solvent molecules and S_N2 transition states is developed and a *Solvation rule for S_N2 reactions* which rationalizes the different experimental results is explained and justified. Finally, predictions based on the solvation rule are shown to be in agreement with the results of theoretical calculations of solvent effects on S_N2 transition states and secondary α deuterium kinetic isotope effect measurements.

KENNETH CHARLES WESTAWAY. Can. J. Chem. **56**, 2691 (1978).

Deux groupes de recherches ont déjà utilisé les effets isotopiques cinétiques d'atomes lourds agissant comme nucléofuges dans le but de déterminer quel est l'effet d'un changement de solvant sur un état de transition S_N2. Deux ensembles de comportement complètement différents ont pu être observés au cours de ces études. Dans un cas, un faible changement de solvant produit un changement sensible dans l'effet isotopique cinétique du nucléofuge, et par conséquent dans la structure de l'état de transition. Dans l'autre étude, malgré des changements de solvants importants l'effet isotopique cinétique du nucléofuge (ainsi que la structure de l'état de transition) demeure relativement constant. On a développé un modèle décrivant l'interaction entre des molécules de solvants et les états de transition S_N2; on explique aussi, en y apportant les justifications nécessaires, une *Règle de solvatation des réactions S_N2* qui rationalise les différents résultats expérimentaux. Enfin, on montre que des prédictions faites sur la base de la Règle de solvatation sont en bon accord avec les résultats de calcul théoriques des effets de solvants sur les états de transition S_N2 et avec les mesurages de l'effet isotopique cinétique secondaire d'un deuterium en α.

[Traduit par le journal]

Can. J. Chem. Downloaded from www.nrcresearchpress.com by 210.87.254.40 on 09/05/12
For personal use only.

In recent years considerable attention has been focused on the effects of changing the solvent on the rates, products, and mechanisms of organic reactions (1–4). One area of study that has been of particular interest is an investigation of the effect of a solvent change on simple bimolecular nucleophilic substitution reactions (S_N2) at saturated carbon (1, 5). In fact, several workers have attempted to measure and understand the interaction of solvents with reactants and transition states by examining the changes in (*i*) the rates of reaction (1, 6, 7), (*ii*) the thermodynamic properties of both the initial and the transition states (1–3), and most recently (*iii*) the effect of solvent change on the structure of the transition states in S_N2 reactions (8, 9).

Two sets of workers, Hargreaves, Katz, and Saunders (8) and Graczyk, Taylor, and Turnquist (9), have used leaving group heavy atom kinetic isotope effects to examine the effect of changing the solvent on the structure of the transition states of simple bimolecular (S_N2) nucleophilic substitution reactions. At present, the results from these two different groups are in serious conflict. Saunders and co-workers found that both the rate constant and the leaving group heavy atom (sulfur) kinetic isotope effect varied markedly when the composition of the solvent was changed from ethanol to various mixtures of ethanol and dimethylsulfoxide in the S_N2 reaction of ethoxide ion with trimethylsulfonium ion, reaction [1], and concluded that the structure of the transition state is altered significantly when the solvent is changed.

$$[1]\quad C_2H_5O^- + CH_3\text{—}\overset{+}{S}(CH_3)_2 \rightarrow [C_2H_5\overset{\delta-}{O}\text{---}CH_3\text{---}\overset{\delta+}{S}(CH_3)_2] \rightarrow C_2H_5OCH_3 + (CH_3)_2S$$

Taylor and co-workers, on the other hand, observed that although the rate constant changed by three orders of magnitude when the solvent was changed in the S_N2 reaction of thiophenoxide ion with *n*-butylchloride, reaction [2],

$$[2]\quad C_6H_5S^- + n\text{-}C_4H_9Cl \rightarrow [C_6H_5\overset{\delta-}{S}\text{---}\overset{CH_3}{\overset{|}{(CH_2)_2}}\text{---}\overset{\delta-}{Cl}] \rightarrow C_6H_5S(CH_2)_3CH_3 + Cl^-$$

Can. J. Chem. Downloaded from www.nrcresearchpress.com by 210.87.254.40 on 09/05/12
For personal use only.

the leaving group heavy atom (chlorine) kinetic isotope effect, and thus the structure of the transition state, did not change appreciably even over a wide range of protic and aprotic solvents.

The apparent discrepancy between these two studies, in which the structure of the transition state changes markedly with solvent in the one case and remains unchanged in the other case, can be rationalized by the solvation rule presented in this paper.

Development of the Basis for the Solvation Rules

A closer examination of Tables 1 and 2, which present the experimental results obtained for reactions [1] and [2], respectively, shows that the rate constants become larger as the solvent is changed from a protic to a dipolar aprotic solvent. These changes are expected because it is well known that the rate constants of S_N2 reactions become larger as the solvent becomes more aprotic in character (1, 10, 11). The increase in rate constant is the result of two factors. (*1*) Several studies (1, 12, 13) have demonstrated that negatively charged nucleophiles and small, highly charged nucleophiles in particular, are less solvated (higher free energy) in dipolar aprotic solvents than in protic solvents. Changing to a more dipolar aprotic solvent leads to an increase in the free energy of the reactants and thus to an increase in rate. (*2*) Haberfield and co-workers (5, 14–16) and Fuchs and Cole (17) have shown that the free energies of S_N2 transition states that do not have very small highly charged nucleophiles are more highly solvated in dipolar aprotic solvents than in protic solvents regardless of the charges on the nucleophiles in the transition state. In fact, Haberfield concluded that increased solvation of the transition state is the major contributor to the larger rate constants in the dipolar aprotic solvents. In any case, a combination of these two factors easily accounts for the increases observed in the rate constants for the S_N2 reactions in Tables 1 and 2.

TABLE 1. Rate constants and sulfur kinetic isotope effects for the reaction of ethoxide ion with trimethylsulfonium ion in ethanol–dimethylsulfoxide mixtures at 60°C

Mol % DMSO	Rate constant (ℓ/mol s)	k^{32}/k^{34}[a]
0	2.90×10^{-3}	1.0095
17	4.38×10^{-3}	1.0075
25	5.67×10^{-3}	1.0071
35	9.73×10^{-3}	1.0066
55	14.80×10^{-3}	1.0040
65	31.10×10^{-3}	1.0035

[a]The error limits on individual sulfur kinetic isotope effects is $\leq \pm 0.0008$.

TABLE 2. Rate constants and chlorine kinetic isotope effects for the reaction of *n*-butyl chloride and thiophenoxide ion in different solvents at 20°C

Solvent	Rate constant (ℓ/mol s)	k^{35}/k^{37}[a]
DMSO	2.6×10^{-2}	1.00964
DMF	4.1×10^{-2}	1.00953
Tetraglyme	1.1×10^{-2}	1.00942
Diglyme	3.5×10^{-3}	1.00949
n-Amyl alcohol	4.0×10^{-5}	1.00942
n-Propanol	6.2×10^{-5}	1.00931
Methanol	2.2×10^{-5}	1.00930
		Ave. 1.00944 ± 0.00012[b]

[a]Average of two or more values for each solvent. Error limits are ± 0.00015.
[b]Standard deviation.

Haberfield's studies, which indicate that the transition state undergoes large changes in free energy when the solvent is changed, suggest that the structure of the transition state should change when the solvent is altered. If this were the case, the magnitude of the leaving group heavy atom kinetic isotope effect, which is a measure of the carbon–leaving group bond length in the transition state, would be expected to change as the solvent is changed. This is obviously consistent with the results obtained by Hargreaves, Katz, and Saunders (Table 1) but is completely opposite to those of Graczyk, Taylor, and Turnquist who found an almost constant chlorine kinetic isotope effect (1.00944 ± 0.00012, with a maximum error of 0.00015 in each isotope effect) over a wide range of protic and aprotic solvents (Table 2). These unexpectedly constant chlorine kinetic isotope effects suggested that the interaction between solvent and an S_N2 transition state could influence the actual bond lengths in the transition state. The following arguments suggest a mechanism for the stabilization of S_N2 transition states by solvent and lead to a *Solvation rule for S_N2 reactions*. This rule rationalizes the results obtained by both research groups and successfully predicts how the structure of an S_N2 transition state is altered when the solvent is varied.[1]

The first assumption required in this theory of solvent effects on transition state structure is that the solvent influences the free energy of an S_N2 transition state by interacting (solvating) primarily, if not exclusively, with the entering and leaving

[1]Although theoretical calculations of the transition state structure for the reaction $F^- + CH_3F' \rightarrow CH_3F + F'^-$ do not agree in detail, they do indicate that the transition state is a very polar species (18–20). The average amount of positive charge on the α carbon is 0.43 ± 0.15 and the average charge on the fluorides is -0.64 ± 0.2. These results are in general agreement with the charge densities reported in other studies (18, 20).

Can. J. Chem. Downloaded from www.nrcresearchpress.com by 210.87.254.40 on 09/05/12
For personal use only.

groups, which are both nucleophiles. This assumption is reasonable because (*i*) theoretical calculations indicate that the α carbon in an S_N2 transition state bears a relatively small positive charge, whereas the nucleophiles are more highly charged (18–21),[1] and because (*ii*) the smaller positive charge on the α carbon in the transition state is shielded from solvent. The electron deficient α carbon is bonded to three hydrogens and/or bulky alkyl or aryl groups in addition to the attacking nucleophile and the leaving group. As a result, the partial positive charge on the α carbon is surrounded or buried in the pentavalent transition state and any interaction with the solvent would be expected to be small,[2] especially compared to the interaction between solvent and the more highly charged, less sterically crowded nucleophiles at the axial positions of the trigonal bipyramid. Thus, the substantial amount of negative charge on the nucleophiles in an S_N2 transition state, coupled with the steric hindrance to solvation of the smaller positive charge on the α carbon, strongly suggests that the solvent interacts mainly, if not exclusively, with the entering and leaving nucleophiles. This hypothesis is supported by the chlorine kinetic isotope effects measured by Cromartie and Swain (22, 23) as well as theoretical calculations of chlorine leaving group kinetic isotope effects for an S_N1 reaction by Sims and co-workers (24, 25). Both sets of workers have concluded from work on different S_N reactions that the interaction between the solvent and the nucleophiles in the transition state is very important.

In considering the interaction between the solvent and the nucleophiles in an S_N2 transition state, it was apparent that there are two different types of transition states. First, there is the case where both the attacking nucleophile, N, and the leaving group, L, have the same charge, i.e., both are negatively charged or both are neutral, reactions [3] and [4], respectively. These reactions are identified as Type I S_N2 reactions.

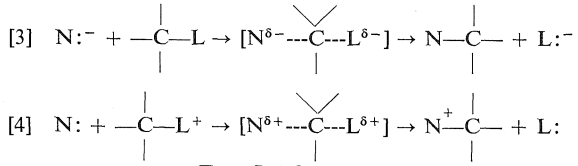

Type I S_N2 Reactions

A Type II S_N2 reaction is defined as one involving a neutral and a negatively charged nucleophile, reactions [5] and [6].

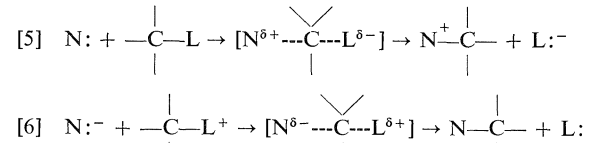

Type II S_N2 Reactions

If the transition state of a Type I S_N2 reaction, with both nucleophiles negatively charged, is transferred from the gas phase to solution, the solvent will interact with the two partially charged nucleophiles, $N^{\delta-}$ and $L^{\delta-}$, and lower the free energy of the transition state. If this transition state were then transferred to a different solvent, the interaction between the partially charged nucleophiles, $N^{\delta-}$ and $L^{\delta-}$, and the solvent (solvation energies) would be different. The free energy of the transition state will vary from one solvent to another depending on the solvation energies of N and L and the rate constant should change with solvent. This is observed (1, 8, 9).

A second assumption required by this theory is that the change in the solvation energy of the negatively charged nucleophiles in the transition state resulting from a change in solvent will be equal or very nearly equal. This is reasonable because both N and L will have the same kind of partial charge in the transition state and may even have approximately the same charge density.[3] If this is the case, each new solvent will interact either more or less strongly with each nucleophile but whether the change in solvent lowers the free energy by solvating (bonding) more tightly or strongly with the nucleophiles or increases the free energy by solvating the nucleophiles less strongly (i.e., either more loosely, by shedding solvent molecules, or by a different mechanism such as a weak anion–dipole interaction in a dipolar aprotic solvent rather than the stronger hydrogen bonding in a protic solvent) the change in the interaction between the negatively charged nucleophiles in the transition state and the solvent will be the same or virtually the same for both nucleophiles. As a result, the *relative* electron density or nucleophilicity of N and L would not be altered by a change of solvent and the structure of the transition state would not be changed even though its free energy had been changed.

It might be expected that the absolute electron density on both N and L would be changed by a variation in solvent and that this should cause a

[2]Any interaction between the more polarized α carbon–hydrogen bonds of the transition state and the solvent would also be small.

[3]This suggests that the lengths of the N—C_α and the C_α—L bonds are such that the charge density on N and L will be approximately the same in the transition state. Although this may be the case, there is no firm evidence to establish this point. In any case, the charge on N and L should be reasonably close for most reactions. (See the section on Limitations of Applying the Solvation Rule.)

Can. J. Chem. Downloaded from www.nrcresearchpress.com by 210.87.254.40 on 09/05/12
For personal use only.

tightening or loosening of the transition state. This would not occur, however, since the solvent would only interact with the electron density at the back of the nucleophiles but not with the electron density in the area between N and L and along the N---C---L bond axis. The electron density in the area between the nucleophiles is held very strongly by the positively charged N, C_α, and L nuclei and would only be altered by a large change in the electron density at N, at L, or at both N and L. Since solvent molecules only interact with the less sterically crowded and more loosely held electron density at the back of the nucleophiles, and since this would occur equally at N and L, the change in electron density at N and L resulting from a change in solvation would not be sufficient to alter the more strongly held electron density in the area between N and L. Consequently, the structure of the transition state would not be altered by a change in solvent. This theory should also apply to the case where both the attacking nucleophile and the leaving group are neutral species since the two nucleophiles in the transition state would again have the same charge and interact similarly with a given solvent.

In a Type II S_N2 transition state, on the other hand, a neutral nucleophile and a negatively charged nucleophile are present. Here the charges on the two nucleophiles are different, and thus the solvation energies of the two nucleophiles would be quite different. For example, if the reaction involved a negatively charged nucleophile and a neutral leaving group (reaction [6]) then a protic solvent would interact with the partial negative charge on the attacking nucleophile, $N^{\delta-}$, via a strong hydrogen bonding interaction, whereas it would solvate the partial positive charge on the leaving nucleophile, $L^{\delta+}$, by a much weaker ion–dipole type of interaction. If the solvent were changed to a dipolar aprotic solvent, the two nucleophiles would again interact with solvent in a different fashion. The partially negative nucleophile, $N^{\delta-}$, would now be solvated by an ion–dipole interaction involving the positive end of the solvent dipole whereas the partially positive nucleophile, $L^{\delta+}$, would be solvated by an ion–dipole interaction with the negative end of the solvent dipole.

Thus the solvation energies of the two nucleophiles would be substantially different in every solvent. Of even greater importance, however, is the fact that changing from a protic to a dipolar aprotic solvent, for example, will result in a very large difference in the relative solvation energies of the two nucleophiles in the transition state. In these circumstances, the change in the solvation energies at the two nucleophiles $N^{\delta-}$ and $L^{\delta+}$ would be large enough to cause a shift in the electron density in the area between the N and L atoms along the N---C_α---L bond axis of an S_N2 transition state. As a result, the structure of the transition state would be altered. Obviously this prediction should apply to the equivalent case in which the attacking nucleophile is a neutral species and the leaving group is negatively charged.

Finally, a *Solvation Rule for S_N2 Reactions* can be formulated. It states that *A change in solvent will not lead to a change in the structure of an S_N2 transition state if the charges on the two nucleophiles in the transition state are the same* (a Type I reaction), *but will lead to a change in the structure of the transition state when a negatively charged nucleophile and a neutral nucleophile* (a Type II reaction) *are present in the transition state.*

The *Solvation rule for S_N2 reactions* can be applied to the reactions shown in [1] and [2]. Reaction [1], in which a neutral nucleophile, dimethylsulfide, is displaced by a negatively charged nucleophile, ethoxide ion, is an example of a Type II S_N2 reaction. The solvation rule predicts that a change in solvent will lead to a change in structure of the transition state for Type II reactions and this is what is observed. The sulfur leaving group kinetic isotope effects decrease markedly from almost 1% in ethanol to a third of this value, 0.35%, in 65 mol% DMSO. Since theoretical calculations have shown that the magnitude of the leaving group kinetic isotope effect increases linearly with the amount of C_α---S bond rupture in the transition state (26), it must be concluded that the C_α---S bond is substantially shorter in the more dipolar aprotic solvent and that the structure of the transition state changed significantly when the solvent was varied over even a reasonably small range.

The solvation rule for S_N2 reactions is also consistent with the results reported by Graczyk, Taylor, and Turnquist for the Type I S_N2 reaction in which a negatively charged attacking nucleophile, thiophenoxide ion, displaces a negatively charged leaving group, chloride ion, from *n*-butyl chloride (reaction [2], Table 2). In this case, the chlorine kinetic isotope effects do not change over a very wide range of solvents and thus the length of the C_α---Cl bond in the transition state is not altered significantly by a change of solvent. Since it is unlikely that the structure of the transition state could shift without a change in the C_α---Cl bond length, it was concluded that a change in solvent did not lead to a change in the structure of the transition state, as the rule predicts.

Justification for the Solvation Rule

A better understanding of the solvation rule can be obtained by examining the ionic free energy of transfer between protic and dipolar aprotic solvents

Can. J. Chem. Downloaded from www.nrcresearchpress.com by 210.87.254.40 on 09/05/12
For personal use only.

(ΔG_{tr}). Cox (12) has recently reported the ionic enthalpies and entropies of transfer of ions from water to dimethylsulfoxide (DMSO). The corresponding ionic free energies of transfer calculated from these values are shown in Table 3. The cations are all more strongly solvated (lower free energy) in DMSO and a comparison of these data with those of Parker (1), Choux and Benoit (13), and others (27–29) suggests that all monovalent cations have very similar ionic free energies of transfer. This means that the average cationic species is 3.1 ± 0.6 kcal/mol more stable in a dipolar aprotic solvent and this average value can be used in the following calculations without introducing a substantial error. Anions, on the other hand, are less solvated in DMSO than in water, and the differences in the solvation energies are larger, i.e., the average value based on the nucleophiles in Table 3 and others (1, 17) would appear to be about 6.1 ± 3 kcal/mol. In fact, most of the nucleophiles used in S_N2 reactions have ionic free energies of transfer of about 6 kcal/mol.

The effect of changing the solvent from water to DMSO on a Type II S_N2 transition state can be estimated in the following manner. The polar transition state can be approximated by a three atom molecule with a positively charged atom at one end, a neutral atom in the middle, and a negatively charged atom at the other end. If this species were transferred from water to DMSO, the free energy of the positively charged atom would be lowered (more strongly solvated) on the average by 3.1 kcal/mol. The average anion in the model transition state would be less strongly solvated by 6.1 kcal/mol in DMSO. The total (absolute) difference in solvation between the two ionic species in the model of the transition state would be large, i.e., approximately 9.2 kcal/mol for the average nucleophile. The extreme differences are 12.3 kcal/mol for chloride ion (the least solvated anion in DMSO) and 6.3 kcal/mol for iodide (the most strongly solvated anion in DMSO).[4] This simplified approach illustrates the direction of the difference in solvation energies of the partially charged nucleophiles but overestimates the magnitude of this difference for two reasons. First, the nucleophiles are only partially charged in the transition state and, secondly, only the backside of the nucleophile is free to interact with solvent molecules. As a result, only a portion of the total difference in energy described above should be observed for a real transition state. For example, if the magnitude of the effect is arbitrarily taken as

[4]Some other anions such as fluoride and hydroxide ions would lead to even larger values than 12.3 kcal/mol. Iodide ion has the smallest ionic free energy of transfer of all the anions.

TABLE 3. Free energies of transfer of ions from water to dimethylsulfoxide at 25°C (12)

Cation	ΔG_{tr} (kcal mol^{-1})	Anion	ΔG_{tr} (kcal mol^{-1})
Li^+	−3.5	Cl^-	9.2
Na^+	−3.5	Br^-	6.1
K^+	−2.9	I^-	3.2
Rb^+	−2.6	N_3^-	5.7
Cs^+	−3.0		Ave. 6.1
	Ave. −3.1		

25% of that calculated for the fully charged totally free ions, the differences in the free energy of solvation between the two nucleophiles, $N^{\delta+}$ and $L^{\delta-}$, in a transition state would be between 3.1 and 1.6 kcal/mol with most values near 2.3 kcal/mol. In Type II S_N2 transition states these differences in free energies of solvation of the nucleophiles is large enough to cause a distortion in the electron density between the nucleophiles in the transition state and, as a result, the structure of the transition state should change when the solvent is changed.

For a Type I S_N2 transition state with both nucleophiles negatively charged, the change in the solvation energy of the two nucleophiles, $N^{\delta-}$ and $L^{\delta-}$, is much smaller. It can be seen from Table 3 that the maximum difference in the solvation energies associated with a change in solvent from water to DMSO would occur when the nucleophiles in the transition state were chloride and iodide ions. In this case the difference in solvation energies in the two solvents is only 6.0 kcal/mol. For any other combination of nucleophiles the difference would be less than 2.5 kcal/mol and, for most combinations, the difference would be less than 1 kcal/mol. If the magnitude of the difference in free energy of solvation of the two nucleophiles in the transition state is again taken as 25% of that for the free ions, the *maximum* difference expected for a Type I S_N2 transition state is 1.5 kcal/mol and most reactions would have a difference in the range of 0.6–0.2 kcal/mol. Obviously the difference in the solvation energies of two neutral nucleophiles, which would bear partial positive charges in the transition state, would be very small (<0.2 kcal/mol). Because the differences in the solvation free energies of the nucleophiles in a Type I S_N2 transition state are only about one fourth of those found in Type II S_N2 transition state, it follows that solvent variations would not distort the more strongly held electron density in the area between the nucleophiles significantly. As a result, the structure of the transition state would not change appreciably when the solvent is varied.

It is worth re-examining reactions [1] and [2] in the light of the above discussion. The free energies of transfer of the ethoxide ion and the trimethyl-

Can. J. Chem. Downloaded from www.nrcresearchpress.com by 210.87.254.40 on 09/05/12
For personal use only.

sulfonium ion involved in reaction [1], as well as the thiophenoxide ion used in reaction [2], can be estimated from data published by Parker (1). The free energy of transfer from water to DMSO for the ethoxide ion should be slightly less than that observed for chloride ion, i.e., about 8 kcal/mol, while the value for the trimethylsulfonium ion should be near that for the rubidium cation (−2.6 kcal/mol). Using the method described above, the difference in the solvation energies of the nucleophiles in water and in DMSO for the transition state of reaction [1] would be approximately $|8.0 - (-2.6)| \times 25/100 = 2.7$ kcal/mol. This is near the upper limit predicted for a Type II S_N2 reaction and it is, therefore, not surprising that Saunders and co-workers found that the structure of the transition state was extremely sensitive to a change in solvent.

The free energy of transfer from water to DMSO for the thiophenoxide ion used in reaction [2] should be approximately equal to that observed for bromide ion (1), i.e., about 6 kcal/mol. The change in the solvation energies of the nucleophiles expected when the S_N2 transition state for reaction [2] is transferred from water to DMSO would be approximately $|9.2 - 6| \times 25/100 = 0.8$ kcal/mol. This difference in solvation energies is larger than that expected for most Type I S_N2 reactions. The observation that a large change in solvent does not lead to a change in the structure of the transition state for a Type I reaction even when the difference in solvation energies of the nucleophiles is large, suggests that the *Solvation rule for S_N2 reactions* will be very successful in predicting the effects of changing the solvent on the structure of the transition state.

Finally, if enough information on the free energies of transfer of ionic species from water to DMSO were available, it should be possible to determine the minimum value for the difference in solvation energies of the nucleophiles which would lead to a change in structure of the transition state when the solvent is changed. At present this value cannot be determined, although the results obtained for reaction [2] suggest that a value significantly greater than 0.8 kcal/mol would be required before the structure of the transition state would respond to a change in solvent.

Theoretical Calculations of Solvent Effects on Transition State Structure

Simonetta and co-workers (20, 30) have estimated the solvent effect on transition state structure by using *ab initio* and CNDO 2 calculations to define the structure of a transition state in different solvents. In particular, the structure of the transition states for two Type I S_N2 reactions, hydride ion with methane, reaction [7], and fluoride ion with methyl fluoride, reaction [8], have been calculated in both the gas phase and in an approximation of an aqueous medium

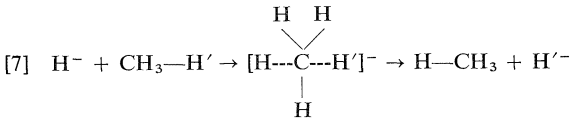

[7] $H^- + CH_3—H' \rightarrow [H---C(H)(H)---H']^- \rightarrow H—CH_3 + H'^-$

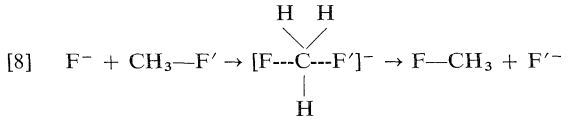

[8] $F^- + CH_3—F' \rightarrow [F---C(H)(H)---F']^- \rightarrow F—CH_3 + F'^-$

In both cases the structure of the transition state did not change substantially when the solvent was changed. The C---H bonds in the transition state of reaction [7] were 1.225 Å when no solvent was present and when each hydride ion was solvated by one water molecule. The methyl fluoride transition state was essentially the same in the gas phase and in solution where each fluoride ion was solvated by four water molecules. In fact, the only difference in the structure of the transition state was that the C---F bonds were 1.8% longer (1.466 Å from 1.439 Å) in solution. The observation of a virtually constant C---F bond length is especially important in this system because eight very strong hydrogen bonds are formed and the energy of the transition state is decreased by over 100 kcal/mol. In fact, the solvent change in this calculation probably represents a greater change in solvent than could be realized experimentally in a kinetic study. Finally, the fact that the carbon–nucleophile and the carbon – leaving group bonds in the transition state are not changed significantly by large changes in solvent in these systems is strong support for the *Solvation rule for S_N2 reactions* which predicts that Type I S_N2 transition states should be independent of solvent.

Implications on Theoretical Calculations of Transition State Structure

The solvation rule has important implications for those calculating the structure of the transition states for S_N2 reactions. The solvation rule states that Type I S_N2 transition states are not altered by a change in solvent. This means that theoretical calculations will give accurate structures for the transition states of these reactions whether they are carried out in gas phase or in solution. As a result, theoretical calculations should provide a valuable contribution to our understanding of this important class of reaction.

Unfortunately, this does not apply to all S_N2 reactions since the structure of a Type II S_N2 transition state is strongly solvent dependent. Thus theoretical (gas phase) calculations can only provide a very crude approximation of the structure of the

TABLE 4. Secondary α deuterium kinetic isotope effects for Type I and Type II S_N2 reactions

Reaction	$(k_H/k_D)_\alpha$	Solvent	Reference
	Type II reactions		
$C_6H_5CH_2OBs + H_2O \xrightarrow{25°C} C_6H_5CH_2OH$	1.153±0.002	80% aq. EtOH	34
	1.132±0.002	90% aq. EtOH	
	1.109±0.002	95% aq. EtOH	
	Ave. 1.131±0.022[a]		
$p\text{-}CF_3C_6H_4CH_2OBs + H_2O \xrightarrow{25°C} p\text{-}CF_3C_6H_4CH_2OBs$	1.084±0.002	70% aq. TFE[b]	34
	1.032±0.002	80% aq. EtOH	
	1.028±0.002	95% aq. EtOH	
	Ave. 1.048±0.031[a]		
$p\text{-}NO_2C_6H_4CH_2OBs + H_2O \xrightarrow{25°C} p\text{-}NO_2C_6H_4CH_2OH$	1.053±0.002	97% aq. TFE[b]	34
	1.022±0.002	80% aq. EtOH	
	1.004±0.002	95% aq. EtOH	
	Ave. 1.026±0.025[a]		
$C_6H_5CH_2\overset{+}{N}(CH_3)_2C_6H_5 + Br^- \xrightarrow{30°C} C_6H_5CH_2Br$	1.194[c]	Acetone	35[e]
	1.255[c]	$CHCl_3$	
$CH_3I + C_5H_5N \xrightarrow{50°C} C_5H_5\overset{+}{N}CH_3I^-$	0.919±0.002	Benzene	36
	0.891±0.008	Nitrobenzene	
	0.857±0.010	2-Butanone	
	0.882±0.006	Ethanol	
	Type I reactions		
$C_6H_5CH_2Cl + Cl^{-*} \xrightarrow{35°C} C_6H_5CH_2Cl^{*}$[d]	1.098±0.016	DMSO	37
	1.084±0.012	DMF	
	1.119±0.017	*n*-BuOH	
	Ave. 1.100±0.018[a]		

[a]These error limits are the standard deviations corresponding to the average value of the isotope effects.
[b]2,2,2-Trifluoroethanol.
[c]The error limits for these isotope effects were not given. These values were obtained from rate constants obtained using a conductometric method of analysis and should have errors of approximately ±0.002.
[d]This isotope effect was determined for $C_6H_5CH_2Cl$ and $C_6D_5CD_2Cl$. The isotope effect for ring deuteration in these S_N2 reactions would be extremely small and the total isotope effect observed can be attributed to the α deuterium atoms.
[e]Unpublished results from this laboratory indicate that this reaction proceeds by an S_N2 mechanism within a triple ion of the form $[(R_4N^+)_2Br^-]^+$.

transition state for reactions in solution and theoretical calculations will be of little use in studying these reactions.

Evidence Based on Secondary α Deuterium Kinetic Isotope Effects

Secondary α deuterium kinetic isotope effects $(k_H/k_D)_\alpha$ have been measured for several S_N2 reactions in different solvents. Although the relationship between the magnitude of these isotope effects and transition state structure is not known, current theory states that these isotope effects arise primarily from changes that occur in the C_α—H out-of-plane bending vibrations when the substrate is converted into the transition state (31, 32). A change of solvent does not alter the force constants for the C_α—H bending vibrations in the substrate significantly (33) and the same should be true for the transition state provided that the structure of the transition state is the same in the two solvents.[2] If this were the case, the changes in the C_α—H out-of-plane bending vibrations would be identical and the magnitude of the secondary α deuterium kinetic isotope effect would be the same in the two solvents. If the structure of the transition state was different in the two solvents, the changes in the C_α—H out-of-plane bending vibrations would be different and the magnitude of the isotope effect would change with solvent. Thus, the magnitudes of the secondary α deuterium kinetic isotope effect in different solvents can be used to indicate if the structure of the transition state is altered by a change in solvent. As a result, these isotope effects can be used to test the validity of the *Solvation rule for S_N2 reactions.*

An examination of the isotope effects in Table 4 shows that the results are consistent with the predictions of the solvation rule. The magnitudes of the secondary α deuterium kinetic isotope effects for the Type II S_N2 reactions of the *para*-substituted benzylbrosylates change significantly over a relatively narrow range of protic solvents. In all but one case, the isotope effects differ by at least ten times the standard deviations for the individual isotope effects. Thus, each isotope effect is significantly different and it must be concluded that the structure of the transition state is altered by a change in solvent. The isotope effect for the reaction between bromide ion and benzyldimethylphenylammonium ion also

Can. J. Chem. Downloaded from www.nrcresearchpress.com by 210.87.254.40 on 09/05/12
For personal use only.

Can. J. Chem. Downloaded from www.nrcresearchpress.com by 210.87.254.40 on 09/05/12
For personal use only.

changes markedly even though the two solvents are closely related dipolar aprotic solvents. The structure of the transition state for this reaction is also very sensitive to a change in solvent. A similar variation is observed in the inverse isotope effects (transition state structure) measured for the S_N2 reaction between methyl iodide and pyridine. The very high precision of these isotope effects forces one to conclude that the structure of the transition state in Type II S_N2 reactions is altered by a change in solvent. This is predicted by the solvation rule.

Type II S_N2 reactions, which require either a neutral nucleophile or a neutral leaving group, can be monitored by measuring the conductivity of the reaction mixture (34–36). This method has produced the most accurate rate constants reported and leads to very precise kinetic isotope effects. Unfortunately, conductivity cannot be used to study Type I S_N2 reactions where both nucleophiles are negatively charged. This means that the isotope effects for these reactions are less precise and thus provide a less stringent test of the solvation rule. The results for the Type I reactions of benzyl chloride illustrate this point. The standard deviations for the individual isotope effects are two to nine times larger than those of the Type II reactions. Within these limitations, however, the magnitudes of the secondary α deuterium kinetic isotope effects are the same. This indicates that the structure of the transition state is not altered by a change in solvent. This conclusion is justified for two reasons. First, the difference between the maximum and minimum values of the isotope effects is less (3.5%) than those observed for the Type II reactions (4.4, 5.6, 4.9, and 6.1%). The second reason is that the isotope effects for the Type I reaction are constant over a much broader range of solvent, i.e. the solvent is changed from the dipolar aprotic solvents, DMSO and DMF, to the protic solvent, *n*-BuOH. In the Type II reactions, larger changes in isotope effect are observed over a relatively narrow range of protic (34) and over a very narrow range of dipolar aprotic solvents (35, 36). Finally, although the case is weaker for Type I reactions, the results for all six reactions are consistent with the predictions of the solvation rule.

Possible Limitations in Applying the Solvation Rule for S_N2 Reactions

It is possible to conceive some circumstances in which the *Solvation rule for S_N2 reactions* might fail to predict the experimental result correctly. For example, a problem could arise if one of the partially charged nucleophiles in the transition state were much more sterically shielded from the solvent than the other in a Type I S_N2 transition state. In this case, a change in solvent would probably produce large differences in the solvation energies of the two nucleophiles in the transition state (a result opposite to that predicted by the *Solvation rule for S_N2 reactions*) and a change in the transition state might be observed.

The solvation rule could also fail if an ionic group which interacted strongly with solvent was either on the α carbon or on a group bonded to the α carbon. For example, if one of the groups on the α carbon were a phenoxide ion, the solvation of this group would be different in each solvent, and could alter the charge density on the α carbon in the transition state. If this occurred, a substantial and unexpected change in the structure of the transition state might result.

Another area of concern is for a Type I S_N2 reaction with a very small highly charged anion such as fluoride ion or hydroxide ion, and a large polarizable anion such as iodide ion, in the transition state. The differences in the solvation energies of the anions in water and a dipolar aprotic solvent could easily be as large for the $F^{\delta-}$---C---$I^{\delta-}$ transition state as for a Type II S_N2 transition state.[5] In these circumstances, a change of solvent may well lead to a change of structure in the transition state.

A similar problem might be expected with very reactant-like (early) or very product-like (late) Type I S_N2 transition states. One nucleophile is essentially neutral while the other is almost fully charged in these transition states and the difference between the solvation energies of the nucleophiles will be large. In fact, the difference in solvation energies could be large enough to cause the structure of the transition state to change with a change in solvent. Although the solvation rule would be expected to fail in these circumstances, there is some evidence to suggest that this is not probable. The leaving group heavy atom kinetic isotope effects measured for a wide variety of S_N2 reactions are reasonably large; their magnitude varies from approximately 30 to 70% of the theoretical maximum isotope effect (8, 9, 24, 38–41). This means that the α carbon – leaving group bond is substantially, but not nearly completely, broken in the transition state (26). The nucleophile – α carbon bond is also fairly long in three related S_N2 transition states (41). If this is a general phenomenon, S_N2 transition states are close to the symmetrical model on which the solvation rule is based and exceptions to the rule should be rare.

Finally, extensive aggregation or ion-pairing of salts in aprotic solvents could lead to incorrect

[5]If the free energy of transfer (ΔG_{tr}) of a fluoride ion is 10 kcal/mol, the difference in the solvation energies of the transition states would be $|10 - 3.2| \times 25/100 = 1.7$ kcal/mol. This value is in the range predicted for Type II S_N2 reactions.

Can. J. Chem. Downloaded from www.nrcresearchpress.com by 210.87.254.40 on 09/05/12
For personal use only.

predictions by the solvation rule. Many ionic compounds are only sparingly soluble in aprotic solvents and exist primarily, if not completely, as ion-pairs in solution (42). In cases where ion-pairing is important, incorrect predictions might result from the solvation rule because the properties of a nucleophile would be expected to be quite different when it is tied together with a cation in an ion-pair than when it exists as a totally free ion in solution. Thus, when extensive ion-pairing accompanied a change in solvent, the nucleophile would, in effect, be changed. This would be equivalent to a change in one of the reacting species and a change in the structure of the transition state would be expected regardless of the predictions of the solvation rule. Unfortunately, there are no experimental results which clearly illustrate this or the other possible limitations in applying the solvation rule.

In conclusion, the *Solvation rule for S_N2 reactions* provides a model for the interaction between S_N2 transition states and the solvent and predicts how the structure of the transition state will be altered by a change in solvent. Finally, the results of two studies involving leaving group heavy atom kinetic isotope effects, six studies using secondary α deuterium kinetic isotope effects, and two theoretical studies of S_N2 reactions are in complete agreement with the predictions based on the solvation rule. The extension of the *Solvation rule for S_N2 reactions* to S_N reactions involving carbonium ion intermediates will be discussed in a subsequent paper.

Acknowledgements

Part of this manuscript was prepared during the year the author spent on sabbatical leave at the University of Wisconsin, Madison. The hospitality extended by Professor James W. Taylor and the receipt of one month's salary from Professor Taylor's NSF grant MPS 75-21059 are gratefully acknowledged. The author also wishes to thank the National Research Council of Canada for support during the preparation of this manuscript.

1. A. J. Parker. Chem. Rev. **69**, 1 (1969).
2. M. H. Abraham. J. Chem. Soc. Perkin II, 1343 (1972).
3. E. M. Arnett, W. G. Bentrude, J. J. Burke, and P. McC. Duggleby. J. Am. Chem. Soc. **87**, 1541 (1965).
4. G. J. Frisone and E. R. Thornton. J. Am. Chem. Soc. **90**, 1211 (1968).
5. P. Haberfield, A. Nudelman, A. Bloom, R. Romm, and H. Ginsberg. J. Org. Chem. **36**, 1792 (1971).
6. P. R. Wells. Linear free energy relationships. Academic Press, New York. 1968. pp. 57–88.
7. J. March. Advanced organic chemistry: reactions, mechanisms and structure. McGraw Hill Co., New York. 1968. p. 295.
8. R. T. Hargreaves, A. M. Katz, and W. H. Saunders, Jr. J. Am. Chem. Soc. **98**, 2614 (1976).
9. D. G. Graczyk, J. W. Taylor, and C. R. Turnquist. J. Am. Chem. Soc. In press.
10. A. J. Parker. Q. Rev. London, **16**, 163 (1962).
11. E. Buncel and H. Wilson. Advances in physical organic chemistry. Vol. 14. Academic Press, New York. 1977. pp. 133–203.
12. B. G. Cox. Ann. Rep. Prog. Chem. **70**, 256 (1973).
13. G. Choux and R. L. Benoit. J. Am. Chem. Soc. **91**, 6221 (1969).
14. P. Haberfield, A. Nudelman, A. Bloom, R. Romm, H. Ginsberg, and P. Steinherz. Chem. Commun. 194 (1968).
15. P. Haberfield, L. Clayman, and J. S. Cooper. J. Am. Chem. Soc. **91**, 787 (1969).
16. P. Haberfield. J. Am. Chem. Soc. **93**, 2091 (1971).
17. R. Fuchs and L. L. Cole. J. Am. Chem. Soc. **95**, 3194 (1973).
18. C. D. Ritchie and G. A. Chappell. J. Am. Chem. Soc. **92**, 1819 (1970).
19. R. F. W. Bader, A. J. Duke, and R. R. Messer. J. Am. Chem. Soc. **95**, 7715 (1973).
20. P. Cremaschi, A. Gamba, and M. Simonetta. Theor. Chim. Acta, Berlin, **25**, 237 (1972).
21. J. J. Dannenberg. J. Am. Chem. Soc. **98**, 6261 (1976).
22. T. H. Cromartie and C. G. Swain. J. Am. Chem. Soc. **98**, 2962 (1976).
23. T. H. Cromartie and C. G. Swain. J. Am. Chem. Soc. **98**, 545 (1976).
24. G. W. Burton, L. B. Sims, J. C. Wilson, and A. Fry. J. Am. Chem. Soc. **99**, 3371 (1977).
25. K. Reppond. Ph.D. Dissertation, University of Arkansas, Fayetteville, AR. 72701. 1974.
26. W. H. Saunders, Jr. Chem. Scr. **8**, 27 (1975).
27. R. F. Rodewald, K. Mahendran, J. L. Bear, and R. Fuchs. J. Am. Chem. Soc. **90**, 6698 (1968).
28. J. I. Padova. Modern aspects of electrochemistry. Vol. 7. *Edited by* B. E. Conway and J. O'M. Bockris. Butterworths, London. 1971. pp. 8–21.
29. R. Fuchs, J. L. Bear, and R. F. Rodewald. J. Am. Chem. Soc. **91**, 5797 (1969).
30. P. Cremaschi and M. Simonetta. Theor. Chim. Acta, Berlin, **37**, 341 (1975).
31. V. J. Shiner, Jr. Isotope effects in chemical reactions. Am. Chem. Soc. Monograph 166. *Edited by* C. J. Collins and M. S. Newman. Van Nostrand Reinhold, New York. 1971. Chapt. 2, pp. 104–137.
32. V. J. Shiner, Jr., M. W. Rapp, E. A. Halevi, and M. Wolfsberg. J. Am. Chem. Soc. **90**, 7171 (1968).
33. R. C. Williams and J. W. Taylor. J. Am. Chem. Soc. **95**, 1710 (1973).
34. V. J. Shiner, Jr., M. W. Rapp, and H. R. Pinnick, Jr. J. Am. Chem. Soc. **92**, 232 (1970).
35. E. F. C. Ko and K. T. Leffek. Can. J. Chem. **49**, 129 (1971).
36. K. T. Leffek and A. F. Matheson. Can. J. Chem. **50**, 982 (1972).
37. H. Strecker and H. Elias. Chem. Ber. **102**, 1270 (1969).
38. K. C. Westaway and R. A. Poirier. Can. J. Chem. **53**, 3216 (1975).
39. J. W. Taylor. Unpublished results.
40. M. P. Friedberger and E. R. Thornton. J. Am. Chem. Soc. **98**, 2861 (1976).
41. S. F. Ali. M.Sc. Dissertation, Laurentian University, Sudbury, Ont., Canada P3E 2C6. 1976.
42. J. March. Advanced organic chemistry; Reactions, mechanisms and structure. McGraw-Hill Inc., NY. 1968. pp. 288–289.

Can. J. Chem. Downloaded from www.nrcresearchpress.com by 210.87.254.6 on 09/05/12
For personal use only.

Stereospecific synthesis of (−)-α-multistriatin from D-glucose

PHAIK-ENG SUM AND LARRY WEILER[1]

Department of Chemistry, University of British Columbia, Vancouver, B.C., Canada V6T 1W5

Received July 24, 1978

PHAIK-ENG SUM and LARRY WEILER. Can. J. Chem. **56**, 2700 (1978).

A totally stereospecific synthesis of the insect pheromone, (−)-α-multistriatin, is reported starting from D-glucose.

PHAIK-ENG SUM et LARRY WEILER. Can. J. Chem. **56**, 2700 (1978).

On rapporte la synthèse totalement stéréospécifique de la phéromone d'insecte, la (−)-α-multistriatine, à partir du D-glucose.

[Traduit par le journal]

α-Multistriatin (**1**) is one of the essential components of the aggregation pheromone of the European elm bark beetle, *Scolytus multistriatus*, which is the principal vector of Dutch elm disease in North America (1). The severe devastation of elm populations in eastern North America has resulted in extensive studies on the isolation (2), structure elucidation (3), synthesis (4), and field utilization (5) of α-multistriatin. The three other diastereomers of **1** have been

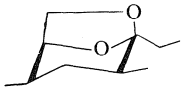

1

found to be biologically ineffective as attractants (5); however, all previous syntheses (4) of α-multistriatin have been nonstereoselective and have led to formation of the diastereomers of **1** in various amounts. We report a fully stereoselective synthesis of naturally occurring (−)-α-multistriatin with the relative and absolute configuration shown in **1**.

The epoxide **3** (6), prepared from D-glucose (**2**), gave a 75% yield of the 2-deoxy sugar **4** (7) on treatment with dimethyllithium cuprate. The alcohol **4** was converted into the corresponding xanthate **5** (7) in 94% yield and the resulting xanthate was deoxygenated with tri-*n*-butylstannane (8) to yield compound **6**, $[\alpha]_D^{28}$ +82.7° (142 mg/ml, ether), mp 70–72°C, in 90% yield from **5**. The benzylidene group in **6** was hydrolyzed (7) in 91% yield to give the diol **7** which was converted into the trityl ether **8**, $[\alpha]_D^{26}$ +26.0° (200 mg/ml, chloroform), mp 147–149°C, in 87% yield (9). Alcohol **8** was oxidized with chromium trioxide – pyridine (10) producing ketone **9**, $[\alpha]_D^{28}$ +98.8° (200 mg/ml, chloroform), ir 1730 cm^{-1}, as a white solid, mp 88–89°C, in 85% yield. A Wittig reaction (11) of **9** proceeded in 80% yield to give the alkene **10** which showed the appearance of two new vinyl hydrogens in the nmr spectrum at ca. δ 4.5. Compound **10** was also a crystalline solid, mp 153–154°C, $[\alpha]_D^{22}$ +45.4° (74 mg/ml, chloroform).

In the next very crucial step the 1,3-diaxial methyl system was generated in a stereoselective hydrogenation of **10** using Wilkinson's catalyst (12) to produce **11**, mp 140–142°C, $[\alpha]_D^{24}$ +27.0° (66 mg/ml, chloroform), in 81% yield. The nmr spectrum ($CDCl_3$) of **11** had the following features: δ 0.70 (d, J = 6 Hz, 3H), 0.94 (d, J = 7 Hz, 3H), 1–2 (m, 4H), 3.1 (m, 2H), 3.47 (s, 3H), 4.0 (br t, 1H), 4.23 (d, J = 5 Hz, 1H), and 7–7.6 (m, 15H). The new high-field, three-proton doublet clearly showed that reduction of the exocyclic double bond had occurred and the low-field doublet at δ 4.23 due to the hydrogen on the anomeric carbon indicated that **11** retained the chair conformation shown although the 5 Hz coupling with the hydrogen on C-2 did point to some flattening of the pyranose ring due to the 1,3-diaxial methyl interaction. It was clear from an examination of molecular models of the two possible chair conformations of **10** that the α-face of the olefin was the more accessible. This steric effect should be amplified with the bulky Wilkinson's catalyst. It has been established that axial methyl goups in cyclohexane rings normally have ^{13}C signals at δ 15–18 whereas the corresponding equatorial methyl groups are usually found at δ 18–25 (13). The ^{13}C nmr spectrum of **11** showed *only two* signals above δ 30, at 15.93 and 18.30 ppm from TMS. This would suggest that the methyl groups in **11** are both axial. Thus carbons 2,4 and 5 in **11** have the correct relative and absolute stereochemistry for conversion into natural (−)-α-multistriatin.

[1]Author to whom correspondence may be addressed.

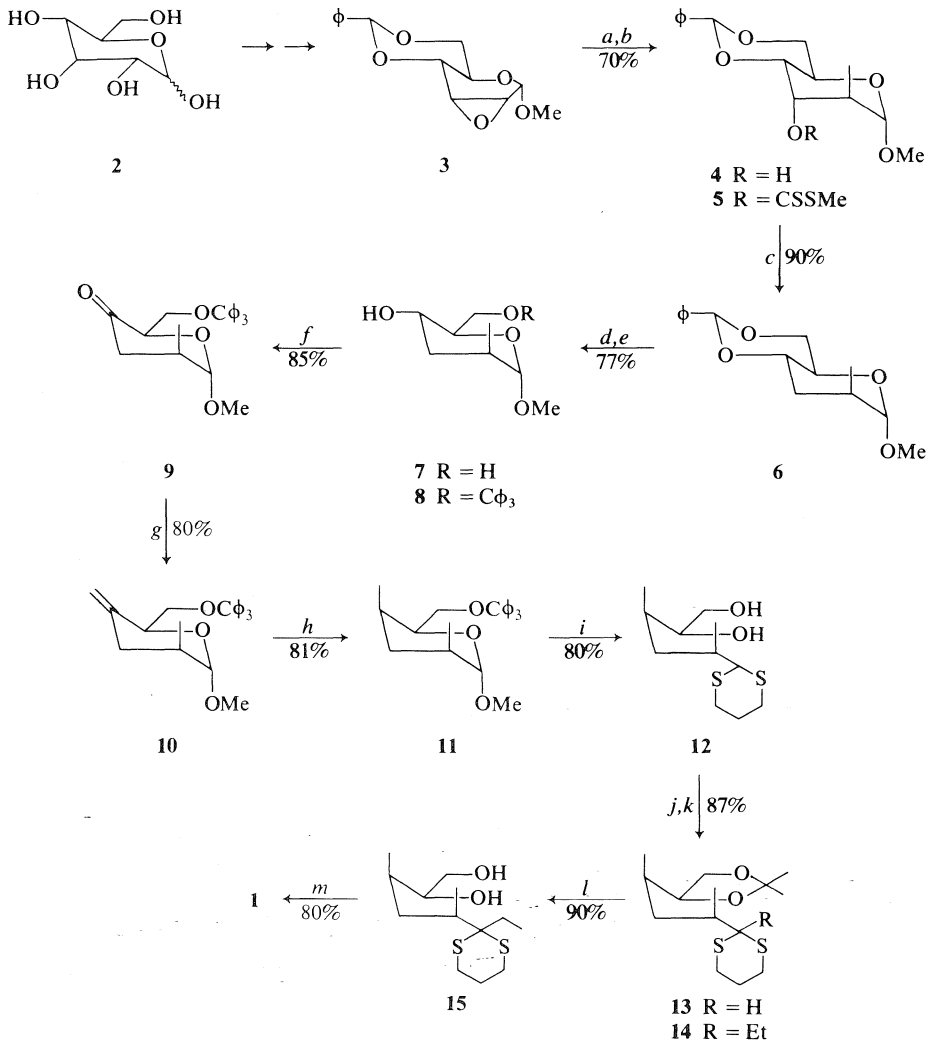

(*a*) Me_2CuLi, ether; (*b*) NaH, CS_2, MeI, ether; (*c*) $(nBu)_3SnH$, toluene; (*d*) TsOH, methanol; (*e*) trityl chloride, pyridine; (*f*) $CrO_3 \cdot 2Py$, dichloromethane; (*g*) $\phi_3\overset{+}{P}-\bar{C}H_2$, ether; (*h*) H_2, $(\phi_3P)_3RhCl$, benzene; (*i*) $HS(CH_2)_3SH$, $BF_3 \cdot Et_2O$, dichloromethane; (*j*) TsOH, 2,2-dimethoxypropane; (*k*) *tert*-butyllithium, hexane followed by iodoethane, HMPA; (*l*) TsOH, methanol; (*m*) $HgCl_2$, HgO, acetonitrile.

The synthesis of **1** was completed using a sequence of reactions which should prove useful in the synthesis of more complex carbohydrates and in the utilization of carbohydrates as chiral precursors for the synthesis of natural products (14). Treatment of compound **11** with 1,3-propanedithiol and boron trifluoride etherate (15*a*) led to cleavage of the trityl group and formation of the dithioacetal **12** in 80% yield. The resulting diol was protected by formation (16) of the isopropylidene **13**, $[\alpha]_D^{25}$ $-6.2°$ (150 mg/ml, ether), bp 120°C/0.1 Torr, in almost quantitative yield. We were unsuccessful in generating the anion of **13** using alkyllithium reagents in ether solvents (15). However, when the dithiane **13** was treated with *tert*-butyllithium in hexane at -20°C for 2 h and -10°C for 6 h a white precipitate formed. This mixture was alkylated with iodoethane in HMPA to produce **14**, $[\alpha]_D^{24}$ $-28.0°$ (50 mg/ml, ether), bp 128°C/0.1 Torr, in 80% yield. The isopropylidene group in **14** was cleaved in 90% yield to give **15**, $[\alpha]_D^{24}$ $-42.6°$ (50 mg/ml, chloroform), as a colourless oil.

Many of the previous syntheses of α-multistriatin involve an acid catalyzed cyclization of an epoxy ketone or a keto diol to generate the bicyclic ketal of **1**. These conditions lead to epimerization of the methyl group adjacent to the carbonyl. Hence we felt that it would be advantageous if we could

Can. J. Chem. Downloaded from www.nrcresearchpress.com by 210.87.254.6 on 09/05/12
For personal use only.

cyclize **15** without epimerization of carbon 4 in **15**. A solution of dithioketal **15** in *anhydrous* acetonitrile containing mercuric chloride and mercuric oxide (17) was refluxed for 4 h to yield **1** in 80% yield. The structure of our synthetic material was fully confirmed by comparison of the spectral data of our synthetic material with that reported for α-multistriatin (3, 4). The nmr spectrum (4*a*) is particularly diagnostic in distinguishing the isomers of multistriatin. Our synthetic material had an optical rotation $[\alpha]_D^{24}$ −46.0° (10 mg/ml, hexane) compared with a rotation $[\alpha]_D^{25}$ −47° (1.9 mg/ml, hexane) for the natural material (1, 4*b*). Finally vpc analysis of our synthetic (−)-α-multistriatin with a 3% OV 101 column, under a variety of conditions which separated the multistriatin isomers, demonstrated that our product was >99.7% pure and no trace of the other multistriatin isomers could be detected. This confirms the absolute configuration of the natural (−)-α-multistriatin as that shown in **1** (4*b*, *d*, *e*).

Acknowledgements

We are grateful to the National Research Council of Canada for financial support and to Professor L. D. Hall for a generous gift of methyl α-D-glucoside.

1. G. N. LANIER, R. M. SILVERSTEIN, and J. W. PEACOCK. *In* Perspectives in forest entomology. *Edited by* J. F. Anderson and H. K. Kaya. Academic Press, New York, NY. 1976. Chapt. 12.
2. J. W. PEACOCK, R. A. CUTHBERT, W. E. GORE, G. N. LANIER, G. T. PIERCE, and R. M. SILVERSTEIN. J. Chem. Ecol. **1**, 149 (1975).
3. G. T. PEARCE, W. E. GORE, R. M. SILVERSTEIN, J. W. PEACOCK, R. A. CUTHBERT, G. N. LANIER, and J. B. SIMEONE. J. Chem. Ecol. **1**, 115 (1975).
4. (*a*) W. E. GORE, G. T. PEARCE, and R. M. SILVERSTEIN. J. Org. Chem. **40**, 1705 (1975); (*b*) G. T. PEARCE, W. E. GORE, and R. M. SILVERSTEIN. J. Org. Chem. **41**, 2797 (1976); (*c*) W. J. ELLIOTT and J. FRIED. J. Org. Chem. **41**, 2475 (1976); (*d*) K. MORI. Tetrahedron, **32**, 1979 (1976); (*e*) G. J. CERNIGLIARO and P. J. KOCIENSKI. J. Org. Chem. **42**, 3622 (1977).
5. G. N. LANIER, W. E. GORE, G. T. PEARCE, J. W. PEACOCK, and R. M. SILVERSTEIN. J. Chem. Ecol. **3**, 1 (1977).
6. N. K. RICHTMYER. Methods Carbohydr. Chem. **1**, 107 (1962).
7. D. R. HICKS and B. FRASER-REID. Can. J. Chem. **53**, 2017 (1975).
8. D. H. R. BARTON and S. W. MCCOMBIE. J. Chem. Soc. Perkin I, 1574 (1975).
9. N. L. HOLDER and B. FRASER-REID. Can. J. Chem. **51**, 3357 (1973).
10. R. RATCLIFFE and R. RODEHORST. J. Org. Chem. **35**, 4000 (1970).
11. G. WITTIG and U. SCHOELLKOPF. Org. Syn. Coll. Vol. V, 751 (1973).
12. J. A. OSBORN, F. N. JARDINE, J. F. YOUNG, and G. WILKINSON. J. Chem. Soc. A, 1711 (1966).
13. (*a*) P. CREWS and E. KHO-WISEMAN. Tetrahedron Lett. 2483 (1978); (*b*) J. B. STOTHERS. *In* Carbon-13 nmr spectroscopy. Academic Press, New York, NY. 1972. Chapt. 3.
14. B. FRASER-REID. Acc. Chem. Res. **8**, 192 (1975).
15. (*a*) D. SEEBACH and E. J. COREY. J. Org. Chem. **40**, 231 (1975); (*b*) D. SEEBACH. Synthesis, **1**, 17 (1969).
16. B. R. BROWN and J. A. H. MCBRIDE. J. Chem. Soc. 3822 (1964).
17. H. TANAKA and S. TORII. J. Org. Chem. **40**, 462 (1978).

Can. J. Chem. Downloaded from www.nrcresearchpress.com by 210.87.254.6 on 09/05/12
For personal use only.

Canadian Journal of Chemistry
Published by
THE NATIONAL RESEARCH COUNCIL OF CANADA

Journal canadien de chimie
Publié par
LE CONSEIL NATIONAL DE RECHERCHES DU CANADA

Volume 56 Number 21 November 1, 1978

Volume 56 numéro 21 1 novembre 1978

La formation des liaisons éthériques lors de la production du polytéréphthalate d'éthylène glycol

VLADIMIR HORNOF ET LEOŠ ZEMAN[1]

Département de génie chimique, Université d'Ottawa, Ottawa (Ont.), Canada K1N 6N5

Reçu le 29 décembre 1977

VLADIMIR HORNOF et LEOŠ ZEMAN. Can. J. Chem. **56**, 2703 (1978).

Des liaisons du type éther sont formées comme sous-produits lors de la préparation du polytéréphthalate d'éthylène glycol à partir du téréphthalate de diméthyle et de l'éthylène glycol. Incorporées par la suite dans la chaîne du polymère, ces liaisons influencent ses propriétés physiques et mécaniques telles que la force de rupture à la tension, le point de fusion et la résistance à l'oxydation. Une méthode chimique d'analyse a été perfectionnée permettant la détermination quantitative des liaisons éthériques dans les fibres polyesters avec une bonne précision. Basée sur l'oxydation sélective de l'éthylène glycol avec de l'acide périodique, cette méthode se sert d'une hydrolyse par l'eau sous pression pour décomposer le polymère. La méthode a été utilisée pour l'étude de la dépendence de la formation des éthers sur la concentration du catalyseur de la polycondensation.

VLADIMIR HORNOF and LEOŠ ZEMAN. Can. J. Chem. **56**, 2703 (1978).

Ether-type linkages are formed as by-products during the preparation of polyethylene terephthalate from dimethyl terephthalate and ethylene glycol. Incorporated in the polymer, these linkages affect its physical and mechanical properties such as tensile strength, melting point, and resistance to oxidation. An improved chemical method of analysis has been developed allowing an accurate determination of ether bonds in polyester fibers. The method is based on the selective oxidation of ethylene glycol with periodic acid and takes advantage of hydrolysis with water under pressure to decompose the polymer. The method has been employed to study the effect of the concentration of polycondensation catalyst on the formation of ethers.

Introduction

Les fibres du type polyester occupent à l'heure actuelle une place très importante dans l'industrie de textiles. Le plus important membre de la famille de polyesters, le téréphthalate d'éthylène glycol, est normalement préparé à partir du téréphthalate de diméthyle et de l'éthylène glycol (1). La présence d'un catalyseur est nécessaire pour atteindre un bon rendement du polymère. L'activité de différents catalyseurs métalliques a été étudiée par Tomita et Ida (2). Leurs résultats indiquent que les catalyseurs actifs dans la polycondensation peuvent également promouvoir la formation de sous-produits.

Parmi les sous-produits est peut-être le plus important le diéthylène glycol, dont l'incorporation dans la chaîne apporte un effet nuisible à la qualité des fibres. La détermination analytique du diéthylène glycol dans le polyester est donc très importante. Les méthodes chimiques d'analyse sont en général basées sur l'oxydation sélective d'α-glycols par l'acide périodique (3). Francis (4) s'est servi de cette réaction pour analyser des faibles quantités de diéthylène glycol dans l'éthylène glycol. Plus récemment, Mifune et Ishida (5) et puis Kirby, Baldwin et Heidner (6) ont développés des méthodes analytiques permettant la détermination du diéthylène glycol dans les fibres polyesters.

La recherche discutée ici a été entreprise avec le but d'étudier l'influence de différents catalyseurs et de leurs concentrations sur la teneur en diéthylène glycol dans le polyester. Puisque les résultats obtenus en utilisant les méthodes analytiques déjà publiées n'avaient pas été satisfaisantes, il a été nécessaire de

[1]Adresse actuelle: 10 Marchant Road, Winchester, MA 01890, U.S.A.

Can. J. Chem. Downloaded from www.nrcresearchpress.com by 210.87.254.105 on 09/05/12
For personal use only.

Can. J. Chem. Downloaded from www.nrcresearchpress.com by 210.87.254.105 on 09/05/12
For personal use only.

les modifier. L'article présenté ici décrit la nouvelle procédure et son application à l'analyse de quelques séries de polyesters.

Méthode analytique

Procédure

On pèse à peu près 0.2 g de fibres avec la précision de 0.0001 g. Les fibres sont placés dans une ampoule ou un petit autoclave où ils sont décomposés avec de l'eau distillée à 200°C. Après 48 h d'hydrolyse, l'acide téréphthalique est enlevé par filtration et le filtrat est subi à l'oxydation par de l'acide périodique en utilisant 0.3 g de ce dernier pendant 20 min. Ensuite, l'excès de HIO_4 est réduit à l'iodide par du dioxyde de souffre. L'iodide produit par la réduction est précipité par l'addition de 0.25 g du carbonate d'argent. Le précipitat est enlevé par filtration et le liquide est mis dans un ballon 250 ml et dilué à 200 ml avec de l'eau distillée. Le ballon est fourni d'un condenseur et on en distille le liquide jusqu'à ce que le volume est réduit à 30 ml. On ajoute encore 100 ml d'eau et continue la distillation jusqu'à ce qu'il n'y est plus d'aldéhydes dans le distillat.[2] Ensuite, le résidu est refroidi à la température de chambre et transféré quantitativement dans un bocal volumétrique 100 ml. Après l'ajustement du volume à la marque avec de l'eau distillé, on pipette 50 ml (ou un autre volume aliquot) dans un Erlenmeyer 500 ml. On ajoute 20 ml de 0.1 N $K_2Cr_2O_7$ et 70 ml de l'acide sulfurique concentré. Le mélange est laissé à refluxer pendant 45 min et finalement, l'excédant du dichromate est déterminé par la titration iodométrique avec du thiosulfate de sodium.

Calculs

Selon Whitman et Roecker (7) c'est 20 équivalents du dichromate de potassium qui réagissent avec 1 mol du diglycol. La teneur en diéthylène glycol de l'échantillon (DEG) peut être calculée selon l'équation [1]:

$$[1] \qquad \text{DEG (mol)} = 0.050\,\frac{(B - A)N_{TS}}{1000X}$$

ou B est consommation de la solution de $Na_2S_2O_3$ pour le témoin; A est consommation de la solution de $Na_2S_2O_3$ pour l'échantillon; N_{TS} est normalité exacte de la solution de $Na_2S_2O_3$; et X est partie aliquote prise pour l'analyse (par exemple, si l'on prend 50 ml à partir de 100 ml, $X = 0.5$).

Le pourcentage molaire du diethylène glycol dans le polyester peut être calculé selon la formule dérivée par Kirby *et al.* (6):

$$[2] \qquad \%\text{DEG} = \frac{192.2\text{DEG}}{W - 44.0\text{DEG}} \times 100$$

ou W est poids de l'échantillon des fibres (g); DEG est moles de diéthylène glycol trouvées dans W g de l'échantillon.

Résultats et discussion

Méthode analytique

La procédure analytique comprend deux phases importantes: dans la première, la fibre est hydrolysée pour donner une solution des glycols; cette dernière est analysée dans la seconde phase en utilisant l'oxydation sélective par de l'acide périodique. L'oxydation par l'acide périodique sert à enlever l'éthylène glycol mais elle ne peut enlever d'autres produits organiques qui pourrait être présents dans le mélange après l'hydrolyse. Par exemple, la méthode analytique développée par Kirby *et al.* (6) utilise de l'hydroxyde de potassium alcoolique pour décomposer les fibres. Ceci résulte dans l'introduction d'une substance oxydable, à savoir l'éthanol, dans le mélange. L'éthanol pourrait par la suite intervenir lors de la détermination du diglycol.

Mifune et Ishida (5) ont évité ce problème en faisant le décomposition des fibres avec de l'hydroxyde de baryum. Après la décomposition, l'excès de l'hydroxyde a été précipité avec de l'acide sulfurique. Cette procédure diminuait la précision des résultats, probablement à cause de l'adsorption du diéthylène glycol sur le précipitat volumineux du sulfate de baryum.

Dans le travail actuel, les fibres ont été décomposées par de l'eau sous pression à 200°C. L'avantage de cette méthode est évident en ce qu'elle n'introduit aucune contamination; elle exige cependant plus longtemps pour complèter l'hydrolyse. Pour une analyse plus rapide, il serait possible de faire la décomposition dans un autoclave à une température encore plus élevée.

Essais de contrôle

Quelques échantillons-modèles ont été analysés afin de vérifier l'applicabilité de la procédure. Les résultats de ces essais sont assemblés dans le tableau 1.

Essai 1 démontre qu'une certaine quantité de diéthylène glycol est détectée même si l'on n'en a pas ajouté. Ce fond peut être attribué au diéthylène glycol présent dans l'éthylène glycol comme l'impureté, aussi bien qu'à d'autres impuretés oxydables qui peuvent se présenter dans l'éthylène glycol ou dans l'acide téréphthalique et qui ne sont pas enlevées par la procédure. De même on trouve un peu de diéthylène glycol dans l'essai 2.

Dans l'essai 3, on a analysé un mélange éthylène glycol – diéthylène glycol (9:1 par mol) en présence de l'acide téréphthalique. Le résultat obtenu a été un peu plus élevé que la valeur exigée (% DEG = 10). Pourtant cette déviation peut être diminuée si l'on soustrait la quantité trouvée dans l'essai 1 du résultat de l'essai 3. L'utilisation des essais-témoins semble d'être la meilleure méthode pour éliminer les erreurs systématiques dues aux impuretés.

Le dernier essai a été fait avec un échantillon du bis-β,β′-(hydroxyethyl) téréphthalate. Ce dernier a été préparé par la réestérification du téréphthalate de diméthyl avec de l'éthylène glycol à 190°C en présence du catalyseur ($Zn(OCOCH_3)_2$). Il est évident que cette étape préliminaire de polycondensation résulte déjà dans la formation du diéthylène glycol.

[2]Vérifié à l'aide de la réaction indicatrice avec de la fuchsine.

Can. J. Chem. Downloaded from www.nrcresearchpress.com by 210.87.254.105 on 09/05/12
For personal use only.

TABLEAU 1. Essais de contrôle

Essai No.	Substances dosées	DEG (μmol) Calculé	DEG (μmol) Trouvé	% DEG Calculé	% DEG Trouvé
1	Éthylène glycol (0.1232 g) Acide téréphthalique (0.3297 g)	0	5.0	0	0.25
2	Éthylène glycol (0.1511 g) Téréphthalate de diméthyl (0.2369 g)	0	7.0	0	0.29
3	Éthylène glycol (0.1038 g) Diéthylène glycol (0.0197 g) Acide téréphthalique (0.3086 g)	186.0	193.0	10.00	10.38
4	Bis-β,β′-(hydroxyethyl) téréphthalate (0.2848 g)	0	12.0	0	0.54

Reproductibilité d'analyse

La reproductibilité de la méthode analytique a été vérifiée sur deux échantillons de polytéréphthalate d'éthylène glycol. Le tableau 2 démontre les résultats obtenus avec un polyester industriel (Tesil 11), tandis que les résultats compilés dans le tableau 3 appartiennent à un polytéréphthalate d'éthylène glycol préparé au laboratoire. Les deux séries de données démontrent que la précision obtenu avec la nouvelle méthode est très satisfaisante, la déviation standarde étant de 0.04 dans le premier cas et de 0.06 dans l'autre.

Effet du catalyseur sur l'éthérification

La méthode analytique décrite ci-haut a été employée pour étudier la dépendance de formation des liaisons éthériques sur la concentration du catalyseur durant la polycondensation. Avec ce but, une série de neuf polyesters a été préparée en variant la concentration de l'acétate de zinc comme catalyseur. Dans tous les cas, la réestérification a été effectuée à 180°C, puis la température a été augmentée à 280°C pour commencer la polycondensation. La réaction a été arrêtée après 10 h.

Les résultats obtenus avec les concentrations du catalyseur entre 5×10^{-4} et 5×10^{-3} mol par rapport à 1 mol du téréphthalate de diméthyl sont démontrés dans le tableau 4. Il est évident que la teneur en diéthylène glycol dans le polyester augmente légèrement avec l'augmentation de la concentration du catalyseur.

TABLEAU 2. Reproductibilité d'analyse (Tesil 11)[a,b]

Poids W (g)	0.05 N Na_2SO_3 (ml)	DEG (μmol)	% DEG
0.2872	18.8	46.5	3.13
0.2857	19.4	45.0	3.05
0.3642	14.5	57.0	3.02
0.2225	23.3	35.0	3.04
0.2814	19.1	45.5	3.12
0.3119	16.9	51.0	3.15
0.4124	11.1	65.5	3.08
0.2929	18.5	47.0	3.09
0.3056	17.9	48.5	3.06
0.2733	19.9	43.5	3.07

[a]% DEG (moyenne) = 3.08.
[b]Déviation standarde σ = 0.04.

TABLEAU 3. Reproductibilité d'analyse (polyester préparé au laboratoire)[a,b]

Poids W (g)	0.05 N $Na_2S_2O_3$ (ml)	DEG (μmol)	% DEG
0.2691	17.9	48.5	3.49
0.2136	22.3	37.5	3.42
0.2358	20.5	42.0	3.45
0.3464	11.7	64.0	3.58
0.3215	13.9	58.5	3.54
0.3001	15.3	55.0	3.54
0.2778	17.3	50.0	3.48
0.2763	17.9	48.5	3.41
0.3118	14.3	57.5	3.57
0.3557	11.7	64.0	3.49

[a]% DEG (moyenne) = 3.50.
[b]Déviation standarde σ = 0.06.

TABLEAU 4. Dépendance de la teneur en diéthylène glycol sur la concentration du catalyseur[a,b]

Catalyseur mol/mol DMT[d] × 10^4	% DEG[c]	Point de fusion (°C)
5	2.94	262.0
8	2.84	263.0
12	3.05	261.0
20	3.17	263.0
27	3.17	264.5
32	3.20	263.0
37	3.30	258.5
43	3.46	258.5
50	3.53	259.5

[a]Catalyseur: $Zn(OCOCH_3)_2$.
[b]Temps de polycondensation: 10 h.
[c]Moyenne de trois déterminations.
[d]Téréphthalate de diméthyl.

La dernière colonne du tableau 4 compile les points de fusion des fibres qui correspondent à ces différents échantillons de polyesters. Il a été suggéré par Yoda (8) qu'une augmentation de la teneur en diéthylène glycol dans les fibres provoquerait une chute de point de fusion. De même, dans la publication de Jannsen *et al.* (9) on trouve que le point de fusion des fibres tombe de 270°C à 250°C en allant de 0.60% à 3.64% du diéthylène glycol. Les résultats obtenus dans ce travail démontrent que le point de fusion est presque constant pour les échantillons étudiés, bien qu'on observe une légère baisse de ce dernier lorsque la teneur en diéthylène glycol est plus élevée. On s'aperçoit cependant d'une inconsistance assez importante lorsqu'on compare les trois travaux. Dans le travail de Yoda (8) par exemple, la teneur en diéthylène glycol obtenue avec de l'acétate de zinc comme catalyseur est 7.5%; le point de fusion correspondant est 259°C. Presque le même point de fusion est obtenu dans le présent travail pour des polyesters dont la teneur en diéthylène glycol n'est que de 3.5%. Ce désaccord avec la variation très importante du point de fusion décrite par Jannsen *et al.* (9) indique la nécessité de la recherche supplémentaire pour mieux caractériser ce système.

1. J. R. WHINFIELD et J. T. DICKSON. Brit. Pat. 732–786.
2. K. TOMITA et H. IDA. Polymer, **16**, 185 (1975).
3. I. MALAPRADE. Bull. Soc. Chim. **4**, 683 (1928).
4. C. V. FRANCIS. Anal. Chem. **21**, 1238 (1949).
5. A. MIFUNE et S. ISHIDA. Kogyo Kagaku Zasshi, **65**, 824 (1962).
6. J. R. KIRBY, A. J. BALDWIN et R. H. HEIDNER. Anal. Chem. **37**, 1306 (1965).
7. C. L. WHITMAN et G. W. ROECKER. Anal. Chem. **33**, 781 (1961).
8. K. YODA. Kobunshi Kagaku, **24**, 472 (1967).
9. R. JANNSEN, H. RUYSSCHAERT et R. VROOM. Makromol. Chem. **77**, 153 (1964).

Can. J. Chem. Downloaded from www.nrcresearchpress.com by 210.87.254.105 on 09/05/12
For personal use only.

Apparent molal volumes and heat capacities of low molecular weight peptides in water at 25°C

CARMEL JOLICOEUR AND JEANNINE BOILEAU

Department of Chemistry, University of Sherbrooke, Sherbrooke, P.Q., Canada J1K 2R1

Received June 26, 1978

CARMEL JOLICOEUR and JEANNINE BOILEAU. Can. J. Chem. **56**, 2707 (1978).

The apparent molal volumes ϕ_v and heat capacities ϕ_c of oligopeptides of glycine, alanine, and serine have been determined in water at 25°C by flow densimetry and flow microcalorimetry. The data are reported for the homologous series: glycine to pentaglycine, L-alanine to tetra-L-alanine and L-serine to tri-L-serine. From the limiting ϕ_v^0 and ϕ_c^0 values of the glycine oligomers, the contributions of the glycyl residue in an extended polypeptide chain has been evaluated as: $\Delta\phi_v^0$(glycyl) = 38.0 ± 0.5 cm^3 mol^{-1} and $\Delta\phi_c^0$(glycyl) = 98 ± 5 J K^{-1} mol^{-1}. The data for the other peptides are discussed in terms of contributions from the amino acid side chains, i.e. —CH_3 and —CH_2OH, and end-group hydration effects. Some necessary conditions for obtaining useful additivity schemes for predicting ϕ_v^0 and ϕ_c^0 of extended polypeptides and proteins are indicated.

CARMEL JOLICOEUR et JEANNINE BOILEAU. Can. J. Chem. **56**, 2707 (1978).

Nous avons déterminé, à l'aide d'un densimètre et d'un microcalorimètre dynamiques, le volume molal apparent ϕ_v et la capacité calorifique molale apparente ϕ_c d'oligopeptides en solution aqueuse à 25°C. L'étude a porté sur les séries homologues suivantes: glycine à pentaglycine, L-alanine à tetra-L-alanine et L-serine à tri-L-serine. A partir des valeurs de ϕ_v^0 et ϕ_c^0 (dilution infinie) des oligomères de la glycine, nous avons pu évaluer la contribution du groupe glycyl dans une chaine polypeptidique allongée: $\Delta\phi_v^0$(glycyl) = 38.0 ± 0.5 cm^3 mol^{-1} et $\Delta\phi_c^0$(glycyl) = 98 ± 5 J K^{-1} mol^{-1}. Les données sur les autres peptides sont discutées en termes de la contribution due aux chaines latérales (—CH_3 ou —CH_2OH) des acides aminés et de l'influence de l'hydratation des groupes terminaux. L'examen des résultats suggère quelques conditions essentielles à l'établissement d'une échelle de valeurs de groupes utile à la prédiction de ϕ_v^0 et ϕ_c^0 de polypeptides et protéines dépliés.

Introduction

The thermodynamic stability of the native structure of proteins has provided one of the great challenges in biochemistry and currently remains the subject of extensive investigations (1). Although the structural features of proteins are being progressively elucidated through amino acid sequencing, X-ray diffraction, and active site studies, important questions persist concerning the thermodynamic quantities which characterize the various levels of structural organisation of proteins in solution.

In an idealistic approach, the thermodynamic information would be obtained by measuring the changes associated with the unfolding of the protein, from its native state (one specified native state if there are many) to a reference state. The latter should be independent of the initial state of the protein and, hopefully, would be accessible to all proteins. Presumably, a suitable reference state would be one where the protein is extended in such a way that there remains minimal interactions between amino acid side chains and each constituent amino acid is optimally accessible to the solvent. An obvious obstacle to this simple procedure, however, is that known means of inducing protein unfolding (temperature, pressure, addition of chemicals) usually do not lead to the required well defined final state (1*b*, 3). In the case of chemical denaturation, further complication arises since the comparison of initial and final states reflects thermodynamic changes due to the changes in solvent composition as well as from the protein structural modifications.

In another idealized approach, one could calculate some of the thermodynamic properties of 'extended' proteins in solution using group contributions derived from the properties of constituent amino acids and peptides. By comparing these results with measured values on the native proteins, the changes for the unfolding process could also be obtained. This procedure, as already applied to the apparent specific volumes of proteins (ref. 4, p. 374 *ff*), requires that appropriate additivity rules be established with good accuracy.

The present work was undertaken in relation to the latter strategy, namely, to investigate the additivity of amino acid contributions to apparent molal volumes and heat capacities of oligopeptides in solution. Since apparent molal heat capacities have been shown to be highly sensitive to hydration effects (e.g. discriminating between the hydration of ionic, polar, and apolar groups), it should provide a critical assessment of the group contribution approach. The

study was initiated on low molecular weight oligopeptides of glycine, alanine, and serine, chosen as to emphasize the influence of side chains having similar size, but different solvation effects.

Experimental

The amino acids glycine, L-alanine, and L-serine, as well as the homopeptides of glycine and alanine were purchased from Sigma. Di- and triserine were obtained from Vega Fox Biochemicals. Except for the latter two peptides, the compounds were recrystallized in various alcohol–water mixtures and tested to give a single TLC spot. The materials were dried several days in vacuum over P_2O_5 and their moisture content was assessed by Karl Fisher titration. With di- and triserine, the amount of material available was minimal and only the drying procedure was followed.

All solutions were prepared by weight in molality using distilled, deionized water (Continental deionizer). In the case of the higher peptides, the dissolution sometimes required hours of vigorous agitation in a thermostated shaker bath.

The solution densities d, and volumetric specific heats σ, were measured using a flow digital densimeter and a flow microcalorimeter described elsewhere (5, 6). For most of this study, the instruments were used under their highest sensitivity conditions, detection limits being respectively 10^{-6} g cm^{-3} and 10^{-5} J K^{-1} cm^{-3}. The flow densimeter and microcalorimeter were connected in series so both d and σ of each sample could be measured simultaneously. Since the common circulating thermostat was set at 25.00°C, and since the temperature rise during the heat capacity measurements was 2.0°C, the specific heat data are obtained at the mean temperature of 26.0°C.

Results

The apparent molal volumes ϕ_v and heat capacities ϕ_c were calculated from the solution densities and specific heats using the standard expressions (7):

$$[1] \qquad \phi_v = \frac{M_2}{d} - \frac{1000(d - d_0)}{mdd_0}$$

and

$$[2] \qquad \phi_c = \phi_v\sigma_0 + \frac{1000(\sigma - \sigma_0)}{c}$$

where M_2 is the molecular weight of the solute, and m and c represent the molal and molar concentrations. Since ϕ_v and ϕ_c were found to vary linearly with concentration, the results were fitted by least-squares method to equations of the form:

$$[3] \qquad \phi_v = \phi_v^0 + B_v c$$

and

$$[4] \qquad \phi_c = \phi_c^0 + B_c c$$

The resulting ϕ^0 and B parameters are reported in Table 1 along with the concentration range investigated and the number of data for each compound.[1]

[1]Detailed values of d, σ, ϕ_v, and ϕ_c are available, at a nominal charge, from the Depository of Unpublished Data, CISTI, National Research Council of Canada, Ottawa, Ont., Canada K1A 0S2.

The standard deviation on the results are also given in parentheses below each parameter. For the tetrapeptides (or higher homologs) the slopes were obtained over a very narrow range of concentration, so their reliability is questionable.

A comparison of the present results with several literature data is presented in Table 2. For the ϕ_v^0 data, the present results are in good agreement with those of previous authors, though several discrepancies are found in the comparisons of ϕ_c^0 data. Except for the data on diglycine however, these discrepancies are within the uncertainties of the methods used by previous investigators. For diglycine, the values reported here are believed to be more reliable than earlier data, since they could be reproduced within 1 J K^{-1} mol^{-1} at a one year interval, using different batches of the compound.

Discussion

In dilute aqueous solutions, amino acids and linear peptides are present in the form of dipolar ions. The ratio of the dipolar ion species to the neutral species is usually many orders of magnitude (ref. 4, p. 96) so, for the present purpose, we may consider only the zwitterionic state of the molecules.

The solution conformation of low molecular weight peptides has been, in many cases, thoroughly investigated using nmr, dielectric, and optical methods (21). Studies on oligopeptides of increasing lengths have shown that the formation of α-helix (or other) structure generally requires a minimum number of 6 to 12 amino acid units, depending on both the amino acids and the solvent. Below this minimum number, the non-cyclic peptides retain considerable conformational mobility, so preferred conformations cannot be identified, i.e. the peptide molecule undergoes rapid conversion among its many possible conformational states. Hence, the peptides studied here may be envisaged as dipolar ions, having conformations sufficiently extended so that each portion of the molecule is accessible to the solvent.

The thermodynamic properties of the amino acids and peptides are, of course, highly influenced by hydration of their ionic end groups. Recent studies on partial molal volumes and heat capacities of nonelectrolytes (22, 24) and various amino acids (8–10, 13, 15, 16, 25) offer important information pertaining to the present investigation. First, with ω-aminocarboxylic acids ($H_2N(CH_2)_nCOOH$) which also exist mainly as dipolar ions, the hydration of the $-NH_3^+$ and $-COO^-$ ions may be considered independent only when there are ca. six methylene groups separating these two ions (9, 13). For shorter alkyl chains, hydration of the end groups interferes with the hydration of the methylene groups, and the incremental

TABLE 1. Apparent molal volumes and heat capacities of amino acids and peptides in water at 25°C[a]

Amino acid	ϕ_v^0 ($cm^3\ mol^{-1}$)	B_v	ϕ_c^0 ($J\ K^{-1}\ mol^{-1}$)	B_c	Concentration range (mol kg^{-1} (H_2O))	No. of data
Glycine	43.25	0.89	39.2	18.5	0.05 –0.9	26
	(0.01)	(0.02)	(0.4)	(0.9)		
Diglycine	76.27	2.07	105.0	40.2	0.02 –0.82	43
	(0.01)	(0.03)	(0.4)	(1.0)		
Triglycine	111.81	3.5	185.9	103	0.01 –0.21	23
	(0.01)	(0.1)	(0.9)	(7)		
Tetraglycine	149.7	26	283	0	0.003–0.019	25
	(0.1)	(13)	(2)	(253)		
Pentaglycine	187.1	515	373	−3000	0.002–0.0033	34
	(0.2)	(84)	(6)	(2600)		
Alanine	60.45	0.70	141.4	9.7	0.06 –1.0	18
	(0.01)	(0.01)	(0.2)	(0.5)		
Dialanine	110.30	2.2	330.8	25	0.04 –0.23	11
	(0.03)	(0.2)	(0.4)	(2.8)		
Trialanine	163.80	4.9	526	69	0.014–0.095	11
	(0.05)	(0.9)	(1)	(17)		
Tetraalanine	220.1	30	733.4	206	0.005–0.024	26
	(0.1)	(7)	(0.9)	(62)		
Serine	60.62	1.27	117.4	21.6	0.06 –0.6	17
	(0.01)	(0.02)	(0.1)	(0.3)		
Diserine	111.8	11	259.9	−15	0.007–0.05	7
	(0.1)	(5)	(1.5)	(54)		
Triserine	166.0	4	398	126	0.004–0.04	6
	(0.2)	(7)	(2)	(87)		

[a]Standard deviations in parentheses.

TABLE 2. Comparison of several ϕ_v^0 and ϕ_c^0 data with earlier results

Amino acid	ϕ_v^0 ($cm^3\ mol^{-1}$)	ϕ_c^0 ($J\ K\ mol^{-1}$)
Glycine	43.25 (43.39,[a] 43.5,[b] 43.19[c])	39.2 (31,[g] 61,[h] 43.9,[i] 36.8,[j] 36.7[a])
Diglycine	76.27 (76.34,[d] 77.2[e])	105.0 (159,[g] 167[k])
Triglycine	111.81 (113.5[e])	185.9 (218[k])
Alanine	60.45 (60.47,[f] 60.62,[a] 60.3,[b] 60.43[c])	141.4 (148,[g] 146,[i] 141,[l] 145.6,[a] 142.5[f])
Dialanine	110.30	330.8 (360[k])
Serine	60.62 (60.3,[b] 60.8[g])	117.4 (115,[g] 125.1[i])

[a]Reference 8.
[b]Reference 9.
[c]Reference 10.
[d]Reference 11.
[e]Reference 12.
[f]Reference 13.
[g]Reference 14.
[h]Reference 15.
[i]Refefence 16.
[j]Reference 17.
[k]Reference 18.
[l]Reference 19.

contribution of the latter to ϕ_c^0, i.e., $\Delta\phi_c^0(CH_2)$, is much lower than that found in homologous series of monofunctional aliphatic molecules (24). On this basis, we must expect similar end-group effects for peptides and, presumably, a minimum of six C—C or C—N bonds will be required to minimize interference in the hydration of the end groups, or influence of the latter on the hydration of the center portion of the peptide.

A second important result can be recalled from studies on a series of α-aminoacids containing aliphatic residues of increasing size (e.g. glycine, alanine, valine, leucine). The contribution of these side chains to ϕ_c^0 are remarkably close to those found in other series of polar molecules or organic ions. This suggests that, in contrast to methylene groups located between the ionic end groups, the hydration of hydrocarbon side chain is not too strongly perturbed by the terminal ions. Analysis of the peptide data reported here will show both analogies and differences in the additivity effects observed with α- and ω-amino acids.

(1) Additivity of Amino Acid Contributions to ϕ_v^0 and ϕ_c^0 in Peptides

To evaluate the incremental contribution of amino

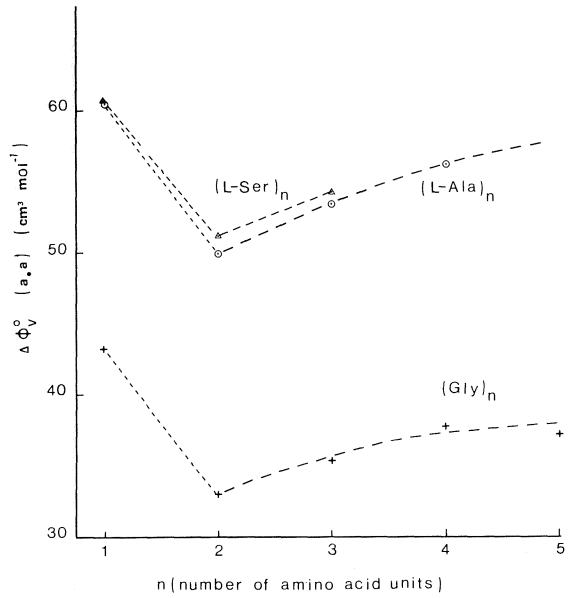

FIG. 1. Incremental contributions of amino acids to ϕ_v^0 of oligopeptides in water at 25°C.

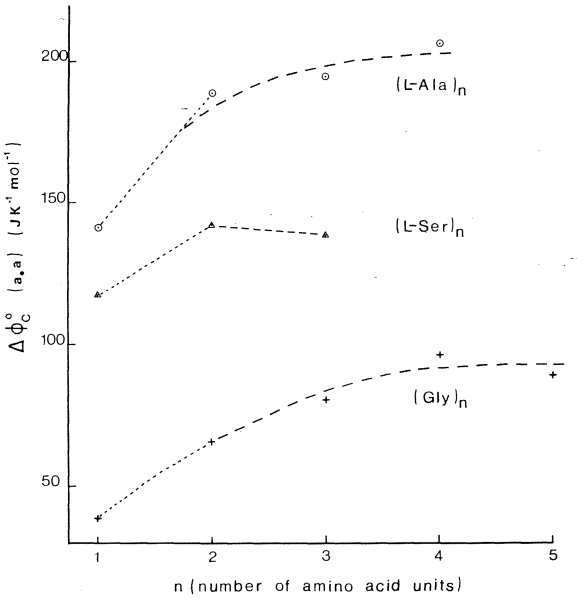

FIG. 2. Incremental contributions of amino acids to ϕ_c^0 of oligopeptides in water at 25°C.

acids to ϕ_v^0 and ϕ_c^0 ($\Delta\phi^0$(a.a)) in each homologous series, we have plotted the increments of these properties against the number of amino acids (n) in the peptides (Figs. 1 and 2). It is apparent from these data that the variation of $\Delta\phi_v^0$(a.a) with n is remarkably similar in each series, while significantly different behaviours are found with $\Delta\phi_c^0$(a.a). The origin of these differences will be discussed below (Section 3).

The results for glycine and its oligomers show that the apparent molal volume of the second amino acid is much smaller than that of the monomer. Hydration of ionic groups such as $-NH_3^+$ and $-COO^-$ will decrease ϕ_v^0 of the monomer (4, 9) and, to first order, this effect is constant within a series of peptides. On the other hand, the formation of the peptide bond decreases $\Delta\phi_v^0$(a.a) assigned to the second amino acid. Clearly the latter effect is dominant. The contribution of further glycyl units increases regularly, tending to a constant value for n between 4 and 6. This behavior most certainly reflects the decreasing influence of end group hydration on $\Delta\phi_v^0$ of the central glycyl units. In peptides, the number of atoms separating the $-NH_3^+$ and $-COO^-$ groups is given as $(3n - 2)$ so it can be expected from the earlier discussion that $\Delta\phi_v^0$ will reach its 'unperturbed' value for the tripeptide and higher homologs. If, as is appropriate in the present case, we neglect the backbone atoms of the glycyl unit considered, the number of atoms separating the end groups is $(3n - 5)$ and, hence, the tetramer will be required to eliminate end-group effects on $\Delta\phi_v^0$(a.a). The levelling-off of $\Delta\phi_v^0$(a.a) at $n \simeq 4$ supports this interpretation and allows the evaluation of the volume of the glycyl residue in the polypeptide chain as: $\Delta\phi_v^0$(glycyl) = 38.0 ± 0.5 cm^3 mol^{-1}. The large uncertainty on this value is due mainly to the difficulty in obtaining accurate data for tetra- and pentaglycine.

With the oligopeptides of L-serine and L-alanine, $\Delta\phi_v^0$(a.a) do not reach a constant value within the series investigated. However, the similar variations of $\Delta\phi_v^0$(a.a) in the three series suggest that side chain/side chain interactions do not contribute significantly to ϕ_v^0; hence L-seryl and L-alanyl group contributions could be extrapolated in a way analogous to the data for the glycine oligomers. Alternately it could be obtained from $\Delta\phi_v^0$(glycyl), if the side chain contributions (CH_3 and CH_2OH) can be assessed reliably.

The $\Delta\phi_c^0$(a.a) data exhibit a common behavior for the three series of peptides, namely a marked increase for the second amino acid compared to the monomer. This might be expected since most 1:1 electrolytes (26) have negative apparent molal heat capacities. As for the ϕ_v^0 data discussed above, this effect will reduce ϕ_c^0(monomer), whereas formation of the peptide bond will reduce the $\Delta\phi_c^0$ assigned to the second glycyl residue. By contrast to ϕ_v^0 data, however, the difference in ϕ_c^0 of glycine and of the glycyl unit originates mainly in hydration effects.

From the data for the higher glycine oligomers, $\Delta\phi_c^0$(a.a) is seen to reach a constant value at $n \simeq 4$, 5, leading to a glycyl unit contribution of 95 ± 5 J K^{-1} mol^{-1}. For the other peptides, $\Delta\phi_c^0$(a.a) is not readily extrapolated to larger n values. Variations of

TABLE 3. Side chain contributions ($H \rightarrow CH_3$) and ($H \rightarrow CH_2OH$) to ϕ_v^0 and ϕ_c^0 of amino acids and peptides[a]

Parameter	Value for n = 1	2	3	4
$\Delta\phi_v^0$ ($H \rightarrow CH_3$)/cm^3 mol^{-1}	17.2	16.8	18.0	18.4
$\Delta\phi_v^0$ ($H \rightarrow CH_2OH$)/cm^3 mol^{-1}	17.4	18.2	18.7	
$\Delta\phi_c^0$ ($H \rightarrow CH_3$)/J K^{-1} mol^{-1}	102	124	114	110
$\Delta\phi_c^0$ ($H \rightarrow CH_2OH$)/J K^{-1} mol^{-1}	78	77	57	

[a]Results tabulated from differences in the incremental values of glycyl, alanyl, and seryl as a function of n.

$\Delta\phi_c^0$(a.a) within the series (L-alanine)$_n$ and (glycine)$_n$ appear related, though different from the behavior of the L-serine peptides.

(2) Additivity of Side Chain Contributions

Having established a reasonable basis for calculating ϕ_v^0 and ϕ_c^0 of 'extended' polyglycine molecules in water, we turn to examine the side chain contributions in the L-alanine and L-serine peptides. These contributions can be expressed as the changes in ϕ_v^0 and ϕ_c^0 for the substitution of a glycyl C—H by a —CH_3 or a —CH_2OH group: $\Delta\phi^0(H \rightarrow CH_3)$ and $\Delta\phi^0(H \rightarrow CH_2OH)$. The latter quantities were obtained as a function of n from appropriate differences of the data in Figs. 1 and 2 and are reported in Table 3. (Because these data are differences between incremental values ($\Delta\phi^0$(a.a)), their uncertainty is expected to increase with n.)

It is readily seen from the data in Fig. 1 or Table 3 that the magnitudes of $\Delta\phi_v^0(H \rightarrow CH_3)$ and $\Delta\phi_v^0(H \rightarrow CH_2OH)$, as well as their variation with n, are very similar. This is in accordance with the rather general observation that $\Delta\phi_v^0(CH_3 \rightarrow CH_2OH) \simeq 0$ cm^3 mol^{-1}; the latter is usually true within 1 cm^3 mol^{-1}, and appears quite independent of the nature of neighboring substituents (23, 27, 28).

The variation of $\Delta\phi_v^0(H \rightarrow CH_3)$ and $\Delta\phi_v^0(H \rightarrow CH_2OH)$ with n indicates some influence of the ionic end groups on the hydration of the side chains.[2] Hence, the $\Delta\phi_v^0(H \rightarrow CH_3, CH_2OH)$ obtained from comparison of the amino acid ϕ_v^0 data are lower (by $\sim$1 cm^3 mol^{-1}) than the values derived from $\Delta\phi_v^0$(a.a) at larger n. It thus seems preferable for predictive purposes, to obtain the side chain contributions from peptide data or, perhaps, from data on analogous non-electrolytes as suggested in early studies (4).

The side chain contributions to the heat capacities $\Delta\phi_c^0(H \rightarrow CH_2OH)$ and $\Delta\phi_c^0(H \rightarrow CH_3)$ exhibit sharp differences in their magnitudes as well as in their variations as a function of n. Judging from the data in Table 3, $\Delta\phi_c^0(H \rightarrow CH_3)$ levels-off at $\sim$105 J K^{-1} mol^{-1} for $n \simeq 4, 5$. This value is remarkably close to that obtained directly by comparing $\Delta\phi_c^0$ of glycine and alanine, i.e. 102 J K^{-1} mol^{-1}, in accordance with the results quoted at the beginning of this discussion, i.e. $\Delta\phi_c^0$ of aliphatic residues on α-amino acids. However, in view of the end group influence upon $\Delta\phi_v^0(H \rightarrow CH_3)$, this agreement may be fortuitous resulting from the opposite effects of ionic and apolar groups on ϕ_c^0. Possibly, the apolar side chain hinders the hydration of the ionic groups (29), thereby increasing ϕ_c^0 of the amino acids.

The values obtained for $\Delta\phi_c^0(H \rightarrow CH_2OH)$ decrease for $n > 2$ and a linear extrapolation from the di- and triserine data yields $\Delta\phi_c^0(H \rightarrow CH_2OH) \simeq 40$ J K^{-1} mol^{-1} for the tetrapeptide. This is only one-half the value obtained directly from ϕ_c^0 of the amino acids, indicating important end-group effects. Qualitatively, this behavior can be rationalized from data on various other compounds.

With aliphatic alcohols (23), the $H \rightarrow CH_2OH$ substitution (e.g. *n*-propanol $\rightarrow$ 1,4-butanediol) leads to $\Delta\phi_c^0(H \rightarrow CH_2OH) \simeq 0$ J K^{-1} mol^{-1}, i.e. the —OH hydration effects cancel out the methylene group contribution (88 J K^{-1} mol^{-1}) to ϕ_c^0. Contrastingly, the same substitution occurring α to a charged nitrogen center (e.g. $CH_3\overset{+}{N}H_3 \rightarrow HOCH_2$-$CH_2\overset{+}{N}H_3$) leads to a $\Delta\phi_c^0$ of 54 J K^{-1} mol^{-1} (2). Clearly, the presence of the neighboring ionic charge has a strong influence on ϕ_c^0 of the —CH_2OH group, an effect which again can be interpreted as due to interference between the hydration of the polar and ionic group. In the case of amino acids, both the NH_3^+ and COO^- can interfere with the hydration of the CH_2OH side chain, and this could explain the large $\Delta\phi_c^0(H \rightarrow CH_2OH)$ found here. An important consequence of these findings is that for the amino acids having polar groups on their side chains, the contribution of the latter to ϕ_c^0 should be derived from polypeptide data, or possibly, from data on non-electrolyte analogues. Contributions obtained by straightforward differences among amino acid data could be grossly misleading.

[2]The effects involved here must be related to those invoked for explaining ϕ_v^0 data in homologous series of aliphatic monofunctional compounds (20), but probably in a still more complex way.

(3) Contribution of the Peptide Linkage

The contribution of the peptide bond (CO—NH) constitutes a fundamental quantity for predicting the properties of the polypeptide backbone in proteins. Both, $\Delta\phi_v^0$(CO—NH) and $\Delta\phi_c^0$(CO—NH) have been estimated previously from data on non-electrolytes, mainly amides and dipeptides.

For the $\Delta\phi_v^0$ contribution, estimates based on early volume data (4) have yielded 20.0 cm^3 mol^{-1} for the —CO—NH— group and 36.3 cm^3 mol^{-1} for the —CH_2—CO—NH(glycyl) residue. The present result $\Delta\phi_v^0(CH_2—CO—NH) = 38.0 \pm 0.5$ cm^3 mol^{-1} confirms the earlier value within the uncertainty expected from the group additivity scheme used in previous studies. The glycyl contribution derived directly from polypeptide data should be a more representative quantity and, in that sense, is more reliable.

The magnitude of $\Delta\phi_c^0$(CO—NH) has also been obtained by Nichols *et al.* (24) from group additivity analysis of data for aqueous amides; the result is $\Delta\phi_c^0(CO—NH) = -61$ J K^{-1} mol^{-1}. From similar considerations on data for cyclic mono- and dipeptides, Cabani *et al.* (18) reported that $\Delta\phi_c^0$(CO—NH) should be near 0 J K^{-1} mol^{-1}. These authors also remarked that this group contribution behaves differently in cyclic compared to linear peptides. Presumably, this indicates that with such complex molecules, detailed group additivity rules are accurate only within categories of similar compounds or homologous series.

As reported above, we have determined for the glycyl unit $\Delta\phi_c^0(CH_2—CO—NH) = 98 \pm 5$ J K^{-1} mol^{-1} which can be compared with the estimates obtained by Krescheck and Benjamin (14) from dipeptides (128 ± 25 J K^{-1} mol^{-1}) and by Cabani *et al.* (18) from di- and triglycine (50 ± 21 J K^{-1} mol^{-1}). Since it was shown that $\Delta\phi_c^0$(a.a) varies significantly with n, the previous estimates should be compared with the corresponding di- and tripeptide data reported here. For such comparison, the present results agree reasonably with those of Cabani *et al.* but differ significantly from the data of Krescheck and Benjamin.

Finally, it is interesting to compare the glycyl contribution to ϕ_v^0 and ϕ_c^0 of peptides with that of an aliphatic hydrocarbon. The apparent molal volume of the glycyl unit is ca. 2.4 times larger than the methylene group contribution in an alkyl chain (16.0 cm^3 mol^{-1} (23)). On the other hand, its apparent molal heat capacity is only ca. 1.1 times $\Delta\phi_c^0(CH_2)$ in homologous series of non-electrolytes (88 J K^{-1} mol^{-1} (24)). Hence, if the methylene group in the glycyl unit is assigned the same contribution as in alkyl chains, the peptide bond indeed appears to have a very minor contribution to ϕ_c^0(ca. 7 J K^{-1} mol^{-1}) in agreement with the suggestion of Cabani *et al.* (18).

Conclusions

The results of this investigation show that ϕ_v^0 and ϕ_c^0 of the low molecular weight oligopeptides vary in a regular fashion with n, and that a minimum value of $n = 4$ is required before the incremental contribution of the amino acid becomes constant. This is taken as evidence for interference of the ionic end groups of the peptides upon the hydration of its middle portion and side chains, an effect noted previously in other homologous series (20). Although contributions from segmental motions or conformational changes as a function of n cannot be ignored, there is no indication that such effects have a significant influence on ϕ_v^0 and ϕ_c^0 of the peptides studied here.

The glycyl group contribution to ϕ_v^0 and ϕ_c^0 derived from the data, together with an additivity scheme for side chain contributions, should provide a basis for predicting ϕ_v^0 and ϕ_c^0 of extended polypeptides and proteins in solution. However, the reliability of such calculations will depend on a proper evaluation of side chain effects; the data reported here show that in some cases, side chain contributions should not be taken directly from amino acid data. This is particularly clear from the ϕ_c^0 data for amino acids having a side chain functional group.

Acknowledgements

The authors gratefully acknowledge financial assistance from the National Research Council of Canada and the Ministère de l'Education du Québec. The assistance of Mr. J. C. Mercier and Mr. P. Bolduc with the experiments and of Dr. P. A. Leduc for data treatment are also acknowledged.

1. S. N. Timasheff and G. D. Fasman (*Editors*). Structure and stability of biological macromolecules. Marcel Dekker Inc., New York. 1969. (*a*) Chapt. 2, p. 65; (*b*) Chapt. 3, p. 213.
2. C. Jolicoeur and J. C. Mercier. To be published.
3. C. Tanford. Advances in protein chemistry. Vol. 23. *Edited by* C. B. Anfinsen, M. L. Anson, K. Bailey, and J. T. Edsall. Academic Press, New York. 1968. pp. 121 and 218.
4. E. J. Cohn and J. T. Edsall. Proteins, amino acids and peptides. American Chemical Society Monographs. Hafner Publishing Co., New York. 1965.
5. P. Picker, E. Tremblay, and C. Jolicoeur. J. Solution Chem. **3**, 377 (1974).
6. P. Picker, P. A. Leduc, P. R. Philip, and J. E. Desnoyers. J. Chem. Thermodyn. **3**, 631 (1971).
7. J. L. Fortier, P. A. Leduc, and J. E. Desnoyers. J. Solution Chem. **3**, 323 (1974).
8. G. Di Paola and B. Belleau. Can. J. Chem. In press.

9. F. SHAHIDI and P. G. FARRELL. J. Chem. Soc. Faraday I. In press.
10. F. J. MILLERO, A. LO SURDO, and C. SHIN. J. Phys. Chem. **82**, 784 (1978).
11. H. D. ELLERTON, G. REINFELDS, D. E. MULCAHY, and P. J. DUNLOP. J. Phys. Chem. **68**, 398 (1964).
12. E. J. COHN, T. L. MCMEEKIN, J. T. EDSALL, and M. H. BLANCHARD. J. Am. Chem. Soc. **56**, 784 (1934).
13. J. D. C. AHLUWALIA, C. OSTIGUY, G. PERRON, and J. E. DESNOYERS. Can. J. Chem. **55**, 3364 (1977).
14. G. C. KRESCHECK and L. BENJAMIN. J. Phys. Chem. **68**, 2476 (1964).
15. S. CABANI, G. CONTI, E. MATTEOLI, and A. TANI. J. Chem. Soc. Faraday I, **73**, 476 (1977).
16. C. H. SPINK and I. WADSO. J. Chem. Thermodyn. **7**, 561 (1975).
17. F. T. GUCKER, W. L. FORD, and C. E. MOSER. J. Phys. Chem. **43**, 153 (1939).
18. S. CABANI, G. CONTI, and E. MATTEOLI. Quatrième Conférence Internationale de Thermodynamique Chimique (Montpellier, France, 1975). Vol. 5, p. 27; Biopolymers, **16**, 465 (1977).
19. F. T. GUCKER and T. W. ALLEN. J. Am. Chem. Soc. **64**, 191 (1942).
20. R. ZANA. J. Phys. Chem. **81**, 1817 (1977).
21. V. J. HRUBY. The chemistry and biology of amino acids, peptides, and proteins. Vol. 3. Marcel Dekker, New York. 1974. p. 2 and references cited therein.
22. J. KONICEK and I. WADSO. Acta Chem. Scand. **25**, 1541 (1970).
23. C. JOLICOEUR and G. LACROIX. Can. J. Chem. **54**, 624 (1976).
24. N. NICHOLS, R. SKOLD, J. SUURKUUSK, and I. WADSO. J. Chem. Thermodyn. **8**, 1081 (1976).
25. K. P. PRASAD and J. C. AHLUWALIA. J. Solution Chem. **5**, 491 (1976).
26. J. E. DESNOYERS, C. DE VISSER, G. PERRON, and P. PICKER. J. Solution Chem. **5**, 605 (1976).
27. F. FRANKS, M. A. J. QUICKENDEN, D. S. REID, and B. WATSON. Trans. Faraday Soc. **66**, 582 (1970).
28. J. T. EDWARD, P. G. FARRELL, and F. SHAHIDI. J. Chem. Soc. Faraday I, **73**, 705 (1977).

Photoelectron spectra of 4-substituted stilbenes

E. J. McAlduff[1] and Tammy Chan

Department of Chemistry, St. Francis Xavier University, Antigonish, N.S., Canada B2G 1C0

Received April 13, 1978

E. J. McAlduff and Tammy Chan. Can. J. Chem. **56**, 2714 (1978).

The photoelectron spectra of stilbene and 4-R-stilbene (R = CH_3O, CH_3, F, Cl, NO_2) has been determined and the five highest π ionization potentials assigned. By considering the stilbenes to be formally constituted by union of a styrene and substituted benzene the influence of substituent on molecular orbital energies has been rationalized. The data suggest that the stilbenes exist in a planar or nearly planar configuration in the gas phase. CNDO/2 calculations have been performed on a wider variety of 4-R-stilbenes (R = NH_2, CH_3, OH, F, CN, CF_3, NO_2) and it is suggested that planar configurations also predominate for those stilbenes. First ionization potentials of some of the stilbenes are correlated with bromination and ozonolysis rate data.

E. J. McAlduff et Tammy Chan. Can. J. Chem. **56**, 2714 (1978).

On a déterminé les spectres photoélectroniques du stilbène et de stilbènes substitués par un groupe R en position 4 (R = CH_3O, CH_3, F, Cl, NO_2) et on a attribué les cinq potentiels d'ionisation π les plus élevés. En faisant l'hypothèse que les stilbènes sont constitués d'une façon formelle par l'union d'un styrène et d'un benzène substitué, on a rationalisé l'influence des substituants sur les énergies des orbitales moléculaires. Les données suggèrent que les stilbènes existent à l'état gazeux dans une configuration plane ou presque plane. On a effectué des calculs CNDO/2 sur plusieurs stilbènes substitués en position 4 par un groupe R (R = NH_2, CH_3, OH, F, CN, CF_3, NO_2) et ces calculs suggèrent que les configurations planes prédominent aussi dans ces stilbènes. On a relié les premiers potentiels d'ionisation de quelques-uns de ces stilbènes avec des données de vitesse de bromation et d'ozonolyse.

[Traduit par le journal]

Introduction

As part of a continuing investigation of the influence of substituents on the photoelectron spectra of benzene derivatives, the PE spectra of a series of monosubstituted *trans*-stilbenes has been determined. A study of the PE spectra of stilbenes provides an opportunity to study the interaction between benzene rings through an intervening ethylene group. In addition, monosubstituted stilbenes may be regarded as formally constituted by union of a substituted benzene with styrene. The extent of this interaction may be studied by comparing the PE spectra of stilbenes and analogous substituted benzenes. Semi-empirical MO calculations (CNDO/2) can be used as an aid to assignment of molecular orbitals even though their qualitative predicting ability of molecular orbital energies is not good.

Maier and Turner (1) have shown that certain bands in the PE spectra of diphenylethylenes are sensitive to conformational changes. Distefano *et al.* (2) determined the PE spectra of *trans*-styrylpyridines and noted the effect of α-methyl addition which had the result of distorting the benzene and pyridine rings from coplanarity. Novak *et al.* (3) determined the PE spectra of several *trans*-dipyridylethylenes but were unable to determine their conformations in the gas phase. However, their results indicated that the angle of twist between the pyridine rings was probably less than 30°.

Introduction of a substituent on benzene removed the degeneracy of the benzene e_{1g} orbitals. Electron releasing substituents interact conjugatively with the phenyl orbital via a high lying occupied lone pair orbital to produce a new π ionization (Ph_S) substantially shifted to lower IP. The other phenyl orbital, Ph_A, is found essentially unchanged from its position in benzene. Electron withdrawing groups shift both bands to higher IP. The PE spectrum of styrene has been determined by a number of workers (1, 4*a*)[2]. In styrene, the conjugation between the ethylenic and phenyl π electrons split the degeneracy of the phenyl π orbitals, shifting the b_1 component by ~1 eV to lower energy while the a_2 component remains essentially unperturbed. The ethylenic π orbital is shifted to higher energy by ~0.04 eV as a result of this conjugation. Thus the highest occupied molecular orbital (IP 8.48 eV) can be regarded as an anti-bonding combination of the Ph_S orbital of benzene and the vinyl π ($Ph_S - \pi$). The second highest occupied orbital in styrene (IP 9.28 eV) is the Ph_A orbital which is confined to the phenyl moiety. The third highest occupied orbital (IP 10.55 eV) is the bonding

[1]To whom correspondence should be addressed.

[2]More extensive discussion on the PE spectra of styrene can be found in ref. 4*b*.

Can. J. Chem. Downloaded from www.nrcresearchpress.com by 210.87.254.6 on 09/05/12
For personal use only.

Can. J. Chem. Downloaded from www.nrcresearchpress.com by 210.87.254.6 on 09/05/12
For personal use only.

combination of Ph_S and π (π + Ph_S). This orbital will be more vinyl-like whereas the HOMO will be more phenyl-like. Interaction of the styryl moiety with the phenyl moiety in the stilbenes will produce the five highest occupied π orbitals of the stilbene.

Results and Discussion

The interactions between the doubly degenerate HOMO of benzene with the three highest occupied orbitals of styrene to produce the five highest orbitals of *trans*-stilbene are shown in Fig. 1. The HOMO of stilbene (π_7) results from an anti-bonding combination of Ph_S − π of styrene with Ph_S of the benzene. π_6 is a Ph_A-type orbital which is confined mainly to the substituted ring and is an orbital with high electron density at the *ortho* and *meta* positions and a node at the position of substitution and *para* to it. For purposes of this discussion, it will be designated Ph_A(sub). π_5 is also a Ph_A-type orbital but resides primarily on the unsubstituted benzene ring. Substituents should have only a secondary effect on its IP and, therefore, its value should change to a lesser extent than the other orbitals.

π_4 is a composite orbital made up of the bonding combination of Ph_S − π of styrene plus Ph_S benzene. In addition, it contains a contribution from the anti-bonding combination of π + Ph_S of styrene and Ph_S of benzene. The combination of these two types of orbitals produces a molecular orbital which has a node on the ethylenic portion of the stilbene and Ph_S-like character on both benzene rings. It will be termed Ph_S − Ph_S in this discussion.

π_3 is the last distinguishable π orbital and is made up of the bonding combination of the π + Ph_S of styrene and Ph_S of benzene. It will be designated Ph_S + π + Ph_S in this discussion but probably also contains some minor contribution from the lower lying phenyl orbital of benzene. Figure 2 shows the PE spectra of stilbene and the five mono-substituted stilbenes (4-CH_3O, 4-CH_3, 4-F, 4-Cl, 4-NO_2). The IP's and assignments are listed in Table 1. The stilbene spectrum shows a band centred at 7.96 eV which is assigned to Ph_S − π − Ph_S(π_7), the larger band at 9.19 eV is assumed to contain both Ph_A orbitals (Ph_A(sub) and Ph_A(unsub)) which are degenerate in the absence of substituents. The shoulder on this band at 9.51 eV is assigned to the Ph_S − Ph_s band (π_4). The third band which is well separated from the

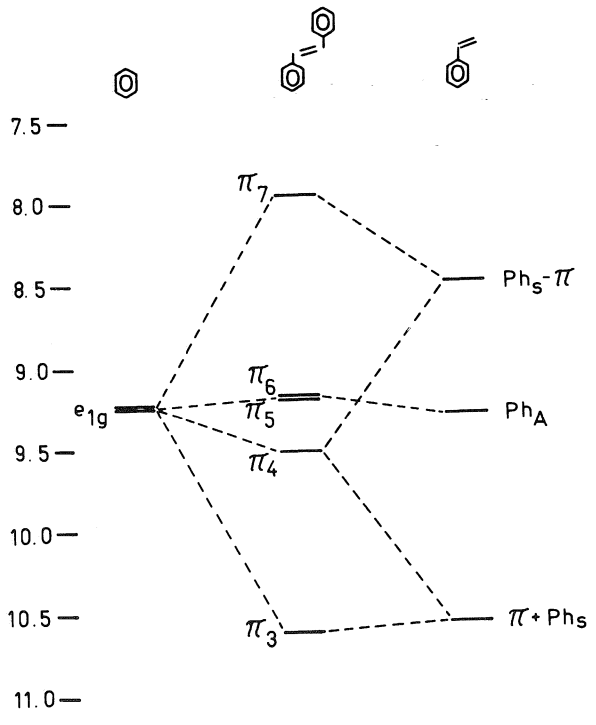

FIG. 1. Interaction of benzene HOMO with three highest orbitals of styrene to produce five highest orbitals of stilbene.

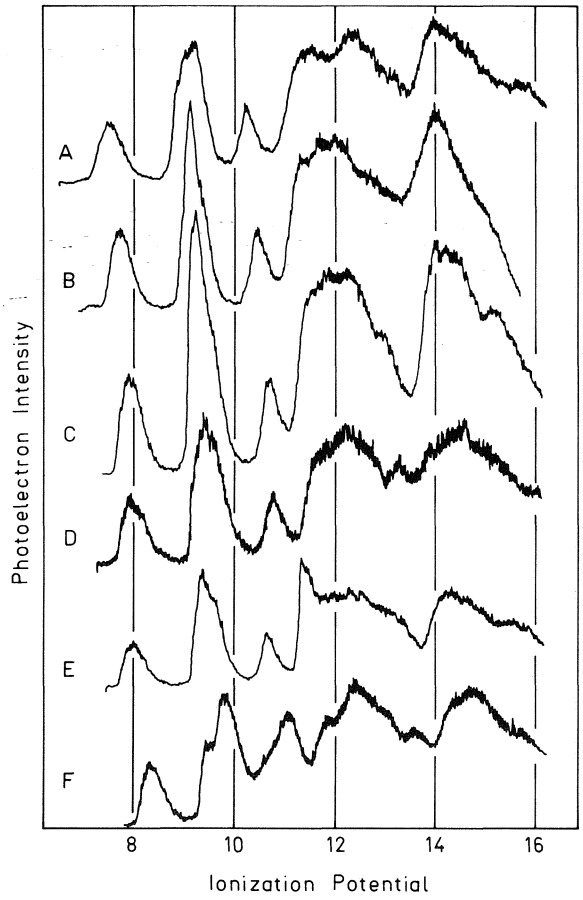

FIG. 2. Photoelectron spectra of stilbenes: *A*, OCH_3; *B*, CH_3; *C*, stilbene; *D*, F; *E*, Cl; *F*, NO_2.

Can. J. Chem. Downloaded from www.nrcresearchpress.com by 210.87.254.6 on 09/05/12
For personal use only.

TABLE 1. Ionization potentials in eV (±0.05) and assignments

	OCH_3	CH_3	H	F	Cl	NO_2
$Ph_S - \pi - Ph_S$ (π_7)	7.57	7.77	7.96	7.96	8.01	8.36
Ph_A(sub) (π_6)	8.86	9.06	9.19	9.37	9.31	9.78
Ph_A(unsub) (π_5)	9.15	9.06	9.19	9.37	9.31	9.48
$Ph_S - Ph_S$ (π_4)	9.15	9.33	9.51	9.60	9.55	9.78
$Ph_S + \pi + Ph_S$ (π_3)	10.21	10.41	10.61	10.66	10.54	10.99
$\pi_7 - \pi_3$	2.64	2.64	2.65	2.70	2.53	2.63
$\pi_7 - \pi_4$	1.58	1.56	1.55	1.64	1.54	1.42

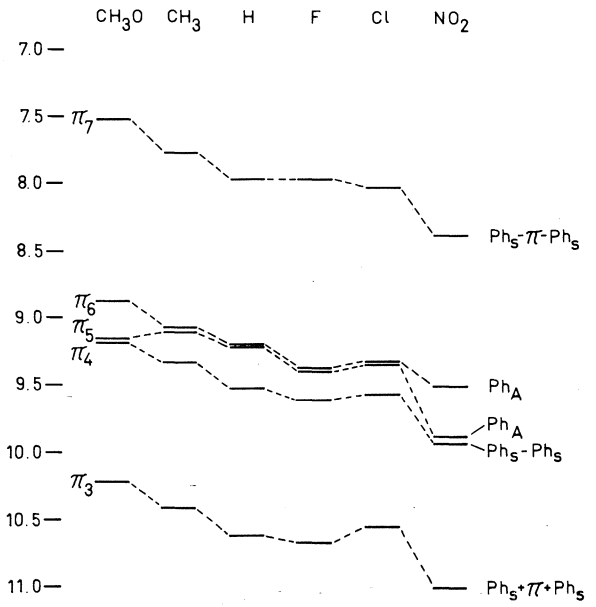

FIG. 3. Correlation diagram of five highest IP's in stilbene and substituted stilbenes.

others at 10.61 eV is assigned to $Ph_S + \pi + Ph_S$. These assignments and IP values agree within experimental error to those already reported for stilbene (1, 2). Figure 3 is a correlation diagram showing the effect of substituents on each of the five highest π levels of stilbene. The assignment for each of these five IP's and the nature of substituent effects will be discussed separately for each orbital.

$Ph_S - \pi - Ph_S$

This IP is clearly separated from the nearest ones for each substituted stilbene and can be seen (Table 1) to vary from 7.57 eV in 4-OCH_3 stilbene to 8.36 eV in 4-NO_2 stilbene. As found for substituted benzenes, electron releasing groups (OCH_3, CH_3) decrease the IP from its value in stilbene and an electron withdrawing group (NO_2) increases the IP.[3]

[3]Substituted benzene IP's used in this investigation and their sources: R = CH_3O, 8.39 eV; CH_3, 8.85 eV (5*a*); R = Cl, 9.06 eV; F, 9.19 eV (5*b*); R = H, 9.24 eV (5*c*); R = NO_2, 9.99 eV (5*d*).

Figure 4 shows a plot of $Ph_s - \pi - Ph_S$ IP for substituted stilbenes vs. Ph_S IP for substituted benzenes. A linear relationship such as this has been obtained for several series of disubstituted benzene IP's vs. monosubstituted benzene IP's (6). Similar behavior has been reported for the relationship between substituted styrylpyridine IP's and substituted benzene IP's (2). The slope of Fig. 4 is ~0.5 which indicates that the sensitivity of the stilbene system to the substituent is much lower than that of benzene. Furthermore the stilbene HOMO at 7.96 eV is at a considerably higher energy than the benzene HOMO at 9.24 eV and hence less influenced by interaction with donor orbitals. In contrast the low lying vacant orbitals of the acceptor groups are now closer in energy to stilbene than they were to benzene and hence produce a larger interaction. The smaller slope can then be considered to result from both decreased interaction by donor groups and enhanced interaction by acceptor groups on stilbene in comparison to benzene.

CNDO/2 calculations (7) have been performed on several monsubstituted stilbenes including four of the ones studied here (4-CH_3, 4-F, 4-NO_2, and stilbene). The results of these calculations are listed in Table 2. Standard geometries were used throughout and all calculations were done assuming planar molecules. The calculation overestimates the ionization potential by several electron volts in each case which is a common occurrence for this type of calculations. Nevertheless, a linear relationship is obtained be-

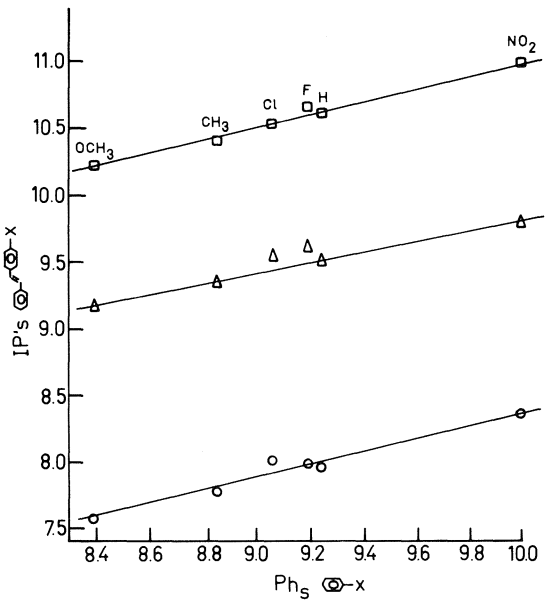

FIG. 4. IP's stilbenes vs. Ph_S IP benzenes (5); ○, $Ph_S - \pi - Ph_S$; △, $Ph_S - Ph_S$; □, $Ph_S + \pi + Ph_S$.

TABLE 2. CNDO/2 calculated ionization potentials for 4-substituted stilbenes

	NH_2	OH	CH_3	F	H	CN	CF_3	NO_2
π_7	9.80	10.24	10.38	10.57	10.64	10.67	11.02	11.21
π_6	13.94	14.10	13.90	14.31	13.98	14.21	14.46	14.78
π_5	13.75	13.84	13.88	13.95	13.87	14.01	14.09	14.24
π_4	12.77	13.52	13.82	14.11	14.48	13.94	14.83	14.90
π_3	16.48	17.27	17.69	17.99	18.46	17.44	18.56	18.58

tween calculated and experimental first IP's which suggests that this overestimation is by a constant amount for each stilbene and, hence, the CNDO/2 calculations can be used as a qualitative aid for the assignment of the ionization potentials.

$Ph_A(sub)$ (π_6) and $Ph_A(unsub)$ (π_5)

These two levels are degenerate in stilbene and are located in the large band at 9.19 eV. This degeneracy is not removed by substitution of CH_3, F, or Cl. It is only for the cases of the strongest donor group (OCH_3) and the strongest acceptor group (NO_2) that the two Ph_A levels are separated. In the case of 4-MeO stilbene Ph_A(sub) has been destabilized to 8.86 eV whereas Ph_A(unsub) is located at 9.15 eV virtually unchanged from its value in stilbene. As expected the electron withdrawing NO_2 group also separates these two IP's with Ph_A(sub) being stabilized to 9.78 eV and Ph_A(unsub) to a lesser extent to 9.48 eV. The change in Ph_A(sub) from stilbene to 4-NO_2 stilbene (0.59 eV) is larger than the change in $Ph_S - \pi - Ph_S$ from stilbene to 4-NO_2 stilbene (0.40 eV). This is analogous to what is observed from benzene to nitrobenzene where Ph_S changes by 0.75 eV and Ph_A by 1.08 eV.[3]

The Ph_A orbital associated with the unsubstituted phenyl ring undergoes the least change in IP of any of the five π orbitals across the series of substituents from CH_3O to NO_2 (0.33 eV) which is to be expected as the substituents are remote from this orbital. Ph_A(sub) undergoes a change in IP of 0.92 eV over the same range of substituents. A comparison between the effect of substituent on Ph_A(sub) and the corresponding effect on Ph_A of benzenes is illustrated in Fig. 5 where Ph_A(sub) IP is plotted against Ph_A of substituted benzenes. A good linear relationship results with the exception of the parent stilbene and the OCH_3 substituent.

$Ph_S - Ph_S$

Figure 4 shows a plot of $Ph_S - Ph_S$ (π_4) IP's vs. Ph_S for substituted benzenes. A linear relationship is observed with a slope of ~0.4. This is of the same order of magnitude to that observed for the plot of $Ph_S - \pi - Ph_S$ IP vs. Ph_S of substituted benzenes indicating that the sensitivity of the stilbene system to substituents is much lower than that of benzene,

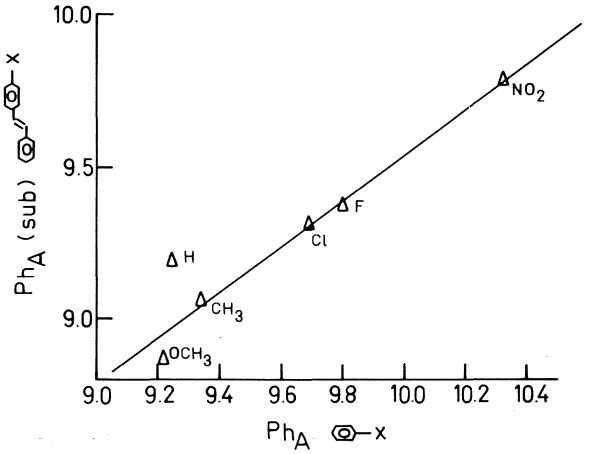

FIG. 5. Ph_A(sub) stilbenes vs. Ph_A benzenes.

which is due in part to the fact that the substituent effect spreads out over a larger π system.

The assignments arrived at here for π_6, π_5, and π_4 are subject to some uncertainty due to the overlapping of the bands involved. However, in postulating the above assignments consideration has been taken into account of the effects of these substituents on Ph_S and Ph_A orbitals of benzene (5) and the relationships observed in Figs. 4 and 5.

$Ph_S + \pi + Ph_S$

The IP's of $Ph_S + \pi + Ph_S$ (π_3) are tabulated in Table 1. From Fig. 3 it can be seen that this band is located in the region of 10–11 eV for each of the stilbenes and is well separated from the broad band containing π_6, π_5, and π_4 and also from the higher energy σ bands. Figure 4 also contains a plot of $Ph_S + \pi + Ph_S$ IP vs. Ph_S IP for substituted benzenes. A linear relationship with a slope similar to that obtained for π_7 and π_4 is observed.

Conformational Effects

π_7 and π_3 represent the anti-bonding and bonding interactions between the styryl and phenyl moieties. The difference between these two levels has been used as an indication (1, 2) of the extent of interaction between these moieties and, hence, as an indication of the extent of departure of the system from coplanarity. As can be seen from Table 1 this difference

Can. J. Chem. Downloaded from www.nrcresearchpress.com by 210.87.254.6 on 09/05/12
For personal use only.

Can. J. Chem. Downloaded from www.nrcresearchpress.com by 210.87.254.6 on 09/05/12
For personal use only.

is virtually constant (2.63–2.70 eV) for all substituents except Cl (2.53 eV). Thus this difference is essentially constant wthin experimental error and is taken to be evidence of the coplanarity of the phenyl rings in the stilbenes. Table 1 also lists the difference in IP between π_7 and π_4. This difference should also provide information about the conformation of the stilbenes since it represents a measure of the extent of interaction between the phenyl groups. Hence, any change in coplanary of the phenyl rings should result in a difference in the separation between π_7 and π_4. With the exception of 4-NO_2 stilbene the difference between π_7 and π_4 is constant within experimental error. Therefore, the relatively constant difference between π_7 and π_3 and between π_7 and π_4 for the substituents suggests that all the stilbenes studied here are planar or nearly planar species. Further confirmation of this comes from the linear relationship between calculated and experimental $Ph_S - \pi - Ph_S$ IP's. All calculations were performed using planar configurations and hence maximum interaction between the phenyl rings through the intervening ethylene. If any of the substituted stilbenes existed in non-planar conformations, this fact should have resulted in less correlation between experimental and calculated IP.

Calculations

CNDO/2 calculations (7) have been performed for a variety of monosubstituted stilbenes and the calculated IPs are listed in Table 2. Three common deficiencies of CNDO/2 calculations are demonstrated by the results: overestimation of the ionization potentials, incorrect order of energy levels, and orbitals placed at too high energies. An attempt has been made to compare the calculated π_7 IP's in Table 2 for those compounds for which the PE spectra have not been determined to some experimental quantity. Thus, Fig. 6 contains a plot of π_7 or $Ph_S - \pi - Ph_S$ IP (calcd) vs. Ph_S IP (expt) of the corresponding substituted benzenes. A linear relationship is obtained except for 4-CN stilbene. This suggests that when the PE spectra are determined for those compounds in Table 2 which have not been previously investigated that the first IP will be found to follow the same linear relationship observed in Fig. 4. In addition, it is predicted that the conformation of 4-NH_2, 4-OH, 4-CF_3 stilbene is the same as that for the stilbenes investigated here. There seems to be no obvious reason why the 4-CN stilbene deviates from the other stilbenes in Table 2.

Reactivity Correlations

The effect of substituent on the kinetics of bromination (8) and ozonolysis (9) of stilbenes are two examples of a large number of reactions of stilbenes

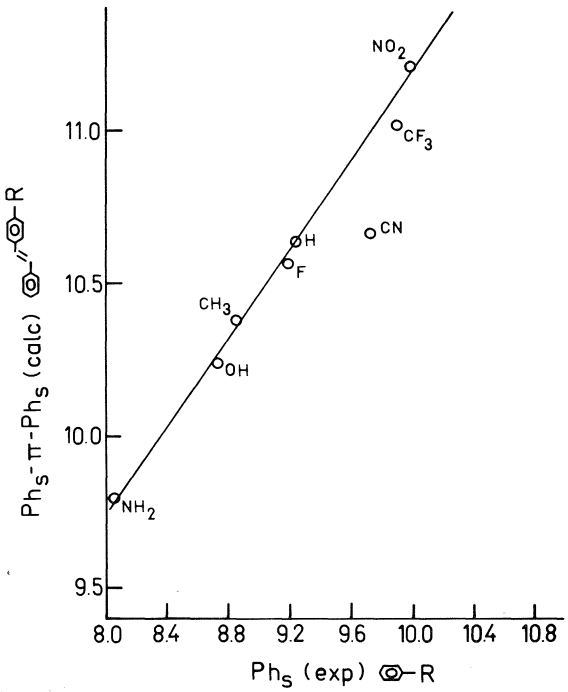

FIG. 6. $Ph_S - \pi - Ph_S$ IP (calcd) vs. Ph_S IP benzenes.

for which reactivity data are available. In this study an attempt has been made to correlate the observed kinetic parameters with ionization potential data. Figure 7 shows a plot of log. k vs. IP (π_7) for four of the substituted stilbenes studied. Both the bromination reaction (upper curve) and ozonolysis (lower curve) show linear relationships between log k and IP. Both reactions are electrophilic so that any substituent which increases the electron density on the ethylenic moiety should increase the rate. This is observed since both curves show negative slopes with the rate decreasing with IP. A more precise method of depicting the reactivity pattern might be to plot log k against some weighted average of π_7 and π_3 since the latter orbital also contains significant electron density on the ethylenic carbons and the magnitude of this electron density is influenced by the substituent. Another way to consider the bromination reaction is that since the intermediate species is postulated to go through either a carbonium or bromonium ion transition state (8) then any substituent which stabilizes this state such as a donor group is going to enhance the rate. For the ozonolysis reaction (9) the initial electrophilic attack is assumed to proceed rapidly via an irreversible 1,3-dipolar cycloaddition to give the final product. Thus, any substituent which causes an increase in the polarizability of the ethylenic C—C bond should enhance its dipolarophilic nature (10).

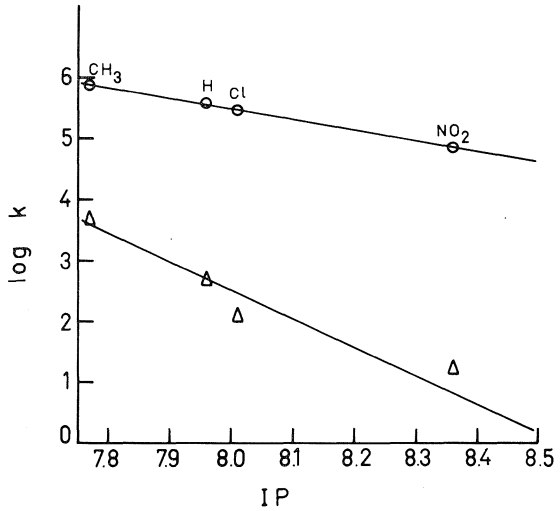

FIG. 7. log k vs. IP ($Ph_s - \pi - Ph_s$) stilbenes: ○, bromination rate data (8); △, ozonolysis rate data (9).

Further studies are in progress on the photoelectron spectra of a wider variety of substituted stilbenes with a view to investigating the influence of the number and location of substituents on the electronic structure and conformation of the stilbenes.

Experimental

The stilbenes were synthesized by a standard procedure (11) and purified by recrystallization. Photoelectron spectra were determined on a Perkin-Elmer PS-18 photoelectron spectrometer with heated probe. Xenon and argon were used as internal standards and the resolution as measured on the 15.76 eV peak of Ar was 25–35 meV. Peak positions listed in Table 1 are the average of at least five determinations.

Acknowledgements

The authors gratefully acknowledge the financial support of the National Research Council of Canada and the St. Francis Xavier University Council for Research. The photoelectron spectra were determined in the laboratory of Professor K. N. Houk of Louisiana State University to whom the authors are indebted for his assistance and co-operation.

1. J. P. MAIER and D. W. TURNER. J. Chem. Soc. Faraday Trans. II, **69**, 196 (1973).
2. G. DISTEFANO, U. MAZZUCATO, A. MODELLI, S. PIGNATARO, and G. ORLANDI. J. Chem. Soc. Faraday Trans. II, **71**, 1588 (1975).
3. I. NOVAK, L. KLASINC, and J. V. KNOP. Z. Naturforsch. **32**a, 886 (1977).
4. (*a*) J. W. RABALAIS and R. J. COLTON. J. Electron Spectrosc. **1**, 83 (1972/73); (*b*) J. W. RABALAIS. Principles of photoelectron spectroscopy. Wiley-Interscience. 1977.
5. (*a*) T. KOBAYASKI and S. NAGAKURA. Bull. Chem. Soc. Jpn. **47**, 2563 (1974); (*b*) D. W. TURNER, C. BAKER, A. D. BAKER, and C. R. BRUNDLE. Molecular photoelectron spectroscopy. Wiley Interscience, New York. 1970; (*c*) L. ASBRINK, E. LINDHOLM, and O. EDQVIST. Chem. Phys. Lett. **5**, 609 (1972); (*d*) J. W. RABALAIS. J. Chem. Phys. **57**, 960 (1972).
6. E. J. MCALDUFF, B. M. LYNCH, and K. N. HOUK. Can. J. Chem. **56**, 495 (1978).
7. G. A. SEGAL. Carnegie Institute of Technology, QCPE Program No. 91.
8. M.-F. RUASSE and J.-E. DUBOIS. J. Org. Chem. **39**, 2441 (1974).
9. H. HENRY, M. ZADOR, and S. FLISZAR. Can. J. Chem. **51**, 3398 (1973).
10. R. HUISGEN. Angew. Chem. Int. Ed. Engl. **2**, 565 (1963); **2**, 633 (1963).
11. J. R. DAVY, P. J. JESSUP, and J. A. REISS. J. Chem. Ed. **52**, 747 (1975).

Can. J. Chem. Downloaded from www.nrcresearchpress.com by 210.87.254.6 on 09/05/12
For personal use only.

β-Lactams. II. The synthesis of *cis*-*N*-(2′-carboxyphenyl)-3-*N*-phenylacetamido-4-methoxymethyl-2-azetidinone

GEORGE JUST AND ROBERT ZAMBONI[1]
Department of Chemistry, McGill University, Montreal, P.Q., Canada H3A 2K6
Received May 8, 1978

GEORGE JUST and ROBERT ZAMBONI. Can. J. Chem. **56**, 2720 (1978).
The synthesis of the β-lactam **19** from anthranilic acid is described.

GEORGE JUST ET ROBERT ZAMBONI. Can. J. Chem. **56**, 2720 (1978).
La synthèse du β-lactame **19** à partir de l'acide anthranilique est décrite.

Can. J. Chem. Downloaded from www.nrcresearchpress.com by 210.87.254.105 on 09/05/12
For personal use only.

The essential features of the classical β-lactam antibiotics penicillin **A** and cephalosporin **B** (1) are (*a*) a *cis*-fused β-lactam ring; (*b*) an acylamino side chain which can be considerably varied; (*c*) an acidic function, the nature of which is not critical since the carboxylic acid can be replaced by a phosphonic acid; (*d*) a five-membered ring or six-membered ring containing a double bond conjugated with the β-lactam nitrogen conferring enough ring strain so as to raise the β-lactam frequency to ≥ 1765 cm^{-1}. It has been shown that the sulphur atom can be replaced by oxygen or carbon without substantial loss of antimicrobial activity, (ref. 2 and references therein).

In this and the following paper, we wish to describe the synthesis of β-lactams identical to penicillin and cephalosporin in points *a* and *b* but differing in that the acidic function is attached to an aromatic ring (see **C** and **D**), and in which the strain of

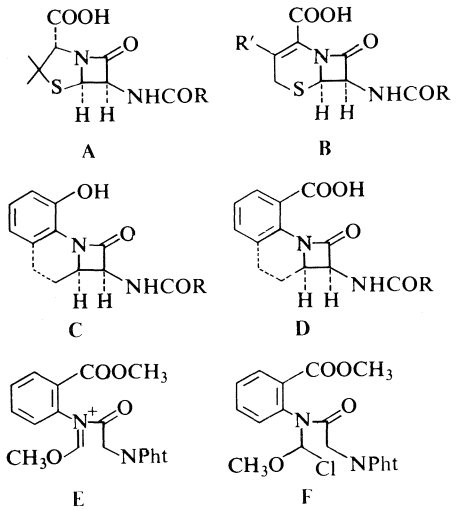

the β-lactam is generated by electron withdrawing groups attached to the benzene ring, and/or by fusing the aromatic and β-lactam rings by an additional ring as indicated.

Whilst this work was in progress Doyle published the synthesis of bicyclic compounds of type **C** (3), in which the phenolic group was in the 3-position and which exhibited 'weak' antimicrobial activity.

In the first paper, we shall deal with the synthesis of bicyclic compounds of type **D**, and in the following papers, the synthesis of the tricyclic compounds of type **C** and **D** will be described.

As a model compound, the known benzylidene anthranilic acid **1** (4) was condensed with phthalimidoacetyl chloride (5). Instead of the expected β-lactam, a crystalline compound, the spectral data of which were consistent with **2**, was obtained. When Schiff base **1** was silylated *in situ* (6) before the addition of the phthalimidoacetyl chloride, the trans β-lactam **3** was obtained in 70% yield. Its structure followed from its spectral and analytical data and the stereochemistry of the ring junction from the fact that $J_{3,4} = 2$ Hz (7).

The acid was characterized as its *p*-methoxybenzyl ester, obtained by reacting **3** with *p*-methoxybenzyl alcohol and 1.2 equiv. of dineopentylformamide acetal in acetonitrile (8). The benzyl ester **3***a* was converted to the free amine **4** by means of hydrazine. We next attempted to isomerize the amine function using the method described by Christensen and co-workers (9) which involves the formation of the *p*-nitrobenzylidene Schiff base **5**, followed by carbanion formation using phenyl lithium, and kinetic protonation at low temperature. We were not successful in effecting the transformation and only recovered approximately 20% of **5**. An adaptation of the method described by Yanagisawa *et al.* (10) which involved formation of Schiff base **6**, followed by oxidation to the quinone methine and quenching with $ZnBH_4$, was equally unsuccessful.

We suspected that the difficulties in obtaining a *cis*-β-lactam may have been due to the relatively bulky phenyl group and therefore performed a

[1]Holder of a NRCC Scholarship, 1974–1978.

Can. J. Chem. Downloaded from www.nrcresearchpress.com by 210.87.254.105 on 09/05/12
For personal use only.

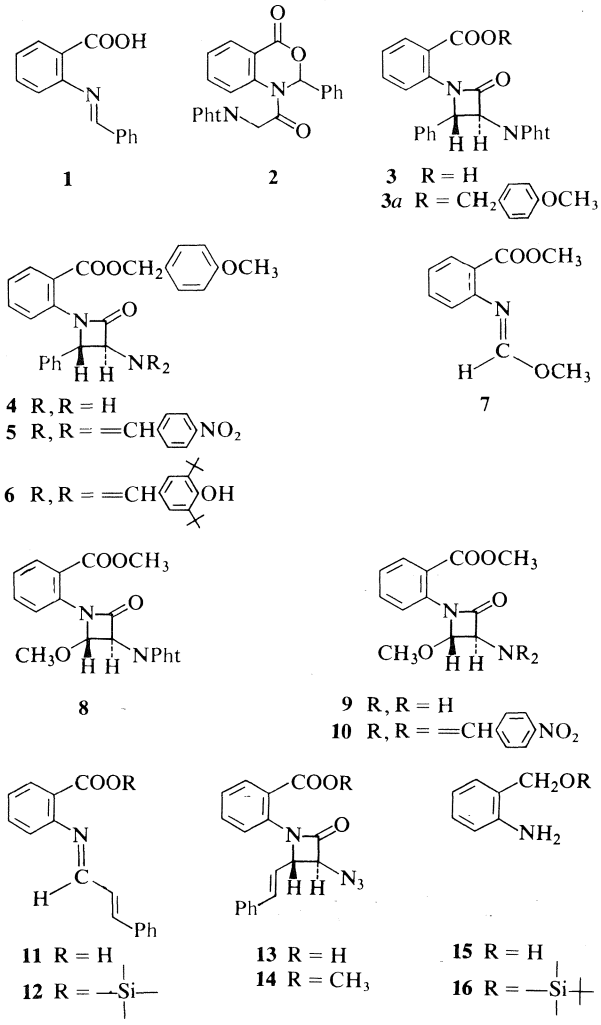

similar series of reactions using imino ether **7** as the starting material. Considerable difficulty was experienced preparing **7** and the reaction conditions described in the Experimental are critical for its obtention. Addition of phthalimidoacetyl chloride to imino ether **7** afforded a 35% yield of β-lactam **8** when the reaction was allowed to proceed for 24 h. When the reaction was stopped after 2 h, a 1:1 mixture of β-lactam **8** and of methyl *N*-phthalimidoacetyl anthranilate was obtained in 30% overall yield. This suggested that the reaction did not proceed through a 2 + 2 addition of phthalimido ketene and the imine **7**, but in two stages, the first intermediate having structure **E** suggested by Doyle *et al.* (1), which is trapped presumably as the chloride **F** (13). Quenching of **F** with water during work-up would give methyl *N*-phthalimidoacetyl anthranilate, whereas a prolonged reaction time may lead to further formation of β-lactam. No β-lactam was obtained when imine **7** was treated with azidoacetyl chloride. Hydrolysis of the phthalimide function in **8** gave a low yield of amine **9**. Isomerization of *trans*-β-lactam **9** to its *cis* isomer via Schiff base **10** was unsuccessful.

Not having been able to prepare a *cis*-fused β-lactam using the approaches described, we next investigated the method recently published by Doyle *et al.* (1), which consisted in reacting azidoacetyl chloride with cinnamylidene Schiff bases, which has been reported to afford *exclusively cis*-β-lactams. Reaction of the silylated cinnamylidene Schiff base of anthranilic acid **12** with azidoacetyl chloride gave a 15–20% yield of *trans*-β-lactam **13**, characterized as its methyl ester **14**. Since cinnamylidene Schiff bases of electron-rich anilines seemed to consistently give *cis*-β-lactams in high yield,[2] it was decided to use the readily available *o*-aminobenzyl alcohol **15** as a starting material, and to oxidize the alcohol to the carboxylic acid at a later stage. Silylation of **15** gave, in quantitative yield, silyl ether **16**, which was converted to Schiff base **17**. Treatment with azido acetyl chloride gave *cis*-β-lactam **18**, mp 91–92°C, in excellent yield. Reduction with hydrogen sulfide – triethyl amine (1) followed by acylation with phenylacetyl chloride and triethylamine gave **19**, mp 108.5–109°C, $\nu_{C=O}$ 1750 cm^{-1}, in 60% yield based on **18**. Ozonolysis of **19** gave a poorly defined mixture of oxidation products. However, ozonolysis of azide **18** in redistilled isopropanol or CH_2Cl_2–ethanol (1:5) at −78°C, followed by sodium borohydride reduction at −50°C, gave, after work-up with pH 4.5 buffer, azido alcohol **20**, mp 95–96°C, $\nu_{C=O}$ 1755 cm^{-1}, in 76% yield. To differentiate the two alcohol functions, **20** was converted to its methyl ether **21** by means of diazomethane – boron trifluoride etherate. Reduction and acylation of the azide function gave amide **22**, $\nu_{C=O}$ 1750, 1665 cm^{-1}, which was converted to alcohol **23**, using aqueous trifluoroacetic acid. Alcohol **23** was easily oxidized to aldehyde **24** with pyridinium chlorochromate (11). Oxidation of **24** with silver oxide – sodium cyanide (12) in methanol led to opening of the β-lactam ring. Carboxylic acid **25** could be obtained in low yield from **23** using chromic acid in acetic acid – water. Its structure followed from its spectral data and the stereochemistry of the ring junction from the fact that $J_{3,4} = 5$ Hz (7). The mass spectrum of the corresponding methyl ester **26** showed a molecular ion, a peak at $M^+ - 31$ which is consistent with a methyl ester, and peaks at *m/e* 205 and 177 for the fragmentation shown on **25**. This fragmentation is characteristic of β-lactams. Carboxylic acid **25** showed no activity toward a variety of bacteria. This is not unexpected if we consider that $\nu_{C=O}$ of **25** is only 1755 cm^{-1},

[2]A. Ugolini and R. Zamboni. Unpublished results.

Can. J. Chem. Downloaded from www.nrcresearchpress.com by 210.87.254.105 on 09/05/12
For personal use only.

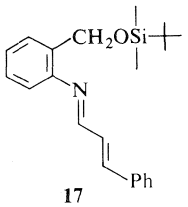

17

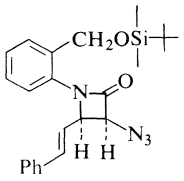

18

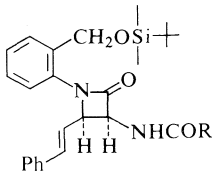

19 R = CH_2Ph

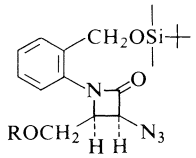

20 R = H
21 R = CH_3

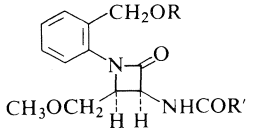

22 R = —Si—, R′ = CH_2Ph
23 R = H, R′ = CH_2Ph

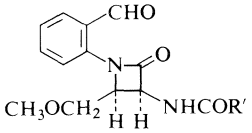

24 R′ = CH_2Ph

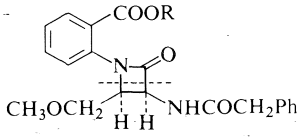

25 R = H
26 R = CH_3

whereas known active cephalosporins have $\nu_{C=O}$ of at least 1765 cm^{-1}.

Experimental

Solvents were of reagent grade unless otherwise specified. Infrared spectra were run on Unicam SP1000 and P.E. 257 spectrophotometers. Nuclear magnetic resonance spectra were run on Varian T-60, T-60A, or Brucker 90 MHz FT spectrophotometers. Mass spectra were taken on an AEI-MS-902 mass spectrometer using the direct sample inlet system with a 70 eV ionization energy or on a LKB 9000 mass spectrometer. Melting points were determined on a Gallenkamp block in open capillary tubes and are uncorrected. Merck SI60 silica gel was used for column chromatography. Merck silica gel HF_{254} was used for thick-layer chromatography (1 mm) on glass plates (20 × 20 cm). Elemental analyses were performed by Heterocyclic Chemical Corporation, Missouri, or Midwest Microlab Ltd., Indianapolis, IN.

Lactone **2**

To a solution of benzylidene anthranilic acid **1** (900 mg) in dry benzene (25 ml) containing triethylamine (0.8 g) was added dropwise a solution of phthalimidoacetyl chloride in dry benzene (6 ml) over a period of 20 min. The reaction mixture was stirred for 1 h more and the salt filtered off. The filtrate was washed with 1% HCl (2 × 10 ml), dried, and evaporated. Chromatography of the filtrate on thick-layer plates using $CHCl_3$–ether 3:1 as eluent afforded ~100 mg of lactone **2**, mp 185°C (dec.); ^{1}Hmr ($DCCl_3$) δ: 4.9 (q, 2H, CH_2), 7.0–8.0 ppm (m, 14H, aromatic + OC*H*Ph); ir ($HCCl_3$) ν_{max}: 1780 (weak), 1740 cm^{-1}; ms *m/e*: 412 (M^+).

Phthalimido β*-Lactam* **3**

To Schiff base **1** (1.7 g, 7.6 mmol) and triethylamine (1.8 g, 18 mmol) in dry CH_2Cl_2 (50 ml) was added quickly trimethylchlorosilane (1.75 g, 16 mmol) in CH_2Cl_2 (5 ml). The mixture was stirred for 5–10 min and then triethylamine (0.8 g, 8 mmol) was added. To the solution was added over 1.5 h a solution of phthalimidoacetyl chloride (1.7 g, 7.6 mmol) in dry CH_2Cl_2 (100 ml). After the addition was complete the mixture was stirred for 2 h more. After the addition of methanol (3 ml), the solution was washed with H_2O (50 ml), saturated NaCl solution (50 ml), dried ($MgSO_4$), and evaporated. The resulting solid was chromatographed on 60 g silica gel activity III. Elution with CH_2Cl_2 and then ethyl ether – chloroform (1:1) afforded, after crystallization with $CHCl_3$–CCl_4, 1.7 g (55%) of β-lactam **3**, mp 214–215°C; ^{1}Hmr ($DCCl_3$) δ: 5.3 (d, 1H, CH, J = 2.5 Hz), 5.6 (d, 1H, CH, J = 2.5 Hz), 6.9–8.0 (m, 13H, C_6H_4 + C_6H_5), 11.2 ppm (bs, 1H, COOH); ir (Nujol) ν_{max}: 2300–3500 (COOH), 1770 (β-lactam), 1720 (phthalimide), 1690 cm^{-1} (COOH); ms: *m/e*: 412 (M^+), 249, 225, 187, 163. *Anal.* calcd. for $C_{24}H_{16}N_2O_5$: C 69.90, H 3.91, N 6.79; found: C 70.29, H 4.09, N 7.03.

Ester **3**a

To acid **3** (2.47 g, 6 mmol) in dry acetonitrile (60 ml) was added methoxybenzyl alcohol (0.91 g, 6.6 mmol) and dineopentyl *N,N*-dimethylformamide acetal (2.04 g, 8.7 mmol). After sealing the flask under nitrogen, the solution was stirred at room temperature 24 h. Concentration down to 20 ml and filtration afforded 2.1 g (66%) of pure ester **3***a*, mp 189–190°C; ^{1}Hmr ($DCCl_3$) δ: 3.7 (s, 3H, OCH_3), 5.0 (d, 1H, CH, J = 2.5 Hz), 5.6 (d, 1H, CH, J = 2.5 Hz), 5.1 (bs, 2H, CH_2), 6.4–7.8 ppm (m, 17H, aromatic); ir (Nujol) ν_{max}: 1780 (β-lactam), 1720 cm^{-1} (ester and phthalimido).

Amine **4**

To ester **3***a* (1.59 g, 3 mmol) in CH_2Cl_2 (75 ml) was added hydrazine (120 μl, 3.8 mmol). The solution was stirred 48 h at room temperature and the solid that formed was filtered off. Evaporation of the solvent afforded an oil which was chromatographed on silica gel activity III using first $CHCl_3$–CH_2Cl_2 1:1 as eluant. Elution with chloroform–ether (3:1) afforded 0.66 g (50%) of amine **4** as an oil; ^{1}Hmr ($DCCl_3$) δ: 1.9 (bs, 2H, NH_2), 3.9 (d, 1H, C*H*NH_2, J = 2.5 Hz), 4.8 (d, 1H, *CH*Ph, J = 2.5 Hz), 5.2 (s, 2H, CH_2), 6.6–7.7 ppm (m, 13H, aromatic); ir ($CHCl_3$) ν_{max}: 3400 (NH_2), 1770 (β-lactam), 1730 (ester), 1120 cm^{-1}.

Schiff Base **5**

A solution of amine **4** (210 mg, 0.52 mmol) and *p*-nitrobenzaldehyde (78 mg, 0.52 mmol) in benzene (50 ml) was refluxed 1.5 h using a Dean–Stark trap. Removal of benzene afforded Schiff base **5** in quantitative yield; ^{1}Hmr ($DCCl_3$) δ: 3.8 (s, 3H, OCH_3), 4.7 (m, 1H, *CH*—N=C), 5.3 (bs, 2H, CH_2), 5.5 (s, 1H, CHPh, J = 2.5 Hz), 6.7–7.5 (m, 13H, C_6H_4 and C_6H_5), 8.0 (q, 4H, $NO_2C_6H_4$), 8.4 ppm (s, 1H, HC=N); ir ($CHCl_3$) ν_{max}: 1775 (β-lactam), 1730 cm^{-1} (ester and phthalimido).

Formimidate **7**

Into methyl anthranilate (10 g, 66 mmol) and trimethyl orthoformate (15 g, 141 mmol) was bubbled HCl gas for a few seconds. The mixture was heated at 110°C and the methanol formed distilled off. Near the end of the distillation a few crys-

Can. J. Chem. Downloaded from www.nrcresearchpress.com by 210.87.254.105 on 09/05/12
For personal use only.

tals of TsOH were added. When 4 g of methanol was collected, the distillation was stopped and 2 g of anhydrous K_2CO_3 was added. Excess orthoformate was then distilled off at ~60°C/60 Torr. Fractional distillation of the residue gave 5.5 g (43%) of almost colourless formimidate **7**; ^{1}Hmr ($DCCl_3$) δ: 3.7 (s, 3H, OCH_3), 3.8 (s, 3H, OCH_3), 6.4–7.8 (m, 5H, C_6H_4 and HC=N); ir (neat) ν_{max}: 3000, 1730 (C=O), 1660 cm^{-1} (C=N); ms *m/e*: 193 (M^+).

β-*Lactam Ester* ***8***

To formimidate **7** (9 g, 46 mmol) in CH_2Cl_2 (150 ml) and triethylamine (5.0 g, 50 mmol) under N_2 was added dropwise over 2 h phthalimidoacetyl chloride (12.25 g, 54 mmol) in CH_2Cl_2 (100 ml). After 24 h, the solution was washed with H_2O (2 × 100 ml), dried ($MgSO_4$), and evaporated. Crystallization from $CHCl_3$–hexane, afforded 6 g (33%) of β-lactam **8**, mp 175–176.5°C; ^{1}Hmr ($CDCl_3$) δ: 3.3 (s, 3H, OCH_3), 3.81 (s, 3H, $COOCH_3$), 5.4 (s, 1H, CH, J = 2 Hz), 5.9 (s, 1H, CH, J = 2 Hz), 7.0–7.8 ppm (m, 8H, C_6H_4); ir ($CHCl_3$) ν_{max}: 1775 (β-lactam), 1730 (ester), 1400 cm^{-1}; ms *m/e*: 380 (M^+).

When the reaction was stopped after 2 h, a crystalline side product, methyl *N*-phthalimidoacetylanthranilate, could be isolated by repeated chromatography on SiO_2 activity III and recrystallization from $CHCl_3$–hexane, mp 188–190°C; ^{1}Hmr ($DCCl_3$) δ: 3.8 (s, 3H, OCH_3), 4.7 (s, 2H, CH_2), 7.0–9.0 (m, 8H, C_6H_4), 11.5 ppm (s, 1H, NH); ir ($CHCl_3$) ν_{max}: 3300 (NH), 1780, 1725 (phthalimido, ester), 1690 cm^{-1} (amide).

Amine β-*Lactam* ***9***

To β-lactam **8** (2.7 g, 7.1 mmol) in CH_2Cl_2 (50 ml) was added hydrazine (0.246 ml, 7.6 mmol). After stirring at room temperature for 3 days, the orange solid was filtered off and washed with CH_2Cl_2. The filtrate was extracted with ice-cold 1% HCl (2 × 100 ml). After neutralization with 1 *N* NaOH, the aqueous phase was extracted with chloroform (2 × 200 ml). Drying ($MgSO_4$) and evaporation afforded 500 mg (28%) of amine **9** as an orange gum; ^{1}Hmr ($DCCl_3$) δ: 1.8 (s, 2H, NH_2), 3.4 (s, 3H, OCH_3), 3.8 (s, 3H, $COOCH_3$), 4.1 (bs, 1H, *CH*NH_2), 5.2 (bs, 1H, *CH*OMe), 7.0–7.8 (m, 4H, C_6H_4); ir ($CHCl_3$) ν_{max}: 3400 (NH), 1770 (β-lactam), 1730 cm^{-1} ($COOCH_3$); ms *m/e*: 250 (M^+), 192.

Schiff Base ***10***

A solution of amine β-lactam **9** (125 mg, 0.5 mmol) and *p*-nitrobenzaldehyde (76 mg, 0.5 mmol) in benzene (30 ml) was heated at reflux for 2 h using a Dean–Stark trap. Evaporation of benzene afforded Schiff base **10**; ^{1}Hmr ($DCCl_3$) δ: 3.3 (s, 3H, OCH_3), 3.7 (s, 3H, CO_2CH_3), 4.8 (t, 1H, *CH*N=C), 5.5 (d, 1H, *CH*OCH_3), 7.0–8.1 (m, 8H, C_6H_4), 8.3 ppm (bs, 1H, N=*CH*); ir (neat) ν_{max}: 1775 (β-lactam), 1730 (ester), 1620 cm^{-1} (C=N).

β-*Lactams* ***13*** *and* ***14***

Anthranilic acid (2.7 g, 20 mmol) and cinnamaldehyde (2.64 g, 20 mmol) was heated for 4 h using a Dean–Stark trap, and the solvent evaporated. To the resulting Schiff base **11** was added triethylamine (6 g, 60 mmol) in dry CH_2Cl_2 (200 ml) and then dropwise trimethyl silyl chloride (4 g, 37 mmol) in CH_2Cl_2 (10 ml) at −5°C. After stirring for 10 min a solution of azidoacetyl chloride (2.4 g, 20 mmol) in CH_2Cl_2 (50 ml) was added at −5°C. After stirring 30 min more at room temperature, methanol (5 ml) was added. The solution was washed with H_2O (2 × 100 ml), dried, and evaporated. Chromatography on SiO_2 (200 g) activity III using first CH_2Cl_2 and then ether afforded 1 g of impure acid **13**. An ethereal solution of **13** was treated with CH_2N_2. Chromatography on SiO_2 activity III (20 g) using $CHCl_3$ as eluent gave 250 mg of ester **14** as a red oil; ^{1}Hmr ($CDCl_3$) δ: 3.8 (s, 3H, OCH_3), 4.5 (d, 1H, CHN_3, J = 2 Hz), 4.7 (q, 1H, C*H*—CH=CH—Ph, J_1 = 2 Hz, J_2 = 7 Hz), 6.0 (q, 1H, J_1 = 7 Hz, J_2 = 18 Hz, CH*CH*=CHPh), 6.7 (d, 1H, HC=C*H*Ph, J = 18 Hz), 6.9–7.5 ppm (m, 8H, C_6H_5 and C_6H_3); ir ($CHCl_3$ ν_{max}: 1760 (β-lactam), 1725 cm^{-1} (ester); ms *m/e*: 320 (M^+).

Silylether Amine ***16***

To *o*-aminobenzyl alcohol **15** (1.23 g, 10 mmol) in dry DMF (15 ml) was added imidazole (1.75 g, 25 mmol) and *tert*-butyldimethylsilyl chloride (1.65 g, 11 mmol). The solution was stirred at room temperature and partitioned between H_2O (50 ml) and ether (100 ml). The ether layer was washed with water (4 × 50 ml), dried, and evaporated. A quantitative yield of silylether amine **16** was obtained; ^{1}Hmr ($DCCl_3$) δ: 0.05 (s, 6H, Si(CH_3)$_2$), 0.9 (s, 9H, Si*t*Bu), 4.0 (bs, 2H, NH_2), 4.6 (s, 2H, *CH*$_2$OH), 6.9–7.0 ppm (m, 4H, C_6H_4); ir (film) ν_{max}: 3460, 3370, 2910, 1630, 1420, 1050 cm^{-1}.

Schiff Base ***17***

A solution of amine **16** (4.72 g, 20 mmol) and cinnamaldehyde (2.7 g, 20 mmol) in benzene (50 ml) was heated at reflux for 8 h using a Dean–Stark trap. Evaporation of benzene afforded a quantitative yield of Schiff base **17** as a yellow oil; ^{1}Hmr ($DCCl_3$) δ: 0.05 (s, 6H, $SiMe_2$), 0.9 (s, 9H, Si*t*Bu), 4.9 (s, 2H, —CH_2O—), 6.8–7.4 (m, 9H, aromatic), 7.9 ppm (t, 1H, *HC*=NPh); ir (film) ν_{max}: 2910, 1640 (C=N) cm^{-1}.

β-*Lactam Azide* ***18***

To a solution of Schiff base **17** (7.0 g) and triethylamine (2.4 g, 1.2 equiv.) in CH_2Cl_2 (200 ml) at −20°C under nitrogen was added dropwise over 1 h azidoacetyl chloride (2.8 g, 1.15 equiv.) in CH_2Cl_2 (100 ml). The solution was stirred for 1 h at room temperature, washed with H_2O (2 × 100 ml), dried ($MgSO_4$), and evaporated. Treatment of the red oil with charcoal in ether gave, after crystallization from pentane, 6.0 g (74%) of β-lactam **18** as a white solid, mp 91–92°C; ^{1}Hmr ($DCCl_3$) δ: 0.1 (s, 6H, $SiMe_2$), 0.95 (s, 9H, Si*t*Bu), 4.6 (s, 2H, *CH*$_2$O), 4.6–5.0 (m, 2H, C*H*—*CH*N_3), 5.8–6.6 ppm (m, 2H, PhC*H*=*CH*—); ir (KBr) ν_{max}: 2900, 2100 (N_3), 1745 cm^{-1} (C=O); ms *m/e*: 434 (M^+), 406 ($M^+ - N_2$), 377 ($M^+ - 57$). *Anal.* calcd. for $C_{24}H_{30}N_4O_2Si$: C 66.40, H 6.97, N 12.92; found: C 66.31, H 6.85, N 12.91.

β-*Lactam Amide* ***19***

Hydrogen sulphide was bubbled into a solution of azide **18** (450 mg, 1.1 mmol) and triethylamine (150 mg, 1.5 mmol) in CH_2Cl_2 (20 ml) at 0°C. After 1 h, the solution was purged with N_2, washed with H_2O (2 × 20 ml), dried, and evaporated. To the crude product in CH_2Cl_2 (20 ml) and triethylamine (150 mg, 1.5 mmol) was added dropwise phenylacetyl chloride (0.237 g, 1.5 mmol) in CH_2Cl_2 (1 ml). After stirring for 30 min more, the solution was washed with pH 4.5 buffer (20 ml), water (20 ml), dried ($MgSO_4$), and evaporated. The crude product was chromatographed on SiO_2 (20 g) activity III using first CH_2Cl_2 as eluent. Elution with $CHCl_3$–ether 1:1 afforded after crystallization from pentane–chloroform 300 mg (60%) of amide **20** as a white solid, mp 108.5–109°C; ^{1}Hmr ($DCCl_3$) δ: 0.1 (s, 6H, $SiMe_2$), 0.95 (s, 9H, Si*t*Bu), 3.4 (s, 2H, —CH_2Ph), 4.8 (s, 2H, CH_2OTBDMS), 4.9 (q, 1H, *CH*CH—CHϕ, J_1 = 7 Hz, J_2 = 5 Hz), 5.6 (q, 1H, C*H*NH, J_1 = 5 Hz, J_2 = 7 Hz), 6.2 (q, 1H, C*H*=CHPh, J_1 = 7 Hz, J_2 = 18 Hz), 6.5 (d, CH=C*H*Ph, 1H, J = 18 Hz), 7.0–7.5 ppm (m, 10H, C_6H_5, C_6H_4, and NH); ir ($HCCl_3$) ν_{max}: 3450 (NH), 2900 (N_3), 1750 (β-lactam), 1680 (amide), 1080 cm^{-1}; ms *m/e*: 524 (M^+), 467 ($M^+ - 57$).

Alcohol ***20***

Ozone was passed for 1.5 h through a solution of azide **18** (4 g) in CH_2Cl_2 (80 ml) and ethanol (160 ml) at −78°C. After

Can. J. Chem. Downloaded from www.nrcresearchpress.com by 210.87.254.105 on 09/05/12
For personal use only.

purging with N_2, $NaBH_4$ (0.8 g) was added and the solution allowed to warm up to room temperature (2 h). The reaction was quenched with pH 4.5 buffer (150 ml), evaporated, and partitioned between $CHCl_3$ (200 ml) and H_2O (100 ml). Evaporation and drying ($MgSO_4$) afforded, after crystallization from hexane–CCl_4, 2.5 g of alcohol **20** (76%), mp 95–96°C; ^{1}Hmr ($DCCl_3$) δ: 0.15 (s, 6H, $SiMe_2$), 0.9 (s, 9H, Si*tBu*), 2.6 (bs, 1H, OH), 3.8 (bs, 2H, CH_2OH), 4.3 (q, 1H, CH), 4.7 (s, 2H, CH_2OTBDMS), 4.8 (d, 1H, CHN_3, J = 5 Hz), 7.0–7.4 ppm (m, 4H, C_6H_4); ir ($HCCl_3$) ν_{max}: 3350 (OH), 2900, 2100 (N_3), 1755 (C=O), 1050 cm^{-1}.

Methyl Ether ***21***

To a solution of alcohol **20** (450 mg) in dry CH_2Cl_2 (50 ml) at 0°C was added 5 drops of a solution containing 0.5 ml $BF_2{\cdot}Et_2O$ in ether (25 ml). To this pink solution was added excess (~10 equiv.) of CH_2N_2 in ether over 30 min. After stirring for an additional hour, the suspension was filtered, washed with H_2O (25 ml), dried ($MgSO_4$), and evaporated. Chromatography of the residue on SiO_2 activity III (20 g) using chloroform as eluent afforded 340 mg (74%) of methyl ether **21** as a clear colorless syrup; ^{1}Hmr ($DCCl_3$) δ: 0.1 (s, 6H, $SiMe_2$), 0.95 (s, 9H, Si*tBu*), 3.2 (s, 3H, OCH_3), 3.3–3.7 (m, 2H, CH_2OCH_3), 4.3 (q, 1H, $CHCH_2OCH_3$), 4.5 (q, 2H, CH_2 OTBDMS), 4.6 (d, 1H, CHN_3, J = 5 Hz), 6.9–7.4 ppm (m, 4H, C_6H_4); ir (neat) ν_{max}: 2900, 2100 (N_3), 1760 (C=O) cm^{-1}.

Methoxy Amide ***22***

Into a solution of methoxy azide **21** (340 mg, 0.9 mmol) in CH_2Cl_2 (20 ml) and Et_3N (0.25 ml, 1.8 mmol) at 0°C was bubbled hydrogen sulfide for 5 min. The ice bath was removed and the solution let stand 1 h, washed with H_2O (2 × 25 ml), dried (Na_2SO_4), and evaporated. To the crude product in CH_2Cl_2 (10 ml) was added pyridine (0.5 ml, 6 mmol) and then phenylacetylchloride (0.2 ml, 1.5 mmol). After stirring at room temperature for 20 min, the solution was washed with pH 4.5 buffer (25 ml), dried ($MgSO_4$), and evaporated. The crude product after chromatography on SiO_2 activity III using chloroform as eluent afforded 280 mg (65%) of amide **22** as a yellow syrup; ^{1}Hmr ($DCCl_3$) δ: 0.15 (6H, d, $SiMe_2$), 0.9 (s, 9H, Si*tBu*), 2.9 (3H, s, OMe), 3.2–3.6 (m, 2H, CH_2OCH_3), 4.2–4.4 (m, 1H, $CHCH_2OMe$), 4.8 (q, 2H, CH_2OTBDMS), 5.7 (q, 1H, $CHNH$, J_1 = 5 Hz, J_2 = 7 Hz), 7.0–7.5 ppm (m, 10H, C_6H_5, C_6H_4 + CHN*H*); ir ($HCCl_3$) ν_{max}: 3350, 2900, 1750 (β-lactam), 1665 (amide), 1100 cm^{-1}.

Benzyl Alcohol ***23***

To a solution of amide **22** (280 mg) in THF (10 ml) – H_2O (2 ml) was added dropwise trifluoroacetic acid (2 ml). After stirring 10 min at room temperature the solution was poured onto 5% $NaHCO_3$ (50 ml) and extracted with ethyl acetate (2 × 50 ml). Drying ($MgSO_4$), evaporation, and chromatography on thick-layer plates (SiO_2, 20 × 20 cm) using ether – ethyl acetate (2:1) as eluent afforded 110 mg (52%) of alcohol **23** as a colourless syrup; ^{1}Hmr ($DCCl_3$) δ: 2.95 (s, 3H, OCH_3), 3.2–3.6 (m, 2H, CH_2OCH_3), 3.7 (s, 2H, CH_2Ph), 3.8–4.2 (m, 1H, CH_2OH), 4.3–4.5 (m, 1H, $CHCH_2OCH_3$), 4.6 (s, 2H, CH_2OH), 5.7 (q, 1H, $CHNH$, J_1 = 5 Hz, J_2 = 7 Hz), 6.7–7.6 ppm (m, 10H, NH, aromatic); ir ($CHCl_3$) ν_{max}: 3350 (NH), 1745 (C=O), 1670 cm^{-1} (C=O of amide).

Aldehyde ***24***

To a slurry of pyridinium chlorochromate (100 mg, 0.46 mmol) and NaOAc (24 mg, 0.3 mmol) in CH_2Cl_2 (2 ml) was added a solution of alcohol **23** (100 mg, 0.3 mmol) in CH_2Cl_2 (1 ml). After stirring for 1 h, the reaction mixture was poured into ether (50 ml). The solution was filtered (Celite), washed with H_2O (2 × 50 ml), and dried (Na_2SO_4). Evaporation of ether gave 70 mg (70%) of aldehyde **24**, mp 137–138°C; ^{1}Hmr ($CDCl_3$) δ: 2.9 (s, 3H, OCH_3), 3.4 (m, 2H, CH_2OMe), 3.7 (s, 2H, CH_2Ph), 4.4–4.7 (m, 1H, $CHCH_2OMe$), 5.8 (q, 1H, $CHNH$, J_1 = 5 Hz, J_2 = 7 Hz), 6.7 (bd, 1H, NH, J = 7 Hz), 7.0–8.0 (m, 9H, aromatic), 10 ppm (s, 1H, CHO); ir (KBr) ν_{max}: 3300, 2880, 1755 (β-lactam), 1680 cm^{-1} (amide and aldehyde); ms *m/e*: 352 (M^+), 351 ($M^+ - 1$), 205, 146.

Carboxylic Acid ***25*** *and Methyl Ester* ***26***

To a solution of alcohol **23** (85 mg) in acetic acid (4 ml) was added 1 ml of a solution of CrO_3 (800 mg) in AcOH (9 ml) and H_2O (1 ml). The solution was stirred overnight at room temperature, poured into H_2O (50 ml), and extracted with $HCCl_3$ (3 × 50 ml). The organic phase was washed with water (2 × 20 ml) and then extracted with $NaHCO_3$ (2 × 50 ml). Neutralization of the $NaHCO_3$ extracts with dilute HCl to pH 1 and extraction with chloroform (2 × 100 ml) afforded after drying ($MgSO_4$) and evaporation 25 mg of acid **26**; ^{1}Hmr ($DCCl_3$) δ: 2.9 (s, 3H, OCH_3), 3.2 (bd, 2H, CH_2OCH_3), 3.6 (s, 2H, CH_2Ph), 4.3 (bd, 1H, $CHCH_2OCH_3$), 5.6 (q, 1H, $CHNH$, J_1 = 5 Hz, J_2 = 7 Hz), 6.8 (d, 1H, NH, J = 7 Hz), 6.8–7.8 ppm (m, 9H, C_6H_5 and C_6H_4); ir ($HCCl_3$) ν_{max}: 2500–3500 (NH, OH), 1755 (β-lactam), 1710 (COOH), 1670 cm^{-1} (C=O amide). Treatment with diazomethane in ether gave methyl ester **26**; ms *m/e*: 382 (M^+), 351 ($M^+ - 31$), 205 (base peak), 177.

Acknowledgements

We would like to thank the National Research Council of Canada and Lederle Laboratories for financial assistance, and Ms. N. Kuck, Lederle Laboratories, for antibacterial tests. One of us (R.Z.) would like to thank the NRCC for a postgraduate scholarship.

1. T. Doyle, B. Belleau, B.-Y. Luh, C. F. Ferrari, and M. P. Cunningham. Can. J. Chem. **55**, 468 (1977).
2. R. A. Firestone, J. L. Fahey, N. S. Maciejewicz, G. S. Pater, and B. G. Christensen. J. Med. Chem. **20**, 551 (1977).
3. T. W. Doyle. Can. J. Chem. **55**, 2714 (1977).
4. G. Stacy and R. Morath. J. Am. Chem. Soc. **74**, 3885 (1952).
5. J. Sheehan and V. S. Frank. J. Am. Chem. Soc. **71**, 1856 (1949).
6. A. K. Bose, S. D. Sharma, J. C. Kapur, and M. S. Manhas. Synthesis, 216 (1973).
7. H. B. Kagan, J. J. Basselier, and J. L. Lucke. Tetrahedron Lett. 941 (1964).
8. H. Büchi, K. Steen, and A. Eschenmoser. Helv. Chim. Acta, **48**, 1746 (1965).
9. J. Firestone, N. Maciejewicz, R. W. Ratcliffe, and B. G. Christensen. J. Org. Chem. **39**, 437 (1974).
10. H. Yanagisawa, M. Fukushima, A. Ando, and H. Nakao. Tetrahedron Lett. 2705 (1975).
11. E. J. Corey and J. W. Suggs. Tetrahedron Lett. 2647 (1975).
12. E. J. Corey, N. W. Gilman, and B. E. Ganem. J. Am. Chem. Soc. **90**, 5616 (1968).
13. H. Moore, L. Hernandez, Jr., and R. Chambers. J. Am. Chem. Soc. **100**, 2245 (1978).

β-Lactams. III. The synthesis of 7-β-phenylacetamido-3′-carboxybenzo[3,4]-*O*-2-isocephem

GEORGE JUST AND ROBERT ZAMBONI[1]

Department of Chemistry, McGill University, Montreal, P.Q., Canada H3A 2K6

Received May 8, 1978

GEORGE JUST and ROBERT ZAMBONI. Can. J. Chem. **56**, 2725 (1978).

The synthesis of the β-lactam **34** from 3-methoxy-2-nitrobenzaldehyde is described.

GEORGE JUST et ROBERT ZAMBONI. Can. J. Chem. **56**, 2725 (1978).

La synthèse du β-lactame **34** à partir du 3-methoxy-2-nitrobenzaldehyde est décrite.

Can. J. Chem. Downloaded from www.nrcresearchpress.com by 210.87.254.40 on 09/05/12
For personal use only.

In the preceding paper we described the synthesis of bicyclic anthranyl azetidinones, in which the β-lactam frequency was 1755 cm^{-1}, and which, not surprisingly, showed no significant anti-microbial activity. To raise the β-lactam frequency it was decided to prepare the tricyclic anthranyl azetidinone **34**, which we expected to absorb at considerably higher frequency and which should therefore be similar to classical β-lactams, except for the position of the carboxylic acid (1).

The commercially available 3-methoxy-2-nitrobenzoic acid (**1**) was reduced to amine **2** with PtO_2 in ethanol and the resulting aminobenzoic acid **2** transformed to its methyl ester **3** with diazomethane. Attempts to convert **3** to its cinnamylidene Schiff base failed. The free amino acid **2** was therefore directly converted to Schiff base **4** by reaction with cinnamaldehyde in benzene using a Dean–Stark apparatus. Reaction of **4** with trimethylsilyl chloride – triethylamine in CH_2Cl_2, followed by azidoacetyl chloride (2) gave, after methylation with diazomethane and extensive chromatography, a mixture of

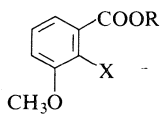

1 X = NO_2, R = H
2 X = NH_2, R = H
3 X = NH_2, R = CH_3
4 X = N=CH—CH=CHPh, R = H

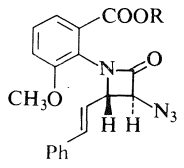

5 R = H
6 R = CH_3

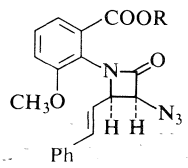

7 R = H
8 R = CH_3

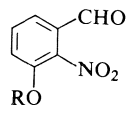

9 R = CH_3
10 R = H
11 R = CH_2Ph

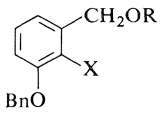

12 R = H, X = NO_2
13 R = H, X = NH_2
14 R = TBDMS, X = NH_2
15 R = TBDMS, X = N=CH—CH=CHPh

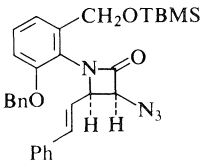

16

17 R = H, R′ = TBDMS
18 R = SO_2CH_3, R′ = TBDMS
19 R = SO_2CH_3, R′ = H

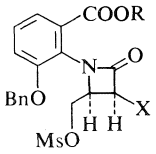

20 X = N_3, R = H
21 X = N_3, R = $CHPh_2$
22 X = $NHCOCH_2Ph$, R = $CHPh_2$

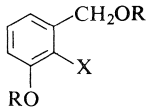

23 R = H, X = NO_2
24 R = TBDMS, X = NH_2
25 R = TBDMS, X = N=CH—CH=CHPh

[1]Holder of a NRCC Scholarship, 1974–1978.

Can. J. Chem. Downloaded from www.nrcresearchpress.com by 210.87.254.40 on 09/05/12
For personal use only.

trans- and *cis*-β-lactams **6** and **8** in approximately 25% yield. The nmr spectrum after addition of $Eu(fod)_3$ clearly showed the presence of the *cis* isomer **8**, $J_{3,4} = 5$ Hz, and of the *trans* isomer **6**, $J_{3,4} = 2$ Hz, in addition to all other appropriate signals.

It was therefore decided to reduce the electron withdrawing carboxyl function, which was responsible for the low yield of the reaction and the formation of the *trans* isomer, to an alcohol before carrying out the cyclo addition, and to eventually reoxidize the benzyl alcohol to the corresponding benzoic acid. 3-Methoxy-2-nitrobenzaldehyde **9** was quantitatively demethylated with BBr_3 (3) in CH_2Cl_2 to phenol **10**, which was benzylated to benzyl ether **11**, mp 77–79°C. $NaBH_4$ reduction gave alcohol **12** which was transformed to aniline **13** by means of catalytic hydrogenation (PtO_2). Silylation with *tert*-butyldimethylsilyl chloride gave 2-amino-3-benzyloxybenzyl alcohol *tert*-butyldimethylsilyl ether **14** in 40% yield, based on **9**. Aniline **14** was transformed to its cinnamylidene Schiff base **15**, which gave *cis*-β-lactam **16** in 84% yield upon reaction with azidoacetyl chloride and triethylamine in CH_2Cl_2 at −20°C. Ozonolysis of **16** in ethanol – methylene chloride (3:1) at −78°C, followed by sodium borohydride reduction at low temperature gave alcohol **17**, which was transformed to mesylate **18**. Treatment of **18** with trifluoroacetic acid – THF – water and oxidation of the resulting alcohol **19** with CrO_3 in acetic acid – water gave a 30% yield of acid **20**, mp 153–155°C. Treatment of **20** with diphenyldiazomethane gave the benzhydryl ester **21**. Reduction of the azido group of **21**, followed by acylation of the resulting amine function gave β-lactam amide ester **22**, mp 128–129°C. Attempts to remove the benzyl groups by catalytic hydrogenation and to cyclize the resulting phenol mesylate with DBU or triethylamine failed, as evidenced by nmr which showed the presence of the mesylate group.

Since we had indications, based on model studies, that the desired cyclization proceeded well, when it was effected on a silyl phenol mesylate of type **28**, the sequence was repeated with a *tert*-butyldimethylsilyl ether instead of the benzyl ether. Reduction of **10** first with $NaBH_4$ in ethanol and then catalytically (PtO_2) afforded, after silylation with *tert*-butyldimethylsilyl chloride, amine **24** in 68% yield from **9**. Aniline **24** was transformed to its cinnamylidene Schiff base **25**, which gave *cis*-β-lactam **26** in approximately 80% yield. Ozonolysis of **26** in ethanol–CH_2Cl_2 (5:1) followed by reduction with $NaBH_4$ afforded, after chromatography, crystalline alcohol **27**, mp 112–112.5°C, in 53% yield. It was transformed

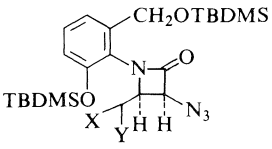

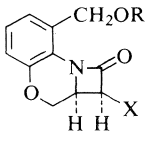

26 X, Y = CH=CHPh
27 X, Y = H, OH
28 X, Y = H, OSO_2CH_3

29*a* R = TBDMS, X = N_3
29*b* R = TBDMS, X = $NHCOCH_2Ph$
30 R = H, X = N_3
31 R = H, X = $NHCOCH_2Ph$

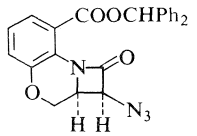

32

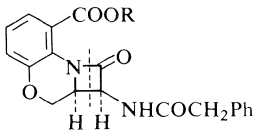

33 R = $CHPh_2$
34 R = H
35 R = CH_3

to its mesylate **28** with MsCl–Et_3N. Cyclization of **28** with 1 equiv. of freshly prepared tetra-*n*-butylammonium fluoride in THF, or better still, with approximately 2 equiv. of KF and 18-crown-6 (0.3 equiv.), gave a 90–95% yield of cyclized product **29***a*, $\nu_{C=O}$ 1775 cm^{-1}, as an oil. Reduction of the azide group with NEt_3–H_2S followed by acylation with phenylacetyl chloride – NEt_3 and deblocking with TFA–H_2O–THF gave amide **31**. Attempts to oxidize the benzyl alcohol **31** with RuO_2–$NaIO_4$, CrO_3–AcOH–H_2O, and $KMnO_4$–pyridine only gave the corresponding aldehyde and no acid **34**. Since the oxidation did not give the desired product we next attempted to oxidize azide benzyl alcohol **30**, obtained from the silyl ether **29***a* by acid treatment. Oxidation with CrO_3–AcOH–H_2O gave the desired carboxylic acid, which was converted to the benzhydryl ester **32** by means of diphenyldiazomethane in acetonitrile. NEt_3–H_2S reduction followed by acylation gave the desired amide **33**. Attempts to remove the benzhydryl ester with TFA–anisole at 0°C failed and resulted in decomposition of the β-lactam ester **33**. However, catalytic hydrogenation, using Pd/C in ethanol, gave the desired acid **34** as a light yellow powder, $\nu_{C=O}$(KBr) 1780, 1685, and 1650 cm^{-1}, fully characterized as its methyl ester **35**. Its structure followed from its spectral data and the stereochemistry of the ring junction from the fact that $J_{3,4} = 4.8$ Hz (4). The mass spectrum of methyl ester **35** showed a molecular ion, a peak at $M^+ - 31$ which is consistent with a methyl ester and peaks at m/e 175 and 192 typical of the fragmentation of β-lactams as indicated on structure **35** (5).

Carboxylic acid **34** showed no activity toward a variety of bacteria. It therefore seems that the position of the carboxyl function in cephalosporins is critical for antimicrobial activity.

Can. J. Chem. Downloaded from www.nrcresearchpress.com by 210.87.254.40 on 09/05/12
For personal use only.

Experimental

Solvents are of reagent grade unless otherwise specified. Infrared spectra were run on Unicam SP1000 and P.E. 257 spectrophotometers. Nuclear magnetic resonance spectra were run on Varian T-60, T-60A or Brucker FT-90 spectrophotometers. Mass spectra were taken on a AE1 MS-902 or on a LKB 9000 mass spectrophotometer using the direct sample inlet system with a 70 eV ionization energy. Melting points were determined on a Gallenkamp block in open capillary tubes and are uncorrected. Merck silica gel 60 was used for column chromatography. Merck silica gel HF 254 was used for thick-layer chromatography (1 mm) on glass plates (20 × 20 cm). Elemental analyses were performed by Midwest Microlab Ltd., Indianapolis, IN.

*β-Lactams **6** and **8***

3-Methoxyanthranilic acid (0.8 g, 5 mmol) and cinnamaldehyde (0.66 g, 5 mmol) in 50 ml benzene were heated at reflux for 24 h using a Dean–Stark trap. After evaporation of the benzene, Me_3SiCl (0.65 ml, 5.1 mmol) in 10 ml CH_2Cl_2 was added dropwise to a solution of **4** in 50 ml CH_2Cl_2 containing Et_3N (1.4 g, 15 mmol). The mixture was then cooled to −20°C and azidoacetyl chloride (0.6 g, 5 mmol) in CH_2Cl_2 (10 ml) was added dropwise over 15 min. The reaction mixture was stirred for an additional 30 min and after the usual work-up, the crude product was chromatographed on SiO_2 activity III (40 g). Elution with CH_2Cl_2 and then with $CHCl_3$–ether (1:1) afforded crude acid **5** and **7** as a mixture. An ethereal solution of the acid was methylated with CH_2N_2, washed with 5% HCl (4 × 50 ml) to remove anthranilic acid, and purified by thick-layer plates (20 × 20 × 1 mm, SiO_2) using $CHCl_3$–ether (5:1), yield 300 mg; ^{1}Hmr ($CHCl_3$) δ: 3.8 (d, 6H, OCH_3), 4.2–5.0 (m, 2H, CH and CHN_3), 6.0–6.6 (m, 2H, PhCH=CH), 6.8–7.5 ppm (m, 8H, C_6H_3 and C_6H_5); ir ($CHCl_3$) ν_{max}: 1750, 1730 cm^{-1}; addition of Eu(fod)$_3$ separated doublet at 3.8 into four singlets and multiplets at 4.2–5.0 to a doublet (1 H) for CHN_3 of the *cis* isomer ($J_{3,4}$ = 5 Hz) and doublet (1 H) for CHN_3 of the *trans* isomer ($J_{3,4}$ = 2 Hz).

*3-Hydroxy-2-nitrobenzaldehyde (**10**)*

To a suspension of 3-methoxy-2-nitrobenzaldehyde (12 g, 66 mmol) in CH_2Cl_2 (300 ml) at −78°C was added dropwise over ½ h a solution of BBr_3 (20 ml, 210 mmol) in CH_2Cl_2 (200 ml). After the addition was complete, the Dry Ice – acetone bath was removed and the red solution allowed to warm up to 20°C (3 h). The red solution was poured into crushed ice (500 g) and extracted with ethyl acetate (1 ℓ). Drying ($MgSO_4$) and evaporation *in vacuo* afforded 11 g (94%) of crude 3-hydroxy-2-nitrobenzaldehyde, mp 140°C (dec.); ^{1}Hmr (DMSO-d_6) δ: 7.4–7.8 (m, 3H, C_6H_3), 10.4, (s, 1H, *CHO*), 11.4 ppm (s, C_6H_3OH); ir (CH_2Cl_2) ν_{max}: 3300(OH), 3000, 1710(C=O), 1610 cm^{-1}.

*3-Benzyloxy-2-nitrobenzaldehyde (**11**)*

To 3-hydroxy-2-nitrobenzaldehyde (5 g, 29 mmol) in DMSO (17 ml) was added benzyl bromide (5 g, 29 mmol) and K_2CO_3 (5 g, 36 mmol). The suspension was stirred overnight at room temperature. The reaction mixture was poured into water (500 ml) and extracted with ether (2 × 300 ml). The ether layer was washed with water (4 × 100 ml). Drying ($MgSO_4$) and evaporation afforded 7 g of crude benzyl ether. Crystallization from chloroform–ether afforded 3.6 g (50%) of **11**, mp 77–79°C; ^{1}Hmr ($CDCl_3$) δ: 5.2 (s, 2H, CH_2O), 7.0–7.5 (m, 8H, C_6H_5 and C_6H_3), 9.8 ppm (s, 1H, CHO); ir (KBr): ν_{max} 3000, 2900, 1705 cm^{-1} (CHO).

*3-Benzyloxy-2-nitrobenzyl Alcohol (**12**)*

To aldehyde **11** (8 g, 48 mmol) suspended in EtOH (300 ml) and MeOH (50 ml) at 0°C was added $NaBH_4$ (0.4 g, 41 mmol) in portions. After stirring for 1 h, excess $NaBH_4$ was destroyed with acetic acid (2 ml). The residue, after evaporation of the solvent, was partitioned between 1% HCl (200 ml) and ethyl acetate (300 ml). Drying ($MgSO_4$) and evaporation afforded in quantitative yield alcohol **12**; ^{1}Hmr (acetone-d_6) δ: 2.8 (bs, 1H, CH_2OH), 4.4 (s, 2H, CH_2OH), 5.1 (s, 2H, $PhCH_2O$), 6.4–7.2 (m, 3H, C_6H_3), 7.3 ppm (s, 5H, C_6H_5); ir (film) ν_{max}: 3550, 3350 (OH), 2900 cm^{-1}.

*Amine **14***

A solution of alcohol **12** (5.2 g) and PtO_2 (400 mg) was hydrogenated at 40 psi, using a Parr hydrogenator, for 2 h. The residue, after filtration of catalyst through Celite and evaporation, was dissolved in ethyl acetate (200 ml) and washed with 5% NaOH (2 × 100 ml). Drying ($MgSO_4$) and evaporation of the ethyl acetate afforded 3.7 g (16 mmol) of almost colourless amine **13** as a semisolid. The amine in DMF (75 ml) was immediately treated with *tert*-butyldimethylsilyl chloride (3.0 g, 20 mmol) and imidazole (3.3 g, 48 mmol). After stirring overnight at room temperature, the solution was partitioned between ether (200 ml) and water (500 ml). The ether layer was washed with water (4 × 100 ml) and dried ($MgSO_4$). Evaporation afforded a quantitative yield of silyl amine **14**; ^{1}Hmr ($CDCl_3$) δ: 0.05 (s, 6H, $SiMe_2$), 0.90 (s, 9H, Si*t*Bu), 4.4 (bs, 2H, NH_2), 4.7 (s, 2H, $CH_2OTBDMS$), 5.0 (s, 2H, $PhCH_2O$), 6.6–6.8 (m, 3H, C_6H_3), 7.4 ppm (s, 5H, C_6H_5); ir (film) ν_{max}: 3370, 3460 (NH_2), 2960, 2940 cm^{-1}.

*Azide β-Lactam **16***

A solution of cinnamaldehyde (3.3 g, 25 mmol), amine **14** (8.3 g, 24 mmol), and a few crystals of TsOH in benzene (200 ml) was heated at reflux overnight using a Dean–Stark trap. Evaporation of the solvent afforded Schiff base **15** as a light yellow oily solid. To the Schiff base dissolved in CH_2Cl_2 (200 ml) and triethylamine (3.3 g, 33 mmol) at −20°C under N_2 was added dropwise over 1 h azidoacetyl chloride (3.6 g, 30 mmol) in CH_2Cl_2 (100 ml). The red brown solution was stirred at −20°C for 1 h more. Washing with water (2 × 100 ml), drying ($MgSO_4$), and evaporation afforded, after treatment with charcoal and filtration through Al_2O_3 (300 g) using CH_2Cl_2 as eluent, 11 g (84%) of fairly pure azido β-lactam **16** as an orange oil; ir (film) ν_{max}: 2900, 2100(N_3), 1770 cm^{-1} (C=O).

*Alcohol **17***

Ozone (8 mmol/h) was bubbled through a solution of crude β-lactam **16** (1.7 g) in EtOH (100 ml) and methylene chloride (20 ml) at −78°C for 35 min. Excess ozone was removed with N_2 and $NaBH_4$ (850 mg) was added. After warming to room temperature (2 h), 100 ml of pH 4.5 buffer was added. Removal of solvent on a rotary evaporator and extraction with CH_2Cl_2 (2 × 300 ml) afforded, after drying ($MgSO_4$) and evaporation, crude alcohol (1.6 g). Careful column chromatography on SiO_2 activity III (30 g) using chloroform as eluent afforded 850 mg (58%) of pure alcohol **17**; ^{1}Hmr ($DCCl_3$ + D_2O) δ: 0.1 (s, 6H, s, $SiMe_2$), 0.95 (s, 9H, Si*t*Bu), 3.7 (d, 2H, CH_2OH), 4.2–4.5 (m, 1H, $CHCH_2OH$), 4.6 (d, 1H, CHN_3, J = 5 Hz), 4.71 (q, 2H, $CH_2OTBDMS$), 5.0 (s, 2H, $PhCH_2$), 6.8–7.3 (m, 3H, C_6H_3), 7.4 ppm (s, 5H, C_6H_5); ir (film) ν_{max}: 3400 (OH), 2900, 2100 (N_3), 1760 (C=O), 1240, 1100 cm^{-1}; ms *m/e*: 411 (M^+ − 57). *Anal.* calcd. for $C_{24}H_{32}N_4O_4Si$: C 61.54, H 6.84, N 11.95; found: C 61.41, H 7.12, N 12.17.

*Mesylate **18***

To alcohol **17** (130 mg) in CH_2Cl_2 (10 ml) and triethylamine (80 μl) at −78°C was added methanesulphonyl chloride (35 μl).

Can. J. Chem. Downloaded from www.nrcresearchpress.com by 210.87.254.40 on 09/05/12
For personal use only.

After warming to 20°C, usual work-up afforded a quantitative yield of mesylate **18**; ^{1}Hmr ($DCCl_3$) δ: 0.15 (s, 6H, $SiMe_2$), 1.0 (s, 9H, Si*tBu*), 2.6 (s, 3H, SO_2CH_3), 4.5 (d, 2H, $CH_2OSO_2CH_3$), 4.8 (q, 1H, $CHCH_2$), 4.8 (s, 2H, $CH_2OTBDMS$), 4.9 (d, 1H, CHN_3, J = 5 Hz), 5.1 (s, 2H, OCH_2Ph), 6.9–7.3 (m, 3H, C_6H_3), 7.4 ppm (s, 5H, C_6H_5); ir ($CHCl_3$) ν_{max}: 2900, 2100 (N_3), 1770 cm^{-1} (C=O).

Benzyl Alcohol ***19***

To mesylate **18** (850 mg) in THF (25 ml) and H_2O (10 ml) was added dropwise trifluoroacetic acid (3 ml). The homogeneous solution was stirred at room temperature 20 min and poured into 5% $NaHCO_3$ (200 ml). Extraction with ethyl acetate (2 × 200 ml), drying ($MgSO_4$), and evaporation afforded crude mesylate benzyl alcohol **19**. The crude benzyl alcohol was chromatographed on SiO_2, activity III, using first $CHCl_3$–ether (1:1) as eluent. Elution with ether afforded 470 mg (72%) of alcohol as a colorless syrup; ^{1}Hmr ($DCCl_3$) δ: 2.7 (s, 3H, CH_3), 3.2 (bs, 1H, CH_2OH), 4.4 (d, 2H, CH_2OMs), 4.6 (s, 2H, CH_2OH), 4.7 (q, 1H, CH—CH_2), 4.9 (d, 1H, CHN_3, J = 5 Hz), 5.1 (s, 2H, CH_2Ph), 6.8–7.4 (m, 3H, C_6H_3), 7.4 ppm (s, 5H, C_6H_5); ir (film) ν_{max}: 3450 (OH), 2900, 2100 (N_3), 1770 (C=O), 1350, 1180, 1100 cm^{-1}.

Carboxylic Acid ***20***

Alcohol **19** (440 mg, 1 mmol) was dissolved in acetic acid and 4.4 ml (2.6 mmol) of a CrO_3 solution (600 mg CrO_3 in 9 ml AcOH, 1 ml H_2O) was added. After stirring overnight at room temperature, most of the acetic acid was evaporated. The residue was poured into pH 1.8 buffer (30 ml) and extracted with $CHCl_3$ (3 × 100 ml). Drying ($MgSO_4$), evaporation of $CHCl_3$, and trituration with ether, afforded 190 mg (42%) of acid **20** as a nearly white solid, mp 153–155°C; ^{1}Hmr ($CDCl_3$) δ: 2.7 (s, 3H, SO_2CH_3), 4.3–4.7 (m, 3H, $CHCH_2$), 4.9 (bd, 1H, CHN_3), 5.1 (s, 2H, CH_2OPh), 7–7.4 (m, 8H, C_6H_3 and C_6H_5), 10.8 ppm (s, 1H, CO_2H); ir ($CHCl_3$) ν_{max}: 2700–3200 (CO_2H), 2080(N_3), 1775 (β-lactam), 1720 cm^{-1} (acid); ir (KBr) ν_{max}: 1740 cm^{-1} (b, C=O).

Ester ***21***

Acid **20** (400 mg, 0.9 mmol) was suspended in CH_3CN (20 ml) and treated with a 1 *M* solution of Ph_2CHN_2 in CH_3CN (1 ml). After stirring 1 h at room temperature a few drops of acetic acid were added. Chromatography of the crude product, on thick layer plates (20 × 20 cm) using $CHCl_3$–ether (5:1) as eluent, afforded 420 mg (77%) of ester **21** as a white foam; ^{1}Hmr ($CDCl_3$) δ: 2.6 (s, 3H, SO_2CH_3), 4.2–4.6 (m, 4H, $CHCH_2$ and CHN_3), 5.1 (s, 2H, OCH_2Ph), 7.2–7.6 ppm (m, 14H, $CHPh_2$ and C_6H_3); ir ($CHCl_3$) ν_{max}: 2100 (N_3), 1780 (β-lactam), 1730 cm^{-1} (ester).

Amide ***22***

H_2S was bubbled into a solution of **21** (390 mg, 0.6 mmol) in 20 ml CH_2Cl_2 and Et_3N (0.1 ml, 0.7 mmol) at 0°C for 5 min. After stirring 1 h at 20°C, the solution was purged with nitrogen (5 min). The reaction mixture was washed with H_2O (20 × 20 ml), dried, and evaporated. To the crude product in CH_2Cl_2 (10 ml) and Et_3N (0.1 ml, 0.7 mmol) was added dropwise a solution of phenylacetyl chloride (108 mg, 0.7 mmol) in CH_2Cl_2 (2 ml). After stirring for 1 h at 0°C, the solution was washed with H_2O (2 × 20 ml), dried, and evaporated. Chromatography of the residue on SiO_2 activity III (20 g) afforded, after elution with ether, 275 mg (64%) of amide **22**, mp 128–129°C (dec.); ^{1}Hmr ($CDCl_3$—DMSO-d_6) δ: 2.90 (s, 3H, CH_3), 3.75 (s, 2H, $COCH_2Ph$), 4.7 (m, 3H, $CHCH_2$, 5.4 (s, 2H, OCH_2Ph), 5.4 (m, 1H, CHNH), 7.25 (s, 1H, $CHPh_2$), 7.25–8.0 ppm (m, 13H, aromatic); ir (KBr) ν_{max}: 3300 (NH), 1770 (β-lactam), 1720 (ester), 1660 cm^{-1} (amide).

3-Hydroxy-2-nitrobenzyl Alcohol ***23***

Crude phenol **10** (11 g, 65 mmol) was dissolved in absolute ethanol (500 ml) and cooled to 0°C. $NaBH_4$ (5g, 131 mmol) was added in portions. The ice bath was removed and the red slurry stirred for 2 h at 20°C. Acetic acid (5 ml) was added and the ethanol was removed on a rotary evaporator. The residue was dissolved in water (200 ml) and acidified with HCl to pH < 1. Extraction with ethyl acetate (2 × 300 ml), drying ($MgSO_4$), and evaporation afforded 10 g (90%) of 3-hydroxy-2-nitrobenzyl alcohol, mp 104–110°C (dec.); ^{1}Hmr (acetone-d_6) δ: 4.6 (s, 2H, CH_2OH), 4.5 (bs, 1H, CH_2OH), 6.8–7.5 (m, 3H, C_6H_3), 10.4 ppm (bs, 1H, C_6H_3OH).

Amine ***24***

Alcohol **23** (10 g, 57 mmol) was dissolved in ethanol (200 ml) and PtO_2 (0.7 g) was added. The mixture was hydrogenated for 2 h in a Parr hydrogenator at 40 psi and filtered through Celite. Evaporation of the filtrate afforded 8 g of the amine as a brown semicrystalline solid. The amine was added to a solution of *tert*-butyldimethylsilyl chloride (21 g, 136 mmol) and imidazole (23.5 g, 350 mmol) in dry DMF (75 ml). The solution was stirred overnight at room temperature and partitioned between ether (300 ml) and water (750 ml). The ether layer was washed with water (4 × 200 ml), dried ($MgSO_4$) and evaporated. The crude product was chromatographed on SiO_2, activity III (300 g). Elution with methylene chloride afforded 16 g (77%) of amine **24**; ^{1}Hmr ($CHCl_3$) δ: 0.05 (s, 6H, $Si(CH_3)_2$), 0.25 (s, 6H, $Si(CH_3)_2$), 0.9 (s, 9H, Si*t*Bu), 1.0 (s, 9H, Si*t*Bu), 4.2 (bs, 2H, NH_2), 4.6 (s, 2H, CH_2O), 6.3–6.8 ppm (m, 3H, C_6H_3); ir (film) ν_{max}: 3500, 3400(NH_2), 3000, 1630 cm^{-1}.

Azide β-Lactam ***26***

Amine **24** (4.4 g, 11 mmol) and cinnamaldehyde (1.6 g, 12 mmol) and a few crystals of TsOH dissolved in dry benzene (150 ml) were refluxed overnight using a Dean–Stark trap to remove the water formed. The crude product, after evaporation of benzene, was dissolved in CH_2Cl_2 (100 ml) and Et_3N (1.8 ml, 13 mmol). To the solution under N_2 at −20°C was added dropwise azidoacetyl chloride (1.5 g, 13 mmol) in CH_2Cl_2 (80 ml) over 1 h. The reaction mixture was stirred for 1 h more and washed with H_2O (2 × 50 ml). Drying ($MgSO_4$) and evaporation afforded the crude product. Filtration through 100 g of Al_2O_3, activity III, using CH_2Cl_2 as eluent afforded 5.5 g (81%) of β-lactam azide **26**, suitable for the next reaction; ir (film) ν_{max}: 2900, 2100 (N_3), 1770 cm^{-1} (C=O).

Alcohol ***27***

Into a solution of crude azide **26** (2.8 g) in ethanol (150 ml) and CH_2Cl_2 (30 ml) at −78°C was passed ozone (8 mmol/h) for 45 min. After removing excess ozone with nitrogen (15 min), $NaBH_4$ (400 mg) was added. The solution was allowed to warm up to room temperature over a period of 2 h. To the slightly yellow solution was added pH 4.5 buffer (150 ml). The ethanol was removed on a rotary evaporator and the residue extracted with $CHCl_3$ (2 × 100 ml). Drying ($MgSO_4$) and evaporation afforded 2.5 g of crude alcohol. Chromatography of the crude alcohol on SiO_2, activity III (45 g), using $CHCl_3$ as eluent, afforded, after crystallization from pentane, 1.3 g (53%) of pure alcohol **27**, mp 112–112.5°C; ^{1}Hmr ($CDCl_3$) δ: 0.05 (d, 6H, $SiMe_2$), 0.25 (d, 6H, $SiMe_2$), 0.90 (s, 9H, Si*t*Bu), 1.0 (s, 9H, Si*t*Bu), 3.1 (bs, 1H, OH), 3.7 (bd, 2H, CH_2OH), 4.2–4.4 (m, 1H, $CHCH_2OH$), 4.7 (q, 2H, $CH_2OTBDMS$), 4.7 (d, 1H, CHN_3, J = 5 Hz), 6.6–7.2 ppm (m, 3H, C_6H_3); ir (KBr) ν_{max}: 3450 (OH), 2900, 2150 (N_3), 1770 (C=O), 1600 cm^{-1} (C=C); ms m/e: 435 (M^+ − 57), 407 (M^+ − 57 − 28). *Anal.* calcd. for $C_{24}H_{40}N_4O_4Si$: C 56.06, H 8.18, N 11.36; found: C 55.95, H 8.03, N 11.38.

Can. J. Chem. Downloaded from www.nrcresearchpress.com by 210.87.254.40 on 09/05/12
For personal use only.

Mesylate ***28***

To alcohol **27** (2 g, 4.1 mmol) in CH_2Cl_2 (50 ml) and Et_3N (0.8 ml, 0.56 mmol) at −78°C was added dropwise MsCl (0.35 ml, 4.5 mmol) in CH_2Cl_2 (5 ml). The solution was stirred for 30 min at −78°C and allowed to warm up to room temperature (1 h). The reaction mixture, after washing with water (2 × 50 ml), drying ($MgSO_4$), and evaporation *in vacuo*, afforded 2.2 g (95%) of mesylate **28** as an oily solid; ^{1}Hmr ($CDCl_3$) δ: 0.05 (d, 6H, $SiMe_2$), 0.25 (d, 6H, $SiMe_2$), 0.9 (s, 9H, Si*t*Bu), 1.0 (s, 9H, Si*t*Bu), 2.75 (s, 3H, CH_3), 4.4 (m, 2H, $CH_2OSO_2CH_3$), 4.7 (m, 1H, CH_2CH), 4.7 (s, 2H, CH_2OTBDMS), 5.0 (d, 1H, CHN_3, J = 5 Hz), 6.7–7.4 ppm (m, 3H, C_6H_3).

Azido β-Lactam ***29****a*

To mesylate **28** (1 g, 1.7 mmol) in CH_3CN (20 ml) was added KF (116 mg, 2 mmol) and 18-crown-6 (75 mg, 0.3 mmol). After stirring 5 h at room temperature, more KF (50 mg) and 18-crown-6 (75 mg) were added. After 4 h more at room temperature, the reaction mixture was poured into water (200 ml) and extracted with CH_2Cl_2 (2 × 200 ml). Drying ($MgSO_4$) and evaporation afforded crude product contaminated with 18-crown-6. Chromatography on SiO_2, activity III (20 g), using CH_2Cl_2 as eluent, afforded 580 mg (92%) of cyclized β-lactam ***29****a* as a colourless oil; ^{1}Hmr (benzene-d_6) δ: 0.2 (s, 6H, $SiMe_2$), 1.1 (s, 9H, Si*t*Bu), 3.0–4.0 (m, 3H, OCH_2CH), 4.2 (d, 1H, CHN_3, J = 5 Hz), 5.4 (q, 2H, CH_2OTBDMS, J = 16 Hz), 6.6–7.6 (m, 3H, C_6H_3); ir ($CHCl_3$) ν_{max}: 2900, 2100 (N_3), 1780 (C=O), 1600 cm^{-1} (C=C).

Benzyl Alcohol ***30***

To azide ***29****a* (580 mg) in THF (20 ml) and H_2O (6 ml) was added dropwise trifluoroacetic acid (3 ml). After stirring for 20 min at room temperature the reaction mixture was poured into 5% $NaHCO_3$ (200 ml) and extracted with CH_2Cl_2 (2 × 100 ml). The combined organic phases were dried ($MgSO_4$) and evaporated. Trituration of the oily residue with ether afforded 300 mg (75%) of alcohol **30**, mp 128–129°C; ^{1}Hmr ($CDCl_3$–DMSO-d_6, few drops D_2O) δ: 3.8–4.4 (m, 3H, CH_2CH), 4.8 (q, 2H, CH_2OH, J = 17 Hz), 5.6 (d, 1H, CHN_3, J = 5 Hz), 7.0 ppm (m, 3H, C_6H_3); ir (KBr): ν_{max} 3380 (OH), 2900, 2100 (N_3), 1775 cm^{-1} (C=O); ms *m/e*: 246 (M^+), 218 (M^+ − 28). *Anal.* calcd. for $C_{11}H_{10}N_4O_3$: C 53.66, H 4.09, N 22.76; found: C 53.57, H 4.32, N 22.44.

Ester ***32***

To alcohol **30** (420 mg, 1.7 mmol) in AcOH (5 ml) was added 4.5 ml of CrO_3 solution (1 g CrO_3 in 1 ml H_2O and 9 ml AcOH). After stirring at 20°C for 24 h, more CrO_3 solution (2.5 ml) was added. After a total time of 48 h the acetic acid was evaporated at 20°C. The residue was partitioned between pH 1.8 buffer (20 ml) and chloroform (100 ml). The aqueous phase was extracted again with $CHCl_3$ (2 × 50 ml). The combined $CHCl_3$ extracts were washed with pH 1.8 buffer (2 × 20 ml), dried ($MgSO_4$), and evaporated. To the crude acid, 260 mg dissolved in CH_3CN (20 ml), was added 9 ml (1.8 mmol) of a solution of diphenyldiazomethane in CH_3CN (2 g Ph_2CN_2 in 100 ml CH_3CN). The red reaction mixture was stirred 1 h at room temperature and quenched with acetic acid (3 drops). The crude product after evaporation of the solvent was chromatographed on thick-layer plates (SiO_2) using $CHCl_3$–ether (9:1) as eluent. Extraction of band with $R_f \simeq 0.7$ afforded 280 mg (39%) of ester **32** as a colourless foam; ^{1}Hmr (C_6D_6, 90 MHz) δ: 3.2–3.4 (m, 1H, CH_2CH), 3.3 (t, 1H, $CHHCH$, $J_1 = J_2$ = 10 Hz), 3.8 (q, 1H, $CHHCH$, J_1 = 3, J_2 = 10 Hz), 4.2 (d, 1H, CHN_3, J = 5 Hz), 6.4–7.6 ppm (m, 13H, aromatic); ir ($CHCl_3$) ν_{max}: 3000, 2100 (N_3), 1795 (β-lactam), 1730 (ester); ms *m/e*: 426 (M^+), 397 (M^+ − 28), 343 (M^+ − N_3-CHCO), 215 (M^+ − CO_2CHPh_2).

Amide ***33***

Hydrogen sulphide was bubbled into a solution of ester **32** (250 mg, 0.6 mmol) and Et_3N (0.1 ml, 0.7 mmol) in CH_2Cl_2 at 0°C for 5 min. The ice bath was removed and the orange solution stirred at room temperature. After 1 h, excess H_2S was purged with nitrogen. The yellow solution was washed with H_2O (2 × 25 ml), dried ($MgSO_4$), and evaporated. To the resulting yellow gum dissolved in CH_2Cl_2 (20 ml) and Et_3N (0.1 ml, 0.7 mmol) was added at 0°C phenylacetyl chloride (90 μl, 0.68 mmol). After stirring for 1 h at 0°C, the solution was washed with pH 4.5 buffer (2 × 25 ml). Drying ($MgSO_4$), evaporation, and chromatography on thick-layer plates using $CHCl_3$–ether (10:1) afforded 235 mg (77%) of amide **33** as a slightly yellow foam; ^{1}Hmr ($CDCl_3$, 90 MHz) δ: 3.5 (s, 2H, CH_2Ph), 3.7 (t, 1H, $CHHCH$, $J_1 = J_2$ = 10 Hz), 4.0–4.5 (m, 2H, $CHHCH$), 5.4 (q, 1H, $CHNH$, J_1 = 4.5, J_2 = 7 Hz), 6.8 (d, 1H, NH, J = 7 Hz), 7.0–7.6 ppm (m, 19H, aromatic and $CHPh_2$); ir ($CHCl_3$) ν_{max}: 3400 (NH), 2900, 1785 (β-lactam), 1730 (ester), 1690 cm^{-1} (amide).

Alcohol Amide ***31***

To amide ***29****b* (180 mg) in THF (5 ml) and H_2O (2 ml) was added dropwise trifluoroacetic acid (0.8 ml). After stirring at room temperature 15 min, the solution was poured onto 10% $NaHCO_3$ and extracted with chloroform (2 × 50 ml). Drying ($MgSO_4$), evaporation, and trituration with ether afforded 80 mg (60%) of alcohol amide **31** as white solid, mp 183–185°C; ^{1}Hmr (acetone-d_6) δ: 3.6 (s, 2H, $CH_2\phi$), 4.0–4.6 (m, 3H, CH_2CH), 4.8 (bs, 3H, CH_2OH), 5.6 (q, 1H, $CHNH$, J_1 = 4.5, J_2 = 7 Hz), 6.6–7.2 (m, 3H, C_6H_3), 7.2 ppm (s, 5H, C_6H_5); ir (KBr) ν_{max}: 3400(OH), 3350(NH), 1775 (C=O of β-lactam), 1660 cm^{-1} (C=O of amide), ms *m/e*: 338(M^+).

Amide ***29****b*

Into azide **29** (500 mg, 1.4 mmol) dissolved in CH_2Cl_2 (20 ml) and Et_3N (0.2 ml, 1.4 mmol) at 0°C was bubbled H_2S for 5 min. After stirring for 1 h at room temperature, the solution was washed with H_2O (2 × 20 ml), dried ($MgSO_4$), and evaporated. To the crude product at 0°C in CH_2Cl_2 (20 ml) and Et_3N (0.2 ml, 1.3 mmol) was added dropwise phenylacetyl chloride (0.23 g, 1.5 mmol) in CH_2Cl_2 (2 ml) over a period of 5 min. After stirring for 1 h at room temperature, the solution was washed with pH 4.5 buffer (30 ml) and H_2O (30 ml), dried ($MgSO_4$), and evaporated. Chromatography of the residue on SiO_2 activity II (20 g) using CH_2Cl_2 up to CH_2Cl_2–ether (1:1) afforded 530 mg (80%) of amide ***29****b* as a colourless foam; ^{1}Hmr ($CDCl_3$) δ: 0.05 (s, 6H, Si(CH_3)$_2$), 0.90 (s, 9H, Si*t*Bu), 4.3 (s, 2H, $CH_2\phi$), 3.6–4.6 (3H, m, CH_2CH), 6.6–7.2 (m, 3H, C_6H_3), 7.3 ppm (bs, 6H, C_6H_5 and NH); ir ($CHCl_3$) ν_{max}: 3400(NH), 2900, 1765 (β-lactam C=O), 1680 cm^{-1} (amide C=O).

Ester ***35*** *and Acid* ***34***

Ester **33** (250 mg) in EtOH (50 ml) containing 10% Pd/C (250 mg) was hydrogenated for 1 h at 40 psi using a Parr hydrogenator. Filtration through Celite and evaporation of the ethanol gave the crude acid. Trituration of the residue with ether afforded (65%) of acid **34** as a pale yellow solid, mp 140°C (dec); ir (KBr) ν_{max}: 3350 (NH), 2500–3600 (OH), 1780 (β-lactam), 1685 (acid), 1650 (amide), 1380 cm^{-1}.

Treatment with ethereal CH_2N_2 and chromatography on thick-layer plates using $CHCl_3$–ether (1:1) afforded, after crystallization from benzene (70%) of ester **35** as a solid, mp (148–150°C); ^{1}Hmr ($CDCl_3$, 90 MHz) δ: 3.6 (s, 2H, CH_2Ph), 3.7 (t, 1H, $CHHCH$, J = 10 Hz), 3.9 (s, 3H, OCH_3), 4.0–4.4 (m, 1H, CH_2CH), 4.5 (q, 1H, $CHHCH$, J_1 = 3.5, J_2 = 10 Hz), 5.5 (q, 1H, $CHNH$, J_1 = 4.5, J_2 = 7 Hz), 6.8 (bd, 1H, NH, J = 7 Hz), 7.0–7.6 ppm (m, 8H, C_6H_3 and C_6H_5); ir ($CHCl_3$)

ν_{max}: 3300, 1780 (β-lactam), 1730 (ester), 1680 cm^{-1} (amide); ms *m/e*: 366 (M^+), 335 ($M^+ - 31$), 192, 175, 160. *Anal.* calcd. for $C_{20}H_{18}N_2O_5$: C 65.56, H 4.95, N 7.65; found: C 65.59, H 5.45, N 7.09.

Acknowledgements

We would like to thank the National Research Council of Canada and Lederle Laboratories for financial assistance, and Mrs. N. A. Kuck, Lederle Laboratories, for biological testing. One of us (R.Z.) would like to thank the NRCC for a postgraduate scholarship.

1. T. N. DOYLE, B. BELLEAU, B. Y. LUH, C. F. FERRARI, and M. P. CUNNINGHAM. Can. J. Chem. **55**, 468 (1977).
2. A. K. BOSE, S. D. SHARMA, J. C. KAPUR, and M. S. MANHAS. Synthesis, 216 (1973).
3. S. F. W. MCOMIE, M. L. WATTS, and D. E. WEST. Tetrahedron, **24**, 2289 (1968).
4. H. B. KAGAN, J. J. BASSELIER, and J. L. LUCKE. Tetrahedron Lett. 941 (1964).
5. M. S. MANHAS and A. K. BOSE. Synthesis of penicillin, cephalosporin C and analogs. Marcel Decker, New York, NY. 1969. pp. 23–26.

Can. J. Chem. Downloaded from www.nrcresearchpress.com by 210.87.254.40 on 09/05/12
For personal use only.

Synthèse de cétones encombrées via réduction de nitriles tertiaires en présence de métaux alcalins

JEAN-PAUL MAZALEYRAT
Groupe de Recherche No 12, C.N.R.S., 94320-Thiais, France

Reçu le 28 mars 1978

JEAN-PAUL MAZALEYRAT. Can. J. Chem. **56**, 2731 (1978).

L'action d'un métal alcalin sur un nitrile possédant un C_α tertiaire peut conduire, après protonation, à une imine. Par hydrolyse de cette dernière on obtient une cétone possédant des carbones α-tertiaires. Cette réaction implique des radicaux anions intermédiaires et constitue une méthode simple de synthèse de cétones symétriques encombrées.

JEAN-PAUL MAZALEYRAT. Can. J. Chem. **56**, 2731 (1978).

The reaction of alkali metals with tertiary alkyl nitriles eventually gives, after protonation, an imine. α-*tert*-Alkylketones are produced by the hydrolysis of these imines. This reaction, involving radical anion intermediates, is a simple method for the synthesis of highly hindered symmetric ketones.

Can. J. Chem. Downloaded from www.nrcresearchpress.com by 210.87.254.105 on 09/05/12
For personal use only.

Il existe différentes voies de synthèse de cétones encombrées (réf. 1 et références citées), mais ces méthodes ne permettent que très rarement d'obtenir un composé possédant deux carbones tertiaires en α du groupement carbonyle. L'obstacle est soit dû à la méthode de synthèse, qui aboutit nécessairement à la présence d'un hydrogène sur un des deux carbones α, soit d'ordre stérique (1; réf. 2 et références citées).

Nous nous sommes intéressés à une voie de préparation très peu exploitée jusqu'à présent (3), faisant appel à la réduction des nitriles tertiaires par les métaux alcalins.

Il est connu que les métaux alcalins dans l'ammoniac liquide ou le HMPT, provoquent la rupture de la liaison C—CN des nitriles et conduisent à l'hydrocarbure correspondant (4*a*). Les mêmes réductions peuvent être réalisées par voie électrochimique (4*b*). Le mécanisme de ces réactions fait intervenir la formation intermédiaire d'un radical alcoyle R·, formé certainement par décomposition d'un radical anion nitrile $RCN^{\bullet -}$, et qui subit ensuite une réduction en anion R^- (schéma 1).

$$RCN \xrightarrow{e^-} RCN^{\bullet -} \longrightarrow R^\bullet \xrightarrow{e^-} R^- \xrightarrow{H^+} RH$$

SCHÉMA 1

Cependant, le comportement de la combinaison anthracène–lithium dans l'éther éthylique vis à vis des nitriles tertiaires **1** apporte des informations supplémentaires sur le comportement des nitriles en présence de réactifs donneurs d'électrons (5). A cause de la grande affinité électronique de l'anthracène, cette réaction n'aboutit pas à la réduction du nitrile en hydrocarbure RH, mais à la formation d'un alcoyl-9 dihydro-9,10 anthracène **2** résultant de la recombinaison entre un radical alcoyle R· et un radical anion anthracène (schéma 2). Toutefois, on enregistre également dans cette réaction la formation d'une imine **3**, et si ce composé provient, comme on peut le supposer, de la recombinaison entre un radical anion anthracène et un radical anion nitrile, cela suggère qu'un tel radical anion nitrile $RCN^{\bullet -}$ possède une durée de vie suffisante pour donner une réaction autre que sa décomposition en R· et CN^-.

Si cette hypothèse est juste, on doit s'attendre à ce que dans certaines conditions, le radical alcoyle R· puisse se recombiner avec le radical anion nitrile présent dans le milieu pour conduire, après hydrolyse, à une imine symétrique **4** (schéme 3).

Effectivement, il est connu que certains α-aminonitriles tertiaires, pour lesquels le radical anion $RCN^{\bullet -}$ a une durée de vie suffisante pour être observable en RPE (6), donnent une réaction tout à fait similaire (schéma 3, R = $(CH_3)_2\overset{|}{C}—N(CH_3)_2$; $(CH_3)_2\overset{|}{C}—N$ ⟨⟩) et conduisent après hydrolyse à une aminoimine correspondant à **4** (7, 8).

Cependant, dans le cas des nitriles ordinaires, on ne connaissait jusqu'à présent qu'un seul exemple de ce type de réaction: celui du pivalonitrile **1***a* qui, traité par le sodium dans le pentane, conduit à la di-*tert*-butyl cétimine **4***a* avec de très bons rendements (3).

Comme les additions radicalaires sont souvent moins sensibles aux contraintes stériques que les réactions ioniques correspondantes (9), un tel schéma est a priori susceptible de constituer une méthode de synthèse d'imines et de cétones encombrées à partir des nitriles tertiaires, et c'est la raison pour laquelle nous avons examiné si cette réaction pouvait être étendue à d'autres composés que le pivalonitrile.

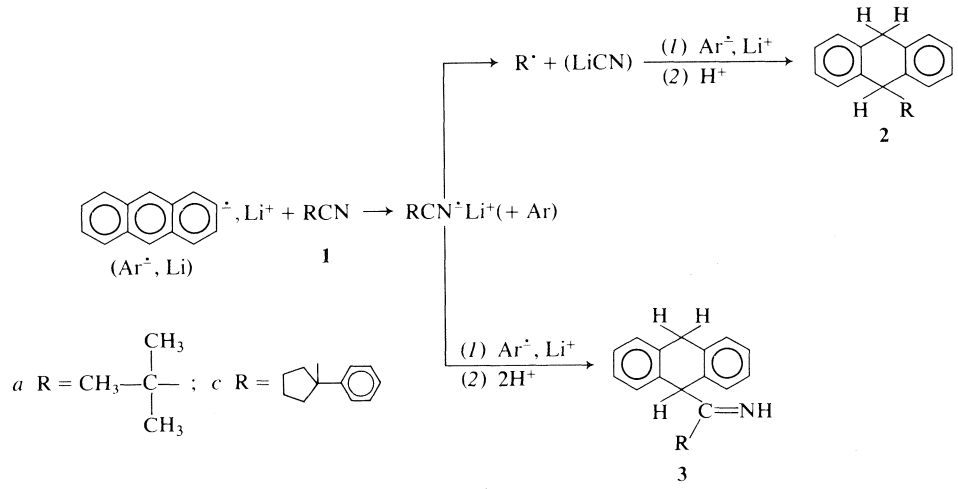

SCHÉMA 2

Résultats et discussion

Considérations générales

Les réactions ont été conduites avec une série de nitriles **1***a–g* (schéma 4), en présence de métaux alcalins, sodium ou lithium, dans différents solvants. Les imines **4** éventuellement formées sont obtenues à l'état pur par simple extraction acido-basique, et converties ensuite en cétones **5** correspondantes, par hydrolyse acide.

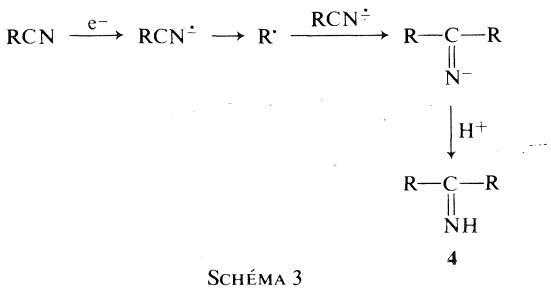

SCHÉMA 3

Le tableau 1 montre que les rendements en imines sont très variables et dépendent beaucoup du nitrile mis en jeu. Le métal alcalin et le solvant ont également une grande influence (voir *b* et *c*). Ils doivent être recherchées dans chaque cas particulier, selon la structure du nitrile, mais il semble cependant que l'utilisation du lithium dans l'éther éthylique constitue un bon choix pour les nitriles **1***c–f* dans lesquels le groupement CN est en position benzylique.

Les variations de rendement enregistrées en fonction des conditions expérimentales sont certainement liées à l'intervention de la réaction de réduction totale du nitrile en hydrocarbure (schéma 1). Nous avons mis en évidence les composés RH provenant de cette réaction compétitive, à chaque fois que nous les avons recherchés dans les parties neutres. La formation d'un hydrocarbure de structure R—R a également été observée lors de la réduction du nitrile **1***c*.

La réduction totale est responsable des mauvais rendements, ou même de l'absence de l'imine **4**, parfois enrégistrés. Avec le nitrile **1***c*, elle est la seule à intervenir lorsque le métal alcalin est le sodium, ou lorsque le solvant est le THF. De même dans le cas du nitrile **1***g*, le diphényl 1,1-éthane est obtenu quantitativement, et l'absence d'imine **4***g* est bien due à l'évolution rapide de la réaction vers la réduction en anions R^-, car l'hydrolyse du mélange réactionnel par D_2O conduit au deutéro-1 diphényl-1,1 éthane (schéma 5). Il est concevable qu'il soit difficile de maîtriser la réduction totale afin de faire évoluer le système dans le sens voulu. Pour que le rendement en imine soit bon, il faut que la réduction de R· en anion R^- soit plus lente que le couplage de ce radical avec un radical anion $RCN^{\cdot-}$, il faut de plus que la rupture de $RCN^{\cdot-}$ soit assez lente. Les vitesses de ces diverses réactions ne sont pas nécessairement influencées de la même façon par la structure de R, le métal alcalin et le solvant, d'où la difficulté de déterminer les conditions expérimentales qui soient

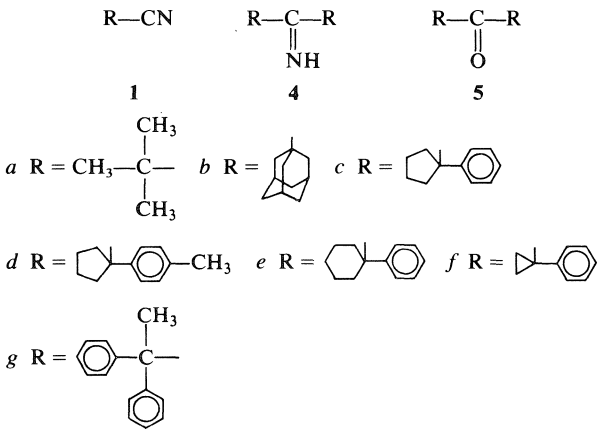

SCHÉMA 4

Can. J. Chem. Downloaded from www.nrcresearchpress.com by 210.87.254.105 on 09/05/12
For personal use only.

TABLEAU 1. Rendements en composé brut **4**

R	Métal et solvant	Rendement en **4** (%)
tert-Butyle (*a*)	Na, pentane	68
1-Adamantyle (*b*)	Na, pentane-éther	0
	Li, éther	15
	Li, THF	65
Phényl-1-cyclopentyle (*c*)	Na, pentane	0
	Na, éther	0
	Na, THF	0
	Li, THF	0
	Li, éther	34
	Li, éther-diphényle	34
p-Tolyl-1 cyclopentyle (*d*)	Li, éther	85
Phényl-1 cyclohexyle (*e*)	Li, éther	28
Phényl-1 cyclopropyle (*f*)	Li, éther	98
α-Méthyl benzhydryle (*g*)	Li, pentane-éther	0
	Li, éther	0

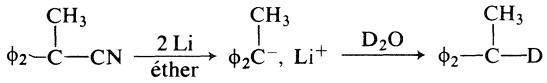

SCHÉMA 5

générales. Il est possible aussi que le couplage radical – radical anion soit toujours la réaction la plus rapide et que l'évolution vers l'anion R^- n'intervienne qu'à cause de la réversibilité de ce couplage, dont nous discutons plus loin.

Enfin, il existe une autre alternative mécanistique que nous n'avons pas considéré jusqu'à présent, selon laquelle l'imine **4** résulterait de l'addition d'un anion R^- sur une molécule de nitrile. Cet anion R^- peut être formé soit directement par réduction d'un radical anion $RCN^{\cdot-}$, accompagnée par le départ de l'ion cyanure (schéma 6*a*), soit par réduction d'un radical R· intermédiaire (schéma 6*b*). Cependant la chute des rendements observée lors de l'addition des organolithiens sur des nitriles encombrés (réf. 10 et références citées) est en defaveur du mécanisme du schéma 6, mais on ne peut l'exclure complétement

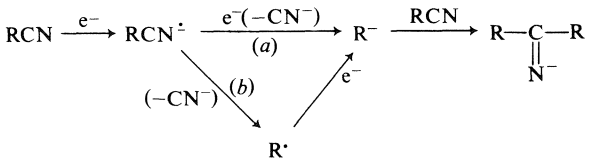

SCHÉMA 6

car l'addition du *tert*-butyl lithium sur le pivalonitrile **1***a* peut bien avoir lieu (11).

La réversibilité de la réaction

Un autre aspect du mécanisme de cette réaction est mis en lumière par l'expérience suivante, au cours de laquelle nous avons réduit le nitrile **3***c* par le lithium dans l'éther éthylique en présence d'un excès de chlorure de *tert*-butyle, avec l'idée que le radical anion du phényl-1 cyclopentane nitrile, en présence de radicaux *tert*-butyle, se recombinerait avec un de ces derniers avant que la rupture de la liaison C—CN intervienne, conduisant à l'anion **A**, ce qui permettrait d'obtenir l'imine mixte **4***h* (schéma 7).

En fait, après hydrolyse, l'imine **4***h* est seulement isolée à l'état de traces, les parties basiques étant constituées essentiellement de l'imine **4***a*. Ce résultat montre que la recombinaison radical – radical anion[1] qui conduit à l'anion **A** est réversible. La réaction inverse peut soit redonner le radical anion **3***c* et le radical *tert*-butyle, soit conduire au radical phényl-cyclopentyle et au radical anion du pivalonitrile **3***a*. Ce radical anion se trouvant en présence de radicaux *tert*-butyle conduit alors à l'anion **B**, avec un degré de réversibilité certainement moindre que dans le cas de **A**, vu l'absence de stabilisation par un noyau phényle des entités $t\text{BuCN}^{\cdot-}$ et $t\text{Bu}^{\cdot}$. La suite d'équilibres étant ainsi déplacée vers **B** explique l'obtention largement prépondérante de l'imine **4***a* après hydrolyse.

Une réversibilité semblable existe également dans l'addition des radicaux anions anthracène sur les nitriles (5), et a été démontrée dans certains cas pour l'addition des organolithiens sur ces mêmes composés (12).

D'un point de vue synthétique, la réversibilité de la formation de l'anion précurseur de l'imine présente à la fois un désavantage et un intérêt. L'inconvénient réside dans la possibilité d'un degré de réversibilité très élevé pour des structures admettant l'existence de radicaux très stables, interdisant alors l'obtention de l'imine à moins de réussir à piéger l'anion correspondant au fur et à mesure de sa formation. Cela pourrait expliquer par exemple l'absence d'imine à l'issue de la réaction dans le cas de la structure **3***g* (schéma 8).

[1]Par souci de clarté, nous ne considérons pas ici l'alternative précédemment envisagée dans le schéma 6, mais la même explication demeure si l'anion **A** est formé par addition de R^- sur le nitrile.

Can. J. Chem. Downloaded from www.nrcresearchpress.com by 210.87.254.105 on 09/05/12
For personal use only.

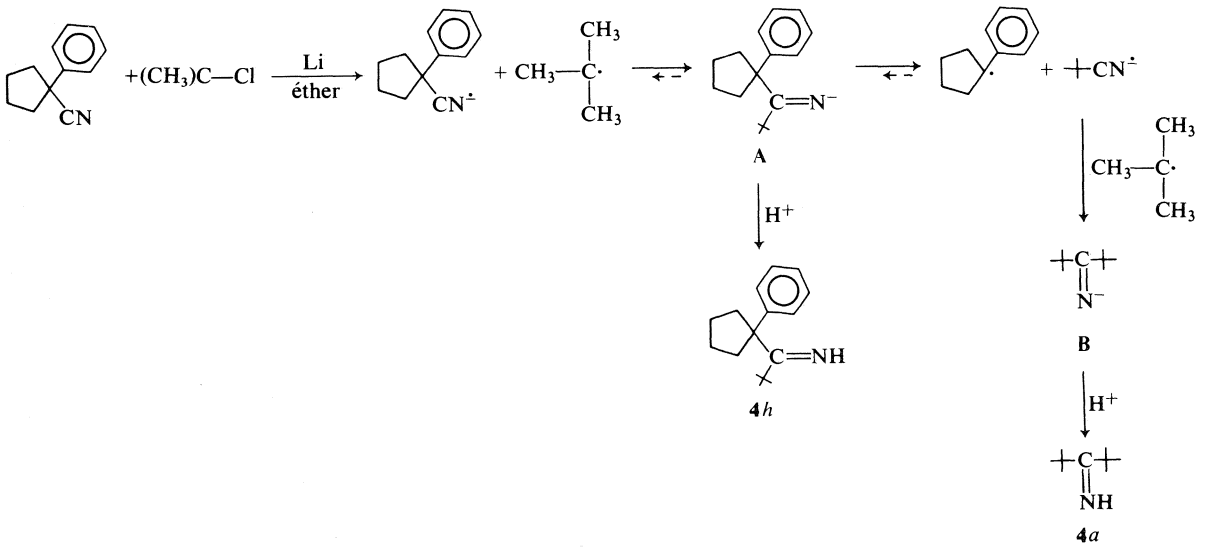

SCHÉMA 7

L'intérêt peut résider en la possibilité d'obtenir une cétone encombrée $(R_1)_2C{=}O$ à partir de l'halogénure correspondant R_1X (lequel peut être plus accessible que le nitrile), en présence d'un nitrile

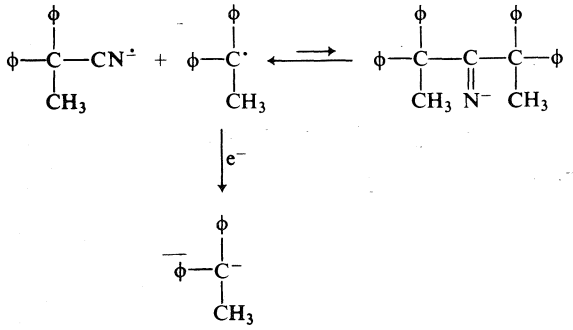

SCHÉMA 8

donnant un grand degré de réversibilité, selon une évolution correspondant au schéma 7.

Conclusion

En définitive, il apparaît que l'action des métaux alcalins sur les nitriles tertiaires n'aboutit pas nécessairement à la réduction totale en hydrocarbure correspondant, mais peut dans des conditions appropriées, constituer une méthode de synthèse d'imines symétriques encombrées, facilement hydrolysables en cétones correspondantes. Ces imines sont obtenues à un haut degré de pureté, par simple extraction acido–basique, ce qui les rend très facilement accessibles, même dans les cas où les rendements sont faibles. En outre, étant donné la grande similitude entre les réductions réalisées par action des réactifs donneurs d'électrons tels que les métaux alcalins ou les combinaisons métaux alcalins – hydrocarbures aromatiques, et les réductions cathodiques (4*b*, 13), on peut supposer que des synthèses similaires pourront être réalisées par voie électrochimique.

Partie expérimentale

Les points de fusion ont été déterminés en tubes capillaires, sur un appareil Tottoli. Les spectres infrarouge ont été enregistrés sur un spectromètre EPI 62 Hitachi. Les spectres de rmn ont été enregistrés sur un spectromètre Varian T 60 pour le proton et sur un spectromètre Varian CFT 20 pour le carbone-13, le tétraméthylsilane étant pris comme référence interne. Les analyses élémentaires et les spectres de masses ont été effectués par le Centre de Microanalyse de Thiais.

Les nitriles **1***a–g* sont commerciaux. Les réactions sont effectuées à température ambiante, sous atmosphère d'azote, par action directe d'un excès de métal alcalin dans un solvant donné. Après hydrolyse, la phase organique est décantée, lavée à l'eau puis traitée par un excès d'acide chlorhydrique "pur" (environ 11 *M*). La phase acide est lavée à l'éther et les phases organiques réunies lavées à l'eau et séchées fournissent les parties neutres du mélange réactionnel brut. La phase acide est neutralisée par la soude ou la potasse diluée, jusqu'à pH fortement basique. L'extraction à l'éther fournit les parties basiques du mélange réactionnel. Dans ces conditions d'extraction, les imines **4** ne subissent pratiquement pas d'hydrolyse acide, la présence des cétones correspondantes n'étant pas détectée dans les parties neutres.

Di-tert-*butyl cétimine* **4**a

Par action de 4 g (0.048 mol) de pivalonitrile **1***a* sur 1.5 g (0.065 at-g) de sodium dans 30 cm^3 de pentane, pendant 48 h, on obtient 2.39 g (68%) de parties basiques correspondant au composé **4***a* déjà connu (3); ir: 3400 cm^{-1}, ^1H rmn ($CDCl_3$) : 1.24 ppm (s).

Di-tert-*butyl cétone* **5**a *(2, 3)*

On obtient le composé **5***a* quantitativement par chauffage au reflux de **4***a* dans un mélange benzène–HCl 20%; ir: 1680 cm^{-1}.

Can. J. Chem. Downloaded from www.nrcresearchpress.com by 210.87.254.105 on 09/05/12
For personal use only.

Can. J. Chem. Downloaded from www.nrcresearchpress.com by 210.87.254.105 on 09/05/12
For personal use only.

Di-(adamantyl-1) cétimine **4**b

Par action de 4.5 g (0.028 mol) de cyano-1 adamantane **1***b* sur 2 g (0.09 at-g) de sodium dans un mélange pentane–éther 1 : 2 pendant 48 h, on obtient 1.2 g de parties basiques dont le spectre de rmn ($CDCl_3$): 2H à 2.33 (s), 2H à 2.00 (m) 15H à 1.70 (m) et 1.47 ppm (m), et le spectre ir (3300–3400 cm^{-1}) sont en accord avec une structure $R—CH_2NH_2$ provenant sans doute de la réduction du nitrile **1***b* par le sodium dans l'éthanol ajouté en fin de réaction.

Par action de 8 g (0.05 mol) de **1***b* sur 1 g (0.15 at. g) de lithium dans 100 cm^3 d'éther éthylique pendant 7 h, on obtient 1.16 g (15%) de parties basiques constituées de l'imine **4***b*. Les parties neutres sont constituées essentiellement du nitrile de départ **1***b* inchangé, l'hydrolyse ayant été effectuée après prélèvement de la solution à la seringue, en l'absence de l'excès de lithium.

Par action de 4 g (0.025 mol) de **1***b* sur 0.5 g (0.075 at-g) de lithium dans 75 cm^3 de THF, pendant 24 h, on obtient 2.4 g (65%) de parties basiques constituées de **4***b*. Le spectre ir des parties neutres montre l'absence de bande CN à 2220 cm^{-1} correspondant au nitrile **1***b*. **4***b*: pf (acétone) 126–127°C; ^1H rmn ($CDCl_3$): 1H à 8 (m), 30H à 1.74 et 2.02 ppm (m); ir: 3300, 1595 cm^{-1}; ^{13}C rmn ($CDCl_3$): 194.08 (s), 44.97 (s), 44.19 (t), 36.81 (t), 28.94 (d); sm (70 eV): pic moléculaire à *m/e* 297. *Anal.* calc. pour $C_{21}H_{31}N$: C 84.78, H 10.50, N 4.71; trouvé: C 84.43, H 10.51, N 4.28.

Diadamantyl-1 cétone **5**b

Obtenue quantitativement par chauffage au reflux de **4***b* pendant 48 h dans 30 cm^3 de benzène et 50 cm^3 de HCl 40%; pf (acétone) 175–178°C; ^1H rmn ($CDCl_3$): 2.00 et 1.74 ppm (m); ^{13}C rmn ($CDCl_3$): 216.93 (s); 49.32 (s); 39.42 (t); 36.80 (t); 28.54 (d); ir: 1660 cm^{-1}; sm (70 eV): pic moléculaire à *m/e* 298. *Anal.* calc. pour $C_{21}H_{30}O$: C 84.51, H 10.13, O 5.36; trouvé: C 84.21, H 10.10, O 5.79.

Di(phényl-1 cyclopentyl) cétimine **4**c

Par action du phényl-1 cyclopentane **1***c* sur un excès de sodium dans le pentane, l'éther ou le THF, ou de lithium dans le THF, le milieu prend une forte coloration rouge brun caractéristique de l'anion phénylcyclopentyle, et après hydrolyse, on n'obtient aucune partie basique. Le nitrile **1***c* est absent des parties neutres qui sont constituées principalement de phénylcyclopentane.

Par action de 1.7 g (0.01 mol) de nitrile **1***c* sur 0.21 g (0.03 at-g) de lithium dans 100 cm^3 d'éther pendant 3 h, on obtient 0.53 g (34%) de parties basiques constituées de l'imine **4***c*. Les parties neutres (0.51 g) sont constituées d'un mélange de cristaux et de liquide.

Cristaux: pf (pentane) 134–136°C; ^1H rmn ($CDCl_3$): 10H à 7.08 (m), 16H entre 0.8 et 2.5 ppm (m); ^{13}C rmn ($CDCl_3$): 148.09 (s), 132.43 (d), 130.75 (d), 129.28 (d), 61.87 (s), 37.69 (t), 26.35 (t); sm (70 eV): pic moléculaire à *m/e* 290. *Anal.* calc. pour $C_{22}H_{26}$: C 90.98, H 9.02; trouvé: C 90.94, H 9.07. L'ensemble de ces caractéristiques est en accord avec la structure du (diphényl-1,1′)-bicyclopentyle.

Liquide: En cpg, par comparaison avec des échantillons témoins, on observe que le liquide est constitué principalement de phénylcyclopentane, accompagné de (diphényl-1,1′) bicyclopentyle ainsi que de nitrile de départ **1***c* en faible proportion. Les rendements respectifs de ces différents composés n'ont pas été déterminés.

Dans une autre réaction menée parallèlement dans les mêmes conditions, en présence de 0.7 g (0.005 mol) de diphényle, on obtient 0.54 g (34%) de parties basiques constituées de l'imine **4***c*: pf (pentane) 86–88°C; ^1H rmn ($CDCl_3$): 1H à 9.63 (m), 10H à 7.17 (m), 16H à 1.95 et 1.40 ppm (m); sm (70 eV): pic moléculaire à *m/e* 317. *Anal.* calc. pour $C_{23}H_{27}N$: C 87.01, H 8.57, N 4.41; trouvé: C 86.99, H 8.76, N 4.31.

Di(phényl-1 cyclopentyl) cétone **5**c

Obtenue quantitativement par chauffage au reflux de **4***c* pendant 4 jours, dans 50 cm^3 de benzène et 25 cm^3 de HCl 20%; pf (EtOH) 94–97°C; ^{13}C rmn ($CDCl_3$): 211.91 (s), 142.31 (s), 128.11 (d), 127.07 (d), 126.33 (d), 66.03 (s), 36.55 (t), 22.71 (t); sm (70 eV): pic moléculaire à *m/e* 318. *Anal.* calc. pour $C_{23}H_{26}O$: C 86.74, H 8.23, O 5.02; trouvé: C 86.71, H 8.29, O 5.04.

*Di(*p*-tolyl-1 cyclopentyl) cétimine* **4**d

Par action de 18.5 g (0.1 mol) de *p*-tolyl-1 cyclopentane nitrile **1***d* sur 2.1 g (0.3 at-g) de lithium dans 250 cm^3 d'éther, pendant 4 h, 30 min, on obtient 14.63 g (85%) de parties basiques constituées de l'imine **4***d*; pf (EtOH) 126–128°C; ^1H rmn ($CDCl_3$): 1H à 8.64 (m), 8H à 7.09 (m), 6H à 2.30 (s), 16H à 1.97 et 1.41 ppm (m); ^{13}C rmn ($CDCl_3$): 189.19 (s), 141.04 (s), 135.42 (s), 128.66 (d), 126.79 (d), 61.76 (s), 37.22 (t), 22.22 (t), 20.90 (q); ir: 3400, 1595 cm^{-1}; sm (70 eV): pic moléculaire à *m/e* 345. *Anal.* calc. pour $C_{25}H_{31}N$: C 86.90, H 9.04, N 4.05; trouvé: C 86.51, H 9.02, N 3.85.

*Di(*p*-tolyl-1 cyclopentyl) cétone* **5**d

Obtenue quantitativement par chauffage au reflux de **4***c* pendant 2 jours dans 50 cm^3 de benzène et 100 cm^3 de HCl 50%; pf (acétone) 133–135°C; ^1H rmn ($CDCl_3$): 8H à 7.10 (m), 6H à 2.32 (s), 16H à 2.06 et 1.33 ppm (m); ^{13}C rmn ($CDCl_3$): 212.09 (s), 139.23 (s), 135.74 (s), 128.72 (d), 126.89 (d), 65.55 (s), 36.44 (t), 22.65 (t), 20.88 (q); ir: 1670 cm^{-1}; sm (70 eV): pic moléculaire à *m/e* 346. *Anal.* calc. pour $C_{25}H_{30}O$: C 86.65, H 8.73, O 4.62; trouvé: C 86.45, H 8.72, O 4.35.

Di(phényl-1 cyclohexyl)cétone **5**e

Par action de 18.5 g (0.1 mol) de phényl-1 cyclohexane nitrile **1***e* sur 2.1 (0.3 at-g) de lithium dans 250 cm^3 d'éther pendant 24 h on obtient 4.83 g (28%) de parties basiques constituées de di(phényl-1 cyclohexyl) cétimine **4***e*. Les parties neutres sont constituées pour environ 80% (d'après les surfaces de pics en cpg) de nitrile de départ **1***e* et pour environ 20% de phénylcyclohexane résultant de la réduction totale. (L'hydrolyse a été effectuée ici en absence de l'excès de lithium.) Le composé **4***e* (pf (EtOH) 103–105°C) présente des données spectrales correctes: en ^1H rmn: 1H à 9.00 (m), 10H à 7.25 (m), 20H à 2.00 et 1.25 ppm (m); ir: 3350 et 1590 cm^{-1}; sm (70 eV): pic moléculaire à 345. Cependant son analyse centésimale (85.88 pour C calculé 86.90) indique la présence d'une impureté qui reste présente après plusieurs cristallisations. Ce composé par chauffage à reflux en présence de 20 cm^3 de benzène et 50 cm^3 de HCl 40% pendant 3 jours conduit à la cétone **5***e*; pf (acétone) 150–152°C; ^1H rmn ($CDCl_3$): 10H à 7.18 (m), 20H à 1.95 et 1.22 ppm (m); ^{13}C rmn ($CDCl_3$): 211.92 (s), 141.71 (s), 128.24 (d), 127.95 (d), 126.22 (d), 58.03 (s), 35.52 (t), 25.88 (t), 22.64 (t); ir: 1675 cm^{-1}; sm (70 eV): pic moléculaire à *m/e* 346. *Anal.* calc. pour $C_{25}H_{30}O$: C 86.65, H 8.73, O 4.62; trouvé: C 86.79, H 8.45, O 4.74.

Di(phényl-1 cyclopropyl) cétimine **4**f

Par action de 15.3 g (0.107 mol) de phényl-1 cyclopropane nitrile **1***f* sur 2.1 (0.3 at-g) de lithium dans 250 cm^3 d'éther, pendant 5 h, on obtient 13.78 g (98%) de parties basiques constituées de **4***f*. Le composé **4***f* est un liquide qui se décompose[2] en cours de distillation (pé 128–132°C/0.05 Torr). Les constantes physiques indiquées ci-dessous pour **4***f* sont celles des parties basiques brutes, sans aucun traitement; ^1H rmn

[2]Le spectre de rmn indique qu'il se produit une ouverture du (des) cyclopropane.

Can. J. Chem. Downloaded from www.nrcresearchpress.com by 210.87.254.105 on 09/05/12
For personal use only.

($CDCl_3$): 1H à 8.75 (m), 10H à 7.08 (m), 8H à 1.08 ppm (m); ^{13}C rmn ($CDCl_3$): 185.59 (s), 141.31 (s), 129.21 (d), 127.98 (d), 126.52 (d), 33.88 (s), 15.30 (t); ir: 1595 et 1610 cm^{-1}; sm (70 eV): pic moléculaire à *m/e* 261. *Anal.* calc. pour $C_{19}H_{19}N$: C 87.31, H 7.33, N 5.36; trouvé: C 87.04, H 7.47, N 5.32.

Di(phényl-1 cyclopropyl) cétone **5**f

Par chauffage au reflux de **4***f* en présence de 20 cm^3 de benzène et 50 cm^3 de HCl 40% pendant 15 h, on obtient la cétone **5***f* accompagnée d'une forte proportion de produits de décomposition.[2] Afin d'effectuer l'hydrolyse dans des conditions plus douces, le chlorhydrate de l'imine **4***f* est préparé en additionnant à **4***f* (parties basiques brutes) en solution dans de l'éther anhydre, un très léger excès de HCl "pur" 11 *M*. On obtient un précipité. Après addition de 50 cm^3 d'éthanol absolu, et élimination des solvants à l'évaporateur rotatif (bain-marie à 70°C environ), on obtient une poudre jaune-marron qui est abondamment lavée à l'acétone, sur Büchner. On obtient une poudre blanche (chlorhydrate d'imine; **4***f*·HCl); pf 122–123°C; ^1H rmn ($CDCl_3$): 2H à 12.50 (m), 10H à 7.10 (m), 8H à 1.73 ppm (m); ^{13}C rmn ($CDCl_3$): 199.53 (s), 137.52 (s), 129.83 (d), 128.39 (d), 127.80 (d), 33.66 (s), 19.96 (t); sm (70 eV): pic *M* − HCl à *m/e* 261. *Anal.* calc. pour $C_{19}H_{20}NCl$: C 76.62, H 6.77, N 4.70, Cl 11.91; trouvé: C 76.55, H 6.90, N 4.48, Cl 12.43.

Par agitation à température ambiante, des cristaux **4***f*·*HCl* dans un mélange d'eau distillée et de benzène, pendant une semaine, on obtient la cétone **5***f* exempte de produits de décomposition; pf (pentane) 63–65°C; ^1H rmn ($CDCl_3$): 10H à 7.04 (m) et 6.75 (m), 8H à 1.23 ppm (m); ^{13}C rmn ($CDCl_3$): 208.31 (s), 139.83 (s), 129.44 (d), 127.81 (d), 126.09 (d), 36.74 (s); 17.20 (t); sm: pic moléculaire à *m/e* 262. *Anal.* calc. pour $C_{19}H_{18}O$: C 86.98, H 6.92, O 6.10; trouvé: C 87.22, H 7.01, O 5.98.

Cas du nitrile **1**g

Par action de 20.7 g (0.1 mol) de 2,2-diphénylpropionitrile **1***g* sur 2.1 g (0.3 at-g) de lithium dans 300 cm^3 d'éther, pendant 4h, on obtient une coloration rouge brun intense. L'hydrolyse effectuée en l'absence de l'excès de lithium, ne fournit aucune partie basique. Les parties neutres (16.45 g) sont constituées uniquement de 1,1-diphényléthane; ^1H rmn ($CDCl_3$): 10H à 7.16, 1H à 4.10 (q, J = 7 Hz), 3H à 1.56 ppm (d, J = 7 Hz). Dans une expérience identique, mais en effectuant l'hydrolyse par D_2O, le spectre rmn ($CDCl_3$) des parties neutres montre la disparition totale du quadruplet à 4.10 ppm et la transformation du doublet à 1.56 ppm en singulet élargi.

Une expérience similaire effectuée en présence de lithium dans un mélange pentane–éther 4:1 pendant 30 h, ne fournit aucune partie basique. Les parties neutres sont constituées de diphényl-1,1 éthane et de nitrile de départ **1***g*.

Réaction en présence de chlorure de tert-*butyle*

Par action d'un mélange de 1.73 g (0.01 mol) de phényl-1 cyclopentane nitrile **1***e* et de 9.34 g (0.1 mol) de chlorure de *tert*-butyle, sur 0.7 g (0.1 at-g) de lithium dans 100 cm^3 d'éther, pendant 20 h, on obtient 1.22 g de parties basiques, dont le spectre de rmn ($CDCl_3$) indique qu'elles sont constituées en très grande majorité de l'imine **4***a*. (Présence d'un signal du groupement *tert*-butyle très largement prépondérant à 1.24 ppm). Le composé **4***a* est isolé par distillation des parties basiques (pé 45–46°C/10 Torr). Par chromatographie sur plaques du résidu de distillation (support: Kieselgel 60 F 254 Merck; éluant pentane 80% – acétate d'éthyle 20%) on isole en quantités très faibles l'imine **4***c*, ainsi qu'un composé dont le spectre de rmn ($CDCl_3$) est compatible avec la structure de l'imine mixte **4***h*: 1H à 8.57 (m), 5H à 7.26 (m), 9H entre 1.1 et 2.2 (m), 9H à 0.96 ppm (s). D'autres composés non identifiés sont présents à l'état de traces dans les autres fractions chromatographiques. Dans les parties neutres, on isole des cristaux correspondant au (diphényl-1,1′)-bicyclopentyl déjà caractérisé précédemment.

1. J. E. Dubois, F. Hennequin et M. Boussu. Bull. Soc. Chim. Fr. 3615 (1969).
2. J. J. Katz, J. E. Dubois et C. Lion. Bull. Soc. Chim. Fr. 683 (1977).
3. V. L. Hansley. U.S. Patent No. 2,742,503 citée dans Chem. Abstr. **50**, 16830i (1956).
4. (*a*) T. Cuvigny, M. Larcheveque et H. Normant. Bull. Soc. Chim. Fr. 1174 (1973); P. G. Arapakos. J. Am. Chem. Soc. **89**, 6794 (1967); L. H. Baldinger et J. A. Newland. J. Am. Chem. Soc. **55**, 2851 (1933); L. I. Smith and L. J. Spillane. J. Am. Chem. Soc. **65**, 206 (1943); (*b*) P. G. Arapakos et M. K. Scott. Tetrahedron Lett. 1975 (1968).
5. J. P. Mazaleyrat. Can. J. Chem. **53**, 3158 (1975).
6. C. Fabre, M. Hadj Ali Salem, Z. Welvart, P. Ackermann, J. P. Germain et H. Robert. Bull. Soc. Chim. Fr. 3814 (1972).
7. C. Fabre et Z. Welvart. Tetrahedron Lett. 3801 (1967).
8. O. Eisenstein, J. P. Mazaleyrat, M. Tordeux et Z. Welvart. J. Am. Chem. Soc. **99**, 2230 (1977).
9. N. Kornblum. Angew. Chem. Int. Ed. Engl. **14**, 734 (1975).
10. B. J. Wakefield. *Dans* The chemistry of organolithium compounds. Pergamon Press. 1974. pp. 116–121.
11. B. Samuel, R. Snaith, C. Summerford et K. Wade. J. Chem. Soc. A, 2019 (1970); J. E. Dubois, B. Leheup, F. Hennequin et P. Bauer. Bull. Soc. Chim. Fr. 1150 (1967); W. C. Percival, R. B. Wagner et N. C. Cook. J. Am. Chem. Soc. **75**, 3731 (1953).
12. D. J. Berry et B. J. Wakefield. J. Organometal. Chem. **23**, 1 (1970).
13. J. Simonet, M. A. Michel et H. Lund. Acta Chem. Scand. B, **29**, 489 (1975).

The line-shape analysis of nuclear magnetic resonance peaks broadened by the presence of a 'hidden' exchange partner

NANCY OKAZAWA AND TED S. SORENSEN

Department of Chemistry, University of Calgary, Calgary, Alta., Canada T2N 1N4

Received April 6, 1978

NANCY OKAZAWA and TED S. SORENSEN. Can. J. Chem. **56**, 2737 (1978).

In nmr spectroscopy involving organic substrates, one often has a situation in which there is a dominant species in rapid equilibrium with one or more minor components. In general, one knows, a priori, neither the population of these minor components nor the rate constants involved in the equilibrium process. In fact, from the physical appearance of these spectra, one cannot normally even deduce that such an equilibrium exists. For example, in cases involving ^{13}C nmr spectroscopy, this minor component may not be observable under slow exchange nmr conditions because of signal-to-noise ratio problems and hence is referred to as a 'hidden' exchange partner. In this paper, we have analyzed the extent of nmr line broadening to be expected from a two-component system of this type, varying the populations, chemical shift separations, and intrinsic line widths. Thus, the presence of a 'hidden' partner can sometimes be detected by a characteristic, but often very subtle, peak broadening–resharpening sequence involving first of all the 'averaged' peak and finally the peak of the dominant component, these peaks being virtually identical in area and very similar in chemical shift so that one is not easily alerted. Assuming there is some experimental line broadening, equations developed in this paper, together with chemical shift estimates for this 'hidden' partner, allow one to quickly estimate both the amount of the minor partner and the rate constant involved. Three 'real life' situations are subsequently analyzed.

NANCY OKAZAWA et TED S. SORENSEN. Can. J. Chem. **56**, 2737 (1978).

En spectroscopie rmn impliquant des substrats organiques, on se trouve souvent en face de la situation où une espèce dominante est en équilibre avec un ou plusieurs composants minoritaires. D'une manière générale, on ne connaît à priori ni la population de ces composants minoritaires ni les constantes de vitesse impliquées dans le processus d'équilibre. De fait, en se basant sur l'apparence physique de ces spectres, on ne peut normalement pas déduire qu'un tel équilibre existe. Par exemple dans les cas impliquant la spectroscopie rmn du ^{13}C, il est possible, à cause de problèmes du rapport signal-à-bruit, que ce composé minoritaire ne puisse pas être observable dans des conditions de rmn impliquant des échanges lents; on réfère souvent à ces composés comme des partenaires d'échanges "masqués." Dans cette publication, nous avons analysé jusqu'à quel point on peut s'attendre à un élargissement des raies de rmn dans des systèmes à deux composants de ce type; à cette fin, nous avons fait varier les populations, les séparations des déplacements chimiques et les largeurs intrinsèques des raies. Ainsi la présence d'un partenaire "masqué" peut quelquefois être mise en évidence par une séquence caractéristique mais subtile d'un élargissement et d'affinement des raies impliquant en premier lieu la raie "pondérée" et finalement la raie du composant principal: ces raies pouvant être virtuellement identiques en superficie et très semblables en déplacements chimiques et il est quelquefois difficile de les remarquer. Faisant l'hypothèse qu'il se produit un certain élargissement des bandes expérimentales, il est possible, grâce aux équations développées dans cette publication prises de concert avec les évaluations des déplacements chimiques pour le partenaire "masqué," d'évaluer rapidement la quantité du partenaire minoritaire ainsi que la constante de vitesse impliquée. On a subséquemment analysé trois situations réelles.

[Traduit par le journal]

Introduction

The use of dynamic nmr spectroscopy for studying the kinetics of chemical reactions is a well-known and well-reviewed process (1). Briefly, these can be broken down into two distinct types: (*i*) degenerate processes, e.g., $A \rightleftarrows A'$, naturally involving equal populations, and (*ii*) reactions $A \rightleftarrows B$, where the equilibrium constant (K) is not generally 1.

For either situation, total line-shape analysis and matching ultimately provides the most reliable method for determining the rate constant corresponding to a particular line-shape and is almost mandatory for Arrhenius $\Delta H^{\ddagger}$ evaluation. However, for various practical reasons, there are many instances when one wants a simple procedure from which one can obtain a reasonably accurate *single* rate measurement, usually then converted to a free energy of activation barrier $\Delta G^{\ddagger}$. Of the various simplified procedures for the $A \rightleftarrows A'$ case, the most widely used is the restricted Gutowsky–Holm coa-

Can. J. Chem. Downloaded from www.nrcresearchpress.com by 210.87.254.42 on 09/05/12
For personal use only.

Can. J. Chem. Downloaded from www.nrcresearchpress.com by 210.87.254.42 on 09/05/12
For personal use only.

lescence line-shape relationship (2), where $\delta\nu$ is the chemical shift separation of the two sites under slow exchange or 'frozen-out' conditions and k is the

$$k = \pi\delta\nu/\sqrt{2} \quad [1]$$

rate constant. This coalescence behavior has been extended to nonequal populations using a graphical procedure (ref. 3*a*; for examples of various other expressions see ref. 3*b*) but, in general, A $\rightleftarrows$ B ($K \neq 1$) processes are treated by total line-shape analysis.

Particularly with the recent advent of routine ^{13}C nmr spectroscopy, a somewhat different situation can arise. A typical scenario would be the following: In a compound where the *possibility* exists for an equilibrium process with another (minor) isomer, conformer, etc., one obtains a ^{13}C nmr spectrum at some particular temperature at which the equilibrium rate constants are expected to be very large (complete averaging). This spectrum looks quite 'normal' in terms of both the expected chemical shifts and the line width of the signals. Suppose one now cools down the sample so that the equilibrium rate constants (if they exist) might be expected to be in the nmr intermediate exchange region. The basic question we wish to pose is the following: What concentration of this minor equilibrium partner is then needed in order to see an observable line-broadening effect? Or the corollary of this: What is the maximum possible concentration of this minor equilibrium partner if one *does not observe* any line-shape changes?

Our analysis is further based on the premise that one may not always be able to see the 'frozen-out' minor partner nmr spectrum. This is particularly true in ^{13}C nmr spectroscopy where signal-to-noise ratio problems can occur. An unfavorable Boltzmann factor further hinders one in this regard. However, one has no comparable problems with measuring ^{13}C nmr line widths and it is possible to detect (and thus verify) the presence of exchange phenomena by simply focusing on the changes which occur to the observable 'major peak' as one varies the exchange rate (usually by varying the temperature). We use quotation marks because the line-shape changes involve going from the averaged peak to a situation where we see only the major species. However, the minor component may be so small in concentration that this change will cause no detectable area change in the peak one sees and any small chemical shift changes which may occur can be easily overlooked. In this paper, we have examined this problem with a view to determining what range of values of K, $\delta\nu$, intrinsic peak half-width, and rate constants result in observable effects and have developed several simple *empirical* equations which apply to these situations. Subsequently we show how these equations can be used to treat particular problems. One involves a cyclooctane conformation analysis study by Anet (4), in which this situation arises, another involves a carbocation equilibrium.

Results

In any phenomenon involving line-shape changes, it is advantageous to have some well-defined, *experimentally determinable*, parameter which can then be compared to some theoretical results, this theoretical result having been determined for changes in K, $\delta\nu$ etc. We believe that minimum intensity (MI) or maximum line width (MLW) are the two most readily obtained parameters. Because of the complexity of the GH expression, an analytical solution for such quantities as the half-width at half-height of the maximally broadened single peak was not attempted. Instead, an empirical approach was used in the solution. Three Fortran IV computer programs were devised, their difference being the particular line-shape characteristic chosen: (*i*) a minimum intensity with the further stipulation that only one peak maximum is allowed (MI,1); (*ii*) a minimum intensity with the further stipulation of only two inflection points (MI,2); (*iii*) a maximum line width at half-height with the stipulation of only one peak maximum (MLW).

Since most ^{13}C nmr applications involve single (uncoupled) peaks and two site exchange, we have restricted our analysis to these cases. The standard exchange equation of Gutowsky and Holm (GH) was used (2,5). This general solution involves some standard assumptions, e.g., $T_{2A} = T_{2B}$, slow passage, negligible lifetimes during site exchange. The variables in each case were the 'frozen-out' frequency separation of A and B ($\delta\nu$, in Hz), the natural line width in the absence of exchange (W^0), the fractional population of B (p_B) and the rate constant (k_A). In practise, one begins with large rate constants and gradually reduces these until the particular result is obtained. The computer program automatically reduces the Δk_A increments in the critical region.

Interdependence of k_A, $\delta\nu$, *and* p_B

$$k_A$$

For the process A $\rightleftharpoons$ B, we have arbitrarily chosen to use the forward rate constant k_A. Fractional populations are expressed in terms of p_B, where $p_A > p_B$, and were varied from $p_B = 0.001$ to 0.5. Frequency separations varying from 10–10 000 Hz were used for $\delta\nu$.

A value for $p_B = 0.5$ corresponds, of course, to equal populations of A and B and was used so that

Can. J. Chem. Downloaded from www.nrcresearchpress.com by 210.87.254.42 on 09/05/12
For personal use only.

we could tie our results in with the GH coalescence eq. [1]. As well, by choosing some relatively large p_B values, one can better show the range of p_B values over which our results are useful.

Plots of k_A (i.e., that k_A characterizing the specific line-shape solutions) vs. $\delta\nu$ give straight lines intersecting at the origin (or with very slight deviations). The only exception to this behavior was found in the MLW results between $p_B = 0.35 - 0.40$. The cause of this discrepancy will be commented on later. This leads to the empirical relationship:

$$[2] \qquad k_A \text{ (characteristic)} = c''_{(p_B)}\,\delta\nu$$

where c'' is a proportionality constant for fixed values of p_B. The form of this equation is identical to the GH coalescence expression (eq. 1). For $p_B = 0.5$, we find $c''_{(p_B)} = 2.19$. This differs by only 1.4% from the GH constant of $\pi/\sqrt{2}$ (2.22) and the source of this small difference relates to the GH definition of coalescence, i.e., where $\nu_A = \nu_B$, which characterizes a single peak which is not quite at maximum half-width or minimum intensity.

One can replace $c''_{(p_B)}$ by incorporating p_B into the expression:

$$[3] \qquad k_A \text{ (characteristic)} = c'_{(p_B)} p_B \delta\nu$$

where $c'_{(p_B)}$ is a new proportionality constant dependent on p_B (the zero-order Taylor expansion term is zero since $c'' \to 0$ as $p_B \to 0$).

We have plotted the proportionality constant $c'_{(p_B)}$ against p_B and these results are shown in Fig. 1 for the three line-shape criteria. The dashed region in the MLW curve corresponds to the region where the k_A vs. $\delta\nu$ plot, although linear, does not intersect at the origin. For values of $p_B \leq 0.2$, the Fig. 1 relationship is nearly linear, although the slope varies slightly depending upon whether the MLW or MI criteria are used. Making appropriate substitution in eq. [3] gives:

$$[4] \qquad k_A \text{ (characteristic)} = c_0' p_B \delta\nu - c p_B^2 \delta\nu$$

where $c = 3.90$ and $c_0' = 6.32$, for the MLW case, where k_A is expressed in s^{-1}. For the MI case, $c = 5.94$ and $c_0' = 6.19$. The MLW criterion will be used in the actual examples described at the end of this paper. For values of $p_B \leq 0.02$, one can neglect the second term, therefore k_A (characteristic) = 6.32 $p_B\delta\nu$, rather close to $k_A = 2\pi p_B\delta\nu$. A drawback to an empirical approach is that the origin of proportionality constants is lost.

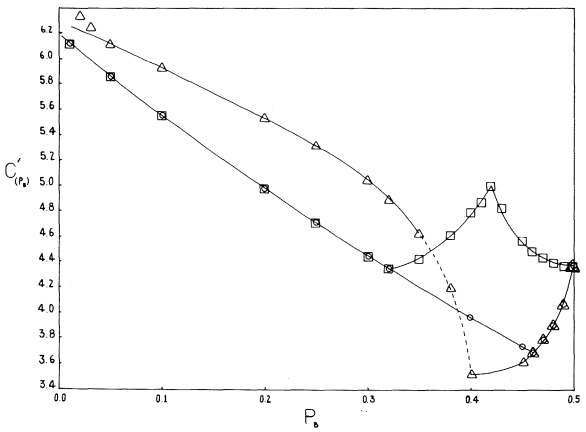

FIG. 1. The behavior of the proportionality constant $c'_{(p_B)}$ as a function of the population of the minor isomer p_B. The proportionality constant $c'_{(p_B)}$ is derived from the linear plot of k_A and $\delta\nu$. The - - - line region is discussed in the text.

The Nonlinear Deviations in Figure 1

Although we are primarily concerned with p_B values of ≤ 0.2, we will briefly discuss the region from $p_B = 0.2$–0.5. In the MI,1 case, the slope change deviations in Fig. 1 result from an abrupt change in the two criteria characteristic of this case. As one lowers k_A from high (complete coalescence) values, the intensity will decrease and then at some further point, start to increase. However, one may also have the situation where the (major) peak intensity is still decreasing but a second maximum occurs and this criterion then determines the k_A value. From $p_B = 0.46$ to 0.5, this second criterion is met first, whereas for $p_B < 0.46$, the first criterion applies. In the MLW case, similar situations arise. An additional complication occurs when the 'single peak' shoulder from the B isomer moves from just above half-height to just below half-height of the curve as a whole. In this region, the k_A vs. $\delta\nu$ plot, although linear, does not intersect at the origin. In the MI,2 case, between $p_B = 0.32$ and 0.5, the 'no more than two inflection points' criteria is met before the minimum intensity one, whereas for $p_B < 0.32$, the results are identical to the MI,1 results. In general, the MI,2 results should mimic closest the true coalescence ($\nu_A = \nu_B$) behavior for the system.

In our further analysis, we will restrict our treatment to cases where $p_B \leq 0.2$ and in most experimental situations, in fact, p_B will be less than 0.1. The observable curve characterizing such p_B values should show the following experimental behavior as one lowers the rate (reduces the temperature): (*i*) the intensity will decrease or the peak half-width will increase; (*ii*) a minimum intensity or a maximum peak half-width will be reached; (*iii*) the peak intensity will then increase or the peak half-width decrease. Observation number three is very *important* in practical situations since observations *i* and *ii* could be due to viscosity broadening or a gradual field

Can. J. Chem. Downloaded from www.nrcresearchpress.com by 210.87.254.42 on 09/05/12
For personal use only.

homogeneity deterioration. In addition to the above observations, the averaged peak position will change because of the Boltzmann distribution factor (discussed subsequently).

Interdependence of the Maximum Line Width (W_{max}), $\delta\nu$, *and the Intrinsic Line Widths* (W^0)

From eq. 4, one could calculate a single k_A (at a particular temperature and hence $\Delta G^{\ddagger}$) *if* one knew the values for p_B, ν_A and ν_B. The value for ν_A can be easily obtained since this is simply the chemical shift position of the 'observable' peak after the 'resharpening' observation discussed in the previous section. Thus $\delta\nu$ is a single variable. To define allowable values for p_B and $\delta\nu$, one must make numerical use of the actual maximum width of the observed peak (denoted as W_{max}). This numerical value will depend of course on the natural peak line width in the absence of exchange (denoted W^0). Plots of W_{max} (MLW criterion) vs. $\delta\nu$ are linear, with an intercept equal to W^0 (except for $0.35 \leq p_B \leq 0.4$, i.e., the region of shoulder inclusion–exclusion, where the plot is linear but the intercept is not W^0). This leads to the relationship:

$$[5] \qquad W_{max} = b_{(p_B)}\delta\nu + W^0$$

where $b_{(p_B)}$ is a proportionality constant for a particular value of p_B. A plot of $b_{(p_B)}$ vs. p_B is shown in Fig. 2. At small values of p_B, this relationship is nearly linear and with close to unit slope, i.e., $b_{(p_B)} \sim p_B$. This observation helps one in empirically fitting the curve in Fig. 2 and the following approximations can be formulated:

$$[6] \qquad W_{max} = \delta\nu(p_B + p_B^2/2p_A^2) + W^0$$

or

$$[7] \qquad W_{max} = \delta\nu(p_A p_B + p_B^2/p_A^2) + W^0$$

where $p_A = 1 - p_B$. Equation [6] appears to be slightly superior. Both of these simplify to eq. [8] when p_B is small.

$$[8] \qquad W_{max} = \delta\nu p_B + W^0$$

or

$$W_{max} - W^0 = \delta\nu p_B$$

(a type of uncertainty relationship)

The Boltzmann Distribution Factor

The equations derived in this work give p_B values applicable *only* at the temperature corresponding to the W_{max} condition. From the Boltzmann equation, p_B will decrease with decreasing temperature, adding in fact to the difficulty in detecting *B* under 'frozen-out spectra' temperature conditions. The Boltzmann factor can also lead to detectable chemical shift changes in an averaged peak as one lowers the temperature. This behavior continues, of course, even in the broadening region covered by our analysis and is a characteristic experimental observation which can be used to further collaborate that one has indeed an equilibrium situation. This shift is, of course, unrelated to the rate processes, i.e., k_A, our primary concern. It should also be noted that ν_B (and hence $\delta\nu$) and p_B are related, since the $\nu_{AV} - \nu_A$ value, in combination with either ν_B or p_B, will define the other. However, this p_B value is not so easily determined at the temperature corresponding to W_{max}, since the peak is broadened.

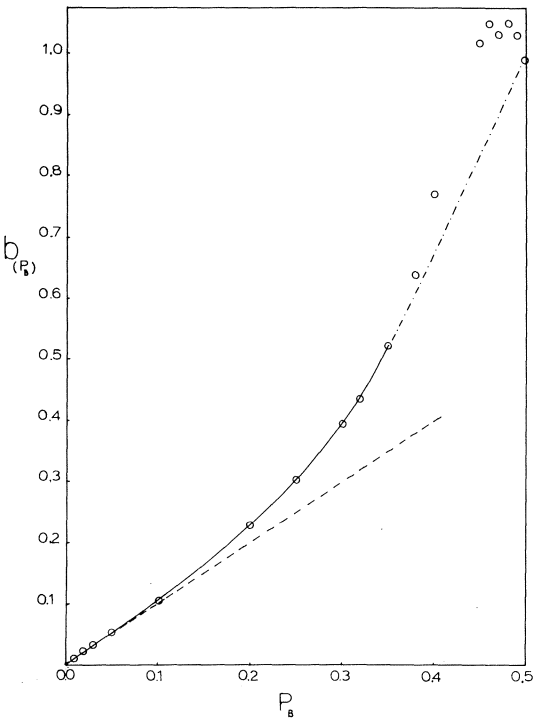

FIG. 2. The behavior of the proportionality constant $b_{(p_B)}$ as a function of the population of the minor isomer p_B. The proportionality constant $b_{(p_B)}$ is derived from the linear plot of W_{max} and $\delta\nu$. The dashed line - - - represents the case where $p_B = b_{(p_B)}$. The reason for the ····· line is commented on in the text.

Practical Applications

The major unknown quantity is k_A and this will be calculated using eq. [4]. It is also evident from eq. [8] that an experimental value of $W_{max} - W^0$ will characterize a particular $\delta\nu p_B$ product and this may be of use in some cases. In practise, the following situations might arise:

(I) For the larger p_B situation, one might determine ν_B (and hence $\delta\nu$) experimentally from 'frozen-out spectra.' From the ν_{AV} position *or* by using eqs. [6–8] (but not from the 'frozen-out spectra') one can ap-

Can. J. Chem. Downloaded from www.nrcresearchpress.com by 210.87.254.42 on 09/05/12
For personal use only.

proximately determine p_B for the temperature corresponding to W_{max}. Equation [4] can then be used to calculate k_A.

(II) From model systems etc., one may be able to estimate a value for ν_B. The remaining steps follow as in I above.

(III) For a given experimental value of W^0, one may wish to calculate the minimum population of B(p_B) which could result in an experimentally observable result, if we have reason to believe, from model systems etc., that our temperature range has spanned the applicable kinetic region.

The latter two situations will now be examined using actual experimental data. Since the last one is hypothetical, this will be treated first.

Case III

In a ^{13}C nmr spectrum of a carbocation, one observes a 'single' peak of $W^0 = 5$ Hz, characteristic of a particular carbon in the 'major' isomer. From model system comparisons, a possible 'minor' isomer would have this same carbon at approximately 4000 Hz separation, i.e., $\delta\nu \sim 4000$ Hz (24 kG field). If we can accept a $W_{max} - W^0$ value of 4 Hz as being observable, then one should be able to detect a p_B value of 0.001, using eq. [8]. This corresponds to $k_A = 24.7\ s^{-1}$, using eq. [4]. A more usual situation in neutral molecules might have $\delta\nu = 200$ Hz, whereby $p_B = 0.020$. At 72 kG fields, the first listed p_B values will be lowered to 0.0003 and 0.007, respectively, and the advantages of superconducting magnets is readily apparent. In any case, we note that rather *minor concentrations of equilibrium partners can lead to experimentally detectable results.*

Case I

Anet and Basus (4)[1], in a ^{13}C study of the cyclooctane ring, report that the single sharp line observed at 25°C gradually broadens to a maximum half-width of 9 Hz at −45°C, whereupon the line resharpens as one goes to lower temperatures. The minor conformer could be observed at −89°C, 367 Hz downfield from the main peak. Using eq. 8, and assuming their W^0 to be about 2 Hz, one obtains:

$$p_B = (9 - 2)/367 \sim 2\%$$

Using eq. 4, $k_A = 6.32 \times 0.02 \times 367 \sim 46\ s^{-1}$ at −45°C ($\Delta G^* = 11.5$ kcal/mol). These values are essentially as reported, using the general GH expression. One should note that this case is an unusually favorable one for seeing minor components since 25% solutions were used.

Case II

The previously reported (6) carbocation, **1**, can exist (in theory) in two conformers, **1***a* and **1***b*, respectively. In both conformers, the cyclopropyl ring is expected to be in the 'bisected' orientation, in which the plane of the ring is at right angles to the paper.

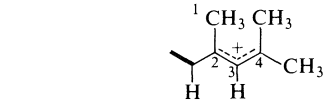

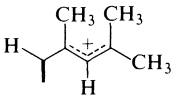

— ≡ Cyclopropyl ring

1*a* **1***b*

In the ^1H nmr spectrum, the C-3 proton signal shifts to lower field on cooling, eventually broadens, and finally resharpens. At this lower temperature, no new signals for a second conformer could be detected under our particular signal-to-noise conditions. The ^{13}C nmr spectrum of this cation has recently been obtained (7). In this case, two of the carbon signals are particularly broadened, the C-3 carbon and the C-1 methyl. In addition, the former shifts to lower field while the latter moves upfield as one lowers the temperature through the line broadening and into the resharpening temperature region. Once again, none of the ^{13}C peaks for this second conformer could be observed in the 'frozen-out spectrum.' Both these ^1H and ^{13}C nmr observations fit our second category. One can show that the observed chemical shifts are consistent with **1***a* being the major isomer, although this fact is basically irrelevant to the analysis.

In the ^1H case, maximum broadness (15 Hz) occurred at −80°C, with $W^0 = 3$ Hz. From eq. [6] $12 = (p_B + p_B^2/2p_A^2)\delta\nu$. From this, one could draw a graph of permissible p_B and $\delta\nu$ values and this is shown in Fig. 3. Note that the spectrometer signal-to-noise characteristics will allow one to set an approximate upper limit for permissible p_B values (i.e., B will be directly observed if p_B is large enough) and thus narrow the range of possible combinations. In practise however, one would not normally plot a graph of this type. Instead, one would estimate $\delta\nu$ by whatever means possible, and in the present instance, one can estimate $\delta\nu$ as ~70 Hz (7) from a comparison to closely related systems where both conformers are detectable. Solving numerically for p_B gives 0.155. For the ^{13}C spectra, $W_{max} - W^0$ is about 27 Hz and we can estimate $\delta\nu$ as 200 Hz (6). This gives $p_B = 0.125$ from eq. 6. Using $p_B = 0.125$ (which seems more reasonable, in that isomer B is

[1]After completion of this study, we became aware that Anet and co-workers had developed essentially the same limiting equations from an actual mathematical solution of the GH equation (8,9). However, our parallel approach allows one to clearly see what range of p_B values apply to these limiting cases.

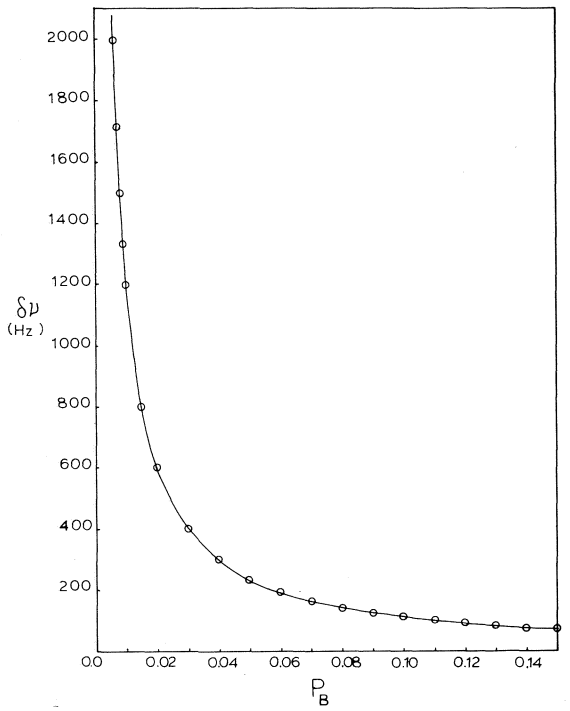

FIG. 3. A graph showing the permissible p_B and δν(H-3 protons) values for the equilibrium mixture of the two cations **1***a* and **1***b*, at the temperature of maximum line broadening.

not detectable at low temperatures), k_A is calculated as 146 s^{-1} from eq. [4], $\Delta G^{\ddagger} = 8.9$ kcal/mol. To reckon the change in p_B from the W_{max} temperature condition to a temperature corresponding to slow exchange kinetics, i.e., 'frozen-out spectra,' requires two basic assumptions (7). The first assumes $\Delta S^{\ddagger} = 0$, which allows one to make $\Delta G^{\ddagger}$ a constant and hence automatically to calculate rates for a series of lower and lower temperatures. The second assumes $\Delta S = 0$, which allows one to define p_B with the only variable again being temperature, i.e., ΔG is treated as a constant in the expression, $\Delta G = -RT \ln K$. In the present case, the above calculations show that p_B will be <0.1 under the low temperature 'frozen-out spectrum' conditions where one could expect to see sharp **1***b* peaks.

We have done this latter calculation only as an illustration of the expected p_B variation. It is in no way a requirement in the analysis.

Concluding Remarks

In conclusion, we would like to emphasize several practical points:

(*i*) The experimental observation of a line broadening–resharpening phenomena can be easily missed if the temperature jumps between sequentially taken spectra are too large.

(*ii*) It may be impractical to obtain ^{13}C spectra corresponding 'exactly' to maximum line width but this will have a rather small effect on a $\Delta G^{\ddagger}$ determination.

(*iii*) Only eq. [4] and [8] are needed in the analysis, for the usual case where $p_B \leq 0.1$.

(*iv*) If one can obtain 'frozen-out' spectra but still 'see' no minor peak, one can plot on the actual observed spectrum, on the basis of eq. [8], the permissible p_B and ν_B values. Where this line enters the noise region of the spectrum will determine the minimum δν separation for A and B and the maximum possible p_B value.

Acknowledgements

The authors thank the National Research Council of Canada for generous financial support. We also wish to thank Drs. R. Paul and T. Okazawa for their helpful advice.

1. (*a*) L. M. JACKMAN and F. A. COTTON (*Editors*). Dynamic nuclear magnetic resonance spectroscopy. Academic Press, New York, NY. 1975; (*b*) I. O. SUTHERLAND. Annu. Rep. NMR Spectrosc. **4**, 71 (1971); (*c*) G. BINSCH. Top. Stereochem. **3**, 97 (1968); (*d*) C. JOHNSON. Adv. Magn. Reson. **1**, 33 (1965); (*e*) L. W. REEVES. Adv. Phys. Org. Chem. **3**, 187 (1965); (*f*) H. KESSLER. Angew. Chem. Int. Ed. Engl. **9**, 219 (1970).
2. H. GUTOWSKY and C. HOLM. J. Chem. Phys. **25**, 1128 (1956).
3. (*a*) H. SHANAN-ATIDI and K. H. BAR-ELI. J. Phys. Chem. **74**, 961 (1970); (*b*) N. M. SERGEYEV, G. I. AURAMENKO, A. V. KISIN, V. A. KORENEVSKY, and YU. A. USTYNYUK. J. Organomet. Chem. **32**, 55 (1971).
4. F. A. L. ANET and V. J. BASUS. J. Am. Chem. Soc. **95**, 4424 (1973).
5. (*a*) H. GUTOWSKY, D. MCCALL, and C. SLICHTER. J. Chem. Phys. **21**, 279 (1953); (*b*) H. MCCANNELL. J. Chem. Phys. **28**, 430 (1958).
6. T. S. SORENSEN and K. RAJESWARI. J. Am. Chem. Soc. **93**, 4222 (1971).
7. N. OKAZAWA and T. S. SORENSEN. Can. J. Chem. In press.
8. F. A. L. ANET, I. YAVARI, I. J. FERGUSON, A. R. KATRITZKY, M. MORENO-MAÑAS, and M. J. T. ROBINSON. J. Chem. Soc. Chem. Commun. 399 (1976).
9. F. A. L. ANET and V. J. BASUS. J. Magn. Reson. In press.

Can. J. Chem. Downloaded from www.nrcresearchpress.com by 210.87.254.42 on 09/05/12
For personal use only.

Aminocyclitols. II. Synthesis of thioanalogues of 2,5-dideoxystreptamine

GERRY KAVADIAS[1] AND ROBERT DROGHINI

Bristol Laboratories of Canada, 100 Industrial Boulevard, Candiac, P.Q., Canada J5R 1J1

Received March 28, 1978

GERRY KAVADIAS and ROBERT DROGHINI. Can. J. Chem. **56**, 2743 (1978).

N,N'-Dibenzoyl-2,5-dideoxystreptamine (**8***b*) reacted with thionyl chloride to form the bisoxazoline **9** and the latter compound was treated with thiobenzoic acid to produce the dithiobenzoate **10***a*. Removal of the protective groups in **10***a* afforded (1,3/4,6)-4,6-diamino-1,3-cyclohexanedithiol (**1**) dihydrochloride. Reaction of **8***b* with triethyl orthoacetate in the presence of boron trifluoride yielded the monooxazoline **12** which, on reaction with thiobenzoic acid followed by deprotection of the resulting **13***a*, afforded (*d,l*)-(1,3/4,6)-4,6-diamino-3-hydroxycyclohexanethiol (**2**) dihydrochloride. Similarly, 3-*N*-benzoyl-1-*N*-ethoxycarbonyl-2,5-dideoxystreptamine (**15**) and 1-*N*-benzoyl-3-*N*-ethoxycarbonyl-2,5-dideoxystreptamine (**20**) were converted via their respective oxazolines **17***a* and **22***a*, to the enantiomeric aminothiols **3** and **4**. Protected derivatives of **1**–**4** are also described.

GERRY KAVADIAS et ROBERT DROGHINI. Can. J. Chem. **56**, 2743 (1978).

La *N,N'*-dibenzoyldidéoxy-2,5 streptamine (**8***b*) réagit avec le chlorure de thionyle pour former la bisoxazoline **9** et ce dernier composé, par traitement avec de l'acide thiobenzoïque, produit le dithiobenzoate **10***a*. L'enlèvement des groupes protecteurs de **10***a* conduit au dichlorhydrate du (1,3/4,6) diamino-4,6 cyclohexanedithiol-1,3 (**1**). La réaction de **8***b* avec l'orthoacétate de triéthyle en présence de trifluorure de bore conduit à la mono-oxazoline **12** qui, par réaction avec l'acide thiobenzoïque suivie par une déprotection du composé **13***a* qui en résulte, fournit le (*d,l*)(1,3/4,6) diamino-4,6 hydroxy-3 cyclohexanethiol (**2**) sous forme de dichlorhydrate. De la même manière, la *N*-benzoyl-3 *N*-éthoxycarbonyl-1 didéoxy-2,5 streptamine (**15**) et la *N*-benzoyl-1 *N*-éthoxycarbonyl-3 didéoxy-2,5 streptamine (**20**) ont pu être transformés, par l'intermédiaire de leurs oxazolines **17***a* et **22***a* respectives, en aminothiols énantiomères **3** et **4**. On décrit aussi la préparation des dérivés protégés **1**–**4**.

[Traduit par le journal]

In a research project directed at the synthesis of thioanalogues of aminoglycoside antibiotics (kanamycins, gentamycins, tobramycin etc., in which the C-5 hydroxyl group is replaced by a hydrogen atom and one or both of the glycosidic oxygens are replaced by sulfur(s)), the aminothiols **1**–**4**, properly protected, were needed as the aglycon components in the glycosidation reactions. In addition, the aminothiols **1**–**4** were needed for biosynthetic studies. In recent years, deoxystreptamine-negative mutants from a number of aminoglycoside-antibiotic-producing microorganisms have been used to obtain novel antibiotics by the addition of 2-deoxystreptamine analogues to the fermentation broth (1–7).

The present paper describes the synthesis of the aminothiols **1**–**4** and their derivatives and gives evidence for their assigned structures. The easily available 2,5-dideoxystreptamine (**8***a*) (8) served as the starting material in these syntheses.

Our first approach to the syntheses of these compounds involved inversion of one or both of the hydroxyls in **8***a*, conversion of the inverted hydroxyl(s) to tosylate(s) and replacement of the latter group(s) with a sulfur nucleophile such as the thiocyanate, thioacetate and thiobenzoate anions. This approach was unsuccessful and soon abandoned, mainly because the major product in the replacement step was an olefin. For example, the reaction of the tosylates **I***a* and **I***b* with sodium thioacetate yielded the olefins **II***a* and **II***b*, respectively.[2]

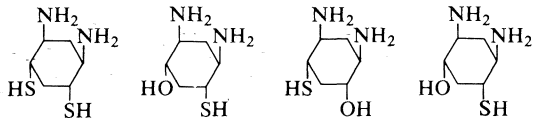

1 **2** (*d,l*) **3** **4**

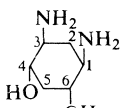

8*a*

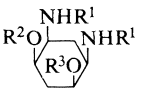

I

a R^1 = Ac, R^2 = H, R^3 = Ts
b R^1 = R^2 = R^3 = Ts

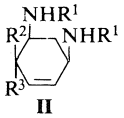

II

a R^1 = Ac, R^2 = OH, R^3 = H
b R^1 = Ts, R^2 = H, R^3 = SAc

[1]Author to whom correspondence should be addressed.

[2]A detailed account of these results will be presented in another publication.

Can. J. Chem. Downloaded from www.nrcresearchpress.com by 210.87.254.105 on 09/05/12
For personal use only.

Can. J. Chem. Downloaded from www.nrcresearchpress.com by 210.87.254.105 on 09/05/12
For personal use only.

A most promising potential route for the conversion of **8***a* to the aminothiols **1**–**4** and, in general, for the conversion of a *trans*-1,2-aminoalcohol to *trans*-1,2-aminothiol with the same configuration appeared to be a process involving the following steps: (*a*) Conversion of the *trans*-1,2-aminoalcohol to *trans*-1,2-benzamidoalcohol; (*b*) conversion of the latter to *cis*-oxazoline; (*c*) ring-opening reaction of the oxazoline with thiobenzoic acid to *trans*-1,2-benzamidothiol benzoate; and (*d*) removal of the protective groups. It is well established that when a benzamido group is *trans* oriented, diaxially or diequatorially to a leaving group at the C-2 position, *cis*-oxazolines are formed by intramolecular replacement of the leaving group by an attack of the oxygen of the benzamido function (9–14). Reaction of 2-oxazolines with thiobenzoic acid causes ring opening and amide formation, with addition of the thiobenzoxy group to the original oxazoline ring (15). For example, the reaction of 2-phenyl-2-oxazoline with thiobenzoic acid produced 2-benzamidoethylthiol benzoate in high yield (15*a*). To examine the practicality of this approach and to establish workable experimental conditions for the conversion of **8***a* to the aminothiols **1**–**4**, *trans*-2-benzamidocyclohexanol (**5**) was used as a model.

Reaction of **5** with thionyl chloride at the reflux temperature gave the known (11) oxazoline **6** in yields varying with the reaction time. A maximum yield of 85% was obtained after 3 min refluxing and was thereafter reduced to 30% after 1 h.

Treatment of the oxazoline **6** with thiobenzoic acid (2 h, 100°C) caused ring opening of the oxazoline and produced *trans*-2-benzamidocyclohexanethiol benzoate (**7***a*) in 85% yield. Alkaline hydrolysis of **7***a* yielded the known *trans*-2-benzamidocyclohexanethiol (**7***b*) (16) which afforded *trans*-2-aminocyclohexanethiol hydrochloride (**7***c*) (16) upon acidic hydrolysis (Scheme 1).

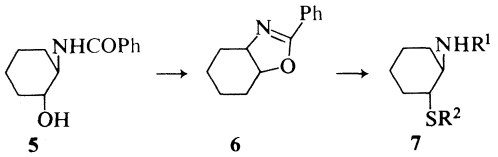

5 **6** **7**

a $R^1 = R^2 = Bz$
b $R^1 = Bz, R^2 = H$
c $R^1 = R^2 = H$

Bz = C_6H_5CO—; Ph = C_6H_5

SCHEME 1

Treatment of **8***b* with thionyl chloride at the reflux temperature for 3 min produced the crystalline bisoxazoline **9** in 72% yield (Scheme 2). The yield of **9** was reduced as the refluxing period was increased and was nil after 45 min. Treatment of the bisoxazoline **9** with excess thiobenzoic acid in DMF (2 h, 115°C) opened both of the oxazoline rings and formed **10***a* in 63% yield. Removal of the protective groups in **10***a* to form **1** was best effected in a two stage hydrolysis: alkaline hydrolysis of **10***a* removed the *S*-benzoyl groups and yielded **10***b* which was then hydrolyzed by refluxing in a hydrochloric acid – acetic acid mixture to produce the dihydrochloride salt of **1**. The structure of **1** was confirmed by ^{1}Hmr spectroscopy. The ^{1}Hmr spectrum of the dihydrochloride salt of **1** showed a two-proton double triplet at δ 3.32 with coupling constants of 11.0 and 3.8 Hz which were assigned to the magnetically equivalent protons at the carbons attached to the amino groups. It also showed a two-proton double triplet at δ 2.88 with coupling constants of 11.0 and 3.8 Hz which were assigned to the protons at the carbons attached to the thio groups. Thus, all the substituents in **1** are equatorially oriented as expected.

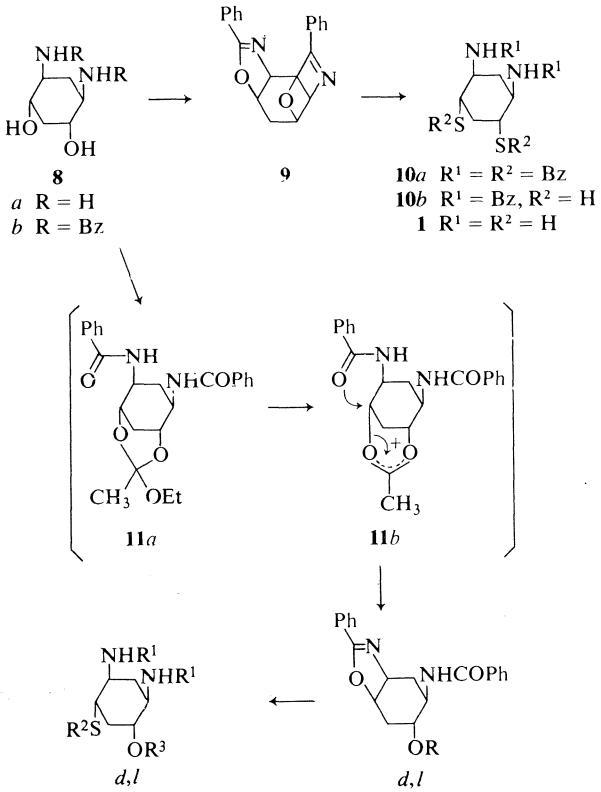

8 **9** **10***a* $R^1 = R^2 = Bz$
a R = H **10***b* $R^1 = Bz, R^2 = H$
b R = Bz **1** $R^1 = R^2 = H$

11*a* **11***b*

d,l *d,l*

13*a* $R^1 = R^2 = Bz, R^3 = Ac$ **12** R = Ac
13*b* $R^1 = Bz, R^2 = R^3 = H$
13*c* $R^1 = R^2 = Bz, R^3 = H$
2 $R^1 = R^2 = R^3 = H$

Bz = C_6H_5CO; Ac = CH_3CO; Ph = C_6H_5

SCHEME 2

In the synthesis of **2** (Scheme 2), the intermediate oxazoline **12** (R = Ac or other protective group) was required. The preparation of **12** by the process

Can. J. Chem. Downloaded from www.nrcresearchpress.com by 210.87.254.105 on 09/05/12
For personal use only.

discussed above would involve the difficult task of protecting one of the two hydroxyls in **8***b* before reaction with thionyl chloride. A more promising route for the synthesis of **12** appeared to be the reaction of **8***b* with triethyl orthoacetate in the presence of an acid catalyst. It was anticipated that the ortho ester **11***a* would be formed initially and, in the presence of the acid catalyst, would be converted to the 1,3-dioxan-2-ylium cation **11***b* (see ref. 17 for a review of 1,3-dioxan-2-ylium cations) which would suffer ring opening by an attack of the oxygen of the benzamido group to form the oxazoline **12**. Indeed, reaction of **8***b* with triethyl orthoacetate in DMF in the presence of boron trifluoride at room temperature did produce **12** in 80% yield. Treatment of the oxazoline **12** with thiobenzoic acid gave the thiobenzoate **13***a* in 79% yield. The acetyl group in **13***a* was selectively removed by controlled acid hydrolysis to produce **13***c*. Compound **13***c*, with all its functional groups protected except the hydroxyl group, could be used in glycosidation reactions. Alkaline hydrolysis of **13***a* removed the *O*-acetyl and the *S*-benzoyl groups and produced **13***b* which was then converted to the dihydrochloride salt of the aminothiol **2** by acidic hydrolysis. The structure of **2** which can be deduced from simple mechanistic considerations was confirmed by ^{1}Hmr spectroscopy. Thus, the characteristic ^{1}Hmr absorptions of **2** hydrochloride at δ 3.78 (d of t, O—C—H—, J_1 = 10.4, J_2 = 4.5 Hz), 3.36 (d of t, N—C—H, J_1 = 10.4, J_2 = 4.5 Hz), 3.28 (d of t, N—C—H, J_1 = 10.4, J_2 = 4.5 Hz), and 3.08 (d of t, S—C—H, J_1 = 10.4, J_2 = 4.5 Hz) indicate that all the substituents in **2** are in equatorial orientations.

Attempts to resolve **2** into the optical isomers **3** and **4** with optically active acids such as *d*- and *l*-tartaric acids and *d*- and *l*-2-nitrotartranilic acids were unsuccessful.

The syntheses of **3** and **4** and their derivatives were accomplished by the routes outlined in Schemes 3 and 4, respectively. 1-*N*-Ethoxycarbonyl-2,5-dideoxystreptamine (**14**) (8) was *N*-benzoylated to give **15**. Treatment of **15** with triethyl orthoacetate in DMF in the presence of boron trifluoride produced, presumably via the intermediate **16**, the oxazoline **17***a* ($[\alpha]_D^{25}$ −64.2) in 78.5% yield. Reaction of the oxazoline **17***a* with thiobenzoic acid gave the thiobenzoate **18***a* ($[\alpha]_D^{25}$ −9.7) in 76.5% yield which, by alkaline hydrolysis, was converted to **18***b* ($[\alpha]_D^{25}$ +32.9). Acid hydrolysis of **18***b* (hydrochloric acid-acetic acid) afforded the dihydrochloride salt of **3** ($[\alpha]_D^{25}$ +2.8). Assignment of the absolute configuration to **3** was based on the mode of its synthesis and the mechanisms of the reactions involved. Since it was derived from the aminocyclitol **14** of known

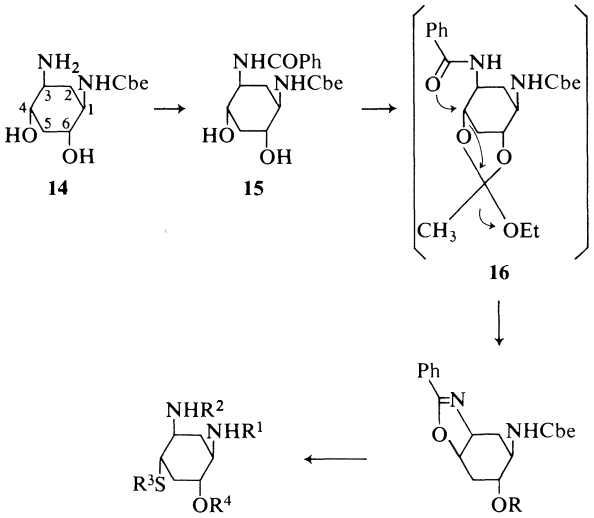

18*a* R^1 = Cbe, R^2 = R^3 = Bz, R^4 = Ac
18*b* R^1 = Cbe, R^2 = Bz, R^3 = R^4 = H
18*c* R^1 = Cbe, R^2 = R^3 = Bz, R^4 = H
3 R^1 = R^2 = R^3 = H

a R = Ac
b R = H

Bz = C_6H_5CO; Cbe = $CO_2C_2H_5$; Ac = CH_3CO; Ph = C_6H_5

SCHEME 3

absolute configuration (8) by replacement of the hydroxyl group at C-4 with a thiol group with an overall retention of the configuration of this carbon center, it follows that the absolute configuration of **3** must be as shown in the formula.

It was possible to remove the acetyl group in **17***a* and form **17***b* without affecting the oxazoline ring. This was accomplished by treatment of **17***a* in

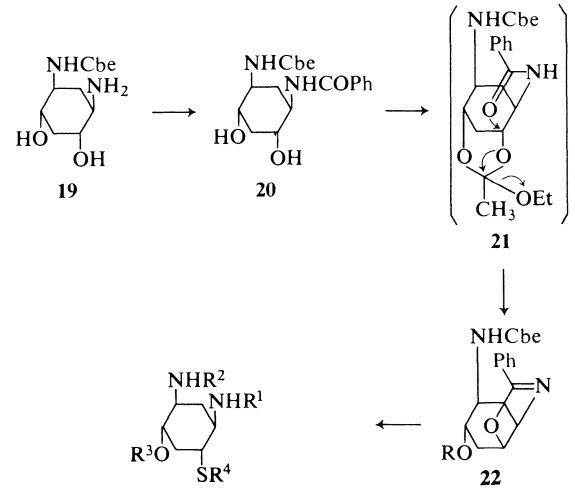

23*a* R^1 = R^4 = Bz, R^2 = Cbe, R^3 = Ac
23*b* R^1 = Bz, R^2 = Cbe, R^3 = R^4 = H
23*c* R^1 = R^4 = Bz, R^2 = Cbe, R^3 = H
4 R^1 = R^2 = R^3 = R^4 = H

a R = Ac
b R = H

Ac = CH_3CO; Bz = C_6H_5CO; Cbe = $CO_2C_2H_5$

SCHEME 4

Can. J. Chem. Downloaded from www.nrcresearchpress.com by 210.87.254.105 on 09/05/12
For personal use only.

ethanol with a catalytic amount of sodium ethoxide at room temperature. The oxazoline **17***b* ($[\alpha]_D^{25}$ −98.6) thus obtained was reacted with thiobenzoic acid to give the thiobenzoate **18***c* ($[\alpha]_D^{25}$ +45.2) in 71% yield. Compound **18***c* has all its functional groups protected except the hydroxyl group and can be used in glycosidation reactions.

The aminothiol **4** was prepared in a manner analogous to that described for the synthesis of its enantiomer **3**. 3-*N*-Ethoxycarbonyl-2,5-dideoxystreptamine (**19**) (8) was *N*-benzoylated to give **20**. Reaction of **20** with triethyl orthoacetate in DMF in the presence of boron trifluoride produced, presumably via the intermediate **21**, the oxazoline **22***a* ($[\alpha]_D^{25}$ +63.7) in 88% yield. The acetyl group in **22***a* was removed by saponification (sodium ethoxide in ethanol) and the oxazoline **22***b* ($[\alpha]_D^{25}$ +100.6) thus obtained was reacted with thiobenzoic acid to give the thiobenzoate **23***c* ($[\alpha]_D^{25}$ −46.3) in 63% yield. Compound **23***c* has all its functional groups protected except the hydroxyl group and can be used in glycosidation reactions. Alkaline hydrolysis of **23***c* yielded **23***b* which by acid hydrolysis afforded the dihydrochloride salt of **4** ($[\alpha]_D^{25}$ −2.8).

In summary then, we have shown that aminothiols of known configuration are readily obtained by a combination of internal and external displacement reactions.

Experimental

The melting points were determined on a Mel-Temp melting point apparatus and are not corrected. The ir spectra were recorded on a Unicam SP-200G grating ir spectrometer. ^{1}Hmr spectra were taken with a Varian EM-360A 60 MHz spectrometer. Tetramethylsilane (for solutions other than deuterium oxide) and sodium 4,4-dimethyl-4-silapentane-1-sulfonate (for solutions of deuterium oxide) were used as internal standards. Thin-layer chromatography (tlc) was carried out on microscope slides coated with silica gel and the spots were visualized with perchloric or sulfuric acid. Optical rotations were measured with a Perkin-Elmer Model 141 polarimeter. The analyses were performed by Micro-Tech Laboratories, Skokie, Ill.

d,l-cis-*2-Phenyl-4,5-cyclohexanooxazoline (**6**)*

A mixture of 9.0 g (41 mmol) of *d,ℓ-trans*-2-benzamidocyclohexanol (9) and 45 ml thionyl chloride was stirred at room temperature for 3 min and then heated on a steam bath for 2 min. The solution was cooled in an ice bath and then evaporated to dryness on a rotary evaporator at 30°C. The residue, on trituration with dry ether (100 ml), solidified. The ether phase was decanted and the grey oxazoline hydrochloride was treated with ether once more. After removal of the ether phase by decantation, the solid residue was partitioned between 6% aqueous sodium hydroxide (140 ml) and ether (140 ml). The ether phase was separated and the aqueous phase was extracted with ether (100 ml). The combined ethereal extracts, after drying, were evaporated to dryness to give 6.96 g (85%) of crystalline oxazoline **6**, mp 45–47°C (lit. (11) mp 45–47°C). Thin-layer chromatography with ether showed, under uv, a major spot of R_f 0.66 (**6**) and a trace of starting material (R_f 0.28); ir ($CHCl_3$): 1640, 1570 cm^{-1}.

When the heating time was extended to 1 h, the yield of **6** was reduced to 30%.

d,l-trans-*2-Benzamidocyclohexanethiol Benzoate (**7**a)*

Into a flame-dry and nitrogen-purged, 100 ml, three-neck flask, equipped with condenser, magnetic stirrer, and nitrogen inlet and outlet tubes, was added 7.30 g (53 mmol) thiobenzoic acid (Aldrich Chemical Co., Inc.) and placed under a slow stream of nitrogen. The flask was slightly warmed to melt the thiobenzoic acid, oxazoline **6** (4.9 g, 24.4 mmol) was added and the mixture was stirred at room temperature until it became a homogeneous solution (5–10 min) and then heated on a steam bath for 2 h. A solid material was formed. After cooling to room temperature, ether (50 ml) was added and stirred to break the lumps into a fine powder. Filtration gave 6.97 g (84.5%) of *d,ℓ-trans*-2-benzamidocyclohexanethiol benzoate, mp 156–158°C. Thin-layer chromatography (ether) showed, under uv, a single spot (R_f 0.71). Recrystallization from ethanol afforded the analytical sample, mp 158–159°C; ir ($CHCl_3$): 3400, 1650, 1640, 1570, 1530 cm^{-1}. *Anal.* calcd. for $C_{20}H_{21}NO_2S$: C 70.76, H 6.24, N 4.13, S 9.45; found: C 70.59, H 6.24, N 4.03, S 9.47.

d,l-trans-*2-Benzamidocyclohexanethiol (**7**b)*

To a solution of 2.0 g sodium hydroxide in 50 ml of 80% ethanol was added 5.76 g (17 mmol) of *d,ℓ-trans*-2-benzamidocyclohexylthiol benzoate and the suspension was stirred at room temperature under nitrogen for 2 h. (After 15 min, it became a clear solution). The reaction mixture was neutralized with carbon dioxide and evaporated to dryness. The residue was treated with water (50 ml) and extracted with chloroform (3 × 50 ml). The chloroform solution, after drying, was evaporated to dryness to give 3.87 g (97%) of *d,ℓ-trans*-2-benzamidocyclohexanethiol, mp 159–162°C. Thin-layer chromatography (10% ethanol–chloroform) showed, under uv, one spot of R_f 0.46. Recrystallization from ethanol (13 ml) gave 3.0 g of **7***b*, mp 162–163°C (lit. (16), mp 161–162°C). *Anal.* calcd. for $C_{13}H_{17}NOS$: C 66.34, H 7.28, N 5.95, S 13.62; found: C 66.38, H 7.29, N 5.84, S 13.40.

d,l-trans-*2-Aminocyclohexanethiol (**7**c) Hydrochloride*

A solution of 2.0 g (8.5 mmol) of *trans*-2-benzamidocyclohexanethiol (**7***b*) in glacial acetic acid (15 ml) was diluted with an equal volume of concentrated hydrochloric acid (15 ml) and refluxed under nitrogen for 17 h. After removal of the solvent by evaporation, the residue was dissolved in water (40 ml) and extracted with ether (2 × 40 ml) to remove the benzoic acid. The aqueous phase was evaporated to dryness to give 1.35 g (95%) of **7***c* hydrochloride, mp 220–222°C (EtOH) (lit. (16) mp 225°C, (18) mp 226–227°C). *Anal.* calcd. for $C_6H_{13}NS\cdot HCl$: C 42.97, H 8.41, N 8.35, S 19.12; found: C 42.97, H 8.65, N 8.28, S 18.91.

N,N′-*Dibenzoyl-2,5-dideoxystreptamine (**8**b)*

To an ice-cold solution of 17.8 g (122 mmol) of 2,5-dideoxystreptamine (**8***a*) (8) and 35 g (330 mmol) of sodium carbonate in 210 ml water and 70 ml methanol, was added dropwise (15 min) with stirring, a solution of 44.4 g (305 mmol) of benzoyl chloride in 70 ml dry acetone. After stirring at 0°C for 30 min and at room temperature for 1 h, the reaction mixture was diluted with water (400 ml). The resulting precipitate was collected by filtration, washed successively with water (2 × 130 ml), ethanol (100 ml) and ether (2 × 130 ml), and dried to give 40.8 g of **8***b*, mp 278–282°C. This product was stirred in boiling ethanol and filtered to give 39.0 g (90%) of **8***b*, mp 280–282°C (dec.). This material was used in the next reaction. The analytical sample was prepared by recrystallization from DMF–EtOH(1:1), mp 283–285°C, resolidified, and melted at 294–295°C; ir (Nujol): 3400, 3300, 1625, 1615,

Can. J. Chem. Downloaded from www.nrcresearchpress.com by 210.87.254.105 on 09/05/12
For personal use only.

1575, 1565 cm^{-1}. *Anal.* calcd. for $C_{20}H_{22}N_2O_4$: C 67.78, H 6.25, N 7.90; found: C 67.70, H 6.26, N 8.03.

Bisoxazoline ***9***

Powdered **8***b* (20.0 g, 56.4 mmol) was added to 100 ml of thionyl chloride and the mixture was stirred at room temperature for 3 min and then heated on a steam bath for 3 min. The solution was cooled in an ice bath and then evaporated to dryness at 30°C. The residue, on trituration with ether (150 ml), solidified. The ether phase was decanted and the crystalline oxazoline dihydrochloride was treated with 6% aqueous sodium hydroxide (250 ml) and extracted with chloroform (250 ml). The chloroform solution, after drying, was evaporated to dryness to give 15.3 g of crude **9**. Thin-layer chromatography (10% ethanol–chloroform) showed, under uv, one major spot of R_f 0.23 (compound **9**) and four minor spots of R_f 0, 0.37, 0.43, and 0.50. The crude product was boiled and stirred with 70 ml acetone (5–10 min) and then cooled in an ice bath and filtered to give 12.8 g (72%) of the bisoxazoline **9**, mp 191–195°C. Thin-layer chromatography showed one major spot (R_f 0.23) and a trace of the spot with R_f 0.37. This material was used in the next reaction. The analytical sample was obtained by recrystallization from ethanol (twice), mp 196–198°C; ir ($CHCl_3$): 1650, 1585, 1500 cm^{-1}. *Anal.* calcd. for $C_{20}H_{18}N_2O_2$: C 75.45, H 5.70, N 8.80; found: C 75.68, H 5.75, N 8.69.

When the heating period was extended to 45 min, no oxazoline **9** was detected (tlc) in the product.

*(1,3|4,6)-4,6-Dibenzamido-1,3-cyclohexanedithiol Dibenzoate (**10**a)*

A mixture of 3.50 g (11.0 mmol) of bisoxazoline **9**, 7.90 g (57 mmol) of thiobenzoic acid, 50 mg of anhydrous *p*-toluenesulfonic acid, and 3.5 ml of dry DMF was heated in an oil bath at 115°C under nitrogen with stirring. The reaction mixture, upon heating, became a clear solution and then solidified. At this point, stirring was discontinued and heating was continued for 2 h. After cooling to room temperature, ether (60 ml) was added and the mixture was stirred to break the lumps. The fine suspension was filtered off, washed with ether, and dried to give 4.81 g of **10***a*, mp 300–310°C. The crude product was dissolved in DMF (30 ml), the solution diluted with chloroform (60 ml) and allowed to crystallize at room temperature. The crystalline product was collected by filtration, washed with ethanol (15 ml) and ether (30 ml) and dried to give 4.14 g (63%) of **10***a*, mp 308–310°C; ir (Nujol): 3250, 1670, 1660, 1640, 1630, 1560, 1540 cm^{-1}. *Anal.* calcd. for $C_{34}H_{30}N_2O_4S_2$: C 68.66, H 5.08, N 4.71, S 10.78; found: C 68.33, H 5.11, N 4.67, S 11.02.

*(1,3|4,6)-4,6-Dibenzamido-1,3-cyclohexanedithiol (**10**b)*

A suspension of 7.90 g (13.3 mmol) of **10***a* in 2 *N* sodium hydroxide in 80% ethanol (70 ml) was heated under reflux under nitrogen with stirring until it became a clear solution (5 min). Heating was then discontinued and the reaction mixture was stirred at room temperature for 1.5 h. The reaction mixture was diluted with water (140 ml) and the clear solution was neutralized with carbon dioxide. The crystalline precipitate was collected by filtration, washed with water, and dried to give 4.8 g (93.5%) of **10***b*, mp 289–290°C; ir (Nujol): 3300 (NH), 1640, and 1550 cm^{-1}. *Anal.* calcd. for $C_{20}H_{22}N_2O_2S_2$: C 62.14, H 5.74, N 7.25, S 16.59; found: C 62.21, H 5.68, N 7.23, S 16.38.

*(1,3|4,6)-4,6-Diamino-1,3-cyclohexanedithiol (**1**) Dihydrochloride*

Compound **10***b* (4.5 g, 11.6 mmol) was hydrolyzed with a 1:1 mixture of glacial acetic acid – concentrated hydrochloric acid (170 ml), as in the procedure given for the hydrolysis of **7***b*, to yield 2.90 g of crystalline product. Thin-layer chromatography with H_2O–NH_4OH–MeOH–$CHCl_3$ (1:1:4:1) sprayed with ninhydrin, showed one major spot of R_f 0.64 (compound **1**) and a minor of R_f 0.52. The crude product was stirred with boiling ethanol (25 ml), the mixture cooled to room temperature, and the insoluble dihydrochloride of **1** was collected by filtration (2.68 g, 92%), mp 305–307°C (dec.); ^{1}Hmr (D_2O) δ: 3.32 (d of t, 2H, N—C—H, J_1 = 11.0, J_2 = 3.8 Hz), 2.88 (d of t, 2H, S—C—H, J_1 = 11.0, J_2 = 3.8 Hz), 2.90–2.46 (m, 2H, H_e of CH_2), 2.11–1.50 (m, 2H, H_a of CH_2). *Anal.* calcd. for $C_6H_{14}N_2S_2 \cdot 2HCl$: C 28.68, H 6.42, N 11.15, S 25.52; found: C 28.60, H 6.61, N 10.95, S 25.47.

Oxazoline ***12***

To a suspension of 14.2 g (40 mmol) of **8***b* in 80 ml dry DMF, was added 30 ml of triethyl orthoacetate and 10 ml of boron trifluoride etherate and the mixture, protected from moisture, was stirred at room temperature for 24 h. (After about 1 h, compound **8***b* had dissolved.) On tlc with ether–ethanol (10:1) the solution showed a major spot of R_f 0.55 (**12**). The reaction mixture was poured into a cold solution of 8% sodium bicarbonate (500 ml) and the precipitate was collected and washed with water (3 × 100 ml). After drying, the crystalline product was dissolved in chloroform (200 ml), filtered to remove some insoluble matter, and the filtrate evaporated to dryness. The solid residue was treated with a 1:1 ether – petroleum ether solution (60 ml) and filtered to give 12.1 g, mp 186–189°C. Recrystallization from ethanol (200 ml) gave 10.2 g of **12**, mp 189–190°C. A further 1.1 g of **12** was recovered from the mother liquor after evaporation and recrystallization from ethanol (30 ml). The two crops were combined to a total of 11.3 g (75%); ir (Nujol): 3350, 1740, 1660, 1530 cm^{-1}. *Anal.* calcd. for $C_{22}H_{22}N_2O_4$: C 69.83, H 5.85, N 7.40; found: C 69.80, H 5.86, N 7.34.

*(d,l)-(1,3|4,6)-3-Acetoxy-4,6-dibenzamidocyclohexanethiol Benzoate (**13**a)*

The procedure described above for the preparation of **10***a* was used. Thus, a mixture of 6.4 g (17 mmol) of **12**, 7.20 g (52 mmol) of thiobenzoic acid, 5.0 ml of dry DMF, and 100 mg of anhydrous *p*-toluenesulfonic acid was heated at 115°C for 1.5 h. Work-up as in **10***a* gave 7.93 g of crude **13***a*, mp 268–276°C. Thin-layer chromatography with 5% EtOH in ether showed, under uv, one major spot of R_f 0.34 (**13***a*) and a minor of R_f 0.60. Recrystallization from DMF (24 ml) – ethyl acetate (50 ml) gave 6.9 g (79%) of **13***a*, mp 276.5–277.5°C; ir (Nujol): 3300, 1735, 1660, 1640, and 1540 cm^{-1}. *Anal.* calcd. for $C_{29}H_{28}N_2O_5S$: C 67.42, H 5.46, N 5.42, S 6.20; found: C 67.29, H 5.48, N 5.35, S 5.97.

The yield of **13***a* was reduced (45–50%) when the reaction was carried out without DMF.

*(d,l)-(1,3|4,6)-4,6-Dibenzamido-3-hydroxycyclohexanethiol (**13**b)*

A suspension of 2.07 g (4.0 mmol) of **13***a* in 20 ml 1 *N* sodium hydroxide (80% ethanol–water) was stirred at room temperature under nitrogen for 1.5 h. The solution was neutralized with carbon dioxide and the product isolated as in the synthesis of **10***b* above to give 1.40 g (95%) of **13***b*, mp 289–292°C (dec.). Thin-layer chromatography (10% ethanol–ether) showed (uv or $HClO_4$) one spot of R_f 0.50; ir (Nujol): 3300, 1640, 1540 cm^{-1}. *Anal.* calcd. for $C_{20}H_{22}N_2O_3S$: C 64.83, H 5.98, N 7.56, S 8.65; found: C 64.68, H 5.86, N 7.45, S 8.45.

*(d,l)-(1,3|4,6)-4,6-Dibenzamido-3-hydroxycyclohexanethiol Benzoate (**13**c)*

A suspension of 2.0 g (3.9 mmol) of **13***a* in 33 ml glacial acetic acid and 8 ml concentrated hydrochloric acid was heated

Can. J. Chem. Downloaded from www.nrcresearchpress.com by 210.87.254.105 on 09/05/12
For personal use only.

under reflux under nitrogen. When all **13***a* had dissolved, the solution was diluted with 33 ml of water and refluxed for 15 min. After cooling to room temperature, the crystalline precipitate was collected, washed with water, and dried to give 1.37 g (75%) of **13***c*, mp 254–257°C. Thin-layer chromatography (20% ethanol–ether) showed, under uv, one major spot of R_f 0.38 and a trace of another compound of R_f 0.73; ir (Nujol): 3400, 3300, 1665, 1640, 1540 cm^{-1}. *Anal.* calcd. for $C_{27}H_{26}N_2O_4S$: C 68.33, H 5.52, N 5.90, S 6.76; found: C 68.43, H 5.55, N 5.74, S 6.86.

*(d,l)-(1,3/4,6)-4,6-Diamino-3-hydroxycyclohexanethiol (**2**) Dihydrochloride*

A hot solution of 3.20 g (8.5 mmol) of **13***b* in 40 ml glacial acetic acid was diluted with an equal volume of concentrated hydrochloric acid and the solution was heated under reflux under nitrogen for 17 h. Work-up, as in the synthesis of **1** above, gave 2.02 g (100%) crude **2** dihydrochloride. Thin-layer chromatography with water – ammonium hydroxide – methanol – chloroform (1:1:4:1) sprayed with ninhydrin showed one major spot of R_f 0.54 (**2**) and a minor of R_f 0.35. Recrystallization from water (4 ml) – ethanol (28 ml) gave 1.33 g of **2** dihydrochloride, mp 341–345°C (dec.) (it turned brown at 265°C and started to decompose at 302°C); ^{1}Hmr (D_2O) δ: 3.78 (d of t, 1H, O—C—H, J_1 = 10.4, J_2 = 4.5 Hz), 3.36 (d of t, 1H, N—C—H, J_1 = 10.4, J_2 = 4.5 Hz), 3.28 (d of t, 1H, N—C—H, J_1 = 10.4, J_2 = 4.5 Hz), 3.08 (d of t, 1H, S—C—H, J_1 = 10.4, J_2 = 4.5 Hz), 2.76–2.38 (m, 2H, H_e of CH_2), 2.11–1.44 (m, 2H, H_a of CH_2). *Anal.* calcd. for $C_6H_{14}N_2O{\cdot}2HCl$: C 30.63, H 6.84, N 11.91, S 13.63; found: C 30.38, H 6.98, N 11.82, S 13.50.

*3-N-Benzoyl-1-N-ethoxycarbonyl-2,5-dideoxystreptamine (**15**)*

To a solution of 7.81 g (35.6 mmol) of **14** (8) ($[\alpha]_D^{25}$ −38.0) and 5.04 g (60 mmol) of sodium bicarbonate in 40 ml water, was added 40 ml acetone and 5 ml methanol and the mixture was cooled in an ice bath while stirring. A solution of 7.03 g (50 mmol) of benzoyl chloride in 15 ml dry acetone was added dropwise. After the addition (15 min), the reaction mixture was stirred at room temperature for 1.5 h and then evaporated *in vacuo*. The residue was treated with water (50 ml) and the solid product collected by filtration, washed with water (2 × 30 ml) and ether (50 ml), and dried first at room temperature, then at 100°C, to give 8.90 g of **15**, mp 254–256°C. The aqueous filtrate was extracted continuously with ethyl acetate to give 2.2 g of **15**, mp 254–256°C. The two crops were combined to a total of 11.1 g (96.5%). A sample was recrystallized from ethanol–ether (1:3), mp 240–245°C, solidified and remelted at 254–256°C; $[\alpha]_D^{25}$ −18.6 (*c* 0.8, EtOH); ir (Nujol): 3350, 1700, 1650, 1550 cm^{-1}. *Anal.* calcd. for $C_{16}H_{22}N_2O_5{\cdot}\frac{1}{2}H_2O$: C 57.99, H 6.99, N 8.45; found: C 57.66, H 6.90, N 8.19.

*Oxazoline **17**a*

To a solution of 37.1 g (112 mmol) of **15** in dry DMF, (110 ml) was added 50 ml triethyl orthoacetate and 15 ml boron trifluoride etherate and the solution, protected from moisture, was stirred at room temperature for 20 h. The mixture was then poured into a cold solution of 8% sodium bicarbonate (1 ℓ) and extracted with ether (4 × 350 ml). The ether solution was washed with water (2 × 250 ml), dried ($MgSO_4$), and evaporated to dryness to yield a syrup which crystallized on trituration with ether to give 31.2 g (78.5%) of **17***a*, mp 108–112°C. Thin-layer chromatography with 5% ethanol–ether showed, under uv, a major spot of R_f 0.54 (**17***a*) and a minor one of R_f 0.85. This material was used in the next experiment without further purification. A small sample was recrystallized from ethyl acetate-petroleum ether (1:3), mp 111–113°C; $[\alpha]_D^{25}$ −64.2 (*c* 1.0, EtOH); ir (Nujol): 3350, 1730, 1690, 1660, 1640, 1540 cm^{-1}. *Anal.* calcd. for $C_{18}H_{22}N_2O_5$: C 62.41, H 6.40, N 8.09; found: C 62.54, H 6.43, N 7.95.

*Oxazoline **17**b*

To a solution of 2.0 g (5.8 mmol) of **17***a* in 25 ml dry ethanol, was added 25 mg sodium hydride (a 55% suspension in oil from which the oil was removed by washing with benzene) and stirred at room temperature for 30 min. The solution was filtered to remove some insoluble matter, the filtrate was neutralized with carbon dioxide and evaporated to dryness. The residue was taken up in chloroform (30 ml) and the solution washed with water (2 × 30 ml), dried, and evaporated to yield 1.75 g (100%) **17***b*, mp 147–150°C. Recrystallization from benzene (6 ml) – petroleum ether (10 ml) gave 1.42 g, mp 149–150°C; tlc (5% ethanol–ether, uv) showed a single spot of R_f 0.55; $[\alpha]_D^{25}$ −98.6 (*c* 1.0, EtOH); ir (Nujol): 3300, 3200, 1700, 1645, 1610 cm^{-1}. *Anal.* calcd. for $C_{16}H_{20}N_2O_4$: C 63.14, H 6.62, N 9.20; found: C 63.39, H 6.81, N 8.47.

*(1S,2S,4R,5R)-5-Acetoxy-2-benzamido-4-ethoxycarbonylaminocyclohexanethiol Benzoate (**18**a)*

The procedure was the same as in the synthesis of **10***a* above except that no *p*-toluenesulfonic acid was added. Thus, a mixture of 31.0 g (89.5 mmol) of powdered **17***a*, 35.0 g (250 mmol) of thiobenzoic acid and 24 ml of dry DMF was heated in an oil bath at 115°C under nitrogen for 1.5 h. Work-up as in **10***a* gave 33.2 g (76.5%) of **18***a*, mp 240–247°C; $[\alpha]_D^{25}$ −9.7 (*c* 1.0, $CHCl_3$); ir (Nujol): 3350, 1730, 1700, 1665, 1585, 1540 cm^{-1}. *Anal.* calcd. for $C_{25}H_{28}N_2O_6S$: C 61.97, H 5.82, N 5.71, S 6.62; found: C 61.81, H 5.86, N 5.84, S 6.66.

*(1S,2S,4R,5R)-2-Benzamido-4-ethoxycarbonylamino-5-hydroxycyclohexanethiol (**18**b)*

A suspension of 32.8 g (68 mmol) of **18***a* in 330 ml of a 1 *N* solution of sodium hydroxide in 80% ethanol–water was stirred under nitrogen at room temperature for 1.5 h. Work-up as in the cases of **10***b* and **13***b* above gave 21.2 g (92%) of **18***b*, mp 260–265°C (dec.) (decomposition started at 252°C with an offensive odor). Thin-layer chromatography with 20% ethanol–ether showed one spot (R_f 0.38). This material was used in the next experiment. A sample was recrystallized from ethanol, mp 266–270°C (dec.); $[\alpha]_D^{25}$ +32.9 (*c* 1.0, pyridine); ir (Nujol): 3300, 1735, 1640, 1550 cm^{-1}. *Anal.* calcd. for $C_{16}H_{22}N_2O_4S$: C 56.78, H 6.55, N 8.82, S 9.47; found: C 56.50, H 6.35, N 8.14, S 9.24.

*(1S,2S,4R,5R)-2-Benzamido-4-ethoxycarbonylamino-5-hydroxycyclohexanethiol Benzoate (**18**c)*

This compound was prepared by the procedure given above for the synthesis of **10***a*. A mixture of 2.41 g (7.9 mmol) of **17***b*, 5.5 g (50 mmol) of thiobenzoic acid and 2.0 ml of DMF was heated at 115°C for 1.5 h and the product isolated as above to give 2.49 g (71%) of **18***c*, mp 225–230°C. Recrystallization from ethanol (85 ml) yielded 1.96 g, mp 230–232°C. Thin-layer chromatography with 5% ethanol–chloroform showed one spot of R_f 0.49; $[\alpha]_D^{25}$ +45.2 (*c* 1.0, DMF); ir (Nujol): 3400, 1700, 1660, 1640, 1540 cm^{-1}. *Anal.* calcd. for $C_{23}H_{26}N_2O_5S$: C 62.42, H 5.92, N 6.33, S 7.24; found: C 62.45, H 5.96, N 6.36, S 7.32.

*(1S,2S,4R,5R)-2,4-Diamino-5-hydroxycyclohexanethiol (**3**) Dihydrochloride*

Compound **18***b* (6.0 g, 17.8 mmol) was hydrolyzed with hydrochloric acid as in the procedure given for **2** to yield 3.64 g (87%) of **3** dihydrochloride, mp: decomposes above 290°C (turns black) with an offensive smell. Thin-layer chro-

matography (H_2O–NH_4OH–MeOH–$CHCl_3$, sprayed with ninhydrin) showed a single spot; $[\alpha]_D^{25}$ +2.8 (*c* 1.0, H_2O); ^{1}Hmr (D_2O) δ: 3.78 (d of t, 1H, O—C—H, J_1 = 10.4, J_2 = 4.5 Hz), 3.36 (d of t, 1H, N—C—H, J_1 = 10.4, J_2 = 4.5 Hz), 3.28 (d of t, 1H, N—C—H, J_1 = 10.4, J_2 = 4.5 Hz), 3.08 (d of t, 1H, S—C—H, J_1 = 10.4, J_2 = 4.5 Hz), 2.76–2.38 (m, 2H, H_e of CH_2), 2.11–1.44 (m, 2H, H_a of CH_2). *Anal.* calcd. for $C_6H_{14}N_2OS \cdot 2HCl$: C 30.64, H 6.86, N 11.91, S 13.63; found: C 30.33, H 6.92, N 11.61, S 13.25.

*1-N-Benzoyl-3-N-ethoxycarbonyl-2,5-dideoxystreptamine (**20**)*

Compound **19** (8) ($[\alpha]_D^{25}$ +37.3) was *N*-benzoylated by the procedure described above for the synthesis of **15** to give **20** (91%), mp 244°C, resolidified and melted at 254–256°C; $[\alpha]_D^{25}$ +17.6 (*c* 0.8, EtOH); ir (Nujol): 3350, 1700, 1650, 1550 cm^{-1}. *Anal.* calcd. for $C_{16}H_{22}N_2O_5$: C 59.61, H 6.88, N 8.69; found: C 59.65, H 7.01, N 8.70.

Oxazoline **22**a

Compound **20**, (6.0 g, 18.2 mmol) was reacted with triethyl orthoacetate (9 ml) and boron trifluoride etherate (2.0 ml) in dry DMF (19 ml), as described in the preparation of **17***a*, to give 5.5 g (88%) crude **22***a* as a solid. Thin-layer chromatography with 5% ethanol–ether showed one major spot of R_f 0.53 and a minor one of R_f 0.90. This material was used in the next reaction. The analytical sample was obtained after three recrystallizations from ethyl acetate (1.5 ml/g) – petroleum ether (6 ml/g), mp 111–113°C; one spot on tlc; $[\alpha]_D^{25}$ +63.7 (*c* 1.0, EtOH); ir (Nujol): 3350, 1745, 1700, 1655, 1550 cm^{-1}. *Anal.* calcd. for $C_{18}H_{22}N_2O_5$: C 62.41, H 6.40, N 8.09; found: C 62.35, H 6.43, N 8.09.

Oxazoline **22**b

Compound **22***a* (5.4 g, 15.6 mmol) was treated with a catalytic amount of sodium ethoxide in ethanol, following the procedure described in the preparation of **17***b*, to give 4.5 g (95%) of **22***b*, mp 145–150°C; one spot on tlc (5% methanol–ether) of R_f 0.61. Recrystallization from benzene (3.5 ml/g) – petroleum ether (4.5 ml/g) gave the analytical sample, mp 148–150°C; $[\alpha]_D^{25}$ +100.6 (*c* 1.0, EtOH); ir ($CHCl_3$): 3450, 1735, 1640, 1550 cm^{-1}. *Anal.* calcd. for $C_{16}H_{20}N_2O_4$: C 63.14, H 6.62, N 9.20; found: C 63.39, H 6.81, N 8.47.

*(1R,2R,4S,5S)-2-Benzamido-4-ethoxycarbonylamino-5-hydroxycyclohexanethiol Benzoate (**23**c)*

This compound was prepared by the procedure described above for the synthesis of **18***c*. A mixture of 3.7 g (12.2 mmol) of **22***b*, 8.0 g of thiobenzoic acid, and 2.5 ml of DMF was heated at 115°C for 1.5 h and the product isolated as above to give 3.4 g (63%) of **23***c*, mp 225–231°C. Recrystallization from ethanol yielded 3.0 g, mp 230–231°C; $[\alpha]_D^{25}$ −46.3 (*c* 1.0, DMF); ir (Nujol): 3300, 1700, 1660, 1640, 1540 cm^{-1}. *Anal.* calcd. for $C_{23}H_{26}N_2O_5S$: C 62.42, H 5.92, N 6.33, S 7.24; found: C 62.49, H 5.96, N 6.36, S 7.37.

*(1R,2R,4S,5S)-2-Benzamido-4-ethoxycarbonylamino-5-hydroxycyclohexanethiol (**23**b)*

A mixture of 300 mg of **23***c* and 3.3 ml of 1 *N* sodium hydroxide in 80% ethanol was stirred at room temperature under nitrogen for 1 h. It was then diluted with water (7 ml), neutralized with carbon dioxide (gas), and the crystalline precipitate was collected by filtration and washed with water (3 × 5 ml). Drying at 100°C under vacuum, gave 200 mg of **23***b*, mp 268–272°C; $[\alpha]_D^{25}$ −33.0 (*c* 1.0, pyridine); ir (Nujol): 3250, 3310, 1690, 1640, 1540 cm^{-1}.

*(1R,2R,4S,5S)-2,4-Diamino-5-hydroxycyclohexanethiol (**4**) Dihydrochloride*

Compound **23***b* was hydrolyzed with a hydrochloric acid – acetic acid mixture as in the procedure given for **2** to yield the dihydrochloride of **4**, mp: decomposes above 290°C with an offensive smell; $[\alpha]_D^{25}$ −2.8; ^{1}Hmr (D_2O) δ: 3.78 (d of t, 1H, O—C—H, J_1 = 10.4, J_2 = 4.5 Hz), 3.36 (d of t, 1H, N—C—H, J_1 = 10.4, J_2 = 4.5 Hz), 3.28 (d of t, 1H, N—C—H, J_1 = 10.4, J_2 = 4.5 Hz), 3.08 (d of t, 1H, S—C—H, J_1 = 10.4, J_2 = 4.5 Hz), 2.76–2.38 (m, 2H, H_e of CH_2), 2.11–1.44 (m, 2H, H_a of CH_2).

1. W. T. Shier, K. L. Rinehart, Jr., and D. Gottlieb. Proc. Natl. Acad. Sci. U.S.A. **63**, 198 (1969).
2. W. T. Shier, K. L. Rinehart, Jr., and D. Gottlieb. U.S. Patent No. 2,669,838 (June 13, 1972); Chem. Abstr. **77**, 150584x (1972).
3. M. Kojima and A. Satoh. J. Antibiot. **26**, 784 (1973).
4. C. A. Claridge, J. A. Bush, M. D. Defuria, and K. E. Price. Dev. Ind. Microbiol. **15**, 101 (1974).
5. K. Nogaoka and A. L. Demain. Bacteriol. Proc. **19**, (1974).
6. R. T. Testa, G. H. Wagman, P. J. L. Daniels, and M. J. Weinstein. J. Antibiot. **27**, 917 (1974).
7. W. T. Shier, P. C. Schaefer, D. Gottleib, and K. L. Rinehart, Jr. Biochemistry, **13**, 5073 (1974).
8. G. Kavadias, S. Velkof, and B. Belleau. Can. J. Chem. **56**, 404 (1978).
9. G. E. McCasland, R. K. Clark, Jr., and H. E. Carter. J. Am. Chem. Soc. **71**, 637 (1949).
10. S. Winstein and R. Boschan. J. Am. Chem. Soc. **72**, 4669 (1950).
11. W. S. Johnson and E. N. Schubert. J. Am. Chem. Soc. **72**, 2187 (1950).
12. H. E. Khadem. Adv. Carbohydr. Chem. **25**, 351 (1970).
13. L. Goodman. Adv. Carbohydr. Chem. **22**, 109 (1967).
14. J. A. Frump. Chem. Rev. **71**, 483 (1971).
15. (*a*) E. M. Fry. J. Org. Chem. **15**, 802 (1950); (*b*) R. F. Lambert and C. E. Kristofferson. J. Org. Chem. **30**, 3938 (1965); (*c*) C. R. Bresson. U.S. Patent No. 3,351,664 (November, 1967); Chem. Abstr. **68**, 95331 (1968).
16. T. Taguchi and M. Kojima. J. Am. Chem. Soc. **78**, 1464 (1956).
17. C. V. Pittman, Jr., S. P. McManus, and J. W. Larsen. Chem. Rev. **72**, 357 (1972).
18. R. P. Louthan, C. R. Bresson, and R. L. Cobb. U.S. Patent No. 3,257,301 (June 21, 1966); Chem. Abstr. **65**, 13573g (1966).

Can. J. Chem. Downloaded from www.nrcresearchpress.com by 210.87.254.105 on 09/05/12
For personal use only.

Field desorption mass spectrometry of carboxylate salts: characteristic spectra and effects of added complexing agents[1]

GORDON WALTER WOOD,[2] EMILY JANE OLDENBURG, AND PUI-YAN LAU
Department of Chemistry, University of Windsor, Windsor, Ont., Canada N9B 3P4

Received May 12, 1978

GORDON WALTER WOOD, EMILY JANE OLDENBURG, and PUI-YAN LAU. Can. J. Chem. **56**, 2750 (1978).

Field desorption mass spectra are reported for a series of sodium carboxylates. Above 20 mA the major ions in the spectra belong to the series $[x\mathrm{Na}^+ + (x - 1)\mathrm{RCOO}^-]^+$ with values of x normally extending throughout the measurable mass range. Desorption characteristics and spectral composition have been shown to be strongly modified by the addition of fructose and other polyhydroxy compounds. Thus, the sodium acetate spectrum is more intense and contains higher aggregates when 0.1–0.2 mol of fructose is added. With further additions the ionized free acid, $\mathrm{AcOH}^{+}\cdot$, becomes the base peak in a low intensity spectrum recorded at 17–18 mA. The main ion from fructose is the sodium complex which does not exceed 20% of the base peak. Added fructose also has a beneficial effect on sodium 12-hydroxystearate but the improvement is less dramatic and there are some complications in the interpretation. A sample of technical lithium stearate contains the usual complexes up to $[\mathrm{Li}_4(\mathrm{RCOO})_3]^+$ and the presence of important amounts of palmitate gives rise to all possible combinations of the two carboxylate anions in these complexes. Smaller amounts of $\mathrm{Li}_2\mathrm{Na}$, $\mathrm{Li}_3\mathrm{Na}$, and $\mathrm{Li}_3\mathrm{K}$ complexed with the appropriate number of anions give evidence of alkali metal impurity.

GORDON WALTER WOOD, EMILY JANE OLDENBURG et PUI-YAN LAU. Can. J. Chem. **56**, 2750 (1978).

On rapporte les spectres de masse par désorption de champs d'une série de carboxylates de sodium. Au-dessus de 20 mA, les ions prépondérants dans le spectre de masse proviennent des séries $[(x\mathrm{Na}^+ + (x - 1)\mathrm{RCOO}^-)]^+$ dans lesquelles les valeurs de x s'étendent normalement à travers toutes les masses pouvant être mesurées. On a montré que les caractéristiques de désorption et les compositions spectrales sont fortement modifiées par l'addition de fructose et d'autres composés polyhydroxylés. Ainsi le spectre de l'acétate de sodium est plus intense et contient des agrégats supérieurs si l'on additionne 0.1–0.2 mol de fructose. Si l'on effectue des additions supplémentaires, l'acide libre ionisée $\mathrm{AcOH}^{+}\cdot$ devient le pic prépondérant dans le spectre à basse intensité enregistré à 17–18 mA. L'ion principal du fructose est un complexe de sodium qui ne représente pas plus de 20% du pic prépondérant. L'addition de fructose conduit aussi à un effet bénifique sur l'hydroxy-12 stéarate de sodium mais l'amélioration est moins dramatique et amène quelques complications dans l'interprétation. Un échantillon de stéarate de lithium de qualité technique contient les complexes habituels allant jusqu'à $[\mathrm{Li}_4(\mathrm{RCOO})_3]^+$ et la présence de quantités importantes de palmitate donne lieu à toutes les combinaisons possibles des deux anions carboxylate dans ces complexes. Des quantités plus faibles de $\mathrm{La}_2\mathrm{Na}$, $\mathrm{Li}_2\mathrm{Na}$ et $\mathrm{Li}_3\mathrm{K}$ complexés avec un nombre approprié d'anions indiquent que les métaux alcalins sont impurs.

[Traduit par le journal]

Introduction

Mixtures of long chain carboxylic acids and their salts are common commercial materials whose properties depend critically on their composition. In a previous paper (1) we have reported on the application of field desorption mass spectrometry (fdms) to analysis of mixtures and impure samples of such carboxylic acids. We now report fdms results on a variety of carboxylate salts, mainly sodium. Although fdms is particularly suited for the handling of non-volatile samples (2–5), early work on sodium acetate (6) and other alkali metal salts (7) showed that collection of useful data from these compounds presented a considerable challenge. For example, the fd spectrum originally reported for sodium acetate (6) was obtained at very high temperature (30–32 mA) and contained few ions of structural significance. We have shown that some improvement in the characteristics of this compound may be obtained by complexation of the sodium ion with a cryptand (8). The present work examines the behavior of a variety of carboxylate salts and the effect on fdms of added complexing agents, especially fructose.

Experimental

The instrumental parameters and methods of sample introduction have been described previously (1).

Fructose, inositol, and other polyhydroxy compounds were

[1]Taken in part from the M.Sc. thesis of E.J.O., University of Windsor, Windsor, Ont., 1977.

[2]To whom correspondence should be addressed.

Can. J. Chem. Downloaded from www.nrcresearchpress.com by 210.87.254.40 on 09/05/12
For personal use only.

TABLE 1. Field desorption mass spectra of some sodium carboxylates, RCOONa[a]

Compound	R	Solvent	ahc[b]	Ions $[xNa^+ + (x-1)RCOO^-]^+$ $x=1$	$x=2$	$x=3$	$x=4$
Na acetate[c]	CH_3	H_2O	22	*100*	21	16	16
Na caproate	C_5H_{11}	CH_3OH	20.5	27	9	36	*100*
Na heptanoate	C_6H_{13}	CH_3OH	21.5	26	8	34	*100*
Na stearate[d]	$C_{17}H_{35}$	CH_3OH	23	—	*100*	12	
		H_2O	23	*100*	14		
Na 12-OHstearate		$CHCl_3/CH_3OH$	20.5	99	100	1	

[a]Intensities are expressed as % of base peak.
[b]Anode heating current (mA).
[c]For this low formula weight salt, the high-mass cutoff is arbitrary. Thus the ion with $x = 5$ amounts to as much as 5% in some scans and traces of $x = 6$, $x = 7$ generally are present.
[d]Evidence that this salt is impure is found in ions *m/e* 301 (up to 18%) and traces of *m/e* 357, 385. These peaks are assigned as the $x = 2$ complexes of C_{16}, C_{20}, and C_{22} salts, respectively.

purchased from Aldrich Chemical. Cryptands (Krypto fixes) were purchased from EM Laboratories, Elmsford, NY. Carboxylate salts were kindly donated by Imperial Oil Enterprises Ltd., Sarnia.

All solvents and other reagents were ACS grade and were used without further purification.

Results and Discussion

In addition to some preliminary experiments with sodium salts which ultimately led to the work reported in this paper, a few measurements were made on calcium propionate and calcium hexanoate. Although both of these salts gave ions which appeared to be the usual net monopositive complexes, i.e. *m/e* 299 for the propionate corresponding to $3CH_3CH_2COO^- + 2Ca^{2+}$, a number of complications led us to postpone further work on salts of divalent metals. Our sample of calcium propionate was significantly contaminated with both sodium and potassium ions. Further, this material gave fd mass spectra containing ions of unknown composition at all anode temperatures tried (23.5, 32, 44 mA). At the highest temperature the only significant ions corresponded to Ca^+ (*m/e* 40, 100; 42, 1.4; 43, 1.1; 44, 3.1), which raises questions as to its origin and possible presence in complex ions at lower temperatures.

Carboxylates related to the univalent, monoisotopic sodium ion are considerably simpler, as the examples in Table 1 show. The major ions for each of the five salts all belong to the series $[xNa^+ + (x-1)RCOO^-]^+$. Since the relative intensity of the various complexes is very sensitive to temperature, duplication of the exact values shown is difficult. Another factor which influences the spectrum is the solvent used. For example, deposition of sodium stearate from a water suspension gives Na^+ as base peak. In general the degree of complexation appears to be a function of solvent, with methanol favoring formation of aggregates more than water.

We have tried a number of strategies to improve on the high desorption temperatures, low ion intensities, and short-time fluctuations of ion current characteristic of sodium salts under fdms conditions. Following our earlier approach using ligands for sodium ion complexation (8), we determined the fd spectrum of an equimolar mixture of sodium 12-hydroxystearate and [2.2.1]-cryptand. As expected desorption occurred smoothly and at lower temperature (12 mA). The base peak at *m/e* 355 corresponds to the cryptate Na^+ + ligand. Ions at *m/e* 654 (cryptate + 12-OHstearate) and *m/e* 610 (decarboxylation product of *m/e* 654) were about 2–3% relative intensity and thus not easily reproduced. Combination of the same cryptand with sodium stearate yielded either empty cryptand, cryptate, or free sodium ion as base peak, depending on the temperature. No peaks of significance contained the carboxylate portion of the salt. A similar experiment with the [2.2.1]-cryptand and sodium acetate in chloroform solution gave some evidence of cryptate formation, but the main effect noted was a lower desorption temperature. We therefore turned to other potential complexing agents for the sodium ion, with the aim of finding a ligand less easily desorbed so that ions related to the carboxylate portion of the salt would be of greater relative intensity.

Of several sugars and related compounds evaluated, fructose appeared most promising. Table 2 presents the results obtained for a series of sodium acetate samples to which up to equimolar amounts of fructose have been added. By comparison with the first column for pure sodium acetate, it can be seen that 0.1:1 molar ratio of fructose-to-salt increases the overall intensity almost threefold and, more importantly, increases the intensity of the structurally significant $[Na_2OAc]^+$ on a relative basis. At 0.2:1 molar ratio of fructose-to-salt, the next member of this series of complexes, $[Na_3OAc_2]^+$, becomes the base peak and the total intensity again increases almost threefold. Notice should be taken at this stage that the first evidence of fructose in the sample appears as *m/e* 203 (Na^+ + fructose) with intensity of 1%. The only other fructose-related peaks ob-

Can. J. Chem. Downloaded from www.nrcresearchpress.com by 210.87.254.40 on 09/05/12
For personal use only.

TABLE 2. Field desorption mass spectra of sodium acetate/fructose mixtures[a]

	Molar ratio of fructose:salt					
	0:1	0.1:1	0.2:1	0.5:1	1:1	
ahc[b]	22	24.5	23	18	17	
int.[c]	120	340	850	0.5	0.7	
m/e						Assignment
23	*100*	93	47	35	18	Na^+
60				*100*	*100*	$AcOH^+\cdot$
102				22	?	$Ac_2O^+\cdot$
105	21	*100*	85	8		Na_2OAc^+
187	15	17	*100*			$Na_3OAc_2^+$
203			1	18	4	Na^+ + fructose
269	16	8	52			$Na_4OAc_3^+$
351	3	1	4			$Na_5OAc_4^+$

[a]Sample was loaded from aqueous solution. Intensities are expressed as % of base peak. All *m/e* values are reported where at least one mixture consistently gave a peak of 1% or more. At fructose levels below 0.5:1, minor peaks were also found for Na_6OAc_5, Na_7OAc_6, and Na_8OAc_7. Other minor peaks appeared to derive from sodium formate and propionate (see text).
[b]Anode heating current (mA).
[c]Total ion beam intensity in an arbitrary unit roughly equivalent to 1000 ions.

served correspond to dehydration (*m/e* 162, 144, etc.) and are very weak. With 0.5:1 or more molar ratio of fructose-to-salt, there is a dramatic change in the result. Spectra are now obtained at much lower temperatures and with much lower intensity. The base peak at molar ratios of fructose-to-salt at 0:5:1 and 1:1 is *m/e* 60, $[AcOH]^+\cdot$! The complexed fructose ion *m/e* 203 is relatively important and is found as base peak for 1:1 mixture below 13 mA, but the usual complexes of sodium and acetate ions have almost disappeared. In summary, the addition of 0.1–0.5 mole of fructose per mole of sodium acetate has been shown to significantly increase the relative amount of structurally significant ions, largely at the expense of Na^+, and with virtually no interference from the fructose. The formation of the conjugate acid of the original anion at 0.5:1 molar ratio of fructose-to-salt and above is interesting, and raises the possibility that with a less volatile compound this process would yield more useful ion intensities. With this point in mind we have repeated the series of fructose additions with sodium stearate. The free acid (*m/e* 284) is the base peak in some scans with 0.5:1 or 1:1 molar ratio of fructose-to-salt, and there is evidence for the formation of $Na_x(RCOO)_{x-1}$ complexes at least as far as the mass-scale cut-off ($x = 3$). However, apparent decarboxylation and oligomer formation complicates the results.

In the sodium acetate/fructose mixtures we observed minor ions at *m/e* 91, 119, 173, 201, 255, 337 which we assign to two series as follows:

$$[Na_2OOCH]^+ + x(NaOAc) = 91, 173, 255, 337 \quad \text{for } x = 0, 1, 2, 3$$

$$[Na_2OOCCH_2CH_3]^+ + x(NaOAc) = 119, 201 \quad \text{for } x = 0, 1$$

Intensities of these ions are quite variable, and rarely greater than 1% of base peak. However, the presence of *m/e* 74 in some scans of the 0.5:1 mixture at moderate ahc values suggests that these ions may reflect sodium formate and sodium propionate in the original sample. An alternate interpretation which considers the above complexes to be "products of thermally field-induced decomposition reactions" (2) appears to us unlikely in view of the apparent lack of field or temperature dependence. Experiments designed to resolve the discrepancies among previous reports on sodium acetate behavior (2, 6, 7) and to clarify the structural assignments are in progress.

Addition of varying amounts of fructose to a series of 12-OH stearate samples gave the results in Table 3. Although in some respects the results here are less dramatic than for sodium acetate, the presence of structurally important ions from 0.2–1.0 molar ratio of fructose-to-salt must be viewed in the context of the result for the original sample. The base peak at *m/e* 345 and the ion at *m/e* 667 belong to the usual prominent series of complex ions, $[xNa^+ + (x - 1)RCOO^-]^+$. Apparent loss of 2H from the hydroxyanions of *m/e* 667 gives *m/e* 665 and the ions at *m/e* 183, 184 present complications for identification. We suggest that the latter may represent doubly charged ions of mass 368, 366 which would then correspond to $[3Na^+ + RCOO^-]^{2+}$ and a similar ion with two less H atoms. The mode of loss of these H atoms is unknown, but ions at *m/e* 345, 343 and 506, 505 appear to be other pairs where this process is occurring, the former from singly charged species and the latter from $[5Na^+ + 3RCOO^-]^{2+}$. Whereas the formation of doubly charged ions may be associated with coordination of an extra sodium ion at the hydroxyl function, the as yet unexplained

Can. J. Chem. Downloaded from www.nrcresearchpress.com by 210.87.254.40 on 09/05/12
For personal use only.

TABLE 3. Field desorption mass spectra of sodium 12-hydroxystearate/fructose[a]

	Molar ratio of fructose:salt				
	0:1	0.2:1	0.5:1	1:1	
ahc[b]	20.5	19.5	19	20	
int.[c]	0.5	3.4	28	3.9	
m/e					Assignment
23	99			75[d]	Na^+
183		2	23	4	
184		27	51	39	$[Na_3RCOO]^{2+}$
329		2	9		$[Na_2R'COO]^{+}$[e]
343		18	21	15	
345	*100*	*100*	*100*	*100*	$[Na_2RCOO]^+$
505		2	2	2	
506		2	2	1	$[Na_5(RCOO)_3]^{2+}$
651		3	5	2	$[Na_3(RCOO)(R'COO)]^{+}$[e]
665		14	13	11	
667	1	87	29	43	$[Na_3(RCOO)_2]^+$
828			4		$[Na_7(RCOO)_5]^{2+}$

[a]Sample was loaded from aqueous solution. Intensities are expressed as % of base peak.
[b]Anode heating current (mA).
[c]Total ion beam intensity in an arbitrary unit roughly equivalent to 1000 ions.
[d]Lower temperature scans contained less sodium as well as less variety of complex ions.
[e]R'COO = stearate, an apparent impurity in this sample.

presence of doubly charged ions in technical grade samples of the free acid (1) where no sodium is involved provides the possibility of another mechanism. Another result of this experiment is the identification of minor ions *m/e* 329, 651, apparently from the presence of sodium stearate impurity in the samples.

An attempt to compare cation effects on stearate spectra was largely frustrated by poor desorption characteristics of calcium and ammonium stearates. Both gave very weak spectra, the former not readily interpreted and the latter showing only *m/e* 284, 283, apparently $M^{+\cdot}$ and $[M - 1]^+$ for stearic acid. Clarification of these results and those for lithium stearate will require scrupulously pure samples. However, the technical lithium salt gave a number of assignable ions as shown in Scheme 1. Note that in addition to sodium and potassium ion impurities, there is sufficient apparent C_{16} homologue that the base peak in each of the three most intense scans contains the species $C_{15}H_{31}COO$. It is also striking that for both the prominent Li_3 and Li_4 species all possible combinations of the two carboxylates are found.

The behavior of mixtures of sodium acetate with inositol (the common *myo* isomer) was quite different from that found with the fructose mixtures. Considering that inositol appears to bind to Na^+ at least as strongly as most polyhydroxy compounds and that fructose is not known to form particularly stable complexes (9, 10), our results may suggest that the effects we are observing should properly be considered as matrix effects rather than the direct result of complexation. Further study of this point is in progress. Our inositol sample gave extremely weak spectra with the maximum intensity of M at 14–16 mA. Later scans showed dehydration peaks and, above 25 mA, M + Na (*m/e* 203). Addition of 0.2, 0.5, and 1.0 mol of inositol to 1.0 mol of sodium acetate gave spectra of intermediate intensity in

Na^+, K^+

$[Li_2C_{17}H_{35}COO]^+$, $[Li_2C_{15}H_{31}COO]^+$

$[Li_3(C_{17}H_{35}COO)_2]^+$, $[Li_3(C_{15}H_{31}COO)_2]^+$, $[Li_3(C_{17}H_{35}COO)(C_{15}H_{31}COO)]^+$

$[Li_4(C_{17}H_{35}COO)_3]^+$, $[Li_4(C_{15}H_{31}COO)_3]^+$, $[Li_4(C_{17}H_{35}COO)_2(C_{15}H_{31}COO)]^+$, $[Li_4(C_{17}H_{35}COO)(C_{15}H_{31}COO)_2]^+$

$[Li_3Na(C_{17}H_{35}COO)_2(C_{15}H_{31}COO)]^+$, $[Li_3K(C_{17}H_{35}COO)_2(C_{15}H_{31}COO)]^+$

$[Li_2Na(C_{17}H_{35}COO)(C_{15}H_{31}COO)]^+$

SCHEME 1. Principal ionic species in fdms of technical lithium stearate. Ions in italics were base peaks in individual scans (21–23 mA)

Can. J. Chem. Downloaded from www.nrcresearchpress.com by 210.87.254.40 on 09/05/12
For personal use only.

Can. J. Chem. Downloaded from www.nrcresearchpress.com by 210.87.254.40 on 09/05/12
For personal use only.

which the acetic acid ion was prominent. For example, the 0.2:1 mixture showed *m/e* 60 as base peak up to 20 mA. At 19 mA and a total intensity of 0.8 units (see Table 2, footnote *c*) the spectrum consisted of: *m/e* (%) 60 (100); 203 (8). At higher temperatures *m/e* 23 quickly became the base peak, but the usual complex ions were not very important. Thus, at 26 mA *m/e* 23 (100); 105 (6); 187 (2); 269 (0.4). With 0.5:1 mixtures *m/e* 60 was marginally stronger: 16 mA, intensity 1.1 units gave *m/e* 60 (100); 23 (62); 203 (41). The acetic acid ion was also more persistent in this mixture, so that at 20 mA where *m/e* 23 was base peak, *m/e* 60 (10) still accounted for 3.0 units. Increasing the inositol level to 1:1 generally gave more *m/e* 60 ions at lower ahc values: at 14.5 mA, *m/e* 60 (100, 0.8 units); 203 (5), 126 (2). In the next scan, 16 mA, *m/e* 23 appeared and the apparent dehydration product of inositol, *m/e* 126, increased to 13%. In summary, inositol is more effective than fructose in generating the conjugate acid, *m/e* 60, from sodium acetate but much less effective in promoting complexation reactions.

The considerable complications in obtaining useful spectra from sodium carboxylates have somewhat dimmed our hopes of analyzing mixtures containing these salts in combination with free acids. However, one brief study was done on a technical mixture of stearic acid and its sodium salt. At 9 mA the two most important ions are *m/e* 284, 285 ($M^{+\cdot}$ and $M + 1^+$ for the acid). At 27 mA *m/e* 23, 329, and 635 no doubt represent $[Na_x(C_{17}H_{35}COO)_{x-1}]^+$ with $x = 1$, 2, and 3. However, the presence of equally intense ions *m/e* 357, 691 strongly suggests the presence of a C_{20} homologue and an ion *m/e* 522 at intermediate temperatures may even represent a stearyl stearate ester. These uncertainties could no doubt be resolved by preparation of authentic mixtures for comparison with this technical product. However, one is left with a broad range of desorption temperatures, all of which would have to be monitored and the appropriate ion intensities summed in order to arrive at an estimate of the composition of the original mixture. The necessary techniques should not be too different from those employed for quantitation of a mixture introduced via the direct probe in electron impact mass spectrometry.

Acknowledgements

Support of this work by an Imperial Oil Limited University Research Grant and by the National Research Council of Canada is gratefully acknowledged. Helpful discussions with Dr. Gordon Alexander, Imperial Oil Enterprises Ltd., Sarnia, who also provided samples of technical grade salts, are acknowledged with thanks.

1. G. W. Wood, E. J. Oldenburg, P.-Y. Lau, and D. L. Wade. Can. J. Chem. **56**, 1372 (1978).
2. H. D. Beckey. Principles of field ionization and field desorption mass spectrometry. Pergamon, Oxford. 1977.
3. H. D. Beckey and H.-R. Schulten. Angew. Chem. Int. Ed. Engl. **14**, 403 (1975).
4. A. L. Burlingame, B. J. Kimble, and P. J. Derrick. Anal. Chem. **48**, 368R (1976).
5. R. A. W. Johnstone (*Editor*). Mass spectrometry. Vol. 4. Specialist Periodical Report, The Chemical Society, London. 1977. pp. 107, 138.
6. H.-R. Schulten and H. D. Beckey. Org. Mass Spectrom. **6**, 885 (1972).
7. H.-R. Schulten and F. W. Röllgen. Org. Mass Spectrom. **10**, 649 (1975).
8. G. W. Wood, P.-Y. Lau, and N. Mak. Biomed. Mass Spectrom. **1**, 425 (1974).
9. S. J. Angyal. Pure Appl. Chem. **35**, 131 (1973).
10. C. Detellier, J. Grandjean, and P. Laszlo. J. Am. Chem. Soc. **98**, 3375 (1976).

Nitration and bromination of 1,1-diphenyl-2-(2-thienyl)ethylene

FRANCESCO A. BOTTINO, GIUSEPPE C. PAPPALARDO, GIUSEPPE SCARLATA, DOMENICO SCIOTTO, AND MICHELE TORRE

Istituto Dipartimentale di Chimica e Chimica Industriale, Universita' di Catania, Viale A. Doria 8, 95125 Catania, Italy

Received March 29, 1978

FRANCESCO A. BOTTINO, GIUSEPPE C. PAPPALARDO, GIUSEPPE SCARLATA, DOMENICO SCIOTTO, and MICHELE TORRE. Can. J. Chem. **56**, 2755 (1978).

The behaviour of 1,1-diphenyl-2-(2-thienyl)ethylene towards electrophilic agents (Br_2, HNO_3) has been investigated and the structure of reaction products assigned by uv, ^1H nmr spectra, and dipole moment measurements.

FRANCESCO A. BOTTINO, GIUSEPPE C. PAPPALARDO, GIUSEPPE SCARLATA, DOMENICO SCIOTTO et MICHELE TORRE. Can. J. Chem. **56**, 2755 (1978).

On a étudié le comportement du diphényl-1,1 (thiényl-2)-2 éthylène vis-à-vis les agents électrophiles (Br_2, HNO_3) et on a attribué la structure des produits de réaction sur la base des spectres uv et rmn ^1H et de moments dipolaires.

[Traduit par le journal]

Can. J. Chem. Downloaded from www.nrcresearchpress.com by 210.87.254.105 on 09/05/12
For personal use only.

Introduction

In connection with our previous work on reactivity and stereochemistry of stilbene systems containing heterocyclic rings (1–10), we here report the results of an investigation on the nitration and bromination of 1,1-diphenyl-2-(2-thienyl)ethylene (**1***a*).

An isomeric product of **1***a*, whose geometrical configuration has not been determined (**2***a*), has been reported by Nam *et al.* (ref. 11, and references cited therein), the bromination of which, in contrast with these results, leads to dibromo derivative **2***b*.

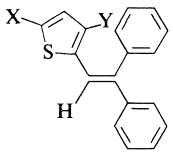

1

a X = Y = H
b X = NO_2, Y = H
c X = Y = Br

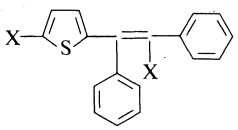

2

a X = H
b X = Br

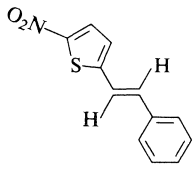

3

Results and Discussion

1,1-Diphenyl-2-(2-thienyl)ethylene (**1***a*) was prepared by a Wittig reaction from benzophenone and 2-thienylmethyltriphenyl-phosphonium chloride (see Experimental).

The nitration of **1***a* with nitric acid (slight molar excess) in acetic anhydride at 0°C gave a mono-nitration product (elemental analysis). The bromination with bromine (1 mol) in acetic acid afforded a mixture of products not yet identified; bromination with excess bromine at 0–5°C gave, in good yields, a dibromo compound as indicated by elemental analysis.

Ultraviolet Spectra

The electronic spectral data (λ_{max}, log ε) in 95% ethanol of the compounds investigated are reported in the Depository of Unpublished Data.[1]

The conjugation band of 1,1-diphenyl-2-(2-thienyl)ethylene (**1***a*) is located at higher wavelengths in comparison with that of triphenylethylene (12) owing to the presence of the heterocyclic ring ($\Delta\lambda$ = 23 nm), as already observed in the analogous diarylethylenes (2). The substitution in the thiophene ring shifts the absorption to longer wavelengths.

The strict similarity between absorption data of the nitration compound and *trans*-5-nitro-2-styryl-thiophene (**3**) is consistent with the proposed structure **1***b* for the former, as subsequently confirmed by ^1H nmr spectrum.

^1H Nuclear Magnetic Resonance Spectra

The analytical combustion data of the bromination product reveal the presence of two bromine atoms in the molecule (see Experimental). The ^1H nmr spectrum is available from the Depository of Unpublished Data.[1] The ratio between the integrated intensities of the sharp singlet at δ 6.83 and the complex signal in the range δ 7.1–7.5, is 1:11. ^1H nmr features are in agreement only with structure **1***c* where the thiophene nucleus for steric reasons is biased in the *s-trans*

[1]Photocopies are available, at a nominal charge, from the Depository of Unpublished Data, CISTI, National Research Council of Canada, Ottawa, Ont., Canada K1A 0S2.

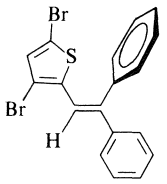

1*c*
s-trans

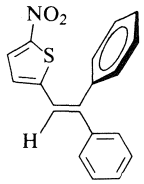

1*b*
s-trans

conformation. The assignment of the signal at δ 6.83 is still ambiguous between H_4 and the olefinic proton. All structures without bromine atoms on the thiophene nucleus can be excluded because of the absence in the ^1H nmr spectrum of ABX or AMX pattern of three heterocyclic protons. The absence of the characteristic AB or AM pattern of the heterocyclic protons on the ^1H nmr spectrum excludes the structure with only one bromine atom on the thiophene. Both bromine atoms are then situated on the heterocyclic ring. If the 3-position were free the signal at δ 6.83, which should be attributed to H_3 or H_{o1}, should resonate as doublet because of long-range coupling between H_3 and H_{o1} (9).

Likewise if the 5-position were free we should notice on the same signal a characteristic stereospecific W_5 plan coupling between H_5 and H_{o1} according to the *trans*-coplanar disposition of the H_{o1} and H_5 in the *s-trans* rotamer (9, 10). Consequently the sharp singlet at δ 6.83 can be interpreted only with structure **1***c*.

The analysis of the ^1H nmr spectrum of the mononitration compound is in agreement with structure **1***b*.[1] In fact the spectrum shows the pattern AMX respectively of the protons H_4, H_{o1}, and H_3, with the characteristic value (13) of the thiophene coupling constants between H_4 and H_3. The failure of the stereospecific W_5 plan coupling between H_4 and H_{o1} ($J^5_{H_4-H_{o1}} = 0.0$ Hz) (9) suggests that the *s-trans* conformation of the heterocyclic nucleus is preferred.

Electric Dipole Moments

Theoretical dipole moments for the three possible isomers of the bromination compound bearing Br atoms in 4,5-, 3,4-, and 3,5-position of the thiophene ring were calculated by means of the chemical vector addition method. The component moments used were the measured moment of **1***a* and the $\overrightarrow{C-Br}$ group moment assumed as 1.57 D (14).

By considering the very small difference between the experimental moments of **1***a* and thiophene (0.53 D) (14) moieties, we assumed the direction of action of the resultant moment of **1***a* to be the same as in thiophene, i.e., from the ring to the hetero atom. The geometry of the thiophene fragment was deduced from microwave spectroscopic data (15).

The occurrence of the possible structures 4,5- and 3,4-Br-substituted was thus ruled out on the basis of the large difference observed between the calculated theoretical moments for these structural isomers (2.42 and 2.15 D, respectively) and the measured value of 1.11 D.

Conversely, the calculated dipole moment for the remaining isomer bearing the Br atoms in 3,5-positions (0.85 D) agrees with the experimental value within the limit of accuracy of the vector addition method (±0.2–0.3 D). This dipole moment evidence thus allows us to decide unambiguously in favour of the 3,5-isomer as reaction product (**1***c*), consistent with above discussed ^1H nmr spectroscopic data.

Experimental

Melting points were taken on a Büchi melting point apparatus and are uncorrected. Ultraviolet absorption spectra were determined on a Hitachi Perkin-Elmer Model EPS-3T recording spectrometer in 95% ethanol solutions (1×10^{-5} mol). Proton magnetic resonance spectra were recorded with a Varian A-60D instrument in deuteriochloroform, using tetramethylsilane as internal standard. Electric dipole moments of **1***a* and of its brominated compound **1***c* were measured in benzene solutions at 25°C (±0.01°C) using apparatus and techniques described earlier in detail (16). The Halverstadt–Kumler method (17) was employed for calculating the total polarization ($P_{2\infty}$). The sum of the electronic and atomic polarizations ($P_E + P_A$) required for the calculation was assumed to be equal to the measured molar refraction (R_D, sodium D line). The estimated error in the measured dipole moment values (μ, Debye units) is ±0.03 D. The experimental results are available from the Depository of Unpublished Data.[1]

*1,1-Diphenyl-2-(2-thienyl)ethylene (***1***a)*

To a solution of 12 g of 2-thienylmethyltriphenylphosphonium chloride (18) (from 2-chloromethylthiophene (19) and triphenylphosphine in chloroform) and 3.64 g of benzophenone in 30 ml of ethanol, under nitrogen, was added portionwise with stirring a solution of EtONa (0.7 g of sodium in 25 ml of ethanol). The reaction mixture was refluxed for 6 h and then poured into water (50 ml). After cooling, the solid precipitate was filtered off and recrystallized from aqueous acetic acid (68% yield), mp 59°C. *Anal.* calcd. for $C_{18}H_{14}S$: C 82.40, H 5.38; found: C 82.50, H 5.22.

*Nitration of 1,1-Diphenyl-2-(2-thienyl)ethylene (***1***a)*

A solution of 1.3 g of olefin in 15 ml of acetic anhydride was nitrated at 0–5°C with nitric acid (1 g) in acetic acid (5 ml). The precipitate obtained was filtered off and washed with water; crystallization from ethanol gave a yellow product of mononitration (**1***b*) (65% yield), mp 153°C. *Anal.* calcd. for $C_{18}H_{13}NO_2S$: C 70.34, H 4.26, N 4.56; found: C 70.31, H 4.30, N 4.25.

*Bromination of 1,1-Diphenyl-2-(2-thienyl)ethylene (***1***a)*

A solution of bromine (1.6 g) in acetic acid (10 ml) was added to a cooled solution (10°C) of **1***a* (1.3 g) in the same solvent (20 ml) and the mixture kept for 24 h at room tem-

Can. J. Chem. Downloaded from www.nrcresearchpress.com by 210.87.254.105 on 09/05/12
For personal use only.

perature. The precipitate was collected, washed with water, and crystallized from ethanol to give 1.45 g (70%) of dibromo compound (**1***c*), mp 91°C. *Anal.* calcd. for $C_{18}H_{12}Br_2S$: C 51.45, H 2.88, Br 38.04; found: C 51.56, H 2.80, Br 38.11.

Acknowledgment

This investigation was supported by the Italian National Research Council (CNR), Rome, Italy.

1. S. Fisichella, G. Scarlata, and D. Sciotto. Ann. Chim. (Rome), **63**, 55 (1973).
2. A. Arcoria, S. Fisichella, G. Scarlata, and M. Torre. J. Heterocycl. Chem. **10**, 643 (1973).
3. S. Fisichella, G. Mineri, G. Scarlata, and D. Sciotto. Ann. Chim. (Rome), **63**, 779 (1973).
4. S. Gruttadauria, G. C. Pappalardo, G. Scarlata, and M. Torre. J. Chem. Soc. Perkin Trans. 2, 1580 (1974).
5. S. Fisichella, G. Scarlata, and M. Torre. Gazz. Chim. Ital. **104**, 1237 (1974).
6. S. Gruttadauria, G. C. Pappalardo, G. Scarlata, and M. Torre. Bull. Chem. Soc. Jpn. **48**, 1681 (1975).
7. S. Fisichella, G. Mineri, G. Scarlata, and D. Sciotto. Tetrahedron, **31**, 2445 (1975).
8. G. Scarlata and M. Torre. J. Heterocycl. Chem. **13**, 1193 (1976).
9. F. A. Bottino, G. Mineri, and D. Sciotto. Tetrahedron. In press.
10. A. Arcoria, F. A. Bottino, and D. Sciotto. J. Heterocycl. Chem. **14**, 1353 (1977).
11. N. H. Nam, N. P. Buu-Hoi, and N. D. Xuong. J. Chem. Soc. 1690 (1954).
12. H. Suzuki. Bull. Chem. Soc. Jpn. **33**, 389 (1960).
13. F. A. Bovey. Nuclear magnetic resonance spectroscopy. Academic Press, New York, NY. 1969. p. 350.
14. A. L. McClellan. Tables of experimental dipole moments. Rahara Enterprises, New York, NY. 1973.
15. B. Bak, D. Christensen, L. Hansen-Nygaard, and J. Rastrup-Andersen. J. Mol. Spectrosc. **7**, 58 (1961).
16. G. C. Pappalardo and S. Pistara. J. Chem. Eng. Data, **17**, 2 (1972).
17. I. F. Halverstadt and W. D. Kumler. J. Am. Chem. Soc. **64**, 2988 (1942).
18. K. Schlogl and H. Egger. Justus Liebigs' Ann. Chem. **676**, 76 (1964).
19. P. Cagniant. Bull. Soc. Chim. Fr. 847 (1949).

Downloaded from www.nrcresearchpress.com by 210.87.254.105 on 09/05/12
For personal use only.

Stereochemistry and mechanisms of the reactions of acylsilanes with alkoxides

ADRIAN G. BROOK, TEUNIS J. D. VANDERSAR, AND WILLIAM LIMBURG
Department of Chemistry, University of Toronto, Toronto, Ont., Canada M5S 1A1

Received May 15, 1978

ADRIAN G. BROOK, TEUNIS J. D. VANDERSAR, and WILLIAM LIMBURG. Can. J. Chem. **56**, 2758 (1978).

Using chiral NpPhMeSiCOMe it is shown that the 'cleavage' pathway for the reaction of alkoxides with acylsilanes involves nucleophilic attack at the carbonyl group, followed by subsequent rearrangements which result in optically active NpPhMeSiOR and aldehyde. The 'rearrangement' pathway involves stereospecific migrations of the naphthyl and phenyl groups from silicon to different faces of the adjacent carbonyl group, resulting in chiral naphthylethanol and phenylethanol of opposite absolute configurations.

ADRIAN G. BROOK, TEUNIS J. D. VANDERSAR et WILLIAM LIMBURG. Can. J. Chem. **56**, 2758 (1978).

Faisant appel au NpPhMeSiCOMe chiral, on a montré que les réactions des alcoolates avec les acylsilanes qui se produisent par clivage impliquent une attaque nucléophile au niveau du groupe carbonyle qui est suivie par des transpositions subséquentes qui conduisent à un NpPhMeSiOR optiquement actif et un aldéhyde. Les réactions qui se produisent par transposition impliquent des migrations stéréospécifiques des groupes naphtyle et phényle du silicium vers différentes faces du groupement carbonyle adjacent et conduisent à des naphtyle- et phényléthanols chiraux de configurations absolues opposées.

[Traduit par le journal]

Can. J. Chem. Downloaded from www.nrcresearchpress.com by 210.87.254.5 on 09/05/12
For personal use only.

Interest in the process whereby acylsilanes were readily hydrolyzed by aqueous base to silanol and aldehyde (1) (eq. [1]) led us to attempt to shed light

$$[1] \qquad R_3SiC(=O)R' \xrightarrow[H_2O]{OH^-} R_3SiOH + HC(=O)R'$$

on the process by replacing the aqueous base with alcoholic alkoxide. Under these conditions we were able to observe two distinct reaction pathways (2). One of these, 'rearrangement,' clearly involves the migration of a group (aryl ≫ alkyl) originally attached to silicon to the neighbouring carbonyl carbon atom (see **2** → **3** in Scheme 1 which uses benzoyltriphenylsilane and ethoxide ion as an example). This migration logically is followed by a second step in which the anion **3** undergoes the well-known silylcarbinol → alkoxysilane rearrangement (3, 4) via carbanion **4** yielding the bis(alkoxy)silane **5**, which subsequently, in part, undergoes alkoxide exchange giving **6** and **7**. Thus this overall process converts acylsilane **1** to a mixture of **5**, **6**, and **7**. The last step of the process, **5** → **6** + **7**, was shown independently to occur under the reaction conditions (2, 5).

The second pathway, 'cleavage' (previously called 'displacement' (2)), followed by acylsilane **1** was the direct counterpart of the originally observed hydrolysis; for example, benzoylsilane (**1**) yielded triphenylethoxysilane (**8**) and benzaldehyde (**10**). Two pathways appeared possible for this latter reaction: (*a*) the original pentavalent intermediate **2** formed ethoxysilane **8** by loss of acyl anion **9**, which on protonation yielded benzaldehyde (**10**) or (*b*) attack of alkoxide ion on the carbonyl carbon of the acylsilane yielded the oxyanion **11**, which then underwent the silylcarbinol → alkoxysilane type rearrangement yielding carbanion **12** which on protonation gave **13**. Alkoxide exchange involving **13**, which would be expected to occur easily, would yield the observed ethoxysilane **8** and benzaldehyde (**10**).

The following experiments using chiral acylsilanes confirm proposals previously made and lead to a clearer understanding both of the stereochemistry associated with the 'rearrangement' component of the reaction and of the manner by which the 'cleavage' reaction occurs.

Consider first the 'rearrangement' process. Treatment of (−)-acetylnaphthylphenylmethylsilane (**14**) (6) having the absolute configuration shown in Scheme 2, with alkoxide (tBuO$^-$ will be used as the example, other alkoxides should behave similarly) can lead to the intermediate **15**, from which naphthyl, phenyl, or methyl migration to the carbonyl carbon could occur. Previous observations suggest little or no methyl migration will occur in the presence of aryl groups (2) and none was detected. The experimental observations described below are explained if naphthyl migration occurs primarily to the back face of the C=O group as depicted, giving alkoxide **16**, which following the known inversion chemistry previously observed on rearrangement and protona-

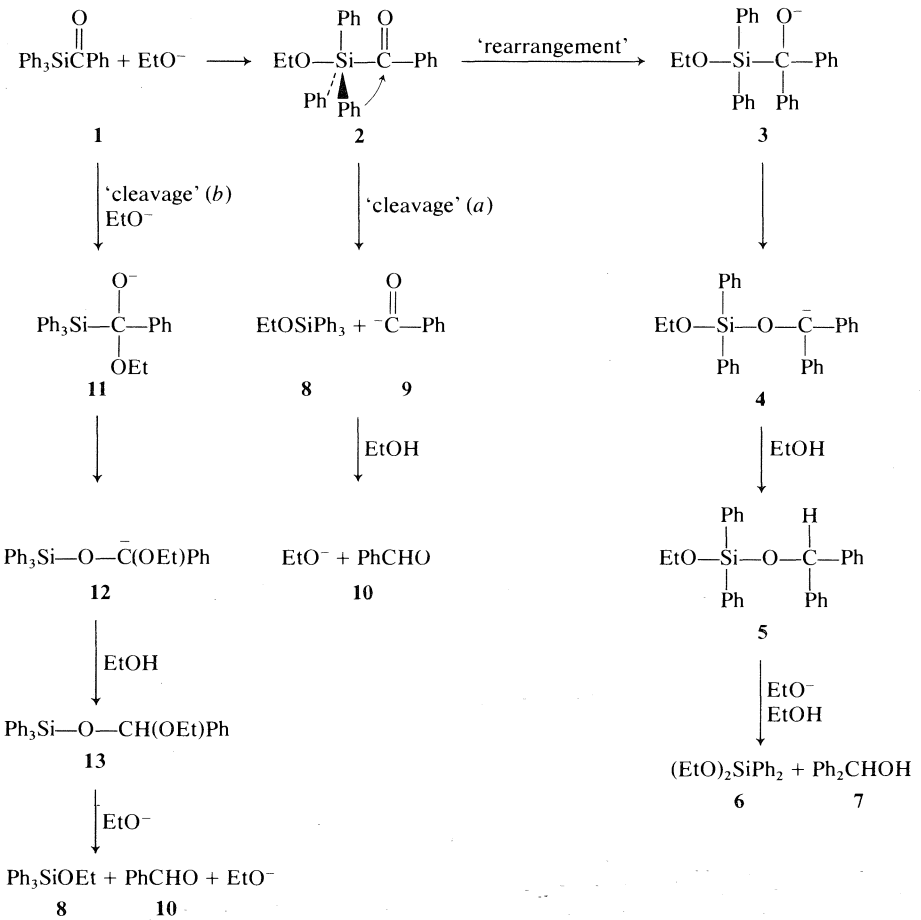

1 2 3 11 8 9 4 5 12 10 13 8 10 6 7

SCHEME 1. Rearrangement and cleavage reactions of acylsilanes with alkoxides.

tion (7, 8) gives **17**. Reduction of **17** under conditions known to cleave silicon–oxygen bonds (9) without affecting the configuration at carbon, would lead to the (−)-enantiomer of 1-naphthylethanol and phenyl methylsilane (**19**), as depicted and observed.

Phenyl migration appears to occur primarily to the top face of the carbonyl group of **15** giving **20**, which on rearrangement and protonation with inversion, as observed previously (7), would give **21**. Reduction of **21** would lead to (+)-1-phenylethanol and naphthylmethylsilane as isolated.

Alkoxides **17** and **21** are expected to be susceptible to alkoxide exchange which, if it occurs, would also lead to the formation of carbinols with retention of configuration at the chiral carbon centres and, in addition, to the formation of di-*tert*-butoxysilanes.

At the conclusion of these reactions but before reduction, a complex mixture of products would be present which would be difficult to separate. However, by reducing the entire reaction mixture, the products of greatest interest, **18** and **22** (and **25**, see below) which carry with them a record of the overall stereochemistry from the sequence of reactions, could be readily isolated by glc and their yields and optical purities determined. These results are found in Table 1.

It is significant that the predominant enantiomers of 1-phenylethanol, ((+)-**22**) and of 1-naphthylethanol, ((−)-**18**) isolated are of opposite relative configuration, consistent with the migrating aryl groups preferentially attacking the opposite faces of the carbonyl group. With sodium ethoxide the optical purities of both the 1-phenylethanol ($\simeq 56\%$ optical purity) and naphthylethanol ($\simeq 35\%$ optical purity) are quite high at either 9 or $-60°C$, and it appears that temperature has little effect on the stereochemical course in terms of specificity. However, temperature does have a significant effect on the relative amounts of phenyl vs. naphthyl migration, phenyl migration being favoured at both temperatures but being relatively more favoured at the lower temperature since the migration ratio of phenyl

Can. J. Chem. Downloaded from www.nrcresearchpress.com by 210.87.254.5 on 09/05/12
For personal use only.

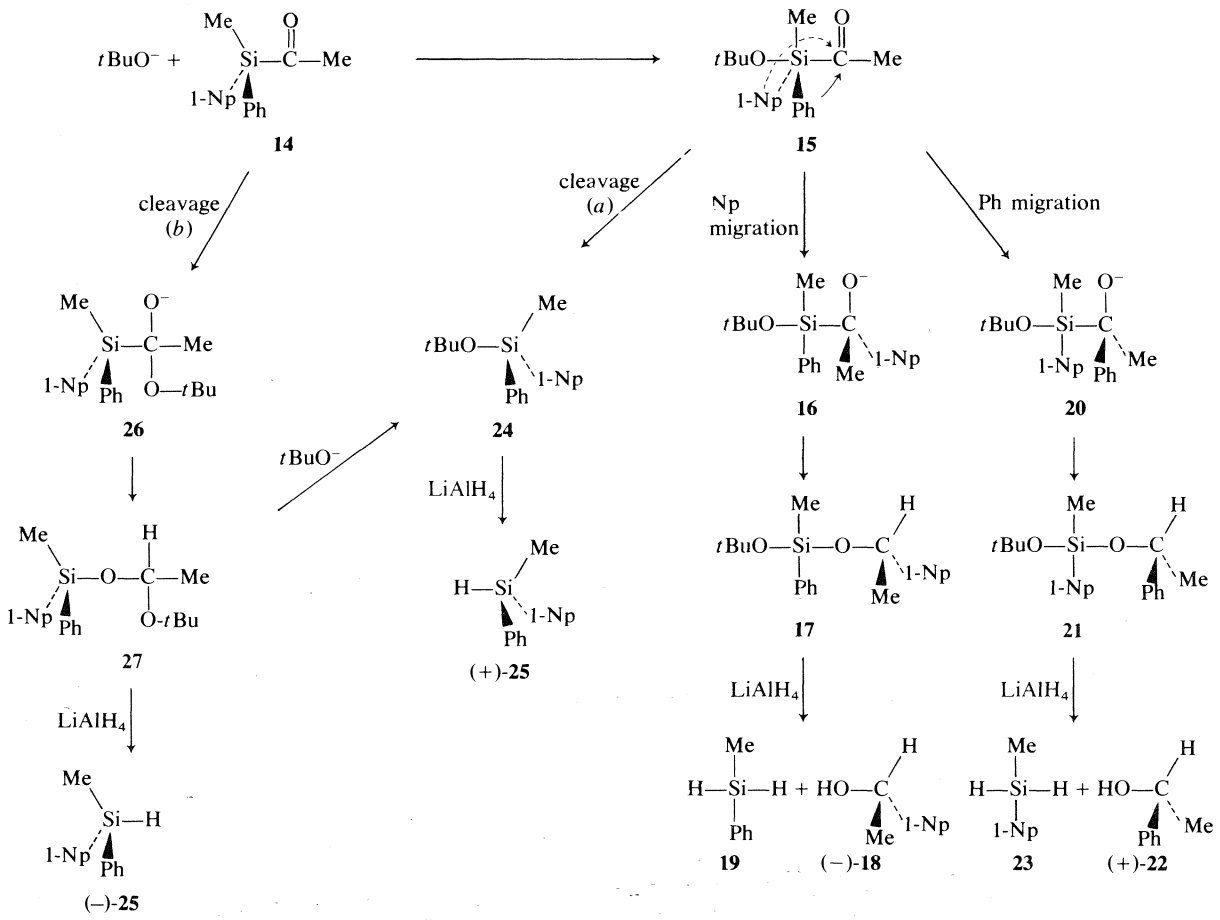

SCHEME 2. Reactions of (−)-acetylsilane with *tert*-butoxide ion.

to naphthyl rose from 6.7:1 to 29:1 on going from +9 to −60°C. This seems reasonable because the bulkier 1-naphthyl group can be expected to have more severe steric effects to overcome in achieving the transition state.

The 'cleavage' process also occurs at the same time that the above 'rearrangements' are occurring. The stereochemical consequences of the two proposed reaction pathways are also described in Scheme 2. If 'cleavage' arises from **15**, then the *tert*-butoxysilane **24** should be formed with effective overall inversion of configuration at silicon relative to **14**. Reduction of **24** would lead, with retention of configuration, to the (+)-silane **25**, although experiments have shown that under the reaction conditions employed, this reduction is at best very slow (9); thus, since *tert*-butoxysilane could not be detected among the products of reduction, it seems probable that little if any of it was ever formed. If nucleophilic attack of the alkoxide ion on the carbonyl group of **14** occurred, the ion formed, **26**, would rearrange to **27** with retention of configuration at silicon, as found previously (4). Reduction of **27** with lithium aluminum hydride would yield (−)-naphthylphenylmethylsilane, the opposite enantiomer to that expected from the route involving **15** → **24**. (In principle some **24** could arise from **17** by alkoxide exchange but this seems very unlikely, in view of the lack of evidence for the formation of *tert*-butoxysilane **24**.) It follows then that the configuration of the naphthylphenylmethylsilane isolated can distinguish between the two proposed pathways for 'cleavage.' The results are given in Table 1. In each reaction carried out the (−)-enantiomer was the predominant naphthylphenylmethylsilane formed. Greater optical purities were observed at lower temperatures (22% at 9°C vs. 35% at −60°C) and with the bulkier alkoxide (EtO⁻ gave 22% optical purity; tBuO⁻ gave 65%.) Thus these results are fully consistent with a pathway which involves nucleophilic attack by the alkoxide at the carbonyl group as the predominant route by which 'cleavage' occurs.

It is also evident that the relative proportions of 'cleavage' to 'rearrangement' depend on the steric

Can. J. Chem. Downloaded from www.nrcresearchpress.com by 210.87.254.5 on 09/05/12
For personal use only.

TABLE 1. Reactions of (−)-1-NpPhMeSiCOMe and alkoxide ions

Reaction conditions	% rearrangement	% cleavage	Migration ratio Ph/Np	OH Np—Me H (−) Relative purity	OH Np—Me H (−) Optical* purity	OH Me—Ph H (+) Relative purity	OH Me—Ph H (+) Optical purity	Me Ph—Si—H 1-Np (−) Relative purity	Me Ph—Si—H 1-Np (−) Optical purity
EtO^- 9°C	92	8	6.7	12	39	80	56	8	22
EtO^- −60°C	90	10	29	3	34	87	56	10	35
$tBuO^-$ 9°C	36	64	3.4	8	34	28	12	64	65

*Optical purity based on 1-phenylethanol, $[\alpha]_D$ +54.1°, 1-naphthylethanol, $[\alpha]_D$ +93.9° (ref. 11), and NpPhMeSiH, $[\alpha]_D$ +34.4° (ref. 12).

bulk of the alkoxide, the proportions changing from about 8:92 with EtO^- to 60:40 with $iPrO^-$ to 72:28 with $tBuO^-$ in further experiments done under identical standard conditions with each alkoxide. This suggests that bulkier alkoxides find it more difficult to attack at silicon to give the intermediate **15** and consequently, attack at the carbonyl group becomes relatively easier, favouring 'cleavage' rather than 'rearrangement.'

An experiment using (+)-benzoyl-1-naphthylphenylmethylsilane provides interesting complementary results (see Scheme 3). After reacting with *tert*-butoxide ion in toluene – *tert*-butyl alcohol at 0°C for 4 days, by which time the acylsilane had disappeared, followed by reduction with excess lithium aluminum hydride as described above, and work-up by a combination of distillation and column chromatography, 'rearrangement' of both phenyl and 1-naphthyl groups was observed, since both benzhydrol and (+)-naphthylphenylcarbinol with a maximum specific rotation of 11.7° were obtained in yields of about 50 and 10%, respectively (ratio of phenyl to naphthyl migrations, 5:1). Neither the absolute configuration of (+)-1-naphthylphenylcarbinol nor its maximum specific rotation appears to be known but application of Brewster's rules (10) predicts that the *R* enantiomer should be (+)-rotatory (at the sodium D line). If the configurational assignment is correct, these results suggest that the predominant direction of attack on the carbonyl group by naphthyl is as shown in Scheme 3 and opposite to that observed with the acetylsilane.

About 13% 'cleavage' accompanied the observed 60% overall 'rearrangement' (ratio 4.4:1) and the 1-naphthylphenylmethylsilane isolated was again the (−)-enantiomer having an optical purity of about 41%. The amount of 'cleavage' effected by $tBuO^-$ was significantly less than observed with the acetylsilane but the results of these experiments with the benzoylsilane are quantitatively less reliable. How-

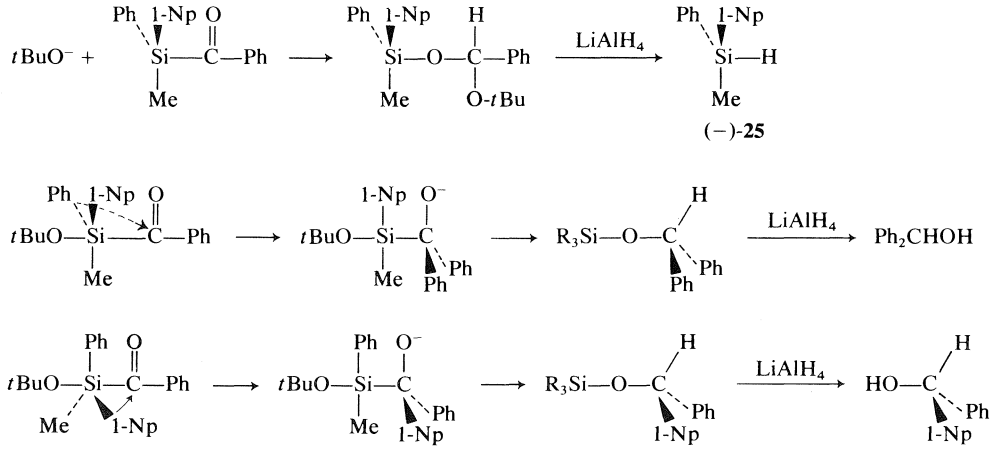

SCHEME 3

Can. J. Chem. Downloaded from www.nrcresearchpress.com by 210.87.254.5 on 09/05/12
For personal use only.

Can. J. Chem. Downloaded from www.nrcresearchpress.com by 210.87.254.5 on 09/05/12
For personal use only.

ever, it is clear that the stereochemistry and approximate optical purity of the $R_3\overset{*}{S}iH$ product from the benzoylsilane are the same as observed from the acetylsilane, so that their modes and stereochemistries of formation almost certainly follow the same general reaction pathway, as illustrated by **14** → **26** → **27** → (−)-**25**.

Based on the above results, it is clear that the observed 'cleavage' reactions arise from attack of alkoxide at the carbonyl group. The manner by which the optically active 'rearrangement' products are formed via nucleophilic attack of alkoxide ion at silicon is more speculative and obviously other conformations or configurations of a pentavalent intermediate such as **15** (or its benzoyl analog) may be involved; the above proposals represent the most concise interpretation of the observations and further speculation is not warranted at this time.

Experimental

Identification of Reaction Products and Their Proportions

The complex mixtures of compounds were quantitatively estimated by glc using two techniques (*a*) internal standard method (using 3-phenylpropanol) and (*b*) calibration graphs, employing a Varian Aerograph Model 202-B Gas Chromatograph with linear temperature programming between 150 and 330°C at a constant heating rate of 10°/min: injection port 250°C; dual-thermal conductivity detector 350°C; column, 5 ft 20% SE-30 on 60–80 acid-washed Chromosorb W. Under these conditions retention times were: 1-phenylethanol, 2.6 min; 3-phenylpropanol, 4.9 min; 1-naphthylmethylsilane, 7.1 min; 1-naphthylethanol, 10.4 min; 1-naphthylphenylmethylsilane, 14.4 min. Under the conditions of work-up, phenylmethylsilane was generally removed with the volatile solvents. Percentages of various components were calculated using the formula

$$\%X = A_X W_{is} 100 / A_{is} W_s$$

where A_X = area under peak of component X
A_{is} = area under peak for 3-phenylpropanol
W_{is} = weight of 3-phenylpropanol injected
W_s = weight of sample injected

Since the above method is strictly applicable only for homologous series of compounds, the results were also determined from calibration curves prepared from known weights of compound injected in 9.5 μl of benzene plotted against peak area from the resulting chromatograph peak for the three compounds of greatest interest, 1-phenylethanol, 1-naphthylethanol, and 1-naphthylphenylmethylsilane. The calibration curves were linear for the ranges 0–130 × 10^{-5} g/9.5 μl of benzene solution injected. This latter method, which was judged to be the more reliable, gave results close to those obtained by the internal standard technique.

By passage of the various optically active components through a preparative glc column under the same conditions used for analysis of the mixtures and then isolation, it was demonstrated that each was optically stable and did not undergo racemization.

In some cases it was convenient to separate large quantities of reaction products into two fractions by chromatography on a 18 in. × ½ in. alumina column. A 50:50 cyclohexane–benzene solvent mixture eluted a mixture of naphthylphenylmethylsilane and naphthylmethylsilane, and subsequent elution with ether yielded a mixture of 1-phenylethanol and 1-naphthylethanol.

Rearrangement of (−)-Acetyl-1-naphthylphenylmethylsilane with Potassium tert-*Butoxide at 9°C*

To a solution of 5.0 g (0.018 mol) of (−)-acetylsilane (6) in 80 ml of dry toluene at −10°C was added 3.0 ml of *tert*-butyl alcohol containing 0.179 g (9.7 × 10^{-4} mol) of potassium *tert*-butoxide. After 5 h stirring under nitrogen at 9°C, the reaction mixture was still yellow, indicating the reaction was incomplete, so an additional 0.120 g (6.6 × 10^{-4} mol) of potassium *tert*-butoxide in *tert*-butyl alcohol was added. After a total of 24 h stirring, an infrared spectrum of the mixture still showed the acetylsilane carbonyl stretch at 6.08 μ, indicative of unreacted acylsilane so an additional 0.129 g (9.7 mmol) of potassium *tert*-butoxide (total KO*t*Bu added = 2.6 × 10^{-3} mol) was added. After 24 h further stirring, all of the acylsilane had reacted and the reaction mixture was poured into water and was extracted with ether. Removal of the solvents left a viscous red oil which was reduced with 2.5 g of lithium aluminum hydride in 175 ml of diisopropyl ether and 50 ml of diethyl ether under reflux (58–60°C) for 24 h. The composition of the reduction mixture obtained after work-up with 10% HCl, a yellow liquid, was determined by glc as described above. The results are listed in Table 1.

Rearrangement of (−)-Acetyl-1-naphthylphenylmethylsilane with Sodium Ethoxide at 9°C

To a solution of 5.0 g (0.018 mol) of acetylsilane in 80 ml of dry toluene cooled to −10°C was added 4.0 ml of absolute ethanol containing 8.9 × 10^{-3} mol of sodium ethoxide. The reaction mixture immediately turned olive green in colour and then slowly changed to opaque brown while being stirred for 24 h at 9°C (cold water bath), after which time a sample showed the absence of the 6.08 μ C=O absorption band of the acetylsilane. The reaction mixture was poured onto water, which was ether extracted. After drying, removal of the ether layer gave a pale yellow oil which was refluxed with 2.5 g of lithium aluminum hydride in 175 ml of diisopropyl ether and 50 ml of diethyl ether for 48 h. Work-up with 10% HCl and ether extraction gave, after removal of the ether, a yellow liquid which was analyzed by glc as described above. The results are listed in Table 1.

A similar rearrangement was also carried out at −60°C, using Dry Ice – CCl_4 as the cooling mixture.

Synthesis and Attempted Reduction of 1-Naphthylphenylmethyl tert-*Butoxysilane*

To 2.0 g (0.012 mol) of (+)-1-naphthylphenylmethylsilane $[\alpha]_D$ +31.0° (*c* 7.7, C_6H_{12}) (90% optical purity) in 20 ml of dry *tert*-butyl alcohol was added 1.64 g (8.8 × 10^{-3} mol) of potassium *tert*-butoxide. The solution was heated at 82°C for 4.5 h and, after addition of pentane, was treated with water. The dried pentane extracts gave, on distillation at 162–165°C/0.13 Torr, (−)-naphthylphenylmethyl-*tert*-butoxysilane, as a clear colourless liquid $[\alpha]_D^{28}$ −23.1° (*c* 3.2 pentane) (lit. $[\alpha]_D$ −28° (9)).

A suspension of 0.5 g of lithium aluminum hydride in 35 ml of diisopropyl ether and 10 ml of diethyl ether and 1.00 g (3.13 × 10^{-3} mol) of the above *tert*-butoxysilane was refluxed for 24 h at 58–60°C. The excess hydride was decomposed with acetone and work-up gave a material whose nmr spectrum showed *tert*-butoxysilane signals but which showed no signal at δ 5.30 ppm, indicating that less than 1–2% of naphthylphenylmethylsilane, the potential reduction product, was present.

Racemization of 1-Naphthylphenylmethylethoxysilane

(−)-1-Naphthylphenylmethylethoxysilane, $[\alpha]_D^{27}$ −9.14° (*c* 10.1, pentane) 89% optically pure, was prepared from 1.5 g of (+)-naphthylphenylmethylsilane, $[\alpha]_D^{28}$ +31.0° (*c* 7.7, cyclohexane) (90% optical purity), 0.8 ml (0.014 mol) of absolute ethanol, and 0.13 g of 5% Pd-on-C in 13 ml dry pentane, using chromatography on silica gel to remove a trace of silanol contaminant.

To 0.24 g (8.2×10^{-4} mol) of the above ethoxysilane in 40 ml of dry toluene was added 5.6×10^{-3} mol of sodium ethoxide in 2 ml of ethanol. After stirring at 6°C for 17.5 h, aqueous work-up gave ethoxysilane with $[\alpha]_D$ −6.02° (*c* 2.2, pentane), corresponding to 58% optical purity, a decrease of 31%.

Rearrangement of Racemic Benzoyl-1-naphthylphenylmethylsilane with Potassium tert-*Butoxide*

A solution of 4.7 g (0.0133 mol) of racemic acylsilane in 95 ml of toluene at −15°C was treated with 5 ml of *tert*-butyl alcohol containing 0.0077 mol of potassium *tert*-butoxide. After 2 days at 0°C, the mixture was poured into 100 ml of 2.5% hydrochloric acid and the ether extracts were dried over sodium sulphate. Removal of the solvents left 5.8 g of oily residue which was dissolved in 25 ml ether and was treated with 2.0 g (0.3 equiv.) of lithium aluminum hydride in 50 ml of ether and 30 ml of di-*n*-butyl ether. The mixture was refluxed and diethyl ether was removed until the contents of the flask reached 83°C, at which temperature they were heated for 20 h. Cooling and normal work-up gave an oil, with strong 2.75 μ (OH) and 4.65 μ (Si–H) infrared absorption, which was distilled under reduced pressure to give the following compounds, identified by infrared, nmr, and mixture melting point: bp 44–62°C/0.07 Torr, a mixture of naphthylmethylsilane and phenylmethylsilane; 100–108°C/0.07 Torr, benzhydrol, mp 67–68°C, 26%; 138–143°C/0.05 Torr, naphthylphenylmethylsilane, 10%; 144–149°C/0.05 Torr, naphthylphenylcarbinol, mp 81–83°C, 7%.

Rearrangement of (+)-Benzoyl-1-naphthylphenylmethylsilane with Potassium tert-*Butoxide*

A solution of 10.0 g (0.028 mol) of (+)-benzoylsilane (4) $[\alpha]_D^{23}$ +5.94° (*c* 8.26, benzene) in 240 ml of toluene at −10°C was treated with 10 ml of *tert*-butyl alcohol containing 0.0077 mol of potassium *tert*-butoxide. After 4 days at 0°C, work-up as described above gave 10.6 g of a yellow material, $[\alpha]_D^{23}$ −0.07° (*c* 7.8, benzene). No residual benzoylsilane could be detected in the infrared spectra (C=O at 6.18 μ absent). Reduction as above with 4.0 g (0.61 equiv.) of lithium aluminum hydride in diethyl ether plus dibutyl ether for 17 h at 83°C, followed by work-up gave 8.9 g of oily residue which was distilled to give 12 fractions of which the following were important: bp 104–114°C/0.005 Torr, benzhydrol, 2.23 g (49.7%); bp 127–129°C/0.005 Torr, 1-naphthylphenylmethylsilane, $[\alpha]_D^{23}$ −13.55° (*c* 2.3, C_6H_{12}), 0.95 g (13.4%); 135–148°C/0.001 Torr, 1-naphthylphenylcarbinol, $[\alpha]_D^{25}$ +5.91° (*c* 3.0, chloroform), 0.65 g (9.9%), which after chromatography on silica gel, eluting with 1:1 hexane–benzene had $[\alpha]_D^{25}$ +11.7° (*c* 1.1, chloroform).

Rearrangement of Racemic Acetylsilane with Various Alkoxides

Using the general conditions described above samples of racemic naphthylphenylmethylsilane in toluene were treated with equal amounts of either sodium ethoxide in ethanol, sodium isopropoxide in isopropyl alcohol or potassium *tert*-butoxide in *tert*-butyl alcohol. On completion of the reactions, work-up indicated the following total amounts of aryl migration: from EtO^-, 92%; from $iPrO^-$, 40%; from $tBuO^-$, 28%.

Acknowledgement

This research was supported by the National Research Council of Canada.

1. A. G. Brook. J. Am. Chem. Soc. **79**, 4373 (1957).
2. A. G. Brook and N. V. Schwartz. J. Org. Chem. **27**, 2311 (1962).
3. A. G. Brook, G. E. LeGrow, and D. M. MacRae. Can. J. Chem. **45**, 239 (1967).
4. A. G. Brook, C. M. Warner, and W. W. Limburg. Can. J. Chem. **45**, 1231 (1967).
5. A. G. Brook. J. Org. Chem. **25**, 1072 (1960).
6. A. G. Brook, J. M. Duff, P. F. Jones, and N. R. Davis. J. Am. Chem. Soc. **89**, 431 (1967).
7. A. G. Brook and J. D. Pascoe. J. Am. Chem. Soc. **93**, 6224 (1971).
8. M. S. Biernbaum and H. S. Mosher. J. Am. Chem. Soc. **93**, 6221 (1971).
9. L. H. Sommer, C. L. Frye, and G. A. Parker. J. Am. Chem. Soc. **86**, 3276 (1964).
10. J. H. Brewster. J. Am. Chem. Soc. **81**, 5475 (1959).
11. R. H. Pickard and J. Kenyon. J. Chem. Soc. **105**, 1126 (1914).
12. L. H. Sommer and H. Fujimoto. J. Am. Chem. Soc. **90**, 982 (1968).

Can. J. Chem. Downloaded from www.nrcresearchpress.com by 210.87.254.5 on 09/05/12
For personal use only.

Complex fluoroanions in solution. IX. BF_3–anion complexes and their disproportionation[1]

S. BROWNSTEIN AND G. LATREMOUILLE

Division of Chemistry, National Research Council of Canada, Ottawa, Ont., Canada K1A 0R9

Received May 2, 1978

S. BROWNSTEIN and G. LATREMOUILLE. Can. J. Chem. **56**, 2764 (1978).

Complex fluoroanions have been prepared with boron trifluoride and perchlorate, nitrate, nitrite, acetate, formate, azide, cyanide, cyanate, thiocyanate, and thiophenolate ions. The complexes formed from the anions of the strong acids, except the hydrogen halides, do not disproportionate to $BF_2(anion)_2^-$. Complexes of anions of weaker acids may disproportionate and, or, complex a second molecule of BF_3. Regularities in fluorine–boron coupling constants are tabulated.

S. BROWNSTEIN et G. LATREMOUILLE. Can. J. Chem. **56**, 2764 (1978).

On a préparé des fluoroanions complexes du trifluorure de bore avec les ions perchlorate, nitrate, nitrite, acétate, formate, azoture, cyanure, cyanate et thiocyanate et thiophénolate. Les complexes qui se forment à partir des anions des acides forts, à l'exception des halogénures d'hydrogène, ne donnent pas lieu à une disproportionation conduisant au $BF_2(anion)_2^-$. Les complexes des anions des acides plus faibles peuvent donner lieu à une disproportionation et, ou à une complexation d'une deuxième molécule de BF_3. On rapporte un tableau présentant les régularités dans les constantes de couplage fluor–bore.

[Traduit par le journal]

Introduction

Mixed boron haloanions have been prepared and undergo slow exchange and disproportionation reactions (1). Complex formation and disproportionation has been observed with the trifluoroacetate ion (2), but only complex formation is found with fluorosulfate and trifluoromethane sulfonate ions (3). This study is an attempt to determine the effect of the anion upon the fluorine chemical shift, boron–fluorine spin coupling constant and extent of disproportionation of the 1:1 adduct between BF_3 and an anion. More than one equivalent of BF_3 is complexed by fluoride ion (4) and trifluoroacetate ion (2) but not by fluorosulfate nor trifluoromethanesulfonate ions (3). When all volatile materials are pumped off under vacuum no BF_3 beyond a 1:1 ratio is retained in the solid phase with the above anions. It is of interest to determine if other mixed anions are capable of complexing a second molecule of BF_3 and if any of them can retain the extra BF_3 in the solid phase.

Experimental

Fluorine resonance spectra were obtained at 94.18 MHz with a Varian Associates XL-100A spectrometer equipped with a Nicolet Instruments TT100A Fourier transform accessory. Spectral widths of 20 kHz were observed using a 5 μs pulse and storing the data in 16K memory channels. Normally the accumulation of 400 transients gave a good signal-to-noise ratio. Chemical shifts are reported in ppm with respect to $CFCl_3$ as zero and with shifts to high field considered negative. Infrared spectra of the tetramethylammonium salts dispersed in potassium bromide pellets were recorded on a Beckman Acculab 4 spectrometer. Ultra-violet spectra were obtained with a Cary 14 spectrometer. Vapor pressure studies were done in a manner previously described except for pressure measurement by a Baratron diaphragm manometer rather than a constant volume mercury manometer (4). Samples were prepared with great care to exclude moisture using standard vacuum line and dry box techniques. Boron trifluoride, sulfur dioxide, and methylene chloride were purified and stored as previously described (4). Tetramethylammonium perchlorate, nitrate, acetate, formate, and cyanide were prepared by neutralization of a tetramethylammonium hydroxide solution with the corresponding acid followed by evaporation of all volatile material under vacuum. The reaction of equivalent quantities of a tetramethylammonium hydroxide solution with one of ammonium thiocyanate followed by evaporation to remove ammonia and water produced tetramethylammonium thiocyanate. Tetramethylammonium and tetrabutylammonium nitrites were prepared by reaction of a solution of the corresponding chloride with one of silver nitrite, removal of the silver chloride, and concentration of the resultant solution. A similar procedure using silver cyanate gave tetramethylammonium cyanate. Tetramethylammonium thiophenolate was prepared by the literature method (5). Most of the tetramethylammonium salts were recrystallized from methanol–water. Tetrabutylammonium azide was purchased from Fluka A.G. All the salts have been reported previously in the literature.

Results and Discussion

The chemical shift of the fluorines in complex fluoborate ions is sensitive to temperature, concentration, and the nature of the solvent. For the purposes of this work all chemical shifts were measured with a 0.34 *m* solution of tetramethylammonium salt in sulfur dioxide as solvent at 203 K except for nitrite, azide, and the mixed haloanions already reported (1). In these cases the shift of BF_4^- was taken to be that used in the present study and

[1]NRCC No. 16916.

Can. J. Chem. Downloaded from www.nrcresearchpress.com by 210.87.254.105 on 09/05/12
For personal use only.

Can. J. Chem. Downloaded from www.nrcresearchpress.com by 210.87.254.105 on 09/05/12
For personal use only.

the other chemical shifts adjusted accordingly. The chemical shifts are listed in Table 1. There is no well established trend for fluorine chemical shifts nor boron–fluorine spin coupling constants with K_a of the parent acid of the anion nor whether it is 'hard' or 'soft'. The correlation between fluorine chemical shifts and boron–fluorine spin coupling constants observed previously (1) is also observed with the present series of mixed anions. This is illustrated in Fig. 1. Deviations from this correlation are probably due to anomalies in chemical shift values since there appears to be a constant contribution to boron–fluorine spin coupling with each additional substituent on boron. For those anions with the largest shift to high field the correlation would be improved if the spin coupling constant were of opposite sign, as suggested previously (6). The spin coupling constant may be expressed by $J_{B-F} = nJ_i$, where J_i is the contribution from substituent i and n is the number of these substituents bonded to boron. Values of J_i are listed in Table 2. The above approach is similar in principle but different in detail from that originally presented by Vladimiroff and Malinowski (7) and applied by Hartman and co-workers (1, 6). These results, taken together with those of ref. 6, suggest that co-ordination of BF_3 and NO_2^- is via nitrogen rather than oxygen.

TABLE 1. Chemical shifts and fluorine–boron spin coupling constants for some complex fluoborate anions

Ion	δ_F	J_{B-F}[a]	Reference
BF_4^-	−139.8		This work
BF_3Cl^-	−113.1	25.2	1
$BF_2Cl_2^-$	−92.6	54.2	1
$BFCl_3^-$	−82.5	79.4	1
BF_3Br^-	−102.3		1
$BF_2Br_2^-$	−76.7	76.1	1
$BFBr_3^-$	−67.1	113.3	1
$BF_3CH_3COO^-$	−135.6	7.3	This work
$BF_2(CH_3COO)_2^-$	−135.2	15.9	This work
$BF(CH_3COO)_3^-$	−136.9	22	This work
$BF_3CF_3COO^-$	−141.0	4.5	2
$BF_2(CF_3COO)_2^-$	−142.3	9	2
$BF_3NO_2^-$	−112.2	25.1	This work
$BF_2(NO_2)_2^-$	−92	55.1	This work
BF_3HCOO^-	−137.4	6	This work
$BF_2(HCOO)_2^-$	−138.9	14.8	This work
$BF_3CF_3SO_3^-$	−137.5		3
$BF_3FSO_3^-$	−140.2		3
$BF_3ClO_4^-$	−141.0		This work
$BF_3NO_3^-$	−141.7		This work
BF_3CN^-	−127.5	26.8	This work
$BF_2(CN)_2^-$	−132.7	Not resolved	This work
BF_3SCN^-	−125.9		This work
BF_3OCN^-	−136.9		This work
$BF_3SC_6H_5^-$	−135.4		This work
$BF_3(N_3)^-$	−134.9	Not resolved	This work
$BF_2(N_3)_2^-$	−133.0	18	This work

[a]In Hz.

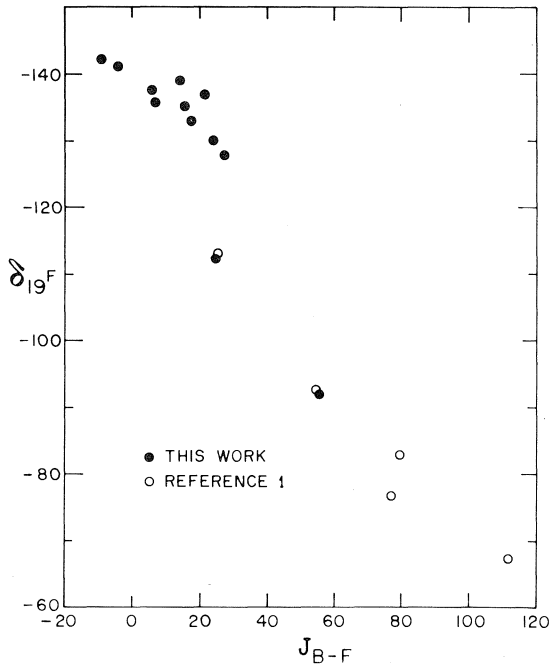

FIG. 1. Variation of ^{19}F chemical shifts and ^{11}B–^{19}F coupling constants in mixed fluoborate anions.

TABLE 2. Contribution of a substituent to boron–fluorine spin coupling in mixed fluoborate anions

Substituent	J_i	Reference
Cl	26.3	1
Br	37.6	1
CF_3COO	−4.5	2
CH_3COO	7.5	This work
NO_2	26.4	This work
HCOO	6.7	This work

If disproportionation of BF_3A^- proceeds by way of reactions [1] to [4],

$$[1] \qquad BF_3 + A \rightarrow BF_3A^-$$

$$[2] \qquad 2BF_3A^- \rightleftharpoons BF_4^- + BF_2A_2^-$$

$$[3] \qquad 3BF_3A^- \rightleftharpoons 2BF_4^- + BFA_3^-$$

$$[4] \qquad 4BF_3A^- \rightleftharpoons 3BF_4^- + BA_4^-$$

that is, with no displacement which produces fluoride ion in the solution, then the ratio of the concentrations of the substituted anions should be independent of the concentration of A^- provided that reaction [1] goes to completion. It was found that with trifluoroacetate, nitrite, cyanide, and acetate the extent of disproportionation is independent of the excess of added anion.

If disproportionation and redistribution of the ligands in BF_3A^- were completely random one would

TABLE 3. Extent of disproportionation of BF_3A^-

Substituent	% BF_4^-	% BF_3A^-	% $BF_2A_2^-$	% BFA_3^-	% BA_4^-	K_2
Theoretical	32	42	21	5	0	0.38
CF_3COO	15	70	15			0.05
NO_2	26	62	12			0.08
CN	6	85	9			0.007
CH_3COO	23	46	31	Trace		0.34
N_3	50	Trace	50			

obtain the proportions of the various species listed in Table 3 (8). None of the systems studied show random behaviour. In every case except azide there is less disproportionation than if it were random. Equilibrium constants for reaction [2] are also listed in Table 3.

Solutions containing the anions cyanide, acetate, and thiophenolate complex more than one equivalent of BF_3. In methylene chloride at 0°C from vapor pressure measurements it is found that complexing of one equivalent of BF_3 is at least 99.4% complete for both cyanide and acetate when only one equivalent of BF_3 has been added. With the addition of two equivalents of BF_3 complexing to give the 2:1 species is 93% complete with cyanide and 89% complete with acetate. Upon evaporation of all volatile materials under vacuum and repetition of the vapor pressure measurements with the residues no further uptake of BF_3 is observed. This indicates that the complexes containing two equivalents of BF_3 are stable towards dissociation even in the absence of gaseous BF_3. The vapor pressure results also exclude, in these cases with an excess of BF_3, disproportionation according to reactions [2] to [4]. Although BF_4^- reacts with BF_3 to produce $B_2F_7^-$ the reaction is readily reversible, while the vapor pressure measurements indicate an irreversible uptake of BF_3.

The vapor pressure results were confirmed, in the case of cyanide ion, by X-ray powder patterns which were different for the starting material and the residues from evaporation of solutions containing one and two equivalents of BF_3. For acetate ion a similar confirmation of different products with one and two equivalents of BF_3 was done by infrared spectroscopy of the residues. Also from the infrared spectra of the residues it was found that the BF_3 complexes of perchlorate, nitrate, fluorosulfate, and trifluoromethanesulfonate ions are stable upon evaporation, under vacuum, of all volatile material.

In solutions containing one equivalent of BF_3 for each cyanide or acetate there is no evidence from fluorine resonance spectra for formation of any complex containing two molecules of BF_3. Therefore reaction [5] does not proceed to any significant degree.

$$[5] \qquad 2BF_3A^- \rightarrow A^- + (BF_3)_2A^-$$

The fluorine resonance spectrum of a sulfur dioxide solution with one equivalent of thiophenoxide ion and BF_3 has signals from both the 1:1 and the 2:1 BF_3 complexes. A sulfur dioxide solution of tetramethylammonium thiophenoxide is yellow because of an interaction between the thiophenoxide ion and the solvent. When complex formation with BF_3 is complete the solution has no visible color. The maximum in the absorption curve for the thiophenoxide – sulfur dioxide complex is masked by the cutoff of the solvent at 3200 Å. Nevertheless the absorption of a shoulder of this complex at 3500 Å is easily measured with the molar extinction co-efficient (ε) of 9 600. From the change in absorptions at this wavelength, with addition of BF_3, an equilibrium constant of 0.15 ± 0.09 at 298 K was calculated for reaction [5]. The relative areas of the fluorine resonance peaks at 203 K, for a solution 250 times more concentrated gave an equilibrium constant of 0.18. If the reaction were statistically random an equilibrium constant of 0.25 would be expected, therefore this reaction behaves in an essentially random fashion with the thiopenolate ion.

The fluorine resonance spectra of the complexes containing two equivalents of BF_3 for each acetate or thiophenolate ion have only a single peak from fluorine bonded to boron. Therefore the two BF_3 moieties are either identical or undergo rapid exchange on the nmr time scale. Their chemical shifts are −136.7 for acetate and −140.2 for thiophenolate. Separate peaks are observed for the two complexed BF_3 species with cyanide ion. A comparison of the spin coupling constants for the 1:1

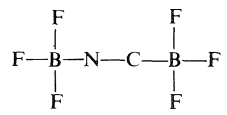

1

Can. J. Chem. Downloaded from www.nrcresearchpress.com by 210.87.254.105 on 09/05/12
For personal use only.

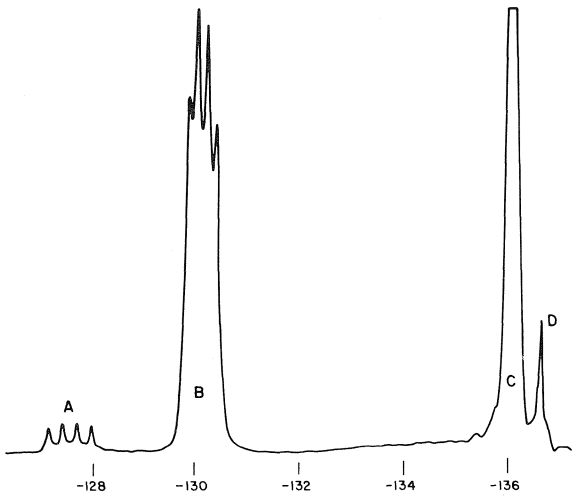

FIG. 2. Fluorine resonance spectrum of a sulfur dioxide solution of tetramethylammonium cyanide and two equivalents of boron trifluoride: (*a*) BF_3CN^-; (*b*) BF_3 co-ordinated to N; (*c*) BF_3 co-ordinated to C; (*d*) BF_4^-.

and 2:1 complexes with those of other BF_3 complexes suggests that boron is co-ordinated to nitrogen in the 1:1 complex. Structure **1** is proposed for the 2:1 complex with the fluorines of BF_3 co-ordinated to nitrogen having a chemical shift of −130.1 and a boron–fluorine coupling constant of 24.4 Hz. The chemical shift of the fluorines on boron co-ordinated to carbon is −136.1 and the ratio of areas of the two peaks is 1.03 to 1.00. A spectrum is shown in Fig. 2.

Conclusions

Complexing of boron trifluoride with anions appears to be a general phenomenon and disproportionation of the resultant complexes is widespread. In some cases room temperature stable complexes containing more than one boron trifluoride may be obtained.

1. J. S. HARTMAN and G. J. SCHROBILGEN. Inorg. Chem. **11**, 940 (1972).
2. S. BROWNSTEIN. Can. J. Chem. **56**, 343 (1978).
3. S. BROWNSTEIN, J. BORNAIS, and G. LATREMOUILLE. Can. J. Chem. **56**, 1419 (1978).
4. S. BROWNSTEIN and J. PAASIVIRTA. Can. J. Chem. **43**, 1645 (1965).
5. R. EHRLICH, A. R. YOUNG, and D. PERRY. Inorg. Chem. **4**, 758 (1965).
6. J. S. HARTMAN and J. M. MILLER. Inorg. Chem. **13**, 1467 (1974).
7. T. VLADIMIROFF and E. R. MALINOWSKI. J. Chem. Phys. **46**, 1830 (1967).
8. G. CALINGAERT and H. A. BEATTY. J. Am. Chem. Soc. **61**, 2748 (1939).

Can. J. Chem. Downloaded from www.nrcresearchpress.com by 210.87.254.105 on 09/05/12
For personal use only.

The synthesis of oligoribonucleotides. II.[1] The use of silyl protecting groups in nucleoside and nucleotide chemistry. VII[2]

KELVIN K. OGILVIE, SERGE L. BEAUCAGE, ARIA L. SCHIFMAN, NICOLE Y. THERIAULT, AND KRISHAN L. SADANA

Department of Chemistry, McGill University, Montreal, P.Q., Canada H3A 2K6

Received May 1, 1978

KELVIN K. OGILVIE, SERGE L. BEAUCAGE, ARIA L. SCHIFMAN, NICOLE Y. THERIAULT, and KRISHAN L. SADANA. Can. J. Chem. **56**, 2768 (1978).

The synthesis of oligonucleotides derived from uridine and adenosine using the *tert*-butyldimethylsilyl protecting group and the trichloroethylphosphorodichloridite condensation procedure is described. These procedures involve rapid preparation of protected starting materials and equally rapid condensation of units to form nucleotides. Optimum yields using collidine as base in tetrahydrofuran as solvent are between 65 and 80%. The utility of the procedure is rendered complete by the capability to remove both the phosphate protecting groups and the alkylsilyl groups in a single 30 min step using tetrabutylammonium fluoride in tetrahydrofuran.

KELVIN K. OGILVIE, SERGE L. BEAUCAGE, ARIA L. SCHIFMAN, NICOLE Y. THERIAULT et KRISHAN L. SADANA. Can. J. Chem. **56**, 2768 (1978).

On décrit la synthèse d'oligonucléotides dérivés de l'uridine et de l'adénosine utilisant le groupe protecteur *tert*-butyldiméthylsilyle et la méthode de condensation faisant appel à la trichloroéthylphosphorodichloridite. Ces méthodes impliquent une préparation rapide des produits de départ protégés et une condensation également rapide des unités conduisant aux nucléotides. Les meilleurs rendements sont obtenus en faisant appel à la collidine comme base dans le tétrahydrofuranne utilisé comme solvant et ils sont de l'ordre de 65 à 80%. L'utilité de cette méthode est rendue complète par sa capacité d'enlever à la fois les groupes protecteurs phosphates et les groupes alkylsilyles dans une seule étape de 30 m utilisant le fluorure de tétrabutylammonium dans le tétrahydrofuranne.

[Traduit par le journal]

Introduction

There are two important challenges in the chemical synthesis of oligonucleotides: the synthesis of oligodeoxynucleotides leading ultimately to the synthesis of genetic material and the synthesis of oligoribonucleotides leading to the synthesis of molecules such as transfer RNA and messenger RNA. Developments in these two areas are similar in that the methods used to date to condense protected monomers into oligomers are virtually the same for both cases. However, they differ greatly in the availability of suitably protected monomers. The lack of procedures for the rapid synthesis of suitably protected ribonucleosides is the major reason that while the chemical synthesis of oligodeoxynucleotides has contributed significantly to the synthesis of a gene (7) no development of equivalent magnitude has occurred in the ribose area.

Of the numerous attempts to prepare oligoribonucleotides only three main approaches have led to significant developments. Khorana developed the diester approach for ribonucleotides (8) but this method suffers from the limits on quantities used and the complexity of protection–deprotection procedures. Reese (9) extensively explored acyl and tetrahydropyranyl protecting groups in ribonucleotide synthesis and van Boom *et al.* (10) have succeeded in extending this work using the triester approach. Werstiuk and Neilson (11) have also had some success with extending the Reese approach reaching a nonanucleotide. Ikehara and co-workers (12) have employed photolabile protecting groups with both the diester and triester methods in successfully preparing a trinucleotide.

For some time we have been exploring new methods for protection–deprotection of ribonucleosides and methods of condensation. Our efforts in exploiting the alkyl silyl protecting groups for ribonucleosides and use of fluoride ion to not only remove silyl groups but phosphate protecting groups as well (5, 13), when combined with the Letsinger phosphite condensation procedure (14), have allowed us to present (6) a new and versatile route to oligoribonucleotides. We believe this method offers the first practical procedure for the chemical synthesis of a transfer RNA. In this manuscript we wish to detail the procedures for the synthesis of protected adenosine and uridine nucleosides and their condensation to nucleotides. In developing this series we will

[1]For Part I in this series, see ref. 6.
[2]For Parts I–VI, see refs. 1–6.

Can. J. Chem. Downloaded from www.nrcresearchpress.com by 210.87.254.40 on 09/05/12
For personal use only.

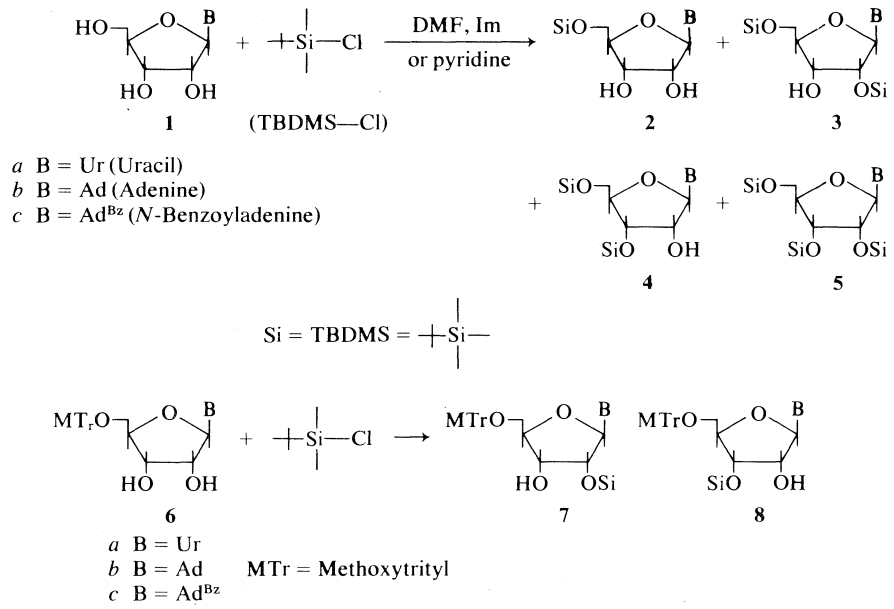

SCHEME 1

present the first complete set of fully protected ribonucleosides of synthetic utility using a single protecting group for all the ribonucleosides.

This manuscript details all of the isomeric derivatives of uridine and adenosine using the *tert*-butyldimethylsilyl (TBDMS) protecting group promoted by Corey and Venkateswarlu (15) in the prostaglandin area. While we have also developed (3, 4) other more stable silyl groups such as the triisopropylsilyl and *tert*-butyltetramethylenesilyl groups, the *tert*-butyldimethylsilyl chloride reagent is commercially available (Aldrich Chemical Co.). The other silyl groups offer unique advantages of stability and will soon be available commercially from the same supplier. Methods described herein for the TBDMS group are directly applicable to the other silylating reagents.

Preparation of the Silylated Nucleosides

The major advantage of the TBDMSCl reagent is that it rapidly converts the ribonucleoside (Scheme 1) into derivatives that can be directly used in forming nucleotides. We have compared two solvent systems for these reactions: (*i*) dimethylformamide and imidazole (DMF + Im) and (*ii*) pyridine. The DMF–Im system seems to give the most rapid rates with the reaction being over in a matter of minutes in most cases. Pyridine reactions are slower but give much more selectivity in derivatization of the 2′-hydroxyl vs. the 3′-hydroxyl. Such selectivity in pyridine has been observed by Blackburne *et al.* (16) in other systems. Although the reactions in DMF with imidazole are over very quickly some slight changes in product distribution may occur with time. Table 1 lists the conditions we have found that lead to optimum yields of compounds **2**, **3**, and **4**.

One excellent synthetic feature of the silylated nucleosides is that isomeric compounds, e.g., **3** and **4**, separate very cleanly on silica gel chromatography (see Table 2). Consequently the products can rapidly be obtained by thick-layer chromatography or by short column chromatography often in solvents such as ether and hexane. Products containing silyl groups on exocyclic amino groups are not obtained in any quantity in these reactions. It appears that *N*-silylated adenosines may be intermediates in the reactions but they either act as silylating agents themselves (i.e., transferring the *N*-silyl to a hydroxyl) or are hydrolyzed during work-up.

We have tried many ways of mixing reagents together but the procedures described give nearly maximum results and are based on direct addition of the silylating agent to the dissolved nucleoside.

Since there are several phosphorylating procedures that require *N*-protection we have also prepared the silylated derivatives of *N*-benzoyl adenosine. From Table 2 it can be seen that *N*-protection causes a remarkable increase in the separation of isomers such as **3***c* and **4***c*. The silyl groups are also completely compatible with the methoxytrityl group and together they provide an ideal protection system for nucleosides. These derivatives (**7** and **8**) are fully described.

Hydrolysis of Silyl Groups

Acid

Another very useful feature of the silylated

Can. J. Chem. Downloaded from www.nrcresearchpress.com by 210.87.254.40 on 09/05/12
For personal use only.

TABLE 1. Preparation of silylated nucleosides*

Starting material	TBDMS-Cl (mequiv.)	Imidazole (mequiv.)	Solvent	Time (h)	Isomer yields (%) 5′-	2′,5-	3′,5-	2′,3′,5′-
Uridine	1.25	2.5	DMF	2	80	7	6	—
Uridine	1.25	0	Pyridine	3	83	5	2	—
Uridine	2.2	4.4	DMF	2	—	46	32	6
Uridine	2.2	4.4	DMSO	2	—	35	36	1
Uridine	3	0	Pyridine	48	—	65	14	2
Uridine	7.0	14	DMF	8	—	15	12	85
MTr-U (*6a*)	1.25	2.5	DMF	18	—	51	36	11
MTr-U (*6a*)	3	0	Pyridine	48	—	64	18	7
Adenosine	1.3	2.6	DMF	21	55	10	15	—
Adenosine	1.25	0	Pyridine	4	78	7	5	—
Adenosine	2.2	4.4	DMF	5	10	37	49	4
Adenosine	3	0	Pyridine	48	12	50	26	4
Adenosine	4.4	8.8	DMF	24	—	—	—	93
MTr-A (*6b*)	1.5	3.1	DMF	1	—	35	42	11
MTr-A (*6b*)	3	0	Pyridine	43	—	32	22	5
$^{Bz}_{A}$(*1c*)	2.2	4.5	DMF	20	66	3	8	—
$^{Bz}_{A}$(*1c*)	2	0	Pyridine	24	67	—	—	—
$^{Bz}_{A}$(*1c*)	3	6	DMF	1.2	15	28	35	5
$^{Bz}_{A}$(*1c*)	4	0	Pyridine	48	17	40	35	—
MTr-$^{Bz}_{A}$(*6c*)	1.7	3.3	DMF	2.5	—	33	48	6
MTr-$^{Bz}_{A}$(*6c*)	3.0	0	Pyridine	48	—	37	41	7

*For details see Experimental.

nucleosides is the fact that the 5′-silyl group is much more labile toward acid than either the 2′- or 3′-silyl (Scheme 2). Consequently compounds **3** and **4** can be treated with 80% HOAc either at room temperature or on heating to give yields of **9** and **10** up to 75%. These results are summarized in Table 3. The 5′-methoxytrityl group can be removed from **7** or **8** to give yields of **9** and **10** as high as 98%.

When the 2′- and 3′-positions both bear silyl groups as in the case of **5**, the 5′-silyl can be removed to give good yields of the 2′,3′-disilylated nucleosides **9***c* and **10***c*. All the silyls can be removed within 2 h using 0.1 *N* methanolic HCl at room temperature. It is clear from these experiments that in multisilylated nucleosides, each silyl is more resistant toward hydrolysis than in the monosilylated compounds. For example, **2***a* is 95% converted to uridine after heating with 80% HOAc for 15 min at 100°C whereas in **3***a* and **4***a*, 10% of the 5′-silyl is still intact after 30 min. Compound **2***a* is 98% converted to uridine after 18 h with 80% HOAc at room temperature whereas **5***a* was 32% intact after 28 h under the same conditions. The silyl groups on adenosine appear to be slightly more resistant to acid than in the uridine case.

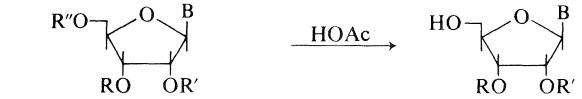

3 R = H; R′ = R″ = Si
4 R = R″ = Si; R′ = H
5 R = R″ = R′ = Si
7 R″ = MTr; R = H; R′ = Si
8 R″ = MTr; R = Si; R′ = H

a B = Ur
b B = Ad

9 B = Ur
10 B = Ad

a R = H; R′ = Si
b R = Si; R′ = H
c R = R′ = Si

SCHEME 2

Bases

Silyl groups can be removed from the 5′- and 2′- or 3′-positions (**2**, **3**, **4**) with base. However it is very difficult to remove either or both silyl groups from a molecule such as **5** where both 2′- and 3′-positions are protected. Furthermore the 2′- or 3′-silyls are more sensitive to base hydrolysis than the 5′-position. For example with 9 *M* NH_4OH in ethanol at 70°C, **9***a* is 90% converted to uridine in 4 h while after 3 h under these conditions **2***a* is unaffected. Compound **9***c* was unaffected by these conditions even after 55 h. Compound **3***a* was 35% converted to **2***a* under these conditions showing once more the effect of poly-substitution. Compound **4***a* was only 10% converted to **2***a* after 5 h under the same conditions indicating that the 3′-silyl is more stable than the 2′-silyl. Using 0.5 *N* NaOH (dioxane–H_2O, 1:1) we found that compounds **3***a* and **3***b* could be completely converted to the parent nucleoside within 36 h.

Can. J. Chem. Downloaded from www.nrcresearchpress.com by 210.87.254.40 on 09/05/12
For personal use only.

TABLE 2. Properties of silylated nucleosides

Compound	Melting point* (°C)	λ_{max} (λ_{min})† (nm in 95% EtOH)	R_f(tlc)‡
2*a* (5′-SiU)	136–139	262(231)	0.05[c], 0.36[f]
3*a* (2′,5′-DiSiU)	121–122	262(231)	0.25[a], 0.59[b]
4*a* (3′,5′-DiSiU)	136–137	262(231)	0.12[a], 0.47[b]
5*a* (2′,3′,5′-TriSiU)	Hard gum	263(231)	0.54[a], 0.80[b]
9*a* (2′-SiU)	189–194	262(231)	0.27[c], 0.17[b]
9*b* (3′-SiU)	204–206	262(231)	0.26[c], 0.17[b]
9*c* (2′,3′-DiSiU)	224–226	262(231)	0.21[a], 0.57[b]
7*a* (MTr-U^{Si}_{OH})	106–109	262, 231(249)	0.28[a], 0.68[b]
8*a* (MTr-U^{OH}_{Si})	115–118	262, 231(249)	0.07[a], 0.50[b]
2*b* (5′-SiA)	178–180	259(227)	0.04[c], 0.40[d]
3*b* (2′,5′-DiSiA)	174–177	259(227)	0.24[b], 0.57[c]
4*b* (3′,5′-DiSiA)	203–204	259(227)	0.08[b], 0.38[c]
5*b* (2′,3′,5′-TriSiA)	142–144	259(227)	0.42[a], 0.74[b]
10*a* (2′-SiA)	214–216	259(227)	0.21[c], 0.60[d]
10*b* (3′-SiA)	216–218	259(227)	0.16[c], 0.58[d]
10*c* (2′,3′-DiSiA)	250–254	260(225)	0.12[b], 0.56[c]
7*b* (MTr-A^{Si}_{OH})	164–167	260, 234(245)	0.15[b], 0.52[c]
8*b* (MTr-A^{OH}_{Si})	176–178	260, 234(245)	0.12[b], 0.32[c]
2*c* (5′-Si^{Bz}_{A})	105–112	278, 259sh, 230sh(248)	0.08[c], 0.28[d]
3*c* (2′,5′-$DiSi^{Bz}_{A}$)	80–85	280, 260sh, 231sh(249)	0.15[b], 0.43[e]
4*c* (3′,5′-$DiSi^{Bz}_{A}$)	66–70	280, 262sh, 232sh(249)	0.13[b], 0.31[e]
7*c* (MTr-$^{Bz\ Si}_{A\ OH}$)	93–97	281, 232, 263sh(253)	0.16[b], 0.48[e]
8*c* (MTr-$^{Bz\ OH}_{A\ Si}$)	97–101	281, 232, 260sh(253)	0.07[b], 0.28[e]

*Fisher-Johns melting point apparatus, uncorrected.
†Cary 17 spectrophotometer.
‡Eastman chromagram sheets 6060. Solvents used were (*a*) ether–hexane (2:1); (*b*) ether; (*c*) ethyl acetate; (*d*) tetrahydrofuran; (*e*) ethyl acetate – ether (1:1); (*f*) chloroform–ethanol (9:1).

*Tetra-*n*-butylammonium Fluoride (TBAF)*

Silyl groups, regardless of their position or number were completely cleaved within 30 min by TBAF in tetrahydrofuran as solvent. A mixture of pyridine–THF–water (1:8:1) was also very effective as a solvent. TBAF is less reactive in pure methanol solutions probably owing to the solvation of fluoride ions. When **3***a* was treated with 20 molar equiv. of TBAF in THF–MeOH (5:3), there was present after 24 h ~50% of 5′-OTBDMSU and the remainder was uridine. Clearly the 2′-silyl group was cleaved more rapidly than the 5′-silyl. This may reflect a hydrogen bonding between the fluoride ion and the 3′-hydroxyl, thus increasing the rate of fluoride attack at the 2′-silyl due to the proximity effect. Such H-bond interactions have recently been exploited by Clark and Miller (17).

The rate of fluoride ion attack can also be moderated by the presence of acetic acid (5) and under such conditions no 2′–3′ isomerization is observed in the unhydrolyzed material after 5 h.

2′–3′ Isomerization of Silyl Groups

Although the silyl groups seem to be stable in most pure solvents we have observed some conditions under which the silyl groups will migrate between 2′- and 3′-positions. For example when preparative tlc plates were allowed to stand for 4 h or longer after development, the eluted products **3** and **4** were no longer pure but contained traces of the other isomer. If the contact time was 24 h at room temperature or 3 h at 100°C up to 20% of the disilyl derivative had isomerized. Although this provides a method to convert more of the 3′,5′-isomer (**4**) into the generally more useful compound **3**, it represents a feature that must be taken into account during work-up.

We have not been able to detect any isomerization during acid treatment of **3** or **4** using either acetic acid or methanolic HCl under a variety of conditions. Similarly these compounds are stable to anhydrous pyridine or triethylamine solutions for at least 24 h. This is in marked contrast to the rapid isomerization of acyl derivatives (18). However, the presence of water with these amines can cause isomerization. For example in pyridine containing 10% water **4***a* was 40% converted to **3***a* after 24 h. Compounds **3***a* and **4***a* are, however, stable in solutions of pyridine–water

Can. J. Chem. Downloaded from www.nrcresearchpress.com by 210.87.254.40 on 09/05/12
For personal use only.

TABLE 3. Acid hydrolysis* of silyl and methoxytrityl groups from the 5′-position of nucleosides and nucleotides

Compound	Temperature (°C)	Time (h)	Yield† (%)
2*a*	22	24	**1***a*(40)
2*a*	100	0.25	**1***a*(95)
3*a*	22	21	**9***a*(82); **1***a*(6)
3*a*	100	0.5	**9***a*(75); **1***a*(14)
3*b*	22	20	**10***a*(70)
3*b*	100	0.6	**10***a*(58)
4*a*	22	28	**9***b*(69); **1***a*(26)
4*a*	100	0.5	**9***b*(75); **1***a*(15)
4*b*	22	28	**10***b*(67); **1***b*(6)
4*b*	100	0.6	**10***b*(55); **1***b*(2)
5*a*	22	28	**9***c*(62); **9***a* + **9***b*(2)
5*a*	100	0.75	**9***c*(75); **1***a*(8) **9***a* + **9***b*(15)
5*b*	100	3	**10***c*(82)
7*a*	22	4	**9***a*(98); **1***a*(2)
7*a*	90	0.25	**9***a*(93)
7*b*	90	0.25	**10***a*(93)
8*a*	90	0.25	**9***b*(83)
8*b*	90	0.25	**10***b*(99)
9*a*	22	22	**1***a*(100)
$SiU_p^{Si}(TCE)U_{Si}^{Si}$ (**11***b*)	90	3	$HOU_p^{Si}(TCE)U_{Si}^{Si}$(55)‡
$SiU_p^{Si}(TCE)U_{Si}^{Si}$ (**11***b*)	22	70	$HOU_p^{Si}(TCE)U_{Si}^{Si}$(65) **11***b*(21)
$MTr\text{-}U_p^{Si}(TCE)U_{Si}^{Si}$(**11***d*)	90	0.25	$HOU_p^{Si}(TCE)U_{Si}^{Si}$(87)
$MTr\text{-}A_p^{Si}(TCE)A_{Si}^{Si}$(**13***d*)	80	0.25	$HOA_p^{Si}(TCE)A_{Si}^{Si}$(93)

*80% HOAc except for entry **9***a* where 0.1 *M* HCl in CH_3OH was used.
†Balance is unreacted starting material unless otherwise indicated.
‡The remainder consisted of a mixture of unreacted starting material and several nucleotides with more than one silyl removed.

when either triisopropylbenzenesulfonic acid or its chloride are added. Isomerization occurs rapidly in DMF and DMF–imidazole mixtures. For example, **3***a* is about 30% isomerized in 17 h at room temperature. This undoubtedly explains some of the differences in product distribution between pyridine and DMF. We have found that on standing in 95% EtOH about 10% isomerization occurs in 7 days whereas in DMSO there is about 20% isomerization observed on standing for 24 h.

Isomerization does not appear to occur during any of the conditions of phosphorylation in anhydrous pyridine using sulfonyl chlorides or their derivatives as condensing agents. However when dicyclohexylcarbodiimide is used in the absence of phosphorylating agent nearly 40% of **3***a* isomerizes after 24 h in dry pyridine. No isomerization is observed during phosphorylations using phosphoryl chlorides.

Characterization of Derivatives

Because the silyl derivatives represent a new class of protected ribonucleosides it was necessary to characterize the products in detail. This was done by chemically converting the new derivatives into known derivatives of uridine and adenosine. In addition satisfactory elemental analyses were obtained on all new compounds and the mass spectra were obtained for all the silylated nucleosides. We have found that the position of silylation can be determined directly from the ^{13}C spectra.[3] Proton nmr is not quite as generally useful as ^{13}C but does serve to distinguish some isomers very well and this will be discussed later below. The nmr results are summarized in Table 4.

Uridine

5′-SiU (**2***a*) was easily characterized by conversion to the 2′,3′-dibenzoyl derivative and subsequent removal of the silyl group to leave 2′,3′-dibenzoyluridine of known structure (19). Compounds **3***a* and **4***a* were sulfonylated in separate experiments with *p*-toluenesulfonyl chloride. On removal of the silyl

[3]Unpublished results.

Can. J. Chem. Downloaded from www.nrcresearchpress.com by 210.87.254.40 on 09/05/12
For personal use only.

Can. J. Chem. Downloaded from www.nrcresearchpress.com by 210.87.254.40 on 09/05/12
For personal use only.

TABLE 4. Chemical shifts of methyl and *tert*-butyl protons on TBDMS groups at 90 MHz in CD_3COCD_3

Compound	δ (ppm)	
	CH_3	$(CH_3)_3C$
5′-SiU (**2***a*)	0.15(6)	0.95(9)
3′-SiU (**9***b*)	0.17(6)	0.95(9)
2′-SiU (**9***a*)	0.11(6)	0.91(9)
3′,5′-DiSiU (**4***a*)	0.16(6); 0.18(6)	0.95(9); 0.96(9)
2′,5′-DiSiU (**3***a*)	0.12(6); 0.17(6)	0.91(9); 0.97(9)
2′,3′-DiSiU (**9***c*)	0.10(3); 0.11(3) 0.14(3); 0.15(3)	0.91(9); 0.94(9)
5′-SiA (**2***b*)	0.11(6)	0.92(9)
3′-SiA (**10***b*)	0.20(6)	0.97(9)
2′-SiA (**10***a*)	−0.13(3); −0.29(3)	0.78(9)
3′,5′-DiSiA (**4***b*)	0.08(3); 0.10(3) 0.21(6)	0.92(9); 0.98(9)
2′,5′-DiSiA (**3***b*)	−0.08(3); 0.01(3) 0.15(6)	0.84(9); 0.96(9)
2′,3′-DiSiA (**10***c*)	−0.50(3); −0.10(3) 0.18(6)	0.78(9); 0.98(9)

groups from the product from **3***a*, the known 3′-*O*-*p*-toluenesulfonyluridine (20) was obtained. However from the sulfonated product of **4***a*, O^2,2′-anhydrouridine was obtained. This was not an unexpected product since the ready formation of the 2′-anhydro compound has been well documented (21, 22). These reactions clearly establish the structures of **2***a*, **3***a*, and **4***a*.

Compound **9***c* was characterized by conversion to the 5′-methoxytrityl derivative and subsequent removal of the silyl groups to yield the known 5′-*O*-monomethoxytrityluridine (23). Compounds **7***a* and **8***a* were acetylated and after removal of the methoxytrityl groups they yielded the same compounds as produced by acetylating **3***a* and **4***a*, respectively, and subsequently removing the 5′-silyl group selectively with 80% acetic acid. The trisilylated compound **5***a* was not obtained crystalline and was characterized by high resolution mass spectrometry.

Although there was little doubt as to the identity of **9***a* and **9***b* (since isomerization does not occur under the acid conditions used to produce them) they were nevertheless derivatized by methoxytrityl chloride to produce, respectively, the compounds **7***a* and **8***a* characterized above.

Adenosine

Compound **2***b* was converted to its 2′,3′-ditosyl derivative which after removal of the silyl group, yielded the known 2′,3′-ditosyladenosine (24). Compound **4***b* was converted in the same manner to 2′-*O*-tosyladenosine (24*b*). Compound **3***b* was tosylated to produce a compound isomeric to the 3′,5′-disilyl-2′-tosyladenosine produced from **4***b*. Because of the analogy to the uridine system and the lack of isomerization during acid hydrolysis of the 5′-silyl group, the structures of **10***a*, **10***b*, and **10***c* were not in question. Their mass spectra and ^{1}Hmr spectra fully supported the proposed structures and the ^{13}C spectra[3] were conclusive (Table 4).

Synthesis of Nucleotides

The silylated nucleosides are easy to prepare. They are also easily coupled together to form nucleotides. The Letsinger chlorophosphite procedure (14) which does not require *N*-protection (25), is uniquely suited to the silylated nucleosides. We have adapted the procedure making changes in duration of reaction and ratio of reactants. The general approach is outlined in Scheme 3 and the results are summarized in Table 5.

We have found that nearly optimum yields are obtained using ratios of reactants of initial nucleoside (5′-protected): trichloroethylphosphorodichloridite ($TCEOPCl_2$): second nucleoside (5′-open) which are 1:1.1:0.8 (or 0.9). These are higher ratios than used in the deoxy series (14). We have also consistently used times of 1 h at −78°C followed by warming to room temperature for 1 h during the condensation step involving the second nucleoside component (5′-open). The subsequent oxidation with iodine and treatment with sodium bisulfite are as previously described (14). All protected nucleotides were isolated as solids from preparative tlc.

We have gravitated toward collidine as the base used during condensation procedures. Yields using pyridine were generally lower. Lutidine gave good but not consistent results and difficulties of solubility arise at −78°C with this base. Collidine on the other hand gave consistently high yields with no experimental difficulties.

From Table 5 it can be seen that yields in the 50–70% range are general although yields of nucleotides

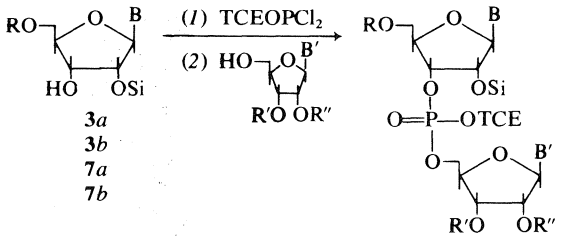

3*a*
3*b*
7*a*
7*b*

11 B = B′ = Ur
12 B = Ad; B′ = Ur
13 B = B′ = Ad
a R = R″ = Si; R′ = H
b R = R′ = R″ = Si
c R = MTr; R′ = R″ = Isopropylidene
d R = MTr; R′ = R″ = Si
e R = MTr; R′ = H; R″ = Si

SCHEME 3

Can. J. Chem. Downloaded from www.nrcresearchpress.com by 210.87.254.40 on 09/05/12
For personal use only.

TABLE 5. Summary of nucleotide condensation reactions*

Starting material	$TCEOPCL_2$ (molar ratio)	Base (mequiv.)	Time of 1st step (min)	Second component (molar ratio)	Product	Yield (%)
MTr-U^{Si}_{OH} (**7***a*)	0.9	Lutidine (3.6)	15	U^{Si}_{OH} (**9***a*, 0.5)	MTr-U^{Si}_{p}(TCE)U^{Si}_{OH} (**11***e*)	35
7*a*	0.9	Pyridine (3.6)	15	**9***a* (0.6)	**11***e*	25
7*a*	1.1	5-Chloro-1-methylimidazole (5.8)	15	**9***a* (0.6)	**11***e*	8
7*a*	1.1	Collidine (4)	30	**9***a* (0.6)	**11***e*	49
7*a*	1.1	Lutidine (3.4)	30	**9***a* (0.6)	**11***e*	53
7*a*	1.1	Collidine (4)	30	U_{ISP} (0.6)	MTr-U^{Si}_{p}(TCE)U_{ISP} (**11***c*)	60
7*a*	1.1	Collidine (4)	30	U_{ISP} (0.8)	**11***c*	69
7*a*	1.1	Collidine (4)	30	U_{ISP} (0.9)	**11***c*	67
SiU^{Si}_{OH} (**3***a*)	1.1	Collidine (4)	30	U^{Si}_{Si} (**9***c*, 0.9)	SiU^{Si}_{p}(TCE)U^{Si}_{Si} (**11***b*)	65
3*a*	1.0	Collidine (4)	45	**9***c* (0.9)	**11***b*	72
3*a*	1.1	Lutidine (4)	15	**9***a* (0.6)	SiU^{Si}_{p}(TCE)U^{Si}_{OH} (**11***a*)	55
MTr-U^{Si}_{OH} (**7***a*)	1.0	Collidine (4)	45	**9***c* (0.9)	MTr-U^{Si}_{p}(TCE)U^{Si}_{Si} (**11***d*)	60
MTr-A^{Si}_{OH} (**7***b*)	1.1	Lutidine (4)	45	A^{Si}_{Si} (**10***c*, 0.6)	MTr-A^{Si}_{p}(TCE)A^{Si}_{Si} (**13***d*)	69
7*b*	1.1	Collidine (4)	45	**10***c* (0.9)	**13***d*	80
Si-A^{Si}_{OH} (**3***b*)	1.1	Collidine (4)	45	**10***c* (0.9)	SiA^{Si}_{p}(TCE)A^{Si}_{Si} (**13***b*)	46
3*b*	0.9	Lutidine (4)	10	U_{ISP} (0.5)	SiA^{Si}_{p}(TCE)U_{ISP}	63
SiU^{Si}_{OH} (**3***a*)	1.1	Lutidine (4)	30	U^{Si}_{p}(TCE)U^{Si}_{OH} (0.6)	SiU^{Si}_{p}(TCE)U^{Si}_{p}(TCE)U^{Si}_{OH}	56
MTr-U^{Si}_{p}(TCE)U^{Si}_{OH}	1.1	Pyridine (4)	15	U^{Si}_{p}(TCE)U^{Si}_{OH} (0.6)	MTrU^{Si}_{p}(TCE)U^{Si}_{p}(TCE)U^{Si}_{p}(TCE)U^{Si}_{OH}	40
MTr-A^{Si}_{OH} (**7***b*)	1.1	Collidine (4)	45	U^{Si}_{p}(TCE)U^{Si}_{Si} (**14***a*, 0.9)	MTrA^{Si}_{p}(TCE)U^{Si}_{p}(TCE)U^{Si}_{Si} (**16***a*)	66
MTr-A^{Si}_{OH} (**7***b*)	1.1	Collidine (4)	45	A^{Si}_{p}(TCE)U^{Si}_{p}(TCE)U^{Si}_{Si} (**16***b*, 0.8)	MTrA^{Si}_{p}(TCE)A^{Si}_{p}(TCE)U^{Si}_{p}(TCE)U^{Si}_{Si} (**17**)	57

*The general procedure is fully described in the experimental. Ratios of all reactants are relative to the starting material. The solvent in all cases was tetrahydrofuran at −78°C. The time of the second step was 1 h at −78°C followed by 1 h at room temperature in all cases.

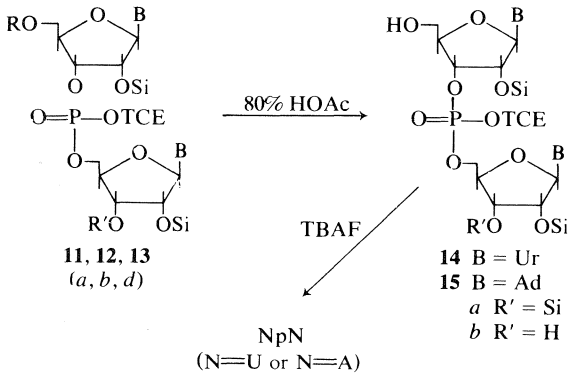

SCHEME 4

containing adenosine are consistently high and are very easy to work up.

The synthesis of dinucleotides such as **11***a* and **11***b* illustrate nucleotide synthesis using a single protecting group. The condensation of 2′,5′-diTBDMSuridine (**3***a*) with 2′-TBDMSuridine (**9***a*, prepared directly from **3***a*) gives a good yield of **11***a*. As will be shown below all of the protecting groups from **11***a* (**11***b* etc.) can be removed in a single 30 min treatment with TBAF to produce uridylyl-3′,5′-uridine.

The methoxytrityl group is an ideal protecting group to use with the silyl groups. A methoxytrityl group on the 5′-position in a growing nucleotide chain also serves as a label because of the coloration which arises with acid spray. Yields of nucleotides using the methoxytrityl group on the 5′-position are often between 69% (**11***c*) and 80% (**13***d*). Because *N*-protection is not required for adenosine, methoxytrityl groups and silyl groups can be removed from the 5′-position with acid without cleavage of the adenine ring. The methoxytrityl group can be cleaved from **11***d* and **13***d* in high yield to give **14***a* and **15***a*, respectively. By contrast the 5′-silyl group can be removed from **11***b* to give only a 65% yield of **14***a* (Scheme 4).

The ease of removal of the 5′-protecting group allows for chain extension to occur in a stepwise fashion. The synthesis of the protected tetranucleotide MTr-A_p^{Si}(TCE)A_p^{Si}(TCE)U_p^{Si}(TCE)U_{Si}^{Si} (**17**) is shown in Scheme 5. Yields are good at each stage of the synthesis with **16***a* (MTr-A_p^{Si}(TCE)U_p^{Si}(TCE)U_{Si}^{Si}) being obtained in 66% yield. Detritylation gives **16***b* in 83% yield from which the tetranucleotide **17** is obtained in 57% yield.

Block syntheses are also viable and the condensation between **11***e* (MTr-U_p^{Si}(TCE)U_{OH}^{Si}) and **14***b* (HO-U_p^{Si}(TCE)U_{OH}^{Si}) produced the protected tetranucleotide of uridine in 40% yield. We feel that in general it is best to protect the 3′-hydroxyl during chain extension, whether units are being added one at a time or in blocks. The reason for this is that on repeated reaction and work up via chromatography some migration of the 2′-silyl group to the 3′-position is bound to occur at the terminal nucleoside. For stepwise chain extension the use of compounds **9***c* and **10***c* containing silyl groups on both 2′- and 3′-positions at the 3′-terminus of the growing chain is ideal as described for the synthesis of **16** and **17**. However for multiple block condensations other 3′-protecting groups which are compatible with the silyl groups will be necessary and will be described in later publications.

Deprotection of Nucleotides

The removal of trityl (or other acid labile) protecting groups is easily carried out since *N*-protection on adenosine is not necessary. The silyl and trichloroethyl groups are both removed within 30 min using the TBAF in THF reagent. In some cases after this treatment we have noticed <5% of material containing a silyl group on the 2′-position adjacent to a 3′-phosphodiester. Apparently if a trace of moisture is present and the protected phosphate group is converted to a *p*-O^- group before the removal of an

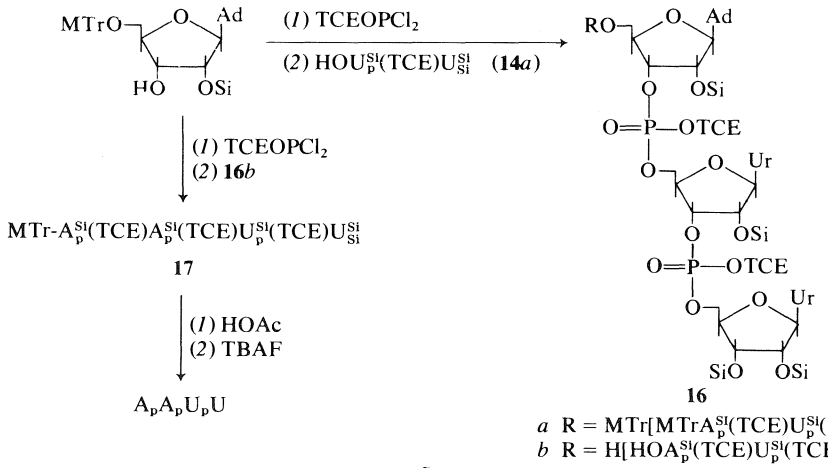

SCHEME 5

Can. J. Chem. Downloaded from www.nrcresearchpress.com by 210.87.254.40 on 09/05/12
For personal use only.

adjacent silyl group, fluoride attack at that silyl position is severely retarded. Such a silyl group can easily be removed by mild acid (26).

All of the free nucleotides had paper chromatographic and electrophoretic mobilities consistent with their structures. These nucleotides were completely degraded by snake venom, and spleen phosphodiesterases and uridine containing nucleotides were degraded with pancreatic ribonuclease.

Conclusion

The *tert*-butyldimethylsilyl group provides an excellent method of protecting the hydroxyl functions of nucleosides which can then be easily condensed via the chlorophosphite procedure to produce nucleotides. This represents the first general procedure whereby ribonucleosides can be directly converted, often in a single step, into derivatives which can be immediately incorporated into nucleotide chains. This feature along with the facile removal of silyl groups and phosphate protecting groups in a single 30 min step at room temperature makes this procedure complete.

This manuscript demonstrates the procedures used to produce the protected derivatives of uridine and adenosine. Similar procedures for the incorporation of cytidine and guanosine will be described in the next article in this series.

Experimental

General Methods

Descending paper chromatography was carried out using Whatman 3MM paper. The solvent systems employed were: solvent *A*, isopropyl alcohol – concentrated ammonium hydroxide – water (7:1:2); solvent *B*, *n*-butanol – acetic acid – water (5:2:3); solvent *B'*, *n*-butanol – ethanol – water (4:1:5, organic phase); solvent *C*, 1 *M* ammonium acetate – ethanol (3:7); solvent *E*, 0.5 *M* ammonium acetate – ethanol (3:7, adjusted to pH 3.5 with acetic acid); solvent *F*, *n*-propanol – concentrated ammonium hydroxide – water (55:10:35). The solvents were prepared on a volume basis. Thin-layer chromatography was carried out employing the ascending technique in closed jars which were not coated with absorbent paper. All thin-layer chromatography was run on Eastman chromagram sheets 13181 (formerly 6060), silica gel with fluorescent indicator, on strips 10 cm × 2 cm. Thick-layer chromatography was carried out on glass plates (20 cm × 20 cm) coated with a 1-mm thick layer of silica gel DSF-5 (Terrochem Laboratories). Paper electrophoresis was performed using Whatman 3MM paper in a Savant Flat Plate electrophoretic chamber with a Savant Model HB power supply operated at 2000 V for 1 h; the solution was a triethylammonium bicarbonate buffer (0.05 *M*, pH 7.5), prepared by making 15.15 g triethylamine up to 31 volume with water and then bubbling 20 g carbon dioxide through the solution. Nucleosides and their derivatives were detected on paper chromatograms, thin- and thick-layer sheets using a uv light source (Mineralite, output ~254 nm). Compounds containing trityl or *p*-monomethoxytrityl groups were detected on chromatography by spraying with 10% perchloric acid solution and drying them in a stream of warm air. Imidazole was detected by placing the tlc in a jar containing iodine whereupon imidazole turns black very rapidly (within 3 min).

Spectra

All uv spectra reported were obtained on a Cary 17 recording spectrophotometer. Routine mass spectra were obtained on a Finnigan 1015 RF quadrupole mass spectrometer, a Hitachi-Perkin Elmer RMU-6D single focussing mass spectrometer and an AEI, MS-9. High resolution spectra were obtained on a CEC-110-B double-focussing mass spectrometer (the Upjohn Co., Kalamazoo, Michigan). Proton magnetic resonance spectra were recorded on a Bruker WH-90 FT nmr.

Melting points were determined on a Fisher-Johns melting point apparatus and are reported uncorrected. Elemental analyses were performed by Galbraith Laboratories Inc., Knoxville, Tennessee and by the Analytical Laboratory, H. C. Ørsted Institute, Copenhagen, Denmark. All new compounds reported gave satisfactory elemental analyses. Samples submitted were prepared by crystallization, lyophilization, or precipitation from tetrahydrofuran with hexane followed by heating in a drying apparatus over P_2O_5.

Reagents and Chemicals

Reagent grade pyridine and lutidine were distilled first from *p*-toluenesulfonyl chloride, redistilled from calcium hydride, and stored over molecular sieves (Type 4A). *N,N*-Dimethylformamide and collidine were dried by distillation from calcium hydride and stored over molecular sieves (Type 4A). Tetrahydrofuran was refluxed with benzophenone and sodium for 3 h under nitrogen and distilled directly onto molecular sieves (Type 4A) and stored in the dark.

2,2,2-Trichloroethylphosphorodichloridite was prepared from phosphorus trichloride and 2,2,2-trichloroethanol as described in the literature (27). Nucleosides were obtained from Sigma Chemical Co. 5-*O*-Methoxytrityluridine (mp 103–105°C) (23), isopropylideneuridine (mp 159–160°C) (28), *N*-benzoyladenosine (mp 159–164°C) (29), 5'-*O*-methoxytrityladenosine (mp 189–191°C) (30), and 5'-*O*-methoxytrityl-*N*-benzoyladenosine (mp 133–137°C) (31) were all prepared according to literature procedures.

Enzyme Assays

(a) Spleen Phosphodiesterase

Lyophilized spleen phosphodiesterase (10–15 units) obtained from Nutritional Biochemicals Corp. was dissolved in 1 ml of 0.01 *M* sodium pyrophosphate buffer adjusted to pH 6.5 with phosphoric acid. An aliquot (0.1 ml) of this solution, 0.2 ml of 0.05 *M* ammonium acetate (adjusted to pH 6.5 with acetic acid), and 0.1–1 mg of the nucleotide substrate were incubated at 37°C. The solution was then applied to Whatman 3MM paper as a band and developed with solvent A. Nucleoside and nucleotide bands were cut out, eluted with water, and diluted to a volume of 10 ml. Absorbances were adjusted by using blanks cut from papers treated in the same way as the sample material. The term od unit refers to the extinction of the absorbing material in 1 ml of neutral solution in a quartz cell with a 1-cm path length.

(b) Snake Venom Phosphodiesterase

Two hundred units of snake venom phosphodiesterase obtained from Calbiochem were dissolved in 1 ml of tris(hydroxymethyl)aminomethane buffer (adjusted to pH 9.2 with 0.1 *N* HCl). An aliquot (0.2 ml) of the enzyme solution was added to the nucleotide material (~1 mg) and incubated at 37°C. The same procedure as in section *a* was then followed.

(c) Pancreatic Ribonuclease A

The enzyme (5 mg, protease free, Type XII A, Sigma

Can. J. Chem. Downloaded from www.nrcresearchpress.com by 210.87.254.40 on 05/05/12
For personal use only.

Can. J. Chem. Downloaded from www.nrcresearchpress.com by 210.87.254.40 on 09/05/12
For personal use only.

Chemical Co.) was dissolved in 1 ml of Tris buffer (pH 7.8). About 30 μl of the enzyme solution was added to 0.1–0.5 mg of the nucleotide in 0.2 ml of Tris buffer (pH 7.5) and the solution was incubated at 37°C for 3 h. The procedure described in section *a* was then followed.

Silylating Conditions

DMF

The ribonucleoside and imidazole were dissolved in DMF and the TBDMS-Cl was then added. In general 1 ml of DMF is used per millimole of ribonucleoside and 2 molar equiv. of imidazole are used for each mol of TBDMS-Cl.

Reactions are all carried out at room temperature for various times although most reactions seem to be complete within 30 min. Yields under the best conditions used are described in Table 1. Compounds were isolated in all cases by chromatography on tlc plates usually employing three plates per millimole of starting nucleoside. The solvents used to separate the desired product are shown in Table 6.

Pyridine

The nucleoside was dissolved in pyridine (2 ml/mmol of nucleoside) and the TBDMS-Cl was added to the solution which was stirred at room temperature. Yields and product distributions are shown in Table 1. Products were again isolated by tlc using the solvents in Table 6.

Preparative Hydrolysis of 5′-TBDMS and 5′-Methoxytrityl Groups from Silylated Nucleosides

These reactions were all carried out in 80% acetic acid (10 ml/mmol) either at room temperature or with heating. Products were isolated after removal of the solvents at reduced pressure followed by tlc purification. Product yields are given in Table 3 while properties of the products are listed in Table 2.

Stability of Silyl Groups Toward Acid, Base, and TBAF

Acid

Various conditions for the removal of a 5′-silyl group with acetic acid are summarized in Table 3. In addition we found that 2′- or 3′-TBDMS groups can be removed with 0.1 *M* methanolic HCl within 2 h at room temperature. No isomerization of 2′ or 3′-TBDMS groups has been observed under any acid condition tried to date.

Base

5′-Silyl groups are very stable to basic conditions requiring about 36 h with 0.5 *M* NaOH in dioxane–water (1:1) at room temperature. Using 7 *M* ammonia in ethanol at 70°C, 2′- or 3′-TBDMS groups are ~90% cleaved from **9***a* and **9***b* whereas as the TBDMS groups are completely unaffected in **2***a* and **9***c* under these conditions. The latter compound is stable for at least 55 h. Under these same conditions **3***a* is 35% isomerized after 5 h and 35% hydrolyzed to **2***a*.

TBAF in THF

This reagent has been prepared in several ways which seem to give similar results. We regularly prepare the reagent as follows. After titration of a dilute (~10%) aqueous solution of tetra-*n*-butylammonium hydroxide with a dilute (~5%) aqueous solution of HF, the neutral solution is lyophilized. The colorless and hydroscopic solid is shattered to a powder (simply by shaking the flask) and dried further over P_2O_5 for periods up to 24 h without heating. The dry powder is then dissolved in freshly distilled THF and stored over molecular sieves (Type 4A) in a tightly stoppered plastic bottle as a 0.7 *M* solution.

An alternate procedure has been published by Kuwajima *et al.* (32). We have modified the procedure by lyophilizing the clathrate and then drying as above. The activity of the reagent is the same as prepared above. Pless (33) has described a procedure which involves ion-exchange chromatography and other preparations have been described by Wen *et al.* (34) and Makosza and Bialecka (35).

TABLE 6. Solvent systems used to develop tlc plates during the isolation of silylated nucleosides

Compound isolated	Solvent used	Number of developments
2*a*	Chloroform–ethanol (9:1)	1
3*a*, **4***a*	Ether–hexane (4:1)	1
5*a*	Ether–hexane (2:1)	1
2*b*	Ethyl acetate – THF (1:1)	1
3*b*, **4***b*	Ether	3
5*b*	Ether–hexane (2:1)	1
2*c*	Ethyl acetate	1
3*c*, **4***c*	Ether	2
7*a*, **8***a*	Ether–hexane (3:2)	2
7*b*, **8***b*	Ethyl acetate	1
7*c*, **8***c*	Ether	2

The general use of this reagent has been described previously (5, 13). Some additional solvent tests studied during the course of this work are as follows: (*i*) **9***a* was treated with 3 molar equiv. of TBAF in a solution of pyridine–THF–water (1:8:1, v/v/v). Complete desilylation to uridine was observed after 30 min; (*ii*) **9***a* was treated with TBAF in acetic acid – water – THF (20:16:1, molar ratio) and after 24 h 50% conversion to uridine was observed; (*iii*) **3***a* was treated with the standard reagent in methanol (1:4; v/v) and after 24 h the solution contained uridine and **2***a* in about equal amounts.

Conversion of **2**a *to 2′,3′-Di-O-benzoyluridine*

Compound **2***a* was treated with a 10-fold molar excess of benzoic anhydride in pyridine at room temperature for 24 h. The reaction mixture was poured into ice water which was extracted with chloroform. The chloroform extracts were concentrated at reduced pressure and applied to tlc plates which were developed in ether–hexane (2:1). The desired product was eluted with ether and crystallized from ether–hexane (98% yield, mp 184–186°C, *m/e* 509 *M* − 57). This product was heated with 80% HOAc for 40 min on a steam bath and the solvents were removed at reduced pressure. The residue was applied to tlc plates which were developed twice in ether to separate the product from the unreacted starting material. 2′,3′-Di-*O*-benzoyluridine crystallized from ether–hexane with a melting point of 194–195°C (lit. (19) mp 195–197°C). The compound had λ_{max} 257 nm (95% EtOH) and showed a prominent peak at *m/e* 341 (*M* − base).

Conversion of **3**a *to 3′-O-Toluenesulfonyluridine*

Compound **3***a* was treated with a five-fold excess of *p*-toluenesulfonyl chloride (TsCl) in pyridine at 5°C for 36 h. After addition of methanol and evaporation of solvents, the residue was applied to tlc plates developed in benzene–ether (2:1). The product was eluted with ether to yield a white solid (65%, λ_{max} (EtOH) 262, 224 nm; *m/e* 569 (*M* − 57)).

The above compound was treated with 8 molar equiv. of TBAF reagent in THF and after 45 min the solution was applied to a tlc plate which on development in THF yielded a product which on crystallization from absolute ethanol produced 3′-*O*-*p*-toluenesulfonyluridine of mp 204–206°C (lit. (20) mp 205–206°C) and showing λ_{max} (EtOH) at 261 and 225 nm with the parent ion at *m/e* 398 in the mass spectrum.

Conversion of **4**a *to* O^2*,2′-Anhydrouridine*

Compound **4***a* was treated exactly as above for **3***a*. The

initial product, 3′,5′-DiTBDMS-2′-*p*-toluenesulfonyluridine (66%; mp 121–125°C; *m/e* 569 (*M* − 57)) on treatment with TBAF produced O^2,2′-anhydrouridine (λ_{max} (EtOH) 249, 224 nm, identical to an authentic sample).

Conversion of **9***c to 5′-Methoxytrityluridine*

Compound **9***c* was treated with 1.5 molar equiv. of methoxytrityl chloride in pyridine for 20 h. After work-up on tlc plates in ether–hexane (2:1) the fully protected compound was obtained (74%, mp 101–105°C). On treatment with TBAF in THF in the usual manner the material was completely converted to 5′-*O*-methoxytrityluridine, identical to an authentic sample (23).

3′-O-Acetyl-2′-O-TBDMSuridine

Method A

Compound **7***a* was treated with an excess of acetic anhydride in pyridine for 16 h. After evaporation of the solvents and treatment with 80% HOAc for 5 h at 20°C, the title compound was isolated from tlc plates developed in ether–hexane (2:1). The product (60%) crystallized from ether–hexane (mp 201–203°C, *m/e* 343 (*M* − 57); R_f 0.27 (ether–hexane; 2:1)).

Method B

Compound **3***a* was treated in the same manner as **7***a* above except that the acetic acid treatment was on a steam bath for 2 h. The title compound was obtained in 70% yield (mp 200–202°C, undepressed when mixed with the product from method *A*.

2′-O-Acetyl-3′-O-TBDMSuridine

Method A

Compound **8***a* was treated in a manner identical to **7***a* above to yield 2′-*O*-acetyl-3′-*O*-TBDMSuridine in 68% yield (mp 207–209°C, *m/e* 343 (*M* − 57); R_f 0.17 (ether–hexane; 2:1)).

Method B

Compound **4***a* was treated in a manner identical to **3***a* above to yield (60%) of the title compound (mp 209–211°C, undepressed when mixed with the product from method *A*).

*2′,3′,5′-TriTBDMSuridine (***5***a)*

This compound could not be obtained crystalline but a high resolution mass spectrum along with the data in Table 2 confirm its identity. The first fragment ion (*M* − 57) was observed at 529.258 (calcd. for $C_{23}H_{45}Si_3N_2O_6$: 529.259).

*5′-O-Monomethoxytrityl-2′-O-TBDMSuridine (*7a*)*

Compound **9***a* (prepared from **3***a*) was treated with methoxytrityl chloride in pyridine under the usual conditions. Work-up on tlc plates (ether–hexane; 1:1) gave **7***a* which crystallized from benzene–hexane (mp 141–143°C, 70%) and was identical in all respects to the major compound isolated from the silylation of methoxytrityluridine (see Tables 1 and 2).

*5′-O-Monomethoxytrityl-3′-O-TBDMSuridine (***8***a)*

Compound **9***b* (prepared from **4***a*) was treated with methoxytrityl chloride as for **9***a* above to yield **8***a* (mp 109–112°C) identical to the minor product obtained on the silylation of methoxytrityl uridine.

Conversion of **2**b *to 2′,3′-Di-*O-p-*Toluenesulfonyladenosine*

Compound **2***b* was treated with 8 molar equiv. of TsCl in pyridine at room temperature for 14 h. Work-up in the usual manner including chromatography on tlc plates in ether–benzene (2:1) gave the 5′-*O*-TBDMS-2′,3′-di-*O*-*p*-toluenesulfonyladenosine (mp 157–159°C; λ_{max} (CH_3OH) 260, 236, 272 (5h) nm; *m/e* 674 (*M* − 15) and 632 (*M* − 57). This compound was treated with 80% HOAc on a steam bath for 1 h. Work-up on tlc plates in ether gave the known 2′,3′-di-*O*-*p*-toluenesulfonyluridine, mp 205–207°C (lit. (24) mp 207–209°C).

Conversion of **4**b *to 2′-*O-p-*Toluenesulfonyladenosine*

Compound **4***b* was treated with 5 molar equiv. of TsCl at 0°C for 64 h in pyridine. Work-up as above using ether–benzene (1:1) gave 3′,5′-DiTBDMS-2′-*O*-*p*-toluenesulfonyladenosine (78%, mp 173–176°C; λ_{max} (EtOH) 261, 228 nm; *m/e* 592 (*M* − 57)). This product was treated with TBAF in THF for 35 min and the product was isolated on tlc plates developed in ethyl acetate – THF (1:1). The product, 2′-*O*-*p*-toluenesulfonyladenosine was crystallized from methanol–water (92%, mp 227–229°C (lit. (25) mp 229–230°C); λ_{max} (EtOH) 261, 228 nm).

Conversion of **3**b *to 2′,5′-DiTBDMS-3′-*O-p-*Toluenesulfonyladenosine*

Compound **3***b* was treated exactly as above for **4***b* to produce the title compound in 65% yield. Its mass spectral characteristics were very similar to the isomeric compound produced above from **4***b* but its R_f in ether–benzene (1:1) was 0.43 compared to 0.50 for the isomeric compound.

General Procedure for the Synthesis of Dinucleotides

The general procedure can best be illustrated by the synthesis of MTr-U_p^{Si}(TCE)U_{ISP} (**11***c*). The experiments with isopropylideneuridine were initial experiments undertaken to determine optimum conditions. Reactions were carried out in tubes or flasks closed by a rubber septum. Reagents in solution were injected via syringe. A syringe filled with magnesium perchlorate was used to equalize the pressure in reaction vessels.

To a cold solution (−78°C) of collidine (2.46 mmol) in THF (0.75 ml) was added trichloroethylphosphorodichloridite (90 μl, 0.61 mol). A solution of MTr-U_{OH}^{Si} (**7***a*, 0.558 mmol) dissolved in THF (0.75 ml) was added dropwise over a period of 5 min. The reaction mixture was stirred at −78°C for an additional 30 min. At this point a solution of isopropylideneuridine (143 mg) dissolved in THF (1.0 ml) was added and stirring was continued at −78°C for 1 h followed by warming to room temperature for an additional 1 h. A solution of iodine (0.61 mmol) in a mixture of THF (2 ml) and water (1.0 ml) was added followed by 0.5 ml of collidine. After 15 min at 22°C the solution was concentrated at reduced pressure and the residue was dissolved in chloroform (20 ml). The chloroform solution was washed with an aqueous sodium bisulfite solution (4 ml of saturated sodium bisulfite solution in 20 ml of water). The aqueous phase was separated and back-extracted twice with chloroform (20 ml each). The combined chloroform extracts were concentrated to a small volume and the residue was applied to tlc plates which were developed twice in ether–hexane (4:1). The desired product was eluted with ethyl acetate which on concentration yielded 375 mg (67%) of MTr-U_p^{Si}(TCE)U_{ISP} (**11***c*).

All of the reactions reported in Table 5 were carried out in this fashion. Yields are based on the limiting nucleoside (isopropylideneuridine in the above example). The physical properties of the fully protected nucleotides are described in Table 7. Their structures were further established by completely deprotecting the compounds to the known free nucleotides which were completely degradable by snake venom and spleen enzymes. The uridine nucleotides were also degraded by pancreatic ribonuclease.

It should be noted that 5′-5′ and 3′-3′ linked dinucleotides were obtained as byproducts and were easily separated on tlc. In the above illustration we obtained a 17% yield of the nucleotide formed by coupling two molecules of **7***a* and a 16% yield of the 5′-5′-linked dinucleotide formed by coupling 2 molecules of isopropylideneuridine. Such by-products were obtained in varying amounts in all condensation reactions.

Can. J. Chem. Downloaded from www.nrcresearchpress.com by 210.87.254.40 on 09/05/12
For personal use only.

Can. J. Chem. Downloaded from www.nrcresearchpress.com by 210.87.254.40 on 09/05/12
For personal use only.

TABLE 7. Properties of protected dinucleotides

Compound	Melting point (°C)	λ_{max} (λ_{min}) (nm)	R_f*
$SiU_p^{Si}(TCE)U_{OH}^{Si}$(**11***a*)	106–112	260(228)	0.05[a], 0.55[b], 0.74[c]
$SiU_p^{Si}(TCE)U_{Si}^{Si}$(**11***b*)	107–112	260(229)	0.05[a], 0.41[b], 0.91[c]
$SiU_p^{Si}(TCE)U_{ISP}$	121–125	258(228)	0.08[a], 0.69[b], 0.71[c]
$MTrU_p^{Si}(TCE)U_{ISP}$ (**11***c*)	121–126	259, 236 (245)	0.05[a], 0.35[b], 0.71[c]
$MTrU_p^{Si}(TCE)U_{Si}^{Si}$ (**11***d*)	118–123	261, 234 (245)	0.07[a], 0.45[b], 0.91[c]
$MTrU_p^{Si}(TCE)U_{OH}^{Si}$ (**11***e*)	118–121	260, 236 (245)	0.00[a], 0.25[b], 0.72[c]
$U_p^{Si}(TCE)U_{Si}^{Si}$ (**14***a*)	121–127	261(230)	0.00[a], 0.13[b], 0.76[c]
$U_p^{Si}(TCE)U_{OH}^{Si}$ (**14***b*)	142–146	261(230)	0.00[a], 0.05[b], 0.40[c]
$SiA_p^{Si}(TCE)A_{Si}^{Si}$ (**13***b*)	98–102	259(229)	0.15[a], 0.32[b], 0.77[c]
$MTrA_p^{Si}(TCE)A_{Si}^{Si}$ (**13***d*)	105–111	259, 236 (242)	0.15[a], 0.34[b], 0.78[c]
$A_p^{Si}(TCE)A_{Si}^{Si}$ (**15***a*)	109–113	260(228)	0.07[a], 0.17[b], 0.66[c]
$SiA_p^{Si}(TCE)U_{ISP}$	115–119	259(229)	0.00[a], 0.56[b], 0.75[c]

*Eastman chromagram sheets; solvents used: (*a*) ether, (*b*) ethyl acetate, (*c*) tetrahydrofuran.

Removal of Protecting Groups

Selective Removal of 5′-Protecting Groups

We have found that the most efficient way to remove the 5′-silyl group from a dinucleotide is to stir the nucleotide (e.g., **11***b*) in 80% HOAc for 3 days. In this way a 65% yield of **14***a* is obtained and 21% of the starting **11***b* was recovered. Heating **11***b* at 90°C for 3 h led to a 55% yield of **14***a* with several other multiply deprotected by-products being formed. The methoxytrityl group can be removed by heating for example **13***d* in 80% HOAc for 15 min at 80°C. Work-up on tlc yielded **15***a* in 93%. Yields are nearly always of the order of 90% in these reactions (see Table 3).

Complete Removal of Silyls and Trichloroethyl Groups

Both of these protecting groups are removed within 30 min on treating 10–50 mg of the protected nucleotide with 1 ml of the standard TBAF reagent. At the end of this period the solution is applied to Whatman 3MM paper and developed in solvent *A*. The pure nucleotide is always the major product. There are sometimes traces (< 5%) of material containing a silyl group, presumably on the 2′-position adjacent to the internucleotide linkage.

The pure nucleotides obtained in this fashion were all fully characterized by comparison to authentic standards on paper chromatography and electrophoresis. They were also shown to contain only 3′-5′ linkages by their complete enzymatic degradation using snake venom, spleen and pancreatic ribonuclease.

Synthesis of the Trinucleotide $SiU_p^{Si}(TCE)U_p^{Si}(TCE)U_{OH}^{Si}$

To a solution of lutidine (0.11 ml) in THF (0.35 ml) at −78°C was added $TCEOPCl_2$ (42 µl) followed by a solution of **3***a* (118 mg) in THF (0.9 ml). The solution was stirred an additional 30 min at −78°C whereupon a solution of **14***b* (135 mg) in THF (1 ml) was added. The solution was stirred for 1 h at −78°C and allowed to warm to room temperature for an additional 1 h. The system was treated with iodine and worked up in the general manner. The product was isolated from tlc plates which were developed twice in ether–hexane (4:1). $SiU_p^{Si}(TCE)U_p^{Si}(TCE)U_{OH}^{Si}$ (131 mg) was isolated in 56% yield (mp 145–150°C; λ_{max} (EtOH) 259 nm; R_f 0.76 (THF)).

Synthesis of the Tetranucleotide MTr-$U_p^{Si}(TCE)U_p^{Si}(TCE)U_p^{Si}$-$(TCE)U_{OH}^{Si}$

To a solution of pyridine (72 µl) in the THF (0.5 ml) was added $TCEOPCl_2$ (32 µl) followed by a solution of **11***e* (0.2 mmol) in THF (0.75 ml). The suspension was stirred for a further 10 min at −78°C whereupon **14***b* (105 mg, 0.115 mmol) in THF (0.5 ml) was added. After stirring at −78°C for 1 h followed by 1 h at room temperature the reaction was worked up with iodine in the usual manner. The product was isolated on tlc plates developed first in ether–hexane (3:1) and then in ether–hexane (4:1). The product was not further characterized at this point but was completely deprotected first with 80% HOAc at 80°C for 15 min and then with TBAF for 30 min to produce the nucleotide $U_pU_pU_pU$ (40% overall) which was fully characterized (R_f^A 0.01, R_f^F 0.27, R_m^{Tp} 0.79; λ_{max} (H_2O) 259 nm).

*Synthesis of MTr-$A_p^{Si}(TCE)U_p^{Si}(TCE)U_{Si}^{Si}$(**16**a)*

To a solution of collidine (0.14 ml) in THF (0.35 ml) at −78°C was added $TCEOPCl_2$ (39 µl) followed by a solution of **7***b* (156 mg) in THF (0.5 ml). The solution was stirred a total of 45 min at −78°C whereupon a solution of **14***b* (220 mg) in THF (0.75 ml) was added. The solution was stirred for 1 h at −78°C and allowed to warm to room temperature during the next hour. The solution was treated with iodine and worked up in the usual manner. The product was isolated from tlc plates (4) which were developed in ether – ethyl acetate (3:1, three times). The product was eluted from the plates with chloroform–ethanol (2:1) and on evaporation of the solvents 266 mg of **16***a* (66%, mp 140–144°C; λ_{max} (EtOH) 260, 238 nm (sh)); R_f 0.85 (THF)) was obtained.

*Preparation of HO-$A_p^{Si}(TCE)U_p^{Si}(TCE)U_{Si}^{Si}$(**16**b)*

Compound **16***a* (225 mg) was heated at 80°C in 80% acetic acid (6 ml) for 15 min. The solvent was removed at reduced pressure and the residue was applied to four tlc plates developed in chloroform–ethanol (9:1). The product band was eluted with $CHCl_3$–EtOH (2:1) and on evaporation of the solvent 159 mg of **16***b* (83%, mp 150–155°C; R_f 0.6 (THF); λ_{max} (EtOH) 260 nm) was obtained.

Synthesis of the Tetranucleotide MTr-A_p^{Si}(TCE)A_p^{Si}(TCE)U_p^{Si}-(TCE)U_{Si}^{Si}(17)

To a solution of collidine (44 μl) in THF (0.11 ml) at −78°C was added $TCEOPCl_2$ (12 μl) followed by a solution of **7***b* (49 mg) in THF (0.11 ml). The solution was stirred a total of 45 min at −78°C (whereupon a solution of **16***b* (96 mg) in THF (0.5 ml) was added. The solution was stirred for 1 h at −78°C and allowed to warm to room temperature during the next hour. The solution was treated with iodine and worked-up in the usual manner. The product was isolated from tlc plates which were developed in chloroform–ethanol (9:1, two times) and the product **17** was eluted with chloroform–ethanol (2:1) and on evaporation of the solvents 84 mg of **17** (57%, R_f 0.8 (THF), λ_{max} (EtOH)) 259, 238 nm (sh). The structure of the compound was further proven by removal of the methoxytrityl group followed by the TBDMS and trichloroethyl groups to give $A_pA_pU_pU$.

Acknowledgements

We gratefully acknowledge financial support from the National Research Council of Canada and the Quebec Education Ministry. We are also indebted to Dr. G. Hamer and Dr. A. Perlin for ^{1}Hmr spectra. We wish to especially acknowledge the assistance from Dr. M. Quilliam and Dr. J. B. Westmore in providing and interpreting mass spectra.

1. K. K. Ogilvie and D. J. Iwacha. Tetrahedron Lett. 317 (1973).
2. K. K. Ogilvie. Can. J. Chem. **51**, 3799 (1973).
3. K. K. Ogilvie, K. L. Sadana, E. A. Thompson, M. A. Quilliam, and J. B. Westmore. Tetrahedron Lett. 2861 (1974).
4. K. K. Ogilvie, E. A. Thompson, M. A. Quilliam, and J. B. Westmore. Tetrahedron Lett. 2865 (1974).
5. K. K. Ogilvie, S. L. Beaucage, D. W. Entwistle, E. A. Thompson, M. A. Quilliam, and J. B. Westmore. J. Carbohydr. Nucleosides, Nucleotides, **3**, 197 (1976).
6. K. K. Ogilvie, N. Theriault, and K. Sadana. J. Am. Chem. Soc. **99**, 7741 (1977).
7. H. G. Khorana *et al.* J. Biol. Chem. **251**, 565 (1976).
8. R. Lohrmann, D. Söll, H. Hayatsu, E. Ohtsuka, and H. G. Khorana. J. Am. Chem. Soc. **88**, 819 (1966).
9. C. B. Reese. Phosphorus Sulfur, **1**, 245 (1976).
10. J. H. van Boom, P. M. H. Burgers, G. van der Marel, C. H. M. Verdegaal, and G. Wille. Nucl. Acids Res. **4**, 1047 (1977).
11. E. S. Werstiuk and T. Neilson. Can. J. Chem. **54**, 2689 (1976).
12. E. Ohtsuka, S. Tanaka, and M. Ikehara. Chem. Pharm. Bull. **25**, 949 (1977).
13. K. K. Ogilvie, S. L. Beaucage, and D. W. Entwistle. Tetrahedron Lett. 1255 (1976).
14. R. L. Letsinger and W. B. Lunsford. J. Am. Chem. Soc. **98**, 3655 (1976).
15. E. J. Corey and A. Venkateswarlu. J. Am. Chem. Soc. **94**, 6190 (1970).
16. I. D. Blackburne, D. M. Fredericks, and R. D. Guthrie. Aust. J. Chem. **29**, 381 (1976).
17. J. H. Clark and J. M. Miller. J. Chem. Soc. Perkin I, 1743 (1977); 2063 (1977).
18. C. B. Reese and D. R. Trentham. Tetrahedron Lett. 2459 (1965).
19. R. Lohrmann and H. G. Khorana. J. Am. Chem. Soc. **86**, 4188 (1964).
20. D. M. Brown, D. B. Parihar, A. Todd, and S. Varadarajan. J. Chem. Soc. 3028 (1958).
21. D. M. Brown, A. R. Todd, and S. Varadarajan. J. Chem. Soc. 2388 (1956).
22. N. C. Yung and J. J. Fox. J. Am. Chem. Soc. **83**, 3060 (1961).
23. M. Smith, D. H. Rammler, I. N. Goldberg, and H. G. Khorana. J. Am. Chem. Soc. **84**, 430 (1962).
24. (*a*) T. Sasaki, K. Minamoto, and S. Tanizawa. J. Org. Chem. **38**, 2896 (1973); (*b*) D. Wagner, J. P. H. Verheyden, and J. G. Moffatt. J. Org. Chem. **39**, 24 (1974).
25. R. L. Letsinger, J. L. Finnan, S. A. Jacobs, B. A. Juodka, and A. K. Varshney. Proc. Int. Conf. Transfer RNA, Poznan, Poland, October 1976. pp. 145–155.
26. F. Ramirez, P. V. Ioannou, J. F. Marecek, M. Nowakowski, B. T. Golding, and G. H. Dodd. Synthesis, 483 (1976).
27. W. Gerrard, W. J. Green, and R. J. Phillips. J. Chem. Soc. 1148 (1954).
28. P. A. Levene and R. S. Tipson. J. Biol. Chem. **106**, 113 (1934).
29. R. H. Hall. Biochemistry, **3**, 769 (1964).
30. R. Lohrmann and H. G. Khorana. J. Am. Chem. Soc. **86**, 4188 (1964).
31. H. Schaller, G. Weimann, B. Lerch, and H. G. Khorana. J. Am. Chem. Soc. **85**, 3821 (1963).
32. I. Kuwajima, T. Murofushi, and E. Nakamura. Synthesis, **9**, 602 (1976).
33. J. Pless. J. Org. Chem. **39**, 2644 (1974).
34. W. Y. Wen, S. Saito, and C. Lee. J. Phys. Chem. **70**, 1244 (1966).
35. M. Makosza and F. Bialecka. Synth. Commun. **6**, 313 (1976).

Can. J. Chem. Downloaded from www.nrcresearchpress.com by 210.87.254.40 on 09/05/12
For personal use only.

Triplet–triplet absorption of some aryl-substituted 1,3,4-oxadiazoles

CLAUDE RULLIÈRE AND JEAN-CLAUDE RAYEZ
Laboratoire de Chimie Physique A, Université de Bordeaux I, F-33405 Talence, France
AND
PIERRE C. ROBERGE
Groupe de Dynamique Moléculaire, Département de Chimie, Université Laval (Qué.), Canada G1K 7P4

Received March 20, 1978

CLAUDE RULLIÈRE, JEAN-CLAUDE RAYEZ, and PIERRE C. ROBERGE. Can. J. Chem. **56**, 2781 (1978).

The triplet–triplet absorption spectra of three naphthyl-1,3,4 oxadiazoles have been measured from 400 to 620 nm. The spectra are analyzed in terms of naphthalene perturbed in the α or β position using a theoretical simulation of the perturbation based on Pariser–Parr–Pople approximation. It is concluded that the lowest triplet state of these molecules must involve an important contribution of charge transfer configurations.

CLAUDE RULLIÈRE, JEAN-CLAUDE RAYEZ et PIERRE C. ROBERGE. Can. J. Chem. **56**, 2781 (1978).

Les spectres d'absorption triplet–triplet de trois dérivés naphtyles du 1,3,4 oxadiazole ont été obtenus dans le domaine de 400 à 620 nm. Ces spectres présentent des similitudes avec ceux de naphtalènes perturbés en position α ou β. La perturbation en position α ou β est simulée en utilisant la méthode Pariser–Parr–Pople. Il semble que l'interprétation des spectres triplet–triplet doive faire intervenir une importante contribution de configurations de transfert de charge dans le premier état triplet de ces molécules.

Can. J. Chem. Downloaded from www.nrcresearchpress.com by 210.87.254.105 on 09/05/12
For personal use only.

Introduction

Aryl-substituted 1,3,4-oxadiazoles are extensively used as laser dyes (1). In the framework of a general search for the best candidates for laser action, we study the substituent effects on triplet–triplet (T–T) absorption in these compounds. We report here preliminary results on the following naphthyl oxadiazoles: 2-(1-naphthyl)-5-phenyl-1,3,4-oxadiazole (αNPD), 2-(2-naphthyl)-5-phenyl-1,3,4-oxadiazole (βNPD) and 2,5-di-(1-naphthyl)-1,3,4-oxadiazole (αNND). The structural formulas of these compounds are given as inserts in Figs. 1 and 2.

The $S_n \leftarrow S_0$ absorption spectra of these molecules (2) indicate a strong interaction between the different fragments (phenyl, naphthyl, and oxadiazole) in the ground state. The β compounds show more resolved vibrational structure than the α compounds. However, in all cases, the fluorescence spectra exhibit a well resolved vibrational structure. This result can be related to a planar or near planar configuration in the first singlet excited state. Berlman has already suggested the occurrence of hydrogen bonding with the nitrogen atoms of the oxadiazole ring in these compounds (3). According to his analysis, 2,3-diphenyl-1,3,4-oxadiazole (PPD) would present the strongest hydrogen bonding, followed by βNND, αNND, and, finally, αNPD. SCF MO calculations show that in the ground state the bond order of the ring–ring bonds and the electronic density on the nitrogen atoms are not significantly different in all these compounds (4). So, hydrogen bonding strength should be mainly dependent on geometrical factors. The β compounds (and PPD which present the same ring–ring geometry) should present a less preferable geometry for hydrogen bonding (five-membered cycle) than the α compounds (six-membered cycle with a closest approach of the hydrogen atom to the nitrogen atom). This is contrary to Berlman's statement. Korneeva and Kuzina (5) have shown that the introduction of a hydroxy group in the 2 position of the phenyl ring in PPD narrows the corresponding absorption band and attributed this effect to a restriction of rotation around the ring–ring bond due to hydrogen bonding. This suggestion offers another explanation of Berlman's results: in PPD and in the β compounds, rotation of the phenyl and/or naphthyl groups is not as restricted by steric hindrance as it is in α-naphthyl compounds. It would appear from the vibrational structure of the $S_n \leftarrow S_0$ spectra, and also by comparison of calculated and experimental oscillator strengths in these compounds (4) that β compounds are more nearly planar in the ground state than α compounds. However, it cannot be excluded that the loss of vibrational structure and the lowering of the expected oscillator strengths in the α compounds are due to intramolecular hydrogen bonding. In any case, it seems quite clear that the interaction between hydrogen and nitrogen atoms

Can. J. Chem. Downloaded from www.nrcresearchpress.com by 210.87.254.105 on 09/05/12
For personal use only.

(steric hindrance or hydrogen bonding) is more important in the α compounds than in the β compounds.

Experimental

The compounds αNND, αNPD, and βNPD were all Koch-Light products; chromatography on silica gel did not show any impurity and so they were used as received. Cyclohexane (Fisher spectroanalyzed) was used as the solvent without further purification. The description of the flash apparatus used for the T–T absorption measurements and the procedure for outgassing the solutions have already been described elsewhere (6). Each spectrum given here is the result of more than 400 flashes on different solutions.

Results and Discussion

Analysis of the Absorption Spectra

The T–T absorption spectra of αNND, αNPD, and βNPD are assembled in Figs. 1 and 2. The behavior of the short wavelength band in these spectra shows close similarity to that of the short wavelength band in quinoline and isoquinoline (7): it is broader and of lower extinction coefficient in the α compounds (quinoline type) than in the β compounds (isoquinoline type). This result might suggest that the T–T spectra of these substituted oxadiazoles can be interpreted in terms of naphthalene perturbed in the α or β position. The short wavelength band in the spectra of the three substituted oxadiazoles would correspond to an overlap of possibly up to three transitions as in the quinolines (7).

The energy of the first two transitions, which are clearly discernible in the spectrum of αNND, are compared in Fig. 1*a* with the energy of the $^3A_g^+ \leftarrow {}^3B_{2u}^+$ and $^3B_{3u}^- \leftarrow {}^3B_{2u}^+$ transitions[1] in naphthalene as calculated by Meyer *et al.* (8). The agreement is good. Intensification of the transitions towards the $^3B_{3u}^-$ and $^3A_g^+$ states could be explained by a lowering of the symmetry in the αNND molecule (C_{2v} at the most). The total oscillator strength for the three transitions (0.14) is close to the oscillator strength of the $^3B_{1g}^- \leftarrow {}^3B_{2u}^+$ transition in naphthalene (0.12).

The spectrum of αNPD, when compared to the one of αNND, shows an increase of the intensity in the red part of the spectrum (Fig. 1*b*). This would not be inconsistent with an intensification of the $^3A_g^+ \leftarrow {}^3B_{2u}^+$ transition due to the destruction of pairing in the naphthalene fragment (the symmetry of αNPD being at the most C_s). The total oscillator strength for all of the observed transitions in αNPD (0.19) is, however, larger than in naphthalene.

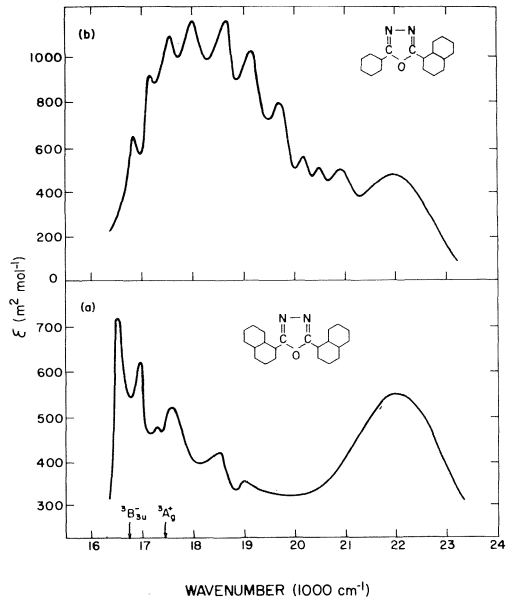

FIG. 1. Triplet–triplet absorption spectra in cyclohexane at room temperature: (*a*) αNND, (*b*) αNPD. The energies of the $^3B_{3u}^- \leftarrow {}^3B_{2u}^+$ and $^3A_g^+ \leftarrow {}^3B_{2u}^+$ transitions in naphthalene are indicated by the arrows at the bottom of the figure.

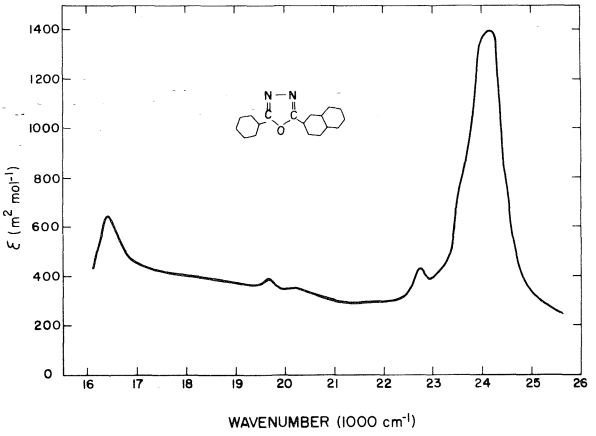

FIG. 2. Triplet–triplet absorption spectrum of βNPD in cyclohexane at room temperature.

The T–T spectrum of βNPD (Fig. 2) could also be interpreted in terms of naphthalene perturbed in the β position. The intensification of the $^3A_g^+ \leftarrow {}^3B_{2u}^+$ transition, polarized along the short axis of naphthalene, should be much less important than in the α compounds. The total oscillator strength of the observed transitions in βNPD (0.15) is also close

[1]The spectroscopic notations for naphthalene correspond to Pariser's choice of axis (as in refs. 7 or 8): *y* along the short axis and *x* along the long axis of naphthalene.

Can. J. Chem. Downloaded from www.nrcresearchpress.com by 210.87.254.105 on 09/05/12
For personal use only.

to the oscillator strength of the ${}^3B_{1g}^- \leftarrow {}^3B_{2u}^+$ transition in naphthalene.

The preceding analysis of the T–T spectra of the naphthyl oxadiazoles is based on the hypothesis that the loss of symmetry and the related destruction of pairing in the naphthalene fragment upon substitution induce an intensity increase of sign forbidden and symmetry forbidden transitions. In the case of quinoline and isoquinoline, Lavalette and co-workers (7) concluded on the basis of theoretical and experimental evidence that spectral dilution by interaction with the ${}^3B_{1g}^-$ state of naphthalene did not cause any perceptible absorption in the region of the first ${}^3A_g^+$ or ${}^3B_{3u}^-$. However, the perturbation of naphthalene by oxadiazole or phenyl oxadiazole group is much more important than the perturbation introduced by the nitrogen atom in the case of quinoline and isoquinoline. A larger perturbation might induce an intensification of the sign and/or symmetry forbidden transitions towards low lying states. Theoretical calculation should be able to show if this interpretation is correct.

Theoretical Calculations

We decided to simulate perturbations in the α or β position of naphthalene using the Pariser–Parr–Pople (P.P.P.) method. To simulate a perturbation of variable strength, the value of the atomic valence state ionization potential (W_{2p}) for the α or β carbon atom was varied from the normal value of −11.22 eV in naphthalene up to a value of −29 eV. The effect of the perturbation on the other parameters entering into the P.P.P. calculation was considered as a second order effect and neglected. The parameters used were: $R_{C-C} = 1.40$ Å; $W_{2p} = -11.22$ eV for all carbon atoms except the α or β ones; $\beta_{CC} = -2.39$ eV; $\alpha_{CC} = 10.53$ eV; γ_{pq} as computed from Nishimoto-Mataga relation (9). All the singly excited configurations with respect to the ground state were included in the configuration interaction. The results of this calculation are shown in Figs. 3 and 4.

It can be seen that for $|W_{2p}| > 23$ eV, there appear transitions with important oscillator strengths in the region of the naphthalene ${}^3A_g^+$ and ${}^3B_{3u}^-$ in both of the α- and β-perturbed systems.

A possible assignment of the observed spectra of αNND and αNPD in terms of naphthalene perturbed in the α position is given in Table 1. Considering the crudeness of the theoretical approach, the agreement between theory and experiment could be considered satisfactory. The physical meaning of the high values of W_{2p} needed to account for the αNND ($W_{2p} \simeq -25$ eV) and αNPD ($W_{2p} \simeq -23$ eV) spectra is questionable. Such a strong perturbation would

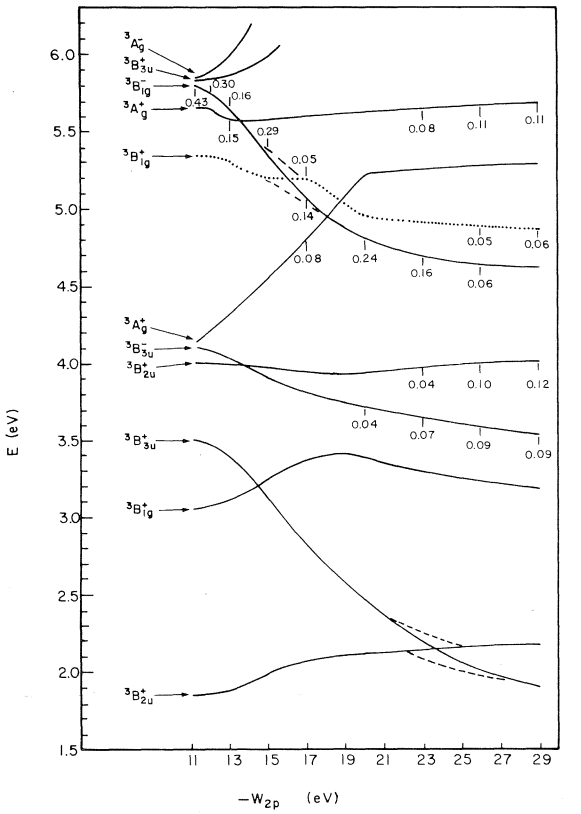

FIG. 3. The calculated energies of the lowest triplet states relative to the ground-state energy, as a function of W_{2p} of the α carbon atom of naphthalene. Oscillator strengths are indicated when larger than 0.04.

surely indicate a planar or quasiplanar lowest triplet state. In contrast to the $S_n \leftarrow S_0$ spectra, the $T_n \leftarrow T_1$ spectra of both αNND and αNPD show well resolved vibrational structure with progressions of ~500 and ~350 cm^{-1}. This observation is surely consistent with planar or quasiplanar lowest triplet state for both of these molecules. However according to Table 1, one would expect an observable transition at ca. 800 nm in αNND and αNPD. The spectral study of αNND was extended to 900 nm but we did not observe any transition in the range 600–900 nm. Moreover the calculation shows that as a result of the perturbation the naphthalene ${}^3B_{1g}^-$ state interacts with adjacent forbidden levels. Such an interaction, as expected in a naphthalene molecule of reduced symmetry (7), leads to the dilution of the intensity of the ${}^3B_{1g}^- \leftarrow {}^3B_{2u}^+$ transition over a group of transitions formerly forbidden in naphthalene. This dilution process requires that the total oscillator strength for all of the observed transitions in αNPD

TABLE 1. Experimental T–T transition energies and oscillator strengths compared to calculated values for α- or β-perturbed naphthalene

αNND			αNPD			βNPD		
Transition energies[a] (eV)			Transition energies[a] (eV)			Transition energies[a] (eV)		
Observed	Calculated[b]	Origin[e]	Observed	Calculated[c]	Origin	Observed	Calculated[d]	Origin[e]
—	1.56(0.08)	$1B_{3u}^-$	—	1.56(0.07)	$1B_{3u}^-$	—	1.82(0.02)	$1B_{3u}^-$
2.06(0.04)	1.95(0.08)	$1B_{2u}^+$	2.08 } (0.13)	1.89(0.04)	$1B_{2u}^+$	2.03(0.04)	2.34(0.07)	$1A_g^+$
2.18(0.04)	2.62(0.09)	$1B_{1g}^+$	~2.2 }	2.62(0.16)	$1B_{1g}^-$	2.44(0.02)	2.90(0.18)	$2B_{1g}^+$
—	2.84(0.03)	$2B_{1g}^+$	2.50(0.02)	2.83(0.02)	$2B_{1g}^+$	—	3.20(0.03)	$1B_{2u}^+$
2.73(0.06)	3.62(0.10)	$2A_g^+$	2.73(0.04)	3.56(0.08)	$2A_g^+$	3.00(0.09)	3.55(0.19)	$2A_g^+$

[a]Oscillator strengths (f) are given in parenthesis.
[b]α-Perturbed naphthalene $W_{2p} = -25$ eV.
[c]α-Perturbed naphthalene $W_{2p} = -23$ eV.
[d]β-Perturbed naphthalene $W_{2p} = -21$ eV.
[e]Original state in unperturbed triplet naphthalene.

or αNND is not much larger than 0.10.[2] The total experimental oscillator strength for αNPD (0.19) is twice this expected value.

The absorption spectrum of βNPD does not show much vibrational structure, which could indicate a nonplanar lowest triplet state for this molecule. The perturbation of the naphthalene fragment by the phenyl oxadiazole fragment would necessarily be less important than in αNPD. However, there is no way to explain the long wavelength absorption band of αNPD in terms of a weakly perturbed naphthalene (see Fig. 4). A rather strong perturbation would be needed. Such a perturbation, ca. $W_{2p} \simeq -21$ eV, would in turn be associated with a strong absorption band in the region 450–500 nm (see Table 1) which is not observed experimentally. So there seems to be no way to explain the T–T absorption spectrum of βNPD in terms of a β perturbed naphthalene molecule.

It is thus believed that the long wavelength absorption band of βNPD is due to an important contribution of charge transfer configurations due to a delocalization of π electrons over the entire molecule. Therefore contribution of charge transfer configurations in the more nearly planar αNND and αNPD triplets should be even more important.

Conclusions

The apparent similarity between the calculated T–T spectrum of a strongly α perturbed naphthalene and the T–T spectra of αNND and αNPD is probably accidental. An understanding of the T–T spectra of aryl-substituted 1,3,4-oxadiazoles will necessitate consideration of π electron delocalization over

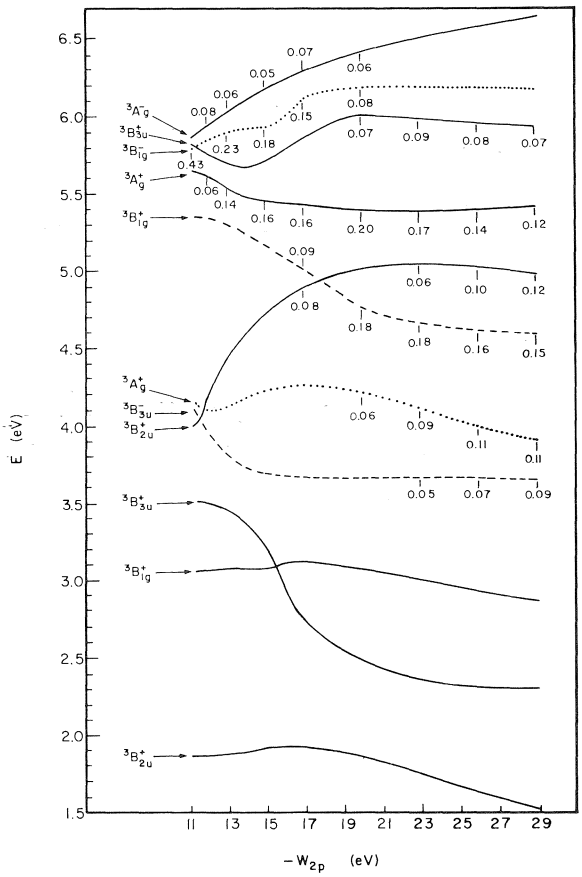

FIG. 4. The calculated energies of the lowest triplet states relative to the ground-state energy, as a function of W_{2p} of the β carbon atom of naphthalene. Oscillator strengths are indicated when larger than 0.04.

[2]One has to remember that the present calculation overestimates the energy of the transitions in the blue part of the spectrum and the oscillator strength of the transitions. The $^3B_{1g}^- \leftarrow {}^3B_{2u}^+$ transition in naphthalene is observed at 3.0 eV ($f = 0.12$) (8). The present calculation would predict it at 3.9 eV ($f = 0.43$). A large part of the discrepancy is due to the omission in our calculation of the excited configurations which are doubly excited with respect to the ground state but singly excited with respect to the first triplet state.

Can. J. Chem. Downloaded from www.nrcresearchpress.com by 210.87.254.105 on 09/05/12
For personal use only.

the entire molecule. SCF MO CI calculations as a function of the interplanar angles for the triplet manifold are in progress.

Acknowledgement

Part of this investigation was made possible due to France–Quebec cooperation (integrated project No. 0101 12).

1. K. D. DREXAGE. Dye lasers. Springer. Berlin, Heidelberg, New York. 1973.
2. I. B. BERLMAN. Handbook of fluorescence spectra of aromatic molecules. Academic Press Inc., New York, NY. 1965.
3. I. B. BERLMAN. Chem. Phys. Lett. **3**, 61 (1969).
4. C. RULLIÈRE, J. C. RAYEZ, and P. C. ROBERGE. To be published.
5. O. G. KORNEEVA and L. M. KUZINA. Zh. Prikl. Spektrosk. **18**, 834 (1973).
6. C. RULLIÈRE, E. C. COLSON, and P. C. ROBERGE. Can. J. Chem. **53**, 3269 (1975).
7. C. TETREAU, D. LAVALETTE, and F. PERADEJORDI. Chem. Phys. Lett. **20**, 379 (1973).
8. Y. H. MEYER, R. ASTIER, and J. M. LECLERCQ. J. Chem. Phys. **56**, 801 (1972).
9. N. NISHIMOTO and N. MATAGA. Z. Phys. Chem. (Frankfurt am Main), **12**, 335 (1957).

Can. J. Chem. Downloaded from www.nrcresearchpress.com by 210.87.254.105 on 09/05/12
For personal use only.

Can. J. Chem. Downloaded from www.nrcresearchpress.com by 210.87.254.42 on 09/05/12
For personal use only.

A new regiospecific synthesis of α,β-unsaturated ketones via acetylene derivatives[1]

JOHN HOOZ AND RICHARD D. MORTIMER

Department of Chemistry, University of Alberta, Edmonton, Alta., Canada T6G 2G2

Received July 18, 1978

JOHN HOOZ and RICHARD D. MORTIMER. Can. J. Chem. **56**, 2786 (1978).

The reaction of trialkylalkynylborate salts with benzeneselenenyl chloride, followed by selective oxidation, provides a new synthetic pathway from acetylenes to acyclic *trans*-α,β-unsaturated ketones. The method is especially useful for preparing unsymmetric acyclic enones which are difficultly accessible using current procedures.

JOHN HOOZ et RICHARD D. MORTIMER. Can. J. Chem. **56**, 2786 (1978).

La réaction de sels trialcylakynlborates avec le chlorure de benzènesélénenyl et l'oxidation sélective subséquente offre une nouvelle voie pour la synthèse de cétones acyclics *trans*-α,β-insaturés à partir des acétylènes. La méthode est particulièrement utile pour la préparation d'énones acyclic asymétriques qui sont difficiles à obtenir par les méthodes connues présentement.

[Traduit par le journal]

The direct approach to α,β-enone synthesis (i.e., oxidation of the corresponding saturated ketone) frequently involves as the initial step the requirement of specific enol(ate) formation, and in the case of *unsymmetric* acyclic ketones, is often problematic[2] (proton transfer, etc.). We have previously reported that trialkylalkynylborate salts **1** (easily available from R_3B and $R'CH_2C{\equiv}CLi$) react stereoselectively with certain electrophiles (Sn, Se) and that this process can be useful for di- and tri-substituted olefin synthesis (5). We now wish to describe the application of reagents **1** to the synthesis of *trans*-α,β-unsaturated ketones which avoids the aforementioned problems.

The solution is outlined in the conversion **1** → **5**. This scheme owes its success to the extremely rapid rearrangement of salts **1** induced by benzeneselenenyl chloride and the selective unmasking of an α-keto-selenide **3** by initial oxidation at boron of the mixed vinyl organometallic **2**. *trans*-Enones **5** are then formed in good yield by subsequent oxidation at selenium and precedented fragmentation (6) of the intermediate ketoselenoxides **4**. In several cases we have isolated intermediates **2** and **3**; however, the entire sequence may be conveniently performed in a single reaction vessel by appropriately treating the crude mixture with the reagents sequentially.

Since the process specifically preassembles masked enones **2** directionally, it is especially applicable to synthesis of acyclic unsymmetric enones. To illustrate the method, a solution of tricyclopentylborane (3 mmol) in ether[3] (15 ml) was added to a solution of 1-lithiohexyne (from 10 mmol 1-hexyne and 10 mmol *n*-butyllithium in hexane (Alfa)) at −25°C under nitrogen with magnetic stirring. The cold bath was removed and stirring was continued for ca. 30 min. The reaction mixture was then cooled to ca. −116°C (ether – liquid N_2 slush) before the dropwise addition of the red-brown solution of C_6H_5SeCl (10.5 mmol) in 12 ml ether.[3,4]

[1]Dedicated to Professor Herbert C. Brown on the occasion of his 66th birthday.

[2]Summaries of the problems and solutions relating to the traditional method, α-bromination–dehydrobromination, appear in refs. 1–4.

[3]All organoboranes were prepared by hydroboration of the corresponding olefin with $H_3B{\cdot}DMS$ (Aldrich) in ether (7).

[4]Hydroboration with $H_3B{\cdot}THF$ and subsequent reaction with C_6H_5SeCl in THF results in significant *inter*molecular transfer of R groups from **1** (31% C_6H_5SeEt from **1**, R = Et, R′ = nC_4H_9).

Can. J. Chem. Downloaded from www.nrcresearchpress.com by 210.87.254.42 on 09/05/12
For personal use only.

Here, as in all examples described, the reaction is essentially instantaneous at ca. −116°C as judged by the immediate discharge of color. The solution was warmed to room temperature by removing the cold bath and **6** (mp 38–39.5°C) was isolated[5] (89%)

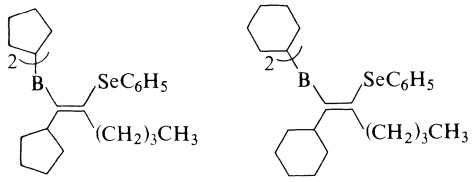

6 **7**

by chromatography (silica gel, hexane elution). Cyclohexyl analog **7**[5] was isolated (82%) similarly.

Successful conversion of intermediates **2** to enones depends dramatically on the choice of oxidant.[6] Compound **6**, for example, was converted to butylcyclopentylacetylene (70%) on treatment with 3 *N* NaOAc–H_2O_2 or H_2O_2 (pH 7), presumably via initial oxidation at Se and subsequent *cis*-elimination.[7] On the other hand, selective oxidation at boron is achieved with anhydrous trimethylamine *N*-oxide[8] (9) to provide the corresponding selenoketone. This

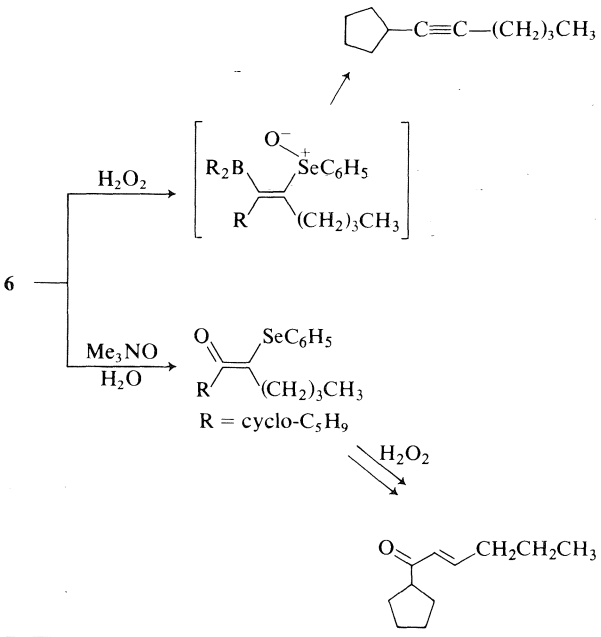

may be isolated[9] if desired (79%),[5] or the mixture further oxidized *in situ* (30% H_2O_2 (10), room temperature, 1.5 h) to the enone (69%), bp (Kugelrohr) 90°C 0.1 Torr; ir[10] (neat): 3030, 1695, 1669, 1630, 980 cm^{-1}; ^{1}Hmr ($CDCl_3$) δ: 7.01, 6.73 (1H, dt, J = 16, 6.5 Hz), 6.26, 5.99 (1H, dt, J = 16, 1.2 Hz), 3.05 (1H, m), 2.15 (2H, br q), 1.9–1.2 (10H, m), 0.92 (3H, br t); ms (*m/e*) 166. *Anal.* calcd. for $C_{11}H_{18}O$: C 79.52, H 10.84; found: C 79.30, H 11.06.

α,β-Unsaturated ketones **8**, **9**, and **10** were similarly obtained[5] (71, 75, and 61%, respectively) from their corresponding organoborane and lithioalkyne precursors.

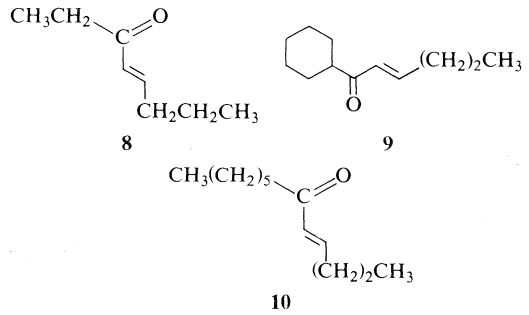

8 **9**

10

An example of its application to the synthesis of a positional isomeric pair is the preparation of **11** (64%) and **12** (60%), substrates which are inaccessible by methods relying on specific enol(ate) formation (1, 3, 4, 12).

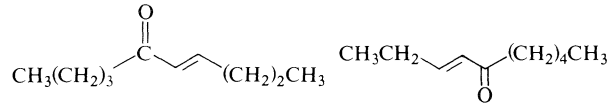

11 **12**

In view of the mildness and unambiguity of the method, it should augment considerably the range of enone structures available from selenoxide fragmentation.[11]

Acknowledgement

We thank the National Research Council of Canada for financial support.

[5]Characterized by acceptable compositional analysis and/or precise mass measurement and compatible spectral (ir, nmr, mass spectral) data.

[6]Reagents which proved unsatisfactory include *m*-chloroperbenzoic acid, $NaIO_4$, $Na_2Cr_2O_7$, $Ca(OCl)_2$, $K_2S_2O_8$, $NaClO_4$, and NaOH–H_2O_2.

[7]An analogous *cis*-fragmentation has been proposed for presumed intermediate boraethylenic sulfoxides (8) as a preparative route to internal acetylenes.

[8]The dihydrate (Aldrich) was dried by azeotropic removal of water in boiling toluene.

[9]Isolation of the selenoketone eliminates the alternative a priori plausible pathway for enone formation, viz.

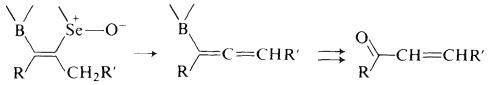

[10]All enones exhibited ir (C=O) absorption bands indicative of *S-cis* ⇄ *S-trans* (11).

[11]An alternate 'preassembly–fragmentation' synthesis of enones employs acetylenes and α-chloroaldonitrones (13).

1. H. O. HOUSE. Modern synthetic reactions. 2nd ed. W. A. Benjamin, New York, NY. 1972. Chapt. 8.
2. J. HOOZ and J. N. BRIDSON. Can. J. Chem. **50**, 2387 (1972).
3. H. J. REICH, J. M. RENGA, and I. L. REICH. J. Am. Chem. Soc. **97**, 5434 (1975).
4. B. M. TROST, T. N. SALZMANN, and K. HIROI. J. Am. Chem. Soc. **98**, 4887 (1976).
5. J. HOOZ and R. MORTIMER. Tetrahedron Lett. 805 (1976).
6. D. N. JONES, D. MUNDY, and R. D. WHITEHOUSE. Chem. Commun. 86 (1970).
7. C. F. LANE. J. Org. Chem. **39**, 1437 (1974).
8. M NARUSE, K. UTIMOTO, and H. NOZAKI. Tetrahedron Lett. 1847 (1973).
9. R. KÖSTER and Y. MORITA. Justus Liebigs Ann. Chem. **704**, 70 (1967).
10. K. B. SHARPLESS and R. F. LAUER. J. Am. Chem. Soc. **94**, 7154 (1972).
11. K. NOACK and R. N. JONES. Can. J. Chem. **39**, 2225 (1961).
12. H. J. REICH, I. L. REICH, and J. M. RENGA. J. Am. Chem. Soc. **95**, 5813 (1973); D. L. J. CLIVE. Chem. Commun. 695 (1973); K. B. SHARPLESS, R. F. LAUER, and A. Y. TERANISHI. J. Am. Chem. Soc. **95**, 6139 (1973).
13. S. SHATZMILLER and A. ESCHENMOSER. Helv. Chim. Acta, **56**, 2975 (1973).

Can. J. Chem. Downloaded from www.nrcresearchpress.com by 210.87.254.42 on 09/05/12
For personal use only.

The heat of mixing of hydrogen cyanide and hydrogen fluoride in the liquid phase

JOHN L. COLLISTER AND HUW O. PRITCHARD
Chemistry Department, York University, Downsview, Ont., Canada M3J 1P3

Received June 27, 1978

JOHN L. COLLISTER and HUW O. PRITCHARD. Can. J. Chem. **56**, 2788 (1978).

An approximate measurement is reported for the heat of mixing of hydrogen cyanide and hydrogen fluoride in the liquid phase.

JOHN L. COLLISTER et HUW O. PRITCHARD. Can. J. Chem. **56**, 2788 (1978).

On rapporte une mesure approximative de la chaleur dégagée lorsque sont mêlés, en phase liquide, le cyanure d'hydrogen et le fluorure d'hydrogen.

[Traduit par le journal]

There has been considerable interest recently in hydrogen-bonded dimers, both experimentally and theoretically. In the case of the gas-phase redistribution reaction

$$(HCN)_2 + (HF)_2 \rightarrow 2HCN{\cdot}HF$$

the available experimental data (1–3) would suggest an endothermicity of about 1.0 kcal mol^{-1} (of HCN·HF product) whereas *ab initio* calculations predict that the reaction might be as much as 1.5 kcal mol^{-1} exothermic (4, 5). In considering this problem, we noticed that there is no experimental information available for liquid mixtures of HCN and HF, and we have conducted a brief exploration which shows that the liquids are miscible in all proportions, and that the temperature rise on mixing can exceed 50°C.

Liquid samples of hydrogen cyanide (mp −14°C) and hydrogen fluoride (mp −92°C) were mixed at −10°C in all rational volume ratios from 1:9 to 9:1, and the instantaneous temperature rises were measured by using a Teflon-coated thermocouple. The sum of the initial volumes of HCN and HF was always 10 ml, measured with an accuracy of about ±5% by syringe. Mixing was conducted in a polythene tube of 20 ml capacity supported in an air space held at −10°C by thermostat, and in view of the suddenness of the temperature rise, heat losses were considered to be small. The measured temperature rises, which were reproducible to better than ±2°C, are listed in column 2 of Table 1; those temperature rises which exceed 40°C are probably slightly underestimated since the final temperature was then higher than the boiling points of the two liquids, 27°C and 20°C, respectively, and vigorous boiling ensued.

We note in passing that, as with HCl and HBr (6, 7), liquid HF appears to be miscible with liquid HCN in all proportions, and no phase separation occurs when 50/50 v/v HCN/HF mixtures are cooled to −80°C.

Columns 3, 4, and 5 of Table 1 give respectively

TABLE 1. Mixing of hydrogen cyanide and hydrogen fluoride in the liquid phase at −10°C

Volume ratio HCN:HF	ΔT (°C)	Mole fraction x_{HCN}	$-\Delta H$ (cal g^{-1})	$-\Delta H$ (cal mol^{-1})
1:9	20.4	0.05	12.3	250
2:8	25.7	0.11	15.6	323
3:7	35.8	0.17	21.7	460
4:6	43.0	0.25	23.5	568
5:5	51.7	0.33	31.6	706
6:4	51.0	0.43	31.3	721
7:3	46.3	0.54	28.6	681
8:2	38.1	0.66	23.7	583
9:1	25.2	0.82	15.8	404

1. H. O. HOUSE. Modern synthetic reactions. 2nd ed. W. A. Benjamin, New York, NY. 1972. Chapt. 8.
2. J. HOOZ and J. N. BRIDSON. Can. J. Chem. **50**, 2387 (1972).
3. H. J. REICH, J. M. RENGA, and I. L. REICH. J. Am. Chem. Soc. **97**, 5434 (1975).
4. B. M. TROST, T. N. SALZMANN, and K. HIROI. J. Am. Chem. Soc. **98**, 4887 (1976).
5. J. HOOZ and R. MORTIMER. Tetrahedron Lett. 805 (1976).
6. D. N. JONES, D. MUNDY, and R. D. WHITEHOUSE. Chem. Commun. 86 (1970).
7. C. F. LANE. J. Org. Chem. **39**, 1437 (1974).
8. M NARUSE, K. UTIMOTO, and H. NOZAKI. Tetrahedron Lett. 1847 (1973).
9. R. KÖSTER and Y. MORITA. Justus Liebigs Ann. Chem. **704**, 70 (1967).
10. K. B. SHARPLESS and R. F. LAUER. J. Am. Chem. Soc. **94**, 7154 (1972).
11. K. NOACK and R. N. JONES. Can. J. Chem. **39**, 2225 (1961).
12. H. J. REICH, I. L. REICH, and J. M. RENGA. J. Am. Chem. Soc. **95**, 5813 (1973); D. L. J. CLIVE. Chem. Commun. 695 (1973); K. B. SHARPLESS, R. F. LAUER, and A. Y. TERANISHI. J. Am. Chem. Soc. **95**, 6139 (1973).
13. S. SHATZMILLER and A. ESCHENMOSER. Helv. Chim. Acta, **56**, 2975 (1973).

Can. J. Chem. Downloaded from www.nrcresearchpress.com by 210.87.254.42 on 09/05/12
For personal use only.

The heat of mixing of hydrogen cyanide and hydrogen fluoride in the liquid phase

JOHN L. COLLISTER AND HUW O. PRITCHARD
Chemistry Department, York University, Downsview, Ont., Canada M3J 1P3

Received June 27, 1978

JOHN L. COLLISTER and HUW O. PRITCHARD. Can. J. Chem. **56**, 2788 (1978).

An approximate measurement is reported for the heat of mixing of hydrogen cyanide and hydrogen fluoride in the liquid phase.

JOHN L. COLLISTER et HUW O. PRITCHARD. Can. J. Chem. **56**, 2788 (1978).

On rapporte une mesure approximative de la chaleur dégagée lorsque sont mêlés, en phase liquide, le cyanure d'hydrogen et le fluorure d'hydrogen.

[Traduit par le journal]

There has been considerable interest recently in hydrogen-bonded dimers, both experimentally and theoretically. In the case of the gas-phase redistribution reaction

$$(HCN)_2 + (HF)_2 \rightarrow 2HCN{\cdot}HF$$

the available experimental data (1–3) would suggest an endothermicity of about 1.0 kcal mol^{-1} (of HCN·HF product) whereas *ab initio* calculations predict that the reaction might be as much as 1.5 kcal mol^{-1} exothermic (4, 5). In considering this problem, we noticed that there is no experimental information available for liquid mixtures of HCN and HF, and we have conducted a brief exploration which shows that the liquids are miscible in all proportions, and that the temperature rise on mixing can exceed 50°C.

Liquid samples of hydrogen cyanide (mp −14°C) and hydrogen fluoride (mp −92°C) were mixed at −10°C in all rational volume ratios from 1:9 to 9:1, and the instantaneous temperature rises were measured by using a Teflon-coated thermocouple. The sum of the initial volumes of HCN and HF was always 10 ml, measured with an accuracy of about ±5% by syringe. Mixing was conducted in a polythene tube of 20 ml capacity supported in an air space held at −10°C by thermostat, and in view of the suddenness of the temperature rise, heat losses were considered to be small. The measured temperature rises, which were reproducible to better than ±2°C, are listed in column 2 of Table 1; those temperature rises which exceed 40°C are probably slightly underestimated since the final temperature was then higher than the boiling points of the two liquids, 27°C and 20°C, respectively, and vigorous boiling ensued.

We note in passing that, as with HCl and HBr (6, 7), liquid HF appears to be miscible with liquid HCN in all proportions, and no phase separation occurs when 50/50 v/v HCN/HF mixtures are cooled to −80°C.

Columns 3, 4, and 5 of Table 1 give respectively

TABLE 1. Mixing of hydrogen cyanide and hydrogen fluoride in the liquid phase at −10°C

Volume ratio HCN:HF	ΔT (°C)	Mole fraction x_{HCN}	$-\Delta H$ (cal g^{-1})	$-\Delta H$ (cal mol^{-1})
1:9	20.4	0.05	12.3	250
2:8	25.7	0.11	15.6	323
3:7	35.8	0.17	21.7	460
4:6	43.0	0.25	23.5	568
5:5	51.7	0.33	31.6	706
6:4	51.0	0.43	31.3	721
7:3	46.3	0.54	28.6	681
8:2	38.1	0.66	23.7	583
9:1	25.2	0.82	15.8	404

the mole fraction of HCN and the estimated values for the heat of mixing on a cal g^{-1} and cal mol^{-1} (of liquid mixture) basis; these estimates are made from the densities of the liquids, i.e. HCN, liq., $\rho \simeq 0.7$ g cm^{-3}, HF, liq., $\rho \simeq 1.0$ g cm^{-3}, and their heat capacities, i.e., HCN, liq., $C_p \simeq 17$ cal deg^{-1} mol^{-1} (8), HF, liq., $C_p \simeq 12$ cal deg^{-1} mol^{-1} (9), assuming additivity. In view of these approximations, taken together with the experimental uncertainties, the mixing heats are probably reliable to within $\pm 20\%$.

Acknowledgements

This work was supported by the National Research Council of Canada, and we acknowledge help from W. F. J. Yared.

1. H. D. METTEE. J. Phys. Chem. **77**, 1762 (1973).
2. C. E. VANDERZEE and W. W. RODENBURG. J. Chem. Thermodyn. **2**, 461 (1970).
3. A. C. LEGON, D. J. MILLEN, P. J. MJÖBERG, and S. C. ROGERS. Chem. Phys. Lett. **55**, 157 (1978).
4. P. KOLLMAN, J. MCKELVEY, A. JOHANSSON, and S. ROTHENBERG. J. Am. Chem. Soc. **97**, 955 (1975).
5. W. L. JORGENSEN and M. E. COURNOYER. J. Am. Chem. Soc. **100**, 4942 (1978) and references therein.
6. A. W. FRANCIS. J. Phys. Chem. **63**, 753 (1959).
7. A. W. FRANCIS. Critical solution temperatures. ACS Adv. Chem. Ser., No. 31, 1969. pp. 104–105.
8. P. D. MONTGOMERY. *In* Kirk–Othmer encyclopedia of chemical technology. Vol. 6. 2nd ed. John Wiley, New York. 1965. p. 574.
9. J. F. GALL. *In* Kirk–Othmer encyclopedia of chemical technology. Vol. 9. 2nd ed. John Wiley, New York. 1966. p. 610.

Can. J. Chem. Downloaded from www.nrcresearchpress.com by 210.87.254.42 on 09/05/12
For personal use only.

Canadian Journal of Chemistry
Published by
THE NATIONAL RESEARCH COUNCIL OF CANADA

Journal canadien de chimie
Publié par
LE CONSEIL NATIONAL DE RECHERCHES DU CANADA

Volume 56 Number 22 November 15, 1978

Volume 56 numéro 22 15 novembre 1978

Can. J. Chem. Downloaded from www.nrcresearchpress.com by 210.87.254.105 on 09/05/12
For personal use only.

Allene–methylacetylene isomerization over silica-supported cobalt and iron catalysts

C. P. KHULBE[1] AND R. S. MANN
Department of Chemical Engineering, University of Ottawa, Ottawa, Ont., Canada K1N 6N5

Received February 20, 1978

C. P. KHULBE and R. S. MANN. Can. J. Chem. **56**, 2791 (1978).

Equilibrium between allene and methylacetylene was studied over iron catalyst in the temperature range of 165 to 200°C, with allene or methylacetylene as the initial reactant. In both cases similar equilibrium product-distribution (allene 16% and methylacetylene 84%), fairly close to the calculated value, is observed.

Kinetics of allene–methylacetylene isomerization was studied between 70 and 165°C. The order of reaction was always one and temperature independent. Both activity and calculated energy of activation (11.8 and 11.2 kcal/mol over iron and cobalt respectively) were similar for the two catalysts, suggesting that active sites for the reaction were also similar. This similarity, as well as the first order kinetics, are fully explained by a reaction mechanism based on adsorbate migration.

C. P. KHULBE et R. S. MANN. Can. J. Chem. **56**, 2791 (1978).

On a étudié l'équilibre entre l'allène et le méthylacétylène sur un catalyseur de fer à des températures allant de 165 à 200°C; on a utilisé soit l'allène soit le méthylacétylène comme produit de départ. Dans les deux cas, on a pu observer des distributions de produits à l'équilibre qui sont semblables soit 16% d'allène et 84% de méthylacétylène; ces valeurs sont en bon accord avec celles qui avaient été calculées.

On a étudié la cinétique de l'isomérisation allène–méthylacétylène entre 70 et 165°C. L'ordre de la réaction est toujours égale à l'unité et est indépendante de la température. L'activité ainsi que l'énergie d'activation calculées (11.8 et 11.2 kcal/mol respectivement pour le fer et le cobalt) sont semblables pour les deux catalyseurs; ces résultats suggèrent que les sites actifs pour la réaction sont aussi semblables. Cette similarité de même que la cinétique du premier ordre sont expliquées par un mécanisme réactionnel basé sur une migration du produit adsorbé.
[Traduit par le journal]

Introduction

While the isomerization (double bond migration) of olefins, diolefins, and substituted diolefins (1–9) has been studied extensively, very little has been reported about acetylene–allene isomerization.

On treatment of acetylenic compounds with a base, hydrogen from a propargylic methylene group migrates to the triple bond carbon atom, thus giving allenic compounds or, on further migration, a mixture of acetylenic compounds including allene derivatives. The alkoxide-catalyzed rearrangement of ethylacetylene to dimethylacetylene was described as a prototropic rearrangement with methylallene as an intermediate (9). The postulation of an allenic intermediate in this process was supported by the rearrangement of isopropylacetylene to 3-methylbuta-1,2-diene catalyzed by KOH–ETOH at 170°C, the subsequent formation of 2-alkyne being impossible in this case by the fact that *tert*-butylacetylene was unchanged under comparable conditions (10). In his review, Iwai (11) has summarized acetylene–allene isomerization.

Kamentzy and Markovich (12) calculated equilibrium data for the isomerization of allene

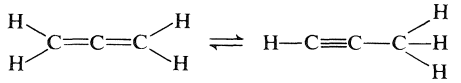

[1]Present address: Energy Research Laboratories, Canada Centre for Mineral and Energy Technology, Department of Energy, Mines and Resources, c/o 555 Booth Street, Ottawa, Canada.

Can. J. Chem. Downloaded from www.nrcresearchpress.com by 210.87.254.105 on 09/05/12
For personal use only.

TABLE 1. Equilibrium constants for allene–methylacetylene isomerization (ref. 12)

T (°C)	κ	% of allene
82	15.5	6.0
200	9.9	10.0
400	5.5	15.3
500	4.7	17.4
600	4.2	19.2

at different temperatures by the statistical method using spectroscopic data obtained by Linnett and Avery (13) for allene, and by Crawford (14) for methylacetylene, and the heat of hydrogenation obtained by Kistiakowsky and co-workers (15). Table 1 shows the equilibrium constants and percentage of allene in equilibrium mixture at various temperatures.

On the basis of equilibrium data calculated by Kamentzy and Markovich (12), Bond and Sheridan (16) suggested that the reaction should occur on supported or unsupported metals. In the hydrogenation of allene on pumice-supported nickel, palladium, and platinum (16), they could not obtain even traces of methylacetylene. Though the rearrangement of allenes and acetylenes could be obtained by different means, nothing has been reported about the allene–methylacetylene isomerization reaction catalyzed by supported or unsupported metals.

Chang and Kokes (17) studied the isomerization of methylacetylene over zinc oxide. The kinetics of the first half of allene isomerization to methylacetylene could be represented fairly well by first order. The infrared studies show a similarity between the adsorbed state of allene and methylacetylene, indicating the same adsorbed species for both the compounds.

Preliminary studies of allene isomerization over unsupported and silica-supported copper, nickel–copper alloy, and the transition metals of Group VIII showed that only silica-supported iron and cobalt were active for the isomerization reaction. The present paper deals with the equilibrium and kinetic studies and mechanism of allene–methylacetylene isomerization over silica supported cobalt and iron catalysts.

Experimental

The experiments were performed in a constant volume static conventional high vacuum system. The details of the apparatus are given elsewhere (18).

Metal catalysts containing 5% metal were prepared using Fisher Scientific Co. certified $Co(NO_3)_2 \cdot 6H_2O$ and $Fe(NO_3)_2 \cdot 9H_2O$, which in turn contained less than 0.05 wt.% metals as impurity. Silica (EH-5), supplied by Cabot Corporation, Boston, was heated at 650°C for about 12 h and then mixed with a solution of about 0.5 g of the desired compound in about 100 cm^3 of acetone. The slurry thus obtained was stirred and dried at room temperature. The impregnated catalyst was then crushed into fine powder.

The reaction vessel containing the catalyst was sealed and evacuated until a high vacuum (10^{-4} Torr) was obtained. A stream of hydrogen (80 cm^3/min) was passed through the reactor and the temperature raised slowly to 400°C in about 12 h and then maintained constant for 24 h. The hydrogen stream was stopped and the reaction vessel allowed to cool to room temperature in about 200 mm Hg of hydrogen. Following hydrogenation the catalyst was reduced again and evacuated for 4 h at 450°C and then cooled to room temperature under vacuum for isomerization studies.

To stabilize its activity the catalyst was aged by introducing allene (50 mm) at room temperature. The reactor was connected to the liquid nitrogen trap after 30 min. Allowing sufficient time for condensation, the trap was disconnected and the gases were analyzed with the help of a Hewlett-Packard Research Gas Chromatograph employing 16 ft × 1/4 in. column at 35°C, packed with 30% dimethylsulpholane on acid washed 20–60 mesh chromosorb P using helium (25 cm^3/min) as the carrier gas. After about ten treatments when a constant activity (same distribution) was obtained, the desired temperature was maintained with the help of a temperature controller. A definite amount of allene (50 mm Hg) was introduced into the reactor and the gas was analyzed after a certain time. The same amount of gas was introduced again and the analysis made at different time intervals. Runs were made for different allene pressures, to obtain the order of reaction with respect to initial allene pressure, and at several temperatures.

Results and Discussion

Equilibrium Studies

Equilibrium between allene and methylacetylene was studied over silica-supported 5% iron (weight = 0.67585 g) catalysts between 165 and 200°C. Starting with a 50 mm sample of pure allene, the distribution of isomers was followed by analyzing the samples at various time intervals, and that at 185°C in Fig. 1 is shown. The analysis showed that equilibrium could be obtained in about 12 h and that equilibrium values were nearly constant (5.275 ± 0.025) within the studied temperature range. Similar values were obtained for the equilibrium distribution (κ = 5.393 ± 0.143) when methylacetylene was taken as the reactant and samples were analyzed after a time interval of 12, 24, and 36 h.

At 200°C, the equilibrium mixture should contain about 90% methylacetylene (12). Slobodine (19) studied the equilibrium of allene–methylacetylene isomerization by passing these substances over "Floridine" between 167 and 350°C. With methylacetylene as the initial substance, the resulting mixture contained about 61.5 to 67.8% methylacetylene at 325°C. On the other hand, with allene as the initial substance, except at 325°C, the resulting mixture contained a much lower percentage of methylacetylene. No direct determination of the allene content of the mixtures were carried out. The polymeri-

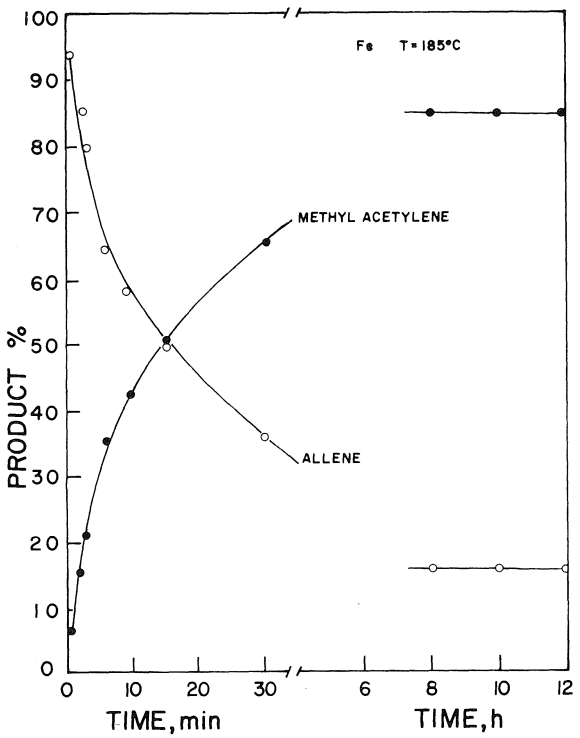

FIG. 1. Allene–methylacetylene distribution on silica supported iron catalyst.

zation and decomposition reactions must have proceeded to a considerable extent and their products diluting the resulting mixture. It seems, therefore, quite natural that the methylacetylene contents of the mixture were, in all cases, lower than the theoretical value. Cordes and Gungler (20) obtained an equilibrium mixture containing 20% allene and 80% methylacetylene at 300°C by heating these isomers as the initial substance in the presence of activated charcoal. In the present study, starting with allene or methylacetylene, an equilibrium mixture containing about 16% allene and 84% methylacetylene was obtained in the studied temperature range. This is fairly close to the calculated values (12).

Kinetics

Varying amounts of allene were introduced into the reactor and the samples analyzed after various time intervals. As no pressure change was observed during the reaction polymerization could not have occurred. Analysis showed that only allene and methylacetylene were present in the products and thus neither isomer could have been fragmented. To established the kinetics, results were analyzed using two different approaches. In one case, the initial rate of allene isomerization was calculated assuming a first order reversible reaction. In another case the initial rate of methylacetylene was obtained using the initial rate method. The initial rate of allene isomerization was always equal to the initial rate of methylacetylene formation.

Initial Rate of Allene Isomerization

Assuming a first order reversible reaction for allene–methylacetylene isomerization, the following equation was developed

$$[1] \qquad r_i = (1 - y_e)\frac{P}{t}\ln\left(\frac{1 - y_e}{y - y_e}\right)$$

where r_i = initial rate of allene isomerization mm/min; y = fraction of allene left after time t; y_e = fraction of allene at equilibrium; P = initial pressure of allene in mm; and t = time in min.

For all calculations y_e value obtained in the present study was used. At a particular initial pressure and temperature, r_i was calculated using product analysis values at different time intervals and eq. [1]. The initial rate calculated was found to be constant (Table 2). This indicates that the assumption of a first order reversible reaction is valid.

Initial Rate Method

Partial pressures of methylacetylene were plotted against time. Initial rate, at a particular initial allene pressure and temperature, was obtained by drawing a tangent on the pressure time curve at $t = 0$ (Figs. 2 and 3). The slope of the tangent gave the initial rate of methylacetylene formation (r_G values, Table 2), which was always equal to the calculated initial rate of allene isomerization.

TABLE 2. Kinetics of isomerization on iron catalyst at 135°C

Initial pressure (mm)	Reaction time (min)	Initial rate (mm^{-1}) Using eq. [1]	Average r_i	Initial rate method r_G
50 ± 2	0.5	0.62		
	3.0	0.75		
	5.0	0.72	0.69	0.70
	7.5	0.67		
	10.0	0.68		
75 ± 2	2.0	0.74		
	4.0	0.78		
	6.0	0.81	0.77	0.80
	8.0	0.78		
	15.0	0.74		
100 ± 2	2.0	1.06		
	4.0	1.04		
	6.0	0.97	0.99	0.98
	8.0	0.88		
125 ± 2	2.5	1.28		
	4.0	1.20	1.13	1.15
	6.0	1.07		
	10.0	0.98		

Can. J. Chem. Downloaded from www.nrcresearchpress.com by 210.87.254.105 on 09/05/12
For personal use only.

Can. J. Chem. Downloaded from www.nrcresearchpress.com by 210.87.254.105 on 09/05/12
For personal use only.

Figures 2 and 3 show the pressure–time curves for methylacetylene on Fe and Co respectively. Using these curves or eq. [1] the isomerization reaction was observed to be of first order and temperature independent on both catalysts. Hence the initial rate expression for allene isomerization can be written as

$$[2] \qquad r_0 = kP_{\text{allene}}$$

The energy of activation was calculated to be 11.8 and 11.2 kcal/mol for Fe and Co, respectively. The activity (defined as the rate constant per g of catalyst for initial allene pressure of 50 mm Hg at 127°C) was nearly equal for iron ($k_{127} = 0.0250$ min^{-1}/g) and cobalt ($k_{127} = 0.0253$ min^{-1}/g) catalysts. No direct comparison can be made with other catalysts or their physical characteristics as only iron and cobalt were active for the isomerization reaction.

In the hydrogenation of allene on silica-supported cobalt catalysts, traces of methylacetylene were observed at higher allene pressures (18). No such mention is made by previous workers on the hydrogenation of allene or methylacetylene (16, 21–23). However, Kokes *et al.* (24, 25) observed a first order methylacetylene–allene isomerization reaction catalyzed by ZnO.

Reaction Mechanism

The infrared studies of allene adsorbed on cobalt/silica catalyst revealed the presence of only

$$CH_2{=}C{-}CH_2$$
$$\quad\;\; |\quad\; |$$
$$\quad\;\; *\quad\; *$$

species (18) on the surface of the catalyst. No absorption bands assigned to the $-CH_3$ group was observed. On the addition of hydrogen to allene

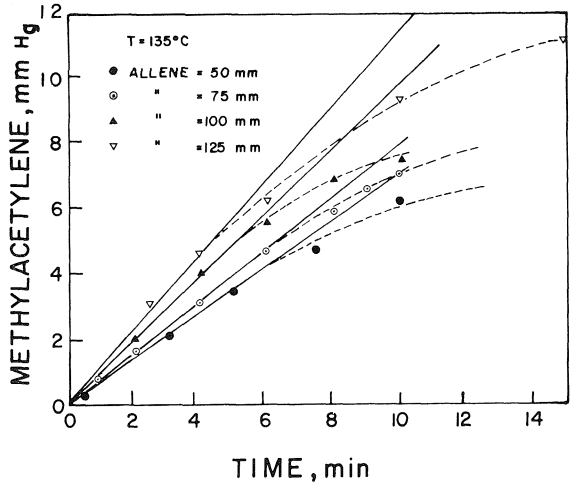

FIG. 2. Formation of methylacetylene (Fe catalyst).

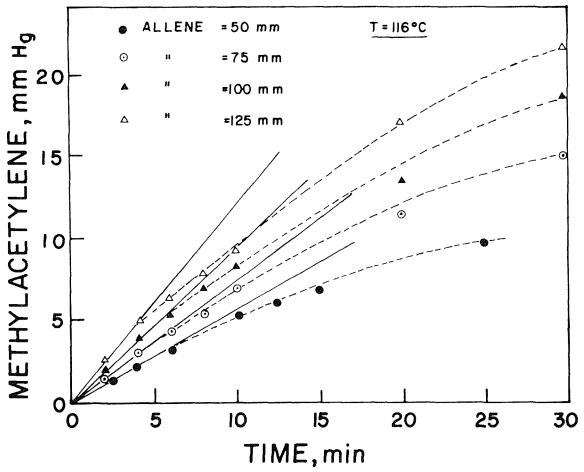

FIG. 3. Formation of methylacetylene (Co catalyst).

exposed catalyst, the

$$CH_2{=}C{-}CH_2$$
$$\quad\;\; |\quad\; |$$
$$\quad\;\; *\quad\; *$$

species converted to $CH_3{-}CH_2{-}CH_2{-}M$ species, indicating that the dissociative adsorption of allene was not taking place and any methylacetylene formed was not retained on the catalyst surface.

In the hydrogenation of allene over Co–silica catalyst at higher allene pressures (allene/H_2 ratio of 3.0 or more) traces of methylacetylene were observed. At an allene/H_2 ratio of 2.5 or less, no methylacetylene was observed in the product. This indicates that probably hydrogenation and isomerization reactions were taking place at different active sites and the rate of hydrogenation was much higher than the rate of allene isomerization.

Though unsupported Fe and Co and other supported or unsupported catalysts were active for allene hydrogenation they were inactive for allene isomerization, possibly because of the irreversible adsorption of allene or methylacetylene on the catalyst surface. It is logical to assume that unsupported Fe and Co were inactive for isomerization reaction as they were active for allene or methylacetylene hydrogenation (16, 18, 21, 22). If the inability of Fe and Co for allene–methylacetylene isomerization was due to irreversible adsorption of allene or methylacetylene, these catalysts should not be active for allene or methylacetylene hydrogenation. In the present study Fe–silica catalyst deactivated continuously on hydrogenation of allene, probably because of the formation of surface carbides. This is also an indication that the isomerization reaction was not occurring on the metal surface as the Fe–silica catalyst was active and stable for the isomerization reaction.

Can. J. Chem. Downloaded from www.nrcresearchpress.com by 210.87.254.105 on 09/05/12
For personal use only.

The nearly equal activity and energy of activation for the two catalysts suggests that the isomerization reaction was occurring on the same active sites, probably the silica surface, and the rate-determining step was the same. In the present study silica showed no activity for the isomerization reaction.

For many years, it was generally believed that the support was inert and simply acted as a carrier for the metal in a finely divided high area form. There is now growing evidence that the support may not be inert but may influence the catalytic activity in any of several ways: it may interact chemically with the metal thereby modifying the properties of the metal; the support may exert an influence on the actual structure of the metal; or the support may act either as a source of reactive intermediates or as a seat of reaction, through the migration of adsorbed species between metal and support.

The phenomenon of surface migration between metal and support, "Spill-over" (27), has been shown to be of particular importance with hydrogen on supported metals. Altham and Webb (28), who used tritium and radioactive approach to monitor the extent of hydrogen spill-over on platinum–silica and platinum—alumina catalysts, observed that in the absence of platinum, neither alumina nor silica was active for olefin exchange at temperatures below 250°C. However, when the metal was present, both silica and alumina possessed an appreciable activity for olefin and hydrogen exchange at ambient temperatures, although neither oxide was active for olefin hydrogenation.

Evidence for the participation of the support in the reaction of olefins and acetylenes over supported metals has been obtained by the use of catalyst poisons. Webb and MacNabb (29) studied the hydrogenation, hydroisomerization, and deuterium exchange of 1-butene over rhodium–silica in the temperature range 0–69°C. The results have been satisfactorily interpreted by considering the hydrogenation and 1-butene exchange to be confined to the surface of metals only, and the isomerization occurring on the support and involving the migration of hydrocarbon from the metal to the support. Since, in the absence of rhodium, silica itself showed no isomerization activity in the temperature range studied and the reversible adsorption of 1–butene on silica did not occur to any appreciable extent, rhodium must have therefore activated the surface of silica by adsorbing the hydrocarbon which then migrated to the support before undergoing reaction.

On the basis of present observations and related literature, it can be assumed that the isomerization of allene to methylacetylene was occurring on the surface of silica activated by Fe and Co. It is possible that other metals are not active for the surface migration of allene from metal to silica support.

The thermal isomerization of alkadienes apparently involves "detachment" of hydrogen (26)

$$H_2C{=}C{=}CH_2 \rightleftarrows [\dot{H}C{=}C{-}\dot{C}H_2 + H] \rightleftarrows HC{\equiv}C{-}CH_3$$

$$H_2C{=}C{=}\underset{\displaystyle CH_3}{\underset{|}{C}}{-}CH_3 \rightleftarrows [\dot{H}_2C{=}C{-}\underset{\displaystyle CH_3}{\underset{|}{\dot{C}}}{-}\dot{C}H_2 + H]$$

$$\uparrow\downarrow$$

$$H_2C{=}\underset{\displaystyle H}{\underset{|}{C}}{-}\underset{\displaystyle CH_3}{\underset{|}{C}}{=}CH_2$$

When allene was heated with ether and sodium at 100°C, allene yielded the sodium derivative of methylacetylene (19). Allene treated for 12 h at 160 to 170°C with alcoholic potash gave methylacetylene and ethyl isopropenyl ether (intermediate product) together with unreacted allene (10).

$$H_2C{=}C{=}CH_2 + C_2H_5OH \rightleftarrows H_2C{=}\underset{\displaystyle OC_2H_5}{\underset{|}{C}}{-}CH_3$$

$$\rightleftarrows HC{\equiv}C{-}CH_3 + C_2H_5OH$$

The reaction path for the base catalyzed acetylene–allene isomerization is presumed to be (11):

$$RCH_2{-}C{\equiv}CH + B^- \rightleftharpoons \dot{R}\dot{C}H{-}\dot{C}{=}\dot{C}H + HB$$

$$\downarrow\uparrow$$

$$RCH{=}C{=}CH_2 + B^-$$

Though in the present study there is no evidence of hydrogen detachment from the allene molecule, for simplicity it can be assumed that on the silica surface the reaction was occurring as base catalyzed allene–methylacetylene isomerization. Considering the above-mentioned assumptions the overall reaction mechanism can be represented as follows

$$\text{Allene (g)} \rightleftarrows \text{allene (adsorbed on metal)}$$

$$\downarrow\uparrow$$

$$[\dot{C}H_2{-}\dot{C}{=}CH] \underset{+H}{\overset{-H}{\rightleftharpoons}} \text{allene (adsorbed on silica)}$$

$$+H\downarrow\uparrow -H$$

$$CH_3{-}C{\equiv}CH \text{ (adsorbed on silica)} \rightleftarrows CH_3{-}C{\equiv}CH \text{ (adsorbed on metal)}$$

$$\downarrow\uparrow$$

$$CH_3{-}C{\equiv}CH \text{ (gas)}$$

To confirm the isomerization reaction mechanism, further work is in progress.

Acknowledgement

The authors are indebted to the National Research Council of Canada for financial support of the project (A-1125).

1. J. J. PHILLIPSON and P. B. WELLS. Proc. Chem. Soc. 227 (1964).
2. V. RAGAINI. J. Catal. **34**, 1 (1974).
3. D. BALLAIVET, D. BARTHOEUF, and Y. TRAMBOUZE. J. Catal. **34**, 423 (1974).
4. G. GATI and H. KNOZINGER. 5th International Congress on Catalysis. 1972. Paper 57.
5. J. W. HIGHTOWER and K. HALL. Trans. Faraday Soc. **66**, 477 (1970).
6. Y. AMENOMIYA. J. Res. Inst. Catal. Hokkaido Univ. **9**, 1 (1961).
7. J. I. MACNAB and G. WEBB. J. Catal. **10**, 19 (1968).
8. G. C. BOND, G. WEBB, and P. B. WELLS. Trans. Faraday Soc. **64**, 3077 (1968).
9. T. L. JACOBS, R. AKAWIE, and R. G. COOPER. J. Am. Chem. Soc. **73**, 1273 (1951).
10. A. FAVORSKY. J. Prakt. Chem. **37**, 382 (1888); **44**, 208 (1891).
11. I. IWAI. Mechanism of molecular migrations. Vol. 2. *Edited by* B. S. Thyagarajan. Wiley, New York. 1969.
12. D. A. F. KAMENTZY and MARKOVICH. Acta Phys. Chim. USSR, **17**, 308 (1942).
13. J. W. LINNETT and W. H. AVERY. J. Chem. Phys. **58**, 146 (1936).
14. J. CRAWFORD. J. Chem. Phys. **7**, 140 (1939).
15. G. B. KISTIAKOWSKY, RUHOFF, SMITH, and VAUGHAN. J. Am. Chem. Soc. **58**, 146 (1936).
16. G. C. BOND and J. SHERIDAN. Trans. Faraday Soc. **48**, 651 (1952); **48**, 658 (1952).
17. C. C. CHANG and R. J. KOKES. J. Catal. **28**, 92 (1973).
18. C. P. KHULBE. Ph.D. Thesis. University of Ottawa, Ottawa, Ont., Canada. 1976.
19. Y. M. SLOBODINE. J. Gen. Chem. (USSR), **6**, 1892 (1936); **9**, 272 (1939); **7**, 1664 (1937).
20. J. F. CORDES and H. GUNZLER. Z. Naturforsch. **156**, 933 (1966).
21. R. S. MANN and D. E. TO. Can. J. Chem. **46**, 161 (1968).
22. R. S. MANN and D. E. TIU. Can. J. Chem. **46**, 3249 (1968).
23. R. S. MANN and A. M. SHAH. Can. J. Chem. **48**, 3324 (1970); **50**, 1793 (1972).
24. R. J. KOKES. Acc. Chem. Res. **6**, 262 (1973).
25. R. J. KOKES, A. L. DENT, C. C. CHENG, and L. T. DIXON. J. Am. Chem. Soc. **94**, 4429 (1972).
26. G. EGLOFF, G. HULLA, and V. I. KOMAREWOKY. Isomerization of pure hydrocarbons. Am. Chem. Soc. Monograph, Reinhold Pub. Co., New York. 1942. Chapt. 2, p. 70.
27. P. A. SERMON and G. C. BOND. Catal. Rev. **8**, 211 (1974).
28. J. A. ALTHAM and G. WEBB. J. Catal. **18**, 133 (1970).
29. G. WEBB and J. I. MACNAB. J. Catal. **26**, 226 (1972).

Can. J. Chem. Downloaded from www.nrcresearchpress.com by 210.87.254.105 on 09/05/12
For personal use only.

The nature of green alkaline iron sulfide solutions and the preparation of sodium iron(III) sulfide, $NaFeS_2$

PETER TAYLOR AND DAVID W. SHOESMITH

Research Chemistry Branch, Whiteshell Nuclear Research Establishment, Pinawa, Man., Canada R0E 1L0

Received April 12, 1978

PETER TAYLOR and DAVID W. SHOESMITH. Can. J. Chem. **56**, 2797 (1978).

The intense emerald green solutions formed by the reaction of iron salts with alkali metal sulfides at pH 11–13 have been found to contain colloidal $MFeS_2$, M = Li, Na, K. Solid $KFeS_2$ and $NaFeS_2$ have been recovered from these systems. X-ray powder diffraction studies confirmed the identity of $KFeS_2$, and showed $NaFeS_2$ to have a structure different from those of other $MFeS_2$ compounds, and related to that of the mineral rasvumite, $K_3Fe_9S_{14}$. Some aspects of the crystal structures and chemistry of different $MFeS_2$ compounds are discussed. A mechanism for the formation of colloidal $MFeS_2$ is proposed on the basis of kinetic data. It is likely that colloidal $NaFeS_2$ is responsible for the colour of the "green liquor" of the pulp and paper industry.

PETER TAYLOR et DAVID W. SHOESMITH. Can. J. Chem. **56**, 2797 (1978).

On a trouvé que les solutions d'un vert émeraude intense qui se forment par réaction des sels de fer avec les sulfures des métaux alcalins à des pH de 11–13 contiennent du $MFeS_2$, M = Li, Na, K à l'état colloïdal. On a pu récupérer du $KFeS_2$ et du $NaFeS_2$ à l'état solide à partir de ces systèmes. Des études de diffraction de rayons-X sur des poudres ont confirmé l'identité du $KFeS_2$ et ont démontré que le $NaFeS_2$ possède une structure différente de celle des autres composés $MFeS_2$ et qu'elle est reliée à celle de la rasvumite minérale, $K_3Fe_9S_{14}$. On discute de quelques aspects des structures cristallines et de la chimie des différents composés $MFeS_2$. On propose un mécanisme pour la formation du $MFeS_2$ à l'état colloïdal en se basant sur les données cinétiques. Il est vraisemblable que le $NaFeS_2$ à l'état colloïdal soit responsable pour la couleur de la "liqueur verte" de l'industrie des pâtes et papiers.

[Traduit par le journal]

Introduction

The existence of an intense green iron sulfide species in alkaline solution has been known since 1801 (1). It was reported extensively in the early literature on iron sulfide chemistry, and a compilation of many of these observations is given by Mellor (ref. 2, pp. 144–183). It does not appear to have been characterized satisfactorily, and has been variously identified as colloidal ferrous sulfide (ref. 2, p. 146), $FeS{\cdot}4Na_2S$ (ref. 2, p. 166, ref. 3), hydrated ferric sulfide (ref. 2, p. 181), colloidal $MFeS_2$, M = K, NH_4 (ref. 2, p. 182, ref. 4), $Na_3[Fe(S)(OH)_3]$ (5, 6), and even colloidal sulfur (7). We first observed the green species in the course of an electrochemical study of the reaction of aqueous sodium sulfide solutions with iron (8), performed as part of an investigation of carbon steel corrosion by aqueous hydrogen sulfide in heavy water plants. It was desirable to establish the identity of the green material, in order to understand the electrochemical processes involved, and to resolve the confusion in the literature. It is curious that there are few references to this material in the recent literature when it was so commonly encountered, but not satisfactorily characterized, by earlier workers.

Results and Discussion

Preparation and Identification of the Green Species

Intense green solutions giving similar visible spectra have been obtained from reactions of a variety of iron-containing materials with excess MSH (M = Li, Na, K) in aqueous solution at pH 11 to 12. The green species formed rapidly with ferric nitrate, but with ferrous salts it appeared more slowly, and only on exposure to the air. It was also produced electrochemically under conditions appropriate for the generation of Fe^{3+} at an iron electrode (8).

For M = Na or K, the green material could be precipitated as a green–black solid by the addition of an equal volume either of acetone, or of 1 mol dm^{-3} MOH or MCl. Total, irreversible precipitation occurred, indicating that flocculation of colloidal material, rather than precipitation by depression of solubility or a common ion effect, had occurred. This is consistent with the many early references (ref. 2, pp. 144–183) to the green material as a colloid. For M = Li, the colloid was more difficult to flocculate, and its chemical stability was lower, so that the lithium-containing solid was not readily isolable, and was not studied further.

Can. J. Chem. Downloaded from www.nrcresearchpress.com by 210.87.254.6 on 09/05/12
For personal use only.

Can. J. Chem. Downloaded from www.nrcresearchpress.com by 210.87.254.6 on 09/05/12
For personal use only.

TABLE 1. X-ray powder diffraction data for $NaFeS_2$ (d in pm)

hkl	d_{calcd}[a]	d_{obsd}[b]	I/I_1[c]	hkl	d_{calcd}	d_{obsd}	I/I_1
110	692.7	695	100	222	218.1	218.2	5
200	534.0	536	75	421	214.9	215.1	2
020	455.0	456	25	331	214.8		
111	436.2	436	15	$31\bar{2}$	208.2	208.3	5
$11\bar{1}$	426.0	426	5	510	207.9		
220	346.3	346.4	20	501	201.7	201.3	10
310	331.5	331.3	10	132	201.3		
$12\bar{1}$	330.9			322	199.4	199.6	10
221	296.4	296.3	20	$13\bar{2}$	199.2		
$22\bar{1}$	290.0	289.6	70	402	195.3	195.5	5
400	267.0	266.8	5	$40\bar{2}$	188.2	188.1	5
321	252.9	253.0	10	422	179.5		
202	248.5	248.1	5	150	179.4	179.3	2
022	235.5	235.4	5	332	179.1		
330	230.9	230.9	15	042	175.4	175.1	15
420	230.3			440	173.2	173.3	15
					(Plus 15 weak, broad lines to 104 pm)		

[a]Monoclinic, $a = 1069$, $b = 910$, $c = 551$ pm, $\beta = 92.1°$; the trial unit cell was refined using a least-squares program written by D. E. Appleman and H. T. Evans, Jr., U.S. Geological Survey, Geologic Division, Washington, DC 20244. The resulting de Wolff reliability index (24) was 13.1.
[b]Debye–Scherrer photographic data.
[c]Measured photometrically.

TABLE 2. X-ray powder diffraction data for $NaFeS_2$ prepared by various methods*

	A		B		C		D
hkl	d_{obsd}	I/I_1	d_{obsd}	I/I_1	d_{obsd}	I/I_1	d_{obsd}
110	695	100	690	100	700	7	695
200	536	75	534	70	534	6	536
020	456	25	455	40	457	4	457
220	346.4	20	347	35	—	—	348
$22\bar{1}$	289.6	70	290	100	289	6	292
330, 420	230.9	15	231	30	231	2	231
501, 132	201.3	10	201	15	—	—	202
322, $13\bar{2}$	199.6	10					
042	175.1	15	—	—	—	—	175
440	173.3	15					

*A, major lines from pattern in Table 1; B, diffractometer data for material prepared on 200 mg scale and heated to 400°C *in vacuo* (major lines only); C, unidentified material prepared by Erd *et al.* (12); D, material prepared by Böttcher (footnote 1 in text) and analyzed as $Na_{0.95}Fe_{0.96}S_2.1.84\ H_2O$; no intensities were given.

The solid recovered from potassium-containing solutions was identified by X-ray powder diffraction (9) as poorly crystallized $KFeS_2$. Larger scale reactions, using a modified experimental procedure, showed that conversion of $Fe(NO_3)_3 \cdot 9H_2O$ to $KFeS_2$ was quantitative. Sodium-containing solutions yielded a solid with a diffraction pattern completely different from that of $KFeS_2$ or any other ABS_2 solid listed in the file of the Joint Committee for Powder Diffraction Standards up to volume 27 (1977). Diffraction lines are broad, as a consequence of small crystallite size, but reproducible, and the pattern has been indexed satisfactorily on the basis of a monoclinic unit cell ($a = 1069$, $b = 910$, $c = 551$ pm, $\beta = 92.1°$) (Table 1) similar to the orthorhombic cell ($a = 1108$, $b = 912$, $c = 547$ pm) of the mineral rasvumite (10), $K_3Fe_9S_{14}$. The diffraction pattern is also very similar to those obtained by Bronger (11) and Böttcher[1] from material prepared in attempts to synthesize $NaFeS_2$ from Na_2S_2, Fe, and S or Na_2CO_3, Fe, and S, and by Erd *et al.* (12) from material prepared by the reaction between solutions of $FeCl_3$ and NaSH at pH 11 (Table 2). The apparent structural similarity between the sodium salt and rasvumite, $K_3Fe_9S_{14}$ (ref. 9, card 25-263, ref. 10) suggests that the former is $Na_3Fe_9S_{14}$ rather than $NaFeS_2$, but this is not consistent with the preparative evidence discussed below. It is easier to reconcile the $K_3Fe_9S_{14}$-like structure with the $NaFeS_2$ stoichiometry if $K_3Fe_9S_{14}$ is formulated as a salt of the FeS_2^- anion, $K_3(Fe^{II})_2(Fe^{III}S_2)_7$, with four alkali metal atoms in an $MFeS_2$ structure replaced by two Fe^{II} atoms and two vacant sites.

The preparation of the sodium salt parallels

[1]P. Böttcher. Private communication.

Can. J. Chem. Downloaded from www.nrcresearchpress.com by 210.87.254.6 on 09/05/12
For personal use only.

exactly that of $KFeS_2$, which strongly suggests that it is $NaFeS_2$; this conclusion is supported by the similarity of the visible spectra. Freshly flocculated $KFeS_2$ and $NaFeS_2$ in suspension gave the same spectrum as the colloidal suspensions, although less well defined due to the increase in particle size. After filtration, the solid appears black, but dried thin films remain intense green in transmitted light, so it is unlikely that any structural change occurs during the process of flocculation and isolation of the solid. Although the weights of sodium salt obtained from larger-scale preparations were consistent with the formulation $NaFeS_2 \cdot 2H_2O$, this water was removed by continuous pumping at ca. 100°C without any observable change in the diffraction pattern. Further heating *in vacuo* at 450°C for 88 h produced no change in the diffraction pattern, other than sharpening of the peaks due to improved crystallinity, and the appearance of peaks attributable to pyrite (cubic FeS_2) and pyrrhotite ($Fe_{1-x}S$). These phases may have been present as impurities, or arisen from partial decomposition of the sample. There are three possible interpretations of the lack of major changes in the diffraction pattern upon dehydration. The water may occupy channels within the $NaFeS_2$ structure; it may be adsorbed or occluded rather than incorporated in the crystal structure, or it is possible that the initial product consisted in part of an X-ray amorphous hydrated salt $NaFeS_2 \cdot xH_2O$. It is not possible to distinguish between these three models without more detailed structural data, although the consistent formation of material with the approximate stoichiometry $NaFeS_2 \cdot 2H_2O$ favours the first model. Schneider (ref. 2, p. 183) reported the synthesis of $NaFeS_2 \cdot 4H_2O$ under conditions analogous to those he used to prepare $KFeS_2$, and the products prepared by Bronger (11) and Böttcher[1] analyzed as $Na_{1+x}Fe_{1-x}S_2 \cdot yH_2O$, with $0.19 \geq x \geq -0.08$ and $2 \geq y \geq 1.4$. Elemental analyses of the very finely divided, air-sensitive material produced in this work were irreproducible. However, three separate preparative experiments yielded iron content, based on weights of starting material and product, of 37.3, 38.2, and 40.9% (calcd. for $NaFeS_2$, 39.1%), while sulfur analysis of freshly prepared material gave a mean value for five determinations of 41.0% (calcd. 44.9%). The combination of preparative, spectroscopic, crystallographic, and analytical data thus strongly supports the identity of the material as $NaFeS_2$, although the nature of its hydration is uncertain.

It is interesting that $NaFeS_2$ adopts a different structure from the other alkali metal thioferrates, $MFeS_2$, M = K, Rb, Cs, all three of which have closely related structures. The similar visible spectra of $NaFeS_2$ and $KFeS_2$ indicate that the anion has the same structure in both salts. $KFeS_2$ is known (14) to consist of infinite linear di-μ-sulfido-bridged polymeric chains, each iron being tetrahedrally coordinated by sulfur while each potassium has eight neighboring sulfur atoms. It is likely that $NaFeS_2$ consists of similar $(FeS_2)_n^{n-}$ chains, but that they are constrained to a different crystal packing arrangement by the preference of the smaller sodium ion for a lower coordination number than potassium. A more detailed structural discussion is not possible without single crystal data for $NaFeS_2$.

Teder (15) has prepared green solutions by dissolving sodium sulfide (prepared by reduction of reagent grade sodium sulfate with hydrogen in an alumina tube at 500°C) in water, and the spectra he observed are very similar to those we obtained from samples of colloidal $MFeS_2$. He attributed these spectra, and hence the "green liquor" obtained by dissolution of sodium sulfide/carbonate mixtures prepared in recovery furnaces in the pulp and paper industry, to some unidentified sulfide species, but it is likely that they arise from traces of colloidal $MFeS_2$. The colour of "green liquor" had been previously, and we believe correctly, attributed to iron compounds (16).

The Chemistry of Formation of Colloidal $MFeS_2$

A series of experiments was performed to study the rate of formation of $NaFeS_2$ as a function of NaSH and $Fe(NO_3)_3$ concentration at pH = 11 to 13, maintaining constant ionic strength by addition of $NaNO_3$ solution. Below pH ≃ 11, colloidal $MFeS_2$ was not formed, while above pH ≃ 13, it tended to flocculate. The three peaks in the visible spectrum at 640 nm (ε = 11 600), 530 nm (ε = 5300), and 435 nm (ε = 7000) developed in unison (Fig. 1), confirming that all three peaks arise from the same species. Extinction coefficients were obtained from

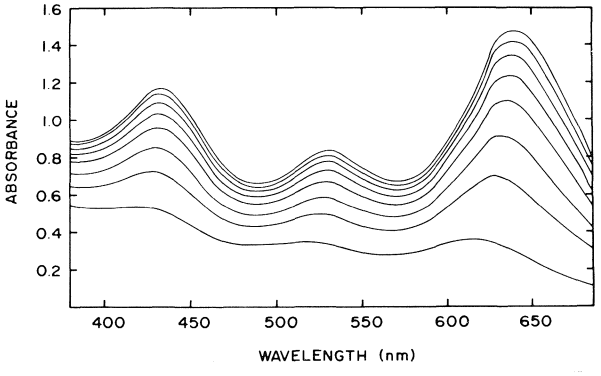

FIG. 1. Development of the spectrum of colloidal $NaFeS_2$ during a typical kinetic experiment ($[Fe^{3+}] = 2.12 \times 10^{-4}$ mol dm^{-3}; $[SH^-] = 2 \times 10^{-2}$ mol dm^{-3}); pH 11; first scan started 1 min after mixing; subsequent scans at 2 min intervals but alternate scans omitted.

Can. J. Chem. Downloaded from www.nrcresearchpress.com by 210.87.254.6 on 09/05/12
For personal use only.

the spectra of solutions in which the reaction was complete, and are based on iron concentrations. The high values of these coefficients indicate that all three features arise from charge transfer transitions. The initial appearance of the spectrum occurred with approximately first order reaction kinetics in both iron and sulfide concentrations (Figs. 2 and 3), but a lack of knowledge of the relationship between extinction coefficient and polymer chain length of the product anion precludes a detailed treatment of the initial kinetics.

Assuming only that the initial iron moiety is monomeric and that the final product is the polymeric anion, $(FeS_2)_n^{n-}$, the reaction must involve the coordination of two SH^- or S^{2-} ions to each Fe, a polymerization process, and the elimination of hydroxide ions and water molecules. Dissociation data for H_2S (17, 18) and ferric ion (19) indicate

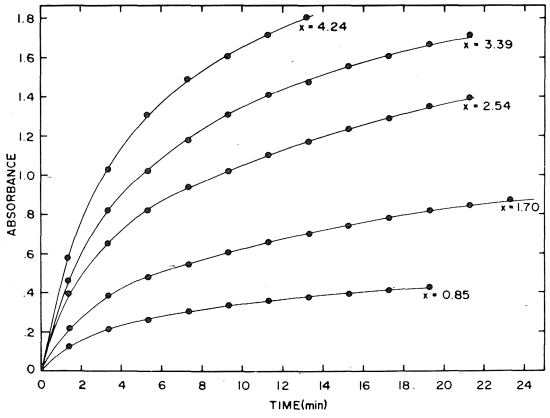

FIG. 2. Plots of absorbance at the maximum of the peak at ca. 630 nm as a function of time; pH 11; $[SH^-] = 10^{-2}$ mol dm^{-3}; $[Fe^{3+}] = 10^{-4}x$ mol dm^{-3}.

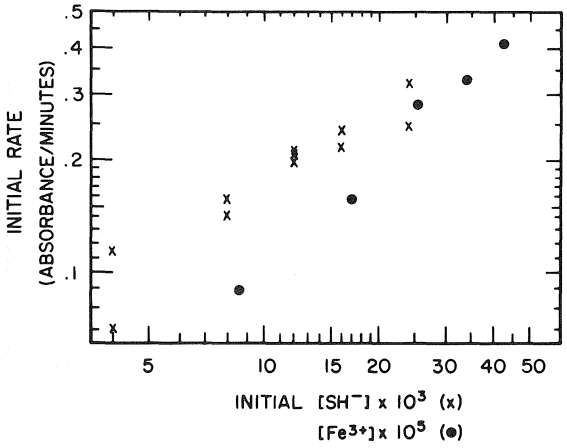

FIG. 3. Plots of initial rate of reaction as a function of (*a*) initial $[Fe^{3+}]$ at an initial $[SH^-]$ of 10^{-2} mol dm^{-3}; (*b*) initial $[SH^-]$ at an initial $[Fe^{3+}]$ of 2.12×10^{-4} mol dm^{-3}.

that SH^- and $Fe(OH)_4^-$ are the predominant sulfur and iron species, respectively, present under our reaction conditions. Reaction rates were similar at both pH 11 and 13, consistent with SH^- and $Fe(OH)_4^-$ being the reactive species. The reaction rate was reduced when the ferric solution was permitted to stand after the addition of NaOH to adjust the pH, but before addition of NaSH, for as little as 5 s. After longer periods of aging of the ferric solution, an induction period became apparent (Fig. 4). This can be attributed to retardation of the formation of $NaFeS_2$ by polymerization of the initial ferric species. We were constrained by the stability and detection limits of $NaFeS_2$ to work with supersaturated iron solutions.

No significant difference in rate or final yield of $NaFeS_2$ was observed between reactions performed in N_2-saturated and air-saturated solutions. If the redox reaction between Fe^{3+} and SH^- was competitive with the formation of $MFeS_2$, then a higher yield of $MFeS_2$ would accrue from the reaction in the presence of air, in which ferric ion would be regenerated. This result implies that the polymerization process is very fast, since the redox reaction is facile.

A slight shift of the spectral peaks to longer wavelength as the reaction proceeds is consistent with a progressive increase in polymer chain length of the product. When $NaFeS_2$ was prepared electrochemically, it was formed rapidly by generation of Fe^{3+} at an electrode surface, and continually swept into solution, where reaction ceased, since Fe^{3+} was absent (12). Under these circumstances, no shift in the spectrum with increasing $NaFeS_2$ concentration was observed.

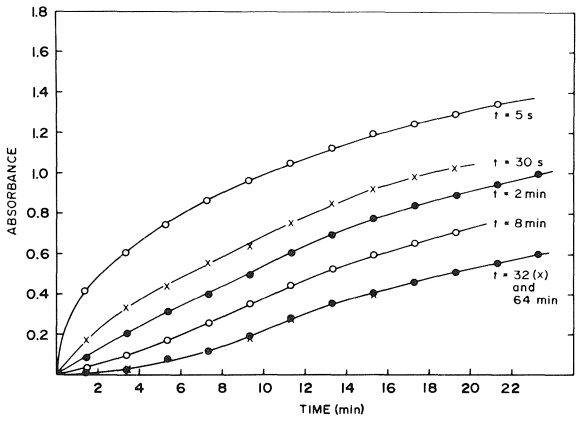

FIG. 4. Plots of absorbance at the maximum of the peak at ca. 630 nm as a function of time, showing the variation of reaction rate with the time interval, *t*, between making the iron solution alkaline, and adding the sulfide solution. $[Fe^{3+}] = 2.12 \times 10^{-4}$ mol dm^{-3}; $[SH^-] = 2 \times 10^{-2}$ mol dm^{-3}; pH 11.

Can. J. Chem. Downloaded from www.nrcresearchpress.com by 210.87.254.6 on 09/05/12
For personal use only.

A plausible simplified mechanism for the formation of $MFeS_2$, which is consistent with all of these observations, is outlined by reactions [1] and [2], the first reaction being rate determining. The unit $RFe(OH)_2$ represents $Fe(OH)_4^-$ initially, and growing polymeric species of the type 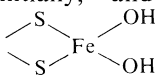 in the subsequent stages of reaction.

[1] $[RFe(OH)_2]^{n-} + SH^- \rightarrow [RFe(OH)(SH)]^{n-} + OH^-$

[2] $[RFe(OH)(SH)]^{n-} + [R'Fe(OH)(SH)]^{m-}$

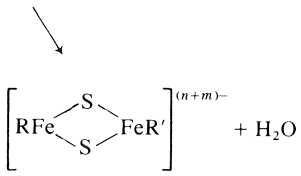

We note that a large number of compounds with

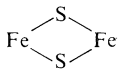

linkages have been prepared as model compounds for ferredoxins (20) and that $KFeS_2$ has been of some interest in this regard (21).

Decomposition of $MFeS_2$

Both $NaFeS_2$ and $KFeS_2$ decompose rapidly in acid solution with production of H_2S and sulfur (ref. 2, p. 183, ref. 5). This reaction can be represented by the overall stoichiometry [3], and probably proceeds by protonation of the S-bridges [4] and

[3] $2MFeS_2 + 6H^+ \rightarrow 2M^+ + 2Fe^{2+} + 3H_2S + \frac{1}{8}S_8$

[4] 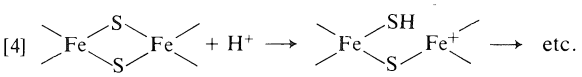

subsequent redox reaction of Fe^{III}—SH groups. At pH 11 or greater the $MFeS_2$ salts are stable in the presence of SH^-, without special precautions to exclude air. In the absence of SH^-, the salts decompose quite rapidly. At 80°C, $NaFeS_2$ decomposes rapidly in alkaline solution in the absence of air, even in the presence of SH^-, with production of polysulfides, identified by uv–visible spectroscopy (22). These observations suggest that $[FeS_2]_n^{n-}$ is somewhat susceptible to nucleophilic attack by base, [5]

[5] 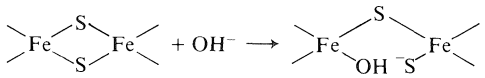

and subsequent redox reaction, and that this reaction is suppressed by SH^-. The evidence that terminal Fe^{III}—SH or Fe^{III}—S^- groups readily undergo redox reaction supports the conclusion that the postulated polymerization steps [2] in the formation of $MFeS_2$ must be rapid. The stability of the $[FeS_2]_n^{n-}$ structure towards internal redox reaction is further exemplified by the high thermal stability of $MFeS_2$, M = K, Rb, Cs, which are prepared by fusion reactions at 800°C (5, 11); $KFeS_2$ also occurs as a by-product in cement furnaces (23). This is in sharp contrast with ferric sulfide itself, the very existence of which is open to question (13), and which is constrained by its stoichiometry to have a structure quite different from the $[FeS_2]_n^{n-}$ anion.

Finally, a rather remarkable reaction occurred when dry solid $NaFeS_2$ or $KFeS_2$ was added to 1 mol dm^{-3} lithium hydroxide solution. An intense green colour developed rapidly in the solution, the spectrum of which showed the three characteristic $MFeS_2$ peaks. The colour persisted only for a few minutes, after which a brown precipitate, presumably a ferric oxide/hydroxide, appeared. In corresponding reactions with 1 mol dm^{-3} NaOH, only a very faint green colour was observed, but a brown solid was formed, and the solution turned yellow overnight. The solution was shown by its uv–visible spectrum to contain polysulfides. The reason for the redispersal of $MFeS_2$ in LiOH is not clear, but it may involve electrophilic attack on sulfur bridges by Li^+, [6], analogous to the protonation reaction [4], with consequent fragmentation of the polymer and redox reaction between Fe^{3+} and sulfide.

[6] 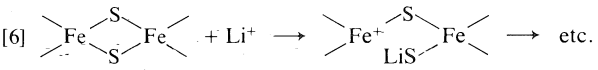

Experimental

Reagent grade salts were used without further purification, as was Matheson C.P. grade H_2S. Solutions were prepared with double-distilled water. Alkali metal sulfide solutions were prepared by purging 1 mol dm^{-3} solutions of the appropriate hydroxide with nitrogen, saturating with H_2S and repurging with nitrogen; they were diluted immediately before use. Electrochemical experiments in which $MFeS_2$ salts were observed are described elsewhere (8). Mackinawite was prepared by electrochemical oxidation of iron in 1 mol dm^{-3} NaSH, saturated with H_2S, at an anodic current density of 5 mA cm^{-2}. Most preparations were performed in screw-top polypropylene bottles without taking special precautions to exclude air, as preliminary experiments indicated that colloidal suspensions of $MFeS_2$ are stable to air in the presence of excess sulfide for several weeks in a stoppered bottle. Visible–uv spectra were obtained with a Unicam SP800 spectrometer. X-ray diffraction data were obtained with a 114.6 mm diameter Debye–Scherrer camera and Co K_α radiation, and with a Philips model PW-1050 diffractometer, equipped with a diffracted beam monochromator, using Cu K_α radiation.

Preparation of $MFeS_2$ (M = Na, K; mg Scale)

In a typical experiment, 100 cm^3 each of ca. 4×10^{-4} mol dm^{-3} ferric nitrate and 2×10^{-2} mol dm^{-3} MOH solutions were mixed and 10 cm^3 of 1 mol dm^{-3} MSH solution was added. The solution was allowed to stand overnight, after

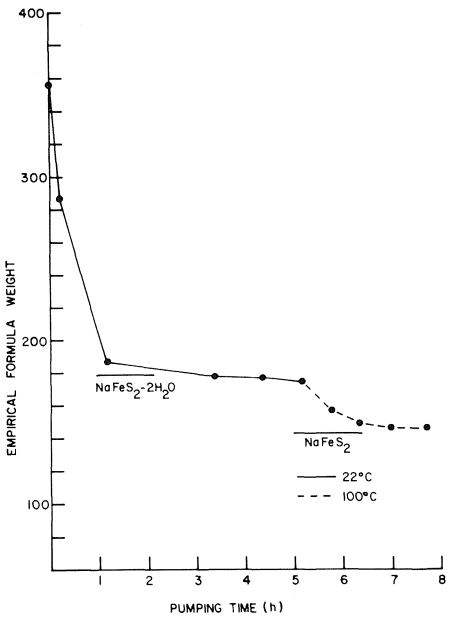

FIG. 5. Plot of weight loss vs. time of pumping for dehydration of sample of $NaFeS_2$.

which the green material was precipitated by addition of an equal volume of 1 mol dm^{-3} MOH, 1 mol dm^{-3} MCl or acetone, filtered, washed with 10^{-2} mol dm^{-3} MOH and then with acetone. Samples were stored under nitrogen in sealed glass vials, as they were quite susceptible to air oxidation. Syntheses of $NaFeS_2$ were also carried out using ferrous and ferric ammonium sulfates and synthetic mackinawite (13) (tetragonal FeS_{1-x}) as starting materials. As mackinawite is comparatively insoluble, it was added to the reaction mixture as a solid.

Preparation of $KFeS_2$ (100 mg Scale)

In a typical experiment, $Fe(NO_3)_3 \cdot 9H_2O$ (0.698 g, 1.73 mmol) was dissolved in water (80 cm^3) and 10 cm^3 each of 5 mol dm^{-3} KOH and 1 mol dm^{-3} KSH were added. After addition of KOH a flocculent brown precipitate of $Fe(OH)_3$ formed; this turned black instantly on addition of KSH. After standing overnight a black solid had settled; this was filtered, washed with 10^{-2} mol dm^{-3} KOH and acetone, dried, and identified as $KFeS_2$ by X-ray diffraction (0.277 g, 1.74 mmol). The supernatant liquor contained less than 0.1 mg of iron.

Preparation of $NaFeS_2$ (100 mg Scale)

These preparations were carried out paralleling exactly the synthesis of $KFeS_2$, above, but the weight of product recovered indicated that it contained a considerable amount of water; it was also much bulkier than a corresponding amount of $KFeS_2$. The water was removed by continuous pumping at about 10 Pa, first at room temperature, then at ca. 100°C; a plot of weight vs. time of pumping for one experiment is shown in Fig. 5. At room temperature, after initial rapid loss, the weight levelled out at a value corresponding approximately to the formulation $NaFeS_2 \cdot 2H_2O$, with only a very slow further weight loss. On heating to 100°C very rapid loss occurred again, leading to a final constant weight in reasonable agreement with the stoichiometry $NaFeS_2$ (for three experiments, calcd. 0.669, 0.511, 0.395 g; obsd. 0.640, 0.522, 0.415 g). It was difficult to obtain this material in a high degree of purity, due to its sensitivity to oxidation and hydrolysis, and the observation of pyrrhotite and pyrite in material heated at 450°C suggests that these may have been present as impurities in the initial product.

Kinetic Experiments

Aliquots of stock solutions of $Fe(NO_3)_3$, $NaNO_3$, NaOH, and NaSH were mixed to give the appropriate concentrations. Unless otherwise stated, NaOH was added to an acidic solution of $Fe(NO_3)_3$ to adjust the pH immediately before the addition of NaSH. A portion of the mixed solution was transferred rapidly to the uv–visible spectrometer cell, and the spectrum was recorded at 2-min intervals over the wavelength range 700 to 400 nm.

1. L. N. VAUQUELIN. Ann. Phys. Leipzig, **9**, 40 (1801).
2. J. W. MELLOR. A comprehensive treatise on inorganic and theoretical chemistry. Vol. XIV. Longmans, London. 1935.
3. S. M. HORSCH. Bull. Soc. Chim. **27**, 777 (1920).
4. H. MALFATTI. Z. Anal. Chem. **48**, 352 (1909).
5. J. L. DEUTSCH and H. B. JONASSEN. Inorg. Synth. **6**, 170 (1960).
6. H. GRUBITSCH. Anorganisch-praparativen Chemie. Springer-Verlag, Vienna. 1950. p. 391.
7. D. T. RICKARD. Am. J. Sci. **274**, 941 (1974).
8. D. W. SHOESMITH, P. TAYLOR, M. G. BAILEY, and B. IKEDA. Electrochim. Acta. In press.
9. Joint Committee on Powder Diffraction Standards, Swarthmore, Pennsylvania.
10. M. N. SOKOLOVA, M. G. DOBROVOL'SKAYA, N. I. ORGANOVA, and A. L. DMITRIK. Am. Mineral. **56**, 1121 (1971); Zap. Vses. Mineral. Obshchh. **99**, 712 (1970).
11. W. BRONGER. Naturwissenschaften, **52**, 158 (1965).
12. R. C. ERD, H. T. EVANS, and D. H. RICHTER. Am. Mineral. **42**, 309 (1957).
13. J. C. WARD. Rev. Pure Appl. Chem. **20**, 175 (1970).
14. J. W. BOON and C. H. MACGILLAVRY. Recl. Trav. Chim. Pays-Bas, **61**, 910 (1942); W. BRONGER. Z. Anorg. Allg. Chem. **359**, 225 (1968).
15. A. TEDER. Svensk. Papperstidn. **71**, 447 (1968).
16. J. P. CASEY. Pulp and paper chemistry and technology. 2nd ed. Interscience, New York. 1960. Part 1, p. 271.
17. A. J. ELLIS and W. GIGGENBACH. Geochim. Cosmochim. Acta, **35**, 247 (1971).
18. W. GIGGENBACH. Inorg. Chem. **10**, 1333 (1971).
19. C. F. BAES, JR. and R. E. MESMER. The hydrolysis of cations. Wiley, New York. 1976. pp. 226–237.
20. M. A. BOBRIK, K. O. HODGSON, and R. H. HOLM. Inorg. Chem. **16**, 1851 (1977).
21. D. O. COWAN, G. PASTERNAK, and F. KAUFMAN. Proc. Natl. Acad. Sci. **66**, 837 (1970).
22. A. TEDER. Acta Chem. Scand. **25**, 1722 (1971); W. F. GIGGENBACH. Inorg. Chem. **11**, 1201 (1972).
23. F. TROJER. Am. Ceram. Soc. Bull. **47**, 630 (1968).
24. P. M. DE WOLFF. J. Appl. Crystallogr. **1**, 108 (1968).

Can. J. Chem. Downloaded from www.nrcresearchpress.com by 210.87.254.6 on 09/05/12
For personal use only.

Thermal expansivities of water + tetrahydrofuran mixtures at 298.15 K[1]

OSAMU KIYOHARA,[2] PATRICK J. D'ARCY, AND GEORGE C. BENSON

Division of Chemistry, National Research Council of Canada, Ottawa, Ont., Canada K1A 0R6

Received May 29, 1978

OSAMU KIYOHARA, PATRICK J. D'ARCY, and GEORGE C. BENSON. Can. J. Chem. **56**, 2803 (1978).

Densities of water + tetrahydrofuran mixtures were measured at 5 K intervals of temperature from 288.15 to 308.15 K. Excess thermal expansion coefficients and partial molar excess thermal expansivities at 298.15 K over the whole mole fraction range were derived from the results. The significance of the expansivities is discussed in terms of the structural changes accompanying the formation of the mixture.

OSAMU KIYOHARA, PATRICK J. D'ARCY et GEORGE C. BENSON. Can. J. Chem. **56**, 2803 (1978).

On a mesuré la densité de mélanges d'eau et de tétrahydrofuranne à tous les 5 K entre les températures de 288.15 et 308.15 K. On a déduit de ces résultats les coefficients d'expansion thermique d'excès et les expansivités thermiques molaires partielles d'excès à 298.15 K pour le domaine complet de fractions molaires. On discute de la signification des expansivités en rapport avec les changements de structure qui accompagnent la formation du mélange.

[Traduit par le journal]

Can. J. Chem. Downloaded from www.nrcresearchpress.com by 210.87.254.42 on 09/05/12
For personal use only.

Excess enthalpies and volumes of water + tetrahydrofuran (THF) mixtures were reported in a previous paper (1). As an extension of the investigation of the thermodynamic properties of this system, excess thermal expansion coefficients at 298.15 K were obtained from measurements of density at various temperatures around 298.15 K. These values are needed to derive isothermal compressibilities and heat capacities at constant volume from measurements of ultrasonic velocities and heat capacities at constant pressure, which are currently in progress in our laboratory.

Experimental

Materials

The source and purification of the THF were the same as in our previous work (1). Mixtures with deionized distilled water were prepared by mass taking into account the effect of buoyancy. The error of the mole fractions is estimated to be less than $\pm 2 \times 10^{-5}$.

Measurements of Density

Densities of the mixtures were determined with a flow type oscillating tube densimeter (Sodev Inc., Model 02D). Details of the apparatus and its operating procedure have been described by Picker *et al.* (2). Briefly, the density of a fluid is obtained by measuring the resonant frequency of a U-shaped stainless steel tube filled with the fluid. The equation

$$[1] \qquad \rho = A + B\tau^2$$

relates the density ρ to the period τ of the oscillator. A and B are constants of the instrument which can be determined by calibration with fluids of known densities.[3]

For the present work, calibration of the densimeter was based on measurements for water and THF at each temperature, and densities of the mixtures were obtained from the equation

$$[2] \qquad \rho - \rho(H_2O) = \frac{[\tau^2 - \tau^2(H_2O)][\rho(H_2O) - \rho(THF)]}{[\tau^2(H_2O) - \tau^2(THF)]}$$

where $\rho(H_2O)$ and $\rho(THF)$ are the densities of water and THF, and $\tau(H_2O)$ and $\tau(THF)$ are the corresponding periods. Values of the density of water were taken from the review by Kell (5), and densities of THF were determined in our Anton Paar densimeter. The latter was calibrated at each temperature by measurements on a series of solvents.

The temperature of the Picker densimeter was monitored with a calibrated quartz thermometer and was kept constant by a Sodev programmable circulating thermostat. Temperature differences are believed to be accurate to ± 0.002 K in the range 283.15 to 303.15 K. The uncertainty of the values of the density is estimated to be less than $\pm 3 \times 10^{-5}$ g cm^{-3}.

Results and Discussion

Densities of the mixtures and pure components at

[1]NRCC No. 16939.

[2]NRCC Research Associate from 1975.

[3]The manual for the densimeter recommends the use of distilled water and dry nitrogen gas for this purpose. Originally we attempted to calibrate the densimeter by measuring nitrogen gas, water, and several organic solvents whose densities had been determined in our Anton Paar densimeter (3). However, it was found that the point for water deviated considerably from the calibration line (by nearly 7×10^{-4} g cm^{-3} at 298.15 K), and that the amount of the deviation depended on the temperature. Although the reason for this anomaly is not clear, the discrepancies could be eliminated by readjusting the driving power applied to the oscillator tube at each temperature (4). This mode of operation proved to be inconvenient since drifts of the oscillator frequency necessitated frequent checks of the calibration and readjustments of the driving power. Nevertheless, because of its quick response and good thermal stability within ± 10 K of the ambient temperature we found the Picker densimeter to be more suitable than the Anton Paar densimeter for the precise determinations of density differences required in our present work.

Can. J. Chem. Downloaded from www.nrcresearchpress.com by 210.87.254.42 on 09/05/12
For personal use only.

Table 1. Densities and molar excess volumes of $H_2O(1)$ + THF(2) mixtures at 288.15, 293.15, 298.15, 303.15 and 308.15 K

x_1	ρ/g cm^{-3}	$\bar{V}^E$/cm^3 mol^{-1}	x_1	ρ/g cm^{-3}	$\bar{V}^E$/cm^3 mol^{-1}
		T = 288.15 K			
0.0	0.892876	0.0	0.90182	0.986923	-0.5549
0.05579	0.895336	-0.0930	0.90257	0.987021	-0.5513
0.08291	0.896713	-0.1462	0.91070	0.988343	-0.5179
0.13422	0.899547	-0.2507	0.91776	0.989434	-0.4865
0.19701	0.903380	-0.3776	0.92753	0.990816	-0.4387
0.25531	0.907231	-0.4854	0.94331	0.992710	-0.3509
0.30551	0.910813	-0.5706	0.94369	0.992745	-0.3485
0.36550	0.915397	-0.6580	0.94956	0.993332	-0.3125
0.40275	0.918466	-0.7063	0.96119	0.994365	-0.2374
0.45171	0.922766	-0.7605	0.97187	0.995262	-0.1661
0.48730	0.926135	-0.7947	0.97634	0.995671	-0.1366
0.55076	0.932701	-0.8421	0.97851	0.995878	-0.1224
0.61174	0.939803	-0.8697	0.98609	0.996721	-0.0746
0.63945	0.943317	-0.8751	0.98922	0.997140	-0.0560
0.70058	0.951877	-0.8721	0.99064	0.997345	-0.0478
0.74482	0.958771	-0.8515	0.99476	0.998027	-0.0253
0.79792	0.967913	-0.8016	1.0	0.999100[a]	0.0
0.85621	0.978690	-0.6963			
		T = 293.15 K			
0.0	0.887436	0.0	0.79608	0.963116	-0.7786
0.04015	0.889173	-0.0635	0.84132	0.971791	-0.7065
0.08655	0.891483	-0.1499	0.90272	0.983755	-0.5346
0.15430	0.895327	-0.2857	0.91240	0.985539	-0.4969
0.19616	0.897928	-0.3678	0.92166	0.987139	-0.4565
0.25496	0.901847	-0.4757	0.93303	0.988910	-0.4001
0.29946	0.905033	-0.5504	0.94031	0.989960	-0.3610
0.36802	0.910317	-0.6495	0.94821	0.991009	-0.3155
0.39892	0.912897	-0.6894	0.95958	0.992370	-0.2455
0.42206	0.914890	-0.7155	0.97097	0.993650	-0.1718
0.44644	0.917102	-0.7424	0.97423	0.994026	-0.1506
0.49504	0.921744	-0.7861	0.98135	0.994910	-0.1050
0.55341	0.927933	-0.8273	0.98469	0.995366	-0.0842
0.60775	0.934284	-0.8477	0.98917	0.996045	-0.0573
0.63958	0.938391	-0.8545	0.99255	0.996632	-0.0381
0.68887	0.945282	-0.8510	0.99578	0.997273	-0.0210
0.76595	0.957702	-0.8107	1.0	0.998204[a]	0.0
		T = 298.15 K			
0.0	0.881968[b]	0.0	0.74020	0.948571	-0.8079
0.03494	0.883462	-0.0523	0.79663	0.958772	-0.7573
0.07640	0.885485	-0.1260	0.83914	0.967198	-0.6910
0.10979	0.887276	-0.1900	0.86223	0.971975	-0.6412
0.15579	0.889963	-0.2814	0.88997	0.977742	-0.5637
0.19649	0.892517	-0.3606	0.91198	0.982206	-0.4855
0.25838	0.896702	-0.4739	0.92393	0.984483	-0.4346
0.26594	0.897237	-0.4868	0.93375	0.986258	-0.3882
0.35326	0.903842	-0.6215	0.94567	0.988228	-0.3252
0.42053	0.909508	-0.7033	0.95077	0.989010	-0.2961
0.44276	0.911522	-0.7265	0.95317	0.989392	-0.2825
0.48139	0.915207	-0.7622	0.95855	0.990149	-0.2496
0.48712	0.915782	-0.7672	0.95898	0.990212	-0.2470
0.54760	0.922233	-0.8098	0.96990	0.991738	-0.1786
0.56343	0.923968	-0.8173	0.97153	0.991967	-0.1682
0.57527	0.925403	-0.8225	0.97744	0.992816	-0.1307
0.58834	0.926888	-0.8265	0.97748	0.992820	-0.1304
0.66079	0.936306	-0.8349	0.98992	0.994856	-0.0542
0.66607	0.937051	-0.8343	0.99227	0.995310	-0.0407
0.69579	0.941432	-0.8283	0.99564	0.996012	-0.0222
0.73121	0.947073	-0.8135	1.0	0.997045[a]	0.0

Table 1 (Concluded)

x_1	ρ/g cm^{-3}	$\bar{V}^E$/cm^3 mol^{-1}	x_1	ρ/g cm^{-3}	$\bar{V}^E$/cm^3 mol^{-1}
		T = 303.15 K			
0.0	0.876489[b]	0.0	0.85365	0.966015	-0.6420
0.05741	0.879037	-0.0870	0.90252	0.976806	-0.5086
0.06803	0.879566	-0.1057	0.91274	0.979025	-0.4714
0.16415	0.884989	-0.2891	0.92151	0.980877	-0.4361
0.16564	0.885088	-0.2925	0.93338	0.983289	-0.3830
0.16907	0.885290	-0.2982	0.94051	0.984670	-0.3480
0.25972	0.891348	-0.4653	0.94232	0.984993	-0.3383
0.28475	0.893158	-0.5070	0.95227	0.986789	-0.2842
0.30979	0.895051	-0.5476	0.95829	0.987826	-0.2495
0.38802	0.901362	-0.6549	0.95923	0.987977	-0.2437
0.43475	0.905516	-0.7077	0.97273	0.990203	-0.1609
0.51540	0.913466	-0.7749	0.97438	0.990480	-0.1506
0.55227	0.917503	-0.7955	0.98189	0.991775	-0.1038
0.59727	0.922839	-0.8114	0.98527	0.992392	-0.0830
0.64610	0.929222	-0.8166	0.98935	0.993182	-0.0585
0.74894	0.945284	-0.7812	0.99271	0.993915	-0.0396
0.75228	0.945872	-0.7786	1.0	0.995647[a]	0.0
0.80302	0.955442	-0.7277			
		T = 308.15 K			
0.0	0.870945[b]	0.0	0.80021	0.950248	-0.7122
0.04246	0.872770	-0.0589	0.85507	0.962150	-0.6239
0.07232	0.874210	-0.1072	0.90064	0.972755	-0.5040
0.15620	0.878949	-0.2655	0.90914	0.974788	-0.4761
0.17489	0.880112	-0.3013	0.92027	0.977336	-0.4337
0.25045	0.885178	-0.4397	0.93208	0.979992	-0.3837
0.31286	0.889809	-0.5419	0.94320	0.982322	-0.3294
0.35591	0.893260	-0.6045	0.95283	0.984280	-0.2786
0.39905	0.896938	-0.6590	0.96008	0.985692	-0.2375
0.43638	0.900329	-0.6999	0.97176	0.987902	-0.1675
0.44157	0.900821	-0.7053	0.97557	0.988627	-0.1441
0.49671	0.906235	-0.7505	0.98022	0.989534	-0.1155
0.54732	0.911710	-0.7801	0.98714	0.990989	-0.0740
0.60180	0.918241	-0.7979	0.99137	0.991870	-0.0479
0.64823	0.924433	-0.8006	0.99169	0.991946	-0.0461
0.70106	0.932338	-0.7890	0.99554	0.992863	-0.0241
0.75093	0.940788	-0.7606	1.0	0.994032[a]	0.0

[a] From reference 5

[b] Values of ρ/g cm^{-3} for pure THF from the literature are: 0.88194 (6), 0.88436 (7) at 298.15 K; 0.8730 (8) at 303.15 K; 0.87333 (7) at 308.15 K.

288.15, 293.15, 298.15, 303.15, and 308.15 K are summarized in Table 1, where x_1 is the mole fraction of water. Literature values of the density of pure THF (6–8) are given in the footnote of the table for comparison. Molar excess volumes $\bar{V}^E(T)$ calculated from the results are also listed.

The difficulty in finding a suitable smoothing function to represent $\bar{V}^E$ has been pointed out previously (1). In order to estimate thermal expansion coefficients for the mixtures at 298.15 K, smoothed values of $\bar{V}^E$ (298.15) were obtained by fitting the results at that temperature with a set of least-squares cubic splines. Deviations of the results at other temperatures were fitted with the smoothing equation

$$[3]\quad \Delta\bar{V}^E(T) = \bar{V}^E(T) - \bar{V}^E(298.15) = x_1(1-x_1)\sum_{i=1}^{n}\sum_{j=1}^{2} a_{ij}(T-298.15)^j(1-x_1)^{(i-1)/2}$$

Can. J. Chem. Downloaded from www.nrcresearchpress.com by 210.87.254.42 on 09/05/12
For personal use only.

Can. J. Chem. Downloaded from www.nrcresearchpress.com by 210.87.254.42 on 09/05/12
For personal use only.

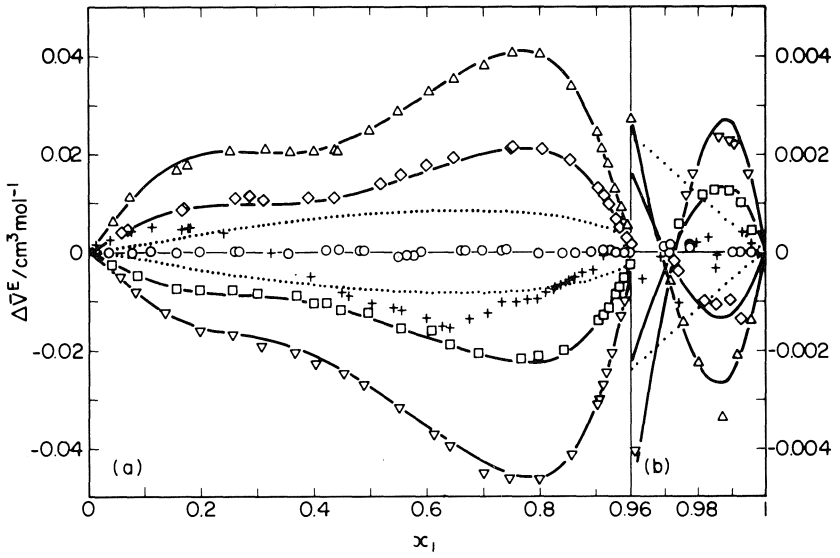

FIG. 1. Deviations of excess volumes for $H_2O(1)$ + THF(2) mixtures at various temperatures from smoothed results at 298.15 K: ▽, 288.15 K; □, 293.15 K; ○, 298.15 K; ◇, 303.15 K; △, 308.15 K; +, 298.15 K from ref. 1; —, calculated from eq. [3] with coefficients from Table 2; ···, ±1% deviation. Note that different scales are used in (*a*) and (*b*).

where a quadratic form of temperature dependence is assumed. The values of the coefficients a_{ij} calculated by the method of least squares with all points weighted equally are listed in Table 2.

A plot of the experimental values of $\Delta\overline{V}^E(T)$ and their smoothed representations by [3] is given in Fig. 1. Also shown are the deviations of the results of our previous dilatometric studies at 298.15 K (1). Most of these deviations fall within the 1% limits shown in the figure but some amount to nearly 2%. Although the values of $\overline{V}^E$ derived from our dilatometric studies are believed to be more accurate, the present results should provide good estimates of the temperature variation of $\overline{V}^E$.

The excess thermal expansion coefficient α^E is defined by

$$[4] \qquad \alpha^E = \alpha - \sum\phi_i\alpha_i^0$$

where α is the thermal expansion coefficient of the mixture, ϕ_i is the volume fraction of component i referred to the unmixed state, and α_i^0 is the thermal expansion coefficient of pure component i. At 298.15 K the value of α_1^0 is 0.257 kK^{-1} (5), and our densities of THF lead to a value of 1.243 kK^{-1} for α_2^0. The latter may be compared with the values 1.33 kK^{-1} (9), 1.085 kK^{-1} (10), and 1.226 kK^{-1} (11) given in the literature. Values of α^E for mixtures at 298.15 K were calculated from the relation

$$[5] \qquad \alpha^E = \frac{1}{\overline{V}}\left[\frac{\partial\Delta\overline{V}^E}{\partial T} - \overline{V}^E\sum\phi_i\alpha_i^0\right]$$

where $\overline{V}$ is the molar volume of the mixture. The value of $\partial\Delta\overline{V}^E/\partial T$ was obtained from [3], and $\overline{V}$ and $\overline{V}^E$ were calculated from the densities of the components and the smoothing equation for $\overline{V}^E$ given in ref. 1. In Fig. 2, the plot of α^E against x_1 is highly skewed and rises approximately linearly to a maximum near $x_1 = 0.8$. This corresponds roughly to the mole fraction at which there is a minimum of the excess enthalpy (1).

Values of the partial molar excess thermal expansivities defined by

$$[6] \qquad \bar{E}_i^E = (\partial\overline{V}_i^E/\partial T)_p$$

where $\overline{V}_i^E$ is the partial molar excess volume of component i, are shown in Fig. 3. For the most part, these were calculated from eq. [3], however, that representation is not suitable for evaluating $\bar{E}_2^E$ in very dilute THF mixtures since it implies an infinite limiting slope for the curve for $\bar{E}_2^E$ against x_1. Polynomial forms in x_1 were used to smooth the

TABLE 2. Coefficients for least-squares representation of $\Delta\overline{V}^E$ by eq. [3][a]

i	a_{i1}/cm^3 mol^{-1} K^{-1}	a_{i2}/cm^3 mol^{-1} K^{-2}
1	−0.020025	0.0002153
2	−0.754320	0.0051480
3	10.8699	−0.112429
4	−48.5126	0.584174
5	106.4688	−1.380297
6	−126.749	1.68357
7	78.690	−1.03290
8	−19.983	0.25280

[a]Standard deviation of fit σ = 0.00011 cm^3 mol^{-1}.

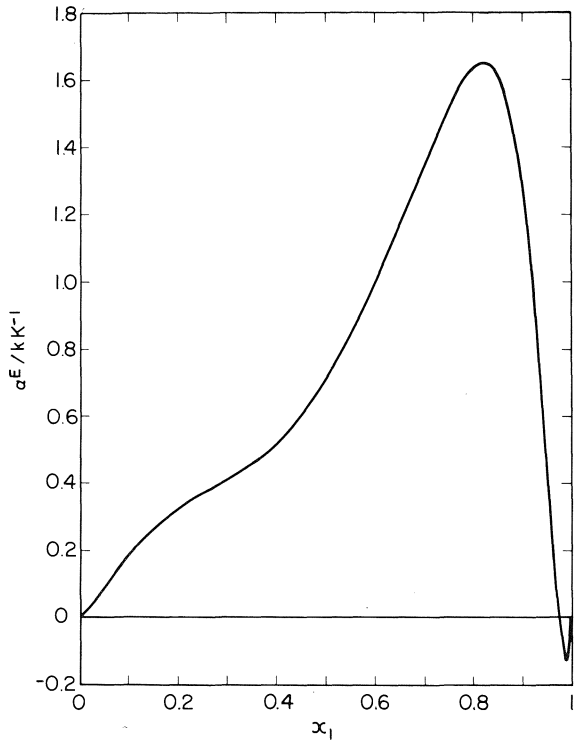

FIG. 2. Excess thermal expansion coefficient of $H_2O(1)$ + THF(2) mixtures at 298.15 K.

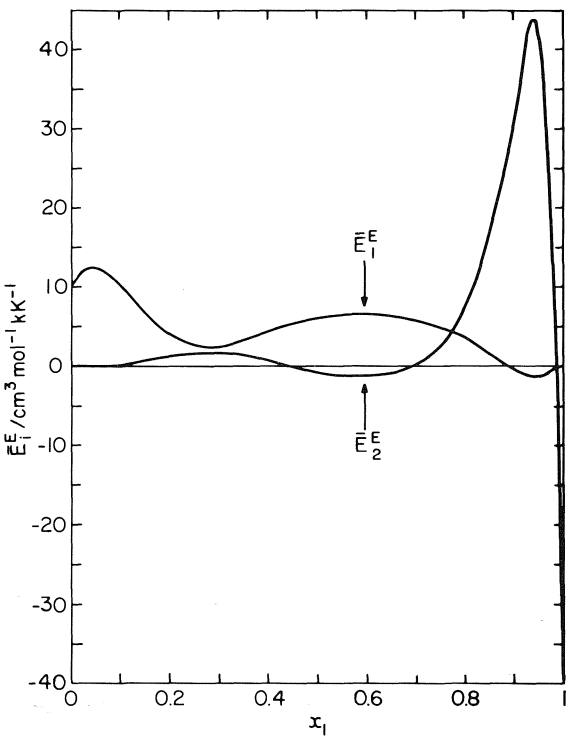

FIG. 3. Partial molar excess thermal expansivities of $H_2O(1)$ + THF(2) at 298.15 K.

$\Delta\bar{V}^E$ results at high dilutions of THF, and to evaluate $\bar{E}_2^E$. In this range it appears that THF molecules severely restrict mutual molecular motions within the mixture, and lead to negative values of both $\bar{E}_1^E$ and $\bar{E}_2^E$. However, with increasing THF concentration, $\bar{E}_2^E$ increases rapidly, becoming positive and reaching a maximum at $x_1 = 0.94$. The molecular significance of this peak is not clear, but similar behavior has been reported for *tert*-butyl alcohol + water mixtures (12).

Previously we found that the partial molar excess enthalpies of H_2O + THF mixtures are nearly constant over the central range of mole fractions (1). The variations of the partial molar excess expansivities are also relatively minor in this range. This finding supports the suggestion that the system consists of stabilized water clusters in equilibrium with a random mixture of H_2O and THF molecules (1). The small broad peak of $\bar{E}_1^E$ in the THF-rich region may be due to hydrogen bonding between unlike species in the mixture.

Several previous authors have studied the volumetric behavior of highly dilute H_2O + THF mixtures. Our results lead to a value of $\phi_E^0 = 62.5$ cm^3 mol^{-1} kK^{-1} at 298.15 K for the apparent molar expansivity of THF at infinite dilution. This appears reasonable in comparison with the literature values $\phi_E(0.153\ m) = 62.0$ cm^3 mol^{-1} kK^{-1} (11) and $\phi_E(0.39\ m) = 68.6$ cm^3 mol^{-1} kK^{-1} (13).

Acknowledgement

We are indebted to Mr. C. J. Halpin for purifying the THF used in this investigation.

1. O. KIYOHARA and G. C. BENSON. Can. J. Chem. **55**, 1354 (1977).
2. P. PICKER, E. TREMBLAY, and C. JOLICOEUR. J. Solution Chem. **3**, 377 (1974).
3. O. KIYOHARA and G. C. BENSON. Can. J. Chem. **51**, 2489 (1973).
4. P. PICKER. Private communication.
5. G. S. KELL. J. Chem. Eng. Data, **20**, 97 (1975).
6. W. HAYDUK, H. LAUDIE, and O. H. SMITH. J. Chem. Eng. Data, **18**, 373 (1973).
7. D. D. DESHPANDE, L. G. BHATGADDE, S. OSWAL, and C. S. PRABHU. J. Chem. Eng. Data, **16**, 469 (1971).
8. L. G. SCHORNACK and C. A. ECKERT. J. Phys. Chem. **74**, 3014 (1970).
9. D. J. METZ and A. GLINES. J. Phys. Chem. **71**, 1158 (1967).
10. C. CARVAJAL, K. J. TÖLLE, J. SMID, and M. SZWARC. J. Am. Chem. Soc. **87**, 5548 (1965).
11. J. L. NEAL and D. A. I. GORING. J. Phys. Chem. **74**, 658 (1970).
12. C. DE VISSER, G. PERRON, and J. E. DESNOYERS. Can. J. Chem. **55**, 856 (1977).
13. S. CABANI, G. CONTI, and E. MATTEOLI. J. Solution Chem. **5**, 751 (1976).

Can. J. Chem. Downloaded from www.nrcresearchpress.com by 210.87.254.42 on 09/05/12
For personal use only.

The heat capacities and volumes of some low molecular weight amides, ketones, esters, and ethers in water over the whole solubility range

GENEVIÈVE ROUX,[1] GÉRALD PERRON, AND JACQUES E. DESNOYERS[2]

Department of Chemistry, University of Sherbrooke, Sherbrooke, P.Q., Canada J1K 2R1

Received May 9, 1978

GENEVIÈVE ROUX, GÉRALD PERRON, and JACQUES E. DESNOYERS. Can. J. Chem. **56**, 2808 (1978).

The densities and heat capacities per unit volume of aqueous solutions of propionamide, methylacetate, ethylacetate, methylethylketone and diethylketone, and bis(2-ethoxyethyl)ether were measured over the whole solubility range with a flow densimeter and a flow microcalorimeter. Most systems were studied at 10, 25, and 40°C. Properties of the pure liquids were also measured whenever possible. The derived apparent molal volumes ϕ_V all decrease with concentration in the water-rich region, except with ethyl acetate which increases at high temperature. In general the more hydrophobic the solute the more negative the initial slope. All apparent molal heat capacities ϕ_C decrease as a function of concentration and the decrease is more important for more hydrophobic solutes. The apparent molal expansibilities ϕ_E are obtained from $\Delta\phi_V/\Delta T$. They are positive for all solutes but, at low concentrations, they are smaller than the corresponding molar value of the pure liquid. Various factors affecting hydrophobic interactions are examined.

GENEVIÈVE ROUX, GÉRALD PERRON et JACQUES E. DESNOYERS. Can. J. Chem. **56**, 2808 (1978).

Les masses volumiques et capacités calorifiques des solutions aqueuses de proprionamide, d'acétates de méthyle et d'éthyle, des diéthyl et méthyléthyl cétone et du bis(2-éthoxy éthyl) éther ont été mesurées sur tout le domaine de solubilité avec un densimètre et un microcalorimètre à écoulement continu. La plupart des systèmes ont été étudiés à 10, 25 et 40°C. Lorsque possible les propriétés des liquides purs ont aussi été mesurées. A l'exception de l'acétate d'éthyle, les volumes molaires apparents ϕ_V décroissent avec la concentration dans la région riche en eau et en général les pentes initiales sont plus négatives les plus hydrophobes sont les solutés. Toutes les capacités calorifiques molaires apparentes décroissent en fonction de la concentration et l'effet augmente avec le caractère hydrophobe du soluté. Les expansibilités molaires apparentes ϕ_E, obtenues à partir de $d\phi_V/dT$, sont toutes positives mais sont aux basses concentrations inférieures aux valeurs molaires des liquides purs. Différents facteurs influençant les interactions hydrophobes sont discutés.

Introduction

Recent work in this laboratory (1–3) has been concerned with transitions in aqueous liquid mixtures. Through heat capacity measurements the apparent molal heat capacity ϕ_C of many simple liquids which are completely miscible in water, such as dimethylformamide (4), dimethylsulfoxide (5), and dioxane (6), decreases in a regular way from the standard (infinite dilution) partial molal heat capacity, $\phi_C^0 = \bar{C}_p^0$, to the molar heat capacity of the pure organic liquid C_p^0. On the other hand, with some liquids such as *tert*-butylalcohol (1), piperidine (6), triethylamine (7), and 2-*n*-butoxyethanol (3), ϕ_C goes through a maximum and then decreases sharply to C_p^0. The changes are much sharper if partial molal heat capacities $\bar{C}_p$ are plotted (2) and the concentration dependence of $\bar{C}_p$ suggests the existence of some pseudo-phase transition in the water region analogous to micellization.

The exact reason why some liquid mixtures show these sharp changes in ϕ_C and $\bar{C}_p$ is not clear and could be related to the hydrophobic character, the tendency of these systems to unmix, the geometry of the molecules, or the nature of the polar group on the molecule. The present study was undertaken to throw some light on the importance of some of these factors. Therefore amides, ketones, and esters of similar geometries were examined as a function of temperature and whenever possible over the whole solubility range. A polyether which unmixes at high temperatures was also investigated.

Heat capacities measured by flow microcalorimetry require the simultaneous determination of the solution densities. From the densities, obtained with a flow densimeter, apparent molal volumes ϕ_V were derived, and from their temperature dependence apparent molal expansibilities were calculated, $\phi_E = d\phi_V/dT$.

Experimental

The origin and purification procedure of the chemicals are as follows. Propionamide, from Baker Chemicals, was recrystallized from acetone and dried under vacuum over P_2O_5.

[1]On leave of absence from Laboratoire de thermodynamique et cinétique chimique, Université de Clermont, 63170 Aubière, France.

[2]To whom correspondence should be addressed.

Can. J. Chem. Downloaded from www.nrcresearchpress.com by 210.87.254.105 on 09/05/12
For personal use only.

Can. J. Chem. Downloaded from www.nrcresearchpress.com by 210.87.254.105 on 09/05/12
For personal use only.

Methylacetate, from Baker Chemicals, ethylacetate and methylethylketone, both from Fisher Scientific (Certified A.C.S.), were used as such. Diethylketone, from Aldrich, was redistilled and the central fraction (30%) was collected. Bis(2-ethoxyethyl)ether, from Baker Chemicals and Eastman Kodak, was redistilled under vacuum with a fine stream of nitrogen.

The purity of all chemicals was verified to be better than 99.8% with vapor phase chromatography on carbowax 20 *M* at 10% or SE 30 at 10%, and all liquids were kept over 4 Å molecular sieves. All solutions were prepared by weight with distilled deionized water (Continental Deionized Water System).

The densities d and heat capacities per unit volume σ of the solutions were measured relative to pure water, d_0 and σ_0, with a SODEV flow digital densimeter (8) and a Picker flow microcalorimeter (9, 10). Differences in densities $d - d_0$ were measured to $\pm 3 \times 10^{-6}$ g cm^{-3} and differences in heat capacities $\sigma - \sigma_0$ to $\pm 7 \times 10^{-5}$ J K^{-1} cm^{-3}. The flow rate in the microcalorimeter was maintained at about 0.45 cm^3 min^{-1} and the basic power at 21.5 mW causing an increase in temperature during the measurements of 0.7 K. The absolute temperature was determined to ± 0.01 K with a Hewlett-Packard quartz thermometer. The general procedure and uncertainties at other temperatures have been described elsewhere (1, 10).

Results

The apparent molal volumes and heat capacities are calculated in the usual way from the differences in densities $d - d_0$ and specific heat capacities $c_p - c_{p0}$;

$$[1] \qquad \phi_V = \frac{M}{d} - \frac{1000(d - d_0)}{mdd_0}$$

and

$$[2] \qquad \phi_C = Mc_p + \frac{1000(c_p - c_{p0})}{m}$$

where M is the solute molecular weight and m the molality. The data for pure water were taken from Kell (11) and Stimson (12). The difference $c_p - c_{p0}$ is calculated from

$$[3] \qquad c_p - c_{p0} = c_{p0}\left\{\frac{\sigma - \sigma_0}{\sigma_0} + 1\right\}\frac{d_0}{d} - c_{p0}$$

where $\sigma_0 = d_0 c_{p0}$.

The original data for Δd and $\Delta\sigma/\sigma_0$ and the derived values ϕ_V and ϕ_C are given elsewhere (13). The measurements were made over the whole mole fraction range whenever the liquids were completely miscible and up to saturation in the other cases. In the dilute range, the apparent molal quantities ϕ_Y can be fitted with an expression of the type

$$[4] \qquad \phi_Y = \phi_Y^{\theta} + A_Y m$$

where Y refers to V or C_p. The linear region where eq. [4] applies varies with the system and temperature. The values of $\bar{V}^{\theta}$, $\bar{C}_p^{\theta}$, A_V, and A_C, obtained from a least-squares analysis, and the concentration limit of the linear region are given in Table 1. Similar data for other related systems taken from the literature are also given. The molar values V^0 and C_p^0 for the pure liquids are also given whenever they were measured.

With bis(2-ethoxyethyl)ether two samples were used. The sample from Baker was taken in the measurements at 25°C and that from Eastman Kodak at 10 and 40°C. Some densities were also repeated at 25°C with the Eastman Kodak chemical and the ϕ_V fell on the same curve as the data obtained with the Baker sample.

Relatively few measurements of densities were made previously over the whole concentration range with the present aqueous systems. On the other hand some relatively good $\bar{V}^{\theta}$ and V^0 are available at 25°C in the literature and can be used to verify the accuracy of the present measurements.

For proprionamide $\bar{V}^{\theta}$ was determined by Herskowits and Kelly (14) as 70.9 cm^3 mol^{-1} and by Dunstan and Mussell (15) as 71 cm^3 mol^{-1}. Shahidi *et al.* (16) calculated $\bar{V}^{\theta}$ from the intrinsic volumes of the solute and interaction terms taking into account the geometry of the molecule and found, depending on the relation used, to be 72.0 or 71.3 cm^3 mol^{-1}. The present $\bar{V}^{\theta}$, 71.47 cm^3 mol^{-1}, agrees with these values.

For ethyl acetate Edwards *et al.* (17) obtained 88.8 $\pm$ 0.3 cm^3 mol^{-1} compared with the present 88.97 cm^3 mol^{-1}. The densities of pure ethyl acetate were also studied by various authors (18) and the present V^0 agrees inside the experimental uncertainty with these.

Methylethylketone was studied by Bøje and Hvidt (19) and by Edwards *et al.* (17). Their $\bar{V}^{\theta}$ values (82.5 and 82.9 cm^3 mol^{-1} respectively) are comparable with the present value of 82.52 cm^3 mol^{-1} Bøje and Hvidt also determined ϕ_V over the whole mole fraction range and their data, inside their quoted uncertainty, agree with ours. The suggested value for V^0, 90.14 cm^3 mol^{-1} is identical to ours.

Edwards *et al.* (17) obtained 165.0 $\pm$ 0.3 cm^3 mol^{-1} for $\bar{V}^{\theta}$ of bis(2-ethoxyethyl)ether which compares with the present value of 164.16 cm^3 mol^{-1}.

The precision of the $\bar{V}^{\theta}$ data is of the order of ± 0.05 cm^3 mol^{-1} and the generally good agreement with literature data fixes the accuracy at ± 0.5 cm^3 mol^{-1} or better.

To our knowledge there are no data in the literature on the heat capacities of the present organic aqueous mixtures. Pure methylethylketone was studied as a function of temperature by Sinke and Oetting (20) and by Andon *et al.* (21) and their C_p^0 are in good agreement with ours at 25°C but significant differences (a few percent) are observed at other temperatures. However, the generally good agreement of $\bar{V}^{\theta}$ and V^0 with the literature and the proven

TABLE 1. Apparent molal volumes and heat capacities of several solutes in water

Solute	T (°C)	$\bar{V}^{\theta}$ ($cm^3\ mol^{-1}$)	A_V ($cm^3\ mol^{-2}\ kg$)	Max mol ($mol\ kg^{-1}$)	V^{o} ($cm^3\ mol^{-1}$)	$\bar{C}_p^{\theta}$ ($J\ K^{-1}\ mol^{-1}$)	A_C ($J\ K^{-1}\ mol^{-2}\ kg$)	Max mol ($mol\ kg^{-1}$)	C_p^{o} ($J\ K^{-1}\ mol^{-1}$)
Acetamide*	25	55.61	−0.12			162.4	−1.4		
Propionamide	25	71.47	−0.33	1		253.6	−4.5	2.5	
Methylacetate	25	72.46	−0.10	0.7	80.10	298.2	−15.5	1.2	
Ethylacetate	10	87.35	−0.60	0.6	96.53	409.6	−23.4	0.9	164.2
	25	88.97	+0.08	0.9	98.50	396.6	−22.1	0.9	169.5
	40	90.72	+0.46	0.8	100.58	390.9	−30.8	0.8	173.9
Acetone*	25	66.92	−0.37			240.5	−7.6		
Methylethylketone	4	80.83	−1.49	0.55	87.74	335.3	−17.5	1.5	152.8
	10	81.33	−1.41	0.55	88.40	335.8	−13.1	2.5	153.4
	25	82.52	−0.75	0.55	90.14	336.6	−10.4	2	158.4
	40	83.60	−0.11	1	91.95	335.1	−9.7	1	161.6
Diethylketone	25	98.08	−1.10	0.5	106.43	428.3	−18.0	0.5	
Bis(2-ethoxyethyl)-ether	10	162.72	−4.50	0.5	176.95	693.7	−39.2	2	344.7
	25	164.16	−2.21	0.6	179.59	697.8	−16.7	1.5	347.5
	40	166.49	−1.73	0.3	182.55	703.6	−8.5	1.3	352.0
2 Methoxyethanol†	25	75.11	−0.47	0.8	79.25	286.7	−8.7	4	176.4
2 Ethoxyethanol†	25	90.97	−0.86	0.6	97.15	383.5	−11.7	3.4	210.3

*Reference 31.
†Reference 3.

reliability of the flow microcalorimetric technique for the measurement of heat capacities lead us to believe that the present data on ϕ_C are accurate to 1 $J\ K^{-1}\ mol^{-1}$ or better, at least in the water-rich region.

Discussion

Standard Quantities

The standard partial molal quantities $\bar{C}_p^{\theta}$ and $\bar{V}^{\theta}$ are useful in predicting the temperature and pressure dependence of equilibrium quantities and give information on solute–solvent interactions. For this purpose it is important to develop additivity schemes from which the properties of complex molecules can be predicted from those of simpler ones. Data exist in the literature on $\bar{V}^{\theta}$ of ketones, ethers, esters, and amides in water but little is known about their $\bar{C}_p^{\theta}$.

Various additivity schemes (16, 17, 22–25) have been proposed recently for $\bar{V}^{\theta}$ and $\bar{C}_p^{\theta}$. Nichols *et al.* (22) have made a fairly exhaustive study of $\bar{C}_p^{\theta}$ of molecules of biological interest and Perron and Desnoyers (23) made a similar study of aromatic molecules. The main difference in these two schemes lies in the value given to the H atom. The scheme of Perron and Desnoyers is an extension of the approach of Jolicoeur and Lacroix (24) and has the advantage of being applicable to $\bar{V}^{\theta}$ also. Recently Guthrie (25) has proposed a much more sophisticated group additivity scheme which can in principle yield a much better agreement between the predicted and experimental $\bar{C}_p^{\theta}$ but requires up to 49 parameters. With the present state of knowledge it is better to concentrate on the simpler additivity schemes of Nichols *et al.* and of Perron and Desnoyers. Also Edwards and co-workers (16, 17) have proposed a relatively simple theory for the prediction of $\bar{V}^{\theta}$ from van der Waals volumes corrected for void space and interactions, but this is not, strictly speaking, an additivity scheme.

The main group contributions to $\bar{C}_p^{\theta}$ and $\bar{V}^{\theta}$ of Nichols *et al.* and Perron and Desnoyers are summarized in Table 2. Assuming these contributions correct, average values for the —C(=O)—, —CO—, and —CNH_2 group were derived and are also given in Table 2. The average deviations between the calculated and measured $\bar{C}_p^{\theta}$ and $\bar{V}^{\theta}$ for the data in Table 1 are 5 $J\ K^{-1}\ mol^{-1}$ for the $\bar{C}_p^{\theta}$ schemes of both Nichols *et al.* and Perron and Desnoyers and 0.5 $cm^3\ mol^{-1}$ for the $\bar{V}^{\theta}$ scheme of Perron and Desnoyers. The agreement is worse with the molecules which contain more than one polar group, e.g., with the polyether. This has been noted before (22, 26).

The expansibilities $\bar{E}^{\theta}$ can be estimated from $\Delta\bar{V}^{\theta}/\Delta T$ and for ethyl acetate, methylethylketone, and bis(2-ethoxyethyl)ether the values are found to be 0.112, 0.076, and 0.126 $cm^3\ K^{-1}\ mol^{-1}$, respectively, at 25°C. On the other hand, if we calculate $\bar{E}^{\theta} - E^{o}$, the values are now −0.022, −0.046, and −0.060. This indicates that the expansibility of an organic molecule surrounded by water is less than that of an organic molecule surrounded by similar organic molecules. This is consistent with models which suggest that hydrophobic hydration occurs with a reduction of free space near the solute.

Can. J. Chem. Downloaded from www.nrcresearchpress.com by 210.87.254.105 on 09/05/12
For personal use only.

Can. J. Chem. Downloaded from www.nrcresearchpress.com by 210.87.254.105 on 09/05/12
For personal use only.

TABLE 2. Group contributions to $\bar{C}_p^\theta$ and $\bar{V}^\theta$ of aliphatic molecules at 25°C

Group	$\bar{C}_p^\theta$ (Wadsö) ($J\,K^{-1}\,mol^{-1}$)	$\bar{C}_p^\theta$ (Perron) ($J\,K^{-1}\,mol^{-1}$)	$\bar{V}^\theta$ (Perron) ($cm^3\,mol^{-1}$)
$-CH_3$	157	178	26.7
$-CH_2$	90	88	16.0
—H	67	90	10.7
O ‖ —C—	−67	−105	13.1
O ‖ —CO—	−10	−50	19.4
—OH	−4	12	12
$-CONH_2$	5	−14	28.8
—O—	−57	−72	4.1

Depending on the solute, the values of $\bar{C}_p^\theta$ increase or decrease with temperature. On the other hand $\bar{C}_p^\theta - C_p^0$ decreases with temperature with most systems suggesting that hydrophobic hydration is largest near the freezing temperature of water. Bis(2-ethoxyethyl)ether is an exception to this rule since $\bar{C}_p^\theta - C_p^0$ is approximately independent of T.

Concentration Dependence

The main objective of the present study was to examine some of the factors that could influence the concentration dependence of ϕ_C and ϕ_V of organic molecules in water. Some amines and alcohols show anomalous ϕ_C or $\bar{C}_p$ which suggests the existence of transitions similar to micellization although molecules like *tert*-butylalcohol and triethylamine could hardly be considered surfactants. The maximum observed in the ϕ_C of these molecules occurs around 0.05 mole fraction and is very temperature dependent. Unfortunately much of the data in the literature were aimed at deriving additivity schemes and were limited to 25°C and low concentrations or else were aimed at the measurement of excess functions and only mole fractions between 0.1 and 0.9 were considered. In order to throw some light on this problem ϕ_C and ϕ_V of a series of ketones, esters, amides, and ethers of similar geometries and sizes are compared in Fig. 1. The initial slopes are given in Table 1. With all these solutes A_C is negative and the order is very nearly inversely proportional to the value of $\bar{C}_p^\theta$. In none of these systems do we observe maxima in ϕ_C as in the case of alcohols (1), some amines (6, 7), and larger alkoxyethanols (3). It would therefore appear that with the present system the leading effect giving the sign and magnitude of A_C is the reduction of hydrophobic hydration as the concentration increases. This is consistent with the destructive cosphere overlap models (7).

The parameter A_V follows the same order as A_C

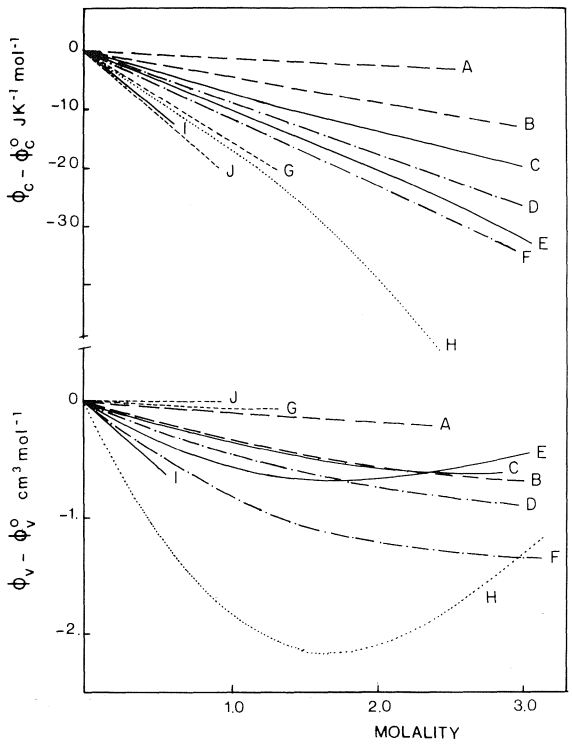

FIG. 1. Apparent molal heat capacities and volumes of various polar solutes in water in the water-rich region at 25°C: *A*, acetamide; *B*, propionamide; *C*, acetone; *D*, 2-methoxyethanol; *E*, methylethylketone; *F*, 2-ethoxyethanol; *G*, methylacetate; *H*, bis(2-ethoxyethyl)ether; *I*, diethylketone; *J*, ethyl acetate.

with the exception of the two esters. The volumes have the general trends of most organic liquids in water; ϕ_V decreases with concentration and, if the solubility is high enough, goes through a minimum and reaches a value V^0 which is larger than $\bar{V}^\theta$. The temperature dependence of ϕ_C and ϕ_V of ethyl acetate is shown in Fig. 2. As seen the initial slope A_V is even positive at 40°C. At present we have no explanation for the anomalous concentration dependences of ϕ_V of the esters.

The concentration dependence of ϕ_C and ϕ_V of methylethylketone at various temperatures is given in Fig. 3. Here the trends are fairly typical of this class of solutes except for 40°C. A_C and A_V are negative and become less negative as the temperature increases. Also, except at high temperature, ϕ_V goes through a minimum.

The present investigation therefore shows that the maximum in ϕ_C is not a general effect since most types of molecules do not show any anomalous concentration dependence. With alcohols, amines and amine salts (27) additional interactions, such as hydrogen bonding, could be responsible for the positive contribution to ϕ_C.

Can. J. Chem. Downloaded from www.nrcresearchpress.com by 210.87.254.105 on 09/05/12
For personal use only.

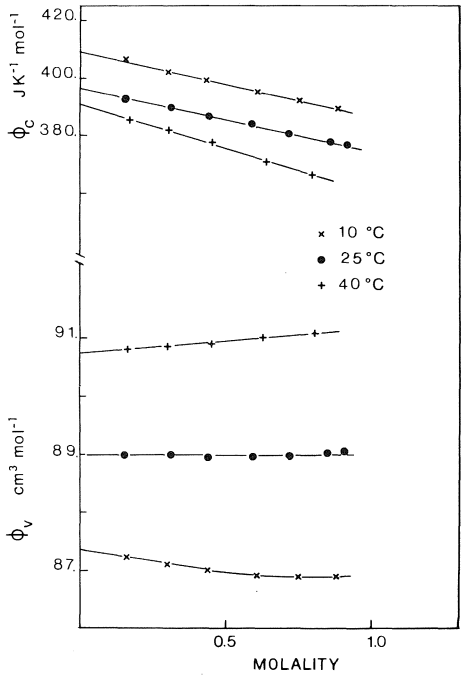

FIG. 2. Apparent molal heat capacities and volumes of ethyl acetate at various temperatures.

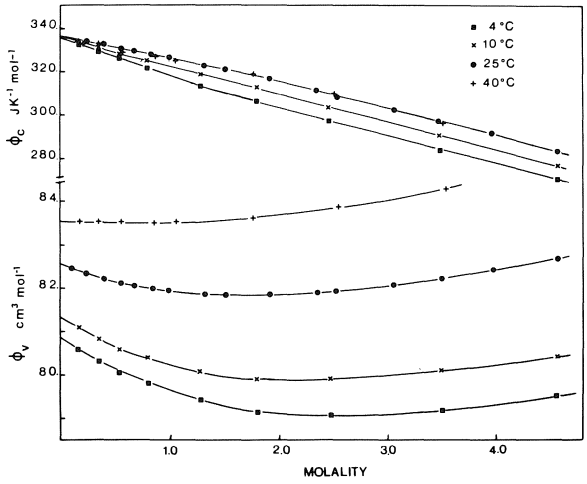

FIG. 3. Apparent molal heat capacities and volumes of methylethylketone at various temperatures.

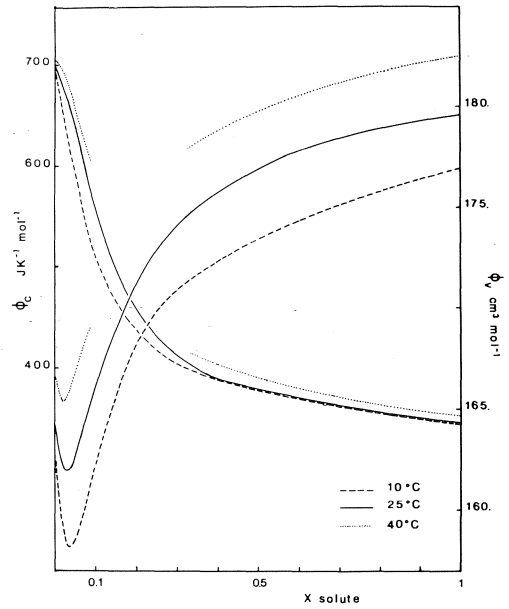

FIG. 4. Apparent molal heat capacities and volumes of bis(2-ethoxyethyl)ether at various temperatures.

The ϕ_C and ϕ_V of bis(2-ethoxyethyl)ether was investigated since this aqueous system shows a lower critical solution temperature at 28°C (28, 29). It is therefore possible to study its properties very close to the unmixing region. The ϕ_C and ϕ_V are plotted against the mole fraction at temperatures above and below the critical solution temperature in Fig. 4. Although the initial slopes A_V and A_C fall in a general pattern with the other liquid mixtures (Fig. 1), the large drop in ϕ_C and large increase in ϕ_V beyond the minimum suggests that a transition is occurring beyond 0.05 mole fraction. In this respect this ether resembles alcohols, etheralcohols, amines, and carboxylic acids at high concentration. The $\bar{C}_p$ and $\bar{V}$ rapidly tend to the values of C_p^0 and V^0 beyond 0.1 mole fractions indicating that an additional molecule will only see other ether molecules when added to the solution. On the other hand there is no anomaly in ϕ_C in the water-rich region contrary to alcohols and amines. ϕ_C decreases in a regular way to C_p^0. The slight hump in the concentration dependence of ϕ_C at high temperature does not appear very significant. On the other hand, if ϕ_C is plotted against the volume fraction X_V (Fig. 5), a different picture emerges. It was shown that with liquids such as dimethylformamide (7) ϕ_C is nearly linear in volume fraction. Therefore, if we consider the straight line between $\phi_C - \phi_C^\theta$ and C_p^0 as the ideal behavior, then it seems that the anomalies occur mainly in the water-rich region and increase with temperature.

The most interesting feature of bis(2-ethoxyethyl)-ether is that data were obtained very close to the phase separation region. At 25°C we are at 3° from the lower critical solution temperature and at 40°C measurements were made on both sides of the phase diagram. All these data near the two phase region are qualitatively very similar to the data at lower temperatures and a smooth curve can be drawn joining the data points at 40°C (see Figs. 4 and 5). This was also observed with 2-butoxyethanol (3).

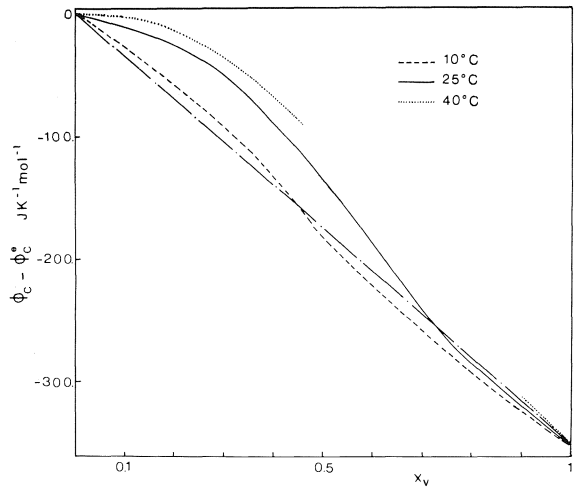

FIG. 5. Apparent molal heat capacities of bis(2-ethoxyethyl)ether as a function of volume fraction at various temperatures.

The positive deviation observed in Fig. 5 at high temperature might be due to anomalous energy fluctuations near the two phase region but these deviations are certainly small compared with those observed with alcohols, etheralcohols, and amines (1–3, 6, 7). This does not rule out the possibility that pseudo-transitions in aqueous organic mixtures may be related to the existence of an *upper* critical solution temperature since recent studies (30) suggest that 2-butoxyethanol has such a critical temperature below 0°C and the anomalies in ϕ_C are largest at the lowest temperature investigated (2, 3).

Since ϕ_V data are available as a function of temperature and concentration it is possible to calculate ϕ_E as a function of concentration. This was done in Fig. 6 for bis(2-ethoxyethyl)ether and methylethylketone at 17.5°C. These have the same general shape as alcohols in water (1, 3) although the maximum is not quite as sharp.

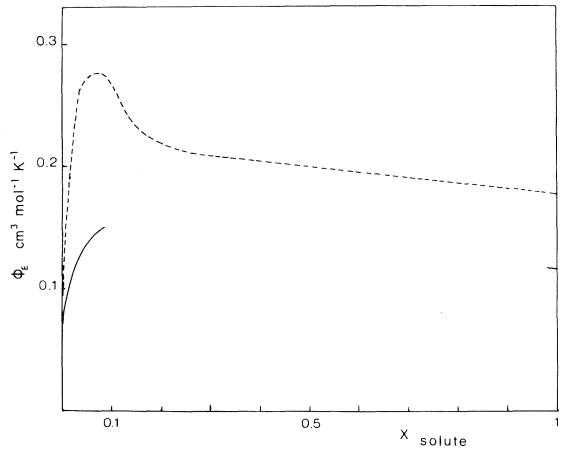

FIG. 6. Apparent molal expansibilities of bis(2-ethoxyethyl)ether (---) and methylethylketone at 17.5°C.

The present study eliminates some of the possible factors that could be responsible for the anomalous concentration dependence of ϕ_C of some organic molecules or ions in water. Polar molecules which do not contain alcohol or amine (and possibly carboxyl) groups show little anomaly. Also there is no increase in anomaly near the lower critical solution temperature. The hydrophobic character certainly plays an important role in this non-ideality and it is quite possible that the existence of strong hydrogen bonding or ionizing groups like alcohols and amines enhances the solubility of hydrophobic molecules more than other polar groups. On the other hand bis(2-ethoxyethyl)ether appears to be more hydrophobic than *tert*-butylalcohol or butoxyethanol but its non-ideality is much smaller.

The geometry of the molecules probably has some influence on the non-ideality but this effect has not been properly investigated yet.

Finally the maximum and the large decrease in ϕ_C is certainly related to some structural changes taking place in the solution. Heat capacity is related to the shift in equilibrium of the system during a unit increase in temperature. This shift in equilibrium contribution to ϕ_C will probably be larger if the corresponding changes in enthalpies are large. For example, current work on the enthalpy of dilution of 2-butoxyethanol in water indicates that the increase in relative enthalpy is very large with this system in the region where ϕ_C shows extrema. Unfortunately not sufficient data are available at present on the enthalpy of other organic aqueous mixtures in the water-rich region to establish such a correspondence.

Acknowledgements

The authors would like to thank the Quebec Ministry of Education for financial assistance and the France–Québec exchange program for the award of a post-doctorate fellowship to one of us (G.R.).

1. C. DE VISSER, G. PERRON, and J. E. DESNOYERS. Can. J. Chem. **55**, 856 (1977).
2. G. ROUX, G. PERRON, and J. E. DESNOYERS. J. Phys. Chem. **82**, 966 (1978).
3. G. ROUX, G. PERRON, and J. E. DESNOYERS. J. Solution Chem. **7**, 639 (1978).
4. C. DE VISSER, G. PERRON, J. E. DESNOYERS, W. J. M. HEUVELSLAND, and G. SOMSEN. J. Chem. Eng. Data, **22**, 74 (1977).
5. C. DE VISSER, W. J. M. HEUVELSLAND, L. A. DUNN, and G. SOMSEN. J. Chem. Soc. Faraday Trans. I, **74**, 1159 (1978).
6. O. KIYOHARA, G. PERRON, and J. E. DESNOYERS. Can. J. Chem. **53**, 2591 (1975).

Can. J. Chem. Downloaded from www.nrcresearchpress.com by 210.87.254.105 on 09/05/12
For personal use only.

7. C. DE VISSER, G. PERRON, and J. E. DESNOYERS. J. Am. Chem. Soc. **99**, 5894 (1977).
8. P. PICKER, E. TREMBLAY, and C. JOLICOEUR. J. Solution Chem. **3**, 377 (1974).
9. P. PICKER, P. A. LEDUC, P. R. PHILIP, and J. E. DESNOYERS. J. Chem. Thermodyn. **3**, 361 (1971).
10. J. E. DESNOYERS, C. DE VISSER, G. PERRON, and P. PICKER. J. Solution Chem. **5**, 605 (1976).
11. G. S. KELL. J. Chem. Eng. Data, **12**, 66 (1967).
12. H. F. STIMSON. Am. J. Phys. **23**, 614 (1955).
13. G. ROUX, G. PERRON, and J. E. DESNOYERS. Int. Data Ser. B. To be published.
14. T. T. HERSKOWITS and T. M. KELLY. J. Phys. Chem. **77**, 381 (1973).
15. A. E. DUNSTAN and A. G. MUSSEL. J. Chem. Soc. 1935 (1910).
16. F. SHAHIDI, P. G. FARRELL, and J. T. EDWARDS. J. Chem. Soc. Faraday Trans. I, **73**, 715 (1977).
17. J. T. EDWARDS, P. G. FARRELL, and F. SHAHIDI. J. Chem. Soc. Faraday Trans. I, **73**, 705 (1977).
18. T. ABRAHAM, V. BERY, and A. P. KUDCHADKER. J. Chem. Eng. Data, **16**, 355 (1971).
19. L. BØJE and A. HVIDT. J. Chem. Thermodyn. **3**, 663 (1971).
20. G. C. SINKE and F. L. OETTING. J. Phys. Chem. **68**, 1354 (1964).
21. J. L. ANDON, J. F. COUNSELL, and J. F. MARTIN. J. Chem. Soc. A, 1894 (1968).
22. N. NICHOLS, R. SKÖLD, C. SPINK, J. SUURKUUSK, and I. WADSÖ. J. Chem. Thermodyn. **8**, 1081 (1976).
23. G. PERRON and J. E. DESNOYERS. Fluid Phase Equil. In press.
24. C. JOLICOEUR and G. LACROIX. Can. J. Chem. **54**, 624 (1976).
25. J. P. GUTHRIE. Can. J. Chem. **55**, 3700 (1977).
26. C. OSTIGUY, J. C. AHLUWALIA, G. PERRON, and J. E. DESNOYERS. Can. J. Chem. **55**, 3368 (1977).
27. G. PERRON, N. DESROSIERS, and J. E. DESNOYERS. Can. J. Chem. **54**, 2163 (1976).
28. N. TAKENAKA and K. ARAKAWA. Bull. Chem. Soc. Jpn. **47**, 566 (1974).
29. W. SCHNEIDER, R. VOGEL, and E. MOKHTARI-NYAD. Ber. Bunsenges. Phys. Chem. **81**, 1076 (1977).
30. J. E. DESNOYERS, R. BEAUDOIN, G. PERRON, and G. ROUX. Chemistry for energy. *Edited by* M. Tomlinson. Am. Chem. Soc. Symposium Series. In press.
31. O. KIYOHARA, G. PERRON, and J. E. DESNOYERS. Can. J. Chem. **53**, 3263 (1975).

Can. J. Chem. Downloaded from www.nrcresearchpress.com by 210.87.254.105 on 09/05/12
For personal use only.

Memory impairment in flowing suspensions. I. Some theoretical considerations

A. OKAGAWA, G. J. ENNIS, AND S. G. MASON
Pulp and Paper Research Institute of Canada, Montreal, P.Q., Canada H3A 2A7
and
Department of Chemistry, McGill University, Montreal, P.Q., Canada H3A 2A7

Received April 5, 1978

A. OKAGAWA, G. J. ENNIS, and S. G. MASON. Can. J. Chem. **56**, 2815 (1978).

When a suspension of nearly monodisperse rigid axisymmetric particles in a Newtonian liquid is sheared, the orientation distributions of the particle undergo damped oscillations of frequency twice that of the rotating particles. If the flow is stopped and then reversed, the oscillations regrow under certain restricted conditions until the initial state is fully restored: the system has perfect memory. Removing some of the restrictions causes imperfect recovery of the initial orientation distribution, so that when the flow is reversed cyclically back and forth, the orientation distribution eventually becomes time-independent: the system has lost all of its memory. A number of sources of memory impairment are considered theoretically, several of which are amenable to experimental verification and are illustrated by numerical calculation.

A. OKAGAWA, G. J. ENNIS et S. G. MASON. Can. J. Chem. **56**, 2815 (1978).

Lorsqu'on applique un cisaillement à une suspension de particules rigides axisymétriques presque monodispersées se trouvant dans un liquide newtonien, les distributions d'orientations des particules subissent des oscillations atténuées dont la fréquence est le double de celle des particules en rotation. Si l'on stoppe l'écoulement et qu'on en change le sens alors que certaines conditions critiques sont remplies, les oscillations recommencent à croître jusqu'à ce que le système reprenne tout à fait son était initial: le système possède une mémoire parfaite. Lorsque certaines de ces restrictions sont levées, le système ne reprend qu'imparfaitement la distribution initiale d'orientations et si l'on change alternativement le sens de l'écoulement, la distribution d'orientations devient éventuellement indépendante du temps: le système a complètement perdu la mémoire. On examine d'un point de vue théorique plusieurs causes de perte de mémoire, dont certaines peuvent être soumises à une vérification expérimentale et décrites au moyen de calculs numériques.

[Traduit par le journal]

Introduction

In a fluid suspension undergoing simple shear flow, each particle rotates, translates, and interacts with others. When the velocity field is reversed, the translational and rotational loci of each particle can be exactly retraced under certain restricted conditions (1–5): the system thus shows perfect memory. In this paper we extend earlier work on the statistical mechanics of flowing dispersions (6–9) and examine some aspects of memory impairment in dilute suspensions of rigid spheroids. In the following paper (10) we present experimental evidence which confirms and extends these principles.

Qualitative demonstrations of such reversibility have been given by Heller (11), in a cine-film by Taylor (12), by Goldsmith and Mason (13), and others. For example, letters of a dyed liquid inscribed in the annulus between two concentric cylinders filled with the same undyed liquid were made to disappear by rotating one of the cylinders for a number of turns and then to reappear, slightly blurred by diffusion of the dye, on rotating the same number of turns backwards (4). Okagawa and Mason (3, 6) demonstrated reversible orientation distributions in dilute suspensions of nearly monodisperse rigid rods in a Newtonian liquid: when shear was applied the orientation distribution functions exhibited damped oscillations of frequency twice that of the individually rotating particles; on reversing flow the oscillations regrew perfectly reversibly until the initial conditions were fully restored. For a system with perfect memory, this process can be repeated indefinitely. However, if the system does not satisfy the reversibility requirements, some of the memory is lost during each reversal. This loss is cumulative and eventually it becomes complete so that the orientation distribution is time-independent.

The same behavior will be exhibited by any macroscopic property which depends upon particle orientation, for example, the rheological (7), optical (14), and electrical (15) properties. The same is true of properties determined wholly or in part by spatial distributions, although we will not consider these further since they appear to be much less important.

The formal theory of time-reversal in fluid flow has been given by Bretherton (1), Slattery (2), and elaborated for suspension rheology by Cox (16). The

general requirements for perfect reversibility of particle translation and rotation in a suspension are: (*i*) the fluid motion is given by the linearized form of the Navier–Stokes equation (i.e., for the regime of creeping flow), and (*ii*) the boundary conditions are identical for both forward and backward flows. Specifically these conditions require that the particles are rigid, their surfaces are smooth and free of singularities (17), non-sedimenting, have no interaction forces or torques such as those arising from Coulombic and/or molecular dispersion forces, possess no thermal (Brownian) motion so that the behavior is truly orthokinetic (5), and are suspended in a viscous Newtonian fluid flowing at effectively zero Reynolds number (3, 6, 8, 9). Relaxing any of these conditions introduces some irreversibility, as can be realized, for example, by applying an external electric field, using non-Newtonian suspending media, or using particles with appreciable Brownian motion, all of which we have done in the experiments on spheroidal-like particles described in the following paper (10).

In this paper, we consider a number of pertinent theoretical principles for dilute suspensions of rigid spheroids suspended in a Newtonian dielectric liquid of the same density.

We first discuss briefly the motion of single spheroids in a simple shear flow and the resulting oscillations of the orientation distribution functions in dilute suspension thereof. In the systems with perfect memory, we consider the effects of dispersion in particle shape and of 2-body hydrodynamic interactions. In the final part, various disturbances which may cause memory loss are considered, several of which are illustrated numerically.

Perfect Memory

When the conditions mentioned above are satisfied, reversibility occurs in any general laminar flow; we shall, however, limit our treatment to simple shear (or Couette) flow whose undisturbed velocity components v_i in a space-fixed Cartesian coordinate system x_i are

$$[1] \qquad v_1 = v_2 = 0, \quad v_3 = Gx_2$$

where v_i is the velocity of undisturbed fluid along the X_i axis and G is the velocity gradient or rate of shear; when flow is reversed $v_3 = -Gx_2$. It is to this flow that the calculations in this and the experiments described in the following paper (10) apply.

(a) Single Particles

Since we will be concerned primarily with effects of particle rotation it is convenient to eliminate translation by placing a single spheroid at the origin of the coordinate system shown in Fig. 1. If the axis

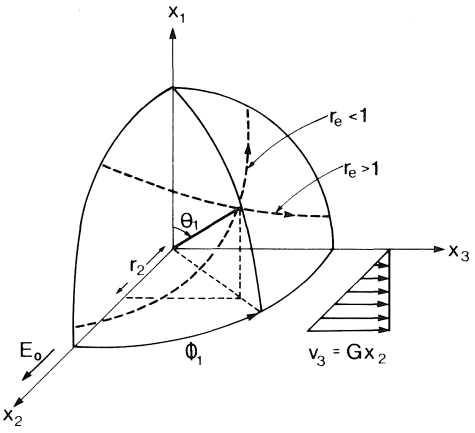

FIG. 1. Coordinate system x_i and spherical polar angles θ_1 and ϕ_1 for unit length of the axis of revolution of a spheroid in simple shear flow $v_3 = \pm Gx_2$. In some instances, an electric field of strength E_0 is also applied along the X_2-axis. Typical rotational orbits (spherical ellipses) of the ends of the axis of revolution of a prolate spheroid ($r_e > 1$) and an oblate spheroid ($r_e < 1$) in shear flow alone ($E_0 = 0$) are indicated by the dashed lines. The relative projected length r_2 of the semi-axis on the X_2-axis is also indicated.

of revolution of the spheroid is on x_1' of the particle-fixed Cartesian coordinate system x_i', the particle surface is given by

$$[2] \qquad \frac{x_1'^2}{a^2} + \frac{x_2'^2}{b^2} + \frac{x_3'^2}{b^2} = 1$$

where a is the semi-axis of revolution and b is the other semi-axis. The orientation is given by the spherical polar angles θ_1, ϕ_1, and the spin angle ψ_1 of the axis of revolution. However, we will ignore further consideration of ψ_1 since for spheroids (and other bodies of revolution) it is difficult to measure and is of little importance in our experiments, although in principle it can be treated quantitatively in ways similar to those considered below for θ_1 and ϕ_1. The rotation of the axis of the particle of revolution, first described by Jeffery (18), is given by

$$[3a] \qquad \omega = \frac{d\phi_1}{dt} = \frac{G}{(r_e^2 + 1)}(r_e^2 \cos^2 \phi_1 + \sin^2 \phi_1)$$

$$[3b] \qquad \frac{d\theta_1}{dt} = \frac{G}{4}\frac{(r_e^2 - 1)}{(r_e^2 + 1)} \sin 2\theta_1 \sin 2\phi_1$$

which integrate to yield

$$[4a] \qquad \tan \theta_1 = \frac{Cr_e}{(r_e^2 \cos^2 \phi_1 + \sin^2 \phi_1)^{1/2}}$$

$$[4b] \qquad \tan \phi_1 = r_e \tan\left(\frac{2\pi t}{T} + \kappa\right)$$

where C and κ are the orbit constant and phase angle (7), $r_e = a/b$ is the ellipsoidal axis ratio, t is time, and T, the period of one complete rotation about the

vorticity axis X_1 through $\phi_1 = 2\pi$, is

$$[5] \qquad T = \frac{2\pi}{G}(r_e + r_e^{-1})$$

The particle axis thus rotates periodically in a closed spherical elliptical orbit at a fixed C and κ, the locus of an end in one quadrant being shown in Fig. 1. Due to the linearity of the equations of motion of the particle and the surrounding medium (18), [3]–[5] are also valid when the flow is reversed so that the particle retraces exactly the forward rotational (and when appropriate, translational) path. The rotations described by [3] and [4] have been confirmed experimentally using rigid rods which behave like prolate spheroids, $r_e > 1$ (19), and discs like oblate spheroids, $r_e < 1$ (20) when r_e is calculated from the measured T by means of [5] is used in [3] and [4].

(b) Dilute Suspensions

Consider now an infinitely dilute suspension of monodisperse spheroids with each particle rotating according to [3] and [4] at a fixed C and κ determined by its initial orientation. The instantaneous orientation probability distribution $p_t(\theta_1,\phi_1)$ for an initially randomly oriented population is (7):

$$[6] \qquad p_t(\theta_1, \phi_1) = \frac{\sin\theta_1}{4\pi(\cos^2\theta_1 + \chi^2 \sin^2\theta_1)^{3/2}}$$

where

$$[7a] \qquad \chi^2 = \chi_1 \sin^2\phi_1 + \chi_2 \sin\phi_1 \cos\phi_1 + \chi_3 \cos^2\phi_1$$

$$[7b] \qquad \chi_1 = \frac{1}{2}\left\{1 + r_e^{-2} + (1 - r_e^{-2}) \cos\frac{4\pi t}{T}\right\}$$

$$[7c] \qquad \chi_2 = (r_e^{-1} - r_e) \sin\frac{4\pi t}{T}$$

$$[7d] \qquad \chi_3 = \frac{1}{2}\left\{1 + r_e^{2} + (1 - r_e^{2}) \cos\frac{4\pi t}{T}\right\}$$

Since each χ_i is an oscillating function with a period of $T/2$, $p_t(\theta_1,\phi_1)$ for a specified r_e and θ_1, ϕ_1 oscillates with a frequency of $2/T$ as long as shear is applied. As shown in [3] the rotational velocity of each particle is linear in G and hence reversible, so that $p_t(\theta_1,\phi_1)$ is also reversible when flow is reversed.[1]

[1]The magnitudes of $+G$ (forward) and $-G$ need not be identical, nor constant. The critical quantity for perfect restoration is the amount of shear strain of the suspension which should be identical in both directions so that the net macroscopic strain is zero. Thus the initial conditions are restored after shearing at an arbitrary rate $G_1(t)$ from 0 to t_1' and then reversing at $-G_2(t)$ from t_1' to t_2' such that

$$\int_0^{t_1'} G_1(t)\,dt - \int_{t_1'}^{t_2'} G_2(t)\,dt = 0$$

As a matter of convenience, and without ambiguity, we generally employ as the measure of shear strain the mean number of particle rotations $t/\overline{T}$ through $\phi_1 = \pm 2\pi$.

A convenient single measure of the distribution of orientation is a mean projected linear dimension, for example, the projection $r_2 = \sin\theta_1 \cos\phi_1$ of unit length of the axis of revolution on the X_2-axis (Fig. 1). The mean $\overline{r_2}$, averaged over all particles is thus given by

$$[8] \qquad \overline{r_2} = \overline{S_{13}} = \int_0^{2\pi} \int_0^{\pi} \sin\theta_1 |\cos\phi_1| p_t(\theta_1, \phi_1)\,d\theta_1\,d\phi_1$$

where S_{13} is defined below.

Integration of [8] yields complicated elliptic functions (7) which we do not reproduce here. Although $\overline{r_2}$ can be used for all $0 < r_e < \infty$, it is best employed only for $r_e > 1$. With oblate spheroids ($r_e < 1$) a mean projected area, for example, the projection $S_{13} = \sin\theta_1 \cos\phi_1$ of unit area of the equatorial cross section on the X_1X_3-plane is more convenient (7). Since the two are identical, i.e., $r_2 = S_{13}$, [8] is thus valid for all r_e's; in this paper we limit considerations to prolate spheroids ($r_e > 1$) and hence employ $\overline{r_2}$ but it should be remembered that the same principles and many equations apply to oblate spheroids ($r_e < 1$ and S_{13}) which, incidentally, are used in some of the experiments to be described (10). For initially random orientations $\overline{r_2} = \overline{S_{13}} = 0.5$, both quantities oscillate at constant amplitude with minima at $t/\overline{T} = 0.25$, 0.75, etc. and maxima at $t/\overline{T} = 0.5$, 1.0, etc.

In practice, however, the oscillations of $p_t(\theta_1,\phi_1)$ are usually damped and the suspension assumes a steady state $p_\infty(\theta_1,\phi_1)$ which is time-independent (3, 6, 7). Although the oscillations are damped, there are certain cases which are completely reversible and thus exhibit perfect memory. Two of these are now considered.

The most obvious cause of reversible damping is the dispersion of r_e, inevitable in real systems, which causes variations in TG and hence mixing of phase angles κ as shear proceeds (7, 21); $p_t(\theta_1,\phi_1)$ is then given by averaging over all r_e's. If the probability distribution of r_e is denoted by $g(r_e)$, the mean projected length is now given by the integral:

$$[9] \qquad \overline{r_{2\sigma}} = \int_0^{\infty} \overline{r_2} g(r_e)\,dr_e$$

where the subscript σ designates the value due to variations in r_e. The oscillations of $\overline{r_{2\sigma}}$ become damped as shear proceeds but can be exactly restored to their forward ($+G$) values when flow is reversed ($G < 0$) (3, 7). Thus the system has perfect memory.

This is demonstrated by the numerical example in Fig. 2, in which the distribution of r_e is assumed to

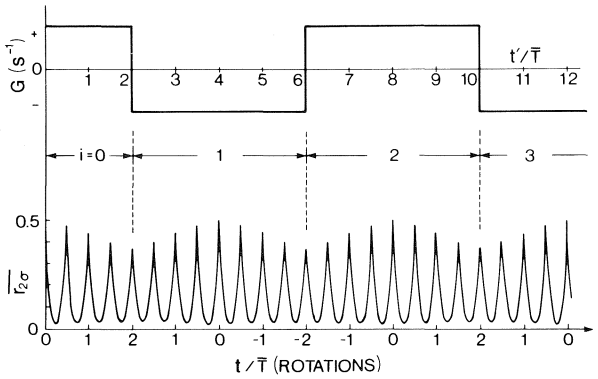

FIG. 2. Perfect memory in an initially isotropic ($r_{2\sigma 0} = 1/2$) suspension of non-interacting prolate spheroids of $\bar{r}_e = 10$ and $\sigma_e = 0.2$ calculated and drawn by computer using [9], for square-wave cycles $\pm G$ with flow reversal at real dimensionless times $t'/\bar{T} = 2, 6, 10$, etc. (upper part) for $i = 3$ reversals after $R_T = 2$ mean particle rotations during each 1/2 cycle about the X_1 (vorticity) axis of flow. The corresponding damped oscillation of $\bar{r}_{2\sigma}$ are shown by the computer calculated and drawn curves in the bottom portion, and show perfect memory even when $R_T, i \to \infty$. Since the time scale is dimensionless, the magnitude of G is immaterial as long as the flow regime is creeping and thermal (Brownian) motion is absent, i.e., $Br_r \to \infty$.

be Gaussian:

$$[10] \qquad g(r_e) = \frac{1}{\sqrt{2\pi}\sigma_e} \exp\left[\frac{-(r_e - \bar{r}_e)^2}{2\sigma_e^2}\right]$$

where σ_e is the standard deviation of r_e from the mean $\bar{r}_e$. Numerical calculations from [8]–[10] were made for an initially isotropic ($\bar{r}_{2\sigma} = 1/2$) dilute suspensions of non-interacting prolate spheroids of $\bar{r}_e = 10$, and $\sigma_e = 0.2$ (numerical values selected to correspond to previous calculations (7)) subjected to square-wave cycles of $\pm G$ in which the initial $G(>0)$ is applied until $t'/\bar{T} = 2$, where t' is the actual time and which corresponds to 4 semi-rotations of the mean-sized particle, and reversed ($G < 0$) until $t'/\bar{T} = 6$, then restored to $G > 0$ and so on indefinitely. The changes in $\bar{r}_{2\sigma}$ are shown by the computer drawn curves at the bottom of Fig. 2. It is seen that the amplitude of the oscillations of $\bar{r}_{2\sigma}$ at constant G decreases until flow is reversed and then increases reproducibly to the initial value at $t/\bar{T} = 0$ (where t now can have either positive or negative values relative to the initial time ($t = 0$) indicated in Fig. 2) or $t'/\bar{T} = 4, 8, 12$, etc. This process can be repeated indefinitely even when the flow is reversed at very large $t/\bar{T}$ where the amplitude of the oscillations becomes vanishingly small. For the more general case in which R_T is the mean number of particle rotations before the flow is reversed and i is the number of flow reversals, we note that even when R_T and/or $i \to \infty$ the system will show perfect memory.

The damped oscillations of $\bar{r}_{2\sigma}$ can be characterized by a relaxation time τ_1 during which the amplitude is reduced to e^{-1} of the undamped oscillation observed in a monodisperse suspension of $r_e = \bar{r}_e$ (i.e., $\sigma_e = 0$). A detailed analysis (7) of such damping, which has been confirmed experimentally (6), for a spread given by [10] yields:

$$[11] \qquad \tau_1 = \frac{(\bar{r}_e^2 + 1)^2}{\sqrt{2}G\sigma_e|\bar{r}_e^2 - 1|} \qquad \text{for } r_e \gtrless 1$$

A second mechanism for reversibly damped oscillations is shear-induced particle interactions: when two or more rigid particles pass in close proximity C and κ of each particle can change reversibly (22, 23). It is difficult to estimate the changes even for 2-body interactions, but an approximate analysis for long slender rods (7), also confirmed experimentally (6), yields a relaxation time τ_2:

$$[12] \qquad \tau_2 = \frac{\ln r_e}{GNl^3}$$

where N is the number density of particles and $l = 2a$, and is valid for $r_e \gg 1$. When both mechanisms operate simultaneously, the effects are reciprocally additive, i.e., $\tau_{net}^{-1} = \tau_1^{-1} + \tau_2^{-1}$ (6, 7). For n-body interactions, where $n > 2$, the analysis is thus far intractable; these interactions should nevertheless be reversible as has been demonstrated experimentally with rigid spheres, rods, and discs (22–24).

A third mechanism is non-uniform shear G such as that occurring in Poiseuille flow, e.g., between fixed parallel plates or through a circular tube, where the variation in G causes reversible mixing of phase angles κ. This should produce reversible damping similar to that considered above but with the added feature of a superimposed reversible pulse of lower frequency. Cox *et al.* discuss this interesting phenomenon elsewhere (25).

Memory Loss

We now consider several causes of partial or complete irreversibility with resulting impairment of memory of orientation distributions which have been studied experimentally; several of these have been examined further by numerical analysis.

(a) Electric Fields

When an external electrical field is superimposed on the suspension as it undergoes shear flow, each particle experiences an electrical torque which introduces an additional term involving the electric field strength E_0 on the right hand side of each of [3*a*, *b*], and hence modification of [4*a*, *b*] (26–28).

Thus when E_0 is applied across the flow, i.e., along the X_2-axis as in Fig. 1, a prolate spheroid experiences an algebraically greater ($d\theta_1/dt$) and smaller ($d\phi_1/dt$)

than given by [3*a*, *b*]; for example $(d\phi_1/dt)$ is decreased when $0 \leq \phi_1 \leq \pi/4$ and increased when $\pi/4 \leq \phi_1 \leq \pi/2$, a pattern which is repeated in alternate quadrants. Integration of the rotational equations yields the analogues of [4] and [5] for a single spheroid of dielectric constant K_1 suspended in a dielectric medium of K_2 (28):

$$[13] \quad \tan\theta_1 = \frac{C_0 r_e}{(r_e^2\cos^2\phi_1 + \sin^2\phi_1 - f r_e \sin 2\phi_1)^{1/2}} \times \exp\left[\frac{-K_2 E_0^2 P(q,r_e)}{\eta} t\right]$$

$$[14] \quad \tan\phi_1 = r_e(1-f^2)^{1/2}\tan\left(\frac{2\pi t}{T_1} + \kappa_1\right) + f r_e$$

and the period of rotation T_1 by

$$[15] \quad T_1 = \frac{2\pi}{G(1-f^2)^{1/2}}(r_e + r_e^{-1})$$

where C_0 (orbit) and κ_1 (phase angle) are integration constants analogous to C and κ in [4] and the dimensionless parameter

$$[16] \quad f = \frac{-K_2 E_0^2 P(q,r_e)(r_e^2+1)}{G\eta r_e}$$

gives the ratio of the electrical to hydrodynamic torques. For the remaining quantities in [13]–[16]: η is the viscosity of the suspending medium, $P(q,r_e)$ a known analytic function of r_e (> 0 for $r_e < 1$, < 0 for $r_e > 1$) and $q = K_1/K_2$ is the dielectric ratio.

When $f^2 < 1$, it follows from [15] that T_1 is real and finite; thus a particle executes complete rotations through $\phi_1 = 2\pi$. However, when $f^2 \geq 1$, corresponding to a supercritical electrical field (26, 28), it assumes a steady calculable orientation. Although all values of f are amenable to analysis, for simplicity we consider only the case of sub-critical electric fields $f^2 < 1$ when a particle rotates in a spiral orbit which drifts towards $\theta_1 = \pi/2$ when $r_e > 1$, and 0 when $r_e < 1$. Since [13]–[16] contain G and E_0^2, the sign of E_0 does not affect the rotations whereas that of G does. Thus applying $\pm E_0$ (and indeed applying an ac field and using the rms E_0 in the equations (28)) regardless of the sign of G causes each particle to drift to the limiting θ_1. As will be seen this causes memory loss.

As in the experiments (10) and in the numerical calculations below we consider only prolate spheroids ($r_e > 1$) at very low concentrations where interactions (especially electrical) are negligible although similar methods can be employed with oblate spheroids ($r_e < 1$). We examine the effect of an electric field which is applied in two ways: first with constant f^2 and then with occasional shocks administered at the point of flow reversal. Since it is so experimentally convenient (10), the particles are initially aligned along the X_2-axis so that $\overline{r_2} = 1$ and $\kappa = 0$. Memory retention (or loss) on reversing flow can then be expressed by the change in $\overline{r_2}$.

(b) Steady Electrical Fields

For continuous application of E_0 at constant f integration of [14], the details of which we omit, yields for $\sigma_e = 0$

$$[17] \quad \overline{r_2} = \left[1 + \left\{r_e(1-f^2)^{1/2}\tan\left(\frac{2\pi t}{T_1} + \kappa_1\right) + f r_e\right\}^2\right]^{-1/2}$$

where $\kappa_1 = \tan^{-1}(-f(1-f^2)^{-1/2})$ which oscillates at constant E_0, G with a period $T_1/2$ between $\overline{r_2} = 0$ and 1. The oscillations are undamped but it should be noted from [17] that they are not symmetrical about the maxima ($\phi_1 = 0, \pi/2$, etc.) or minima ($\phi_1 = \pi/4, 3\pi/4$, etc.); they are, however, identical in alternate 1/2 cycles. Thus, strictly speaking, the waves are not truly reversible except when they coincide at $\overline{r_2} = 1$ or 0 but can be made so by shifting the time scale by $\pm T_1/4$ after each reversal of flow.

In the case we are considering here $p_0(\theta_1,\phi_1) = \delta(\phi_1)\delta(\theta_1 - \pi/2)$ using the Dirac δ-function. For distributions in which there are particles with $0 < \theta_1 < \pi/2$, including initially random orientations $p_0(\theta_1,\phi_1) = \sin\theta_1/4\pi$ (as in Fig. 2), $\overline{r_2}$ undergoes oscillations of frequency $2/T_1$ whose amplitude changes, often increasing, as a result of the drift of all particles towards $\theta_1 = \pi/2$ until a steady state is reached at which the amplitude asymptotically reaches a constant value < 1 (28). Such systems are therefore irreversible and will exhibit memory loss. We do not discuss these examples further here, although we note that the same principles may be applied for numerical computations.

Returning to our case in which $p_0(\pi/2,\phi_1) = \delta(\phi_1)$ but now with $\sigma_e > 0$ as in some of our experiments (10), we calculate $\overline{r_{2\sigma}}$ by means of [9] and [17] for square-wave cycles $\pm G$ as in Fig. 2 but with $0 < f^2 < 1$. Because of the spread in r_e, phase mixing occurs as at $f = 0$ but at an enhanced rate (10), and damped oscillations occur (Fig. 3). The oscillations (now of frequency $2/T_1$) are similar to those in Fig. 2 except that they are not reversible. Thus during the first half cycle ($i = 0$, Fig. 3*a*) the oscillations are damped as in Fig. 2 except that the initial values of $\overline{r_{2\sigma}}$ are different (1/2 in Fig. 2, and 1 in Fig. 3*a*) because of the different initial orientation distributions. On reversing flow, however, the oscillations of

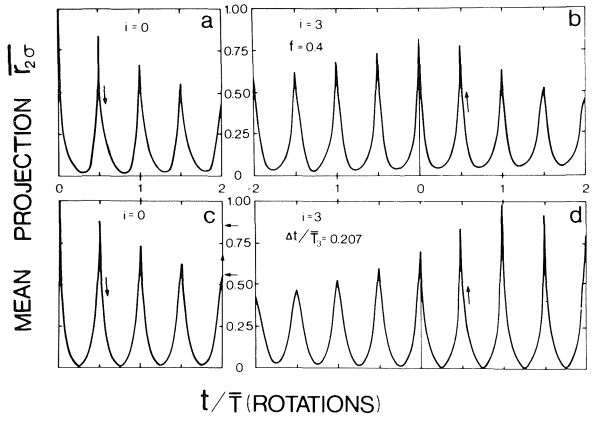

FIG. 3. (*a*) Oscillations at $f = 0.4$ of $\overline{r}_{2\sigma}$ calculated from [9] and [17] for the first-half cycle of the system shown in Fig. 2, but with the particles initially aligned so that $r_{2\sigma 0} = 1$. (*b*) As for (*a*) but during 3rd cycle of G (Fig. 2). Note that at $t/T_1 = 0$ the maximum $\overline{r}_{2\sigma 3}$ has decreased from 1 to 0.822 and that the left-hand portion ($t/T_1 < 0$) is not a mirror image of the right. (*c*) Oscillations of $\overline{r}_{2\sigma}$ at $f = 0$ for the same system as in part (*a*). On stopping flow at $R_T = 2$ and applying a shock at $\Delta t/T_3 = 0.2073$, $\overline{r}_{2\sigma}$ increased from 0.553 to 0.863 (shown by the horizontal arrows on the right ordinate scale). (*d*) Oscillations of $\overline{r}_{2\sigma}$ for the same system as in part (*c*) after $i = 3$ with the application of an electric shock at $\Delta t/T_3 = 0.207$ between each flow reversal. Note that the maximum $\overline{r}_{2\sigma}$ (< 1) in this case occurs at $t/T = +1$.

$\overline{r}_{2\sigma}$ increase in amplitude to reach a maximum < 1 at $t/T_1 = 0$, and then on continuing into negative time yield damped oscillations which are not mirror images of those in positive time. This is illustrated in Fig. 3*b* where the third cycle ($i = 3$) is shown corresponding to $G < 0$ (see Fig. 2, top): the maximum $\overline{r}_{2\sigma} = 0.822$ at $t/T_1 = 0$.

On increasing i the maximum $\overline{r}_{2\sigma}$ continues to change. It should be noted that the asymmetry about the maxima (and minima) $\overline{r}_{2\sigma}$ is generally too small to be discernible in Fig. 3 because of the small values of f.

A convenient measure of the memory retained by the suspension under this mode of cycling is given by (3):

$$[18] \qquad M_i = \frac{\overline{r}_{2\sigma i} - \overline{r}_{2\sigma\infty}}{\overline{r}_{2\sigma 0} - \overline{r}_{2\sigma\infty}}$$

where $\overline{r}_{2\sigma i}$ is the value at $t/T_1 = 0$ after i reversals of G, $\overline{r}_{2\sigma 0}$ is the initial value and $\overline{r}_{2\sigma\infty}$ the equilibrium value. While this definition is useful in the present context it has some serious limitations for general use. It is not a continuous function of time but is defined only for discrete values $(t/T)_i = 0$, and is applicable only when $\overline{r}_{2\infty}$ is time-independent. Thus $M_i = 1$ and 0 correspond respectively to complete retention and complete loss of memory; and $(1 - M_i)$ is the fractional memory loss.

When the suspension assumes a steady value of $\overline{r}_{2\infty}$, as is the case for $\sigma_e \neq 0$ and all values of $0 \leq f^2 < 1$, a steady state orientation is established given by (26):

$$[19] \qquad p_\infty(\phi_1, \pi/2) = \frac{r_e(1 - f^2)^{1/2}}{2\pi(r_e^2 \cos^2\phi_1 + \sin^2\phi_1 - f r_e \sin 2\phi_1)}$$

from which the mean $\overline{r}_{2\sigma\infty}$ can be obtained by the integral:

$$[20] \qquad \overline{r}_{2\sigma\infty} = \int_0^{2\pi} |\cos\phi_1| p_\infty(\phi_1, \pi/2)\, d\phi_1$$

Equation [20], whose solution is $\frac{1}{2}B_0$ given in analytic form by [93]-(7) and numerically in Table II-(7),[2] is used to calculate $\overline{r}_{2\infty}$ for use in [18].

Calculated values of M_i for the system in Fig. 3*a*, *b* are shown in Fig. 4*a* for various values of i at $1 > f^2 > 0$. Because of limitations in defining M_i and the lack of symmetry of ω ($= d\phi_1/dt$) about the X_2-axis (e.g., the maximum ω occurs at $\phi_1 = 0$ for $f = 0$ and $-\pi/8 < \phi_1 < 0$ for $f^2 > 0$ (10)), M_i shows fluctuations at small values of i and then a steady decline. For the largest f ($= 0.6$) M_i decreases to almost 1/2 after the first reversal. In all cases considered in Fig. 4*a*, $M_\infty = 0$; further calculations (not given here) show that this applies for all values of $R_T > 1$, i.e., the memory eventually becomes completely lost.

(c) Electric Shocks

We now consider a square-wave variation of G as in Fig. 2 except that at each reversal the flow is stopped for an interval Δt during which a field of strength E_0 is applied along the X_2-axis thus causing rotation of each particle in accord with (28)

$$[21] \qquad \tan\theta_1 = \frac{C_E}{\sqrt{\sin 2\phi_1}} \exp\left(\frac{\pi t}{T_3}\right)$$

$$[22] \qquad \tan\phi_1 = \exp\left(\frac{2\pi t}{T_3} + \kappa_E\right)$$

where C_E and κ_E are the orbit constant and phase angle, and T_3 is a characteristic time-scale:

$$[23] \qquad T_3 = \frac{\pi\eta}{K_2 E_0^2 |P(q,r_e)|}$$

Since $P(q,r_e) < 0$ for $r_e > 1$, the X_1' axes of prolate spheroids rotate toward the direction of E_0 (i.e., X_2), whereas those of oblate spheroids ($r_e < 1$) for which $P(q,r_e) > 0$ move toward the normal to E_0 (i.e., towards the X_1X_3 plane). After removal of E_0, the flow is then reversed at $f = 0$.

Using the same system as before numerical calculations of $\overline{r}_{2\sigma}$ are shown for $i = 0$ and 3 in Fig. 3*c*, *d*.

[2]Designating eq. [93] and Table II of ref. 7.

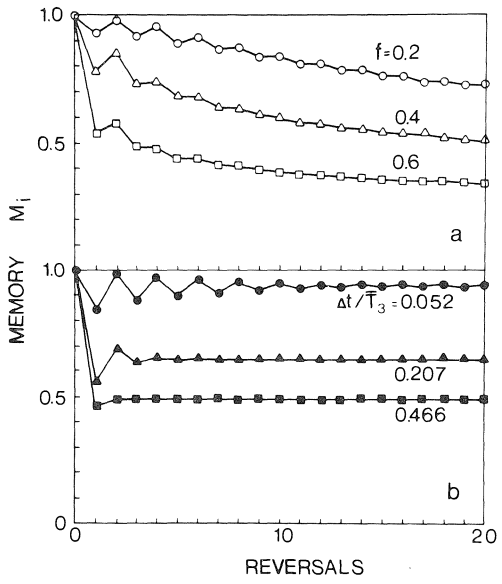

FIG. 4. Variation of M_i with i calculated from [18] for the same system as in Fig. 3*a* for various values of f (steady fields, part *a*) and for various electric shocks of magnitude $\Delta t/T_3$ (part *b*). Note that in (*a*) M_i initially fluctuates and then diminishes steadily until $M_\infty = 0$ (see text), while in (*b*) $M_\infty > 0$, i.e., the memory is not completely lost when shocks are applied although the loss increases from 0 as $\Delta t/T_3$ increases from 0 (the case corresponding to Fig. 2).

When $i = 0$, $\overline{r_2}$ for a particular value of r_e in a suspension of mean $\overline{r_e}$ is, from [4],

$$[24] \quad \overline{r_2} = \left[1 + r_e^2 \tan^2 \left\{\frac{2\pi t(\overline{r_e} + \overline{r_e}^{-1})}{\overline{T}(r_e + r_e^{-1})}\right\}\right]^{1/2}$$

from which $\overline{r_{2\sigma}}$ is calculated by means of [9]. When flow is stopped at $t/\overline{T} = 2$, the κ_E for each r_e is calculated from the final ϕ_1 given by [4*b*] using [22] and setting $t = 0$. When an electric shock corresponding to the dimensionless value $\Delta t/\overline{T}_3 = 0.2073$ is applied, the mean $\overline{r_2}$ for a particular r_e can readily be shown from [21]–[23] to be

$$[25] \quad \overline{r_2} = [1 + \exp(4\pi\Delta t/T_3 + 2\kappa_E)]^{-1/2}$$

which with the aid of [9] is used to calculate $\overline{r_{2\sigma}}$. Applying this shock after $R_T = 2$ causes $\overline{r_{2\sigma}}$ to increase from 0.553 to 0.863 (Fig. 3*c*).

For $i = 1$, the new phase angle κ for each r_e is then obtained using [4] with $t = 0$ from the final orientation given by [22], and during the reverse flow, $\overline{r_2}$ for a given r_e can then be calculated by adding κ to the bracketed argument for $\tan^2$ in [24] from which new equation $\overline{r_{2\sigma}}$ is calculated again with the aid of [9]. This process is continued for successive cycles.

The result for $i = 3$ shown in Fig. 3*d* is typical for all values of $i > 0$. In Fig. 3*d* the amplitude increases to a maximum at $t/T = 1$ (rather than 0) and then decreases as t/T decreases to -2; similar behavior is shown at all odd values of i, with the oscillations diminishing in amplitude as i increases; when i (> 0) is even the maxima occur at $t/T = -1$. M_i is calculated from [18] as before with $\overline{r_{2\sigma\infty}}$ evaluated by means of [19] and [20] at $f = 0$, yielding

$$[26] \quad \overline{r_{2\sigma\infty}} = \frac{1}{\pi\sqrt{\overline{r_e}^2 - 1}} \ln \frac{\overline{r_e} + \sqrt{\overline{r_e}^2 - 1}}{\overline{r_e} - \sqrt{\overline{r_e}^2 - 1}}$$

which gives $\overline{r_{2\sigma\infty}} = 0.1915$ for the system.

The same procedure can be followed for other values of $\Delta t/T_3$, with the results shown in Fig. 4*b* which shows initial fluctuations which then damp out and reach a constant asymptotic value $M_\infty \neq 0$, i.e., the memory is never completely lost although for the values shown the eventual memory loss increases from 0 at $f = 0$ (which is identical to the case considered in Fig. 2 except for the initial orientation $p_0(\phi_1,\theta_1)$) to about 1/2 for $\Delta t/T_3 = 0.466$. If we take the maximum value of $\overline{r_{2\sigma}}$ obtained during each 1/2 cycle of G, which incidentally occurs at $t/T = \pm 1/2$, ± 1, ± 2 for $\Delta t/T_3 = 0.0518$, 0.2073, and 0.4663, respectively, with $\pm$ for odd and even values of i, respectively, and use it instead of $\overline{r_{2\sigma i}}$ at $t/T = 0$ the steady-state memories $M_\infty' = 0.964$, 0.991, and 0.95, respectively, are appreciably greater than those shown in Fig. 4*b*. It is curious that for the three values of $\Delta t/T_3$ employed, the M_∞' is greatest for the intermediate value, a result for which we have no explanation. It is clear from these examples that there are limitations to the definition of M_i in [18] but the results given here show, nevertheless, that applying electric shocks causes only partial memory loss.

(d) Brownian Rotation

If the particles are small enough to exhibit Brownian movement, [3] and [4] are disturbed by superimposed random displacements which are totally irreversible. The effect of Brownian rotation on the rotation in shear is determined by the dimensionless rotary Brenner number Br_r (5)

$$[27] \quad Br_r = G/2D_r$$

where D_r is the rotary diffusion coefficient of a particle about its axis of revolution; Br_r is thus a measure of the ratio of orthokinetic (and reversible) and perikinetic (irreversible) rotations (5).

Translational Brownian motion also influences the spatial distribution by an amount determined by the translational Br_t (5) which is analogous to [27]. However, as already mentioned, these effects are not important in the present context and are not considered further.

The time-dependent orientation distribution function for spheroidal particles with Brownian rotation

is given by the Fokker–Planck equation in the form

$$[28]\quad \frac{\partial p_t(\theta_1,\phi_1)}{\partial t} = -\nabla\cdot\boldsymbol{\omega} p_t(\theta_1,\phi_1) + D_r\nabla^2 p_t(\theta_1,\phi_1)$$

where $\boldsymbol{\omega}$ (which is proportional to G) is the angular velocity vector for the axis of revolution of particles in shear alone. The general solution of [28], which clearly involves Br_r, is not available, but is for several specific cases.

When $Br_r = \infty$, e.g., when $D_r = 0$, the solution for an initially isotropic suspension is [6]. A semi-quantitative solution has been found for small $D_r \neq 0$, i.e. large but finite Br_r, and $r_e \gg 1$ (29) which predicts that the oscillations of $p_t(\theta_1,\phi_1)$ are damped with two successive relaxation modes. In the first, rapid diffusion occurs with a relaxation time $\tau = 0(D_r r_e^4)^{-1}$ in which phase mixing dominates; this is followed by the second mode with $\tau = O(D_r r_e^2)^{-1}$ due to a redistribution of particle orbits C so that a steady state orientation distribution $p_\infty(\theta_1,\phi_1)$ is eventually achieved; in this condition it is clear that all memory would be lost.

The general solution for $p_\infty(\theta_1,\phi_1)$, which is important, e.g., in the theory of streaming double refraction, obtained by setting the right hand side of [28] equal to zero, is given by a series expansion (29). On the other hand Brownian diffusion alone (or $Br_r = 0$) is predicted to cause an exponential decay to random orientations (30) with $\tau = O(6D_r)^{-1}$. Since Brownian rotations are random, they are independent of shear rotations over short time intervals. Therefore when flow is reversed, particle rotation is not retraced exactly, thus causing some loss of memory.

Thus on the basis of these considerations we would expect that at $0 < Br_r < \infty$, M_i would decrease with increasing i and asymptotically approach zero.

We can illustrate the effect by an example, admittedly somewhat artificial, in which in lieu of the electric shocks administered at each flow reversal considered above, the particles are allowed to undergo identical bursts of randomization of the phase angle κ (in a manner similar to the administration of electric shocks described above), corresponding to bursts of rotary Brownian diffusion in the X_2X_3 plane. As before, we take an infinitely dilute suspension with $\overline{r_e} = 10$, $\sigma_e = 0.2$ initially aligned along the X_2 axis and assume that all the particles remain in the orbit $C = \infty$ so that the equilibrium orientation is given by [19] with $f = 0$; the corresponding probability distribution of κ is random (7), i.e.,

$$[29a]\quad p_\infty(\kappa) = 1/2\pi$$

Since all the particles are initially aligned at $\phi_1 = 0$, $\theta_1 = \pi/2$, the initial distribution is

$$[29b]\quad p_0(\kappa) = \delta(\kappa)$$

At the point of flow reversal after R_T mean rotations κ becomes randomized according to a Gaussian distribution $g(\kappa)$ as in [10] except that κ and σ_{κ_1} replace r_e and σ_κ respectively, σ_{κ_1} being the standard deviation from $\overline{\kappa_1}$ $(= 0)$ after the first flow reversal. Flow is then reversed as in Fig. 1 until $t/T = -R_T$ when a similar random burst in κ occurs which when added to the first burst yields $\sigma_{\kappa_2} = \sqrt{2}\sigma_{\kappa_1}$. After i similar reversals $\sigma_{\kappa_i} = \sqrt{i}\sigma_{\kappa_1}$. At any point during flow $\overline{r}_{2\sigma}$ is calculated from the integral

$$[30]\quad \overline{r}_{2\sigma} = \int_0^\infty \int_{-\infty}^\infty \overline{r}_2 g(r_e) g(\kappa_i)\, d\kappa_i\, dr_e$$

Figure 5 shows the numerical values calculated from [30] for the same system as in Fig. 2 but with $\sigma_{\kappa_1} = 0.2$ radian and $R_T = 9$. Similar results, which we do not give here, are obtained for other values of σ_{κ_1} and R_T for the same system and, as might be

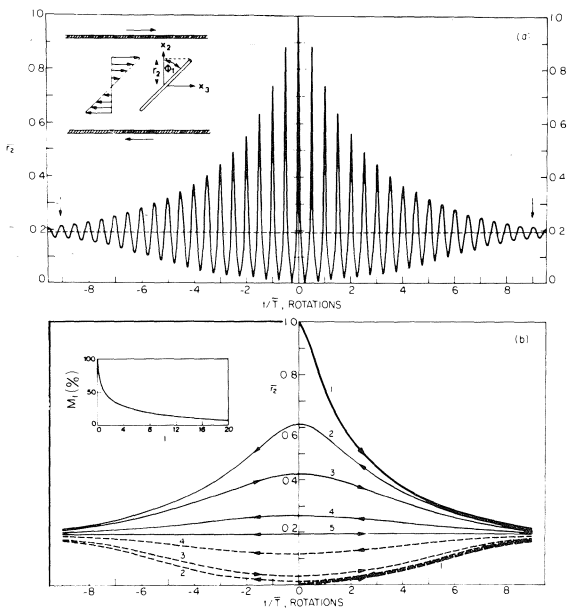

FIG. 5. (*a*) Damped oscillations similar to the same system as in Fig. 2 but for $R_T = 9$ mean particle rotations and $r_{2\sigma 0} = 1$. The broken line indicates the equilibrium value $r_{2\sigma\infty} = 0.1915$ calculated from [26]. (*b*) The envelope of the maxima and minima of the oscillations in $\overline{r_2}$ after random bursts of κ at the points shown by the arrows for $\sigma_{\kappa_1} = 0.2$ radians shown as solid and broken lines respectively obtained by numerical integration of [30]. Curve *1* corresponds to the oscillations shown in part *a*. Curves *2*, *3*, *4* are for the first, fourth, and sixteenth reversals following perturbations of κ at $t/T = \pm 9$, and curve *5* (which is flat) is the equilibrium value $r_{2\sigma\infty}$. The memory of the system M_i vs. i calculated from [18] is shown by the inset and asymptotically approaches 0 when all memory is lost.

expected, show that M_i decreases monotonically (but not exponentially) with i at a rate which increases with increasing σ_{κ_1} and R_T, and asymptotically approaches zero, i.e., all memory is lost as $i \to \infty$.

Thus even though we are not yet able to perform the calculations for continuous 3-dimensional Brownian (random) displacement ($Br_r < \infty$) it is reasonable to conclude that eventually all memory would be destroyed (31). This has been confirmed experimentally (10).

(e) Other Disturbances

Several other disturbances are known to cause memory loss. With the exception of hydrodynamic interactions of spheres and to a limited extent with rods and discs cited below they have not yet been analyzed theoretically. As will be seen in the following paper (10) it is exceedingly difficult to avoid memory impairment in theoretically reversible systems because of unavoidable effects such as buoyancy due to small (but never zero) density differences between particles and suspending medium, convection due to thermal gradients, and most important of all irreversible hydrodynamic interactions.

Hydrodynamic interactions between geometrically perfect rigid spheres, rods, and discs have been shown to be reversible (8, 20, 22, 23) for $Br = \infty$ as would be expected when the reversibility conditions cited in the Introduction are satisfied. Recent careful observations, however, of 2-body interactions in which a pair of spheres (9) or rods (17) approach each other very closely are not strictly reversible as a result of small but inevitable surface asperities and, additionally with rods, sharp edges. Another cause of irreversibility is inertia which introduces a non-linear term into the Navier–Stokes equation and strictly speaking invalidates [3] and [4] at non-zero Reynolds numbers R_e, but at $Br_r = \infty$ have been shown (32) to cause a drift in the orbit constant defined in [4] towards $C = 0, \infty$ for single rigid discs ($r_e < 1$) and rods ($r_e > 1$). The rate and direction of the drift are independent of the sign of G, so that any oscillations in $\overline{r_2}$ would be partially irreversible. This drift has been analyzed theoretically, but only with partial success (32). Similar drifts occur at $R_e = 0$, $Br_r = \infty$ for rigid rods and discs in various non-Newtonian media (33–36). Recently (37) theoretical calculations for long slender rods ($r_e \gg 1$) in a second order fluid have predicted a drift towards $C = 0$, i.e., memory impairment should occur.

Some of these effects are, in addition to those considered earlier, examined experimentally in the following paper (10).

1. F. P. Bretherton. J. Fluid Mech. **14**, 284 (1962).
2. J. C. Slattery. J. Fluid Mech. **19**, 625 (1964).
3. A. Okagawa and S. G. Mason. Science, **181**, 159 (1973).
4. S. G. Mason. Chem. Can. **23**, 29 (1973).
5. S. G. Mason. J. Colloid Interface Sci. **58**, 275 (1977).
6. A. Okagawa and S. G. Mason. J. Colloid Interface Sci. **45**, 330 (1973).
7. A. Okagawa, R. G. Cox, and S. G. Mason. J. Colloid Interface Sci. **45**, 303 (1973).
8. P. A. Arp and S. G. Mason. J. Colloid Interface Sci. **61**, 21 (1977).
9. P. A. Arp and S. G. Mason. J. Colloid Interface Sci. **61**, 44 (1977).
10. G. J. Ennis, A. Okagawa, and S. G. Mason. Can. J. Chem. This issue.
11. J. P. Heller. Am. J. Phys. **28**, 348 (1960).
12. G. I. Taylor. Low Reynolds Number Flow (16 mm cine film), Educational Service Inc., Newton, MA. 1966.
13. H. L. Goldsmith and S. G. Mason. Rheology: theory and applications. Vol. 4. *Edited by* F. R. Eirich. Academic Press, New York. 1967. p. 85.
14. A. Okagawa and S. G. Mason. Can. J. Chem. **55**, 4243 (1977).
15. A. Okagawa, R. G. Cox, and S. G. Mason. J. Chem. Soc. Faraday I, **74**, 1242 (1978).
16. R. G. Cox. The motion of small particles in a moving fluid. Post Graduate Research Laboratory Report No. 25, Pulp and Paper Research Institute of Canada, Pointe Claire, P.Q., Canada. 1970.
17. P. A. Arp and S. G. Mason. J. Colloid Interface Sci. **59**, 378 (1977).
18. G. B. Jeffery. Proc. R. Soc. London, A**102**, 161 (1922).
19. B. J. Trevelyan and S. G. Mason. J. Colloid Sci. **6**, 354 (1951).
20. H. L. Goldsmith and S. G. Mason. J. Fluid Mech. **12**, 88 (1962).
21. G. K. Batchelor. Ann. Rev. Fluid Mech. **6**, 227 (1974).
22. A. Karnis, H. L. Goldsmith, and S. G. Mason. J. Colloid Interface Sci. **22**, 531 (1966).
23. E. Anczurowski, R. G. Cox, and S. G. Mason. J. Colloid Interface Sci. **23**, 547 (1967).
24. C. L. Darabaner and S. G. Mason. Rheol. Acta, **6**, 273 (1967).
25. R. G. Cox, A. Okagawa, and S. G. Mason. J. Colloid Interface Sci. In press.
26. S. T. Demetriades. J. Chem. Phys. **29**, 1054 (1958).
27. R. S. Allan and S. G. Mason. Proc. R. Soc. A**267**, 62 (1962).
28. A. Okagawa, R. G. Cox, and S. G. Mason. J. Colloid Interface Sci. **47**, 536 (1974).
29. E. J. Hinch and L. G. Leal. J. Fluid Mech. **57**, 753 (1973).
30. H. Benoit. Ann. Phys. **12**, 561 (1951).
31. M. Zuzovsky, Z. Priel, and S. G. Mason. To be published.
32. A. Karnis, H. L. Goldsmith, and S. G. Mason. Can. J. Chem. Eng. **44**, 181 (1966).
33. A. Karnis and S. G. Mason. Trans. Soc. Rheol. **10**, 571 (1966).
34. F. Gauthier, H. L. Goldsmith, and S. G. Mason. Rheol. Acta, **10**, 344 (1971).
35. F. Gauthier, H. L. Goldsmith, and S. G. Mason. Trans. Soc. Rheol. **15**, 297 (1971).
36. E. Bartram, H. L. Goldsmith, and S. G. Mason. Rheol. Acta, **14**, 776 (1975).
37. L. G. Leal. J. Fluid Mech. **69**, 305 (1975).

Memory impairment in flowing suspensions. II. Experimental results

G. J. ENNIS, A. OKAGAWA, AND S. G. MASON
Pulp and Paper Research Institute of Canada, Montreal, P.Q., Canada H3A 2A7
and
Department of Chemistry, McGill University, Montreal, P.Q., Canada H3A 2A7

Received April 5, 1978

G. J. ENNIS, A. OKAGAWA, and S. G. MASON. Can. J. Chem. **56**, 2824 (1978).

Experiments on the reversibility of particle orientation distributions in suspensions of nearly monodisperse rigid rods and hardened red blood cells (HRBC) subjected to cyclic shearing are described.

The orientation distributions of initially aligned rods measured by direct observation exhibited a gradual loss in memory as flow was reversed back and forth which was attributed mainly to non-reversible particle interactions. When an electric field was applied continuously during cyclic shear flow, the rate of memory loss was increased. However, if an electrical shock was applied momentarily between each reversal of flow, the suspension maintained some memory. These results are generally in agreement with the theory presented in the preceding paper.

With suspensions of HRBC, the particles were initially randomly oriented and the light transmittance across the planes of shear was used to measure changes in orientation distribution. Since HRBC are small enough to exhibit appreciable rotary Brownian motion, memory loss was inevitable and increased with the duration of each shear cycle and the cell concentration.

Memory loss was also observed for rods and HRBC in non-Newtonian media and was attributed to drift in the rotational orbit constants of the particles.

G. J. ENNIS, A. OKAGAWA et S. G. MASON. Can. J. Chem. **56**, 2824 (1978).

On décrit certaines expériences portant sur la réversibilité des distributions d'orientations de particules dans des suspensions de globules rouges durcis et de bâtonnets rigides presque monodispersés, qu'on soumet alternativement à des cisaillements dans des sens opposés.

On a mesuré par observation directe les distributions d'orientations de bâtonnets initialement alignés et l'on a noté qu'un changement alternatif du sens de l'écoulement provoque une perte graduelle de mémoire, qu'on a principalement attribuée à des interactions irréversibles entre les particules. Si un champs électrique était maintenu durant l'écoulement cisaillé alternatif, le système perdrait la mémoire plus rapidement. Cependant, si la suspension recevait une secousse électrique momentanée entre chaque changement de sens de l'écoulement, elle conserverait la mémoire dans une certaine mesure. En général, ces résultats sont en accord avec la théorie exposée dans le mémoire précédent.

Dans les suspensions de globules rouges durcis, les particules étaient initialement orientées au hasard et la lumière transmise au travers des plans de cisaillement servait à mesurer les variations dans la distribution d'orientations. Etant donné que les globules sont assez petits pour donner lieu à un mouvement Brownien rotationnel appréciable, la perte de mémoire était inévitable et elle s'accentuait avec la durée de chaque cycle de cisaillement et la concentration des globules.

Dans les milieux non-Newtoniens, les bâtonnets et les globules subissaient une perte de mémoire qu'on a attribuée à la dérive des constantes rotationnelles orbitales des particules.

[Traduit par le journal]

Introduction

In the preceding paper (1) we considered some theoretical aspects of memory loss in dilute suspensions of spheroids of nearly uniform size subjected to alternating cycles of simple shear flow. In this paper we present some experimental tests of the theory using two different methods: one lengthy and tedious, based on microscopic measurements of the mean orientation distributions of individual rods (used to model prolate spheroids, $r_e > 1$ (2) at $Br_r = \infty$[1]) and the other rapid and simple using macroscopic measurements of the turbidity of hardened red blood cells (HRBC) (used to model oblate spheroids, $r_e < 1$, $0 < Br_r < \infty$ (3)). The rods were initially aligned in one direction ($\theta_1 = 90°$ and $\phi_1 = 0°$ or $p_0(\theta_1,\phi_1) = \delta(\theta_1 - \pi/2)\delta\phi_1$ and $\kappa = 0$) by applying an external electric field along the X_2-axis (Fig.

[1]Most of the symbols used in this paper are the same as in the preceding paper (1) and will generally be used here without further definition.

Can. J. Chem. Downloaded from www.nrcresearchpress.com by 210.87.254.40 on 09/05/12
For personal use only.

Can. J. Chem. Downloaded from www.nrcresearchpress.com by 210.87.254.40 on 09/05/12
For personal use only.

1-(1))[2] prior to applying cyclic shear flow. From the measurements of θ_1 and ϕ_1 of each particle at $Br_r = \infty$ at any given time t, the mean value $\overline{r_2}$ was determined and used as a single measure of orientation (4, 5); thus $\overline{r_2} = 1, 1/2, 0$ correspond respectively to complete alignment along the X_2-axis (Fig. 1-(1)), three-dimensional random orientation, and complete orientation in the direction of flow (i.e., the X_3-axis). In general $\overline{r_2}$ shows damped oscillations when the suspension is first subjected to shear, which are restored with varying degrees of perfection when the shear is reversed. The change of particle orientation distribution on restoring the initially zero shear strain (1) is taken as the memory loss, a convenient, although not perfect, definition of which is $(1 - M_i)$, where [18]-(1):

$$[1] \qquad M_i = \frac{\overline{r_{2\sigma i}} - \overline{r_{2\sigma\infty}}}{\overline{r_{2\sigma 0}} - \overline{r_{2\sigma\infty}}}$$

The effect of an electric field on M_i of rods was studied by subjecting them to combined shear and sinusoidal electric fields ($f^2 < 1$ (1)) and to shock, i.e., an electric field E_0 (at $G = 0$) for an interval Δt between each flow reversal. The rods were also suspended in an elastico-viscous solution and subjected to cyclic shear flow, causing the orbits C to drift and hence, as expected, memory loss.

With HRBC which scatter light, or silvered HRBC (AgHRBC) which absorb it, an initially random orientation was obtained due to Brownian rotation at $Br_r = 0$ and the optical transmittance at $Br_r \geq 0$ along the X_2-axis was used as a single measure of orientation distribution (6, 7). The transmittance T' (not to be confused with the periods T, T_1, T_3 defined in ref. 1 and also used later) decreases with increase in the optical scattering cross section C_{sca} for scattering particles (HRBC) and the geometrical cross section S for absorbing particles (AgHRBC) (7); for spheroids (and discs) C_{sca}, S pass through maxima when the light beam impinges on the particle when it is edge-on and face-on respectively. Since only relative changes in T' were measured, the memory retained was calculated from the maxima for HRBC or of the minima for AgHRBC using the analogue of [1]:

$$[2] \qquad M_i' = \frac{T_i' - T_\infty'}{T_0' - T_\infty'}$$

where T_i' is the maximum or minimum transmittance at $t/\overline{T} = 0$ after i flow reversals (Fig. 2-(1)) and T_∞' is the equilibrium value after the amplitude of the oscillations approach zero.

[2]Designating Fig. 1 of ref. 1; a similar convention is adopted for designating numbered equations for referenced papers.

Various effects on M_i' were examined, e.g., by changing the medium viscosity, particle concentration, the velocity gradient G, and by using a non-Newtonian medium. As will be seen, the experimental findings were, with one unaccountable exception, in qualitative agreement with the theory (1).

Before presenting the results, it should be pointed out that the quantities M_i and M_i' are expressed as 'point' values at $t/T = 0$ and not continuous functions of time. Therefore in the graphical displays of M_i, M_i', vs. t, no attempts were made to draw best fit lines for any given set of experimental points; lines were drawn merely to connect points and such illustrations are really histograms although we have not drawn them in conventional histogram form.

Experimental Materials

(a) Suspensions of Rods

Electrically conductive rods (so chosen to facilitate electrical alignment and to simplify the electrical calculations (8, 9)) as uniform as possible in length (900 μm) were prepared by microtoming A1-coated Nylon monofilaments (175 μm diameter) embedded in blocks of wax (Tissuemat, Fisher, mp = 67°C) thus obtaining rods of mean axis ratio $\overline{r_p} = 5.14$ with a nearly Gaussian distribution of standard deviation $\sigma_p = 0.11$ (2.1%). The equivalent prolate spheroidal axis ratios r_e (2) were calculated from the measured period of rotation T at known G using [5]-(1); for 60 particles $\overline{r_e} = 3.95$ and $\overline{\sigma_e} = 0.15$ (3.8%). The rods were suspended in two kinds of fluid at concentrations $N = 20\ ml^{-1}$ (volume fraction $c = 0.43 \times 10^{-3}$). One medium was oxidized castor oil which proved to have a Newtonian viscosity $\eta = 4.90$ Pa s up to $G = 100\ s^{-1}$; the other was an elastico-viscous solution of 3% polyisobutylene (PIB) in decalin (10). To avoid particle sedimentation over periods of several days tetrabromoethane was added to the media to match the particle and fluid densities.

(b) Suspensions of HRBC

The cells were prepared from fresh human blood erythrocytes by fixing them with glutaraldehyde by the method of Goldsmith and Marlow (3) slightly modified (11) to minimize cell destruction. They were rigid biconcave discs of mean diameter 5.0 μm and maximum thickness 1.3 μm with $\overline{r_p} = 0.26$ and $\sigma_p = 0.014$ (5.4%). The HRBC were also rendered opaque (and light absorbing) by silvering their surfaces in an aqueous solution of $AgNO_3$ and NH_4OH (11) following a standard procedure for silvering cellulose fibers (12). The AgHRBC thus obtained were slightly larger (average diameter 5.6 μm, thickness 1.8 μm) with $\overline{r_p} = 0.31$ and $\sigma_p = 0.027$ (8.7%) measured from scanning electron micrographs, and $\overline{r_e} = 0.49$ from measured values of TG (1). Both the HRBC and AgHRBC were suspended in various concentrations of aqueous glycerol (Newtonian) to which $SnCl_4$ was added to match densities. Concentrations were determined by counting cells using a Spencer hemacytometer (Fisher) and ranged from $N = (0.4 \text{ to } 1.4) \times 10^8$ cells/cm^3 corresponding to volume fractions $c = (2 \text{ to } 3.5) \times 10^{-3}$.

As a non-Newtonian elastico-viscous medium, an aqueous polyacrylamide (PAA) solution (2.5% wt./vol.) was used (10).

The properties of all the suspensions used are summarized in Table 1.

TABLE 1. Description of suspensions, temperature = 21.0 ± 0.5°C

	Rods		Discs		
	A1-coated nylon		HRBC	AgHRBC	
d (μm)	175		5.0	5.6	
l (μm)	900		1.3	1.76	
r_p	5.14(3.1)[a]		0.26	0.31	
r_e[b]	3.95(3.8)[a]		0.45	0.49	
Medium	Pale 4 oil[c] + $C_2H_2Br_4$	3% PIB[d] in decalin	67% glycerine in H_2O	75% glycerine in H_2O	2.5% PAA[e] in H_2O
η (Pa s)[f]	4.92	0.32	0.077	0.125	0.149
N (ml^{-1})	20		1.38×10^{8}	0.46×10^{8} to 0.54×10^{8}	0.36×10^{8}
c	4.33×10^{-2}		3.52×10^{-3}	2.00×10^{-3} to 2.34×10^{-3}	1.56×10^{-3}
D_r (s^{-1})[g]			2.6×10^{-4}	1.56×10^{-4}	
Br_r	∞	—	3×10^{3}	3.5×10^{3} to 1×10^{4}	4×10^{3}[h] to 12×10^{3}

[a]Standard deviation (%) from means in parentheses.
[b]From [5]-(1) using T' from period of oscillation of rods and of $T' = T/2$ for discs.
[c]Oxidized castor oil, Frank E. Dempsey and Sons Ltd.
[d]Polyisobutylene, Vistanex, Enjay Co.
[e]Polyacrylamide, Cyanamer P250, American Cyanamid Co.
[f]Extrapolated zero-shear viscosity.
[g]Calculated from [32]-(7).
[h]Based on η at $G = 0$ (10).

Experimental Methods

(a) Direct Observations

The experiments on rods were performed in a Couette apparatus (a modified version of that described in (13)) which provides simple shear flow by means of two counter-rotating concentric metal cylinders. The outer cylinder (diameter 30.47 cm) is electrically insulated from the inner one (diameter 26.71 cm and grounded) so that an electric field can be applied across the annulus. The suspensions of rods in the annulus were floated on a much less viscous and insoluble layer of a denser liquid (e.g., glycerine) to avoid end effects which would distort the flow field (8). Applying an electric field (1.06 kV/cm at 60 Hz) for a few minutes across the cylinders caused the rods to align close to the direction of the field, i.e., along the X_2-axis (Fig. 1-(1)), so that $\theta_1 = 90°$ and $\phi_1 = 0°$ approx.; there was no evidence of electrical field distortion by the interface between the two liquid layers. After removing the electric field, a shear flow was applied (with or without a superimposed 60 Hz external electric field E_0 along the X_2-axis) and photographs of the rods were taken at regular time intervals of 1 to 5 s^{-1} along the X_1-axis using an automatic camera (Robot motor recorder 36 ME) equipped with a Tessovar lens (Carl Zeiss). The time of each frame was recorded from a digital clock through a separate lens on the camera on the upper right corner of each photographic frame. The two quantities, the projected length l_{23} on the X_2X_3-plane and the angle ϕ_1 of each rod were measured from the photographs which were projected frame-by-frame on an analyzing table. The angle ϕ_1 of each rod was calculated from the geometrical relationship $\sin\phi_1 = l_{23}/\bar{l}$ where $\bar{l}$ is the mean rod length; since σ_p was small, using $\bar{l}$ instead of l of each rod introduced a negligible error in determining θ_1. The orientations were also described by the projected length $r_2 = \sin\theta_1 \cos\phi_1$ along the X_2-axis (1, 4, 5). To obtain the mean projected length $\bar{r}_2$ of 100 to 200 rods, it was necessary to photograph several different fields of view since each frame contained only about 50 rods.

(b) Rheo-optical Measurements

The optical transmittance T' of the HRBC and AgHRBC suspensions was measured in a second Couette apparatus (14) equipped with transparent concentric cylinders (of outer and inner radii 5.455 and 5.725 cm so that the gap width = 0.270 cm) by passing white light from a tungsten microscope illuminator with an ir heat filter from the inside cylinder through the annulus, i.e., along the X_2-axis of the flow field (Fig. 1-(1)). The transmitted light was measured by a silicon photocell through a Tessovar lens (Carl Zeiss) focussed from the outside cylinder on the suspension so as to cover a 1 cm^2 area of the light beam. The photocell output was displayed on a power meter (Coherent Radiation, Model 212) and recorded through an amplifier on a chart recorder (Keithley, Model 370). To eliminate end effects, the suspensions were floated in a Freon substrate. A shear rate $G = \pm0.5$ to 3 s^{-1} was applied by rotating the inner cylinder with the outer one stationary. In both sets of experiments (*a*) and (*b*) the ratios of particle

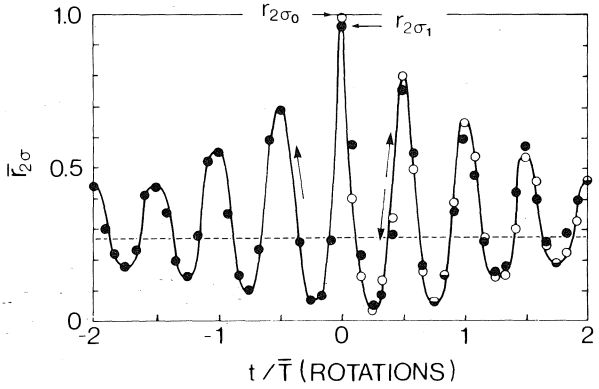

FIG. 1. Oscillations in $\bar{r}_{2\sigma}$ of rods ($\bar{r}_e = 3.95$, $\bar{\sigma}_e = 0.15$) showing nearly perfect memory of particle orientations after reversing the flow at $t/\bar{T} = 2$. Values for forward flow ($G > 0$, open circles) are nearly the same as for $G < 0$, and the damped oscillations at $t \leq 0$ are nearly the mirror images of those at $t \geq 0$. Note that on returning to $t = 0$ after the first flow reversal $i = 1$, $\bar{r}_{2\sigma 0} = 0.997$ and $\bar{r}_{2\sigma 1} = 0.964$ (indicated by the arrows) there is a slight loss of memory during the first cycle. The equilibrium value $\bar{r}_{2\sigma\infty} = 0.270$ for $p(C) = \delta(\infty)$ calculated from [20]-(1) is shown by the horizontal dashed line, so that in this experiment $M_1 = 0.955$. $G = \pm0.44$ s^{-1}, $N = 20$ ml^{-1}, and $E_0 = 0$.

Can. J. Chem. Downloaded from www.nrcresearchpress.com by 210.87.254.40 on 09/05/12
For personal use only.

Can. J. Chem. Downloaded from www.nrcresearchpress.com by 210.87.254.40 on 09/05/12
For personal use only.

dimensions to gap widths were such that wall effects were negligible (26).

Results and Discussion

(a) Rods

(i) Simple Shear (f = 0; $Br_r = \infty$)

In simple shear ($+G$) the rods, initially aligned very closely to $\phi_1 = 0°$, $\theta_1 = 90°$, i.e., with $\overline{r_{2\sigma 0}} = 1$, $C = \infty$, $\kappa = 0$ (1, 5), exhibited the damped oscillations of $\overline{r_2}$ as expected (1, 4, 5) with θ_1 remaining close to $\pi/2$ (i.e., $C = \infty$) over several particle rotations. As shown in Fig. 1, on reversing to $-G$ after $R_T = 2$ mean particle rotations, the oscillations were almost perfectly restored, with $\overline{r_{2\sigma 1}}$ reaching 0.96. On continuing the reversed flow during $i = 1$ to $t/\overline{T} < 0$, i.e., into 'negative' time, the damped oscillations were approximately the mirror images of those at $t \geq 0$. As the flow was cycled back and forth between $R_T = \pm 2$ (see Fig. 2-(1)), the amplitudes of these oscillations gradually diminished, but were still clearly discernible at $i > 15$. However, eventually they disappeared until a constant $\overline{r_{2\sigma\infty}}$ was reached when the memory of the initial state was completely lost.

The spread in orientation at $t/\overline{T} = 0$ after various values of the reversal number i for this series of experiments is illustrated by the integral distributions $P(\phi_1)$ in Fig. 2. Initially all of the rods were aligned in the region of $\phi_1 = \pm 10°$, but after only 3 flow reversals this was reduced to less than 40%. As G was cycled back and forth, θ_1 remained constant at $\pi/2$ (i.e., $C = \infty$) and $P(\phi_1)$ went through that corresponding to random orientations and approached the steady state orientation distribution $P_\infty(\phi)$ calculated from the integration of the probability distribution $P_\infty(\phi_1)$ ([19]-(1) for $f = 0$): which yields

$$[3] \qquad P_\infty(\phi_1) = \int_0^{\phi_1} p_\infty(\phi_1)\, d\phi_1 = \frac{1}{2\pi} \tan^{-1}\left(\frac{\tan \phi_1}{r_e}\right)$$

Values of M_i of the system calculated by means of [1] with $\overline{r_{2\sigma 0}} = 0.997$ (measured) and $\overline{r_{2\sigma 0}} = 0.270$ (calculated from [20]-(1)) are shown in Fig. 3 for cyclic flows of $R_T = 1$, 2, and 4 rotations from $t/T = 0$. It is seen that the memory of the suspension gradually faded. Thus, for example, the memory loss $(1 - M_i)$ after 7 flow reversals was 0.12, 0.26, and 0.52 for $R_T = 1$, 2, and 4 respectively, i.e., the memory loss was roughly doubled with each doubling of R_T. This suggests that under these conditions M_i was determined by the total real elapsed time of shear flow whether or not the flow was reversed. However, when M_i was plotted against real time t'/T (Fig. 3, bottom) the points did not fall on a single line.

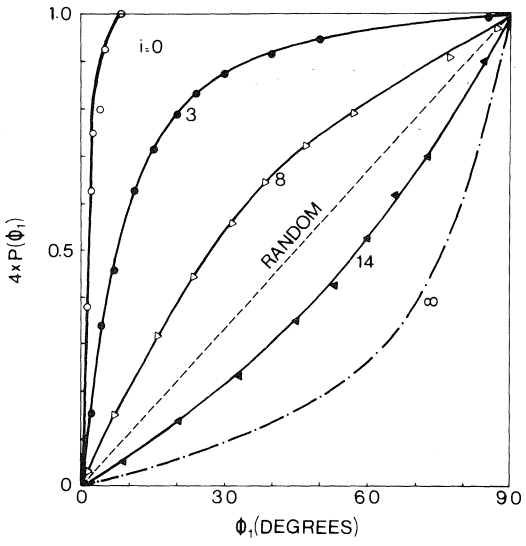

FIG. 2. Integral distributions of particle orientations $P(\phi_1)$, the fraction of particles oriented above ϕ_1, for the same experiment as in Fig. 1 at $t/\overline{T} = 0$ for various values of i showing the change from initial to final alignment, the measured values being shown as points. The straight (broken) line represents isotropic (or random) values of ϕ_1, and that for $i = \infty$ is calculated from [3]. Since the distributions are identical in all quadrants between $0 < \phi_1 < 2\pi$ the range of ϕ_1 in the graph is restricted to the first quadrant.

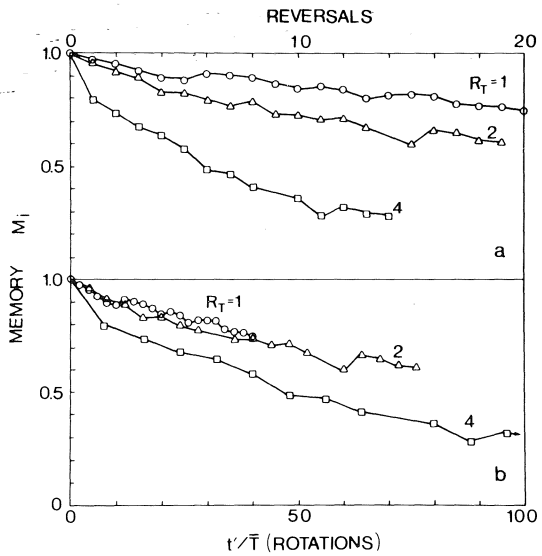

FIG. 3. Change in M_i of rods ($\overline{r_e} = 3.95$, $N = 20\ ml^{-1}$) calculated from [1] from the measured $\overline{r_2}$ at $t/\overline{T} = 0$ when the flow ($G = \pm 0.44\ s^{-1}$) is reversed at $R_T = 1$ (open circles), 2 (open triangles), and 4 (open squares) are plotted against the number of flow reversals i (upper part) and against $t'/\overline{T}$ (lower part). M_i decreased nearly monotonically with i at rates which increased with R_T. When plotted against total time elapsed $t'/\overline{T}$, the points did not fall onto a single line.

Can. J. Chem. Downloaded from www.nrcresearchpress.com by 210.87.254.40 on 09/05/12
For personal use only.

Possible mechanisms for memory loss in these experiments have been discussed in the preceding paper (1). For particles of the dimensions used in these experiments the interparticle forces (which would lead to irreversibility) were negligible compared to the reversible hydrodynamic forces (15), and $D_r \simeq 10^{-13}$ s^{-1} which would lead to a calculated (1) diffusional relaxation time of 10^6 years whereas the longest experiment in this series took only 100 min. Thermal convection due to fluctuations in room temperature was examined by observing the suspension at rest in the apparatus. The measured $\overline{r_2}$ showed no appreciable change from $\overline{r_2} = 0.997$ over 1 h which corresponds to 60 particle rotations at the G employed in experiments, and 2.5 h later was still $\overline{r_2} = 0.93$. Therefore, these three mechanisms for memory loss clearly do not explain these observations.

As already mentioned the particle orbits did not change appreciably from $C = \infty$ during the experiments, so that the memory loss observed was due entirely to the change in the probability distribution $p_i(\kappa)$ of phase angles κ. It is interesting to compare the observations of memory impairment due to disturbances in κ with the calculations given in ref. 1 in which M_i decreased monotonically (Fig. 5*b*-(1)) with i in a manner similar to that shown in Fig. 3.

From earlier studies of shear-induced interactions between rigid particles in the creeping flow regime, it was concluded that they were reversible (2, 16–18). More recently (19), however, careful examination of 2-body interactions of rods showed that this was not exactly true for very close approach presumably as a result of surface asperities over the whole surface and sharp edges at the ends of the rods. Calculations, following ref. 17, show that the number of close collisions was about 10 per flow cycle of $R_T = \pm 2$ for the 150 particles of the mean populations taken for each measurement of $\overline{r_{2\sigma}}$ in this series of experiments so that, for example, for $i = 20$ (Fig. 3) each particle could have undergone at least 1 close collision each of which would cause a substantial change in κ and hence $p(\kappa)$ of the assembly.

We conclude, therefore, that the memory losses in these experiments were due to interactions, mostly 2-body (2), due to imperfections in the surfaces of the particles. Reducing surface roughness of the rods to molecular dimensions and eliminating any sharp edges (e.g., rounding the ends) should eliminate the losses (15); this, however, would be very difficult in practice for systems in which $Br_r = \infty$ which generally require that the particles be large.

(ii) Effects of Electric Fields

(1) Steady Electric Fields

When a cyclic shear of $G = \pm 0.44$ s^{-1} and an ac electric field of rms $E_0 = 280$ V/cm corresponding to $f = 0.024$ were applied to an initially aligned suspension of rods ($\overline{r_e} = 3.95$), the $\overline{r_2}$ at $i = 0$ showed damped oscillations similar to those shown in Fig. 1. Since $f = 0.024$ corresponds to an increase of only 0.03% in the period of rotation given by [15]-(1)[3] over $f = 0$, the effect of the electric field was small. However, when the flow was reversed, the recovery of the initial $\overline{r_{2\sigma}}$ was less than that at $f = 0$ and the difference increased with the number of cycles. This is shown in Fig. 4 where for $R_T = 1$ and 2 are compared with $f = 0$. It is seen that memory impairment was increased by applying the electric field, and that at corresponding values of i, the losses $(1 - M_i)$ for $R_T = 2$ were nearly double those for $R_T = 1$.

From the theory given in the preceding paper (1), the calculated values M_i (Fig. 4*a*-(1)) showed practically no change up to 10 reversals indicating nearly perfect memory at this small value of f; as f increases the theory predicts increasing memory loss. Clearly there is a discrepancy between theory and experiment, much larger than for $f = 0$; again we attribute it to particle interactions. In the theory for $f > 0$ both hydrodynamic and electric interactions were neglected. Theoretically hydrodynamic interactions should not cause any memory loss (1), but as shown above they do in practice. Electric interactions resulting from intense Coulombic attraction (and in certain cases repulsion) between dipoles induced on the particles (20–22) cause cumulative memory loss even under conditions when none occurs at $f = 0$. The theory of memory loss taking interactions into account for $f > 0$ has not yet been worked out, however, and will prove to be complicated except possibly for dilute suspensions of electrically conducting spheres where the equations describing two-body interactions have been derived (21) and confirmed experimentally (22). However, it is safe to predict that the memory loss at $1 > f^2 > 0$ (1) will increase with increasing f, r_e, and c and that eventually $M_\infty = 0$ (1).

(2) Electric Shocks

In these experiments with the rods, the principles of which are given in ref. 1, electric shocks $E_0 = 2$ kV/cm corresponding to $T_3 = 82.7$ s ([23]-(1)) were applied at each flow reversal.

With the initially aligned rods damped oscillations

[3]Strictly speaking, for non-spheroidal particles such as the rods of particle axis ratio $r_p = 5.14$ used, we should employ r_{eH} and r_{eE} (with $r_{eE} > r_p > r_{eH}$), the hydrodynamically and electrically equivalent spheroidal axis ratios (9), in [13]-(1) and related equations. In the calculations presented here we do not distinguish between the two r_e's and, in effect, simply use $r_{eH} = r_{eE} = r_e$ where r_e is determined from the period of rotation T at $E_0 = 0$ using [5]-(1).

Can. J. Chem. Downloaded from www.nrcresearchpress.com by 210.87.254.40 on 09/05/12
For personal use only.

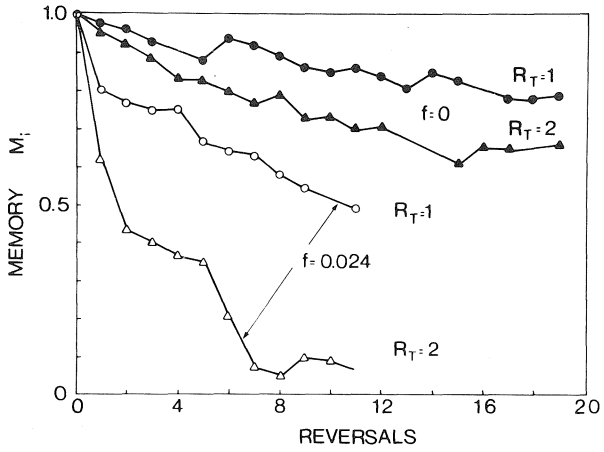

FIG. 4. Change in M_i of the same suspension as in Fig. 3 at $f = 0$ (solid points) and at $f = 0.024$ (open points) when flow is reversed at $R_T = 1$ (circles) and $R_T = 2$ (triangles). As predicted (1) there is an enhanced memory loss in the presence of a steady electric field.

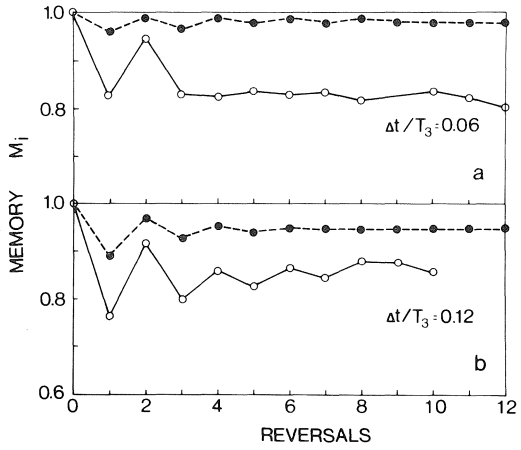

FIG. 5. Change in M_i for the same suspension as Fig. 1 when subjected to electric shocks $\Delta t/T_3 = 0.06$ (part *a*) and 0.12 (part *b*) when the flow was stopped after $R_T = 1$ for an interval Δt before resuming flow in the reverse direction. The broken lines correspond to the theory developed in ref. 1 for suspensions without hydrodynamic or electric interactions of the rods.

of $\overline{r_2}$ at $i = 0$ were similar to those shown in Fig. 1. When the flow was stopped at $R_T = 1$ the E_0 applied for an interval Δt, each rod rotated toward the X_2-axis (8, 9) so that $\overline{r_{2\sigma}}$ increased from 0.592 to 0.810 after $\Delta t = 10$ s in qualitative accord with [69*b*]-(8). Upon reversing flow, the amplitude of the oscillation increased first to $\overline{r_{2\sigma}} = 0.965$ at $t/\overline{T} = 0.5$, then decreased to yield $\overline{r_{2\sigma 1}} = 0.837$ at $t/\overline{T} = 0$ similarly to Fig. 3*d*-(1) corresponding to a memory loss $(1 - M_1) = 0.24$. Changes of M_i for $R_T = 1$ with 5 and 10 s electric bursts, corresponding to $\Delta t/T_3 = 0.0605$ and 0.1209 are shown in Fig. 5. It is seen that initially M_i fluctuated with increasing i but then appeared to approach steady non-zero value. This behavior differs considerably from that observed at $f = 0$ and 0.024 (Fig. 4) where $M_\infty = 0$. Theoretical values of M_i calculated (1) for these experiments are shown by broken lines in Fig. 5 with M_i showing initial fluctuations and then approaching constant non-zero values considerably higher than those observed experimentally. Although the absolute values of M_i from theory and the experiments differ considerably, the general variations of M_i with i and $\Delta t/T_3$ parallel one another. It is safe to conclude, however, that just as with $f^2 \geq 0$ discussed earlier, the differences can be attributed to irreversible hydrodynamic and electric interactions between the rods used.

(iii) Elastico-viscous Medium

In PIB/decalin, damped oscillations of $\overline{r_{2\sigma}}$ similar to those in Fig. 1 were observed, but as expected (1) with a much higher rate of damping. Values of M_i calculated from measured $\overline{r_{2\sigma}}$ at $t/\overline{T}$ for $R_T = 1$, 2, and 3 are shown in Fig. 6. To calculate M_i from [1],

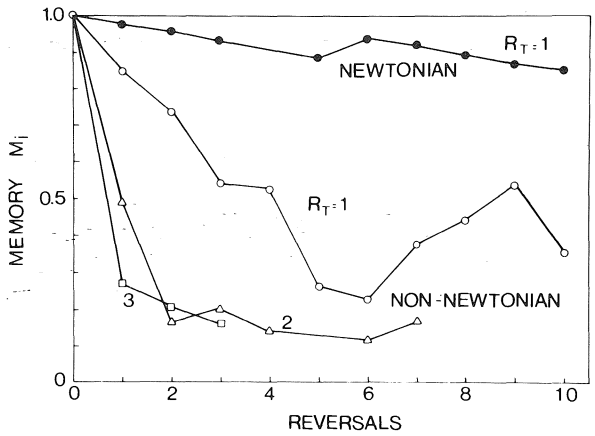

FIG. 6. M_i of rods ($\overline{r_e} = 3.95$, $N = 20\ \text{ml}^{-1}$) suspended in 3% PIB/decalin solution at $R_T = 1$ (open circles), 2 (open triangles), and 3 (open squares) compared with the results for the Newtonian fluid (Fig. 3*a*) at $R_T = 1$ (closed circles). No explanation can be offered for the wide fluctuations at $R_T = 1$ in the non-Newtonian fluid.

$\overline{r_{2\sigma\infty}} = 0.138$ (somewhat less than calculated for the Newtonian medium, Fig. 1) obtained from the measured steady state orientation distribution achieved after several hundred particle rotations in a steady non-cyclic shear was used. It is seen from Fig. 6 that M_i decreased more rapidly than with the Newtonian medium. For $R_T = 1$, M_i after $i = 5$ fluctuated widely for no apparent reason. For $R_T = 2$ and 3, M_i decreased rapidly up to $i = 2$, then slowly decreased over the range of i. The memory loss observed in these experiments can be attributed to two causes: orbital drift and particle interaction, both

Can. J. Chem. Downloaded from www.nrcresearchpress.com by 210.87.254.40 on 09/05/12
For personal use only.

irreversible. It has been shown that a single rod in the medium used here at $f = 0$ and low G rotated with respect to ϕ_1 as in a Newtonian fluid but showed a drift of orbit constant toward $C = 0$, i.e., $\theta_1 = 0$ and $r_2 = 0$ (23). Since the rate and direction of drift of C were independent of the flow direction, $\overline{r}_{2\sigma}$ of the suspension continued to decrease gradually to the steady value, causing M_i to decrease as the rods drifted toward $C = 0$. We believe that the irreversible interactions are primarily the consequence of irreversible drift in C and only secondarily due to imperfections in the rods noted earlier (17). Thus, combining the orbit drift and interaction effects caused the system to lose memory much more rapidly than in Newtonian fluids (Fig. 6).

(b) Red Blood Cells

(i) Simple Shear ($Br_r < \infty$)

Unlike the experiments with the rods considered above, here the particles had sufficient rotary Brownian motion so that the initial orientations were random, i.e., $\overline{r}_{2\sigma 0} = 1/2$. Also the measurements of turbidity T' were macroscopic (on a large population of cells) and rapid, rather than microscopic (on a large number of individuals rods) and tedious.

Typical examples of the variation of T' for HRBC and AgHRBC for cyclic shear flows and at $G = 0$ ($Br_r = 0$) are shown in Fig. 7.

For HRBC (Fig. 7*a*) T' initially increased rapidly to a maximum when shear was applied and was followed by damped oscillations qualitatively similar to Fig. 1. This is in accord with the rheoptical theory of light scattering by oblate spheroids (7) which

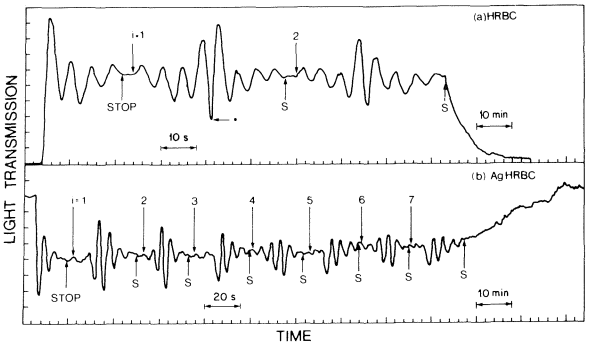

FIG. 7. Typical recorder charts of the light transmittance T' (arbitrary linear scale) for aqueous glycerine suspensions of HRBC (part *a*) and AgHRBC (part *b*) sheared at $G = \pm 1.53$ s^{-1}. Note that initially T' increased for HRBC and decreased for AgHRBC in accord with theory (7). Stopping flow (at $+G$) is indicated by the upward arrows (labelled STOP and *S*) and reversing at $-G$ by the downward arrows at various values of *i*. Gradual decay (part *a*) or recovery (part *b*) in T' occurred when flow stopped between flow reversals and at the end of each experiment (i.e., after the last 5) as a result of rotary Brownian motion of the particles.

relates changes in T' to the changes in orientation distribution due to flow at $Br_r > 0$. When flow was stopped (indicated by vertical arrows in Fig. 7*a*) and after a short interval reversed in direction ($i = 1$) regrowth of the oscillations in the first half of the shearing cycle (corresponding to $t/T > 0$, Fig. 1) and decay in the second half ($t/T < 0$) were observed. As indicated in Fig. 7*a* by the horizontal asterisked arrow, T' did not decrease to the initial value corresponding to random orientation, thus indicating some memory loss. Upon reversing flow again ($i = 2$), behavior similar to the cycle for $i = 1$ was exhibited but with still lower amplitudes. This process could be repeated many times with reducing amplitudes in successive cycles, reaching zero amplitude after some 50 reversals when the memory was completely lost (cf. curve *5* in Fig. 5*b*-(1)).

The suspension of opaque AgHRBC showed similar behavior except, as predicted (7), T' first decreased (Fig. 7*b*).

As with $\overline{r}_{2\sigma}$ for rods the period of oscillation of T' corresponds to $\overline{T}/2$ from which mean axis ratio of particles was calculated to yield $\overline{r_e} = 0.45$ and 0.49 for HRBC and AgHRBC. This is in reasonably good agreement with $\overline{r_e} = 0.38$ obtained by direct measurements of $\overline{TG}$ on individual HRBC's from another sample (3).

Upon stopping flow permanently (at the point indicated by the last *S* in Fig. 7) both suspensions showed the gradual recovery in T' to the initial level for random orientation as a result of rotary Brownian motion; this has been discussed elsewhere (7) and will not be considered further here except to point out that $Br_r = 0$ leads to complete loss of memory as $t \to \infty$ (1).

Values of M_i' for AgHRBC calculated from measured values of T_i' using [2] for $R_T = 0.5$, 1, and 2 are shown in Fig. 8. It is evident that as in Fig. 3 for rods the rate of memory loss increased with increasing R_T. In the experiments with rods the major contribution to memory loss was attributed to partially irreversible particle interactions, also a possible mechanism here. However, in the present case, what immediately comes to mind as the main source of the loss was rotary Brownian motion (1) for which $D_r = 1.6 \times 10^{-4}\ s^{-1}$ when calculated from [32]-(7) for oblate spheroids of the same overall dimensions as those used in these experiments, so that for $G = 1.53\ s^{-1}$, $Br_r = 4.9 \times 10^3$. Recent calculations (24) of the effect of continuous Brownian rotation on the particle orientation distribution shows that for a given $Br_r \gg 1$ the memory of the suspension should be independent of R_T and depends only on the total elapsed time. In Fig. 8*b*, M_i' is plotted against the dimensionless real time

Can. J. Chem. Downloaded from www.nrcresearchpress.com by 210.87.254.40 on 09/05/12
For personal use only.

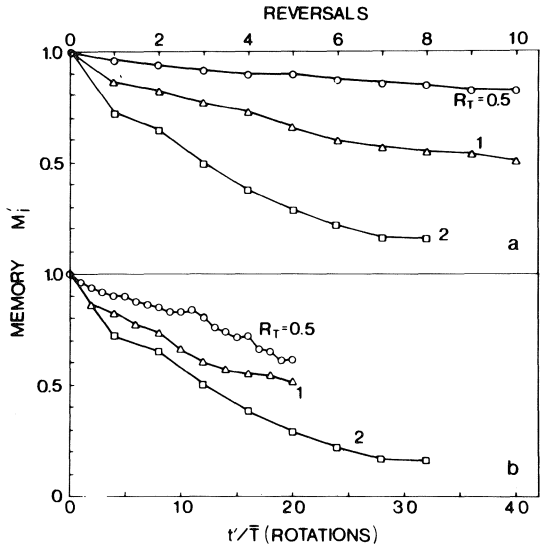

FIG. 8. Memory M_i' for AgHRBC at $N = 0.46 \times 10^8$ ml^{-1} suspended in 75% aqueous glycerine with $R_T = 0.5$, 1, 2 plotted against i (upper) and $t'/\bar{T}$ (lower) at $G = \pm 1.53$ s^{-1}. $Br_r = 4900$.

scale $t'/\bar{T}$. As with the rods (Fig. 3) the points for the different R_T's did not fall on a single line. Contrary to the prediction (24) based solely on rotary Brownian motion we attribute the difference to particle interactions. It should be mentioned that, strictly speaking, these two mechanisms are not independent of each other, since Brownian motion influences both translational and rotational motions of particles in a shear flow, so that all types of particle interaction should become irreversible when flow is reversed. Thus the memory loss effect is enhanced in two ways by the Brownian motion.

(ii) Effect of Concentration

The effect of cell concentration is illustrated in Fig. 9 for $R_T = 1$ at $Br_r = 4900$, where M_i' is plotted against number concentration N for various i's, showing linear variation up to $i = 5$. As N increased, the collision frequency between particles also increased (8) to that the memory loss from imperfections in the particles is expected to be greater (1, 15). The linearity of M_i' with respect to N suggests that the dominant interactions involved are 2-body (4, 17) and that n-body interactions where $n \geq 3$ are not significant over the concentration range studied.

(iii) Effect of Velocity Gradient

M_i' of AgHRBC at $N = 0.41 \times 10^8$ ml^{-1} at $G = 1.07$, 1.61, and 3.25 s^{-1} when the flow was reversed at $R_T = 2$ is shown in Fig. 10 where M_i' is plotted against G for various i. It is seen that M_i' decreased linearly and at nearly identical rates for all $i \leq 8$. When G (and hence Br_r) increased at given D_r, the

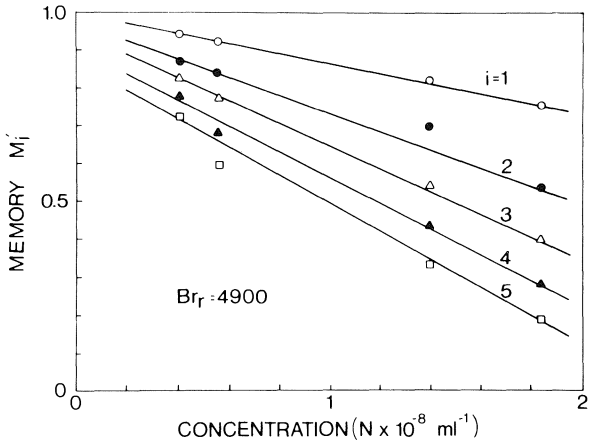

FIG. 9. Memory M_i' vs. N for AgHRBC when flow was reversed at $R_T = 1$ with $G = \pm 1.53$ s^{-1}. (When $i > 5$, the linearity between M_i' and N was lost and these data are omitted.)

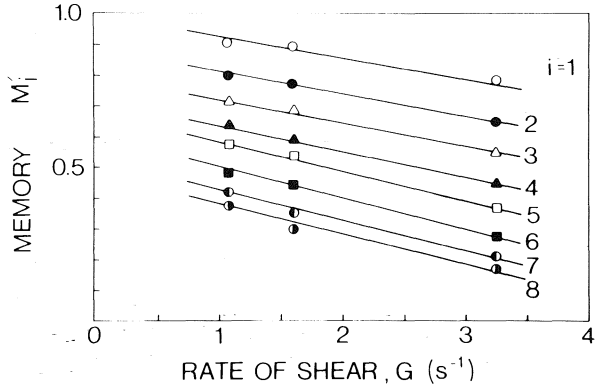

FIG. 10. M_i' vs. G for AgHRBC at $N = 0.41 \times 10^8$ ml^{-1} with $R_T = 2$ for various i over a range of $Br_r = (3.5\text{–}10) \times 10^3$. The decrease of M_i' with G was unexpected and is not understood.

effect of rotary Brownian motion on particle orientation distributions and hence memory loss should become smaller (1, 4, 5). To our surprise the opposite occurred, although it should be noted that Br_r in these experiments was high ((3.5 to 10) $\times 10^3$). Other possible causes for this behavior are (*i*) the development of secondary flows (25), and (*ii*) fluid and particle inertia (26).

In the experimental arrangement used here, secondary flows would only be expected at values of $G\,10^4 \times$ those employed and, in any case, could never be detected in the experiments; they do not provide an explanation. The effects of inertia were discussed in (1) and would be expected to show appreciable memory impairment at particle Reynolds numbers $Re_G (= 4b^2 G\rho_2/\eta$, ρ_2 being the density of the medium) above 10^{-2} (26). In the present experiments Re_G was of the order 10^{-7}, much too low to account

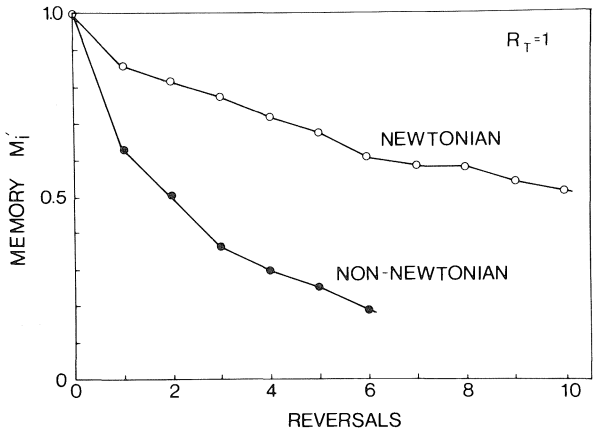

FIG. 11. Effect of non-Newtonian suspending medium (2.5% PAA solution) on the memory of suspensions of AgHRBC at $N = 0.36 \times 10^8$ ml^{-1} when flow is reversed at $R_T = 1$, $G = \pm 0.51$ s^{-1}. The corresponding points for the Newtonian medium (from Fig. 8, $R_T = 1$, $N = 0.46 \times 10^8$ ml^{-1}) show that the rate of memory impairment is roughly 3 times as great in the non-Newtonian medium even though N was less.

for the results. The unexpected variation of M_i' with G is inexplicable.

(iv) Non-Newtonian Medium

M_i' for AgHRBC at $N = 0.36 \times 10^{-8}$ ml^{-1} in the elastico-viscous PAA was measured as above for $R_T = 1$. It is clearly seen from Fig. 11 that the memory loss was much more rapid (about 3×) than in the Newtonian medium even though N was less. As observed with rods (Fig. 6) the memory loss in PAA was primarily due to drift in particle orbits (23) of the disc-shaped cells toward $C = \infty$ (27, 28). At $C = \infty$, the AgHRBC preferentially faced toward the incident light beam thus reducing T' (7) and causing M_i' to decrease, reaching 0 as $i \rightarrow \infty$. This process was probably accelerated by interactions as in the non-Newtonian media (Fig. 8).

(c) Concluding Remarks

To a large extent the experimental findings confirm, qualitatively at least, all of the theoretical predictions presented in ref. 1. A number of additional effects, with one exception (Fig. 10), can be attributed to particle interactions which are too complicated to evaluate theoretically at this stage. As indicated in the previous paper similar behavior will be exhibited by all macroscopic properties which are governed by particle orientations, in addition to the optical properties considered here.

1. A. OKAGAWA, G. J. ENNIS, and S. G. MASON. Can. J. Chem. This issue.
2. H. L. GOLDSMITH and S. G. MASON. Rheology: theory and application. Vol. 4. *Edited by* F. R. Eirich. Academic Press, New York. 1967. p. 85.
3. H. L. GOLDSMITH and J. MARLOW. Proc. R. Soc. B**182**, 351 (1972).
4. A. OKAGAWA, R. G. COX, and S. G. MASON. J. Colloid Interface Sci. **45**, 303 (1973).
5. A. OKAGAWA and S. G. MASON. J. Colloid Interface Sci. **45**, 330 (1973).
6. M. M. FROJMOVIC, A. OKAGAWA, and S. G. MASON. Biochem. Biophys. Res. Commun. **62**, 17 (1975).
7. A. OKAGAWA and S. G. MASON. Can. J. Chem. **55**, 4243 (1977).
8. A. OKAGAWA, R. G. COX, and S. G. MASON. J. Colloid Interface Sci. **47**, 536 (1974).
9. A. OKAGAWA and S. G. MASON. J. Colloid Interface Sci. **47**, 568 (1974).
10. E. BARTRAM, H. L. GOLDSMITH, and S. G. MASON. Rheol. Acta, **14**, 776 (1975).
11. G. J. ENNIS. M.Sc. Thesis, McGill University, Montreal, P.Q., Canada. 1978. Appendix II.
12. B. L. BROWNING. Tappi, **33**, 410 (1950).
13. W. BARTOK and S. G. MASON. J. Colloid Sci. **12**, 243 (1957).
14. C. L. DARABANER, J. K. RAASCH, and S. G. MASON. Can. J. Chem. Eng. **45**, 3 (1967).
15. P. A. ARP and S. G. MASON. J. Colloid Interface Sci. **61**, 44 (1977).
16. A. KARNIS, H. L. GOLDSMITH, and S. G. MASON. J. Colloid Interface Sci. **22**, 531 (1966).
17. E. ANCZUROWSKI, R. G. COX, and S. G. MASON. J. Colloid Interface Sci. **23**, 547 (1967).
18. C. L. DARABANER and S. G. MASON. Rheol. Acta, **6**, 273 (1967).
19. P. A. ARP and S. G. MASON. J. Colloid Interface Sci. **59**, 378 (1977).
20. I. Y. Z. ZIA, R. G. COX, and S. G. MASON. Proc. R. Soc. A**300**, 421 (1967).
21. P. A. ARP and S. G. MASON. Colloid Polym. Sci. **255**, 566 (1977).
22. P. A. ARP and S. G. MASON. Colloid Polym. Sci. **255**, 980 (1977).
23. A. KARNIS and S. G. MASON. Trans. Soc. Rheol. **10**, 571 (1966).
24. M. ZUZOVSKY, Z. PRIEL, and S. G. MASON. To be published.
25. G. I. TAYLOR. Phil. Trans. A**223**, 289 (1923).
26. A. KARNIS, H. L. GOLDSMITH, and S. G. MASON. Can. J. Chem. Eng. **44**, 181 (1966).
27. F. GAUTHIER, H. L. GOLDSMITH, and S. G. MASON. Rheol. Acta, **10**, 334 (1971).
28. F. GAUTHIER, H. L. GOLDSMITH, and S. G. MASON. Trans. Soc. Rheol. **15**, 297 (1971).

Can. J. Chem. Downloaded from www.nrcresearchpress.com by 210.87.254.40 on 09/05/12
For personal use only.

Crystal and molecular structures of 2,2,4,4,6,8,8-heptamethyl-6-methylamino-1,3,5-triaza-2,4,6,8(P^V)-tetraphosphorin and 2,2,4,4,6,8,8-heptamethyl-6-methylamino-7-benzoyl-1,3,5-triaza-2,4,6,8(P^V)- tetraphosphorin

HARRY P. CALHOUN, RICHARD T. OAKLEY, NORMAN L. PADDOCK, STEVEN J. RETTIG, AND JAMES TROTTER[1]

Department of Chemistry, University of British Columbia, 2075 Westbrook Mall, Vancouver, B.C., Canada V6T 1W5

Received July 4, 1978

Can. J. Chem. Downloaded from www.nrcresearchpress.com by 210.87.254.6 on 09/05/12
For personal use only.

HARRY P. CALHOUN, RICHARD T. OAKLEY, NORMAN L. PADDOCK, STEVEN J. RETTIG, and JAMES TROTTER. Can. J. Chem. **56**, 2833 (1978).

Crystals of 2,2,4,4,6,8,8-heptamethyl-6-methylamino-1,3,5-triaza-2,4,6,8(P^V)-tetraphosphorin are monoclinic, $a = 11.639(4)$, $b = 11.957(7)$, $c = 12.114(4)$ Å, $\beta = 94.07(2)°$, $Z = 4$, space group $P2_1/n$. The structure was solved by direct methods and was refined by full-matrix least-squares procedures to $R = 0.032$ and R_w of 0.041 for 2012 reflections with $I \geq 3\sigma(I)$. Crystals of 2,2,4,4,6,8,8-heptamethyl-6-methylamino-7-benzoyl-1,3,5-triaza-2,4,6,8(P^V)-tetraphosphorin are triclinic, $a = 15.513(1)$, $b = 8.422(1)$, $c = 8.933(1)$ Å, $\alpha = 89.24(1)$, $\beta = 100.18(1)$, $\gamma = 107.30(1)°$, $Z = 2$, space group $P\bar{1}$. The structure was solved by Patterson and Fourier syntheses and was refined to a final R of 0.041 and R_w of 0.044 for 3654 reflections with $I \geq 3\sigma(I)$. The eight-membered P_4N_3C rings in both structures have 'tub' conformations. The mean bond lengths (corrected for libration) are: P—N(*endo*), 1.609(9), P—N(*exo*), 1.679(2), P—C(*endo*), 1.717(2), and P—C(*exo*), 1.815(8) Å for $Me_7(MeNH)P_4N_3CH$ and 1.595(4), 1.655(2), 1.763(4), and 1.804(5) Å respectively for $Me_7(MeNH)P_4N_3CC(O)Ph$. The near-equivalence of the endocyclic P—N bond lengths in the azaphosphorins is discussed in terms of opposing changes in the in-plane and out-of-plane π-systems.

HARRY P. CALHOUN, RICHARD T. OAKLEY, NORMAN L. PADDOCK, STEVEN J. RETTIG et JAMES TROTTER. Can. J. Chem. **56**, 2833 (1978).

Les cristaux de l'heptaméthyl-2,2,4,4,6,8,8 méthylamino-6 triaza-1,3,5 tétraphosphorine-2,4,6,8(P^V) sont monocliniques, $a = 11.639(4)$, $b = 11.957(7)$, $c = 12.114(4)$ Å, $\beta = 94.07(2)°$, $Z = 4$, groupe d'espace $P2_1/n$. La structure a été résolue par méthodes directes et l'affinement par moindres carrés (matrice complète), effectué sur 2012 réflexions ayant $I \geq 3\sigma(I)$, a conduit aux valeurs finales de $R = 0.032$ et $R_w = 0.041$. Les cristaux de l'heptaméthyl-2,2,4,4,6,8,8 méthylamino-6 benzoyl-7 triaza-1,3,5 tétraphosphorine-2,4,6,8(P^V) sont tricliniques, $a = 15.513(1)$, $b = 8.422(1)$, $c = 8.933(1)$ Å, $\alpha = 89.24(1)$, $\beta = 100.18(1)$, $\gamma = 107.30(1)°$, $Z = 2$, groupe d'espace $P\bar{1}$. La structure a été résolue au moyen de synthèses de Patterson et de Fourier, et l'affinement, effectué sur 3654 réflexions ayant $I \geq 3\sigma(I)$, a conduit aux valeurs finales $R = 0.041$ et $R_w = 0.044$. Dans les deux structures, le cycle P_4N_3C à huit atomes possède une conformation "tub". Les valeurs moyennes des longueurs de liaisons (corrigées pour la libration) sont: P—N(*endo*), 1.609(9), P—N(*exo*), 1.679(2), P—C(*endo*), 1.717(2), et P—C(*exo*), 1.815(8) Å pour $Me_7(MeNH)P_4N_3CH$ et 1.595(4), 1.655(2), 1.763(4) et 1.804(5) Å, respectivement, pour $Me_7(MeNH)P_4N_3CC(O)Ph$. On discute de la quasi-équivalence des longueurs de liaisons P—N endocycliques dans les azaphosphorines en fonction des changements compétitifs dans les systèmes π dans le plan et hors du plan.

[Traduit par le journal]

Introduction

Many studies have been made of the structural changes which occur upon perturbing the π-electron distribution in cyclic phosphazenes, either by inhomogeneous substitution of the phosphorus atoms or by complexation at nitrogen. In the azaphosphorins **1**, **2** (1) a third type of perturbation is found, in which one nitrogen atom of the N_3P_3 or N_4P_4 skeleton is replaced by a $\equiv$CH group. Substitution is possible both at the ring carbon atom and at the exocyclic nitrogen atom, and the structure of the *N*-benzoyl-*C*-benzoyl derivative **3** has been determined (2). Structural relationships in tetrameric phosphazenes are often especially informative, and we have therefore determined the crystal and molecular structures of the parent azaphosphorin **2** and its *C*-benzoyl derivative **4**.

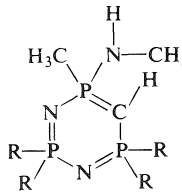

1

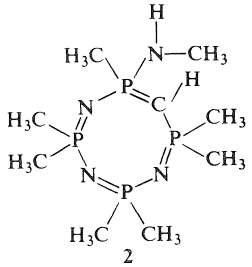

2

[1]To whom correspondence should be addressed.

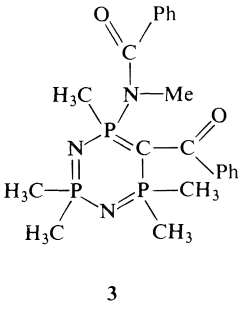

3

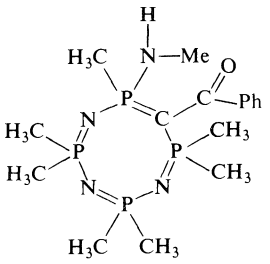

4

Experimental

2,2,4,4,6,8,8-Heptamethyl-6-methylamino-1,3,5-triaza-2,4,6,8(P^V)-tetraphosphorin (2)

Colourless crystals of 2,2,4,4,6,8,8-heptamethyl-6-methylamino-1,3,5-triaza-2,4,6,8(P^V)-tetraphosphorin were grown from *n*-hexane (1). The crystals were handled in a dry box, as the compound is extremely sensitive to atmospheric moisture. The crystal, sealed in a Lindemann glass capillary, was mounted with *b* parallel to the goniostat axis and had dimensions of ca. 0.5 × 0.9 × 0.4 mm. Unit-cell parameters were refined by least-squares on 2 sin θ/λ values for 17 reflections measured on a diffractometer with MoK_α radiation (λ = 0.71069 Å). Crystal data (at 22°C) are:

$C_9H_{26}N_4P_4$ fw = 314.23

Monoclinic, a = 11.639(4), b = 11.957(7), c = 12.114(4) Å, β = 94.07(2)°, V = 1682(1) Å^3, Z = 4, ρ_c = 1.241 g cm^{-3}, $F(000)$ = 672, $\mu(MoK_\alpha)$ = 4.4 cm^{-1}. Absent reflections: $0k0$, $k \neq 2n$ and $h0l$, $h + l \neq 2n$ define uniquely the space group $P2_1/n$ (non-standard setting of $P2_1/c$, C_{2h}^5, No. 14).

Intensities were measured with zirconium-filtered MoK_α radiation on a Datex-automated General Electric XRD-6 diffractometer. A θ–2θ scan at 2° min^{-1} over a range of (1.80 + 0.86 tan θ) degrees in 2θ was employed. 20 s background counts were measured at each end of the scan. Data were measured to 2θ = 50°. The intensities of the check reflections, measured every 30 reflections throughout the data collection, remained constant to within ±3%. After data reduction, an absorption correction was applied using the Gaussian integration method (3, 4). Transmission factors ranged from 0.802 to 0.850. Of the 2965 independent reflections measured, 2012 (68%) had intensities greater than 3σ(I) above background where $\sigma^2(I) = S + B + (0.04S)^2$ with S = scan count and B = time-averaged background count.

The structure was solved by direct methods (5). The positions of the eight ring atoms and two of the methyl carbon atoms were determined from an *E*-map. The remaining non-hydrogen atoms and 22 of the 26 hydrogen atoms were located from subsequent difference syntheses. Refinement of the ordered model converged at R = 0.065. Possible disorder of P(1) and its exocyclic substituents was suggested both by the appearance of a large peak (2.4 e Å^{-1}) between N(1) and C(2) on a difference map and by the anisotropic thermal parameters for P(1), N(1), C(2), and C(9) which were inconsistent with those for the other atoms. Careful examination of a Fourier map led to a twofold disordered model with unbalanced site occupancies of 0.7 and 0.3 estimated from relative peak heights. The site occupancies were kept fixed throughout the refinement, but the final thermal parameters of the disordered atoms indicate that these values are quite satisfactory. The disordered non-hydrogen atoms were included in the refinement first with isotropic, then with anisotropic thermal parameters, reducing R to 0.036. A difference map gave positions for all of the disordered hydrogen atoms which were included (with isotropic thermal parameters) in all subsequent cycles of refinement. The scattering factors of ref. 6 were used for non-hydrogen atoms and those of ref. 7 for hydrogen atoms. Anomalous scattering factors from ref. 8 were used for the phosphorus atoms. The weighting scheme ($w = (|F_o|/7.5)^2$ if $|F_o| < 7.5$, $w = 1.0$ if $7.5 \leq |F_o| \leq 20.0$, $w = (20.0/|F_o|)^2$ if $|F_o| > 20.0$, and $w = 0.0625$ for the unobserved reflections) gave uniform average values of $w(|F_o| - |F_c|)^2$ over ranges of $|F_o|$ and was employed in the final stages of refinement. A type I anisotropic extinction correction (Thornley–Nelmes definition of mosaic anisotropy with a Lorentzian distribution) was applied (9–11). Extinction parameters are given in Table 1. Convergence was reached at R = 0.032 and R_w of 0.041 for 2012 reflections with $I \geq 3\sigma(I)$. For all 2965 reflections R = 0.051 and R_w = 0.043.

On the final cycle of refinement the mean and maximum parameter shifts corresponded to 0.10 and 0.92σ respectively. The mean error in an observation of unit weight was 0.5698.

2,2,4,4,6,8,8-Heptamethyl-6-methylamino-7-benzoyl-1,3,5-triaza-2,4,6,8(P^V)-tetraphosphorin (4)

The preparation of this compound has been described previously (1). The crystal used for data collection was mounted with b^* parallel to the goniostat axis and had dimensions of ca. 0.18 × 0.20 × 0.36 mm. Twenty planes measured with CuK_α radiation (λ = 1.5418 Å) were used in the refinement of the unit-cell parameters. Crystal data are:

$C_{16}H_{30}N_4OP_4$ fw = 418.34

Triclinic, a = 15.513(1), b = 8.422(1), c = 8.933(1) Å, α = 89.24(1), β = 100.18(1), γ = 107.30(1)°, V = 1095.8(2) Å^3, Z = 2, ρ_c = 1.268 g cm^{-3}, $F(000)$ = 636, $\mu(CuK_\alpha)$ = 32.4 cm^{-1}. Space group $P\bar{1}$ (C_i^1, No. 2).

The intensity of the check reflection remained constant to within ±4% during the data collection. Of 4385 independent reflections measured (to 2θ = 146°, CuK_α radiation), 3679 (84%) had intensities greater than 3σ(I) above background. The data were corrected for absorption, transmission factors ranging from 0.44 to 0.67.

The centrosymmetric space group $P\bar{1}$ was strongly indicated by the $|E|$ statistics. The structure was solved by Patterson and Fourier syntheses. Full-matrix least-squares refinement of the non-hydrogen atoms with isotropic, then with anisotropic thermal parameters proceeded routinely to convergence at R = 0.088. A difference map then gave the positions of all 30 hydrogen atoms which were included in all subsequent cycles of refinement with isotropic thermal parameters. The entire

TABLE 1

(*a*) Anisotropic extinction parameters Lorentzian-type I

Y	Thornley–Nelmes (× 10^{-8})
11	2.7(7)
22	1.5(2)
33	10.8(21)
12	1.7(3)
13	3.5(9)
23	3.1(6)

(*b*) Principal axes of mosaic spread (seconds of arc) and directions in orthogonal Å space referred to a, b, c^*

η_1	1.5	0.46	−0.87	0.14
η_2	4.4	0.83	0.39	−0.38
η_3	11.6	0.28	0.29	0.91

Can. J. Chem. Downloaded from www.nrcresearchpress.com by 210.87.254.6 on 09/05/12
For personal use only.

TABLE 2. Final positional parameters (fractional: O, N, and C × 10^4, P × 10^5, H × 10^3) with estimated standard deviations in parentheses

Atom	x	y	z	Atom	x	y	z
	Compound **2**				Compound **4**		
(equivalent positions: $\pm(x, y, z; 1/2 - x, 1/2 + y, 1/2 - z)$				P(1)	41454(4)	65151(7)	22955(7)
P(1b)	37452(19)	22635(14)	67550(18)	P(2)	22286(4)	43339(7)	8313(7)
P(1a)	38376(44)	26902(33)	66089(40)	P(3)	15078(4)	72041(7)	6679(7)
P(2)	15169(5)	21102(6)	53638(5)	P(4)	34306(4)	90439(7)	6654(7)
P(3)	25504(5)	33724(5)	36738(5)	O	3963(1)	3833(2)	4428(2)
P(4)	45974(5)	22013(5)	45140(5)	N(1)	4526(1)	7506(3)	3975(3)
N(1b)	4440(3)	3316(3)	7417(3)	N(2)	1490(1)	5319(2)	624(3)
N(1a)	4146(6)	2186(8)	7885(6)	N(3)	2445(1)	8661(2)	1126(3)
N(2)	1665(2)	2459(2)	4094(2)	N(4)	3959(1)	7682(2)	945(2)
N(3)	3900(2)	3251(2)	3997(2)	C(1)	3155(1)	4836(3)	2362(3)
N(4)	4355(2)	1774(2)	5724(2)	C(2)	5111(2)	5855(4)	2024(4)
C(1)	2369(2)	2710(2)	6408(2)	C(3)	1569(2)	2184(3)	888(4)
C(2b)	3865(15)	1193(15)	7819(10)	C(4)	2685(2)	4330(5)	−889(4)
C(2a)	4531(35)	3996(21)	6806(36)	C(5)	798(3)	7436(5)	1967(6)
C(3)	44(3)	2395(4)	5667(3)	C(6)	890(2)	7533(5)	−1149(5)
C(4)	1604(4)	594(3)	5365(3)	C(7)	4104(2)	10980(4)	1637(5)
C(5)	2165(3)	4773(3)	4072(3)	C(8)	3390(2)	9468(5)	−1320(4)
C(6)	2310(3)	3354(3)	2190(2)	C(9)	3895(2)	7898(5)	4816(4)
C(7)	6089(3)	2569(4)	4463(3)	C(10)	3212(2)	3879(3)	3686(3)
C(8)	4423(4)	995(3)	3628(3)	C(11)	2377(2)	3004(3)	4346(3)
C(9b)	4561(18)	4385(9)	6867(16)	C(12)	2319(2)	1479(4)	4996(4)
C(9a)	3713(29)	1110(37)	8146(21)	C(13)	1592(3)	725(5)	5718(4)
H(N1b)	514(4)	311(4)	790(4)	C(14)	933(3)	1471(6)	5823(4)
H(N1a)	497(7)	208(7)	821(7)	C(15)	985(3)	2974(7)	5196(5)
H(1)	201(3)	309(3)	681(3)	C(16)	1705(2)	3739(5)	4447(4)
H(2a)	460(4)	100(4)	805(4)	H(N1)	491(3)	723(4)	449(4)
H(2b)	342(5)	142(4)	848(5)	H(2a)	494(3)	528(5)	105(5)
H(2c)	343(4)	54(4)	758(4)	H(2b)	560(3)	673(5)	204(4)
H(2d)	556(9)	400(9)	702(8)	H(2c)	525(2)	524(5)	274(4)
H(2e)	430(10)	433(10)	610(10)	H(3a)	121(2)	192(4)	−9(4)
H(2f)	441(13)	495(11)	744(11)	H(3b)	196(2)	154(4)	97(3)
H(3a)	−7(3)	208(3)	640(3)	H(3c)	123(2)	202(4)	166(4)
H(3b)	2(3)	321(3)	576(3)	H(4a)	309(3)	540(5)	−97(4)
H(3c)	−46(4)	204(4)	508(4)	H(4b)	218(3)	410(4)	−178(4)
H(4a)	235(4)	41(4)	525(4)	H(4c)	293(3)	349(5)	−90(4)
H(4b)	108(3)	28(3)	477(3)	H(5a)	109(2)	726(4)	300(4)
H(4c)	136(3)	31(3)	599(4)	H(5b)	22(3)	663(5)	168(4)
H(5a)	134(3)	496(3)	385(3)	H(5c)	76(3)	849(5)	201(5)
H(5b)	232(3)	484(3)	489(3)	H(6a)	26(2)	687(4)	−126(4)
H(5c)	268(4)	527(4)	377(4)	H(6b)	124(3)	725(6)	−188(6)
H(6a)	149(3)	347(3)	198(3)	H(6c)	87(3)	856(5)	−118(4)
H(6b)	284(3)	384(3)	195(3)	H(7a)	378(3)	1177(5)	139(4)
H(6c)	266(3)	264(3)	201(3)	H(7b)	468(2)	1139(4)	129(4)
H(7a)	650(3)	198(3)	474(3)	H(7c)	417(2)	1087(4)	269(4)
H(7b)	621(3)	273(3)	368(3)	H(8a)	308(2)	1024(4)	−162(4)
H(7c)	622(3)	320(3)	492(3)	H(8b)	394(3)	977(5)	−157(4)
H(8a)	470(3)	117(3)	296(3)	H(8c)	304(3)	848(5)	−192(4)
H(8b)	486(3)	41(3)	394(3)	H(9a)	340(3)	810(4)	416(4)
H(8c)	367(3)	78(3)	355(3)	H(9b)	365(3)	696(6)	549(5)
H(9a)	521(6)	482(6)	723(6)	H(9c)	423(3)	884(6)	549(6)
H(9b)	483(6)	440(6)	619(6)	H(12)	275(2)	102(4)	481(4)
H(9c)	376(8)	478(8)	700(8)	H(13)	153(4)	−50(7)	611(6)
H(9d)	285(9)	92(8)	798(8)	H(14)	35(3)	96(5)	624(4)
H(9e)	396(10)	97(10)	889(11)	H(15)	58(4)	347(7)	529(6)
H(9f)	407(10)	22(9)	761(8)	H(16)	169(2)	474(4)	388(4)

structure was refined for four cycles giving a final R value of 0.041 and R_w of 0.044 for 3654 reflections with $I \geq 3\sigma(I)$ (25 planes which had $|F_o| - |F_c| \geq 3\sigma(F)$ were treated as unobserved in the final stages of refinement; instrumental error was suspected for these reflections). For all 4385 reflections $R = 0.051$ and $R_w = 0.048$. An isotropic secondary extinction correction was approximated by minimizing $\Sigma w[|F_o| - |F_c|/(1 + gI)|]^2$ where I is the uncorrected intensity; the final value of g was $9.1(1) \times 10^{-8}$. The weighting scheme used was: $w = (|F_o|/11.3)^2$ if $|F_o| < 11.3$, $w = (11.3/|F_o|)^2$ if $|F_o| \geq 11.3$, and $w = 0.12$ for the unobserved reflections.

On the final cycle of refinement the mean and maximum

Can. J. Chem. Downloaded from www.nrcresearchpress.com by 210.87.254.6 on 09/05/12
For personal use only.

Can. J. Chem. Downloaded from www.nrcresearchpress.com by 210.87.254.6 on 09/05/12
For personal use only.

TABLE 3. Final thermal parameters and their estimated standard deviations

(*a*) Anisotropic thermal parameters ($U_{ij} \times 10^3$, P $\times 10^4$ Å^2)*

Atom	U_{11}	U_{22}	U_{33}	U_{12}	U_{13}	U_{23}
			Compound **2**			
P(1b)	390(6)	429(10)	316(7)	19(8)	38(5)	19(7)
P(1a)	406(16)	524(26)	259(15)	37(20)	39(10)	16(19)
P(2)	368(3)	533(4)	387(3)	−33(3)	42(2)	28(3)
P(3)	396(3)	350(3)	400(3)	9(3)	4(2)	27(3)
P(4)	366(3)	402(3)	336(3)	27(3)	24(2)	−19(3)
N(1b)	49(2)	56(2)	49(2)	−1(2)	−2(2)	−4(2)
N(1a)	39(4)	73(6)	33(4)	−2(4)	2(3)	6(4)
N(2)	43(1)	51(1)	38(1)	−7(1)	−1(1)	2(1)
N(3)	40(1)	41(1)	55(1)	−2(1)	1(1)	8(1)
N(4)	46(1)	54(1)	35(1)	10(1)	6(1)	1(1)
C(1)	40(1)	62(2)	37(1)	8(1)	5(1)	−7(1)
C(2b)	58(5)	69(5)	41(6)	3(4)	11(4)	13(5)
C(2a)	74(11)	52(16)	63(10)	−6(14)	−3(7)	−14(15)
C(3)	40(2)	107(3)	63(2)	−1(2)	8(1)	0(2)
C(4)	83(3)	56(2)	64(2)	−19(2)	8(2)	10(2)
C(5)	64(2)	44(2)	77(2)	10(2)	0(2)	−4(2)
C(6)	48(2)	63(2)	42(1)	1(2)	3(1)	9(1)
C(7)	41(1)	89(3)	53(2)	2(2)	5(1)	6(2)
C(8)	93(3)	45(2)	42(2)	7(2)	6(2)	−8(1)
C(9b)	91(5)	47(7)	61(5)	−21(6)	11(4)	−7(6)
C(9a)	43(10)	82(13)	46(16)	0(8)	11(11)	8(14)
			Compound **4**			
P(1)	254(3)	322(3)	393(3)	80(2)	34(2)	22(2)
P(2)	285(3)	275(3)	441(3)	95(2)	−15(2)	−9(2)
P(3)	271(3)	289(3)	555(4)	98(2)	76(2)	56(2)
P(4)	286(3)	299(3)	537(4)	64(2)	60(2)	69(2)
O	38(1)	64(1)	58(1)	15(1)	−5(1)	19(1)
N(1)	36(1)	46(1)	47(1)	11(1)	−1(1)	−6(1)
N(2)	29(1)	32(1)	75(2)	11(1)	−5(1)	0(1)
N(3)	30(1)	33(1)	71(1)	7(1)	11(1)	−1(1)
N(4)	35(1)	38(1)	46(1)	13(1)	8(1)	10(1)
C(1)	29(1)	33(1)	41(1)	7(1)	2(1)	3(1)
C(2)	38(1)	52(2)	51(2)	20(1)	8(1)	4(1)
C(3)	39 (1)	29(1)	72(2)	10(1)	−7(1)	−3(1)
C(4)	57(2)	61(2)	51(2)	15(2)	5(1)	−7(1)
C(5)	55(2)	54(2)	105(3)	11(2)	38(2)	−5(2)
C(6)	53(2)	52(2)	89(3)	13(2)	−10(2)	23(2)
C(7)	41(2)	35(1)	100(3)	3(1)	5(2)	−5(1)
C(8)	55(2)	66(2)	68(2)	24(2)	13(2)	28(2)
C(9)	58(2)	71(2)	58(2)	22(2)	7(2)	−19(2)
C(10)	36(1)	37(1)	46(1)	8(1)	1(1)	5(1)
C(11)	39(1)	50(1)	44(1)	1(1)	2(1)	10(1)
C(12)	62(2)	59(2)	69(2)	5(2)	6(2)	24(2)
C(13)	83(3)	81(3)	71(2)	−12(2)	14(2)	30(2)
C(14)	61(2)	119(4)	63(2)	−23(2)	14(2)	11(2)
C(15)	53(2)	120(3)	77(3)	13(2)	22(2)	1(2)
C(16)	47(2)	78(2)	65(2)	14(1)	14(1)	10(2)

(*b*) Isotropic thermal parameters ($U \times 10^3$)

Atom	U (Å^2)	Atom	U (Å^2)	Atom	U (Å^2)
			Compound **2**		
H(1)	62(9)	H(6b)	78(11)	H(9d)	38(24)
H(3a)	81(11)	H(6c)	71(10)	H(9e)	68(35)
H(3b)	69(10)	H(7a)	78(11)	H(9f)	58(29)
H(3c)	111(15)	H(7b)	84(11)	H(N1b)	56(11)
H(4a)	109(15)	H(7c)	85(12)	H(N1a)	32(20)
H(4b)	83(11)	H(8a)	91(12)	H(2a)	60(13)
H(4c)	91(12)	H(8b)	72(10)	H(2b)	51(20)

TABLE 3 (*Concluded*)

Atom	U (Å^2)	Atom	U (Å^2)	Atom	U (Å^2)
H(5a)	88(11)	H(8c)	81(12)	H(2c)	49(11)
H(5b)	69(9)	H(9a)	118(23)	H(2d)	53(27)
H(5c)	111(15)	H(9b)	80(22)	H(2e)	55(30)
H(6a)	76(10)	H(9c)	142(36)	H(2f)	59(37)
		Compound **4**			
H(N1)	78(11)	H(5a)	62(10)	H(8b)	85(11)
H(2a)	105(14)	H(5b)	83(10)	H(8c)	81(12)
H(2b)	97(13)	H(5c)	97(13)	H(9a)	81(11)
H(2c)	80(11)	H(6a)	68(9)	H(9b)	103(14)
H(3a)	76(10)	H(6b)	113(18)	H(9c)	126(17)
H(3b)	54(8)	H(6c)	98(12)	H(12)	63(9)
H(3c)	66(9)	H(7a)	77(11)	H(13)	135(18)
H(4a)	86(12)	H(7b)	73(9)	H(14)	84(11)
H(4b)	77(10)	H(7c)	74(11)	H(15)	131(21)
H(4c)	81(12)	H(8a)	70(10)	H(16)	72(10)

*The anisotropic thermal parameters employed in the refinement are U_{ij} in the expression: $f = f^0 \exp(-2\pi^2 \Sigma_i \Sigma_j U_{ij} h_i h_j a_i^* a_j^*)$. For isotropic atoms: $f = f^0 \exp(-8\pi^2 U \sin^2\theta/\lambda^2)$.

parameter shifts corresponded to 0.28 and 1.04σ respectively. The mean error in an observation of unit weight was 0.3796.

The final positional and thermal parameters for both compounds appear in Tables 2 and 3 respectively; measured and calculated structure factors have been placed in the Depository of Unpublished Data.[2]

The thermal motions of both molecules have been analysed in terms of rigid-body modes of translation, libration, and screw motion (12) using the computer program MGTLS. For compound **2** (rms $\sigma U_{ij} = 0.0017$ Å^2 for ordered atoms) analysis of each of the phosphorus tetrahedra gave physically reasonable results (rms $\Delta U_{ij} = 31, 25, 14, 8$, and 10×10^{-4} Å^2 for P(1b)—P(4) respectively). For molecule **4** (rms $\sigma U_{ij} = 0.0016$ Å^2) analyses were successful for the four phosphorus tetrahedra and for the phenyl group (rms $\Delta U_{ij} = 11, 13, 16, 12$, and 19×10^{-4} Å^2 respectively). The appropriate bond distances have been corrected for libration (13), using shape parameters q^2 of 0.08 for all atoms involved. Corrected bond lengths appear in Table 4 along with the uncorrected values. Changes in bond angles were less than 1σ, thus only the uncorrected values are given in Table 5.

Results and Discussion

General views of the two isomers of **2** and the molecule **4**, with their crystallographic numbering schemes, are shown in Fig. 1, and the packing arrangements in Fig. 2. The crystal structure of 2,2,4,4,6,8,8 - heptamethyl - 6 - methylamino - 1,3,5 - triaza-2,4,6,8(P^V)-tetraphosphorin (**2**) consists of discrete molecules each linked to two others (related by the *n* glide plane) by N—H...N hydrogen bonds (Fig. 2*a*), a situation which occurs for both positions of the disordered group P(1)N(1)C(9). The hydrogen bond geometry is more favourable for the 30% occupied site HN(1a)Me (see Table 6). In the crystal structure of the *C*-benzoyl derivative (**4**), the molecules associate via weak N—H...O hydrogen bonds (N...O = 3.024(3) Å) and weak C—H...O interactions to form centrosymmetric dimers (Fig. 2*b*). There are weak intramolecular C—H...O (and N) interactions present as well. Details are given in Table 6. Other intermolecular distances in all three structures correspond to normal van der Waals interactions, and justify discussion of the structures in molecular terms.

The molecular conformations are closely related; intra-annular torsion angles defining them are given in Table 7. The two slightly different ring conformations of the azaphosphorins **2***a* and **2***b* (Fig. 1*a*, *b*) can both be regarded as tubs. The tub conformation ($\bar{4}$) is known to be flexible, and can be inverted, as Fig. 3 shows, by torsional motion about the ring bonds, only small changes in non-bonded interactions being involved. The transformation proceeds through the saddle conformation ($\bar{4}2m$) (Fig. 3*b*), in which the four phosphorus atoms are coplanar, a structure closely approached by the parent molecule $N_4P_4Me_8$ (14).

The two azaphosphorins *a* and *b* differ in two ways. They are primarily configurational isomers, P(1) being an asymmetric centre. They can be interconverted by a reflection, followed by conformational inversion, in the sense of Fig. 3*a–c*, the two molecules then being nearly superposable, but with the NMe group on different sides of the ring.

This last feature causes slight changes in ring geometry arising from steric interactions. The cross-ring distance C(5)C(2) in *a* is maintained at 4.26 Å in *b* (C(5)C(9)) by an outward rotation of the C(2)P(1)N(1)C(9) group (in *b*) about an axis through C(1)N(4).

The ring in the *C*-benzoyl derivative **4** is less regular again, principally because the N(2)P(3)C(5)-C(6) grouping is displaced away from the phenyl

[2]The structure factor table is available, at a nominal charge, from the Depository of Unpublished Data, CISTI, National Research Council of Canada, Ottawa, Ont., Canada K1A 0S2.

Can. J. Chem. Downloaded from www.nrcresearchpress.com by 210.87.254.6 on 09/05/12
For personal use only.

TABLE 4. Bond lengths (Å) with estimated standard deviations in parentheses

(*a*) Non-hydrogen atoms

Bond	Length		Bond	Length	
	Uncorr.	Corr.		Uncorr.	Corr.
			Compound **2**		
P(1b)—N(1b)	1.670(4)	1.678	P(1b)—C(2b)	1.81(1)	1.82
P(1b)—N(4)	1.591(3)	1.598	P(1b)—C(1)	1.713(3)	1.719
P(1a)—N(1a)	1.674(8)	1.681	P(1a)—C(2a)	1.77(3)	1.78
P(1a)—N(4)	1.675(5)	1.683	P(1a)—C(1)	1.710(5)	1.717
P(2) —N(2)	1.615(2)	1.623	P(2) —C(1)	1.708(3)	1.715
P(3) —N(2)	1.608(2)	1.616	P(2) —C(3)	1.811(3)	1.819
P(3) —N(3)	1.598(2)	1.604	P(2) —C(4)	1.816(4)	1.826
P(4) —N(3)	1.598(2)	1.607	P(3) —C(5)	1.808(3)	1.819
P(4) —N(4)	1.596(2)	1.604	P(3) —C(6)	1.799(3)	1.807
N(1b)—C(9b)	1.45(1)	1.46	P(4) —C(7)	1.797(3)	1.808
N(1a)—C(9a)	1.43(4)	1.43	P(4) —C(8)	1.801(3)	1.814
			Compound **4**		
P(1) —N(1)	1.650(2)	1.655	P(3) —C(6)	1.796(3)	1.806
P(1) —N(4)	1.587(2)	1.592	P(4) —C(7)	1.791(3)	1.799
P(2) —N(2)	1.588(2)	1.595	P(4) —C(8)	1.798(4)	1.806
P(3) —N(2)	1.581(2)	1.589	O —C(10)	1.245(3)	1.252
P(3) —N(3)	1.591(2)	1.596	N(1) —C(9)	1.447(4)	1.449
P(4) —N(3)	1.592(2)	1.599	C(1) —C(10)	1.427(3)	1.434
P(4) —N(4)	1.590(2)	1.596	C(10)—C(11)	1.503(3)	1.508
P(1) —C(1)	1.762(2)	1.767	C(11)—C(12)	1.387(4)	1.397
P(1) —C(2)	1.799(3)	1.804	C(11)—C(16)	1.377(4)	1.388
P(2) —C(1)	1.753(2)	1.759	C(12)—C(13)	1.383(5)	1.388
P(2) —C(3)	1.800(3)	1.806	C(13)—C(14)	1.365(7)	1.375
P(2) —C(4)	1.803(3)	1.810	C(14)—C(15)	1.363(7)	1.372
P(3) —C(5)	1.784(3)	1.795	C(15)—C(16)	1.391(5)	1.396

(*b*) Bonds involving hydrogen atoms

Bond	Length	Weighted mean
	Compound **2**	
N—H	1.00(5), 1.02(8)	
C(1)—H	0.80(3)	
C(methyl)—H	0.89–1.39(3–14)	0.96(6)
	Compound **4**	
N—H	0.78(4)	
C(aromatic)—H	0.86–1.07(3–5)	0.97(9)
C(methyl)—H	0.86–1.01(3–5)	0.94(4)

group. The C(16)C(5) and C(16)C(9) distances are 4.23, 4.06 Å respectively, the C(5)C(9) cross-ring distance being lengthened to 4.93 Å. The interaction is not large enough to distort the phenyl group, which is planar within experimental error ($\chi^2 = 6.4$), and the mean phenyl C—C distance of 1.386(10) Å is as expected. The P—Me distances (**2**, 1.807–1.826; **4**, 1.795–1.810 Å) are slightly longer than those in the trimeric derivative (mean 1.796(4) Å (2)) but similar to those in the methylphosphazenes $(NPMe_2)_{3-8}$ (14–19), where mean distances range from 1.801 to 1.811 Å. There is an especially close relationship to $N_4P_4Me_8$ (14).

The introduction of a carbon atom into the ring evidently causes no profound conformational change, but it has an unexpected effect on the bond lengths, which is discussed first for the azaphosphorins **2**. In $Ph_3P{=}CH_2$, P=C = 1.661 Å (20) and the mean endocyclic P—C bond length of 1.717(2) Å in **2** can reasonably be taken to correspond to the change from a 2-centre to a 3-centre bond; as expected, the bond lengths are similar to those in a Wittig intermediate (21). The P—N bond lengths present more of a problem. One of them (P(1a)N(4) in **2***a*) is excessively long (1.683(5) Å), partly because of hybridization differences which alone would cause this bond to be about 0.03 Å longer than its counterpart P(1b)—N(4) (1.598(3) Å). The much larger

Can. J. Chem. Downloaded from www.nrcresearchpress.com by 210.87.254.6 on 09/05/12
For personal use only.

Can. J. Chem. Downloaded from www.nrcresearchpress.com by 210.87.254.6 on 09/05/12
For personal use only.

TABLE 5. Bond angles (deg) with estimated standard deviations in parentheses

(*a*) Non-hydrogen atoms

Bonds	Angle (deg)	Bonds	Angle (deg)
	Compound **2**		
N(1b)—P(1b)—N(4)	115.2(2)	N(2) —P(3) —C(5)	111.6(2)
N(1b)—P(1b)—C(1)	107.2(2)	N(2) —P(3) —C(6)	104.5(1)
N(1b)—P(1b)—C(2b)	100.4(6)	N(3) —P(3) —C(5)	106.1(1)
N(4) —P(1b)—C(1)	112.5(2)	N(3) —P(3) —C(6)	108.9(1)
N(4) —P(1b)—C(2b)	106.4(6)	C(5) —P(3) —C(6)	104.7(2)
C(1) —P(1b)—C(2b)	114.7(5)	N(3) —P(4) —N(4)	119.5(1)
N(1a)—P(1a)—N(4)	107.0(4)	N(3) —P(4) —C(7)	105.1(2)
N(1a)—P(1a)—C(1)	106.5(4)	N(3) —P(4) —C(8)	111.3(1)
N(1a)—P(1a)—C(2a)	97.3(14)	N(4) —P(4) —C(7)	110.2(1)
N(4) —P(1a)—C(1)	108.6(3)	N(4) —P(4) —C(8)	105.7(1)
N(4) —P(1a)—C(2a)	118.9(15)	C(7) —P(4) —C(8)	104.1(2)
C(1) —P(1a)—C(2a)	116.7(13)	P(1b)—N(1b)—C(9b)	120.2(7)
N(2) —P(2) —C(1)	120.1(1)	P(1a) —N(1a)—C(9a)	118.3(13)
N(2) —P(2) —C(3)	108.1(2)	P(2) —N(2) —P(3)	126.2(1)
N(2) —P(2) —C(4)	104.4(2)	P(3) —N(3) —P(4)	129.1(1)
C(1) —P(2) —C(3)	106.2(2)	P(1a) —N(4) —P(4)	136.1(2)
C(1) —P(2) —C(4)	112.9(2)	P(1b)—N(4) —P(4)	118.2(2)
C(3) —P(2) —C(4)	104.0(2)	P(1a) —C(1) —P(2)	122.3(2)
N(2) —P(3) —N(3)	120.1(1)	P(1b)—C(1) —P(2)	128.4(2)
	Compound **4**		
N(1) —P(1) —N(4)	113.7(1)	N(4) —P(4) —C(7)	111.0(1)
N(1) —P(1) —C(1)	110.0(1)	N(4) —P(4) —C(8)	104.7(1)
N(1) —P(1) —C(2)	101.7(1)	C(7) —P(4) —C(8)	104.4(2)
N(4) —P(1) —C(1)	110.8(1)	P(1) —N(1) —C(9)	120.3(2)
N(4) —P(1) —C(2)	107.5(1)	P(2) —N(2) —P(3)	136.4(1)
C(1) —P(1) —C(2)	112.9(1)	P(3) —N(3) —P(4)	133.5(1)
N(2) —P(2) —C(1)	120.7(1)	P(1) —N(4) —P(4)	135.3(1)
N(2) —P(2) —C(3)	104.6(1)	P(1) —C(1) —P(2)	121.1(1)
N(2) —P(2) —C(4)	110.7(1)	P(1) —C(1) —C(10)	114.4(2)
C(1) —P(2) —C(3)	109.7(1)	P(2) —C(1) —C(10)	124.3(2)
C(1) —P(2) —C(4)	107.7(1)	O —C(10)—C(1)	121.8(2)
C(3) —P(2) —C(4)	101.8(2)	O —C(10)—C(11)	116.2(2)
N(2) —P(3) —N(3)	121.3(1)	C(1) —C(10)—C(11)	121.7(2)
N(2) —P(3) —C(5)	107.9(2)	C(10)—C(11)—C(12)	119.2(3)
N(2) —P(3) —C(6)	105.9(2)	C(10)—C(11)—C(16)	121.8(3)
N(3) —P(3) —C(5)	105.7(2)	C(12)—C(11)—C(16)	118.7(3)
N(3) —P(3) —C(6)	111.1(1)	C(11)—C(12)—C(13)	119.9(4)
C(5) —P(3) —C(6)	103.4(2)	C(12)—C(13)—C(14)	120.9(4)
N(3) —P(4) —N(4)	118.9(1)	C(13)—C(14)—C(15)	119.8(4)
N(3) —P(4) —C(7)	105.4(1)	C(14)—C(15)—C(16)	120.0(4)
N(3) —P(4) —C(8)	111.7(1)	C(11)—C(16)—C(15)	120.6(4)

(*b*) Angles involving hydrogen atoms

Bonds	Angle (deg)	Mean
	Compound **2**	
C/P—N—H	98–122(2–5)	113(9)
P—C(1)—H	113–123(2)	118(5)
N—C(methyl)—H	102–121(4–7)	113(7)
P—C(methyl)—H	99–137(2–7)	108(3)
H—C(methyl)—H	91–120(3–9)	110(6)
	Compound **4**	
C/P—N—H	113(3), 114(3)	
C—C(aromatic)—H	114–126(2–4)	120(4)
N—C(methyl)—H	108–111(2–3)	110(2)
P—C(methyl)—H	103–113(2–3)	109(2)
H—C(methyl)—H	105–116(3–4)	110(4)

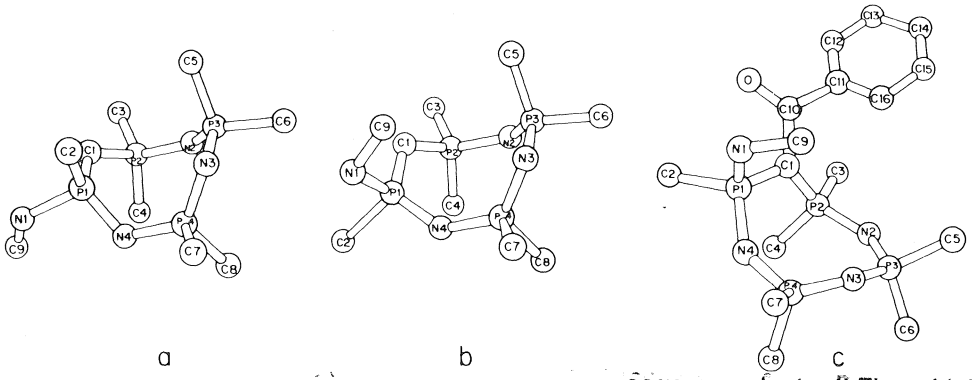

Fig. 1.

Molecular structures of (*a*), **2***a* (occupancy factor 0.3); (*b*), **2***b* occupancy factor 0.7); and (*c*), **4**.

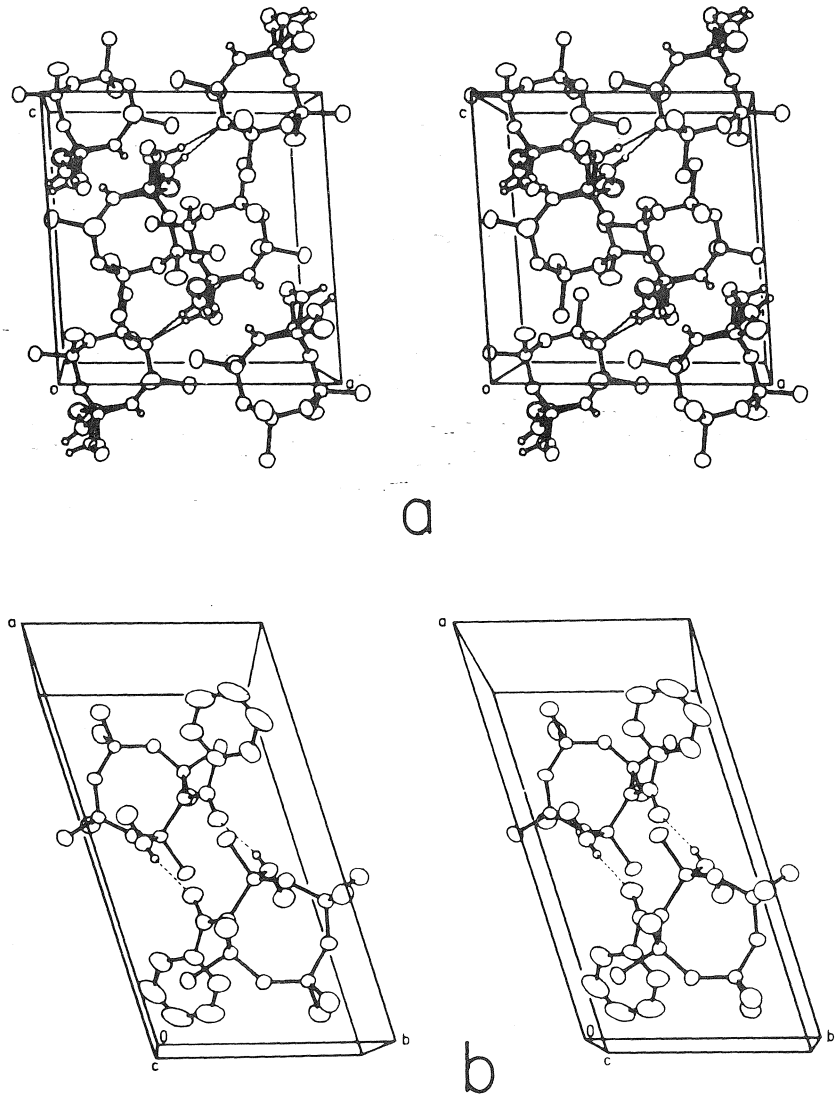

FIG. 2. Stereo views of the packing arrangements of **2** (*a*) and **4** (*b*). Broken or fine lines represent hydrogen bonds.

Can. J. Chem. Downloaded from www.nrcresearchpress.com by 210.87.254.6 on 09/05/12
For personal use only.

Can. J. Chem. Downloaded from www.nrcresearchpress.com by 210.87.254.6 on 09/05/12
For personal use only.

TABLE 6. Hydrogen-bond and C—H...O/N interaction data* (distances in Å and angles in deg)

D—H...A	H...A	D...A	∠DHA	∠XAH
		Compound **2**		
N(1a)—H...N(2)[1]	2.31(4)	3.309(4)	176(3)	119(1), 113(1)
N(1b)—H...N(2)[1]	2.24(9)	3.212(8)	158(7)	104(2), 112(2)
		Compound **4**		
N(1)—H(N1)...O[2]	2.25(4)	3.024(3)	169(3)	159(1)
C(2)—H(2c)...O	2.70(4)	3.183(4)	117(3)	107(1)
C(2)—H(2c)...O[2]	2.62(4)	3.220(4)	128(3)	113(1)
C(4)—H(4a)...N(4)	2.49(4)	3.197(4)	132(3)	96(1), 105(1)

*Superscripts refer to atoms at positions: [1] $1/2 + x, 1/2 - y, 1/2 + z$; [2] $1 - x, 1 - y, 1 - z$.

TABLE 7. Torsion angles in the azaphosphorin ring

	Angle (deg)			
Bond	**2***a*	**2***b*	**4**	$P_4N_4Me_8$
P(1)—C(1)	−10.2(3)	30.5(2)	14.5(1)	31.1
C(1)—P(2)	−59.4(2)	−81.0(2)	−81.7(1)	−54.5
P(2)—N(2)	−1.4(2)	−1.4(2)	47.1(1)	−31.1
N(2)—P(3)	56.7(1)	56.7(1)	−5.3(1)	54.5
P(3)—N(3)	13.1(1)	13.1(1)	45.0(1)	31.1
N(3)—P(4)	−64.4(1)	−64.4(1)	−56.7(1)	−54.5
P(4)—N(4)	−25.5(2)	−16.2(2)	−44.3(1)	−31.1
N(4)—P(1)	86.8(3)	53.8(2)	75.7(1)	54.5

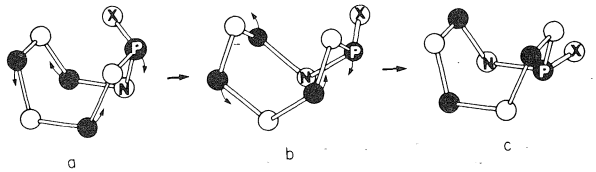

FIG. 3. Conformational inversion path in $(NPX_2)_4$, $\bar{4}$ symmetry. The change takes place by torsional motion about the ring bonds in the sense of the arrows. The diagram shows the change in conformation of one X-group from *endo* to *exo*.

actual difference may either be real or a result of some inadequacy in the disordered model used in the refinement of the structure of **2**. It should be noted, however, that N(4) showed no signs of being disordered. An additional point of interest in the structure of **2** is the involvement of the ring atom N(2) in the hydrogen bonding which increases the mean N(2)—P distance to 1.620(4) Å compared to a mean N(3)—P distance of 1.606(2) Å, a significant increase in bond length.

Apart from these two features, the PN bonds in the ring are nearly equal among themselves, and their lengths are close to that of the PN bond in $N_4P_4Me_8$ (1.596 Å) (14). At first sight, the equality is surprising. Modification of the electronic structure of a cyclic phosphazene, either by inhomogeneous substitution at phosphorus (22), or protonation (23) or alkylation (24) at nitrogen, or by a perturbation at both centres (25) leads to pronounced bond length inequalities which have been interpreted in terms of the effect of the substituent on a double π-system, and the substitution of carbon for nitrogen is equally drastic. As explained below, the substitution has only a small structural effect because it has opposite and compensating effects on the in-plane and out-of-plane π-systems.

In $N_4P_4Me_8H^+$, the proton localises two electrons on nitrogen, so that the in-plane π-system is confined to the P_4N_3 fragment, leading to inequalities of bond order in the sense of the bond lengths shown in Fig. 4 (23). The single $p\pi$-orbital at the protonated nitrogen atom then makes a normal contribution to the out-of-plane π-system. In the azaphosphorin, **2**, two electrons are again localised, now in a covalent bond from the endocyclic carbon atom to hydrogen, and the in-plane π-system formed by the P_4N_3 fragment is therefore similar to that in the $N_4P_4Me_8H^+$ ion, and by itself would be expected to induce the same bond length inequalities. However, the out-of-plane system of **2** differs from that of $N_4P_4Me_8H^+$, in that the substitution of the less electronegative carbon for nitrogen in the ring concentrates electron density in the bonds to carbon, primarily at the expense of the neighbouring bonds to nitrogen, so that the changes in the two π-systems tend to compensate one another, an effect not previously found in phosphazene chemistry.

Can. J. Chem. Downloaded from www.nrcresearchpress.com by 210.87.254.6 on 09/05/12
For personal use only.

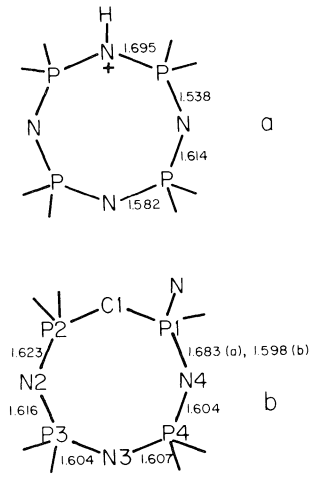

FIG 4. (*a*) Mean bond lengths in $N_4P_4Me_8H^+$; (*b*) ring bond lengths in **2**, showing the approximate cancellation of the inequalities in (*a*) as a result of the substitution of carbon for nitrogen.

The equality of the P—N bond lengths in **2** can then be understood in terms of calculations on a simple planar model, in which the phosphorus atoms are assumed to be homogeneously substituted, and the Coulomb parameter of carbon is taken to be the mean of those of phosphorus and nitrogen. HMO calculations then show that the π-bond order of P(1)N(1) is modified in two ways. In the out-of-plane system, the concentration of π-electron density in the P—C bond weakens the adjacent P—N bond. In the in-plane system, this P—N bond is especially strong, because it is a terminal bond in the P_4N_3 fragment. The qualitative compensation of the two effects, which in detail depends on the assumed parameters, improves with increasing distance from the perturbing centre.

The structure of the benzoyl compound **4** confirms and extends these results. Moderate conjugative electron withdrawal by the benzoyl group is suggested by the near planarity of the environments of C(1) and C(10) (both atoms are within ±0.04 Å of the mean planes of their substituents) and by the comparatively short exocyclic C(1)—C(10) bond (1.434(3) Å, compared to the 1.485 Å expected for a $C(sp^2)$—$C(sp^2)$ single bond (26)). The interaction is perhaps a little weaker than that in the trimeric derivative **3** (2), in agreement with the torsion angles about the CC bond to the azaphosphorin ring (**4**, 29.5°; **3**, 7.7°). The large torsion angle about the C—Ph bond (41.5°) and the length of the C(10)—C(11) bond (1.508(3) Å) both indicate that conjugation with the phenyl group is negligible.

In simple ylids, the P=C bond is lengthened by the attachment of electron-withdrawing substituents to carbon, as can be seen by a comparison of the structures of $Ph_3P{=}CH_2$ (P=C = 1.661 Å (20)) and $Ph_3P{=}CClC(O)Ph$ (P=C = 1.736 Å (27)). In the latter molecule, the partial positive charge on carbon induced (in different ways) by the two substituents increases the electronegativity difference between the phosphorus and carbon atoms and decreases the bond order, as shown by the increase in the length of the P=C bond.[3] In the same way, the benzoyl group in **4** lengthens the endocyclic P—C bonds, and causes a further electronic migration, which appears to be delocalised over the entire ring. The mean endocyclic P—C distance of 1.717(2) Å in **2** is significantly increased to 1.763(4) Å in **4**, and the mean endocyclic P—N bond is decreased correspondingly from 1.609(9) Å in **2**[4,5] to 1.595(4) Å in **4**. Calculations similar to those referred to above show that an increase of electronegativity of C(1) decreases the order of the ring P—C bonds, and increases the mean order of the ring P—N bonds.

The geometry and the electronic interactions of the exocyclic MeNH group are also of interest. The exocyclic PN distances in **2** and **4** are similar to those found in the dimethylaminophosphazenes $(NP(NMe_2)_2)_{3,4,6,8}$ (28–31), in which exocyclic π-bonding seems established. In agreement, the *exo*-PN bond in **4** is slightly shorter than in **2**, reflecting the increase in exocyclic π-bonding that occurs as electron-withdrawing substituents are introduced elsewhere. Quantitatively, the *exo*-π-bonding may be weaker than these geometrical features would suggest. Simple calculations show that if it were strong, it would measurably lengthen the P(1)N(4) bond relative to the others (this may indeed occur to some extent, see above). Experimentally, the coordination round N(1) is significantly non-planar, the mean bond angles at this atom being 113° (**2***a*), 116.4° (**2***b*), 116.1° (**4**). The (limited) π-bonding is evidently easily displaced, because in **3** the *exo*-PN distance is long (1.742 Å) and the amide ν(C=O) is low (1), showing that the *N*-benzoyl group competes effectively with the phosphazene ring for electron density.

A further feature is common to all the molecules. The C(2)P(1)N(1)C(9) groups are rigorously planar within experimental error in **2** and nearly planar in **4** (Fig. 1), the torsion angles about the P(1)N(1) bond being respectively 178(2)°, −179.8(9)°, and −164.8(2)°. The possibility that this is predominantly a π-electron effect is countered by the argument

[3]The secondary effect of *d*-orbital stabilisation is less important.

[4]Here and elsewhere in this report mean values refer to weighted means with rms deviations from the mean in parentheses.

[5]This does not include the distance P(1a)—N(4) (see above).

above, and by the fact that the same relationship holds in the *N*-benzoyl derivative **3** (2), in which the torsion angle is 177.6(2)°. It is likely that exocyclic π-bonding has some effect, but non-bonded (including polar) interactions appear to be decisive.

Acknowledgements

We thank the National Research Council of Canada for financial support, and for NRCC Scholarships (to H.P.C. and R.T.O.), and the University of British Columbia Computing Centre for assistance.

1. R. T. OAKLEY and N. L. PADDOCK. Can. J. Chem. **55**, 3651 (1977).
2. R. T. OAKLEY, N. L. PADDOCK, S. J. RETTIG, and J. TROTTER. Can. J. Chem. **55**, 2534 (1977).
3. P. COPPENS, L. LEISEROWITZ, and D. RABINOVICH. Acta Crystallogr. **18**, 1035 (1965).
4. W. R. BUSING and H. A. LEVY. Acta Crystallogr. **22**, 457 (1967).
5. R. E. LONG. Ph.D. Thesis, University of California at Los Angeles, Los Angeles. 1965.
6. D. T. CROMER and J. B. MANN. Acta Crystallogr. Sect. A, **24**, 321 (1968).
7. R. F. STEWART, E. R. DAVIDSON, and W. T. SIMPSON. J. Chem. Phys. **42**, 3175 (1965).
8. D. T. CROMER and D. LIBERMAN. J. Chem. Phys. **53**, 1891 (1970).
9. P. J. BECKER and P. COPPENS. Acta Crystallogr. Sect. A, **30**, 129 (1974); **30**, 148 (1974); **31**, 417 (1975).
10. P. COPPENS and W. C. HAMILTON. Acta Crystallogr. Sect. A, **26**, 71 (1970).
11. F. R. THORNLEY and R. J. NELMES. Acta Crystallogr. Sect. A, **30**, 748 (1974).
12. V. SCHOMAKER and K. N. TRUEBLOOD. Acta Crystallogr. Sect. B, **24**, 63 (1969).
13. D. W. J. CRUICKSHANK. Acta Crystallogr. **9**, 747 (1956); **9**, 754 (1956); **14**, 896 (1961).
14. M. W. DOUGILL. J. Chem. Soc. 5471 (1961).
15. R. T. OAKLEY, N. L. PADDOCK, S. J . RETTIG, and J. TROTTER. Can. J. Chem. **55**, 4206 (1977).
16. M. W. DOUGILL and B. SHELDRICK. Acta Crystallogr. Sect. B, **33**, 295 (1977).
17. R. T. OAKLEY, N. L. PADDOCK, S. J. RETTIG, and J. TROTTER. Can. J. Chem. **55**, 3118 (1977).
18. R. T. OAKLEY, N. L. PADDOCK, S. J. RETTIG, and J. TROTTER. Can. J. Chem. **55**, 2530 (1977).
19. K. D. GALLICANO, R. T. OAKLEY, N. L. PADDOCK, S. J. RETTIG, and J. TROTTER. Can. J. Chem. **55**, 304 (1977).
20. J. C. J. BART. J. Chem. Soc. Sect. B, 350 (1969).
21. G. CHIOCCOLA and J. J. DALY. J. Chem. Soc. Sect. A, 568 (1968).
22. W. C. MARSH and J. TROTTER. J. Chem. Soc. Sect. A, 573 (1971); T. N. RANGANATHAN, S. M. TODD, and N. L. PADDOCK. Inorg. Chem. **12**, 316 (1973).
23. J. TROTTER and S. H. WHITLOW. J. Chem. Soc. Sect. A, 455 (1970).
24. H. P. CALHOUN and J. TROTTER. J. Chem. Soc. Dalton Trans. 377 (1974).
25. H. P. CALHOUN, N. L. PADDOCK, and J. TROTTER. J. Chem. Soc. Dalton Trans. 2708 (1973).
26. M. J. S. DEWAR and H. N. SCHMEISING. Tetrahedron, **11**, 96 (1960).
27. F. S. STEPHENS. J. Chem. Soc. 5640 (1965); 5658 (1965).
28. S. J. RETTIG and J. TROTTER. Can. J. Chem. **51**, 1295 (1973).
29. G. J. BULLEN. J. Chem. Soc. 3193 (1962).
30. A. J. WAGNER and A. VOS. Acta Crystallogr. Sect. B, **24**, 1423 (1968).
31. H. P. CALHOUN, N. L. PADDOCK, and J. TROTTER. J. Chem. Soc. Dalton Trans. 38 (1976).

Can. J. Chem. Downloaded from www.nrcresearchpress.com by 210.87.254.6 on 09/05/12
For personal use only.

Horseradish peroxidase. XXIX. Reactions in water and deuterium oxide: cyanide binding, compound I formation, and reactions of compounds I and II with ferrocyanide[1]

H. BRIAN DUNFORD, W. DONALD HEWSON,[2] AND HÅKAN STEINER[3]

Department of Chemistry, University of Alberta, Edmonton, Alta., Canada T6G 2G2

Received August 30, 1977[4]

H. BRIAN DUNFORD, W. DONALD HEWSON, and HÅKAN STEINER. Can. J. Chem. **56**, 2844 (1978).

The kinetics of the reactions of hydrogen peroxide and cyanide with native horseradish peroxidase, as well as reactions of compounds I and II with ferrocyanide have been studied in ordinary water and in deuterium oxide at 25°C and ionic strength 0.11 using a stopped-flow apparatus. Rate constants for all reactions were measured over a wide range of acidity in both solvents from which equilibrium and kinetic isotope effects were evaluated. Protonation of an ionizable group on the enzyme with a pK_a value of 4.15 ± 0.05 in water inhibits the reactions with both hydrogen peroxide and cyanide. A significant kinetic isotope effect, k_H/k_D = 1.6 ± 0.1, was measured for compound I formation whereas no significant kinetic isotope effect was found for cyanide binding. On the basis of these findings, a partial mechanism for compound I formation is proposed in which the group of pK_a 4.15 plays a crucial role. The pH dependencies of the ferrocyanide reaction in the pH interval 4.5–10.8 confirmed the role of an acid group with a pK_a of 5.2 for compound I and for compound II a pK_a of 8.6 and another with a value lower than that encompassed by the pH range of the study. Equilibrium isotope effects were found but no kinetic isotope effects for either the reaction of compound I or of compound II. This suggests that there are no rate-limiting proton transfers in the reactions between ferrocyanide and compounds I and II of horseradish peroxidase. The only reducing substrates which exhibit positive k_H/k_D values possess a labile proton.

H. BRIAN DUNFORD, W. DONALD HEWSON et HÅKAN STEINER. Can. J. Chem. **56**, 2844 (1978).

Faisant appel à un appareil à flux stoppé, on a étudié la cinétique des réactions du peroxyde d'hydrogène et du cyanure avec le peroxydase naturelle du raifort, de même que les réactions du composé I et II avec le ferrocyanure dans l'eau ordinaire et dans l'oxyde de deutérium à 94% à 25°C et une force ionique de 0.11. On a mesuré les constantes de vitesse pour toutes les réactions dans les deux solvants à divers degrés d'acidité, en se basant sur ces constantes de vitesse, on a pu évaluer l'équilibre et les effets isotopiques cinétiques. Dans l'eau la protonation d'un groupe ionisable de l'enzyme, pK_a de 4.15 ± 0.05 inhibe les réactions tant avec le peroxyde d'hydrogène qu'avec le cyanure. On a mesuré un effet isotopique cinétique important, k_H/k_D = 1.6 ± 0.1, pour la formation du composé I alors que l'on n'a pas trouvé d'effet isotopique cinétique pour la fixation du cyanure. Sur la base de ces données, on propose un mécanisme partiel pour la formation du composé I dans lequel le groupe pK_a 4.15 joue un rôle crucial. Le fait que la réaction du ferrocyanure dépend du pH dans l'intervalle de 4.5–10.8 confirme qu'un groupe acide de pK_a = 5.2 joue un rôle pour le composé I; dans le cas du composé II, il existerait deux groupes acides l'un de pK_a 8.6 et l'autre avec une valeur plus faible que celle couverte par l'intervalle de pH étudié. On a trouvé les effets isotopiques d'équilibre mais l'on n'a trouvé aucun effet isotopique cinétique pour les réactions soit du composé I soit du composé II. Ceci suggère qu'il n'y a pas de transfert du proton qui détermine la vitesse des réactions entre le ferrocyanure et les composés I et II de la peroxydase du raifort. Les seuls substrats réducteurs qui présentent des valeurs positives de k_H/k_D possèdent un proton labile.

[Traduit par le journal]

Introduction

Near neutral pH, compound I formation is a fast reaction with an Arrhenius activation energy similar in magnitude to the activation energy of diffusion in aqueous solution (1); however, this reaction rate was shown not to be diffusion controlled by studies in solutions of high viscosity (2). The same conclusion has been reached for compound I formation from cytochrome c peroxidase (3). It has been shown that the rates of compound I formation and cyanide binding are both inhibited by ethanol, which probably acts as a ligand in the sixth coordination position of the heme iron (2), and that cyanide inhibits compound I formation (4, 5). The main purpose of the present kinetic study of these two reactions in water and deuterium oxide was under-

[1]Supported by a grant from the National Research Council of Canada. The previous three papers in this series are refs. 2, 28, and 45.

[2]Currently holder of an NRCC Postdoctoral Fellowship. Present address: Department of Biochemistry, University of Illinois, Urbana, IL 61801, U.S.A.

[3]Recipient of a travel grant from the Swedish National Research Council. Present address: Mikrobiologiska Institutionen, Stockholms Universitet, S-106 91 Stockholm 50, Sweden.

[4]Revision received July 11, 1978.

Can. J. Chem. Downloaded from www.nrcresearchpress.com by 210.87.254.105 on 09/05/12
For personal use only.

Can. J. Chem. Downloaded from www.nrcresearchpress.com by 210.87.254.105 on 09/05/12
For personal use only.

taken for further comparisons between these two reactions in the hope of obtaining a more detailed picture of their mechanisms. A study of the ionic strength dependence for the rate of compound I formation was undertaken as a further test as to whether hydrogen peroxide, or its conjugate base, is the diffusing substrate.

The kinetics of the reactions of compounds I and II with several different reducing substrates have been studied in our laboratory (6–11). The pH dependencies of reaction rates have indicated that an acid group with a pK around 5.2 is important in compound I catalyzed reactions. In compound II two groups, one with pK 8.6, the other with a very low pK, have varying influence on reaction rates. To gain further insight into the mechanisms of proton transfer in these redox reactions the effect of changing from water to deuterium oxide was studied (12, 13). A preliminary study involved the oxidation of iodide, *p*-cresol, and ferrocyanide by compound II in deuterium oxide which represented the first attempt to get kinetic and equilibrium H/D ratios for peroxidase reactions (12). *p*-Aminobenzoic acid (PABA) has a pH–rate profile similar to that of ferrocyanide in its reaction with compound II; in later more intensive studies the reactions of PABA with both compound I and compound II were examined in both water and deuterium oxide (10, 13). A self-consistent and rather detailed picture emerged of the mechanisms, particularly of the compound II reactions (12–16). However, there remained certain anomalies about the ferrocyanide reaction with compound II. The present kinetic isotopic study conducted over a wide range of pH (pD) was undertaken to resolve details about the reaction of ferrocyanide ion with compound II and to extend the results to its reaction with compound I.

Experimental

Horseradish peroxidase (E.C.1.11.1.7 donor–H_2O_2–oxidoreductase) was purchased from Sigma as a lyophilized salt-free powder (Type VI, lot 25C-9570) and from Boehringer-Mannheim as purified ammonium sulfate precipitates (lots 7315529, 1366531, and 1067433). The enzyme was prepared for use by extensive dialysis against multiply distilled water (17) followed by Millipore filtration. After dialysis the purity numbers, the ratio of absorbance at 403 to 280 nm, for the four lots were 3.1, 3.3, 3.4, and 3.5. It has been determined that isozyme C (18, 19) is the major component of many commercial preparations (20, 21).

Deuterium oxide was purchased from Diaprep and Columbia Organic Chemicals, Co. with stated isotopic purities of 99.7% or greater. All other chemicals were reagent grade and used without further purification.

Absorbance spectra and measurements were obtained with a Cary 14 spectrophotometer. Kinetic measurements were obtained with a Gibson-Durrum stopped-flow apparatus model D-110. Greater than a 10-fold excess of hydrogen peroxide, cyanide, or ferrocyanide relative to the enzyme concentration was used which ensured pseudo-first-order kinetics. The enzyme concentration for all kinetic experiments was 0.6–0.8 μM. Reaction rates were monitored at 403 nm for compound I formation and 420 nm for cyanide binding. Because of the big difference in reaction rates of compounds I and II with ferrocyanide both reactions could be studied by starting with compound I which was prepared using slightly less than a molar equivalent of hydrogen peroxide. First the compound I reaction was followed at 410 nm, the isobestic wavelength between compound II and native HRP. Then the monochromator was reset at 422 nm and the compound II reaction was followed. For most experiments both drive syringes of the stopped-flow apparatus contained 0.1 M potassium nitrate and buffer of an ionic strength of 0.01 for a total ionic strength of 0.11. However, to avoid the denaturation of the enzyme in acidic solutions below pH 3.7 a pH jump method was used in which only the drive syringe containing the substrate held the buffer with an ionic strength of 0.02. This pH jump method is viable since the rate of compound I formation or cyanide binding is faster than the rate of denaturation but slower than the rate of protonation of the enzyme when mixed with the buffer. At most pH values one substrate concentration was used and between 5 and 10 traces were collected in the absorbance mode. The best parameters for the recorded single exponentials were found from a non-linear least-squares analysis as earlier described (11). The reported second-order rate constants are mean values obtained by dividing the first-order constant by the substrate concentration, which for compound II reactions had been corrected for the decrease caused by converting compound I to II.

The concentration of horseradish peroxidase was determined spectrophotometrically at 403 nm using a molar absorptivity of $1.02 \times 10^5\ M^{-1}\ cm^{-1}$ (22) and that of hydrogen peroxide was checked weekly using the horseradish peroxidase assay (9). Potassium cyanide solutions were prepared immediately before the experiments were carried out and were not used for more than a few hours.

The acidity of the solutions in ordinary water and 94% deuterium oxide was measured with a Fisher 420 digital pH meter equipped with a Fisher combination glass electrode calibrated to ± 0.03 pH units. Measurements of pD were made using this glass electrode in the deuterium oxide solutions (23, 24). The usual equation of Glasoe and Long was modified to account for solutions less than 100% deuterium oxide. In eq. [1] pH_{obs} is the observed meter reading in the deuterium

$$[1] \qquad pD = pH_{obs} + 0.38$$

oxide solution when the glass electrode had been calibrated with standard buffers in ordinary water. The pH (pD) measurements were made using the purged solutions from the stopped-flow apparatus.

Results

Compound I Formation

The values of the apparent second-order rate constants, k_a, for compound I formation in ordinary water and 94% deuterium oxide are plotted against pH (pD) in Fig. 1. Seven of the values of k_a in ordinary water from pH 3.19 to 9.76 were obtained as slopes of linear plots of k_{obs} vs. the concentration of hydrogen peroxide, which had zero intercepts (25). These order-with-respect-to-concentration data were obtained with the preparation of horseradish peroxidase from the Sigma Chemical Company. The agreement among the rate constants determined for

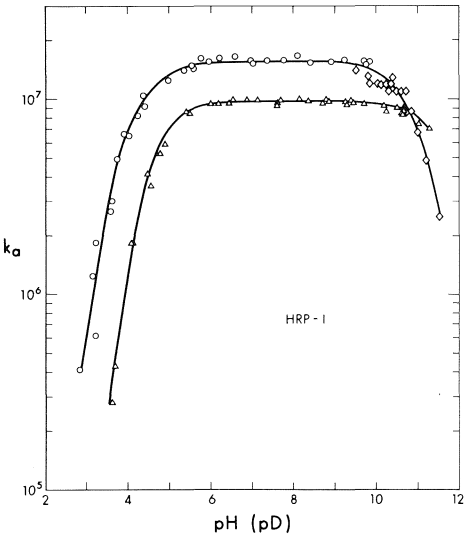

FIG. 1. Compound I formation as a function of pH (pD). Semilogarithmic plots of the apparent second-order rate constant in ordinary water (○, this work); (◇, taken from ref. 28) and 94% deuterium oxide (△). The curves were calculated using eq. [3] which yielded the constants in Table 1.

this enzyme from separate sources, Sigma and Boehringer-Mannheim, is excellent.

The rate of compound I formation has been studied carefully at lower pH values in light water, with two acid groups of pK_a values 3.2 and 3.9 appearing to influence the kinetics (26). The alkaline transition of peroxidases is also well documented (27–33) which leads to reaction [2] for which K_1

$$\begin{array}{lcl} & EH_3 & \\ & \uparrow\downarrow & \\ & EH_2 & \\ & {\scriptstyle K_2}\uparrow\downarrow & \\ [2] \quad & EH + H_2O_2 \xrightarrow{k_a} & \text{Compound I} \\ & {\scriptstyle K_1}\uparrow\downarrow & \\ & E & \end{array}$$

represents the alkaline transition of HRP and K_2 an acid ionization in the active site. From the results of the present study the influence of the most acid group could not be detected, so that values for the three parameters only, labelled in eq. [2], are quoted. The restricted kinetic scheme based upon [2] leads to [3].

$$[3] \qquad k_{app} = \frac{k_a}{1 + \frac{K_1}{[H^+]} + \frac{[H^+]}{K_2}}$$

Above pH 10 saturation kinetics are observed in water, so that a more complicated analysis is required. The values of k_{app} quoted in (28) are also plotted in Fig. 1 and were used in the nonlinear least-squares analysis of [3]. The study in D_2O was terminated at pD = 11.28 and the decrease in rate at the highest pD values should be fairly accurately defined, although order-with-respect-to-concentration plots were not conducted in this region. The values of K_1, K_2, and k_a, obtained for both water and deuterium oxide, are compiled in Table 1 and were used to calculate the smooth curves in Fig. 1. The substrate species which diffuses to the enzyme is uncharged hydrogen peroxide, as indicated by absence of any ionic strength dependence (Table 2) which confirms the results obtained using the diffusion-controlled limit rule (14).

Much of the hydrogen in a protein is readily exchanged with deuterium when the protein is dissolved in deuterium oxide (34–37). However, longer incubation times are required to exchange the less labile amide hydrogen of the protein backbone (35). To determine the effect of the extent of deuterium exchange upon the rate of compound I formation, solutions at pD values of 5.45, 7.59, and 9.41 were incubated for 1.2 hours at 25°C in 94% deuterium oxide. The normal incubation time ranged from 15 to 20 min. No slowly exchanging hydrogen had an effect upon the rate of compound I formation at these pD values.

The hydrogen in hydrogen peroxide can also exchange with deuterium as demonstrated using nuclear magnetic resonance. The resonance peak of hydrogen peroxide, which was observed when 50 μl of 98% hydrogen peroxide were dissolved in 0.4 ml of acetone-d_6, disappeared when the hydrogen peroxide was dissolved in a readily exchangeable solvent such as acetic acid-d_4. The exchangeability of hydrogen in hydrogen peroxide has been proven by other methods (38).

Cyanide Binding

The values of the apparent second-order rate constants for cyanide binding to horseradish peroxidase in ordinary water and in 94% deuterium oxide are plotted semilogarithmically against pH (pD) in Fig. 2. In acid solution the binding of cyanide has been carefully studied in ordinary water with the influence of acid groups of pK_a values of 2.9 and 3.9 being detected (26). The reaction is also inhibited by the ionization of hydrocyanic acid near pH 9 and by the alkaline ionization of HRP (28, 39). There also is a barely discernible inhibition between pH 6 and 7 which was deduced previously by applying the principle of detailed balancing (39). However, this ionizable group is not adequately defined in 94% deuterium oxide and it has been ignored in the

Can. J. Chem. Downloaded from www.nrcresearchpress.com by 210.87.254.105 on 09/05/12
For personal use only.

Can. J. Chem. Downloaded from www.nrcresearchpress.com by 210.87.254.105 on 09/05/12
For personal use only.

TABLE 1. Compound I formation. Kinetic parameters obtained by a nonlinear least-squares analysis of the data in Fig. 1 (according to eq. [3])

Parameter[a]	Value		
	H_2O	94% D_2O	Comparison
k_a ($M^{-1}s^{-1}$)	$(1.55\pm0.05)\times10^7$	$(9.7\pm0.2)\times10^6$	$k_H/k_D = 1.6\pm0.1$
pK_1	10.90 ± 0.06	11.7 ± 0.1	$\Delta pK_1 = 0.8\pm0.2$
pK_2	4.11 ± 0.03	4.56 ± 0.03	$\Delta pK_2 = 0.45\pm0.06$

[a]Errors are standard deviations computed by the nonlinear least-squares analysis.

TABLE 2. Second-order rate constants for compound I formation as a function of total ionic strength in phosphate buffer pH 7.04 at 40°C

$10^{-7}\times k_{app}$ ($M^{-1}s^{-1}$)	Total ionic strength
1.99 ± 0.05	0.01
1.96 ± 0.05	0.02
2.04 ± 0.06	0.03
2.00 ± 0.07	0.04
1.94 ± 0.07	0.05
1.93 ± 0.07	0.06
2.02 ± 0.07	0.07
2.04 ± 0.07	0.08
2.00 ± 0.1	0.09
1.99 ± 0.06	0.10
2.03 ± 0.10	0.11

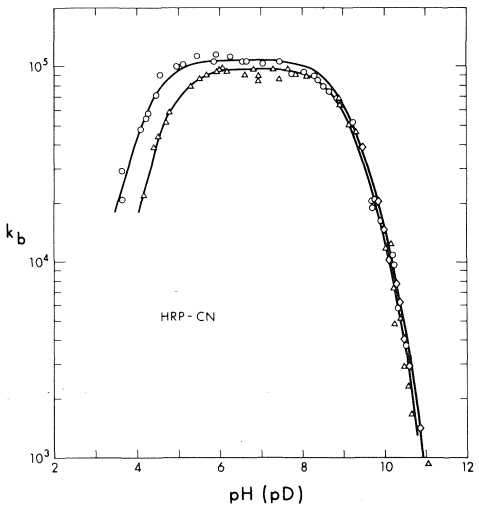

FIG. 2. Cyanide binding as a function of pH (pD). Semi-logarithmic plots of the apparent second-order rate constant in ordinary water (○, this work); (◇, taken from ref. 28) and 94% deuterium oxide (△). The curves were calculated using eq. [5] which resulted in the constants listed in Table 3.

present analysis. Thus the pH profile for the rate of cyanide binding in ordinary water involves a minimum of three ionizations on the enzyme and the ionization of hydrocyanic acid. This leads to the kinetic scheme [4] where K_3 and K_4 are acid dissocia-

[4]
$$\begin{array}{ccccc} EH_3 & & & & \\ \uparrow\downarrow & & & & \\ EH_2 & & & & \\ K_4\uparrow\downarrow & & & & \\ EH & + HCN & \xrightarrow{k_b} & ECN & + H^+ \\ K_3\uparrow\downarrow & & \uparrow\downarrow K_5 & & \\ E & & CN^- & & \end{array}$$

tion constants of the enzyme, K_5 is the acid dissociation constant of hydrocyanic acid, and k_b is the pH independent second-order rate constant. Our data do not extend to sufficiently acid solutions to duplicate earlier measurements of the most acid ionization (26). Using only the above parameters, [4] leads to [5].

[5]
$$k_{app} = \frac{k_b}{\left(\frac{K_3}{[H^+]} + 1 + \frac{[H^+]}{K_4}\right)\left(1 + \frac{K_5}{[H^+]}\right)}$$

Further cyanide kinetic results for the alkaline region in H_2O were added to the analysis (28). The experimental data are displayed in Fig. 2 along with the best-fit curves computed on the basis of nonlinear least-squares analysis of eq. [5] and its analog for deuterium oxide. The best-fit parameters are listed in Table 3.[5]

A sample of the enzyme was incubated in 94% deuterium oxide for 1.2 h at 25°C and at pD 6.92, and reacted with cyanide at the same rate as a sample incubated at this pD for only 15 min.

Reactions of Compounds I and II with Ferrocyanide

The reactions under all conditions are first order with respect to ferrocyanide and enzyme as shown earlier (8, 9, 12). The second-order rate constants as a function of pH in light and heavy water for the reaction of ferrocyanide with compounds I and II

[5]All of the experimental data in Figs. 1 and 2 are available upon request, at a nominal charge, from the Depository of Unpublished Data, CISTI, National Research Council of Canada, Ottawa, Ont., Canada K1A 0S2.

Can. J. Chem. Downloaded from www.nrcresearchpress.com by 210.87.254.105 on 09/05/12
For personal use only.

TABLE 3. Cyanide binding. Parameters obtained by a nonlinear least-squares analysis of the data in Fig. 3 (according to eq. [5])

Parameter[a]	Value		
	H_2O	94% D_2O	Comparison
k_b ($M^{-1}s^{-1}$)	$(1.06\pm0.04) \times 10^5$	$(9.6 \pm0.3) \times 10^4$	$k_H/k_D = 1.1 \pm0.1$
pK_3	10.8 ± 0.3	11.1 ± 0.5	
pK_4	4.20 ± 0.05	4.70 ± 0.06	$\Delta pK_4 = 0.5 \pm0.1$
pK_5	9.14 ± 0.05	9.21 ± 0.05	$\Delta pK_5 = 0.07\pm0.10$

[a]Errors are standard deviations computed by the nonlinear least-squares analysis.

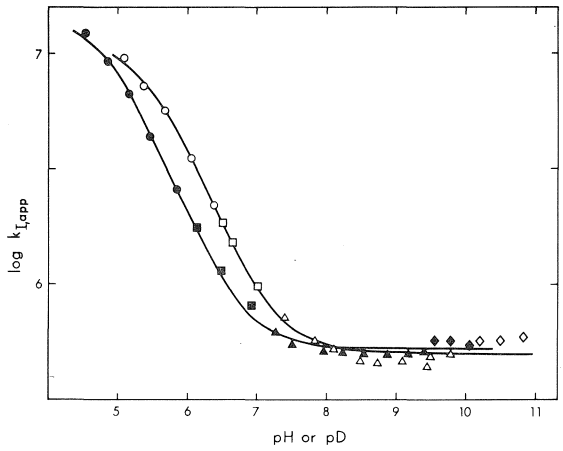

FIG. 3. Plot of the logarithm of the second-order rate constant, $k_{I,app}$, for the reaction of HRP-I with $Fe(CN)_6^{4-}$ vs. pH (solid symbols) and pD (open symbols). The curves were generated by a nonlinear least-squares fit of eq. [7]. The buffers were: acetate, ○ and ●; phosphate, □ and ■; Tris, △ and ▲; bicarbonate, ◇ and ◆.

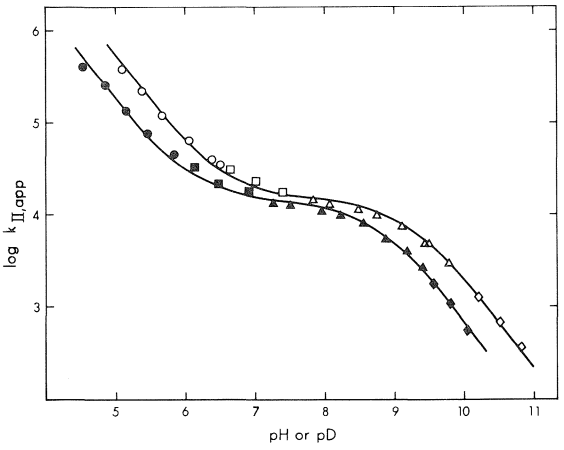

FIG. 4. Plot of the logarithm of the second-order rate constant, $k_{II,app}$, for the reaction of HRP-II with $Fe(CN)_6^{4-}$ vs. pH (solid symbols) and pD (open symbols). The curves were generated by a nonlinear least-squares fit of eq. [9]. Buffers as in Fig. 3.

are given in Figs. 3 and 4. The results in ordinary water are in good agreement with the earlier studies.

For compound I the following model was used. EH and E represent HRP-I with a catalytically important group protonated and deprotonated; K_6 is the corresponding acid dissociation constant and k_1 and k_2 are second-order rate constants.

[6]
$$\begin{array}{ccc} EH + S & \xrightarrow{k_1} & \text{products} \\ H^+\uparrow\downarrow K_6 & & \\ E + S & \xrightarrow{k_2} & \text{products} \end{array}$$

The apparent second-order rate constant, $k_{I,app}$, is given by eq. [7] which gave a best fit to the experimental data with the parameter values given in Table 4. The model seems equally appropriate in both H_2O and D_2O.

[7]
$$k_{I,app} = \frac{k_1 + k_2\dfrac{K_6}{[H^+]}}{1 + \dfrac{K_6}{[H^+]}}$$

For compound II reaction [8] expressed in terms of ionization of the native enzyme adequately describes the observed rates. An alternative but equivalent explanation in terms of a transition state ionization constant has been given (9).

[8]
$$\begin{array}{ccc} EH_2 + S & \xrightarrow{k_3} & \text{products} \\ H^+\uparrow\downarrow K_7 & & \\ EH + S & \xrightarrow{k_4} & \text{products} \\ H^+\uparrow\downarrow K_8 & & \\ E & & \end{array}$$

EH_2, EH, and E are three differently protonated forms of HRP-II; K_7 and K_8 are the corresponding molecular acid dissociation constants and k_3 and k_4 are second-order rate constants. The apparent second-order rate constant, $k_{II,app}$, for this scheme

TABLE 4. Parameters obtained from the pH dependencies of the second-order rate constant for the reduction of HRP-I by ferrocyanide in H_2O and D_2O

Parameter	Value[a]		
	H_2O	97.3% D_2O	Ratio of parameter in H_2O/D_2O
k_1 ($M^{-1}s^{-1}$)	1.4×10^7 ($\pm$6.8%)	1.1×10^7 ($\pm$9.1%)	1.2 ($\pm$16%)
k_2 ($M^{-1}s^{-1}$)	5.2×10^5 ($\pm$2.0%)	5.0×10^7 ($\pm$2.7%)	1.0 ($\pm$4.8%)
K_6 (M)	7.5×10^{-6} ($\pm$11%)	2.3×10^{-6} ($\pm$15%)	3.3 ($\pm$26%)

[a]The errors are given as $\pm$ the relative standard deviation.

TABLE 5. Parameters obtained from the pH dependencies of the second-order rate constant for the reduction of HRP-II by ferrocyanide in H_2O and D_2O

Parameter	Value[a]		
	H_2O	97.3% D_2O	Ratio of parameter in H_2O/D_2O
k_4 ($M^{-1}s^{-1}$)	1.4×10^4 ($\pm$6.1%)	1.5×10^4 ($\pm$4.8%)	0.95 ($\pm$11%)
K_8 (M)	1.9×10^{-9} ($\pm$10%)	6.5×10^{-10} ($\pm$8.0%)	2.9 ($\pm$18%)
k_3/K_8 ($M^{-2}s^{-1}$)	1.8×10^{10} ($\pm$6.7%)	5.2×10^{10} ($\pm$5.4%)	0.34 ($\pm$12%)

[a]The errors are given as $\pm$ the relative standard deviation.

is given by [9] and the best fit parameters and

$$[9]\qquad k_{II,app} = \frac{\frac{k_3[H^+]}{K_7} + k_4}{1 + \frac{K_8}{[H^+]}}$$

isotope effects are shown in Table 5.

Discussion

Reactions of Cyanide and Hydrogen Peroxide

In ordinary water the protonation of an ionizable group with a pK_a value of 4.15 $\pm$ 0.05 inhibits both compound I formation and cyanide binding (see Table 2, pK_2, for hydrogen peroxide and Table 4, pK_4, for cyanide) in reasonable agreement with previous results (26). In 94% deuterium oxide, pK_2 has shifted to 4.56 for compound I formation and pK_4 to 4.70 for cyanide binding, the same within their standard deviations. Therefore, pK_2 and pK_4 likely refer to the same ionizable group on the enzyme.

Both reactions have pH independent apparent rate constants near neutral pH, with an exception for the small effect of $pK_a = 6.4$ for cyanide binding in light water (39); the latter effect has been detected by nmr (40). For compound I formation, this pH independent region extends approximately from pH 5.5 to 9.5. In the case of cyanide binding, the apparent rate constant decrease in the alkaline region is readily attributed to the ionization of hydrocyanic acid, $pK_5 = 9.14$. The rate constant for cyanide binding is not sufficiently large to invoke the diffusion controlled limit rule unequivocally (14) but one does obtain an abnormally large rate constant if it is assumed that CN^- is the diffusing reactant (26).

Only the data for compound I formation were obtained with sufficient accuracy to quantify the equilibrium isotope effect on the pK_a value of the ionizable group responsible for the conversion of horseradish peroxidase to its alkaline form. From Table 5, a pK_1 value of 10.89 agrees well with previous values determined by kinetic and other methods (27–33). With the exception of the negligible ΔpK_5 for hydrocyanic acid, discussed elsewhere (58), conventional magnitudes for the equilibrium isotope effects are observed (41–44).

Since compound I formation and cyanide binding have large regions where the k_{app} is pH independent, it is possible to draw certain conclusions about the kinetic isotope effects. For k_a of compound I formation, the value of k_H/k_D is 1.6. Therefore the rate of compound I formation is influenced by the rate of proton (deuteron) transfer. This provides another piece of evidence that the rate of compound I formation at neutral pH is not diffusion controlled (2). In contrast, the binding of cyanide shows no appreciable kinetic isotope effect.

The finding of a kinetic isotope effect for compound I formation supports a partial mechanism which involves the heterolytic breaking and forming of oxygen–hydrogen covalent bonds (45). Com-

Can. J. Chem. Downloaded from www.nrcresearchpress.com by 210.87.254.105 on 09/05/12
For personal use only.

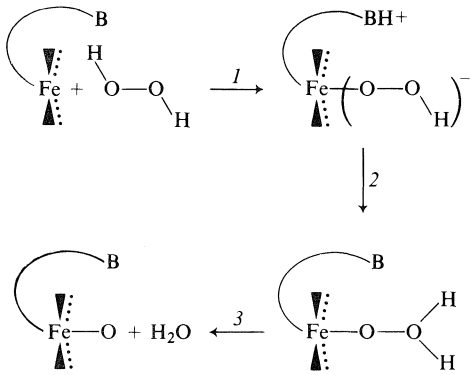

FIG. 5. Schematic representation of compound I formation. The basic group B on the enzyme has a pK_a of 4.15 ± 0.05 in H_2O. The kinetic isotope effect might occur in reaction *1*, where H_2O_2 is converted into the excellent nucleophile OOH^-, or in reaction *2* where a hydroxide ion is converted into the much better leaving group H_2O.

pound I formation results in no net gain or loss of protons (46) and a proposed mechanism involves proton transfer from hydrogen peroxide to the enzyme, formation of an iron–oxygen bond, followed by proton transfer to the bound HO_2^- ion and departure of water as illustrated in Fig. 5. It is not possible to ascertain which of the two proton transfers in this mechanism is part of the rate-determining step, since supporting evidence can be found for either of the two possibilities. In either case, the small magnitude of the kinetic isotope effect would indicate either that the proton transfer is not the sole rate-limiting step but that it is occurring in concert with a second process or there is a considerable isotope effect in the transition state cancelling the zero point energy difference of the initial reactants (47).

The first proton transfer (reaction *1* in Fig. 5) from hydrogen peroxide to the enzyme results in formation of the excellent nucleophile HO_2^- so that the first proton transfer and the initial binding step to the ferric ion might be concerted processes. An essential feature of acid–base catalysis is that there is a large shift in the pK_a values during the course of the reaction (48, 49) and a large downward shift would occur in the pK_a value of hydrogen peroxide as it binds to the ferric ion. Appropriate positioning of the basic group B could facilitate compound I formation from the bent hydrogen peroxide molecule and retard cyanide binding from the linear HCN molecule. (There is a 100-fold difference in rate.) The second proton transfer (reaction *2*, Fig. 5), which has no counterpart in cyanide binding, converts hydroxide ion into the much better leaving group H_2O, so that again there may be two processes occurring in a concerted fashion. Evidence is accumulating that the product release is often the rate-determining step in an enzymatic reaction (50). The partial mechanism outlined in Fig. 4 shows the transfer of two oxidizing equivalents by an oxygen atom to the iron center of the heme. It does not take into account the ultimate formation of free radical and Fe(IV) species. (For a review, see ref. 16.) The absence of a kinetic isotope effect for cyanide binding could indicate that a step such as transfer of the hydrocyanic acid molecule from the outer to the inner coordination sphere of the ferric ion is rate limiting.

The role of a basic group in facilitating the initial peroxide binding step has been discussed (51). The pH–rate profile for HRP (26) and turnip peroxidase (52) and the present isotope study provide evidence as to the actual nature of the group. A pK_a of 4.0 ± 0.1 could indicate a carboxyl group and there are many aspartate and glutamate residues present. However, studies on peroxidases with modified prosthetic groups suggest that a propionate side chain of the hemin group may be involved (53, 54). Although both propionate groups are hydrogen bonded to protein residues in other heme proteins, and thus contribute to the tightness of the heme binding to apoprotein, there is at present no direct evidence of a similar situation for peroxidase. The hemin vinyl groups of peroxidase are deeply buried in a hydrophobic region and they may contribute to the stability of binding of the prosthetic group (55). Space-filling models show that a propionate group may be positioned appropriately to act as both proton acceptor and donor. A related role for a propionate group had been postulated for metmyoglobin ligand binding reactions (56).

Compounds I and II Plus Ferrocyanide

The two substrates of intermediate reactivity with compound II, i.e. ferrocyanide and PABA, have pH–rate profiles consistent with a combined mechanism in which they are oxidized according to a general acid catalysis mechanism at high pH (group of pK_a 8.6) and a specific acid catalysis mechanism at low pH (group of pK_a ~ 0). In the PABA case the isotope effects were completely consistent with this combined mechanism (13). For the ferrocyanide reaction with compound II the same equilibrium isotope effect was found at low pH but in the neutral and basic regions both the equilibrium and kinetic isotope effects appeared small and reversed (12). The present intensive study in both water and deuterium oxide confirms the equilibrium effect with a reasonable pK isotopic shift for the group with pK ~ 0. It also indicates a reasonable equilibrium isotopic shift for the group with pK of 8.6 and no kinetic

Can. J. Chem. Downloaded from www.nrcresearchpress.com by 210.87.254.105 on 09/05/12
For personal use only.

Can. J. Chem. Downloaded from www.nrcresearchpress.com by 210.87.254.105 on 09/05/12
For personal use only.

isotope effect in neutral or basic solutions. The lack of a kinetic isotope effect could be due to the fact that complete or partial proton transfer is not part of the reaction or at least not rate limiting. The fact that the ferrocyanide does not differ from the product ferricyanide in proton content should not be taken as evidence for protons not taking part in the reaction. There is a net uptake of one proton by the enzyme when ferrocyanide is reducing compound II as well as compound I (46). The participation of protons is also obvious from the influence on reaction rates of differently protonated enzyme species. A possible alternative explanation of the lack of a kinetic isotope effect is that there is a rate-limiting proton transfer but the transition state resembles the reactants. For a partial proton transfer as has been suggested (12) this explanation would mean the same as no proton transfer at all. The present studies do not bring support to the idea of a rate-limiting, partial proton transfer from a distal group to a ligand in compound II with ferrocyanide as a substrate. The rate of an internal proton transfer between two groups in the enzyme should not be influenced to this extent by changing the substrate but merely be set by the difference in pK between the two groups if $pK_{donor} - pK_{acceptor}$ is positive (57). Part of the problem in the original explanation of the HRP-II–ferrocyanide isotope effects was caused by trying to attribute all effects in the neutral and alkaline regions to one acid group on the enzyme; the proton balance work shows clearly that another proton is involved.

The pD–rate profile for compound I reduction with $Fe(CN)_6^{4-}$ in D_2O is identical with the one obtained in H_2O except for a normal pK_a shift of 0.52 ± 0.11. This behaviour is a further indication that the obtained pK_a value reflects a single group being titrated and not more complex prototropic equilibria.

The PABA study (13) and the present one of ferrocyanide are the only complete studies of isotope effects as a function of pH for both compounds I and II. A further comparison of the two sets of results seems worthwhile. The pH–rate profiles for compound II are similar for both substrates. So are the profiles for compound I except that there are some special features at low pH for the PABA reaction, most likely owing to protonation of the substrate. The parallelism between compounds I and II with respect to the behaviour upon isotopic substitution is remarkable: a kinetic isotope effect for both reactions when PABA is employed as a substrate and no kinetic effect for either of them when ferrocyanide is the substrate. It is not less remarkable when considering the fact that the proton transfers are rate limiting with the less reactive substrate, PABA, and not for ferrocyanide which reacts 100 times faster. The two behaviours appear to emanate from a fundamental difference in the mechanism of reaction of the substrates. The most striking difference that could be the cause is the protons carried on the amino group of PABA (or the proton on the phenolic group of *p*-cresol). Removal of a proton from these functional groups could be the rate-limiting step for the reactions of compounds I and II with both of these substrates. For ferrocyanide the proton needed in the overall reaction could be derived from the solvent after a rate-limiting electron transfer.

In summary, the most self-consistent explanation of all of the results on PABA and ferrocyanide to date is that two acid groups in compound II and one in compound I facilitate electron transfer to the enzyme through proton equilibria. When a positive k_H/k_D effect is observed the required proton for conversion of compound I to II or II to the native enzyme (46) is derived from the substrate in a rate-controlling step; where there is no kinetic isotope effect the proton is derived from the solvent in a non rate-controlling step.

Acknowledgement

We thank Miss I. Ralston who performed much of the computer analysis.

1. W. D. Hewson and H. B. Dunford. Can. J. Chem. **53**, 1928 (1975).
2. W. D. Hewson and H. B. Dunford. Biochemistry, **16**, 2949 (1977).
3. S. Loo and J. E. Erman. Biochim. Biophys. Acta, **481**, 279 (1977).
4. B. Chance. J. Cell. Comp. Physiol. **22**, 33 (1943).
5. M. L. Cotton, H. B. Dunford, and J. M. T. Raycheba. Can. J. Chem. **51**, 627 (1973).
6. R. Roman and H. B. Dunford. Biochemistry, **11**, 2076 (1972).
7. R. Roman and H. B. Dunford. Can. J. Chem. **51**, 588 (1973).
8. B. B. Hasinoff and H. B. Dunford. Biochemistry, **9**, 4930 (1970).
9. M. L. Cotton and H. B. Dunford. Can. J. Chem. **51**, 582 (1973).
10. H. B. Dunford and M. L. Cotton. J. Biol. Chem. **250**, 2920 (1975).
11. R. Roman, H. B. Dunford, and M. Evett. Can. J. Chem. **49**, 3059 (1971).
12. J. E. Critchlow and H. B. Dunford. J. Biol. Chem. **247**, 3714 (1972).
13. C. D. Hubbard, H. B. Dunford, and W. D. Hewson. Can. J. Chem. **53**, 1563 (1975).
14. H. B. Dunford. J. Theor. Biol. **46**, 467 (1974).
15. H. B. Dunford. Physiol. Vég. **12**, 13 (1974).
16. H. B. Dunford and J. S. Stillman. Coord. Chem. Rev. **19**, 187 (1976).
17. W. D. Hewson and H. B. Dunford. J. Biol. Chem. **251**, 6036 (1976).

18. L. M. SHANNON, E. KAY, and J. Y. LEW. J. Biol. Chem. **241**, 2166 (1966).
19. K.-G. PAUL and T. STIGBRAND. Acta Chem. Scand. **24**, 3607 (1970).
20. H. DELINCÉE and B. J. RADOLA. Biochim. Biophys. Acta, **200**, 404 (1970).
21. P. F. HOLLENBERG, T. RAND-MEIR, and L. P. HAGER. J. Biol. Chem. **249**, 5186 (1974).
22. G. R. SCHONBAUM and S. LO. J. Biol. Chem. **247**, 3353 (1972).
23. P. K. GLASOE and F. A. LONG. J. Phys. Chem. **64**, 188 (1960).
24. A. K. COVINGTON, M. PAABO, R. A. ROBINSON, and K. G. BATES. Anal. Chem. **40**, 700 (1968).
25. B. CHANCE and V. LEGALLIS. Discuss. Faraday Soc. **17**, 123 (1954).
26. D. DOLMAN, G. A. NEWELL, M. D. THURLOW, and H. B. DUNFORD. Can. J. Biochem. **53**, 495 (1975).
27. H. THEORELL, Ark. Kemi Mineral. Geol. Band **16A**, No. 3, (1942).
28. D. JOB and H. B. DUNFORD. Can. J. Chem. **56**, 1327 (1978).
29. H. KIHARA, S. SAIGO, T. IIZUKA, and Y. ISHIMURA. Biochem. Biophys. Acta, **533**, 112 (1978).
30. T. ARAISO and I. YAMAZAKI. Biochemistry, **17**, 942 (1978).
31. T. IIZUKA, S. OGAWA, T. INUBUSHI, T. YONEZAWA, and I. MORISHIMA. FEBS Lett. **64**, 156 (1976).
32. M. EPSTEIN and A. SCHEJTER. FEBS Lett. **25**, 46 (1972).
33. A. LANIR and A. SCHEJTER. Biochem. Biophys. Res. Commun. **62**, 199 (1975).
34. A. HVIDT and S. O. NIELSON. Adv. Protein Chem. **21**, 287 (1966).
35. A. HVIDT and K. LINDERSTRØM-LANG. Biochim. Biophys. Acta, **14**, 574 (1954).
36. S. J. EDELSTEIN and H. K. SCHACHMAN. J. Biol. Chem. **242**, 306 (1967).
37. W. G. MARTIN, C. A. WINKLER, and W. H. COOK. Can. J. Chem. **37**, 1662 (1959).
38. H. ERYLENMEYER and H. GÄRTNER. Helv. Chim. Acta, **17**, 970 (1934).
39. W. D. ELLIS and H. B. DUNFORD. Biochemistry, **7**, 2054 (1968).
40. R. J. P. WILLIAMS, P. E. WRIGHT, G. MAZZA, and J. R. RICARD. Biochim. Biophys. Acta, **412**, 127 (1975).
41. C. K. RULE and V.K. LA MER. J. Am. Chem. Soc. **60**, 1974 (1938).
42. C. A. BUNTON and V. J. SHINER, JR. J. Am. Chem. Soc. **83**, 42 (1961).
43. N. C. LI, P. TANG, and R. MATHUR. J. Phys. Chem. **65**, 1074 (1961).
44. R. P. BELL and A. T. KUHN. Trans. Faraday Soc. **59**, 1789 (1963).
45. P. JONES and H. B. DUNFORD. J. Theor. Biol. **69**, 457 (1977).
46. H. YAMADA and I. YAMAZAKI. Arch. Biochem. Biophys. **165**, 728 (1974).
47. F. WESTHEIMER. Chem. Rev. **61**, 265 (1961).
48. W. P. JENCKS and J. M. SAYER. Faraday Symp. Chem. Soc. **10**, 41 (1975).
49. W. P. JENCKS. Acc. Chem. Res. **9**, 425 (1976).
50. W. W. CLELAND. Acc. Chem. Res. **8**, 145 (1975).
51. P. NICHOLLS. J. Gen. Physiol. **49**, 131 (1965).
52. D. JOB, J. RICARD, and H. B. DUNFORD. Can. J. Biochem. **56**, 702 (1978).
53. A. C. MAEHLY. Nature, **192**, 630 (1961).
54. M. TAMURA, T. ASAKURA, and T. YONETANI. Biochim. Biophys. Acta, **268**, 292 (1972).
55. R. K. DINELLO and D. DOLPHIN. Biochem. Biophys. Res. Commun. **80**, 698 (1978).
56. D. E. GOLDSACK, W. S. EBERLEIN, and R. A. ALBERTY. J. Biol. Chem. **241**, 2653 (1966).
57. M. EIGEN. Angew. Chem. Int. Ed. Engl. **3**, 1 (1964).
58. H. B. DUNFORD and W. D. HEWSON. J. Phys. Chem. Submitted; J. BIGELEISEN. J. Phys. Chem. Submitted.

Can. J. Chem. Downloaded from www.nrcresearchpress.com by 210.87.254.105 on 09/05/12
For personal use only.

Selective reduction of a carboxyl group with diborane. Synthesis of specifically carbon-14 labelled D,L-2-Amino-4-(2-aminoethoxy)butanoic acid

YU-YING LIU, EDNA THOM, AND ARNOLD A. LIEBMAN
Chemical Research Department, Hoffmann-La Roche Inc., Nutley, NJ 07110, U.S.A.

Received May 23, 1978

YU-YING LIU, EDNA THOM, and ARNOLD A. LIEBMAN. Can. J. Chem. **56**, 2853 (1978).

Specific labelling of the title compound was achieved through intermediate **3***a*, methyl 2-(2-phthalimidoethoxy)acetate, derived from methyl bromoacetate-*2*-^{14}C. Conversion to the corresponding acid (**4**) was followed with selective diborane reduction which provided 2-(2-phthalimidoethoxy)ethanol-*2*-^{14}C (**5**). Treatment with thionyl chloride yielded the chloride **6** which is identical with the intermediate used in the nonlabelled synthesis and reaction with sodium ethyl phthalimidomalonate provided the title compound after hydrolytic work-up.

YU-YING LIU, EDNA THOM et ARNOLD A. LIEBMAN. Can. J. Chem. **56**, 2853 (1978).

On a réalisé le marquage spécifique du composé mentionné dans le titre par l'intermédiaire de **3***a*, le (phtalimido-2 éthoxy)-2 acétate de méthyle à partir du bromoacétate-*2*-^{14}C de méthyle. On a effectué la transformation en acide correspondant (**4**) par une réduction sélective avec le diborane qui a fourni le (phtalimido-2 éthoxy)-2 étanol-*2*-^{14}C (**5**). Par réaction avec le chlorure de thionyle, ce composé conduit au chlorure **6** qui est identique avec l'intermédiaire utilisé dans les synthèses non-marquées; la réaction avec le sel de sodium du phtalimidomalonate d'éthyle conduit au composé mentionné dans le titre après une extraction impliquant une hydrolyse.

[Traduit par le journal]

L-2-Amino-4-(2-aminoethoxy)butanoic acid (**7**) is an amino acid isolated from a fermentation broth of *Streptomyces* sp. x-11,085. It was shown (1) to be identical with the chemical reduction product of L-2-amino-4-(2-aminoethoxy)-*trans*-but-3-enoic acid, an antimetabolite antibiotic previously isolated from this unclassified species of *Streptomyces* (2). Synthesis of the saturated compound was effected by condensation of 2-(2-phthalimidoethoxy)ethyl chloride with sodium ethyl phthalimidomalonate followed by hydrolytic removal of protecting groups and decarboxylation. Enzymatic resolution then provided the L-amino acid (1).

These compounds possess interesting biological activities among which is their effect on ethylene production and subsequent ripening of fruits (2) when applied to these fruits. We wished to prepare the saturated amino acid specifically carbon-14 labelled at C-3 or C-4 for testing as a possible ethylene precursor, as such or after enzymatic resolution and/or enzymatic conversion to the Δ^3 dehydro analog. Since the starting material used in the normotopic synthesis, bischloroethyl ether, if labelled, would lead to a multiple labelled product because of symmetry, alternate starting materials and routes to this compound were investigated.

In a projected labelling synthesis, formation of the ether linkage could be achieved by the reaction of a suitably protected 2-aminoethanol with an ester of bromoacetic-*1*-^{14}C acid. Reduction of the resulting aminoethoxy ester **3** to the alcohol **5** (Scheme 1) and conversion to the corresponding chloride **6** provides an intermediate that would be closely related, if not identical to that used in the nonlabelling synthesis and could be carried on to the final product using established procedures. This sequence would allow labelling at C-2 from malonate or C-3 or C-4 from acetate as indicated.

It appeared that the *N*-phthalimido protecting group was necessary to the success of the conversion of **6** → **7** and we investigated its use at the outset. Susceptibility of the phthalimide group to reduction under the conditions effecting ester reduction required that **3** first be converted to the acid **4**. The carboxyl group is readily reduced with borane and in the presence of the phthalimide group selective reduction occurred only at the carboxyl carbon to yield alcohol **5** quantitatively. The acid **4** could be formed by the action of lithium iodide on the methyl ester **3***a* or in better yield by hydrogenolysis of the benzyl ester **3***b*.

By these procedures, **7** was prepared specifically labelled at C-4 using bromoacetic-*2*-^{14}C acid as the starting material and at C-2 using ethyl phthalimidomalonate-*2*-^{14}C for inserting the label. Because of the quantities required, these materials were prepared from barium carbonate-^{14}C according to literature procedures.

Experimental

Melting points were determined on a Thomas–Hoover capillary melting point apparatus and are uncorrected. Radio-

Can. J. Chem. Downloaded from www.nrcresearchpress.com by 210.87.254.6 on 09/05/12
For personal use only.

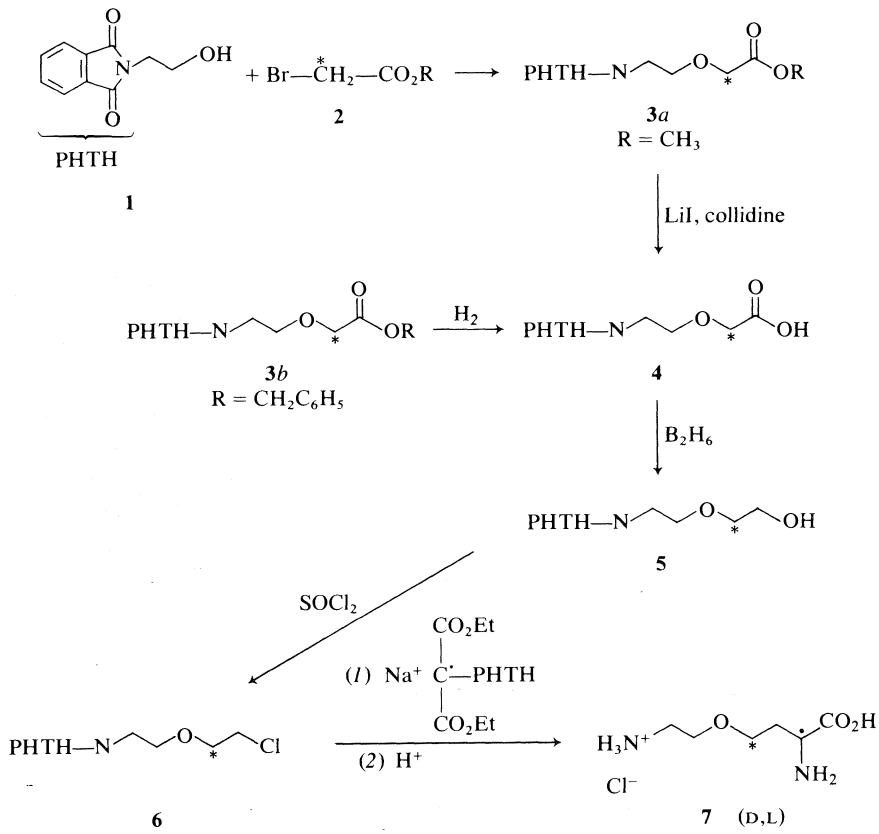

SCHEME 1. Preparation of carbon-14 labelled **7**.

chemical purity was determined on thin-layer chromatograms (Brinkmann pre-coated silica gel F-254) with a Packard Model 7201 Radiochromatogram Scanner System and radioactivity was measured by the liquid scintillation technique with a Packard Tricarb Model 2010 spectrometer. Spectral measurements were recorded as follows: infrared on either Perkin Elmer Model 137 or Model 621 or Beckman Model IR-9 spectrometers, ultraviolet on Carey 14 and 15 spectrophotometers, nmr on Varian T-60A, A-60 and HA-100 spectrometers and mass spectra on CEC 110-21B and JEOL Co. 015G double focusing and Hitachi RMU 6L single focus spectrometers.

*Methyl 2-(2-Phthalimidoethoxy)acetate (**3**a)*

Two millimoles (282 mg) of 2-phthalimidoethanol in 20 ml of anhydrous benzene was added to a suspension of sodium hydride (84 mg, 2 mmol of 57% mineral oil dispersion in benzene) and the resulting mixture was stirred and heated under reflux for 2 h. After cooling, 153 mg (1 mmol) of methyl bromoacetate was added and again the mixture was stirred under reflux for 2 h, then cooled, treated with 20 ml of water, and extracted with several portions of methylene chloride. The combined organic extracts were concentrated, *in vacuo*, and the residue purified by column chromatography on 25 g of silica gel using chloroform–acetone, 6:1 elution. The yield of **3***a* was 171 mg (0.65 mmol, 65%) of white solid, mp 142–144°C; ^{1}Hmr ($CDCl_3$) δ: 3.64 (s, 3H,—OCH_3), 3.85 (m, 4H,—CH_2—CH_2—), 4.08 (s, 2H,—O—CH_2—CO—), 7.75 (m, 4H, Ar). *Anal.* calcd. for $C_{13}H_{13}NO_5$: C 59.3, H 5.0, N 5.3; found: C 59.6, H 5.1, N 5.5.

*Benzyl 2-(2-Phthalimidoethoxy)acetate (**3**b)*

In a similar manner, the benzyl ester was also prepared on a 1 mmol scale. Reflux was continued for 20 h after the addition of benzyl bromoacetate and the product was purified by hplc on silica gel (E. Merck 60) with a chloroform – ethyl acetate gradient elution to yield 203 mg (60%) of white solid, mp 97–98°C. *Anal.* calcd. for $C_{19}H_{17}NO_5$: C 67.3, H 5.1, N 4.1; found: C 67.4, H 5.0, N 4.2.

*2-(2-Phthalimidoethoxy)acetic Acid (**4**)*

*By Hydrolysis of **3**a*

A 526 mg (2 mmol) sample of **3***a* and 798 mg (5.96 mmol) of lithium iodide were heated under reflux in 3 ml of collidine for 2 h. After cooling, the entire mixture was dissolved in chloroform which was then extracted with 30 ml of 2 *N* HCl. A chloroform wash of the acidic extract was combined with the original organic solution which was washed several times with water. Evaporation then afforded the crude product which was purified by crystallization from ethanol–water yielding 230 mg (0.92 mmol, 46%) of **4**, mp 167–168°C; ^{1}Hmr ($CDCl_3$) δ: 3.75 (m, 6H), 7.56 (m, 4H, Ar), 9.50 (s, 1H, COO*H*). *Anal.* calcd. for $C_{12}H_{11}NO_5$: C 57.8, H 4.5, N 5.6; found: C 57.7, H 4.5, N 5.6.

*By Hydrogenolysis of **3**b*

A solution of **3***b*, 678 mg (2 mmol) in 15 ml of ethyl acetate was hydrogenated over 160 mg of 10% Pd/C at room temperature and 1 atm until uptake of hydrogen ceased. The catalyst was removed by filtration and concentration of the filtrate, *in vacuo*, left pure **4**, 482 mg, (1.93 mmol, 96.7%).

Can. J. Chem. Downloaded from www.nrcresearchpress.com by 210.87.254.6 on 09/05/12
For personal use only.

Can. J. Chem. Downloaded from www.nrcresearchpress.com by 210.87.254.6 on 09/05/12
For personal use only.

*2-(2-Phthalimidoethoxy)ethanol (**5**)*

A solution of 3.5 ml of 0.97 *M* diborane in tetrahydrofuran was added to a stirred solution of **4**, (425 mg, 1.7 mmol) in 2 ml of dry tetrahydrofuran. The addition was carried out under N_2 and at 0°C, conditions which were maintained for an additional hour. Methanol, 1 ml, was then added and the resulting mixture was evaporated to dryness, treated with 10 ml of water, and then extracted with chloroform. The organic extracts were combined, dried ($MgSO_4$), filtered and concentrated *in vacuo* to yield pure **5**, 385 mg (96.3%), mp 59–60°C; ir (3% $CHCl_3$ solution): 3600, 1775, 1710 cm^{-1}; ^{1}Hmr ($CDCl_3$) δ: 3.3 (s, 1H, —O*H*), 3.56 (s, 4*H*, —CH_2—O—CH_2—), 3.76 (m, 4H, N—CH_2—OH), 7.64 (m, 4H, Ar). *Anal.* calcd. for $C_{12}H_{13}NO_4$: C 61.3, H 5.6, N 5.6; found: C 61.3, H 5.7, N 5.9.

2-(2-Phthalimidoethoxy)ethanol-2-^{14}C [**5**-*(2-*^{14}C*)*]

The sequence described above was carried out using methyl bromoacetate-*2-*^{14}*C* (**2**) derived from $Ba^{14}CO_3$ (200 mCi) using literature procedures (ref. 3, p. 326).

2-(2-Phthalimidoethoxy)ethyl-2-^{14}C *Chloride* [**6**-*(2-*^{14}C*)*]

On a 0.4 mmol scale, 95 mg of alcohol [**5**-*(2-*^{14}*C)*] prepared as described above, was treated with 0.2 ml thionyl chloride and 0.25 ml pyridine in 2.5 ml benzene under reflux for 2.5 h. After cooling, the mixture was concentrated *in vacuo* and the residue was chromatographed over silica gel using a gradient elution of chloroform, chloroform–ethyl acetate (1:1) resulting in 92 mg of product (0.36 mmol, 91%), mp 68°C (lit. (4) mp 70°C) which was homogeneous by tlc and >99% radiochemically pure.

D,L-*2-Amino-4-(2-aminoethoxy)butanoic-4-*^{14}C *Acid Hydrochloride* [*7-(4-*^{14}C*)*]

The chloro derivative **6**-*(2-*^{14}*C)*, 253 mg (1 mmol), sodium ethylphthalimido malonate (5), 327 mg, (1 mmol), and potassium iodide (0.2 mmol) were dissolved in 2 ml of anhydrous DMF and the resulting solution was heated at 155°C for 4 h. After cooling, 20 ml of water was added and the resulting clear solution was decanted from the brown precipitate and co-distillation with several portions of chloroform–ethanol effectively concentrated the solution to a solid residue. This was chromatographed on a 25 g silica gel column with chloroform to provide 189 mg (36.2%) of adduct which was >95% radiochemically pure. Treatment with hydrazine hydrate, 100 mg of 98% material, in 3 ml of ethanol under reflux for 2 h yielded a white solid after removing excess hydrazine. This was heated with 4 ml of 6 *N* HCl for 2 h under reflux then cooled and filtered. The filtrate was concentrated *in vacuo* and the residue, dissolved in water, was applied to 10 g of Bio Rad AG 50W-X8 (80–100 mesh) cation exchange resin (H^+). Elution was accomplished first with 100 ml of water, then 80 ml of 20% pyridine in water, then 100 ml of 1 *N* NH_4OH. The latter was concentrated to a small volume and the pH then adjusted to 3.5 with 0.1 *N* HCl. The resulting product was recrystallized from ethanol to yield 47.7 mg (66% from **6**) of **7**-*(4-*^{14}*C)* with specific activity of 18.6 μCi/mg. Radiochemical purity was >99% and the radiochemical yield from methyl bromoacetate-*2-*^{14}*C* (**2**) was 2.4%. Dilution with nonradioactive intermediates was effected at several stages of the synthesis.

Specific activity of **7** ^{14}C-labelled at C-2 was 57.7 μCi/mg. The preparation was carried out as described above using ethyl phthalimidomalonate-*2-*^{14}*C* as the ^{14}C carrier. This was prepared from ethyl malonate-*2-*^{14}*C* derived from $Ba^{14}CO_3$ via literature procedures (ref. 3, pp. 40, 438, 453, and 899).

Acknowledgements

We thank Dr. R. P. W. Scott and his staff in our Physical Chemistry Department, in particular, Dr. W. Benz for mass spectra, Dr. F. Scheidl for microanalyses, Dr. V. Toome for uv spectra, Mr. S. Traiman for ir spectra, and Dr. T. Williams for nmr spectra.

1. J. P. Scannel, D. L. Pruess, H. A. Ax, A. Jacoby, M. Kellett, and A. Stempel. J. Antibiot. **29**, 38 (1976).
2. D. L. Pruess, J. P. Scannel, M. Kellett, H. A. Ax, J. Janeck, T. H. Williams, A. Stempel, and J. Berger. J. Antibiot. **27**, 229 (1974).
3. A. Murray and D. L. Williams. Organic synthesis with isotopes. Interscience, New York, NY. 1958.
4. F. P. Dwyer, N. S. Gill, E. C. Gyarfas, and F. Lions. J. Am. Chem. Soc. **75**, 1526 (1953).
5. G. Barger and T. E. Weichselbaum. *In* Organic synthesis. Coll. Vol. II. *Edited by* A. H. Blatt. J. Wiley and Sons, New York, NY. 1943. p. 384.

Heats of mixing of trialkylamines: disorder and steric hindrance contributions

ROBERT PHILIPPE

Université de Lyon I, Laboratoire de Chimie Analytique, 43, Boulevard du 11 novembre 1918, 69621-Villeurbanne, France

AND

GENEVIÈVE DELMAS AND PHUONG NGUYEN HONG

Département de chimie, Université du Québec à Montréal, C.P. 8888, Montréal (Qué.), Canada H3C 3P8

Received May 24, 1978

Can. J. Chem. Downloaded from www.nrcresearchpress.com by 210.87.254.6 on 09/05/12
For personal use only.

ROBERT PHILIPPE, GENEVIÈVE DELMAS, and PHUONG NGUYEN HONG. Can. J. Chem. **56**, 2856 (1978).

Nine trialkylamines, triethyl- to trihexylamine trioctyl-, tridodecyl, tri(methyl-2-butyl)-, and dimethyldodecylamine have been used for heats of mixing of the following systems at 298 K: *A*, fourteen systems made of all the possible binary mixtures (except one) of the six shorter amines; *B*, twelve systems made of a long chain amine, trioctyl-, tridodecyl- or dimethyldodecylamine with the four shorter members of the series; *C*, two systems consisting of the mixture of two long-chain compounds, trioctylamine with tridodecyl- and dimethyldodecylamine. Heats for the class *A* systems are less than or equal to 40 J/mol, indicating no net effect of the small polarity of the shorter members of the series. The experimental H^E of these mixtures are compared with two theories. The Monte Carlo approach gives good predictions but the heats calculated with the Snider–Herrington theory are too negative. Heats of the class *B* systems are suitable for the investigation of two new contributions to the heats of mixing, the positive heat of disordering of long-chains H^E(dis.) and the negative heat found in systems where one of the components is sterically hindered, H^E(ster.hindr.). H^E(dis.) found with the long-chain amines indicates an orientational order larger than in the case of the *n*-alkane of the same chain-length but equivalent to that found in the tetraalkyltin compounds of the same length. Recent work has shown that the tetrapropyl and tetraethyltin derivatives when mixed with long-chain alkanes or tin derivatives give rise to a H^E(ster.hindr.) contribution. From this work and the present study, the steric hindrance contributions of five sterically hindered compounds tetraethyltin and tetrapropyltin, triethyl- and tripropylamine, and 3,3-diethylpentane mixed with different second components are calculated. The steric hindrance contribution is found proportional to the volume of the second component and increasing in the following order of the sterically hindered component: triethyl- < tripropylamine < tetraethyl- < tetrapropyltin < 3,3-diethylpentane. Heats of the class *C* systems are small without significant contribution of H^E(dis.) due to the fitting of the long-chains in solution.

ROBERT PHILIPPE, GENEVIÈVE DELMAS et PHUONG NGUYEN HONG. Can. J. Chem. **56**, 2856 (1978).

Neuf trialkylamines, triethyl à trihexylamine, trioctyl, tridodecyl-, tri(methyl-2-butyl)- et dimethyldocecyl amine ont été utilisées pour la mesure de chaleurs de mélange des systèmes suivants à 298 K: *A*, quatorze systèmes faits de toutes les combinaisons binaires possible (sauf une) des six plus petites amines; *B*, douze systèmes faits d'une amine à longue chaine trioctyl-, tridodecyl-, ou diméthyldodecylamine avec les quatre plus petites amines; *C*, deux systèmes consistant du mélange de deux composés à longue chaine. Les chaleurs de mélanges des systèmes *A* sont toutes inférieures ou égales à 40 J/mol ce qui indique un effet global nul de la faible polarité des plus petites amines. Les valeurs expérimentales de H^E de ces mélanges sont comparées avec les théories. La méthode de Monte Carlo donne de bonne prédictions mais les chaleurs calculées avec la théorie de Snider–Herrington sont trop négatives. Les chaleurs des systèmes de la classe *B* permettent d'obtenir des informations au sujet de deux contributions aux chaleurs de mélange, la contribution positive de désordre des longues chaines H^E(dis.) et la contribution négative trouvée dans les systèmes dont un des constituants est empêché stériquement, H^E(ster.hind.). H^E(dis.) trouvé avec les amines à longues chaines indique que les corrélations d'orientations sont plus importantes que dans les alcanes ayant la même longeur mais sont semblables à celles des composés tétraalkylés. Des mesures de chaleurs sur les dérivés tétraalkylés de l'étain ont montré que le dérivé ethylé et propylé donnent une contribution d'empêchement stérique. A partir de ces résultats, les contributions d'empêchement stérique à H^E de cinq composés empêchés stériquement, les dérivés éthylés et propylés de l'étain et de l'azote et le 3,3-diéthylpentane sont obtenues quand ils sont mélangés à différents deuxièmes constituants. On a trouvé que la contribution d'empêchement stérique est proportionnelle au volume de deuxième constituant et croit dans l'ordre suivant du composé stériquement empêché triéthyl- < tripropylamine tetraethyl- < tetrapropylétain < 3,3-diéthylpentane. Les chaleurs de mélange de la classe *C* sont petites puisque l'adaptation des corrélations d'orientations des longues chaines en solution ne donne pas lieu à un H^E(dis.).

Can. J. Chem. Downloaded from www.nrcresearchpress.com by 210.87.254.6 on 09/05/12
For personal use only.

Introduction

Heats of mixing of non-polar systems depend on the energy of unlike contacts compared with that of like contacts. This first contribution H^E(chem.) is positive and has been recognized since early on (1). It can be predicted by current theories based on the analysis of heats by group interactions (2). The second contribution, H^E(f.v.) is negative and is derived from the difference in degree of thermal expansion or free volume of the two components. In most non-polar systems, the first contribution is larger than the second one, so that the total heat is positive. However, in mixtures of atactic non-polar polymers with non-polar solvents, the second contribution is larger than in mixtures of small molecules and therefore the experimental heat is quite often negative (3, 4). H^E(f.v.) can be calculated from the state of expansion of the liquids. Different models have been used by Prigogine (5), Delmas and Patterson (3, 6), and Orwell and Flory (7). The Van der Waals model of Flory is widely used because of its simplicity and because of the good results it gives. Recent and systematic measurements of heats of mixing of linear and branched alkanes (8), tetraalkyltin derivatives (9), and trialkylamines (10) with branched and linear alkanes and mixtures of tetraalkyl tin derivatives (11) have shown that two additional contributions arise from molecular shape. The origin of the third contribution H^E(dis.) is to be found in the correlations of orientations present in the pure state in some liquids, e.g. *n*-alkanes. Systematic comparison of the thermodynamical and optical (12) properties of linear alkanes with those of branched alkanes was instrumental in the recognition of the importance of orientational order in liquids. The correlations of orientations are destroyed when ordered liquids are mixed with globular molecules, and this gives rise to H^E(dis.). H^E(dis.) does not occur or occurs to a lesser extent in two cases: when the two liquids mixed are both composed either of globular molecules (since their more isotropic shape does not favour correlations of orientations) or of ordered molecules (since the solution is as ordered as the pure liquids).

The fourth contribution to H^E, H^E(ster.hindr.) has been recognized only recently (11, 12*a*). Unexpectedly, it is negative (13) but cannot be explained by a free volume difference and seems to be related to the presence of one sterically hindered molecule among the two liquids mixed. It was given the name condensation contribution (12*a*), alternatively it may be called a steric hindrance (11) contribution. More details will be given later. Analysis of the heats of mixing of liquids which are similar in volatility and chemical nature but whose molecules have different shapes shows that H^E(dis.), or H^E(ster.hindr.), or a combination of both, are the main contributions to the experimental heats. Examples of the first two cases are (*1*) the system tetrabutyltin + n-C_{16} for which the experimental heat of mixing is 360 J/mol (9), a value which corresponds to the heat of disordering of n-C_{16}, and (*2*) the system 3,3-diethylpentane + n-C_8 (20) for which the experimental heat of mixing (-82 J/mol) corresponds to H^E(ster.hindr.) due to 3,3-diethylpentane.

Heats of mixing measurements of trialkylamines with other trialkylamines is a study similar to that made on mixtures of tetraalkyltin derivatives (10). Some of the aims of the present work are similar to those we had then, i.e. to obtain more information on the disorder and steric hindrance contributions (systems involving long-chain compounds) and to compare the experimental heats with those predicted by the theories (mixtures of the globular short-chain compounds). The heats of trialkylamine systems may give some further information concerning (*a*) the effect on the heats of the small polarity of the shorter members of the series, (*b*) the possibility of *intra*-molecular correlations of orientations in the tetraalkyl- and trialkyl-derivatives which would not occur in linear alkanes, and (*c*) the generality of the result found on the tetraalkyltin derivatives, i.e. the ethyl and propyl derivatives seem much more sterically hindered than those of methyl and butyl.

The nine compounds used were all trialkylamines. For eight of them, the central nitrogen atom bore three identical alkyl radicals. In seven cases, these were straight-chain radicals with 2, 3, 4, 5, 6, 8, and and 12 carbon atoms while the other was the methyl-2-butyl radical. The remaining amine was dimethyldodecylamine. Heats of mixing were measured at 298 K on the following systems: *A*, fourteen systems of all the possible binary combinations (except one) of the five short-chain amines: triethylamine to trihexylamine and tri(methyl-2-butyl)amine (The system not measured was tripropylamine + tri(methyl-2-butyl)amine.); *B*, twelve systems where one of the components is a long-chain amine (four systems mixing tridodecylamine with the four shorter members of the series, four systems with trioctylamine, and the same four systems with dimethyldodecylamine); *C*, two systems with long-chain compounds mixed together: trioctylamine mixed with tridodecylamine and with dimethyldodecylamine.

To simplify matters, the following abbreviations are used in the text and the tables: NEt_3, NPr_3, $NBut_3$, $NPent_3$, $NHex_3$, $NOct_3$, and $NDodec_3$, corresponding to the radicals in 2, 3, 4, 5, 6, 8, and 12 carbon atoms. The dimethyldodecylamine and the tri(methyl-2-butyl)amine are replaced by NMe_2-

TABLE 1. Physico-chemical parameters for the pure components at 25°C

Compound	d	α (10^3 K^{-1})	P^* (J cm^{-3})	V^* (cm^3 mol^{-1})	$s = S/V$ (Å^{-1})	$\tilde{v}^a$	$\tilde{T}_{11}{}^b$	$\xi_{(\alpha)}{}^c$	$\xi_{(\Delta H_V)}{}^d$
NEt_3	0.7234	1.290	459.2	107.3	0.94	1.3042	0.71058	0.50215	0.499
NPr_3	0.7524	1.064	409.6	151.1	0.90	1.2606	0.64466	0.54113	0.540
$NBut_3$	0.7746	0.970	442.3	192.8	0.88	1.2414	0.61428	0.56036	0.569
$NPent_3$	0.7870	0.920	441.2	234.8	0.86	1.2310	0.59725	0.57145	0.589
$NHex_3$	0.7964	0.879	442.1	276.9	0.85	1.2223	0.58283	0.58106	
$NOct_3$	0.8105	0.832	450.5	359.9	0.84	1.2121	0.56573	0.59267	0.633
$NDodec_3$	0.8211	0.787	475.5	528.7	0.83	1.2022	0.54873	0.60445	0.668
NMe_2Dodec	0.7846	0.910	457.1	221.3	0.92	1.2290	0.59377		0.600
$N(Me\text{-}2\text{-}But)_3$	0.7790	0.956	419.2	235.7	0.86	1.2385	0.60956		

[a]From $\tilde{v}^{1/3} = ((4/3)\alpha T + 1)/(\alpha T + 1)$.
[b]From αT and equation in the text under parameters for the pure components.
[c]From eq. [14].
[d]From eq. [13].

Dodec and $N(Me\text{-}2\text{-}But)_3$. $NDodec_3$ has been used instead of $NLaur_3$ in previous work.

Experimental

Apparatus

The heats of viscous systems and in particular the heats for mixtures of two components having a relatively large difference of densities and viscosities ($NOct_3$ and $NDodec_3$ with the shorter members of the series) have been obtained with a tilting Tian–Calvet calorimeter to assure good mixing. Details of the instrument, the cells, and the calibration can be found in refs. 4 and 9. Agreement was better than 2% with the reference system, benzene + carbon tetrachloride (14). For each system, seven to ten runs were made in order to obtain the value of the maximum and the concentration dependence of the heat.

The other systems were measured with the Picker Flow Microcalorimeter (15) Technеurop Inc., Montreal. As shown by Grolier and Inglese (16), the best results are obtained when measurements are taken at a constant flow ratio of the two constituents. Curves are also obtained at about seventeen flow ratios. Heats by the Calvet or Picker calorimeters gave good agreement (better than 1%) with non-viscous mixtures. For viscous systems, the heats measured by the flow calorimeter were smaller (10 to 30%) than those measured by the static calorimeter.

Chemicals

The amines come from the same sources as in previous work (10, 17), namely, the Eastman, Aldrich Companies and the Chemical Procurement Laboratories. Densities of the compounds were measured as a test of their purities and can be found in Table 1.

Calculation of the Free Volume Contribution

We have chosen to apply the approximate form (8, 12) of the Prigogine theory which separates the interactional and free volume contribution. H^E(f.v.) is given by eq. [1]

$$[1]\quad H^E(\text{f.v.})/(x_1U_1^* + x_2U_2^*) = \tilde{C}_p(\tilde{T}_U)[\psi_1\tilde{T}_1 + \psi_2\tilde{T}_2 - \tilde{T}_U]$$

Here, $\tilde{T}_U$ is an average reduced temperature for the solution appropriate to the energy, U, and is defined by:

$$[2]\quad \tilde{U}(\tilde{T}_U) = \psi_1\tilde{U}(\tilde{T}_1) + \psi_2\tilde{U}(\tilde{T}_2)$$

The reducing parameter for the energy U^*, ($\tilde{U} = U/U^*$), can be obtained from experimental data since $U^* = P^*\cdot V^*$. In the Van der Waals model used by Flory, $\tilde{U} = -1/\tilde{v}$, so that eq. [2] becomes $1/\tilde{v}_U = \psi_1/\tilde{v}_1 + \psi_2/\tilde{v}_2$. The ψ's are energy fractions, i.e. $\psi_1 = x_1U_1^*/(x_1U^* + x_2U_2^*)$. The reduced volumes of the pure components are obtained from their expansion coefficients α and

$$\tilde{v}^{1/2} = (\tfrac{4}{3}\alpha T + 1)/(\alpha T + 1)$$

and their reduced temperatures $\tilde{T}_1$ and $\tilde{T}_2$ by

$$\tilde{T} = \tilde{v}^{-1}(1 - \tilde{v}^{-1/3})$$

$\tilde{C}_p(\tilde{T}_U)$ in eq. [1] is $(\frac{4}{3}\tilde{v}_U{}^{-1/3} - 1)^{-1}$. The interactional contribution expressed in terms of the Flory parameter X_{12} is obtained from the experimental heat and H^E(f.v.):

$$[3]\quad \frac{[H^E(\text{exp}) - H^E(\text{f.v.})]}{(x_1U_1^* + x_2U_2^*)} = X_{12}\psi_1\frac{\theta_2}{P_1^*}f(\tilde{v}_U)$$

$f(\tilde{v}_U) = (4\tilde{v}_U - 3\tilde{v}_U{}^{4/3})^{-1}$ corresponds to $[-\tilde{U}(\tilde{T}_U) + \tilde{T}_U\tilde{C}_p(\tilde{T}_U)]$ in the Van der Waals model. Its value is not far from 1. θ_2 is a surface fraction defined by $x_2V_2^*s_2/(x_2V_2^*s_2 + x_1V_1^*s_1)$. The s's are surface-to-volume ratios used in the Flory theory to characterize the shape of the molecule. The values of s depend to some extent on the model used but the X_{12} parameter does not. The parameter $X_{12}s_1{}^{-1}$ has been tabulated instead of X_{12} because it does not depend on which compound has been chosen as the first component ($X_{12}s_1{}^{-1} = X_{21}s_2{}^{-1}$).

Parameters for the Pure Components

The densities (d), expansion coefficients (α), and thermal pressure coefficients (γ) necessary to obtain $\tilde{v}$, V^*, P^* have been measured (17) or are obtained from literature (17). d, α, P^*, V^* are reported in Table 1. In the van der Waals model, $P^* = \gamma\tilde{v}^2T$. The surface-to-volume ratios, calculated by methods usual for the alkanes (7), are given in Table 1. The reduced volumes, $\tilde{v}$, of the pure components necessary for the calculation of the free volume contribution, the reduced temperature, $\tilde{T}_{11}$, used in the Monte Carlo approach, and the ξ parameters of the Snider–Herrington theory have been added in the last four columns.

Results and Discussion

Table 2 summarizes the results for all the systems. The experimental heats H^E have been fitted to the equation:

$$[4]\quad H^E = x_1x_2\sum_{i=0}A_i(x_1 - x_2)^i$$

where x is the mole fraction.

Can. J. Chem. Downloaded from www.nrcresearchpress.com by 210.87.254.6 on 09/05/12
For personal use only.

TABLE 2. Heats of mixing and calculated parameters for mixtures of trialkylamines NR_3 + NR'_3 at 25°C[a]

System (1)	(2)	Class	H^E_{max} (J mol^{-1})	x_{1max}	A_0	A_1	A_2	A_3	H^E_v (J cm^{-3})	$H^E_{f.v.}$ (J mol^{-1})	$X_{12}s_1^{-1}$ (J cm^{-3} Å)
NEt_3	+NPr_3	A	10.6	0.572	41.46	11.80	2.74	0.64	0.084	−11.5	0.72
	+$NBut_3$	A	16.3	0.565	64.08	16.00	6.31	−5.21	0.112	−26.8	1.28
	+$NPent_3$	A	30.7	0.567	120.38	32.92	6.46		0.189	−39.5	1.95
	+$NHex_3$[b]	A	40.0	0.600	159.20	72.14	−64.16		0.228	−53.2	2.41
	+$NOct_3$[b]	B	86.0	0.600	329.92	199.70	−183.60		0.413	−73.6	3.81
	+$NDodec_3$[b]	B	296.0	0.625	1107.59	477.44	265.17		1.093	−102.5	8.32
NPr_3	+$NBut_3$	A	17.5	0.480	69.96	−4.59	−5.26	5.57	0.112	−2.6	0.51
	+$NPent_3$	A	10.5	0.547	41.55	6.79	5.09	7.68	0.055	−7.2	0.41
	+$NHex_3$	A	18.1	0.565	71.13	20.70	−4.58	−2.51	0.088	−13.2	0.69
	+$NOct_3$[b]	B	92.0	0.600	328.54	119.68	149.48		0.392	−24.0	2.30
	+$NDodec_3$[b]	B	225.0	0.600	872.55	328.18	69.58		0.745	−40.0	4.61
$NBut_3$	+$NPent_3$	A	0.0	(0.5)					0	−1.1	0.02
	+$NHex_3$	A	19.9	0.532	79.09	10.83			0.079	−4.2	0.46
	+$NOct_3$[b]	B	104.0	0.550	408.90	88.30	67.41		0.388	−11.1	2.01
	+$Dodec_3$[b]	B	260.0	0.600	986.40	319.94	555.17		0.795	−23.7	4.27
$NPent_3$	+$NHex_3$	A	11.0	0.532	44.05	6.78	−7.70	−15.44	0.043	−0.9	0.21
	+$NOct_3$[b]	B	78.1	0.600	292.27	114.48	61.06		0.274	−5.2	1.33
	+$NDodec_3$[b]	B	216.0	0.525	837.83	255.03	−181.86		0.577	−14.2	3.18
$NOct_3$	+$NDodec_3$[b]	C	50.0	0.500	205.63	−14.67	+75.90		0.126	−2.2	0.64
NMe_2Dodec	+NEt_3	B	70.1	0.472	279.62	−29.65	4.04		0.435	−40.8	3.11
	+NPr_3	B	75.8	0.492	303.11	−8.42	30.48		0.408	−8.2	1.98
	+$NBut_3$	B	111.7	0.510	466.89	12.97	66.80		0.539	−1.6	2.38
	+$NPent_3$	B	98.6	0.510	394.24	14.97	39.25	−45.6365	0.433	−0.05	1.88
	+$NOct_3$	C	40.6	0.540	161.12	29.64	−14.42	−1.3739	0.142	−4.1	0.71
$N(Me\text{-}2\text{-}But)_3$	+NEt_3	A	24.8	0.432	97.37	−27.69	3.94	5.8210	0.152	−31.2	1.54
	+$NBut_3$	A	7.1	0.487	28.43	−0.90	6.55	−3.6341	0.033	−0.1	0.15
	+$NPent_3$	A	44.5	0.487	117.86	−7.79	26.94	21.6076	0.189	−0.6	0.86
	+$NHex_3$[b]	B	72.0	0.500	287.63	21.64	−30.83		0.281	−3.3	1.34

[a]All A's in J mol^{-1}.
[b]Systems measured with the tilting Tian–Calvet calorimeter.

The first two columns of Table 2 list the maximum of the heats and the concentration of the maximum. The next four columns give the parameters A_i of eq. [1]. The average difference between the actual experimental points and the calculated values is about 0.6% for all the systems. The next column indicates the heat per cm^3 calculated through the equation:

$$[5] \qquad H_v^E = H^E/(x_1V_1^* + x_2V_2^*)$$

The denominator of eq. [5] is the average core volume of the pure components in the solution. To compare heats of systems for which the molar volume is quite different, the heat of mixing per unit volume is more suited than H^E. The results of the comparison would not be significantly different if the molar volumes were used instead of the core volumes. The last two columns list the calculated free volume term in the Van der Waals model and the corresponding $X_{12}s_1^{-1}$ parameter of the Flory theory.

The diverse contributions described in the Introduction have different weights in the experimental heats. The qualitative or semi-quantitative analysis of the H^E will show if one contribution is dominant in a given system. Figures for H^E listed in Table 2 indicate that in the mixtures made up of NR_3 + NR_3', where R and R′ are taken from the ethyl to hexyl radicals (class A in Table 2), thirteen out of the fourteen systems have heats smaller than 40 J/mol. These results show that none of the contributions described previously is very large. In particular, the small polarity of NEt_3 is not revealed in non-polar surroundings. A similar result was found when the same compounds were mixed with alkanes (10). In this class of systems, no separation of contributions is possible, and these mixtures may better be analysed with theories which predict global heats from parameters on the pure components, as will be done later.

Disorder Contribution

The system which does not fit its own class A (made of mixtures of globular, less-oriented molecules) is $N(Me\text{-}2\text{-}But)_3$ + $NHex_3$. Its heat of mixing is large (75 J/mol) compared to that of the very similar system, $NPent_3$ + $NHex_3$ (11 J/mol). The interpretation of this difference is that the two methyl groups at the end of the alkyl chain in $N(Me\text{-}2\text{-}But)_3$ prevent a good fitting between the chains of the two compounds. $N(Me\text{-}2\text{-}But)_3$ acts as an order-breaker of the small orientational order of $NHex_3$ while $NPent_3$ does not.

For eleven systems (class B in Table 2), consisting of a globular and one long-chain molecule (trioctyl or tridodecyl and dimethyldodecylamines), the heats are larger, between 70 and 290 J/mol. They increase with the chain length of the long-chain component while varying less with the size of the globular component. The heat per cm^3, H_v^E, follows the same trend as can be seen in Fig. 1. This increase cannot be due to the change in free volume since the difference in size and expansion coefficient of the two components becomes increasingly negative, so that the free volume contribution would tend to lower the total heat. The interpretation of this increase in the

Can. J. Chem. Downloaded from www.nrcresearchpress.com by 210.87.254.6 on 09/05/12
For personal use only.

TABLE 3. H^E(dis.) of dodecyl and octyl chains with different order-breakers in the approximation H^E(exp) $\simeq$ H^E(dis.) in J/cm^3

	H^E(dis.) for order-breaker equals[a]								
Compound	NEt_3	NPr_3	$NBut_3$	br-C_8	br-C_{12}	br-C_{16}	$SnEt_4$	$SnPr_4$	$SnBut_4$
$NDodec_3$	1.1	(0.74)	(0.80)	1.14	1.17	1.12			
$SnDodec_4$				1.22	1.25	1.22	1.28	(0.97)	1.24
n-C_{12}	1.4	(0.70)	(0.63)	0.84	0.72	0.68			
NMe_2Dodec	0.43	0.41	0.53						
$NOct_3$	0.41	0.39	0.39	0.46	0.39	0.42			
$SnOct_4$									0.67
n-C_8		0.21	0.23	0.18	0.15	0			0.21

[a]The systems for which H^E(dis.) is in parentheses have a steric hindrance contribution which lowers H^E(dis.).

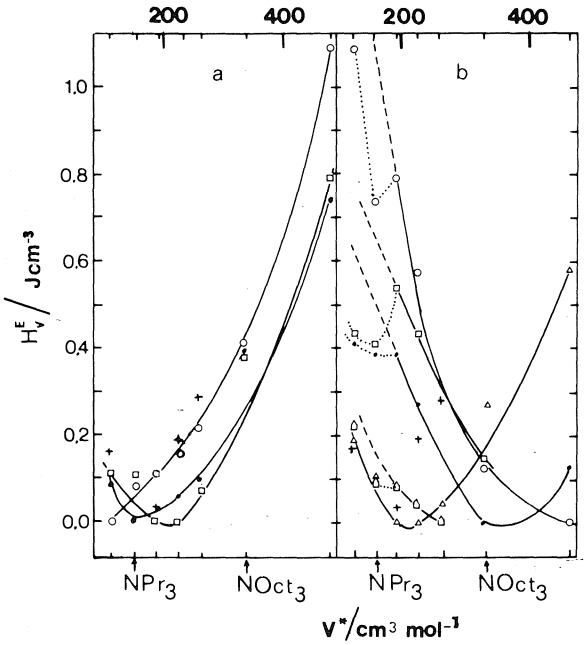

FIG. 1. Heats of mixing H_v^E in J/cm^3 vs. the core volume of one constituent. (*a*) For the shorter amines: (○) NEt_3, (●) NPr_3, (□) $NBut_3$, (+) N(Me-2-But)$_3$ with the series. (*b*) For the longer amines: (○) $NDodec_3$, (●) $NOct_3$, (□) NMe_2-Dodec, (⌒) $NHex_3$, (△) $NPent_3$, (+) N(Me-2-But)$_3$ with the series. The H^E(ster.hindr.) contribution is the difference between the dashed line and the dotted line. The higher values with N(Me-2-But)$_3$ (+) compared to $NPent_3$ (△) illustrate the nonfitting of branched and linear chains.

experimental heats is that the trend of the heats versus the molar or chain length of the second component is due mainly to the H^E(dis.) contribution. A finer separation of the contribution in H^E(chem.), H^E(dis.), and eventually H^E(ster.hindr.) is, in principle, difficult but may be made easier in practice by simple considerations. The free volume contribution is maximum for the NEt_3 + $NDodec_3$ mixture where the calculated value (penultimate column of Table 2) reaches a quarter of all the other contributions. For the other systems in this class, the free volume term is a smaller fraction of the total heat because the calculated value drops rapidly when the difference of expansion coefficients diminishes. A more definite validation of the assumption in the type *B* systems that H^E(exp) $\simeq$ H^E(dis.) is the reasonable range found within this approximation for H^E(dis.) of the same component with different order-breakers. Table 3 gives such values for the dodecyl chain in NR_3, SnR_4, n-C_{12}, and dimethyldodecylamine in J/cm^3. One sees that with most of the order-breakers, the heat of disordering is 1.15 J/cm^3 for $NDodec_3$ and 1.25 J/cm^3 for $SnDodec_4$. The values in parentheses correspond to the sterically hindered order-breakers for which H^E(dis.) is found to be lower due to the negative steric hindrance contribution. Dodecane appears to be less ordered by about one-third than the tri- or tetradodecyl chains due to its greater mobility. The lower values of H^E(dis.) for NMe_2Dodec may be due to the presence of the two CH_3's which prevent at one extremity of the molecule the correlation of orientations of neighbouring molecules. The last three rows of the table seem to indicate that the octyl chain in $NOct_3$ and $SnOct_4$ has about twice as intense correlation of orientations as n-octane. Rayleigh scattering measurements on alkanes show that orientational order is negligible in n-heptane but measurable in n-octane. These measurements have not been undertaken on NR_3 or SnR_4 compounds. It has been found previously, as seen in Table 3, that volatile order-breakers like NEt_3 give higher heats of disordering. H^E(dis.) have been obtained with similar results for hexadecane chains (10).

The third class of systems (class *C* in Table 2) corresponds to mixtures of two ordered compounds, both of which are ordered in the pure state and whose heats are small because there is no extensive destruction of correlation of orientations in the solution by contact with unlike molecules in the solution. Two systems, $NOct_3$ with $NDodec_3$ and $NOct_3$ with NMe_2Dodec, belong to this group.

Figure 1*a* shows H_v^E for the *A* and *B* type systems. The left part of the diagram indicates the small heats for mixtures of globular molecules, the right-hand side corresponding to large heats when the chain-

Can. J. Chem. Downloaded from www.nrcresearchpress.com by 210.87.254.6 on 09/05/12
For personal use only.

Can. J. Chem. Downloaded from www.nrcresearchpress.com by 210.87.254.6 on 09/05/12
For personal use only.

length of the second component increases. The curves are drawn by joining the points for the same order-breaker. The points for NMe_2Dodec and the shorter amines have not been inserted in the graph. To illustrate more clearly the irregularities of the heats in the series and for the discussion on the steric hindrance contribution, the heats for one long-chain amine have been plotted in Fig. 1*b* versus the core volume of the order-breaker and lines are drawn through the heats for the same long-chain compounds. This diagram is intended to show two features: the lower heats with NPr_3 and NEt_3 which do not have the values expected from the tributyl, tripentyl points (downward part of the curve). Note the difference between the dashed and dotted lines in the four series (○, □, ●, ⌓). The lower part of the figure indicates the extent of the fitting of the chains for mixtures of compounds different in size. For instance, $NPent_3$ (△) and probably $NHex_3$ (⌓) can fit their chains onto molecules in the series between NEt_3 and about $NOct_3$ and consequently these systems show small heats. The non-fitting of the linear and branched chains are indicated by the higher heats for the branched isomer of $NPent_3$, $N(Me\text{-}2\text{-}But)_3$. Compare the sixteenth result of Table 2 with the last two ones.

Steric Hindrance Contribution

There are a few examples of heats of mixing of non-polar compounds whose heats are too negative to be explained by the free volume contribution. An interesting case is the system *n*-C_8 + 3,3-diethylpentane (DEP) whose heat of mixing measured by Mathot and Prigogine (13) was found to be −82 J/mol. Recent measurements of other systems involving 3,3-diethylpentane have shown that the heats of mixing are smaller than expected. If the second component of the mixture with DEP is a long chain, there will be a disorder contribution added to the H^E(ster.hindr.) so that the total experimental heat will be less positive than expected rather than negative. Recent measurements of such systems have confirmed this possibility (12). We think that a similar effect occurs in the systems measured here. The kink downwards seen in Fig. 1*b* when NPr_3 is mixed with $NDodec_3$, NMe_2Dodec, $NOct_3$, and even $NHex_3$ would be explained by the fact that H^E(ster.hindr.) is larger for NPr_3 than for $NBut_3$.

Criteria for a Steric Hindrance Contribution

The first component is the sterically hindered molecule, i.e. NEt_3 and NPr_3 in the case of the present systems. The second component is one not sterically hindered. In previous work, linear alkanes have constituted the second components while long-chain triamines are used in this work. Globular molecules, such as cyclohexane and $SnBut_4$, seem to give a much smaller contribution. The molecular origin of the effect is not clear except that the sign of the heat corresponds to a diminution of the mobility or to a better fitting of the molecules in solution compared to the state in the pure components. It is not sure whether the compound, whose mobility is changed by contact with the unlike molecule, is the sterically hindered compound or the second component, or both. Probably non-thermodynamic data could give information on this.

Comparison of H^E(ster.hindr.) for Different Systems

An estimation of H^E(ster.hindr.) can be obtained from the difference between the expected value and the measured value of the heats of mixing. The expected value can be found in Fig. 1*b* on the dashed line drawn by extrapolation of the points for the higher amines at the abscissa corresponding to the core volume of the sterically hindered compound, for example, NPr_3. Because the heats with NMe_3 as first component were not measurable, the last point on the dashed line is lacking. This diminishes the reliability of the position of the expected value. However, since diagrams similar to Fig. 1*b* had been made on the SnR_4 + SnR_4' compounds and SnR_4 + alkanes with greater confidence because the heats with $SnMe_4$ were available and since data were also available with DEP, it was thought worthwhile to compare data on H^E(ster.hindr.) at this point. Figure 2 gives H^E(ster.hindr.) with five sterically hindered compounds versus the molar volume of the second component. The lines are drawn through the points corresponding to the same sterically hindered compound. The results for NEt_3 and NPr_3 with the trialkylamines as second component come from this work (curves *1* and *2*). The other points are calculated from previous work on the systems NPr_3 + alkanes (curve *5*), $SnPr_4$ + SnR_4' (curve *4*), $SnPr_4$ + alkanes (curve *6*), and DEP + alkanes (curve *7*). Details on the curve with DEP will be given since H^E(ster.hindr.) are not obtained in exactly the same way as they are with the series. Heats of mixing of *n*-C_{16} with many branched nonanes vary considerably with the number and position of the methyl groups on the chain. For instance, the molar heat at its maximum is 235 J/mol with 2,2,4,4-tetramethylpentane and 78 J/mol with 2,3,3,4-tetramethylpentane. Since the value with 2,2,5-trimethylhexane is about the largest for all the isomers, 315 J/mol, this compound is chosen as the one having little steric hindrance contribution. As the other contributions, chemical, disorder, and free volume must be about the same for the two isomers, the steric hindrance contribution of 2,3,3,4-tetramethylpentane would be equal to the difference 78 − 315, i.e. = −237 J/mol. Since the effect is larger with the ethyl-substituted

Can. J. Chem. Downloaded from www.nrcresearchpress.com by 210.87.254.6 on 09/05/12
For personal use only.

nonane isomer DEP, and since that compound (DEP or CEt_4) has a structure similar to $SnEt_4$ and similar enough to NEt_3, the corresponding point has been inserted in Fig. 2. H^E(*n*-C_{16} + DEP) is 18 J/mol, and by the same argument H^E(ster.hindr.) is 18 − 316 = −298 J/mol. With *n*-C_8, the heats with 2,2,5-trimethylhexane and DEP being respectively +82 J/mol and −83 J/mol, H^E(ster.hindr.) for this system is −165 J/mol, the value of which is about half that with *n*-C_{16} as second component. With the same sterically hindered compound, H^E(ster.hindr.) seems proportional to the volume of the second component, as seen in Fig. 2. However, if the second component becomes globular when its size diminishes, as in the case of the SnR_4 and NR_3 compounds, H^E(ster. hindr.) becomes zero (curves *1–4*). For the alkanes, on the other hand, H^E(ster.hindr.) becomes zero only when $V^* = 0$ since curves *5–7* extrapolate to the origin. Curves *1–4* will superpose with curves *5–7* if the plots are made with the 'useful' volume ($V^* - 200$) cm^3, rather than V^*. This would indicate that linear chains in the second component as well as a sterically hindered compound are necessary to have the steric hindrance contribution. The difference between curves *1–4* and *5–7* should not arise from the way H^E(ster.hindr.) has been obtained because the method is identical for an alkane or a long-chain trialkylamine as a second component. The sterically hindered character decreases in the following order: DEP, $SnPr_4$, $SnEt_4$, NPr_3, NEt_3. Due to their small size and the uncertainty in extrapolation, data for NEt_3 and NPr_3 are less dependable than the others. It is realized that there is perhaps a subjective and approximate element in this evaluation by supposing that other contributions are very similar for the sterically hindered and non-sterically hindered molecules. However, the apparent consistency of the data presented in Fig. 2, particularly the fact that H^E(ster.hindr.), when expressed per cm^3, do seem to depend only on the sterically hindered component and not on the second component, would give some confidence in this analysis. Furthermore, such semi-quantitative evaluation of steric hindrance as seen by calorimetry may be useful for comparison of steric hindrance observed by other methods.

Evaluation of the disordering and steric hindrance contributions has been done directly on H^E. In Fig. 3, the $X_{12}s_1^{-1}$ of the systems measured in this work have been plotted with the same coordinate as Fig. 1 *a* and *b*. Since the general trends of the curves in Figs. 1 and 3 are the same, a qualitative discussion of the contributions to the heats, except for the free volume contribution, could be made on the X_{12} parameters. X_{12}(dis.) positive and X_{12}(ster.hindr.) negative could be obtained. However, as some of the X_{12} are made very large by a very negative calculated free volume contribution (note the NEt_3 + $NDodec_3$ system), it was not thought that an analysis of the disordering and steric hindrance contributions in terms of X_{12}, while less direct than that made on H^E, would give either greater physical insight in the present systems or even more comparable values between the systems. The magnitude of the steric hindrance contribution to the $X_{12}s_2^{-1}$ parameter in J cm^{-3} Å calculated as was done for H^E(ster.hindr.) is small for the amine systems (between −0.6 and −1.6), larger for the SnR_4 systems, reaching possibly −6.0 for 3,3-diethylpentane with *n*-C_{16}. It is interesting to note that the global X_{12} parameter has been found negative only for very few non-polar systems. The conditions necessary for this occurrence are: no disordering contribution, no large free volume, and one sterically hindered compound in the mixture. $X_{12}s_1^{-1}$ has been found to be −0.89 for $SnBut_4$ + br-C_{16} (2,2,4,4,6,8,8-heptamethylnonane) and −2.0 for $SnPr_4$ + br-C_{16} (10).

Comparison with Predictions of Theories

Theories of liquids and mixtures are developed usually for simple molecules. In applying them to mixtures of molecules of different size, one should not expect a quantitative agreement with the experimental data. However, the effect of the size and energy parameters and of the mixing rules on the predictions may be analysed and compared with interest with the experimental data.

A. Use of a State Equation Generated by the Monte Carlo Calculation Method

The simplest description for a solution is that of a pure liquid (one-fluid model) for which the parameters of size σ_m and energy ε_m are an average of those of the components.

Excess thermodynamic properties such as heats can be obtained from either a model or from experimental values of the energy for a reference component.

The size and energy difference between the two components are expressed by two parameters. Keeping only the terms in squares of the parameters in the expansion, one obtains (18)

$$[6]\quad \frac{H^E}{x_1x_2} = \frac{-\Delta\varepsilon}{x_1x_2\varepsilon_{12}^{0}}(-U + TC_p) - 2\delta^2T^2\frac{dC_p}{dT}$$

The first term corresponds to H^E(chem.), the second to H^E(f.v.), and $\Delta\varepsilon$ is a function of the two parameters η and δ.

$$[7]\qquad \eta = \frac{\sigma_{11}}{\sigma_{12}^{0}} - 1 \qquad \delta = \frac{\varepsilon_{11}}{\varepsilon_{12}^{0}} - 1$$

where σ is the hard sphere diameter. Liquid 1 is compared to a reference liquid which follows the

Can. J. Chem. Downloaded from www.nrcresearchpress.com by 210.87.254.6 on 09/05/12
For personal use only.

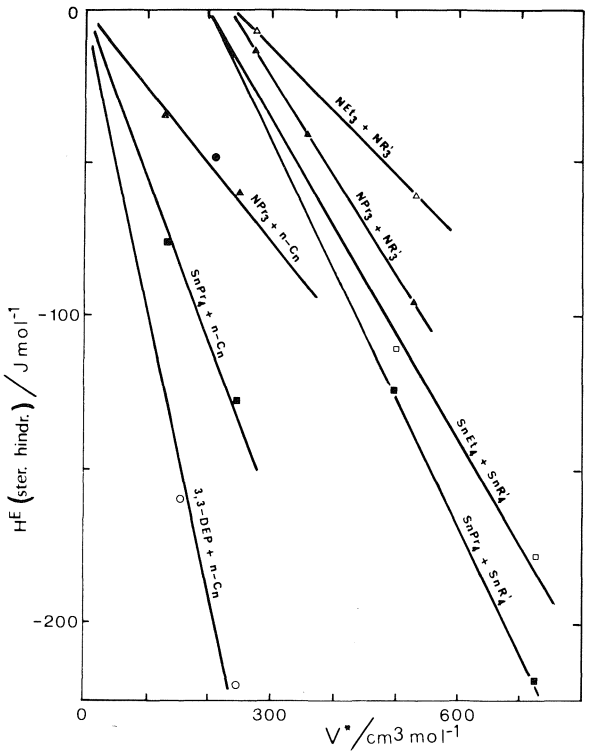

FIG. 2. Estimated values of the steric hindrance contribution in J/mol with five sterically hindered molecules (△) NEt_3, (▲) NPr_3, (□) $SnEt_4$, (■) $SnPr_4$, (○) 3,3-diethylpentane (DEP) vs. the core volume of the second component. Lines are drawn through the points corresponding to systems with the same first component and second components as indicated on the lines. One point (●) corresponds to the system $NPr_3 + NMe_2Dodec$.

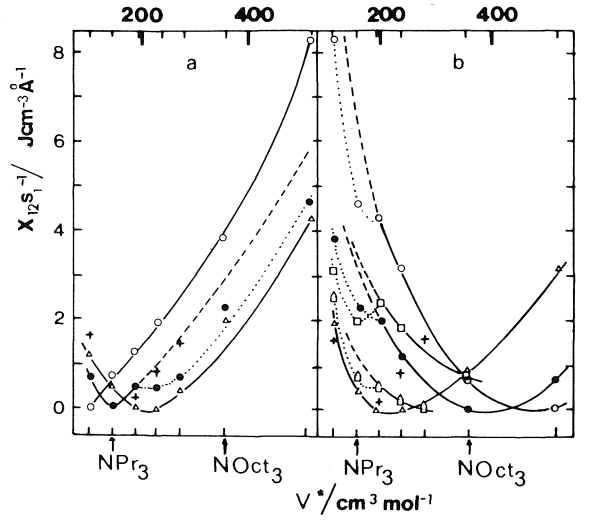

FIG. 3. $X_{12}S_1^{-1}$ in J/cm^3 Å. (*a*) For the three shorter amines: (○) NEt_3, (●) NPr_3, (△) $NBut_3$, (+) N(Me-2-But)$_3$ with the series. (*b*) For the longer amines: (○) $NDodec_3$, (●) $NOct_3$, (□) NMe_2Dodec, (⌓) $NHex_3$, (△) $NPent_3$, (+) N(Me-2-But)$_3$ with the series.

Berthelot–Lorentz rules:

$$[8] \qquad \varepsilon_{12}^{0} = \varepsilon_{11}^{1/2}\varepsilon_{22}^{1/2}$$

$$\sigma_{12}^{0} = (\sigma_{11} + \sigma_{22})/2$$

From the Monte Carlo calculations, Singer and Singer (18) give the following expression for H

$$[9] \quad H = RT^*(-8.6961 + 0.3042\tilde{T} + 0.7854\tilde{T}^2)$$

From the first and second derivatives of H, it is possible to obtain C_p and dC_p/dT required in eq. [6]. After some simple arrangement, H^E can be calculated as follows:

$$[10] \quad \frac{H^E}{x_1x_2RT} = (\sigma - 2\eta)^2\left(\frac{9.6961}{\tilde{T}} + 0.7854\tilde{T}\right) - 2\delta^2(1.5708\tilde{T})$$

Using the Flory combining rule, $(\delta - 2\eta)^2$ has been used for $-\Delta\varepsilon/\varepsilon_{12}^{0}$. In eq. [10], $\tilde{T}$ represents the reference liquid, in eq. [9], $\tilde{T}^* = T/\tilde{T}$ and $\tilde{T}$ is calculated from α.

Parameters for the Pure Components

The reduced volume and reduced temperature can be obtained from αT in the two equations

$$\alpha T = (-0.1648\tilde{T} - 0.4130\tilde{T}^2) \times (1.068 - 0.1648\tilde{T} - 0.2065\tilde{T}^2)^{-1}$$

and

$$\tilde{v} = (1.068 - 0.1648\tilde{T} - 0.2065\tilde{T}^2)^{-1}$$

The size parameter σ can be calculated from $\tilde{v}$ and the molar volume. ε is $kT/\tilde{T}$ and ε_{12}^{0} from eq. [8]. Table 1 gives the pure component reduced temperatures $\tilde{T}_{11}$. The parameter $\tilde{T}_{12}$ corresponds to the reference liquid, and the difference parameters η and δ are reported in Table 4 as well as H^E_{calcd} and H^E_{exp}.

The predictions of the Monte Carlo calculations are fairly good but not as good as with the $SnR_4 + SnR_4'$ systems with quite similar parameters. The less good agreement may come from the fact that experimental heats with the amine systems are much smaller even when compared by cm^3. For example, $SnBut_4 + SnDodec_4 = 1.24$ J/cm^3 while $NBut_3 + NDodec_3 = 0.79$ J/cm^3. The physical reason for this difference is not clear. One can speculate that the amines in solution lose less of their cohesive energy than the tin derivatives because there is more room to fit the three alkyl chains of one molecule with the alkyl chains of other surrounding molecules than it is with four alkyl chains on the same atom. The greater flexibility of the first N—C bond compared to the Sn—C bond may help the stacking in solution.

B. The Snider–Herrington Theory

A new equation of state was developed by Snider and Herrington (19) and applied successfully to

Can. J. Chem. Downloaded from www.nrcresearchpress.com by 210.87.254.6 on 09/05/12
For personal use only.

TABLE 4. Calculated heats using the Monte Carlo simulated equation of state and the Snider–Herrington treatment

System		Monte Carlo						Snider–Herrington				
(1)	(2)	$\tilde{T}_{12}$	η	δ	$H^{E}_{(r.v.)calcd}$ (J mol^{-1})	H^{E}_{calcd} (J mol^{-1})	H^{E}_{exp} (J mol^{-1})	H^{E}_{calcd} [a] (J mol^{-1})	V^{E}_{calcd} [a] (cm^3 mol^{-1})	k_{12} [b]	V^{E}_{calcd} [c] (cm^3 mol^{-1})	H^{E}_{calcd} [d] (J mol^{-1})
NPr_3	$+NEt_3$	0.676818	0.05702	0.049884	−3.2	30.2	10.5	−153	−0.125	0.99404	0.050	−165
$NBut_3$	$+NEt_3$	0.660678	0.097284	0.075532	−7.2	110.8	16.3	−419	−0.307	0.98522	0.185	−546
$NPent_3$	$+NEt_3$	0.651455	0.129631	0.090758	−10.2	228.9	30.7	−623	−0.289	0.97742	0.398	−1010
$NHex_3$	$+NEt_3$											
$NOct_3$	$+NEt_3$	0.634032	0.199052	0.120732	−17.2	632.6	86.0	−1156	−0.520	0.95804	0.958	−2712
$NDodec_3$	$+NEt_3$	0.624433	0.259294	0.137960	−21.7	1190.6	290.0	−1378	−0.702	0.94219	1.658	−5014
$NBut_3$	$+NPr_3$	0.629287	0.040489	0.024429	−0.7	27.6	17.5	−50	0.014	0.99744	0.027	−109
$NPent_3$	$+NPr_3$	0.620502	0.073153	0.038932	−1.8	100.8	10.5	−139	−0.002	0.99548	0.139	−366
$NHex_3$	$+NPr_3$	0.612965	0.100353	0.051706	−3.1	195.1	18.1	−251	−0.031	0.99163	0.180	—
$NOct_3$	$+NPr_3$	0.603907	0.143664	0.067482	−5.1	422.11	92.0	−398	−0.100	0.98544	0.372	−1647
$NDodec_3$	$+NPr_3$	0.594764	0.205311	0.083892	−7.8	894.3	225.0	−449	−0.526	0.98063	0.395	−3730
$NPent_3$	$+NBut_3$	0.605705	0.032720	0.014156	−0.2	24.0	0	−28	−0.050	0.99928	−0.020	−7.4
$NHex_3$	$+NBut_3$	0.598348	0.060107	0.026626	−0.8	80.2	19.9	−56	0.290	0.99789	0.097	—
$NOct_3$	$+NBut_3$	0.589505	0.103775	0.042026	−2.0	253.5	104.0	−147	−0.162	0.99401	0.757	−933
$NDodec_3$	$+NBut_3$	0.580581	0.166203	0.058044	−3.6	686.8	260.0	−60	−0.382	0.99141	—	—
$NDodec_3$	$+NOct_3$	0.557165	0.063521	0.015372	−0.2	123.6	56.0	86	−0.125	> 1	—	—
$NDodec_3$	$+NPent_3$	0.572476	0.134173	0.043275	−2.1	487.2	216.0	41	−0.300	0.9955	—	—
$NOct_3$	$+NPent_3$	0.581276	0.071259	0.027480	−0.8	120.4	78.1	−426	−2.100	0.99698	0.146	−440
$NHex_3$	$+NPent_3$	0.589996	0.027401	0.012295	−0.2	16.5	11.1	−28	−0.069	0.99949	0.053	—
NMe_2Dodec	$+NEt_3$	0.649554	0.11994	0.093949	−11.11	171.5	70.10	−639	−0.377	0.97529	0.275	−934
NMe_2Dodec	$+NBut_3$	0.603938	0.02292	0.017124	−0.34	7.2	75.8	−18	−0.032	0.99591	0.088	−38
NMe_2Dodec	$+NPr_3$	0.618692	0.06335	0.061872	−2.04	60.4	111.7	−187	−0.126	0.99283	0.185	−340
$NPent_3$	$+NMe_2Dodec$	0.595507	0.00984	−0.002917	−0.01	4.7	98.6	29	0.045	0.99810	0.099	—
$NOct_3$	$+NMe_2Dodec$	0.579580	0.08105	0.024482	−0.67	179.4	40.6	−570	−3.351	1.00022	−0.062	—
$N(Me\text{-}2\text{-}But)_3$	$+NEt_3$	0.658134	0.13037	0.07968	−7.98	265.5	24.8	−475	−0.160	0.98172	0.350	—
$N(Me\text{-}2\text{-}But)_3$	$+NBut_3$	0.611915	0.03351	0.038642	−1.71	5.5	7.1	62	0.018	1.00140	−0.056	—
$N(Me\text{-}2\text{-}But)_3$	$+NPent_3$	0.603374	0.00075	−0.010149	−0.12	1.1	44.5	25	0.021	0.99890	−0.037	—

[a] $k_{12} = 1$ and ξ obtained from α.
[b] k_{12} values which fit the experimental H^E.
[c] Calculated values using for each system the fitted k_{12} (previous column).
[d] $k_{12} = 1$ and ξ obtained from ΔH_{vap}.

Can. J. Chem. Downloaded from www.nrcresearchpress.com by 210.87.254.6 on 09/05/12
For personal use only.

mixtures of simple liquids.

$$[11] \qquad p/nkT = \chi(\xi) - (an/kT)$$

where p is the pressure, n is the number density ($= N_{Avog}/V$), and a is a cohesive energy similar to that used in the Van der Waals equation of state, multiplied by a volume parameter.

$$\xi = \tfrac{1}{6}\pi r^3 n$$

where r is the hard-sphere diameter.

$$[12] \qquad \chi(\xi) = (1 + \xi + \xi^2)/(1 - \xi)^3$$

r and a for the pure components are obtained from ξ: the ξ values from the heats of vaporization:

$$[13] \qquad \triangle H_{vap}/RT = \chi(\xi) + 1$$

or from the expansion coefficient

$$[14] \qquad \alpha T = \frac{[(1 + \xi + \xi^2)(1 - \xi)]}{\left[-1 + 4\left(\xi + \xi^2 + \frac{\xi^3}{2}\right)\right]}$$

are listed in Table 1. Equations [11] and [12] may be generalized for a mixture. The solution hard-sphere diameter is $r_m^3 = x_1 r_1^3 + x_2 r_2^3$. a_m and ξ_m are given by eqs. [8] and [9] of ref. 19. A deviation from the geometrical rule can be introduced by the constant k_{12}. A k_{12} smaller than 1 will make the H^E values more positive.

$$\frac{a_{12}/kT}{r_m^3} = k_{12}\left(\frac{a_{11}/kT}{r_1^3}\right)^{1/2}\left(\frac{a_{22}/kT}{r_2^3}\right)^{1/2}$$

H^E is given by the difference between the $\chi(\xi)$ for the solution and the $\chi(\xi)$ for the pure liquids since p/nkT can be neglected.

$$H^E = RT[-\chi(\xi_m) + x_1\chi(\xi_1) + x_2\chi(\xi_2)]$$

$$\chi(\xi_m) = \frac{(1 + \xi_m + \xi_m^2)}{(1 - \xi_m)^3 - f[(r_1 - r_2), x_1]}$$

One sees that the excess heats will be very sensitive to the curvature of the function $\chi(\xi)$.

The results are the balance of two large terms, one negative due to the difference in free volume between the two components, and the other positive due to the difference in size. With $k_{12} = 0$, the negative term is larger in absolute value, so that the predicted heats are too negative. This is the case for the system consisting of two liquids with a relatively large free volume difference, i.e. mixtures of the globular amines and mixtures of a long-chain compound with a globular one. For the systems having a size difference but a relatively small free volume term, the positive size difference term is larger so that the heats are predicted to be positive. In the next column, the k_{12} value needed to fit the experimental heats has been given. Predicted values of V^E have been added for $k_{12} = 1$ and the k_{12} value which fits the heats. Measurements of V^E are being carried out to investigate whether the fitted k_{12} gives a good prediction for V^E. The diminution of the k_{12} value which fits the heats is not unreasonable physically since the cohesive energy between unlike molecules must diminish when the size difference increases. It was thought that the heats of vaporization would give a better prediction than the expansion coefficient which is a more strenuous test of the theory. However, the H^E calculated from $\xi(\alpha)$ (7th column) are nearer H^E_{exp} than H^E_{calcd} from $\xi(\triangle H_{vap})$ (last column of Table 4).

Acknowledgements

This collaboration between the Université du Québec and the Université de Lyon was supported by the France–Québec scientific programme of exchange. The National Research Council of Canada financed part of this work.

1. J. Hildebrand and R. Scott. The solubility of nonelectrolytes. Dover. 1964. Chapt. VII.
2. J. P. E. Grolier, K. Sosnkowska-Kehiaian, and H. V. Kehiaian. J. Chim. Phys. **70**, 367 (1973).
3. G. Delmas, D. Patterson, and T. Somcynsky. J. Polym. Sci. **57**, 79 (1962).
4. P. Tancrède and G. Delmas. Eur. Polym. J. **9**, 199 (1973).
5. I. Prigogine (with the collaboration of A. Bellemans and V. Mathot). The molecular theory of solutions. North-Holland, Amsterdam. 1957.
6. D. Patterson and G. Delmas. Trans. Faraday Soc. **49**, 1 (1970).
7. R. A. Orwoll and P. J. Flory. J. Am. Chem. Soc. **89**, 6814 (1967).
8. V. T. Lam, P. Picker, D. Patterson, and P. Tancrède. J. Chem. Soc. Faraday II, **70**, 1465 (1974).
9. G. Delmas and S. Turrell. J. Chem. Soc. Faraday I, **70**, 572 (1974).
10. R. Philippe, G. Delmas, and P. N. Hong. Can. J. Chem. In press.
11. G. Delmas and N. T. Thanh. J. Phys. Chem. **81**, 1730 (1977).
12. (*a*) P. Tancrède, P. Bothorel, P. de Saint Romain, and D. Patterson. J. Chem. Soc. Faraday II, **73**, 15 (1977); (*b*) P. Tancrède, P. Bothorel, and D. Patterson. J. Chem. Soc. Faraday II, **73**, 29 (1977).
13. (*a*) I. Prigogine and V. Mathot. J. Chem. Phys. **18**, 765 (1950); (*b*) V. Mathot. Bull. Soc. Chim. Belg. **59**, 111 (1950).
14. K. N. Marsh. Int. Data Ser. Selected Data Mixtures Ser. A, 3 (1973).
15. P. Picker, C. Jolicoeur, and J. E. Desnoyers. J. Chem. Thermodyn. **1**, 469 (1969).
16. (*a*) J. P. E. Grolier and A. Inglese. Can. J. Chem. **54**, 1952 (1976); (*b*) J. P. E. Grolier. Thermochim. Acta, **16**, 27 (1976).
17. R. Philippe, G. Patterson, and M. Couchon. Can. J. Chem. **56**, 370 (1978).
18. J. V. L. Singer and K. Singer. Mol. Phys. **24**, 357 (1972).
19. N. S. Snider and T. M. Herrington. J. Chem. Phys. **47**, 2248 (1967).
20. P. de Saint Romain. Ph.D. Thesis, McGill University, Montréal. 1977.

Rotamers arising from restricted motions and electronic interactions of acetoxymethyl groups in carbohydrates

S. PEREZ,[1] J. ST-PIERRE, AND R. H. MARCHESSAULT

Department of Chemistry, University of Montreal, Montreal, P.Q., Canada H3C 3V1

Received August 30, 1977[2]

S. PEREZ, J. ST-PIERRE, and R. H. MARCHESSAULT. Can. J. Chem. **56**, 2866 (1978).

The two dimensional conformational spaces available for acetoxymethyl groups in carbohydrates are reported. The studies were performed on two molecules differing in their C-4 configurations, i.e. *gluco* and *galacto*. The acetoxymethyl group was assigned a mean geometry derived from the computation of 19 equivalent groups as found in pertinent acetylated carbohydrates. The internal energy calculations were performed by including the partitioned contributions arising from the non-bonded energies, electrostatic interactions, and torsion energy. An instability rating of 3 kcal/mol was assigned to conformations involving *peri* interactions, i.e., *trans–gauche* and *gauche–gauche* forms in *gluco* and *galacto* carbohydrates, respectively. The results which are best described in term of topology show that several conformations corresponding to the *trans* and *gauche* states of the C—O single bond are preferred. However, significant shifts from perfect staggering are observed. The predicted regions of low energy are found to be in good agreement with experimental data from crystal structures of acetylated carbohydrates.

S. PEREZ, J. ST-PIERRE et R. H. MARCHESSAULT. Can. J. Chem. **56**, 2866 (1978).

On présente l'espace conformationnel à deux dimensions accessible aux groupes acétoxyméthyles dans les carbohydrates. Les études ont porté sur deux molécules présentant des conformations différentes à l'atome C-4, soit *gluco* et *galacto*. On a attribué au groupe acétoxyméthyle une géométrie moyenne déduite de calculs effectués sur 19 groupes semblables se trouvant dans des carbohydrates acétylés appropriés. Dans le calcul de l'énergie interne, on a tenu compte des contributions respectives des énergies d'interaction non-liée, des interactions électrostatiques et de l'énergie de torsion. On a attribué une instabilité évaluée à 3 kcal/mol aux conformations faisant intervenir des interactions *péri*, c'est-à-dire les formes *trans–gauche* et *gauche–gauche* dans les carbohydrates *gluco* et *galacto* respectivement. Les résultats, dont on donne une description topologique, montrent une préférence pour certaines conformations correspondant aux états *trans* et *gauche* de la liaison simple C—O. Cependant, il y a des écarts significatifs au décalage parfait. Les prévisions quant aux régions de basses énergies sont en bon accord avec les résultats expérimentaux tirés des structures cristallines de carbohydrates acétylés.

[Traduit par le journal]

Introduction

The allowed torsional angle variations around the inter-glycosidic linkages, usually described in terms of (Φ,ψ) maps, determine the conformation of polysaccharides. Furthermore a knowledge of the most probable conformation of the lateral substituents with respect to the backbone is important for a complete conformational specification. Since many of the naturally occuring polysaccharides are found to be partially acetylated (1, 2), the number of conformational variables is considerable. Although some computation methods can minimize simultaneously a large number of parameters (3, 4), an a priori knowledge of the allowed ranges for certain structural parameters as well as their interdependence is valuable.

An acetate group at the primary hydroxyl of a polysaccharide can adopt various conformations around the *exo*-cyclic C(5)—C(6) bond (torsion angle χ). In aldohexopyranoses the rotamer populations of the C(5)—CH_2OAc group fall into three preferred conformations: *gauche–trans*, *gauche–gauche*, and *trans–gauche* (5). A recent survey (6) of the rotations about the *exo*-cyclic bond of 125 primary hydroxyl and esterified hydroxyl groups from 71 crystal structures of carbohydrates showed that in glucosides, the *gauche–gauche* conformer is preferred (60%) along with the *gauche–trans* (40%) form. In galactosides, the *gauche–trans* (58%) and the *trans–gauche* (34%) are the two favoured conformers. The *gauche–gauche* form which involves *peri* interactions has been found in only two structures, associated with the occurrence of intramolecular hydrogen bonds.

Complete knowledge of the conformation of the primary acetate group requires two other torsion angles: torsion angle ω describing the conformation of the ester group and torsion angle θ around the

[1]Present address: Centre de recherches sur les macromolécules végétales (CNRS), 53X, Grenoble cédex, France.

[2]Revision received August 4, 1978.

Can. J. Chem. Downloaded from www.nrcresearchpress.com by 210.87.254.105 on 09/05/12
For personal use only.

TABLE 1. Crystal structures of acetylated carbohydrates analyzed

Compound	Reference
1,2,3,4,6-Penta-*O*-acetyl-α-D-altropyranose	10
Cellobiose octaacetate	19
Cellotriose undecaacetate	20
Methyl-6-*O*-acetyl-β-D-galactopyranoside	21
2,3,4,6-Tetra-*O*-acetyl-1-cyano-β-D-galactopyranoside	22
3,4,6-Tri-*O*-acetyl-1,2,-*O*-[1-(exoethoxy)ethylidene)]-α-D-glucopyranose	23
Methyl-6-*O*-acetyl-β-D-glucopyranoside	24
1-*O*-(*p*-Bromobenzene-sulphonyl)-4,5,7-tri-*O*-acetyl-2,6-anhydro-3-deoxy-D-glucoheptitol	25
3,1′-Anhydro-2-(4′,6′-di-*O*-acetyl-2,3′-dideoxy-α-D-ribosehexopyranose)-3-hydroxy-5-methyl-2*H*-1,2,6-thiadiazine-1,1-dioxide	26
1,2,3,4,6-Penta-*O*-acetyl-α-D-idopyranose	27
Methyl-2,3,4,6,2′,4′,6′-hepta-*O*-acetyl-β-D-laminarabioside	*
3,4,6-Tri-*O*-acetyl-β-D-mannose-1,2-methyl orthoacetate	28
3,4,6-Tri-*O*-acetyl-2-bromo-2-deoxy-α-D-mannopyranosyl fluoride	29
Tetra-*O*-acetyl-α-D-mannopyranosyl chloride	30
Brominated compound from paeoniflorin	31

*H. Takeda, T. Kaiya, N. Yasuoka, and N. Kasai. Private communication.

C(6)—O(6) bond. It seems well established that the barrier to rotation around the former is very high and that only small departures from planarity of the ester group are possible (7, 8). The conformation around the C(6)—O(6) bond can be rationalized on the basis of non-bonded and electrostatic interactions alone. An analysis of the problem using data for methyl formate has led to the proposal that the torsion potential for this rotation is zero (9).

The purpose of the present study is to establish the allowed variations for rotation around the C(6)—O(6) bond of the acetoxymethyl group in aldohexopyranoses. The theoretically calculated energy minima will be related to experimental evidence from crystal structure determinations of simple acetylated carbohydrates.

Method of Calculation

The purpose of the present work lies in the establishment of the conformationally-allowed region for an acetoxymethyl group in carbohydrates and oligosaccharides. One way to arrive at such a result is to perform a statistical survey of relevant crystal data. The complementary way is to perform a conformational analysis on such a molecular fragment. We choose an empirical method of calculation because it is the one used in all polysaccharide structural determinations (4). Ultimately if the two approaches coincide, i.e. the predicted and observed results (from the crystal data survey) agree, this would confirm the validity (within a given and accepted degree of confidence) for such a method of calculation.

The molecular geometry and conformation for the aldohexopyranose were those found in the crystal structure of 1,2,3,4,6-penta-*O*-acetyl-α-D altropyranose (10). However, the acetoxymethyl group was assigned a mean geometry derived from the computation of 19 equivalent groups as found in pertinent acetylated carbohydrates (Table 1). The bond distances and angles used for the acetoxymethyl group are schematically depicted, Fig. 1*a*, along with the torsion angles relevant for discussion. The sign of torsion angles is in adherence to the IUPAC nomenclature (11). χ will be used to describe the rotations around the C(5)—C(6) bond. When more specific descriptions are needed $\chi^{O(5)}$ (O(5)—C(5)—C(6)—O(6)) and $\chi^{C(4)}$ (C(4)—C(5)—C(6)—O(6)) will be employed.

The potential energy of the molecule was calculated by including the partitioned contributions arising from the non-bonded energies, electrostatic interactions, and torsion energy about the different torsion angles.

The van der Waals interactions between non-bonded atoms were evaluated using 6-12 potential functions with the parameters proposed by Scott and Scheraga (12, 13). The following expression was used:

$$V_{nb} = -\frac{A_{ij}}{R_{ij}^{6}} + \frac{B_{ij}}{R_{ij}^{12}}$$

where R_{ij} is the distance between atoms. The atomic polarizability for the CH_3 group, which was treated as a spherical domain of fixed size, the number of polarizable electrons, and the van der Waals radius are 1.77, 7.0, and 1.9 Å, respectively. The charge distribution in aldohexopyranose pentaacetate was taken from a previous study by Vijayalakshmi and Rao (14). The electrostatic interactions were calcu-

Can. J. Chem. Downloaded from www.nrcresearchpress.com by 210.87.254.105 on 09/05/12
For personal use only.

Can. J. Chem. Downloaded from www.nrcresearchpress.com by 210.87.254.105 on 09/05/12
For personal use only.

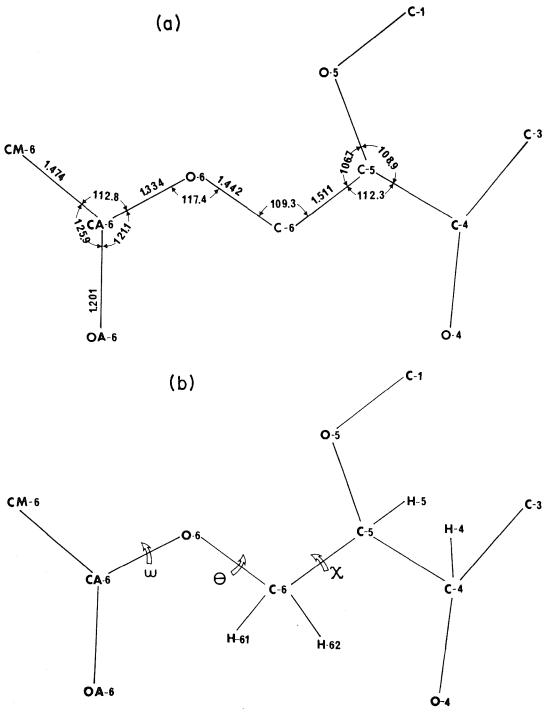

FIG. 1. Schematic representation of the acetoxymethyl group. (*a*) Molecular geometry derived by averaging 19 equivalent groups. (*b*) Torsion angles χ, θ, and ω.

lated using a Coulomb's law potential

$$V_{es} = \frac{332 e_i e_j}{\varepsilon R_{ij}}$$

where R_{ij} is the interatomic distance between atoms i and j, and e_i and e_j are expressed in fraction of electronic charge. ε, which is the effective dielectric constant of the medium, was assigned a value of 2.0 (15, 18). In the calculation of the potential energies there was no limit for the interaction distances for non-bonded and electronic terms. An intrinsic torsional potential with a three-fold barrier of 2.7 kcal/mol was assigned to rotation about C(5)—C(6). For rotation around the C(6)—O(6) bond, torsional angle θ, the value of the torsional potential was taken as zero. Because of resonance within the acetate group, rotation around the O(6)—CA(6) bond (rotation ω) was not allowed. As found in all carbohydrate acetates, the secondary acetate groups were fixed in the position where the carbonyl is coplanar with the hydrogen at the corresponding pyranose ring carbon atom.

The disposition of the substituent at C(4) is known to be one of the parameters fostering preferred conformations around the C(5)—C(6) *exo*-cyclic bond (6). Therefore two iso-energy contour maps were prepared, one corresponding to the *gluco* configuration (O(4)—C(4)—C(5)—O(5) = 180° for $^4C_1$ (*D*) ring) and another one corresponding to the *galacto* configuration (O(4)—C(4)—C(5)—O(5) = −60° for $^4C_1$ (*D*) ring). The conformations involving *peri* interactions, i.e. *trans–gauche* in *gluco* carbohydrates and *gauche–gauche* in *galacto* carbohydrates were systematically assigned an instability rating of 3 kcal/mol (6). The energy maps were calculated at intervals of 5° in χ and θ.

Results and Discussion

Gluco *Carbohydrates: Conformational Map and Comparison with Experimental Data*

It was noticed throughout this work that among the potential energy terms, the non-bonded part as well as the torsion potential about the C(5)—C(6) bond are predominant.

The energy map calculated for rotations of the acetoxymethyl group in *gluco* carbohydrates is given in Fig. 2, while the values of χ and θ angles for all the calculated minima are given in Table 2. The general features of the map arise from a combination of restricted motions around the *gauche–gauche* and *gauche–trans* (χ angle) conformations and a large region of allowed values for θ (about θ = 180°) ranging from −60° to 60°. The two lowest energy minima are found for the *gauche–gauche* conformation at C(5)—C(6). These two minima, [(*gauche–gauche*)–g^-] and [(*gauche–gauche*)–*t*], belong clearly to a large

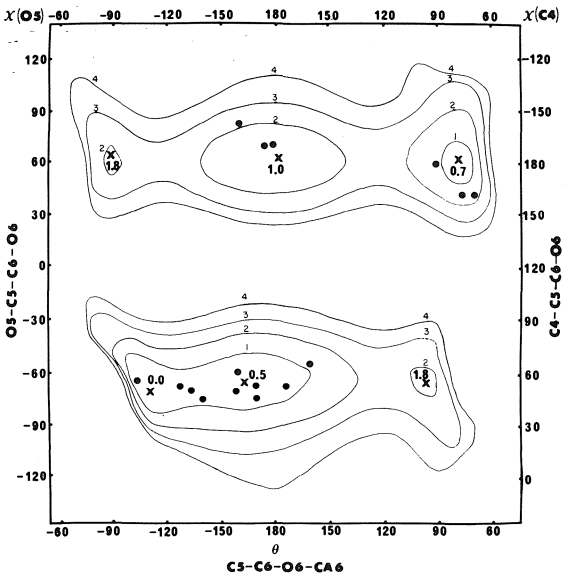

FIG. 2. Energy diagram computed for acetoxymethyl group in *gluco* carbohydrates, in terms of (χ,θ). Contours given at intervals of 1 kcal/mol are expressed relative to the minimum marked by 0.0. ● denotes an observed combination of (χ,θ) as found in simple acetylated carbohydrates in solid state.

Can. J. Chem. Downloaded from www.nrcresearchpress.com by 210.87.254.105 on 09/05/12
For personal use only.

TABLE 2. Preferred conformations and associated energies for the rotations of acetoxymethyl group in *gluco* carbohydrates

χ (deg)		θ		Relative energy
$\chi^{O(5)}$	$\chi^{C(4)}$	(deg)	Symbol	(kcal/mol)
−70	50	−110	[(*gauche–gauche*)–g^-]	0.0
−65	55	165	[(*gauche–gauche*)–*t*]	0.5
−65	55	95	[(*gauche–gauche*)–g^+]	1.8
60	180	85	[(*gauche–trans*)–g^+]	0.7
60	180	180	[(*gauche–trans*)–*t*]	1.0
60	180	−90	[(*gauche–trans*)–g^-]	1.8

valley ranging from $\theta = -100°$ to $\theta = 160°$. The third minimum [(*gauche–gauche*)–g^+] found for this conformation of χ corresponds to a somewhat higher energy. It is noticeable that the calculated values of χ corresponding to the energy minima depart slightly from perfect staggering. This is in agreement with the mean values found for $\chi^{O(5)} = -66.5°$ and $\chi^{C(4)} = 54.8°$ when averaging 61 equivalent *gauche–gauche* conformations in *gluco* carbohydrates (6).

The other low energy minima are found when the *gauche–trans* form around C(5)—C(6) exists. One of these minima is found to correspond to a perfect *trans* conformation around θ [(*gauche–trans*)–*t*]. Another one corresponds to a g^+ form [(*gauche–trans*)–g^+] which is, however, significantly shifted from perfect staggering. The same departure from perfect staggering is observed with the third minimum [(*gauche–trans*)–g^-].

The observed combinations of (χ,θ) as found in crystal structures of simple acetylated *gluco* carbohydrates are represented in the iso-energy map (Fig. 2). Among the six theoretically predicted conformations of low energy, only the four lowest minima are found experimentally. The most populated area corresponds to the low energy valley described previously. All the observed conformations lie within the 1.2 kcal/mol contour. The experimental ranges of χ angles are restricted ($-73° \leq \chi^{O(5)} \leq -52°$; $46° \leq \chi^{C(4)} \leq 64°$), whereas the distribution of θ angle is spread over 90°. The two other types of conformations found in the solid state correspond to the [(*gauche–trans*)–g^+] and [(*gauche–trans*)–*t*] minima. Here again the experimental distribution is in good agreement with the general topology of the calculated low energy regions. The two other calculated minima, which correspond to a somewhat higher energy, are not found in the solid state thus far.

With respect to the conformations displayed around the C(5)—C(6) bond, the statistical distribution found for acetoxymethyl groups (*gauche–gauche* form: 62.5% and *gauche–trans* form: 37.5%) is very comparable to that obtained when considering hydroxymethyl and esterified hydroxymethyl groups together (6).

Galacto *Carbohydrates: Conformational Maps and Comparison with Experimental Data*

The energy map calculated for rotations of the

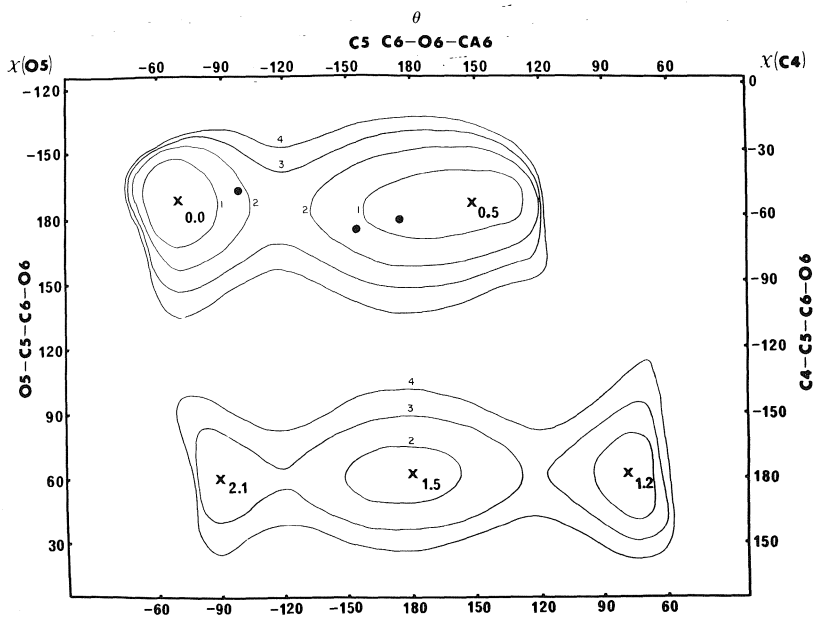

FIG. 3. Energy diagram computed for acetoxymethyl group in *galacto* carbohydrates, in terms of (χ,θ). Contours given at intervals of 1 kcal/mol are expressed relative to the minimum marked by 0.0. ● denotes an observed combination of (χ,θ) as found in simple acetylated carbohydrates in solid state.

TABLE 3. Preferred conformations and associated energies for the rotations of acetoxymethyl group in *galacto* carbohydrates

χ (deg)		θ		Relative energy
$\chi^{O(5)}$	$\chi^{C(4)}$	(deg)	Symbol	(kcal/mol)
−170	−50	−70	[(*trans–gauche*)–g^-]	0.0
−170	−50	150	[(*trans–gauche*)–*t*]	0.5
60	180	80	[(*gauche–trans*)–g^+]	1.2
60	180	−175	[(*gauche–trans*)–*t*]	1.5
60	180	−90	[(*gauche–trans*)–g^-]	2.1

acetoxymethyl group in *galacto* carbohydrates is depicted in Fig. 3. The values of χ and θ angles which correspond to the calculated minima are listed in Table 3.

Here again, the most restricted parameter is the torsion angle χ. The two lowest energy minima are found when the *trans–gauche* conformation around C(5)—C(6) occurs. The lowest minimum corresponds to a g^- conformation of θ angle: [(*trans–gauche*)–g^-]. The second minimum is located in a somewhat extended region of low energy which is spread over 70° along θ.

The three other low energy minima are found for the (*gauche–trans*) form about C(5)—C(6). In term of rotations about θ, these conformations occur around the non-eclipsed forms: [(*gauche–gauche*)–g^+], [(*gauche–trans*)–*t*], and [(*gauche–trans*)–g^-], respectively, with a significant shift from perfect staggering in the case of conformations g^+ and g^-.

The number of observed combinations of (χ,θ) from crystal structures of acetylated *galacto* carbohydrates is limited. Although the favoured conformations of hydroxymethyl groups in galactosides are the *gauche–trans* (58%) and the *trans–gauche* (34%) (6), only the latter form is observed so far when the primary hydroxyl group is acetylated. The reported conformations occur near the two lowest energy regions of the map: [(*trans–gauche*)–g^-] and [(*trans–gauche*)–*t*].

Conclusions

The comparison between the calculated energy minima and the experimental conformations reveals a close agreement. The relatively small number of energy minima can be understood on the basis of the usual partitioned energy method and upon consideration of *peri* interactions. The data and calculations presented here suggest that the conformation of the primary acetate group in an aldohexopyranose is mainly governed by intramolecular forces and that packing interactions play a minor role.

The foregoing analysis will be useful in the conformational understanding of complex polysaccharides. For example, in the *Klebsiella* type 59 polysaccharide, the primary hydroxyl of the mannose residues are reported to be acetylated (16). Similarly in the important commercial polysaccharide from *Xanthomonas compestris*, Xanthan gum (17), mannose is *O*-acetylated at the primary position.

The energy maps in Figs. 2 and 3 provide a probability distribution of conformations for primary acetate groups attached to *gluco* and *galacto* carbohydrates in any poly, oligo, or monosaccharide in solution. Eventually such information should be reconcilable with certain solution property data such as nmr spectra and circular dichroism curves.

Acknowledgements

The authors wish to thank Dr. N. Kasai of the University of Osaka who kindly communicated data prior to publication.

Financial support from the National Research Council of Canada and the Ministère de l'Education du Québec are acknowledged.

One of us (S.P.) benefited from the France–Quebec Exchange Program.

1. H. O. BOUVENG, P. J. GAREGG, and B. LINDBERG. Acta Chem. Scand. **14**, 742 (1960).
2. H. MEIER. Acta Chem. Scand. **15**, 1381 (1961).
3. S. ARNOTT and W. E. SCOTT. J. Chem. Soc. Perkin II, 324 (1972).
4. P. ZUGENMAIER and A. SARKO. Biopolymers, **15**, 2121 (1976).
5. M. SUNDARALINGAM. Biopolymers, **6**, 189 (1968).
6. S. PÉREZ and R. H. MARCHESSAULT. Carbohydr. Res.
7. J. CORNIBERT, N. V. HIEN, F. BRISSE, and R. H. MARCHESSAULT. Can. J. Chem. **52**, 3742 (1974).
8. B. PULLMANN and A. PULLMANN. Adv. Protein Chem. **28**, 347 (1974).
9. J. F. YAN, G. VANDERKOOI, and H. A. SCHERAGA. J. Chem. Phys. **49**, 2713 (1968).
10. J. OLLIS, V. J. JAMES, and J. D. STEVENS. Cryst. Struct. Commun. **4**, 215 (1975).
11. IUPAC-IUB Commission on Biochemical Nomenclature. Arch. Biochem. Biophys. **145**, 405 (1971); J. Mol. Biol. **52**, 1 (1970).
12. R. A. SCOTT and H. A. SCHERAGA. J. Chem. Phys. **44**, 3054 (1966).
13. R. A. SCOTT and H. A. SCHERAGA. J. Chem. Phys. **45**, 2091 (1966).
14. K. S. VIJAYALAKSHMI and V. S. R. RAO. Carbohydr. Res. **29**, 427 (1973).
15. G. N. RAMACHANDRAN. Int. J. Protein Res. **1**, 5 (1969).
16. B. LINDBERG, J. LONNGREN, and U. RUDÉN. Carbohydr. Res. **42**, 83 (1975).
17. P.-E. JANSSON, L. KENNE, and B. LINDBERG. Carbohydr. Res. **45**, 275 (1975).
18. R. A. SCOTT and H. A. SCHERAGA. J. Phys. Chem. **79**, 2361 (1975).

Can. J. Chem. Downloaded from www.nrcresearchpress.com by 210.87.254.105 on 09/05/12
For personal use only.

19. F. LEUNG, H. D. CHANZY, S. PÉREZ, and R. H. MARCHESSAULT. Can. J. Chem. **54**, 1365 (1976).
20. S. PÉREZ and F. BRISSE. Acta Crystallogr. In press.
21. K. B. LINDBERG. Acta Crystallogr. B**32**, 645 (1976).
22. C. FOCES-FOCES, F. H. CANO, and S. GARCIA-BLANCO. Acta Crystallogr. B**32**, 427 (1976).
23. J. A. HEITMANN, G. F. RICHARDS, and L. R. SCHROEDER. Acta Crystallogr. B**30**, 2322 (1974).
24. K. B. LINDBERG. Acta Crystallogr. B**32**, 642 (1976).
25. A. CAMERMAN and J. TROTTER. Acta Crystallogr. **18**, 197 (1965).
26. C. FOCES-FOCES, P. SMITH-VERDIER, F. FLORENCIO-SABATE, and S. GARCIA-BLANCO. Acta Crystallogr. B**31**, 140 (1975).
27. P. LUGER and H. PAULSEN. Carbohydr. Res. **51**, 169 (1976).
28. J. L. FLIPPEN. Cryst. Struct. Commun. **5**, 157 (1976).
29. J. C. CAMPBELL, R. A. DWEK, P. W. KENT, and C. K. PROUT. Carbohydr. Res. **10**, 71 (1969).
30. P. HERPIN, R. FAMERY, J. AUGE, S. DAVID, and L. GUIBE. Acta Crystallogr. B**32**, 209 (1976).
31. M. KANEDA and Y. IITAKA. Acta Crystallogr. B**28**, 1411 (1972).

Downloaded from www.researchpress.com by 210.87.254.105 on 09/05/12
For personal use only.

Synthesis of the 3,3′-dinitro and 3,3′-diamino derivatives of α,α-trehalose and its D-*gluco*,D-*manno* and D-*manno*,D-*manno* isomers[1]

HANS H. BAER AND ANNA J. BELL

Department of Chemistry, University of Ottawa, Ottawa, Ont., Canada K1N 9B4

Received July 12, 1978

HANS H. BAER and ANNA J. BELL. Can. J. Chem. **56**, 2872 (1978).

The tetraaldehyde **2** obtained from α,α-trehalose (**1**) by periodate oxidation was cyclized with nitromethane in the presence of sodium methoxide to give a mixture of 3,3′-dideoxy-3,3′-dinitro disaccharides in good yield. Acetalation of the product with benzaldehyde followed by chromatographic separation of the bisacetals afforded crystalline 4,6;4′,6′-di-*O*-benzylidene derivatives (**3**, **4**, and **5**) of 3-deoxy-3-nitro-α-D-glucopyranosyl 3-deoxy-3-nitro-α-D-glucopyranoside (**6**, 3,3′-dideoxy-3,3′-dinitro-α,α-trehalose), 3-deoxy-3-nitro-α-D-glucopyranosyl 3-deoxy-3-nitro-α-D-mannopyranoside (**7**), and 3-deoxy-3-nitro-α-D-mannopyranosyl 3-deoxy-3-nitro-α-D-mannopyranoside (**8**), respectively. Acid debenzylidenation then gave crystalline **6**–**8**, and these were hydrogenated catalytically to produce the corresponding diamino disaccharide dihydrochlorides **9**–**11**.

HANS H. BAER et ANNA J. BELL. Can. J. Chem. **56**, 2872 (1978).

Le tétraaldéhyde **2**, préparé par oxydation au periodate de l'α,α-tréhalose (**1**), a été cyclisé avec le nitrométhane en présence de méthanolate de sodium. On a obtenu un mélange de 3,3′-didésoxy-3,3′-dinitro disaccharides avec un bon rendement. Par acétalation du mélange avec le benzaldéhyde suivie d'une séparation chromatographique des bis-acétals on a isolé a l'état cristallin les dérivés 4,6;4′,6′-di-*O*-benzylidène (**3**, **4** et **5**) du (3-désoxy-3-nitro-α-D-glucopyranosyl)-3-désoxy-3-nitro-α-D-glucopyranoside (**6**), du (3-désoxy-3-nitro-α-D-glucopyranosyl)-3-désoxy-3-nitro-α-D-mannopyranoside (**7**) et du (3-désoxy-3-nitro-α-D-mannopyranosyl)-3-désoxy-3-nitro-α-D-mannopyranoside (**8**), respectivement. L'hydrolyse acide des groupements benzylidènes a conduit aux composés cristallins **6**–**8**, qui, par hydrogénation catalytique, ont donné les dichlorhydrates des diamino disaccharides correspondants (**9**–**11**).

The disaccharide α,α-trehalose (α-D-glucopyranosyl α-D-glucopyranoside, **1**) is widely distributed in nature and has been isolated from such diversified sources as bacteria, fungi and yeasts, algae, insects and other invertebrates, and also from some higher plants. Its chemistry (2) and more recently its metabolism (3) have been reviewed. The biological significance of the disaccharide is emphasized by its varied roles as a structural component (e.g., in the cord factor of mycobacteria), as a reserve supply of energy (e.g., in insects during flight), and as a possible intermediate in glucose resorption. Among the facets that continue to draw much attention is the mechanism of action of the hydrolytic enzyme, trehalase, which is present not only in the types of organisms mentioned but also in mammals including man. Further interest in trehalose chemistry arose from the discovery of the 2-amino-2-deoxy derivative (trehalosamine) (4) and 2-amino-2-deoxy-α-D-glucopyranosyl α-D-mannopyranoside (5) as antibiotically active metabolites of *Streptomyces* species.

In continuation of our synthetic work (1, 6) on nitrogenous carbohydrates of potential biological interest we have decided to attempt the preparation of some new trehalose-type sugars for possible evaluation in biochemical studies. This was prompted by a suggestion of Dr. J. Defaye (Grenoble) whose laboratory in collaboration with that of J. E. Courtois (Paris) is engaged in detailed studies (7–11) of structure–activity relationships in the mechanism of trehalase action, for which there is a need for structurally and stereochemically modified trehalose analogs to be evaluated as substrates or inhibitors. A number of such compounds have been synthesized and assayed jointly by the French teams (7–11) while comprehensive work on the chemical modification of the disaccharide has also been performed by a group of British authors (12*a*–*j*). Several synthetic amino, diamino, and tetraamino analogs have been described. These include the 2-amino-2-deoxy (13) and 6-amino-6-deoxy (14) derivatives of trehalose and the 3-amino-3-deoxy-D-*altro* isomer (12*e*) as well as 6,6′-diamino-6,6′-dideoxytrehalose (15), the 2,2′-diamino-2,2′-dideoxy-D-*altro*,D-*altro* isomer (12*e*), the 4,4′,6,6′-tetraamino analog of D-*galacto*,D-*galacto* configuration (12*i*), and various 2,2′, 3,3′, 4,4′, 6,6′, and 4,4′,6,6′ diamines and tetraamines having additional deoxy functions (12*d*, *f*–*h*). However, no nitro derivatives of α,α-trehalose or its stereoisomers

[1]Part 18 in a series on cyclizations of dialdehydes with nitromethane. For Part 17 see ref. 1.

Can. J. Chem. Downloaded from www.nrcresearchpress.com by 210.87.254.42 on 09/05/12
For personal use only.

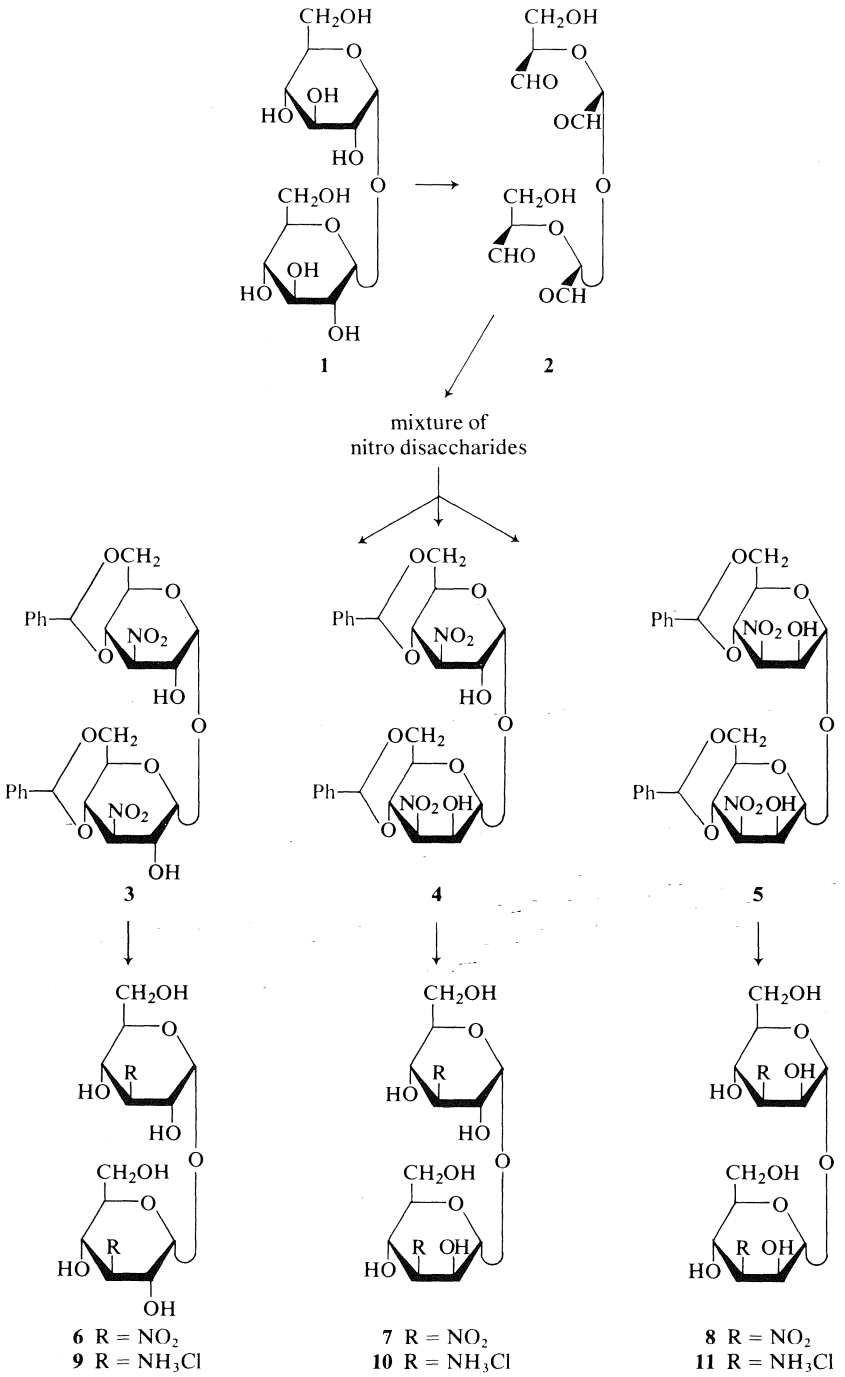

are known although we previously prepared (16) a structurally related nitro disaccharide (and the corresponding amine) which contained a β-linked heptuloside moiety. We have now employed the same method, starting with **1**, and obtained 3,3′-dideoxy-3,3′-dinitro-α,α-trehalose and two stereoisomers as well as the corresponding diamino sugars.

The tetraaldehyde **2**, quantitatively produced (17) from commercial **1** by periodate oxidation, was doubly cyclized with nitromethane in the presence of sodium methoxide according to the general procedure previously elaborated for sugar dialdehydes (18–20). Although a large number of stereoisomeric nitro sugars can theoretically arise in the reconstitution of two pyranose rings by this reaction, it was expected on the basis of earlier experiences that the D-*gluco*

Can. J. Chem. Downloaded from www.nrcresearchpress.com by 210.87.254.42 on 09/05/12
For personal use only.

TABLE 1. The 100-MHz nmr data of compounds **3–8**. Chemical shifts (δ, from TMS), with coupling constants (Hz) in parentheses

Compound	Solvent	H-1	H-2[a]	H-3	H-4	H-5,-6,-6′	PhCH	Ar	OH-2[b]	Others
3	$(CD_3)_2SO$	5.16d (3.6)	4.19q (3.6, 10.5)	5.34q (10.5, 9.0)	3.8–4.35m		5.70s	7.37s	6.27d (9)	
4[c]	$(CD_3)_2SO$	5.20d (3.6)	[d]	5.08q (10.5, 9.5)	3.75–4.8m		5.72s	7.40s	6.22d (10)	
		5.09s (<1)	[d]	5.55q (3.5, 10.5)			5.81s	7.40s	6.19d (5)	
5	$(CD_3)_2SO$	5.09d (1.2)	4.48q (1.2, 3.5)	5.37q (3.5, 10.5)	3.72–4.76m		5.82s	7.40s	6.24d (5)	
6	$(CD_3)_2CO$	**5.27d** (3.6)	4.14q (3.6, 10.5)	5.07q (10.5, 9.5)	~4.00q	3.6–3.9m				4.45s[e] 1.8m + 3.64m[f]
7[c]	$CD_3)_2CO$	5.29d (3.5)	4.14q (3.5, 10.5)	4.88q (10.5, 9.7)	3.5–4.0					1.82m + 3.6m[f]
		5.21d (1.5)	4.44q (1.5, 3.5)	5.04q (3.5, 10.2)						
8	$(CD_3)_2SO$	4.99d (1.5)	4.22q (1.5, 3.5)	4.80q (3.5, 10.5)	4.23q (10.5, 10.0)	3.4–3.8m				5.90d (6), 5.55d (6.5)[g]

[a]Multiplicities refer to spectra after D_2O exchange of OH-2.
[b]Signal disappeared after D_2O exchange.
[c]Upper row, *gluco* moiety; lower row, *manno* moiety.
[d]Signal included in unresolved multiplets of δ 4 region.
[e]Six-proton intensity; DOH due to deuterium exchange.
[f]Tetrahydrofuran.
[g]Signals disappeared on D_2O exchange (OH).

and D-*manno* configurations would be favored under the conditions of kinetic control that were employed (16, 18, 19). This proved in fact to be the case. The mixture of nitro disaccharides formed in high yield consisted chiefly of three major components that were identified as 3-deoxy-3-nitro-α-D-glucopyranosyl 3-deoxy-3-nitro-α-D-glucopyranoside (**6**), 3-deoxy-3-nitro-α-D-glucopyranosyl 3-deoxy-3-nitro-α-D-mannopyranoside (**7**), and 3-deoxy-3-nitro-α-D-mannopyranosyl 3-deoxy-3-nitro-α-D-mannopyranoside (**8**). They were accompanied by minor proportions of other products, which were not identified.[2] Since a direct separation of the products could not be achieved the mixture was benzylidenated to give the corresponding bis-4,6-acetals **3**, **4**, and **5** which were isolated in crystalline form by preparative thin-layer chromatography. The yields were 22, 25, and 9% based on the crude acetal mixture which had been obtained in 81% yield. When the D-*gluco*,D-*manno* bisacetal **4** was treated briefly with ethanolic potassium hydroxide at room temperature, it partially incurred epimerization to the thermodynamically more stable D-*gluco*,D-*gluco* isomer **3** which was isolated in 34% yield although no attempts were made to optimize the conditions for this transformation. Similarly, it was demonstrated by means of tlc that the D-*manno*,D-*manno* isomer **5** is in the same fashion convertible into **4** and thence **3**. This facile epimerization, known (21) from studies in analogous monosaccharide derivatives where it was found to be virtually quantitative under appropriate conditions, was to serve at this time only to corroborate the configurational assignments of the products; it could doubtless be used as an aid to improving the yield of **3** in case the latter is the principal target of the synthesis.

The configurations of **3–5** followed clearly from ^1H nmr spectra. Two of the compounds, namely those having the highest and lowest mobilities in tlc, gave relatively simple spectra showing only one signal for each set of positionally identical protons in the two monosaccharidic moieties and thus proved themselves to be symmetrically constituted disaccharides (**3** and **5**). By contrast, the compound of intermediate chromatographic mobility (**4**) exhibited a more complicated spectrum in which most sets of positionally identical protons (except for the aromatic ones) gave, as far as the signals could be discerned, an individual signal for each of the two molecule halves, with differing chemical shifts and coupling constants, thus indicating an unsymmetrical disaccharide structure (Table 1). Compound **3** could readily be assigned the D-*gluco*,D-*gluco* configuration on account of the signal character of H-3, the proton at the nitro-substituted position.[3] The signal was a quartet containing two large splittings (9.0 and 10.5 Hz), re-

[2]Apart from other configurational isomers, by-products might, in this reaction, conceivably be formed by cross cyclization of **2**, with a nitromethane molecule linking C-2 and C-2′ to give a six-membered ring, although there was no evidence for this to have occurred to any large extent.

[3]In 3-deoxy-3-nitro sugar derivatives this signal is normally located without difficulty as we know from a large body of experience (22). Barring *O*-acylation at other ring positions it occurs at lower field than those of the remaining sugar protons, with the possible exception of an equatorial (α-anomeric) H-1 signal which, however, is distinguished by its multiplicity.

Can. J. Chem. Downloaded from www.nrcresearchpress.com by 210.87.254.42 on 09/05/12
For personal use only.

Can. J. Chem. Downloaded from www.nrcresearchpress.com by 210.87.254.42 on 09/05/12
For personal use only.

quiring axial orientation for H-2, H-3, and H-4. In agreement therewith, H-2 gave a quartet (after deuterium exchange of OH-2) showing 10.5 and 3.6 Hz splittings, with the latter corresponding to that present in the anomeric doublet. The analogous signals in **5**, namely an H-3 quartet (J = 10.5 and 3.5 Hz), an H-2 quartet (J = 3.5 and 1.2 Hz), and the anomeric doublet (J = 1.2 Hz) indicated the D-*manno*,D-*manno* configuration. In compound **4**, the lowest-field ring proton signal, a quartet with splittings of 10.5 and 3.5 Hz at δ 5.55, was attributable to H-3 of a D-*manno* moiety, and although the signal of the adjacent H-2 could not be used for confirmation as it was not resolved from other resonances upfield, it became discernible after debenzylidenation of **4** (i.e., in **7**) and was then found to agree with the assignment. (Moreover, the D-*galacto* configuration, the only alternative that would also have been compatible with a similar H-3 quartet, was ruled out by the aforementioned alkali-induced epimerization of **4** to **3**.) Another H-3 signal was located at δ 5.08 as a quartet having two large splittings (10.5 and 9.5 Hz) indicative of the D-*gluco* configuration of the second monosaccharide moiety. Again, this was confirmed by the spectrum of **7**. As a point of incidental interest the chemical shifts of the benzylidene methine protons may be compared (Table 1). It has been observed (23) in 4,6-*O*-benzylidenated methyl 3-nitrohexopyranosides that this shift is a fairly sensitive indicator of over-all configuration. Thus, in DMSO-d_6 solution, it occurred in the methyl α-D-glucoside 0.1 ppm to higher field than in the methyl α-D-mannoside. This phenomenon recurs in **3**–**5**. Finally, it may be worth noting that the hydroxyl protons produced doublets with J = 9–10 Hz in *gluco* moieties (**3** and **4**) and J = 5 Hz in *manno* moieties (**4** and **5**). In summary, a comparison of the three spectra reveals close similarities of the signals present in **4** with the respective ones in **3** and **5**, as should be expected in view of the configurational relation. However, the spectrum of **4** is not an exact superposition of those of its symmetrical isomers. The most notable divergence is associated with the shift position of the H-3 and H-3′ protons in **4**: in the *gluco* entity it is shifted upfield, and in the *manno* entity, it is displaced downfield (by about 0.2 ppm each way), relative to H-3 in the corresponding symmetrical isomers.

The bisacetals **3**–**5** upon de-*O*-benzylidenation by trifluoroacetic acid furnished the crystalline nitro disaccharides **6**–**8** in yields of 72–85%. The ^{1}H nmr spectra of these pure sugars provided full confirmation for the configurations. In every case the signals of H-1, H-2, and H-3 were amenable to analysis and accorded with the expected patterns (Table 1). The molecular rotations of **6**–**8** show a good correspondence with those of the nonnitro analogs. In order to make this comparison, we took cognizance of the fact that substitution of a nitro group for 3-OH in methyl α-D-glucopyranoside increases the $[M]_D$ value by 6370 whereas such substitution in methyl α-D-mannopyranoside decreases it by 5410, and we applied these increments[4] to the molecular rotations of α,α-trehalose and its α-D-*gluco*,α-D-*manno* and α-D-*manno*,α-D-*manno* isomers, for each glycosyl unit present (Table 2). The values so calculated for **6**–**8** deviate from those found by 3–8%.

An interesting feature of the nitrodisaccharides **6**–**8** was their propensity for retaining solvent of crystallization which was difficult to remove by heating *in vacuo*. Thus, **6** and **7** were obtained as solvates incorporating tetrahydrofuran, and **8** crystallized with chloroform. The organic solvent could be dislodged by evaporation with water, but highly stable hydrates were then obtained (see Experimental). Catalytic hydrogenation of **6**–**8** over platinum in the presence of a stoichiometric amount of hydrochloric acid afforded the corresponding diamino sugar dihydrochlorides, 3,3′-diamino-3,3′-dideoxy-α,α-trehalose dihydrochloride (**9**) and its *gluco*,*manno* (**10**) and *manno*,*manno* (**11**) isomers, as analytically pure solids.

NOTE ADDED IN PROOF: Dr. J. Defaye kindly arranged to have compounds **6**–**11** in 20 millimolar concentration tested for hydrolysis by cockchafer trehalase and reported that they show no enzyme affinity. This is in accord with recent findings (7) which indicate that at least one unmodified α-D-glucopyranosyl moiety must be present for recognition.

Experimental

Melting points were taken in glass capillaries in an electrically heated aluminum block apparatus and are not corrected. Optical rotations were determined at room temperature in a Perkin-Elmer 141 automatic polarimeter. Infrared spectra were obtained from KBr discs in a Unicam SP 1100 spectrometer. The nmr data refer to 100-MHz spectra with tetramethylsilane lock signal, obtained on a Varian HA-100 instrument, and the coupling constants were measured at 250 Hz sweep width (Table 1). For qualitative tlc, precoated silica gel plates SIL G-25 UV_{254} (Macherey-Nagel & Co, West Germany) were used and the spots were made visible by spraying with 5% sulfuric acid in ethanol, followed by heating. Preparative tlc was performed on 18 cm × 40 cm glass plates coated with a 1.5-mm layer of MN Kieselgel G/UV_{254} (Macherey-Nagel & Co.). Unless otherwise indicated, solvent systems employed for development were (A), 3:1 chloroform–methanol; (B), 4:1 chloroform – ethyl acetate; and (C), 7:3

[4]The data are tied to the configurations from which they were derived; comparison of other glycosides with their respective 3-nitro derivatives reveals effects on molecular rotation that are similar in trend but different in magnitude.

TABLE 2. Molecular rotations

Compound	Mol. weight	$[\alpha]_D$ in H_2O (ref.)	$[M]_D$ Observed		$[M]_D$ Calculated
Methyl α-D-glucopyranoside	194	+158°(24)	+30650	Δ +6370	
3-deoxy-3-nitro derivative	223	+166°(25)	+37020		
Methyl α-D-mannopyranoside	194	+79°(24)	+15330	Δ −5410	
3-deoxy-3-nitro derivative	223	+44.5°(23)	+9920		
α-D-Glucopyranosyl α-D-glucopyranoside·$2H_2O$	378	+179°(2)	+67660		
3,3′-dideoxy-3,3′-dinitro derivative·H_2O	418	+187°	+78170		+80400
α-D-Glucopyranosyl α-D-mannopyranoside·0.5 H_2O	351	+162°(8)	+56860		
3,3′-dideoxy-3,3′-dinitro derivative·THF	472	+133°	+62780		+57820
α-D-Mannopyranosyl α-D-mannopyranoside	342	+124°(26)	+42410		
3,3′-dideoxy-3,3′-dinitro derivative	400	+83°	+33200		+31590

ether – petroleum ether. Here and elsewhere in the text, petroleum ether refers to the fraction boiling at 30–60°C.

*Periodate Oxidation of α,α-Trehalose (**1**)*

To a solution of α,α-trehalose dihydrate (**1**) (2.05 g, 5.42 mmol) in water (20 ml) was added a solution of sodium metaperiodate (4.87 g, 22.7 mmol, i.e., a 5% excess over 4 molar equiv.) in water (50 ml). The reaction mixture was kept in the dark at room temperature for 24 h, during which the pH value of the medium was periodically adjusted to approximately 6 by the portionwise addition of sodium hydrogen carbonate (0.89 g) in water (20 ml). Examination by tlc (double irrigation with solvent A) showed that the very slow-moving **1** was eventually replaced by a single, fast-moving product, the tetraaldehyde **2**. Several spots having intermediate mobilities were seen during early stages of the oxidation and were attributable to reaction intermediates. For processing, ethanol (30 ml) was added to the reaction mixture and, after cooling with ice water, the inorganic precipitate was filtered off and washed with chilled ethanol. The filtrate was concentrated to a small volume by evaporation and fresh ethanol (30 ml) was added to precipitate further inorganic material, which was removed. This operation was repeated three or four times, with evaporations being conducted to near dryness, until eventually the oxidation product dissolved clearly and was then obtained as a dry, white foam upon solvent evaporation; yield, 1.70 g of **2**.

*Nitromethane Cyclization of **2***

The tetraaldehyde **2** (1.70 g) and nitromethane (1.0 ml) were dissolved in absolute methanol (20 ml), and the mixture was rendered alkaline to pH 10 (measured potentiometrically) by dropwise addition of a dilute, methanolic sodium methoxide solution (freshly prepared from sodium hydride; *c*, 0.5% Na). It was important to avoid an excessive amount of base as this tended to give impure, discolored products; on the other hand, too low an alkalinity caused inconveniently slow reaction. The mixture, which became deep-yellow and deposited some precipitate (nitronate salts), was allowed to stand in a closed vessel at room temperature for 3.5 h. It was then deionized by stirring with a cation exchange resin (3 ml of Amberlite IR-120-H^+ or equivalent) whereby the precipitate dissolved. The resin was filtered off and washed with methanol, and the filtrate was evaporated to give a dry, yellow solid of nitro sugars (2.0 g, about 90% based on **1**). The product mixture was dissolved in ethyl acetate and recovered as an off-white powder (1.67 g, 77%) by precipitation with anhydrous ether.

Benzylidenation and Separation

The above mixture of nitro sugars (1.67 g), benzaldehyde (10 ml), and finely divided anhydrous zinc chloride (2.5 g) were placed under a nitrogen atmosphere in a closed vessel protected from light and vigorously stirred at room temperature for 4.5 days. The reaction mixture was then poured into, and agitated with, crushed ice and an equal amount of petroleum ether. The solid organic product which separated was collected, washed well with petroleum ether, and dried in the air. It was then dissolved in ether and recovered by precipitation, under ice cooling, with chilled petroleum ether. The pale yellow material (1.96 g, 81%) showed three well-separated, major spots in tlc. By triple irrigation with solvent B on a 9-cm plate, these migrated approximately 6, 4, and 2 cm. There were also several minor spots between the fastest and the second, and just above and below the third main spot. The main spots represented compounds **3**, **4**, and **5**, in order of decreasing mobility. These products were then isolated by preparative tlc using two to four successive irrigations with solvent B. Seven plates of 18 cm × 40 cm were used to accommodate 1.82 g of the product mixture. There was obtained, in almost pure condition, crystalline **3** (0.40 g) and **4** (0.46 g), which represented 22 and 25%, respectively, of the mixture applied. The third fraction, which consisted mainly of **5**, was obtained as a gum (0.34 g, 18.7%) that was revealed by tlc (solvent C) to contain small proportions of several contaminants. It yielded crystalline **5** upon purification by a second, preparative tlc (solvent C). Material moving even more slowly than **5**, isolated in the first chromatography and amounting to 0.6 g, was inhomogeneous and not investigated further.

*4,6-O-Benzylidene-3-deoxy-3-nitro-α-D-glucopyranosyl 4,6-O-Benzylidene-3-deoxy-3-nitro-α-D-glucopyranoside (**3**)*

Recrystallized from chloroform, **3** consisted of fine, colorless needles, mp 259°C (dec.); $[\alpha]_D$ +111.6° (*c* 0.4, acetone); $\nu_{max}^{(KBr)}$: 3580 (OH), 1550, 1360 (NO_2), and 760, 703 cm^{-1} (benzylidene). *Anal.* calcd. for $C_{26}H_{28}N_2O_{13}$ (576.5): C 54.16, H 4.90, N 4.86; found: C 54.05, H 4.86, N 4.80.

*4,6-O-Benzylidene-3-deoxy-3-nitro-α-D-glucopyranosyl 4,6-O-Benzylidene-3-deoxy-3-nitro-α-D-mannopyranoside (**4**)*

Recrystallized from chloroform, the fine colorless needles of **4** decomposed at 225°C; $[\alpha]_D$ +81.5° (*c* 0.5, acetone); $\nu_{max}^{(KBr)}$: 3450 (broad, OH), 1552, 1365 (NO_2), and 760, 703 cm^{-1} (benzylidene). *Anal.* calcd. for $C_{26}H_{28}N_2O_{13}$ (576.5): C 54.16, H 4.90, N 4.86; found: C 54.07, H 4.81, N 4.96.

When a sample of **4** (900 mg) was dissolved at room temperature in 12 ml of 0.13 *M* ethanolic potassium hydroxide solution and, after 15 min, deionized by cation exchange, the isomer **3** was a prominent product among remnant **4** and some minor decomposition products, according to tlc (solvent B). By preparative tlc of the reaction mixture, 260 mg of pure **3** could be isolated. The remainder of the material recovered from this operation was subjected to a second, identical

Can. J. Chem. Downloaded from www.nrcresearchpress.com by 210.87.254.42 on 09/05/12
For personal use only.

Can. J. Chem. Downloaded from www.nrcresearchpress.com by 210.87.254.42 on 09/05/12
For personal use only.

treatment with base, and another 50 mg of **3** could subsequently be isolated.

4,6-O-Benzylidene-3-deoxy-3-nitro-α-D-mannopyranosyl 4,6-O-Benzylidene-3-deoxy-3-nitro-α-D-mannopyranoside (5)

Compound **5** as obtained from the chromatography was recrystallized from ethanol – ether – petroleum ether to give fine needles (0.16 g), mp 175–176°C; $[\alpha]_D$ +51.4° (*c* 0.4, acetone); $\nu_{max}^{(KBr)}$: 3550 (broad, OH), 1552, 1365 (NO_2), and 765, 705 cm^{-1} (benzylidene). *Anal.* calcd. for $C_{26}H_{28}N_2O_{13}$ (576.5): C 54.16, H 4.90, N 4.86; found: C 53.98, H 5.04, N 4.74.

Compound **5** was shown by tlc (solvent B) to epimerize to a mixture of **3** and **4** by brief treatment with 0.1 *M* ethanolic potassium hydroxide followed by deionization.

De-O-benzylidenation

Each of the acetals **3**–**5** (0.35–1.0 g) was treated with 90% trifluoroacetic acid (27) at 0°C for 0.5 h. The acid (5 ml) was removed by evaporation *in vacuo* followed by coevaporation with several successive portions of ethanol. The residues were recrystallized as stated below, to furnish pure **6**, **7**, and **8** in yields of 77, 72, and 85%, respectively.

3-Deoxy-3-nitro-α-D-glucopyranosyl 3-Deoxy-3-nitro-α-D-glucopyranoside (6)

Recrystallized from tetrahydrofuran–ether, the white needles of **6**, mp 167–169°C, contained 1 mol of tetrahydrofuran of crystallization as evidenced by the nmr spectrum (multiplets of 4H intensity at δ 1.80 and 3.64). This solvent could not be removed *in vacuo* at 110°C unless the analytical sample was first treated with a small amount of water and then dried (4 h, 110°C). However, **6** then appeared to exist as a monohydrate, according to the elemental analysis. It showed mp 159–161°C, $[\alpha]_D$ +187° (*c* 0.3, water), $\nu_{max}^{(KBr)}$: 3700–3300 (very broad, OH), 1555, 1370 cm^{-1} (NO_2). *Anal.* calcd. for $C_{12}H_{20}N_2O_{13}\cdot H_2O$ (418.3): C 34.45, H 5.30, N 6.70; found: C 34.67, 34.39, H 5.25, 5.28, N 6.61, 6.72.

3-Deoxy-3-nitro-α-D-glucopyranosyl 3-Deoxy-3-nitro-α-D-mannopyranoside (7)

After repeated recrystallizations from tetrahydrofuran–ether, **7** was obtained as a solvate with tetrahydrofuran, according to the nmr spectrum and elemental analysis. It showed mp 145–147°C, $[\alpha]_D$ +133° (*c* 0.3, water), $\nu_{max}^{(KBr)}$: 3700–3300 (very broad, OH), 1560, 1365 cm^{-1} (NO_2). The analytical sample was dried *in vacuo* at 110°C for 4 h. *Anal.* calcd. for $C_{12}H_{20}N_2O_{13}\cdot C_4H_8O$ (472.4): C 40.68, H 5.98, N 5.93; found: C 40.81, H 6.01, N 5.85.

When another analytical sample was evaporated with added water before drying it lost the tetrahydrofuran but analyzed as a hemihydrate. *Anal.* calcd. for $C_{12}H_{20}N_2O_{13}\cdot 0.5\,H_2O$ (409.3): C 35.21, H 5.17, N 6.85; found: C 35.19, H 5.33, N 6.50.

3-Deoxy-3-nitro-α-D-mannopyranosyl 3-Deoxy-3-nitro-α-D-mannopyranoside (8)

Compound **8** was recrystallized from chloroform–methanol; mp 185–192°C (dec.), $[\alpha]_D$ +83° (*c* 0.3, water); $\nu_{max}^{(KBr)}$: 3700–3300 (very broad, OH), 1550, 1370 cm^{-1} (NO_2). The analytical sample, dried *in vacuo* at 110°C for 4 h, retained chloroform of crystallization, which was confirmed by its nmr spectrum in DMSO-d_6. *Anal.* calcd. for $C_{12}H_{20}N_2O_{13}\cdot\frac{1}{3}CHCl_3$ (440.05): C 33.65, H 4.66, N 6.37; found: C 33.66, H 4.98, N 6.37.

Catalytic Hydrogenations

Platinum dioxide catalyst (200 mg) suspended in 0.5 *M* hydrochloric acid (2 ml) was prehydrogenated and a solution of **6** (160 mg) in 0.5 *M* hydrochloric acid (4 ml) was then introduced. With efficient shaking under hydrogen at room temperature and ordinary pressure the hydrogenation was finished within 2 h. The catalyst was removed and washed well with at least seven 10-ml portions of water; the product showed a considerable tendency to remain adsorbed. The combined aqueous solution and washings were evaporated to dryness to give the amino sugar dihydrochloride **9** (140 mg) as a white solid. The isomers **10** and **11** were obtained in the same way from **7** and **8**, respectively. The products gave single spots, indicated by ninhydrin spray, in paper chromatography (descending, on Whatman No. 1 paper) using the Fischer–Dörfel (28) solvent system, 5:5:3:1 pyridine – ethyl acetate – acetic acid – water, with 11:40:6 pyridine – ethyl acetate – water in the bottom of the tank. The $R_{GN\cdot HCl}$ values were 0.43 (**9**), 0.39 (**10**), and 0.35 (**11**). Occasionally, somewhat lower values were found owing to minor fluctuations in solvent composition or temperature, but the ratio was remarkably constant for values obtained in the same run.

3-Amino-3-deoxy-α-D-glucopyranosyl 3-Amino-3-deoxy-α-D-glucopyranoside Dihydrochloride (9)

The crude hydrogenation product was dissolved in a minimum amount of methanol, recovered by careful precipitation with ethyl acetate, dried *in vacuo* at 56°C for 4 h and then represented a somewhat hygroscopic, fine white powder (possibly a microcrystalline hydrate) that decomposed at 230°C; $[\alpha]_D$ +168° (*c* 0.3, water); $\nu_{max}^{(KBr)}$: 3500–3100 (OH, NH_3^+), ~1620 and 1510 cm^{-1} (NH_3^+). For analysis, a sample was dried further, at 80°C and 1 Torr, whereby it lost 6.52% of its weight. *Anal.* calcd. for $C_{12}H_{26}Cl_2N_2O_9$ (413.3): C 34.87, H 6.34, N 6.78; found: C 34.97, H 6.46, N 6.67.

3-Amino-3-deoxy-α-D-glucopyranosyl 3-Amino-3-deoxy-α-D-mannopyranoside Dihydrochloride (10)

Prepared in the same way as just described for **9**, the isomer **10** was similar in appearance and in its ir data; it decomposed at 208°C and showed $[\alpha]_D$ +124.5° (*c* 0.3, water). Dried to constant weight at 80°C and 1 Torr, the analytical sample lost only 3.94% of its weight and then gave values corresponding to a monohydrate. *Anal.* calcd. for $C_{12}H_{26}Cl_2N_2O_9\cdot H_2O$ (431.3): C 33.42, H 6.54, N 6.50; found: C 33.21, H 6.45, N 6.41.

3-Amino-3-deoxy-α-D-mannopyranosyl 3-Amino-3-deoxy-α-D-mannopyranoside Dihydrochloride (11)

The crude product **11** was purified by dissolution in methanol and careful precipitation with ether. The dry white powder showed similar ir bands as **9**. It decomposed at 200–202°C and had $[\alpha]_D$ +84.3° (*c* 0.3, water). When dried to constant weight at 100°C and 2 Torr, it still retained water and analyzed as a dihydrate. *Anal.* calcd. for $C_{12}H_{26}Cl_2N_2O_9\cdot 2H_2O$ (449.3): C 32.08, H 6.73, N 6.24; found: C 32.00, H 6.55, N 6.15.

Acknowledgments

This work was supported financially by the National Research Council of Canada. H.H.B. wishes to express his appreciation to Dr. Jacques Defaye for generous hospitality and stimulating discussions during a sojourn at his laboratory in the Centre de Recherches sur les Macromolécules Végétales, C.N.R.S., Grenoble, France, where the present work was conceived. The National Research Council of Canada and the Centre National de la Recherche Scientifique are thanked for the award of a travel stipend under the auspices of their scientific exchange program.

1. J. KOVÁŘ and H. H. BAER. Carbohydr. Res. **45**, 161 (1975).
2. G. G. BIRCH. Adv. Carbohydr. Chem. **18**, 201 (1963).
3. A. D. ELBEIN. Adv. Carbohydr. Chem. Biochem. **30**, 227 (1974).
4. F. ARCAMONE and F. BIZIOLI. Gazz. Chim. Ital. **87**, 896 (1957); F. ARCAMONE, L. VALENTINI, and M. REGGIANINI. Gazz. Chim. Ital. **87**, 1499 (1957); M. GHIONE and A. SANFILIPPO. G. Microbiol. **3**, 189 (1957).
5. M. URAMOTO, N. OTAKE, and H. YONEHARA. J. Antibiot. (Ser. A), **20**, 236 (1967).
6. H. H. BAER and F. F. Z. GEORGES. Can. J. Chem. **55**, 1348 (1977).
7. E. BAR-GUILLOUX, J. DEFAYE, H. DRIGUEZ, and B. HENRISSAT. IX Internat. Symp. Carbohydr. Chem. London, April 1978. Abstr. C9; 176th Natl. Meeting Am. Chem. Soc. Miami Beach, September 1978. Abstr. CARB 73.
8. E. BAR-GUILLOUX, J. DEFAYE, H. DRIGUEZ, and D. ROBIC. Carbohydr. Res. **45**, 217 (1975).
9. J. LABAT, F. BAUMANN, and J. E. COURTOIS. Biochimie, **56**, 805 (1974); Carbohydr. Res. **26**, 341 (1973).
10. E. R. GUILLOUX, J. DEFAYE, R. H. BELL, and D. HORTON. Carbohydr. Res. **20**, 421 (1971).
11. E. R. GUILLOUX, F. PERCHERON, and J. DEFAYE. Carbohydr. Res. **10**, 267 (1969); E. GUILLOUX, J. E. COURTOIS, and F. PERCHERON. Bull. Soc. Chim. Biol. **50**, 1915 (1968).
12. (*a*) G. G. BIRCH, C. K. LEE, A. C. RICHARDSON, and Y. ALI. Carbohydr. Res. **49**, 153 (1976); (*b*) C. K. LEE. Carbohydr. Res. **42**, 354 (1975); (*c*) G. G. BIRCH, C. K. LEE, and A. C. RICHARDSON. Carbohydr. Res. **36**, 97 (1974); (*d*) A. C. RICHARDSON and E. TARELLI. J. Chem. Soc. Perkin I, 1520 (1973); (*e*) L. HOUGH, P. A. MUNROE, A. C. RICHARDSON, Y. ALI, and S. T. K. BUKHARE. J. Chem. Soc. Perkin I, 287 (1973); (*f*) A. C. RICHARDSON and E. TARELLI. J. Chem. Soc. Perkin I, 949 (1972); (*g*) L. HOUGH, A. C. RICHARDSON, and E. TARELLI. J. Chem. Soc. C, 2122 (1971); (*h*) L. HOUGH, A. C. RICHARDSON, and E. TARELLI. J. Chem. Soc. C, 1732 (1971); (*i*) Y. ALI, L. HOUGH, and A. C. RICHARDSON. Carbohydr. Res. **14**, 181 (1970); (*j*) several further articles in this series in 1970–1973, cited in *d*–*i*.
13. S. UMEZAWA, K. TATSUTA, and R. MUTO. J. Antibiot. (Ser. A), **20**, 388 (1967).
14. S. HANESSIAN and P. LAVALLÉE. J. Antibiot. **25**, 683 (1972).
15. S. UMEZAWA, T. TSUCHIYA, S. NAKADA, and K. TATSUTA. Bull. Chem. Soc. Jpn. **40**, 395 (1967).
16. H. H. BAER and A. AHAMMAD. Can. J. Chem. **44**, 2893 (1966).
17. E. L. JACKSON and C. S. HUDSON. J. Am. Chem. Soc. **61**, 1530 (1939).
18. H. H. BAER and H. O. L. FISCHER. Proc. Natl. Acad. Sci. U.S.A. **44**, 991 (1958); J. Am. Chem. Soc. **81**, 5184 (1959); J. Am. Chem. Soc. **82**, 3709 (1960).
19. H. H. BAER and K. ČAPEK. Can. J. Chem. **47**, 99 (1969).
20. H. H. BAER. Adv. Carbohydr. Chem. Biochem. **24**, 67 (1969).
21. H. H. BAER and W. RANK. Can. J. Chem. **49**, 3197 (1971).
22. H. H. BAER, T. NEILSON, and W. RANK. Can. J. Chem. **45**, 991 (1967); H. H. BAER and K. S. ONG. Can. J. Chem. **46**, 2511 (1968); H. H. BAER and W. RANK. Can. J. Chem. **47**, 2811 (1969); H. H. BAER and F. KIENZLE. Can. J. Chem. **47**, 2819 (1969); H. H. BAER, J. M. J. FRÉCHET, and U. WILLIAMS. Can. J. Chem. **52**, 3337 (1974).
23. H. H. BAER and W. RANK. Can. J. Chem. **50**, 1216 (1972).
24. C. S. HUDSON. J. Am. Chem. Soc. **47**, 268 (1925).
25. H. H. BAER, F. KIENZLE, and T. NEILSON. Can. J. Chem. **43**, 1829 (1965).
26. F. MICHEEL and D. BORMANN. Chem. Ber. **93**, 1143 (1960).
27. J. E. CHRISTENSEN and L. GOODMAN. Carbohydr. Res. **7**, 510 (1968).
28. F. G. FISCHER and H. DÖRFEL. Z. Physiol. Chem. **301**, 224 (1955).

Can. J. Chem. Downloaded from www.nrcresearchpress.com by 210.87.254.42 on 09/05/12
For personal use only.

Nuclear analogs of β-lactam antibiotics. IX.[1] Synthesis of 7-methoxy 2-isocephems and *O*-2 isocephems

JAMES L. DOUGLAS, DONALD E. HORNING, AND TERRY T. CONWAY

Bristol Laboratories of Canada, 100 Industrial Blvd., Candiac, P.Q., Canada J5R 1J1

Received February 23, 1978

JAMES L. DOUGLAS, DONALD E. HORNING, and TERRY T. CONWAY. Can. J. Chem. **56**, 2879 (1978).

The syntheses of 7-methoxy-7-phenoxyacetamido-3-methyl-Δ^3-isocephem-4-carboxylic acid **11***a*, 7-methoxy-7-phenoxyacetamido-3-methyl-Δ^3-*O*-2-isocephem-4-carboxylic acid **11***b* and 7-methoxy-7-(2-thienyl)acetamido-3-acetoxymethyl-Δ^3-*O*-2-isocephem-4-carboxylic acid **11***c* are described. A sequence analogous to that used to prepare 7-methoxy cephalosporins was used: Schiff base anions were thiomethylated and the Schiff bases hydrolyzed to free amines. The amines were acylated and thiomethyl to methoxyl conversion effected with mercuric ion catalysis. Removal of protective esters gave the acids **11***a*, **11***b*, and **11***c*. Compound **11***c* showed a modest level but broad spectrum of antibacterial activity.

JAMES L. DOUGLAS, DONALD E. HORNING et TERRY T. CONWAY. Can. J. Chem. **56**, 2879 (1978).

On décrit les synthèses des acides méthoxy-7 phénoxyacétamido-7 méthyl-3 Δ^3 isocéphem-carboxylique-4 (**11***a*), méthoxy-7 phénoxyacétamido-7 méthyl-3 Δ^3 isocéphem-*O*-2 carboxylique-4 (**11***b*) et méthoxy-7 (thiényl-2)acétamido-7 acétoxyméthyl-3 Δ^3 isocéphem-*O*-2 carboxylique-4 (**11***c*). On a eu recours à une séquence semblable à celle qui a permis de préparer les méthoxy-7 céphalosporines: on a thiométhylé les anions des bases de Schiff et on a hydrolysé les bases de Schiff pour obtenir les amines libres. On a acylé les amines et effectué la conversion du thiométhyl en méthoxyl avec catalyse de l'ion mercurique. Les acides **11***a*, **11***b* et **11***c* ont été obtenus en enlevant les groupes esters. Le composé **11***c* a manifesté une activité antibactérienne modérée, mais étendue.

[Traduit par le journal]

Discussion

In previous communications (1–3) we have described the synthesis of 2-isocephems and *O*-2-isocephems (**1** and **2**). In view of the reported broadening of the antibacterial spectrum of cephalosporins by substitution with a 7-methoxy group (4), we decided to prepare 7-methoxy analogs of the 2-iso- and *O*-2-isocephems (**3** and **4**).

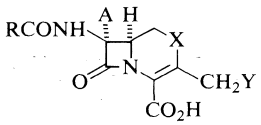

1 X = S, A = H
2 X = O, A = H
3 X = S, A = OMe
4 X = O, A = OMe

Several procedures have been reported for introducing a 7-methoxy substituent into the cephalosporin nucleus. We chose the method of Spitzer and Goodson (5) for introducing a 7-thiomethyl group and Applegate's modification (**6**) for conversion of the thiomethyl to a methoxyl group. In this manner, two simple isocephems substituted with a 7-methoxy group were prepared (Scheme 1, **11***a* and **11***b*). As well, the more highly substituted analog **11***c* was prepared to provide a compound structurally similar to clinically useful antibiotics.

The starting materials **5***a* and **5***b* for the synthesis of **11***a* and **11***b*, respectively, have been reported (1, 2). Starting material **5***c* was prepared from compound **12** (1) by the method previously used to prepare the benzyl ester (3) corresponding to **5***c* (Scheme 2).

The amines **5***a*, **5***b*, and **5***c* were converted to the Schiff bases **6***a*, **6***b*, and **6***c* by treatment with *p*-nitrobenzaldehyde. Anion formation at the 7-position with lithium diisopropylamide followed by treatment with methoxycarbonyl methyl disulfide (syntheses of the ethyl analog are described in ref. 7) gave the 7-thiomethyl derivatives **7***a*, **7***b*, and **7***c*. The Schiff bases were hydrolyzed to give amines **8***a*, **8***b*, and **8***c*. Acylation of the amines with the appropriate carboxylic acid and EEDQ (8) gave the amides **9***a*, **9***b*, and **9***c*. Mercuric acetate in methanol replaced the thiomethyl groups for methoxyl groups (**10***a*, **10***b*, and **10***c*). The ester protecting groups were removed by hydrogenolysis over palladium to give acids **11***a*, **11***b*, and **11***c*.

Spectral[2] and analytical data provide confirmation

[1]For Part VIII of this series, see ref. 3.

[2]Tables of nmr and ir data for compounds reported here are available from the Depository of Unpublished Data. Photocopies may be obtained, at a nominal charge, upon request, from the Depository of Unpublished Data, CISTI, National Research Council of Canada, Ottawa, Ont., Canada K1A 0S2.

Can. J. Chem. Downloaded from www.nrcresearchpress.com by 210.87.254.5 on 09/05/12
For personal use only.

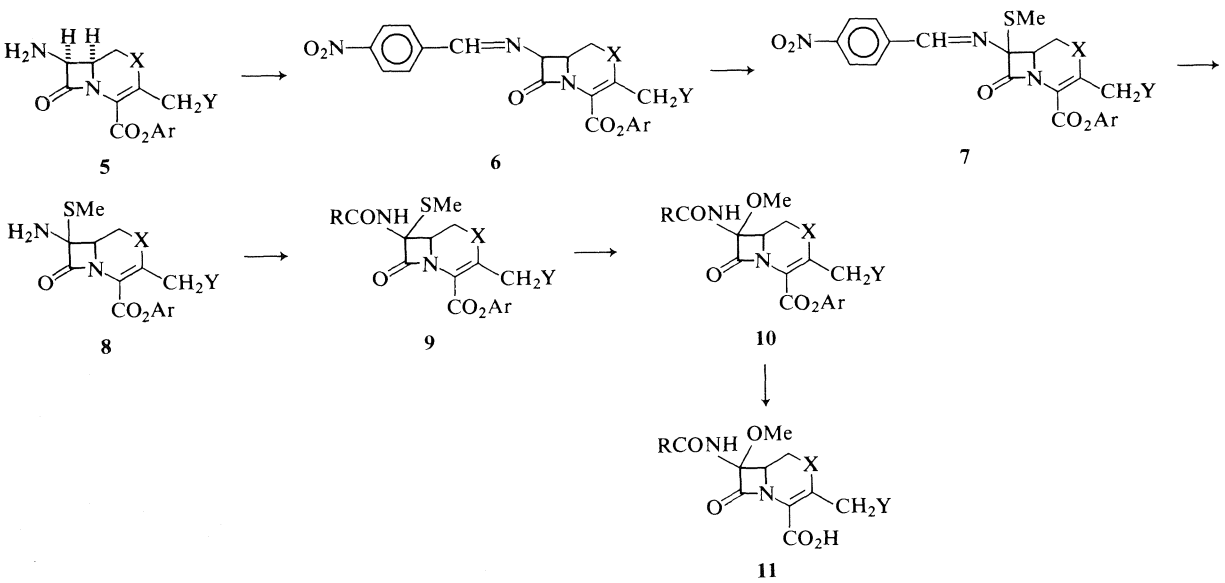

a series: X = S, Y = H, Ar = CH_2—C$_6$H$_4$—NO_2, R = $PhOCH_2$

b series: X = O, Y = H, Ar = CH_2Ph, R = $PhOCH_2$

c series: X = O, Y = $OCOCH_3$, Ar = CH_2—C$_6$H$_4$—NO_2, R = 2-thienylacetyl

SCHEME 1

of the structures proposed for the compounds synthesized. The only point of uncertainty is the stereochemistry of the 7-methoxy group. However, by analogy to 7-methoxy cephalosporins (6) prepared by the same method, it is expected that the 7-methoxy substituent in compounds **11***a*, **11***b*, and **11***c* has the α configuration.

A summary of the antibacterial activity of compounds **11***a*, **11***b*, and **11***c* along with two cephalosporins is given in Table 1. In retrospect, it is not surprising that **11***a* and **11***b* show no antibacterial activity since 7-methoxycephalosporins with a 3-methyl group are also devoid of antibacterial activity (9). A comparison between the 3-acetoxymethyl derivatives **11***c* and **16** shows that the *O*-2-isocephem **11***c* has appreciably poorer activity than the cephalosporin. However, **11***c* does show some activity against the cephalothin resistant *Proteus morganii*.

Experimental

The ir spectra were recorded on a Unicam SP-200G ir spectrophotometer. The uv spectra were recorded on a Unicam SP-800 UV spectrophotometer. The nmr spectra were de-

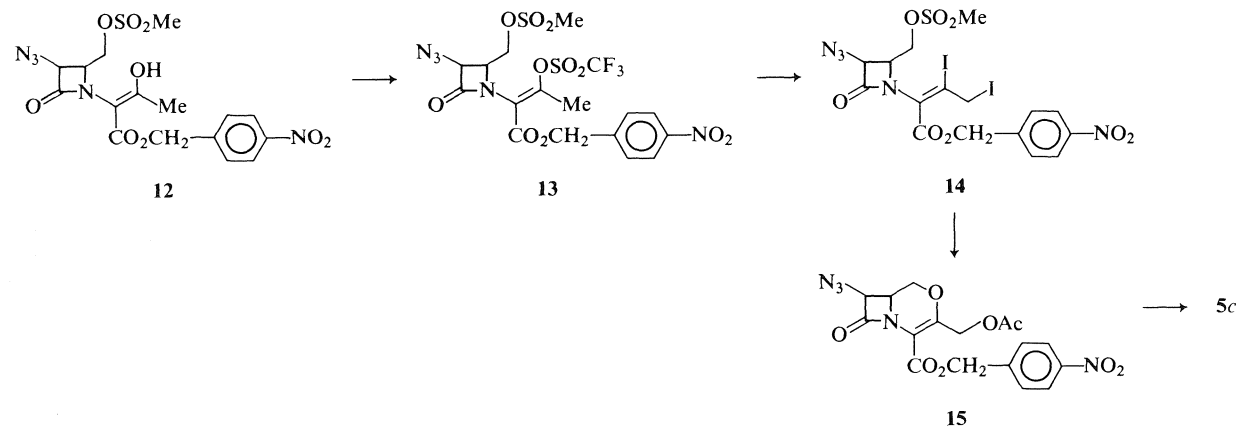

SCHEME 2

Can. J. Chem. Downloaded from www.nrcresearchpress.com by 210.87.254.5 on 09/05/12
For personal use only.

TABLE 1. Biological activities[a]

Compound	*Staphylococcus aureus* Smith	*Staphylococcus aureus* BX1633[b]	*E. coli* 9675	*Proteus mirabilis*	*Proteus morganii*
11*a* and **11***b*	all ≥ 125				
11*c*	2	2	125	8	32
16	1.6	3.1	12.5	3.1	3.1
Cephalothin	0.16	0.3	63	1	>125

[a]Expressed as the minimal inhibitory concentration (μg/ml) and determined by a two-fold serial dilution assay.
[b]Penicillin resistant.

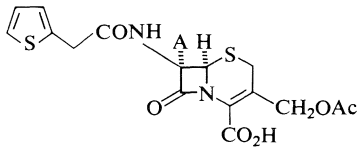

16 A = OMe
Cephalothin A = H

termined in deuteriochloroform solution (unless otherwise noted) on a Varian A60-A spectrometer using tetramethylsilane as an internal standard. Melting points are uncorrected and were determined on a Gallenkamp melting point apparatus. The analyses were performed by Micro-Tech Laboratories, Skokie, Illinois. All reaction solvents were reagent grade and had been stored over molecular sieve before use. Tetrahydrofuran had been distilled from lithium aluminum hydride immediately before use. Anhydrous sodium sulfate was used to dry extraction solutions.

p-*Nitrobenzyl 7-β-Azido-3-acetoxymethyl-Δ³-O-2-isocephem-4-carboxylate (**15**)*

A solution of enol **12** (28.0 g, 61.5 mmol) in 300 ml of dichloromethane was cooled to −10°C and trifluoromethyl sulfonic anhydride (18.0 g, 61.5 mmol) was added. A solution of triethylamine (18.2 ml, 130 mmol) in 50 ml of dichloromethane was added slowly. The resulting solution was allowed to warm to 20°C,[3] then a solution of iodine (13.9 g, 55 mmol) in 300 ml of dichloromethane was added. After remaining for 45 min at 23°C, the solution was washed with water, dilute potassium iodide solution, and saturated sodium chloride (500 ml each). The solution was dried and the solvent was evaporated *in vacuo* to give the crude diiodide (**14**; 42 g) as a brown oil.

A mixture of diiodide **14** (42 g), potassium acetate (18 g, finely powdered), and dimethylformamide (400 ml) was stirred at 23°C for 3½ h. The resulting mixture was poured into 1500 ml of dilute sodium chloride solution and extracted with ether (3 × 400 ml). The combined ether extracts were washed with water four times, then with 10% sodium bicarbonate solution, water, 10% hydrochloric acid, water, and saturated sodium chloride solution (1000 ml each). The ether extract was dried and the solvent was evaporated in vacuo to give an oil, 6.5 g. The oil was chromatographed in 210 g of silica gel (activity 3) by the dry column technique. Elution with ether gave first several by-products then pure *O*-2-isocephem **15** (4.8 g; 19% overall yield from **12**).

[3]The triflate could be isolated at this point (if only 1 equiv. of triethylamine was used) by washing the solution with water and evaporating the solvent *in vacuo* to give the triflate **13** as a yellow oil.

p-*Nitrobenzyl 7-β-Amino-3-acetoxymethyl-Δ³-O-2-isocephem-4-carboxylate (**5***c*)*

Hydrogen sulfide was bubbled vigorously for 1 min into a solution of the azido compound **15** (4.7 g, 11.3 mmol) and triethylamine (1.8 ml, 12.5 mmol) in 200 ml of dichloromethane. The solution was stirred for 30 min, then nitrogen was bubbled through to expel the excess hydrogen sulfide. The solvent was evaporated *in vacuo* and the residue was extracted with 1:1 ether and 10% hydrochloric acid (3 × 50 ml). The acid extracts were neutralized with solid sodium bicarbonate and extracted with dichloromethane (3 × 30 ml). The extract was dried and the solvent was evaporated *in vacuo* to give the amine **5***c* (2.5 g; 58% yield).

p-*Nitrobenzyl 7-(*p-*Nitrophenylimino)-3-methyl-Δ³-isocephem-4-carboxylate (**6**a), Benzyl 7-(*p-*Nitrophenylimino-3-methyl-Δ³-O-2-isocephem-4-carboxylate (**6**b), and* p-*Nitrobenzyl 7-(*p-*Nitrophenylimino)-3-acetoxymethyl-Δ³-O-2-isocephem-4-carboxylate (**6**c)*

A solution of amino compound **5***a*, **5***b*, or **5***c* (10.0 mmol) and *p*-nitrobenzaldehyde (1.51 g, 10.0 mmol) in 150 ml of dichloromethane was heated under reflux under a trap filled with molecular sieve (4 Å) for 2 h. The solvent was evaporated *in vacuo* to give the imine **6***a*, **6***b*, or **6***c* in quantitative yield. The imines could be used in subsequent reactions without purification. Imine **6***b* was purified by chromatography on silica gel (elution with ether) to give material with mp 147–148°C. *Anal.* calcd for $C_{22}H_{19}N_3O_6$: C 62.70, H 4.54, N 9.97; found: C 62.59, H 4.63, N 9.96.

p-*Nitrobenzyl 7-(*p-*Nitrophenylimino)-7-thiomethyl-3-methyl-Δ³-isocephem-4-carboxylate (7*a*), Benzyl 7-(*p-*Nitrophenylimino)-7-thiomethyl-3-methyl-Δ³-O-2-isocephem-4-carboxylate (7*b*), and* p-*Nitrobenzyl 7-(*p-*Nitrophenylimino)-7-thiomethyl-3-acetoxymethyl-Δ³-O-2-isocephem-4-carboxylate 7*c

A solution of *n*-butyllithium in hexane (6.6 ml, 11 mmol) was added with stirring to a solution of diisopropylamine (1.11 g, 11 mmol) in 10 ml of dimethylformamide at −78°C under nitrogen. After 2 min, a solution of imine **6***a*, **6***b*, or **6***c* (10 mmol) in 40 ml of dimethylformamide was added slowly to the lithium diisopropylamide solution. After a further 5 min, a solution of methoxycarbonyl methyl disulfide (2.84 g, 18 mmol) in 20 ml of dimethylformamide was added. The reaction mixture was stirred at −78°C for 15 min then allowed to warm to 23°C. The solution was poured into 300 ml of pH 6.5 buffer (235 ml of 0.1 *M* potassium dihydrogenphosphate plus 65 ml of 0.1 *M* sodium hydroxide solution). This mixture was extracted with dichloromethane (3 × 200 ml). The organic phase was washed with dilute sodium chloride solution (3 × 300 ml), dried, and the solvent was evaporated *in vacuo* to give the crude thiomethyl compounds.

Can. J. Chem. Downloaded from www.nrcresearchpress.com by 210.87.254.5 on 09/05/12
For personal use only.

Can. J. Chem. Downloaded from www.nrcresearchpress.com by 210.87.254.5 on 09/05/12
For personal use only.

Thiomethyl compound **7***a* was purified sufficiently for further reactions by recrystallizing from methanol then benzene and was obtained thus in 50% yield.

Thiomethyl compound **7***b* was purified by chromatography on 250 g of silica gel (activity 3, elution with benzene then ether). Compound **7***b* was obtained in 65.5% yield and was recrystallized from methanol, mp 122.5–123.5°C. *Anal.* calcd. for $C_{23}H_{21}N_3O_6S$: C 59.09, H 4.53, N 8.99; found: C 59.22, H 4.55, N 8.95.

Thiomethyl compound **7***c* was purified by chromatography on 250 g of silica gel (activity 3, elution with ether) and was obtained in 42% yield.

p-*Nitrobenzyl 7-Amino-7-thiomethyl-3-methyl-*Δ^3*-isocephem-4-carboxylate (***8***a), Benzyl 7-Amino-7-thiomethyl-3-methyl-*Δ^3*-O-2-isocephem-4-carboxylate (***8***b), and* p*-Nitrobenzyl-7-amino-7-thiomethyl-3-acetoxymethyl-*Δ^3*-O-2-isocephem-4-carboxylate* ***8***c*

A solution of the imine **7***a*, **7***b*, or **7***c* (3.0 mmol), *p*-toluenesulfonic acid monohydrate (850 mg, 4.5 mmol), and water (0.8 ml, 45 mmol) in 25 ml of ethyl acetate was stirred for ½ h. The precipitate was collected and washed with ethyl acetate and ether to give the pure *p*-toluenesulfonate salts of amines **8***a*, **8***b*, and **8***c*. Salt **8***a* had mp 161–163°C (dec.). *Anal.* calcd. for $C_{16}H_{17}N_3O_5S_2 \cdot C_7H_8O_3S$: C 48.66, H 4.44, N 7.40; found: C 48.74, H 4.31, N 7.47. Salt **8***b* had mp 140–142°C (dec.). *Anal.* calcd. for $C_{16}H_{18}N_2O_4S \cdot C_7H_8O_3S$: C 54.33, H 5.17, N 5.53, S 12.66; found: C 54.66, H 5.19, N 5.62, S 12.56.

The free bases were obtained by treating the salts with an excess of 10% sodium bicarbonate solution and extracting with dichloromethane. The extracts were dried and the solvent was evaporated *in vacuo* to give amine **8***a* (90% yield), **8***b* (67% yield), or **8***c* (53% yield).

p-*Nitrobenzyl 7-Thiomethyl-7-(phenoxyacetamido)-3-methyl-*Δ^3*-isocephem-4-carboxylate (***9***a), Benzyl 7-Thiomethyl-7-(phenoxyacetamido)-3-methyl-*Δ^3*-O-2-isocephem-4-carboxylate (***9***b), and* p*-Nitrobenzyl 7-Thiomethyl-7-(2-thienylacetamido)-3-acetoxymethyl-*Δ^3*-O-2-isocephem-4-carboxylate (***9***c)*

A solution of the amine **8***a*, **8***b*, or **8***c* (1.85 mmol), phenoxyacetic acid (290 mg, 1.9 mmol) or 2-thienylacetic acid (270 mg, 1.9 mmol), EEDQ (518 mg, 1.9 mmol), and dichloromethane (40 ml) was stirred at 23°C for 4 h. The solution was washed with 10% hydrochloric acid, 1% sodium bicarbonate and saturated sodium chloride solutions (40 ml each) then dried, and the solvent was evaporated *in vacuo* to give the amide in sufficient purity for subsequent reactions.

Amide **9***a* was obtained in 90% yield.

Amide **9***b* was obtained in 94% yield and was crystallized from benzene–pentane, mp 153–155°C. *Anal.* calcd. for $C_{24}H_{24}N_2O_6S$: C 61.52, H 5.15, N 5.98, S 6.84; found: C 61.73, H 5.14, N 5.98, S 6.70.

Amide **9***c* was obtained in 96% yield.

p-*Nitrobenzyl 7-Methoxy-7-(phenoxyacetamido)-3-methyl* Δ^3*-isocephem-4-carboxylate (***10***a), Benzyl 7-Methoxy-7-(phenoxyacetamido)-3-methyl-*Δ^3*-O-2-isocephem-4-carboxylate (***10***b), and* p*-nitrobenzyl 7-Methoxy-7-(2-thienylacetamido)-3-acetoxymethyl-*Δ^3*-O-2-isocephem-4-carboxylate (***10***c)*

A mixture of thiomethyl compound **9***a*, **9***b*, or **9***c* (1.0 mmol) and mercuric acetate (319 mg, 1.0 mmol) in 110 ml of methanol was stirred at 23°C for 1 h. The solvent was evaporated *in vacuo* and the residue was mixed with benzene (50 ml). The benzene mixture was washed with water (50 ml), dried, and the solvent was evaporated *in vacuo* to give the crude methoxy compounds which were purified by chromatography on 30 g of silica gel (activity 3).

Compound **10***a* was eluted from the column with benzene–chloroform 1:1 and was obtained in 44% yield.

Compound **10***b* was eluted from the column with the sequence benzene, chloroform, ether and was obtained in 93% yield. It was crystallized from benzene–pentane, mp 150–151°C.

Compound **10***c* was eluted from the column with ether and was obtained in 30% yield.

7-Methoxy-7-(phenoxyacetamido)-3-methyl-Δ^3*-isocephem-4-carboxylic Acid* ***11***a

A mixture of the ester **10***a* (230 mg, 0.45 mmol), tetrahydrofuran (12 ml), methanol (2.3 ml), and 10% palladium-on-charcoal (140 mg) was hydrogenated with shaking for 4 h at 23°C and 50 psi. The catalyst was removed by filtration and the solvent was evaporated *in vacuo*. The residue was dissolved in ethyl acetate (15 ml), washed with 10% hydrochloric acid and water (15 ml each), and extracted with 1% sodium bicarbonate solution (2 × 15 ml). The extract was acidified to pH 2 with 10% hydrochloric acid and extracted with ethyl acetate (2 × 15 ml). The combined ethyl acetate extracts were washed with saturated sodium chloride (15 ml), dried, and the solvent was evaporated *in vacuo* to give the acid **11***a*, 129 mg (77% yield). It was recrystallized from acetonitrile, mp 208–209°C (dec.). *Anal.* calcd. for $C_{17}H_{18}N_2O_6S$: C 53.96, H 4.79, N 7.40, S 8.47; found: C 53.64, H 4.90, N 7.55, S 8.47.

7-Methoxy-7-(phenoxyacetamido)-3-methyl-Δ^3*-O-2-isocephem-4-carboxylic Acid (***11***b)*

A mixture of ester **10***b* (110 mg, 0.244 mmol), tetrahydrofuran (10 ml), and 10% palladium-on-charcoal (55 mg) was hydrogenated at 23°C and atmospheric pressure for 10 min. The catalyst was removed by filtration and the solvent was evaporated in vacuo. The residue was recrystallized from ether to give acid **11***b*, 64 mg (73% yield), mp 190–191°C (dec.); uv λ_{max} (EtOH): 270 nm (ε 7850).

7-Methoxy-7-(2-thienylacetamido)-3-acetoxymethyl-Δ^3*-O-2-isocephem-4-carboxylic Acid (***11***c)*

A mixture of ester **10***c* (212 mg, 0.39 mmol), ethyl acetate (50 ml), *n*-butyl alcohol (12 ml), 1 *M* hydrochloric acid (0.4 ml), and 20% palladium-hydroxide-on-charcoal (212 mg) was hydrogenated with shaking for 3½ h at 23°C and 50 psi. The catalyst was removed by filtration and the solvent was evaporated *in vacuo*. The residue was mixed with ether and extracted with 1% sodium bicarbonate solution (2 × 25 ml) and water (25 ml). The combined aqueous extracts were cooled to 0°C, acidified to pH 2 with 10% hydrochloric acid, and extracted with ethyl acetate (3 × 30 ml). The combined organic extracts were dried and the solvent was evaporated *in vacuo*. The residue was purified by trituration with ether to give acid **11***c*, 32 mg (20% yield), mp 150–155°C (dec.); uv λ_{max} (THF): 270 nm (ε 9340). *Anal.* calcd. for $C_{17}H_{18}N_2O_8S$: C 49.75, H 4.42, N 6.83; found: C 49.63, H 4.59, N 6.89.

Acknowledgements

We would like to thank Dr. M. Ménard of these laboratories, Dr. T. Doyle of Bristol Laboratories, Syracuse, NY, and Dr. B. Belleau of McGill University, Montreal, P.Q. for their comments and suggestions during the course of this work. We thank also M. Misiek of Bristol Laboratories, Syracuse, NY for the microbiological data.

1. T. W. DOYLE, J. L. DOUGLAS, B. BELLEAU, J. MEUNIER, and B. LUH. Can. J. Chem. **55**, 2873 (1977).
2. T. W. DOYLE, B. BELLEAU, B. LUH, T. T. CONWAY, M. MÉNARD, J. L. DOUGLAS, D. T. CHU, G. LIM, L. R. MORRIS, P. RIVEST, and M. CASEY. Can. J. Chem. **55**, 484 (1977).
3. T. T. CONWAY, G. LIM, J. L. DOUGLAS, M. MÉNARD, T. W. DOYLE, P. RIVEST, D. HORNING, L. R. MORRIS, and D. CIMON. Can. J. Chem. **56**, 1335 (1978).
4. A. K. MILLER, E. CELOZZI, B. A. PELAK, E. D. STAPLEY, and D. HENDLIN. Antimicrob. Agents Chemother. **2**, 281 (1972); H. C. NEU. Antimicrob. Agents Chemother. **6**, 170 (1974).
5. W. A. SPITZER and T. GOODSON. Tetrahedron Lett. 273 (1973).
6. H. E. APPLEGATE, J. E. DOLFINI, M. S. PUAR, W. A. SLUSARCHYK, B. TOEPLITZ, and J. Z. GOUGOUTAS. J. Org. Chem. **39**, 2794 (1974).
7. G. ZUMACH and E. KUHLE. Angew. Chem. Int. Ed. Engl. **9**, 54 (1970); S. J. BROIS, J. F. PILOT, and H. W. BARNUM. J. Am. Chem. Soc. **92**, 7629 (1970).
8. B. BELLEAU and G. MALEK. J. Am. Chem. Soc. **90**, 1651 (1968).
9. T. JEN, J. FRAZEE, and J. R. E. HOOVER. J. Org. Chem. **38**, 2857 (1973).

Can. J. Chem. Downloaded from www.nrcresearchpress.com by 210.87.254.5 on 09/05/12
For personal use only.

Reaction of dimethyl sulfoxide with chlorothiolformates, hydrogen chloride, hydrogen fluoride, and hexafluoroisopropanol[1]

ALAN QUEEN, ALBERTA E. LEMIRE, ALEXANDER F. JANZEN, AND MICHAEL N. PADDON-ROW

Department of Chemistry, University of Manitoba, Winnipeg, Man., Canada R3T 2N2

Received May 23, 1978

ALAN QUEEN, ALBERTA E. LEMIRE, ALEXANDER F. JANZEN, and MICHAEL N. PADDON-ROW. Can. J. Chem. **56**, 2884 (1978).

Dimethyl sulfoxide reacts with phenyl chlorothiolformate according to the stoichiometry:

$$2\ PhSCOCl + 3\ Me_2SO \rightarrow PhSSPh + Me_2S + MeSCH_2Cl + Me_2SO{:}HCl + 2\ CO_2$$

p-Chlorophenyl and *tert*-butyl chlorothiolformate appeared to react in a similar manner. The 1:1 hydrogen chloride adduct $Me_2SO{:}HCl$ was characterized by elemental analysis and proton and carbon nmr. A cryoscopic molecular weight determination of the adduct $Me_2SO{:}HOCH(CF_3)_2$ showed it to be monomeric at low concentrations but associated at higher concentrations, suggesting a monomer–dimer equilibrium. The 1:2 adduct $Me_2SO{:}2HF$ is formed by the addition of anhydrous HF to dimethyl sulfoxide.

ALAN QUEEN, ALBERTA E. LEMIRE, ALEXANDER F. JANZEN et MICHAEL N. PADDON-ROW. Can. J. Chem. **56**, 2884 (1978).

Le diméthyl sulfoxyde réagit avec le chlorothiolformiate de phényle selon la stoëchiométrie:

$$2PhSCOCl + 3Me_2SO \rightarrow PhSSPh + Me_2S + MeSCH_2Cl + Me_2SO{:}HCl + 2CO_2$$

Le chlorothiolformiate de *p*-chlorophényle et de *tert*-butyle paraissent réagir de manière analogue. On a caractérisé par l'analyse chimique et par rmn du ^1H et ^{13}C le composé d'addition 1:1 de formule $Me_2SO{:}HCl$. La détermination cryoscopique de la masse moléculaire du composé d'addition $Me_2SO{:}HOCH(CF_3)_2$ indique qu'il se forme une espèce monomère aux faibles concentrations, mais qu'une association se produit aux concentrations supérieures, ce qui laisse supposer l'existence d'un équilibre monomère–dimère. On obtient un composé d'addition 1:2 de formule $Me_2SO{:}2HF$ lors de l'addition de HF anhydre au diméthyl sulfoxyde.

[Traduit par le journal]

Introduction

Sulfonium salts (**1**; Y = O, X = Cl) can be obtained by reacting dimethyl sulfoxide (DMSO) with chloroformate esters (1), hence, it seemed reasonable that the corresponding sulfur analogues (**1**; Y = S, X = Cl) would be produced using DMSO and chlorothiolformate esters **2**. Instead, when these reactions were carried out in an inert solvent, the products were disulfide **3**, chloromethyl methyl sulfide **4**, the HCl adduct of DMSO **5**, dimethyl sulfide, and carbon dioxide. This paper describes the reactions of DMSO with phenyl chlorothiolformate and is also concerned with the structure and reactivity of $Me_2SO{:}HCl$ and the corresponding $Me_2SO{:}HOCH(CF_3)_2$.

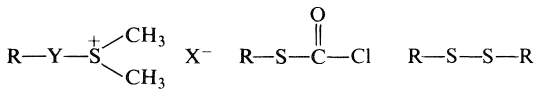

1 **2** **3**

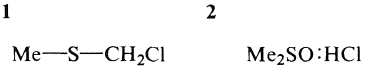

4 **5**

[1]Presented at the 8th International Symposium on Organic Sulfur Chemistry. Portoroz, Yugoslavia, June 18–23, 1978.

Results and Discussion

The overall equation for the reaction of phenyl chlorothiolformate with DMSO can be written as in [1]. The products, with the exception of $Me_2SO{:}HCl$

$$[1]\quad 2PhSCOCl + 3Me_2SO \rightarrow PhSSPh + Me_2S + MeSCH_2Cl + Me_2SO{:}HCl + 2CO_2$$

(*vide infra*), were identified by comparison with authentic samples. To determine the stoichiometry, various ratios of reactants were mixed and the products analyzed (Table 1). In support of [1], it was found that complete conversion of PhSCOCl only occurred when the ratio of DMSO to PhSCOCl exceeded 3:2. For these conditions, the formation of 1 mol of PhSSPh was accompanied by 1 mol of $Me_2SO{:}HCl$, within experimental error. When smaller amounts of DMSO were used, equal but smaller quantities of PhSSPh and $Me_2SO{:}HCl$ were obtained. Nuclear magnetic resonance integration of the reaction mixture showed clearly that the ratio of Me_2S to $MeSCH_2Cl$ was 1:1. The amount of liberated CO_2 was not measured but its presence was confirmed by ir spectroscopy.

Reaction [1] was carried out in CCl_4 because $Me_2SO{:}HCl$ precipitates in this solvent and further

Can. J. Chem. Downloaded from www.nrcresearchpress.com by 210.87.254.105 on 09/05/12
For personal use only.

TABLE 1. Reaction of phenyl chlorothiolformate with DMSO in CCl_4

PhSCOCl (mmol)	DMSO (mmol)	Unreacted PhSCOCl (mmol)	PhSSPh (mmol)	Me_2SO:HCl (mmol)
20	10	9	3.0	2.6
20	20	7	6.5	6.6
20	30	0	9.4	9.6
20	40	0	9.8	9.7

reaction or decomposition of Me_2SO:HCl is prevented.

Reaction [1] is obviously a multistep process but its stoichiometry can be accounted for by [2–5].

[2] $2PhS{-}C(=O){-}Cl + 2Me_2S{=}O \longrightarrow 2\left[\begin{array}{l} Me \\ Me \end{array}\!\!>\!S{-}O{-}C(=O){-}SPh \;\; Cl\right] \longrightarrow 2Me_2S + 2CO_2 + 2ClSPh$

[3] $Me_2S + 2Cl{-}SPh \longrightarrow [Me_2SCl_2] + PhSSPh$

[4] $Me_2S{-}CH_2{-}Cl \xrightarrow[-HCl]{\text{four-center}} [Me_2S{=}CH_2] \xrightarrow{\text{three-center Cl transfer}} MeSCH_2Cl$

[5] $HCl + Me_2SO \longrightarrow Me_2SO{:}HCl$

Equation [2] is analogous to the reaction of DMSO with chloroformate esters (1), whereas [4] is identical to the postulated conversion of Me_2SF_2 to $MeSCH_2F$ (2). In a separate experiment it was found that reaction of Me_2S with PhSCl gave PhSSPh and $MeSCH_2Cl$ in a 1:1 ratio, as required by [3]. Equation [5] was also confirmed in a separate experiment, as described below.

The reactions of DMSO with *p*-chlorophenyl and *tert*-butyl chlorothiolformate were briefly investigated and found to give di-*p*-chlorophenyl disulfide (85%) and di-*tert*-butyl disulfide (87%).

With thiophosgene, Me_2SO:HCl and $MeSCH_2Cl$ were isolated in 63 and 40% yield, respectively, while COS was identified by mass spectrometry suggesting the stoichiometry of [6]. Presumably, the intermediate Me_2SCl_2 reacts further to give $MeSCH_2Cl$ and Me_2SO:HCl, as in [4] and [5].

[6] $Cl_2C{=}S + 2Me_2SO \rightarrow MeSCH_2Cl + Me_2SO{:}HCl + COS$

Me_2SO:HCl, Me_2SO:2HF, and Me_2SO:HOCH$(CF_3)_2$

Previous attempts to characterize Me_2SO:HCl have been only partially successful,[2] although other adducts such as Ar_2SO:HCl (5) or $Me_2SO{:}HNO_3$ (6) are well known. We find that Me_2SO:HCl may be prepared most conveniently by adding anhydrous HCl to DMSO in CCl_4. Under these conditions, Me_2SO:HCl precipitates as a white solid which may be dried under vacuum, mp 56–57°C, 80% yield, and which gave satisfactory elemental analysis.

The addition of anhydrous HF to DMSO gave an oily 1:2 adduct Me_2SO:2HF, identified by NaOH titration (equiv. wt. calcd.: 118.1; found: 117) and ^{19}F and ^1H nmr. On contact with glass, the adduct gave a white solid tentatively assumed to be $Me_2SOH^+SiF_5^-$.

Various structures (**6–10**) have been proposed for $R_2SO{:}HA$ and $R_2SO{:}2HA$ adducts (HA = HCl, HNO_3, H_2SO_4, H_2O, HOR, HSR), mainly on the basis of reactivity, and cryoscopic and spectroscopic studies (5, 7, 8). To gain further structural information about DMSO adducts, we carried out a cryoscopic molecular weight determination of $Me_2SO{:}HOCH(CF_3)_2$. This adduct is soluble and stable in benzene, whereas Me_2SO:2HF is too reactive in glass apparatus and Me_2SO:HCl is insoluble in benzene, cyclohexane and CCl_4 but decomposes in CH_2Cl_2. As seen in Fig. 1, $Me_2SO{:}HOCH(CF_3)_2$ is

$R_2\overset{+}{S}OH\ A^-$ (**6**) $\quad R{-}\overset{O}{\overset{\|}{S}}{}^{+}{-}R\ A^-$ (**7**) $\quad R{-}S{-}R$ (OH, A) (**8**)

$R_2S{=}O\cdots HOH$ (**9**) $\quad R_2S{=}O\cdots HOR$, $\cdots HOR$ (**10**)

[2]The Me_2SO:HCl adduct has been described as a "semi-crystalline mush" (3). In another report (4) the adduct was not dried nor its melting point determined and the chemical analysis was slightly low (HCl calcd.: 31.9%; found: 30.2%.

Can. J. Chem. Downloaded from www.nrcresearchpress.com by 210.87.254.105 on 09/05/12
For personal use only.

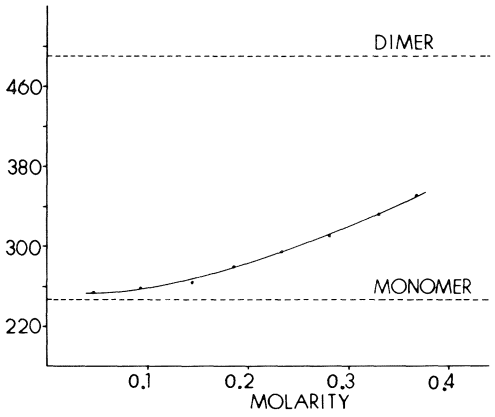

FIG. 1. Cryoscopic molecular weight determination of $Me_2SO{:}HOCH(CF_3)_2$ in benzene as a function of concentration.

essentially monomeric in benzene at low concentration, $\sim 0.2\ M$, but the apparent molecular weight increases at higher concentration suggesting a monomer–dimer equilibrium, perhaps involving the structures depicted in [7].

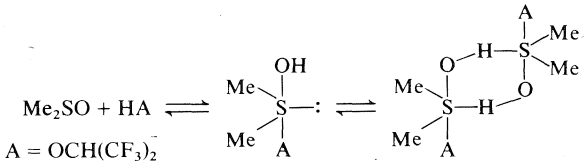

The ^1H nmr spectrum of $Me_2SO{:}HOCH(CF_3)_2$ shows only a single averaged methyl peak at 35°C and the ^{19}F nmr spectrum shows only a single averaged CF_3 group, therefore, the equilibrium of [7] must be rapid on the nmr time scale. Similarly, the ^1H and ^{13}C nmr spectra of $Me_2SO{:}HCl$ show only single methyl peaks, consistent with rapid exchange. DMSO was added to $Me_2SO{:}HCl$ but only a single averaged methyl peak was observed down to −60°C. A comparison of the ^1H and ^{13}C nmr data for $Me_2SO{:}HCl$ and DMSO is shown in Table 2.

DMSO was recovered from $Me_2SO{:}HCl$ by addition of a suitable base, such as pyridine *N*-oxide. Addition of anhydrous HCl to $Me_2SO{:}HCl$ in CH_2Cl_2 produced $MeSCH_2Cl$, presumably via the intermediate Me_2SCl_2, (eq. [4]).

DMSO and Proton Exchange

The addition of DMSO is known to suppress rapid proton exchange in alcohol solutions (9, 10) and this effect has been ascribed to the strong hydrogen bonding of DMSO with hydroxyl groups (ref. 8, p. 35). Another explanation is reasonable, namely, that DMSO forms adducts with trace impurities which are known to catalyze proton exchange, such as H_2O, HF, or HCl (the latter from chlorinated solvents (9)). Removal of these impurities may then suppress catalyzed proton exchange in alcohol solutions. In an analogous situation, rapid fluorine exchange can be suppressed by chemically removing trace impurities such as HF and H_2O (11).

Experimental

General

Volatile materials were handled in a conventional glass vacuum line. Starting compounds were obtained commercially or prepared by literature methods: C_6H_5SCOCl (K & K), *p*-ClC_6H_4SCOCl (K & K), CH_3SSCH_3 (Eastman), $(CH_3)_2SO$ (Fisher), $(CF_3)_2CHOH$ (Aldrich), C_6H_5SH (Aldrich), CH_3SCH_3, $C_6H_5SSC_6H_5$ (12), $(CH_3)_3CSSC(CH_3)_3$ (13), C_6H_5SCl (14), and $(CH_3)_2SO{:}HOCH(CF_3)_2$ (15).

Proton and fluorine nmr spectra were obtained on a Varian A-56/60A spectrometer and carbon nmr spectra on a Varian CFT-20 spectrometer using TMS and $CFCl_3$ as internal references. Mass spectra were obtained on Perkin–Elmer RMU-6D and Finnigan 1015 mass spectrometers. Elemental analyses were performed by Analytische Laboratorien, Engelskirchen, Germany.

Reaction of Phenyl Chlorothiolformate with DMSO

To determine the stoichiometry of the reaction of PhSCOCl with DMSO, various ratios of reactants were mixed and the products analyzed (Table 1). Typically, DMSO in CCl_4 was slowly added to PhSCOCl in CCl_4 at 0°C and the mixture stirred at room temperature for 30 min (solution A). Several methods were then used to isolate and identify the products. Analysis for PhSSPh was carried out by neutralizing solution A with aqueous $NaHCO_3$ followed by removing solvent and volatile products under vacuum. The resulting yellow solid contained PhSSPh which was purified by column chromatography (silica gel), weighed, and identified by mp, ir, nmr, and ms.

To estimate the amount of unreacted PhSCOCl, the yellow solid above was redissolved in CCl_4 and excess diisopropylamine was added to convert PhSCOCl to the less reactive amide derivative *N*-diisopropyl-*S*-phenylthiolcarbamate $(iC_3H_7)_2NCOSC_6H_5$. The ratio of thiolcarbamate to disulfide could be estimated accurately by nmr integration. This procedure was tested by treating known amounts of PhSSPh and PhSCOCl in CCl_4 with excess diisopropylamine. Attempts to separate the disulfide and thiolcarbamate by column chromatography introduced errors of 5–10%. The thiolcarbamate was recrystallized from methanol, mp 93°C. *Anal.* calcd. for $C_{13}H_{19}NSO$: C 65.77, H 8.08, N 5.71, S 13.53; found: C 65.99, H 8.07, N 5.71, S 13.53.

Volatile products were removed under vacuum from solution A and separated by trap-to-trap distillation. The liquid nitrogen trap contained CO_2 which was identified by ir. The acetone – Dry Ice bath contained MeSMe which was redistilled, weighed, and identified by its bp, ir, nmr, and ms.

The ratio of MeSMe to $MeSCH_2Cl$ was conveniently estimated by nmr integration of solution A. The molar ratio was found to be 1:1 irrespective of the ratio of starting compounds PhSCOCl and DMSO.

$Me_2SO{:}HCl$ was found to be insoluble in CCl_4, therefore its yield was estimated by filtering solution A, followed by weighing or titrating with standardized NaOH.

Reaction of p*-Chlorophenyl Thiolchloroformate with DMSO*

DMSO (0.02 mol) in CCl_4 (5 ml) was added to *p*-ClC_6H_4SCOCl (0.01 mol) in CCl_4 (5 ml) at 0°C and the mixture stirred

Can. J. Chem. Downloaded from www.nrcresearchpress.com by 210.87.254.105 on 09/05/12
For personal use only.

TABLE 2. Proton and carbon nmr data for Me_2SO:HCl and DMSO

	δ_{CH_3}	δ_H	δ_C	$^1J_{CH}$	$^3J_{CSCH}$
Me_2SO:HCl[a]	2.87	10.1	37.2	141±0.4	3.7±0.4
Me_2SO	2.5[b]	—	40.4[c]	137.6[d]	4.4±0.1,[e] 4.6[d]

[a]Proton nmr: 10% in CH_2Cl_2 at 35°C on Varian A-56/60A spectrometer. Carbon nmr: saturated CH_2Cl_2 solution on Varian CFT-20 spectrometer at 34°C. Chemical shifts are to low field of internal TMS.
[b]Reference 17.
[c]Concentration dependent (18).
[d]Reference 19.
[e]Reference 20.

at room temperature for 30 min. Neutralization with aqueous $NaHCO_3$ followed by removal of solvent and volatile material left a solid (p-$ClC_6H_4S)_2$, mp 72°C, 85% yield, which was purified by column chromatography (silica gel).

Reaction of tert-*Butyl Thiolchloroformate with DMSO*

DMSO (0.05 mol) in CH_2Cl_2 (2 ml) was added to $Me_3CSCOCl$ (0.03 mol) in CH_2Cl_2 (3 ml) at 0°C and the mixture stirred at room temperature for 3 h. The solution was neutralized with aqueous $NaHCO_3$ and the products extracted with CH_2Cl_2 and dried (Na_2SO_4). Distillation gave $(Me_3CS)_2$ 130°C/150 Torr, 87%, identified by comparison of its ir, nmr, and refractive index with those of an authentic sample.

Reaction of Benzenesulfenyl Chloride with Dimethyl Sulfide

Me_2S (0.19 g, 3.1 mmol) and C_6H_5SCl (0.72 g, 5.0 mmol) in CCl_4 (10 ml) were stirred at room temperature for 12 h. The nmr spectrum indicated that CH_3SCH_2Cl and PhSSPh were produced in a 1:1 ratio. Removal of volatile material left behind a solid identified as PhSSPh on the basis of its nmr and mass spectrum.

Synthesis of Me_2SO:HCl

From HCl and DMSO

Anhydrous HCl was bubbled through a solution of dry DMSO (3.9 g, 0.05 mol) in CCl_4 (20 ml) at 0°C for 3 min. The resultant white precipitate was filtered under vacuum, washed with CCl_4, dried under vacuum for 12 h, and identified as Me_2SO:HCl, mp 56–57°C, 78% yield. *Anal.* calcd. for C_2H_7ClOS: C 20.96, H 6.16; found: C 20.91, H 6.28. Titration with standardized NaOH gave equivalent weight of 112.0 (calcd. 114.6) and potentiometric titration with $AgNO_3$ solution gave chloride 30.5% (calcd. 30.94).

Nuclear magnetic resonance examination of the CCl_4 fraction in the above reaction showed only unreacted DMSO. Me_2SO:HCl is soluble in CH_2Cl_2 but solutions decompose slowly at room temperature giving Me_2S as one of the major decomposition products.

From DMSO and Thiophosgene

Addition of DMSO (10 mmol) to Cl_2CS (5 mmol) in CCl_4 (10 ml) at 0°C gave a precipitate identified as Me_2SO:HCl, 63% yield. The filtrate contained $MeSCH_2Cl$ (2.1 mmol) and a small amount of Me_2S (0.6 mmol). The gas given off during the reaction was identified as COS by mass spectrometry. A uv spectrum of the filtrate showed that all Cl_2CS was consumed.

DMSO and Hexafluoroisopropanol

Me_2SO:$HOCH(CF_3)_2$ was prepared by mixing equimolar amounts of DMSO and $HOCH(CF_3)_2$ (15). Heat was evolved on mixing. The ir spectrum (neat) showed a broad absorption centred at 3100 cm^{-1}, ^1H nmr (neat) δ: 2.58 (s, CH_3), 4.55 (sept, CH), 7.60 (s, OH). The mass spectrum of Me_2SO:$HOCH(CF_3)_2$ was essentially that of DMSO and $HOCH(CF_3)_2$.

The apparent molecular weight of Me_2SO:$HOCH(CF_3)_2$ was determined cryoscopically in benzene over a concentration range 0–0.4 M and the results compared with naphthalene under identical conditions. The temperature of the system was measured with the aid of a thermistor bridge and a recorder. A plot of solute (grams) vs. temperature (arbitrary units) for Me_2SO:$HOCH(CF_3)_2$ and naphthalene was prepared and the apparent molecular weight of Me_2SO:$HOCH(CF_3)_2$ was obtained by comparing the ratio of solute (g) at various temperatures. The results are shown in Fig. 1.

DMSO and HF

Anhydrous HF was bubbled through a solution of DMSO (1.8 g, 0.02 mol) in CCl_4 (10 ml) in a Teflon beaker for 3 min at 0°C to give an oily top layer. The bottom layer was withdrawn with a syringe and the oil washed twice with 5 ml of CCl_4. Volatile material was removed from the oil at reduced pressure (10 cm Hg) and titration of the oil with 0.1 M NaOH, using phenolphthalein as an indicator, gave an equivalent weight of 117 (calcd. for $(CH_3)_2SO$:2HF:118.1). The ^{19}F nmr spectrum in CH_2Cl_2 gave a singlet at 176 ppm, close to that of an HF solution (16), while the ^1H nmr spectrum gave singlets at 8.03 and 2.67 ppm.

If the oil was allowed to come into contact with glass apparatus, a white solid, mp 86–88°C, recrystallized from CH_3CN, was slowly formed. Its ^{19}F nmr spectrum showed a slightly broadened singlet at 142 ppm, close to that of $(nC_3H_7)_4N^+SiF_5^-$ (16), while the ^1H nmr spectrum showed singlets at 8.78 and 2.87 ppm, of relative intensity 1:6.

Acknowledgements

The financial assistance of the National Research Council of Canada is gratefully acknowledged. Dr. R. E. Wasylishen, University of Winnipeg, kindly assisted us with the ^{13}C nmr measurements. We thank Dr. C. E. Burchill for helpful discussions.

1. D. H. R. BARTON, B. J. GARNER, and R. H. WIGHTMAN. J. Chem. Soc. 1855 (1964).
2. R. K. MARAT and A. F. JANZEN. Can. J. Chem. **55**, 3031 (1977).
3. T. TSUCHIYA, S. IRIYAMA, and S. UMEZAWA. Bull. Chem. Soc. Jpn. **37**, 286 (1964).
4. J. A. OLABE, M. C. GIORDANO, and A. J. ARRIA. Electrochim. Acta, **12**, 907 (1967).
5. E. FROMM. Ann. **396**, 75 (1912); K. FRIES and W. VOGT. Ann. **381**, 337 (1911).
6. A. SAYTZEFF. Ann. **144**, 150 (1867); P. NYLEN. Z. Anorg. Allg. Chem. **246**, 227 (1941).
7. R. J. GILLESPIE. Q. Rev. Chem. Soc. **8**, 40 (1954); M. E. PEACH and T. C. WADDINGTON. J. Chem. Soc. 799 (1963); T. J. WALLACE and J. J. MAHON. J. Am. Chem. Soc. **86**, 4099 (1964); G. A. OLAH, A. T. KU, and J. A. OLAH. J. Org.

Can. J. Chem. Downloaded from www.nrcresearchpress.com by 210.87.254.105 on 09/05/12
For personal use only.

Chem. **35**, 3904 (1970); W. WARTHMANN and A. SCHMIDT. Chem. Ber. **108**, 520 (1975); Y. MEHMET and J. B. HYNE. Phosphorus Sulfur, **1**, 47 (1976).
8. H. H. SZMANT. *In* Dimethyl sulfoxide. Vol. 1. *Edited by* S. W. Jacob, E. E. Rosenbaum, and D. C. Wood. Marcel Dekker, New York, NY. 1971. pp. 1–97.
9. O. L. CHAPMAN and R. W. KING. J. Am. Chem. Soc. **86**, 1256 (1964).
10. D. E. MCGREER and M. M. MOCEK. J. Chem. Educ. **40**, 358 (1963); B. CASU, M. REGGIANI, G. G. GALLO, and A. VIGEVANI. Tetrahedron Lett. 2839 (1964).
11. J. A. GIBSON, D. G. IBBOTT, and A. F. JANZEN. Can. J. Chem. **51**, 3203 (1973); R. K. MARAT and A. F. JANZEN. Can. J. Chem. **55**, 1167 (1977).
12. J. CYMERMAN and J. B. WILLIS. J. Chem. Soc. 1332 (1951).
13. A. I. VOGEL and D. M. CONAN. J . Chem. Soc. 16 (1943).
14. H. LECHER and F. HOLSCHNEIDER. Ber. **57**, 755 (1924).
15. A. KIVINEN, J. MURTO, and L. KILPI. Suom. Kemistil. B, **40**, 301 (1967).
16. R. K. MARAT and A. F. JANZEN. Can. J. Chem. **55**, 3845 (1977).
17. J. I. BRAUMAN and N. J. NELSON. J. Am. Chem. Soc. **88**, 2332 (1966).
18. J. B. STOTHERS. Carbon-13 nmr spectroscopy. Academic Press, New York, NY. 1972. p. 49.
19. H. DREESKAMP. Z. Phys. Chem. **59**, 321 (1968).
20. P. F. SWINTON and G. GATTI. Spectrosc. Lett. **4**, 361 (1971).

Can. J. Chem. Downloaded from www.nrcresearchpress.com by 210.87.254.105 on 09/05/12
For personal use only.

Synthesis and stereochemistry of 2-pyrone derivatives related to some fungal metabolites

SUZANNE LESAGE AND ARTHUR S. PERLIN

Department of Chemistry, McGill University, Montreal, P.Q., Canada H3A 2A7

Received June 7, 1978

SUZANNE LESAGE and ARTHUR S. PERLIN. Can. J. Chem. **56**, 2889 (1978).

Some stereochemistry of 'asperlin' (**1**) and related fungal metabolites containing a 5,6-dihydro-2-pyrone moiety, has been deduced through correlation of nmr and ord parameters with those of reference compounds derived from carbohydrates of known stereochemistry. The reference compounds are 4,6-di-*O*-acetyl-2,3-dideoxy-D-*threo*- and -D-*erythro*-hex-2-enono-1,5-lactones obtained by modification of D-galactal and D-glucal, respectively, and the D-enantiomer of **1**, synthesized in a multistep sequence from D-galactose. It is shown that the 5,6-substituents of the pyrone ring of **1** have the L-*threo* configuration and also that the exocyclic epoxypropyl moiety is *trans*.

SUZANNE LESAGE et ARTHUR S. PERLIN. Can. J. Chem. **56**, 2889 (1978).

On a recueilli des renseignements sur la stéréochimie de l'asperlin' (**1**) et de métabolites fongiques apparentés contenant l'ensemble dihydro-5,6 pyrone-2, en établissant des corrélations entre les paramètres tirés de la rmn et de la dro, d'une part, et ceux de composés de référence dérivés de carbohydrates de stéréochimie connue, d'autre part. Les composés de référence sont le di-*O*-acétyl-4,6 didésoxy-2,3 D-*thréo*- et D-*érythro*-hexène-2 lactones-1,5 obtenues par modification du D-galactal et du D-glucal, respectivement, ainsi que l'énantiomère D de **1**, synthétisé par une séquence à plusieurs étapes à partir du D-galactose. On montre que les substituants en position 5 et 6 du cycle pyrone de **1** possèdent la configuration L-*thréo* et que le groupe époxypropyle exocyclique est en position *trans*.

[Traduit par le journal]

Introduction

A large number of natural products contain α,β-unsaturated lactone structures (1). These include compounds of the coumarin series, macrolides, the steroid withaferin, and 2-pyrones of fungal origin. Among the latter group is 5-acetoxy-5,6-dihydro-6-(1,2-epoxypropyl)-2-pyrone (**1**) (2–4), produced by *Aspergillus nidulans* and termed 'asperlin,' which possesses antibiotic and antitumor activity. Asperlin and related metabolites bear a close structural similarity to α,β-unsaturated δ-lactones such as **2**, that are readily accessible from carbohydrates; e.g., **2** has been prepared by the oxidation of aldose **3** with methyl sulfoxide in the presence of pyridine – sulfur trioxide complex and triethylamine (5, 6) or from the δ-lactone corresponding to **3** by a base-catalyzed α,β-elimination (7). Because the absolute configurations of chiral centres in such carbohydrate derivatives are known, it should be feasible to draw stereochemical correlations between the appropriate carbohydrates and the lactones of fungal origin. This is demonstrated, in fact, in the current report, which also furnishes information about the stereochemistry of the epoxypropyl side chain of asperlin (**1**).

Results and Discussion

Stereochemistry of the 2-Pyrone ring of 1. Synthesis of Model Compounds

The lactone ring of **2** differs from that of **1** in having an acetoxyl group at C-2.[1] Presumably, in synthesizing compounds related to asperlin this difference could be removed simply by starting with a 2-deoxy analog of **3**. There was evidence (4) to suggest that an appropriate 2-deoxy sugar should possess the *threo* configuration at C-4, C-5 (rather than the *erythro*, as in **2** and **3**), because $J_{H\text{-}4,H\text{-}5}$ of **1** is small (3.0 Hz). Nevertheless, since this coupling would be determined by the conformation of the lactone ring, an *erythro* isomer also might exhibit a small H-4,H-5 coupling if its 4,5-substituents were quasi-axial (antiperiplanar); indeed, it is known (8) that allylic acetoxyl groups are stable in the axial orientation, due probably to σ*–π orbital overlap (9). Consequently, to circumvent such ambiguity, syntheses in both the *threo* and *erythro* series have been carried out. This has involved application of the oxidation–elimination sequence (5, 6) mentioned above to 3,4,6-tri-*O*-acetyl-2-deoxy-D-*lyxo*-(**4**)- and -D-*arabino*-(**5**)-hexopyranose.

In principle, these latter compounds should be accessible directly by hydration of the corresponding glycal triacetates (**6** and **7**), by analogy with the well-known route to 2-deoxy sugars (10, 11). However, this has proven not to be a practical method for

[1]For consistency in numbering, **1** is regarded below as a lactone related to **2** and analogous compounds. Accordingly, its carbonyl carbon is position-1 rather than, as in the pyrone system, position **2**.

Can. J. Chem. Downloaded from www.nrcresearchpress.com by 210.87.254.105 on 09/05/12
For personal use only.

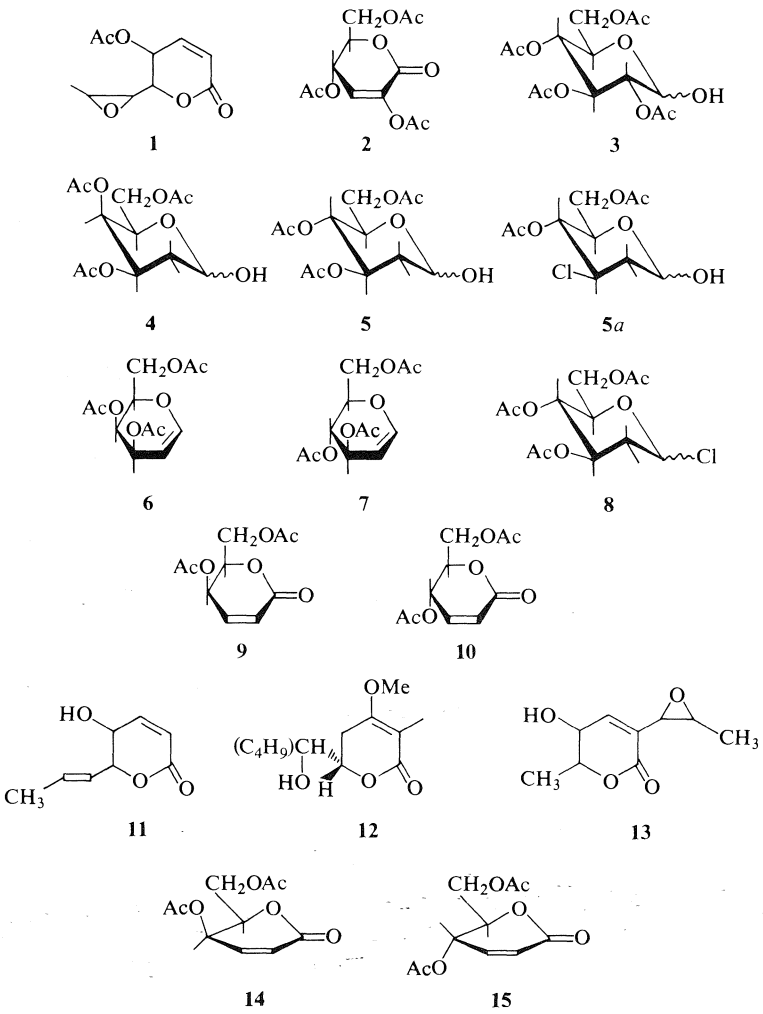

preparation of **4** and **5** because it is accompanied by extensive elimination and rearrangement (12–16). Alternatively, a two-step sequence of reactions was used. Glycals **6** and **7** were each treated with hydrogen chloride in toluene (17) to afford glycosyl chlorides (e.g., **8**), which were converted into the required aldoses (**4** and **5**) with aqueous acetone in the presence of silver carbonate. Product **5** showed ^{1}H nmr spectral properties similar to those of a preparation of **5** from 1,3,4,6-tetra-*O*-acetyl-2-deoxy-D-*arabino*-hexopyranose (18) and also to one obtained via the addition of hydrogen bromide to **7** (19). A second product isolated in this latter reaction appeared (19) to be the allylic hydrobromination product and evidence was obtained that the corresponding chloro derivative (**5***a*) was formed in the present instance.

Compounds **4**, **5**, and **5***a* were then each subjected to oxidation with methyl sulfoxide and pyridine–sulfur trioxide complex in the presence of triethylamine. Two different α,β-unsaturated δ-lactones (**9** and **10**) were obtained, one (**10**) from the two *arabino* isomers (**5** and **5***a*), and the other (**9**) from the *lyxo* isomer (**4**); i.e., the formation of **10** involved the facile elimination of either a 3-acetoxy group (from **5**) or a 3-chloro substituent (from **5***a*). It is possible that **4**, which also was an oil, contained some of the 3-chloro isomer (corresponding to **5***a*), but the material was oxidized without checking this possibility because the same lactone (**9**) as from **4** was to be anticipated, as in the *arabino* series.

A structural resemblance between **9** and **10** and the unsaturated lactone structure of asperlin (**1**) is shown by broad similarities in the ^{1}H and ^{13}C nmr data (Table 1) for the three compounds, as well as their characteristic infrared absorption bands at 1700 and 1645 cm^{-1}. However, there is a much closer correspondence between the spectral properties of asperlin and lactone **9**: as the data of Table 1 imply, signals H-2, -3, and -4 of **1** and **9** are virtually super-

Can. J. Chem. Downloaded from www.nrcresearchpress.com by 210.87.254.105 on 09/05/12
For personal use only.

Can. J. Chem. Downloaded from www.nrcresearchpress.com by 210.87.254.105 on 09/05/12
For personal use only.

TABLE 1. Nuclear magnetic resonance parameters for asperlin (**1**) and synthetic lactones **9** and **10**[a]

	Proton (δ)					
Compound	H-2	H-3	H-4	H-5	H-6	H-6′
1	6.22	7.08	5.33	4.15	~3.1	—
9	6.22	7.03	5.33	4.80	4.39	4.36
10	6.00	6.79	5.54	4.66	4.77	4.37

	J (Hz)						
Compound	2,3	2,4	3,4	4,5	5,6	5,6′	6,6′
1	10.0	—	5.5	3.0	7.0	—	—
9	10.0	—	5.8	2.7	6.0	6.7	—
10	10.0	1.7	3.0	7.5	4.5	4.0	12.0

	Carbon (δ)									
Compound	C-1	C-2	C-3	C-4	C-5	C-6	C-7	C-8	C=O	CH_3
1[b]	161.5	124.7	140.6	62.1	78.3	55.1	53.7	16.9	169.6	20.4
9	161.2	124.7	139.6	61.2	75.6	61.1	—	—	170.0	20.1
									169.4	20.2
10	160.1	122.2	142.9	63.3	77.2	61.8	—	—	170.1	20.4
									169.5	

[a]Proton data at 100 MHz, ^{13}C data at 22.6 MHz; solvent, $CDCl_3$. ^1H nmr parameters for **9** and **10** verified by NMRCAL simulations.
[b]^{13}C assignments from ref. 5.

imposable. Therefore, the lactone ring of asperlin must be configurationally related to **9**, rather than **10**.

Associated with the chiral centers at C-4 and C-5 of **9** is an optical rotation of $[\alpha]_D$ −199° and an ord spectrum exhibiting a negative cotton effect ($\phi = -7.3 \times 10^3$ at 280 nm). By contrast, asperlin exhibits $[\alpha]_D$ 345° and a positive cotton effect ($\phi = +9.2 \times 10^3$ at 280 nm) (4). Hence, since the configuration of **9** is D-*threo*, that of asperlin must be L-*threo*.[2]

A comparison of these ord data with those for several other metabolites should permit the absolute stereochemistry of the latter compounds to be defined as well. Consideration of the ring geometry of an α,β-unsaturated δ-lactone (20) by analogy with the 'octant rule' for cyclohexanones, as in Fig. 1, suggests that the pattern of substitution at C-5 should largely govern the shape of ord curves observed. According to Fig. 2, the exocyclic C-5 side chain of asperlin is located in the upper left quadrant. Analogously, 5-hydroxy-6-(propenyl)-5,6-dihydro-2-pyrone (**11**), which also exhibits a positive Cotton effect (21), should be configurationally related to asperlin. In fact, the latter has been obtained (21) by *O*-acetylation and epoxidation of **11**. By contrast, in

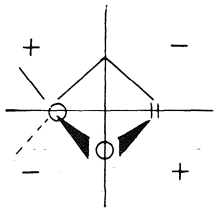

FIG. 1. Quadrant representation for an α,β-unsaturated δ-lactone (5,6-dihydro-2-pyrone), according to Snatzke (20).

(−)-pestalotin (**12**) (22, 23) and 3-(1,2-epoxypropyl)-5,6-dihydro-5-hydroxy-6-methyl-2-pyrone (**13**) (24, 25), each of which shows a negative Cotton effect, the ring substituent at C-5 would be depicted as in the lower left quadrant, as for the CH_2OAc substituent of lactone **9**.

Some information also was obtained about the conformations of asperlin and synthetic lactones **9** and **10**. Long-range coupling (^4J) is observed between H-2 and H-4 of **10**, whereas neither **9** nor asperlin exhibits this long-range effect (Table 1). Since coupling of this type involving an allylic proton varies from 0 to 3 Hz as the dihedral angle (with H-2) varies from 0 to 90° (26), it appears that, on the average, H-4 of **10** is oriented out of plane with respect to the double bond. By contrast, **9** and asperlin favor a conformation in which the C-4, H-4 bond approaches coplanarity with the olefinic bond. The 4-acetoxyl group of **1** or **9** would then be in a *trans*-diaxial relationship with respect to H-5, and that of

[2]According to the *R* and *S* convention, lactone **9** is D-(−)-4*R*,5*R*, whereas asperlin must be designated as L-(+)-4*S*,5*R*. This seeming contradiction for the configuration of C-5 stems from the fact that in asperlin, priority must be given to the epoxypropyl side chain over the atoms of the ring, whereas in **9** the 6-CH_2OAc group has the low priority.

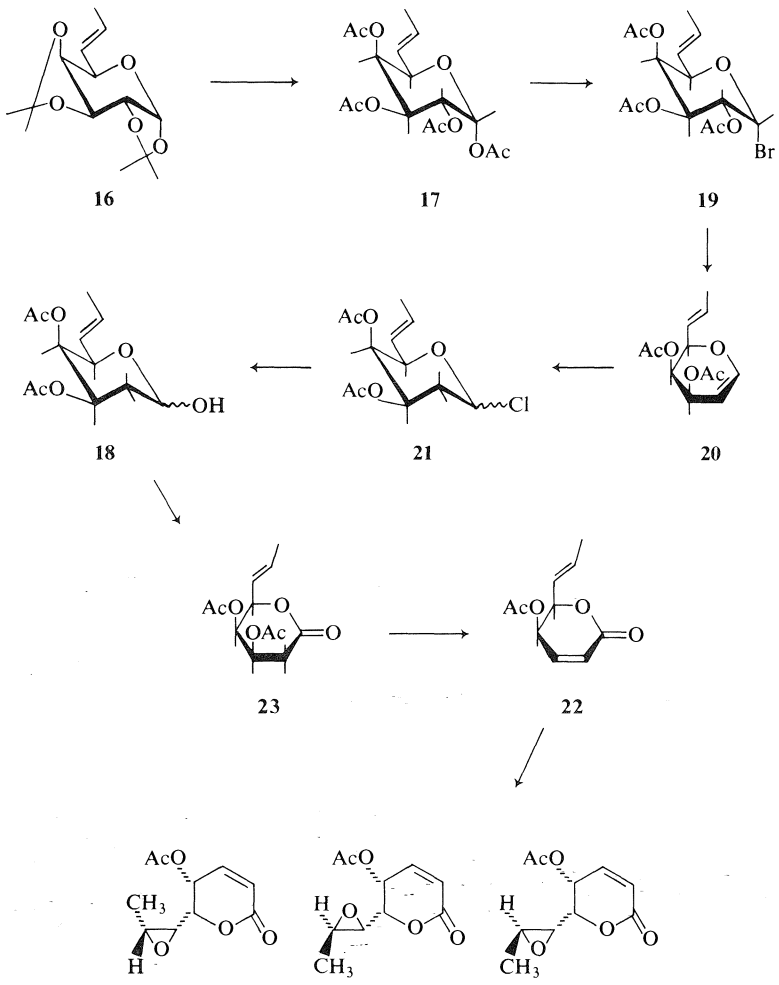

10 would be in a *gauche* relationship, as in **14** and **15**. Turning to the interrelated coupling between H-4 and H-3, it is seen (Table 1) that $J_{3,4}$ for **10** is 3.0 Hz, whereas it is 5.5–5.8 Hz for **1** and **9**. According to a geometric relationship deduced (27) for vicinal allylic coupling in simple olefins, these J values correspond to dihedral angles of ~70 and ~25°, respectively. Although the molecules under consideration here also contain a carbonyl group in conjugation and nearby carbon–oxygen bonds, which might affect the magnitude of J, the conformations depicted in **14** and **15** are compatible with the relatively smaller H-3,H-4 dihedral angle predicted for asperlin and lactone **9**, than for **10**. Hence, the mirror image of **14** should closely represent the lactone ring conformation of asperlin.

Synthesis of the D-*Enantiomer of Asperlin*

Continuing with these structural analogies between asperlin (**1**) and carbohydrate model compounds, a synthesis has been effected of the D-enantiomer of asperlin. This has served not only to confirm the findings above as to the geometry of the lactone ring but also to provide information about the stereochemistry of the epoxypropyl side chain of asperlin.

A comparison of asperlin with a variety of *cis* and *trans* epoxides by ^{13}C nmr spectroscopy has suggested (28) that the epoxypropyl side chain of asperlin has a *trans* configuration. In view of this, the starting point for the synthesis was an eight-carbon sugar derivative having a *trans*-propenyl side chain and a D-*galacto* configuration, i.e., compound **16**. The latter was prepared from the previously known *cis* olefin (29) by photochemical isomerization, because attempts to synthesize **16** directly were unsuccessful. However, about 25% of the *cis* isomer remained unchanged and was not separated out. Subsequent steps were carried out, therefore, with the isomerization mixture. This proved to be feasible because the major products derived from **16** generally

Can. J. Chem. Downloaded from www.nrcresearchpress.com by 210.87.254.105 on 09/05/12
For personal use only.

Can. J. Chem. Downloaded from www.nrcresearchpress.com by 210.87.254.105 on 09/05/12
For personal use only.

were identifiable by nmr spectroscopy without serious interference from their minor *cis* isomers. In the following discussion reference is made, for simplicity, to reactions in the *trans* series, although it is clear that each step was paralleled on a smaller scale in the *cis* series as well.

Acetolysis of **16** with acetic anhydride and boron trifluoride etherate at 0°C (30) for 0.5 h yielded 1,2,3,4-tetra-*O*-acetyl-6,7,8-trideoxy-α-D-*galacto*-oct-6-*trans*-enopyranose (**17**); under these conditions the olefin was essentially unaffected.[3] By analogy with reactions described above, the next step required synthesis of an appropriate 2-deoxyaldose derivative (**18**). Accordingly, compound **17** was treated with hydrogen bromide at 30°C for 1 h to give a glycosyl halide (**19**) which, on reduction with zinc, afforded the glycal (**20**); the 2-deoxyaldose (**18**) was then obtained via the hydrogen chloride adduct (**21**) by reaction of **20** with hydrogen chloride for 10 min at 0°C, followed by hydrolysis in the presence of silver carbonate.

Formation of the α,β-unsaturated lactone (**22**) from **18** was then effected. Unexpectedly, however, the combined oxidation–elimination reaction that had so readily furnished **9** and **10** from **4** and **5**, proved to be very sluggish when applied to **18**. By contrast, oxidation proceeded smoothly when aldose **18** was treated with pyridinium chlorochromate in methylene chloride (31) to give the aldonolactone (**23**) and α,β-elimination to yield **22** was then induced by the introduction of triethylamine.

The reaction of **22** with *m*-chloroperbenzoic acid gave a mixture of diastereomeric epoxides (**24**, **25**). According to the ^1H and ^{13}C nmr spectra of the reaction products, three species were formed on epoxidation, including a minor one from the *cis* olefin corresponding to **22**. Judging from the relative intensities of three signals attributable to H-5, which are particularly well resolved (Fig. 2A), the *trans* isomers (**24**) were present in a ratio of 3:2, whereas only one *cis* epoxide (**25**) had been formed in appreciable yield from the *cis* olefin.

It is evident from the accompanying spectrum of authentic asperlin (Fig. 2B) that the major synthetic product corresponds to the natural material; the spectral identity of the two was confirmed by adding a small proportion of asperlin to the solution of the mixed products, whereupon the relative intensities of the signals ascribed to **24***a* increased. Furthermore, the major group of signals in the ^{13}C spectrum of the mixture corresponds to the ^{13}C spectrum of asperlin. Hence, **24** is the D-enantiomer of asperlin.

[3]These, and other reaction conditions described below, were selected following preliminary model experiments, so as to minimize addition to the exocyclic olefin.

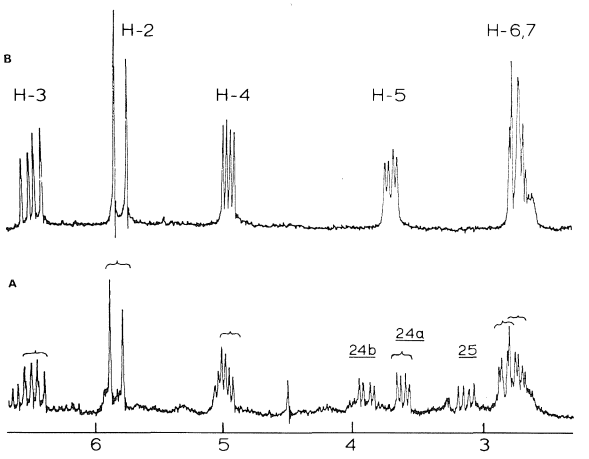

FIG. 2. ^1H nmr spectra at 100 MHz of products (**24***a*,*b* and **25**) obtained from synthesis of the D-enantiomer of asperlin (*A*) and of authentic asperlin (**1**) (*B*). Solvent, C_6D_6. (Upfield signals due to the acetoxyl and 8-CH_3 protons are not shown.) *The introduction of a small portion of authentic asperlin, promoted a commensurate increase in the relative intensities of the bracketed signals, i.e., those of the major product* (designated **24***a*; see Table 2).

TABLE 2. ^{13}C nuclear magnetic resonance data for **24***a*,*b* and asperlin (**1**)[a]

	Chemical shift (δ)		
Carbon	**1**	**24***a*[b]	**24***b*
C-1	161.5	161.3	160.8
C-2	124.7	124.9	124.9
C-3	140.6	140.5	140.8
C-4	62.1	62.1	62.4
C-5	78.3	78.9	—
C-6	55.1	55.0	52.9
C-7	53.7	54.5	52.5
C-8	16.9	17.0	17.0
CH_3	20.4	20.5	20.5

[a]At 22.6 MHz; solvent, $CDCl_3$; the signal assignments given for **24***a* and **24***b* are based on general considerations of ^{13}C chemical shifts, and have not been verified.
[b]Group of strongest signals. Designated by analogy with the strongest signals in Fig. 2*A*.

These results demonstrate that the configuration of the epoxypropyl group of asperlin is *trans*, although which of the two possible diastereomers of **24** it represents, remains to be determined. Moreover, since the starting compound (**16**) has a *galacto* configuration, its conversion into **24** confirms the *threo* configuration at C-4 and C-5 of asperlin. It is worth noting also that the ord spectrum of the mixture of **24** and **25** exhibited a negative Cotton effect ($\phi = -2.8 \times 10^3$ at 280 nm) which, being opposite in sign to that of asperlin, as noted above, emphasizes the fact that the latter contains the L-*threo* configuration.

Can. J. Chem. Downloaded from www.nrcresearchpress.com by 210.87.254.105 on 09/05/12
For personal use only.

Experimental

General Methods

Evaporations were carried out under reduced pressure at or below 60°C (bath temperature). Melting points were determined on a Fisher Johns apparatus. Infrared spectra were measured as liquid films on silver chloride plates, with a Unicam SP200 spectrophotometer. Optical rotary dispersion curves were obtained with a JASCO ORD-UV-5 spectrophotometer. Proton magnetic resonance spectra were determined with a Varian HA-100 spectrometer and carbon-13 magnetic resonance spectra with a Bruker WH-90 spectrometer; in each instance, tetramethylsilane was used as an internal standard. Microanalyses were performed by Dr. C. Daesslé (Organic Microanalyst, Montreal) or by Schwarzkopf Microanalytical Laboratory (New York). Chromatographic columns were packed with silica gel, 0.02–0.05 mm particle size (Macherey Nagel and Co., Germany), or with silica gel 60, 0.60–0.20 particle size (E. Merck, Germany). For thin-layer chromatography (tlc) silica gel G. (Macherey Nagel Co., Germany) was used as adsorbent. The following solvent systems were used: (*A*) CH_2Cl_2–acetone (9:1); (*B*) CH_2Cl_2–acetone (3:1); (*C*) CH_2Cl_2–acetone (1:1). Compounds were detected by spraying with 25% aqueous sulfuric acid and heating at 110°C, or where applicable, by irradiation with uv light.

3,4,6-Tri-O-*acetyl-2-deoxy*-D-arabino-*hexopyranose* (***5***) *and 4,6-Di*-O-*acetyl-3-chloro-2,3-dideoxy*-D-arabino-*hexopyranose* (***5a***)

3,4,6-Tri-*O*-acetyl-1,5-anhydro-1,2-dideoxy-D-*arabino*-hex-1-enitol (**7**) (960 mg) was dissolved in toluene (50 ml) and anhydrous HCl was bubbled in at 0°C. After 1 h, more toluene (100 ml) was added and the solution was neutralized by washing with saturated sodium bicarbonate, followed with water. The toluene was evaporated off and replaced with acetone (50 ml), and the solution was stirred with silver carbonate at room temperature for several hours, after which the suspension was filtered through Celite and the filtrate concentrated. The resulting oil was chromatographed on a column using chloroform as the eluant. Two main fractions were recovered: **5***a* as a syrup (0.20 g) and compound **5** (0.29 g) which was recrystallized from ethyl acetate – petroleum ether, mp 94–97°C (lit. (19) mp 93–95°C); ^{1}Hmr data for **5** δ: 2.0–2.1 (3 × 3H, s, CH_3CO—); 2.0–2.2 (2-H, m, H-2,2′); 4–4.2 (3H, m, H-3,6,6′); 4.8–5.4 (3H, m, H-5,1,4); for **5***a* δ: 2.0–2.1 (2 × 3H, s, CH_3CO—); 2.2–2.7 (2H, m, H-2,2′); 4.0–4.5 (3H, m, H-3,6,6′); 4.6–5.5 (3 overlapping 1H, m, H-1,4,5).

3,4,6-Tri-O-*acetyl-2-deoxy*-D-arabino-*hexopyranose* (***5***)

A saturated solution of HCl in toluene (20 ml) containing 1,3,4,6-tetra-*O*-acetyl-2-deoxy-D-*arabino*-hexopyranose (0.70 g) was stirred at 0°C for 1 h; the reaction was then complete (tlc solvent *A*). The treatment with water and silver carbonate and work-up, were as described above, but only **5** was obtained (0.50 g, 80%), mp 94–97°C.

4,6-Di-O-*acetyl-2,3-dideoxy*-D-erythro-*hex-2-enono-1,5-lactone* (***10***)

(*a*) The triacetate (**5**) (0.26 g) was added to a mixture of methyl sulfoxide (12 ml), triethylamine (1.5 ml), and pyridine – sulfur trioxide complex (0.94 g), the resulting homogeneous solution being stirred for 0.5 h. Cold $CHCl_3$ (100 ml) was added and the organic layer was washed successively with aqueous tartaric acid (100 ml), saturated sodium bicarbonate (100 ml), and water (2 × 100 ml), then it was dried over $MgSO_4$ and concentrated. The yellow oil (**10**) (0.19 g) obtained was distilled at 125–130°C (bath temperature/0.5 Torr); $[\alpha]_D^{25}$ +158° (*c* 5.7, $CHCl_3$); ^{1}Hmr and ^{13}Cmr spectroscopic data are given in Table 1; ir: 1700–1780 (C=O, acetyl and lactone), 1645 cm^{-1} (C=C). *Anal.* calcd. for $C_{10}H_{12}O_6$: C 52.6, H 5.3; found: C 52.4, H 5.9.

(*b*) The 3-chloro-analog of **5** (**5***a*) when subjected to oxidation with pyridine – sulfur trioxide as described above, gave the same lactone (**10**) as confirmed by tlc (solvent *A*) and ^{1}Hmr spectroscopy.

4,6-Di-O-*acetyl-2,3-dideoxy*-D-threo-*hex-2-enono-1,5-lactone* (***9***)

3,4,6-Tri-*O*-acetyl-1,5-anhydro-1,2-dideoxy-D-*lyxo*-hex-1-enitol (**6**) (0.98 g) was hydrochlorinated in toluene as described for the *arabino* isomer (**7**). Similarly, the product was treated with silver carbonate in aqueous acetone. The crude material recovered (presumably a mixture of 3,4,6-tri-*O*-acetyl-2-deoxy-D-*lyxo*-hexopyranose (**4**) and its 3-chloro-3-deoxy analog, according to ^{1}Hmr spectroscopy) was subjected to oxidation, as described above. Lactone **9** was obtained as a pale yellow oil (0.20 g) which was distilled (0.5 Torr, 125–130°C bath temperature); $[\alpha]_D^{25}$ −199° (*c* 5.6, $CHCl_3$); ord: negative Cotton effect (280 mm, $\Phi = 7.3 \times 10^3$); ^{1}Hmr data for **4** δ: 1.95, 2.03, 2.12 (3 × 3H, singlets, CH_3CO—); 2.01, 2.07 (2 × 3H, singlets, CH_3CO—, 3-chloro analog ~25%); 2.0–2.2 (2H, overlapping CH_3, H-2, H-2′); 2.3–2.8 (m, H-2,2′ of 3-chloro analog), 4.0–4.5 (3H, m, H-3,6,6′), 5.2–5.5 (3 × 1H overlapping m, H-1,4,5). *Anal.* calcd. for $C_{10}H_{12}O_6$: C 52.6, H 5.3; found: C 52.9, H 5.7.

Proton and carbon-13 nmr spectroscopic data for **9** are given in Table 1.

6,7,8-Trideoxy-1,2: *3,4-di*-O-*isopropylidene*-α-D-galacto-*oct-6*-trans-*enopyranose* (***16***)

A cyclohexane solution (300 ml) of the *cis* olefin (28, 29) (4.5 g) was irradiated in a water-cooled quartz cell with unfiltered uv light (450 W Hanovia Type of mercury arc lamp, Model 679A) under a stream of N_2 for four to five periods of 2 h. After each treatment polymeric material in suspension was filtered off and a portion of the filtrate (10 ml) was concentrated and monitored (^{1}Hmr) until no further change was observed. The final solution was concentrated to a yellow syrup, which was chromatographed (eluent, CH_2Cl_2) to yield a colourless syrup (4.0 g) containing a mixture (3:1, from ^{1}Hmr spectra) of the *trans* (**16**) and *cis* olefins. ^{1}H nmr data for **15** δ: 1.40 (6H, s, CH_3 isopropylidene); 1.54 (3H, s, CH_3 isopropylidene); 1.59 (3H, s, CH_3 isopropylidene); 1.80 (3H, d, H-8,8′,8″, J = 5 Hz); 4.1–4.4, 4.6–4.8 (4H, overlapping m); 5.60 (1H, d, H-1, J = 5 Hz); 5.68–5.90 (2H, m, H-6, H-7); ^{13}C nmr data for **15** δ: 17.8, (C-1); 24.3, 24.8, 25.9, 26.8 (CH_3-isopropylidene); 69.0 (C-5); 70.9, 73.2 (C-2,3,4); 96.5 (C-1); 108.2, 109.0 (C-isopropylidene); 126.8, (C-6); 129.7, (C-7).

1,2,3,4-Tetra-O-*acetyl-6,7,8-trideoxy*-α-D-*lyxo-oct-6*-trans-*enopyranose* (***17***)

The product of photolysis (olefin **16**) (5.0 g) was dissolved in acetic anhydride (20 ml) and the solution cooled at 0°C. Boron trifluoride – etherate (redistilled over sodium hydride) (10 ml) was added and the solution was stirred for 10 min at 0°C, after which it was poured onto a slurry of ice and NaOH (~5%). This was followed by extraction with ether (3 × 250 ml). The combined extracts were washed with saturated sodium bicarbonate, and water, dried over sodium sulfate, and the solvent was evaporated off. The residual brown syrup (8 g), on purification by column chromatography (eluent, CH_2Cl_2) gave a yellow oil (4.5 g), which was found by ^{1}Hmr to consist of **17**, accompanied by about 25% of the *cis* isomer; ^{1}Hmr data for **17** δ: 1.70 (3-H, dd, H-8,8′,8″, $J_{7,8} \simeq 7$ Hz, $J_{6,8} \simeq 1$ Hz); 1.97, 2.12 (2 × 6H, s, CH_3, acetoxyls); 4.0–5.5 (4H, poorly resolved m, H-2,3,4,5); 5.5–5.9 (2H, overlapped m, H-6,7); 6.36 (1H, d, H-1, $J_{1,2} \simeq 3$ Hz).

Can. J. Chem. Downloaded from www.nrcresearchpress.com by 210.87.254.105 on 09/05/12
For personal use only.

*1,5-Anhydro-3,4-di-*O*-acetyl-1,2,6,7,8-pentadeoxy-*D*-lyxo-oct-1,6-trans-dienitol (**20**)*

The oil obtained above (**17**) (4.5 g) was dissolved in acetic acid (15 ml), HBr (30% in acetic acid; 3.0 ml) was introduced and the solution was stirred at 0°C for 0.5 h. A previously-mixed slurry of Zn (4.5 g), sodium acetate (10 g), and cupric sulfate pentahydrate (0.5 g) in water (12 ml) was then added, and the suspension was stirred vigorously at 0°C for 2–3 h, after which it was filtered and the solid residue was rinsed with cold 50% aqueous acetic acid. The filtrate was extracted with methylene chloride (3 × 250 ml) and the organic layer was washed successively with saturated sodium bicarbonate and water, dried over sodium sulfate, and concentrated. A clear colourless syrup (3.2 g) obtained was found to consist of a mixture of several products (tlc, solvent A). Separation by column chromatography (eluent: CH_2Cl_2) afforded **20** as a colourless syrup (0.62 g). The slower moving components were combined and subjected to the same series of reactions, which provided a further 0.3 g of product; ^{1}Hmr data for **20** (major component; 25% *cis*-isomer present) δ: 1.72 (3H, d, H-8,8′,8″, $J_{7,8} \simeq 7$ Hz; 1.97, 2.10 (2 × 3H, s, CH_3, acetoxyl); 4.64 (1H, q, H-2, $J_{1,2} = 6.5$ Hz, $J_{2,3} = 2$ Hz); 5.3–6.0 (5H, overlapped m, H-3,4,6,7); 6.47 (1H, q, H-1, $J_{1,3} = 2$ Hz); ^{13}Cmr data for **20** δ: 17.4 (C-8); 20.1, 20.2 (CH_3-acetoxyl); 64.3 (C-4); 65.6 (C-3); 75.4 (C-5); 98.0 (C-2); 125.2 (C-7); 130.6 (C-6); 145.6 (C-7); 169.7 and 168.8 (C=O, acetoxyl); ^{13}Cmr data for the 6-*cis*-isomer of **20** δ: 13.1 (C-8); 64.1 (C-4); 65.3 (C-3); 70.7 (C-5); 98.0 (C-2); 124.4 (C-7); 129.9 (C-6); 145.7 (C-1); 169.4, 169.3 (C=O, acetoxyl).

*3,4-Di-*O*-acetyl-2,6,7,8-tetradeoxy-*D*-lyxo-oct-6-trans-enopyranose (**18**)*

The glycal (**20**) (0.92 g) was stirred at 0°C in ether (10 ml) containing 5% HCl for 0.5 h, more ether (100 ml) was added, and the solution was washed with bicarbonate. The rest of the work-up and treatment with silver carbonate in aqueous acetone was performed as described above for preparation of **5**. The 2-deoxy octose (**18**) was obtained as an oil (0.65 g); ^{1}Hmr data for **18** δ: 1.68 (3H, d, H-8,8′,8″, $J_{7,8} = 7$ Hz); 1.94, 2.08 (2 × 3H, s, CH_3-acetoxyls); ~2 (2H, overlapped by CH_3CO, H-2,2′); 4.0–6.0 (6H, overlapping m, H-1,3,4,5,6,7); ^{13}Cmr data for **18** δ: 17.8 (C-8); 20.7, 20.8 (CH_3, acetoxyls); 30.4 (C-2); 66.5 (C-3); 69.4, 69.9 (C-4, C-5); 92.0 (C-1); 125.9 (C-6); 129.0 (C-7); 158.3, 158.8 (C=O, acetoxyls).

*3,4-Di-*O*-acetyl-2,6,7,8-tetradeoxy-*D*-lyxo-oct-6-trans-enono-1,5-lactone (**23**)*

The 2-deoxy aldose derivative (**18**) (0.65 g) was dissolved in dichloromethane (15 ml) to which pyridinium chlorochromate (1.0 g) was added and the mixture was stirred for 2 h at room temperature or until the reaction was complete (tlc, solvent A). Ether (75 ml) was then added, the mixture was filtered through a layer of silica gel, and the solvents were evaporated off. The product was purified by column chromatography (eluent, CH_2Cl_2) affording a clear oil (0.25 g); ^{1}Hmr data for (**23**) δ: 1.70 (3H, d, H-8,8′,8″, $J_{7,8} = 6.5$ Hz, $J_{6,8} = 1$ Hz); 2.00, 2.12 (2 × 3H, s, CH_3, acetoxyls); 2.80 (2H, m, H-2,2′); 4.85 (1H, br d, H-4); 5.1–5.5 (2H, m, H-3,5); 5.5–6.0 (2H, m, H-6,7, $J_{6,7} = 15.5$ Hz, $J_{5,7} = 1.0$ Hz).

*4-*O*-Acetyl-2,3,6,7,8-pentadeoxy-*D*-threo-oct-2,6-trans-dienono-1,5-lactone (**22**)*

Lactone **23** (0.25 g) was dissolved in a 1:1 mixture of dichloromethane and triethylamine (5 ml). After 5 h the solvent was evaporated off, the residue was dissolved in CH_2Cl_2 (75 ml), and the solution was washed with water and dried over $MgSO_4$; removal of the solvent afforded **22** as an oil (0.20 g); ^{1}Hmr data for **22** δ: 1.74 (3H, d, H-8,8′, d, H-8,8′,8″); 2.08 (3H, s, CH_3-acetoxyl); 4.90 (1H, q, H-5, $J_{5,6} = 6.8$ Hz); 5.21 (1H, q, H-4, $J_{4,5} = 3.2$ Hz); 5.4–6.0 (2H, m, H-6,7, $J_{6,7} = 15.5$ Hz, $J_{7,8} = 6.5$ Hz); 6.15 (1H, d of d, H-2, $J_{2,3} = 9.6$ Hz, $J_{2,4} = 1.5$ Hz); 6.90 (1H, d of q, H-3, $J_{3,5} = 1$ Hz).

*Epoxidation of **22**. D-Enantiomer of asperlin (**24**)*

m-Chloroperbenzoic acid (0.20 g) was added to a solution of **22** (0.20 g) in dichloromethane (10 ml) and the solution was stirred at room temperature for 24 h. The volume of solvent was increased (100 ml), the solution was washed with saturated sodium bicarbonate and water, then dried over Na_2SO_4, and the solvent was evaporated. The resulting pale yellow oil (0.14 g), which was purified by column chromatography (eluent, CH_2Cl_2–hexane (3:1)), consisted of a mixture of the diastereomeric *trans*-epoxides (**24***a*,*b*) and ~25% of the *cis*-epoxide (**25**). The ^{1}Hmr spectrum is compared with that of asperlin in Fig. 2, and ^{13}C data for **24***a*,*b* and **1** are compared in Table 2.

Acknowledgements

The authors express their gratitude to the National Research Council of Canada for generous support. They also acknowledge with thanks the kind assistance of Dr. P. G. Farrell, Dr. B. Fraser-Reid, and R. Simoneau and the gift of a sample of 'asperlin' from the Upjohn Co.

1. T. K. Devon and A. I. Scott. Handbook of naturally occurring compounds. Vol. 1. Academic Press, New York, NY. 1975.
2. A. D. Argoudelis, J. H. Coats, and R. R. Herr. Antimicrob. Agents Chemother. 801 (1965).
3. S. P. Owen and B. K. Bhuynan. Antimicrob. Agents Chemother. 804 (1965).
4. A. D. Argoudelis and J. F. Zieserl. Tetrahedron Lett. 1969 (1966).
5. M. Tanabe, T. Hamasaki, D. Thomas, and L. Johnson. J. Am. Chem. Soc. **93**, 273 (1971).
6. G. M. Cree, D. M. Mackie, and A. S. Perlin. Can. J. Chem. **47**, 511 (1969); D. M. Mackie and A. S. Perlin. Carbohydr. Res. **24**, 67 (1972).
7. R. M. de Lederkremer, M. I. Litter, and L. F. Sala. Carbohydr. Res. **36**, 185 (1974).
8. R. J. Ferrier and G. M. Sankey. J. Chem. Soc. C, 2345 (1966).
9. J. Lessard, P. Viet Mink Tan, R. Martino, and J. K. Saunders. Can. J. Chem. **55**, 1015 (1977).
10. W. G. Overend and M. Stacey. Adv. Carbohydr. Chem. **8**, 45 (1953).
11. S. Hanessian. Adv. Carbohydr. Chem. **21**, 143 (1966).
12. B. Helferich. Adv. Carbohydr. Chem. **7**, 210 (1952).
13. R. J. Ferrier. Adv. Carbohydr. Chem. Biochem. **24**, 199 (1969).
14. B. Fraser-Reid and B. Radatus. J. Am. Chem. Soc. **92**, 5288 (1970).
15. S. Yik-Tai Tam and B. Fraser-Reid. Carbohydr. Res. **45**, 29 (1975).
16. F. Gonzalez, S. Lesage, and A. S. Perlin. Carbohydr. Res. **42**, 267 (1975).
17. J. J. K. Novak and F. Sorm. Collect. Czech. Chem. Commun. **27**, 902 (1962).
18. T. Maki and S. Tejima. Chem. Pharm. Bull. **16**, 2242 (1968).
19. T. Maki and S. Tejima. Chem. Pharm. Bull. **15**, 1069 (1967).

20. G. SNATZKE. Angew. Chem. Int. Ed. Engl. **7**, 14 (1968).
21. R. H. EVANS, JR., G. A. ELLSTEAD, and M. P. KUNSTMANN. Tetrahedron Lett. 1791 (1969).
22. Y. KIMURA, K. KATAGIRI, and S. TAMURA. Tetrahedron Lett. 3137 (1971).
23. K. MORI, M. ODA, and M. MATSUI. Tetrahedron Lett. 3173 (1976).
24. S. G. MILLS and W. B. TURNER. J. Chem. Soc. C, 2242 (1967).
25. W. ROSENBROOK, JR. and R. E. CARNEY. Tetrahedron Lett. 1791 (1969).
26. S. STERNHELL. Rev. Pure Appl. Chem. **14**, 15 (1964).
27. E. W. GARBISH. J. Am. Chem. Soc. **86**, 4461 (1964).
28. S. LESAGE. Ph.D. Thesis, McGill University, Montreal, P.Q. 1977; S. LESAGE and A. S. PERLIN. Can. J. Chem. In press.
29. D. G. LANCE, W. A. SZAREK, J. K. N. JONES, and G. B. HOWARTH. Can. J. Chem. **47**, 2871 (1969).
30. C. R. NARAYAN and K. N. IYER. J. Chem. Soc. **30**, 1734 (1965).
31. E. J. COREY and J. N. SUGGS. Tetrahedron Lett. 2647 (1975).

Can. J. Chem. Downloaded from www.nrcresearchpress.com by 210.87.254.105 on 09/05/12
For personal use only.

Synthesis of azapolycyclic compounds by the aminium radical route: rearrangements of *C*-nitroso compounds and their stereoelectronic requirements[1]

ROBERT W. LOCKHART,[2] MASAYUKI KITADANI,[3] FREDERICK W. B. EINSTEIN, AND YUAN L. CHOW

Department of Chemistry, Simon Fraser University, Burnaby, B.C., Canada V5A 1S6

Received March 27, 1978

ROBERT W. LOCKHART, MASAYUKI KITADANI, FREDERICK W. B. EINSTEIN, and YUAN L. CHOW. Can. J. Chem. **56**, 2897 (1978).

The aminium radicals generated from the photolysis of *N*-nitroso-*endo*-2-methylaminomethylbicyclo[2.2.1]hept-5-en and *N*-nitroso-*endo*-2-methylaminomethylbicyclo[2.2.2]oct-5-ene cyclize at the C-6 position, since the relevant reacting centers can achieve excellent orbital overlap with minimum molecular motion in comparison to the alternative cyclization path at the C-5 position. The photolysis of the former compound gave a *C*-nitroso compound which underwent a series of unusual intramolecular cleavages, deoximations, and redox reactions during the work-up. Stereoelectronic requirements for these intramolecular reactions are discussed. Thermolysis of *N*-chloro-*endo*-2-methylaminomethylbicyclo[2.2.2]oct-5-en in methanol also gave the product with azaisotwistane skeleton.

ROBERT W. LOCKHART, MASAYUKI KITADANI, FREDERICK W. B. EINSTEIN et YUAN L. CHOW. Can. J. Chem. **56**, 2897 (1978).

Les radicaux aminium produits par photolyse du *N*-nitroso *endo*-méthylaminométhyl-2 bicyclo[2.2.1]heptène-5 et du *N*-nitroso *endo*-méthylaminométhyl-2 bicyclo[2.2.2]octène-5 se cyclisent à la position C-6, puisque les centres réactifs appropriés peuvent donner lieu à un excellent recouvrement d'orbitales avec un minimum de déplacements moléculaires, ce qui n'est pas le cas pour l'autre voie de cyclisation possible à la position C-5. La photolyse du premier composé a conduit à un composé *C*-nitroso qui a subi une série inhabituelle de clivages intramoléculaires, de désoximations et de réactions d'oxydoréduction pendant qu'on l'isolait. On discute des exigences stéréoélectroniques pour ces réactions intramoléculaires. La thermolyse du *N*-chloro *endo*-méthylaminométhyl-2 bicyclo[2.2.2] octène-5 dans le méthanol a également conduit au produit ayant un squelette azaisotwistane.

[Traduit par le journal]

Introduction

In continuation of our interests in the application of the aminium radical cyclization route in the synthesis of azapolycyclic compounds (2), the photolysis of $\Delta^{4,5}$-alkenyl nitrosamines as a route to azapolycyclic systems has been investigated. It is well established that $\Delta^{4,5}$-alkenyl aminium radicals (**A**) generated from the corresponding nitrosamines and chloramines readily cyclize to yield five- (but not six-) membered ring systems (**B**) by a kinetically controlled process (2). The *C*-radical intermediate **B** then reacts with a radical (·NO or ·Cl or their donors) to give the azacyclic compounds (**C**; X = Cl or NO).

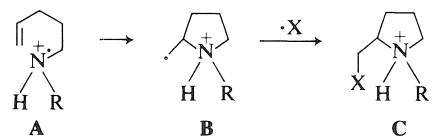

A **B** **C**

Eventually our goal is to define the nature of the orbital overlap requirements in cyclizations initiated by radicals as proposed in our previous publication (2). In this paper intramolecular photoaddition of two bridged bicyclic alkenyl nitrosamines and subsequent rearrangements of the cyclization product are described. The accompanying paper (3) is concerned with the interception of the cyclized *C*-radical intermediates with trapping agents in an effort to modify the synthetic process and obtain other complementary products.

Results

Two alkenylamines, 2-*endo*-methylaminomethylbicyclo[2.2.1]hept-5-ene (**1**) and 2-*endo*-methylaminomethylbicyclo[2.2.2]oct-5-ene (**2**), were prepared by known methods as outlined in the Experimental; the former contained about 30% of the corresponding *exo*-isomer which could not be removed. The corresponding nitrosamines **3** and **4** were readily prepared by nitrosation with dinitrogen tetraoxide or nitrosyl borofluoride.

Photolysis of nitrosamine **3** in acidic methanol solution under nitrogen gave rise to a strong ab-

[1]Some of these results have been published in a preliminary communication (see ref. 1).

[2]NRCC Scholarship holder 1973–1976.

[3]On study leave from College of General Education, Kobe University, Kobe, Japan.

Can. J. Chem. Downloaded from www.nrcresearchpress.com by 210.87.254.6 on 09/05/12
For personal use only.

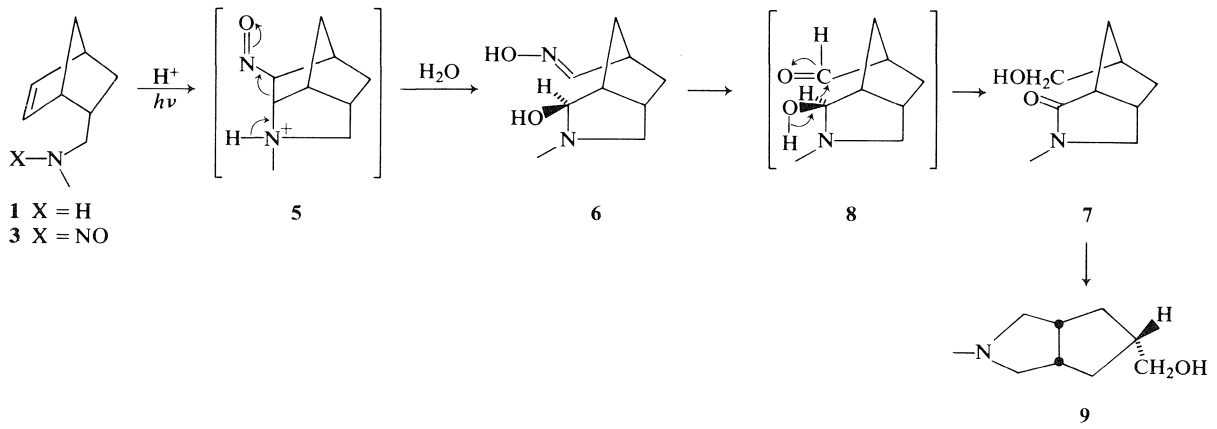

SCHEME 1

sorption at 290 nm typical of a *C*-nitroso dimer (4). The major products were the unstable aldoxime **6** and the water soluble lactam **7** in addition to minor products, some of which were derived from the *exo*-nitrosamine. The structure of the hydroxy lactam (**7**) was suggested by the analytical results and by the ir absorption at 1660 (5) and 3300 cm^{-1}; these absorptions might be interpreted as being due to a γ-lactam group internally hydrogen bonded to the hydroxyl group. The prominent mass spectral peak at *m/e* 98 has been assigned as being that peak characteristic of *N*-methylpyrrolidone derivatives (6). The spectra were in agreement with the proposed structure but were not definitive. Lactam **7** was reduced with sodium bis(2-methoxyethoxy)aluminium hydride to give a tertiary amine (**9**) which showed a sharp doublet at τ 6.38 (J = 5 Hz) for the magnetically equivalent CH_2OH protons in contrast to the complex multiplet for the corresponding CH_2OH protons at τ 6.4 in **7**. This observation indicated that the CH_2OH's were magnetically nonequivalent in **7** and were transformed to magnetically equivalent protons as the result of reduction. From the mechanistic consideration that the formation of **7** arises from photocyclization, cleavage reaction, and intramolecular redox reaction (*vide infra*), the reduction product must be assigned structure **9** which possesses a plane of symmetry cutting across the CH_2OH and N—CH_3 groups.

The nmr signal at τ 2.72 (J = 7 Hz), together with the ir absorption at 3300, 920, 890, and 860 cm^{-1}, suggest that **6** is the *syn*-aldoxime and the broad doublet at τ 5.30 (J = 5.5 Hz) may be assigned to the C—H proton geminal to the OH and amine groups. Attempted deoximation of aldoxime **6** with sodium bisulfite solution led to the formation of lactam **7**, indicating that hydrolysis to an aldehyde group (see **8**) was accompanied by a rarely observed intramolecular redox reaction. This probably occurred during the work-up to give **7**, owing to the proximity of the relevant functional groups. The reaction pattern might be represented as shown in Scheme 1; cleavage of primary products, such as the *C*-nitroso compound **5**, has frequently been found in photoadditions of nitrosamines (7). In the present case, cleavage to give **6** was such a facile process that various measures (such as control of temperature, light source, and/or irradiation time) taken to circumvent the cleavage processes and to obtain the expected tricyclic oxime did not meet with success. It was realized that other approaches had to be used for the synthesis of these azatricyclic compounds (3).

Irradiation of bicyclic alkenyl nitrosamine **4** under nitrogen gave the tricyclic *syn* (53%) and corresponding *anti* (18%) oximes **10** (Scheme 2). Both oximes (**10**), alone or as a mixture, were deoximated with sodium bisulfite to give amino ketone **11** which exhibited an ir absorption at 1720 cm^{-1} and the nmr signal for H_a at τ 6.98 (d, J = 5 Hz). *syn*-Oxime **10** was fairly soluble in water and formed the methylene chloride soluble hydrochloride salt. Oximes **10** exhibited the necessary ir absorption for the oximino group and had similar mass spectra. In agreement with other amino oximes (8), *syn*-**10** showed a doublet at τ 6.02 (J = 4 Hz) for H_a and *anti*-**10** a triplet at τ 6.25 (J = 6.5 Hz) for H_e and a doublet at 6.86 (J = 4.5 Hz) for H_a. In all these tricyclic amines **10** and **11**, a double doublet in the τ 6.7–6.9 region and a partially hidden signal (a doublet) in the τ 7.5 region could be assigned to H_b and H_c, respectively. Although on the basis of the Karplus relation these assignments do not contradict the structural assignment of the azaisotwistane skeletons **10** and **11**, the azatwistane skeleton resulting from the six-membered ring cyclization cannot be entirely ruled out. The hydrochloride of *syn*-oxime **10** was, therefore, in-

Can. J. Chem. Downloaded from www.nrcresearchpress.com by 210.87.254.6 on 09/05/12
For personal use only.

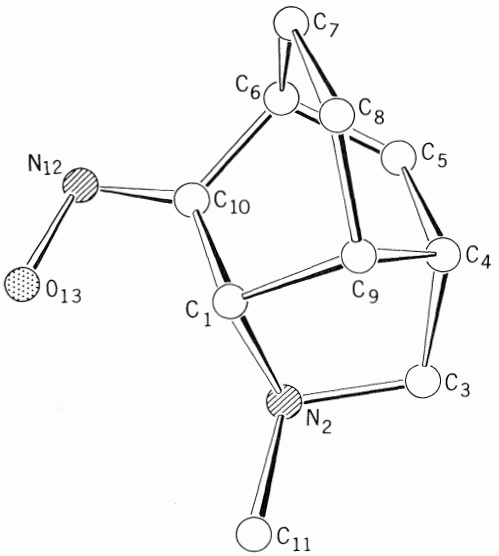

FIG. 1. The proposed crystal structure for the hydrochloride of *syn*-oxime **10**.

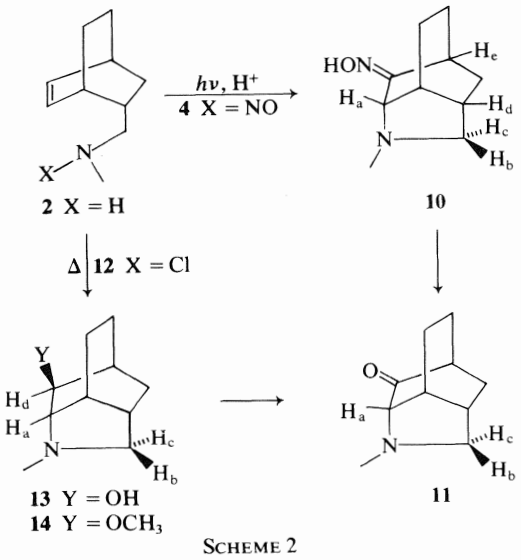

SCHEME 2

vestigated by X-ray structural analysis to confirm the proposed structure[4] as shown in Fig. 1; some relevant data on the dimensions are given in Table 1. Crystal data for the hydrochloride of *syn*-oxime **10**: $(C_{10}H_{17}N_2O)^+Cl^-$, colorless crystals, orthorhombic, space group P_{bca}, $a = 11.655(5)$, $b = 12.574(5)$, $c = 14.947(6)$ Å, $U = 2180.0$ Å^3, $D_m = 1.31$ g cm^{-3}, $Z = 8$, $D_c = 1.32$. The structure has been refined to $R = 0.066$ for 653 observed reflections measured with a computer-controlled diffractometer using single-crystal monochromatized Mo-K_α radiation.

Although the final electron density map could be further refined, particularly around the environment of the oxime function, it is interesting to note the dimensions of 1.41 and 1.30 Å for the C=N and the N—O bonds, respectively: the former is significantly longer than the normal bond length for a C=N bond (1.26 Å) and the latter shorter than that for the N—O bond (1.42 Å) characteristic of oximes (10). These data suggest a significant contribution of the polar resonance form of the oximes e.g., $\rangle C{=}N{-}O{-}H\ldots Cl^- \leftrightarrow \rangle \bar{C}{-}N{=}O\ldots H{-}Cl$, in which the double bond character is distributed across the C—N—O system. The contacts N(2)---Cl (3.11 Å) within the same molecule and O(13)---Cl (3.12 Å) between the adjacent molecules indicate there is a weak hydrogen bond; this is further supported by an examination of the angles (161 and 180°, respectively) subtended at the hydrogen atoms.

Failure to obtain the azatwistane skeleton as indicated above led us to investigate the thermolysis of *N*-chloramines for which nitrenium ions (11) or amine radicals (12) have been proposed as reactive intermediates. On refluxing in dioxane–water, chloramine **12** decomposed quickly (1.25 h as indicated by iodimetric titration) to amino alcohol **13** (12%) and starting amine **2**, in addition to a small yield of chlorine-containing amines. The last fraction was unstable and was shown to contain one chlorine atom but was probably not a homogeneous fraction. Amino alcohol **13** (3) was readily converted to ketone **11** by Jones' oxidation. The thermal decomposition of chloramine **12** in methanol, however, took a considerably longer time (11 h for the disappearance of the positive chlorine) and gave one major product, methoxy amine **14** (59%), and starting amine **2** (6.5%), in addition to two more unidentified products (8%) as shown by gc–ms analysis. The major product was isolated by preparative vpc and was shown to possess structure **14** by X-ray crystallographic analysis of the corresponding picrate (Fig. 2). Some relevant data on the dimensions are given in Table 1. The crystal data for the picrate of **14** are as follows: $C_{17}H_{22}N_4O_8$, yellow needles, monoclinic, space group $P_{2_1/c}$, $a = 7.651(4)$, $b = 12.441(6)$, $c = 19.793(8)$ Å and $B = 94.08°(4)$, $U = 1884.0$ Å^3, $D_m = 1.44$ g cm^{-1}, $Z = 4$, $D_c = 1.44$. The structure was refined to $R = 0.080$ for 1502 observed reflections.

For H_b and H_c, hydroxyamine **13** (3) exhibited signals at 7.44 (dd, $J = 10$ and 4.5 Hz) and 7.26

[4]The details of the method and molecular dimensions are described in ref. 9.

Can. J. Chem. Downloaded from www.nrcresearchpress.com by 210.87.254.6 on 09/05/12
For personal use only.

Can. J. Chem. Downloaded from www.nrcresearchpress.com by 210.87.254.6 on 09/05/12
For personal use only.

TABLE 1. Interatomic distances and angles of the hydrochloride of **10** and the picrate of **14**

	Distance (Å)			Distance (Å)	
Bond	**10**	**14**	Bond	**10**	**14**
C1—N2	1.520(9)	1.54(1)	C5—C6	1.522(11)	1.51(1)
C1—C9	1.529(10)	1.53(1)	C6—C7	1.508(12)	1.53(2)
C1—C10	1.470(11)	1.53(1)	C6—C10	1.486(11)	1.50(1)
N2—C3	1.524(9)	1.52(1)	C7—C8	1.522(13)	1.52(1)
N2—C11	1.526(9)	1.47(1)	C8—C9	1.522(12)	1.52(1)
C3—C4	1.525(11)	1.48(1)	C10—N12	1.414(10)	
C4—C5	1.544(10)	1.54(1)	N12—O13	1.306(7)	
C4—C9	1.528(10)	1.50(1)	C10—O12		1.42(1)
			O12—C13		1.42(1)

	Angles (deg)			Angles (deg)	
Bond	**10**	**14**	Bond	**10**	**14**
C10—C1—C9	105.9(7)	103(1)	C4—C5—C6	111.2(8)	110(1)
C10—C1—N2	108.9(7)	109(1)	C5—C6—C7	110.4(9)	109(1)
C9—C1—N2	102.4(7)	103(1)	C5—C6—C10	104.5(8)	109(1)
C1—N2—C3	107.4(5)	105(1)	C7—C6—C10	106.7(8)	109(1)
C1—N2—C11	112.1(7)	111(1)	C6—C7—C8	109.1(8)	102(1)
C3—N2—C11	112.4(6)	113(1)	C7—C8—C9	112.5(8)	111(1)
N2—C3—C4	102.6(7)	104(1)	C10—N12—O13	100.0(9)	

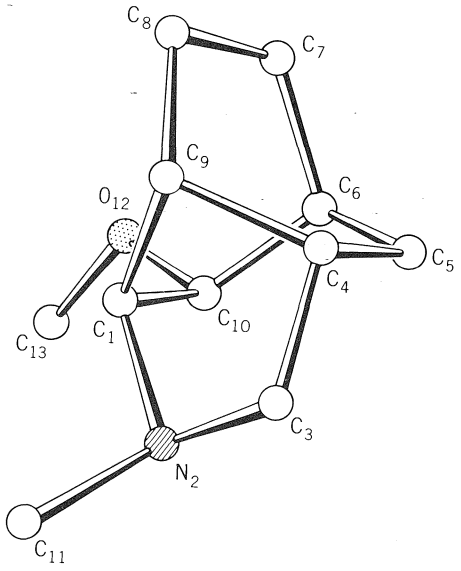

FIG. 2. The proposed crystal structure for the picrate of compound **14**.

(d, J = 10 Hz) whereas methoxy amine **14** displayed them at τ 7.58 (d, J = 9 Hz) and 7.32 (dd, J = 9 and 4.5 Hz) (14). In considering the Karplus relation, it appeared to us that the coupling patterns of **14** were quite different from those of **13**, and that **14** agreed with the azatwistane skeleton when the dihedral angles were measured. This led us to erroneously report in our preliminary communication (1), the structure to be the azatwistane derivative. At about the same time, Waegell and co-workers (13) solvolysed the same chloramine **12** in methanol in the presence of silver oxide to give the methoxy amine for which they postulated structure **14**.[5] More recently, the same group synthesised the parent *N*-methyl-2-azatwistane and *N*-methyl-2-azaisotwistane (14); on the basis of the similarity of the 250 MHz nmr spectra of the latter and those of **14**, the azaisotwistane structure was assigned to **14**.

Discussion

It has been demonstrated that the regiospecificity of the cyclization of $\Delta^{4,5}$-alkenylaminium radicals generated from the photolysis of the corresponding nitrosamines is controlled by the degree of *p*-orbital overlap in the transition state; in every case except one (15) this leads to exclusive formation of the five-membered ring carrying the apparently thermodynamically less stable *C*-radical, i.e., the intramolecular radical attacks are mainly governed by kinetic controls and not, to any significant extent, by the thermodynamic stability of the transition states (2). It is conceivable that in certain cases the energy barrier arising from nonbonded interactions in the transition state might be sufficiently high to retard cyclization to a five-membered ring formation. Such

[5]We are grateful to Professor B. Waegell who has confirmed the identity of our compound by comparison of its ir spectra with those of his sample.

Can. J. Chem. Downloaded from www.nrcresearchpress.com by 210.87.254.6 on 09/05/12
For personal use only.

a case can be seen in the aminium radical cyclization reported by Heusler (15) in which *N*-chloro-*cis*-octahydroisoquinoline cyclizes to the azatwistane structure (six-membered ring formation) instead of cyclizing to the alternative five-membered ring compound commonly observed in other cases.

The aminium radicals derived from **3** and **4** undergo five-membered ring cyclization exclusively as shown by the product patterns. The cyclization of the former aminium radical, a rigid bicyclo[2.2.1] system, to give **5** (as the final product) can be understood in terms of bond formation involving the readily available and better overlapping *p*-orbitals of the C-6 position of the double bond and the radical center. In this case it is also true that the alternative cyclization to the C-5 position is disfavored since it has to overcome considerable strain energy. For the cyclization of the aminium radical **15**, a more flexible bicyclo[2.2.2] system, the kinetically driven attack on the C-6 *p*-orbital has to surmount various 1,2-eclipsing and 1,3-diaxial interactions in the transition state to give **16**; these extra nonbonded interactions would be relieved in the transition state of the alternative attack at the C-5 *p*-orbital leading to **17**, in which the cyclohexane ring systems are staggered. The failure to observe twistane products clearly indicates that these stereochemical barriers are not sufficient to overcome the driving force in the five-membered ring cyclization. The different modes of cyclization for the present isoazatwistane and Heusler's (15) azatwistane product may provide an interesting case for investigation in conformational analysis.

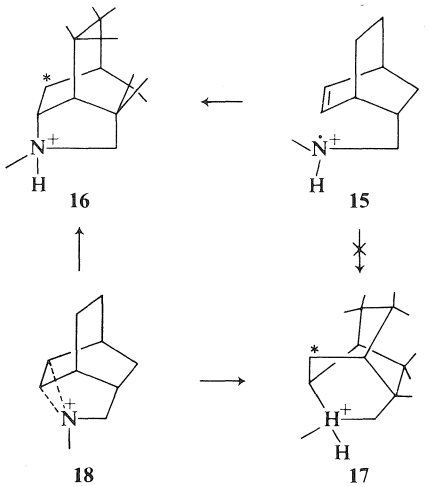

16 **15** **18** **17**

The thermal decomposition of *N*-chloroalkenylamine in neutral hydroxylic solvents has been investigated by various groups (11–13); among them, Edwards *et al.* (12) and other groups (13) have provided good evidence that the reaction follows the homolytic amino radical route initiated by adventitious radicals (16, 17) rather than the nitrenium ion route by assisted ionizations (11). Further, Edwards *et al.* (12) have concluded that *trans*-*C*-halo compounds, such as **13** where Y = Cl, undergo skeletal rearrangements via aziridinium ions, such as **18**, to give more stable *trans*-substituted polycyclic amines. The thermolysis of *N*-chloramine **12** is also expected to follow the homolytic pathway using the amine radical cyclization as the key step which might lead to the formation of the *C*-chloro compound **13** (Y = Cl) as the primary product. If the final products **13** and **14** are assumed to arise from this *C*-chloro compound by a similar solvolytic mechanism as proposed by Edwards *et al.* (12), the opening of aziridinium ion **18** by nucleophilic attack would yield both isoazatwistanes, **13** and **14**, and the alternative azatwistane compounds; on the basis of a conformational analysis similar to that discussed above, the latter formation should be favoured. However, this assumption poses a serious dilemma as it fails to explain the failure to isolate azatwistane derivatives in the thermolysis of **12**. A similar difficulty has been encountered in the solvolysis of **13** (where Y = Br); possible explanations are discussed in the succeeding paper (3). Since the vpc spectrum of the crude oil from the thermolysis of **12** in methanol is considerably simpler than that from the solvolysis of **13** (where Y = Br) (3), it is speculated that CH_3OH (or water in dioxane) might directly participate in the kinetically driven radical cyclization process. The slow thermolysis in methanol indicates that a chain process, such as that observed in the Ag^+-catalysed reaction (13, 14), might be very short.

The complex product pattern observed in the photolysis of nitrosamine **3** is attributed to the cleavage reaction of β-nitroso ammonium salts often observed in the nitrosamine photoreaction (7). The structures of oxime **6**, lactam **7**, and bicyclic amine **9** have been deduced from the spectral data in conjunction with mechanistic considerations. The key to the structural proof rests on the observation that the complex multiplet due to the magnetically nonequivalent CH_2OH in **7** is transformed to a sharp doublet, i.e., the magnetically equivalent CH_2OH in **9**, as the result of the reduction of the γ-lactam ring to the pyrrolidine ring.

The facile cleavage of *C*-nitroso compound **5** stands in contrast to the stability of the corresponding *C*-nitroso compound obtained from photocyclization of **4**; the latter readily tautomerizes to the oximes **10**, a process common to most *C*-nitroso compounds (4). The driving force for the cleavage is most likely derived from the strain energies associated with the rigid bicyclo[2.2.1] system as has been

Can. J. Chem. Downloaded from www.nrcresearchpress.com by 210.87.254.6 on 09/05/12
For personal use only.

demonstrated in the photoaddition of nitrosamines to norbornene (7). Although we have concluded that a coplanar *cis*-orientation of the functional groups is required for the cleavage reaction (7), this configuration could not be confirmed in **5** because of rapid decomposition.

It is suspected that ready hydrolysis of the oxime group in **6** is facilitated by *endo*-OH group participation (the isomer of **6**) under acidic conditions via an intermediate such as **6***a*, leading to the unisolated aldehyde **8** (or its epimer). The intramolecular redox

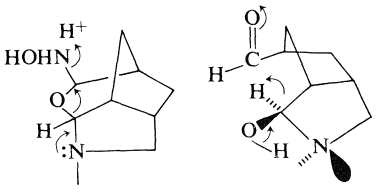

6*a* **8***a*

reaction of an aldehyde and a *gem*-aminoalcohol group requires a stereochemical orientation of the functional groups as shown in **8** for the hydride transfer and may be analogous to the intramolecular redox process of ajaconine derivatives (18). Recently Deslongchamps (19) has elegantly demonstrated that ejection or migration of anionic species from a tetrahedral carbon carrying heteroatomic (nitrogen or oxygen) substituents is stereoelectronically assisted by the lone-pair orbitals oriented antiperiplanar to the departing groups. Although this new stereoelectronic theory is primarily demonstrated in the decomposition of hemiacetals, hemiorthoesters, and hemiorthoamides, the author has suggested that it also applies to the haloform reaction, retro-aldol and allied reactions, various fragmentations involving ejection of anions, the benzylic acid rearrangement, and various other anionoid reactions. The unusual over-the-space redox process is believed to be controlled by stringent stereoelectronic factors; it is the ready orientation of the nitrogen lone-pair orbital antiperiplanar to the C—H bond as in **8***a* that effectively promotes hydride shift.

Experimental

Unless otherwise specified, nmr spectra were recorded with a Varian A56/60 spectrometer in $CDCl_3$ using TMS as the internal standard. Infrared spectra were recorded as Nujol mulls or neat liquids with a Perkin Elmer model 457 grating spectrophotometer, uv spectra with a Unicam SP800 spectrometer, and mass spectra with a Hitachi-Perkin-Elmer RMU-6E instrument at 80 eV. Melting points were recorded with a Fisher Johns hot stage apparatus and were uncorrected. Microanalyses were performed by Mr. M. K. Yang, Department of Biological Sciences, Simon Fraser University.

For the photolyses, Hanovia medium pressure mercury lamps (654A36, 200 W and 8A36, 100 W) were used in conjunction with a Pyrex apparatus equipped with a Nonex filter (50% transmission at 320 nm). The photolysis products were isolated in the usual way (4).

Synthesis of N-*Nitroso-2*-endo-*methylaminomethylbicyclo[2.2.1]hept-5-ene (**3**)*

Allyl bromide (56 g) was treated with cyclopentadiene (25 g) by the described method (18). Distillation of the crude product gave a clear oil (50 g, 70.5%) consisting principally of 2-*endo*-bromomethylbicyclo[2.2.1]hept-5-ene and about 30% of the corresponding *exo*-isomer; ir: 3060(m), 720(s), and 630(s) cm^{-1}.

A solution of methylamine (27 g) and the above sample (25 g) in ether (125 ml) was placed in an autoclave which was heated in an oil bath at 100°C for 67 h. The product was extracted with 1.0 *N* HCl (3 × 50 ml) which was washed with ether. The acidic aqueous phase was basified to pH 10–11 with aqueous NaOH and extracted with CH_2Cl_2 which was dried over $MgSO_4$, filtered, and evaporated to give 2-*endo*-methylaminomethylbicyclo[2.2.1]hept-5-ene (**1**) as a light yellow oil (12.8 g); ir: 3300(w), 3060(m), 1250, and 720(s) cm^{-1}; nmr τ: 3.90 (dd, J = 6 and 3 Hz, 1H), 4.12 (dd, J = 6 and 3 Hz, 1H), 7.20 (m, 2H), 7.40 (d, J = 7 Hz, 0.7H), 7.55 (s, *N*—CH_3, 0.9H), 7.61 (s, *N*—CH_3, 2.1H), 7.80 (m, 2H), 8.68 (m, 2H), 9.04 (s, D_2O exch., 1H), and 9.50 (br d, J = 10 Hz, 0.7H); ms m/e: 137 (M^+, 10), 71(66), 70(61), and 44(100). This oil contains 30% of the *exo*-isomer as shown by the ratio of the *N*—CH_3 signals at τ 7.55(s) and 7.61 which was 0.9:2.1.

The amine (2 g, 0.015 mol) and anhydrous sodium acetate (4 g, 0.5 mol) in CH_2Cl_2 (125 ml) were stirred and cooled in an acetone–ice bath. A cold solution of N_2O_4 (1.5 g, 0.016 mol) in CH_2Cl_2 (50 ml) was added dropwise over 1 h. The mixture was stirred at −10°C for another 10 min, filtered, and washed with dilute Na_2CO_3 (10%). The solvent was dried and evaporated to give an oil (2.4 g) which was purified by chromatography to give nitrosamine **3**: ir: 3060(m), 1430(s), 1270, 1155, 1035(s), and 720(s) cm^{-1}; ms *m/e*: 167(1), 166(M^+, 1), 165(1), 149(22), 136(24), 101(35), 91(40), 82(88), and 66(100); uv (methanol): 344 nm (ε, 97). The olefinic protons appeared in the nmr spectrum as a pair of double doublets at τ 3.75 (J = 6 and 3 Hz) and 3.98 (J = 6 and 3 Hz). The *N*-methyl protons attributed to the *syn*-isomer resonated at τ 6.92(s) and the C8 protons of this isomer appeared as a complex pattern centered at τ 6.0. The *N*-methyl signal of the corresponding *anti*-isomer appeared at τ 6.20(s). The ratio of the *N*-methyl signals for the *syn*- and *anti*-isomers was 81:19. Other resonances appeared at τ 7.20 (m, 3H), 8.10 (m, H3-*exo*), 8.65 (m, 2H), and 9.30 (ddd, J = 11.5, 4, and 2.5 Hz, H3-*endo*). The sample contained about 30% of the *exo*-isomer as shown by the corresponding nmr signals.

Synthesis of N-*Nitroso-2*-endo-*methylaminomethylbicyclo[2.2.2]oct-5-ene (**4**)*

Acrylic acid (30 g) was treated with cyclohexadiene (25 g) as described before (19). Distillation of the reaction product at 148–150°C/13 Torr gave an oily solid which was recrystallized from pentane several times to give 2-*endo*-carboxylbicyclo[2.2.2]oct-5-en (35.4 g, 67%): mp 57–59°C (lit. (19) mp 56–57°C); ir: (Nujol): 3200–2500 (s,br), 1700(s), 1240(s), 940 and 700(s) cm^{-1}.

The acid (10 g, 0.066 *M*) was mixed with pyridine (6.0 g) and thionyl chloride (9.45 g) in dry benzene (200 ml) at 0°C for 20 min. Methylamine was bubbled into this solution until it was basic to moist pH paper. The benzene solution was washed with 10% aqueous Na_2CO_3 solution, and water, dried over $MgSO_4$, filtered, and evaporated to give a solid. Recrystallization from hexane gave white needles of *N*-methyl-2-*endo*-carboxamidobicyclo[2.2.2]oct-5-en (9.1 g, 83%); mp 136–138°C; ir: 3285(s), 3040(w), 1640(s), 1555(s), and 690(m)

Can. J. Chem. Downloaded from www.nrcresearchpress.com by 210.87.254.6 on 09/05/12
For personal use only.

cm^{-1}; nmr τ: 3.70 (m, 2H), 4.2 (br m, D_2O exch.), 7.25 (d, J = 4.5 Hz, 3H), 7.40 (m, 2H), and 8.0–9.0 (unresolved, 6H). *Anal.* calcd. for $C_{10}H_{15}NO$: C 72.69, H 9.15, N 8.48; found: C 72.86, H 9.14, N 8.41.

The amide (8.8 g, 0.053 mol) was added slowly in portions to a stirring suspension of lithium aluminum hydride (4.05 g, 0.1 mol) in ether and the mixture was stirred at room temperature for 20 h. After the usual work-up the ether solvent was distilled through a Vigreaux column leaving 2-*endo*-methylaminomethylbicyclo[2.2.2]oct-5-en (**2**) as a light yellow oil (7.47 g, 94%); ir: 3280(w), 3040(m), 1610(w), 1150, 1130, and 700 cm^{-1}; nmr τ: 3.80 (m, 2H), 7.4–7.8 (unresolved, 3H), 7.61 (s, N—CH_3), 8.0–9.0 (unresolved, 6H), and 9.10 (m, 1H); ms *m/e*: (15 eV) 151 (M^+, 16), 85(75), 83(100), and 44(66).

Amine **2** (5 g, 0.033 mol) was added to a suspension of $NOBF_4$ (6.4 g, 0.055 mol) (2) in CH_2Cl_2 (100 ml) at 0°C. Pyridine (4.32 g, 0.055 mol) in CH_2Cl_2 (50 ml) was added dropwise over 15 min. After 1 h the mixture was filtered then washed with Na_2CO_3 (10%), dilute HCl (0.1 *N*), and then water. The solution was dried and filtered, and the solvent was evaporated to give *N*-nitrosamine **4** (3.64 g); ir: 3040(w), 1430(s), 1330, 1310, 1268, 1155(m), 1030(s), and 700(s) cm^{-1}; ms *m/e*: 180 (M^+, 32), 163(18), 150(35), and 79(100); uv (methanol): 345 nm (ε, 100). The olefinic protons appeared as a two-proton multiplet at τ 3.70. The *N*-methyl protons attributed to the *syn*-isomer appeared at τ 6.97(s) and the C9 protons of this isomer appeared as a complex pattern at τ 6.1. The *N*-methyl signal of the corresponding *anti*-isomer resonated at τ 6.25(s) while the C9 protons appeared as a complex pattern centered at τ 6.7. The ratio of the *N*-methyl signals for the *syn*- and *anti*-isomers was 82:18. The remaining protons appeared as unresolved multiplets at τ 7.3–9.2 (9H). An analytical sample of **4** was prepared by repeated distillation at 25°C/0.05 Torr. *Anal.* calcd. for $C_{10}H_{16}N_2O$: C 66.64, H 8.95, N 15.54; found: C 66.90, H 9.12, N 15.71.

Photolysis of N-*Nitroso-2*-endo-*methylaminomethylbicyclo[2.2.1]hept-5-ene (3)*

A solution of nitrosamine **3** (1.5 g, 0.009 mol) and concentrated HCl (0.8 ml, 0.048 *N*) in methanol (200 ml) was irradiated under N_2 for 1.5 h. The usual work-up gave a neutral fraction (80 mg) and a basic fraction (*A*, 850 mg). The mother liquor was further basified from pH 9 to 13 with NaOH solution then continuously extracted for 5 days with CH_2Cl_2 to yield 200 mg of additional extract, *B*.

A portion of the basic extract *A* (750 mg) was chromatographed on silica gel. Elution with 2% methanol–CH_2Cl_2 gave crystals (237 mg, 22%) which were rechromatographed on a preparative scale tlc plate (silica gel, 10% methanol–CH_2Cl_2) to give *syn*-aldoxime **6**: mp 109–112°C; ir: 3200 (w, br), 3040 (w, br), 1260, 920(s), and 890(s) cm^{-1}; nmr τ: 2.72 (d, J = 7 Hz, 1H), 5.30 (d, J = 5.5 Hz, 1H), 6.55 (br d, J = 8 Hz, 1H), 7.28 (s, N—CH_3), 7.5–8.0 (unresolved, 4H), and 8.5 (m, 3H); ms *m/e*: 184 (M^+, 1), 183(5), 182.1037 (11, calcd. for $C_9H_{14}N_2O_2$: 182.1055), 168(22), 152(17), 82(78), 57(100), and 49(89). *Anal.* calcd. for $C_9H_{16}N_2O_2$: N 15.19; found: N 15.20.

Elution with 5% methanol–CH_2Cl_2 gave a mixture of aldoxime and olefinic material: ir: 3300 (s, br), 3060(w), 920(m), and 870 cm^{-1}; nmr τ: 2.60(m), 3.10 (m, D_2O exchangeable), and 3.90 (t, J = 1.5 Hz).

The material isolated by continuous extraction (*B*) was vacuum distilled (40°C/0.025 Torr) to give hydroxy lactam **7** (29%): ir: 3400 (s, br), 1662(s), 1500(m), 1400, 1300, 1270(m), 1115, 1070, 1045, and 1015(m) cm^{-1}; nmr τ: 6.00 (m, D_2O exchangeable), 6.42 (m, 3H), 6.92 (dd, J = 10 and 1 Hz, 1H), 7.18 (s, N—CH_3) and ~7.8 (m, 7H); ms *m/e*: 169 (M^+, 90), 152(10), 98(100), 86(50) and 84(77). *Anal.* calcd. for $C_9H_{15}NO_2$: C 63.88, H 8.93, N 8.28; found: C 63.51, H 8.83, N 8.39.

An aqueous ethanol (50%) solution of crude aldoxime **6** (600 mg) was refluxed with $NaHSO_3$ (1.3 g) for 4 h (20). The solvent was removed by distillation (78–80°C) and the residue was acidified with dilute HCl (0.1 *N*). Extraction with $CHCl_3$ (3 × 20 ml) gave no neutral extract. The aqueous mother liquor was basified (pH 13) with aqueous NaOH and continuously extracted with CH_2Cl_2 for 5 days to give hydroxy lactam **7** (403 mg; ir 1662 cm^{-1}) containing a small amount of nitrile impurity (ir 2220(w) cm^{-1}).

A mixture of **7** (100 mg, 0.006 mol) and a 70% benzene solution of sodium bis(2-methoxyethoxy)aluminum hydride, 0.43 g, 0.015 mol) in benzene (10 ml) was stirred at 50°C for 0.5 h then at room temperature for another 2 h. The mixture was decomposed with water and filtered. The residual solid was washed with additional benzene and the combined benzene filtrate was dried and evaporated to an oil (45 mg) which was distilled at 25°C/0.5 Torr to give bicyclic amino alcohol **9**; ir: 3300 (s, br), 1150, 1135(w), 1020(m), 985(w), and 865(m) cm^{-1}; nmr τ: 6.38 (d, J = 5 Hz, CH_2OH), 6.84 (s, D_2O exchangeable), 7.39 (d, J = 8.5 Hz, 2H), 7.70, (s, N—CH_3), 7.4–8.1 (m, 6H), and 8.3–9.2 (m, 3H); ms *m/e*: 155 (M^+, 10), 154(17), 124(19), and 57(100). The signal at τ 6.38 was collapsed to a singlet when irradiated at τ 8.6 but the signal was not affected when irradiated at the τ 7.2–8.1 area. The picrate of **9** was recrystallized twice from ethanol to give yellow needles, mp 138–139°C. *Anal.* calcd. for $C_{15}H_{20}N_4O_8$: C 46.88, H 5.52, N 14.58; found: C 46.64, H 5.52, N 14.53.

Photolysis of N-*Nitroso-2*-endo-*methylaminomethylbicyclo[2.2.2]oct-5-ene (4)*

A solution of nitrosamine **4** (1 g, 0.0055 mol) and concentrated HCl (0.5 ml, 0.03 *N*) in methanol (200 ml) was irradiated under nitrogen for 1.5 h. The usual work-up gave a neutral fraction (20 mg) and a basic fraction (620 mg). In addition, continuous liquid–liquid extraction of the basic mother liquor with CH_2Cl_2 gave a semisolid (150 mg).

The basic extract (600 mg) was chromatographed on a silica gel column (40 g). Elution with 5% methanol–CH_2Cl_2 gave crude *syn*-oxime **10** (233 mg, 23%) which was purified by preparative scale tlc (silica gel; 10% methanol–CH_2Cl_2) to give a clear oil: ir: 3220 (s, br) 3060 (m, br), 1660(w), 1285(w), 1130(m), 940(s), and 918(s) cm^{-1}; nmr τ: 3.49 (m, D_2O exchangeable), 6.02 (br d, J = 5 Hz, H_a), 6.98 (dd, J = 9.5 and 4 Hz, H_b), 7.40 (s, N—CH_3), 7.4–7.9 (unresolved, 5H), and 8.30 (m, $W_{1/2}$ = 5.5 Hz, 7H); ms *m/e*: 180 (M^+, 15), 164(24), 163(100), 162(28), 108(24), 94(49), and 82(16). The nmr spectrum of oxime **10** in the presence of $Eu(DPM)_3$ shift reagent (29 mg) showed doublet at τ 6.08 (d, J = 9.5 Hz) which was originally part hidden at τ 7.5. The downfield shifts of H_a and N—CH_3 protons were much faster than others.

Elution with 5–8% methanol–CH_2Cl_2 gave a 1:1 mixture of *syn*-oxime **10** and *anti*-oxime **10** (80 mg, 8%). Crystallization from CH_2Cl_2 gave *anti*-oxime **8** (20 mg); mp 153–154°C; ir: 3180(w), 3060(w), 1600(w), 1210, 1138, 965(s), 920(s), 868, 770, and 720 cm^{-1}; nmr τ: 6.25 (t, J = 6.5 Hz, H_e), 6.72 (dd, J = 11 and 4.5 Hz, H_b), 6.87 (d, J = 4.5 Hz, H_a), 7.40 (part of H_e doublet), 7.50 (s, N—CH_3), 7.70 (m, 3H), and 8.33 (m, 5H); ms *m/e*: 181(7), 180.1249 (M^+, 42, calcd. for $C_{10}H_{16}N_2O$: 180.1263), 179(4), 164(54), 163(100), 162(39), 108(40), 94(55), and 82(22). Irradiation at τ 7.75 resulted in collapse of the double doublet pattern at τ 6.72 (H_b) to a doublet (J = 11 Hz) and the coalescence of the doublet at τ 6.87 (H_a). Irradiation at τ 8.3 collapsed the triplet at τ 6.25 (H_e) to a singlet.

Finally, elution of the silica gel column with 20% methanol–CH_2Cl_2 gave an unidentified olefinic fraction (50 mg); ir: 3040(m) and 750(s) cm^{-1}; nmr τ: 3.66(m).

The semisolid, isolated by continuous extraction, was re-

Can. J. Chem. Downloaded from www.nrcresearchpress.com by 210.87.254.6 on 09/05/12
For personal use only.

crystallized several times from ethanol – ethyl acetate to give the hydrochloride of *syn*-oxime **10**: mp 215–219°C; ir (Nujol): 3125(s), 3060(s), 2660(m), 2580(m), 2550(m), 1040(m), 990, 958(s), 945(s), 905(s), and 745 cm^{-1}; ms *m/e*: 180(s), 163(22), 108(88), 94(18), and 83(100). *Anal.* calcd. for $C_{10}H_{17}N_2OCl$: C 55.42, H 7.91, N 12.92; found: C 55.28, H 8.04, N 12.94.

This compound caused a green flame when subjected to the Beilstein test for halogens. The hydrochloride (600 mg) was dissolved in water, basified to pH 13–14 with aqueous NaOH, and extracted with CH_2Cl_2 (3 × 50 ml) to yield *syn*-oxime **10** (80 mg). Continuous extraction of the aqueous solution with CH_2Cl_2 recovered crystalline hydrochloride of **10** (300 mg).

Treatment of *syn*-oxime **10** (120 mg) with bisulfite gave a ketone (48 mg) containing some nitrile impurity; ir: 2220(w) and 1720(s) cm^{-1}. The bisulfite hydrolysis of a mixture of *syn*-oxime **7** and *anti*-oxime **8** gave the identical mixture which was chromatographed on neutral alumina with CH_2Cl_2 to give amino ketone **11**: ir: 1720(s), 1220, 1130, and 1100 cm^{-1}; nmr τ: 6.78 (dd, J = 9 and 4 Hz, H_b), 6.98 (d, J = 5 Hz, H_a), 7.40 (s, N—CH_3), 7.50 (m, 2H), 7.72 (m, 2H), and 8.12 (m, $W_{1/2}$ = 4.5 Hz, 5H); ms *m/e*: 165.1151 (M^+, 18, calcd. for $C_{10}H_{15}NO$: 165.1154), 137(100), 96(31), 95(47), 94(78), and 82(82).

Thermolysis of N-*Chloro-2*-endo-*methylaminomethylbicyclo*[*2.2.2*]*oct-5-ene* (**12**)

N-Chloramine **12** was prepared by stirring the corresponding amine (0.01 mol) in CH_2Cl_2 (50 ml) with a sodium hypochlorite solution (50 ml, Prefex Bleach®) at 0°C for 1 h. The CH_2Cl_2 solution was worked up to give a crude product: ir: 3040(m), 1615(w), 1180, 1170(m), and 710(s) cm^{-1}; nmr τ: 3.75 (m, 2H), 7.05 (m, 2H), 7.10 (s, 2H), 7.45 (m, 3H), and 8.0–9.2 (m, 7H); uv (methanol): 277 nm (ε, 315). The sample contained >95% of positive chlorine as determined by iodimetric titration.

A solution of a crude chloramine **12** (1.68 g, 0.009 mol) in methanol (150 ml) was refluxed for 10.75 h. Iodimetric titrations showed that the positive chlorine decreased <5% during the first hour and 90% in the following 8 h. The methanol was evaporated and the residue was portioned into neutral (76 mg) and basic fractions (1.07 g). The basic fraction was shown by gc–ms (20% SE30, 155°C) to contain several minor and one major component: peak 1 (2.5%, 5.8 min) had ms fragments at *m/e* 149(25) and 70(100); peak 2 (6.5%, 6.9 min) had the same ms fragmentation pattern as that of authentic amine **2**; peak 3 (5.5%, 10.0 min) had ms fragments at *m/e* 146(57), 145(43), and 44(100); and peak 4 (59%, 11.1 min) had ms fragments at *m/e* 181(28), 167(19), 166(100), 96(20), 95(20), 94(29), and 82(35). The major component of this basic fraction (peak 4) was isolated by preparative scale gc (20% SE30, 135°C) to afford methoxy amine **14**: ir: 2765(m), 1225, 1095(s), 1020, 965, and 830 cm^{-1}; nmr τ: 6.65 (s, OCH_3), 6.71 (d, J = 4.5 Hz, H_d), 7.32 (dd, J = 9 and 4.5 Hz, H_b), 7.49 (s, N—CH_3), 7.65 (high-field portion of H_c doublet), and 7.8–9.0 (unresolved, 11H); ^{13}C nmr in benzene: 84.4(d), 67.3(d), 64.6(t), 55.9(q), 42.0(q), 35.6(d), 34.6(d), 32.8(t), 26.7(d), 19.5(t), and 17.7(t) ppm; ms: the pattern same as that of the peak 4 above. When the proton nmr spectrum was recorded in the presence of $Eu(fod)_3$ shift reagent a signal at τ 5.38, attributed to H_a originally at approximately τ 7.5, began to emerge from beneath the *N*-methyl signal. A doublet originally at τ 7.58 (J = 9 Hz, H_c) was clearly resolved in the presence of shift reagent. The picrate methoxyamine **14** was recrystallized three times from ethanol as yellow needles: mp 171–171.5°C. *Anal.* calcd. for $C_{17}H_{22}N_4O_8$: C 49.76, H 5.40, N 13.65; found: C 49.77, H 5.38, N 13.80.

A solution of *N*-chloramine **12** (2 g, 0.011 mol) in 60% aqueous dioxane was refluxed in the dark for 1.25 h until iodimetric titration showed the major part of **12** had disappeared. The solvent was evaporated and the acidic residue was worked up in the usual manner to give basic extract (1.14 g), a portion (1 g) of which was chromatographed on silica gel using methanol – ethyl acetate as eluent to give three main fractions. The second fraction eluted with 1–10% methanol in ethyl acetate was the starting amine (164 mg). The third fraction eluted with 50% methanol gave the tricyclic amino alcohol **13** (260 mg, 12%). Alcohol **13** was oxidized with a Jones' reagent to give ketone **11** which showed the identical ir, nmr, and mass spectra with those obtained above.

The first fraction (146 mg) eluted with ethyl acetate was rechromatographed to give a colorless oil which was contaminated with a small amount of the starting amine as shown by vpc and gave the following spectra data: ir: 1670(w), 1110(m), 852, 730, and 695 cm^{-1}; nmr τ: 3.75(m), 5.97 (d, J = 6.5 Hz, 1H), 6.35(m), 7.22 (d, J = 8 Hz, 1H), 7.45 (s, 3H), 7.60 (dd, J = 8 and 3 Hz, 1H), 8.0 (m, 2H), and 8.39 (m, 9H); gc–ms *m/e*: 187(10), 186(5), 185 (M^+, 31), 184(5), 150(66), 95(26), 94(100), and 82(49). The picrate of this compound decomposed on attempted recrystallization. The structure was not identified.

Acknowledgements

The authors are grateful to the National Research Council of Canada for financial support and for an NRCC Scholarship (to R.W.L). We would like to thank Professor P. Deslongchamps for a stimulating discussion.

1. R. W. Lockhart, K. Hanaya, F. W. B. Einstein, and Y. L. Chow. J. Chem. Soc. Chem. Commun. 344 (1975).
2. R. A. Perry, S. C. Chen, B. C. Menon, K. Hanaya, and Y. L. Chow. Can. J. Chem. **54**, 2385 (1976).
3. R. W. Lockhart, R. A. Perry, M. Kitadani, and Y. L. Chow. Can. J. Chem. This issue.
4. Y. L. Chow, S. C. Chen, and D. W. L. Chang. Can. J. Chem. **48**, 157 (1970); Y. L. Chow, C. J. Colon, and S. C. Chen. J. Org. Chem. **32**, 2109 (1967).
5. H. Pracejus, M. Kehlen, H. Kehlen, and H. Matschiner. Tetrahedron, **21**, 2257 (1965); W. J. Genller, C. D. Gatsonis, and Q. A. Ahmed. J. Org. Chem. **33**, 2968 (1968); J. W. Huffman, T. Kamiya, and C. B. C. Rao. J. Org. Chem. **32**, 700 (1967).
6. A. M. Duffield, H. Budzikiewicz, and C. Djerassi. J. Am. Chem. Soc. **87**, 2926 (1965).
7. K. S. Pillay, S. C. Chen, T. Mojelsky, and Y. L. Chow. Can. J. Chem. **53**, 3014 (1975).
8. Y. L. Chow and C. J. Colon. J. Org. Chem. **33**, 2958 (1968).
9. W. L. Lockhart. Ph.D. Dissertation. Simon Fraser University, Burnaby, B.C. 1976.
10. W. C. Hamilton and J. A. Ibers. Hydrogen bonding in solids. W. A. Benjamin, Inc., Toronto, Ont. 1968. p. 14; O. Kennard. Molecular structures and dimensions. Vol. A1, Crystallographic Data Center, Cambridge. 1972.
11. P. G. Gassman and J. Digos. J. Am. Chem. Soc. **90**, 2716 (1968).

12. O. E. EDWARDS, G. BERNATH, J. DIXON, J. M. PATON, and D. VOCELLO. Can. J. Chem. **52**, 2123 (1974); O. E. EDWARDS, D. VOCELLO, and J. W. APSIMON. Can. J. Chem. **50**, 1167 (1972).
13. (*a*) R. TADAYONI, J. LACRAMPE, A. HEUMANN, R. FURSTOSS, and B. WAEGELL. Tetrahedron Lett. 735 (1975); (*b*) R. FURSTOSS, R. TADAYONI, and B. WAEGELL. Nouv. J. Chim. **1**, 167 (1977).
14. R. FURSTOSS, R. TADAYONI, and B. WAEGELL. J. Org. Chem. **42**, 2844 (1977).
15. K. HEUSLER. Tetrahedron Lett. 97 (1970).
16. N. C. DENO. Methods Free-Radical Chem. **3**, 135 (1972).
17. R. S. NEALE and M. R. WALSH. J. Am. Chem. Soc. **87**, 1255 (1965).
18. D. DVORNIK and O. E. EDWARDS. Tetrahedron, **14**, 54 (1961).
19. P. DESLONGCHAMPS. Tetrahedron, **31**, 2463 (1976).
20. K. ALDER and E. WINDEMUTH. Ber. **71**, 373 (1938).
21. W. R. BOEHME, E. SCHIPPER, W. G. SCHARPF, and J. NICHOLS. J. Am. Chem. Soc. **80**, 5488 (1958).
22. S. H. PINES, J. M. CHEMERDA, and M. A. KOZLOWSKI. J. Org. Chem. **31**, 3446 (1966).

Downloaded from www.nrcresearchpress.com by 210.87.254.6 on 09/05/12
For personal use only.

Syntheses of azapolycyclic compounds by aminium radical routes: trapping of the radical intermediates[1]

RICHARD A. PERRY, ROBERT W. LOCKHART,[2] MASAYUKI KITADANI,[3] AND YUAN L. CHOW

Department of Chemistry, Simon Fraser University, Burnaby, B.C., Canada V5A 1S6

Received March 27, 1978

RICHARD A. PERRY, ROBERT W. LOCKHART, MASAYUKI KITADANI, and YUAN L. CHOW. Can. J. Chem. **56**, 2906 (1978).

Photolysis of three alkenyl nitrosamines in the presence of oxygen or bromotrichloromethane resulted in the interception of the intermediate *C*-radicals by these radical trapping agents and the reaction pathways were cleanly diverted leading to the formation of the nitrate esters or halides with pyrrolidine rings as the primary products. The *exo*-nitrates in the oxidative photolyses decomposed by secondary ionic pathways; these reactions were hydrolysis, nitrous acid elimination and a cleavage reaction (promoted by a β-amino group), among others. The efficiency of the cleavage reaction is controlled by a stereoelectronic factor that requires the participating bonds and the lone-pair nitrogen orbital be oriented in an antiperiplanar conformation. When such a conformation exists in a rigid or semiflexible framework, cleavage occurs extensively. However, in freely rotating acyclic systems, cleavage does not occur even when the required conformation can be attained. Only halides resistant to intramolecular nucleophilic displacement to form the aziridinium intermediates were isolated in the bromotrichloromethane trapping experiments. Other *exo*-halides underwent solvolysis via aziridinium ion intermediates.

RICHARD A. PERRY, ROBERT W. LOCKHART, MASAYUKI KITADANI et YUAN L. CHOW. Can. J. Chem. **56**, 2906 (1978).

La photolyse de trois alkénylnitrosamines en présence d'oxygène ou de bromotrichlorométhane a donné lieu à l'interception des *C*-radicaux intermédiaires par ces pièges à radicaux et les chemins réactionnels ont été nettement déviés vers la formation d'esters nitrates ou d'halogénures avec des noyaux pyrrolidines comme produits primaires. Les nitrates *exo* en photolyse oxydante se décomposaient par voies ioniques secondaires; ces réactions étaient, entre autres, l'hydrolyse, l'élimination d'acide nitreux ou une réaction de clivage (favorisée par un groupe β-amino). L'efficacité de la réaction de clivage est sous le contrôle d'un facteur stéréoélectronique exigeant que les liaisons participantes et l'orbitale de l'azote renfermant la paire libre se trouvent dans des conformations antipériplanaires. Quand une telle conformation existe dans une structure rigide ou semiflexible, le clivage se produit bien. Cependant, dans les systèmes acycliques en rotation libre, le clivage ne se produit pas, même quand les conformations exigées peuvent exister. Les seuls halogénures isolés ont été ceux qui possèdent une barrière d'énergie élevée pour le déplacement nucléophilique intramoléculaire menant aux intermédiaires aziridinium. Les autres halogénures *exo* ont subi une solvolyse passant par l'intermédiaire de l'ion aziridinium.

[Traduit par le journal]

Introduction

As shown in the preceding report (2), applications of the intramolecular photoaddition of the alkenyl nitrosamines in the synthesis of azatricyclic compounds may be complicated by the ring-opening reaction promoted by a β-ammonium group partly due to cumulative ring strain. Since photoreaction occurs by a stepwise radical addition (3, 4), it is envisaged that the *C*-radical intermediate **B** might be intercepted by a suitable radical trapping reagent so that a stable and isolable azapolycyclic derivative could be obtained.

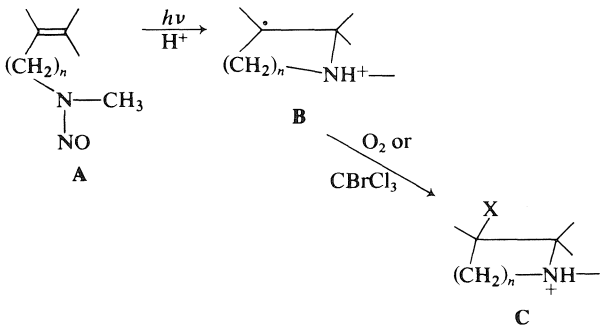

Efficient interception of a *C*-radical intermediate by oxygen in intermolecular photoadditions of nitrosamines (4–7), nitroamines,[4] and tetrazenes (8)

[1]Some of these results have been published in a preliminary communication; see ref. 1.

[2]NRCC Scholarship holder 1973–1976.

[3]On study leave from College of General Education, Kobe University, Kobe, Japan.

[4]Y. L. Chow, H. Richard, and R. W. Snyder. Unpublished results.

Can. J. Chem. Downloaded from www.nrcresearchpress.com by 210.87.254.42 on 09/05/12
For personal use only.

Can. J. Chem. Downloaded from www.nrcresearchpress.com by 210.87.254.42 on 09/05/12
For personal use only.

to olefins has been demonstrated: in the oxidative photoaddition of nitrosamine the mechanism has been assumed to follow [1]–[3] to give nitrate esters (7). The key step is the fast conversion of a *C*-radical to a peroxy radical (eq. [1]); the latter is much less reactive than the former. A peroxynitrite, the primary product in the present case, has recently been shown to rearrange spontaneously to the nitrate ester (eq. [3]) (9), although other decomposition pathways, such as elimination of HNO_2 to form a carbonyl compound, might also occur under the reaction conditions.

[1] $$R^{\bullet} + O_2 \rightarrow R{-}O{-}O$$

[2] $$R{-}O{-}O^{\bullet} + {}^{\bullet}NO \rightarrow R{-}O{-}O{-}NO$$

[3] $$R{-}O{-}O{-}NO \rightarrow R{-}O{-}NO_2$$

A good radical trapping agent in the present case should react sluggishly with electrophilic aminium radicals but vigorously with nucleophilic alkyl radicals. As well as oxygen, shown above, bromotrichloromethane is expected to fill the requirements since it has been shown to be a good bromine atom donor to alkyl radicals (10–14). Furthermore, owing to its polarity, its reaction with aminium radicals may not occur readily. This compound has been used in radical-initiated additions to olefins (15, 16) and brominations of alkyl groups (11–13) in which, under certain conditions (10), the chain carrier is the trichloromethyl radical. In the intramolecular nitrosamine photoaddition sequence, bromotrichloromethane may participate by the following mechanism (eqs. [4]–[5]) to give bromo derivatives and nitrosotrichloromethane as the products. As the trichloromethyl radical possesses electrophilic character, it is not expected to react with a proton-associated nitrosamine to regenerate an aminium radical as in [6].

[4] $$R^{\bullet} + BrCCl_3 \rightarrow RBr + {}^{\bullet}CCl_3$$

[5] $$^{\bullet}CCl_3 + {}^{\bullet}NO \rightarrow ONCCl_3$$

[6] $$^{\bullet}CCl_3 + R_2N{-}NO{-}{-}{-}H^+ \nrightarrow NOCCl_3 + R_2NH^{\ddagger}$$

On the basis of these assumptions, photolyses of some alkenyl nitrosamines possessing a double bond at the C_4—C_5 position were carried out in the presence of oxygen or of bromotrichloromethane.

Results

Trapping experiments with *C*-radical intermediates were first done using previously prepared (17) alkenyl nitrosamine **1** as a model compound. Photolysis, under oxygen, of a methanol solution of **1** in the presence of hydrochloric acid gave *endo*-nitrate **3** (15%), amino ketone **7** (31%), and *exo*-alcohol **4** (20%); the latter two were decomposition products of the primary products, the nitrates (or the pernitrite). Missing in the crude product was *exo*-nitrate **5** which was prepared from *exo*-alcohol **4** and was found to decompose readily on storage to give ketone **7**; decomposition was even faster in basic solution. In contrast, *endo*-nitrate decomposed to ketone **7** only in a sodium hydroxide solution but was stable on storage. Reduction of the crude product with lithium aluminium hydride followed by Jones' oxidation gave ketone **7** in 55% overall yield; the low yield was attributed to the volatility of alcohols **2** and **4** (*vide infra*) and poor yields from the Jones' oxidation. In a photolysis reaction carried out in the presence of perchloric acid, we failed to obtain salts of the amine nitrates by crystallization. This attempt also showed that the nitrate esters decomposed extensively during acid–base treatments of the crude products. A small amount of *endo*-alcohol **2** was also isolated in this reaction.

Both *exo*-alcohol **4** and *endo*-alcohol **2**, particularly the latter, codistilled with the solvents during evaporation and were oxidized readily to previously identified ketone **7** (17). The remarkable volatility of

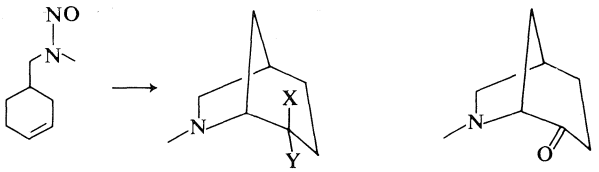

1 **2** X = H; Y = OH; **3** X = H; Y = ONO_2; **4** X = OH; Y = H; **5** X = ONO_2; Y = H; **6** X = H; Y = Br; **7**

endo-alcohol **2** might arise from the *cis* orientation of the proximate functional groups facilitating intramolecular hydrogen bonding; such peculiar properties have been noticed by others (18) in azabicyclic alcohols. The *endo*-nitrate **3** showed the typical ir absorptions for nitrate at 1620, 1275, and 860 cm^{-1} and an nmr signal at τ 5.25 for the axial proton of C*H*—ONO_2. This compound was reduced with lithium aluminium hydride to *endo*-alcohol **2**.

Photolysis of nitrosamine **1** in a mixture of methanol–bromotrichloromethane (25%) containing hydrochloric acid gave rise to a blue solution. The compound showing the blue color (λ_{max} 580 nm) codistilled with the solvents and was assumed to be trichloronitrosomethane monomer (19), by analogy to the assignment made in nitrite photolysis in the presence of this trapping agent (20). The neutral fraction contained a major product having the molecular formula Cl_2CNOH as shown by gc–ms analysis; this species was believed to be phosgene oxime derived from trichloronitrosomethane. The

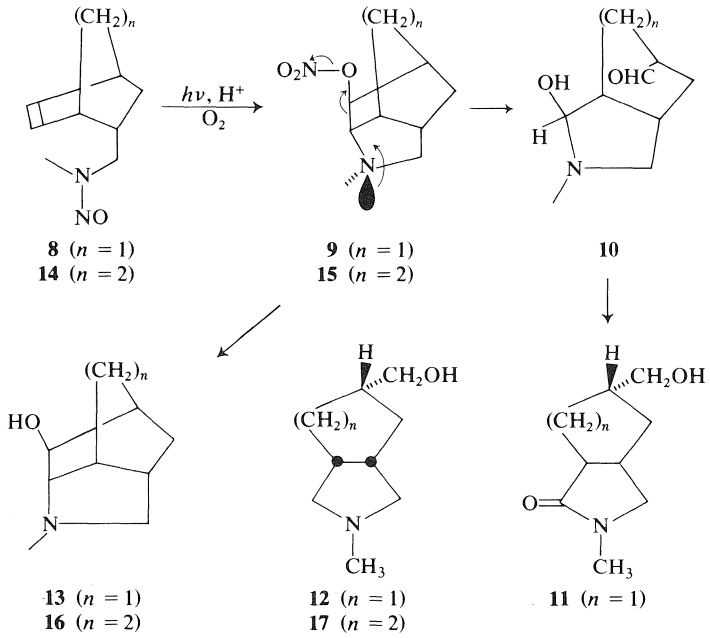

basic fraction was almost pure *endo*-bromide **6** (55%) and exhibited the axial C*H*—Br proton at τ 5.98 as a double doublet of a doublet. The corresponding *exo*-bromide was not obtained in spite of careful searching. These radical-trapping experiments demonstrate that the expected products were formed in the photolysis, as outlined above, but that some of them might have decomposed by secondary pathways.

Photolysis, under oxygen, of *N*-nitroso-2-*endo*-methylaminomethylbicyclo[2.2.1]hept-5-ene (**8**) (2), containing ca. 30% of the corresponding *exo*-isomer, gave a basic fraction exhibiting strong ir absorptions for nitrate at 1620 and 1275 cm^{-1} and for carbonyl at 1720 cm^{-1}; an aldehyde proton nmr signal at τ 0.25 was also observed. Since the basic fraction decomposed gradually, freshly obtained crude product was reduced with lithium aluminium hydride to afford tricyclic alcohol **13** (12%), the known bicyclic alcohol **12** (40%), and some unknown olefinic amines. The OH group in **13** was assumed to be in the *exo*-orientation from the narrow nmr signal at τ 5.90 for the C*H*OH proton which should couple weakly to the vicinal protons (6). Continuous extraction of the aqueous phase of the reduction mixture afforded lactam **11** (2). This indicates that ring scission has occurred, as in **9** → **10**, and is similar to what is observed in the oxidative photoaddition of *N*-nitrosamine to norbornene (6), as well as in the intramolecular redox reaction **10** → **11** (2). It is likely that under strongly basic LAH reduction conditions, aldehyde **10** is rapidly transformed to lactam **11** which is reduced further to **12**. However, direct reduction of **10** → **12** cannot be entirely discounted.

In view of the observed extensive decomposition described above, the crude basic products from the oxidative photolysis of *N*-nitroso-2-*endo*-methylaminomethylbicyclo[2.2.2]oct-5-ene (**14**) were immediately LAH reduced to give tricyclic alcohol **16** (13%) and a compound tentatively assigned as bicyclic alcohol **17** (13%), in addition to some unknown olefinic amines. Alcohol **16** was oxidized to the corresponding ketone which has been synthesized previously (2); the *endo*-orientation of the C*H*OH proton was inferred from the similarity of the coupling pattern to that of the methoxy derivative, the stereochemical structure of which has been determined by X-ray crystallography (2).

Bicyclic alcohol **17** is a homologue of **12** and is believed to be formed by cleavage and redox pathways analogous to those of **9** → **10** → **11** → **12**. However, in the present case the lactam corresponding to **11** was not isolated and a redox process similar to **10** → **11** has not been substantiated. The nmr multiplet at τ 6.50 was attributed to the magnetically nonequivalent CH_2OH protons and that at τ 7.0–7.7 overlapping with the *N*—CH_3 singlet (τ 7.62) was due to the four CH_2—N protons. Although these and the ir data are in agreement with **17** they are not unambiguous proof of the structure.

Photolysis, under nitrogen, of nitrosamine **8** in a heterogeneous mixture of trichlorobromomethane and hydrochloric acid produced the typical blue color and gave a basic fraction which showed a major and minor product on tlc analysis. The nmr spectrum was essentially that of bromoamine **18** with weak signals due to chloroamine **19**. Both compounds **18** and **19** were isolated as oils by chroma-

Can. J. Chem. Downloaded from www.nrcresearchpress.com by 210.87.254.42 on 09/05/12
For personal use only.

Can. J. Chem. Downloaded from www.nrcresearchpress.com by 210.87.254.42 on 09/05/12
For personal use only.

tography but attempts to purify them by preparation of derivatives and/or by distillation caused extensive decomposition. Both **18** and **19** exhibited the strong high resolution ms M^+ peaks corresponding to their molecular formulae and narrow nmr signals at τ 6.15 and 6.25 for the *endo*-protons of the C*H*—X group, in agreement with the corresponding signal for the alcohol **13**. Furthermore, the spectra[5] of **19** were identical with those of the chloro compound obtained from the Ag_2O-catalysed decomposition of *N*-chloramine.

A similar photolysis of nitrosamine **14** in the presence of trichlorobromomethane, followed by the usual basic work-up in aqueous solution, however, gave a low yield of the basic fraction. Analysis by gc–ms showed that the major products were the parent alkenylamine and bromine-containing amines, in addition to some olefinic amine. The amine fraction containing bromine, however, decomposed rapidly during work up. The crude product obtained after evaporation of solvent was examined by nmr in trifluoroacetic acid. That the expected product of bromoamine **20** was formed in a relatively good yield in this acidic photolysis was indicated by the fairly clean nmr spectrum, and a narrow signal at $\tau \sim 5.6$ for the C*H*Br proton. The reaction of this residue with sodium methoxide in methanol, however, gave a low yield of basic fraction which contained methoxy amine **21** (ca 20% yield) as the major product and a number of minor components as shown by a complex vpc spectrum.

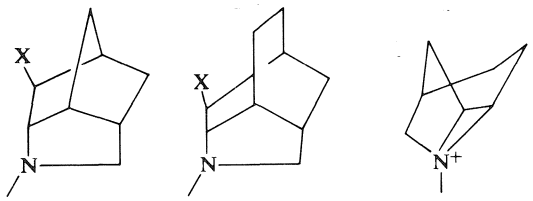

18 X = Br
19 X = Cl

20 X = Br
21 X = OCH_3

22

The substituted azatricyclic compounds **13**, **16**, **18**, **19**, and **21** exhibited nmr signals for the protons vicinal to the nitrogen in the expected range of ca. τ 7.0; a nicely resolved 250 MHz nmr spectrum of **21** has been published by Waegell and co-workers (21). The methine protons of all these compounds were observed as doublets with weak couplings ($J = 4 \sim 4.5$ Hz). The magnetically nonequivalent methylene protons appeared as doublets and double doublets with geminal coupling constants of $8 \sim 10.5$ Hz. However, the chemical shifts of the corresponding protons in these compounds varied considerably depending on the nature of the substituent groups. Correlations of the coupling patterns with structural assignments by application of the Karplus relation were frustrated by the unknown anisotropic factors of the substituents.

The addition of iodine as a radical-trapping agent in the photolysis of **1** was not successful owing to the internal filter effect of iodine which has an intense absorption at ca. 350 nm. Additions of carbon tetrachloride and tributyltin hydride as trapping agents also gave unsatisfactory results.

Discussion

In the photolysis of alkenylnitrosamines in acidic solution, the corresponding aminium radicals cyclize exclusively to form the *C*-radicals with a pyrrolidine ring, presumably owing to better overlapping of the reacting orbitals. This propensity to five-membered ring formation has been well established not only in nitrosamine cyclizations (2, 17) but also in *N*-chloramine cyclizations under acidic conditions (18, 22); only one exception has been reported so far (23). The *C*-radicals are trapped by oxygen or bromotrichloromethane according to the sequence outlined in the Introduction to give the nitrates and bromides. As this is a stepwise radical reaction, both *endo* (*cis*)- and *exo*(*trans*)-isomers of the nitrate and bromide are expected to be formed in photocyclization of nitrosamine **1**. The latter formation is probably favored in view of predominate *trans*-addition of nitrosamines to cyclohexene derivatives under acidic conditions (25). Edwards *et al.* (24) have reported that the thermolysis of *N*-chloro-*N*-methyl-3-cyclohexenylmethylamine (**1**, NO = Cl) in methanol gives both *exo*- and *endo*-chloro derivatives from the five-membered cyclization (i.e., **3**, X = H, Y = Cl; and **5**, Y = Cl, X = H) as the primary products by the amino radical route; the former is believed to rearrange via the aziridinium ion (**22**) (25–27) to give the *exo*-methoxy derivatives with bicyclo[2.2.1] (**3**, X = H, Y = OCH_3) as well as bicyclo[2.2.2] skeletons; the yield of the latter is slightly higher. In the present case, failure to isolate *exo*-nitrate **5** and the *exo*-bromide (**5**, ONO_2 = Br) indicates that these compounds also rearrange via aziridinium intermediate **22** by a mechanism similar to that suggested by Edwards *et al.* (24). The *exo*-bromide from the $CBrCl_3$ trapping experiment may have decomposed extensively during the rearrangement on neutralization with an aqueous sodium carbonate solution. A similar rearrangement (24) of *exo*-nitrate **5** is expected to give **4** and the corresponding amino alcohol with the bicyclo[2.2.2] skeleton when carried out under basic conditions; the latter has not been detected, presumably owing to its solubility in water. Although eliminations of HNO_2 from these types of nitrate esters to form ketones are known (6), the

[5]The authors are grateful to Professor B. Waegell who has compared our spectra with his.

Can. J. Chem. Downloaded from www.nrcresearchpress.com by 210.87.254.42 on 09/05/12
For personal use only.

decomposition of **5** to form ketone **7** might be particularly enhanced by the orientation of the functional group. It is suspected that the proximate amino lone-pair electrons act as the receptor for the departing proton. Although the results are in general agreement with the predictions, there are certain differences between the results observed in the present case and those of Edwards *et al.* (24); these differences could arise from a dissimilarity in the solvolytic conditions.

The isolation of tricyclic haloamines **18** and **19** following photolysis of nitrosamine **8** in the presence of bromotrichloromethane is a useful alternative method of building this tricyclic skeleton because of the facile cleavage pathways in the photolysis under nitrogen and oxygen. While excessive heating of these haloamines causes decomposition, their rigid framework prevents aziridinium ion (**23**, $n = 1$) formation, even though the halo and amino groups are oriented in an *anti*-configuration. By analogy to the acidic photolysis of nitrosamines described in this and the preceding paper, the stable protonated bromoamine **20** was probably formed in good yield, judging from the fairly clean nmr spectrum of the crude residues remaining after evaporation of the photolysates. Neutralization with aqueous sodium carbonate causes extensive rearrangement giving a mixture in low yield. The instability of bromoamine **20**, in contrast to **18** and **19**, might arise from the ease of formation of aziridinium ion **23** ($n = 2$) since the bicyclo[2.2.2] system is relatively flexible. It is envisaged that aziridinium intermediate **23** ($n = 2$), if intercepted by a strong nucleophile such as methoxide anion, might open up to the strain-free azatwistane skeleton **24** ($n = 2$, X = OCH_3) which might be less susceptible to solvolysis (2). As discussed previously (2), the opening of aziridinium ion

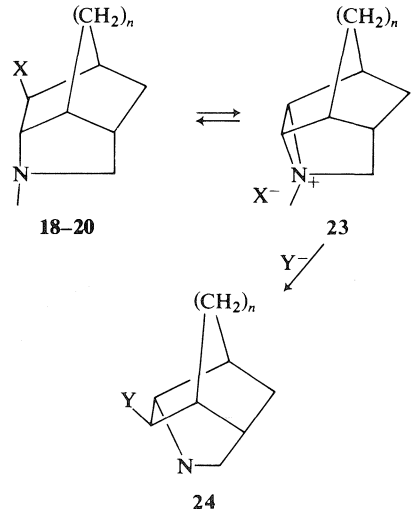

23 ($n = 2$) by methoxide ion is not expected to favor the formation of **21** owing to steric reasons. The low yield of **21** in the solvolysis of **20** is in agreement with this assumption. However, as the major part of the remaining material decomposed to a complex mixture, it might be suspected that methoxy azatwistane **24** (X = OCH_3, $n = 2$) and allied compounds, if formed at all, are susceptible to solvolytic rearrangement under the isolation conditions. Alternatively,[6] it might be speculated that the transition state of a nucleophilic attack on **23** ($n = 2$) shifts (or tunnels) to other energy surfaces before collapsing to **24**. Derivatives of another type of azatwistane have been shown to rearrange readily on solvolysis (19).

The nitrate esters obtained from the oxidative photoreactions of **8** and **14** may have the *exo*-orientation exclusively, since the *endo*-approach of a trapping agent is considerably hindered. The alcohols isolated after LAH reduction in both cases contain only the *exo*-isomers **13** and **16** although the yields are low. The low yields are due to the facile amino-group-assisted cleavage reaction of the nitrates **9** and **15** to give the bicyclic aldehydes **10**, which occurs in the free bases but not in the protonated forms as in the nitrosamine cleavage reaction (2). This reaction is another case of a stereoelectronically assisted rearrangement, the general principles of which have been described by Deslongchamps (29).

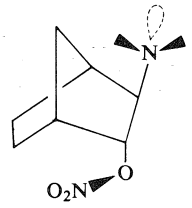

25

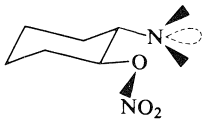

26

In the *exo*-nitrates **9** and **15**, the antiperiplanar orientation of the lone-pair electron orbital of the amine center and the departing NO_2 moiety, with respect to the cleaving C—C bond, satisfies nicely the stereoelectronic requirements for the rearrangement. The photoaddition of *N*-nitrosodimethylamine to norbornane and cyclohexene in the presence of oxygen (6), yields 2-*exo*-dimethylamino-3-*endo*-nitratonorbornene (**25**) and *trans*-1-dimethylamino-2-nitratocyclohexane (**26**), respectively; we have shown that the same cleavage reaction under basic conditions occurs more extensively with the former than

[6]We acknowledge, with appreciation, a referee's suggestion that, in the transition state of the opening of the aziridinium ring, a nucleophile would select *the weaker* bond giving **21** rather than **24** owing to the unsymmetrical nature of the aziridinium ion **23** ($n = 2$). On inspecting the Dreiding Models, it is uncertain which N—C bond is weaker since the bicyclo[2.2.2] system is semiflexible.

Can. J. Chem. Downloaded from www.nrcresearchpress.com by 210.87.254.42 on 09/05/12
For personal use only.

the latter and is facilitated by a *trans* orientation of the functional groups. Again, the antiperiplanar orientation of the relevant electron pairs and bonds in a rigid and a semiflexible framework fulfills the stereoelectronic requirement for ejection of the nitrite group.

For acyclic 1-dimethylamino-2-nitratohexane, obtained from acidic photoaddition, under oxygen,[4] no such cleavage reaction is observed although the functional groups can rotate freely about the relevant bonds to assume an antiperiplanar conformation. It might be concluded that the observed amino-group-assisted cleavage reaction occurs more easily when the nitrogen lone-pair orbital is in the antiperiplanar conformation with respect to the relevant bonds and is held in a rigid framework. Obviously the rigidity decreases in the order **9** > **15** > **25** > **26** and the extent of cleavage also decreases qualitatively in the same order.

Experimental

The general experimental conditions are the same as those described in the preceding paper (2).

N-*Nitroso*-N-*methyl-3-cyclohex-1-ylmethylamine* (**1**) *Under* O_2

(*a*) Nitrosamine **1** (1 g, 6 mmol) (17) in methanol (225 ml) containing concentrated HCl (0.6 ml) was photolyzed for 3.5 h while oxygen gas was bubbled through the solution. The uv spectra showed no *C*-nitroso peak at ca. 290 nm. Following the normal work-up procedure (6, 7), the photolysate was evaporated and the residue was taken up and washed with ether to afford neutral fractions. The aqueous layer was made basic with Na_2CO_3 solution and was extracted with CH_2Cl_2. This gave unreacted nitrosamine (0.18 g) in the acidic fraction and basic material (0.64 g). The remaining basic aqueous solution was continuously extracted with ether to afford only a small amount (< 10 mg) of material.

A portion of the basic material (0.42 g) was chromatographed on basic alumina (50 g) and elution with 1% MeOH–CH_2Cl_2 gave *endo*-nitrate **3** (0.07 g): ir: 2940, 2860, 2790, 1620, 1450, 1275, 860; nmr τ: 5.25 (ddd, J = 10, 6, and 2 Hz, 1H), 6.80 (bd, J = 6.5 Hz, 1H), 7.0–7.6 (m, 2H), 7.53 (s, 3H), 7.6–8.8 (m, 7H); ms (75°C) *m/e* (%): 186 (M^+, 0), 140 (14), 138 (14), 124 (7), 96 (21), 82 (100), 58 (43), 55 (29), 42 (57), 41 (59). The next three fractions (0.18 g), eluted with 1–3% MeOH–CH_2Cl_2, contained aminoketone **7**, with a minor amount of nitrate **3**. Eluted with 10–50% MeOH in CH_2Cl_2 was *exo*-alcohol **4**: 0.1 g; ir: 3350 (b), 2940, 2860, 2790, 1450, 1005; nmr τ: 6.10 (bt, J = 5 Hz, 1H), 6.5 (s, D_2O exchangeable), 6.9–7.4 (m, 3H), 7.50 (s, 3H), 7.51–8.7 (m, 7H); ms 141 (M^+, 18), 96 (15), 82 (100), 42 (15). Jones' oxidation of *exo*-alcohol **4** gave ketone **7** (53%), which was identical with the previously prepared sample (17). The yields after chromatography, based on reacted nitrosamine (0.82 g), were *endo*-nitrate **3**, 15%; ketone **7**, 31%; and *exo*-alcohol **4**, 20%. The yields, estimated from the nmr spectrum of the crude basic fraction, were 15, 35, and 45%, respectively.

The ir absorption (1620 cm^{-1}) of *endo*-nitrate **3** was not significantly decreased relative to that (1720 cm^{-1}) of ketone **7** when a mixture (1:1.6 ratio) was examined either after storage for 2 months (25°C) or after being stirred with 0.5 *N* HCl for 21 h at 25°C. Treatment with 0.7 *N* NaOH aqueous solution for 21 h caused a decrease in the nitrate peak relative to the ketone peak (ir ratio 1:2.2). *endo*-Nitrate **3** was relatively stable in pyridine but decomposed more when treated with 5 *N* NaOH for 1.5 h to give a 1:3 ratio of the nitrate to ketone ir absorption intensities.

Reaction of *exo*-alcohol **2** for 0.75 h with concentrated HNO_3 (0.25 ml) in concentrated H_2SO_4 (0.6 ml), followed by basification and extraction, gave an impure nitrate: ir: 1720 (w), 1620, 1275, 860. The ratio of product ir peaks at 1715 and 1620 cm^{-1} was 1:1.2 after 20 h at 25°C and 3:1 after 2 months.

LAH (0.8 g) reduction of the basic fraction (0.21 g) in ether for 28 h at 25°C, followed by removal of the solvent through a Vigreaux column gave a mixture of *endo*- and *exo*-alcohols **2** and **4** in the ratio of 1:1.25 as shown by vpc analysis. A Jones' oxidation of this mixture (0.059 g) produced ketone **7** (0.032 g, 55%). LAH reduction of *endo*-nitrate **3** (0.05 g) gave *endo*-alcohol **2** (0.020 g) as the hydrochloride after continuous extraction with CH_2Cl_2.

(*b*) Nitrosamine **1** (3 g, 0.019 mol) in MeOH (220 ml) containing 70% $HClO_4$ (3 ml, 0.02 mol) was photolyzed for 4.5 h and the solvent was evaporated. All attempts to crystallize perchlorate salts from a variety of solvents failed.

The crude photolysate was basified, extracted with benzene, and was worked up in the usual manner to give a basic fraction (1.53 g). The aqueous phase was extracted with CH_2Cl_2 and worked up to give a mixture which was separated into ether soluble and CH_2Cl_2 soluble compounds. The ether soluble material (0.11 g) was found by gc (125°C) to contain 50% *endo*-alcohol **2** (12.4 min), 40% *exo*-alcohol **4** (13.5 min), and 10% of an unknown compound. The CH_2Cl_2 soluble fraction was shown to contain the HCl salt of *endo*-alcohol **2**: ir: 3500 (b), 3050 (b, m), 2950, 2880, 2005 (w), 1450, 1100 (b); nmr (D_2O) τ: 6.3 (m, 1H), 6.5–6.8 (m, 2H), 6.88 (s, 3H), 7.4–7.9 (m, 5H), 8.05–8.6 (m, 3H); ms (170°C): 141 (M^+, 28), 97 (26), 96 (37), 82 (100), 55 (11), 42 (26). Jones' oxidation of this salt gave ketone **7** (50%, *vide supra*).

The major basic fraction, obtained above, was chromatographed on neutral alumina (70 g). The fractions eluted with 1% MeOH in CH_2Cl_2 (0.49 g) contained *endo*-nitrate **3** as the major component. Continued elution with the same eluant gave a mixture (0.3 g) of nitrate **3** and ketone **7**. Using 2% MeOH–CH_2Cl_2, a mixture (0.16 g) of nitrate, ketone, and *exo*-alcohol **4** was obtained. The remaining fractions (0.5 g), eluted with 5–50% MeOH–CH_2Cl_2, contained *exo*-alcohol **4** (*vide supra*).

The total yields of the various products were 0.3 g of neutral products, 0.55 g of *endo*-nitrate **3** (15%), 0.3 g of ketone **7** (11%), 0.8 g of *exo*-alcohol **4** (29%), and 0.3 g of the hydrochloride salt of *endo*-alcohol **2** (9%).

Photolysis of **1** *in the Presence of* $BrCCl_3$

Nitrosamine **1** (0.95 g, 6 mmol) and concentrated HCl (1.7 ml) in a mixture of $BrCCl_3$ (42 ml, 100 g) and MeOH (170 ml) were photolyzed for 3 h to give greenish yellow solution. After removal of the solvent through a Vigreaux column, the residue was separated into acidic/neutral material (0.12 g) and basic material (0.69 g) using a Na_2CO_3 solution to make the solution basic in the usual fashion. Further, continuous extraction of the basic aqueous phase with ether yielded a small amount (< 15 mg) of an oil which was discarded. The distilled solvent had a light blue color (λ_{max} 580 nm) which disappeared after 2 weeks of refrigerated storage.

The basic residue contained one major component (> 98%, retention time 12.9 min) and a minor component (retention time 8.7 min) when examined by gc (135°C). The major product also showed one peak on programmed temperature gc and was distilled to give *endo*-bromoamine **6** (55%): ir: 2940, 2860, 2840, 2780, 1450, 765 (m); nmr τ: 5.98 (ddd, J = 9, 7.5,

Can. J. Chem. Downloaded from www.nrcresearchpress.com by 210.87.254.42 on 09/05/12
For personal use only.

and 1.5 Hz, 1H), 6.75–7.2 (m, 2H), 7.47 (s, 3H), 7.4–8.7 (m, 8H); ms: 205 (M^+, ^{81}Br, 22), 203.0304 (M^+, *calcd.* for $C_8H_{14}N^{79}Br$: 203.0310, 22), 124 (56), 82 (100), 42 (27).

The acidic/neutral fraction was shown to be composed of five principal components by gc analysis (120°C), with one being the major (64%) component (2.3 min): gc–ms analysis showed that the major peak could be phosgen oxime: 115 ($^{35,37}Cl$, 65), 113 ($^{35}Cl_2$, 87), 98 (11), 96 (15), 80 (46), 79 (35), 78 (100), 77 (74), 63 (11), 61 (30), 47 (13), 43 (22). The distilled blue solvent showed a peak which corresponded to a minor peak of the neutral fraction and was assumed to be that due to trichloronitrosomethane.

Photolysis of Nitrosamine ***8***

Under Oxygen

A solution of *N*-nitrosamine **8** (2 g, 0.011 mol) and concentrated HCl (1.0 ml, 0.06 *N*) in methanol (200 ml) was photolysed under oxygen for 3 h. The usual work-up gave a neutral fraction (130 mg); ir: 3350 (m, br), 3055 (w), 1715 (w), 1640 (m), 1550 (m) cm^{-1}; nmr τ: 0.20 (d, J = 2.5 Hz), 3.90 (m). The mother liquor was basified and extracted with CH_2Cl_2 (3 × 50 ml) which was dried and evaporated to a crude basic residue (1.8 g): ir: 3300 (w, br), 3060 (w), 1720 (m), 1670 (m), 1620 (s), 1275 (m), and 865 (m) cm^{-1}. After 24 h the ir band at 1720 cm^{-1} became stronger relative to the others.

In a similar experiment the basified mother liquor was extracted with ether (4 × 50 ml); the extracts were dried and immediately treated with LAH (2 g), and on work up gave a yellow oil (*A*, 1.2 g). The aqueous layer was further extracted with CH_2Cl_2 (3 × 50 ml) to give oil *B* (130 mg). Finally, the aqueous layer was continuously extracted with CH_2Cl_2 for 3 days to afford crude hydroxy lactam **11** (180 mg): ir: 3380 (s, br), 1655 (s), 1065, 1040, and 1020 (m) cm^{-1}; nmr τ: 6.45 (m, 3H) and 6.92 (dd, J = 10 and 1 Hz, 1H) (2).

Oil *A* (1.0 g) was chromatographed on neutral alumina (50 g). Elution with 0.4% methanol–CH_2Cl_2 gave a crude olefinic alcohol (110 mg): ir: 3380 (m), 3055 (m), 1660 (w), 1030 (m), 778, and 705 (s) cm^{-1}; ms *m/e*: 124 (8), 106 (6), and 66 (100); nmr τ: 3.93 (m, 2H), 6.40 (dd, J = 6 and 2 Hz, 1H), 7.05 (m, D_2O exchangeable), 7.22 (m, 3H), 7.75 (m, 3H), and 8.70 (m, 5H). Elution with 1% methanol–CH_2Cl_2 gave an unidentified mixture (200 mg). Elution with 2% methanol–CH_2Cl_2 gave an oil (267 mg, 30%) which was distilled at 25°C/0.5 Torr to give bicyclic amino alcohol **12**; the ir, nmr, and mass spectra were superimposable on those of an authentic sample (2). The picrate of **12** was recrystallized twice from ethanol to give yellow needles, mp and mp on admixture with an authentic sample (2) 138–139°C. Continued elution with 3–5% methanol–CH_2Cl_2 gave tricyclic amino alcohol **13** (216 mg, 12.5%): ir: 3350 (s, br), 1650 (w), 1130, 1040 (m), and 1015 (s) cm^{-1}; nmr τ: 6.31 (m, $W_{1/2}$ = 3.5 Hz, H_d), 7.05 (m, D_2O exchangeable), 7.27 (m, 3H), 7.50 (s, N—CH_3), 7.68 (m, 1H), 7.90 (m, 3H), 8.2–9.1 (m, 4H); ms *m/e*: 154 (4), 153 (M^+, 37), 152 (7), 136 (12), 124 (22), 96 (91), 95 (36), 94 (100), 82 (62), 57 (45); nmr (HCl salt) τ: 5.28 (m, D_2O exchangeable), 5.90 (m, $W_{1/2}$ = 3 Hz, H_d), 6.69 (d, J = 5 Hz, H_a), 6.72 (d, J = 10.5 Hz, H_c), 7.02 (dd, J = 10.5 and 5 Hz, H_b), 7.20 (s, N—CH). The picrate of **13** was recrystallized three times from ethanol, mp 185–187°C. *Anal.* calcd. for $C_{15}H_{18}N_4O_8$: C 47.12, H 4.76, N 14.65; found: C 46.84, H 4.66, N 14.55.

Basic extract *B* (95 mg) was reduced with LAH (2 g) in THF (200 ml) and was worked up and purified in the usual manner to give a crude amino alcohol **12** (46 mg, 55%).

In the Presence of Bromotrichloromethane

A mixture of nitrosamine **8** (1 g, 0.006 mol), concentrated HCl (0.55 ml), and $CBrCl_3$ (100 ml) was photolysed under N_2 for 2 h. The fluorescent blue mixture was removed under vacuum and the residue was separated into neutral (350 mg) and basic (666 mg) fractions. The neutral fraction exhibited no *N*-methyl signal in the nmr spectrum. The basic fraction exhibited only one major spot at R_f 0.37 and a faint spot at R_f 0.19 on a silica gel tlc plate (10% methanol–CH_2Cl_2); the nmr spectrum was essentially that of **18** (ca. 90%) with weak signals of **19**. Silicic acid chromatography (1% methanol–CH_2Cl_2) of this fraction (500 mg) afforded an oily bromo amine **18** (148 mg); ir: 1185, 1165 (s), 935 (s), and 6.90 (s) cm^{-1}; nmr τ: 6.15 (m, $W_{1/2}$ = 4 Hz, H_d), 6.56 (d, J = 4.5 Hz, H_a), 7.10 (dd, J = 9.5 and 5 Hz, H_b), 7.50 (d, J = 9.5 Hz, H_c), 7.50 (s, superimposed on doublet, N—CH_3), 7.80 (m, 2H), and 8.4–9.0 (m, 3H); ms *m/e* (%): 217 (16), 215.0310 (M^+, calcd. for $C_9H_{14}N^{79}Br$: 215.0295, 16), 136 (100), 96 (38), 95 (27), 94 (100), and 82 (30).

The bromo amine **18** gave a dark tar on attempted vacuum distillation and the picrate derivative (mp 180–190°C, dec.) decomposed on repeated recrystallization.

The minor component (ca. 5% of the major component) of the basic fraction was isolated by preparative scale vpc (6 ft × ¼ in., 20% SE30, 150°C, retention time 10.8 min) as an oily chloro amine **19**: ir 1630 (vw), 940 (m), and 740 (m) cm^{-1}; nmr τ: 6.25 (m, $W_{1/2}$ = 3.5 Hz, H_d), 6.80 (d, J = 5 Hz, H_a), 7.10 (dd, J = 9.5 and 5 Hz, H_b), 7.50 (d, J = 9.5 Hz, H_c), 7.50 (s, superimposed on the doublet, N—CH_3), 7.80 (m, 3H), and 8.0–9.0 (m, 3H); ms *m/e* (%): 173 (10), 171.0825 (calcd. for $C_9H_{14}NCl$: 171.0814, 30), 136 (85), 96 (46), 95 (29), 94 (100), and 82 (19).

Photolysis of N*-Nitrosamine* ***14***

Under Oxygen

A solution of nitrosamine **14** (2 g, 0.011 mol) and concentrated HCl (1.0 ml, 0.06 *N*) in methanol (200 ml) was photolysed under oxygen for 1.5 h. The work-up gave an oily neutral fraction (80 mg). The aqueous solution was basified and extracted with ether (3 × 50 ml). The ether solution was dried and stirred overnight with LAH (2 g). Work-up in the usual way gave the reduced product (980 mg). The aqueous layer was further extracted with CH_2Cl_2 (3 × 50 ml) to give an additional basic extract (420 mg): ir: 3380 (m, br), 3040 (m), 1700 (s), 1625 (s), 1270 (m), and 1050 (m) cm^{-1}; nmr τ: 6.2 (m), 6.67 (s), 7.15 (m), 7.48 (s), 7.6 (m), and 8.2 (m).

The reduced extract (980 mg) was chromatographed on neutral alumina (50 g). Elution with 0.5% methanol–CH_2Cl_2 gave an olefinic fraction (340 mg); ir: 3040 (m) and 692 (s) cm^{-1}; nmr τ: 3.70 (m). Examination of this fraction by gc–ms (20% SE30, 170°C) showed it to contain the parent amine, **16**, and **17**, and an unknown olefinic compound as the major component. Elution with 1% methanol–CH_2Cl_2 gave bicyclic amino alcohol **17** (254 mg, 13%) which distilled at 30°C/0.05 Torr: ir: 3350 (s, br) and 1040 (s) cm^{-1}; nmr τ: 6.58 (m, 2H), 7.0–7.75 (m, 4H), 7.62 (s, N—CH_3), 7.8–8.2 (m, 2H), and 8.4 (m, 6H); ms *m/e* (%): 169.1446 (M^+, calcd. for $C_{10}H_{19}NO$: 169.1467, 33), 168 (38), 152 (10), 138 (45), and 57 (100). Irradiation at τ 8.4 resulted in collapse of the pattern at τ 6.58 to a broadened singlet ($W_{1/2}$ = 4 Hz). Attempts to prepare the *p*-nitrobenzoate and picrate derivatives of **17** were unsuccessful.

Elution with 2% methanol–CH_2Cl_2 gave *exo*-amino alcohol **16** (269 mg, 13%) as an oil which on sublimation at 30°C/0.05 Torr gave white crystals: mp 73–74°C; ir: 3350 (s, br), 1052 (s), 1025 (s), and 980 cm^{-1}; nmr τ: 6.01 (m, D_2O exchangeable), 6.20 (d, J = 4 Hz, 1H), 7.19 (d, J = 4.5 Hz, 1H), 7.26 (d, J = 10 Hz, 1H), 7.47 (dd, J = 10 and 4.5 Hz, 1H), 7.48 (s, N—CH_3), 8.0 (m, 2H), 8.20 (m, 3H), 8.67 (m, 1H), and 8.85 (m, 1H); ms *m/e* (%): 168 (11), 167.1302 (M^+, calcd. for $C_{10}H_{17}NO$: 167.1310, 77), 166 (29), 150 (16), 110 (71), 97 (17), 96 (21), 95 (60), 94 (100), and 82 (100). Irradiation at τ 8.0 resulted in collapse of the doublet at τ 6.20 to a singlet and coalescence of the doublet at τ 7.19.

Treatment of **16** with a saturated benzene solution of picric

Can. J. Chem. Downloaded from www.nrcresearchpress.com by 210.87.254.42 on 09/05/12
For personal use only.

acid gave a picrate (yellow needles, slow decomposition 160–200°C) which decomposed on repeated attempts at recrystallization. An acetone solution (3 ml) of amino alcohol **16** (65 mg) was treated with CrO_3–H_2SO_4 in acetone at 0°C. The green solution was stirred for 1.5 h. The acetone was evaporated and the residue was basified with aqueous Na_2CO_3 and extracted with CH_2Cl_2 (4 × 15 ml) to give a clear oil (25 mg). The nmr and ir spectra of this oil were identical with those of the corresponding ketone isolated previously (2).

In Bromotrichloromethane

A mixture of nitrosamine **14** (0.5 g, 0.0028 mol), concentrated HCl (0.3 ml), and $CBrCl_3$ (100 ml) was photolysed under N_2 for 2.75 h. The mixture was distilled under vacuum at 20°C and the blue distillate was trapped in a cooled receiver. The neutral extract (204 mg) was a mixture of at least six components as determined by vpc and exhibited no *N*-methyl signal in the nmr. The basic fraction (205 mg) had the following physical constants: ir: 3300 (w, br), 3040 (m), 1720 (w), 1660 (w), 1162, 950, and 700 (m) cm^{-1}; nmr τ: 3.75 (m), 5.60 (m), 5.80 (m, D_2O exchangeable), and 7.0–9.0 (unresolved). Analysis of this fraction by gc–ms (20% SE30, 150°C) showed three peaks in the ratio of 1.2:4.1:1.0; peak 1 (3.2 min) was not identified; peak 2 (3.5 min) exhibited an ms pattern identical to that of the parent amine; and peak 3 (9.3 min) which exhibited ms fragments at *m/e*: 231 (7), 229 (7), 150 (46), 94 (100), and 82 (40). An attempt to isolate the third component by silicic acid chromatography was unsuccessful.

In a separate experiment, a solution consisting of nitrosamine **14** (4.9 g), methanol (120 ml), concentrated hydrochloric acid (3.5 ml), and $CBrCl_3$ (230 ml) was irradiated at −20°C until the absorption maximum at 350 nm disappeared. The photolysate was rapidly evaporated to dryness. The nmr spectrum of this residue in trifluoroacetic acid showed a narrow signal ($W_{1/2}$ = 4 Hz) at τ ~ 5.6. To the residue (4.7 g) taken up in methanol (10 ml) was added with sodium methoxide (10%) in methanol until strongly alkaline to litmus tests. The basic solution was worked up in the usual manner to afford brown crude basic fraction (2.7 g). The vpc spectrum of this crude oil showed one major peak corresponding to **21** (yield, ca. 20%) and at least 40 minor peaks. Chromatography of this oil in benzene–ether gave a forerun (230 mg) followed by a mixture; the forerun was distilled to give methoxy amine **21**; picrate mp and mixture mp 171.5–172.5°C (2).

Acknowledgement

The authors are grateful to the National Research Council of Canada, Ottawa for generous operating grants for the projects.

1. K. S. Pillay, R. W. Lockhart, T. Tezuka, and Y. L. Chow. J. Chem. Soc. Chem. Commun. 80 (1974).
2. R. W. Lockhart, M. Kitadani, F. W. B. Einstein, and Y. L. Chow. Can. J. Chem. This issue.
3. Y. L. Chow, S. C. Chen, and D. W. L. Chang. Can. J. Chem. **49**, 3069 (1971).
4. Y. L. Chow. Acc. Chem. Res. **6**, 354 (1973).
5. Y. L. Chow, J. N. S. Tam, C. J. Colon, and K. S. Pillay. Can. J. Chem. **51**, 2469 (1973).
6. K. S. Pillay, K. Hanaya, and Y. L. Chow. Can. J. Chem. **53**, 3022 (1975).
7. K. S. Pillay and Y. L. Chow. J. Chem. Soc. Perkin II, 93 (1977).
8. L. Magdzinski and Y. L. Chow. J. Am. Chem. Soc. **100**, 2444 (1978).
9. D. H. R. Barton, R. H. Hesse, M. M. Pechet, and L. C. Smith. J. Chem. Soc. Chem. Commun. 754 (1977).
10. D. D. Tanner, R. J. Arhart, E. V. Blackburn, N. C. Das, and N. Wada. J. Am. Chem. Soc. **97**, 2190 (1975); D. D. Tanner and N. Wada. J. Am. Chem. Soc. **97**, 829 (1974).
11. J. H. Hargis. J. Org. Chem. **38**, 346 (1973).
12. G. J. Gleicher. Tetrahedron, **30**, 935 (1974).
13. B. Giese. Angew. Chem. Intern. Ed. (Engl.), **15**, 173 (1976); **15**, 174 (1976); **15**, 688 (1976).
14. F. K. Velichko and L. V. Vinogradova. Izv. Akad. Nauk SSSR Ser. Khim. 1192 (1972).
15. D. I. Davies and L. T. Parfitt. J. Chem. Soc. (C), 1401 (1969); 2691 (1967).
16. G. I. Fray, G. R. Geen, D. I. Davies, L. T. Parfitt, and M. J. Parrott. J. Chem. Soc. Perkin 1, 729 (1974).
17. R. E. Perry, S. C. Chen, B. C. Menon, K. Hanaya, and Y. L. Chow. Can. J. Chem. **54**, 2385 (1976).
18. J. W. Bastable, J. D. Hobson, and W. D. Riddell. J. Chem. Soc. Perkin I, 2205 (1972).
19. W. Prandtle and K. Sennewald. Chem. Ber. **62**, 1754 (1929).
20. M. Akhtar, D. H. R. Barton, and P. G. Sammes. J. Am. Chem. Soc. **87**, 4601 (1965).
21. R. Furstoss, R. Tadayoni, and B. Waegell. J. Org. Chem. **42**, 2844 (1977); R. Furstoss, R. Tadayoni, and B. Waegell. Nouv. J. Chim. **1**, 167 (1977).
22. J. M. Surzur, L. Stella, and P. Nauguter. Tetrahedron Lett. 903 (1971).
23. K. Heusler. Tetrahedron Lett. 97 (1970).
24. O. E. Edwards, G. Bernath, J. Dixon, J. M. Paton, and D. Vocelle. Can. J. Chem. **52**, 2123 (1974).
25. Y. L. Chow, S. C. Chen, K. S. Pillay, and R. A. Perry. Can. J. Chem. **50**, 1057 (1972).
26. G. F. Hennion and A. C. Hazy. J. Org. Chem. **30**, 2650 (1965); C. F. Hammer, M. CaCarthy Ali, and J. D. Weber. Tetrahedron, **29**, 1767 (1972).
27. W. Nagata, S. Hirai, T. Okumura, and K. Kawata. J. Am. Chem. Soc. **91**, 1650 (1969); **89**, 5046 (1967).
28. H. Teufel, E. F. Jenny, and K. Heusler. Tetrahedron Lett. 3413 (1973); H. J. Trede, E. F. Jenny, and K. Heusler. Tetrahedron Lett. 3425 (1973); W. Holick, E. F. Jenny, and K. Heusler. Tetrahedron Lett. 3421 (1973).
29. P. Deslongchamps. Tetrahedron, **31**, 2463 (1975).

Can. J. Chem. Downloaded from www.nrcresearchpress.com by 178.218.224.3 on 09/06/12
For personal use only.

Canadian Journal of Chemistry

Published by
THE NATIONAL RESEARCH COUNCIL OF CANADA

Journal canadien de chimie

Publié par
LE CONSEIL NATIONAL DE RECHERCHES DU CANADA

Volume 56 Number 23 December 1, 1978 Volume 56 numéro 23 1 décembre 1978

Crystal and molecular structure of two *C*-phenyl pentitol derivatives

DOUGLAS C. ROHRER

Medical Foundation of Buffalo, Inc., Buffalo, NY 14203, U.S.A.

AND

JEAN-CLAUDE FISCHER, DEREK HORTON, AND WOLFGANG WECKERLE

Department of Chemistry, The Ohio State University, Columbus, OH 43210, U.S.A.

Received May 9, 1978

DOUGLAS C. ROHRER, JEAN-CLAUDE FISCHER, DEREK HORTON, and WOLFGANG WECKERLE. Can. J. Chem. **56**, 2915 (1978).

Grignard addition of phenylmagnesium bromide to 3,5-*O*-benzylidene-1-deoxy-D-*erythro*-2-pentulose (**1**) affords *C*-phenyl branched-chain pentitols having exclusively either the D-*arabino* (**2**) or D-*ribo* (**5**) stereochemistry according to the mode of substitution of **1**. In order to determine the chirality of these products conclusively, the crystal and molecular structure of the unsubstituted pentitol **6** (from **2**) has been determined. Crystals of 1-deoxy-2-*C*-phenyl-D-arabinitol (**6**; $C_{11}H_{16}O_4$) are orthorhombic, space group $P2_12_12_1$, with cell dimensions $a = 8.9420(6)$, $b = 18.910(1)$, $c = 6.4263(6)$ Å, and $Z = 4$. The structure was solved by multi-solution direct methods and refined to a final discrepancy index of 5.6%. The molecule has an extended, planar zigzag conformation with the phenyl ring nearly perpendicular to this plane. Compound **6** forms one intramolecular (between 2-OH and O-4) and three intermolecular hydrogen bonds. Palladium-catalyzed hydrogenolysis of the 2-phenylcarbamate of **2** results in deoxygenation of the benzylic center with complete inversion of configuration, as established by crystal-structure determination of the product **7**. Crystals of 2(*S*)-4-*O*-acetyl-3,5-*O*-benzylidene-1,2-dideoxy-2-*C*-phenyl-D-*erythro*-pentitol (**7**; $C_{20}H_{22}O_4$) are monoclinic, space group C_2, with cell dimensions $a = 19.102(1)$, $b = 6.1925(5)$, $c = 16.098(1)$ Å, $\beta = 108.325(9)°$, and $Z = 4$. The structure was solved by multi-solution direct methods and refined to a final discrepancy index of 5.9%. The molecule has an almost ideal planar, zigzag backbone conformation which incorporates the 1,3-dioxane ring. Comparison of the conformation observed in the crystal with that calculated from proton–proton coupling constants shows good agreement.

DOUGLAS C. ROHRER, JEAN-CLAUDE FISCHER, DEREK HORTON et WOLFGANG WECKERLE. Can. J. Chem. **56**, 2915 (1978).

La réaction de Grignard du bromure de phénylmagnesium sur le 3,5-*O*-benzylidène-1-désoxy-D-*érythro*-2-pentulose (**1**) conduit à des *C*-phényl pentitols à chaîne ramifiée dont la stéréochimie est exclusivement soit D-*arabino* (**2**) soit D-*ribo* (**5**) selon le mode de substitution de **1**. Dans le but de déterminer sans ambiguité la chiralité de ces produits, on a établi la structure cristalline et moléculaire du pentitol non substitué **6** (obtenue de **2**). Les cristaux de 1-désoxy-2-*C*-phényl-D-arabinitol (**6**; $C_{11}H_{16}O_4$) sont orthorombiques, groupe d'espace $P2_12_12_1$, avec des dimensions de maille $a = 8.9420(6)$, $b = 18.910(1)$, $c = 6.4263(6)$ Å et $Z = 4$. La structure a été résolue à l'aide des méthodes directes, méthode de multi solutions, avec affinement jusqu'à une valeur finale de R de 0.056. La molécule a une conformation allongée et en zigzag, le cycle phényle étant pratiquement perpendiculaire au plan moyen du squelette carboné. Le composé **6** forme une liaison hydrogène intramoléculaire (entre OH-2 et O-4) et trois liaisons hydrogène intermoléculaires. La détermination de la structure des cristaux du produit **7** a établi que l'hydrogénation catalytique sur palladium du 2-phénylcarbamate de **2** conduit à la désoxygénation du centre benzylique avec totale inversion de configuration. Les cristaux de 2(*S*)-4-*O*-acetyl-3,5-*O*-benzylidène-1,2-didésoxy-2-*C*-phényl-D-*érythro*-pentitol (**7**; $C_{20}H_{22}O_4$) sont monocliniques, groupe d'espace C_2, avec des dimensions de maille $a = 19.102(1)$, $b = 6.1925(5)$, $c = 16.098(1)$ Å, $\beta = 108.325(9)°$ et $Z = 4$. La struc-

ture a été résolue à l'aide des méthodes directes, méthode de multi solutions, avec affinement jusqu'à une valeur finale de R de 0.059. Le squellette carboné de la molécule a une conformation pratiquement plane et en zigzag, le cycle 1,3-dioxane se trouvant dans le plan. La conformation de la molécule observée dans le cristal est en bon accord avec celle qui avait été calculée à partir des constantes de couplage entre protons.

Can. J. Chem. Downloaded from www.nrcresearchpress.com by 178.218.224.3 on 09/06/12
For personal use only.

Introduction

Grignard addition of phenylmagnesium bromide to 3,5-*O*-benzylidene-1-deoxy-D-*erythro*-2-pentulose (**1**) afforded (1) a single, *C*-phenyl branched-chain pentitol formulated tentatively as 3,5-*O*-benzylidene-1-deoxy-2-*C*-phenyl-D-arabinitol (**2**). Compound **2** was subsequently converted into the syrupy *tert*-butyldimethylsilyl ether **3** having $[\alpha]_D - 57°$ in chloroform. When the sequence of reactions was reversed, however, with initial silylation of **1** to give **4** and then Grignard addition, a totally different syrupy product (**5**) having $[\alpha]_D + 42°$ in chloroform was obtained exclusively (1), in high yield. Although it is well known (2) that the stereoselectivity of reactions of Grignard reagents with carbonyl-sugar derivatives may be considerably *modified* by change of the reaction conditions or change of a substituent, in this case the mode of addition is evidently *completely reversed* according to the prior mode of substitution (**1** or **4**) of the given substrate (1-deoxy-D-*erythro*-2-pentulose).

This remarkable sequence may prove extremely useful in asymmetric synthesis, as there are many examples of biologically important compounds (such as cholinergic agents (2, 3) and hormones and drugs related to atropine (4) and epinephrine (adrenalin) (5)) that contain an asymmetric, benzylic carbon atom for which these Grignard addition-products may serve as chiral precursors. The potential synthetic utility of these compounds is extended even further by the observation (1) that the tertiary benzylic center can be deoxygenated with complete retention of optical purity, by palladium-catalyzed hydrogenation to give, for example, compound **7**, to which the 2(*S*) configuration was tentatively ascribed.

The configurational assignment of such asymmetric, tertiary alcohols as in **2** generally poses considerable difficulties (6) and the determination of configuration of the chiral benzylic center in **7** is scarcely feasible by standard physical or reasonable chemical methods. We therefore undertook an X-ray diffraction study of the unsubstituted pentitol **6** (obtained (1) from **2** by acid hydrolysis) and the benzylidene acetal **7**, with the objective of providing, first, final proof of their stereochemistry, and second, information on their conformation.

Experimental

For details of synthesis and nmr measurements, see ref. 1.

Experimental Crystal Data for Tertiary Alcohol **6**
1-Deoxy-2-*C*-phenyl-D-arabinitol (**6**)

$C_{11}H_{16}O_4$ fw = 212.2
Orthorhombic, $a = 8.9420(6)$, $b = 18.910(1)$, $c = 6.4263(6)$ Å, $V = 1086.5$ Å^3, $\rho_c = 1.298$ g cm^{-3}, $Z = 4$, room temperature (~20°C), Ni-filtered CuK$_\alpha$, $\lambda = 1.5418$ Å, space group: $P2_12_12_1$, crystal size 0.10 × 0.11 × 0.03 mm^3.

Integrated diffraction intensities for 1313 independent reflections with $2\theta < 150°$ were measured with an Enraf–Nonius CAD-4 diffractometer using ω–2θ scans. Of these, 1045 intensities were determined to be observed above background ($I > 2\sigma_I$).

Phase angles sufficient to locate the nonhydrogen atoms were derived by using the direct-methods program MULTAN (7). The hydrogen atoms were located on a difference electron-density map at an intermediate stage of the least-squares refinement. In the final cycles of full-matrix, least-squares refinement, positional parameters for all atoms, anisotropic thermal parameters for the nonhydrogen atoms, and isotropic thermal parameters for the hydrogen atoms were varied. The quantities $(1/\sigma_F^2)$, where σ_F is as defined by Stout and Jensen (8), but with an instability constant of 0.06, were used to weight the refinement; data determined to be unobserved were given zero weight. The scattering factors used were calculated from the coefficients given in the International Tables for X-ray Crystallography, Vol. IV (9). The final value of the residual, $R = \Sigma||F_o| - |F_c||/\Sigma|F_o|$, was 0.037 for the observed data and 0.056 for all measured data. Final atomic positions are listed in Table 1 and tables of anisotropic thermal parameters and of observed and calculated structure amplitudes are in the Depository of Unpublished Data.[1]

Experimental Crystal Data for the Deoxygenated Product **7**
2(*S*)-4-*O*-Acetyl-3,5-*O*-benzylidene-1,2-dideoxy-2-*C*-phenyl-D-*erythro*-pentitol (**7**)

$C_{20}H_{22}O_4$ fw = 326.4
Monoclinic, $a = 19.102(1)$, $b = 6.1925(5)$, $c = 16.098(1)$ Å, $\beta = 108.325(9)°$, $V = 1807.6$ Å^3, $\rho_c = 1.199$ g cm^{-3}, $Z = 4$, room temperature (~20°C); Ni-filtered CuK$_\alpha$, $\lambda = 1.5418$ Å, space group: C_2, crystal size 0.40 × 0.40 × 0.80 mm^3.

Using the same data-measurement procedure used for **6**, 2033 independent intensities ($2\theta < 150°$) were measured with 1887 intensities determined to be observed above background ($I > 2\sigma_I$).

The atomic positions were determined and refined by the same methods described for **6**. The final value of the residual R was 0.055 for the observed data and 0.059 for all measured data. The final atomic coordinates are listed in Table 2. Tables containing the thermal parameters and the observed and calculated structure-factor amplitudes are in the Depository of Unpublished Data.[1]

Results and Discussion

Figures 1 and 2 show similar three-dimensional views of the two *C*-phenyl pentitols **6** and **7** having

[1]Complete set of data may be obtained, at a nominal charge, from the Depository of Unpublished Data, CISTI, National Research Council of Canada, Ottawa, Ont., Canada K1A 0S2.

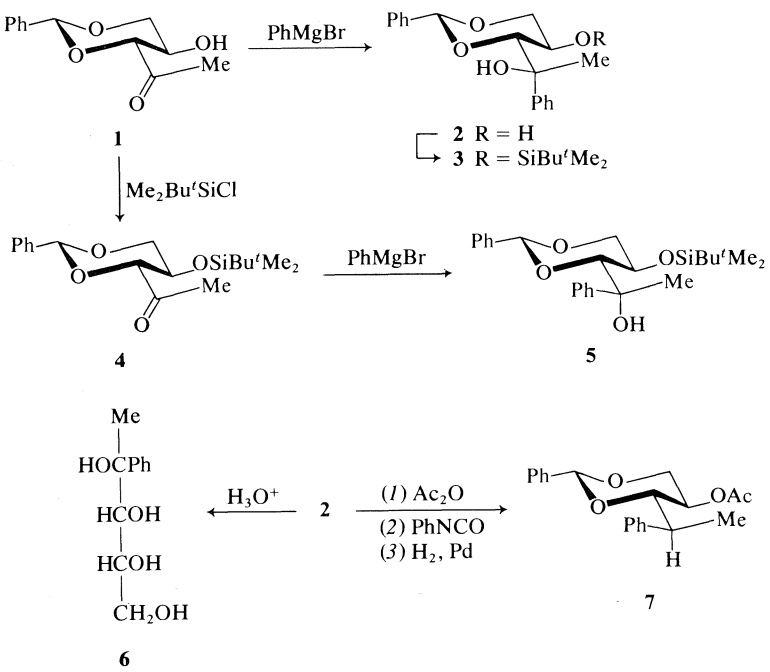

the planar, zigzag arrangement in the plane of the paper. The bond lengths shown in Figs. 1 and 2 and the valence angles given in Tables 3 and 4 are all within the range of values expected for this type of compound. Figure 3 depicts Newman projections along each carbon–carbon and, for **7**, along the relevant carbon–oxygen bonds, to illustrate the torsion angles.

The Structure of the Tertiary Alcohol **6**

The configuration at C-2 of **2**, **3**, and **5** could be predicted, with reasonable confidence, on the basis of mechanistic arguments (compare, for example, ref. 10) regarding the Grignard addition reactions with **1** and its 4-*tert*-butyldimethylsilyl ether **4**, respectively. In the original paper (1), the assignment was convincingly achieved by nuclear Overhauser experiments (after the present investigation had been initiated), with a suitably protected derivative of **2**, thus firmly establishing the D-*arabino* stereochemistry. The D-*ribo* configuration must, therefore, be attributed to the other product (**5**). These earlier results are now unambiguously affirmed and extended by crystal-structure determination of the unprotected pentitol **6**.

The C-6, C-2 → C-5 carbon chain of **6** (Fig. 1) adopts the extended, essentially planar, zigzag arrangement, in accord with the general conforma-

TABLE 1. Final atomic coordinates for molecule **6** (esd in parentheses)

Atom	*X/A*	*Y/B*	*Z/C*	Atom	*X/A*	*Y/B*	*Z/C*
C-1	0.6914(3)	0.73091(14)	0.3971(5)	H-1A	0.765(4)	0.760(2)	0.319(6)
C-2	0.6109(3)	0.67648(11)	0.2632(4)	H-1B	0.602(4)	0.763(2)	0.456(6)
C-3	0.7177(3)	0.61847(11)	0.1782(4)	H-1C	0.750(5)	0.712(2)	0.500(8)
C-4	0.8535(3)	0.64695(12)	0.0588(4)	H-3	0.654(3)	0.589(1)	0.082(5)
C-5	0.9395(3)	0.58839(15)	−0.0514(5)	H-4	0.926(3)	0.667(1)	0.163(4)
C-6	0.4831(3)	0.64054(12)	0.3804(4)	H-5A	1.029(3)	0.606(1)	−0.112(5)
C-7	0.3488(3)	0.62492(13)	0.2830(4)	H-5B	0.982(3)	0.552(2)	0.047(5)
C-8	0.2360(3)	0.58928(16)	0.3872(6)	H-7	0.338(3)	0.641(1)	0.139(5)
C-9	0.2563(4)	0.56687(14)	0.5899(6)	H-8	0.137(4)	0.579(2)	0.319(6)
C-10	0.3885(4)	0.58310(16)	0.6899(5)	H-9	0.176(3)	0.535(2)	0.660(6)
C-11	0.5002(3)	0.61993(15)	0.5881(5)	H-10	0.400(4)	0.570(2)	0.831(6)
O-2	0.5435(2)	0.71130(10)	0.0869(3)	H-11	0.589(4)	0.629(2)	0.656(5)
O-3	0.7774(2)	0.57751(8)	0.3448(3)	H-2O	0.611(3)	0.721(1)	0.007(5)
O-4	0.8070(2)	0.69855(9)	−0.0907(3)	H-3O	0.749(4)	0.538(2)	0.325(7)
O-5	0.8534(3)	0.55346(9)	−0.2056(3)	H-4O	0.874(4)	0.727(1)	−0.103(5)
				H-5O	0.836(4)	0.576(2)	−0.304(6)

Can. J. Chem. Downloaded from www.nrcresearchpress.com by 178.218.224.3 on 09/06/12
For personal use only.

TABLE 2. Final atomic coordinates for molecule **7** (esd in parentheses)

Atom	*X/A*	*Y/B*	*Z/C*	Atom	*X/A*	*Y/B*	*Z/C*
C-1	−0.06353(15)	−0.0822(8)	0.34759(19)	H-1A	−0.054(2)	−0.026(9)	0.411(2)
C-2	0.01148(12)	−0.1060(5)	0.33178(15)	H-1B	−0.098(2)	−0.214(11)	0.325(2)
C-3	0.00023(12)	−0.1640(4)	0.23570(15)	H-1C	−0.091(1)	0.037(8)	0.311(2)
C-4	0.07265(12)	−0.1872(5)	0.21490(14)	H-2	0.034(2)	0.048(8)	0.344(2)
C-5	0.05703(13)	−0.2681(6)	0.12136(15)	H-3	−0.024(1)	−0.056(7)	0.200(2)
C-6	0.06229(11)	−0.2605(5)	0.39579(14)	H-4	0.105(1)	−0.279(6)	0.249(2)
C-7	0.13377(15)	−0.1970(7)	0.44305(20)	H-5A	0.106(2)	−0.323(10)	0.108(3)
C-8	0.17933(16)	−0.3326(11)	0.50489(22)	H-5B	0.038(2)	−0.152(6)	0.090(2)
C-9	0.15678(17)	−0.5334(9)	0.51987(21)	H-7	0.144(2)	−0.040(9)	0.434(2)
C-10	0.08547(19)	−0.6013(7)	0.47222(20)	H-8	0.228(2)	−0.315(13)	0.522(3)
C-11	0.03981(16)	−0.4664(6)	0.41087(17)	H-9	0.180(2)	−0.632(10)	0.553(2)
C-12	0.17980(14)	0.0372(7)	0.24674(18)	H-10	0.068(2)	−0.767(10)	0.476(3)
C-13	0.20443(20)	0.2639(9)	0.25082(33)	H-11	−0.011(2)	−0.519(12)	0.378(3)
C-14	−0.05358(12)	−0.4270(0)	0.12555(13)	H-13A	0.185(2)	0.349(9)	0.297(3)
C-15	−0.10254(11)	−0.6099(4)	0.10276(14)	H-13B	0.263(2)	0.267(13)	0.270(3)
C-16	−0.10568(11)	−0.7317(5)	0.02914(15)	H-13C	0.181(2)	0.336(14)	0.186(3)
C-17	−0.15419(14)	−0.9032(5)	0.00535(18)	H-14	−0.081(1)	−0.294(7)	0.085(2)
C-18	−0.19957(14)	−0.9562(5)	0.05511(19)	H-16	−0.071(2)	−0.692(8)	−0.009(2)
C-19	−0.19700(13)	−0.8339(6)	0.12712(19)	H-17	−0.155(1)	−0.994(6)	−0.050(2)
C-20	−0.14852(13)	−0.6609(5)	0.15172(16)	H-18	−0.220(1)	−1.092(8)	0.047(2)
O-3	−0.03902(7)	−0.3608(3)	0.21439(9)	H-19	−0.230(2)	−0.863(10)	0.162(2)
O-4	0.10540(9)	0.0237(4)	0.22188(13)	H-20	−0.142(1)	−0.557(8)	0.199(2)
O-5	0.01300(8)	−0.4576(4)	0.10775(10)				
O-12	0.21877(11)	−0.1163(7)	0.26199(20)				

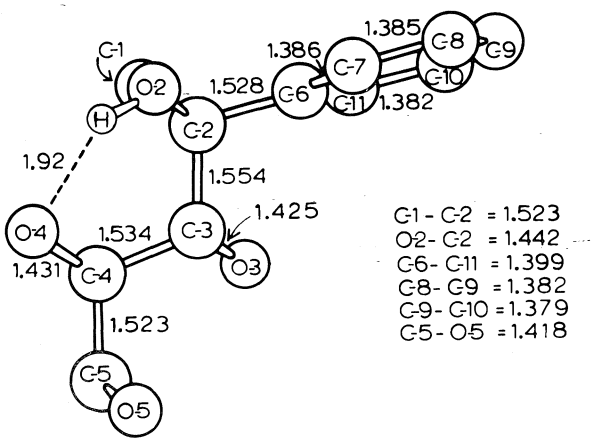

FIG. 1. Three-dimensional drawing of molecule **6** with bond lengths. The average standard deviation is 0.004 Å.

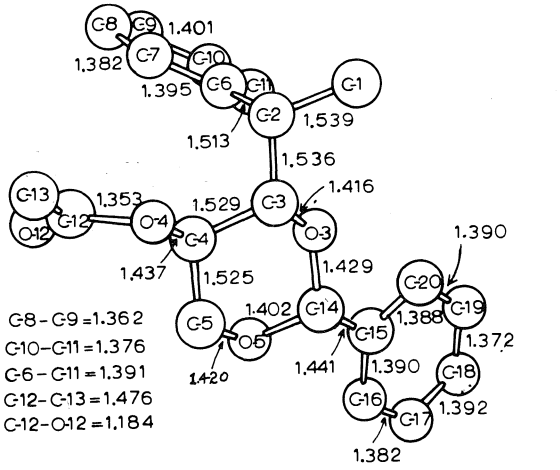

FIG. 2. Three-dimensional drawing of molecule **7** with bond lengths. The average standard deviation is 0.004 Å.

tional predictions that may be made for open-chain sugar derivatives (11–13). The phenyl ring is almost perpendicular to the plane of the carbon backbone, generating (Fig. 3*d*) torsion angles of 83.5° and −94.1°, respectively. Interestingly, C-1, rather than C-6 (namely, the phenyl group), is rotated out-of-plane C-1—C-2—C-3—C-4 by −54.5°. This orientation implies the parallel alignment of the C-2—O-2 and C-4—O-4 bonds (1,3-interaction)[2] that is associated with an estimated[3] instability factor of about 1.5 kcal/mol and is, therefore, generally considered (11, 12, 15) to be unfavorable. In the case of **6**, however, this conformation permits formation of an intramolecular hydrogen-bond (16) involving O-4 and the hydroxyl group at C-2 (O-2 · · · O-4 separation is 2.630 Å, and the 2-OH · · · O-4 distance is 1.92 Å). In any case, this rotamer is definitely of lower energy than the other two staggered C-2—C-3 rotamers, which would have a higher energy as a result of the loss of the hydrogen-bond stabilization and a 1,3 steric interaction between either C-1 or C-6, and O-4, if the planar, zigzag arrangement of atoms C-2 to C-5 is maintained.

[2]For criticism of this term in conformational analysis of acyclic compounds, see ref. 12.

[3]Values from conformational analysis of cyclitols and pyranose sugars in aqueous solution (14).

Can. J. Chem. Downloaded from www.nrcresearchpress.com by 178.218.224.3 on 09/06/12
For personal use only.

TABLE 3. Valence angles in molecule **6**

Bonds			Bond angle[a] (deg)	Bonds			Bond angle[a] (deg)
C-3	C-2	C-1	112.7(2)	C-6	C-2	C-1	112.1(2)
O-2	C-2	C-1	109.4(2)	C-6	C-2	C-3	108.6(2)
O-2	C-2	C-3	107.6(2)	O-2	C-2	C-6	106.1(2)
C-4	C-3	C-2	114.5(2)	O-3	C-3	C-2	110.5(2)
O-3	C-3	C-4	105.7(2)	C-5	C-4	C-3	112.1(2)
O-4	C-4	C-3	110.2(2)	O-4	C-4	C-5	109.3(2)
O-5	C-5	C-4	112.9(2)	C-7	C-6	C-2	121.3(2)
C-11	C-6	C-2	120.9(2)	C-11	C-6	C-7	117.8(2)
C-8	C-7	C-6	121.1(2)	C-9	C-8	C-7	120.6(2)
C-10	C-9	C-8	118.9(2)	C-11	C-10	C-9	120.7(2)
C-10	C-11	C-6	120.9(2)				

[a]Numbers in parentheses are estimated standard deviations.

TABLE 4. Valence angles in molecule **7**

Bonds			Bond angle[a] (deg)	Bonds			Bond angle[a] (deg)
C-3	C-2	C-1	110.3(2)	C-6	C-2	C-1	112.3(2)
C-6	C-2	C-3	113.3(2)	C-4	C-3	C-2	113.1(2)
O-3	C-3	C-2	109.9(2)	O-3	C-3	C-4	108.2(2)
C-5	C-4	C-3	109.7(2)	O-4	C-4	C-3	107.4(2)
O-4	C-4	C-5	108.7(2)	O-5	C-5	C-4	110.3(2)
C-7	C-6	C-2	120.1(2)	C-11	C-6	C-2	122.1(2)
C-11	C-6	C-7	117.8(2)	C-8	C-7	C-6	120.6(3)
C-9	C-8	C-7	121.3(3)	C-10	C-9	C-8	119.0(3)
C-11	C-10	C-9	119.9(3)	C-10	C-11	C-6	121.4(2)
O-4	C-12	C-13	111.3(3)	O-12	C-12	C-13	125.7(3)
O-12	C-12	O-4	123.0(2)	O-3	C-14	C-15	112.8(1)
O-5	C-14	C-15	113.6(1)	O-5	C-14	O-3	109.9(1)
C-16	C-15	C-14	119.6(2)	C-20	C-15	C-14	120.7(2)
C-20	C-15	C-16	119.7(2)	C-17	C-16	C-15	119.9(2)
C-18	C-17	C-16	120.4(2)	C-19	C-18	C-17	119.5(2)
C-20	C-19	C-18	120.7(2)	C-19	C-20	C-15	119.8(2)
C-14	O-3	C-3	114.3(1)	C-12	O-4	C-4	118.1(2)
C-14	O-5	C-5	112.9(2)				

[a]Numbers in parentheses are estimated standard deviations.

The terminal hydroxyl group is also disposed out of the plane of the carbon backbone (see Fig. 3*c*). This conformation is almost certainly determined by the intermolecular hydrogen-bonding (see Table 5). It would be expected, however, that dissolution would permit equilibration to afford almost equal proportions of this rotamer and the extended one; the third staggered rotamer would generate a parallel (*peri*) interaction between O-3 and O-5 and is, therefore, unlikely.

Unfortunately, no coupling constants could be extracted (1) from the very complex nmr spectra of **6** in a variety of solvents. Therefore, no information is available about the conformation of **6** in the liquid state that might have been compared with data for crystalline **6** by way of the Karplus equation (17–19) that correlates spin–spin coupling constants of vicinal protons ($^3J_{H,H}$) with the dihedral angle in the various H—C—C—H units of the molecule.

Molecule **6** forms three intermolecular hydrogen-bonds with symmetry-related molecules and one intramolecular hydrogen-bond between O-2 and O-4, as already mentioned. The details of the hydrogen-bond distances are given in Table 5. The only other intermolecular non-bonded contacts less than 3.5 Å involve C-3 to O-5 (3.396 Å) and C-4 to O-2 (3.309 Å).

Structure of the Deoxygenated Product 7

The stereospecific deoxygenation of the benzylic center (**2** → **7**) is somewhat reminiscent of the palladium-catalyzed hydrogenolysis of phenylurethanes to give (20) arenes. The literature precedent, however, does not involve an asymmetric carbon center. Therefore, in the absence of firm evidence not readily obtainable other than by crystallographic methods, a tentative configurational assignment [2(*S*)] for the benzylic center at C-2 in **7** was made (1) that rested on mechanistic arguments: it is known from a wealth of experimental data (21) that catalytic

Can. J. Chem. Downloaded from www.nrcresearchpress.com by 178.218.224.3 on 09/06/12
For personal use only.

TABLE 5. Hydrogen-bond contact distances and angles for molecule **6**

Donor	Acceptor	Distances (Å) O···O	O—H	H···O	Angle, deg O—H···O	Acceptor symmetry operator
3-O—	H···O-5	2.758	0.80	1.96	170	$\frac{3}{2} - x, 1 - y, \frac{1}{2} + z$
4-O—	H···O-2	2.716	0.81	1.91	170	$\frac{1}{2} + x, \frac{3}{2} - y, -z$
5-O—	H···O-3	3.002	0.78	2.32	148	$x, y, -1+z$
2-O—	H···O-4	2.630	0.81	1.92	147	x, y, z

TABLE 6. Comparison of dihedral angles and ^{1}H nmr coupling data for compound **7**

Vicinal protons	Crystallographic dihedral angle, deg Crystal	Calculated[a]	Calculated[b]	Nmr proton–proton coupling constants, Hz Observed[c]	Calculated[a]	Calculated[b]
2, 3	50.2	49.4	62.3	3.2	3.1	4.8
3, 4	173.5	[d]	[e]	9.8	9.1	9.6
4, 5A	41.8	37.4	45.1	5.0	4.3	5.4
4, 5B	162.2	[d]	171.8	10.0	8.3	9.4

[a]By using the Karplus (17) equation: $^3J_{H,H} = 4.22 - 0.5 \cos\phi + 4.50 \cos 2\phi$.
[b]By using a modified (19) equation: $^3J_{H,H} = (7.8 - \cos\phi + 5.6 \cos 2\phi)(1 - 0.1X)$, where $X = \Sigma_1^4(X_n - X_H)$ and X_n is the electronegativity of substituent n, X_H that of hydrogen.
[c]At 100 MHz in chloroform-*d*.
[d]The unmodified Karplus equation does not allow for vicinal coupling-constants larger than 9.22 Hz.
[e]With the specified mode of substitution, the modified Karplus equation does not provide for vicinal coupling constants larger than 9.69 Hz.

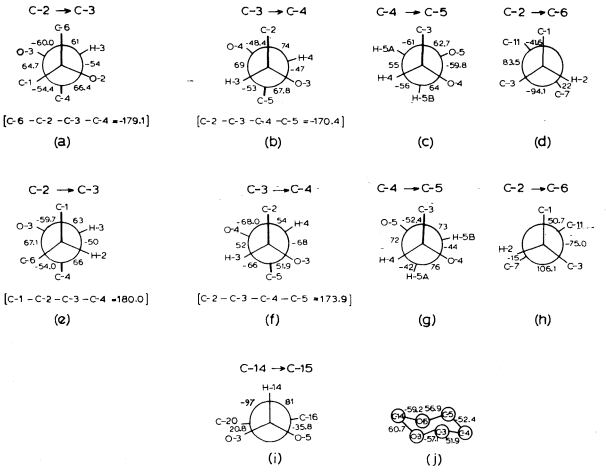

FIG. 3. Newman projections along each carbon–carbon bond and relevant carbon–oxygen bonds for molecule **6** (*a* to *d*) and molecule **7** (*e* to *j*).

hydrogenolysis of benzyl derivatives of the general type Ph—C—X → Ph—C—H shows substantial stereospecificity. Furthermore, depending on the electronegativity of the displaced group X as well as the chemical nature of the catalyst metal, either retention or inversion may occur, and it appears that palladium-catalyzed hydrogenolysis generally proceeds with a high degree of configurational inversion.

In keeping with these arguments, single-crystal X-ray diffraction analysis of **7** now verifies that the product obtained was indeed the one resulting from inversion, namely 2(*S*)-4-*O*-acetyl-3,5-*O*-benzylidene-1,2-dideoxy-2-*C*-phenyl-D-*erythro*-pentitol (**7**). As a view of the crystal structure (Fig. 2) reveals, the carbon backbone of **7** adopts an almost ideal planar zigzag conformation (the torsion angles along C-2—C-3 and C-3—C-4 being 180.0° and 173.9°; see Fig. 3 *e* and *f*) part of which (C-3, C-4, and C-5) is incorporated into the 1,3-dioxane ring. The latter exists in the expected (22) chair conformation, and is indeed more puckered than cyclohexane in the O—C—O region, as manifested by the torsion angles (~60°) along the bonds C-14—O-3 and C-14—O-5 (Fig. 3*j*) that deviate significantly from the value (56°) observed (23) for cyclohexane. On the other hand, and in contrast to a literature report (24) on 2-*p*-chlorophenyl-1,3-dioxane, the two torsion angles in the 'cyclohexane' part (each being 52°) are distinctively smaller than the quoted value for cyclohexane and are indicative of considerable flattening in this region of the molecule.

The acetalic phenyl group at C-14 rotates slightly about the C-14—C-15 bond to generate (Fig. 3*i*) torsion angles of 20.8° and −35.8° involving O-3 with C-20 and O-5 with C-16. This staggered disposition results in the least amount of steric crowding, with both C-16 and C-20 positioned between an oxygen atom and H-14 rather than one between the two oxygen atoms, the other between an oxygen atom and H-14. This conformer is frequently observed in other crystal structures (24, 25) and constitutes an energy-minimum conformation.

Can. J. Chem. Downloaded from www.nrcresearchpress.com by 178.218.224.3 on 09/06/12
For personal use only.

Can. J. Chem. Downloaded from www.nrcresearchpress.com by 178.218.224.3 on 09/06/12
For personal use only.

Molecule **7** has no hydrogen atoms capable of being involved in a hydrogen bond. The only intermolecular nonhydrogen contacts less than 3.5 Å involve C-19 with O-12 (3.364 Å) and O-5 with O-5 (3.346 Å).

The equatorially attached C_2 chain at C-3 of the 1,3-dioxane ring adopts, as a means of relieving non-bonded interaction strain, an orientation (Fig. 3*e*) such that the phenyl group at C-2 is perpendicular to the dioxane ring (compare Fig. 2). Furthermore, the phenyl group rotates about the C-2—C-6 bond (Fig. 3*h*) so that it is disposed broadside to the axial proton at C-4.

Table 6 presents a comparison of proton–proton couplings measured (1) with a solution of **7** in chloroform-*d*, with values calculated from the dihedral angles in the crystal by use of the Karplus equation, either with (19) or without (17) correction for electronegativity effects. In addition, two columns are included listing values for the dihedral angles that were calculated similarly from the observed coupling-constants. The data show reasonable qualitative correlation that is sufficient to assume a conformation of **7** in solution similar to that adopted in the solid state.

Acknowledgments

This work was supported in part by Grant No. GM-11976 (The Ohio State University Research Foundation Project 1820) from the National Institute of General Medical Sciences, U.S. Department of Health, Education and Welfare, and by the Medical Foundation of Buffalo, Inc.

1. J.-C. FISCHER, D. HORTON, and W. WECKERLE. Carbohydr. Res. **59**, 459 (1977).
2. T. D. INCH. Adv. Carbohydr. Chem. Biochem. **27**, 191 (1972).
3. R. W. BRIMBLECOMBE, T. D. INCH, J. WETHERELL, and N. WILLIAMS. J. Pharm. Pharmacol. **23**, 649 (1971), and earlier papers, cited therein.
4. B. V. RAMA SASTRY. *In* Medicinal chemistry. *Edited by* A. Burger. Wiley-Interscience, New York. 1970. p. 1544.
5. D. J. TRIGGLE. *In* Medicinal chemistry. *Edited by* A. Burger. Wiley-Interscience, New York. 1970. p. 1235.
6. S. D. GERO, D. HORTON, A. M. SEPULCHRE, and J. D. WANDER. Tetrahedron, **29**, 2963 (1973); J. Org. Chem. **40**, 1061 (1975).
7. G. GERMAIN, P. MAIN, and M. M. WOOLFSON. Acta Crystallogr. A**22**, 368 (1971).
8. G. H. STOUT and L. H. JENSEN. X-ray structure determination. Macmillan, New York. 1968. p. 457.
9. International Tables for X-ray Crystallography. Vol. IV. Kynoch Press, Birmingham, England. 1974. Table 2.2B.
10. J.-C. FISCHER and D. HORTON. Carbohydr. Res. **59**, 477 (1977).
11. D. HORTON and M. J. MILLER. J. Org. Chem. **30**, 2457 (1965); H. EL KHADEM, D. HORTON, and T. F. PAGE, JR. J. Org. Chem. **33**, 734 (1968); D. HORTON, P. L. DURETTE, and J. D. WANDER. Ann. N.Y. Acad. Sci. **222**, 884 (1973); Adv. Chem. Ser. **117**, 147 (1973); D. HORTON and J. D. WANDER. J. Org. Chem. **39**, 1859 (1974).
12. G. A. JEFFREY and H. S. KIM. Carbohydr. Res. **14**, 207 (1970).
13. A. DUCRUIX, C. PASCARD-BILLY, D. HORTON, and J. D. WANDER. Carbohydr. Res. **29**, 276 (1973).
14. S. J. ANGYAL. Angew. Chem. **81**, 172 (1969); Angew. Chem. Int. Ed. Engl. **8**, 157 (1969); J. A. HIRSCH. *In* Topics in stereochemistry. Vol. 1. *Edited by* N. L. Allinger and E. L. Eliel. Wiley-Interscience, New York. 1967. p. 199.
15. A. DUCRUIX, C. PASCARD-BILLY, S. J. EITELMAN, and D. HORTON. J. Org. Chem. **41**, 2652 (1976).
16. R. L. GIRLING and G. A. JEFFREY. Carbohydr. Res. **18**, 339 (1971); G. A. JEFFREY and E. J. FASISKA. Carbohydr. Res. **21**, 187 (1972).
17. M. KARPLUS. J. Chem. Phys. **30**, 11 (1959).
18. M. KARPLUS. J. Am. Chem. Soc. **85**, 2870 (1963).
19. P. L. DURETTE and D. HORTON. Org. Magn. Reson. **3**, 417 (1971).
20. J. D. WEAVER, E. J. EISENBRAUN, and L. E. HARRIS. Chem. Ind. London, 187 (1973).
21. A. M. KHAN, F. J. MCQUILLIN, and I. JARDINE. J. Chem. Soc. C, 136 (1967).
22. C. ROMERS, C. ALTONA, H. R. BUYS, and E. HAVINGA. *In* Topics in stereochemistry. Vol. 4. *Edited by* E. L. Eliel and N. L. Allinger. Wiley-Interscience, New York. 1969. p. 39; J. F. STODDART. Stereochemistry of carbohydrates. Wiley-Interscience, New York. 1971. p. 186.
23. R. BUCOURT. *In* Topics in stereochemistry. Vol. 8. *Edited by* E. L. Eliel and N. L. Allinger. Wiley-Interscience, New York. 1974. p. 159.
24. A. J. DE KOK and C. ROMERS. Recl. Trav. Chim. Pays-Bas, **89**, 313 (1970).
25. H. T. KLAFF and C. ROMERS. Acta Crystallogr. **20**, 490 (1966); G. M. KELLIE, P. MURRAY-RUST, and F. G. RIDDEL. J. Chem. Soc. Perkin Trans. II, 2384 (1972).

Extraction of cadmium salicylate with some nitrogen-containing organic bases

J. M. SINGH AND S. N. TANDON

Department of Chemistry, University of Roorkee, Roorkee 247672, India

Received January 23, 1978[1]

J. M. SINGH and S. N. TANDON. Can. J. Chem. **56**, 2922 (1978).

$Cd(HSal)_2$ is extracted from aqueous solutions into *n*-butanol, but not into non-hydroxylic solvents (such as benzene and chloroform) at pH 4.5 to 6.0. Addition of N bases, which have no effect alone, causes extraction into the latter solvents, apparently by displacement of co-ordinated water, giving $Cd(HSal)_2 \cdot 2B$. This synergistic effect varies with B (β-picoline > pyridine > quinoline). Formation and distribution constants are given for the experimental conditions.

J. M. SINGH et S. N. TANDON. Can. J. Chem. **56**, 2922 (1978).

De solutions aqueuses entre pH 4.5 et 6.0, on peut extraire $Cd(HSal)_2$ dans le *n*-butanol, mais non pas dans les solvants non-hydroxylés tels que le benzène et le chloroforme. L'addition de bases azotées, qui par elles-mêmes sont sans effet, favorise l'extraction dans ces derniers solvants, en déplaçant probablement l'eau de coordination pour former $Cd(HSal)_2 \cdot 2B$. L'effet synergique varie selon la nature de B (β-picoline > pyridine > quinoline). On rapporte les constantes de formation et de distribution correspondant aux conditions expérimentales utilisées.

[Traduit par le journal]

Introduction

Earlier workers (1–3) have studied the extraction of some bivalent metal salicylates in hydroxylic solvents and identified the extracted species. In contrast to the behaviour of hydroxylic solvents negligible extractions of metal salicylates are observed in non-polar solvents, but the presence of neutral donors like tributyl phosphate in non-polar solvents makes the species less hydrophilic and the extractions are then increased by several orders of magnitude (4). Aggett *et al.* (5–7) carried out extensive studies on the extraction of some metal salicylates in tributyl phosphate. We have studied the extraction of metal salicylates in the presence of organic bases like pyridine, picolines, and quinoline, which will be more effective in displacing water from the coordination sphere so larger synergistic effects may be observed. By using different bases their relative effectiveness as synergists can be obtained.

A survey of literature revealed that practically no work has been done on the extraction of cadmium salicylate either in hydroxylic solvents or in non-polar solvents in the presence of organic bases. The present article reports the extraction behaviour of cadmium salicylate in *n*-butanol and the extracting species is identified. The addition of organic bases to *n*-butanol does not increase the extraction, but the addition of these bases to non-polar solvents like benzene brings about a synergistic enhancement in the extraction. The cadmium salicylate base species has been identified and the extraction and formation constants are calculated. The stability of different mixed complexes is compared.

[1]Revision received August 9, 1978.

Over the pH range studied (4.5–6.0), only the species H_2Sal and $HSal^-$ of salicylic acid need be considered in the aqueous phase. Although dimerization of salicylic acid occurs in benzene, it can reasonably be expected to be small or negligible in polar or hydroxylic solvents (such as *n*-butanol) that can act as acceptors for hydrogen bonds (8).

Experimental

Reagents

A.R. cadmium sulphate was dissolved in doubly distilled water and the solution was standardized by EDTA solution using xylenol orange indicator. Freshly prepared solutions of salicylic acid (BDH, AR) were used throughout the investigations. *n*-Butanol, pyridine, picolines, and quinoline were also of analytical grade. ^{115m}Cd radioisotope supplied by Bhabha Atomic Research Centre, Bombay (India) was used for distribution studies.

Analytical Procedure

In each set equal volumes (10 ml) of the aqueous (10^{-4} *M* cadmium(II) and 0.0125 *M* salicylic acid, or other concentration) and organic phases were shaken at room temperature 30 ± 2.0°C. After equilibration the two phases were separated and the pH of the aqueous phase was determined by a Cambridge bench pH-meter. Suitable aliquots of the two phases were counted using a G.M. counter and the distribution ratio was calculated by the usual method. The optimum pH for the extraction of cadmium(II) in the presence of salicylic acid alone and with the bases extends from 4.0 to 6.0. Optimum concentrations with regard to the bases are 0.5, 1, and 4 *M* for β-picoline, pyridine, and quinoline respectively for maximum extraction with a salicylic acid concentration of 0.025 *M* overall. The ionic strength of the aqueous phase was maintained constant (0.1 *M*) with sodium perchlorate. Bases alone do not influence the extraction of cadmium under the experimental conditions.

For the determination of the distribution ratio of pyridine and β-picoline, 10 ml aqueous solutions of known concentration adjusted to a definite pH by adding either perchloric acid or sodium hydroxide and to an ionic strength of 0.1 *M* with

Can. J. Chem. Downloaded from www.nrcresearchpress.com by 210.87.254.40 on 09/05/12
For personal use only.

Can. J. Chem. Downloaded from www.nrcresearchpress.com by 210.87.254.40 on 09/05/12
For personal use only.

sodium perchlorate, were equilibrated with Analar benzene (10 ml) and shaken for about 20 h at 30 ± 2°C. After separation of both phases, the pH of the aqueous layer was measured. The concentration of pyridine in the aqueous phase was measured by the cyanogen bromide and aniline method (9). For the determination of the β-picoline concentration in the aqueous phase, the bromide–thiocyanate method in the presence of sulphanilic acid (10) was used. Values of partition coefficients (P_β) were calculated from the D-values determined by the above procedures.

For ir studies, the solid complexes were prepared by liquid–liquid extraction. Base (0.02 M pyridine or β-picoline) was added to an aqueous solution of cadmium sulphate (0.01 M) and the mixture was warmed to dissolve all the base. After being cooled, the solution was treated with an aqueous solution of sodium salicylate (0.02 M) when the mixed complex separated. This dissolved when the mixture was extracted with an equal volume of benzene. The benzene layer was separated and allowed to evaporate slowly at room temperature. The colourless crystals of the complex were washed with benzene. The infrared spectra of the ligands and solid complexes were taken in a KBr medium with Beckman IR-20, range 4000–250 cm^{-1}.

Results and Discussion

For the extraction of cadmium(II) into n-butanol with salicylic acid alone plots of log D vs. pH (Fig. 1, curve a) and log D vs. log $[H_2Sal]_{total}$ (Fig. 2, curve a) gave straight lines of slope near 2. This indicates the release of two protons and the utilization of two acid molecules per cadmium atom for complexation. Since the species is not extracted into benzene or any solvent other than alcohol, it is probable that the species is highly hydrophilic and

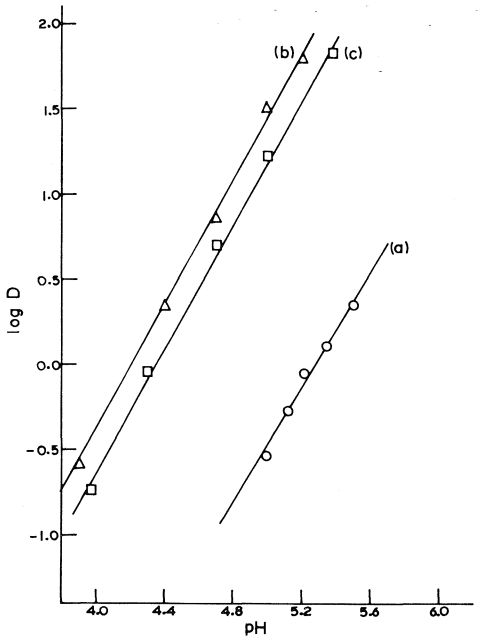

FIG. 1. The effect of pH on the extraction of Cd^{2+} with salicylic acid at constant acid concentration: (*a*) n-butanol; (*b*) benzene–β-picoline; (*c*) benzene–pyridine.

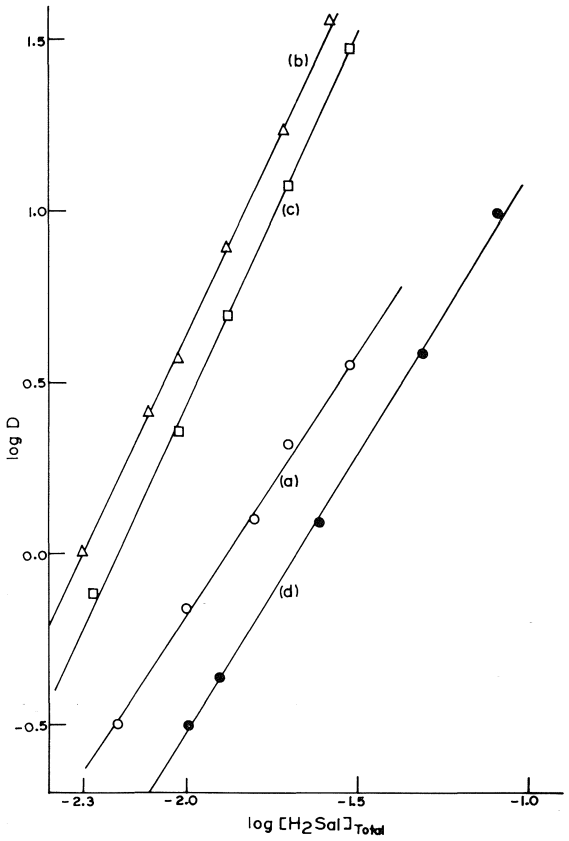

FIG. 2. The effect of salicylic acid concentration on the extraction of Cd^{2+} at constant pH and metal ion concentration: (*a*) n-butanol; (*b*) benzene–β-picoline; (*c*) benzene–pyridine; (*d*) benzene–quinoline.

that only alcohol as solvent can replace water molecules from the coordination sphere. When log D was plotted against log [ROH] using benzene as a neutral diluent (Fig. 3), a straight line of slope near 1 was obtained, suggesting the ratio 1:1 for cadmium-to-alcohol. Thus the species in n-butanol can be represented as $[Cd(HSal)_2 \cdot BuOH \cdot H_2O]$ assuming the coordination number of cadmium to be 4.

Benzene as a neutral diluent produces a negligible extraction of cadmium salicylate, but if it contains pyridine, β-picoline, or quinoline, much higher values of the extraction are obtained due to the replacement of the water molecules from coordination sphere by the neutral donor.

For the extraction of cadmium(II) salicylate into benzene in the presence of organic bases, plots of log D vs. pH (Fig. 1, curves b and c) and log D vs. log $[H_2Sal]_{total}$ (Fig. 2, curves b, c, and d) gave slopes near 2, suggesting the release of two protons and the utilization of two acid molecules per cadmium atom for the formation of the mixed complex also. Again log D was plotted against log $[B]_{total}$ (Fig. 4, curves a, b, and c) and straight lines of slope near 2 were

Can. J. Chem. Downloaded from www.nrcresearchpress.com by 210.87.254.40 on 09/05/12
For personal use only.

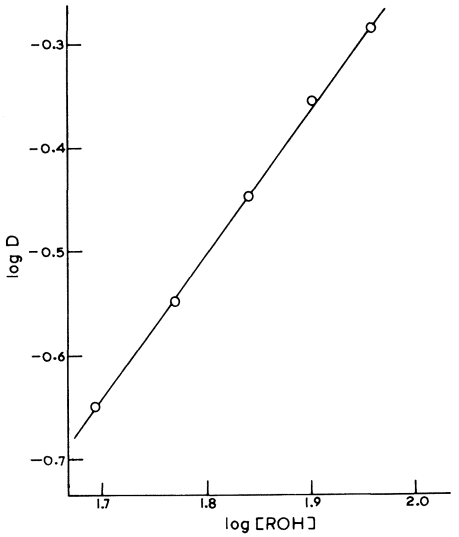

FIG. 3. Effect of *n*-butanol concentration on the extraction of Cd^{2+} with salicylic acid.

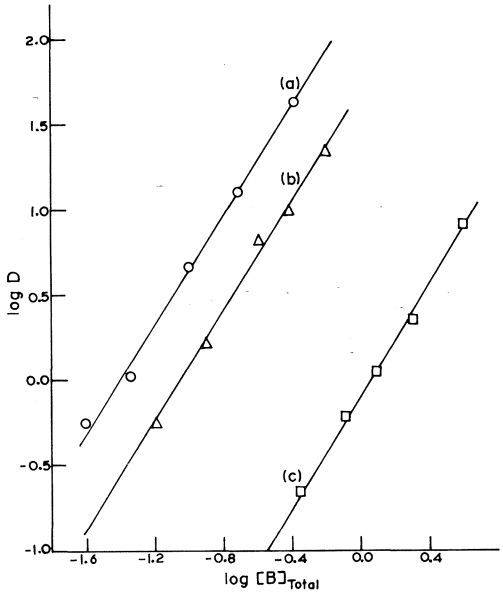

FIG. 4. Effect of base concentration on the extraction of Cd^{2+} with salicylic acid at constant pH and acid concentration: (*a*) benzene–β-picoline; (*b*) benzene–pyridine; (*c*) benzene–quinoline.

obtained suggesting the utilization of two base molecules per cadmium atom. Thus the extracting species may be represented as $[Cd(HSal)_2 \cdot 2B]$. The absence of water molecule in the species is indicated by almost quantitative extractions of cadmium salicylate in the presence of these bases at most of the experimental conditions. It has been noticed that of the different nitrogen-containing organic bases used in the study, α-picoline is quite unable to enhance extractions. This may be due to the poor basicity of α-picoline; steric factors may also play a role.

The equation for the formation of the mixed complex can be represented as:

$$Cd^{2+} + 2HSal^-{}_{aq} + 2B_{aq} \rightleftharpoons Cd(HSal)_2 \cdot 2B$$

The equilibrium constant for the reaction is given by

$$K_{ex} = \frac{[Cd(HSal)_2 \cdot 2B]_0}{[Cd^{2+}]_{aq}[HSal^-]_{aq}{}^2[B]_{aq}{}^2}$$

Hence

$$[1] \quad \log D = \log K_{ex} + 2 \log [HSal^-]_{aq} + 2 \log [B]_{aq}$$

where

$$D = \frac{[Cd(HSal)_2 \cdot 2B]_0}{[Cd^{2+}]_{aq}}$$

The mass balance for salicylic acid is given by the relation

$$\begin{aligned}[H_2Sal]_{total} &= [H_2Sal]_0 + [H_2Sal]_{aq} + [HSal^-]_{aq} \\ &\quad + [Cd(HSal)_2 \cdot 2B]_0 + 2[(H_2Sal)_2]_0 \\ &= [HSal^-]_{aq}\{(ps + 1)([H^+]/K_1) + 1\} \\ &\quad + 2[Cd(HSal)_2 \cdot 2B]_0 \\ &\quad + 2K_{dim}\{[HSal^-]_{aq} ps [H^+]/K_1\}^2\end{aligned}$$

where ps (4) is the partition coefficient, K_1 is the first dissociation constant, and K_{dim} is the dimerization constant of salicylic acid in benzene.

Since the values of $[H_2Sal]_{total} < 1$, the $[HSal^-]_{aq}{}^2$ term can be neglected compared to the $[HSal^-]_{aq}$ term and the above relation simplifies to

$$[2] \quad [HSal^-]_{aq} = \frac{[H_2Sal]_{total} - 2[Cd(HSal)_2 \cdot 2B]_0}{\{(ps + 1)([H^+]/K_1) + 1\}}$$

The mass balance for the base is given by

$$[B]_{total} = [B]_{org} + [B]_{aq} + [BH^+]_{aq} + 2[Cd(HSal)_2 \cdot 2B]_0$$

and hence

$$[3] \quad [B]_{aq} = \frac{[B]_{total} - 2[Cd(HSal)_2 \cdot 2B]_0}{\{P_B + 1 + [H^+]/K_{BH^+}\}}$$

where P_B and K_{BH^+} are the partition coefficient and ionization constant of BH^+ of the base. K_{BH^+} values are taken from the literature (11, 12) and P_B values are calculated by using the expression:

$$\begin{aligned}[B]_{total} &= [B]_{org} + [B]_{aq} + [BH^+]_{aq} \\ &= [B]_{aq}[1 + P_B + [H^+]/K_{BH^+}]\end{aligned}$$

TABLE 1. Variation of $[HSal^-]_{aq}$ at constant $[B]_{total}$ and pH

log $[H_2Sal]_{total}$	log D	log $[HSal^-]_{aq}$	log $[B]_{aq}$	log K_{ex}	log K
(*a*) β-Picoline, $[B]_{total}$ = 0.25 *M* and pH = 5.0					
−2.301	−0.009	−2.319	−1.455		
−2.000	0.563	−2.015	−1.455	7.58	6.50
−1.690	1.229	−1.712	−1.455		
−1.601	1.558	−1.614	−1.455		
(*b*) Pyridine, $[B]_{total}$ = 0.5 *M* and pH = 5.0					
−2.301	−0.104	−2.317	−0.944		
−2.000	0.346	−2.015	−0.944	6.38	5.46
−1.690	1.079	−1.712	−0.944		
−1.523	1.473	−1.534	−0.944		

TABLE 2. Variation of $[B]_{aq}$ at constant $[H_2Sal]_{total}$ and pH

log $[B]_{total}$	log D	log $[B]_{aq}$	log $[HSal^-]_{aq}$	log K_{ex}	log K
(*a*) β-Picoline, $[H_2Sal]_{total}$ = 0.02 *M* and pH 5.0					
−1.602	−0.245	−2.456	−1.712		
−1.301	−0.013	−2.154	−1.712	7.81	6.73
−1.000	0.666	−1.854	−1.712		
−0.301	1.105	−1.552	−1.712		
(*b*) Pyridine, $[H_2Sal]_{total}$ = 0.02 *M* and pH 5.0					
−1.204	−0.244	−1.844	−1.712		
−0.903	0.225	−1.544	−1.712	6.72	5.80
−0.602	0.819	−1.242	−1.712		
−0.426	0.997	−1.066	−1.712		

Thus

$$P_B = \frac{[B]_{total}}{[B]_{aq}} - (1 + [H^+]/K_{BH^+})$$

where

$$P_B = \frac{[B]_{org}}{[B]_{aq}}$$

and

$$K_{BH^+} = \frac{[H^+][B]_{aq}}{[BH^+]_{aq}}$$

The average values of partition coefficients obtained are 1.95 and 1.85 for pyridine and β-picoline respectively.[2] Equilibrium concentrations $[HSal^-]_{aq}$ and $[B]_{aq}$ are calculated using eqs. [2] and [3].

The extraction constant (K_{ex}) is calculated using eq. [1] and the formation constant (K) by the relation log K = log K_{ex} − log P(complex). Partition coefficient values of the complex (P(complex)) are calculated from the limiting values of their percent extraction. The results for β-picoline and pyridine systems are given in Tables 1 and 2. The data for quinoline are not given. As its distribution (11) is highly in favour of organic phase (ps > 100) when compared with other bases, it is quite likely that in this case a mixed complex is formed in the organic phase.

As shown by the extraction data the different bases are effective in synergism in the order β-picoline > pyridine > quinoline. The stabilities of the mixed complexes follow the order β-picoline > pyridine > α-picoline. A similar sequence of stability of complexes has been observed in other systems both the strength of the base and steric factors (13) of which are also considered.

The infrared spectra of cadmium salicylate–pyridine and β-picoline complexes are almost the same. The spectra is quite complicated in the region 1650–400 cm^{-1} and the interpretation is somewhat difficult due to the overlap of frequencies of coordinated bases with those of coordinated salicylate. In 1650–1500 cm^{-1} region both C=N and C=C of pyridine and asymmetric OCO stretching of salicylate ion occur. The peak at 1630 cm^{-1} may be due to the absorption of coordinated pyridine and peak at 1580 cm^{-1} may be assigned to asymmetric OCO absorption. The peak around 1390 cm^{-1} is due to cadmium salicylate complex. However the doublet at 1480 cm^{-1} and 1460 cm^{-1} may be due to sym-

[2]Data for the determination of partition coefficients are available, at a nominal charge, from the Depository of Unpublished Data, CISTI, National Research Council of Canada, Ottawa, Ont., Canada K1A 0S2.

Can. J. Chem. Downloaded from www.nrcresearchpress.com by 210.87.254.40 on 09/05/12
For personal use only.

metric OCO stretching vibrations of the salicylate ion.

As the spectra in the region 1650–400 cm^{-1} gives no conclusive information, attention was concentrated on the hydroxyl absorption region. The following bonding possibilities in the complex may be present: (*i*) the complex may be an ionised salt such as $[Cd(py)_2]^{2+}[HSal^-]_2$; (*ii*) the complex is an adduct of formally neutral complex $[Cd(HSal)_2]\cdot 2py$; (*iii*) all ligands are coordinated $[Cd(HSal)_2\cdot 2py]$.

If the complex is an ionised salt (case (*i*)), the $HSal^-$ would be present as an intramolecularly hydrogen bonded species.

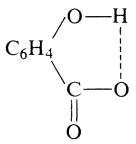

Therefore the spectra of such complex would only show vibrations due to associated OH-groups (O—H...O) at around 3000–2500 cm^{-1} and no peak due to free OH group would be expected. The absence of peak in the region 3000–2500 cm^{-1} rules out the possibility (*i*) where the complex is a simple salt type. It will be difficult to distinguish between the possibilities (*ii*) and (*iii*) where both the salicylate ions are coordinated. In both the cases, strong absorption due to O—H...O should be absent, whereas vibration due to the M—O...H group would be present with lower vibration frequency than that of OH in water. Considerable absorptions occur at $\sim 3420\ cm^{-1}$ and $3080\ cm^{-1}$. These two peaks can safely be assigned to the OH absorption of the bonded (M—O...H) OH groups. No such peak around $3400\ cm^{-1}$ has been observed in case of sodium salicylate, where the phenolic OH group is involved in hydrogen bonding.

Acknowledgement

The financial assistance of University Grants Commission, New Delhi, India is gratefully acknowledged.

1. H. J. De Brium, D. K. Kairaltis, and L. Szego. Aust. J. Chem. **15**, 218 (1962).
2. B. H. Bernstrom. Acta Chem. Scand. **10**, 174 (1956).
3. V. Pandu Ranga Rao and V. V. Rama Sastri. J. Inorg. Nucl. Chem. **36**, 415 (1974).
4. H. M. N. H. Irving and S. P. Sinha. Anal. Chim. Acta, **51**, 39 (1970).
5. J. Aggett and P. Crossley. J. Inorg. Nucl. Chem. **29**, 1113 (1967).
6. J. Aggett, B. T. Evans, and R. Hancock. J. Inorg. Nucl. Chem. **30**, 2529 (1968).
7. J. Aggett, P. Crossley, and R. Hancock. J. Inorg. Nucl. Chem. **31**, 3241 (1969).
8. B. Hok. Kem. Svensk Tidskr. **65**, 182 (1953).
9. F. D. Snell and C. T. Snell. Colorimetric methods of analysis. Vol. IV. D. Van Nostrand Company, Inc., Princeton, NJ. 1962. p. 245.
10. F. D. Snell and C. T. Snell. Colorimetric methods of analysis. Vol. IV. A. D. Van Nostrand Company, Inc., Princeton, NJ. 1967. p. 467.
11. H. M. N. H. Irving and N. S. Al-Niami. J. Inorg. Nucl. Chem. **27**, 1671 (1965).
12. H. Akaiwa and H. Kawamoto. J. Inorg. Nucl. Chem. **29**, 1345 (1967).
13. H. Kawamoto and H. Akaiwa. J. Inorg. Nucl. Chem. **31**, 1141 (1969).

Can. J. Chem. Downloaded from www.nrcresearchpress.com by 210.87.254.40 on 09/05/12
For personal use only.

The crystal structures of $S_7NSN(CH_3)_2$ and $(C_6H_{11})_2NSN(C_6H_{11})_2$

ROBERT B. BRUCE, RONALD J. GILLESPIE,[1] AND DAVID R. SLIM
Department of Chemistry, McMaster University, Hamilton, Ont., Canada L8S 4M1

Received February 1, 1978

ROBERT B. BRUCE, RONALD J. GILLESPIE, and DAVID R. SLIM. Can. J. Chem. **56**, 2927 (1978).

The compound $S_7NSN(CH_3)_2$ has been prepared by the reaction of S_7NH with $S[N(CH_3)_2]_2$. Crystals are orthorhombic with $a = 12.412(4)$, $b = 23.894(6)$, $c = 8.132(2)$ Å, $Z = 8$, space group *Pbca*. The structure was refined to a final agreement index R_1 of 0.051 for 1721 observed reflections. The structure of $S[N(C_6H_{11})_2]$ was also determined for comparison. The crystals are monoclinic with $a = 13.74(2)$, $b = 6.196(8)$, $c = 13.74(2)$ Å, $\beta = 91.26(8)°$, $Z = 2$, space group *I*2. The structure was refined to a final agreement index, R_1, of 0.052 for 1024 observed reflections.

ROBERT B. BRUCE, RONALD J. GILLESPIE et DAVID R. SLIM. Can. J. Chem. **56**, 2927 (1978).

Le composé $S_7NSN(CH_3)_2$ a été preparé par la réaction de S_7NH avec $S[N(CH_3)_2]_2$. Les cristaux sont orthorhombiques $a = 12.412(4)$, $b = 23.894(6)$, $c = 8.132(2)$ Å, $Z = 8$, groupe d'espace *Pbca*. On a raffiné la structure jusqu'à une valeur finale de R_1 de 0.051 pour 1721 réflexions observées. Pour faire une comparaison avec celle de $S_7NSN(CH_3)_2$ la structure de $S[N(C_6H_{11})_2]$ a été aussi determinée. Les cristaux sont monocliniques, $a = 13.74(2)$, $b = 6.196(8)$, $c = 13.75(2)$ Å, $\beta = 91.26(8)°$, $Z = 2$, groupe d'espace *I*2. On a raffiné la structure jusqu'à une finale de R_1 de 0.052 pour 1024 réflexions observées.

Can. J. Chem. Downloaded from www.nrcresearchpress.com by 210.87.254.105 on 09/05/12
For personal use only.

Introduction

As part of a wider investigation of the chemistry of S_7NH, S_4N_4, and other sulfur nitrogen compounds, we have prepared the compound $S_7NSN(CH_3)_2$ and determined its crystal structure by X-ray crystallography. In order to facilitate an understanding of the bonding in the NSN system we have also determined the structure of $S[N(C_6H_{11})_2]_2$ as the only previous study of a compound of the type $S(NR_2)_2$ had been made by electron diffraction (1).

Heptasulfurimide has a remarkably acidic proton which reacts readily even with weak bases. For example, it donates a proton to bis(trimethyl)silylamine to give the trimethylsilyl derivative (2).

$$S_7NH + [(CH_3)_3Si]_2NH \rightarrow S_7NSi(CH_3)_3 + (CH_3)_3SiNH_2$$

A similar reaction occurs with *NN'*-thiobisamines

$$S_7NH + S(NR_2)_2 \rightarrow S_7NSNR_2 + HNR_2$$

The methyl, ethyl, isopropyl, and cyclohexyl derivatives were all prepared by this reaction. They are pale yellow crystalline solids of relatively low melting point. The methyl derivative, which gave the best-shaped crystals, was chosen for X-ray studies.

Experimental

(a) $S_7NSN(CH_3)_2$

Heptasulfurimide was prepared by a method similar to that described by Brauer (3). Dimethylformamide (3.5 ℓ) was saturated with ammonia at −20°C and while ammonia was continually bubbled through the solution, sulfur monochloride (350 ml) was added in 15 ml aliquots below the surface of the solution by means of a syringe. Since the reaction was vigorous the solution was cooled to −20°C before each addition of S_2Cl_2. When all the S_2Cl_2 had been added, the bubbling of ammonia was continued for another 15 min. The deep blue solution was allowed to stand for a further 30 min and then added slowly to 50 ℓ of 1% aqueous HCl with constant stirring. The purple–pink mixture was then neutralised with 10% HCl which caused the colour of the solution to turn slightly brown and then to orange at the equivalence point. The suspension was allowed to settle overnight and the solution was decanted, leaving a yellow solid. After drying in air for 24 h, it was extracted with tetrahydrofuran which was then removed on a rotary extractor and the resultant brown oil dissolved in a minimum of hot methanol. Upon cooling pale yellow plate-like crystals were obtained which were vacuum dried and recrystallised from carbon disulfide to remove traces of sulfur. The typical yield was 30 g of pale yellow rectangular block shaped crystals (mp 113°C, literature 113°C (3)).

Powdered S_7NH (0.01 mol, 2.39 g) and an excess of *NN'*-thiobisdimethylamine (0.03 mol, 11.8 g) were added to benzene (10 ml) at 50°C. After stirring for 90 min a red solution was obtained. The solvent was removed under vacuum leaving a red oil which was separated into its components on a silica gel column using hexane as the eluent. The first fraction off the column gave $S_7NSN(CH_3)_2$ as yellow crystals on evaporation of the hexane (yield 2 g, mp 55°C). *Anal.* calcd. for $S_8N_2C_2H_6$: S 81.54, N 8.91, C 7.63, H 1.92; found: S 81.70, N 8.88, C 7.76, H 1.87. The second fraction, on evaporation of the hexane, gave a yellow oil consisting of a mixture of the compounds $(CH_3)_2NS_xN(CH_3)_2$ where $x > 1$.

(b) NN'-Thiobisdicyclohexylamine

A solution of SCl_2 (0.2 mol, 12.7 ml) in ether (200 ml) was added dropwise to dicyclohexylamine (0.8 mol, 160 ml) in 3 ℓ of ether at 0°C with vigorous stirring. The mixture was allowed to warm to room temperature and, after filtering, the solvent was removed on a rotary extractor. The resultant yellow oil was dissolved in a minimum amount of hot benzene. Pale yellow crystals resulted on cooling and were purified by two further recrystallisations. A typical yield was 30 g of colourless crystals (mp 149–150°C, literature 150°C (4)).

[1]To whom correspondence should be addressed.

Can. J. Chem. Downloaded from www.nrcresearchpress.com by 210.87.254.105 on 09/05/12
For personal use only.

TABLE 1. Positional and thermal parameters* ($\times 10^3$) for $S_7NSN(CH_3)_2$

Atom	x/a	y/b	z/c	U_{11}	U_{22}	U_{33}	U_{12}	U_{13}	U_{23}
S(1)	171.3(1)	404.7(2)	122.1(2)	48.0(8)	64.0(9)	63.1(9)	3.4(7)	12.1(7)	−8.4(8)
S(2)	126.1(1)	333.3(1)	6.9(2)	35.6(6)	61.0(9)	61.9(6)	−3.6(6)	−9.5(6)	8.4(8)
S(3)	182.1(1)	266.3(1)	141.8(2)	34.3(6)	65.2(9)	60.4(9)	−1.8(6)	2.9(6)	16.8(7)
S(4)	322.3(1)	241.2(1)	36.1(2)	50.0(8)	67(1)	69(1)	8.4(7)	7.0(8)	−2.6(8)
S(5)	444.2(1)	281.1(1)	155.3(2)	30.7(6)	96(1)	77(1)	4.8(7)	−2.3(7)	32.2(9)
S(6)	479.7(1)	351.9(1)	23.4(2)	33.9(7)	100(1)	80(1)	−2.1(8)	9.1(8)	28.9(9)
S(7)	405.5(1)	417.9(1)	131.3(2)	56.4(8)	83(1)	66(1)	−19.6(9)	−19.8(8)	−3.7(9)
S(8)	278.6(1)	476.1(1)	−129.1(2)	66.7(9)	43.8(8)	64(1)	0.7(7)	2.2(8)	−0.8(7)
N(1)	286.5(1)	429.8(2)	35.6(6)	37(4)	56(4)	54(3)	−6(3)	−5(3)	−3(3)
N(2)	303.9(4)	444.3(2)	−300.4(6)	45(2)	56(3)	54(3)	1(2)	−1(2)	6(2)
C(1)	414.5(8)	433.1(5)	−347.4(9)	62(5)	134(10)	67(5)	25(6)	19(4)	24(6)
C(2)	222.8(9)	406.6(4)	−369.2(9)	87(6)	77(6)	54(4)	−19(5)	−6(4)	−1(4)

Atom	x/a	y/b	z/c	U
H(1)	460.8(8)	35(4)	194(12)	82(38)
H(2)	426(7)	104(3)	189(10)	46(25)
H(3)	415(6)	74(3)	36(9)	68(21)
H(4)	237(7)	98(3)	19(10)	60(23)
H(5)	228(5)	129(3)	181(8)	33(17)
H(6)	155(9)	77(4)	163(13)	134(47)

*Anisotropic temperature factors (U_{ij}) are given by the expression $\exp[-2\pi^2(a^{*2}h^2U_{11} + b^{*2}k^2U_{22} + c^{*2}l^2U_{33} + 2a^*b^*hkU_{12} + 2a^*c^*hlU_{13} + 2b^*c^*klU_{23})]$.

Crystal Data

$S_7NSN(CH_3)_2$ fw = 314.4
Orthorhombic, a = 12.412(4), b = 23.894(6), c = 8.132(2) Å, U = 2412.3 Å^3, Z = 8, D_c = 1.74 g cm^{-3}, $F(100)$ = 1280, λ(Mo-K$\bar{\alpha}$) = 0.71069 Å, μ(Mo-K$\bar{\alpha}$) = 14 cm^{-1}.

The unit cell parameters were obtained from a least-squares refinement of 15 reflections in the region $20° < 2\theta < 25°$. Weissenberg and precession photographs indicated that reflections were absent for $hk0$ when $h = 2n + 1$, $0kl$ when $k = 2n + 1$, and $h0l$ when $l = 2n + 1$, characteristic of the space group *Pbca* (No. 61 D_{2h}^{15}) (5).

$(C_6H_{11})_2NSN(C_6H_{11})_2$ fw = 392.1
Monoclinic a = 13.74(2), b = 6.196(6), c = 13.75(2) Å, β = 91.26(5)°, U = 1170.2 Å^3, Z = 2, D_c = 1.11 g cm^{-3}, $F(000)$ = 436, λ(Mo-K$\bar{\alpha}$) = 0.71069 Å, μ(Mo-K$\bar{\alpha}$) = 1.6 cm^{-1}.

The unit cell parameters were obtained from a least-squares refinement of 15 reflections in the region $20° < 2\theta < 25°$. Weissenberg and precession photographs indicated that reflections were absent for hkl when $h + k + l = 2n + 1$, characteristic of the space groups $I2$, Im, and $I2/m$. Refinement was successfully completed in the non-standard space group $I2$ which is an alternative setting for the space group $C2$ (No. 7, C_s^2) (5). The equivalent positions of $I2$ are: x, y, z; $\bar{x}, y, \bar{z}$; $1/2 + x, 1/2 + y, 1/2 + z$; $1/2 - x, 1/2 + y, 1/2 - z$.

X-ray Measurements

(a) $S_7NSN(CH_3)_2$

The crystal, which was an approximate cube of side 0.40 mm, was attached to a glass fibre and mounted on a Syntex $P\bar{1}$ diffractometer with the c axis almost coincident with the ϕ axis of the diffractometer. Intensities were measured with graphite monochromated radiation, using a θ–2θ scan, with a scan rate varying from 8.0 to 24.0°/min in 2θ, so that the weaker reflections were examined more slowly to minimize counting errors. Stationary background counts, with a time equal to one-half the scan time for each reflection, were made at each end of the scan range. One standard reflection was regularly checked every 50 reflections to monitor the stability of the crystal and its alignment, but no significant variation was observed. A total of 3980 reflections within a quadrant with $2\theta < 55°$ were measured. Subsequent averaging resulted in a total of 2133 independent reflections, of which 1721 were considered observed at the significance level $I/\sigma(I) = 3$ where $\sigma(I)$ is the standard deviation from counting statistics. Lorentz and polarisation corrections were applied to the observed intensities, but an absorption correction was not considered necessary (μ = 14 cm^{-1}).

(b) $(C_6H_{11})_2NSN(C_6H_{11})_2$

The crystal which was an irregular block of approximate dimensions 0.25 × 0.30 × 0.22 mm was attached to a glass fibre and mounted on a Syntex $P\bar{1}$ diffractometer with its 0.25 mm edge, which was perpendicular to the (110) face almost coincident with the ϕ axis of the diffractometer. Data were collected in a similar manner to that described above.

A total of 1432 reflections within a quadrant with $2\theta < 50°$ were measured and subsequent averaging resulted in 1101 independent reflections of which 1024 were considered observed at the significance level $I/(\sigma)I = 3$ where $\sigma(I)$ is the standard deviation from counting statistics. Lorentz and polarisation corrections were applied but an absorption correction was not considered necessary (μ = 1.6 cm^{-1}).

Structure Determination

(a) $S_7NSN(CH_3)_2$

The structure factors were put on an absolute scale by accurately calculating the distribution of E-values for all intensities. The most consistent set of signs for 138 of the 168 reflections which had E values above 1.8 was determined using the direct methods programs SINGEN and PHASE from the X-ray 71 system (6). The E map, computed using the calculated phases revealed eight large peaks, which were assumed to correspond to sulfur atoms. A full-matrix least-squares refinement, using scattering curves of neutral atoms and position and isotropic thermal parameters gave a value of $R_1 = [(\Sigma|F_o|^2 - |F_c|^2)/\Sigma F_o^2]^{1/2}$ of 0.21. The positions of the two carbon and two nitrogen atoms were located from an electron density map and further refinement reduced R_1 to 0.15. Anisotropic temperature factors were introduced and R_1 was lowered to 0.062. The positions of the six hydrogen atoms

TABLE 2. Positional and thermal parameters* ($\times 10^3$) for $(C_6H_{11})_2NSN(C_6H_{11})_2$

Atom	x/a	y/b	z/c	U_{11}	U_{22}	U_{33}	U_{12}	U_{13}	U_{23}
S	0000	0000	0000	37.4(8)	39.5(9)	40.4(8)	0	−6.9(6)	0
N	34.1(3)	152.0(8)	94.0(3)	30(2)	70(3)	38(2)	−9(2)	−3(2)	−13(2)
C(1)	−34.3(3)	195.5(9)	171.0(3)	29(2)	55(3)	46(3)	0(2)	−1(2)	−4(3)
C(2)	−11.7(3)	65.7(9)	261.4(3)	41(2)	63(4)	44(2)	3(2)	5(2)	7(2)
C(3)	−88.1(4)	100(1)	338.4(4)	58(3)	88(4)	58(4)	−4(4)	22(3)	3(4)
C(4)	−100.4(6)	332.5(9)	360.7(5)	71(4)	87(5)	66(4)	−5(4)	33(3)	15(4)
C(5)	−122.5(4)	464(1)	271.7(5)	49(3)	74(5)	107(4)	10(4)	18(3)	−18(4)
C(6)	−44.7(4)	431.3(9)	194.0(4)	41(3)	54(3)	62(3)	1(2)	−1(2)	−7(2)
C(7)	137.3(3)	209.1(9)	111.8(3)	29(2)	53(3)	39(2)	−6(2)	−4(2)	−6(3)
C(8)	201.6(3)	10.6(9)	106.5(3)	34(2)	55(3)	65(3)	−4(3)	−9(2)	−8(4)
C(9)	307.1(3)	75.0(9)	131.0(4)	35(3)	64(4)	76(4)	5(3)	−13(3)	0(3)
C(10)	341.3(3)	253.4(9)	66.9(4)	33(3)	74(4)	69(4)	−8(3)	4(2)	−19(3)
C(11)	276.6(3)	448.0(9)	73.0(4)	39(3)	57(4)	58(3)	−11(3)	4(2)	−9(3)
C(12)	171.6(3)	387.1(9)	46.8(3)	37(3)	48(3)	54(3)	−7(2)	−4(2)	3(3)

Atom	x/a	y/b	z/c	Atom	x/a	y/b	z/c	Atom	x/a	y/b	z/c
H(1)	−96	138	140	H(9)	−189	422	245	H(16)	350	−55	125
H(2)	54	111	288	H(10)	190	493	218	H(17)	410	293	86
H(3)	−6	−91	244	H(11)	−65	513	132	H(18)	342	201	−2
H(4)	−69	19	400	H(12)	137	263	181	H(19)	280	507	142
H(5)	−153	39	315	H(13)	178	−100	155	H(20)	300	564	28
H(6)	−152	357	410	H(14)	197	−52	40	H(21)	128	516	53
H(7)	−39	392	393	H(15)	313	121	202	H(22)	168	336	−23
H(8)	−128	622	290								

*Anisotropic temperature factors (U_{ij}) are given by the expression exp $[-2\pi^2(a^{*2}h^2U_{11} + b^{*2}k^2U_{22} + c^{*2}l^2U_{33} + 2a^*b^*hkU_{12} + 2a^*c^*hlU_{13} + 2b^*c^*klU_{23})]$.

were located from a three-dimensional difference electron density map. Isotropic temperature factors were introduced for the hydrogen atoms and further least-squares refinement converged to a final R_1 value of 0.064 for the 2133 independent reflections or 0.051 for the 1721 observed reffections and the largest shift Δ/σ in the final cycle was 0.1. A final difference electron density map showed no peak greater than 0.5 e/Å^3. The final positional coordinates and thermal parameters are given in Table 1. The asymmetric unit is shown in Fig. 1 and a projection of the unit cell down the *a* axis is given in Fig. 2.

(b) $(C_6H_{11})_2NSN(C_6H_{11})_2$

Since there are two molecules in the cell then for the space group to be *I*2/*m* the sulfur atom would have to be situated at the origin and the NSN bond angle would have to be 180°. As this is a very improbable bond angle for S(II) this space group was rejected and the space group *I*2 was assumed. Since there were 10 large peaks of similar intensity on the three-dimensional Patterson map, they were assumed to correspond to S—N or S—C vectors. The sulfur atom was placed at 000 and the positions of six light atoms, assumed to be carbon, were located from a sharpened Patterson function. Least-squares refinement of the positional and isotropic thermal parameters, using scattering curves for neutral atoms, gave an R_1 index of 0.37. The positions of the remaining non-hydrogen atoms were located from a three-dimensional electron density map and further refinement reduced R_1 to 0.15. Also the coordinates of all atoms were examined to investigate the possibility of the space group being *Im* but this proved to be unsuccessful. The refinement was continued in *I*2. The positions of the hydrogen atoms were computed assuming tetrahedral HCH bond angles and a C—H bond length of 1.00 Å. The hydrogen atoms were assigned an isotropic temperature factor of $U = 0.09$ and their positions were fixed. Anisotropic temperature factors were introduced for all the non-hydrogen atoms and refinement converged to a final R_1 of 0.056 for the 1101 independent reflections or 0.052 for the 1024 observed reflections. The largest shift Δ/σ was less than 0.1 and a final difference electron density map showed no peak greater than 0.4 e/Å^3. The final positional coordinate and thermal parameters are given in Table 2. The asymmetric unit is shown in Fig. 3 and a projection of the unit cell down the *b* axis is given in Fig. 4.

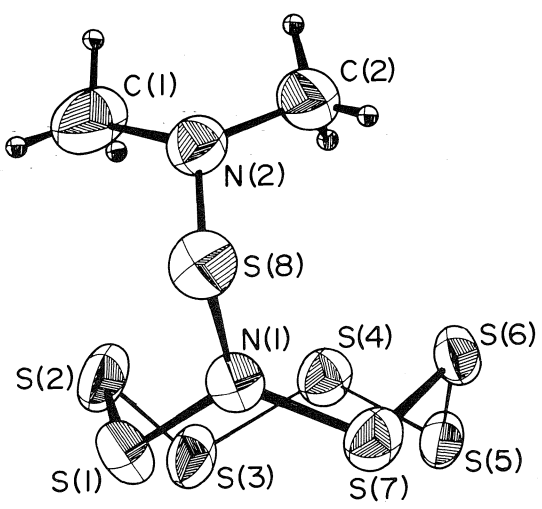

FIG. 1. The $S_7NSN(CH_3)_2$ asymmetric unit.

Tabulations of observed and calculated structure factor tables are available.[2]

[2]Complete sets of tabular data are available, at a nominal charge, from the Depository of Unpublished Data, CISTI, National Research Council of Canada, Ottawa, Ont., Canada K1A 0S2.

Can. J. Chem. Downloaded from www.nrcresearchpress.com by 210.87.254.105 on 09/05/12
For personal use only.

Can. J. Chem. Downloaded from www.nrcresearchpress.com by 210.87.254.105 on 09/05/12
For personal use only.

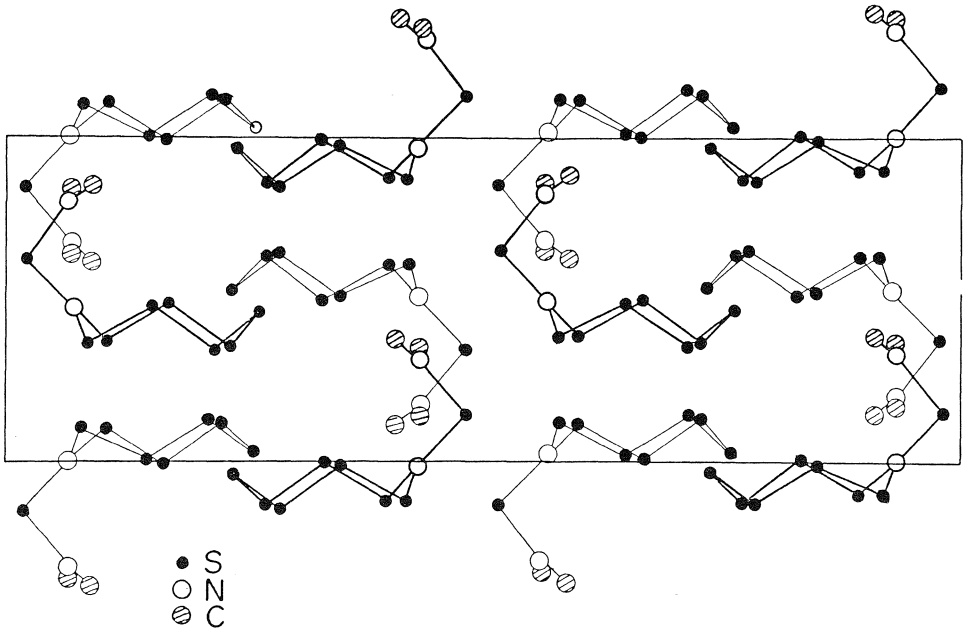

FIG. 2. The projection of the structure of $S_7NSN(CH_3)_2$ down the *a* axis.

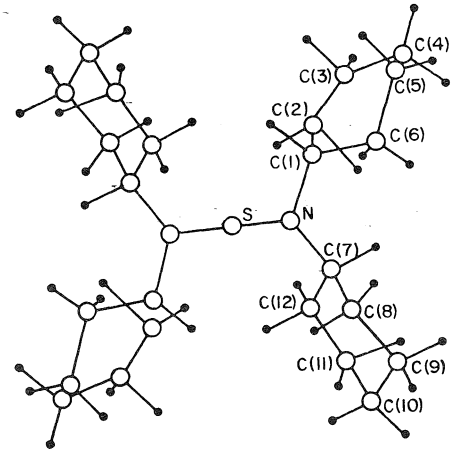

FIG. 3. The molecular unit of $(C_6H_{11})_2NSN(C_6H_{11})_2$.

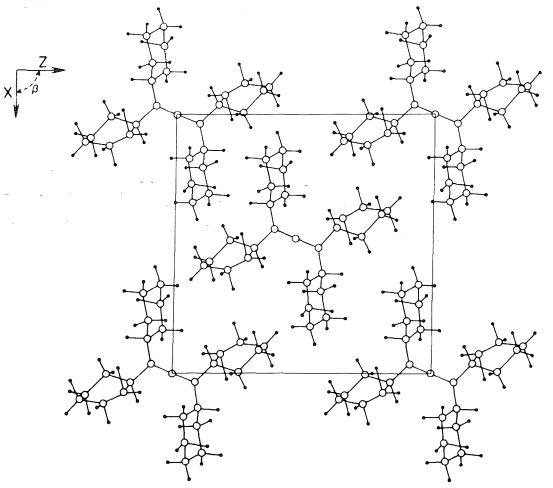

FIG. 4. The projection of the structure of $(C_6H_{11})_2NSN(C_6H_{11})_2$ down the *b* axis.

Discussion

(a) The Structure of $(C_6H_{11})_2NSN(C_6H_{11})_2$

Table 3 lists the interatomic distances and angles for $(C_6H_{11})_2NSN(C_6H_{11})_2$. The most important features of the structure are the near planarity of the three bonds around both nitrogen atoms, the comparatively short N—S distances of 1.657 Å and the NSN bond angle of 110°. These parameters are not significantly different from those observed in an electron diffraction study of $(CH_3)_2NSN(CH_3)_2$ (1). The N—S bond lengths are shorter than the value of 1.74 Å expected for a single bond, and indicate a bond order of approximately 1.2 (7). This shortening, together with the near planarity of the bonds about nitrogen, can be explained if there is delocalisation of the nitrogen lone-pair onto the S atom. This can be described as a $d\pi$–$p\pi$ bond and such delocalisation can be expected whenever a second row element with a filled shell of eight electrons is bonded to a third row element with an incomplete valence shell (8). The enhanced repulsion between these short, partially double, bonds would tend to open up the NSN bond angle from the tetrahedral angle. It is interesting to note that the four carbon atoms C(1), C(7),

TABLE 3. Interatomic distances and angles for $(C_6H_{11})_2NSN(C_6H_{11})_2$

(*a*) Bond lengths < 2.0 Å

Bond	Length	Bond	Length	Bond	Length
S—N	1.657(4)	C(1)—C(2)	1.506(7)	C(7)—C(8)	1.518(8)
N—C(1)	1.456(6)	C(2)—C(3)	1.522(8)	C(8)—C(9)	1.535(7)
—C(7)	1.477(5)	C(3)—C(4)	1.484(11)	C(9)—C(10)	1.495(9)
Mean N—C	1.467	C(4)—C(5)	1.494(10)	C(10)—C(11)	1.503(8)
		C(5)—C(6)	1.541(8)	C(11)—C(12)	1.528(7)
		C(6)—C(1)	1.503(8)	C(12)—C(7)	1.502(7)
		Mean C—C	1.511		

(*b*) Intramolecular contacts < 3.0 Å

Atom pairs	Distance	Atom pairs	Distance
S—C(1)	2.693(5)	C(3) —C(5)	2.477(11)
—C(7)	2.733(4)	—C(6)	2.926(9)
N—C(2)	2.456(6)	C(4) —C(6)	2.505
—C(6)	2.475(7)	C(7) —C(9)	2.488(6)
—C(8)	2.467(6)	—C(10)	2.900(6)
—C(12)	2.485(6)	—C(11)	2.489(7)
C(1)—C(3)	2.502(8)	C(8) —C(10)	2.510(8)
—C(4)	2.904(8)	—C(11)	2.942(9)
—C(5)	2.496(9)	—C(12)	2.506(9)
—C(7)	2.513(6)	C(9) —C(11)	2.478(9)
C(2)—C(4)	2.481(9)	—C(12)	2.908(7)
—C(5)	2.907(10)	C(10)—C(12)	2.487(7)
—C(6)	2.486(8)		

(*c*) Bond angles

Bonds	Angle	Bonds	Angle
N—S —N′	110.7(2)	C(4) —C(5) —C(6)	111.2(5)
S —N—C(1)	119.7(3)	C(5) —C(6) —C(1)	110.1(5)
S —N—C(7)	121.3(3)	C(8) —C(7) —C(12)	112.1(4)
C(1)—N—C(7)	117.9(4)	C(7) —C(8) —C(9)	109.1(5)
C(2)—C(1)—C(6)	111.4(4)	C(8) —C(9) —C(10)	111.9(5)
C(1)—C(2)—C(3)	111.4(4)	C(9) —C(10)—C(11)	111.5(4)
C(2)—C(3)—C(4)	111.2(6)	C(10)—C(11)—C(12)	110.3(5)
C(3)—C(4)—C(5)	112.6(6)	C(11)—C(12)—C(7)	110.4(4)

C(1′), and C(7′) attached to the two nitrogens are coplanar. If it is assumed that a single *d* orbital on the central sulfur atom is used in bonding with the nitrogen *p* orbitals maximum overlap is obtained if the axes of the nitrogen *p* orbitals are parallel which in turn causes the four carbon atoms to be coplanar. The two nitrogen *p* orbitals and the sulfur *d* orbital may be used to construct a bonding, a non-bonding, and an anti-bonding molecular orbital. The bonding and non-bonding orbitals are occupied by the four electrons from the two nitrogen atoms. The N—C bond lengths are shorter than a normal N—C single bond, e.g. ethylenediamine (1.47 Å) (9) which is consistent with a formal positive charge on nitrogen due to the partial double bonding postulated for the N—S bonds. The two C_6H_{11} rings have the expected chair conformation with a mean C—C bond length of 1.511 Å which is similar to that found in cyclohexane (1.52 Å) (10).

(b) The Structure of $S_7NSN(CH_3)_2$

Table 4 lists the bond lengths and angles for $S_7NSN(CH_3)_2$. The structure shows a number of interesting features. Both nitrogen atoms have an almost planar geometry indicating delocalisation of the nitrogen lone-pairs onto sulfur. However, the NSN group is not symmetrical. The bonds between the ring nitrogen and the adjacent ring sulfur atoms are short (mean 1.60 Å) indicating a bond order of 1.5 (7), which suggests essentially complete delocalisation of the lone-pair into the ring. In contrast the N(1)—S(8) bond length (1.73 Å) indicates a single bond. Thus there appears to be a strong tendency for this nitrogen lone-pair to be delocalised into the

Can. J. Chem. Downloaded from www.nrcresearchpress.com by 210.87.254.105 on 09/05/12
For personal use only.

Can. J. Chem. Downloaded from www.nrcresearchpress.com by 210.87.254.105 on 09/05/12
For personal use only.

TABLE 4. Interatomic distances (Å) and angles (deg) for $S_7NSN(CH_3)_2$

(*a*) Bond lengths < 2.1 Å

Bond	Length	Bond	Length
S(1)—S(2)	2.013(2)	N(2)—C(1)	1.345(10)
—N(1)	1.605(6)	—C(2)	1.404(11)
S(2)—S(3)	2.038(2)	C(1)—H(1)	0.98(8)
S(3)—S(4)	1.911(2)	—H(2)	0.94(7)
S(4)—S(5)	1.943(2)	—H(3)	0.96(8)
S(5)—S(6)	2.039(3)	C(2)—H(4)	0.93(8)
S(6)—S(7)	1.993(3)	—H(5)	0.95(6)
S(7)—N(1)	1.588(6)	—H(6)	0.91(10)
S(8)—N(1)	1.734(5)		
—N(2)	1.607(5)		

(*b*) Intramolecular contacts < 3.5 Å

Atom pairs	Distance	Atom pairs	Distance
S(1)—S(3)	3.312(2)	S(5)—S(7)	3.303(3)
—S(7)	2.692(2)	(S6)—N(1)	2.887(6)
—S(8)	2.922(2)	—C(2)	3.312(10)
S(2)—S(4)	3.147(2)	S(7)—S(8)	2.909(2)
S(3)—S(5)	3.014(2)	S(8)—C(1)	2.565(10)
—S(6)	3.197(3)	—C(2)	2.631(9)

(*c*) Bond angles

Bonds	Angle	Bonds	Angle
N(1)—S(1)—S(2)	109.0(2)	N(2)—C(1)—H(1)	105(5)
S(1)—S(2)—S(3)	109.7(1)	N(2)—C(1)—H(2)	103(5)
S(2)—S(3)—S(4)	105.6(1)	N(2)—C(1)—H(3)	109(4)
S(3)—S(4)—S(5)	102.9(1)	N(2)—C(2)—H(4)	111(5)
S(4)—S(5)—S(6)	106.8(1)	N(2)—C(2)—H(5)	112(4)
S(5)—S(6)—S(7)	110.0(1)	N(2)—C(2)—H(6)	100(6)
S(6)—S(7)—N(1)	106.9(2)	H(1)—C(1)—H(2)	123(7)
S(7)—N(1)—S(1)	114.9(3)	H(1)—C(1)—H(3)	117(7)
S(7)—N(1)—S(8)	122.0(3)	H(2)—C(1)—H(3)	99(6)
S(1)—N(1)—S(8)	122.2(3)	H(4)—C(2)—H(5)	107(6)
N(1)—S(8)—N(2)	110.6(3)	H(5)—C(2)—H(6)	119(8)
S(8)—N(2)—C(1)	120.5(6)	H(4)—C(2)—H(6)	109(8)
S(8)—N(2)—C(2)	121.7(5)		
C(1)—N(2)—C(2)	112.3(7)		

ring and not onto the S(8) bridging sulfur. The bonding at the nitrogen in the ring can, therefore, be described in terms of the two resonance structures **1** and **2**.

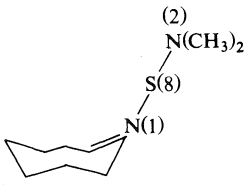

1

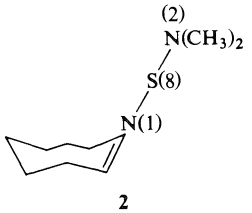

2

The dimethylamino nitrogen N(2) forms a rather short bond with S(8) (1.61 Å) indicating a bond order of approximately 1.5. This bond is stronger than that found in $(C_6H_{11})_2NSN(C_6H_{11})_2$ and appears to compensate for the relatively weak bond formed to the sulfur by N(1). The contraction in the N—C bond lengths (mean 1.37 Å) over those observed in $(C_6H_{11})_2NSN(C_6H_{11})_2$ can also be attributed to the greater formal charge in N resulting from increased delocalisation of the N(2) lone-pair.

Since the two N—S bond lengths in the ring are considerably shorter than those in S_7NH (mean 1.68 Å) (11) it appears that the delocalisation of the nitrogen lone-pair is more extensive in $S_7NSN(CH_3)_2$ than in S_7NH. This can be plausibly attributed to the repulsive effect of the formal negative charge on S(8) which results from the contribution of the resonance form **3**.

The delocalisation of the nitrogen lone-pair seems to have interesting consequences for the structure of

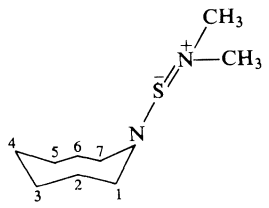

3

the ring. The average S—S bond length (1.99 Å) is very slightly less than that in S_7NH (2.02 Å) (11) and, as in S_7NH, there is a significant alternation of the S—S bond lengths between the nitrogen atom and the opposite sulfur atom. Moreover, the bond angle at S(4) is significantly smaller than the other ring angles, which do not differ significantly from those in S_7NH (11) or in S_8 (12). Unfortunately, at present, we do not understand the nature of the bonding in the S_7NH or S_8 rings sufficiently well to be able to interpret these bond length and bond angle changes in a meaningful way. However, both the relatively high acidity of the hydrogen in S_7NH and the structure of the present compound indicate clearly that there is a strong tendency for delocalisation of the nitrogen lone pair into the sulfur ring, i.e., that this ring is unsaturated in the sense that it is a strong electron pair acceptor and that acceptance of such an electron pair appears to strengthen the bonding in the ring.

1. I. HARGITTAI and M. HARGITTAI. Acta Chim. Acad. Sci. Hung. **75**, 129 (1973).
2. M. GOEHRING. Angew. Chem. **17**, 589 (1961).
3. G. BRAUER (*Editor*). Handbook of preparative inorganic chemistry. 2nd ed. Academic Press. 1965. pp. 370–372.
4. Q. E. THOMPSON. Q. Rep. Sulfur Chem. **5**, 245 (1970).
5. International tables for X-ray crystallography. Vol. 1. Kynoch Press, Birmingham, U.K. 1962.
6. J. M. STEWART, P. A. KUNDELL, and J. C. BALDWIN. X-ray 71 system of crystallography programs. University of Maryland, Technical Report, 1971.
7. R. J. GILLESPIE, P. R. IRELAND, and J. E. VEKRIS. Can. J. Chem. **53**, 21 (1975).
8. R. J. GILLESPIE. Molecular geometry. Van Nostrand Reinhold, London. 1972. p. 109.
9. A. YOKOZEKI and K. KUCHITSU. Bull. Chem. Soc. Jpn. **44**, 2926 (1971).
10. R. KAHN, R. FOURME, D. ANDRE, and M. RENAUD. Acta Crystallogr. Sect. B, **29**, 131 (1973).
11. H. J. HECHT, R. REINHARDT, R. STEUDEL, and H. BRADACZEK. Z. Anorg. Allgem. Chem. **426**, 43 (1976).
12. A. CARON and J. DONOHUE. Acta Crystallogr. **18**, 562 (1965); D. E. SANDS. J. Am. Chem. Soc. **87**, 1395 (1965).

Can. J. Chem. Downloaded from www.nrcresearchpress.com by 210.87.254.105 on 09/05/12
For personal use only.

Temperature dependence of rate constants for the reactions of oxygen atoms, O(^3P), with HBr and HI[1]

D. L. SINGLETON AND R. J. CVETANOVIĆ

Division of Chemistry, National Research Council of Canada, Ottawa, Ont., Canada K1A 0R9

Received May 30, 1978

D. L. SINGLETON and R. J. CVETANOVIĆ. Can. J. Chem. **56**, 2934 (1978).

Rate constants for the reactions O(^3P) + HX → OH + X (X = Br, I) have been determined by a phase shift technique. Oxygen atoms were generated by modulated mercury photosensitized decomposition of nitrous oxide, and were monitored by the chemiluminescence from the reaction with nitric oxide. Over the temperature interval 298–554 K, the rate constants are satisfactorily represented by the Arrhenius expressions $k_{O+HBr} = (8.09 \pm 0.86) \times 10^9 \exp(-3.59 \pm 0.08)/RT$ and $k_{O+HI} = (2.82 \pm 0.27) \times 10^{10} \exp(-1.99 \pm 0.07)/RT$, where the units are ℓ mol^{-1} s^{-1} and kcal mol^{-1}. The indicated uncertainties are one standard deviation. The results of bond energy – bond order calculations, incorporating recently proposed modifications, are discussed.

D. L. SINGLETON et R. J. CVETANOVIĆ. Can. J. Chem. **56**, 2934 (1978).

On a déterminé par la technique du déphasage les constantes de vitesse des réactions O(^3P) + HX → OH + X (où X = Br, I). Les atomes d'oxygène provenaient de la décomposition d'oxyde nitreux photosensibilisée au mercure et ils étaient détectés grâce à chemiluminescence produite par leur réaction avec l'oxyde nitrique. Dans le domaine de température 298–554 K, les constantes de vitesse sont décrites d'une manière satisfaisante par les équations d'Arrhénius $k_{O+HBr} = (8.09 \pm 0.86) \times 10^9 \exp(-3.59 \pm 0.08)/RT$ et $k_{O+HI} = (2.82 \pm 0.27) \times 10^{10} \exp(-1.99 \pm 0.07)/RT$, les unités étant ℓ mol^{-1} s^{-1} et kcal mol^{-1}. Les incertitudes indiquées ci-dessus correspondent à l'écart-type. On discute des résultats de calculs d'énergie de liaison et d'indice de liaisons, en tenant compte de modifications récemment proposées.

[Traduit par le journal]

Introduction

The reactions of ground state oxygen atoms with hydrogen halides are of interest in the chemistry of combustion because of the tendency of halogenated agents to extinguish flames. Also, the reactions of HCl and HBr are of interest in determining the impact of halogen compounds on the chemistry of the stratosphere, particularly with regard to the ozone layer. While there are a few determinations reported for the temperature dependence of the O + HCl reaction (1, 2), there is only one reported for the reaction with HBr (2), and none with HI.

Various attempts have been made to clarify the dynamics of the O(^3P) + HCl → OH($^2\Pi$) + Cl(^2P) reaction. Recently, Macdonald and Moore (3) have concluded that the reaction appears to occur adiabatically on the lowest triplet surface instead of involving a significant crossing of triplet and singlet surfaces (4).

The bond energy – bond order (BEBO) method has been fairly useful as a simple technique for predicting activation energies, at least for many reactions involving the abstraction of hydrogen by doublet species. Recently Gilliom (5, 6) proposed slight modifications in the parameters of the BEBO method, and compared calculated and experimental results for many hydrogen abstractions, although abstractions by O(^3P) were not included. Since the BEBO method generally underestimated activation energies for abstraction by O(^3P) when the older parameters were used, it was of interest in the present work to determine what improvements, if any, result when the modifications proposed by Gilliom are used for the reactions O + HX → OH + X (X = Cl, Br, I).

Experimental

The technique has been described previously (7–9). In a flowing mixture of Hg, N_2O, NO, and HX (X = Br, I), ground state oxygen atoms are formed and react according to the sequence:

$$\mathrm{Hg}(^1S_0) + h\nu(254\ \mathrm{nm}) \rightarrow \mathrm{Hg}(^3P_1)$$

$$\mathrm{Hg}(^3P_1) + \mathrm{N_2O} \rightarrow \mathrm{Hg}(^1S_0) + \mathrm{N_2} + \mathrm{O}(^3P)$$

[1] $$\mathrm{O}(^3P) + \mathrm{HX} \rightarrow \mathrm{OH} + \mathrm{X}$$

[2] $$\mathrm{O}(^3P) + \mathrm{NO} + \mathrm{M} \rightarrow \begin{cases} \mathrm{NO_2}^* + \mathrm{M} \\ \mathrm{NO_2} + \mathrm{M} \end{cases}$$

By modulating the 254 nm light, the oxygen atom concentration is modulated, as is the intensity of chemiluminescence from reaction [2]. The phase difference, ϕ, between the 254 nm light and the chemiluminescence is related to the rates of reactions [1] and [2]:

$$2\pi\nu/\tan\phi = k_1[\mathrm{HX}] + k_2[\mathrm{NO}][\mathrm{M}]$$

where ν is the modulation frequency. The phase angles are

[1]NRCC No. 16976.

Can. J. Chem. Downloaded from www.nrcresearchpress.com by 210.87.254.105 on 09/05/12
For personal use only.

TABLE 1. Rate constants for the reactions O + HBr ([1*a*]), O + HI ([1*b*]), and O + NO + M ([2])[a]

	O + HBr			O + HI			O + NO + M
T (K)	$10^7 k_{1a}$ (ℓ mol^{-1} s^{-1})	$10^{10} k_2$ (ℓ^2 mol^{-2} s^{-1})	Number of points	$10^9 k_{1b}$ (ℓ mol^{-1} s^{-1})	$10^{10} k_2$ (ℓ^2 mol^{-2} s^{-1})	Number of points	$10^{10} k_2$[b] (ℓ^2 mol^{-2} s^{-1})
298	2.12±0.10	4.61±0.09	17	0.954±0.020	4.40±0.13	15	4.84
344	4.17±0.07	3.66±0.06	14	1.69 ±0.06	3.92±0.10	15	3.70
407	9.50±0.13	2.78±0.05	15	2.50 ±0.08	2.97±0.09	14	2.80
499	22.4 ±0.5	1.93±0.11	14	3.69 ±0.08	2.12±0.12	13	2.12
554	30.5 ±1.0	1.93±0.10	18	4.68 ±0.12	1.66±0.08	22	1.87

[a]The indicated uncertainties are one standard deviation.
[b]Calculated from the previously determined (9) Arrhenius expression for this reaction.

measured with photomultipliers and a lock-in amplifier. The photomultiplier viewing the chemiluminescence was fitted with a Corning 3-70 filter. A 7-54 filter and $CoSO_4/NiSO_4$ filter were used to isolate the 254 nm light incident on the reaction cell, and interference filters were attached to the photomultipliers monitoring the incident and transmitted 254 nm light.

Flow rates were measured using a calibrated rotameter for N_2O and calibrated capillaries for NO and HX, with DC-704 oil manometers to measure the pressure drops. Temperatures were measured with a chromel–alumel thermocouple inserted into the reaction cell.

Modulation frequencies were between 1.3 and 6 kHz. The total pressure was varied at each temperature by a factor of two in the range 22–83 Torr. The approximate relative concentrations $[N_2O]/[NO]/[HX]$ were, for HBr, 100/10/(1–10) and, for HI, 100/10/(0.1–1). The residence time of gas in the reaction cell was less than 2.5 s for HBr and less than 0.4 s for HI. Oxygen atoms were generated at the rate of 10^{12} atoms cm^{-3} s^{-1} as determined by gas chromatographic determination of the products of the O(^3P) + 1-butene reaction. The extent of consumption of HX was less than 0.004% for HBr and 0.02% for HI.

The gases had the following stated purity levels (for the liquid phase, except for NO): N_2O, 98.0%; NO, 99.0%; HBr, 99.8%; HI, 98.0%. The NO was passed through Linde 13X molecular sieve to remove traces of NO_2. The HI was degassed at liquid nitrogen temperature to remove H_2 and distilled at −78°C to separate it from I_2. Exposure of the hydrogen halides to light was minimized. Also, HBr and HI were admitted to the N_2O, NO, Hg mixture downstream from the mercury saturator and just prior to the reaction cell. The reaction of Hg with HI is negligibly slow under the present conditions (10).

Results

Determination of Rate Constants

Rate constants were obtained from linear least squares treatment of plots of $2\pi\nu/[HX] \tan\phi$ vs. $[NO][M]/[HX]$. The intercepts give k_1 and the slopes, k_2. A typical plot is shown in Fig. 1. The results at each temperature are given in Table 1. The values of k_2 determined in the present work are always within 10% of the values of k_2 determined previously (9) in mixtures of N_2O, NO, and Hg.

The rate constants can be adequately represented by linear Arrhenius expressions, as shown in Fig. 2. The values of the Arrhenius parameters determined

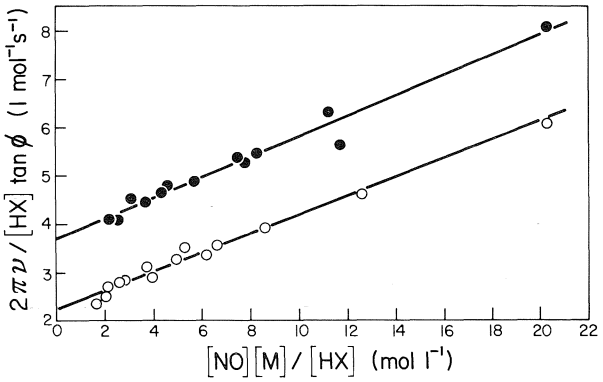

FIG. 1. Plots of $2\pi\nu/[HX] \tan\phi$ vs. $[NO][M]/[HX]$ at 499 K. The scales of the ordinate and abscissa are: for HX = HBr (○), 10^8 and 10^{-3}; for HX = HI (●), 10^9 and 10^{-2}.

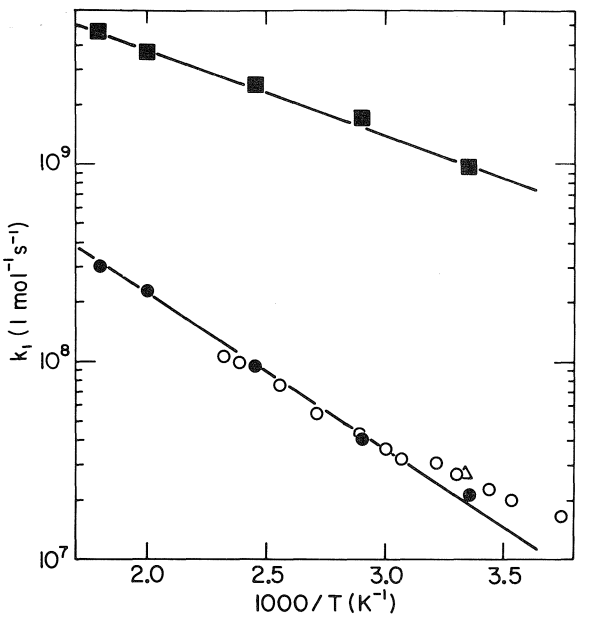

FIG. 2. Arrhenius plots of the rate constants for O + HX → OH + X. HX = HBr: ●, this work; ○, ref. 2; △, ref. 18. HX = HI: ■, this work.

Can. J. Chem. Downloaded from www.nrcresearchpress.com by 210.87.254.105 on 09/05/12
For personal use only.

Can. J. Chem. Downloaded from www.nrcresearchpress.com by 210.87.254.105 on 09/05/12
For personal use only.

TABLE 2. Comparison of rate constants and Arrhenius parameters determined for the reactions O + HBr and O + HI with literature values[a]

$10^8 k_{298}$ (ℓ mol^{-1} s^{-1})	$10^{10}A$ (ℓ mol^{-1} s^{-1})	E (kcal mol^{-1})	Reference
	O + HBr		
0.212±0.010	0.809±0.086	3.59±0.08	This work
0.268±0.012[b]	0.23 ±0.04[c]	2.68±0.10[c]	Brown and Smith (2)
0.27 ±0.06			Takacs and Glass (18)
	O + HI		
9.54	2.82 ±0.27	1.99±0.07	This work
~12			Takacs and Glass (18)

[a]Indicated uncertainties are one standard deviation.
[b]303 K.
[c]Calculated from Brown and Smith's data (2) by weighting k_i values by $(1/\sigma_{k_i})^2$ and using the appropriate transformation of the statistical weights (11).

TABLE 3. Model reaction sequence

	Reaction	k_{298}[a] X = Br	Reference	X = I	Reference
[1]	O + HX → OH + X	2.1×10^7	This work	9.5×10^8	This work
[2]	O + NO + M → NO_2 + M	4.8×10^{10}	9	4.8×10^{10}	9
[3]	OH + HX → H_2O + X	3.1×10^9	12	7.8×10^9	13
[4]	OH + NO + M → HNO_2 + M	5–9 × 10^8 [b]	14	7–13 × 10^8 [b]	14
[5]	X + NO + M → XNO + M	7–17 × 10^6 [b]	15	4–9 × 10^6 [b]	15
[6]	O + XNO → XO + NO	1×10^{10}	Estimate	1×10^{10}	Estimate
[7]	O + HNO_2 → OH + NO_2	1×10^{10}	Estimate	1×10^{10}	Estimate
[8]	O + NO_2 → O_2 + NO	5.5×10^9	16	5.5×10^9	16
[9]	XO + NO → NO_2 + X	1.3×10^{10}	17	1×10^{10}	Estimate
[10]	X + XNO → X_2 + NO	8×10^{10}	Estimate	1.6×10^{10}	15

[a]Units are ℓ mol^{-1} s^{-1} except for reaction [2] for which units are ℓ^2 mol^{-2} s^{-1}.
[b]Bimolecular rate constants applicable over the range of total pressure in these particular experiments. The values for reaction [4] are for M = N_2, and for reaction [5], M = He.

by least squares, with each k_i weighted (11) by $1/\sigma_{k_i}^2$, are given in Table 2.

Estimation of the Extent of Reaction of O(^{3}P) with Reaction Products

In the determination of the rate constants for reaction [1], it is assumed that reaction of oxygen atoms with products of the initial reactions [1] and [2] is negligible. This is a fair assumption because of the low concentration of oxygen atoms. The sequence of reactions considered most important is given in Table 3. Hydroxyl reacts with HX (reaction [3]) and with NO (reaction [4]), and the ratio of the rates of the two reactions is r_3/r_4. In the case of HBr, the conditions are such that $2 < r_3/r_4 < 19$, and for HI, $0.05 < r_3/r_4 < 0.7$ at 298 K. These ratios increase at higher temperatures because of the temperature coefficients of k_3 and k_4. The rate of oxygen atom production is too slow for the reaction O + OH → O_2 + H to compete with reactions [3] and [4]. Thus, each oxygen atom consumed in reaction [1] generates two reactive molecules, either XNO or HNO_2.

An estimate, or upper limit, of the extent of secondary reactions of oxygen atoms can be made by comparing the rates of reactions [1′] and [6′],

$$[1'] \quad O + HX \xrightarrow{(HX, NO)} 2XNO$$

$$[6'] \quad O + XNO \rightarrow \text{products}$$

assuming reactions [3] and [5] dominate over reactions [4] and [7] (although reactions [4] and [7] lead to a similar scheme, and reaction [7] could be represented by reaction [6′]). The ratio $r_{6'}/r_{1'} = k_4[XNO]/k_1[HX]$ is evaluated by taking as an upper limit, $[XNO]/[HX] \leq 2I_0/F_{HX}$, where I_0 is the rate of generation of oxygen atoms and F_{HX} is the flow rate of hydrogen halide (i.e., the ratio of concentrations of two species is equal to the ratio of their flow rates). In the worst case, i.e. at 298 K, the extreme values of F_{HBr} lead to $0.006 \leq r_{6'}/r_{1'} \leq 0.04$. For HI, the ratio is $0.0005 \leq r_{6'}/r_{1'} \leq 0.0014$. A more complicated, but also an approximate scheme, based on reactions in Table 3 and including removal of products by flow, gave values of $(r_6 + r_7)/(r_1 + r_2)$ which were between 1/4 and 1/10 of the values given above for $r_{6'}/r_{1'}$. It is therefore concluded that consumption of oxygen atoms by reactions other than [1] and [2] is negligible.

Can. J. Chem. Downloaded from www.nrcresearchpress.com by 210.87.254.105 on 09/05/12
For personal use only.

There is no interference from chemiluminescence from $X + X + M \rightarrow X_2 + M$, the rate of which is insignificant because of the low concentration of atoms. The faster route to formation of X_2 is reaction [10], and from an analysis similar to that described for secondary reactions, $r_{10}/r_5 = k_{10}[XNO]/k_5[NO][M] \leq 2I_0k_{10}/k_5[M]F_{NO}$, which has maximum values at 298 K of 0.03 and 0.06 for X = Br and X = I, respectively. The reaction $O + X_2 \rightarrow XO + X$, even if it occurred at collision frequency, would, on the time scale of the chemiluminescence measurements, be even less important than reaction [6′], which has already been shown not to be significant.

Discussion

Comparison of k_1 *with Reported Values*

The present results for O + HBr are in reasonable agreement with the results of Brown and Smith (2), as shown in Fig. 2. These authors used a discharge-flow technique and determined the concentration of oxygen atoms using the chemiluminescence from reaction [2]. They made corrections for secondary reactions of oxygen atoms by numerically integrating a set of six reactions. The uncertainties in the rate constants of these reactions and in the wall recombination rate of Br used in their model could possibly account for the differences between their results at lower temperatures and the extrapolated Arrhenius plot in the present work. There could, perhaps, also be a genuine slight curvature in the Arrhenius plot.

The present room temperature value for HBr and the value of Takacs and Glass (18) are within the reported uncertainties. Using a discharge flow system, Takacs and Glass monitored the concentrations of oxygen atoms and bromine atoms by esr spectroscopy and corrected for secondary consumption of oxygen atoms using a model consisting of four reactions.

The only reported value of k_1 for O + HI is an approximate value referred to by Takacs and Glass (18). Their value is in approximate agreement with the presently determined value at room temperature.

Bond Energy – Bond Order (BEBO) Calculations

Brown and Smith (2) have reported the results of BEBO calculations for the O + HCl and O + HBr reactions. The calculated activation energies were much smaller than the experimental values, even when they doubled the triplet repulsion energy term, as originally suggested by Mayer and Schieler (19). In a very recent paper, Brown and Smith (20) reported experimental results and theoretical calculations (BEBO and trajectory) for O + DCl and O + DBr. A quasiclassical trajectory calculation using a LEPS potential proved to be fairly successful in giving rate constants consistent with experimental results for the first three vibrational levels of HCl. On the other hand, since conventional BEBO calculations gave activation energies much too low for these reactions, Brown and Smith (20) arbitrarily varied the BEBO parameter p for HCl and HBr until calculated and observed activation energies were identical, and then used the same values of p for calculations on the deuterated molecules. The agreement between calculated and observed kinetic isotope effects was moderate.

Recently, Gilliom (5, 6), in a reply to Jordan and Kaufman's criticism (21) of the BEBO method, reported that, if in addition to modern values of the inert gas intermolecular potentials, a modified Pauling constant were used, the BEBO method would give good agreement with experimental results, even for some cases where the method had previously failed. Reactions of $O(^3P)$ were not included, however, in the many examples reported. In the present work, we have examined the results of BEBO calculations on reactions of $O(^3P)$ with HCl, HBr, and HI, using Gilliom's parameters.

In the BEBO formulation, taking O + HBr as an example, a value of the potential energy of activation, V^*, is obtained by finding the value of n, the bond order of the breaking H—Br bond, that makes V a maximum, subject to the constraint that the sum of the bond orders of the incipient O—H bond and of the breaking H—Br bond is unity (22).

$$V = D_{HBr}(1 - n^p) - D_{OH}(1 - n)^q + C_1 D_{BrO} B(n - n^2)^\gamma \{1 + B(n - n^2)^\gamma\}$$

where

$$B = 0.5 \exp[-\beta(R_{OH} + R_{HBr} - R_{BrO})]$$

$$\gamma = C_2\beta$$

In these expressions, C_1 is a constant used to scale the Sato anti-Morse function ($C_1 = 1$ in ref. 22), C_2 is the Pauling constant, β is the Morse function parameter for BrO, D and R are the normal single bond energy (corrected for zero point energy) and distance for the indicated molecules. The BEBO parameters p and q are given by

$$p = C_2 \ln(D_{HBr}/D_{HeH})/(R_{HeKr} - R_{HBr})$$

$$q = C_2 \ln(D_{OH}/D_{HeH})/(R_{HeNe} - R_{OH})$$

Gilliom recommended $C_2 = 0.28$, based on data for single, double, and triple carbon–carbon bonds, rather than the older value of 0.26. Also Marschoff and Jatem (23), using the same values of the inert gas intermolecular potentials as Gilliom, did BEBO calculations in which C_2 was varied between 0.23 and 0.29, a range they considered to represent a reasonable uncertainty in C_2. They obtained the best

TABLE 4. Potential energies of activation calculated by BEBO and Zavitsas methods[a]

Method	Parameters	O + HCl	O + HBr	O + HI
BEBO	Old	0.8	0.3	0.07
BEBO	Old modified[b]	2.3	0.9	0.2
BEBO	Gilliom's	2.1	0.7	0.1
BEBO	Gilliom's modified[b]	7.3	2.1	0.4
Zavitsas		0.6	−4.5	−7.0
Experimental		4.5–7.5[c]	3.6[d]	2.0[d]

[a]Units are kcal mol^{-1}.
[b]Triplet repulsion term is twice that of the unmodified procedure.
[c]Arrhenius activation energy, ref. 1.
[d]Arrhenius activation energy, this work.

agreement between calculated and experimental results of 71 reactions using $C_2 = 0.277$.

Zavitsas and Melikian (24) have developed a BEBO-like method which gives good agreement with experimental activation energies in their reported examples, although O(^3P) reactions were not included. This method differs from BEBO in assuming that in the transition state the bond energies of the making and the breaking bonds are equal, and that the bond energies are given by Morse functions. As in BEBO calculations, the Sato anti-Morse function is used to obtain the triplet repulsion energy between, for example, O and Br.

In Table 4 are given the potential energies of activation calculated by the BEBO method using the old ($C_1 = 1$), old-modified ($C_1 = 2$, as suggested by Mayer and Schieler (19)), and Gilliom's parameters ($C_1 = 1.8$ (5, 6) and, modified, $C_1 = 3.6$). Also, the results of the Zavitsas calculation ($C_1 = 1.8$) are shown.[2] For the BEBO calculations, the correction for zero point energy is made using the calculated frequencies of the transition state and the stretching frequency of the reactant. For the Zavitsas model, the correction is made as recommended (24). Comparisons between calculated BEBO potential energies of activation and experimental Arrhenius activation energies are made, although the experimental values have incorporated in them any slight temperature dependence of the pre-exponential factor. Because the calculated bending vibrational frequency of the transition state is very small in most cases in Table 4, a full transition state calculation to obtain an Arrhenius activation energy would not give very meaningful results (2, 25).

With the exception of the calculation using Gilliom's parameters with $C_1 = 3.6$, these models fail to give values of activation energies consistent with the experimental values. The model of Zavitsas gives exceptionally poor agreement, since negative activation energies are predicted for HBr and HI. It would be necessary to use values of C_1 of ~2.9, 5.0, and 9.0 to obtain agreement with the experimental values for HCl, HBr, and HI, respectively. Also, for HI, varying D_{IO}, R_{IO}, or the stretching frequency of IO by 10% raises the calculated activation energy at most to −5.4 kcal mol^{-1}. The failure of the Zavitsas calculation is probably due to the value chosen for the resonance stabilization energy of the activated complex. In the model, −10.6 kcal mol^{-1} is assumed, based on the allyl radical. The stabilization energy is probably much different in the case of O—H—Br type structures, where the relative contributions from resonance structures are likely to be very much different.

A common problem in both the BEBO and the Zavitsas methods is the uncertainty in the magnitude and shape of the triplet repulsion curve. Both approaches scale the Sato anti-Morse function to match particular portions of theoretically calculated curves for triplet H_2. (Calculations using a different form of the triplet repulsion term suggested by Arthur, Donchi, and McDonell (26) did not give improved results.) Mayer and Schieler (19) suggested doubling the triplet repulsion term in cases where the approaching atom is a triplet. Since the BEBO calculations reported by Gilliom (in which the approaching species are doublets) give fairly good agreement with experimental results, it was of interest to try Mayer and Schieler's suggestion, using Gilliom's parameters, for the O(^3P) + HX reactions. As seen in Table 4, this calculation gives the best fit with experimental values for all three hydrogen halides. For HCl, the calculated activation energy is within the range of reported values. Although the calculated values for HBr and HI are about 1.5 kcal mol^{-1} lower than the observed values, the agreement must be considered reasonable for this type of calculation. (It would be necessary to let $C_1 = 5.0$ and 7.9 to match the experimental values for HBr and HI, respectively.)

However, calculations using Gilliom's parameters

[2]The input data for all the calculations and a complete tabulation of the results are available, at a nominal charge, from the Depository of Unpublished Data, CISTI, National Research Council of Canada, Ottawa, Ont., Canada K1A 0S2.

Can. J. Chem. Downloaded from www.nrcresearchpress.com by 210.87.254.105 on 09/05/12
For personal use only.

Can. J. Chem. Downloaded from www.nrcresearchpress.com by 210.87.254.105 on 09/05/12
For personal use only.

were made also for other oxygen atom reactions involving abstractions of hydrogen. Without doubling the triplet repulsion term ($C_1 = 1.8$), for the reactions of oxygen atoms with H_2, H_2O, CH_4, and CH_3CHO, activation energies of 11.3, 20.0, 12.3,[3] and 6.2[3] were calculated. The experimental Arrhenius activation energies are ~9 (28), 18.5 (28), 9.1 (28), and 1.9 (29). For these reactions, the calculated values are all larger than the experimental values, although the discrepancy exceeds 2 kcal mol^{-1} only for the latter two reactions involving C—H bonds. Thus, it does not appear justified to double the triplet repulsion term in the HCl, HBr, and HI reactions.

If Gilliom's correction for zero point energy (6) is used, the disparity between calculated and experimental activation energies is further increased in all cases except for HCl, for which the calculated value is 4.5 kcal mol^{-1} with $C_1 = 1.8$. Evidently the BEBO method does not consistently predict activation energies for hydrogen abstractions by oxygen atoms, even when Gilliom's parameters are used. The exact reasons for the inconsistencies are not certain.

1. A. R. Ravishankara, G. Smith, R. T. Watson, and D. D. Davis. J. Phys. Chem. **81**, 2220 (1977), and references therein.
2. R. D. H. Brown and I. W. M. Smith. Int. J. Chem. Kinet. **7**, 301 (1975).
3. R. G. Macdonald and C. B. Moore. J. Chem. Phys. **68**, 513 (1978).
4. E. E. Nikitin and V. N. Kondrat'ev. Dokl. Acad. Nauk SSSR, **212**, 149 (1973).
5. R. D. Gilliom. J. Chem. Phys. **65**, 5027 (1976).
6. R. D. Gilliom. J. Am. Chem. Soc. **99**, 8399 (1977).

[3]A value of $D_{C-O} = 86.3$ kcal mol^{-1} is used, corresponding to an ether. If 90.4 kcal mol^{-1} is used, corresponding to an alcohol as suggested by Previtali and Neumann (27), values of 14.2 and 7.8 are calculated for CH_4 and CH_3CHO.

7. R. Atkinson and R. J. Cvetanović. J. Chem. Phys. **55**, 659 (1971).
8. S. Furuyama, R. Atkinson, A. J. Colussi, and R. J. Cvetanović. Int. J. Chem. Kinet. **6**, 741 (1974).
9. D. L. Singleton, S. Furuyama, R. J. Cvetanović, and R. S. Irwin. J. Chem. Phys. **63**, 1003 (1975).
10. A. Jeannotte, E. H. Appelman, F. Schreiner, and B. M. Abraham. 174th Am. Chem. Soc. National Meeting, Aug. 28 – Sept. 2, 1977. Paper No. Phys. 90.
11. R. J. Cvetanović and D. L. Singleton. Int. J. Chem. Kinet. **9**, 481 (1977); **9**, 1007 (1977).
12. G. A. Takacs and G. P. Glass. J. Phys. Chem. **77**, 1060 (1973).
13. G. A. Takacs and G. P. Glass. J. Phys. Chem. **77**, 1948 (1973).
14. R. Overend, G. Paraskevopoulos, and C. Black. J. Chem. Phys. **64**, 4149 (1976).
15. H. van den Bergh and J. Troe. J. Chem. Phys. **64**, 736 (1976).
16. R. F. Hampson and D. Garvin (*Editors*). Natl. Bur. Stand. Tech. Note, No. 866. 1975.
17. M. A. A. Clyne and R. T. Watson. J. Chem. Soc. Faraday I, **71**, 336 (1975).
18. G. A. Takacs and G. P. Glass. J. Phys. Chem. **77**, 1182 (1973).
19. S. W. Mayer and L. Schieler. J. Phys. Chem. **72**, 236 (1968).
20. R. D. H. Brown and I. W. M. Smith. Int. J. Chem. Kinet. **10**, 1 (1978).
21. R. M. Jordan and F. Kaufman. J. Chem. Phys. **63**, 1691 (1975).
22. H. S. Johnston. Gas phase reaction rate theory. Ronald Press, New York, NY. 1966.
23. C. M. Marschoff and A. Jatem. Chem. Phys. Lett. **56**, 35 (1978).
24. A. A. Zavitsas and A. A. Melikian. J. Am. Chem. Soc. **97**, 2757 (1975).
25. S. W. Mayer, L. Schieler, and H. S. Johnston. J. Chem. Phys. **45**, 385 (1966).
26. N. L. Arthur, K. F. Donchi, and J. A. McDonell. J. Chem. Phys. **62**, 1585 (1975).
27. C. M. Previtali and M. G. Neumann. Int. J. Chem. Kinet. **9**, 417 (1977).
28. L. G. Anderson. Rev. Geophys. Space Phys. **14**, 151 (1976).
29. D. L. Singleton, R. S. Irwin, and R. J. Cvetanović. Can. J. Chem. **55**, 3321 (1977).

Standard thermodynamic transfer functions from water to water + acetone mixtures for a n-nonylcarbon chain attached to different ionic groups

RAYMOND BURY AND CLAUDE TREINER[1]

Laboratoire d'Electrochimie, Université Pierre et Marie Curie, 4, Place Jussieu 75005 Paris, France

Received April 11, 1978

RAYMOND BURY and CLAUDE TREINER. Can. J. Chem. **56**, 2940 (1978).

The standard enthalpy of transfer of trimethyldecylammonium bromide, tetramethylammonium bromide, methyl and decylsodium sulfate have been determined from water to water + acetone mixtures from calorimetric measurements at 298.15 K. The standard entropy function has been calculated using standard Gibbs free energy of transfer data for the same compounds. It is shown that the standard enthalpy and entropy of transfer of a n-nonylhydrocarbon chain attached to the sulfate or to the trimethylammonium groups are quite different whereas the standard Gibbs free energy functions are practically equal in the mixed solvents. It is concluded that the sign of the charge on the ionic groups is responsible for this behaviour and that the influence of this effect extends to a large number of solvent molecules. It is suggested that a similar effect may contribute to the standard enthalpy of so called reference ions: e.g. tetraphenylboron ion casting some doubt on the reliability of these extrathermodynamic approaches at least in mixed solvents, as far as the standard enthalpy function is concerned.

RAYMOND BURY et CLAUDE TREINER. Can. J. Chem. **56**, 2940 (1978).

L'enthalpie standard de transfert, ΔH_t^0, du bromure de triméthyldécylammonium, du bromure de tétraméthylammonium, des sulfates de méthylsodium et de décylsodium, a été déterminée à 298.15 K à partir de mesures calorimétriques, de l'eau à des mélanges eau + acétone. Connaissant l'enthalpie libre standard de transfert, ΔG_t^0 des mêmes composés, l'entropie standard de transfert, ΔS_t^0 a été calculée. On montre que les valeurs de ΔH_t^0 et ΔS_t^0 pour la chaine n-nonylhydrocarbonée sont très différentes selon que cette chaine est attachée au groupe sulfate ou triméthylammonium, mais que les valeurs de ΔG_t^0 sont pratiquement identiques dans les mélanges eau–acétone. Il est proposé que le signe de la charge de la tête ionique soit responsable de cet effet et que son influence s'étend à un grand nombre de molécules de solvant autour de l'ion. On suggère qu'un effet similaire doit contribuer à la valeur ΔH_t^0 pour les ions dits de référence: ion tétraphénylborure par exemple, ce qui rend suspect les résultats utilisant ces approches extrathermodynamiques, au moins dans les solvants mixtes, en ce qui concerne la fonction enthalpique.

Introduction

The search for group additivity rules for organic molecules or ions is one of the most promising approach to the study of complex molecules in aqueous solutions (1). In particular the methylene group has been the subject of numerous thermodynamic studies through the determination of standard properties of homologous series of compounds differing from each other only by a CH_2 group.

Thus it has been recognized long ago that the thermodynamic properties of the methylene group in aqueous solution may strongly depend on its nearest neighbours on the molecule to which it is attached. In a classical study, Cohn and Edsall (2) had shown that the Gibbs standard free energy of transfer of a CH_2 group from water to ethanol is constituted of additive contributions only when the number of carbon atoms between the amino group and the carboxylic group is equal to or greater than $n = 3$. Numerous examples may be found in the literature to illustrate this behaviour (3). We shall give two striking examples particularly relevant to the present study: (*1*) The enthalpy of micellization ΔH_m^0 of a CH_2 group of a nonionic surfactant in water is negative when it is remote from the head groups, but positive for a methylene group situated between the sulfoxide and the hydroxyl group (4). (*2*) The enthalpy of transfer ΔH_t^0 from water to dimethylsulfoxide (DMSO) of alcohols and tetraalkylammonium compounds is strongly dependent upon the number of carbon atoms on a normal alkylchain whereas ΔH_t^0 is almost constant for alkylsulfonates salts from $n = 2$ to $n = 8$ (15). This means that the properties of a CH_2 group is not only dependent upon its position in a given molecule but also on the structure and shape of the whole molecule itself. We found it interesting to investigate the problem of the influence of polar groups on their nearest neighbours in mixed aqueous solvents by studying the standard free energy entropy and enthalpy of transfer from water

[1]To whom correspondence should be addressed.

Can. J. Chem. Downloaded from www.nrcresearchpress.com by 210.87.254.40 on 09/05/12
For personal use only.

TABLE 1. Characteristic parameters of vapour–liquid equilibrium

Weight (%)	Z_1	m (mol kg^{-1})	P (Torr)	Y†	$\frac{\partial \bar{G}^0}{\partial Z_1}$ (kcal mol^{-1})	$-\Delta G_t^0$ (cal mol^{-1})
		(*a*) *n*-DTMABr in water + acetone mixtures				
0	1.0	—	—	—	10.0*	0
3.966	0.9874	0	44.256	0.49349		
		0.00799	44.182	0.49277		
		0.01613	44.108	0.49204		
		0.02486	44.026	0.49123	11.30 (ave.)	97
8.055	0.9735	0	62.733	0.61330		
		0.00591	62.638	0.61278		
		0.01188	62.542	0.61224		
		0.01747	62.454	0.61175		
		0.02330	62.358	0.61123	11.40 (ave.)	343
10.037	0.9666	0	72.065	0.67555		
		0.01226	71.806	0.67447		
		0.01802	71.688	0.67398		
		0.02404	71.585	0.67356	11.68 (ave.)	405
		(*b*) SDS in water + acetone mixtures				
0	1.0	—	—	—	10.5*	0
6.059	0.9804	0	53.571	0.55486		
		0.00508	53.511	0.55443		
		0.01034	53.444	0.55394		
		0.01479	53.392	0.55356		
		0.01903	53.341	0.55319	10.97 (ave.)	201
7.058	0.9770	0	58.141	0.58588		
		0.00449	58.075	0.58546		
		0.00944	58.008	0.58504		
		0.01431	57.934	0.58456		
		0.01946	57.860	0.58409	11.70 (ave.)	254
11.274	0.9621	0	76.440	0.68703		
		0.00952	76.171	0.68598		
		0.01419	76.053	0.68552		
		0.01922	75.899	0.68491	15.10 (ave.)	441

*Calculated, see ref. 8.
†Vapour phase composition (mole fraction).

to aqueous binary mixtures of compounds with different head-groups.

Let us consider a standard thermodynamic property of transfer from solvent to solvent ΔX_t^0, one can write

$$[1]\quad \Delta X_t^0[(CH_3)_3N{-}(CH_2)_9{-}CH_3Br] \approx \Delta X_t^0[(CH_3)_4NBr] + \Delta X_t^0[(CH_2)_9]$$

$$\Delta X_t^0[(CH_3{-}(CH_2)_9{-}OSO_3Na] \approx \Delta X_t^0[CH_3OSO_3Na] + \Delta X_t^0[(CH_2)_9]$$

We assume then that the standard thermodynamic properties of the two ionic surfactants, trimethyldecylammonium bromide (TMDABr) and sodium decylsulfate (SDS), can be split into, respectively, tetramethylammonium bromide (Me_4NBr) and methylsodiumsulfate ($MeOSO_3Na$), plus two n-nonylhydrocarbon chains. The position of the terminal methyl group is the same for both ionic surfactants and for the classical electrolytes, so that ΔX_t^0-$[(CH_2)_9]$ will measure the remaining influence of the ionic groups on their nearest neighbours.

The standard Gibbs free energy of transfer from water to water + acetone mixtures for the compounds involved in relation [1] are known (6). How-

TABLE 2. Standard Gibbs free energy of transfer of electrolytes from water to water + acetone mixtures at 298.15 K (mole fraction scale, cal mol^{-1})

Weight (%)	ΔG_t^0			
	Me_4NBr	*n*-DTMABr	$MeOSO_3Na$	SDS
0	0	0	0	0
5.00	0	190	120	165
10.00	20	405	255	380
15.00	40	610	400	675
20.00	115	820	555	965
30.00	340	1290	855	1450
40.00	710	1820	1155	1815
60.00	1680	2040	1975	2170
80.00	3595	1250	3525	1330

Can. J. Chem. Downloaded from www.nrcresearchpress.com by 210.87.254.40 on 09/05/12
For personal use only.

Can. J. Chem. Downloaded from www.nrcresearchpress.com by 210.87.254.40 on 09/05/12
For personal use only.

TABLE 3. Enthalpy of solution ΔH_s^0 (kcal mol^{-1}) for electrolytes in water + acetone mixtures at 298.15 K

Weight (%)	ΔH_s^0			
	Me_4NBr†	*n*-DTMABr	SDS‡	$MeOSO_3Na$
0	5.85	7.60	6.67	2.03
5.00	5.90	9.24	7.29	2.14
10.00	5.97	10.61	8.17	2.23
15.00	6.00	11.57	9.17	2.28
20.00	6.00	11.67	9.99	2.41
30.00	5.78	11.60	11.01	2.53
40.00	5.60	11.30	10.22	2.38
60.00	5.17	10.39	5.80	1.78
70.00	—	—	5.12	1.11
80.00	4.65	8.69	4.57	0.48
90.00	—	7.60	4.12	−0.28
95.00	—		4.19	−0.55
100.00	4.75*	7.35	4.27	—

*Calculated, see text.
†ΔH_s^0 = 5.77 kcal mol^{-1} (29), ΔH_s^0 = 5.92 kcal mol^{-1} (30).
‡ΔH_s^0 = 5.7 kcal mol^{-1} (31).

ever, new experimental results have been obtained in the water-rich region which somewhat affect the previously published values. We present in this paper the new results, the corrected ΔG_t^0 values, together with the enthalpy ΔH_t^0 (and hence the entropy ΔS_t^0) of transfer for the four solutes considered in relation [1].

Experimental

Vapour Pressure Measurements

The standard free energy of transfer $\Delta G_t^0{}_{w\to s}$ of both surfactants from water to water + acetone mixtures have been obtained using a vapour pressure method. Full details have been given previously (7). The variation of vapour pressure of the binary solvent with solute concentration are used to determine the rate of change of the change of the standard chemical potential $\bar{G}_0$ of the solute with solvent composition Z_1, $\partial\bar{G}_0/\partial Z_1$. Integration of this quantity for different Z_1 values with respect to Z_1 leads to ΔG_t^0 with water as the reference solvent. Solute molality was always kept below 0.03 mol kg^{-1}. (The critical micelle concentration for TMDABr and SDS at 298.15 K in water are respectively equal to 0.066 and 0.035 mol kg^{-1} and increase with acetone concentrations.)

Table 1 presents the experimental results obtained in the water-rich region. $(\partial\bar{G}_0/\partial Z_1)_{Z_1\to 1}$ has been calculated as described before (8). Using these results and the $\partial\bar{G}_0/\partial Z_1$ values obtained previously for acetone concentrations above 20 wt.% we obtain the integrated ΔG_t^0 results of Table 2. They have been calculated for acetone concentrations corresponding to the enthalpy experiments.

Calorimetric Measurements

The calorimeter and method developed by Bury *et al.* (9) for measuring the heat of solutions of urea in aqueous organic mixtures were used for the present determinations. The accuracy of these measurements were of the order of ±0.5%. Since the final concentrations of electrolytes (0.001–0.005 mol kg^{-1}) were close to infinite dilution, any small concentration dependence of heat of solution ΔH_s being within the experimental error, the heat of solution at infinite dilution ΔH_0 was taken to be the average of a number (2–5) of ΔH_s measurements (Table 3).[2]

Discussion

Thermodynamic Transfer Functions for Ionic Surfactants from Water to Water + Acetone Mixtures

Before discussing the behaviour of the hydrocarbon chains it is useful to briefly consider the results concerning the neutral electrolytes. Their essential features may be summarized as follows:

(*1*) The standard free energies of transfer of both surfactants are very close in the entire solvent composition range studied and similar to that of classical electrolytes with large organic ions (10) (Fig. 1). Differences only appear in the enthalpy and entropy functions. The large endothermic effect in the water-rich region can be attributed to the particular water-like structure of these rather highly organized solvent mixtures (11–13).

(*2*) The difference in standard enthalpy and entropy of transfer between the two surfactants is much larger above $Z_2 = 0.10$ where water structure may be believed to be entirely destroyed.

(*3*) In the acetone-rich mixtures there is a convergence of ΔH_t^0 and ΔS_t^0 of each surfactant with its

[2]This may not always be true. (We are grateful to J. E. Desnoyers for drawing our attention to this point.) At low dielectric constant mixtures a more important dependence of ΔH on concentration may be found. As an example we have measured the heat of dilution of SDS in a 60 wt.% of acetone mixtures using a Calvet microcalorimeter which has been described previously (32). The experimental results were treated by a least-squares method using the extended Debye–Hückel equation; they are presented in Table 4 where ϕ_L^m is the relative apparent molal heat of dilution.

TABLE 4. Enthalpy of solution for SDS in a water + acetone mixture (60.00%) as a function of surfactant concentration

m (mol kg^{-1})	ϕ_L^m (kcal mol^{-1})	ΔH_s^m (kcal mol^{-1})
0.0	0.0	5.695
0.0005	0.056	5.751
0.001	0.079	5.774
0.005	0.141	5.836
0.010	0.175	5.870

Between 0.01 *m* and infinite dilution the variation of ΔH_s^m is 0.175 mol kg^{-1}. Our original result (Table 3) for m_f = 0.00432 mol kg^{-1}, ΔH^0 = 5.80 kcal mol^{-1}, is still compatible with the more precise extrapolation. It is clear, however, that for ΔH^0 values of the utmost precision, measurements down to 0.0005 mol kg^{-1} should be necessary; these are not easy to make. We have thus shown that the small concentration dependence of ΔH_s below 0.005 mol kg^{-1} may introduce a few percent uncertainty in the absolute ΔH_t^0 values (3% in the case just studied).

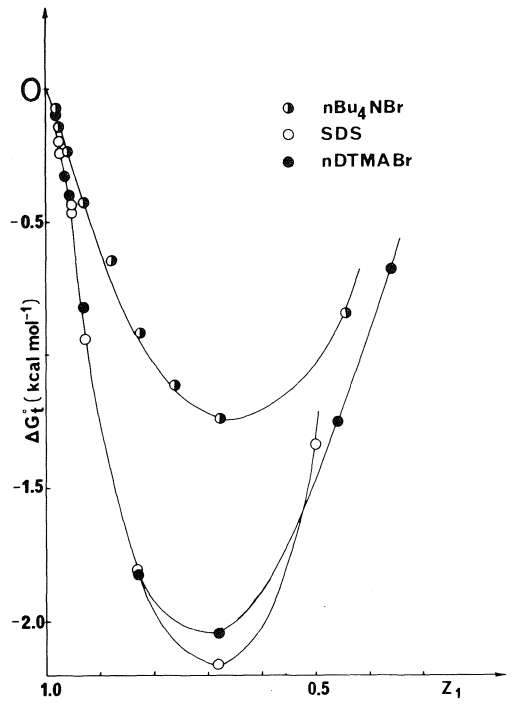

FIG. 1. Gibbs standard free energy of transfer of electrolytes from water to water + acetone mixtures at 298.15 K.

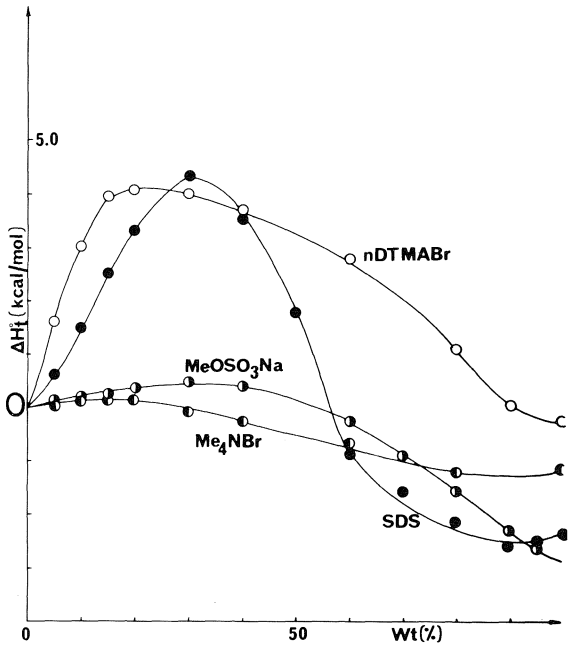

FIG. 2. Standard enthalpy of transfer of electrolytes from water to water + acetone mixtures at 298.15 K.

lower homologue. $MeOSO_3Na$, Me_4NBr, and SDS were not sufficiently soluble in pure acetone for their enthalpy of dissolution to be measured. However, in the case of Me_4NBr, the least soluble solute, a ΔH_t^0 value from water to acetone could be obtained by combination of Abraham's estimate (14) for the standard entropy of transfer ΔS_t^0 and De Ligny's results for ΔG_t^0 (15) ($\Delta S_t^0 = -34$ cal mol^{-1} deg^{-1}. $\Delta G_t^0 = 9.04$ kcal mol^{-1} both on mole fraction basis). Hence $\Delta H_t^0 = -1.10$ kcal mol^{-1}. This value is of course approximate and should be used as such. We observe then that the difference between ΔH_t^0 for TMDABr and Me_4NBr is of the order of +0.8 kcal mol^{-1}. Extrapolation of the results for the more soluble SDS and $MeOSO_3Na$ to pure acetone shows the same convergence with a difference of about +0.5 kcal mol^{-1} only (see Fig. 2). This means that ΔH_t^0 from water to pure acetone is essentially independent of the number of carbon atoms on the linear chain. This is the more noteworthy as usually some dependence is found with chain length at least between the first and the second homologue of a given series even if this dependence almost disappears for the higher homologues. Krishnan and Friedman find the same trend for sulfonates from water to pure DMSO (5) (ΔH_t^0 is almost constant from $n = 2$ to $n = 8$ carbon atoms in the chain); other similar findings have been reported for shorter hydrocarbon chains (16). One interesting feature of these results is that whereas a very large dependence is observed for ΔH_t^0 upon n for the tetraalkylammonium series, such a dependence is not found for the trimethylammonium series studied here. One might suggest that a linear hydrocarbon chain can be more easily accommodated in any structure than a bulky solute.

Behaviour of an n-Nonylhydrocarbon Chain Attached to a Sulfate or a Trimethylammonium Group

If we substract the ΔG_t^0, ΔH_t^0, and ΔS_t^0 results for Me_4NBr and $MeOSO_3Na$ from those for the two surfactants we obtain the contributions of an n-nonylhydrocarbon chain to the transfer functions according to relation [1]. Let us call $(CH_2)_9^{\varepsilon+}$ the hydrocarbon chain obtained from the cationic surfactant and $(CH_2)_9^{\varepsilon-}$ the chain obtained from the anionic one. Figures 3, 4, 5, show that indeed the two chains are not identical and that even with the head-group effects removed, large differences remain on some of the standard thermodynamic transfer functions.

Following previous authors (17, 18) we may consider four different effects contributing to any standard function ΔX_t^0:

$$\Delta X_t^0 = \Delta X_t^0(\text{cav}) + \Delta X_t^0(\text{el}) + \Delta X_t^0(\text{spec}) + \Delta X_t^0(\text{struct})$$

Can. J. Chem. Downloaded from www.nrcresearchpress.com by 210.87.254.40 on 09/05/12
For personal use only.

Can. J. Chem. Downloaded from www.nrcresearchpress.com by 210.87.254.40 on 09/05/12
For personal use only.

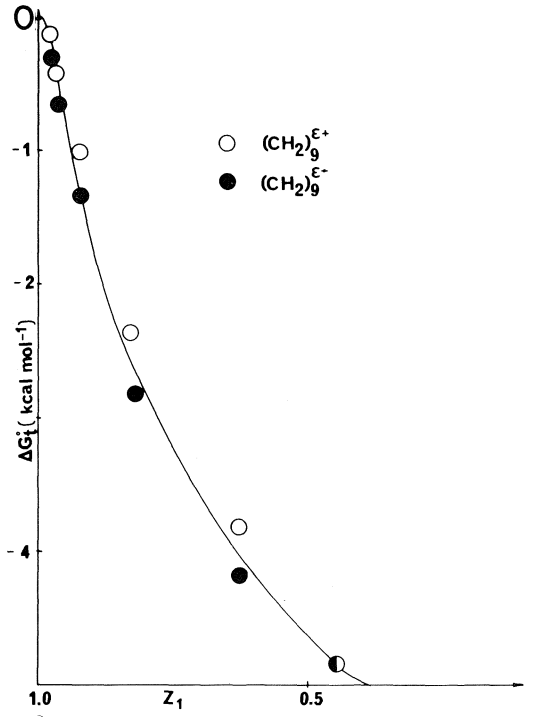

FIG. 3. Gibbs standard free energy of transfer of a n-nonyl carbon chain from water to water + acetone mixtures: ○, cationic; ●, anionic origin.

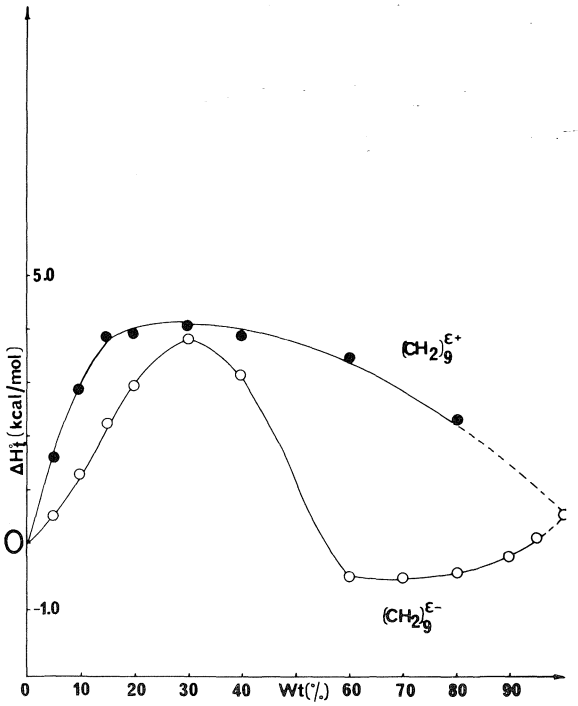

FIG. 4. Standard enthalpy of transfer of n-nonyl carbon chain from water to water + acetone mixtures: ●, cationic; ○, anionic origin.

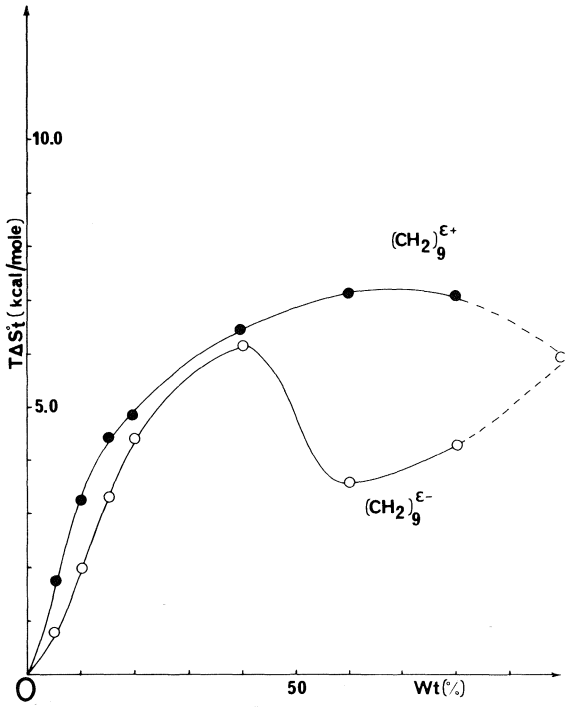

FIG. 5. Standard entropy of transfer of a n-nonyl carbon chain from water to water + acetone mixtures: ●, cationic; ○, anionic origin.

where the subscripts stand for cavity, electric, specific, and structural effects, respectively.

Clearly the work of cavity formation should be exactly the same for the two linear chains. The main part of the electric effect has been subtracted as well as the specific effect. Also geometrical aspects which can be related to structural effects should be similar in both cases. There remains only the effect of the charge on the solvent molecules which surround the methylene groups nearest to the head group; in particular the effect of the sign of the charge needs to be examined. It is now commonly accepted that, in most cases of binary aqueous solvents cation and anion exhibit an opposite behaviour (19). The minimum of ΔG_t^0 for Bu_4NBr and TMDABr in aqueous acetone mixtures has been explained by that opposite effect (6, 10). $\Delta G_t^0(Br^-)$ is positive for the bromide ion because anions are preferentially solvated by water. The work of cavity formation as can be calculated from the scaled-particle theory (20–22) and preferential solvation of most univalent cations by organic molecules (19) explains the negative ΔG_t^0 values ($\Delta G_t^0 = \Delta G_t^{0-} + \Delta G_t^{0+}$). The sum of the two contributions (negative and positive) is responsible for the minimum observed. Furthermore we note that, within experimental error,

$$\Delta G_t^0\{(CH_2)_9^{\varepsilon-}\} \approx \Delta G_t^0\{(CH_2)_9^{\varepsilon+}\}$$

Can. J. Chem. Downloaded from www.nrcresearchpress.com by 210.87.254.40 on 09/05/12
For personal use only.

in the mixed solvents. This near equality rules out the possibility that the electric charge per se still plays a significant role in these cases; it may be considered as another example of the well-known compensation phenomena in aqueous solvents between enthalpy and entropy.

The study of the behaviour of the enthalpy and entropy functions give more information. For example we have pointed out that the difference $\delta\Delta H_t^0$ from water to pure acetone for homologues of each series (sulfate or trimethylammonium) was 0.5 and 0.8 kcal mol^{-1} respectively. Thus

$$\Delta H_t^0\{(CH_2)_9{}^{\varepsilon-}\} \approx \Delta H_t^0\{(CH_2)_9{}^{\varepsilon+}\}$$

The large difference observed especially in the intermediate region must be due to the presence of both acetone and water molecules. It is interesting to compare ΔH_t^0 for Bu_4NBr (22) and TMDABr (Fig. 6). The curve corresponding to Bu_4NBr is shifted to higher endothermic values with respect to TMDABr but the shapes of the curves are very similar. In these cases the electric charge is somewhat shielded from the solvent whereas for the sulfate group the charge is much more exposed to the solvent molecules which surround it. Thus the difference between the enthalpy (and entropy) for $(CH_2)_9{}^{\varepsilon-}$ and $(CH_2)_9{}^{\varepsilon+}$ seems to be essentially due to the orientation of water molecules next to the linear carbon chain induced by the sign of the electrical charge. This effect, which may be called structural, must concern a large number of molecules around the electric charge in order to create such a decrease in enthalpy. It is nonspecific, otherwise it would have showed up somewhat on ΔG_t^0. One may suggest that water dipoles are diluted in acetone which acts as an 'inert' solvent as far as the dipole effect is concerned.

It might be worthwhile to recall a similar behaviour in the case of tetraaryl ions. In order to evaluate single-ion thermodynamic quantities the tetraphenylboron assumption has often been used; it is assumed that the tetraphenylarsonium ion (ϕ_4As^+) and the tetraphenylboron ion (ϕ_4B^-) are weakly solvated to the same extent in different solvents (24, 25). Treiner (26) has shown, using the scaled-particle theory (SPT), that it seems to be the case as far as the ΔG_t^0 function is concerned for ϕ_4As^+ and ϕ_4B^- from water to some pure and mixed aqueous solvents; however, ΔH_t^0 could not be calculated by the SPT. Figure 7 presents ΔH_t^0 for ϕ_4BNa and ϕ_4PBr from water to water–dioxane mixtures (27). The similarity with the shape of curves for $(CH_2)_9{}^{\varepsilon-}$ and $(CH_2)_9{}^{\varepsilon+}$ is real (and also with those corresponding to TMDABr and SDS of course), even if the changes observed are more important in the former than in the latter case. Similar observations can be made with tetraaryl negative and tetraalkyl positive ions in water + *tert*-butanol mixtures (23).

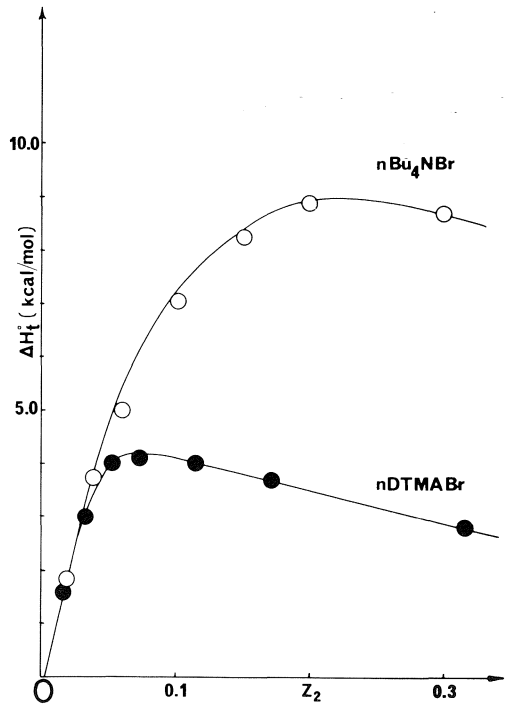

FIG. 6. Standard enthalpy of transfer of a linear and bulky tetraalkylammonium salt from water to water + acetone mixtures at 298.15 K.

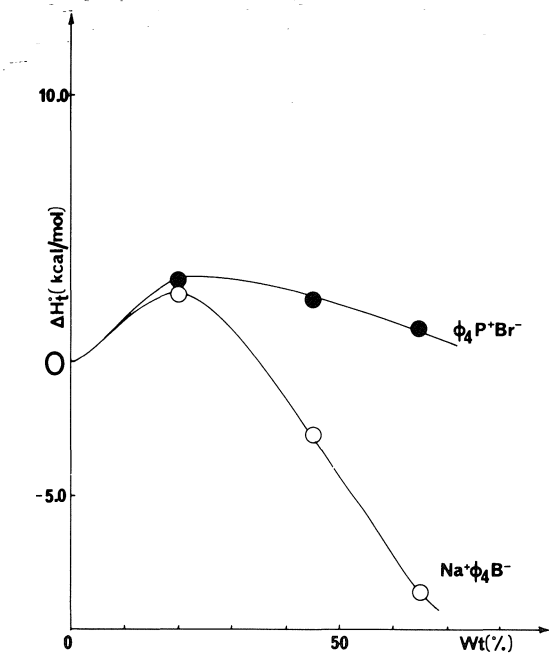

FIG. 7. Standard enthalpy of transfer of tetraaryl salts from water to water + dioxane mixtures at 298.16 K (ref. 27).

The analogies observed lead us to the following suggestion. Part of the large difference in ΔH_t^0 for ϕ_4BNa and ϕ_4AsCl might be due to the different properties of ϕ_4B^- and ϕ_4As^+ because of the effect of the sign of the charge on the surrounding water molecules just like in the case of the hydrocarbon chains where the remaining sign effect contributes heavily to ΔH_t^0.

Finally Feakins *et al.* (28) from their calorimetric study on $Na\phi_4B$ in water + dioxane mixtures conclude that ϕ_4B^- behaves like a small monoatomic ion. This conclusion may be reconciled with ours. For small ions an exothermic effect is predominant ($\Delta H_t^0(spec) < 0$). The scaled-particle theory predicts a large endothermic effect for a neutral particle in these mixed solvents ($\Delta H_t^0(cav) > 0$). If anions are more strongly hydrated than cations, then for two large ions of opposite charges and equal size, $\Delta H_t^0(exp)$ will be less endothermic for the anion than for the cation, in agreement with experimental observation. Hence the comparison between the effect of large and small ions on the binary aqueous solvents studied indicates that in the case of large anions the effect of the charge on water dipole predominates over the nonspecific (cavity) effect; in the case of large cations the nonspecific effect seems predominant.

1. S. CABANI, G. CONTI, and L. LEPORI. Trans. Faraday Soc. **67**, 1933 (1971); J. J. SAVAGE and R. H. WOOD. J. Solution Chem. **5**, 733 (1976).
2. E. J. COHN and J. T. EDSALL. Proteins, amino acids, and pepticles. Rheinhold, New York. NY. 1943.
3. F. FRANKS and D. S. REID. *In* Water, a comprehensive treatise. Vol. II. *Edited by* F. Franks. Plenum. 1973. Chapt. 5; C. V. KRISHNAN and H. L. FRIEDMAN. *In* Solute–solvent interactions. Vol. 2. *Edited by* J. F. Coetzee and C. D. Ritchie. M. Dekker. 1976. Chapt. 1.
4. J. M. CORKILL, J. F. GOODMAN, and S. R. TATE. *In* Hydrogen-bonded solvent systems. *Edited by* A. K. Covington and P. Jones. Taylor and Francis Ltd. 1968.
5. C. V. KRISHNAN and H. L. FRIEDMAN. J. Solution Chem. **2**, 37 (1973).
6. C. TREINER and A. LE BESNERAIS. J. Chem. Soc. Faraday Trans. I, **73**, 44 (1977); J. Chem. Thermodyn. In press.
7. C. TREINER. J. Chim. Phys. **70**, 1183 (1973).
8. C. TREINER, P. TZIAS, and M. CHEMLA. Can. J. Chem. In press.
9. R. BURY, A. MAYAFFRE, and M. CHEMLA. J. Chim. Phys. **78**, 745 (1977).
10. C. TREINER and P. TZIAS. Adv. Chem. Ser. **155**, 303 (1976).
11. C. DE VISSER, G. PERRON, and J. E. DESNOYERS. J. Am. Chem. Soc. **99**, 5894 (1977).
12. E. M. ARNETT and D. R. MC. KELVEY. J. Am. Chem. Soc. **87**, 1393 (1965).
13. E. M. ARNETT and D. R. MC. KELVEY. J. Am. Chem. Soc. **88**, 5031 (1966).
14. M. H. ABRAHAM. J. Chem. Soc. Faraday Trans. I, **69**, 1375 (1973).
15. D. BAX, C. L. DE LIGNY, and A. J. REMINJNSE. Recl. Trav. Chim. **91**, 1225 (1972).
16. C. V. KRISHNAN and H. L. FRIEDMAN. J. Phys. Chem. **75**, 3598 (1961); **75**, 3606 (1971).
17. C. V. KRISHNAN and H. L. FRIEDMAN. J. Phys. Chem. **73**, 1572 (1969).
18. (*a*) C. JOLICOEUR and G. LACROIX. Can. J. Chem. **51**, 3051 (1973); (*b*) C. JOLICOEUR, J. BOILEAU, S. BAZINET, and P. PICKER. Can. J. Chem. **53**, 716 (1975).
19. O. POPOVYCH. Crit. Rev. Anal. Chem. **1**, 73 (1970).
20. R. A. PIEROTTI. J. Phys. Chem. **67**, 1840 (1963).
21. R. A. PIEROTTI. J. Phys. Chem. **69**, 281 (1965).
22. C. TREINER, P. TZIAS, M. CHEMLA, and G. N. POLTORATSKI. J. Chem. Soc. Faraday Trans. I, **72**, 2007 (1976).
23. R. H. MOHANTY, T. S. SARMA, S. SUBRAMANIAN, and J. C. AHLUWALIA. J. Chem. Soc. Faraday Trans. I, **67**, 305 (1971).
24. E. GRUNWALD, G. BAUGHAM, and G. KOHNSTAM. J. Am. Chem. Soc. **82**, 5801 (1960).
25. E. M. ARNETT and D. R. MC. KELVEY. Rec. Chem. Prog. **26**, 185 (1965).
26. C. TREINER. Can. J. Chem. **55**, 682 (1977).
27. OM N. BHATNAGAR. Can. J. Chem. **54**, 3487 (1976).
28. D. FEAKINS and C. T. ALLAN. J. Chem. Soc. Faraday Trans. I, **72**, 314 (1976).
29. P. PAOLETTI. Trans. Faraday Soc. **61**, 219 (1965).
30. Y. C. WU and H. L. FRIEDMAN. J. Phys. Chem. **70**, 2020 (1966).
31. E. HUTCHINSON, K. E. MANCHISTER, and L. WINSLOW. J. Phys. Chem. **58**, 1124 (1954).
32. R. BURY, A. MAYAFFRE, and M. CHEMLA. J. Chim. Phys. **73**, 935 (1976).

Can. J. Chem. Downloaded from www.nrcresearchpress.com by 210.87.254.40 on 09/05/12
For personal use only.

The Raman spectra of tetrachloroantimony(V) dichloro nonafluorodiantimonate(V), tetrachloroantimony(V) undecafluoroantimonate(V), and related molecules

JACK G. BALLARD AND THOMAS BIRCHALL

Department of Chemistry, McMaster University, Hamilton, Ont., Canada L8S 4M1

Received June 27, 1978

JACK G. BALLARD and THOMAS BIRCHALL. Can. J. Chem. **56**, 2947 (1978).

The Raman spectra of $[SbCl_4^+][Sb_2Cl_2F_9^-]$, $[SbCl_4^+][Sb_2F_{11}^-]$, $[AsCl_4^+][SbF_6^-]$, and $SbCl_4F(NbF_5)_x$ are reported. The spectra of all compounds except the last are interpreted in terms of a tetrahedral cation with weak association between the cation and anion. The spectra of the adduct found between $SbCl_4F$ and NbF_5 are interpreted in terms of polymeric fluorine bridged arrangements.

JACK G. BALLARD et THOMAS BIRCHALL. Can. J. Chem. **56**, 2947 (1978).

On rapporte les spectres Raman de $[SbCl_4^+][Sb_2Cl_2F_9^-]$, $[SbCl_4^+][Sb_2F_{11}^-]$, $[AsCl_4^+][SbF_6^-]$ et $SbCl_4F(NbF_5)_x$. On interprète les spectres des trois premiers composés en fonction d'un cation tétraédrique et d'une faible association entre le cation et l'anion. On interprète les spectres du composé d'addition entre $SbCl_4F$ et NbF_5 en fonction d'arrangements polymériques comportant des ponts fluor.

[Traduit par le journal]

Can. J. Chem. Downloaded from www.nrcresearchpress.com by 210.87.254.40 on 09/05/12
For personal use only.

Introduction

Antimony(V) chloride fluorides $SbCl_{5-x}F_x$ have had various structures assigned to them. They have been reported to be trigonal bipyramidal (1), or ionic such as $[SbCl_4^+][F^-]$ for $SbCl_4F$ (2). Antimony(V) dichloride trifluoride has been variously described as ionic, $[SbCl_4^+][SbF_6^-]$ (3), trigonal bipyramidal monomeric (4), and as a halo-bridged species (5). More recently, Preiss (6) has shown $SbCl_4F$ to be a fluorine bridge tetramer and Beattie *et al.* (7) have interpreted the Raman spectrum in terms of this structure. The molecule $SbCl_3F_2$ has recently been shown to be a fluorine bridged tetramer (8) and its Raman spectrum (9) assigned by comparison to that of $SbCl_4F$. In 1972 Preiss (10) repeated the preparation of $SbCl_2F_3$, using Kolditz and Lieth's method (3), and showed that the molecule had the formulation $[SbCl_4^+][Sb_2Cl_2F_9^-]$. Raman data were presented in this paper (10), but these were simply a reassignment of the spectra reported earlier by Dehnicke and Weidlein (4). Since it was not clear that these latter two groups were in fact examining the same molecules we have prepared a sample of $[SbCl_4^+][Sb_2Cl_2F_9^-]$, identified it by X-ray crystallography and Mössbauer spectroscopy (11), and reexamined its Raman spectrum. The Raman spectra of several related compounds are also presented here.

Experimental

$[SbCl_4^+][Sb_2Cl_2F_9^-]$ was prepared by the method of Kolditz (12) and confirmed as being identical to that of Preiss (10) by measurement of the unit cell parameters ($a = 11.7$, $b = 10.4$, $c = 13.2$, $\beta = 94.2°$). The melting point was 49–53°C and ^{121}Mössbauer data have already been reported (11).

$[SbCl_4^+][Sb_2F_{11}^-]$ was prepared by the reaction of a 4:1 mixture of SbF_5 and $SbCl_5$ or by the reaction of $SbCl_4F$ with 2 mol of SbF_5 in liquid SO_2 at 20°C in a sealed tube. The product is a white solid mp 81–82°C. Mössbauer spectra have already been reported (11).

$[AsCl_4^+][SbF_6^-]$ was isolated while attempting to prepare $[SbCl_4^+][AsF_6^-]$ by the reaction of $SbCl_4F$ and AsF_5. Halogen rearrangement occurred and the hexafluoroantimonate(V) salt of $[AsCl_4^+]$ was obtained as a white solid which decomposed before melting.

In a typical preparation of $SbCl_4F{\cdot}NbF_5$ a weighed amount ($\sim$1.0 g) of $SbCl_4F$ was introduced into one arm of a previously dried reaction vessel in a glove box and a stoichiometric amount of NbF_5 was added to a second arm. The vessel was transferred to a vacuum line and evacuated. Sulphur dioxide was then condensed onto the NbF_5, the vessel sealed and allowed to warm to room temperature. The NbF_5 dissolved in the liquid SO_2 and this solution was poured through a frit separating the two arms of the reaction vessel onto the $SbCl_4F$. The mixture was allowed to react overnight after which the SO_2 was removed and the sample washed several times with fresh liquid SO_2. The white adduct melted at 55–57°C.

Raman spectra were recorded using an Ar ion laser (5145 Å) with a Spex 1400 Spectrophotometer system. Samples were contained in carefully dried sealed capillary tubes.

Results and Discussion

The Raman data for $[AsCl_4^+][SbF_6^-]$, $[SbCl_4^+][Sb_2Cl_2F_9^-]$, and $[SbCl_4^+][Sb_2F_{11}^-]$ are shown in Fig. 1 and Table 1.

Weidlein and Dehnicke (13) have reported Raman data for $[AsCl_4^+][AsF_6^-]$ and this is compared to our data for the $[SbF_6^-]$ analogue. The assignments are based on a tetrahedral cation and an octahedral anion. If the cation $[AsCl_4^+]$ has T_d symmetry, then a total of four fundamentals are Raman active. The strongest band in the spectrum at 415 cm^{-1} is assigned to ν_1. This agrees with the assignment made

Can. J. Chem. Downloaded from www.nrcresearchpress.com by 210.87.254.40 on 09/05/12
For personal use only.

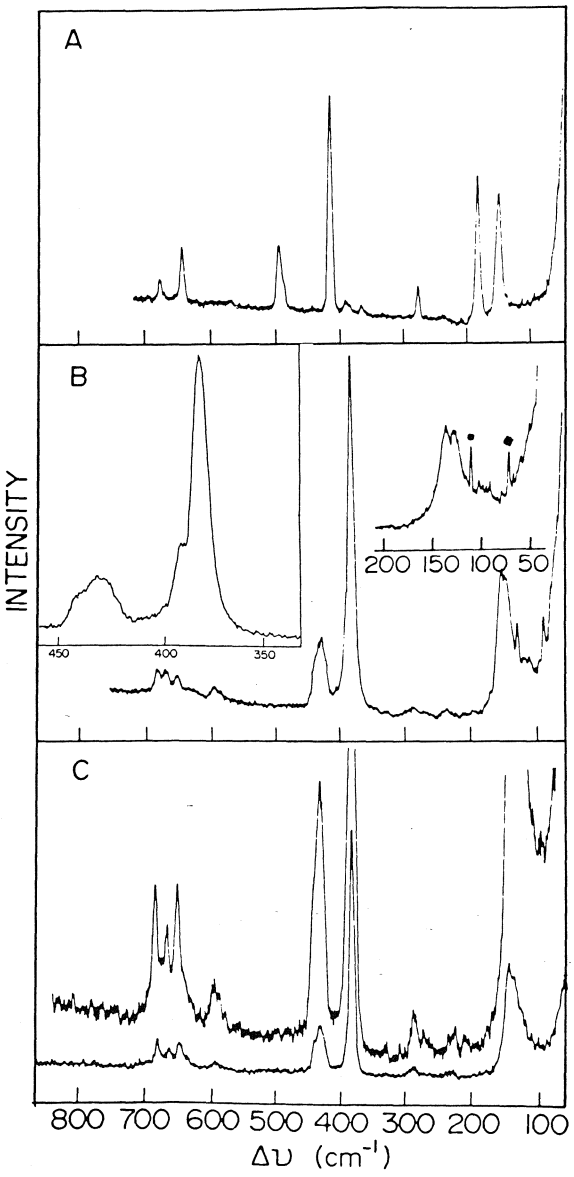

FIG. 1. Raman spectra at 20°C of (*a*) solid $[AsCl_4^+][SbF_6^-]$; (*b*) solid $[SbCl_4^+][Sb_2Cl_2F_9^-]$, inset (450–350 cm^{-1}) region expanded; (*c*) solid $[SbCl_4^+][Sb_2F_{11}^-]$. The spectra were recorded in glass melting point tubes (*glass lines).

for the $[AsF_6^-]$ analogue, where ν_1 is at 422 cm^{-1} (13). The $\nu_2(e)$ vibration is assigned to the band at 149 cm^{-1}; in $[AsCl_4^+][AsF_6^-]$ this occurs at 156 cm^{-1}; ν_3 and ν_4 were assigned to the bands at 490 and 184 cm^{-1}, the 490 cm^{-1} band being split into two bands at 496 and 488 cm^{-1}. This is attributed to cation–anion interaction and evidence for such interaction is also found in the anion spectrum. No corresponding lowering of symmetry was reported in $[AsCl_4^+][AsF_6^-]$ (13).

An undistorted anion having O_h symmetry would have only three Raman active vibrations, namely, $\nu_1(a_{1g})$, $\nu_2(e_g)$, and $\nu_5(t_{2g})$, but there are more than three bands to be assigned to the $[SbF_6^-]$ anion. Cation–anion interaction, alluded to above, would lower the symmetry and allow additional vibrations to be Raman active. These bands are assigned as indicated in Table 1 and agree favourably with the assignments made for the distorted $[SbF_6^-]$ ion in $[Xe_2F_3^+][SbF_6^-]$ (14). No evidence for cation–anion interaction was found in $[PCl_4^+][PCl_6^-]$ (15), $[PCl_4^+][SbCl_6^-]$ (16), or $[AsCl_4^+][AsF_6^-]$ (13). Figure 1 also shows the spectra of $[SbCl_4^+][Sb_2Cl_2F_9^-]$ and $[SbCl_4^+][Sb_2F_{11}^-]$ as solids. One can see the similarity between these spectra and that discussed above in that the strongest bands in each of these spectra arise from the cation. The positions of the bands representing the asymmetric stretch and bend are, of course, appropriately shifted due to the increased mass of the ion. We have assigned the cation bands by analogy to those for the $[AsCl_4^+]$ ion and this has been aided by being able to carry out polarization measurements on the melts. Earlier investigation of "$SbCl_2F_3$" by Dehnicke and Weidlein (4) had resulted in the erroneous conclusion that this molecule was trigonal bipyramidal. A reinterpretation of these data was made by Preiss (10) as a result of his X-ray analysis of this compound, but a complete analysis was not possible at that time. We have been able to observe all four Raman active bands for the $[SbCl_4^+]$ cation and these are listed in Table 1. The band at 385 cm^{-1}, which occurs at 388 cm^{-1} in the melt and is totally polarized, is assigned to $\nu_1(a_1)$. The $\nu_2(e)$ mode, which was not detected by the previous workers, is at 128 cm^{-1} and is broadened. The asymmetric stretch at 436 cm^{-1} is presumably the result of a lowering of symmetry due to cation–anion interaction as suggested by both Mössbauer (11) and X-ray analysis (17). The remaining cation band, $\nu_2(t_2)$ occurs at 137 cm^{-1}. These assignments hold also for the $[Sb_2F_{11}^-]$ analogue. In the melt, the splitting observed for $\nu_3(t_2)$ disappears, while $\nu_2(e)$ becomes sharper, as might have been expected since cation–anion interactions would be reduced in the liquid state. All of these assignments are completely consistent within the $[PCl_4^+]$, $[AsCl_4^+]$, $[SbCl_4^+]$ series, with a steady decrease in frequency of all bands which represent the asymmetric stretch as the mass of the central atom increases. The only notable difference within this series is found in the degree of cation–anion interaction which is most noticeable for $[SbCl_4^+]$, the largest and hence the most easily distorted.

The anion bands of the $[SbCl_4^+]$ compounds are weak by comparison with those of the cation (Fig. 1). This appears to be a general feature of all $[Sb_2F_{11}^-]$ spectra and these are rarely, if ever,

TABLE 1. Vibrational frequencies for group(V) chloride fluoride compounds containing an $[MCl_4^+]$ cation

	$[SbCl_4^+][Sb_2Cl_2F_9^-]$			$[SbCl_4^+][Sb_2F_{11}^-]$				
$[AsCl_4^+][SbF_6^-]$ solid[a]	Solid[a]	Melt[b]	dp ratio	Solid[a]	Melt[b]	dp ratio	Assignment	Description of motion
496(30)	441(13)	436(11)	(0.68)	438(13)	437(11)	(0.69)	T_d $\nu_3(t_2)$	ν_{as}(M—Cl_4) degenerate stretch
488(13)	430(19)			433(20)				
415(100)	385(100)	388(100)	(0.06)	388(100)	386(100)	(0.03)	$\nu_1(a_1)$	ν_{sym}(M—Cl_4)
184(66)	137(40)	144(16)	(0.68)	139(44)	140(22)	(0.78)	$\nu_4(t_2)$	δ_{as}(M—Cl_4) degenerate bend
149(56)	128(36)	126(12)	(0.68)	130(38) 124(24)	123(16)	(0.75)	$\nu_2(e)$	$\delta_{sym}(MCl_4)$
							O_h	
645(25)	646(6)	651(9)		649(10)	651(10)		$\nu_1(a_{1g})$	$\nu_{sym}(MX_6)$
574(2)	591(5)	604(4)		591(3)	599(2)		$\nu_2(e_g)$	ν_{sym}(M—X_4)
678(10)	675(5) 663(6)	674(9)		682(12) 663(8)	678(8)		$\nu_3(t_{1u})$	Degenerate stretch
390(5)[c] 368(4)[c]	392(27)sh[d]			327(1)				
241(2) 218(1)	241(3)			225(2) 210(1)			$\nu_4(t_{1u})$	Degenerate bend
278(15)	287(3) 276(2)			288(4) 271(1)sh	294(3)		$\nu_5(t_{2g})$	M—X angle deformation
120(1) 80(1)								Lattice modes

[a]Solid at 20°C.
[b]Melt at 70°C; p: polarized; dp: depolarized; sh: shoulder.
[c]Sb—Cl impurity.
[d]Sb—Cl band of $[Sb_2Cl_2F_9^-]$ (see Fig. 5 of ref. 10).

assigned. A partial, somewhat tentative assignment is made in Table 1 by comparison with those of the $[SbF_6^-]$ ion. The spectra of the $[Sb_2Cl_2F_9^-]$ and $[Sb_2F_{11}^-]$ anions appear little different. However, the former should have an Sb—Cl stretching vibration and Preiss (10) had in fact assigned the band at 393 cm^{-1} to the Sb—Cl stretch of both the anion $[SbCl_2F_9^-]$ and the $[SbCl_4^+]$ cation. Expansion of the Sb—Cl stretching region shows an additional band, at 392 cm^{-1}, in the spectrum of the $[Sb_2Cl_2F_9^-]$ anion (Fig. 1) which is not present in the $[Sb_2F_{11}^-]$ spectrum which we assign to the anion Sb—Cl stretch. The anion spectra again simplify on melting, for the reasons discussed above, but depolarization ratios could not be measured because of the low intensities of the anion bands.

Raman data recorded for the adduct formed between $SbCl_4F$ and NbF_5 are 98(12), 110(24), 117(24), 139sh, 147(22), 161(36), 232(3), 260(3), 343(100), 370(20)sh, 382(55), 403(12)sh, 651(1), 705sh, 711(6), 740(9), 748sh, 761(11), 784(4). There are a number of possible products of this reaction. Niobium pentafluoride could abstract a fluoride from $SbCl_4F$ to produce $[SbCl_4^+][NbF_6^-]$ or $[SbCl_4^+][Nb_2F_{11}^-]$. A halogen rearrangement could occur, as it did with $SbCl_4F$ and AsF_5, to produce $[NbCl_4^+][SbF_6^-]$. Since both reactants have tetrameric fluorine bridged structures, the third possibility for the structure of the reaction product would be a mixed antimony–niobium fluorine bridged compound, which may be tetrameric in nature. It is apparent, upon examination of the data, that there is a similarity between the spectrum of the adduct and those of the reactants (7). Comparison of the band positions with the data in Table 1 also indicates that neither $[SbCl_4^+]$ nor $[SbF_6^-]$ are present in this compound, nor can any bands be convincingly assigned to a $[NbCl_4^+]$ cation. The first two structures suggested above are therefore ruled out. A fluorine bridged polymer is therefore the most likely possibility. Antimony-121 Mössbauer measurements (18) are also consistent with this suggestion but further work will be necessary to completely characterize this compound.

Acknowledgement

The National Research Council of Canada is thanked for financial support.

1. F. A. COTTON and G. WILKINSON. Advanced inorganic chemistry. 3rd ed. Interscience, New York. 1972. p. 377.
2. K. DEHNICKE and J. WEIDLEIN. Chem. Ber. **98**, 1087 (1965).
3. L. KOLDITZ and W. LIETH. Z. Anorg. Allg. Chem. **310**, 237 (1961).
4. K. DEHNICKE and J. WEIDLEIN. Z. Anorg. Allg. Chem. **323**, 267 (1963).
5. E. L. MUETTERTIES, W. MAHLER, K. J. PACKER, and R. SCHMUTZLER. Inorg. Chem. **3**, 1298 (1964).
6. H. PREISS. Z. Chem. **6**, 350 (1966).

Can. J. Chem. Downloaded from www.nrcresearchpress.com by 210.87.254.40 on 09/05/12
For personal use only.

7. I. R. BEATTIE, K. M. S. LIVINGSTONE, G. A. OZIN, and D. J. REYNOLDS. J. Chem. Soc. A, 958 (1969).
8. J. G. BALLARD, T. BIRCHALL, and D. R. SLIM. J. Chem. Soc. Chem. Commun. 653 (1976).
9. J. G. BALLARD, T. BIRCHALL, and D. R. SLIM. J. Chem. Soc. Dalton Trans. 1469 (1977).
10. H. PREISS. Z. Anorg. Allg. Chem. **389**, 254 (1972).
11. J. G. BALLARD and T. BIRCHALL. J. Phys. Paris, **37**, C6-513 (1976).
12. L. KOLDITZ. Z. Anorg. Allg. Chem. **289**, 218 (1957).
13. J. WEIDLEIN and K. DEHNICKE. Z. Anorg. Allg. Chem. **337**, 113 (1965).
14. R. J. GILLESPIE and B. LANDA. Inorg. Chem. **12**, 1383 (1973).
15. P. REICH and H. PREISS. Z. Chem. **7**, 115 (1967).
16. G. L. CARLSON. Spectrochem. Acta, **19**, 1291 (1963).
17. J. G. BALLARD, T. BIRCHALL, and D. R. SLIM. Can. J. Chem. **55**, 743 (1977).
18. J. G. BALLARD. Ph.D. Thesis, McMaster University, Hamilton, Ont. 1977.

Can. J. Chem. Downloaded from www.nrcresearchpress.com by 210.87.254.40 on 09/05/12
For personal use only.

Interaction of polymers in solution with porous solids. I. Penetration of porous glass by dextran

JOHN C. DAY, BOHUMIL ALINCE, AND A. ALLEN ROBERTSON
Pulp and Paper Research Institute of Canada, Montreal, P.Q., Canada H3A 2A7
and
Department of Chemistry, McGill University, Montreal, P.Q., Canada H3A 2A7

Received May 12, 1978

JOHN C. DAY, BOHUMIL ALINCE, and A. ALLEN ROBERTSON. Can. J. Chem. **56**, 2951 (1978).

Measurements of the penetration of porous substrates (porous glasses) by non-sorbing macromolecules (dextrans) have yielded penetration curves that relate the degree of penetration to molecular size. Combinations of well-characterized polymer fractions with a series of uniformly porous glasses have demonstrated that, in agreement with the theory, the penetration is dependent only on the relative size of the molecule and the pore. Several models differing in the methods of characterizing the sizes of the pores and solute molecules have been compared. The predictions of the shape of the penetration curves are similar for most models and are in similar agreement with the experimental data.

JOHN C. DAY, BOHUMIL ALINCE et A. ALLEN ROBERTSON. Can. J. Chem. **56**, 2951 (1978).

Au moyen de mesures de la pénétration de substrats poreux (verres poreux) par des macromolécules inertes (dextranes), on a déterminé des courbes reliant le degré de pénétration à la taille des molécules. En réunissant des fractions bien caractérisées de polymères et une série de verres uniformément poreux, on a démontré qu'en accord avec la théorie, la pénétration ne dépend que des tailles relatives de la molécule et de la pore. On a comparé plusieurs modèles qui diffèrent quand à la méthode utilisée pour caractériser les tailles des pores et des molécules de soluté. Pour la plupart des modèles, on prévoit pour les courbes de pénétration des allures semblables et on note un accord semblable entre ces prévisions et les résultats expérimentaux.
[Traduit par le journal]

Can. J. Chem. Downloaded from www.nrcresearchpress.com by 210.87.254.40 on 09/05/12
For personal use only.

Introduction

The interaction of polymer molecules in solution with porous substrates depends initially on their ability to penetrate the pores and then on their interaction with the pore walls, which may vary from strong attraction resulting in adsorption to strong repulsion. This study reports the penetration of a porous material by a polymer in solution in which the interaction of the polymer and surface is shown to be minimal. The behaviour is relevant to the mechanism of separation by molecular size in gel permeation chromatography (GPC), and to the determination of pore-size distributions by the degree to which molecules of different sizes are excluded from polydisperse pore systems. It is important, in the context of this work, to an understanding of the mechanism of polymer adsorption on internal surfaces.

During adsorption on a porous material, the concentration of the adsorbate solution in the pores is determined by the bulk concentration, the relative rate of penetration and adsorption, the degree of interaction of the polymer with the pore-wall surface, and the relative size of the polymer and the pore. Using a non-sorbing polymer as the penetrating solute provides a means of identifying and studying the factors affecting the penetration.

The dependence of the ratio of the equilibrium concentration attainable within a pore to the external solution concentration on the relative size of the solute molecules and the pore has been derived by Casassa (1) for the case where the interactive forces between the polymer and the pore wall are negligible. Few data to verify this have been published (2). The influence of interaction has been included in a more general treatment by Pouchly (3), where the chain segment concentration near the pore-wall surface is determined by both the degree of interaction with and the conformational restrictions imposed by the pore wall.

Molecular size separation by the penetration of non-absorbing macromolecules into porous materials was first accomplished using flexible polymer gels (4), then by using rigid polymer gels (5) and porous silica (6). Interest in the mechanism of separation has led to theories based on diffusion or on the degree of penetration and these have been extensively reviewed (4, 7–10). The relative influence of the two mechanisms in GPC procedures was investigated by Yau (ref. 10, p. 105, refs. 11, 12), who found that separation is primarily due to the extent of permeation and that kinetic processes contribute only in a minor way.

The correlation obtained between the penetration

TABLE 1. Characterization data of dextran fractions (supplied by Pharmacia)

Dextran designation	Lot number	$\overline{M}_w$ (LS)	$\overline{M}_n$ (Osm.)	$\overline{M}_w/\overline{M}_n$	Intrinsic viscosity (dl g^{-1})	Equivalent hydrodynamic radius, r_h (nm)
Maltose	—	180	180	1.00	—	0.5 (ref. 13)
T10	3205	9 300	5 700	1.63	0.095	2.41
T20	7968	22 300	15 000	1.49	0.148	3.74
T40	2514	41 800	25 700	1.63	0.210	5.18
T110	5404	100 500	62 000	1.62	0.309	7.90
T500	4024	495 000	195 000	2.54	0.52	15.98

determined by static experiments and the elution of the same polymers from columns packed with the same porous material (11) indicates that the separation is independent of the flow rate of the eluant and is not dependent on the attainment of equilibrium conditions during column operation. In his review, Coll (ref. 10, p. 135) points out that as long as a solute molecule undergoes a large number of exchanges between the mobile phase (bulk solution) and stationary phase (pores) in the column, the elution volume of a molecular species is independent of the flow rate, and the equilibrium model for the partition of the solute between the bulk solution and the pores is applicable. However, a true comparison of the theoretical penetration curves can only be made with the data obtained from static penetration experiments. In this study, the penetration of characterized porous glass by fractionated samples of dextran in water solution is compared with model penetration curves.

Materials and Methods

Dextran

Characterized dextran fractions were obtained from Pharmacia, Uppsala, Sweden. Molecular weights, determined by light scattering and osmometry, and intrinsic viscosities are listed in Table 1. Molecular weight distributions, determined by gel filtration on 'Sephadex' (cross-linked dextran gel), are shown in Fig. 1. All data were supplied by the manufacturer.

The structure (14–16) and the hydrodynamic properties (14, 17–19) of dextran have been extensively studied. The molecules are randomly branched and sedimentation behaviour suggests that the sphere is a reasonable model for the molecule in solution and any asymmetry decreases at higher molecular weights. Several methods (14, 17, 19) have been applied to calculate the dimensions of dextran molecules in solution. For the purpose of the present investigation, the equivalent hydrodynamic radius, r_h (Table 1), was calculated using the Einstein viscosity relation (ref. 20, p. 606).

$$[1] \qquad r_h = (3.0 \times 10^{22} \overline{M}_w[\eta]/N\pi)^{1/3}$$

where r_h is the equivalent hydrodynamic radius (nm), $\overline{M}_w$ is the weight average molecular weight, $[\eta]$ is the intrinsic viscosity (dl g^{-1}), and N is the Avogadro number.

The relation between the equivalent hydrodynamic radius and the root-mean-square radius of gyration of dextran is examined in the Discussion section.

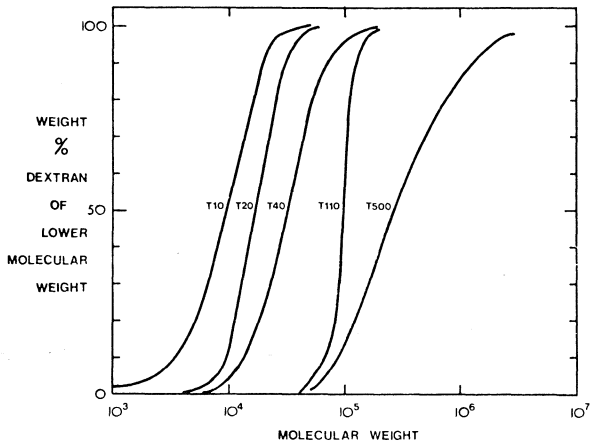

FIG. 1. Molecular weight distributions of dextran fractions (supplied by Pharmacia).

The dextran fractions were stored in air-tight containers to prevent contamination and sorption of moisture from the atmosphere. Since dextran solutions are growth media for micro-organisms, sodium azide (final concentration, 10 mg ℓ^{-1}) was added to prevent degradation of the macromolecule during equilibration. The specific conductance of the distilled water was less than 1.5×10^{-6} ohm^{-1} cm^{-1}. The disaccharide, maltose, provided a probe of smaller effective dimensions in solution, for comparison with the dextran fractions.

Porous Glass

Three different CPG-10 controlled pore glasses (Corning Glass Works, Corning, NY; Electro-Nucleonics Inc., Fairfield, NJ) were used as the porous substrate. After washing the glasses to remove fines and colloidal glass particles from the pore system, the benzene sorption–desorption isotherm of each was determined, from which the values of the parameters required to characterize the pore system were calculated by established methods (21, 22) (Table 2). The surface areas were obtained by BET analysis of the isotherms and were in agreement with areas obtained by nitrogen adsorption. The pore volume was determined from the plateau in the adsorption isotherm above a relative vapour pressure of 0.95 (22) and the mean pore size and pore-size distribution were determined by an analysis of the desorption isotherm, based on the Kelvin equation (21), which gives a Kelvin radius, a, that is interpreted either as the radius of equivalent cylindrical pores or as the separation distance of parallel-walled slits. It is relevant here to consider both alternatives since the porous glass is believed to

Can. J. Chem. Downloaded from www.nrcresearchpress.com by 210.87.254.40 on 09/05/12
For personal use only.

TABLE 2. Characterization data for CPG-10 porous glasses

Designation of glass CPG-10-	Surface area ($m^2\ g^{-1}$)	Pore volume ($cm^3\ g^{-1}$)	Kelvin radius (nm)	Pore size distribution (±%)*
75C	150	0.53	6.85	8
240C	110	1.32	16.6	7
170EN	105	1.49	20.1	14

*Width of distribution (% of Kelvin radius) accounting for 80% of the pore volume.

Can. J. Chem. Downloaded from www.nrcresearchpress.com by 210.87.254.40 on 09/05/12
For personal use only.

have a network of highly interconnected pores with properties intermediate between slits and cylinders.

Procedure

Approximately 2 g of CPG-10 porous glass was accurately weighed in screw-capped glass bottles (capacity 30 cm^3), to which 15 cm^3 of dextran solution was then added. The mixture was equilibrated at 25 ± 1°C tumbling at 10 rpm to keep the glass particles in suspension. Although all measurable concentration change occurred in the first hour, each suspension was allowed to equilibrate for 24 h. Control mixtures consisting of glass and solvent only were simultaneously equilibrated. Exclusion of the polymer from the pore volume results in an increased concentration of the supernatant. The ratio of pore volume to solution was chosen so that the increase in concentration was large enough to be measured accurately.

For all dextran–glass combinations tested, the ratio of the concentrations in the pores and in the bulk solution was independent of the concentration of polymer solution added over the range from 1 g ℓ^{-1} to 20 g ℓ^{-1}. Most of the data were obtained with solutions of initial concentration, 10 g ℓ^{-1}.

The supernatant concentration was compared with that of the original solution in a 10 cm cell in a Hilger–Watts differential refractometer thermostatted at 25°C. Refractive index increments due to changes in dextran concentration and to substances eluted from the glass were found to be additive; the simultaneous control readings were therefore subtracted from those of test mixtures. The refractometer was calibrated with dextran solutions of known concentration; no variation in the calibration with molecular weight of the dextran was found.

To verify that no air was trapped within the pore volume when the dextran solution was added to dry glass, weighed samples of glass were evacuated in the equilibration bottles and then immersed in distilled water before the dextran solution was added. A degree of exclusion equal to that without evacuation was obtained. This result is consistent with the open structure of the pore system of CPG-10 glass (23).

Calculation of Penetration Coefficient

Casassa (1) defines a distribution coefficient, K, as the ratio of the polymer concentration within the pores, C_p, to the concentration in the supernatant solution, C_s.

$$[2] \qquad K = C_p/C_s$$

The system is assumed to consist of monodisperse polymers within monodisperse pores of given geometry, in which the whole pore volume is considered accessible to the polymer, but the concentration attainable within the pores is lower than that in the bulk solution. This is due to conformational entropy restrictions, imposed by the pore walls, which are directly dependent on the relative size of the polymer and the pores (1).

This coefficient equals unity when the relative size is zero, and decreases as the relative size increases. It is therefore directly related to penetration and inversely to exclusion. The term 'penetration coefficient' describes this behaviour logically, and is used throughout this paper for the parameter, K.

When a quantity of porous glass is immersed in a volume of solution, V_0, of concentration, C_0, the solute is partitioned between the pore volume present, V_p, at concentration C_p, and the supernatant solution volume, V_s, at concentration C_s. At equilibrium, the following two relations apply:

$$[3] \qquad V_0 = V_p + V_s$$

$$[4] \qquad C_0V_0 = C_pV_p + C_sV_s$$

Upon substituting V_s from eq. [3] into eq. [4] and re-arranging,

$$C_p = C_s + \frac{V_0}{V_p}(C_0 - C_s)$$

Substituting from eq. [2]

$$[5] \qquad K = 1 - \frac{V_0}{V_p}\left(1 - \frac{C_0}{C_s}\right)$$

All quantities on the right hand side of eq. [5] are measurable, so that K may be calculated directly from experimental observations.

Results and Discussion

Experimental Results

The degree of penetration of three porous glasses (CPG-10-75C, CPG-10-240C, CPG-10-170EN) by five dextran fractions and maltose was measured. The average penetration coefficient and relative size of each combination are presented in Table 3. The relative size of polymer and pore is given by r_h/a and σr_h where r_h is the hydrodynamic radius of the polymer molecules, a is the Kelvin radius of the pores, and σ is the surface area/pore volume ratio. Where sufficient measurements were made, the 95% confidence interval of the penetration coefficient is given. The range of the size ratio which includes 80% of both molecules and pore volume is also listed.

For each glass, the penetration coefficient decreases as the relative size increases (i.e. as the molecular size increases). For the combinations of dextran T110 and T500 with CPG-10-75C, in which the molecular size of the dextran exceeds the pore size (i.e. $r_h/a > 1.0$), the penetration coefficient is close to zero and does not alter significantly as r_h/a increases. This indicates that the pore volume estimated from the benzene sorption isotherms (V_p in eq. [5]) coincides with the maximum volume from which the dextran is excluded.

Can. J. Chem. Downloaded from www.nrcresearchpress.com by 210.87.254.40 on 09/05/12
For personal use only.

TABLE 3. Penetration coefficient and relative size of several combinations of dextran and porous glass

Dextran	Relative size		Penetration coefficient
	r_h/a	σr_h	
	CPG-10-75C		
Maltose	0.07(0.06–0.09)	0.14(0.13–0.15)	0.93
T10	0.35(0.20–0.64)	0.67(0.42–1.08)	0.42(±0.03)
T20	0.55(0.32–0.78)	1.04(0.67–1.32)	0.18(±0.04)
T40	0.76(0.40–1.14)	1.44(0.83–1.93)	0.0
T110	1.15(0.83–1.54)	2.2 (1.69–2.60)	−0.03
T500	2.3 (0.95–4.62)	4.4 (1.96–7.82)	0.0 (±0.07)
	CPG-10-240C		
Maltose	0.03(0.03–0.04)	0.042(0.04–0.05)	0.96
T10	0.14(0.09–0.26)	0.20 (0.18–0.32)	0.79(±0.02)
T20	0.22(0.14–0.32)	0.31 (0.20–0.40)	0.64(±0.03)
T40	0.31(0.17–0.46)	0.43 (0.24–0.58)	0.50(±0.03)
T110	0.48(0.34–0.62)	0.66 (0.51–0.78)	0.34(±0.04)
T500	0.96(0.40–1.86)	1.33 (0.59–2.35)	0.07(±0.015)
	CPG-10-170EN		
Maltose	0.03(0.02–0.04)	0.035(0.03–0.04)	0.99
T10	0.12(0.06–0.25)	0.17 (0.11–0.27)	0.88
T20	0.19(0.10–0.31)	0.26 (0.17–0.34)	0.72
T40	0.26(0.12–0.45)	0.36 (0.21–0.49)	0.64
T110	0.39(0.27–0.61)	0.56 (0.43–0.66)	0.50

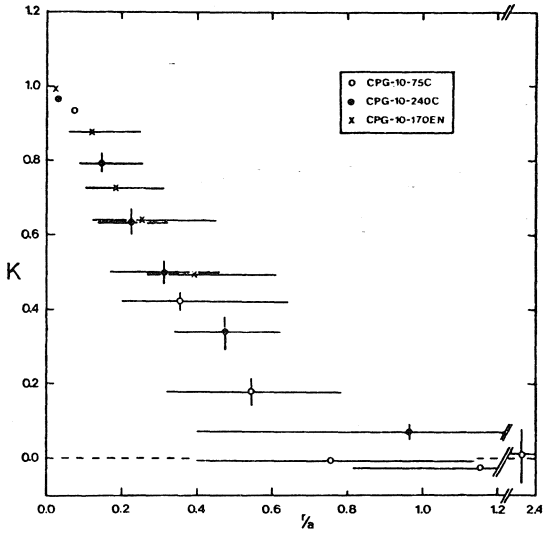

FIG. 2. Effect of relative size on penetration coefficient.

The data in Table 3 including the confidence limits are plotted in Fig. 2. The penetration curves for the three glasses coincide within experimental error. The relative size appears to be the major factor determining the partition of homologous polymer molecules between bulk solution and pore volume, when no adsorption occurs. These data may be compared with theoretical predictions of the variation of the penetration coefficient with relative size.

The equilibration distribution of macromolecules between bulk solution and pores has been discussed in reviews of GPC (e.g. refs. 7, 9) as one of the mechanisms of separation. Static mixing experiments have shown that the penetration of a single porous glass by a series of polystyrene samples decreases as the molecular weight (i.e. molecular size) increases (11). The behaviour parallels that of the series eluted at low flow rates from a column packed with the same material (12). However, no published data have been found which indicate the concurrence of penetration curves when substrates of distinctly different pore size are employed.

Theoretical Models

A number of theoretical models have been developed which employ simple geometric equivalents of the macromolecule and the pore system, and the concept that the penetration coefficient is equal to the fraction of the pore volume available to the molecule. Variation in the shape of the molecule (24) and in the geometric components used to simulate the pore system (ref. 10, p. 119, refs. 25, 26) have resulted in expressions for the penetration coefficient in terms of several combinations of parameters describing the relative size of the molecule and pore (Table 4).

The definition of the penetration coefficient based on the fraction of pore volume available to the molecule is a special case, derived from more general

TABLE 4. Theoretical variation of penetration coefficient with relative size

Curve No.	Geometry: Molecule	Geometry: Pore	Expression for penetration coefficient*	Reference
1	Rigid sphere	Any	$K = 1 - \sigma r$	ref. 10, p. 119
2	Rigid sphere	Slit	$K = 1 - r/a$	ref. 10, p. 119
3	Rigid sphere	Cylinder	$K = 1 - 2r/a$ (at low r/a)	ref. 10, p. 119
4	Rigid sphere	Cylinder	$K = (1 - r/a)^2$ (accounting for curvature)	24
5	Rigid sphere	Isotropic network of randomly oriented planes	$K = \exp(-\sigma r)$	
6	Any rigid shape		$K = \exp(-\sigma \bar{L}/2)$	24
7	Flexible chain	Slit	$K = \frac{8}{\pi^2} \sum_{m=0}^{\infty} \frac{1}{(2m+1)^2} \times \exp\left(-\frac{(2m+1)^2\pi^2(\sigma s)^2}{4}\right)$	ref. 10, p. 119
8	Flexible chain	Cylinder	$K = 4 \sum_{m=1}^{\infty} \frac{1}{\beta_m^2} \exp\left(-\beta_m^2 \frac{s^2}{a^2}\right)$	2
9	Flexible chain	Random solid spheres	$K = \exp\left(-\frac{2}{\sqrt{\pi}}\sigma s + \frac{(\sigma s)^2}{3 \ln f}\right)$	27

*σ = surface area/pore volume ratio ($\sigma = 1/a$ for slits; $\sigma = 2/a$ for cylinders); r = radius of rigid sphere; a = half-separation of parallel planes of slit; cylinder radius; $\bar{L}$ = Mean external length (the average cross-section dimension of the molecule projected in all directions); s = root-mean-square radius of gyration; β_m = mth root of $J_0(\beta) = 0$, where $J_0(\beta)$ is a Bessel function of the first kind, of zero order; f = pore volume fraction of total volume of porous material.

definitions as follows. In statistical thermodynamic terms, the penetration coefficient is defined as the ratio of the partition functions for molecules in pores and in the bulk solution. This becomes the ratio of configuration integrals for a random walk chain in the presence or absence of pore boundaries under the conditions assumed in the models to simplify calculation (ref. 10, p. 119, refs. 24, 27). In practical terms, the penetration coefficient is equal to the ratio of concentrations inside and outside the pores (eq. [2]). For models based on simple rigid geometric components, the number of dimensions over which the configuration integrals must be determined is reduced to those of physical space; the penetration coefficient is then equivalent to the fraction of the pore volume available to the molecule.

Using the statistical thermodynamic approach, Casassa (1) derived expressions for the penetration coefficient of linear chains in slit and cylindrical pores (curves *7*, *8* in Table 4). Doi (27) recently proposed an expression for linear flexible chains in the voids among randomly-distributed, uniform solids (curve *9* in Table 4). In both models, the root-mean-square (rms) radius of gyration is used to describe molecular size.

Theory for linear chains may be inappropriate for dextran because of the effects of branching. Casassa and Tagami (2) have considered the influence of branching on penetration and have shown that the curves derived for polymer molecules of the same molecular weight but different degrees of branching are superposed if the radius of gyration of the equivalent linear chain is multiplied in each case by $g^{1/6}$ where g is defined by the ratio of the unperturbed mean square radius of the branched polymer molecule to that of a linear polymer chain of the same mass.

$$[6] \qquad g = R_{br}^2/R_{lin}^2$$

The evaluation of g is determined, practically, from the intrinsic viscosity ratio of the branched and unbranched polymers which is experimentally found (28–30) to be equal to $g^{0.5(\pm 0.1)}$. Thus if the Flory–Fox equation (31) can be assumed to be valid for both branched and linear polymers,

$$[7] \qquad [\eta] = \phi' s^3 M^{-1}$$

where $[\eta]$ is the intrinsic viscosity, ϕ' is the Flory constant, s is the rms radius of gyration, and M is the molecular weight. The influence of branching on the intrinsic viscosity (and hence on the equivalent hydrodynamic volume) is accounted for by multiplying the rms radius of gyration by $g^{1/6}$. Thus coincidence of the theoretical penetration curves for branched and linear polymers would be expected if the hydrodynamic size determines the partition of polymers between the bulk solution and the pores.

A demonstration of the identity of the equivalent sphere diameter of dextran molecules obtained by

Can. J. Chem. Downloaded from www.nrcresearchpress.com by 210.87.254.40 on 09/05/12
For personal use only.

Can. J. Chem. Downloaded from www.nrcresearchpress.com by 210.87.254.40 on 09/05/12
For personal use only.

viscosity measurements with the minimum diameter of pore that can be penetrated is provided in a recent study by Haller (32). However, it has been pointed out (33) that the hydrodynamic size may provide good agreement between polymers of a similar type (e.g., between linear molecules and those with a limited amount of long-chain branching, such as dextran), but that it should not be extended uncritically to more highly-branched molecules.

Comparison of Theory and Experiment

It is possible to compare directly the data in Table 3, where the molecular size is specified by the equivalent hydrodynamic radius, with curves *1* to *5* in Table 4 in which the molecule is considered to be a rigid sphere and the pores are considered cylindrical, slit-shaped, or equivalent to the voids among randomly-oriented planes. In Fig. 3, the data curve lies slightly above, but has a shape similar to the curve for a rigid sphere in a cylindrical pore when the influence of curvature is considered (curve *4*). If curvature is neglected (curve *3*), a reasonable prediction of the variation of the penetration coefficient is obtained only at relative sizes below $r/a = 0.3$.

Since the position of the data points is dependent on arbitrary molecular size and pore-size parameters, the suitability of a penetration model can only be indicated by a similarity in shape of the theoretical penetration curve to the plot of the experimental data. The chosen molecular size and pore-size diameters do, however, produce an experimental curve lying close to the theoretical curves. This near-coincidence is fortuitous (1), but the theoretical curve may be used to predict with some confidence the degree of penetration of CPG-10 porous glass by dextran, when the experimental system is described by these parameters.

In Fig. 4, the data coincide with the theoretical penetration coefficient for slit geometry (curve *1*) as the relative size increases up to $\sigma r = 0.7$. Above this value, the theoretical penetration coefficient decreases more rapidly than the data. For the model in which the pores are considered as voids among randomly-oriented planes, curve *5* maintains a higher value of the penetration coefficient above $\sigma r = 0.5$ than observed. This pore model is more open than the pore system of CPG-10 glass and is unsuitable as a model for this substrate.

A suitable method is now sought to convert the equivalent hydrodynamic radius, r_h, to the rms radius of gyration, s, to permit comparison of the data with curves *7*, *8*, and *9* in Table 4 that are derived in terms of s.

A factor relating r_h and s may be calculated from the Einstein viscosity relation (eq. [1]) (ref. 20, p. 606) and the Flory–Fox equation (eq. [7]) (31).

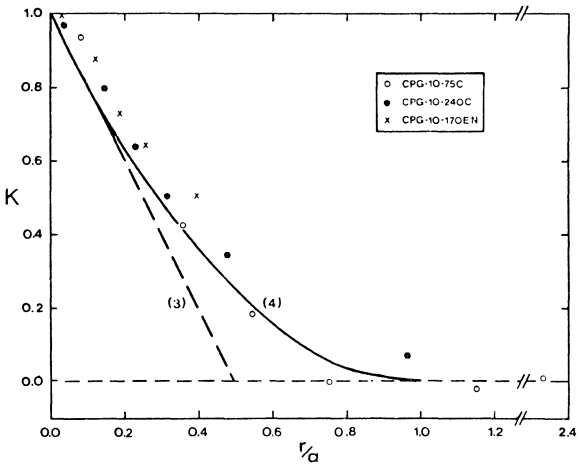

FIG. 3. Comparison of penetration data with a model of rigid sphere molecules in cylindrical pores.

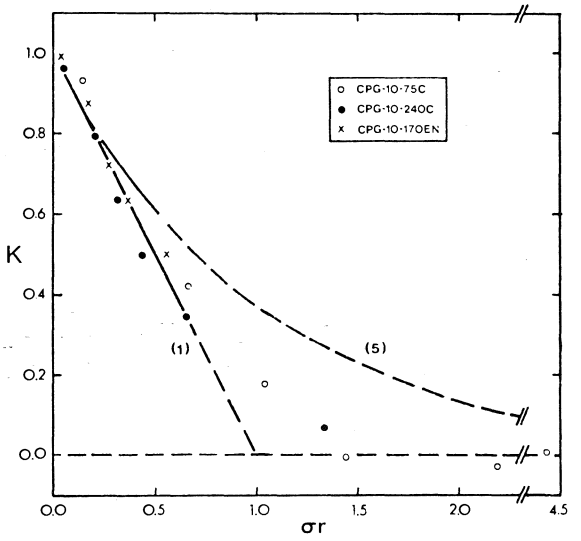

FIG. 4. Comparison of penetration data with models of rigid sphere molecules in slits and random plane pores.

Using the value of the Flory constant, ϕ', given by Senti (55.2×10^{21}) for dextran solutions (19), r_h/s is found to be 0.957.

The effects of branching and departures from θ-conditions have been taken into account by analyzing the results obtained by Wales *et al.* (17) from viscosity measurements. These provided values of $g = 3.47\overline{M}_w^{-0.13}$ and $\alpha = 0.56\overline{M}_w^{0.061}$. The factor α is defined as the ratio of the rms radius of gyration of the polymer under non-θ-conditions (25°C) to that under θ-conditions. These data were, however, based on a Flory constant of 30.8×10^{21} and, for consistency, the above value of g was adjusted by the factor $(30.8/55.2)^{2/3}$ to conform to Senti's value for ϕ'.

Can. J. Chem. Downloaded from www.nrcresearchpress.com by 210.87.254.40 on 09/05/12
For personal use only.

The data from Table 3 were converted to the values shown in Fig. 5 using these factors. An alternative approach by Granath (14) to the study of Pharmacia dextrans was based on the Stockmayer modification of the Flory–Fox equation. This provided another evaluation of g but its use gave similar data to that in Fig. 5 over most of the range and these have not been plotted.

It is seen that the conversion of the molecular size from hydrodynamic terms to statistical terms does not greatly alter the position of the experimental data. Although the data are displaced above the curve for flexible molecules in cylindrical pores (curve *8*) it is evident that they show a similar trend.

In Fig. 6, the comparison of the adjusted data with the curves for models of the flexible chain in slit pores (curve *7*) and the voids among random spheres (curve *9*) is made. As expected from the earlier comparison of the rigid sphere models (Figs. 5 and 6), the similarity of the variation of the data with that of the theoretical curve for slit geometry is as good as with that for cylindrical geometry.

Of all the models in Table 4, the 'voids among random spheres' model of the pore system might be considered, from the description of the structure of CPG-10 porous glass (23) to simulate the pore system most closely. The position and shape of the curves for this model are dependent on the void fraction of the total volume of the porous material (factor, f, in the expression for curve *9* in Table 4). Unless the void fraction is constant, this treatment does not predict that different glass samples would produce coincident penetration curves. However, the difference among the theoretical curves for the three glasses used are not great enough to be distinguishable in the scattered data.

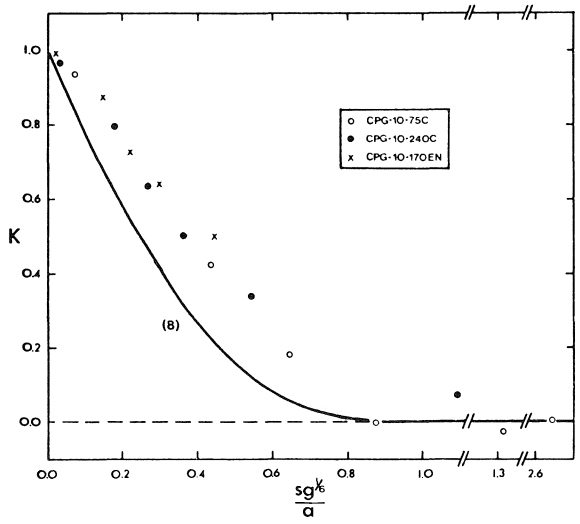

FIG. 5. Comparison of penetration data with a model of flexible chain molecules in cylindrical pores.

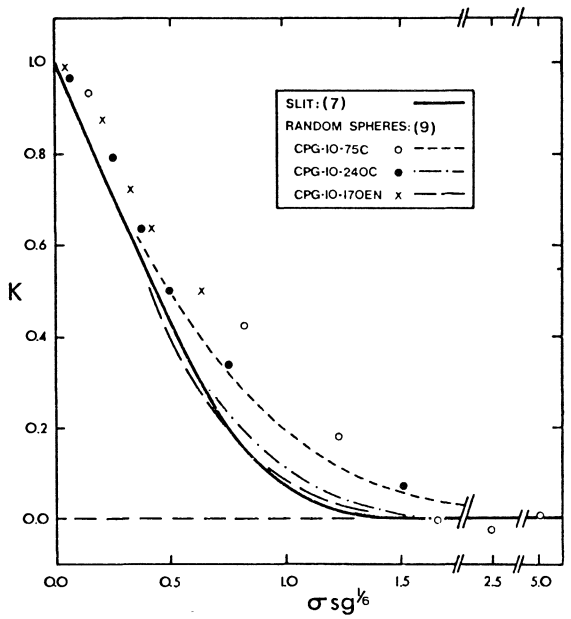

FIG. 6. Comparison of penetration data with models of flexible chain molecules in slit pores and voids among random spheres.

Two major sources of difference remain between the theoretical models and real systems. Although the pore geometry of CPG-10 glass appears to be more uniform than that of many materials previously available, the difference between the actual geometry and that of the models may influence the partition. The concurrence of experimental data with curves based on ideal geometry may support but cannot confirm the mechanism of partition (1).

Secondly, although the polydispersity of both the polymer and the pore system used in this study is low, the condition of monodispersity of both, assumed in the theoretical treatments, is not fulfilled. Scatter in the penetration data of the dextran series for each glass may result from differences in variance and skewness of the dextran molecular weight distributions. Differences in the shape of curves obtained with different glasses are more likely due to differences in the size distributions of the pore systems.

Conclusions

In this study of the penetration of CPG-10 porous glass by dextran fractions, the degree of penetration is expressed as a penetration coefficient, equal to the ratio of the concentration attainable within the pores to that in the bulk solution. The observed behaviour is consistent with theory which predicts that the value of this parameter is determined primarily by the size of the polymer in solution relative to that of the pore.

The penetration curves for this series of dextrans on three CPG-10 glasses of distinctly different pore sizes coincide.

The molecules are assumed to be either solid spheres or random coils and the pore geometry to be cylindrical, slit-shaped, or equivalent to the voids among random spheres. Among these models, the more sophisticated (e.g., random coils in the voids among random spheres) may simulate the actual 'polymer in pore' more realistically. However, the data obtained with components of narrow size distribution do not show a significantly better conformity with any particular model since, except for solid spheres in slit-shaped pores, the curves do not vary markedly in shape. The experimental data lie close to most of the theoretical curves and their position is not greatly influenced by the choice of the relative size parameter. Thus, these theoretical curves can be used to predict the degree of penetration for this system.

1. E. F. Casassa. J. Polym. Sci. B, **5**, 773 (1967).
2. E. F. Casassa and Y. Tagami. Macromolecules, **2**, 14 (1969).
3. J. J. Pouchly. J. Phys. Chem. **52**, 2567 (1970).
4. K. H. Altgelt and J. C. Moore. *In* Polymer fractionation. *Edited by* M. J. R. Cantow. Academic Press, New York, NY. 1967. Chapt. B.4.
5. J. C. Moore. J. Polym. Sci. A, **2**, 835 (1964).
6. W. Haller. Nature, **206**, 693 (1965).
7. K. H. Altgelt. Adv. Chromatogr. **7**, 3 (1968).
8. J. J. Cazes. Chem. Educ. **47**, A461 (1970).
9. D. D. Bly. Science, **168**, 527 (1970).
10. K. H. Altgelt and L. Segal (*Editors*). Gel permeation chromatography. Marcel Dekker, New York, NY. 1971.
11. W. W. Yau, C. P. Malone, and S. W. Fleming. J. Polym. Sci. B, **6**, 803 (1968).
12. W. W. Yau. J. Polym. Sci. A**27**, 483 (1969).
13. J. E. Stone and A. M. Scallan. Cellul. Chem. Technol. **2**, 343 (1968).
14. K. A. Granath. J. Colloid Sci. **13**, 308 (1958).
15. S. Lindberg and S. Swenson. Acta Chem. Scand. **22**, 1907 (1968).
16. A. Jeanes. Carbohyd. Chem. **5**, 127 (1965).
17. M. Wales, P. A. Marshall, and S. G. Weissberg. J. Polym. Sci. **10**, 229 (1953).
18. A. G. Ogston and E. F. Woods. Trans. Faraday Soc. **50**, 635 (1954).
19. F. R. Senti *et al.* J. Polym. Sci. **17**, 527 (1955).
20. P. J. Flory. Principles of polymer chemistry. Cornell University Press, Ithaca, NY. 1953. Chapt. 14.
21. S. J. Gregg and K. S. W. Sing. Adsorption surface area and porosity. Academic Press, London. 1967.
22. L. J. Gurvitsch. J. Phys. Chem. Soc. Russ. **47**, 805 (1915).
23. A. R. Cooper *et al.* J. Appl. Polym. Sci. **15**, 571 (1971).
24. J. C. Giddings *et al.* J. Phys. Chem. **72**, 4397 (1968).
25. A. G. Ogston. Trans. Faraday Soc. II, **54**, 1754 (1958).
26. T. C. Laurent and J. J. Killander. J. Chromatogr. **14**, 317 (1964).
27. M. Doi. Trans. Faraday Soc. II, **71**, 1720 (1975).
28. B. H. Zimm and R. W. Kilb. J. Polym. Sci. **37**, 19 (1959).
29. K. Kamada and H. Sato. Polym. J. **2**, 489 (1971).
30. M. Kurata *et al.* Polym. J. **3**, 729 (1972).
31. P. J. Flory and T. G. Fox, Jr. J. Am. Chem. Soc. **73**, 1904 (1951).
32. W. Haller. Macromolecules, **10**, 83 (1977).
33. E. F. Casassa. Macromolecules, **9**, 182 (1976).

Can. J. Chem. Downloaded from www.nrcresearchpress.com by 210.87.254.40 on 09/05/12
For personal use only.

Factor analysis as a complement to band resolution. V. Complexing of pentachlorophenol and acetone in carbon tetrachloride solution

J. KORPPI-TOMMOLA AND H. F. SHURVELL

Department of Chemistry, Queen's University, Kingston, Ont., Canada K7L 3N6

Received June 27, 1978

J. KORPPI-TOMMOLA and H. F. SHURVELL. Can. J. Chem. **56**, 2959 (1978).

Complex formation between pentachlorophenol and acetone and acetone-d_6 in carbon tetrachloride solution has been studied in both the hydroxyl and carbonyl stretching regions of the infrared spectrum. Factor analysis of the digitized spectra indicates three absorbing components for each set of solutions in the hydroxyl stretching region. Concentration studies revealed roughly linear relationships between the areas of the 'free' ν(OH) band and both of the resolved complex bands, suggesting that two different 1:1 complexes occur in CCl_4 solution. In the ν(CO) region only one band due to complex formation was detected. Equilibrium constants for the isotopically different complexes at about 30°C are reported. In the hydroxyl stretching region, band resolution was also carried out using four components which gave a better fit to the observed spectrum. A set of equilibrium constants were then obtained. However, considerable difficulties were met in the calculations and in the interpretation of these results, so that the three band, two complex model is preferred.

J. KORPPI-TOMMOLA et H. F. SHURVELL. Can. J. Chem. **56**, 2959 (1978).

On a étudié la formation de complexes entre l'acétone ou l'acétone-d_6 et le pentachlorophénol en solution dans le tétrachlorure de carbone, en utilisant les régions du spectre infrarouge correspondant aux vibrations de valence des groupes hydroxyle et carbonyle. Une analyse factorielle des spectres digitalisés indique la présence de trois composantes d'absorbtion dans la région de l'hydroxyle pour chaque série de solutions. Des études en fonction de la concentration révèlent l'existence d'une relation approximativement linéaire entre l'aire de la bande ν(OH) "libre" et celle de chacune des bandes résolues des complexes, ce qui laisse supposer la formation de deux complexes 1:1 distincts dans les solutions de CCl_4. Dans la région ν(CO), on n'a décelé qu'une seule bande attribuable à la formation de complexe. On rapporte des constantes d'équilibre à environ 30°C pour les différentes variétés isotopiques de complexes. Pour la région de l'hydroxyle, on a également réussi à résoudre les bandes en quatre composantes, ce qui a donné un meilleur accord avec les spectres observés. On a obtenu de cette manière une série de constantes d'équilibre. Cependant, les calculs et l'interprétation de ces résultats ont posé de sérieuses difficultés et l'on préfère le modèle à trois bandes et deux complexes.

[Traduit par le journal]

Introduction

Pentachlorophenol (PCP) has three properties which make it very convenient for the study of complex formation: it is a solid alcohol, it does not undergo self-association in solution (1), and it has no CH stretching bands (ν(CH)) to interfere with the broad ν(OH) complex band in the infrared spectrum. Complex formation of PCP and various nitrogen compounds in solution have been studied extensively (2–5). Infrared and Raman spectra of PCP have been published recently (6). A phase transition of solid PCP at about 60°C has been investigated using infrared (1) and Raman (7) spectroscopic methods.

The band contour of the ν(CO) band of acetone has been studied in various solvents (8, 9) and as a function of temperature (10). The interactions between several combination modes (11) and the ν(CO) mode can be considered as an explanation of the different shapes of the ν(CO) band found in various solvents and at various temperatures. However, if only one solvent is used and the acetone concentration is kept below 0.2 *M* the ν(CO) band is a 'good' band for complex formation studies.

The application of factor analysis to digitized infrared spectra leads to the determination of the number of absorbing components in a complex band. This number is an essential input parameter for band resolution and is independent of any assumed band shapes in the subsequent band resolution procedure (12, 13). Band areas of the resolved components can be used to calculate the molar absorption coefficients for the absorbing species if data are available for several solutions. Once the molar absorption coefficients are known, the concentration of each absorbing component can be obtained and various models of complexation can be tested to produce consistent equilibrium constants. In principle, the above procedure gives quantitative as well as qualitative information con-

Can. J. Chem. Downloaded from www.nrcresearchpress.com by 210.87.254.105 on 09/05/12
For personal use only.

Can. J. Chem. Downloaded from www.nrcresearchpress.com by 210.87.254.105 on 09/05/12
For personal use only.

cerning the type of complexation. It has been applied to the study of complex formation of pentachlorophenol and acetone and pentachlorophenol and acetone-d_6 in both the hydroxyl and carbonyl stretching regions. The initial concentration of PCP was kept at about 0.05 *M* for two sets of solutions, i.e. for PCP acetone and PCP acetone-d_6 systems. For one set of PCP acetone solutions the initial PCP concentration was kept at about 0.1 *M*. Acetone concentration was varied from 0.005 to 1.0 *M*. Details of the solutions and of the pathlengths used in the two spectral regions are not given here, but these are available from the authors on request.

Experimental

Pentachlorophenol was purchased from the J. T. Baker Chemical Company. Deuterated acetone (Ac-d_6) was obtained from Merck, Sharp, Dohme (Canada) Ltd. These reagents were used without further purification. Spectroscopic grade acetone and carbon tetrachloride (Fisher Scientific) were stored over molecular sieves (type 4A) for at least 24 h before use. Spectra were recorded using R.I.I.C. variable pathlength cells on a Perkin-Elmer 180 spectrometer. The instrument was flushed with dry air and wavenumber calibration was checked using standard compounds. Pathlengths were determined using the fringe method from 0.05 to 0.2 mm and linearity was assumed over the range used in this work. All spectra were recorded using an absorbance scale. Identical cells with equal pathlengths were placed in both infrared beams. The cell in the reference beam contained the base in CCl_4 at the same initial concentration as in the sample cell. The same solutions were used in both the ν(OH) and ν(CO) regions, with the pathlengths adjusted accordingly. Concentrations were corrected for the thermal expansion of CCl_4 produced by the higher temperature of the sample compartment of the spectrometer.

Computational Techniques

The observed spectra were digitized at 2.5 cm^{-1} intervals in the hydroxyl monomer band region while the rest of the spectrum was digitized at 5.0 cm^{-1} intervals using the manual technique described previously (14). A computer program EXTEND was written to interpolate the ordinate values to make the digitizing interval 2.5 cm^{-1} over the total range, giving about 400 data points. In the ν(CO) region the digitization interval was 2.0 cm^{-1}, which gives about 100 data points per spectrum.

A description of factor analysis can be found in refs. 12–14. The factor analysis programme (CHISQ) was applied to three sets of digitized spectra obtained for the solutions studied. For band resolution a programme originally written by Jones *et al.* (15) was modified to perform the calculations in absorbance units. Baseline subtraction and band area computation subroutines were added to the programme. A standard linear regression programme (LINREG 2, available from Queen's University Computing Centre, Programme Library) was used to solve for the molar absorption coefficients (ε_i). Two sets of ε_i were calculated in the hydroxyl stretching region. One set using three and the other set using four components to reproduce the observed spectrum. It was found that the linear regression programme gives most reliable results if the data are available from more than 20 solutions. Half-band widths were calculated using the PC121 programme from the library of Jones *et al.* (15).

Chemical Equilibrium

Our results in the hydroxyl stretching region suggest that there are two 1:1 pentachlorophenol–acetone complexes in CCl_4 solution. Accordingly, the following equations were used to calculate the equilibrium constants:

$$[1] \quad C_D^T = C_D + C_{11}^{(1)} + C_{11}^{(2)} = (A_D/\varepsilon_D l) + (A_1/\varepsilon_1 l) + (A_2/\varepsilon_2 l)$$

$$[2] \quad C_A = C_A^T - C_D^T + C_D = C_A^T - C_D^T + (A_D/\varepsilon_D l)$$

$$[3] \quad K_{11}^{(i)} = C_{11}^{(i)}/(C_D \times C_A) = (\varepsilon_D/\varepsilon_i)(A_i/A_D)(1/C_A)$$

where C_D^T and C_A^T are the initial concentrations and C_D and C_A are the equilibrium concentrations of the proton donor (PCP) and the proton acceptor (Ac), respectively. $C_{11}^{(i)}$ is the concentration of the *i*th 1:1 complex in the solution. A_D is the band area of the 'free' OH stretching band and ε_D the corresponding molar absorptivity coefficient. A_i refers to the band area of the *i*th resolved complex and ε_i to the corresponding molar absorption coefficient. *l* is the pathlength.

In the ν(CO) region the calculations were made in the same way, except that only one 1:1 complex was assumed to occur in the solution. For comparison, 1:1 equilibrium constants were also calculated using the areas of the 'free' ν(OH) band.

Results and Discussion

A preliminary study of the hydroxyl stretching region of the infrared spectrum of pentachlorophenol in 0.1 *M* CCl_4, CS_2, C_6H_6, and C_6F_6 solutions was made. The spectra are shown in Fig. 1. Each spectrum consists of a strong, singlet monomer band, at 3524, 3515, 3442, and 3537 cm^{-1}, respectively, and each shows traces of a band due to associated species. The monomer band in benzene shows an asymmetric contour, a large shift to lower frequencies, and a half width about three times that in the other solutions. The shift and the large half width might be the result of a solvent–solute interaction. From an examination of Fig. 1 it seems reasonable to assume that neither self-association nor conformational isomerism occurs for PCP in carbon tetrachloride solutions.

Typical behaviour of the OH stretching band of solutions of PCP and acetone in CCl_4 is shown in Fig. 2. For a fixed PCP concentration, the sharp monomer band at 3524 cm^{-1} decreases in intensity relative to the broad complex band on the lower frequency side as the acetone concentration is increased. The broad band in the spectra of PCP/acetone-d_6 solutions (Fig. 2) is a 'pure' complex band, since neither the proton donor nor the proton acceptor has fundamental (CH stretching) modes in the frequency region concerned. Visual inspection would suggest three absorbing components to occur in the region. No traces of an 'end group' band were

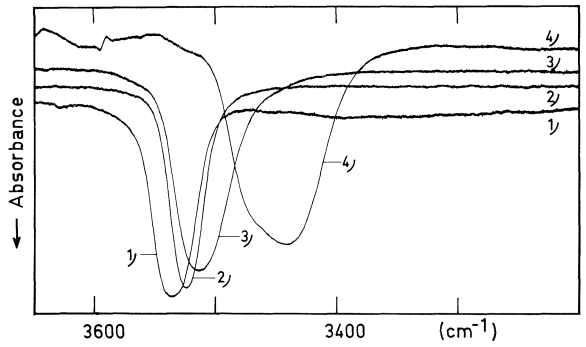

FIG. 1. The hydroxyl stretching band of PCP in various solvents: (*1*) C_6F_6, (*2*) CCl_4, (*3*) CS_2, (*4*) C_6H_6. Concentrations 0.10 *M* and pathlengths 1.00 mm in all solutions.

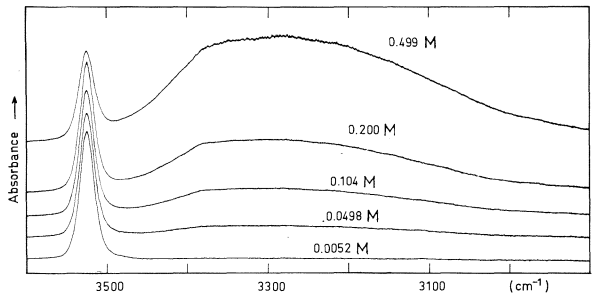

FIG. 2. The hydroxyl stretching band of PCP/acetone-d_6 solutions. Acetone-d_6 concentrations are given in the figure.

detected in the spectrum, which is an expected result for complexing between PCP and acetone.

Factor Analysis

For all three sets of solutions studied, factor analysis indicated three absorbing components in the OH stretching region. The results for the PCP – acetone-d_6 system will be given as an illustration of the method. Similar results were obtained for the other two systems.

The number of absorbing components NC in a complex band is taken as the number of non-zero eigenvalues of the matrix $\mathbf{Q} = \mathbf{A}^T\mathbf{A}$, where $\mathbf{A}$ is the absorbance and $\mathbf{A}^T$ its transpose. Due to experimental error and computational procedures, all calculated eigenvalues are non-zero. However, several statistical tests have been described (12) to determine when an eigenvalue is really non-zero. If an eigenvalue is less than the residual standard deviation or less than the square root of the estimated variance, then it is statistically zero. The results of these tests on the bands of the PCP/acetone-d_6 system are shown in Table 1 for an estimated experimental error in absorbance measurements DA = 0.01. Both criteria clearly indicate only three non-zero eigenvalues.

Another useful test is to regenerate the absorbance

TABLE 1. Factor analysis of eight CCl_4 solutions of PCP and acetone-d_6 in the ν(OH) region using the residual standard deviation and square root of eigenvalue variance criteria

No. of eigenvectors	Eigenvalue	Residual standard deviation[a]	Square root of estimated variance[a]
1	390.82046	0.11542	0.26438
2	42.21191	0.01142	0.14355
3	0.35470	0.00439	0.20714
4	0.04223	0.00246	0.15011
5	0.01211	0.00150	0.13602
6	0.00363	0.00105	0.13594
7	0.00243	0.00059	0.19765
8	0.00107	0.00026	0.10628

[a]Experimental absorbance error DA = 0.01.

matrix $\mathbf{A}$ using from 1 to *m* eigenvectors of $\mathbf{Q}$. The smallest number of eigenvectors to give a satisfactory fit with the experimental $\mathbf{A}$ is then NC. In Table 5 it is seen for DA = 0.01 that three eigenvectors are sufficient to regenerate $\mathbf{A}$. A final criterion is the calculation of χ_m^2 using from one to eight eigenvectors of $\mathbf{Q}$. The results are summarized in the last two columns of Table 2. The expectation values of χ_m^2 are given by $(N_W - m)(N_S - m)$, where N_W is the number of points in a digitized spectrum (400 in the present case) and $N_S = 8$ is the number of solutions. It is seen that χ_3^2 is of the same order of magnitude as the expectation value. Again, three absorbing components are indicated.

In the carbonyl stretching region of the three sets of solutions, factor analysis again indicates three components. However, the interpretation here is different. In the spectra of acetone, there are combination bands which may interact with the ν(CO) fundamental. This interaction gives rise to a broad shoulder on the high frequency side of ν(CO) in acetone, while in acetone-d_6 a Fermi doublet (9–11) is observed in the spectrum (Fig. 3). Thus, with two bands assigned to the 'free' carbonyl stretching vibration we are left with only one absorbing component to be assigned to the complex. This component is found as an asymmetry, which shows a concentration dependence, on the lower frequency side of the ν(CO) band (Fig. 3). According to our results in the hydroxyl stretching region, two complexes should occur in CCl_4 solution, while in the carbonyl stretching region, only one complex is indicated between PCP and acetone. However, it is not unknown that the ν(OH) mode should be more affected by complexing than the ν(CO) mode.

To explain the observation of only one complex band in the ν(CO) stretching region, we suggest that either one of the complexes does not affect the ν(CO) vibration significantly, or that both complexes

Can. J. Chem. Downloaded from www.nrcresearchpress.com by 210.87.254.105 on 09/05/12
For personal use only.

TABLE 2. Factor analysis of eight CCl_4 solutions of PCP and acetone-d_6 in the ν(OH) region. Comparison of observed and regenerated absorbance matrix[a]

No. of eigenvalues	Distribution of misfits (number of points) Number of standard deviations 0–1	1–2	2–3	3–4	4–5	>5	χ^2	Expectation value
1	590	400	376	452	227	1163	426281	2800
2	1786	1285	126	9	1	1	4162	2394
3	3136	63	6	1	2	0	615	1990
4	3168	33	5	2	0	0	193	1588
5	3202	6	0	0	0	0	71	1188
6	3208	0	0	0	0	0	35	790
7	3208	0	0	0	0	0	11	394
8	3208	0	0	0	0	0	0	0

[a]Experimental absorbance error DA = 0.01.

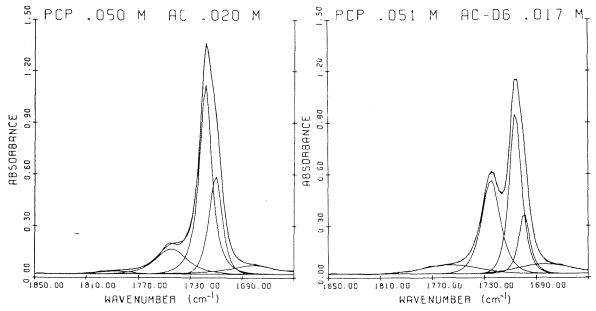

FIG. 3. Band resolution results for PCP/acetone complexes in the carbonyl stretching region.

contribute to the ν(CO) vibration in the same way and we cannot resolve the components in the spectrum.

Band Contour Resolution

As suggested by factor analysis, we carried out band resolution using three Cauchy–Gauss product functions in the hydroxyl stretching region. Plots of typical resolved spectra are shown in Fig. 4. In the top diagram the worst misfits occur from 3200 to 3400 cm^{-1}, with the fit getting better at lower concentrations. In the three component fit the left wing of the lower frequency complex band extends over the monomer ν(OH) band. To reduce the overlap and to improve the fit, we tried adding a fourth component to the resolution procedure. The result is seen in the bottom diagram of Fig. 4. The fit is perfect and although the three complex bands overlap, the overlap between the monomer band and any of the complex bands is negligible. From this result we attempted to calculate the molar absorption coefficients (ε_i) for the four bands. However, no consistent values for ε_i were obtained for the various solutions and, in fact, even negative values were sometimes calculated. Since the four-component model is also chemically unreasonable, we were

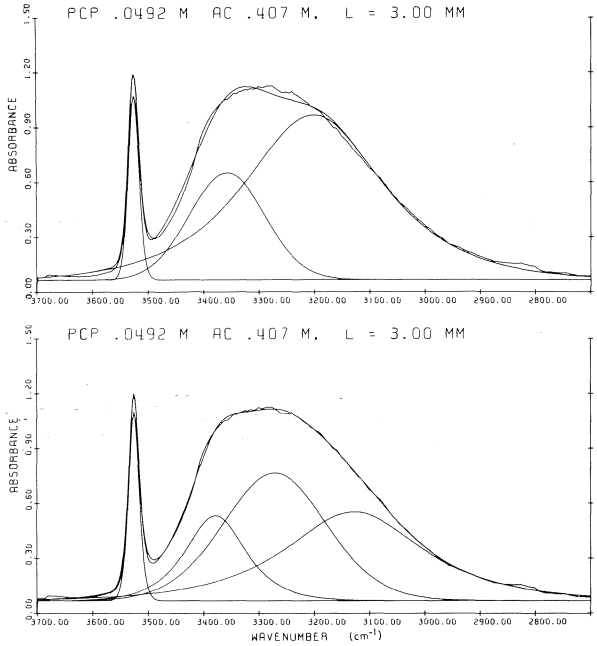

FIG. 4. Band resolution results for PCP/acetone complexes using three and four component fit in the hydroxyl stretching region.

forced to accept the three-component fit. Average wavenumbers and half-widths of the three resolved components are given in Table 3. Both wavenumber and half-width of the ν(OH) monomer band show very small standard deviations in all three sets of solutions. The PCP/acetone-d_6 system shows the most consistent wavenumbers and half-widths, which is expected since there are no CH stretching bands to interfere with the complex band. The wavenumbers of $(1:1)^2$ complex bands for the PCP (0.05 *M*)/Ac and for the PCP (0.05 *M*)/Ac-d_6 systems are almost the same, which means that this frequency does not depend on isotopic substitution

Can. J. Chem. Downloaded from www.nrcresearchpress.com by 210.87.254.105 on 09/05/12
For personal use only.

TABLE 3. Computed average parameters for the ν(OH) band components[a]

System	Component	ν (cm^{-1})	$\Delta\nu_{1/2}$ (cm^{-1})	ε (mol^{-1} m^2)
PCP (0.1 *M*)	Monomer	3524.3 (0.8)	22.5 (0.4)	637
Acetone	$(1:1)^1$-complex	3361 (9)	154 (19)	2786 (500)
(10 solutions)	$(1:1)^2$-complex	3217 (15)	304 (10)	3858 (150)
PCP (0.05 *M*)	Monomer	3524.6 (0.3)	21.9 (0.3)	637
Acetone	$(1:1)^1$-complex	3357 (9)	159 (5)	2786 (500)
(8 solutions)	$(1:1)^2$-complex	3201 (16)	290 (30)	3858 (150)
PCP (0.05 *M*)	Monomer	3524.7 (0.3)	22.1 (0.6)	668
Acetone-d_6	$(1:1)^1$-complex	3353 (3)	166 (4)	2084 (650)
(7 solutions)	$(1:1)^2$-complex	3199 (5)	290 (7)	4548 (900)

[a]The numbers in parentheses are standard deviations.

TABLE 4. Computed average parameters for the ν(CO) band components[a]

System	Component	ν (cm^{-1})	$\Delta\nu_{1/2}$ (cm^{-1})	ε (mol^{-1} m^2)
PCP (0.05 *M*)	Combination	1744.3(0.6)	27.1(1.9)	656(600)
Acetone	Monomer	1717.7(0.3)	11.0(0.2)	744(180)
(8 solutions)	(1:1)-complex	1710.5(1.3)	11.2(1.0)	599(500)
PCP (0.05 *M*)	Monomer, FR comp.	1724.6(0.2)	16.9(0.4)	1035(420)
Acetone-d_6	Monomer, FR comp.	1705.9(0.4)	10.8(0.4)	708(260)
(8 solutions)	(1:1)-complex	1699.5(0.6)	10.7(0.5)	574(150)

[a]The numbers in parentheses are standard deviations. FR refers to Fermi resonance.

in acetone, but rather on the initial concentration of PCP in solution (Table 3).

Band resolution in the ν(CO) region was carried out using a three-component fit for acetone and acetone-d_6 spectra (Fig. 3). Small bands on both sides of the main peaks were added to reproduce the experimental spectra better. These bands were not included in further calculations. Frequency and half-width consistency for the three main bands is excellent, as seen in Table 4. The Δν values for the nearest ν(CO) monomer band and the complex band are 7.2 and 6.4 cm^{-1} for PCP/Ac and PCP/Ac-d_6 complexes, respectively. The ratio of the frequency differences is very close to the mass ratio of the two isotopic acetones.

Molar Absorption Coefficients and Equilibrium Constants

Molar absorption coefficients were calculated by inserting the band areas and total concentrations of the proton donor into eq. [3] and subsequently solving a set of linear equations. For the PCP (0.1 *M*)/acetone and PCP (0.05 *M*)/acetone systems in the ν(OH) region, we assumed equal ε_i's and data from 18 solutions were included. As indicated by standard deviations of the ε_i's (Table 3), the computation is very sensitive to the values of the band areas obtained from the fitting procedure. In the ν(CO) region, three ε_i's were also calculated using the band areas obtained for each set of solutions. These results are shown in Table 4.

To investigate the type of complexing, the complex band areas were plotted as a function of the monomer band areas, i.e. the concentration of the complex is plotted as a function of the concentration of free PCP in solution. The result is seen in Fig. 5, where graphs are shown for the various component band areas in the ν(OH) region. Both complex band areas show linear dependence on the monomer band areas up to an acetone concentration of 0.4 *M* (A_D about 10 000). According to eq. [3], this dependence indicates that both the resolved complex bands arise from (1:1)-complexes. We call the complex corresponding to the higher frequency complex band a $(1:1)^1$-complex and the other complex a $(1:1)^2$-complex. For the solutions where the initial PCP concentration was 0.1 *M* and the acetone concentration over 0.4 *M*, the concentrations of the $(1:1)^1$-complex seem to diminish at the expense of increasing $(1:1)^2$-complex concentration, the corresponding curve shows a maximum at about A_D = 11 000 (Fig. 5). It is also seen that at high acetone concentrations for solutions where the initial PCP concentration is 0.05 *M*, the $(1:1)^1$-complex concentration is relatively higher than for the solutions with double the PCP initial concentration (see the top diagram in Fig. 5).

The equilibrium constants are given in Table 5. Average values were calculated for solutions in which

Can. J. Chem. Downloaded from www.nrcresearchpress.com by 210.87.254.105 on 09/05/12
For personal use only.

TABLE 5. Equilibrium constants[a] (mol^{-1} m^3) at 30 ± 1°C with standard deviations

Complex	ν(OH) band components		ν(CO) band	'free' ν(OH) band
	$K_{11}^1 \times 10^3$	$K_{11}^2 \times 10^3$	$K_{11} \times 10^3$	$K_{11} \times 10^3$
PCP (0.1 *M*)/Ac	2.1(0.5)	4.9(0.7)	—	7.6(0.5)
PCP (0.05 *M*)/Ac	3.2(0.8)	5.4(1.2)	11.0(1.9)	8.8(1.6)
PCP (0.05 *M*)/Ac-d_6	4.0(0.7)	5.5(1.0)	8.9(1.6)	8.9(1.1)

[a] $K_{11} \simeq K_{11}^{(1)} + K_{11}^{(2)}$. The numbers in parentheses are standard deviations.

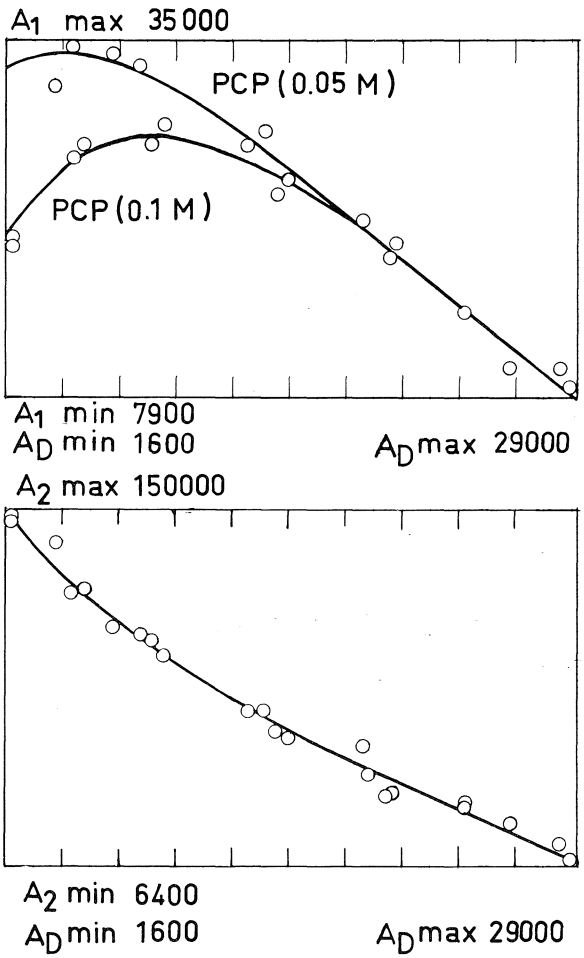

FIG. 5. Band areas (A_1 and A_2) of the resolved complex bands as a function of the area of the monomer ν(OH) band (A_D) for all three sets of solutions studied. The band areas have been normalized to unit pathlength. Areas for the PCP (0.1 *M*) acetone system have been divided by two for this plot.

the acetone concentrations were less than 0.4 *M*. The values of the equilibrium constants indicate that a decrease in initial concentration of PCP favours the formation of the $(1:1)^1$-complex ($K_{11}^{(1)}$). Also, an isotopic effect on the equilibrium is found, acetone-d_6 forms relatively more of the $(1:1)^1$-complex than does the non-deuterated acetone. The $K_{11}^{(2)}$ equilibrium constant, however, seems to be almost independent of the initial PCP concentration and of the isotopic substitution of the proton acceptor.

In the ν(CO) region it was assumed that only one (1:1)-complex occurs in the solution. For these calculations, the free acetone concentration was assumed to be proportional to the sum of the areas of the two highest wavenumber components in the region. The same type of calculation was also performed using the areas of the monomer ν(OH) band. The two equilibrium constants (Table 5) obtained from different parts of the infrared spectrum are comparable and in good agreement with the value $K_{11} = 9.11$ mol^{-1} ℓ previously reported for the PCP/acetone complex in CCl_4 solution (4).

Conclusions

This work clearly shows that hydrogen bonding between PCP and acetone in CCl_4 solution manifests itself much more in the OH stretching region of PCP than in the CO stretching region of acetone. Thus, more information on this system is available from the OH stretching band. The band resolution procedure provides a powerful method for studying complex formation in solution. However, it is seen that an independent technique such as factor analysis is valuable to establish the number of absorbing components in the spectra. This reduces the temptation to add more bands to improve the fit. Matrix isolation spectra, where the broad ν(OH) association or complex band is resolved into several components (16), could also be used to find the number of absorbing components.

In the present study, we used three and four components to reproduce the experimental spectrum in the hydroxyl stretching region. Although the three-component fit does not reproduce the experimental spectrum perfectly, factor analysis clearly indicates that there are only three absorbing components in the band. The present work does not give any information on the structures of the complexes. Nevertheless, it is possible to suggest *two* chemically reasonable structures for PCP/acetone (1:1)-complexes in CCl_4 solution. In one structure, the hydroxyl proton could interact with one of the

Can. J. Chem. Downloaded from www.nrcresearchpress.com by 210.87.254.105 on 09/05/12
For personal use only.

carbonyl lone pairs, while in the other, the interaction could be between the hydroxyl proton and both lone pairs. It is not possible to suggest three chemically reasonable structures for (1 : 1)-complexes. This conclusion, together with the factor analysis result, leads us to reject the four-component model.

Acknowledgements

This work was supported by grants from the National Research Council of Canada. One of the authors (J.K.-T) acknowledges a Fellowship granted under the Cultural Exchange Programme between Canada and Finland.

1. J. W. ROHLEDER and B. JAKUBOWSKI. Acta Phys. Pol. **31**, 1047 (1967).
2. T. GRAMSTAD. Acta Chem. Scand. **16**, 807 (1962).
3. T. GRAMSTAD and G. VAN BINST. Spectrochim. Acta, **22**, 1681 (1966).
4. T. GRAMSTAD. Spectrochim. Acta, **19**, 497 (1963).
5. G. S. DENISOV and V. M. SHREIBER. Spectrosc. Lett. **5**, 377 (1972).
6. J. H. S. GREEN, D. J. HARRISON, and C. P. STOCKLEY. J. Mol. Struct. **33**, 307 (1976).
7. H. F. SHURVELL, J. KORPPI-TOMMOLA, and R. J. C. BROWN. Can. J. Chem. **56**, 359 (1978).
8. J. FRUWERT, G. GEISELER, and D. LUPPA. Z. Chem. **8**, 238 (1968).
9. M. T. FOREL and M. FOUASSIER. Spectrochim. Acta, **23**A, 1977 (1966).
10. M. MAILLOUX, M. J. WEINMAN, and M. S. WEINMAN. C. R. Acad. Sci. Paris, **276**C, 379 (1973).
11. G. DELLEPIANE and J. OVEREND. Spectrochim. Acta, **22**, 593 (1966).
12. J. T. BULMER and H. F. SHURVELL. J. Phys. Chem. **77**, 256 (1973); **77**, 2085 (1973).
13. J. T. BULMER and H. F. SHURVELL. Can. J. Chem. **53**, 1251 (1975).
14. J. T. BULMER and H. F. SHURVELL. Can. J. Spectrosc. **16**, 94 (1971).
15. R. N. JONES *et al.* National Research Council of Canada, Computer Programmes for Infrared Spectroscopy. 1974.
16. J. KORPPI-TOMMOLA. J. Mol. Struct. **40**, 13 (1977).

Can. J. Chem. Downloaded from www.nrcresearchpress.com by 210.87.254.105 on 09/05/12
For personal use only.

Fluorinated alkoxides. Part XIII. The reduction of β-imino-alkoxy complexes to give stable, polydentate, amino-alcohols; their coordination to Co^{2+}, Ni^{2+}, and Cu^{2+}

JOHN W. L. MARTIN AND C. J. WILLIS

Chemistry Department, University of Western Ontario, London, Ont., Canada N6A 5B7

Received March 17, 1978

JOHN W. L. MARTIN and C. J. WILLIS. Can. J. Chem. **56**, 2966 (1978).

The amino-alcohols $HOC(CF_3)_2CH_2CH(CH_3)NH(CH_2)_3NHCH(CH_3)CH_2C(CF_3)_2OH$ and $HOC(CF_3)_2CH_2CH(CH_3)NH(CH_2)_3NH(CH_2)_3NHCH(CH_3)CH_2C(CF_3)_2OH$ have been prepared by reduction of the corresponding imino-alcohols coordinated to, e.g., Cu^{2+}, by use of $LiAlH_4$. The products are capable of acting as polydentate, dinegative, ligands (following ionization of the fluorinated alcohol groups) and the second compound gives stable, neutral, complexes of Co^{2+}, Ni^{2+}, and Cu^{2+} in which the metal atom is five-coordinate.

JOHN W. L. MARTIN et C. J. WILLIS. Can. J. Chem. **56**, 2966 (1978).

On a préparé les amino-alcools $HOC(CF_3)_2CH_2CH(CH_3)NH(CH_2)_3NHCH(CH_3)CH_2C(CF_3)_2OH$ et $HOC(CF_3)_2CH_2CH(CH_3)NH(CH_2)_3NH(CH_2)_3NHCH(CH_3)CH_2C(CF_3)_2OH$ par réduction avec $LiAlH_4$ des imino-alcools correspondants coordonnés à un ion tel que Cu^{2+}. Ces produits peuvent jouer le rôle de ligands polydentates porteurs de deux charges négatives (après ionisation des groupes alcools fluorés) et le second composé forme des complexes neutres stables avec Co^{2+}, Ni^{2+} et Cu^{2+} dans lesquels l'atome métallique est pentacoordonné.

[Traduit par le journal]

Can. J. Chem. Downloaded from www.nrcresearchpress.com by 210.87.254.42 on 09/05/12
For personal use only.

In previous parts of this series, we have reported the preparation of metal complexes in which chelation occurs from an ionized, fluorinated, tertiary alkoxy group, $-C(CF_3)_2O^-$, and a nitrogen donor atom. Such a ligand can be formed in two ways, either by the synthesis and subsequent coordination of a fluorinated amino-alcohol (1), or by template synthesis of β-imino-alkoxy ligands (2). The latter are formed by condensation of hexafluorodiacetone-alcohol, $CH_3COCH_2C(CF_3)_2OH$ (HFDA), with a diamine or triamine in the presence of the metal ion, and variation in the amine used allows the preparation of tetradentate (type **1**) or pentadentate (type **2**) ligands

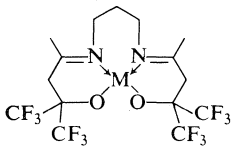

1*a*, M = Ni^{2+}
1*b*, M = Cu^{2+}

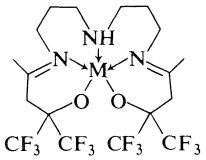

2*a*, M = Ni^{2+}
2*b*, M = Cu^{2+}

Although these neutral complexes are very stable, the unsaturated ligands themselves cannot be displaced without decomposition, so their general applicability to the formation of complexes with a variety of metals cannot be easily tested. We have therefore undertaken a study of the reduction of the above systems in the hope of removing the unsaturation and forming the more stable, isolable, amino-alcohols **3** and **4** from **1** and **2** respectively:

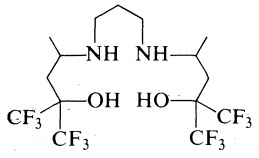

3

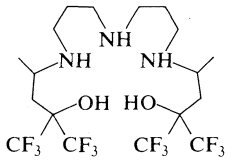

4

Previous workers have reported the reduction of coordinated imino-groups in a number of complexes. Curtis (3) has shown that the cationic nickel complex of the unsaturated tetra-azamacrocyclic ligand **5** may be reduced by H_2/Pt, by $NaBH_4$, by Al/OH^-, or by cathodic reduction, while **6** has been successfully reduced with $NaBH_4$.[1]

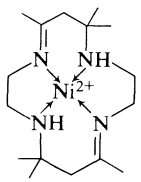

5

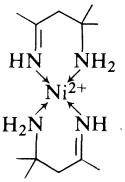

6

In both these systems, reduction of the analogous copper complex led to decomposition and the production of metallic copper, and Busch and co-

[1]N. F. Curtis and J. W. L. Martin. Unpublished results.

Can. J. Chem. Downloaded from www.nrcresearchpress.com by 210.87.254.42 on 09/05/12
For personal use only.

workers (5) have similarly reported success only with nickel complexes in the reduction of a number of macrocycles. All coordination is through nitrogen in the above systems, but a cationic nickel complex of a β-imino alcohol has been successfully reduced by Curtis and Martin (6).

Preparation of Reduced Ligands

The tetradentate ligand **3** was prepared by borohydride reduction of the nickel complex **1***a* in ethanol, followed by treatment with hydrochloric acid to remove the metal; the reduced ligand nickel complex was not isolated. In the case of the copper complex **1***b*, reaction with lithium aluminum hydride (LAH) immediately precipitated a pale yellow material which we assume to be a copper(I) complex. Hydrolysis and work-up with free access of air restored the blue colour characteristic of copper(II), and led to the isolation of the neutral copper complex **7**

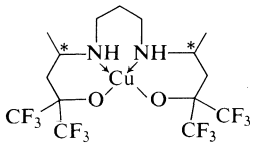

7

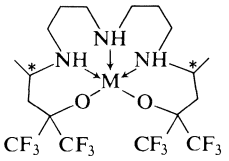

8*a*, M = Co^{2+}
8*b*, M = Ni^{2+}
8*c*, M = Cu^{2+}

The pentadentate ligand **4** was most easily prepared by LAH reduction of the copper complex **2***b* (which was more easily synthesised than its nickel analogue) leading, as before, through an apparent copper(I) complex to the reduced copper(II) complex **8***c*. The ligand **4**, as the hydrochloride, was then isolated from this by treatment with hydrochloric acid. A similar sequence using borohydride in place of LAH for reduction of **2***b* led to the same products, but in poor yield.

The successful use of copper complexes in these imino reduction reactions is surprising, in view of the failures quoted by previous workers. A contributing factor may be the neutral nature of the complexes in the current work, which may be more resistant to decomposition through nucleophilic attack than the cationic complexes studied by previous workers. However, it is also likely that our systems gave more stable copper(I) intermediates which did not tend to disproportionate; it is significant that previous workers have reported metallic copper as a decomposition product.

We have previously reported (1) that molecules containing a fluorinated tertiary alcohol and an amine group exhibit strong interactions between the two, sometimes to the point of complete proton transfer to give zwitterionic structures as **9**:

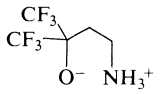

9

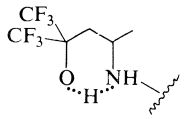

10

The same possibility exists in the compounds now under study, which both contain the partial structure **10**, and studies of their infrared spectra show that a similar interaction is occurring, although hydrogen-bonding seems more likely than complete proton transfer. In neither **3** nor **4** was there an absorption band associated with free —O—H. We have previously reported that the γ-amino fluorinated alcohol **9** shows no $—NH_2$ absorptions above 3200 cm^{-1}, but instead has strong, very broad, absorption in the region 2200–3000 cm^{-1} characteristic of $—NH_3^+$ and similar to glycine, whereas the analogous β-amino fluorinated alcohol shows fairly sharp absorption at 3330 and 3400 cm^{-1}, suggesting an intramolecularly H-bonded structure. In both **3** and **4**, two N—H stretching absorptions are seen; at 3276 and 2450–2750 (broad) for **3** and 3246 and 2740–2780 (broad) for **4**, (as the monohydrochloride) with N—H bending modes at 1519 and 1525 cm^{-1} respectively. A direct comparison with the other amino-alcohols is complicated by the fact that the amine groups are now secondary, and that, with two or three amine groups in the molecule, inter-amino H-bonding may be present.

As would be expected, coordination to a metal ion caused a considerable sharpening in the spectra in this region as H-bonding was removed, and strong, sharp, absorptions in the region 3120–3280 cm^{-1} (Table 1), characteristic of coordinated secondary amine, were now present.

Metal Complex Formation

The tetradentate ligand **3** readily coordinated to copper(II) to give complex **7**. However, attempts to prepare the nickel(II) analogue did not give a stable product. Although an interaction of Ni^{2+} with ligand occurred, giving a red solution consistent with the expected square-planar complex, attempts to isolate and purify a product led only to decomposition. Similarly, we could not isolate the nickel complex which was presumably an intermediate in the reduction of **1***a* to give ligand **3**. This result is surprising, in view of the well-established stability of neutral nickel(II) complexes of this type (1, 2, 7) and no obvious reason for this instability can be given.

The pentadentate ligand **4** proved more versatile.

TABLE 1. Infrared and visible spectra

Compound	ν(N—H)*, cm^{-1}	Visible band maxima, cm^{-1} (ε)	Solvent
7	3126(s)	14 900 (180), 17 900 (sh)	Methanol
		14 900 (170), 18 200 (sh)	Methanol/pyridine
8*a*	3264(s), 3234(m)	13 300 (8), 15 400 (sh), 17 700 (15), 21 000 (14), 22 600 (sh)	Benzene
8*b*	3257(m), 3266(sh)	7 800 (16), 13 300 ((11), 15 000 (43), 21 500 (15), 26 900 (90)	Ethanol
		8 000 (13), 13 000 (sh), 15 800 (40), 22 200 (16), 25 800 (97)	Pyridine
8*c*	3269(s), 3280(sh)	13 800 (108), 16 900 (sh)	Ethanol
		14 100 (83), 16 700 (sh)	Pyridine

*Nujol mulls, s = strong, m = medium, sh = shoulder.

TABLE 2. Analytical data

Compound	Formula	Carbon		Hydrogen		Nitrogen		Melting point (°C)
		Calcd.	Found	Calcd.	Found	Calcd.	Found	
3	$C_{15}H_{22}F_{12}N_2O_2$	36.7	36.7	4.52	4.56	5.71	5.63	82–83
4*	$C_{18}H_{30}ClF_{12}N_3O_2$	37.0	37.0	5.17	5.17	7.19	7.13	—
7	$C_{15}H_{20}CuF_{12}N_2O_2$	32.6	32.3	3.65	3.89	5.07	4.94	273–275
8*a*	$C_{18}H_{27}CoF_{12}N_3O_2$	35.8	35.8	4.50	4.51	6.94	6.97	169–170
8*b*	$C_{18}H_{27}F_{12}N_3NiO_2$	35.8	35.8	4.51	4.57	6.95	7.02	167–169
8*c*	$C_{18}H_{27}CuF_{12}N_3O_2$	35.5	35.7	4.47	4.41	6.89	6.73	146–148

*Analyzed as the hydrochloride.

As noted above, the copper(II) complex **8***c* was readily isolated as a direct product of the reduction; it was also readily re-formed by interaction of the ligand with Cu^{2+} ions. The complex was apparently monomeric in the vapour phase (mass spectrum) and in solution (osmometric in acetonitrile) and there is little reason to doubt that the metal atom is five-coordinate. The visible spectrum (Table 1) was similar to those reported for similar five-coordinate copper complexes (2), although this is not a good discriminator for copper.

With nickel, the picture was clearer. The complex **8***b* formed readily from the ligand and Ni^{2+} and gave stable green crystals. Its visible spectrum was very similar to those previously reported for similar five-coordinate nickel complexes (2), as was its magnetic moment of 3.15 BM.

The cobalt(II) analogue also formed readily. It had magnetic moment 4.64 BM (300 K), typical of high-spin five-coordinate Co^{2+} (8) and was resistant to oxidation to a cobalt(III) complex, either by air or by such oxidizing agents as bromine or hydrogen peroxide. A similar resistance to oxidation in five-coordinate cobalt(II) complexes has been noticed by other workers (4, 10).

No significant change in the visible spectrum of any complex studied occurred in the presence of donor solvent (pyridine), showing that additional coordination was not occurring. We have noted similar effects before (2, 7) with complexes of these bulky fluorinated ligands, where solvation appears to be sterically restricted.

Considerable opportunity for asymmetry exists in these complexes, both through permanent chiral centres on the ligands (marked *) and through co-ordination. No attempt to separate possible isomers has yet been made.

We conclude that reduction of imino-alkoxy complexes, which are readily available through template synthesis reactions, offers a useful synthetic route to polydentate ligands in the fluorinated alcohol field. The considerable stability of this type of complex is demonstrated by the ready in situ hydrogenation of an imino group in a ligand bound to copper, an approach not previously reported to be successful, and we attribute this in part to the neutral nature of the complexes formed by coordination of the ionized alcohols. The applicability of the approach to related systems is being studied.

Experimental

General

Infrared spectra were recorded on a Perkin-Elmer 621 instrument, visible spectra on Cary 14 and 118 spectrometers, mass spectra on a Varian MAT 311A, and molecular weights determined osmometrically on a Hewlett-Packard 301A vapour-pressure osmometer. Magnetic moments were determined by the Gouy method at 300 K. Microanalyses were performed by Malissa-Reuter Laboratories, West Germany; all analytical data are in Table 2.

Reduction of Ligands

(a) Tetradentate

The nickel and copper imino-complexes **1***a* and **1***b* were prepared by the method described previously (2). In the reduction of the nickel complex, **1***a* was dissolved in ethanol and $NaBH_4$ added in a 5:1 molar ratio with constant stirring. The

Can. J. Chem. Downloaded from www.nrcresearchpress.com by 210.87.254.42 on 09/05/12
For personal use only.

Can. J. Chem. Downloaded from www.nrcresearchpress.com by 210.87.254.42 on 09/05/12
For personal use only.

resulting black precipitate was removed by centrifuging and a little more $NaBH_4$ added to the now nearly colourless solution. Aqueous (1:1) hydrochloric acid was added to decompose both the excess borohydride and the nickel complex, and the reduced ligand was extracted from the solution into ether. Evaporation to dryness followed by extraction with dichloromethane gave the free reduced ligand **3**, colourless crystals from hexane, in approximately 60% yield.

The copper complex **1***b* was dissolved in anhydrous ether and $LiAlH_4$ in dry ether added in a 6:1 molar ratio. Immediate reaction occurred to precipitate a yellow solid. On addition of wet ether followed by water to decompose excess hydride, the precipitate went black. The system was left exposed to air for several hours with occasional stirring, during which time the ethereal layer became blue. Ether extraction and aeration of the aqueous layer was continued until no further colour was seen, after which evaporation of the ether solution gave the reduced copper(II) complex **7**, blue crystals from ethanol/chloroform. Molecular weight calcd., 552; parent ion in mass spectrum *m/e* 551.

The free ligand **3** was obtained from the copper complex by decomposing it with excess concentrated hydrochloric acid in ethanol solution, followed by extraction into ether and recrystallization as before.

(b) Pentadentate

The copper complex **2***b* was reduced with $LiAlH_4$ and the product worked up as before to yield the reduced copper(II) complex **8***c*, blue crystals from ethanol. Molecular weight calcd., 609; parent ion in mass spectrum, *m/e* 608.

The free ligand was prepared by adding concentrated hydrochloric acid to an ethanol/*n*-butanol solution of **8***c* followed by neutralization with potassium hydroxide and extraction into ether. Evaporation of the ether followed by recrystallization from hexane gave the reduced pentadentate ligand **4**, overall yield 45–50% from **2***b*. The ligand was isolated in the form of a monohydrochloride which was not deprotonated to the free base even by the use of excess aqueous base in the extraction.

Metal Complexes

Preparation of the copper complex of the tetradentate ligand **3** by direct reduction is described above; the same compound was prepared in virtually quantitative yield by interaction of the ligand with copper(II) chloride in ethanol with addition of potassium hydroxide to precipitate potassium chloride.

Attempts to make the nickel analogue were not successful. Interaction of nickel(II) chloride with ligand **3** in the presence of base produced a red solution, with absorption maxima at 18 800 and 24 600 cm^{-1}, but a green precipitate separated on work-up and no product could be characterized.

With the pentadentate ligand **4** the metal complexes were prepared similarly. A slight molar excess of the ligand was added to the metal chloride (Co^{2+}, Ni^{2+}, or Cu^{2+}) in ethanol and the stoichiometric amount of potassium hydroxide in ethanol added. After removal of precipitated potassium chloride, the solution was evaporated to give the metal complex in high yield: cobalt complex, **8***a*, purple plates from benzene, molecular weight calcd., 604; parent ion peak in mass spectrum, *m/e* 603; copper complex, **8***c*, identical with that obtained by direct reduction.

Acknowledgement

We thank the National Research Council of Canada for a grant in support of this work.

1. I. S. Chang and C. J. Willis. Can. J. Chem. **55**, 2465 (1977).
2. J. W. L. Martin and C. J. Willis. Can. J. Chem. **55**, 2459 (1977).
3. N. F. Curtis. J. Chem. Soc. 2644 (1964); 924 (1965); J. Chem. Soc. C, 1979 (1967).
4. R. Morassi, F. Mani, and L. Sacconi. Inorg. Chem. **12**, 1246 (1973).
5. E. K. Barefield, F. V. Lovecchio, N . E. Tokel, E. Ochiai, and D. H. Busch. Inorg. Chem. **11**, 283 (1972); V. Katovic, L. T. Taylor, F. L. Urbach, W. H. White, and D. H. Busch. Inorg. Chem. **11**, 479 (1972); S. C. Jackels, K. Farmery, E. K. Barefield, N. J. Rose, and D. H. Busch. Inorg. Chem. **11**, 2893 (1972).
6. J. W. L. Martin and N. F. Curtis. J. Chem. Soc. Dalton, 87 (1975).
7. W. S. Cripps and C. J. Willis. Can. J. Chem. **53**, 809 (1975).
8. J. S. Wood. Coord. Chem. Rev. **2**, 403 (1967).
9. M. Ciampolini and G. P. Speroni. Inorg. Chem. **5**, 45 (1966).

Mechanism of bromination of a quaternary pyrimidinium cation. Change of rate determining step with acidity

OSWALD S. TEE,[1] DAVID C. THACKRAY, AND CHARLES G. BERKS
Department of Chemistry, Concordia University, Montreal, P.Q., Canada H3G 1M8

Received June 2, 1978

OSWALD S. TEE, DAVID C. THACKRAY, and CHARLES G. BERKS. Can. J. Chem. **56**, 2970 (1978).

The kinetics of bromination of the 1,2-dihydro-1,3-dimethyl-2-oxopyrimidinium cation (Q^+) in aqueous media (pH 0–5) have been studied using the stopped-flow method. At the higher acidities (pH < 2) the results are consistent with rate determining attack by bromine upon the pseudobase (QOH), whereas at low acidities (pH > 4) it appears that pseudobase formation is rate determining. The change occurs because at high acidity the reversal of the pseudobase QOH to the cation is fast relative to bromine attack, whereas at low acidity the converse is true. Results obtained at intermediate acidities (pH 2–4) are consistent with this interpretation.

A separate kinetic study of pseudobase formation (and decomposition) yielded rate constants in good agreement with those derived from the bromination study.

OSWALD S. TEE, DAVID C. THACKRAY et CHARLES G. BERKS. Can. J. Chem. **56**, 2970 (1978).

Les cinétiques de bromation de l'ion dihydro-1,2-dimethyl-1,3-oxo-2-pyrimidinium (Q^+) dans des solutions aqueuses (pH 0–5) ont été mesurées par la méthode de flux stoppé. Les résultats des aidités plus hautes (pH < 2) indiquent que l'attaque du brome sur la pseudobase (QOH) est déterminante de la vitesse, tandis qu'il paraîtrait que la formation de la pseudobase est déterminante de la vitesse à des acidités plus faibles (pH > 4). Le changement se présente parce que le retour de la pseudobase QOH au cation Q^+ est plus rapide que l'attaque du brome dans les solutions plus acides, mais l'inverse s'obtient dans les solutions moins acides. Il y a un bon accord entre cette interprétation et les résultats qu'on a obtenus aux acidités intermédiaires (pH 2–4).

Une étude distincte des cinétiques de formation (et de décomposition) de la pseudobase a donnée des constantes de vitesse approchant celles de l'étude de bromation.

Introduction

The 1,2-dihydro-1,3-dimethyl-2-oxopyrimidinium cation (Q^+) readily forms its pseudobase (QOH) in neutral aqueous solution (1, 2). Since this species is an enamine it should be very susceptible to electrophilic attack and so we have proposed (3) that the facile aqueous bromination of the cation Q^+ proceeds by way of attack of bromine upon the pseudobase QOH which leads to the observable adduct **1** (Scheme 1) (3). Slow acid-catalyzed dehydration of this adduct leads to the substitution product having a 5-bromo substituent (3). The processes $Q^+ \rightarrow \rightarrow \rightarrow \mathbf{1}$ occur too rapidly in aqueous solution to be followed by conventional spectrophotometry. However, by use of the stopped-flow method we have now obtained sound kinetic evidence for the primary steps of the Scheme 1.

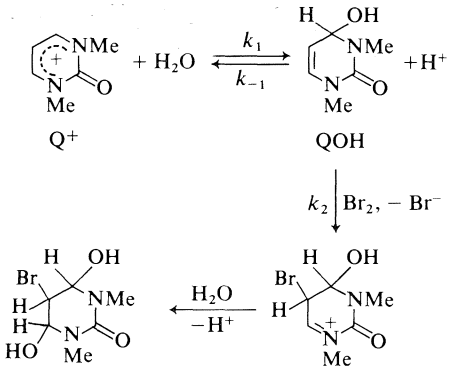

SCHEME 1

Results and Discussion

Our initial experiments, carried out in aqueous sulphuric acid (1 and 0.1 *N*), showed pseudo-first-order kinetics for the disappearance of bromine in the presence of an excess of the cation Q^+. During the course of these experiments Lloyd *et al.* (4) reported to us the observation that in aqueous solution (no acid or buffer) and with an excess of Q^+ the reaction obeyed zero-order kinetics. We hypothesized that the difference between the two observations was due to a change of rate determining step with decreasing acidity. Upon carrying out experiments at much lower acidity (pH = 4.27, 4.80) we observed pseudo-zero-order kinetics, in support of our hypothesis. Finally experiments carried out at inter-

[1]Author to whom correspondence should be addressed.

Can. J. Chem. Downloaded from www.nrcresearchpress.com by 210.87.254.105 on 09/05/12
For personal use only.

Can. J. Chem. Downloaded from www.nrcresearchpress.com by 210.87.254.105 on 09/05/12
For personal use only.

mediate acidities (pH = 2.67, 3.04) showed mixed zero- and first-order kinetics.

These results can be interpreted using a mechanism which involves either preequilibrium formation of, or rate determining formation of the pseudobase QOH. To corroborate this interpretation we also studied the kinetics of pseudobase formation and decomposition.

Our studies required the equilibrium constant for pseudobase formation

[1] $$Q^+ + H_2O \rightleftharpoons QOH + H^+$$

defined as $K_{R^+} = [QOH][H^+]/[Q^+]$ (5). Although values were available from earlier work (1, 2), we redetermined the value under the same conditions of temperature and ionic strength as the kinetic experiments, and found $K_{R^+} = 6.92 \times 10^{-8}$ M ($pK_{R^+} = 7.16$).

pH 0–2

In 0.1 and 1 N sulphuric acid (pH = 1.26, and pH $\simeq H_0 = 0.11$) the disappearance of bromine is strictly first order in the presence of an excess ($\geq$10-fold) of the substrate cation Q^+. First-order rate constants (k_1^{obs}) increase in proportion to the cation concentration (Table 1) and so overall the reaction is second order: first order in cation and first order in bromine. Furthermore, the derived second-order rate constants (k_2^{obs}) increase monotonically with pH (Table 1).

These observations are consistent with the bromination reaction involving rate determining attack of bromine upon the pseudobase QOH (eq. [2])

[2] $$Q^+ + H_2O \underset{}{\overset{K_{R^+}}{\rightleftharpoons}} H^+ + QOH \xrightarrow[Br_2]{k_2} \text{products}$$

This mechanism [2] requires that

[3] $$\text{rate} = -d[Br_2]/dt = k_2K_{R^+}[Q^+][Br_2]/[H^+]$$

Since $[H^+] \gg K_{R^+}$ ($=6.92 \times 10^{-8}$ M), $[Q^+] \simeq$ the stoichiometric concentration of cation Q^+, and eq. [3] is compatible with the experimental results for $k_2^{obs} = k_2K_{R^+}/[H^+]$. Clearly the quantity $k_2^{obs}[H^+]$ should be a constant ($=k_2K_{R^+}$) and the data (Table 1) are in reasonable agreement with this. Accordingly the data suggest $k_2 \simeq 7 \times 10^8$ M^{-1} s^{-1}.

pH 4–5

For experiments carried out in acetate buffers (pH = 4.27 and 4.80) with a 10-fold (or more) excess of cation Q^+ over bromine, the disappearance of the bromine shows zero-order kinetic behaviour for most (>90%) of the reaction. Zero-order rate constants (k_0^{obs}) increase in proportion to $[Q^+]$ (Table 2) suggesting, in fact, that reaction is simply first order in the cation Q^+. In support of this, experiments carried out with cation concentrations more nearly equal to that of bromine showed first-order behaviour with rate constants ($k_1^{obs\prime}$) comparable to those derived from zero-order data (Table 2). Within experimental error, the rate constants are not affected by acidity in this region.

These results suggest that at low acidity the forma-

TABLE 1. Pseudo-first-order rate constants for the bromination of cation Q^+ [a]

pH	$[Q^+] \times 10^3$ (M)	k_1^{obs} (s^{-1})	k_2^{obs} (M^{-1} s^{-1})	$k_2^{obs}[H^+]$ (s^{-1})
0.11[b]	0.5	0.0335	67.0	52[c]
	0.75	0.0491	65.5	41
	1.0	0.0654	65.4	51
			Ave. 66.0	Ave. 51
1.26	0.5	0.443	886	49
	0.7	0.674	963	53
	1.0	0.935	935	51
			Ave. 929	Ave. 51
2.67	0.5	(10.3)[d]	20 600	44
	0.7	(14.6)	20 900	45
	1.0	(19.4)	19 400	41
			Ave. 20 300	Ave. 43
3.04	0.5	(27.0)[d]	54 000	49
	1.0	(48.3)	48 300	44
			Ave. 51 200	Ave. 47

[a]At 30°C, [KBr] = 0.1 M. Each k_1^{obs} is the average of 3–6 runs differing by 5% or less; $k_2^{obs} = k_1^{obs}/[Q^+]$.
[b]Actually a value of H_0.
[c]Assuming $k_2 = 7.0 \times 10^8$ M^{-1} s^{-1}, $K_{R^+} = 6.92 \times 10^8$ M, values in this column should equal $k_2K_{R^+} = 48$ s^{-1}.
[d]Values in parentheses obtained by procedure *a* described in text assuming $k_1 = 1.3$ s^{-1}.

TABLE 2. Pseudo-zero-order rate constants for the bromination of cation Q^+ [a]

pH	$[Q^+] \times 10^3$ (M)	$k_0^{obs} \times 10^4$ (M s^{-1})	$k_1^{obs\prime}$ (s^{-1})
2.67	0.5	(6.55)[b]	1.31
	0.7	(9.03)	1.29
	1.0	(12.4)	1.24
			Ave. 1.28
3.04	0.5	(6.45)[b]	1.29
	1.0	(13.8)	1.38
			Ave. 1.34
4.27	0.5	6.55	1.31
	0.7	8.96	1.28
	1.0	13.1	1.31
			Ave. 1.30
4.80	0.1	—	1.38[c]
	0.2	—	1.33[c]
	1.0	12.1	1.21
			Ave. 1.31

[a]At 30°C, [KBr] = 0.1 M. Each k_0^{obs} is the average of 3–5 runs differing by 5% or less; $k_1^{obs\prime} = k_0^{obs}/[Q^+]$ except where noted.
[b]Values in parentheses obtained by procedure *b* described in text assuming $k_{-1}/k_2 = 0.03$.
[c]By direct measurement of first-order kinetics.

Can. J. Chem. Downloaded from www.nrcresearchpress.com by 210.87.254.105 on 09/05/12
For personal use only.

tion of the pseudobase QOH is rate determining and that attack by bromine occurs in a subsequent very fast step.

$$[4] \quad Q^+ + H_2O \xrightarrow{k_1} H^+ + QOH \xrightarrow[\text{fast}]{Br_2} \text{products}$$

Under these circumstances we simply have

$$[5] \quad \text{rate} = -d[Br_2]/dt = k_1[Q^+]$$

Thus for a large excess of cation zero-order behaviour should be observed with the rate constants $k_0^{obs} = k_1[Q^+]$ being a linear function of the cation concentration. Alternatively, if $[Q^+] \simeq [Br_2]$ the cation and bromine should disappear at comparable rates and the reaction should show first-order behaviour with rate constants $k_1^{obs'} = k_1$, as observed (Table 2). On this basis the formation of the pseudobase QOH has $k_1 \simeq 1.3\ s^{-1}$.

pH 2–4

In this region of acidity mixed-order kinetics are observed which are intermediate between the types described for the previous two pH regions. Employing an excess of the substrate cation Q^+ one observes a gradual change of order from pseudo-zero to pseudo-first during the course of the bromination reaction. Accordingly, analysis of the experimental data is more difficult.

The behaviour in this region of acidity is readily understandable if one assumes a steady state concentration of the pseudobase QOH. Moreover, the equations which result from a steady state treatment can also accommodate the behaviour observed in the other two regions of acidity. For mechanism [6]

$$[6] \quad Q^+ + H_2O \underset{k_{-1}}{\overset{k_1}{\rightleftharpoons}} H^+ + QOH \xrightarrow[Br_2]{k_2} \text{products}$$

assumption of a steady state concentration of QOH leads to

$$[7] \quad \text{rate} = \frac{-d[Br_2]}{dt} = \frac{k_1k_2[Q^+][Br_2]}{k_{-1}[H^+] + k_2[Br_2]}$$

Therefore the observed order of reaction should depend upon the relative magnitudes of the denominator terms $k_{-1}[H^+]$ and $k_2[Br_2]$ of eq. [7], that is, upon the relative rates of pseudobase reversal and of bromine attack.

If $k_{-1}[H^+] \gg k_2[Br_2]$ eq. [7] simplifies to eq. [3], since $K_{R^+} = k_1/k_{-1}$. This situation is consistent with the results obtained at high acidity (pH < 2) and corresponds to the pseudobase QOH reverting to the cation Q^+ faster than it reacts with bromine.

Alternatively, if bromine attack is faster than pseudobase reversal, $k_2[Br_2] \gg k_{-1}[H^+]$, [7] simplifies to [5] in agreement with the results obtained at low acidity (pH > 4). Note, however, that at some stage of the reaction, when sufficient of the bromine has been consumed, the inequality must reverse, and [5] be superceded by [3]. Accordingly, as the reaction proceeds the order changes from pseudo-zero to pseudo-first. At pH > 4 this occurs only after most (>94%) of the bromine has been consumed.

From the experiments carried out at high acidity (pH < 2) it appears that $k_2 \simeq 7 \times 10^8\ M^{-1}\ s^{-1}$. On the other hand, the studies at low acidity (pH > 4) yielded $k_1 \simeq 1.3\ s^{-1}$ and so $k_{-1} \simeq 1.9 \times 10^7\ M^{-1}\ s^{-1}$ since $K_{R^+} = k_1/k_{-1} = 6.92 \times 10^{-8}\ M$. Thus at pH 3, for example, the term $k_{-1}[H^+] = 1.9 \times 10^4\ s^{-1}$, whereas $k_2[Br_2] = 3.5 \times 10^4\ s^{-1}$ initially and thereafter decreases as the bromine is consumed. In other words, around pH 3 the denominator terms of [7] are of comparable magnitude and so mixed-order kinetics are to be expected.

The values of k_1, k_{-1}, and k_2 given above also justify the use of the steady-state approximation inasmuch as the processes which consume the pseudobase QOH are both much faster than that by which it is produced.

For analysis of the experimental data obtained at intermediate acidities (pH = 2.67 and 3.04) the full steady-state equation [7] must be used since the terms $k_{-1}[H^+]$ and $k_2[Br_2]$ are of comparable magnitude for much of the reaction. Integration of [7], assuming $[Q^+]$ is constant, yields [8].

$$[8] \quad \frac{k_{-1}[H^+]}{k_2} \ln \frac{[Br_2]_0}{[Br_2]} + ([Br_2]_0 - [Br_2]) = k_1[Q^+]t$$

This equation contains a first-order term and a zero-order term whose relative importance depends upon $[H^+]$ and $[Br_2]$. The form of the combination of the logarithmic and linear terms precludes simple fitting of [8] to data. We have tried various approaches to this problem and have settled upon the following: (*a*) treat k_1 as known, subtract the zero-order component, find the ratio k_{-1}/k_2 by least-squares fitting, and calculate a first-order rate constant $k_1^{obs} = k_1k_2[Q^+]/k_{-1}[H^+]$; (*b*) assume a value of k_{-1}/k_2, subtract the first-order term, and find a zero-order rate constant $k_0^{obs} = k_1[Q^+]$ by fitting. Both approaches give good fits (correlation coefficients >0.999) up to 90% reaction.

The values of k_1^{obs} obtained by procedure *a*, assuming $k_1 = 1.3\ s^{-1}$, are shown in Table 1 in parentheses. They show the required dependence upon cation concentration and yield values of k_2^{obs} which increase with pH in the same manner as those

Can. J. Chem. Downloaded from www.nrcresearchpress.com by 210.87.254.105 on 09/05/12
For personal use only.

obtained at lower pH. Thus the quantity $k_2^{obs}[H^+]$ remains sensibly constant (Table 1). Procedure *a* yields values of k_{-1}/k_2 in the range 0.026–0.031. By way of comparison, $k_2 = 7.0 \times 10^8\ M^{-1}\ s^{-1}$ and $k_{-1} = 1.9 \times 10^7\ M^{-1} s^{-1}$ (from above) require $k_{-1}/k_2 = 0.027$. This good agreement and the compatibility of all the k_2^{obs} values in Table 1 supports our use of procedure *a*.

Values of k_0^{obs} derived from experimental data by way of procedure *b* and assuming $k_{-1}/k_2 = 0.03$ are shown in parentheses in Table 2. They show the required dependence upon $[Q^+]$ and yield values of k_1^{obs} close to 1.3 s^{-1} which are independent of pH.

In summary, the data obtained at intermediate acidities are of mixed order but may be described by the steady-state equations [7] and [8], and employing the values of the rate constants k_1, k_{-1}, and k_2 derived from the data obtained in the regions of high and low acidity. Altogether the data indicate that as the acidity is decreased there is a change of rate determining step due to a reduction in the acid-catalyzed rate of pseudobase reversal to the cation relative to the rate of bromine attack.

Pseudobase Formation and Decomposition

To provide independent evidence for the validity of the interpretation given above we also studied the kinetics of pseudobase formation and decomposition by the stopped-flow method. The approach used was that which Bunting and co-workers have employed so successfully in their extensive studies of various quaternary heterocyclic cations (ref. 5 and references therein).

A solution of the heterocyclic cation Q^+ (or its pseudobase QOH) was rapidly mixed with a buffer solution of pH > pK_{R^+} (or pH < pK_{R^+}) and the rate at which the system attained a new equilibrium was measured. The approach to equilibrium follows first-order kinetics and the observed rate constant k_{obs} is the sum of the rate constants for formation (k_f) and decomposition (k_d) of the pseudobase QOH. Since $k_f[Q^+]_e = k_d[QOH]_e$ at equilibrium and $K_{R^+} = [QOH]_e[H^+]/[Q^+]_e$ one can write

$$[9] \qquad k_f = k_{obs}K_{R^+}/(K_{R^+} + [H^+])$$

and

$$[10] \qquad k_d = k_{obs}[H^+]/(K_{R^+} + [H^+])$$

Values of k_{obs}, and hence k_f and k_d, were obtained in the pH range 5.5–9.5. Outside this range the equilibrations are too fast to measure. Throughout the experimental conditions were kept as close as possible to those employed in the bromination studies.

The pH dependencies of the rate constants are displayed in Figs. 1 and 2. They may be described by

$$[11] \qquad k_f = k_1 + k_{OH}[OH^-]$$

and

$$[12] \qquad k_d = k + k_{-1}[H^+]$$

where k_1 and k_{-1} have their former meaning (eq. [6]), and k and k_{OH} refer to

$$[13] \qquad Q^+ + OH^- \underset{k}{\overset{k_{OH}}{\rightleftharpoons}} QOH$$

The curves shown in Fig. 2 were calculated from [11] and [12] using $k_1 = 1.5\ s^{-1}$, $k_{-1} = 2.2 \times 10^7\ M^{-1} s^{-1}$, $k = 0.31\ s^{-1}$, and $k_{OH} = 2.1 \times 10^6\ M^{-1} s^{-1}$. The curve for Fig. 1 was then calculated using $k_{obs} = k_f + k_d$.

The values of k_1 and k_{-1} just given, although a little high, are in good agreement with those (1.3 $\times$ s^{-1} and 1.9 $\times$ $10^7\ M^{-1} s^{-1}$) derived from the bromination studies. The magnitude of these values

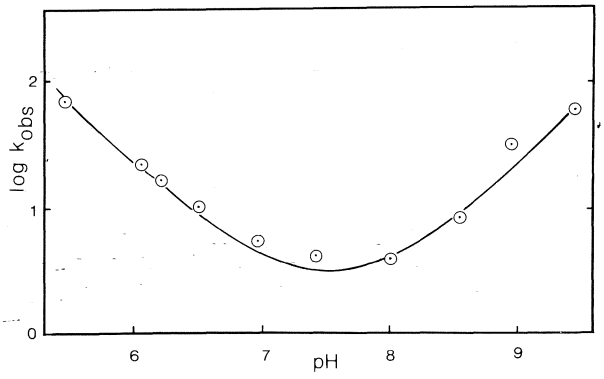

FIG. 1. pH dependence of k_{obs} for formation and decomposition of pseudobase QOH.

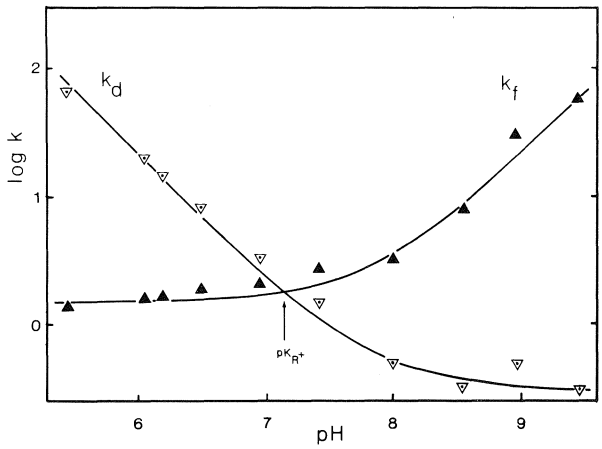

FIG. 2. pH dependence of rate constants for formation (k_f) and decomposition (k_d) of pseudobase QOH.

Can. J. Chem. Downloaded from www.nrcresearchpress.com by 210.87.254.105 on 09/05/12
For personal use only.

and the deviation of points in Figs. 1 and 2 *above* the calculated curves may be due to buffer catalysis. More specifically, pseudobase formation may involve general base-assisted nucleophilic attack by water and the reverse reaction, decomposition, is then general acid-catalyzed [14].

[14] $$Q^+ + H_2O + B^- \rightleftarrows QOH + HB$$

On the basis of buffer catalysis, solvent isotope effects, and entropies of activation, Bunting has concluded that a mechanism like [14] applies to the cation–pseudobase systems he has studied (5, 6). A possible manifestation of [14] in the present work is that at pH = 6.05 we found $k_{obs} = 28.8 \pm 2.0\ s^{-1}$ in a succinate buffer and $k_{obs} = 22.8 \pm 1.0\ s^{-1}$ in a phosphate buffer. Bunting and Meathrel (6) also found that the ratio k_{OH}/k_1 varied little (0.35×10^7 to $4.7 \times 10^7\ M^{-1}$) for a variety of cations whose K_{R^+} values covered a 10^6 range. The observation was rationalized (6) in terms of a mechanism like [14], the constants k_{OH} and k_1 being ascribed to hydroxide ion and a water molecule, respectively, operating as general bases facilitating the nucleophilic attack of water as in mechanism [14]. According to this view the ratio k_{OH}/k_1 largely reflects the relative basicities of hydroxide ion and water rather than their relative nucleophilicities towards a particular cation. For our system the ratio is $0.14 \times 10^7\ M^{-1}$, which is close to those cited above and consistent with the views of Bunting and Meathrel (6).

As a final point we note that our values of k_1 ($1.3\ s^{-1}$ from bromination studies, $1.5\ s^{-1}$ from pseudobase studies) at 30°C agree with the observations of Lloyd.[2] At 25°C he found that $5 \times 10^{-3}\ M$ bromine in the presence of 0.101 M cation Q^+ was consumed in 50 ms.[2] This corresponds to a zero-order rate constant $k_0^{obs} \sim 0.1\ M\ s^{-1}$ and thus a value of $k_1 \sim 1\ s^{-1}$ (at 25°C).

Relative Reactivities

We now consider the reactivity ascribed to the pseudobase QOH in relation to the proposed mechanism (Scheme 1) and the analysis of the data given above. The value of $k_2 = 7 \times 10^8\ M^{-1}\ s^{-1}$ cited previously is based upon the total bromine concentration and does not take into account the depletion of free bromine owing to the formation of tribromide ion. At 30°C the dissociation constant of tribromide $K = [Br_2][Br^-]/[Br_3^-] = 0.0554\ M$ (7) and thus the fraction of free bromine in the presence of 0.1 M bromide ion is $K/(K + [Br^-]) = 0.356$. Thus attack of bromine upon the pseudobase QOH actually has $k_2 = 2 \times 10^9\ M^{-1}\ s^{-1}$, which is close to diffusion controlled.

[2]Details provided by D. Lloyd.

Recently Dubois and Toullec (8) argued that since chlorine, bromine, and iodine all attack the enol of acetone at the same rate they do so at a diffusion controlled rate ($\sim 10^9\ M^{-1}\ s^{-1}$). A simple enamine should be more reactive than this enol for reasons of electronegativity (cf. [15] and [16]). How-

[15] 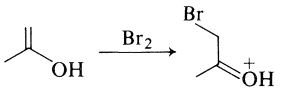

[16] 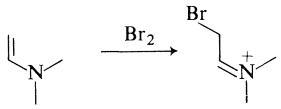

ever, if [15] is diffusion controlled then [16] must be also. The pseudobase QOH contains an enamine moiety attached to a presumably deactivating carbamoyl substituent (—CONMe—). It appears therefore, that the magnitude of the deactivation is insufficient to depress the rate of [16] significantly below the diffusion controlled limit.

The value of $k_2 \simeq 2 \times 10^9\ M^{-1}\ s^{-1}$ for bromine attack upon the pseudobase **2** (X = H) may be compared to values we have obtained for related systems under similar conditions.

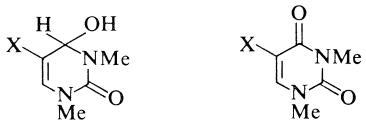

2 **3**

	$k_2\ (M^{-1}s^{-1})$	
X	**2**	**3**
H	2×10^9	10^5
Br	4×10^6	20

By conducting experiments in strong aqueous acid we recently showed that the 5-bromo analogue of cation Q^+ reacts with bromine via its pseudobase **2** (X = Br) with a second-order rate constant of $4 \times 10^6\ M^{-1}\ s^{-1}$ (9). Thus the presence of X = Br in **2** causes a rate retardation of 500. By way of comparison, the same substitution in 1,3-dimethyluracil **3** brings about a reduction in rate of 5000 (10). The large retardations, while partly electronic in origin, probably have a large steric contribution resulting from the fact that attack occurs *ipso* to the 5-bromine when X = Br in **2** or **3**. In contrast, phenol, which has a reactivity ($1.8 \times 10^5\ M^{-1}\ s^{-1}$ at 25°C) close to that of 1,3-dimethyluracil **3** (X = H), is only 56 times as reactive as *p*-bromophenol ($k_2 = 3.2 \times 10^3\ M^{-1}\ s^{-1}$) (11).[3]

[3]The value of k_2 given for *p*-bromophenol in ref. 11 is in error. R. P. Bell, personal communication.

Can. J. Chem. Downloaded from www.nrcresearchpress.com by 210.87.254.105 on 09/05/12
For personal use only.

Finally, with respect to the reactivity of Q^+ and QOH in equilibration, we point out that the rate constants we have obtained are very similar to those which Bunting and Meathrel (12) found for the 2-cyanomethyl-5-nitroisoquinolium cation (**4**) and its pseudobase. Of the many cations they studied, the cation **4** has a value of pK_{R+} most similar to that of Q^+. Again, this may be a consequence of the involvement of mechanism [14].

Cation	pK_{R+}	k_1 (s^{-1})	k_{-1} (M^{-1} s^{-1})	k (s^{-1})	k_{OH} (M^{-1} s^{-1})	Temperature (°C)
Q^+	7.16	1.5	2.2×10^7	0.31	2.1×10^6	30
4	7.26	0.22	6.4×10^6	0.54	1.9×10^6	25

Conclusions

The bromination kinetics lead us to the conclusion that the 1,2-dihydro-1,3-dimethyl-2-oxopyrimidinium cation Q^+ does indeed react with bromine via its pseudobase QOH (Scheme 1). At high pH (>4) the rate of formation of this pseudobase is rate determining [4]. At low pH (<2) the pseudobase undergoes rapid acid-catalyzed decomposition back to Q^+ and the diffusion controlled attack of bromine upon QOH is rate determining [2]. These conclusions are supported by a study of the kinetics of pseudobase formation and decomposition. Furthermore, pseudobase formation is probably general base-catalyzed, and the microscopic reverse, decomposition, general acid-catalyzed as shown in [14].

Experimental

Materials

The 1,2-dihydro-1,3-dimethyl-2-oxopyrimidinium cation was employed as the hydrogen sulphate salt which was prepared as previously (3). Aqueous sulphuric acid solutions (0.1 *N*, pH = 1.26 and 1.0 *N*, H_0 = 0.11 (13)) were made up from volumetric concentrates. Buffer solutions of constant ionic strength (0.01 *M*) were made up following Perrin (14) and checked using a Corning digital 110 pH meter. Since all kinetic solutions were 0.1 *M* in potassium bromide, the total ionic strength was 0.11 *M* for experiments using buffers.

Bromine solutions in sulphuric acid were prepared by use of the bromate–bromide reaction (15). For bromine solutions in buffers, where this reaction is too slow, a relatively concentrated solution was made up by weight and then diluted appropriately. In all the bromination experiments the initial bromine concentration was 5×10^{-5} *M* after 1:1 mixing in the stopped-flow apparatus.

Methods

The value of pK_{R+} appropriate to the conditions of the kinetics experiments ([KBr] = 0.1 *M*, total ionic strength = 0.11 *M*, 30°C) was determined spectrophotometrically (16). Using an analytical wavelength of 239 nm (λ_{max} of QOH) gave 7.15 ± 0.04, whereas using 314 nm (near λ_{max} of Q^+) gave 7.17 ± 0.03. Accordingly, in the text we use pK_{R+} = 7.16.

Kinetics experiments were carried out using an Aminco-Morrow stopped-flow accessory attached to an Aminco DW-2 uv–visible spectrophotometer operating in the dual wavelength mode. Temperature in the observation cell and the drive syringes was maintained at 30.0 ± 0.1°C using a Lauda RC-20B circulating bath. Absorbance changes were recorded using a Biomation 805 waveform recorder and the stored signal was viewed using an oscilloscope. Acceptable traces were plotted out on large graph paper by connecting the Biomation 805 to the X—Y recorder of the Aminco DW-2 through an adjustable dropping resistor.

For bromination studies one drive syringe contained cation Q^+ in the chosen medium, and the other contained bromine (1×10^{-4} *M*) in the same medium. All concentrations given in the text are *after* mixing. Reactions were followed by monitoring the change at 267 nm (λ_{max} Br_3^-) relative to that at 240 nm where there is little or no change. For pH < 2 strictly first-order behaviour was observed for >94% reaction. Pseudo-first-order rate constants (k_1^{obs}) were obtained from least-squares analysis of ln ($A - A_\infty$) vs. time for the first 80–90% of reaction ($r \geq 0.9995$). For pH > 4 and large excess of cation Q^+ zero-order behaviour was observed over much of the reaction. Pseudo-zero-order constants (k_0^{obs}) were obtained by analysis of ($A - A_\infty$) vs. time for the first 50–60% of the reaction ($r \geq 0.9995$). The slope (dA/dt) from this analysis relates to k_0^{obs} through an apparent extinction coefficient ε[4] and the following equations:

$$k_0^{obs} = \frac{-d[Br_2]}{dt} = -\frac{1}{\varepsilon l}\frac{dA}{dt}$$

$$A_0 - A_\infty = \varepsilon[Br_2]_0 l$$

Therefore

$$k_0^{obs} = \frac{[Br_2]_0}{(A_0 - A_\infty)}\frac{dA}{dt}$$

For the first-order disappearance of bromine which results from the first-order disappearance of Q^+ when pH > 4 and $[Q^+]_0$ only slightly greater than $[Br_2]_0$ analysis of the data requires an imaginary (and negative) infinity reading A_∞'. The observed A_∞ corresponds to the actual total consumption of bromine, whereas A_∞' corresponds to the imaginary total consumption of cation Q^+. For an apparent[4] extinction coefficient ε the following relationships hold.

$$A_0 - A_\infty = \varepsilon[Br_2]_0 l \qquad A_0 - A_\infty' = \varepsilon[Q^+]_0 l$$

Therefore

$$A_\infty' = A_0 - (A_0 - A_\infty)[Q^+]_0/[Br_2]_0$$

On this basis we analyzed ln ($A - A_\infty'$) vs. time covering about 90% reaction and obtained good straight lines ($r \geq 0.9995$) whose slopes gave values of $k_1^{obs'}$. Bromination data obtained at pH = 2.67 and 3.04 which are of mixed order were analyzed by procedures *a* and *b* described in the text.

The pseudobase kinetic studies were conducted in the manner of Bunting and Meathrel (6). One drive syringe contained a 5×10^{-4} *M* solution of Q^+ (or QOH) in 0.1 *M* aqueous potassium bromide, while the other contained a buffer of pH > pK_{R+} (or pH < pK_{R+}) also in 0.1 *M* aqueous KBr and of twice the concentration given in Perrin (14). Thus, after mixing; the solution conditions were the same as those in the

[4]Apparent because of contributions to the absorbance from Q^+ as well as Br_3^-. Also because of the nature of a dual wavelength experiment.

bromination studies. The disappearance of Q^+ (or QOH) was monitored at 316 nm (or 239 nm) relative to 270 nm (spectrum minimum). Good first-order behaviour was observed for $>90\%$ reaction and analysis of ln $(A - A_\infty)$ vs. time gave pseudo-first-order rate constants k_{obs} with $r \geq 0.9995$. The reproducibility of k_{obs} depends upon the speed of the reaction. For the fastest runs near the limit of the apparatus it is about 10% but for the slowest runs it is less than 5%.

Acknowledgements

This research was supported by a grant from the National Research Council of Canada. We are particularly grateful to Dr. Douglas Lloyd (University of St. Andrews, Scotland) for providing details of his work. We also thank Professor R. P. Bell for clarifying a published error and Mr. W. Fitch for assistance with drawing the figures.

1. A. R. KATRITZKY, M. KINGSLAND, and O. S. TEE. J. Chem. Soc. B, 1484 (1968).
2. O. S. TEE and M. ENDO. Can. J. Chem. **54**, 2681 (1976).
3. O. S. TEE and S. BANERJEE. Can. J. Chem. **52**, 451 (1974).
4. D. LLOYD, H. MCNAB, and K. S. TUCKER. J. Chem. Soc. Perkin I, 1862 (1977).
5. J. W. BUNTING and D. J. NORRIS. J. Am. Chem. Soc. **99**, 1189 (1977).
6. J. W. BUNTING and W. G. MEATHREL. Can. J. Chem. **51**, 1965 (1973).
7. O. S. TEE and G. V. PATIL. J. Org. Chem. **41**, 828 (1976).
8. J. E. DUBOIS and J. TOULLEC. Tetrahedron, **29**, 2859 (1973).
9. S. BANERJEE, O. S. TEE, and K. D. WOOD. J. Org. Chem. **42**, 3670 (1977).
10. O. S. TEE and C. G. BERKS. In preparation.
11. R. P. BELL and D. J. RAWLINSON. J. Chem. Soc. 63 (1961).
12. J. W. BUNTING and W. G. MEATHREL. Can. J. Chem. **52**, 962 (1974).
13. C. D. JOHNSON, A. R. KATRITZKY, and S. A. SHAPIRO. J. Am. Chem. Soc. **91**, 6654 (1969).
14. D. D. PERRIN. Aust. J. Chem. **16**, 572 (1963).
15. A. E. BURGESS and J. L. LATHAM. J. Chem. Educ. **46**, 370 (1969).
16. A. ALBERT and E. P. SERJEANT. Ionization constants of acids and bases. Methuen, London. 1962.

Can. J. Chem. Downloaded from www.nrcresearchpress.com by 210.87.254.105 on 09/05/12
For personal use only.

The $\{Li(NH_3)_n\}^+$ and $\{Na(NH_3)_n\}^+$ systems. A CNDO/2 study of the Li^+ and Na^+ ion solvation

C. SIEIRO, P. CAÑAS, AND P. MARTINEZ

Centro Coordinado del CSIC, Facultad de Ciencias, Universidad Autónoma, Canto Blanco, Madrid 34, Spain

Received February 13, 1978

C. SIEIRO, P. CAÑAS, and P. MARTINEZ. Can. J. Chem. **56**, 2977 (1978).

We present the CNDO/2 calculations of Li^+ and Na^+ solvation in ammonia solvent. The results indicate a solvation number of $n = 6$ for Li^+ and $n \geq 8$ for Na^+, at equilibrium distances of $Li^+ \ldots N = 2.3$ Å and $Na^+ \ldots N = 2.9$ Å. The charge transfer from ammonia to both ions is analyzed.

C. SIEIRO, P. CAÑAS et P. MARTINEZ. Can. J. Chem. **56**, 2977 (1978).

On présente les calculs selon la méthode CNDO/2 pour la solvatation de Li^+ et Na^+ dans l'ammoniac. Les résultats indiquent un degré de solvatation $n = 6$ pour l'ion Li^+ et $n \geq 8$ pour l'ion Na^+, les distances à l'équilibre étant $Li^+ \ldots N$, 2.3 Å, et $Na^+ \ldots N$, 2.9 Å. On analyse les transferts de charge des molécules d'ammoniac vers ces deux ions.

[Traduit par le journal]

Can. J. Chem. Downloaded from www.nrcresearchpress.com by 210.87.254.42 on 09/05/12
For personal use only.

Introduction

The theoretical study of ion solvation has been, to date, fundamentally realized on the hydration case. In general, studies on solvation with other non-aqueous solvents have not been widely done.

The earlier works on solvation used, fundamentally, the Born model, which is based on the continuum theory of the solvent. The consecutive refinements of this model have reached the limit of usefulness (1–4).

Quantum mechanical studies have recently been carried out using the *ab initio* SCF MO computation on the most simple systems and more extensively the semi-empirical methods (CNDO/2, INDO, EHT, etc.) for the study of the most complex systems in aqueous and non-aqueous media (5–31).

In this paper we present the study of the solvation of the Li^+ and Na^+ ions in ammonia solvent. We consider the primary solvation sheath as being the bulk solvent. In this case, the difference between the total energy of the whole system at infinite distance and the total energy, corresponding to equilibrium, refers to the solvation energy at absolute zero. We omitted the corrections of $\Delta H_{298.16}$ to $\Delta E_{0\ K}$ which were negligible in this particular case.

$$\Delta E = E_{eq} - E_\infty = E_{M^+(MN_3)_n}\,(r = r_{eq}) - E_{M^+(NH_3)_n}\,(r = \infty)$$

or

$$[1] \qquad \Delta E = E_{M^+(NH_3)_n} - (E_{M^+} + nE_{NH_3})$$

where n is the solvation number, $E_{M^+(NH_3)_n}$, E_{M^+}, and E_{NH_3} are the energies of the solvated ion, isolated ion, and the ammonia molecule, respectively.

We have used the by now classical CNDO/2 method in its original parametrization of Pople–Santry–Segal (32, 33). The program used was a modified version of the QCPE 141 program. The geometric input data for the ammonia molecule is the latest available experimental value d(N—H) = 1.014 Å and $\angle$ HNH = 106.7°.

The CNDO/2 method uses only the valence orbitals as "the minimum basis set" and thus the energy of the cation M^+ is zero, consequently:

$$[2] \qquad \Delta E = E_{M^+(NH_3)_n} - nE_{NH_3}$$

We also obtain the stabilization energies considering the diatomic ($M^+ \ldots N$) energy terms for different solvation numbers.

The Solvation Model

As we have mentioned before, the bulk solvent is approximate to a first sheath around the ions. We considered 1 to 8 molecules of ammonia in the geometrically most symmetric orientation around the central ion. In all cases of $M^+ \ldots NH_3$ complexes, the M^+ ion was along the lone-pair direction.

Figure 1 shows the geometrical distribution of ammonia considered for the different numbers of solvation. The potential energy curves of the $\{M(NH_3)_n\}^+$ systems are obtained by varying the $M^+ \ldots N$ distances within the range of 0.5 to 5 Å. At this last distance the interaction energy approaches zero and the whole system is described as being n molecules of ammonia and one ion, all being independent. That is to say this situation corresponds to the above mentioned energy, E_∞.

Gupta and Rao (21) have studied the solvated lithium system for $n = 1$, 2, and 4 molecules of ammonia, but for the last coordination number, they considered a square planar model whereas we have considered a tetrahedral one. The results in all three cases practically coincide with ours.

Can. J. Chem. Downloaded from www.nrcresearchpress.com by 210.87.254.42 on 09/05/12
For personal use only.

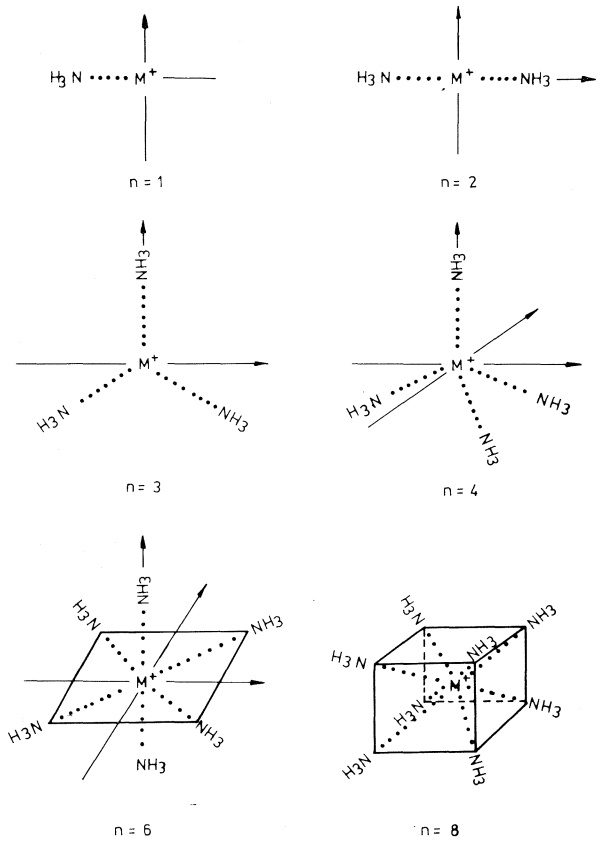

FIG. 1. Coordinate system and solvation model for $M^+(NH_3)_n$ ($M^+ = Li^+$ and Na^+).

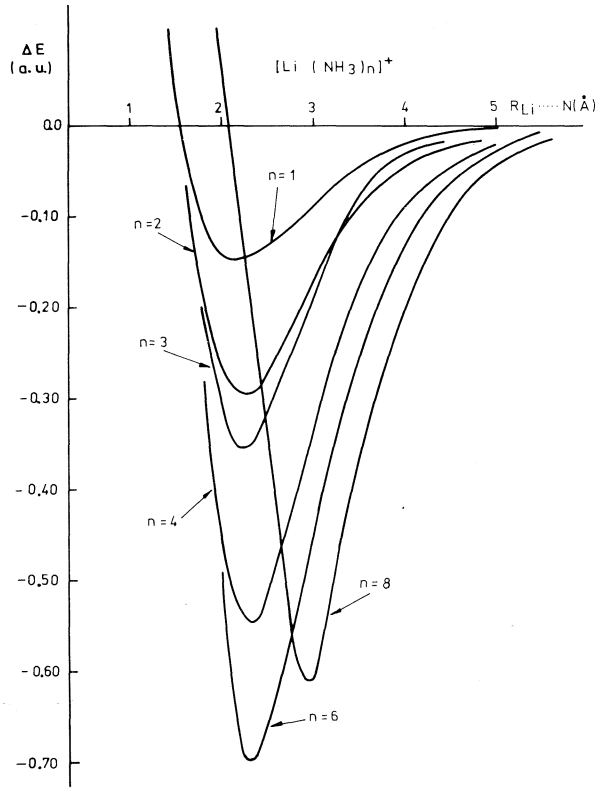

FIG. 2. Potential energy curves for the (LiN) variation of the $Li^+(NH_3)_n$ system.

Results and Discussion

In Figs. 2 and 3, we present the potential energy curves obtained for the $\{Li(NH_3)_n\}^+$ and $\{Na(NH_3)_n\}^+$ systems, respectively, where n = 1, 2, 3, 4, 6, and 8. Table 1 shows the results for the equilibrium N ... M^+ (Li^+ and Na^+) bond length, stabilization energy, diatomic energy terms, and charge transfer for all the complexes studied.

(a) Lithium Solvation

As shown in Fig. 2, all curves show that the interaction of the lithium ion with ammonia molecules stabilize the ion with respect to the subsystems, and furthermore indicate a strong ordering effect of ions on the ammonia molecules. This was the first result of the classical ion-solvent theory. The ordering effect does not mean a static but a dynamic and statistical arrangement.

The ammoniation energies are higher than the hydration ones in all n values studied (see Table 1). The most stable complex corresponds to a value of $n = 6$, but the stabilization energies per Li^+ ... N bond decrease as the solvation number increases. The solvation sheath corresponding to the predicted most stable octahedral system has a radius of 2.3 Å. There are no experimental data for this n value, and the only experimental Li^+ ... N distance available corresponds to the $\{Li(NH_3)_n\}^+$ complex and $R_{Li \ldots N}$ = 1.94 Å (34). The *ab initio* calculation of Støgard (35) for $n = 1$ yields $R_{Li \ldots N}$ = 1.98 Å, which is more exact than the CNDO/2 prediction (see Table 1).

The ammonia is an electron donor molecule and there is a great charge transfer to the lithium ion in all the systems, this charge transfer decreases with increasing solvation number. This feature is a logical consequence of an increase in the Li^+ ... N equilibrium distance with the number of ammonia molecules around the ion. The charge transfer process decreases as the nitrogen lone pair recedes. The unrealistically high values of charge transfer represent a systematic artificial error of the CNDO/2 treatment as a final consequence of the neglect of the inner shell electrons. The alkali ions are represented as screened nuclei and it is not possible to take into account the polarization of the inner shell electrons.

TABLE 1. Solvation number, total energy, sheath radius, stabilization energies, transfer charge, and diatomic energy terms of the lithium and sodium solvated systems*

System	n	E_T (au)	$d_{M^+ \ldots N}$ (Å)	$-\Delta E$ (kcal/mol) Cation–ammonia complex	$-\Delta E$ (kcal/mol) Cation–water complex	q_T	Diatomic energy terms (au)
$\{Li(NH_3)_n\}^+$	1	−14.0198	2.1	93	44	−0.30	−0.378
	2	−28.0342	2.2	92	44	−0.30	−0.359
	3	−42.0370	2.3	88	41	−0.24	−0.315
	4	−56.0259	2.3	85	38	−0.24	−0.295
	6	−83.9200	2.3	72	33	−0.18	−0.240
	8	−111.5818	2.9	48	30	−0.10	−0.130
$\{Na(NH_3)_n\}^+$	1	−14.2238	2.6	220	32	−0.34	−0.663
	2	−28.4234	2.7	213	31	−0.34	−0.622
	3	−42.4331	2.7	173	31	−0.34	−0.619
	4	−56.8608	2.7	215	28	−0.33	−0.618
	6	−85.2274	2.7	208	27	−0.32	−0.585
	8	−113.2337	2.9	177	26	−0.26	−0.487

*ΔE is the average stabilization energy per $Li^+ \ldots N$ bond; E_T of NH_3 is −13.8710 au. The diatomic energy terms refer to energy per $Li^+(Na^+)$—N bond. q_T is the charge transfer per $Li^+(Na^+) \ldots N$ bond.

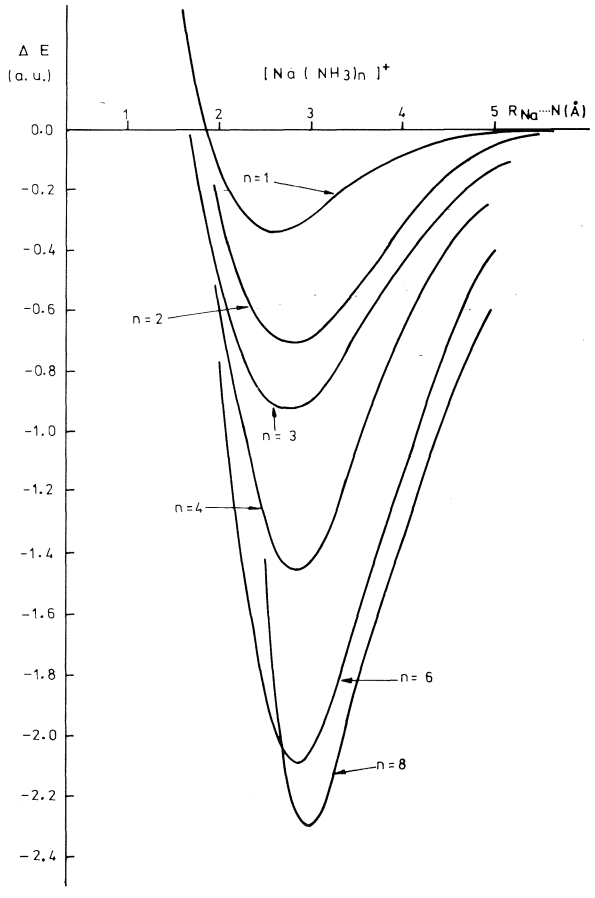

FIG. 3. Potential energy curves for the (NaN) variation of the $Na^+(NH_3)_n$ system.

(b) Sodium Solvation

Figure 3 shows the potential curves obtained for the solvated sodium ion. The stabilization energy increases continually with the coordination number. This result is analogous to that obtained in the hydration case for the Li^+ and Na^+ ions. The equilibrium bond lengths for all n values are higher than the lithium complex systems. There are no experimental data available for this system and the higher solvation number and sheath radius than in the solvated lithium system is consistent with the greater ionic radius of the sodium ion. The charge transfer of the ammonia molecules to the Na^+ ion is larger than in the lithium case and decreases in the same sense.

The two systems studied contain only monovalent cations and the number of surrounding ammonia molecules depends on the ion size and the steric hindrance of the ammonia molecules comprising the solvation sheath. We have also calculated for the H^+ cation case, and obtained four molecules of ammonia for the primary solvent sheath. Figure 4 shows the solvation energy for H^+ and Li^+ in water and ammonia media at different values for n. In the case of H^+ in H_2O solvent, there is a maximum in the stabilization energy at approximately $n = 6$, but in ammonia the stabilization energy is practically the same from $n = 2$ to $n = 5$, due to the greater molecular volume with respect to that of the H_2O. In the $\{Li(NH_3)_n\}^+$ and $\{Na\ NH_3)_n\}^+$ systems the results obtained are analogous. In NH_3 solvent, there is a maximum in the ammoniation energy at $n = 6$ but this maximum does not exist in the range $n = 1$ to $n = 8$ when water solvent is considered.

Can. J. Chem. Downloaded from www.nrcresearchpress.com by 210.87.254.42 on 09/05/12
For personal use only.

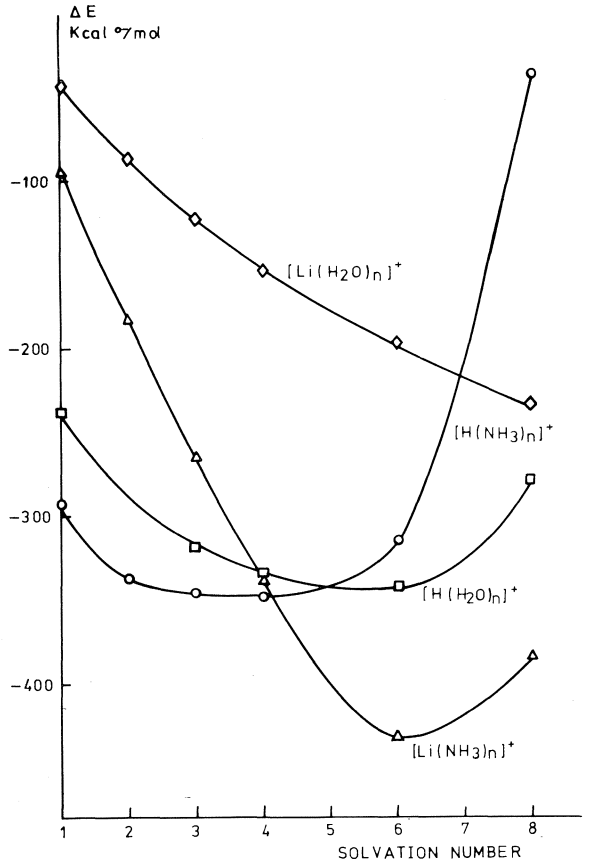

FIG. 4. Variation of the stabilization energies with n for the $Li^+(NH_3)_n$, $Li^+(H_2O)_n$, $H^+(NH_3)_n$, and $H^+(H_2O)$ systems.

We can conclude that the CNDO/2 method predicts a solvation number of 6 and ≥ 8 for Li^+ and Na^+ ions, respectively, as being the energetically most favourable of all the coordinations studied. The solvation energy calculated cannot be compared with the experimental data, but the results in the Na^+ case appear to be excessively high. This is a consequence of the whole CNDO/2 procedure. However, in the case of a hydrated complex (1:1), more accurate calculations obtain poorer results than the CNDO/2 ones, depending on the basis set used (11). Only the extremely accurate calculations of Clementi *et al.* obtain, in the $Li(H_2O)^+$ case, values approximating to the experimental ones. The greater value of the size of the octahedral cation–ammonia complex is also obtained, in the case of hydrated complexes, using more accurate calculations. With cation–ammonia complexes, this value might be due to the steric hindrance among the ammonia molecules. The CNDO/2 results differ considerably from the *ab initio* calculations; however, in the latter, the basis set used is very limited when the complex is great and a definite conclusion cannot be reached. Moreover, the inclusion of a second solvation sheath would probably improve our results. This will constitute a further study.

Acknowledgement

This study was supported by the Comisión Asesora de Investigación Científica y Técnica, Madrid.

1. B. E. CONWAY. Ann. Rev. Phys. Chem. **17**, 481 (1966).
2. M. BORN. Z. Phys. **1**, 45 (1920).
3. K. J. LAIDLER and C. PEGIS. Proc. R. Soc. A**241**, 80 (1957).
4. H. S. FRANK and W. Y. WEN. Discuss. Faraday Soc. **24**, 133 (1957).
5. G. H. F. DIERCKSEN and W. P. KRAEMER. Chem. Phys. Lett. **5**, 570 (1970).
6. H. LISCHKA, TH. PLESSER, and P. SCHUSTER. Chem. Phys. Lett. **5**, 263 (1970).
7. R. E. BURTON and J. DALY. J. Trans. Faraday Soc. **66**, 2408 (1970); **66**, 1281 (1970).
8. P. SCHUSTER. Theor. Chim. Acta, Berlin, **19**, 212 (1970).
9. K. G. BREITSCHWERDT. Chem. Phys. Lett. **6**, 587 (1970).
10. R. E. BURTON and J. DALY. J. Trans. Faraday Soc. **67**, 1219 (1971).
11. P. SCHUSTER and H. PREUSS. Chem. Phys. Lett. **11**, 35 (1971).
12. K. G. BREITSCHWERDT. Ber. Bunsenges. Phys. Chem. **75**, 319 (1971).
13. W. P. KRAEMER and G. H. F. DIERCKSEN. Theor. Chim. Acta, Berlin, **27**, 265 (1970); **23**, 393 (1972).
14. G. H. F. DIERCKSEN and W. P. KRAEMER. Theor. Chim. Acta, Berlin, **23**, 387 (1972).
15. E. CLEMENTI and H. POPKIE. J. Chem. Phys. **57**, 472 (1972).
16. P. RUSSEGGER, H. LISCHKA, and P. SCHUSTER. Theor. Chim. Acta, Berlin, **24**, 191 (1972).
17. K. G. BREITSCHWERDT and H. KISTENMACHER. Chem. Phys. Lett. **14**, 288 (1972).
18. P. RUSSEGGER and P. SCHUSTER. Chem. Phys. Lett. **19**, 254 (1973).
19. H. KISTENMACHER, H. POPKIE, and E. CLEMENTI. J. Chem. Phys. **58**, 5627 (1973); **58**, 1689 (1973).
20. K. BAUGE and A. STØGARD. Acta Chem. Scand. **27**, 2683 (1973).
21. A. GUPTA and C. N. R. RAO. J. Phys. Chem. **77**, 2888 (1973).
22. B. M. RODE. Chem. Phys. Lett. **20**, 366 (1973); **25**, 369 (1974).
23. A. PULLMAN and P. SCHUSTER. Chem. Phys. Lett. **24**, 472 (1974).
24. B. M. RODE and H. PREUSS. Theor. Chim. Acta, Berlin, **35**, 369 (1974).
25. D. A. ZHOGOLEV. Chem. Phys. Lett. **29**, 506 (1974).
26. B. M. RODE, M. BREUSS, and P. SCHUSTER. Chem. Phys. Lett. **32**, 34 (1975).
27. P. SCHUSTER, W. MARIUS, A. PULLMAN, and H. BERTHOD. Theor. Chim. Acta, Berlin, **40**, 323 (1975).
28. H. G. HERTZ, H. WEINGÄRTNER, and B. M. RODE. Ber. Bunsenges. Phys. Chem. **79**, 1190 (1975).
29. M. URBAN, S. PAVLIK, V. KELLO, and J. MARDIAKOVA. Coll. Czech. Chem. Commun. **40**, 587 (1975).
30. G. H. F. DIERCKSEN, W. P. KRAEMER, and B. O. ROSS. Theor. Chim. Acta, Berlin, **36**, 249 (1975).
31. B. M. RODE. Monatsch. Chem. **106**, 339 (1975).
32. J. A. POPLE and G. A. SEGAL. J. Chem. Phys. **44**, 3289 (1966).
33. D. P. SANTRY and G. A. SEGAL. J. Chem. Phys. **47**, 158 (1967).
34. N. MAMMANO and M. J. SIENKO. J. Am. Chem. Soc. **90**, 6322 (1968).
35. A. STØGARD. Acta Chem. Scand. **77**, 2669 (1973).

Can. J. Chem. Downloaded from www.nrcresearchpress.com by 210.87.254.42 on 09/05/12
For personal use only.

Enrichment of nitrogen-15 by the direct laser photolysis of ammonia-d_3 in the $\tilde{A}$–$\tilde{X}$ transition[1]

P. A. HACKETT, R. A. BACK, AND S. KODA[2]

PIE Group, Division of Chemistry, National Research Council of Canada, Ottawa, Ont., Canada K1A 0R6

Received May 24, 1978

P. A. HACKETT, R. A. BACK and S. KODA. Can. J. Chem. **56**, 2981 (1978).

Ammonia-d_3 of differing $^{14}N/^{15}N$ ratios has been photolysed in the $\tilde{A}$–$\tilde{X}$ transition using a narrow-band-width, frequency-doubled, pulsed dye laser. At specific excitation wavelengths, chosen by absorption spectroscopy, the product nitrogen is enriched in ^{15}N, a maximum enrichment factor of 4.8 being attained. The initial isotopic selectivity of excitation is largely retained in the nitrogen product, even though the primary photodissociation forms free radicals and N_2 is formed only after a sequence of secondary reactions. Quantum yields of nitrogen and hydrogen formation have been measured at very low conversions as a function of the time of irradiation. The initial yield of nitrogen appears to be zero and that of hydrogen 0.25.

P. A. HACKETT, R. A. BACK et S. KODA. Can. J. Chem. **56**, 2981 (1978).

On a utilisé un laser à colorant en mode déclenché, de largeur de bande spectrale étroite et doublé en fréquence pour photolyser de l'ammoniaque-d_3 dans la transition $\tilde{A}$–$\tilde{X}$ pour divers rapports $^{14}N/^{15}N$. A certaines longueurs d'ondes d'excitation, choisies d'après le spectre d'absorption, le produit est enrichi en ^{15}N et le facteur d'enrichissement maximum est 4.8. La sélectivité isotopique initiale est presque complètement retenue par le produit azoté même si N_2 n'est produit qu'après une suite de réactions secondaires impliquant les radicaux libres formés dans la photodissociation primaire. On a mesuré les rendements quantiques de formation d'azote et d'hydrogène à très faible niveau de décomposition en fonction des temps d'irradiation. Le rendement quantique initial d'azote est nul et celui de l'hydrogène est 0.25.

Introduction

The identification and characterization of photochemical systems useful for isotope separation is of much immediate interest. Most attention has been paid to infrared multiphoton decomposition and to simple ultraviolet photolysis, although a variety of more complicated 2- or 3-photon schemes have also been studied or proposed. For successful isotope separation by a simple one-photon uv photolysis, the lifetime of the excited state must fall within rather narrow limits. It must be short enough that the quantum yield of decomposition is high, but not so short that the line width of the absorption spectrum is so broadened that optical isotopic selectivity is lost. The photolysis of formaldehyde meets these requirements almost ideally, but few other systems have been successfully demonstrated. The ammonia photolysis (1) provides an example of an excited-state lifetime that is too short; the predissociation broadens the spectrum so much that ^{14}N–^{15}N optical selectivity is completely lost; the NH_3–NDH_2 selectivity is reduced to a maximum value of about 10, and even this modest selectivity would probably be lost in secondary reactions that lead to H–D exchange in the products (2). In ammonia-d_3, however, the predissociation is appreciably slower and the spectrum sharper, showing resolved rotational structure in bands corresponding to the first two vibrational levels of the excited state (3). There appears to be sufficient optical selectivity to permit a useful ^{14}N–^{15}N separation if it is retained in the secondary reactions following dissociation. The present paper describes a study of this isotope separation system.

Experimental

Ammonia-d_3 (99% D, natural abundance $^{14}N/^{15}N$) and $^{15}ND_3$ (98% ^{15}N, 99% D) were obtained from Merck, Sharp and Dohme of Canada Ltd., and were used without further purification. Research grade propane (Matheson) was used without further purification as glc analysis showed negligible olefin content.

High resolution absorption spectra of both ammonias were obtained in the first order of the spectrograph previously described (4). The pathlength was 10 cm, pressures varied from several to several hundred Torr, and temperatures from ambient to 400°C. Line positions were obtained by comparison to lines of a copper arc and band origins were determined by graphical methods.

Following the photographic survey of the absorption spectra, a Molectron DL200 dye laser equipped with potassium pentaborate frequency doubling crystals and pumped by a Molectron UV 1000 pulsed nitrogen laser was used to obtain quantitative absorption spectra in those specific spectral regions where optical selectivity could be expected. The spectra were obtained by comparing the output of two Hammamatsu R788 solar blind photodiodes in a logarithmic ratiometer. One diode monitored a portion of the incident laser intensity, the other monitored the intensity transmitted through a 10 cm

[1]NRCC No. 16977.

[2]Present address: Department of Reaction Chemistry, Faculty of Engineering, University of Tokyo, Hongo, Bunkyo-ku, Tokyo 113, Japan.

Can. J. Chem. Downloaded from www.nrcresearchpress.com by 210.87.254.5 on 09/05/12
For personal use only.

Can. J. Chem. Downloaded from www.nrcresearchpress.com by 210.87.254.5 on 09/05/12
For personal use only.

TABLE 1. ^{14}N, ^{15}N isotope shifts in the $\tilde{A}$–$\tilde{X}$ absorption spectrum of ammonia-d_3

Band	$\nu_0(^{14}ND_3)/cm^{-1}$	$\Delta\nu_0(^{15}N—^{14}N)/cm^{-1}$	$\nu_0(^{14}ND_3)/cm^{-1}$*
$01–00^-$	47 367.05	−4.7	47 367.35
$01–01^-$	46 618.17	+1.37	46 617.88
$01–02^-$	45 937.6	+7.4	45 937.0
$01–04^-$	44 496.4	+27.7	—
$00–00^+$	46 714.3	+1.0	46 713.8
$00–01^+$	45 969.1	+7.7	45 967.4
$00–02^+$	45 355.1	+10.1	45 355.1
$00–03^+$	44 887.7	+15.7	44 887.1

*From ref. 3.

long thermostated cell containing the sample. As the wavelength of the dye laser was scanned, the angle of the frequency doubling crystal was adjusted by a stepping motor locked to the diffraction grating stepping motor through a digital frequency divider. Optimum wavelengths and temperatures to selectively excite $^{15}ND_3$, and the numerical value of this selectivity were determined with this system. The effective linewidth of the ultraviolet laser radiation was estimated by using the system to measure the apparent widths of isolated lines in the (0,0) band of the $A^2\Sigma^+ \leftarrow X^2\Pi$ absorption system of nitric oxide, known to be much narrower than the laser linewidth.

Photolyses were then carried out at 300 Torr pressure of ND_3 in cylindrical quartz cells 10 cm long and 2 cm in diameter with a volume of 46 cm^3, with the laser tuned to an optimum wavelength. After irradiation, ND_3 and N_2D_4 were condensed at −196°C, and the residual pressure of noncondensable gases measured by a sensitive capacitance manometer connected to the cell. These gases were then removed and their composition determined by removing D_2 through a hot palladium thimble and measuring the residual pressure of N_2. The ND_3 and N_2D_4 were then returned to the reaction vessel for further irradiation. Repeated irradiation of the same sample in this way, with irradiation times typically from 5 to 20 min, gave measurements of product yields as a function of total irradiation time. These yields were converted to absolute quantum yields by comparison with the amount of hydrogen produced in the presence of 300 Torr of propane used as a hydrogen atom scavenger ($\Phi_{H_2} = 1$) (2).

The isotopic composition of the product nitrogen was determined in a separate series of experiments. All quartz reaction vessels, equipped with break-seals, and flamed before filling with mixtures of $^{14}ND_3$ and $^{15}ND_3$, were used. The ^{15}N content varied from natural abundance to equimolar and the pressure was 1200 Torr, enough to ensure complete absorption of the ultraviolet radiation in all samples. After irradition noncondensable gases were analysed in a Hitachi-Perkin Elmer RMU-60 mass spectrometer, by observing the peaks *m/e* 28, 29, and 30. The ratios of these peaks were independent of the electron energy (70–20 eV). The isotopic content of the starting mixtures was determined by complete decomposition of a small sample of each by Tesla discharge at low pressure, and subsequent mass spectral analysis of the N_2 product.

Results and Discussion

Each band of $^{15}ND_3$ showed a small isotope shift in the band origin, when compared to the data Douglas (3) on $^{14}ND_3$. The rotational structure of the bands was completely unchanged, however. This is not unreasonable as the upper state is planar, and the ground-state constants C'' for the two species are equal whilst B'' differs only by 0.37%. The observed isotope shifts are tabulated in Table 1.

At first sight, because the bands with $v_2' = 1$ are sharper than those with $v_2' = 0$ (linewidths 0.8 and 2.5 cm^{-1} respectively (3)), better optical selectivity might be expected in the former. However, such ($01–0m^-$) bands are overlapped by the tails of the P and Q branches of the ($00–0m^+$) bands as was seen in a previous study in which high resolution emission spectroscopy showed that the cadmium resonance line at 2144 Å excites both Q(1) of the $01–01^-$ band and P(8) of the $00–00^+$ band (4). The selectivity may be further affected by other sequence bands, by absorption due to the 3% ND_2H present, and perhaps by the weak underlying continuum postulated by Gregory and Lipsky (5). These facts, together with the non-negligible linewidth of the dye laser (1.4 cm^{-1}) made it essential to determine empirically the best wavelengths for selective excitation from the laser absorption spectrum. The best region found for optical selectivity is illustrated in Fig. 1. For excitation near the Q head of the $00–02^+$ band, at 220.39

ERRATA Fig. 2 appears above the caption for Fig. 1

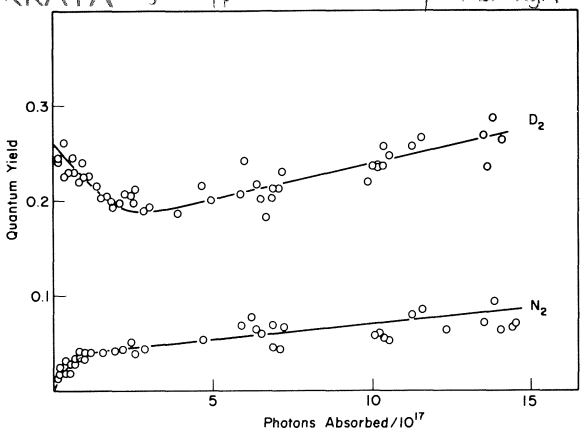

FIG. 1. Laser absorption spectrum of ammonia-d_3. The solid lines refer to $^{14}ND_3$, the dashed line to $^{15}ND_3$. The insert shows a complete spectrum of the band. Band and line assignments for $^{14}ND_3$ were taken from ref. 3 and used as wavelength calibration points. The arrow indicates a region where selective excitation of $^{15}ND_3$ is possible.

TABLE 2. Isotopic content of nitrogen produced in the laser photolysis of ammonia-d_3 at $\lambda_{ex} \simeq 220.39$ nm

Run No.	Initial % ^{15}N	*m/e* peak height I^{28}	I^{29}	I^{30}	Final % ^{15}N	α_1*	α_2†
1	47.5	0	20	120	93	—	13.3
2	0.40	400	13	0	1.7	4.4	—
3	0.40	90	3	0	1.61	4.5	—
4	47.5	0	17	26	80.2	—	3.4
5	32.0	12	56	63	69.0	5.0	4.8
6	15.8	470	730	381	47.2	4.1	5.6
7	23.8	300	910	675	60.0	4.9	4.8

*$\alpha_1 = I^{29}(100 - \text{initial}\%\ ^{15}N)/(2 \times I^{28} \times \text{initial}\%\ ^{15}N)$.
†$\alpha_2 = 2 \times I^{30}(100 - \text{initial}\%\ ^{15}N)/(I^{29} \times \text{initial}\%\ ^{15}N)$.

nm a maximum optical selectivity of 5.18 was obtained at room temperature.

Photolysis at this wavelength yielded N_2 with the isotopic composition given in Table 2. Typically, ultraviolet pulse energies in these experiments were 5×10^{-6} J, pulse repetition rates 10 Hz, and photolysis times 3 h. Conversions were about 0.04%, so that the isotopic composition of the nitrogen product should represent an initial value for the selectivity of the overall photolysis process. It is well established that the initial reactions in the photolysis are:

[1] $$ND_3 + h\nu \rightarrow ND_2 + D$$

[2] $$2ND_2 \xrightarrow{M} N_2D_4$$

[3] $$D + ND_2 \xrightarrow{M} ND_3$$

[4] $$2D \xrightarrow{M} D_2$$

It is generally agreed that N_2 arises from subsequent secondary reactions of N_2D_4 with ND_2 and D, although the precise mechanism is not clear. The average enrichment observed in the N_2 product ($\alpha = 4.5$) is only slightly less than the selectivity of excitation (5.2), which implies that there is little loss of selectivity in the transformation of the initial photofragment ND_2 into the final product nitrogen. Thus exchange of nitrogen atoms between hydrazine and ammonia, and the reaction

[5] $$^{15}ND_2 + {}^{14}ND_3 \rightarrow {}^{15}ND_3 + {}^{14}ND_2$$

or the reaction of D atoms with ammonia

[6] $$D + {}^{14}ND_3 \rightarrow D_2 + {}^{14}ND_2$$

must be unimportant in the present system. This bodes well for the practical separation of nitrogen isotopes by the ammonia photolysis, although the relatively low value of α would require at least 5 stages to achieve a useful enrichment of ^{15}N starting from natural abundance ND_3. However, it may now be worthwhile to exploit the ir-activated hot band

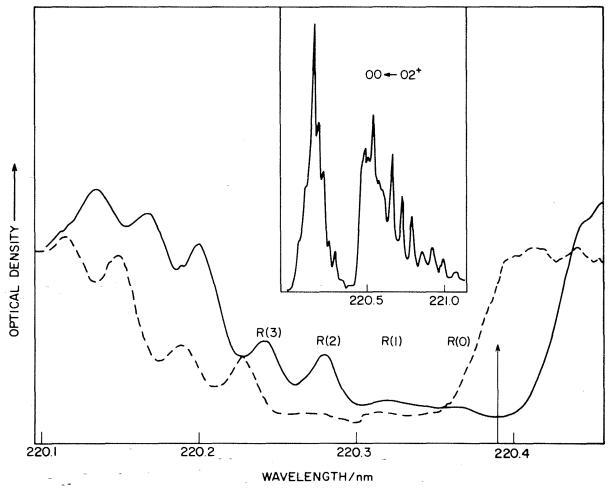

FIG. 2. Dose-dependent quantum yields in the laser photolysis of ammonia-d_3, $\lambda_{ex} \simeq 220.5$ nm.

ERRATA Fig 1 appears above the caption for Fig. 2.

photolysis of ND_3 (6) with the prior knowledge provided by this study that the secondary chemistry retains selectivity.

The time-dependent quantum yields shown in Fig. 2 deserve some comment. The yield of N_2 appears to approach zero at zero time, confirming previous conclusions that N_2 was formed from secondary reactions of hydrazine. The experimental accuracy permits an upper limit for the reaction

[7] $$2ND_2 \rightarrow N_2 + 2D_2$$

a suggested primary source of N_2, of about 5% of reaction [2]; there is no positive evidence that it occurs at all (7, 8).

The initial quantum yield of D_2 reflects the competition between the combination reactions [2], [3], and [4], and the value of about 0.25 suggests an almost statistical ratio of 1:2:1 for the three reactions. Estimates of rates of diffusion and radical lifetimes in the system indicate that these reactions should have been complete within the laser beam

Can. J. Chem. Downloaded from www.nrcresearchpress.com by 210.87.254.5 on 09/05/12
For personal use only.

(diameter 4 mm) and the observed ratio should correspond to homogeneous surface-free reaction

As hydrazine accumulates in the system, the yield of N_2 rises and that of D_2 falls. Reactions involved initially must be

[8] $$D + N_2D_4 \rightarrow D_2 + N_2D_3$$

and

[9] $$ND_2 + N_2D_4 \rightarrow ND_3 + N_2D_3$$

followed by further reactions of N_2D_3 and perhaps other transient intermediates, leading finally to formation of N_2, D_2, and some regeneration of ND_3 in a mechanism that has not yet been fully delineated. Reaction [8] by itself would enhance the yield of D_2, and the observed decrease implies that loss of D atoms in other reactions, probably with N_2D_3, must more than compensate for reaction [8]. As hydrazine concentration builds up further, however, reaction [8] will begin to predominate, and the yield of D_2 will increase again as observed. If enough N_2D_4 were present, the yield of D_2 would become unity; this is stoichiometrically impossible in the present system, and the final value of the D_2 yield when N_2D_4 has reached its steady state will depend on a complex competition between reactions [1], [2], [3], [8], and [9] subsequent further reactions of N_2D_3 and other species. The same competition will also control the final quantum yield of nitrogen which in the steady state must be 1/3 that of D_2. The data in Fig. 2 indicate a final value of about 0.1, so that conversion of the photofragment ND_2 into N_2 is only about 20% efficient.[3] This suggests the use of a scavenger for ND_2 to improve yields for isotope separation. Possible scavengers are O_2, to take advantage of the reaction sequence

[10] $$ND_2 + O_2 \xrightarrow{\text{slow}} NO + D_2O$$

[11] $$ND_2 + NO \xrightarrow{\text{fast}} N_2 + D_2O$$

or ^{15}NO, using reaction [11] alone, which Srinivasan has shown retains selectivity for nitrogen atoms (10). Both systems look promising but might be complicated by reactions of DNO and DO_2 formed from reactions of D with NO and O_2.

In summary, we have demonstrated separation of nitrogen isotopes by simple photolysis of ND_3 at 220.39 nm. The chemistry is clean and the optical selectivity is largely retained in the N_2 product. The separation factor of about 4.5 is limited chiefly by the linewidth of the absorption spectrum, and little improvement can be expected. The quantum yield of N_2 of about 0.1 could probably be improved by suitable scavengers.

Acknowledgements

We would like to thank Dr. A. Douglas of the Herzberg Institute of Astrophysics for the use of the spectrograph and Dr. C. Willis of the Division of Chemistry for many helpful discussions.

1. J. R. McNesby and H. Okabe. Adv. Photochem. **3**, 157 (1964), and references therein.
2. S. Koda and R. A. Back. Can. J. Chem. **55**, 1380 (1977).
3. A. Douglas. Discuss. Faraday Soc. **35**, 158 (1963).
4. P. A. Hackett, R. A. Back, and S. Koda. J. Chem. Phys. **65**, 5103 (1976).
5. T. A. Gregory and S. Lipsky. J. Chem. Phys. **65**, 5469 (1976).
6. R. V. Ambartzumian, V. S. Letokhov, G. N. Makarov, and A. A. Puretskii. Zh. Eksp. Teor. Fiz. Pis'ma Red. **15**, 709 (1972).
7. C. Willis, A. W. Boyd, and A. O. Miller. Can. J. Chem. **47**, 3008 (1969).
8. P. V. Khê, J. C. Soulignac, and R. Lesclaux. J. Phys. Chem. **81**, 210 (1977).
9. W. E. Groth, U. Schurath, and R. N. Schindler. J. Phys. Chem. **72**, 3914 (1968).
10. R. Srinivasan. J. Phys. Chem. **4**, 679 (1960).

[3]Values of $\Phi_{N_2} = 0.18$ have been reported for absorbed doses greater than 10^9, see ref. 9.

Can. J. Chem. Downloaded from www.nrcresearchpress.com by 210.87.254.5 on 09/05/12
For personal use only.

Radical ions in photochemistry. 6. The photosensitized (electron transfer) ring opening of aryloxiranes[1]

ANGELO ALBINI[2] AND DONALD R. ARNOLD[3]

Photochemistry Unit, Department of Chemistry, University of Western Ontario, London, Ont., Canada N6A 5B7

Received May 17, 1978

ANGELO ALBINI and DONALD R. ARNOLD. Can. J. Chem. **56**, 2985 (1978).

The photosensitized (electron transfer) irradiation of *cis*- and *trans*-2,3-diphenyloxirane (**1** and **2**) led to cleavage of the oxirane carbon–carbon bond and subsequent formation of the carbonyl ylide. The resulting carbonyl ylides have been trapped with the dipolarophiles, acrylonitrile, maleonitrile, and fumaronitrile. The resulting isomeric tetrahydrofuran derivatives have been characterized. Sensitizers (electron acceptors) which are effective include 1,4-dicyanonaphthalene, 1,4-dicyanobenzene, dimethyl terephthalate, and methyl 4-cyanobenzoate; 1-cyanonaphthalene was not effective. The proposed mechanism involves formation and cleavage of the oxirane radical cation followed by back electron transfer from the sensitizer radical anion to give the carbonyl ylide. Electrochemical and photophysical evidence which supports the proposed mechanism was obtained.

ANGELO ALBINI et DONALD R. ARNOLD. Can. J. Chem. **56**, 2985 (1978).

L'irradiation photosensibilisée (transfert d'électron) du *cis*- et du *trans*-diphényl-2,3 oxiranne (**1** et **2**) a conduit au clivage de la liaison carbone–carbone de l'oxiranne et la formation subséquente de l'ylure de carbonyle. Les ylures de carbonyle ont été piégés au moyen des dipolarophiles acrylonitrile, maléonitrile et fumaronitrile. On a obtenu des dérivés isomères du tétrahydrofuranne qu'on a caractérisés. Au nombre des sensibilisateurs (accepteurs d'électrons) qui sont efficaces, citons le dicyano-1,4 naphtalène, le dicyano-1,4 benzène, le téréphtalate de diméthyle et le cyano-4 benzoate de méthyle; le cyano-1 naphtalène était inefficace. Le mécanisme proposé implique la formation et le clivage du cation radicalaire oxiranne, puis le transfert d'électron depuis l'anion radicalaire du sensibilisateur pour donner l'ylure de carbonyle. On a obtenu des indices de nature électrochimique et photophysique qui appuient le mécanisme proposé.

[Traduit par le journal]

Introduction

We recently reported the photosensitized (electron transfer) cleavage of acyclic β-phenethyl ethers (1*b*); a typical example is shown in reaction [1].

$$[1]\quad (C_6H_5)_2CHCH_2{-}O{-}CH(CH_3)_2 + CH_3OH \xrightarrow[CH_3CN]{h\nu,\ \text{sensitizer}} (C_6H_5)_2CH_2 + CH_3OCH_2OCH(CH_3)_2$$

sensitizer = 1,4-dicyanonaphthalene
(1-cyanonaphthalene was *ineffective*)

The proposed mechanism for this reaction involves electron transfer from the ether to the excited singlet state of the sensitizer. The ether radical cation then cleaves in the direction which yields the more stable fragments; in this case the diphenylmethyl radical and the α-oxycarbonium ion. The radical is then reduced to the anion by the radical anion of the sensitizer. Protonation of the anion and reaction of the α-oxycarbonium ion with alcohol then account for the observed products.

Since aryloxiranes can be viewed as β-arylethyl ethers is seemed reasonable to expect this type of reaction could be used to cleave these compounds as well. If the reaction takes an analogous course, a useful technique for generating the corresponding carbonyl ylides would result. Carbonyl ylides have been produced from aryloxiranes by both direct (2) and sensitized (triplet–triplet transfer) (3) irradiation, as well as by thermal (4) activation, but there are no examples which have been recognized as involving the photosensitized (electron transfer) process.

In this paper we report (*1*) the *cis–trans* isomerization of the 2,3-diphenyloxiranes by photosensitization (electron transfer); (*2*) the preparation and characterization of the isomeric tetrahydrofuran derivatives which result from the cycloaddition of the carbonyl ylides, generated by the photosensitized (electron transfer) cleavage of the 2,3-diphenyloxiranes, to acrylo-, maleo-, and fumaronitrile; and (*3*) an analysis of photophysical and electrochemical data which support the radical ion mechanism for carbonyl ylide formation.

[1]Contribution No. 188 from the Photochemistry Unit. Part 5 of this series is ref. 1*a*.

[2]On leave (1977) from the Istituto di Chimica Organica dell' Università di Pavia, Pavia, Italy.

[3]To whom correspondence should be addressed.

Can. J. Chem. Downloaded from www.nrcresearchpress.com by 210.87.254.5 on 09/05/12
For personal use only.

Can. J. Chem. Downloaded from www.nrcresearchpress.com by 210.87.254.5 on 09/05/12
For personal use only.

TABLE 1. The photosensitized (electron transfer) isomerization of *cis*- and *trans*-2,3-diphenyloxirane (**1** and **2**)

Sensitizer[a]	Solvent	Composition at equilibrium (**1**:**2**)
1,4-Dicyanonaphthalene (DCN)	Acetonitrile	0.22
1,4-Dicyanonaphthalene (DCN)	Methanol	0.25
1,4-Dicyanonaphthalene (DCN)	Benzene	0.28
1,4-Dicyanobenzene (DCB)	Acetonitrile	0.19
Dimethyl terephthalate (DMT)	Acetonitrile	0.21
Methyl 4-cyanobenzoate (MCB)	Acetonitrile	0.20
Acetone[b]	Acetonitrile	0.22
1-Cyanonaphthalene (MCN)	Acetonitrile	No isomerization
2-Acetonaphthone[c]	Acetonitrile	No isomerization
1,4-Dimethoxynaphthalene	Acetonitrile	No isomerization
Benzophenone[c]	Acetonitrile	No isomerization

[a]The initial concentration of **1** or **2** was 0.15 *M* and the sensitizer concentration was $1–2 \times 10^{-2}$ *M* unless otherwise noted. A Pyrex filter which absorbed wavelengths < ca. 290 nm was used.
[b]2 *M* in sensitizer.
[c]4×10^{-2} *M* in sensitizer.

Results

cis and *trans*-2,3-Diphenyloxirane (**1** and **2**) were prepared by oxidation of the isomeric stilbenes with 3-chloroperbenzoic acid (5). The isomerization of **1** and **2** was studied as a function of sensitizer and solvent. The ratio of isomers was determined by vapor phase chromatography (vpc) and, in those cases where isomerization was observed, the same ratio was obtained starting with either isomer.

Secondary reactions which consume **1** and **2** were relatively minor (<5%), during the irradiation time required to reach equilibrium when acetonitrile or benzene was the solvent. The oxiranes were not stable to prolonged irradiation in methanol (2*b*); however, isomerization was observed. The sensitizer was almost totally recovered in every case. These results are summarized in Table 1.

[2] 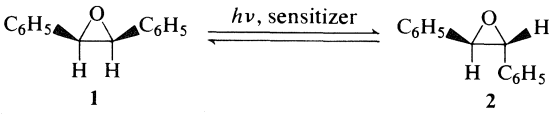

sensitizer = 1,4-dicyanonaphthalene (DCN), 1,4-dicyanobenzene (DCB), dimethyl terephthalate (DMT), methyl 4-cyanobenzoate (MCB), and acetone; 1-cyanonaphthalene (MCN) was ineffective.

The sensitized (electron transfer) irradiation of **1** and **2** in the presence of acrylonitrile leads to the formation of the tetrahydrofuran derivatives **3***a*, *b* and **4***a*, *b* (reaction [3]). All four possible isomeric products have been isolated and characterized. The yields reported in Table 2 were determined by vpc and were in fair agreement with isolated yields following column chromatography. The formation of the cycloaddition products effectively competes with the isomerization of **1** and **2** since little or no isomeric oxirane was observed during the course of the irradiation.

The total yield of adducts was essentially quantitative when 1,4-dicyanonaphthalene was the sensitizer. The ratio of isometric products was not the same starting with **1** or **2**. The ratio of products was also different when acetone was used as sensitizer and when the oxiranes were excited by direct irradiation; however, since the material balance was low in these cases it is more difficult to attach significance to the observed variation. The ratios of products under these different conditions are summarized in Table 2.

The sensitized (electron transfer) irradiation of **1** and **2** in the presence of maleonitrile (**5**) or fumaronitrile (**6**) likewise leads to formation of the analogous tetrahydrofuran derivatives (reaction [4]). In this case, there are six possible isomers and all of them have been isolated and characterized. The configuration of the products now depends upon the configuration of both the oxirane and the dinitrile. These results are summarized in Table 3.

The gross structures assigned to the tetrahydrofurans were based on their spectroscopic (ir and nmr), chemical properties, and elemental analysis. The stereochemical assignments (ignoring chirality) rest largely on the nmr spectral data. Proton–proton coupling constants could not be used since the tetrahydrofuran ring can assume various conformations and the differences between *cis* and *trans* vicinal coupling is not large (4*c*). An analysis of the observed chemical shift data does, however, provide sufficient evidence (Table 4).

Considering first the mono cyano derivatives, the relationship between **3***a* and **3***b* and between **4***a* and **4***b* was established by equilibrating these isomeric pairs upon treatment with base. At equilibrium **3***b*

Can. J. Chem. Downloaded from www.nrcresearchpress.com by 210.87.254.5 on 09/05/12
For personal use only.

TABLE 2. The yields of cycloadducts obtained upon irradiation of **1** or **2** in the presence of acrylonitrile[a]

Oxirane	Sensitizer	Yield 3*a*	3*b*	4*a*	4*b*	Total yield of adducts
1	None[b]	11	10	1	1	23
2	None[b]	2	1	12	10	25
1	DCN	47	40	6	7	ca. 100
2	DCN	38	32	16	16	ca. 100
1	Acetone	25	21	5	6	57
2	Acetone	12	10	10	10	42

[a]Typical conditions were oxirane (0.15 *M*) and sensitizer (DCN 2×10^{-2} *M*; acetone 2 *M*) and acrylonitrile (1 *M*) in acetonitrile solution. Irradiation was through a Pyrex filter. The yields (%) were determined by vpc.
[b]Irradiation through quartz.

TABLE 3. The yields of cycloadducts obtained upon photosensitized (electron transfer) irradiation of **1** and **2** in the presence of maleonitrile (**5**) and fumaronitrile (**6**)[a]

Oxirane	Dinitrile	Yield 3*c*	3*d*	3*e*	4*c*	4*d*	4*f*	Total yield of adducts
1	**6**		87			7	5	ca. 100
2	**6**		75			16	12	ca. 100
1	**5**	53		35	9			97
2	**5**	42		28	21			91

[a]Typical conditions were oxirane (0.15 *M*), dinitrile (0.4 *M*), and 1,4-dicyanonaphthalene (2×10^{-2} *M*) in acetonitrile. Irradiation was through a Pyrex filter. Yields (%) were determined by vpc and were in fair agreement with isolated yields.

and **4***b* predominate (ca. 90%) providing evidence that these are the less hindered isomers where the vicinal phenyl and cyano groups are *trans*. This assignment is consistent with the nmr spectra which show the proton on the carbon bearing the cyano group of **3***b* and **4***b* absorbs at higher field than for **3***a* and **4***a*. Protons *cis* to a vicinal phenyl group in a five-membered ring are well known to appear at higher field (4*c*, 6).

The remaining choice between **3***a*, *b* and **4***a*, *b* cannot be rigorously made from an analysis of the nmr spectra but must rest partially upon the relative product ratios observed from **1** and **2** and reasoning by analogy (see below) with the dicyano derivatives where an unambiguous assignment can be made. However, these assignments are then strengthened by the recognition of a consistent pattern in the nmr spectra of all the isomeric pairs. That is, the protons

[3] **1** or **2** + CH_2=CHCN $\xrightarrow{h\nu \text{ sensitizer}}$ 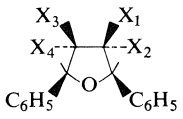 + 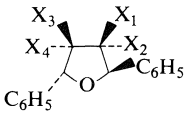

(**3**; phenyl groups *cis*) (**4**; phenyl groups *trans*)

(*a*) X_1 = CN, X_2–X_4 = H
(*b*) X_2 = CN, X_1 = X_3–X_4 = H

[4] **1** or **2** + 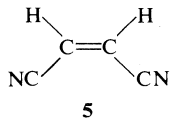 or 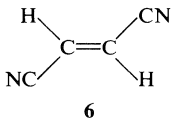 $\xrightarrow{h\nu, \text{ sensitizer}}$

5

6

(*c*) X_1 = X_3 = CN, X_2 = X_4 = H
(*d*) X_1 = X_4 = CN, X_2 = X_3 = H
(*e*) X_2 = X_4 = CN, X_1 = X_3 = H
(*f*) X_2 = X_3 = CN, X_1 = X_4 = H

TABLE 4. Nuclear magnetic resonance spectra of tetrahydrofuran derivatives **3** and **4** (*a–f*)[a]

Compound	H_2	H_5	$X_{1(2)}$	X_3	X_4	$J_{H_2X_{1(2)}}$	$J_{X_{1(2)}X_3}$	$J_{X_{1(2)}X_4}$	$J_{X_3X_4}$	$J_{X_3H_5}$	$J_{X_4H_5}$
3*a*	5.1 d	5.0 dd	3.55 m	2.3 m	2.85 m	6.8	5.8	9	12.7	5	7
3*b*	5.08 d	5.15 dd	2.95 m	2.3 m	2.67 m	7.7	10.2	6	12	7.6	7.6
4*a*	5.4 d	5.6 dd	3.55 m	2.9 m	2.4 m	5.7	3.2	7	12.7	6.8	8.1
4*b*	5.35 d	5.36 dd	3.14 m	2.93 m	2.42 m	8.2	7.2	10.4	12	6	9.2

Compound	H_2	H_5	$X_{1(2)}$	$X_{3(4)}$	$J_{H_2X_{1(2)}}$	$J_{X_{1(2)}X_{3(4)}}$	$J_{X_{3(4)}H_5}$	$J_{H_2X_{3(4)}}$
3*c*[b]	5.33 dd		4.25 dd		4.5			2
3*d*	5.32 d	5.15 d	3.85 dd	3.37 dd	6.5	5.5	7.8	
3*e*	5.31 dd		3.38 dd		5.5			2.5
4*c*	5.69 d	5.53 d	3.51 dd	3.9 dd	8.8	6.5	5.3	
4*d*[b]	5.85 dd		4.28 dd		7.5			2
4*f*	5.47 dd		3.51 dd		5.8			2.5

[a]Chemical shifts (δ ppm) from tetramethylsilane internal, standard coupling constants in Hz. Deuterochloroform solution unless noted otherwise.
[b]Deuteroacetonitrile solution.

on carbon 2 and 5 absorb at considerably lower field when the phenyl groups are *trans* to one another (i.e. **4***a–f*).

While this work was in progress the methyl esters analogous to **3***a*, *b* and **4***a*, *b* were characterized (3*c*). The nmr spectra of the esters are similar to those of the nitriles and the reported structural assignments are consistent.

The stereochemical assignments for the dicyano derivatives **3***c–e* and **4***c*, *d*, and *f* were similarly established from an analysis of their nmr spectra (Table 4). The symmetric isomers were easily distinguished by the A_2B_2 proton coupling pattern. As previously mentioned, protons in the 3 and 4 positions absorb at higher field if they are *cis* to the vicinal phenyl group.

Some electrochemical and photophysical experiments were carried out in order to provide data relevant to the discussion of the proposed electron transfer mechanism for the oxirane ring opening process. The oxidation potentials of **1** ($E_{1/2}^{ox}$ = 1.88 V vs. $Ag/AgNO_3$ in acetonitrile) and **2** (1.89 V) were estimated from cyclic voltammetry measurements. The anodic oxidation process was not reversible (100 mV s^{-1} sweep rate) and so the derived oxidation potentials do not have thermodynamic significance. Nevertheless, reactivity correlations using such data have been shown to be useful (1).

TABLE 5. Fluorescence quenching of 1,4-dicyanonaphthalene (DCN) and 1-cyanonaphthalene (MCN) by **1** and **2** in acetonitrile solution at 20°C

Fluorophore	τ (ns)[a]	Quencher	k_q (s^{-1} M^{-1})
DCN	10.06	**1**	0.98×10^{10}
DCN		**2**	1.16×10^{10}
MCN	8.92	**1**	$< 3 \times 10^{7}$[b]
MCN		**2**	$< 3 \times 10^{7}$[b]

[a]Reference 1*b*.
[b]No decrease (< 2%) in fluorescence intensity was observed with a concentration of **1** or **2** > 0.05 *M*.

Fluorescence quenching studies were performed in order to determine the excited state multiplicity involved in the sensitization process. The fluorescence quenching rate constants were determined from the Stern–Volmer plots of fluorescence intensity versus the concentration of **1** and **2**, and the measured fluorescence lifetime of the sensitizer. These observations are summarized in Table 5.

Discussion

The mechanism we propose for reactions [2]–[4] is summarized in Scheme 1. The first step, excitation of the sensitizer, is assured through the use of a light filter (Pyrex) which prevents direct excitation of the oxiranes. Neither **1** nor **2** absorb at wavelengths longer than 280 nm (0–0 band at 272 nm) (7).

Direct excitation is not occurring since when the oxiranes **1** and **2** are excited by direct irradiation, the major product along with the stereoisomerization is deoxybenzoin which results from cleavage of the carbon–oxygen bond (3*c*). In the reactions reported here, using effective photosensitizers (electron transfer), no deoxybenzoin was detected and the yields of products derived from carbon–carbon bond cleavage were essentially quantitative.

Step *2* leads from the excited singlet state of the photosensitizer to the oxirane radical cation. It seems likely that several intermediate stages (e.g. collision encounter complex, exciplex, radical ion pair) are involved during the electron transfer process; however, we have no evidence for this view. The energy associated with this electron transfer process, within an encounter complex, can be estimated from eq. [5] originally used by Weller and co-workers to correlate fluorescence quenching results (8).

$$[5]\quad \Delta G(\text{kcal mol}^{-1}) = 23.06[E(D/D^+)_V - E(A/A^-)_V - e_0^2/\varepsilon\alpha] - \Delta E_{0-0}(\text{kcal mol}^{-1})$$

The quantity in brackets (the oxidation poten-

Can. J. Chem. Downloaded from www.nrcresearchpress.com by 210.87.254.5 on 09/05/12
For personal use only.

Can. J. Chem. Downloaded from www.nrcresearchpress.com by 210.87.254.5 on 09/05/12
For personal use only.

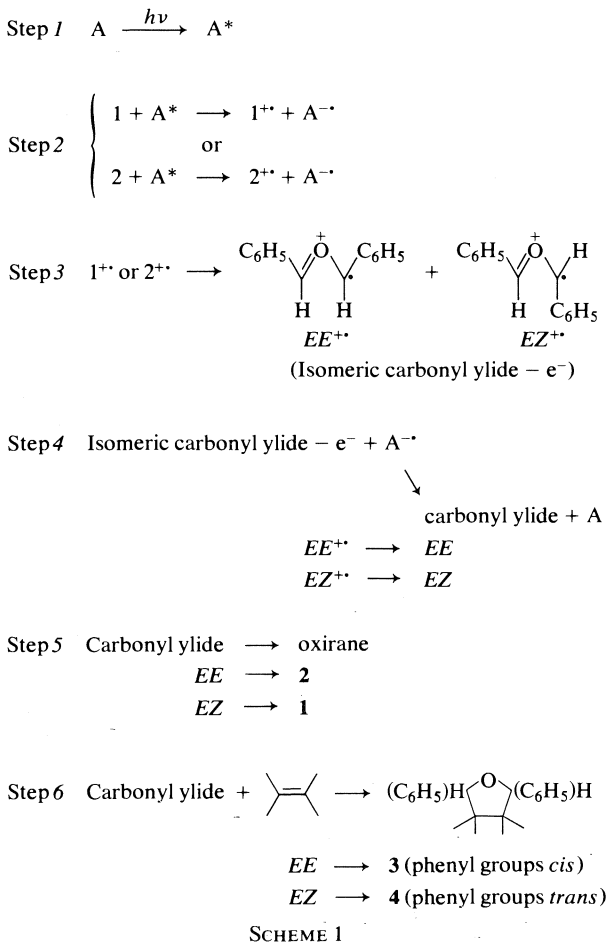

SCHEME 1

tial of the donor, the reduction potential of the acceptor, and a Coulombic attraction term) represents the energy required for the electron transfer process, while the energy available is the sensitizer singlet (or triplet) energy. With the exception of the oxidation potentials of **1** and **2** the necessary data were available in the literature. We therefore determined the required oxidation potentials of **1** and **2** using cyclic voltammetry. The calculated free-energy change (ΔG) for the electron transfer process between **1** and the singlet and triplet states of several potential sensitizers are listed in Table 6. Note that for DCN, DCB, and MCB, all effective sensitizers, the calculated energy for the electron transfer involving the sensitizer singlet is favorable; while for MCN, an ineffective sensitizer, the calculated ΔG is positive.

Fluorescence quenching studies confirm that the sensitizer singlet is the excited state involved. The fluorescence of DCN was quenched by **1** and **2** at almost the diffusion-controlled rate,[4] while the fluorescence of MCN was not measurably quenched by either **1** or **2**.

The ring cleavage of **1** and **2** photosensitized by acetone has recently been reported and was attributed to triplet–triplet transfer (3*c*). This explanation still seems reasonable since the electron transfer process with the acetone singlet or triplet is, according to eq. [5], so unfavorable. Furthermore, triplet–triplet transfer is conceivable because of the relatively high triplet energy of acetone.

It is unlikely that the triplet of DCN, DCB, or MCB could be effective by either the electron transfer process or by triplet–triplet transfer. The calculated free-energies for the electron transfer process involving the sensitizer triplet are positive in every case, and the triplet energies of these sensitizers are undoubtedly too low since acetophenone, with a higher triplet energy (E_T = 72 kcal mol^{-1}), was ineffective (3*c*).

Two additional considerations consistent with the lack of involvement of the triplet in the case of DCN are pertinent. 1,4-Dicyanonaphthalene has a very inefficient intersystem crossing process yet it is an efficient sensitizer. Furthermore, if its triplet were involved we would have observed competitive photosensitized isomerization of maleonitrile and fumaronitrile in those experiments where these dinitriles were present since the isomerization of these dinitriles can be brought about with sensitizers having a triplet energy as low as 49 kcal mol^{-1} (9). In fact, no isomerization of the dinitriles was observed during the course of reaction [4].

Before leaving the discussion of step *2*, Scheme 1, it will be important later on that we consider where the electron is coming from during the electron transfer process; that is, should the oxirane radical cation be viewed largely as an aryl radical cation or as an oxirane (i.e. ether) radical cation? The currently accepted view of aryl substituted three-membered rings maintains there is some conjugative interaction involving the strained ring bonds (Walsh orbitals) and the π-electron system (10). However, from the similarity in the oxidation potential of **1** and **2** and the value we reported (1*b*) for 2,2-diphenylethyl isopropyl ether ($E_{1/2}^{ox}$ = 1.81 V), in connection with our study of reaction [1], we can conclude that any interaction between the phenyl and the oxirane moiety is not evident from the cyclic voltammagrams. Furthermore, the similar distinction between effective (DCN) and ineffective (MCN) sensitizers and the ability of **1**, **2**, and 2,2-diphenylethyl isopropyl ether to quench the fluorescence of DCN but not the fluorescence of MCN indicates that the photosensitized electron transfer process is also insensitive to any interaction between the phenyl group and the oxirane ring which might be present. In our study of

[4]We looked for emission which might have originated from an exciplex in strongly quenched solutions (acetonitrile and benzene solution), however, none was observed.

TABLE 6. Calculated ΔG values, using eq. [5], for the electron transfer process involving the singlet and triplet states of the sensitizer as potential acceptors and **1** ($E_{1/2}^{ox}$ = 1.88 V, Ag/0.1 *M* Ag^+) as donor

Sensitizer	E_s (kcal mol^{-1})[a]	E_T (kcal mol^{-1})[a]	$E_{1/2}^{red}$ (V)[b]	ΔG(S) (kcal mol^{-1})	ΔG(T) (kcal mol^{-1})
1,4-Dicyanonaphthalene (DCN)	86.4	55.5	−1.67	−5.8	+25.1
1,4-Dicyanobenzene (DCB)	97.6	70.1	−2.00	−9.4	+18.1
Methyl 4-cyanobenzoate (MCB)	95.3	72.0	−2.10	−4.8	+18.5
1-Cyanonaphthalene (MCN)	89.4	57.3	−2.33	+6.4	+38.5
Acetone	88[c]	79 (82)[c]	−2.65[d]	+15.2	+24 (+21.2)

[a]Reference 1*b*.
[b]Reduction potential measured versus $Ag/AgNO_3$ (0.1 *M*) in acetonitrile solution (1*b*).
[c]Reference 21.
[d]Reference 22.

reaction [1], we concluded that the electron donated by the ether was in fact from the phenyl moiety (1*b*). The similarities between reaction [1] and reactions [2], [3], and [4] now lead us to suggest that this is also true for **1** and **2**.

There is a recent report which describes the photoaddition of methanol to an aryl oxirane (5) sensitized by ferric ion (reaction [6]) (11).

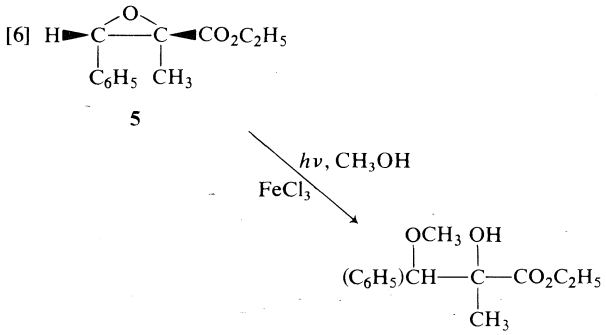

The carbon–oxygen bond of **5** is cleaved in this reaction. It was not possible to detect stereoisomerization of the oxirane since the *Z*-isomer reacted under the reaction conditions even in the dark. The mechanism proposed in this case involves electron transfer from the oxirane moiety to the ferric ion. If this mechanism pertains it seems likely that the ferric ion is in fact partially bonded to the oxygen prior to the cleavage. This would explain the preference for carbon–oxygen bond cleavage. It would obviously be interesting to compare these ferric ion sensitized results with those using DCN.

We next consider step *3* in the proposed Scheme 1, the oxirane ring cleavage process. We first thought of this step as analogous to the previously observed bond cleavage of 2,2-diphenylethyl isopropyl ether (reaction [1]) which in this case would give the isomeric carbonyl ylides $- e^-$. Back electron transfer from the sensitizer anion radical then gives the stereoisomeric carbonyl ylides (step *4*). This simple picture may not be adequate since it ignores the likely possibility that the cleavage process may be influenced by orbital symmetry. It will therefore be of interest to compare the stereochemical behavior of step *3* with the cleavage of **1** and **2** induced by thermal activation, by direct irradiation, and by photosensitization (triplet–triplet transfer).

There are three possible stereoisomeric carbonyl ylides, the *EE*, *EZ*, and the *ZZ* configuration. The *ZZ* isomer must suffer steric repulsion relative to the other isomers and therefore need not be considered. It is known that such isomeric carbonyl ylides are not rapidly equilibrated thermally (4).

The thermal ring cleavage of **1** and **2** requires high temperature (ca. 200°C). There is a strong preference for the orbital symmetry allowed conrotatory ring opening (and closing). This knowledge comes from an elegant study of the *cis–trans* isomerization and the racemization of the optically active *trans*-isomer (12); thermally induced cycloadditions have not been reported with this system; however, 2,3-di(4-nitrophenyl)oxirane has been studied and the carbonyl ylide resulting from conrotatory ring opening has been trapped with dipolarophiles (dimethyl maleate and fumarate) (13).

Direct irradiation of **1** and **2** leads via the orbital symmetry allowed disrotatory opening to the *EE* and *EZ* carbonyl ylides, respectively. Step *6* is well known to occur with retention of stereochemistry in both the carbonyl ylide and the trapping olefin. The direct irradiation of **1** and **2** in the presence of methyl acrylate and maleic anhydride gave the isomeric tetrahydrofurans with stereospecificity as high as 90% (3*c*). In marked contrast the acetone triplet–triplet transfer sensitized ring cleavage gave the same mixture of isomeric tetrahydrofurans from both **1** and **2**.[5] This result can be interpreted in terms of a common intermediate or the relatively rapid equilibration of intermediates preceding the carbonyl ylide (3*c*).

From an analysis of the dependence of the ratio of stereoisomeric products (**3** and **4**) obtained from the

[5]This preliminary communication does not mention if the oxiranes were equilibrated during the irradiation (3*c*).

Can. J. Chem. Downloaded from www.nrcresearchpress.com by 210.87.254.5 on 09/05/12
For personal use only.

Can. J. Chem. Downloaded from www.nrcresearchpress.com by 210.87.254.5 on 09/05/12
For personal use only.

isomeric oxiranes, we conclude that while step *3* does not occur stereospecifically, the isomeric carbonyl ylides $- e^-$ are not formed in equal amounts from **1** and **2** and once formed preserve stereochemical integrity.

With acrylonitrile as the dipolarophile the ratio of (**3***a* + **3***b* : **4***a* + **4***b*) from **1**, divided by this ratio from **2**, is about 3. This factor should be independent of the trapping agent and in fact the observed ratios (2.5 with fumaronitrile and 3 with maleonitrile) are all within experimental error. This indicates there is a small but significant preference for formation of the *EE* relative to the *EZ* isomeric carbonyl ylide $- e^-$ from **1** relative to **2**.

The observed preference for formation of the *EE* carbonyl ylide $- e^-$ from **1** can be attributed to the difference in steric interaction of the vicinal phenyl rings in the oxirane radical cation. The repulsion of the phenyl rings in $\mathbf{1}^{+\cdot}$ directs the ring opening to the less hindered $EE^{+\cdot}$ configuration. Presumably, the carbonyl ylides $- e^-$ are essentially planar and resonance delocalization preserves stereochemical integrity until back electron transfer from the sensitizer radical anion (step *4*) gives the carbonyl ylides.

It is interesting to compare the oxirane radical cation cleavage observed here with the cleavage which results upon electrochemical oxidation of **2** and 2,2,3,3-tetraphenyloxirane (14). Products obtained from the anodic oxidation of **2**, benzophenone (27%), and diphenylacetic acid (17%) indicate some carbon–oxygen bond cleavage. The tetraphenyl derivative gives a good yield of benzophenone (96%) under these conditions which is indicative of carbon–carbon bond cleavage. The difference was attributed to the ability of the initial radical cation of **2** to lose a proton and another electron; the sequence of these steps could not be determined from the data.

If the electrochemical reactions involve a two electron oxidation before the product determining step, the difference between the electrochemical oxidation and the photosensitized (electron transfer) reactions can be readily explained. While transfer of two electrons at the anode is not unlikely, the photosensitized electron transfer can remove only one. The initial oxirane radical cation is of course in a reducing environment; that is, near the sensitizer radical anion.

The cleavage of the oxirane radical cation in the mass spectrometer also occurs via competitive routes (15). The mass spectrum fragmentation pattern of **2** gives evidence of direct cleavage, loss of benzaldehyde (the base peak is $m/e = 90$), and rearrangement followed by fragmentation ($m/e =$ 167 equivalent to $(C_6H_5)_2CH^{+\cdot}$).

It is thus apparent that even though photochemical electron transfer, anodic oxidation, and ionization in the mass spectrometer all involve the formation of the oxirane radical cation, the conditions are so different there is little obvious analogy with regard to ultimate product formation.

Step *5* in the proposed scheme is the well known thermal conrotatory electrocyclic ring closure of the isomeric carbonyl ylides. Since the ring cleavage process is not stereospecific the sequence of steps *4* and *5* results in isomerization of the oxirane. The photostationary state, which favors the *trans*-isomer (**2**) (Table 1), is not markedly dependent upon the sensitizer or solvent used. In fact, the acetone sensitized isomerization, which involves triplet–triplet transfer, gave a similar ratio. We believe this similarity is fortuitous for the limited range of sensitizers employed in this study and for the system **1**–**2**.

The photosensitized (electron transfer) stationary state should depend to some extent upon the relative rates of the fluorescence quenching process, which subsequently leads to electron transfer, by the isomeric oxiranes (**1** and **2**). The measured fluorescence quenching rate constants of DCN with **1** and **2** are essentially diffusion controlled; furthermore, **1** and **2** have similar oxidation potentials so the rate of electron transfer is expected to be similar. This need not be the case in general. We anticipate examples where the photosensitized (electron transfer) isomerization yields an equilibrium mixture quite different from those obtained by other methods of isomerization (i.e., thermal[6] and photochemical by direct and photosensitized (triplet–triplet transfer) irradiation).

To our knowledge, this is the first reported example of the configurational isomerization of an oxirane photosensitized by the electron transfer process. Close analogy can be found in a report of the *cis–trans*-isomerization of the 1,2-diphenylcyclopropanes which was attributed to the electron transfer mechanism (16). Hixson and co-workers found that the fluorescence of 1-cyanonaphthalene (MCN) was quenched by 1,2-diphenylcyclopropane and that MCN was an effective photosensitizer (electron transfer) for the *cis–trans*-isomerization. We must now ask why 1-cyanonaphthalene is an effective sensitizer for the isomerization of the 1,2-diphenylcyclopropanes, but is ineffective in the case of **1** and **2**. The explanation lies in the observation that 1,2-diphenylcyclopropane has a significantly lower oxidation potential ($E_{1/2}{}^{ox} = 1.09$ V vs.

[6]The thermodynamic equilibrium strongly favors **2** over **1** ($k_{eq} = 9.5$) (12).

TABLE 7. Melting points and analytical data of new compounds

Compound	Melting point (°C)	Found C	Found H	Found N	Calculated C	Calculated H	Calculated N
3*a*	82–82.5[a]	81.91	6.16	5.56			
3*b*	77–79[b]	81.71	6.15				
4*a*	104–105[b]	81.74	6.25		81.90	6.06	5.62
4*b*	50–51[b]	82.08	6.20				
3*c*	231–233[c]	78.97	5.07				
3*d*	153–155[d]	78.89	5.12	10.47			
3*e*	189.5–190[d]	79.11	4.88				
4*c*	151–152.5[e]	79.08	5.25		78.81	5.16	10.21
4*d*	228–229[d]	78.79	5.22				
4*f*	121.5–123[e]	78.77	5.41				

Recrystallizing solvent: (*a*) cyclohexane, (*b*) petroleum ether, (*c*) acetone–cyclohexane, (*d*) benzene, (*e*) petroleum ether – benzene.

Ag/Ag^+ in acetonitrile (17)) than **1** or **2**. In fact, the calculated (eq. [5]) free-energy for the electron transfer indicates the process should be spontaneous ($\Delta G = -12$ kcal mol^{-1}).

Step *6* in the proposed scheme is the thermally allowed ($4\pi s + 2\pi s$) cycloaddition reaction (18). This reaction involving the carbonyl ylide has been extensively studied, particularly by Huisgen and co-workers (4). Photosensitization by electron transfer may offer some advantages over the alternative thermal and photochemical modes of formation of the carbonyl ylide. For example, the reaction can be brought about at low temperature and under mild conditions. Relatively long wavelength light can be used to activate the photosensitizer. A sensitizer with a high triplet energy is not required so that possible isomerization of the dipolarophile can be avoided.

It is interesting that the cycloaddition reaction with acrylonitrile, fumaronitrile, and maleonitrile can compete effectively with ring closure (step *5*). It should also be mentioned that in the cycloadditions involving maleonitrile, **3***c*, where the phenyl and cyano groups are all *cis*, is formed in preference (1.5 to 1) to **3***e*. When the *EE* carbonyl ylide, formed by direct irradiation of **2**, was trapped with maleic anhydride the analogous all *cis* adduct was again slightly (1.2 to 1) preferred (3*c*). In contrast, *trans*-2,3-di(4-nitrophenyl)oxirane gives, upon heating in the presence of dimethyl maleate, the isomeric tetrahydrofuran derivatives with the all *cis* configuration the minor (0.7 to 1) product (13). Clearly, neither steric factors involved in the "two-planes orientation complex" (19) nor electronic factors associated with secondary orbital interactions (20) are strong enough to greatly favor one isomer over the other.

Experimental

General

Acetonitrile (Aldrich Gold Label) was refluxed overnight over calcium hydride under a dry nitrogen atmosphere and fractionally distilled. The other solvents (Fischer spectroscopic grade) were used as received. 1-Cyanonaphthalene was sublimed under vacuum. Methyl 4-cyanobenzoate, 1,4-dicyanobenzene, and dimethyl terephthalate were purified by repeated recrystallization. 1,4-Dicyanonaphthalene was prepared by reaction of 1,4-dibromonaphthalene with cuprous cyanide and purified by chromatography on alumina and recrystallization from nitroethane. The stilbene oxides were prepared by oxidation of the corresponding stilbene with 3-chloroperbenzoic acid in chloroform at room temperature, and purified by repeated crystallization first from methanol and then from hexanes. Their purity was checked by vpc (10% SE-30 on Chromosorb W 60/80, 5 ft at 180°C). Fumaronitrile (Aldrich) was freshly sublimed in vacuum. Maleonitrile was prepared from fumaronitrile by heating in the presence of iodine and purified by fractional distillation, column chromatography on alumina, eluting with benzene–hexane, and recrystallization from pentane–ether. Tetramethylammonium perchlorate was recrystallized from ethanol four times and dried under vacuum at 65°C. Silver nitrate, for the reference electrode, was purified by recrystallization from water. Nuclear magnetic resonance spectra were obtained with a Varian HA-100 spectrometer. Infrared spectra were recorded on a Perkin-Elmer 621 spectrometer and mass spectra on a Matt 311A spectrometer. Vapour phase chromatograph analyses were performed on a Varian 90-P instrument. Melting points are corrected. The combustion analyses were performed by Chemalytics, Inc., Tempe, Arizona.

Quenching Experiments

Stern–Volmer plots were obtained using a conventional 90° two-monochromator spectrofluorimeter at room temperature, from the intensity of the spectra at the maximum. The samples were degassed on a mercury-free vacuum line using three freeze–pump–thaw cycles.

Oxidation Potential Measurements

Cyclic voltametric data were obtained using a three-electrode cell with a Princeton Applied Research Electrochemistry System Model 170. The working electrode was a platinum wire. A Ag/Ag^+ (0.1 *M*) electrode was used as a reference electrode and 0.1 *M* tetraethylammonium perchlorate as a supporting electrolyte. The solvent was acetonitrile.

Irradiations

All irradiations were carried out using a General Electric Co. 1 kW medium pressure mercury vapour lamp at 10°C. The progress of the reaction was followed by nmr and/or vpc (15% Apiezon or 10% SE-30 on Chromosorb W). Solutions (0.15 *M*)

Can. J. Chem. Downloaded from www.nrcresearchpress.com by 210.87.254.5 on 09/05/12
For personal use only.

TABLE 8. Diagnostic infrared bands of the new tetrahydrofurans[a]

Compound	Frequency
3*a*	2240 m, 1085 m, 1060 s, 1020 s, 1010 m, 755 s, 725 s, 695 s
3*b*	2235 m, 1080 s, 1055 s, 1030 m, 1015 m, 745 s, 740 s, 690 s
4*a*	2245 m, 1095 m, 1055 s, 1025 m, 960 m, 755 s, 725 s, 695 s
4*b*	2240 m, 1075 m, 1045 s, 1020 m, 745 s, 690 s
3*c*	2245 m, 1085 m, 1060 s, 1020 s, 1010 s, 745 m, 710 s, 690 s
3*d*	2245 m, 1085 m, 1060 m, 1020 s, 740 s, 720 s, 690 s
3*e*	2245 m, 1075 m, 1050 s, 1015 s, 760 m, 740 s, 690 s
4*c*	2245 m, 1080 m, 1050 s, 1020 m, 1005 m, 755 s, 720 s, 690 s
4*d*	2245 m, 1082 m, 1055 s, 1020 m, 740 m, 720 m, 690 s
4*f*	2250 m, 1075 m, 1040 s,br, 1020 m, 965 m, 745 s, 690 s

[a]Taken in KBr disks, cm^{-1} (medium = m, strong = s, broad = br).

of **1** or **2** were used with a 2×10^{-2} *M* concentration of sensitizer in the case of the aromatic sensitizers (1×10^{-2} *M* DCN in methanol or benzene) or 2 *M* in the case of acetone. A 4×10^{-2} *M* concentration of 2-acetonaphthone or benzophenone was used for the attempted triplet sensitization. For the cycloaddition reactions, a 0.4–1 *M* concentration of the olefin was used. The solutions were deoxygenated either by argon bubbling or by three freeze–pump–thaw cycles. Only the sensitizer absorbed light with the Pyrex filter used in these experiments. No reaction took place under these conditions omitting the sensitizer. Products were separated by column chromatography on silica gel, using cyclohexane–benzene mixtures as eluent. Melting point, recrystallization solvents, and analytical data on the new compounds are reported in Table 7. Major ir bands are tabulated in Table 8.

Base Catalyzed Isomerization of **3**a *and* **4**a

Both **3***a* and **4***a* (20 mg) were refluxed 1/2 h in sodium methoxide (0.5 *M*) in methanol, maintaining a nitrogen stream through the reaction vessel. Treatment with water and extraction with benzene gave a mixture containing ~90% of **3***b* and **4***b*, respectively. Similar treatment of **3***b* and **4***b* lead to the same mixture.

Acknowledgements

This work was supported by the National Research Council of Canada. We are also grateful for a NATO fellowship administered by CNR (Rome) to one of us (A.A.).

1. (*a*) A. J. MAROULIS, Y. SHIGEMITSU, and D. R. ARNOLD. J. Am. Chem. Soc. **100**, 535 (1978); (*b*) D. R. ARNOLD and A. J. MAROULIS. J. Am. Chem. Soc. **98**, 5931 (1976).
2. (*a*) G. W. GRIFFIN and A. PADWA. *In* Photochemistry of heterocyclic compounds. *Edited by* O. Buchardt. Wiley-Interscience, New York. 1976. Chapt. 2; (*b*) G. W. GRIFFIN. Angew. Chem. Int. Ed. Engl. **10**, 537 (1971); (*c*) D. R. ARNOLD and L. A. KARNISCHKY. J. Am. Chem. Soc. **92**, 1404 (1970); (*d*) K. NISHIYAMA, K. ISHIKAWA, I. SARKAR, D. C. LANKIN, and G. W. GRIFFIN. Heterocycles, **6**, 1337 (1977).
3. (*a*) D. R. ARNOLD, A. B. EVNIN, and L. A. KARNISCHKY. Pure Appl. Chem. **24**, 523 (1970); (*b*) I. J. LEV, K. ISHIKAWA, N. S. BHACCA, and G. W. GRIFFIN. J. Org. Chem. **41**, 2654 (1976); (*c*) G. A. LEE. J. Org. Chem. **41**, 2656 (1976); personal communication.
4. (*a*) R. HUISGEN. Angew. Chem. Int. Ed. Engl. **16**, 572 (1977); (*b*) H. HAMBERGER and R. HUISGEN. J. Chem. Soc. Chem. Commun. 1190 (1971); (*c*) A. DAHMEN, H. HAMBERGER, R. HUISGEN, and V. MARKOWSKI. J. Chem. Soc. Chem. Commun. 1192 (1971); (*d*) V. MARKOWSKI and R. HUISGEN. J. Chem. Soc. Chem. Commun. 439 (1977); (*e*) A. ROBERT, J. J. POMMERET, E. MARCHAND, and A. FAUCAUD. Tetrahedron, **29**, 463 (1973).
5. D. J. REIF and H. O. HOUSE. Org. Synth. Coll. **4**, 860 (1963).
6. L. M. JACKMAN and S. STERNHELL. Applications of nuclear magnetic resonance spectroscopy in organic chemistry. 2nd ed. Pergamon Press, Toronto. 1969. p. 234.
7. R. S. BECKER, R. O. BOST, J. KOLC, N. R. BERTONIERE, R. L. SMITH, and G. W. GRIFFIN. J. Am. Chem. Soc. **92**, 1302 (1970).
8. (*a*) A. WELLER. *In* Exciplex. *Edited by* M. S. Gordon and W. R. Ware. Academic Press, New York, NY. 1975. Chapt. 2; (*b*) A. WELLER. *In* Nobel symposium 5, fast reactions and primary processes in chemical kinetics. *Edited by* S. Claesson. Almqvist and Widsell, Stockholm. 1967. p. 413.
9. D. R. ARNOLD and P. C. WONG. Unpublished results.
10. (*a*) P. BRUCKMANN and M. KLESSINGER. Chem. Ber. **107**, 1108 (1974); (*b*) R. BENASSI, P. LAZZERETTI, I. MORETTI, F. TADDEI, and G. TORRE. Org. Magn. Reson. **5**, 391 (1973); (*c*) P. LAZZERETTI, I. MORETTI, F. TADDEI, and G. TORRE. Org. Magn. Reson. **5**, 385 (1973).
11. J. KAGAN, P. Y. JUANG, B. E. FIRTH, J. T. PRZYBYTEK, and S. P. SINGH. Tetrahedron Lett. 4289 (1977).
12. H. H. J. MACDONALD and R. J. CRAWFORD. Can. J. Chem. **50**, 428 (1972); personal communication.
13. R. HUISGEN and V. MARKOWSKI. Unpublished results.
14. E. A. MAYEDA, L. L. MILLER, and J. F. WOLF. J. Am. Chem. Soc. **94**, 6812 (1972).
15. M. FETIZON, Y. HENRY, G. ARANDA, H.-E. AUDIER, and H. DE LUZES. Org. Mass Spectrom. **8**, 201 (1974).
16. S. S. HIXSON, J. BOYER, and C. GALLUCCI. J. Chem. Soc. Chem. Commun. 540 (1974).
17. T. SHONO and Y. MATSUMURA. J. Org. Chem. **35**, 4157 (1970).
18. R. B. WOODWARD and R. HOFFMANN. The conservation of orbital symmetry. Verlag Chemie, Weinheim, and Academic Press, New York. 1970.
19. R. HUISGEN. J. Org. Chem. **33**, 2291 (1968).
20. K. N. HOUK, J. SIMS, C. R. WATTS, and L. J. LUSKUS. J. Am. Chem. Soc. **95**, 7301 (1973).
21. S. L. MUROV. Handbook of photochemistry. Marcel Dekker, Inc., New York. 1973.
22. R. O. LOUTFY and R. O. LOUTFY. Can. J. Chem. **50**, 4052 (1972).

Can. J. Chem. Downloaded from www.nrcresearchpress.com by 210.87.254.5 on 09/05/12
For personal use only.

Simultaneous determination of relative and absolute rate constants in racemization studies; applications to kinetic isotope effects

MICHAL TENCER AND ALLAN R. STEIN[1]

Department of Chemistry, Memorial University of Newfoundland, St. John's, Nfld., Canada A1B 3X7

Received May 25, 1978

MICHAL TENCER and ALLAN R. STEIN. Can. J. Chem. **56**, 2994 (1978).

The method reported allows the simultaneous determination of relative and absolute rate constants for two substances in a single kinetic run. The approach is of special interest for kinetic isotope effect determinations where rate ratios are often near one and failure to exactly duplicate reaction conditions can lead to uncertainties in the values calculated from independently measured rate constants. For racemization studies, using two optically active materials with opposite signs of rotation, knowing their initial rotational contribution and having the faster racemizing one in higher concentration, the rates can be calculated if the times required to reach zero net rotation and the extremum value are measured. Other systems to which the method can be extended are suggested.

MICHAL TENCER et ALLAN R. STEIN. Can. J. Chem. **56**, 2994 (1978).

On décrit une méthode qui permet de déterminer simultanément les constantes de vitesse relatives et absolues pour deux substances au cours d'un seul et même essai de cinétique. Cette méthode présente un intérêt particulier pour la détermination de l'effet isotopique cinétique, alors que les rapports entre les vitesses sont souvent voisins de un et que les valeurs calculées au moyen de mesures indépendantes de constantes de vitesse peuvent être entachées d'erreurs si l'on ne réussit pas à reproduire parfaitement les conditions de la réaction. Pour des études de racémisation, si l'on utilise deux substances optiquement actives possédant des rotations de signes opposés, si l'on connaît les contributions initiales respectives de ces substances à la rotation et que la substance qui se racémise le plus rapidement possède la concentration la plus élevée, on peut calculer les vitesses à partir de mesures du temps nécessaire pour que la rotation nette devienne nulle, d'une part, et passe par sa valeur extremum, d'autre part. On suggère d'autres systèmes auxquels la méthode est applicable.

[Traduit par le journal]

Can. J. Chem. Downloaded from www.nrcresearchpress.com by 210.87.254.6 on 09/05/12
For personal use only.

Introduction

Frequently it is not possible to precisely duplicate reaction conditions. Consequently precision and accuracy of rate and rate constant determinations suffer. When it is important to be able to compare rates or reactivities, one commonly used approach is to use a competitive reaction with two or more substrates in the same reaction mixture and to follow the reactions by the appearance of products or the disappearance of starting materials. In this way more reliable relative rates can sometimes be obtained.

It is perhaps in the area of kinetic isotope effects, where rate ratios are often very near unity, that the greatest problems arise. If the isotope effect is to be determined by comparing two independently obtained rates, extreme precision is required. Temperature must be very carefully controlled, solvents and reagents must be equally pure (or impure), concentrations of reagents must be identical or precisely known and so on, conditions which are often difficult to meet and reproducibility becomes a problem (1). Unfortunately, it is in just such systems that the competitive approach is most difficult to apply. Normally isotope-specific methods such as mass spectrometry or nuclear magnetic resonance, methods which frequently are not precise enough for subtle kinetic purposes, must be used to follow the reactions. These methods usually require either very high concentrations of the species (2) or, more commonly, concentration or isolation of the species (3) (or materials derived from them) which may introduce errors due to equilibration and, if recoveries are not quantitative, fractionation. Even such methods are not useable for, for example, secondary deuterium kinetic isotope effects in 'symmetrical' reactions of the type illustrated in reaction [1] where the product and the starting material are the same.

[1] 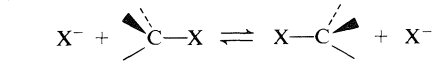

Here the only available methods for following the reaction are *radio*-tracer techniques (e.g., if the nucleophile-leaving group is a halide, a *radio*-halide can be used) (4) and/or racemization kinetics (if optically active starting material is available) (5).

There are a number of cases where considerable kinetic data were extracted from single runs. Thus,

[1]To whom all correspondence should be addressed.

Can. J. Chem. Downloaded from www.nrcresearchpress.com by 210.87.254.6 on 09/05/12
For personal use only.

for example Ahlberg (6) and others have calculated activation parameters from single variable temperature runs and Albery and Robinson (7) developed a differential method for enthalpies and heat capacities of activation. Such sequential or simultaneous measurement eliminates many of the empirical problems associated with independently determining and comparing the rates for two solutions. The method we wish to report is a 'differential' method but is quite different from the Albery and Robinson approach (7) since the two substrates are in a single solution. Using optically active substrates and following the optical rotation as a function of time it is possible to determine relative and absolute rates for the two substances in a single run.

Derivation

For a racemization reaction of the type in reaction [1], the rate expression below applies (8).

$$[2a] \qquad \ln\frac{\alpha_0}{\alpha} = 2kt\,[\mathrm{X}]^q$$

or

$$[2b] \qquad \alpha = \alpha_0 \exp(-2kt[\mathrm{X}]^q)$$

In the equation, α_0 is the initial rotation, α that at time t, [X] is the concentration of the nucleophile/leaving group and is, of course, constant throughout any given run, while the exponent q expresses the order of the reaction with respect to X, i.e. $q = 0$ for a reaction which is first order, that is, the rate depends only upon the concentration of the substrate, $q = 1$ for a second order reaction, and so on. The factor of '2' arises from the fact that inversion of one molecule cancels the rotation of another.

If two compounds with opposite rotations, A and B, are placed in the same cell and A, which is the faster racemizing compound, has the higher absolute initial rotation, the observed rotation α at any time will be the sum of the contributions of each component. One of these rotational contributions will be positive, the other negative; but since it is not specified which is which, absolute values can be used (eq. [3]). Reaction of A and B must, of course, show the same dependence upon nucleophile concentration, i.e. $q_A \equiv q_B \equiv q$.

$$[3a] \qquad \alpha = |\alpha_A| - |\alpha_B|$$

$$[3b] \qquad \alpha = |\alpha_{0A}| \exp(-2k_A t\,[\mathrm{X}]^q) - |\alpha_{0B}| \exp(-2k_B t\,[\mathrm{X}]^q)$$

At some time t_Z, the observed rotation will be zero and

$$|\alpha_{0A}| \exp(-2k_A t_Z[\mathrm{X}]^q) = |\alpha_{0B}| \exp(-2k_B t_Z[\mathrm{X}]^q)$$

from which eq. [4] arises.

$$[4] \qquad k_A - k_B = \frac{1}{2t_Z[\mathrm{X}]^q} \ln\frac{|\alpha_{0A}|}{|\alpha_{0B}|}$$

Later, at time t_E, the observed rotation reaches a minimum (or maximum) value before again approaching zero, this time asymptotically. At this extremum:

$$\frac{d\alpha}{dt} = 0$$

Since $[\mathrm{X}]^q$ is constant, differentiating eq. [3*b*] gives:

$$-2k_A[\mathrm{X}]^q|\alpha_{0A}| \exp(-2k_A t_E[\mathrm{X}]^q) + 2k_B[\mathrm{X}]^q|\alpha_{0B}| \exp(-2k_B t_E[\mathrm{X}]^q) = 0$$

which, on rearranging, gives eq. [5].

$$[5] \qquad \frac{k_A}{k_B} = \frac{|\alpha_{0B}|}{|\alpha_{0A}|}\exp\{2(k_A - k_B)t_E[\mathrm{X}]^q\}$$

Substituting for $k_A - k_B$ from eq. [4] allows derivation of eq. [6].

$$[6a] \qquad \frac{k_A}{k_B} = \frac{|\alpha_{0B}|}{|\alpha_{0A}|}\exp\left\{\frac{t_E}{t_Z}\cdot\ln\frac{|\alpha_{0A}|}{|\alpha_{0B}|}\right\}$$

or

$$[6b] \qquad \frac{k_A}{k_B} = \frac{|\alpha_{0A}|}{|\alpha_{0B}|}(t_E/t_Z - 1)$$

Thus determining the rate ratio requires that the ratio of the initial rotations due to A and B be measured and that t_Z and t_E be determined. To calculate the rate constants themselves using eqs. [4] and [6], the nucleophile concentration and the order of the reaction with respect to the nucleophile, q, must also be known. The values obtained for k_A and k_B will be dependent upon the various uncertainties that affect a single run but at least any resultant errors should be the same or similar for the two components in the simultaneous determination.

Results and Discussion

Typical curves for several runs are shown in Fig. 1 and additional results are tabulated along with data obtained by conventional methods in Table 1. While it is probably in the area of kinetic isotope effects that the approach outlined is most useful, data for other cases are included to illustrate its usefulness over a range of rate ratios. In all the cases reported, the reactions are first order in nucleophile, the bromide ion (i.e. $q = 1$), and the reactants are variously *para*-substituted α-phenylethyl bromides with *deuterium*-substitution, if any, on the α-carbon.

From eqs. [4] and [5], it is apparent that if the ratio of the initial rotations $|\alpha_{0A}|/|\alpha_{0B}|$ is excessive or if

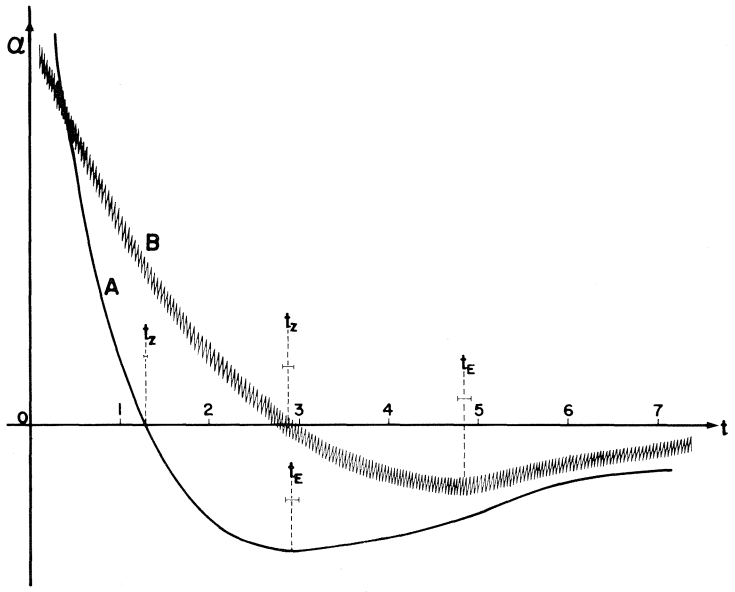

FIG. 1. Rotation as a function of time. Curve *A*: *p*-bromo- vs. unsubstituted 1-bromo-1-phenylethane; time intervals, 4000 s, $|\alpha_{0A}|/|\alpha_{0B}| = 1.866$, [LiBr] = 0.01 *M* in acetone, $T = 313.15$ K. Curve *B*: secondary *deuterium* kinetic isotope effect for 1-bromo-1-phenylethane; time intervals, 1000 s, $|\alpha_{0H}|/|\alpha_{0D}| = 1.138$, [LiBr] = 0.04 *M* in acetone, $T = 318.15$ K.

TABLE 1. Typical results for the single-run determination of relative and actual rate constants

							Independently determined values		
$\lvert\alpha_{0A}\rvert/\lvert\alpha_{0B}\rvert$	t_Z (min)	t_E (min)	k_A/k_B	Range of value[a]	k_A[b]	k_B[b]	k_A/k_B	k_A[b]	k_B[b]
p-Nitro- vs. unsubstituted 1-bromo-1-phenylethane[c]; acetone, 40°C, [LiBr] = 0.0100 *M*									
3.538	64.0	141.0	4.57	3.75–5.57	21.06	4.61			
3.767	70.3	149.3	4.43	3.77–5.14	20.30	4.58	4.52[d]	22.29[d]	4.93[d]
2.077	131.0	43.0	4.46	3.89–5.03	18.81	4.22			
p-Nitro- vs. *p*-methyl-substituted 1-bromo-1-phenylethane; acetone, 40°C, [LiBr] = 0.0100 *M*									
8.761	165.0	218.0	2.01	1.67–2.28	21.84	10.88	1.98[d]	22.29[d]	11.28[d]
p-Bromo- vs. unsubstituted 1-bromo-1-phenylethane; acetone, 40°C, [LiBr] = 0.0100 *M*									
1.866	86.0	195.0	2.205	2.22–2.31	11.06	5.02	2.18[d]	10.75[d]	4.93[d]
1-*Protio*- vs. 1-*deutero*-1-bromo-1-phenylethane[f]; acetone, 45°C									
1.138	48.0	80.7	1.092	1.082–1.101	6.647	6.087		—	—
1.094	79.0	164.0	1.107	1.066–1.150	7.747	7.037	1.08[e,g]	—	—
1.0595	65.0	186.0	1.114	1.096–1.132	7.263	6.522		7.328	—

[a]Estimated by taking the highest and lowest acceptable t_Z/t_E ratios from the recorder traces and calculating k_A/k_B. Value reported for the rate constant ratio is that for the 'best' times.
[b]The units are $\times 10^{-3}$ ℓ/mol s in every case.
[c]Three determinations using different solutions.
[d]Unpublished data of A. R. Stein, E. A. Seymour, and J. Sweet.
[e]Unpublished data of A. R. Stein, M. Tencer, and R. Dawe.
[f]In order, the [LiBr] = 0.0400, 0.0133, 0.0100 *M* for the three runs.
[g]Average value for [LiBr] = 0.00200 *M* over the temperature range 25–45°C.

the concentration of the nucleophile [X] is too low, a long, flat curve results and extracting t_Z and, especially, t_E is difficult. Instrument instability also increases uncertainties in such long runs. On the other hand, very fast runs (i.e. $|\alpha_{0A}|/|\alpha_{0B}| \gtrsim 1.0$ and high [X]) exaggerate uncertainties due to the zero time (t_0) value (see Experimental) and result in low rotations unless very high concentrations of the reactant are used. As expected from the above considerations, the best curves are obtained by choosing concentrations of the two reactants such that $|\alpha_{0A}|/|\alpha_{0B}|$ is approximately equal to the expected k_A/k_B value.

As can be seen from Fig. 1, there is some uncertainty in the graphically determined t_Z and t_E values. These uncertainties are greater for the deuterium isotope effect determination with 1-bromo-1-phenylethane (curve *B*) than for the rate of the *para*-bromo-

Can. J. Chem. Downloaded from www.nrcresearchpress.com by 210.87.254.6 on 09/05/12
For personal use only.

Can. J. Chem. Downloaded from www.nrcresearchpress.com by 210.87.254.6 on 09/05/12
For personal use only.

versus the unsubstituted case (curve *A*) because the very low initial rotation resulted in a poor signal-to-noise ratio in the former case. Calculated k_A/k_B values, k_H/k_D values in this case, are quite insensitive to errors in t_Z and t_E since the ratio of the initial rotations is near unity. Thus relatively small changes in the value k_H/k_D are observed with changes in the power to which the initial rotation ratio is raised (see eq. [6*b*]). When the rate constants differ greatly, much larger rotation changes are possible. The curves look much better (curve *A*) but because of the larger $|\alpha_{0A}|/|\alpha_{0B}|$ values, calculated rate ratios are much more sensitive to errors in t_Z and t_E.

As is apparent from Table 1, the rate constant ratios and the absolute rate constants obtained with the single-run method are generally in good agreement with the independently determined values. Discrepancies can be attributed to the lack of exact reproducibility of experimental conditions from one run to the next. This would affect the independently determined values and the rate constants (but hopefully not the rate ratio) from the single run method. Errors in initial time, t_Z and t_E estimation, are other possible sources of discrepancies.

While the described approach has so far only been applied to symmetrical racemization reactions in which the nucleophile and the leaving group are the same, it is not limited to such systems. Any reactions involving loss of optical activity can be used. Eliminations forming achiral alkenes from chiral substrates and rearrangements from chiral to achiral substrates are among the systems amenable to study. For such systems, of course, the equations would have to be modified by eliminating the '2' first introduced in eq. [2].

The inability to use linear regression analysis on the single-run data reduces its reliability. This last problem could largely be overcome by using more data points and calculating the best curve fit by successive approximations of k_A and k_B. In fact, by curve-fitting techniques, the empirical problems associated with obtaining curves of the type illustrated can be eliminated but this approach also eliminates a major advantage of the described method: the rate constants and ratios can be readily calculated without recourse to a computer facility.

Experimental

Synthesis and resolution of the compounds used was by the procedures (8) or by procedures analogous to those already described.[2] The *deuterium*, if any, was introduced by $LiAlD_4$ reduction of the corresponding ketone. The resultant alcohol was resolved and converted to the labelled bromide by essentially the same procedures as were used for the unlabelled analogue.

Reagent grade acetone which was freshly distilled from molecular sieves under dried nitrogen was used as a solvent for the runs reported in the Table. Reagent grade lithium bromide was oven-dried at 250°C. All manipulations, transfers and dilutions of the solutions, were done in a dry nitrogen-filled glove bag.

The initial rotations, α_{0A} and α_{0B}, were determined in acetone solutions. Two millilitres of each solution and the amount of the lithium bromide in acetone required to give the desired concentration were mixed and the 10 cm cell of the polarimeter quickly filled in the glove bag. The stoppered cell was transferred to the Perkin-Elmer Model 141 recording polarimeter used for this study and time measured from the instant the circulating, constant temperature bath was connected to the cell. Thus the errors introduced due to racemization starting at the instant of mixing and the time required for the solution to equilibrate at the higher bath temperature at least partially compensate for each other.

Acknowledgments

The authors thank Memorial University of Newfoundland and the National Research Council of Canada for financial assistance.

1. W. A. PRYOR, M. IINO, and G. R. NEWKOME. J. Am. Chem. Soc. **99**, 6003 (1977).
2. V. A. STOUTE and M. A. WINNIK. Can. J. Chem. **53**, 3503 (1975); H. KWART and T. J. GEORGE. J. Am. Chem. Soc. **99**, 5214 (1977).
3. R. H. BETTS, J. BRON, W. D. BUCHANNON, and K.-Y. D. WU. Can. J. Chem. **55**, 2966 (1977); J. W. HILL and A. FRY. J. Am. Chem. Soc. **84**, 2763 (1962); M. P. FRIEDBERGER and E. R. THORNTON. J. Am. Chem. Soc. **98**, 2861 (1976); H. J. SHINE, G. H. HENDERSON, A. CU, and P. SCHMID. J. Am. Chem. Soc. **99**, 3719 (1977).
4. (*a*) A. R. STEIN. Tetrahedron Lett. **47**, 4145 (1974); (*b*) A. HOLMGREN. Acta Chem. Scand. A**31**, 539 (1977) and references therein; (*c*) J. L. GLEAVE, E. D. HUGHES, and C. K. INGOLD. J. Chem. Soc. 236 (1935).
5. (*a*) A. R. STEIN. J. Org. Chem. **41**, 519 (1976); (*b*) E. D. HUGHES, F. JULIUSBURGER, A. D. SCOTT, B. TOPLEY, and J. WEISS. J. Chem. Soc. 1173 (1936).
6. P. AHLBERG. Chem. Scr. **4**, 41 (1973) and references therein.
7. W. J. ALBERY and B. H. ROBINSON. Trans. Faraday Soc. **65**, 980 (1969).
8. A. R. STEIN. J. Org. Chem. **38**, 4022 (1973) and references therein.

[2]A. R. Stein, E. A. Seymour, J. Sweet, M. Tencer, and R. Dawe. Unpublished results.

Stéréochimie de β-diols et de leurs dérivés cycliques. X.[1] Etude structurale en résonance magnétique nucléaire du proton de dioxanne-1,3-4-spirocyclohexanes : méthyl-2 dioxanne-1,3-4-spiro-*tert*-butyl-4′ cyclohexanes-*cis* et -*trans* (série I)

LOUIS CAZAUX, JEAN-PIERRE GORRICHON, PIERRE MARONI ET MARCEL PERRY
Laboratoire de Synthèse et Physicochimie organique, ERA no 686 du CNRS, 118, route de Narbonne, 31077 Toulouse Cédex, France

Reçu le 3 mars 1978

LOUIS CAZAUX, JEAN-PIERRE GORRICHON, PIERRE MARONI et MARCEL PERRY. Can. J. Chem. **56**, 2998 (1978).

Les deux composés du titre sont des modèles pour l'étude structurale ultérieure de deux séries plus complexes. Leur analyse spectrale à haut champ a permis de caractériser par la technique INDOR ou par effet de solvant à peu près tous les protons et de déterminer les structures en conformation double chaise. Enfin, les déplacements chimiques dans CCl_4 ont été utilisés pour évaluer l'influence des oxygènes intracycliques sur les résonances des protons 2′ et 6′ du spirobicyclohexane.

LOUIS CAZAUX, JEAN-PIERRE GORRICHON, PIERRE MARONI, and MARCEL PERRY. Can. J. Chem. **56**, 2998 (1978).

The two title compounds serve as models for an eventual structural study of two more complex series. High field nmr spectral analysis using INDOR or solvent effects allows us to assign nearly all proton signals and to propose that these compounds exist in the double chair conformation. Finally, chemical shifts in CCl_4 have been used to evaluate the effect of the intracyclic oxygen atoms on the 2′ and 6′ proton nmr resonances of the spirobicyclohexane.
[Journal translation]

Les spirodioxannes en position 2 et 5 ont fait l'objet de plusieurs études d'inversion de cycle en rmn (2, 5). A notre connaissance, les composés à jonction spiro en 4 ont été, en revanche peu étudiés (6). Dans le cadre d'un travail portant sur l'addition de dérivés magnésiens (7, 8) ou zinciques (8, 9) à des cétones conformationnellement homogènes, nous avons pu obtenir ce type de molécules. Elles proviennent de β-cétols ou de β-hydroxyesters tertiaires, par réduction en β-diols au moyen de $LiAlH_4$, puis acétalisation de ces derniers par l'éthanal (schéma 1). Tous les composés étudiés sont des liquides qui ont été séparés par chromatographie sur couche mince préparative. Les spectres de rmn du proton pour les divers spirodioxannes ainsi synthétisés sont relativement complexes. Les protons de la partie

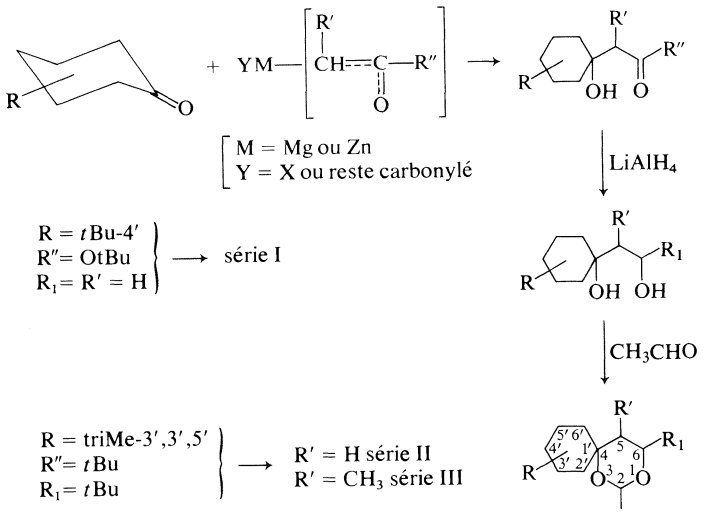

SCHÉMA 1. Synthèse des dioxanne-1,3-4-spirocyclohexanes.

[1]Pour la partie IX, voir réf. 1.

Can. J. Chem. Downloaded from www.nrcresearchpress.com by 210.87.254.40 on 09/05/12
For personal use only.

Can. J. Chem. Downloaded from www.nrcresearchpress.com by 210.87.254.40 on 09/05/12
For personal use only.

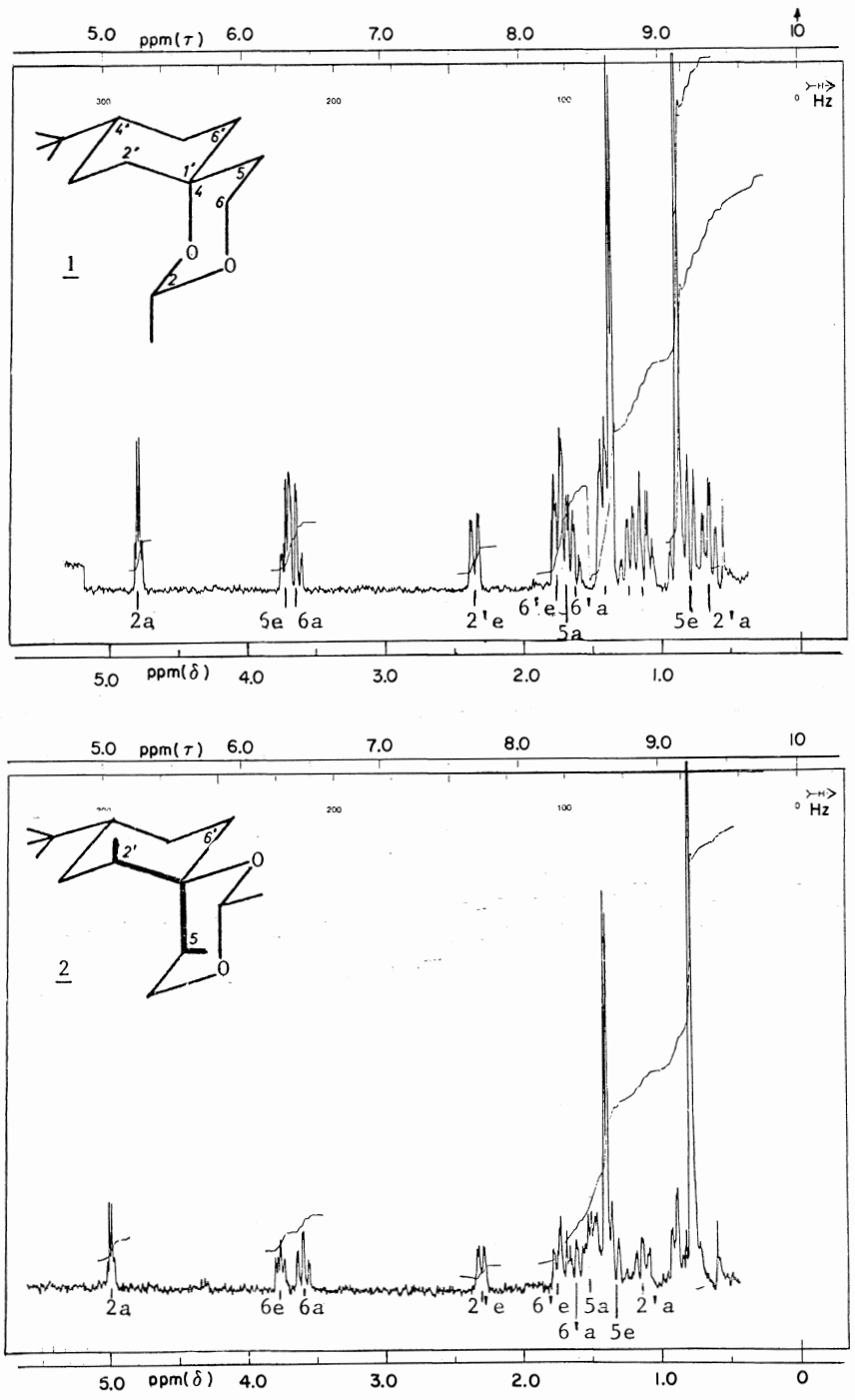

FIG. 1. Spectres rmn à 300 MHz des spirodioxannes **1** et **2** dans le benzène.

dioxannique sont cependant facilement localisés. En revanche, l'attribution des résonances est beaucoup plus compliquée pour la partie cyclohexanique.

Un des problèmes importants posés par ces composés lorsqu'ils comportent plusieurs molécules isomères est la détermination de configuration au niveau notamment du carbone C_4 de jonction spiro. Sa résolution permet de remonter aux structures des β-diols et β-cétols précurseurs. Avant son extension à des cas plus complexes, nous l'avons résolu par l'étude des spectres rmn du proton des deux méthyl-2-dioxannes-1,3-4-spiro-*tert*-butyl-4′ cyclohexanes-

Can. J. Chem. Downloaded from www.nrcresearchpress.com by 210.87.254.40 on 09/05/12
For personal use only.

TABLEAU 1. Déplacements chimiques (δ ppm/TMS) et constantes de couplages (*J* en Hz) des composés **1** et **2**

No	Solvant	H_{2a}	Me_{2e}	H_{5a}	H_{5e}	H_{6a}	H_{6e}	$H_{2'a}$	$H_{2'e}$	$H_{3'a}$	$H_{3'e}$	$H_{4'a}$	$tBu_{4'e}$	$H_{5'a}$	$H_{5'e}$	$H_{6'a}$	$H_{6'e}$
1	C_6H_6*	4.73	1.36	1.71	0.78	3.62	3.71	0.65	2.33	~1.10	~1.40	~0.9	0.88	~1.20	~1.40	1.63	1.73
cis	CCl_4†	4.74	1.15	1.73	1.06	3.75	3.75	0.85	2.54	~1.15	~1.45	—	0.83	~1.15	~1.45	1.45	1.64
					J_{5a5e} = −13.2			$J_{2'a2'e}$ = −14.0							$J_{6'a6'e}$ = −13.0		
					J_{6a6e} = −11.5			$J_{3'a3'e}$ = −12.5 à 13.5							$J_{5'a5'e}$ = −12.5 à 13.5		
			$J_{H\text{-}Me}$ = 5		J_{6e5a} = 6.0			$J_{2'e3'a}$ = 3							$J_{6'e5'a}$ = 3.5		
					J_{6e5e} = 1.4			$J_{2'e3'e}$ = 3							$J_{6'e5'e}$ = 3.5		
					J_{6a5a} = 12.6			$J_{2'a3'e}$ = 3.6 = $J_{4'a3'e}$							$J_{6'a5'e}$ = 3.2 = $J_{4'a5'e}$		
					J_{6a5e} = 2.5			$J_{2'a3'a}$ = 13.8			$J_{2'e6'e}$ = 3				$J_{6'a5'a}$ = 12.0		
2	C_6H_6*	4.98	1.40	1.50	1.33	3.58	3.75	1.13	2.29	~0.9	~1.5	~0.8	0.77	~0.9	~1.5	1.60	1.74
trans	CCl_4†	4.86	1.13	1.51	1.63	3.60	3.78	1.14	2.45	~1.0$_5$	~1.7	~0.9	0.84	~1.0$_5$	~1.7	1.41	1.62
					J_{5a5e} = −13.1			$J_{2'e2'a}$ = −12.7							$J_{6'e6'a}$ = −13.0		
					J_{6a6e} = −11.2			$J_{2'e3'a}$ = 3.2							$J_{6'e5'a}$ = 3		
					J_{6e5a} = 5.3			$J_{2'a3'e}$ = 3.2							$J_{6'e5'e}$ = 3		
			$J_{H\text{-}Me}$ = 5		J_{6e5e} = 1.6			$J_{2'a3'e}$ = 4							$J_{6'a5'e}$ = 3.6		
					J_{6a5a} = 13.0			$J_{2'a3'a}$ = 13.5							$J_{6'a5'a}$ = 13.0		
					J_{6a5e} = 2.6												
						$J_{5a2'a}$ = 1.7		$J_{2'a5a}$ = 1.7			$J_{2'e6'e}$ = 3						

*Spectres enregistrés à 300 MHz.
†Spectres enregistrés à 250 MHz.

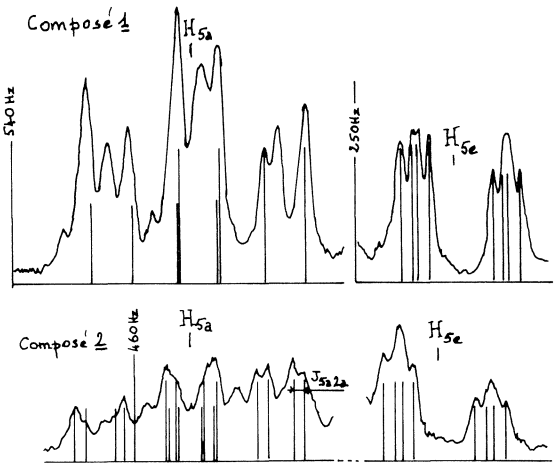

FIG. 2. Agrandissements des résonances des protons H_{5a} et H_{5e} des deux isomères **1** et **2**.

cis (**1**) et -*trans* (**2**) (série I, schéma 1) qui fait l'objet du présent mémoire. Ces deux isomères[2] sont représentés dans leur conformation préférentielle sur la fig. 1 et par un seul énantiomère.

Spectres à 300 MHz dans le benzène

Nous avons enregistré les spectres de rmn de ces composés sur un appareil Varian HR 300.[3] Afin de différencier le plus possible les hydrogènes de la partie cyclohexanique, nous avons utilisé le benzène comme solvant (fig. 1). Les résultats de l'analyse de ces spectres sont rassemblés dans le tableau 1.

L'attribution des résonances des protons dioxanniques H_{2a}, H_{6a} et H_{6e} ne pose aucun problème. Comme dans les dioxannes, les signaux correspondants sont fortement déblindés par la présence des oxygènes.

La connaissance des constantes de couplage J_{56}, déterminées sur la partie du spectre concernant H_{6e} et H_{6a}, permet de prévoir la forme des signaux relatifs aux protons H_{5e} et H_{5a} et de les localiser sur le spectre (fig. 2).

On remarque sur le proton H_{5a} de **2**, un dédoublement des raies lié à une constante de couplage à distance avec le proton $H_{2'a}$ (voir figs 1 et 2).

Nous avons conduit de façon similaire, l'étude de la partie cyclohexanique. A partir des valeurs des constantes de couplage déterminées pour des cyclohexanes méthylés (10) on peut attendre, pour les protons $H_{2'e}$ et $H_{6'e}$, un quadruplet ($^3J_{ea} \sim {}^3J_{ee} \sim {}^4J_{ee} \sim 3$ Hz) dédoublé par une grande constante

[2]L'énergie conformationnelle du groupement méthyle en 2 étant de l'ordre de 4.1 kcal, seuls les diastéréoisomères ayant ce substituant équatorial ont été isolés.

[3]Nous remercions très vivement MM. Anteunis et Tavernier, Professeurs à l'Université de Gand, pour l'enregistrement de ces spectres et pour de fructueuses discussions.

Can. J. Chem. Downloaded from www.nrcresearchpress.com by 210.87.254.40 on 09/05/12
For personal use only.

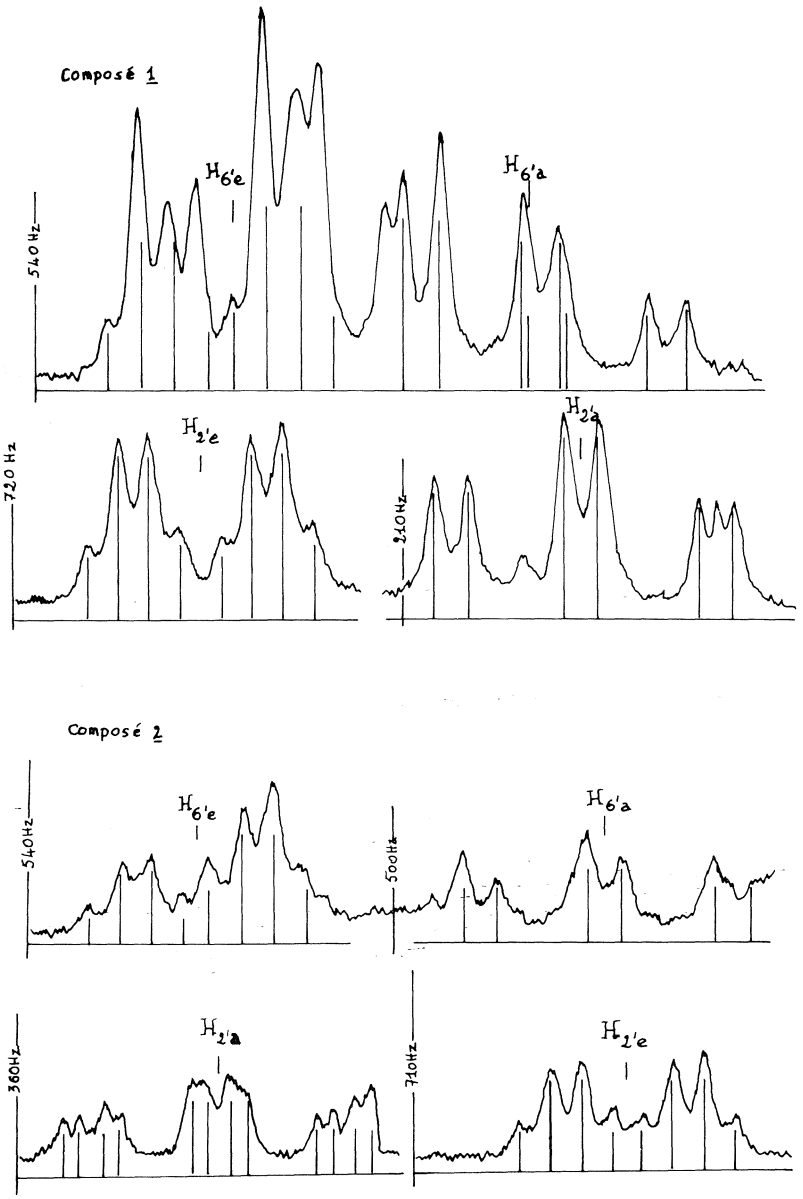

FIG. 3. Agrandissements des résonances des protons $H_{2'e}$, $H_{2'a}$, $H_{6'e}$ et $H_{6'a}$ des composés **1** et **2**.

($^2J_{gem} \sim$ 13–14 Hz), pour les protons $H_{2'a}$ et $H_{6'a}$ un triplet à grande constante ($^2J_{gem} \sim {}^3J_{aa} \sim$ 13–14 Hz) dédoublé par une petite constante ($^3J_{ae}$). Nous avons pu, sur des agrandissements réalisés à partir des spectres complets, trouver de telles figures de résonance (fig. 3).

Comme nous l'avons déjà remarqué pour H_{5a}, seul le proton $H_{2'a}$ du composé **2** possède un couplage en W (1.7 Hz). Sa résonance est modifiée en conséquence et *ce seul fait permet de distinguer les deux isomères* et d'attribuer au proton $H_{2'a}$ le signal à champ fort dans l'isomère **2**; une expérience d'irradiation INDOR permet d'associer à ce proton le signal à champ faible (δ = 2.29 ppm) comme étant celui de $H_{2'e}$.

La disposition des liaisons C—C et C—O du cycle dioxannique est la même dans les deux isomères vis à vis de $H_{2'e}$ et $H_{2'a}$ d'une part, de $H_{6'e}$ et $H_{6'a}$ d'autre part. En effet, la seule différence entre les deux isomères est le changement de position de l'oxygène O_3 mais il reste dans le plan de symétrie du cycle cyclohexanique. Pour cette raison, nous avons attribué à $H_{2'a}$ et $H_{2'e}$ de l'isomère **1**, respectivement les résonances à champ le plus fort et le plus faible.

Les déplacements chimiques des hydrogènes

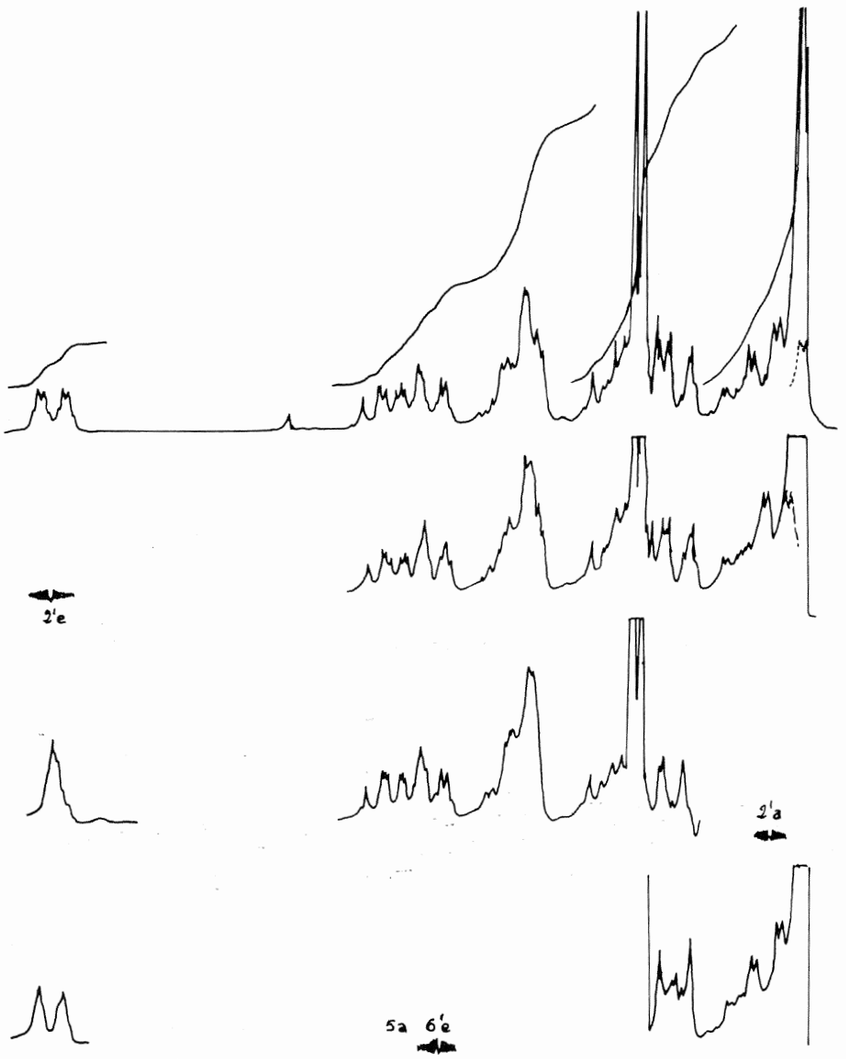

FIG. 4. Expériences d'irradiation pour le composé **1** dans CCl_4.

portés par les carbones 3′ et 5′ ont été déterminés par les mêmes méthodes. Toutefois, certaines incertitudes (notamment pour le composé **2**) demeurent du fait de la complication apportée par leur couplage avec le proton $H_{4'a}$.

Les valeurs des constantes de couplage, relevées sur ces spectres et réunies dans le tableau 1, confirment que la conformation préférentielle de telles molécules est bien la double chaise.

Spectres à 250 MHz dans le tétrachlorure de carbone

Dans ce solvant, le recouvrement des massifs relatifs aux protons cyclohexaniques ne permet pas l'interprétation directe des spectres. Pour résoudre ce problème nous nous sommes servis des résultats de l'étude précédente et de la technique d'irradiation mise en oeuvre sur un appareil CAMECA travaillant à 250 MHz.

Isomère 1

On localise facilement le proton $H_{2'e}$ (quadruplet dédoublé) à 2.54 ppm. L'irradiation du massif correspondant permet de situer les résonances de $H_{6'e}$ (disparition de la constante $^4J_{2'e6'e}$: quadruplet dédoublé → triplet dédoublé) et de $H_{2'a}$ (disparition de la constante $^2J_{gem} \sim 13$ Hz : triplet de doublets → doublet de doublets). Une irradiation vers 225 Hz confirme le déplacement chimique de $H_{2'a}$ (δ = 0.85 ppm.). En effet, on obtient pour $H_{2'e}$ la dis-

TABLEAU 2. Influence des liaisons O—C sur le δ des protons en fonction de leurs orientations mutuelles (les valeurs pour les cyclohexanols sont relevées dans la réf. 15; pour les dioxannes voir la réf. 16)

Conformation	Composé	δ	δ	Composé	δ
$[G^-G^+]_o$		+0.61 ($H_{2'e}$ de **1**)	+0.52 ($H_{2'e}$ de **2**)		+0.46
$[TG^-]_o$	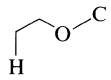	+0.19 ($H_{6'e}$ de **1**)	+0.17 ($H_{6'e}$ de **2**) +0.23 ($H_{6'a}$ de **2**)	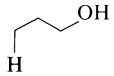	+0.07
$[G^-T]_o$	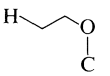	+0.03 ($H_{2'a}$ de **1**)	−0.20 (H_{5e} du dioxanne) −0.20 (H_{5e} de **1**) −0.15 (H_{5e} de **2**)	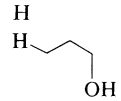	−0.27
$[G^+G^+]_o$		+0.32 ($H_{2'a}$ de **2**)	+0.41 (H_{5a} du dioxanne) +0.28 (H_{5a} de **1**) +0.35 (H_{5a} de **2**)	—	
$[TT]_o$	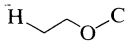	+0.27 ($H_{6'a}$ de **1**)		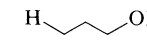	+0.01

parition de $^2J_{gem}$ conduisant à un singulet très élargi (cf. fig. 4).

Pour ces deux irradiations, on note en outre, des modifications dans les massifs situés vers 1.45 et 1.15 ppm. D'après la forme de ces signaux on peut y situer respectivement $H_{3'e}$ et $H_{3'a}$.

En irradiant $H_{6'e}$ (δ = 1.65 ppm), on vérifie que ce proton est bien couplé avec $H_{2'e}$. On irradie aussi le massif proche (δ = 1.7 ppm) attribuable à H_{5a} (comme le prouve l'observation des signaux de H_{6e} et H_{6a} vers 3.75 ppm) et on modifie le quadruplet dédoublé situé à 1.06 ppm. On a ainsi localisé H_{5a} et H_{5e} (cf. fig. 4).

On peut alors penser que $H_{5'e}$ et $H_{5'a}$ ont des résonances voisines de celles de $H_{3'e}$ et $H_{3'a}$ respectivement et que le proton $H_{4'a}$ se trouve masqué par le signal du groupement tertiobutyle comme c'est le cas dans les *tert*-butylcyclohexanes (10). Par différence, nous pensons que $H_{6'a}$ résonne vers 1.45 ppm.

Isomère 2

On trouve $H_{2'e}$ à 2.45 ppm. L'irradiation de ce massif modifie les signaux situés autour de 1.7 et 1.1 ppm. En irradiant alors à 286 Hz (1.14 ppm) et 405 Hz (1.62 ppm) et en observant les modifications apportées au massif du proton $H_{2'e}$, on localise sans ambiguité respectivement $H_{2'a}$ et $H_{6'e}$.

On détermine d'autre part, par irradiation de H_{6e} et H_{6a} (δ_{irr} = 3.66 ppm), les positions de H_{5e} (1.63 ppm) et de H_{5a} (1.51 ppm). Notons que l'on observe bien, sur le massif correspondant à ce dernier proton le dédoublement dû au couplage à distance avec $H_{2'a}$.

Nous situons finalement $H_{3'a}$ et $H_{5'a}$, $H_{3'e}$ et $H_{5'e}$ respectivement vers 1.05 et 1.7 ppm. En effet, compte tenu des effets des groupes méthyles situés en γ, les protons axiaux doivent être blindés par rapport à ceux de l'isomère **1** alors que les équatoriaux ne subissent qu'une faible influence (voir tableau 2 et fig. 5).

Comme précédemment $H_{4'a}$ doit être masqué par le signal du groupement tertiobutyle; on peut alors, par différence, trouver $H_{6'a}$ à 1.41 ppm.

Influence des oxygènes intracycliques sur les déplacements chimiques des protons du spirobicyclohexane

Dans les dioxannes-1,3, il est connu que les résonances des protons H_{5e} et H_{5a} sont, en général,

Can. J. Chem. Downloaded from www.nrcresearchpress.com by 210.87.254.40 on 09/05/12
For personal use only.

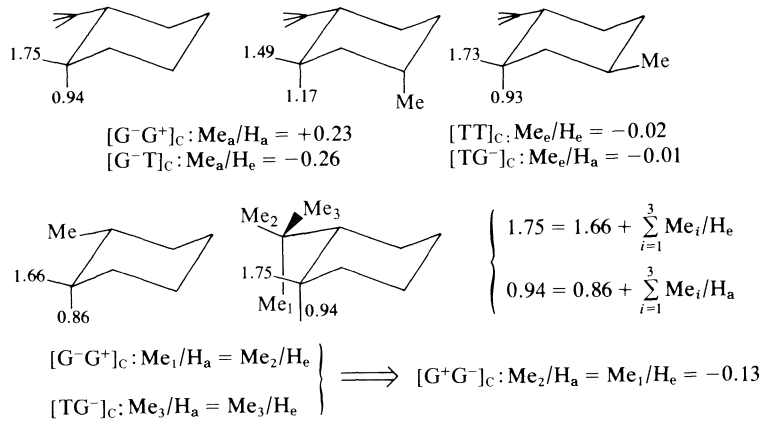

FIG. 5. Incréments d'effets γ (en ppm dans CCl_4) pour divers enchaînements.

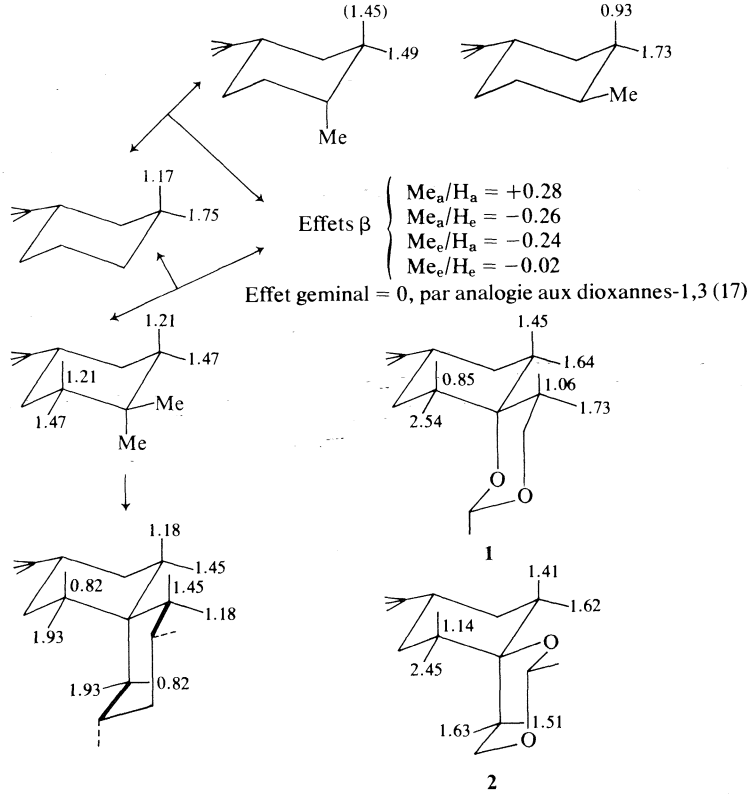

FIG. 6. Calcul des δ dans CCl_4 du *tert*-butyl-4′ méthyl-3 spirobicyclohexane et valeurs expérimentales de **1** et **2**.

inversées par rapport à celles des mêmes protons dans les cyclohexanes (11–13). Cette anomalie, liée à la présence des oxygènes dans le cycle, n'a pas reçu d'explication satisfaisante (14).

Pour tenter de mieux comprendre les phénomènes qui agissent sur les déplacements chimiques du proton, en présence d'oxygènes intracycliques, nous avons déduit l'effet du remplacement d'un groupement méthylénique par un oxygène, de la comparaison des deux spirodioxannes étudiés **1** et **2** et du *tert*-butyl-4′ méthyl-3 spirobicyclohexane (fig. 6). Malheureusement, aucune donnée n'apparaît dans la littérature pour ce composé; nous avons donc tenté d'obtenir les valeurs de δ nécessaires, à partir du *tert*-butyl cyclohexane et d'incréments déterminés à partir de résultats de la littérature (10) (voir fig. 5).

Can. J. Chem. Downloaded from www.nrcresearchpress.com by 210.87.254.40 on 09/05/12
For personal use only.

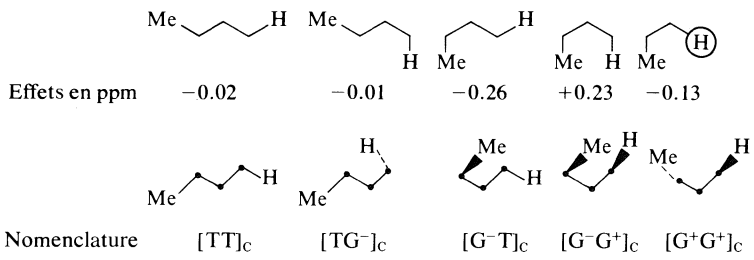

Incréments d'effet γ

Plusieurs enchaînements entre groupement méthyle et proton sont à considérer. Nous les avons représentés ci-dessous.[4]

Ces divers effets sont déterminés à partir des *tert*-butylcyclohexanes (10) dans la fig. 5. Ces incréments ont des valeurs proches de celles déjà données dans la littérature (10) sauf pour l'arrangement $[G^-T]_C$ pour lequel une valeur voisine de zéro a aussi été proposée (18). Le paramètre correspondant à l'enchaînement $[G^+G^+]_C$ n'avait pas été déterminé.

Déplacements chimiques des protons du tert-*butyl-4' méthyl-3 spirobicyclohexane*

Ce calcul est résumé dans la fig. 6.

Effets de la liaison C—O

En supposant raisonnablement les effets du deuxième hétéroatome négligeables vis à vis des protons du cycle cyclohexanique, nous avons déterminé l'influence du remplacement d'un CH_2 par un oxygène. Les résultats sont rassemblés dans le tableau 2. Nous y donnons également les orientations des liaisons C—O vis à vis des protons considérés et à titre de comparaison les effets de la liaison C—O dans les alcools cycliques (15).

Les enchaînements $[TG^-]_O$ et $[G^-G^+]_O$ ont des effets comparables dans les spirodioxannes et les cyclohexanols, notamment en ce qui concerne $[G^-G^+]_O$ pour lequel on retrouve un fort déblindage lié à une disposition diaxiale-1,3. L'arrangement $[G^+G^+]_O$ conduit à une influence tout à fait semblable à celle déterminée pour le proton H_{5a} des dioxannes (16, 17).

En revanche, on note pour l'enchaînement plan $[TT]_O$, un effet de +0.27 ppm. Dans les hydrocarbures et alcools cycliques, cet effet est pratiquement nul. Ceci est peut être lié à l'orientation particulière d'une des orbitales de l'oxygène (en W plan par rapport au proton étudié).

D'autre part, on relève aussi un désaccord entre les influences de l'enchaînement $[G^-T]_O$ dans les spirodioxannes (+0.03) et les dioxannes (−0.20 ppm sur H_{5e}). Cette "anomalie" pourrait trouver une explication, soit dans un effet particulier dû à la présence de deux oxygènes (dans les dioxannes), soit plus sûrement dans une estimation erronée du paramètre correspondant à l'enchaînement $[G^-T]_C$. En effet, la valeur de ce paramètre est contestée dans la littérature (−0.26 selon réf. 10; ∼0 selon réf. 18).

[4]Les conformations sont repérées par les orientations "*trans*" (T) ou "*gauche*" (G) du méthyle et de l'hydrogène en γ considérées par rapport à la chaise carbonée et notées dans l'ordre Me, H (19).

1. P. Maroni, L. Cazaux, G. Chassaing, I. Prejzner et L. T. Tran. Bull. Soc. Chim. Fr. 1258 (1975).
2. J. E. Anderson. J. Chem. Soc. Chem. Commun. 669 (1969).
3. G. E. Eccleston et E. Wyn-Jones. J. Chem. Soc. B, 2469 (1971).
4. A. Greenberg et P. Laszlo. Tetrahedron Lett. 2641 (1970).
5. D. Tavernier, M. Anteunis et N. Hosten. Tetrahedron Lett. 75 (1973).
6. D. Tavernier, M. Anteunis et E. Bernaert. Bull. Soc. Chim. Belg. **83**, 497 (1974); **83**, 357 (1974).
7. Y. Koudsi. Thèse de Doctorat ès-Sciences, Université Paul Sabatier Toulouse, no 666, 1975.
8. M. Perry et Y. Maroni-Barnaud. Bull. Soc. Chim. Fr. 2372 (1969).
9. J. Pansard et M. Gaudemar. Bull. Soc. Chim. Fr. 3472 (1973).
10. D. Danneels et M. Anteunis. Org. Magn. Reson. **6**, 617 (1974).
11. H. Booth. Progress in nmr spectroscopy. Vol. 5. Pergamon Press, Oxford. 1969. pp. 231–381.
12. J. Delmau, J. C. Duplan et M. Davidson. Tetrahedron, **23**, 4371 (1967).
13. M. Anteunis, D. Tavernier et F. Borremans. Bull. Soc. Chim. Belg. **75**, 396 (1966).
14. E. L. Eliel, V. S. Rao, F. W. Vierhapper et G. Z. Juaristi. Tetrahedron Lett. 4399 (1975).
15. G. Danneels et M. Anteunis. Tetrahedron Lett. 687 (1975).
16. P. Maroni et J. P. Gorrichon. Bull. Soc. Chim. Fr. 785 (1972).
17. P. Maroni, L. Cazaux, J. P. Gorrichon, P. Tisnes et J. G. Wolf. Org. Magn. Reson. **5**, 517 (1973).
18. H. Werner, H. J. Köhler, M. Mühlstädt, A. Zschurka et G. Mann. Org. Magn. Reson. **5**, 119 (1973).
19. P. E. McMahon et W. C. Tincher. J. Mol. Spectrosc. **15**, 180 (1965).

Can. J. Chem. Downloaded from www.nrcresearchpress.com by 210.87.254.40 on 09/05/12
For personal use only.

Stéréochimie de β-diols et de leurs dérivés cycliques. XIII.[1] Etude structurale en résonance magnétique nucléaire du proton de dioxanne-1,3-4-spirocyclohexanes : *tert*-butyl-6-*c* méthyl-2-*r* (série II) et diméthyl-2-*r*, 5-*t* ou 5-*c* (série III) dioxanne-1,3-4-*t* ou -*c*-spirotriméthyl-3′,3′,5′-cyclohexanes-*trans* ou -*cis*

LOUIS CAZAUX, JEAN-PIERRE GORRICHON, YAHIA KOUDSI ET PIERRE MARONI

Laboratoire de Synthèse et Physicochimie organique, ERA no 686 du CNRS, 118 route de Narbonne, 31077 Toulouse Cédex, France

Reçu le 3 mars 1978

LOUIS CAZAUX, JEAN-PIERRE GORRICHON, YAHIA KOUDSI et PIERRE MARONI. Can. J. Chem. **56**, 3006 (1978).

Les spectres de deux séries de quatre et huit diastéréoisomères des dioxannes-1,3-4-spirocyclohexanes du titre sont analysés à 60, 100 et 250 MHz dans CCl_4. A l'aide notamment du calcul empirique des déplacements chimiques, les structures ont été déterminées sans ambiguité en dehors de toute filiation chimique; à deux exceptions près, les conformations sont des double chaises. Dans ces molécules les effets γ intercycles des groupes méthyles en position 5 sont calculés.

LOUIS CAZAUX, JEAN-PIERRE GORRICHON, YAHIA KOUDSI, and PIERRE MARONI. Can. J. Chem. **56**, 3006 (1978).

The nmr spectra at 60, 100, and 250 MHz in CCl_4 of two series of four and eight diastereoisomers of the title 1,3-dioxanespiro-4-cyclohexanes have been analysed. In particular, use of the empirical calculation of chemical shifts allows for the unambiguous determination of structure without the need for chemical methods. With two exceptions, these compounds exist in the double chair conformation. In these molecules the γ intercyclic effect of the methyl groups in position 5 have been calculated.

[Journal translation]

Can. J. Chem. Downloaded from www.nrcresearchpress.com by 210.87.254.42 on 09/05/12
For personal use only.

Nous avons synthétisé, outre les deux composés de la série I, **1** et **2** décrite dans le mémoire précédent (partie X, réf. 1) et les quatre composés **3** à **6** étudiés dans le suivant (partie XIV) deux séries de spirodioxannes (schéma 1) à partir de la triméthyl-3,3,5

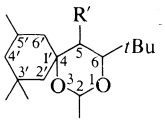

SCHÉMA 1. Spirodioxannes des séries II (R′ = H) et III (R′ = CH_3).

cyclohexanone et de dérivés magnésiens de la diméthyl-3,3 butanone-2 (R′ = H, série II) ou de la diméthyl-2,2 pentanone-3 (R′ = CH_3, série III). Ces deux séries comportent respectivement quatre et huit diastéréoisomères (schéma 2).[2] Ce sont des produits liquides qui ont été séparés par chromatographie sur couche mince préparative.

Nous déterminons les structures de ces molécules indépendamment de toute filiation chimique, en utilisant les déplacements chimiques des protons dans le tétrachlorure de carbone. Les conformations sont alors connues en appliquant les résultats du calcul empirique des déplacements chimiques (2). De plus, les écarts observés entre valeurs calculées et expérimentales de ces paramètres, sont révélateurs de modification de la conformation des cycles (3).

Le passage des β-cétols aux dioxannes, lors de la synthèse, ne modifie pas la configuration des carbones C_4, C_5 et C_6. La détermination de structure des β-cétols de départ et des β-diols intermédiaires peut donc être traitée (4) comme application de ce travail.

Notation

Nous avons représenté dans le schéma 2, les divers isomères obtenus : les carbones asymétriques y sont nommés dans l'ordre successif où ils apparaissent au cours de la synthèse: $C_{5'}$, $C_{spiro(1'\text{ ou }4)}$, $C_{5(cétols)}$, $C_{6(diols)}$ et $C_{2(dioxannes)}$. Dans la série III, les notations "a" et "e" se réfèrent à l'orientation axiale ou équatoriale du groupement méthyle en 5. Il y a dans cette série, une inversion de nomenclature du carbone 5 quand on passe du cétol au diol, par suite de la modification de l'ordre séquentiel des substituants. Quelques relations topologiques simples entre les divers isomères permettent de construire facilement les modèles moléculaires. Dans la série II, ou dans un même type a ou e de la série III, on peut passer de **7** aux isomères **8**, **9** et **10**, en faisant subir au cycle cyclohexanique et aux substituants méthyles en 3′ et 5′, les changements respectifs: **7** → $\bar{\mathbf{8}}$: passage de $Me_{3'a}$ en $Me_{5'a}$; **7** → $\bar{\mathbf{9}}$: passage de $Me_{5'e}$

[1]Partie précédente, voir réf. 1.

[2]L'énergie conformationnelle du méthyle en position 2 étant de 4.1 kcal mol^{-1} (11) seuls les diastéréoisomères pour lesquels ce méthyle est équatorial ont été isolés.

Can. J. Chem. Downloaded from www.nrcresearchpress.com by 210.87.254.42 on 09/05/12
For personal use only.

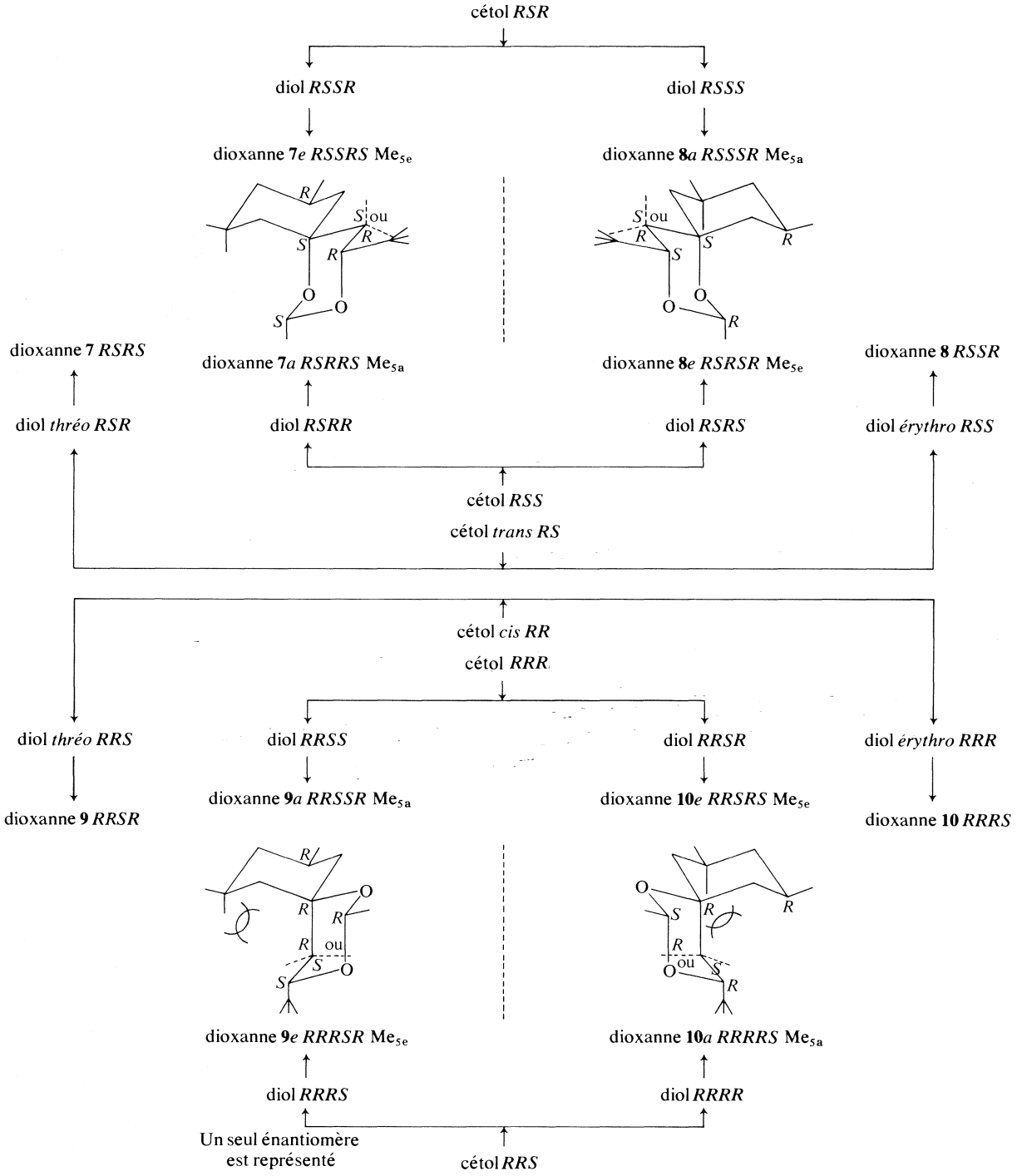

SCHÉMA 2. Filiation chimique conduisant aux spirodioxannes non substitués en 5, **7** à **10** (série II) et monométhylés en 5, **7***ae* à **10***ae* (série III).

en $Me_{5'a}$ et inversion du cycle cyclohexanique; **7** → **10**: passage de $Me_{3'e}$ en $Me_{5'a}$ et inversion du cycle cyclohexanique.[3]

Abstraction faite du méthyle axial en 3′, il faut noter, enfin, que les composés **7** et **8** sont images l'un de l'autre, ainsi que **9** et **10** (schéma 2).

Etude conformationnelle

Si l'on excepte les composés **9***e* et **10***e*, la conformation préférentielle de ces molécules devrait être la double chaise.

Partie cyclohexanique

Les composés de type **7** et **8** présentent une interaction diaxiale-1,3 $Me_{3'a}\cdots C_4O_3$ d'environ 2.5 kcal mol^{-1} (5) et les composés **9** et **10**, une interaction diaxiale-1,3, $Me_{3'a}\cdots C_4—C_5$ de l'ordre de 3.7 kcal mol^{-1} (6). Dans tous les isomères étudiés, on trouve une interaction $Me_{3'a}\cdots H$ estimée à 0.8–0.9 kcal mol^{-1} (7). Mais ces tensions n'apparaissent pas suffisantes pour déplacer l'équilibre conformationnel vers une forme croisée.[4] Les contraintes précédentes demeurent, en effet, inférieures aux enthalpies ΔH^0 entre conformations chaise et croisée déterminées pour le cyclohexane lui-même, 4.8 à 7.9 kcal mol^{-1} (7). On doit aussi tenir compte du facteur entropique qui conduirait selon Anteunis *et al.* (6) à une enthalpie libre $\Delta G^0 \sim 5.1$ kcal mol^{-1} dans le cas du cyclohexane pour un $\Delta H^0 = 6$ kcal mol^{-1}. Mais les molécules qui nous intéressent sont dissymétriques et la variation d'entropie doit être plus faible.

D'après la littérature (9) on constate aussi, que les constantes de couplage homologues demeurent très voisines dans les triméthyl-3,3,5 et tétraméthyl-3,3,5,5 cyclohexylamines (schéma 3). Cette similitude montre que l'interaction diaxiale-1,3 présente dans le composé tétraméthylé n'introduit que des modifications négligeables dans la géométrie du cycle. L'analyse des δ conduit au même résultat: l'effet Δδ exercé par le groupe méthyle axial en 5, sur les protons H_A, H_B et H_X est respectivement −0.42, +0.25 et +0.13 ppm. Ces valeurs sont tout à fait comparables à celles déterminées pour des cyclohexanols ne comportant pas d'interaction diaxiale-1,3 soit −0.40, +0.19 et +0.18 ppm (réf. 2 et références citées).

Partie dioxannique

Pour le dioxanne-1,3 non substitué, la valeur élevée de la différence d'enthalpie chaise-croisée ΔH^0 (6 à 8 kcal mol^{-1}) (10) est très défavorable à une conformation croisée. De plus les substituants tertiobutyle en 6 et méthyle en 2 sont tous les deux

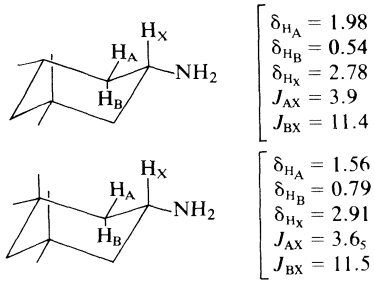

SCHÉMA 3. Déplacements chimiques (en ppm) et constantes de couplage (en Hz) pour des cyclohexylamines.

équatoriaux sur le cycle puisque leurs énergies conformationnelles sont respectivement >5 kcal mol^{-1} et d'environ 4.1 kcal mol^{-1} (11).

Toutes ces considérations permettent d'admettre que, dans les spirodioxannes, la conformation privilégiée est la double chaise.

En revanche, pour les isomères **9***e* et **10***e* de la série III, il devient nécessaire d'envisager une conformation non chaise. Il y a en effet une contrainte considérable (voir schéma 2) entre le méthyle équatorial en 5 et le cycle cyclohexanique. Cette interaction entre méthyles 5e et 3′a est analogue à une interaction diaxiale-1,3 entre substituants méthyle et tertiobutyle. Elle est en tout état de cause, très supérieure à l'énergie conformationnelle d'un tertiobutyle axial sur un cyclohexane (≥ 5.8 kcal mol^{-1}). L'inversion de la chaise cyclohexanique n'est pas suffisante car elle fait apparaître trois interactions diaxiales-1,3, une $Me\cdots C—CH_2$ et deux $Me\cdots C—O$ ce qui correspond à une énergie d'environ 8.7 kcal mol^{-1} (5, 6).

Analyse des spectres dans CCl_4

Les spectres des composés de la série II ont été enregistrés à 60 et 100 MHz sur des appareils Varian A-60 et HA-100 pour des solutions à 20% dans CCl_4. Ceux des composés de la série III ont été enregistrés à 60 et 100 MHz sur les mêmes appareils et à 250 MHz sur un appareil Cameca pour des solutions à 20% dans CCl_4. Les déplacements chimiques des différents protons et groupes de protons ainsi que les constantes de couplage sont rassemblés dans les tableaux 1 et 2.

Protons méthyliques (2e, 5e ou 5a, 3′e, 3′a, 5′e)

Les groupements méthyles en position 2e, 5e, 5a et 5′e apparaissent sous forme de doublets. On les distingue (*i*) par leurs constantes de couplage avec le proton géminé: Me_{2e} (5 Hz), $Me_{5e\ ou\ 5a}$ (7 Hz) et $Me_{5'e}$ (6 Hz). Ces valeurs sont normales pour des composés dioxanniques (12 et références citées) et

[3] $\bar{n}$ désigne l'énantiomère de *n*.

[4] La forme croisée du cyclohexane est plus stable que la forme bateau d'environ 1.6 kcal mol^{-1} (8).

Can. J. Chem. Downloaded from www.nrcresearchpress.com by 210.87.254.42 on 09/05/12
For personal use only.

TABLEAU 1. Déplacements chimiques (en ppm/TMS) et constantes de couplages (en Hz) pour les spirodioxannes de la série II dans CCl_4*

Composé	δ(J)											
	Me_{2e}	H_{2a}	tBu_{6e}	H_{6a}	H_5	$H_{2'e}$	$H_{2'a}$	$Me_{3'e}$	$Me_{3'a}$	$Me_{5'e}$	$H_{6'e}$	$H_{6'a}$
7	1.19 (5.0)	4.82 (5.0)	0.85	3.31 (10.7 et 3.5)	—	2.24 (−14.4)	~0.65 (−14.4)	0.89	1.01	0.87 (6.2)	1.65 (−13.4 et 2.2)	—
8	1.20 (5.0)	4.78 (5.0)	0.85	3.30 (11.1 et 3.0)	—	~1.45 —	—	0.94	1.06	0.87 (6.2)	2.42 (−13.4 et 2.2)	~0.40
9	1.16 (5.0)	4.95 (5.0)	0.88	3.27 (11.5 et 2.8)	5e ~1.8 5a ~1.3	2.17 (−13.2)	—	0.92	0.98	0.90 (6.2)	~1.55 (—)	—
10	1.15 (5.0)	4.92 (5.0)	0.88	3.22 (11.5 et 2.8)	5e ~1.65 5a ~1.25	1.43 (—)	—	0.91	0.95	0.93 (—)	2.32 (−12.2 et 2.2)	~0.70

*Spectres enregistrés sur des appareils Varian A 60 et HA 100.

cyclohexaniques (13). Signalons que la résonance du Mc_{5a} est élargie (par rapport à celle du Me_{5e}) par un couplage en W avec H_{6a}; (*ii*) par leurs déplacements chimiques : le méthyle en 2e est le plus déblindé (12).

Les méthyles en 3′a et 3′e sont des singulets; dans tous les cas, le signal de $Me_{3'a}$ (toujours le plus déblindé) a la plus grande largeur à mi-hauteur en raison de couplages longue distance avec les protons $H_{2'a}$ et $H_{4'a}$.

Protons dioxanniques (2a, 5a ou 5e, 6a)

Le signal du proton H_{2a} se présente sous la forme d'un quadruplet et celui de H_{6a} comme un doublet de doublet (série II) ou un doublet unique (série III). Ces deux protons axiaux ont des déplacements chimiques normaux (2), environ 5 ppm pour H_{2a} et 3 ppm pour H_{6a}. Les protons H_{5e} et H_{5a} ont pu être repérés, grâce aux constantes de couplage.

Protons cyclohexaniques (2′e, 2′a, 6′e, 6′a)

Les protons $H_{2'e}$ et $H_{2'a}$ constituent les parties A et B d'un système AB; $H_{6'e}$ et $H_{6'a}$ respectivement les parties A (ou X) et X (ou A) de systèmes ABX ou AMX, B ou M étant le proton $H_{5'a}$.

De plus, sur les signaux des protons $H_{2'e}$ et $H_{6'e}$, on relève deux constantes de couplage à longue distance d'environ 2 Hz, puisqu'ils sont en situation W coplanaire entre eux et avec le proton $H_{4'e}$.

Dans tous les isomères étudiés, nous avons pu situer les protons $H_{2'e}$ et $H_{6'e}$. Les protons axiaux correspondants sont, en revanche, plus difficilement localisables.

La fig. 1 présente un exemple caractéristique de spectre à 60 MHz et l'allure des massifs représentatifs des protons $H_{2'e}$ et $H_{6'e}$.

Correlation structure: déplacements chimiques

Composés de la série II

Calcul empirique des δ des protons $H_{2'e}$, $H_{2'a}$, $H_{6'e}$ et $H_{6'a}$

Ce calcul a été effectué à partir des résultats obtenus dans le cas des méthyl-2 dioxanne-1,3-4-spiro-*tert*-butyl-4′ cyclohexanes *cis* et *trans* **1** et **2** (série I (2)).

Nous avons d'abord déduit de la comparaison des méthyl- et *tert*-butylcyclohexanes et d'incréments déjà déterminés (13), l'influence d'un tertiobutyle sur les protons en γ.

Nous résumons dans la fig. 3 le résultat du calcul des déplacements chimiques dans les quatre diastéréoisomères de la série II.

Identification des diastéréoisomères

En comparant les valeurs des déplacements chimiques calculées et expérimentales, il apparait que l'identification des isomères est possible sans ambiguité.

Les protons les plus déblindés ($H_{2'e}$ et $H_{6'e}$) permettent un classement en deux groupes distincts: **7** et **9** d'une part, **8** et **10** de l'autre. Il faut noter que les δ des protons $H_{2'e}$ sont calculés avec une excellente précision ($\leq$0.02 ppm) alors que l'écart est plus grand pour $H_{6'e}$ (~0.1 ppm).

Les protons $H_{2'a}$ (ou $H_{6'a}$) différencient **7** de **9** et **8** de **10**; on retrouve en effet entre leurs déplacements chimiques le même écart d'environ 0.30 ppm qui existe déjà dans les composés **1** et **2**.

Sur les protons dioxanniques, si on examine les modèles moléculaires on remarque que H_{2a} de **7** et **8** est dans une situation semblable du point de vue de

Can. J. Chem. Downloaded from www.nrcresearchpress.com by 210.87.254.42 on 09/05/12
For personal use only.

Can. J. Chem. Downloaded from www.nrcresearchpress.com by 210.87.254.42 on 09/05/12
For personal use only.

TABLEAU 2. Déplacements chimiques (en ppm/TMS) et constantes de couplage (en Hz) pour les spirodioxannes de la série III dans CCl_4*

Composé	δ(*J*)																
	Me_{2e}	H_{2a}	H_{5a}	Me_{5e}	H_{5e}	Me_{5a}	tBu_{6e}	H_{6a}	$H_{2'e}$	$H_{2'a}$	$Me_{3'e}$	$Me_{3'a}$	$H_{4'e}$	$H_{4'a}$	$Me_{5'e}$	$H_{6'e}$	$H_{6'a}$
7*a*	1.17 (5.0)	4.90			1.11 (1.4 et 7.0)	0.95 (7.0)	0.93	3.55 (1.4)	2.48 (−14.4)	0.57	0.88	0.98	1.36	0.70	0.88 (6.0)	1.80 (−13.0 et 2.2)	0.50
7*e*	1.13 (5.0)	4.87	1.51 (10.0 et 7.0)	0.78 (7.0)			0.93	3.04 (10.0)	1.89 (−14.2)	0.85	0.87	0.98	—	0.68	0.85 (6.1)	1.35 (−12.6 et 2.2)	—
8*a*	1.19 (5.0)	4.87			1.11 (1.4 et 7.0)	0.94 (7.0)	0.93	3.56 (1.4)	1.62 (−14.4)	0.72	0.86	0.98	1.38	0.72	0.88 (6.2)	2.65 (−13.6 et 2.2)	0.40
8*e*	1.16 (5.0)	4.81	1.54 (10.0 et 7.0)	0.78 (7.0)			0.92	3.02 (10.0)	1.20 (−14.3)	—	0.85	1.03	1.36	0.69	0.86 (6.2)	2.04 (−13.2 et 2.2)	0.61
9*a*	1.18 (5.0)	4.98			1.77 (1.8 et 7.0)	0.97 (7.0)	0.95	3.53 (1.8)	2.38 (−13.4)	1.06	0.87	0.96	—	—	0.90 (6.0)	1.86 (−13.2 et 2.2)	0.73
9*e*	1.18 (5.0)	4.83	1.69 (8.0 et 7.0)	0.82 (7.0)			0.95	2.92 (8.0)	1.49 (−13.4)	0.95	0.87	0.95	1.21	1.08	0.90 (6.0)	2.08 (−13.1 et 5.1)	—
10*a*	1.15 (5.0)	5.00			1.64 (1.9 et 7.0)	0.96 (7.0)	0.95	3.52 (1.9)	1.82 (−14.0)	—	0.90	1.05	—	—	0.90 (6.0)	2.55 (−12.8 et 2.2)	—
10*e*	1.16 (5.1)	4.81	1.60 (9.2 et 7.0)	0.78 (7.0)			0.93	2.87 (9.2)	1.60 (−13.9)	—	0.88	1.01	—	—	0.92 (6.0)	—	—

*Spectres enregistrés sur un appareil Cameca 250.

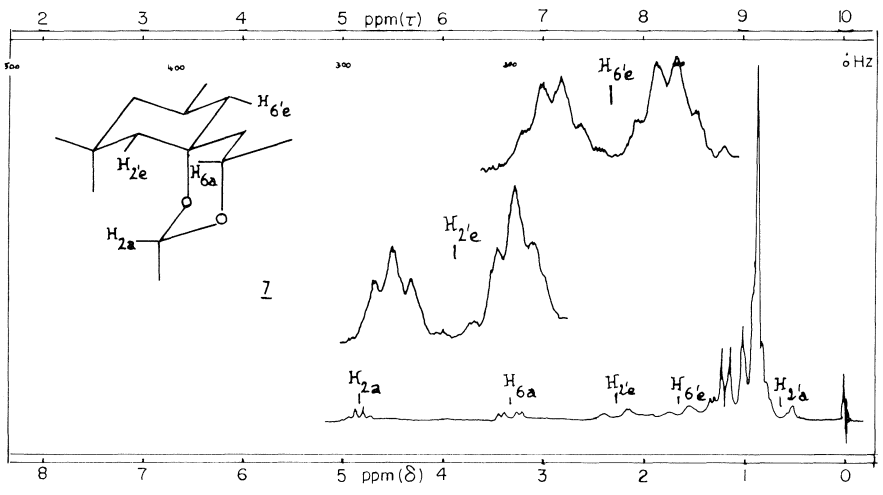

FIG. 1. Spectre à 60 MHz du composé **7**.

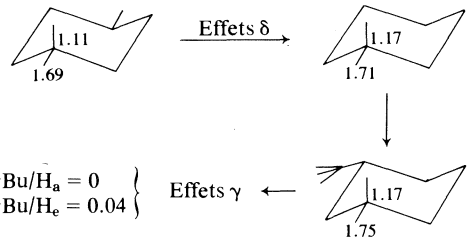

FIG. 2. Incréments d'effet γ d'un groupement tertiobutyle.

l'environnement spatial, notamment vis à vis de la liaison $C_{2'}$—$C_{3'}$, à celle du proton H_{6a} dans **9** et **10**. H_{2a} de **9** et **10** et H_{6a} de **7** et **8** ne devraient pas subir la même influence.

Si on se refère aux δ de ces divers protons (tableau 1) on constate que $\delta_{H_{2a}}$ (**7** et **8**) $-\delta_{H_{2a}}$ (**9** et **10**) $\simeq -0.13$ ppm et $\delta_{H_{6a}}$ (**9** et **10**) $- \delta_{H_{6a}}$ (**7** et **8**) $\simeq -0.06$ ppm. On a donc là aussi un moyen de connaitre l'isomérie portant sur l'orientation de la liaison C_4—O_3. Ceci est encore confirmé par les différences notées pour les spirodioxannes **1** et **2**. En effet $\delta_{H_{2a}}(\mathbf{1}) - \delta_{H_{2a}}(\mathbf{2}) = -0.12$ ppm et $\delta_{H_{6a}}(\mathbf{2}) - \delta_{H_{6a}}(\mathbf{1}) = -0.15$ ppm.

Composés de la série III

Les résultats acquis pour la série II au niveau du cycle cyclohexanique sont maintenant perturbés par les influences intercycles (effet γ) des groupements méthyles substitués sur le carbone 5. Ces effets γ étant peu décrits dans la littérature, nous avons, avec ces molécules, un moyen de les déterminer. Pour différencier les diastéréoisomères de cette série, nous avons aussi effectué un calcul de déplacement chimique des protons dioxanniques.

Calcul empirique des δ des protons H_{2a} et H_{6a}

Ce calcul a été réalisé à partir des déplacements chimiques expérimentaux des protons analogues dans la série II (cf. tableau 1). En raison de l'influence non négligeable des interactions gauches Me···*t*Bu, sur les incréments Δδ déjà décrits (2), liés à un méthyle en position 5, nous sommes conduits à déterminer de nouveaux paramètres. Pour cela, nous avons extrapolé les δ du *tert*-butyl-6 diméthyl-4,4 dioxanne-1,3 à partir de ceux du *tert*-butyl-4 dioxanne-1,3 (3) et d'incréments connus (2). Nous rappelons aussi les δ des protons dans les *tert*-butyl-6 triméthyl-4,4,5 dioxannes-1,3 *cis* et *trans* (14). La comparaison de ces diverses valeurs fournit les incréments cherchés (fig. 4). Les déplacements chimiques des protons H_{2a} et H_{6a} des huit diastéréoisomères de la série III, sont alors obtenus en ajoutant ces paramètres aux δ des protons correspondants des spirodioxannes de la série II (tableau 3).

Attribution de configuration

Les différences de déplacements chimiques du proton 6a (tableau 3) et les valeurs des constantes de couplage J_{5a6a} et J_{5e6a} (tableau 2) permettent de distinguer la série e de la série a. A partir des calculs du tableau 3, on peut alors, attribuer à chacun des huit isomères un couple de valeurs de façon que l'écart $\delta_{calc} - \delta_{exp}$ soit minimal. On a ainsi un moyen d'identifier chaque isomère et de remonter à la configuration des produits dont ils sont issus. Cependant les variations de δ entre isomères, ne différant que par la substitution méthylée sur le cycle cyclohexanique restent dans les limites de l'incertitude expérimentale. L'attribution faite sur 2a et 6a a donc du être confirmée par l'analyse des effets intercycles des Me_5 sur les protons 2′e et 6′e qui sont soumis directement à l'influence des $Me_{3'}$ et du $Me_{5'}$ (*vide infra*).

Les résultats obtenus justifient les hypothèses

Can. J. Chem. Downloaded from www.nrcresearchpress.com by 210.87.254.42 on 09/05/12
For personal use only.

Can. J. Chem. Downloaded from www.nrcresearchpress.com by 210.87.254.42 on 09/05/12
For personal use only.

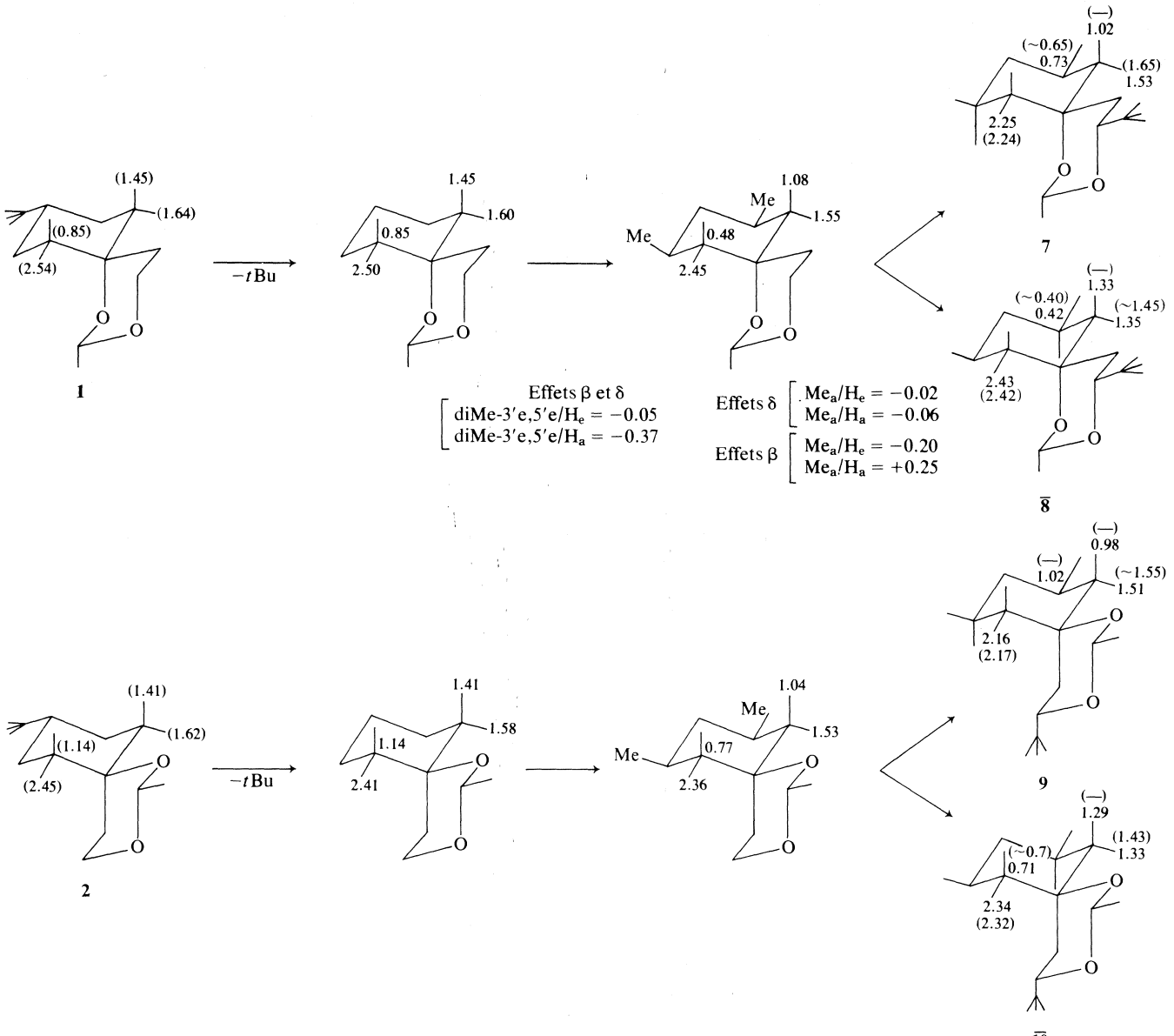

FIG. 3. Calcul empirique du déplacement chimique des protons $H_{2'e}$, $H_{2'a}$, $H_{6'e}$ et $H_{6'a}$ des composés **7**, **8**, **9** et **10**. Entre parenthèses figurent les valeurs expérimentales.

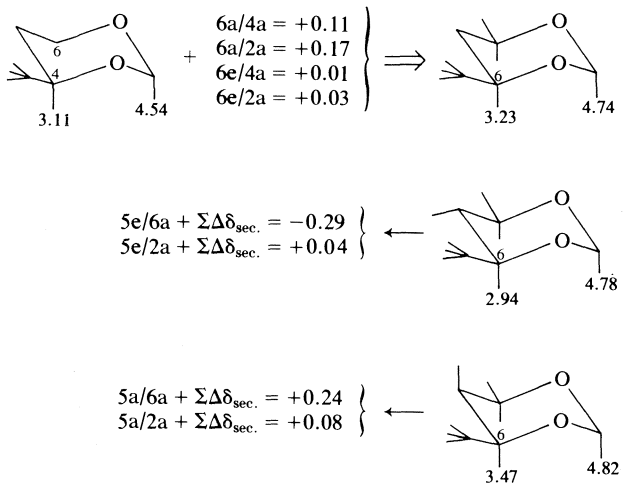

FIG. 4. Incréments des substituants méthyles en position 5 d'un dioxanne-1,3 en présence d'un *gem*-diméthyle-4,4 et d'un tertiobutyle-6.

TABLEAU 3. Déplacements chimiques des protons 2a et 6a calculés et expérimentaux dans les spirodioxannes de la série III

Spirodioxanne	H	δ_{calc}	δ_{exp}	$\Delta\delta$ ($\delta_{calc} - \delta_{exp}$)
7*a*	2a	4.90	4.90	0
	6a	3.55	3.55	0
7*e*	2a	4.86	4.87	−0.01
	6a	3.02	3.04	−0.02
8*a*	2a	4.86	4.87	−0.01
	6a	3.54	3.56	−0.02
8*e*	2a	4.82	4.81	+0.01
	6a	3.01	3.02	−0.01
9*a*	2a	5.03	4.98	+0.05
	6a	3.51	3.53	−0.02
9*e*	2a	4.99	4.83	+0.16
	6a	2.98	2.92	+0.06
10*a*	2a	5.00	5.00	0
	6a	3.46	3.52	−0.06
10*e*	2a	4.96	4.81	+0.15
	6a	2.93	2.87	+0.06

faites sur les conformations de ces molécules; en particulier seuls les composés **9***e* et **10***e* présentent un écart $\Delta\delta$ important (>0.1 ppm) que nous pouvons corréler à une modification conformationnelle (3).

Conformations des composés **9**e *et* **10**e

Spirodioxanne **9**e—Nous observons sur le spectre rmn enregistré dans CCl_4, un massif de quatre bandes centrées à 2.08 ppm et un doublet à 1.49 ppm que nous attribuons respectivement à $H_{6'e}$ et $H_{2'e}$. L'allure particulière de ces signaux est probablement due à une plus faible amplitude des couplages à distance que dans le cas des autres isomères (cf. fig. 5). Nous lisons sur le doublet, la constante $^2J_{2'} = -13.4$ Hz et sur le multiplet (partie X d'un système ABX) la somme $|^2J_{6'} + {}^3J_{6'e5'a}| = 18.2$ Hz. La première constante est normale pour un couplage géminé dans les cyclohexanes. En prenant pour $^2J_{6'}$ une valeur de −13.1 Hz (moyenne des valeurs relevées pour les composés en conformation chaise, tableau 2) nous en déduisons $^3J_{6'e5'a} \sim 5.1$ Hz. Cette forte valeur ($^3J_{6'e5'a} = 2.2$ Hz dans les autres isomères) et la diminution des couplages à longue distance $^4J_{2'e4'e}$, $^4J_{2'e6'e}$ et $^4J_{6'e4'e}$ impliquent une déformation importante de la partie cyclohexanique.

La valeur de la constante $^3J_{5a6a} = 8$ Hz (cette constante est de l'ordre de 10 Hz dans les composés sous forme chaise) indique également une modification conformationnelle de la partie dioxannique.

Spirodioxanne **10**e—Seul le signal du proton $H_{2'e}$ est visible à 1.60 ppm ($^2J_{2'} = -13.9$ Hz). Dans ce cas aussi, les couplages en W ne sont pas apparents et nous pouvons en conclure que la partie cyclohexanique est déformée. Le cycle dioxannique ne serait que peu perturbé puisque la constante $^3J_{5a6a} = 9.2$ Hz.

Qu'il y ait participation de formes croisées dans les conformations de ces deux molécules apparaît encore très nettement sur les valeurs d'incréments d'effets γ intercycles dont nous abordons la détermination dans le paragraphe suivant (cf. tableau 4).

Effets γ intercycles des groupes méthyles en position 5a et 5e

Nous avons vu (schéma 2) que si l'on ne tient pas compte du substituant $Me_{3'a}$, les spirodioxannes **7***a* et **8***a*, **7***e* et **8***e*, **9***a* et **10***a*, **9***e* et **10***e* sont images dans un miroir. Il en résulte que la comparaison de chaque molécule de la série III au composé correspondant de la série II permet de définir deux fois le même effet du groupement méthyle 5 sur les protons $H_{2'e}$ et $H_{6'e}$. Nous donnons dans le tableau 4 les valeurs ainsi calculées avec l'enchaînement impliqué.

L'enchaînement $[G^-G^+]$ correspond à l'influence d'un méthyle axial sur un proton axial en situation diaxiale-1,3. Les valeurs relevées dans le tableau 4 (+0.15 à +0.40 ppm) sont en grandeur et en signe comparables à celles observées dans les cyclohexanes (+0.27 ppm (13)), les cyclohexanols (+0.18 à 0.23 ppm (15)) et les dioxannes (+0.11 à +0.20 ppm (2)) pour un même arrangement méthyl–proton.

La valeur de $[TG^-]$ (+0.23 ppm en moyenne) est très forte vis à vis de celle notée dans les cyclohexanes (+0.01 ppm (13)). En revanche, l'enchaînement $[G^+G^+]$ dans **7***e* et **8***e* a une valeur moyenne (−0.32 ppm) de même signe mais plus grande que celle que nous avons déterminée à partir du tertiobutylcyclohexane (cf. fig. 4 dans réf. 1, $[G^+G^+]_c =$

Can. J. Chem. Downloaded from www.nrcresearchpress.com by 210.87.254.42 on 09/05/12
For personal use only.

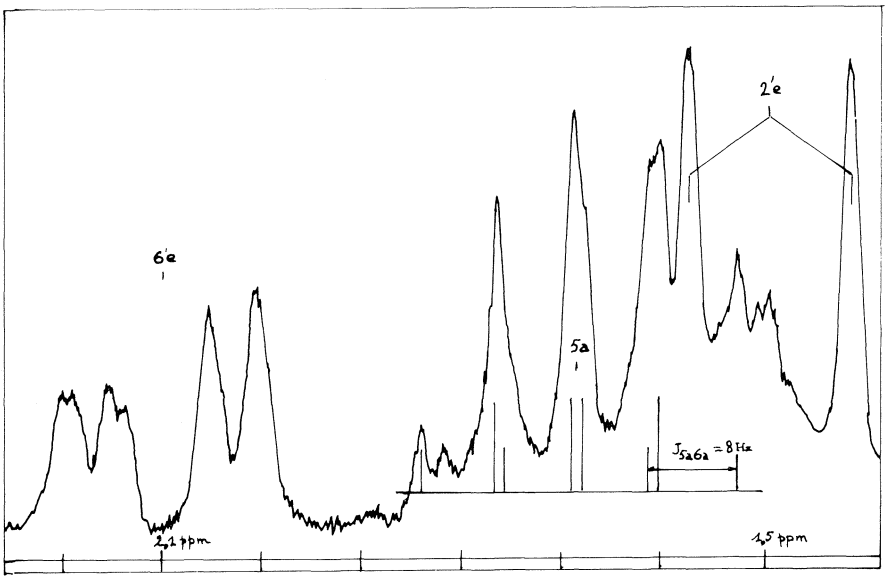

FIG. 5. Résonances des protons $H_{6'e}$, $H_{2'e}$ et H_{5a} du composé **9***e* à 100 MHz.

TABLEAU 4. Incréments d'effets γ intercycles $Me_5/H_{2'\text{ ou }6'}$ dans les spirodioxannes

Substituant	Proton (no du composé)	$Me_{5/H}$	Enchaînement
Me_{5a}	2'e (**7***a*)	+0.24	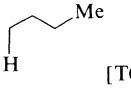 [TG⁻]
	6'e (**8***a*)	+0.23	
	2'e (**9***a*)	+0.21	
	6'e (**10***a*)	+0.23	
	6'e (**7***a*)	+0.15	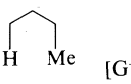 [G⁻G⁺]
	2'e (**8***a*)	~+0.17	
	6'e (**9***a*)	~+0.31	
	2'e (**10***a*)	~+0.39	
Me_{5e}	2'e (**7***e*)	−0.35	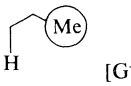 [G⁺G⁺]
	6'e (**8***e*)	−0.38	
	2'e (**9***e*)	~−0.68	
	6'e (**7***e*)	−0.30	
	2'e (**8***e*)	−0.25	
	6'e (**9***e*)	~+0.53	
	2'e (**10***e*)	~+0.17	
	2'a (**7***e*)	~+0.20	[G⁻G⁺]
	6'a (**8***e*)	~+0.20	

−0.13 ppm). On observe donc, un bon accord entre les diverses valeurs d'un même incrément d'effet γ intercycle pour les composés **7***a* à **10***a* et **7***e*, **8***e*. En revanche, les forts écarts notés pour les produits **9***e* et **10***e*, renforcent l'hypothèse de la présence de conformations croisées pour l'un ou l'autre (ou les deux) cycle(s).

Dans le cas où les méthyles en 3' et 5' seraient inversés (**7**ae → **8**ae, **9**ae → **10**ae), les effets intercycles deviennent aberrants: TG^- (−0.35 à −0.62), G^-G^+ (+0.95 à +1.00) et G^+G^+ (+0.44 à −1.07). De plus la dispersion de ces résultats et l'homogénéité de ceux qui découlent des attributions précédentes confirment notre analyse structurale.

1. L. CAZAUX, J. P. GORRICHON, P. MARONI et M. PERRY. Can. J. Chem. **56**, 2998 (1978).
2. P. MARONI, L. CAZAUX, J. P. GORRICHON, P. TISNES et J. G. WOLF. Org. Magn. Reson. **5**, 517 (1973).
3. P. MARONI, L. CAZAUX, J. P. GORRICHON, P. TISNES et J. G. WOLF. Org. Magn. Reson. **5**, 523 (1973).

Can. J. Chem. Downloaded from www.nrcresearchpress.com by 210.87.254.42 on 09/05/12
For personal use only.

4. Y. KOUDSI. Thèse de doctorat ès-Sciences, Université Paul Sabatier Toulouse, No 666, 1975.
5. S. J. ANGYAL, V. A. PICKLES et R. AHLLIWALIA. Carbohydr. Res. **1**, 365 (1966).
6. M. ANTEUNIS, D. TAVERNIER et F. BORREMANS. Heterocycles, **4**, 357 (1976).
7. G. M. KELLIE et F. G. RIDDELL. Top. Stereochem. **8**, 225 (1974).
8. J. B. HENDRICKSON. J. Am. Chem. Soc. **83**, 4537 (1961).
9. H. BOOTH. Progress in nmr spectroscopy. Vol. 5. Pergamon Press, Oxford. 1969. pp. 303–304.
10. M. ANTEUNIS, D. TAVERNIER et F. BORREMANS. Heterocycles, **4**, 293 (1976).
11. E. L. ELIEL et F. NADER. J. Am. Chem. Soc. **92**, 3050 (1970).
12. P. MARONI et J. P. GORRICHON. Bull. Soc. Chim. Fr. 785 (1972).
13. D. DANNEELS et M. ANTEUNIS. Org. Magn. Reson. **6**, 617 (1974).
14. P. MARONI, J. P. MAFFRAND et J. P. GORRICHON. C.R. Acad. Sci. Ser. C **270**, 740 (1970).
15. E. L. ELIEL, M. H. GIANNI, T. H. WILLIAMS et J. B. STOTHERS. Tetrahedron Lett. 741 (1962).

Downloaded from www.nrcresearchpress.com by 210.87.254.42 on 09/05/12
For personal use only.

Stéréochimie de β-diols et de leurs dérivés cycliques. XIV.[1] Analyse structurale de dioxanne-1,3-4-spirocyclohexanes par résonance magnétique nucléaire du ^{13}C

LOUIS CAZAUX, JEAN-PIERRE GORRICHON ET PIERRE MARONI

Laboratoire de Synthèse et Physicochimie organique, ERA no 686 du CNRS, 118, route de Narbonne, 31077 Toulouse Cédex, France

Reçu le 3 mars 1978

LOUIS CAZAUX, JEAN-PIERRE GORRICHON et PIERRE MARONI. Can. J. Chem. **56**, 3016 (1978).

Le calcul empirique du déplacement chimique en rmn du ^{13}C selon Grant et Saunders est envisagé dans cinq séries de dioxanne-1,3-4-spirocyclohexanes dont une comporte huit diastéréoisomères. Les incréments nécessaires à ce calcul sont déduits de la littérature ou établis à partir de molécules modèles et leur application conduit à des attributions de structure non ambiguës.

LOUIS CAZAUX, JEAN-PIERRE GORRICHON, and PIERRE MARONI. Can. J. Chem. **56**, 3016 (1978).

Following the methods of Grant and Saunders the empirical calculation of the ^{13}C chemical shift in five series of 1,3-dioxanespiro-4-cyclohexanes, including one with eight diastereoisomers, is reported. The increments used in these calculations have been derived from the literature or determined from model compounds and their use leads to unambiguous structural assignments.

[Journal translation]

Introduction

Dans les mémoires précédents (1, 2), nous avons utilisé le calcul empirique du déplacement chimique en rmn du proton (3, 4) pour l'étude conformationnelle de dioxanne-1,3-4-spirocyclohexanes. Nous poursuivons ce travail en rmn du ^{13}C à partir de deux méthodes de calcul proposées dans la littérature, l'une par Grant et coll. (5–8), l'autre par Saunders et coll. (9–12).

La structure spirodioxannique des composés étudiés impose la définition préalable de nouveaux incréments que nous avons testés par ailleurs sur des hydrocarbures, alcools cycliques et dioxannes-1,3 de conformation connue (25). Dans ce mémoire nous établissons, dans un premier temps, les systèmes d'incréments des deux méthodes pour les molécules choisies comme modèles; puis nous les appliquons au calcul des déplacements chimiques des dioxannes-1,3-4-spirocyclohexanes schématisés dans le tableau 1 et à l'analyse conformationnelle de ces dérivés indépendamment de l'étude précédente (1, 2) en rmn du proton.

Systèmes d'incréments utilisés

Méthode de Grant

Hydrocarbures cycliques à six chaînons

A partir d'une investigation systématique de 15 cyclohexanes méthylés, Dalling et Grant (5) ont caractérisé les effets de la substitution d'un hydrogène par un groupement méthyle sur les carbones du cycle. Ces résultats ont été développés et les paramètres réajustés dans une publication plus récente de ces auteurs (6). Malgré les difficultés rencontrées pour justifier telle valeur des paramètres par un phénomène physique bien défini, on peut néanmoins prédire le déplacement chimique de carbones dans ces cycles à partir de formules simples: $\delta_{C/TMS} = 27.1 + \sum A$ pour les carbones du cycle; $\delta_{C/TMS} = 23.1 + \sum B$ pour les groupements méthyles (27.1 est la valeur expérimentale pour la résonance des carbones du cyclohexane; 23.1 la valeur moyenne expérimentale pour un groupe méthyle équatorial sur le cyclohexane). Les valeurs des incréments A et B sont données dans les réfs 5 et 6.

Alcools cycliques

Les travaux de Roberts et coll. (13) sur les alcools linéaires et les cyclohexanols d'une part, de Grover et Stothers (14) d'autre part, permettent de déterminer les effets du substituant hydroxyle[2] en prenant comme base $\delta_0 = 27.1$ ppm pour les cyclohexanols et les δ des carbones de la décaline-*trans* pour les décalols.

Dioxannes-1,3

Effets des substituants méthyles—Kellie et Riddell (15, 16) ont mesuré le déplacement chimique des carbones cycliques de 25 dioxannes-1,3. Ces auteurs déterminent les incréments liés à l'effet de groupes méthyles d'une manière analogue à celle utilisée par Grant pour les cyclohexanes. Ces paramètres ne sont pas les mêmes suivant la position du substituant

[1]Pour la partie XIII, voir réf. 2.

[2]Nous avons vérifié (25) que dans le cas des cyclohexanols, la présence d'un groupe hydroxyle ne modifiait pas les paramètres d'effet du groupement méthyle définis par Grant pour les cyclohexanes. Nous n'avons évidemment examiné que le cas où n'existe aucune interaction (géminée ou vicinale) entre ces deux substituants.

Can. J. Chem. Downloaded from www.nrcresearchpress.com by 210.87.254.5 on 09/05/12
For personal use only.

Can. J. Chem. Downloaded from www.nrcresearchpress.com by 210.87.254.5 on 09/05/12
For personal use only.

puisque les carbones 2,4 ou 6 et 5 dans un dioxanne-1,3 ne sont pas équivalents. Les bases sont les déplacements chimiques des carbones 2, 4 et 5 du dioxanne-1,3 lui-même.

Effets des oxygènes—L'effet α des oxygènes intracycliques est très important. Par comparaison du dioxanne-1,3 et du cyclohexane on peut le chiffrer à environ +39 ppm pour un oxygène (δ_{C_4} = 66.2 ppm, $\delta_{C(cyclohexane)}$ = 27.1 ppm) et à +66 ppm pour deux oxygènes (δ_{C_2} = 93.1). L'additivité de ces effets n'est donc pas respectée.

Quelques résultats de la littérature (17, 18) permettent de préciser l'effet γ pour des enchaînements O—C_α—C_β—C_γ gauche ou antipériplanaire. Pour des liaisons C_β—C_γ et O—C_α *gauche*, l'effet est relativement faible (−2.1 à −3.3 ppm dans les dioxannes) en revanche pour un enchaînement antipériplanaire l'effet paraît très sensible à la substitution du carbone étudié et peut devenir important (−1.4 à −2.3 ppm pour un $\geq$C—, −8.3 pour un CH_2, −11 pour un méthyle-5 équatorial).

Nous avons entrepris pour notre part (25) la détermination des incréments liés à l'effet β de ces oxygènes à la fois en fonction de l'orientation des hétéroatomes (enchaînements C—O—C_α—C_β *gauche* ou *anti*) et du degré de substitution du carbone C_α. Les résultats de cette étude sont rassemblés dans les tableaux 2 et 5.

On constate tout d'abord que la valeur de l'incrément *A* est tout à fait comparable à la différence d'effet β existant entre des substituants hydroxyle et méthyle ($\delta_C^{ROH}(\beta) - \delta_C^{RCH_3}(\beta) = -0.5$ ppm; cf. réf. 13). Ceci montrerait encore que l'effet β est peu sensible à la nature d'un substituant (19–21), un groupement O—CH_2 intracyclique ayant la même influence qu'un groupe hydroxyle exocyclique.

Les différences observées entre les incréments *A* et *B*, *B* et *C* d'une part, *D* et *E* d'autre part pourraient s'expliquer par une modification de l'effet inducteur des groupes méthyles portés par le carbone α en raison de la polarisation de la liaison O—C_α. Les écarts (~1.5 et 0.5 ppm respectivement) et le nombre d'exemples sont cependant trop faibles pour caractériser un tel effet de façon sûre. Il faut noter que l'on retrouve une différence d'environ 1.5 ppm entre les effets β_e et β_a déterminés pour des méthyles substitués sur le cyclohexane (9.0 et 5.4 ppm) et ceux substitués en 4 sur le dioxanne (7.3 et 3.7 ppm).

Il semble donc que, pour l'effet β d'oxygènes intracycliques, l'effet de substitution soit plus important que celui d'orientation.

Méthode de Saunders

Hydrocarbures à six chaînons

A partir des résultats obtenus par Grant pour les décalines (7) et d'une mise en cause de la signification réelle de l'effet β, qui ne serait pas une contribution inductive, Saunders et Beierbeck (9) proposent une interprétation en fonction des interactions gauches présentes dans les molécules étudiées.

L'effet α, en général non additif d'après ces auteurs, est éliminé du calcul en utilisant comme "bases" les déplacements chimiques des carbones primaire, secondaire, tertiaire et quaternaire respectivement dans l'éthane, le propane, l'isobutane et le néopentane. Quatre incréments suffisent alors pour calculer les déplacements chimiques suivant la formule:

$$\delta_C = A + \sum I$$

Les valeurs de ces incréments sont fournies dans la réf. 9.

Alcools cycliques

Les effets à longue distance (δ, ε) du groupement hydroxyle dans les décalols sont faibles (14). On peut donc admettre que, pour les carbones situés dans ces positions, les incréments déterminés par Beierbeck et Saunders (9) pour les décalines sont encore valables.

Pour les carbones situés en β ou γ du substituant hydroxyle, il est nécessaire d'introduire quatre nouveaux incréments, définis dans les réfs 10 et 25, tenant compte d'interactions dues à la présence de l'oxygène.

Dioxannes-1,3

Nous avons déterminé les incréments d'interaction nécessaire au calcul de l'effet β par cette méthode soit sur le carbone non substitué en position 5 dans le cycle dioxannique, soit sur les carbones de méthyles équatoriaux ou axiaux en position 4. On peut, pour ces carbones, conserver les valeurs de base (16.1 et 5.9 ppm respectivement) déjà utilisées par Saunders pour éliminer l'effet α.

Nous avons tout d'abord choisi comme modèles les molécules représentées dans la fig. 1. A partir des déplacements chimiques expérimentaux des carbones de ces molécules, on peut écrire:

$$25.2 = 16.1 + 2HO + 2CO''$$

$$33.6 = 16.1 + 2HO + 2CO'' + 2HC$$

$$21.6 = 5.9 + 2HO + 2HC$$

$$35.9 = 16.1 + 2HO + 2CO'' + 3HC + 1CC'$$

Les notations des incréments sont les mêmes que dans le cas des cyclohexanes et cyclohexanols. Elles sont précisées dans la fig. 2. Les trois premières valeurs ne sont pas fondamentalement différentes de celles déterminées dans les cyclohexanes et cyclohexanols. Les valeurs numériques des paramètres HC et HO sont seulement plus faibles dans le cas des

TABLEAU 1. Déplacements chimiques (en ppm/TMS) des carbones $C_{2'}$, $C_{6'}$ et C_5 des composés **1**–**10***a* à 15.08 MHz dans $CDCl_3$

	δ										
	C_5					$C_{2'}$			$C_{6'}$		
		Calc.					Calc.			Calc.	
Composé	Exp.	Grant	Saunders	$C_{5\alpha}$ Exp.	$C_{5\alpha'}$ Exp.	Exp.	Grant	Saunders	Exp.	Grant	Saunders
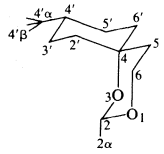 *cis*-**1**	36.2	36.3	37.8			29.6	30.5	31.7	40.6	40.1	41.9
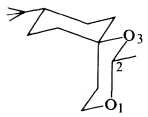 *trans*-**2**	30.6	31.3	30.9			30.8	30.5	31.5	41.3	40.1	41.7
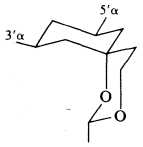 *cis-cis*-**3**	36.8	36.3	37.8			38.3	38.6	41.1	48.9	48.2	51.3
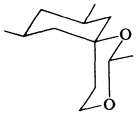 *trans-trans*-**4**	32.4	31.3	30.9			39.0	38.6	41.0	49.7	48.2	51.2
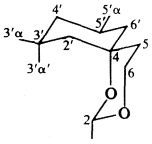 **5**	37.4	36.3	37.8			40.3	42.7	47.6*	48.8	48.2	51.3
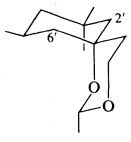 **6**	36.8	36.3	37.8			51.7	52.3	57.8*	38.1	38.6	41.1
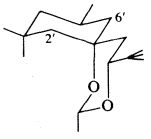 **7**	37.3	36.3	35.3			41.0	42.7	47.6*	48.9	48.2	51.3
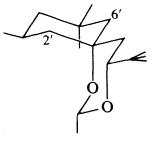 **8**	36.8	36.3	35.3			52.0	52.3	57.8*	39.0	38.6	41.1

Can. J. Chem. Downloaded from www.nrcresearchpress.com by 210.87.254.5 on 09/05/12
For personal use only.

TABLEAU 1 (*Concluded*)

Composé	δ								
	C_5			$C_{5\alpha}$	$C_{5\alpha'}$	$C_{2'}$		$C_{6'}$	
		Calc.					Calc.		Calc.
	Exp.	Grant	Saunders	Exp.	Exp.	Exp.	Grant Saunders	Exp.	Grant Saunders
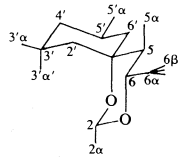 **7*e***	42.1	41.3		15.1		35.5	38.6	46.2	44.2
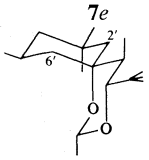 **8*e***	41.1	41.3		15.2		48.0	48.3	34.2	34.6
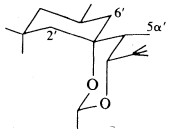 **7*a***	39.7	38.0			9.8	32.4	42.7	46.0	44.2
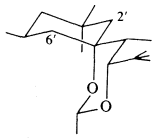 **8*a***	39.5	38.0			9.7	48.8	48.3	40.3	38.6
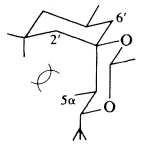 **9*e***	38.1	36.3		17.6		40.6		47.6	
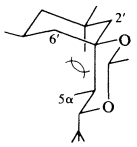 **10*e***	36.4	36.3		15.7		46.6		40.2	
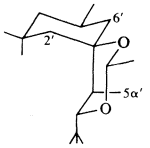 **9*a***	34.0	33.0			10.0	45.5	42.7	45.5	44.2
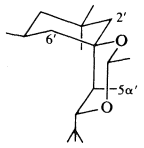 **10*a***	34.9	33.0			10.5	47.7	48.3	42.0	38.6

*Voir texte.

Can. J. Chem. Downloaded from www.nrcresearchpress.com by 210.87.254.5 on 09/05/12
For personal use only.

Can. J. Chem. Downloaded from www.nrcresearchpress.com by 210.87.254.5 on 09/05/12
For personal use only.

TABLEAU 2. Incréments d'effets β d'oxygènes intracyclique dans les dioxannes-1,3 en fonction de l'orientation et de la substitution

Composé	Paramètre	Valeur
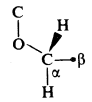	*A*	−0.5±0.4 (7 valeurs)
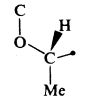	*B*	−2.0±0.4 (7 valeurs)
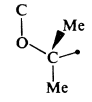	*C*	−3.4±0.1 (4 valeurs)
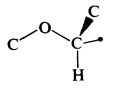	*D*	−1.6±0.3 (5 valeurs)
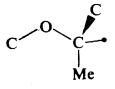	*E*	−2.1 (1 valeur)

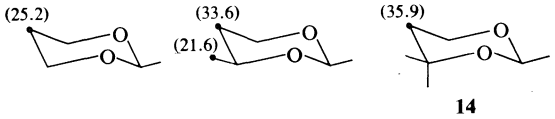

14

FIG. 1. Déplacements chimiques des carbones des dioxannes "modèles" relevés sur des spectres enregistrés dans $CDCl_3$ avec le TMS pour référence interne (réf. 24 et tableau 3).

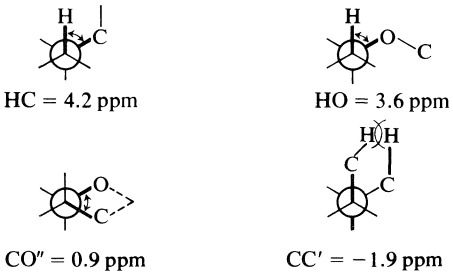

FIG. 2. Incréments d'interactions pour les dioxannes-1,3.

dioxannes-1,3. L'incrément d'interaction *gauche* intracyclique (CO″) n'est plus nul comme dans le cas de deux liaisons C—C (CC″ = 0). La valeur de l'incrément CC′ est plus surprenante (elle est de +1.74 ppm dans les cyclohexanes et cyclohexanols). Il faut noter qu'elle correspond à une interaction avec un méthyle axial en 4 sur le cycle dioxannique. Le fait que ce groupement présente une interaction de type diaxiale-1,3 avec l'hydrogène synaxial en 2 plus

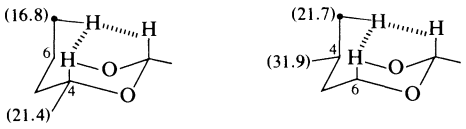

FIG. 3. Déplacements chimiques des carbones des groupes méthyles du triméthyl-2-*r*,4-*c*,6-*t* dioxanne-1,3 (24) et du triméthyl-2,4,4 dioxanne-1,3 (**14** dans le tableau 3). Incréments d'effet γ.

forte que dans le cas des cyclohexanes, pourrait être responsable de ce changement.

Il nous reste à déterminer un dernier paramètre: celui qui tient compte d'une situation diaxiale-1,3 de la liaison portant le carbone étudié vis-à-vis de deux hydrogènes synaxiaux portés par des carbones en γ (γ_{HH}). Pour cela nous avons comparé les résonances des carbones de groupements méthyles équatoriaux (pris comme références puisqu'on peut les calculer à l'aide des incréments précédents) et axiaux dans les deux dioxannes de la fig. 3.

La différence entre ces deux valeurs de $2\gamma_{HH}$ est probablement liée au degré de substitution du carbone en position 4 ou 6, Dalling et Grant (6) avait déjà noté et étudié un tel phénomène dans les cyclohexanes, décalines et spirobicyclohexane. Des déformations de cycle ou d'angle, augmentant les énergies d'éclipsage entre liaisons, pourraient être responsables de ces variations. Le cas des dioxannes-1,3 est un peu particulier. La différence de longueurs entre liaisons C—C et C—O laisse prévoir deux valeurs possibles pour ces effets γ_{HH} (voir fig. 4). L'hydrogène axial en position 2 est, en effet, plus proche dans l'espace du groupement méthyle étudié que l'hydrogène axial en 4. La valeur de $2\gamma_{HH}$ (−4.6 ppm) relevée pour le premier dioxanne est faible. Elle peut s'expliquer essentiellement par des déformations de la molécule (comme dans le cas des cyclohexanes). Dans le dioxanne diméthylé en 4, l'effet Thorpe–Ingold diminue les possibilités de déformations et la valeur de l'incrément est considérablement augmentée. Nous avons rassemblé dans la fig. 5 quelques résultats expérimentaux relatifs aux effets $2\gamma_{HH}$ pour des méthyles axiaux dans les modèles étudiés.

Applications à l'étude structurale de dioxanne-1,3-4-spirocyclohexanes

Méthyl-2 dioxanne-1,3-4-spiro-tert-*butyl-4′ cyclohexane*-cis *et* -trans *(1 et 2) et Méthyl-2 dioxanne-1,3-4-spiro-1′*-r *diméthyl-3′*-c,*5′*-c *ou 3′*-t,*5′*-t *(3 et 4)*

Nous avons représenté dans le tableau 1, un énantiomère de chacun des deux diastéréoisomères *cis* et *trans* existant pour ces types de composés et ce, dans leur conformation préférentielle.

FIG. 4. Interactions γ_{HH} dans les dioxannes-1,3 (pour un méthyle 4 axial).

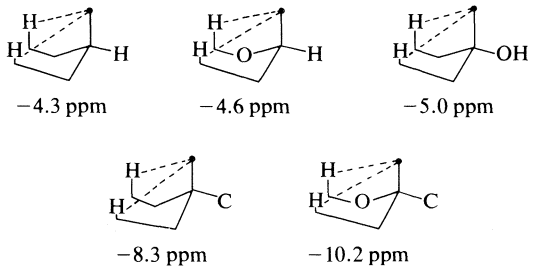

FIG. 5. Effets $2\gamma_{HH}$ pour des carbones de méthyles axiaux seuls ou *gem*-diméthylés (ces valeurs sont les différences expérimentales entre résonances des méthyles équatoriaux et axiaux portés par le même carbone).

Nous avons vu, au cours de l'étude préliminaire, que l'effet β des oxygènes (tableau 2), pour une substitution donnée, dépendait de l'orientation anti ou *gauche* des liaisons O—C par rapport à la liaison C_α—C_β. Pour le carbone 2′ (liaison O_3—C_2 *gauche* par rapport à C_1′—C_2′; incrément $C = -3.4$ du tableau 2) l'influence de O_3 sera la même pour les quatre composés étudiés. Il en est de même pour le carbone 6′ (liaison O_3—C_2 anti par rapport à C_1′—C_6′; incrément $D = -2.1$ du tableau 2). L'environnement de ce premier oxygène et la présence du deuxième hétéroatome n'apporteront qu'une différenciation très faible, difficile à chiffrer.

Le carbone en position 5, dans le cycle dioxannique occupe en revanche, une situation particulière. Il est équatorial sur le cycle cyclohexanique dans les isomères **1** et **3**, axial pour **2** et **4**. Ce seul fait devrait permettre de différencier les spirodioxannes *cis* et *trans*.

Méthode de Grant

(i) Déplacements chimiques des carbones C_2′ et C_6′

Nous avons voulu reconstruire les spirodioxannes (cf. fig. 6) à l'aide des paramètres établis dans la première partie et de la valeur δ_0 des carbones du cyclohexane (27.1 ppm). Nous avons donc tout d'abord introduit la *gem*-diméthylation sur le cyclohexane (cycle A), fermé le deuxième cycle B (spirobicyclohexane) puis introduit les oxygènes (spirodioxanne) et enfin les substituants sur les deux cycles. Nous calculons donc les $\delta_{C_2'}$ et $\delta_{C_6'}$ du spirocyclohexane en les assimilant pour commencer aux δ_{C_2} et δ_{C_6} du diméthyl-1,1 cyclohexane soit

$$\delta_{C_2} = \delta_{C_6} = 27.1 + 9.0 + 5.4 - 1.3G_\beta = 40.2 \text{ ppm}$$

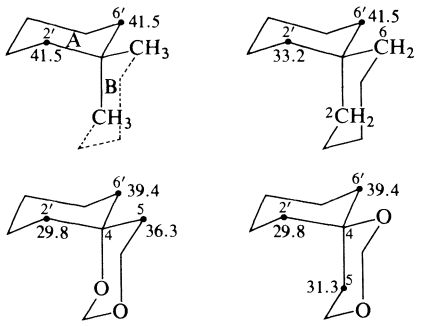

FIG. 6. Spirobicyclohexane et spirodioxannes non substitués.

Toutefois, les hydrogènes des groupes méthyléniques en 2′ et 6′ ont une orientation bien déterminée du fait des contraintes imposées par le reste du cycle A. De plus, leur polarisabilité est bien plus faible que celle des groupements méthyles. Pour ces raisons l'incrément G_β ne semble plus représentatif et peut être négligé (22). Par conséquent:

$$\delta_{C_2'} = \delta_{C_6'} = 27.1 + 9.0 + 5.4 = 41.5 \text{ ppm}$$

Pour tenir compte de la partie du cycle B à refermer (en pointillés sur la fig. 6), on considère les carbones C_2′ et C_6′, comme substituants respectivement axial et équatorial sur ce cycle B. D'autre part on constate que $\delta_{C(\text{Me eq cyclohexane})} = 23.1$ ppm est très voisin de $\delta_{C(\text{Me isobutane})} = 24.5$ ppm; le reste du cycle n'a donc que très peu d'influence sur $\delta_{C(\text{Me eq})}$. En revanche, le fait qu'un substituant méthyle soit axial rend la résonance de son carbone très sensible aux interactions *gauches* avec les liaisons du cycle et à la substitution du carbone en α (cf. fig. 5). Ainsi, le passage d'un méthyle seul de la position équatoriale à la position axiale se traduit par un blindage de −4.3 ppm alors qu'entre les méthyles géminés du triméthyl-1,1,4 cyclohexane on observe une différence de −8.3 ppm (cf. fig. 5). Dans le spirobicyclohexane, on peut alors écrire:

$$\delta_{C_2'} = 41.5 - 8.3 = 33.2 \text{ ppm}$$

($\delta_{exp} = 32.0$ selon réf. 6 à basse température)

$$\delta_{C_6'} = 41.5 - 0 = 41.5 \text{ ppm}$$

($\delta_{exp} = 43.2$ selon réf. 6 à basse température)

En introduisant ensuite les incréments qui se réfèrent à l'influence des oxygènes (tableau 2), on détermine les déplacements chimiques pour un spirodioxanne non substitué:

$$\delta_{C_2'} = 33.2 - 3.4 = 29.8$$

et

$$\delta_{C_6'} = 41.5 - 2.1 = 39.4$$

Can. J. Chem. Downloaded from www.nrcresearchpress.com by 210.87.254.5 on 09/05/12
For personal use only.

TABLEAU 3. Déplacements chimiques (en ppm) en rmn du ^{13}C de quelques dioxannes-1,3

Composé	C_2	$C_{2\alpha}$	C_4	$C_{4\alpha}$	$C_{4\alpha'}$	C_5		C_6	$C_{6\alpha}$	$C_{6\beta}$
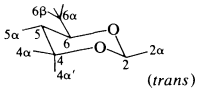 (*trans*) **11**	92.3	21.6	75.6	29.5	18.5	40.9	$C_{5\alpha}$ 14.0	84.5	35.2	27.6
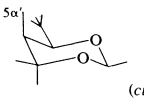 (*cis*) **12**	93.5	21.6	75.3	27.5	24.0	37.6	$C_{5\alpha'}$ 9.6	81.8	34.2	27.3
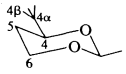 **13**	98.6	21.3	83.8	33.4	$C_{4\beta}$ 25.1	25.1	—	66.0	—	—
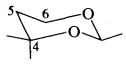 **14**	92.6	21.7	78.4	31.9	21.7	35.9	—	63.1	—	—

La comparaison des δ des carbones en position 3 sur le cyclohexane (27.1 ppm) et le *tert*-butyl-1 cyclohexane (27.8 selon réf. 13) fournit l'incrément du tertiobutyle: $t\text{Bu}/C_\gamma = +0.7$. L'application des incréments de Grant (5, 6) donne celui du groupement diméthyl-3,5: $\beta_e + \delta_e = 8.8$ ppm.

Nous avons rassemblé les valeurs δ_{calc} et δ_{exp} dans le tableau 1. L'écart maximal observé est de 1.5 ppm. On confirme ainsi l'attribution des carbones $C_{2'}$ et $C_{6'}$, mais ce calcul ne permet pas de différencier les deux isomères dans chaque série, cette différenciation étant faite sur le carbone C_5.

(ii) Déplacements chimiques des carbones C_5

A partir du déplacement chimique du carbone en position 2 sur le diméthyl-1,1 cyclohexane (40.2 ppm) et en tenant compte des incréments du tableau 2, on calcule le déplacement chimique du carbone 5 du triméthyl-2,4,4 dioxanne-1,3:

$$\delta_{C_5} = 40.2 - 3.4 - 0.5 = 36.3 \text{ ppm}$$

$$(\delta_{exp} = 35.9)$$

Lorsque l'on referme le cycle (à partir du *gem*-diméthyl-4,4) tout se passe comme si le carbone 5 de la partie dioxannique (cf. fig. 6) était celui d'un groupement méthyle soit équatorial soit axial sur le cycle cyclohexanique. En effet la différence $\Delta\delta = -5.0$ ppm entre les méthyles axial et équatorial en 1 des deux triméthyl-1,3,5 cyclohexanols est très proche de celle observée pour la même situation dans les cyclohexanes. D'autre part l'influence des substituants alkyles en γ ou δ portés par le cycle cyclohexanique peut être considérée comme nulle. Le déplacement chimique du carbone 5 est donc de 36.3 ppm dans les spirodioxannes *cis* et de 36.3 − 5.0 ppm = 31.3 ppm dans leurs isomères *trans*. On peut donc, sans ambiguité, caractériser chacun des isomères dans les deux couples de composés étudiés.

Méthode de Saunders

Les résultats précédents ont été confirmés par cette deuxième méthode. Nous détaillons ci-dessous, à titre d'exemple le calcul dans le cas du composé **2** (cf. tableau 1). Les interactions relatives au carbone $C_{2'}$ peuvent être représentées comme suit:

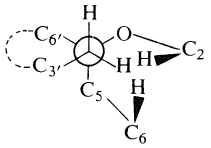

projection selon $C_{2'}$—$C_{1'}$

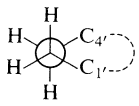

projection selon $C_{2'}$—$C_{3'}$

On peut alors écrire:

$$\delta_{C_{2'}} = 16.1 + 3HC + 2HO + 2CC'' + 1CC' + 2\gamma_{HH}$$

$$= 31.5 \text{ ppm}^3$$

$$(\delta_{exp} = 30.8)$$

Pour le carbone $C_{6'}$, on peut écrire de la même façon:

$$\delta_{C_{6'}} = 16.1 + 3HC + 2HO + 2CC'' + 1CC'$$

$$= 41.7 \text{ ppm}$$

$$(\delta_{exp} = 41.3)$$

[3]Nous avons choisi pour $2\gamma_{HH}$, la valeur (−10.2) déterminée pour un carbone de groupement méthyle axial géminé en 4 sur le cycle dioxannique (cf. fig. 5) puisque la situation de $C_{2'}$ est analogue.

Can. J. Chem. Downloaded from www.nrcresearchpress.com by 210.87.254.5 on 09/05/12
For personal use only.

La représentation des interactions relatives au carbone C_5 permet d'écrire:

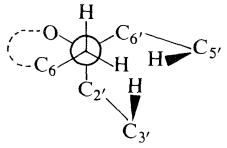

projection selon C_5—C_4

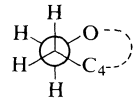

projection selon C_5—C_6

$$\delta_{C_5} = 16.1 + 3HC + 2HO + 2CO'' + 1CC' + 2\gamma_{HH}$$

$$= 30.9 \text{ ppm}^4$$

$$(\delta_{exp} = 30.6)$$

Méthyl-2 dioxanne-1,3-trans *ou* -cis-*4-spiro-triméthyl-3',3',5' cyclohexanes*-trans *(5 et 6) et* tert-*butyl-6*-c *méthyl-2*-r *dioxanne-1,3-4*-t *ou* -c-*spiro-triméthyl-3',3',5' cyclohexanes*-trans *(7 et 8)*

Ces différents composés sont représentés dans le tableau 1. Comme nous l'avons noté dans l'étude en rmn du proton, l'introduction d'un groupe méthyle axial en position 3' conduit à une asymétrie supplémentaire et donc à quatre diastéréoisomères. Cependant, nous n'avons étudié, en rmn du ^{13}C que les composés issus des diols ayant un groupe hydroxyle axial sur le cycle cyclohexanique car nous disposions de quantités trop faibles des spirodioxannes isomères (liaison C_4—O_3 équatoriale) pour pouvoir enregistrer les spectres; de ce fait les conséquences de l'isomérie de position de la liaison C_4—O_3 sur les déplacements chimiques ne peuvent plus être atteintes par comparaison directe. Toutefois les déplacements chimiques du carbone 5 des composés **5**, **6**, **7** et **8** peuvent être atteints à partir du composé **3** puisqu'un méthyle 3' axial n'a pas d'influence sur ce carbone (effet δ_a des réfs 5 et 6). Ainsi, les dérivés tétraméthylés **5** et **6** possèdent bien une liaison C_4—O_3 axiale sur le cycle cyclohexanique puisque les déplacements chimiques trouvés pour le carbone 5 sont respectivement 37.4 et 36.8 ppm en parfait accord avec les valeurs expérimentales et calculées pour le composé **3** (tableau 1). Le fait que, dans les composés analogues **7** et **8**, tertiobutylés en 6, le carbone 5 résonne aussi vers 37 ppm et donc que le substituant tertiobutyle semble n'avoir que peu d'influence sur le carbone en β, peut paraître surprenant. Pour le vérifier nous avons synthétisé le *tert*-butyl-4-*c* méthyl-2-*r* dioxanne-1,3 **13** et enregistré son spectre (tableau 3). Il s'avère que δ_{C_5} égale 25.1 ppm, valeur identique à celle du même carbone dans le méthyl-2 dioxanne-1,3 (15).

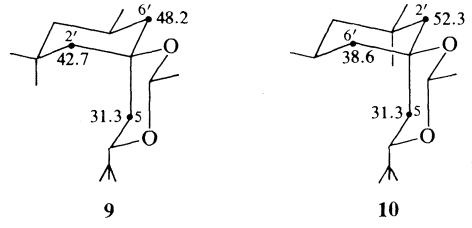

9 **10**

FIG. 7. Déplacements chimiques calculés pour les carbones $C_{2'}$ et $C_{6'}$ des isomères **9** et **10** dont les spectres n'ont pu être enregistrés. Nous avons également fait figurer la valeur de δ_{C_5} extrapolée à partir du composé **4**.

Il faut alors différencier **5** de **6** et **7** de **8**. En ajoutant aux valeurs calculées pour $\delta_{C_{2'}}$ et $\delta_{C_{6'}}$, dans le composé **3**, l'incrément β relatif à un groupe méthyle axial géminé (cf. réfs 5 et 6: $\beta_a + G_\beta$), on obtient les déplacements chimiques de ces mêmes carbones dans les quatre composés étudiés. Nous avons rassemblé les résultats de ce calcul dans le tableau 1. La comparaison avec les valeurs expérimentales permet la caractérisation non ambiguë des différents isomères. On peut également prévoir les déplacements chimiques de ces mêmes carbones dans les isomères **9** et **10** (fig. 7).

La méthode de Saunders conduit à de bons résultats (cf. tableau 1) pour les $\delta_{C_{6'}}$ et δ_{C_5} de **5**, **6**, **7** et **8**; il n'en est pas de même pour $\delta_{C_{2'}}$, dont l'écart peut atteindre 7 ppm. Nous avons trouvé un tel écart en calculant le δ_{C_2} dans le tétraméthyl-1,3,3,5-*t* cyclohexanol-1-*r* (25). On peut penser que l'interaction diaxiale-1,3 entre le groupe méthyle en position 3' et la liaison C_4—O_3 est responsable de la variation de certains paramètres de calcul ou qu'elle nécessiterait l'introduction d'un nouvel incrément $\delta_{OHH} \sim -4.0$ ppm (compte tenu des erreurs du calcul).

tert-*Butyl-6*-c *diméthyl-2*-r, *5*-t *ou 5*-c *dioxanne-1,3-4*-t *ou* -c-*spiro-triméthyl-3',3',5' cyclohexanes*-trans *(7*e, *7*a, *8*e, *8*a*) ou* -cis *(9*e, *9*a, *10*e, *10*a*)*

Nous savons que dans cette série, il existe huit isomères puisque la présence d'un groupe méthyle en position 5 introduit une asymétrie supplémentaire (cf. schéma dans la réf. 2). Nous avons pu enregistrer les spectres[5] pour ces huit composés.

L'application de la méthode de Saunders conduit à de mauvais résultats. Ceci était prévisible du fait des fortes interactions entre groupements méthyle en 5 et tertiobutyle en 6 sur le cycle dioxannique dont on ne peut tenir compte avec les incréments déter-

[4]Dans ce cas pour tenir compte de la présence de la liaison C—O portée par le carbone $C_{1'}$, nous avons utilisé la valeur de $2\gamma_{HH} = -5.0$ ppm déterminée à partir des cyclohexanols (cf. fig. 5).

[5]Nous remercions vivement M. Jean-Yves Lallemand, Laboratoire de Chimie de l'E.N.S. Paris, pour l'enregistrement de ces spectres.

Can. J. Chem. Downloaded from www.nrcresearchpress.com by 210.87.254.5 on 09/05/12
For personal use only.

Can. J. Chem. Downloaded from www.nrcresearchpress.com by 210.87.254.5 on 09/05/12
For personal use only.

TABLEAU 4. Déplacements chimiques (en ppm) en rmn du ^{13}C des composés **1–10***a* (solutions à 20% dans $CDCl_3$ avec le TMS comme référence interne)*

	δ														
Composé	C_2	$C_{2\alpha}$	$C_{4\text{ ou }1'}$	C_6	$C_{6\alpha}$	$C_{6\beta}$	$C_{3'}$	$C_{3'\alpha}$	$C_{3'\alpha'}$	$C_{4'}$	$C_{4'\alpha}$	$C_{4'\beta}$	$C_{5'}$	$C_{5'\alpha}$
1	91.7	21.4	71.0	62.5	—	—	21.7	—	—	48.1	32.4	27.6	21.7	—
2	91.8	21.8	73.5	62.7	—	—	[24.0]	—	—	48.0	32.3	27.6	[23.1]	—
3	92.0	[22.2]	73.5	62.9	—	—	27.1	[23.0]	—	44.5	—	—	27.1	[22.8]
4	91.6	[22.0]	74.0	62.7	—	—	(29.5)	[22.8]	—	44.1	—	—	(28.2)	[22.6]
5	92.4	[21.3]	73.8	62.8	—	—	31.6	34.5	26.1	49.1	—	—	23.1	[22.5]
6	91.6	[21.8]	74.0	62.8	—	—	31.6	34.5	27.5	49.2	—	—	23.6	[22.6]
7	92.4	[21.2]	73.9	79.3	33.7	25.7	31.7	34.6	26.1	49.5	—	—	23.6	[22.5]
8	91.7	[21.6]	74.1	79.4	33.7	25.7	31.7	34.5	27.5	49.5	—	—	23.7	[22.7]
7*e*	92.4	[22.0]	78.6	84.2	35.9	28.2	32.2	35.5	27.3	49.7	—	—	24.3	[23.3]
7*a*	93.6	[22.1]	77.7	81.9	34.8	28.2	32.6	35.4	26.9	49.3	—	—	24.6	[23.6]
8*e*	91.6	[22.5]	78.8	84.7	36.1	28.4	32.4	35.7	28.4	50.1	—	—	24.1	[23.6]
8*a*	92.8	[22.5]	77.6	81.8	34.9	28.2	32.4	35.7	28.7	49.8	—	—	24.4	[23.6]
9*e*	95.1	[23.2]	78.2	88.1	35.6	27.6	31.6	(33.7)	(30.7)	48.1	—	—	27.1	[23.7]
9*a*	93.1	[22.5]	78.4	82.1	35.0	28.1	33.0	36.0	29.0	49.3	—	—	25.0	[23.1]
10*e*	93.5	[23.0]	78.9	86.2	35.8	28.1	31.3	(33.8)	(32.6)	48.3	—	—	27.1	[23.4]
10*a*	93.0	[22.5]	78.6	81.6	34.6	28.0	32.6	34.9	(26.7)	49.9	—	—	(26.3)	[23.5]

*Les valeurs entre crochets ou parenthèses peuvent être échangées.

minés plus haut. En revanche la méthode de Grant semble mieux adaptée puisqu'elle permet de compléter le système d'incréments pour évaluer les interactions nouvelles créées par le nombre grandissant de substitutions.

Dans ce but, nous avons enregistré les spectres des *tert*-butyl-6-*c* tétraméthyl-2-*r*, 4,4,5-*c* et 5-*t* dioxannes-1,3 (**11** et **12** (tableau 3)). On remarque tout d'abord, que les carbones des groupements méthyles axial 5α′ (isomère *cis*) ou équatorial 5α (isomère *trans*) résonnent respectivement à 9.6 et 14.0 ppm. On a donc un moyen de distinguer, dans la série de spirodioxannes étudiée, les isomères qui relèvent de ce changement d'orientation.

D'autre part, nous avons déjà noté que le groupement tertiobutyle en position 6 n'apporte aucune perturbation au δ_{C_5}. La comparaison directe du triméthyl-2,4, et des *tert*-butyl-6-*c* tétraméthyl-2-*r*, 4,4,5 dioxannes-1,3-*cis* et -*trans* nous conduit à l'évaluation des effets α d'un groupe méthyle en 5:

$$\alpha_e = 40.9 - 35.9 = +5.0$$

$$\alpha_a = 37.6 - 35.9 = +1.7$$

Ces deux valeurs tiennent compte des effets secondaires dus aux substituants vicinaux en 4 et 6 ce qui explique qu'elles soient différentes de celles relevées par ailleurs ($\alpha_e = \alpha_a = 3.1$ ppm (15, 16)).

On peut alors déterminer δ_{C_5} pour les huit composés étudiés à partir des valeurs calculées lues pour ce carbone dans le tableau 1 (**7** et **8**) et la fig. 7 (**9** et **10**) et classer les huit diastéréoisomères en quatre groupes de deux composés chacun: liaison C_4—O_3 axiale: Me_{5e} (**7***e*, **8***e*) → $\delta_{C_5} = 36.3 + 5.0 = 41.3$; Me_{5a} (**7***a*, **8***a*) → $\delta_{C_5} = 36.3 + 1.7 = 38.0$; liaison C_4—O_3 équatoriale: Me_{5e} (**9***e*, **10***e*) → $\delta_{C_5} = 31.3 + 5.0 = 36.3$; Me_{5a} (**9***a*, **10***a*) → $\delta_{C_5} = 31.3 + 1.7 = 33.0$. Le classement ainsi obtenu est en accord avec la remarque précédente sur les valeurs de δ des groupements méthyles 5α et 5α′.

Nous avons vu dans la série non méthylée en 5, comment l'on pouvait distinguer les isomères dans ces groupes de deux, par le calcul de $\delta_{C_{2'}}$ et $\delta_{C_{6'}}$. Dans le cas présent, il suffit de connaître les incréments d'effets intercycles liés à la présence du groupe méthyle en 5. Bien que ces effets soient très sensibles à toutes variations de géométrie dans les molécules étudiées (6), on peut toutefois utiliser les paramètres suivants de la fig. 8.

Les déplacements chimiques ainsi déterminés en ajoutant les incréments de la fig. 8 aux valeurs de $\delta_{C_{2'}}$ et $\delta_{C_{6'}}$ des composés **7**, **8**, **9** et **10** (tableau 1 et fig. 7) figurent dans le tableau 1. Ils ont permis de distinguer sans ambiguité **7***e* de **8***e*, **7***a* de **8***a* et **9***a* de **10***a*.

Les écarts observés (parfois supérieurs à 2.5 ppm)

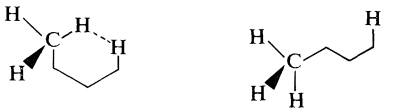

FIG. 8. Incréments d'effets intercycles déduits des résultats de la réf. 6.

sont plus grands que ceux notés précédemment. Ceci provient, à notre avis, d'une part de l'accumulation des erreurs lorsque l'on utilise un nombre toujours plus grand d'incréments et de la variation des incréments utilisés pour ce dernier calcul.

Les composés **9***e* et **10***e* posent un problème conformationnel. Si l'on admet la conformation double chaise, la présence d'un méthyle équatorial en 5 crée une interaction très importante avec le méthyle axial en 3′. On doit alors envisager une conformation croisée pour l'un ou l'autre (ou les deux) cycle(s) de ces molécules. Les spectres de rmn du ^{13}C pour ces deux isomères sont très voisins. L'attribution faite dans le tableau 1 n'a pu l'être qu'à partir des analyses des spectres de rmn du proton et des filiations chimiques établies lors de la synthèse (23) de ces deux produits.

On peut toutefois noter que: (*i*) dans le composé **9***e*, les fortes valeurs des résonances des carbones C_2, C_5, C_6 et $C_{5\alpha}$ suggèrent une légère déformation du cycle dioxannique. Les valeurs relevées pour les mêmes carbones dans **10***e* semblent plus "normales." (*ii*) Dans les deux composés: les résonances des carbones $C_{3'\alpha}$ et $C_{3'\alpha'}$ sont très proches alors que dans **9***a* et **10***a*, $\Delta\delta_{C_{3'\alpha}-C_{3'\alpha'}} \simeq 7$ ppm (cf. tableau 4); on trouve pour les carbones $C_{2'}$ et $C_{6'}$ comparables des valeurs de déplacements chimiques pratiquement identiques.

$$\delta_{C_{2'}}(\mathbf{9}e) = \delta_{C_{6'}}(\mathbf{10}e) \simeq 40.5 \text{ ppm}$$

et

$$\delta_{C_{6'}}(\mathbf{9}e) = \delta_{C_{2'}}(\mathbf{10}e) \simeq 47 \text{ ppm}$$

Ces remarques, et celles déjà notées lors de l'étude en rmn du proton, conduisent à proposer pour ces deux molécules des structures où le cycle cyclohexanique se trouverait en conformation croisée; le cycle dioxannique ne serait que peu (**9***e*) ou pas (**10***e*) déformé.

Conclusion

Au cours du présent travail, nous avons établi des systèmes d'incréments permettant le calcul empirique du déplacement chimique en rmn du ^{13}C. Ces paramètres, déterminés à partir de nos propres résultats et de ceux de la littérature, peuvent être employés, indépendamment de tout autre technique, à la détermination de structure de molécules complexes.

Toute méthode de calcul empirique peut être envisagée, soit à partir de l'expérience par un traitement statistique des données (Dalling et Grant (5–8) ont opéré de cette façon dans le cas des cyclohexanes polyméthylés), soit en donnant une signification précise au phénomène que l'on étudie et en déterminant les incréments correspondants (c'est le procédé choisi par Saunders et coll. (9–12) dans une étude des effets β en série décalinique).

Nous avons, pour des cycles à six chaînons, les

TABLEAU 5. Incréments d'effets β d'oxygènes intracycliques en fonction de l'orientation et de la substitution dans les dioxannes-1,3

Substituants	δ_C (C étudié)	δ réf.*	n_A	n_B	n_C	n_D	n_E
Sans	26.9 (C_5)†	27.1	2	0	0	0	0
Méthyl-2	25.2 (C_5)†	26.9	2	0	0	0	0
Diméthyl-2,2	25.8 (C_5)†	27.0	2	0	0	0	0
Méthyl-4	34.0 (C_5)†	36.1	1	1	0	0	0
Diméthyl-2-*r*,4-*c*	33.6 (C_5)†	35.7	1	1	0	0	0
	21.7 (C_{Me4e})†	23.1	0	0	0	1	0
Diméthyl-4-*r*,6-*c*	40.9 (C_5)‡	45.0	0	2	0	0	0
	21.6 (C_{Me4e})‡	23.1	0	0	0	1	0
Triméthyl-2-*r*,4-*c*,6-*c*	40.8 (C_5)‡	44.5	0	2	0	0	0
	21.4 (C_{Me4e})‡	22.9	0	0	0	1	0
Triméthyl-2-*r*,4-*c*,6-*t*	36.2 (C_5)‡	41.2	0	2	0	0	0
	21.4 (C_{Me4e})‡	23.4	0	0	0	1	0
	16.8 (C_{Me4a})‡	19.2	0	1	0	0	0
Diméthyl-4,4	36.7 (C_5)	40.1	1	0	1	0	0
Triméthyl-2,4,4	35.9 (C_5)	39.8	1	0	1	0	0
	31.9 (C_{Me4c})	34.0	0	0	0	0	1
	21.7 (C_{Me4a})	25.2	0	0	1	0	0
Triméthyl-4,4,6	44.2 (C_5)†	49.7	0	1	1	0	0
Diméthyl-4-*r*,5-*t*	19.0 (C_{Me4e})	20.5	0	0	0	1	0

*Valeurs du $\delta^{13}C$ dans le cyclohexane correspondant (5, 6).
†Voir réfs 15 et 16.
‡Réference 24.

Can. J. Chem. Downloaded from www.nrcresearchpress.com by 210.87.254.5 on 09/05/12
For personal use only.

cyclohexanols et les dioxannes, appliqué ces deux méthodes à la détermination des influences de substituants méthyles et d'oxygènes intra ou exocycliques. De cette étude il ressort que (*i*) la méthode de Grant conduit à des valeurs de δ en excellent accord avec l'expérience. En effet, on peut généralement trouver un incrément pour décrire une situation nouvelle. Le système comporte donc un grand nombre de paramètres dont la signification réelle reste toutefois à préciser; (*ii*) la méthode de Saunders, en revanche, ne nécessite qu'un petit nombre de paramètres reliés aux interactions gauches et spatiales entre liaisons. Il est alors plus difficile d'introduire de nouveaux incréments et on ne rend pas compte de toutes les situations possibles.

Dans le cas particulier des dioxannes-1,3-4-spirocyclohexanes, ces modes de calcul du déplacement chimique permettent des attributions de structure non ambiguës. En ce qui concerne l'analyse conformationnelle de tels dérivés, les renseignements obtenus par l'étude des déplacements chimiques des carbones sont comparables à ceux atteints en rmn du proton.

1. L. Cazaux, J. P. Gorrichon, M. Perry et P. Maroni. Can. J. Chem. **56**, 2998 (1978).
2. L. Cazaux, J. P. Gorrichon, Y. Koudsi et P. Maroni. Can. J. Chem. **56**, 3006 (1978).
3. P. Maroni, L. Cazaux, J. P. Gorrichon, P. Tisnes et J. G. Wolf. Org. Magn. Reson. **5**, 517 (1973).
4. P. Maroni, L. Cazaux, J. P. Gorrichon, P. Tisnes et J. G. Wolf. Org. Magn. Reson. **5**, 523 (1973).
5. D. K. Dalling et D. M. Grant. J. Am. Chem. Soc. **89**, 6612 (1967).
6. D. K. Dalling et D. M. Grant. J. Am. Chem. Soc. **94**, 5318 (1972).
7. D. K. Dalling, D. M. Grant et E. G. Paul. J. Am. Chem. Soc. **95**, 3718 (1973).
8. D. K. Dalling et D. M. Grant. J. Am. Chem. Soc. **96**, 1827 (1974).
9. H. Beierbeck et J. K. Saunders. Can. J. Chem. **53**, 1307 (1975).
10. H. Beierbeck et J. K. Saunders. Can. J. Chem. **54**, 632 (1976).
11. H. Beierbeck et J. K. Saunders. Can. J. Chem. **54**, 2985 (1976).
12. H. Beierbeck, J. K. Saunders et J. W. ApSimon. Can. J. Chem. **55**, 2813 (1977).
13. J. D. Roberts, F. J. Weigert, J. I. Kroschwitz et H. J. Reich. J. Am. Chem. Soc. **92**, 1338 (1970).
14. S. H. Grover et J. B. Stothers. Can. J. Chem. **52**, 870 (1974).
15. G. M. Kellie et F. G. Riddell. J. Chem. Soc. B, 1030 (1971).
16. F. G. Riddell. J. Chem. Soc. B, 331 (1970).
17. E. L. Eliel, W. F. Bailey, L. D. Kopp, R. L. Willer, D. M. Grant, R. Bertrand, K. A. Christensen, D. L. Dalling, M. W. Duch, E. Wenkert, F. M. Schell et D. W. Cochran. J. Am. Chem. Soc. **97**, 322 (1975).
18. A. J. Jones, E. L. Eliel, D. M. Grant, Sr., M. C. Knoeber et W. F. Bailey. J. Am. Chem. Soc. **93**, 4772 (1971).
19. N. S. Bhacca, D. D. Gianini, N. S. Jankowski et M. E. Wolff. J. Am. Chem. Soc. **95**, 8421 (1973); **96**, 5462 (1974).
20. L. Simeral et G. E. Maciel. J. Phys. Chem. **77**, 1590 (1973).
21. E. Lipmaa, T. Pehk, J. Paasivirta, N. Belikova et A. Plate. Org. Magn. Reson. **2**, 581 (1970); **3**, 783 (1971).
22. D. Zimmermann, R. Ottinger, J. Reisse, H. Christol et J. Brugidou. Org. Magn. Reson. **6**, 346 (1974).
23. Y. Koudsi. Thèse de Doctorat ès-Sciences, Université Paul Sabatier, Toulouse, no 666, 1975.
24. K. Bock et L. Wiebe. Acta Chem. Scand. **27**, 2676 (1973).
25. J. P. Gorrichon. Thèse de Doctorat ès-Sciences, Université Paul Sabatier, Toulouse, no 713, 1976.

Can. J. Chem. Downloaded from www.nrcresearchpress.com by 210.87.254.5 on 09/05/12
For personal use only.

Polar substituents in barrelene photochemistry: mechanistic aspects of the photochemistry of 2-cyanobenzobarrelene

CHRISTOPHER OWEN BENDER, DEE W. BROOKS, WILLIAM CHENG, DOUGLAS DOLMAN, SEAMUS F. O'SHEA, AND SIDNEY S. SHUGARMAN

Department of Chemistry, University of Lethbridge, Lethbridge, Alta., Canada T1K 3M4

Received June 19, 1978

CHRISTOPHER OWEN BENDER, DEE W. BROOKS, WILLIAM CHENG, DOUGLAS DOLMAN, SEAMUS F. O'SHEA, and SIDNEY S. SHUGARMAN. Can. J. Chem. **56**, 3027 (1978).

The direct photolysis of 2-cyanobenzobarrelene (**4**) yields 5- and 7-cyanobenzocyclooctatetraene (**6**, $\Phi = 0.08$ and **7**, $\Phi = 0.25$) and 1-cyanobenzosemibullvalene (**8**, $\Phi = 0.05$), whereas the acetophenone sensitized irradiation of **4** yields only **8** ($\Phi = 0.35$). Deuterium labelling studies suggest that **7** derives from an initial $2\pi + 2\pi$ cycloaddition between the vinyl and vinylcyano bridges of **4**, whereas **8**, resulting from direct or sensitized irradiations of **4**, derives from di-π-methane rearrangement involving initial vinyl–vinylcyano bridging. The observed initial bonding preferences of the $2\pi + 2\pi$ cycloadditions and di-π-methane rearrangement of **4** are in accord with predictions based upon CNDO-CI calculations of changes in atom–atom interaction energies between possible bridging sites in singlet and triplet excited states of **4**.

CHRISTOPHER OWEN BENDER, DEE W. BROOKS, WILLIAM CHENG, DOUGLAS DOLMAN, SEAMUS F. O'SHEA et SIDNEY S. SHUGARMAN. Can. J. Chem. **56**, 3027 (1978).

La photolyse directe du cyano-2 benzobarrelène (**4**) conduit au cyano-5 et -7 benzocyclooctatetraène (**6**, $\Phi = 0.08$ et **7**, $\Phi = 0.25$) et au cyano-1 benzo semi-bullvalène (**8**, $\Phi = 0.05$), tandis que l'irradiation sensibilisée par l'acétophenone de **4** conduit à **8** uniquement ($\Phi = 0.35$). Des études de marquages au deuterium suggerènt que **7** dérive d'une réaction initiale de cycloaddition $2\pi + 2\pi$ qui procède par liaison entre les ponts vinyle et vinylcyano de **4**, tandis que **8**, resultant de la photolyse directe ou sensibilisée de **4**, provient d'un réarrangement di-π-méthane qui procède par liaison entre les ponts vinyle et vinylcyano de **4**. Les liaisons initiales observées des cycloadditions $2\pi + 2\pi$ et du réarrangement di-π-méthane sont en accord avec les prédictions qui proviennent de calculs des changements d'énergies d'interactions atome–atome entre les sites de liaisons possibles de l'état excité singulet et triplet de **4**.

Introduction

Zimmerman and co-workers (1) have reported that benzobarrelene (**1**) undergoes two types of photochemical rearrangement, one leading to cyclooctatetraene (COT) product **2**, which was rationalized as proceeding from the singlet excited state of **1** via $2\pi + 2\pi$ cycloaddition, and the other leading to semibullvalene (SB) product **3** from the triplet excited state via di-π-methane rearrangement (1). Furthermore, deuterium labelling studies revealed that of the two bonding routes (Scheme 1, routes *i* and *ii*) which could a priori furnish the COT product (**2**), the benzo–vinyl pathway (Scheme 1, route *i*) was mainly utilized, while the SB product (**3**) which could also arise a priori from two bonding routes (Scheme 1, routes *iii* and *iv*) was uniquely provided by the vinyl–vinyl pathway (Scheme 1, route *iii*).

Within the perspective of these two rearrangement types, the potential for mechanistic variation and hence challenge to theoretical predictions can, in principle, be maximized by the introduction of a substituent in a vinyl location, so that the symmetry of the benzobarrelene skeleton is destroyed and hence the number of possible initial bonding modes is increased to three $2\pi + 2\pi$ cycloadditions and six di-π-methane rearrangements. In this paper we report on the mechanistic aspects of the photochemistry of 2-cyanobenzobarrelene (**4**) and comment on the ability of some predictive methods to rationalize the product formations.[1]

Results

2-Cyanobenzobarrelene (**4**) was prepared by the addition of benzyne to bromobenzene, followed by treatment of the bromobarrelene **5** with cuprous cyanide (see Scheme 2). The structure of **4** follows from the mode of synthesis, the similarity of the nmr spectrum to that of the naphtho analogue (**9**) of **4**, and the observation that it undergoes retro-Diels–Alder reaction in the presence of lithium cyclohexylamide to yield naphthalene (45%) (cf. the formation of anthracene from **9** under similar conditions; ref. 5).

The direct irradiation of **4** yields three primary photoproducts isomeric with the starting material: 5- and 7-cyanobenzo-COT (**6** and **7**) and 1-cyanobenzotricyclo[3.3.0.$0^{2,8}$]octa-3,6-diene (i.e., 1-cyanobenzosemibullvalene (**8**)) (see Scheme 3). The photoproducts were separated by chromatography and were obtained in crystalline form.

[1]Some preliminary details of the photochemistry of **4** have appeared in two communications (2, 3).

Can. J. Chem. Downloaded from www.nrcresearchpress.com by 210.87.254.6 on 09/05/12
For personal use only.

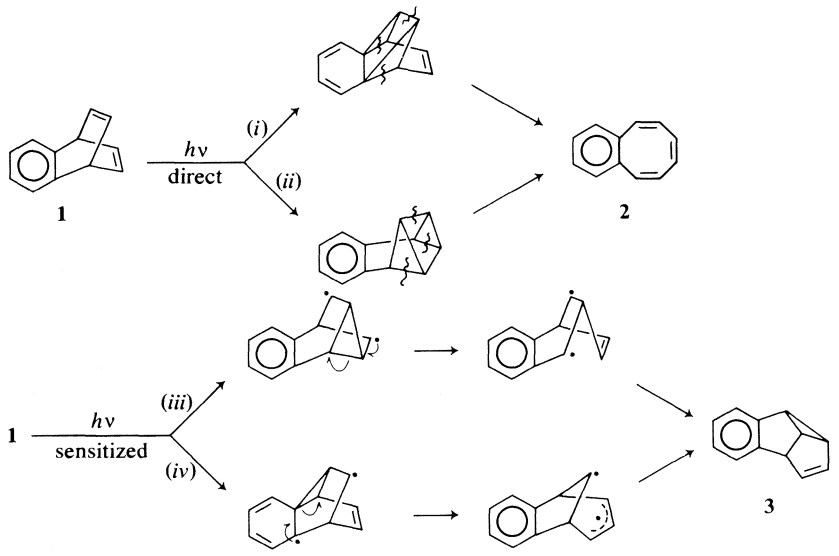

SCHEME 1

The structures of **6** and **7** were deduced from nmr spectral evidence. As expected for COT derivatives only absorptions in the aromatic-olefinic region of the spectra were observed. The nmr data are shown in Table 1 and for the purposes of comparison also

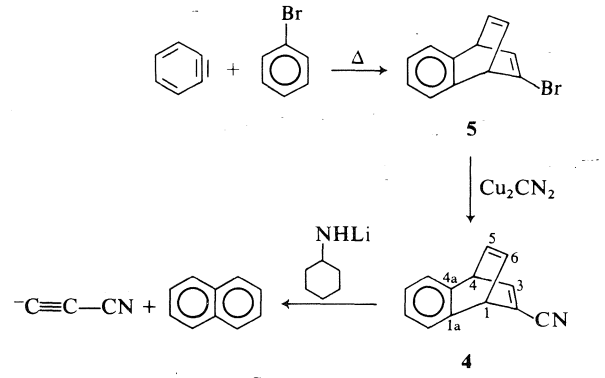

SCHEME 2

included are those of the known COT's **2** (1) and **10** (5). Additional support for the assigned structures comes from spin-decoupling experiments (see footnotes in Table 1) and, in the case of **6**, from examination of the nmr spectrum of the 8-deuterio derivative **17** (see Table 1), unambiguously provided by the direct irradiation of 5-deuterio-2-cyanobenzobarrelene (**15**) (*vide infra*; see Scheme 5).

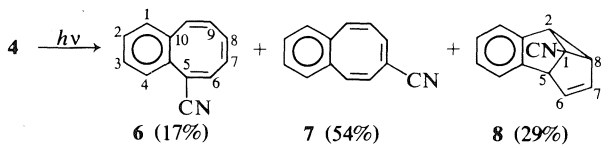

SCHEME 3

The structure of the SB product **8** was ascertained from the nmr spectrum (see Experimental) which was closely similar to that reported for **11** (5). Further evidence in favour of the assignment stems from the observation that **8** isomerizes to 6-cyanobenzo-COT (**13**) upon direct irradiation (cf. the photoisomeriza-

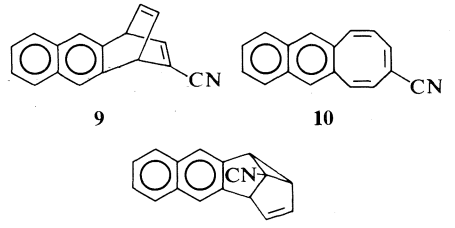

tion of **3** to **2** (1)) (see Scheme 4). The nmr data for **13** are given in Table 1. Assistance with the signal assignments was obtained from examination of the nmr spectrum of the 8-deuterio derivative **14**. Compound **14** was prepared from the direct irradiation of 7-deuterio-1-cyanobenzo-SB (**12**) (*vide infra*), envisaged, by analogy to observations with perdeuteriobenzo-SB (1), to result from cleavage of the C-2—C-8 and C-1—C-5 bonds.

In accord with the assigned structures, the deshielding effect of the cyano group on the adjacent

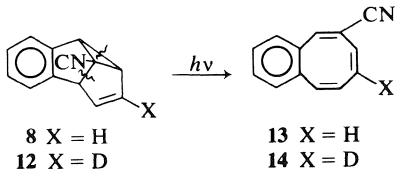

SCHEME 4

Can. J. Chem. Downloaded from www.nrcresearchpress.com by 210.87.254.6 on 09/05/12
For personal use only.

TABLE 1. The nmr data of aromatic and vinyl protons of cyclooctatetraenes[a]

Assignment	Description and signal position, τ						
	7[b,e]	13[b,f]	14[b,g]	6[b,h]	17[b,i]	10[c]	2[d]
Aromatic	2.72–3.15 m	2.70–3.12 m	2.71–3.13 m	2.67–3.13 m	2.64–3.16 m	2.10–2.60 m	2.72–3.27 m
H-5	3.32 d,$J_{5,6}$ = 11.5	2.78[j] s	2.79[j] s	—	—	3.05 d,$J_{5,6}$ = 11.5	3.53 d,$J_{5,6}$ = 10.5
H-6	4.11 d,$J_{5,6}$ = 11.5	—	—	3.25 dd,$J_{6,7}$ = 4, $J_{6,9}$ = 1.25	3.22 dd,$J_{6,7}$ = 4, $J_{6,9}$ = 1.25	3.94 d,$J_{5,6}$ = 11.5	4.08 d,$J_{5,6}$ = 10.5
H-7	—	4.25 d,$J_{7,8}$ = 11	4.23 s	3.90–4.17 m	4.14 br d,$J_{6,7}$ = 4	—	4.19 s
H-8	3.46 d,$J_{8,9}$ = 4.5	3.85–4.05 m	—		—	3.33 d,$J_{8,9}$ = 3.5	4.19 s
H-9	4.03 dd,$J_{8,9}$ = 4.5, $J_{9,10}$ = 11.5		3.97 d,$J_{9,10}$ = 11.5		4.01 br d,$J_{9,10}$ = 11	3.86 dd,$J_{9,10}$ = 11.5, $J_{8,9}$ = 3.5	4.08 d,$J_{5,6}$ = 10.5
H-10	3.35 d,$J_{9,10}$ = 11.5	3.45 d,$J_{9,10}$ = 11.5	3.46 d,$J_{9,10}$ = 11.5	3.41 d,$J_{9,10}$ = 11	3.39 d,$J_{9,10}$ = 11	3.05 d,$J_{9,10}$ = 11.5	3.53 d,$J_{5,6}$ = 10.5

[a]Run on HA-100 MHz nmr in CCl_4 with TMS as internal standard; coupling constants are given in hertz.
[b]This work.
[c]Reference 5.
[d]Reference 1.
[e]Irradiation of H-8 collapsed H-9 to a d ($J_{9,10}$ = 11.5).
[f]Irradiation at centre of H-8,9 m collapsed H-10 and H-7 to singlets; irradiation of H-10 left H-7 unchanged.
[g]Irradiation of H-10 collapsed H-9 to an s; irradiation of H-9 collapsed H-10 to an s; irradiation of H-7 left H-9 unchanged.
[h]Irradiation of the H-7,8,9 m at τ 4.01 collapsed H-10 to an s; irradiation at τ 4.14 collapsed H-6 to an s.
[i]Irradiation of H-6 collapsed H-7 to a br s and sharpened the H-9 d ($J_{9,10}$ = 11); irradiation of H-10 collapsed H-9 to a br s; irradiation of H-9 collapsed H-7 to a sharp d ($J_{6,7}$ = 4) and H-10 to an s; irradiation of H-7 collapsed H-6 to a br s.
[j]Signal position determined by LIS.

TABLE 2. Quantum yield data[a]

Compound	Sensitizer	Conversion (%)	Products			
			6	7	8	13
4	None[b]	10.5	0.09	0.28	0.06	—
4	None[b]	31	0.07	0.23	0.05	—
4	PhCOMe[c,d]	14.5	—	—	0.32	—
4	PhCOMe[c,d]	18	—	—	0.39	—
8	None[b]	7	—	—	—	0.14
8	None[b]	8.5	—	—	—	0.12
7	None[b]	9.0	—	—	<0.003	—
7	Ph_2CO[c,d]	0	—	—	<0.000	—

[a]Cyclohexane solvent.
[b]Light of 276 nm was used for direct irradiations.
[c]Light of 328 nm was used for sensitized irradiations.
[d]Sensitizer absorbing >95% of light.

coplanar vinyl protons of **6** (H-6), **7** (H-8), and **13** (H-5) relative to the corresponding protons in **2** lies within the range 0.73–0.83 ppm and compares well with the reported chemical shift substituent constant of 0.8 for the *cis*-proton of acrylonitrile (6).

The COT's **6** and **7** were irradiated separately under the same conditions as used for **4** in order to examine for secondary photochemical processes. Both were found to be reasonably stable and long irradiation times were required to cause any disappearance of starting material. In the case of **6**, identifiable product was not obtained. Semibullvalene **8** (18% yield), however, was formed from COT **7** together with much polymeric material. The sensitized irradiation of **7** with benzophenone at 328 nm did not lead to detectable amounts of SB **8**. Since the photoreduction of benzophenone was efficiently quenched in the presence of **7**, it seems certain that triplet energy transfer to the COT had been successful; **8**, therefore, derives from the singlet excited state of **7**.

In contrast to the direct irradiation of **4**, sensitization with acetophenone leads cleanly to the formation of a single product, 1-CN-SB (**8**). The quantum yields for this and other transformations observed in this study are given in Table 2. In the case of the conversion of **8** to **13** attempts to sensitize the reaction with either acetophenone or acetone failed; the starting material slowly disappeared to give unidentified products but the formation of **13** was shown to be absent by nmr and tlc.

Singlet and Triplet Energies of 4

The singlet energy of **4** in cyclohexane solution at room temperature was determined to be 96 kcal mol^{-1} from intersection of the absorption and fluorescence spectra. The triplet energy of **4** could not

Can. J. Chem. Downloaded from www.nrcresearchpress.com by 210.87.254.6 on 09/05/12
For personal use only.

TABLE 3. Observed and theoretical hydrogen distribution of deuterated 7-CN-COT from the photolysis of **15**[a]

	Aromatic	H-10 + H-5	H-8	H-6 + H-9
Route *i*, calcd.[b]	4.00	1.07±0.06	1.00	2.00
Route *iii*, calcd.[b]	4.00	2.00	1.00	1.07±0.06
Found[c]	4.00	1.97±0.04	1.01±0.04	1.06±0.03

[a]CCl_4 solvent.
[b]Corrected for 93 ± 6% d_1 at C-5 in reactant **15**.
[c]Errors estimated from scatter of nmr signal integrations.

Can. J. Chem. Downloaded from www.nrcresearchpress.com by 210.87.254.6 on 09/05/12
For personal use only.

be obtained spectrometrically since no phosphorescence in isopentane – methylcyclohexane glass at 77 K could be detected. However, an 'effective' triplet energy at room temperature in benzene solution of $> 56 < 59$ kcal mol^{-1} was determined from triplet sensitization experiments: the triplet sensitizers acetophenone (74 kcal mol^{-1}), benzophenone (69 kcal mol^{-1}), thioxanthone (65 kcal mol^{-1}), Michler's ketone (61 kcal mol^{-1}), and 2-acetonaphthone (59 kcal mol^{-1}) gave $\Phi_8 = 0.33 \pm 0.03$, whereas 1-acetonaphthone (56 kcal mol^{-1}) gave $\Phi_8 \simeq 0.00$.

Mechanistic Considerations

Inspection of the possible modes of $2\pi + 2\pi$ cycloadditions available to barrelene **4** shows that whereas **6** can derive from only one route (Scheme 5, route *i*), that involving initial bridging between the benzo and vinylcyano group, there are two a priori cycloaddition pathways that can account for the formation of **7**: initial benzo-vinyl bridging (Scheme 5, route *ii*) and initial vinyl–vinylcyano bridging (Scheme 5, route *iii*).

To evaluate the relative importance of routes *ii* and *iii* the direct irradiation of the deuterated barrelene **15** (93% d_1 at C-5; prepared as in the case of **4** but replacing the bromobenzene by *p*-deuteriobromobenzene) was investigated. The nmr spectrum of the deuterated 7-CN-COT product isolated from the photolysate was consistent only with the β-labelled compound **22**; the olefinic region of the nmr spectrum showed a doublet centered at τ 3.32 (H-5, $J = 11.5$ Hz), a singlet at τ 3.35 (H-10), a singlet at τ 3.46 (H-8), and a doublet at τ 4.11 (H-6, $J = 11.5$ Hz). (See Table 3 for H-distributions.) Thus 7-CN-COT (**7**) is uniquely provided by the vinyl–vinylcyano pathway (Scheme 5, route *iii*).

As anticipated for the single $2\pi + 2\pi$ cycloaddition pathway capable of leading to **6** (Scheme 5, route *i*), the deuterated material isolated from the photolysis of **15** contained exclusive labelling at C-8 (see Table 1 for nmr data) and hence is **17**.

Nuclear magnetic resonance examination of the labelled SB product **12** from either the direct or the sensitized irradiations of barrelene **15** showed the deuterium to be located at C-7 (see Scheme 6). However, this labelling does not allow delineation of a unique pathway for the di-π-methane rearrangement of the barrelene since there are two routes which could furnish **12**: route *i* (Scheme 6), which commences with aromatic–vinylcyano bonding (between C-3 and C-4*a*), and route *ii* (Scheme 6), initiating with vinyl–vinylcyano bonding (between C-3 and C-5).

A means of determining the occurrence of routes *i* and/or *ii* (Scheme 6) was obtained by examining the photolysis of the mixture of deuterated barrelenes **23***b*. The mixture consisted of an equal amount of two singly labelled isomers, one incorporating deuterium

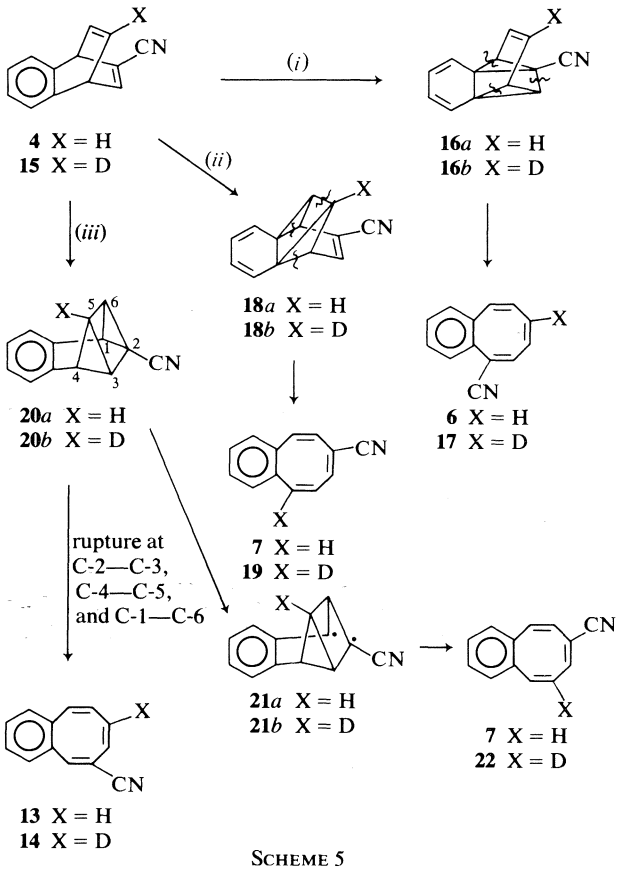

SCHEME 5

TABLE 4. Observed and theoretical hydrogen distributions of labelled semibullvalene mixtures

Case	Label distribution[a] H-2	H-5	H-6	H-7	H-8	ArH
(*A*) Distributions calculated and found for deuterated semibullvalenes from photolyses of **23***b*						
1. Mechanism *i*, calcd.[b]	1.00	1.00	0.54±0.04	1.00	0.54±0.04	4.00
2. Mechanism *ii*, calcd.[b]	0.54±0.04	1.00	0.54±0.04	1.00	1.00	4.00
3. Direct, exptl.[c]	0.57±0.04	0.97±0.03	0.55±0.03	1.01±0.04	0.96±0.04	4.00
4. Acetophenone sensitized, exptl.[c]	0.56±0.03	1.02±0.03	0.53±0.04	0.97±0.04	1.03±0.04	4.00
5. 2-Acetonaphthone sensitized, exptl.[c]	0.57±0.03	1.01±0.02	0.55±0.04	0.98±0.02	0.98±0.04	4.00
(*B*) Distributions found for recovered labelled semibullvalenes from photolysis of **28***b*						
6. Direct, exptl.[c]	0.54±0.03	0.97±0.04	0.54±0.02	1.04±0.04	0.99±0.05	4.00
7. Sensitized, exptl.[c]	0.56±0.03	1.00±0.02	0.56±0.04	0.96±0.03	1.01±0.04	4.00

[a] Acetone-d_6 solvent.
[b] Corrected for equal amounts of the two singly labelled isomers in mixture **23***b*, one containing 94 ± 3% d_1 at C-4 and the other 92 ± 4% d_1 at C-6.
[c] Errors estimated from scatter of nmr signal integrations.

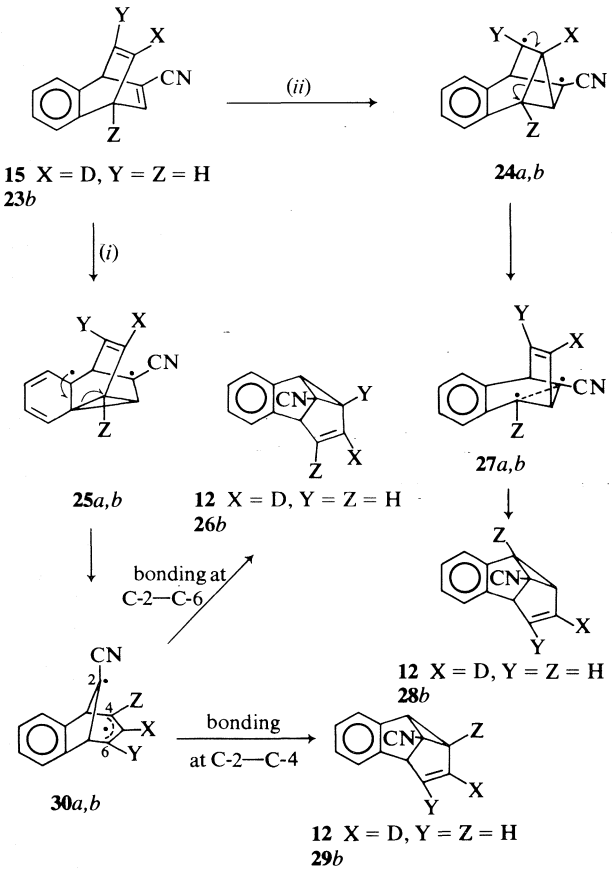

SCHEME 6. For series *a*, X = D, Y = Z = H. For series *b*, individual structures represent an approximately 50:50 mixture of two component compounds, each singly labelled with deuterium at the positions designated by Y and Z; X = H.

(94 ± 3%) at C-4 and the other deuterium (92 ± 4%) at C-6, and was prepared as in the case of **4** but replacing the bromobenzene by *m*-deuteriobromobenzene. Within experimental error, no deuterium isotope effects were discernible in the benzyne addition stage or in the subsequent photoisomerizations.

The hydrogen distributions of the 1-CN-SB material isolated from the direct, acetophenone, and 2-acetonaphthone sensitized irradiations of deuterobarrelene mixture **23***b* are the same within experimental error (see Table 4); half of the deuterium is located at C-2 and half at C-6 (i.e., consistent with **28***b*). Thus route *ii* (Scheme 6) alone accounts for the di-π-methane rearrangement of barrelene **4** during the formation of SB product from direct or sensitized irradiations of **4**.

With the SB mixture **28***b* at hand, it was pertinent to investigate its photolysis to ascertain whether a vinylcyclopropane rearrangement leading to the SB mixture **31** occurs. Such a photoisomerization with the dicarbomethoxy-SB **33** has previously been found to yield **34** (see Scheme 7) (7). The nmr spectrum of the SB material recovered from the direct irradiation of mixtures **28***b* (>80% loss of starting material, 63% being converted to deuterated mixture **32**, containing equal amounts of deuterium at C-5 and C-9) was essentially identical to that of the starting material (see Table 4, case *6*). Irradiation with acetone as sensitizer resulted in the slow disappearance of **28***b* to give unidentified products but again there was no

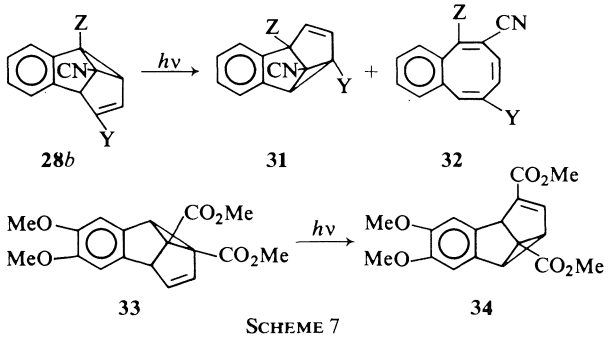

SCHEME 7

Can. J. Chem. Downloaded from www.nrcresearchpress.com by 210.87.254.6 on 09/05/12
For personal use only.

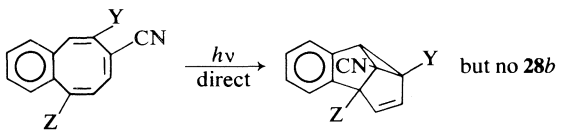

35 36

SCHEME 8. Individual structures represent an approximately 50:50 mixture of two component compounds, each singly labelled with deuterium at the positions designated by Y and Z.

detectable change in the labelling pattern in the recovered starting material after >80% consumption (see Table 4, case *7*). Thus the photochemical vinylcyclopropane rearrangement does not operate in 1-CN-SB (**8**).

Finally, the direct irradiation of COT **35** (**35** was isolated as the major product of the direct irradiation of **23***b*) was carried out. This was important to do because of the possibility that some of the SB **8** formed during the direct irradiation of barrelene **4** derives, in part, from the secondary photolysis of the primary COT **7** photoproduct. That this is not so, was demonstrated by the fact that COT **35** leads to SB **36**, containing a different labelling pattern than SB **28***b* formed from the direct irradiation of **23***b*, i.e., in **36**, the available deuterium is located at C-5 (50%) and at C-8 (50%); no SB product containing deuterium at C-6 and C-1 was observable (see Scheme 8). Thus SB **8** formed from the direct irradiation of **4** appears to be due entirely to the primary photolysis of **4**, under the conditions of irradiation used in this study. Since the quantum yield for the formation of **8** from **7** is so low and the formation of intermediates has not been excluded, mechanistic speculation as to the production of **8** is deferred.

Discussion

The excited state of **4**, yielding SB **8** upon sensitization with sensitizers of triplet energy ranging from 59 to 74 kcal mol^{-1}, can reasonably be assigned to T_1 since (*a*) the quantum yields for the formation of **8** remain essentially constant over the sensitizer energy range and (*b*) the deuterated barrelene mixture **23***b*, employed in runs with the lowest and highest sensitizers (i.e., 2-acetonaphthone and acetophenone), gives SB product containing the same label distributions in both cases (see Table 4). The excited state responsible for the formation of COT's **6** and **7** upon direct irradiation of **4** with 276 nm light (103 kcal mol^{-1}) is attributed to S_1 ($E_{s_1} \simeq 97$ kcal mol^{-1}); they are not formed during sensitized runs. In the case of **8**, when generated from the direct irradiation of **4**, T_1 may be involved since the deuterated barrelene mixture **23***b* leads to SB material (**28***b*) containing the same label distributions from direct and sensitized irradiations. Furthermore, the quantum yield data (Table 2) show the formation of **8** from the direct irradiation of **4** to be much less efficient than from sensitized runs as expected for a process involving intersystem crossing. However, these data do not rule out the possibility that the S_1 excited state of **4** provides **8** since it is not known that S_1 would have followed an alternative mechanistic course.

With respect to the COT formations from **4**, the results from the labelling experiments with **15** (see Table 3 and Scheme 5) reveal a dramatic substitution effect on the initial $2\pi + 2\pi$ bonding preferences. Thus for benzobarrelene itself Zimmerman and his co-workers (1) have shown that the benzo–vinyl bonding pathway (Scheme 1, route *i*) predominates to the extent of $94 \pm 2\%$ (1). In the present case bridging to the benzo moiety constitutes only a minor route (24%, Scheme 5, route *i*) and then only to the more substituted ethylene.

This result was of considerable interest when first reported by us (2) because it did not support the pericyclic formulations proposed by Epiotis. Epiotis (8) had reasoned that polar $2\pi + 2\pi$ cyclizations occurring from the first excited singlet state are expected to be [s + a] stereoselective and that in systems where geometric constraints demand an [s + s] cyclization mode, the reaction is pericyclically forbidden. Extension of this concept to the case of barrelene **4**, where there are three different $2\pi + 2\pi$ initial bridging options, would lead to the conclusion that bonding between the least polar bridges (i.e., route *ii*, Scheme 5) should be the most favored. This is not seen to be the case for **4** nor for any of the polar benzobarrelene examined to date (2, 7, 9). Epiotis has subsequently pointed out to us that revised and more detailed calculations indicate that for *intramolecular* photocycloadditions, the skeletal restrictions prohibit the introduction of a sufficient number of donor and/or acceptor groups to render the reaction 'highly polar.'[2] Thus previous examples suggested by Epiotis to be in accord with prediction are now inappropriate (8).

Another predictive method is also rendered inutile by the present work. We had previously reported, in connection with the photochemistry of dimethyl 2,3-benzobicyclo[2.2.2]octatetraene-5,6-dicarboxylate, and its 10-methoxy derivative, that alterations in initial $2\pi + 2\pi$ bonding preferences of polarly substituted benzobarrelenes seem to be related to changes in donor–acceptor, (i.e., charge–transfer) properties of the addend–addend complexes engendered in the bridging process (7, 9). However, the limiting factor that invalidates this interpretation in the case of **4**, is that for models approximating the individual addends

[2]We thank the author for a preprint of his manuscript (10).

Can. J. Chem. Downloaded from www.nrcresearchpress.com by 210.87.254.6 on 09/05/12
For personal use only.

Can. J. Chem. Downloaded from www.nrcresearchpress.com by 210.87.254.6 on 09/05/12
For personal use only.

(e.g., benzene, IP_V = 9.25 eV (11), ethylene, IP_V = 10.51 eV (11), and acrylonitrile, IP_V = 10.88 eV (12)), the aromatic moiety always has a smaller vertical ionization potential (IP_V) than the noncyanolated vinyl bridge, at any consistent level of substitution (e.g., *o*-xylene, IP_V = 8.57 eV (11) and *cis*-2-butene, IP_V = 9.13 eV (12); or tetralin, IP_V = 8.44 eV (11) and cyclohexene, IP_V = 9.12 eV (11)). Thus, contrary to observation, excited-state charge–transfer interaction, and hence bonding, involving the aromatic addend would erroneously be predicted to be favored.

A rationale which is in accord with observations derives from CNDO-CI calculations of changes in atom–atom interaction energies between possible bridging sites resulting from excitation to the singlet excited state of **4**. The total molecular energy calculated by NDO-type methods can be rewritten in terms of a sum of one-atom energies plus a sum of two-atom interaction energies for all distinct pairs of atoms in the molecule (14); this is a consequence of the neglect of all three- and four-centre electron interaction integrals which, in *ab initio* calculations give rise to interaction energies involving three and four atoms simultaneously. Naively, one can say that the changes in atom–atom interaction energies that result from electron excitation give rise to forces which make the atoms move. By resolving the excitation energy into atom–atom components one can make predictions about the initial motions and, in rigid systems, the possible product.

Related approaches using the changes in the bond-order matrix elements provide the basis for the Woodward–Hoffman rules and a similar scheme which is based on orbital–orbital interaction energies was recently reported by Zimmerman *et al.* (13). Both the bond-order and orbital–orbital energy approaches were investigated for the present system. However, it was felt that the additional difficulty introduced by the nonplanar structure gives rise to ambiguities; for example, the changes in the 16 orbital–orbital interaction energies for a given pair of atoms are not all of the same sign, unlike the case of planar conjugated systems where one need only consider the effects of the interaction of the π orbitals belonging to the atoms in question. The atom–atom energy, the sum of all orbital–orbital interactions between the pair of atoms, seems better suited to the discussion of nonplanar molecules, where the strict σ–π separation is lost. The extension of the atom–atom analysis to excitation energies follows in a straightforward (but tedious) way from the method used for ground states; details are available from the authors.

This approach has a number of strengths and weaknesses. It is simple to implement and understand. The interpretations of the results is reasonably straightforward: atom pairs for which the change in interaction energy is attractive tend to move towards one another and atoms which are repelled from one another move apart.

There is no ambiguity about the geometry of the molecule, an important consideration since the molecular energy is a sensitive function of the geometry, and there are no difficulties relating to partitioning the molecule. On the other hand the CNDO method is an approximation, and our assumption of the relationship between the changes in the atom–atom energies and the reaction coordinate is questionable; a more extensive study of this point is underway.

The predictions for the product distributions of the photolyses of the parent benzobarrelene and the 2-cyanobenzobarrelene are given in Table 5 for both the singlet and triplet (*vide infra*) mediated reactions. The calculations refer to the structure which minimizes the ground-state molecular energy in the CNDO/2 approximation;[3] the CI calculations for the excited state were performed in three different parameterizations: theoretical (14), Pariser, and Mataga (ref. 15 and references cited therein), the last two being designed to give the best descriptions of the triplet and singlet states respectively. For the singlet excited state (S_1) the results suggest the formation of the intermediate **20**, and hence the product **22**, as the most probable pathway with the intermediate **16**, and product **6**, as the next most probable pathway, in agreement with the experimental findings. As may also be seen from Table 5, the pathway predicted by this method to be most probable in the singlet photolysis of benzobarrelene (**1**) is again consistent with experimental results (1).

Finally with respect to the singlet cycloadditions of **4**, the observation that **7** but no **13** is formed from the proposed intermediate **20***a* can be attributed to the preferred rupture of the C-1—C-2 bond of **20***a*, since favorable stabilization from the cyano and benzo groups is afforded both radical centres in the ensuing species **21***a*. An alternative explanation is provided by the fact that in cyclopropanes, electron withdrawing substituents (here, the cyano group in **20***a*), strengthen the bond opposite, while weakening the bonds adjacent (16).

Turning now to the triplet excited state of **4**, the main reactivity appears to be similar to that of benzobarrelene (*1*), namely, efficient semibullvalene formation (cf. Φ = 0.35 for **8** and 0.52 for **3** (17)), deriving from di-π-methane rearrangement involving initial bridging between the vinyl bridges (Scheme 6,

[3]Calculations were performed using a modified and extended version of the CNDO/M program (QCPE #315) originally written by Jaffé and co-workers (21).

TABLE 5. Changes in atom–atom energies (eV) accompanying electronic excitation to the lowest singlet (S_1) and triplet (T_1) states of **1** and **4**[a]

Atoms bridging		S_1			T_1		
		T	P	M	T	P	M
		(*A*) for benzobarrelene (**1**)					
2	6	0.283	0.233	−0.114	−1 226	−0.954	−0.831
1(a)	6	−0.825	−0.992	−0.687	0.040	−0.056	−0.045
		(*B*) for 2-cyanobenzobarrelene (**4**)					
1(a)	2	0.019	0.091	0.044	−0.113	−0.121	−0.120
1(a)	6	0.118	0.138	0.122	0 023	0.040	0.036
2	6	−0.031	−0.346	−0.095	−0 225	−0.279	−0.272
3	4(a)	0.186	0.216	0.203	−0.172	−0.166	−0.128
3	5	0.183	0.288	0.093	−0.267	−0.290	−0.254
4(a)	5	0.207	0.253	0.234	0.027	0.063	0.070

[a]Calculated by the CNDO/CI method using the theoretical (T), Pariser (P), and Mataga (M) parameterizations. The underlined values are the most enhanced interactions calculated for the given transition using the specified integral.

route *ii*). The regiospecificity observed in the vinyl–vinylcyano bonding in the case of **4** can be attributed to the availability of stabilization of the radical centre at C-2 in species **24** via the cyano group.

Recently Santiago and Houk (18) reported a molecular orbital model to account for the direction of preferred di-π-methane bridging in polarly substituted benzonorbornadienes and for barrelene **4**. In this approach, CNDO-CI calculations were performed on a model transition state consisting of a stacked, parallel plane of addends approximating the individual bridging moieties. Although the correct bridging preferences were obtained for the benzonorbornadienes, the predictions for **4** were found to be incorrect (3). The atom–atom interaction energies for the triplet state of **4**, resulting from our rigid model calculations (*vide supra*), Table 5, suggest that the formation of intermediate **24** leading to the product **12** is the preferred pathway, in agreement with experiment. The second most probable pathway involves bridging between C-2 and C-6 and would lead to products which are not observed. The Mataga parameterization predicts a slight preference for this pathway over that involving **24** but this discrepancy is not too disturbing since the Mataga integrals are optimized with respect to the singlet calculation. For the parent benzobarrelene (**1**) the predicted most probable pathway for the triplet excited-state reaction is also consistent with experimental results (1) (see Table 5). In view of the simplicity of the approach the agreement between the predictions and the observed results is encouraging; it remains to be seen if the method is useful under more general conditions.

Experimental

The nmr spectra were recorded on Varian HA-100 or A-60 instruments with TMS as internal standard. The ir spectra were recorded on a Perkin-Elmer Model 337 spectrophotometer, the uv spectra on a Cary 15 spectrophotometer, and the mass spectra on an MS 9 (A.E.I.). All melting points are uncorrected. Elemental analyses were performed by Galbraith Labs. Inc., Knoxville, TN. Cyclohexane and benzene solvents were prepared for photolyses by scrubbing with 10% of their volume of 30% fuming sulfuric acid, followed by washing with 10% aqueous sodium hydroxide, drying ($MgSO_4$), and finally distilling from calcium hydride. Solid triplet sensitizers were sublimed and recrystallized before use and liquid sensitizers were distilled. Nuclear magnetic resonance chemical shifts are given in τ units and *J* values in hertz; uv maxima are given in nanometres (ε); ir bands are given in reciprocal centimetres. Thin-layer chromatographic separations were carried out on Merck plates, 20 cm × 20 cm, 0.25 mm layer of Silica Gel 60 F-254.

2-Bromo-1,4-dihydro-1,4-ethenonaphthalene (5)

A 12.5 ml portion of isoamyl nitrite was added to a stirred, ice-cooled mixture of 6.85 g (49.95 mmol) of anthranilic acid and 0.08 g of trifluoroacetic acid in 75 ml of dioxane. The stirred mixture was allowed to warm to room temperature during 80 min. The benzene diazonium carboxylate salt was centrifuged and the supernatant liquid discarded. The salt was then washed via centrifugation, twice with dioxane and once with bromobenzene. The salt, slurried in bromobenzene (30 ml), was added to 500 ml of bromobenzene and stirred at 45°C for 24 h under a dry nitrogen atmosphere. The mixture was concentrated *in vacuo* and the residue, dissolved in 10 ml of benzene, was column chromatographed on silicic acid (100–200 mesh). Elution with cyclohexane gave crude **5** from early fractions and crystallization from ethanol gave 187 mg (1.6%) of colorless crystals, mp 50–51°C: uv (cyclohexane): 246 sh (1050), 260 (760), 268 (720), and 277 (640); nmr (60 MHz, CCl_4): 2.80–3.45 (m, 7H, aromatic and vinyl), and 5.12–5.52 (m, 2H, bridgehead). *Anal.* calcd. for $C_{12}H_9Br$: C 61.83, H 3.98, Br 34.28; found: C 61.79, H 3.90, Br 34.20.

2-Cyano-1,4-dihydro-1,4-ethenonaphthalene (4)

A solution of 187 mg (0.80 mmol) of **5** and 171 mg (0.86 mmol) of cuprous cyanide in 40 ml of dry DMF was stirred under reflux for 4 h. The cooled mixture was diluted with 200 ml of benzene and extracted in turn with 5% aqueous $FeCl_3$ (2 × 50 ml), 5% aqueous NaOH (50 ml), and water (50 ml). The benzene solution was concentrated *in vacuo* and the residue column chromatographed on silica gel (60–200 mesh). Elution with cyclohexane removed unreacted starting

Can. J. Chem. Downloaded from www.nrcresearchpress.com by 210.87.254.6 on 09/05/12
For personal use only.

Can. J. Chem. Downloaded from www.nrcresearchpress.com by 210.87.254.6 on 09/05/12
For personal use only.

material. Elution with 1% ether–cyclohexane gave crude **4** and crystallization from ethanol gave 126.5 mg (74%) of colorless crystals, mp 66–67°C: ir (KBr): 2210, C≡N; uv (cyclohexane): 266 sh (1080), 268 (1120), 273 (1090), 276 (1080), and 283 sh (710); nmr (100 MHz, CCl_4): 2.62 (dd, 1H, H-3, $J_{3,4} = 6$, $J_{1,3} = 2$), 2.78–3.36 (m, 6H, aromatics, H-5 and H-6), 4.95–5.23 (m, 2H, bridgeheads); LIS nmr (100 MHz) with 16.0 mg of **4** and 35.4 mg of Eu(fod)$_3$ d_{30} in 0.25 ml CCl_4: 1.74 (dd, 1H, H-3, $J_{3,4} = 6$, $J_{1,3} = 1.5$), 2.46–3.13 (m, 6H, aromatic, H-5 and H-6), 4.23 (dt, 1H, H-1, $J_{1,6} = 5$, $J_{1,3} = J_{1,5} = 2.0$), and 4.66 (dt, 1H, H-4, $J_{3,4} = J_{4,5} = 6$, $J_{4,6} = 2$); spin-decoupling experiments on LIS spectra: irradiation of H-3 left aromatics, H-5, H-6 m unchanged, collapsed H-1 to a dd ($J_{1,6} = 5$, $J_{1,5} = 2$), and collapsed H-4 to a dd ($J_{4,5} = 6$, $J_{4,6} = 2$); irradiation of H-1 left H-4 unchanged, collapsed H-3 to a d ($J_{3,4} = 6$), and modified the aromatics, H-5, H-6 m; irradiation of H-4 collapsed H-3 to a d ($J_{1,3} = 2$), modified the aromatic H-5, H-6 m, and left H-1 unchanged. *Anal.* calcd. for $C_{13}H_9N$: C 87.12, H 5.06, N 7.82; found: C 87.10, H 5.10, N 7.80.

Action of Lithium Cyclohexylamide on Cyanobarrelene ***4***

A solution of 293.8 mg (1.48 mmol) of **4**, 45 ml of cyclohexylamine (CaH_2 dried and distilled), and 4 ml (8.0 mmol) of 2 *M* butyllithium hexane was stirred at 85–90°C for 48 h in a nitrogen atmosphere. The cooled mixture was quenched with 50 ml of water, diluted with 250 ml of benzene, and extracted with 10% HCl (2 × 100 ml) and then with water (2 × 100 ml). The benzene solution was dried ($MgSO_4$), concentrated *in vacuo*, and the residue column chromatographed on silicic acid (100–200 mesh) with cyclohexane solvent. Crystallization of the contents of the initial bands from ethanol gave 96.2 mg (45%) of colorless crystals, mp 78–80°C, which were shown by tlc, ir, and mixture mp to be identical to naphthalene.

Preparative Photolysis Apparatus

The apparatus consisted of a 450W Hanovia medium-pressure mercury arc surrounded by a water-cooled quartz immersion well. For direct irradiations the light was filtered through a Corex sleeve. For acetone and acetophenone sensitized irradiations a Pyrex sleeve was used. Sample solutions were deoxygenated by flushing with argon, before and during irradiations.

Direct Irradiation of Cyanobarrelene ***4***

A solution of 103.5 mg (0.58 mmol) of **4** in 250 ml of cyclohexane was photolysed directly for 15 min. The photolysate was concentrated *in vacuo* and the residue chromatographed on a silicic acid column with 1% ether–cyclohexane. The first band contained 55.3 mg (53%) of a mixture of the COT's **6** and **7**, and crystallization from ethanol gave 26.1 mg (25%) of pale yellow **7**, mp 102–103°C; ir (KBr): 2205, C≡N; uv (cyclohexane): 227 sh (15 700), 241 (15 200), and 288 (1050); nmr, see Table 1. *Anal.* found: C 87.28, H 5.09, N 7.80.

The mother liquors were concentrated and applied in equal portions to two tlc plates; four irrigations with 8% ether–hexane gave complete separation of **6** and **7**. The first band contained 12.3 mg (12%) of **7**. The second band contained 12.8 mg (12%) of **6** which, after crystallization from ethanol, gave 7.2 mg of colorless **6**, mp 66–68°C; ir (KBr): 2200, C≡N; uv (cyclohexane): 237 (11 250) and 274 (815); nmr, see Table 1. Mass spectrum (70 eV, direct inlet) showed molecular ion at *m/e* 179.0740 (79%), $C_{13}H_9N$ requires 179.0735.

Crystallization (ethanol) of the contents of the second band from the column chromatography yielded 5.6 mg (5%) of **8** as a colorless solid, mp 95–96°C; ir (KBr): 2230, C≡N; uv (cyclohexane): 259 sh (290), 266 (410), 272 (560), and 279 (590); nmr (100 MHz, $CDCl_3$): the aliphatic-olefinic region comprises an ABMXY spin system, 2.56–3.00 (m, 4H, aromatics), 4.30 (*A*BM q, 1H, H-6, $J_{5,6} = 2.5$, $J_{6,7} = 5$), 4.80 (A*B*X q, 1H, H-7, $J_{6,7} = 5$, $J_{7,8} = 2.5$), 5.78 (A*M* d, 1H, H-5, $J_{5,6} = 2.5$), 6.34 (X*Y* d, 1H, H-2, $J_{2,8} = 7$), and 6.67 (B*XY* q, 1H, H-8, $J_{7,8} = 2.5$, $J_{2,8} = 7$). *Anal.* found: C 87.22, H 4.98, N 7.87.

The mother liquors from the crystallization were concentrated *in vacuo* and applied in equal portions to two tlc plates; four irrigations with 8% ether–hexane gave complete separation of **8** and starting material (**4**). The first band contained 36.9 mg (36%) of **4** and the second 2.7 mg (3%) of **8**.

Sensitized Photolysis of Cyanobarrelene ***4***

A solution of 101.2 mg (0.57 mmol) of **4** and 1 ml of acetophenone in 250 ml of cyclohexane was photolysed for 20 min. The photolysate was concentrated *in vacuo* and the acetophenone was removed by short-path distillation (40°C/0.1 Torr). The residue was crystallized from ethanol to give 40.3 mg (40%) of **8**. The mother liquors were concentrated and applied in equal portions to two tlc plates; after four irrigations with 8% ether–hexane 41.6 mg (41%) of starting material (**4**) and 10.2 mg (10%) of **8** were obtained from the first and second bands, respectively.

*5-Deuteriocyanobarrelene (**15**) and the 4- and 6-Deuteriocyanobarrelene Mixture **23**b*

The deuterated compound **15** and the deuterated mixture **23***b* were obtained in ≃1.5% overall yields (based on benzyne precursor) using essentially the same method as that used to prepare **4**, except that bromobenzene was replaced by *p*-deuteriobromobenzene (5) in the case of **15** and by *m*-deuteriobromobenzene (5) in the case of **23***b*. For **15**, mp 66–67°C, nmr (100 MHz, CCl_4): 2.55 (dd, 1.00H, H-3, $J_{1,3} = 2$, $J_{3,4} = 6$), 2.73–3.25 (m, 5.07 ± 0.06H, aromatics, H-6 and residual H-5), 4.96–5.12 (m, 1.97 ± 0.04H, bridgeheads), i.e., 93 ± 6% deuteration at C-5 based on the assumption of 0% d_1 at H-3. For **23***b*, LIS nmr (100 MHz): with 7.1 mg of **23***b* and 12.7 mg of Eu(fod)$_3$-d_{30} in 0.25 ml CCl_4: 2.04–2.18 (m, 1.03 ± 0.04H, aromatics, H-5, and residual H-6), 4.51–4.68 (m, 0.97 ± 0.05H, H-1), 4.78–4.94 (m, 0.53 ± 0.03H, H-4), i.e., this corresponds to an approximately 50:50 mixture of two component compounds one containing 94 ± 3% d_1 at C-4 and the other 92 ± 4% d_1 at C-6.

*Direct Photolysis of 5-Deuteriocyanobarrelene (**15**)*

A solution of 119.0 mg (0.66 mmol) of **15** in 250 ml of cyclohexane was photolysed for 20 min. The photolysate was worked up as previously described for the direct irradiation of **4** and yielded a total of 55.1 mg (46%) of **22**, mp 101–103°C, 18.1 mg (15%) of **17**, mp 66–68°C, 12.3 mg (10%) of **12**, mp 94–96°C, and 7.2 mg (6%) of starting material (**15**). The nmr spectrum of **22** is described in Table 2 and the results section and that of **17** in Table 1; the nmr of **12** (100 MHz, CCl_4): 2.60–3.03 (m, 4.00H, aromatics), 4.30 (d, 1.04 ± 0.05H, H-6, $J_{5,6} = 2.5$), 4.40–5.70 (no discernible signal, 0.05 ± 0.5H, residual H-7), 5.80 (d, 1.01 ± 0.05H, H-5, $J_{5,6} = 2.5$), 6.35 (d, 1.0 ± 0.04H, H-2, $J_{2,8} = 7$), and 6.70 (d, 0.06 ± 0.04H, H-8, $J_{2,8} = 7$).

*Sensitized Photolysis of 5-Deuteriocyanobarrelene (**15**)*

A solution of 35.8 mg (0.20 mmol) of **15** and 1.0 ml of acetophenone in 250 ml of cyclohexane was photolysed for 7 min. The photolysate was worked up as previously described for the sensitized irradiation of **4** and yielded a total of 14.6 mg (41%) of **12**, mp 94–96°C, and 16.3 mg (46%) of starting material (**15**). The nmr spectrum of **12** is essentially the same as that described for **12** obtained from the direct irradiation of **15**.

*Direct Photolysis of 1-Cyanobenzosemibullvalene (**8**)*

A solution of 82.6 mg (0.46 mmol) of **8** in 250 ml of cyclohexane was photolysed directly for 41 min. The photolysate

Can. J. Chem. Downloaded from www.nrcresearchpress.com by 210.87.254.6 on 09/05/12
For personal use only.

was concentrated *in vacuo* and the residue was chromatographed on a silicic acid column; elution was with 1% ether–cyclohexane. Crystallization from ethanol of the contents of the first band gave 39.2 mg (47%) of colorless **13**, mp 73–74°C; ir (KBr): 2220, C≡N; uv (cyclohexane): 241 (22 700) and 281 (1530); nmr see Table 1; mass spectrum (70 eV, direct inlet) showed molecular ion at *m/e* 179.0744 (75%).

The second band contained 38.4 mg (46%) of recovered starting material.

*Direct Photolysis of 8-Deuterio-2-cyanosemibullvalene (**12**)*

A solution of 17.6 mg (0.10 mmol) of **12** in 250 ml of cyclohexane was photolysed directly for 12 min. The photolysate was worked up as previously described for the undeuterated case to give 6.2 mg (35% of **14**, mp 73–74°C, and 8.1 mg (46%) of recovered starting material; see Table 1 for nmr data of **14**.

*Direct Photolysis of Deuterated Barrelene Mixture **23**b*

A solution of 216.4 mg (1.21 mmol) of mixture **23***b* in 250 ml of cyclohexane was photolysed directly for 8 min. From the photolysate, which was worked up as in the deuterated case, 179.2 mg (82%) of **23***b* was recovered and 1.2 mg (0.6%) of SB mixture **28***b* was obtained, mp 95–96°C; see Table 4 (case *3*) for the nmr H distributions. In addition, 15.2 mg (7%) of **35** was isolated from crystallization of the COT fraction, mp 101–103°C; nmr (100 MHz, $CDCl_3$): 2.62–3.07 (m, 4.00H aromatics), 3.16–3.37 (m, 2.53 ± 0.04H, H-5, -10, and -8), and 3.86–4.11 (m, 1.55 ± 0.05H, H-6 and -9). That the available deuterium was located 50% at C-6 and 50% at C-10 is suggested by the following nmr details: H-10 (τ 3.26) occurs as a doublet ($J_{9,10}$ = 11.5), as does H-8 (τ 3.32, $J_{8,9}$ = 4.0) and H-6 (τ 4.04, $J_{5,6}$ = 11.5). For H-5 there are two types of signals since C-6 is 50% deuterated: a doublet with limbs at τ 3.17 and 3.29 ($J_{5,6}$ = 11.5) and a singlet at τ 3.23. For H-9 there are also two types of spin systems discernible, since H-10 is 50% deuterated: two doublets centred at τ 3.88 and 4.00 ($J_{8,9}$ = 4.0, $J_{9,10}$ = 11.5), and broad lines between the inner limbs of the two doublets (τ 3.92–3.97). There are no lines between the doublet centred at τ 3.88, indicating the total absence of deuterium at C-8 (Note: the doublet centred at τ 4.00 is partially coincidental with the H-6 doublet).

*Sensitized Photolysis of Deuterated Barrelene Mixture **23**b*

(a) With Acetophenone

A solution of 32.6 mg (0.18 mmol) of mixture **23***b* and 1 ml of acetophenone in 250 ml of cyclohexane was photolysed for 9 min. The photolysate was worked up as in the undeuterated case to give 14.3 mg (44%) of starting material and 14.7 mg (45%) of deuterated semibullvalene mixture **28***b*, mp 95–96°C; see Table 4 (case *4*) for the nmr H distributions.

(b) With 2-Acetonaphthone

A solution of 34.0 mg (0.19 mmol) of mixture **23***b* and 176.3 mg of 2-acetonaphthone in 35 ml of cyclohexane was photolysed with light of wavelength 328 nm for 105 min in the 'merry-go-round' apparatus. The photolysate was submitted to column chromatography on silicic acid with 1% ether–cyclohexane was eluting agent. The sensitizer came off first, followed by a band containing **23***b* and **28***b*. This second band was concentrated *in vacuo* and applied in equal portions to two tlc plates; after four irrigations with 8% ether–hexane, 21.6 mg (64%) of **23***b* and 9.6 mg (28%) of **28***b* were obtained from the first and second bands, respectively. See Table 4 (case *5*) for the nmr H distributions of **28***b*.

*Direct Photolysis of Deuterated Semibullvalene Mixture **28**b*

A solution of 17.7 mg (0.10 mmol) of mixture **28***b* in 250 ml cyclohexane was irradiated directly for 30 min. The photolysate was worked up as in the undeuterated case to give 3.5 mg (20%) of recovered starting material (see Table 4, case *7*, for nmr H distributions) and 11.2 mg (63%) of deuterated COT mixture **32**, mp 72–74°C; nmr (100 MHz, Me_2CO-d_6): 2.52 (s, 0.50 ± 0.04H, H-5), 2.55–2.97 (m, 4.00H, aromatics), 3.33 (d and s, 0.99 ± 0.03H, H-10, $J_{9,10}$ = 11.5), 3.72–3.94 (m, 1.56 ± 0.03H, H-8, -9), and 4.13 (d, 0.97 ± 0.03H, H-7, $J_{7,8}$ = 11.5).

*Sensitized Photolysis of Deuterated Semibullvalene Mixture **28**b*

A solution of 9.7 mg (0.05 mmol) of **28***b* and 1 ml of acetone in 250 ml of cyclohexane was photolysed for 20 min. The photolysate was concentrated *in vacuo* and the residue was applied to a tlc plate; three irrigations with 8% ether–hexane led to the recovery of 1.6 mg (16.5%) of starting material; no COT products could be detected on the tlc plate. The nmr H distributions for the recovered starting material are given in Table 4 (case *7*).

*Direct Photolysis of COT **7***

A solution of 135.2 mg (0.76 mmol) of **7** in 250 ml of cyclohexane was photolysed directly for 370 min. The photolysate was concentrated *in vacuo* and the residue chromatographed on a silicic acid column with 1% ether–cyclohexane. The first band contained 113.2 mg (84%) of recovered **7**. The second band contained mostly SB **8** but the tlc showed several other minor components to be present. The contents of the second band were applied to a tlc plate; after two irrigations with 8% ether–hexane, 4.0 mg (3%) of **8** was obtained from the first band. Crystallization from ethanol gave 2.8 mg of pure **8**, mp 94–96°C.

*Direct Photolysis of Deuterated COT **35***

A solution of 42.8 mg (0.24 mmol) of **35** in 250 ml of cyclohexane was photolysed directly for 339 min. The photolysate was worked up as in the undeuterated case to give 32.8 mg (77%) of recovered **35** and 3.1 mg (7%) of SB **36**, mp 94–96°C; nmr (100 MHz, $CDCl_3$): 2.58–2.96 (m, 4.00H, aromatics), 4.23–4.34 (m, 1.01 ± 0.03H, H-6), 4.74–4.84 (m, 0.98 ± 0.04H, H-7) 5.78 (d, 0.56 ± 0.04H, H-5, $J_{5,6}$ = 2.5), 6.26–6.38 (m, 1.01 ± 0.02H, H-2), and 6.67 (dd, 0.58 ± 0.04H, H-8, $J_{7,8}$ = 2.5, $J_{2,8}$ = 7).

*Direct Photolysis of COT **6***

A solution of 48.9 mg (0.27 mmol) of **6** in 250 ml of cyclohexane was photolysed directly for 150 min. The photolysate was concentrated *in vacuo* and the residue chromatographed on a silicic acid column with 1% ether–cyclohexane. The first band contained 41.9 mg (86%) of **6** and the second contained 0.5 mg of a mixture of compounds. The nmr spectrum and tlc of the contents of the second band showed that **8** was not present.

Quantum Yield Determinations

Quantum yields were determined on a 'merry-go-round' fitted with a 450 W Hanovia medium pressure mercury arc and surrounded by a water-cooled quartz immersion well. Light of wavelength 276 nm was isolated by a two compartment quartz cell fitting concentrically around the immersion well. The first compartment contained a 2.0-cm path length of a solution of 533 g of nickel sulfate hexahydrate and 300 g of cobaltous sulfate heptahydrate per litre of 5% aqueous H_2SO_4. The second compartment contained a 0.2-cm path length of a solution of 1 g of bismuth trichloride per 0.5 litre of 10% aqueous HCl; transmittance was 263–290 nm with a maximum at 276 nm (8%).

For sensitized irradiations at 328 nm, the solution used in the first compartment was diluted with 0.5 ℓ of 5% aqueous H_2SO_4; the solution used in the second compartment was replaced by one prepared from 10.4 g of cupric chloride dihydrate per litre of 10% aqueous HCl. This combination showed transmittance between 304–357 nm with a maximum at 328 nm (32%).

Can. J. Chem. Downloaded from www.nrcresearchpress.com by 210.87.254.6 on 09/05/12
For personal use only.

Light of wavelength 312 nm was isolated by using a solution of 310 g of cobaltous sulfate heptahydrate per litre of water in the first compartment and a solution of 1 g of potassium chromate in 300 ml of water in the second. This combination showed transmittance between 301–325 nm with a maximum at 312 nm (26%).

Before irradiation, solutions of reactants (ca. 0.50 mmol) (and acetophenone, ca. 5.5 mmol or acetone, ca. 7.0 mmol, if any) in cyclohexane solvent (ca. 35 ml) contained in calibrated (for differences in light transmittance) 20 mm × 150 mm quartz test-tube-like photolysis cells were deoxygenated by flushing with argon. The tubes were sealed under a positive pressure of argon which was maintained throughout the course of the irradiation. The lamp output was determined by potassium ferrioxalate actinometry (19). For the direct photolysis of **4**, the photolysates were concentrated *in vacuo* and chromatographed on silicic acid (*vide supra*). The first fraction (containing **6** and **7**) was weighed and analyzed by nmr as was the second fraction (containing **8** and unreacted starting material). Otherwise photolysates were concentrated *in vacuo* and acetophenone sensitizer, if any, removed by short-path distillation at 40°C/0.1 Torr, a known amount of β-naphthyl methyl ketone was added as internal standard, and the product compositions were determined by nmr analysis. In all cases nmr peak areas were calibrated against authentic mixtures of similar constitution. The product appearance quantum yield data are given in Table 2; $\Phi_{dis} < 0.05$ was found for both the acetone and acetophenone sensitized irradiations of **8**.

Phosphorescence and Fluorescence Studies of Barrelene ***4***

The fluorescence spectrum of **4** was measured in cyclohexane solution at room temperature on an Aminco-Bowman Spectrometer. Intersection of the fluorescence (λ_{max} = 340 nm) and absorption spectra of **4** occurred at 296 nm, suggesting a singlet energy of 97 kcal mol^{-1}.

The phosphorescence study was carried out on a modified Aminco-Bowman apparatus (20) in an isopentane–methylcyclohexane (1:4) glass at 77 K. No detectable phosphorescence peak could be observed.

Effective Triplet Energy of ***4***

Sensitization studies were carried out on the 'merry-go-round' apparatus, set up for quantum yield determinations, using light of 328 nm wavelength. The procedure and concentrations of reactants used in the runs were similar to those described for other quantum yield determinations (*vide supra*), except that benzene solvent was used instead of cyclohexane, and after photolyses, the photolysates were chromatographed on silicic acid to remove the sensitizer (acetophenone sensitizer was removed by short-path distillation); product compositions were determined by nmr as before. The quantum yields for the appearance of **8** from **4** were acetophenone, 0.36; benzophenone, 0.34; thioxanthone, 0.36; Michler's ketone, 0.31; 2-acetonaphthone, 0.33; 1-acetonaphthone, <0.001. The conversions were kept below 20%. The cut-off for the sensitized formation of **8** on going from 2- to 1-acetonaphthone indicates the effective triplet energy of **4** to lie between 56–59 kcal mol^{-1}.

Acknowledgements

The authors thank the Spectroscopic Services Laboratory of the University of Alberta for the 100-MHz nmr and mass spectra, Professor Brian Henry of the University of Manitoba for phosphorescence studies, and the University of Lethbridge Computing Centre for use of facilities. Financial support from the National Research Council of Canada and the University of Lethbridge Research Committee is gratefully acknowledged.

1. H. E. Zimmerman, R. S. Givens, and R. M. Pagni. J. Am. Chem. Soc. **90**, 6096 (1968).
2. C. O. Bender and S. S. Shugarman. J. Chem. Soc. Chem. Commun. 934 (1974).
3. C. O. Bender and E. H. King-Brown. J. Chem. Soc. Chem. Commun. 878 (1976).
4. H. E. Zimmerman and C. O. Bender. J. Am. Chem. Soc. **92**, 4366 (1970).
5. C. O. Bender and H. D. Burgess. Can. J. Chem. **51**, 3486 (1973).
6. C. Pascual, J. Meir, and W. Simon. Helv. Chim. Acta, **49**, 164 (1966).
7. C. O. Bender and J. Wilson. Helv. Chim. Acta, **59**, 1469 (1976).
8. N. D. Epiotis. Angew. Chem. Int. Ed. Eng. **13**, 751 (1974).
9. C. O. Bender and D. W. Brooks. Can. J. Chem. **53**, 1684 (1975).
10. N. D. Epiotis. Theory of organic reactions. Springer-Verlag, New York, NY. 1978.
11. F. Brogli, E. Giovannini, E. Heilbronner, and R. Schurter. Chem. Ber. **106**, 961 (1973).
12. D. Bryce-Smith, A. Gilbert, B. Orger, and H. Tyrrell. J. Chem. Soc. Chem. Commun. 334 (1974).
13. (*a*) H. E. Zimmerman, W. T. Gruenbaum, R. T. Klun, M. G. Steinmetz, and T. R. Welter. J. Chem. Soc. Chem. Commun. 228 (1978); (*b*) H. E. Zimmerman and M. G. Steinmetz. J. Chem. Soc. Chem. Commun. 230 (1978).
14. J. A. Pople and D. L. Beveridge. Approximate molecular orbital theory. McGraw-Hill, New York, NY. 1971.
15. J. Del Bene and H. H. Jaffé. J. Chem. Phys. **50**, 1126 (1969).
16. H. Gunther. Tetrahedron Lett. 5173 (1970).
17. H. E. Zimmerman, R. J. Boettcher, N. E. Buehler, G. E. Keck, and M. G. Steinmetz. J. Am. Chem. Soc. **98**, 7680 (1976).
18. C. Santiago and K. N. Houk. J. Am. Chem. Soc. **98**, 3380 (1976).
19. C. G. Hatchard and C. A. Parker. Proc. R. Soc. London, Ser. A, **235**, 518 (1956).
20. B. Henry and J. Morrison. J. Mol. Spectrosc. **55**, 311 (1975).
21. J. Del Bene and H. H. Jaffé. J. Chem. Phys. **48**, 1807 (1968); **48**, 4050 (1968); **49**, 1221 (1968); **50**, 1126 (1969).

Canadian Journal of Chemistry
Published by
THE NATIONAL RESEARCH COUNCIL OF CANADA

Journal canadien de chimie
Publié par
LE CONSEIL NATIONAL DE RECHERCHES DU CANADA

Volume 56 Number 24 December 15, 1978 Volume 56 numéro 24 15 décembre 1978

Can. J. Chem. Downloaded from www.nrcresearchpress.com by 210.87.254.6 on 09/05/12
For personal use only.

Notes for authors of papers presenting the results of X-ray crystal-structure analysis

The crystallographic nomenclature should correspond to that given in the *International tables for X-ray crystallography, Vol. I* (1).

The following primary crystallographic data should be given: chemical formula, formula weight, unit cell dimensions, unit cell volume, observed density, number of formula units in cell, calculated density, working temperature, and the assumed value for the wavelength or other reference parameter used in calculating the cell dimensions. All measured quantities should be accompanied by an estimate of the accuracy, and the basis for the estimate should be stated. The crystal data should be presented in a condensed form such as:

$C_6H_4N_2O_4$ fw = 168.1
Orthorhombic, $a = 13.20(3)$, $b = 13.97(3)$, $c = 3.800(5)$ Å, $V = 700.7$ Å^3, $\rho_o = 1.57(1)$, $Z = 4$, $\rho_c = 1.583$ (20°C; CuKα_1, $\lambda = 1.54050$ Å).

Authors are reminded that for presentation in such compilations as *Crystal data* (2), certain conventions regarding the choice of unit cell are mandatory. Confusion in the literature can be avoided if these conventions are adopted in primary publication. Full details are given in *Crystal data*, and in the *International tables for X-ray crystallography, Vol. II* (1).

The space group should be reported in the Hermann–Mauguin notation. If the setting differs from the standard setting in the *International tables for X-ray crystallography, Vol. I* (1), the corresponding Schoenflies symbol and the systematic absences should be given also. If there is any ambiguity in the choice of space group, the manner of its resolution should be stated. It must be emphasized that the space-group symbol given, and the origin implied by the symbol, should correspond to the setting and origin actually used.

The following information pertaining to the measurement of intensity data should be given: method of recording and measurement, the region of reciprocal space explored, and the number of accessible and observed reflections in this region, specimen size and shape, the radiation used, and details of any special corrections such as absorption or extinction.

The final refinement should be reported in sufficient detail to enable the reader to assess its reliability and completeness and, if necessary, to repeat or extend it. The origin of the scattering factors used should be specified, together with details of any corrections for anomalous scattering. A suitable table of observed and calculated structure amplitudes must accompany the paper. This table will not be published, but will be placed in the Depository of Unpublished Data, which will supply copies on request; it must, therefore, be suitable for limited duplication and circulation. The existence of this table, and of any other deposited material, is indicated in the printed article by a footnote in the following format: 'Tables of observed and calculated structure factor amplitudes, of temperature factors (and of ---) are available, at a nominal charge, from the Depository of Unpublished Data, CISTI, National Research Council of Canada, Ottawa, Ont., Canada K1A 0S2'. A final agreement index ($R = \sum||F_o| - |F_c||/\sum|F_o|$) should be given and defined with respect to the treatment of unobserved reflections. For least-squares refinement, any approximation (e.g., block-diagonal) should be specified, as should the quantity minimized. The weighting scheme should be given, and should include a statement of any reflections assigned zero weight. Where possible, the correctness of the reported structure should be checked by a method independent of that used for refinement (e.g., by a difference-Fourier synthesis) and the result of this procedure briefly reported.

The final positional parameters should be given in a single table, with the coordinates expressed as fractions of the cell edges. If the space-group setting is non-standard, a statement of the equivalent positions should be given also. The table should preferably include, or at least be accompanied by, an estimate of the standard deviations of the parameters. The asymmetric unit defined by the coordinates should, where possible, specify a single molecule or

other appropriate chemical entity. Atoms of the same chemical species should be distinguished by appended arabic numerals in parentheses. Subscripts are not acceptable, as they may lead to confusion in chemical contexts. Temperature factors should normally be placed in the Depository.

Bond lengths and angles may be given in a table or on a diagram. However, extensive tables of normal bond lengths and angles (particularly those involving hydrogen atoms) should be placed in the Depository, as should extensive tables of intermolecular distances and deviations of atoms from mean planes.

The volume of information required for compliance with these notes is formidable, and it is essential that the presentation be concise and relevant. It should not be a narrative account of the progress of the analysis, or a discussion of method, unless these elements have a direct bearing on the chemical conclusions.

1. International tables for X-ray crystallography. Vols. I–IV. Kynoch Press, Birmingham. 1952, 1959, 1962, 1974.
2. Crystal data, determinative tables, 3ième édition. NBS et JCPDS. 1972, 1973.

Can. J. Chem. Downloaded from www.nrcresearchpress.com by 210.87.254.6 on 09/05/12
For personal use only.

Can. J. Chem. Downloaded from www.nrcresearchpress.com by 210.87.254.6 on 09/05/12
For personal use only.

Recommandations aux auteurs d'articles décrivant la détermination de structures cristallines par diffraction des rayons X

La nomenclature cristallographique doit se conformer à celle qu'on trouve dans les *International tables for X-ray crystallography, Vol. I* (1).

Les données cristallographiques suivantes doivent être fournies: la formule chimique, la masse moléculaire correspondante, les dimensions de la maille, le volume de la maille, la densité observée, le nombre de motifs par maille, la densité calculée, la température, ainsi que la valeur employée pour la longueur d'onde ou pour tout autre paramètre de référence lors du calcul des dimensions de la maille. On évaluera la précision de toutes les quantités mesurées et on indiquera les critères sur lesquels se fonde cette évaluation. Les données cristallographiques doivent être présentées sous une forme condensée telle que:

$C_6H_4N_2O_4$ m = 168.1
Orthorhombique, $a = 13.20(3)$, $b = 13.97(3)$, $c = 3.800(5)$ Å, $V = 700.7$ Å^3, $\rho_o = 1.57(1)$, $Z = 4$, $\rho_c = 1.583$ (20°C; CuKα_1, $\lambda = 1.54050$ Å).

On rappelle aux auteurs que les résultats devant figurer dans des tables comme les *Crystal Data* (2) doivent correspondre à une maille définie selon certaines conventions. On évitera de la confusion dans la littérature si l'on adopte ces conventions dès la publication initiale. On trouvera tous les détails à ce sujet dans les *Crystal data* et dans les *International tables for X-ray crystallography, Vol. II* (1).

On doit rapporter le groupe d'espace dans la notation de Hermann–Mauguin. Si l'on a adopté une définition qui diffère de la définition conventionnelle des *International tables for X-ray crystallography, Vol. I* (1), on doit en outre spécifier le symbole de Schoenflies correspondant et énumer les extinctions systématiques. S'il existe une ambiguïté dans le choix du groupe d'espace, on indiquera la façon dont elle a été résolue. Il faut insister sur le fait que le symbole du groupe d'espace et l'origine qu'il implique doivent correspondre à la définition du groupe et à l'origine qui ont de fait été utilisées.

On donnera aussi les informations suivantes concernant la mesure des intensités diffractées: la méthode d'enregistrement et de mesure, la portion de l'espace réciproque qui a été explorée, le nombre de réflexions accessibles et le nombre de réflexions observées dans cette portion, les dimensions et la forme du spécimen, le rayonnement utilisé et les détails touchant toute correction particulière, telle que l'absorption ou l'extinction.

La description de l'affinement doit être suffisamment détaillée pour permettre au lecteur de déterminer s'il est complet et satisfaisant, et au besoin, de le répéter ou de le prolonger. On doit aussi spécifier la source des facteurs de diffusion atomique utilisés, de même que les détails relatifs aux corrections apportées pour la dispersion anomale. La publication doit être accompagnée d'un tableau des valeurs observées et calculées des amplitudes des facteurs de structure. Ce tableau ne sera pas publié, mais il sera confié au "Dépôt de données non publiées," qui en fournira des copies sur demande; il doit donc être sous une forme qui se prête à une duplication et à une mise en circulation limitées. L'existence de ce tableau et de tout autre matériel déposé doit être indiquée dans l'article même par une note en bas de page rédigée comme suit: "Les tableaux des amplitudes des facteurs de structure, des facteurs d'agitation thermique (et de ---) sont disponibles. On peut les obtenir à un prix nominal en s'adressant au Dépôt de données non publiées, ICIST, Conseil national de recherches du Canada, Ottawa (Ont.), Canada K1A 0S2." On donnera un indice d'accord final ($R = \sum||F_o| - |F_c||/\sum|F_o|$), en définissant de quelle manière on a tenu compte des réflexions non observées. En ce qui a trait à l'affinement par moindres carrés, on doit indiquer la fonction minimisée et signaler toute approximation (comme les blocs diagonaux) qu'on aurait utilisée. On décrira la méthode de pondération et on indiquera les critères sur lesquels on s'est basé pour attribuer un poids nul à certaines réflexions. Dans la mesure du possible, on vérifiera si la structure rapportée est juste, à l'aide d'une méthode indépendante de celle utilisée pour l'affinement (comme une synthèse de Fourier différence), et l'on décrira brièvement le résultat de cette vérification.

On réunira dans un même tableau les coordonnées atomiques finales, qui seront exprimées sous forme de fractions de l'arête de la maille. Si l'on a utilisé pour le groupe d'espace une définition non conventionnelle, on dressera en plus la liste des positions équivalentes. Une évaluation de l'écart-type sur ces paramètres devrait faire partie de ce tableau. Le motif asymétrique défini par les coordonnées doit, si possible, spécifier une seule et même molécule ou autre entité chimique appropriée. On distinguera les atomes de même nature par des chiffres arabes ajoutés entre parenthèses. L'emploi d'indices est inacceptable puisque ceux-ci peuvent prêter à confusion dans un contexte chimique. On doit normalement placer en dépôt les facteurs d'agitation thermique.

On peut présenter les longueurs de liaisons et les angles soit dans un tableau, soit dans un diagramme. Toutefois, on mettra en dépôt tout tableau renfer-

mant un grand nombre de valeurs normales de longueurs et d'angles de liaisons (en particulier ceux qui impliquent les atomes d'hydrogène); on fera de même pour les grands tableaux des distances intermoléculaires et des écarts entre atomes et plans moyens.

Pour se conformer à ces recommandations, les auteurs devront réunir une quantité imposante d'informations, mais il est essentiel que la présentation en soit concise et au point. On évitera les longs exposés sur les principes des méthodes utilisées ou sur le déroulement de la résolution de la structure, à moins que ces éléments n'aient une relation directe avec les conclusions d'ordre chimique.

1. International tables for X-ray crystallography. Vols. I–IV. Kynoch Press, Birmingham. 1952, 1959, 1962, 1974.
2. Crystal data, determinative tables, 3ième édition. NBS et JCPDS. 1972, 1973.

Can. J. Chem. Downloaded from www.nrcresearchpress.com by 210.87.254.6 on 09/05/12
For personal use only.

Substituent and steric effects in the oxidation of alkyl aryl sulfides by peroxydisulfate

C. SRINIVASAN, P. KUTHALINGAM, AND N. ARUMUGAM
School of Chemistry, Madurai University, Madurai 625 021, India

Received January 21, 1978[1]

C. SRINIVASAN, P. KUTHALINGAM, and N. ARUMUGAM. Can. J. Chem. **56**, 3043 (1978).

The kinetics of oxidation of a number of alkyl aryl sulfides with potassium peroxydisulfate in aqueous ethanol have been investigated. The effect of substituents on the oxidation has been studied by employing a number of *p*- and *m*-substituted phenyl methyl sulfides: the reaction is accelerated by electron-releasing and retarded by electron-withdrawing substituents, indicating a rate-determining electrophilic attack by the peroxydisulfate ion at the reaction site, sulfur. A good correlation is found to exist between the rate constants and the Hammett σ^+/σ^- constants, the ρ^+ value for the reaction being -0.56 with a correlation coefficient of 0.979. The activation parameters have also been determined.

Studies with different alkyl phenyl sulfides clearly indicate that the reaction is quite sensitive to steric congestion around the reaction site. The results obtained in this study are compared with those found for the oxidation of the same set of sulfides with different oxidants.

C. SRINIVASAN, P. KUTHALINGAM et N. ARUMUGAM. Can. J. Chem. **56**, 3043 (1978).

On a examiné la cinétique de l'oxydation de plusieurs sulfures d'alkyle et d'aryle avec le peroxydisulfate de potassium dans l'éthanol aqueux. On a étudié l'influence des substituants sur la réaction d'oxydation à l'aide d'une série de sulfures possédant un groupe alkyle et un groupe phényle substitué aux positions *méta* et *para*. Les substituants électro-donneurs accélèrent la réaction, tandis que les substituants électro-attracteurs la ralentissent. Cet effet indique que l'étape déterminante est une attaque électrophile de l'ion peroxydisulfate sur la site de réaction, soit le soufre. On observe une bonne corrélation entre les constantes de vitesse et les constantes σ^+/σ^- de Hammett; on obtient pour cette réaction une valeur de ρ^+ de -0.56 avec un coefficient de corrélation de 0.979. On a également déterminé les paramètres d'activation.

Des études sur différents sulfures d'alkyle et de phényle montrent clairement que la réaction est grandement influencée par l'encombrement stérique au voisinage du site réactionnel. On compare les résultats recueillis dans le présent travail avec ceux qui ont été rapportés pour l'oxydation de la même série de sulfures avec différents oxydants.

[Traduit par le journal]

Introduction

In our earlier paper (1), we have proposed that the oxidation of alkyl aryl sulfides with peroxydisulfate in 50% aqueous ethanol (v/v) proceeds by a rate-determining electrophilic attack of the peroxydisulfate ion [1] at sulfur of the sulfide to form sulfoxide.

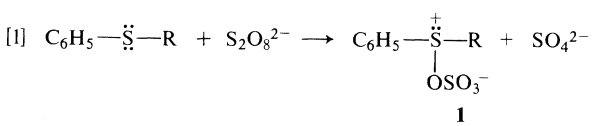

1

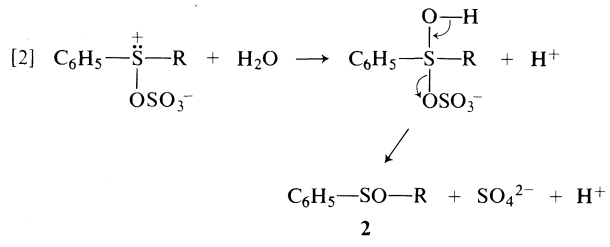

2

The intermediate **1** may decompose to give the sulfoxide **2** by the attack of water as indicated in [2] or according to the step [3] which is very similar to that proposed by Ogata and Akada (2) in the kinetics of peroxydisulfate oxidation of *p*-nitrosophenol.

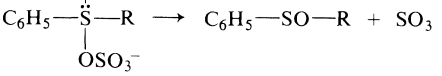

However, the question regarding the origin of the sulfoxide oxygen, whether from water or from peroxydisulfate ion, has not been solved. The present work describes the substituent and steric effects on the reaction of alkyl aryl sulfides with peroxydisulfate.

The sulfides studied are listed in Tables 1 and 2. Twelve *m*- and *p*-substituted phenyl methyl sulfides are used to study the effect of structure on reactivity by keeping the steric effects constant at the reaction centre (Table 1). Five alkyl phenyl sulfides are chosen to study the steric effects and in these sulfides there is a gradual increase in the size of the alkyl group attached to sulfur (Table 2).

[1]Revision received August 10, 1978.

Can. J. Chem. Downloaded from www.nrcresearchpress.com by 210.87.254.42 on 09/05/12
For personal use only.

Can. J. Chem. Downloaded from www.nrcresearchpress.com by 210.87.254.42 on 09/05/12
For personal use only.

TABLE 1. Second-order rate constants, enthalpies, and entropies of activation for substituted phenyl methyl sulfides*

Sulfides	$k_2 \times 10^3$ ℓ mol^{-1} s^{-1} 35°C	40°C	45°C	$\Delta H^{\ddagger}$ kcal/mol	$\Delta S^{\ddagger}$ (eu) at 40°C
p-Methoxyphenyl methyl sulfide	12.6	16.8†	22.0	10.3	−34.1
Methyl *p*-tolyl sulfide	6.44	8.64†	11.5	10.8	−33.5
p-Isopropylphenyl methyl sulfide	5.86	7.74	10.3	10.3	−35.0
p-Fluorophenyl methyl sulfide	5.60	7.39	9.75	10.6	−35.3
Methyl *m*-tolyl sulfide	5.00	6.84	9.15	11.4	−31.8
Methyl phenyl sulfide	4.54†	6.13†	8.24†	11.1	−33.2
m-Methoxyphenyl methyl sulfide	4.35	6.06	8.13	11.7	−31.3
p-Chlorophenyl methyl sulfide	3.99	5.48	7.24	11.0	−33.8
p-Bromophenyl methyl sulfide	3.83	5.20	7.07	11.4	−32.7
m-Chlorophenyl methyl sulfide	2.24	3.26	4.08	11.4	−33.2
p-Methylthioacetophenone	1.71	2.32†	3.12	11.1	−35.3
Methyl *p*-nitrophenyl sulfide	1.26	1.91	2.53	13.2	−29.3
p-Methylthiobenzoic acid	1.15	1.64	2.23	12.7	−36.2

*General conditions: [sulfide]:[$S_2O_8^{2-}$] = 10:1 in 50% aqueous ethanol (v/v) at a constant ionic strength of 0.015 *M*. $\Delta H^{\ddagger}$ values were evaluated graphically.
†Values from ref. 1.

TABLE 2. Second-order rate constants for the oxidation of alkyl phenyl sulfides with peroxydisulfate ion at 40°C and relative rates of oxidation*

Sulfide	$k_2 \times 10^3$ (ℓ mol^{-1} s^{-1})	Relative rates of oxidation by $S_2O_8^{2-}$	Br_2†	H_2O_2‡	Chloramine-T§
Methyl phenyl sulfide	6.13	100	100	100	100
Ethyl phenyl sulfide	2.44	39.1	109	108	123
n-Propyl phenyl sulfide	1.97	32.1	71	88	86
Isopropyl phenyl sulfide	0.938	15.3	3.6	95	179
tert-Butyl phenyl sulfide‖	0.104	1.70	—	60	241

*General reaction conditions: [sulfide]:[$S_2O_8^{2-}$] = 10:1 in 50% aqueous ethanol (v/v) at a constant ionic strength of 0.015 *M*.
†Values from ref. 31.
‡Values from ref. 32.
§Values from ref. 33.
‖Since the rate is very slow k_2 value has been calculated from the initial rates.

Experimental

Materials

Potassium peroxydisulfate (G.R., E. Merck) was used after recrystallization from double distilled water. Methyl phenyl sulfide, *p*-methoxyphenyl methyl sulfide, methyl *p*-tolyl sulfide, and *p*-methylthioacetophenone were prepared as described earlier (1). *p*-Chlorophenyl methyl sulfide and *p*-bromophenyl methyl sulfide were prepared by the methylation of the corresponding benzenethiols obtained by the reduction of their respective benzenesulfonyl chlorides (3). *p*-Isopropylphenyl methyl sulfide was prepared by the methylation of *p*-isopropylbenzenethiol (4). The procedure adopted by Baliah, Shanmuganathan, and Varadachari (5) was employed for the preparation of *p*-methylthiobenzoic acid. Methyl *p*-nitrophenyl sulfide (6), *p*-fluorophenyl methyl sulfide (7), methyl *m*-tolyl sulfide (8), *m*-chlorophenyl methyl sulfide (9), and *m*-methoxyphenyl methyl sulfide (10) were prepared as described in literature.

Ethyl phenyl sulfide (11) was prepared by using benzenethiol and diethyl sulfate. Phenyl *n*-propyl and phenyl isopropyl sulfides (12) were prepared by the alkylation of benzenethiol with the appropriate alkyl bromides in the presence of sodium ethoxide. *tert*-Butyl phenyl sulfide was obtained by passing isobutylene (13) into sulfuric acid followed by the addition of benzenethiol (12).

Kinetic Measurements

The procedure employed for the kinetic studies was essentially the same as described in our earlier paper (1). Measurements were carried out under pseudo first-order conditions in 50% aqueous ethanol (v/v) at constant ionic strength (14, 15).[2] All the reactions were homogeneous. The rate of the reaction was followed by estimating the unreacted peroxydisulfate by the iodometric procedure of Kolthoff and Carr (16). The kinetics were generally followed up to 60–70% of the reaction. The second-order rate constants were calculated from the pseudo first-order rate constants as described in ref. 1. The rate constants were confirmed in each substrate by performing at least a set of duplicate runs in all of them at all the temperatures mentioned here (Table 1).

Product Analysis

TLC analysis showed that alkyl phenyl sulfides are oxidised

[2]Oxidation of 50% aqueous ethanol (v/v) by peroxydisulfate is found to be negligible in our experimental conditions. See also refs. 14 and 15.

Can. J. Chem. Downloaded from www.nrcresearchpress.com by 210.87.254.42 on 09/05/12
For personal use only.

by peroxydisulfate solely to their sulfoxides (see also ref. 1). Product analyses were carried out with the same initial concentration of the reactants employed in the kinetic measurements.

Results and Discussion

Substituent Effects

The results of the kinetic studies with substituted phenyl methyl sulfides show that the reaction is first-order in peroxydisulfate and in sulfide for over 60–70% of the reaction. From the data in Table 1, it is evident that electron-releasing substituents accelerate and electron-withdrawing substituents retard the rate of the reaction.

It is generally known that the linear free-energy relationships apply to a reaction series in which either the entropies of activation for the series are constant or in which the variation in activation entropy is linearly related to changes in enthalpy of activation (17–20). An examination of the activation parameters in Table 1 shows clearly that the reaction under investigation has nearly constant entropies of activation, favouring a linear free-energy relationship.

Hence the reactivity pattern is brought out by two different correlations[3] at 40°C; one, log k_2 with σ and the other log k_2 with σ^+/σ^-. Since sulfur can act as an electron-donor or an electron-acceptor depending on the substituent present *para* to the methylthio group (21), we have used both σ^+ and σ^- simultaneously in the latter correlation. It may be pointed out here that in some reactions (22), both σ^+ and σ^- are employed simultaneously. A fair correlation (23) is obtained with Hammett's σ constants ($\rho = -0.87$, $r = 0.930$, $s = 0.11$); but a good correlation is found to exist when σ^+/σ^- values are plotted against the logarithms of rate constants. The ρ^+ value obtained for the latter correlation by the method of least squares is -0.56 ($r = 0.979$ and $s = 0.06$).

The negative ρ^+ value indicates that the nucleophilic sulfur atom of the sulfide is more positively charged in the transition state of the rate-determining step of the oxidation reaction than it is in the reactant. This is consistent with step [1] being the rate-determining. The small ρ^+ value obtained in our case may be attributed to the fact that the dinegative peroxydisulfate ion is not a typical electrophilic reagent (27). Such small ρ values are commonly observed in most studies of other electrophilic reactions at sulfur centre. For instance, ρ value of -1.13 has been observed in the oxidation of aryl alkyl sulfides by hydrogen peroxide (28). But the higher ρ value observed in the reactions of aryl alkyl sulfides with chloramine-T (29) and bromine (30) may be due to the strong electrophilic character of the attacking species.

Steric Effects in the Oxidation of Alkyl Phenyl Sulfides

The steric effect on the oxidation of sulfides with peroxydisulfate was also studied by changing the alkyl moiety from methyl to *tert*-butyl in a series of alkyl phenyl sulfides. The rate data are given in Table 2. The rate decreases in the order PhSMe > PhSEt > PhSPr^n > PhSPr^i > PhSBu^t.

The results show that the reaction is sensitive to steric congestion at the reaction centre. It is evident from Table 2, which exhibits the results obtained by us and those of Modena (31, 32) and Oae and coworkers (33) with other oxidizing agents, that the steric retardation in the oxidation of alkyl phenyl sulfides depends on the nature and size of the oxidizing agent. The rate constants in the present study (Table 2) decreased monotonically with the increasing bulkiness of the alkyl groups. The retardation observed here is larger than those found for the oxidation of the same sulfides by bromine (31), hydrogen peroxide (32), and chloramine-T (33). This is probably due to the larger size of the peroxydisulfate ion. This is also supported by the observation that steric effect is almost absent in the chloramine-T oxidation (33) of these sulfides, which is presumably due to the smaller size of the attacking species Cl^+.

Acknowledgements

One of the authors (P.K.) thanks the U.G.C., New Delhi, and the Madurai University, for the award of a Fellowship under the Faculty Improvement Programme. P.K. also wishes to thank the Principal and Management of Aditanar College of Arts and Science, Tiruchendur, for making it possible for him to accept the Fellowship mentioned. Our thanks are also due to referees of this paper for their helpful and constructive comments.

[3]We have used σ_p and σ_m values (24) for the log $k_2 - \sigma$ correlation. In the log $k_2 - \sigma^+/\sigma^-$ correlation, σ_p^+ values (24) have been used for *p*-methoxy, *p*-methyl, *p*-isopropyl, *p*-chloro, *p*-bromo, and *p*-fluoro substituents. σ_p^- values (25) are used for *p*-acetyl and *p*-carboxylic groups. σ^- value given by Bordwell and Andersen (26) has been used for *p*-nitro group. σ_m^+ values were used for the *meta* substituents (24).

1. N. ARUMUGAM, C. SRINIVASAN, and P. KUTHALINGAM. Indian J. Chem. **16**A, 478 (1978).
2. Y. OGATA and T. AKADA. Tetrahedron, **28**, 15 (1972).
3. H. MEERWEIN, G. DITTMAR, R. GOLLNER, K. HAFNER, F. MENSCH, and O. STEINFORT. Chem. Ber. **90**, 841 (1957).
4. H. GILMAN and H. S. BROADBENT. J. Am. Chem. Soc. **69**, 2054 (1947).

5. V. BALIAH, SP. SHANMUGANATHAN, and R. VARADACHARI. J. Phys. Chem. **61**, 1013 (1957).
6. C. C. PRICE and G. W. STACY. J. Am. Chem. Soc. **68**, 499 (1946).
7. H. ZAHN and H. ZUBER. Chem. Ber. **86**, 180 (1953).
8. D. S. TARBELL and D. K. FUKUSHIMA. J. Am. Chem. Soc. **68**, 1458 (1946).
9. G. LEANDRI, A. MANGINI, and R. PASSERINI. Gazz. Chim. Ital. **84**, 3 (1954).
10. F. G. BORDWELL and P. J. BOUTON. J. Am. Chem. Soc. **79**, 717 (1957).
11. H. GILMAN and N. J. BEABER. J. Am. Chem. Soc. **47**, 1450 (1925).
12. V. N. IPATIEFF, H. PINES, and B. S. FRIEDMAN. J. Am. Chem. Soc. **60**, 2731 (1938).
13. C. BARKENBUS and B. KELLEY. J. Chem. Ed. **22**, 356 (1945).
14. L. R. SUBBARAMAN and M. SANTAPPA. Proc. Indian Acad. Sci. **64**, 345 (1966).
15. A. SABESAN and N. VENKATASUBRAMANIAN. Aust. J. Chem. **24**, 1633 (1971).
16. I. M. KOLTHOFF and E. M. CARR. Anal. Chem. **25**, 298 (1953).
17. P. R. WELLS. Chem. Rev. **63**, 171 (1963).
18. J. LEFFLER. J. Org. Chem. **20**, 1202 (1955).
19. R. W. TAFT, JR. *In* Steric effects in organic chemistry. *Edited by* M. S. Newman. John Wiley and Sons, Inc., New York. 1956. p. 660.
20. L. L. SCHALEGER and F. A. LONG. Adv. Phys. Org. Chem. **1**, 1 (1963).
21. V. BALIAH and M. UMA. Tetrahedron, **19**, 455 (1963).
22. O. EXNER. *In* Advances in linear free-energy relationships. *Edited by* N. B. Chapman and J. Shorter. Plenum Press, New York. 1972. p. 34.
23. J. SHORTER. Correlation analysis in organic chemistry: an introduction to linear free-energy relationships. Oxford University Press, Oxford. 1973. p. 105.
24. H. C. BROWN and Y. OKAMOTO. J. Am. Chem. Soc. **80**, 4979 (1958).
25. J. SHORTER. Correlation analysis in organic chemistry: an introduction to linear free-energy relationships. Oxford University Press, Oxford. 1973. p. 14.
26. F. G. BORDWELL and H. M. ANDERSEN. J. Am. Chem. Soc. **75**, 6019 (1953).
27. E. J. BEHRMAN. J. Am. Chem. Soc. **85**, 3478 (1963).
28. G. MODENA and L. MAIOLI. Gazz. Chim. Ital. **87**, 1306 (1957).
29. F. RUFF and A. KUCSMAN. J. Chem. Soc. Perkin II, 509 (1975).
30. U. MIOTTI, G. MODENA, and L. SEDEA. J. Chem. Soc. B, 802 (1970).
31. U. MIOTTI and G. MODENA. Boll. Sci. Fac. Chim. Ind-Bologna. **27**, 381 (1969).
32. G. MODENA. Gazz. Chim. Ital. **89**, 834 (1959).
33. F. RUFF, K. KOMOTO, N. FURUKAWA, and S. OAE. Tetrahedron, **32**, 2763 (1976).

Can. J. Chem. Downloaded from www.nrcresearchpress.com by 210.87.254.42 on 09/05/12
For personal use only.

Absolute rate constants for hydrocarbon autoxidation. 25. Rate constants for hydrogen atom abstraction from alkanes by the *tert*-butylperoxy radical[1]

J. H. B. CHENIER, S. B. TONG,[2] AND J. A. HOWARD[3]

Division of Chemistry, National Research Council of Canada, Ottawa, Ont., Canada K1A 0R9

Received May 29, 1978

J. H. B. CHENIER, S. B. TONG, and J. A. HOWARD. Can. J. Chem. **56**, 3047 (1978).

Rate constants for abstraction of secondary and tertiary hydrogens from structurally different alkanes by the *tert*-butylperoxy radical in solution at 30°C have been determined by competitive experiments in the presence of *tert*-butyl hydroperoxide. Rate constants fall in the range 1×10^{-4} to 9×10^{-4} and $1 \times 10^{-3} - 2 \times 10^{-2}$ M^{-1} s^{-1} for secondary and tertiary aliphatic C—H bonds, respectively. The most reactive secondary hydrogen is, therefore, almost as reactive as the least reactive tertiary hydrogen. Differences in reactivity within a type of aliphatic C—H bond are governed by differences in steric hindrance to attack by the peroxy radical and by relief of steric strain upon removal of the labile hydrogen. Rate constants for reaction of perdeuterated methylcyclohexane and 3-methylpentane are much smaller than the values calculated from the maximum primary kinetic isotope effect for this reaction.

J. H. B. CHENIER, S. B. TONG et J. A. HOWARD. Can. J. Chem. **56**, 3047 (1978).

Certaines expériences de compétition effectuées en solution à 30°C en présence d'hydroperoxyde de *tert*-butyle ont permis de déterminer les constantes de vitesse correspondant à l'arrachement, par le radical *tert*-butylperoxy, d'atomes d'hydrogène secondaires et tertiaires présents dans des alcanes de différentes structures. Les constantes de vitesse se situent dans les domaines de $1 \times 10^{-4} - 9 \times 10^{-4}$ et $1 \times 10^{-3} - 2 \times 10^{-2}$ M^{-1} s^{-1} pour les liaisons C—H aliphatiques secondaires et tertiaires respectivement. L'hydrogène secondaire le plus réactif est donc presque aussi réactif que l'hydrogène tertiaire le moins réactif. A l'intérieur d'une même catégorie de liaisons C—H aliphatiques, les différences de réactivité sont régies par des différences d'empêchement stérique lors de l'attaque du radical peroxy et par une diminution de la tension stérique lors de l'arrachement de l'atome d'hydrogène labile. Les constantes de vitesses correspondant aux réactions du méthylcyclohexane et du méthyl-3 pentane perdeutérés sont beaucoup inférieures aux valeurs prévues en supposant le maximum de l'effet isotopique primaire pour cette réaction.

[Traduit par le journal]

Can. J. Chem. Downloaded from www.nrcresearchpress.com by 210.87.254.40 on 09/05/12
For personal use only.

Introduction

Most of the rate constants for reactions of alkylperoxy radicals (ROO·) with oxidizable substrates (RH), reaction [1], reported in this series (1) have been determined *directly* by solving

$$\text{[1]} \qquad \mathrm{ROO^{\cdot} + RH \xrightarrow{k_p} ROOH + R^{\cdot}\ (or\ ROORH^{\cdot})}$$

the rate expression [2]

$$\text{[2]} \qquad \frac{-\mathrm{d[O_2]}}{\mathrm{d}t} = \frac{k_p[\mathrm{RH}]R_i^{1/2}}{(2k_t)^{1/2}}$$

where $-\mathrm{d[O_2]}/\mathrm{d}t$ is the rate of autoxidation of RH, R_i is the rate of free-radical chain initiation, and k_p and $2k_t$ are the rate controlling propagation and termination rate constants.

Very often more accurate values of the relative reactivity of two substrates AH and BH to a common peroxy radical can be obtained from competitive experiments in which the relative amounts of AH and BH consumed or the yields of the hydroperoxides AOOH and BOOH produced after co-oxidation are measured (2).

The number of substrates that can usefully be studied by the co-oxidation method can be greatly increased by performing the reactions in the presence of >0.5 M *tert*-butyl hydroperoxide. This is because substrates that are resistant to autoxidation oxidize with significant chain lengths in the presence of this hydroperoxide. Furthermore, kinetic analysis is simplified because of a substantial decrease in the number of elementary reactions. In this paper we report rate constants for reaction of the *tert*-butylperoxy radical with a variety of structurally different alkanes in solution which were determined by this technique.

Experimental

Materials

The hydrocarbons and most of the alcohols were obtained from commercial sources and were usually >99% pure by glc. Purification of the hydrocarbons was achieved by percolation down a column of basic alumina and distillation while the alcohols, which were used as glc standards, were used without further purification. 2,4-Dihydroxy-2,4-dimethylpentane

[1]NRCC No. 16979.

[2]Research Associate 1977–1978.

[3]To whom all correspondence should be addressed.

Can. J. Chem. Downloaded from www.nrcresearchpress.com by 210.87.254.40 on 09/05/12
For personal use only.

was prepared by the thermally initiated (di-*tert*-butyl peroxide, 1 *M*) autoxidation of 2,4-dimethylpentane at 100°C and 10 atm of oxygen. The reaction was taken to about 10% conversion and the hydroperoxides produced were reduced with triphenylphosphine. The diol was then isolated from the reaction mixture by preparative glc. *tert*-Butyl hydroperoxide was purified as described previously (1) and di-*tert*-butyl hyponitrite was prepared by the method of Kiefer and Traylor (3).

Procedures

Binary mixtures of hydrocarbons were oxidized in the presence of α,α′-azobisisobutyronitrile (0.06 *M*) and *tert*-butyl hydroperoxide (0.5–2.0 *M*) to 1–5% conversion. The total hydroperoxide was then reduced with triphenylphosphine and the hydrocarbons and alcohols were distilled from AIBN, $(C_6H_5)_3P$, and $(C_6H_5)_3PO$ by vacuum distillation. Alcohol yields were determined by glc techniques using a Varian 2800 Chromatograph equipped with 12 ft 12% OV-101 and 12% FFAP on Chromosorb W columns and flame ionization detectors.

Steady-state concentrations of *tert*-butylperoxy radicals produced during *tert*-butyl hyponitrite initiated autoxidation of the alkanes in the presence of *tert*-butyl hydroperoxide were determined by epr spectroscopy relative to a standard solution of 1,1-diphenyl-2-picrylhydrazyl.

Results and Discussion

The simplest reaction scheme that describes the α,α′-azobisisobutyronitrile (In_2) initiated co-oxidation of two alkanes, R_1H and R_2H, in the presence of *tert*-butyl hydroperoxide is

Initiation

[3] $$In_2 \xrightarrow{O_2} InO_2\cdot \xrightarrow{t\text{-BuOOH}} t\text{-}BuO_2\cdot$$

Propagation

[4] $$t\text{-}BuO_2\cdot + R_1H \xrightarrow{k_p^{(1)}} t\text{-BuOOH} + R_1\cdot$$

[5] $$t\text{-}BuO_2\cdot + R_2H \xrightarrow{k_p^{(2)}} t\text{-BuOOH} + R_2\cdot$$

[6] $$R_1\cdot + O_2 \rightarrow R_1O_2\cdot$$

[7] $$R_2\cdot + O_2 \rightarrow R_2O_2\cdot$$

Chain Transfer

[8] $$t\text{-}BuO_2\cdot + t\text{-}BuO_2\cdot \rightarrow 2t\text{-}BuO\cdot + O_2$$

[9] $$t\text{-}BuO\cdot + t\text{-BuOOH} \rightarrow t\text{-BuOH} + t\text{-}BuO_2\cdot$$

[10] $$R_1O_2\cdot + t\text{-BuOOH} \rightarrow R_1OOH + t\text{-}BuO_2\cdot$$

[11] $$R_2O_2\cdot + t\text{-BuOOH} \rightarrow R_2OOH + t\text{-}BuO_2\cdot$$

Termination

[12] $$2t\text{-}BuO_2\cdot \rightarrow t\text{-BuOOBu-}t + O_2$$

Provided that R_1OOH and R_2OOH are only formed in reactions [10] and [11] and that conversion is low (< 1%) the ratio of rate constants $k_p^{(1)}/k_p^{(2)}$ can be calculated from

[13] $$\frac{k_p^{(1)}}{k_p^{(2)}} = \frac{[R_1OOH]_t[R_2H]_0}{[R_2OOH]_t[R_1H]_0}$$

where $[R_1OOH]_t$ and $[R_2OOH]_t$ are the yields of the hydroperoxides and $[R_1H]_0$ and $[R_2H]_0$ are the initial hydrocarbon concentrations. In practice mixtures of hydroperoxides are best analyzed after quantitative reduction to the alcohols with triphenylphosphine.

[14] $$R_1OOH + (C_6H_5)_3P \rightarrow R_1OH + (C_6H_5)_3PO$$

The majority of the competitive experiments reported in this work were performed using 3-methylpentane as one of the reactants because absolute rate constants for abstraction of the secondary and tertiary hydrogens from this substrate by $t\text{-}BuO_2\cdot$ are known (1). Furthermore, keeping one reactant constant reduces cumulative errors although some relative reactivities were checked by 'circular' experiments. For instance the relative reactivities of cyclohexane and cyclopentane to 3-methylpentane were confirmed by co-oxidations of cyclohexane and cyclopentane and the relative reactivities of the various positions in an alkane were checked by autoxidation of the alkane in the absence of a second substrate.

Secondary Aliphatic C—H Bonds

Yields of secondary alcohols formed by co-oxidations of alkanes containing reactive secondary C—H bonds with 3-methylpentane are summarized in Table 1. Cyclopentane and cyclohexane have only one type of secondary C—H bond and gave only one alcohol whereas *n*-hexane and 2-methylpentane gave two secondary alcohols. Although methylcyclopentane should give two secondary alcohols (2- and 3-methylcyclopentanol) they were not separated by our analytic technique while two of the three secondary alcohols from methylcyclohexane were resolved.

In some experiments low yields of 2- and 3-hexanone and cyclohexanone were observed in co-oxidations containing *n*-hexane and cyclohexane although cyclopentanone was not detected from co-oxidations containing cyclopentane. These ketones could be formed in a cross-termination reaction [15], or by autoxidation of the secondary hydroperoxide, reaction [16] (4).

[15] 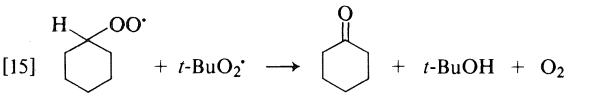

[16] 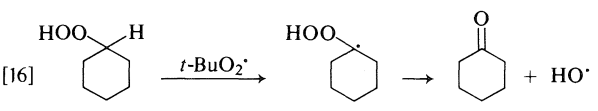

We were able to demonstrate that reaction [15] is unimportant by measuring the steady-state alkylperoxy radical concentration, $[RO_2\cdot]_{ss}$, for di-*tert*-butyl hyponitrite initiated autoxidations of *n*-hexane

Can. J. Chem. Downloaded from www.nrcresearchpress.com by 210.87.254.40 on 09/05/12
For personal use only.

TABLE 1. Yields of secondary alcohols (R_1OH) and relative and absolute rate constants for secondary aliphatic C—H bonds obtained from co-oxidations in the presence of *tert*-butyl hydroperoxide (1–2 *M*) at 30°C

Substrate, R_1H (*M*)	3-Methylpentane concentration (*M*)	$10^2[R_1OH]$ (*M*)	$10^2[R_2OH]$[a] (*M*)	$k_p^{(1)}$[b] / $k_p^{(2)}$	$10^4 k_p$[c] (M^{-1} s^{-1})
2-Methylpentane (3.41)	3.53	0.13[d]	4.5	0.03	1.0
		0.43[e]		0.1	3.3
2-Methylpentane (4.55)	2.35	0.15[d]	3.0	0.026	—
		0.46[e]	—	0.09	—
2-Methylbutane (7.59)	—	0.23	5.2[f]	0.044	1.5
Methylcyclohexane (4.7)	2.35	0.17[g]	0.73	0.12	2.0
		0.5[h]	—	0.34	4.0
Methylcyclohexane (2.35)	4.7	0.085[g]	1.57	0.11	—
		0.27[h]	—	0.35	—
Cyclohexane (6.15)	1.73	2.8	1.8	0.44	2.6
Cyclohexane (4.1)	3.47	1.06	2.0	0.45	—
n-Hexane (4.6)	2.4	0.32[i]	0.8	0.21	3.5
		0.47[j]	—	0.31	5.5
n-Hexane (2.3)	4.8	0.18[i]	2.0	0.19	—
		0.3[j]	—	0.31	—
Methylcyclopentane (5.35)	2.3	0.47[k]	0.29	0.7	6.0
Methylcyclopentane (2.67)	4.63	0.29[k]	0.82	0.6	—
Cyclopentane (6.42)	2.4	4.5	1.4	1.2	8.7
Cyclopentane (3.21)	4.8	2.9	3.3	1.3	—

[a]3-Methyl-3-pentanol unless stated otherwise.
[b]$k_p^{(1)}$ refers to overall *s*-C—H reactivity.
[c]Average absolute reactivity per active H relative to $k_p^{(2)}$ per *t*-C—H = 0.007 M^{-1} s^{-1} for 3-methylpentane.
[d]4-Methylpentan-3-ol.
[e]4-Methylpentan-2-ol.
[f]2-Methylbutan-2-ol.
[g]2-Methylcyclohexanol.
[h]A mixture of 3- and 4-methylcyclohexanol.
[i]Hexan-3-ol.
[j]Hexan-2-ol.
[k]A mixture of 2- and 3-methylcyclopentanol.

TABLE 2. Measured and calculated steady-state peroxy radical concentrations for di-*tert*-butyl hyponitrite initiated autoxidation of alkanes in the presence of *tert*-butyl hydroperoxide at 30°C

Alkane	[DTBH][a] (*M*)	[*t*-BuOOH] (*M*)	$10^5[RO_2\cdot]_{ss}^{obsd}$ (*M*)	$10^5[RO_2\cdot]_{ss}^{calcd}$ (*M*)
n-Hexane	0.107	0.67	1.54	2.2
n-Hexane	0.027	0.67	0.90	1.0
n-Hexane	0.13	2.0	1.84	2.3
n-Hexane	0.033	2.0	1.0	1.1
Cyclohexane	0.0127	0.67	1.3	2.3
Cyclohexane	0.032	0.67	0.64	1.1
Cyclohexane	0.11	2.0	1.0	2.2
Cyclohexane	0.027	2.0	0.53	1.1
3-Methylpentane	0.10	0.67	1.6	2.1
3-Methylpentane	0.025	0.67	0.86	1.0

[a]Di-*tert*-butyl hyponitrite.

and cyclohexane containing *tert*-butyl hydroperoxide at 30°C. Values of $[RO_2\cdot]_{ss}$ are listed in Table 2 and are close to the values predicted from rates of initiation and our best value of 1.2×10^3 M^{-1} s^{-1} for the termination rate constant for *tert*-butylperoxy radicals (5). The occurrence of reaction [15] would significantly reduce $[RO_2\cdot]_{ss}$ because the rate constant for reaction [15] is expected to be about three orders of magnitude larger than the termination rate constant for *t*-$BuO_2\cdot$ (6, 7).

With regards to reaction [16] Hendry *et al.* (4) have demonstrated that cyclohexyl hydroperoxide is ~13 times more reactive than cyclohexane (per molecule) towards *t*-$BuO_2\cdot$ at 80°C. The yields of secondary alcohols could, therefore, be reduced by this reaction. Because of this we have only considered experiments in which the yield of ketone was less than one tenth the yield of the corresponding alcohol.

Absolute rate constants for secondary aliphatic C—H bonds fall in the rage 1×10^{-4} to 9×10^{-4}

Can. J. Chem. Downloaded from www.nrcresearchpress.com by 210.87.254.40 on 09/05/12
For personal use only.

M^{-1} s^{-1} per active hydrogen (Table 1). Although some of this difference in reactivity must be due to experimental error there is no doubt that the secondary hydrogens of *n*-hexane are more reactive than the secondary hydrogens of 3-methylpentane (k_p/H = 0.0002 M^{-1} s^{-1}) and that those attached to the penultimate carbon are more reactive than those on C-3 (structure **1**). A similar difference in the reactivity of the secondary hydrogens attached to C-2 and C-3 of a *n*-alkane towards abstraction by alkylperoxy radicals has been found in the autoxidation of dodecane (8) and hexadecane[4,5] at higher temperatures while other radicals show a preference for the secondary hydrogens on C-2 (7, 9). The two types of secondary hydrogens in 2-methylpentane exhibit the same difference in reactivity towards *t*-BuOO$^\bullet$ although both positions are less reactive than the corresponding sites in *n*-hexane.

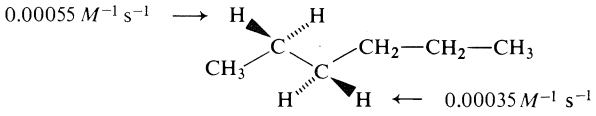

1

The hydrogens in cyclohexane are somewhat less reactive than the two types of secondary hydrogens in *n*-hexane and are slightly more reactive than the somewhat more protected secondary hydrogens in 3-methylpentane. Not unexpectedly cyclopentane is more reactive (per hydrogen) than cyclohexane to *t*-$BuO_2^\bullet$, a situation that is found for other free radicals such as Br$^\bullet$, $C_6H_5^\bullet$, and $CCl_3^\bullet$ (10, 11).

The overall rate constant (per H) for abstraction of a secondary hydrogen from methylcyclopentane is slightly smaller than the value for cyclopentane while the reactivity of the secondary hydrogens of methylcyclohexane depends to some extent on the distance from the methyl group (structure **2**).

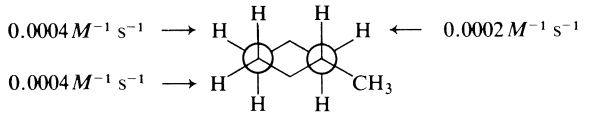

2

Tertiary Aliphatic C—H Bonds

The yields of the tertiary alcohols produced by co-oxidation of alkanes containing reactive tertiary C—H bonds and 3-methylpentane in the presence of *tert*-butyl hydroperoxide at 30°C are summarized in Table 3. All these alkanes gave only one tertiary alcohol with the exception of 2,3-dimethylpentane which gave 2- and 3-hydroxy-2,3-dimethylpentane. 2,4-Dimethylpentane could, in principle, give 2,4-dihydroxy-2,4-dimethylpentane by intramolecular hydrogen abstraction (12, 13). It would, however, appear that in the presence of 1.0 *M tert*-butyl hydroperoxide this reaction does not compete with abstraction of the hydroperoxidic hydrogen.

Absolute rate constants for tertiary aliphatic C—H bonds fall in the rage $1 \times 10^{-3} - 2 \times 10^{-2}$ M^{-1} s^{-1} (Table 3) depending on the structure of the alkane. These rate constants along with the Neuman projections of the hydrocarbons are presented in Scheme 1.

It is possible to draw two general conclusions from an examination of Scheme 1. First, the reactivity of a tertiary aliphatic C—H bond to *t*-$BuO_2^\bullet$ depends on the size of the alkyl substituent on the adjacent carbon. Thus reactivity increases in the order 2,2,4-trimethylpentane < 2,4-dimethylpentane < 2-methylpentane ~ 2-methylbutane which is consistent with a decrease in reactivity with an increase in size.

Secondly, the reactivity of a *t*-C—H bond is less sensitive to the bulk of an alkyl group attached to the carbon bearing the reactive hydrogen than it is to the size of the alkyl group on the adjacent carbon. Thus 2,2,3-trimethylpentane is more than twice as reactive as 2,2,4-trimethylpentane, a difference that is almost certainly due to the relief of steric strain on removal of a hydrogen atom from a sterically crowded sp^3 carbon.

In addition the tertiary hydrogens of methylcyclopentane and methylcyclohexane exhibit the expected enhanced reactivity with methylcyclopentane more reactive than methylcyclohexane.

Arrhenius Parameters

Arrhenius parameters for selected alkanes relative to the parameters for abstraction of the tertiary C—H in 3-methylpentane by *t*-$BuO_2^\bullet$ were determined from co-oxidations conducted from 30 to 80°C and the results are listed in Table 4. In general these parameters serve to demonstrate that differences in reactivity are the result of differences in both the entropy and enthalpy of activation. More specifically the high *A*-factors for cyclohexane and the secondary hydrogens in methylcyclohexane are consistent with the suggestion that there is an increase in entropy upon conversion of a tight cyclohexane ring to a looser cyclohexyl radical while the high activation energy for this compound arises because an unstrained sp^3 hybridized carbon is converted to a strained sp^2 carbon (10).

The *A*-factor for cyclopentane is similar to the *A*-factor for an acyclic aliphatic *s*-C—H which means that the enhanced reactivity of this substrate is entirely due to a low activation energy. A low acti-

[4]B. Mile. Private communication.
[5]S. Korcek and L. R. Mahoney. Private communication.

TABLE 3. Yields of tertiary alcohols and relative and absolute rate constants for tertiary aliphatic C—H bonds obtained from co-oxidations in the presence of *tert*-butyl hydroperoxide (1–2 *M*) at 30°C

Substrate R_1H (*M*)	3-Methylpentane concentration (*M*)	$10^2[R_1OH]$ (*M*)	$10^2[R_2OH]$[a] (*M*)	$k_p^{(1)}/k_p^{(2)}$[b]	$10^3 k_p^{(1)}$[c] (M^{-1} s^{-1})
2,2,4-Trimethylpentane (3.63)	2.4	0.67	2.0	0.22	1.5
2,2,4-Trimethylpentane (1.8)	4.8	0.23	2.8	0.22	
2,4-Dimethylpentane (2.05)	4.64	0.8	2.4	0.75	2.5
2,4-Dimethylpentane (4.1)	2.32	1.7	1.3	0.75	
2,4-Dimethylpentane (3.0)	3.4	1.9	3.2	0.67	
2,2,3-Trimethylpentane (1.88)	4.63	0.18	1.0	0.44	3.2
2,2,3-Trimethylpentane (3.76)	2.3	0.26	0.34	0.47	
2,3-Dimethylpentane (3.09)	3.49	1.4[d]	2.1	0.75	5.5
		2.3[e]		1.2	8.9
2,3-Dimethylpentane (2.0)	4.7	1.1[d]	3.2	0.81	
		1.8[e]		1.3	
2-Methylbutane (5.16)	2.35	4.8	2.2	1.0	7.0
2-Methylbutane (2.53)	4.7	2.2	4.3	0.95	
2-Methylpentane (3.41)	3.53	4.3	4.5	1.0	7.0
2-Methylpentane (4.55)	2.35	5.3	3.0	0.91	
2,3-Dimethylbutane (4.65)	2.4	28.8	5.5	2.7	9.3
2,3-Dimethylbutane (3.49)	3.6	3.35	1.32	2.6	
2,2,3-Trimethylbutane (2.07)	4.63	1.26	1.9	1.5	13
2,2,3-Trimethylbutane (3.1)	3.47	1.3	0.73	2.0	
2,2,3-Trimethylbutane (3.45)	3.08	1.87	0.82	2.0	
Methylcyclohexane (4.7)	2.35	2.0	0.73	1.4	10
Methylcyclohexane (2.35)	4.7	1.3	1.6	1.6	
Methylcyclopentane (5.35)	2.3	5.1	0.69	3.2	21
Methylcyclopentane (2.67)	4.63	2.7	1.7	2.8	

[a]3-Methyl-3-pentanol.
[b]Overall relative reactivity for *t*-C—H's.
[c]Absolute reactivity per H relative to k_p per *t*-C—H = 0.007 M^{-1} s^{-1} for 3-methylpentane.
[d]2,3-Dimethylpentan-2-ol.
[e]2,3-Dimethylpentan-3-ol.

vation energy probably reflects the relief of strain upon removal of a H-atom from cyclopentane. It is interesting to note that the activation energy difference, $E_p^{c\text{-}C_6H_{12}} - E_p^{c\text{-}C_5H_{10}} = 2.75$ kcal mol^{-1}, is very similar to the difference in activation energies for reaction of Br• with these cyclanes obtained by Ferguson and Whittle ($\Delta E_{Br\bullet} = 2.1$ kcal mol^{-1}) (10) and Bunce and Hadley ($\Delta E_{Br\bullet} = 2.7$ kcal mol^{-1}) (11).

In the case of the tertiary C—H bonds 2,2,4-trimethylpentane is less reactive than 3-methylpentane because $\Delta S^{\ddagger}_{3MP} - \Delta S^{\ddagger}_{2,2,4\text{-}TMP} = 6$ cal deg^{-1} mol^{-1} which more than compensates for $E_{3MP} - E_{2,2,4TMP} = 0.8$ kcal mol^{-1}. The low reactivity of 2,2,4-trimethylpentane to autoxidation has been noted previously (2) and attributed to shielding of the tertiary hydrogen from peroxy radical attack.

It is interesting to note that the *t*-C—H bond in 2,2,3-trimethylbutane is 1.5 times more reactive than the *t*-C—H in 3-methylpentane despite a lower entropy of activation. In this case the decrease in activation energy of 3 kcal mol^{-1} because of relief of steric strain upon removal of the tertiary hydrogen more than compensates for the difference in entropy of activation.

In summary it would appear that a bulky group near the reaction centre either accelerates the rate of transfer of a hydrogen atom to a peroxy radical because of the relief of steric strain or decreases the rate by lowering the probability of forming the activated complex. Furthermore when the bulky group is attached to the β-carbon the decrease in rate because of a decrease in $\Delta S^{\ddagger}$ more than compensates for the increase in rate due to a decrease in E while the reverse is operative when the bulky group is attached to the α-carbon.

TABLE 4. Arrhenius parameters[a] for reaction of alkanes with the *tert*-butylperoxy radical

Alkane		$\log(A_p/M^{-1}\ s^{-1})$[a]	E_p/(kcal mol^{-1})
3-Methylpentane	3°	9.5±0.5	16.3 ±0.7
	2°	8.9±0.7	17.5 ±0.8
Cyclohexane	2°	10.4±0.5	19.5 ±0.7
Cyclopentane	2°	8.8±1	16.75±1
2,2,4-Trimethylpentane	3°	8.3±1	15.5 ±1
2,2,3-Trimethylbutane	3°	7.5±0.6	13.2 ±0.8
Methylcyclohexane	3°	9.7±0.7	16.3 ±1.0
	2°[b]	9.7±0.7	18.7 ±1.0
	2°[c]	9.6±0.7	17.9 ±1.0

[a]Per active C—H bond relative to the parameters for the tertiary hydrogen in 3-methylpentane.
[b]Abstraction of a hydrogen atom from C-2.
[c]Abstraction of a hydrogen atom from C-3 and C-4.

Can. J. Chem. Downloaded from www.nrcresearchpress.com by 210.87.254.40 on 09/05/12
For personal use only.

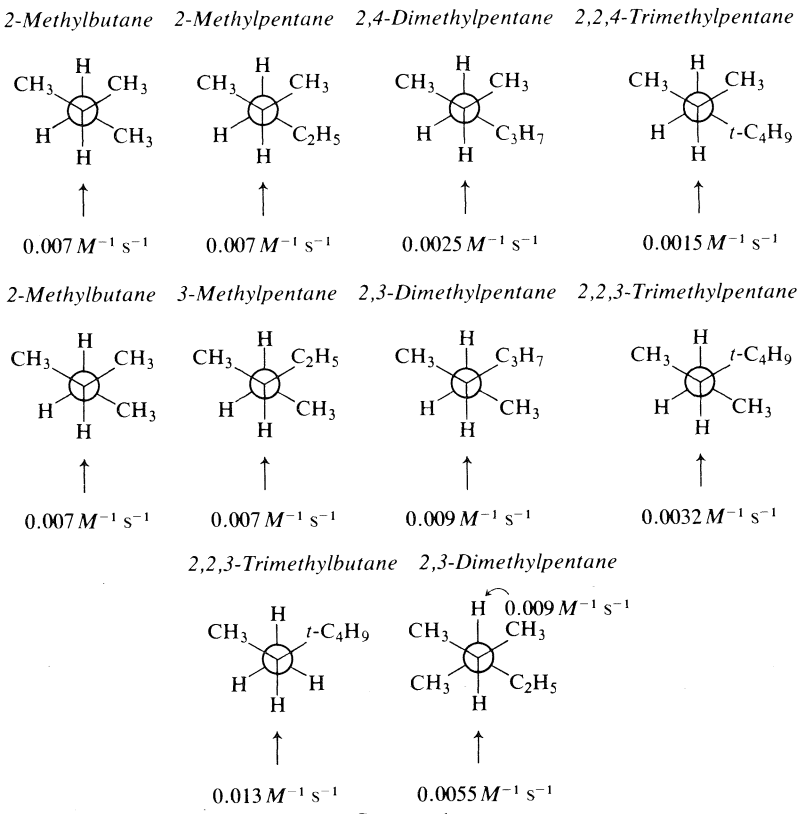

SCHEME 1

Aliphatic C—D Bonds

Rate constants and Arrhenius parameters for reaction of perdeuterated methylcyclohexane and 3-methylpentane with the *tert*-butylperoxy radical are gathered in Table 5. The kinetic data for methylcyclohexane-d_{14} were obtained relative to 3-methylpentane while the data for 3-methylpentane-d_{14} were obtained relative to 2,2,4-trimethylpentane. The kinetic isotope effects (k_p^H/k_p^D) of 24–28 are significantly larger than the isotope effects that we obtained for reaction of t-$BuO_2^\bullet$ with aralkanes, cyclohexane, and tetrahydrothiophene (14). Furthermore an isotope effect of ~25 is well above the theoretical limit of 9.5 for breaking a C—H bond (15) which suggests that factors other than complete loss of zero-point energies of stretching and bending vibrations in the transition state influence the magnitude of k_p^H/k_p^D. There could, of course, be additional contributions to this ratio because of secondary deuterium isotope effects. These are, however, usually small and it is unlikely that they would increase the isotope effect from 9.5 to 25.

Relative reactivities for methylcyclohexane-d_{14} were determined over a temperature range and the estimated activation parameters are compared with the values for protiated methylcyclohexane in the last two columns in Table 5. For the tertiary and secondary hydrogens $A_p^D = 3\text{–}5 \times A_p^H$ and $E_p^D = E_p^H + 2.5$ to 3.1 kcal mol^{-1}. These activation parameters suggest an entropy of activation difference of ~3 cal deg^{-1} mol^{-1} in favor of the fully deuterated compound and an enthalpy of activation difference of ca. 1.5 kcal mol^{-1} above the maximum. Clearly further work on the reactivity of deuterated alkanes to t-$BuO_2^\bullet$ is needed to clarify these anomalous differences.

Comparison with Other Work

We have previously (5) used the direct method to measure rate constants for reaction of cyclohexane, tridecane, and hexadecane with t-$BuO_2^\bullet$ and where a comparison can be made the two methods give results that are in excellent agreement. For instance the direct method gave k_p(overall) = 0.0031 M^{-1} s^{-1} for cyclohexane at 30°C while the competitive method gives an identical value. Hendry and coworkers (4) have also used the direct method to measure the reactivity of this cyclane to t-$BuO_2^\bullet$ and report a value of 0.175 M^{-1} s^{-1} at 80°C. Our value at this temperature calculated from the Arrhenius

Can. J. Chem. Downloaded from www.nrcresearchpress.com by 210.87.254.40 on 09/05/12
For personal use only.

TABLE 5. Rate constants[a] for reaction of deuterated alkanes with the *tert*-butylperoxy radical

Alkane		$10^4 k_p^D$ (M^{-1} s^{-1})	k_p^H/k_p^D	log (A_p^D/M^{-1} s^{-1})	E_p^D (kcal mol^{-1})	A_p^H/A_p^D	$E_p^D - E_p^H$ (kcal mol^{-1})
Methylcyclohexane(*d*-14)	3°	3.6	28	10 ±1	18.8±1	0.32	2.5
	2°[b]	0.08	25	10.4±1	21.6±1	0.2	2.9
	2°[c]	0.15	27	10.2±1	21 ±1	0.25	3.1
3-Methylpentane(*d*-14)	3°	2.5	28	—	—	—	—
	2°	0.08	25	—	—	—	—

[a]Per active H-atom relative to the *t*-C—H in 3-methylpentane.
[b]C-2.
[c]Averages for C-3 and C-4.

parameters in Table 4 is 0.25 M^{-1} s^{-1}. The direct method has been used by Niki and Kamiya (16) to determine overall reactivities of several alkanes to *t*-$BuO_2^{\bullet}$ at 90°C and their results and the rate constants estimated from our Arrhenius parameters are in satisfactory agreement. For instance, we estimate that the overall reactivity of 3-methyloctane should be ~0.7 M^{-1} s^{-1} at 90°C while Niki and Kamiya report a value of 0.66 to 0.74 M^{-1} s^{-1}.

Acknowledgements

We should like to thank Dr. K. U. Ingold, Dr. F. R. Mayo, and Dr. B. Mile for the helpful comments made on a preliminary version of this manuscript.

1. J. A. HOWARD, J. H. B. CHENIER, and D. A. HOLDEN. Can. J. Chem. **56**, 170 (1978) and previous papers in this series.
2. G. A. RUSSELL. *In* Free radicals. Vol. 1. *Edited by* J. K. Kochi. Wiley, New York, NY. 1973. Chapt. 7.
3. H. KIEFER and T. G. TRAYLOR. Tetrahedron Lett. 6163 (1966).
4. D. G. HENDRY, C. W. GOULD, D. SCHULTZLE, M. G. SYZ, and F. R. MAYO. J. Org. Chem. **41**, 1 (1976).
5. S. KORCEK, J. H. B. CHENIER, J. A. HOWARD, and K. U. INGOLD. Can. J. Chem. **50**, 2285 (1972).
6. J. A. HOWARD, W. J. SCHWALM, and K. U. INGOLD. Adv. Chem. Ser. **75**, 6 (1968).
7. J. E. BENNETT, D. M. BROWN, and B. MILE. Trans. Faraday Soc. **66**, 397 (1970).
8. B. D. Boss and R. N. HAZLETT. Can. J. Chem. **47**, 4175 (1969).
9. S. E. FULLER, J. R. LINDSAY-SMITH, and R. O. C. NORMAN. Abstracts of the 2nd International Symposium on Organic Free Radicals, Aix-en-Provence. 1977.
10. K.-C. FERGUSON and E. WHITTLE. Trans. Faraday Soc. **67**, 2618 (1971).
11. N. J. BUNCE and M. HADLEY. J. Org. Chem. **39**, 2271 (1974).
12. F. RUST. J. Am. Chem. Soc. **79**, 4000 (1957).
13. T. MILL and G. MONTORSI. Int. J. Chem. Kinet. **5**, 119 (1973).
14. J. A. HOWARD. *In* Free radicals. Vol. 2. *Edited by* J. K. Kochi. Wiley, New York, NY. 1973. Chapt. 1.
15. G. BRUNTON, D. GRILLER, L. R. C. BARCLAY, and K. U. INGOLD. J. Am. Chem. Soc. **98**, 6803 (1976) and references therein.
16. E. NIKI and Y. KAMIYA. Bull. Chem. Soc. Jpn. **48**, 3226 (1975).

Can. J. Chem. Downloaded from www.nrcresearchpress.com by 210.87.254.40 on 09/05/12
For personal use only.

Synthesis of two in vivo metabolites of *N*-(*n*-propyl)phentermine

RONALD T. COUTTS, ABRAHAM BENDERLY, ALLAN L. C. MAK, AND WESLEY G. TAYLOR
Faculty of Pharmacy and Pharmaceutical Sciences, University of Alberta, Edmonton, Alta., Canada T6G 2N8

Received April 26, 1978

RONALD T. COUTTS, ABRAHAM BENDERLY, ALLAN L. C. MAK, and WESLEY G. TAYLOR. Can. J. Chem. **56**, 3054 (1978).

The phenolic metabolite, 1-(4-hydroxyphenyl)-2-methyl-2-(*n*-propylamino)propane (**1***e*) was prepared by a Ritter reaction from either 3-(4-methoxyphenyl)-2-methyl-1-propene or 3-(4-methoxyphenyl)-2-methyl-2-propanol and propionitrile. Three other products of the Ritter reaction were isolated and identified by interpretation of their mass spectra. Another phenolic metabolite, 1-(4-hydroxy-3-methoxyphenyl)-2-methyl-2-(*n*-propylamino)propane (**1***f*) could not be prepared by a Ritter reaction but was obtained from the product of the reaction between 3-(4-benzyloxy-3-methoxyphenyl)-2-methyl-1-propene and iodine isocyanate.

RONALD T. COUTTS, ABRAHAM BENDERLY, ALLAN L. C. MAK et WESLEY G. TAYLOR. Can. J. Chem. **56**, 3054 (1978).

On a préparé le métabolite phénolique (hydroxy-4 phényl)-1 méthyl-2 (*n*-propylamino)-2 propane (**1***e*) par réaction de Ritter à partir du propionitrile et du (méthoxy-4 phényl)-3 méthyl-2 propène-1 ou du (méthoxy-4 phényl)-3 méthyl-2 propanol-2. On a isolé trois autres produits de la réaction de Ritter et on les a identifiés par interprétation de leurs spectres de masse. Un autre métabolite phénolique, l'(hydroxy-4 méthoxy-3 phényl)-1 méthyl-2 (*n*-propylamino)-2 propane (**1***f*), qu'on n'a pas réussi à préparer par réaction de Ritter, a été obtenu à partir du produit de la réaction entre l'isocyanate d'iode et le (benzyloxy-4 méthoxy-3 phényl)-3 méthyl-2 propène-1.

[Traduit par le journal]

Can. J. Chem. Downloaded from www.nrcresearchpress.com by 210.87.254.6 on 09/05/12
For personal use only.

In a continuation of studies on the effect on in vitro and in vivo metabolism of increasing the length of the *N*-alkyl chain of clinically useful drugs (1, 2), *N*-(*n*-propyl)phentermine (**1***d*, NPP), a higher homolog of the anorectic sympathomimetic drug mephentermine (**2***b*) was metabolized in vivo in the rat and two major phenolic metabolites were isolated.[1] Interpretation of their mass spectra suggested that these new metabolites were 1-(4-hydroxyphenyl)-2-methyl-2-(*n*-propylamino)propane (**1***e*) and 1-(4-hydroxy-3-methoxyphenyl)-2-methyl-2-(*n*-propylamino)propane (**1***f*). Conclusive identification of the metabolites was not possible in the absence of authentic samples of **1***e* and **1***f*. Both metabolites were also required for quantitative analysis studies. This note describes our approaches to the synthesis of **1***e* and **1***f*.

Phentermines are not as readily obtained synthetically as amphetamines (1). Patented procedures for the synthesis of phentermine (**2***a*) and mephentermine (**2***b*) are complex (3) and are not easily applicable to phenolic derivatives of phentermine. The Ritter reaction (4), however, provides a direct synthetic route to these compounds. Treatment of the alkene (**3**) or the tertiary alcohol (**4**) with propionitrile under Ritter conditions was more complex than anticipated and gave four products which were readily separated by gc. The mass spectra of the two major products were readily interpretable in terms of

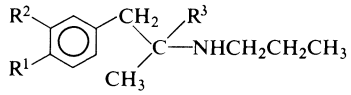

1

a $R^1 = R^2 = R^3 = H$
b $R^1 = OH, R^2 = R^3 = H$
c $R^1 = OH, R^2 = OCH_3, R^3 = H$
d $R^1 = R^2 = H, R^3 = CH_3$
e $R^1 = OH, R^2 = H, R^3 = CH_3$
f $R^1 = OH, R^2 = OCH_3, R^3 = CH_3$

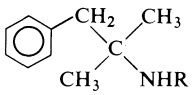

2

a R = H
b R = CH_3

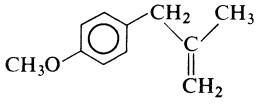

3

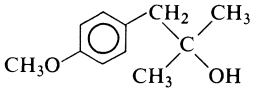

4

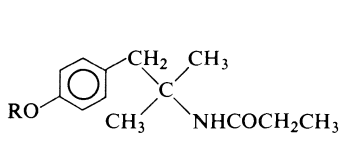

5

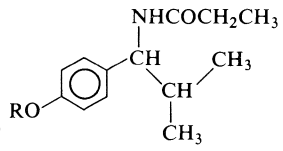

6

a R = H *b* R = CH_3

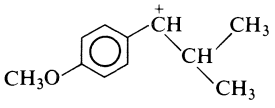

7

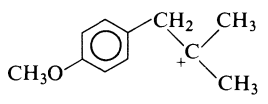

8

[1]R. T. Coutts and W. G. Taylor. Unpublished results.

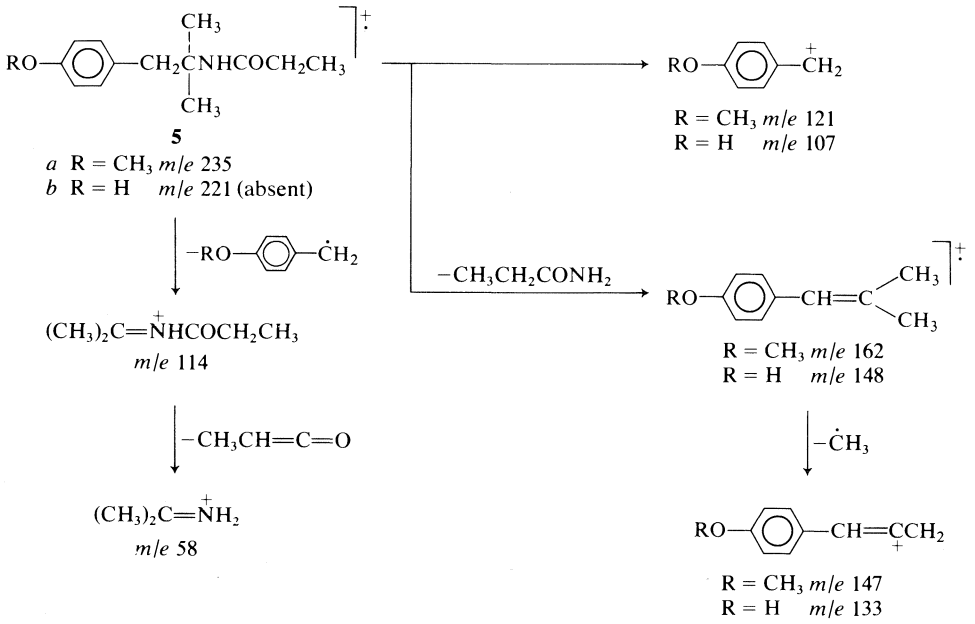

SCHEME 1

structures **5***a* and **5***b* (Scheme 1). Comparable fragmentation patterns are observed in the spectra of structurally related methoxylated and phenolic amines (5). The two minor products had very simple mass spectra, each containing only three ions. These spectra were also readily interpreted (Scheme 2) and indicated that the structures of the minor reaction products were **6***a* and **6***b*. The formation of the latter two products is consistent with the formation of significant quantities of the benzylic carbonium ion (**7**) in addition to the expected tertiary ion (**8**) during the course of the Ritter reaction.

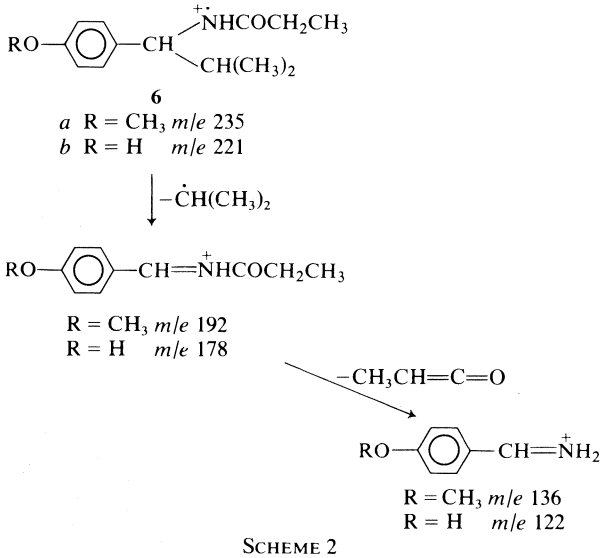

SCHEME 2

An effort was made to improve the yield of the desired compound (**5***a*) by altering the conditions of the Ritter reaction. The ratio of sulfuric acid to glacial acetic acid used proved to be critical; by suitably altering this ratio, either the phenol (**5***a*) or the methyl ether (**5***b*) was the major product of the reaction with **3** or **4** (Table 1). The phenolic compounds **5***a* and **6***a* were separated from **5***b* and **6***b* by alkaline extraction and from each other by column chromatography or fractional crystallization. Reduction of **5***a* with diborane (6) gave the desired 1-(4-hydroxyphenyl)-2-methyl-2-(*n*-propylamino)propane (**1***e*).

The Ritter reaction was not applicable to the synthesis of 1-(4-hydroxy-3-methoxyphenyl)-2-methyl-2-(*n*-propylamino)propane (**1***f*). The presence of the electron-donating group at the C-3 position of **9** promoted ring closure (3) to a mixture of the 3,4-dihydroisoquinoline derivative (**10***a*), the corresponding phenol (**10***b*) and the phenol acetate (**10***c*) (Scheme 3). An alternative method of synthesizing **1***f* was sought. It is well documented that iodine isocyanate (INCO) adds regioselectively to unsymmetrical alkenes, whereby the isocyanate function appears at the more substituted double-bond carbon atom (7). When this reagent and the unsymmetrical alkene (**9**) were allowed to react, the desired addition occurred and 4-benzyloxy-3-methoxyphentermine (**12**, R = H) was subsequently obtained as illustrated in Scheme 4. The *N*-propionyl derivative (**12**, R = $COCH_2CH_3$) was prepared and reduced with diborane to 1-(4-benzyloxy-3-methoxyphenyl)-2-

Can. J. Chem. Downloaded from www.nrcresearchpress.com by 210.87.254.6 on 09/05/12
For personal use only.

TABLE 1. Preparation of isomeric amides **5***a* and **6***a*, **5***b* and **6***b* by the Ritter reaction

Starting material	H_2SO_4 to CH_3COOH ratio (vol)	Products (%)*				Total gc yield (%)
		5*a*	**5***b*	**6***a*	**6***b*	
4	1:1.2	87.1	4.0	3.7	5.3	75
4	1:1.5	39.0	30.0	12.6	16.4	46
4	1:4.4	15.5	66.5	8.5	10.1	85
3	1:1.2	62.0	11.6	17.0	9.4	74
3	1:4.0	1.7	84.3	3.3	8.3	56

*Based on peak areas.

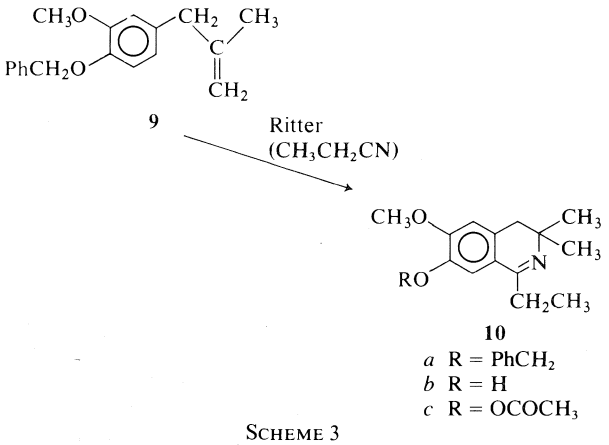

SCHEME 3

methyl-2-*n*-propylamino)propane (**12**, R = $CH_2CH_2CH_3$), which was catalytically hydrogenated to the required **1***f* (Scheme 4).

The synthetic compounds **1***e* and **1***f* were identical in gc and gc–ms behavior to the two phenolic in vivo metabolites of NPP.

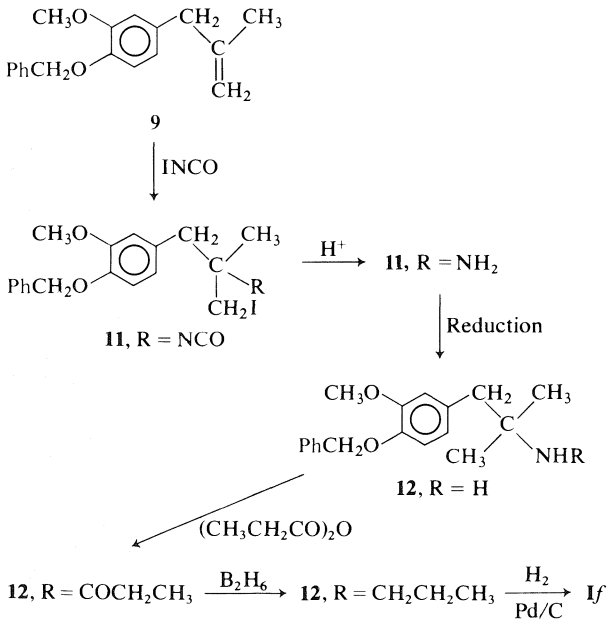

SCHEME 4

Experimental

Melting points are uncorrected. The ^{1}Hmr spectra were determined for solutions in deuteriochloroform with a Varian Associates EM 360A (60 MHz) spectrometer, with TMS as internal standard. Combined gc–ms was performed on a Hewlett Packard 5710A gas chromatograph – Hewlett Packard 5980A mass spectrometer using a glass column, 0.85 m long, 4 mm id, packed with 5% OV-101 on Chromosorb 750 at 160°C, helium flow rate 60 ml/min. Accurate mass measurements were made on an A.E.I., MS-9 or MS-12 mass spectrometer at an ionizing potential of 70 eV. The starting materials, 1-(4-benzyloxy-3-methoxy)phenyl-2-propanone and 1-(4-methoxy)-phenyl-2-propanone were prepared by a reported procedure (8).

*1-(4-Methoxyphenyl)-2-methyl-2-propanol (**4**)*

A benzene solution (40 ml) of 1-(4-methoxy)phenyl-2-propanone (19.2 g, 0.1 mol) was added dropwise (40 min) to an ether solutions of methyllithium (Alfa Inorganic, Inc., 250 ml of 0.6 *M*) at −65°C under N_2. After stirring for 2 h and warming up to room temperature (1 h), the reaction mixture was quenched with 5% aqueous NH_4Cl (100 ml) and extracted with ether (3 × 50 ml). The organic phase was then dried (Na_2SO_4) and concentrated. Bulb-to-bulb distillation of the residue (70°C/0.02 Torr) provided 17 g (95%) of **4** as a colorless solid, mp 37.5–38.5°C; ^{1}Hmr δ: 1.22 (6H, s, $C(CH_3)_2$), 1.6 (1H, s, br, OH), 3.8 (3H, s, CH_3), 7.0 (4H, q, *J* = 8–9 Hz, C_6H_4); ms *m/e* (% relative abundance): 181 (1), 180 (9), 165 (9), 123 (10), 122 (100), 121 (38), 107 (18), 92 (4), 91 (11), 79 (5), 78 (11), 65 (5), 59 (66). *Exact mass* calcd. for $C_{11}H_{16}O_2$: 180.1146; found: 180.1152. *Anal.* calcd. for $C_{11}H_{16}O_2$: C 73.30, H 8.95; found: C 73.04, H 8.81.

*3-(4-Benzyloxy-3-methoxyphenyl)-2-methyl-1-propene (**9**)*

To a magnetically-stirred suspension of triphenylphosphonium bromide (10.49 g, 0.029 mol) in THF (50 ml) at −78°C was added dropwise, *n*-butyllithium solution (18.5 ml, 1.55 *M* in hexane) under N_2. The reaction mixture was allowed to warm up to room temperature and it was maintained at this temperature for 2 h. The solution was cooled again to −78°C and the ketone, 1-(4-benzyloxy-3-methoxyphenyl)-2-propanone (7.2 g, 0.029 mol) in THF (70 ml) was then added dropwise (1 h). The reaction mixture was warmed up to room temperature (1 h), stirred at this temperature for 2 h then at reflux temperature for 20 h. After cooling, the mixture was concentrated and 40 ml of ether–pentane (5:1) solution was added. The resulting precipitate of triphenylphosphine oxide was filtered off. Elution chromatography of the concentrated filtrate on silica gel (cyclohexane–ether, 4:1) afforded 7.2 g (94%) of **9**. Molecular distillation (70°C/0.02 Torr) resulted in a colorless oil which solidified on standing, mp 29–30°C; ^{1}Hmr δ: 1.63 (3H, s, CH_3), 3.3 (2H, s, $ArCH_2$), 3.9 (3H, s, OCH_3), 4.85 (2H, s, br, $C{=}CH_2$), 5.25 (2H, s, OCH_2), 6.8 (3H, m, C_6H_3), 7.6 (5H, m, C_6H_5); ms *m/e* (% relative abun-

Can. J. Chem. Downloaded from www.nrcresearchpress.com by 210.87.254.6 on 09/05/12
For personal use only.

Can. J. Chem. Downloaded from www.nrcresearchpress.com by 210.87.254.6 on 09/05/12
For personal use only.

dance): 268 (33), 177 (27), 117 (7), 107 (5), 91 (100), 55 (5). *Exact mass* calcd. for $C_{18}H_{20}O_2$: 268.1458; found: 268.1463. *Anal.* calcd. for $C_{18}H_{20}O_2$: C 80.56, H 7.51; found: C 80.40, H 7.50.

*3-(4-Methoxyphenyl)-2-methyl-1-propene (**3**)*

Using a procedure similar to that employed in the preparation of **9**, 1-(4-methoxy)phenyl-2-propanone (3.3 g) was reacted to give 3.05 g (94%) of the alkene **3**, bp 44–45°C 0.12 Torr; ^{1}Hmr δ: 1.63 (3H, s, CH_3), 3.25 (2H, s, $ArCH_2$), 3.8 (3H, s, OCH_3), 4.75 (2H, s, br, $C{=}CH_2$), 7.0 (4H, q, J = 8–9 Hz, C_6H_4); ms *m/e* (% relative abundance): 163 (22), 162 (100), 161 (10), 149 (7), 147 (88), 137 (16), 135 (5), 121 (56), 117 (9), 115 (10), 103 (8), 91 (26), 78 (14), 77 (13). *Exact mass* calcd. for $C_{11}H_{14}O$: 162.1040; found: 162.1048. *Anal.* calcd. for $C_{11}H_{14}O$: C 81.44, H 8.70; found: C 81.78, H 8.66.

N-*[1-(4-Hydroxyphenyl)-2-methyl-2-propyl]propionamide (5a)*

Concentrated H_2SO_4 (3 ml, Baker, 96%) was added to a stirred solution of propionitrile (0.66 g, 0.012 mol) in glacial acetic acid (2.5 ml) at ice bath temperature. The alcohol (**4**) (1.8 g, 0.01 mol) dissolved in acetic acid (1 ml) was added dropwise and the mixture was stirred at room temperature for 18 h, neutralized with 10% Na_2CO_3 and extracted (3 × 20 ml) with ether – methylene chloride (14:11). Gas chromatographic analysis showed four peaks, the retention times of which were **5***b*, 10.51 min; **6***b*, 12.66 min; **5***a*, 13.94 min; **6***a*, 14.88 min; gc–ms *m/e* (% relative abundance) **5***b*: 235 (5), 162 (65), 147 (12), 121 (30), 114 (42), 58 (100); **6***b*, m/e 235 (5), 192 (74), 136 (100); **5***a*, m/e 148 (41), 133 (21), 114 (50), 77 (14), 58 (100); **6***a*: 221 (12), 178 (81), 122 (100).

To separate the phenolic compounds, the organic layer was washed with 10% NaOH. After acidification, the aqueous layer was extracted with CH_2Cl_2 and the combined extracts were washed with brine and dried (Na_2SO_4). Removal of the solvent produced 0.98 g (42%) of **5***a*, mp 138–139°C (from ether–hexane); ^{1}Hmr δ: 1.0–1.5 (9H, m, $C(CH_3)_2$, CH_2CH_3), 2.0 (2H, q, J = 7 Hz, CH_2), 3.0 (2H, s, $ArCH_2$), 5.2 (H, s, br, OH), 6.4 (4H, q, J = 8–9 Hz, C_6H_4). *Exact mass* calcd. for $C_{13}H_{19}NO_2$: 221.1411; found: 221.1413. *Anal.* calcd. for $C_{13}H_{19}NO_2$: C 70.56, H 8.65, N 6.33; found: C 70.59, H 8.72, N 6.02.

*1-(4-Hydroxyphenyl)-2-methyl-2-(*n*-propylamino)propane (**1e**)*

To a solution of borane in THF (8 ml, 0.10 *M*) in a 50 ml flask equipped with a reflux condenser, dropping funnel, and a magnetic stirring bar and maintained under N_2, was added 0.5 g (2.3 mmol) of the amide (**5***a*) in THF (8 ml) over 15 min. The temperature was maintained at 0°C during the addition. The colorless solution was then refluxed for 10 h, cooled to room temperature, and treated with 6 *N* HCl (5 ml). After stirring for 0.5 h, the aqueous layer was separated, washed with ether, basified with 20% Na_2CO_3 (pH 9–9.5), and extracted (2 × 15 ml) with ether–CH_2Cl_2 (14:11). The combined extract was washed with brine and dried (Na_2SO_4). Removal of the solvent gave 0.4 g (86%) of **1***e*, mp 89.5–90.5°C (from hexane–CCl_4); ^{1}Hmr δ: 0.7–1.9 (11H, m, $C(CH_3)_2$, $CH_2CH_2CH_3$), 2.4–3.0 (4H, m, $ArCH_2$, $CH_2CH_2CH_3$), 5.3 (2H, s, br, NH, OH), 6.9 (4H, q, J = 8–9 Hz, C_6H_4); ms *m/e* (% relative abundance): 192 (2), 101 (7), 100 (100), 58 (60). *Exact mass* calcd. for $C_{12}H_{18}NO$ $(M - CH_3)^+$: 192.1384; found: 192.1386. *Anal.* calcd. for $C_{13}H_{21}NO$: C 75.32, H 10.21, N 6.76; found: C 75.11, H 10.03, N 6.67.

*1-Ethyl-7-hydroxy-6-methoxy-3,3-dimethyl-3,4-dihydroisoquinoline (**10**b)*

Concentrated H_2SO_4 (14 ml) was added to a stirred mixture of glacial acetic acid (40 ml) and propionitrile (1.3 ml, 0.018 mol) at 0°C. The alkene (**9**) (4 g, 0.015 mol) in glacial acetic acid (10 ml) was added dropwise at ice-bath temperature. The resulting mixture was stirred at room temperature for 15 h. The mixture was neutralized with 20% Na_2CO_3, then extracted with methylene chloride (2 × 30 ml) and the combined extracts were dried and evaporated *in vacuo*. The residue (4.05 g) was shown by ^{1}Hmr to be a mixture of **10***b* (60%), **10***a* (24%), and **10***c* (16%). The phenolic compound **10***b* was separated from the remainder (3 g) of the mixture (**10***a–c*) as described for **5***a* and 1.5 g of **10***b* was obtained, mp 146–148°C (from chloroform); ^{1}Hmr δ: 1.0–1.5 (9H, m, $C(CH_3)_2$, CH_2CH_3), 2.4–2.9 (4H, m, $ArCH_2$, CH_2CH_3), 3.9 (3H, s, OCH_3), 6.7 (1H, s, C_6H), 7.2 (1H, s, C_6H), 8.9 (1H, s, br, OH); ms *m/e* (% relative abundance): 234 (13), 233 (79), 232 (41), 219 (16), 218 (100), 216 (10), 204 (8), 203 (16), 191 (36), 190 (23), 177 (6), 164 (9), 163 (10), 161 (11), 145 (8), 117 (10), 91 (12). *Exact mass* calcd. for $C_{14}H_{19}NO_2$: 233.1411; found: 233.1412.

*1-(4-Benzyloxy-3-methoxyphenyl)-2-iodomethyl-2-propylisocyanate (**11**, R = NCO)*

A slurry of iodine (9 g, 0.035 mol) and freshly prepared silver isocyanate (6.88 g, 0.046 mol) in dry ether (10 ml) was stirred for 1 h at 25°C under dry N_2. The mixture was then cooled to −20°C and the alkene (**9**) (6.7 g, 0.025 mol) in ether (25 ml) was added dropwise. After stirring at room temperature for 36 h, the reaction mixture was filtered through Celite and washed with a saturated Na_2SO_3 solution to remove excess iodine. The ether layer was then washed with brine, dried (Na_2SO_4), and evaporated, to yield 9.18 g of a pale yellow oil (mixture by ^{1}Hmr of 73% **11**, R = NCO and 20% **9**); ir (neat) ν_{max} 2250 (NCO) cm^{-1}; ^{1}Hmr of **11**, R = NCO δ: 1.45 (3H, s, CH_3), 2.85 (2H, s, CH_2I), 3.3 (2H, s, $ArCH_2$), 3.85 (3H, s, OCH_3), 5.2 (2H, s, OCH_2), 6.8 (3H, m, C_6H_3), 7.5 (5H, m, C_6H_5).

*1-(4-Benzyloxy-3-methoxyphenyl)-2-methyl-2-aminopropane (**12**, R = H)*

To the crude iodoisocyanate (**11**, R = NCO) (9.18 g, containing 20% of **9**) in ether (100 ml) was added dropwise concentrated HCl (35 ml). The mixture was stirred for 6 h, and the precipitate of the iodoamine (**11**, R = NH_2) hydrochloride salt which formed was filtered and washed with ether (5.6 g, 68%).

To a suspension of LAH (2 g) in dry DME (125 ml) under N_2 the dried hydrochloride salt of **11**, R = NH_2 (5.6 g) was added portionwise. After refluxing for 36 h, the mixture was cooled to 0°C and was treated with 40 ml of 4 *N* HCl. The mixture was stirred (3 h), filtered through Celite, and washed with water. The resulting solution was basified with solid NaOH, and extracted with ether (3 × 50 ml). Evaporation of the combined ether extracts gave 2.1 g (57%) of **12**, R = H, as a colorless solid; ^{1}Hmr δ: 1.2 (6H, s, $C(CH_3)_2$), 1.6 (2H, s, br, NH_2), 2.65 (2H, s, $ArCH_2$), 3.9 (3H, s, OCH_3), 5.25 (2H, s, OCH_2), 6.8 (3H, m, C_6H_3), 7.5 (5H, m, C_6H_5); ms *m/e* (% relative abundance): 286 (1), 285 (3), 270 (4), 229 (4), 228 (24), 137 (6), 107 (8), 91 (61), 65 (20), 59 (23), 58 (100), 51 (5). *Exact mass* calcd. for $C_{18}H_{23}NO_2$: 285,1727; found: 285.1728. The hydrochloride of the title compound had mp 178–179°C. *Anal.* calcd. for $C_{18}H_{24}ClNO_2$: C 67.17, H 7.52, N 4.35, Cl 11.02; found: C 67.13, H 7.30, N 4.14, Cl 11.15.

*1-(4-Benzyloxy-3-methoxyphenyl)-2-methyl-2-(*n*-propylamino)propane (**12**, R = $CH_2CH_2CH_3$)*

To a solution of **12**, R = H (2.10 g, 7.37 mmol) in dry THF (40 ml) and triethylamine (3.1 ml, 22.1 mmol) was added dropwise and with stirring, a solution of propionic anhydride (1.5 ml, 11 mmol) in THF (10 ml). Stirring was continued for

15 h then a solution of 2 *N* NaOH (10 ml) was added and the mixture was stirred for a further 2 h. The organic layer was separated and the aqueous layer extracted with CH_2Cl_2 (2 × 25 ml). The combined organic extracts were dried (Na_2SO_4) and evaporated to provide the amide (**12**, R = $COCH_2CH_3$) as a colorless oil 2.4 g (97%) which solidified on standing, mp 80–82°C (diethyl ether).

A solution of the amide **12**, R = $COCH_2CH_3$ (2 g, 5.87 mmol) in THF (15 ml) was reduced with diborane (23.5 ml, 1 *M* in THF) according to the procedure described in the preparation of **1***e*, and **12**, R = $CH_2CH_2CH_3$ (1.51 g, 79%) was obtained as the hydrochloride salt, mp 190°C; ^{1}Hmr of base δ: 0.8–1.2 (9H, m, $C(CH_3)_2$, $CH_2CH_2CH_3$), 1.4 (2H, m, $CH_2CH_2CH_3$), 2.4–2.8 (5H, m, $ArCH_2$, NH, $RNHCH_2R$), 3.95 (3H, s, OCH_3), 5.2 (2H, s, OCH_2), 6.7 (3H, m, C_6H_3), 7.5 (5H, m, C_6H_5); ms *m/e* (% relative abundance): 327 (2), 268 (6), 223 (5), 177 (6), 150 (5), 149 (31), 114 (16), 101 (43), 100 (100), 92 (4), 91 (64), 70 (8), 58 (69). *Exact mass* calcd. for $C_{21}H_{29}NO_2$: 327.2190; found: 327.2193.

*1-(4-Hydroxy-3-methoxyphenyl)-2-methyl-2-(*n*-propylamino)propane (**1***f*)*

A solution of the amine (**12**, R = $CH_2CH_2CH_3$) (1.5 g, 4.59 mmol) in ethanol (100 ml) was hydrogenated over palladium–charcoal (2.7 g) at 40 psi for 17 h. The mixture was filtered through Celite and concentrated to give 0.7 g (82%) of **1***f*; ^{1}Hmr δ: 0.8–1.2 (9H, m, $C(CH_3)_2$, $CH_2CH_2CH_3$), 1.8 (2H, m, $CH_2CH_2CH_3$), 2.6–2.8 (4H, m, $ArCH_2$, $CH_2CH_2CH_3$), 3.85 (3H, s, OCH_3), 5.5 (2H, s, br, NH, OH), 6.8 (3H, m, C_6H_3); ms *m/e* (% relative abundance): 222 (1), 137 (5), 122 (2), 116 (1), 100 (100), 98 (2), 94 (2), 91 (2), 77 (2), 71 (1), 58 (27). *Exact mass* calcd. for $C_{13}H_{20}NO_2(M - CH_3)^+$: 222.1489; found: 222.1492. A sample for analysis was purified by gc (Varian aerograph 90-P instrument) and the product with retention time 9.1 min on a 180 cm × 4 mm id stainless steel column containing 3% OV-101 on Chromosorb W (column temperature 160°C; He flow rate 60 ml/min) was collected as colorless needles, mp 114–115°C. *Anal.* calcd. for $C_{14}H_{23}NO_2$: C 70.85, H 9.77, N 5.90; found: C 70.38, H 9.68, N 5.86.

Acknowledgements

Financial assistance from the Medical Research Council of Canada (grant No. MT-2993 to R.T.C.) is acknowledged with thanks. Useful discussions with Dr. G. R. Jones are also acknowledged.

1. R. T. Coutts, G. W. Dawson, C. W. Kazakoff, and J. Y. Wong. Drug Metab. Dispos. **4**, 256 (1976).
2. R. T. Coutts, G. W. Dawson, and A. H. Beckett. J. Pharm. Pharmacol. **28**, 815 (1976).
3. L. L. Abell, W. F. Bruce, and J. Seifter (to Wyeth Inc.). U.S. Patent No. 2,590,079 (March 25, 1952); Chem. Abstr. **46**, 10200e (1952).
4. J. J. Ritter and F. X. Murphy. J. Am. Chem. Soc. **74**, 763 (1952).
5. K. K. Midha, J. K. Cooper, I. J. McGilveray, R. T. Coutts, and R. Dawe. Drug Metab. Dispos. **4**, 568 (1976).
6. H. C. Brown and P. Heim. J. Org. Chem. **38**, 912 (1973).
7. A. Hassner, R. P. Hoblitt, C. Heathcock, J. E. Kropp, and M. Lorber. J. Am. Chem. Soc. **92**, 1326 (1970).
8. I. A. Pearl and D. L. Beyer. J. Org. Chem. **16**, 221 (1951).

Can. J. Chem. Downloaded from www.nrcresearchpress.com by 210.87.254.6 on 09/05/12
For personal use only.

Inductive substituent constants from dissociation of methyl-substituted 2-picolinium ions[1]

ALFRED FISCHER, MURRAY JOHN KING, AND FRANK PRICE ROBINSON
Department of Chemistry, University of Victoria, Victoria, B.C., Canada V8W 2Y2

Received April 20, 1978

ALFRED FISCHER, MURRAY JOHN KING, and FRANK PRICE ROBINSON. Can. J. Chem. **56**, 3059 (1978).

The dissociation constants of a series of 28 α-substituted 2-methylpyridinium ions in water at 25°C have been measured by potentiometric and spectrophotometric methods. Correlation of the $-pK$ values with σ_I values gives slope $\rho_I = 5.45$, intercept $-pK_0 = -5.81$, correlation coefficient $r = 0.991$, and enables new σ_I values to be evaluated. Dissociation constants for the 2-pyridinylmethylammonium ion and its *N*-methyl and *N,N*-dimethyl derivatives are also reported.

ALFRED FISCHER, MURRAY JOHN KING et FRANK PRICE ROBINSON. Can. J. Chem. **56**, 3059 (1978).

Faisant appel à des méthodes potentiométrique et spectrophotométrique, on a mesuré à 25°C pour des solutions aqueuses, les constantes de dissociation d'une série de 28 ions méthyl-2 pyridinium substitués en α. La corrélation des valeurs de $-pK$ avec les valeurs σ_I fournit une pente $\rho_I = 5.45$, une ordonnée à l'origine $-pK_0 = -5.81$, un coefficient de corrélation $r = 0.991$ et elle permet d'évaluer de nouvelles valeurs σ_I. On rapporte aussi les constantes de dissociation de l'ion méthylammonium-2 pyridinyle et de ses dérivés *N*-méthyle et *N,N*-diméthyle.

[Traduit par le journal]

Introduction

The analysis of substituent electronic effects in aromatic systems has been carried out using both single substituent parameter and dual substituent parameter treatments. The single substituent parameter approach involves the use of the Hammett equation (1–5).

$$\log (k/k_o) = \rho\sigma$$

In this approach the substituent constant (σ) is a function of both the substituent and its position, i.e., *meta* and *para* substituents have different σ values, whereas the reaction constant (ρ), a susceptibility measure, is independent of the position of the substituent within the aromatic ring. As Taft has pointed out (6) the Hammett equation is a polar (inductive) effect relationship,[2] substituent constants measuring the inductive effect of the substituents *m,p*-XC_6H_4, relative to that of C_6H_5, operating across the Ar—Y bond in the general reaction:

$$Ar—Y + Ph—Y' \rightleftharpoons Ar—Y' + Ph—Y$$

A common cause of deviation from the Hammett equation, most evident in the case of *para*-substituted phenyl groups, is the existence of π delocalization (resonance) effects operating across the Ar—Y bond. Additional classes of substituent constants have been developed in attempts to allow for the situations where the π acceptor properties of Y and Y′ differ significantly (σ^+) and, in the converse situations, where the π donor properties of Y and Y′ are different (σ^-) (2, 9). Although the use of modified substituent constants (σ^+, σ^-) in addition to the purely inductive substituent constants (σ^0) does extend the number of successful reactivity correlations, it has long been evident (10, 11) that aromatic reactivities do not fall neatly into three classes and dual substituent parameter treatments have been developed in attempts to accommodate this reality. One approach, initially developed by Yukawa and Tsuno (12, 13), has followed that of the single substituent parameter treatment in regarding the aryl group as the substituent and using Hammett type substituent constants to measure its inductive (σ^0) and resonance ($\sigma^+ - \sigma^0$, $\sigma^- - \sigma^0$) effects. An alternative approach, most thoroughly exploited by Taft and his co-workers, considers the group X as the substituent and the C_6H_4Y group as the reaction centre (6, 11, 14, 15). In this approach the inductive (σ_I) and resonance (σ_R) effects of the X group operating across the X—C_6H_4 bond are the quanti-

[1]From the Ph.D. Thesis of Murray John King, University of Victoria, Victoria, B.C., 1973.

[2]There is a considerable variation in the use of nomenclature concerning substituent effects (7). We use the terms 'polar' and 'inductive' to refer to that part of the substituent electronic effect not dependent on π delocalization across the R—Y bond (R is a substituent; Y is a reaction centre). Use of the term 'inductive' is not intended to imply that the effect is necessarily transmitted by the classical bond-relay mechanism: field effects may be important or dominant but would still be included in the 'inductive' effect. That part of the substituent electronic effect which is dependent on π delocalization across the R—Y bond we describe as a π delocalization or 'resonance' effect (often called the mesomeric effect, following Ingold (8)).

Can. J. Chem. Downloaded from www.nrcresearchpress.com by 210.87.254.6 on 09/05/12
For personal use only.

Can. J. Chem. Downloaded from www.nrcresearchpress.com by 210.87.254.6 on 09/05/12
For personal use only.

ties of interest and the correlation equation takes the form:

$$\log (k/k_o) = \sigma_I\rho_I + \sigma_R\rho_R$$

In this treatment *meta* and *para* substituents have the same σ_I and σ_R values and the difference in their effect on reactivity is accommodated by a change in the susceptibility coefficients, ρ_I and ρ_R.

Values of σ_I were derived by Taft from rates of acid- and base-catalysed hydrolysis of substituted acetate esters. Since Taft's initial work additional data have become available on reactivities of rigid aliphatic systems which provide good data sets for the evaluation of σ_I values. Such systems include 4-substituted bicyclo[2.2.2]octane-1-carboxylic acids (16–19), 4-substituted *trans*-cyclohexanecarboxylic acids (20, 21), 3-substituted adamantane 1-carboxylic acids (22), α-substituted *meta*- and *para*-toluic acids (23), and 4-substituted quinuclidines (24, 25). Charton (26) has evaluated a set of σ_I values from the dissociation constants of substituted acetic acids, on the assumption that steric effects are negligible.

In this paper we report the dissociation constants of an extensive set of α-substituted 2-picolinium ions (substituted 2-methylpyridinium ions). Subsequent papers will deal with the α-substituted 3- and 4-picolinium ions. The picolyl system is an excellent probe for the investigation of the inductive effects of substituents because (*a*) it meets the requirement of separating function centre and substituent by a rigid structure; (*b*) the reaction is particularly sensitive to substituent effects: compare $\rho = 6.0$ for dissociation of pyridinium ions (27) with $\rho = 1.4$ for ionization of benzoic acids in 50% ethanol and $\rho = 1.6$ for dissociation of benzoic acids in 80% aqueous methyl cellosolve (15), the conditions used by Exner for the study of the substituted toluic acids (23); (*c*) a large number of substituted derivatives is available without great difficulty; (*d*) it is possible to study substituted 2-, 3-, and 4-picolines and thus obtain three independent values of σ_I for each substituent. In contrast with the situation in the benzene series, reactivity studies of substituted pyridines have not been extensively investigated. The substituted picolines are of course pyridine derivatives and, focussing attention on the XCH_2 group as the substituent, our study provides additional data on the dissociation of substituted pyridines.

Experimental

Preparation of Compounds

Melting points were determined on a Bock-Monoscop hot-stage microscope and are uncorrected. The nmr spectra, in CCl_4 with TMS as internal standard, were obtained with Varian HA-60-IL or Perkin-Elmer R-12A spectrometers unless specified otherwise. Mass spectra were obtained on a Hitachi Perkin-Elmer RMU-7 mass spectrometer. Analyses were performed by the Microanalysis Laboratory, Toronto or by Dr. D. McGillivray, University of Victoria.

The purities of the substituted methylpyridines whose hydrochlorides could satisfactorily be prepared were, for the most part, verified by sharp melting points and the absence of impurity peaks in the nmr spectra. However, for some compounds the hydrochlorides were too hygroscopic for satisfactory melting points to be obtained. The purities of these compounds along with the compounds whose hydrochlorides could not be prepared, were verified by glc using one of the following columns: PEGA, QF1, FFAP, or SE30. Still other hydrochlorides melted over a 5–10°C range but elemental analysis gave values in good agreement with those calculated.

Benzoic acid (Fisher, 'Primary Standard') was used without further purification. Pyridine (Fisher, Certified) was distilled from potassium hydroxide pellets and stored over molecular sieves, bp 117°C (lit. (28) bp 115°C). The hydrochloride was prepared by dissolving the base in ether and bubbling in dry hydrogen chloride until precipitation was complete. The hygroscopic hydrochloride was recrystallized from chloroform – ethyl acetate. The following substituted 2-picolines were commercially available: 2-picoline (Aldrich, hydrochloride hygroscopic), 2-ethylpyridine (Reilly, hydrochloride hygroscopic), 2-*n*-propylpyridine (Reilly, hydrochloride mp 127.5–128.5°C), 2-benzylpyridine (Reilly, hydrochloride mp 106–108°C), 2-picolylamine (2-pyridinemethanamine, Aldrich, monohydrochloride mp 128–129°C), 2-chloromethylpyridine hydrochloride (Baker, mp 121–122.5°C), 2-pyridylcarbinol (2-pyridinemethanol, Aldrich, hydrochloride mp 107–108.5°C). 2-Trimethylsilylpyridine was supplied by Dr. M. W. Morgan, University of Victoria. Hydrochlorides were prepared as described above for pyridine and were purified by recrystallization from chloroform – ethyl acetate or from methanol – ethyl acetate and/or by sublimation. These liquid compounds which were used in the free base form in the p*K* measurements were distilled and middle fractions collected.

2-Bromomethylpyridine hydrobromide was prepared by reacting 2-pyridylcarbinol with PBr_3 (29). After recrystallization from anhydrous ethanol followed by sublimation the hydrobromide had mp 147–148.5°C (lit. (29) mp 145–146°C).

Phenyl 2-picolyl sulfone was prepared in 78% yield from 2-chloromethylpyridine hydrochloride by reaction with sodium benzene sulfinate (30). The product was recrystallized from anhydrous ethanol, mp 110–112.5°C (lit. (30) mp 111.5–112.5°C); nmr ($CDCl_3$) τ: 1.58 (m, 1, 6-*H*), 2.40 (m, 8, C_6H_5, 3-*H*, 4-*H* and 5-*H*), 5.44 (s, 2, CH_2).

2-Pyridinemethanethiol. A solution of 2-chloromethylpyridine hydrochloride (16.5 g) and thiourea (81 g) in ethanol (75 cm^3) was refluxed for 6 h. Filtration and recrystallization from methanol afforded 2-pyridylmethyl isothiuronium chloride hydrochloride in 84% yield. A solution of the hydrochloride (18 g) in water (25 cm^3) was treated with sodium hydroxide and then acidified to pH 6 with acetic acid. The solution was extracted with ether and the 2-pyridinemethanethiol was obtained in 18% yield after distillation at 35–40°C under reduced pressure (lit. (31) bp 57–58°C/80 Pa); nmr τ: 1.60 (m, 1, 6-*H*), 2.73 (m, 3, 3-*H*, 4-*H* and 5-*H*), 6.3 (d, 2, $J = 13.0$ Hz, CH_2, becomes singlet on D_2O exchange), 7.95 (t, 1, S*H*, removed on D_2O exchange); mass spectrum (70 eV) *m*/*e* (relative intensity): 125 (41, M_r (C_6H_7NS) = 125), 124(27), 93(100), 92(27), 66(37), 65(24), 39(25). The hydrochloride was sublimed but was too hygroscopic to give a sharp mp.

2-Pyridylmethyl acetate (2-pyridinemethanol acetate ester). 2-Pyridylcarbinol (21.8 g, 0.2 mol) was heated with acetic anhydride (61.2 g, 0.6 mol) for 3 h at 145°C. The resulting solution was concentrated, diluted with water (50 cm^3), and

Can. J. Chem. Downloaded from www.nrcresearchpress.com by 210.87.254.6 on 09/05/12
For personal use only.

then made weakly basic with solid potassium carbonate. Following extraction with $CHCl_3$, the acetate was distilled at 80–90°C under reduced pressure (lit. (32) bp 103–104°C/2 kPa) and was obtained in 78% yield; nmr τ: 1.50 (m, 1, 6-*H*), 2.41 (m, 1, 4-*H*), 2.81 (m, 2, 3-*H* and 5-*H*), 4.88 (s, 2, CH_2), 7.95 (s, 3, CH_3); mass spectrum (70 eV) *m/e* (relative intensity): 109(63), 108(100, $M - COCH_3$), 92(13), 80(12), 79(16), 78(14), 65(12), 43(28). Attempts at the preparation of the hydrochloride resulted in decomposition of the compound.

Ethyl-2-pyridylacetate was prepared by esterification of 2-pyridylacetic acid hydrochloride (33). The acid hydrochloride was added to a cold mixture of concentrated sulfuric acid and absolute ethanol. The product was obtained in 75% yield after distillation at 95°C under reduced pressure (lit. (34) bp 109–112°C/0.8 kPa); nmr τ: 1.54 (m, 1, 2-*H*), 2.46 (m, 1, 4-*H*), 2.91 (m, 2, 3-*H* and 5-*H*), 5.90 (q, 2, $J = 7.0$ Hz, CH_2CH_3), 6.29 (s, 2, CH_2CO), 8.82 (t, 3, CH_2CH_3); mass spectrum (70 eV) *m/e* (relative intensity): 165 (27, M_r ($C_9H_{11}NO_2$) = 165), 20(38), 93(100), 92(86), 65(23), 39(18), 29(46). The attempted preparation of the hydrochloride resulted in partial hydrolysis of the compound.

Methyl 2-pyridylacetate was prepared by a similar method to that used for the ethyl ester. It was obtained in 67% yield after distillation at 100°C under reduced pressure (lit. (34) bp 122–125°C/2.8 kPa); nmr τ: 1.54 (m, 1, 6-*H*), 2.40 (m, 1, 4-*H*), 2.83 (m, 2, 3-*H* and 5-*H*), 6.28 (s, 2, CH_2), 6.41 (s, 3, CH_3). The hydrochloride was recrystallized from methanol – ethyl acetate and had mp 163–164°C; mass spectrum (70 eV) *m/e*: (relative intensity) 151 (3, M_r ($C_8H_9NO_2$) = 151), 136(3), 120(6), 119(5), 106(10), 93(76), 92(100), 79(15), 65(95), 39(50).

Methyl 2-picolyl sulfone. Methanesulfonyl chloride (114 g, 1 mol) was treated successively with hydrazine hydrate (50 g, 1 mol) and a solution of sodium hydroxide (80 g, 2 mol) in water (500 cm^3) (35). The reaction mixture was evaporated to dryness and the residue was dissolved in anhydrous ethanol and refluxed for 2 h. The sodium chloride formed was removed by filtration and the filtrate evaporated to give the sodium salt of methanesulfinic acid (62 g). A mixture of methanesulfinic acid sodium salt (13 g), sodium acetate (16 g) 2-chloromethylpyridine hydrochloride (16.4 g), and 1-butanol (70 cm^3) was refluxed for 5 h. After cooling, the mixture was poured into water (700 cm^3) and extracted with chloroform. After removal of the chloroform and 1-butanol, the residue was recrystallized from anhydrous ethanol. Sublimation gave methyl 2-picolyl sulfone (60%), mp 121–122°C; nmr ($CDCl_3$) τ: 1.40 (m, 1, 6-*H*), 2.49 (m, 3, 3-*H*, 4-*H*, and 5-*H*), 5.55 (s, 2, CH_2), 7.10 (s, 3, CH_3); mass spectrum (70 eV) *m/e* (relative intensity): 156.008 (19, M_r ($^{12}C_6{}^1H_6{}^{14}N^{32}S^{16}O_2$) = 156.012, $M - CH_3$), 93(26), 92(100), 65(33), 39(15). *Anal.* calcd. for $C_7H_9NSO_2$: C 49.07, H 5.31, N 8.19; found: C 49.16, H 5.23, N 7.93.

Ethyl 2-picolyl sulfone. The sodium salt of ethanesulfinic acid was prepared in the same manner as the methane derivative. Reaction with 2-chloromethylpyridine hydrochloride and sodium acetate afforded the sulfone in 48% yield after recrystallization from anhydrous ethanol, followed by sublimation. The sulfone had mp 104–105°C (lit. (31) mp 105°C); nmr ($CDCl_3$) τ: 1.40 (m, 1, 6-*H*), 2.48 (m, 3, 3-*H*, 4-*H* and 5-*H*), 5.70 (s, 2, CH_2), 6.99 (q, 2, $J = 7.6$ Hz, CH_2CH_3), 8.62 (t, 3, CH_2CH_3); mass spectrum (70 eV) *m/e* (relative intensity): 156.009 (12, M_r ($^{12}C_6{}^1H_6{}^{14}N^{32}S^{16}O_2$) = 156.012, $M - C_2H_5$), 93(56), 92(100), 65(20), 39(14).

2-Pyridylacetonitrile was prepared by the reaction of 2-chloromethylpyridine hydrochloride with sodium cyanide in DMSO (36) and was obtained in 36% yield after distillation at 88–90°C under reduced pressure (lit. (36) bp 118–120°C/1.7 kPa); nmr τ: 1.49 (m, 1, 6-*H*), 2.52 (m, 3, 3-*H*, 4-*H* and 5-*H*), 6.12 (s, 2, CH_2). The hydrochloride was prepared and recrystallized from anhydrous ethanol and then sublimed. The compound decomposed on heating above 125°C and had mass spectrum (70 eV) *m/e* (relative intensity): 118 (64, M_r ($C_7H_6N_2$) = 118), 91(26), 78(100), 64(23), 51(57), 36(68). *Anal.* calcd. for $C_7H_7H_2Cl$: C 54.35, N 18.13, H 4.56; found: C 54.13, N 18.32, H 4.49.

2-Methoxymethylpyridine was prepared from 2-chloromethylpyridine hydrochloride by refluxing with sodium methoxide (37). It was obtained in 43% yield after distillation at 24–26°C under reduced pressure (lit. (37) bp 76–78°C/2.4 kPa); nmr τ: 1.55 (m, 1, 6-*H*), 2.68 (m, 3, 3-*H*, 4-*H*, and 5-*H*), 5.50 (s, 2, CH_2), 6.61 (s, 3, OCH_3); mass spectrum (70 eV) *m/e* (relative intensity): 93(100), 92(14), 78(15), 66(15), 65(19). The hydrochloride was prepared and sublimed but was too hygroscopic to obtain a satisfactory melting point.

2-Pyridylacetone (1-(2-pyridinyl)-2-propanone). Phenyllithium was prepared under a N_2 atmosphere in 80% yield, from lithium (14.7 g, 2.1 mol) and bromobenzene (157 g, 1 mol). A solution of diisopropylamine (101 g, 1 mol) in anhydrous ether (50 cm^3) was added at such a rate that the ether refluxed gently. A solution of 2-picoline (93 g, 1 mol), previously dried over KOH pellets, in ether (50 cm^3) was added, followed by a solution of methyl acetate (74 g, 1 mol) in ether (50 cm^3). The reaction mixture was then refluxed for an additional 3 h. Water (250 cm^3) was added and the mixture was extracted several times with ether. After drying the combined extracts ($MgSO_4$) and evaporation of the ether, 2-pyridylacetone (34 g) was obtained in 26% yield after distillation under reduced pressure (lit. (38) bp 101°C/1.3 kPa). The hydrochloride was prepared and purified by recrystallization from anhydrous ethanol, followed by sublimation. It had mp 125–126°C; nmr (CF_3CO_2H) τ: 1.6 (m, 4, 3-*H*, 4-*H*, 5-*H* and 6-*H*), 5.43 (s, 2, CH_2), 7.47 (s, 3, CH_3); mass spectrum (70 eV) *m/e* (relative intensity): 135 (15, M_r (C_8H_9NO) = 135), 120(14), 93(100), 92(27), 66(18), 65(18), 43(30), 36(18).

2-Phenacylpyridine (1-phenyl-2-(2-pyridinyl)ethanone) was prepared by the reaction of the 2-picolyl anion, formed from 2-picoline and phenyllithium, with methylbenzoate. The liquid was distilled at 150–155°C under reduced pressure (lit. (39) bp 145–153°C/0.3 kPa) to give a heavy yellow liquid which solidified on standing. The product was recrystallized from petroleum ether and then sublimed. It had mp 50–52°C (lit. (39) mp 52.5–54°C); nmr τ: 1.60 (m, 1, 6-*H*), 2.6 (m, 8, C_6H_5, 3-*H*, 4-*H* and 5-*H*), 4.0 (s, 1, $CH{=}C$, removed after prolonged D_2O exchange), 5.59 (s, 1, OH, removed on D_2O exchange).

C-Methylation product of 2-phenacylpyridine. A solution of 2-phenacylpyridine (10 g, 0.05 mol) in methanol was added to a solution of sodium methoxide (from 1.25 g of sodium) and to this mixture methyl iodide (7.0 g) was added. After refluxing the solution on a water bath for 1 h the methanol was evaporated. After the addition of water, the solution was extracted (×3) with ether. The ether was evaporated and the α-benzoyl-2-ethylpyridine distilled at 115–120°C under reduced pressure; nmr τ: 5.08 (q, 1, $J = 7.0$ Hz, $CHCH_3$), 8.50 (d, 3, $CHCH_3$).

O-Methylation product of 2-phenacylpyridine. Potassium *tert*-butoxide (5.6 g, 0.05 mol) was dissolved in anhydrous DMSO (100 cm^3). After addition of 2-phenacylpyridine (10 g, 0.05 mol) and dimethyl sulfate (6.3 g, 0.05 mol) the mixture was stirred for 2 h. Water was added and the mixture was extracted several times with methylene chloride. The combined extracts were dried ($MgSO_4$) and after evaporation of the solvent a heavy dark oil remained. On standing for 3 days α-methoxy-β-2-pyridylstyrene separated and was recrystallized from anhydrous ethanol. It had mp 125–126°C; nmr ($CDCl_3$) τ: 4.40 (s, 1, CH), 6.61 (s, 3, $O{-}CH_3$).

Can. J. Chem. Downloaded from www.nrcresearchpress.com by 210.87.254.6 on 09/05/12
For personal use only.

2-Thiocyanatomethylpyridine hydrochloride. A solution of 2-chloromethylpyridine hydrochloride (8.2 g) in benzene (8 cm^3) was added to a boiling solution of potassium thiocyanate (5 g) in acetone (50 cm^3) and the mixture was heated on a steam bath for 2.5 h (31). The precipitated potassium chloride and excess potassium thiocyanate were filtered from the hot mixture. On cooling the filtrate, 2-thiocyanatomethylpyridine hydrochloride separated and was recrystallized from methanol mp 163–165°C (lit. (40) mp 167–170°C). *Anal.* calcd. for $C_7H_7N_2SCl$: C 45.01, N 15.02, H 3.78; found: C 44.87, N 15.37, H 3.78.

2-Methylthiomethylpyridine. Methanethiol (9.8 g, 0.2 mol) and 2-chloromethylpyridine hydrochloride (16.4 g, 0.1 mol) were added to a solution of sodium ethoxide (from 4.6 g, 0.2 mol sodium) in ethanol (100 cm^3) and the mixture was heated on a steam bath for 2 h. After removal of the solvent, the residue was distilled at 90°C under reduced pressure (lit. (41) bp 100–105°C/2.3 kPa) to give a 73% yield of product which had nmr τ: 1.60 (m, 1, 6-*H*), 2.69 (m, 3, 3-*H*, 4-*H* and 5-*H*), 6.31 (s, 2, CH_2), 8.04 (s, 3, CH_3). The hydrochloride was prepared and recrystallized from methanol, mp 137–138.5°C; mass spectrum (70 eV) *m/e* (relative intensity): 93(100), 92(15), 65(23), 64(17), 39(17), 36(13).

2-Acetamidomethylpyridine (N-2-pyridinylmethylacetamide). Acetic anhydride (30 cm^3) was added to cold 2-aminomethylpyridine (18 g). The resulting solution was poured into water and then extracted with chloroform. After evaporation of the chloroform and distillation at 145°C under reduced pressure, 2-acetamidomethylpyridine was obtained in 56% yield (lit. (42) bp 160–163°C/0.7 kPa). The product solidified upon standing and was recrystallized from benzene – petroleum ether, mp 56.5–57°C (lit. (42) mp 59–60°C); nmr ($CDCl_3$) τ: 1.51 (m, 1, 6-*H*), 1.78 (m, 1, N*H*), 2.38 (m, 1, 4-*H*), 2.77 (m, 2, 3-*H* and 5-*H*), 5.50 (d, 2, J = 5.5 Hz, CH_2), 8.04 (s, 3, CH_3); mass spectrum (70 eV) *m/e* (relative intensity): 150 (20, M_r ($C_8H_{10}N_2O$) = 150), 149(24), 135(12), 107(100), 92(33), 80(17), 79(15), 43(14).

2-Methylaminomethylpyridine (N-methyl-2-pyridinemethanamine). A solution of 2-chloromethylpyridine hydrochloride (46.8 g) in ethanol (300 cm^3) was added to an ice-cold 40% aqueous solution of methylamine (300 g) and the resulting solution was stirred at room temperature for 1 h and then heated at 90°C for 1 h. The solution was saturated with solid potassium hydroxide and extracted with ether–chloroform. The product was obtained in 70% yield after distillation at 70–73°C under reduced pressure. It had nmr τ: 1.50 (s, 1, 6-*H*), 2.71 (m, 3, 3-*H*, 4-*H* and 5-*H*), 6.23 (s, 2, CH_2), 7.65 (s, 3, CH_3), 8.18 (s, 1, N*H*, removed by D_2O); mass spectrum (70 eV) *m/e* (relative intensity): 119(29), 93(100), 92(38), 80(22), 65(18), 44(40). The dipicrate was recrystallized from 95% ethanol, mp 178–180°C. *Anal.* calcd. for $C_{19}H_{16}N_8O_{14}$: C 39.30, N 19.31, H 2.78; found: C 39.04, N 19.24, H 2.60.

2-Dimethylaminomethylpyridine (N,N-dimethyl-2-pyridinemethanamine) was prepared from 2-aminomethylpyridine by reaction with 90% formic acid and 37% aqueous formaldehyde solution according to the method described for the 3-isomer (43). The product was obtained in 38% yield after distillation at 56–58°C under reduced pressure (lit. (44) bp 195°C); nmr τ: 1.58 (m, 1, 6-*H*), 2.52 (m, 2, 3-*H*, 4-*H*), 2.93 (m, 1, 5-*H*), 6.43 (s, 2, CH_2), 7.80 (s, 6, CH_3); mass spectrum (70 eV) *m/e* (relative intensity): 93(100), 92(23), 65(18), 58(36), 42(14).

2-Phenylthiomethylpyridine was prepared from 2-chloromethylpyridine hydrochloride and benzenethiol in the presence of base (45) and was obtained in 86% yield after distillation at 145–150°C under reduced pressure (lit. (45) bp 123–127°C/0.5 kPa); nmr τ: 1.66 (m, 1, 6-*H*), 2.80 (m, 8, 3-*H*, 4-*H*, 5-*H* and C_6H_5), 5.83 (s, 2, CH_2). The hydrochloride was recrystallized from anhydrous ethanol–ether, followed by sublimation, mp 128–130°C (lit. (45) mp 137–138°C).

2-Phenoxymethylpyridine was prepared from 2-chloromethylpyridine hydrochloride by reaction with sodium phenoxide in methanol (46). It was distilled at 165°C under reduced pressure (lit. (46) bp 140–143°C/70 Pa). The product solidified on standing. The hydrochloride was purified by sublimation and had mp 90–92°C; nmr (CF_3CI_2H) τ: 1.55 (m, 2, 3-*H*, 6-*H*), 2.35 (m, 2, 4-*H*, 5-*H*) 3.30 (m, 5, C_6H_5). 4.90 (s, 2, CH_2); mass spectrum (70 eV) *m/e* (relative intensity): 185 (4, M_r ($C_{12}H_{11}NO$) = 185), 184(4), 94(33), 92(48), 78(45), 66(27), 65(63), 51(35), 39(51), 36(100).

2-N-Acetylmethylaminomethylpyridine (N-methyl-N-2-pyridinylmethylacetamide). 2-Methylaminomethylpyridine (12 g) was heated with acetic anhydride (15 cm^3) for 30 min. The solution was diluted with water, made strongly alkaline with solid sodium hydroxide and then extracted with chloroform. The product was obtained in 75% yield after distillation at 140–145°C under reduced pressure and had mass spectrum (70 eV) *m/e* (relative intensity): 121(17), 94(21), 93(100), 92(18), 65(12), 44(17). The picrate was recrystallized from 95% ethanol, mp 158–160°C. *Anal.* calcd. for $C_{15}H_{15}N_5O_8$: C 45.78, N 17.81, H 3.84; found: C 45.58, N 18.02, H 3.74.

The hydrochloride was sublimed and had mp 127–129°C; nmr (CF_3CO_2H) τ: 1.70 (m, 2, 3-*H* and 6-*H*), 2.35 (m, 2, 4-*H* and 5-*H*), 5.36 (s, 2, CH_2), 7.17 (s, 3, N-CH_3), 8.03 (s, 3, $COCH_3$).

2-Nitromethylpyridine. Sodium 2-picolylnitronate was prepared from 2-picoline, sodium amide, and *n*-propylnitrate (47). The crude sodium salt was acidified with glacial acetic acid and the product was extracted with chloroform. Distillation of the chloroform extract under reduced pressure resulted in a violent explosion. In a subsequent preparation the compound was purified by chromatography on silica gel and elution with ether–chloroform (1:1 v/v) before distillation at 90–95°C under reduced pressure (lit. (47) bp 70°C/30 Pa). On standing a few days the compound darkened considerably and was chromatographed again before use. The picrate was recrystallized from 95% ethanol and had mp 136–138°C (lit. (47) mp 152°C). *Anal.* calcd. for $C_{12}H_9N_5O_9$: C 39.24, N 19.07, H 2.47; found: C 39.02, N 18.72, H 2.47.

Apparatus

Potentiometric titrations were carried out in aqueous solution at 25.0 ± 0.1°C using a glass electrode (Beckman #39000) and a calomel reference electrode (Beckman #39071). Water from a Calora constant temperature bath was circulated through the water jacket of the titration cell to maintain constant temperature during a titration. Electromotive force values were measured using an electrometer (Keithley model 610C) fitted with a pH electrode adaptor (Keithley model 6107) and the values are read out using a digital voltmeter (Vidar 520). The titrant was added from an autoburette (Radiometer model ABU11). Standardization of electrode potentials was carried out using the buffers (48): saturated potassium hydrogen tartrate (pH 3.557 at 25°C), potassium hydrogen phthalate (0.05 mol kg^{-1}, pH 4.008 at 25°C), equimolar potassium dihydrogen phosphate – disodium hydrogen phosphate (each 0.025 mol kg^{-1}, pH 6.865 at 25°C), borax (0.01 mol kg^{-1}, pH 9.180 at 25°C), and potassium tetroxalate (0.05 mol kg^{-1}, pH 1.679 at 25°C). Before and after each potentiometric titration the emf readings of buffers which encompassed the range of pH values to be measured were determined and the mean of the before and after readings used in the pH calculation (below). Normally the emf values for the standard buffers before and after a run agreed to within a few tenths of

Can. J. Chem. Downloaded from www.nrcresearchpress.com by 210.87.254.6 on 09/05/12
For personal use only.

a millivolt. If the values differed by more than 1 mV or if the emf differences between the two standard buffers differed by more than 1 mV the run was discarded. The pH values were obtained from [1] where pH_1 and E_1 are the pH value and emf reading of standard buffer 1, pH_2 and E_2 are the pH value and emf reading of standard buffer 2, and pH_3 is the unknown pH value and E_3 the emf reading of the titration solution:

$$[1] \quad pH_3 = pH_1 + (pH_2 - pH_1)(E_3 - E_1)(E_2 - E_1)^{-1}$$

The pK values of those compounds which could not be measured by potentiometric titration were determined by uv spectrophotometry at 25.0 ± 0.2°C. Absorbance values were measured with a Cary model 17 uv spectrometer.

Solutions

Potassium tetroxalate and potassium hydrogen phthalate were BDH AnalaR. Potassium hydrogen tartrate, disodium hydrogen phosphate and potassium dihydrogen phosphate were Fisher Certified and sodium borate was Baker Analyzed. Solutions were prepared in distilled deionized water of conductivity < 0.2 mS m^{-1} (48). A small amount of thymol was added to the tartrate solution to retard mold growth. Buffer solutions were freshly prepared every 4 weeks.

Sodium hydroxide and hydrochloric acid solutions (0.5 mol dm^{-3}) used in potentiometric titrations were prepared from concentrated volumetric solutions (BDH) and standardized against potassium hydrogen phthalate and anhydrous sodium carbonate, respectively.

Formic acid (BDH AnalaR) was stirred with boric anhydride and then distilled, bp 100–101°C (lit. (28) bp 100.5°C). Acetic acid (Baker Analyzed) was purified by heating with chromium trioxide and acetic anhydride (49) and fractionally distilled, bp 118–119°C (lit. (49) bp 118°C). Aqueous solutions (0.1 mol dm^{-3}) were prepared by weight and standardized with sodium hydroxide (0.1 mol dm^{-3}). For each acid seven buffer solutions were prepared containing 10 mmol dm^{-3} of the formate (acetate) and from 3–40 mmol dm^{-3} of formic acid (acetic acid) by combining the calculated weights of the standard solution of the acid with a fixed weight of standard sodium hydroxide. Succinic acid (BDH AnalaR) was recrystallized twice from acetone and dried under reduced pressure (49). A series of 10 buffers was prepared by dissolving 5 mmol of the acid in 60–100 cm^3 of aqueous sodium hydroxide (0.1 mol dm^{-3}) followed by dilution to 500 cm^3. These acidic buffers were used in the spectrophotometric pK determinations.

A series of 15 aqueous hydrochloric acid solutions of known concentrations ranging from 0.6–400 mmol dm^{-3} was prepared by dilution from concentrated volumetric solution (BDH). These solutions were used in the spectrophotometric pK determinations of those picolinium ions which were too acidic to be measured by the potentiometric method.

*Measurement of p*K *Values*

For dissociation of the acid HB in aqueous solution pK is given by [2]:

$$[2] \quad pK_{HB} = -\log a_H - \log([B]/[HB]) - \log f_B + \log f_{HB}$$

Most pK values were determined by potentiometric titration (50) but some values not accessible by this method were determined by spectrophotometry (50). In the majority of cases titration of an aqueous solution (100 cm^3) of the picoline hydrochloride (1 mmol) with standard sodium hydroxide (0.5 mol dm^{-2}) was preferred to titration of the picoline with hydrochloric acid because (in these cases) the hydrochloride could be readily purified on a small scale by vacuum sublimation immediately before use. The free bases were liquids and small scale distillation was less convenient than sublimation. In some other cases the substituent group, e.g., ethoxycarbonyl, was not stable to hydrogen chloride gas under the conditions used for preparation of the hydrochlorides. In such cases and other cases where the hydrochloride could not be obtained pure (most diacidic bases) the picoline, if sufficiently soluble in water, was titrated with hydrochloric acid. Some picolines were not soluble at 10 mmol dm^{-3} and concentrations of 5 mmol dm^{-3} or 2.5 mmol dm^{-3} were used. For less soluble compounds the potentiometric titration method is unsuitable and pK values of these picolines were determined by the spectrophotometric method using appropriate buffers. For those compounds whose pK values were well beyond the limits of the potentiometric method (p$K < 2.5$) the value was determined by the spectrophotometric method in hydrochloric acid solutions.

In the titration the emf of the cell containing the solution being titrated was measured after each successive addition of 0.2 cm^3 of titrant until 1.8 cm^3 had been added. In the cases in which the hydrochloride was titrated with sodium hydroxide the solution was finally titrated to three emf values in the range 125–175 mV past the half-neutralization emf reading and the pair of consistent (±0.5%) titre values from this set were averaged to give the end-point titre (t_f). Generally this value agreed with that calculated from the known weight of hydrochloride taken to about 1%. The small discrepancy is attributed to the difficulty in accurately weighing the hygroscopic hydrochlorides and the value of t_f, rather than the initial weight of hydrochloride, was used in deriving the pK value.

In the calculation of the pK value from the emf readings and titration values it was assumed that $-\log a_H = pH$, that activity coefficients were given by the Güntelberg extension of the Debye–Hückel limiting law (51), [3] (I is ionic strength), and that $f_0 = 1$, $f_- = f_+$, $f_{+2} = 4f_+$.

$$[3] \quad -\log f_+ = 0.509\, I^{1/2}/(1 + I^{1/2})$$

It follows that the H^+ and OH^- concentrations are given by [4] and [5]

$$[4] \quad [H^+] = f_+^{-1}\, 10^{-pH}$$

$$[5] \quad [OH^-] = f_+^{-1}\, 10^{(pH - 14)}$$

From the condition for electroneutrality of the titrated solution, the conservation of the sum of the amounts of B and HB, the fact that $[OH^-]$ is negligible for $pH < 7$ and that $[H^+]$ is negligible for $pH > 7$ expressions were derived relating I, [B], and [HB] to the titration values. These expressions take different forms, according to whether a neutral acid (p$K < 7$) is titrated with sodium hydroxide (I), a univalent cationic acid (p$K < 7$) is titrated with sodium hydroxide (II), a univalent cationic acid (p$K > 7$) is titrated with sodium hydroxide (II*a*), a neutral base (p$K < 7$) is titrated with hydrochloric acid (III), a neutral diacidic base ($pK_1 < 7 < pK_2$) is titrated with hydrochloric acid (IV), or a divalent cationic dibasic acid ($pK_1 < 7 < pK_2$) is titrated with sodium hydroxide (V). For case I, applicable to benzoic acid, the relevant expressions are as follows where n = concentration (mol dm^{-3}) of titrant, t = volume (cm^3) of titrant added, t_f is the end-point titre, v = initial volume (cm^3) of the solution being titrated:

$$I = nt/(v + t) + [H^+]$$

$$[B] = nt/(v + t) + [H^+]$$

$$[HB] = n(t_f - t)/(v + t) - [H^+]$$

Related expressions apply to the other cases cited. For each emf/titre pair I was calculated by an iterative method starting

Can. J. Chem. Downloaded from www.nrcresearchpress.com by 210.87.254.6 on 09/05/12
For personal use only.

with the assumption that $[H^+] = 0$ (or $[OH^-] = 0$, as appropriate) and then calculating $[H^+]$ from [4] (or $[OH^-]$ from [5]) and repeating the cycle until the difference between successive values of I was insignificant: the final value of I was then used to calculate $[H^+]$ from [4] (or $[OH^-]$ from [5]), [B], [HB], and finally pK_{HB}.

Each titration run generated nine pairs of emf readings and titre values from which nine values of the pK could be calculated. The calculations were carried out on a computer. The program determined the mean pK value for the run, the deviations of the individual pK values, and rejected the pK value corresponding to the largest deviation if the modulus of the latter was greater than 0.03, recalculated a new mean and new deviations, and repeated this cycle until no deviation was larger than 0.03. In only 53 of 265 titration runs (involving $9 \times 265 = 2385$ pK calculations) was more than one value rejected.[3] The majority of the 53 runs involved situations in which a lower precision could be expected such as determination of the second pK of a dibasic acid or determination of a pK value close to the limit of the potentiometric method (~ 2.5). Thus although measurements were made over the range of [B]/[HB] from 9:1 to 1:9 excellent precision was achieved. A minimum of three titration runs was made for each compound. There was excellent agreement between the pK values determined in triplicate. In 88 sets of triplicate pK values two sets covered a range of 0.04 pK units and two a range of 0.03 pK units. Three of these sets involved the determination of second pK values of dibasic divalent cationic acids. For all other sets the pK values covered a range of 0.02 or less. The root-mean-square deviation of all pK values measured by the potentiometric method was less than 0.01.

For spectrophotometric pK determinations a solution of known concentration of the acid HB (or base B) was prepared in distilled deionized water. To obtain the spectra of both acid and base forms of the pyridine, absorbances were measured for the compound in hydrochloric acid (5 mmol dm^{-3}) and sodium hydroxide (5 mmol dm^{-3}) over the range 200–300 nm, and the wavelength at which the two spectra differed the most was chosen as the analytical wavelength. Equal volumes (5 cm^3) of the solutions of the pyridine and acid (10 mmol dm^{-3}) were mixed and the absorbance of the solution at the analytical wavelength was recorded. This was repeated twice more and the mean of the three values was taken as the absorbance of the protonated form D_{HB}. A similar procedure using sodium hydroxide solution[4] gave the absorbance of the basic form, D_B. Finally, the absorbance (D) of the pyridine in a series of buffer solutions whose pH encompassed the pK of HB was determined. From the indicator ratio, $i = [B]/[HB^+] = (D - D_{HB})/(D_B - D)$, the individual values of [B] and $[HB^+]$ could be obtained since the sum of the concentrations was known. From the electroneutrality condition, the fact that $[OH^-]$ is negligible ($pH < 7$) the conservation of the sum of the amounts of the buffer acid HA and its conjugate base A, the expressions for the dissociation of the indicator acid HB and the buffer acid HA, expressions for I, $[H^+]$, the buffer ratio [A]/[HA] and pK_{HB} can be derived. A number of cases can arise requiring different forms for the equations depending upon the charge type of HA and HB and whether HB or B is added to the buffer mixture. For the case of neutral substrate base B and neutral buffer acid HA (acetic and formic acids were used) eqs. [6], [7], and [8] are applicable (the superscript asterisk denote a stoichiometric concentration).

$$[6] \qquad I = [{}^*A^-] + [HB^+] + [H^+]$$

$$[7] \qquad [H^+] = f_+^{-1} f_-^{-1} 10^{-pK_{HA}} [HA]/[A^-]$$

$$[8] \qquad pK_{HB} = pK_{HA} + \log([A^-]/[HA]) - \log([B]/[HB^+]) + \log f_- + \log f_+$$

The buffer ratio is given by [9], for the case (VI) where the picoline was added as its hydrochloride, and by [10] for case (VI*a*) when the picoline itself was the substrate

$$[9] \qquad [A^-]/[HA] = ([{}^*A^-] - [B] + [H^+])/([{}^*HA] + [B] - [H^+])$$

$$[10] \qquad [A^-]/[HA] = ([{}^*A^-] + [HB^+] + [H^+])/([{}^*HA] - [HB^+] - [H^+])$$

The values of I and $[H^+]$ can be determined by iteration over the cycle [6], [9], [7] (or [6], [10], [7]), starting from $[H^+] = 0$, although in practice the cycle [6], [7] was used since I was determined with sufficient accuracy if $[H^+]$ was evaluated from [7] on the assumption that $[HA]/[A^-] = [{}^*HA]/[{}^*A^-]$. The calculations were carried out on a computer and individual pK values which deviated by more than 0.05 from the mean pK value for a run were rejected and a new mean calculated. Runs were carried out in duplicate.

The buffer action of the second dissociation of succinic acid was used in determining the pK values of the trimethylsilylpyridines (case VII). In principle it is possible to calculate pK_{HB} from an equation similar to [8] where HA and A are the monoanion and dianion, respectively, of succinic acid. However, a complicated set of iterations is necessary to take account of the effect of the first dissociation equilibrium for succinic acid on the concentrations of the mono- and dianions. In practice the pH of the succinic acid buffers was determined by the potentiometric method and pK_{HB} was then evaluated from [11]

$$[11] \qquad pK_{HB} = pH - \log([B]/[HB^+]) + \log f_+$$

A few calculations were also carried out using the measured pH and the first dissociation constant to evaluate the ratio of succinic acid to monoanion and then using the electroneutrality condition and the conservation of succinic acid plus its two anions to evaluate the concentrations of the mono- and dianions. These values on substitution into [8] gave pK_{HB} values which agreed with those evaluated from [11] to better than 0.01 pK units.[5]

For those picolinium ions for which pK was less than 2.5, standard solutions of hydrochloric acid were used to fix the hydrogen ion concentration (case VIII). The indicator ratios (D_{HB} was measured in hydrochloric acid of concentration 1 mol dm^{-3} and D_B was measured in phosphate buffer) were determined and pK_{HB} evaluated from [12]

$$[12] \qquad pK_{HB} = -\log[H^+] - \log([B]/[HB]) - \log(f_B/f_{HB})$$

The pK obtained using activity coefficients derived from the Güntelberg extension of Debye–Hückel limiting law were regressed against I to find pK_{HB} at $I = 0$.

Results

The pK values determined for benzoic acid and for

[3]The statistics relate to data for α-substituted 2-, 3-, and 4-picolines. There was no noticeable variation of the precision between the three series.

[4]In the case of dibasic acids for which $pK_1 < 7 < pK_2$ the absorbance of the base form for pK_1 (the half acid) was determined in phosphate buffer.

[5]For succinic acid $pK_1 = 4.21$, $pK_2 = 5.64$ (52).

Can. J. Chem. Downloaded from www.nrcresearchpress.com by 210.87.254.6 on 09/05/12
For personal use only.

pyridinium ion, from individual runs, are shown in Table 1 and pK values for substituted 2-picolines are shown in Table 2. 2-Thiocyanatomethylpyridine reacted with water, as indicated by emf and uv readings which changed rapidly with time. Its pK value could not be determined.

Accuracy of pK *Values*

The validity of the assumption that $-\log a = \text{pH}$ is limited to ± 0.02 pH units and this in turn sets a similar limit to the accuracy of pK values derived by the potentiometric method. The precision of the potentiometric pK values is rather better than this (see Experimental). Dissociation constants measured by uv spectrophotometry in buffer solutions were reproducible to ± 0.02 pK units. However, 2-trimethylsilylmethylpyridine reacted in solution and was particularly unstable in acid solution. The concentrations of the hydrochloric acid and sodium hydroxide solutions used for determining D_{HB} and D_B were reduced to 1 mmol dm^{-3} and absorbance readings, which changed with time, were recorded over 2 min and extrapolated back to zero time. The pK of this compound is therefore of lower reliability (± 0.1). The pK values measured in hydrochloric acid solutions were determined by an extrapolation technique. Because of a significant variation in the calculated pK values with ionic strength, these values are also less accurate (± 0.1) although the reproductivity of the measurements was rather better than this. As a check on the accuracy of the potentiometric method, the pK value of benzoic acid was determined (Table 1). The mean value (4.22) agrees with the accepted literature value (4.20) to within the limits of accuracy (± 0.02). The literature value is the mean of eight thermodynamic values measured by conductance and eight thermodynamic values measured by potentiometry (53).

The measurement of the acid dissociation constant of pyridinium ion (Table 1) by potentiometric titration of the hydrochloride with sodium hydroxide (5.20) potentiometric titration of the free base with hydrochloric acid (5.18) and by uv spectrophotometry (5.19) provides a check on the reproducibility of the pK values obtained by different methods. This reproducibility is further established by the pK value for ethyl 2-picolyl sulfone measured by titration of the hydrochloride (2.52) and by titration of the free base (2.51) and by that for 2-pyridinemethanethiol for which the corresponding values are 4.40 and 4.39.

Inductive Substituent Constants (σ_I Values)

Correlation of the $-$pK values with σ_I values (15) gave, for $n = 13$, slope $\rho_I = 5.449$, intercept $-pK_0 = -5.81$, correlation coefficient $r = 0.991$, standard deviation $s = 0.15$, standard deviation of the slope $s_\rho = 0.23, f = 0.07$.[6] The points for the trimethylsilyl and nitropicolines were left out of the correlation because of the relatively large error (± 0.1) in the pK measurements and because, in the case of the nitro point, of the large deviation from the linear relation-

TABLE 1. pK values of benzoic acid and pyridinium ion

Compound	pK	No. of values in set	Method
Benzoic acid	4.22	9	I
	4.21	9	I
	4.22	9	I
Pyridine	5.20	9	II
	5.20	9	II
	5.20	9	II
	5.17	9	III
	5.20	8	III
	5.17	9	III
	5.18	6	VI
	5.20	5	VI

TABLE 2. Dissociation of substituted 2-picolinium ions, 2-$XCH_2C_5H_4NH^+$: pK values and derived $\bar{\sigma}$ values

X	pK	Method	$\bar{\sigma}_I$[a]	σ_I[b]
H	5.95	II	−0.03	0.00
CH_3	5.93	II	−0.02	−0.04
CH_2CH_3	5.93	II	−0.02	
C_6H_5	5.10	II	0.13	0.10
CN	2.58	II	0.59	0.56
$COCH_3$	4.49	II	0.24	0.28
COC_6H_5	5.06	VIa	0.14	
CO_2CH_3	4.10	II	0.31	0.30[c]
$CO_2C_2H_5$	4.15	III	0.30	0.30[c]
$Si(CH_3)_3$	6.6	VII	−0.14	−0.10
NH_3^+	1.6	VIII	0.77	
$NH_2CH_3^+$	1.4	VIII	0.81	
$NH(CH_3)_2^+$	0.9	VIII	0.90	
$NHCOCH_3$	4.23	III	0.29	0.26
$N(CH_3)COCH_3$	3.99	II	0.33	
NO_2	1.2	VIII	0.85	0.65
OH	4.85	II	0.18	
OCH_3	4.40	II	0.26	0.27
OC_6H_5	3.97	II	0.34	0.38
$OCOCH_3$	3.65	III	0.40	
SH	4.40	II, III	0.26	
SCH_3	4.50	II	0.24	0.23
SC_6H_5	4.42	II	0.26	
SO_2CH_3	2.48	III	0.61	0.59
$SO_2C_2H_5$	2.51	II, III	0.61	
$SO_2C_6H_5$	2.4	VIII	0.63	
Cl	3.42	II	0.44	0.46
Br	3.51	II	0.42	0.44

[a]This work.
[b]Reference 15.
[c]Value for CO_2R.

[6] $f \equiv$ root-mean-square of the deviations/root-mean-square of ($pK_H - pK$). A correlation of good precision has $f \leq 0.1$ (14, 15).

Can. J. Chem. Downloaded from www.nrcresearchpress.com by 210.87.254.6 on 09/05/12
For personal use only.

ship (see below). The mean of the pK values for the methyl and ethyl 2-pyridyl acetates was used in the correlation, since Taft only lists a σ_I value for CO_2R. The linear correlation is excellent, as is shown by the high value of the correlation coefficient and low value of the standard deviation, the latter equivalent to 0.03 in the σ value, the limit of precision found in other well-behaved systems (6). Our basic assumption, that the substituent effects measured in the substituted 2-picoline system reflect inductive effects alone, is therefore validated. Further confirmation of this is provided by the results of a dual substituent parameter correlation using σ_I and σ_R^0 (15). This gave $\rho_I = 5.43$ $\rho_R = 0.17$, $\lambda(\equiv \rho_R/\rho_I) = 0.03$, $s = 0.16$.[7] The very low value of λ and the lack of any improvement in the fit of the data as compared with that of the single substituent parameter equation, point to the absence of resonance effects in this system.

Derived $\bar{\sigma}_I$ values, evaluated from the relationship $\bar{\sigma}_I = (5.81 - pK)/5.45$ are shown in Table 2 together with Taft's values for σ_I. There are twelve substituents not listed by Taft for which σ_I values are obtained from the present study. With the exception of the value for the nitro group, there is good agreement between Taft's σ_I values and those determined in the present work for the common substituents. This agreement confirms that steric interaction between the substituent and reaction centre is not a complicating factor in the dissociation of substituted 2-picolinium ions. For the nitro group $\bar{\sigma}_I$ is 0.2 units larger than Taft's value, corresponding to a pK value for the nitropicolinium ion approximately one unit more acidic than would be predicted. Feuer and Lawrence have shown that the 2-nitromethylpicoline is present to the extent of 9% as the nitronate tautomer in dimethylsulfoxide solution (47). Such tautomerism would affect the measured pK value and could have a particularly serious effect on the pK value determined by spectrophotometry if the extinction coefficient of the nitronate tautomer was markedly different from that of the nitro tautomer. They obtained $pK = 3.92$ by potentiometric titration but this value would lead to $\bar{\sigma}_I = 0.35$, a result even more deviant (in the opposite direction) than that of Table 2. Clearly, further study of this system is required.

The $\bar{\sigma}_I$ value of the benzoyl group is 0.1 unit lower than that derived from the corresponding 3- and 4-phenacylpyridine. 2-Phenacylpyridine exists as the enol **1** in the solid state and predominantly as the enol in both ethanol and cyclohexane solution (54); the intramolecular hydrogen bond contributes to an enhanced stability. We confirmed the previous report that methylation of the sodio derivative with methyl iodide in methanol gives the *C*-methylation product (55). This exists in the keto form **2***b* as

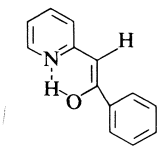

1

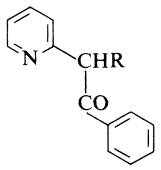

2
a R = H
b R = CH_3

shown by the ir carbonyl stretch at 1700 cm^{-1} and the τ 8.50 doublet (CH_3) and 5.08 quartet (CH) in the nmr spectrum. Replacement of the vinylic hydrogen in **1** by the more bulky methyl group would result in the introduction of steric strain, the consequence of which is that the hydrogen bonded enol form is forced out of the favourable planar state. Alkylation with dimethyl sulfate in dimethyl sulfoxide gave the *O*-methyl product: nmr τ: 6.61 (OCH_3), 4.40 (CH), both singlets. 2-Phenacylpyridine underwent D_2O exchange in two steps to give first **1** with the hydroxylic hydrogen replaced by deuterium and subsequently **1** with both the hydroxylic hydrogen and the vinylic hydrogen replaced by deuterium. It is evident that 2-phenacylpyridine exists predominantly as its tautomer **1** and that the measured pK is therefore not that of the benzoyl form.

Dissociation of 2-Picolylammonium Ions

pK values of 2-picolylammonium ion and its *N*-methyl and *N*,*N*-dimethyl derivates are shown in Table 3. The pK values for methylammonium ion dimethylammonium ion and trimethylammonium ion are 10.62, 10.77, and 9.80, respectively (56). Thus, introduction of the 2-pyridyl substituent into a methyl group of the methylammonium ion and its dimethyl and trimethyl counterparts, lowers the pK value by ca. 2 units. Compared to hydrogen the

TABLE 3. Dissociation of 2-picolylammonium ions

Ion	pK	Method
$C_5H_5NCH_2NH_3^+$	8.57	II
$C_5H_5NCH_2NH_2CH_3^+$	8.88	IV
$C_5H_5NCH_2NH(CH_3)_2^+$	8.16	IV

[7]The data are for the dual substituent parameter equation in the variable intercept form ($n = 13$, $-pK_0 = -5.49$, $f = 0.07$) for comparison with the Hammett equation correlation (above), which was also carried out, as is normal, using a variable intercept parameter. For the dual substituent parameter equation in the nonvariable intercept form the correlation gave for $n = 12$, $\rho_I = 5.79$, $\rho_R = 0.01$, $\lambda = 0.002$, $s = 0.18$, $f = 0.08$.

Can. J. Chem. Downloaded from www.nrcresearchpress.com by 210.87.254.6 on 09/05/12
For personal use only.

2-pyridinyl substituent is electron withdrawing. It is also electron-withdrawing compared to the phenyl substituent: the pK of benzylammonium ion is 9.38 (57). From the Hammett correlation of the data for dissociation of benzylammonium ions (57) and the measured dissociation constants of 2-picolylammonium ion the σ^0 value for the 2-aza substituent is obtained as 0.78, closely similar to the mean σ value (0.77) derived from hydrolysis of methyl and ethyl picolinates in aqueous methanol, aqueous ethanol, aqueous acetone and aqueous dioxan (58) and to the σ^0 value of 0.81 from hydrolysis of 2-pyridylmethyl acetate in aqueous acetone (59).

1. L. P. HAMMETT. J. Am. Chem. Soc. **59**, 96 (1937).
2. L. P. HAMMETT. Physical organic chemistry. McGraw-Hill, New York, NY. 1940. Chapt. 7.
3. H. H. JAFFÉ. Chem. Rev. **53**, 191 (1953).
4. O. EXNER. *In* Advances in linear free energy relationships. *Edited by* N. B. Chapman and J. Shorter. Plenum, London, England. 1972. Chapt. 1.
5. C. D. JOHNSON. The Hammett equation. Cambridge University Press, Cambridge, England. 1973.
6. R. W. TAFT. J. Phys. Chem. **64**, 1805 (1960).
7. A. R. KATRITZKY and R. D. TOPSOM. J. Chem. Educ. **48**, 427 (1971).
8. C. K. INGOLD and E. H. INGOLD. J. Chem. Soc. 1310 (1926).
9. H. C. BROWN and Y. OKAMOTO. J. Am. Chem. Soc. **80**, 4979 (1958).
10. H. VAN BEKKUM, P. E. VERKADE, and B. M. WEPSTER. Recl. Trav. Chim. Pays-Bas, **78**, 815 (1959).
11. R. W. TAFT and I. C. LEWIS. J. Am. Chem. Soc. **81**, 5343 (1959).
12. Y. YUKAWA and Y. TSUNO. Bull. Chem. Soc. Jpn. **39**, 2274 (1966).
13. Y. YUKAWA, Y. TSUNO, and S. SAWADA. Bull. Chem. Soc. Jpn. **39**, 2274 (1966).
14. P. R. WELLS, S. EHRENSON, and R. W. TAFT. *In* Progress in physical organic chemistry. Vol. 6. *Edited by* A. Streitweiser, Jr. and R. W. Taft. Interscience, New York, NY. 1968. p. 147.
15. S. EHRENSON, R. T. C. BROWNLEE, and R. W. TAFT. *In* Progress in physical organic chemistry. Vol. 10. *Edited by* A. Streitweiser, Jr. and R. W. Taft. Interscience, New York, NY. 1973. p. 1.
16. J. D. ROBERTS and W. T. MORELAND. J. Am. Chem. Soc. **75**, 2167 (1953).
17. C. D. RITCHIE and E. S. LEWIS. J. Am. Chem. Soc. **84**, 591 (1962).
18. H. D. HOLTZ and L. M. STOCK. J. Am. Chem. Soc. **86**, 5188 (1964).
19. C. F. WILCOX and J. S. MCINTYRE. J. Org. Chem. **30**, 777 (1965); C. F. WILCOX and C. LEUNG. J. Am. Chem. Soc. **90**, 336 (1968).
20. S. SIEGEL and J. M. KOMARMY. J. Am. Chem. Soc. **82**, 2547 (1960).
21. N. B. CHAPMAN, J. SHORTER, and K. J. TOYNE. J. Chem. Soc. 1077 (1964).
22. H. STETTER and J. MAYER. Chem. Ber. **95**, 667 (1962).
23. O. EXNER. Coll. Czech. Chem. Commun. **31**, 65 (1966).
24. J. PALECEK and J. HLAVATY. Z. Chem. **9**, 428 (1969).
25. C. A. GROB and M. G. SCHLAGETER. Helv. Chim. Acta, **59**, 264 (1976).
26. M. CHARTON. J. Org. Chem. **29**, 1222 (1964).
27. A. FISCHER, W. J. GALLOWAY, and J. VAUGHAN. J. Chem. Soc. 3591 (1964).
28. L. F. FEISER and M. FEISER. Reagents for organic synthesis. Vols. 1 and 2. Wiley, New York, NY. 1967.
29. K. WINTERFELD and K. FLICK. Arch. Pharm. **26**, 448 (1956).
30. S. GOLDING, A. R. KATRITZKY, and H. Z. KUCHARSKA. J. Chem. Soc. 3090 (1965).
31. E. MARUSZENSKA-WIECZORKOWSKA and J. MICHALSKI. Rocz. Chem. **31**, 543 (1957).
32. K. B. AUGUSTINSSNON and H. HASSELGUIST. Acta Chem. Scand. **18**, 1009 (1964).
33. F. B. LAFORGE. J. Am. Chem. Soc. **50**, 2477 (1928).
34. R. B. WOODWARD and E. C. KORNFELD. Org. Syn. **29**, 44 (1949).
35. H. LEHMANN and H. KLOES. Ger. Patent No. 1,145,168; Chem. Abstr. **59**, 9799c (1963).
36. W. SCHULZE. J. Prakt. Chem. **19**, 94 (1962).
37. T. NAITO and K. UENO. Yakugaku Zasshi, **79**, 1277 (1959).
38. J. BUCHI, F. KRACHER, and G. SCHMIDT. Helv. Chim. Acta, **42**, 729 (1952).
39. N. N. GOLDBERG, L. B. BARKLEY, and R. LEVINE. J. Am. Chem. Soc. **73**, 4301 (1951).
40. W. MATHES and A. WOLF. U.S. Patent No. 2,848,457; Chem. Abstr. **53**, 1384i (1959).
41. K. KOHMANN, H. SIGEL, and H. ERLENMEYER. Helv. Chim. Acta, **47**, 1754 (1964).
42. J. D. BOWER and G. R. RAMAGE. J. Chem. Soc. 2834 (1955).
43. H. ERDTMAN, F. HAGLID, and I. WELLINGS. Acta Chem. Scand. **17**, 1717 (1963).
44. T. MORIKAWA. J. Pharm. Soc. Jpn. **75**, 593 (1955).
45. L. BAUER and L. GARDELLA. J. Org. Chem. **28**, 1323 (1963).
46. I. SUZUKI. Pharm. Bull. **4**, 211 (1956).
47. H. FEUER and J. P. LAWRENCE. J. Org. Chem. **37**, 3662 (1972).
48. R. G. BATES. Determination of pH. 2nd ed. Wiley, New York, NY. 1973.
49. D. D. PERRIN, W. L. F. ARMAREGO, and D. R. PERRIN. Purification of laboratory chemicals. Pergamon, Oxford. 1966.
50. A. ALBERT and E. P. SERJEANT. Ionization constants of acids and bases. Methuen, London. 1962.
51. E. A. GUGGENHEIM. Thermodynamics. North Holland Publishing Co., Amsterdam. 1957. p. 314.
52. G. D. PINCHING and R. G. BATES. J. Res. Natl. Bur. Stand. **45**, 322 (1950); **45**, 444 (1950).
53. D. H. MCDANIEL and H. C. BROWN. J. Org. Chem. **23**, 420 (1958).
54. R. F. BRANCH, A. H. BECKETT, and D. B. COWELL. Tetrahedron, **19**, 401 (1963).
55. A. H. BECKETT and K. A. KERRIDGE. J. Chem. Soc. 2998 (1954).
56. D. H. EVERETT and W. F. K. WYNNE-JONES. Proc. R. Soc. A, **177**, 499 (1941).
57. L. F. BLACKWELL, A. FISCHER, I. J. MILLER, R. D. TOPSOM, and J. VAUGHAN. J. Chem. Soc. 3588 (1964).
58. H. H. JAFFE and H. L. JONES. Adv. Heterocycl. Chem. **3**, 209 (1964); A. D. CAMPBELL, S. Y. CHOOI, L. W. DEADY, and R. A. SHANKS. Aust. J. Chem. **23** 203 (1970); L. W. DEADY and R. A. SHANKS. Aust. J. Chem. **25**, 2363 (1972).
59. L. W. DEADY and R. A. SHANKS. Aust. J. Chem. **25**, 431 (1972).

Inductive substituent constants from dissociation of methyl-substituted 3-picolinium ions

ALFRED FISCHER, MURRAY JOHN KING, AND FRANK PRICE ROBINSON
Department of Chemistry, University of Victoria, Victoria, B.C., Canada V8W 2Y2

Received April 25, 1978

ALFRED FISCHER, MURRAY JOHN KING, and FRANK PRICE ROBINSON. Can. J. Chem. **56**, 3068 (1978).

The dissociation constants of 30 α-substituted 3-methylpyridinium ions in water at 25°C have been measured by potentiometric and spectrophotometric methods. Correlation of the pK values with σ_I values gives, for $n = 16$, slope $\rho_I = 3.044$, intercept $-pK_0 = -5.59$, correlation coefficient $r = 0.993$, and enables new σ_I values to be evaluated. Application of the dual substituent parameter equation gives $\lambda(\equiv \rho_R/\rho_I) = 0.04$, confirming that resonance effects are negligible in this series. Dissociation constants of the 3-pyridinylmethylammonium ion and its *N*-methyl and *N,N*-dimethyl derivatives are also reported.

ALFRED FISCHER, MURRAY JOHN KING et FRANK PRICE ROBINSON. Can. J. Chem. **56**, 3068 (1978).

Faisant appel à des méthodes potentiométrique et spectrophotométrique, on a mesuré à 25°C et pour des solutions aqueuses, les constantes de dissociation de 30 ions méthyl-3 pyridinium substitués en α. La corrélation des valeurs de pK avec les valeurs σ_I fournit, pour $n = 16$, une pente ρ_I 3.044, une ordonnée à l'origine $-pK_0 = -5.59$, un coefficient de corrélation $r = 0.993$ et elle permet aussi d'évaluer de nouvelles valeurs de σ_I. Une application de l'équation pour paramètres à doubles substituants conduit à un $\lambda(\equiv \rho_R/\rho_I) = -0.04$, ce qui confirme que, dans cette série, les effets de résonance sont négligeables. On rapporte aussi les constantes de dissociation de l'ion méthylammonium-3 pyridinyle et de ses dérivés *N*-méthyle et *N,N*-diméthyle.

[Traduit par le journal]

In a previous paper we reported the dissociation constants of a series of α-substituted 2-picolinium ions (α-substituted 2-methylpyridinium ions) and a set of σ_I values derived from the dissociation constants (1). We now report the dissociation constants of an extensive set of α-substituted 3-picolinium ions, measured as described in the earlier paper.

The pK values for the 3-picolines are shown in Table 1. The values are estimated to be accurate to ± 0.02. None of the 3-picolinium ions is sufficiently acidic to require measurement of the dissociation constant in hydrochloric acid solutions. This is fortunate since, in the 2-picolinium ion series, pK values measured in hydrochloric acid solutions were of lower accuracy (± 0.1). Thus the values for the 3-picolinium ions containing the substituents NH_3^+, $NH_2CH_3^+$, $NH(CH_3)_2^+$, NO_2, and $SO_2C_6H_5$ are more accurate than those of the correspondingly substituted 2-picolinium ions. 2-Nitromethylpyridine (and presumably also 2-nitromethylpyridinium ion) is tautomeric (2). As a result of the tautomeric equilibrium (or equilibria) the measured dissociation constant is not simply that of the nitropicolinium ion to nitropicoline. 2-Phenacylpyridine is likewise tautomeric, existing predominantly in the intramolecularly hydrogen-bonded enol form (3). The corresponding 3-picoline derivatives are not tautomeric since the resonance interaction which stabilizes the nitronate form of 2-nitromethylpyridine is absent in the 3-isomer and there is no strong intramolecular hydrogen bond to stabilize the enol form of 3-phenacylpyridine. Thus the measured pK values of the 3-nitromethyl- and 3-phenacylpyridines are, in each case, attributable to the equilibrium between the picolinium ion and the pyridine plus hydrogen ion.

Correlation of the $-pK$ values with the σ_I values (4) listed in the righthand column of Table 1 gave, for $n = 16$, slope $\rho_I = 3.044$, intercept $-pK_0 = -5.59$, correlation coefficient $r = 0.993$, standard deviation $s = 0.08$, standard deviation of the slope $s_\rho = 0.10$, root-mean-square deviations/root-mean-square of $(pK_H - pK)\,f = 0.07$. Derived $\bar{\sigma}_I$ values, evaluated from the relationship $\bar{\sigma}_I = (5.59 - pK)/3.044$, are also shown in column 4 of Table 1.

There is excellent agreement between the $\bar{\sigma}_I$ values determined in the present work and Taft's σ_I values, for common substituents. The largest difference between the pairs of values is 0.05 and the standard deviation is 0.03. This is about the limit to which the σ values are 'constant' from one reaction series to another.[1] The accuracy of the 3-picolinium ion dissociation constant data is such that the $\bar{\sigma}_I$ values are measured to ± 0.01. Thus, in this work, the limiting factor in the determination of $\bar{\sigma}_I$ values is the reliability of the assumption that σ values are constants.

Taft has argued against the introduction of a

[1]Compare with Table xxv (p. 54) of ref. 4.

Can. J. Chem. Downloaded from www.nrcresearchpress.com by 210.87.254.6 on 09/05/12
For personal use only.

TABLE 1. Dissociation of substituted 3-picolinium ions, 3-$XCH_2C_5H_4NH^+$: pK values and substituent constants

X	pK	Method[a]	$\bar{\sigma}_I$[b]	$\bar{\sigma}_I$[c]	$\bar{\sigma}^0$[d]	σ_I[e]
H	5.67	II	−0.02	(0.00)	−0.08	0.00
CH_3	5.71	II	−0.04	−0.01	−0.09	−0.04
CH_2CH_3	5.70	II	−0.03	−0.01	−0.08	
C_6H_5	5.20	II	0.13	0.15	0.00	0.10
CN	3.97	II	0.53	0.53	0.20	0.56
$COCH_3$	4.85	II	0.24	0.26	0.06	0.28
COC_6H_5	4.84	II	0.25	0.26	0.06	
CO_2CH_3	4.67	II	0.30	0.31	0.09	
$CO_2C_2H_5$	4.68	II	0.30	0.31	0.08	0.30[f]
$Si(CH_3)_3$	5.93	VII	−0.11	−0.08	−0.12	−0.10
NH_3^+	3.24	IV	0.77	0.76	0.32	
$NH_2CH_3^+$	3.02	IV	0.85	0.83	0.36	
$NH(CH_3)_2^+$	2.75	V	0.93	0.91	0.41	
$NHCOCH_3$	4.70	III	0.29	0.30	0.08	0.26
$N(CH_3)COCH_3$	4.56	II	0.34	0.35	0.10	
NO_2	3.63	III	0.65	0.64	0.26	0.65
OH	4.93	II	0.22	0.23	0.04	
OCH_3	4.69	II	0.30	0.31	0.08	0.27
OC_6H_5	4.55	II	0.34	0.35	0.11	0.38
$OCOCH_3$	4.43	II	0.38	0.39	0.13	
SH	4.87	III	0.24	0.25	0.05	
SCH_3	4.83	II	0.25	0.26	0.06	0.23
SC_6H_5	4.81	II	0.26	0.27	0.06	
SCN	4.01	II	0.52	0.52	0.20	
SO_2CH_3	3.65	III	0.64	0.63	0.26	0.59
$SO_2C_2H_5$	3.65	III	0.64	0.63	0.26	
$SO_2C_6H_5$	3.71	VIa	0.62	0.61	0.25	
Cl	4.28	II	0.43	0.43	0.15	0.46
Br	4.27	II	0.44	0.44	0.15	0.44
I	4.39	II	0.40	0.40	0.13	0.39

[a]Reference 6.
[b]From (5.594 − pK)/3.044.
[c]From (5.67 − pK)/3.21.
[d]From (5.19 − pK)/6.01 (6).
[e]From ref. 4.
[f]Value for CO_2R. The mean pK value for X = CO_2CH_3 and $CO_2C_2H_5$ was used in the correlations.

variable intercept parameter in correlation analysis of substituent effects (4). Correlation of (pK_H − pK) with σ_I with this constraint gave $\rho_I = 3.210$, $s = 0.10$, $f = 0.08$. Values of $\bar{\sigma}_I$ calculated from (pK_H − pK)/3.21 are listed in column 5 of Table 1. They are not significantly different from the values obtained using the Hammett equation in the variable intercept form (column 4).

The excellent correlation obtained with σ_I values in the single substituent parameter (Hammett) equation clearly indicates that the substituents in the methyl group exhibit only inductive effects on the dissociation of the 3-picolinium ions. Further confirmation that this is so is provided by the results of a correlation using the dual substituent parameter equation (σ_I and σ_R^0). This gives $\rho_I = 3.191$, $\rho_R = -0.141$, $s = 0.09$, $f = 0.07$. The value of λ ($\equiv \rho_R/\rho_I$) = −0.04 is not significantly different from zero, and a factor of 10 smaller than the value ~0.4 observed generally for *meta* reactivities and, specifically, the value of 0.43 observed for dissociation of 3-X-pyridinium ions (4).

The dissociation of 3-X-pyridinium ions conforms with good precision to the Hammett equation, using σ^0 values (5) as the measure of substituent effect, and gives $\rho = 6.01$, $pK_0 = 5.19$ (6). This is also shown by the results of the dual substituent parameter analysis using σ_R^0 which gives a good fit with $\lambda = 0.43$. Accordingly it is possible to derive substituent constants (σ^0 values) for the XCH_2 groups from the expression $\bar{\sigma}^0 = (5.19 - pK)/6.01$. These values are shown in column 6 of Table 1 and encompass the range from −0.12 ($CH_2Si(CH_3)_3$) to +0.41 ($CH_2NH(CH_3)_2^+$).

Table 2 lists pK values of the 3-picolylammonium ion (3-pyridinemethanamine conjugate acid) and its *N*-methyl and *N*,*N*-dimethyl derivatives. The substituent constant (σ^0) for the 3-aza substituent (i.e., 3-pyridinyl relative to phenyl) evaluated from the fit of the pK value for the picolylammonium ion to the

Can. J. Chem. Downloaded from www.nrcresearchpress.com by 210.87.254.6 on 09/05/12
For personal use only.

Can. J. Chem. Downloaded from www.nrcresearchpress.com by 210.87.254.6 on 09/05/12
For personal use only.

TABLE 2. Dissociation of 3-picolylammonium ions

Ion	pK	Method
$C_5H_5NCH_2NH_3^+$	8.60	II
$C_5H_5NCH_2NH_2CH_3^+$	8.83	IV
$C_5H_5NCH_2NH(CH_3)_2^+$	7.97	V

Hammett plot for benzylammonium ions (7) is 0.75. The value is in satisfactory agreement with the σ^0 value of 0.72, from hydrolysis of benzyl acetates in aqueous acetone (8) and is somewhat larger than the mean σ value of 0.65 from hydrolysis of methyl and ethyl picolinates in aqueous methanol, aqueous ethanol, aqueous acetone, and aqueous dioxan (9).

Experimental

General experimental methods are described in the previous paper (1). The following substituted 3-picolines were commercially available: 3-picoline (Aldrich, hydrochloride hygroscopic), 3-ethylpyridine (Reilly, hydrochloride hygroscopic), 3-picolylamine (3-pyridinemethanamine, Reilly, monohydrochloride mp 162–163°C), 3-pyridyleacetonitrile (Aldrich, hydrochloride mp 158–160°C), 3-chloromethylpyridine hydrochloride (Aldrich, mp 135–137°C), 3-pyridylcarbinol (3-pyridinemethanol, Aldrich, hydrochloride mp 113–114.5°C). 3-Trimethylsilylmethylpyridine was supplied by Dr. M. W. Morgan (10).

The following substituted 3-picolines were prepared by methods similar to those described for their 2-isomers (1). Phenyl 3-picolyl sulfone, mp 129–130°C (lit. (11) mp 134.5–135.5°C); nmr ($CDCl_3$) τ: 1.42 (m, 1, 2-*H*), 1.79 (m, 1, 6-*H*), 2.50 (m, 7, C_6H_5, 4-*H* and 5-*H*), 5.70 (s, 2, CH_2). 3-Pyridinemethanethiol (12); nmr τ: 1.60 (m, 2, 2-*H* and 6-*H*), 2.39 (m, 1, 4-*H*), 2.89 (m, 1, 5-*H*), 6.30 (d, 2, J = 7.5 Hz, CH_2, becomes singlet on D_2O exchange), 8.09 (t, 1, S*H*, removed on D_2O exchange); mass spectrum (70 eV) *m/e* (relative intensity): 125 (46, M_r (C_6H_7NS) = 125), 93(27), 92(100), 65(50), 39(25). 3-Pyridylmethylacetate (3-pyridinemethanol acetate ester), nmr τ: 1.50 (m, 2, 2-*H* and 6-*H*), 2.40 (m, 1, 4-*H*), 2.81 (m, 1, 5-*H*), 4.94 (s, 2, CH_2), 8.80 (s, 3, CH_3); hydrochloride (recrystallized from methanol – ethyl acetate), mp 95–97°C (lit. (13) mp 96–98°C); mass spectrum (70 eV) *m/e* (relative intensity): 151 (4, M_r ($C_8H_9NO_2$) = 151), 136 (2), 109(17), 108(11), 92(27), 91(25), 80(22), 65(36), 43(100), 39(50), 36(87). Ethyl 3-pyridylacetate, nmr τ: 1.54 (m, 2, 2-*H* and 6-*H*), 2.43 (m, 1, 4-*H*), 2.86 (m, 1, 5-*H*), 5.96 (q, 2, J = 7 Hz, CH_2CH_3), 6.49 (s, 2, CH_2CO), 8.84 (t, 3, CH_2CH_3); hydrochloride (from methanol–ethyl acetate), mp 142.5–144.5°C; mass spectrum (70 eV) *m/e* (relative intensity): 165 (34, M_r ($C_9H_{11}NO_2$) = 165), 121(13), 120(11), 93(40), 92(100), 65(35), 39(33), 36(42), 29(54). Methyl 3-pyridylacetate (H_2SO_4 catalyst (14)), nmr τ: 1.56 (m, 2, 2-*H* and 6-*H*), 2.42 (m, 1, 4-*H*), 2.88 (m, 1, 5-*H*), 6.39 (s, 3, CH_3), 6.46 (s, 2, CH_2); hydrochloride (sublimed), mp 116.5–118.5°C; mass spectrum (70 eV) *m/e* (relative intensity): 151 (95, M_r ($C_8H_9NO_2$) = 151), 92(100) 65(45), 39(28), 36(75). Methyl 3-picolyl sulfone, mp 124.5–125.5°C; nmr ($CDCl_3$) τ: 1.38 (m, 2, 2-*H* and 6-*H*), 2.11 (m, 1, 4-*H*), 2.61 (m, 1, 5-*H*), 5.73 (s, 2, CH_2), 7.19 (s, 3, CH_3); mass spectrum (70 eV) *m/e* (relative intensity): 171.037 (8, M_r ($^{12}C_7{}^1H_9{}^{14}N^{32}S^{16}O_2$) = 171.035), 93(9), 92(100), 65(35), 39(25). *Anal.* calcd. for $C_7H_9NSO_2$: C 49.07, H 5.31, N 8.19; found: C 49.04, H 5.50, N 8.18. Ethyl 3-picolyl sulfone, mp 70–71°C; nmr ($CDCl_3$) τ: 1.38 (m, 2, 2-*H* and 6-H), 2.12 (m, 1, 4-H), 2.60 (m, 1, 5-*H*), 5.78 (s, 2, CH_2), 7.07 (q, 2, J = 7.8 Hz, CH_2CH_3), 8.62 (t, 3, CH_3); mass spectrum (70 eV) *m/e* (relative intensity): 185.056 (15, M_r ($^{12}C_8{}^1H_{11}{}^{14}N^{32}S^{16}O_2$) = 185.051), 121(3), 93(12), 92(100), 65(20), 63(4), 39(13). *Anal.* calcd. for $C_8H_{11}NSO_2$: C 51.84, H 6.00, N 7.57; found: C 52.05, H 5.97, N 7.54. 3-Methoxymethylpyridine, nmr τ: 1.52 (m, 2, 2-*H* and 6-*H*), 2.42 (m, 1, 4-*H*), 2.86 (m, 1, 5-*H*), 5.62 (s, 2, CH_2), 6.69 (s, 3, OCH_3); hydrochloride (from methanol) mp 101–103°C; mass spectrum (70 eV) *m/e* (relative intensity): 123 (32, M_r (C_7H_9NO) = 123), 108(64), 93(45), 92(80), 80(42), 65(76), 53(30), 51(30), 45(41), 39(82), 36(100). 3-Methylthiomethylpyridine, nmr τ: 1.69 (m, 2, 2-*H* and 6-*H*), 2.41 (m, 1, 4-*H*), 2.82 (m, 1, 5-*H*), 6.40 (s, 2, CH_2), 8.19 (s, 3, CH_3); hydrochloride (from methanol), mp 134–135°C; mass spectrum (70 eV) *m/e* (relative intensity): 139 (9, M_r (C_7H_9NS) = 139), 93(9), 92(82), 65(58), 39(60), 38(32), 36(100). 3-Acetamidomethylpyridine (*N*-3-pyridinylmethylacetamide), nmr ($CDCl_3$) τ: 1.56 (m, 3, 2-*H*, 6-*H* and N*H*), 2.37 (m, 1, 4-*H*), 2.77 (m, 1, 5-*H*), 5.63 (d, 2, J = 6.0 Hz, CH_2), 8.07 (s, 3, CH_3); mass spectrum (70 eV) *m/e* (relative intensity): 150 (90, M_r ($C_8H_{10}N_2O$) = 150), 149(48), 135(55), 107(100), 92(32), 80(40), 43(57). 3-Methylaminomethylpyridine (*N*-methyl-3-pyridinemethanamine), nmr τ: 1.59 (m, 2, 2-*H* and 6-*H*), 2.38 (m, 1, 4-*H*), 2.81 (m, 1, 5-*H*), 6.34 (s, 2, CH_2), 7.69 (s, 3, CH_3), 8.52 (s, 1, N*H*, removed by D_2O); mass spectrum (70 eV) *m/e* (relative intensity): 122 (54, M_r ($C_7H_{10}N_2$) = 122), 121(59), 92(46), 80(100), 79(39), 65(30), 44(81). 3-Dimethylaminomethylpyridine (*N*,*N*-dimethyl-3-pyridinemethanamine), nmr τ: 1.55 (m, 2, 2-*H* and 6-*H*), 2.41 (m, 1, 4-*H*), 2.82 (m, 1, 5-*H*), 6.62 (s, 2, CH_2), 7.83 (s, 6, CH_3); mass spectrum (70 eV) *m/e* (relative intensity): 136 (43, M_r ($C_8H_{12}N_2$) = 136), 135(21), 92(32), 58(100), 42(14), 39(12); dihydrochloride (from methanol), mp 188–189°C (lit. (15) mp 179–180°C). 3-Phenylthiomethylpyridine, nmr τ: 1.68 (m, 2, 2-*H* and 6-*H*), 2.74 (m, 7, 4-*H*, 5-*H* and C_6H_5), 6.10 (s, 2, CH_2); hydrochloride (recrystallized from absolute ethanol – ether, followed by sublimation), mp 111–113°C; mass spectrum (70 eV) *m/e* (relative intensity): 201 (97, M_r ($C_{12}H_{11}NS$) = 201), 93(15), 92(100), 65(42), 39(20). *Anal.* calcd. for $C_{12}H_{12}NSCl$: C 60.60, N 5.90, H 5.09; found: C 60.54, N 5.70, H 4.90. 3-Phenoxymethylpyridine, nmr τ: 1.50 (m, 2, 2-*H* and 6-*H*), 2.32 (m, 1, 4-*H*), 2.97 (m, 6, 5-*H* and C_6H_5), 5.06 (s, 2, CH_2); hydrochloride (sublimed), mp 100–102°C; mass spectrum (70 eV) *m/e* (relative intensity): 185 (42, M_r ($C_{12}H_{11}NO$) = 185), 92(100), 65(37), 39(20), 36(39): *Anal.* calcd. for $C_{12}H_{12}NOCl$: C 64.99, N 6.32, H 5.46; found: C 64.97, N 6.32, H 5.41. 3-*N*-Acetylmethylaminomethylpyridine (*N*-methyl-*N*-3-pyridinylmethylacetamide), nmr τ: 1.66 (m, 2, 2-*H* and 6-*H*), 2.55 (m, 1, 4-*H*), 2.85 (m, 1, 5-*H*), 5.56 (s, 2, CH_2), 7.12 (s, 3, N-CH_3), 8.00 (s, 3, $COCH_3$); mass spectrum (70 eV) *m/e* (relative intensity): 164 (76, M_r ($C_9H_{12}N_2O$) = 164), 121(50), 107(100), 93(39), 92(47), 44(42); picrate (from 95% ethanol), mp 92.5–93.5°C. *Anal.* calcd. for $C_{15}H_{15}N_5O_8$: C 45.78, N 17.81, H 3.84; found: C 45.54, N 17.90, H 3.79. The hydrochloride was sublimed, mp 114–117°C.

3-Propylpyridine was prepared by alkylation of the anion of 3-picoline, itself generated from 3-picoline using sodamide in ammonia, with ethyl bromide (16). After distillation at 30–40°C under reduced pressure the 3-propylpyridine was obtained in 31% yield and had nmr τ: 1.68 (m, 2, 2-*H* and 6-*H*), 2.62 (m, 1, 4-*H*), 2.96 (m, 1, 5-*H*), 7.42 (t, 2, J = 8.8 Hz, CH_2CH_2-CH_3), 8.37 (m, 2, $CH_2CH_2CH_3$), 9.08 (t, 3, J = 6.9 Hz, $CH_2CH_2CH_3$). The hydrochloride was recrystallized from chloroform – ethyl acetate, mp 135–136°C; mass spectrum (70 eV) *m/e* relative intensity): 121 (30, M_r ($C_8H_{11}N$) = 121), 106(9), 93(19), 92(100), 65(26), 51(12), 39(40), 36(37).

3-Benzylpyridine was prepared from 3-chloromethylpyridine hydrochloride by a Friedel–Crafts reaction using benzene and powdered $AlCl_3$ (17). The product was obtained in 55% yield after distillation at 110°C under reduced pressure and solidified on standing; nmr τ: 1.56 (m, 2, 2-*H* and 6-*H*), 2.79 (m, 7, 4-*H*, 5-*H*, and C_6H_5), 6.05 (s, 2, CH_2). The hydrochloride was recrystallized from chloroform – ethyl acetate, mp 146.5–148.5°C; mass spectrum (70 eV) *m/e* (relative intensity): 169 (25, M_r ($C_{12}H_{11}N$) = 169), 168(26), 115(13), 91(16), 65(25), 51(23), 39(39), 39(30), 36(100).

3-Bromomethylpyridine hydrobromide was prepared by refluxing 3-pyridylcarbinol (40 g) with 48% HBr (360 cm^3) for 4 h. Concentration of the solution, dilution with ethanol (200 cm^3) and cooling gave the hydrobromide (64.7 g, 70%) which was recrystallized from methanol and then sublimed, mp 147.5–149°C (lit. (18) mp 148–149°C).

3-Pyridylacetone (1-(3-pyridinyl)-2-propanone) was prepared by condensation of 3-pyridylacetic acid with acetic anhydride followed by decarboxylation of the resulting β-keto acid (19) and was obtained in 13% yield after distillation at 130–140°C under reduced pressure; nmr τ: 1.61 (m, 2, 2-*H* and 6-*H*), 2.53 (m, 1, 4-*H*), 2.82 (m, 1, 5-*H*), 6.34 (s, 2, CH_2), 7.98 (s, 3, CH_3). The hydrochloride after sublimation had mp 143–145°C; mass spectrum (70 eV) *m/e* (relative intensity): 135 (15, M_r (C_8H_9NO) = 135), 93(100), 92(20), 65(14), 43(45), 39(16).

3-Phenacylpyridine (1-phenyl-2-(3-pyridinyl) ethanone) was prepared by reaction of the anion of 3-picoline, formed by reaction of 3-picoline with lithium diisopropylamide, with methyl benzoate. After distillation at 160°C under reduced pressure, the product had nmr ($CDCl_3$) τ: 1.41 (m, 2, 2-*H* and 6-*H*), 1.93 (m, 2, 4-*H* and 5-*H*), 2.48 (m, 5, C_6H_5), 5.72 (s, 2, CH_2). The hydrochloride was recrystallized from methanol and than sublimed but a sharp melting point was not obtained. *Anal.* calcd. for $C_{13}H_{12}NOCl$: C 66.82, N 6.00, H 5.18: found: C 66.65, N 5.84, H 5.16.

3-Thiocyanatomethylpyridine thiocyanate. A solution of 3-chloromethylpyridine hydrochloride (8.2 g, 0.05 mol) in methanol (50 cm^3) was mixed with potassium thiocyanate (9.7 g, 0.1 mol) and refluxed for 2 h. The precipitated potassium chloride was filtered off and the product crystallized from the filtrate on cooling, in 89% yield. Recrystallization from methanol followed by sublimation gave mp 100.5–102°C, (lit. (20) mp 110°C); mass spectrum (70 eV) *m/e* relative intensity): 150 (34, M_r ($C_7H_6N_2S$) = 150), 93(19), 92(100), 65(40), 59(15), 39(31), 31(84).

3-Iodomethylpyridine hydriodide. 3-Pyridylcarbinol (20 g) was refluxed for 20 h with 55% hydriodic acid (180 cm^3) and a trace of red phosphorus. The solution was concentrated on the rotary evaporator and the solid product (22.1 g, 50% yield) was filtered and recrystallized from 95% ethanol, mp 177–179°C; mass spectrum (70 eV) *m/e* (relative intensity): 219 (17, M_r (C_6H_6NI) = 219), 128(33), 127(20), 92(100), 65(32), 39(17). *Anal.* calcd. for $C_6H_7NI_2$: C 20.76, N 4.04, H 2.04; found: C 20.98, N 4.20, H 2.04.

3-Nitromethylpyridine was prepared by the method of Feuer and Lawrence (2), except that *n*-propyl nitrate was used in place of the suggested ethyl nitrate. It was purified by chromatography on silica gel, eluting with $CHCl_3$; nmr ($CDCl_3$) τ: 1.34 (m, 2, 2-*H* and 6-*H*), 2.20 (m, 1, 4-*H*), 2.66 (m, 1, 5-*H*), 4.59 (s, 2, CH_2). The picrate was recrystallized from 95% EtOH, mp 147–149°C (lit. (2) mp 150–151°C).

1. A. Fischer, M. J. King, and F. P. Robinson. Can. J. Chem. **56**, 3059 (1978).
2. H. Feuer and J. P. Lawrence. J. Org. Chem. **37**, 3662 (1972).
3. R. F. Branch, A. H. Beckett, and D. B. Cowell. Tetrahedron, **19**, 401 (1963).
4. S. Ehrenson, R. T. C. Brownlee, and R. W. Taft. *In* Progress in physical organic chemistry. Vol. 10. *Edited by* A. Streitwieser, Jr. and R. W. Taft. Interscience, New York, NY. 1973. p. 1.
5. R. W. Taft. J. Phys. Chem. **64**, 1805 (1960).
6. A. Fischer, W. J. Galloway, and J. Vaughan. J. Chem. Soc. 3951 (1964).
7. L. F. Blackwell, A. Fischer, I. J. Miller, R. D. Topsom, and J. Vaughan. J. Chem. Soc. 3588 (1964).
8. L. W. Deady and R. A. Shanks. Aust. J. Chem. **25**, 431 (1972).
9. H. H. Jaffé and H. L. Jones. Adv. Heterocycl. Chem. **3**, 209 (1964); A. D. Campbell, S. Y. Chooi, L. W. Deady, and R. A. Shanks. Aust. J. Chem. **23**, 203 (1970); L. W. Deady and R. A. Shanks. Aust. J. Chem. **25**, 2363 (1972).
10. A. Fischer, M. W. Morgan, and C. Eaborn. J. Organomet. Chem. **136**, 323 (1977).
11. S. Golding, A. R. Katritzky, and H. Z. Kucharska. J. Chem. Soc. 3090 (1965).
12. Z. J. Vejdelek and M. Protiva. Chem. Listy, **45**, 451 (1952).
13. K. Augustinsson and H. Hasselguist. Acta Chem. Scand. **18**, 1009 (1964).
14. F. B. LaForge. J. Am. Chem. Soc. **50**, 2477 (1928).
15. H. Erdtman, F. Haglid, and I. Wellings. Acta Chem. Scand. **17**, 1717 (1963).
16. E. Hardeggar and E. Nikles. Helv. Chim. Acta, **39**, 505 (1956).
17. R. Kuhn. Chem. Ber. **93**, 2966 (1960).
18. R. G. Coombes, M. D. Johnson, and N. Winterton. J. Chem. Soc. 7029 (1965).
19. A. Burger and C. Walter. J. Am. Chem. Soc. **72**, 1988 (1950).
20. W. Mathes and A. Wolf. U.S. patent No. 2,848,457; Chem. Abstr. **53**, 1384i (1959).

Can. J. Chem. Downloaded from www.nrcresearchpress.com by 210.87.254.6 on 09/05/12
For personal use only.

Inductive substituent constants from dissociation of methyl-substituted 4-picolinium ions[1]

ALFRED FISCHER, MURRAY JOHN KING, AND FRANK PRICE ROBINSON

Department of Chemistry, University of Victoria, Victoria, B.C., Canada V8W 2Y2

Received May 31, 1978[2]

ALFRED FISCHER, MURRAY JOHN KING, and FRANK PRICE ROBINSON. Can. J. Chem. **56**, 3072 (1978).

The dissociation constants of 29 α-substituted 4-methylpyridinium ions in water at 25°C have been measured by potentiometric or spectrophotometric methods. Correlation of the log K values with σ_I values gives, for $n = 13$, slope $\rho = 2.922$, intercept log $K_0 = 5.93$, correlation coefficient $r = 0.990$. Effective σ_I values evaluated from the dissociation of substituted 4-picolinium ions are in good agreement with those calculated from dissociation of substituted 2- and 3-picolinium ions and with literature values. pK values of the 4-pyridinylmethylammonium ion and its *N*-methyl and *N*,*N*-dimethyl derivatives are 8.22, 8.48, and 7.63, respectively.

ALFRED FISCHER, MURRAY JOHN KING et FRANK PRICE ROBINSON. Can. J. Chem. **56**, 3072 (1978).

Au moyen de méthodes potentiométriques et spectrophotométriques, on a mésure dans l'eau à 25°C les constantes de dissociation de 29 ions méthyl-4 pyridinium substitués en position α. De la relation entre les valeurs de log K et celles de σ_I, on tire pour $n = 13$, une pente ρ de 2.922, une ordonnée à l'origine log K_0 de 5.93 et un coefficient de corrélation r de 0.990. Les valeurs effectives de σ_I évaluées au moyen de la dissociation des ions picolinium-4 substitués sont en bon accord avec celles qu'on calcule à partir de la dissociation des ions picolinium-2 et -3 substitués et avec les valeurs de la littérature. Les valeurs de pK de l'ion pyridinyl-4 méthylammonium et de ses dérivés *N*-méthyl et *N*,*N*-diméthyl sont de 8.22, 8.48 et 7.43, respectivement.

[Traduit par le journal]

In this paper we report the dissociation constants of a series of α-substituted 4-picolinium ions (α-substituted 4-methylpyridinium ions) and derived σ_I values. The latter are compared with values derived from the 2- and 3-picolinium ion series (1, 2) and with literature values.

The pK values for the 4-picolines are shown in Table 1. Values are estimated to be accurate to ±0.02 although the precision and, presumably, the relative accuracy of the values measured by potentiometry is rather better than this. 4-Trimethylsilylmethylpyridine reacted in solution (as did its 2-isomer) and the extinction coefficients had to be determined by an extrapolation technique (1). For this reason its pK value is less accurate, ±0.1.

Correlation of values of ($pK_H - pK$) with σ_I values (3) gave, for $n = 13$, slope $\rho = 2.922$, intercept 0.074, correlation coefficient $r = 0.990$, standard deviation $s = 0.09$, standard deviation of the slope $s_\rho = 0.13$, root-mean-square deviations/root-mean-square observations $f = 0.07$.[3] Effective σ values evaluated from the relation $\bar{\sigma}_I = (pK_H - pK - 0.074)/2.922$ are shown in Table 1 and are repeated in Table 2 for comparison with similar values from the 2- and 3-picolinium ion series and other values evaluated from literature data or taken directly from the literature.

For the picolinium ions the accuracy with which pK values are generally determined, ±0.02, is much greater than the precision with which the values correlate with σ_I values, for which s ranges from 0.08 (3-picolinium ions) to 0.15 (2-picolinium ions). Thus the limiting factor in the determination of $\bar{\sigma}_I$ values is not generally the accuracy of the pK data but the precision with which substituent effects are proportional from one reaction series to another. The measure of the precision with which $\bar{\sigma}_I$ values are determined is given by s/ρ and this ranges from 0.027 (3-picolinium ions) to 0.030 (4-picolinium ions). The same limiting precision (0.03) was found by Taft for σ^0 reactivities (8).

The trimethylsilylmethyl group appears to be a much better electron donor in the 4-picolinium ion series than in the 3-picolinium ion series and in the other reactivities. It is possible that this is a consequence of the error in the pK value resulting from the problems in this measurement (see above). It is more likely that the enhanced $\bar{\sigma}_I$ value reflects the powerful resonance (hyperconjugative) effect of the trimethylsilylmethyl group. It is a basic assumption of our analysis that the resonance effect, on the pyridinium ion – pyridine equilibrium, of methyl and

[1]From the Ph.D. Thesis of Murray John King, University of Victoria, Victoria, B.C., 1973.

[2]Revision received August 9, 1978.

[3]The Hammett equation in the variable intercept parameter form was used. The data for the substituents NO_2 and $Si(CH_3)_3$ were not used in the correlation and the mean pK value (5.00) for the 4-picolinic acid esters was used as a single datum. The dual substituent parameter correlation with nonvariable intercept and using σ_I and σ_R^0 (3) gave, for $n = 12$, $\rho_I = 3.11$, $\rho_R = 0.035$, λ ($\equiv \rho_R/\rho_I$) $= 0.01$, $s = 0.10$, $f = 0.08$.

Can. J. Chem. Downloaded from www.nrcresearchpress.com by 210.87.254.105 on 09/05/12
For personal use only.

Can. J. Chem. Downloaded from www.nrcresearchpress.com by 210.87.254.105 on 09/05/12
For personal use only.

TABLE 1. Dissociation of substituted 4-picolinium ions, 4-$XCH_2C_5H_4NH^+$: pK values and derived σ_I values

X	pK	Method[a]	$\bar{\sigma}_I$[b]
H	6.00	II	−0.03
CH_3	6.01	II	−0.03
CH_2CH_3	6.04	II	−0.04
C_6H_5	5.56	II	0.13
CN	4.32	II	0.55
$COCH_3$	5.14	II	0.27
COC_6H_5	5.13	II	0.27
CO_2CH_3	4.94	II	0.34
$CO_2C_2H_5$	5.06	VIa	0.30
$Si(CH_3)_3$	6.5	VII	−0.20
NH_3^+	3.62	IV	0.79
$NH_2CH_3^+$	3.38	IV	0.87
$NH(CH_3)_2^+$	3.05	IV	0.98
$NHCOCH_3$	5.13	III	0.27
$N(CH_3)COCH_3$	5.04	III	0.30
NO_2	2.87	III	1.05
OH	5.35	II	0.20
OCH_3	5.10	II	0.28
OC_6H_5	4.98	II	0.32
$OCOCH_3$	4.83	II	0.38
SH	5.28	III	0.22
SCH_3	5.23	II	0.24
SC_6H_5	5.20	II	0.25
SCN	4.40	II	0.52
SO_2CH_3	4.04	III	0.65
$SO_2C_2H_5$	4.04	III	0.65
$SO_2C_6H_5$	4.04	VIa	0.65
Cl	4.68	II	0.43
Br	4.66	II	0.43

[a]Described in ref. 1.
[b]Calculated from $\bar{\sigma}_I = (5.926 - pK)/2.922$.

substituted methyl groups is either constant or proportional to the inductive effect of the substituent of the substituted methyl group. This assumption is likely to be violated for the trimethylsilylmethyl group since the trimethylsilylmethyl group has a much stronger electron-donating resonance effect than does methyl (9).

The $\bar{\sigma}_I$ value for the nitro group is substantially greater in the 4-picolinium ion series than in the 3-picolinium ion series which itself is in excellent agreement with literature values. 4-Nitromethylpyridinium ion is 1.16 pK units stronger as an acid than predicted by the σ_I for the nitro group of 0.65. This is similar to the behaviour of 2-nitromethylpyridinium ion and the same explanation presumably applies: tautomerism of the nitromethylpyridine results in the formation of a more weakly basic nitronate form (Fig. 1). If this is the correct explanation for the observation that 4-nitromethylpyridine is a weaker base than expected then 93% of the nitromethylpyridine must exist in the nitronate form. Feuer and Lawrence (10) have shown that the nitronate form is present to the extent of 33% in dimethyl sulfoxide solution and it is not unreasonable that even more of this (polar) form should be present in aqueous solution.

The reduced basicity of 2-phenacylpyridine has been commented on (1). For all other substituents with the exception of $NH(CH_3)_2^+$ there is excellent agreement between the $\bar{\sigma}_I$ values derived from the three picolinium ion series. In the case of the $NH(CH_3)_2^+$ substituent the range of values is 0.08 and the somewhat greater range in this instance is probably a consequence of the greater error in the pK value of the 2-picolinium ion derivative, measured in hydrochloric acid solutions (1).

Mean $\bar{\sigma}_I$ values from the dissociation of picolinium ions are shown in column 5 of Table 2. In deriving these mean $\bar{\sigma}_I$ values deviant individual values were rejected (the values derived from 2- and 4-nitromethylpyridine, 2- and 4-trimethylsilylmethylpyridine, 2-phenacylpyridine) and the values derived from the less accurate pK values (such as in the case of the $NH(CH_3)_2^+$ substituent from the 2-picoline series) were assigned proportionately lower (20%) weights. Also shown in Table 2 are $\bar{\sigma}_I$ values calculated from literature pK data for 4-substituted quinuclidines (column 6), substituted acetic acids (column 7), 4-substituted bicyclo[2.2.2]octane-1-carboxylic acids (column 8), 4-substituted bicyclo[2.2.2]-oct-2-ene-1-carboxylic acids (column 9), α-substituted 4-toluic acids (column 10), and Taft's σ_I values (column 11). All of the $\bar{\sigma}_I$ values were obtained from linear correlation of pK with σ_I with a variable intercept parameter. Only data for those substituents common to two or more reaction series have been included in Table 2. Extensive tables of σ_I values evaluated from ^{19}F nmr shifts and also from aromatic reactivities are available (11) but we have restricted our comparisons to acid dissociation reactions in order to assess the constancy of $\bar{\sigma}_I$ values in a similar set of reactivities. Other data for other acid dissociation reactions are available from which $\bar{\sigma}_I$ values may be determined but have not been included in Table 2 either because a too restricted range of substituents is encompassed (dissociation of 3-substituted adamantane-1-carboxylic acids (12)) or too few (<6) substituents for which σ_I values are listed in the primary set have been studied (dissociation of *trans*-4-substituted cyclohexane-1-carboxylic acids (13)) or because the correlation is of lower precision with $s/\rho > 0.03$ (dissociation of substi-

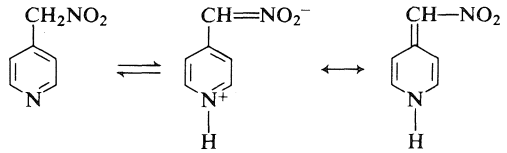

FIG. 1. Tautomerism of 4-nitromethylpyridine.

TABLE 2. Inductive substituent constants from dissociation of picolinium ions and other acid dissociation reactions[a]

X	$\bar{\sigma}_I$[b]	$\bar{\sigma}_I$[c]	$\bar{\sigma}_I$[d]	$\bar{\sigma}_I$[e]	$\bar{\sigma}_I$[f]	$\bar{\sigma}_I$[g]	$\bar{\sigma}_I$[h]	$\bar{\sigma}_I$[i]	$\bar{\sigma}_I$[j]	$\bar{\sigma}_I$[k]
H	−0.03	−0.02	−0.03	−0.03	−0.10	−0.01	−0.01	−0.03	0.02	0.00
CH_3	−0.02	−0.04	−0.03	−0.03	−0.08	−0.04	−0.02	0.00		−0.04
C_2H_5	−0.02	−0.03	−0.04	−0.03	−0.10	−0.02	−0.03			
iC_3H_7					−0.12					
tC_4H_9					−0.13	−0.07				
$CH{=}CH_2$					0.02	0.09				
$C{\equiv}CH$					0.25	0.34				
C_6H_5	0.13	0.13	0.13	0.13	0.10	0.10			0.10	0.10
CN	0.59	0.53	0.55	0.56	0.56	0.55	0.58	0.59	0.53	0.56
CF_3						0.41	0.39	0.42		0.45
CH_2OH					0.04	0.05	0.03			
CH_2OCH_3					0.04	0.06				
$COCH_3$	0.24	0.24	0.27	0.25	0.27	0.28				0.28
COC_6H_5	(0.14)	0.25	0.27	0.26						
$CONH_2$					0.29	0.27		0.31		
CO_2^-					0.02	−0.16	−0.20	−0.13		
CO_2H						0.39	0.29	0.31		
CO_2CH_3	0.31	0.30	0.34	0.32	0.27	0.34				0.30
$CO_2C_2H_5$	0.30	0.30	0.30	0.30	0.27	0.34	0.29	0.29		0.30
$Si(CH_3)_3$	(−0.14)	−0.11	(−0.20)	−0.11		−0.12			−0.13	−0.10
NH_2					0.11					0.12
$NHCH_3$					0.07					
$N(CH_3)_2$					0.11					0.06
NH_3^+	0.77	0.77	0.79	0.78		0.58				
$NH_2CH_3^+$	0.81	0.85	0.87	0.86		0.58				
$NH(CH_3)_2^+$	0.90	0.93	0.98	0.95		0.68				
$N(CH_3)_3^+$						0.71	0.95	0.98		
$NHCOCH_3$	0.29	0.29	0.27	0.28	0.24	0.26				0.26
$N(CH_3)COCH_3$	0.33	0.34	0.30	0.32						
NO_2	(0.85)	0.65	(1.05)	0.65	0.65	(0.75)	0.66			0.65
OH	0.18	0.22	0.20	0.20	0.26	0.22	0.22			
OCH_3	0.26	0.30	0.28	0.28	0.29	0.28	0.29		0.31	0.27
OC_6H_5	0.34	0.34	0.32	0.33		0.38			0.38	0.38
$OCOCH_3$	0.40	0.38	0.38	0.39	0.36					
SH	0.26	0.24	0.22	0.24		0.26				
SCH_3	0.24	0.25	0.24	0.24	0.26	0.25				0.23
SC_6H_5	0.26	0.26	0.25	0.26		0.30				
SCN		0.52	0.52	0.52		0.54				
SO_2CH_3	0.61	0.64	0.65	0.63	0.60	0.58				0.59
$SO_2C_2H_5$	0.61	0.64	0.65	0.63						
$SO_2C_6H_5$	0.63	0.62	0.65	0.63		0.56				
F					0.46	0.52				0.50
Cl	0.44	0.43	0.43	0.43	0.44	0.46	0.46	0.46	0.45	0.46
Br	0.42	0.44	0.43	0.43	0.47	0.45	0.46		0.45	0.44
I		0.40		0.40	0.41	0.38			0.40	0.39

[a]For each reaction series ($pK_H - pK$) was correlated with σ_I (3) to give ρ and ($pK_H - pK_0$). Values of $\bar{\sigma}_I$ were obtained from $\bar{\sigma}_I = ((pK_H - pK) - (pK_H - pK_0))/\rho \equiv (pK_0 - pK)/\rho$. Values in parentheses unreliable as a measure of inductive effect (see text).
[b]From dissociation of 2-picolinium ions (1).
[c]From dissociation of 3-picolinium ions (2).
[d]From dissociation of 4-picolinium ions (Table 1).
[e]'Mean' values for dissociation of picolinium ions (see text).
[f]From dissociation of quinuclidinium ions (4): $n = 16$, $\rho = 4.601$, $(pK_H - pK_0) = 0.467$, $s = 0.13$, $f = 0.05$.
[g]From dissociation of acetic acids at 25°C (5): $n = 17$, $\rho = 4.082$, $(pK_H - pK_0) = 0.031$, $s = 0.08$, $f = 0.05$.
[h]From dissociation of bicyclo[2.2.2]octane-1-carboxylic acids (6): $n = 9$, $\rho = 1.565$, $(pK_H - pK_0) = 0.021$, $s = 0.05$, $f = 0.06$.
[i]From dissociation of bicyclo[2.2.2]oct-2-ene-1-carboxylic acids (6): $n = 6$, $\rho = 1.692$, $(pK_H - pK_0) = 0.048$, $s = 0.05$, $f = 0.07$.
[j]From dissociation of α-substituted 4-toluic acids in 50% ethanol (7): $n = 9$, $\rho = 0.966$, $(pK_H - pK_0) = -0.015$, $s = 0.02$, $f = 0.06$.
[k]Reference 3.

tuted 3-toluic acids (7) and of substituted 4-toluic acids in 80% methyl cellosolve (7*b*)).

In general, within the precision implied by the standard deviation (s/ρ) of 0.03 for the individual reaction series, there is excellent agreement between the $\bar{\sigma}_I$ values determined from dissociation of picolinium ions, the values calculated from other dissociation reactions and Taft's σ_I values. Grob and Schlageter (4) state that the correlation of the quinuclidine data (of $\sigma_I^q \equiv pK_H - pK$) with σ_I is only fair with $r = 0.906$. Examination of their plot reveals that the correlation is good but there is a very marked deviation in the case of the CO_2^- substituent, which, according to the quinuclidine p*K*

Can. J. Chem. Downloaded from www.nrcresearchpress.com by 210.87.254.105 on 09/05/12
For personal use only.

Can. J. Chem. Downloaded from www.nrcresearchpress.com by 210.87.254.105 on 09/05/12
For personal use only.

value, is *electron attracting* whereas the $\bar{\sigma}_I$ values from the carboxylic and dissociation series show that it is quite strongly electron repelling. Substituent effects of charged groups can show marked variations from one reaction series to another and it is inappropriate to place much weight on the marked deviation of the CO_2^- substituent in the quinuclidine series. For the same correlation, restricting our choice of σ_I values to Taft's primary set (3) which, significantly, does not include a value for CO_2^-, we obtained $r = 0.988$, for $n = 17$. The datum point for X = H was significantly deviant with $\bar{\sigma}_H = -0.08$. When the correlation was repeated without this point ($n = 16$) an even better correlation was obtained with $r = 0.992$, $s = 0.13$, $s/\rho = 0.027$, $f = 0.05$ and the point for X = H was even more deviant with $\bar{\sigma}_H = -0.10$. We conclude that the quinuclidine data exhibit an excellent correlation with σ_I (although the hydrogen datum point is deviant) and that it is unnecessary (and indeed undesirable) to introduce a set of σ_I^q values. In the analysis of the quinuclidine (and other) data we have used a variable intercept parameter. Taft has argued against the introduction of a variable intercept parameter, particularly in the application of the dual substituent parameter equation (3). In the case of the quinuclidine dissociation, where analysis using the variable intercept parameter form of the single substituent parameter (Hammett) equation shows the hydrogen datum point is significantly deviant, it seems unreasonable to assume that this point is 'correct' as would be implied by application of the equation without a variable intercept parameter. It is noteworthy that, like hydrogen, the alkyl substituents appear to be more strongly electron donating ($\bar{\sigma}_I$ more negative) in the quinuclidines than in the acetic acids. It is possible that this reflects a specific difference between the two systems. Alternatively it may represent the incursion of a systematic error of measurement in the high pH range.

There are marked discrepancies between the substituent effects of the positively charged ammonio and substituted ammonio groups in the picolines and in the acetic acids. For these groups the $\bar{\sigma}_I$ values from the acetic acids are 0.20–0.28 units smaller than the values from the picolines, i.e., the ammonio-substituted acetic acids are 0.8–1.1 pK units weaker than would be predicted from the $\bar{\sigma}_I$ values derived from the dissociation of picolinium ions. We are unable to account for this. It is of interest that $\bar{\sigma}_I$ for the trimethylammonio substituent which, at 0.71, is consistent with other ammonio and methylammonio values derived from the acetic acid series, is 0.95, from bicyclooctane carboxylic acids, and 0.98, from bicyclooctene carboxylic acids, consistent with the values for the other ammonio substituents derived from the picolines. This suggests that the values obtained from the acetic acid series are anomalous. The $\bar{\sigma}_I$ values for the ammonio, methylammonio, and dimethylammonio substituents derived from the picolines increase in that order. Successive replacement of hydrogen of the ammonio group by methyl should result in increased dispersal of the positive charge and a smaller substituent effect of the substituted ammonio group. However if the ammonio group is extensively solvated through hydrogen bonding its positive charge will be extensively distributed into the solvent. Successive replacement of hydrogen by methyl will then reduce such solvation and increase the concentration of positive charge on the substituent. Evidently the latter factor, the reduction in solvation, is more important than the former, the electron-donating effect of the methyl group.

For dissociation of substituted 2-, 3-, and 4-picolines ρ_I values are 5.449, 3.044, and 2.922, respectively. Qualitatively, these results confirm the conclusion based on the results of the analysis of the pK data for substituted pyridines, in terms of the dual substituent parameter equation (3), that the inductive effect of substituents, as measured by ρ_I is much greater at the 2 position than at the 3 and 4 positions. More quantitatively, the ratio of the ρ_I values for dissociation of substituted picolines and pyridines is 0.51 at the 2 position, 0.51 at the 3 position, and 0.57 at the 4 position. These values measure the attenuation of the inductive effect of substituents produced by the interposition of a methylene group. The attenuation appears to be independent of position and is somewhat smaller (the fall-off factor is closer to unity) than the value often cited, a fall-off factor across a methylene group of 1/2.8 (14). However similar fall-off factors have apparently been observed in some other systems.[4]

The pK values of the 4-picolylammonium ion (4-pyridinemethanamine conjugate acid) and its *N*-methyl and *N*,*N*-dimethyl derivatives are shown in Table 3. The values parallel those of the 2 and 3 isomers and as in those cases the introduction of the first methyl group increases the pK value whereas the second methyl group lowers the pK. The substituent constant (σ^0) for the 4-aza substituent (4-pyridinyl

TABLE 3. Dissociation of 4-picolylammonium ions

Ion	pK	Method[a]
$C_5H_5NCH_2NH_3^+$	8.22	IV
$C_5H_5NCH_2NH_2CH_3^+$	8.48	IV
$C_5H_5NCH_2NH(CH_3)_2^+$	7.63	IV

[a]Described in ref. 1.

[4]Compare with footnote 89 in ref. 11.

Can. J. Chem. Downloaded from www.nrcresearchpress.com by 210.87.254.105 on 09/05/12
For personal use only.

relative to phenyl) evaluated from the pK value for 4-picolylammonium ion is 1.12. This is significantly larger than the value of 0.95, from hydrolysis of benzyl acetates in aqueous acetone (15) and which itself is in excellent agreement with the mean σ value of 0.96 obtained from hydrolysis of methyl and ethyl picolinates in aqueous methanol, aqueous ethanol, aqueous acetone, and aqueous dioxan (16).

Experimental

General experimental methods are described in a previous paper (1).

The following compounds were commercially available: 4-picoline (Aldrich, hydrochloride hygroscopic), 4-*n*-propylpyridine (Baker, hydrochloride mp 158–163°C, dec.), 4-benzylpyridine (Reilly, hydrochloride mp 142–144°C), 4-picolylamine (4-pyridinemethanamine, Reilly), 4-chloromethylpyridine hydrochloride (Aldrich, transformation at 160°C but no melting occurred), 4-pyridylcarbinol (4-pyridinemethanol, Reilly, hydrochloride mp 183–184°C). 4-Trimethylsilylmethylpyridine was supplied by Dr. M. W. Morgan (17).

The following substituted 4-picolines were prepared by methods similar to those described for their 2-isomers (1). Phenyl 4-picolyl sulfone, mp 199–200.5°C (lit. (18) mp 203–204°C); nmr ($CDCl_3$) τ: 1.46 (m, 2, 2-*H* and 6-*H*), 2.93 (d, 2, 3-*H* and 5-*H*), 2.40 (m, 5, C_6H_5), 5.71 (s, 2, CH_2). 4-Pyridinemethanethiol, nmr τ: 1.55 (m, 2, 2-*H* and 6-*H*), 2.83 (m, 2, 3-*H* and 5-*H*), 6.36 (d, 2, J = 8.0 Hz, CH_2, becomes singlet on D_2O exchange), 8.22 (t, 1, S*H*, removed on D_2O exchange); ms (70 eV) *m/e* (relative intensity): 125 (98, M_r (C_6H_7NS) = 125), 93(55), 92(100), 66(24), 65(61), 39(51); picrate (recrystallized from 95% ethanol) mp 153–154°C, *anal.* calcd. for $C_{12}H_{10}N_4O_7S$: C 40.66, N 15.82, H 2.85; found: C 40.89, N 16.35, H 2.74; hydrochloride (recrystallized from methanol – ethyl acetate), mp 154.5–155.5°C; *anal.* calcd. for C_6H_8NSCl: C 44.55, N 8.67, H 4.99; found: C 44.11, N 8.94, H 4.88. 4-Pyridylmethyl acetate (4-pyridinemethanol acetate ester), nmr τ: 1.50 (m, 2, 2-*H* and 6-*H*), 2.82 (m, 2, 3-*H* and 5-*H*), 4.98 (s, 2, CH_2), 7.97 (s, 3, CH_3); hydrochloride (recrystallized from methanol), mp 159–160°C (lit. (19) mp 154–156°C); ms (70 eV) *m/e* (relative intensity); 151 (9, M_r ($C_8H_9NO_2$) = 151), 109(43), 108(20), 92(14), 80(23), 65(18), 43(100), 39(23), 38(28), 36(83). Methyl 4-picolyl sulfone, mp 133.5–134.5°C; nmr ($CDCl_3$) τ: 1.30 (m, 2, 2-*H* and 6-*H*), 2.61 (m, 2, 3-*H* and 5-*H*), 5.75 (s, 2, CH_2), 7.20 (s, 3, CH_3); ms (70 eV) *m/e* (relative intensity): 171.027 (26, M_r ($^{12}C_7{}^1H_9{}^{14}N^{32}S^{16}O_2$) = 171.035), 93(9), 92(100), 65(34), 39(23). *Anal.* calcd. for $C_7H_9NSO_2$: C 49.07, H 5.31, N 8.19; found: C 49.01, H 5.24, N 7.89. Ethyl 4-picolyl sulfone, mp 86–87.5°C; nmr ($CDCl_3$) τ: 1.31 (m, 2, 2-*H* and 6-*H*), 2.60 (m, 2, 3-*H* and 5-*H*), 5.77 (s, 2, CH_2), 7.03 (q, 2, J = 7.0 Hz, CH_2CH_3), 8.63 (t, 3, CH_2CH_3); ms (70 eV) *m/e* (relative intensity): 185.056 (74, M_r ($^{12}C_8{}^1H_{11}{}^{14}N^{32}S^{16}O_2$) = 185.051), 93(35), 92(100), 65(48), 39(22). *Anal.* calcd. for $C_8H_{11}NSO_2$: C 51.84, H 6.00, N 7.57; found: C 51.71, H 5.96, N 7.46. 4-Methoxymethylpyridine, nmr τ: 1.42 (m, 2, 2-*H* and 6-*H*), 2.85 (d, 2, 3-*H* and 5-*H*), 5.63 (s, 2, CH_2), 6.67 (s, 3, OCH_3); hydrochloride (recrystallized from methanol – ethyl acetate), mp 134.5–135.5°C; ms (70 eV) *m/e* (relative intensity): 123 (45, M_r (C_7H_9NO) = 123), 108(41), 93(64), 92(41), 80(48), 65(55), 51(43), 45(78), 39(100), 36(91). 4-Pyridylacetone (1-(4-pyridinyl)2-propanone), hydrochloride (sublimed), mp 149–151°C; nmr (CF_3CO_2H) τ: 1.20 (m, 2, 2-*H* and 6-*H*), 1.94 (d, 2, 3-*H* and 5-*H*), 5.59 (s, 2, CH_2), 7.48 (s, 3, CH_3); ms (70 eV) *m/e* (relative intensity): 135 (18, M_r (C_8H_9NO) = 135), 93(100), 92(20), 65(14), 43(45), 36(29). 4-Phenacylpyridine (1-phenyl-2-(3-pyridinyl)ethanone), mp 114–117°C (lit. (20) mp 112–113°C); nmr ($CDCl_3$) τ: 1.40 (m, 2, 2-*H* and 6-*H*), 2.00 (m, 2, 3-*H* and 5-*H*), 2.60 (m, 5, C_6H_5), 5.71 (s, 2, CH_2); ms (70 eV) *m/e* (relative intensity): 197 (22, M_r ($C_{13}H_{11}NO$ = 197), 105(100), 77(54), 51(18), 39(9); hydrochloride (sublimed), mp 192–195°C. 4-Methylthiomethylpyridine, nmr τ: 1.50 (m, 2, 2-*H* and 6-*H*), 2.83 (m, 2, 3-*H* and 5-*H*), 6.45 (s, 2, CH_2), 8.09 (s, 3, CH_3); hydrochloride (sublimed), mp 144–146°C; ms (70 eV) *m/e* (relative intensity): 139 (100, M_r (C_7H_9NS) = 139), 124(34), 93(53), 92(77), 65(48), 36(56); *anal.* calcd. for $C_7H_{10}NSCl$: C 47.83, N 7.98, H 5.74; found: C 47.77, N 7.83, H 5.80. 4-Acetamidomethylpyridine (*N*-4-pyridinylmethylacetamide), mp 86.5–88°C; nmr ($CDCl_3$) τ: 1.54 (m, 3, 2-*H*, 6-*H* and N*H*), 2.82 (m, 2, 3-*H* and 5-*H*), 5.63 (d, 2, J = 6.0 Hz, CH_2), 8.03 (s, 3, CH_3); ms (70 eV) *m/e* (relative intensity): 150 (100, M_r ($C_8H_{10}N_2O$) = 150), 108(40), 107(67), 92(15), 80(23), 79(25), 43(34). *Anal.* calcd. for $C_8H_{10}N_2O$: C 63.95, N 18.66, H 6.73; found: C 63.72, N 18.71, H 6.64. 4-Methylaminomethylpyridine (*N*-methyl-4-pyridinemethanamine), nmr τ: 1.61 (q, 2, 2-*H* and 6-*H*), 2.82 (m, 2, 3-*H* and 5-*H*), 6.31 (s, 2, CH_2), 7.67 (s, 3, CH_3), 8.19 (s, 1, N*H*, removed by D_2O); ms (70 eV) *m/e* (relative intensity): 122 (85, M_r ($C_7H_{10}N_2$) = 122), 121(57), 107(35), 93(82), 92(50), 80(73), 79(62), 58(70), 44(100). 4-Dimethylaminomethylpyridine (*N,N*-dimethyl-4-pyridinemethanamine), nmr τ: 1.53 (q, 2, 2-*H* and 6-*H*), 2.82 (m, 2, 3-*H* and 5-*H*), 6.62 (s, 2, CH_2), 7.82 (s, 6, CH_3); ms (70 eV) *m/e* (relative intensity): 136 (19, M_r ($C_8H_{12}N_2$) = 136), 135(9), 92(13), 65(9), 58(100), 42(11); dipicrate (recrystallized from 95% ethanol), mp 215–216°C; *anal.* calcd. for $C_{20}H_{18}N_8O_{14}$: C 40.39, N 18.86, H 3.05; found: C 40.40, N 19.06, H 3.01. 4-Phenylthiomethylpyridine, mp 44–45.5°C (lit. (21) mp 48–51°C); nmr τ: 1.62 (m, 2, 2-*H* and 6-*H*), 2.80 (m, 7, 3-*H*, 5-*H* and C_6H_5), 6.14 (s, 2, CH_2); hydrochloride (recrystallized from absolute ethanol – ether and sublimed), mp 135–137°C (lit. (21) mp 142–144°C). 4-Phenoxymethylpyridine; hydrochloride (recrystallized from methanol–ether), mp 153–156°C; nmr (D_2O) τ: 0.90 (d, 2, 2-*H* and 6-*H*), 1.52 (d, 2, 3-*H* and 5-*H*), 2.39 (m, 5, C_6H_5), 4.22 (s, 2, CH_2); ms (70 eV) *m/e* (relative intensity): 185 (100, M_r ($C_{12}H_{11}NO$) = 185), 94(78), 92(91), 65(50), 39(27), 36(40). 4-*N*-Acetylmethylaminomethylpyridine (*N*-methyl-4-pyridinylmethylacetamide), mp 48–49.5°C; nmr τ: 1.55 (m, 2, 2-*H* and 6-*H*), 2.95 (d, 2, 3-*H* and 5-*H*), 5.55 (s, 2, CH_2), 7.08 (s, 3, N—CH_3), 7.91 (s, 3, $COCH_3$); ms (70 eV) *m/e* (relative intensity): 164 (100, M_r ($C_9H_{12}N_2O$) = 164), 121(69), 107(75), 93(31), 92(30), 79(37), 44(70), 43(55). *Anal.* calcd. for $C_9H_{12}N_2O$: C 65.80, N 17.07, H 7.38; found: C 65.86, N 16.99, H 7.38. 4-Nitromethylpyridine, mp 119–120°C (lit. (10) mp 97°C). *Anal.* calcd. for $C_6H_6N_2O_2$: C 52.15, N 20.29, H 4.38; found: C 52.39, N 20.07, H 4.38.

The following substituted 4-picolines were prepared by methods similar to those described for their 3-isomers. 4-Bromomethylpyridine hydrobromide (recrystallised from absolute ethanol and sublimed), did not melt on slow heating but fast heating gave a mp of 200°C (lit. (22) mp 185–187°C). *Anal.* calcd. for $C_6H_7NBr_2$: C 28.47, H 2.80, N 5.54; found: C 28.35, H 2.78, N 5.68. 4-Thiocyanatomethylpyridine thiocyanate mp 115–116.5°C (lit. (23) mp 120°C); ms (70 eV) *m/e* relative intensity): 150 (7, M_r ($C_7H_6N_2S$) = 150), 92(63), 65(61), 59(72), 39(100), 32(68).

Methyl 4-pyridyl acetate. Carbonation of 4-picolyllithium (from 4-picoline and phenyllithium) gave the lithium salt of 4-pyridylacetic acid. Dissolution of the latter in methanol followed by saturation with hydrogen chloride gave the ester which was distilled at 105–110°C under reduced pressure, nmr τ: 1.54 (m, 2, 2-*H* and 6-*H*), 2.89 (m, 2, 3-*H* and 5-*H*), 6.41

(s, 3, CH_3), 6.50 (s, 2, CH_2); hydrochloride (recrystallized from methanol), mp 204.5–207°C; ms (70 eV) *m/e* (relative intensity): 151 (100, M_r ($C_8H_9NO_2$) = 151), 107(25), 106(25), 92(87), 65(44), 59(42), 39(25), 36(41). Ethyl 4-pyridylacetate was prepared similarly, nmr τ: 1.55 (m, 2, 2-*H* and 6-*H*), 2.88 (m, 2, 3-*H* and 5-*H*), 5.90 (q, 2, J = 7.0 Hz, CH_2CH_3), 6.50 (s, 2, CH_2CO), 8.82 (t, 3, CH_2CH_3); ms (70 eV) *m/e* (relative intensity): 165 (100, M_r ($C_9H_{11}NO_2$) = 165), 154(81), 106(40), 93(77), 92(81), 65(38), 29(55). The hydrochloride could not be satisfactorily prepared.

4-Pyridylacetonitrile was prepared by refluxing 4-chloromethylpyridine hydrochloride with potassium cyanide in aqueous methanol. After distillation at 100°C under reduced pressure the product solidified on standing, and was obtained in 25% yield. The hydrochloride was prepared and recrystallized from absolute ethanol. It decomposed on heating above 255°C (lit. (24) mp 270–272°C); nmr (CF_3COOH) τ: 1.61 (m, 2, 2-*H* and 6-*H*), 2.43 (d, 2, 3-*H* and 5-*H*), 6.14 (s, 2, CH_2); ms (70 eV) *m/e* (relative intensity): 118 (100, M_r ($C_7H_6N_2$) = 118), 91(39), 78(27), 64(42), 51(54), 38(29), 36(83). *Anal.* calcd. for $C_7H_7N_2Cl$: C 54.35, N 18.13, H 4.56; found: C 54.48, N 18.31, H 4.55.

The methods for determining the pK values have been described (1).

Acknowledgements

We thank the National Research Council of Canada and the University of Victoria Committee on Research and Travel for generous financial support and for the award of a National Research Council of Canada Post-graduate Bursary and a University of Victoria Post-graduate Scholarship to M.J.K.

1. A. Fischer, M. J. King, and F. P. Robinson. Can. J. Chem. **56**, 3059 (1978).
2. A. Fischer, M. J. King, and F. P. Robinson. Can. J. Chem. **56**, 3068 (1978).
3. S. Ehrenson, R. T. C. Brownlee, and R. W. Taft. *In* Progress in physical organic chemistry. Vol. 10. *Edited by* A. Streitwieser, Jr. and R. W. Taft. Interscience, New York, NY. 1973. p. 1.
4. C. A. Grob and M. G. Schlageter. Helv. Chim. Acta, **59**, 264 (1976).
5. M. Charton. J. Org. Chem. **29**, 1222 (1964).
6. H. D. Holtz and L. M. Stock. J. Am. Chem. Soc. **86**, 5188 (1964); F. W. Baker, R. C. Parish, and L. M. Stock. J. Am. Chem. Soc. **89**, 5677 (1967).
7. (*a*) O. Exner and J. Jonáš. Coll. Czech. Chem. Commun. **27**, 2296 (1962); (*b*) O. Exner. Coll. Czech. Chem. Commun. **31**, 65 (1966).
8. R. W. Taft. J. Phys. Chem. **64**, 1805 (1960).
9. C. Eaborn. Organosilicon compounds. Butterworths, London, U.K. 1960. pp. 102 and 149.
10. H. Feuer and J. P. Lawrence. J. Org. Chem. **37**, 3662 (1972).
11. R. T. Taft, E. Price, I. R. Fox, I. C. Lewis, K. K. Andersen, and G. T. Davies. J. Am. Chem. Soc. **85**, 709 (1963).
12. H. Stetter and J. Mayer. Chem. Ber. **95**, 667 (1962).
13. S. Siegel and J. M. Komarmy. J. Am. Chem. Soc. **82**, 2547 (1960).
14. G. E. K. Branch and M. Calvin. The theory of organic chemistry. Prentice-Hall, New York, NY. 1941. p. 204.
15. L. W. Deady and R. A. Shanks. Aust. J. Chem. **25**, 431 (1972).
16. H. H. Jaffé and H. L. Jones. Adv. Heterocycl. Chem. **3**, 209 (1964); A. D. Campbell, S. Y. Chooi, L. W. Deady, and R. A. Shanks. Aust. J. Chem. **23**, 203 (1970); L. W. Deady and R. A. Shanks. Aust. J. Chem. **25**, 2363 (1972).
17. A. Fischer, M. W. Morgan, and C. Eaborn. J. Organometal. Chem. **136**, 323 (1977).
18. S. Golding, A. R. Katritzky, and H. Z. Kucharska. J. Chem. Soc. 3090 (1965).
19. K. Augustinsson and H. Hasselguist. Acta Chem. Scand. **18**, 1009 (1964).
20. C. Osuch and R. Levine. J. Org. Chem. **22**, 939 (1957).
21. L. Bauer and L. Gardella. J. Org. Chem. **28**, 1323 (1963).
22. R. L. Bixler and C. Niemann. J. Org. Chem. **23**, 575 (1958).
23. W. Mathes and A. Wolf. U.S. patent No. 2,848,457; Chem. Abstr. **53**, 1384i (1959).
24. B. E. Betts and W. Davey. J. Chem. Soc. 3339 (1961).

Can. J. Chem. Downloaded from www.nrcresearchpress.com by 210.87.254.105 on 09/05/12
For personal use only.

The oxygen exchange from $O_2/C^{18}O_2$ with surfaces of vanadium pentoxide and alkali metal-promoted vanadium pentoxide catalysts

DAVID VICTOR FIKIS, KEITH WALTER HECKLEY, WILLIAM JOHN MURPHY,[1] AND ROBERT ANDERSON ROSS

Department of Chemistry, Lakehead University, Thunder Bay, Ont., Canada P7B 5E1

Received July 7, 1978

DAVID VICTOR FIKIS, KEITH WALTER HECKLEY, WILLIAM JOHN MURPHY, and ROBERT ANDERSON ROSS. Can. J. Chem. **56**, 3078 (1978).

The oxygen exchange reaction between $O_2/C^{18}O_2$ and the surfaces of vanadium pentoxide and promoted vanadium pentoxide catalysts has been studied in a circulation system using a quartz differential reactor. Isotopic compositions were analysed with an in-line mass spectrometer. Alkali metal sulphates, Li to Cs, were added to the pentoxide as individual promoters at a concentration level of 9 mol% and the effect of variation of promoter concentration was examined with melts containing potassium sulphate at additional levels of 1, 2, and 5 mol%. The structures of the solids were studied by X-ray diffraction and by ATR and transmission infrared spectroscopy. The latter results have been used to explain the two activity series for the exchange rates: (*i*) V_2O_5 < Na < Li < K < Rb < Cs (melts) and (*ii*) V_2O_5 < 1 mol% < 2 mol% < 5 mol% < 9 mol% (K), in terms of additive effects on the relative abundance and strength of identified vanadium/oxygen linkages in the surfaces of the catalysts.

DAVID VICTOR FIKIS, KEITH WALTER HECKLEY, WILLIAM JOHN MURPHY et ROBERT ANDERSON ROSS. Can. J. Chem. **56**, 3078 (1978).

On a étudié dans un système à circulation muni d'un réacteur différentiel en quartz, les réactions d'échange d'oxygène entre $O_2/C^{18}O_2$ et les surfaces de catalyseurs de pentoxyde de vanadium et de pentoxyde de vanadium activé. Un spectromètre de masse en série analysait les compositions isotopiques. On a effectué des expériences en utilisant à titre de seul promoteur le sulfate d'un métal alcalin, de Li à Cs, qu'on ajoutait au pentoxyde à une concentration de 9 mol%. On a examiné l'influence d'une variation de la concentration du promoteur à l'aide d'autres échantillons contenant du sulfate de potassium à raison de 1, 2, et 5 mol%. On a étudié la structure des solides en utilisant la diffraction des rayons X, ainsi que la spectroscopie infrarouge par transmission et par RTA. Les vitesses d'échange ont conduit au classement de l'activité des systèmes selon les séries suivantes: (*i*) V_2O_5 < Na < Li < K < Rb < Cs et (*ii*) V_2O_5 < 1 mol% < 2 mol% < 5 mol% < 9 mol% (K). Les résultats des méthodes énumérées ci-dessus ont permis de relier ces deux séries aux effets conjugués de l'abondance et de la force relatives des liens vanadium/oxygène se trouvant sur la surface des catalyseurs.

[Traduit par le journal]

Introduction

Vanadium pentoxide and vanadium pentoxide promoted with alkali metal sulphates have been used extensively as oxidation catalysts. The addition of these promoters has been shown to influence catalyst activity in oxygen exchange (1, 2), sulphuric acid production (3), and sulphur dioxide oxidation (4) in accord with the activity series:

$$V_2O_5\,(\text{none}) < (Li_2SO_4) < (Na_2SO_4) < (K_2SO_4) < (Rb_2SO_4) < (Cs_2SO_4)$$

A similar series has been reported for the reducibility of the catalysts by hydrogen (5). Catalyst activity increases also with increase in the concentration level of the additive up to 50 mol% (6).

These observations have been attributed to changes in the mobility of the catalyst oxygen (1, 2, 6, 7) which, in turn, has been related to the relative abundance of V^{4+} sites in the surface (2, 7, 8). This latter feature has also been reported to influence the activity of similar materials, vanadium bronzes, in the heterogeneous decomposition of 2-propanol (9).

Although relationships between activities and such properties as electrical conductivity have been explored (1, 9, 10), very few data are available, particularly for the promoted samples, regarding surface chemical factors which might influence catalyst activity. Infrared spectroscopic observations have shown that various changes occur in the spectra of vanadium pentoxide on mixing with alkali metal sulphates (11) and initiated the proposal that

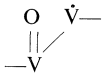

species is the active centre for oxygen exchange on vanadium pentoxide (12).

These investigations have now been extended to

[1]Present address: Research Department, Imperial Oil Ltd., Sarnia, Ont.

Can. J. Chem. Downloaded from www.nrcresearchpress.com by 210.87.254.5 on 09/05/12
For personal use only.

include a kinetic and mechanistic study of the oxygen exchange reaction between oxygen, carbon dioxide, and vanadium pentoxide as well as vanadium pentoxide modified by the addition of alkali metal sulphates. The solids have also been examined by ATR and transmission infrared spectroscopy in an attempt to identify active catalytic sites and any variation in site distribution which might be affected by addition of 1.01, 2.00, 4.98, and 9.09 mol% potassium sulphate and also by a change of the atomic number of the alkali metal additive at a fixed concentration, 9.09 mol%.

Experimental

Apparatus and Procedure

The kinetic measurements were carried out in an all-glass circulation apparatus described previously (13) using a quartz differential reactor. Total volume of the circulation loop of the apparatus was 507 ml. Analysis of the isotopic compositions of the gaseous mixture was obtained from a Vacuum Generator Micromass mass spectrometer, incorporating lanthanum hexaboride coated tungsten filaments. This unit was attached to the circulation loop via a capillary leak and operated at $\sim 3 \times 10^{-6}$ Torr.

Samples were pretreated at 500°C for 4 h in dry circulating oxygen at 10 Torr (1.33 kN m^{-2}) in order to remove adsorbed gases and to stabilise the oxygen content of the surface. Rubidium- and caesium-promoted samples were pretreated at 420°C. Experiments were performed primarily at partial pressures of 10 Torr oxygen and 2 Torr carbon dioxide. These pressures were varied between 2 and 3 Torr and 0.66 and 4.2 Torr, respectively, for rate order determinations. The catalyst charge was 10 g in all runs.

Materials

Vanadium pentoxide was >99.9% pure (Ventron, Boston). Samples containing alkali metal sulphates (Ventron, >99.9% pure) were prepared by mixing vanadium pentoxide powder and the corresponding weight of the appropriate additive in a ball mill for 2 h. This mixture was then heated at 700°C for 4 h in a quartz dish. The liquid melts were cooled rapidly, ground, and pelletized in a 1.27 cm die (ram pressure 3 tons) for 2 min. These pellets, and the pellets of pure vanadium pentoxide which were prepared in a similar manner, were calcined at 500°C for 10 h with the exception of the caesium and rubidium sulphate melts which were calcined at 430°C. The pellets were crushed and sieved to a particle diameter between 1 and 2 mm for the catalytic studies.

Oxygen (research purity grade, 99.995%) was supplied by Matheson Ltd., Toronto and the $C^{18}O_2$ (Lot 1876; >99%) was purchased from Stohler Isotope Chemicals, Montreal.

The surface areas of the catalysts (BET, krypton, σ = 21.1 Å^2) were 0.75, 0.58, 0.40, 0.86, 0.48, and 0.24 $m^2\ g^{-1}$ for the V_2O_5 and the catalysts containing 9.09 mol% Li_2SO_4, Na_2SO_4, K_2SO_4, Rb_2SO_4, and Cs_2SO_4, respectively. The surface areas of the 1.01, 2.00, and 4.98 mol% K_2SO_4-promoted catalysts were 0.52, 0.88, and 0.51 $m^2\ g^{-1}$, respectively. No change in surface area was observed after reaction. Chemical analyses of the various melts showed a maximum residual sulphate level of ~1 ppm prior to use in catalysis. This value was similar to that found with pure vanadium pentoxide samples, ~1 ppm in agreement with previous work (14).

The ir spectra reported were obtained by the KBr technique using a Beckman IR 12 IR spectrometer and X-ray analyses were conducted with Philips equipment.

Results

The exchange rates were studied from 400 to 500°C with the exception of samples promoted with Rb_2SO_4 and Cs_2SO_4 which were examined from 320 to 420°C. These latter catalysts evolved oxygen above 440°C.

Figure 1 shows a typical product distribution for the exchange reaction. All ^{18}O species exchanged with the surface or bulk oxygen of the catalysts in agreement with the literature (15, 16). No change in the ^{18}O content of molecular oxygen was observed during reaction and the reaction products were free of carbon monoxide.

The rates of exchange, R, at the various temperatures shown in Table 1 were determined from the expression (17)

$$[1] \qquad R = \frac{2.3 N_{O_2} N_{CO_2}}{S\tau(N_{O_2} + N_{CO_2})} \log (1 - F)$$

where S is the total surface area of the catalyst (in m^2); N_{O_2} is the amount of oxygen in the O_2 form (in g); N_{CO_2} is the amount of oxygen in CO_2 (in g); $F = (C_0 - C)/(C_0 - C_\infty)$ where C_0 is the initial concentration of ^{18}O (in %) in CO_2, C is the concentration of ^{18}O at the time of exchange, τ; and C_∞ is the equilibrium concentration of ^{18}O in the CO_2 (<2%). Applicability of eq. [1] to each exchange condition was demonstrated by plots of $-\log (1 - F)$ vs. τ. All gave straight lines with a typical correlation coefficient ~0.995.

The reaction rate was independent of both oxygen and carbon dioxide partial pressures in general agreement with current literature (15, 16) on similar systems.

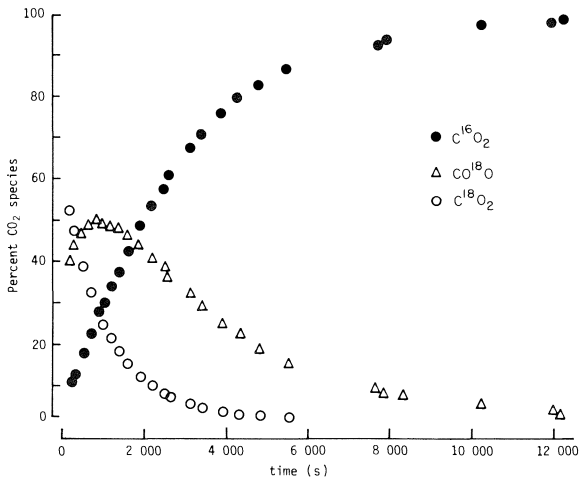

FIG. 1. Carbon dioxide product distribution at 500°C for the exchange of $^{16}O_2$, $C^{18}O_2$, and V_2O_5 promoted with 9.09 mol% Li_2SO_4.

Can. J. Chem. Downloaded from www.nrcresearchpress.com by 210.87.254.5 on 09/05/12
For personal use only.

TABLE 1. Rate of exchange of oxygen from CO_2 in g O_2 m^{-2} s^{-1} ($\times 10^7$)

	Rate							Activation energy (kJ/mol)
	340°C	370°C	400°C	420°C	450°C	480°C	500°C	
V_2O_5	—	—	—	0.94	1.38	2.67	3.02	4.3
1.01 mol% $K_2SO_4.V_2O_5$	—	—	—	1.74	3.35	4.93	6.61	4.2
2.00 mol% $K_2SO_4.V_2O_5$	—	—	—	4.90	9.00	10.10	14.20	3.0
4.98 mol% $K_2SO_4.V_2O_5$	—	—	—	7.23	10.29	14.40	16.60	2.9
9.09 mol% $K_2SO_4.V_2O_5$	—	—	—	11.00	16.03	22.00	28.20	2.8
9.09 mol% $Li_2SO_4.V_2O_5$	—	—	—	2.90	3.78	4.54	6.12	2.3
9.09 mol% $Na_2SO_4.V_2O_5$	—	—	—	1.45	1.97	3.69	4.90	3.9
9.09 mol% $Rb_2SO_4.V_2O_5$	4.08	9.10	16.0	20.90	—	—	—	4.1
9.09 mol% $Cs_2SO_4.V_2O_5$	6.99	18.50	52.3	76.00	—	—	—	6.4

Figure 2 shows the transmission infrared spectra of V_2O_5 and V_2O_5 promoted with alkali metal sulphates. Three major peaks are evident in the spectrum of V_2O_5 at 1020, 825, and 450 to 600 cm^{-1}. The first two have been identified respectively (12) as the V=O stretching vibration (1020 cm^{-1}) (18, 19) and the V—O—V stretching vibration (825 cm^{-1}). The nature of the vibration giving rise to the band at 450 to 600 cm^{-1} is uncertain but may be due to V—O—V rocking vibrations. Figure 2 further shows that with increase in the atomic number of the alkali metal additive, the V=O band splits into a multiplet. A similar but less marked effect is observed with the V—O—V stretch.

Figure 3 shows the infrared spectra of V_2O_5 and V_2O_5 promoted with the various levels of potassium sulphate. Again, the V=O peak splits and although the V—O—V band does not split, a destabilisation down scale is observed with increasing concentration level of the additive. Parallel experiments using

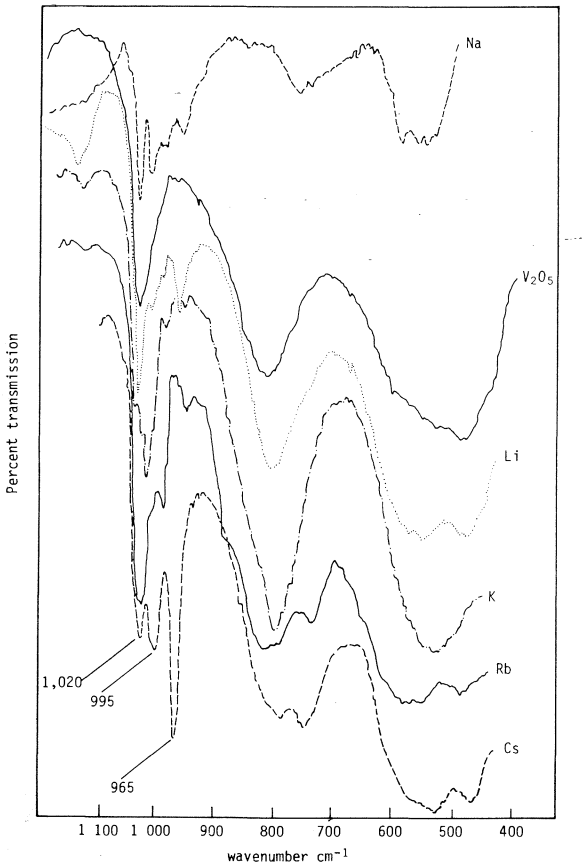

FIG. 2. Transmission infrared spectra of V_2O_5 promoted with 9.09 mol% alkali metal sulphates.

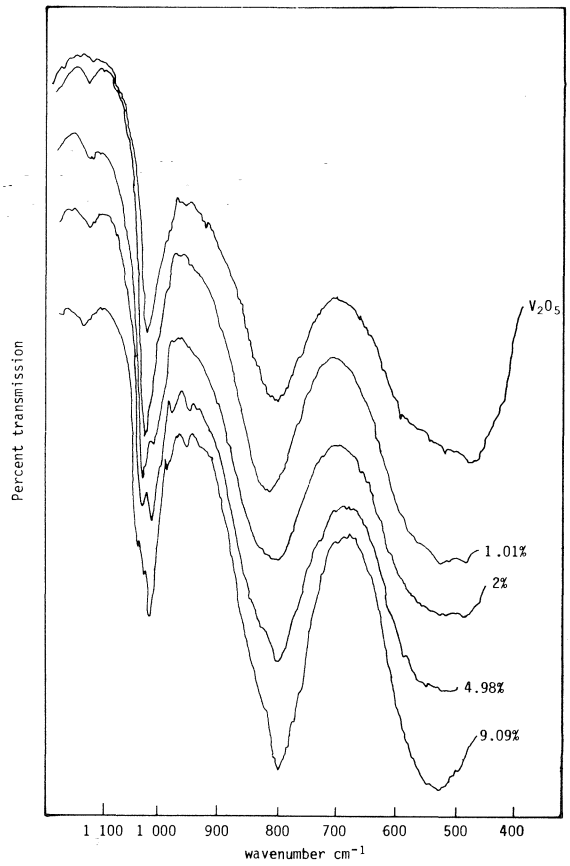

FIG. 3. Transmission infrared spectra of V_2O_5 and V_2O_5 containing various concentration levels of potassium sulphate.

Can. J. Chem. Downloaded from www.nrcresearchpress.com by 210.87.254.5 on 09/05/12
For personal use only.

Can. J. Chem. Downloaded from www.nrcresearchpress.com by 210.87.254.5 on 09/05/12
For personal use only.

infrared ATR spectroscopy were performed and although the results showed similar behaviour, spectra were not so well defined.

Discussion

The solid solution of an alkali metal in vanadium pentoxide is known to modify the host lattice in a manner related to the atomic number and concentration of the added metal (20, 21). Thus, lithium, sodium, and potassium form a series of bronzes of general formula $M_xV_2O_5$ (9) which at low concentrations (Li, $0 < x \leq 0.13$; Na, $0 \leq x \leq 0.02$; K, $0 < x \leq 0.006$) are isostructural with orthorhombic vanadium pentoxide, α-bronzes. At higher concentrations of lithium ($0.22 \leq x \leq 0.62$) and sodium ($0.22 \leq x \leq 0.40$) the β-phase is formed with a monoclinic unit cell (9, 21). With the exception of the sodium promoted samples, all of the present catalysts gave X-ray diffraction patterns indistinguishable from that for vanadium pentoxide.

The catalysts containing sodium formed β-vanadium bronzes. In all of these solid solutions, the alkali metal atom occupies interstitial positions in tunnels or channels between V—O—V layers in the pentoxide lattice (21), as shown in Fig. 4.

The oxidation state of vanadium in vanadium pentoxide can influence catalyst activity (2, 7–9) and esr studies have indicated that the occurrence of the 4+ oxidation state is enhanced by alkali metal promotion (9). In some V_2O_5 glasses the V^{4+}/V^{5+} ratio can reach a level of 50% (22–24).

Table 1 shows two activity series for the exchange rates:

$$V_2O_5 < Na < Li < K < Rb < Cs \text{ (melts)}$$

and

$$V_2O_5 < 1.01 \text{ mol\%} < 2.00 \text{ mol\%} < 4.98 \text{ mol\%} < 9.09 \text{ mol\% (K)}$$

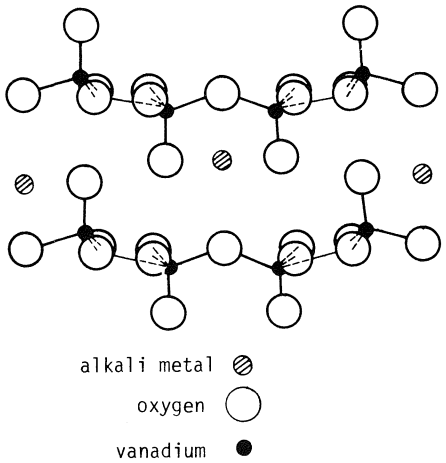

FIG. 4. Projection of the structure of V_2O_5 in the (001) plane.

A comparison of these data with results recorded for similar catalysts in oxidation (4, 5) and oxygen-exchange studies (1, 2) shows that the second series is similar but the positions of Na and Li are reversed in the first. Earlier series have been related to both oxygen mobility and V^{4+} concentrations in the oxides (2, 7, 8). However, for β-vanadium bronzes it has also been reported that electron transfer reactions within the solid are more preponderant than for the other solid solutions. Specifically, a higher concentration of V^{4+} ions are formed (10, 25, 26). Thus the decrease in activity of the sodium-promoted catalyst in this study may somehow be inversely related to the preponderance of the 4+ oxidation state.

A mechanism of the type shown in Scheme 1 may

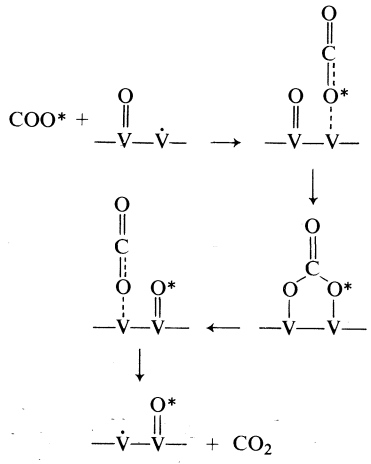

SCHEME 1

be applicable to the exchange reaction of O_2, CO_2, and V_2O_5, with carbon dioxide adsorbing to form a surface carbonate species. The scheme is similar to that of Hirota *et al.* (15) proposed for V_2O_5 alone but differs regarding the inclusion of the bidentate carbonate type intermediate.

The active sites are the adjacent $\begin{matrix}O\\\|\\-V-\dot{V}-\end{matrix}$ species and —V̇— represents V^{4+}. The V=O and the V—O—V stretching frequencies have been identified by transmission ir spectroscopy as occurring at 1020 cm^{-1} and 820 cm^{-1} (12).

Figure 2 shows that as the atomic number of the alkali metal promoter is increased the V=O stretching frequency band at 1020 cm^{-1} splits into a number of components with splitting increasing as the atomic number increases. This may be attributed to the destabilisation of V=O bands. A similar but less pronounced effect is observed with the V—O—V net stretch at 820 cm^{-1}. For the sodium-promoted catalyst although splitting and destabilisation of the V=O peak is observed, the population of such spe-

Can. J. Chem. Downloaded from www.nrcresearchpress.com by 210.87.254.5 on 09/05/12
For personal use only.

cies is very small when compared to the other members of the series. There is a corresponding destabilisation of the V—O—V stretching frequency from 820 to 750 cm^{-1}. Comparison of the relative populations of the V=O and destabilised V=O species with the activity series suggests that correlations may be possible.

Thus, the rates of reaction on the V_2O_5 and sodium-promoted catalysts may be dependent on two factors: (*a*) the population of all V=O species and (*b*) the percentage of the population of the weaker V=O species on the surface. And although the V=O species peak in the sodium-promoted catalyst is weaker than that in V_2O_5, the weaker V=O species in the sodium catalyst (1000 cm^{-1}), which is not present in the V_2O_5, may be contributing to catalyst activity.

Figure 3 provides information as to how the relative populations of the V=O and weakened V=O species might affect activity in the potassium series. As the additive percentage increases from 0 to 9.09 mol%, a gradual increase in the relative abundances of the weaker V=O species over the 'normal' V=O species may be noted in direct parallel with the trend in activities.

The zero order dependence of the reaction rate on carbon dioxide concentration indicates that the rate-determining step is invoked in the surface reaction and, acknowledging the data of Figs. 2 and 3, a mechanism may be proposed which recognises the influence of the polarity of the V=O species:

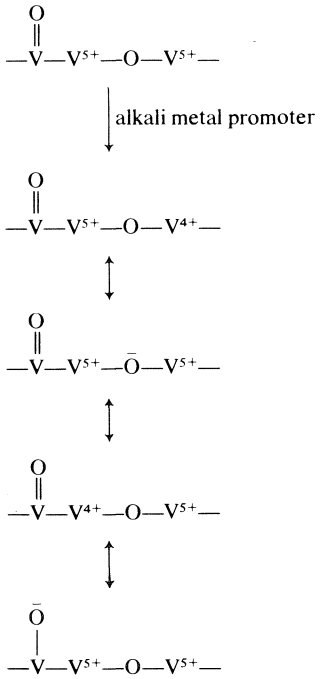

A measure of delocalisation may be expected through the interaction of the 3*d* orbital electron in V^{4+} with adjacent *p* orbitals of surface oxygen species. Since the added level of sodium caused a change in crystal structure from orthorhombic to monoclinic, the perturbation of the V—O—V network may be expected to modify in a direction which decreases the extent of delocalisation.

Since no change in the ^{18}O content of molecular oxygen was observed during reaction and since the exchange of oxygen between O_2 and the surface is slower (7) than that with CO_2, the formation of complexes by stepwise associative mechanisms involving CO_2 and O_2 would appear to be ruled out (16). Furthermore, no carbon monoxide was detected during the course of reaction which may indicate that a carbon–surface bond is likely to form before oxygen–carbon bond scission during the adsorption of carbon dioxide.

The activation energies are in good agreement with values reported for similar reactions (16, 17) and also exhibit a monotonic compensation effect with the rates. This latter feature provides some confirmation of the proposal regarding the location of rate control (27).

The increase in activation energy for the series Li < K < Rb < Cs may be related to the stability of the transient carbonate-type intermediate shown in Scheme 1 or in the following structure,

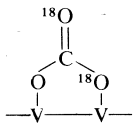

which would result from non-dissociative adsorption of CO_2. Both may occur since each may be regarded as a transient intermediate of the same basic adsorbed state and are indistinguishable in the present study.

Table 1 shows that the exchange rate over the sodium-promoted catalyst is lower than that for the lithium melt. This is consistent with a decrease in the population of V=O species while the faster rate measured for the same catalyst when compared with V_2O_5 may be related to a comparative decrease in electron delocalisation over the V—O—V network. The presence of some weakened V=O species, ~1000 cm^{-1}, indicates that some delocalisation does occur perhaps through modifications of surface forms, such as:

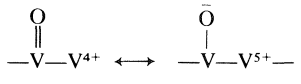

which could result in bond stabilisation during the formation of a carbonate-like intermediate. It could

be postulated that the latter would be more stable on vanadium pentoxide than on the samples containing Li or K, say, if the charge on the V^{4+} centre was of reduced range. Similarly, the higher activation energy for exchange on vanadium pentoxide may be a feature of effective delocalisation confined to limited areas of the surface.

1. A. P. DZISYAK, G. K. BORESKOV, L. A. KASATKINA, and V. E. KOCHURIKHIN. Kinet. Catal. **2**, 655 (1961).
2. V. N. BIBIN and L. A. KASATKINA. Kinet. Catal. **15**, 653 (1964).
3. G. K. BORESKOV. Catalysis in sulphuric acid production (in Russian). State press for Chemical Literature, Moscow. 1954.
4. P. JIRU, D. TOMKOVA, V. JARA, and J. WANKOVA. Z. Anorg. Allg. Chem. **121**, 303 (1960).
5. D. G. KLISSURSKI and N. Ts. ABADZHIEVA. Khim. Ind. Sofia, **46**, 250 (1974).
6. L. A. KASATKINA, G. K. BORESKOV, and P. N. SOKOLOV. Russ. J. Phys. Chem. **34**, 168 (1960).
7. G. K. BORESKOV, L. A. KASATKINA, V. V. POPOVSKII, and YU A. BALOVNEV. Kinet. Catal. **1**, 207 (1960).
8. O. V. KRYLOV. Catalysis by nonmetals. Academic Press, New York. 1970. p. 174.
9. D. K. CHAKRABARTY, D. GUHA, and A. B. BISWAS. J. Solid State Chem. **22**, 263 (1977).
10. D. K. CHAKRABARTY, D. GUHA, I. K. BHATNAGAR, and A. B. BISWAS. J. Catal. **45**, 305 (1976).
11. P. JIRU. Vanadieye Katalizatory Dlya Kontaktn. Proizv. Sernoi Kisloty, Nauchn. Issled. Inst. Udobr i Insektofung., S.B. State i. 1963. p. 21.
12. Y. KERA and K. HIROTA. J. Phys. Chem. **73**, 973 (1969).
13. V. V. POPOVSKII and G. K. BORESKOV. Kinet. Catal. **1**, 566 (1960).
14. D. V. FIKIS, W. J. MURPHY, and R. A. ROSS. Can. J. Chem. **56**, 2530 (1978).
15. K. HIROTA, Y. KERA, and S. TERATAINI. J. Phys. Chem. **72**, 3133 (1968).
16. G. K. BORESKOV and V. S. MUZYKANTOV. N.Y. Acad. Sci. Ann. **213**, 137 (1973).
17. L. A. KASATKINA and G. V. ANTOSHIN. Kinet. Catal. **2**, 252 (1963).
18. H. I. EICHHOFF and F. WEIGEL. Z. Anorg. Allg. Chem. **275**, 267 (1954).
19. R. A. MILLAR and L. R. COUSINS. J. Chem. Phys. **26**, 329 (1957).
20. A. A. FOTIEV and B. V. SLOBODIAN. Russ. J. Chem. **10**, 80 (1965).
21. P. HAGENMULLER. Comprehensive inorganic chemistry. Vol. 4. *Edited by* A. F. Trotman-Dickenson. Pergamon Press, Oxford, England. 1973. p. 572.
22. M. MUNAKATA. Solid-State Electron. **1**, 159 (1960).
23. H. H. NESTER and W. D. KINGERY. *In* VII International Congress on Glass. Brussels. 1965. Paper No. 106.
24. H. ROWSON. Inorganic glass-forming systems. Academic Press, New York. 1967. p. 195.
25. J. H. PERLSTEIN. J. Solid State Chem. **3**, 317 (1971).
26. J. H. PERLSTEIN and M. J. SIENKO. J. Chem. Phys. **48**, 174 (1968).
27. A. K. GALWEY. Adv. Catal. **26**, 247 (1977).

Can. J. Chem. Downloaded from www.nrcresearchpress.com by 210.87.254.5 on 09/05/12
For personal use only.

The standard enthalpy of ionization of water at 298 K from calorimetric measurements on iodine pentoxide

PAUL J. CERUTTI, HON CHUNG KO, KEITH G. MCCURDY, AND LOREN G. HEPLER

Department of Chemistry, University of Lethbridge, Lethbridge, Alta., Canada T1K 3M4

Received July 7, 1978

PAUL J. CERUTTI, HON CHUNG KO, KEITH G. MCCURDY, and LOREN G. HEPLER. Can. J. Chem. **56**, 3084 (1978).

We have made calorimetric measurements of the enthalpies of reaction of I_2O_5(c) with water and with a small excess of OH^-(aq) and have combined the results to obtain $\Delta H^0 = 13.34_0$ kcal mol^{-1} for the standard enthalpy of ionization of water. It is suggested that this approach can be applied usefully to investigation of the enthalpy of ionization of D_2O for which there are still unresolved differences between reported values.

PAUL J. CERUTTI, HON CHUNG KO, KEITH G. MCCURDY et LOREN G. HEPLER. Can. J. Chem. **56**, 3084 (1978).

On a mesuré par calorimétrie l'enthalpie des réactions de I_2O_5(c) avec l'eau, d'une part, et avec un léger excès de OH^-(aq), d'autre part; à l'aide de ces résultats réunis, on a établi que l'enthalpie standard d'ionisation de l'eau est $\Delta H^0 = 13.34_0$ kcal mol^{-1}. On signale l'intérêt que peut présenter cette méthode pour l'étude de l'enthalpie d'ionisation de D_2O, enthalpie pour laquelle il existe entre les valeurs rapportées dans la littérature des écarts d'origine encore mal connue.

[Traduit par le journal]

Introduction

Reliable information about the self-ionization of water represented by

[1] $$H_2O(liq) \rightleftharpoons H^+(aq) + OH^-(aq)$$

is required for investigations of aqueous acids and bases, and also for other investigations that involve aqueous solutions. More specifically, we need to know the equilibrium constant K_ω and related thermodynamic quantities such as ΔG_ω^0, ΔH_ω^0, ΔS_ω^0, ΔC_p^0, ΔV^0, etc. It now appears that K_ω and ΔG_ω^0 are very well known at 25°C and 1 atm, and are pretty well known over a wide range of temperature and pressure (1–4). On the other hand, in spite of a considerable number of previous investigations, small but important uncertainties persist in the various other thermodynamic properties at 25°C and 1 atm, with generally larger uncertainties at other temperatures and pressures.

Because we are here concerned with ΔH_ω^0 at 25°C for the reaction represented by [1], we now focus our attention on some previous results that illustrate the need for still one more investigation of this old problem.

Our most reliable ΔH_ω^0 values for [1] appear to come from calorimetric investigations that are all of the same type in which the enthalpy of mixing a strong acid (usually HCl or $HClO_4$) with a strong base (usually NaOH) is measured at finite concentrations; results are either combined with enthalpies of dilution or extrapolated to zero concentration to obtain the desired standard state enthalpy represented by ΔH_ω^0. Procedures for using enthalpies of dilution (5, 6) and for extrapolation (7) have been published. The best results obtained this way (1–4) appear to range from $\Delta H_\omega^0 = 13.33$ to 13.36 kcal mol^{-1}, with $\Delta H_\omega^0 = 13.34$ kcal mol^{-1} commonly being selected for further use.

Another common way to obtain the desired ΔH_ω^0 is by application of d ln $K_\omega/dT = \Delta H_\omega^0/RT^2$ to K_ω values obtained at several temperatures. Possibly the most often quoted value obtained in this way is $\Delta H_\omega^0 = 13.526$ kcal mol^{-1} as calculated by Covington, Robinson, and Bates (8) from the earlier emf results of Harned and Robinson (9). Although the more recent thorough investigation by Covington and co-workers (10) indicates that small systematic errors in the emf results are the probable source of the discrepancy between ΔH_ω^0 values, we note that there is some calorimetric support (cited in refs. 1–4) for ΔH_ω^0 values at least 0.10 kcal mol^{-1} larger than the commonly selected value cited in the paragraph above.

Because of the possibility of small but important systematic errors (10) in K_ω values at different temperatures and thence in ΔH_ω^0 values obtained by application of d ln $K_\omega/dT = \Delta H_\omega^0/RT^2$ and also because of the less likely but still possible presence of systematic errors in the conventional calorimetric investigations, alternative approaches are desirable.

The first such alternative approach was originated by Larson (11), who calculated $\bar{S}^0 = -2.7_0$ cal K^{-1} mol^{-1} for OH^-(aq) from the thermodynamic properties of $NaOH \cdot H_2O$(c), NaCl(c), and solutions of these compounds. It is important to recognize that

Can. J. Chem. Downloaded from www.nrcresearchpress.com by 210.87.254.105 on 09/05/12
For personal use only.

Can. J. Chem. Downloaded from www.nrcresearchpress.com by 210.87.254.105 on 09/05/12
For personal use only.

this entropy is not based in any way on enthalpies of neutralization or on K_ω for water. Use of this entropy for $OH^-(aq)$ with $\bar{S}^0 = 0$ for $H^+(aq)$ and the well known entropy of $H_2O(liq)$ leads to $\Delta S_\omega^0 = -19.4_1$ cal K^{-1} mol^{-1} for the entropy of ionization of water as in [1]. Further combination of this ΔS_ω^0 with the well known ΔG_ω^0 of ionization leads to $\Delta H_\omega^0 = 13.31$ kcal mol^{-1} for the desired enthalpy of ionization.

Now, in this paper, we present results of our measurements on iodine pentoxide and our derived enthalpy of ionization of water.

Experimental

All calorimetric measurements were made with an LKB Precision Calorimetry System. The standard LKB 100 ml glass reaction vessel was used with solid samples contained in 1 ml glass ampoules. All calorimetric results apply to 25.00 ± 0.05°C and are reported in terms of the defined thermochemical calorie (1 cal = 4.184 J).

Several batches of $I_2O_5(c)$ were prepared according to the procedure first described by Lamb, Bray, and Geldard (12). For analysis, weighed samples were dissolved in water and then either titrated with standardized NaOH or reduced with excess I^- and then titrated with standardized thiosulfate; all titres were within 0.15% of values calculated on the basis of pure samples of $I_2O_5(c)$.

Results

We have measured enthalpies of reaction of $I_2O_5(c)$ with water and also with 0.0188 *m* aqueous sodium hydroxide (a small excess), as represented by the following equations:

[2] $\frac{1}{2}I_2O_5(c) + \frac{1}{2}H_2O(liq) = H^+(aq) + IO_3^-(aq)$ ΔH_2

[3] $\frac{1}{2}I_2O_5(c) + OH^-(aq) = IO_3^-(aq) + \frac{1}{2}H_2O(liq)$ ΔH_3

Results of our measurements, all expressed in terms of kcal mol^{-1} of iodate formed, are given in Tables 1 and 2.

We have combined our ΔH_2 values (Table 1) with calorimetrically measured (13) enthalpies of dilution of aqueous iodic acid solutions to obtain the corresponding standard state ΔH_2^0 values that are also listed in Table 1. Because of the electrical symmetry of the solutes in reaction [3], it is expected and observed that there is negligible dependence of ΔH_3 on concentration; we have therefore taken each ΔH_3 value to be the same as the desired ΔH_3^0. Average values of ΔH_2^0 and ΔH_3^0 are listed in Table 3 for each sample of $I_2O_5(c)$; the tabulated ± values are standard deviations.

Differences between ΔH_2^0 and ΔH_3^0 values for the various samples are larger than the reproducibilities indicated by the standard deviations. We suspect that these differences are due to the presence of different polymorphic forms of $I_2O_5(c)$. Whatever the cause, these differences are of little importance for our purposes because our analyses showed that all samples corresponded very closely to the com-

TABLE 1. Enthalpies of reaction of $I_2O_5(c)$ with water

Sample No.	g I_2O_5/100 ml	ΔH_2/ kcal (mol IO_3^-)$^{-1}$	ΔH_2^0/ kcal (mol IO_3^-)$^{-1}$
1	0.2259	0.418	0.334
1	0.2287	0.356	0.272
1	0.2425	0.512	0.426
1	0.2595	0.506	0.417
1	0.3075	0.498	0.401
2	0.323205	0.353	0.254
2	0.328846	0.352	0.252
2	0.337953	0.392	0.291
2	0.348177	0.347	0.244
3	0.210203	0.263	0.182
3	0.229344	0.285	0.201
3	0.229598	0.300	0.216
3	0.245483	0.292	0.205
3	0.245928	0.276	0.189
3	0.254519	0.257	0.169
4	0.123076	0.236	0.173
4	0.151490	0.247	0.178
4	0.182320	0.248	0.173
4	0.234174	0.251	0.166
4	0.275844	0.255	0.162
4	0.310193	0.266	0.169
4	0.343771	0.277	0.175
4	0.385838	0.288	0.181
5	0.097983	0.298	0.244
5	0.136268	0.299	0.233
5	0.176876	0.306	0.232
5	0.228136	0.304	0.220
5	0.271294	0.312	0.221

TABLE 2. Enthalpies of reaction of $I_2O_5(c)$ with excess $OH^-(aq)$

Sample No.	g I_2O_5/100 ml	ΔH_3/kcal (mol IO_3^-)$^{-1}$
1	0.2343	−12.94
1	0.2631	−12.92
1	0.2957	−13.02
2	0.136395	−13.101
2	0.186049	−12.958
3	0.205679	−13.103
3	0.225967	−13.119
3	0.241433	−13.137
3	0.242702	−13.146
3	0.247002	−13.128
3	0.247101	−13.189
3	0.250927	−13.136
4	0.069195	−13.262
4	0.082892	−13.227
4	0.096555	−13.172
4	0.111059	−13.159
4	0.128440	−13.252
4	0.141883	−13.251
4	0.183809	−13.204
5	0.098948	−13.120
5	0.120409	−13.142
5	0.142841	−13.096
5	0.161214	−13.054
5	0.182023	−13.080
5	0.205383	−13.057

Can. J. Chem. Downloaded from www.nrcresearchpress.com by 210.87.254.105 on 09/05/12
For personal use only.

position represented by I_2O_5, which justifies use of equations [2] and [3] to represent the calorimetric reactions. We therefore limit our use of these results to combination of each ΔH_2^0 value with the ΔH_3^0 value for the same sample of I_2O_5(c) to obtain the desired enthalpy of ionization of water as

$$[4] \qquad \Delta H_\omega^0 = \Delta H_2^0 - \Delta H_3^0$$

The resulting ΔH_ω^0 values are given in Table 3, where the cited $\pm$ values are based on the standard deviations.

We had only small amounts of samples #1 and #2 left after completing the necessary analyses, hence the small number of calorimetric runs with these samples. Following completion of these runs we took extra care with subsequent preparations to make sure that each sample was well mixed and therefore homogeneous, and also made more calorimetric runs with each sample.

We obtain what we consider to be the best enthalpy of ionization of water from our results by assigning relative weights of one to the ΔH_ω^0 values (Table 3) from samples #1 and #2 and relative weights of three to ΔH_ω^0 values from samples #3, #4, and #5; the resulting weighted average is $\Delta H_\omega^0 = 13.34_0$ kcal mol^{-1}. We estimate the *total* uncertainty (chemicals, calorimetry, data treatment) to be ± 0.05 kcal mol^{-1}.

It is clear that the results of the present investigation, along with Larson's (11) derived ΔH_ω^0 cited earlier, all support the traditional calorimetric $\Delta H_\omega^0 = 13.34$ kcal mol^{-1} rather than some larger value as obtained from $\mathrm{d}\ln K_\omega/\mathrm{d}T = \Delta H_\omega^0/RT^2$ and from a few calorimetric investigations.

We now suggest that measurements of the enthalpies of ionization of I_2O_5(c) with D_2O(liq) and with excess OD^- (in D_2O) might help resolve present uncertainties in the thermodynamics of ionization of D_2O(liq).

It is interesting to note that the spread in reported values for the enthalpy of ionization of D_2O(liq) at 298 K is even larger than for H_2O(liq). The early measurements of Wynne-Jones (14) led to pK values at three temperatures, from which Goldberg and Hepler (6) calculated $\Delta H^0 = 14.49$ kcal mol^{-1}. Later more extensive measurements of pK at 10 temperatures from 5–50°C led Covington, Robinson, and Bates (8) to obtain $\Delta H^0 = 14.311$ kcal mol^{-1}. Calorimetric measurements of the enthalpy of reaction of DCl with NaOD in D_2O led Goldberg and Hepler (6) to obtain $\Delta H^0 = 14.488$ kcal mol^{-1}. Finally, measurements of pK at 10 temperatures from 25–225°C by Shoesmith and Lee (15) led to $\Delta H^0 = 14.548$ kcal mol^{-1}; in connection with this last value it should be noted that an alternative method of calculation also led Shoesmith and Lee (15) to obtain $\Delta H^0 = 14.18$ kcal mol^{-1}. We now suggest that the spread from 14.18 to 14.55 kcal mol^{-1} in all these results might best be resolved by further calorimetric measurements of enthalpies of reaction of strong acid with strong base in D_2O *and* measurements on I_2O_5(c) in D_2O and OD^- along the lines of the present investigation.

TABLE 3. Standard state enthalpies of reactions [2] and [3] and derived standard enthalpy of ionization of water

Sample No.	ΔH_2^0/kcal (mol IO_3^-)$^{-1}$	ΔH_3^0/kcal (mol IO_3^-)$^{-1}$	ΔH_ω^0/kcal mol^{-1}
1	0.370±0.066	−12.96 ±0.05	13.33±0.08
2	0.260±0.021	−13.03 ±0.10	13.29±0.10
3	0.194±0.017	−13.137±0.027	13.33±0.03
4	0.172±0.006	−13.218±0.041	13.39±0.04
5	0.230±0.010	−13.092±0.035	13.32±0.04

Acknowledgements

We are grateful to the National Research Council of Canada for support of this research, to Elaine King-Brown for help with preparations of I_2O_5(c), and to Ingemar Dellien for helpful discussions.

1. J. J. CHRISTENSEN, L. D. HANSEN, and R. M. IZATT. Handbook of proton ionization heats and related thermodynamic quantities. John Wiley and Sons, New York. 1976.
2. G. OLOFSSON and L. G. HEPLER. J. Solution Chem. **4**, 127 (1975).
3. L. G. HEPLER and E. M. WOOLLEY. *In* Water: a comprehensive treatise. Vol. 3. *Edited by* F. Franks. Plenum Press, New York. 1973. Chapt. 3.
4. J. W. LARSON and L. G. HEPLER. *In* Solute–solvent interactions. *Edited by* J. F. Coetzee and C. D. Ritchie. Marcel Dekker, New York. 1969. Chapt. 1.
5. C. E. VANDERZEE and J. A. SWANSON. J. Phys. Chem. **67**, 2608 (1963).
6. R. N. GOLDBERG and L. G. HEPLER. J. Phys. Chem. **72**, 4654 (1968).
7. J. D. HALE, R. M. IZATT, and J. J. CHRISTENSEN. J. Phys. Chem. **67**, 2605 (1963).
8. A. K. COVINGTON, R. A. ROBINSON, and R. G. BATES. J. Phys. Chem. **70**, 3820 (1966).
9. H. S. HARNED and R. A. ROBINSON. Trans. Faraday Soc. **36**, 973 (1940).
10. C. P. BEZBORUAH, M. F. G. F. C. CAMOES, A. K. COVINGTON, and J. V. DOBSON. J. Chem. Soc. Faraday Trans. I, **69**, 949 (1973).
11. J. W. LARSON. J. Phys. Chem. **74**, 685 (1970).
12. A. B. LAMB, W. C. BRAY, and W. J. GELDARD. J. Am. Chem. Soc. **42**, 1636 (1920).
13. E. M. WOOLLEY, J. O. HILL, W. K. HANNAN, and L. G. HEPLER. J. Solution Chem. **7**, 385 (1978).
14. W. F. K. WYNNE-JONES. Trans. Faraday Soc. **32**, 1397 (1936).
15. D. W. SHOESMITH and W. LEE. Can. J. Chem. **54**, 3553 (1976).

2,3-(1′-Pyrazolino-3′,4′) hexopyranosides and their products of decomposition[1]

HANS H. BAER, FRIEDRICH LINHART, AND HANNA R. HANNA

Department of Chemistry, University of Ottawa, Ottawa, Ont., Canada K1N 9B4

Received June 7, 1978

HANS H. BAER, FRIEDRICH LINHART, and HANNA R. HANNA. Can. J. Chem. **56**, 3087 (1978).

The methyl 4,6-*O*-benzylidene-2,3-dideoxy-3-nitrohex-2-enopyranosides having the β-D-*erythro* (**1**), α-D-*erythro* (**2**), β-D-*threo* (**3**), and α-D-*threo* (**4**) configurations reacted with diazomethane to give high yields of 2,3-(1′-pyrazolino-3′,4′) derivatives (**5**–**8**). The pyrazolines **5** and **6** (from **1** and **2**) were deduced on the basis of nuclear magnetic resonance and optical rotatory dispersion data to possess the β- and α-D-*gluco* configurations, and **7** and **8** (from **3** and **4**), to have the β- and α-D-*ido* configurations, respectively. Thermolysis of **5**, **6**, and **8** led to the methyl-branched, nitroolefinic glycosides **9**, **10**, and **11** (the 2-*C*-methyl derivatives of **1**, **2**, and **4**), whereas **7** afforded the corresponding 2,3-*C*-methylene derivative **12**, a cyclopropano sugar. The α-anomeric cyclopropano derivative **13** was obtained from **8** by decomposition on silica gel.

HANS H. BAER, FRIEDRICH LINHART et HANNA R. HANNA. Can. J. Chem. **56**, 3087 (1978).

Par réaction avec le diazométhane les méthyl-4,6-*O*-benzylidène-2,3-didésoxy-3-nitrohex-2-énopyranosides ayant les configurations β-D-*érythro* (**1**), α-D-*érythro* (**2**), β-D-*thréo* (**3**) et α-D-*thréo* (**4**) ont donné avec de bons rendements les dérivés 2,3-(1′-pyrazolino-3′,4′) **5**–**8**. A l'aide de données de résonance magnétique nucléaire et de dispersion rotatoire on a déduit que les pyrazolines **5** et **6** (préparées à partir de **1** et **2**) possèdent, respectivement, les configurations β- et α-D-*gluco*, et **7** et **8** (préparées à partir de **3** et **4**) les configurations β- et α-D-*ido*. Par thermolyse de **5**, **6** et **8** on obtient les glycosides insaturés à branchement méthyle **9**, **10** et **11** (les dérivés 2-*C*-méthylés de **1**, **2** et **4**) alors que **7** donne un sucre cyclopropanique, le dérivé 2,3-*C*-méthylène **12**. Le dérivé cyclopropanique α-anomérique **13** a été obtenu par décomposition de **8** sur gel de silice.

The chemical literature contains a very large number of reports on the synthesis of carbohydrate derivatives that bear a nitrogen heterocycle fused to the sugar chain (3). The great variety of the fused-ring systems described and their manifold uses in synthetic work are matched by the number of different approaches to their preparation. However, it appears that few pyrazolines and pyrazoles derived from sugars are known, apart from some which originate from mono- and bis(phenylhydrazones) and no longer possess the structural feature of a pyranose or furanose ring. We now record the synthesis of some methyl hexopyranoside derivatives which carry a pyrazoline ring fused to the 2,3-position. The work was undertaken with the expectation that compounds of this type might be useful intermediates in the synthesis of branched-chain sugars.

One of the classical ways of pyrazoline synthesis is the 1,3-dipolar addition of diazoalkanes to olefins (4–6). Our special interest was focused on α-nitroalkenes as substrates which, by virtue of the nitro group, not only promised to be good dipolarophiles (5, 7) but also would lead to products having an additional functionality as a key to further transformations. It was therefore decided to study reactions between the four readily available, stereoisomeric methyl 4,6-*O*-benzylidene-2,3-dideoxy-3-nitrohex-2-enopyranosides (**1**–**4**) and diazomethane. An extension of the work using methyl diazoacetate as a dipolar reagent will be described in a subsequent paper.

The nitroolefinic glycosides **1**–**4** reacted smoothly with a moderate excess of diazomethane in ether–tetrahydrofuran solution, giving high yields (80–95%) of the pyrazolines **5**–**8**. The reactions of the D-*erythro* glycosides **1** and **2** were performed at an initial temperature of 0°C for 1 h and went to completion at room temperature during an additional 30 min. The D-*threo* glycosides **3** and **4** (especially the latter) proved even more reactive and under the conditions just mentioned gave rise to by-products. However, good results were obtained by treating the β-glycoside **3** with diazomethane at −5°C for 20 min and the α-glycoside **4** at −20°C for 5 min. (Compound **4** can literally be titrated with diazomethane solution.) The products **5**, **6**, and **7** crystallized readily whereas **8** was obtained as a colorless, amorphous solid. They displayed limited stability and tended to decompose on storage but could be kept under refrigeration for some weeks or months. Although progress of the

[1]Part 41 in a series on reactions of nitro sugars. For part 40 see ref. 1. The essential results of this work were obtained in 1971 by F.L. during a sojourn as a postdoctorate fellow in this laboratory, and were communicated by us (2) in 1972. Publication of a full account was postponed until certain stereochemical details that awaited clarification were investigated by H.R.H. in the course of doctoral studies.

Can. J. Chem. Downloaded from www.nrcresearchpress.com by 210.87.254.105 on 09/05/12
For personal use only.

Can. J. Chem. Downloaded from www.nrcresearchpress.com by 210.87.254.105 on 09/05/12
For personal use only.

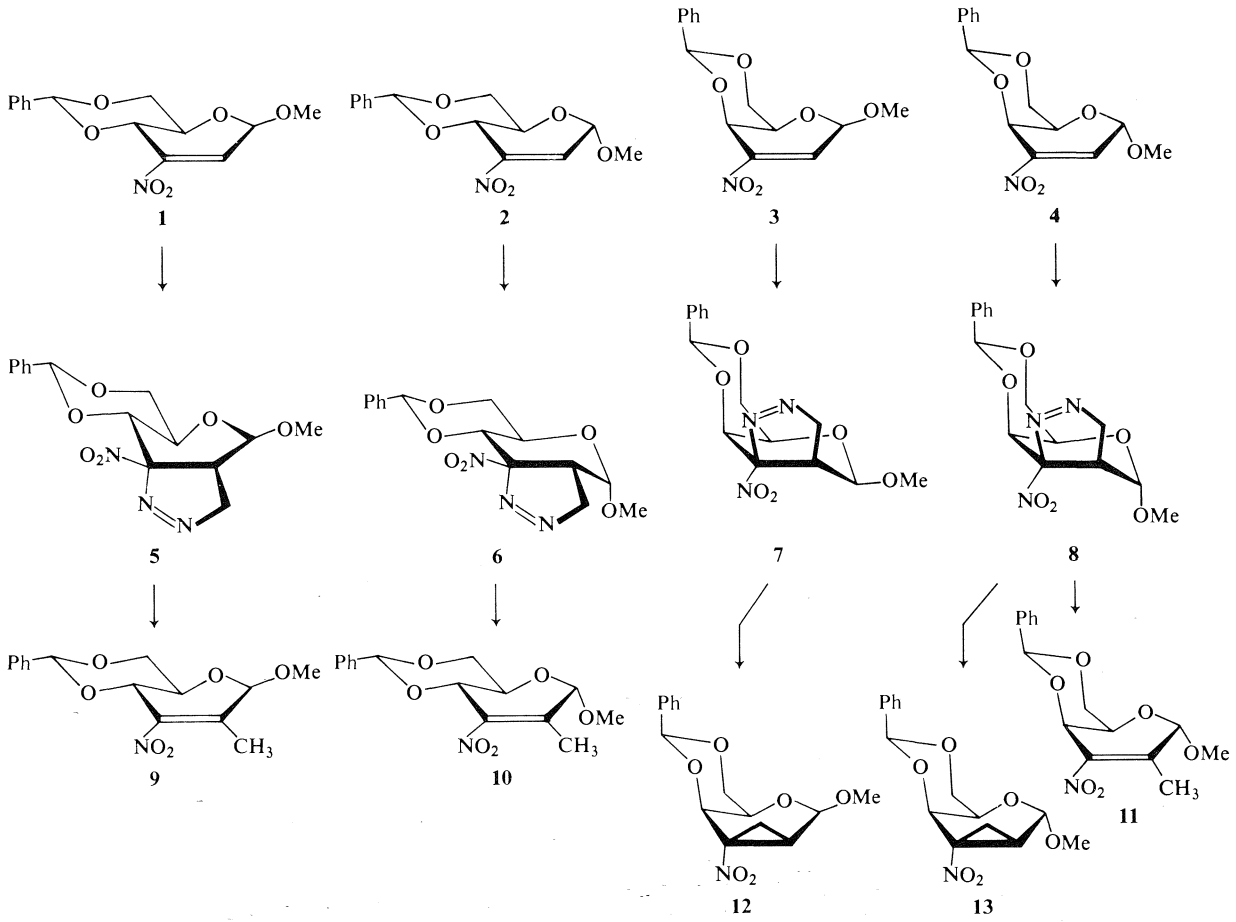

reactions and purification procedures could be monitored by tlc, **7** and **8** in particular exhibited a certain sensitivity towards silica gel which caused in some instances the appearance of a minor spot owing to a degradation product. This point will be referred to again in a subsequent paragraph.

The constitution of the pyrazolines was revealed by elemental analysis and spectral evidence. There was no infrared absorption above 3000 cm^{-1}, which indicated absence of N—H. Strong nitro bands were present at 1555–1560 cm^{-1}, and these showed shoulders around 1530–1540 cm^{-1} presumably owing to N=N vibrations of the 1-pyrazoline structure (8, 9). The typical benzylidene acetal bands occurred in the 700–800 cm^{-1} region. The compounds showed low-intensity ultraviolet absorption near 325 nm as do 1-pyrazolines generally (8, 9). The nmr spectrum of each product contained a 1-proton, highfield multiplet attributable to H-2 of the pyranose ring. The multiplet showed splittings owing to coupling with H-1 and the two methylene protons of the fused ring. These methylene protons were deshielded by the adjacent azo group, giving well-separated AB signals of an ABX system at medium field (δ 5–6 region). The spectral features thus established the heterocycles to be 1-pyrazolines as expected, rather than 2-pyrazolines as might have resulted from tautomerization, and indicated the orientation of ring fusion, i.e., attachment of the azomethylene bridge to C-2 and C-3 of the pyranose ring through CH_2 and N, respectively. This mode of 1,3-dipolar addition of diazomethane to α-nitroalkenes was in line with expectations based on previous findings and general considerations (4–7). All the remaining ^1H nmr signals could also be accounted for in terms of the constitution depicted (Table 1). The discussion of configuration is reserved for later paragraphs.

When **5**, **6**, and **8** were refluxed at 130°C in chlorobenzene, they underwent pyrolysis yielding mainly methyl 4,6-*O*-benzylidene-2,3-dideoxy-2-*C*-methyl-3-nitrohex-2-enopyranosides (**9**, **10**, and **11**, respectively), isolated crystalline in 51–67% yields. By contrast, the pyrazoline **7** on similar treatment afforded in 71% yield the crystalline cyclopropano sugar **12**. According to the nmr spectrum the crude **12** seemed to contain a minor proportion of what may have been the corresponding 2-*C*-methyl olefin (i.e., the β-anomer of **11**), but this could not be verified

Can. J. Chem. Downloaded from www.nrcresearchpress.com by 210.87.254.105 on 09/05/12
For personal use only.

TABLE 1. The 100 MHz ^{1}H nuclear magnetic resonance data for compounds **5**–**13** in chloroform-*d*

	Chemical shifts (δ)[a]											
Compound[b]	H-1	H-2	H-4	H-5	H-6$_e$	H-6$_a$	H-7$_{exo}$	H-7$_{endo}$	*PhC*-H	1-OMe	2-Me	Ph
5	4.40d	2.79sp	5.45d	3.24sx	4.33q	3.74t	4.98q	4.71q	5.71s	3.42s	—	7.3–7.6m
6	4.76d	2.97sx	5.04d	3.64sx	4.35q	3.85t	4.13q	5.23q	5.73s	3.28s	—	7.3–7.6m
7	4.92d	2.65m	4.88d	3.73m	4.37q	4.12q	5.02q	4.50q	5.53s	3.55s	—	7.3s
8	5.03d	2.74sx	5.20m	4.03	4.39q	4.21q	5.11q	4.40q	5.57s	3.38s	—	7.3s
9	5.22d	—	4.75oc	←4.35q, 3.7–4.1m(2H)→			—	—	5.64s	3.47s	1.92d	7.3–7.6m
10	4.85s	—	4.68q	←4.34q, 3.75–4.2m(2H)→			—	—	5.62s	3.48s	1.92d	7.25–7.50m
11	5.07s	—	4.99d	3.88m	←4.34dq(2H)→		—	—	5.63s	3.49s	2.13s	7.3–7.6m
12	4.76d	2.54sp	5.48d	3.19m	←4.3m(2H)→		←1.99d(2H)[c]→		5.66s	3.53s	—	7.3–7.6m
13	4.90s	2.44q	5.59d	3.68m	←4.24d(2H)→		1.74q	2.01q	5.68s	3.35s	—	7.3–7.6m

	Observed splittings (Hz)								
Compound	$J_{1,2}$	$J_{2,7_{exo}}$	$J_{2,7_{endo}}$	$J_{4,5}$	$J_{5,6_e}$	$J_{5,6_a}$	$J_{6_e,6_a}$	$J_{7_{exo},7_{endo}}$	Others
5	3.4	8.3	5.3	10.5	5.0	10.0	10.5	18.7	
6	6.0	6.7	1.3	9.7	4.8	9.8	10.0	17.7	
7	3.7	8.5	10.5	1.3	1.7	1.7	12.8	17.5	
8	~1.5	9	10.5	~2	1.8	1.7	12.5	16.5	$J_{2,4}$ ~1
9	—	—	—	10.5			~10	—	$^5J_{4,Me}$ 2; $^5J_{1,4}$ 2.5
10	—	—	—	9			~9	—	$^5J_{4,Me}$ 2
11	—	—	—	~1	2.5	2.5	~13	—	
12	2	8	8	2.3				0[c]	
13	0	8.3	10.3	2.3				5.5	

[a]Multiplicities are indicated as s, singlet; d, doublet; t, triplet; q, quartet; sx, sextet; sp, septet; oc, octet; m, multiplet.
[b]Note that, in **5**–**8** and **12** and **13**, H-7$_{exo}$ is situated *cis* to H-2 and H-7$_{endo}$ is *trans* to H-2.
[c]By coincidence the H-7 protons are magnetically equivalent; they give rise to a doublet (A_2 part of an A_2B system) owing to coupling with H-2, and no geminal coupling is observed.

Can. J. Chem. Downloaded from www.nrcresearchpress.com by 210.87.254.105 on 09/05/12
For personal use only.

by isolation. Conversely, in the pyrolysis of **8** the corresponding cyclopropane **13** apparently was a minor by-product. The cyclopropanes **12** and **13** were also formed slowly on exposure of **7** and **8**, respectively, to silica gel. This observation, first made during chromatographic tests, could be utilized to produce crystalline **13** on a preparative scale in high yield.

The structure of the unsaturated glycosides **9**–**11** was proved by their nmr spectra which contained a 3-proton signal near δ 2 owing to the 2-*C*-methyl group. In **9** and **10**, this signal was a narrow doublet because of long-range coupling with H-4 ($^5J_{4,Me}$ = 2 Hz). The H-4 signal occurred near δ 4.7 and, in the case of **9**, showed long-range coupling also with H-1 ($^5J_{1,4}$ = 2.5 Hz). No long-range coupling was evident in the corresponding signals of **11**. These findings were consistent with the geometry of the protons involved, in relation to the olefinic double bond (10). The three products gave infrared bands at 1530 cm^{-1} as expected for nitroalkenes.

The cyclopropano derivatives **12** and **13** were characterized by high-field signals (δ 1.7–2.5) for the two methylene protons of the cyclopropane ring and H-2 of the pyranose ring, in addition to well-separated signals at lower field that accounted for the remaining protons required of these structures. Assignment of configuration was possible on the basis of chemical shift and coupling parameters in comparison with the various, structurally analogous 2,3-anhydro-3-nitro glycoside stereoisomers obtained earlier in this laboratory (11) and with the 2,3-cyclopropano glycosides described by Horton and coworkers (12) and Radatus and Fraser-Reid (13). Thus, the H-4 signals of **12** and **13** were found at quite similar, conspicuously low field positions (δ 5.48 and 5.59, respectively). Considering that pyranose ring protons are noticeably deshielded by vicinal, *trans* oriented oxirane (11, 14) or cyclopropane (13) rings but shielded by such rings in *cis* orientation, one may conclude that **12** and **13** bear their cyclopropane rings on the same side, most likely *trans* to H-4. In the 2,3-anhydro-3-nitro glycoside of α-D-*talo* configuration (the analog of **13**), the H-4 resonance is at δ 5.63 whereas in all its stereoisomers studied (11) the range was δ 4.0–5.05. Furthermore, the H-1 signals of **12** and **13** also showed very similar chemical shifts (δ 4.76 and 4.90); the difference of only 0.14 ppm is unusually small for a pair of anomeric protons but is readily explained on the same basis. Thus, a cyclopropane ring located on the upper face of the pyranose will deshield the axial, β-anomeric proton situated *trans* to it but shield the equatorial, α-anomeric proton and thereby diminish the shift difference normally characteristic for the two. The configuration shown was strongly supported in the α-glycoside **13** by zero coupling between H-1 and H-2 as has previously been observed in analogous, benzylidenated 2,3-anhydro (11, 12, 15) and (non-nitro) cyclopropano (13) structures having an H-1,2 *trans* arrangement (i.e., the α-D-*talo* or α-D-*manno* configuration). In conformity with $J_{1,2}$ = 0 Hz, the H-2 signal of **13** was a quartet, split only by H-7_{exo} and H-7_{endo}. In the event of an opposite, downward orientation of the cyclopropane ring (H-1,2 *cis*) one would expect a large $J_{1,2}$ value as indeed was found (12, 13) for a non-nitro analog having the α-D-*allo* configuration ($J_{1,2}$ = 5–6 Hz). That the 3-*C*-nitro substituent does not have much influence can be seen from the value of 6.3 Hz observed in methyl 4,6-*O*-benzylidene-2,3-dideoxy-2,3-*C*-methylene-3-nitro-α-D-'allopyranoside,' a stereoisomer of our compounds recently obtained in a different way by Sakakibara and Sudoh (16).[2] Hence the designation of **13** as methyl 4,6-*O*-benzylidene-2,3-dideoxy-2,3-*C*-methylene-3-nitro-α-D-idopyranoside appears to be secure. The β-glycoside **12** showed $J_{1,2}$ = 2 Hz, and the H-2 signal at δ 2.54 was a septet reflecting that splitting. This coupling constant compares well with those in 2,3-anhydro and cyclopropano analogs having an H-1,2 *cis* structure as in the β-D-*manno* configuration, for which was found (11) 0.8 and (13) 3.5 Hz. For β-glycosidic 2,3-anhydro analogs possessing the D-*allo* and D-*gulo* configurations we found (11) $J_{1,2}$ = 0 Hz, and $J_{1,2}$ = 1 Hz was reported (13) for the β-D-*allo* cyclopropano analog. Despite some ambiguity present in these comparisons we believe the data to support the view that **12** is the anomer of **13**, i.e., it bears the ring in like disposition and is to be designated as a β-D-*ido* compound. As will be seen from the following discussion, the anomeric relationship is borne out by a consideration of the structure of the pyrazoline precursors from which **12** and **13** arose by extrusion of nitrogen, most certainly without inversion at C-2.

To begin with, some problems were encountered in the allocation of configurations to the pyrazolino derivatives **5**–**8**. From the origin of the compounds by 1,3-dipolar cycloaddition, *cis* fusion of the heterocycle to the pyranose ring could be inferred with

[2]The authors based their assignment, correctly no doubt, on the similarity of their $J_{1,2}$ value with that of the non-nitro analog (12, 13) having the α-D-*allo* configuration. However, their adoption of the same configurational prefix *allo* is unfortunate since substitution of H-3 by the nitro group implies, in terms of nomenclature, an inverted configuration so that the *gluco* designation should be applied. Compare the usage in other branched-chain sugars containing quaternary centers; see also footnotes 2 in refs. 17*a* and *b*.

TABLE 2. The ^{13}C chemical shifts (ppm from tetramethylsilane) for compounds **5–8** in chloroform[a]

Compound	C-1	C-2	C-3	C-4	C-5	C-6	C-7	Ph-CHO_2	O-CH_3
5	99.3	44.1	119.8	75.0	63.8	69.7	81.1	102.4	56.0
6	96.0	43.2	118.1	76.7	58.6	69.1	77.1	102.7	55.5
7	99.3	40.5	119.3	70.9	67.2	68.8	77.2	101.1	57.1
8	95.6	41.3	116.4	69.2	59.2	69.0	78.9	100.9	55.4

[a]In addition to the resonances listed, all compounds showed the appropriate signals for the phenyl ring carbon atoms in the range 123–136 ppm.

Can. J. Chem. Downloaded from www.nrcresearchpress.com by 210.87.254.105 on 09/05/12
For personal use only.

certitude, but its upward or downward orientation in each individual case was difficult to establish. Although all the required ^1H nmr data were available (Table 1), they did not yield unambiguous information right away in this regard. This is so because, for each of the products, a reasonable conformation (distorted chair, half-chair, or skew form) that is consistent with the data can be constructed for *either* configuration. Nevertheless, some of the parameters were helpful in corroborating the configurations determined by other means, as will be mentioned below. Next, ^{13}C nmr spectra of **5–8** were evaluated. The ^{13}C chemical shifts obtained from proton-decoupled spectra (Table 2) clearly confirmed the constitution of the products and suggested at least a partial answer to the question of configuration. In the latter regard, inspection of the data reveals certain significant trends when the compounds are compared with each other, even though the over-all spectra are very similar. Thus, the normally expected increases in shielding of C-1 and C-5, and to a lesser degree of C-2 and C-4, are observed on going from a β-glycoside (**5** or **7**) to the respective α-glycoside (**6** or **8**). There are few conspicuous differences otherwise. It has been pointed out by Perlin and co-workers (18–20) that the sums of all ^{13}C chemical shifts occurring in each member of a set of diastereomers mirror the total steric interactions and should therefore bear relation to the overall configurations. For compounds **5** and **6** such summation (leaving out the phenyl group) gives $\sum_5 = 711.0$ and $\sum_6 = 697.9$ ppm, and the difference of 13.1 ppm is very nearly the same as that (13.6 ppm) derived from the reported (21) shifts of the anomeric methyl 4,6-*O*-benzylidene-D-glucopyranosides. This fact suggests that the steric influences exerted upon the molecules **5** and **6** by the structural features surrounding C-2 and C-3 must be quite similar, which in turn justifies the conclusion that the pyrazoline rings are attached in like orientations, causing the two compounds to be a pair of anomers. Similarly for **7** and **8**, the difference of the sums $\sum_7 = 701.4$ and $\sum_8 = 685.9$ ppm is 15.5 ppm. Although data of comparison for the corresponding methyl 4,6-*O*-benzylidene-D-galactopyranoside anomeric pair were unavailable, the difference is close to that (14.4 ppm) of the methyl β- and α-D-galactopyranosides (18), which supports the assumption of **7** and **8** being anomers also. This result fits the aforementioned indication that the degradation products **12** and **13** represent an anomeric pair. It should be noted, however, that the deductions based on the ^{13}C chemical shifts do not interrelate the pairs **5**/**6** and **7**/**8** configurationally; they merely advocate anomerism and leave open the C-2,3 configuration of either pair. Additional evidence was needed and this was provided by optical rotatory dispersion measurements.

It was found that the absorption band near 325 nm is associated with a negative Cotton effect in **5** and **6**, and with a positive one in **7** and **8**. To assess the significance of this, let us consider some analogies. It is known that the Cotton effect is determined largely by chirality in the immediate environment of the chromophore. Thus, in the structurally related methyl 2,3-anhydro-4,6-*O*-benzylidene-3-nitro-D-hexopyranosides, which also display an effect in that region (11), the sign is independent of the anomeric configuration and determined only by the configurations at C-3 and C-4. (The configuration of C-2, being by necessity linked to that of C-3, need not be considered separately here.) Figure 1 shows Newman projections of these nitroepoxides viewed along the C-3,4 bond.[3] The Cotton effect appears to obey the following empirical rule: when the C-3 nitro group is written at the top of the projection and O-4 then appears on its right-hand side, the sign is positive (cases A, B, and C); if O-4 appears on the left-hand side, the sign is negative (case D). The same was found to hold for the nitroalkenes **1–4** and **9–11**, although in these unsaturated sugars (λ_{max} 325–330 nm) C-3 is achiral and the sole determinant for the sign of the Cotton effect is C-4. The sign is negative in the α- and β-D-*erythro* compounds (Fig. 1, case E) and positive in the α- and β-D-*threo* compounds (case F). On the grounds of these observations the pyrazolino sugars **5** and **6**, if indeed they are anomers as indicated by the ^{13}C nmr data, may be ascribed the configuration represented by D (with

[3]Absence of perfect staggering is a consequence of the half-chair conformation in which these compounds must exist.

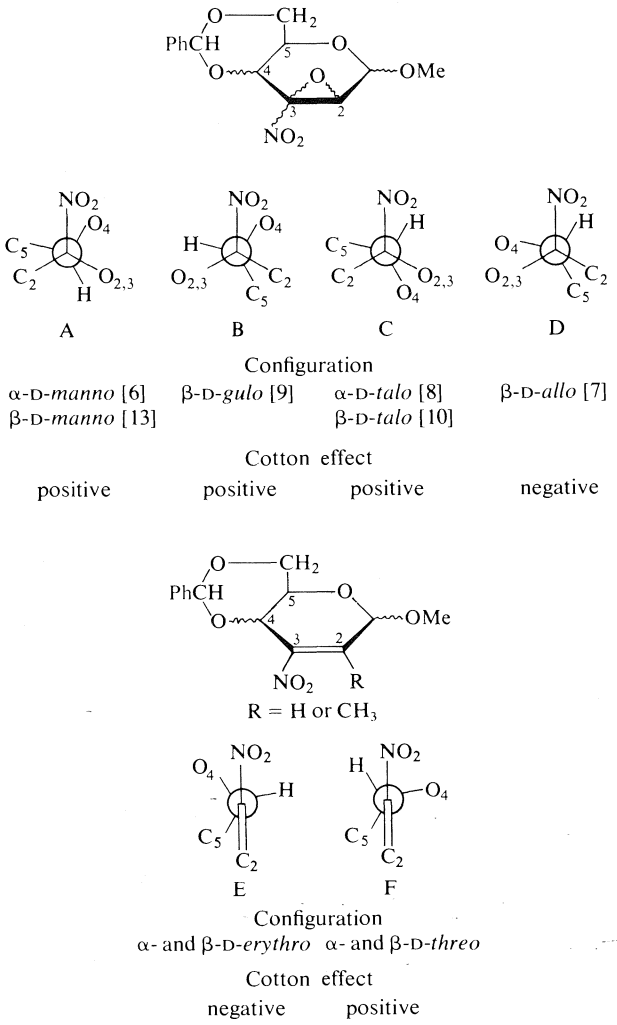

FIG. 1. Newman projections of methyl 2,3-anhydro-4,6-*O*-benzylidene-3-nitro-D-hexopyranosides (top) and methyl 4,6-*O*-benzylidene-2,3-dideoxy-3-nitro-D-hex-2-enopyranosides and 2-*C*-methyl derivatives (bottom). The numbers in brackets are the compound numbers in ref. 11. The molecules are viewed along the C-3—C-4 bond.

CH_2—N=N— replacing $O_{2,3}$). The alternate possibility, corresponding to A, should be associated with a positive Cotton effect. We therefore designate **5** and **6** as β- and α-D-*gluco* isomers, respectively.[4] As for the isomers **7** and **8**, which would correspond to B or C (Fig. 1), their positive effect is in accord with the rule elaborated above but evidently cannot afford a distinction between these possibilities.[5] However, since the configuration of the cyclopropano derivative **13** is well supported by the nmr spectrum, the same α-D-*ido* configuration follows for its progenitor **8**, and with the additional evidence for an anomeric relationship, **7** can be accorded the β-D-*ido* configuration.

Given the configurations of **5**–**8** so assigned, one may now review the ^{1}H nmr data of Table 1 and be satisfied that these are consistent with a conformation close to the $_5H^4$ half-chair for **5**, and with distorted $_1C^4$ chair conformations for **6**, **7**, and **8**, as is best visualized with the aid of molecular models. It is worth noting, in particular, that the splitting values of 16.5–17.7 Hz for the geminally coupled pyrazoline protons at C-7 in **6**–**8**, and also the large vicinal couplings between both of these protons and H-2 in **7** and **8**, are in good agreement with corresponding data reported (9) for simple pyrazolines. The smaller $J_{2,7}$ couplings present in **5** and **6** likewise accord with the dihedral angles occurring in models of the conformations mentioned. The slightly increased $J_{7,7'}$ value (18.7 Hz) for **5** could be a consequence of change in the pyrazoline ring shape caused by its fusion to a pyranose half-chair. That **5** appears to stand apart conformationally from its three isomers is also suggested by the chemical shifts of the C-7 protons. These protons are influenced primarily by the anisotropy of the N=N double bond (9, 22). Thus, groups pseudoaxially oriented with respect to the plane of the double bond are placed in the shielding cone and are shifted to higher field (22). This applies to H_{7exo} in **6** and to H_{7endo} in **7** and **8**, which are shielded quite strongly relative to their geminal partners (Table 1). The difference is small in **5**, implying a more nearly equal space arrangement of the C-7 protons with respect to the double bond, and this accords with a more planar five-membered ring as would result from fusion to a half-chair. In the latter situation there is little puckering possible, contrary to the case of fusion to a (distorted) chair.

[4]The nitro group, as the substituent of highest configurational priority at the geminally disubstituted C-3, is thought of as replacing the hydroxyl group in the parent sugar, D-glucose. Note that the analogous epoxide having like orientations of the nitro group and fused hetero ring is termed a D-*allo* compound.

[5]The nitroepoxy and nitroolefinic glycosides just mentioned exhibit a second Cotton effect at shorter wavelengths (approximately 275 and 285–290 nm, respectively). The same appears to apply to **5**–**8** although technical difficulties prevented us from obtaining accurate determinations. At any rate, it has not yet been possible to correlate these second effects with configuration. Whether the rule for the first Cotton effect is in fact valid for the pyrazolino analogs as we are assuming in this discussion, and holds perhaps even more generally for any similar 2,3-fused systems, is of course a critical point that begs confirmation by other examples. Unfortunately, the cyclopropano sugars **12** and **13** cannot serve as such since they do not have an absorption maximum in the same region.

Can. J. Chem. Downloaded from www.nrcresearchpress.com by 210.87.254.105 on 09/05/12
For personal use only.

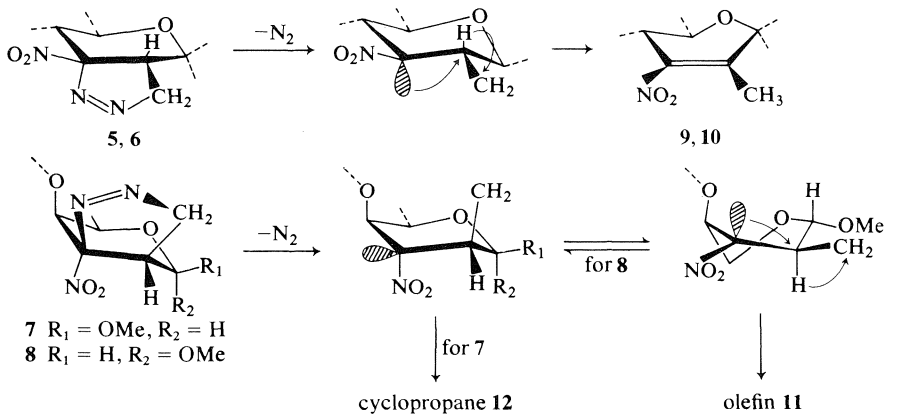

SCHEME 1

The highly stereoselective nature of diazomethane addition to each of the nitroolefins **1**–**4** invites comment. One might perhaps have anticipated at first sight that the orientation of the anomeric methoxyl group would influence the approach of the reagent to C-2; this is normally observed in kinetically controlled, nucleophilic additions (11, 17*b*, 23, 24). However, such is evidently not the case. Instead, a directing effect is associated with the orientation of O-4, and it seems possible that coordination of the diazomethane molecule precedes, and facilitates, addition which then produces the pyrazoline ring *cis* to this acetal oxygen. This might also explain why in **3** and **4**, wherein O-4 is in a better geometric position for this purpose, the reaction proceeds faster than in **1** and **2**.

Concerning the differential behavior of the pyrazolines in thermal decomposition, one may suggest that in **5** and **6** the geometry emerging concomitant with the loss of N_2 favors hydrogen migration from C-2 to C-7, leading exclusively to olefins as depicted in partial formulas in Scheme 1 (upper sequence). On the other hand, in **7** and **8** the same process may require, for a facile hydrogen shift, transition through a skew conformation. In the case of **8** such conformational change could be attained relatively easily; indeed, it would be promoted by relief of a severe 1,3-diaxial interaction between the nitro and methoxy group present in the normal chair. Hence, the olefin **11** is favored as the main product (Scheme 1, lower sequence). The same driving force for conformational change does not exist in **7**; moreover, attainment of the skew form would likely be opposed by the β-glycosidic methoxyl coming into interaction with O-4. Ring closure to give the cyclopropane **12** thus appears to be a reasonable alternative. Finally, it should be noted in this context that the decomposition of pyrazolines to cyclopropanes, a much-investigated subject (8, 22, 25–27, and further references cited therein), frequently involves configurational inversion at the carbon atoms adjacent to the azo bridge. However, the *central* pyrazoline carbon (C-2 in our derivatives) is not affected by this complication and consequently, the orientation of ring fusion in the cyclopropano sugars must remain the same as in the parent pyrazolines.

Experimental

For general procedures and instrumental techniques see preceding papers of this series (1, 11, 17). Optical rotations were determined at approximately 25°C in a Perkin-Elmer 141 automatic polarimeter. Cotton effects were measured with a Jasco ORD/UV-5 instrument. The ^{1}H nmr data were obtained from 100-MHz spectra of $CDCl_3$ solutions containing tetramethylsilane as internal standard, and signal assignments were confirmed, where feasible, by double irradiation. The ^{13}C nmr spectra, also of $CDCl_3$ solutions with TMS, were measured in a Varian CFT-20 instrument and assignments were aided by the SFORD technique. The methyl 4,6-*O*-benzylidene-2,3-dideoxy-3-nitrohex-2-enopyranosides **1** (28, 29), **2** (29, 30), **3** (28, 31), and **4** (30, 32) were prepared as previously described. Diazomethane was generated from *N*-methyl-*N*-nitroso-*p*-toluenesulfonamide (Diazald®).

Methyl 4,6-O-Benzylidene-2,3-dideoxy-2,3-methyleneazo-3-nitro-β-D-glucopyranoside (5)[6]

To a solution of potassium hydroxide (3 g) in water (5 ml) and 95% ethanol (15 ml), contained in a distillation flask immersed in a water bath of 65°C, was added dropwise a solution of Diazald (3 g) in ether (30 ml). The emerging mixture of diazomethane and ether vapor was passed through a condenser and the yellow condensate was allowed to react, in the receiver, with a solution of **1** (1.0 g) in dry tetrahydrofuran (10 ml, spectroscopy grade) and dry ether (17 ml) which was maintained at 0°C in an ice-water bath. After completion of the diazomethane production the reaction mixture was kept at 0°C (for a total of 1 h) and then at room temperature for

[6]Chemical Abstracts Service advises that **5** will be indexed as 3*H*-[1,3]dioxino[4′,5′:5,6]pyrano[4,3-*c*]pyrazole, 3a,4,5a,-6,9a,9b-hexahydro-4-methoxy-9b-nitro-8-phenyl-, [3a*R*-(3aα,-4α,5aβ,8β,9aα,9bα)]-.

Can. J. Chem. Downloaded from www.nrcresearchpress.com by 210.87.254.105 on 09/05/12
For personal use only.

Can. J. Chem. Downloaded from www.nrcresearchpress.com by 210.87.254.105 on 09/05/12
For personal use only.

another 0.5 h. The solution was evaporated *in vacuo* to give a yellow syrup which solidified upon trituration with a few drops of fresh, anhydrous ether. The material was chilled under ether (5 ml) for 3 h and then isolated as nearly colorless crystals (1.1 g), mp 115–116°C (with dec.). Recrystallized twice from anhydrous ether, the colorless product (0.81 g, 71%) showed an unchanged melting point; $[\alpha]_D$ −157.8°, $[\alpha]_{578}$ −163.9°, $[\alpha]_{546}$ −194.2°, $[\alpha]_{436}$ −429.6°, $[\alpha]_{365}$ −1307° (*c* 0.7, chloroform); ν_{max}(Nujol): 1563, with shoulder at 1535–1540 cm^{-1} (NO_2, N=N); λ_{max}(MeOH): 325 nm (ε 160); ord (*c* 0.4, methanol): $[\Phi]_{337}$ −8400°. *Anal.* calcd. for $C_{15}H_{17}N_3O_6$ (335.3): C 53.73, H 5.11, N 12.53; found: C 53.66, H 5.06, N 12.52.

*Methyl 4,6-O-Benzylidene-2,3-dideoxy-2,3-methyleneazo-3-nitro-α-D-glucopyranoside (**6**)*

The reaction was carried out as described above for **1**, on approximately 1/3 scale, using 300 mg of **2** dissolved in tetrahydrofuran (20 ml). Complete conversion of **2** into a single, faster-moving product was indicated by tlc with 1:2 ethyl acetate – petroleum ether (bp 30–60°C). Processing as described furnished colorless, crystalline **6** that was recrystallized once from ethyl acetate – anhydrous ether; yield 328 mg (95%), mp 179°C with dec.; $[\alpha]_D$ −2.2°, $[\alpha]_{578}$ −1.7°, $[\alpha]_{546}$ −5.8°, $[\alpha]_{436}$ −56°, $[\alpha]_{365}$ −400° (*c* 2.7, chloroform); ν_{max}(Nujol): 1560, with shoulders at about 1530 cm^{-1} (NO_2, N=N); ord (*c* 0.14, methanol): $[\Phi]_{352}$ −720°. *Anal.* calcd. for $C_{15}H_{17}N_3O_6$ (335.3): C 53.73, H 5.11, N 12.53; found: C 53.73, H 5.06, N 12.55.

*Methyl 4,6-O-Benzylidene-2,3-dideoxy-2,3-methyleneazo-3-nitro-β-D-idopyranoside (**7**)*

Diazomethane from 0.3 g of Diazald in ether (3 ml) was allowed to react with a solution of **3** (100 mg) in tetrahydrofuran (5 ml) maintained at —5°C. The reaction was complete within 20 min after the end of the diazomethane distillation, according to tlc (1:2 ethyl acetate – petroleum ether, bp 30–60°C). The solution was immediately evaporated to give a yellowish oil which solidified upon trituration with a little anhydrous ether. The crude product (92 mg, 81%) contained a very minor contaminant that moved slightly more slowly than the main product (tlc). Whereas recrystallization from ethyl acetate – petroleum ether or tetrahydrofuran–ether failed to remove the impurity, a pure sample of **7** was obtained by slow recrystallization from ethyl acetate – chlorocyclohexane at −15°C. The white needles had mp 115°C (with dec.); $[\alpha]_D$ +34.3°, $[\alpha]_{578}$ +40°, $[\alpha]_{546}$ +56.7°, $[\alpha]_{436}$ +265°, $[\alpha]_{365}$ +1548° (*c* 1.2, chloroform); ν_{max}(Nujol): 1563, with shoulder at 1540 cm^{-1} (NO_2, N=N); λ_{max}(MeOH): 323 nm (ε 260); ord (*c* 0.12, methanol): $[\Phi]_{333}$ +14000°. *Anal.* calcd. for $C_{15}H_{17}N_3O_6$ (335.3): C 53.73, H 5.11, N 12.53; found: C 53.65, H 5.20, N 12.39.

*Methyl 4,6-O-Benzylidene-2,3-dideoxy-2,3-methyleneazo-3-nitro-α-D-idopyranoside (**8**)*

A distilled, ethereal solution of diazomethane was prepared from Diazald (0.5 g) and ether (5 ml). This was added from a buret to a solution of **4** (100 mg) in tetrahydrofuran (5 ml), chilled by swirling in a bath of −20°C. The diazomethane was consumed rapidly and visibly. Within 5 min a yellow coloration began to persist in the reaction mixture, and the solvent was then immediately removed by evaporation at low temperature in an oil-pump vacuum. The residue was co-evaporated once with a portion of added ether, and the resulting, colorless foam was dried *in vacuo*; yield 114 mg. Attempts at crystallization from various common solvents failed; $[\alpha]_D$ +158.7°, $[\alpha]_{578}$ +168.2°, $[\alpha]_{546}$ +202.5°, $[\alpha]_{436}$ +516.6°, $[\alpha]_{365}$ +1820° (*c* 2.2, chloroform); ν_{max}(Nujol): 1560, with shoulder at about 1535 cm^{-1} (NO_2, N=N); λ_{max}(MeOH): 323 nm (ε 225); ord (*c* 0.2, methanol): $[\Phi]_{330}$ +15000°. To obtain a pure product it is important to observe the above reaction conditions carefully. Prolonged exposure of **4** to excess diazomethane, or a higher reaction temperature, tends to lead to side products whereas insufficient exposure may cause some **4** to remain unreacted as seen by the occurrence of minor nmr peaks due to its presence.

*Methyl 4,6-O-Benzylidene-2,3-dideoxy-2-C-methyl-3-nitro-β-D-erythro-hex-2-enopyranoside (**9**)*

The pyrazolino sugar **5** (582 mg) was boiled under reflux in chlorobenzene (15 ml) for 6 h, after which it was largely replaced by a faster-moving product (tlc). The solvent was evaporated and the residue chromatographed on a column of silica gel (20 g) by means of 4:1 carbon tetrachloride – ethyl acetate. The main fractions containing **9** together with some impurities were collected and evaporated to give 270 mg (51%) of **9**, mp 180–183°C, raised to 185–187°C by recrystallization from ether at low temperature. The colorless needles showed $[\alpha]_D$ −248.5° (*c* 1.06, chloroform); ν_{max}(Nujol): 1530 cm^{-1} (nitroalkene); cd: $[\theta]_{327}$ −16500 (0.0017 *M* in dioxane). *Anal.* calcd. for $C_{15}H_{17}NO_6$ (307.3): C 58.63, H 5.58, N 4.56; found: C 58.53, H 5.66, N 4.50.

*Methyl 4,6-O-Benzylidene-2,3-dideoxy-2-C-methyl-3-nitro-α-D-erythro-hex-2-enopyranoside (**10**)*

The pyrazolino sugar **6** (330 mg) was boiled under reflux in chlorobenzene (10 ml) for 6 h, after which time no **9** was left, according to tlc. The solvent was evaporated and the dry residue (304 mg) was recrystallized from ethyl acetate – petroleum ether to give 197 mg (65%) of colorless needles, mp 181–182°C, unchanged on a further recrystallization from ether at low temperature; $[\alpha]_D$ −117.8° (*c* 1.1, chloroform); ν_{max}(Nujol): 1525 cm^{-1} (nitroalkene); cd $[\theta]_{328}$ −18600 (0.0025 *M* in dioxane). *Anal.* calcd. for $C_{15}H_{17}NO_6$ (307.3): C 58.63, H 5.58, N 4.56; found: C 58.67, H 5.63, N 4.70.

*Methyl 4,6-O-Benzylidene-2,3-dideoxy-2-C-methyl-3-nitro-α-D-threo-hex-2-enopyranoside (**11**)*

A solution of the pyrazolino sugar **8** (122 mg) in chlorobenzene (5 ml) was boiled under reflux for 1 h and then evaporated to dryness. The tlc (1:2 ethyl acetate – petroleum ether) indicated that the residue contained a major product (**11**) together with a slightly faster migrating, minor product (the cyclopropano derivative **13**). The nmr spectrum of the crude product was also consistent with this. The material was recrystallized twice from ether and then weighed 75 mg (67%) and had mp 212–213°C but was not completely pure. It was further purified by chromatography on a column of silica gel (15 g) by use of 4:1 carbon tetrachloride – ethyl acetate as the eluent and by another recrystallization from ethyl acetate – ether, after which it showed mp 214–215°C; $[\alpha]_D$ +109° (*c* 1.04, chloroform); ν_{max}(Nujol): 1520 cm^{-1} (NO_2); cd: $[\theta]_{330}$ +11500 (0.0048 *M* in dioxane). *Anal.* calcd. for $C_{15}H_{17}NO_6$ (307.3): C 58.63, H 5.58, N 4.56; found: C 58.48, H 5.66, N 4.68.

*Methyl 4,6-O-Benzylidene-2,3-dideoxy-2,3-C-methylene-3-nitro-β-D-idopyranoside (**12**)*

A solution of the pyrazolino sugar **7** (200 mg) in toluene (10 ml) was refluxed for 16 h. Completion of the reaction was checked by tlc. The crystalline residue resulting from evaporation of the solvent was recrystallized from methylcyclohexane to yield 130 mg (71%) of **12**, mp 115–116°C; $[\alpha]_D$ −40°, $[\alpha]_{578}$ −43°, $[\alpha]_{546}$ −46.8°, $[\alpha]_{436}$ −43.6°, $[\alpha]_{365}$ −43.6° (*c* 2.3, chloroform); ν_{max}(Nujol): 1545 cm^{-1} (NO_2); mass spectrum: *m/e* 307. *Anal.* calcd. for $C_{15}H_{17}NO_6$ (307.3): C 58.63, H 5.58, N 4.56; found: C 58.50, H 5.46, N 4.46.

*Methyl 4,6-O-Benzylidene-2,3-dideoxy-2,3-C-methylene-3-nitro-α-D-idopyranoside (**13**)*

In the preparation of **11** (see a preceding section), the formation of a minor by-product that moved slightly faster in tlc was noted. The same spot, attributed to **13**, was sometimes observed on tlc of the starting pyrazoline **8**. Its strength was variable and seemed to depend on incidental conditions of manipulation, one of which appeared to be the time elapsed between sample spotting and irrigation. This led us to consider that action of silica gel upon **8** was responsible for an accelerated formation of **13**, which was borne out by the following preparative experiment.

A sample of **8** (520 mg) dissolved in a small amount of 4:1 carbon tetrachloride – ethyl acetate was allowed to drain into the top of a column (diameter, 1 cm) of silica gel (20 g) moistened with the same solvent mixture. The sample was kept stationary in the top of the column overnight, during which period a slow evolution of gas took place. Trapped bubbles were released by careful stirring of the upper layer with a rod and elution of the column using the above solvent mixture was then commenced. The main fractions containing **13** were evaporated to give 348 mg (75%) of white crystals of **13** contaminated by a small proportion of **11** (tlc and nmr). The material was recrystallized twice from ether to give pure **13** as colorless needles, mp 169–171°C; $[\alpha]_D$ +87°, $[\alpha]_{578}$ +91°, $[\alpha]_{546}$ +104.5°, $[\alpha]_{436}$ +200°, $[\alpha]_{365}$ +395° (*c* 2.0, chloroform); ν_{max}(Nujol): doublet 1550–1530 cm^{-1}, ν_{max}($CHCl_3$): singlet 1540 cm^{-1}. *Anal.* calcd. for $C_{15}H_{17}NO_6$ (307.3): C 58.63, H 5.58, N 4.56; found: C 58.52, H 5.56, N 4.62.

*Circular Dichroism Data of Compounds **1–4***

Ellipticities are given for the first extremum in dioxane solution, with molar concentrations in parentheses: **1**, $[\theta]_{330}$ −11700 (0.0026); **2**, $[\theta]_{330}$ −12100 (0.0023); **3**, $[\theta]_{325}$ +2120 (0.0036); **4**, $[\theta]_{330}$ +3370 (0.005).

Acknowledgments

This work was supported by grant A-1350 from the National Research Council of Canada. The authors are indebted to Professor A. S. Perlin for an evaluation of the ^{13}C nmr data.

1. H. H. Baer and C. B. Madumelu. Carbohydr. Res. **67**, 329 (1978).
2. H. H. Baer, C. W. Chiu, S. H. L. Chiu, F. Linhart, W. Rank, and D. Shields. 8th Int. Symp. Chem. Natural Products. New Delhi, India, February 1972. Abstr. E 31.
3. H. El Khadem. Adv. Carbohydr. Chem. Biochem. **25**, 351 (1970).
4. R. Huisgen. Proc. Chem. Soc. London, 357 (1961).
5. C. H. Jarbo. *In* The chemistry of heterocyclic compounds. Pyrazoles, pyrazolines, pyrazolidines, indazoles and condensed rings. *Edited by* A. Weissberger. Interscience Publishers, New York, NY. 1967. pp. 195–205.
6. P. A. S. Smith. The chemistry of open-chain organic nitrogen compounds. Vol. II. W. A. Benjamin, Inc., New York, NY. 1966. pp. 239–242.
7. W. E. Parham and W. Rhasek. J. Am. Chem. Soc. **76**, 799 (1954).
8. T. V. Van Auken and K. L. Rinehart, Jr. J. Am. Chem. Soc. **84**, 3736 (1962).
9. R. J. Crawford, A. Mishra, and R. J. Dummel. J. Am. Chem. Soc. **88**, 3959 (1966).
10. M. Barfield. J. Chem. Phys. **48**, 4463 (1968); M. Barfield, R. J. Spear, and S. Sternhell. J. Am. Chem. Soc. **93**, 5322 (1971).
11. H. H. Baer and W. Rank. Can. J. Chem. **49**, 3192 (1971).
12. E. L. Albano, D. Horton, and J. H. Lauterbach. Carbohydr. Res. **9**, 149 (1969).
13. B. Radatus and B. Fraser-Reid. Can. J. Chem. **50**, 2909 (1972).
14. R. J. Ferrier and N. Prasad. J. Chem. Soc. C, 575 (1969).
15. D. H. Buss, L. Hough, L. D. Hall, and J. F. Manville. Tetrahedron, **21**, 69 (1965).
16. T. Sakakibara and R. Sudoh. J. Chem. Soc. Chem. Commun. 7 (1977).
17. (*a*) H. H. Baer and W. Rank. Can. J. Chem. **51**, 2001 (1973); (*b*) H. H. Baer and W. Rank. Can. J. Chem. **52**, 2257 (1974).
18. A. S. Perlin, B. Casu, and H. J. Koch. Can. J. Chem. **48**, 2596 (1970).
19. A. S. Perlin and H. J. Koch. Can. J. Chem. **48**, 2639 (1970).
20. A. S. Perlin. Internat. Rev. Sci. Org. Chem. Ser. 2, **7**, 1 (1975).
21. E. Conway and R. D. Guthrie. Tetrahedron Lett. 4879 (1972).
22. D. E. McGreer and J. W. McKinley. Can. J. Chem. **49**, 105 (1971).
23. H. Paulsen and W. Greve. Chem. Ber. **107**, 3013 (1974); T. Sakakibara and R. Sudoh. Chem. Commun. 69 (1974); T. Sakakibara and R. Sudoh. J. Org. Chem. **40**, 2823 (1975).
24. P. M. Collins, D. Gardiner, S. Kumar, and W. G. Overend. J. Chem. Soc. Perkin I, 2596 (1972); P. M. Collins, W. G. Overend, and V. M. Racz. Carbohydr. Res. **45**, 127 (1975).
25. D. E. McGreer, N. W. K. Chiu, M. G. Vinje, and K. C. K. Wong. Can. J. Chem. **43**, 1407 (1965).
26. R. J. Crawford and A. Mishra. J. Am. Chem. Soc. **88**, 3963 (1966); A. Mishra and R. J. Crawford. Can. J. Chem. **47**, 1515 (1969); M. P. Schneider and R. J. Crawford. Can. J. Chem. **48**, 628 (1970); R. J. Crawford and M. Ohno. Can. J. Chem. **52**, 3134, 4112 (1974); R. J. Crawford, H. Tokunaga, L. H. M. C. Schrijver, and J. C. Godard. Can. J. Chem. **56**, 998 (1978).
27. T. C. Clarke, L. A. Wendling, and R. G. Bergman. J. Am. Chem. Soc. **97**, 5638 (1975).
28. H. H. Baer. Methods Carbohydr. Chem. **6**, 302 (1972).
29. H. H. Baer and F. F. Z. Georges. J. Org. Chem. **41**, 3474 (1976).
30. H. H. Baer and F. Kienzle. Can. J. Chem. **45**, 983 (1967).
31. H. H. Baer, F. Kienzle, and T. Neilson. Can. J. Chem. **43**, 1829 (1965).
32. H. H. Baer and W. Rank. Can. J. Chem. **50**, 1216 (1972).

Can. J. Chem. Downloaded from www.nrcresearchpress.com by 210.87.254.105 on 09/05/12
For personal use only.

Studies on nucleation phenomena occurring in aqueous solutions supersaturated with calcium sulfate. II. The induction time

DOUGLAS MARTIN KELLER, RONALD E. MASSEY, AND O. E. HILEMAN, JR.

Department of Chemistry, McMaster University, Hamilton, Ont., Canada L8S 4M1

Received June 22, 1978

DOUGLAS MARTIN KELLER, RONALD E. MASSEY, and O. E. HILEMAN, JR. Can. J. Chem. **56**, 3096 (1978).

The results of a set of experiments designed to delineate the effects of changes in temperature and supersaturation levels on the length of the time interval between establishing those levels and the detection of a steady-state nucleation rate of $CaSO_4 \cdot 2H_2O$ from solution are reported. The data were obtained using the droplet technique coupled with *in situ* generation of SO_4^{2-} at such a rate that the system experienced a near step function change in the driving force with time. A theoretical model for the length of the time interval is derived and compared with the data. Empirical modeling studies led to a rather different functional relationship that is compared with a theoretical model discussed in the literature by Frisch and Carlier. The functional form of an equation relating together the lag time and the subsequent nucleation rate exhibited by a given system is proposed.

DOUGLAS MARTIN KELLER, RONALD E. MASSEY et O. E. HILEMAN, JR. Can. J. Chem. **56**, 3096 (1978).

On rapporte les résultats d'une série d'expériences ayant pour but de délimiter les effets de changements de température et de niveaux de sursaturation sur l'intervalle de temps qui existe entre le moment de l'établissement de ces niveaux et celui de la détection d'un état stationnaire pour la vitesse de nucléation du $CaSO_4 \cdot 2H_2O$ à partir d'une solution. On a obtenu ces résultats en faisant appel à la technique des gouttelettes de concert avec une génération *in situ* de SO_4^{2-} à une vitesse telle que le système subit, avec le temps, un changement de fonction incrémentielle de sa force motrice. On a déduit un modèle théorique pour la longueur de l'intervalle de temps et on l'a comparé avec ces dernières. Les études sur des modèles empiriques ont conduit à une relation fonctionnelle assez différente que l'on compare à un modèle théorique discuté dans la littérature par Frisch et Cartier. On propose la forme fonctionnelle d'une équation reliant le décalage de temps et la vitesse de nucléation subséquente d'un système donné.

[Traduit par le journal]

Can. J. Chem. Downloaded from www.nrcresearchpress.com by 210.87.254.40 on 09/05/12
For personal use only.

Introduction

Equation [1], which summarizes the results of classical nucleation theory, does not lead one to expect the observed time gap between the establishment of a given supersaturation within a system and the attainment of the resultant time independent rate of appearance of particles of the new phase within it.

$$[1] \qquad J = A \exp\left[-\delta\sigma^3 v^2 (kT)^{-3} (\ln S)^{-2}\right]$$

where J is the rate of nucleation expressed as the number of new nuclei s^{-1} cm^{-3}; δ is a shape factor; σ is the surface energy in ergs cm^{-2}; v is the monomer volume in the newly forming phase in cm^3; S is the supersaturation defined as the $\{[Ca^{2+}][SO_4^{2-}]/K_{sp}\}^{1/2}$; A is some collection of constant and exponential terms assumed to be constant; and k and T have their usual meanings. These time gaps, variously called induction times or time lags, are quite long in the metastable region of the Ostwald diagram but shorten as the supersaturation approaches the metastable/labile boundary and then goes beyond into the labile region.

The observed induction time, τ', is usually considered to be comprised of one or more of the following: t_d, the time required for development of a steady-state embryo distribution; t_n, the time required for the attainment of a steady-state nucleation rate; and t_g, the growth time required to bring the critical nuclei to some detectable size (see eq. [2]).

$$[2] \qquad \tau' = f(t_d, t_n, t_g)$$

In literature reports of laboratory studies on nucleation phenomena, authors have suggested the use of either the first detection of the new phase or the attainment of a steady-state rate of appearance of discrete units of the new phase as suitable signals of the end of the induction period. Examples of each are illustrated by the schematic plots of Fig. 1 where both n_t, the observed number of new particles and J_e', the rate of particle nucleation calculated from it, are plotted as a function of t, the lapsed time after a time independent driving force has been established in the system.

In Fig. 1, Λ denotes the time of first detection of the new phase and τ the attainment of the time independent rate of its formation. A conclusion one

Can. J. Chem. Downloaded from www.nrcresearchpress.com by 210.87.254.40 on 09/05/12
For personal use only.

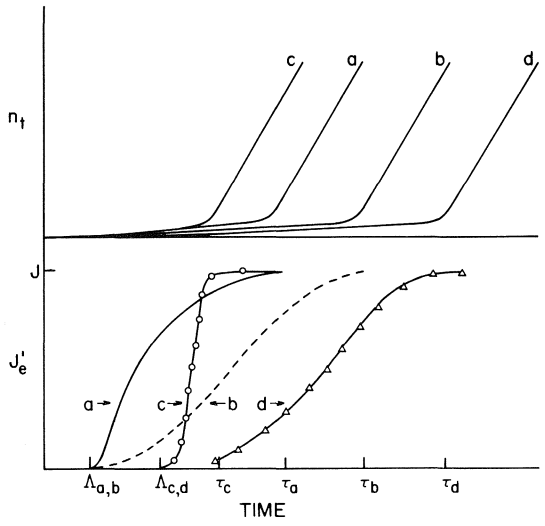

FIG. 1. Schematic representation of n_t and J_e' as functions of time during a nucleation from solution experiment.

can draw from a study of Fig. 1 is that it is rather difficult to sort out the relative impacts of t_d, t_n, and t_g on τ' using the data supplied by use of either Λ or τ alone or in concert.

Time dependent rates of nucleation have been considered from a theoretical point of view by several authors (1–14). Most start with the Zeldovich–Frenkel equation and attempt a solution of that equation under specific boundary conditions and approximations that give an overall time to the point where the rate is no longer a function of t. This, of course, ignores the additional time contribution to the experimentally observed τ that is required to bring the initially formed nuclei to crystals of detectable size. Thus, experimental verification of any theoretical model is difficult unless one assumes that the growth time is some negligible fraction of the observed time lag. Since values of both of these are non-linear functions of the supersaturation the validity of such an assumption may be suspect.

In this paper we report the results of some of our studies on the influence of variations in temperature and supersaturation levels on the observed time gap between the establishment of a given $CaSO_4 \cdot 2H_2O$ supersaturation level and the subsequent attainment of a steady-state nucleation rate of that compound from aqueous solution. Starting from the Zeldovich (1) modification of the Becker–Döring (18) equation and following the methods used by Frisch (8) we develop a theoretical model showing the expected dependency and this is compared with that experimentally observed. Several empirical models are also considered. Additionally a relationship is shown between the observed lag time and nucleation rate.

Experimental Details

Vonnegut's droplet technique coupled with *in situ* generation of the sparingly soluble $CaSO_4 \cdot 2H_2O$ from very soluble precursors (DTiGS) and photomicroscopy were used as experimental tools in the study (15, 16). A DTiGS experiment can be divided into a sequential series of steps, namely: preparation of an aqueous solution containing the precursors for generation of the supersaturation, dispersion of a small known amount of this solution in an immiscible oil, selection and subsequent preparation of a population of droplets for microscopic observation, generation of the supersaturation, notation of 'number–time' data, and then data analysis and interpretation. Additionally, the rate of formation of the supersaturation and the equilibrium solubility of the crystalline product in aqueous medium must be measured.

The reaction between $S_2O_8^{2-}$ and I^- was used to generate SO_4^{2-} *in situ*, in the presence of Ca^{2+}. Initial conditions used are shown in Table 1. Supersaturation data for a droplet population were inferred from results of 'beaker' experiments carried out in parallel. The appearance of crystals within the droplet population was recorded photomicrographically. For subsequent analysis, the 'number–time' data were separated on the basis of narrow droplet volume ranges. For explicit details of the procedure see ref. 17. A summary of the results pertinent to this paper is shown in Table 2 and as a contour plot of τ vs. T and S in Fig. 2.

Discussion

The Zeldovich (1) modification of the Becker–Döring (18) theory of nucleation may be used to develop equations describing solid formation within a supersaturated mother liquor.

The concentration of embryos composed of n monomers at time t is denoted by the function $f(n,t)$. The fundamental kinetic equation of the new phase formation is (18)

$$[3] \qquad \partial f_n/\partial_t = I_n - I_{n+1}$$

I_n is the net number of embryos of size n formed per unit time from embryos of size $n-1$, often labelled the 'flux of embryos', and is given by

$$[4] \qquad I_n = f_{n-1} a_{n-1} \beta_{n-1} - f_n a_n \alpha_n$$

where a_n is the surface area of an embryo composed of n monomers, β_n is the rate of addition per unit area of monomers to an embryo composed of n monomers, and α_n is the rate of departure per unit area of monomers from an embryo of size n.

From these equations Frenkel (2) obtains

$$[5] \qquad \frac{\partial f}{\partial t} = \frac{\partial}{\partial n}\left(D \frac{\partial f}{\partial n}\right) + \frac{1}{kT} \frac{\partial}{\partial n}\left(Df \frac{\partial \Delta G}{\partial n}\right)$$

where ΔG is the free energy change accompanying the embryo formation and D is given by $D = a\beta$ in the Becker–Döring theory.

The definition of lag time used in this paper is that introduced by Daynes (19) in diffusion theory: the intersection with the time axis of the asymptote to

Can. J. Chem. Downloaded from www.nrcresearchpress.com by 210.87.254.40 on 09/05/12
For personal use only.

TABLE 1. Experimental variables used in the constant driving force experiments*

Variables	E_4	E_5	E_6	E_7	E_8	E_9	E_{10}	E_{11}	E_{12}	E_{13}	E_{14}	E_{15}
T (±1 K)	295.0	301.3	307.5	313.6	295.0	301.3	307.5	313.6	295.0	301.3	307.5	313.6
$[Ca^{2+}]_i$	0.175	0.175	0.175	0.175	0.204	0.204	0.204	0.204	0.233	0.233	0.233	0.233
$[SO_4^{2-}]_f$	0.175	0.175	0.175	0.175	0.204	0.204	0.204	0.204	0.233	0.233	0.233	0.233
$[S_2O_8^{2-}]_i$	0.0875	0.0875	0.0875	0.0875	0.102	0.102	0.102	0.102	0.117	0.117	0.117	0.117
$[K^+]$	0.175	0.175	0.175	0.175	0.204	0.204	0.204	0.204	0.233	0.233	0.233	0.233
$[NO_3^-]$	0.350	0.350	0.350	0.350	0.408	0.408	0.408	0.408	0.466	0.466	0.466	0.466
μ_f	1.23	1.23	1.23	1.23	1.37	1.37	1.37	1.37	1.52	1.52	1.52	1.52

*$[SO_4^{2-}]_f$ = final sulfate concentration, μ = final ionic strength, pH = 3.23, NH_4I = 0.350 M, $[Ca^{2+}]/[SO_4^{2-}]$ = 1.00.

the function $Q(t)$. This function is defined as the number of embryos of the new phase of size N formed to time t where N is greater than n^* (the critical embryo size defined by the extremum of ΔG, i.e., $((d\Delta G/dn)_{n=n^*} = 0)$ such that the probability of decomposition for these embryos is virtually zero (2).

To solve [5] requires the specification of the initial distribution of f. This was often taken to be the steady distribution introduced by Becker and Döring (16)

$$f(n) = \text{constant for } n = 0$$

$$f(n) = 0 \text{ for } n > 0$$

If the $\Delta G(n)$ function possesses a narrow enough extremus peak a more realistic distribution which does not ignore the local fluctuations of monomer density is given in ref. 8 as

$$f_s(n) - f(n, 0) \simeq 0 \text{ for } 0 < n < n^* - \left(\frac{kT}{\gamma}\right)^{1/2}$$

$$\simeq f_s(n^*) \text{ for } n^* - \left(\frac{kT}{\gamma}\right)^{1/2} < n < n^* + \left(\frac{kT}{\gamma}\right)^{1/2}$$

$$\simeq 0 \text{ for } n^* < n < N$$

where the subscript s indicates steady-state, $\gamma = -(\partial^2 \Delta G(n)/\partial n^2)_{n=n^*}$, and $(kT/\gamma)^{1/2}$ is a measure of the width of the peak of $\Delta G(n)$.

Following the methods used by Frisch and Carlier (14) and Courtney (9) in their treatment of the equation resulting from the Zeldovich–Becker–Döring theory (eqs. [3] through [5]) and using the latter distribution results in the following expression for the lag time

$$[6] \qquad L \simeq \frac{(2\pi)^{1/2} kT}{D(n^*)\gamma}$$

Recalling that $D = a\beta$ and $\gamma = -(\partial^2 \Delta G(n)/\partial n^2)_{n=n^*}$ expressions for a, β, and ΔG appropriate to our system are required. The embryo will be assumed to be of spherical shape, hence

$$a = 4\pi r_n^2$$

where r_n is the radius of an embryo composed of n monomers and

$$\Delta G(n) = n(\mu_n - \mu_m) + a\sigma$$

$$= n(\mu_n - \mu_m) + (4\pi)^{1/3}(3v)^{2/3} n^{2/3}\sigma$$

where μ_n is the chemical potential of a monomer within the embryo, μ_m is the chemical potential of a monomer in the mother phase, and σ is the surface

TABLE 2. A summary of J_f',* τ, and S values for four temperatures and three ion product levels

Ion product	Parameter	Value at 295.0 K	301.3 K	307.5 K	313.6 K
0.03063	J_f' (s^{-1} cm^{-3})	5.80×10^{3}	4.67×10^{4}	2.22×10^{6}	3.67×10^{6}
	τ (s)	1.56×10^{4}	5.40×10^{3}	9.80×10^{2}	4.2×10^{1}
	S (±0.01)	4.49	4.44	4.38	4.32
0.04162	J_f' (s^{-1} cm^{-3})	1.90×10^{5}	4.27×10^{6}	3.25×10^{7}	5.77×10^{7}
	τ (s)	6.40×10^{3}	7.03×10^{2}	1.00×10^{2}	2.1×10^{1}
	S (±0.01)	5.24	5.18	5.10	5.03
0.05429	J_f' (s^{-1} cm^{-3})	5.27×10^{6}	1.36×10^{7}	1.23×10^{8}	3.14×10^{8}
	τ (s)	1.85×10^{3}	2.30×10^{2}	2.7×10^{1}	1.3×10^{1}
	S (±0.01)	5.98	5.91	5.83	5.75

*J_f' is the best fit nucleation rate (17).

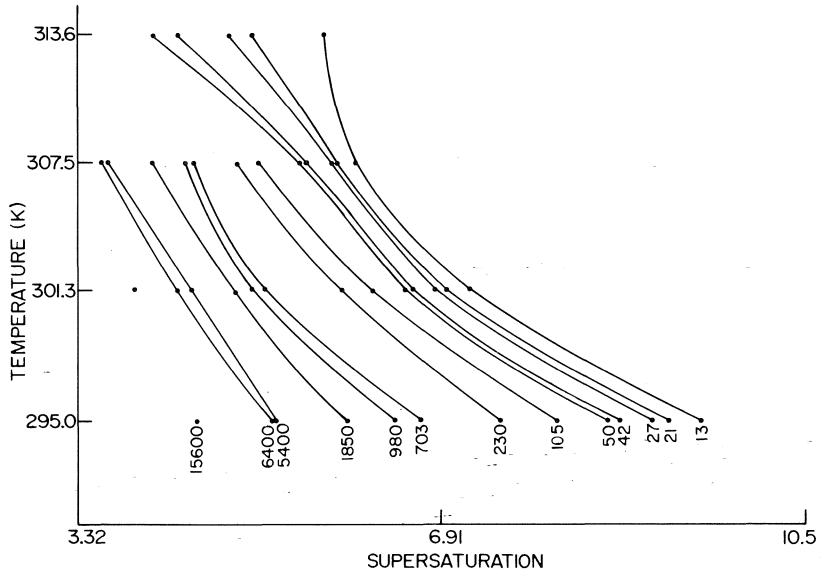

FIG. 2. A contour map of τ vs. T and S for the nucleation of $CaSO_4{\cdot}2H_2O$ from solution.

tension between the mother liquor and the embryo. This gives

$$\left(\frac{\partial^2 \Delta G}{\partial n^2}\right)_{n=n^*} = \frac{\mu_n - \mu_m}{3n^*}$$

For liquid solutions (2)

$$\beta = c_m \left(\frac{kT}{2\pi m}\right)^{1/2} \exp\left(\frac{-\Delta G_D}{kT}\right)$$

$$= sSN_0{}^{3/2} \left(\frac{kT}{2\pi m}\right)^{1/2} \exp\left(\frac{-\Delta G_D}{kT}\right)$$

where c_m is the concentration of free monomers, m is the monomeric mass, ΔG_D is the free energy of activation of diffusion (2), s is the equilibrium solubility of the solid phase in mol cm^{-3}, S is the supersaturation ratio, N_0 is Avogadro's number, and M is the molecular weight of the monomer in g mol^{-1}. Equation [7], resulting from the above expressions substituted into eq. [6], expresses L in terms of physical observables.

$$[7] \qquad L = \frac{4\pi\sigma M^{1/2} \exp\left(\frac{\Delta G_D}{kT}\right)}{(N_0 kT)^{3/2} sS \ln^2 S}$$

A contour plot of L values, generated with eq. [7] and the data of Table 3, as a function of T and S levels available in our laboratory studies is shown as Fig. 3. Contour lines of various equal L values have been drawn in Fig. 3 to facilitate comparison with Fig. 2, a similar contour plot showing the data obtained from the experimental program. Although the surface shapes are similar: a dished, tilted surface of sharply rising gradient that tends to ∞ at the

Can. J. Chem. Downloaded from www.nrcresearchpress.com by 210.87.254.40 on 09/05/12
For personal use only.

Can. J. Chem. Downloaded from www.nrcresearchpress.com by 210.87.254.40 on 09/05/12
For personal use only.

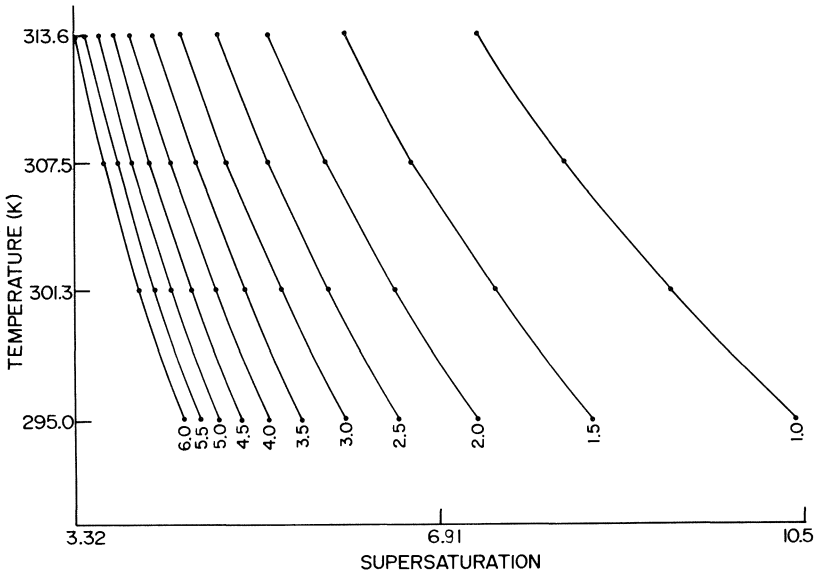

FIG. 3. A contour map of $L \times 10^6$ vs. T and S generated by use of eq. [7].

stable limit of the Ostwald diagram and to zero at high values of S, a comparison of the τ and L values shows that the generated surface lies much below the experimental surface reaching L levels approaching the reported τ levels only at values of S near to one (1.0001). Also, the extent of variation across the L values is much less than that for the experimental data. That is, the generated surface is rather like a rising plateau of low gradient whereas the experimental surface exhibits a much larger gradient. Taken together, these qualitative observations lead one to suspect the validity of the functional relationships suggested by the theoretical model. Thus, we turned to empirical modeling to search out the best functional relationship between τ, S, and T.

The search program was comprised of a selection of several equations from each of the following six general functional relationships: (*1*) $\tau = f(S,T)$; (*2*) $\tau = f(S) + g(T)$; (*3*) $\tau = f(S,T) + g(S)$, $\tau = f(S,T) + g(T)$, $\tau = f(S,T) + g(S,T)$; (*4*) $\ln \tau = f(S,T)$; (*5*) $\ln \tau = f(S) + g(T)$; (*6*) $\ln \tau = f(S,T) + g(S)$, $\ln \tau = f(S,T) + g(T)$, $\ln \tau = f(S,T) + g(S,T)$. Those equations screened representing groups

TABLE 3. Parameter values used in eq. [7] to calculate the values of L and S in Fig. 3

T (K)	$S \times 10^5$ (mol cm^{-3})	σ (ergs cm^{-2})	$\Delta G_D \times 10^{13}$ (ergs molecule^{-1})
295.0	3.896	23.92	3.128
301.3	3.941	23.13	3.128
307.5	3.997	22.35*	3.128
313.6	4.055	21.59	3.128

*Calculated from $\sigma = 26.64 - 0.125t$, where t is temperature in °C.

(*1*) through (*4*) exhibited values of the square of the multiple correlation coefficient (r^2) less than 0.71, those from group (*5*) had r^2 values less than 0.97 while representatives from group (*6*) showed r^2 values greater than 0.97. Thus further attention was focussed on the latter functional relationship as being the most promising for describing the observed lag times in our studies on $CaSO_4 \cdot 2H_2O$.

Shown in Table 4 is a listing of the set of equations [8]–[18] from group (*6*) screened along with the best values of the adjustable parameters and r^2 for each. r^2 is not a measure of goodness of fit although it is frequently used in this manner. A true goodness of fit parameter, Mallow's CP statistic, indicates that a significant difference exists between the various members of the listing. They are presented in Table 4 in descending order of goodness of fit. Values for r^2 are quoted rather than Mallow's CP statistic since the r^2 statistic is much more familiar and in this case directly parallels the level of goodness of fit.

Figure 4 shows a contour map of calculated $\ln \tau$ values as a function of S and T resulting from use of the uppermost tabular equation. For comparison the experimental $\ln \tau$ values are also shown in Fig. 4. The sum of the square of the residuals is 1.90 and is a further indication that the model fits the data rather well. We suggest, then, that reasonable estimates of the lag time for $CaSO_4 \cdot 2H_2O$ nucleation from solution can be obtained by use of eq. [19].

$$[19] \quad \ln \tau = \frac{-871.5}{\ln S} + \frac{5.115 \times 10^3}{\ln T \ln S} - 0.8346$$

Note that [18] of Table 4 has the form of eq.

TABLE 4. Equations representing group (*6*) used in the multiple regression screening program

Equation number and form		a	b	c	r^2
[8]	$\ln \tau = \frac{a}{\ln S} + \frac{b}{\ln T \ln S} + c$	-871.5	5.115×10^3	-8.346	0.9713
[9]	$\ln \tau = \frac{a}{T \ln S} + \frac{b}{\ln S} + c$	4.758×10^4	-133.3	-8.344	0.9712
[10]	$\ln \tau = \frac{a}{T \ln S} + \frac{b}{\ln T \ln S} + c$	5.617×10^4	-924.0	-8.345	0.9711
[11]	$\ln \tau = \frac{a}{T \ln S} + \frac{b}{S} + c$	4.763×10^4	-258.1	-39.77	0.9708
[12]	$\ln \tau = \frac{a}{T \ln S} + \frac{b}{S \ln T} + c$	5.257×10^4	-1655	-43.59	0.9707
[13]	$\ln \tau = \frac{a}{\ln T} + \frac{b}{T^3 S} + c$	2.295×10^3	1.254×10^9	-404.3	0.9706
[14]	$\ln \tau = \frac{a}{\ln^2 T} + \frac{b}{T^3 S} + c$	6.561×10^9	1.254×10^9	-203.6	0.9705
[15]	$\ln \tau = \frac{a}{T} + \frac{b}{T^3 S} + c$	2.135×10^4	1.254×10^9	-73.09	0.9704
[16]	$\ln \tau = \frac{a}{T^3 \ln^2 S} + \frac{b}{\ln T} + c$	5.222×10^8	2.463×10^3	-432.0	0.9704
[17]	$\ln \tau = \frac{a}{T^3 \ln^2 S} + \frac{b}{\ln^2 T}$	5.222×10^8	7.040×10^3	-216.6	0.9703
[18]	$\ln \tau = \frac{a}{T^3 \ln^2 S} + \frac{b}{T} + c$	5.222×10^8	2.290×10^4	-76.52	0.9701
*		1.140×10^9	-1.974×10^3	-20.66	
†	$L = \frac{a \exp \frac{b}{T}}{T^{3/2} S \ln^2 S} + c$	5.712×10^5	2.200×10^3	-8992	0.6600

[III.6] of ref. 14; i.e.,

$$[20] \quad \ln L_1 \cong \frac{16\pi\sigma^3 v^2}{3k^3 T^3 \ln^2 S} - \frac{(4\pi)^{1/3}(3v)^{2/3}\sigma}{kT} + \ln\left[\left(\frac{\pi d}{4\sigma v}\right)^{1/2} \frac{1}{N_0 s}\right]$$

Using averaged values for $CaSO_4 \cdot 2H_2O$ of σ (22.75 ergs cm^{-2}) and s (3.972×10^{-5} mol cm^{-3}) across the temperature range the 'constant' terms in eq. [20] were calculated. The results are listed in Table 4 (entry *) below the corresponding parameter estimates for the empirical equation. The most significant distinction between the two sets of results is the sign difference on b. The first two terms of the fitted equation work in concert to decrease τ as T increases; whereas in eq. [20] the second term provides a small negative correction to τ as T increases. Equation [20], using a least-squares criterion, appears as a poorly optimized version of that particular functional relationship but it could provide insight into the physical significance of the parameters in the analogous empirical equation.

Historically, the results of the application of fluctuation theory to the problem of the lag time in nucleation phenomena have led to expressions that have the form of eq. [7] (entry † in Table 4). Our attempts to fit equations of that form and of the forms represented in groups (*1*) through (*3*) to the data obtained from studies on $CaSO_4 \cdot 2H_2O$ nucleation failed. Surprisingly, empirical equations analogous in form to that examined by Frisch and Carlier (ref. 14, eq. [III.6]), but discarded by them, lead to data fits that are far superior; these were discarded because they represented an unrealistic initial boundary condition for vapour–liquid nucleation experiments under the usual experimental conditions. The results of our modeling program indicate that future efforts in the derivation of models of lag times in nucleation from solution should be concentrated on relationships of the form of group (*6*).

A term by term comparison of eqs. [1] and [20] leads to the suggestion that there could be a functional relationship between J and L_1 of the form shown as eq. [21]. Equations of this form were tested

$$[21] \quad \ln J \cong \ln L_1^{-1} + \ln T - \frac{(4\pi)^{1/3}(3Md)^{2/3}\sigma}{N^{2/3}kT} + \ln\left\{\frac{Akd}{2K_{sp}}\left[\frac{\pi N_0}{\sigma M}\right]^{1/2}\right\}$$

Can. J. Chem. Downloaded from www.nrcresearchpress.com by 210.87.254.40 on 09/05/12
For personal use only.

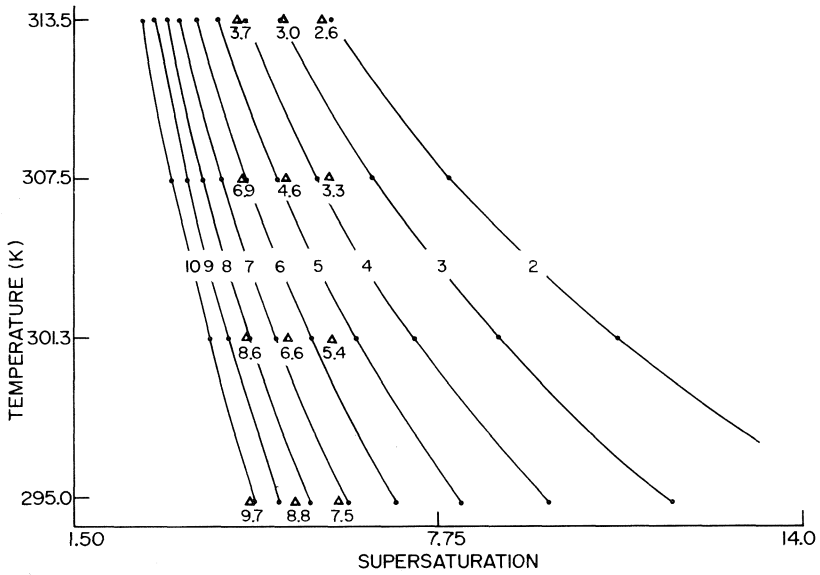

FIG. 4. A contour map of ln τ vs. T and S generated by use of eq. [19]. Experimental τ values shown by Δ's.

TABLE 5. Various functional relationships between J, L, and T evaluated with the multiple regression program

	Equation number and form	a	b	c	d	r^2
[23]	$\ln J = a \ln L^{-1} + bT + cT^{-1} + d$	1.827	-3.110	-2.654×10^5	1.845×10^3	0.8998
[24]	$\ln J = a \ln L^{-1} + b \ln T^{-1} + cT^{-1} + d$	1.827	1.874×10^3	-5.478×10^5	1.254×10^3	0.8997
[25]	$\ln J = a \ln L^{-1} + b \ln T^{-1} + cT + d$	1.827	-1.738×10^3	-5.953	-8.098×10^3	0.8997
[26]	$\ln J = a \ln L^{-1} + bT + c$	1.820	-0.2379	9.827×10^1	—	0.8862

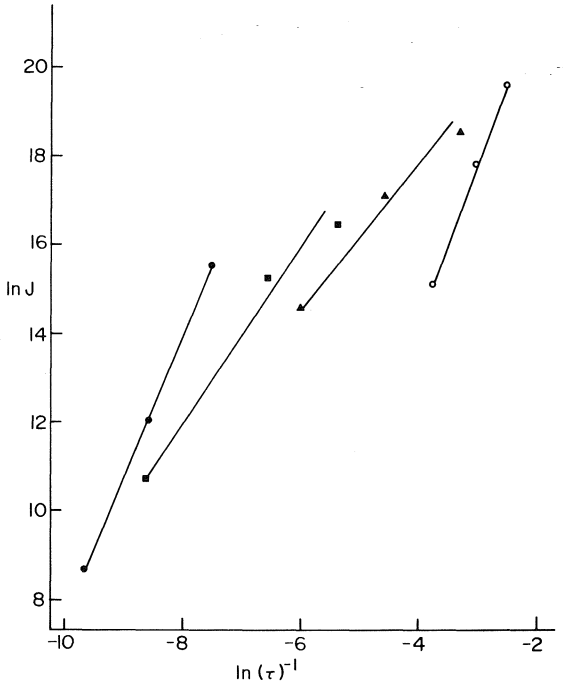

FIG. 5. Plots of ln J vs. ln τ^{-1} for twelve levels of supersaturation distributed over four temperatures. ●, 295.0 K; ■, 301.3 K; ▲, 307.5 K; ○, 313.6 K.

by comparison with the experimentally determined J, τ, and T values using a multiple regression screening program. The results are shown in Table 5 and plots of ln J vs. ln τ^{-1} at various temperatures are included as Fig. 5. Each result suggests that a relationship between the rate, lag time, and temperature can be represented by eq. [22].

$$[22]\quad \ln J = 1.827 \ln \tau^{-1} - 1.874 \times 10^3 \ln T - 5.478 \times 10^5 T^{-1} + 1.254 \times 10^4$$

This linear relationship between ln J and ln τ^{-1} at constant temperature is very important in that it demonstrates that the lag time, as defined, is a real nucleation response. Thus, measurements of it can be used to estimate σ, A, and S^* for systems in which measurements of J are difficult or impossible to obtain.

Acknowledgements

The authors acknowledge the financial assistance provided by the National Advisory Committee on Water Resources Research of the Department of Energy, Mines and Resources, and by the National Research Council of Canada.

Can. J. Chem. Downloaded from www.nrcresearchpress.com by 210.87.254.40 on 09/05/12
For personal use only.

1. J. B. ZELDOVICH. (*a*) J. Expt. Theoret. Phys. USSR, **12**, 525 (1942); (*b*) Acta Physicochim. URSS, **18**, 1 (1943).
2. J. I. FRENKEL. Kinetic theory of liquids. Oxford University Press, London. 1946. p. 382*ff*.
3. D. TURNBULL. Metals Tech. June 1948.
4. R. F. PROBSTEIN. Time lag in the self nucleation of a supersaturated vapor. Princeton Univ. Aero. Engrs. Lab Report No. 168. November 27, 1950.
5. A. KANTROWITZ. J. Chem. Phys. **19**, 1097 (1951).
6. H. WAKESHIMA. J. Chem. Phys. **22**, 1614 (1954).
7. F. C. COLLINS. Z. Elektrochem. **59**, 404 (1955).
8. H. L. FRISCH. J. Chem. Phys. **27**, 90 (1957).
9. W. G. COURTNEY. J. Chem. Phys. **36**, 2018 (1962).
10. R. P. ANDRES and M. BOUDART. J. Chem. Phys. **42**, 2057 (1965).
11. B. K. CHAKRAVERTY. Surface Sci. **4**, 205 (1966).
12. D. KASCHIEV. Surface Sci. **14**, 209 (1969).
13. R. P. ANDRES. *In* Nucleation. *Edited by* A. C. Zettlemoyer. Marcel Dekker, New York. 1969.
14. H. L. FRISCH and C. C. CARLIER. J. Chem. Phys. **54**, 4326 (1971).
15. B. VONNEGUT. J. Colloid Sci. **3**, 563 (1948).
16. O. E. HILEMAN, JR. Talanta, **14**, 139 (1967).
17. D. M. KELLER, RONALD E. MASSEY, and O. E. HILEMAN, JR. Can. J. Chem. **56**, 831 (1978).
18. R. BECKER and W. DÖRING. Ann. Phys. **24**, 719 (1935).
19. H. A. DAYNES. Proc. R. Soc. London, A**97**, 286 (1920).

Can. J. Chem. Downloaded from www.nrcresearchpress.com by 210.87.254.40 on 09/05/12
For personal use only.

Nuclear magnetic resonance studies of the solution chemistry of metal complexes. XV. Trimethyllead complexes of inorganic ligands

EMIKO K. MILLAR, CHRISTOPHER A. EVANS, AND DALLAS L. RABENSTEIN[1]

Department of Chemistry, University of Alberta, Edmonton, Alta., Canada T6G 2G2

Received May 8, 1978

EMIKO K. MILLAR, CHRISTOPHER A. EVANS, and DALLAS L. RABENSTEIN. Can. J. Chem. **56**, 3104 (1978).

The formation constants of the trimethyllead(IV) complexes of SO_3^{2-}, SeO_3^{2-}, $S_2O_3^{2-}$, SCN^-, HPO_4^{2-}, CO_3^{2-}, Cl^-, Br^-, and I^- have been determined in aqueous solution by ^1H nuclear magnetic resonance spectroscopy. The formation constants are in general fairly small and the extent to which complexes form is strongly dependent on pH. At high pH $(CH_3)_3PbOH$ forms while at low pH protonation of those ligands which are the conjugate bases of weak acids competes with complex formation. There is no indication of high selectivity in the binding of trimethyllead(IV) by a particular ligand type, and calculations indicate that trimethyllead(IV) is likely to be distributed among a variety of ligands in biological fluids, including chloride which forms uncharged and presumably lipid soluble $(CH_3)_3PbCl$.

EMIKO K. MILLAR, CHRISTOPHER A. EVANS et DALLAS L. RABENSTEIN. Can. J. Chem. **56**, 3104 (1978).

Faisant appel à la spectroscopie rmn ^1H, on a déterminé les constantes de formation des complexes du triméthylplomb(IV) avec SO_3^{2-}, SeO_3^{2-}, $S_2O_3^{2-}$, SCN^-, HPO_4^{2-}, CO_3^{2-}, Cl^-, Br^- et I^- en solution aqueuse. Les constantes de formation sont généralement assez faibles et le degré de formation des complexes est fortement influencé par le pH. A des pH élevés, il y a formation de $(CH_3)_3PbOH$ alors qu'à des pH faibles, la protonation des ligands qui sont des bases conjuguées d'acides faibles sont en compétition avec la formation du complexe, On n'a relevé aucune indication concernant une grande sélectivité pour la liaison du triméthylplomb(IV) avec un type particulier de ligand; les calculs indiquent que le triméthylplomb(IV) est vraisemblablement distribué entre une variété de ligands dans les fluides biologiques, y compris le chlorure qui forme du $(CH_3)_3PbCl$ qui ne porte pas de charge et qui est vraisemblablement soluble dans les lipides.

[Traduit par le journal]

Can. J. Chem. Downloaded from www.nrcresearchpress.com by 210.87.254.42 on 09/05/12
For personal use only.

Introduction

Even though the organometallic chemistry of trialkyllead(IV) compounds has been the subject of much study, little is known about their coordination chemistry in aqueous solution. In this paper, we report the results of a study of the complexation of trimethyllead by sulfite, selenite, thiocyanate, thiosulfate, phosphate, carbonate, and the halides. Some results are also presented for the complexation of trimethyllead by sulfide. The complexation was studied by ^1H nuclear magnetic resonance spectroscopy. Previous studies have shown that the chemical shift of trimethyllead provides a sensitive probe of complex formation (1).

At the present time, there is considerable interest in the behavior of lead and its compounds in the environment, and in the toxicology of these compounds. Of the various organometallic forms, the trialkyllead(IV) species are of particular importance. For example, it has long been recognized that inhalation or absorption of tetraalkyllead compounds results in the presence of trialkyllead(IV) salts in the fluids and tissues of the body (2). More recently, interest has focussed on the trimethyllead(IV) species as a result of reports on the methylation of lead by microorganisms (3–5). It seems likely that the behavior of trialkyllead(IV) compounds in the environment and in biological systems will depend to some extent on their coordination chemistry. The research described in this paper forms the second part (1) of a continuing program directed towards characterizing the aqueous solution chemistry of trimethyllead and its complexes.

[1]To whom all correspondence should be addressed.

Experimental

Chemicals

Trimethyllead acetate (Alfa Inorganics) was used as the source of trimethyllead. Because acetate forms a complex with $(CH_3)_3Pb^+$ in aqueous solution, it was converted to a stock solution of trimethyllead perchlorate by an ion exchange procedure described previously (1). The stock solution was standardized by potentiometric titration (1).

Sodium selenite (Alfa Inorganics) was purified by first filtering an aqueous solution and then recrystallization. Stock solutions prepared from the purified solid were standardized by adding an excess of $HClO_4$ and then titration with NaOH. The selenite concentration was determined from the volume of NaOH between the first and second endpoints. Disodium hydrogen phosphate (B.D.H.) solutions were standardized by a similar titration procedure. Sodium hydrogen sulfite and

Can. J. Chem. Downloaded from www.nrcresearchpress.com by 210.87.254.42 on 09/05/12
For personal use only.

sodium sulfide (J. T. Baker) solutions were standardized by literature procedures (6). The other ligands were obtained as reagent grade sodium salts, and were used as received.

pH Measurements and Nuclear Magnetic Resonance Measurements

pH measurements and nmr measurements were made as described previously (1). Spectra were recorded at a probe temperature of 25 ± 1°C. Chemical shifts were measured relative to the *tert*-butyl resonance of *tert*-butanol (TBA), but are reported relative to the methyl resonance of sodium 2,2-dimethyl-2-silapentane-5-sulphonic acid (DSS). Positive shifts correspond to resonances of protons less shielded than the methyl protons of DSS. The TBA resonance is 1.243 ppm downfield from the methyl resonance of DSS. The ^1H nmr spectrum of trimethyllead consists of a singlet flanked symmetrically by two small satellites due to those methyl groups bonded to the ^{207}Pb isotope ($I = \frac{1}{2}$, natural abundance = 21.1%). Previous studies have shown the magnitude of $J_{^{207}Pb-^1H}$ to be relatively insensitive to complex formation (1).

Solution Preparation

The experiments were of two types: (*a*) measurement of the chemical shift of trimethyllead in solutions having a constant $[ligand]_{total}/[(CH_3)_3Pb]_{total}$ ratio as a function of pH and (*b*), measurement of the chemical shift of trimethyllead in solutions having a range of $[ligand]_{total}/[(CH_3)_3Pb]_{total}$ ratios at constant pH. In experiments of the first type, a solution was prepared from trimethyllead stock solution, either solid ligand or ligand stock solution, and enough solid $NaClO_4$ to give a constant ionic strength of 0.30 *M*. The pH was then adjusted with concentrated $HClO_4$ or carbonate-free NaOH, and ~0.4 ml samples withdrawn at the appropriate pH values. Samples were taken at closely spaced pH intervals (typically every 0.3–0.5 pH unit), generally over the pH range 2–12. Nuclear magnetic resonance spectra were recorded immediately after sample preparation. Solutions of those ligands which are easily oxidized were prepared in an argon atmosphere.

In experiments of the second type, individual solutions were prepared at each of the desired $[ligand]_{total}/[(CH_3)_3Pb]_{total}$ ratios from the stock trimethyllead solution, the solid ligand, and $NaClO_4$. In all experiments except those involving NaSCN, the ionic strength was kept constant at 0.30 *M* by adding $NaClO_4$. In studying the $(CH_3)_3Pb$–SCN system, an ionic strength of 1.5 *M* was used to permit a wider range of $[NaSCN]_{total}/[(CH_3)_3Pb]_{total}$ ratios to be used at constant ionic strength.

Trimethyllead concentrations of $2 \times 10^{-3} - 5 \times 10^{-3}$ *M* were used.

Results

The formation constants listed in Table 1 were calculated from the chemical shift of the methyl protons of $(CH_3)_3Pb(IV)$ in solutions containing known amounts of $(CH_3)_3Pb(IV)$ and ligand. For example, Fig. 1 shows the chemical shift as a function of pH for an aqueous solution of trimethyllead perchlorate and for an aqueous solution containing trimethyllead perchlorate and disodium hydrogen phosphate. Figure 2 shows chemical shift data as a function of the $[NaX]_{total}/[(CH_3)_3Pb]_{total}$ ratio for the NaI, NaBr, and NaCl systems. In both Figs. 1 and 2, the presence of ligand causes the chemical shift to change, indicating the formation of trimethyllead complexes.

TABLE 1. Acid dissociation constants and formation constants of the trimethyllead complexes of selected inorganic ligands, and the ^1H chemical shifts of the trimethyllead complexes

Ligand	pK_a[a]	$\delta_{complex}$[b]	K_f[a] $(CH_3)_3PbX$
HPO_4^{2-}	6.71	1.435	75 ± 3
SO_3^{2-}	6.79	1.407	18.8 ± 1.6
SeO_3^{2-}	7.83	1.425	90 ± 4
$S_2O_3^{2-}$		1.504	138 ± 3
SCN^-		1.709	0.38 ± 0.03[c]
CO_3^{2-}	10.30	1.347	396 ± 32
I^-		1.867	1.89 ± 0.13
Br^-		1.692	1.95 ± 0.19
Cl^-		1.595	1.22 ± 0.39

[a]At 25°C and 0.30 *M* ionic strength (with $NaClO_4$) unless otherwise noted.
[b]In ppm vs. DSS.
[c]1.50 *M* ionic strength ($NaClO_4$).

Formation constants for the phosphate, sulfite, selenite, thiosulfate, and carbonate complexes were calculated from data of the type shown in Fig. 1. For each of these systems, exchange averaged resonances were observed for the trimethyllead, indicating exchange of trimethyllead among its various species to be rapid on the nmr time scale. Consequently, separate resonances were not observed for the complexed $(CH_3)_3Pb(IV)$ and it was necessary to calculate the formation constants by curve fitting procedures. The general procedure will be described with reference to the phosphate complex.

The pH dependence of the chemical shift of $(CH_3)_3Pb(IV)$ in aqueous solution is due to the following pH-dependent equilibria (1):

[1] $$(CH_3)_3Pb^+ + OH^- \rightleftarrows (CH_3)_3PbOH$$

$$K_1 = \frac{[(CH_3)_3PbOH]}{[(CH_3)_3Pb^+][OH^-]} = 7.34 \times 10^4\ M^{-1}$$

[2] $$(CH_3)_3Pb^+ + (CH_3)_3PbOH \rightleftarrows ((CH_3)_3Pb)_2OH^+$$

$$K_2 = \frac{[((CH_3)_3Pb)_2OH^+]}{[(CH_3)_3Pb^+][(CH_3)_3PbOH]} = 3.12 \times 10\ M^{-1}$$

where waters of hydration are omitted. In the solution containing phosphate, some $(CH_3)_3Pb(IV)$ also is present in complexed form. Of the various models tested for the complexation equilibria, the best fit was obtained for one in which the $(CH_3)_3Pb(IV)$ and HPO_4^{2-} form a simple one-to-one complex.

[3] $$(CH_3)_3Pb^+ + HPO_4^{2-} \rightleftarrows (CH_3)_3Pb(HPO_4)^-$$

$$K_f = \frac{[(CH_3)_3Pb(HPO_4)^-]}{[(CH_3)_3Pb^+][HPO_4^{2-}]}$$

Because exchange is rapid, the observed chemical

Can. J. Chem. Downloaded from www.nrcresearchpress.com by 210.87.254.42 on 09/05/12
For personal use only.

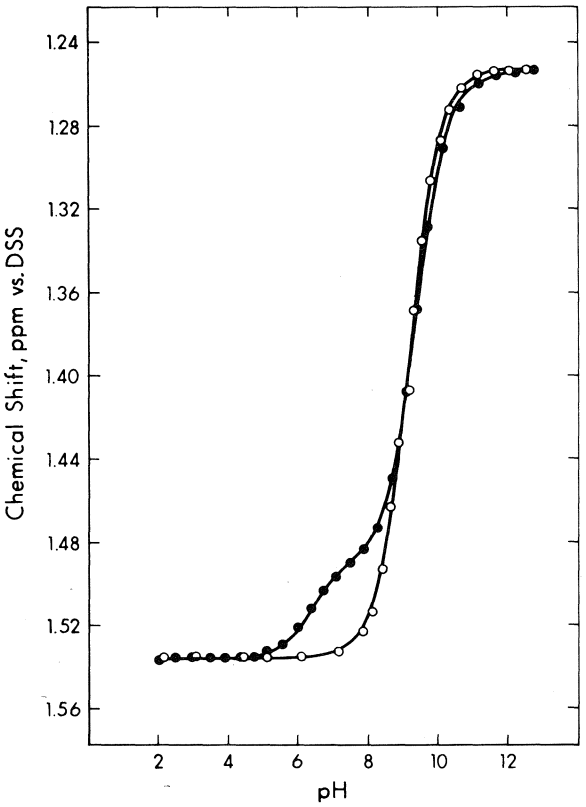

FIG. 1. pH dependence of the chemical shift of the methyl protons of trimethyllead(IV) in aqueous solutions containing 5.00×10^{-3} M $(CH_3)_3Pb(ClO_4)$ (open points) and containing 5.00×10^{-3} M $(CH_3)_3Pb(ClO_4)$ and 1.35×10^{-2} M Na_2HPO_4 (solid points). The ionic strength was 0.30 M ($NaClO_4$ as required).

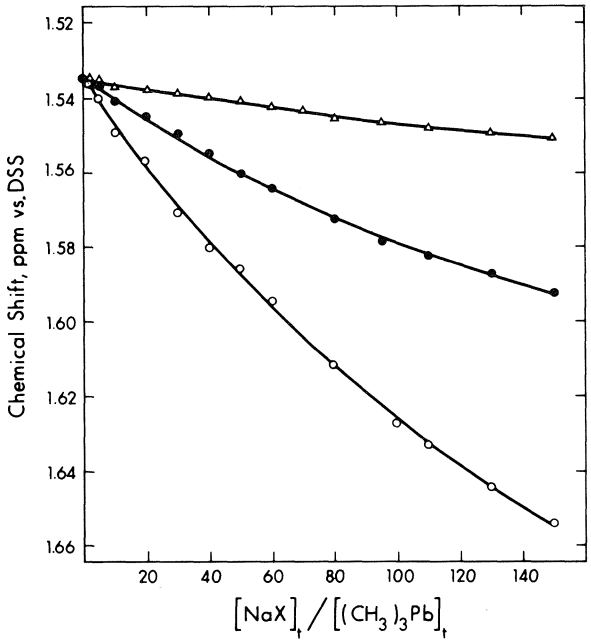

FIG. 2. The chemical shift of the methyl protons of trimethyllead(IV) in aqueous solutions containing 2.00×10^{-3} M $(CH_3)_3Pb(ClO_4)$ and sodium halide as a function of the ligand-to-trimethyllead ratio at pH 4.00. Sodium chloride (△), sodium bromide (●), and sodium iodide (○). The ionic strength was 0.30 M ($NaClO_4$ as required).

shift, δ_{obs}, is the weighted average of the chemical shifts of the various species present.

$$[4] \quad \delta_{obs} = P_{TML}\delta_{TML} + P_{(TML)_2OH}\delta_{(TML)_2OH} + P_{TMLOH}\delta_{TMLOH} + P_C\delta_C$$

where P represents the fractional concentration of trimethyllead in the form indicated by the subscript, δ the chemical shift of that form, and TML represents $(CH_3)_3Pb^+$.

K_f for $(CH_3)_3Pb(HPO_4)^-$ was obtained by curve fitting chemical shift data to eq. [4]. The procedure involved (*i*) estimating initial values for K_f and δ_C, (*ii*) calculating the fractional concentration of each species at the pH of the given data point using this estimate for K_f, the values for K_1 and K_2 given above, and the total $(CH_3)_3Pb(IV)$ and ligand concentrations, (*iii*) predicting a value for the averaged chemical shift ($\delta_{i,pred}$) at the particular pH from these fractional concentrations, the initial estimate for δ_C, and the known values (1) for δ_{TML}, $\delta_{(TML)_2OH}$, and δ_{TMLOH}. Steps (*i*)–(*iii*) are then repeated for each data point using the initial estimates for K_f and δ_C. In step (*iv*), the nonlinear least-squares program KINET (7) compares the set of predicted chemical shifts with the observed values by calculating the sum of the squares of the residuals (SSR) and then (*v*), KINET adjusts K_f and δ_C to minimize the SSR. Steps (*i*)–(*v*) are then repeated until the best values for K_f and δ_C are obtained from the particular experimental data as indicated by a minimum in the SSR.

The K_f value obtained for $(CH_3)_3Pb(HPO_4)^-$ by this procedure using data in the pH region 2 to 13 is 75.1 ± 3, where the uncertainty is a linear estimate of the standard deviation (7). The solid curve through the experimental points in Fig. 1 for the trimethyllead–phosphate system is predicted from the values obtained for K_f and δ_C. There was no indication of complexes formed with other phosphate species; at high pH where PO_4^{3-} forms, hydroxide ion competes with the phosphate ligand and $(CH_3)_3PbOH$ forms while at low pH there is a competitive equilibrium between protonation and complexation of HPO_4^{2-}. The data in Fig. 1 indicate no complexation by $H_2PO_4^-$, which also is weak as a conjugate base. The pH dependence of the formation of $(CH_3)_3Pb(HPO_4)^-$ is shown in Fig. 3.

The formation constants in Table 1 for the sulfite, selenite, thiosulfate, and carbonate complexes were determined by the same procedure. For the sulfite

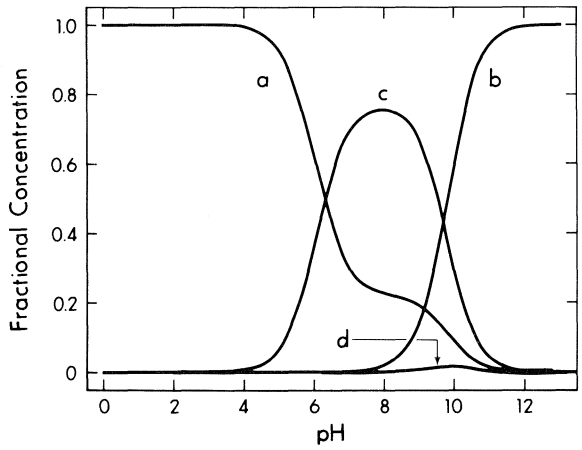

FIG. 3. pH dependence of the distribution of trimethyllead among its various forms in a solution containing 5.00×10^{-3} *M* $(CH_3)_3Pb(ClO_4)$ and 1.35×10^{-2} *M* Na_2HPO_4. $(CH_3)_3Pb^+$ (*a*), $(CH_3)_3PbOH$ (*b*), $(CH_3)_3Pb(HPO_4)^-$ (*c*), and $((CH_3)_3Pb)_2OH^+$ (*d*).

and selenite systems, chemical shift data in the pH ranges 7 to 12.7 and 8 to 12.7 respectively were fit to models in which $(CH_3)_3Pb(SO_3)^-$ and $(CH_3)_3Pb(SeO_3)^-$ are the only complexes. Attempts to fit data at pH < 7 to these models were unsuccessful. At pH < 7, both ligands are protonated, suggesting the formation of other complexes; however, it has not been possible to determine the nature of the complexes. The simple model in Table 1 for thiosulfate describes its complexation equilibria with $(CH_3)_3Pb(IV)$ over the pH range 2 to 13, and that for carbonate over the range 9 to 13.

Formation constants for the chloride, bromide, iodide, and thiocyanate complexes were obtained from data of the type shown in Fig. 2 by similar curve fitting procedures. The results are given in Table 1. A constant pH of 4 was used in the halide studies and 5 in the thiocyanate studies to minimize competition from OH^- for the $(CH_3)_3Pb^+$. Even though ligand-to-metal ratios as high as 150 and 300 were used in the halide and thiocyanate studies, respectively, all of the data for each system could be fit with good precision to a model involving a simple one-to-one $(CH_3)_3PbX$ complex.

Similar data were taken for fluoride; however, precipitation precluded a determination of the formation constant for the fluoride complex.

Data of the type shown in Fig. 1 were taken for solutions containing $(CH_3)_3Pb(IV)$ and sodium sulfide over the pH range 7–13. The data indicate formation of strong complexes, apparently with both S^{2-} and HS^-; however, it has not been possible to obtain reliable values for the formation constants. This may be related to the apparent decomposition of trialkyllead compounds in the presence of sulfide (4).

Discussion

The coordination geometry around the lead atom of $(CH_3)_3Pb(IV)$ in aqueous solution is thought to be trigonal bipyramidal, with the three methyl groups and the lead atom in the planar trigonal unit and the two water molecules in axial positions (8, 9)[2]. The trimethyllead complexes studied in this work probably form from $(CH_3)_3Pb^+$ by substitution of one H_2O ligand. Their formation constants are small, indicating the affinity of the trimethyllead moiety for these ligands not to be large relative to that for water. There is no evidence of complexes having a ligand-to-metal ratio greater than 1:1 with these ligands, indicating an even smaller tendency to replace the second water molecule. This is expected since the formation constants for the stepwise formation of complexes generally decrease as the ligand-to-metal ratio increases.

The only literature result available for comparison with the formation constants determined in this work is the value of 630 obtained by Bertazzi by anion exchange techniques for the $(CH_3)_3PbSCN$ complex (10). This value is considerably larger than that determined in this work, and much too large to be compatible with the chemical shift data.

The results in Table 1 together with other results from our studies on the coordination chemistry of trimethyllead (1) suggest that trimethyllead does not show a strong preference for any particular type of donor group.[3] The largest formation constants appear to be with the deprotonated sulfhydryl groups of organic thiol ligands.[3] For example, with mercaptoethanol the formation constants of the complexes formed are[3]

[5] $$(CH_3)_3Pb^+ + RS^- \rightleftarrows (CH_3)_3PbSR$$
$$K_{f1} = 9.1 \times 10^5$$

[6] $$(CH_3)_3Pb^+ + (CH_3)_3PbSR \rightleftarrows ((CH_3)_3Pb)_2SR^+$$
$$K_{f2} = 14.0$$

This is of particular interest with respect to the chemistry of trimethyllead in biological fluids, where there is an abundance of potential ligands, including carboxylate groups, carbonate, inorganic and organic phosphate, chloride, and the sulfhydryl groups of peptides and proteins. Because of the different pH dependence of the extent to which the various complexes form and the relative abundances of the different ligands, the formation constants predict that, at physiological pH, there will be a significant fraction of $(CH_3)_3Pb(IV)$ complexed even by those ligands having small formation constants.

[2]C. A. Evans and D. L. Rabenstein. Unpublished results.

[3]S. Backs, C. A. Evans, and D. L. Rabenstein. Unpublished results.

Can. J. Chem. Downloaded from www.nrcresearchpress.com by 210.87.254.42 on 09/05/12
For personal use only.

Can. J. Chem. Downloaded from www.nrcresearchpress.com by 210.87.254.42 on 09/05/12
For personal use only.

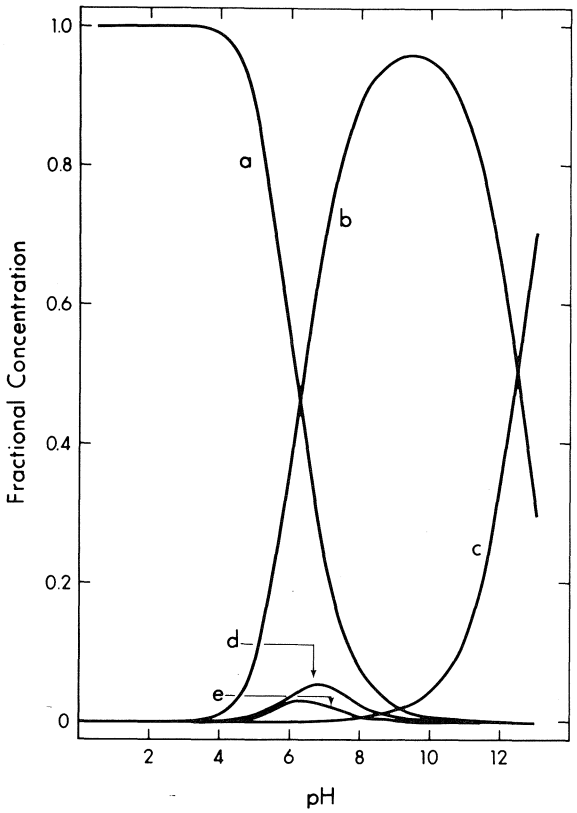

FIG. 4. pH dependence of the distribution of trimethyllead among its various forms in an aqueous solution containing $(CH_3)_3PbClO_4$, 2-mercaptoethanol, and sodium phosphate, each at a total concentration of 5.00×10^{-3} *M*. $(CH_3)_3Pb^+$ (*a*), $(CH_3)_3Pb(SCH_2CH_2OH)$ (*b*), $(CH_3)_3PbOH$ (*c*), $(CH_3)_3Pb(HPO_4)^-$ (*d*), $((CH_3)_3Pb)_2SCH_2CH_2OH^+$ (*e*).

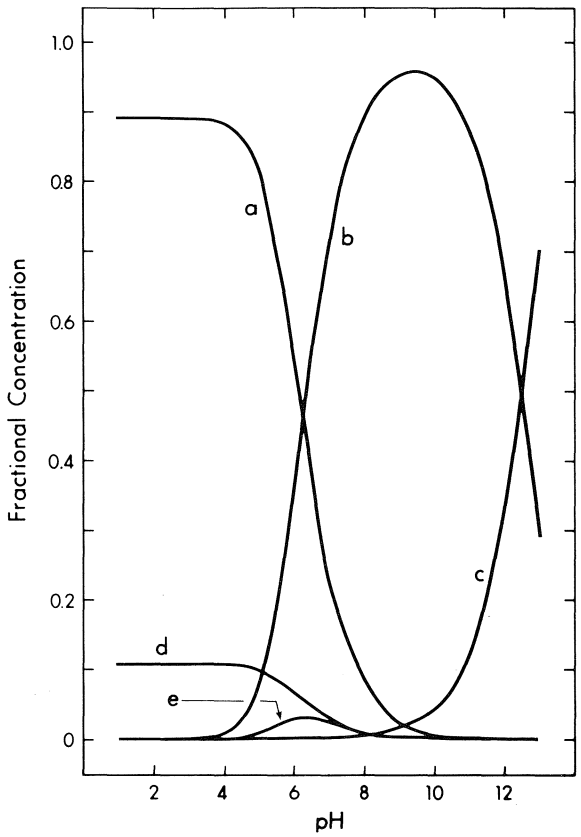

FIG. 5. pH dependence of the distribution of trimethyllead among its various forms in an aqueous solution containing 5.00×10^{-3} *M* $(CH_3)_3PbClO_4$ and 2-mercaptoethanol and 0.10 *M* NaCl. $(CH_3)_3Pb^+$ (*a*), $(CH_3)_3Pb(SCH_2CH_2OH)$ (*b*), $(CH_3)_3PbOH$ (*c*), $(CH_3)_3PbCl$ (*d*), and $((CH_3)_3Pb)_2SCH_2CH_2OH^+$ (*e*).

To illustrate, the pH dependence calculated for the fractional concentrations of the various trimethyllead species in solutions containing 2-mercaptoethanol and phosphate and in solutions containing 2-mercaptoethanol and chloride are shown in Figs. 4 and 5. Even though K_f for the $(CH_3)_3Pb(HPO_4)^-$ and $(CH_3)_3PbCl$ complexes are several orders of magnitude less than that for the 2-mercaptoethanol complex, some $(CH_3)_3Pb(HPO_4)^-$ and $(CH_3)_3PbCl$ form because of the competitive protonation of the sulfhydryl ligand. This situation is in marked contrast to that for $CH_3Hg(II)$, which shows such an extreme affinity for sulfhydryl ligands that, in biological systems, essentially all of the $CH_3Hg(II)$ is assumed to be complexed by the sulfhydryl groups of peptides and proteins (11). The presence of even a small fraction of $(CH_3)_3Pb(IV)$ as $(CH_3)_3PbCl$ is of particular interest because this complex has electroneutrality and most likely is lipid soluble. $(CH_3)_3Pb^+$ complexes of HPO_4^{2-}, Cl^-, and CO_3^{2-} are probably even more important in the environment where the concentration of sulfhydryl ligands can be expected to be low.

Acknowledgements

This research was supported in part by a Water Resources Research Support Program Grant from the Inland Waters Directorate, Environment Canada, and by the University of Alberta.

1. T. L. SAYER, S. BACKS, C. A. EVANS, E. K. MILLAR, and D. L. RABENSTEIN. Can. J. Chem. **55**, 3255 (1977).
2. J. E. CREMER. Brit. J. Ind. Med. **16**, 191 (1959).
3. P. T. S. WONG, Y. K. CHAU, and P. L. LUXON. Nature, **253**, 263 (1975).
4. A. W. P. JARVIE, R. N. MARKALL, and H. R. POTTER. Nature, **255**, 217 (1975).
5. U. SCHMIDT and F. HUBER. Nature, **259**, 157 (1976).
6. D. L. RABENSTEIN, M. C. TOURANGEAU, and C. A. EVANS. Can. J. Chem. **54**, 2517 (1976).
7. J. L. DYE and V. A. NICELY. J. Chem. Educ. **48**, 443 (1971).
8. P. GOGGIN. D. Phil. Thesis, Oxford. 1960. p. 156.
9. I. R. BEATTIE. Q. Rev. **17**, 382 (1963).
10. N. BERTAZZI. Z. Anorg. Allg. Chem. **410**, 316 (1974).
11. D. L. RABENSTEIN. Acc. Chem. Res. **11**, 100 (1978).

A conformational study of methyl β-cellobioside-d_8 by ^{13}C nuclear magnetic resonance spectroscopy: dihedral angle dependence of $^3J_{C-H}$ in $^{13}C—O—C—^1H$ arrays

GORDON K. HAMER, FELIPE BALZA, NATSUKO CYR, AND ARTHUR S. PERLIN

Department of Chemistry, McGill University, Montreal, P.Q., Canada H3A 2A7

Received May 2, 1978

GORDON K. HAMER, FELIPE BALZA, NATSUKO CYR, and ARTHUR S. PERLIN. Can. J. Chem. **56**, 3109 (1978).

Methyl β-cellobioside (**2**) has been deuterated at positions C-2, -3, -3′, -4, -6, and -6′ by ^1H–^2H exchange with deuterium oxide in the presence of Raney nickel catalyst. The resulting simplification in the ^{13}C nmr spectrum of this isotopically-labelled compound has facilitated the measurement of interresidue ^{13}C–^1H coupling, as a means of determining the orientation of the glycosidic linkage in **2**. Three-bond coupling across the linkage between ^{13}C-1 and H-4′ is found to be 4.3 Hz and that between ^{13}C-4′ and H-1, 4.2 Hz. By reference to other ^{13}C–^1H coupling data, which exhibit a Karplus type of relationship between the magnitude of $^3J_{C-H}$ and dihedral angle in $^{13}C—O—C—^1H$ arrays of bonded atoms, it appears that torsion angles ϕ and ψ of the disaccharide in aqueous solution are in the region of 25–30°, i.e., close to the angles of crystalline **2**. Corresponding data for the hepta-*O*-acetyl derivative indicate that ψ is smaller by ~10° and ϕ is unchanged. An analysis of the ^1H-coupled ^{13}C spectrum of cyclohexaamylose-2,3,6,6′-d_4 is presented in relation to these findings. Computer simulations of the observed spectra have been used to determine coupling constants and to assess the importance of second-order effects on the measurement of J_{C-H}.

GORDON K. HAMER, FELIPE BALZA, NATSUKO CYR et ARTHUR S. PERLIN. Can. J. Chem. **56**, 3109 (1978).

On a deutéré le β-cellobioside de méthyle (**2**) aux positions C-2, -3, -3′, -4, -6 et -6′ par échange ^1H–^2H avec l'oxyde de deutérium en présence de catalyseur de nickel de Raney. Ce produit du marquage isotopique possède un spectre rmn de ^{13}C simplifié qui facilite la mesure du couplage ^{13}C–^1H entre les résidus, ce qui permet de déterminer l'orientation du lien glycosidique dans **2**. On trouve pour le couplage sur trois liaisons dans le lien glycosidique, des valeurs de 4.3 Hz entre ^{13}C-1 et H-4′ et de 4.2 Hz entre ^{13}C-4′ et H-1. Si l'on se reporte à d'autres mesures de couplage ^{13}C-^1H, qui manifestent une relation du type Karplus entre la valeur de $^3J_{C-H}$ et l'angle dièdre dans la séquence $^{13}C—O—C—^1H$ d'atomes liés, on déduit que les angles de torsion ϕ et ψ du disaccharide en solution aqueuse se situent aux environs de 25–30°C, soit tout près des angles observés dans le composé **2** cristallin. Les données correspondantes pour le dérivé hepta-*O*-acétylé n'indique aucun changement sur ϕ et une diminution de ~10° sur ψ. On présente, en rapport avec ces nouveaux résultats, une analyse du spectre de ^{13}C avec couplage ^1H pour la cyclohexaamylose-2,3,6,6′-d_4. On a utilisé la reconstitution des spectres par ordinateur pour déterminer les constantes de couplage et évaluer l'importance des effets de second ordre sur les mesures de J_{C-H}.

[Traduit par le journal]

Can. J. Chem. Downloaded from www.nrcresearchpress.com by 210.87.254.105 on 09/05/12
For personal use only.

Introduction

As an aid in studying conformations of disaccharides and oligosaccharides in solution, measurements of interresidue spin–spin coupling (^3J) between a ^{13}C nucleus of one residue and the nearest ^1H of the adjacent residue (**1**) are being made from natural abundance, ^1H-coupled ^{13}C nmr spectra (1–3). That is, the conformation of the glycosidic region represented by **1** should be reflected in the magnitude of ^3J between the ^{13}C and ^1H nuclei, inasmuch as ^3J is dependent upon the dihedral angle relating these nuclei in space (4–6). A number of α-D-glucopyranosides have been examined in this way, including maltose and cyclohexaamylose (1–3). For the latter compounds, the observed interresidue coupling of ^{13}C-1 with H-4′ (or H-4) and of ^{13}C-4′ (or C-4) with H-1 is interpreted (2) as evidence that torsion (dihedral) angles ϕ (C′—O—C—H) and ψ (C—O—C′—H′) (**1**) of their glycosidic bonds, correspond to conformations in solution that are somewhat more staggered than in the solid state.

Here, we deal with the orientation of the glycosidic bond in methyl β-cellobioside (**2**). Cellobiose itself was examined initially (1), although strong overlap between the α- and β-anomeric pairs of C-1 and C-4′ signals interfered with measurements of their line widths. Judging from the results to be presented, our estimates (1) of interresidue coupling in cellobiose are low. By choosing a single glycosidic form (**2**), this source of difficulty has now been avoided. In addition, however, the present measurements of interresidue coupling in **2** have been greatly facilitated by the availability of an octa-*C*-deuterio analog of the glycoside, i.e., **3**, because of a marked

Can. J. Chem. Downloaded from www.nrcresearchpress.com by 210.87.254.105 on 09/05/12
For personal use only.

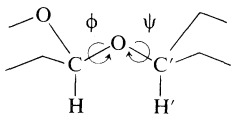

1

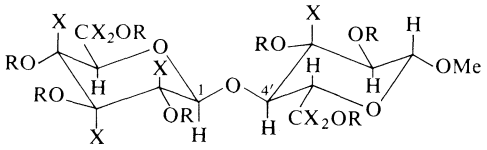

2 X = H, R = D
3 X = D, R = D
7 X = D, R = Ac

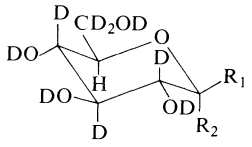

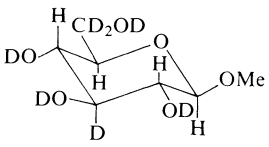

4 R_1 = OD, R_2 = H
6*a* R_1 = H, R_2 = OD
6*b* R_1 = OD, R_2 = H

5

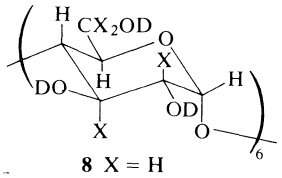

8 X = H
9 X = D

simplification in the ^{1}H-coupled ^{13}C nmr spectrum of **3** as compared with that of **2**.

Results and Discussion

^{13}C Nuclear Magnetic Resonance Spectra of Methyl β-Cellobioside-d_8

Compound **3** was prepared (7) by treating methyl β-cellobioside with deuterium oxide at 100°C for 24 h in the presence of Raney nickel catalyst, a procedure shown (8) to extensively *C*-deuterate simpler glycosides. Deuterium was incorporated into all positions except 1, 5, 1′, 2′, 4′, and 5′, as shown by a comparison of the ^{13}C nmr spectra of **2** and **3** (Figs. 1*A* and 1*B*). This ^{2}H distribution is consistent with general observations (7, 8) on glycosides under these conditions, in that only protons α to a free hydroxyl group undergo appreciable ^{1}H–^{2}H exchange. Most of the signal assignments for **2** and **3** in Fig. 1 are based on the reports of earlier workers (9, 10), although our results call (7) for a reversal of their designations for C-3 and C-5 and also C-3′ and C-5′ (see Experimental). The resistance of H-2′ in glycoside **2** to exchange is analogous to the relatively low reactivity found for H-2 of methyl β-D-glucopyranoside, which appears to be even greater in the disaccharide owing, presumably, to the presence nearby of the linkage at position-4′.

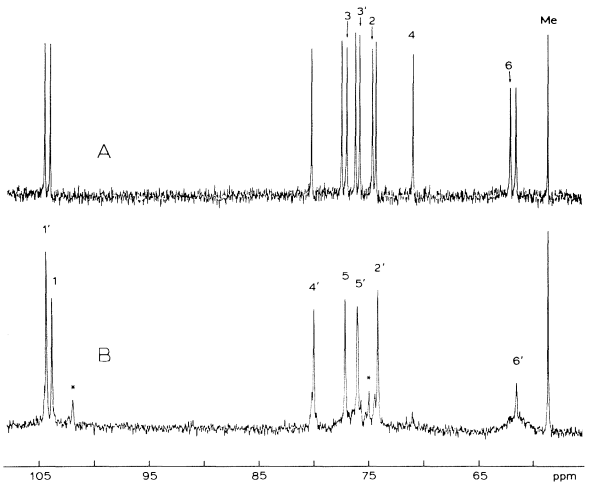

FIG. 1. 22.63 MHz ^{1}H-decoupled ^{13}C nmr spectrum of (*A*) methyl β-cellobioside (**2**) and (*B*) methyl β-cellobioside-d_8 (**3**); recorded in D_2O solution at 35°C. Signals indicated by asterisks are due to isomerization product(s) formed during ^{1}H–^{2}H exchange (see Experimental).

Of particular significance is the fact that in the preparation of **3**, positions-1 and -4′ remain intact; hence also, the 1- and 4′-carbon signals essential for a study of ^{13}C–^{1}H coupling across the glycosidic bond, remain among those readily observable in Fig. 1*B*.

The substantial simplification of spectrum 1*A*, achieved in 1*B* through the introduction of deuterium is magnified in the ^{1}H-coupled spectra of **2** and **3**. An example of this is found in examining the signals of the two anomeric carbons. The C-1 and C-1′ signals of **2** overlap extensively (Fig. 2*A*), whereas with the deuterated compound (**3**) the individual signals are clearly visible (Fig. 2*B*); reasons for this are considered later (see footnote 2). It is to be noted that Figs. 2*A* and *B* represents only half of these signals, the other half being separated by the magnitude of one-bond coupling with H-1 or H-1′.[1] This type of presentation emphasizes fine structure due to two- and three-bond couplings and is used below as well in dealing with other signals.

If there were *no* appreciable interresidue coupling in **2** between C-1 and H-4′, the C-1 signal should exhibit a splitting pattern similar to that of C-1 of β-D-glucose. The latter has the appearance of a doublet of doublets ($^1J_{C\text{-}1\text{–}H\text{-}1}$ = 161 Hz, $^2J_{C\text{-}1\text{–}H\text{-}2}$ = −5.7 Hz (1, 11, 12)). As seen in Fig. 2*D*, a 2 Hz coupling (^3J) with H-5 (6) is not resolved but introduces some line broadening; this becomes more evident (Fig. 2*E*) when H-5 of β-D-glucose is replaced (1) by deuterium (the effect of long-range coupling

[1] $^1J_{C\text{–}H}$ is approximately 160 Hz in each instance, in accord with (4, 6) the β-D-*gluco* configuration of each residue in **2** (Table 1).

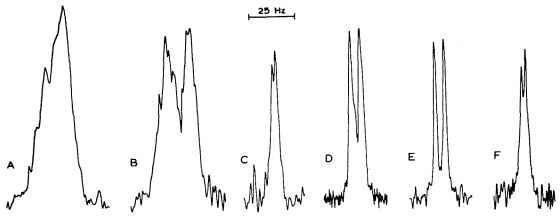

FIG. 2. One-half of the 22.63 MHz ^{1}H-coupled ^{13}C nmr spectrum of (*A*) C-1 of methyl β-cellobioside (**2**), (*B*) C-1 of methyl β-cellobioside-d_8 (**3**), (*C*) C-1 of β-D-glucose-2,3,4,6,6′-d_5 (**6***b*) formed by enzymic hydrolysis of **3**, (*D*) C-1 of β-D-glucose, (*E*) C-1 of β-D-glucose-5,6,6′-d_3, (*F*) C-1 of β-D-glucose-2,3,4,6,6′-d_5 (**4**) prepared by acid hydrolysis of methyl α-D-glucopyranoside-2,3,4,6,6′-d_5. Spectra recorded in D_2O solution at 35°C.

with H-3 and -4 is small). With the deuterated cellobioside (**3**), the fact that H-2 (as well as -3 and -4) has been exchanged[2] should give a C-1 signal in which only the couplings with H-1 and H-5 are evident (although slight broadening is to be expected owing to coupling with ^{2}H-2[3]), *again assuming that interresidue coupling is negligible*. A model for this is the C-1 signal of β-D-glucose-2,3,4,6,6′-d_5 (**4**) (Fig. 2*F*) (prepared by acid hydrolysis of the corresponding methyl α-D-glycoside (7, 8)), which exhibits a splitting of 2.2 Hz, due to the H-5 remaining.

It is clear from the C-1 signal of **3**, however, that in addition to the expected spacing of ~2 Hz associated with H-5, an additional spacing of ~4 Hz is present (Fig. 2*B*). The latter is attributed to interresidue coupling with H-4′. This has been demonstrated by treatment of **3** with a β-glucosidase from *Aspergillus phoenicis*, an enzyme shown by Reese and co-workers (14) to be highly selective in liberating the nonreducing end residue of methyl β-cellobioside. Hydrolysis of **3** proceeded almost quantitatively to give a mixture of two products, characterized by ^{13}C nmr spectroscopy as methyl β-D-glucopyranoside-3,6,6′-d_3 (**5**) and α,β-D-glucose-2,3,4,6,6′-d_5 (**6**). As seen in Fig. 2*C*, $^3J_{C\text{-}1-H\text{-}5}$ of the β-anomer of **6** is 2.0 Hz, which is close to that found (Fig. 2*F*) in **4**. Since the C-1 signal no longer exhibits the ~4 Hz spacing evident before hydrolysis, interresidue coupling of C-1 with H-4′ in the intact glycoside must have accounted for this splitting. By computer simulation, the value of $^3J_{C\text{-}1-H\text{-}4'}$ was determined to be 4.3 Hz and $^3J_{C\text{-}1-H\text{-}5}$, 2.2 Hz (Table 1).

[2]An accompanying decrease in line width undoubtedly contributes to the greater signal separation for C-1 and C-1′ in spectrum 2*B* as compared with 2*A*. Another probable factor is an upfield β-isotope displacement (13 and references cited therein) of the C-1 signal relative to that of C-1′ (−0.04 ppm) due to the deuterium at position-2.

[3] ^{13}C–^{2}H coupling was not resolved in any of the spectra examined here. Undoubtedly, however, ^{2}H-decoupling would be an advantage by giving more sharply resolved signals.

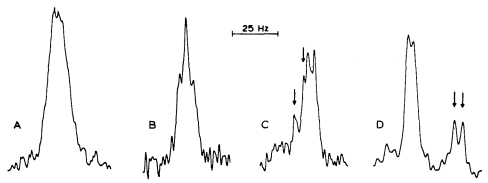

FIG. 3. One-half of the 22.63 MHz ^{1}H-coupled ^{13}C nmr spectrum of (*A*) C-4′ of methyl β-cellobioside (**2**), (*B*) C-4′ of methyl β-cellobioside-d_8 (**3**), (*C*) C-4 of methyl β-D-glucoside-3,6,6′-d_3 (**5**) formed by enzymic hydrolysis of **3**, (*D*) C-4 of **5** recorded in 70% C_5D_5N–D_2O solution (see Experimental); except for (*D*), spectra recorded in D_2O solution at 35°C. Signals indicated by arrows ((*C*) and (*D*)) arise from the aglycon CH_3 of **5**.

The C-4′ signal of **2** is a multiplet (Fig. 3A) comprised in part of splittings owing to two-bond coupling with H-3′ and H-5′, which are expected (12) to be 3–4 Hz. However, these and other possible spacings are not discernible. Through removal of the coupling with H-3′ (4.5 Hz in β-D-glucose (12)) by deuteration, the C-4′ signal of **3** (Fig. 3B) becomes a broad triplet comprised of spacings of about 4 Hz each. One of these splittings must be due to H-5′. Since the contribution of H-2′ should be small ($^3J < 1$ Hz), because it is *gauche* with respect to C-4′ (6), the only other possible source of the ~4 Hz spacing is interresidue coupling with H-1. Now, during the enzymic hydrolysis of **3** described above, the C-4′ signal virtually disappeared, to be replaced by the C-4 resonance of newly-liberated methyl β-D-glucoside-3,6,6′-d_3 (**5**). This latter signal is essentially a doublet with a spacing of 3.5 Hz (Fig. 3*C*); computer simulation gave $^2J_{C\text{-}4-H\text{-}5} = -3.0$ Hz.[4] Thus, it is clear that the extra splitting of about 4 Hz in Fig. 3*B* is due to coupling between C-4′ and H-1 of the nonreducing end residue of **3**. Based on a computer simulation of the C-4′ signal, the interresidue coupling amounts to 4.2 Hz, whereas $^2J_{C\text{-}4'-H\text{-}5'}$ is −3.0 Hz (Table 1).

A recent study of octa-*O*-acetyl-β-cellobiose-1-^{13}C by ^{1}H nmr spectroscopy has shown (15) that C-1 engages in coupling with H-4′ to the extent of 5.5 Hz, which is appreciably larger than the corresponding value now found for the unsubstituted methyl β-cellobioside (**3**). *O*-Acetyl derivatives are of general interest in the context of comparing solution geometries with those of crystalline materials, because they eliminate the possible role of interresidue hydrogen bonding that characterizes these molecules in the solid state (16, 17), as well as in methyl sulfoxide solution (18). Accordingly, measurements have been made on the heptaacetate of **3**

[4]Note that because of second order effects, the magnitude of ^2J is not equal to the observed spacing. By analogy with other measurements of two-bond coupling in pyranose sugars (6, 11, 12), the sign of ^2J is taken to be negative.

Can. J. Chem. Downloaded from www.nrcresearchpress.com by 210.87.254.105 on 09/05/12
For personal use only.

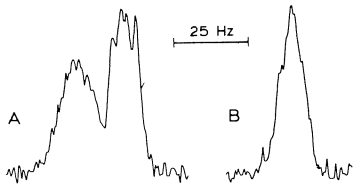

FIG. 4. One-half of the 22.63 MHz ^{1}H-coupled ^{13}C nmr spectrum of (*A*) C-1 of methyl hepta-*O*-acetyl-β-cellobioside-d_8 (**7**), (*B*) C-4′ of **7**; recorded in $CDCl_3$ solution at 35°C.

(**7**), for comparison with **3** itself, and also to see how closely analogous its C-1–H-4′ coupling is with that of β-cellobiose octaacetate (coupling between C-4′ and H-1 in the latter compound has not previously been examined).

As found in comparing the spectrum of **3** with that of **2**, the C-1 and C-4′ signals of **7** exhibited a much clearer splitting pattern than the corresponding signals before ^{1}H–^{2}H exchange. The coupling constants determined for the C-1 signal (Fig. 4*A*) by computer simulation, are 5.2 and 3.0 Hz (Table 1). Since the latter must be due to coupling with H-5, a value for $^3J_{C\text{-}1\text{–}H\text{-}4'}$ of 5.2 Hz is obtained; this is close to the 5.5 Hz interresidue coupling reported (15) for the β-octaacetate. Although the resolution of the C-4′ signal of **7** (Fig. 4*B*) is relatively poorer than that of C-4′ in **3**, the signals are virtually superimposable ($\Delta\nu^{1/2}$ is 9 Hz in both cases). Assuming that $^2J_{C\text{-}4'\text{–}H\text{-}5'}$ is the same in both compounds, then $^3J_{C\text{-}4'\text{–}H\text{-}1}$ for **7** is estimated to be 4.2 Hz.

Dihedral Angle Dependence of $^3J_{C-H}$*, and the Conformation of Methyl* β*-Cellobioside*

X-ray crystallographic data for methyl β-cellobioside show (16) that φ and ψ are 25 and −38°, respectively. For β-cellobiose, the corresponding angles are noticeably different (17, 19, 20), i.e., 44.6 and −13.7°.[5] According to optical rotatory studies (21, 22), these latter angles closely describe the orientation of the glycosidic bond of β-cellobiose, as well as of the β-glycoside (**2**), in aqueous solution.

To compare the results of the present measurements with these others, reference may be made to ^{13}C–^{1}H coupling in model compounds of known conformation. Although there is ample experimental (4–6) and theoretical (23, 24) evidence that a 'Karplus-type' of relationship exists between $^3J_{C-H}$ and torsional angle, values reported (6) for sp^3 carbons in carbohydrate molecules exhibit a considerable scatter. However, *interresidue* coupling involves sp^3 carbons contained in a specific sequence of nuclei, namely ^{13}C—O—C—^{1}H. Data obtained from monosaccharides for this type of array are plotted in Fig. 5, and although a relatively small number of points are represented, the well-known Karplus curve shape is evident in the solid line shown. Unfortunately, experimental values for the 0 to 60° range are difficult to find, because there can be few model compounds containing fixed ^{13}C—O—C—^{1}H angles of the appropriate size. Yet, as shown by the experimental findings and theoretical calculations (26, 27) on the conformation of cellobiose and its derivatives, it is in terms of this region that the present results need to be evaluated.

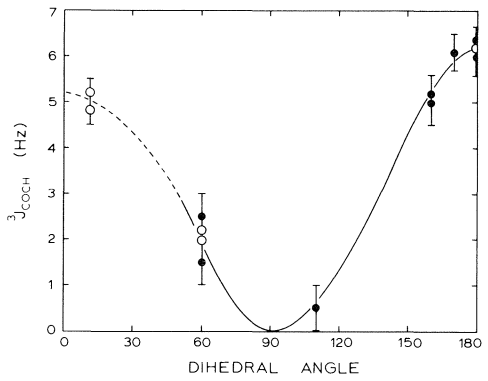

FIG. 5. Relationship between $^3J_{C-O-C-H}$ and the ^{13}C—O—C—^{1}H dihedral angle. Data represented by filled circles taken from refs. 6, 7, and 25; data represented by open circles, this work.

To help complete the curve in Fig. 5, data for cyclohexaamylose (**8**) may be considered. X-ray studies (28) of several complexes of this cyclic oligosaccharide show that φ and ψ are close to ±10°, on the average, and angles of the same magnitude are predicted by theoretical studies (29). Slightly larger values, i.e., ±20°, have been reported (22) for aqueous solutions of **8** on the basis of optical rotatory measurements.[6] We have estimated recently (2) that the interresidue couplings in **8** between ^{13}C-1 and H-4 and between ^{13}C-4 and H-1 are in the region of 4–5 Hz. These couplings have now been remeasured in the spectrum of the compound (**9**) after ^{1}H–^{2}H exchange (at carbons 2, 3, and 6) because the C-1 and C-4 signals (Fig. 6) exhibit more clearly defined splittings than could be observed (2) in the spectrum before deuteration. Analysis of the C-1 signal, with the aid of computer simulation, has afforded a ^3J value of 4.8 Hz for interresidue coupling between C-1 and H-4. Similarly, simulation of the C-4

[5]Its conformation appears to change little when the compound is dissolved in methyl sulfoxide, inasmuch as the hydrogen bond that occurs between OH-3′ and O-5 in the crystal is retained in solution (18).

[6]Alternatively, it is possible that instead of the conformation being symmetrical, one of the glycosyl residues is substantially folded away from the axis of the ring (21), as is found (29) in crystalline cyclohexaamylose hexahydrate. Such a distinction would not be apparent in the time-averaged nmr measurements.

Can. J. Chem. Downloaded from www.nrcresearchpress.com by 210.87.254.105 on 09/05/12
For personal use only.

TABLE 1. ^{13}C–^{1}H coupling data for methyl β-D-cellobioside-d_8, cyclohexaamylose-d_4, and related compounds[a]

Compound	Signal observed	^{1}J (Hz)[b]	^{2}J (Hz)[b]	^{3}J (Hz)[b]
Methyl β-cellobioside-d_8 (**3**)	C-1	162.1(H-1)		4.3(H-4′) 2.2(H-5)
	C-4′	147.4(H-4′)	−3.0(H-5′)	4.2(H-1)
	C-5′	143.5(H-5′)	−3.5(H-4′)	
Methyl β-cellobioside-d_8 heptaacetate (**7**)	C-1	161.8(H-1)		5.2(H-4′) 3.0(H-5)
	C-4′	148.4(H-4′)	−3.0(H-5′)	4.2(H-1)
Methyl β-glucoside-d_3 (**5**)	C-4	146(H-4)[c]	−3.0(H-5)[d]	
β-D-Glucose-d_5 (**4**)	C-1	161.9(H-1)		2.2(H-5)
(**6***b*)	C-1	161(H-1)[e]		2.0(H-5)
Cyclohexaamylose-d_4 (**9**)	C-1	169.1(H-1)		4.8(H-4)
	C-4	145.8(H-4)	−3.5(H-5)	5.2(H-1)
	C-5	146.5(H-5)	−2.9(H-4)	6.2(H-1)

[a]Determined by computer simulation. The sign of ^{2}J is assumed to be negative by analogy with ^{2}J in related compounds (6, 11, 12).
[b]The coupled proton is indicated in parentheses.
[c]Approximate value, owing to partial overlap with C-5.
[d]In 70% C_5D_5N–D_2O, $^{2}J = -2.8$ Hz (see Experimental).
[e]Approximate value, owing to partial overlap with C-1 of **5**.

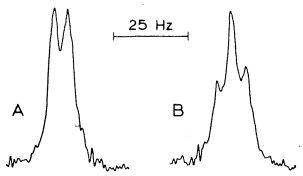

FIG. 6. One-half of the 22.63 MHz ^{1}H-coupled ^{13}C nmr spectrum of (*A*) C-1 of cyclohexaamylose-d_4 (**9**), (*B*) C-4 of **9**; recorded in D_2O solution at 50°C.

signal gives a value of −3.5 Hz for $^{2}J_{C\text{-}4\text{–}H\text{-}5}$, i.e., close to that of **5**, and a value of 5.2 Hz for the interresidue coupling with H-1 (Table 1).

Using this information, the plot in Fig. 5 has been extended (broken line) so as to permit an approximation of torsional angles in the cellobioside (**3**) in aqueous solution. Accordingly, the observed values for interresidue ^{13}C–^{1}H couplings of 4.3 and 4.2 Hz (in **3**) correspond to torsional angles of about 25–30°. Although these values reflect a thermodynamically-averaged conformation, they suggest that both φ and ψ are of the same order as their values in the solid state. By contrast, on the basis of optical rotations (21, 22) it has been suggested that the solution and crystalline conformations differ appreciably. We cannot account for this discrepancy between the results of the optical measurements, and our own results; perhaps it is a reflection of uncertainties in both sets of data.

An examination of **7**, the heptaacetate of **3**, in chloroform shows that interresidue coupling between C-1 and H-4′ increases by ~1 Hz, whereas that between C-4′ and H-1 remains the same as for the nonesterified compound. On this basis, the orientation of the glycosidic bond in **7** (in chloroform) may be represented by a geometry in which ψ is 10–20° smaller than in **3** (in water).[7] It is noteworthy in this context that acetylation may have a substantial effect on ψ in the solid state: X-ray data show (20) that ψ changes from −13.7° in β-cellobiose to +15.7° in its octaacetate, whereas φ remains constant. This variation has been attributed (20) to the loss of a hydrogen bond between O-5 and OH-3′ through acetylation. However, it is possible that the difference between **3** and **7** in *solution* is related not so much to changes in interresidue hydrogen bonding, as in solvation patterns and substituent size. Conceivably, these latter changes could be compatible with a major conformational variation. Theoretical calculations (26) predict a subsidiary minimum for cellobiose, in which ψ is ~180. Since the C-1,H-4′ coupling of 5.2 Hz in **7** is not inconsistent with a large value of ψ (Fig. 5), there remains the possibility that **7** represents a conformation related to this alternate energy minimum.

Further Comments on the Measurement of ^{13}C–^{1}H Coupling Constants. Second-order Effects

It was pointed out above that the observed splitting patterns have been reproduced by computer simulation. This procedure was adopted primarily because some second order effects were to be expected (30). For example, the C-4′ signal of **3** has

[7]This parallels the results of our earlier comparison (2) of the conformation of methyl β-maltoside and its heptaacetate.

Can. J. Chem. Downloaded from www.nrcresearchpress.com by 210.87.254.105 on 09/05/12
For personal use only.

Can. J. Chem. Downloaded from www.nrcresearchpress.com by 210.87.254.105 on 09/05/12
For personal use only.

the general appearance (Fig. 2*B*) of a symmetrical triplet comprised of spacings of ~4 Hz each. However C-4′ is part of an ABMX spin system also containing H-4′ (A) and H-5′ (B), which are strongly coupled ($^3J_{H\text{-}4'\text{–}H\text{-}5'}$ = 9.5 Hz). A simple first-order treatment, therefore, could give rise (30) to substantial disagreement between observed and calculated ^{13}C–^1H coupling involving C-4′. In fact, computer calculation of the spectrum shows that the C-4′–H-5′ coupling is smaller than the observed spacing by ~1 Hz, i.e., $^2J_{C\text{-}4'\text{–}H\text{-}5'} = -3.0$ Hz. As shown by the simulated spectrum (Fig. 7*B*), use of the latter value together with $^3J_{C\text{-}4'\text{–}H\text{-}1}$ = 4.2 Hz closely reproduces the experimentally observed C-4′ signal.

Second-order effects arise also in dealing with interresidue coupling between C-1 and H-4′ of **3**. Although C-1 is not coupled to H-5′, the latter couples strongly with H-4′ ($^3J_{H\text{-}4'\text{–}H\text{-}5'}$ = 9.5 Hz), and $\Delta\nu_{4',5'}$ is small (3 Hz). Treating C-1 as the X part of an ABMRX spin system in which J_{BX} ($J_{C\text{-}1\text{–}H\text{-}5'}$) = 0, gives the complex multiplet shown in Fig. 7*A*, which closely reproduces the experimentally observed signal. Similar considerations apply to C-1 of **7** and **9**, although the second order effects are not as apparent because, here, $\Delta\nu_{4',5'}$ is larger (16.7 and 21.2 Hz, respectively).

Among other signals examined were those of C-5′ of **3** and C-5 of cyclohexaamylose-d_4 (**9**); these signals were of particular interest because ^2J values involving C-5 and H-4 of pyranose sugars could not be measured in earlier studies (6, 11, 12). The C-5 signal of the oligosaccharide (**9**) (Fig. 7*C*) is a doublet of doublets in which the larger spacing is attributable to three-bond coupling with antiperiplanar H-1. As with C-4′ of **3** above, however, a large value of $^3J_{H\text{-}4\text{–}H\text{-}5}$ introduces a second order correction (30) for $^2J_{C\text{-}5\text{–}H\text{-}4}$, giving a value of −2.9 Hz (whereas the spacing observed is 3.7 Hz). The calculation also affords a value of 6.2 Hz for $^3J_{C\text{-}5\text{–}H\text{-}1}$, as compared with the observed coupling of 6.3 Hz (7) for the analogous pathway in methyl α-D-glucopyranoside-2,3,4,6,6′-d_5. Similarly, $^2J_{C\text{-}5'\text{–}H\text{-}4'}$ in methyl β-cellobioside-d_8 was calculated to be −3.5 Hz (Table 1).

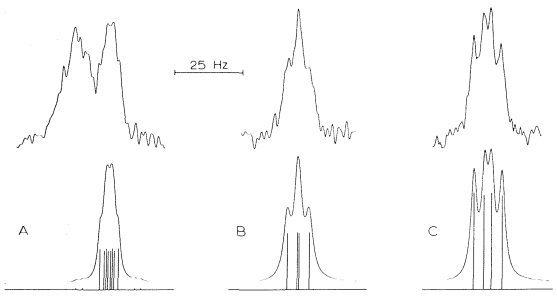

FIG. 7. One-half of the observed (upper) and theoretical (lower) ^1H-coupled ^{13}C nmr spectra of (*A*) C-1 of methyl β-cellobioside-d_8 (**3**), (*B*) C-4′ of **3**, (*C*) C-5 of cyclohexaamylose-d_4 (**9**). Theoretical spectra calculated from the parameters given in Tables 1 and 2.

Experimental

^{13}C Nuclear Magnetic Resonance Spectra

^{13}C nmr spectra were recorded on a Bruker WH-90 Ft spectrometer operating at 22.63 MHz. Except for methyl β-cellobioside-d_8 heptaacetate (**7**), samples were prepared in D_2O (200–400 mg/ml) containing several drops of CH_3OH as an internal standard; chemical shifts referenced to CH_3OH are expressed relative to external TMS ($\delta_C(CH_3OH)$ = 50.4 ppm). The heptaacetate **7** was run in $CDCl_3$ with TMS as an internal reference. In the ^1H-coupled spectrum of the enzyme hydrolysate (mixture of **5** and **6**), the C-4 signal of **5** is partially overlapped by the lowest field signal of the methyl quartet (Fig. 3*C*). By recording the spectrum in 70% C_5D_5N–D_2O, the CH_3 resonance was shifted 1.4 ppm to higher field (Fig. 3*D*) thus permitting clear observation of the C-4 doublet. Unless stated otherwise, the nmr probe temperature was 35 ± 1°C. Owing to its lower solubility, cyclohexaamylose-d_4 (**9**) was run at 50°C.

Proton-coupled ^{13}C spectra were recorded with gated ^1H-irradiation essentially as previously described (2). Spectral widths of 1000–1500 Hz were used, giving a digital resolution of 0.24–0.37 Hz after Fourier transformation (4K real data points). For **7**, a spectral width of 2000 Hz was required (resolution, 0.49 Hz).

Analysis of ^1H-coupled Spectra

Spectra were analyzed by computer simulation using the ITRCAL program (31) run on a Nicolet B-NC 12 model computer interfaced to the WH-90 spectrometer. First-order AMX analyses were made for the C-1 spectra of **4** and **6***b*. Second-order analyses (ABMRX, ABMX, or ABX) were carried out for C-1 (**3**, **7**, **9**), C-4 (**5**, **9**), C-4′ (**3**, **7**), C-5 (**9**), and C-5′ (**3**) signals. The required ^1H nmr parameters (J_{AB} and $\Delta\nu_{AB}$) were taken from the literature (**5**) or calculated from spectra (**3**, **7**, **9**) recorded on the WH-90 at 90.0 MHz (Table 2). In each case the analysis involved a systematic variation of the appropriate $J_{C\text{–}H}$ values together with the line-width to obtain the best visual fit between simulated and observed spectra. Where the multiplet structure was well resolved (e.g., C-5 of **9**), the ITRCAL program was run in iterative mode (31). It is estimated that the error in the values of ^2J and ^3J listed in Table 1 is ±0.2–0.4 Hz.

Preparation of Deuterated Compounds

Methyl β-Cellobioside-d_8 (3)

A solution of methyl β-cellobioside (**2**) (0.40 g) in D_2O (99.5%, 25 ml) containing Raney nickel (7, 33) (3.9 g wet weight, preexchanged with D_2O) was heated under reflux for 24 h. The solution was filtered through Celite, passed through a short column of Chelex-100 ion-exchange resin (Na^+ form) to ensure removal of paramagnetic ions and concentrated to a volume of 1.0 ml. ^{13}C nmr analysis of the solution (Fig. 1*B*) showed seven major signals attributable to **3** (the product was characterized as its heptaacetate, **7** (see below)) and several minor signals from an unidentified product, most probably an isomer of **3** arising from epimerization(s) of the nonreducing glucose residue (7, 8). ^{13}C nmr data for **2**: δ_C 104.4 (C-1′), 103.9 (C-1), 80.1 (C-4′), 77.3 (C-5), 76.9 (C-3), 76.1 (C-5′), 75.7 (C-3′), 74.5 (C-2), 74.2 (C-2′), 70.8 (C-4), 62.0 (C-6), 61.5 (C-6′), 58.5 (CH_3); ^{13}C nmr data for **3**: δ_C 104.4 (C-1′), 103.8 (C-1), 80.0 (C-4′), 77.1 (C-5), 76.0 (C-5′), 74.1

TABLE 2. ^{1}H nuclear magnetic resonance data used in ABMRX, ABMX, and ABX spectrum simulations[a]

Compound	X	A	B	M	R	J_{AB}(Hz)	$\lvert\Delta\nu_{AB}\rvert$(Hz)[b]
3	C-1	H-4′	H-5′[c]	H-1	H-5	9.5	3.0
	C-4′	H-4′	H-5′	H-1	—	9.5	3.0
	C-5′	H-4′	H-5′	—	—	9.5	3.0
5[d]	C-4	H-4	H-5	—	—	9.4	7.7
7	C-1	H-4′	H-5′[c]	H-1	H-5	9.9	16.7
	C-4′	H-4′	H-5′	H-1	—	9.9	16.7
9	C-1	H-4	H-5[c]	H-1	—	9.9	21.2
	C-4	H-4	H-5	H-1	—	9.9	21.2
	C-5	H-4	H-5	—	—	9.9	21.2

[a] J_{AM}, J_{BM}, J_{AR}, J_{BR} = 0.
[b] At 90.0 MHz.
[c] J_{BX} = 0.
[d] Reference 32.

(C-2′), 61.5 (undeuterated C-6′, residual signal), 58.5 (CH_3). Signal assignments are based on the work of Dorman and Roberts (9) and Usui *et al.* (10); however, a comparison of the data for **2** and **3** (specifically, the absence in **3** of signals at 76.9 and 75.7 ppm) requires the reversal of their assignments (9, 10) for C-3 and C-5 and also C-3′ and C-5′. The small upfield displacement of most signals of **3** relative to those of **2** reflects the β-isotope effect (13) due to deuteration of adjacent carbons. In the case of C-5, which is flanked by deuterium at both C-4 and C-6, the shift is particularly large (−0.24 ppm).

Methyl Hepta-O-acetyl-β-Cellobioside-d_8 *(7)*

The solution of **3** (above) was concentrated and the residue was acetylated by heating with acetic anhydride and anhydrous sodium acetate. The product, methyl hepta-*O*-acetyl-β-cellobioside-d_8 (**7**) was recrystallized from ethanol; mp 183–185°C (lit. (34) mp for undeuterated **7**, 187°C); ^{13}C nmr δ_C: 170.5, 170.3, 170.2, 169.8, 169.7, 169.3, 169.0 ($COCH_3$); 101.5 (C-1′); 100.8 (C-1); 76.5 (C-4′); 72.7 (C-5′); 71.8 (C-5); 71.6 (C-2′); 62.0 (C-6′, residual signal); 57.0 (CH_3); 20.8 (1C), 20.7 (1C), 20.5 (5C) ($COCH_3$).

Enzymic Hydrolysis of Methyl β-*Cellobioside-*d_8

A solution of **3** (0.30 g) in 1.0 ml of H_2O–D_2O (3:1) was prepared in a 10-mm nmr tube and 1–2 mg of *A. phoenicis* β-glucosidase (14) added. The progress of the hydrolytic reaction was monitored at 20 min intervals by ^{13}C nmr spectroscopy (probe temperature, 50°C). When the intensity of the C-4 signal of the liberated methyl β-D-glucoside-d_3 (**5**) became essentially constant, the solution was heated at 100°C for 10 min, centrifuged, and filtered. ^{13}C nmr analysis showed that the hydrolysate consisted of methyl β-D-glucoside-3,6,6′-d_3 (**5**) and α,β-D-glucose-2,3,4,6,6′-d_5 (**6**) together with a small amount of unreacted disaccharide; ^{13}C nmr data for **5**: δ_C 104.7 (C-1), 77.2 (C-5), 74.5 (C-2), 71.1 (C-4), 58.6 (CH_3); ^{13}C nmr data for **6**: δ_C 97.4 (C-1β), 93.6 (C-1α), 77.2 (C-5β), 72.7 (C-5α).

A sample of β-D-glucose-2,3,4,6,6′-d_5 (**4**) was also prepared chemically by acid hydrolysis of methyl α-D-glucoside-2,3,4,6,6′-d_5 (7, 8); ^{13}C nmr data for **4**: δ_C 97.3 (C-1), 77.2 (C-5).

Cyclohexaamylose-2,3,6,6′-d_4 *(9)*

Cyclohexaamylose (**8**) (0.50 g) was dissolved in D_2O (25 ml), Raney nickel (5.0 g wet weight, preexchanged with D_2O) introduced, and the suspension refluxed for 72 h. After filtration and treatment with Chelex-100 resin ^{13}C nmr analysis of the product showed >95% ^{2}H–^{1}H exchange at C-2, C-3, and C-6 (note that after 24 h, H-3 is only ~50% exchanged (7)); ^{13}C nmr data for **8**: δ_C 102.9 (C-1), 82.7 (C-4), 74.8 (C-3), 73.5 (C-5), 73.2 (C-2), 61.9 (C-6); ^{13}C nmr data for **9**: δ_C 102.8 (C-1), 82.6 (C-4), 73.4 (C-5). These results confirm the cyclohexaamylose signal assignments given by Colson *et al.* (35); thus, the earlier assignments of Usui *et al.* (10) for C-2 and C-5 should be reversed.

Acknowledgments

The authors express their gratitude to the Pulp and Paper Research Institute of Canada and the National Research Council of Canada for generous support. They also acknowledge the assistance of A. Parfondry and helpful discussions with H. J. Koch and R. S. Stuart. E. T. Reese kindly furnished the sample of *A. phoenicis* β-glucosidase, and W. R. Grace and Co., samples of Raney nickel catalyst.

1. A. S. PERLIN, N. CYR, R. G. S. RITCHIE, and A. PARFONDRY. Carbohydr. Res. **37**, C1 (1974).
2. A. PARFONDRY, N. CYR, and A. S. PERLIN. Carbohydr. Res. **59**, 299 (1977).
3. A. S. PERLIN. MTP Internat. Rev. Sci., Org. Chem., Series 2, Vol. 2. *Edited by* G. O. Aspinall. Butterworths, London. 1976. p. 1.
4. A. S. PERLIN and B. CASU. Tetrahedron Lett. 2921 (1969).
5. R. U. LEMIEUX, T. L. NAGABHUSHAN, and B. PAUL. Can. J. Chem. **50**, 773 (1972).
6. J. A. SCHWARCZ and A. S. PERLIN. Can. J. Chem. **50**, 3667 (1972); J. A. SCHWARCZ. Ph.D. Thesis, McGill University, Montreal, P.Q., August, 1974.
7. F. BALZA, N. CYR, G. K. HAMER, A. S. PERLIN, H. J. KOCH, and R. S. STUART. Carbohydr. Res. **59**, C7 (1977); F. BALZA. M.Sc. Thesis, McGill University, Montreal, P.Q., December, 1977.
8. H. J. KOCH and R. S. STUART. Carbohydr. Res. **59**, C4 (1977).
9. D. E. DORMAN and J. D. ROBERTS. J. Am. Chem. Soc. **93**, 4463 (1971).
10. T. USUI, N. YAMAOKA, K. MATSUDA, K. TUZIMURA, H. SUGIYAMA, and S. SETO. J. Chem. Soc. Perkin Trans. I, 2425 (1973).
11. J. A. SCHWARCZ, N. CYR, and A. S. PERLIN. Can. J. Chem. **53**, 1872 (1975).

Can. J. Chem. Downloaded from www.nrcresearchpress.com by 210.87.254.105 on 09/05/12
For personal use only.

12. N. CYR, G. K. HAMER, and A. S. PERLIN. Can. J. Chem. **56**, 297 (1978).
13. P. A. J. GORIN and M. MAZUREK. Can. J. Chem. **53**, 1212 (1975).
14. D. STERNBERG, P. VIJAYAKUMAR, and E. T. REESE. Can. J. Microbiol. **23**, 139 (1977).
15. G. EXCOFFIER, D. Y. GAGNAIRE, and F. R. TARAVEL. Carbohydr. Res. **56**, 229 (1977).
16. J. T. HAM and D. G. WILLIAMS. Acta Crystallogr. B, **26**, 1373 (1970).
17. S. S. CHU and G. A. JEFFREY. Acta Crystallogr. B, **24**, 830 (1968).
18. B. CASU, M. REGGIANI, G. G. GALLO, and A. VIGEVANI. Tetrahedron, **22**, 3061 (1966); **24**, 803 (1968).
19. D. A. REES and R. J. SKERRETT. Carbohydr. Res. **7**, 334 (1968).
20. F. LEUNG, H. D. CHANZY, S. PEREZ, and R. H. MARCHESSAULT. Can. J. Chem. **54**, 1365 (1976).
21. D. A. REES and D. THOM. J. Chem. Soc. Perkin Trans. II, 191 (1977).
22. D. A. REES. J. Chem. Soc. B, 877 (1970).
23. R. WASYLISHEN and T. SCHAEFER. Can. J. Chem. **50**, 2710 (1972).
24. A. S. PERLIN, N. CYR, H. J. KOCH, and B. KORSCH. Ann. N.Y. Acad. Sci. **222**, 935 (1973).
25. K. BOCK and C. PEDERSEN. Acta Chem. Scand. B, **31**, 354 (1977).
26. D. A. REES and P. J. C. SMITH. J. Chem. Soc. Perkin Trans. II, 836 (1975); M. GIACOMINI, B. PULLMAN, and B. MAIGRET. Theor. Chim. Acta, **19**, 347 (1970).
27. B. K. SATHYANARAYANA and V. S. R. RAO. Biopolymers, **10**, 1605 (1971).
28. A. HYBL, R. E. RUNDLE, and D. E. WILLIAMS. J. Am. Chem. Soc. **87**, 2779 (1965); P. C. MANOR and W. SAENGER. J. Am. Chem. Soc. **96**, 3630 (1974); W. SAENGER. *In* Environmental effects on molecular structure and properties. The Jerusalem Symposia on Quantum Chemistry and Biochemistry VIII. *Edited by* E. D. Bergmann and B. Pullman. The Israel Academy of Sciences and Humanities, Jerusalem. 1975.
29. P. R. SUNDARARAJAN and V. S. R. RAO. Carbohydr. Res. **13**, 351 (1970).
30. N. CYR, R. G. S. RITCHIE, T. M. SPOTSWOOD, and A. S. PERLIN. Can. J. Spectrosc. **19**, 190 (1974).
31. ITRCAL. Nicolet Instrument Corporation, Madison, WI. 1974.
32. S. J. PERKINS, L. N. JOHNSON, D. C. PHILLIPS, and R. A. DWEK. Carbohydr. Res. **59**, 19 (1977).
33. A. A. PAVLIC and H. ADKINS. J. Am. Chem. Soc. **68**, 1471 (1946).
34. C. S. HUDSON and R. SAYRE. J. Am. Chem. Soc. **38**, 1867 (1916).
35. P. COLSON, H. J. JENNINGS, and I. C. P. SMITH. J. Am. Chem. Soc. **96**, 8081 (1974).

Can. J. Chem. Downloaded from www.nrcresearchpress.com by 210.87.254.105 on 09/05/12
For personal use only.

^{13}C-nuclear magnetic resonance spectra of oxiranes. Configuration of 1,2-epoxypropyl side chains in fungal metabolites

SUZANNE LESAGE AND ARTHUR S. PERLIN

Department of Chemistry, McGill University, Montreal, P.Q., Canada H3A 2A7

Received June 20, 1978

SUZANNE LESAGE and ARTHUR S. PERLIN. Can. J. Chem. **56**, 3117 (1978).

^{13}C nmr data indicate that the epoxypropyl side chain of 'asperlin' (**1**) has a *trans* configuration. This assignment follows from associated measurements on model compounds, showing that the ^{13}C chemical shift of an epoxypropyl CH_3 group is close to either 17 ppm (*trans* isomers) or 13 ppm (*cis* isomers). Synthesized as oxirane derivatives related to **1** are diastereomeric pairs of 8-deoxy-6,7-*cis*- and -*trans*-epoxy-1,2:3,4-di-*O*-isopropylidene-α-D-*galacto*-octopyranoses.

SUZANNE LESAGE et ARTHUR S. PERLIN. Can. J. Chem. **56**, 3117 (1978).

Les résultats de la rmn du ^{13}C indiquent que la chaîne latérale époxypropyle de l'"asperlin" (**1**) possède une configuration *trans*. Cette attribution fait suite à des mesures connexes effectuées sur des composés modèles, qui montrent le déplacement chimique du ^{13}C pour le groupe CH_3 de l'époxypropyle se situe soit vers 17 ppm (isomère *trans*), soit vers 13 ppm (isomère *cis*). On a synthétisé des dérivés oxirannes reliés à **1**, soit les paires diastéréomériques des désoxy-8 *cis*- et désoxy-8 *trans*-époxy-6,7 di-*O*-isopropylidène-1,2:3,4 α-D-*galacto*-octopyrannoses.

[Traduit par le journal]

Can. J. Chem. Downloaded from www.nrcresearchpress.com by 210.87.254.40 on 09/05/12
For personal use only.

Introduction

The oxirane ring is found in a variety of natural products (1). This article is concerned with the configuration of the oxirane moiety in asperlin (**1**), an antibiotic and antitumor compound produced by *Aspergillus nidulans* (2–4).

^{13}C nmr spectra of *cis*- and *trans*-2,3-epoxybutane and higher homologs indicate (5) that geometric isomers are distinguishable, by the fact that the ring carbons of *cis* oxiranes generally resonate upfield of those of the corresponding *trans* isomers. In attempting to utilize these observations to determine the configuration of the epoxypropyl side chain of asperlin, compounds more closely akin in structure to **1** than the simpler epoxides cited above, have been synthesized as reference molecules and their ^{13}C nmr spectra have been obtained for comparison with that of **1**.

Results and Discussion

The compounds synthesized, represented by **2**, are 8-carbon sugar derivatives containing a pyranose ring moiety and an epoxypropyl side chain. 1,2:5,6-Di-*O*-isopropylidene-α-D-galactopyranose (**3**) was oxidized with pyridinium chlorochromate (6) in dichloromethane, affording syrupy dialdose **4**[1] in 75% yield. A Wittig reaction between **4** and ethylidene triphenylphosphorane in the presence of *n*-butyllithium produced 6,7,8-trideoxy-1,2:3,4-di-*O*-isopropylidene-α-D-*galacto*-oct-6-*cis*-enopyranose (**5**) (9, 10).[2] From the latter, a 3:1 mixture of diastereomeric *cis* epoxides (**6**, **7**) was obtained in the form of an analytically pure mixed crystal, by oxidation with *m*-chloroperbenzoic acid.

Although the corresponding *trans* isomers also were required for this study, none of the *trans* olefin (**8**) appeared to have been formed together with **5**, nor had it been detected (9, 10) under the conditions of the earlier syntheses of **5**. Modifications of the Wittig reaction that have been known to alter *cis* to *trans* ratios, also failed to yield product **8**: i.e., acid isomerization of the intermediate betaine (11) was tried, as well as the use of a crown ether (12). However, isomerization of the isolated *cis* olefin (**5**), proved to be successful: uv irradiation of **5** in cyclohexane resulted in its conversion into **8** to the extent of about 75%.[3] Then, oxidation of **8** with *m*-chloroperbenzoic acid afforded a 2:1 mixture of the diastereomeric *trans* oxiranes (**9**, **10**).

Paulson *et al.* (5) have shown that chemical shifts for the ring carbons of isomeric oxiranes are generally predictable, because in the *cis* isomers (**11**) these nuclei are more strongly shielded than in the *trans* isomers (**12**). This difference appears to be analogous to the 'steric compression' effect that has been

[1]Dialdose **4** is available also by methylsulfoxide oxidation of **3** (7, 8) but its isolation from that reaction is less convenient.

[2]Sodamide was employed in these earlier syntheses of **5**, whereas *n*-butyllithium proved to be more satisfactory in the present instance.

[3]Another isomerization procedure tried, i.e., thermally in the presence of triphenylphosphine (13), had virtually no effect on **5**.

Can. J. Chem. Downloaded from www.nrcresearchpress.com by 210.87.254.40 on 09/05/12
For personal use only.

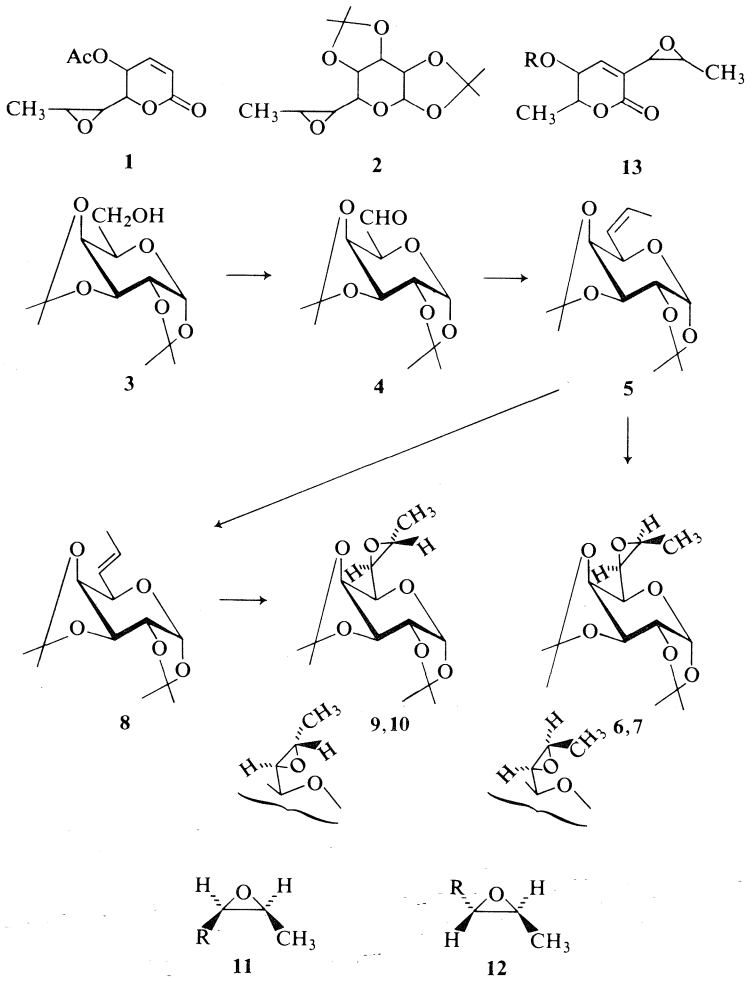

observed with a wide variety of stereoisomeric compounds (14, 15). Similarly, the C-6 and C-7 signals[4] of the synthetic *cis* oxiranes (**6**, **7**) are upfield (on the average) of those of their *trans* isomers (**9**, **10**) (Table 1). Shielding influences (16, 17) owing to substituents appended to an epoxide ring have been evaluated by Paulson *et al.* (5) but the number of substituent parameters obtained is insufficient for calculating the C-7, C-8 chemical shifts of **1** and the model epoxides synthesized. Furthermore, shielding contributions of the pyrone ring of **1** are such that the chemical shifts of C-6 and C-7 overlap the range of values for the corresponding carbons in **6**, **7**, **9**, and **10** (Table 1). This precludes using these data from the model compounds, as well as from the simpler epoxides, for determining the configuration of the oxirane ring of asperlin.

By contrast, the methyl groups of these various compounds show a large, and consistent, difference in chemical shift. Among the data of Paulson *et al.* (5) are values for several pairs of geometric isomers containing an epoxypropyl grouping. For these, and also for the pairs **6**, **7** and **9**, **10**, the CH_3 signals of all *cis* isomers appear at 13–14 ppm, whereas those of *trans* isomers are found substantially downfield, at 17–18 ppm (Table 1).[5] Consequently, the observed value of 16.9 ppm for C-8 of asperlin shows that the epoxypropyl side chain of the metabolite has a *trans* configuration.

It is well known (20, 21) that *cis* and *trans* oxiranes may be differentiated by ^1H nmr spectroscopy, because vicinal coupling between the ring protons of *cis* isomers is usually larger than that for *trans*. How-

[4]Owing to differences in the system of numbering, C-6 and C-7 of the reference compounds correspond to C-7 and C-8 of **1**.

[5]A similar configurational difference is exhibited (14, 15) in the alkene series: e.g., the allylic methyl groups in the series 2-butene to 2-decene have chemical shifts of 11.4–12.8 ppm (*cis* isomers) or 16.8–18.0 (*trans* isomers) (18). It is noteworthy that corresponding values for olefins **5** and **8** are 13.6 and 17.8 ppm, respectively.

Can. J. Chem. Downloaded from www.nrcresearchpress.com by 210.87.254.40 on 09/05/12
For personal use only.

TABLE 1. ^{13}C chemical shifts for epoxypropyl moieties of **1** and related compounds[a]

Compound	δ[a] C-7[b]	C-8[b]	CH_3
1	55.1	53.7	16.9
6,7	53.7	52.6	13.2
	55.5	51.2	14.2
9,10	56.8	54.7	17.3
	58.2	52.9	17.3
11	—	—	13.0–13.4[c]
12	—	—	17.5–17.8[c]
13	54.6	59.1	17.5
13 (acetate)	54.3	58.7	17.5

[a]In ppm relative to TMS; solvent, $CDCl_3$.
[b]Assignments for **1** and **13** are taken from ref. 19*a* and *b*, respectively. The other signal assignments are given by analogy with those of **1**; carbons-6 and -7 of **6**, **7**, **9**, **10** correspond to C-7 and C-8 of **1**.
[c]Data from ref. 5.

ever, the ranges of $^3J_{cis}$ and $^3J_{trans}$ overlap in the 2.2–2.5 Hz region, so that a coupling of this magnitude could be ambiguous, particularly if both isomers are not available and/or coupling with other protons introduces second-order effects. With deuteriochloroform as solvent, the H-6 and H-7 signals of asperlin overlap (4). In deuteriobenzene, however, good separation has been obtained (δ 2.87 and 2.67, respectively) and, measured from a 220 MHz spectrum, the observed spacing is 1.7 Hz. Since this value is appreciably *less* than 2.2 Hz, the result is consistent with the *trans* configuration assigned above. It is in agreement also with results obtained through synthesis (22) of an enantiomeric form of asperlin.

A pyrone metabolite related to asperlin, i.e., **13** (R = H), contains a 1,2-epoxypropyl side chain at position-2 (23, 24). The terminal methyl group of this compound has a chemical shift of 17.6 ppm and that of its acetate (**13**, R = Ac) 17.5 ppm, showing that the oxirane moiety of this class of metabolite also possesses a *trans* configuration. Earlier (22), **13** had been designated a *trans* isomer on the basis of a coupling of 2.0 Hz between the two epoxide protons. Although this value is in the region of overlap for geometric isomers, the present ^{13}C data serve to substantiate the original conclusions.

It is seen, therefore, that the 1,2-epoxypropyl side chains of both metabolites (**1** and **13**), although located at different positions of the pyrone ring, have the same (*trans*) configuration. The present data also serve as a further illustration of the usefulness of ^{13}C nmr spectroscopy for the characterization of oxiranes.

Experimental

Evaporations were carried out under reduced pressure at or below 60°C. The adsorbent for column chromatography was silica gel, 0.02–0.05 mm particle size (Macherey Nagel and Co., Germany). Microanalyses were performed by Dr. C. Daessle (Montreal). Carbon-13 magnetic resonance spectra were obtained with a Bruker WH-90 spectrometer; proton spectra were obtained with a Varian HA-100 spectrometer, those at 220 MHz being furnished by Dr. A. A. Grey (220 MHz Centre, Toronto, Ont.).

1,2:3,4-Di-O-*isopropylidene*-α-D-galacto-*hexodialdo-1,5-pyranose* (*4*)

To a solution of 1,2:3,4-di-*O*-isopropylidene-α-D-galactopyranose (**3**) (prepared according to Singh *et al.* (25)) (12 g, 0.05 mol) in dichloromethane (100 ml) was added pyridinium chlorochromate reagent (21.5 g, 0.01 mol) prepared as described by Corey and Suggs (6). The reaction mixture was stirred at room temperature for 4–5 h, ether (500 ml) was added, and the solution was filtered through Silica Gel, then concentrated. After column chromatography with methylene chloride as eluant, aldehyde **4** (8 g, 75%) was obtained as a pale yellow syrup, which had spectroscopic properties indistinguishable from those described by Horton *et al.* (7).

6,7,8-Trideoxy-1,2:3,4-di-O-*isopropylidene*-α-D-galacto-*oct-6*-cis-*enopyranose* (*5*)

(*a*) *n*-Butyllithium (5 ml, 15% in hexane) was added to ether (150 ml) under N_2, followed by ethyltriphenylphosphonium bromide (3 g), and the orange solution was refluxed (0.5 h). Aldehyde **4** (1.9 g) in ether (10 ml) was then added dropwise; the reaction mixture became colourless and a white precipitate separated. After refluxing (0.5 h), the precipitate was filtered off and rinsed with ether (50 ml); the organic layer was washed with 5% H_2SO_4 (2 × 50 ml), and water, dried over sodium sulfate, and concentrated to an oil (**5**) (1.5 g, 75%) which had physical and ^1Hmr spectroscopic properties similar to those described by Lance and Szarek (9); ^{13}Cmr data for **5**: δ: 13.6 (C-8); 24.5, 25.0, 26.1 (×2) (CH_3-isopropylidene); 63.7 (C-5); 70.4, 71.1 (C-2, C-3); 73.4 (C-4); 96.7 (C-1); 108.3, 109.1 (C-isopropylidene); 126.5 (C-6); 128.4 (C-7).

(*b*) The same olefin (**5**) was obtained by heating under reflux for 3–4 h a methylene chloride (50 ml) solution of aldehyde **4** (6 g) and ethyltriphenylphosphonium bromide (11 g), to which potassium *tert*-butoxide (3 g) and crown ether (18-crown-6, 0.5 g) (12) were added. The solvent was evaporated off and the residue extracted with cyclohexane (5 × 100 ml), the extract was concentrated, and the syrup obtained was then chromatographed with CH_2Cl_2 as eluant to yield olefin **5** as a colourless oil (4.5 g), indistinguishable from the product obtained in *a*.

(*c*) Since the latter method has been known to yield different ratios of *cis* and *trans* isomers in different solvents, the reaction was repeated using tetrahydrofuran as solvent (12) but only the *cis* olefin (**5**) was detected.

8-Deoxy-6,7-cis-*epoxy-1,2:3,4-di*-O-*isopropylidene*-α-D-galacto-*octopyranoses* (*6*, *7*)

A solution of the *cis* olefin (**5**) (0.43 g, 1.58 mmol) and *m*-chloroperbenzoic acid (0.30 g, 1.75 mmol) in methylene chloride (15 ml) was stirred at room temperature for 24 h. On work-up, as described by Lewis (26), a colourless syrup (0.43 g) was obtained, which proved to be a 3:1 mixture of diastereomers **6** and **7** (^{13}Cmr evidence). It crystallized and was recrystallized from ethanol–water, mp 76–77°C; $[\alpha]_D^{25}$ −79°C (c 1.58, $CHCl_3$); ^1Hmr data for **6**,**7**: δ: 1.32, 1.46 (12H, s, isopropylidene), 1.5 (3H, H-8, 8′, 8″); 3.0–3.3 (2H, m, H-6, H-7); 3.50 (1H, q); 4.2–4.7 (3H, m); 5.48 (1-H, d, H-1, J = 5 Hz); ^{13}Cmr data, major component: δ: 13.3 (C-8); 24.4, 24.8, 26.0 (×2), (CH_3-isopropylidene); 52.6 (C-7); 53.7

(C-6); 65.6 (C-5); 70.6, 70.7, 71.6 (C-2,3,4); 96.4 (C-1); 108.4, 109.4 (*C*-isopropylidene); minor component: δ: 14.2 (C-8); 24.4, 24.8, 26.0 (×2), (CH_3-isopropylidene); 51.2 (C-7); 55.5 (C-6); 67.9 (C-7); 70.3, 70.8, (C-2,3,4); 96.9 (C-1); 108.7, 109.9 (*C*-isopropylidene). *Anal.* calcd. for $C_{14}H_{22}O_6$: C 58.72, H 7.75; found: C 58.5, H 7.5.

6,7,8-Trideoxy-1,2:3,4-di-O-*isopropylidene*-α-D-galacto-*oct-6*-trans-*enopyranose* (***8***)

A cyclohexane solution (300 ml) of the *cis* olefin (**5**) (4.5 g) was irradiated in a water-cooled quartz cell with unfiltered uv light (450 W Hanovia Type of mercury-arc lamp, Model 679A) under a stream of N_2 for five periods of 2 h. After each treatment polymeric material in suspension was filtered off. The final solution was concentrated to a yellow syrup which was chromatographed (eluant, CH_2Cl_2) to yield a colourless syrup (4.0 g) consisting of a mixture (3:1, from ^{1}Hmr spectra) of the *trans* (**8**) and *cis* (**5**) olefins; ^{1}Hmr data for **8**: δ: 1.40 (6H, s, CH_3-isopropylidene); 1.54 (3H, s, CH_3 isopropylidene); 1.54 (3H, s, CH_3-isopropylidene); 1.80 (3H, d, H-8, 8′, 8″. J = 5 Hz); 4.1–4.4, 4.6–4.8 (4H, overlapping m); 5.60 (1H, d, H-1, J = 5 Hz); 5.68–5.90 (2H, m, H-6, H-7); ^{13}Cmr data: δ: 17.8, (C-8); 24.3, 24.8, 25.9, 26.8 (CH_3-isopropylidene); 69.0 (C-5); 70.4, 70.9, 73.2 (C-2,3,4); 96.5 (C-1); 108.2, 109.0 (C-isopropylidene); 126.8, (C-6); 129.7 (C-7).

8-Deoxy-6,7-trans-*epoxy-1,2:3,4-di*-O-*isopropylidene*-α-D-galacto-*octopyranoses* (***9***, ***10***)

A sample of syrupy oxiranes **9** and **10** was obtained by subjecting olefin **8** (0.15 g) to the conditions described above for olefin **5**; ^{1}Hmr data for **9**,**10**: δ: 1.45, 1.49, 1.61 (12H, s, CH_3-isopropylidene): ~1.5 (3H, H-8, 8′, 8″); 5.0–5.5 (2H, m, H-6, H-7); 5.5–5.65 (1H; m); 4.3–4.8 (3H, m); 5.65 (1H, br d, H-1); ^{13}Cmr data, major component: δ: 17.3 (C-8); 24.4, 24.9, 26.0 (CH_3-isopropylidene); 54.7 (C-7); 56.8 (C-6); 68.8 (C-5); 70.6, 70.7, 71.4 (C-2,3,4); 96.2 (C-1); 108.7, 109.6 (*C*-isopropylidene); minor component (some peaks were poorly resolved and/or lost in the noise): δ: 17.3 (C-8); 51.2 (C-6); 55.5 (C-7); 69.7 (C-5); 70.8, 71.0, 71.6 (C-2,3,4); 96.4 (C-1).

Acknowledgments

The authors express their gratitude to the National Research Council of Canada for generous support. They also acknowledge with thanks the kind assistance of Dr. N. Cyr and Dr. P. G. Farrell, and the gift of a sample of 'asperlin' from the Upjohn Co.

1. T. K. Devon and A. J. Scott. Handbook of naturally occurring compounds. Vol. 1. Academic Press, New York, NY. 1975.
2. A. D. Argoudelis, J. H. Coats, and R. R. Herr. Antimicrob. Agents Chemother. 801 (1965).
3. S. P. Owen and B. K. Bhuynan. Antimicrob. Agents Chemother. 804 (1965).
4. A. D. Argoudelis and J. F. Zierserl. Tetrahedron Lett. 1969 (1966).
5. D. R. Paulson, T. Y. N. Tang, G. F. Moran, A. S. Murray, B. P. Pelka, and E. M. Vasquez. J. Org. Chem. **40**, 184 (1975).
6. E. J. Corey and J. N. Suggs. Tetrahedron Lett. 2647 (1975).
7. D. Horton, M. Nadakate, and J. M. J. Tronchet. Carbohydr. Res. **7**, 56 (1968).
8. G. M. Cree, D. M. Mackie, and A. S. Perlin. Can. J. Chem. **47**, 511 (1969).
9. D. G. Lance and W. A. Szarek. Carbohydr. Res. **10**, 306 (1969).
10. D. G. Lance, W. A. Szarek, J. K. N. Jones, and G. B. Howarth. Can. J. Chem. **47**, 2871 (1969).
11. M. Schlosser and K. F. Christmann. Angew. Chem. Int. Ed. Eng. **5**, 126 (1966).
12. R. M. Boden. Synthesis, 784 (1975).
13. W. Theilheimer. Synth. Methods Org. Chem. **20**, 441 (1966).
14. N. Wilson and J. B. Stothers. Topics Stereochem. **8**, 1 (1974).
15. A. S. Perlin. *In* Isotopes in organic chemistry. Vol. 3. *Edited by* E. Buncel and C. C. Lee. Elsevier, New York, NY. 1977. p. 171.
16. H. Spiesecke and W. G. Schneider. J. Chem. Phys. **35**, 722 (1961).
17. D. M. Grant and E. G. Paul. J. Am. Chem. Soc. **86**, 2984 (1964).
18. D. E. Dorman, M. Jautelat, and J. D. Roberts. J. Org. Chem. **36**, 2757 (1971); W. de Haan and L. J. M. van de Ven. Org. Magn. Reson. **5**, 147 (1973).
19. (*a*) M. Tanabe, T. Hamasaki, D. Thomas, and L. Johnson. J. Am. Chem. Soc. **93**, 273 (1971); (*b*) T. J. Simpson. Tetrahedron Lett. 175 (1975).
20. L. M. Jackman and S. Sternhell. Applications of nmr spectroscopy in organic chemistry. 2nd ed. Pergamon, Oxford. 1969.
21. K. L. Williamson, C. L. Langford, and C. R. Nicholson. J. Am. Chem. Soc. **86**, 762 (1964); G. C. Lyle and L. K. Keefer. J. Org. Chem. **31**, 3921 (1966).
22. S. Lesage and A. S. Perlin. Can. J. Chem. **56**, 2889 (1978).
23. S. D. Mills and W. B. Turner. J. Chem. Soc. C, 2242 (1967).
24. W. Rosenbrook, Jr. and R. E. Carney. Tetrahedron Lett. 1867 (1970).
25. P. P. Singh, M. M. Gharia, F. Dagupta, and H. C. Srivastava. Tetrahedron Lett. 439 (1977).
26. S. N. Lewis. *In* Oxidation: techniques and applications in organic synthesis. *Edited by* R. L. Augustine. Dekker, New York, NY. 1966. p. 226.

Can. J. Chem. Downloaded from www.nrcresearchpress.com by 210.87.254.40 on 09/05/12
For personal use only.

^{13}C nuclear magnetic resonance spectra of some C-19-hydroxy, C-5,6 epoxy, C-24 ethyl, and C-19-norsteroids

HERBERT L. HOLLAND, PETER R. P. DIAKOW, AND GREGG J. TAYLOR

Department of Chemistry, Brock University, St. Catharines, Ont., Canada L2S 3A1

Received April 17, 1978

HERBERT L. HOLLAND, PETER R. P. DIAKOW, and GREGG J. TAYLOR. Can. J. Chem. **56**, 3121 (1978).

The carbon magnetic resonance spectra of a series of C-19 hydroxy, C-5β,6β epoxy, C-5α,6α epoxy, and C-24 ethyl steroids have been assigned. Shift parameters for the C-19 hydroxyl function are listed. The data presented has led to a reassignment of the published spectra of several C5α,6α epoxy steroids. In addition, ^{13}Cmr spectral data for several bicyclic enones and a $\Delta^{5(10)}$-3-estrone are presented.

HERBERT L. HOLLAND, PETER R. P. DIAKOW et GREGG J. TAYLOR. Can. J. Chem. **56**, 3121 (1978).

On a fait l'attribution des signaux des spectres de résonnance magnétique nucléaire de ^{13}C pour une série de stéroides portant un hydroxyle en C-19, un époxyde en C-(5,6)β, un époxyde en C-(5,6)α ou un éthyle en C-24. On donne une liste de paramètres de déplacement pour la fonction hydroxyle en C-19. A la lumière des présents résultats, on a repris les attributions dans le cas de spectres déjà publiés pour plusieurs époxystéroides-C(5,6)α. On présente en outre des résultats de spectres rmn du ^{13}C pour certaines énones bicycliques et pour la $\Delta^{5(10)}$-estrone-3.

[Traduit par le journal]

Can. J. Chem. Downloaded from www.nrcresearchpress.com by 210.87.254.42 on 09/05/12
For personal use only.

In spite of continuing interest in the carbon magnetic resonance of steroids, culminating in the recent publication of the first truly comprehensive review of the subject (1), several important groups of steroids remain to be examined by this technique. In this study, we have used standard methods of ^{13}C magnetic resonance spectroscopy to assign the carbon resonances of a series of C-19 hydroxy ,C-5,6 epoxy, and C-24 ethyl steroids, as well as those of $\Delta^{5,10}$-3-estrone and several bicyclic model compounds.

Our study began with the bicyclic enone **1***a* (Table 1). Resonances at C-1, -2, and -8a were readily assignable by comparison with the ^{13}C spectra of Δ^4-3-keto steroids (1); the remaining resonances were assigned as follows. Comparison of the ^{13}Cmr spectra of 19-nor-Δ^4-3-keto steroids and corresponding steroids carrying the C-10 methyl substituent (1) enabled us to calculate a substituent effect for the removal of the C-19 methyl on the resonances of carbons 1–10 of the steroid system. Average values from a series of such comparisons are listed under 'Δppm' in Table 1. Application of these parameters to the spectrum of **1***b* (2) now allowed unambiguous assignment of the resonances of carbons 4, 6, and 7 of **1***a*.

The remaining resonances were assigned following the synthesis of the deuterium labelled compounds **1***d* and **1***e*. Base-catalysed deuterium exchange of Δ^4-3-keto steroids is known to occur principally at the C-2 position (3). Application of a similar procedure to **1***a* led to the isolation of a labelled enone

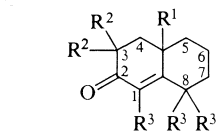

1

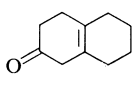

2

a $R^1 = R^2 = R^3 = H$
b $R^1 = CH_3$, $R^2 = R^3 = H$
c $R^1 = CH_2OH$, $R^2 = R^3 = H$
d $R^1 = R^3 = H$, $R^2 = D$
e $R^1 = R^2 = R^3 = D$

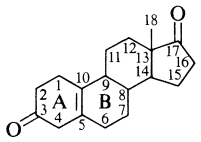

3

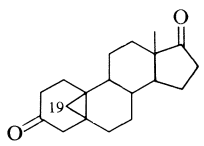

4

1*d* in which the resonance at 36.6 ppm was apparently absent. Mass spectral analysis indicated that the principal component was a dideuterated species, although substantial amounts of d_4, d_3, and d_1 species were also present. In confirmation of this, a reduction in the intensity of peaks at 35.5 and 37.9 ppm in **1***d* of ca. 30% with respect to the corresponding peaks in the spectrum of **1***a* was observed.

The above data confirm the assignment of C-3 at 36.6 ppm and suggest that the other enolic carbons, C-4a and -8, resonate at 37.9 and 35.5 ppm. The latter was confirmed following the synthesis of **1***e* in which exchange has occurred at all the enolic carbons (3). The spectrum of **1***e* shows only four signals in

TABLE 1. ^{13}C chemical shifts of estr-5(10)-ene-3,17-dione (**3**) and related compounds

	δ (ppm)					
Carbon[a]	**1***a*	**2**	**3**	**4**	**1***b* (2)	Δppm (1)
1 (4)	29.3	30.0*	24.9	31.8*	38.1	−8.8
2 (3)	36.6	39.0	39.0	36.2	34.0	+2.7
3 (2)	199.2	210.0	210.5	212.1	199.1	+0.3
4 (1)	124.3	44.5	44.6	46.9	123.9	+0.6
5 (8a)	166.9	124.5**	126.8	18.8	170.2	−4.6
6 (8)	35 5	30.9*	32.0	26.6**	32.8	+3.5
7 (7)	27.1	22.6	27.5	26.2**	27.2	−0.2
8 (6)	25.6	23.1	38.8	35.5	21.8	+4.2
9 (5)	34.6	30.0*	46.3	48.3	41.6	−4.6
10 (4a)	37.9	124.3**	130.8	25.3	36.0	+4.1
11			25.9	24.7		
12			30.7	31.7*		
13			48.3	46.9		
14			50.3	50.3		
15			21.5	21.7		
16			35.8	35.8		
17			220.1	220.7		
18			14.0	14.1		
19				18.1	22.1	

[a]To aid comparison, the numbering of the bicyclic enones is also included in parentheses. Chemical shifts marked with asterisks may be interchanged.

the aliphatic region of the spectrum, those of C-4, -5, -6, and -7.

With the assignments of C-4a at 37.9 ppm (calcd. 40.1 ppm) and C-8 at 35.5 ppm (calcd. 36.3 ppm) now secure, assignment of the remaining resonance at 34.6 ppm to C-5 is unambiguous.

The β,γ-unsaturated ketone **2** was next examined as a model for rings A and B of estr-5(10)-ene-3,17-dione (**3**) but only the resonances at C-1, -2, and -3 were uniquely assignable (Table 1): the chemical shift of C-2 is analogous to those of similar β,γ-unsaturated carbonyl carbons (4). The corresponding steroid **3** is significant in that it contains the $\Delta^{5(10)}$-3-keto functionality present in commercial birth control hormones (5). The resonances of carbons 11–18 of **3** (Table 1) were readily assigned by comparison with the published spectra of estr-4-ene-3,17-dione (1, 6) and those of C-2, -3, -4, -5, -8, -9, and -10 by analysis of the off-resonance spectrum and comparison with the spectrum of **2**. Assignment of C-10 to the lower field olefinic resonance at 130.8 ppm follows from the presence of a β substituent (C-11) not present in **2**. The resonances of C-6 and -7 were assigned by the aid of parameters derived from a comparison of the spectrum of **1***a* with that of the corresponding steroid estr-4-ene-3,17-dione (1, 6) (C-6, +0.1; C-7, +4.9) and the remaining resonance of **3** at 24.9 assigned to C-1.

An interesting comparison with **3** is provided by the C-5β,19-cyclopropyl steroid **4**. Resonances of carbons 2–4, 7, 9, and 11–18 of **4** were assigned by comparison with other 3,17-diketosteroids (1), whereas those of C-5, -10, and -19 follow from their presence in a cyclopropyl ring. Of the two remaining methylene resonances (26.6 and 31.8 ppm), the former has been tentatively assigned to C-6 and the latter to C-1. Although close comparison of **4** with other 5β steroids may not be fully justified, since the geometry of the AB ring junction is different (*vide infra*), it is nevertheless interesting to note that both C-4 and -6 resonate at lower field than the corresponding carbons of other 5β-androstan-3-ones (1), an effect which may be due to the presence of the extra β-C substituent at C-5. That the resonance of C-1 at 31.8 ppm, is upfield from the corresponding value of C-1 in 5β-androstan-3-ones (1) may be attributed to the removal of the C-5β hydrogen (7). The resonance of C-9 of **4** at 48.3 ppm is well downfield from that characteristic of 5β steroids (1, 8–10), owing to a distortion of **4** from normal 5β steroid geometry by the cyclopropyl system. Such a distortion would be expected to reduce the steric interactions between the C-9 hydrogen and the C-2α and -4α hydrogens which are responsible for the shift of C-9 to higher field in 5β steroids (9).

Before commencing an analysis of the ^{13}Cmr spectra of the C-19 alcohols **5***b–d*, and **6***b* and **6***c*, we recorded the spectra of the corresponding C-19 unsubstituted steroids **5***a*, **6***a*, and **6***d* in the solvent ($CDCl_3$) used for the subsequent study (Table 2). Assignments were straightforward and were made by comparison with literature values for related steroids and solvents (1).

Examination of the C-19 alcohols began with the

Can. J. Chem. Downloaded from www.nrcresearchpress.com by 210.87.254.42 on 09/05/12
For personal use only.

TABLE 2. ^{13}C chemical shifts of C-19-hydroxysteroids and related compounds

	δ (ppm)								
Carbon[a]	**5***a*	**6***a*	**1***c*	**5***b*	**5***c*[b]	**5***d*	**6***b*	**6***c*	**6***d*
1 (4)	35.8	37.2	33.0*	33.6	33.4*	33.6	33.5	33.4	37.1
2 (3)	34.0	31.5	34.3	35.0	35.1	35.0	31.9*	28.2	27.8
3 (2)	199.3	71.4	200.8	199.6	200.4	200.1	71.3	73.5	74.0
4 (1)	124.1	42.2	126.6	127.3	126.1	127.1	42.3	38.3	38.2
5 (8a)	170.8	141.3	168.3	165.6	168.5	166.9	136.0	134.8	139.7
6 (8)	32.7	120.8	33.4*	33.6	33.5*	33.6	126.5	128.2	122.7
7 (7)	31.6	31.5	27.1	31.9	31.9	31.8	31.8*	31.3	31.9
8 (6)	35.5	31.5	21.8	36.1	36.2	36.2	33.0	33.1	31.9
9 (5)	53.8	50.3	35.7	54.3	54.2	54.0	50.6	50.4	50.1
10 (4a)	38.7	36.7	41.6	43.9	44.0	44.0	41.7	41.6	36.6
11	20.6	20.4		21.0	21.2	21.2	21.0	21.8	21.0
12	36.8	30.8		31.0	36.9	37.2	30.2	40.0	39.8
13	42.9	47.5		47.7	42.9	43.1	47.8	42.6	42.4
14	50.4	51.8		51.5	50.9	50.9	52.5	57.6	56.7
15	23.6	21.8		21.8	23.2	23.6	21.8	24.1	24.3
16	27.8	35.8		35.8	30.2	27.7	35.8	28.2	28.2
17	83.0	221.3		220.0	80.9	83.0	221.1	56.2	56.2
18	12.3	13.5		13.9	11.3	12.4	13.9	12.2	11.9
19 (9)	17.5	19.4	63.4	66.1	65.1	66.0	62.9	62.8	19.3
20								35.8	35.8
21								18.7	18.7
22								36.2	36.2
23								23.8	23.9
24								39.6	39.6
25								28.0	28.0
26								22.6	22.6
27								22.8	22.8
Other	128.4					128.5		21.4	21.4
	129.6					129.6		170.5	170.5
	130.8					130.8			
	132.9					132.9			
	166.5					166.6			

[a]The numbering of the bicyclic enones is in parentheses. Chemical shifts marked with asterisks may be interchanged.
[b]Solvent $CDCl_3$–DMSO-d_6.

model compound **1***c*, the assignments for which followed directly from a consideration of the α, β, and γ oxygen substituent effects of primary alcohols (11) and the spectrum of **1***b* (Table 1), and are shown in Table 2. The spectra of 19-hydroxyandrost-4-ene-3,17-dione (**5***b*) and the related Δ^4-3-ketones **5***c* and **5***d* are also assigned in Table 2: carbons 3–5, 7, 8, and 11–18 were assigned by comparison with C-19 unsubstituted steroids (**5***a* and refs. 1 and 6). Carbons 9, 10, and 19 were assigned from off-resonance data and 1, 2, and 6 on the basis of parameters derived by a comparison of the spectra of the model compounds **1***b* and **1***c*. With the assignments for **5***b–d* secure, the spectra of the Δ^5-3β,19-diols **6***b* and **6***c* could be assigned by comparison with the data for **6***a* and **6***d*.

The shift parameters for carbons 1–11 and 19 observed for the introduction of an hydroxyl function at C-19 of the steroids are presented in Table 3. In the series **5***b–d*, C-4 is deshielded and C-5 shielded whereas for **6***b* and **6***c*, C-6 is deshielded, C-5 shielded, and C-4 unaffected. These shifts may be ascribed to a polarization of the π electrons by the oxygen atom at C-19; this effect also caused a slight downfield shift at C-3 in **5***b–d*.

As a basis for the examination of the ^{13}Cmr spectra of C-5α,6α and C-5β,6β epoxy steroids **8** and **9**, respectively, we have used the corresponding Δ^5 olefins. The assignments for the latter are presented here (**6***a*, Table 2, **7***a–c*, Table 4) for those examples not available in the literature (1). The assignments for **6***a* have been discussed (*vide supra*) and those for **7***c* follow directly from related steroids (1). The spectrum of testosterone ethylene ketal (**7***a*) was readily interpreted by comparison with the spectra of testosterone (1, 6) and **6***a* (Table 2); only carbons 1 and 12 have not been uniquely assigned. Similarly, the resonances of **7***b* were assigned by comparison with the spectrum of **6***a*.

The spectra of the β-epoxides **9***a* and **9***b* were assigned by comparison with the corresponding olefins **6***a* and **7***a*, respectively. Carbon 8 of **9***a* and **9***b* was unambiguously assignable in the off-resonance

Can. J. Chem. Downloaded from www.nrcresearchpress.com by 210.87.254.42 on 09/05/12
For personal use only.

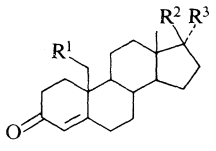

5

a $R^1 = R^3 = H, R^2 = OBz$
b $R^1 = OH, R^2 + R^3 = O$
c $R^1 = R^2 = OH, R^3 = H$
d $R^1 = OH, R^2 = OBz, R^3 = H$

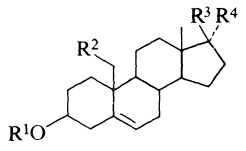

6

a $R^1 = R^2 = H, R^3 + R^4 = O$
b $R^1 = H, R^2 = OH, R^3 + R^4 = O$
c $R^1 = Ac, R^2 = OH, R^3 = C_8H_{17}$,* $R^4 = H$
d $R^1 = Ac, R^2 = R^4 = H, R^3 = C_8H_{17}$
*C_8H_{17} refers to the cholesterol side chain

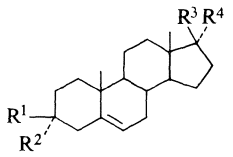

7

a $R^1 + R^2 = OCH_2CH_2O, R^3 = OH, R^4 = H$
b $R^1 = OH, R^2 = H, R^3 + R^4 = OCH_2CH_2O$
c $R^1 = OAc, R^2 = R^4 = H, R^3 = COCH_3$

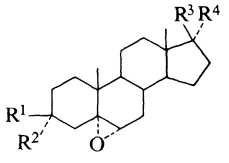

8

a $R^1 + R^2 = OCH_2CH_2O, R^3 = OH, R^4 = H$
b $R^1 = OH, R^2 = H, R^3 + R^4 = OCH_2CH_2O$
c $R^1 = OAc, R^2 = R^4 = H, R^3 = COCH_3$
d $R^1 = OH, R^2 = H, R^3 + R^4 = O$
e $R^1 = OAc, R^2 = H, R^3 + R^4 = O$
f $R^1 = R^3 = OAc, R^2 = R^4 = H$

spectra, whereas the assignment of C-6 of **9***a* was confirmed following specific decoupling from the C-6α hydrogen at δ 3.2. The chemical shift differences (with the exception of those for C-5 and C-6) between the Δ^5 olefin and the corresponding β epoxide are small, being greatest at the γ carbons 3, 8, and 19 (ca. −2 ppm, see Table 4). In particular, the lack of an appreciably shift difference between carbons 1–4 and 9 in **9***a* and **9***b* vs. **6***a* and **7***b*, may be indicative of little change of relative geometry of the A/B ring junction in the two systems. The values observed in the epoxides are much different from those of the corresponding A and B ring carbons of normal 5β steroids (1), especially at C-9 (8–10). The lack of an appreciable upfield γ shift at C-1, such as that observed in the C-5α,6α epoxides (*vide infra*) may be attributed to a fixed C-1—C-5 oxygen dihedral angle of close to 180°.

Carbons 8–19 of the C-5α,6α epoxy steroids **8***a–f* (and C-20 and -21 of **8***c*) were assigned by analysis of the off-resonance spectra and comparison with the spectra of the corresponding olefins (1) (Tables 4 and 5). Of the remaining carbons, carbons 3–6 were readily assignable. Carbons 1, 2, and 7 were then assigned as follows. Carbon 7 should not vary appreciably across the series **8***a–f*, whereas carbons 1 and 2 of **8***b–f* should show shifts consistent with the substitution (OH or OAc) at C-3β (1). In addition the resonance of C-2 would be expected to correspond closely with that of the corresponding olefin

TABLE 3. Shift parameters for the C-19-hydroxyl substituent

	δ (ppm)					
Carbon	**5***b*	**5***c*	**5***d*	**6***b*	**6***c*	**1***c*
1	−1.9	−2.2	−2.2	−3.7	−3.7	−5.1
2	+0.6	+1.2	+1.0	+0.4	+0.4	+0.4
3	+0.7	+1.0	+0.8	−0.1	−0.5	+1.7
4	+3.4	+2.5	+3.0	+0.1	+0.1	+2.1
5	−4.5	−2.5	−3.9	−5.3	−4.9	−1.9
6	+1.3	+1.8	+0.9	+5.7	+5.5	+0.6
7	+0.8	+0.4	+0.2	+0.3	−0.6	−0.1
8	+1.2	+1.2	+0.7	+1.5	+1.1	0.0
9	+0.7	+0.3	+0.2	+0.3	+0.3	−5.9
10	+5.5	+5.4	+5.3	+5.0	+5.0	+5.6
11	+0.9	+0.6	+0.6	+0.6	+0.8	
19	+48.9	+47.8	+48.5	+43.0	+43.5	+44.0

Downloaded from www.nrcresearchpress.com by 210.87.254.42 on 09/05/12
For personal use only.

Can. J. Chem. Downloaded from www.nrcresearchpress.com by 210.87.254.42 on 09/05/12
For personal use only.

TABLE 4. ^{13}C chemical shifts of Δ^5-steroids **7***a–c* and C-5β,6β-epoxysteroids **9***a* and *b*[a]

	δ (ppm)				
Carbon	**7***a*	**7***b*	**7***c*	**9***a*	**9***b*
1	36.6*	37.3	37.1	37.2	36.7
2	31.1	31.3*	27.8	31.5	30.9
3	109.5	71.7	73.9	69.2	109.5
4	41.8	42.3	38.1	42.1	41.5
5	140.4	140.9	139.8	63.1	63.1
6	121.9	121.5	122.4	64.4	63.1
7	31.4	31.6*	31.8	31.5	31.9
8	32.0	32.2	31.5	29.5	29.8
9	49.9	50.0	50.0	51.2	50.2
10	36.6	36.6	36.6	35.2	35.2
11	20.7	20.5	21.0	21.3	21.5
12	36.4*	30.6	38.8	31.0	35.7
13	42.8	45.8	44.0	47.5	42.8
14	51.4	50.7	56.9	51.6	50.9
15	23.5	22.8	24.5	21.8	23.4
16	30.6	34.2	22.9	35.8	30.5
17	81.9	119.6	63.7	221.0	81.8
18	11.0	14.2	13.2	13.5	10.9
19	18.9	19.4	19.3	17.1	17.2
20			209.4		
21			31.8		
Other	64.2	64.6	21.4		64.1
	64.4	65.2	170.5		64.3

[a]Chemical shifts marked with asterisks may be interchanged.

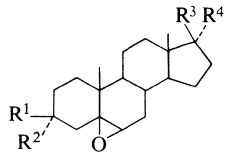

9

a $R^1 = OH, R^2 = H, R^3 + R^4 = O$
b $R^1 + R^2 = OCH_2CH_2O, R^3 = OH, R^4 = H$

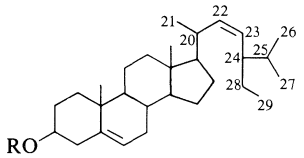

10

a R = H
b R = Ac

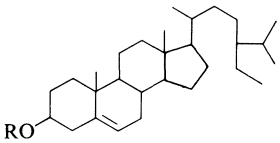

11

a R = H
b R = Ac

and other C-5α steroids (1). The assignments which follow from this approach are given in Table 5. They differ in the assignments of C-2 and -7 from the published data on related C-5α,6α epoxy steroids (12); the latter were however derived from a consideration of the small effect of a C-11α-hydroxyl group on the shift of C-1 and C-2, and without the more definitive data arising from acetylation at C-3 available to us.

TABLE 5. ^{13}C chemical shifts of C-5α,6α-epoxysteroids **8***a–f*[a]

	δ (ppm)					
Carbon	**8***a*	**8***b*	**8***c*	**8***d*	**8***e*	**8***f*
1	31.4	32.5	32.3	32.6	32.2	32.2
2	31.1	31.0	27.2	31.0	27.2	27.2*
3	109.0	68.5	71.3	68.4	71.2	71.3
4	39.2	39.9	36.1	39.8	36.1	36.2**
5	64.1	65.7	65.2	65.9	65.2	65.2
6	57.3	59.1	59.0	58.9	58.7	58.9
7	28.2	28.2	28.7	27.8	27.8	28.4
8	30.0	30.2	29.9	29.6	29.6	29.6
9	42.5	42.5	42.5	42.9	42.8	42.5
10	35.2	35.0	35.1	35.1	35.2	35.1
11	20.4	20.1	21.4	20.1	20.0	20.1
12	36.4	30.2	38.6	31.2	31.2	36.5**
13	43.0	45.8	44.0	47.7	47.6	42.5
14	51.7	50.8	57.1	51.9	51.9	51.2
15	23.3	22.6	24.3	21.8	21.7	23.4
16	30.4	34.1	22.8	35.8	35.7	27.4*
17	81.6	119.2	63.4	220.8	220.3	82.5
18	11.1	14.2	13.2	13.6	13.6	11.9
19	15.7	15.9	15.9	15.9	15.9	15.9
20			209.4			
21			31.5			
Other	64.4	64.4	20.7			21.1
	64.6	65.2	170.3			21.3
						170.2
						171.1

[a]Chemical shifts marked with asterisks may be interchanged.

Can. J. Chem. Downloaded from www.nrcresearchpress.com by 210.87.254.42 on 09/05/12
For personal use only.

A striking feature of the spectra of **8***a–f* relative to the corresponding olefins is the upfield γ shifts of C-1 and C-9 absent for the corresponding β epoxides: models reveal fixed C-1–C-5 oxygen and C-1–C-9 oxygen dihedral angles of $<90°$. Similar downfield shifts at C-1 and -9 occur in C-5α hydroxy steroids (1).

The last group of steroids to be examined in the present study comprises the 24-ethyl steroids stigmasterol (**10***a*), β-sitosterol (**11***a*), and the corresponding acetates **10***b* and **11***b* (Table 6). Carbons 1–19 of this series correspond closely with the same carbon resonances of cholesterol (1) and cholesteryl acetate (**6***d*, Table 2). Carbons 20–22 of **10***a* and **10***b* were assigned by comparison with ergosterol (1), while the chemical shifts of carbons 23–28 were calculated from a consideration of the effect of addition of a methyl group (C-29) to C-28 of ergosterol (calcd. C-23, 129.3; C-24, 51.2; C-25, 31.5; C-26, 19.7; C-27, 20.0; C-28, 26.7 ppm). Carbons 20 and 21 of **11***a* and **11***b* exhibit chemical shifts very similar to those of the corresponding carbons of cholesterol (1) and cholesteryl acetate (**6***d*): the chemical shifts of carbons 22–27 were calculated by considering the effect of ethyl substitution (C-28 + C-29) at C-24 of cholesterol (calcd. C-22, 33.7; C-23, 28.3; C-24, 48.5; C-25, 25.4; C-26, 19.0; C-27, 19.2). The remaining resonances are then assignable to C-28 and -29. With the exception of C-18 and -29 of **10***a* and **10***b*, all the assignments of this series are unambiguous.

TABLE 6. ^{13}C chemical shifts of stigmasterol (**10***a*) stigmasteryl acetate (**10***b*), β-sitosterol (**11***a*), and β-sitosteryl acetate (**11***b*)[a]

	δ (ppm)			
Carbon	**10***a*	**10***b*	**11***a*	**11***b*
1	37.4	37.1	37.3	37.1
2	31.7	27.9	31.8	27.8
3	71.8	74.1	71.9	74.1
4	42.4	38.3	42.4	38.2
5	140.9	139.8	140.9	139.8
6	121.7	122.8	121.8	122.7
7	31.9	32.0	32.0	32.0
8	31.9	32.0	32.0	32.0
9	50.3	50.3	50.3	50.2
10	36.6	36.7	36.6	36.6
11	21.1	21.1	21.1	21.0
12	39.8	39.8	39.9	39.8
13	42.4	42.3	42.4	42.3
14	57.0	56.9	56.8	56.7
15	24.4	24.5	24.3	24.3
16	28.9	28.9	28.2	28.3
17	56.0	56.1	56.2	56.1
18	12.2*	12.2*	11.9	11.9
19	19.4	19.3	19.4	19.3
20	40.5	40.6	36.2	36.2
21	21.1	21.1	19.1	19.1
22	138.4	138.5	34.0	34.0
23	129.4	129.5	29.3	29.3
24	51.3	51.4	50.3	50.0
25	31.9	32.0	26.2	26.2
26	19.0	19.0	18.8	18.8
27	21.1	21.1	19.8	19.8
28	25.4	25.5	23.1	23.1
29	12.0*	12.1*	11.9	11.9
Other		21.3		21.4
		170.5		170.5

[a]Chemical shifts marked with asterisks may be interchanged.

Experimental

Apparatus, Methods, and Materials

Natural abundance ^{13}C nuclear magnetic resonance spectra were recorded on a Bruker WP-60 Fourier transform spectrometer at 15.08 MHz. Samples were 0.15–0.3 *M* in $CDCl_3$; TMS was used as internal reference. 8K FID's were collected, yielding transformed spectra of 4096 data points giving an accuracy of 0.92 Hz per point. The following compounds were prepared in this laboratory by established procedures and gave satisfactory spectral and analytical data: 4,4a,5,6,7,8-hexahydro-2(3*H*)-naphthalenone (**1***a*) (13), 4a-hydroxymethyl-4,4a,5,6,7,8-hexahydro-2(3*H*)-naphthalenone (**1***c*) (13, 14), 3,4,5,6,7,8-hexahydro-2(1*H*)-naphthalenone (**2**) (15), 3,3-ethylenedioxy-17β-hydroxyandrost-5-ene (**7***a*) (16), 17,17-ethylenedioxy-3β-hydroxyandrost-5-ene (**7***b*) (17), (5,6)α-epoxy-3,3-ethylenedioxy-17β-hydroxy-5α-androstane (**8***a*) (16), (5,6)α-epoxy-17,17-ethylenedioxy-3β-hydroxy-5α-androstane (**8***b*) (18), 3β-acetyloxy-(5,6)α-epoxy-5α-pregnan-20-one (**8***c*) (19), (5,6)α-epoxy-3β-hydroxy-5α-androstan-17-one (**8***d*) (20), 3β-acetyloxy-(5,6)α-epoxy-5α-androstan-17-one (**8***e*) (21), 3β,17β-diacetyloxy-(5,6)α-epoxy-5α-androstane (**8***f*) (22), (5,6)β-epoxy-3β-hydroxyandrostan-17-one (**9***a*) (20), (5,6)β-epoxy-3,3-ethylenedioxy-17β-hydroxy-5β-androstane (**9***b*) (16), 3β-hydroxystigmast-5-ene (β-sitosterol (**11***a*)) (23), and 3β-acetyloxystigmast-5-ene (**11***b*) (23).

(5β,19)-Cycloandrostan-3,17-dione (**4**) was kindly supplied by Dr. M. Gut of the Worcester Foundation for Experimental Biology. The other steroids used in this study were commercial samples.

*4,4a,5,6,7,8-Hexahydro-2(3*H*)-naphthalenone*-3,3-d_2 (*1*d)

Sodium (0.7 g) was dissolved in dioxan (50 ml) containing deuterium oxide (12 ml) and the enone **1***a* (2 g) added to this solution. The resulting mixture was stirred at room temperature for 72 h and then poured onto phosphate buffer (pH 7, 50 ml). The mixture was extracted with ether and the extract dried and evaporated. The residue was distilled at 70–75°C/0.7 Torr, to give **1***d* (0.6 g). Mass spectral analysis indicated the isotopic composition to be d_4, 17%; d_3, 26%; d_2, 35%; d_1, 15%; d_0, 5%.

*4,4a,5,6,7,8-Hexahydro-2(3*H*)-naphthalenone*-1,3,3,4a,8,8-d_6 (*1*e)

The enone **1***a* (2 g) was dissolved in dioxan (20 ml) containing deuterium oxide (10 ml). *p*-Toluenesulphonic acid (0.5 g) was then added and the mixture heated under reflux for 4 days. The product **1***e* (1.7 g) was isolated as described above; ms: isotopic composition d_6, 54%; d_5, 30%; d_4, 10%; d_3, 5%.

Acknowledgements

We thank the National Research Council for Financial Support and Dr. M. Gut for a sample of **4**. We are also grateful to T. Jones and E. Kelusky for

their aid in recording spectra and to Dr. K. N. Scott for helpful correspondence concerning the assignments of compound **3**.

1. J. W. BLUNT and J. B. STOTHERS. Org. Magn. Reson. **9**, 439 (1977).
2. G. I. BIRNBAUM, A. STOESSL, S. H. GROVER, and J. B. STOTHERS. Can. J. Chem. **52**, 993 (1974).
3. S.K. MALHOTRA and H. J. RINGOLD. J. Am. Chem. Soc. **86**, 1997 (1964).
4. GURUDATA and J. B. STOTHERS. Can. J. Chem. **47**, 3601 (1969).
5. R. WEICHERT. Angew. Chem. Int. Ed. Engl. **16**, 506 (1977).
6. H. J. REICH, M. JAUTELAT, M. T. MESSE, F. J. WEIGERT, and J. D. ROBERTS. J. Am. Chem. Soc. **91**, 7445 (1969).
7. H. BEIERBECK and J. K. SAUNDERS. Can. J. Chem. **54**, 2985 (1976).
8. B. BALOGH, D. M. WILSON, and A. L. BURLINGAME. Nature, **233**, 261 (1971).
9. D. LEIBFRITZ and J. D. ROBERTS. J. Am. Chem. Soc. **95**, 4996 (1973).
10. J. W. BLUNT, J. M. COXON, N. B. LINDLEY, and G. A. LANE. Aust. J. Chem. **29**, 967 (1976).
11. J. D. ROBERTS, F. J. WEIGERT, J. I. KROSCHWITZ, and H. J. REICH. J. Am. Chem. Soc. **92**, 1338 (1970).
12. S. LANG, D. N. LINCOLN, and V. WRAY. J. Chem. Soc. Perkin 2, 344 (1975).
13. D. I. SCHUSTER and D. F. BRIZZOLARA. J. Am. Chem. Soc. **92**, 4357 (1970).
14. G. STORK, P. ROSEN, N. GOLDMAN, R. V. COOMBS, and J. TSUJI. J. Am. Chem. Soc. **87**, 275 (1965).
15. J. H. FASSNACHT and N. A. NELSON. J. Org. Chem. **27**, 1885 (1962).
16. J. A. CAMPBELL, J. C. BABCOCK, and J. A. HOGG. J. Am. Chem. Soc. **80**, 4717 (1959).
17. L. F. FIESER. J. Am. Chem. Soc. **76**, 1945 (1954).
18. J. S. MIHINA. U.S. Patent No. 2,992,241 (July 11, 1961); Chem. Abstr. **55**, 26041a (1961).
19. A. BOWERS, and H. J. RINGOLD. Tetrahedron, **3**, 14 (1958).
20. H. L. HOLLAND and P. R. P. DIAKOW. Can. J. Chem. **56**, 694 (1978).
21. H. B. MACPHILLAMY and C. R. SHOLZ. J. Am. Chem. Soc. **74**, 5512 (1952).
22. M. ACKROYD, W. J. ADAMS, B. ELLIS, V. PETROW, and I. A. STUART-WEBB. J. Chem. Soc. 4099 (1957).
23. J. A. STEELE and E. MOSETTIG. J. Org. Chem. **28**, 571 (1963).

Can. J. Chem. Downloaded from www.nrcresearchpress.com by 210.87.254.42 on 09/05/12
For personal use only.